

# PTEP

## Progress of Theoretical and Experimental Physics

### Review of Particle Physics

P.A. Zyla *et al.* (Particle Data Group), *Prog. Theor. Exp. Phys.* 2020, 083C01 (2020)

**PDG**  
particle data group

Downloaded from <https://academic.oup.com/ptep/article/2020/8/083C01/5891211> by guest on 12 November 2020



*The Physical Society of Japan*

**OXFORD**  
UNIVERSITY PRESS

# REVIEW OF PARTICLE PHYSICS\*

Particle Data Group

## *Abstract*

The *Review* summarizes much of particle physics and cosmology. Using data from previous editions, plus 3,324 new measurements from 878 papers, we list, evaluate, and average measured properties of gauge bosons and the recently discovered Higgs boson, leptons, quarks, mesons, and baryons. We summarize searches for hypothetical particles such as supersymmetric particles, heavy bosons, axions, dark photons, etc. Particle properties and search limits are listed in Summary Tables. We give numerous tables, figures, formulae, and reviews of topics such as Higgs Boson Physics, Supersymmetry, Grand Unified Theories, Neutrino Mixing, Dark Energy, Dark Matter, Cosmology, Particle Detectors, Colliders, Probability and Statistics. Among the 120 reviews are many that are new or heavily revised, including a new review on High Energy Soft QCD and Diffraction and one on the Determination of CKM Angles from B Hadrons.

The *Review* is divided into two volumes. Volume 1 includes the Summary Tables and 98 review articles. Volume 2 consists of the Particle Listings and contains also 22 reviews that address specific aspects of the data presented in the Listings.

The complete *Review* (both volumes) is published online on the website of the Particle Data Group ([pdg.lbl.gov](http://pdg.lbl.gov)) and in a journal. Volume 1 is available in print as the *PDG Book. A Particle Physics Booklet* with the Summary Tables and essential tables, figures, and equations from selected review articles is available in print and as a web version optimized for use on phones as well as an Android app.

The 2020 edition of the *Review of Particle Physics* should be cited as:  
P.A. Zyla *et al.* (Particle Data Group), *Prog. Theor. Exp. Phys.* **2020**, 083C01 (2020)

DOI: 10.1093/ptep/ptaa104

For the online version see [pdg.lbl.gov](http://pdg.lbl.gov):



©2020 Regents of the University of California

\*The publication of the *Review of Particle Physics* is supported by the Director, Office of Science, Office of High Energy Physics of the U.S. Department of Energy under Contract No. DE-AC02-05CH11231; by the European Laboratory for Particle Physics (CERN); by an implementing arrangement between the governments of Japan (MEXT: Ministry of Education, Culture, Sports, Science and Technology) and the United States (DOE) on cooperative research and development; by the Italian National Institute of Nuclear Physics (INFN); and by the Physical Society of Japan (JPS). Individual collaborators receive support for their PDG activities from their respective funding agencies.



## Particle Data Group

P.A. Zyla,<sup>1</sup> R.M. Barnett,<sup>1</sup> J. Beringer,<sup>1</sup> O. Dahl,<sup>1</sup> D.A. Dwyer,<sup>1</sup> D.E. Groom,<sup>1</sup> C.-J. Lin,<sup>1</sup> K.S. Lugovsky,<sup>1,2</sup> E. Pianori,<sup>1</sup> D.J. Robinson,<sup>1</sup> C.G. Wohl,<sup>1</sup> W.-M. Yao,<sup>1</sup> K. Agashe,<sup>3</sup> G. Aielli,<sup>4</sup> B.C. Allanach,<sup>5</sup> C. Amsler,<sup>6</sup> M. Antonelli,<sup>7</sup> E.C. Aschenauer,<sup>8</sup> D.M. Asner,<sup>8</sup> H. Baer,<sup>9</sup> Sw. Banerjee,<sup>10</sup> L. Baudis,<sup>11</sup> C.W. Bauer,<sup>1</sup> J.J. Beatty,<sup>12</sup> V.I. Belousov,<sup>2</sup> S. Bethke,<sup>13</sup> A. Bettini\*,<sup>14</sup> O. Biebel,<sup>15</sup> K.M. Black,<sup>16</sup> E. Blucher,<sup>17</sup> O. Buchmüller,<sup>18</sup> V. Burkert,<sup>19</sup> M.A. Bychkov,<sup>20</sup> R.N. Cahn,<sup>1</sup> M. Carena,<sup>21,17,22</sup> A. Ceccucci,<sup>23</sup> A. Cerri,<sup>24</sup> D. Chakraborty,<sup>25</sup> R. Sekhar Chivukula,<sup>26</sup> G. Cowan,<sup>27</sup> G. D'Ambrosio,<sup>28</sup> T. Damour,<sup>29</sup> D. de Florian,<sup>30</sup> A. de Gouvêa,<sup>31</sup> T. DeGrand,<sup>32</sup> P. de Jong,<sup>33</sup> G. Dissertori,<sup>34</sup> B.A. Dobrescu,<sup>21</sup> M. D'Onofrio,<sup>35</sup> M. Doser,<sup>23</sup> M. Drees,<sup>36</sup> H.K. Dreiner,<sup>36</sup> P. Eerola,<sup>37</sup> U. Egede,<sup>38</sup> S. Eidelman,<sup>39,40</sup> J. Ellis,<sup>41,23</sup> J. Erler,<sup>42,43</sup> V.V. Ezhela,<sup>2</sup> W. Fetscher,<sup>34</sup> B.D. Fields,<sup>44,45</sup> B. Foster,<sup>46,47,48</sup> A. Freitas,<sup>49</sup> H. Gallagher,<sup>50</sup> L. Garren,<sup>21</sup> H.-J. Gerber†,<sup>34</sup> G. Gerbier,<sup>51</sup> T. Gershon,<sup>52</sup> Y. Gershtein,<sup>53</sup> T. Gherghetta,<sup>54</sup> A.A. Godizov,<sup>2</sup> M.C. Gonzalez-Garcia,<sup>55,56,57</sup> M. Goodman,<sup>58</sup> C. Grab,<sup>34</sup> A.V. Gritsan,<sup>59</sup> C. Grojean,<sup>60,61</sup> M. Grünewald,<sup>62</sup> A. Gurtu,<sup>63,23</sup> T. Gutsche,<sup>64</sup> H.E. Haber,<sup>65</sup> C. Hanhart,<sup>66</sup> S. Hashimoto,<sup>67</sup> Y. Hayato,<sup>68</sup> A. Hebecker,<sup>69</sup> S. Heinemeyer,<sup>70,71,72</sup> B. Heltsley,<sup>73</sup> J. J. Hernández-Rey‡,<sup>74</sup> K. Hikasa,<sup>75</sup> J. Hisano,<sup>76</sup> A. Höcker,<sup>23</sup> J. Holder,<sup>77,78</sup> A. Holtkamp,<sup>23</sup> J. Huston,<sup>79</sup> T. Hyodo,<sup>80</sup> K.F. Johnson,<sup>81</sup> M. Kado,<sup>82,83,84</sup> M. Karliner,<sup>85</sup> U.F. Katz,<sup>86</sup> M. Kenzie,<sup>52</sup> V.A. Khoze,<sup>87,88</sup> S.R. Klein,<sup>89,90</sup> E. Klempt,<sup>91</sup> R.V. Kowalewski,<sup>92</sup> F. Krauss,<sup>87</sup> M. Kreps,<sup>52</sup> B. Krusche,<sup>93</sup> Y. Kwon,<sup>94</sup> O. Lahav,<sup>95</sup> J. Laiho,<sup>96</sup> L.P. Lellouch,<sup>97</sup> J. Lesgourgues,<sup>98</sup> A. R. Liddle,<sup>99,100</sup> Z. Ligeti,<sup>1</sup> C. Lippmann,<sup>101</sup> T.M. Liss,<sup>102</sup> L. Littenberg,<sup>8</sup> C. Lourenço,<sup>23</sup> S.B. Lugovsky,<sup>2</sup> A. Lusiani,<sup>103,104</sup> Y. Makida,<sup>67</sup> F. Maltoni,<sup>105,106</sup> T. Mannel,<sup>107</sup> A.V. Manohar,<sup>26</sup> W.J. Marciano,<sup>8</sup> A. Masoni,<sup>108</sup> J. Matthews,<sup>109</sup> U.-G. Meißner,<sup>91,66</sup> M. Mikhasenko,<sup>23</sup> D.J. Miller,<sup>110</sup> D. Milstead,<sup>111</sup> R.E. Mitchell,<sup>112</sup> K. Mönig,<sup>113</sup> P. Molaro,<sup>114</sup> F. Moortgat,<sup>23,115</sup> M. Moskovic,<sup>23</sup> K. Nakamura,<sup>116,67</sup> M. Narain,<sup>117</sup> P. Nason,<sup>118,119</sup> S. Navas†,<sup>120</sup> M. Neubert,<sup>121</sup> P. Nevski§,<sup>8</sup> Y. Nir,<sup>122</sup> K.A. Olive,<sup>54</sup> C. Patrignani,<sup>123</sup> J.A. Peacock,<sup>124</sup> S.T. Petcov,<sup>125,116,126</sup> V.A. Petrov,<sup>2</sup> A. Pich,<sup>74</sup> A. Piepke,<sup>127</sup> A. Pomarol,<sup>128,129</sup> S. Profumo,<sup>65</sup> A. Quadt,<sup>130</sup> K. Rabbertz,<sup>131</sup> J. Rademacker,<sup>132</sup> G. Raffelt,<sup>133</sup> H. Ramani,<sup>1</sup> M. Ramsey-Musolf,<sup>134,135,136</sup> B.N. Ratcliff,<sup>137</sup> P. Richardson,<sup>87</sup> A. Ringwald,<sup>47</sup> S. Roesler,<sup>23</sup> S. Rolli,<sup>138</sup> A. Romaniouk,<sup>139</sup> L.J. Rosenberg,<sup>140</sup> J.L. Rosner,<sup>17</sup> G. Rybka,<sup>140</sup> M. Ryskin,<sup>88</sup> R.A. Ryutin,<sup>2</sup> Y. Sakai,<sup>67</sup> G.P. Salam,<sup>23,141,142</sup> S. Sarkar,<sup>142</sup> F. Sauli§,<sup>23</sup> O. Schneider,<sup>143</sup> K. Scholberg,<sup>144</sup> A.J. Schwartz,<sup>145</sup> J. Schwiening,<sup>101</sup> D. Scott,<sup>146</sup> V. Sharma,<sup>26</sup> S.R. Sharpe,<sup>140</sup> T. Shutt,<sup>137</sup> M. Silari,<sup>23</sup> T. Sjöstrand,<sup>147</sup> P. Skands,<sup>38</sup> T. Skwarnicki,<sup>96</sup> G.F. Smoot,<sup>148,149,90,1</sup> A. Soffer,<sup>85</sup> M.S. Sozzi,<sup>150</sup> S. Spanier,<sup>151</sup> C. Spiering,<sup>113</sup> A. Stahl,<sup>152</sup> S.L. Stone,<sup>96</sup> Y. Sumino,<sup>75</sup> T. Sumiyoshi,<sup>153</sup> M.J. Syphers,<sup>25,21</sup> F. Takahashi,<sup>75</sup> M. Tanabashi,<sup>154,76</sup> J. Tanaka,<sup>155</sup> M. Taševský,<sup>156</sup> K. Terashi,<sup>155</sup> J. Terning,<sup>157</sup> U. Thoma,<sup>91</sup> R.S. Thorne,<sup>95</sup> L. Tiator,<sup>158</sup> M. Titov,<sup>51</sup> N.P. Tkachenko,<sup>2</sup> D.R. Tovey,<sup>159</sup> K. Trabelsi,<sup>84</sup> P. Urquijo,<sup>160</sup> G. Valencia,<sup>38</sup> R. Van de Water,<sup>21</sup> N. Varelas,<sup>161</sup> G. Venanzoni,<sup>104</sup> L. Verde,<sup>57,56</sup> M.G. Vincter,<sup>162</sup> P. Vogel,<sup>163</sup> W. Vogelsang,<sup>64</sup> A. Vogt,<sup>164</sup> V. Vorobyev,<sup>39,40</sup> S.P. Wakely,<sup>17,22</sup> W. Walkowiak,<sup>107</sup> C.W. Walter,<sup>144</sup> D. Wands,<sup>165</sup> M.O. Wascko,<sup>18</sup> D.H. Weinberg,<sup>166</sup> E.J. Weinberg,<sup>167</sup> M. White,<sup>90,1</sup> L.R. Wiencke,<sup>168</sup> S. Willocq,<sup>136</sup> C.L. Woody,<sup>8</sup> R.L. Workman,<sup>169</sup> M. Yokoyama,<sup>170,116</sup> R. Yoshida,<sup>19</sup> G. Zanderighi,<sup>13</sup> G.P. Zeller,<sup>21</sup> O.V. Zenin,<sup>2,171</sup> R.-Y. Zhu,<sup>172</sup> S.-L. Zhu,<sup>173</sup> F. Zimmermann<sup>23</sup>

Technical Associates: J. Anderson,<sup>1</sup> T. Basaglia,<sup>23</sup> V.S. Lugovsky,<sup>2</sup> P. Schaffner,<sup>1</sup> W. Zheng,<sup>174</sup>

1. *Physics Division, Lawrence Berkeley National Laboratory, Berkeley, CA, USA*
2. *Institute for High Energy Physics, COMPAS Group, Protvino, Russia*
3. *University of Maryland, Department of Physics, College Park, MD, USA*
4. *Università degli Studi di Roma "Tor Vergata", Rome, Italy*
5. *Department of Applied Mathematics and Theoretical Physics, University of Cambridge, Cambridge, UK*
6. *Stefan Meyer Institute for Subatomic Physics, Austrian Academy of Sciences, Vienna, Austria*
7. *Lab. Nazionali di Frascati dell'INFN, Frascati, Italy*
8. *Brookhaven National Laboratory, Nuclear and Particle Physics Directorate, Upton, NY, USA*
9. *University of Oklahoma, Department of Physics and Astronomy, Norman, OK, USA*
10. *University of Louisville, Louisville, KY, USA*
11. *Universität Zürich, Physik-Institut, Zürich, Switzerland*
12. *Ohio State University, Department of Physics, Columbus, OH, USA*
13. *Max-Planck-Institute of Physics, Munich, Germany*
14. *INFN and Dipartimento di Fisica e Astronomia, Università di Padova, Padova, Italy*
15. *Ludwig-Maximilians-Universität, Fakultät für Physik, München, Germany*
16. *University of Wisconsin, Department of Physics, Madison, WI, USA*
17. *University of Chicago, Enrico Fermi Institute and Department of Physics, Chicago, IL, USA*

\* Coordination activities supported directly by INFN.

† Deceased.

‡ Support from Programa Estatal de Generación de Conocimiento MCIU, Spain and ERDF of the European Union (PGC2018-096663-B-C41 and C44).

§ Retired.

18. *Imperial College, High Energy Physics Group, Blackett Laboratory, London, UK*
19. *Jefferson Lab, Newport News, VA, USA*
20. *University of Virginia, Department of Physics, Charlottesville, VA, USA*
21. *Fermi National Accelerator Laboratory, Batavia, IL, USA*
22. *University of Chicago, Kavli Institute for Cosmological Physics, Chicago, IL, USA*
23. *CERN, European Organization for Nuclear Research, Genève, Switzerland*
24. *Department of Physics and Astronomy, University of Sussex, Brighton, UK*
25. *Department of Physics, Northern Illinois University, DeKalb, IL, USA*
26. *Department of Physics, University of California at San Diego, La Jolla, CA, USA*
27. *Department of Physics, Royal Holloway, University of London, London, UK*
28. *INFN Sezione di Napoli, Napoli, Italy*
29. *Institut des Hautes Etudes Scientifiques, Bures-sur-Yvette, France*
30. *UNSAM - Universidad Nacional de San Martín, International Center for Advanced Studies (ICAS) and Instituto de Ciencias Físicas (ICIFI), Buenos Aires, Argentina*
31. *Northwestern University, Department of Physics and Astronomy, Evanston, IL, USA*
32. *University of Colorado at Boulder, Department of Physics, Boulder, CO, USA*
33. *Nikhef and University of Amsterdam, Amsterdam, The Netherlands*
34. *ETH Zurich, Institute for Particle Physics and Astrophysics, Zurich, Switzerland*
35. *University of Liverpool, Department of Physics, Liverpool, UK*
36. *Universität Bonn, Physikalisches Institut, Bonn, Germany*
37. *University of Helsinki, Department of Physics, Helsinki, Finland*
38. *Monash University, School of Physics and Astronomy, Melbourne, Australia*
39. *Budker Institute of Nuclear Physics SB RAS, Novosibirsk, Russia*
40. *Novosibirsk State University, Novosibirsk, Russia*
41. *King's College London, Department of Physics, London, UK*
42. *Universidad Nacional Autónoma de México, Departamento de Física Teórica, Instituto de Física, México, Mexico*
43. *Helmholtz Institute Mainz, Johannes Gutenberg-University, Mainz, Germany*
44. *University of Illinois, Department of Astronomy, Urbana, IL, USA*
45. *University of Illinois, Department of Physics, Urbana, IL, USA*
46. *University of Hamburg, Hamburg, Germany*
47. *Deutsches Elektronen-Synchrotron DESY, Hamburg, Germany*
48. *University of Oxford, Denys Wilkinson Building, Department of Physics, Oxford, UK*
49. *University of Pittsburgh, Department of Physics and Astronomy, Pittsburgh, PA, USA*
50. *Tufts University, Department of Physics and Astronomy, Medford, MA, USA*
51. *CEA Saclay, DSM/IRFU/SPP, Gif-sur-Yvette, France*
52. *University of Warwick, Department of Physics, Coventry, UK*
53. *Department of Physics and Astronomy, Rutgers University, NJ, USA*
54. *University of Minnesota, School of Physics and Astronomy, Minneapolis, MN, USA*
55. *CN Yang Institute for Theoretical Physics, Stony Brook University, Stony Brook, NY, USA*
56. *Institució Catalana de Recerca i Estudis Avancats, Barcelona, Spain*
57. *Instituto de ciencias del Cosmos (ICC), University of Barcelona, Barcelona, Spain*
58. *Argonne National Laboratory, Argonne, IL, USA*
59. *Johns Hopkins University, Baltimore, MD, USA*
60. *Theoriegruppe, Deutsches Elektronen-Synchrotron DESY, Hamburg, Germany*
61. *Institut für Physik, Humboldt-Universität zu Berlin, Berlin, Germany*
62. *University College Dublin, School of Physics, Dublin, Ireland*
63. *Physics Department, Kyung Hee University, Seoul 02447, Republic of Korea*
64. *Universität Tübingen, Institut für Theoretische Physik, Tübingen, Germany*
65. *Santa Cruz Institute for Particle Physics, University of California, Santa Cruz, CA, USA*
66. *Institut für Kernphysik and Institute for Advanced Simulation, Forschungszentrum Jülich, Jülich, Germany*
67. *KEK, High Energy Accelerator Research Organization, Tsukuba, Japan*
68. *Kamioka Observatory, ICRP, The University of Tokyo, Tokyo, Japan*
69. *Heidelberg University, Institute for Theoretical Physics, Heidelberg, Germany*
70. *Instituto de Física Teórica (UAM/CSIC), Universidad Autónoma de Madrid, Madrid, Spain*

71. *Campus of International Excellence UAM+CSIC, Universidad Autónoma de Madrid, Madrid, Spain*
72. *Instituto de Física de Cantabria, CSIC-UC, Santander, Spain*
73. *Cornell University, Laboratory of Elementary-Particle Physics, Ithaca, NY, USA*
74. *IFIC — Instituto de Física Corpuscular, Universitat de València — C.S.I.C., Valencia, Spain*
75. *Tohoku University, Department of Physics, Sendai, Japan*
76. *Nagoya University, Kobayashi-Maskawa Institute, Nagoya, Japan*
77. *University of Delaware, Department of Physics and Astronomy, Newark, DE, USA*
78. *University of Delaware, Bartol Research Institute, Newark, DE, USA*
79. *Michigan State University, Dept. of Physics and Astronomy, East Lansing, MI, USA*
80. *Department of Physics, Tokyo Metropolitan University, Tokyo, Japan*
81. *Florida State University, Department of Physics, Tallahassee, FL, USA*
82. *Dipartimento di Fisica, Sapienza Università di Roma, Rome, Italy*
83. *INFN Sezione di Roma, Rome, Italy*
84. *IJCLab, CNRS/IN2P3, Université Paris-Saclay, Orsay, France*
85. *Department of Particle Physics, Tel-Aviv University, Tel Aviv, Israel*
86. *Friedrich-Alexander University of Erlangen-Nürnberg, Erlangen Centre for Astroparticle Physics, Erlangen, Germany*
87. *University of Durham, Institute for Particle Physics Phenomenology, Department of Physics, Durham, UK*
88. *Petersburg Nuclear Physics Institute, Petersburg, Russia*
89. *Nuclear Science Division, Lawrence Berkeley National Laboratory, Berkeley, CA, USA*
90. *University of California, Department of Physics, Berkeley, CA, USA*
91. *Universität Bonn, Helmholtz-Institut für Strahlen- und Kernphysik, Bonn, Germany*
92. *University of Victoria, Victoria, BC, Canada*
93. *University of Basel, Institute of Physics, Basel, Switzerland*
94. *Yonsei University, Department of Physics, Seoul, Republic of Korea*
95. *University College London, Department of Physics and Astronomy, London, UK*
96. *Syracuse University, Department of Physics, Syracuse, NY, USA*
97. *Aix-Marseille Univ, Université de Toulon, CNRS, CPT, Marseille, France*
98. *Institute of Theoretical Particle Physics and Cosmology (TTK), RWTH, Aachen, Germany*
99. *Perimeter Institute for Theoretical Physics, Waterloo, Canada*
100. *Instituto de Astrofísica e Ciências do Espaço, Universidade de Lisboa, Lisbon, Portugal*
101. *GSI, Helmholtzzentrum für Schwerionenforschung, Darmstadt, Germany*
102. *Division of Science, City College of New York, New York, NY, USA*
103. *Scuola Normale Superiore, Pisa, Italy*
104. *INFN Sezione di Pisa, Pisa, Italy*
105. *Université catholique de Louvain, Centre for Cosmology, Particle Physics and Phenomenology (CP<sup>3</sup>), Louvain-la-Neuve, Belgium*
106. *Università di Bologna and INFN, Dipartimento di Fisica e Astronomia, Bologna, Italy*
107. *Universität Siegen, Department für Physik, Siegen, Germany*
108. *INFN Sezione di Cagliari, Monserrato, Italy*
109. *Louisiana State University, Department of Physics and Astronomy, Baton Rouge, LA, USA*
110. *University of Glasgow, School of Physics and Astronomy, Glasgow, UK*
111. *Stockholms Universitet, AlbaNova University Centre, Fysikum, Stockholm, Sweden*
112. *Indiana University, Department of Physics, Bloomington, IN, USA*
113. *DESY, Zeuthen, Germany*
114. *INAF-OATS, Trieste, Italy*
115. *University of Ghent, Dept. of Physics and Astronomy, Ghent, Belgium*
116. *University of Tokyo, Kavli IPMU (WPI), The University of Tokyo Institutes for Advanced Study, Kashiwa, Japan*
117. *Brown University, Department of Physics, Providence, RI, USA*
118. *INFN Sezione di Milano-Bicocca, Piazza della Scienza, Milano, Italy*
119. *Dip. di Fisica "G. Occhialini", Università di Milano-Bicocca, Milano, Italy*
120. *Universidad de Granada, Dpto. de Física Teórica y del Cosmos & C.A.F.P.E., Granada, Spain*
121. *Johannes Gutenberg University, PRISMA Cluster of Excellence and Mainz Institute for Theoretical Physics, Mainz, Germany*
122. *Department of Particle Physics and Astrophysics, Weizmann Institute of Science, Rehovot, Israel*

123. *Università di Bologna and INFN, Dip. Scienze per la Qualità della Vita, Rimini, Italy*
124. *University of Edinburgh, Royal Observatory, Institute for Astronomy, Edinburgh, UK*
125. *SISSA/INFN, Trieste, Italy*
126. *INRNE, Bulgarian Academy of Sciences, Sofia, Bulgaria*
127. *University of Alabama, Department of Physics and Astronomy, Tuscaloosa, AL, USA*
128. *Universitat Autònoma de Barcelona, Departament de Física, Barcelona, Spain*
129. *IFAE, Universitat Autònoma de Barcelona, Barcelona, Spain*
130. *Georg-August-Universität Göttingen, II. Physikalisches Institut, Göttingen, Germany*
131. *Karlsruhe Institute of Technology, Karlsruhe, Germany*
132. *University of Bristol, HH Wills Physics Laboratory, Bristol, UK*
133. *Max-Planck-Institut für Physik (Werner-Heisenberg-Institut), München, Germany*
134. *Tsung-Dao Lee Institute, Shanghai Jiao Tong University, Shanghai, China*
135. *Shanghai Jiao Tong University, Shanghai, China*
136. *University of Massachusetts, Department of Physics, Amherst, MA, USA*
137. *SLAC National Accelerator Laboratory, Menlo Park, CA, USA*
138. *DOE, Washington, DC, USA*
139. *National Research Nuclear University "MEPhI", Moscow, Russia*
140. *University of Washington, Department of Physics, Seattle, WA, USA*
141. *LPTHE, UPMC Université de Paris 6, Paris, France*
142. *University of Oxford, Rudolf Peierls Centre for Theoretical Physics, Oxford, UK*
143. *Institute of Physics, Ecole Polytechnique Fédérale de Lausanne (EPFL), Lausanne, Switzerland*
144. *Duke University, Physics Department, Durham, NC, USA*
145. *University of Cincinnati, Department of Physics, Cincinnati, OH, USA*
146. *University of British Columbia, Department of Physics and Astronomy, Vancouver, BC, Canada*
147. *Lund University, Department of Astronomy and Theoretical Physics, Lund, Sweden*
148. *The Hong Kong University of Science and Technology, Kowloon, Hong Kong*
149. *Paris Centre for Cosmological Physics, APC (CNRS), Université de Paris, Paris, France*
150. *Pisa University, Pisa, Italy*
151. *University of Tennessee, Department of Physics and Astronomy, Knoxville, TN, USA*
152. *III. Physikalisches Institut, Physikzentrum, RWTH Aachen University, Aachen, Germany*
153. *Tokyo Metropolitan University, High Energy Physics Laboratory, Tokyo, Japan*
154. *Department of Physics, Nagoya University, Nagoya, Japan*
155. *International Center for Elementary Particle Physics (ICEPP), University of Tokyo, Tokyo, Japan*
156. *Institute of Physics, Czech Academy of Sciences, Prague, Czech Republic*
157. *Department of Physics, University of California, Davis, CA, USA*
158. *Institut für Kernphysik, Johannes Gutenberg University, Mainz, Germany*
159. *University of Sheffield, Department of Physics and Astronomy, Sheffield, UK*
160. *University of Melbourne, School of Physics, Victoria, Australia*
161. *University of Illinois at Chicago, Chicago, IL, USA*
162. *Carleton University, Department of Physics, Ottawa, ON, Canada*
163. *California Institute of Technology, Kellogg Radiation Laboratory, Pasadena, CA, USA*
164. *The University of Liverpool, Division of Theoretical Physics, Department of Mathematical Sciences, Liverpool, UK*
165. *University of Portsmouth, Institute of Cosmology and Gravitation, Portsmouth, UK*
166. *Ohio State University, Department of Astronomy and CCAPP, Columbus, OH, USA*
167. *Columbia University, Department of Physics, New York, NY, USA*
168. *Dept. of Physics, Colorado School of Mines, Golden, CO, USA*
169. *George Washington University Virginia Campus, Department of Physics, Ashburn, VA, USA*
170. *University of Tokyo, Department of Physics, Tokyo, Japan*
171. *Moscow Institute of Physics and Technology, Dolgoprudny, Russia*
172. *California Institute of Technology, High Energy Physics, Pasadena, CA, USA*
173. *School of Physics, Peking University, Beijing, China*
174. *Institute of High Energy Physics, Beijing, China*

## HIGHLIGHTS OF THE 2020 EDITION OF THE REVIEW OF PARTICLE PHYSICS

All PDG data and review articles are available online at [pdg.lbl.gov](http://pdg.lbl.gov).

878 new papers with 3,324 new measurements

120 reviews (most are revised)

- 411 new papers from *LHC* experiments (ATLAS, CMS and LHCb).
  - Extensive up-to-date *Higgs boson* coverage from 117 new papers with 201 measurements, including latest results on mass, couplings, decay width and branching ratios, plus searches for other neutral and charged Higgs bosons.
  - *Supersymmetry*: 83 new papers with major exclusions.
  - *Top quark*: 36 new papers provide latest results on mass, coupling, and constraints on various models of physics beyond the Standard Model involving top-quark production and decay.
  - Latest from *B-meson physics*: 85 papers and 356 measurements, including observations of new excited  $\Lambda_b$  baryons and new pentaquark states.
  - 5 new sections including limits of cross sections in *WIMP and Dark Matter Searches* for masses in the GeV range (65 new entries, including also older results).
  - *Heavy Neutral Lepton* Listings reorganized and extended.
  - New *proton charge radius* measurements appear to resolve charge radius puzzle.
- New reviews on:
    - *High Energy Soft QCD and Diffraction*.
    - *Determination of CKM Angles from B Hadrons*.
  - Significant update/revision to reviews on:
    - Major revision of *Physical Constants* following the 2019 redefinition of units in the International System of Units.
    - *Electroweak Model* and *CKM* reviews provide latest fits of Standard Model parameters.
    - *Structure Functions* review includes new discussion on transverse momentum dependent distributions (TMDs).
    - *Top Quark* review summarizes latest results and constraints on new physics from top quark.
    - $D^0$ - $\bar{D}^0$  *Mixing* summarizes latest results and discusses implications of first observation of CP violation in  $D^0$  decays.
    - Completely rewritten review on *Neutrino Masses, Mixing and Oscillations* discusses latest results from solar, atmospheric, reactor and accelerator-based neutrino experiments and provides global fit values for mixing parameters and mass spectrum.
    - *Pentaquarks* review updated based on new LHCb measurement of hidden-charm pentaquarks.
    - *Monte Carlo Neutrino Generators* includes new extensive discussion on nuclear scattering.
    - Completely rewritten review on *Dark Matter*.
    - *Experimental Tests of Gravitational Theory* revised and extended to include gravitational waves.

## VOLUME 1: SUMMARY TABLES AND REVIEWS

Highlights	6	<b>Experimental Methods and Colliders</b>	
Introduction	11	31. Accelerator physics of colliders (rev.)	521
History plots	19	32. High-energy collider parameters (rev.)	529
Online particle physics information (rev.)	20	33. Neutrino beam lines at high-energy proton synchrotrons (rev.)	534
<b>SUMMARY TABLES</b>		34. Passage of particles through matter (rev.)	535
Gauge and Higgs bosons	31	35. Particle detectors at accelerators (rev.)	551
Leptons	34	36. Particle detectors for non-accelerator phys. (rev.)	589
Quarks	37	37. Radioactivity and radiation protection (rev.)	612
Mesons	38	38. Commonly used radioactive sources (rev.)	618
Meson quick reference table	91		
Baryon quick reference table	92	<b>Mathematical Tools</b>	
Baryons	93	39. Probability (rev.)	621
Searches not in Other Sections	111	40. Statistics (rev.)	626
Tests of conservation laws	113	41. Monte Carlo techniques (rev.)	642
		42. Monte Carlo event generators	646
<b>REVIEWS, TABLES, AND PLOTS</b>		43. Monte Carlo neutrino event generators (rev.)	657
<b>Constants, Units, Atomic and Nuclear Properties</b>		44. Monte Carlo particle numbering scheme (rev.)	661
1. Physical constants (rev.)	137	45. Clebsch-Gordan coefficients, spherical harmonics, and $d$ functions	665
2. Astrophysical constants (rev.)	138	46. SU(3) isoscalar factors and representation matrices	666
3. International system of units (SI)	140	47. SU( $n$ ) multiplets and Young diagrams	667
4. Periodic table of the elements (rev.)	141		
5. Electronic structure of the elements	142	<b>Kinematics, Cross-Section Formulae, and Plots</b>	
6. Atomic and nuclear properties of materials	144	48. Kinematics (rev.)	671
7. Electromagnetic relations	146	49. Resonances (rev.)	675
8. Naming scheme for hadrons (rev.)	148	50. Cross-section formulae for specific processes (rev.)	682
<b>Standard Model and Related Topics</b>		51. Neutrino cross section measurements (rev.)	691
9. Quantum chromodynamics (rev.)	153	52. Plots of cross sections and related quantities (rev.)	696
10. Electroweak model and constraints on new physics (rev.)	180		
11. Higgs boson physics, status of (rev.)	203	<b>Particle Properties</b>	
12. CKM quark-mixing matrix (rev.)	261	<u>Gauge Bosons</u>	
13. $CP$ violation in the quark sector (rev.)	271	53. Mass and width of the $W$ boson (rev.)	715
14. Neutrino masses, mixing, and oscillations (new)	285	54. $Z$ boson	717
15. Quark model (rev.)	312	<u>Charged Leptons</u>	
16. Heavy-quark & soft-collinear effective theory (rev.)	325	55. Muon anomalous magnetic moment (rev.)	722
17. Lattice quantum chromodynamics (rev.)	333	56. Muon decay parameters (rev.)	725
18. Structure functions (rev.)	347	57. $\tau$ branching fractions (rev.)	728
19. Fragmentation functions in $e^+e^-$ , $ep$ and $pp$ collisions (rev.)	368	58. $\tau$ -lepton decay parameters	731
20. High Energy Soft QCD and Diffraction (new)	385	<u>Quarks</u>	
<b>Astrophysics and Cosmology</b>		59. Quark masses (rev.)	733
21. Experimental tests of gravitational theory (rev.)	409	60. Top quark (rev.)	741
22. Big-Bang cosmology (rev.)	422		
23. Inflation (rev.)	435		
24. Big-Bang nucleosynthesis (rev.)	451		
25. Cosmological parameters (rev.)	458		
26. Neutrinos in cosmology (rev.)	467		
27. Dark matter (new)	474		
28. Dark energy (rev.)	490		
29. Cosmic microwave background (rev.)	499		
30. Cosmic rays (rev.)	510		

(Continued on next page.)



Mesons

61. Form factors for radiative pion & kaon decays (rev.)	762
62. Scalar mesons below 2 GeV (rev.)	764
63. Pseudoscalar and pseudovector mesons in the 1400 MeV region (rev.)	771
64. Rare kaon decays (rev.)	774
65. <i>CPT</i> invariance tests in neutral kaon decay (rev.)	779
66. $V_{ud}$ , $V_{us}$ , Cabibbo angle, and CKM unitarity (rev.)	781
67. <i>CP</i> -violation in $K_L$ decays	784
68. Review of multibody charm analyses (rev.)	788
69. $D^0$ - $\bar{D}^0$ mixing (rev.)	792
70. $D_s^+$ branching fractions (rev.)	801
71. Leptonic decays of charged pseudoscalar mesons (rev.)	803
72. Production and decay of $b$ -flavored hadrons (rev.)	814
73. Polarization in $B$ decays (rev.)	824
74. $B^0$ - $\bar{B}^0$ mixing (rev.)	828
75. Semileptonic $B$ decays, $V_{cb}$ and $V_{ub}$ (rev.)	835
76. CKM angles from $B$ hadrons, determination of (new)	849
77. Spectroscopy of mesons containing two heavy quarks (rev.)	854
78. Non- $q\bar{q}$ mesons (rev.)	861
<u>Baryons</u>	
79. Baryon decay parameters	868
80. $N$ and $\Delta$ resonances (rev.)	869
81. Baryon magnetic moments	874
82. $\Lambda$ and $\Sigma$ resonances (rev.)	875
83. Pole structure of the $\Lambda(1405)$ region (rev.)	878
84. Charmed baryons (rev.)	879
85. Pentaquarks (rev.)	881

**Hypothetical Particles and Concepts**

86. Extra dimensions (rev.)	889
87. $W'$ -boson searches (rev.)	897
88. $Z'$ -boson searches (rev.)	900
89. Supersymmetry: theory (rev.)	905
90. Supersymmetry: experiment (rev.)	923
91. Axions and other similar particles (rev.)	939
92. Quark and lepton compositeness, searches for (rev.)	953
93. Dynamical electroweak symmetry breaking: implications of the $H(0)$ (rev.)	958
94. Grand unified theories (rev.)	971
95. Leptoquarks (rev.)	986
96. Magnetic monopoles (rev.)	989

**VOLUME 2: PARTICLE LISTINGS**  
(available online only)**Illustrative key and abbreviations**

Illustrative key	999
Abbreviations	1000

**Gauge and Higgs bosons**

( $\gamma$ , gluon, graviton, $W$ , $Z$ , Higgs, Axions)	1013
--	------

**Leptons**

( $e$ , $\mu$ , $\tau$ , Heavy-charged lepton searches, Neutrino properties, Number of neutrino types, Double- $\beta$ decay, Neutrino mixing, Heavy-neutral lepton searches)	1101
---	------

**Quarks**

( $u$ , $d$ , $s$ , $c$ , $b$ , $t$ , $b'$ , $t'$ ( $4^{th}$ gen.), Free quarks)	1173
--	------

**Mesons**

Light unflavored ( $\pi$ , $\rho$ , $a$ , $b$ ) ( $\eta$ , $\omega$ , $f$ , $\phi$ , $h$ )	1209
Other light unflavored	1332
Strange ( $K$ , $K^*$ )	1337
Charmed ( $D$ , $D^*$ )	1391
Charmed, strange ( $D_s$ , $D_s^*$ , $D_{sJ}$ )	1448
Bottom ( $B$ , $V_{cb}/V_{ub}$ , $B^*$ , $B_J^*$ )	1465
Bottom, strange ( $B_s$ , $B_s^*$ , $B_{sJ}^*$ )	1640
Bottom, charmed ( $B_c$ )	1664
$c\bar{c}$ ( $\eta_c$ , $J/\psi(1S)$ , $\chi_c$ , $h_c$ , $\psi$ )	1668
$b\bar{b}$ ( $\eta_b$ , $\Upsilon$ , $\chi_b$ , $h_b$ )	1782

**Baryons**

$N$	1825
$\Delta$	1878
$\Lambda$	1902
$\Sigma$	1927
$\Xi$	1959
$\Omega$	1971
Charmed ( $\Lambda_c$ , $\Sigma_c$ , $\Xi_c$ , $\Omega_c$ )	1974
Doubly charmed ( $\Xi_{cc}$ )	1996
Bottom ( $\Lambda_b$ , $\Sigma_b$ , $\Xi_b$ , $\Omega_b$ , $b$ -baryon admixture)	1997
Exotic baryons ( $P_c$ pentaquarks)	2014

**Searches not in Other Sections**

Magnetic monopole searches	2017
Supersymmetric particle searches	2019
Technicolor	2062
Searches for quark and lepton compositeness	2063
Extra dimensions	2067
WIMP and dark matter searches	2073
Other particle searches	2085

## INTRODUCTION

1. Overview . . . . .	11
2. Particle Listings responsibilities . . . . .	11
3. Consultants . . . . .	12
4. Naming scheme for hadrons . . . . .	15
5. Procedures . . . . .	15
5.1 Selection and treatment of data . . . . .	15
5.2 Averages and fits . . . . .	15
5.2.1 Treatment of errors . . . . .	15
5.2.2 Unconstrained averaging . . . . .	16
5.2.3 Constrained fits . . . . .	16
5.3 Rounding . . . . .	17
5.4 Discussion . . . . .	17
History plots . . . . .	19

## ONLINE PARTICLE PHYSICS INFORMATION

1. Introduction . . . . .	20
2. Particle Data Group (PDG) resources . . . . .	20
3. Particle physics information platforms . . . . .	20
4. Literature databases . . . . .	20
5. Particle physics journals and conference proceedings series . . . . .	21
6. Conference databases . . . . .	21
7. Research institutions . . . . .	21
8. People . . . . .	21
9. Experiments . . . . .	21
10. Jobs . . . . .	21
11. Software repositories . . . . .	22
12. Data repositories . . . . .	22
13. Data preservation . . . . .	24
14. Particle physics education and outreach sites . . . . .	24



# Introduction

## 1 Overview

The *Review of Particle Physics* is a comprehensive review of the field of Particle Physics and of related areas in Cosmology. It is divided into two volumes. Volume 1 includes the “Summary Tables” and “Reviews, Tables, and Plots”. Volume 2 consists of the “Particle Listings”.

The *Review* is updated each year and made available on the PDG website (pdg.lbl.gov). In even-numbered years, the *Review* is also published in a journal and printed as the *PDG Book* together with an abridged *Particle Physics Booklet* containing Summary Tables and essential tables, figures, and equations from selected review articles. This edition is an updating through January 2020.

The Summary Tables give our best values and limits for particle properties such as masses, widths or lifetimes, and branching fractions, as well as an extensive summary of searches for hypothetical particles and a summary of experimental tests of conservation laws.

The 96 review articles in Reviews, Tables and Plots cover a wide variety of theoretical and experimental topics. Together with the Summary Tables they provide a quick reference for the practicing particle physicist. Two more review articles, Online Particle Physics Information and Tests of Conservation Laws, can be found in the Introduction and Summary Tables, respectively.

The Particle Listings are a compilation/evaluation of data on particle properties. They contain all the data used to get the values given in the Summary Tables. They also give information on unconfirmed particles and particle searches. In this edition, the Particle Listings include 3,324 new measurements from 878 papers, in addition to the 41,371 measurements from 11,322 papers that first appeared in previous editions [1]. 22 review articles are part of the Particle Listings and address specific aspects of the data presented in the Listings. Because of the large quantity of data, the Particle Listings are not an archive of all published data on particle properties. We refer interested readers to earlier editions for data now considered to be obsolete.

We organize the particles into six categories:

- Gauge and Higgs bosons
- Leptons
- Quarks
- Mesons
- Baryons
- Searches not in other sections

The last category only includes searches for particles that do not belong to the previous groups. For example, it includes searches for supersymmetric particles, compositeness and extra dimensions, while searches for heavy charged leptons and massive neutrinos are with the leptons.

In Sec. 2 of this Introduction, we list the main areas of responsibility of the authors of the Particle Listings. Our many consultants, without whom we would not have been able to produce this *Review*, are acknowledged in Sec. 3. In Sec. 4, we mention briefly the naming scheme for hadrons, which was extended in the previous edition [1]. In Sec. 5, we discuss our procedures for choosing among measurements of particle properties and for obtaining best values of the properties from the measurements.

The accuracy and usefulness of this *Review* depend in large part on interaction between its users and the authors. We appreciate comments, criticisms, and suggestions for improvements of any kind. Please send them to the appropriate author, according to the list of responsibilities in Sec. 2 below, or to pdg@lbl.gov.

In addition to the online publication at pdg.lbl.gov, the *Review* is available in different formats:

- The printed *PDG Book* includes volume 1 only, *i.e.* it contains the Summary Tables and most review articles. Since the 2016 edition [2] the detailed tables from the Particle Listings are no longer printed.
- The *Particle Physics Booklet* includes the Summary Tables plus essential tables, figures, and equations from selected review articles. Starting with the Booklets of the 2018 edition,

we have excluded most text and explanations in order to revert back to a more pocket-sized format. The Booklet is available in print and as a web version optimized for use on phones as well as an Android app (see pdg.lbl.gov/booklet).

- *pdgLive* (pdgLive.lbl.gov) is a web application giving more interactive access to PDG data than the static web pages and PDF files that are also available.
- Files that can be downloaded from the PDG website include a table of masses, widths, and PDG Monte Carlo particle ID numbers; PDF files of volume 1 (PDG Book), volume 2 (Particle Listings) and Booklet; individual review articles; all figures; and an archive file containing the complete PDG website (except for pdgLive).

Copies of the *PDG Book* or the *Particle Physics Booklet* can be ordered from our website or directly at pdg.lbl.gov/order. For special requests only, please email pdg@lbl.gov in North and South America, Australia, and the Far East, and pdg-products@cern.ch in all other areas.

This *Review* is considered to be a single comprehensive review of particle physics and related areas. Therefore we prefer that it be cited as a whole, rather than citing *e.g.* an individual review article that is part of this *Review*. For the 2020 edition, the proper citation is:

P.A. Zyla *et al.* (Particle Data Group), Prog. Theor. Exp. Phys. **2020**, 083C01 (2020).

If you wish to refer to a specific part of the *Review*, for example to the Higgs boson review article, the following form should be used:

*Status of Higgs Boson Physics* in P.A. Zyla *et al.* (Particle Data Group), Prog. Theor. Exp. Phys. **2020**, 083C01 (2020).

## 2 Particle Listings responsibilities

\* Asterisk indicates the people to contact with questions or comments about Particle Listings sections.

### • Gauge and Higgs bosons

$\gamma$	A. Bettini, D.E. Groom*
Gluons	R.M. Barnett,* A.V. Manohar
Graviton	A. Bettini,* D.E. Groom
$W, Z$	M. Grünewald,* A. Gurtu*
Higgs bosons	S. Heinemeyer,* K. Hikasa, J. Tanaka
Heavy bosons	R.M. Barnett,* K.A. Olive, M. Tanabashi
Axions	K.A. Olive, G. Raffelt,* F. Takahashi

### • Leptons

Neutrinos	M. Goodman, C.-J. Lin,* K. Nakamura, K.A. Olive, A. Piepke, P. Vogel
$e, \mu$	A. Bettini,* C. Grab
$\tau$	A. Lusiani, K. Mönig*

### • Quarks

Quarks	R.M. Barnett,* A.V. Manohar
Top quark	R.M. Barnett,* Y. Sumino
$b', t'$	R.M. Barnett,* Y. Sumino
Free quark	A. Bettini,* C.-J. Lin

### • Mesons

$\pi, \eta$	A. Bettini,* C. Grab
Unstable mesons	C. Amsler, M. Doser,* S. Eidelman,* T. Gutsche, C. Hanhart, J.J. Hernández-Rey, C. Lourenco, A. Masoni, M. Mikhasenko, R.E. Mitchell, S. Navas, C. Patrignani, S. Spanier, G. Venanzoni, V. Vorobyev
$K$ (stable)	G. D'Ambrosio, C.-J. Lin*
$D$ (stable, no mix.)	J. Rademacker, D. Robinson*
$D^0$ mixing	D.M. Asner, W.-M. Yao*
$B$ (stable)	A. Cerri,* P. Eerola, M. Kreps, Y. Kwon, W.-M. Yao*

- Baryons
  - Stable baryons C. Grab, D. Robinson\*
  - Unstable baryons V. Burkert, E. Klempt, U. Thoma,  
L. Tiator, R.L. Workman\*
  - Charmed baryons J. Rademacker, D. Robinson\*
  - Bottom baryons A. Cerri,\* P. Eerola, M. Kreps,  
Y. Kwon, W.-M. Yao\*
- Miscellaneous searches
  - Monopole A. Bettini,\* D. Milstead
  - Supersymmetry M. D’Onofrio, H.K. Dreiner,\*  
A. de Gouvêa, F. Moortgat  
K.A. Olive
  - Technicolor K. Agashe,\* K.A. Olive, M. Tanabashi
  - Compositeness M. Tanabashi, J. Terning\*
  - Extra Dimensions T. Gherghetta, K.A. Olive,  
D. Robinson\*
  - WIMP, DM, Other H. Baer, A. Bettini,\* W.-M. Yao\*

### 3 Consultants

The Particle Data Group benefits greatly from the assistance of hundreds of physicists who are asked to referee review articles and verify every piece of data entered into this *Review*. Of special value is the advice of the PDG Advisory Committee, which meets biennially and thoroughly reviews all aspects of our operation. The members of the 2020 committee are:

- S. Demers (Yale)
- D. d’Enterria (CERN)
- J. Frieman (FNAL)
- L. Hall (UC Berkeley/LBNL)
- T. Nakada (EPFL)
- M. Yokoyama (Tokyo)
- Q. Zhao (IHEP Beijing)

We have especially relied on the expertise of the following people for advice on particular topics:

- I. Abt (MPI Munich)
- M. Achasov (Budker Inst., Novosibirsk)
- M. Albrow (FNAL)
- A. Antognini (ETH Zurich)
- F. Anulli (INFN, Rome)
- E. Aprile (Columbia U.)
- G. Arduini (CERN)
- E. Armengaud (CEA Saclay, DSM/IRFU/SPP)
- M. Artuso (Syracuse U.)
- P. Azzurri (INFN, Pisa)
- H. Bachacou (IRFU, Saclay)
- K. Backes (Yale U.)
- A. Barabash (ITEP)
- E. Barberis (FNAL)
- M. Bardeen (FNAL)
- W. Barter (Imperial Coll. London)
- M. Battaglieri (U. di Genova)
- G. Bell (Siegen U.)
- V. Belyaev (ITEP)
- S. Benson (CERN)
- Z. Berezhiani (INFN, LNGS)
- F. Bernlochner (Karlsruhe U.)
- E. Berti (Johns Hopkins U.)
- V. Bertone (NIKHEF)
- M. Bettler (CERN)
- M. Beznogov (Astro. Inst. UNAM)
- M. Borsato (CERN)
- J. Bramante (Queen’s U.)
- J.E. Brau (Oregon U.)
- T. Bringmann (Oslo U.)
- J. Brod (Cincinnati U.)
- G. Brooijmans (Columbia U.)
- R. Bruce (CERN)
- T. Brune (TU)
- O. Bruning (CERN)
- D.A. Bryman (TRIUMF)
- J. Butterworth (UCL)
- F. Calore (LAPTH)
- F. Canelli (Zurich U.)
- A. Canto (CERN)
- J. Cao (IHEP Beijing)
- L. Cardani (INFN, Rome)
- V. Cavaliere (BNL)
- G. Cavallero (CERN)
- M. Cepeda (CIEMAT)
- F. Cerutti (LBNL)
- M. Charles (CNRS)
- M. Chen (Queen’s U.)
- K. Cheung (Tsinghua U.)
- G. Chiarelli (INFN, Pisa)
- V. Chobanova (CERN)
- J. Chou (Rutgers U.)
- S. Choudhury (Indian Inst. Tech., Mumbai)
- R. Ciesielski (Rockefeller U.)
- G. Colangelo (Bern U.)
- J.I. Collar (Chicago U.)
- G. Compère (ULB, Brussels)
- M. Crisler (FNAL)
- A. Czarnecki (Alberta U.)
- G. D’Ambrosio (INFN, Napoli)
- A. Danilov (INR, Moscow)
- M. Daum (PSI)
- I. David (Glasgow U.)
- C. Davies (Glasgow U.)
- B. Dawson (Adelaide U.)
- J. De Blas (INFN, Padua)
- P. Decowski (NIKHEF)
- G. de Lellis (INFN, Napoli)
- M. Della Morte (SDU)
- S. Demidov (INR, Moscow)
- D. Denisov (FNAL)
- D. d’Enterria (CERN)
- A.V. Derbin (Petersburg Nuclear Phys. Inst.)
- S. Derenzo (LBNL)
- S. Desai (Boston U.)
- U. De Sanctis (Rome U. Tor Vergata)
- S. Descotes-Genon (Paris-Sud U.)
- B. Dey (CERN)
- M. Diamond (Toronto U.)
- A. Di Domenica (INFN, Rome)
- F. Dordei (CERN)
- K. Dundas (Columbia U.)
- S.R. Elliott (LANL)
- K. Ellis (Durham U.)
- C. Englert (Glasgow U.)
- D. Epifanov (Budker Inst., Novosibirsk)
- M. Escudero (King’s Coll. London)
- S. Esen (CERN)
- R. Essig (YITP, Stony Brook)
- P. Everaerts (MIT)

- V. Ezhov (NRC Kurchatov Inst. PNPI)
- S. Fang (IHEP Beijing)
- P. Fayet (LPTENS)
- M. Fedderke (Stanford U.)
- A. Ferrari (CERN)
- W. Fischer (BNL)
- J. Formaggio (MIT)
- J. Fortin (UC San Diego)
- T. Fujita (Kyoto U.)
- T. Gaisser (Delaware U., Bartol Inst.)
- P. Gambino (INFN, Torino)
- A. Gangapshev (INR, Moscow)
- J. Gao (IHEP Beijing)
- R. Garisto (APS)
- A. Gasparian (Jefferson Lab)
- C. Gatti (INFN, LNF)
- A. Geiser (DESY, Hamburg)
- M. Genest (CNRS)
- M. Gersabeck (Manchester U.)
- L. Gironi (INFN, Milano-Bicocca)
- C. Glasman (U. Autònoma de Madrid)
- S.N. Gninenko (Russian Academy of Sciences)
- T. Golling (Geneva U.)
- B. Golob (Jozef Stefan Inst.)
- J. Gomez Cadenas (DIPIC)
- j. goodman (Maryland U.)
- P. Grabmayr (Tübingen U.)
- P. Grafstroem (INFN, Bologna)
- L. Grandi (Chicago U.)
- E. Grauges (ICC, U. of Barcelona)
- R. Gray (U. Washington)
- G. Greene (Tennessee U.)
- Y. Grossman (Cornell U.)
- Y. Guo (KPH, JGU Mainz)
- C. Gwilliam (Liverpool U.)
- C. Ha (Northwestern U.)
- F. Halzen (Wisconsin U.)
- S. Harnew (Oxford U.)
- F.A. Harris (Hawaii U.)
- A. Hasenfratz (Colorado U., Boulder)
- K.M. Heeger (Yale U.)
- A. Hinzmann (Hamburg U.)
- A. Hoang (HEPHY, Vienna)
- Y. Hochberg (Racah Inst. Hebrew U.)
- T. Huege (KIT)
- A. Ianni (INFN, LNGS)
- N. Ilic (NIKHEF)
- I.G. Irastorza (U. de Zaragoza)
- A. Jafari (DESY, Zeuten)
- N. Jafari (DESY, Zeuten)
- P. Janot (CERN)
- L. Jeanty (Oregon U.)
- X. Ji (SJTU)
- C. Joram (CERN)
- J. Jowett (CERN)
- A. Jung (Purdue U.)
- K. Kaadze (CERN)
- H. Kamano (Osaka U.)
- J. Kamenik (Jozef Stefan Inst.)
- J. Kaminski (Bonn U.)
- D. Karlen (Victoria U.)
- S. Karshenboim (Pulkovo Obs., St.Petersburg)
- E.T. Kearns (Boston U.)
- V. Kekelidze (JINR, Dubna)
- J. Kile (CFTP)
- S. Kim (Seoul National U.)
- K. Kirch (ETH Zurich)
- M. Kitaguchi (Nagoya U.)
- R. Klanner (DESY, Hamburg)
- S. Klaver (CERN)
- S. Knirck (Werner-Heisenberg-Inst.)
- R. Kogler (Hamburg U.)
- A. Kopylov (INR, Moscow)
- E. Kovetz (Ben-Gurion U.)
- A. Krasznahorkay (Hungarian Academy of Sciences)
- P. Krokovny (Budker Inst., Novosibirsk)
- A. Kronfeld (FNAL)
- B. Kubis (Bonn U.)
- A. Kupsc (Uppsala U.)
- M. Kuzniak (Carleton U.)
- G. Landsberg (Brown U.)
- C. Lange (CERN)
- G. Latyshev (COMPAS Group, IHEP)
- H. Lee (ANL)
- H. Lee (BNL)
- L.B. Leinson (Russian Academy of Sciences)
- G.P. Lepage (Cornell U.)
- O. Leroy (CPPM Marseille)
- J. Libby (Indian Inst. Tech., Madras)
- Z. Ligeti (LBNL)
- E. Lisi (INFN, Bari)
- Y. Liu (Lanzhou U.)
- S. Lloyd (Phys. Dep. Durham U.)
- H. Long (Inst. of Physics, Vietnamese Academy of Science & Technology)
- P.T. Lukens (FNAL)
- O. Lupton (Warwick U.)
- X. Lyu (UCAS, Beijing)
- H. Ma (IHEP Beijing)
- P. Maksimovic (Johns Hopkins U.)
- B. Malaescu (CNRS)
- S. Malde (Oxford U.)
- Y. Mambrini (Paris-Sud U.)
- G. Mandaglio (Messina U.)
- D.M. Manley (Kent U.)
- M. Margoni (INFN, Padova)
- Z. Marshall (LBNL)
- S.P. Martin (Northern Illinois U.)
- G. Martinelli (INFN, Rome)
- M. Martinelli (CERN)
- A. Masiero (INFN, Padua)
- R. Massarczyk (LANL)
- K. Matchev (Florida U.)
- A. Mathad (ETH Zurich)
- V. Matiunin (CERN)
- N. Mavromatos (King's Coll. London)
- M. Mazziotta (INFN, Bari)
- P. Mcdonald (LBNL)
- S. Meinel (Arizona U.)
- W. Melnitchouk (Jefferson Lab)
- F. Meloni (CERN)
- E. Meoni (CERN)



- P. Merkel (FNAL)
- P.D. Meyers (Princeton U.)
- T. Mibe (KEK)
- I. Mikulec (Austrian Academy of Sciences)
- V. Mitsou (IFIC, Valencia)
- R.N. Mohapatra (Maryland U.)
- S. Moosavi (Ryerson U.)
- M. Morello (SNS, Pisa)
- O. Moreno (SLAC)
- S. Moretti (Southampton U.)
- S. Moriyama (ICRR)
- M. Mulder (CERN)
- S. Murgia (UC Irvine)
- W. Murray (Warwick U.)
- B. Nachman (LBNL)
- R. Nahnauer (DESY, Hamburg)
- T. Nakadaira (KEK)
- T. Nakaya (Kyoto U.)
- S. Narison (Montpellier U.)
- A. Nelles (DESY, Zeuten)
- P. Newman (IFAE)
- V. Obraztsov (IHEP, Protvino)
- H.B. O'Connell (Chicago U.)
- K. Oide (KEK)
- Y. Onishi (KEK)
- G. Orebi Gann (LBNL)
- A. Orso Maria Iorio (INFN, Napoli)
- P. Osland (Bergen U.)
- S. Ostapchenko (Frankfurt U.)
- C. Palomba (INFN, Rome)
- T. Papadopoulou (Athens U.)
- E. Passemar (Indiana U.)
- S. Paul (TU)
- C. Paus (MIT)
- F. Petricca (MPI Munich)
- G. Petrucciani (CERN)
- G. Piacquadio (NYU)
- L. Piilonen (Virginia Tech)
- P. Piminov (Budker Inst., Novosibirsk)
- I. Polyakov (Syracuse U.)
- A. Poon (NSD LBNL)
- N. Porayako (MPIK)
- W. QIAN (IHEP Beijing)
- S. Rakshit (Indian Inst. of Technology)
- K. Ramanathan (Chicago U.)
- A. Rana (Delhi U.)
- A. Rebhan (TU Vienna)
- M. Redi (CERN)
- C.F. Redmer (IKP)
- J. Richard (IP2I, Lyon)
- W. Richard (Dep. of Phys. Texas Tech U.)
- J. Rico (ICREA, Barcelona; SISSA/INFN, Trieste)
- A. Ritz (Victoria U.)
- A. Rodas (UCM, Madrid)
- G. Ross (Oxford U.)
- M. Rotondo (INFN, Frascati)
- G. Ruggiero (Lancaster U.)
- C.T. Sachrajda (Southampton U.)
- R. Salerno (CNRS)
- M. Santimaria (INFN, LNF)
- V. Sanz (Sussex U.)
- N. Saoulidou (Athens U.)
- A.V. Sarantsev (Bonn U.)
- E. Sarkisyan-Grinbaum (Texas U.)
- A. Saunders (LANL)
- M. Schmaltz (Boston U.)
- B. Schmidt (CERN)
- F. Schroeder (Delaware U.)
- C. Schwanda (HEPHY, Vienna)
- R. Schwienhorst (Michigan State U.)
- B. Schwingenheur (MPIK)
- D. Scott (U. of British Columbia)
- R. Seidl (BNL)
- I. Seong (UC Irvine)
- S. Seon-Hee (IBS, Daejeon)
- A.P. Serebrov (Petersburg Nuclear Phys. Inst.)
- S. Serednyakov (Budker Inst., Novosibirsk)
- E. Shabalina (Georg August U. Goettingen)
- L. Shchutska (ETH Zurich)
- V. Shiltsev (FNAL)
- Y. Shirman (UC Irvine)
- D. Shwartz (Budker Inst., Novosibirsk)
- P. Sikivie (Florida U.)
- L. Silvestrini (INFN, Rome)
- S. Simula (INFN, Rome)
- A. Soffer (Tel Aviv U.)
- F. Spano (RHUL)
- H. Spiesberger (JGU, Mainz)
- M. Spira (PSI)
- Y. Stadnik (New South Wales U.)
- O. Stelzer-Chilton (TRIUMF)
- I.W. Stewart (MIT)
- A. Szczepaniak (Indiana U.)
- F. Tackmann (DESY, Zeuten)
- K. Tackmann (DESY, Hamburg)
- T.M. Tait (UC Irvine)
- A. Tapper (Imperial Coll. London)
- C. Ternes (IFIC, Valencia)
- R. Tesarek (FNAL)
- A. Thomas (KPH, JGU Mainz)
- J. Thomas (NSD LBNL)
- J. Timmermans (NIKHEF)
- K. Todyshev (Budker Inst., Novosibirsk)
- S. Trifinopoulos (Zurich U.)
- J. Uzan (CNRS)
- P.L. Vahle (William and Mary Coll.)
- K.A. van Bibber (UC Berkeley)
- R.G. Van De Water (LANL)
- C. van Eldik (Erlangen U.)
- R. Van Kooten (Indiana U.)
- A. Vartak (UC San Diego)
- C. Vincenzo (LANL)
- B. von Krosigk (DESY, Hamburg)
- A. Vossen (Duke U.)
- W. Wagner (Wuppertal U.)
- J. Walder (Lancaster U.)
- D. Wang (School of Physics, Peking U.)
- Y. Wang (JGU, Mainz)
- G. Watt (Durham U.)
- B. Webber (Cambridge U.)
- R. Wendell (Kyoto U.)
- N. Wex (MPIFR, Bonn)

- M. Whitehead (RWTH Aachen)
- M. Williams (Manchester U.)
- J.S. Wilson (FNAL)
- M. Wing (UCL)
- H.T. Wong (Academia Sinica, Inst. of Physics)
- G. Wormser (U. Paris-Saclay)
- Z. Xia (PMO, Nanjing)
- C. Yaguna (UPTC)
- T. Yamanaka (Osaka U.)
- T. Yamazaki (Tokyo U.)
- W. Yan (USTC China)
- W. Yan (Beihang U.)
- L. Yang (UC San Diego)
- S. Youn (IBS, Daejeon)
- A. Young (NCSU)
- C. Yuan (IHEP Beijing)
- C. Yue (Liaoning Normal U.)
- Q. Yue (Tsinghua U.)
- V. Zacek (U. de Montreal)
- A. Zakharov (ITEP)
- L. Zani (INFN, Pisa)
- D. Zerwas (LAL Orsay)
- C. Zhang (IHEP Beijing)
- Y. Zhang (Phys. Dep. Oxford U.)
- B. Zheng (South China U.)
- A. Zhevlakov (Tamsk State U.)
- K. Zhu (IHEP Beijing)
- J. Zupan (Cincinnati U.)
- R.M. Zwaska (FNAL)

#### 4 Naming scheme for hadrons

We introduced in the 1986 edition [3] a new naming scheme for the hadrons. Changes from older terminology affected mainly the heavier mesons made of  $u$ ,  $d$ , and  $s$  quarks. Otherwise, the only important change to known hadrons was that the  $F^\pm$  became the  $D_s^\pm$ . None of the lightest pseudoscalar or vector mesons changed names, nor did the  $c\bar{c}$  or  $b\bar{b}$  mesons (we do, however, now use  $\chi_c$  for the  $c\bar{c}$   $\chi$  states), nor did any of the established baryons. The Summary Tables give both the new and old names whenever a change has occurred.

In the previous edition [1] the naming scheme was extended to address the naming of charmonium and bottomonium states that are commonly referred to as X, Y or Z states in the literature. The current scheme is described in “Naming Scheme for Hadrons” (p. 1) of this *Review*. A table details the correspondence between the names newly adopted by the PDG and those that have appeared in the literature.

We give here our conventions on type-setting style. Particle symbols are italic (or slanted) characters:  $e^-$ ,  $p$ ,  $\Lambda$ ,  $\pi^0$ ,  $K_L$ ,  $D_s^+$ ,  $b$ . Charge is indicated by a superscript:  $B^-$ ,  $\Delta^{++}$ . Charge is not normally indicated for  $p$ ,  $n$ , or the quarks, and is optional for neutral isosinglets:  $\eta$  or  $\eta^0$ . Antiparticles and particles are distinguished by charge for charged leptons and mesons:  $\tau^+$ ,  $K^-$ . Otherwise, distinct antiparticles are indicated by a bar (overline):  $\bar{\nu}_\mu$ ,  $\bar{t}$ ,  $\bar{p}$ ,  $\bar{K}^0$ , and  $\bar{\Sigma}^+$  (the antiparticle of the  $\Sigma^-$ ).

### 5 Procedures

#### 5.1 Selection and treatment of data

The Particle Listings contain all relevant data known to us that are published in journals. With very few exceptions, we do not include results from preprints or conference reports. Nor do we include data that are of historical importance only (the Listings are not an archival record). We search every volume of 20 journals through our cutoff date for relevant data. We also include later published papers that are sent to us by the authors (or others).

In the Particle Listings, we clearly separate measurements that are used to calculate or estimate values given in the Summary Tables from measurements that are not used. We give explanatory

comments in many such cases. Among the reasons a measurement might be excluded are the following:

- It is superseded by or included in later results.
- No error is given.
- It involves assumptions we question.
- It has a poor signal-to-noise ratio, low statistical significance, or is otherwise of poorer quality than other data available.
- It is clearly inconsistent with other results that appear to be more reliable. Usually we then state the criterion, which sometimes is quite subjective, for selecting “more reliable” data for averaging. See Sec. 5.4.
- It is not independent of other results.
- It is not the best limit (see below).
- It is quoted from a preprint or a conference report.

In some cases, *none* of the measurements is entirely reliable and no average is calculated. For example, the masses of many of the baryon resonances, obtained from partial-wave analyses, are quoted as estimated ranges thought to probably include the true values, rather than as averages with errors. This is discussed in the Baryon Particle Listings.

For upper limits, we normally quote in the Summary Tables the strongest limit. We do not average or combine upper limits except in a very few cases where they may be re-expressed as measured numbers with Gaussian errors.

As is customary, we assume that particle and antiparticle share the same spin, mass, and mean life. The Tests of Conservation Laws table, following the Summary Tables, lists tests of  $CPT$  as well as other conservation laws.

We use the following indicators in the Particle Listings to tell how we get values from the tabulated measurements:

- OUR AVERAGE —From a weighted average of selected data.
- OUR FIT —From a constrained or overdetermined multiparameter fit of selected data.
- OUR EVALUATION —Not from a direct measurement, but evaluated from measurements of related quantities.
- OUR ESTIMATE —Based on the observed range of the data. Not from a formal statistical procedure.
- OUR LIMIT —For special cases where the limit is evaluated by us from measured ratios or other data. Not from a direct measurement.

An experimentalist who sees indications of a particle will of course want to know what has been seen in that region in the past. Hence we include in the Particle Listings all reported states that, in our opinion, have sufficient statistical merit and that have not been disproved by more reliable data. However, we promote to the Summary Tables only those states that we feel are well established. This judgment is, of course, somewhat subjective and no precise criteria can be given. For more detailed discussions, see the minireviews in the Particle Listings.

#### 5.2 Averages and fits

We divide this discussion on obtaining averages and errors into three sections: (1) treatment of errors; (2) unconstrained averaging; (3) constrained fits.

##### 5.2.1 Treatment of errors

In what follows, the “error”  $\delta x$  means that the range  $x \pm \delta x$  is intended to be a 68.3% confidence interval about the central value  $x$ . We treat this error as if it were Gaussian. Thus when the error *is* Gaussian,  $\delta x$  is the usual one standard deviation ( $1\sigma$ ). Many experimenters now give statistical and systematic errors separately, in which case we usually quote both errors, with the statistical error first. For averages and fits, we then add the two errors in quadrature and use this combined error for  $\delta x$ .

When experimenters quote asymmetric errors  $(\delta x)^+$  and  $(\delta x)^-$  for a measurement  $x$ , the error that we use for that measurement in making an average or a fit with other measurements is a continuous function of these three quantities. When the resultant average or fit  $\bar{x}$  is less than  $x - (\delta x)^-$ , we use  $(\delta x)^-$ ; when it is

greater than  $x + (\delta x)^+$ , we use  $(\delta x)^+$ . In between, the error we use is a linear function of  $x$ . Since the errors we use are functions of the result, we iterate to get the final result. Asymmetric output errors are determined from the input errors assuming a linear relation between the input and output quantities.

In fitting or averaging, we usually do not include correlations between different measurements, but we try to select data in such a way as to reduce correlations. Correlated errors are, however, treated explicitly when there are a number of results of the form  $A_i \pm \sigma_i \pm \Delta$  that have identical systematic errors  $\Delta$ . In this case, one can first average the  $A_i \pm \sigma_i$  and then combine the resulting statistical error with  $\Delta$ . One obtains, however, the same result by averaging  $A_i \pm (\sigma_i^2 + \Delta_i^2)^{1/2}$ , where  $\Delta_i = \sigma_i \Delta [\sum (1/\sigma_j^2)]^{1/2}$ . This procedure has the advantage that, with the modified systematic errors  $\Delta_i$ , each measurement may be treated as independent and averaged in the usual way with other data. Therefore, when appropriate, we adopt this procedure. We tabulate  $\Delta$  and invoke an automated procedure that computes  $\Delta_i$  before averaging and we include a note saying that there are common systematic errors.

Another common case of correlated errors occurs when experimenters measure two quantities and then quote the two and their difference, e.g.,  $m_1$ ,  $m_2$ , and  $\Delta = m_2 - m_1$ . We cannot enter all of  $m_1$ ,  $m_2$  and  $\Delta$  into a constrained fit because they are not independent. In some cases, it is a good approximation to ignore the quantity with the largest error and put the other two into the fit. However, in some cases correlations are such that the errors on  $m_1$ ,  $m_2$  and  $\Delta$  are comparable and none of the three values can be ignored. In this case, we put all three values into the fit and invoke an automated procedure to increase the errors prior to fitting such that the three quantities can be treated as independent measurements in the constrained fit. We include a note saying that this has been done.

### 5.2.2 Unconstrained averaging

To average data, we use a standard weighted least-squares procedure and in some cases, discussed below, increase the errors with a "scale factor." We begin by assuming that measurements of a given quantity are uncorrelated, and calculate a weighted average and error as

$$\bar{x} \pm \delta\bar{x} = \frac{\sum_i w_i x_i}{\sum_i w_i} \pm \left( \sum_i w_i \right)^{-1/2}, \quad (1)$$

where

$$w_i = 1/(\delta x_i)^2.$$

Here  $x_i$  and  $\delta x_i$  are the value and error reported by the  $i$ th experiment, and the sums run over the  $N$  experiments. We then calculate  $\chi^2 = \sum w_i (\bar{x} - x_i)^2$  and compare it with  $N - 1$ , which is the expectation value of  $\chi^2$  if the measurements are from a Gaussian distribution.

If  $\chi^2/(N - 1)$  is less than or equal to 1, and there are no known problems with the data, we accept the results.

If  $\chi^2/(N - 1)$  is very large, we may choose not to use the average at all. Alternatively, we may quote the calculated average, but then make an educated guess of the error, a conservative estimate designed to take into account known problems with the data.

Finally, if  $\chi^2/(N - 1)$  is greater than 1, but not greatly so, we still average the data, but then also do the following:

(a) We increase our quoted error,  $\delta\bar{x}$  in Eq. (1), by a scale factor  $S$  defined as

$$S = [\chi^2/(N - 1)]^{1/2}. \quad (2)$$

Our reasoning is as follows. The large value of the  $\chi^2$  is likely to be due to underestimation of errors in at least one of the experiments. Not knowing which of the errors are underestimated, we assume they are all underestimated by the same factor  $S$ . If we scale up all the input errors by this factor, the  $\chi^2$  becomes  $N - 1$ , and of course the output error  $\delta\bar{x}$  scales up by the same factor. See Ref. [4].

When combining data with widely varying errors, we modify this procedure slightly. We evaluate  $S$  using only the experiments with smaller errors. Our cutoff or ceiling on  $\delta x_i$  is arbitrarily chosen to be

$$\delta_0 = 3N^{1/2} \delta\bar{x},$$

where  $\delta\bar{x}$  is the unscaled error of the mean of all the experiments. Our reasoning is that although the low-precision experiments have little influence on the values  $\bar{x}$  and  $\delta\bar{x}$ , they can make significant contributions to the  $\chi^2$ , and the contribution of the high-precision experiments thus tends to be obscured. Note that if each experiment has the same error  $\delta x_i$ , then  $\delta\bar{x}$  is  $\delta x_i/N^{1/2}$ , so each  $\delta x_i$  is well below the cutoff. (More often, however, we simply exclude measurements with relatively large errors from averages and fits: new, precise data chase out old, imprecise data.)

Our scaling procedure has the property that if there are two values with comparable errors separated by much more than their stated errors (with or without a number of other values of lower accuracy), the scaled-up error  $\delta\bar{x}$  is approximately half the interval between the two discrepant values.

We emphasize that our scaling procedure for *errors* in no way affects central values. And if you wish to recover the unscaled error  $\delta\bar{x}$ , simply divide the quoted error by  $S$ .

(b) If the number  $M$  of experiments with an error smaller than  $\delta_0$  is at least three, and if  $\chi^2/(M - 1)$  is greater than 1.25, we show in the Particle Listings an ideogram of the data. Figure 1 is an example. Sometimes one or two data points lie apart from the main body; other times the data split into two or more groups. We extract no numbers from these ideograms; they are simply visual aids, which the reader may use as he or she sees fit.

Each measurement in an ideogram is represented by a Gaussian with a central value  $x_i$ , error  $\delta x_i$ , and area proportional to  $1/\delta x_i$ . The choice of  $1/\delta x_i$  for the area is somewhat arbitrary. With this choice, the center of gravity of the ideogram corresponds to an average that uses weights  $1/\delta x_i$  rather than the  $(1/\delta x_i)^2$  actually used in the averages. This may be appropriate when some of the experiments have seriously underestimated systematic errors. However, since for this choice of area the height of the Gaussian for each measurement is proportional to  $(1/\delta x_i)^2$ , the peak position of the ideogram will often favor the high-precision measurements at least as much as does the least-squares average. See our 1986 edition [3] for a detailed discussion of the use of ideograms.

### 5.2.3 Constrained fits

In some cases, such as branching ratios or masses and mass differences, a constrained fit may be needed to obtain the best values of a set of parameters. For example, most branching ratios and rate measurements are analyzed by making a simultaneous least-squares fit to all the data and extracting the partial decay fractions  $P_i$ , the partial widths  $\Gamma_i$ , the full width  $\Gamma$  (or mean life), and the associated error matrix.

Assume, for example, that a state has  $m$  partial decay fractions  $P_i$ , where  $\sum P_i = 1$ . These have been measured in  $N_r$  different ratios  $R_r$ , where, e.g.,  $R_1 = P_1/P_2$ ,  $R_2 = P_1/P_3$ , etc. [We can handle any ratio  $R$  of the form  $\sum \alpha_i P_i / \sum \beta_i P_i$ , where  $\alpha_i$  and  $\beta_i$  are constants, usually 1 or 0. The forms  $R = P_i/P_j$  and  $R = (P_i/P_j)^{1/2}$  are also allowed.] Further assume that *each* ratio  $R$  has been measured by  $N_k$  experiments (we designate each experiment with a subscript  $k$ , e.g.,  $R_{1k}$ ). We then find the best values of the fractions  $P_i$  by minimizing the  $\chi^2$  as a function of the  $m - 1$  independent parameters:

$$\chi^2 = \sum_{r=1}^{N_r} \sum_{k=1}^{N_k} \left( \frac{R_{rk} - R_r}{\delta R_{rk}} \right)^2, \quad (3)$$

where the  $R_{rk}$  are the measured values and  $R_r$  are the fitted values of the branching ratios.

In addition to the fitted values  $\bar{P}_i$ , we calculate an error matrix  $(\delta\bar{P}_i \delta\bar{P}_j)$ . We tabulate the diagonal elements of  $\delta\bar{P}_i = \langle \delta\bar{P}_i \delta\bar{P}_i \rangle^{1/2}$  (except that some errors are scaled as discussed below). In the Particle Listings, we give the complete correlation matrix; we also calculate the fitted value of each ratio, for comparison with the input data, and list it above the relevant input, along with a simple unconstrained average of the same input.

Three comments on the example above:

(1) There was no connection assumed between measurements of the full width and the branching ratios. But often we also have information on partial widths  $\Gamma_i$  as well as the total width  $\Gamma$ . In this case we must introduce  $\Gamma$  as a parameter in the fit, along

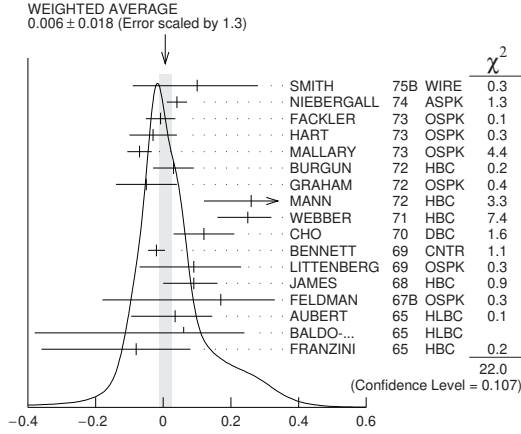


Figure 1: A typical ideogram. The arrow at the top shows the position of the weighted average, while the width of the shaded pattern shows the error in the average after scaling by the factor  $S$ . The column on the right gives the  $\chi^2$  contribution of each of the experiments. Note that the next-to-last experiment, denoted by the incomplete error flag ( $\perp$ ), is not used in the calculation of  $S$  (see the text).

with the  $P_i$ , and we give correlation matrices for the widths in the Particle Listings.

(2) We try to pick those ratios and widths that are as independent and as close to the original data as possible. When one experiment measures all the branching fractions and constrains their sum to be one, we leave one of them (usually the least well-determined one) out of the fit to make the set of input data more nearly independent. We now do allow for correlations between input data.

(3) We calculate scale factors for both the  $R_r$  and  $P_i$  when the measurements for any  $R$  give a larger-than-expected contribution to the  $\chi^2$ . According to Eq. (3), the double sum for  $\chi^2$  is first summed over experiments  $k = 1$  to  $N_k$ , leaving a single sum over ratios  $\chi^2 = \sum \chi_r^2$ . One is tempted to define a scale factor for the ratio  $r$  as  $S_r^2 = \chi_r^2 / \langle \chi_r^2 \rangle$ . However, since  $\langle \chi_r^2 \rangle$  is not a fixed quantity (it is somewhere between  $N_k$  and  $N_{k-1}$ ), we do not know how to evaluate this expression. Instead we define

$$S_r^2 = \frac{1}{N_k} \sum_{k=1}^{N_k} \frac{(R_{rk} - \bar{R}_r)^2}{\langle (R_{rk} - \bar{R}_r)^2 \rangle}. \quad (4)$$

With this definition the expected value of  $S_r^2$  is one. We can show that

$$\langle (R_{rk} - \bar{R}_r)^2 \rangle = \langle (\delta R_{rk})^2 \rangle - (\delta \bar{R}_r)^2, \quad (5)$$

where  $\delta \bar{R}_r$  is the fitted error for ratio  $r$ .

The fit is redone using errors for the branching ratios that are scaled by the larger of  $S_r$  and unity, from which new and often larger errors  $\delta \bar{P}'_i$  are obtained. The scale factors we finally list in such cases are defined by  $S_i = \delta \bar{P}'_i / \delta \bar{P}_i$ . However, in line with our policy of not letting  $S$  affect the central values, we give the values of  $\bar{P}_i$  obtained from the original (unscaled) fit.

There is one special case in which the errors that are obtained by the preceding procedure may be changed. When a fitted branching ratio (or rate)  $\bar{P}_i$  turns out to be less than three standard deviations ( $\delta \bar{P}'_i$ ) from zero, a new smaller error ( $\delta \bar{P}''_i$ ) is calculated on the low side by requiring the area under the Gaussian between  $\bar{P}_i - (\delta \bar{P}''_i)^-$  and  $\bar{P}_i$  to be 68.3% of the area between zero and  $\bar{P}_i$ . A similar correction is made for branching fractions that are within three standard deviations of one. This keeps the quoted errors from overlapping the boundary of the physical region.

### 5.3 Rounding

While the results shown in the Particle Listings are usually exactly those published by the experiments, the numbers that

appear in the Summary Tables (means, averages and limits) are subject to a set of rounding rules.

The basic rule states that if the three highest order digits of the error lie between 100 and 354, we round to two significant digits. If they lie between 355 and 949, we round to one significant digit. Finally, if they lie between 950 and 999, we round up to 1000 and keep two significant digits. In all cases, the central value is given with a precision that matches that of the error. So, for example, the result (coming from an average)  $0.827 \pm 0.119$  would appear as  $0.83 \pm 0.12$ , while  $0.827 \pm 0.367$  would turn into  $0.8 \pm 0.4$ .

Rounding is not performed if a result in a Summary Table comes from a single measurement, without any averaging. In that case, the number of digits published in the original paper is kept, unless we feel it inappropriate. Note that, even for a single measurement, when we combine statistical and systematic errors in quadrature, rounding rules apply to the result of the combination. It should be noted also that most of the limits in the Summary Tables come from a single source (the best limit) and, therefore, are not subject to rounding.

Finally, we should point out that in several instances, when a group of results come from a single fit to a set of data, we have chosen to keep two significant digits for all the results. This happens, for instance, for several properties of the  $W$  and  $Z$  bosons and the  $\tau$  lepton.

### 5.4 Discussion

The problem of averaging data containing discrepant values is nicely discussed by Taylor in Ref. [5]. He considers a number of algorithms that attempt to incorporate inconsistent data into a meaningful average. However, it is difficult to develop a procedure that handles simultaneously in a reasonable way two basic types of situations: (a) data that lie apart from the main body of the data are incorrect (contain unreported errors); and (b) the opposite—it is the main body of data that is incorrect. Unfortunately, as Taylor shows, case (b) is not infrequent. He concludes that the choice of procedure is less significant than the initial choice of data to include or exclude.

We place much emphasis on this choice of data. Often we solicit the help of outside experts (consultants). Sometimes, however, it is simply impossible to determine which of a set of discrepant measurements are correct. Our scale-factor technique is an attempt to address this ignorance by increasing the error. In effect, we are saying that present experiments do not allow a precise determination of this quantity because of unresolvable discrepancies, and one must await further measurements. The reader is warned of this situation by the size of the scale factor, and if he or she desires can go back to the literature (via the Particle Listings) and redo the average with a different choice of data.

Our situation is less severe than most of the cases Taylor considers, such as estimates of the fundamental constants like  $\hbar$ , *etc.* Most of the errors in his case are dominated by systematic effects. For our data, statistical errors are often at least as large as systematic errors, and statistical errors are usually easier to estimate. A notable exception occurs in partial-wave analyses, where different techniques applied to the same data yield different results. In this case, as stated earlier, we often do not make an average but just quote a range of values.

A brief history of early Particle Data Group averages is given in Ref. [4]. On the following page, our History Plots show the time evolution of some of our values of a few particle properties. Sometimes large changes occur. These usually reflect the introduction of significant new data or the discarding of older data. Older data are discarded in favor of newer data when it is felt that the newer data have smaller systematic errors, or have more checks on systematic errors, or simply have much smaller errors. Sometimes, the scale factor becomes large near the time at which a large jump takes place, reflecting the uncertainty introduced by the new and inconsistent data. By and large, however, a full scan of our history plots shows a dull progression toward greater precision at central values quite consistent with the first data points shown.

We conclude that the reliability of the combination of experimental data and our averaging procedures is usually good, but it

is important to be aware that fluctuations outside of the quoted errors can and do occur.

#### **ACKNOWLEDGMENTS**

The publication of the *Review of Particle Physics* is supported by the Director, Office of Science, Office of High Energy Physics of the U.S. Department of Energy under Contract No. DE-AC02-05CH11231; by the European Laboratory for Particle Physics (CERN); by an implementing arrangement between the governments of Japan (MEXT: Ministry of Education, Culture, Sports, Science and Technology) and the United States (DOE) on cooperative research and development; by the Italian National Institute of Nuclear Physics (INFN); and by the Physical Society of Japan (JPS). Individual collaborators receive support for their PDG activities from their respective funding agencies.

We thank all those who have assisted in the many phases of preparing this *Review*. We particularly thank the many who have responded to our requests for verification of data entered in the Listings, and those who have made suggestions or pointed out errors.

We are grateful to the staff at CERN, IHEP Beijing, KEK, and LBNL who take care of the mailing and distribution of our

products.

This work used resources of the National Energy Research Scientific Computing Center, a DOE Office of Science User Facility supported by the Office of Science of the U.S. Department of Energy under Contract No. DE-AC02-05CH11231.

#### **References**

- [1] The previous edition was: M. Tanabashi *et al.* (Particle Data Group), *Phys. Rev.* **D98**, 030001 (2018).
- [2] C. Patrignani *et al.* (Particle Data Group), *Chin. Phys.* **C40**, 10, 100001 (2016).
- [3] M. Aguilar-Benitez *et al.* (Particle Data Group), *Phys. Lett.* **170B**, 1 (1986).
- [4] A. H. Rosenfeld, *Ann. Rev. Nucl. Part. Sci.* **25**, 555 (1975).
- [5] B.N. Taylor, “Numerical Comparisons of Several Algorithms for Treating Inconsistent Data in a Least-Squares Adjustment of the Fundamental Constants,” U.S. National Bureau of Standards NBSIR 81-2426 (1982).

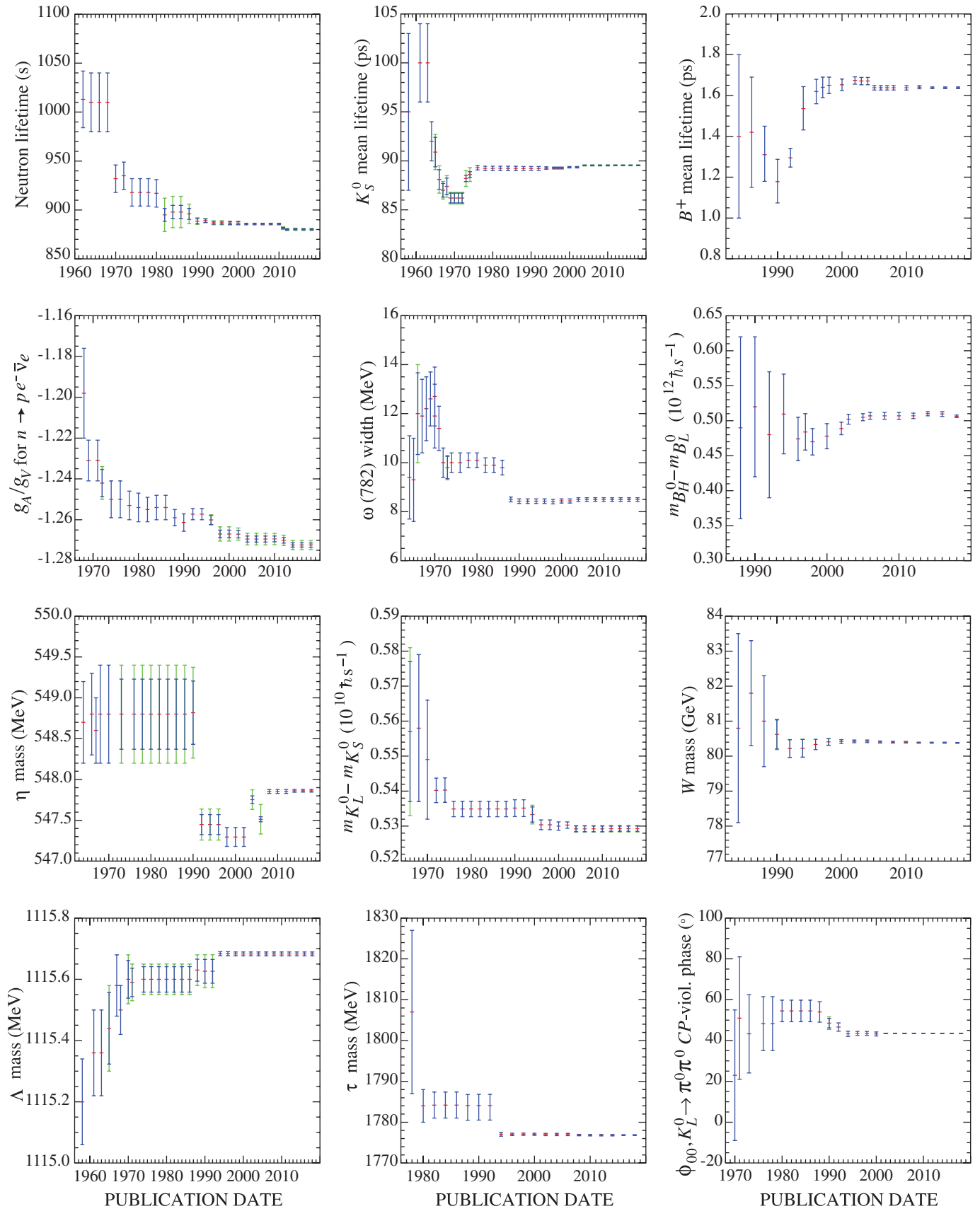


**Figure 1:** A historical perspective of values of a few particle properties tabulated in this *Review* as a function of date of publication of the *Review*. A full error bar indicates the quoted error; a thick-lined portion indicates the same but without the “scale factor.”



## Online Particle Physics Information

1	Introduction . . . . .	20
2	Particle Data Group (PDG) resources . . . . .	20
3	Particle Physics Information Platforms . . . . .	20
4	Literature Databases . . . . .	20
5	Particle Physics Journals and Conference Proceedings Series . . . . .	21
6	Conference Databases . . . . .	21
7	Research Institutions . . . . .	21
8	People . . . . .	21
9	Experiments . . . . .	21
10	Jobs . . . . .	21
11	Software Packages and Repositories . . . . .	22
11.1	Particle Physics Software . . . . .	22
11.2	Astrophysics Software . . . . .	22
11.3	Web Apps . . . . .	23
11.4	Mobile Apps . . . . .	23
12	Data repositories . . . . .	23
12.1	Particle Physics . . . . .	23
12.2	Astrophysics . . . . .	23
12.3	General Physics . . . . .	23
13	Data preservation activities . . . . .	24
13.1	Particle Physics . . . . .	24
13.2	Astrophysics . . . . .	24
14	Particle Physics Education and Outreach Sites . . . . .	24
14.1	Science Educators' Networks . . . . .	24
14.2	Physics Courses . . . . .	24
14.3	Masterclasses . . . . .	24
14.4	General Sites . . . . .	25
14.5	General Physics Activities . . . . .	25
14.6	Particle Physics Activities . . . . .	25
14.7	Lab Education Offices . . . . .	26
14.8	Educational Programs of Experiments . . . . .	27
14.9	News . . . . .	27
14.10	Art in Physics . . . . .	28
14.11	Blogs and Twitter . . . . .	28

Revised August 2019 by M. Moskvic (CERN).

### 1 Introduction

The collection of online information resources in particle physics and related areas presented in this chapter is of necessity incomplete. An expanded and regularly updated online version can be found at:

[http://library.cern/particle\\_physics\\_information](http://library.cern/particle_physics_information)  
 Suggestions for additions and updates are very welcome.<sup>1</sup>

### 2 Particle Data Group (PDG) resources

- **Review of Particle Physics (RPP):** A comprehensive report on the fields of particle physics and related areas of cosmology and astrophysics, including both review articles and a compilation/evaluation of data on particle properties. The review section includes articles, tables and plots on a wide variety of theoretical and experimental topics of interest to particle physicists and astrophysicists. The particle properties section provides tables of published measurements as well as the Particle Data Group's best values and limits for particle properties such as masses, widths, lifetimes, and branching fractions, as well as an extensive summary of searches for hypothetical particles. RPP is published as a large book every two years, with partial updates made available once each year on the web.

All the contents of the book version of RPP are available online:

<http://pdg.lbl.gov>

The printed book can be ordered:

http:

[//pdg.lbl.gov/2019/html/receive\\_our\\_products.html](http://pdg.lbl.gov/2019/html/receive_our_products.html)

Of historical interest is the complete RPP collection which can be found online:

<http://pdg.lbl.gov/rpp-archive/>

[http://library.cern/PDG\\_publications/review\\_particle\\_physics](http://library.cern/PDG_publications/review_particle_physics)

- **Particle Physics booklet:** An abridged version of the Review of Particle Physics, available as a pocket-sized 250-page booklet. It is one of the most useful summaries of physics data. The booklet contains an abbreviated set of reviews and the summary tables from the most recent edition of the Review of Particle Physics.

The PDF file of the booklet can be downloaded:

<http://pdg.lbl.gov/current/booklet.pdf>

The printed booklet can be ordered:

http:

[//pdg.lbl.gov/2019/html/receive\\_our\\_products.html](http://pdg.lbl.gov/2019/html/receive_our_products.html)

- **PDGLive:** A web application for browsing the contents of the PDG database that contains the information published in the Review of Particle Physics. It allows one to navigate to a particle of interest, see a summary of the information available, and then proceed to the detailed information published in the Review of Particle Physics. Data entries are directly linked to the corresponding bibliographic information in INSPIRE.

<http://pdglive.lbl.gov>

- **Computer-readable files:** Data files that can be downloaded from the PDG include tables of particle masses and widths, PDG Monte Carlo particle numbers, and cross-section data. The files are updated with each new edition of the Review of Particle Physics.

[http://pdg.lbl.gov/current/html/computer\\_read.html](http://pdg.lbl.gov/current/html/computer_read.html)

### 3 Particle Physics Information Platforms

- **INSPIRE:** INSPIRE serves as a one-stop information platform for the particle physics community, comprising 8 interlinked databases on literature, conferences, institutions, journals, researchers, experiments, jobs and data. Run in collaboration by CERN, DESY, Fermilab, IHEP, IN2P3, and SLAC, it has been serving the scientific community for almost 50 years. Previously known as SPIRES, it was the first website outside Europe and the first database on the web. Close interaction with the user community and with arXiv, ADS, HEPData, ORCID, PDG and publishers is the backbone of INSPIRE's evolution.

<http://inspirehep.net/>

In 2019, INSPIRE launched INSPIRE beta, featuring all-new literature search, author profiles and job postings. INSPIRE beta is running in parallel with the current platform and it will fully replace it in the future. The INSPIRE beta site is available at:

<http://beta.inspirehep.net>

– Blog: <http://blog.inspirehep.net/>

– Twitter: @inspirehep

### 4 Literature Databases

- **ADS:** The SAO/NASA Astrophysics Data System is a Digital Library portal offering access to 13 million bibliographic records in Astronomy and Physics. The ADS search engine also indexes the full-text for approximately four million publications in this collection and tracks citations, which now amount to over 80 million links. The system also provides access and links to a wealth of external resources, including electronic articles hosted by publishers and arXiv, data catalogs and a variety of data products hosted by the astronomy archives worldwide. The ADS can be accessed at:

<http://ads.harvard.edu/>

- **arXiv.org:** A repository of full-text articles in physics, astronomy, mathematics, computer science, statistics, nonlinear sciences, quantitative finance, quantitative biology, electrical engineering and systems science, and economics. Papers are submitted by registered authors to arXiv, often as preprints in advance of submission to a journal for publication; includes postprints, working papers, and other relevant material. Established in 1991, the repository is interlinked

<sup>1</sup>Please send comments and corrections to [micha.moshe.moskvic@cern.ch](mailto:micha.moshe.moskvic@cern.ch)

with ADS and INSPIRE, among others. Readers can browse subject categories or search by author, title, abstract, date, and other fields. Receive daily update alerts for subfields by email or RSS.

<https://arXiv.org>

- Blog: <https://blogs.cornell.edu/arXiv>
- Twitter: @arxiv

- **CDS:** The CERN Document Server contains records of about 700,000 CERN and non-CERN articles, preprints, theses. It includes records for internal and technical notes, official CERN committee documents, and multimedia objects. CDS is planning to focus on its role as an institutional repository covering all CERN material from the early 50s and reflecting the holdings of the CERN library. Non-CERN particle and accelerator physics content is in the process of being exported to INSPIRE.

<http://cds.cern.ch>

- **INSPIRE HEP:** The HEP collection, the flagship of the INSPIRE suite, serves more than 1.3 million bibliographic records with a growing number of full-text articles attached and metadata including author affiliations, abstracts, references, experiments, keywords as well as links to arXiv, ADS, PDG, HEPData, publisher platforms and other servers. It provides fast metadata and full-text searches, plots extracted from full text, author disambiguation, author profile pages and citation analysis and is expanding its content to, e.g., experimental notes.

<http://inspirehep.net>

- **JACoW:** The Joint Accelerator Conference Website publishes the proceedings of several accelerator conferences held around the world. A custom interface allows searching based on keywords, titles, authors, and in the full text.

<http://www.jacow.org/>

- **KEK Library Preprints and Reports Database:** This database contains bibliographic records of preprints and technical reports held in the KEK library, with links to the full-text images of more than 100,000 papers scanned from their worldwide preprint collection. Particularly useful for older scanned preprints. Links to it are included in INSPIRE HEP.

[https://www.i-repository.net/il/meta\\_pub/engG0000128Lib](https://www.i-repository.net/il/meta_pub/engG0000128Lib)

- **MathSciNet:** This database of almost 3 million items provides reviews, abstracts and bibliographic information for much of the mathematical sciences literature. Over 100,000 new items, most of them classified according to the Mathematics Subject Classification, and more than 80,000 reviews of the current published literature are added each year. Author identification allows users to search for publications by author and citation data allows users to track the history and influence of research publications.

<http://www.ams.org/mathscinet>

- **OSTI.GOV:** A portal to free, publicly available DOE-sponsored R&D results including technical reports, bibliographic citations, journal articles, conference papers, books, multimedia and data information. It consolidates OSTI's home page and the now-retired primary search tool SciTech Connect. It contains over 3 million records, including citations to 1.5 million journal articles, 1 million of which have digital object identifiers (DOIs) linking to full-text articles on publishers' websites.

<https://www.osti.gov>

## 5 Particle Physics Journals and Conference Proceedings Series

- **CERN Journal List:** This list of journals and conference series publishing particle physics content provides information on Open Access, copyright policies and terms of use.

<http://library.cern/oa/where-publish>

- **INSPIRE Journals:** The database contains over 3,600 journals publishing HEP-related articles.

<http://inspirehep.net/collection/journals>

## 6 Conference Databases

- **INSPIRE Conferences:** The database of more than 23,000 past, present, and future conferences, schools, and meetings relevant to high-energy physics and related fields is searchable by title, acronym, series, date and location. Included are information about published proceedings, links to conference contributions in the INSPIRE HEP database, and links to the conference website when available. New conferences can be submitted from the entry page.

<http://inspirehep.net/conferences>

## 7 Research Institutions

- **INSPIRE Institutions:** INSPIRE Institutions contains over 11,500 institutes, laboratories, and universities, where research on particle physics and astrophysics is led. Every record includes, whenever possible, as detailed information, such as address, web links, experiments, and links to INSPIRE papers authored by people affiliated to that institution. One can search for a particular institution by name, acronym, and location.

<http://inspirehep.net/institutions>

## 8 People

- **INSPIRE HEPNames:** Searchable worldwide database of over 125,000 active, departed, retired, and deceased people associated with particle physics and related fields. The affiliation history of these researchers, their e-mail addresses, ORCIDs, web pages, experiments they participated in, PhD advisor, information on their graduate students and links to their papers in the INSPIRE HEP, arXiv and ADS databases are provided, as well as a user interface to update this information.

<http://inspirehep.net/hepnames>

- **ORCID:** Registry providing persistent digital identifiers allowing to unambiguously identify researchers. Through integration in key research workflows such as manuscript and grant submission, it supports automated linkages between scientists and their professional activities ensuring that their work is recognized.

<https://orcid.org>

## 9 Experiments

- **INSPIRE Experiments:** Contains more than 3,500 past, present, and future experiments in particle physics. Lists both accelerator and non-accelerator experiments. Includes official experiment name and number, location, and collaboration lists. Simple searches by participant, title, experiment number, institution, date approved, accelerator, or detector, return a description of the experiment, including a complete list of authors, title, overview of the experiment's goals and methods, and a link to the experiment's web page if available. Recently, it has expanded its scope to include particle accelerators besides experiments and to link them together.

<http://inspirehep.net/Experiments>

- **Cosmic ray/Gamma ray/Neutrino and similar experiments:** This extensive collection of experiment websites is organized by focus of study and by location. Additional sections link to educational materials, organizations, and other useful resources. The site is maintained at the Max Planck Institute for Nuclear Physics, Heidelberg.

<http://www.mpi-hd.mpg.de/hfm/CosmicRay/CosmicRaySites.html>

## 10 Jobs

- **AAS Job Register:** The American Astronomical Society publishes once a month graduate, postgraduate, faculty and other positions mainly in astronomy and astrophysics.

<http://jobregister.aas.org/>

- **Academic Jobs Online:** A full-service online recruiting site for academic institutions worldwide in all disciplines and areas.

<https://academicjobsonline.org/ajo>

- **APS Careers:** A gateway for physicists, students, and physics enthusiasts to information about physics jobs and careers. It contains Physics job listings, career advice, upcoming workshops and meetings, and career and job-related resources provided by the American Physical Society.  
<http://www.aps.org/careers/employment>
- **brightrecruits.com:** A recruitment service run by IOP Publishing that connects employers from different industry sectors with jobseekers who have a background in physics and engineering.  
<http://brightrecruits.com/>
- **IOP Careers:** Career information and resources primarily aimed at university students are provided by the UK Institute of Physics.  
<http://www.iop.org/careers/>
- **INSPIRE HEPJobs:** Lists academic and research jobs in high energy physics, nuclear physics, accelerator physics and astrophysics with the option to post a job or to receive email notices of new job listings. About 500 jobs are currently listed.  
<http://inspirehep.net/jobs>
- **Physics Today Jobs:** Online recruitment advertising website for Physics Today magazine, published by the American Institute of Physics. Physics Today Jobs is the managing partner of the AIP Career Network, an online job board network for the physical science, engineering, and computing disciplines. Over 6,000 resumes are currently available, and nearly 5,000 jobs were posted in 2018.  
<http://www.physicstoday.org/jobs>

## 11 Software Packages and Repositories

Most relevant software is hosted by general-purpose repositories like GitHub, GitLab or BitBucket, but here are a few specific repositories focused on astrophysics or HEP. ## Repositories

- **ASCL:** The Astrophysics Source Code Library (ASCL) is a free online registry for source codes of interest to astronomers and astrophysicists. It lists codes that have been used in research that has appeared in, or been submitted to, peer-reviewed publications.  
<http://ascl.net>
- **GenSer:** The Generator Services project collaborates with Monte Carlo (MC) generator authors and with LHC experiments in order to prepare validated LCG compliant code for both theoretical and experimental communities at the LHC, sharing the user support duties, providing assistance for the development of the new object-oriented generators, and guaranteeing the maintenance of the older packages on the LCG supported platforms. The project consists of the generators repository, validation, HepMC record and MCDB event databases.  
<http://ep-dep-sft.web.cern.ch/project/generator-service-project-genser>
- **Hepforge:** A development environment for high-energy physics software projects, in particular housing many event-generator related projects, that offers a ready-made, easy-to-use set of web-based tools, including shell account with up-to-date development tools, web page hosting, subversion, git and Mercurial code management systems, mailing lists, bug tracker and wiki system.  
<http://www.hepforge.org/>

### 11.1 Particle Physics Software

- **FastJet:** This is a software package for jet finding in  $pp$  and  $e^+e^-$  collisions. It includes fast native implementations of many sequential recombination clustering algorithms, plugins for access to a range of cone jet finders and tools for advanced jet manipulation.  
<http://fastjet.fr/>
- **GAMBIT:** A global fitting code for generic Beyond the Standard Model theories, designed to allow fast and easy definition of new models, observables, likelihoods, scanners and

backend physics codes.

- <http://gambit.hepforge.org>
  - **Geant4:** This is a toolkit for the simulation of the passage of particles through matter. Its areas of application include high energy, nuclear and accelerator physics, as well as studies in medical and space science.  
<http://geant4.web.cern.ch/geant4/>
  - **LHAPDF:** HEP community standard library for parton distribution function interpolation, including official collection of PDF data sets.  
<http://lhpdf.hepforge.org/>
  - **QUDA:** Library for performing calculations in lattice QCD on GPUs using NVIDIA's CUDA platform. The current release includes optimized solvers for Wilson, Clover-improved Wilson, Twisted mass, Staggered, Improved staggered, Domain wall and Mobius fermion actions.  
<http://lattice.github.io/quda/>
  - **Rivet:** The Rivet toolkit, a system for validation of Monte Carlo event generators, provides a large set of experimental analyses useful for MC generator development, validation, and tuning.  
<http://rivet.hepforge.org/>
  - **ROOT:** This framework for data processing in high-energy physics, born at CERN, offers applications to store, access, process, analyze and represent data or perform simulations.  
<http://root.cern.ch>
  - **Scikit-HEP:** This is a community-driven and community-oriented project with the aim of providing Particle Physics at large with an ecosystem for data analysis in Python. The project started in Autumn 2016 and is under active development. It focuses on providing core and common tools for the community but also on improving the interoperability between HEP tools and the scientific ecosystem in Python as well as the discoverability of utility packages and projects.  
<http://scikit-hep.org>
  - **tmLQCD:** This freely available software suite provides a set of tools to be used in lattice QCD simulations, mainly a HMC implementation for Wilson and Wilson twisted mass fermions and inverter for different versions of the Dirac operator.  
<https://github.com/etmc/tmLQCD>
  - **USQCD:** The software suite enables lattice QCD computations to be performed with high performance across a variety of architectures. The page contains links to the project web pages of the individual software modules, as well as to complete lattice QCD application packages which use them.  
<http://usqcd-software.github.io>
  - **Software lists:** A list of Monte Carlo generators may be found at:  
<http://cmsdoc.cern.ch/cms/PRS/gentools/www/geners/collection/>
- The homepage of the SUSY Les Houches Accord contains links to codes relevant for supersymmetry calculations and phenomenology.  
<http://skands.physics.monash.edu/slha/>
- A variety of codes and algorithmic tools for analysing supersymmetric phenomenology is described in  
<http://arxiv.org/abs/0805.2088>
- G. Cowan's list provides links to HEP software, general statistics and data analysis links.  
<http://www.pp.rhul.ac.uk/~cowan/sda/statlinks.html>
- An extended list of more specialized HEP-related software can be found in the online version of this review:  
[http://library.cern/particle\\_physics\\_information#sof](http://library.cern/particle_physics_information#sof)

### 11.2 Astrophysics Software

- **Astropy:** The Astropy Project is a community effort to develop a single core package for Astronomy in Python and foster interoperability between Python astronomy packages.  
<http://www.astropy.org>
- **Starlink:** Starlink was a UK Project supporting astronomi-

cal data processing. It was shut down in 2005 but its open-source software continued to be developed at the Joint Astronomy Centre until March 2015. It is currently maintained by the East Asian Observatory. The open-source software products are a collection of applications and libraries, usually focused on a specific aspect of data reduction or analysis.

<http://starlink.eao.hawaii.edu/starlink>

- Links to a large number of astronomy software archives are listed at:

<http://heasarc.nasa.gov/docs/heasarc/astro-update/>

### 11.3 Web Apps

- **APFEL Web:** This online parton density function plotter allows to compare predictions for different PDF fits.  
<https://apfel.mi.infn.it/>
- **ColliderReach:** A tool to give a simple estimate of the relation between the mass reaches of different proton-proton collider configurations.  
<http://collider-reach.web.cern.ch/>
- **TMDplotter:** Allows to plot TMDs and PDFs as a function of different variables.  
<http://tmdplotter.desy.de/>

### 11.4 Mobile Apps

- **arXiv eXplorer:** Android app for browsing and searching arXiv.org, and for reading, saving and sharing articles.  
<https://play.google.com/store/apps/details?id=com.gbeatty.arxiv>
- **Collider:** This mobile app allows users to see data from the ATLAS experiment at the LHC.  
<http://collider.physics.ox.ac.uk/>
- **LHSee:** This smartphone app allows users to see collisions from the Large Hadron Collider.  
<http://www2.physics.ox.ac.uk/about-us/outreach/public/lhsee>
- **The Particles:** App for Apple iPad, Windows 8 and Microsoft Surface. Allows users to browse a wealth of real “event” images and videos, read popular “biographies” of each of the particles and explore the A-Z of particle physics with its details and definitions of key concepts, laboratories and physicists. Developed by Science Photo Library in partnership with Prof. Frank Close.  
<http://www.sciencephoto.com/apps/particles.html>

## 12 Data repositories

Data is increasingly deposited in general-purpose repositories like Zenodo (<https://zenodo.org/>), figshare (<https://figshare.com/>) or the Open Science Framework (<https://osf.io/>), but here are a few specific repositories focused on physics.

### 12.1 Particle Physics

- **HEPData:** The HEPData project, funded by the STFC (UK) and based at Durham University, has been built up over the past four decades as a unique repository for scattering data from experimental particle physics papers. It currently comprises the data points from plots and tables related to several thousand publications including those from the LHC. The data from HEPData can also be accessed through INSPIRE. A new enhanced service was recently developed in collaboration with CERN.  
<https://hepdata.net>
- **CERN Open Data:** The CERN Open Data portal provides data from real collision events, as well as simulated and simplified datasets, produced by the experiments at the LHC, virtual machines to reproduce the analysis environment, and software to process the data. It serves over 2 PB of data in total and encourages their use for both educational and research purposes.  
<http://opendata.cern.ch>
- **HepSim:** A repository with Monte Carlo simulations for particle-collision experiments. It contains predictions from

parton shower models and includes Monte Carlo events after fast and full detector simulations and event reconstruction.

<http://atlaswww.hep.anl.gov/hepsim/>

- **ILDG:** The International Lattice Data Grid is an international organization which provides standards, services, methods and tools that facilitate the sharing and interchange of lattice QCD gauge configurations among scientific collaborations by uniting their regional data grids. It offers semantic access with local tools to worldwide distributed data.  
<http://www.usqcd.org/ildg/>
- **MCDB - Monte Carlo Database:** This central database of MC events aims to facilitate communication between Monte-Carlo experts and users of event samples in LHC collaborations. Having these events stored in a public place along with the corresponding documentation allows for direct cross checks of the performances on reference samples.  
<http://mcdb.cern.ch/>
- **MCPLOTS:** MCPLOTS is a repository of Monte Carlo plots comparing High Energy Physics event generators to a wide variety of available experimental data. The website is supported by the LHC Physics Centre at CERN.  
<http://mcplots.cern.ch/>

### 12.2 Astrophysics

- **CfA Dataverse:** This astronomy data repository at Harvard is open to all scientific data from astronomical institutions worldwide.  
<https://dataverse.harvard.edu/dataverse/cfa>
- **NASA’s HEASARC:** The High Energy Astrophysics Science Archive Research Center (HEASARC) is the primary archive for NASA’s (and other space agencies’) missions dealing with electromagnetic radiation from extremely energetic phenomena ranging from black holes to the Big Bang.  
<http://heasarc.gsfc.nasa.gov/>
- **NASA archives:** The NASA archives provide access to raw and processed datasets from numerous NASA missions. Mikulski Archive for Space Telescopes (MAST): Hubble telescope, other missions (UV, optical):  
<http://archive.stsci.edu/>  
NASA/IPAC Infrared Science Archive: Spitzer, Herschel, Planck telescope, other missions:  
<http://irsa.ipac.caltech.edu/>
- **NASA/IPAC Extragalactic Database (NED):** An astronomical database that collates and cross-correlates information on extragalactic objects. It contains their positions, basic data, and names as well as bibliographic references to published papers, and notes from catalogs and other publications. NED supports searches for objects and references, and offers browsing capabilities for abstracts of articles of extragalactic interest.  
<http://ned.ipac.caltech.edu/>
- **SIMBAD:** The SIMBAD astronomical database provides basic data, cross-identifications, bibliography and measurements for astronomical objects outside the solar system. It can be queried by object name, coordinates and various criteria. Lists of objects and scripts can be submitted.  
<http://simbad.u-strasbg.fr/simbad/>
- **VizieR:** VizieR provides access to the most complete library of published astronomical catalogues and data tables, available online organized in a self-documented database. Query tools allow users to select relevant data tables and extract and format records matching given criteria. Currently, more than 19,000 catalogues are available.  
<http://vizier.u-strasbg.fr/>

### 12.3 General Physics

- **NIST Physical Measurement Laboratory:** The National Institute of Standards and Technology provides access to physical reference data (physical constants, atomic spectroscopy data, x-ray and gamma-ray data, radiation dosimetry data, nuclear physics data and more) and measurements

and calibrations data (dimensional and electromagnetic measurements).

<https://www.nist.gov/pml/>

- **Springer Materials - The Landolt-Börnstein Database:** Landolt-Börnstein is a data collection covering all areas of physical sciences and engineering, such as particle physics, electronic structure and transport, magnetism, superconductivity. International experts scan the primary literature in more than 8,000 peer-reviewed journals and evaluate and select the most valid information to be included in the database. It includes more than 130,000 online documents, 1.2 million references, and covers 250,000 chemical substances. SpringerMaterials Interactive allows to visualise and analyse data. The search functionality is freely accessible and the search results are displayed in their context, whereas the full text is secured to subscribers.

<http://materials.springer.com>

## 13 Data preservation activities

### 13.1 Particle Physics

- **CERN Analysis Preservation:** CERN Analysis Preservation is a platform for preserving knowledge and assets of individual physics analyses in LHC collaborations. Its aim is to capture and document all the elements needed to understand and rerun an analysis even several years later: data, software, environment, workflow, context, and documentation. This platform is currently in a pilot stage. It is accessible by LHC experimental groups (standard collaboration access restrictions are applied).

<https://analysispreservation.cern.ch>

- **DASPOS:** A collective effort to explore the realisation of a viable data, software and algorithm preservation architecture in High Energy Physics

<https://daspos.crc.nd.edu>

- **DPHEP:** DPHEP coordinates the efforts to define and implement Data Preservation and Long Term Analysis in HEP. DPHEP, which was initiated as a study group in 2008-2009, includes all major HEP experiments and labs. In 2014, it has become a Collaboration through the signature of a Collaboration Agreement by a number of large funding agencies. The group is endorsed by the International Committee for Future Accelerators (ICFA).

DPHEP regularly organizes workshops, creates status reports, and maintains links with similar activities in other disciplines. Details of the organizational structure, the objectives, workshops and publications can be found on the website.

<http://dphep.org>

- **REANA:** REANA (REusable ANALyses) is a system for instantiating research data analyses on the cloud using container-based solutions. It complements CERN Analysis Preservation permitting the reuse and revalidation of preserved analyses. It is being developed in close collaboration with DASPOS and RECAST.

<http://reanahub.io/>

- **RECAST:** Building on analysis preservation and re-use infrastructure of the LHC experiments, RECAST acts as a science gateway allowing theorists to suggest new reinterpretations of archived analyses of the LHC dataset. Experiments review suggestions and, if approved, simulate the proposed models and re-run the archived analysis to determine their viability. Such reinterpretation results are then appended to the records of the original publication in the relevant digital archives.

<https://recast.cern.ch>

### 13.2 Astrophysics

More formal and advanced data preservation activity is ongoing in the field of Experimental Astrophysics, including:

- Fermi Data  
<https://fermi.gsfc.nasa.gov/ssc/data>

- IVOA (International Virtual Observatory Alliance)  
<http://www.ivoa.net/astronomers/applications.html>
- GWOSC (Gravitational Wave Open Science Center)  
<https://www.gw-openscience.org/about/>
- PLA (Planck Legacy Archive)  
<http://pla.esac.esa.int/pla/>
- SDSS (Sloan Digital Sky Survey)  
<http://sdss.org>

## 14 Particle Physics Education and Outreach Sites

A useful list of resources can also be found at

<http://www.stfc.ac.uk/research/particle-physics-and-particle-astronautics/particle-physics-resources/>

### 14.1 Science Educators' Networks

- **IPPOG:** The International Particle Physics Outreach Group is a network of scientists, science educators and communication specialists working across the globe in informal science education and outreach for particle physics. The IPPOG collaboration comprises 30 members: 24 countries, 5 experiments and CERN as an international laboratory.

<http://ippog.web.cern.ch>

- **Interactions.org:** Designed to serve as a central resource for communicators of particle physics. The daily updated website provides links to current particle physics news from the world's press, high-resolution photos and graphics from the particle physics laboratories of the world; links to education and outreach programs; information about science policy and funding; a glossary; and links to many educational sites.

<http://www.interactions.org>

- **QuarkNet:** The QuarkNet Collaboration is a national program that partners high school science teachers with particle physicists working in experiments at CERN or Fermilab. The network consists of over 50 centers at research groups in universities and labs across the United States. About 100,000 students from 500+ U.S. high schools learn fundamental physics as they participate in inquiry-oriented investigations and analyze authentic data online. QuarkNet is supported in part by the National Science Foundation and Fermilab.

<https://quarknet.org/>

- **Netzwerk Teilchenwelt:** Behind the project are about 200 researchers from 30 institutes and universities doing research in particle physics, astroparticle physics and hadron and nuclear physics in Germany. Exciting young scientists throughout Germany for particle physics and accompanying them from school to top-level particle physics research—that's what they have set their sights on.

<https://www.teilchenwelt.de>

### 14.2 Physics Courses

- **MIT OpenCourseWare - Physics:** These MIT course materials reflect almost all the undergraduate and graduate subjects taught at MIT. In addition to physics courses, supplementary educational resources are also available.

<http://ocw.mit.edu/courses/physics/>

- **OnlineCourses.com:** A collection of online tests, video lectures, and related course materials from mostly prestigious universities around the world.

<http://www.onlinecourses.com/physics/>

### 14.3 Masterclasses

- **Cosmic Ray Studies:** There are more than 12 projects around the world that address young people and teachers giving them an opportunity to explore cosmic particles, collecting, uploading and analyzing data and sharing results. Two annual events include International Cosmic Day and International Muon Week.

<https://icd.desy.de>

<https://quarknet.org/content/international-muon-week>

- **Hands-On Universe:** This program enables students to investigate the Universe while applying tools and concepts from science, math and technology.

<http://handsonuniverse.org/>

- **HYPATIA:** HYPATIA (Hybrid Pupil's Analysis Tool for Interactions in ATLAS) is a tool for high school students to inspect the graphic visualization of particle collision products in the ATLAS detector at CERN.

<http://hypatia.phys.uoa.gr/>

- **International Masterclasses:** Each year about 13,000 high school students in 55 countries come to one of about 225 nearby universities or research centres for a day to unravel the mysteries of particle physics. Lectures from active scientists give insight in topics and methods of basic research enabling the students to perform measurements on real data from one of seven experiments. At the end of the day, like an international research collaboration, participants join a video conference for discussion and combination of results. The program is coordinated from Institut für Kern- und Teilchenphysik at TU Dresden and the Notre Dame University QuarkNet Center within the framework of the International Particle Physics Outreach Group (IPPOG). CERN, Fermilab and TRIUMF support videoconferences.

<https://physicsmasterclasses.org>

World Wide Data Day is an annual event.

<https://quarknet.org/content/world-wide-data-day>

- **LHC physics Masterclasses:** Lectures from active scientists give insight into methods of basic research, enabling the students to perform measurements on real data from LHC experiments. Like in a real research collaboration, the participants then discuss their results and compare with expectations.

<http://cms.web.cern.ch/content/cms-physics-masterclass>

<http://lhcb-public.web.cern.ch/lhcb-public/en/LHCb-outreach/masterclasses/en>

<http://alice.physicsmasterclasses.org/MasterClassWebpage.html>

<http://atlas-minerva.web.cern.ch/atlas-minerva>

- **IceCube Masterclass:** The program is inspired by the International Masterclasses program started by IPPOG and is coordinated by the Wisconsin IceCube Particle Astrophysics Center with support from QuarkNet.

<https://masterclass.icecube.wisc.edu/>

#### 14.4 General Sites

- **Contemporary Physics Education Project (CPEP):** Provides charts, brochures, Web links, and classroom activities. Online interactive courses include: Fundamental Particles and Interactions; Plasma Physics and Fusion; History and Fate of the Universe; and Nuclear Science.

<http://www.cpepweb.org/>

- **PhysicsCentral:** This site maintained by the American Physical Society provides information about current research and people in physics, experiments that can be performed at home or at school and the possibility to get physics questions answered by physicists.

<http://www.physicscentral.com>

#### 14.5 General Physics Activities

- **HyperPhysics:** An exploration environment for concepts in physics employing concept maps and other linking strategies and providing opportunities for numerical exploration.

<http://hyperphysics.phy-astr.gsu.edu/hbase/hph.html>

- **PhET Interactive Simulations:** Founded in 2002 by Nobel Laureate Carl Wieman, the PhET Interactive Simulations project at the University of Colorado Boulder creates free interactive math and science simulations. PhET sims are based on extensive education research and engage students through an intuitive, game-like environment where students learn through exploration and discovery.

<https://phet.colorado.edu/en/simulations/category/physics>

#### 14.6 Particle Physics Activities Citizen Science

- **Higgs Hunters:** A web-based citizen science project to help search for unknown exotic particles in the LHC data.

<http://HiggsHunters.org>

- **LHC @ home:** Volunteer computing platform to help physicists compare theory with experiment, in the search for new fundamental particles and answers to questions about the Universe.

<http://lhcatome.web.cern.ch>

#### Classroom Activities Collections

- **Contemporary Physics Education Project - Fundamental particle and interactions:**

<http://www.cpepphysics.org/particles.html>

- **Fermilab Physical Science/Physics Resources:**

<https://ed.fnal.gov/home/educators1000-physics.shtml>

- **IceCube Activities:**

<https://icecube.wisc.edu/outreach/activities>

- **IPPOG Resources:**

<http://ippog.org/resources>

- **Jefferson Lab Teacher Resources:**

<https://education.jlab.org/indexpages/teachers.html>

- **LIGO Classroom Activities:**

<https://www.ligo.caltech.edu/page/classroom-activities>

- **MINERvA Neutrinos in the Classroom:**

<https://neutrino-classroom.org>

- **Perimeter Institute Educational Resources:**

<https://resources.perimeterinstitute.ca>

- **Quarked Lesson Plans:**

<http://www.quarked.org/parents/lessonplans.html>

- **QuarkNet Data Activities Portfolio:**

<https://quarknet.org/data-portfolio>

- **Sanford Lab curriculum materials:**

<https://sanfordlab.org/educators/curriculum-modules>

#### Interactive Sites

- **CAMELIA:** CAMELIA (Cross-platform Atlas Multimedia Educational Lab for Interactive Analysis) is a discovery tool for the general public, based on computer gaming technology.

<https://www.atlasexperiment.org/camelia.html>

- **CERNland:** With a range of games, multimedia applications and films CERNland is a virtual theme park developed to bring the excitement of CERN's research to a young audience aged between 7 and 12. CERNland is designed to show children what is being done at CERN and inspire them with some physics.

<http://www.cernland.net/>

- **In particular:** Podcast and more about physics and the process of discovering physics at the ATLAS experiment.

<https://inparticular.web.cern.ch/>

- **Lancaster Particle Physics:** Suitable for 16+ students, this site offers a number of simulations and explanations of particle physics, including a section on the LHC.

<http://www.lppp.lancs.ac.uk/>

- **Quarked!** - Adventures in the Subatomic Universe: This project, targeted to kids aged 7-12 (and their families), brings subatomic physics to life through a multimedia project including an interactive website, a facilitated program for museums and schools, and an educational outreach program.

<http://www.quarked.org/>



**Planetarium Show**

- **Phantom of the Universe:** A planetarium show about dark matter that covers astrophysics, an underground experiment, and the LHC. It is distributed to planetariums for free.

<http://phantomoftheuniverse.com/>

**Video/Film**

- **Angels and Demons:** With the aim of looking at the myth versus reality of antimatter and science at CERN this site describes the science behind the story including a set of videos.  
<http://angelsanddemons.web.cern.ch/>
- **CollidingParticles:** A series of films following a team of physicists involved in research at the LHC.  
<http://www.collidingparticles.com/>
- **Rewarding Learning videos about CERN:** The three videos based on interviews with scientists and engineers at CERN introduce pupils to CERN and the type of research and work undertaken there and are accompanied by teachers' notes.  
<http://www.nicurriculum.org.uk/STEMWorks/resources/cern/index.asp>
- **Videos by Don Lincoln:** Short YouTube videos on basic particle physics and cosmology.  
<https://www.youtube.com/playlist?list=PLCfRa7MXBEsoJuAM8s6D8oKDPyBepBosS>

**Websites \* Cambridge Relativity and Cosmology:** Materials for the greater public to learn about the Origins of the Universe, including information on black holes, string theory, M-theory, the cosmic microwave background and the structure of the Universe.

<http://www.damtp.cam.ac.uk/research/gr/public/index.html>

\* **Imagine the Universe:** This site is for students age 14 and up and for anyone interested in learning about the Universe.

<http://imagine.gsfc.nasa.gov/home.html>

\* **Particle Adventure:** An interactive tour of quarks, neutrinos, antimatter, extra dimensions, dark matter, accelerators and particle detectors from the Particle Data Group of Lawrence Berkeley National Laboratory. Simple elegant graphics and translations into 16 languages.

<http://particleadventure.org/>

**14.7 Lab Education Offices**

- **Argonne National Laboratory (ANL) Educational Programs:** Connecting today's world-class research to tomorrow's STEM problem solvers.  
<http://www.anl.gov/education/>
- **Brookhaven National Laboratory (BNL) Educational Programs:** The Office of Educational Programs mission is to design, develop, implement, and facilitate workforce development and education initiatives that support the scientific mission at Brookhaven National Laboratory and the Department of Energy.  
<http://www.bnl.gov/education/>
- **CERN's education programmes:** CERN's education and outreach programmes cover all ages from high-school students to university students. Specifically, CERN offers the tailor-made High-School Students Internship Programme several times per year and the Beamline for Schools Competition, challenging high-school students from around the world to propose an experiment to carry out at a real research laboratory. The Laboratory also runs residential programmes for high-school teachers from around the world and a summer programme for undergraduate students.  
<https://home.cern/about/what-we-do/our-educational-programmes>
- **DESY Education:** DESY Hamburg offers a regular series of public lectures and the DESY Science Café for young and old alike.  
[https://fortbildung.desy.de/index\\_eng.html](https://fortbildung.desy.de/index_eng.html)

- **DESY Zeuthen Outreach:** Posters, photos, lectures, videos and blogs. Projects for teachers and students include School Labs, Cosmic@Web, Teilchenwelt and International Cosmic Day.

<https://astro.desy.de/outreach>

- **Fermilab Office of Education and Public Outreach:** Provides education resources and information about activities for 's, physicists, students and visitors to the Lab. In addition to information about 25 programs, the website provides online data-based investigations for high school students, online versions of exhibits in the Lederman Science Center, links to particle physics discovery resources, web-based instructional resources, tips for education and outreach, and links to the Lederman Science Center and the Teacher Resource Center.

<http://ed.fnal.gov/>

- **Perimeter Institute Outreach:** Perimeter Institute shares ideas with students, teachers, and like-minded people through programs and resources that communicate the power, joy, and mystery of science. Perimeter's award-winning Outreach team brings science to life and raises scientific literacy through classroom resources, public lectures, teacher workshops, an educator network, and a summer school where students interact with Perimeter researchers.

<https://www.perimeterinstitute.ca/outreach>

- **Science Education at Jefferson Lab:** Jefferson Lab's long-term commitment to science education continues to focus on increasing the number of teachers with a substantial background in math and science, strengthening the motivation and preparation of all students, especially minorities and females, and addressing the serious under representation of minorities and females in science, math, engineering and technology careers.

<http://education.jlab.org/>

- **Joint Institute for Nuclear Research Education (JINR):** The JINR educational portal has resources, programs for teachers and school students and lab tours.

<http://www.jinr.ru/schoolstudents-teachers-en/>

- **Laboratori Nazionali di Frascati Educational (INFN):** INFN educational programs are addressed to students, teachers and general audiences of every age, from Italy and abroad. Insights and education about the INFN-LNF research are offered thanks to the organization of guided tours and open days, stages for students, refresher courses for teachers, seminars and divulgation events. The aim is to create a constant exchange between the research world and society, thanks to direct contact and via the internet and other social media.

<http://edu.lnf.infn.it/about/?lang=en>

- **Laboratori Nazionali del Gran Sasso Outreach Activities:** The Lab offers pupils the opportunity to approach the fascinating world of Physics and Science in general through stages, summer schools and training camps. It makes young researchers' skills and competences available to people both in public events, such as the Open Day and the European Researchers' Night, and in guided tours to visit the underground experimental halls.

<https://www.lngs.infn.it/en/outreach-activities>

- **Lawrence Berkeley National Laboratory (LBNL) Workforce Development and Education:** Working with our partners both within and outside Berkeley Lab, LBNL promotes equal access to scientific and technical careers for students from all backgrounds, supports STEM teachers, and build scientific literacy through innovative education programs. The lab also supports educational outreach efforts from Berkeley Lab's divisions by providing program development assistance, materials, funding, volunteers, project management, marketing, and administrative support.

<https://education.lbl.gov/>

- **Sanford Underground Research Facility Education and Outreach:** Leveraging research being conducted underground at Sanford Lab, staff provide training, teaching

tools and materials for teachers so they can inspire and challenge students.

<https://sanfordlab.org/educators>

- **SNOLAB Outreach:** The goal at SNOLAB is to develop new educational material that fosters an appreciation of the field of astroparticle physics. The education team endeavours to facilitate an exchange of knowledge with the public and scientists from around the world to better understand our solar system. The desired outcome of the educational work is to have a network of healthy and resilient community partners with informed and active citizens better equipped to understand the goals here at SNOLAB now and in the future.

<https://www.snolab.ca/outreach>

- **TRIUMF High School Programs:** TRIUMF offers outreach programs for high-school students, teachers, and the general public with a mission of promoting science and research in the public arena. TRIUMF's outreach activities are also designed to tell Canadian students, teachers, and the public about the excitement of curiosity-driven research and about how a laboratory like TRIUMF adds value to Canada in new technologies, medical applications, and highly qualified people.

<https://www.triumf.ca/for-public/high-school-programs>

- **LBL Workforce Development and Education:** This group carries out Berkeley Lab's mission to inspire and prepare the next generation of scientists, engineers, and technicians.

<https://education.lbl.gov/>

#### 14.8 Educational Programs of Experiments

- **ATLAS Education:** The ATLAS Experiment has a wide range of educational resources available for students and teachers. Categories include primary and secondary school students, university students, teachers, citizen science, and multimedia and resources.

<https://atlas.cern/resources/education>

- **CMS Education and Outreach Resources:** Access to 110 resources from Activities and Artworks to Visualizations.

<https://cds.cern.ch/collection/CMS%20Education%20and%20Outreach%20Resources?ln=en>

- **HiSPARC at UCU:** HiSPARC is an outreach, educational and research experiment on cosmic rays detection, which was initiated in the Netherlands in 2004. It brings together secondary school students and teachers, undergraduate students and university researchers in the quest to understand the origin of the most energetic particles in our universe. HSPARC has stations in the Netherlands, the United Kingdom, Denmark and Namibia.

<https://www.uu.nl/en/organisation/university-college-utrecht/hisparc-at-ucu>

- **IceCube Education and Outreach:** IceCube is committed to bringing science to a wider audience. Learning opportunities for high school students, research experiences for teachers and undergraduates, learning activities for the classroom or at home, and webcasts.

<https://icecube.wisc.edu/outreach>

- **KASCADE and KASCADE-Grande KDC:** The aim of the project KDC (KASCADE Cosmic Ray Data Centre) is the installation and establishment of a public data centre for high-energy astroparticle physics based on the data of the KASCADE experiment.

<https://kdc.ipk.kit.edu>

- **LIGO Education Resources:** Something fun and educational for K-12 educators, parents and interested students.

<https://www.ligo.caltech.edu/page/educational-resources>

- **MINERvA Neutrinos in the Classroom:** Information and educational materials provide high school physics students with an in-depth hands-on interactive experience with real high-energy particle physics. The materials should be

suitable for a 1-2 weeks module on particle physics as it's done by professional scientists.

<https://neutrino-classroom.org>

- **VIRGO Educational Resources:** Useful resources (websites, texts, videos) for teachers and students related to gravitational waves and the interferometers like Virgo.

<http://public.virgo-gw.eu/educational-resources/>

- **Pierre Auger Observatory's Educational Pages:** The site offers information about cosmic rays and their detection, and provides material for students and teachers.

<https://www.auger.org/index.php/edu-outreach>

#### 14.9 News

- **Asimmetrie:** Bimonthly magazine about particle physics published by INFN, the Istituto Nazionale di Fisica Nucleare (in Italian).

<http://www.asimmetrie.it/>

- **CERN Courier:**

– Website: <https://cerncourier.com>

– Twitter: @cerncourier

- **DESY inForm:**

– Website: [http://www.desy.de/news/desy\\_inform/index\\_eng.html](http://www.desy.de/news/desy_inform/index_eng.html)

– Twitter: @desy

- **Fermilab News:**

– Website: <https://news.fnal.gov>

– Twitter: @Fermilab

- **LC Newsline:** The newsletter of the Linear Collider community.

<http://newsline.linearcollider.org/>

– Twitter: @LCnewsline

- **IOP News:**

<http://www.iop.org/news/>

- **JINR News:**

[http://www1.jinr.ru/News/Jinrnews\\_index.html](http://www1.jinr.ru/News/Jinrnews_index.html)

- **News at Interactions.org:** The Interactions site provides news and press releases on particle physics.

<http://www.interactions.org/news-center>

– Twitter: @particlnews

- **Perimeter Institute News:**

– Website: <https://www.perimeterinstitute.ca/news>

– Twitter: @perimeter

- **Sanford News and Events:**

– Website: <https://sanfordlab.org/news-and-events>

– Twitter: @SanforLab

- **SLAC Signals:** This email newsletter reports about cutting-edge science, major SLAC milestones and other lab information. It has replaced SLAC Today in November 2013. Its signup page can be found at

<http://eepurl.com/IqP11>

- **SNOLAB News and Headline:**

<https://www.snolab.ca/news>

- **Symmetry:** This magazine about particle physics and its connections to other aspects of life and science, from interdisciplinary collaborations to policy to culture is published 6 times per year by Fermilab and SLAC.

<http://www.symmetrymagazine.org/>

– Twitter: @symmetrymag

- **TRIUMF on NewsWise:**

<https://www.newswise.com/institutions/newsroom/19528>

#### 14.10 *Art in Physics*

- **Arts@CERN - When Art Meets Science:** Arts at CERN is the leading art and science programme promoting the dialog between artists and particle physicists. Programmes include Art Commissions and Exhibitions, Collide, Accelerate and Guest Artists.

<https://arts.cern>

The Collide@CERN residency programme aims to develop expert knowledge in the arts through the connection with fundamental science. Since 2011 the COLLIDE award calls to artists to win a fully funded residency for up to 3 months.

<https://arts.cern/programme/collide>

Accelerate@CERN is a country specific one-month research award for artists who have never spent time at a science lab before.

<https://arts.cern/programme/accelerate>

- **Art of Physics Competition:** The Canadian Association of Physicists organizes this competition, the first was launched in 1992, with the aim of stimulating interest, especially among non-scientists, in some of the captivating imagery associated with physics. The challenge is to capture photographically a beautiful or unusual physics phenomenon and explain it in less than 200 words in terms that everyone can understand.

<https://www.cap.ca/programs/art-physics/>

- **Fermilab Art Gallery:** The convergence of art and science occurs daily in the Fermilab Art Gallery open to the public. To initiate and stimulate communication and interactions among scientists, artists and the public, the laboratory hosts an artist-in-residence program. The artist-in-residence interacts with scientists to learn about their research and how it connects to society. They use this information to create a body of work, leading to presentations in the community and possibly an exhibition of the artwork at Fermilab.

<http://events.fnal.gov/art-gallery/>

- **TRIUMF Science through Art:** TRIUMF's Science through Art initiatives explore the space where art and science collide. These programs bring artists and TRIUMF researchers, engineers, technicians, tradespeople, and students together to explore new ways of thinking about science, discovery, creativity, and our universe.

<https://www.triumf.ca/science-through-art>

#### 14.11 *Blogs and Twitter*

Lists of active blogs and tweets can be found on INSPIRE:

- **Scientist blogs:**  
<http://tinyurl.com/nmku27s>
- **Scientists with twitter accounts:**  
<http://tinyurl.com/nrg5k63>
- **Experiments with twitter accounts:**  
<http://tinyurl.com/q86kma8>
- **Institutions with twitter accounts:**  
<http://tinyurl.com/mzcm3nw>

List of physicists on Twitter at TrueSciPhi:

<http://truesciphi.org/phy.html>

Some selected particle physics related blogs:

- **ATLAS blog:**  
<https://atlas.cern/updates/blog>
- **Life and Physics:** Jon Butterworth's blog in the Guardian.  
<http://www.guardian.co.uk/science/life-and-physics>
- **Of Particular Significance:** Conversations about science, with a current focus on particle physics, with theoretical physicist Matt Strassler.  
<http://profmattstrassler.com/>
- **Particle People:** This interactions.org page highlights a new blogger involved in particle physics research each month.  
<http://www.interactions.org/particle-people>
- **Preposterous Universe:** Theoretical physicist Sean Carroll's blog.  
<https://www.preposterousuniverse.com/blog/>
- **Quantum diaries:** Thoughts on work and life from particle physicists from around the world, from 2005 to 2016.  
<http://www.quantumdiaries.org/>
- **Quantum diaries survivor:** Experimental particle physicist Tommaso Dorigo's blog.  
[https://www.science20.com/quantum\\_diaries\\_survivor](https://www.science20.com/quantum_diaries_survivor)
- **Science blogs:** Launched in January 2006, ScienceBlogs features bloggers from a wide array of scientific disciplines, including physics.  
<http://scienceblogs.com/channel/physical-science/>
- **AstroBetter:** Blog with tips and tricks for professional astronomers.  
<https://www.astrobetter.com/>

## SUMMARY TABLES OF PARTICLE PHYSICS

Gauge and Higgs bosons . . . . .	31
Leptons . . . . .	34
Quarks . . . . .	37
Mesons . . . . .	38
Baryons . . . . .	93
Searches not in Other Sections* . . . . .	111
Tests of conservation laws . . . . .	113
Meson Quick Reference Table . . . . .	91
Baryon Quick Reference Table . . . . .	92

\* There are also search limits in the Summary Tables for the Gauge and Higgs Bosons, the Leptons, the Quarks, and the Mesons.



## SUMMARY TABLES OF PARTICLE PROPERTIES

Extracted from the Particle Listings of the  
*Review of Particle Physics*

P.A. Zyla *et al.* (Particle Data Group),  
Prog. Theor. Exp. Phys. **2020**, 083C01 (2020)

Available at <http://pdg.lbl.gov>

## Particle Data Group

P.A. Zyla, R.M. Barnett, J. Beringer, O. Dahl, D.A. Dwyer, D.E. Groom, C.-J. Lin, K.S. Lugovsky, E. Pianori, D.J. Robinson, C.G. Wohl, W.-M. Yao, K. Agashe, G. Aielli, B.C. Allanach, C. Amsler, M. Antonelli, E.C. Aschenauer, D.M. Asner, H. Baer, Sw. Banerjee, L. Baudis, C.W. Bauer, J.J. Beatty, V.I. Belousov, S. Bethke, A. Bettini, O. Biebel, K.M. Black, E. Blucher, O. Buchmuller, V. Burkert, M.A. Bychkov, R.N. Cahn, M. Carena, A. Ceccucci, A. Cerri, D. Chakraborty, R. Sekhar Chivukula, G. Cowan, G. D'Ambrosio, T. Damour, D. de Florian, A. de Gouvêa, T. DeGrand, P. de Jong, G. Dissertori, B.A. Dobrescu, M. D'Onofrio, M. Doser, M. Drees, H.K. Dreiner, P. Eerola, U. Egede, S. Eidelman, J. Ellis, J. Erler, V.V. Ezhela, W. Fetscher, B.D. Fields, B. Foster, A. Freitas, H. Gallagher, L. Garren, H.-J. Gerber, G. Gerbier, T. Gershon, Y. Gershtein, T. Gherghetta, A.A. Godizov, M.C. Gonzalez-Garcia, M. Goodman, C. Grab, A.V. Gritsan, C. Grojean, M. Grünewald, A. Gurtu, T. Gutsche, H.E. Haber, C. Hanhart, S. Hashimoto, Y. Hayato, A. Hebecker, S. Heinemeyer, B. Heltsley, J. J. Hernández-Rey, K. Hikasa, J. Hisano, A. Höcker, J. Holder, A. Holtkamp, J. Huston, T. Hyodo, K.F. Johnson, M. Kado, M. Karliner, U.F. Katz, M. Kenzie, V.A. Khoze, S.R. Klein, E. Klempt, R.V. Kowalewski, F. Krauss, M. Kreps, B. Krusche, Y. Kwon, O. Lahav, J. Laiho, L.P. Lellouch, J. Lesgourgues, A. R. Liddle, Z. Ligeti, C. Lippmann, T.M. Liss, L. Littenberg, C. Lourenço, S.B. Lugovsky, A. Lusiani, Y. Makida, F. Maltoni, T. Mannel, A.V. Manohar, W.J. Marciano, A. Masoni, J. Matthews, U.-G. Meißner, M. Mikhasenko, D.J. Miller, D. Milstead, R.E. Mitchell, K. Mönig, P. Molaro, F. Moortgat, M. Moskvic, K. Nakamura, M. Narain, P. Nason, S. Navas, M. Neubert, P. Nevski, Y. Nir, K.A. Olive, C. Patrignani, J.A. Peacock, S.T. Petcov, V.A. Petrov, A. Pich, A. Piepke, A. Pomarol, S. Profumo, A. Quadt, K. Rabbertz, J. Rademacker, G. Raffelt, H. Ramani, M. Ramsey-Musolf, B.N. Ratcliff, P. Richardson, A. Ringwald, S. Roesler, S. Rolli, A. Romaniouk, L.J. Rosenberg, J.L. Rosner, G. Rybka, M. Ryskin, R.A. Ryutin, Y. Sakai, G.P. Salam, S. Sarkar, F. Sauli, O. Schneider, K. Scholberg, A.J. Schwartz, J. Schwiening, D. Scott, V. Sharma, S.R. Sharpe, T. Shutt, M. Silari, T. Sjöstrand, P. Skands, T. Skwarnicki, G.F. Smoot, A. Soffer, M.S. Sozzi, S. Spanier, C. Spiering, A. Stahl, S.L. Stone, Y. Sumino, T. Sumiyoshi, M.J. Syphers, F. Takahashi, M. Tanabashi, J. Tanaka, M. Tañasevský, K. Terashi, J. Terning, U. Thoma, R.S. Thorne, L. Tiator, M. Titov, N.P. Tkachenko, D.R. Tovey, K. Trabelsi, P. Urquijo, G. Valencia, R. Van de Water, N. Varelas, G. Venanzoni, L. Verde, M.G. Vincter, P. Vogel, W. Vogelsang, A. Vogt, V. Vorobyev, S.P. Wakely, W. Walkowiak, C.W. Walter, D. Wands, M.O. Wascko, D.H. Weinberg, E.J. Weinberg, M. White, L.R. Wiencke, S. Willocq, C.L. Woody, R.L. Workman, M. Yokoyama, R. Yoshida, G. Zanderighi, G.P. Zeller, O.V. Zenin, R.-Y. Zhu, S.-L. Zhu, F. Zimmermann

## Technical Associates:

J. Anderson, T. Basaglia, V.S. Lugovsky, P. Schaffner, W. Zheng

©2020 Regents of the University of California  
(Approximate closing date for data: January 15, 2020)

## GAUGE AND HIGGS BOSONS

 $\gamma$  (photon)

$$I(J^{PC}) = 0.1(1^{--})$$

Mass  $m < 1 \times 10^{-18}$  eV  
Charge  $q < 1 \times 10^{-46}$  e (mixed charge)  
Charge  $q < 1 \times 10^{-35}$  e (single charge)  
Mean life  $\tau = \text{Stable}$

 $g$   
or gluon

$$I(J^P) = 0(1^-)$$

Mass  $m = 0$  [a]  
SU(3) color octet

## graviton

$$J = 2$$

Mass  $m < 6 \times 10^{-32}$  eV

 $W$ 

$$J = 1$$

Charge =  $\pm 1$  e  
Mass  $m = 80.379 \pm 0.012$  GeV  
 $W/Z$  mass ratio =  $0.88147 \pm 0.00013$   
 $m_Z - m_W = 10.809 \pm 0.012$  GeV  
 $m_{W^+} - m_{W^-} = -0.029 \pm 0.028$  GeV  
Full width  $\Gamma = 2.085 \pm 0.042$  GeV  
 $\langle N_{\pi^\pm} \rangle = 15.70 \pm 0.35$   
 $\langle N_{K^\pm} \rangle = 2.20 \pm 0.19$   
 $\langle N_p \rangle = 0.92 \pm 0.14$   
 $\langle N_{\text{charged}} \rangle = 19.39 \pm 0.08$

$W^-$  modes are charge conjugates of the modes below.

$W^+$ DECAY MODES	Fraction ( $\Gamma_i/\Gamma$ )	Confidence level	$\rho$ (MeV/c)
$\ell^+ \nu$	[b] (10.86 ± 0.09) %		–
$e^+ \nu$	(10.71 ± 0.16) %		40189
$\mu^+ \nu$	(10.63 ± 0.15) %		40189
$\tau^+ \nu$	(11.38 ± 0.21) %		40170
hadrons	(67.41 ± 0.27) %		–
$\pi^+ \gamma$	< 7	$\times 10^{-6}$	95% 40189
$D_s^+ \gamma$	< 1.3	$\times 10^{-3}$	95% 40165
$cX$	(33.3 ± 2.6) %		–
$c\bar{s}$	(31 $^{+13}_{-11}$ ) %		–
invisible	[c] (1.4 ± 2.9) %		–
$\pi^+ \pi^+ \pi^-$	< 1.01	$\times 10^{-6}$	95% 40189

 $Z$ 

$$J = 1$$

Charge = 0  
Mass  $m = 91.1876 \pm 0.0021$  GeV [d]  
Full width  $\Gamma = 2.4952 \pm 0.0023$  GeV  
 $\Gamma(\ell^+ \ell^-) = 83.984 \pm 0.086$  MeV [b]  
 $\Gamma(\text{invisible}) = 499.0 \pm 1.5$  MeV [e]  
 $\Gamma(\text{hadrons}) = 1744.4 \pm 2.0$  MeV  
 $\Gamma(\mu^+ \mu^-)/\Gamma(e^+ e^-) = 1.0001 \pm 0.0024$   
 $\Gamma(\tau^+ \tau^-)/\Gamma(e^+ e^-) = 1.0020 \pm 0.0032$  [f]

## Average charged multiplicity

$$\langle N_{\text{charged}} \rangle = 20.76 \pm 0.16 \quad (S = 2.1)$$

## Couplings to quarks and leptons

$$g_V^\ell = -0.03783 \pm 0.00041$$

$$g_V^u = 0.266 \pm 0.034$$

$$g_V^d = -0.38^{+0.04}_{-0.05}$$

$$g_A^\ell = -0.50123 \pm 0.00026$$

$$g_A^u = 0.519^{+0.028}_{-0.033}$$

$$g_A^d = -0.527^{+0.040}_{-0.028}$$

$$g^{V\ell} = 0.5008 \pm 0.0008$$

$$g^{Ve} = 0.53 \pm 0.09$$

$$g^{V\mu} = 0.502 \pm 0.017$$

## Gauge &amp; Higgs Boson Summary Table

## Asymmetry parameters [8]

$$\begin{aligned}
A_e &= 0.1515 \pm 0.0019 \\
A_\mu &= 0.142 \pm 0.015 \\
A_\tau &= 0.143 \pm 0.004 \\
A_s &= 0.90 \pm 0.09 \\
A_c &= 0.670 \pm 0.027 \\
A_b &= 0.923 \pm 0.020
\end{aligned}$$

## Charge asymmetry (%) at Z pole

$$\begin{aligned}
A_{FB}^{(0\ell)} &= 1.71 \pm 0.10 \\
A_{FB}^{(0u)} &= 4 \pm 7 \\
A_{FB}^{(0s)} &= 9.8 \pm 1.1 \\
A_{FB}^{(0c)} &= 7.07 \pm 0.35 \\
A_{FB}^{(0b)} &= 9.92 \pm 0.16
\end{aligned}$$

Z DECAY MODES	Fraction ( $\Gamma_i/\Gamma$ )	Scale factor/ Confidence level	$p$ (MeV/c)
$e^+e^-$	[h] ( 3.3632±0.0042) %		45594
$\mu^+\mu^-$	[h] ( 3.3662±0.0066) %		45594
$\tau^+\tau^-$	[h] ( 3.3696±0.0083) %		45559
$\ell^+\ell^-$	[b,h] ( 3.3658±0.0023) %		—
$\ell^+\ell^-\ell^+\ell^-$	[j] ( 4.63 ±0.21 ) × 10 <sup>-6</sup>		45594
invisible	[h] (20.000 ±0.055) %		—
hadrons	[h] (69.911 ±0.056) %		—
( $u\bar{u}+c\bar{c}$ )/2	(11.6 ±0.6) %		—
( $d\bar{d}+s\bar{s}+b\bar{b}$ )/3	(15.6 ±0.4) %		—
$c\bar{c}$	(12.03 ±0.21) %		—
$b\bar{b}$	(15.12 ±0.05) %		—
$b\bar{b}b\bar{b}$	( 3.6 ±1.3 ) × 10 <sup>-4</sup>		—
$g g g$	< 1.1 %	CL=95%	—
$\pi^0\gamma$	< 2.01 × 10 <sup>-5</sup>	CL=95%	45594
$\eta\gamma$	< 5.1 × 10 <sup>-5</sup>	CL=95%	45592
$\rho^0\gamma$	< 2.5 × 10 <sup>-5</sup>	CL=95%	45591
$\omega\gamma$	< 6.5 × 10 <sup>-4</sup>	CL=95%	45590
$\eta'(958)\gamma$	< 4.2 × 10 <sup>-5</sup>	CL=95%	45589
$\phi\gamma$	< 9 × 10 <sup>-7</sup>	CL=95%	45588
$\gamma\gamma$	< 1.46 × 10 <sup>-5</sup>	CL=95%	45594
$\pi^0\pi^0$	< 1.52 × 10 <sup>-5</sup>	CL=95%	45594
$\gamma\gamma\gamma$	< 2.2 × 10 <sup>-6</sup>	CL=95%	45594
$\pi^\pm W^\mp$	[j] < 7 × 10 <sup>-5</sup>	CL=95%	10167
$\rho^\pm W^\mp$	[j] < 8.3 × 10 <sup>-5</sup>	CL=95%	10142
$J/\psi(1S)X$	( 3.51 <sup>+0.23</sup> <sub>-0.25</sub> ) × 10 <sup>-3</sup>	S=1.1	—
$J/\psi(1S)\gamma$	< 1.4 × 10 <sup>-6</sup>	CL=95%	45541
$\psi(2S)X$	( 1.60 ±0.29 ) × 10 <sup>-3</sup>		—
$\psi(2S)\gamma$	< 4.5 × 10 <sup>-6</sup>	CL=95%	45519
$J/\psi(1S)J/\psi(1S)$	< 2.2 × 10 <sup>-6</sup>	CL=95%	45489
$\chi_{c1}(1P)X$	( 2.9 ±0.7 ) × 10 <sup>-3</sup>		—
$\chi_{c2}(1P)X$	< 3.2 × 10 <sup>-3</sup>	CL=90%	—
$\Upsilon(1S)X + \Upsilon(2S)X$ + $\Upsilon(3S)X$	( 1.0 ±0.5 ) × 10 <sup>-4</sup>		—
$\Upsilon(1S)X$	< 3.4 × 10 <sup>-6</sup>	CL=95%	—
$\Upsilon(1S)\gamma$	< 2.8 × 10 <sup>-6</sup>	CL=95%	45103
$\Upsilon(2S)X$	< 6.5 × 10 <sup>-6</sup>	CL=95%	—
$\Upsilon(2S)\gamma$	< 1.7 × 10 <sup>-6</sup>	CL=95%	45043
$\Upsilon(3S)X$	< 5.4 × 10 <sup>-6</sup>	CL=95%	—
$\Upsilon(3S)\gamma$	< 4.8 × 10 <sup>-6</sup>	CL=95%	45006
$\Upsilon(1, 2, 3S) \Upsilon(1, 2, 3S)$	< 1.5 × 10 <sup>-6</sup>	CL=95%	—
( $D^0/\bar{D}^0$ )X	(20.7 ±2.0) %		—
$D^\pm X$	(12.2 ±1.7) %		—
$D^*(2010)^\pm X$	[j] (11.4 ±1.3) %		—
$D_{s1}(2536)^\pm X$	( 3.6 ±0.8 ) × 10 <sup>-3</sup>		—
$D_{sJ}(2573)^\pm X$	( 5.8 ±2.2 ) × 10 <sup>-3</sup>		—
$D^*(2629)^\pm X$	searched for		—
$B^+X$	[k] ( 6.08 ±0.13 ) %		—
$B_s^0 X$	[k] ( 1.59 ±0.13 ) %		—
$B_c^\pm X$	searched for		—
$A_c^\pm X$	( 1.54 ±0.33 ) %		—
$\Xi_c^0 X$	seen		—
$\Xi_c^\pm X$	seen		—
b-baryon X	[k] ( 1.38 ±0.22 ) %		—
anomalous $\gamma$ + hadrons	[j] < 3.2 × 10 <sup>-3</sup>	CL=95%	—
$e^+e^-\gamma$	[j] < 5.2 × 10 <sup>-4</sup>	CL=95%	45594
$\mu^+\mu^-\gamma$	[j] < 5.6 × 10 <sup>-4</sup>	CL=95%	45594

$\tau^+\tau^-\gamma$	[j] < 7.3	× 10 <sup>-4</sup>	CL=95%	45559
$\ell^+\ell^-\gamma\gamma$	[n] < 6.8	× 10 <sup>-6</sup>	CL=95%	—
$q\bar{q}\gamma\gamma$	[n] < 5.5	× 10 <sup>-6</sup>	CL=95%	—
$\nu\bar{\nu}\gamma\gamma$	[n] < 3.1	× 10 <sup>-6</sup>	CL=95%	45594
$e^\pm\mu^\mp$	LF [j] < 7.5	× 10 <sup>-7</sup>	CL=95%	45594
$e^\pm\tau^\mp$	LF [j] < 9.8	× 10 <sup>-6</sup>	CL=95%	45576
$\mu^\pm\tau^\mp$	LF [j] < 1.2	× 10 <sup>-5</sup>	CL=95%	45576
$\rho e$	L,B < 1.8	× 10 <sup>-6</sup>	CL=95%	45589
$\rho\mu$	L,B < 1.8	× 10 <sup>-6</sup>	CL=95%	45589

**H<sup>0</sup>**

J = 0

Mass  $m = 125.10 \pm 0.14$  GeVFull width  $\Gamma < 0.013$  GeV, CL = 95% (assumes equal on-shell and off-shell effective couplings)**H<sup>0</sup> Signal Strengths in Different Channels**

Combined Final States = 1.13 ± 0.06

 $WW^* = 1.19 \pm 0.12$  $ZZ^* = 1.20^{+0.12}_{-0.11}$  $\gamma\gamma = 1.11^{+0.10}_{-0.09}$  $c\bar{c}$  Final State < 110, CL = 95% $b\bar{b} = 1.04 \pm 0.13$  $\mu^+\mu^- = 0.6 \pm 0.8$  $\tau^+\tau^- = 1.15^{+0.16}_{-0.15}$  $Z\gamma < 6.6$ , CL = 95%

top Yukawa coupling &lt; 1.7, CL = 95%

 $t\bar{t}H^0$  Production = 1.28 ± 0.20 $H^0$  Production Cross Section in  $pp$  Collisions at  $\sqrt{s} = 13$  TeV = 59 ± 5 pb**H<sup>0</sup> DECAY MODES**

H <sup>0</sup> DECAY MODES	Fraction ( $\Gamma_i/\Gamma$ )	Confidence level	$p$ (MeV/c)
$e^+e^-$	< 3.6 × 10 <sup>-4</sup>	95%	62550
$J/\psi\gamma$	< 3.5 × 10 <sup>-4</sup>	95%	62511
$J/\psi J/\psi$	< 1.8 × 10 <sup>-3</sup>	95%	62473
$\psi(2S)\gamma$	< 2.0 × 10 <sup>-3</sup>	95%	62495
$\Upsilon(1S)\gamma$	< 4.9 × 10 <sup>-4</sup>	95%	62192
$\Upsilon(2S)\gamma$	< 5.9 × 10 <sup>-4</sup>	95%	62148
$\Upsilon(3S)\gamma$	< 5.7 × 10 <sup>-4</sup>	95%	62121
$\Upsilon(nS) \Upsilon(mS)$	< 1.4 × 10 <sup>-3</sup>	95%	—
$\rho(770)\gamma$	< 8.8 × 10 <sup>-4</sup>	95%	62547
$\phi(1020)\gamma$	< 4.8 × 10 <sup>-4</sup>	95%	62546
$e\mu$	LF < 6.1 × 10 <sup>-5</sup>	95%	62550
$e\tau$	LF < 4.7 × 10 <sup>-3</sup>	95%	62537
$\mu\tau$	LF < 2.5 × 10 <sup>-3</sup>	95%	62537
$\gamma$ invisible	< 4.6 %	95%	—

**Neutral Higgs Bosons, Searches for****Mass limits for heavy neutral Higgs bosons ( $H_2^0, A^0$ ) in the MSSM** $m > 389$  GeV, CL = 95% ( $\tan\beta = 10$ ) $m > 863$  GeV, CL = 95% ( $\tan\beta = 20$ ) $m > 1157$  GeV, CL = 95% ( $\tan\beta = 30$ ) $m > 1341$  GeV, CL = 95% ( $\tan\beta = 40$ ) $m > 1496$  GeV, CL = 95% ( $\tan\beta = 50$ ) $m > 1613$  GeV, CL = 95% ( $\tan\beta = 60$ )**Charged Higgs Bosons ( $H^\pm$  and  $H^{\pm\pm}$ ), Searches for****Mass limits for  $m_{H^\pm} < m(\text{top})$**  $m > 155$  GeV, CL = 95%**Mass limits for  $m_{H^\pm} > m(\text{top})$**  $m > 181$  GeV, CL = 95% ( $\tan\beta = 10$ ) $m > 249$  GeV, CL = 95% ( $\tan\beta = 20$ ) $m > 390$  GeV, CL = 95% ( $\tan\beta = 30$ ) $m > 894$  GeV, CL = 95% ( $\tan\beta = 40$ ) $m > 1017$  GeV, CL = 95% ( $\tan\beta = 50$ ) $m > 1103$  GeV, CL = 95% ( $\tan\beta = 60$ )

**New Heavy Bosons  
( $W'$ ,  $Z'$ , leptoquarks, etc.),  
Searches for**

**Additional  $W$  Bosons**

- $W'$  with standard couplings  
Mass  $m > 5200$  GeV, CL = 95% ( $pp$  direct search)  
 $W_R$  (Right-handed  $W$  Boson)  
Mass  $m > 715$  GeV, CL = 90% (electroweak fit)

**Additional  $Z$  Bosons**

- $Z'_{SM}$  with standard couplings  
Mass  $m > 4.500 \times 10^3$  GeV, CL = 95% ( $pp$  direct search)  
 $Z_{LR}$  of  $SU(2)_L \times SU(2)_R \times U(1)$  (with  $g_L = g_R$ )  
Mass  $m > 630$  GeV, CL = 95% ( $p\bar{p}$  direct search)  
Mass  $m > 1162$  GeV, CL = 95% (electroweak fit)  
 $Z_\chi$  of  $SO(10) \rightarrow SU(5) \times U(1)_\chi$  (with  $g_\chi = e/\cos\theta_W$ )  
Mass  $m > 4.100 \times 10^3$  GeV, CL = 95% ( $pp$  direct search)  
 $Z_\psi$  of  $E_6 \rightarrow SO(10) \times U(1)_\psi$  (with  $g_\psi = e/\cos\theta_W$ )  
Mass  $m > 3900$  GeV, CL = 95% ( $pp$  direct search)  
 $Z_\eta$  of  $E_6 \rightarrow SU(3) \times SU(2) \times U(1) \times U(1)_\eta$  (with  $g_\eta = e/\cos\theta_W$ )  
Mass  $m > 3.900 \times 10^3$  GeV, CL = 95% ( $pp$  direct search)

**Scalar Leptoquarks**

- $m > 1050$  GeV, CL = 95% (1st gen., pair prod.,  $B(\tau t)=1$ )  
 $m > 1755$  GeV, CL = 95% (1st gen., single prod.,  $B(\tau b)=1$ )  
 $m > 1420$  GeV, CL = 95% (2nd gen., pair prod.,  $B(\mu t)=1$ )  
 $m > 660$  GeV, CL = 95% (2nd gen., single prod.,  $B(\mu q)=1$ )  
 $m > 900$  GeV, CL = 95% (3rd gen., pair prod.,  $B(e q)=1$ )  
 $m > 740$  GeV, CL = 95% (3rd gen., single prod.,  $B(e q)=1$ )  
(See the Particle Listings for assumptions on leptoquark quantum numbers and branching fractions.)

**Diquarks**

- Mass  $m > 6000$  GeV, CL = 95% ( $E_6$  diquark)

**Axiguon**

- Mass  $m > 6100$  GeV, CL = 95%

**Axions ( $A^0$ ) and Other  
Very Light Bosons, Searches for**

See the review on "Axions and other similar particles."

The best limit for the half-life of neutrinoless double beta decay with Majoron emission is  $> 7.2 \times 10^{24}$  years (CL = 90%).

NOTES

In this Summary Table:

When a quantity has "(S = ...)" to its right, the error on the quantity has been enlarged by the "scale factor"  $S$ , defined as  $S = \sqrt{\chi^2/(N-1)}$ , where  $N$  is the number of measurements used in calculating the quantity. We do this when  $S > 1$ , which often indicates that the measurements are inconsistent. When  $S > 1.25$ , we also show in the Particle Listings an ideogram of the measurements. For more about  $S$ , see the Introduction.

A decay momentum  $p$  is given for each decay mode. For a 2-body decay,  $p$  is the momentum of each decay product in the rest frame of the decaying particle. For a 3-or-more-body decay,  $p$  is the largest momentum any of the products can have in this frame.

- [a] Theoretical value. A mass as large as a few MeV may not be precluded.  
[b]  $\ell$  indicates each type of lepton ( $e$ ,  $\mu$ , and  $\tau$ ), not sum over them.  
[c] This represents the width for the decay of the  $W$  boson into a charged particle with momentum below detectability,  $p < 200$  MeV.  
[d] The  $Z$ -boson mass listed here corresponds to a Breit-Wigner resonance parameter. It lies approximately 34 MeV above the real part of the position of the pole (in the energy-squared plane) in the  $Z$ -boson propagator.  
[e] This partial width takes into account  $Z$  decays into  $\nu\bar{\nu}$  and any other possible undetected modes.  
[f] This ratio has not been corrected for the  $\tau$  mass.  
[g] Here  $A \equiv 2g_V g_A / (g_V^2 + g_A^2)$ .  
[h] This parameter is not directly used in the overall fit but is derived using the fit results; see the note "The  $Z$  boson" and ref. LEP-SLC 06 (Physics Reports (Physics Letters C) **427** 257 (2006)).  
[i] Here  $\ell$  indicates  $e$  or  $\mu$ .  
[j] The value is for the sum of the charge states or particle/antiparticle states indicated.  
[k] This value is updated using the product of (i) the  $Z \rightarrow b\bar{b}$  fraction from this listing and (ii) the  $b$ -hadron fraction in an unbiased sample of weakly decaying  $b$ -hadrons produced in  $Z$ -decays provided by the Heavy Flavor Averaging Group (HFLAV, <http://www.slac.stanford.edu/xorg/hflav/osc/PDG.2009/#FRACZ>).  
[l] See the  $Z$  Particle Listings for the  $\gamma$  energy range used in this measurement.  
[n] For  $m_{\gamma\gamma} = (60 \pm 5)$  GeV.



## Lepton Summary Table

## LEPTONS

<b>e</b>	$J = \frac{1}{2}$
Mass $m = (548.5799070 \pm 0.000000016) \times 10^{-6}$ u	
Mass $m = 0.5109989461 \pm 0.0000000031$ MeV	
$ m_{e^+} - m_{e^-} /m < 8 \times 10^{-9}$ , CL = 90%	
$ q_{e^+} + q_{e^-} /e < 4 \times 10^{-8}$	
Magnetic moment anomaly	
$(g-2)/2 = (1159.65218091 \pm 0.00000026) \times 10^{-6}$	
$(g_{e^+} - g_{e^-}) / g_{\text{average}} = (-0.5 \pm 2.1) \times 10^{-12}$	
Electric dipole moment $d < 0.11 \times 10^{-28}$ ecm, CL = 90%	
Mean life $\tau > 6.6 \times 10^{28}$ yr, CL = 90% [a]	

<b><math>\mu</math></b>	$J = \frac{1}{2}$
Mass $m = 0.1134289257 \pm 0.0000000025$ u	
Mass $m = 105.6583745 \pm 0.0000024$ MeV	
Mean life $\tau = (2.1969811 \pm 0.0000022) \times 10^{-6}$ s	
$\tau_{\mu^+}/\tau_{\mu^-} = 1.00002 \pm 0.00008$	
$c\tau = 658.6384$ m	
Magnetic moment anomaly $(g-2)/2 = (11659209 \pm 6) \times 10^{-10}$	
$(g_{\mu^+} - g_{\mu^-}) / g_{\text{average}} = (-0.11 \pm 0.12) \times 10^{-8}$	
Electric dipole moment $ d  < 1.8 \times 10^{-19}$ ecm, CL = 95%	

## Decay parameters [b]

$\rho = 0.74979 \pm 0.00026$
$\eta = 0.057 \pm 0.034$
$\delta = 0.75047 \pm 0.00034$
$\xi P_{\mu} = 1.0009^{+0.0016}_{-0.0007}$ [c]
$\xi P_{\mu} \delta / \rho = 1.0018^{+0.0016}_{-0.0007}$ [c]
$\xi' = 1.00 \pm 0.04$
$\xi'' = 0.98 \pm 0.04$
$\alpha/A = (0 \pm 4) \times 10^{-3}$
$\alpha'/A = (-10 \pm 20) \times 10^{-3}$
$\beta/A = (4 \pm 6) \times 10^{-3}$
$\beta'/A = (2 \pm 7) \times 10^{-3}$
$\overline{\eta} = 0.02 \pm 0.08$

$\mu^+$  modes are charge conjugates of the modes below.

$\mu^-$ DECAY MODES	Fraction ( $\Gamma_i/\Gamma$ )	Confidence level	$\rho$ (MeV/c)
$e^- \overline{\nu}_e \nu_{\mu}$	$\approx 100\%$		53
$e^- \overline{\nu}_e \nu_{\mu} \gamma$	[d] $(6.0 \pm 0.5) \times 10^{-8}$		53
$e^- \overline{\nu}_e \nu_{\mu} e^+ e^-$	[e] $(3.4 \pm 0.4) \times 10^{-5}$		53
<b>Lepton Family number (LF) violating modes</b>			
$e^- \nu_e \overline{\nu}_{\mu}$	LF [f] $< 1.2$	%	90% 53
$e^- \gamma$	LF $< 4.2$	$\times 10^{-13}$	90% 53
$e^- e^+ e^-$	LF $< 1.0$	$\times 10^{-12}$	90% 53
$e^- 2\gamma$	LF $< 7.2$	$\times 10^{-11}$	90% 53

<b><math>\tau</math></b>	$J = \frac{1}{2}$
Mass $m = 1776.86 \pm 0.12$ MeV	
$(m_{\tau^+} - m_{\tau^-})/m_{\text{average}} < 2.8 \times 10^{-4}$ , CL = 90%	
Mean life $\tau = (290.3 \pm 0.5) \times 10^{-15}$ s	
$c\tau = 87.03$ $\mu\text{m}$	
Magnetic moment anomaly $> -0.052$ and $< 0.013$ , CL = 95%	
$\text{Re}(d_{\tau}) = -0.220$ to $0.45 \times 10^{-16}$ ecm, CL = 95%	
$\text{Im}(d_{\tau}) = -0.250$ to $0.0080 \times 10^{-16}$ ecm, CL = 95%	

## Weak dipole moment

$\text{Re}(d_{\tau}^W) < 0.50 \times 10^{-17}$ ecm, CL = 95%
$\text{Im}(d_{\tau}^W) < 1.1 \times 10^{-17}$ ecm, CL = 95%

## Weak anomalous magnetic dipole moment

$\text{Re}(\alpha_{\tau}^W) < 1.1 \times 10^{-3}$ , CL = 95%
$\text{Im}(\alpha_{\tau}^W) < 2.7 \times 10^{-3}$ , CL = 95%
$\tau^{\pm} \rightarrow \pi^{\pm} K_S^0 \nu_{\tau}$ (RATE DIFFERENCE) / (RATE SUM) = $(-0.36 \pm 0.25)\%$

## Decay parameters

See the  $\tau$  Particle Listings for a note concerning  $\tau$ -decay parameters.

$\rho(e \text{ or } \mu) = 0.745 \pm 0.008$
$\rho(e) = 0.747 \pm 0.010$
$\rho(\mu) = 0.763 \pm 0.020$
$\xi(e \text{ or } \mu) = 0.985 \pm 0.030$
$\xi(e) = 0.994 \pm 0.040$
$\xi(\mu) = 1.030 \pm 0.059$
$\eta(e \text{ or } \mu) = 0.013 \pm 0.020$
$\eta(\mu) = 0.094 \pm 0.073$
$(\delta\xi)(e \text{ or } \mu) = 0.746 \pm 0.021$
$(\delta\xi)(e) = 0.734 \pm 0.028$
$(\delta\xi)(\mu) = 0.778 \pm 0.037$
$\xi(\pi) = 0.993 \pm 0.022$
$\xi(\rho) = 0.994 \pm 0.008$
$\xi(a_1) = 1.001 \pm 0.027$
$\xi(\text{all hadronic modes}) = 0.995 \pm 0.007$
$\overline{\eta}(\mu)$ PARAMETER = $-1.3 \pm 1.7$
$\xi_{\kappa}(e)$ PARAMETER = $-0.4 \pm 1.2$
$\xi_{\kappa}(\mu)$ PARAMETER = $0.8 \pm 0.6$

$\tau^+$  modes are charge conjugates of the modes below. " $h^{\pm}$ " stands for  $\pi^{\pm}$  or  $K^{\pm}$ . " $e^{\pm}$ " stands for  $e$  or  $\mu$ . "Neutrals" stands for  $\gamma$ 's and/or  $\pi^0$ 's.

$\tau^-$ DECAY MODES	Fraction ( $\Gamma_i/\Gamma$ )	Scale factor / Confidence level	$\rho$ (MeV/c)
<b>Modes with one charged particle</b>			
particle $^- \geq 0$ neutrals $\geq 0K^0 \nu_{\tau}$ ("1-prong")	$(85.24 \pm 0.06) \%$		-
particle $^- \geq 0$ neutrals $\geq 0K_L^0 \nu_{\tau}$	$(84.58 \pm 0.06) \%$		-
$\mu^- \overline{\nu}_{\mu} \nu_{\tau}$	[g] $(17.39 \pm 0.04) \%$		885
$\mu^- \overline{\nu}_{\mu} \nu_{\tau} \gamma$	[e] $(3.67 \pm 0.08) \times 10^{-3}$		885
$e^- \overline{\nu}_e \nu_{\tau}$	[g] $(17.82 \pm 0.04) \%$		888
$e^- \overline{\nu}_e \nu_{\tau} \gamma$	[e] $(1.83 \pm 0.05) \%$		888
$h^- \geq 0K_L^0 \nu_{\tau}$	$(12.03 \pm 0.05) \%$		883
$h^- \nu_{\tau}$	$(11.51 \pm 0.05) \%$		883
$\pi^- \nu_{\tau}$	[g] $(10.82 \pm 0.05) \%$		883
$K^- \nu_{\tau}$	[g] $(6.96 \pm 0.10) \times 10^{-3}$		820
$h^- \geq 1$ neutrals $\nu_{\tau}$	$(37.01 \pm 0.09) \%$		-
$h^- \geq 1\pi^0 \nu_{\tau}$ (ex. $K^0$ )	$(36.51 \pm 0.09) \%$		-
$h^- \pi^0 \nu_{\tau}$	$(25.93 \pm 0.09) \%$		878
$\pi^- \pi^0 \nu_{\tau}$	[g] $(25.49 \pm 0.09) \%$		878
$\pi^- \pi^0$ non- $\rho(770) \nu_{\tau}$	$(3.0 \pm 3.2) \times 10^{-3}$		878
$K^- \pi^0 \nu_{\tau}$	[g] $(4.33 \pm 0.15) \times 10^{-3}$		814
$h^- \geq 2\pi^0 \nu_{\tau}$	$(10.81 \pm 0.09) \%$		-
$h^- 2\pi^0 \nu_{\tau}$	$(9.48 \pm 0.10) \%$		862
$h^- 2\pi^0 \nu_{\tau}$ (ex. $K^0$ )	$(9.26 \pm 0.10) \%$		862
$\pi^- 2\pi^0 \nu_{\tau}$ (ex. $K^0$ )	[g] $(9.32 \pm 0.10) \%$		862
$\pi^- 2\pi^0 \nu_{\tau}$ (ex. $K^0$ ), scalar	$< 9$	$\times 10^{-3}$ CL=95%	862
$\pi^- 2\pi^0 \nu_{\tau}$ (ex. $K^0$ ), vector	$< 7$	$\times 10^{-3}$ CL=95%	862
$K^- 2\pi^0 \nu_{\tau}$ (ex. $K^0$ )	[g] $(6.5 \pm 2.2) \times 10^{-4}$		796
$h^- \geq 3\pi^0 \nu_{\tau}$	$(1.34 \pm 0.07) \%$		-
$h^- \geq 3\pi^0 \nu_{\tau}$ (ex. $K^0$ )	$(1.25 \pm 0.07) \%$		-
$h^- 3\pi^0 \nu_{\tau}$	$(1.18 \pm 0.07) \%$		836
$\pi^- 3\pi^0 \nu_{\tau}$ (ex. $K^0$ )	[g] $(1.04 \pm 0.07) \%$		836
$K^- 3\pi^0 \nu_{\tau}$ (ex. $K^0$ ), $\eta$	[g] $(4.8 \pm 2.1) \times 10^{-4}$		765
$h^- 4\pi^0 \nu_{\tau}$ (ex. $K^0$ )	$(1.6 \pm 0.4) \times 10^{-3}$		800
$h^- 4\pi^0 \nu_{\tau}$ (ex. $K^0, \eta$ )	[g] $(1.1 \pm 0.4) \times 10^{-3}$		800
$a_1(1260) \nu_{\tau} \rightarrow \pi^- \gamma \nu_{\tau}$	$(3.8 \pm 1.5) \times 10^{-4}$		-
$K^- \geq 0\pi^0 \geq 0K^0 \geq 0\gamma \nu_{\tau}$	$(1.552 \pm 0.029) \%$		820
$K^- \geq 1(\pi^0 \text{ or } K^0 \text{ or } \gamma) \nu_{\tau}$	$(8.59 \pm 0.28) \times 10^{-3}$		-
<b>Modes with <math>K^0</math>'s</b>			
$K_S^0(\text{particles})^- \nu_{\tau}$	$(9.43 \pm 0.28) \times 10^{-3}$		-
$h^- K^0 \nu_{\tau}$	$(9.87 \pm 0.14) \times 10^{-3}$		812
$\pi^- K^0 \nu_{\tau}$	[g] $(8.38 \pm 0.14) \times 10^{-3}$		812
$\pi^- \overline{K}^0 \nu_{\tau}$	$(5.4 \pm 2.1) \times 10^{-4}$		812
$(\text{non-}K^*(892)^- \nu_{\tau})$			
$K^- K^0 \nu_{\tau}$	[g] $(1.486 \pm 0.034) \times 10^{-3}$		737
$K^- K^0 \geq 0\pi^0 \nu_{\tau}$	$(2.99 \pm 0.07) \times 10^{-3}$		737
$h^- \overline{K}^0 \pi^0 \nu_{\tau}$	$(5.32 \pm 0.13) \times 10^{-3}$		794
$\pi^- \overline{K}^0 \pi^0 \nu_{\tau}$	[g] $(3.82 \pm 0.13) \times 10^{-3}$		794
$\overline{K}^0 \rho^- \nu_{\tau}$	$(2.2 \pm 0.5) \times 10^{-3}$		612

# Lepton Summary Table

$K^- K^0 \pi^0 \nu_\tau$	[g]	$(1.50 \pm 0.07) \times 10^{-3}$	685	$K^- K^+ K^- \pi^0 \nu_\tau$	< 4.8	$\times 10^{-6}$ CL=90%	345
$\pi^- \bar{K}^0 \geq 1 \pi^0 \nu_\tau$		$(4.08 \pm 0.25) \times 10^{-3}$	-	$\pi^- K^+ \pi^- \geq 0$ neut. $\nu_\tau$	< 2.5	$\times 10^{-3}$ CL=95%	794
$\pi^- \bar{K}^0 \pi^0 \pi^0 \nu_\tau$ (ex. $K^0$ )	[g]	$(2.6 \pm 2.3) \times 10^{-4}$	763	$e^- e^- e^+ \bar{\nu}_e \nu_\tau$	$(2.8 \pm 1.5) \times 10^{-5}$		888
$K^- K^0 \pi^0 \pi^0 \nu_\tau$		< 1.6	$\times 10^{-4}$ CL=95%	$\mu^- e^- e^+ \bar{\nu}_\mu \nu_\tau$	< 3.2	$\times 10^{-5}$ CL=90%	885
$\pi^- K^0 \bar{K}^0 \nu_\tau$		$(1.55 \pm 0.24) \times 10^{-3}$	682	$\pi^- \mu^- \mu^+ \nu_\tau$	< 1.14	$\times 10^{-5}$ CL=90%	870
$\pi^- K_S^0 K_S^0 \nu_\tau$	[g]	$(2.35 \pm 0.06) \times 10^{-4}$	682	<b>Modes with five charged particles</b>			
$\pi^- K_S^0 K_L^0 \nu_\tau$	[g]	$(1.08 \pm 0.24) \times 10^{-3}$	682	$3h^- 2h^+ \geq 0$ neutrals $\nu_\tau$	$(9.9 \pm 0.4) \times 10^{-4}$		794
$\pi^- K_L^0 K_L^0 \nu_\tau$		$(2.35 \pm 0.06) \times 10^{-4}$	682	(ex. $K_S^0 \rightarrow \pi^- \pi^+$ )			
$\pi^- K^0 \bar{K}^0 \pi^0 \nu_\tau$		$(3.6 \pm 1.2) \times 10^{-4}$	614	("5-prong")			
$\pi^- K_S^0 K_S^0 \pi^0 \nu_\tau$	[g]	$(1.82 \pm 0.21) \times 10^{-5}$	614	$3h^- 2h^+ \nu_\tau$ (ex. $K^0$ )	$(8.29 \pm 0.31) \times 10^{-4}$		794
$K^* K^0 \pi^0 \nu_\tau \rightarrow$		$(1.08 \pm 0.21) \times 10^{-5}$	-	$3\pi^- 2\pi^+ \nu_\tau$ (ex. $K^0, \omega$ )	$(8.27 \pm 0.31) \times 10^{-4}$		794
$\pi^- K_S^0 K_S^0 \pi^0 \nu_\tau$				$3\pi^- 2\pi^+ \nu_\tau$ (ex. $K^0, \omega$ , $f_1(1285)$ )	[g] $(7.75 \pm 0.30) \times 10^{-4}$		-
$f_1(1285) \pi^- \nu_\tau \rightarrow$		$(6.8 \pm 1.5) \times 10^{-6}$	-	$K^- 2\pi^- 2\pi^+ \nu_\tau$ (ex. $K^0$ )	[g] $(6 \pm 12) \times 10^{-7}$		716
$\pi^- K_S^0 K_S^0 \pi^0 \nu_\tau$				$K^+ 3\pi^- \pi^+ \nu_\tau$	< 5.0	$\times 10^{-6}$ CL=90%	716
$f_1(1420) \pi^- \nu_\tau \rightarrow$		$(2.4 \pm 0.8) \times 10^{-6}$	-	$K^+ K^- 2\pi^- \pi^+ \nu_\tau$	< 4.5	$\times 10^{-7}$ CL=90%	528
$\pi^- K_S^0 K_S^0 \pi^0 \nu_\tau$				$3h^- 2h^+ \pi^0 \nu_\tau$ (ex. $K^0$ )	$(1.65 \pm 0.11) \times 10^{-4}$		746
$\pi^- K_S^0 K_L^0 \pi^0 \nu_\tau$	[g]	$(3.2 \pm 1.2) \times 10^{-4}$	614	$3\pi^- 2\pi^+ \pi^0 \nu_\tau$ (ex. $K^0$ )	$(1.63 \pm 0.11) \times 10^{-4}$		746
$\pi^- K_L^0 K_L^0 \pi^0 \nu_\tau$		$(1.82 \pm 0.21) \times 10^{-5}$	614	$3\pi^- 2\pi^+ \pi^0 \nu_\tau$ (ex. $K^0, \eta$ , $f_1(1285)$ )	$(1.11 \pm 0.10) \times 10^{-4}$		-
$K^- K_S^0 K_S^0 \nu_\tau$	< 6.3	$\times 10^{-7}$ CL=90%	466	$3\pi^- 2\pi^+ \pi^0 \nu_\tau$ (ex. $K^0, \eta$ , $\omega$ , $f_1(1285)$ )	[g] $(3.8 \pm 0.9) \times 10^{-5}$		-
$K^- K_S^0 K_L^0 \nu_\tau$	< 4.0	$\times 10^{-7}$ CL=90%	337	$K^- 2\pi^- 2\pi^+ \pi^0 \nu_\tau$ (ex. $K^0$ )	[g] $(1.1 \pm 0.6) \times 10^{-6}$		657
$K^0 h^+ h^- h^- \geq 0$ neutrals $\nu_\tau$	< 1.7	$\times 10^{-3}$ CL=95%	760	$K^+ 3\pi^- \pi^+ \pi^0 \nu_\tau$	< 8	$\times 10^{-7}$ CL=90%	657
$K^0 h^+ h^- h^- \nu_\tau$	[g]	$(2.5 \pm 2.0) \times 10^{-4}$	760	$3h^- 2h^+ 2\pi^0 \nu_\tau$	< 3.4	$\times 10^{-6}$ CL=90%	687
<b>Modes with three charged particles</b>							
$h^- h^- h^+ \geq 0$ neutrals $\geq 0 K_L^0 \nu_\tau$		$(15.20 \pm 0.06) \%$	861	<b>Miscellaneous other allowed modes</b>			
$h^- h^- h^+ \geq 0$ neutrals $\nu_\tau$		$(14.55 \pm 0.06) \%$	861	$(5\pi)^- \nu_\tau$	$(7.8 \pm 0.5) \times 10^{-3}$		800
(ex. $K_S^0 \rightarrow \pi^+ \pi^-$ )				$4h^- 3h^+ \geq 0$ neutrals $\nu_\tau$	< 3.0	$\times 10^{-7}$ CL=90%	682
("3-prong")				("7-prong")			
$h^- h^- h^+ \nu_\tau$		$(9.80 \pm 0.05) \%$	861	$4h^- 3h^+ \nu_\tau$	< 4.3	$\times 10^{-7}$ CL=90%	682
$h^- h^- h^+ \nu_\tau$ (ex. $K^0$ )		$(9.46 \pm 0.05) \%$	861	$4h^- 3h^+ \pi^0 \nu_\tau$	< 2.5	$\times 10^{-7}$ CL=90%	612
$h^- h^- h^+ \nu_\tau$ (ex. $K^0, \omega$ )		$(9.43 \pm 0.05) \%$	861	$X^- (S=-1) \nu_\tau$	$(2.92 \pm 0.04) \%$		-
$\pi^- \pi^+ \pi^- \nu_\tau$		$(9.31 \pm 0.05) \%$	861	$K^*(892)^- \geq 0$ neutrals $\geq$	$(1.42 \pm 0.18) \%$	S=1.4	665
$\pi^- \pi^+ \pi^- \nu_\tau$ (ex. $K^0$ )		$(9.02 \pm 0.05) \%$	861	$0 K^0 \nu_\tau$			
$\pi^- \pi^+ \pi^- \nu_\tau$ (ex. $K^0$ ),	< 2.4	%	CL=95%	$K^*(892)^- \nu_\tau$	$(1.20 \pm 0.07) \%$	S=1.8	665
non-axial vector				$K^*(892)^- \nu_\tau \rightarrow \pi^- \bar{K}^0 \nu_\tau$	$(7.82 \pm 0.26) \times 10^{-3}$		-
$\pi^- \pi^+ \pi^- \nu_\tau$ (ex. $K^0, \omega$ )	[g]	$(8.99 \pm 0.05) \%$	861	$K^*(892)^0 K^- \geq 0$ neutrals $\nu_\tau$	$(3.2 \pm 1.4) \times 10^{-3}$		542
$h^- h^- h^+ \geq 1$ neutrals $\nu_\tau$		$(5.29 \pm 0.05) \%$	-	$K^*(892)^0 K^- \nu_\tau$	$(2.1 \pm 0.4) \times 10^{-3}$		542
$h^- h^- h^+ \geq 1\pi^0 \nu_\tau$ (ex. $K^0$ )		$(5.09 \pm 0.05) \%$	-	$\bar{K}^*(892)^0 \pi^- \geq 0$ neutrals $\nu_\tau$	$(3.8 \pm 1.7) \times 10^{-3}$		655
$h^- h^- h^+ \pi^0 \nu_\tau$		$(4.76 \pm 0.05) \%$	834	$\bar{K}^*(892)^0 \pi^- \nu_\tau$	$(2.2 \pm 0.5) \times 10^{-3}$		655
$h^- h^- h^+ \pi^0 \nu_\tau$ (ex. $K^0$ )		$(4.57 \pm 0.05) \%$	834	$(\bar{K}^*(892) \pi)^- \nu_\tau \rightarrow$	$(1.0 \pm 0.4) \times 10^{-3}$		-
$h^- h^- h^+ \pi^0 \nu_\tau$ (ex. $K^0, \omega$ )		$(2.79 \pm 0.07) \%$	834	$\pi^- \bar{K}^0 \pi^0 \nu_\tau$			
$\pi^- \pi^+ \pi^- \pi^0 \nu_\tau$		$(4.62 \pm 0.05) \%$	834	$K_1(1270)^- \nu_\tau$	$(4.7 \pm 1.1) \times 10^{-3}$		447
$\pi^- \pi^+ \pi^- \pi^0 \nu_\tau$ (ex. $K^0$ )		$(4.49 \pm 0.05) \%$	834	$K_1(1400)^- \nu_\tau$	$(1.7 \pm 2.6) \times 10^{-3}$	S=1.7	335
$\pi^- \pi^+ \pi^- \pi^0 \nu_\tau$ (ex. $K^0, \omega$ )	[g]	$(2.74 \pm 0.07) \%$	834	$K^*(1410)^- \nu_\tau$	$(1.5 \pm 1.4) \times 10^{-3}$		326
$h^- h^- h^+ \geq 2\pi^0 \nu_\tau$ (ex. $K^0$ )		$(5.17 \pm 0.31) \times 10^{-3}$	-	$K_S^0(1430)^- \nu_\tau$	< 5	$\times 10^{-4}$ CL=95%	317
$h^- h^- h^+ 2\pi^0 \nu_\tau$		$(5.05 \pm 0.31) \times 10^{-3}$	797	$K_S^0(1430)^- \nu_\tau$	< 3	$\times 10^{-3}$ CL=95%	315
$h^- h^- h^+ 2\pi^0 \nu_\tau$ (ex. $K^0$ )		$(4.95 \pm 0.31) \times 10^{-3}$	797	$\eta \pi^- \nu_\tau$	< 9.9	$\times 10^{-5}$ CL=95%	797
$h^- h^- h^+ 2\pi^0 \nu_\tau$ (ex. $K^0, \omega, \eta$ )	[g]	$(10 \pm 4) \times 10^{-4}$	797	$\eta \pi^- \pi^0 \nu_\tau$	[g] $(1.39 \pm 0.07) \times 10^{-3}$		778
$h^- h^- h^+ 3\pi^0 \nu_\tau$		$(2.13 \pm 0.30) \times 10^{-4}$	749	$\eta \pi^- \pi^0 \pi^0 \nu_\tau$	[g] $(2.0 \pm 0.4) \times 10^{-4}$		746
$2\pi^- \pi^+ 3\pi^0 \nu_\tau$ (ex. $K^0$ )		$(1.95 \pm 0.30) \times 10^{-4}$	749	$\eta K^- \nu_\tau$	[g] $(1.55 \pm 0.08) \times 10^{-4}$		719
$2\pi^- \pi^+ 3\pi^0 \nu_\tau$ (ex. $K^0, \eta$ , $f_1(1285)$ )		$(1.7 \pm 0.4) \times 10^{-4}$	-	$\eta K^*(892)^- \nu_\tau$	$(1.38 \pm 0.15) \times 10^{-4}$		511
$2\pi^- \pi^+ 3\pi^0 \nu_\tau$ (ex. $K^0, \eta$ , $\omega$ , $f_1(1285)$ )	[g]	$(1.4 \pm 2.7) \times 10^{-5}$	-	$\eta K^- \pi^0 \nu_\tau$	[g] $(4.8 \pm 1.2) \times 10^{-5}$		665
$K^- h^+ h^- \geq 0$ neutrals $\nu_\tau$		$(6.29 \pm 0.14) \times 10^{-3}$	794	$\eta K^- \pi^0$ (non- $K^*(892)) \nu_\tau$	< 3.5	$\times 10^{-5}$ CL=90%	-
$K^- h^+ \pi^- \nu_\tau$ (ex. $K^0$ )		$(4.37 \pm 0.07) \times 10^{-3}$	794	$\eta \bar{K}^0 \pi^- \nu_\tau$	[g] $(9.4 \pm 1.5) \times 10^{-5}$		661
$K^- h^+ \pi^- \pi^0 \nu_\tau$ (ex. $K^0$ )		$(8.6 \pm 1.2) \times 10^{-4}$	763	$\eta \bar{K}^0 \pi^- \pi^0 \nu_\tau$	< 5.0	$\times 10^{-5}$ CL=90%	590
$K^- \pi^+ \pi^- \geq 0$ neutrals $\nu_\tau$		$(4.77 \pm 0.14) \times 10^{-3}$	794	$\eta K^- K^0 \nu_\tau$	< 9.0	$\times 10^{-6}$ CL=90%	430
$K^- \pi^+ \pi^- \geq 0\pi^0 \nu_\tau$ (ex. $K^0$ )		$(3.73 \pm 0.13) \times 10^{-3}$	794	$\eta \pi^+ \pi^- \pi^- \geq 0$ neutrals $\nu_\tau$	< 3	$\times 10^{-3}$ CL=90%	744
$K^- \pi^+ \pi^- \nu_\tau$		$(3.45 \pm 0.07) \times 10^{-3}$	794	$\eta \pi^- \pi^+ \pi^- \nu_\tau$ (ex. $K^0$ )	[g] $(2.20 \pm 0.13) \times 10^{-4}$		744
$K^- \pi^+ \pi^- \nu_\tau$ (ex. $K^0$ )		$(2.93 \pm 0.07) \times 10^{-3}$	794	$\eta \pi^- \pi^+ \pi^- \nu_\tau$ (ex. $K^0, f_1(1285)$ )	$(9.9 \pm 1.6) \times 10^{-5}$		-
$K^- \pi^+ \pi^- \nu_\tau$ (ex. $K^0, \omega$ )	[g]	$(2.93 \pm 0.07) \times 10^{-3}$	794	$\eta a_1(1260)^- \nu_\tau \rightarrow \eta \pi^- \rho^0 \nu_\tau$	< 3.9	$\times 10^{-4}$ CL=90%	-
$K^- \rho^0 \nu_\tau \rightarrow$		$(1.4 \pm 0.5) \times 10^{-3}$	-	$\eta \eta \pi^- \nu_\tau$	< 7.4	$\times 10^{-6}$ CL=90%	637
$K^- \pi^+ \pi^- \pi^- \nu_\tau$		$(1.31 \pm 0.12) \times 10^{-3}$	763	$\eta \eta \pi^- \pi^0 \nu_\tau$	< 2.0	$\times 10^{-4}$ CL=95%	559
$K^- \pi^+ \pi^- \pi^0 \nu_\tau$ (ex. $K^0$ )		$(7.9 \pm 1.2) \times 10^{-4}$	763	$\eta \eta K^- \nu_\tau$	< 3.0	$\times 10^{-6}$ CL=90%	382
$K^- \pi^+ \pi^- \pi^0 \nu_\tau$ (ex. $K^0, \eta$ )		$(7.6 \pm 1.2) \times 10^{-4}$	763	$\eta'(958) \pi^- \nu_\tau$	< 4.0	$\times 10^{-6}$ CL=90%	620
$K^- \pi^+ \pi^- \pi^0 \nu_\tau$ (ex. $K^0, \omega$ )		$(3.7 \pm 0.9) \times 10^{-4}$	763	$\eta'(958) \pi^- \pi^0 \nu_\tau$	< 1.2	$\times 10^{-5}$ CL=90%	591
$K^- \pi^+ \pi^- \pi^0 \nu_\tau$ (ex. $K^0, \omega, \eta$ )	[g]	$(3.9 \pm 1.4) \times 10^{-4}$	763	$\eta'(958) K^- \nu_\tau$	< 2.4	$\times 10^{-6}$ CL=90%	495
$K^- \pi^+ K^- \geq 0$ neut. $\nu_\tau$	< 9	$\times 10^{-4}$ CL=95%	685	$\phi \pi^- \nu_\tau$	$(3.4 \pm 0.6) \times 10^{-5}$		585
$K^- K^+ \pi^- \geq 0$ neut. $\nu_\tau$		$(1.496 \pm 0.033) \times 10^{-3}$	685	$\phi K^- \nu_\tau$	[g] $(4.4 \pm 1.6) \times 10^{-5}$		445
$K^- K^+ \pi^- \nu_\tau$	[g]	$(1.435 \pm 0.027) \times 10^{-3}$	685	$f_1(1285) \pi^- \nu_\tau$	$(3.9 \pm 0.5) \times 10^{-4}$	S=1.9	408
$K^- K^+ \pi^- \pi^0 \nu_\tau$	[g]	$(6.1 \pm 1.8) \times 10^{-5}$	618	$f_1(1285) \pi^- \nu_\tau \rightarrow$	$(1.18 \pm 0.07) \times 10^{-4}$	S=1.3	-
$K^- K^+ K^- \nu_\tau$		$(2.2 \pm 0.8) \times 10^{-5}$	472	$\eta \pi^- \pi^+ \pi^- \nu_\tau$			
$K^- K^+ K^- \nu_\tau$ (ex. $\phi$ )	< 2.5	$\times 10^{-6}$ CL=90%	-	$f_1(1285) \pi^- \nu_\tau$	[g] $(5.2 \pm 0.4) \times 10^{-5}$		-
				$3\pi^- 2\pi^+ \nu_\tau$			
				$\pi(1300)^- \nu_\tau \rightarrow (\rho\pi)^- \nu_\tau \rightarrow$	< 1.0	$\times 10^{-4}$ CL=90%	-
				$(3\pi)^- \nu_\tau$			

## Lepton Summary Table

$\pi(1300)^- \nu_\tau \rightarrow$	$< 1.9$	$\times 10^{-4}$ CL=90%	-
$((\pi\pi)_{S\text{-wave}} \pi)^- \nu_\tau \rightarrow$			
$(3\pi)^- \nu_\tau$			
$h^- \omega \geq 0$ neutrals $\nu_\tau$	$(2.40 \pm 0.08) \%$		708
$h^- \omega \nu_\tau$	$(1.99 \pm 0.06) \%$		708
$\pi^- \omega \nu_\tau$	[g] $(1.95 \pm 0.06) \%$		708
$K^- \omega \nu_\tau$	[g] $(4.1 \pm 0.9) \times 10^{-4}$		610
$h^- \omega \pi^0 \nu_\tau$	[g] $(4.1 \pm 0.4) \times 10^{-3}$		684
$h^- \omega 2\pi^0 \nu_\tau$	$(1.4 \pm 0.5) \times 10^{-4}$		644
$\pi^- \omega 2\pi^0 \nu_\tau$	[g] $(7.2 \pm 1.6) \times 10^{-5}$		644
$h^- 2\omega \nu_\tau$	$< 5.4$	$\times 10^{-7}$ CL=90%	250
$2h^- h^+ \omega \nu_\tau$	$(1.20 \pm 0.22) \times 10^{-4}$		641
$2\pi^- \pi^+ \omega \nu_\tau$ (ex. $K^0$ )	[g] $(8.4 \pm 0.6) \times 10^{-5}$		641

## Lepton Family number (LF), Lepton number (L), or Baryon number (B) violating modes

L means lepton number violation (e.g.  $\tau^- \rightarrow e^+ \pi^- \pi^-$ ). Following common usage, LF means lepton family violation and not lepton number violation (e.g.  $\tau^- \rightarrow e^- \pi^+ \pi^-$ ). B means baryon number violation.

$e^- \gamma$	LF	$< 3.3$	$\times 10^{-8}$ CL=90%	888
$\mu^- \gamma$	LF	$< 4.4$	$\times 10^{-8}$ CL=90%	885
$e^- \pi^0$	LF	$< 8.0$	$\times 10^{-8}$ CL=90%	883
$\mu^- \pi^0$	LF	$< 1.1$	$\times 10^{-7}$ CL=90%	880
$e^- K_S^0$	LF	$< 2.6$	$\times 10^{-8}$ CL=90%	819
$\mu^- K_S^0$	LF	$< 2.3$	$\times 10^{-8}$ CL=90%	815
$e^- \eta$	LF	$< 9.2$	$\times 10^{-8}$ CL=90%	804
$\mu^- \eta$	LF	$< 6.5$	$\times 10^{-8}$ CL=90%	800
$e^- \rho^0$	LF	$< 1.8$	$\times 10^{-8}$ CL=90%	719
$\mu^- \rho^0$	LF	$< 1.2$	$\times 10^{-8}$ CL=90%	715
$e^- \omega$	LF	$< 4.8$	$\times 10^{-8}$ CL=90%	716
$\mu^- \omega$	LF	$< 4.7$	$\times 10^{-8}$ CL=90%	711
$e^- K^*(892)^0$	LF	$< 3.2$	$\times 10^{-8}$ CL=90%	665
$\mu^- K^*(892)^0$	LF	$< 5.9$	$\times 10^{-8}$ CL=90%	659
$e^- \bar{K}^*(892)^0$	LF	$< 3.4$	$\times 10^{-8}$ CL=90%	665
$\mu^- \bar{K}^*(892)^0$	LF	$< 7.0$	$\times 10^{-8}$ CL=90%	659
$e^- \eta'(958)$	LF	$< 1.6$	$\times 10^{-7}$ CL=90%	630
$\mu^- \eta'(958)$	LF	$< 1.3$	$\times 10^{-7}$ CL=90%	625
$e^- f_0(980) \rightarrow e^- \pi^+ \pi^-$	LF	$< 3.2$	$\times 10^{-8}$ CL=90%	-
$\mu^- f_0(980) \rightarrow \mu^- \pi^+ \pi^-$	LF	$< 3.4$	$\times 10^{-8}$ CL=90%	-
$e^- \phi$	LF	$< 3.1$	$\times 10^{-8}$ CL=90%	596
$\mu^- \phi$	LF	$< 8.4$	$\times 10^{-8}$ CL=90%	590
$e^- e^+ e^-$	LF	$< 2.7$	$\times 10^{-8}$ CL=90%	888
$e^- \mu^+ \mu^-$	LF	$< 2.7$	$\times 10^{-8}$ CL=90%	882
$e^+ \mu^- \mu^-$	LF	$< 1.7$	$\times 10^{-8}$ CL=90%	882
$\mu^- e^+ e^-$	LF	$< 1.8$	$\times 10^{-8}$ CL=90%	885
$\mu^+ e^- e^-$	LF	$< 1.5$	$\times 10^{-8}$ CL=90%	885
$\mu^- \mu^+ \mu^-$	LF	$< 2.1$	$\times 10^{-8}$ CL=90%	873
$e^- \pi^+ \pi^-$	LF	$< 2.3$	$\times 10^{-8}$ CL=90%	877
$e^+ \pi^- \pi^-$	L	$< 2.0$	$\times 10^{-8}$ CL=90%	877
$\mu^- \pi^+ \pi^-$	LF	$< 2.1$	$\times 10^{-8}$ CL=90%	866
$\mu^+ \pi^- \pi^-$	L	$< 3.9$	$\times 10^{-8}$ CL=90%	866
$e^- \pi^+ K^-$	LF	$< 3.7$	$\times 10^{-8}$ CL=90%	813
$e^- \pi^- K^+$	LF	$< 3.1$	$\times 10^{-8}$ CL=90%	813
$e^+ \pi^- K^-$	L	$< 3.2$	$\times 10^{-8}$ CL=90%	813
$e^- K_S^0 K_S^0$	LF	$< 7.1$	$\times 10^{-8}$ CL=90%	736
$e^- K^+ K^-$	LF	$< 3.4$	$\times 10^{-8}$ CL=90%	738
$e^+ K^- K^-$	L	$< 3.3$	$\times 10^{-8}$ CL=90%	738
$\mu^- \pi^+ K^-$	LF	$< 8.6$	$\times 10^{-8}$ CL=90%	800
$\mu^- \pi^- K^+$	LF	$< 4.5$	$\times 10^{-8}$ CL=90%	800
$\mu^+ \pi^- K^-$	L	$< 4.8$	$\times 10^{-8}$ CL=90%	800
$\mu^- K_S^0 K_S^0$	LF	$< 8.0$	$\times 10^{-8}$ CL=90%	696
$\mu^- K^+ K^-$	LF	$< 4.4$	$\times 10^{-8}$ CL=90%	699
$\mu^+ K^- K^-$	L	$< 4.7$	$\times 10^{-8}$ CL=90%	699
$e^- \pi^0 \pi^0$	LF	$< 6.5$	$\times 10^{-6}$ CL=90%	878
$\mu^- \pi^0 \pi^0$	LF	$< 1.4$	$\times 10^{-5}$ CL=90%	867
$e^- \eta \eta$	LF	$< 3.5$	$\times 10^{-5}$ CL=90%	699
$\mu^- \eta \eta$	LF	$< 6.0$	$\times 10^{-5}$ CL=90%	653
$e^- \pi^0 \eta$	LF	$< 2.4$	$\times 10^{-5}$ CL=90%	798
$\mu^- \pi^0 \eta$	LF	$< 2.2$	$\times 10^{-5}$ CL=90%	784
$p \mu^- \mu^-$	L,B	$< 4.4$	$\times 10^{-7}$ CL=90%	618
$\bar{p} \mu^+ \mu^-$	L,B	$< 3.3$	$\times 10^{-7}$ CL=90%	618
$\bar{p} \gamma$	L,B	$< 3.5$	$\times 10^{-6}$ CL=90%	641
$\bar{p} \pi^0$	L,B	$< 1.5$	$\times 10^{-5}$ CL=90%	632
$\bar{p} 2\pi^0$	L,B	$< 3.3$	$\times 10^{-5}$ CL=90%	604
$\bar{p} \eta$	L,B	$< 8.9$	$\times 10^{-6}$ CL=90%	475
$\bar{p} \pi^0 \eta$	L,B	$< 2.7$	$\times 10^{-5}$ CL=90%	360
$\Lambda \pi^-$	L,B	$< 7.2$	$\times 10^{-8}$ CL=90%	525

$\bar{\Lambda} \pi^-$	L,B	$< 1.4$	$\times 10^{-7}$ CL=90%	525
$e^-$ light boson	LF	$< 2.7$	$\times 10^{-3}$ CL=95%	-
$\mu^-$ light boson	LF	$< 5$	$\times 10^{-3}$ CL=95%	-

## Heavy Charged Lepton Searches

 $L^\pm$  – charged lepton

Mass  $m > 100.8$  GeV, CL = 95% [h] Decay to  $\nu W$ .

 $L^\pm$  – stable charged heavy lepton

Mass  $m > 102.6$  GeV, CL = 95%

## Neutrino Properties

See the note on “Neutrino properties listings” in the Particle Listings.

Mass  $m < 1.1$  eV, CL = 90% (tritium decay)

Mean life/mass,  $\tau/m > 300$  s/eV, CL = 90% (reactor)

Mean life/mass,  $\tau/m > 7 \times 10^9$  s/eV (solar)

Mean life/mass,  $\tau/m > 15.4$  s/eV, CL = 90% (accelerator)

Magnetic moment  $\mu < 0.28 \times 10^{-10} \mu_B$ , CL = 90% (solar + radiochemical)

## Number of Neutrino Types

Number  $N = 2.996 \pm 0.007$  (Standard Model fits to LEP-SLC data)

Number  $N = 2.92 \pm 0.05$  ( $S = 1.2$ ) (Direct measurement of invisible Z width)

## Neutrino Mixing

The following values are obtained through data analyses based on the 3-neutrino mixing scheme described in the review “Neutrino Masses, Mixing, and Oscillations.”

$$\sin^2(\theta_{12}) = 0.307 \pm 0.013$$

$$\Delta m_{21}^2 = (7.53 \pm 0.18) \times 10^{-5} \text{ eV}^2$$

$$\sin^2(\theta_{23}) = 0.547 \pm 0.021 \text{ (Inverted order)}$$

$$\sin^2(\theta_{23}) = 0.545 \pm 0.021 \text{ (Normal order)}$$

$$\Delta m_{32}^2 = (-2.546^{+0.034}_{-0.040}) \times 10^{-3} \text{ eV}^2 \text{ (Inverted order)}$$

$$\Delta m_{32}^2 = (2.453 \pm 0.034) \times 10^{-3} \text{ eV}^2 \text{ (Normal order)}$$

$$\sin^2(\theta_{13}) = (2.18 \pm 0.07) \times 10^{-2}$$

$$\delta, \text{ CP violating phase} = 1.36 \pm 0.17 \pi \text{ rad}$$

$$\langle \Delta m_{21}^2 - \Delta \bar{m}_{21}^2 \rangle < 1.1 \times 10^{-4} \text{ eV}^2, \text{ CL} = 99.7\%$$

$$\langle \Delta m_{32}^2 - \Delta \bar{m}_{32}^2 \rangle = (-0.12 \pm 0.25) \times 10^{-3} \text{ eV}^2$$

## NOTES

In this Summary Table:

When a quantity has “(S = . . .)” to its right, the error on the quantity has been enlarged by the “scale factor” S, defined as  $S = \sqrt{\chi^2/(N-1)}$ , where N is the number of measurements used in calculating the quantity. We do this when  $S > 1$ , which often indicates that the measurements are inconsistent. When  $S > 1.25$ , we also show in the Particle Listings an ideogram of the measurements. For more about S, see the Introduction.

A decay momentum p is given for each decay mode. For a 2-body decay, p is the momentum of each decay product in the rest frame of the decaying particle. For a 3-or-more-body decay, p is the largest momentum any of the products can have in this frame.

[a] This is the best limit for the mode  $e^- \rightarrow \nu \gamma$ . The best limit for Nuclear de-excitation experiments is  $6.4 \times 10^{24}$  yr.

[b] See the review on “Muon Decay Parameters” for definitions and details.

[c]  $P_\mu$  is the longitudinal polarization of the muon from pion decay. For V–A coupling,  $P_\mu = 1$  and  $\rho = \delta = 3/4$ .

[d] This only includes events with energy of  $e > 45$  MeV and energy of  $\gamma > 40$  MeV. Since the  $e^- \bar{\nu}_e \nu_\mu$  and  $e^- \bar{\nu}_e \nu_\mu \gamma$  modes cannot be clearly separated, we regard the latter mode as a subset of the former.

[e] See the relevant Particle Listings for the energy limits used in this measurement.

[f] A test of additive vs. multiplicative lepton family number conservation.

[g] Basis mode for the  $\tau$ .

[h]  $L^\pm$  mass limit depends on decay assumptions; see the Full Listings.

## Quark Summary Table

## QUARKS

The  $u$ -,  $d$ -, and  $s$ -quark masses are estimates of so-called “current-quark masses,” in a mass-independent subtraction scheme such as  $\overline{\text{MS}}$  at a scale  $\mu \approx 2$  GeV. The  $c$ - and  $b$ -quark masses are the “running” masses in the  $\overline{\text{MS}}$  scheme. This can be different from the heavy quark masses obtained in potential models.

**u**

$$I(J^P) = \frac{1}{2}(\frac{1}{2}^+)$$

$$m_u = 2.16^{+0.49}_{-0.26} \text{ MeV} \quad \text{Charge} = \frac{2}{3} e \quad I_z = +\frac{1}{2}$$

$$m_u/m_d = 0.47^{+0.06}_{-0.07}$$

**d**

$$I(J^P) = \frac{1}{2}(\frac{1}{2}^+)$$

$$m_d = 4.67^{+0.48}_{-0.17} \text{ MeV} \quad \text{Charge} = -\frac{1}{3} e \quad I_z = -\frac{1}{2}$$

$$m_s/m_d = 17-22$$

$$\overline{m} = (m_u + m_d)/2 = 3.45^{+0.55}_{-0.15} \text{ MeV}$$

**s**

$$I(J^P) = 0(\frac{1}{2}^+)$$

$$m_s = 93^{+11}_{-5} \text{ MeV} \quad \text{Charge} = -\frac{1}{3} e \quad \text{Strangeness} = -1$$

$$m_s / ((m_u + m_d)/2) = 27.3^{+0.7}_{-1.3}$$

**c**

$$I(J^P) = 0(\frac{1}{2}^+)$$

$$m_c = 1.27 \pm 0.02 \text{ GeV} \quad \text{Charge} = \frac{2}{3} e \quad \text{Charm} = +1$$

$$m_c/m_s = 11.72 \pm 0.25$$

$$m_b/m_c = 4.577 \pm 0.008$$

$$m_b - m_c = 3.45 \pm 0.05 \text{ GeV}$$

**b**

$$I(J^P) = 0(\frac{1}{2}^+)$$

$$m_b = 4.18^{+0.03}_{-0.02} \text{ GeV} \quad \text{Charge} = -\frac{1}{3} e \quad \text{Bottom} = -1$$

**t**

$$I(J^P) = 0(\frac{1}{2}^+)$$

$$\text{Charge} = \frac{2}{3} e \quad \text{Top} = +1$$

Mass (direct measurements)  $m = 172.76 \pm 0.30$   
GeV <sup>[a,b]</sup> (S = 1.2)

Mass (from cross-section measurements)  $m = 162.5^{+2.1}_{-1.5}$  GeV <sup>[a]</sup>

Mass (Pole from cross-section measurements)  $m = 172.4 \pm 0.7$   
GeV

$$m_t - m_{\bar{t}} = -0.16 \pm 0.19 \text{ GeV}$$

$$\text{Full width } \Gamma = 1.42^{+0.19}_{-0.15} \text{ GeV} \quad (S = 1.4)$$

$$\Gamma(Wb)/\Gamma(Wq(q = b, s, d)) = 0.957 \pm 0.034 \quad (S = 1.5)$$

**t-quark EW Couplings**

$$F_0 = 0.687 \pm 0.018$$

$$F_- = 0.320 \pm 0.013$$

$$F_+ = 0.002 \pm 0.011$$

$$F_{V+A} < 0.29, \text{ CL} = 95\%$$

<b>DECAY MODES</b>	Fraction ( $\Gamma_i/\Gamma$ )	Confidence level	$\frac{p}{(\text{MeV}/c)}$
$Wq(q = b, s, d)$			—
$Wb$			—
$e\nu_e b$	(11.10 ± 0.30) %		—
$\mu\nu_\mu b$	(11.40 ± 0.20) %		—
$\tau\nu_\tau b$	(11.1 ± 0.9) %		—
$q\bar{q}b$	(66.5 ± 1.4) %		—
$\gamma q(q = u, c)$	[c] < 1.8	$\times 10^{-4}$	95%
<b><math>\Delta T = 1</math> weak neutral current (T1) modes</b>			
$Zq(q = u, c)$	T1 [d] < 5	$\times 10^{-4}$	95%
$Hu$	T1 < 1.2	$\times 10^{-3}$	95%
$Hc$	T1 < 1.1	$\times 10^{-3}$	95%
$\ell^+ \bar{q}q' (q = d, s, b; q' = u, c)$	T1 < 1.6	$\times 10^{-3}$	95%

 **$b'$  (4<sup>th</sup> Generation) Quark, Searches for**

$$\text{Mass } m > 190 \text{ GeV, CL} = 95\% \quad (p\bar{p}, \text{ quasi-stable } b')$$

$$\text{Mass } m > 1130 \text{ GeV, CL} = 95\% \quad (B(b' \rightarrow Zb) = 1)$$

$$\text{Mass } m > 1350 \text{ GeV, CL} = 95\% \quad (B(b' \rightarrow Wt) = 1)$$

$$\text{Mass } m > 46.0 \text{ GeV, CL} = 95\% \quad (e^+ e^-, \text{ all decays})$$

 **$t'$  (4<sup>th</sup> Generation) Quark, Searches for**

$$m(t'(2/3)) > 1280 \text{ GeV, CL} = 95\% \quad (B(t' \rightarrow Zt) = 1)$$

$$m(t'(2/3)) > 1295 \text{ GeV, CL} = 95\% \quad (B(t' \rightarrow Wb) = 1)$$

$$m(t'(2/3)) > 1310 \text{ GeV, CL} = 95\% \quad (\text{singlet } t')$$

$$m(t'(5/3)) > 1350 \text{ GeV, CL} = 95\%$$

**Free Quark Searches**

All searches since 1977 have had negative results.

## NOTES

- [a] A discussion of the definition of the top quark mass in these measurements can be found in the review “The Top Quark.”
- [b] Based on published top mass measurements using data from Tevatron Run-I and Run-II and LHC at  $\sqrt{s} = 7$  TeV. Including the most recent unpublished results from Tevatron Run-II, the Tevatron Electroweak Working Group reports a top mass of  $173.2 \pm 0.9$  GeV. See the note “The Top Quark” in the Quark Particle Listings of this Review.
- [c] This limit is for  $\Gamma(t \rightarrow \gamma q)/\Gamma(t \rightarrow Wb)$ .
- [d] This limit is for  $\Gamma(t \rightarrow Zq)/\Gamma(t \rightarrow Wb)$ .

## Meson Summary Table

### LIGHT UNFLAVORED MESONS ( $S = C = B = 0$ )

For  $I = 1$  ( $\pi, b, \rho, a$ ):  $u\bar{d}, (u\bar{u}-d\bar{d})/\sqrt{2}, d\bar{u}$ ;  
for  $I = 0$  ( $\eta, \eta', h, h', \omega, \phi, f, f'$ ):  $c_1(u\bar{u} + d\bar{d}) + c_2(s\bar{s})$

 **$\pi^\pm$** 

$$I^G(J^{PC}) = 1^-(0^-)$$

Mass  $m = 139.57039 \pm 0.00018$  MeV ( $S = 1.8$ )  
Mean life  $\tau = (2.6033 \pm 0.0005) \times 10^{-8}$  s ( $S = 1.2$ )  
 $c\tau = 7.8045$  m

$\pi^\pm \rightarrow \ell^\pm \nu \gamma$  form factors [a]

$F_V = 0.0254 \pm 0.0017$   
 $F_A = 0.0119 \pm 0.0001$   
 $F_V$  slope parameter  $a = 0.10 \pm 0.06$   
 $R = 0.059^{+0.009}_{-0.008}$

$\pi^-$  modes are charge conjugates of the modes below.

For decay limits to particles which are not established, see the section on Searches for Axions and Other Very Light Bosons.

$\pi^\pm$ DECAY MODES	Fraction ( $\Gamma_i/\Gamma$ )	Confidence level	$p$ (MeV/c)
$\mu^+ \nu_\mu$	[b] (99.98770 $\pm$ 0.00004) %		30
$\mu^+ \nu_\mu \gamma$	[c] ( 2.00 $\pm$ 0.25 ) $\times 10^{-4}$		30
$e^+ \nu_e$	[b] ( 1.230 $\pm$ 0.004 ) $\times 10^{-4}$		70
$e^+ \nu_e \gamma$	[c] ( 7.39 $\pm$ 0.05 ) $\times 10^{-7}$		70
$e^+ \nu_e \pi^0$	( 1.036 $\pm$ 0.006 ) $\times 10^{-8}$		4
$e^+ \nu_e e^+ e^-$	( 3.2 $\pm$ 0.5 ) $\times 10^{-9}$		70
$e^+ \nu_e \nu \bar{\nu}$	< 5 $\times 10^{-6}$	90%	70
<b>Lepton Family number (LF) or Lepton number (L) violating modes</b>			
$\mu^+ \bar{\nu}_e$	L [d] < 1.5 $\times 10^{-3}$	90%	30
$\mu^+ \nu_e$	LF [d] < 8.0 $\times 10^{-3}$	90%	30
$\mu^- e^+ e^+ \nu$	LF < 1.6 $\times 10^{-6}$	90%	30

 **$\pi^0$** 

$$I^G(J^{PC}) = 1^-(0^{++})$$

Mass  $m = 134.9768 \pm 0.0005$  MeV ( $S = 1.1$ )  
 $m_{\pi^\pm} - m_{\pi^0} = 4.5936 \pm 0.0005$  MeV  
Mean life  $\tau = (8.52 \pm 0.18) \times 10^{-17}$  s ( $S = 1.2$ )  
 $c\tau = 25.5$  nm

For decay limits to particles which are not established, see the appropriate Search sections ( $A^0$  (axion) and Other Light Boson ( $X^0$ ) Searches, etc.).

$\pi^0$ DECAY MODES	Fraction ( $\Gamma_i/\Gamma$ )	Scale factor/ Confidence level	$p$ (MeV/c)
$2\gamma$	(98.823 $\pm$ 0.034) %	S=1.5	67
$e^+ e^- \gamma$	( 1.174 $\pm$ 0.035 ) %	S=1.5	67
$\gamma$ positronium	( 1.82 $\pm$ 0.29 ) $\times 10^{-9}$		67
$e^+ e^+ e^- e^-$	( 3.34 $\pm$ 0.16 ) $\times 10^{-5}$		67
$e^+ e^-$	( 6.46 $\pm$ 0.33 ) $\times 10^{-8}$		67
$4\gamma$	< 2 $\times 10^{-8}$	CL=90%	67
$\nu \bar{\nu}$	[e] < 2.7 $\times 10^{-7}$	CL=90%	67
$\nu_e \bar{\nu}_e$	< 1.7 $\times 10^{-6}$	CL=90%	67
$\nu_\mu \bar{\nu}_\mu$	< 1.6 $\times 10^{-6}$	CL=90%	67
$\nu_\tau \bar{\nu}_\tau$	< 2.1 $\times 10^{-6}$	CL=90%	67
$\gamma \nu \bar{\nu}$	< 1.9 $\times 10^{-7}$	CL=90%	67
<b>Charge conjugation (C) or Lepton Family number (LF) violating modes</b>			
$3\gamma$	C < 3.1 $\times 10^{-8}$	CL=90%	67
$\mu^+ e^-$	LF < 3.8 $\times 10^{-10}$	CL=90%	26
$\mu^- e^+$	LF < 3.4 $\times 10^{-9}$	CL=90%	26
$\mu^+ e^- + \mu^- e^+$	LF < 3.6 $\times 10^{-10}$	CL=90%	26

 **$\eta$** 

$$I^G(J^{PC}) = 0^+(0^{-+})$$

Mass  $m = 547.862 \pm 0.017$  MeV  
Full width  $\Gamma = 1.31 \pm 0.05$  keV

**C-nonconserving decay parameters**

$\pi^+ \pi^- \pi^0$  left-right asymmetry =  $(0.09^{+0.11}_{-0.12}) \times 10^{-2}$   
 $\pi^+ \pi^- \pi^0$  sextant asymmetry =  $(0.12^{+0.10}_{-0.11}) \times 10^{-2}$   
 $\pi^+ \pi^- \pi^0$  quadrant asymmetry =  $(-0.09 \pm 0.09) \times 10^{-2}$   
 $\pi^+ \pi^- \gamma$  left-right asymmetry =  $(0.9 \pm 0.4) \times 10^{-2}$   
 $\pi^+ \pi^- \gamma$   $\beta$  ( $D$ -wave) =  $-0.02 \pm 0.07$  ( $S = 1.3$ )

**CP-nonconserving decay parameters**

$\pi^+ \pi^- e^+ e^-$  decay-plane asymmetry  $A_\phi = (-0.6 \pm 3.1) \times 10^{-2}$

**Other decay parameters**

$\pi^0 \pi^0 \pi^0$  Dalitz plot  $\alpha = -0.0288 \pm 0.0012$  ( $S = 1.1$ )  
Parameter  $\Lambda$  in  $\eta \rightarrow \ell^+ \ell^- \gamma$  decay =  $0.716 \pm 0.011$  GeV/ $c^2$

$\eta$ DECAY MODES	Fraction ( $\Gamma_i/\Gamma$ )	Scale factor/ Confidence level	$p$ (MeV/c)
<b>Neutral modes</b>			
neutral modes	(72.12 $\pm$ 0.34) %	S=1.2	-
$2\gamma$	(39.41 $\pm$ 0.20) %	S=1.1	274
$3\pi^0$	(32.68 $\pm$ 0.23) %	S=1.1	179
$\pi^0 2\gamma$	( 2.56 $\pm$ 0.22 ) $\times 10^{-4}$		257
$2\pi^0 2\gamma$	< 1.2 $\times 10^{-3}$	CL=90%	238
$4\gamma$	< 2.8 $\times 10^{-4}$	CL=90%	274
invisible	< 1.0 $\times 10^{-4}$	CL=90%	-
<b>Charged modes</b>			
charged modes	(27.89 $\pm$ 0.29) %	S=1.2	-
$\pi^+ \pi^- \pi^0$	(22.92 $\pm$ 0.28) %	S=1.2	174
$\pi^+ \pi^- \gamma$	( 4.22 $\pm$ 0.08 ) %	S=1.1	236
$e^+ e^- \gamma$	( 6.9 $\pm$ 0.4 ) $\times 10^{-3}$	S=1.3	274
$\mu^+ \mu^- \gamma$	( 3.1 $\pm$ 0.4 ) $\times 10^{-4}$		253
$e^+ e^-$	< 7 $\times 10^{-7}$	CL=90%	274
$\mu^+ \mu^-$	( 5.8 $\pm$ 0.8 ) $\times 10^{-6}$		253
$2e^+ 2e^-$	( 2.40 $\pm$ 0.22 ) $\times 10^{-5}$		274
$\pi^+ \pi^- e^+ e^- (\gamma)$	( 2.68 $\pm$ 0.11 ) $\times 10^{-4}$		235
$e^+ e^- \mu^+ \mu^-$	< 1.6 $\times 10^{-4}$	CL=90%	253
$2\mu^+ 2\mu^-$	< 3.6 $\times 10^{-4}$	CL=90%	161
$\mu^+ \mu^- \pi^+ \pi^-$	< 3.6 $\times 10^{-4}$	CL=90%	113
$\pi^+ e^- \bar{\nu}_e + c.c.$	< 1.7 $\times 10^{-4}$	CL=90%	256
$\pi^+ \pi^- 2\gamma$	< 2.1 $\times 10^{-3}$		236
$\pi^+ \pi^- \pi^0 \gamma$	< 5 $\times 10^{-4}$	CL=90%	174
$\pi^0 \mu^+ \mu^- \gamma$	< 3 $\times 10^{-6}$	CL=90%	210

**Charge conjugation (C), Parity (P),  
Charge conjugation  $\times$  Parity (CP), or  
Lepton Family number (LF) violating modes**

DECAY MODES	C	[f] <	Confidence level	$p$ (MeV/c)
$\pi^0 \gamma$	C	< 9	$\times 10^{-5}$	CL=90% 257
$\pi^+ \pi^-$	$P, CP$	< 1.3	$\times 10^{-5}$	CL=90% 236
$2\pi^0$	$P, CP$	< 3.5	$\times 10^{-4}$	CL=90% 238
$2\pi^0 \gamma$	C	< 5	$\times 10^{-4}$	CL=90% 238
$3\pi^0 \gamma$	C	< 6	$\times 10^{-5}$	CL=90% 179
$3\gamma$	C	< 1.6	$\times 10^{-5}$	CL=90% 274
$4\pi^0$	$P, CP$	< 6.9	$\times 10^{-7}$	CL=90% 40
$\pi^0 e^+ e^-$	C	[g] < 8	$\times 10^{-6}$	CL=90% 257
$\pi^0 \mu^+ \mu^-$	C	[g] < 5	$\times 10^{-6}$	CL=90% 210
$\mu^+ e^- + \mu^- e^+$	LF	< 6	$\times 10^{-6}$	CL=90% 264

 **$f_0(500)$** 

$$I^G(J^{PC}) = 0^+(0^{++})$$

also known as  $\sigma$ ; was  $f_0(600)$

See the review on "Scalar Mesons below 2 GeV."

Mass (T-Matrix Pole  $\sqrt{s}$ ) =  $(400-550) - i(200-350)$  MeV  
Mass (Breit-Wigner) =  $(400-550)$  MeV  
Full width (Breit-Wigner) =  $(400-700)$  MeV

$f_0(500)$ DECAY MODES	Fraction ( $\Gamma_i/\Gamma$ )	$p$ (MeV/c)
$\pi \pi$	seen	-
$\gamma \gamma$	seen	-

 **$\rho(770)$** 

$$I^G(J^{PC}) = 1^+(1^{--})$$

See the note in  $\rho(770)$  Particle Listings.

Mass  $m = 775.26 \pm 0.25$  MeV  
Full width  $\Gamma = 149.1 \pm 0.8$  MeV  
 $\Gamma_{ee} = 7.04 \pm 0.06$  keV

## Meson Summary Table

$\rho(770)$ DECAY MODES	Fraction ( $\Gamma_i/\Gamma$ )	Scale factor/ Confidence level	$p$ (MeV/c)
$\pi^+\pi^-$	$\sim 100$ %		363
<b><math>\rho(770)^\pm</math> decays</b>			
$\pi^\pm\gamma$	( 4.5 $\pm$ 0.5 ) $\times 10^{-4}$	S=2.2	375
$\pi^\pm\eta$	< 6 $\times 10^{-3}$	CL=84%	152
$\pi^\pm\pi^+\pi^-\pi^0$	< 2.0 $\times 10^{-3}$	CL=84%	254
<b><math>\rho(770)^0</math> decays</b>			
$\pi^+\pi^-\gamma$	( 9.9 $\pm$ 1.6 ) $\times 10^{-3}$		362
$\pi^0\gamma$	( 4.7 $\pm$ 0.6 ) $\times 10^{-4}$	S=1.4	376
$\eta\gamma$	( 3.00 $\pm$ 0.21 ) $\times 10^{-4}$		194
$\pi^0\pi^0\gamma$	( 4.5 $\pm$ 0.8 ) $\times 10^{-5}$		363
$\mu^+\mu^-$	[h] ( 4.55 $\pm$ 0.28 ) $\times 10^{-5}$		373
$e^+e^-$	[h] ( 4.72 $\pm$ 0.05 ) $\times 10^{-5}$		388
$\pi^+\pi^-\pi^0$	( 1.01 $\pm$ 0.54 $\pm$ 0.34 ) $\times 10^{-4}$		323
$\pi^+\pi^-\pi^+\pi^-$	( 1.8 $\pm$ 0.9 ) $\times 10^{-5}$		251
$\pi^+\pi^-\pi^0\pi^0$	( 1.6 $\pm$ 0.8 ) $\times 10^{-5}$		257
$\pi^0e^+e^-$	< 1.2 $\times 10^{-5}$	CL=90%	376

 **$\omega(782)$** 

$$I^G(J^{PC}) = 0^-(1^{--})$$

Mass  $m = 782.65 \pm 0.12$  MeV (S = 1.9)Full width  $\Gamma = 8.49 \pm 0.08$  MeV $\Gamma_{ee} = 0.60 \pm 0.02$  keV

$\omega(782)$ DECAY MODES	Fraction ( $\Gamma_i/\Gamma$ )	Scale factor/ Confidence level	$p$ (MeV/c)
$\pi^+\pi^-\pi^0$	(89.3 $\pm$ 0.6) %		327
$\pi^0\gamma$	( 8.40 $\pm$ 0.22 ) %	S=1.8	380
$\pi^+\pi^-$	( 1.53 $\pm$ 0.06 ) %		366
neutrals (excluding $\pi^0\gamma$ )	( 7 $\pm$ 4 ) $\times 10^{-3}$	S=1.1	-
$\eta\gamma$	( 4.5 $\pm$ 0.4 ) $\times 10^{-4}$	S=1.1	200
$\pi^0e^+e^-$	( 7.7 $\pm$ 0.6 ) $\times 10^{-4}$		380
$\pi^0\mu^+\mu^-$	( 1.34 $\pm$ 0.18 ) $\times 10^{-4}$	S=1.5	349
$e^+e^-$	( 7.36 $\pm$ 0.15 ) $\times 10^{-5}$	S=1.5	391
$\pi^+\pi^-\pi^0\pi^0$	< 2 $\times 10^{-4}$	CL=90%	262
$\pi^+\pi^-\gamma$	< 3.6 $\times 10^{-3}$	CL=95%	366
$\pi^+\pi^-\pi^+\pi^-$	< 1 $\times 10^{-3}$	CL=90%	256
$\pi^0\pi^0\gamma$	( 6.7 $\pm$ 1.1 ) $\times 10^{-5}$		367
$\eta\pi^0\gamma$	< 3.3 $\times 10^{-5}$	CL=90%	162
$\mu^+\mu^-$	( 7.4 $\pm$ 1.8 ) $\times 10^{-5}$		377
$3\gamma$	< 1.9 $\times 10^{-4}$	CL=95%	391

**Charge conjugation (C) violating modes**

$\eta\pi^0$	C < 2.2 $\times 10^{-4}$	CL=90%	162
$2\pi^0$	C < 2.2 $\times 10^{-4}$	CL=90%	367
$3\pi^0$	C < 2.3 $\times 10^{-4}$	CL=90%	330
invisible	< 7 $\times 10^{-5}$	CL=90%	-

 **$\eta'(958)$** 

$$I^G(J^{PC}) = 0^+(0^{-+})$$

Mass  $m = 957.78 \pm 0.06$  MeVFull width  $\Gamma = 0.188 \pm 0.006$  MeV

$\eta'(958)$ DECAY MODES	Fraction ( $\Gamma_i/\Gamma$ )	Confidence level	$p$ (MeV/c)
$\pi^+\pi^-\eta$	(42.5 $\pm$ 0.5) %		232
$\rho^0\gamma$ (including non-resonant $\pi^+\pi^-\gamma$ )	(29.5 $\pm$ 0.4) %		165
$\pi^0\pi^0\eta$	(22.4 $\pm$ 0.5) %		239
$\omega\gamma$	( 2.52 $\pm$ 0.07 ) %		159
$\omega e^+e^-$	( 2.0 $\pm$ 0.4 ) $\times 10^{-4}$		159
$\gamma\gamma$	( 2.307 $\pm$ 0.033 ) %		479
$3\pi^0$	( 2.50 $\pm$ 0.17 ) $\times 10^{-3}$		430
$\mu^+\mu^-\gamma$	( 1.13 $\pm$ 0.28 ) $\times 10^{-4}$		467
$\pi^+\pi^-\mu^+\mu^-$	< 2.9 $\times 10^{-5}$	90%	401
$\pi^+\pi^-\pi^0$	( 3.61 $\pm$ 0.17 ) $\times 10^{-3}$		428
$(\pi^+\pi^-\pi^0)$ S-wave	( 3.8 $\pm$ 0.5 ) $\times 10^{-3}$		428
$\pi^\mp\rho^\pm$	( 7.4 $\pm$ 2.3 ) $\times 10^{-4}$		106
$\pi^0\rho^0$	< 4 %	90%	111
$2(\pi^+\pi^-)$	( 8.4 $\pm$ 0.9 ) $\times 10^{-5}$		372
$\pi^+\pi^-2\pi^0$	( 1.8 $\pm$ 0.4 ) $\times 10^{-4}$		376
$2(\pi^+\pi^-)$ neutrals	< 1 %	95%	-

$2(\pi^+\pi^-)\pi^0$	< 1.8 $\times 10^{-3}$	90%	298
$2(\pi^+\pi^-)2\pi^0$	< 1 %	95%	197
$3(\pi^+\pi^-)$	< 3.1 $\times 10^{-5}$	90%	189
$K^\pm\pi^\mp$	< 4 $\times 10^{-5}$	90%	334
$\pi^+\pi^-e^+e^-$	( 2.4 $\pm$ 1.3 $\pm$ 1.0 ) $\times 10^{-3}$		458
$\pi^+e^-\nu_e$ + c.c.	< 2.1 $\times 10^{-4}$	90%	469
$\gamma e^+e^-$	( 4.91 $\pm$ 0.27 ) $\times 10^{-4}$		479
$\pi^0\gamma\gamma$	( 3.20 $\pm$ 0.24 ) $\times 10^{-3}$		469
$\pi^0\gamma\gamma$ (non resonant)	( 6.2 $\pm$ 0.9 ) $\times 10^{-4}$		-
$\eta\gamma\gamma$	< 1.33 $\times 10^{-4}$	90%	322
$4\pi^0$	< 3.2 $\times 10^{-4}$	90%	380
$e^+e^-$	< 5.6 $\times 10^{-9}$	90%	479
invisible	< 6 $\times 10^{-4}$	90%	-

**Charge conjugation (C), Parity (P),  
Lepton family number (LF) violating modes**

$\pi^+\pi^-$	$P, CP$ < 1.8 $\times 10^{-5}$	90%	458
$\pi^0\pi^0$	$P, CP$ < 4 $\times 10^{-4}$	90%	459
$\pi^0e^+e^-$	C [g] < 1.4 $\times 10^{-3}$	90%	469
$\eta e^+e^-$	C [g] < 2.4 $\times 10^{-3}$	90%	322
$3\gamma$	C < 1.0 $\times 10^{-4}$	90%	479
$\mu^+\mu^-\pi^0$	C [g] < 6.0 $\times 10^{-5}$	90%	445
$\mu^+\mu^-\eta$	C [g] < 1.5 $\times 10^{-5}$	90%	273
$e\mu$	LF < 4.7 $\times 10^{-4}$	90%	473

 **$f_0(980)$** 

$$I^G(J^{PC}) = 0^+(0^{++})$$

See the review on "Scalar Mesons below 2 GeV."

Mass  $m = 990 \pm 20$  MeVFull width  $\Gamma = 10$  to 100 MeV

$f_0(980)$ DECAY MODES	Fraction ( $\Gamma_i/\Gamma$ )	$p$ (MeV/c)
$\pi\pi$	seen	476
$K\bar{K}$	seen	36
$\gamma\gamma$	seen	495

 **$a_0(980)$** 

$$I^G(J^{PC}) = 1^-(0^{++})$$

See the review on "Scalar Mesons below 2 GeV."

Mass  $m = 980 \pm 20$  MeVFull width  $\Gamma = 50$  to 100 MeV

$a_0(980)$ DECAY MODES	Fraction ( $\Gamma_i/\Gamma$ )	$p$ (MeV/c)
$\eta\pi$	seen	319
$K\bar{K}$	seen	†
$\rho\pi$	not seen	137
$\gamma\gamma$	seen	490

 **$\phi(1020)$** 

$$I^G(J^{PC}) = 0^-(1^{--})$$

Mass  $m = 1019.461 \pm 0.016$  MeVFull width  $\Gamma = 4.249 \pm 0.013$  MeV (S = 1.1)

$\phi(1020)$ DECAY MODES	Fraction ( $\Gamma_i/\Gamma$ )	Scale factor/ Confidence level	$p$ (MeV/c)
$K^+K^-$	(49.2 $\pm$ 0.5) %	S=1.3	127
$K_L^0K_S^0$	(34.0 $\pm$ 0.4) %	S=1.3	110
$\rho\pi + \pi^+\pi^-\pi^0$	(15.24 $\pm$ 0.33) %	S=1.2	-
$\eta\gamma$	( 1.303 $\pm$ 0.025 ) %	S=1.2	363
$\pi^0\gamma$	( 1.30 $\pm$ 0.05 ) $\times 10^{-3}$		501
$l^+l^-$	-		510
$e^+e^-$	( 2.973 $\pm$ 0.034 ) $\times 10^{-4}$	S=1.3	510
$\mu^+\mu^-$	( 2.86 $\pm$ 0.19 ) $\times 10^{-4}$		499
$\eta e^+e^-$	( 1.08 $\pm$ 0.04 ) $\times 10^{-4}$		363
$\pi^+\pi^-$	( 7.3 $\pm$ 1.3 ) $\times 10^{-5}$		490
$\omega\pi^0$	( 4.7 $\pm$ 0.5 ) $\times 10^{-5}$		172
$\omega\gamma$	< 5 %	CL=84%	209
$\rho\gamma$	< 1.2 $\times 10^{-5}$	CL=90%	215
$\pi^+\pi^-\gamma$	( 4.1 $\pm$ 1.3 ) $\times 10^{-5}$		490
$f_0(980)\gamma$	( 3.22 $\pm$ 0.19 ) $\times 10^{-4}$	S=1.1	29
$\pi^0\pi^0\gamma$	( 1.12 $\pm$ 0.06 ) $\times 10^{-4}$		492
$\pi^+\pi^-\pi^+\pi^-$	( 3.9 $\pm$ 2.8 $\pm$ 2.2 ) $\times 10^{-6}$		410

## Meson Summary Table

$\pi^+\pi^+\pi^-\pi^-\pi^0$	< 4.6	$\times 10^{-6}$	CL=90%	342
$\pi^0 e^+ e^-$	( 1.33 $\pm$ 0.07 $\phantom{\pm 0.10}$ )	$\times 10^{-5}$		501
$\pi^0 \eta \gamma$	( 7.27 $\pm$ 0.30 )	$\times 10^{-5}$	S=1.5	346
$a_0(980) \gamma$	( 7.6 $\pm$ 0.6 )	$\times 10^{-5}$		39
$K^0 \bar{K}^0 \gamma$	< 1.9	$\times 10^{-8}$	CL=90%	110
$\eta'(958) \gamma$	( 6.22 $\pm$ 0.21 )	$\times 10^{-5}$		60
$\eta \pi^0 \pi^0 \gamma$	< 2	$\times 10^{-5}$	CL=90%	293
$\mu^+ \mu^- \gamma$	( 1.4 $\pm$ 0.5 )	$\times 10^{-5}$		499
$\rho \gamma \gamma$	< 1.2	$\times 10^{-4}$	CL=90%	215
$\eta \pi^+ \pi^-$	< 1.8	$\times 10^{-5}$	CL=90%	288
$\eta \mu^+ \mu^-$	< 9.4	$\times 10^{-6}$	CL=90%	321
$\eta U \rightarrow \eta e^+ e^-$	< 1	$\times 10^{-6}$	CL=90%	-
invisible	< 1.7	$\times 10^{-4}$	CL=90%	-

## Lepton Family number (LF) violating modes

$e^\pm \mu^\mp$	LF	< 2	$\times 10^{-6}$	CL=90%	504
-----------------	----	-----	------------------	--------	-----

 **$h_1(1170)$** 

$$I^G(J^{PC}) = 0^-(1^+ -)$$

Mass  $m = 1166 \pm 6$  MeV  
Full width  $\Gamma = 375 \pm 35$  MeV

$h_1(1170)$ DECAY MODES	Fraction ( $\Gamma_i/\Gamma$ )	$\rho$ (MeV/c)
$\rho \pi$	seen	305

 **$b_1(1235)$** 

$$I^G(J^{PC}) = 1^+(1^+ -)$$

Mass  $m = 1229.5 \pm 3.2$  MeV (S = 1.6)  
Full width  $\Gamma = 142 \pm 9$  MeV (S = 1.2)

$b_1(1235)$ DECAY MODES	Fraction ( $\Gamma_i/\Gamma$ )	Confidence level	$\rho$ (MeV/c)
$\omega \pi$	seen		348
	[D/S amplitude ratio = 0.277 $\pm$ 0.027]		
$\pi^\pm \gamma$	( 1.6 $\pm$ 0.4 )	$\times 10^{-3}$	607
$\eta \rho$	seen		†
$\pi^+\pi^+\pi^-\pi^0$	< 50	%	84%
$K^*(892)^\pm K^\mp$	seen		†
$(K\bar{K})^\pm \pi^0$	< 8	%	90%
$K_S^0 K_L^0 \pi^\pm$	< 6	%	90%
$K_S^0 K_S^0 \pi^\pm$	< 2	%	90%
$\phi \pi$	< 1.5	%	84%

 **$a_1(1260)$  [1]**

$$I^G(J^{PC}) = 1^-(1^+ +)$$

Mass  $m = 1230 \pm 40$  MeV [1]  
Full width  $\Gamma = 250$  to 600 MeV

$a_1(1260)$ DECAY MODES	Fraction ( $\Gamma_i/\Gamma$ )	$\rho$ (MeV/c)
$3\pi$	seen	577
$(\rho\pi)_{S\text{-wave}}, \rho \rightarrow \pi\pi$	seen	353
$(\rho\pi)_{D\text{-wave}}, \rho \rightarrow \pi\pi$	seen	353
$(\rho(1450)\pi)_{S\text{-wave}}, \rho \rightarrow \pi\pi$	seen	†
$(\rho(1450)\pi)_{D\text{-wave}}, \rho \rightarrow \pi\pi$	seen	†
$f_0(500)\pi, f_0 \rightarrow \pi\pi$	seen	-
$f_0(980)\pi, f_0 \rightarrow \pi\pi$	not seen	179
$f_0(1370)\pi, f_0 \rightarrow \pi\pi$	seen	†
$f_2(1270)\pi, f_2 \rightarrow \pi\pi$	seen	†
$\pi^+\pi^-\pi^0$	seen	576
$\pi^0\pi^0\pi^0$	not seen	577
$KK\pi$	seen	250
$K^*(892)K$	seen	†
$\pi\gamma$	seen	608

 **$f_2(1270)$** 

$$I^G(J^{PC}) = 0^+(2^+ +)$$

Mass  $m = 1275.5 \pm 0.8$  MeV  
Full width  $\Gamma = 186.7^{+2.2}_{-2.5}$  MeV (S = 1.4)

$f_2(1270)$ DECAY MODES	Fraction ( $\Gamma_i/\Gamma$ )	Scale factor/ Confidence level	$\rho$ (MeV/c)
$\pi\pi$	( 84.2 $\pm$ 2.9 $\phantom{\pm 0.9}$ ) %	S=1.1	623
$\pi^+\pi^-2\pi^0$	( 7.7 $\pm$ 1.1 $\phantom{\pm 3.2}$ ) %	S=1.2	563

 **$K\bar{K}$** 

$K\bar{K}$	( 4.6 $\pm$ 0.5 $\phantom{\pm 0.4}$ ) %	S=2.7	404
$2\pi^+2\pi^-$	( 2.8 $\pm$ 0.4 ) %	S=1.2	560
$\eta\eta$	( 4.0 $\pm$ 0.8 ) $\times 10^{-3}$	S=2.1	326
$4\pi^0$	( 3.0 $\pm$ 1.0 ) $\times 10^{-3}$		565
$\gamma\gamma$	( 1.42 $\pm$ 0.24 ) $\times 10^{-5}$	S=1.4	638
$\eta\pi\pi$	< 8	$\times 10^{-3}$	CL=95%
$K^0 K^- \pi^+ + \text{c.c.}$	< 3.4	$\times 10^{-3}$	CL=95%
$e^+ e^-$	< 6	$\times 10^{-10}$	CL=90%

 **$f_1(1285)$** 

$$I^G(J^{PC}) = 0^+(1^+ +)$$

Mass  $m = 1281.9 \pm 0.5$  MeV (S = 1.8)  
Full width  $\Gamma = 22.7 \pm 1.1$  MeV (S = 1.5)

 **$f_1(1285)$  DECAY MODES**

$f_1(1285)$ DECAY MODES	Fraction ( $\Gamma_i/\Gamma$ )	Scale factor/ Confidence level	$\rho$ (MeV/c)
$4\pi$	( 32.7 $\pm$ 1.9 ) %	S=1.2	568
$\pi^0\pi^0\pi^+\pi^-$	( 21.8 $\pm$ 1.3 ) %	S=1.2	566
$2\pi^+2\pi^-$	( 10.9 $\pm$ 0.6 ) %	S=1.2	563
$\rho^0\pi^+\pi^-$	( 10.9 $\pm$ 0.6 ) %	S=1.2	336
$\rho^0\rho^0$	seen		†
$4\pi^0$	< 7	$\times 10^{-4}$	CL=90%
$\eta\pi^+\pi^-$	( 35 $\pm$ 15 ) %		479
$\eta\pi\pi$	( 52.2 $\pm$ 2.0 ) %	S=1.2	482
$a_0(980)\pi$ [ignoring $a_0(980) \rightarrow K\bar{K}$ ]	( 38 $\pm$ 4 ) %		238
$\eta\pi\pi$ [excluding $a_0(980)\pi$ ]	( 14 $\pm$ 4 ) %		482
$K\bar{K}\pi$	( 9.0 $\pm$ 0.4 ) %	S=1.1	308
$K\bar{K}^*(892)$	not seen		†
$\pi^+\pi^-\pi^0$	( 3.0 $\pm$ 0.9 ) $\times 10^{-3}$		603
$\rho^\pm\pi^\mp$	< 3.1	$\times 10^{-3}$	CL=95%
$\gamma\rho^0$	( 6.1 $\pm$ 1.0 ) %	S=1.7	406
$\phi\gamma$	( 7.4 $\pm$ 2.6 ) $\times 10^{-4}$		236
$e^+ e^-$	< 9.4	$\times 10^{-9}$	CL=90%

 **$\eta(1295)$** 

$$I^G(J^{PC}) = 0^+(0^- +)$$

See the review on "Pseudoscalar and pseudovector mesons in the 1400 MeV region."

Mass  $m = 1294 \pm 4$  MeV (S = 1.6)  
Full width  $\Gamma = 55 \pm 5$  MeV

 **$\eta(1295)$  DECAY MODES**

$\eta(1295)$ DECAY MODES	Fraction ( $\Gamma_i/\Gamma$ )	$\rho$ (MeV/c)
$\eta\pi^+\pi^-$	seen	487
$a_0(980)\pi$	seen	248
$\eta\pi^0\pi^0$	seen	490
$\eta(\pi\pi)_{S\text{-wave}}$	seen	-

 **$\pi(1300)$** 

$$I^G(J^{PC}) = 1^-(0^- +)$$

Mass  $m = 1300 \pm 100$  MeV [1]  
Full width  $\Gamma = 200$  to 600 MeV

 **$\pi(1300)$  DECAY MODES**

$\pi(1300)$ DECAY MODES	Fraction ( $\Gamma_i/\Gamma$ )	$\rho$ (MeV/c)
$\rho\pi$	seen	404
$\pi(\pi\pi)_{S\text{-wave}}$	seen	-

 **$a_2(1320)$** 

$$I^G(J^{PC}) = 1^-(2^+ +)$$

Mass  $m = 1316.9 \pm 0.9$  MeV (S = 1.9)  
Full width  $\Gamma = 107 \pm 5$  MeV [1]

 **$a_2(1320)$  DECAY MODES**

$a_2(1320)$ DECAY MODES	Fraction ( $\Gamma_i/\Gamma$ )	Scale factor/ Confidence level	$\rho$ (MeV/c)
$3\pi$	( 70.1 $\pm$ 2.7 ) %	S=1.2	623
$\eta\pi$	( 14.5 $\pm$ 1.2 ) %		535
$\omega\pi\pi$	( 10.6 $\pm$ 3.2 ) %	S=1.3	364
$K\bar{K}$	( 4.9 $\pm$ 0.8 ) %		436
$\eta'(958)\pi$	( 5.5 $\pm$ 0.9 ) $\times 10^{-3}$		287
$\pi^\pm\gamma$	( 2.91 $\pm$ 0.27 ) $\times 10^{-3}$		651
$\gamma\gamma$	( 9.4 $\pm$ 0.7 ) $\times 10^{-6}$		658
$e^+ e^-$	< 5	$\times 10^{-9}$	CL=90%

## Meson Summary Table

 **$f_0(1370)$** 

$$I^G(J^{PC}) = 0^+(0^{++})$$

See the review on "Scalar Mesons below 2 GeV."

Mass  $m = 1200$  to  $1500$  MeV  
Full width  $\Gamma = 200$  to  $500$  MeV

$f_0(1370)$ DECAY MODES	Fraction ( $\Gamma_i/\Gamma$ )	$\rho$ (MeV/c)
$\pi\pi$	seen	672
$4\pi$	seen	617
$4\pi^0$	seen	617
$2\pi^+2\pi^-$	seen	612
$\pi^+\pi^-2\pi^0$	seen	615
$\rho\rho$	seen	†
$2(\pi\pi)_{S\text{-wave}}$	seen	–
$\pi(1300)\pi$	seen	†
$a_1(1260)\pi$	seen	35
$\eta\eta$	seen	411
$K\bar{K}$	seen	475
$K\bar{K}\eta\pi$	not seen	†
$6\pi$	not seen	508
$\omega\omega$	not seen	†
$\gamma\gamma$	seen	685
$e^+e^-$	not seen	685

 **$\pi_1(1400)$  [k]**

$$I^G(J^{PC}) = 1^-(1^{-+})$$

See the review on "Non- $q\bar{q}$  Mesons."Mass  $m = 1354 \pm 25$  MeV ( $S = 1.8$ )  
Full width  $\Gamma = 330 \pm 35$  MeV

$\pi_1(1400)$ DECAY MODES	Fraction ( $\Gamma_i/\Gamma$ )	$\rho$ (MeV/c)
$\eta\pi^0$	seen	557
$\eta\pi^-$	seen	556
$\rho(770)\pi$	not seen	442

 **$\eta(1405)$** 

$$I^G(J^{PC}) = 0^+(0^{-+})$$

See the review on "Pseudoscalar and Pseudovector Mesons in the 1400 MeV Region."

Mass  $m = 1408.8 \pm 2.0$  MeV ( $S = 2.2$ )  
Full width  $\Gamma = 50.1 \pm 2.6$  MeV ( $S = 1.7$ )

$\eta(1405)$ DECAY MODES	Fraction ( $\Gamma_i/\Gamma$ )	Confidence level	$\rho$ (MeV/c)
$K\bar{K}\pi$	seen		424
$\eta\pi\pi$	seen		562
$a_0(980)\pi$	seen		345
$\eta(\pi\pi)_{S\text{-wave}}$	seen		–
$f_0(980)\pi^0 \rightarrow \pi^+\pi^-\pi^0$	not seen		–
$f_0(980)\eta$	seen		†
$4\pi$	seen		639
$\rho\rho$	<58 %	99.85%	†
$\rho^0\gamma$	seen		491
$K^*(892)K$	seen		123

 **$h_1(1415)$** 

$$I^G(J^{PC}) = 0^-(1^{+-})$$

was  $h_1(1380)$ Mass  $m = 1416 \pm 8$  MeV ( $S = 1.5$ )  
Full width  $\Gamma = 90 \pm 15$  MeV **$f_1(1420)$** 

$$I^G(J^{PC}) = 0^+(1^{++})$$

See the review on "Pseudoscalar and Pseudovector Mesons in the 1400 MeV Region."

Mass  $m = 1426.3 \pm 0.9$  MeV ( $S = 1.1$ )  
Full width  $\Gamma = 54.5 \pm 2.6$  MeV

$f_1(1420)$ DECAY MODES	Fraction ( $\Gamma_i/\Gamma$ )	$\rho$ (MeV/c)
$K\bar{K}\pi$	seen	438
$K\bar{K}^*(892) + c.c.$	seen	163

 $\eta\pi\pi$   
 $\phi\gamma$ possibly seen  
seen573  
349 **$\omega(1420)$  [l]**

$$I^G(J^{PC}) = 0^-(1^{--})$$

Mass  $m = 1410 \pm 60$  MeV [l]  
Full width  $\Gamma = 290 \pm 190$  MeV [l]

$\omega(1420)$ DECAY MODES	Fraction ( $\Gamma_i/\Gamma$ )	$\rho$ (MeV/c)
$\rho\pi$	seen	480
$\omega\pi\pi$	seen	437
$b_1(1235)\pi$	seen	112
$e^+e^-$	seen	705

 **$a_0(1450)$** 

$$I^G(J^{PC}) = 1^-(0^{++})$$

See the review on "Scalar Mesons below 2 GeV."

Mass  $m = 1474 \pm 19$  MeV  
Full width  $\Gamma = 265 \pm 13$  MeV

$a_0(1450)$ DECAY MODES	Fraction ( $\Gamma_i/\Gamma$ )	$\rho$ (MeV/c)
$\pi\eta$	$0.093 \pm 0.020$	627
$\pi\eta'(958)$	$0.033 \pm 0.017$	410
$K\bar{K}$	$0.082 \pm 0.028$	547
$\omega\pi\pi$	<b>DEFINED AS 1</b>	484
$a_0(980)\pi\pi$	seen	342
$\gamma\gamma$	seen	737

 **$\rho(1450)$** 

$$I^G(J^{PC}) = 1^+(1^{--})$$

See the note in  $\rho(1450)$  Particle Listings.Mass  $m = 1465 \pm 25$  MeV [l]  
Full width  $\Gamma = 400 \pm 60$  MeV [l]

$\rho(1450)$ DECAY MODES	Fraction ( $\Gamma_i/\Gamma$ )	$\rho$ (MeV/c)
$\pi\pi$	seen	720
$\pi^+\pi^-$	seen	719
$4\pi$	seen	669
$e^+e^-$	seen	732
$\eta\rho$	seen	311
$a_2(1320)\pi$	not seen	58
$K\bar{K}$	seen	541
$K^+K^-$	seen	541
$K\bar{K}^*(892) + c.c.$	possibly seen	229
$\eta\gamma$	seen	630
$f_0(500)\gamma$	not seen	–
$f_0(980)\gamma$	not seen	398
$f_0(1370)\gamma$	not seen	92
$f_2(1270)\gamma$	not seen	177

 **$\eta(1475)$** 

$$I^G(J^{PC}) = 0^+(0^{-+})$$

See the review on "Pseudoscalar and Pseudovector Mesons in the 1400 MeV Region."

Mass  $m = 1475 \pm 4$  MeV ( $S = 1.4$ )  
Full width  $\Gamma = 90 \pm 9$  MeV ( $S = 1.6$ )

$\eta(1475)$ DECAY MODES	Fraction ( $\Gamma_i/\Gamma$ )	$\rho$ (MeV/c)
$K\bar{K}\pi$	seen	477
$K\bar{K}^*(892) + c.c.$	seen	244
$a_0(980)\pi$	seen	396
$\gamma\gamma$	seen	738
$K_S^0 K_S^0 \eta$	possibly seen	†
$\gamma\phi(1020)$	possibly seen	385

 **$f_0(1500)$** 

$$I^G(J^{PC}) = 0^+(0^{++})$$

See the reviews on "Scalar Mesons below 2 GeV" and on "Non- $q\bar{q}$  Mesons".Mass  $m = 1506 \pm 6$  MeV ( $S = 1.4$ )  
Full width  $\Gamma = 112 \pm 9$  MeV



## Meson Summary Table

$f_0(1500)$ DECAY MODES	Fraction ( $\Gamma_i/\Gamma$ )	Scale factor	$\rho$ (MeV/c)
$\pi\pi$	(34.5±2.2) %	1.2	741
$\pi^+\pi^-$	seen		740
$2\pi^0$	seen		741
$4\pi$	(48.9±3.3) %	1.2	692
$4\pi^0$	seen		692
$2\pi^+2\pi^-$	seen		687
$2(\pi\pi)_{S\text{-wave}}$	seen		–
$\rho\rho$	seen		†
$\pi(1300)\pi$	seen		145
$a_1(1260)\pi$	seen		219
$\eta\eta$	( 6.0±0.9) %	1.1	517
$\eta\eta'(958)$	( 2.2±0.8) %	1.4	20
$K\bar{K}$	( 8.5±1.0) %	1.1	569
$\gamma\gamma$	not seen		753

$$f_2'(1525) \quad I^G(J^{PC}) = 0^+(2^{++})$$

Mass  $m = 1517.4 \pm 2.5$  MeV ( $S = 2.8$ )  
 Full width  $\Gamma = 86 \pm 5$  MeV ( $S = 2.2$ )

$f_2'(1525)$ DECAY MODES	Fraction ( $\Gamma_i/\Gamma$ )	Scale factor	$\rho$ (MeV/c)
$K\bar{K}$	(87.6±2.2) %	1.1	576
$\eta\eta$	(11.6±2.2) %	1.1	525
$\pi\pi$	( 8.3±1.6) $\times 10^{-3}$		747
$\gamma\gamma$	( 9.5±1.1) $\times 10^{-7}$	1.1	759

$$\pi_1(1600) \quad I^G(J^{PC}) = 1^-(1^{+-})$$

See the review on "Non- $q\bar{q}$  Mesons" and a note in PDG 06, Journal of Physics **G33** 1 (2006).

Mass  $m = 1660^{+15}_{-11}$  MeV ( $S = 1.2$ )  
 Full width  $\Gamma = 257 \pm 60$  MeV ( $S = 1.9$ )

$\pi_1(1600)$ DECAY MODES	Fraction ( $\Gamma_i/\Gamma$ )	$\rho$ (MeV/c)
$\pi\pi\pi$	seen	802
$\rho^0\pi^-$	seen	640
$f_2(1270)\pi^-$	not seen	316
$b_1(1235)\pi$	seen	355
$\eta'(958)\pi^-$	seen	542
$f_1(1285)\pi$	seen	312

$$a_1(1640) \quad I^G(J^{PC}) = 1^-(1^{++})$$

Mass  $m = 1655 \pm 16$  MeV ( $S = 1.2$ )  
 Full width  $\Gamma = 254 \pm 40$  MeV ( $S = 1.8$ )

$a_1(1640)$ DECAY MODES	Fraction ( $\Gamma_i/\Gamma$ )	$\rho$ (MeV/c)
$\pi\pi\pi$	seen	800
$f_2(1270)\pi$	seen	314
$\sigma\pi$	seen	–
$\rho\pi_{S\text{-wave}}$	seen	638
$\rho\pi_{D\text{-wave}}$	seen	638
$\omega\pi\pi$	seen	607
$f_1(1285)\pi$	seen	309
$a_1(1260)\eta$	not seen	†

$$\eta_2(1645) \quad I^G(J^{PC}) = 0^+(2^{-+})$$

Mass  $m = 1617 \pm 5$  MeV  
 Full width  $\Gamma = 181 \pm 11$  MeV

$\eta_2(1645)$ DECAY MODES	Fraction ( $\Gamma_i/\Gamma$ )	$\rho$ (MeV/c)
$a_2(1320)\pi$	seen	243
$K\bar{K}\pi$	seen	580
$K^*\bar{K}$	seen	404
$\eta\pi^+\pi^-$	seen	685
$a_0(980)\pi$	seen	499
$f_2(1270)\eta$	not seen	†

$$\omega(1650) [n] \quad I^G(J^{PC}) = 0^-(1^{--})$$

Mass  $m = 1670 \pm 30$  MeV [J]  
 Full width  $\Gamma = 315 \pm 35$  MeV [J]

$\omega(1650)$ DECAY MODES	Fraction ( $\Gamma_i/\Gamma$ )	$\rho$ (MeV/c)
$\rho\pi$	seen	647
$\omega\pi\pi$	seen	617
$\omega\eta$	seen	500
$e^+e^-$	seen	835
$\pi^0\gamma$	not seen	830

$$\omega_3(1670) \quad I^G(J^{PC}) = 0^-(3^{--})$$

Mass  $m = 1667 \pm 4$  MeV  
 Full width  $\Gamma = 168 \pm 10$  MeV

$\omega_3(1670)$ DECAY MODES	Fraction ( $\Gamma_i/\Gamma$ )	$\rho$ (MeV/c)
$\rho\pi$	seen	645
$\omega\pi\pi$	seen	615
$b_1(1235)\pi$	possibly seen	361

$$\pi_2(1670) \quad I^G(J^{PC}) = 1^-(2^{-+})$$

Mass  $m = 1670.6^{+2.9}_{-1.2}$  MeV ( $S = 1.3$ )  
 Full width  $\Gamma = 258^{+8}_{-9}$  MeV ( $S = 1.2$ )

$\pi_2(1670)$ DECAY MODES	Fraction ( $\Gamma_i/\Gamma$ )	Confidence level	$\rho$ (MeV/c)
$3\pi$	(95.8±1.4) %		808
$f_2(1270)\pi$	(56.3±3.2) %		327
$\rho\pi$	(31 ± 4) %		647
$\sigma\pi$	(10 ± 4) %		–
$\pi(\pi\pi)_{S\text{-wave}}$	( 8.7±3.4) %		–
$\pi^\pm\pi^+\pi^-$	(53 ± 4) %		806
$K\bar{K}^*(892) + c.c.$	( 4.2±1.4) %		453
$\omega\rho$	( 2.7±1.1) %		302
$\pi^\pm\gamma$	( 7.0±1.2) $\times 10^{-4}$		829
$\gamma\gamma$	< 2.8 $\times 10^{-7}$	90%	835
$\eta\pi$	< 5 %		739
$\pi^\pm 2\pi^+ 2\pi^-$	< 5 %		735
$\rho(1450)\pi$	< 3.6 $\times 10^{-3}$	97.7%	145
$b_1(1235)\pi$	< 1.9 $\times 10^{-3}$	97.7%	364
$f_1(1285)\pi$	possibly seen		322
$a_2(1320)\pi$	not seen		292

$$\phi(1680) \quad I^G(J^{PC}) = 0^-(1^{--})$$

Mass  $m = 1680 \pm 20$  MeV [J]  
 Full width  $\Gamma = 150 \pm 50$  MeV [J]

$\phi(1680)$ DECAY MODES	Fraction ( $\Gamma_i/\Gamma$ )	$\rho$ (MeV/c)
$K\bar{K}^*(892) + c.c.$	seen	462
$K_S^0 K\pi$	seen	621
$K\bar{K}$	seen	680
$e^+e^-$	seen	840
$\omega\pi\pi$	not seen	623
$K^+K^-\pi^+\pi^-$	seen	544
$\eta\phi$	seen	290
$\eta\gamma$	seen	751

$$\rho_3(1690) \quad I^G(J^{PC}) = 1^+(3^{--})$$

Mass  $m = 1688.8 \pm 2.1$  MeV  
 Full width  $\Gamma = 161 \pm 10$  MeV ( $S = 1.5$ )

$\rho_3(1690)$ DECAY MODES	Fraction ( $\Gamma_i/\Gamma$ )	Scale factor	$\rho$ (MeV/c)
$4\pi$	(71.1 ± 1.9) %		790
$\pi^\pm\pi^+\pi^-\pi^0$	(67 ± 22) %		787
$\omega\pi$	(16 ± 6) %		655
$\pi\pi$	(23.6 ± 1.3) %		834
$K\bar{K}\pi$	( 3.8 ± 1.2) %		629
$K\bar{K}$	( 1.58 ± 0.26) %	1.2	685
$\eta\pi^+\pi^-$	seen		727

## Meson Summary Table

$\rho(770)\eta$	seen	520
$\pi\pi\rho$	seen	633
$a_2(1320)\pi$	seen	308
$\rho\rho$	seen	335

 **$\rho(1700)$** 

$$I^G(J^{PC}) = 1^+(1^- -)$$

See the note in  $\rho(1700)$  Particle Listings.

Mass  $m = 1720 \pm 20$  MeV [1] ( $\eta\rho^0$  and  $\pi^+\pi^-$  modes)  
 Full width  $\Gamma = 250 \pm 100$  MeV [1] ( $\eta\rho^0$  and  $\pi^+\pi^-$  modes)

$\rho(1700)$ DECAY MODES	Fraction ( $\Gamma_i/\Gamma$ )	$\rho$ (MeV/c)
$2(\pi^+\pi^-)$	seen	803
$\rho\pi\pi$	seen	653
$\rho^0\pi^+\pi^-$	seen	651
$\rho^\pm\pi^\mp\pi^0$	seen	652
$a_1(1260)\pi$	seen	404
$h_1(1170)\pi$	seen	450
$\pi(1300)\pi$	seen	349
$\rho\rho$	seen	372
$\pi^+\pi^-$	seen	849
$\pi\pi$	seen	849
$K\bar{K}^*(892) + c.c.$	seen	496
$\eta\rho$	seen	545
$a_2(1320)\pi$	not seen	335
$K\bar{K}$	seen	704
$e^+e^-$	seen	860
$\pi^0\omega$	seen	674
$\pi^0\gamma$	not seen	855

 **$a_2(1700)$** 

$$I^G(J^{PC}) = 1^-(2^+ +)$$

Mass  $m = 1705 \pm 40$  MeV  
 Full width  $\Gamma = 258 \pm 40$  MeV

$a_2(1700)$ DECAY MODES	Fraction ( $\Gamma_i/\Gamma$ )	$\rho$ (MeV/c)
$\eta\pi$	$(3.7 \pm 1.0) \%$	758
$\gamma\gamma$	$(1.16 \pm 0.27) \times 10^{-6}$	852
$\rho\pi$	seen	668
$f_2(1270)\pi$	seen	356
$K\bar{K}$	$(1.9 \pm 1.2) \%$	695
$\omega\pi^-\pi^0$	seen	638
$\omega\rho$	seen	346

 **$f_0(1710)$** 

$$I^G(J^{PC}) = 0^+(0^+ +)$$

See the review on "Non- $q\bar{q}$  Mesons."

Mass  $m = 1704 \pm 12$  MeV  
 Full width  $\Gamma = 123 \pm 18$  MeV

$f_0(1710)$ DECAY MODES	Fraction ( $\Gamma_i/\Gamma$ )	$\rho$ (MeV/c)
$K\bar{K}$	seen	694
$\eta\eta$	seen	652
$\pi\pi$	seen	841
$\gamma\gamma$	seen	852
$\omega\omega$	seen	337

 **$\pi(1800)$** 

$$I^G(J^{PC}) = 1^-(0^- +)$$

Mass  $m = 1810^{+9}_{-11}$  MeV ( $S = 2.2$ )  
 Full width  $\Gamma = 215^{+7}_{-8}$  MeV

$\pi(1800)$ DECAY MODES	Fraction ( $\Gamma_i/\Gamma$ )	$\rho$ (MeV/c)
$\pi^+\pi^-\pi^-$	seen	878
$f_0(500)\pi^-$	seen	-
$f_0(980)\pi^-$	seen	624
$f_0(1370)\pi^-$	seen	366
$f_0(1500)\pi^-$	not seen	247
$\rho\pi^-$	not seen	731

$\eta\eta\pi^-$	seen	660
$a_0(980)\eta$	seen	471
$a_2(1320)\eta$	not seen	†
$f_2(1270)\pi^-$	not seen	441
$f_0(1370)\pi^-$	not seen	366
$f_0(1500)\pi^-$	seen	247
$\eta\eta'(958)\pi^-$	seen	373
$K_0^*(1430)K^-$	seen	†
$K^*(892)K^-$	not seen	568

 **$\phi_3(1850)$** 

$$I^G(J^{PC}) = 0^-(3^- -)$$

Mass  $m = 1854 \pm 7$  MeV  
 Full width  $\Gamma = 87^{+28}_{-23}$  MeV ( $S = 1.2$ )

$\phi_3(1850)$ DECAY MODES	Fraction ( $\Gamma_i/\Gamma$ )	$\rho$ (MeV/c)
$K\bar{K}$	seen	785
$K\bar{K}^*(892) + c.c.$	seen	602

 **$\eta_2(1870)$** 

$$I^G(J^{PC}) = 0^+(2^- +)$$

Mass  $m = 1842 \pm 8$  MeV  
 Full width  $\Gamma = 225 \pm 14$  MeV

$\eta_2(1870)$ DECAY MODES	Fraction ( $\Gamma_i/\Gamma$ )	$\rho$ (MeV/c)
$\gamma\gamma$	seen	921

 **$\pi_2(1880)$** 

$$I^G(J^{PC}) = 1^-(2^- +)$$

Mass  $m = 1874^{+26}_{-5}$  MeV ( $S = 1.6$ )  
 Full width  $\Gamma = 237^{+33}_{-30}$  MeV ( $S = 1.2$ )

$f_2(1950)$ DECAY MODES	Fraction ( $\Gamma_i/\Gamma$ )	$\rho$ (MeV/c)
$K^*(892)\bar{K}^*(892)$	seen	377
$\pi^+\pi^-$	seen	958
$\pi^0\pi^0$	seen	959
$4\pi$	seen	921
$\eta\eta$	seen	798
$K\bar{K}$	seen	833
$\gamma\gamma$	seen	968
$\rho\bar{\rho}$	seen	238

 **$a_4(1970)$** 

$$I^G(J^{PC}) = 1^-(4^+ +)$$

was  $a_4(2040)$ 

Mass  $m = 1967 \pm 16$  MeV ( $S = 2.1$ )  
 Full width  $\Gamma = 324^{+15}_{-18}$  MeV

$a_4(1970)$ DECAY MODES	Fraction ( $\Gamma_i/\Gamma$ )	$\rho$ (MeV/c)
$K\bar{K}$	seen	851
$\pi^+\pi^-\pi^0$	seen	959
$\rho\pi$	seen	825
$f_2(1270)\pi$	seen	559
$\omega\pi^-\pi^0$	seen	801
$\omega\rho$	seen	601
$\eta\pi$	seen	902
$\eta'(958)\pi$	seen	743

 **$f_2(2010)$** 

$$I^G(J^{PC}) = 0^+(2^+ +)$$

Mass  $m = 2011^{+60}_{-80}$  MeV  
 Full width  $\Gamma = 202 \pm 60$  MeV

$f_2(2010)$ DECAY MODES	Fraction ( $\Gamma_i/\Gamma$ )	$\rho$ (MeV/c)
$\phi\phi$	seen	†
$K\bar{K}$	seen	876

## Meson Summary Table

$$f_4(2050) \quad I^G(J^{PC}) = 0^+(4^{++})$$

Mass  $m = 2018 \pm 11$  MeV ( $S = 2.1$ )  
Full width  $\Gamma = 237 \pm 18$  MeV ( $S = 1.9$ )

$f_4(2050)$ DECAY MODES	Fraction ( $\Gamma_i/\Gamma$ )	$\rho$ (MeV/c)
$\omega\omega$	seen	637
$\pi\pi$	(17.0 ± 1.5) %	1000
$K\bar{K}$	( 6.8 <sup>+3.4</sup> <sub>-1.8</sub> ) × 10 <sup>-3</sup>	880
$\eta\eta$	( 2.1 ± 0.8) × 10 <sup>-3</sup>	848
$4\pi^0$	< 1.2 %	964
$a_2(1320)\pi$	seen	568

$$\phi(2170) \quad I^G(J^{PC}) = 0^-(1^{--})$$

Mass  $m = 2160 \pm 80$  MeV [1]  
Full width  $\Gamma = 125 \pm 65$  MeV [1]

$\phi(2170)$ DECAY MODES	Fraction ( $\Gamma_i/\Gamma$ )	$\rho$ (MeV/c)
$e^+e^-$	seen	1080
$\phi f_0(980)$	seen	396
$K^+K^-f_0(980) \rightarrow$ $K^+K^-\pi^+\pi^-$	seen	-
$K^+K^-f_0(980) \rightarrow K^+K^-\pi^0\pi^0$	seen	-
$K^{*0}K^\pm\pi^\mp$	not seen	759
$K^*(892)^0\bar{K}^*(892)^0$	not seen	609

$$f_2(2300) \quad I^G(J^{PC}) = 0^+(2^{++})$$

Mass  $m = 2297 \pm 28$  MeV  
Full width  $\Gamma = 149 \pm 40$  MeV

$f_2(2300)$ DECAY MODES	Fraction ( $\Gamma_i/\Gamma$ )	$\rho$ (MeV/c)
$\phi\phi$	seen	529
$K\bar{K}$	seen	1037
$\gamma\gamma$	seen	1149

$$f_2(2340) \quad I^G(J^{PC}) = 0^+(2^{++})$$

Mass  $m = 2345^{+50}_{-40}$  MeV  
Full width  $\Gamma = 322^{+70}_{-60}$  MeV

$f_2(2340)$ DECAY MODES	Fraction ( $\Gamma_i/\Gamma$ )	$\rho$ (MeV/c)
$\phi\phi$	seen	580
$\eta\eta$	seen	1037

## STRANGE MESONS ( $S = \pm 1, C = B = 0$ )

$K^+ = u\bar{s}, K^0 = d\bar{s}, \bar{K}^0 = \bar{d}s, K^- = \bar{u}s,$  similarly for  $K^{*s}$

$$K^\pm \quad I(J^P) = \frac{1}{2}(0^-)$$

Mass  $m = 493.677 \pm 0.016$  MeV [0] ( $S = 2.8$ )  
Mean life  $\tau = (1.2380 \pm 0.0020) \times 10^{-8}$  s ( $S = 1.8$ )  
 $c\tau = 3.711$  m

### CPT violation parameters ( $\Delta =$ rate difference/sum)

$$\Delta(K^\pm \rightarrow \mu^\pm \nu_\mu) = (-0.27 \pm 0.21)\%$$

$$\Delta(K^\pm \rightarrow \pi^\pm \pi^0) = (0.4 \pm 0.6)\% [b]$$

### CP violation parameters ( $\Delta =$ rate difference/sum)

$$\Delta(K^\pm \rightarrow \pi^\pm e^+ e^-) = (-2.2 \pm 1.6) \times 10^{-2}$$

$$\Delta(K^\pm \rightarrow \pi^\pm \mu^+ \mu^-) = 0.010 \pm 0.023$$

$$\Delta(K^\pm \rightarrow \pi^\pm \pi^0 \gamma) = (0.0 \pm 1.2) \times 10^{-3}$$

$$\Delta(K^\pm \rightarrow \pi^\pm \pi^+ \pi^-) = (0.04 \pm 0.06)\%$$

$$\Delta(K^\pm \rightarrow \pi^\pm \pi^0 \pi^0) = (-0.02 \pm 0.28)\%$$

### T violation parameters

$$K^+ \rightarrow \pi^0 \mu^+ \nu_\mu \quad P_T = (-1.7 \pm 2.5) \times 10^{-3}$$

$$K^+ \rightarrow \mu^+ \nu_\mu \gamma \quad P_T = (-0.6 \pm 1.9) \times 10^{-2}$$

$$K^+ \rightarrow \pi^0 \mu^+ \nu_\mu \quad \text{Im}(\xi) = -0.006 \pm 0.008$$

### Slope parameter $g^{[q]}$

(See Particle Listings for quadratic coefficients and alternative parametrization related to  $\pi\pi$  scattering)

$$K^\pm \rightarrow \pi^\pm \pi^+ \pi^- \quad g = -0.21134 \pm 0.00017$$

$$K^\pm \rightarrow \pi^\pm \pi^0 \pi^0 \quad g = 0.626 \pm 0.007$$

$$(\mathcal{G}_+ - \mathcal{G}_-) / (\mathcal{G}_+ + \mathcal{G}_-) = (-1.5 \pm 2.2) \times 10^{-4}$$

$$(\mathcal{G}_+ - \mathcal{G}_-) / (\mathcal{G}_+ + \mathcal{G}_-) = (1.8 \pm 1.8) \times 10^{-4}$$

### $K^\pm$ decay form factors [a,r]

Assuming  $\mu$ -e universality

$$\lambda_+(K_{\mu 3}^+) = \lambda_+(K_{e 3}^+) = (2.959 \pm 0.025) \times 10^{-2}$$

$$\lambda_0(K_{\mu 3}^+) = (1.76 \pm 0.25) \times 10^{-2} \quad (S = 2.7)$$

Not assuming  $\mu$ -e universality

$$\lambda_+(K_{e 3}^+) = (2.956 \pm 0.025) \times 10^{-2}$$

$$\lambda_+(K_{\mu 3}^+) = (3.09 \pm 0.25) \times 10^{-2} \quad (S = 1.5)$$

$$\lambda_0(K_{\mu 3}^+) = (1.73 \pm 0.27) \times 10^{-2} \quad (S = 2.6)$$

$K_{e 3}$  form factor quadratic fit

$$\lambda'_+(K_{e 3}^\pm) \text{ linear coeff.} = (2.59 \pm 0.04) \times 10^{-2}$$

$$\lambda''_+(K_{e 3}^\pm) \text{ quadratic coeff.} = (0.186 \pm 0.021) \times 10^{-2}$$

$$\lambda'_+(K_{\mu 3}^\pm) \text{ FORM FACTOR FROM QUADRATIC FIT}$$

$$= (24 \pm 4) \times 10^{-3}$$

$$\lambda''_+(K_{\mu 3}^\pm) \text{ FORM FACTOR} = (1.8 \pm 1.5) \times 10^{-3}$$

$$M_V \text{ (VECTOR POLE MASS FOR } K_{e 3}^\pm \text{ DECAY)} = 890.3 \pm 2.8 \text{ MeV}$$

$$M_V \text{ (VECTOR POLE MASS FOR } K_{\mu 3}^\pm \text{ DECAY)} = 878 \pm 12 \text{ MeV}$$

$$M_S \text{ (SCALAR POLE MASS FOR } K_{\mu 3}^\pm \text{ DECAY)} = 1215 \pm 50 \text{ MeV}$$

$$\Lambda_+ \text{ (DISPERSIVE VECTOR FORM FACTOR IN } K_{e 3}^\pm \text{ DECAY)} = (2.460 \pm 0.017) \times 10^{-2}$$

$$\Lambda_+ \text{ (DISPERSIVE VECTOR FORM FACTOR IN } K_{\mu 3}^\pm \text{ DECAY)} = (25.4 \pm 0.9) \times 10^{-3}$$

$$\ln(C) \text{ (DISPERSIVE SCALAR FORM FACTOR IN } K_{\mu 3}^\pm \text{ decays)} = (182 \pm 16) \times 10^{-3}$$

$$K_{e 3}^+ \quad |f_S/f_+| = (-0.08^{+0.34}_{-0.40}) \times 10^{-2}$$

$$K_{e 3}^+ \quad |f_T/f_+| = (-1.2^{+1.3}_{-1.1}) \times 10^{-2}$$

$$K_{\mu 3}^+ \quad |f_S/f_+| = (0.2 \pm 0.6) \times 10^{-2}$$

$$K_{\mu 3}^+ \quad |f_T/f_+| = (-0.1 \pm 0.7) \times 10^{-2}$$

$$K^+ \rightarrow e^+ \nu_e \gamma \quad |F_A + F_V| = 0.133 \pm 0.008 \quad (S = 1.3)$$

$$K^+ \rightarrow \mu^+ \nu_\mu \gamma \quad |F_A + F_V| = 0.165 \pm 0.013$$

$$K^+ \rightarrow e^+ \nu_e \gamma \quad |F_A - F_V| < 0.49, \text{ CL} = 90\%$$

$$K^+ \rightarrow \mu^+ \nu_\mu \gamma \quad |F_A - F_V| = -0.153 \pm 0.033 \quad (S = 1.1)$$

### Charge radius

$$\langle r \rangle = 0.560 \pm 0.031 \text{ fm}$$

### Forward-backward asymmetry

$$A_{FB}(K_{\pi\mu}^\pm) = \frac{\Gamma(\cos(\theta_{K\mu}) > 0) - \Gamma(\cos(\theta_{K\mu}) < 0)}{\Gamma(\cos(\theta_{K\mu}) > 0) + \Gamma(\cos(\theta_{K\mu}) < 0)} < 2.3 \times 10^{-2}, \text{ CL} = 90\%$$

$K^-$  modes are charge conjugates of the modes below.

$K^+$ DECAY MODES	Fraction ( $\Gamma_i/\Gamma$ )	Scale factor / Confidence level (MeV/c)	$\rho$
<b>Leptonic and semileptonic modes</b>			
$e^+ \nu_e$	( 1.582 ± 0.007 ) × 10 <sup>-5</sup>		247
$\mu^+ \nu_\mu$	( 63.56 ± 0.11 ) %	S=1.2	236
$\pi^0 e^+ \nu_e$	( 5.07 ± 0.04 ) %	S=2.1	228
Called $K_{e 3}^+$ .			

## Meson Summary Table

$\pi^0 \mu^+ \nu_\mu$ Called $K_{\mu 3}^+$	( 3.352 ± 0.033 ) %	S=1.9	215
$\pi^0 \pi^0 e^+ \nu_e$	( 2.55 ± 0.04 ) × 10 <sup>-5</sup>	S=1.1	206
$\pi^+ \pi^- e^+ \nu_e$	( 4.247 ± 0.024 ) × 10 <sup>-5</sup>		203
$\pi^+ \pi^- \mu^+ \nu_\mu$	( 1.4 ± 0.9 ) × 10 <sup>-5</sup>		151
$\pi^0 \pi^0 \pi^0 e^+ \nu_e$	< 3.5 × 10 <sup>-6</sup>	CL=90%	135
<b>Hadronic modes</b>			
$\pi^+ \pi^0$	( 20.67 ± 0.08 ) %	S=1.2	205
$\pi^+ \pi^0 \pi^0$	( 1.760 ± 0.023 ) %	S=1.1	133
$\pi^+ \pi^+ \pi^-$	( 5.583 ± 0.024 ) %		125
<b>Leptonic and semileptonic modes with photons</b>			
$\mu^+ \nu_\mu \gamma$	[s,t] ( 6.2 ± 0.8 ) × 10 <sup>-3</sup>		236
$\mu^+ \nu_\mu \gamma (SD^+)$	[a,u] ( 1.33 ± 0.22 ) × 10 <sup>-5</sup>		–
$\mu^+ \nu_\mu \gamma (SD^+ INT)$	[a,u] < 2.7 × 10 <sup>-5</sup>	CL=90%	–
$\mu^+ \nu_\mu \gamma (SD^- + SD^- INT)$	[a,u] < 2.6 × 10 <sup>-4</sup>	CL=90%	–
$e^+ \nu_e \gamma$	( 9.4 ± 0.4 ) × 10 <sup>-6</sup>		247
$\pi^0 e^+ \nu_e \gamma$	[s,t] ( 2.56 ± 0.16 ) × 10 <sup>-4</sup>		228
$\pi^0 e^+ \nu_e \gamma (SD)$	[a,u] < 5.3 × 10 <sup>-5</sup>	CL=90%	228
$\pi^0 \mu^+ \nu_\mu \gamma$	[s,t] ( 1.25 ± 0.25 ) × 10 <sup>-5</sup>		215
$\pi^0 \pi^0 e^+ \nu_e \gamma$	< 5 × 10 <sup>-6</sup>	CL=90%	206
<b>Hadronic modes with photons or <math>\ell\bar{\ell}</math> pairs</b>			
$\pi^+ \pi^0 \gamma (INT)$	( - 4.2 ± 0.9 ) × 10 <sup>-6</sup>		–
$\pi^+ \pi^0 \gamma (DE)$	[s,v] ( 6.0 ± 0.4 ) × 10 <sup>-6</sup>		205
$\pi^+ \pi^0 e^+ e^-$	( 4.24 ± 0.14 ) × 10 <sup>-6</sup>		205
$\pi^+ \pi^0 \pi^0 \gamma$	[s,t] ( 7.6 ± 3.0 ) × 10 <sup>-6</sup>		133
$\pi^+ \pi^+ \pi^- \gamma$	[s,t] ( 7.1 ± 0.5 ) × 10 <sup>-6</sup>		125
$\pi^+ \gamma \gamma$	[s] ( 1.01 ± 0.06 ) × 10 <sup>-6</sup>		227
$\pi^+ 3\gamma$	[s] < 1.0 × 10 <sup>-4</sup>	CL=90%	227
$\pi^+ e^+ e^- \gamma$	( 1.19 ± 0.13 ) × 10 <sup>-8</sup>		227
<b>Leptonic modes with <math>\ell\bar{\ell}</math> pairs</b>			
$e^+ \nu_e \nu\bar{\nu}$	< 6 × 10 <sup>-5</sup>	CL=90%	247
$\mu^+ \nu_\mu \nu\bar{\nu}$	< 2.4 × 10 <sup>-6</sup>	CL=90%	236
$e^+ \nu_e e^+ e^-$	( 2.48 ± 0.20 ) × 10 <sup>-8</sup>		247
$\mu^+ \nu_\mu e^+ e^-$	( 7.06 ± 0.31 ) × 10 <sup>-8</sup>		236
$e^+ \nu_e \mu^+ \mu^-$	( 1.7 ± 0.5 ) × 10 <sup>-8</sup>		223
$\mu^+ \nu_\mu \mu^+ \mu^-$	< 4.1 × 10 <sup>-7</sup>	CL=90%	185
<b>Lepton family number (LF), Lepton number (L), <math>\Delta S = \Delta Q</math> (SQ) violating modes, or <math>\Delta S = 1</math> weak neutral current (S1) modes</b>			
$\pi^+ \pi^+ e^- \bar{\nu}_e$	SQ < 1.3 × 10 <sup>-8</sup>	CL=90%	203
$\pi^+ \pi^+ \mu^- \bar{\nu}_\mu$	SQ < 3.0 × 10 <sup>-6</sup>	CL=95%	151
$\pi^+ e^+ e^-$	S1 ( 3.00 ± 0.09 ) × 10 <sup>-7</sup>		227
$\pi^+ \mu^+ \mu^-$	S1 ( 9.4 ± 0.6 ) × 10 <sup>-8</sup>	S=2.6	172
$\pi^+ \nu\bar{\nu}$	S1 ( 1.7 ± 1.1 ) × 10 <sup>-10</sup>		227
$\pi^+ \pi^0 \nu\bar{\nu}$	S1 < 4.3 × 10 <sup>-5</sup>	CL=90%	205
$\mu^- \nu e^+ e^+$	LF < 2.1 × 10 <sup>-8</sup>	CL=90%	236
$\mu^+ \nu_e$	LF [d] < 4 × 10 <sup>-3</sup>	CL=90%	236
$\pi^+ \mu^+ e^-$	LF < 1.3 × 10 <sup>-11</sup>	CL=90%	214
$\pi^+ \mu^- e^+$	LF < 5.2 × 10 <sup>-10</sup>	CL=90%	214
$\pi^- \mu^+ e^+$	L < 5.0 × 10 <sup>-10</sup>	CL=90%	214
$\pi^- e^+ e^+$	L < 2.2 × 10 <sup>-10</sup>	CL=90%	227
$\pi^- \mu^+ \mu^+$	L < 4.2 × 10 <sup>-11</sup>	CL=90%	172
$\mu^+ \bar{\nu}_e$	L [d] < 3.3 × 10 <sup>-3</sup>	CL=90%	236
$\pi^0 e^+ \bar{\nu}_e$	L < 3 × 10 <sup>-3</sup>	CL=90%	228
$\pi^+ \gamma$	[x] < 2.3 × 10 <sup>-9</sup>	CL=90%	227

 **$K^0$** 

$$I(J^P) = \frac{1}{2}(0^-)$$

50%  $K_S$ , 50%  $K_L$ Mass  $m = 497.611 \pm 0.013$  MeV (S = 1.2) $m_{K^0} - m_{K^\pm} = 3.934 \pm 0.020$  MeV (S = 1.6)**Mean square charge radius**

$$\langle r^2 \rangle = -0.077 \pm 0.010 \text{ fm}^2$$

**T-violation parameters in  $K^0$ - $\bar{K}^0$  mixing [r]**Asymmetry  $A_T$  in  $K^0$ - $\bar{K}^0$  mixing =  $(6.6 \pm 1.6) \times 10^{-3}$ **CP-violation parameters**

$$\text{Re}(\epsilon) = (1.596 \pm 0.013) \times 10^{-3}$$

**CPT-violation parameters [r]**

$$\text{Re } \delta = (2.5 \pm 2.3) \times 10^{-4}$$

$$\text{Im } \delta = (-1.5 \pm 1.6) \times 10^{-5}$$

$$\text{Re}(y), K_{e3} \text{ parameter} = (0.4 \pm 2.5) \times 10^{-3}$$

$$\text{Re}(x_-), K_{e3} \text{ parameter} = (-2.9 \pm 2.0) \times 10^{-3}$$

$$|m_{K^0} - m_{\bar{K}^0}| / m_{\text{average}} < 6 \times 10^{-19}, \text{CL} = 90\% [\nu]$$

$$(\Gamma_{K^0} - \Gamma_{\bar{K}^0}) / m_{\text{average}} = (8 \pm 8) \times 10^{-18}$$

**Tests of  $\Delta S = \Delta Q$** 

$$\text{Re}(x_+), K_{e3} \text{ parameter} = (-0.9 \pm 3.0) \times 10^{-3}$$

 **$K_S^0$** 

$$I(J^P) = \frac{1}{2}(0^-)$$

Mean life  $\tau = (0.8954 \pm 0.0004) \times 10^{-10}$  s (S = 1.1) Assuming CPTMean life  $\tau = (0.89564 \pm 0.00033) \times 10^{-10}$  s Not assuming CPT

$$c\tau = 2.6844 \text{ cm} \text{ Assuming CPT}$$

**CP-violation parameters [z]**

$$\text{Im}(\eta_{+-0}) = -0.002 \pm 0.009$$

$$\text{Im}(\eta_{000}) = -0.001 \pm 0.016$$

$$|\eta_{000}| = |A(K_S^0 \rightarrow 3\pi^0) / A(K_L^0 \rightarrow 3\pi^0)| < 0.0088, \text{CL} = 90\%$$

$$\text{CP asymmetry } A \text{ in } \pi^+ \pi^- e^+ e^- = (-0.4 \pm 0.8)\%$$

 **$K_S^0$  DECAY MODES**

	Fraction ( $\Gamma_i/\Gamma$ )	Scale factor / Confidence level	$p$ (MeV/c)
<b>Hadronic modes</b>			
$\pi^0 \pi^0$	(30.69 ± 0.05) %		209
$\pi^+ \pi^-$	(69.20 ± 0.05) %		206
$\pi^+ \pi^- \pi^0$	( 3.5 ± 1.1 / -0.9 ) × 10 <sup>-7</sup>		133
<b>Modes with photons or <math>\ell\bar{\ell}</math> pairs</b>			
$\pi^+ \pi^- \gamma$	[t,aa] ( 1.79 ± 0.05 ) × 10 <sup>-3</sup>		206
$\pi^+ \pi^- e^+ e^-$	( 4.79 ± 0.15 ) × 10 <sup>-5</sup>		206
$\pi^0 \gamma \gamma$	[aa] ( 4.9 ± 1.8 ) × 10 <sup>-8</sup>		230
$\gamma \gamma$	( 2.63 ± 0.17 ) × 10 <sup>-6</sup>	S=3.0	249
<b>Semileptonic modes</b>			
$\pi^\pm e^\mp \nu_e$	[bb] ( 7.04 ± 0.08 ) × 10 <sup>-4</sup>		229
<b>CP violating (CP) and <math>\Delta S = 1</math> weak neutral current (S1) modes</b>			
$3\pi^0$	CP < 2.6 × 10 <sup>-8</sup>	CL=90%	139
$\mu^+ \mu^-$	S1 < 8 × 10 <sup>-10</sup>	CL=90%	225
$e^+ e^-$	S1 < 9 × 10 <sup>-9</sup>	CL=90%	249
$\pi^0 e^+ e^-$	S1 [aa] ( 3.0 ± 1.5 / -1.2 ) × 10 <sup>-9</sup>		230
$\pi^0 \mu^+ \mu^-$	S1 ( 2.9 ± 1.5 / -1.2 ) × 10 <sup>-9</sup>		177

 **$K_L^0$** 

$$I(J^P) = \frac{1}{2}(0^-)$$

$$m_{K_L} - m_{K_S}$$

$$= (0.5293 \pm 0.0009) \times 10^{10} \hbar \text{ s}^{-1} \text{ (S = 1.3) Assuming CPT}$$

$$= (3.484 \pm 0.006) \times 10^{-12} \text{ MeV Assuming CPT}$$

$$= (0.5289 \pm 0.0010) \times 10^{10} \hbar \text{ s}^{-1} \text{ Not assuming CPT}$$

$$\text{Mean life } \tau = (5.116 \pm 0.021) \times 10^{-8} \text{ s (S = 1.1)}$$

$$c\tau = 15.34 \text{ m}$$

**Slope parameters [q]**

(See Particle Listings for other linear and quadratic coefficients)

$$K_L^0 \rightarrow \pi^+ \pi^- \pi^0: g = 0.678 \pm 0.008 \text{ (S = 1.5)}$$

$$K_L^0 \rightarrow \pi^+ \pi^- \pi^0: h = 0.076 \pm 0.006$$

$$K_L^0 \rightarrow \pi^+ \pi^- \pi^0: k = 0.0099 \pm 0.0015$$

$$K_L^0 \rightarrow \pi^0 \pi^0 \pi^0: h = (0.6 \pm 1.2) \times 10^{-3}$$

 **$K_L$  decay form factors [r]**Linear parametrization assuming  $\mu$ -e universality

$$\lambda_+(K_{\mu 3}^0) = \lambda_+(K_{e 3}^0) = (2.82 \pm 0.04) \times 10^{-2} \text{ (S = 1.1)}$$

$$\lambda_0(K_{\mu 3}^0) = (1.38 \pm 0.18) \times 10^{-2} \text{ (S = 2.2)}$$

# Meson Summary Table

Quadratic parametrization assuming  $\mu$ - $e$  universality

$$\lambda'_+(K_{\mu 3}^0) = \lambda'_+(K_{e 3}^0) = (2.40 \pm 0.12) \times 10^{-2} \quad (S = 1.2)$$

$$\lambda''_+(K_{\mu 3}^0) = \lambda''_+(K_{e 3}^0) = (0.20 \pm 0.05) \times 10^{-2} \quad (S = 1.2)$$

$$\lambda_0(K_{\mu 3}^0) = (1.16 \pm 0.09) \times 10^{-2} \quad (S = 1.2)$$

Pole parametrization assuming  $\mu$ - $e$  universality

$$M_V^\mu(K_{\mu 3}^0) = M_V^e(K_{e 3}^0) = 878 \pm 6 \text{ MeV} \quad (S = 1.1)$$

$$M_S^\mu(K_{\mu 3}^0) = 1252 \pm 90 \text{ MeV} \quad (S = 2.6)$$

Dispersive parametrization assuming  $\mu$ - $e$  universality

$$\Lambda_+ = (2.51 \pm 0.06) \times 10^{-2} \quad (S = 1.5)$$

$$\ln(C) = (1.75 \pm 0.18) \times 10^{-1} \quad (S = 2.0)$$

$$K_{e 3}^0 \quad |f_S/f_+| = (1.5 \pm 1.4) \times 10^{-2}$$

$$K_{e 3}^0 \quad |f_T/f_+| = (5 \pm 4) \times 10^{-2}$$

$$K_{\mu 3}^0 \quad |f_T/f_+| = (12 \pm 12) \times 10^{-2}$$

$$K_L \rightarrow \ell^+ \ell^- \gamma, K_L \rightarrow \ell^+ \ell^- \ell'^+ \ell'^-: \alpha_{K^*} = -0.205 \pm 0.022 \quad (S = 1.8)$$

$$K_L^0 \rightarrow \ell^+ \ell^- \gamma, K_L^0 \rightarrow \ell^+ \ell^- \ell'^+ \ell'^-: \alpha_{DIP} = -1.69 \pm 0.08 \quad (S = 1.7)$$

$$K_L \rightarrow \pi^+ \pi^- e^+ e^-: a_1/a_2 = -0.737 \pm 0.014 \text{ GeV}^2$$

$$K_L \rightarrow \pi^0 2\gamma: a_V = -0.43 \pm 0.06 \quad (S = 1.5)$$

## CP-violation parameters [z]

$$A_L = (0.332 \pm 0.006)\%$$

$$|\eta_{00}| = (2.220 \pm 0.011) \times 10^{-3} \quad (S = 1.8)$$

$$|\eta_{+-}| = (2.232 \pm 0.011) \times 10^{-3} \quad (S = 1.8)$$

$$|\epsilon| = (2.228 \pm 0.011) \times 10^{-3} \quad (S = 1.8)$$

$$|\eta_{00}/\eta_{+-}| = 0.9950 \pm 0.0007^{[cc]} \quad (S = 1.6)$$

$$\text{Re}(\epsilon'/\epsilon) = (1.66 \pm 0.23) \times 10^{-3}^{[cc]} \quad (S = 1.6)$$

Assuming  $CPT$

$$\phi_{+-} = (43.51 \pm 0.05)^\circ \quad (S = 1.2)$$

$$\phi_{00} = (43.52 \pm 0.05)^\circ \quad (S = 1.3)$$

$$\phi_\epsilon = \phi_{SW} = (43.52 \pm 0.05)^\circ \quad (S = 1.2)$$

$$\text{Im}(\epsilon'/\epsilon) = -(\phi_{00} - \phi_{+-})/3 = (-0.002 \pm 0.005)^\circ \quad (S = 1.7)$$

Not assuming  $CPT$

$$\phi_{+-} = (43.4 \pm 0.5)^\circ \quad (S = 1.2)$$

$$\phi_{00} = (43.7 \pm 0.6)^\circ \quad (S = 1.2)$$

$$\phi_\epsilon = (43.5 \pm 0.5)^\circ \quad (S = 1.3)$$

$$CP \text{ asymmetry } A \text{ in } K_L^0 \rightarrow \pi^+ \pi^- e^+ e^- = (13.7 \pm 1.5)\%$$

$$\beta_{CP} \text{ from } K_L^0 \rightarrow e^+ e^- e^+ e^- = -0.19 \pm 0.07$$

$$\gamma_{CP} \text{ from } K_L^0 \rightarrow e^+ e^- e^+ e^- = 0.01 \pm 0.11 \quad (S = 1.6)$$

$$j \text{ for } K_L^0 \rightarrow \pi^+ \pi^- \pi^0 = 0.0012 \pm 0.0008$$

$$f \text{ for } K_L^0 \rightarrow \pi^+ \pi^- \pi^0 = 0.004 \pm 0.006$$

$$|\eta_{+-\gamma}| = (2.35 \pm 0.07) \times 10^{-3}$$

$$\phi_{+-\gamma} = (44 \pm 4)^\circ$$

$$|\epsilon'_{+-\gamma}|/\epsilon < 0.3, \text{ CL} = 90\%$$

$$|\bar{g}_{E1}| \text{ for } K_L^0 \rightarrow \pi^+ \pi^- \gamma < 0.21, \text{ CL} = 90\%$$

## T-violation parameters

$$\text{Im}(\xi) \text{ in } K_{\mu 3}^0 = -0.007 \pm 0.026$$

## CPT invariance tests

$$\phi_{00} - \phi_{+-} = (0.34 \pm 0.32)^\circ$$

$$\text{Re}(\frac{2}{3}\eta_{+-} + \frac{1}{3}\eta_{00}) - \frac{A}{2} = (-3 \pm 35) \times 10^{-6}$$

## $\Delta S = -\Delta Q$ in $K_{23}^0$ decay

$$\text{Re } x = -0.002 \pm 0.006$$

$$\text{Im } x = 0.0012 \pm 0.0021$$

## $K_L^0$ DECAY MODES

	Fraction ( $\Gamma_i/\Gamma$ )	Scale factor/ Confidence level (MeV/c)	$\rho$
<b>Semileptonic modes</b>			
$\pi^\pm e^\mp \nu_e$ Called $K_{e 3}^0$ .	[bb] (40.55 $\pm$ 0.11) %	S=1.7	229
$\pi^\pm \mu^\mp \nu_\mu$ Called $K_{\mu 3}^0$ .	[bb] (27.04 $\pm$ 0.07) %	S=1.1	216
$(\pi \mu \text{ atom}) \nu$	(1.05 $\pm$ 0.11) $\times 10^{-7}$		188
$\pi^0 \pi^\pm e^\mp \nu$	[bb] (5.20 $\pm$ 0.11) $\times 10^{-5}$		207
$\pi^\pm e^\mp \nu e^+ e^-$	[bb] (1.26 $\pm$ 0.04) $\times 10^{-5}$		229
<b>Hadronic modes, including Charge conjugation <math>\times</math> Parity Violating (CPV) modes</b>			
$3\pi^0$	(19.52 $\pm$ 0.12) %	S=1.6	139
$\pi^+ \pi^- \pi^0$	(12.54 $\pm$ 0.05) %		133
$\pi^+ \pi^-$	CPV [dd] (1.967 $\pm$ 0.010) $\times 10^{-3}$	S=1.5	206
$\pi^0 \pi^0$	CPV (8.64 $\pm$ 0.06) $\times 10^{-4}$	S=1.8	209
<b>Semileptonic modes with photons</b>			
$\pi^\pm e^\mp \nu_e \gamma$	[t,bb,ee] (3.79 $\pm$ 0.06) $\times 10^{-3}$		229
$\pi^\pm \mu^\mp \nu_\mu \gamma$	(5.65 $\pm$ 0.23) $\times 10^{-4}$		216
<b>Hadronic modes with photons or <math>\ell\bar{\ell}</math> pairs</b>			
$\pi^0 \pi^0 \gamma$	< 2.43 $\times 10^{-7}$	CL=90%	209
$\pi^+ \pi^- \gamma$	[t,ee] (4.15 $\pm$ 0.15) $\times 10^{-5}$	S=2.8	206
$\pi^+ \pi^- \gamma (\text{DE})$	(2.84 $\pm$ 0.11) $\times 10^{-5}$	S=2.0	206
$\pi^0 2\gamma$	[ee] (1.273 $\pm$ 0.033) $\times 10^{-6}$		230
$\pi^0 \gamma e^+ e^-$	(1.62 $\pm$ 0.17) $\times 10^{-8}$		230
<b>Other modes with photons or <math>\ell\bar{\ell}</math> pairs</b>			
$2\gamma$	(5.47 $\pm$ 0.04) $\times 10^{-4}$	S=1.1	249
$3\gamma$	< 7.4 $\times 10^{-8}$	CL=90%	249
$e^+ e^- \gamma$	(9.4 $\pm$ 0.4) $\times 10^{-6}$	S=2.0	249
$\mu^+ \mu^- \gamma$	(3.59 $\pm$ 0.11) $\times 10^{-7}$	S=1.3	225
$e^+ e^- \gamma \gamma$	[ee] (5.95 $\pm$ 0.33) $\times 10^{-7}$		249
$\mu^+ \mu^- \gamma \gamma$	[ee] (1.0 $\pm$ 0.8 $\pm$ 0.6) $\times 10^{-8}$		225
<b>Charge conjugation <math>\times</math> Parity (CP) or Lepton Family number (LF) violating modes, or <math>\Delta S = 1</math> weak neutral current (S1) modes</b>			
$\mu^+ \mu^-$	S1 (6.84 $\pm$ 0.11) $\times 10^{-9}$		225
$e^+ e^-$	S1 (9 $\pm$ 6 $\pm$ 4) $\times 10^{-12}$		249
$\pi^+ \pi^- e^+ e^-$	S1 [ee] (3.11 $\pm$ 0.19) $\times 10^{-7}$		206
$\pi^0 \pi^0 e^+ e^-$	S1 < 6.6 $\times 10^{-9}$	CL=90%	209
$\pi^0 \pi^0 \mu^+ \mu^-$	S1 < 9.2 $\times 10^{-11}$	CL=90%	57
$\mu^+ \mu^- e^+ e^-$	S1 (2.69 $\pm$ 0.27) $\times 10^{-9}$		225
$e^+ e^- e^+ e^-$	S1 (3.56 $\pm$ 0.21) $\times 10^{-8}$		249
$\pi^0 \mu^+ \mu^-$	CP,S1 [ff] < 3.8 $\times 10^{-10}$	CL=90%	177
$\pi^0 e^+ e^-$	CP,S1 [ff] < 2.8 $\times 10^{-10}$	CL=90%	230
$\pi^0 \nu \bar{\nu}$	CP,S1 [gg] < 3.0 $\times 10^{-9}$	CL=90%	230
$\pi^0 \pi^0 \nu \bar{\nu}$	S1 < 8.1 $\times 10^{-7}$	CL=90%	209
$e^\pm \mu^\mp$	LF [bb] < 4.7 $\times 10^{-12}$	CL=90%	238
$e^\pm e^\pm \mu^\mp \mu^\mp$	LF [bb] < 4.12 $\times 10^{-11}$	CL=90%	225
$\pi^0 \mu^\pm e^\mp$	LF [bb] < 7.6 $\times 10^{-11}$	CL=90%	217
$\pi^0 \pi^0 \mu^\pm e^\mp$	LF < 1.7 $\times 10^{-10}$	CL=90%	159

## $K_0^*(700)$

$$I(J^P) = \frac{1}{2}(0^+)$$

also known as  $\kappa$ ; was  $K_0^*(800)$

$$\text{Mass (T-Matrix Pole } \sqrt{s}) = (630-730) - i(260-340) \text{ MeV}$$

$$\text{Mass (Breit-Wigner)} = 824 \pm 30 \text{ MeV}$$

$$\text{Full width (Breit-Wigner)} = 478 \pm 50 \text{ MeV}$$

## $K_0^*(700)$ DECAY MODES

	Fraction ( $\Gamma_i/\Gamma$ )	$\rho$ (MeV/c)
$K\pi$	100 %	240

## $K^*(892)$

$$I(J^P) = \frac{1}{2}(1^-)$$

$$K^*(892)^\pm \text{ hadroproduced mass } m = 891.66 \pm 0.26 \text{ MeV}$$

$$K^*(892)^\pm \text{ in } \tau \text{ decays mass } m = 895.5 \pm 0.8 \text{ MeV}$$

$$K^*(892)^0 \text{ mass } m = 895.55 \pm 0.20 \text{ MeV} \quad (S = 1.7)$$

$$K^*(892)^\pm \text{ hadroproduced full width } \Gamma = 50.8 \pm 0.9 \text{ MeV}$$

$$K^*(892)^\pm \text{ in } \tau \text{ decays full width } \Gamma = 46.2 \pm 1.3 \text{ MeV}$$

$$K^*(892)^0 \text{ full width } \Gamma = 47.3 \pm 0.5 \text{ MeV} \quad (S = 1.9)$$

## Meson Summary Table

<b>K*(892) DECAY MODES</b>	Fraction ( $\Gamma_i/\Gamma$ )	Confidence level	$\rho$ (MeV/c)
$K\pi$	$\sim 100$	%	289
$K^0\gamma$	$(2.46 \pm 0.21) \times 10^{-3}$		307
$K^\pm\gamma$	$(9.9 \pm 0.9) \times 10^{-4}$		309
$K\pi\pi$	$< 7$	$\times 10^{-4}$	95% 223

**K<sub>1</sub>(1270)**

$$I(J^P) = \frac{1}{2}(1^+)$$

Mass  $m = 1253 \pm 7$  MeV [*l*] (S = 2.2)  
 Full width  $\Gamma = 90 \pm 20$  MeV [*l*]

<b>K<sub>1</sub>(1270) DECAY MODES</b>	Fraction ( $\Gamma_i/\Gamma$ )	$\rho$ (MeV/c)
$K\rho$	(42 $\pm$ 6 ) %	†
$K^*_0(1430)\pi$	(28 $\pm$ 4 ) %	†
$K^*(892)\pi$	(16 $\pm$ 5 ) %	286
$K\omega$	(11.0 $\pm$ 2.0) %	†
$Kf_0(1370)$	(3.0 $\pm$ 2.0) %	†
$\gamma K^0$	seen	528

**K<sub>1</sub>(1400)**

$$I(J^P) = \frac{1}{2}(1^+)$$

Mass  $m = 1403 \pm 7$  MeV  
 Full width  $\Gamma = 174 \pm 13$  MeV (S = 1.6)

<b>K<sub>1</sub>(1400) DECAY MODES</b>	Fraction ( $\Gamma_i/\Gamma$ )	$\rho$ (MeV/c)
$K^*(892)\pi$	(94 $\pm$ 6 ) %	402
$K\rho$	(3.0 $\pm$ 3.0) %	293
$Kf_0(1370)$	(2.0 $\pm$ 2.0) %	†
$K\omega$	(1.0 $\pm$ 1.0) %	284
$K^*_0(1430)\pi$	not seen	†
$\gamma K^0$	seen	613

**K\*(1410)**

$$I(J^P) = \frac{1}{2}(1^-)$$

Mass  $m = 1414 \pm 15$  MeV (S = 1.3)  
 Full width  $\Gamma = 232 \pm 21$  MeV (S = 1.1)

<b>K*(1410) DECAY MODES</b>	Fraction ( $\Gamma_i/\Gamma$ )	Confidence level	$\rho$ (MeV/c)
$K^*(892)\pi$	$> 40$	%	95% 410
$K\pi$	(6.6 $\pm$ 1.3) %		612
$K\rho$	$< 7$	%	95% 305
$\gamma K^0$	$< 2.3$	$\times 10^{-4}$	90% 619

**K<sup>\*</sup><sub>0</sub>(1430) [*hh*]**

$$I(J^P) = \frac{1}{2}(0^+)$$

Mass  $m = 1425 \pm 50$  MeV  
 Full width  $\Gamma = 270 \pm 80$  MeV

<b>K<sup>*</sup><sub>0</sub>(1430) DECAY MODES</b>	Fraction ( $\Gamma_i/\Gamma$ )	$\rho$ (MeV/c)
$K\pi$	(93 $\pm$ 10 ) %	619
$K\eta$	(8.6 $\pm$ 2.7 / 3.4) %	486
$K\eta'(958)$	seen	†

**K<sup>\*</sup><sub>2</sub>(1430)**

$$I(J^P) = \frac{1}{2}(2^+)$$

$K^*_2(1430)^\pm$  mass  $m = 1427.3 \pm 1.5$  MeV (S = 1.3)  
 $K^*_2(1430)^0$  mass  $m = 1432.4 \pm 1.3$  MeV  
 $K^*_2(1430)^\pm$  full width  $\Gamma = 100.0 \pm 2.1$  MeV  
 $K^*_2(1430)^0$  full width  $\Gamma = 109 \pm 5$  MeV (S = 1.9)

<b>K<sup>*</sup><sub>2</sub>(1430) DECAY MODES</b>	Fraction ( $\Gamma_i/\Gamma$ )	Scale factor/ Confidence level	$\rho$ (MeV/c)
$K\pi$	(49.9 $\pm$ 1.2) %		620
$K^*(892)\pi$	(24.7 $\pm$ 1.5) %		420
$K^*(892)\pi\pi$	(13.4 $\pm$ 2.2) %		373
$K\rho$	(8.7 $\pm$ 0.8) %	S=1.2	320
$K\omega$	(2.9 $\pm$ 0.8) %		313
$K^\pm\gamma$	(2.4 $\pm$ 0.5) $\times 10^{-3}$	S=1.1	628

$K\eta$	$(1.5^{+3.4}_{-1.0}) \times 10^{-3}$	S=1.3	488
$K\omega\pi$	$< 7.2$	$\times 10^{-4}$	CL=95% 106
$K^0\gamma$	$< 9$	$\times 10^{-4}$	CL=90% 627

**K\*(1680)**

$$I(J^P) = \frac{1}{2}(1^-)$$

Mass  $m = 1718 \pm 18$  MeV  
 Full width  $\Gamma = 322 \pm 110$  MeV (S = 4.2)

<b>K*(1680) DECAY MODES</b>	Fraction ( $\Gamma_i/\Gamma$ )	$\rho$ (MeV/c)
$K\pi$	(38.7 $\pm$ 2.5) %	782
$K\rho$	(31.4 $\pm$ 5.0 / 2.1) %	571
$K^*(892)\pi$	(29.9 $\pm$ 2.2 / 5.0) %	618
$K\phi$	seen	387

**K<sub>2</sub>(1770) [*ll*]**

$$I(J^P) = \frac{1}{2}(2^-)$$

Mass  $m = 1773 \pm 8$  MeV  
 Full width  $\Gamma = 186 \pm 14$  MeV

<b>K<sub>2</sub>(1770) DECAY MODES</b>	Fraction ( $\Gamma_i/\Gamma$ )	$\rho$ (MeV/c)
$K\pi\pi$		794
$K^*_2(1430)\pi$	seen	287
$K^*(892)\pi$	seen	654
$Kf_2(1270)$	seen	53
$K\phi$	seen	441
$K\omega$	seen	607

**K<sup>\*</sup><sub>3</sub>(1780)**

$$I(J^P) = \frac{1}{2}(3^-)$$

Mass  $m = 1776 \pm 7$  MeV (S = 1.1)  
 Full width  $\Gamma = 159 \pm 21$  MeV (S = 1.3)

<b>K<sup>*</sup><sub>3</sub>(1780) DECAY MODES</b>	Fraction ( $\Gamma_i/\Gamma$ )	Confidence level	$\rho$ (MeV/c)
$K\rho$	(31 $\pm$ 9 ) %		613
$K^*(892)\pi$	(20 $\pm$ 5 ) %		656
$K\pi$	(18.8 $\pm$ 1.0) %		813
$K\eta$	(30 $\pm$ 13 ) %		719
$K^*_2(1430)\pi$	$< 16$	%	95% 290

**K<sub>2</sub>(1820) [*ll*]**

$$I(J^P) = \frac{1}{2}(2^-)$$

Mass  $m = 1819 \pm 12$  MeV  
 Full width  $\Gamma = 264 \pm 34$  MeV

<b>K<sub>2</sub>(1820) DECAY MODES</b>	Fraction ( $\Gamma_i/\Gamma$ )	$\rho$ (MeV/c)
$K^*_2(1430)\pi$	seen	328
$K^*(892)\pi$	seen	683
$Kf_2(1270)$	seen	191
$K\omega$	seen	640
$K\phi$	seen	483

**K<sup>\*</sup><sub>4</sub>(2045)**

$$I(J^P) = \frac{1}{2}(4^+)$$

Mass  $m = 2048^{+8}_{-9}$  MeV (S = 1.1)  
 Full width  $\Gamma = 199^{+27}_{-19}$  MeV

<b>K<sup>*</sup><sub>4</sub>(2045) DECAY MODES</b>	Fraction ( $\Gamma_i/\Gamma$ )	$\rho$ (MeV/c)
$K\pi$	(9.9 $\pm$ 1.2) %	960
$K^*(892)\pi\pi$	(9 $\pm$ 5 ) %	804
$K^*(892)\pi\pi\pi$	(7 $\pm$ 5 ) %	770
$\rho K\pi$	(5.7 $\pm$ 3.2) %	744
$\omega K\pi$	(5.0 $\pm$ 3.0) %	740
$\phi K\pi$	(2.8 $\pm$ 1.4) %	597
$\phi K^*(892)$	(1.4 $\pm$ 0.7) %	368

## Meson Summary Table

### CHARMED MESONS ( $C = \pm 1$ )

$$D^+ = c\bar{d}, D^0 = c\bar{u}, \bar{D}^0 = \bar{c}u, D^- = \bar{c}d, \text{ similarly for } D^{*s}$$

 **$D^\pm$** 

$$J(P) = \frac{1}{2}(0^-)$$

$$\begin{aligned} \text{Mass } m &= 1869.65 \pm 0.05 \text{ MeV} \\ \text{Mean life } \tau &= (1040 \pm 7) \times 10^{-15} \text{ s} \\ c\tau &= 311.8 \mu\text{m} \end{aligned}$$

**c-quark decays**

$$\begin{aligned} \Gamma(c \rightarrow \ell^+ \text{ anything}) / \Gamma(c \rightarrow \text{ anything}) &= 0.096 \pm 0.004 \text{ [kk]} \\ \Gamma(c \rightarrow D^*(2010)^+ \text{ anything}) / \Gamma(c \rightarrow \text{ anything}) &= 0.255 \pm 0.017 \end{aligned}$$

**CP-violation decay-rate asymmetries**

$$\begin{aligned} A_{CP}(\mu^\pm \nu) &= (8 \pm 8)\% \\ A_{CP}(K_S^0 e^\pm \nu) &= (-0.6 \pm 1.6)\% \\ A_{CP}(K_S^0 \pi^\pm) &= (-0.41 \pm 0.09)\% \\ A_{CP}(K_L^0 K^\pm) \text{ in } D^\pm \rightarrow K_L^0 K^\pm &= (-4.2 \pm 3.4) \times 10^{-2} \\ A_{CP}(K^\mp 2\pi^\pm) &= (-0.18 \pm 0.16)\% \\ A_{CP}(K^\mp \pi^\pm \pi^\pm \pi^0) &= (-0.3 \pm 0.7)\% \\ A_{CP}(K_S^0 \pi^\pm \pi^0) &= (-0.1 \pm 0.7)\% \\ A_{CP}(K_S^0 \pi^\pm \pi^+ \pi^-) &= (0.0 \pm 1.2)\% \\ A_{CP}(\pi^\pm \pi^0) &= (2.4 \pm 1.2)\% \\ A_{CP}(\pi^\pm \eta) &= (1.0 \pm 1.5)\% \quad (S = 1.4) \\ A_{CP}(\pi^\pm \eta'(958)) &= (-0.6 \pm 0.7)\% \\ A_{CP}(\bar{K}^0 / K^0 K^\pm) &= (0.11 \pm 0.17)\% \\ A_{CP}(K_S^0 K^\pm) &= (-0.01 \pm 0.07)\% \\ A_{CP}(K_S^0 K^\pm \pi^0) \text{ in } D^\pm \rightarrow K_S^0 K^\pm \pi^0 &= (1 \pm 4) \times 10^{-2} \\ A_{CP}(K_L^0 K^\pm \pi^0) \text{ in } D^\pm \rightarrow K_L^0 K^\pm \pi^0 &= (-1 \pm 4) \times 10^{-2} \\ A_{CP}(K^+ K^- \pi^\pm) &= (0.37 \pm 0.29)\% \\ A_{CP}(K^\pm K^*0) &= (-0.3 \pm 0.4)\% \\ A_{CP}(\phi \pi^\pm) &= (0.01 \pm 0.09)\% \quad (S = 1.8) \\ A_{CP}(K^\pm K_0^*(1430)^0) &= (8 \pm 7)\% \\ A_{CP}(K^\pm K_2^*(1430)^0) &= (43 \pm 20)\% \\ A_{CP}(K^\pm K_0^*(700)) &= (-12 \pm 13)\% \\ A_{CP}(a_0(1450)^0 \pi^\pm) &= (-19 \pm 14)\% \\ A_{CP}(\phi(1680) \pi^\pm) &= (-9 \pm 26)\% \\ A_{CP}(\pi^+ \pi^- \pi^\pm) &= (-2 \pm 4)\% \\ A_{CP}(K_S^0 K^\pm \pi^+ \pi^-) &= (-4 \pm 7)\% \\ A_{CP}(K^\pm \pi^0) &= (-4 \pm 11)\% \end{aligned}$$

 **$\chi^2$  tests of CP-violation (CPV)**

$$\begin{aligned} \text{Local CPV in } D^\pm \rightarrow \pi^+ \pi^- \pi^\pm &= 78.1\% \\ \text{Local CPV in } D^\pm \rightarrow K^+ K^- \pi^\pm &= 31\% \end{aligned}$$

**CP violating asymmetries of P-odd (T-odd) moments**

$$A_T(K_S^0 K^\pm \pi^+ \pi^-) = (-12 \pm 11) \times 10^{-3} \text{ [ll]}$$

 **$D^+$  form factors**

$$\begin{aligned} f_+(0) |V_{cs}| \text{ in } \bar{K}^0 \ell^+ \nu_\ell &= 0.719 \pm 0.011 \quad (S = 1.6) \\ r_1 \equiv a_1/a_0 \text{ in } \bar{K}^0 \ell^+ \nu_\ell &= -2.13 \pm 0.14 \\ r_2 \equiv a_2/a_0 \text{ in } \bar{K}^0 \ell^+ \nu_\ell &= -3 \pm 12 \quad (S = 1.5) \\ f_+(0) |V_{cd}| \text{ in } \pi^0 \ell^+ \nu_\ell &= 0.1407 \pm 0.0025 \\ r_1 \equiv a_1/a_0 \text{ in } \pi^0 \ell^+ \nu_\ell &= -2.00 \pm 0.13 \\ r_2 \equiv a_2/a_0 \text{ in } \pi^0 \ell^+ \nu_\ell &= -4 \pm 5 \\ f_+(0) |V_{cd}| \text{ in } D^+ \rightarrow \eta e^+ \nu_e &= (8.3 \pm 0.5) \times 10^{-2} \\ r_1 \equiv a_1/a_0 \text{ in } D^+ \rightarrow \eta e^+ \nu_e &= -5.3 \pm 2.7 \quad (S = 1.9) \\ r_\nu \equiv V(0)/A_1(0) \text{ in } D^+ \rightarrow \omega e^+ \nu_e &= 1.24 \pm 0.11 \\ r_2 \equiv A_2(0)/A_1(0) \text{ in } D^+ \rightarrow \omega e^+ \nu_e &= 1.06 \pm 0.16 \\ r_\nu \equiv V(0)/A_1(0) \text{ in } D^+, D^0 \rightarrow \rho e^+ \nu_e &= 1.64 \pm 0.10 \quad (S = 1.2) \\ r_2 \equiv A_2(0)/A_1(0) \text{ in } D^+, D^0 \rightarrow \rho e^+ \nu_e &= 0.84 \pm 0.06 \\ r_\nu \equiv V(0)/A_1(0) \text{ in } \bar{K}^*(892)^0 \ell^+ \nu_\ell &= 1.49 \pm 0.05 \quad (S = 2.1) \\ r_2 \equiv A_2(0)/A_1(0) \text{ in } \bar{K}^*(892)^0 \ell^+ \nu_\ell &= 0.802 \pm 0.021 \\ r_3 \equiv A_3(0)/A_1(0) \text{ in } \bar{K}^*(892)^0 \ell^+ \nu_\ell &= 0.0 \pm 0.4 \\ \Gamma_L/\Gamma_T \text{ in } \bar{K}^*(892)^0 \ell^+ \nu_\ell &= 1.13 \pm 0.08 \\ \Gamma_+/ \Gamma_- \text{ in } K^*(892)^0 \ell^+ \nu_\ell &= 0.22 \pm 0.06 \quad (S = 1.6) \end{aligned}$$

Most decay modes (other than the semileptonic modes) that involve a neutral  $K$  meson are now given as  $K_S^0$  modes, not as  $\bar{K}^0$  modes. Nearly always it is a  $K_S^0$  that is measured, and interference between Cabibbo-allowed and doubly Cabibbo-suppressed modes can invalidate the assumption that  $2\Gamma(K_S^0) = \Gamma(\bar{K}^0)$ .

<b><math>D^+</math> DECAY MODES</b>	Fraction ( $\Gamma_i/\Gamma$ )	Scale factor/ Confidence level	$p$ (MeV/c)
<b>Inclusive modes</b>			
$e^+$ semileptonic	$(16.07 \pm 0.30) \%$		—
$\mu^+$ anything	$(17.6 \pm 3.2) \%$		—
$K^-$ anything	$(25.7 \pm 1.4) \%$		—
$\bar{K}^0$ anything + $K^0$ anything	$(61 \pm 5) \%$		—
$K^+$ anything	$(5.9 \pm 0.8) \%$		—
$K^*(892)^- \text{ anything}$	$(6 \pm 5) \%$		—
$\bar{K}^*(892)^0 \text{ anything}$	$(23 \pm 5) \%$		—
$K^*(892)^0 \text{ anything}$	$< 6.6 \%$	CL=90%	—
$\eta$ anything	$(6.3 \pm 0.7) \%$		—
$\eta'$ anything	$(1.04 \pm 0.18) \%$		—
$\phi$ anything	$(1.12 \pm 0.04) \%$		—
<b>Leptonic and semileptonic modes</b>			
$e^+ \nu_e$	$< 8.8$	$\times 10^{-6}$ CL=90%	935
$\gamma e^+ \nu_e$	$< 3.0$	$\times 10^{-5}$ CL=90%	935
$\mu^+ \nu_\mu$	$(3.74 \pm 0.17) \times 10^{-4}$		932
$\tau^+ \nu_\tau$	$(1.20 \pm 0.27) \times 10^{-3}$		90
$\bar{K}^0 e^+ \nu_e$	$(8.73 \pm 0.10) \%$		869
$\bar{K}^0 \mu^+ \nu_\mu$	$(8.76 \pm 0.19) \%$		865
$K^- \pi^+ e^+ \nu_e$	$(4.02 \pm 0.18) \%$	S=3.2	864
$\bar{K}^*(892)^0 e^+ \nu_e, \bar{K}^*(892)^0 \rightarrow K^- \pi^+$	$(3.77 \pm 0.17) \%$		722
$(K^- \pi^+) [0.8-1.0] \text{ GeV } e^+ \nu_e$	$(3.39 \pm 0.09) \%$		864
$(K^- \pi^+)_{S\text{-wave}} e^+ \nu_e$	$(2.28 \pm 0.11) \times 10^{-3}$		—
$\bar{K}^*(1410)^0 e^+ \nu_e$	$< 6$	$\times 10^{-3}$ CL=90%	—
$\bar{K}^*(1410)^0 \rightarrow K^- \pi^+$			—
$\bar{K}_2^*(1430)^0 e^+ \nu_e$	$< 5$	$\times 10^{-4}$ CL=90%	—
$\bar{K}_2^*(1430)^0 \rightarrow K^- \pi^+$			—
$K^- \pi^+ e^+ \nu_e$ nonresonant	$< 7$	$\times 10^{-3}$ CL=90%	864
$\bar{K}^*(892)^0 e^+ \nu_e$	$(5.40 \pm 0.10) \%$	S=1.1	722
$K^- \pi^+ \mu^+ \nu_\mu$	$(3.65 \pm 0.34) \%$		851
$\bar{K}^*(892)^0 \mu^+ \nu_\mu$	$(3.52 \pm 0.10) \%$		717
$\bar{K}^*(892)^0 \rightarrow K^- \pi^+$			—
$K^- \pi^+ \mu^+ \nu_\mu$ nonresonant	$(1.9 \pm 0.5) \times 10^{-3}$		851
$\bar{K}^*(892)^0 \mu^+ \nu_\mu$	$(5.27 \pm 0.15) \%$		717
$K^- \pi^+ \pi^0 \mu^+ \nu_\mu$	$< 1.5$	$\times 10^{-3}$ CL=90%	825
$\bar{K}_1^*(1270)^0 e^+ \nu_e, \bar{K}_1^0 \rightarrow K^- \pi^+ \pi^0$	$(1.06 \pm 0.15) \times 10^{-3}$		—
$\bar{K}_0^*(1430)^0 \mu^+ \nu_\mu$	$< 2.3$	$\times 10^{-4}$ CL=90%	380
$\bar{K}^*(1680)^0 \mu^+ \nu_\mu$	$< 1.5$	$\times 10^{-3}$ CL=90%	105
$\pi^0 e^+ \nu_e$	$(3.72 \pm 0.17) \times 10^{-3}$	S=2.0	930
$\pi^0 \mu^+ \nu_\mu$	$(3.50 \pm 0.15) \times 10^{-3}$		927
$\eta e^+ \nu_e$	$(1.11 \pm 0.07) \times 10^{-3}$		855
$\pi^- \pi^+ e^+ \nu_e$	$(2.45 \pm 0.10) \times 10^{-3}$		924
$f_0(500)^0 e^+ \nu_e, f_0(500)^0 \rightarrow \pi^+ \pi^-$	$(6.3 \pm 0.5) \times 10^{-4}$		—
$\rho^0 e^+ \nu_e$	$(2.18 \pm 0.17) \times 10^{-3}$		774
$\rho^0 \mu^+ \nu_\mu$	$(2.4 \pm 0.4) \times 10^{-3}$		770
$\omega e^+ \nu_e$	$(1.69 \pm 0.11) \times 10^{-3}$		771
$\eta'(958) e^+ \nu_e$	$(2.0 \pm 0.4) \times 10^{-4}$		690
$a(980)^0 e^+ \nu_e, a(980)^0 \rightarrow \eta \pi^0$	$(1.7 \pm 0.8) \times 10^{-4}$		—
$\phi e^+ \nu_e$	$< 1.3$	$\times 10^{-5}$ CL=90%	657
$D^0 e^+ \nu_e$	$< 1.0$	$\times 10^{-4}$ CL=90%	5
<b>Hadronic modes with a <math>\bar{K}</math> or <math>\bar{K}K\bar{K}</math></b>			
$K_S^0 \pi^+$	$(1.562 \pm 0.031) \%$	S=1.7	863
$K_L^0 \pi^+$	$(1.46 \pm 0.05) \%$		863
$K^- 2\pi^+$	$[nn] (9.38 \pm 0.16) \%$	S=1.6	846
$(K^- \pi^+)_{S\text{-wave}} \pi^+$	$(7.52 \pm 0.17) \%$		846
$\bar{K}_0^*(1430)^0 \pi^+, \bar{K}_0^*(1430)^0 \rightarrow K^- \pi^+$	$[oo] (1.25 \pm 0.06) \%$		382
$\bar{K}^*(892)^0 \pi^+$	$(1.04 \pm 0.12) \%$		714
$\bar{K}^*(892)^0 \rightarrow K^- \pi^+$			—
$\bar{K}^*(1410)^0 \pi^+, \bar{K}^*0 \rightarrow$	not seen		381
$K^- \pi^+ \pi^+$			—
$\bar{K}_2^*(1430)^0 \pi^+, \bar{K}_2^*(1430)^0 \rightarrow K^- \pi^+$	$[oo] (2.3 \pm 0.7) \times 10^{-4}$		371

# Meson Summary Table

$\bar{K}^*(1680)^0 \pi^+$ , $\bar{K}^*(1680)^0 \rightarrow K^- \pi^+$	[ $oo$ ]	$(2.2 \pm 1.1) \times 10^{-4}$	58	$K^+ \bar{K}_0^*(1430)^0$ , $\bar{K}_0^*(1430)^0 \rightarrow K^- \pi^+$	$(1.82 \pm 0.35) \times 10^{-3}$	-
$K_S^0 \pi^+ \pi^0$	[ $nn$ ]	$(7.36 \pm 0.21) \%$	845	$K^+ \bar{K}_2^*(1430)^0$ , $\bar{K}_2^* \rightarrow$ $K^- \pi^+$	$(1.6 \pm \frac{1.2}{0.8}) \times 10^{-4}$	-
$K_S^0 \rho^+$		$(6.14 \pm \frac{0.60}{0.35}) \%$	677	$K^+ \bar{K}_0^*(700)$ , $\bar{K}_0^* \rightarrow$ $K^- \pi^+$	$(6.8 \pm \frac{3.5}{2.1}) \times 10^{-4}$	-
$K_S^0 \rho(1450)^+$ , $\rho^+ \rightarrow \pi^+ \pi^0$		$(1.5 \pm \frac{1.2}{1.4}) \times 10^{-3}$	-	$a_0(1450)^0 \pi^+$ , $a_0^0 \rightarrow$ $K^+ K^-$	$(4.5 \pm \frac{7.0}{1.8}) \times 10^{-4}$	-
$\bar{K}^*(892)^0 \pi^+$ , $\bar{K}^*(892)^0 \rightarrow K_S^0 \pi^0$		$(2.64 \pm 0.32) \times 10^{-3}$	714	$\phi(1680) \pi^+$ , $\phi \rightarrow$ $K^+ K^-$	$(4.9 \pm \frac{4.0}{1.9}) \times 10^{-5}$	-
$\bar{K}_0^*(1430)^0 \pi^+$ , $\bar{K}_0^{*0} \rightarrow$ $K_S^0 \pi^0$		$(2.7 \pm 0.9) \times 10^{-3}$	-	$K_S^0 K_S^0 \pi^+$	$(2.70 \pm 0.13) \times 10^{-3}$	741
$\bar{K}_0^*(1680)^0 \pi^+$ , $\bar{K}_0^{*0} \rightarrow$ $K_S^0 \pi^0$		$(10 \pm \frac{7}{-10}) \times 10^{-4}$	-	$K_S^+ K_S^0 \pi^+ \pi^-$	$(1.74 \pm 0.18) \times 10^{-3}$	678
$\bar{\pi}^0 \pi^+$ , $\bar{\pi}^0 \rightarrow K_S^0 \pi^0$		$(6 \pm \frac{5}{-4}) \times 10^{-3}$	-	$K_S^0 K^- 2\pi^+$	$(2.38 \pm 0.17) \times 10^{-3}$	678
$K_S^0 \pi^+ \pi^0$ nonresonant		$(3 \pm 4) \times 10^{-3}$	845	$K^+ K^- 2\pi^+ \pi^-$	$(2.3 \pm 1.2) \times 10^{-4}$	601
$K_S^0 \pi^+ \pi^0$ nonresonant and $\bar{\pi}^0 \pi^+$		$(1.37 \pm \frac{0.21}{0.40}) \%$	-	A few poorly measured branching fractions:		
$(K_S^0 \pi^0)_{S\text{-wave}} \pi^+$		$(1.27 \pm \frac{0.27}{0.33}) \%$	845	$\phi \pi^+ \pi^0$	$(2.3 \pm 1.0) \%$	619
$K_S^0 \pi^+ \eta'(958)$		$(1.90 \pm 0.21) \times 10^{-3}$	481	$\phi \rho^+$	$< 1.5 \%$ CL=90%	260
$K^- 2\pi^+ \pi^0$	[ $pp$ ]	$(6.25 \pm 0.18) \%$	816	$K^+ K^- \pi^+ \pi^0$ non- $\phi$	$(1.5 \pm \frac{0.7}{0.6}) \%$	682
$K_S^0 2\pi^+ \pi^-$	[ $pp$ ]	$(3.10 \pm 0.09) \%$	814	$K^*(892)^+ K_S^0$	$(1.7 \pm 0.8) \%$	612
$K^- 3\pi^+ \pi^-$	[ $nn$ ]	$(5.7 \pm 0.5) \times 10^{-3}$	772	<b>Doubly Cabibbo-suppressed modes</b>		
$\bar{K}^*(892)^0 2\pi^+ \pi^-$ , $\bar{K}^*(892)^0 \rightarrow K^- \pi^+$		$(1.2 \pm 0.4) \times 10^{-3}$	645	$K^+ \pi^0$	$(2.08 \pm 0.21) \times 10^{-4}$	S=1.4 864
$\bar{K}^*(892)^0 \rho^0 \pi^+$ , $\bar{K}^*(892)^0 \rightarrow K^- \pi^+$		$(2.3 \pm 0.4) \times 10^{-3}$	239	$K^+ \eta$	$(1.25 \pm 0.16) \times 10^{-4}$	S=1.1 776
$\bar{K}^*(892)^0 a_1(1260)^+$	[ $qq$ ]	$(9.3 \pm 1.9) \times 10^{-3}$	†	$K^+ \eta'(958)$	$(1.85 \pm 0.20) \times 10^{-4}$	571
$K^- \rho^0 2\pi^+$		$(1.72 \pm 0.28) \times 10^{-3}$	524	$K^+ \pi^+ \pi^-$	$(4.91 \pm 0.09) \times 10^{-4}$	846
$K^- 3\pi^+ \pi^-$ nonresonant		$(4.0 \pm 2.9) \times 10^{-4}$	772	$K^+ \rho^0$	$(1.9 \pm 0.5) \times 10^{-4}$	679
$K^+ 2K_S^0$		$(2.54 \pm 0.13) \times 10^{-3}$	545	$K^*(892)^0 \pi^+$ , $K^*(892)^0 \rightarrow$ $K^+ \pi^-$	$(2.3 \pm 0.4) \times 10^{-4}$	714
$K^+ K^- K_S^0 \pi^+$		$(2.4 \pm 0.5) \times 10^{-4}$	436	$K^+ f_0(980)$ , $f_0(980) \rightarrow$ $\pi^+ \pi^-$	$(4.4 \pm 2.6) \times 10^{-5}$	-
<b>Pionic modes</b>				$K_2^*(1430)^0 \pi^+$ , $K_2^*(1430)^0 \rightarrow$ $K^+ \pi^-$	$(3.9 \pm 2.7) \times 10^{-5}$	-
$\pi^+ \pi^0$		$(1.247 \pm 0.033) \times 10^{-3}$	925	$K^+ \pi^+ \pi^-$ nonresonant	not seen	846
$2\pi^+ \pi^-$		$(3.27 \pm 0.18) \times 10^{-3}$	909	$2K^+ K^-$	$(6.14 \pm 0.11) \times 10^{-5}$	550
$\rho^0 \pi^+$		$(8.3 \pm 1.5) \times 10^{-4}$	767	$\phi(1020)^0 K^+$	$< 2.1 \times 10^{-5}$ CL=90%	-
$\pi^+ (\pi^+ \pi^-)_{S\text{-wave}}$		$(1.83 \pm 0.16) \times 10^{-3}$	909	$K^+ \phi(1020)$ , $\phi \rightarrow$ $K^+ K^-$	$(4.4 \pm 0.6) \times 10^{-6}$	-
$\sigma \pi^+$ , $\sigma \rightarrow \pi^+ \pi^-$		$(1.38 \pm 0.12) \times 10^{-3}$	-	$K^+ (K^+ K^-)_{S\text{-wave}}$	$(5.77 \pm 0.12) \times 10^{-5}$	550
$f_0(980) \pi^+$ , $f_0(980) \rightarrow \pi^+ \pi^-$		$(1.56 \pm 0.33) \times 10^{-4}$	669	<b><math>\Delta C = 1</math> weak neutral current (<math>CI</math>) modes, or Lepton Family number (<math>LF</math>) or Lepton number (<math>L</math>) violating modes</b>		
$f_0(1370) \pi^+$ , $f_0(1370) \rightarrow \pi^+ \pi^-$		$(8 \pm 4) \times 10^{-5}$	-	$\pi^+ e^+ e^-$	$CI < 1.1 \times 10^{-6}$ CL=90%	930
$f_2(1270) \pi^+$ , $f_2(1270) \rightarrow \pi^+ \pi^-$		$(5.0 \pm 0.9) \times 10^{-4}$	485	$\pi^+ \pi^0 e^+ e^-$	$< 1.4 \times 10^{-5}$ CL=90%	925
$\rho(1450)^0 \pi^+$ , $\rho(1450)^0 \rightarrow \pi^+ \pi^-$		$< 8 \times 10^{-5}$ CL=95%	338	$\pi^+ \phi$ , $\phi \rightarrow e^+ e^-$	[ $rr$ ] $(1.7 \pm \frac{1.4}{0.9}) \times 10^{-6}$	-
$f_0(1500) \pi^+$ , $f_0(1500) \rightarrow \pi^+ \pi^-$		$(1.1 \pm 0.4) \times 10^{-4}$	-	$\pi^+ \mu^+ \mu^-$	$CI < 7.3 \times 10^{-8}$ CL=90%	918
$f_0(1710) \pi^+$ , $f_0(1710) \rightarrow \pi^+ \pi^-$		$< 5 \times 10^{-5}$ CL=95%	-	$\pi^+ \phi$ , $\phi \rightarrow \mu^+ \mu^-$	[ $rr$ ] $(1.8 \pm 0.8) \times 10^{-6}$	-
$f_0(1790) \pi^+$ , $f_0(1790) \rightarrow \pi^+ \pi^-$		$< 7 \times 10^{-5}$ CL=95%	-	$\rho^+ \mu^+ \mu^-$	$CI < 5.6 \times 10^{-4}$ CL=90%	757
$(\pi^+ \pi^+)_{S\text{-wave}} \pi^-$		$< 1.2 \times 10^{-4}$ CL=95%	909	$K^+ e^+ e^-$	[ $ss$ ] $< 1.0 \times 10^{-6}$ CL=90%	870
$2\pi^+ \pi^-$ nonresonant		$< 1.1 \times 10^{-4}$ CL=95%	909	$K^+ \pi^0 e^+ e^-$	$< 1.5 \times 10^{-5}$ CL=90%	864
$\pi^+ 2\pi^0$		$(4.7 \pm 0.4) \times 10^{-3}$	910	$K_S^0 \pi^+ e^+ e^-$	$< 2.6 \times 10^{-5}$ CL=90%	-
$2\pi^+ \pi^- \pi^0$		$(1.16 \pm 0.08) \%$	883	$K_S^0 K^+ e^+ e^-$	$< 1.1 \times 10^{-5}$ CL=90%	-
$3\pi^+ 2\pi^-$		$(1.66 \pm 0.16) \times 10^{-3}$	845	$K^+ \mu^+ \mu^-$	[ $ss$ ] $< 4.3 \times 10^{-6}$ CL=90%	856
$\eta \pi^+$		$(3.77 \pm 0.09) \times 10^{-3}$	848	$\pi^+ e^+ \mu^-$	$LF < 2.9 \times 10^{-6}$ CL=90%	927
$\eta \pi^+ \pi^0$		$(1.38 \pm 0.35) \times 10^{-3}$	831	$\pi^+ e^- \mu^+$	$LF < 3.6 \times 10^{-6}$ CL=90%	927
$\omega \pi^+$		$(2.8 \pm 0.6) \times 10^{-4}$	764	$K^+ e^+ \mu^-$	$LF < 1.2 \times 10^{-6}$ CL=90%	866
$\eta'(958) \pi^+$		$(4.97 \pm 0.19) \times 10^{-3}$	681	$K^+ e^- \mu^+$	$LF < 2.8 \times 10^{-6}$ CL=90%	866
$\eta'(958) \pi^+ \pi^0$		$(1.6 \pm 0.5) \times 10^{-3}$	654	$\pi^- 2e^+$	$L < 1.1 \times 10^{-6}$ CL=90%	930
<b>Hadronic modes with a <math>K\bar{K}</math> pair</b>				$\pi^- 2\mu^+$	$L < 2.2 \times 10^{-8}$ CL=90%	918
$K^+ K_S^0$		$(3.04 \pm 0.09) \times 10^{-3}$	S=2.2 793	$\pi^- e^+ \mu^+$	$L < 2.0 \times 10^{-6}$ CL=90%	927
$K_L^0 K^+$		$(3.21 \pm 0.16) \times 10^{-3}$	793	$\rho^- 2\mu^+$	$L < 5.6 \times 10^{-4}$ CL=90%	757
$K_S^0 K^+ \pi^0$		$(5.07 \pm 0.30) \times 10^{-3}$	744	$K^- 2e^+$	$L < 9 \times 10^{-7}$ CL=90%	870
$K_L^0 K^+ \pi^0$		$(5.24 \pm 0.31) \times 10^{-3}$	744	$K_S^0 \pi^- 2e^+$	$< 3.3 \times 10^{-6}$ CL=90%	863
$K^+ K^- \pi^+$	[ $nn$ ]	$(9.68 \pm 0.18) \times 10^{-3}$	744	$K^- \pi^0 2e^+$	$< 8.5 \times 10^{-6}$ CL=90%	864
$\phi \pi^+$		$(5.70 \pm 0.14) \times 10^{-3}$	647	$K^- 2\mu^+$	$L < 1.0 \times 10^{-5}$ CL=90%	856
$\phi \pi^+$ , $\phi \rightarrow K^+ K^-$		$(2.69 \pm \frac{0.07}{0.08}) \times 10^{-3}$	647	$K^- e^+ \mu^+$	$L < 1.9 \times 10^{-6}$ CL=90%	866
$K^+ \bar{K}^*(892)^0$ , $\bar{K}^*(892)^0 \rightarrow K^- \pi^+$		$(2.49 \pm \frac{0.08}{0.13}) \times 10^{-3}$	613	$K^*(892)^- 2\mu^+$	$L < 8.5 \times 10^{-4}$ CL=90%	703

**$D^0$**

$$I(J^P) = \frac{1}{2}(0^-)$$

Mass  $m = 1864.83 \pm 0.05$  MeV

$m_{D^\pm} - m_{D^0} = 4.822 \pm 0.015$  MeV

Mean life  $\tau = (410.1 \pm 1.5) \times 10^{-15}$  s

$c\tau = 122.9 \mu\text{m}$



# Meson Summary Table

## Mixing and related parameters

$$\begin{aligned}
 |m_{D_1^0} - m_{D_2^0}| &= (0.95_{-0.44}^{+0.41}) \times 10^{10} \text{ h s}^{-1} \\
 (\Gamma_{D_1^0} - \Gamma_{D_2^0})/\Gamma &= 2\gamma = (1.29_{-0.18}^{+0.14}) \times 10^{-2} \\
 |q/p| &= 0.92_{-0.09}^{+0.12} \\
 A_\Gamma &= (-0.125 \pm 0.526) \times 10^{-3} \\
 \phi_{K_S^0 \pi \pi} &= -0.09_{-0.13}^{+0.10} \\
 K^+ \pi^- \text{ relative strong phase: } \cos \delta &= 0.97 \pm 0.11 \\
 K^- \pi^+ \pi^0 \text{ coherence factor } R_{K \pi \pi^0} &= 0.82 \pm 0.06 \\
 K^- \pi^+ \pi^0 \text{ average relative strong phase } \delta^{K \pi \pi^0} &= (199 \pm 14)^\circ \\
 K^- \pi^- 2\pi^+ \text{ coherence factor } R_{K 3\pi} &= 0.53_{-0.21}^{+0.18} \\
 K^- \pi^- 2\pi^+ \text{ average relative strong phase } \delta^{K 3\pi} &= (125_{-14}^{+22})^\circ \\
 D^0 \rightarrow K^- \pi^- 2\pi^+, R_{K 3\pi} (\gamma \cos \delta^{K 3\pi} - x \sin \delta^{K 3\pi}) &= (-3.0 \pm 0.7) \times 10^{-3} \text{ TeV}^{-1} \\
 K_S^0 K^+ \pi^- \text{ coherence factor } R_{K_S^0 K \pi} &= 0.70 \pm 0.08 \\
 K_S^0 K^+ \pi^- \text{ average relative strong phase } \delta^{K_S^0 K \pi} &= (0 \pm 16)^\circ \\
 K^* K \text{ coherence factor } R_{K^* K} &= 0.94 \pm 0.12 \\
 K^* K \text{ average relative strong phase } \delta^{K^* K} &= (-17 \pm 18)^\circ
 \end{aligned}$$

## CP-violation decay-rate asymmetries (labeled by the $D^0$ decay)

$$\begin{aligned}
 A_{CP}(K^+ K^-) &= (-0.07 \pm 0.11)\% \\
 A_{CP}(2K_S^0) &= (0.4 \pm 1.4)\% \\
 A_{CP}(\pi^+ \pi^-) &= (0.13 \pm 0.14)\% \\
 A_{CP}(\pi^0 \pi^0) &= (0.0 \pm 0.6)\% \\
 A_{CP}(\rho \gamma) &= (6 \pm 15) \times 10^{-2} \\
 A_{CP}(\phi \gamma) &= (-9 \pm 7) \times 10^{-2} \\
 A_{CP}(\overline{K}^*(892)^0 \gamma) &= (-0.3 \pm 2.0) \times 10^{-2} \\
 A_{CP}(\pi^+ \pi^- \pi^0) &= (0.3 \pm 0.4)\% \\
 A_{CP}(\rho(770)^+ \pi^- \rightarrow \pi^+ \pi^- \pi^0) &= (1.2 \pm 0.9)\% \text{ [tt]} \\
 A_{CP}(\rho(770)^0 \pi^0 \rightarrow \pi^+ \pi^- \pi^0) &= (-3.1 \pm 3.0)\% \text{ [tt]} \\
 A_{CP}(\rho(770)^- \pi^+ \rightarrow \pi^+ \pi^- \pi^0) &= (-1.0 \pm 1.7)\% \text{ [tt]} \\
 A_{CP}(\rho(1450)^+ \pi^- \rightarrow \pi^+ \pi^- \pi^0) &= (0 \pm 70)\% \text{ [tt]} \\
 A_{CP}(\rho(1450)^0 \pi^0 \rightarrow \pi^+ \pi^- \pi^0) &= (-20 \pm 40)\% \text{ [tt]} \\
 A_{CP}(\rho(1450)^- \pi^+ \rightarrow \pi^+ \pi^- \pi^0) &= (6 \pm 9)\% \text{ [tt]} \\
 A_{CP}(\rho(1700)^+ \pi^- \rightarrow \pi^+ \pi^- \pi^0) &= (-5 \pm 14)\% \text{ [tt]} \\
 A_{CP}(\rho(1700)^0 \pi^0 \rightarrow \pi^+ \pi^- \pi^0) &= (13 \pm 9)\% \text{ [tt]} \\
 A_{CP}(\rho(1700)^- \pi^+ \rightarrow \pi^+ \pi^- \pi^0) &= (8 \pm 11)\% \text{ [tt]} \\
 A_{CP}(f_0(980) \pi^0 \rightarrow \pi^+ \pi^- \pi^0) &= (0 \pm 35)\% \text{ [tt]} \\
 A_{CP}(f_0(1370) \pi^0 \rightarrow \pi^+ \pi^- \pi^0) &= (25 \pm 18)\% \text{ [tt]} \\
 A_{CP}(f_0(1500) \pi^0 \rightarrow \pi^+ \pi^- \pi^0) &= (0 \pm 18)\% \text{ [tt]} \\
 A_{CP}(f_0(1710) \pi^0 \rightarrow \pi^+ \pi^- \pi^0) &= (0 \pm 24)\% \text{ [tt]} \\
 A_{CP}(f_2(1270) \pi^0 \rightarrow \pi^+ \pi^- \pi^0) &= (-4 \pm 6)\% \text{ [tt]} \\
 A_{CP}(\sigma(400) \pi^0 \rightarrow \pi^+ \pi^- \pi^0) &= (6 \pm 8)\% \text{ [tt]} \\
 A_{CP}(\text{nonresonant } \pi^+ \pi^- \pi^0) &= (-13 \pm 23)\% \text{ [tt]} \\
 A_{CP}(a_1(1260)^+ \pi^- \rightarrow 2\pi^+ 2\pi^-) &= (5 \pm 6)\% \\
 A_{CP}(a_1(1260)^- \pi^+ \rightarrow 2\pi^+ 2\pi^-) &= (14 \pm 18)\% \\
 A_{CP}(\pi(1300)^+ \pi^- \rightarrow 2\pi^+ 2\pi^-) &= (-2 \pm 15)\% \\
 A_{CP}(\pi(1300)^- \pi^+ \rightarrow 2\pi^+ 2\pi^-) &= (-6 \pm 30)\% \\
 A_{CP}(a_1(1640)^+ \pi^- \rightarrow 2\pi^+ 2\pi^-) &= (9 \pm 26)\% \\
 A_{CP}(\pi_2(1670)^+ \pi^- \rightarrow 2\pi^+ 2\pi^-) &= (7 \pm 18)\% \\
 A_{CP}(s_0^*(1370) \rightarrow 2\pi^+ 2\pi^-) &= (-15 \pm 19)\% \\
 A_{CP}(s_0^*(770)^0 \rightarrow 2\pi^+ 2\pi^-) &= (3 \pm 27)\% \\
 A_{CP}(2\rho(770)^0 \rightarrow 2\pi^+ 2\pi^-) &= (-6 \pm 6)\% \\
 A_{CP}(2f_2(1270) \rightarrow 2\pi^+ 2\pi^-) &= (-28 \pm 24)\% \\
 A_{CP}(K^+ K^- \pi^0) &= (-1.0 \pm 1.7)\% \\
 A_{CP}(K^*(892)^+ K^- \rightarrow K^+ K^- \pi^0) &= (-0.9 \pm 1.3)\% \text{ [tt]} \\
 A_{CP}(K^*(1410)^+ K^- \rightarrow K^+ K^- \pi^0) &= (-21 \pm 24)\% \text{ [tt]} \\
 A_{CP}((K^+ \pi^0)_{S\text{-wave}} K^- \rightarrow K^+ K^- \pi^0) &= (7 \pm 15)\% \text{ [tt]} \\
 A_{CP}(\phi(1020) \pi^0 \rightarrow K^+ K^- \pi^0) &= (1.1 \pm 2.2)\% \text{ [tt]} \\
 A_{CP}(f_0(980) \pi^0 \rightarrow K^+ K^- \pi^0) &= (-3 \pm 19)\% \text{ [tt]} \\
 A_{CP}(a_0(980)^0 \pi^0 \rightarrow K^+ K^- \pi^0) &= (-5 \pm 16)\% \text{ [tt]} \\
 A_{CP}(f_2'(1525) \pi^0 \rightarrow K^+ K^- \pi^0) &= (0 \pm 160)\% \text{ [tt]} \\
 A_{CP}(K^*(892)^- K^+ \rightarrow K^+ K^- \pi^0) &= (-5 \pm 4)\% \text{ [tt]} \\
 A_{CP}(K^*(1410)^- K^+ \rightarrow K^+ K^- \pi^0) &= (-17 \pm 29)\% \text{ [tt]} \\
 A_{CP}((K^- \pi^0)_{S\text{-wave}} K^+ \rightarrow K^+ K^- \pi^0) &= (-10 \pm 40)\% \text{ [tt]} \\
 A_{CP}(K_S^0 \pi^0) &= (-0.20 \pm 0.17)\% \\
 A_{CP}(K_S^0 \eta) &= (0.5 \pm 0.5)\% \\
 A_{CP}(K_S^0 \eta') &= (1.0 \pm 0.7)\% \\
 A_{CP}(K_S^0 \phi) &= (-3 \pm 9)\% \\
 A_{CP}(K^- \pi^+) &= (0.2 \pm 0.5)\% \\
 A_{CP}(K^+ \pi^-) &= (-0.9 \pm 1.4)\%
 \end{aligned}$$

$$\begin{aligned}
 A_{CP}(D_{CP(\pm 1)} \rightarrow K^\mp \pi^\pm) &= (12.7 \pm 1.5)\% \\
 A_{CP}(K^- \pi^+ \pi^0) &= (0.1 \pm 0.5)\% \\
 A_{CP}(K^+ \pi^- \pi^0) &= (0 \pm 5)\% \\
 A_{CP}(K_S^0 \pi^+ \pi^-) &= (-0.1 \pm 0.8)\% \\
 A_{CP}(K^*(892)^- \pi^+ \rightarrow K_S^0 \pi^+ \pi^-) &= (0.4 \pm 0.5)\% \\
 A_{CP}(K^*(892)^+ \pi^- \rightarrow K_S^0 \pi^+ \pi^-) &= (1 \pm 6)\% \\
 A_{CP}(\overline{K}^0 \rho^0 \rightarrow K_S^0 \pi^+ \pi^-) &= (-0.1 \pm 0.5)\% \\
 A_{CP}(\overline{K}^0 \omega \rightarrow K_S^0 \pi^+ \pi^-) &= (-13 \pm 7)\% \\
 A_{CP}(\overline{K}^0 f_0(980) \rightarrow K_S^0 \pi^+ \pi^-) &= (-0.4 \pm 2.7)\% \\
 A_{CP}(\overline{K}^0 f_2(1270) \rightarrow K_S^0 \pi^+ \pi^-) &= (-4 \pm 5)\% \\
 A_{CP}(\overline{K}^0 f_0(1370) \rightarrow K_S^0 \pi^+ \pi^-) &= (-1 \pm 9)\% \\
 A_{CP}(\overline{K}^0 \rho^0(1450) \rightarrow K_S^0 \pi^+ \pi^-) &= (-4 \pm 10)\% \\
 A_{CP}(\overline{K}^0 f_0(600) \rightarrow K_S^0 \pi^+ \pi^-) &= (-3 \pm 5)\% \\
 A_{CP}(K^*(1410)^- \pi^+ \rightarrow K_S^0 \pi^+ \pi^-) &= (-2 \pm 9)\% \\
 A_{CP}(K_0^*(1430)^- \pi^+ \rightarrow K_S^0 \pi^+ \pi^-) &= (4 \pm 4)\% \\
 A_{CP}(K_0^*(1430)^+ \pi^- \rightarrow K_S^0 \pi^+ \pi^-) &= (12 \pm 15)\% \\
 A_{CP}(K_2^*(1430)^- \pi^+ \rightarrow K_S^0 \pi^+ \pi^-) &= (3 \pm 6)\% \\
 A_{CP}(K_2^*(1430)^+ \pi^- \rightarrow K_S^0 \pi^+ \pi^-) &= (-10 \pm 32)\% \\
 A_{CP}(K^- \pi^+ \pi^+ \pi^-) &= (0.2 \pm 0.5)\% \\
 A_{CP}(K^+ \pi^- \pi^+ \pi^-) &= (-2 \pm 4)\% \\
 A_{CP}(K^+ K^- \pi^+ \pi^-) &= (1.3 \pm 1.7)\% \\
 A_{CP}(K_1^*(1270)^+ K^- \rightarrow K^+ K^- \pi^+ \pi^-) &= (-2.3 \pm 1.7)\% \\
 A_{CP}(K_1^*(1270)^+ K^- \rightarrow K^*0 \pi^+ K^-) &= (-1 \pm 10)\% \\
 A_{CP}(K_1^*(1270)^- K^+ \rightarrow \overline{K}^*0 \pi^- K^+) &= (-10 \pm 32)\% \\
 A_{CP}(K_1^*(1270)^- K^+ \rightarrow K^+ K^- \pi^+ \pi^-) &= (1.7 \pm 3.5)\% \\
 A_{CP}(K_1^*(1270)^+ K^- \rightarrow \rho^0 K^+ K^-) &= (-7 \pm 17)\% \\
 A_{CP}(K_1^*(1270)^- K^+ \rightarrow \rho^0 K^- K^+) &= (10 \pm 13)\% \\
 A_{CP}(K_1(1400)^+ K^- \rightarrow K^+ K^- \pi^+ \pi^-) &= (-4.4 \pm 2.1)\% \\
 A_{CP}(K^*(1410)^+ K^- \rightarrow K^*0 \pi^+ K^-) &= (-20 \pm 17)\% \\
 A_{CP}(K^*(1410)^- K^+ \rightarrow \overline{K}^*0 \pi^- K^+) &= (-1 \pm 14)\% \\
 A_{CP}(K^*(1680)^+ K^- \rightarrow K^+ K^- \pi^+ \pi^-) &= (-17 \pm 29)\% \\
 A_{CP}(K^*0 \overline{K}^*0) \text{ in } D^0, \overline{D}^0 \rightarrow K^*0 \overline{K}^*0 &= (-5 \pm 14)\% \\
 A_{CP}(K^*0 \overline{K}^*0 \text{ S-wave}) &= (-3.9 \pm 2.2)\% \\
 A_{CP}(\phi \rho^0) \text{ in } D^0, \overline{D}^0 \rightarrow \phi \rho^0 &= (1 \pm 9)\% \\
 A_{CP}(\phi \rho^0 \text{ S-wave}) &= (-3 \pm 5)\% \\
 A_{CP}(\phi \rho^0 \text{ D-wave}) &= (-37 \pm 19)\% \\
 A_{CP}(\phi(\pi^+ \pi^-)_{S\text{-wave}}) &= (6 \pm 6)\% \\
 A_{CP}(K^*(892)^0 (K^- \pi^+)_{S\text{-wave}}) &= (-10 \pm 40)\% \\
 A_{CP}(K^+ K^- \pi^+ \pi^- \text{ non-resonant}) &= (8 \pm 20)\% \\
 A_{CP}((K^- \pi^+)_{P\text{-wave}} (K^+ \pi^-)_{S\text{-wave}}) &= (3 \pm 11)\% \\
 A_{CP}(K^+ K^- \mu^+ \mu^-) \text{ in } D^0, \overline{D}^0 \rightarrow K^+ K^- \mu^+ \mu^- &= (0 \pm 11)\% \\
 A_{CP}(\pi^+ \pi^- \mu^+ \mu^-) \text{ in } D^0, \overline{D}^0 \rightarrow \pi^+ \pi^- \mu^+ \mu^- &= (5 \pm 4)\%
 \end{aligned}$$

## CP-even fractions (labeled by the $D^0$ decay)

$$\begin{aligned}
 \text{CP-even fraction in } D^0 \rightarrow \pi^+ \pi^- \pi^0 \text{ decays} &= (97.3 \pm 1.7)\% \\
 \text{CP-even fraction in } D^0 \rightarrow K^+ K^- \pi^0 \text{ decays} &= (73 \pm 6)\% \\
 \text{CP-even fraction in } D^0 \rightarrow \pi^+ \pi^- \pi^+ \pi^- \text{ decays} &= (76.9 \pm 2.3)\% \\
 \text{CP-even fraction in } D^0 \rightarrow K_S^0 \pi^+ \pi^- \pi^0 \text{ decays} &= (23.8 \pm 1.7)\% \\
 \text{CP-even fraction in } D^0 \rightarrow K^+ K^- \pi^+ \pi^- \text{ decays} &= (75 \pm 4)\%
 \end{aligned}$$

## CP-violation asymmetry difference

$$\Delta A_{CP} = A_{CP}(K^+ K^-) - A_{CP}(\pi^+ \pi^-) = (-0.154 \pm 0.029)\%$$

## $\chi^2$ tests of CP-violation (CPV) p-values

$$\begin{aligned}
 \text{Local CPV in } D^0, \overline{D}^0 \rightarrow \pi^+ \pi^- \pi^0 &= 4.9\% \\
 \text{Local CPV in } D^0, \overline{D}^0 \rightarrow \pi^+ \pi^- \pi^+ \pi^- &= (0.6 \pm 0.2)\% \\
 \text{Local CPV in } D^0, \overline{D}^0 \rightarrow K_S^0 \pi^+ \pi^- &= 96\% \\
 \text{Local CPV in } D^0, \overline{D}^0 \rightarrow K^+ K^- \pi^0 &= 16.6\% \\
 \text{Local CPV in } D^0, \overline{D}^0 \rightarrow K^+ K^- \pi^+ \pi^- &= 9.1\%
 \end{aligned}$$

## T-violation decay-rate asymmetry

$$\begin{aligned}
 A_T(K^+ K^- \pi^+ \pi^-) &= (2.9 \pm 2.2) \times 10^{-3} \text{ [fl]} \\
 A_{T\text{viol}}(K_S \pi^+ \pi^- \pi^0) \text{ in } D^0, \overline{D}^0 \rightarrow K_S \pi^+ \pi^- \pi^0 &= (-0.3_{-1.6}^{+1.4}) \times 10^{-3}
 \end{aligned}$$

## CPT-violation decay-rate asymmetry

$$A_{CP T}(K^\mp \pi^\pm) = 0.008 \pm 0.008$$

## Form factors

$$\begin{aligned}
 r_V &\equiv V(0)/A_1(0) \text{ in } D^0 \rightarrow K^*(892)^- \ell^+ \nu_\ell = 1.46 \pm 0.07 \\
 r_2 &\equiv A_2(0)/A_1(0) \text{ in } D^0 \rightarrow K^*(892)^- \ell^+ \nu_\ell = 0.68 \pm 0.06 \\
 f_+(0) &\text{ in } D^0 \rightarrow K^- \ell^+ \nu_\ell = 0.736 \pm 0.004 \\
 f_+(0) |V_{cs}| &\text{ in } D^0 \rightarrow K^- \ell^+ \nu_\ell = 0.7166 \pm 0.0030 \\
 r_1 &\equiv a_1/a_0 \text{ in } D^0 \rightarrow K^- \ell^+ \nu_\ell = -2.40 \pm 0.16 \\
 r_2 &\equiv a_2/a_0 \text{ in } D^0 \rightarrow K^- \ell^+ \nu_\ell = 5 \pm 4 \\
 f_+(0) &\text{ in } D^0 \rightarrow \pi^- \ell^+ \nu_\ell = 0.637 \pm 0.009 \\
 f_+(0) |V_{cd}| &\text{ in } D^0 \rightarrow \pi^- \ell^+ \nu_\ell = 0.1436 \pm 0.0026 \quad (S = 1.5) \\
 r_1 &\equiv a_1/a_0 \text{ in } D^0 \rightarrow \pi^- \ell^+ \nu_\ell = -1.97 \pm 0.28 \quad (S = 1.4) \\
 r_2 &\equiv a_1/a_0 \text{ in } D^0 \rightarrow \pi^- \ell^+ \nu_\ell = -0.2 \pm 2.2 \quad (S = 1.7)
 \end{aligned}$$

## Meson Summary Table

Most decay modes (other than the semileptonic modes) that involve a neutral  $K$  meson are now given as  $K_S^0$  modes, not as  $\bar{K}^0$  modes. Nearly always it is a  $K_S^0$  that is measured, and interference between Cabibbo-allowed and doubly Cabibbo-suppressed modes can invalidate the assumption that  $2\Gamma(K_S^0) = \Gamma(\bar{K}^0)$ .

$D^0$ DECAY MODES	Fraction ( $\Gamma_i/\Gamma$ )	Scale factor/ Confidence level (MeV/c)	$p$
<b>Topological modes</b>			
0-prongs	[uu] (15 ± 6) %	–	–
2-prongs	(71 ± 6) %	–	–
4-prongs	[vv] (14.6 ± 0.5) %	–	–
6-prongs	[xx] (6.5 ± 1.3) × 10 <sup>-4</sup>	–	–
<b>Inclusive modes</b>			
$e^+$ anything	[yy] (6.49 ± 0.11) %	–	–
$\mu^+$ anything	(6.8 ± 0.6) %	–	–
$K^-$ anything	(54.7 ± 2.8) %	S=1.3	–
$\bar{K}^0$ anything + $K^0$ anything	(47 ± 4) %	–	–
$K^+$ anything	(3.4 ± 0.4) %	–	–
$K^*(892)^-$ anything	(15 ± 9) %	–	–
$\bar{K}^*(892)^0$ anything	(9 ± 4) %	–	–
$K^*(892)^+$ anything	< 3.6 %	CL=90%	–
$K^*(892)^0$ anything	(2.8 ± 1.3) %	–	–
$\eta$ anything	(9.5 ± 0.9) %	–	–
$\eta'$ anything	(2.48 ± 0.27) %	–	–
$\phi$ anything	(1.08 ± 0.04) %	–	–
invisibles	< 9.4 × 10 <sup>-5</sup>	CL=90%	–
<b>Semileptonic modes</b>			
$K^- e^+ \nu_e$	(3.542 ± 0.035) %	S=1.3	867
$K^- \mu^+ \nu_\mu$	(3.41 ± 0.04) %	–	864
$K^*(892)^- e^+ \nu_e$	(2.15 ± 0.16) %	–	719
$K^*(892)^- \mu^+ \nu_\mu$	(1.89 ± 0.24) %	–	714
$K^- \pi^0 e^+ \nu_e$	(1.6 ± 1.3 / 0.5) %	–	861
$\bar{K}^0 \pi^- e^+ \nu_e$	(1.44 ± 0.04) %	–	860
$(\bar{K}^0 \pi^-)_{S-wave} e^+ \nu_e$	(7.9 ± 1.7) × 10 <sup>-4</sup>	–	860
$K^- \pi^+ \pi^- e^+ \nu_e$	(2.8 ± 1.4 / 1.1) × 10 <sup>-4</sup>	–	843
$K_1(1270)^- e^+ \nu_e$	(7.6 ± 4.0 / 3.1) × 10 <sup>-4</sup>	–	511
$K^- \pi^+ \pi^- \mu^+ \nu_\mu$	< 1.3 × 10 <sup>-3</sup>	CL=90%	821
$(\bar{K}^*(892)^0 \pi^-) \mu^+ \nu_\mu$	< 1.5 × 10 <sup>-3</sup>	CL=90%	692
$\pi^- e^+ \nu_e$	(2.91 ± 0.04) × 10 <sup>-3</sup>	–	927
$\pi^- \mu^+ \nu_\mu$	(2.67 ± 0.12) × 10 <sup>-3</sup>	S=1.3	924
$\pi^- \pi^0 e^+ \nu_e$	(1.45 ± 0.07) × 10 <sup>-3</sup>	–	922
$\rho^- e^+ \nu_e$	(1.50 ± 0.12) × 10 <sup>-3</sup>	S=1.9	771
$a(980)^- e^+ \nu_e, a^- \rightarrow \eta \pi^-$	(1.33 ± 0.34 / 0.30) × 10 <sup>-4</sup>	–	–
<b>Hadronic modes with one <math>\bar{K}</math></b>			
$K^- \pi^+$	(3.950 ± 0.031) %	S=1.2	861
$K_S^0 \pi^0$	(1.240 ± 0.022) %	–	860
$K_1^0 \pi^0$	(10.0 ± 0.7) × 10 <sup>-3</sup>	–	860
$K_S^0 \pi^+ \pi^-$	[nn] (2.80 ± 0.18) %	S=1.1	842
$K_S^0 \rho^0$	(6.3 ± 0.6 / 0.8) × 10 <sup>-3</sup>	–	674
$K_S^0 \omega, \omega \rightarrow \pi^+ \pi^-$	(2.0 ± 0.6) × 10 <sup>-4</sup>	–	670
$K_S^0 (\pi^+ \pi^-)_{S-wave}$	(3.3 ± 0.8) × 10 <sup>-3</sup>	–	842
$K_S^0 f_0(980), f_0 \rightarrow \pi^+ \pi^-$	(1.20 ± 0.40 / 0.23) × 10 <sup>-3</sup>	–	549
$K_S^0 f_0(1370), f_0 \rightarrow \pi^+ \pi^-$	(2.8 ± 0.9 / 1.3) × 10 <sup>-3</sup>	†	–
$K_S^0 f_2(1270), f_2 \rightarrow \pi^+ \pi^-$	(9 ± 10 / 6) × 10 <sup>-5</sup>	–	262
$K^*(892)^- \pi^+, K^{*-} \rightarrow K_S^0 \pi^-$	(1.64 ± 0.14 / 0.17) %	–	711
$K_0^*(1430)^- \pi^+, K_0^{*-} \rightarrow K_S^0 \pi^-$	(2.67 ± 0.40 / 0.33) × 10 <sup>-3</sup>	–	378
$K_2^*(1430)^- \pi^+, K_2^{*-} \rightarrow K_S^0 \pi^-$	(3.4 ± 1.9 / 1.0) × 10 <sup>-4</sup>	–	367
$K^*(1680)^- \pi^+, K^{*-} \rightarrow K_S^0 \pi^-$	(4.4 ± 3.5) × 10 <sup>-4</sup>	–	46
$K^*(892)^+ \pi^-, K^{*+} \rightarrow K_S^0 \pi^+$	[zz] (1.13 ± 0.60 / 0.34) × 10 <sup>-4</sup>	–	711
$K_0^*(1430)^+ \pi^-, K_0^{*+} \rightarrow K_S^0 \pi^+$	[zz] < 1.4 × 10 <sup>-5</sup>	CL=95%	–

$K_2^*(1430)^+ \pi^-, K_2^{*+} \rightarrow K_S^0 \pi^+$	[zz] < 3.4 × 10 <sup>-5</sup>	CL=95%	–
$K_S^0 \pi^+ \pi^-$ nonresonant	(2.5 ± 6.0 / 1.6) × 10 <sup>-4</sup>	–	842
$K^- \pi^+ \pi^0$	[nn] (14.4 ± 0.5) %	S=2.0	844
$K^- \rho^+$	(11.3 ± 0.7) %	–	675
$K^- \rho(1700)^+, \rho^+ \rightarrow \pi^+ \pi^0$	(8.2 ± 1.8) × 10 <sup>-3</sup>	–	†
$K^*(892)^- \pi^+, K^*(892)^- \rightarrow K^- \pi^0$	(2.31 ± 0.40 / 0.20) %	–	711
$\bar{K}^*(892)^0 \pi^0, \bar{K}^*(892)^0 \rightarrow K^- \pi^+$	(1.95 ± 0.24) %	–	711
$K_0^*(1430)^- \pi^+, K_0^{*-} \rightarrow K^- \pi^0$	(4.8 ± 2.2) × 10 <sup>-3</sup>	–	378
$\bar{K}_0^*(1430)^0 \pi^0, \bar{K}_0^{*0} \rightarrow K^- \pi^+$	(5.9 ± 5.0 / 1.6) × 10 <sup>-3</sup>	–	379
$K^*(1680)^- \pi^+, K^{*-} \rightarrow K^- \pi^0$	(1.9 ± 0.7) × 10 <sup>-3</sup>	–	46
$K^- \pi^+ \pi^0$ nonresonant	(1.15 ± 0.60 / 0.20) %	–	844
$K_S^0 2\pi^0$	(9.1 ± 1.1) × 10 <sup>-3</sup>	S=2.2	843
$K_S^0 (2\pi^0)_{S-wave}$	(2.6 ± 0.7) × 10 <sup>-3</sup>	–	–
$\bar{K}^*(892)^0 \pi^0, \bar{K}^{*0} \rightarrow K_S^0 \pi^0$	(8.1 ± 0.7) × 10 <sup>-3</sup>	–	711
$\bar{K}^*(1430)^0 \pi^0, \bar{K}^{*0} \rightarrow K_S^0 \pi^0$	(4 ± 23) × 10 <sup>-5</sup>	–	–
$\bar{K}^*(1680)^0 \pi^0, \bar{K}^{*0} \rightarrow K_S^0 \pi^0$	(1.0 ± 0.4) × 10 <sup>-3</sup>	–	–
$K_S^0 f_2(1270), f_2 \rightarrow 2\pi^0$	(2.3 ± 1.1) × 10 <sup>-4</sup>	–	–
$2K_S^0, \text{one } K_S^0 \rightarrow 2\pi^0$	(3.2 ± 1.1) × 10 <sup>-4</sup>	–	–
$K^- 2\pi^+ \pi^-$	[nn] (8.23 ± 0.14) %	S=1.1	813
$K^- \pi^+ \rho^0$ total	(6.87 ± 0.31) %	–	609
$K^- \pi^+ \rho^0$ 3-body	(6.1 ± 1.6) × 10 <sup>-3</sup>	–	609
$\bar{K}^*(892)^0 \rho^0, \bar{K}^{*0} \rightarrow K^- \pi^+$	(1.01 ± 0.05) %	–	416
$\bar{K}^*(892)^0 \rho^0$ transverse, $\bar{K}^{*0} \rightarrow K^- \pi^+$	(1.2 ± 0.4) %	–	417
$K^- a_1(1260)^+, a_1^+ \rightarrow \rho^0 \pi^+$	(4.33 ± 0.32) %	–	327
$K_1(1270)^- \pi^+, K_1^- \rightarrow K^- \pi^+ \pi^-$ total	(3.9 ± 0.4) × 10 <sup>-3</sup>	–	–
$K_1(1270)^- \pi^+, K_1^- \rightarrow \bar{K}^*(892)^0 \pi^-, \bar{K}^{*0} \rightarrow K^- \pi^+$	(6.6 ± 2.3) × 10 <sup>-4</sup>	–	484
$K^- 2\pi^+ \pi^-$ nonresonant	(1.81 ± 0.07) %	–	813
$K_S^0 \pi^+ \pi^- \pi^0$	[aaa] (5.2 ± 0.6) %	–	813
$K_S^0 \eta, \eta \rightarrow \pi^+ \pi^- \pi^0$	(1.17 ± 0.03) × 10 <sup>-3</sup>	–	772
$K_S^0 \omega, \omega \rightarrow \pi^+ \pi^- \pi^0$	(9.9 ± 0.6) × 10 <sup>-3</sup>	–	670
$K^- \pi^+ 2\pi^0$	(8.86 ± 0.23) %	–	815
$K^- 2\pi^+ \pi^- \pi^0$	(4.3 ± 0.4) %	–	771
$\bar{K}^*(892)^0 \pi^+ \pi^- \pi^0, \bar{K}^{*0} \rightarrow K^- \pi^+$	(1.3 ± 0.6) %	–	643
$K^- \pi^+ \omega, \omega \rightarrow \pi^+ \pi^- \pi^0$	(2.8 ± 0.5) %	–	605
$\bar{K}^*(892)^0 \omega, \bar{K}^{*0} \rightarrow K^- \pi^+, \omega \rightarrow \pi^+ \pi^- \pi^0$	(6.5 ± 3.0) × 10 <sup>-3</sup>	–	410
$K_S^0 \eta \pi^0$	(5.7 ± 1.1) × 10 <sup>-3</sup>	–	721
$K_S^0 a_0(980), a_0 \rightarrow \eta \pi^0$	(6.8 ± 2.1) × 10 <sup>-3</sup>	–	–
$\bar{K}^*(892)^0 \eta, \bar{K}^{*0} \rightarrow K_S^0 \pi^0$	(1.7 ± 0.5) × 10 <sup>-3</sup>	–	–
$K_S^0 2\pi^+ 2\pi^-$	(2.66 ± 0.30) × 10 <sup>-3</sup>	–	768
$K_S^0 \rho^0 \pi^+ \pi^-, \text{no } K^*(892)^-$	(1.1 ± 0.7) × 10 <sup>-3</sup>	–	–
$K^*(892)^- 2\pi^+ \pi^-, K^*(892)^- \rightarrow K_S^0 \pi^-$	(5 ± 7) × 10 <sup>-4</sup>	–	642
$K^*(892)^- \rho^0 \pi^+, K^*(892)^- \rightarrow K_S^0 \pi^-$	(1.6 ± 0.6) × 10 <sup>-3</sup>	–	230
$K_S^0 2\pi^+ 2\pi^-$ nonresonant	< 1.2 × 10 <sup>-3</sup>	CL=90%	768
$K^- 3\pi^+ 2\pi^-$	(2.2 ± 0.6) × 10 <sup>-4</sup>	–	713

Fractions of some of the following modes with resonances have already appeared above as submodes of particular charged-particle modes. These nine modes below are all corrected for unseen decays of the resonances.

$K_S^0 \eta$	(5.09 ± 0.13) × 10 <sup>-3</sup>	–	772
$K_S^0 \omega$	(1.11 ± 0.06) %	–	670
$K_S^0 \eta'(958)$	(9.49 ± 0.32) × 10 <sup>-3</sup>	–	565
$\bar{K}^*(892)^0 \pi^+ \pi^- \pi^0$	(1.9 ± 0.9) %	–	643
$K^- \pi^+ \omega$	(3.1 ± 0.6) %	–	605

## Meson Summary Table

$\bar{K}^*(892)^0 \omega$	( 1.1 ± 0.5 ) %	410	Resonant $(\pi^+ \pi^-) \pi^+ \pi^-$	( 1.51 ± 0.12 ) × 10 <sup>-3</sup>	-
$K^- \pi^+ \eta'(958)$	( 6.43 ± 0.34 ) × 10 <sup>-3</sup>	479	3-body total		
$K_S^0 \eta'(958) \pi^0$	( 2.52 ± 0.27 ) × 10 <sup>-3</sup>	479	$\sigma \pi^+ \pi^-$	( 6.2 ± 0.9 ) × 10 <sup>-4</sup>	-
$\bar{K}^*(892)^0 \eta'(958)$	< 1.0 × 10 <sup>-3</sup>	CL=90% 119	$\sigma \rho(770)^0$	( 5.0 ± 2.5 ) × 10 <sup>-4</sup>	-
<b>Hadronic modes with three K's</b>			$f_0(980) \pi^+ \pi^-, f_0 \rightarrow$	( 1.8 ± 0.5 ) × 10 <sup>-4</sup>	-
$K_S^0 K^+ K^-$	( 4.42 ± 0.32 ) × 10 <sup>-3</sup>	544	$\pi^+ \pi^-$		
$K_S^0 a_0(980)^0, a_0^0 \rightarrow K^+ K^-$	( 2.9 ± 0.4 ) × 10 <sup>-3</sup>	-	$f_2(1270) \pi^+ \pi^-, f_2 \rightarrow$	( 3.7 ± 0.6 ) × 10 <sup>-4</sup>	-
$K^- a_0(980)^+, a_0^+ \rightarrow$	( 5.9 ± 1.8 ) × 10 <sup>-4</sup>	-	$\pi^+ \pi^-$		
$K^+ K_S^0$			$2f_2(1270), f_2 \rightarrow \pi^+ \pi^-$	( 1.6 ± 1.8 ) × 10 <sup>-4</sup>	-
$K^+ a_0(980)^-, a_0^- \rightarrow$	< 1.1 × 10 <sup>-4</sup>	CL=95% -	$f_0(1370) \sigma, f_0 \rightarrow$	( 1.6 ± 0.5 ) × 10 <sup>-3</sup>	-
$K^- K_S^0$			$\pi^+ \pi^- 2\pi^0$	( 1.02 ± 0.09 ) %	882
$K_S^0 f_0(980), f_0 \rightarrow K^+ K^-$	< 9 × 10 <sup>-5</sup>	CL=95% -	$\eta \pi^0$	[bbb] ( 6.3 ± 0.6 ) × 10 <sup>-4</sup>	S=1.1 846
$K_S^0 \phi, \phi \rightarrow K^+ K^-$	( 2.03 ± 0.15 ) × 10 <sup>-3</sup>	520	$\omega \pi^0$	[bbb] ( 1.17 ± 0.35 ) × 10 <sup>-4</sup>	761
$K_S^0 f_0(1370), f_0 \rightarrow K^+ K^-$	( 1.7 ± 1.1 ) × 10 <sup>-4</sup>	-	$\omega \eta$	( 1.98 ± 0.18 ) × 10 <sup>-3</sup>	S=1.1 648
$3K_S^0$	( 7.5 ± 0.7 ) × 10 <sup>-4</sup>	S=1.4 539	$2\pi^+ 2\pi^- \pi^0$	( 4.2 ± 0.5 ) × 10 <sup>-3</sup>	844
$K^+ 2K^- \pi^+$	( 2.25 ± 0.32 ) × 10 <sup>-4</sup>	434	$\eta \pi^+ \pi^-$	[bbb] ( 1.09 ± 0.16 ) × 10 <sup>-3</sup>	827
$K^+ K^- \bar{K}^*(892)^0, \bar{K}^{*0} \rightarrow$	( 4.5 ± 1.8 ) × 10 <sup>-5</sup>	†	$\omega \pi^+ \pi^-$	[bbb] ( 1.6 ± 0.5 ) × 10 <sup>-3</sup>	738
$K^- \pi^+$			$\eta 2\pi^0$	( 3.8 ± 1.3 ) × 10 <sup>-4</sup>	829
$K^- \pi^+ \phi, \phi \rightarrow K^+ K^-$	( 4.1 ± 1.7 ) × 10 <sup>-5</sup>	422	$3\pi^+ 3\pi^-$	( 4.3 ± 1.2 ) × 10 <sup>-4</sup>	795
$\phi \bar{K}^*(892)^0, \phi \rightarrow K^+ K^-,$	( 1.08 ± 0.21 ) × 10 <sup>-4</sup>	†	$\eta'(958) \pi^0$	( 9.2 ± 1.0 ) × 10 <sup>-4</sup>	678
$\bar{K}^{*0} \rightarrow K^- \pi^+$			$\eta'(958) \pi^+ \pi^-$	( 4.5 ± 1.7 ) × 10 <sup>-4</sup>	650
$K^+ 2K^- \pi^+$ nonresonant	( 3.4 ± 1.5 ) × 10 <sup>-5</sup>	434	$2\eta$	( 2.11 ± 0.19 ) × 10 <sup>-3</sup>	S=2.2 754
$2K_S^0 K^\pm \pi^\mp$	( 5.9 ± 1.3 ) × 10 <sup>-4</sup>	427	$2\eta \pi^0$	( 7.3 ± 2.2 ) × 10 <sup>-4</sup>	699
<b>Pionic modes</b>			$3\eta$	< 1.3 × 10 <sup>-4</sup>	CL=90% 421
$\pi^+ \pi^-$	( 1.455 ± 0.024 ) × 10 <sup>-3</sup>	S=1.3 922	$\eta \eta'(958)$	( 1.01 ± 0.19 ) × 10 <sup>-3</sup>	537
$2\pi^0$	( 8.26 ± 0.25 ) × 10 <sup>-4</sup>	923	<b>Hadronic modes with a <math>K\bar{K}</math> pair</b>		
$\pi^+ \pi^- \pi^0$	( 1.49 ± 0.06 ) %	S=2.1 907	$K^+ K^-$	( 4.08 ± 0.06 ) × 10 <sup>-3</sup>	S=1.6 791
$\rho^+ \pi^-$	( 1.01 ± 0.04 ) %	764	$2K_S^0$	( 1.41 ± 0.05 ) × 10 <sup>-4</sup>	S=1.1 789
$\rho^0 \pi^0$	( 3.86 ± 0.23 ) × 10 <sup>-3</sup>	764	$K_S^0 K^- \pi^+$	( 3.3 ± 0.5 ) × 10 <sup>-3</sup>	S=1.1 739
$\rho^- \pi^+$	( 5.15 ± 0.25 ) × 10 <sup>-3</sup>	764	$\bar{K}^*(892)^0 K_S^0, \bar{K}^{*0} \rightarrow$	( 8.2 ± 1.6 ) × 10 <sup>-5</sup>	608
$\rho(1450)^+ \pi^-, \rho^+ \rightarrow \pi^+ \pi^0$	( 1.6 ± 2.1 ) × 10 <sup>-5</sup>	-	$K^- \pi^+$		
$\rho(1450)^0 \pi^0, \rho^0 \rightarrow \pi^+ \pi^-$	( 4.5 ± 2.0 ) × 10 <sup>-5</sup>	-	$K^*(892)^+ K^-, K^{*+} \rightarrow$	( 1.89 ± 0.30 ) × 10 <sup>-3</sup>	-
$\rho(1450)^- \pi^+, \rho^- \rightarrow \pi^- \pi^0$	( 2.7 ± 0.4 ) × 10 <sup>-4</sup>	-	$K_S^0 \pi^-$		
$\rho(1700)^+ \pi^-, \rho^+ \rightarrow \pi^+ \pi^0$	( 6.1 ± 1.5 ) × 10 <sup>-4</sup>	-	$\bar{K}^*(1410)^0 K_S^0, \bar{K}^{*0} \rightarrow$	( 1.3 ± 1.9 ) × 10 <sup>-4</sup>	-
$\rho(1700)^0 \pi^0, \rho^0 \rightarrow \pi^+ \pi^-$	( 7.4 ± 1.8 ) × 10 <sup>-4</sup>	-	$K^- \pi^+$		
$\rho(1700)^- \pi^+, \rho^- \rightarrow \pi^- \pi^0$	( 4.8 ± 1.1 ) × 10 <sup>-4</sup>	-	$K^*(1410)^+ K^-, K^{*+} \rightarrow$	( 3.2 ± 1.9 ) × 10 <sup>-4</sup>	-
$f_0(980) \pi^0, f_0 \rightarrow \pi^+ \pi^-$	( 3.7 ± 0.9 ) × 10 <sup>-5</sup>	-	$K_S^0 \pi^+$		
$f_0(500) \pi^0, f_0 \rightarrow \pi^+ \pi^-$	( 1.22 ± 0.22 ) × 10 <sup>-4</sup>	-	$(K^- \pi^+)_{S\text{-wave}} K_S^0$	( 6.0 ± 2.9 ) × 10 <sup>-4</sup>	739
$f_0(1370) \pi^0, f_0 \rightarrow \pi^+ \pi^-$	( 5.5 ± 2.1 ) × 10 <sup>-5</sup>	-	$(K_S^0 \pi^+)_{S\text{-wave}} K^-$	( 3.9 ± 1.0 ) × 10 <sup>-4</sup>	739
$f_0(1500) \pi^0, f_0 \rightarrow \pi^+ \pi^-$	( 5.8 ± 1.6 ) × 10 <sup>-5</sup>	-	$a_0(980)^- \pi^+, a_0^+ \rightarrow K_S^0 K^-$	( 1.3 ± 1.4 ) × 10 <sup>-4</sup>	-
$f_0(1710) \pi^0, f_0 \rightarrow \pi^+ \pi^-$	( 4.6 ± 1.6 ) × 10 <sup>-5</sup>	-	$a_0(1450)^- \pi^+, a_0^- \rightarrow$	( 2.5 ± 2.0 ) × 10 <sup>-5</sup>	-
$f_2(1270) \pi^0, f_2 \rightarrow \pi^+ \pi^-$	( 1.97 ± 0.21 ) × 10 <sup>-4</sup>	-	$K_S^0 K^-$		
$\pi^+ \pi^- \pi^0$ nonresonant	( 1.3 ± 0.4 ) × 10 <sup>-4</sup>	907	$a_2(1320)^- \pi^+, a_2^- \rightarrow$	( 5 ± 5 ) × 10 <sup>-6</sup>	-
$3\pi^0$	( 2.0 ± 0.5 ) × 10 <sup>-4</sup>	908	$K_S^0 K^-$		
$2\pi^+ 2\pi^-$	( 7.56 ± 0.20 ) × 10 <sup>-3</sup>	880	$\rho(1450)^- \pi^+, \rho^- \rightarrow K_S^0 K^-$	( 4.6 ± 2.5 ) × 10 <sup>-5</sup>	-
$a_1(1260)^+ \pi^-, a_1^+ \rightarrow$	( 4.54 ± 0.31 ) × 10 <sup>-3</sup>	-	$K_S^0 K^+ \pi^-$	( 2.17 ± 0.34 ) × 10 <sup>-3</sup>	S=1.1 739
$2\pi^+ \pi^-$ total			$K^*(892)^0 K_S^0, K^{*0} \rightarrow$	( 1.12 ± 0.21 ) × 10 <sup>-4</sup>	608
$a_1(1260)^+ \pi^-, a_1^+ \rightarrow$	( 3.14 ± 0.21 ) × 10 <sup>-3</sup>	-	$K^+ \pi^-$		
$\rho^0 \pi^+$ S-wave			$K^*(892)^- K^+, K^{*-} \rightarrow$	( 6.2 ± 1.0 ) × 10 <sup>-4</sup>	-
$a_1(1260)^+ \pi^-, a_1^+ \rightarrow$	( 1.9 ± 0.5 ) × 10 <sup>-4</sup>	-	$K_S^0 \pi^-$		
$\rho^0 \pi^+$ D-wave			$K^*(1410)^0 K_S^0, K^{*0} \rightarrow$	( 5 ± 8 ) × 10 <sup>-5</sup>	-
$a_1(1260)^+ \pi^-, a_1^+ \rightarrow$	( 6.4 ± 0.7 ) × 10 <sup>-4</sup>	-	$K^+ \pi^+$		
$\sigma \pi^+$			$K^*(1410)^- K^+, K^{*-} \rightarrow$	( 2.6 ± 2.0 ) × 10 <sup>-4</sup>	-
$a_1(1260)^- \pi^+, a_1^- \rightarrow$	( 2.3 ± 0.9 ) × 10 <sup>-4</sup>	-	$K_S^0 \pi^-$		
$\rho^0 \pi^-$ S-wave			$(K^+ \pi^-)_{S\text{-wave}} K_S^0$	( 3.7 ± 1.9 ) × 10 <sup>-4</sup>	739
$a_1(1260)^- \pi^+, a_1^- \rightarrow \sigma \pi^-$	( 6.1 ± 3.4 ) × 10 <sup>-5</sup>	-	$(K_S^0 \pi^-)_{S\text{-wave}} K^+$	( 1.4 ± 0.6 ) × 10 <sup>-4</sup>	739
$\pi(1300)^+ \pi^-, \pi(1300)^+ \rightarrow$	( 5.1 ± 2.7 ) × 10 <sup>-4</sup>	-	$a_0(980)^+ \pi^-, a_0^+ \rightarrow K_S^0 K^+$	( 6 ± 4 ) × 10 <sup>-4</sup>	-
$\sigma \pi^+$			$a_0(1450)^+ \pi^-, a_0^+ \rightarrow$	( 3.2 ± 2.5 ) × 10 <sup>-5</sup>	-
$\pi(1300)^- \pi^+, \pi(1300)^- \rightarrow$	( 2.3 ± 2.2 ) × 10 <sup>-4</sup>	-	$K_S^0 K^+$		
$\sigma \pi^-$			$\rho(1700)^+ \pi^-, \rho^+ \rightarrow K_S^0 K^+$	( 1.1 ± 0.6 ) × 10 <sup>-5</sup>	-
$a_1(1640)^+ \pi^-, a_1^+ \rightarrow$	( 3.2 ± 1.6 ) × 10 <sup>-4</sup>	-	$K^+ K^- \pi^0$	( 3.42 ± 0.14 ) × 10 <sup>-3</sup>	743
$\rho^0 \pi^+$ D-wave			$K^*(892)^+ K^-, K^*(892)^+ \rightarrow$	( 1.52 ± 0.07 ) × 10 <sup>-3</sup>	-
$a_1(1640)^+ \pi^-, a_1^+ \rightarrow \sigma \pi^+$	( 1.8 ± 1.4 ) × 10 <sup>-4</sup>	-	$K^+ \pi^0$		
$\pi_2(1670)^+ \pi^-, \pi_2^+ \rightarrow$	( 2.0 ± 0.9 ) × 10 <sup>-4</sup>	-	$K^*(892)^- K^+, K^*(892)^- \rightarrow$	( 5.4 ± 0.4 ) × 10 <sup>-4</sup>	-
$f_2(1270)^0 \pi^+, f_2^0 \rightarrow$			$K^- \pi^0$		
$\pi^+ \pi^-$			$(K^+ \pi^0)_{S\text{-wave}} K^-$	( 2.43 ± 0.18 ) × 10 <sup>-3</sup>	743
$\pi_2(1670)^+ \pi^-, \pi_2^+ \rightarrow \sigma \pi^+$	( 2.6 ± 1.0 ) × 10 <sup>-4</sup>	-	$(K^- \pi^0)_{S\text{-wave}} K^+$	( 1.3 ± 0.5 ) × 10 <sup>-4</sup>	743
$2\rho^0$ total	( 1.85 ± 0.13 ) × 10 <sup>-3</sup>	518	$f_0(980) \pi^0, f_0 \rightarrow K^+ K^-$	( 3.6 ± 0.6 ) × 10 <sup>-4</sup>	-
$2\rho^0$ , parallel helicities	( 8.3 ± 3.2 ) × 10 <sup>-5</sup>	-	$\phi \pi^0, \phi \rightarrow K^+ K^-$	( 6.6 ± 0.4 ) × 10 <sup>-4</sup>	-
$2\rho^0$ , perpendicular helicities	( 4.8 ± 0.6 ) × 10 <sup>-4</sup>	-	$2K_S^0 \pi^0$	< 5.9 × 10 <sup>-4</sup>	740
$2\rho^0$ , longitudinal helicities	( 1.27 ± 0.10 ) × 10 <sup>-3</sup>	-	$K^+ K^- \pi^+ \pi^-$	( 2.47 ± 0.11 ) × 10 <sup>-3</sup>	677
$2\rho(770)^0$ , S-wave	( 1.8 ± 1.3 ) × 10 <sup>-4</sup>	-	$\phi(\pi^+ \pi^-)_{S\text{-wave}}, \phi \rightarrow$	( 10 ± 5 ) × 10 <sup>-5</sup>	614
$2\rho(770)^0$ , P-wave	( 5.3 ± 1.3 ) × 10 <sup>-4</sup>	-	$K^+ K^-$		
$2\rho(770)^0$ , D-wave	( 6.2 ± 3.0 ) × 10 <sup>-4</sup>	-	$(\phi \rho^0)_{S\text{-wave}}, \phi \rightarrow K^+ K^-$	( 6.9 ± 0.6 ) × 10 <sup>-4</sup>	250
			$(\phi \rho^0)_{P\text{-wave}}, \phi \rightarrow K^+ K^-$	( 4.0 ± 1.9 ) × 10 <sup>-5</sup>	-

## Meson Summary Table

$(\phi\rho^0)_{D\text{-wave}}, \phi \rightarrow K^+K^-$	$(4.2 \pm 1.4) \times 10^{-5}$	-	$\pi^+\pi^-\mu^+\mu^-$	CI	$(9.6 \pm 1.2) \times 10^{-7}$	894	
$(K^*(892)^0\bar{K}^*(892)^0)_{S\text{-wave}}, K^{*0} \rightarrow K^\pm\pi^\mp$	$(2.24 \pm 0.13) \times 10^{-4}$	-	$\pi^+\pi^-\mu^+\mu^-$ (non-res)		$< 5.5 \times 10^{-7}$	CL=90% -	
$(K^*(892)^0\bar{K}^*(892)^0)_{P\text{-wave}}, K^* \rightarrow K^\pm\pi^\mp$	$(1.20 \pm 0.08) \times 10^{-4}$	-	$\rho^0\mu^+\mu^-$	CI	$< 2.2 \times 10^{-5}$	CL=90% 754	
$(K^*(892)^0\bar{K}^*(892)^0)_{D\text{-wave}}, K^* \rightarrow K^\pm\pi^\mp$	$(4.7 \pm 0.4) \times 10^{-5}$	-	$\omega e^+e^-$	CI	$< 6 \times 10^{-6}$	CL=90% 768	
$K^*(892)^0(K^-\pi^+)_{S\text{-wave}}, 3\text{-body}, K^{*0} \rightarrow K^+\pi^-$	$(1.4 \pm 0.6) \times 10^{-4}$	-	$\omega\mu^+\mu^-$	CI	$< 8.3 \times 10^{-4}$	CL=90% 751	
$K_1(1270)^+K^-, K_1^+ \rightarrow K^0\pi^+$	$(1.4 \pm 0.9) \times 10^{-4}$	-	$K^-K^+e^+e^-$	CI	$< 1.1 \times 10^{-5}$	CL=90% 791	
$K_1(1270)^+K^-, K_1^+ \rightarrow K^*(1430)^0\pi^+, K^{*0} \rightarrow K^+\pi^-$	$(1.5 \pm 0.5) \times 10^{-4}$	-	$\phi e^+e^-$	CI	$< 5.2 \times 10^{-5}$	CL=90% 654	
$K_1(1270)^+K^-, K_1^+ \rightarrow K^*(1430)^0\pi^+, K^{*0} \rightarrow K^+\pi^-$	$(2.2 \pm 0.6) \times 10^{-4}$	-	$K^-K^+\mu^+\mu^-$	CI	$(1.54 \pm 0.32) \times 10^{-7}$	710	
$K_1(1270)^+K^-, K_1^+ \rightarrow K^*(1430)^0\pi^+, K^{*0} \rightarrow K^+\pi^-$	$(1.5 \pm 1.2) \times 10^{-5}$	-	$K^-K^+\mu^+\mu^-$ (non-res)		$< 3.3 \times 10^{-5}$	CL=90% -	
$K_1(1270)^-K^+, K_1^- \rightarrow \rho^0K^-$	$(4.6 \pm 0.4) \times 10^{-4}$	-	$\phi\mu^+\mu^-$	CI	$< 3.1 \times 10^{-5}$	CL=90% 631	
$K_1(1400)^+K^-, K_1^+ \rightarrow K^*(892)^0\pi^+, K^{*0} \rightarrow K^+\pi^-$	$(2.7 \pm 0.6) \times 10^{-4}$	-	$\bar{K}^0 e^+e^-$	[ss]	$< 2.4 \times 10^{-5}$	CL=90% 866	
$K^*(1410)^-K^+, K^{*-} \rightarrow K^+\pi^-$	$(7.0 \pm 1.1) \times 10^{-5}$	-	$\bar{K}^0\mu^+\mu^-$	[ss]	$< 2.6 \times 10^{-4}$	CL=90% 852	
$K_1(1680)^+K^-, K_1^+ \rightarrow K^0\pi^-$	$(8.9 \pm 3.2) \times 10^{-5}$	-	$K^-\pi^+e^+e^-, 675 < m_{ee} < 875 \text{ MeV}$		$(4.0 \pm 0.5) \times 10^{-6}$	-	
$2K_S^0\pi^+\pi^-$	$(1.22 \pm 0.23) \times 10^{-3}$	673	$K^-\pi^+e^+e^-, 1.005 < m_{ee} < 1.035 \text{ GeV}$		$< 5 \times 10^{-7}$	CL=90% -	
$K^+K^-\pi^+\pi^-$ non-resonant	$(2.7 \pm 0.6) \times 10^{-4}$	-	$\bar{K}^*(892)^0 e^+e^-$	[ss]	$< 4.7 \times 10^{-5}$	CL=90% 719	
$K_S^0 K^- 2\pi^+ \pi^-$	$< 1.4 \times 10^{-4}$	CL=90% 595	$K^-\pi^+\mu^+\mu^-$	CI	$< 3.59 \times 10^{-4}$	CL=90% 829	
$K^+ K^- \pi^+ \pi^- \pi^0$	$(3.1 \pm 2.0) \times 10^{-3}$	600	$K^-\pi^+\mu^+\mu^-, 675 < m_{\mu\mu} < 875 \text{ MeV}$		$(4.2 \pm 0.4) \times 10^{-6}$	-	
Other $K\bar{K}X$ modes. They include all decay modes of the $\phi, \eta,$ and $\omega$ .							
$\phi\pi^0$	$(1.17 \pm 0.04) \times 10^{-3}$	645	$\bar{K}^*(892)^0\mu^+\mu^-$	[ss]	$< 2.4 \times 10^{-5}$	CL=90% 700	
$\phi\eta$	$(1.8 \pm 0.5) \times 10^{-4}$	489	$\pi^+\pi^-\pi^0\mu^+\mu^-$	CI	$< 8.1 \times 10^{-4}$	CL=90% 863	
$\phi\omega$	$< 2.1 \times 10^{-3}$	CL=90% 238	$\mu^\pm e^\mp$	LF [bb]	$< 1.3 \times 10^{-8}$	CL=90% 929	
<b>Radiative modes</b>							
$\rho^0\gamma$	$(1.82 \pm 0.32) \times 10^{-5}$	771	$\pi^0 e^\pm\mu^\mp$	LF [bb]	$< 8.6 \times 10^{-5}$	CL=90% 924	
$\omega\gamma$	$< 2.4 \times 10^{-4}$	CL=90% 768	$\eta e^\pm\mu^\mp$	LF [bb]	$< 1.0 \times 10^{-4}$	CL=90% 848	
$\phi\gamma$	$(2.81 \pm 0.19) \times 10^{-5}$	654	$\pi^+\pi^- e^\pm\mu^\mp$	LF [bb]	$< 1.5 \times 10^{-5}$	CL=90% 911	
$\bar{K}^*(892)^0\gamma$	$(4.2 \pm 0.7) \times 10^{-4}$	719	$\rho^0 e^\pm\mu^\mp$	LF [bb]	$< 4.9 \times 10^{-5}$	CL=90% 767	
<b>Doubly Cabibbo suppressed (DC) modes or <math>\Delta C = 2</math> forbidden via mixing (C2M) modes</b>							
$K^+\ell^-\bar{\nu}_\ell$ via $\bar{D}^0$	$< 2.2 \times 10^{-5}$	CL=90% -	$\omega e^\pm\mu^\mp$	LF [bb]	$< 1.2 \times 10^{-4}$	CL=90% 764	
$K^+$ or $K^*(892)^+$ $e^-\bar{\nu}_e$ via $\bar{D}^0$	$< 6 \times 10^{-5}$	CL=90% -	$K^-K^+e^\pm\mu^\mp$	LF [bb]	$< 1.8 \times 10^{-4}$	CL=90% 754	
$K^+\pi^-$ DC	$(1.50 \pm 0.07) \times 10^{-4}$	S=3.0 861	$\phi e^\pm\mu^\mp$	LF [bb]	$< 3.4 \times 10^{-5}$	CL=90% 648	
$K^+\pi^-$ via DCS	$(1.364 \pm 0.026) \times 10^{-4}$	-	$\bar{K}^0 e^\pm\mu^\mp$	LF [bb]	$< 1.0 \times 10^{-4}$	CL=90% 863	
$K^+\pi^-$ via $\bar{D}^0$	$< 1.6 \times 10^{-5}$	CL=95% 861	$K^-\pi^+e^\pm\mu^\mp$	LF [bb]	$< 5.53 \times 10^{-4}$	CL=90% 848	
$K_S^0\pi^+\pi^-$ in $D^0 \rightarrow \bar{D}^0$	$< 1.8 \times 10^{-4}$	CL=95% -	$\bar{K}^*(892)^0 e^\pm\mu^\mp$	LF [bb]	$< 8.3 \times 10^{-5}$	CL=90% 714	
$K^*(892)^+\pi^-, K^{*+} \rightarrow K_S^0\pi^+$	$(1.13 \pm_{0.34}^{0.60}) \times 10^{-4}$	711	$2\pi^-2e^+$ + c.c.	L	$< 1.12 \times 10^{-4}$	CL=90% 922	
$K_S^0(1430)^+\pi^-, K_S^{*+} \rightarrow K_S^0\pi^+$	$< 1.4 \times 10^{-5}$	-	$2\pi^-2\mu^+$ + c.c.	L	$< 2.9 \times 10^{-5}$	CL=90% 894	
$K_2^*(1430)^+\pi^-, K_2^{*+} \rightarrow K_S^0\pi^+$	$< 3.4 \times 10^{-5}$	-	$K^-\pi^-2e^+$	L	$< 2.8 \times 10^{-6}$	CL=90% 861	
$K^+\pi^-\pi^0$ DC	$(3.06 \pm 0.15) \times 10^{-4}$	844	$K^-\pi^-2\mu^+$ + c.c.	L	$< 3.9 \times 10^{-4}$	CL=90% 829	
$K^+\pi^-\pi^0$ via $\bar{D}^0$	$(7.6 \pm_{0.6}^{0.5}) \times 10^{-4}$	-	$2K^-2e^+$ + c.c.	L	$< 1.52 \times 10^{-4}$	CL=90% 791	
$K^+\pi^+2\pi^-$ via DCS	$(2.49 \pm 0.07) \times 10^{-4}$	-	$2K^-2\mu^+$ + c.c.	L	$< 9.4 \times 10^{-5}$	CL=90% 710	
$K^+\pi^+2\pi^-$ DC	$(2.65 \pm 0.06) \times 10^{-4}$	813	$\pi^-\pi^-e^+\mu^+$ + c.c.	L	$< 7.9 \times 10^{-5}$	CL=90% 911	
$K^+\pi^+2\pi^-$ via $\bar{D}^0$	$(7.9 \pm 3.0) \times 10^{-6}$	812	$K^-\pi^-e^+\mu^+$ + c.c.	L	$< 2.18 \times 10^{-4}$	CL=90% 848	
$\mu^-$ anything via $\bar{D}^0$	$< 4 \times 10^{-4}$	CL=90% -	$2K^-e^+\mu^+$ + c.c.	L	$< 5.7 \times 10^{-5}$	CL=90% 754	
<b><math>\Delta C = 1</math> weak neutral current (CI) modes, Lepton Family number (LF) violating modes, Lepton (L) or Baryon (B) number violating modes</b>							
$\gamma\gamma$	CI	$< 8.5 \times 10^{-7}$	$p e^-$	L,B [ccc]	$< 1.0 \times 10^{-5}$	CL=90% 696	
$e^+e^-$	CI	$< 7.9 \times 10^{-8}$	$\bar{p} e^+$	L,B [ddd]	$< 1.1 \times 10^{-5}$	CL=90% 696	
$\mu^+\mu^-$	CI	$< 6.2 \times 10^{-9}$					
$\pi^0 e^+e^-$	CI	$< 4 \times 10^{-6}$					
$\pi^0\mu^+\mu^-$	CI	$< 1.8 \times 10^{-4}$					
$\eta e^+e^-$	CI	$< 3 \times 10^{-6}$					
$\eta\mu^+\mu^-$	CI	$< 5.3 \times 10^{-4}$					
$\pi^+\pi^-e^+e^-$	CI	$< 7 \times 10^{-6}$					
$\rho^0 e^+e^-$	CI	$< 1.0 \times 10^{-4}$					

 **$D^*(2007)^0$** 

$$I(J^P) = \frac{1}{2}(1^-)$$

$I, J, P$  need confirmation.

Mass  $m = 2006.85 \pm 0.05 \text{ MeV}$  ( $S = 1.1$ )  
 $m_{D^{*0}} - m_{D^0} = 142.014 \pm 0.030 \text{ MeV}$  ( $S = 1.5$ )  
 Full width  $\Gamma < 2.1 \text{ MeV}$ , CL = 90%

$\bar{D}^*(2007)^0$  modes are charge conjugates of modes below.

 **$D^*(2007)^0$  DECAY MODES**

$D^*(2007)^0$ DECAY MODES	Fraction ( $\Gamma_i/\Gamma$ )	$\rho$ (MeV/c)
$D^0\pi^0$	$(64.7 \pm 0.9) \%$	43
$D^0\gamma$	$(35.3 \pm 0.9) \%$	137

 **$D^*(2010)^\pm$** 

$$I(J^P) = \frac{1}{2}(1^-)$$

$I, J, P$  need confirmation.

Mass  $m = 2010.26 \pm 0.05 \text{ MeV}$   
 $m_{D^*(2010)^+} - m_{D^+} = 140.603 \pm 0.015 \text{ MeV}$   
 $m_{D^*(2010)^+} - m_{D^0} = 145.4257 \pm 0.0017 \text{ MeV}$   
 Full width  $\Gamma = 83.4 \pm 1.8 \text{ keV}$

$D^*(2010)^-$  modes are charge conjugates of the modes below.

 **$D^*(2010)^\pm$  DECAY MODES**

$D^*(2010)^\pm$ DECAY MODES	Fraction ( $\Gamma_i/\Gamma$ )	$\rho$ (MeV/c)
$D^0\pi^+$	$(67.7 \pm 0.5) \%$	39
$D^+\pi^0$	$(30.7 \pm 0.5) \%$	38
$D^+\gamma$	$(1.6 \pm 0.4) \%$	136

## Meson Summary Table

 **$D_0^*(2300)^0$** 

$$I(J^P) = \frac{1}{2}(0^+)$$

was  $D_0^*(2400)^0$ 

Mass  $m = 2300 \pm 19$  MeV  
 Full width  $\Gamma = 274 \pm 40$  MeV

$D_0^*(2300)^0$ DECAY MODES	Fraction ( $\Gamma_i/\Gamma$ )	$\rho$ (MeV/c)
$D^+ \pi^-$	seen	369

 **$D_1(2420)^0$** 

$$I(J^P) = \frac{1}{2}(1^+)$$

Mass  $m = 2420.8 \pm 0.5$  MeV ( $S = 1.3$ )  
 $m_{D_1^0} - m_{D^{*+}} = 410.6 \pm 0.5$  MeV ( $S = 1.3$ )  
 Full width  $\Gamma = 31.7 \pm 2.5$  MeV ( $S = 3.5$ )

 $\bar{D}_1(2420)^0$  modes are charge conjugates of modes below.

$D_1(2420)^0$ DECAY MODES	Fraction ( $\Gamma_i/\Gamma$ )	$\rho$ (MeV/c)
$D^*(2010)^+ \pi^-$	seen	353
$D^0 \pi^+ \pi^-$	seen	425
$D^+ \pi^-$	not seen	472
$D^{*0} \pi^+ \pi^-$	not seen	279

 **$D_2^*(2460)^0$** 

$$I(J^P) = \frac{1}{2}(2^+)$$

 $J^P = 2^+$  assignment strongly favored.

Mass  $m = 2460.7 \pm 0.4$  MeV ( $S = 3.1$ )  
 $m_{D_2^{*0}} - m_{D^{*+}} = 591.0 \pm 0.4$  MeV ( $S = 2.9$ )  
 $m_{D_2^0} - m_{D^{*+}} = 450.4 \pm 0.4$  MeV ( $S = 2.9$ )  
 Full width  $\Gamma = 47.5 \pm 1.1$  MeV ( $S = 1.8$ )

 $\bar{D}_2^*(2460)^0$  modes are charge conjugates of modes below.

$D_2^*(2460)^0$ DECAY MODES	Fraction ( $\Gamma_i/\Gamma$ )	$\rho$ (MeV/c)
$D^+ \pi^-$	seen	505
$D^*(2010)^+ \pi^-$	seen	389
$D^0 \pi^+ \pi^-$	not seen	462
$D^{*0} \pi^+ \pi^-$	not seen	324

 **$D_2^*(2460)^\pm$** 

$$I(J^P) = \frac{1}{2}(2^+)$$

 $J^P = 2^+$  assignment strongly favored.

Mass  $m = 2465.4 \pm 1.3$  MeV ( $S = 3.1$ )  
 $m_{D_2^*(2460)^\pm} - m_{D_2^*(2460)^0} = 2.4 \pm 1.7$  MeV  
 Full width  $\Gamma = 46.7 \pm 1.2$  MeV

 $D_2^*(2460)^\mp$  modes are charge conjugates of modes below.

$D_2^*(2460)^\pm$ DECAY MODES	Fraction ( $\Gamma_i/\Gamma$ )	$\rho$ (MeV/c)
$D^0 \pi^+$	seen	513
$D^{*0} \pi^+$	seen	396
$D^+ \pi^+ \pi^-$	not seen	462
$D^{*+} \pi^+ \pi^-$	not seen	326

**CHARMED, STRANGE MESONS**  
**( $C = S = \pm 1$ )** $D_s^+ = c\bar{s}$ ,  $D_s^- = \bar{c}s$ , similarly for  $D_s^{*}$ 's **$D_s^\pm$** 

$$I(J^P) = 0(0^-)$$

Mass  $m = 1968.34 \pm 0.07$  MeV  
 $m_{D_s^\pm} - m_{D^\pm} = 98.69 \pm 0.05$  MeV  
 Mean life  $\tau = (504 \pm 4) \times 10^{-15}$  s ( $S = 1.2$ )  
 $c\tau = 151.2$   $\mu\text{m}$

**CP-violating decay-rate asymmetries**

$$\begin{aligned}
 A_{CP}(\mu^\pm \nu) &= (5 \pm 6)\% \\
 A_{CP}(K^\pm K_S^0) &= (0.09 \pm 0.26)\% \\
 A_{CP}(K^\pm K_L^0) \text{ in } D_s^\pm \rightarrow K^\pm K_L^0 &= (-1.1 \pm 2.7) \times 10^{-2} \\
 A_{CP}(K^+ K^- \pi^\pm) &= (-0.5 \pm 0.9)\% \\
 A_{CP}(\phi \pi^\pm) &= (-0.38 \pm 0.27)\% \\
 A_{CP}(K^\pm K_S^0 \pi^0) &= (-2 \pm 6)\% \\
 A_{CP}(2K_S^0 \pi^\pm) &= (3 \pm 5)\% \\
 A_{CP}(K^+ K^- \pi^\pm \pi^0) &= (0.0 \pm 3.0)\% \\
 A_{CP}(K^\pm K_S^0 \pi^+ \pi^-) &= (-6 \pm 5)\% \\
 A_{CP}(K_S^0 K^\mp 2\pi^\pm) &= (4.1 \pm 2.8)\% \\
 A_{CP}(\pi^+ \pi^- \pi^\pm) &= (-0.7 \pm 3.1)\% \\
 A_{CP}(\pi^\pm \eta) &= (1.1 \pm 3.1)\% \\
 A_{CP}(\pi^\pm \eta') &= (-0.9 \pm 0.5)\% \\
 A_{CP}(\eta \pi^\pm \pi^0) &= (-1 \pm 4)\% \\
 A_{CP}(\eta' \pi^\pm \pi^0) &= (0 \pm 8)\% \\
 A_{CP}(K^\pm \pi^0) &= (-27 \pm 24)\% \\
 A_{CP}(\bar{K}^0 / K^0 \pi^\pm) &= (0.4 \pm 0.5)\% \\
 A_{CP}(K_S^0 \pi^\pm) &= (0.20 \pm 0.18)\% \\
 A_{CP}(K^\pm \pi^+ \pi^-) &= (4 \pm 5)\% \\
 A_{CP}(K^\pm \eta) &= (9 \pm 15)\% \\
 A_{CP}(K^\pm \eta'(958)) &= (6 \pm 19)\%
 \end{aligned}$$

**CP violating asymmetries of P-odd (T-odd) moments**

$$A_T(K_S^0 K^\pm \pi^+ \pi^-) = (-14 \pm 8) \times 10^{-3} [11]$$

 **$D_s^+ \rightarrow \phi \ell^+ \nu_\ell$  form factors**

$$\begin{aligned}
 r_2 &= 0.84 \pm 0.11 \quad (S = 2.4) \\
 r_V &= 1.80 \pm 0.08 \\
 \Gamma_L/\Gamma_T &= 0.72 \pm 0.18 \\
 f_+(0) |V_{cs}| \text{ in } D_s^+ \rightarrow \eta e^+ \nu_e &= 0.446 \pm 0.007 \\
 f_+(0) |V_{cs}| \text{ in } D_s^+ \rightarrow \eta' e^+ \nu_e &= 0.48 \pm 0.05
 \end{aligned}$$

**CP violating asymmetries of P-odd (T-odd) moments**

$$\begin{aligned}
 f_+(0) |V_{cd}| \text{ in } D_s^+ \rightarrow K^0 e^+ \nu_e &= 0.162 \pm 0.019 \\
 r_V \equiv V(0)/A_1(0) \text{ in } D_s^+ \rightarrow K^*(892)^0 e^+ \nu_e &= 1.7 \pm 0.4 \\
 r_2 \equiv A_2(0)/A_1(0) \text{ in } D_s^+ \rightarrow K^*(892)^0 e^+ \nu_e &= 0.77 \pm 0.29 \\
 f_{D_s^+}^+ |V_{cs}| \text{ in } D_s^+ \rightarrow \mu^+ \nu_\mu &= 246 \pm 5 \text{ MeV}
 \end{aligned}$$

Unless otherwise noted, the branching fractions for modes with a resonance in the final state include all the decay modes of the resonance.  $D_s^-$  modes are charge conjugates of the modes below.

$D_s^\pm$ DECAY MODES	Fraction ( $\Gamma_i/\Gamma$ )	Scale factor/ Confidence level	$\rho$ (MeV/c)
-----------------------	--------------------------------	-----------------------------------	-------------------

Inclusive modes			
$e^+$ semileptonic	[eee]	( 6.5 $\pm$ 0.4 ) %	—
$\pi^+$ anything		(119.3 $\pm$ 1.4 ) %	—
$\pi^-$ anything		( 43.2 $\pm$ 0.9 ) %	—
$\pi^0$ anything		(123 $\pm$ 7 ) %	—
$K^-$ anything		( 18.7 $\pm$ 0.5 ) %	—
$K^+$ anything		( 28.9 $\pm$ 0.7 ) %	—
$K_S^0$ anything		( 19.0 $\pm$ 1.1 ) %	—
$\eta$ anything	[fff]	( 29.9 $\pm$ 2.8 ) %	—
$\omega$ anything		( 6.1 $\pm$ 1.4 ) %	—
$\eta'$ anything	[ggg]	( 10.3 $\pm$ 1.4 ) %	S=1.1
$f_0(980)$ anything, $f_0 \rightarrow \pi^+ \pi^-$		< 1.3	CL=90%
$\phi$ anything		( 15.7 $\pm$ 1.0 ) %	—
$K^+ K^-$ anything		( 15.8 $\pm$ 0.7 ) %	—
$K_S^0 K^+$ anything		( 5.8 $\pm$ 0.5 ) %	—
$K_S^0 K^-$ anything		( 1.9 $\pm$ 0.4 ) %	—
$2K_S^0$ anything		( 1.70 $\pm$ 0.32 ) %	—
$2K^+$ anything		< 2.6	$\times 10^{-3}$ CL=90%
$2K^-$ anything		< 6	$\times 10^{-4}$ CL=90%

**Leptonic and semileptonic modes**

$e^+ \nu_e$	< 8.3	$\times 10^{-5}$	CL=90%	984
$\mu^+ \nu_\mu$	( 5.49 $\pm$ 0.16 )	$\times 10^{-3}$		981
$\tau^+ \nu_\tau$	( 5.48 $\pm$ 0.23 ) %			182
$\gamma e^+ \nu_e$	< 1.3	$\times 10^{-4}$	CL=90%	984
$K^+ K^- e^+ \nu_e$	—			851
$\phi e^+ \nu_e$	[hhh]	( 2.39 $\pm$ 0.16 ) %	S=1.3	720
$\phi \mu^+ \nu_\mu$	( 1.9 $\pm$ 0.5 ) %			715

## Meson Summary Table

$\eta e^+ \nu_e + \eta'(958) e^+ \nu_e$	[hhh]	( 3.03 ± 0.24 ) %	-	908
$\eta e^+ \nu_e$	[hhh]	( 2.32 ± 0.08 ) %	-	751
$\eta'(958) e^+ \nu_e$	[hhh]	( 8.0 ± 0.7 ) × 10 <sup>-3</sup>	-	905
$\eta \mu^+ \nu_\mu$		( 2.4 ± 0.5 ) %	-	747
$\eta'(958) \mu^+ \nu_\mu$		( 1.1 ± 0.5 ) %	-	829
$\omega e^+ \nu_e$	[iii]	< 2.0 × 10 <sup>-3</sup>	CL=90%	921
$K^0 e^+ \nu_e$		( 3.4 ± 0.4 ) × 10 <sup>-3</sup>	-	782
$K^*(892)^0 e^+ \nu_e$	[hhh]	( 2.15 ± 0.28 ) × 10 <sup>-3</sup>	S=1.1	
<b>Hadronic modes with a <math>K\bar{K}</math> pair</b>				
$K^+ K_S^0$		( 1.46 ± 0.04 ) %	S=1.1	850
$K^+ K^0$		( 1.49 ± 0.06 ) %	-	850
$K^+ \bar{K}^0$		( 2.95 ± 0.14 ) %	-	850
$K^+ K^- \pi^+$	[nn]	( 5.39 ± 0.15 ) %	S=1.2	805
$\phi \pi^+$	[hhh, jii]	( 4.5 ± 0.4 ) %	-	712
$\phi \pi^+, \phi \rightarrow K^+ K^-$	[jii]	( 2.24 ± 0.08 ) %	-	712
$K^+ \bar{K}^*(892)^0, \bar{K}^{*0} \rightarrow$		( 2.58 ± 0.08 ) %	-	416
$K^- \pi^+$			-	732
$f_0(980) \pi^+, f_0 \rightarrow K^+ K^-$		( 1.14 ± 0.31 ) %	-	732
$f_0(1370) \pi^+, f_0 \rightarrow K^+ K^-$		( 7 ± 5 ) × 10 <sup>-4</sup>	-	-
$f_0(1710) \pi^+, f_0 \rightarrow K^+ K^-$		( 6.6 ± 2.8 ) × 10 <sup>-4</sup>	-	198
$K^+ \bar{K}_0^*(1430)^0, \bar{K}_0^* \rightarrow$		( 1.8 ± 0.4 ) × 10 <sup>-3</sup>	-	218
$K^+ K_S^0 \pi^0$		( 1.52 ± 0.22 ) %	-	805
$2K_S^0 \pi^+$		( 7.7 ± 0.6 ) × 10 <sup>-3</sup>	-	802
$K^0 K^0 \pi^+$		-	-	802
$K^*(892)^+ \bar{K}^0$	[hhh]	( 5.4 ± 1.2 ) %	-	683
$K^+ K^- \pi^+ \pi^0$		( 6.2 ± 0.6 ) %	S=1.1	748
$\phi \rho^+$	[hhh]	( 8.4 ± 1.9 ) %	-	401
$K_S^0 K^- 2\pi^+$		( 1.65 ± 0.10 ) %	-	744
$K^*(892)^+ \bar{K}^*(892)^0$	[hhh]	( 7.2 ± 2.6 ) %	-	417
$K^+ K_S^0 \pi^+ \pi^-$		( 9.9 ± 0.8 ) × 10 <sup>-3</sup>	-	744
$K^+ K^- 2\pi^+ \pi^-$		( 8.6 ± 1.5 ) × 10 <sup>-3</sup>	-	673
$\phi 2\pi^+ \pi^-$	[hhh]	( 1.21 ± 0.16 ) %	-	640
$\phi \rho^0 \pi^+, \phi \rightarrow K^+ K^-$		( 6.5 ± 1.3 ) × 10 <sup>-3</sup>	-	181
$\phi a_1(1260)^+, \phi \rightarrow$		( 7.4 ± 1.2 ) × 10 <sup>-3</sup>	-	†
$K^+ K^-, a_1^+ \rightarrow$			-	
$\rho^0 \pi^+$			-	
$\phi 2\pi^+ \pi^-$ non- $\rho$ , $\phi \rightarrow$		( 1.8 ± 0.7 ) × 10 <sup>-3</sup>	-	-
$K^+ K^-$			-	
$K^+ K^- \rho^0 \pi^+$ non- $\phi$	< 2.6	× 10 <sup>-4</sup>	CL=90%	249
$K^+ K^- 2\pi^+ \pi^-$ nonresonant	( 9 ± 7 )	× 10 <sup>-4</sup>	-	673
$2K_S^0 2\pi^+ \pi^-$	( 8.4 ± 3.5 )	× 10 <sup>-4</sup>	-	669
<b>Hadronic modes without <math>K</math>'s</b>				
$\pi^+ \pi^0$	< 3.4	× 10 <sup>-4</sup>	CL=90%	975
$2\pi^+ \pi^-$	( 1.08 ± 0.04 ) %	S=1.1	-	959
$\rho^0 \pi^+$	( 1.9 ± 1.2 ) × 10 <sup>-4</sup>	-	-	825
$\pi^+ (\pi^+ \pi^-)_{S\text{-wave}}$	[kkk]	( 9.0 ± 0.4 ) × 10 <sup>-3</sup>	-	959
$f_2(1270) \pi^+, f_2 \rightarrow \pi^+ \pi^-$		( 1.09 ± 0.20 ) × 10 <sup>-3</sup>	-	559
$\rho(1450)^0 \pi^+, \rho^0 \rightarrow \pi^+ \pi^-$		( 3.0 ± 1.9 ) × 10 <sup>-4</sup>	-	421
$\pi^+ 2\pi^0$		( 6.5 ± 1.3 ) × 10 <sup>-3</sup>	-	961
$2\pi^+ \pi^- \pi^0$		-	-	935
$\eta \pi^+$	[hhh]	( 1.68 ± 0.10 ) %	S=1.2	902
$\omega \pi^+$	[hhh]	( 1.92 ± 0.30 ) × 10 <sup>-3</sup>	-	822
$3\pi^+ 2\pi^-$		( 7.9 ± 0.8 ) × 10 <sup>-3</sup>	-	899
$2\pi^+ \pi^- 2\pi^0$		-	-	902
$\eta \rho^+$	[hhh]	( 8.9 ± 0.8 ) %	-	724
$\eta \pi^+ \pi^0$		( 9.5 ± 0.5 ) %	-	885
$\eta (\pi^+ \pi^0)_{P\text{-wave}}$		( 5.1 ± 3.1 ) × 10 <sup>-3</sup>	-	885
$a_0(980)^0 \pi^0, a_0(980)^0 \rightarrow \eta \pi^0$		( 2.2 ± 0.4 ) %	-	-
$\omega \pi^+ \pi^0$	[hhh]	( 2.8 ± 0.7 ) %	-	802
$3\pi^+ 2\pi^- \pi^0$		( 4.9 ± 3.2 ) %	-	856
$\omega 2\pi^+ \pi^-$	[hhh]	( 1.6 ± 0.5 ) %	-	766
$\eta'(958) \pi^+$	[ggg, hhh]	( 3.94 ± 0.25 ) %	-	743
$3\pi^+ 2\pi^- 2\pi^0$		-	-	803
$\omega \eta \pi^+$	[hhh]	< 2.13 %	CL=90%	654
$\eta'(958) \rho^+$	[ggg, hhh]	( 5.8 ± 1.5 ) %	-	465
$\eta'(958) \pi^+ \pi^0$		( 5.6 ± 0.8 ) %	-	720
$\eta'(958) \pi^+ \pi^0$ nonresonant	< 5.1	%	CL=90%	720
<b>Modes with one or three <math>K</math>'s</b>				
$K^+ \pi^0$		( 6.1 ± 2.1 ) × 10 <sup>-4</sup>	-	917
$K_S^0 \pi^+$		( 1.19 ± 0.05 ) × 10 <sup>-3</sup>	-	916
$K^+ \eta$	[hhh]	( 1.72 ± 0.34 ) × 10 <sup>-3</sup>	-	835
$K^+ \omega$	[hhh]	( 8.7 ± 2.5 ) × 10 <sup>-4</sup>	-	741
$K^+ \eta'(958)$	[hhh]	( 1.7 ± 0.5 ) × 10 <sup>-3</sup>	-	646

$K^+ \pi^+ \pi^-$		( 6.5 ± 0.4 ) × 10 <sup>-3</sup>	-	900
$K^+ \rho^0$		( 2.5 ± 0.4 ) × 10 <sup>-3</sup>	-	745
$K^+ \rho(1450)^0, \rho^0 \rightarrow \pi^+ \pi^-$		( 6.9 ± 2.4 ) × 10 <sup>-4</sup>	-	-
$K^*(892)^0 \pi^+, K^{*0} \rightarrow$		( 1.41 ± 0.24 ) × 10 <sup>-3</sup>	-	775
$K^+ \pi^-$			-	-
$K^*(1410)^0 \pi^+, K^{*0} \rightarrow$		( 1.23 ± 0.28 ) × 10 <sup>-3</sup>	-	-
$K^+ \pi^-$			-	-
$K^*(1430)^0 \pi^+, K^{*0} \rightarrow$		( 5.0 ± 3.5 ) × 10 <sup>-4</sup>	-	-
$K^+ \pi^-$			-	-
$K^+ \pi^+ \pi^-$ nonresonant		( 1.03 ± 0.34 ) × 10 <sup>-3</sup>	-	900
$K^0 \pi^+ \pi^0$		( 1.00 ± 0.18 ) %	-	899
$K_S^0 2\pi^+ \pi^-$		( 3.0 ± 1.1 ) × 10 <sup>-3</sup>	-	870
$K^+ \omega \pi^0$	[hhh]	< 8.2 × 10 <sup>-3</sup>	CL=90%	684
$K^+ \omega \pi^+ \pi^-$	[hhh]	< 5.4 × 10 <sup>-3</sup>	CL=90%	603
$K^+ \omega \eta$	[hhh]	< 7.9 × 10 <sup>-3</sup>	CL=90%	366
$2K^+ K^-$		( 2.16 ± 0.20 ) × 10 <sup>-4</sup>	-	628
$\phi K^+, \phi \rightarrow K^+ K^-$		( 8.8 ± 2.0 ) × 10 <sup>-5</sup>	-	-
<b>Doubly Cabibbo-suppressed modes</b>				
$2K^+ \pi^-$		( 1.28 ± 0.04 ) × 10 <sup>-4</sup>	-	805
$K^+ K^*(892)^0, K^{*0} \rightarrow$		( 6.0 ± 3.4 ) × 10 <sup>-5</sup>	-	-
$K^+ \pi^-$			-	-
<b>Baryon-antibaryon mode</b>				
$p \bar{n}$		( 1.22 ± 0.11 ) × 10 <sup>-3</sup>	-	295
$p \bar{p} e^+ \nu_e$	< 2.0	× 10 <sup>-4</sup>	CL=90%	296
<b><math>\Delta C = 1</math> weak neutral current (C1) modes, Lepton family number (LF), or Lepton number (L) violating modes</b>				
$\pi^+ e^+ e^-$	[ss]	< 1.3 × 10 <sup>-5</sup>	CL=90%	979
$\pi^+ \phi, \phi \rightarrow e^+ e^-$	[rr]	( 6 ± 8 ) × 10 <sup>-6</sup>	-	-
$\pi^+ \mu^+ \mu^-$	[ss]	< 4.1 × 10 <sup>-7</sup>	CL=90%	968
$K^+ e^+ e^-$	C1	< 3.7 × 10 <sup>-6</sup>	CL=90%	922
$K^+ \mu^+ \mu^-$	C1	< 2.1 × 10 <sup>-5</sup>	CL=90%	909
$K^*(892)^+ \mu^+ \mu^-$	C1	< 1.4 × 10 <sup>-3</sup>	CL=90%	765
$\pi^+ e^+ \mu^-$	LF	< 1.2 × 10 <sup>-5</sup>	CL=90%	976
$\pi^+ e^- \mu^+$	LF	< 2.0 × 10 <sup>-5</sup>	CL=90%	976
$K^+ e^+ \mu^-$	LF	< 1.4 × 10 <sup>-5</sup>	CL=90%	919
$K^+ e^- \mu^+$	LF	< 9.7 × 10 <sup>-6</sup>	CL=90%	919
$\pi^- 2e^+$	L	< 4.1 × 10 <sup>-6</sup>	CL=90%	979
$\pi^- 2\mu^+$	L	< 1.2 × 10 <sup>-7</sup>	CL=90%	968
$\pi^- e^+ \mu^+$	L	< 8.4 × 10 <sup>-6</sup>	CL=90%	976
$K^- 2e^+$	L	< 5.2 × 10 <sup>-6</sup>	CL=90%	922
$K^- 2\mu^+$	L	< 1.3 × 10 <sup>-5</sup>	CL=90%	909
$K^- e^+ \mu^+$	L	< 6.1 × 10 <sup>-6</sup>	CL=90%	919
$K^*(892)^- 2\mu^+$	L	< 1.4 × 10 <sup>-3</sup>	CL=90%	765

 $D_s^{*\pm}$  $I(J^P) = 0(?)^?$  $J^P$  is natural, width and decay modes consistent with  $1^-$ .Mass  $m = 2112.2 \pm 0.4$  MeV $m_{D_s^{*\pm}} - m_{D_s^\pm} = 143.8 \pm 0.4$  MeVFull width  $\Gamma < 1.9$  MeV, CL = 90% $D_s^{*-}$  modes are charge conjugates of the modes below. **$D_s^{*+}$  DECAY MODES**Fraction ( $\Gamma_i/\Gamma$ ) $p$  (MeV/c)

$D_s^{*+} \gamma$	(93.5 ± 0.7) %	139
$D_s^{*+} \pi^0$	( 5.8 ± 0.7 ) %	48
$D_s^{*+} e^+ e^-$	( 6.7 ± 1.6 ) × 10 <sup>-3</sup>	139

 $D_{s0}^{*+}(2317)^\pm$  $I(J^P) = 0(0^+)$  $J, P$  need confirmation. $J^P$  is natural, low mass consistent with  $0^+$ .Mass  $m = 2317.8 \pm 0.5$  MeV $m_{D_{s0}^{*+}(2317)^\pm} - m_{D_s^\pm} = 349.4 \pm 0.5$  MeVFull width  $\Gamma < 3.8$  MeV, CL = 95% $D_{s0}^{*+}(2317)^-$  modes are charge conjugates of modes below. **$D_{s0}^{*+}(2317)^\pm$  DECAY MODES**Fraction ( $\Gamma_i/\Gamma$ )

Confidence level

 $p$  (MeV/c)

$D_s^{*+} \pi^0$	(100 ± 20) %	298
$D_s^{*+} \gamma$	< 5 %	90%
$D_s^{*+}(2112)^+ \gamma$	< 6 %	90%

# Meson Summary Table

$D_s^+ \gamma \gamma$	< 18	%	95%	323
$D_s^*(2112)^+ \pi^0$	< 11	%	90%	–
$D_s^+ \pi^+ \pi^-$	< 4	$\times 10^{-3}$	90%	194
$D_s^+ \pi^0 \pi^0$	not seen			205

## $D_{s1}(2460)^\pm$

$$I(J^P) = 0(1^+)$$

Mass  $m = 2459.5 \pm 0.6$  MeV ( $S = 1.1$ )  
 $m_{D_{s1}(2460)^\pm} - m_{D_s^\pm} = 347.3 \pm 0.7$  MeV ( $S = 1.2$ )  
 $m_{D_{s1}(2460)^\pm} - m_{D_s^\pm} = 491.2 \pm 0.6$  MeV ( $S = 1.1$ )  
 Full width  $\Gamma < 3.5$  MeV, CL = 95%

$D_{s1}(2460)^-$  modes are charge conjugates of the modes below.

$D_{s1}(2460)^+$ DECAY MODES	Fraction ( $\Gamma_i/\Gamma$ )	Scale factor/ Confidence level	$\rho$ (MeV/c)
$D_s^{*+} \pi^0$	(48 ± 11) %		297
$D_s^+ \gamma$	(18 ± 4) %		442
$D_s^+ \pi^+ \pi^-$	(4.3 ± 1.3) %	S=1.1	363
$D_s^{*+} \gamma$	< 8 %	CL=90%	323
$D_{s0}^*(2317)^+ \gamma$	(3.7 $^{+5.0}_{-2.4}$ ) %		138

## $D_{s1}(2536)^\pm$

$$I(J^P) = 0(1^+)$$

$J, P$  need confirmation.

Mass  $m = 2535.11 \pm 0.06$  MeV  
 Full width  $\Gamma = 0.92 \pm 0.05$  MeV

$D_{s1}(2536)^-$  modes are charge conjugates of the modes below.

$D_{s1}(2536)^+$ DECAY MODES	Fraction ( $\Gamma_i/\Gamma$ )	Confidence level	$\rho$ (MeV/c)
$D^*(2010)^+ K^0$	0.85 ± 0.12		149
$(D^*(2010)^+ K^0)_{S\text{-wave}}$	0.61 ± 0.09		149
$D^+ \pi^- K^+$	0.028 ± 0.005		176
$D^*(2007)^0 K^+$	<b>DEFINED AS 1</b>		167
$D^+ K^0$	< 0.34	90%	381
$D^0 K^+$	< 0.12	90%	391
$D_s^{*+} \gamma$	possibly seen		388
$D_s^+ \pi^+ \pi^-$	seen		437

## $D_{s2}^*(2573)$

$$I(J^P) = 0(2^+)$$

$J^P$  is natural, width and decay modes consistent with  $2^+$ .

Mass  $m = 2569.1 \pm 0.8$  MeV ( $S = 2.4$ )  
 Full width  $\Gamma = 16.9 \pm 0.7$  MeV

$D_{s2}^*(2573)^-$  modes are charge conjugates of the modes below.

$D_{s2}^*(2573)^+$ DECAY MODES	Fraction ( $\Gamma_i/\Gamma$ )	$\rho$ (MeV/c)
$D^0 K^+$	seen	431
$D^*(2007)^0 K^+$	not seen	238

## $D_{s1}^*(2700)^\pm$

$$I(J^P) = 0(1^-)$$

Mass  $m = 2708.3^{+4.0}_{-3.4}$  MeV  
 Full width  $\Gamma = 120 \pm 11$  MeV

## BOTTOM MESONS ( $B = \pm 1$ )

$B^+ = u\bar{b}, B^0 = d\bar{b}, \bar{B}^0 = \bar{d}b, B^- = \bar{u}b$ , similarly for  $B^{*s}$

### B-particle organization

Many measurements of  $B$  decays involve admixtures of  $B$  hadrons. Previously we arbitrarily included such admixtures

in the  $B^\pm$  section, but because of their importance we have created two new sections: “ $B^\pm/B^0$  Admixture” for  $\Upsilon(4S)$  results and “ $B^\pm/B^0/B_s^0/b$ -baryon Admixture” for results at higher energies. Most inclusive decay branching fractions and  $\chi_b$  at high energy are found in the Admixture sections.  $B^0\text{-}\bar{B}^0$  mixing data are found in the  $B^0$  section, while  $B_s^0\text{-}\bar{B}_s^0$  mixing data and  $B\text{-}\bar{B}$  mixing data for a  $B^0/B_s^0$  admixture are found in the  $B_s^0$  section.  $CP$ -violation data are found in the  $B^\pm, B^0$ , and  $B^\pm/B^0$  Admixture sections.  $b$ -baryons are found near the end of the Baryon section.

The organization of the  $B$  sections is now as follows, where bullets indicate particle sections and brackets indicate reviews.

- $B^\pm$   
mass, mean life,  $CP$  violation, branching fractions
- $B^0$   
mass, mean life,  $B^0\text{-}\bar{B}^0$  mixing,  $CP$  violation, branching fractions
- $B^\pm/B^0$  Admixtures  
 $CP$  violation, branching fractions
- $B^\pm/B^0/B_s^0/b$ -baryon Admixtures  
mean life, production fractions, branching fractions
- $B^*$   
mass
- $B_1(5721)^+$   
mass
- $B_1(5721)^0$   
mass
- $B_2^*(5747)^+$   
mass
- $B_2^*(5747)^0$   
mass
- $B_3^*(5970)^+$   
mass
- $B_3^*(5970)^0$   
mass
- $B_s^0$   
mass, mean life,  $B_s^0\text{-}\bar{B}_s^0$  mixing,  $CP$  violation, branching fractions
- $B_s^*$   
mass
- $B_{s1}(5830)^0$   
mass
- $B_{s2}^*(5840)^0$   
mass
- $B_c^\pm$   
mass, mean life, branching fractions

At the end of Baryon Listings:

- $\Lambda_b$   
mass, mean life, branching fractions
- $\Lambda_b(5912)^0$   
mass, mean life
- $\Lambda_b(5920)^0$   
mass, mean life
- $\Sigma_b$   
mass
- $\Sigma_b^*$   
mass
- $\Xi_b^0, \Xi_b^-$   
mass, mean life, branching fractions
- $\Xi_b'(5935)^-$   
mass

- $\Xi_b(5945)^0$   
mass
- $\Xi_b(5955)^-$   
mass
- $\Omega_b^-$   
mass, branching fractions
- $b$ -baryon Admixture  
mean life, branching fractions

**B<sup>±</sup>**

$$I(J^P) = \frac{1}{2}(0^-)$$

$I, J, P$  need confirmation. Quantum numbers shown are quark-model predictions.

Mass  $m_{B^\pm} = 5279.34 \pm 0.12$  MeV  
 Mean life  $\tau_{B^\pm} = (1.638 \pm 0.004) \times 10^{-12}$  s  
 $c\tau = 491.1 \mu\text{m}$

**CP violation**

$A_{CP}(B^+ \rightarrow J/\psi(1S)K^+) = (1.8 \pm 3.0) \times 10^{-3}$ (S = 1.5)	$A_{CP}(B^+ \rightarrow [K^+ K^-]_D K^+ \pi^- \pi^+) = -0.04 \pm 0.06$
$A_{CP}(B^+ \rightarrow J/\psi(1S)\pi^+) = (1.8 \pm 1.2) \times 10^{-2}$ (S = 1.3)	$A_{CP}(B^+ \rightarrow [\pi^+ \pi^-]_D K^+ \pi^- \pi^+) = -0.05 \pm 0.10$
$A_{CP}(B^+ \rightarrow J/\psi \rho^+) = -0.05 \pm 0.05$	$A_{CP}(B^+ \rightarrow [K^- \pi^+]_D K^+ \pi^- \pi^+) = 0.013 \pm 0.023$
$A_{CP}(B^+ \rightarrow J/\psi K^*(892)^+) = -0.048 \pm 0.033$	$A_{CP}(B^+ \rightarrow [K^+ K^-]_D \pi^+ \pi^- \pi^+) = -0.019 \pm 0.015$
$A_{CP}(B^+ \rightarrow \eta_c K^+) = 0.01 \pm 0.07$ (S = 2.2)	$A_{CP}(B^+ \rightarrow [\pi^+ \pi^-]_D \pi^+ \pi^- \pi^+) = -0.013 \pm 0.019$
$A_{CP}(B^+ \rightarrow \psi(2S)\pi^+) = 0.03 \pm 0.06$	$A_{CP}(B^+ \rightarrow [K^- \pi^+]_D \pi^+ \pi^- \pi^+) = -0.002 \pm 0.011$
$A_{CP}(B^+ \rightarrow \psi(2S)K^+) = 0.012 \pm 0.020$ (S = 1.5)	$A_{CP}(B^+ \rightarrow \bar{D}^{*0} \pi^+) = 0.0010 \pm 0.0028$
$A_{CP}(B^+ \rightarrow \psi(2S)K^*(892)^+) = 0.08 \pm 0.21$	$A_{CP}(B^+ \rightarrow (D_{CP(+1)}^*)^0 \pi^+) = 0.016 \pm 0.010$ (S = 1.2)
$A_{CP}(B^+ \rightarrow \chi_{c1}(1P)\pi^+) = 0.07 \pm 0.18$	$A_{CP}(B^+ \rightarrow (D_{CP(-1)}^*)^0 \pi^+) = -0.09 \pm 0.05$
$A_{CP}(B^+ \rightarrow \chi_{c0} K^+) = -0.20 \pm 0.18$ (S = 1.5)	$A_{CP}(B^+ \rightarrow D^{*0} K^+) = -0.001 \pm 0.011$ (S = 1.1)
$A_{CP}(B^+ \rightarrow \chi_{c1} K^+) = -0.009 \pm 0.033$	$A_{CP}(B^+ \rightarrow D_{CP(+1)}^{*0} K^+) = -0.11 \pm 0.08$ (S = 2.7)
$A_{CP}(B^+ \rightarrow \chi_{c1} K^*(892)^+) = 0.5 \pm 0.5$	$A_{CP}(B^+ \rightarrow D_{CP(-1)}^{*0} K^+) = 0.07 \pm 0.10$
$A_{CP}(B^+ \rightarrow D^0 \ell^+ \nu_\ell) = (-0.14 \pm 0.20) \times 10^{-2}$	$A_{CP}(B^+ \rightarrow D_{CP(+1)} K^*(892)^+) = 0.08 \pm 0.06$
$A_{CP}(B^+ \rightarrow \bar{D}^0 \pi^+) = -0.007 \pm 0.007$	$A_{CP}(B^+ \rightarrow D_{CP(-1)} K^*(892)^+) = -0.23 \pm 0.22$
$A_{CP}(B^+ \rightarrow D_{CP(+1)} \pi^+) = -0.0080 \pm 0.0026$	$A_{CP}(B^+ \rightarrow D_S^+ \phi) = 0.0 \pm 0.4$
$A_{CP}(B^+ \rightarrow D_{CP(-1)} \pi^+) = 0.017 \pm 0.026$	$A_{CP}(B^+ \rightarrow D_S^+ \bar{D}^0) = (-0.4 \pm 0.7)\%$
$A_{CP}([K^\mp \pi^\pm \pi^\pm \pi^-]_D \pi^+) = 0.02 \pm 0.05$	$A_{CP}(B^+ \rightarrow D_S^{*+} \bar{D}^{*0}) = -0.15 \pm 0.11$
$A_{CP}(B^+ \rightarrow [\pi^+ \pi^+ \pi^- \pi^-]_D K^+) = 0.10 \pm 0.04$	$A_{CP}(B^+ \rightarrow D^{*+} \bar{D}^0) = -0.06 \pm 0.13$
$A_{CP}(B^+ \rightarrow [\pi^+ \pi^- \pi^+ \pi^-]_D K^*(892)^+) = 0.02 \pm 0.11$	$A_{CP}(B^+ \rightarrow D^+ \bar{D}^{*0}) = 0.13 \pm 0.18$
$A_{CP}(B^+ \rightarrow \bar{D}^0 K^+) = -0.017 \pm 0.005$	$A_{CP}(B^+ \rightarrow D^+ \bar{D}^0) = 0.016 \pm 0.025$
$A_{CP}([K^\mp \pi^\pm \pi^\pm \pi^-]_D K^+) = -0.31 \pm 0.11$	$A_{CP}(B^+ \rightarrow K_S^0 \pi^+) = -0.017 \pm 0.016$
$A_{CP}(B^+ \rightarrow [\pi^+ \pi^+ \pi^- \pi^-]_D \pi^+) = (-4 \pm 8) \times 10^{-3}$	$A_{CP}(B^+ \rightarrow K^+ \pi^0) = 0.037 \pm 0.021$
$A_{CP}(B^+ \rightarrow [K^- \pi^+]_D K^+) = -0.58 \pm 0.21$	$A_{CP}(B^+ \rightarrow \eta' K^+) = 0.004 \pm 0.011$
$A_{CP}(B^+ \rightarrow [K^- \pi^+ \pi^0]_D K^+) = 0.07 \pm 0.30$ (S = 1.5)	$A_{CP}(B^+ \rightarrow \eta' K^*(892)^+) = -0.26 \pm 0.27$
$A_{CP}(B^+ \rightarrow [K^+ K^- \pi^0]_D K^+) = 0.30 \pm 0.20$	$A_{CP}(B^+ \rightarrow \eta' K_S^0(1430)^+) = 0.06 \pm 0.20$
$A_{CP}(B^+ \rightarrow [\pi^+ \pi^- \pi^0]_D K^+) = 0.05 \pm 0.09$	$A_{CP}(B^+ \rightarrow \eta' K_S^0(1430)^+) = 0.15 \pm 0.13$
$A_{CP}(B^+ \rightarrow \bar{D}^0 K^*(892)^+) = -0.007 \pm 0.019$	<b><math>A_{CP}(B^+ \rightarrow \eta K^+) = -0.37 \pm 0.08</math></b>
$A_{CP}(B^+ \rightarrow [K^- \pi^+]_D K^*(892)^+) = -0.75 \pm 0.16$	$A_{CP}(B^+ \rightarrow \eta K^*(892)^+) = 0.02 \pm 0.06$
$A_{CP}(B^+ \rightarrow [K^- \pi^+ \pi^- \pi^+]_D K^*(892)^+) = -0.45 \pm 0.25$	$A_{CP}(B^+ \rightarrow \eta K_S^0(1430)^+) = 0.05 \pm 0.13$
$A_{CP}(B^+ \rightarrow [K^- \pi^+]_D \pi^+) = 0.00 \pm 0.09$	$A_{CP}(B^+ \rightarrow \eta K_S^0(1430)^+) = -0.45 \pm 0.30$
$A_{CP}(B^+ \rightarrow [K^- \pi^+ \pi^0]_D \pi^+) = 0.35 \pm 0.16$	$A_{CP}(B^+ \rightarrow \omega K^+) = -0.02 \pm 0.04$
$A_{CP}(B^+ \rightarrow [K^+ K^- \pi^0]_D \pi^+) = -0.03 \pm 0.04$	$A_{CP}(B^+ \rightarrow \omega K^{*+}) = 0.29 \pm 0.35$
$A_{CP}(B^+ \rightarrow [\pi^+ \pi^- \pi^0]_D \pi^+) = -0.016 \pm 0.020$	$A_{CP}(B^+ \rightarrow \omega(K\pi)_0^{*+}) = -0.10 \pm 0.09$
$A_{CP}(B^+ \rightarrow [K^- \pi^+]_{(D\pi)} \pi^+) = -0.09 \pm 0.27$	$A_{CP}(B^+ \rightarrow \omega K_S^0(1430)^+) = 0.14 \pm 0.15$
$A_{CP}(B^+ \rightarrow [K^- \pi^+]_{(D\gamma)} \pi^+) = -0.7 \pm 0.6$	$A_{CP}(B^+ \rightarrow K^{*0} \pi^+) = -0.04 \pm 0.09$ (S = 2.1)
$A_{CP}(B^+ \rightarrow [K^- \pi^+]_{(D\pi)} K^+) = 0.8 \pm 0.4$	$A_{CP}(B^+ \rightarrow K^*(892)^+ \pi^0) = -0.39 \pm 0.21$ (S = 1.6)
$A_{CP}(B^+ \rightarrow [K^- \pi^+]_{(D\gamma)} K^+) = 0.4 \pm 1.0$	<b><math>A_{CP}(B^+ \rightarrow K^+ \pi^- \pi^+) = 0.027 \pm 0.008</math></b>
$A_{CP}(B^+ \rightarrow [\pi^+ \pi^- \pi^0]_D K^+) = -0.02 \pm 0.15$	$A_{CP}(B^+ \rightarrow K^+ K^- K^+ \text{nonresonant}) = 0.06 \pm 0.05$
$A_{CP}(B^+ \rightarrow [K_S^0 K^+ \pi^-]_D K^+) = 0.04 \pm 0.09$	$A_{CP}(B^+ \rightarrow f(980)^0 K^+) = -0.08 \pm 0.09$
$A_{CP}(B^+ \rightarrow [K_S^0 K^- \pi^+]_D K^+) = 0.23 \pm 0.13$	<b><math>A_{CP}(B^+ \rightarrow f_2(1270) K^+) = -0.68^{+0.19}_{-0.17}</math></b>
$A_{CP}(B^+ \rightarrow [K_S^0 K^- \pi^+]_D \pi^+) = -0.052 \pm 0.034$	$A_{CP}(B^+ \rightarrow f_0(1500) K^+) = 0.28 \pm 0.30$
$A_{CP}(B^+ \rightarrow [K_S^0 K^+ \pi^-]_D \pi^+) = -0.025 \pm 0.026$	$A_{CP}(B^+ \rightarrow f_2'(1525)^0 K^+) = -0.08^{+0.05}_{-0.04}$
$A_{CP}(B^+ \rightarrow [K^*(892)^- K^+]_D K^+) = 0.03 \pm 0.11$	<b><math>A_{CP}(B^+ \rightarrow \rho^0 K^+) = 0.37 \pm 0.10</math></b>
$A_{CP}(B^+ \rightarrow [K^*(892)^+ K^-]_D K^+) = 0.34 \pm 0.21$	$A_{CP}(B^+ \rightarrow K^0 \pi^+ \pi^0) = 0.07 \pm 0.06$
$A_{CP}(B^+ \rightarrow [K^*(892)^+ K^-]_D \pi^+) = -0.05 \pm 0.05$	$A_{CP}(B^+ \rightarrow K_S^0(1430)^0 \pi^+) = 0.061 \pm 0.032$
$A_{CP}(B^+ \rightarrow [K^*(892)^- K^+]_D \pi^+) = -0.012 \pm 0.030$	$A_{CP}(B^+ \rightarrow K_S^0(1430)^+ \pi^0) = 0.26^{+0.18}_{-0.14}$
<b><math>A_{CP}(B^+ \rightarrow D_{CP(+1)} K^+) = 0.120 \pm 0.014</math> (S = 1.4)</b>	$A_{CP}(B^+ \rightarrow K_S^0(1430)^0 \pi^+) = 0.05^{+0.29}_{-0.24}$
$A_{ADS}(B^+ \rightarrow D K^+) = -0.40 \pm 0.06$	$A_{CP}(B^+ \rightarrow K^+ \pi^0 \pi^0) = -0.06 \pm 0.07$
$A_{ADS}(B^+ \rightarrow D \pi^+) = 0.100 \pm 0.032$	$A_{CP}(B^+ \rightarrow K^0 \rho^+) = -0.03 \pm 0.15$
$A_{ADS}(B^+ \rightarrow [K^- \pi^+]_D K^+ \pi^- \pi^+) = -0.33 \pm 0.35$	$A_{CP}(B^+ \rightarrow K^{*+} \pi^+ \pi^-) = 0.07 \pm 0.08$
$A_{ADS}(B^+ \rightarrow [K^- \pi^+]_D \pi^+ \pi^- \pi^+) = -0.01 \pm 0.09$	$A_{CP}(B^+ \rightarrow \rho^0 K^*(892)^+) = 0.31 \pm 0.13$
$A_{CP}(B^+ \rightarrow D_{CP(-1)} K^+) = -0.10 \pm 0.07$	$A_{CP}(B^+ \rightarrow K^*(892)^+ f_0(980)) = -0.15 \pm 0.12$
	$A_{CP}(B^+ \rightarrow a_1^+ K^0) = 0.12 \pm 0.11$
	$A_{CP}(B^+ \rightarrow b_1^+ K^0) = -0.03 \pm 0.15$
	$A_{CP}(B^+ \rightarrow K^*(892)^0 \rho^+) = -0.01 \pm 0.16$
	$A_{CP}(B^+ \rightarrow b_1^0 K^+) = -0.46 \pm 0.20$
	$A_{CP}(B^+ \rightarrow K^0 K^+) = 0.04 \pm 0.14$
	$A_{CP}(B^+ \rightarrow K_S^0 K^+) = -0.21 \pm 0.14$
	$A_{CP}(B^+ \rightarrow K^+ K_S^0 K_S^0) = 0.025 \pm 0.031$
	<b><math>A_{CP}(B^+ \rightarrow K^+ K^- \pi^+) = -0.122 \pm 0.021</math></b>
	$A_{CP}(B^+ \rightarrow K^+ K^- \pi^+ \text{nonresonant}) = -0.11 \pm 0.06$
	$A_{CP}(B^+ \rightarrow K^+ \bar{K}^*(892)^0) = 0.12 \pm 0.10$
	$A_{CP}(B^+ \rightarrow K^+ \bar{K}_0^*(1430)^0) = 0.10 \pm 0.17$
	$A_{CP}(B^+ \rightarrow \phi \pi^+) = 0.1 \pm 0.5$
	$A_{CP}(B^+ \rightarrow \pi^+(K^+ K^-)_{S\text{-wave}}) = -0.66 \pm 0.04$
	<b><math>A_{CP}(B^+ \rightarrow K^+ K^- K^+) = -0.033 \pm 0.008</math></b>
	$A_{CP}(B^+ \rightarrow \phi K^+) = 0.024 \pm 0.028$ (S = 2.3)
	$A_{CP}(B^+ \rightarrow X_0(1550) K^+) = -0.04 \pm 0.07$
	$A_{CP}(B^+ \rightarrow K^{*+} K^+ K^-) = 0.11 \pm 0.09$
	$A_{CP}(B^+ \rightarrow \phi K^*(892)^+) = -0.01 \pm 0.08$
	$A_{CP}(B^+ \rightarrow \phi(K\pi)_0^{*+}) = 0.04 \pm 0.16$



## Meson Summary Table

$A_{CP}(B^+ \rightarrow \phi K_1(1270)^+) = 0.15 \pm 0.20$
$A_{CP}(B^+ \rightarrow \phi K_2^*(1430)^+) = -0.23 \pm 0.20$
$A_{CP}(B^+ \rightarrow K^+ \phi) = -0.10 \pm 0.08$
$A_{CP}(B^+ \rightarrow K^+ [\phi \phi]_{\eta_c}) = 0.09 \pm 0.10$
$A_{CP}(B^+ \rightarrow K^*(892)^+ \gamma) = 0.014 \pm 0.018$
$A_{CP}(B^+ \rightarrow X_S \gamma) = 0.028 \pm 0.019$
$A_{CP}(B^+ \rightarrow \eta K^+ \gamma) = -0.12 \pm 0.07$
$A_{CP}(B^+ \rightarrow \phi K^+ \gamma) = -0.13 \pm 0.11 \quad (S = 1.1)$
$A_{CP}(B^+ \rightarrow \rho^+ \gamma) = -0.11 \pm 0.33$
$A_{CP}(B^+ \rightarrow \pi^+ \pi^0) = 0.03 \pm 0.04$
$A_{CP}(B^+ \rightarrow \pi^+ \pi^- \pi^+) = 0.057 \pm 0.013$
$A_{CP}(B^+ \rightarrow \rho^0 \pi^+) = 0.009 \pm 0.019$
$A_{CP}(B^+ \rightarrow f_2(1270) \pi^+) = 0.40 \pm 0.06$
$A_{CP}(B^+ \rightarrow \rho^0(1450) \pi^+) = -0.11 \pm 0.05$
$A_{CP}(B^+ \rightarrow \rho_3(1690) \pi^+) = -0.80 \pm 0.28$
$A_{CP}(B^+ \rightarrow \mathbf{f}_6(1370) \pi^+) = 0.72 \pm 0.22$
$A_{CP}(B^+ \rightarrow \pi^+ \pi^- \pi^+ \text{ nonresonant}) = -0.14^{+0.23}_{-0.16}$
$A_{CP}(B^+ \rightarrow \rho^+ \pi^0) = 0.02 \pm 0.11$
$A_{CP}(B^+ \rightarrow \rho^+ \rho^0) = -0.05 \pm 0.05$
$A_{CP}(B^+ \rightarrow \omega \pi^+) = -0.04 \pm 0.05$
$A_{CP}(B^+ \rightarrow \omega \rho^+) = -0.20 \pm 0.09$
$A_{CP}(B^+ \rightarrow \eta \pi^+) = -0.14 \pm 0.07 \quad (S = 1.4)$
$A_{CP}(B^+ \rightarrow \eta \rho^+) = 0.11 \pm 0.11$
$A_{CP}(B^+ \rightarrow \eta' \pi^+) = 0.06 \pm 0.16$
$A_{CP}(B^+ \rightarrow \eta' \rho^+) = 0.26 \pm 0.17$
$A_{CP}(B^+ \rightarrow b_1^0 \pi^+) = 0.05 \pm 0.16$
$A_{CP}(B^+ \rightarrow \rho \bar{\rho} \pi^+) = 0.00 \pm 0.04$
$A_{CP}(B^+ \rightarrow \rho \bar{\rho} K^+) = 0.00 \pm 0.04 \quad (S = 2.2)$
$A_{CP}(B^+ \rightarrow \rho \bar{\rho} K^*(892)^+) = 0.21 \pm 0.16 \quad (S = 1.4)$
$A_{CP}(B^+ \rightarrow \rho \bar{\Lambda} \gamma) = 0.17 \pm 0.17$
$A_{CP}(B^+ \rightarrow \rho \bar{\Lambda} \pi^0) = 0.01 \pm 0.17$
$A_{CP}(B^+ \rightarrow K^+ \ell^+ \ell^-) = -0.02 \pm 0.08$
$A_{CP}(B^+ \rightarrow K^+ e^+ e^-) = 0.14 \pm 0.14$
$A_{CP}(B^+ \rightarrow K^+ \mu^+ \mu^-) = 0.011 \pm 0.017$
$A_{CP}(B^+ \rightarrow \pi^+ \mu^+ \mu^-) = -0.11 \pm 0.12$
$A_{CP}(B^+ \rightarrow K^* e^+ e^-) = -0.09 \pm 0.14$
$A_{CP}(B^+ \rightarrow K^* \mu^+ \mu^-) = -0.12 \pm 0.24$
$\gamma = (71.1^{+4.6}_{-5.3})^\circ$
$\Gamma_B(B^+ \rightarrow D^0 K^+) = 0.0993 \pm 0.0046$
$\delta_B(B^+ \rightarrow D^0 K^+) = (129.6^{+5.0}_{-6.0})^\circ$
$\Gamma_B(B^+ \rightarrow D^0 K^{*+}) = 0.076 \pm 0.020$
$\delta_B(B^+ \rightarrow D^0 K^{*+}) = (98^{+18}_{-37})^\circ$
$\Gamma_B(B^+ \rightarrow D^{*0} K^+) = 0.140 \pm 0.019$
$\delta_B(B^+ \rightarrow D^{*0} K^+) = (319.2^{+7.7}_{-8.7})^\circ$

$B^-$  modes are charge conjugates of the modes below. Modes which do not identify the charge state of the  $B$  are listed in the  $B^\pm/B^0$  ADMIXTURE section.

The branching fractions listed below assume 50%  $B^0 \bar{B}^0$  and 50%  $B^+ B^-$  production at the  $\Upsilon(4S)$ . We have attempted to bring older measurements up to date by rescaling their assumed  $\Upsilon(4S)$  production ratio to 50:50 and their assumed  $D, D_s, D^*$ , and  $\psi$  branching ratios to current values whenever this would affect our averages and best limits significantly.

Indentation is used to indicate a subchannel of a previous reaction. All resonant subchannels have been corrected for resonance branching fractions to the final state so the sum of the subchannel branching fractions can exceed that of the final state.

For inclusive branching fractions, e.g.,  $B \rightarrow D^\pm X$ , the values usually are multiplicities, not branching fractions. They can be greater than one.

$B^+$ DECAY MODES	Fraction ( $\Gamma_i/\Gamma$ )	Scale factor/ Confidence level (MeV/c)	$\rho$
<b>Semileptonic and leptonic modes</b>			
$\ell^+ \nu_\ell X$	[III] ( 10.99 ± 0.28 ) %		–
$e^+ \nu_e X_c$	( 10.8 ± 0.4 ) %		–
$D \ell^+ \nu_\ell X$	( 9.7 ± 0.7 ) %		–
$\bar{D}^0 \ell^+ \nu_\ell$	[III] ( 2.35 ± 0.09 ) %	2310	
$\bar{D}^0 \tau^+ \nu_\tau$	( 7.7 ± 2.5 ) × 10 <sup>-3</sup>	1911	
$\bar{D}^*(2007)^0 \ell^+ \nu_\ell$	[III] ( 5.66 ± 0.22 ) %	2258	
$\bar{D}^*(2007)^0 \tau^+ \nu_\tau$	( 1.88 ± 0.20 ) %	1839	
$D^- \pi^+ \ell^+ \nu_\ell$	( 4.4 ± 0.4 ) × 10 <sup>-3</sup>	2306	

$\bar{D}_0^*(2420)^0 \ell^+ \nu_\ell, \bar{D}_0^{*0} \rightarrow$	( 2.5 ± 0.5 ) × 10 <sup>-3</sup>	–
$\bar{D}_2^*(2460)^0 \ell^+ \nu_\ell, \bar{D}_2^{*0} \rightarrow$	( 1.53 ± 0.16 ) × 10 <sup>-3</sup>	2065
$D^{(*)-} n \pi \ell^+ \nu_\ell (n \geq 1)$	( 1.88 ± 0.25 ) %	–
$D^{*-} \pi^+ \ell^+ \nu_\ell$	( 6.0 ± 0.4 ) × 10 <sup>-3</sup>	2254
$\bar{D}_1(2420)^0 \ell^+ \nu_\ell, \bar{D}_1^0 \rightarrow$	( 3.03 ± 0.20 ) × 10 <sup>-3</sup>	2084
$\bar{D}_1^*(2430)^0 \ell^+ \nu_\ell, \bar{D}_1^{*0} \rightarrow$	( 2.7 ± 0.6 ) × 10 <sup>-3</sup>	–
$\bar{D}_2^*(2460)^0 \ell^+ \nu_\ell,$	( 1.01 ± 0.24 ) × 10 <sup>-3</sup>	S=2.0 2065
$\bar{D}_2^{*0} \rightarrow D^{*-} \pi^+$		
$\bar{D}^0 \pi^+ \pi^- \ell^+ \nu_\ell$	( 1.7 ± 0.4 ) × 10 <sup>-3</sup>	2301
$\bar{D}^{*0} \pi^+ \pi^- \ell^+ \nu_\ell$	( 8 ± 5 ) × 10 <sup>-4</sup>	2248
$D^{(*)-} K^+ \ell^+ \nu_\ell$	( 6.1 ± 1.0 ) × 10 <sup>-4</sup>	–
$D_s^- K^+ \ell^+ \nu_\ell$	( 3.0 ± 1.4 ) × 10 <sup>-4</sup>	2242
$D_s^{*-} K^+ \ell^+ \nu_\ell$	( 2.9 ± 1.9 ) × 10 <sup>-4</sup>	2185
$\pi^0 \ell^+ \nu_\ell$	( 7.80 ± 0.27 ) × 10 <sup>-5</sup>	2638
$\eta \ell^+ \nu_\ell$	( 3.9 ± 0.5 ) × 10 <sup>-5</sup>	2611
$\eta' \ell^+ \nu_\ell$	( 2.3 ± 0.8 ) × 10 <sup>-5</sup>	2553
$\omega \ell^+ \nu_\ell$	[III] ( 1.19 ± 0.09 ) × 10 <sup>-4</sup>	2582
$\rho^0 \ell^+ \nu_\ell$	[III] ( 1.58 ± 0.11 ) × 10 <sup>-4</sup>	2583
$\rho \bar{\rho} \ell^+ \nu_\ell$	( 5.8 ± 2.6 ) × 10 <sup>-6</sup>	2467
$\rho \bar{\rho} \mu^+ \nu_\mu$	< 8.5 × 10 <sup>-6</sup>	CL=90% 2446
$\rho \bar{\rho} e^+ \nu_e$	( 8.2 ± 4.0 ) × 10 <sup>-6</sup>	2467
$e^+ \nu_e$	< 9.8 × 10 <sup>-7</sup>	CL=90% 2640
$\mu^+ \nu_\mu$	2.90 × 10 <sup>-07</sup> to 1.07 × 10 <sup>-06</sup>	CL=90% 2639
$\tau^+ \nu_\tau$	( 1.09 ± 0.24 ) × 10 <sup>-4</sup>	S=1.2 2341
$\ell^+ \nu_\ell \gamma$	< 3.0 × 10 <sup>-6</sup>	CL=90% 2640
$e^+ \nu_e \gamma$	< 4.3 × 10 <sup>-6</sup>	CL=90% 2640
$\mu^+ \nu_\mu \gamma$	< 3.4 × 10 <sup>-6</sup>	CL=90% 2639
$\mu^+ \mu^- \mu^+ \nu_\mu$	< 1.6 × 10 <sup>-8</sup>	CL=95% 2634

## Inclusive modes

$D^0 X$	( 8.6 ± 0.7 ) %	–
$\bar{D}^0 X$	( 79 ± 4 ) %	–
$D^+ X$	( 2.5 ± 0.5 ) %	–
$D^- X$	( 9.9 ± 1.2 ) %	–
$D_s^+ X$	( 7.9 ± 1.4 ) %	–
$D_s^- X$	( 1.10 ± 0.40 ) %	–
$\Lambda_c^+ X$	( 2.1 ± 0.9 ) %	–
$\bar{\Lambda}_c^- X$	( 2.8 ± 1.1 ) %	–
$\bar{c} X$	( 97 ± 4 ) %	–
$c X$	( 23.4 ± 2.2 ) %	–
$c/\bar{c} X$	( 120 ± 6 ) %	–

 $D, D^*$ , or  $D_s$  modes

$\bar{D}^0 \pi^+$	( 4.68 ± 0.13 ) × 10 <sup>-3</sup>	2308
$D_{CP(+1)} \pi^+$	[nnn] ( 2.05 ± 0.18 ) × 10 <sup>-3</sup>	–
$D_{CP(-1)} \pi^+$	[nnn] ( 2.0 ± 0.4 ) × 10 <sup>-3</sup>	–
$\bar{D}^0 \rho^+$	( 1.34 ± 0.18 ) %	2237
$\bar{D}^0 K^+$	( 3.63 ± 0.12 ) × 10 <sup>-4</sup>	2281
$D_{CP(+1)} K^+$	[nnn] ( 1.80 ± 0.07 ) × 10 <sup>-4</sup>	–
$D_{CP(-1)} K^+$	[nnn] ( 1.96 ± 0.18 ) × 10 <sup>-4</sup>	–
$D^0 K^+$	( 3.57 ± 0.35 ) × 10 <sup>-6</sup>	2281
$[K^- \pi^+]_D K^+$	[ooo] < 2.8 × 10 <sup>-7</sup>	CL=90% –
$[K^+ \pi^-]_D K^+$	[ooo] < 1.5 × 10 <sup>-5</sup>	CL=90% –
$[K^- \pi^+ \pi^0]_D K^+$	seen	–
$[K^+ \pi^- \pi^0]_D K^+$	seen	–
$[K^- \pi^+ \pi^+ \pi^-]_D K^+$	seen	–
$[K^+ \pi^- \pi^+ \pi^-]_D K^+$	seen	–
$[K^- \pi^+]_D \pi^+$	[ooo] ( 6.3 ± 1.1 ) × 10 <sup>-7</sup>	–
$[K^+ \pi^-]_D \pi^+$	( 1.78 ± 0.32 ) × 10 <sup>-4</sup>	–
$[K^- \pi^+ \pi^0]_D \pi^+$	seen	–
$[K^+ \pi^- \pi^0]_D \pi^+$	seen	–
$[K^- \pi^+ \pi^+ \pi^-]_D \pi^+$	seen	–
$[K^+ \pi^- \pi^+ \pi^-]_D \pi^+$	seen	–
$[\pi^+ \pi^- \pi^0]_D K^-$	( 4.6 ± 0.9 ) × 10 <sup>-6</sup>	–
$[K_S^0 K^+ \pi^-]_D K^+$	seen	–
$[K_S^0 K^- \pi^+]_D K^+$	seen	–
$[K^*(892)^+ K^-]_D K^+$	seen	–
$[K_S^0 K^- \pi^+]_D \pi^+$	seen	–

## Meson Summary Table

$[K^*(892)^+ K^-]_D \pi^+$	seen	-	$\bar{D}'_1(2427)^0 \pi^+$	$(5.0 \pm 1.2) \times 10^{-4}$	-
$[K^*_S K^+ \pi^-]_D \pi^+$	seen	-	$\times B(\bar{D}'_1(2427)^0 \rightarrow D^{*-} \pi^+)$		
$[K^*(892)^- K^+]_D \pi^+$	seen	-	$\bar{D}_1(2420)^0 \pi^+ \times B(\bar{D}'_1 \rightarrow$	$< 6$	$\times 10^{-6}$ CL=90% 2082
$\bar{D}^0 K^*(892)^+$		$(5.3 \pm 0.4) \times 10^{-4}$	$\bar{D}^{*0} \pi^+ \pi^-)$		
$D_{CP(-1)} K^*(892)^+$	[nnn]	$(2.7 \pm 0.8) \times 10^{-4}$	$\bar{D}^*_1(2420)^0 \rho^+$	$< 1.4$	$\times 10^{-3}$ CL=90% 1996
$D_{CP(+1)} K^*(892)^+$	[nnn]	$(6.2 \pm 0.7) \times 10^{-4}$	$\bar{D}^*_2(2460)^0 \pi^+$	$< 1.3$	$\times 10^{-3}$ CL=90% 2063
$D^0 K^*(892)^+$		$(3.1 \pm 1.6) \times 10^{-6}$	$\bar{D}^*_2(2460)^0 \pi^+ \times B(\bar{D}^{*0} \rightarrow$	$< 2.2$	$\times 10^{-5}$ CL=90% 2063
$\bar{D}^0 K^+ \pi^+ \pi^-$		$(5.2 \pm 2.1) \times 10^{-4}$	$\bar{D}^{*0} \pi^+ \pi^-)$		
$\bar{D}^0 K^+ \bar{K}^0$		$(5.5 \pm 1.6) \times 10^{-4}$	$\bar{D}^*_1(2680)^0 \pi^+, \bar{D}^*_1(2680)^0 \rightarrow$	$(8.4 \pm 2.1) \times 10^{-5}$	-
$\bar{D}^0 K^+ \bar{K}^*(892)^0$		$(7.5 \pm 1.7) \times 10^{-4}$	$D^- \pi^+$		
$\bar{D}^0 \pi^+ \pi^+ \pi^-$		$(5.6 \pm 2.1) \times 10^{-3}$	$\bar{D}^*_3(2760)^0 \pi^+,$	$(1.00 \pm 0.22) \times 10^{-5}$	-
$\bar{D}^0 \pi^+ \pi^+ \pi^-$ nonresonant		$(5 \pm 4) \times 10^{-3}$	$\bar{D}^*_3(2760)^0 \pi^+ \rightarrow D^- \pi^+$		
$\bar{D}^0 \pi^+ \rho^0$		$(4.2 \pm 3.0) \times 10^{-3}$	$\bar{D}^*_2(3000)^0 \pi^+,$	$(2.0 \pm 1.4) \times 10^{-6}$	-
$\bar{D}^0 a_1(1260)^+$		$(4 \pm 4) \times 10^{-3}$	$\bar{D}^*_2(3000)^0 \pi^+ \rightarrow D^- \pi^+$		
$\bar{D}^0 \omega \pi^+$		$(4.1 \pm 0.9) \times 10^{-3}$	$\bar{D}^*_2(2460)^0 \rho^+$	$< 4.7$	$\times 10^{-3}$ CL=90% 1977
$D^*(2010)^- \pi^+ \pi^+$		$(1.35 \pm 0.22) \times 10^{-3}$	$\bar{D}^0 D^+_S$	$(9.0 \pm 0.9) \times 10^{-3}$	1815
$D^*(2010)^- K^+ \pi^+$		$(8.2 \pm 1.4) \times 10^{-5}$	$D^*_{S0}(2317)^+ \bar{D}^0, D^*_{S0} \rightarrow$	$(8.0 \pm \frac{1.6}{1.3}) \times 10^{-4}$	1605
$\bar{D}_1(2420)^0 \pi^+, \bar{D}^0_1 \rightarrow$		$(5.2 \pm 2.2) \times 10^{-4}$	$D^+_S \pi^0$		
$D^*(2010)^- \pi^+$			$D_{S0}(2317)^+ \bar{D}^0 \times$	$< 7.6$	$\times 10^{-4}$ CL=90% 1605
$D^- \pi^+ \pi^+$		$(1.07 \pm 0.05) \times 10^{-3}$	$B(D_{S0}(2317)^+ \rightarrow D^*_S \gamma)$		
$D^- K^+ \pi^+$		$(7.7 \pm 0.5) \times 10^{-5}$	$D_{S0}(2317)^+ \bar{D}^*(2007)^0 \times$	$(9 \pm 7) \times 10^{-4}$	1511
$D^0_0(2300)^0 K^+, D^0_0 \rightarrow$		$(6.1 \pm 2.4) \times 10^{-6}$	$B(D_{S0}(2317)^+ \rightarrow D^+_S \pi^0)$		
$D^- \pi^+$			$D_{sJ}(2457)^+ \bar{D}^0$	$(3.1 \pm \frac{1.0}{0.9}) \times 10^{-3}$	-
$D^*_2(2460)^0 K^+, D^*_2 \rightarrow$		$(2.32 \pm 0.23) \times 10^{-5}$	$D_{sJ}(2457)^+ \bar{D}^0 \times$	$(4.6 \pm \frac{1.3}{1.1}) \times 10^{-4}$	-
$D^- \pi^+$			$B(D_{sJ}(2457)^+ \rightarrow D^+_S \gamma)$		
$D^*_1(2760)^0 K^+, D^*_1 \rightarrow$		$(3.6 \pm 1.2) \times 10^{-6}$	$D_{sJ}(2457)^+ \bar{D}^0 \times$	$< 2.2$	$\times 10^{-4}$ CL=90% -
$D^+ K^0$		$< 2.9$	$B(D_{sJ}(2457)^+ \rightarrow D^+_S \pi^+ \pi^-)$		
$D^+ K^+ \pi^-$		$(5.6 \pm 1.1) \times 10^{-6}$	$D_{sJ}(2457)^+ \bar{D}^0 \times$	$< 2.7$	$\times 10^{-4}$ CL=90% -
$D^*_2(2460)^0 K^+, D^*_2 \rightarrow$		$< 6.3$	$B(D_{sJ}(2457)^+ \rightarrow D^+_S \pi^0)$	$< 9.8$	$\times 10^{-4}$ CL=90% -
$D^+ \pi^-$			$B(D_{sJ}(2457)^+ \rightarrow D^*_S \gamma)$		
$D^+ K^{*0}$		$< 4.9$	$D_{sJ}(2457)^+ \bar{D}^0 \times$	$(1.20 \pm 0.30) \%$	-
$D^+ \bar{K}^{*0}$		$< 1.4$	$D_{sJ}(2457)^+ \bar{D}^*(2007)^0 \times$	$(1.4 \pm \frac{0.7}{0.6}) \times 10^{-3}$	-
$\bar{D}^*(2007)^0 \pi^+$		$(4.90 \pm 0.17) \times 10^{-3}$	$B(D_{sJ}(2457)^+ \rightarrow D^+_S \gamma)$		
$\bar{D}^{*0}_{CP(+1)} \pi^+$	[ppp]	$(2.7 \pm 0.6) \times 10^{-3}$	$\bar{D}^0 D_{S1}(2536)^+ \times$	$(4.0 \pm 1.0) \times 10^{-4}$	1447
$D^{*0}_{CP(-1)} \pi^+$	[ppp]	$(2.4 \pm 0.9) \times 10^{-3}$	$B(D_{S1}(2536)^+ \rightarrow$		
$\bar{D}^*(2007)^0 \omega \pi^+$		$(4.5 \pm 1.2) \times 10^{-3}$	$D^*(2007)^0 K^+ +$		
$\bar{D}^*(2007)^0 \rho^+$		$(9.8 \pm 1.7) \times 10^{-3}$	$D^*(2010)^+ K^0)$		
$\bar{D}^*(2007)^0 K^+$		$(3.97 \pm \frac{0.31}{0.28}) \times 10^{-4}$	$\bar{D}^0 D_{S1}(2536)^+ \times$	$(2.2 \pm 0.7) \times 10^{-4}$	1447
$\bar{D}^{*0}_{CP(+1)} K^+$	[ppp]	$(2.60 \pm 0.33) \times 10^{-4}$	$B(D_{S1}(2536)^+ \rightarrow$		
$\bar{D}^{*0}_{CP(-1)} K^+$	[ppp]	$(2.19 \pm 0.30) \times 10^{-4}$	$D^*(2007)^0 K^+$		
$D^*(2007)^0 K^+$		$(7.8 \pm 2.2) \times 10^{-6}$	$D^*(2007)^0 K^+)$		
$\bar{D}^*(2007)^0 K^*(892)^+$		$(8.1 \pm 1.4) \times 10^{-4}$	$\bar{D}^0 D_{S1}(2536)^+ \times$	$(5.5 \pm 1.6) \times 10^{-4}$	1339
$\bar{D}^*(2007)^0 K^+ \bar{K}^0$		$< 1.06$	$B(D_{S1}(2536)^+ \rightarrow$		
$\bar{D}^*(2007)^0 K^+ \bar{K}^*(892)^0$		$(1.5 \pm 0.4) \times 10^{-3}$	$D^*(2007)^0 K^+)$		
$\bar{D}^*(2007)^0 K^+ \pi^+ \pi^-$		$(1.03 \pm 0.12) \%$	$\bar{D}^0 D_{S1}(2536)^+ \times$	$(2.3 \pm 1.1) \times 10^{-4}$	1447
$\bar{D}^*(2007)^0 a_1(1260)^+$		$(1.9 \pm 0.5) \%$	$B(D_{S1}(2536)^+ \rightarrow D^{*+} K^0)$		
$\bar{D}^*(2007)^0 \pi^- \pi^+ \pi^+ \pi^0$		$(1.8 \pm 0.4) \%$	$\bar{D}^0 D_{sJ}(2700)^+ \times$	$(5.6 \pm 1.8) \times 10^{-4}$	S=1.7 -
$\bar{D}^{*0} 3\pi^+ 2\pi^-$		$(5.7 \pm 1.2) \times 10^{-3}$	$B(D_{sJ}(2700)^+ \rightarrow D^0 K^+)$		
$D^*(2010)^+ \pi^0$		$< 3.6$	$\bar{D}^{*0} D_{S1}(2536)^+, D^+_{S1} \rightarrow$	$(3.9 \pm 2.6) \times 10^{-4}$	1339
$D^*(2010)^+ K^0$		$< 9.0$	$D^{*+} K^0$		
$D^*(2010)^- \pi^+ \pi^+ \pi^0$		$(1.5 \pm 0.7) \%$	$\bar{D}^0 D_{sJ}(2573)^+, D^+_{sJ} \rightarrow$	$(8 \pm 15) \times 10^{-6}$	-
$D^*(2010)^- \pi^+ \pi^+ \pi^+ \pi^-$		$(2.6 \pm 0.4) \times 10^{-3}$	$D^0 K^+$		
$\bar{D}^{*0} \pi^+$	[qqq]	$(5.7 \pm 1.2) \times 10^{-3}$	$\bar{D}^{*0} D_{sJ}(2573), D^+_{sJ} \rightarrow$	$< 2$	$\times 10^{-4}$ CL=90% 1306
$\bar{D}^*_1(2420)^0 \pi^+$		$(1.5 \pm 0.6) \times 10^{-3}$	$D^0 K^+$		
$\bar{D}_1(2420)^0 \pi^+ \times B(\bar{D}^0_1 \rightarrow$		$(2.5 \pm \frac{1.6}{1.4}) \times 10^{-4}$	$\bar{D}^{*0} D_{sJ}(2573), D^+_{sJ} \rightarrow$	$< 5$	$\times 10^{-4}$ CL=90% 1306
$\bar{D}^0 \pi^+ \pi^-)$			$D^0 K^+$		
$\bar{D}_1(2420)^0 \pi^+ \times B(\bar{D}^0_1 \rightarrow$		$(2.2 \pm 1.0) \times 10^{-4}$	$\bar{D}^0 D^*_{S^+}$	$(7.6 \pm 1.6) \times 10^{-3}$	1734
$\bar{D}^0 \pi^+ \pi^-$ (nonresonant))			$\bar{D}^*(2007)^0 D^+_S$	$(8.2 \pm 1.7) \times 10^{-3}$	1737
$\bar{D}^*_2(2462)^0 \pi^+$		$(3.56 \pm 0.24) \times 10^{-4}$	$\bar{D}^*(2007)^0 D^+_S$	$(1.71 \pm 0.24) \%$	1651
$\times B(\bar{D}^*_2(2462)^0 \rightarrow D^- \pi^+)$			$D^{(*)+} \bar{D}^{*0}$	$(2.7 \pm 1.2) \%$	-
$\bar{D}^*_2(2462)^0 \pi^+ \times B(\bar{D}^{*0} \rightarrow$		$(2.2 \pm 1.0) \times 10^{-4}$	$\bar{D}^*(2007)^0 D^*(2010)^+$	$(8.1 \pm 1.7) \times 10^{-4}$	1713
$\bar{D}^0 \pi^- \pi^+)$			$\bar{D}^0 D^*(2010)^+ +$	$< 1.30$	$\%$ CL=90% 1792
$\bar{D}^0 \pi^- \pi^+ \pi^-$ (nonresonant))		$< 1.7$	$\bar{D}^*(2007)^0 D^+$		
$\bar{D}^*_2(2462)^0 \pi^+ \times B(\bar{D}^{*0} \rightarrow$		$(2.2 \pm 1.1) \times 10^{-4}$	$\bar{D}^0 D^*(2010)^+$	$(3.9 \pm 0.5) \times 10^{-4}$	1792
$D^*(2010)^- \pi^+)$			$\bar{D}^0 D^+$	$(3.8 \pm 0.4) \times 10^{-4}$	1866
$\bar{D}^*_0(2400)^0 \pi^+$		$(6.4 \pm 1.4) \times 10^{-4}$	$\bar{D}^0 D^+ K^0$	$(1.55 \pm 0.21) \times 10^{-3}$	1571
$\times B(\bar{D}^*_0(2400)^0 \rightarrow D^- \pi^+)$			$D^+ \bar{D}^*(2007)^0$	$(6.3 \pm 1.7) \times 10^{-4}$	1791
$\bar{D}_1(2421)^0 \pi^+$		$(6.8 \pm 1.5) \times 10^{-4}$	$\bar{D}^*(2007)^0 D^+ K^0$	$(2.1 \pm 0.5) \times 10^{-3}$	1475
$\times B(\bar{D}_1(2421)^0 \rightarrow D^{*-} \pi^+)$			$\bar{D}^0 D^*(2010)^+ K^0$	$(3.8 \pm 0.4) \times 10^{-3}$	1476
$\bar{D}^*_2(2462)^0 \pi^+$		$(1.8 \pm 0.5) \times 10^{-4}$	$\bar{D}^*(2007)^0 D^*(2010)^+ K^0$	$(9.2 \pm 1.2) \times 10^{-3}$	1362
$\times B(\bar{D}^*_2(2462)^0 \rightarrow D^{*-} \pi^+)$			$\bar{D}^0 D^0 K^+$	$(1.45 \pm 0.33) \times 10^{-3}$	S=2.6 1577

## Meson Summary Table

$\bar{D}^*(2007)^0 D^0 K^+$	$(2.26 \pm 0.23) \times 10^{-3}$	1481	$X(3915) K^+$	$< 2.8$	$\times 10^{-4}$	CL=90%	1103			
$\bar{D}^0 D^*(2007)^0 K^+$	$(6.3 \pm 0.5) \times 10^{-3}$	1481	$X(3915)^0 K^+, X^0 \rightarrow \eta_c \eta$	$< 4.7$	$\times 10^{-5}$	CL=90%	-			
$\bar{D}^*(2007)^0 D^*(2007)^0 K^+$	$(1.12 \pm 0.13) \%$	1368	$X(3915)^0 K^+, X^0 \rightarrow \eta_c \pi^0$	$< 1.7$	$\times 10^{-5}$	CL=90%	-			
$D^- D^+ K^+$	$(2.2 \pm 0.7) \times 10^{-4}$	1571	$X(4014)^0 K^+, X^0 \rightarrow \eta_c \eta$	$< 3.9$	$\times 10^{-5}$	CL=90%	-			
$D^- D^*(2010)^+ K^+$	$(6.3 \pm 1.1) \times 10^{-4}$	1475	$X(4014)^0 K^+, X^0 \rightarrow \eta_c \pi^0$	$< 1.2$	$\times 10^{-5}$	CL=90%	-			
$D^*(2010)^- D^+ K^+$	$(6.0 \pm 1.3) \times 10^{-4}$	1475	$Z_c(3900)^0 K^+, Z_c^0 \rightarrow$	$< 4.7$	$\times 10^{-5}$	CL=90%	-			
$D^*(2010)^- D^*(2010)^+ K^+$	$(1.32 \pm 0.18) \times 10^{-3}$	1363	$\eta_c \pi^+ \pi^-$							
$(\bar{D} + \bar{D}^*)(D + D^*) K$	$(4.05 \pm 0.30) \%$	-	$X(4020)^0 K^+, X^0 \rightarrow$	$< 1.6$	$\times 10^{-5}$	CL=90%	-			
$D_s^+ \pi^0$	$(1.6 \pm 0.5) \times 10^{-5}$	2270	$\eta_c \pi^+ \pi^-$							
$D_s^{*+} \pi^0$	$< 2.6$	$\times 10^{-4}$	CL=90%	2215	$\chi_{c1}(3872) K^*(892)^+, \chi_{c1} \rightarrow$	$< 4.8$	$\times 10^{-6}$	CL=90%	939	
$D_s^+ \eta$	$< 4$	$\times 10^{-4}$	CL=90%	2235	$J/\psi \gamma$					
$D_s^{*+} \eta$	$< 6$	$\times 10^{-4}$	CL=90%	2178	$\chi_{c1}(3872) K^*(892)^+, \chi_{c1} \rightarrow$	$< 2.8$	$\times 10^{-5}$	CL=90%	939	
$D_s^+ \rho^0$	$< 3.0$	$\times 10^{-4}$	CL=90%	2197	$\psi(2S) \gamma$					
$D_s^{*+} \rho^0$	$< 4$	$\times 10^{-4}$	CL=90%	2138	$\chi_{c1}(3872)^+ K^0, \chi_{c1}^+ \rightarrow$	[rrr]	$< 6.1$	$\times 10^{-6}$	CL=90%	-
$D_s^+ \omega$	$< 4$	$\times 10^{-4}$	CL=90%	2195	$J/\psi(1S) \pi^+ \pi^0$					
$D_s^{*+} \omega$	$< 6$	$\times 10^{-4}$	CL=90%	2136	$\chi_{c1}(3872) K^0 \pi^+, \chi_{c1} \rightarrow$	$(1.06 \pm 0.31) \times 10^{-5}$				-
$D_s^+ a_1(1260)^0$	$< 1.8$	$\times 10^{-3}$	CL=90%	2079	$J/\psi(1S) \pi^+ \pi^-$					
$D_s^{*+} a_1(1260)^0$	$< 1.3$	$\times 10^{-3}$	CL=90%	2015	$Z_c(4430)^+ K^0, Z_c^+ \rightarrow J/\psi \pi^+$	$< 1.5$	$\times 10^{-5}$	CL=95%	-	
$D_s^+ K^+ K^-$	$(7.2 \pm 1.1) \times 10^{-6}$	2149	$Z_c(4430)^+ K^0, Z_c^+ \rightarrow$	$< 4.7$	$\times 10^{-5}$	CL=95%				-
$D_s^+ \phi$	$< 4.2$	$\times 10^{-7}$	CL=90%	2141	$\psi(2S) \pi^+$					
$D_s^{*+} \phi$	$< 1.2$	$\times 10^{-5}$	CL=90%	2079	$\psi(4260)^0 K^+, \psi^0 \rightarrow$	$< 1.56$	$\times 10^{-5}$	CL=95%	-	
$D_s^+ \bar{K}^0$	$< 8$	$\times 10^{-4}$	CL=90%	2242	$J/\psi \pi^+ \pi^-$					
$D_s^{*+} \bar{K}^0$	$< 9$	$\times 10^{-4}$	CL=90%	2185	$X(3915) K^+, X \rightarrow J/\psi \gamma$	$< 1.4$	$\times 10^{-5}$	CL=90%	-	
$D_s^+ \bar{K}^*(892)^0$	$< 4.4$	$\times 10^{-6}$	CL=90%	2172	$X(3915) K^+, X \rightarrow$	$< 3.8$	$\times 10^{-5}$	CL=90%	-	
$D_s^{*+} \bar{K}^*(892)^0$	$< 3.5$	$\times 10^{-6}$	CL=90%	2172	$\chi_{c1}(1P) \pi^0$					
$D_s^{*+} \bar{K}^*(892)^0$	$< 3.5$	$\times 10^{-4}$	CL=90%	2112	$X(3930)^0 K^+, X^0 \rightarrow J/\psi \gamma$	$< 2.5$	$\times 10^{-6}$	CL=90%	-	
$D_s^- \pi^+ K^+$	$(1.80 \pm 0.22) \times 10^{-4}$	2222	$J/\psi(1S) K^+$	$(1.006 \pm 0.027) \times 10^{-3}$	1684					
$D_s^{*-} \pi^+ K^+$	$(1.45 \pm 0.24) \times 10^{-4}$	2164	$J/\psi(1S) K^0 \pi^+$	$(1.14 \pm 0.11) \times 10^{-3}$	1651					
$D_s^{*-} \pi^+ K^*(892)^+$	$< 5$	$\times 10^{-3}$	CL=90%	2138	$J/\psi(1S) K^+ \pi^+ \pi^-$	$(8.1 \pm 1.3) \times 10^{-4}$	S=2.5	1612		
$D_s^{*-} \pi^+ K^*(892)^+$	$< 7$	$\times 10^{-3}$	CL=90%	2076	$J/\psi(1S) K^+ K^- K^+$	$(3.37 \pm 0.29) \times 10^{-5}$		1252		
$D_s^- K^+ K^+$	$(9.7 \pm 2.1) \times 10^{-6}$	2149	$X(3915) K^+, X \rightarrow \rho \bar{\rho}$	$< 7.1$	$\times 10^{-8}$	CL=95%	-			
$D_s^{*-} K^+ K^+$	$< 1.5$	$\times 10^{-5}$	CL=90%	2088	$J/\psi(1S) K^*(892)^+$	$(1.43 \pm 0.08) \times 10^{-3}$		1571		
					$J/\psi(1S) K(1270)^+$	$(1.8 \pm 0.5) \times 10^{-3}$		1402		
					$J/\psi(1S) K(1400)^+$	$< 5$	$\times 10^{-4}$	CL=90%	1308	
					$J/\psi(1S) \eta K^+$	$(1.24 \pm 0.14) \times 10^{-4}$		1510		
					$\chi_{c1-odd}(3872) K^+,$	$< 3.8$	$\times 10^{-6}$	CL=90%	-	
					$\chi_{c1-odd} \rightarrow J/\psi \eta$					
					$\psi(4160) K^+, \psi \rightarrow J/\psi \eta$	$< 7.4$	$\times 10^{-6}$	CL=90%	-	
					$J/\psi(1S) \eta K^+$	$< 8.8$	$\times 10^{-5}$	CL=90%	1273	
					$J/\psi(1S) \phi K^+$	$(5.0 \pm 0.4) \times 10^{-5}$		1227		
					$J/\psi(1S) K_1(1650), K_1 \rightarrow$	$(6 \pm 10/6) \times 10^{-6}$		-		
					$\phi K^+$					
					$J/\psi(1S) K^*(1680)^+, K^* \rightarrow$	$(3.4 \pm 1.9/2.2) \times 10^{-6}$		-		
					$\phi K^+$					
					$J/\psi(1S) K_2^*(1980), K_2^* \rightarrow$	$(1.5 \pm 0.9/0.5) \times 10^{-6}$		-		
					$\phi K^+$					
					$J/\psi(1S) K(1830)^+,$	$(1.3 \pm 1.3/1.1) \times 10^{-6}$		-		
					$K(1830)^+ \rightarrow \phi K^+$					
					$\chi_{c1}(4140) K^+, \chi_{c1} \rightarrow$	$(10 \pm 4) \times 10^{-6}$		-		
					$J/\psi(1S) \phi$					
					$\chi_{c1}(4274) K^+, \chi_{c1} \rightarrow$	$(3.6 \pm 2.2/1.8) \times 10^{-6}$		-		
					$J/\psi(1S) \phi$					
					$\chi_{c0}(4500) K^+, \chi_c^0 \rightarrow$	$(3.3 \pm 2.1/1.7) \times 10^{-6}$		-		
					$J/\psi(1S) \phi$					
					$\chi_{c0}(4700) K^+, \chi_{c0} \rightarrow$	$(6 \pm 5/4) \times 10^{-6}$		-		
					$J/\psi(1S) \phi$					
					$J/\psi(1S) \omega K^+$	$(3.20 \pm 0.60/0.32) \times 10^{-4}$		1388		
					$\chi_{c1}(3872) K^+, \chi_{c1} \rightarrow$	$(6.0 \pm 2.2) \times 10^{-6}$		1141		
					$J/\psi \omega$					
					$X(3915) K^+, X \rightarrow J/\psi \omega$	$(3.0 \pm 0.9/0.7) \times 10^{-5}$		1103		
					$J/\psi(1S) \pi^+$	$(3.87 \pm 0.11) \times 10^{-5}$		1728		
					$J/\psi(1S) \pi^+ \pi^+ \pi^+ \pi^- \pi^-$	$(1.16 \pm 0.13) \times 10^{-5}$		1635		
					$\psi(2S) \pi^+ \pi^+ \pi^-$	$(1.9 \pm 0.4) \times 10^{-5}$		1304		
					$J/\psi(1S) \rho^+$	$(4.1 \pm 0.5) \times 10^{-5}$	S=1.4	1611		
					$J/\psi(1S) \pi^+ \pi^0$ nonresonant	$< 7.3$	$\times 10^{-6}$	CL=90%	1717	
					$J/\psi(1S) a_1(1260)^+$	$< 1.2$	$\times 10^{-3}$	CL=90%	1415	
					$J/\psi(1S) \rho \bar{\rho} \pi^+$	$< 5.0$	$\times 10^{-7}$	CL=90%	643	
					$J/\psi(1S) p \bar{p}$	$(1.46 \pm 0.12) \times 10^{-5}$		567		
					$J/\psi(1S) \Sigma^0 p$	$< 1.1$	$\times 10^{-5}$	CL=90%	-	
					$J/\psi(1S) D^+$	$< 1.2$	$\times 10^{-4}$	CL=90%	871	
					$J/\psi(1S) \bar{D}^0 \pi^+$	$< 2.5$	$\times 10^{-5}$	CL=90%	665	
					$\psi(2S) \pi^+$	$(2.44 \pm 0.30) \times 10^{-5}$		1347		
					$\psi(2S) K^+$	$(6.19 \pm 0.22) \times 10^{-4}$		1284		
					$\psi(2S) K^*(892)^+$	$(6.7 \pm 1.4) \times 10^{-4}$	S=1.3	1116		

## Meson Summary Table

$\psi(2S)K^+\pi^+\pi^-$	$(4.3 \pm 0.5) \times 10^{-4}$	1179	$f_0(1370)^0K^+ \times$	$< 1.07$	$\times 10^{-5}$	CL=90%	-
$\psi(2S)\phi(1020)K^+$	$(4.0 \pm 0.7) \times 10^{-6}$	417	$B(f_0(1370)^0 \rightarrow \pi^+\pi^-)$				
$\psi(3770)K^+$	$(4.9 \pm 1.3) \times 10^{-4}$	1218	$\rho^0(1450)K^+ \times$	$< 1.17$	$\times 10^{-5}$	CL=90%	-
$\psi(3770)K^+, \psi \rightarrow D^0\bar{D}^0$	$(1.5 \pm 0.5) \times 10^{-4}$	S=1.4 1218	$B(\rho^0(1450) \rightarrow \pi^+\pi^-)$				
$\psi(3770)K^+, \psi \rightarrow D^+D^-$	$(9.4 \pm 3.5) \times 10^{-5}$	1218	$f_2'(1525)K^+ \times$	$< 3.4$	$\times 10^{-6}$	CL=90%	2394
$\psi(3770)K^+, \psi \rightarrow \rho\bar{\rho}$	$< 2$	$\times 10^{-7}$	$B(f_2'(1525) \rightarrow \pi^+\pi^-)$				
$\psi(4040)K^+$	$< 1.3$	$\times 10^{-4}$	$K^+\rho^0$	$(3.7 \pm 0.5) \times 10^{-6}$			2559
$\psi(4160)K^+$	$(5.1 \pm 2.7) \times 10^{-4}$	868	$K_S^0(1430)^0\pi^+$	$(3.9 \pm 0.6) \times 10^{-5}$		S=1.4	2445
$\psi(4160)K^+, \psi \rightarrow \bar{D}^0D^0$	$(8 \pm 5) \times 10^{-5}$	-	$K_0^*(1430)^+\pi^0$	$(1.19 \pm 0.20) \times 10^{-5}$			-
$\chi_{c0}\pi^+, \chi_{c0} \rightarrow \pi^+\pi^-$	$< 1$	$\times 10^{-7}$	$K_2^*(1430)^0\pi^+$	$(5.6 \pm 2.2) \times 10^{-6}$			2445
$\chi_{c0}K^+$	$(1.50 \pm 0.15) \times 10^{-4}$	1478	$K^*(1410)^0\pi^+$	$< 4.5$	$\times 10^{-5}$	CL=90%	2448
$\chi_{c0}K^*(892)^+$	$< 2.1$	$\times 10^{-4}$	$K^*(1680)^0\pi^+$	$< 1.2$	$\times 10^{-5}$	CL=90%	2358
$\chi_{c1}(1P)\pi^+$	$(2.2 \pm 0.5) \times 10^{-5}$	1468	$K^+\pi^0\pi^0$	$(1.62 \pm 0.19) \times 10^{-5}$			2610
$\chi_{c1}(1P)K^+$	$(4.85 \pm 0.33) \times 10^{-4}$	S=1.5 1412	$f_0(980)K^+ \times B(f_0 \rightarrow \pi^0\pi^0)$	$(2.8 \pm 0.8) \times 10^{-6}$			2522
$\chi_{c1}(1P)K^*(892)^+$	$(3.0 \pm 0.6) \times 10^{-4}$	S=1.1 1265	$K^-\pi^+\pi^+$	$< 4.6$	$\times 10^{-8}$	CL=90%	2609
$\chi_{c1}(1P)K^0\pi^+$	$(5.8 \pm 0.4) \times 10^{-4}$	1370	$K^-\pi^+\pi^+$ nonresonant	$< 5.6$	$\times 10^{-5}$	CL=90%	2609
$\chi_{c1}(1P)K^+\pi^0$	$(3.29 \pm 0.35) \times 10^{-4}$	1373	$K_1(1270)^0\pi^+$	$< 4.0$	$\times 10^{-5}$	CL=90%	2489
$\chi_{c1}(1P)K^+\pi^+\pi^-$	$(3.74 \pm 0.30) \times 10^{-4}$	1319	$K_1^*(1400)^0\pi^+$	$< 3.9$	$\times 10^{-5}$	CL=90%	2451
$\chi_{c1}(2P)K^+, \chi_{c1}(2P) \rightarrow$	$< 1.1$	$\times 10^{-5}$	$K^0\pi^+\pi^0$	$< 6.6$	$\times 10^{-5}$	CL=90%	2609
$\pi^+\pi^-\chi_{c1}(1P)$			$K^0\rho^+$	$(7.3 \pm 1.0) \times 10^{-6}$			2558
$\chi_{c2}K^+$	$(1.1 \pm 0.4) \times 10^{-5}$	1379	$K^*(892)^+\pi^+\pi^-$	$(7.5 \pm 1.0) \times 10^{-5}$			2557
$\chi_{c2}K^+, \chi_{c2} \rightarrow \rho\bar{\rho}\pi^+\pi^-$	$< 1.9$	$\times 10^{-7}$	$K^*(892)^+\rho^0$	$(4.6 \pm 1.1) \times 10^{-6}$			2504
$\chi_{c2}K^*(892)^+$	$< 1.2$	$\times 10^{-4}$	$K^*(892)^+f_0(980)$	$(4.2 \pm 0.7) \times 10^{-6}$			2466
$\chi_{c2}K^0\pi^+$	$(1.16 \pm 0.25) \times 10^{-4}$	1336	$a_1^+K^0$	$(3.5 \pm 0.7) \times 10^{-5}$			-
$\chi_{c2}K^+\pi^0$	$< 6.2$	$\times 10^{-5}$	$b_1^+K^0 \times B(b_1^+ \rightarrow \omega\pi^+)$	$(9.6 \pm 1.9) \times 10^{-6}$			-
$\chi_{c2}K^+\pi^+\pi^-$	$(1.34 \pm 0.19) \times 10^{-4}$	1284	$K^*(892)^0\rho^+$	$(9.2 \pm 1.5) \times 10^{-6}$			2504
$\chi_{c2}(3930)\pi^+, \chi_{c2} \rightarrow \pi^+\pi^-$	$< 1$	$\times 10^{-7}$	$K_1(1400)^+\rho^0$	$< 7.8$	$\times 10^{-4}$	CL=90%	2388
$h_c(1P)K^+$	$(3.7 \pm 1.2) \times 10^{-5}$	1401	$K_2^*(1430)^+\rho^0$	$< 1.5$	$\times 10^{-3}$	CL=90%	2381
$h_c(1P)K^+, h_c \rightarrow \rho\bar{\rho}$	$< 6.4$	$\times 10^{-8}$	$b_1^0K^+ \times B(b_1^0 \rightarrow \omega\pi^0)$	$(9.1 \pm 2.0) \times 10^{-6}$			-
			$b_1^+K^* \times B(b_1^+ \rightarrow \omega\pi^+)$	$< 5.9$	$\times 10^{-6}$	CL=90%	-
			$b_1^0K^* \times B(b_1^0 \rightarrow \omega\pi^0)$	$< 6.7$	$\times 10^{-6}$	CL=90%	-
<b>K or K* modes</b>			$K^+\bar{K}^0$	$(1.31 \pm 0.17) \times 10^{-6}$		S=1.2	2593
$K^0\pi^+$	$(2.37 \pm 0.08) \times 10^{-5}$	2614	$\bar{K}^0K^+\pi^0$	$< 2.4$	$\times 10^{-5}$	CL=90%	2578
$K^+\pi^0$	$(1.29 \pm 0.05) \times 10^{-5}$	2615	$K^+K_S^0K_S^0$	$(1.05 \pm 0.04) \times 10^{-5}$			2521
$\eta'K^+$	$(7.04 \pm 0.25) \times 10^{-5}$	2528	$f_0(980)K^+, f_0 \rightarrow K_S^0K_S^0$	$(1.47 \pm 0.33) \times 10^{-5}$			-
$\eta'K^*(892)^+$	$(4.8 \pm 1.8) \times 10^{-6}$	2472	$f_0(1710)K^+, f_0 \rightarrow K_S^0K_S^0$	$(4.8 \pm 4.0) \times 10^{-7}$			-
$\eta'K_S^0(1430)^+$	$(5.2 \pm 2.1) \times 10^{-6}$	-	$K^+K_S^0K_S^0$ nonresonant	$(2.0 \pm 0.4) \times 10^{-5}$			2521
$\eta'K_2^*(1430)^+$	$(2.8 \pm 0.5) \times 10^{-5}$	2346	$K_S^0K_S^0\pi^+$	$< 5.1$	$\times 10^{-7}$	CL=90%	2577
$\eta K^+$	$(2.4 \pm 0.4) \times 10^{-6}$	S=1.7 2588	$K^+K^-\pi^+$	$(5.2 \pm 0.4) \times 10^{-6}$			2578
$\eta K^*(892)^+$	$(1.93 \pm 0.16) \times 10^{-5}$	2534	$K^+K^-\pi^+$ nonresonant	$(1.68 \pm 0.26) \times 10^{-6}$			2578
$\eta K_S^0(1430)^+$	$(1.8 \pm 0.4) \times 10^{-5}$	-	$K^+\bar{K}^*(892)^0$	$(5.9 \pm 0.8) \times 10^{-7}$			2540
$\eta K_2^*(1430)^+$	$(9.1 \pm 3.0) \times 10^{-6}$	2414	$K^+\bar{K}_0^0(1430)^0$	$(3.8 \pm 1.3) \times 10^{-7}$			2421
$\eta(1295)K^+ \times B(\eta(1295) \rightarrow$	$(2.9 \pm 0.8) \times 10^{-6}$	2455	$\pi^+(K^+K^-) s\text{-wave}$	$(8.5 \pm 0.9) \times 10^{-7}$			2578
$\eta\pi\pi)$			$K^+K^+\pi^-$	$< 1.1$	$\times 10^{-8}$	CL=90%	2578
$\eta(1405)K^+ \times B(\eta(1405) \rightarrow$	$< 1.3$	$\times 10^{-6}$	$K^+K^+\pi^-$ nonresonant	$< 8.79$	$\times 10^{-5}$	CL=90%	2578
$\eta\pi\pi)$			$f_2'(1525)K^+$	$(1.8 \pm 0.5) \times 10^{-6}$		S=1.1	2394
$\eta(1405)K^+ \times B(\eta(1405) \rightarrow$	$< 1.2$	$\times 10^{-6}$	$K^*+\pi^+K^-$	$< 1.18$	$\times 10^{-5}$	CL=90%	2524
$K^*K)$			$K^*(892)^+K^*(892)^0$	$(9.1 \pm 2.9) \times 10^{-7}$			2485
$\eta(1475)K^+ \times B(\eta(1475) \rightarrow$	$(1.38 \pm 0.21) \times 10^{-5}$	2407	$K^*+K^+\pi^-$	$< 6.1$	$\times 10^{-6}$	CL=90%	2524
$K^*K)$			$K^+K^-K^+$	$(3.40 \pm 0.14) \times 10^{-5}$		S=1.4	2523
$f_1(1285)K^+$	$< 2.0$	$\times 10^{-6}$	$K^+\phi$	$(8.8 \pm 0.7) \times 10^{-6}$		S=1.1	2516
$f_1(1420)K^+ \times B(f_1(1420) \rightarrow$	$< 2.9$	$\times 10^{-6}$	$f_0(980)K^+ \times B(f_0(980) \rightarrow$	$(9.4 \pm 3.2) \times 10^{-6}$			2522
$\eta\pi\pi)$			$K^+K^-)$				
$f_1(1420)K^+ \times B(f_1(1420) \rightarrow$	$< 4.1$	$\times 10^{-6}$	$a_2(1320)K^+ \times$	$< 1.1$	$\times 10^{-6}$	CL=90%	2449
$K^*K)$			$B(a_2(1320) \rightarrow K^+K^-)$				
$\phi(1680)K^+ \times B(\phi(1680) \rightarrow$	$< 3.4$	$\times 10^{-6}$	$X_0(1550)K^+ \times$	$(4.3 \pm 0.7) \times 10^{-6}$			-
$K^*K)$			$B(X_0(1550) \rightarrow K^+K^-)$				
$f_0(1500)K^+$	$(3.7 \pm 2.2) \times 10^{-6}$	2398	$\phi(1680)K^+ \times B(\phi(1680) \rightarrow$	$< 8$	$\times 10^{-7}$	CL=90%	2344
$\omega K^+$	$(6.5 \pm 0.4) \times 10^{-6}$	2558	$K^+K^-)$				
$\omega K^*(892)^+$	$< 7.4$	$\times 10^{-6}$	$f_0(1710)K^+ \times B(f_0(1710) \rightarrow$	$(1.1 \pm 0.6) \times 10^{-6}$			2336
$\omega(K\pi)_0^{*+}$	$(2.8 \pm 0.4) \times 10^{-5}$	-	$K^+K^-)$				
$\omega K_0^*(1430)^+$	$(2.4 \pm 0.5) \times 10^{-5}$	-	$K^+K^-\pi^+$ nonresonant	$(2.38 \pm 0.28) \times 10^{-5}$			2523
$\omega K_2^*(1430)^+$	$(2.1 \pm 0.4) \times 10^{-5}$	2379	$K^*(892)^+K^+K^-$	$(3.6 \pm 0.5) \times 10^{-5}$			2466
$a_0(980)^+K^0 \times B(a_0(980)^+ \rightarrow$	$< 3.9$	$\times 10^{-6}$	$K^*(892)^+\phi$	$(10.0 \pm 2.0) \times 10^{-6}$		S=1.7	2460
$\eta\pi^+)$			$\phi(K\pi)_0^{*+}$	$(8.3 \pm 1.6) \times 10^{-6}$			-
$a_0(980)^0K^+ \times B(a_0(980)^0 \rightarrow$	$< 2.5$	$\times 10^{-6}$	$\phi K_1(1270)^+$	$(6.1 \pm 1.9) \times 10^{-6}$			2380
$\eta\pi^0)$			$\phi K_1(1400)^+$	$< 3.2$	$\times 10^{-6}$	CL=90%	2339
$K^*(892)^0\pi^+$	$(1.01 \pm 0.08) \times 10^{-5}$	2562	$\phi K^*(1410)^+$	$< 4.3$	$\times 10^{-6}$	CL=90%	-
$K^*(892)^+\pi^0$	$(6.8 \pm 0.9) \times 10^{-6}$	2563	$\phi K_0^*(1430)^+$	$(7.0 \pm 1.6) \times 10^{-6}$			-
$K^+\pi^-\pi^+$	$(5.10 \pm 0.29) \times 10^{-5}$	2609	$\phi K_2^*(1430)^+$	$(8.4 \pm 2.1) \times 10^{-6}$			2332
$K^+\pi^-\pi^+$ nonresonant	$(1.63 \pm 0.21) \times 10^{-5}$	2609	$\phi K_2^*(1770)^+$	$< 1.50$	$\times 10^{-5}$	CL=90%	-
$\omega(782)K^+$	$(6 \pm 9) \times 10^{-6}$	2558					
$K^+f_0(980) \times B(f_0(980) \rightarrow$	$(9.4 \pm 1.0) \times 10^{-6}$	2522					
$\pi^+\pi^-)$							
$f_2(1270)^0K^+$	$(1.07 \pm 0.27) \times 10^{-6}$	-					



## Meson Summary Table

$K^+ \mu^+ \mu^-$ nonresonant	$B1$	$(4.37 \pm 0.27) \times 10^{-7}$	2612
$K^+ \tau^+ \tau^-$	$B1$	$< 2.25 \times 10^{-3}$	CL=90% 1687
$K^+ \bar{\nu} \nu$	$B1$	$< 1.6 \times 10^{-5}$	CL=90% 2617
$\rho^+ \nu \bar{\nu}$	$B1$	$< 3.0 \times 10^{-5}$	CL=90% 2583
$K^*(892)^+ \ell^+ \ell^-$	$B1$	$(1.01 \pm 0.11) \times 10^{-6}$	S=1.1 2564
$K^*(892)^+ e^+ e^-$	$B1$	$(1.55 \pm_{0.31}^{0.40}) \times 10^{-6}$	2564
$K^*(892)^+ \mu^+ \mu^-$	$B1$	$(9.6 \pm 1.0) \times 10^{-7}$	2560
$K^*(892)^+ \nu \bar{\nu}$	$B1$	$< 4.0 \times 10^{-5}$	CL=90% 2564
$K^+ \pi^+ \pi^- \mu^+ \mu^-$	$B1$	$(4.3 \pm 0.4) \times 10^{-7}$	2593
$\phi K^+ \mu^+ \mu^-$	$B1$	$(7.9 \pm_{1.7}^{2.1}) \times 10^{-8}$	2490
$\bar{\Lambda} \rho \nu \bar{\nu}$	$< 3.0 \times 10^{-5}$	CL=90%	2430
$\pi^+ e^+ \mu^-$	$LF$	$< 6.4 \times 10^{-3}$	CL=90% 2637
$\pi^+ e^- \mu^+$	$LF$	$< 6.4 \times 10^{-3}$	CL=90% 2637
$\pi^+ e^\pm \mu^\mp$	$LF$	$< 1.7 \times 10^{-7}$	CL=90% 2637
$\pi^+ e^+ \tau^-$	$LF$	$< 7.4 \times 10^{-5}$	CL=90% 2338
$\pi^+ e^- \tau^+$	$LF$	$< 2.0 \times 10^{-5}$	CL=90% 2338
$\pi^+ e^\pm \tau^\mp$	$LF$	$< 7.5 \times 10^{-5}$	CL=90% 2338
$\pi^+ \mu^+ \tau^-$	$LF$	$< 6.2 \times 10^{-5}$	CL=90% 2333
$\pi^+ \mu^- \tau^+$	$LF$	$< 4.5 \times 10^{-5}$	CL=90% 2333
$\pi^+ \mu^\pm \tau^\mp$	$LF$	$< 7.2 \times 10^{-5}$	CL=90% 2333
$K^+ e^+ \mu^-$	$LF$	$< 7.0 \times 10^{-9}$	CL=90% 2615
$K^+ e^- \mu^+$	$LF$	$< 6.4 \times 10^{-9}$	CL=90% 2615
$K^+ e^\pm \mu^\mp$	$LF$	$< 9.1 \times 10^{-8}$	CL=90% 2615
$K^+ e^+ \tau^-$	$LF$	$< 4.3 \times 10^{-5}$	CL=90% 2312
$K^+ e^- \tau^+$	$LF$	$< 1.5 \times 10^{-5}$	CL=90% 2312
$K^+ e^\pm \tau^\mp$	$LF$	$< 3.0 \times 10^{-5}$	CL=90% 2312
$K^+ \mu^+ \tau^-$	$LF$	$< 4.5 \times 10^{-5}$	CL=90% 2298
$K^+ \mu^- \tau^+$	$LF$	$< 2.8 \times 10^{-5}$	CL=90% 2298
$K^+ \mu^\pm \tau^\mp$	$LF$	$< 4.8 \times 10^{-5}$	CL=90% 2298
$K^*(892)^+ e^+ \mu^-$	$LF$	$< 1.3 \times 10^{-6}$	CL=90% 2563
$K^*(892)^+ e^- \mu^+$	$LF$	$< 9.9 \times 10^{-7}$	CL=90% 2563
$K^*(892)^+ e^\pm \mu^\mp$	$LF$	$< 1.4 \times 10^{-6}$	CL=90% 2563
$\pi^- e^+ e^+$	$L$	$< 2.3 \times 10^{-8}$	CL=90% 2638
$\pi^- \mu^+ \mu^+$	$L$	$< 4.0 \times 10^{-9}$	CL=95% 2634
$\pi^- e^+ \mu^+$	$L$	$< 1.5 \times 10^{-7}$	CL=90% 2637
$\rho^- e^+ e^+$	$L$	$< 1.7 \times 10^{-7}$	CL=90% 2583
$\rho^- \mu^+ \mu^+$	$L$	$< 4.2 \times 10^{-7}$	CL=90% 2578
$\rho^- e^+ \mu^+$	$L$	$< 4.7 \times 10^{-7}$	CL=90% 2582
$K^- e^+ e^+$	$L$	$< 3.0 \times 10^{-8}$	CL=90% 2617
$K^- \mu^+ \mu^+$	$L$	$< 4.1 \times 10^{-8}$	CL=90% 2612
$K^- e^+ \mu^+$	$L$	$< 1.6 \times 10^{-7}$	CL=90% 2615
$K^*(892)^- e^+ e^+$	$L$	$< 4.0 \times 10^{-7}$	CL=90% 2564
$K^*(892)^- \mu^+ \mu^+$	$L$	$< 5.9 \times 10^{-7}$	CL=90% 2560
$K^*(892)^- e^+ \mu^+$	$L$	$< 3.0 \times 10^{-7}$	CL=90% 2563
$D^- e^+ e^+$	$L$	$< 2.6 \times 10^{-6}$	CL=90% 2309
$D^- e^+ \mu^+$	$L$	$< 1.8 \times 10^{-6}$	CL=90% 2307
$D^- \mu^+ \mu^+$	$L$	$< 6.9 \times 10^{-7}$	CL=95% 2303
$D^{*-} \mu^+ \mu^+$	$L$	$< 2.4 \times 10^{-6}$	CL=95% 2251
$D_s^- \mu^+ \mu^+$	$L$	$< 5.8 \times 10^{-7}$	CL=95% 2267
$\bar{D}^0 \pi^- \mu^+ \mu^+$	$L$	$< 1.5 \times 10^{-6}$	CL=95% 2295
$\Lambda^0 \mu^+$	$L, B$	$< 6 \times 10^{-8}$	CL=90%
$\Lambda^0 e^+$	$L, B$	$< 3.2 \times 10^{-8}$	CL=90%
$\bar{\Lambda}^0 \mu^+$	$L, B$	$< 6 \times 10^{-8}$	CL=90%
$\bar{\Lambda}^0 e^+$	$L, B$	$< 8 \times 10^{-8}$	CL=90%

 **$B^0$** 

$$I(J^P) = \frac{1}{2}(0^-)$$

$I, J, P$  need confirmation. Quantum numbers shown are quark-model predictions.

$$\text{Mass } m_{B^0} = 5279.65 \pm 0.12 \text{ MeV}$$

$$m_{B^0} - m_{B^\pm} = 0.31 \pm 0.05 \text{ MeV}$$

$$\text{Mean life } \tau_{B^0} = (1.519 \pm 0.004) \times 10^{-12} \text{ s}$$

$$c\tau = 455.4 \mu\text{m}$$

$$\tau_{B^+}/\tau_{B^0} = 1.076 \pm 0.004 \quad (\text{direct measurements})$$

 **$B^0$ - $\bar{B}^0$  mixing parameters**

$$\chi_d = 0.1858 \pm 0.0011$$

$$\Delta m_{B^0} = m_{B_H^0} - m_{B_L^0} = (0.5065 \pm 0.0019) \times 10^{12} \hbar \text{ s}^{-1}$$

$$= (3.334 \pm 0.013) \times 10^{-10} \text{ MeV}$$

$$\chi_d = \Delta m_{B^0}/\Gamma_{B^0} = 0.769 \pm 0.004$$

$$\text{Re}(\lambda_{CP} / |\lambda_{CP}|) \text{ Re}(z) = 0.047 \pm 0.022$$

$$\Delta\Gamma \text{ Re}(z) = -0.007 \pm 0.004$$

$$\text{Re}(z) = (-4 \pm 4) \times 10^{-2} \quad (S = 1.4)$$

$$\text{Im}(z) = (-0.8 \pm 0.4) \times 10^{-2}$$

**CP violation parameters**

$$\text{Re}(\epsilon_{B^0})/(1+|\epsilon_{B^0}|^2) = (-0.5 \pm 0.4) \times 10^{-3}$$

$$A_{T/CP}(B^0 \leftrightarrow \bar{B}^0) = 0.005 \pm 0.018$$

$$A_{CP}(B^0 \rightarrow D^*(2010)^+ D^-) = 0.037 \pm 0.034$$

$$A_{CP}(B^0 \rightarrow [K^+ K^-]_D K^*(892)^0) = -0.05 \pm 0.10$$

$$A_{CP}(B^0 \rightarrow [K^+ \pi^-]_D K^*(892)^0) = 0.047 \pm 0.029$$

$$A_{CP}(B^0 \rightarrow [K^+ \pi^- \pi^+ \pi^-]_D K^*(892)^0) = 0.037 \pm 0.034$$

$$A_{CP}(B^0 \rightarrow [K^- \pi^+]_D K^*(892)^0) = 0.19 \pm 0.19$$

$$A_{CP}(B^0 \rightarrow [K^- \pi^+ \pi^+ \pi^-]_D K^*(892)^0) = -0.01 \pm 0.24$$

$$R_d^+ = \Gamma(B^0 \rightarrow [\pi^+ K^-]_D K^{*0}) / \Gamma(B^0 \rightarrow [\pi^- K^+]_D K^{*0}) = 0.064 \pm 0.021$$

$$R_d^- = \Gamma(\bar{B}^0 \rightarrow [\pi^- K^+]_D K^{*0}) / \Gamma(\bar{B}^0 \rightarrow [\pi^+ K^-]_D K^{*0}) = 0.095 \pm 0.021$$

$$A_{CP}(B^0 \rightarrow [\pi^+ \pi^-]_D K^*(892)^0) = -0.18 \pm 0.14$$

$$A_{CP}(B^0 \rightarrow [\pi^+ \pi^- \pi^+ \pi^-]_D K^*(892)^0) = -0.03 \pm 0.15$$

$$R_d^+ = \Gamma(B^0 \rightarrow [\pi^+ K^- \pi^+ \pi^-]_D K^{*0}) / \Gamma(B^0 \rightarrow [\pi^- K^+ \pi^+ \pi^-]_D K^{*0}) = 0.074 \pm 0.026$$

$$R_d^- = \Gamma(\bar{B}^0 \rightarrow [\pi^- K^+ \pi^+ \pi^-]_D K^{*0}) / \Gamma(\bar{B}^0 \rightarrow [\pi^+ K^- \pi^+ \pi^-]_D K^{*0}) = 0.072 \pm 0.025$$

$$A_{CP}(B^0 \rightarrow K^+ \pi^-) = -0.083 \pm 0.004$$

$$A_{CP}(B^0 \rightarrow \eta' K^*(892)^0) = -0.07 \pm 0.18$$

$$A_{CP}(B^0 \rightarrow \eta' K_0^*(1430)^0) = -0.19 \pm 0.17$$

$$A_{CP}(B^0 \rightarrow \eta' K_2^*(1430)^0) = 0.14 \pm 0.18$$

$$A_{CP}(B^0 \rightarrow \eta' K^*(892)^0) = 0.19 \pm 0.05$$

$$A_{CP}(B^0 \rightarrow \eta K_0^*(1430)^0) = 0.06 \pm 0.13$$

$$A_{CP}(B^0 \rightarrow \eta K_2^*(1430)^0) = -0.07 \pm 0.19$$

$$A_{CP}(B^0 \rightarrow b_1 K^+) = -0.07 \pm 0.12$$

$$A_{CP}(B^0 \rightarrow \omega K^{*0}) = 0.45 \pm 0.25$$

$$A_{CP}(B^0 \rightarrow \omega(K\pi)_0^{*0}) = -0.07 \pm 0.09$$

$$A_{CP}(B^0 \rightarrow \omega K_2^*(1430)^0) = -0.37 \pm 0.17$$

$$A_{CP}(B^0 \rightarrow K^+ \pi^- \pi^0) = (0 \pm 6) \times 10^{-2}$$

$$A_{CP}(B^0 \rightarrow \rho^- K^+) = 0.20 \pm 0.11$$

$$A_{CP}(B^0 \rightarrow \rho(1450)^- K^+) = -0.10 \pm 0.33$$

$$A_{CP}(B^0 \rightarrow \rho(1700)^- K^+) = -0.4 \pm 0.6$$

$$A_{CP}(B^0 \rightarrow K^+ \pi^- \pi^0 \text{ nonresonant}) = 0.10 \pm 0.18$$

$$A_{CP}(B^0 \rightarrow K^0 \pi^+ \pi^-) = -0.01 \pm 0.05$$

$$A_{CP}(B^0 \rightarrow K^*(892)^+ \pi^-) = -0.27 \pm 0.04$$

$$A_{CP}(B^0 \rightarrow (K\pi)_0^{*+} \pi^-) = 0.02 \pm 0.04$$

$$A_{CP}(B^0 \rightarrow K_2^*(1430)^+ \pi^-) = -0.29 \pm 0.24$$

$$A_{CP}(B^0 \rightarrow K^*(1680)^+ \pi^-) = -0.07 \pm 0.14$$

$$A_{CP}(B^0 \rightarrow \bar{f}_0(980) K_S^0) = 0.28 \pm 0.31$$

$$A_{CP}(B^0 \rightarrow (K\pi)_0^{*0} \pi^0) = -0.15 \pm 0.11$$

$$A_{CP}(B^0 \rightarrow K^{*0} \pi^0) = -0.15 \pm 0.13$$

$$A_{CP}(B^0 \rightarrow K^*(892)^0 \pi^+ \pi^-) = 0.07 \pm 0.05$$

$$A_{CP}(B^0 \rightarrow K^*(892)^0 \rho^0) = -0.06 \pm 0.09$$

$$A_{CP}(B^0 \rightarrow K^{*0} \bar{f}_0(980)) = 0.07 \pm 0.10$$

$$A_{CP}(B^0 \rightarrow K^+ \rho^-) = 0.21 \pm 0.15$$

$$A_{CP}(B^0 \rightarrow K^*(892)^0 K^+ K^-) = 0.01 \pm 0.05$$

$$A_{CP}(B^0 \rightarrow a_1^- K^+) = -0.16 \pm 0.12$$

$$A_{CP}(B^0 \rightarrow K^0 K^0) = -0.6 \pm 0.7$$

$$A_{CP}(B^0 \rightarrow K^*(892)^0 \phi) = 0.00 \pm 0.04$$

$$A_{CP}(B^0 \rightarrow K^*(892)^0 K^- \pi^+) = 0.2 \pm 0.4$$

$$A_{CP}(B^0 \rightarrow \phi(K\pi)_0^{*0}) = 0.12 \pm 0.08$$

$$A_{CP}(B^0 \rightarrow \phi K_2^*(1430)^0) = -0.11 \pm 0.10$$

$$A_{CP}(B^0 \rightarrow K^*(892)^0 \gamma) = -0.006 \pm 0.011$$

$$A_{CP}(B^0 \rightarrow K_2^*(1430)^0 \gamma) = -0.08 \pm 0.15$$

$$A_{CP}(B^0 \rightarrow X_S \gamma) = -0.009 \pm 0.018$$

$$A_{CP}(B^0 \rightarrow \rho^+ \pi^-) = 0.13 \pm 0.06 \quad (S = 1.1)$$

$$A_{CP}(B^0 \rightarrow \rho^- \pi^+) = -0.08 \pm 0.08$$

$$A_{CP}(B^0 \rightarrow a_1(1260)^\pm \pi^\mp) = -0.07 \pm 0.06$$

$$A_{CP}(B^0 \rightarrow b_1^- \pi^+) = -0.05 \pm 0.10$$

$$A_{CP}(B^0 \rightarrow \rho \bar{K}^*(892)^0) = 0.05 \pm 0.12$$

$$A_{CP}(B^0 \rightarrow \rho \bar{\Lambda} \pi^-) = 0.04 \pm 0.07$$

$$A_{CP}(B^0 \rightarrow K^{*0} \ell^+ \ell^-) = -0.05 \pm 0.10$$

$$A_{CP}(B^0 \rightarrow K^{*0} e^+ e^-) = -0.21 \pm 0.19$$

$$A_{CP}(B^0 \rightarrow K^{*0} \mu^+ \mu^-) = -0.034 \pm 0.024$$

$$C_{D^+ D^+} (B^0 \rightarrow D^*(2010)^- D^+) = -0.01 \pm 0.11$$

$$S_{D^+ D^+} (B^0 \rightarrow D^*(2010)^- D^+) = -0.72 \pm 0.15$$

$$C_{D^{++} D^-} (B^0 \rightarrow D^*(2010)^+ D^-) = 0.00 \pm 0.13 \quad (S = 1.3)$$

$$S_{D^{++} D^-} (B^0 \rightarrow D^*(2010)^+ D^-) = -0.73 \pm 0.14$$

$$C_{D^{*-} D^{*-}} (B^0 \rightarrow D^{*-} D^{*-}) = 0.01 \pm 0.09 \quad (S = 1.6)$$

## Meson Summary Table

$S_{D^{*+}D^-} (B^0 \rightarrow D^{*+}D^-) = -0.59 \pm 0.14$ (S = 1.8)	$S_{\pi\pi} (B^0 \rightarrow \pi^+\pi^-) = -0.65 \pm 0.04$
$C_+ (B^0 \rightarrow D^{*+}D^-) = 0.00 \pm 0.10$ (S = 1.6)	$C_{\rho^0\pi^0} (B^0 \rightarrow \rho^0\pi^0) = -0.33 \pm 0.22$
$S_+ (B^0 \rightarrow D^{*+}D^-) = -0.73 \pm 0.09$	$C_{\rho\pi} (B^0 \rightarrow \rho^+\pi^-) = -0.03 \pm 0.07$ (S = 1.2)
$C_- (B^0 \rightarrow D^{*+}D^-) = 0.19 \pm 0.31$	$S_{\rho\pi} (B^0 \rightarrow \rho^+\pi^-) = 0.05 \pm 0.07$
$S_- (B^0 \rightarrow D^{*+}D^-) = 0.1 \pm 1.6$ (S = 3.5)	$\Delta C_{\rho\pi} (B^0 \rightarrow \rho^+\pi^-) = 0.27 \pm 0.06$
$C (B^0 \rightarrow D^*(2010)^+D^*(2010)^-K_S^0) = 0.01 \pm 0.29$	$\Delta S_{\rho\pi} (B^0 \rightarrow \rho^+\pi^-) = 0.01 \pm 0.08$
$S (B^0 \rightarrow D^*(2010)^+D^*(2010)^-K_S^0) = 0.1 \pm 0.4$	$C_{\rho^0\pi^0} (B^0 \rightarrow \rho^0\pi^0) = 0.27 \pm 0.24$
$C_{D^+D^-} (B^0 \rightarrow D^+D^-) = -0.22 \pm 0.24$ (S = 2.5)	$S_{\rho^0\pi^0} (B^0 \rightarrow \rho^0\pi^0) = -0.23 \pm 0.34$
$S_{D^+D^-} (B^0 \rightarrow D^+D^-) = -0.76^{+0.15}_{-0.13}$ (S = 1.2)	$C_{a_1\pi} (B^0 \rightarrow a_1(1260)^+\pi^-) = -0.05 \pm 0.11$
$C_{J/\psi(1S)\pi^0} (B^0 \rightarrow J/\psi(1S)\pi^0) = 0.03 \pm 0.17$ (S = 1.5)	$S_{a_1\pi} (B^0 \rightarrow a_1(1260)^+\pi^-) = -0.2 \pm 0.4$ (S = 3.2)
$S_{J/\psi(1S)\pi^0} (B^0 \rightarrow J/\psi(1S)\pi^0) = -0.88 \pm 0.32$ (S = 2.2)	$\Delta C_{a_1\pi} (B^0 \rightarrow a_1(1260)^+\pi^-) = 0.43 \pm 0.14$ (S = 1.3)
$C (B^0 \rightarrow J/\psi(1S)\rho^0) = -0.06 \pm 0.06$	$\Delta S_{a_1\pi} (B^0 \rightarrow a_1(1260)^+\pi^-) = -0.11 \pm 0.12$
$S (B^0 \rightarrow J/\psi(1S)\rho^0) = -0.66^{+0.16}_{-0.12}$	$C (B^0 \rightarrow b_1^-K^+) = -0.22 \pm 0.24$
$C_{D_{CP}^{(*)}h^0} (B^0 \rightarrow D_{CP}^{(*)}h^0) = -0.02 \pm 0.08$	$\Delta C (B^0 \rightarrow b_1^-K^+) = -1.04 \pm 0.24$
$S_{D_{CP}^{(*)}h^0} (B^0 \rightarrow D_{CP}^{(*)}h^0) = -0.66 \pm 0.12$	$C_{\rho^0\rho^0} (B^0 \rightarrow \rho^0\rho^0) = 0.2 \pm 0.9$
$C_{K^0\pi^0} (B^0 \rightarrow K^0\pi^0) = 0.00 \pm 0.13$ (S = 1.4)	$S_{\rho^0\rho^0} (B^0 \rightarrow \rho^0\rho^0) = 0.3 \pm 0.7$
$S_{K^0\pi^0} (B^0 \rightarrow K^0\pi^0) = 0.58 \pm 0.17$	$C_{\rho\rho} (B^0 \rightarrow \rho^+\rho^-) = 0.00 \pm 0.09$
$C_{\eta'(958)K_S^0} (B^0 \rightarrow \eta'(958)K_S^0) = -0.04 \pm 0.20$ (S = 2.5)	$S_{\rho\rho} (B^0 \rightarrow \rho^+\rho^-) = -0.14 \pm 0.13$
$S_{\eta'(958)K_S^0} (B^0 \rightarrow \eta'(958)K_S^0) = 0.43 \pm 0.17$ (S = 1.5)	$ \lambda  (B^0 \rightarrow J/\psi K^*(892)^0) < 0.25$ , CL = 95%
$C_{\eta'K^0} (B^0 \rightarrow \eta'K^0) = -0.06 \pm 0.04$	$\cos 2\beta (B^0 \rightarrow J/\psi K^*(892)^0) = 1.7^{+0.7}_{-0.9}$ (S = 1.6)
$S_{\eta'K^0} (B^0 \rightarrow \eta'K^0) = 0.63 \pm 0.06$	$\cos 2\beta (B^0 \rightarrow [K_S^0\pi^+\pi^-]_{D^{(*)}h^0}) = 0.91 \pm 0.25$
$C_{\omega K_S^0} (B^0 \rightarrow \omega K_S^0) = 0.0 \pm 0.4$ (S = 3.0)	$(S_+ + S_-)/2 (B^0 \rightarrow D^{*-}\pi^+) = -0.039 \pm 0.011$
$S_{\omega K_S^0} (B^0 \rightarrow \omega K_S^0) = 0.70 \pm 0.21$	$(S_- - S_+)/2 (B^0 \rightarrow D^{*-}\pi^+) = -0.009 \pm 0.015$
$C (B^0 \rightarrow K_S^0\pi^0\pi^0) = -0.21 \pm 0.20$	$(S_+ + S_-)/2 (B^0 \rightarrow D^-\pi^+) = -0.046 \pm 0.023$
$S (B^0 \rightarrow K_S^0\pi^0\pi^0) = 0.89^{+0.27}_{-0.30}$	$(S_- - S_+)/2 (B^0 \rightarrow D^-\pi^+) = -0.022 \pm 0.021$
$C_{\rho^0 K_S^0} (B^0 \rightarrow \rho^0 K_S^0) = -0.04 \pm 0.20$	$S_+ (B^0 \rightarrow D^-\pi^+) = 0.058 \pm 0.023$
$S_{\rho^0 K_S^0} (B^0 \rightarrow \rho^0 K_S^0) = 0.50^{+0.17}_{-0.21}$	$S_- (B^0 \rightarrow D^+\pi^-) = 0.038 \pm 0.021$
$C_{f_0 K_S^0} (B^0 \rightarrow f_0(980)K_S^0) = 0.29 \pm 0.20$	$(S_+ + S_-)/2 (B^0 \rightarrow D^-\rho^+) = -0.024 \pm 0.032$
$S_{f_0 K_S^0} (B^0 \rightarrow f_0(980)K_S^0) = -0.50 \pm 0.16$	$(S_- - S_+)/2 (B^0 \rightarrow D^-\rho^+) = -0.10 \pm 0.06$
$S_{f_2 K_S^0} (B^0 \rightarrow f_2(1270)K_S^0) = -0.5 \pm 0.5$	$C_{\eta_c K_S^0} (B^0 \rightarrow \eta_c K_S^0) = 0.08 \pm 0.13$
$C_{f_2 K_S^0} (B^0 \rightarrow f_2(1270)K_S^0) = 0.3 \pm 0.4$	$S_{\eta_c K_S^0} (B^0 \rightarrow \eta_c K_S^0) = 0.93 \pm 0.17$
$S_{f_x K_S^0} (B^0 \rightarrow f_x(1300)K_S^0) = -0.2 \pm 0.5$	$C_{c\bar{c}K^{(*)0}} (B^0 \rightarrow c\bar{c}K^{(*)0}) = (0.5 \pm 1.7) \times 10^{-2}$
$C_{f_x K_S^0} (B^0 \rightarrow f_x(1300)K_S^0) = 0.13 \pm 0.35$	$\sin(2\beta) = 0.695 \pm 0.019$
$S_{K^0\pi^+\pi^-} (B^0 \rightarrow K^0\pi^+\pi^- \text{ nonresonant}) = -0.01 \pm 0.33$	$C_{J/\psi(nS)K^0} (B^0 \rightarrow J/\psi(nS)K^0) = (0.5 \pm 2.0) \times 10^{-2}$
$C_{K^0\pi^+\pi^-} (B^0 \rightarrow K^0\pi^+\pi^- \text{ nonresonant}) = 0.01 \pm 0.26$	$S_{J/\psi(nS)K^0} (B^0 \rightarrow J/\psi(nS)K^0) = 0.701 \pm 0.017$
$C_{K_S^0 K_S^0} (B^0 \rightarrow K_S^0 K_S^0) = 0.0 \pm 0.4$ (S = 1.4)	$C_{J/\psi K^{*0}} (B^0 \rightarrow J/\psi K^{*0}) = 0.03 \pm 0.10$
$S_{K_S^0 K_S^0} (B^0 \rightarrow K_S^0 K_S^0) = -0.8 \pm 0.5$	$S_{J/\psi K^{*0}} (B^0 \rightarrow J/\psi K^{*0}) = 0.60 \pm 0.25$
$C_{K^+K^-K_S^0} (B^0 \rightarrow K^+K^-K_S^0 \text{ nonresonant}) = 0.06 \pm 0.08$	$C_{\chi_{c0} K_S^0} (B^0 \rightarrow \chi_{c0} K_S^0) = -0.3^{+0.5}_{-0.4}$
$S_{K^+K^-K_S^0} (B^0 \rightarrow K^+K^-K_S^0 \text{ nonresonant}) = -0.66 \pm 0.11$	$S_{\chi_{c0} K_S^0} (B^0 \rightarrow \chi_{c0} K_S^0) = -0.7 \pm 0.5$
$C_{K^+K^-K_S^0} (B^0 \rightarrow K^+K^-K_S^0 \text{ inclusive}) = 0.01 \pm 0.09$	$C_{\chi_{c1} K_S^0} (B^0 \rightarrow \chi_{c1} K_S^0) = 0.06 \pm 0.07$
$S_{K^+K^-K_S^0} (B^0 \rightarrow K^+K^-K_S^0 \text{ inclusive}) = -0.65 \pm 0.12$	$S_{\chi_{c1} K_S^0} (B^0 \rightarrow \chi_{c1} K_S^0) = 0.63 \pm 0.10$
$C_{\phi K_S^0} (B^0 \rightarrow \phi K_S^0) = 0.01 \pm 0.14$	$\sin(2\beta_{\text{eff}})(B^0 \rightarrow \phi K^0) = 0.22 \pm 0.30$
$S_{\phi K_S^0} (B^0 \rightarrow \phi K_S^0) = 0.59 \pm 0.14$	$\sin(2\beta_{\text{eff}})(B^0 \rightarrow \phi K_S^0(1430)^0) = 0.97^{+0.03}_{-0.52}$
$C_{K_S K_S K_S} (B^0 \rightarrow K_S K_S K_S) = -0.23 \pm 0.14$	$\sin(2\beta_{\text{eff}})(B^0 \rightarrow [K_S^0\pi^+\pi^-]_{D^{(*)}h^0}) = 0.80 \pm 0.16$
$S_{K_S K_S K_S} (B^0 \rightarrow K_S K_S K_S) = -0.5 \pm 0.6$ (S = 3.0)	$\beta_{\text{eff}} (B^0 \rightarrow [K_S^0\pi^+\pi^-]_{D^{(*)}h^0}) = (22 \pm 5)^\circ$
$C_{K_S^0\pi^0\gamma} (B^0 \rightarrow K_S^0\pi^0\gamma) = 0.36 \pm 0.33$	$2\beta_{\text{eff}} (B^0 \rightarrow J/\psi\rho^0) = (42^{+10}_{-11})^\circ$
$S_{K_S^0\pi^0\gamma} (B^0 \rightarrow K_S^0\pi^0\gamma) = -0.8 \pm 0.6$	$ \lambda  (B^0 \rightarrow [K_S^0\pi^+\pi^-]_{D^{(*)}h^0}) = 1.01 \pm 0.08$
$C_{K_S^0\pi^+\pi^-\gamma} (B^0 \rightarrow K_S^0\pi^+\pi^-\gamma) = -0.39 \pm 0.20$	$ \sin(2\beta + \gamma)  > 0.40$ , CL = 90%
$S_{K_S^0\pi^+\pi^-\gamma} (B^0 \rightarrow K_S^0\pi^+\pi^-\gamma) = 0.14 \pm 0.25$	$2\beta + \gamma = (83 \pm 60)^\circ$
$C_{K^{*0}\gamma} (B^0 \rightarrow K^*(892)^0\gamma) = -0.04 \pm 0.16$ (S = 1.2)	$\alpha = (84.9^{+5.1}_{-4.5})^\circ$
$S_{K^{*0}\gamma} (B^0 \rightarrow K^*(892)^0\gamma) = -0.15 \pm 0.22$	$x_+ (B^0 \rightarrow DK^{*0}) = 0.04 \pm 0.17$
$C_{\eta K^0\gamma} (B^0 \rightarrow \eta K^0\gamma) = 0.1 \pm 0.4$ (S = 1.4)	$x_- (B^0 \rightarrow DK^{*0}) = -0.16 \pm 0.14$
$S_{\eta K^0\gamma} (B^0 \rightarrow \eta K^0\gamma) = -0.5 \pm 0.5$ (S = 1.2)	$y_+ (B^0 \rightarrow DK^{*0}) = -0.68 \pm 0.22$
$C_{K^0\phi\gamma} (B^0 \rightarrow K^0\phi\gamma) = -0.3 \pm 0.6$	$y_- (B^0 \rightarrow DK^{*0}) = 0.20 \pm 0.25$ (S = 1.2)
$S_{K^0\phi\gamma} (B^0 \rightarrow K^0\phi\gamma) = 0.7^{+0.7}_{-1.1}$	$r_{B^0} (B^0 \rightarrow DK^{*0}) = 0.220^{+0.041}_{-0.047}$
$C (B^0 \rightarrow K_S^0\rho^0\gamma) = -0.05 \pm 0.19$	$\delta_{B^0} (B^0 \rightarrow DK^{*0}) = (194^{+30}_{-22})^\circ$
$S (B^0 \rightarrow K_S^0\rho^0\gamma) = -0.04 \pm 0.23$	
$C (B^0 \rightarrow \rho^0\gamma) = 0.4 \pm 0.5$	
$S (B^0 \rightarrow \rho^0\gamma) = -0.8 \pm 0.7$	
$C_{\pi\pi} (B^0 \rightarrow \pi^+\pi^-) = -0.32 \pm 0.04$	

$\bar{B}^0$  modes are charge conjugates of the modes below. Reactions indicate the weak decay vertex and do not include mixing. Modes which do not identify the charge state of the  $B$  are listed in the  $B^\pm/B^0$  ADMIXTURE section.

The branching fractions listed below assume 50%  $B^0\bar{B}^0$  and 50%  $B^+B^-$  production at the  $\Upsilon(4S)$ . We have attempted to bring older measurements up to date by rescaling their assumed  $\Upsilon(4S)$  production ratio to 50:50 and their assumed  $D, D_s, D^*$ , and  $\psi$  branching ratios to current values whenever this would affect our averages and best limits significantly.

## Meson Summary Table

Indentation is used to indicate a subchannel of a previous reaction. All resonant subchannels have been corrected for resonance branching fractions to the final state so the sum of the subchannel branching fractions can exceed that of the final state.

For inclusive branching fractions, e.g.,  $B \rightarrow D^{\pm} X$ , the values usually are multiplicities, not branching fractions. They can be greater than one.

$B^0$ DECAY MODES	Fraction ( $\Gamma_i/\Gamma$ )	Scale factor / Confidence level	$\rho$ (MeV/c)
$\ell^+ \nu_\ell X$	[III] ( 10.33 ± 0.28 ) %	-	-
$e^+ \nu_e X_c$	( 10.1 ± 0.4 ) %	-	-
$D \ell^+ \nu_\ell X$	( 9.4 ± 0.9 ) %	-	-
$D^- \ell^+ \nu_\ell$	[III] ( 2.31 ± 0.10 ) %	2309	-
$D^- \tau^+ \nu_\tau$	( 1.08 ± 0.23 ) %	1909	-
$D^*(2010)^- \ell^+ \nu_\ell$	[III] ( 5.05 ± 0.14 ) %	2257	-
$D^*(2010)^- \tau^+ \nu_\tau$	( 1.57 ± 0.09 ) %	S=1.1 1838	-
$\overline{D}^0 \pi^- \ell^+ \nu_\ell$	( 4.1 ± 0.5 ) × 10 <sup>-3</sup>	2308	-
$D_0^*(2300)^- \ell^+ \nu_\ell, D_0^{*-} \rightarrow$	( 3.0 ± 1.2 ) × 10 <sup>-3</sup>	S=1.8 -	-
$\overline{D}^0 \pi^-$			
$D_2^*(2460)^- \ell^+ \nu_\ell, D_2^{*-} \rightarrow$	( 1.21 ± 0.33 ) × 10 <sup>-3</sup>	S=1.8 2065	-
$\overline{D}^0 \pi^-$			
$\overline{D}^{(*)} n \pi \ell^+ \nu_\ell$ ( $n \geq 1$ )	( 2.3 ± 0.5 ) %	-	-
$\overline{D}^{*0} \pi^- \ell^+ \nu_\ell$	( 5.8 ± 0.8 ) × 10 <sup>-3</sup>	S=1.4 2256	-
$D_1(2420)^- \ell^+ \nu_\ell, D_1^- \rightarrow$	( 2.80 ± 0.28 ) × 10 <sup>-3</sup>	-	-
$\overline{D}^{*0} \pi^-$			
$D_1'(2430)^- \ell^+ \nu_\ell, D_1'^- \rightarrow$	( 3.1 ± 0.9 ) × 10 <sup>-3</sup>	-	-
$\overline{D}^{*0} \pi^-$			
$D_2^*(2460)^- \ell^+ \nu_\ell, D_2^{*-} \rightarrow$	( 6.8 ± 1.2 ) × 10 <sup>-4</sup>	2065	-
$\overline{D}^{*0} \pi^-$			
$D^- \pi^+ \pi^- \ell^+ \nu_\ell$	( 1.3 ± 0.5 ) × 10 <sup>-3</sup>	2299	-
$D^{*-} \pi^+ \pi^- \ell^+ \nu_\ell$	( 1.4 ± 0.5 ) × 10 <sup>-3</sup>	2247	-
$\rho^- \ell^+ \nu_\ell$	[III] ( 2.94 ± 0.21 ) × 10 <sup>-4</sup>	2583	-
$\pi^- \ell^+ \nu_\ell$	[III] ( 1.50 ± 0.06 ) × 10 <sup>-4</sup>	2638	-
$\pi^- \tau^+ \nu_\tau$	< 2.5 × 10 <sup>-4</sup>	CL=90% 2339	-
<b>Inclusive modes</b>			
$K^{\pm} X$	( 78 ± 8 ) %	-	-
$D^0 X$	( 8.1 ± 1.5 ) %	-	-
$\overline{D}^0 X$	( 47.4 ± 2.8 ) %	-	-
$D^+ X$	< 3.9 %	CL=90%	-
$D^- X$	( 36.9 ± 3.3 ) %	-	-
$D_s^+ X$	( 10.3 ± 2.1 ) %	-	-
$D_s^- X$	< 2.6 %	CL=90%	-
$\Lambda_c^+ X$	< 3.1 %	CL=90%	-
$\overline{\Lambda}_c^- X$	( 5.0 ± 2.1 ) %	-	-
$\overline{c} X$	( 95 ± 5 ) %	-	-
$c X$	( 24.6 ± 3.1 ) %	-	-
$\overline{c}/c X$	( 119 ± 6 ) %	-	-
<b>D, D*, or D<sub>s</sub> modes</b>			
$D^- \pi^+$	( 2.52 ± 0.13 ) × 10 <sup>-3</sup>	S=1.1 2306	-
$D^- \rho^+$	( 7.6 ± 1.2 ) × 10 <sup>-3</sup>	2235	-
$D^- K^0 \pi^+$	( 4.9 ± 0.9 ) × 10 <sup>-4</sup>	2259	-
$D^- K^*(892)^+$	( 4.5 ± 0.7 ) × 10 <sup>-4</sup>	2211	-
$D^- \omega \pi^+$	( 2.8 ± 0.6 ) × 10 <sup>-3</sup>	2204	-
$D^- K^+$	( 1.86 ± 0.20 ) × 10 <sup>-4</sup>	2279	-
$D^- K^+ \pi^+ \pi^-$	( 3.5 ± 0.8 ) × 10 <sup>-4</sup>	2236	-
$D^- K^+ \overline{K}^0$	< 3.1 × 10 <sup>-4</sup>	CL=90% 2188	-
$D^- K^+ \overline{K}^*(892)^0$	( 8.8 ± 1.9 ) × 10 <sup>-4</sup>	2070	-
$\overline{D}^0 \pi^+ \pi^-$	( 8.8 ± 0.5 ) × 10 <sup>-4</sup>	2301	-
$D^*(2010)^- \pi^+$	( 2.74 ± 0.13 ) × 10 <sup>-3</sup>	2255	-
$\overline{D}^0 K^+ K^-$	( 5.9 ± 0.5 ) × 10 <sup>-5</sup>	2191	-
$D^- \pi^+ \pi^+ \pi^-$	( 6.0 ± 0.7 ) × 10 <sup>-3</sup>	S=1.1 2287	-
$(D^- \pi^+ \pi^+ \pi^-)$ nonresonant	( 3.9 ± 1.9 ) × 10 <sup>-3</sup>	2287	-
$D^- \pi^+ \rho^0$	( 1.1 ± 1.0 ) × 10 <sup>-3</sup>	2206	-
$D^- a_1(1260)^+$	( 6.0 ± 3.3 ) × 10 <sup>-3</sup>	2121	-
$D^*(2010)^- \pi^+ \pi^0$	( 1.5 ± 0.5 ) %	2248	-
$D^*(2010)^- \rho^+$	( 6.8 ± 0.9 ) × 10 <sup>-3</sup>	2180	-
$D^*(2010)^- K^+$	( 2.12 ± 0.15 ) × 10 <sup>-4</sup>	2226	-
$D^*(2010)^- K^0 \pi^+$	( 3.0 ± 0.8 ) × 10 <sup>-4</sup>	2205	-
$D^*(2010)^- K^*(892)^+$	( 3.3 ± 0.6 ) × 10 <sup>-4</sup>	2155	-
$D^*(2010)^- K^+ \overline{K}^0$	< 4.7 × 10 <sup>-4</sup>	CL=90% 2131	-
$D^*(2010)^- K^+ \overline{K}^*(892)^0$	( 1.29 ± 0.33 ) × 10 <sup>-3</sup>	2007	-
$D^*(2010)^- \pi^+ \pi^+ \pi^-$	( 7.21 ± 0.29 ) × 10 <sup>-3</sup>	2235	-
$(D^*(2010)^- \pi^+ \pi^+ \pi^-)$ non-resonant	( 0.0 ± 2.5 ) × 10 <sup>-3</sup>	2235	-
$D^*(2010)^- \pi^+ \rho^0$	( 5.7 ± 3.2 ) × 10 <sup>-3</sup>	2150	-

$D^*(2010)^- a_1(1260)^+$	( 1.30 ± 0.27 ) %	2061
$\overline{D}_1(2420)^0 \pi^- \pi^+, \overline{D}_1^0 \rightarrow$	( 1.47 ± 0.35 ) × 10 <sup>-4</sup>	-
$D^{*-} \pi^+$		
$D^*(2010)^- K^+ \pi^- \pi^+$	( 4.7 ± 0.4 ) × 10 <sup>-4</sup>	2181
$D^*(2010)^- \pi^+ \pi^+ \pi^- \pi^0$	( 1.76 ± 0.27 ) %	2218
$D^{*-} 3\pi^+ 2\pi^-$	( 4.7 ± 0.9 ) × 10 <sup>-3</sup>	2195
$D^*(2010)^- \omega \pi^+$	( 2.46 ± 0.18 ) × 10 <sup>-3</sup>	S=1.2 2148
$\overline{D}_1(2430)^0 \omega, \overline{D}_1^0 \rightarrow$	( 2.7 ± 0.8 ) × 10 <sup>-4</sup>	1992
$D^{*-} \pi^+$		
$D^{*-} \rho(1450)^+, \rho^+ \rightarrow \omega \pi^+$	( 1.07 ± 0.40 ) × 10 <sup>-3</sup>	-
$\overline{D}_1(2420)^0 \omega, \overline{D}_1^0 \rightarrow$	( 7.0 ± 2.2 ) × 10 <sup>-5</sup>	1995
$D^{*-} \pi^+$		
$\overline{D}_2^*(2460)^0 \omega, \overline{D}_2^0 \rightarrow$	( 4.0 ± 1.4 ) × 10 <sup>-5</sup>	1975
$D^{*-} \pi^+$		
$D^{*-} b_1(1235)^+, b_1^+ \rightarrow$	< 7 × 10 <sup>-5</sup>	CL=90% -
$\overline{D}^{*-} \pi^+$		
$\overline{D}^{*-} \pi^+$ [qqq]	( 1.9 ± 0.9 ) × 10 <sup>-3</sup>	-
$D_1(2420)^- \pi^+, D_1^- \rightarrow$	( 9.9 ± 2.0 ) × 10 <sup>-5</sup>	-
$D^- \pi^+ \pi^-$		
$D_1(2420)^- \pi^+, D_1^- \rightarrow$	< 3.3 × 10 <sup>-5</sup>	CL=90% -
$D^{*-} \pi^+ \pi^-$		
$\overline{D}_2^*(2460)^- \pi^+, (D_2^*)^- \rightarrow$	( 2.38 ± 0.16 ) × 10 <sup>-4</sup>	2062
$D^0 \pi^-$		
$\overline{D}_0^*(2400)^- \pi^+, (D_0^*)^- \rightarrow$	( 7.6 ± 0.8 ) × 10 <sup>-5</sup>	2090
$D^0 \pi^-$		
$D_2^*(2460)^- \pi^+, (D_2^*)^- \rightarrow$	< 2.4 × 10 <sup>-5</sup>	CL=90% -
$D^{*-} \pi^+ \pi^-$		
$\overline{D}_2^*(2460)^- \rho^+$	< 4.9 × 10 <sup>-3</sup>	CL=90% 1974
$D^0 \overline{D}^0$	( 1.4 ± 0.7 ) × 10 <sup>-5</sup>	1868
$D^{*0} \overline{D}^0$	< 2.9 × 10 <sup>-4</sup>	CL=90% 1794
$D^- D^+$	( 2.11 ± 0.18 ) × 10 <sup>-4</sup>	1864
$D^\pm D^{*\mp}$ (CP-averaged)	( 6.1 ± 0.6 ) × 10 <sup>-4</sup>	-
$D^- D_s^+$	( 7.2 ± 0.8 ) × 10 <sup>-3</sup>	1812
$D^*(2010)^- D_s^+$	( 8.0 ± 1.1 ) × 10 <sup>-3</sup>	1735
$D^- D_s^{*+}$	( 7.4 ± 1.6 ) × 10 <sup>-3</sup>	1732
$D^*(2010)^- D_s^{*+}$	( 1.77 ± 0.14 ) %	1649
$D_{s0}(2317)^- K^+, D_{s0}^- \rightarrow$	( 4.2 ± 1.4 ) × 10 <sup>-5</sup>	2097
$D_s^- \pi^0$		
$D_{s0}(2317)^- \pi^+, D_{s0}^- \rightarrow$	< 2.5 × 10 <sup>-5</sup>	CL=90% 2128
$D_s^- \pi^0$		
$D_{sJ}(2457)^- K^+, D_{sJ}^- \rightarrow$	< 9.4 × 10 <sup>-6</sup>	CL=90% -
$D_s^- \pi^0$		
$D_{sJ}(2457)^- \pi^+, D_{sJ}^- \rightarrow$	< 4.0 × 10 <sup>-6</sup>	CL=90% -
$D_s^- \pi^0$		
$D_s^- D_s^+$	< 3.6 × 10 <sup>-5</sup>	CL=90% 1759
$D_s^- D_s^+$	< 1.3 × 10 <sup>-4</sup>	CL=90% 1674
$D_s^- D_s^+$	< 2.4 × 10 <sup>-4</sup>	CL=90% 1583
$D_s^* D_s^{*+}$	< 2.4 × 10 <sup>-4</sup>	CL=90% 1583
$D_{s0}^*(2317)^+ D^-, D_{s0}^{*+} \rightarrow$	( 1.06 ± 0.16 ) × 10 <sup>-3</sup>	S=1.1 1602
$D_s^+ \pi^0$		
$D_{s0}(2317)^+ D^-, D_{s0}^+ \rightarrow$	< 9.5 × 10 <sup>-4</sup>	CL=90% -
$D_s^{*+} \gamma$		
$D_{s0}(2317)^+ D^*(2010)^-,$	( 1.5 ± 0.6 ) × 10 <sup>-3</sup>	1509
$D_{s0}^+ \rightarrow D_s^+ \pi^0$		
$D_{sJ}(2457)^+ D^-$	( 3.5 ± 1.1 ) × 10 <sup>-3</sup>	-
$D_{sJ}(2457)^+ D^-, D_{sJ}^+ \rightarrow$	( 6.5 ± 1.7 ) × 10 <sup>-4</sup>	-
$D_s^+ \gamma$		
$D_{sJ}(2457)^+ D^-, D_{sJ}^+ \rightarrow$	< 6.0 × 10 <sup>-4</sup>	CL=90% -
$D_s^{*+} \gamma$		
$D_{sJ}(2457)^+ D^-, D_{sJ}^+ \rightarrow$	< 2.0 × 10 <sup>-4</sup>	CL=90% -
$D_s^+ \pi^+ \pi^-$		
$D_{sJ}(2457)^+ D^-, D_{sJ}^+ \rightarrow$	< 3.6 × 10 <sup>-4</sup>	CL=90% -
$D_s^+ \pi^0$		
$D^*(2010)^- D_{sJ}(2457)^+$	( 9.3 ± 2.2 ) × 10 <sup>-3</sup>	-
$D_{sJ}(2457)^+ D^*(2010)^-, D_{sJ}^+ \rightarrow$	( 2.3 ± 0.9 ) × 10 <sup>-3</sup>	-
$D_s^+ \gamma$		
$D^- D_{s1}(2536)^+, D_{s1}^- \rightarrow$	( 2.8 ± 0.7 ) × 10 <sup>-4</sup>	1444
$D^{*0} K^+ + D^{*+} K^0$		
$D^- D_{s1}(2536)^+, D_{s1}^- \rightarrow$	( 1.7 ± 0.6 ) × 10 <sup>-4</sup>	1444
$D^{*0} K^+$		
$D^- D_{s1}(2536)^+, D_{s1}^- \rightarrow$	( 2.6 ± 1.1 ) × 10 <sup>-4</sup>	1444
$D^{*+} K^0$		



## Meson Summary Table

$D^*(2010)^- D_{s1}(2536)^+$ , $D_{s1}^+ \rightarrow D^{*0} K^+ + D^{*+} K^0$	$(5.0 \pm 1.4) \times 10^{-4}$	1336	$D^*(2010)^- D^0 K^+$	$(2.47 \pm 0.21) \times 10^{-3}$	1479
$D^*(2010)^- D_{s1}(2536)^+$ , $D_{s1}^+ \rightarrow D^{*0} K^+$	$(3.3 \pm 1.1) \times 10^{-4}$	1336	$D^*(2010)^- D^*(2007)^0 K^+$ $D^- D^+ K^0$	$(1.06 \pm 0.09) \%$ $(7.5 \pm 1.7) \times 10^{-4}$	1366 1568
$D^{*-} D_{s1}(2536)^+$ , $D_{s1}^+ \rightarrow$ $D^{*+} K^0$	$(5.0 \pm 1.7) \times 10^{-4}$	1336	$D^*(2010)^- D^+ K^0 +$ $D^- D^*(2010)^+ K^0$	$(6.4 \pm 0.5) \times 10^{-3}$	1473
$D^- D_{sJ}(2573)^+$ , $D_{sJ}^+ \rightarrow$ $D^0 K^+$	$(3.4 \pm 1.8) \times 10^{-5}$	1414	$D^*(2010)^- D^*(2010)^+ K^0$ $D^{*-} D_{s1}(2536)^+$ , $D_{s1}^+ \rightarrow$ $D^{*+} K^0$	$(8.1 \pm 0.7) \times 10^{-3}$ $(8.0 \pm 2.4) \times 10^{-4}$	1360 1336
$D^*(2010)^- D_{sJ}(2573)^+$ , $D_{sJ}^+ \rightarrow D^0 K^+$	$< 2 \times 10^{-4}$ CL=90%	1304	$\bar{D}^0 D^0 K^0$	$(2.7 \pm 1.1) \times 10^{-4}$	1574
$D^- D_{sJ}(2700)^+$ , $D_{sJ}^+ \rightarrow$ $D^0 K^+$	$(7.1 \pm 1.2) \times 10^{-4}$	-	$\bar{D}^0 D^*(2007)^0 K^0 +$ $\bar{D}^*(2007)^0 D^0 K^0$	$(1.1 \pm 0.5) \times 10^{-3}$	1478
$D^+ \pi^-$	$(7.4 \pm 1.3) \times 10^{-7}$	2306	$\bar{D}^*(2007)^0 D^*(2007)^0 K^0$	$(2.4 \pm 0.9) \times 10^{-3}$	1365
$D_s^+ \pi^-$	$(2.16 \pm 0.26) \times 10^{-5}$	2270	$(\bar{D} + \bar{D}^*)(D + D^*) K$	$(3.68 \pm 0.26) \%$	-
$D_s^+ \pi^-$	$(2.1 \pm 0.4) \times 10^{-5}$ S=1.4	2215	<b>Charmonium modes</b>		
$D_s^+ \rho^-$	$< 2.4 \times 10^{-5}$ CL=90%	2197	$\eta_c K^0$	$(8.0 \pm 1.1) \times 10^{-4}$	1751
$D_s^+ \rho^-$	$(4.1 \pm 1.3) \times 10^{-5}$	2138	$\eta_c(1S) K^+ \pi^-$	$(6.0 \pm 0.7) \times 10^{-4}$	1722
$D_s^+ a_0^-$	$< 1.9 \times 10^{-5}$ CL=90%	-	$\eta_c(1S) K^+ \pi^-$ (NR)	$(6.2 \pm 1.3) \times 10^{-5}$	-
$D_s^+ a_0^-$	$< 3.6 \times 10^{-5}$ CL=90%	-	$X(4100)^- K^+, X^- \rightarrow$	$(2.0 \pm 1.0) \times 10^{-5}$	-
$D_s^+ a_1(1260)^-$	$< 2.1 \times 10^{-3}$ CL=90%	2080	$\eta_c \pi^-$	-	-
$D_s^+ a_1(1260)^-$	$< 1.7 \times 10^{-3}$ CL=90%	2015	$\eta_c(1S) K^*(1410)^0$	$(1.9 \pm 1.5) \times 10^{-4}$	1395
$D_s^+ a_2^-$	$< 1.9 \times 10^{-4}$ CL=90%	-	$\eta_c(1S) K_0^*(1430)^0$	$(1.6 \pm 0.4) \times 10^{-4}$	1387
$D_s^+ a_2^-$	$< 2.0 \times 10^{-4}$ CL=90%	-	$\eta_c(1S) K_2^*(1430)^0$	$(4.9 \pm \frac{2.2}{2.7}) \times 10^{-5}$	1386
$D_s^- K^+$	$(2.7 \pm 0.5) \times 10^{-5}$ S=2.7	2242	$\eta_c(1S) K^*(1680)^0$	$(3 \pm 4) \times 10^{-5}$	1166
$D_s^{*-} K^+$	$(2.19 \pm 0.30) \times 10^{-5}$	2185	$\eta_c(1S) K_0^*(1950)^0$	$(4.4 \pm \frac{2.9}{4.0}) \times 10^{-5}$	-
$D_s^- K^*(892)^+$	$(3.5 \pm 1.0) \times 10^{-5}$	2172	$\eta_c K^*(892)^0$	$(5.2 \pm \frac{0.7}{0.8}) \times 10^{-4}$ S=1.5	1646
$D_s^{*-} K^*(892)^+$	$(3.2 \pm \frac{1.5}{1.3}) \times 10^{-5}$	2112	$\eta_c(2S) K_S^0$ , $\eta_c \rightarrow \rho \bar{\rho} \pi^+ \pi^-$	$(4.2 \pm \frac{1.4}{1.2}) \times 10^{-7}$	-
$D_s^- \pi^+ K^0$	$(9.7 \pm 1.4) \times 10^{-5}$	2222	$\eta_c(2S) K^*0$	$< 3.9 \times 10^{-4}$ CL=90%	1159
$D_s^{*-} \pi^+ K^0$	$< 1.10 \times 10^{-4}$ CL=90%	2164	$h_c(1P) K_S^0$	$< 1.4 \times 10^{-5}$	1401
$D_s^- K^+ \pi^+ \pi^-$	$(1.7 \pm 0.5) \times 10^{-4}$	2198	$h_c(1P) K^*0$	$< 4 \times 10^{-4}$ CL=90%	1253
$D_s^- \pi^+ K^*(892)^0$	$< 3.0 \times 10^{-3}$ CL=90%	2138	$J/\psi(1S) K^0$	$(8.68 \pm 0.30) \times 10^{-4}$	1683
$D_s^{*-} \pi^+ K^*(892)^0$	$< 1.6 \times 10^{-3}$ CL=90%	2076	$J/\psi(1S) K^+ \pi^-$	$(1.15 \pm 0.05) \times 10^{-3}$	1652
$\bar{D}^0 K^0$	$(5.2 \pm 0.7) \times 10^{-5}$	2280	$J/\psi(1S) K^*(892)^0$	$(1.27 \pm 0.05) \times 10^{-3}$	1571
$\bar{D}^0 K^+ \pi^-$	$(8.8 \pm 1.7) \times 10^{-5}$	2261	$J/\psi(1S) \eta K_S^0$	$(5.4 \pm 0.9) \times 10^{-5}$	1508
$\bar{D}^0 K^*(892)^0$	$(4.5 \pm 0.6) \times 10^{-5}$	2213	$J/\psi(1S) \phi K_S^0$	$< 2.5 \times 10^{-5}$ CL=90%	1271
$\bar{D}^0 K_0^*(1430)^0$	$< 6.7 \times 10^{-5}$ CL=90%	2062	$J/\psi(1S) \phi K^0$	$(4.9 \pm 1.0) \times 10^{-5}$ S=1.3	1224
$\bar{D}^0 K_0^*(1430)^0$	$(7 \pm 7) \times 10^{-6}$	2058	$J/\psi(1S) \omega K^0$	$(2.3 \pm 0.4) \times 10^{-4}$	1386
$\bar{D}^0 K_2^*(1430)^0$	$(2.1 \pm 0.9) \times 10^{-5}$	2057	$\chi_{c1}(3872) K^0$ , $\chi_{c1} \rightarrow$ $J/\psi \omega$	$(6.0 \pm 3.2) \times 10^{-6}$	1140
$D_0^*(2300)^- K^+$ , $D_0^{*-} \rightarrow$ $\bar{D}^0 \pi^-$	$(1.9 \pm 0.9) \times 10^{-5}$	-	$X(3915)$ , $X \rightarrow J/\psi \omega$	$(2.1 \pm 0.9) \times 10^{-5}$	1102
$D_2^*(2460)^- K^+$ , $D_2^{*-} \rightarrow$ $\bar{D}^0 \pi^-$	$(2.03 \pm 0.35) \times 10^{-5}$	2029	$J/\psi(1S) K(1270)^0$	$(1.3 \pm 0.5) \times 10^{-3}$	1402
$D_3^*(2760)^- K^+$ , $D_3^{*-} \rightarrow$ $\bar{D}^0 \pi^-$	$< 1.0 \times 10^{-6}$ CL=90%	-	$J/\psi(1S) \pi^0$	$(1.66 \pm 0.10) \times 10^{-5}$	1728
$\bar{D}^0 K^+ \pi^-$ nonresonant	$< 3.7 \times 10^{-5}$ CL=90%	2261	$J/\psi(1S) \eta$	$(1.08 \pm 0.23) \times 10^{-5}$ S=1.5	1673
$[K^+ K^-]_D K^*(892)^0$	$(4.2 \pm 0.7) \times 10^{-5}$	-	$J/\psi(1S) \pi^+ \pi^-$	$(3.94 \pm 0.17) \times 10^{-5}$	1716
$[\pi^+ \pi^-]_D K^*(892)^0$	$(6.0 \pm 1.1) \times 10^{-5}$	-	$J/\psi(1S) \pi^+ \pi^-$ nonresonant	$< 1.2 \times 10^{-5}$ CL=90%	1716
$[\pi^+ \pi^- \pi^+ \pi^-]_D K^*0$	$(4.6 \pm 0.9) \times 10^{-5}$	-	$J/\psi(1S) f_0(500)$ , $f_0 \rightarrow \pi \pi$	$(8.8 \pm \frac{1.2}{1.6}) \times 10^{-6}$	-
$\bar{D}^0 \pi^0$	$(2.63 \pm 0.14) \times 10^{-4}$	2308	$J/\psi(1S) f_2$	$(3.3 \pm 0.5) \times 10^{-6}$ S=1.5	-
$\bar{D}^0 \rho^0$	$(3.21 \pm 0.21) \times 10^{-4}$	2237	$J/\psi(1S) \rho^0$	$(2.55 \pm \frac{0.18}{0.16}) \times 10^{-5}$	1612
$\bar{D}^0 f_2$	$(1.56 \pm 0.21) \times 10^{-4}$	-	$J/\psi(1S) f_0(980)$ , $f_0 \rightarrow$ $\pi^+ \pi^-$	$< 1.1 \times 10^{-6}$ CL=90%	-
$\bar{D}^0 \eta$	$(2.36 \pm 0.32) \times 10^{-4}$ S=2.5	2274	$J/\psi(1S) \rho(1450)^0$ , $\rho^0 \rightarrow$ $\pi \pi$	$(2.9 \pm \frac{1.6}{0.7}) \times 10^{-6}$	-
$\bar{D}^0 \eta'$	$(1.38 \pm 0.16) \times 10^{-4}$ S=1.3	2198	$J/\psi(1700)^0$ , $\rho^0 \rightarrow \pi^+ \pi^-$	$(2.0 \pm 1.3) \times 10^{-6}$	-
$\bar{D}^0 \omega$	$(2.54 \pm 0.16) \times 10^{-4}$	2235	$J/\psi(1S) \omega$	$(1.8 \pm \frac{0.7}{0.5}) \times 10^{-5}$	1609
$D^0 \phi$	$< 2.3 \times 10^{-6}$ CL=95%	2183	$J/\psi(1S) K^+ K^-$	$(2.50 \pm 0.35) \times 10^{-6}$	1534
$D^0 K^+ \pi^-$	$(5.3 \pm 3.2) \times 10^{-6}$	2261	$J/\psi(1S) a_0(980)$ , $a_0 \rightarrow$ $K^+ K^-$	$(4.7 \pm 3.4) \times 10^{-7}$	-
$D^0 K^*(892)^0$	$(2.2 \pm \frac{0.9}{1.0}) \times 10^{-6}$	2213	$J/\psi(1S) \phi$	$< 1.9 \times 10^{-7}$ CL=90%	1520
$\bar{D}^{*0} \gamma$	$< 2.5 \times 10^{-5}$ CL=90%	2258	$J/\psi(1S) \eta'(958)$	$(7.6 \pm 2.4) \times 10^{-6}$	1546
$\bar{D}^*(2007)^0 \pi^0$	$(2.2 \pm 0.6) \times 10^{-4}$ S=2.6	2256	$J/\psi(1S) K^0 \pi^+ \pi^-$	$(4.3 \pm 0.4) \times 10^{-4}$	1611
$\bar{D}^*(2007)^0 \rho^0$	$< 5.1 \times 10^{-4}$ CL=90%	2182	$J/\psi(1S) K^0 K^- \pi^+ +$ c.c.	$< 2.1 \times 10^{-5}$ CL=90%	1467
$\bar{D}^*(2007)^0 \eta$	$(2.3 \pm 0.6) \times 10^{-4}$ S=2.8	2220	$J/\psi(1S) K^0 K^+ K^-$	$(2.5 \pm 0.7) \times 10^{-5}$ S=1.8	1249
$\bar{D}^*(2007)^0 \eta'$	$(1.40 \pm 0.22) \times 10^{-4}$	2141	$J/\psi(1S) K^0 \rho^0$	$(5.4 \pm 3.0) \times 10^{-4}$	1390
$\bar{D}^*(2007)^0 \pi^+ \pi^-$	$(6.2 \pm 2.2) \times 10^{-4}$	2249	$J/\psi(1S) K^*(892)^+ \pi^-$	$(8 \pm 4) \times 10^{-4}$	1515
$\bar{D}^*(2007)^0 K^0$	$(3.6 \pm 1.2) \times 10^{-5}$	2227	$J/\psi(1S) \pi^+ \pi^- \pi^+ \pi^-$	$(1.42 \pm 0.12) \times 10^{-5}$	1670
$\bar{D}^*(2007)^0 K^*(892)^0$	$< 6.9 \times 10^{-5}$ CL=90%	2157	$J/\psi(1S) f_1(1285)$	$(8.4 \pm 2.1) \times 10^{-6}$	1385
$D^*(2007)^0 K^*(892)^0$	$< 4.0 \times 10^{-5}$ CL=90%	2157	$J/\psi(1S) K^*(892)^0 \pi^+ \pi^-$	$(6.6 \pm 2.2) \times 10^{-4}$	1447
$D^*(2007)^0 \pi^+ \pi^+ \pi^- \pi^-$	$(2.7 \pm 0.5) \times 10^{-3}$	2219	$\chi_{c1}(3872)^- K^+$	$< 5 \times 10^{-4}$ CL=90%	-
$D^*(2010)^+ D^*(2010)^-$	$(8.0 \pm 0.6) \times 10^{-4}$	1711	$\chi_{c1}(3872)^- K^+$ , [rrr]	$< 4.2 \times 10^{-6}$ CL=90%	-
$\bar{D}^*(2007)^0 \omega$	$(3.6 \pm 1.1) \times 10^{-4}$ S=3.1	2180	$\chi_{c1}(3872)^- \rightarrow$ $J/\psi(1S) \pi^- \pi^0$	-	-
$D^*(2010)^+ D^-$	$(6.1 \pm 1.5) \times 10^{-4}$ S=1.6	1790	$\chi_{c1}(3872) K^0$ , $\chi_{c1} \rightarrow$ $J/\psi \pi^+ \pi^-$	$(4.3 \pm 1.3) \times 10^{-6}$	1140
$D^*(2007)^0 \bar{D}^*(2007)^0$	$< 9 \times 10^{-5}$ CL=90%	1715	$\chi_{c1}(3872) K^0$ , $\chi_{c1} \rightarrow J/\psi \gamma$	$< 2.4 \times 10^{-6}$ CL=90%	1140
$D^- D^0 K^+$	$(1.07 \pm 0.11) \times 10^{-3}$	1574			
$D^- D^*(2007)^0 K^+$	$(3.5 \pm 0.4) \times 10^{-3}$	1478			

## Meson Summary Table

$\chi_{c1}(3872)K^*(892)^0, \chi_{c1} \rightarrow J/\psi\gamma$	$< 2.8 \times 10^{-6}$	CL=90%	940	$\omega(K\pi)_0^{*0}$	$(1.84 \pm 0.25) \times 10^{-5}$	-
$\chi_{c1}(3872)K^0, \chi_{c1} \rightarrow \psi(2S)\gamma$	$< 6.62 \times 10^{-6}$	CL=90%	1140	$\omega K_0^*(1430)^0$	$(1.60 \pm 0.34) \times 10^{-5}$	2380
$\chi_{c1}(3872)K^*(892)^0, \chi_{c1} \rightarrow \psi(2S)\gamma$	$< 4.4 \times 10^{-6}$	CL=90%	940	$\omega K_2^*(1430)^0$	$(1.01 \pm 0.23) \times 10^{-5}$	2380
$\chi_{c1}(3872)K^0, \chi_{c1} \rightarrow D^0\bar{D}^0\pi^0$	$(1.7 \pm 0.8) \times 10^{-4}$		1140	$\omega K^+\pi^-$ nonresonant	$(5.1 \pm 1.0) \times 10^{-6}$	2542
$\chi_{c1}(3872)K^0, \chi_{c1} \rightarrow \bar{D}^{*0}D^0$	$(1.2 \pm 0.4) \times 10^{-4}$		1140	$K^+\pi^-\pi^0$	$(3.78 \pm 0.32) \times 10^{-5}$	2609
$\chi_{c1}(3872)K^+\pi^-, \chi_{c1} \rightarrow J/\psi\pi^+\pi^-$	$(7.9 \pm 1.4) \times 10^{-6}$		-	$K^+\rho^-$	$(7.0 \pm 0.9) \times 10^{-6}$	2559
$\chi_{c1}(3872)K^*(892)^0, \chi_{c1} \rightarrow J/\psi\pi^+\pi^-$	$(4.0 \pm 1.5) \times 10^{-6}$		-	$K^+\rho(1450)^-$	$(2.4 \pm 1.2) \times 10^{-6}$	-
$\chi_{c1}(3872)\gamma, \chi_{c1} \rightarrow J/\psi\pi^+\pi^-$	$< 5.1 \times 10^{-7}$	CL=90%	-	$K^+\rho(1700)^-$	$(6 \pm 7) \times 10^{-7}$	-
$Z_c(4430)^\pm K^\mp, Z_c^\pm \rightarrow \psi(2S)\pi^\pm$	$(6.0 \pm_{-2.4}^{3.0}) \times 10^{-5}$		583	$(K^+\pi^-\pi^0)$ nonresonant	$(2.8 \pm 0.6) \times 10^{-6}$	2609
$Z_c(4430)^\pm K^\mp, Z_c^\pm \rightarrow J/\psi\pi^\pm$	$(5.4 \pm_{-1.2}^{4.0}) \times 10^{-6}$		583	$(K\pi)_0^{*+}\pi^-, (K\pi)_0^{*+} \rightarrow$	$(3.4 \pm 0.5) \times 10^{-5}$	-
$Z_c(3900)^\pm K^\mp, Z_c^\pm \rightarrow J/\psi\pi^\pm$	$< 9 \times 10^{-7}$		-	$(K\pi)_0^{*0}\pi^0, (K\pi)_0^{*0} \rightarrow$	$(8.6 \pm 1.7) \times 10^{-6}$	-
$Z_c(4200)^\pm K^\mp, X^\pm \rightarrow J/\psi\pi^\pm$	$(2.2 \pm_{-0.8}^{1.3}) \times 10^{-5}$		-	$K^+\pi^-$		
$J/\psi(1S)p\bar{p}$	$(4.5 \pm 0.6) \times 10^{-7}$		862	$K_2^*(1430)^0\pi^0$	$< 4.0 \times 10^{-6}$	CL=90% 2445
$J/\psi(1S)\gamma$	$< 1.5 \times 10^{-6}$	CL=90%	1732	$K_x^*(1680)^0\pi^0$	$< 7.5 \times 10^{-6}$	CL=90% 2358
$J/\psi(1S)\bar{D}^0$	$< 1.3 \times 10^{-5}$	CL=90%	877	$K_x^0\pi^0$	$(6.1 \pm 1.6) \times 10^{-6}$	-
$\psi(2S)\pi^0$	$(1.17 \pm 0.19) \times 10^{-5}$		1348	$K^0\pi^+\pi^-$	$(4.97 \pm 0.18) \times 10^{-5}$	2609
$\psi(2S)K^0$	$(5.8 \pm 0.5) \times 10^{-4}$		1283	$K^0\pi^+\pi^-$ nonresonant	$(1.39 \pm_{-0.18}^{0.26}) \times 10^{-5}$	S=1.6 2609
$\psi(3770)K^0, \psi \rightarrow \bar{D}^0D^0$	$< 1.23 \times 10^{-4}$	CL=90%	1217	$K^0\rho^0$	$(3.4 \pm 1.1) \times 10^{-6}$	S=2.3 2558
$\psi(3770)K^0, \psi \rightarrow D^-D^+$	$< 1.88 \times 10^{-4}$	CL=90%	1217	$K^*(892)^+\pi^-$	$(7.5 \pm 0.4) \times 10^{-6}$	2563
$\psi(2S)\pi^+\pi^-$	$(2.21 \pm 0.35) \times 10^{-5}$		1331	$K_0^*(1430)^+\pi^-$	$(3.3 \pm 0.7) \times 10^{-5}$	S=2.0 -
$\psi(2S)K^+\pi^-$	$(5.8 \pm 0.4) \times 10^{-4}$		1239	$K_x^{*+}\pi^-$	$(5.1 \pm 1.6) \times 10^{-6}$	-
$\psi(2S)K^*(892)^0$	$(5.9 \pm 0.4) \times 10^{-4}$		1116	$K^*(1410)^+\pi^-, K^{*+} \rightarrow$	$< 3.8 \times 10^{-6}$	CL=90% -
$\chi_{c0}K^0$	$(1.11 \pm_{-0.21}^{0.24}) \times 10^{-6}$		1477	$K^0\pi^+$		
$\chi_{c0}K^*(892)^0$	$(1.7 \pm 0.4) \times 10^{-4}$		1342	$(K\pi)_0^{*+}\pi^-, (K\pi)_0^{*+} \rightarrow$	$(1.62 \pm 0.13) \times 10^{-5}$	-
$\chi_{c1}\pi^0$	$(1.12 \pm 0.28) \times 10^{-5}$		1468	$K^0\pi^+$		
$\chi_{c1}K^0$	$(3.95 \pm 0.27) \times 10^{-4}$		1411	$f_0(980)K^0, f_0 \rightarrow \pi^+\pi^-$	$(8.1 \pm 0.8) \times 10^{-6}$	S=1.3 2522
$\chi_{c1}\pi^-K^+$	$(4.97 \pm 0.30) \times 10^{-4}$		1371	$K^0f_0(500)$	$(1.6 \pm_{-1.6}^{2.5}) \times 10^{-7}$	-
$\chi_{c1}K^*(892)^0$	$(2.38 \pm 0.19) \times 10^{-4}$	S=1.2	1265	$K^0f_0(1500)$	$(1.3 \pm 0.8) \times 10^{-6}$	2397
$X(4051)^-K^+, X^- \rightarrow \chi_{c1}\pi^-$	$(3.0 \pm_{-1.8}^{4.0}) \times 10^{-5}$		-	$f_2(1270)K^0$	$(2.7 \pm_{-1.2}^{1.3}) \times 10^{-6}$	2459
$X(4248)^-K^+, X^- \rightarrow \chi_{c1}\pi^-$	$(4.0 \pm_{-1.0}^{20.0}) \times 10^{-5}$		-	$f_x(1300)K^0, f_x \rightarrow \pi^+\pi^-$	$(1.8 \pm 0.7) \times 10^{-6}$	-
$\chi_{c1}\pi^+\pi^-K^0$	$(3.2 \pm 0.5) \times 10^{-4}$		1318	$K^*(892)^0\pi^0$	$(3.3 \pm 0.6) \times 10^{-6}$	2563
$\chi_{c1}\pi^-\pi^0K^+$	$(3.5 \pm 0.6) \times 10^{-4}$		1321	$K_2^*(1430)^+\pi^-$	$(3.65 \pm 0.34) \times 10^{-6}$	2445
$\chi_{c2}K^0$	$< 1.5 \times 10^{-5}$	CL=90%	1379	$K^*(1680)^+\pi^-$	$(1.41 \pm 0.10) \times 10^{-5}$	2358
$\chi_{c2}K^*(892)^0$	$(4.9 \pm 1.2) \times 10^{-5}$	S=1.1	1228	$K^+\pi^-\pi^+\pi^-$	$< 2.3 \times 10^{-4}$	CL=90% 2600
$\chi_{c2}\pi^-K^+$	$(7.2 \pm 1.0) \times 10^{-5}$		1338	$\rho^0K^+\pi^-$	$(2.8 \pm 0.7) \times 10^{-6}$	2543
$\chi_{c2}\pi^+\pi^-K^0$	$< 1.70 \times 10^{-4}$	CL=90%	1282	$f_0(980)K^+\pi^-, f_0 \rightarrow \pi\pi$	$(1.4 \pm_{-0.6}^{0.5}) \times 10^{-6}$	2506
$\chi_{c2}\pi^-\pi^0K^+$	$< 7.4 \times 10^{-5}$	CL=90%	1286	$K^+\pi^-\pi^+\pi^-$ nonresonant	$< 2.1 \times 10^{-6}$	CL=90% 2600
$\psi(4660)K^0, \psi \rightarrow \Lambda_c^+\Lambda_c^-$	$< 2.3 \times 10^{-4}$	CL=90%	-	$K^*(892)^0\pi^+\pi^-$	$(5.5 \pm 0.5) \times 10^{-5}$	2557
$\psi(4260)^0K^0, \psi^0 \rightarrow J/\psi\pi^+\pi^-$	$< 1.7 \times 10^{-5}$	CL=90%	-	$K^*(892)^0\rho^0$	$(3.9 \pm 1.3) \times 10^{-6}$	S=1.9 2504
<b>K or K* modes</b>				$K^*(892)^0f_0(980), f_0 \rightarrow \pi\pi$	$(3.9 \pm_{-1.8}^{2.1}) \times 10^{-6}$	S=3.9 2466
$K^+\pi^-$	$(1.96 \pm 0.05) \times 10^{-5}$		2615	$K_1(1270)^+\pi^-$	$< 3.0 \times 10^{-5}$	CL=90% 2489
$K^0\pi^0$	$(9.9 \pm 0.5) \times 10^{-6}$		2615	$K_1(1400)^+\pi^-$	$< 2.7 \times 10^{-5}$	CL=90% 2451
$\eta'K^0$	$(6.6 \pm 0.4) \times 10^{-5}$	S=1.4	2528	$a_1(1260)^-K^+$	$(1.6 \pm 0.4) \times 10^{-5}$	2471
$\eta'K^*(892)^0$	$(2.8 \pm 0.6) \times 10^{-6}$		2472	$K^*(892)^+\rho^-$	$(1.03 \pm 0.26) \times 10^{-5}$	2504
$\eta'K_0^*(1430)^0$	$(6.3 \pm 1.6) \times 10^{-6}$		2346	$K_0^*(1430)^+\rho^0$	$(2.8 \pm 1.2) \times 10^{-5}$	-
$\eta'K_2^*(1430)^0$	$(1.37 \pm 0.32) \times 10^{-5}$		2346	$K_1(1400)^0\rho^0$	$< 3.0 \times 10^{-3}$	CL=90% 2388
$\eta K^0$	$(1.23 \pm_{-0.24}^{0.27}) \times 10^{-6}$		2587	$K_0^*(1430)^0\rho^0$	$(2.7 \pm 0.6) \times 10^{-5}$	2381
$\eta K^*(892)^0$	$(1.59 \pm 0.10) \times 10^{-5}$		2534	$K_0^*(1430)^0f_0(980), f_0 \rightarrow \pi\pi$	$(2.7 \pm 0.9) \times 10^{-6}$	-
$\eta K_0^*(1430)^0$	$(1.10 \pm 0.22) \times 10^{-5}$		2415	$K_2^*(1430)^0f_0(980), f_0 \rightarrow \pi\pi$	$(8.6 \pm 2.0) \times 10^{-6}$	-
$\eta K_2^*(1430)^0$	$(9.6 \pm 2.1) \times 10^{-6}$		2414	$K^+K^-$	$(7.8 \pm 1.5) \times 10^{-8}$	2593
$\omega K^0$	$(4.8 \pm 0.4) \times 10^{-6}$		2557	$K^0\bar{K}^0$	$(1.21 \pm 0.16) \times 10^{-6}$	2593
$a_0(980)^0K^0, a_0^0 \rightarrow \eta\pi^0$	$< 7.8 \times 10^{-6}$	CL=90%	-	$K^0K^-\pi^+$	$(6.7 \pm 0.5) \times 10^{-6}$	2578
$b_1^0K^0, b_1^0 \rightarrow \omega\pi^0$	$< 7.8 \times 10^{-6}$	CL=90%	-	$K^*(892)^\pm K^\mp$	$< 4 \times 10^{-7}$	CL=90% 2540
$a_0(980)^\pm K^\mp, a_0^\pm \rightarrow \eta\pi^\pm$	$< 1.9 \times 10^{-6}$	CL=90%	-	$\bar{K}^{*0}K^0 + K^{*0}\bar{K}^0$	$< 9.6 \times 10^{-7}$	CL=90% -
$b_1^-K^+, b_1^- \rightarrow \omega\pi^-$	$(7.4 \pm 1.4) \times 10^{-6}$		-	$K^+K^-\pi^0$	$(2.2 \pm 0.6) \times 10^{-6}$	2579
$b_1^0K^{*0}, b_1^0 \rightarrow \omega\pi^0$	$< 8.0 \times 10^{-6}$	CL=90%	-	$K_S^0K_S^0\pi^0$	$< 9 \times 10^{-7}$	CL=90% 2578
$b_1^-K^{*+}, b_1^- \rightarrow \omega\pi^-$	$< 5.0 \times 10^{-6}$	CL=90%	-	$K_S^0K_S^0\eta$	$< 1.0 \times 10^{-6}$	CL=90% 2515
$a_0(1450)^\pm K^\mp, a_0^\pm \rightarrow \eta\pi^\pm$	$< 3.1 \times 10^{-6}$	CL=90%	-	$K_S^0K_S^0\eta'$	$< 2.0 \times 10^{-6}$	CL=90% 2453
$K_S^0X^0$ (Familon)	$< 5.3 \times 10^{-5}$	CL=90%	-	$K^0K^+K^-$	$(2.68 \pm 0.11) \times 10^{-5}$	2522
$\omega K^*(892)^0$	$(2.0 \pm 0.5) \times 10^{-6}$		2503	$K^0\phi$	$(7.3 \pm 0.7) \times 10^{-6}$	2516
				$f_0(980)K^0, f_0 \rightarrow K^+K^-$	$(7.0 \pm_{-3.0}^{3.5}) \times 10^{-6}$	-
				$f_0(1500)K^0$	$(1.3 \pm_{-0.5}^{0.7}) \times 10^{-5}$	2397
				$f_2'(1525)^0K^0$	$(3 \pm_{-4}^5) \times 10^{-7}$	-
				$f_0(1710)K^0, f_0 \rightarrow K^+K^-$	$(4.4 \pm 0.9) \times 10^{-6}$	-
				$K^0K^+K^-$ nonresonant	$(3.3 \pm 1.0) \times 10^{-5}$	2522
				$K_S^0K_S^0K_S^0$	$(6.0 \pm 0.5) \times 10^{-6}$	S=1.1 2521
				$f_0(980)K^0, f_0 \rightarrow K_S^0K_S^0$	$(2.7 \pm 1.8) \times 10^{-6}$	-
				$f_0(1710)K^0, f_0 \rightarrow K_S^0K_S^0$	$(5.0 \pm_{-2.6}^{5.0}) \times 10^{-7}$	-
				$f_2(2010)K^0, f_2 \rightarrow K_S^0K_S^0$	$(5 \pm 6) \times 10^{-7}$	-
				$K_S^0K_S^0K_S^0$ nonresonant	$(1.33 \pm 0.31) \times 10^{-5}$	2521



$\bar{\Lambda}_c^- p \pi^+ \pi^- \pi^0$	< 5.07	$\times 10^{-3}$	CL=90%	1883
$\bar{\Lambda}_c^- p \pi^+ \pi^- \pi^+ \pi^-$	< 2.74	$\times 10^{-3}$	CL=90%	1821
$\bar{\Lambda}_c^- p \pi^+ \pi^-$ (nonresonant)	( 5.5 ± 1.0 )	$\times 10^{-4}$	S=1.3	1934
$\bar{\Sigma}_c(2520)^- p \pi^+$	( 1.02 ± 0.18 )	$\times 10^{-4}$		1860
$\bar{\Sigma}_c(2520)^0 p \pi^-$	< 3.1	$\times 10^{-5}$	CL=90%	1860
$\bar{\Sigma}_c(2455)^0 p \pi^-$	( 1.08 ± 0.16 )	$\times 10^{-4}$		1895
$\bar{\Sigma}_c(2455)^0 N^0, N^0 \rightarrow$ $\rho \pi^-$	( 6.4 ± 1.7 )	$\times 10^{-5}$		-
$\bar{\Sigma}_c(2455)^- p \pi^+$	( 1.83 ± 0.24 )	$\times 10^{-4}$		1895
$\Lambda_c^- p K^+ \pi^-$	( 3.4 ± 0.7 )	$\times 10^{-5}$		1786
$\bar{\Sigma}_c(2455)^- p K^+, \bar{\Sigma}_c^- \rightarrow$ $\bar{\Lambda}_c^- \pi^-$	( 8.8 ± 2.5 )	$\times 10^{-6}$		1754
$\Lambda_c^- p K^*(892)^0$	< 2.42	$\times 10^{-5}$	CL=90%	1647
$\Lambda_c^- p K^+ K^-$	( 2.0 ± 0.4 )	$\times 10^{-5}$		1588
$\Lambda_c^- p \phi$	< 1.0	$\times 10^{-5}$	CL=90%	1567
$\Lambda_c^- p \bar{p} p$	< 2.8	$\times 10^{-6}$		677
$\bar{\Lambda}_c^- \Lambda K^+$	( 4.8 ± 1.1 )	$\times 10^{-5}$		1767
$\bar{\Lambda}_c^- \Lambda^+$	< 1.6	$\times 10^{-5}$	CL=95%	1319
$\bar{\Lambda}_c(2593)^- / \bar{\Lambda}_c(2625)^- p$	< 1.1	$\times 10^{-4}$	CL=90%	-
$\bar{\Xi}_c^- \Lambda_c^+$	( 1.2 ± 0.8 )	$\times 10^{-3}$		1147
$\bar{\Xi}_c^- \Lambda_c^+, \bar{\Xi}_c^- \rightarrow \Xi^+ \pi^- \pi^-$	( 2.4 ± 1.1 )	$\times 10^{-5}$	S=1.8	1147
$\bar{\Xi}_c^- \Lambda_c^+, \bar{\Xi}_c^- \rightarrow \bar{p} K^+ \pi^-$	( 5.3 ± 1.7 )	$\times 10^{-6}$		-
$\bar{\Xi}_c^- \Lambda_c^+ K^0$	( 4.0 ± 0.9 )	$\times 10^{-4}$		732
$\bar{\Xi}_c(2930)^- \Lambda_c^+, \bar{\Xi}_c^- \rightarrow \Lambda_c^- K^0$	( 2.4 ± 0.6 )	$\times 10^{-4}$		-

**Lepton Family number (LF) or Lepton number (L) or Baryon number (B) violating modes, or/and  $\Delta B = 1$  weak neutral current (BI) modes**

$\gamma\gamma$	BI	< 3.2	$\times 10^{-7}$	CL=90%	2640
$e^+ e^-$	BI	< 8.3	$\times 10^{-8}$	CL=90%	2640
$e^+ e^- \gamma$	BI	< 1.2	$\times 10^{-7}$	CL=90%	2640
$\mu^+ \mu^-$	BI	( 1.1 ± 1.4 )	$\times 10^{-10}$	S=1.6	2638
$\mu^+ \mu^- \gamma$	BI	< 1.6	$\times 10^{-7}$	CL=90%	2638
$\mu^+ \mu^- \mu^+ \mu^-$	BI	< 6.9	$\times 10^{-10}$	CL=95%	2629
$S P, S \rightarrow \mu^+ \mu^-,$ $P \rightarrow \mu^+ \mu^-$	BI [aaaa]	< 6.0	$\times 10^{-10}$	CL=95%	-
$\tau^+ \tau^-$	BI	< 2.1	$\times 10^{-3}$	CL=95%	1952
$\pi^0 \ell^+ \ell^-$	BI	< 5.3	$\times 10^{-8}$	CL=90%	2638
$\pi^0 e^+ e^-$	BI	< 8.4	$\times 10^{-8}$	CL=90%	2638
$\pi^0 \mu^+ \mu^-$	BI	< 6.9	$\times 10^{-8}$	CL=90%	2634
$\eta \ell^+ \ell^-$	BI	< 6.4	$\times 10^{-8}$	CL=90%	2611
$\eta e^+ e^-$	BI	< 1.08	$\times 10^{-7}$	CL=90%	2611
$\eta \mu^+ \mu^-$	BI	< 1.12	$\times 10^{-7}$	CL=90%	2607
$\pi^0 \nu \bar{\nu}$	BI	< 9	$\times 10^{-6}$	CL=90%	2638
$K^0 \ell^+ \ell^-$	BI [III]	( 3.1 ± 0.8 )	$\times 10^{-7}$		2616
$K^0 e^+ e^-$	BI	( 1.6 ± 1.0 )	$\times 10^{-7}$		2616
$K^0 \mu^+ \mu^-$	BI	( 3.39 ± 0.34 )	$\times 10^{-7}$		2612
$K^0 \nu \bar{\nu}$	BI	< 2.6	$\times 10^{-5}$	CL=90%	2616
$\rho^0 \nu \bar{\nu}$	BI	< 4.0	$\times 10^{-5}$	CL=90%	2583
$K^*(892)^0 \ell^+ \ell^-$	BI [III]	( 9.9 ± 1.2 )	$\times 10^{-7}$		2565
$K^*(892)^0 e^+ e^-$	BI	( 1.03 ± 0.19 )	$\times 10^{-6}$		2565
$K^*(892)^0 \mu^+ \mu^-$	BI	( 9.4 ± 0.5 )	$\times 10^{-7}$		2560
$\pi^+ \pi^- \mu^+ \mu^-$	BI	( 2.1 ± 0.5 )	$\times 10^{-8}$		2626
$K^*(892)^0 \nu \bar{\nu}$	BI	< 1.8	$\times 10^{-5}$	CL=90%	2565
invisible	BI	< 2.4	$\times 10^{-5}$	CL=90%	-
$\nu \bar{\nu} \gamma$	BI	< 1.7	$\times 10^{-5}$	CL=90%	2640
$\phi \nu \bar{\nu}$	BI	< 1.27	$\times 10^{-4}$	CL=90%	2541
$e^\pm \mu^\mp$	LF [bb]	< 1.0	$\times 10^{-9}$	CL=90%	2639
$\pi^0 e^\pm \mu^\mp$	LF	< 1.4	$\times 10^{-7}$	CL=90%	2637
$K^0 e^\pm \mu^\mp$	LF	< 2.7	$\times 10^{-7}$	CL=90%	2615
$K^*(892)^0 e^+ \mu^-$	LF	< 1.6	$\times 10^{-7}$	CL=90%	2563
$K^*(892)^0 e^- \mu^+$	LF	< 1.2	$\times 10^{-7}$	CL=90%	2563
$K^*(892)^0 e^\pm \mu^\mp$	LF	< 1.8	$\times 10^{-7}$	CL=90%	2563
$e^\pm \tau^\mp$	LF [bb]	< 2.8	$\times 10^{-5}$	CL=90%	2341
$\mu^\pm \tau^\mp$	LF [bb]	< 1.4	$\times 10^{-5}$	CL=95%	2339
$\Lambda_c^+ \mu^-$	L,B	< 1.4	$\times 10^{-6}$	CL=90%	2143
$\Lambda_c^+ e^-$	L,B	< 4	$\times 10^{-6}$	CL=90%	2145

**$B^\pm/B^0$  ADMIXTURE**

**CP violation**

$A_{CP}(B \rightarrow K^*(892)\gamma)$	= -0.003 ± 0.011
$A_{CP}(B \rightarrow s\gamma)$	= 0.015 ± 0.011
$A_{CP}(B \rightarrow (s+d)\gamma)$	= 0.010 ± 0.031
$A_{CP}(B \rightarrow X_s \ell^+ \ell^-)$	= 0.04 ± 0.11
$A_{CP}(B \rightarrow X_s \ell^+ \ell^-)$	(1.0 < q <sup>2</sup> < 6.0 GeV <sup>2</sup> /c <sup>4</sup> ) = -0.06 ± 0.22
$A_{CP}(B \rightarrow X_s \ell^+ \ell^-)$	(10.1 < q <sup>2</sup> < 12.9 or q <sup>2</sup> > 14.2 GeV <sup>2</sup> /c <sup>4</sup> ) = 0.19 ± 0.18
$A_{CP}(B \rightarrow K^* e^+ e^-)$	= -0.18 ± 0.15
$A_{CP}(B \rightarrow K^* \mu^+ \mu^-)$	= -0.03 ± 0.13
$A_{CP}(B \rightarrow K^* \ell^+ \ell^-)$	= -0.04 ± 0.07
$A_{CP}(B \rightarrow \eta \text{anything})$	= -0.13 <sup>+0.04</sup> <sub>-0.05</sub>
$\Delta A_{CP}(X_s \gamma) = A_{CP}(B^\pm \rightarrow X_s \gamma) - A_{CP}(B^0 \rightarrow X_s \gamma)$	= 0.041 ± 0.023
$\bar{A}_{CP}(B \rightarrow X_s \gamma) = (A_{CP}(B^+ \rightarrow X_s \gamma) + A_{CP}(B^0 \rightarrow X_s \gamma))/2$	= 0.009 ± 0.012
$\Delta A_{CP}(B \rightarrow K^* \gamma) = A_{CP}(B^+ \rightarrow K^{*+} \gamma) - A_{CP}(B^0 \rightarrow K^{*0} \gamma)$	= 0.024 ± 0.028
$\bar{A}_{CP}(B \rightarrow K^* \gamma) = (A_{CP}(B^+ \rightarrow K^{*+} \gamma) + A_{CP}(B^0 \rightarrow K^{*0} \gamma))/2$	= -0.001 ± 0.014

The branching fraction measurements are for an admixture of  $B$  mesons at the  $\Upsilon(4S)$ . The values quoted assume that  $B(\Upsilon(4S) \rightarrow B\bar{B}) = 100\%$ .

For inclusive branching fractions, e.g.,  $B \rightarrow D^\pm \text{anything}$ , the treatment of multiple  $D$ 's in the final state must be defined. One possibility would be to count the number of events with one-or-more  $D$ 's and divide by the total number of  $B$ 's. Another possibility would be to count the total number of  $D$ 's and divide by the total number of  $B$ 's, which is the definition of average multiplicity. The two definitions are identical if only one  $D$  is allowed in the final state. Even though the "one-or-more" definition seems sensible, for practical reasons inclusive branching fractions are almost always measured using the multiplicity definition. For heavy final state particles, authors call their results inclusive branching fractions while for light particles some authors call their results multiplicities. In the  $B$  sections, we list all results as inclusive branching fractions, adopting a multiplicity definition. This means that inclusive branching fractions can exceed 100% and that inclusive partial widths can exceed total widths, just as inclusive cross sections can exceed total cross section.

$\bar{B}$  modes are charge conjugates of the modes below. Reactions indicate the weak decay vertex and do not include mixing.

<b>B DECAY MODES</b>	Fraction ( $\Gamma_i/\Gamma$ )	Scale factor / Confidence level (MeV/c)	$p$
<b>Semileptonic and leptonic modes</b>			
$\ell^+ \nu_\ell \text{anything}$	[III,bbaa]	( 10.86 ± 0.16 ) %	-
$D^- \ell^+ \nu_\ell \text{anything}$	[III]	( 2.6 ± 0.5 ) %	-
$\bar{D}^0 \ell^+ \nu_\ell \text{anything}$	[III]	( 7.3 ± 1.5 ) %	-
$\bar{D} \ell^+ \nu_\ell$		( 2.42 ± 0.12 ) %	2310
$D^{*-} \ell^+ \nu_\ell \text{anything}$	[ccaa]	( 6.7 ± 1.3 ) $\times 10^{-3}$	-
$D^* \ell^+ \nu_\ell$	[ddaa]	( 4.95 ± 0.11 ) %	2257
$\bar{D}^{*+} \ell^+ \nu_\ell$	[III,eeaa]	( 2.7 ± 0.7 ) %	-
$\bar{D}_1(2420) \ell^+ \nu_\ell \text{anything}$		( 3.8 ± 1.3 ) $\times 10^{-3}$	S=2.4
$D \pi \ell^+ \nu_\ell \text{anything} + D^* \pi \ell^+ \nu_\ell \text{anything}$		( 2.6 ± 0.5 ) %	S=1.5
$D \pi \ell^+ \nu_\ell \text{anything}$		( 1.5 ± 0.6 ) %	-
$D^* \pi \ell^+ \nu_\ell \text{anything}$		( 1.9 ± 0.4 ) %	-
$\bar{D}_2^*(2460) \ell^+ \nu_\ell \text{anything}$		( 4.4 ± 1.6 ) $\times 10^{-3}$	-
$D^{*-} \pi^+ \ell^+ \nu_\ell \text{anything}$		( 1.00 ± 0.34 ) %	-
$\bar{D} \pi^+ \pi^- \ell^+ \nu_\ell$		( 1.62 ± 0.32 ) $\times 10^{-3}$	2301
$\bar{D}^* \pi^+ \pi^- \ell^+ \nu_\ell$		( 9.4 ± 3.2 ) $\times 10^{-4}$	2247
$D_s^- \ell^+ \nu_\ell \text{anything}$	[III]	< 7	$\times 10^{-3}$ CL=90%
$D_s^- \ell^+ \nu_\ell K^+ \text{anything}$	[III]	< 5	$\times 10^{-3}$ CL=90%
$D_s^- \ell^+ \nu_\ell K^0 \text{anything}$	[III]	< 7	$\times 10^{-3}$ CL=90%
$X_c \ell^+ \nu_\ell$		( 10.65 ± 0.16 ) %	-
$X_{cb} \ell^+ \nu_\ell$		( 2.13 ± 0.30 ) $\times 10^{-3}$	-
$K^+ \ell^+ \nu_\ell \text{anything}$	[III]	( 6.3 ± 0.6 ) %	-
$K^- \ell^+ \nu_\ell \text{anything}$	[III]	( 10 ± 4 ) $\times 10^{-3}$	-
$K^0 / \bar{K}^0 \ell^+ \nu_\ell \text{anything}$	[III]	( 4.6 ± 0.5 ) %	-
$\bar{D} \tau^+ \nu_\tau$		( 9.9 ± 1.2 ) $\times 10^{-3}$	1911
$D^* \tau^+ \nu_\tau$		( 1.50 ± 0.08 ) %	1838

## Meson Summary Table

<b>D, D*, or D<sub>s</sub> modes</b>				<b>ρ<sup>0</sup> anything</b>			
D <sup>±</sup> anything	( 23.1 ± 1.2 ) %	-	-	( 21 ± 5 ) %	-	-	-
D <sup>0</sup> / $\bar{D}^0$ anything	( 61.5 ± 2.9 ) %	S=1.3	-	< 81 %	CL=90%	-	-
D*(2010) <sup>±</sup> anything	( 22.5 ± 1.5 ) %	-	-	φ anything	( 3.43 ± 0.12 ) %	-	-
D*(2007) <sup>0</sup> anything	( 26.0 ± 2.7 ) %	-	-	φ K*(892)	< 2.2 × 10 <sup>-5</sup>	CL=90%	2460
D <sub>s</sub> <sup>±</sup> anything	[bb] ( 8.3 ± 0.8 ) %	-	-	π <sup>+</sup> gluon (charmless)	( 3.7 ± 0.8 ) × 10 <sup>-4</sup>	-	-
D <sub>s</sub> <sup>*±</sup> anything	( 6.3 ± 1.0 ) %	-	-	<b>Baryon modes</b>			
D <sub>s</sub> <sup>*±</sup> $\bar{D}^*$	( 3.4 ± 0.6 ) %	-	-	Λ <sub>c</sub> <sup>+</sup> / $\bar{\Lambda}_c^-$ anything	( 3.6 ± 0.4 ) %	-	-
$\bar{D}^0 D_{s0}(2317)$	seen	1605	-	Λ <sub>c</sub> <sup>+</sup> anything	< 1.3 %	CL=90%	-
$\bar{D}^0 D_{sJ}(2457)$	seen	-	-	$\bar{\Lambda}_c^-$ anything	< 7 %	CL=90%	-
D(*) $\bar{D}^*$ K <sup>0</sup> + D(*) $\bar{D}^*$ K <sup>±</sup>	[bb, ffaa] ( 7.1 ± 2.7 / -1.7 ) %	-	-	$\bar{\Lambda}_c^- \ell^+$ anything	< 9 × 10 <sup>-4</sup>	CL=90%	-
b → c $\bar{c}$ s	( 22 ± 4 ) %	-	-	$\bar{\Lambda}_c^- e^+$ anything	< 1.8 × 10 <sup>-3</sup>	CL=90%	-
D <sub>s</sub> (* $\bar{D}^*$ )	[bb, ffaa] ( 3.9 ± 0.4 ) %	-	-	$\bar{\Lambda}_c^- \mu^+$ anything	< 1.4 × 10 <sup>-3</sup>	CL=90%	-
D* D*(2010) <sup>±</sup>	[bb] < 5.9 × 10 <sup>-3</sup>	CL=90%	1711	$\bar{\Lambda}_c^- p$ anything	( 2.04 ± 0.33 ) %	-	-
D* D*(2010) <sup>±</sup> + D* D <sup>±</sup>	[bb] < 5.5 × 10 <sup>-3</sup>	CL=90%	-	$\bar{\Lambda}_c^- p e^+ \nu_e$	< 8 × 10 <sup>-4</sup>	CL=90%	2021
DD <sup>±</sup>	[bb] < 3.1 × 10 <sup>-3</sup>	CL=90%	1866	$\bar{\Sigma}_c^-$ anything	( 3.3 ± 1.7 ) × 10 <sup>-3</sup>	-	-
D <sub>s</sub> (* $\bar{D}^*$ ) X (nπ <sup>±</sup> )	[bb, ffaa] ( 9 ± 5 / -4 ) %	-	-	$\bar{\Sigma}_c^-$ anything	< 8 × 10 <sup>-3</sup>	CL=90%	-
D*(2010)γ	< 1.1 × 10 <sup>-3</sup>	CL=90%	2257	$\bar{\Sigma}_c^0$ anything	( 3.7 ± 1.7 ) × 10 <sup>-3</sup>	-	-
D <sub>s</sub> <sup>+</sup> π <sup>-</sup> , D <sub>s</sub> <sup>+</sup> π <sup>0</sup> , D <sub>s</sub> <sup>+</sup> ρ <sup>-</sup> , D <sub>s</sub> <sup>+</sup> ρ <sup>0</sup> , D <sub>s</sub> <sup>+</sup> η, D <sub>s</sub> <sup>+</sup> η, D <sub>s</sub> <sup>+</sup> ρ <sup>0</sup> , D <sub>s</sub> <sup>+</sup> ρ <sup>+</sup> , D <sub>s</sub> <sup>+</sup> ω	[bb] < 4 × 10 <sup>-4</sup>	CL=90%	-	$\bar{\Sigma}_c^0 N (N = p \text{ or } n)$	< 1.2 × 10 <sup>-3</sup>	CL=90%	1938
D <sub>s1}(2536)<sup>+</sup> anything</sub>	< 9.5 × 10 <sup>-3</sup>	CL=90%	-	$\Xi_c^0$ anything, $\Xi_c^0 \rightarrow \Xi^- \pi^+$	( 1.93 ± 0.30 ) × 10 <sup>-4</sup>	S=1.1	-
<b>Charmonium modes</b>				$\Xi_c^+$ , $\Xi_c^+ \rightarrow \Xi^- \pi^+ \pi^+$	( 4.5 ± 1.3 / -1.2 ) × 10 <sup>-4</sup>	-	-
J/ψ(1S) anything	( 1.094 ± 0.032 ) %	S=1.1	-	p/ $\bar{p}$ anything	[bb] ( 8.0 ± 0.4 ) %	-	-
J/ψ(1S) (direct) anything	( 7.8 ± 0.4 ) × 10 <sup>-3</sup>	S=1.1	-	p/ $\bar{p}$ (direct) anything	[bb] ( 5.5 ± 0.5 ) %	-	-
ψ(2S) anything	( 3.07 ± 0.21 ) × 10 <sup>-3</sup>	-	-	$\bar{p} e^+ \nu_e$ anything	< 5.9 × 10 <sup>-4</sup>	CL=90%	-
χ <sub>c1</sub> (1P) anything	( 3.55 ± 0.27 ) × 10 <sup>-3</sup>	S=1.3	-	Λ/ $\bar{\Lambda}$ anything	[bb] ( 4.0 ± 0.5 ) %	-	-
χ <sub>c1</sub> (1P) (direct) anything	( 3.08 ± 0.19 ) × 10 <sup>-3</sup>	-	-	Λ anything	seen	-	-
χ <sub>c2</sub> (1P) anything	( 10.0 ± 1.7 ) × 10 <sup>-4</sup>	S=1.6	-	$\bar{\Lambda}$ anything	seen	-	-
χ <sub>c2</sub> (1P) (direct) anything	( 7.5 ± 1.1 ) × 10 <sup>-4</sup>	-	-	$\Xi^- / \bar{\Xi}^+$ anything	[bb] ( 2.7 ± 0.6 ) × 10 <sup>-3</sup>	-	-
η <sub>c</sub> (1S) anything	< 9 × 10 <sup>-3</sup>	CL=90%	-	baryons anything	( 6.8 ± 0.6 ) %	-	-
Kχ <sub>c1</sub> (3872), χ <sub>c1</sub> → D <sup>0</sup> $\bar{D}^0$ π <sup>0</sup>	( 1.2 ± 0.4 ) × 10 <sup>-4</sup>	-	1141	ρ $\bar{p}$ anything	( 2.47 ± 0.23 ) %	-	-
Kχ <sub>c1</sub> (3872), χ <sub>c1</sub> → D <sup>0</sup> $\bar{D}^0$	( 8.0 ± 2.2 ) × 10 <sup>-5</sup>	-	1141	Λ $\bar{p}$ / $\bar{\Lambda}p$ anything	[bb] ( 2.5 ± 0.4 ) %	-	-
KX(3940), X → D* <sup>0</sup> D <sup>0</sup>	< 6.7 × 10 <sup>-5</sup>	CL=90%	1084	ΛΛ anything	< 5 × 10 <sup>-3</sup>	CL=90%	-
KX(3915), X → ωJ/ψ	[ggaa] ( 7.1 ± 3.4 ) × 10 <sup>-5</sup>	-	1103	<b>Lepton Family number (LF) violating modes or ΔB = 1 weak neutral current (B<sub>1</sub>) modes</b>			
<b>K or K* modes</b>				s e <sup>+</sup> e <sup>-</sup>	B <sub>1</sub> ( 6.7 ± 1.7 ) × 10 <sup>-6</sup>	S=2.0	-
K <sup>±</sup> anything	[bb] ( 78.9 ± 2.5 ) %	-	-	sμ <sup>+</sup> μ <sup>-</sup>	B <sub>1</sub> ( 4.3 ± 1.0 ) × 10 <sup>-6</sup>	-	-
K <sup>+</sup> anything	( 66 ± 5 ) %	-	-	sℓ <sup>+</sup> ℓ <sup>-</sup>	B <sub>1</sub> [III] ( 5.8 ± 1.3 ) × 10 <sup>-6</sup>	S=1.8	-
K <sup>-</sup> anything	( 13 ± 4 ) %	-	-	πℓ <sup>+</sup> ℓ <sup>-</sup>	B <sub>1</sub> < 5.9 × 10 <sup>-8</sup>	CL=90%	2638
K <sup>0</sup> / $\bar{K}^0$ anything	[bb] ( 64 ± 4 ) %	-	-	π e <sup>+</sup> e <sup>-</sup>	B <sub>1</sub> < 1.10 × 10 <sup>-7</sup>	CL=90%	2638
K*(892) <sup>±</sup> anything	( 18 ± 6 ) %	-	-	π μ <sup>+</sup> μ <sup>-</sup>	B <sub>1</sub> < 5.0 × 10 <sup>-8</sup>	CL=90%	2634
K*(892) <sup>0</sup> / $\bar{K}^*(892)^0$ anything	[bb] ( 14.6 ± 2.6 ) %	-	-	K e <sup>+</sup> e <sup>-</sup>	B <sub>1</sub> ( 4.4 ± 0.6 ) × 10 <sup>-7</sup>	-	2617
K*(892)γ	( 4.2 ± 0.6 ) × 10 <sup>-5</sup>	-	2565	K*(892) e <sup>+</sup> e <sup>-</sup>	B <sub>1</sub> ( 1.19 ± 0.20 ) × 10 <sup>-6</sup>	S=1.2	2565
η Kγ	( 8.5 ± 1.8 / -1.6 ) × 10 <sup>-6</sup>	-	2588	K μ <sup>+</sup> μ <sup>-</sup>	B <sub>1</sub> ( 4.4 ± 0.4 ) × 10 <sup>-7</sup>	-	2612
K <sub>1</sub> (1400)γ	< 1.27 × 10 <sup>-4</sup>	CL=90%	2454	K*(892) μ <sup>+</sup> μ <sup>-</sup>	B <sub>1</sub> ( 1.06 ± 0.09 ) × 10 <sup>-6</sup>	-	2560
K <sub>2</sub> <sup>*</sup> (1430)γ	( 1.7 ± 0.6 / -0.5 ) × 10 <sup>-5</sup>	-	2447	Kℓ <sup>+</sup> ℓ <sup>-</sup>	B <sub>1</sub> ( 4.8 ± 0.4 ) × 10 <sup>-7</sup>	-	2617
K <sub>2</sub> <sup>*</sup> (1770)γ	< 1.2 × 10 <sup>-3</sup>	CL=90%	2342	K*(892) ℓ <sup>+</sup> ℓ <sup>-</sup>	B <sub>1</sub> ( 1.05 ± 0.10 ) × 10 <sup>-6</sup>	-	2565
K <sub>3</sub> <sup>*</sup> (1780)γ	< 3.7 × 10 <sup>-5</sup>	CL=90%	2341	Kν $\bar{\nu}$	B <sub>1</sub> < 1.6 × 10 <sup>-5</sup>	CL=90%	2617
K <sub>4</sub> <sup>*</sup> (2045)γ	< 1.0 × 10 <sup>-3</sup>	CL=90%	2243	K*ν $\bar{\nu}$	B <sub>1</sub> < 2.7 × 10 <sup>-5</sup>	CL=90%	-
Kη'(958)	( 8.3 ± 1.1 ) × 10 <sup>-5</sup>	-	2528	πν $\bar{\nu}$	B <sub>1</sub> < 8 × 10 <sup>-6</sup>	CL=90%	2638
K*(892)η'(958)	( 4.1 ± 1.1 ) × 10 <sup>-6</sup>	-	2472	ρν $\bar{\nu}$	B <sub>1</sub> < 2.8 × 10 <sup>-5</sup>	CL=90%	2583
Kη	< 5.2 × 10 <sup>-6</sup>	CL=90%	2588	s e <sup>±</sup> μ <sup>∓</sup>	LF [bb] < 2.2 × 10 <sup>-5</sup>	CL=90%	-
K*(892)η	( 1.8 ± 0.5 ) × 10 <sup>-5</sup>	-	2534	π e <sup>±</sup> μ <sup>∓</sup>	LF < 9.2 × 10 <sup>-8</sup>	CL=90%	2637
Kφ	( 2.3 ± 0.9 ) × 10 <sup>-6</sup>	-	2306	ρ e <sup>±</sup> μ <sup>∓</sup>	LF < 3.2 × 10 <sup>-6</sup>	CL=90%	2582
$\bar{b} \rightarrow \bar{s}\gamma$	( 3.49 ± 0.19 ) × 10 <sup>-4</sup>	-	-	K e <sup>±</sup> μ <sup>∓</sup>	LF < 3.8 × 10 <sup>-8</sup>	CL=90%	2616
$\bar{b} \rightarrow \bar{d}\gamma$	( 9.2 ± 3.0 ) × 10 <sup>-6</sup>	-	-	K*(892) e <sup>±</sup> μ <sup>∓</sup>	LF < 5.1 × 10 <sup>-7</sup>	CL=90%	2563
$\bar{b} \rightarrow \bar{s}$ gluon	< 6.8 %	CL=90%	-	<b>B<sup>±</sup>/B<sup>0</sup>/B<sub>s</sub><sup>0</sup>/b-baryon ADMIXTURE</b>			
η anything	( 2.6 ± 0.5 / -0.8 ) × 10 <sup>-4</sup>	-	-	These measurements are for an admixture of bottom particles at high energy (LHC, LEP, Tevatron, Sp $\bar{P}$ S).			
η' anything	( 4.2 ± 0.9 ) × 10 <sup>-4</sup>	-	-	Mean life τ = (1.5668 ± 0.0028) × 10 <sup>-12</sup> s			
K <sup>+</sup> gluon (charmless)	< 1.87 × 10 <sup>-4</sup>	CL=90%	-	Mean life τ = (1.72 ± 0.10) × 10 <sup>-12</sup> s Charged b-hadron admixture			
K <sup>0</sup> gluon (charmless)	( 1.9 ± 0.7 ) × 10 <sup>-4</sup>	-	-	Mean life τ = (1.58 ± 0.14) × 10 <sup>-12</sup> s Neutral b-hadron admixture			
<b>Light unflavored meson modes</b>				τ <sup>charged b-hadron</sup> /τ <sup>neutral b-hadron</sup> = 1.09 ± 0.13			
ργ	( 1.39 ± 0.25 ) × 10 <sup>-6</sup>	S=1.2	2583	Δτ <sub>b</sub>  /τ <sub>b,<math>\bar{b}</math></sub> = -0.001 ± 0.014			
ρ/ωγ	( 1.30 ± 0.23 ) × 10 <sup>-6</sup>	S=1.2	-	The branching fraction measurements are for an admixture of B mesons and baryons at energies above the T(4S). Only the highest energy results (LHC, LEP, Tevatron, Sp $\bar{P}$ S) are used in the branching fraction averages. In the following, we assume that the production fractions are the same at the LHC, LEP, and at the Tevatron.			
π <sup>±</sup> anything	[bb, hhaa] ( 358 ± 7 ) %	-	-	For inclusive branching fractions, e.g., B → D <sup>±</sup> anything, the values usually are multiplicities, not branching fractions. They can be greater than one.			
π <sup>0</sup> anything	( 235 ± 11 ) %	-	-				
η anything	( 17.6 ± 1.6 ) %	-	-				

## Meson Summary Table

The modes below are listed for a  $\bar{b}$  initial state.  $b$  modes are their charge conjugates. Reactions indicate the weak decay vertex and do not include mixing.

**$\bar{b}$  DECAY MODES** Fraction ( $\Gamma_i/\Gamma$ ) Scale factor/  
Confidence level  $p$  (MeV/c)

## PRODUCTION FRACTIONS

The production fractions for weakly decaying  $b$ -hadrons at high energy have been calculated from the best values of mean lives, mixing parameters, and branching fractions in this edition by the Heavy Flavor Averaging Group (HFLAV) as described in the note “ $B^0$ - $\bar{B}^0$  Mixing” in the  $B^0$  Particle Listings. We no longer provide world averages of the  $b$ -hadron production fractions, where results from LEP, Tevatron and LHC are averaged together; indeed the available data (from CDF and LHCb) shows that the fractions depend on the kinematics (in particular the  $p_T$ ) of the produced  $b$  hadron. Hence we would like to list the fractions in  $Z$  decays instead, which are well-defined physics observables. The production fractions in  $p\bar{p}$  collisions at the Tevatron are also listed at the end of the section. Values assume

$$\begin{aligned} \text{B}(\bar{b} \rightarrow B^+) &= \text{B}(\bar{b} \rightarrow B^0) \\ \text{B}(\bar{b} \rightarrow B^+) + \text{B}(\bar{b} \rightarrow B^0) + \text{B}(\bar{b} \rightarrow B_s^0) + \text{B}(b \rightarrow b\text{-baryon}) &= 100\%. \end{aligned}$$

The correlation coefficients between production fractions are also reported:

$$\begin{aligned} \text{cor}(B_c^0, b\text{-baryon}) &= 0.064 \\ \text{cor}(B_s^0, B^{\pm} = B^0) &= -0.633 \\ \text{cor}(b\text{-baryon}, B^{\pm} = B^0) &= -0.813. \end{aligned}$$

The notation for production fractions varies in the literature ( $f_d$ ,  $d_{B^0}$ ,  $f(b \rightarrow \bar{B}^0)$ ,  $\text{Br}(b \rightarrow \bar{B}^0)$ ). We use our own branching fraction notation here,  $\text{B}(\bar{b} \rightarrow B^0)$ .

Note these production fractions are  $b$ -hadronization fractions, not the conventional branching fractions of  $b$ -quark to a  $B$ -hadron, which may have considerable dependence on the initial and final state kinematic and production environment.

$B^+$	( 40.8 ± 0.7 ) %	—
$B^0$	( 40.8 ± 0.7 ) %	—
$B_s^0$	( 10.0 ± 0.8 ) %	—
$b$ -baryon	( 8.4 ± 1.1 ) %	—

## DECAY MODES

## Semileptonic and leptonic modes

$\nu$ anything	( 23.1 ± 1.5 ) %	—
$\ell^+ \nu_\ell$ anything	[III] ( 10.69 ± 0.22 ) %	—
$e^+ \nu_e$ anything	( 10.86 ± 0.35 ) %	—
$\mu^+ \nu_\mu$ anything	( 10.95 ± 0.29 ) %	—
$D^- \ell^+ \nu_\ell$ anything	[III] ( 2.2 ± 0.4 ) %	S=1.9
$D^- \pi^+ \ell^+ \nu_\ell$ anything	( 4.9 ± 1.9 ) × 10 <sup>-3</sup>	—
$D^- \pi^- \ell^+ \nu_\ell$ anything	( 2.6 ± 1.6 ) × 10 <sup>-3</sup>	—
$\bar{D}^0 \ell^+ \nu_\ell$ anything	[III] ( 6.79 ± 0.34 ) %	—
$\bar{D}^0 \pi^- \ell^+ \nu_\ell$ anything	( 1.07 ± 0.27 ) %	—
$\bar{D}^0 \pi^+ \ell^+ \nu_\ell$ anything	( 2.3 ± 1.6 ) × 10 <sup>-3</sup>	—
$D^{*-} \ell^+ \nu_\ell$ anything	[III] ( 2.75 ± 0.19 ) %	—
$D^{*-} \pi^- \ell^+ \nu_\ell$ anything	( 6 ± 7 ) × 10 <sup>-4</sup>	—
$D^{*-} \pi^+ \ell^+ \nu_\ell$ anything	( 4.8 ± 1.0 ) × 10 <sup>-3</sup>	—
$\bar{D}_j^0 \ell^+ \nu_\ell$ anything ×	[III, iiaa] ( 2.6 ± 0.9 ) × 10 <sup>-3</sup>	—
$\text{B}(\bar{D}_j^0 \rightarrow D^{*+} \pi^-)$		—
$D_j^- \ell^+ \nu_\ell$ anything ×	[III, iiaa] ( 7.0 ± 2.3 ) × 10 <sup>-3</sup>	—
$\text{B}(D_j^- \rightarrow D^0 \pi^-)$		—
$\bar{D}_2^*(2460)^0 \ell^+ \nu_\ell$ anything	< 1.4 × 10 <sup>-3</sup> CL=90%	—
× $\text{B}(\bar{D}_2^*(2460)^0 \rightarrow D^{*-} \pi^+)$		—
$D_2^*(2460)^- \ell^+ \nu_\ell$ anything	( 4.2 ± 1.5 ) × 10 <sup>-3</sup>	—
× $\text{B}(D_2^*(2460)^- \rightarrow D^0 \pi^-)$		—
$\bar{D}_2^*(2460)^0 \ell^+ \nu_\ell$ anything	( 1.6 ± 0.8 ) × 10 <sup>-3</sup>	—
× $\text{B}(\bar{D}_2^*(2460)^0 \rightarrow D^- \pi^+)$		—
charmless $\ell \bar{\nu}_\ell$	[III] ( 1.7 ± 0.5 ) × 10 <sup>-3</sup>	—
$\tau^+ \nu_\tau$ anything	( 2.41 ± 0.23 ) %	—
$D^{*-} \tau \nu_\tau$ anything	( 9 ± 4 ) × 10 <sup>-3</sup>	—
$\bar{c} \rightarrow \ell^- \bar{\nu}_\ell$ anything	[III] ( 8.02 ± 0.19 ) %	—
$c \rightarrow \ell^+ \nu_\ell$ anything	( 1.6 ± 0.5 ) %	—

## Charmed meson and baryon modes

$\bar{D}^0$ anything	( 58.7 ± 2.8 ) %	—
$D^0 D_s^\pm$ anything	[bb] ( 9.1 ± 4.0 ) %	—
$D^\mp D_s^\pm$ anything	[bb] ( 4.0 ± 2.3 ) %	—
$\bar{D}^0 D^0$ anything	[bb] ( 5.1 ± 2.0 ) %	—
$D^0 D^\pm$ anything	[bb] ( 2.7 ± 1.8 ) %	—
$D^\pm D^\mp$ anything	[bb] < 9 × 10 <sup>-3</sup> CL=90%	—
$D^-$ anything	( 22.7 ± 1.6 ) %	—
$D^*(2010)^+$ anything	( 17.3 ± 2.0 ) %	—
$D_1(2420)^0$ anything	( 5.0 ± 1.5 ) %	—
$D^*(2010)^\mp D_s^\pm$ anything	[bb] ( 3.3 ± 1.6 ) %	—
$D^0 D^*(2010)^\pm$ anything	[bb] ( 3.0 ± 0.9 ) %	—
$D^*(2010)^\pm D^\mp$ anything	[bb] ( 2.5 ± 1.2 ) %	—
$D^*(2010)^\pm D^*(2010)^\mp$ anything	[bb] ( 1.2 ± 0.4 ) %	—
$\bar{D} D$ anything	( 10 ± 11 ) %	—
$D_2^*(2460)^0$ anything	( 4.7 ± 2.7 ) %	—
$D_s^-$ anything	( 14.7 ± 2.1 ) %	—
$D_s^+$ anything	( 10.1 ± 3.1 ) %	—
$\Lambda_c^+$ anything	( 7.7 ± 1.1 ) %	—
$\bar{c}/c$ anything	[hhaa] (116.2 ± 3.2) %	—

## Charmonium modes

$J/\psi(1S)$ anything	( 1.16 ± 0.10 ) %	—
$\psi(2S)$ anything	( 2.86 ± 0.28 ) × 10 <sup>-3</sup>	—
$\chi_{c0}(1P)$ anything	( 1.5 ± 0.6 ) %	—
$\chi_{c1}(1P)$ anything	( 1.4 ± 0.4 ) %	—
$\chi_{c2}(1P)$ anything	( 6.2 ± 2.9 ) × 10 <sup>-3</sup>	—
$\chi_c(2P)$ anything, $\chi_c \rightarrow \phi\phi$	< 2.8 × 10 <sup>-7</sup> CL=95%	—
$\eta_c(1S)$ anything	( 4.5 ± 1.9 ) %	—
$\eta_c(2S)$ anything, $\eta_c \rightarrow \phi\phi$	( 3.2 ± 1.7 ) × 10 <sup>-6</sup>	—
$\chi_{c1}(3872)$ anything, $\chi_{c1} \rightarrow \phi\phi$	< 4.5 × 10 <sup>-7</sup> CL=95%	—
$X(3915)$ anything, $X \rightarrow \phi\phi$	< 3.1 × 10 <sup>-7</sup> CL=95%	—

## K or K\* modes

$\bar{3}\gamma$	( 3.1 ± 1.1 ) × 10 <sup>-4</sup>	—
$\bar{3}\bar{p}\nu$	< 6.4 × 10 <sup>-4</sup> CL=90%	—
$K^\pm$ anything	( 74 ± 6 ) %	—
$K_S^0$ anything	( 29.0 ± 2.9 ) %	—

## Pion modes

$\pi^\pm$ anything	( 397 ± 21 ) %	—
$\pi^0$ anything	[hhaa] (278 ± 60) %	—
$\phi$ anything	( 2.82 ± 0.23 ) %	—

## Baryon modes

$p/\bar{p}$ anything	( 13.1 ± 1.1 ) %	—
$\Lambda/\bar{\Lambda}$ anything	( 5.9 ± 0.6 ) %	—
$b$ -baryon anything	( 10.2 ± 2.8 ) %	—

## Other modes

charged anything	[hhaa] (497 ± 7) %	—
hadron <sup>+</sup> hadron <sup>-</sup>	( 1.7 ± 1.0 ) × 10 <sup>-5</sup>	—
charmless	( 7 ± 21 ) × 10 <sup>-3</sup>	—

 $\Delta B = 1$  weak neutral current ( $B1$ ) modes

$\mu^+ \mu^-$ anything	$B1$ < 3.2 × 10 <sup>-4</sup> CL=90%	—
------------------------	--------------------------------------	---

 **$B^*$** 

$$I(J^P) = \frac{1}{2}(1^-)$$

$I, J, P$  need confirmation.

Quantum numbers shown are quark-model predictions.

$$\begin{aligned} \text{Mass } m_{B^*} &= 5324.70 \pm 0.21 \text{ MeV} \\ m_{B^*} - m_B &= 45.21 \pm 0.21 \text{ MeV} \\ m_{B^{*+}} - m_{B^+} &= 45.37 \pm 0.21 \text{ MeV} \end{aligned}$$

**$B^*$  DECAY MODES** Fraction ( $\Gamma_i/\Gamma$ )  $p$  (MeV/c)

$B\gamma$	seen	45
-----------	------	----

 **$B_1(5721)^+$** 

$$I(J^P) = \frac{1}{2}(1^+)$$

$I, J, P$  need confirmation.

$$\begin{aligned} \text{Mass } m &= 5725.9^{+2.5}_{-2.7} \text{ MeV} \\ m_{B_1^+} - m_{B^{*0}} &= 401.2^{+2.4}_{-2.7} \text{ MeV} \\ \text{Full width } \Gamma &= 31 \pm 6 \text{ MeV} \quad (S = 1.1) \end{aligned}$$

## Meson Summary Table

$B_1(5721)^+$ DECAY MODES	Fraction ( $\Gamma_i/\Gamma$ )	$\rho$ (MeV/c)
$B^{*0}\pi^+$	seen	363

$B_1(5721)^0$	$I(J^P) = \frac{1}{2}(1^+)$ <i>I, J, P need confirmation.</i>
$B_1(5721)^0$ MASS = $5726.1 \pm 1.3$ MeV ( $S = 1.2$ )	
$m_{B_1^0} - m_{B^+} = 446.7 \pm 1.3$ MeV ( $S = 1.2$ )	
$m_{B_1^0} - m_{B^{*+}} = 401.4 \pm 1.2$ MeV ( $S = 1.2$ )	
Full width $\Gamma = 27.5 \pm 3.4$ MeV ( $S = 1.1$ )	

$B_1(5721)^0$ DECAY MODES	Fraction ( $\Gamma_i/\Gamma$ )	$\rho$ (MeV/c)
$B^{*+}\pi^-$	seen	363

$B_2^*(5747)^+$	$I(J^P) = \frac{1}{2}(2^+)$ <i>I, J, P need confirmation.</i>
Mass $m = 5737.2 \pm 0.7$ MeV	
$m_{B_2^{*+}} - m_{B^0} = 457.5 \pm 0.7$ MeV	
Full width $\Gamma = 20 \pm 5$ MeV ( $S = 2.2$ )	

$B_2^*(5747)^+$ DECAY MODES	Fraction ( $\Gamma_i/\Gamma$ )	$\rho$ (MeV/c)
$B^0\pi^+$	seen	418
$B^{*0}\pi^+$	seen	374

$B_2^*(5747)^0$	$I(J^P) = \frac{1}{2}(2^+)$ <i>I, J, P need confirmation.</i>
$B_2^*(5747)^0$ MASS = $5739.5 \pm 0.7$ MeV ( $S = 1.4$ )	
$m_{B_2^0} - m_{B^0} = 13.4 \pm 1.4$ MeV ( $S = 1.3$ )	
$m_{B_2^0} - m_{B^+} = 460.2 \pm 0.6$ MeV ( $S = 1.4$ )	
Full width $\Gamma = 24.2 \pm 1.7$ MeV	

$B_2^*(5747)^0$ DECAY MODES	Fraction ( $\Gamma_i/\Gamma$ )	$\rho$ (MeV/c)
$B^+\pi^-$	seen	421
$B^{*+}\pi^-$	seen	376

$B_J(5970)^+$	$I(J^P) = \frac{1}{2}(?^?)$ <i>I, J, P need confirmation.</i>
Mass $m = 5964 \pm 5$ MeV	
$m_{B_J(5970)^+} - m_{B^0} = 685 \pm 5$ MeV	
Full width $\Gamma = 62 \pm 20$ MeV	

$B_J(5970)^+$ DECAY MODES	Fraction ( $\Gamma_i/\Gamma$ )	$\rho$ (MeV/c)
$B^0\pi^+$	possibly seen	632
$B^{*0}\pi^+$	seen	591

$B_J(5970)^0$	$I(J^P) = \frac{1}{2}(?^?)$ <i>I, J, P need confirmation.</i>
Mass $m = 5971 \pm 5$ MeV	
$m_{B_J(5970)^0} - m_{B^+} = 691 \pm 5$ MeV	
Full width $\Gamma = 81 \pm 12$ MeV	

$B_J(5970)^0$ DECAY MODES	Fraction ( $\Gamma_i/\Gamma$ )	$\rho$ (MeV/c)
$B^+\pi^-$	possibly seen	638
$B^{*+}\pi^-$	seen	596

## BOTTOM, STRANGE MESONS

### ( $B = \pm 1, S = \mp 1$ )

$$B_s^0 = s\bar{b}, \bar{B}_s^0 = \bar{s}b, \text{ similarly for } B_s^{*s}$$

$B_s^0$	$I(J^P) = 0(0^-)$
---------	-------------------

*I, J, P need confirmation. Quantum numbers shown are quark-model predictions.*

$$\text{Mass } m_{B_s^0} = 5366.88 \pm 0.14 \text{ MeV}$$

$$m_{B_s^0} - m_B = 87.38 \pm 0.16 \text{ MeV}$$

$$\text{Mean life } \tau = (1.515 \pm 0.004) \times 10^{-12} \text{ s}$$

$$c\tau = 454.2 \mu\text{m}$$

$$\Delta\Gamma_{B_s^0} = \Gamma_{B_{sL}^0} - \Gamma_{B_{sH}^0} = (0.085 \pm 0.004) \times 10^{12} \text{ s}^{-1}$$

#### $B_s^0\text{-}\bar{B}_s^0$ mixing parameters

$$\Delta m_{B_s^0} = m_{B_{sH}^0} - m_{B_{sL}^0} = (17.749 \pm 0.020) \times 10^{12} \hbar \text{ s}^{-1}$$

$$= (1.1683 \pm 0.0013) \times 10^{-8} \text{ MeV}$$

$$\chi_s = \Delta m_{B_s^0} / \Gamma_{B_s^0} = 26.89 \pm 0.07$$

$$\chi_s = 0.499312 \pm 0.000004$$

#### CP violation parameters in $B_s^0$

$$\text{Re}(\epsilon_{B_s^0}) / (1 + |\epsilon_{B_s^0}|^2) = (-0.15 \pm 0.70) \times 10^{-3}$$

$$C_{KK}(B_s^0 \rightarrow K^+K^-) = 0.14 \pm 0.11$$

$$S_{KK}(B_s^0 \rightarrow K^+K^-) = 0.30 \pm 0.13$$

$$r_B(B_s^0 \rightarrow D_s^\mp K^\pm) = 0.37 \pm_{0.09}^{0.10}$$

$$\delta_B(B_s^0 \rightarrow D_s^\pm K^\mp) = (358 \pm 14)^\circ$$

$$\text{CP Violation phase } \beta_s = (2.55 \pm 1.15) \times 10^{-2} \text{ rad}$$

$$|\lambda| (B_s^0 \rightarrow J/\psi(1S)\phi) = 1.012 \pm 0.017$$

$$|\lambda| = 0.999 \pm 0.017$$

$$A, \text{ CP violation parameter} = -0.75 \pm 0.12$$

$$C, \text{ CP violation parameter} = 0.19 \pm 0.06$$

$$S, \text{ CP violation parameter} = 0.17 \pm 0.06$$

$$A_{CP}^L(B_s \rightarrow J/\psi \bar{K}^*(892)^0) = -0.05 \pm 0.06$$

$$A_{CP}^{\parallel}(B_s \rightarrow J/\psi \bar{K}^*(892)^0) = 0.17 \pm 0.15$$

$$A_{CP}^{\perp}(B_s \rightarrow J/\psi \bar{K}^*(892)^0) = -0.05 \pm 0.10$$

$$A_{CP}(B_s \rightarrow \pi^+ K^-) = 0.221 \pm 0.015$$

$$A_{CP}(B_s^0 \rightarrow [K^+ K^-]_D \bar{K}^*(892)^0) = -0.04 \pm 0.07$$

$$A_{CP}(B_s^0 \rightarrow [\pi^+ K^-]_D K^*(892)^0) = -0.01 \pm 0.04$$

$$A_{CP}(B_s^0 \rightarrow [\pi^+ \pi^-]_D K^*(892)^0) = 0.06 \pm 0.13$$

$$S(B_s^0 \rightarrow \phi\gamma) = 0.43 \pm 0.32$$

$$C(B_s^0 \rightarrow \phi\gamma) = 0.11 \pm 0.31$$

$$A^\Delta(B_s \rightarrow \phi\gamma) = -0.7 \pm 0.4$$

$$\Delta a_\perp < 1.2 \times 10^{-12} \text{ GeV}, \text{ CL} = 95\%$$

$$\Delta a_\parallel = (-0.9 \pm 1.5) \times 10^{-14} \text{ GeV}$$

$$\Delta a_\chi = (1.0 \pm 2.2) \times 10^{-14} \text{ GeV}$$

$$\Delta a_\gamma = (-3.8 \pm 2.2) \times 10^{-14} \text{ GeV}$$

$$\text{Re}(\xi) = -0.022 \pm 0.033$$

$$\text{Im}(\xi) = 0.004 \pm 0.011$$

These branching fractions all scale with  $B(\bar{B} \rightarrow B_s^0)$ .

The branching fraction  $B(B_s^0 \rightarrow D_s^- \ell^+ \nu_\ell \text{ anything})$  is not a pure measurement since the measured product branching fraction  $B(\bar{B} \rightarrow B_s^0) \times B(B_s^0 \rightarrow D_s^- \ell^+ \nu_\ell \text{ anything})$  was used to determine  $B(\bar{B} \rightarrow B_s^0)$ , as described in the note on " $B^0\text{-}\bar{B}^0$  Mixing"

For inclusive branching fractions, e.g.,  $B \rightarrow D^\pm \text{ anything}$ , the values usually are multiplicities, not branching fractions. They can be greater than one.

$B_s^0$ DECAY MODES	Fraction ( $\Gamma_i/\Gamma$ )	Scale factor/ Confidence level	$\rho$ (MeV/c)
$D_s^-$ anything	(93 $\pm$ 25 ) %		—
$\ell \nu_\ell X$	( 9.6 $\pm$ 0.8 ) %		—
$e^+ \nu X^-$	( 9.1 $\pm$ 0.8 ) %		—
$\mu^+ \nu X^-$	(10.2 $\pm$ 1.0 ) %		—
$D_s^- \ell^+ \nu_\ell \text{ anything}$	[ <i>jja</i> ] ( 8.1 $\pm$ 1.3 ) %		—
$D_s^{*-} \ell^+ \nu_\ell \text{ anything}$	( 5.4 $\pm$ 1.1 ) %		—
$D_{s1}(2536)^- \mu^+ \nu_\mu, D_{s1}^- \rightarrow D^{*-} K_S^0$	( 2.7 $\pm$ 0.7 ) $\times 10^{-3}$		—

## Meson Summary Table

$D_{s1}(2536)^- X \mu^+ \nu, D_{s1}^- \rightarrow \bar{D}^0 K^+$	$(4.4 \pm 1.3) \times 10^{-3}$	-	$J/\psi(1S) f_2'(1525)_{\parallel}, f_2' \rightarrow \pi^+ \pi^-$	$(1.3 \pm \frac{2.7}{0.9}) \times 10^{-7}$	-	
$D_{s2}(2573)^- X \mu^+ \nu, D_{s2}^- \rightarrow \bar{D}^0 K^+$	$(2.7 \pm 1.0) \times 10^{-3}$	-	$J/\psi(1S) f_2'(1525)_{\perp}, f_2' \rightarrow \pi^+ \pi^-$	$(5 \pm 4) \times 10^{-7}$	-	
$D_s^- \pi^+$	$(3.00 \pm 0.23) \times 10^{-3}$	2320	$J/\psi(1S) f_0(1790), f_0 \rightarrow \pi^+ \pi^-$	$(5.0 \pm \frac{11.0}{1.1}) \times 10^{-6}$	-	
$D_s^- \rho^+$	$(6.9 \pm 1.4) \times 10^{-3}$	2249	$J/\psi(1S) \pi^+ \pi^-$ (nonresonant)	$(1.8 \pm \frac{1.1}{0.4}) \times 10^{-5}$	1775	
$D_s^- \pi^+ \pi^+ \pi^-$	$(6.1 \pm 1.0) \times 10^{-3}$	2301	$J/\psi(1S) \bar{K}^0 \pi^+ \pi^-$	$< 4.4 \times 10^{-5}$	CL=90% 1675	
$D_{s1}(2536)^- \pi^+, D_{s1}^- \rightarrow D_s^- \pi^+ \pi^-$	$(2.5 \pm 0.8) \times 10^{-5}$	-	$J/\psi(1S) K^+ K^-$	$(7.9 \pm 0.7) \times 10^{-4}$	1601	
$D_s^{\mp} K^{\pm}$	$(2.27 \pm 0.19) \times 10^{-4}$	2293	$J/\psi(1S) K^0 K^- \pi^+ + c.c.$	$(9.2 \pm 1.3) \times 10^{-4}$	1538	
$D_s^- K^+ \pi^+ \pi^-$	$(3.2 \pm 0.6) \times 10^{-4}$	2249	$J/\psi(1S) \bar{K}^0 K^+ K^-$	$< 1.2 \times 10^{-5}$	CL=90% 1333	
$D_s^+ D_s^-$	$(4.4 \pm 0.5) \times 10^{-3}$	1824	$J/\psi(1S) f_2'(1525)$	$(2.6 \pm 0.6) \times 10^{-4}$	1310	
$D_s^- D^+$	$(2.8 \pm 0.5) \times 10^{-4}$	1875	$J/\psi(1S) p \bar{p}$	$(3.6 \pm 0.4) \times 10^{-6}$	982	
$D^+ D^-$	$(2.2 \pm 0.6) \times 10^{-4}$	1925	$J/\psi(1S) \gamma$	$< 7.3 \times 10^{-6}$	CL=90% 1790	
$D^0 \bar{D}^0$	$(1.9 \pm 0.5) \times 10^{-4}$	1930	$J/\psi(1S) \pi^+ \pi^- \pi^+ \pi^-$	$(7.8 \pm 1.0) \times 10^{-5}$	1731	
$D_s^{*-} \pi^+$	$(2.0 \pm 0.5) \times 10^{-3}$	2265	$J/\psi(1S) f_1(1285)$	$(7.2 \pm 1.4) \times 10^{-5}$	1460	
$D_s^{*\mp} K^{\pm}$	$(1.33 \pm 0.35) \times 10^{-4}$	-	$\psi(2S) \eta$	$(3.3 \pm 0.9) \times 10^{-4}$	1338	
$D_s^{*-} \rho^+$	$(9.6 \pm 2.1) \times 10^{-3}$	2191	$\psi(2S) \eta'$	$(1.29 \pm 0.35) \times 10^{-4}$	1158	
$D_s^{*+} D_s^- + D_s^{*-} D_s^+$	$(1.39 \pm 0.17) \%$	1742	$\psi(2S) \pi^+ \pi^-$	$(7.1 \pm 1.3) \times 10^{-5}$	1397	
$D_s^{*+} D_s^{*-}$	$(1.44 \pm 0.21) \%$	S=1.1 1655	$\psi(2S) \phi$	$(5.4 \pm 0.6) \times 10^{-4}$	1120	
$D_s^{*(*)+} D_s^{*(*)-}$	$(4.5 \pm 1.4) \%$	-	$\psi(2S) K^- \pi^+$	$(3.1 \pm 0.4) \times 10^{-5}$	1310	
$\bar{D}^{*0} \bar{K}^0$	$(2.8 \pm 1.1) \times 10^{-4}$	2278	$\psi(2S) \bar{K}^*(892)^0$	$(3.3 \pm 0.5) \times 10^{-5}$	1196	
$\bar{D}^0 \bar{K}^0$	$(4.3 \pm 0.9) \times 10^{-4}$	2330	$\chi_{c1} \phi$	$(2.04 \pm 0.30) \times 10^{-4}$	1274	
$\bar{D}^0 K^- \pi^+$	$(1.04 \pm 0.13) \times 10^{-3}$	2312	$\pi^+ \pi^-$	$(7.0 \pm 1.0) \times 10^{-7}$	2680	
$\bar{D}^0 \bar{K}^*(892)^0$	$(4.4 \pm 0.6) \times 10^{-4}$	2264	$\pi^0 \pi^0$	$< 2.1 \times 10^{-4}$	CL=90% 2680	
$\bar{D}^0 \bar{K}^*(1410)$	$(3.9 \pm 3.5) \times 10^{-4}$	2117	$\eta \pi^0$	$< 1.0 \times 10^{-3}$	CL=90% 2654	
$\bar{D}^0 \bar{K}_0^*(1430)$	$(3.0 \pm 0.7) \times 10^{-4}$	2113	$\eta \eta$	$< 1.5 \times 10^{-3}$	CL=90% 2627	
$\bar{D}^0 \bar{K}_2^*(1430)$	$(1.1 \pm 0.4) \times 10^{-4}$	2112	$\rho^0 \rho^0$	$< 3.20 \times 10^{-4}$	CL=90% 2569	
$\bar{D}^0 \bar{K}^*(1680)$	$< 7.8 \times 10^{-5}$	CL=90% 1997	$\eta' \eta'$	$(3.3 \pm 0.7) \times 10^{-5}$	2507	
$\bar{D}^0 \bar{K}_0^*(1950)$	$< 1.1 \times 10^{-4}$	CL=90% 1890	$\eta' \phi$	$< 8.2 \times 10^{-7}$	CL=90% 2495	
$\bar{D}^0 \bar{K}_3^*(1780)$	$< 2.6 \times 10^{-5}$	CL=90% 1971	$\phi f_0(980), f_0(980) \rightarrow \pi^+ \pi^-$	$(1.12 \pm 0.21) \times 10^{-6}$	-	
$\bar{D}^0 \bar{K}_4^*(2045)$	$< 3.1 \times 10^{-5}$	CL=90% 1835	$\phi f_2(1270), f_2(1270) \rightarrow \pi^+ \pi^-$	$(6.1 \pm \frac{1.8}{1.5}) \times 10^{-7}$	-	
$\bar{D}^0 K^- \pi^+$ (non-resonant)	$(2.1 \pm 0.8) \times 10^{-4}$	2312	$\phi \rho^0$	$(2.7 \pm 0.8) \times 10^{-7}$	2526	
$D_{s2}^*(2573)^- \pi^+, D_{s2}^* \rightarrow \bar{D}^0 K^-$	$(2.6 \pm 0.4) \times 10^{-4}$	-	$\phi \pi^+ \pi^-$	$(3.5 \pm 0.5) \times 10^{-6}$	2579	
$D_{s1}^*(2700)^- \pi^+, D_{s1}^* \rightarrow \bar{D}^0 K^-$	$(1.6 \pm 0.8) \times 10^{-5}$	-	$\phi \phi$	$(1.87 \pm 0.15) \times 10^{-5}$	2482	
$D_{s1}^*(2860)^- \pi^+, D_{s1}^* \rightarrow \bar{D}^0 K^-$	$(5 \pm 4) \times 10^{-5}$	-	$\phi \phi \phi$	$(2.2 \pm 0.7) \times 10^{-6}$	2165	
$D_{s3}^*(2860)^- \pi^+, D_{s3}^* \rightarrow \bar{D}^0 K^-$	$(2.2 \pm 0.6) \times 10^{-5}$	-	$\pi^+ K^-$	$(5.8 \pm 0.7) \times 10^{-6}$	2659	
$\bar{D}^0 K^+ K^-$	$(5.5 \pm 0.8) \times 10^{-5}$	2243	$K^+ K^-$	$(2.66 \pm 0.22) \times 10^{-5}$	2638	
$\bar{D}^0 f_0(980)$	$< 3.1 \times 10^{-6}$	CL=90% 2242	$K^0 \bar{K}^0$	$(2.0 \pm 0.6) \times 10^{-5}$	2637	
$\bar{D}^0 \phi$	$(3.0 \pm 0.5) \times 10^{-5}$	2235	$K^0 \pi^+ \pi^-$	$(9.5 \pm 2.1) \times 10^{-6}$	2653	
$\bar{D}^{*0} \phi$	$(3.7 \pm 0.6) \times 10^{-5}$	2178	$K^0 K^{\pm} \pi^{\mp}$	$(8.4 \pm 0.9) \times 10^{-5}$	2622	
$D^{*\mp} \pi^{\pm}$	$< 6.1 \times 10^{-6}$	CL=90%	$K^*(892)^- \pi^+$	$(2.9 \pm 1.1) \times 10^{-6}$	2607	
$\eta_c \phi$	$(5.0 \pm 0.9) \times 10^{-4}$	1663	$K^*(892)^{\pm} K^{\mp}$	$(1.9 \pm 0.5) \times 10^{-5}$	2585	
$\eta_c \pi^+ \pi^-$	$(1.8 \pm 0.7) \times 10^{-4}$	1840	$K_0^*(1430)^{\pm} K^{\mp}$	$(3.1 \pm 2.5) \times 10^{-5}$	-	
$J/\psi(1S) \phi$	$(1.08 \pm 0.08) \times 10^{-3}$	1588	$K_2^*(1430)^{\pm} K^{\mp}$	$(1.0 \pm 1.7) \times 10^{-5}$	-	
$J/\psi(1S) \phi \phi$	$(1.24 \pm \frac{0.17}{0.19}) \times 10^{-5}$	764	$K^*(892)^0 \bar{K}^0 + c.c.$	$(2.0 \pm 0.6) \times 10^{-5}$	2585	
$J/\psi(1S) \pi^0$	$< 1.2 \times 10^{-3}$	CL=90% 1787	$K_0^*(1430) \bar{K}^0 + c.c.$	$(3.3 \pm 1.0) \times 10^{-5}$	2468	
$J/\psi(1S) \eta$	$(4.0 \pm 0.7) \times 10^{-4}$	S=1.4 1733	$K_2^*(1430)^0 \bar{K}^0 + c.c.$	$(1.7 \pm 2.2) \times 10^{-5}$	2467	
$J/\psi(1S) K_S^0$	$(1.88 \pm 0.15) \times 10^{-5}$	1743	$K_S^0 \bar{K}^*(892)^0 + c.c.$	$(1.6 \pm 0.4) \times 10^{-5}$	2585	
$J/\psi(1S) \bar{K}^*(892)^0$	$(4.1 \pm 0.4) \times 10^{-5}$	1637	$K^0 K^+ K^-$	$(1.3 \pm 0.6) \times 10^{-6}$	2568	
$J/\psi(1S) \eta'$	$(3.3 \pm 0.4) \times 10^{-4}$	1612	$\bar{K}^*(892)^0 \rho^0$	$< 7.67 \times 10^{-4}$	CL=90% 2550	
$J/\psi(1S) \pi^+ \pi^-$	$(2.09 \pm 0.23) \times 10^{-4}$	S=1.3 1775	$\bar{K}^*(892)^0 K^*(892)^0$	$(1.11 \pm 0.27) \times 10^{-5}$	2531	
$J/\psi(1S) f_0(500), f_0 \rightarrow \pi^+ \pi^-$	$< 4 \times 10^{-6}$	CL=90%	$\phi K^*(892)^0$	$(1.14 \pm 0.30) \times 10^{-6}$	2507	
$J/\psi(1S) \rho, \rho \rightarrow \pi^+ \pi^-$	$< 4 \times 10^{-6}$	CL=90%	$p \bar{p}$	$< 1.5 \times 10^{-8}$	CL=90% 2514	
$J/\psi(1S) f_0(980), f_0 \rightarrow \pi^+ \pi^-$	$(1.28 \pm 0.18) \times 10^{-4}$	S=1.7	$p \bar{p} K^+ K^-$	$(4.5 \pm 0.5) \times 10^{-6}$	2231	
$J/\psi(1S) f_2(1270), f_2 \rightarrow \pi^+ \pi^-$	$(1.1 \pm 0.4) \times 10^{-6}$	-	$p \bar{p} K^+ \pi^-$	$(1.39 \pm 0.26) \times 10^{-6}$	2355	
$J/\psi(1S) f_2(1270)_0, f_2 \rightarrow \pi^+ \pi^-$	$(7.5 \pm 1.8) \times 10^{-7}$	-	$p \bar{p} \pi^+ \pi^-$	$(4.3 \pm 2.0) \times 10^{-7}$	2454	
$J/\psi(1S) f_2(1270)_{\parallel}, f_2 \rightarrow \pi^+ \pi^-$	$(1.09 \pm 0.34) \times 10^{-6}$	-	$p \bar{p} K^- + c.c.$	$(5.5 \pm 1.0) \times 10^{-6}$	2358	
$J/\psi(1S) f_2(1270)_{\perp}, f_2 \rightarrow \pi^+ \pi^-$	$(1.3 \pm 0.8) \times 10^{-6}$	-	$\Lambda_c^- \Lambda \pi^+$	$(3.6 \pm 1.6) \times 10^{-4}$	1979	
$J/\psi(1S) f_0(1370), f_0 \rightarrow \pi^+ \pi^-$	$(4.5 \pm \frac{0.7}{4.0}) \times 10^{-5}$	-	$\Lambda_c^- \Lambda_c^+$	$< 8.0 \times 10^{-5}$	CL=95% 1405	
$J/\psi(1S) f_0(1500), f_0 \rightarrow \pi^+ \pi^-$	$(2.11 \pm \frac{0.40}{0.29}) \times 10^{-5}$	-	<b>Lepton Family number (LF) violating modes or <math>\Delta B = 1</math> weak neutral current (BI) modes</b>			
$J/\psi(1S) f_2'(1525)_0, f_2' \rightarrow \pi^+ \pi^-$	$(1.07 \pm 0.24) \times 10^{-6}$	-	$\gamma \gamma$	BI	$< 3.1 \times 10^{-6}$	CL=90% 2683
			$\phi \gamma$	BI	$(3.4 \pm 0.4) \times 10^{-5}$	2587
			$\mu^+ \mu^-$	BI	$(3.0 \pm 0.4) \times 10^{-9}$	2681
			$e^+ e^-$	BI	$< 2.8 \times 10^{-7}$	CL=90% 2683
			$\tau^+ \tau^-$	BI	$< 6.8 \times 10^{-3}$	CL=95% 2011
			$\mu^+ \mu^- \mu^+ \mu^-$	BI	$< 2.5 \times 10^{-9}$	CL=95% 2673
			$S P, S \rightarrow \mu^+ \mu^-$	BI	[aaaa] $< 2.2 \times 10^{-9}$	-
			$P \rightarrow \mu^+ \mu^-$			
			$\phi(1020) \mu^+ \mu^-$	BI	$(8.2 \pm 1.2) \times 10^{-7}$	2582
			$\bar{K}^*(892)^0 \mu^+ \mu^-$		$(2.9 \pm 1.1) \times 10^{-8}$	2605
			$\pi^+ \pi^- \mu^+ \mu^-$	BI	$(8.4 \pm 1.7) \times 10^{-8}$	2670



## Meson Summary Table

$\phi\nu\bar{\nu}$	$BI$	$< 5.4$	$\times 10^{-3}$	CL=90%	2587
$e^\pm\mu^\mp$	$LF$	$[bb] < 5.4$	$\times 10^{-9}$	CL=90%	2682
$\mu^\pm\tau^\mp$		$< 4.2$	$\times 10^{-5}$	CL=95%	2388

 **$B_s^*$** 

$$I(J^P) = 0(1^-)$$

$I, J, P$  need confirmation. Quantum numbers shown are quark-model predictions.

$$\text{Mass } m = 5415.4^{+1.8}_{-1.5} \text{ MeV } (S = 2.9)$$

$$m_{B_s^*} - m_{B_s} = 48.6^{+1.8}_{-1.5} \text{ MeV } (S = 2.9)$$

$B_s^*$ DECAY MODES	Fraction ( $\Gamma_i/\Gamma$ )	$\rho$ (MeV/c)
$B_s\gamma$	seen	48

 **$B_{s1}(5830)^0$** 

$$I(J^P) = 0(1^+)$$

$I, J, P$  need confirmation.

$$\text{Mass } m = 5828.70 \pm 0.20 \text{ MeV}$$

$$m_{B_{s1}^0} - m_{B^{*+}} = 504.00 \pm 0.17 \text{ MeV}$$

$$\text{Full width } \Gamma = 0.5 \pm 0.4 \text{ MeV}$$

$B_{s1}(5830)^0$ DECAY MODES	Fraction ( $\Gamma_i/\Gamma$ )	$\rho$ (MeV/c)
$B^{*+}K^-$	seen	97

 **$B_{s2}(5840)^0$** 

$$I(J^P) = 0(2^+)$$

$I, J, P$  need confirmation.

$$\text{Mass } m = 5839.86 \pm 0.12 \text{ MeV}$$

$$m_{B_{s2}^0} - m_{B^{*+}} = 560.52 \pm 0.14 \text{ MeV}$$

$$\text{Full width } \Gamma = 1.49 \pm 0.27 \text{ MeV}$$

$B_{s2}(5840)^0$ DECAY MODES	Fraction ( $\Gamma_i/\Gamma$ )	$\rho$ (MeV/c)
$B^+K^-$	<b>DEFINED AS 1</b>	252
$B^{*+}K^-$	0.093 ± 0.018	141
$B^0K_S^0$	0.43 ± 0.11	245
$B^{*0}K_S^0$	0.04 ± 0.04	–

## BOTTOM, CHARMED MESONS ( $B = C = \pm 1$ )

$$B_c^+ = c\bar{b}, B_c^- = \bar{c}b, \text{ similarly for } B_c^{* \pm}$$

 **$B_c^+$** 

$$I(J^P) = 0(0^-)$$

$I, J, P$  need confirmation.

Quantum numbers shown are quark-model predictions.

$$\text{Mass } m = 6274.9 \pm 0.8 \text{ MeV}$$

$$\text{Mean life } \tau = (0.510 \pm 0.009) \times 10^{-12} \text{ s}$$

$B_c^-$  modes are charge conjugates of the modes below.

$B_c^+$ DECAY MODES $\times B(\bar{b} \rightarrow B_c)$	Fraction ( $\Gamma_i/\Gamma$ )	Confidence level	$\rho$ (MeV/c)
---	--------------------------------	------------------	----------------

The following quantities are not pure branching ratios; rather the fraction  $\Gamma_i/\Gamma \times B(\bar{b} \rightarrow B_c)$ .

$J/\psi(1S)\ell^+\nu_\ell\text{anything}$	$(8.1 \pm 1.2) \times 10^{-5}$	–	–
$J/\psi(1S)\pi^+$	seen	2371	–
$J/\psi(1S)K^+$	seen	2341	–
$J/\psi(1S)\pi^+\pi^+\pi^-$	seen	2350	–
$J/\psi(1S)a_1(1260)$	$< 1.2$	$\times 10^{-3}$	90%
$J/\psi(1S)K^+K^-\pi^+$	seen	2203	–
$J/\psi(1S)\pi^+\pi^+\pi^+\pi^-\pi^-$	seen	2309	–
$\psi(2S)\pi^+$	seen	2052	–
$J/\psi(1S)D^0K^+$	seen	1539	–
$J/\psi(1S)D^*(2007)^0K^+$	seen	1412	–
$J/\psi(1S)D^*(2010)^+K^{*0}$	seen	920	–
$J/\psi(1S)D^+K^{*0}$	seen	1123	–
$J/\psi(1S)D^+$	seen	1822	–
$J/\psi(1S)D_s^{*+}$	seen	1728	–
$J/\psi(1S)D_s^+\pi^+$	seen	1792	–

$\chi_c^0\pi^+$	$(2.4^{+0.9}_{-0.8}) \times 10^{-5}$	2205	
$\rho\bar{\rho}\pi^+$	not seen	2970	
$D^0K^+$	$(3.8^{+1.2}_{-1.1}) \times 10^{-7}$	2837	
$D^0\pi^+$	$< 1.6$	$\times 10^{-7}$	95%
$D^{*0}\pi^+$	$< 4$	$\times 10^{-7}$	95%
$D^{*0}K^+$	$< 4$	$\times 10^{-7}$	95%
$D_s^+\bar{D}^0$	$< 1.4$	$\times 10^{-7}$	90%
$D_s^+D^0$	$< 6$	$\times 10^{-8}$	90%
$D_s^+\bar{D}^0$	$< 3.0$	$\times 10^{-6}$	90%
$D^+D^0$	$< 1.9$	$\times 10^{-6}$	90%
$D^*(2010)^+\bar{D}^0$	$< 6.2$	$\times 10^{-3}$	90%
$D_s^{*+}\bar{D}^*(2007)^0$	$< 1.7$	$\times 10^{-6}$	90%
$D_s^{*+}D^*(2007)^0$	$< 3.1$	$\times 10^{-6}$	90%
$D^*(2010)^+\bar{D}^*(2007)^0$	$< 1.0$	$\times 10^{-4}$	90%
$D^*(2010)^+D^*(2007)^0$	$< 2.0$	$\times 10^{-5}$	90%
$D^+K^{*0}$	$< 0.20$	$\times 10^{-6}$	90%
$D^+K^{*0}$	$< 0.16$	$\times 10^{-6}$	90%
$D_s^+K^{*0}$	$< 0.28$	$\times 10^{-6}$	90%
$D_s^+K^{*0}$	$< 0.4$	$\times 10^{-6}$	90%
$D_s^+\phi$	$< 0.32$	$\times 10^{-6}$	90%
$K^+K^0$	$< 4.6$	$\times 10^{-7}$	90%
$B_s^0\pi^+ / B(\bar{b} \rightarrow B_s)$	$(2.37^{+0.37}_{-0.35}) \times 10^{-3}$	–	

## $c\bar{c}$ MESONS (including possibly non- $q\bar{q}$ states)

 **$\eta_c(1S)$** 

$$I^G(J^PC) = 0^+(0^-)$$

$$\text{Mass } m = 2983.9 \pm 0.5 \text{ MeV } (S = 1.3)$$

$$\text{Full width } \Gamma = 32.0 \pm 0.7 \text{ MeV}$$

$\eta_c(1S)$ DECAY MODES	Fraction ( $\Gamma_i/\Gamma$ )	Confidence level	$\rho$ (MeV/c)
--------------------------	--------------------------------	------------------	----------------

### Decays involving hadronic resonances

$\eta'(958)\pi\pi$	$(4.1 \pm 1.7) \%$	1323	
$\rho\rho$	$(1.8 \pm 0.5) \%$	1275	
$K^*(892)^0K^-\pi^+ + \text{c.c.}$	$(2.0 \pm 0.7) \%$	1278	
$K^*(892)\bar{K}^*(892)$	$(7.0 \pm 1.3) \times 10^{-3}$	1196	
$K^*(892)^0\bar{K}^*(892)^0\pi^+\pi^-$	$(1.1 \pm 0.5) \%$	1073	
$\phi K^+K^-$	$(2.9 \pm 1.4) \times 10^{-3}$	1104	
$\phi\phi$	$(1.77 \pm 0.19) \times 10^{-3}$	1089	
$\phi 2(\pi^+\pi^-)$	$< 4$	$\times 10^{-3}$	90%
$a_0(980)\pi$	$< 2$	$\%$	90%
$a_2(1320)\pi$	$< 2$	$\%$	90%
$K^*(892)K + \text{c.c.}$	$< 1.28$	$\%$	90%
$f_2(1270)\eta$	$< 1.1$	$\%$	90%
$\omega\omega$	$(2.9 \pm 0.8) \times 10^{-3}$	1270	
$\omega\phi$	$< 2.5$	$\times 10^{-4}$	90%
$f_2(1270)f_2(1270)$	$(9.8 \pm 2.5) \times 10^{-3}$	774	
$f_2(1270)f_2'(1525)$	$(9.7 \pm 3.2) \times 10^{-3}$	524	
$f_0(980)\eta$	seen	1264	
$f_0(1500)\eta$	seen	1025	
$f_0(2200)\eta$	seen	498	
$a_0(980)\pi$	seen	1327	
$a_0(1320)\pi$	seen	–	
$a_0(1450)\pi$	seen	1123	
$a_0(1950)\pi$	seen	860	
$K_0^*(1430)\bar{K}$	seen	–	
$K_2^*(1430)\bar{K}$	seen	–	
$K_0^*(1950)\bar{K}$	seen	–	

### Decays into stable hadrons

$K\bar{K}\pi$	$(7.3 \pm 0.4) \%$	1381	
$K\bar{K}\eta$	$(1.36 \pm 0.15) \%$	1265	
$\eta\pi^+\pi^-$	$(1.7 \pm 0.5) \%$	1428	
$\eta 2(\pi^+\pi^-)$	$(4.4 \pm 1.3) \%$	1386	
$K^+K^-\pi^+\pi^-$	$(6.9 \pm 1.0) \times 10^{-3}$	1345	
$K^+K^-\pi^+\pi^-\pi^0$	$(3.5 \pm 0.6) \%$	1304	
$K^0K^-\pi^+\pi^-\pi^+ + \text{c.c.}$	$(5.6 \pm 1.5) \%$	–	
$K^+K^-2(\pi^+\pi^-)$	$(7.5 \pm 2.4) \times 10^{-3}$	1254	
$2(K^+K^-)$	$(1.46 \pm 0.30) \times 10^{-3}$	1056	
$\pi^+\pi^-\pi^0$	$< 5$	$\times 10^{-4}$	90%

## Meson Summary Table

$\pi^+\pi^-\pi^0\pi^0$	( 4.7 ± 1.0 ) %	1460
$2(\pi^+\pi^-)$	( 9.7 ± 1.2 ) × 10 <sup>-3</sup>	1459
$2(\pi^+\pi^-\pi^0)$	(16.1 ± 2.0 ) %	1409
$3(\pi^+\pi^-)$	( 1.8 ± 0.4 ) %	1407
$\rho\bar{\rho}$	( 1.45 ± 0.14 ) × 10 <sup>-3</sup>	1160
$\rho\bar{\rho}\pi^0$	( 3.6 ± 1.3 ) × 10 <sup>-3</sup>	1101
$\Lambda\bar{\Lambda}$	( 1.07 ± 0.24 ) × 10 <sup>-3</sup>	991
$K^+\bar{p}\Lambda + c.c.$	( 2.6 ± 0.4 ) × 10 <sup>-3</sup>	772
$\bar{\Lambda}(1520)\Lambda + c.c.$	( 3.1 ± 1.4 ) × 10 <sup>-3</sup>	694
$\Sigma^+\bar{\Sigma}^-$	( 2.1 ± 0.6 ) × 10 <sup>-3</sup>	901
$\Xi^-\bar{\Xi}^+$	( 9.0 ± 2.6 ) × 10 <sup>-4</sup>	692
$\pi^+\pi^-\rho\bar{\rho}$	( 5.3 ± 1.8 ) × 10 <sup>-3</sup>	1027

## Radiative decays

$\gamma\gamma$	( 1.58 ± 0.11 ) × 10 <sup>-4</sup>	1492
----------------	------------------------------------	------

Charge conjugation (C), Parity (P),  
Lepton family number (LF) violating modes

$\pi^+\pi^-$	$P, CP < 1.1$	× 10 <sup>-4</sup>	90%	1485
$\pi^0\pi^0$	$P, CP < 4$	× 10 <sup>-5</sup>	90%	1486
$K^+K^-$	$P, CP < 6$	× 10 <sup>-4</sup>	90%	1408
$K_S^0K_S^0$	$P, CP < 3.1$	× 10 <sup>-4</sup>	90%	1407

**J/ψ(1S)**

$$I^G(J^{PC}) = 0^-(1^{--})$$

Mass  $m = 3096.900 \pm 0.006$  MeV  
 Full width  $\Gamma = 92.9 \pm 2.8$  keV ( $S = 1.1$ )  
 $\Gamma_{ee} = 5.53 \pm 0.10$  keV  
 $\Gamma_{ee} < 5.4$  eV, CL = 90%

J/ψ(1S) DECAY MODES	Fraction ( $\Gamma_i/\Gamma$ )	Scale factor/ Confidence level (MeV/c)	$p$
hadrons	(87.7 ± 0.5 ) %	-	-
virtual $\gamma \rightarrow$ hadrons	(13.50 ± 0.30 ) %	-	-
$ggg$	(64.1 ± 1.0 ) %	-	-
$\gamma gg$	( 8.8 ± 1.1 ) %	-	-
$e^+e^-$	( 5.971 ± 0.032 ) %	-	1548
$e^+e^-\gamma$	[kkaa] ( 8.8 ± 1.4 ) × 10 <sup>-3</sup>	-	1548
$\mu^+\mu^-$	( 5.961 ± 0.033 ) %	-	1545
<b>Decays involving hadronic resonances</b>			
$\rho\pi$	( 1.69 ± 0.15 ) %	$S=2.4$	1448
$\rho^0\pi^0$	( 5.6 ± 0.7 ) × 10 <sup>-3</sup>	-	1448
$\rho(770)^\mp K^\pm K_S^0$	( 1.9 ± 0.4 ) × 10 <sup>-3</sup>	-	-
$\rho(1450)\pi \rightarrow \pi^+\pi^-\pi^0$	( 2.3 ± 0.7 ) × 10 <sup>-3</sup>	-	-
$\rho(1450)^\pm \pi^\mp \rightarrow K_S^0 K^\pm \pi^\mp$	( 3.5 ± 0.6 ) × 10 <sup>-4</sup>	-	-
$\rho(1450)^0 \pi^0 \rightarrow K^+ K^- \pi^0$	( 2.7 ± 0.6 ) × 10 <sup>-4</sup>	-	-
$\rho(1450)\eta'(958) \rightarrow$ $\pi^+\pi^-\eta'(958)$	( 3.3 ± 0.7 ) × 10 <sup>-6</sup>	-	-
$\rho(1700)\pi \rightarrow \pi^+\pi^-\pi^0$	( 1.7 ± 1.1 ) × 10 <sup>-4</sup>	-	-
$\rho(2150)\pi \rightarrow \pi^+\pi^-\pi^0$	( 8 ± 40 ) × 10 <sup>-6</sup>	-	-
$a_2(1320)\rho$	( 1.09 ± 0.22 ) %	-	1124
$\omega\pi^+\pi^+\pi^-\pi^-$	( 8.5 ± 3.4 ) × 10 <sup>-3</sup>	-	1392
$\omega\pi^+\pi^-\pi^0$	( 4.0 ± 0.7 ) × 10 <sup>-3</sup>	-	1418
$\omega\pi^+\pi^-$	( 7.2 ± 1.0 ) × 10 <sup>-3</sup>	-	1435
$\omega f_2(1270)$	( 4.3 ± 0.6 ) × 10 <sup>-3</sup>	-	1142
$K^*(892)^0 \bar{K}^*(892)^0$	( 2.3 ± 0.6 ) × 10 <sup>-4</sup>	-	1266
$K^*(892)^\pm K^*(892)^\mp$	( 1.00 ± 0.22 ) × 10 <sup>-3</sup>	-	1266
$K^*(892)^\pm K^*(700)^\mp$	( 1.1 ± 1.0 ) × 10 <sup>-3</sup>	-	-
$K_S^0 \pi^- K^*(892)^+ + c.c.$	( 2.0 ± 0.5 ) × 10 <sup>-3</sup>	-	1342
$K_S^0 \pi^- K^*(892)^+ + c.c. \rightarrow$ $K_S^0 K_S^0 \pi^+ \pi^-$	( 6.7 ± 2.2 ) × 10 <sup>-4</sup>	-	-
$K_S^0 K^*(892)^0 \rightarrow \gamma K_S^0 K_S^0$	( 6.3 ± 0.6 ) × 10 <sup>-6</sup>	-	-
$K_2^*(1430)^+ K^- + c.c. \rightarrow$ $K^+ K^- \pi^0$	( 2.69 ± 0.25 ) × 10 <sup>-4</sup>	-	-
$K_2^*(1980)^+ K^- + c.c. \rightarrow$ $K^+ K^- \pi^0$	( 1.10 ± 0.60 ) × 10 <sup>-5</sup>	-	-
$K_4^*(2045)^+ K^- + c.c. \rightarrow$ $K^+ K^- \pi^0$	( 6.2 ± 2.9 ) × 10 <sup>-6</sup>	-	-
$\eta K^*(892)^0 \bar{K}^*(892)^0$	( 1.15 ± 0.26 ) × 10 <sup>-3</sup>	-	1003
$\eta' K^+ K^-$	( 1.48 ± 0.13 ) × 10 <sup>-3</sup>	-	-
$\eta' K^+ \bar{K}^0 + c.c.$	( 1.66 ± 0.21 ) × 10 <sup>-3</sup>	-	1000
$\eta' h_1(1415) \rightarrow \eta' K^* \bar{K} + c.c.$	( 2.16 ± 0.31 ) × 10 <sup>-4</sup>	-	-
$\eta' h_1(1415) \rightarrow \eta' K^* K^\mp$	( 1.51 ± 0.23 ) × 10 <sup>-4</sup>	-	-
$K^*(1410) \bar{K} + c.c. \rightarrow$ $K^\pm K^\mp \pi^0$	( 7 ± 4 ) × 10 <sup>-5</sup>	-	-

$K^*(1410) \bar{K} + c.c. \rightarrow$ $K_S^0 K^\pm \pi^\mp$	( 8 ± 6 ) × 10 <sup>-5</sup>	-	-
$K_2^*(1430) \bar{K} + c.c. \rightarrow$ $K^\pm K^\mp \pi^0$	( 1.0 ± 0.5 ) × 10 <sup>-4</sup>	-	-
$K_2^*(1430) \bar{K} + c.c. \rightarrow$ $K_S^0 K^\pm \pi^\mp$	( 4.0 ± 1.0 ) × 10 <sup>-4</sup>	-	-
$K^*(892)^0 \bar{K}_2^*(1430)^0 + c.c.$	( 4.66 ± 0.31 ) × 10 <sup>-3</sup>	-	1011
$K^*(892)^+ K_2^*(1430)^- + c.c.$	( 3.4 ± 2.9 ) × 10 <sup>-3</sup>	-	1011
$K^*(892)^+ K_2^*(1430)^- + c.c. \rightarrow$ $K^*(892)^+ K_S^0 \pi^- + c.c.$	( 4 ± 4 ) × 10 <sup>-4</sup>	-	-
$K^*(892)^0 \bar{K}_2^*(1770)^0 + c.c. \rightarrow$ $K^*(892)^0 K^- \pi^+ + c.c.$	( 6.9 ± 0.9 ) × 10 <sup>-4</sup>	-	-
$\omega K^*(892) \bar{K} + c.c.$	( 6.1 ± 0.9 ) × 10 <sup>-3</sup>	-	1097
$\bar{K} K^*(892) + c.c. \rightarrow$ $K_S^0 K^\pm \pi^\mp$	( 5.0 ± 0.5 ) × 10 <sup>-3</sup>	-	-
$K^+ K^*(892)^- + c.c.$	( 6.0 ± 0.8 ) × 10 <sup>-3</sup>	$S=2.9$	1373
$K^+ K^*(892)^- + c.c. \rightarrow$ $K^+ K^- \pi^0$	( 2.69 ± 0.13 ) × 10 <sup>-3</sup>	-	-
$K^+ K^*(892)^- + c.c. \rightarrow$ $K^0 K^\pm \pi^\mp + c.c.$	( 3.0 ± 0.4 ) × 10 <sup>-3</sup>	-	-
$K^0 \bar{K}^*(892)^0 + c.c.$	( 4.2 ± 0.4 ) × 10 <sup>-3</sup>	-	1373
$K^0 \bar{K}^*(892)^0 + c.c. \rightarrow$ $K^0 K^\pm \pi^\mp + c.c.$	( 3.2 ± 0.4 ) × 10 <sup>-3</sup>	-	-
$K_1(1400)^\pm K^\mp$	( 3.8 ± 1.4 ) × 10 <sup>-3</sup>	-	1170
$\bar{K}^*(892)^0 K^+ \pi^- + c.c.$	( 7.7 ± 1.6 ) × 10 <sup>-3</sup>	-	1343
$K^*(892)^\pm K^\mp \pi^0$	( 4.1 ± 1.3 ) × 10 <sup>-3</sup>	-	1344
$K^*(892)^0 K_S^0 \pi^0$	( 6 ± 4 ) × 10 <sup>-4</sup>	-	1343
$\omega\pi^0\pi^0$	( 3.4 ± 0.8 ) × 10 <sup>-3</sup>	-	1436
$\omega\pi^0\eta$	( 3.4 ± 1.7 ) × 10 <sup>-4</sup>	-	1363
$b_1(1235)^\pm \pi^\mp$	[bb] ( 3.0 ± 0.5 ) × 10 <sup>-3</sup>	-	1300
$\omega K^\pm K_S^0 \pi^\mp$	[bb] ( 3.4 ± 0.5 ) × 10 <sup>-3</sup>	-	1210
$b_1(1235)^0 \pi^0$	( 2.3 ± 0.6 ) × 10 <sup>-3</sup>	-	1300
$\eta K^\pm K_S^0 \pi^\mp$	[bb] ( 2.2 ± 0.4 ) × 10 <sup>-3</sup>	-	1278
$\phi K^*(892) \bar{K} + c.c.$	( 2.18 ± 0.23 ) × 10 <sup>-3</sup>	-	969
$\omega K \bar{K}$	( 1.9 ± 0.4 ) × 10 <sup>-3</sup>	-	1268
$\omega f_0(1710) \rightarrow \omega K \bar{K}$	( 4.8 ± 1.1 ) × 10 <sup>-4</sup>	-	878
$\phi_2(\pi^+\pi^-)$	( 1.60 ± 0.32 ) × 10 <sup>-3</sup>	-	1318
$\Delta(1232)^{++} \bar{p}\pi^-$	( 1.6 ± 0.5 ) × 10 <sup>-3</sup>	-	1030
$\omega\eta$	( 1.74 ± 0.20 ) × 10 <sup>-3</sup>	$S=1.6$	1394
$\omega\eta'\pi^+\pi^-$	( 1.12 ± 0.13 ) × 10 <sup>-3</sup>	-	1173
$\phi K \bar{K}$	( 1.77 ± 0.16 ) × 10 <sup>-3</sup>	$S=1.3$	1179
$\phi K_S^0 K_S^0$	( 5.9 ± 1.5 ) × 10 <sup>-4</sup>	-	1176
$\phi f_0(1710) \rightarrow \phi K \bar{K}$	( 3.6 ± 0.6 ) × 10 <sup>-4</sup>	-	875
$\phi K^+ K^-$	( 8.3 ± 1.2 ) × 10 <sup>-4</sup>	-	1179
$\phi f_2(1270)$	( 3.2 ± 0.6 ) × 10 <sup>-4</sup>	-	1036
$\Delta(1232)^{++} \bar{\Delta}(1232)^{--}$	( 1.10 ± 0.29 ) × 10 <sup>-3</sup>	-	938
$\Sigma(1385)^- \bar{\Sigma}(1385)^+ (or c.c.)$	[bb] ( 1.16 ± 0.05 ) × 10 <sup>-3</sup>	-	697
$\Sigma(1385)^0 \bar{\Sigma}(1385)^0$	( 1.07 ± 0.08 ) × 10 <sup>-3</sup>	-	697
$K^+ K^- f_2'(1525)$	( 1.05 ± 0.35 ) × 10 <sup>-3</sup>	-	897
$\phi f_2'(1525)$	( 8 ± 4 ) × 10 <sup>-4</sup>	$S=2.7$	877
$\phi\pi^+\pi^-$	( 9.4 ± 1.5 ) × 10 <sup>-4</sup>	$S=1.7$	1365
$\phi\pi^0\pi^0$	( 5.0 ± 1.0 ) × 10 <sup>-4</sup>	-	1366
$\phi K^\pm K_S^0 \pi^\mp$	[bb] ( 7.2 ± 0.8 ) × 10 <sup>-4</sup>	-	1114
$\omega f_1(1420)$	( 6.8 ± 2.4 ) × 10 <sup>-4</sup>	-	1062
$\phi\eta$	( 7.4 ± 0.8 ) × 10 <sup>-4</sup>	$S=1.5$	1320
$\Xi^0 \Xi^0$	( 1.17 ± 0.04 ) × 10 <sup>-3</sup>	-	818
$\Xi(1530)^- \bar{\Xi}^+ + c.c.$	( 3.18 ± 0.08 ) × 10 <sup>-4</sup>	-	600
$\rho K^- \bar{\Sigma}(1385)^0$	( 5.1 ± 3.2 ) × 10 <sup>-4</sup>	-	646
$\omega\pi^0 \rightarrow \pi^+\pi^-\pi^0$	( 4.5 ± 0.5 ) × 10 <sup>-4</sup>	$S=1.4$	1446
$\phi\eta'(958)$	( 1.7 ± 0.8 ) × 10 <sup>-5</sup>	-	-
$\phi f_0(980)$	( 4.6 ± 0.5 ) × 10 <sup>-4</sup>	$S=2.2$	1192
$\phi f_0(980) \rightarrow \phi\pi^+\pi^-$	( 3.2 ± 0.9 ) × 10 <sup>-4</sup>	$S=1.9$	1178
$\phi f_0(980) \rightarrow \phi\pi^0\pi^0$	( 2.59 ± 0.34 ) × 10 <sup>-4</sup>	-	-
$\phi f_0(980) \rightarrow \phi\pi^0\pi^0$	( 1.8 ± 0.5 ) × 10 <sup>-4</sup>	-	-
$\phi\eta\eta'$	( 2.32 ± 0.17 ) × 10 <sup>-4</sup>	-	885
$\phi\pi^0 f_0(980) \rightarrow \phi\pi^0\pi^+\pi^-$	( 4.5 ± 1.0 ) × 10 <sup>-6</sup>	-	-
$\phi\pi^0 f_0(980) \rightarrow \phi\pi^0\rho^0\pi^0$	( 1.7 ± 0.6 ) × 10 <sup>-6</sup>	-	1045
$\eta\phi f_0(980) \rightarrow \eta\phi\pi^+\pi^-$	( 3.2 ± 1.0 ) × 10 <sup>-4</sup>	-	-
$\phi a_0(980)^0 \rightarrow \phi\eta\pi^0$	( 4.4 ± 1.4 ) × 10 <sup>-6</sup>	-	-
$\Xi(1530)^0 \Xi^0$	( 3.2 ± 1.4 ) × 10 <sup>-4</sup>	-	608
$\Sigma(1385)^- \bar{\Sigma}^+ (or c.c.)$	[bb] ( 3.1 ± 0.5 ) × 10 <sup>-4</sup>	-	855
$\phi f_1(1285)$	( 2.6 ± 0.5 ) × 10 <sup>-4</sup>	-	1032
$\phi f_1(1285) \rightarrow$ $\phi\pi^0 f_0(980) \rightarrow$ $\phi\pi^0\pi^+\pi^-$	( 9.4 ± 2.8 ) × 10 <sup>-7</sup>	-	952

## Meson Summary Table

$\phi f_1(1285) \rightarrow$	$(2.1 \pm 2.2) \times 10^{-7}$		955	$p\bar{p}\omega$	$(9.8 \pm 1.0) \times 10^{-4}$	S=1.3	768
$\phi\pi^0 f_0(980) \rightarrow$				$p\bar{p}\eta'(958)$	$(1.29 \pm 0.14) \times 10^{-4}$	S=2.0	596
$\phi\pi^0\pi^0\pi^0$				$p\bar{p}a_0(980) \rightarrow p\bar{p}\pi^0\eta$	$(6.8 \pm 1.8) \times 10^{-5}$		-
$\eta\pi^+\pi^-$	$(3.8 \pm 0.7) \times 10^{-4}$		1487	$p\bar{p}\phi$	$(5.19 \pm 0.33) \times 10^{-5}$		527
$\eta\rho$	$(1.93 \pm 0.23) \times 10^{-4}$		1396	$n\bar{n}$	$(2.09 \pm 0.16) \times 10^{-3}$		1231
$\omega\eta'(958)$	$(1.89 \pm 0.18) \times 10^{-4}$		1279	$n\bar{n}\pi^+\pi^-$	$(4 \pm 4) \times 10^{-3}$		1106
$\omega f_0(980)$	$(1.4 \pm 0.5) \times 10^{-4}$		1267	$\Sigma^+\Sigma^-$	$(1.50 \pm 0.24) \times 10^{-3}$		992
$\rho\eta'(958)$	$(8.1 \pm 0.8) \times 10^{-5}$		S=1.6 1281	$\Sigma^0\bar{\Sigma}^0$	$(1.172 \pm 0.032) \times 10^{-3}$	S=1.4	988
$a_2(1320)\pm\pi^\mp$	[bb] < 4.3	$\times 10^{-3}$	CL=90%	1264	$2(\pi^+\pi^-)K^+K^-$	$(3.1 \pm 1.3) \times 10^{-3}$	1320
$K\bar{K}_2^*(1430)+c.c.$	< 4.0	$\times 10^{-3}$	CL=90%	1158	$p\bar{p}\pi^-$	$(2.12 \pm 0.09) \times 10^{-3}$	1174
$K_1(1270)\pm K^\mp$	< 3.0	$\times 10^{-3}$	CL=90%	1240	$nN(1440)$	seen	978
$K_1(1270)K_S^0 \rightarrow \gamma K_S^0 K_S^0$	$(8.5 \pm 2.5) \times 10^{-7}$			$nN(1520)$	seen		928
$K_S^0\pi^- K_S^*(1430)^+ + c.c.$	$(3.6 \pm 1.8) \times 10^{-3}$		1116	$nN(1535)$	seen		917
$K_2^*(1430)^0\bar{K}_2^*(1430)^0$	< 2.9	$\times 10^{-3}$	CL=90%	601	$\Xi^-\Xi^+$	$(9.7 \pm 0.8) \times 10^{-4}$	S=1.4 807
$\phi\pi^0$	$3 \times 10^{-6}$ or $1 \times 10^{-7}$		1377	$\Lambda\bar{\Lambda}$	$(1.89 \pm 0.09) \times 10^{-3}$	S=2.8	1074
$\phi\eta(1405) \rightarrow \phi\eta\pi^+\pi^-$	$(2.0 \pm 1.0) \times 10^{-5}$		946	$\Lambda\bar{\Sigma}^-\pi^+$ (or c.c.)	[bb] $(8.3 \pm 0.7) \times 10^{-4}$	S=1.2	950
$\omega f_2'(1525)$	< 2.2	$\times 10^{-4}$	CL=90%	1007	$pK^-\bar{\Lambda}+c.c.$	$(8.7 \pm 1.1) \times 10^{-4}$	876
$\omega X(1835) \rightarrow \omega p\bar{p}$	< 3.9	$\times 10^{-6}$	CL=95%	-	$2(K^+K^-)$	$(7.2 \pm 0.8) \times 10^{-4}$	1131
$\omega X(1835), X \rightarrow \eta'\pi^+\pi^-$	< 6.2	$\times 10^{-5}$		-	$pK^-\bar{\Sigma}^0$	$(2.9 \pm 0.8) \times 10^{-4}$	819
$\phi X(1835) \rightarrow \phi p\bar{p}$	< 2.1	$\times 10^{-7}$	CL=90%	-	$K^+K^-$	$(2.86 \pm 0.21) \times 10^{-4}$	1468
$\phi X(1835) \rightarrow \phi\eta\pi^+\pi^-$	< 2.8	$\times 10^{-4}$	CL=90%	578	$K_S^0 K_L^0$	$(1.95 \pm 0.11) \times 10^{-4}$	S=2.4 1466
$\phi X(1870) \rightarrow \phi\eta\pi^+\pi^-$	< 6.13	$\times 10^{-5}$	CL=90%	-	$\Lambda\bar{\Lambda}\pi^+\pi^-$	$(4.3 \pm 1.0) \times 10^{-3}$	903
$\eta\phi(2170) \rightarrow \eta\phi f_0(980) \rightarrow$	$(1.2 \pm 0.4) \times 10^{-4}$		628	$\Lambda\bar{\Lambda}\eta$	$(1.62 \pm 0.17) \times 10^{-4}$		672
$\eta\phi\pi^+\pi^-$				$\Lambda\bar{\Lambda}\pi^0$	$(3.8 \pm 0.4) \times 10^{-5}$		998
$\eta\phi(2170) \rightarrow$	< 2.52	$\times 10^{-4}$	CL=90%	-	$\bar{\Lambda}nK_S^0 + c.c.$	$(6.5 \pm 1.1) \times 10^{-4}$	872
$\eta K^*(892)^0\bar{K}^*(892)^0$				$\pi^+\pi^-$	$(1.47 \pm 0.14) \times 10^{-4}$		1542
$\Sigma(1385)^0\bar{\Lambda} + c.c.$	< 8.2	$\times 10^{-6}$	CL=90%	912	$\Lambda\bar{\Sigma} + c.c.$	$(2.83 \pm 0.23) \times 10^{-5}$	1034
$\Delta(1232)^+\bar{p}$	< 1	$\times 10^{-4}$	CL=90%	1100	$K_S^0 K_S^0$	< 1.4	$\times 10^{-8}$ CL=95% 1466
$\Lambda(1520)\bar{\Lambda} + c.c. \rightarrow \gamma\Lambda\bar{\Lambda}$	< 4.1	$\times 10^{-6}$	CL=90%	-			
$\bar{\Lambda}(1520)\Lambda + c.c.$	< 1.80	$\times 10^{-3}$	CL=90%	807			
$\Theta(1540)\bar{\Theta}(1540) \rightarrow$	< 1.1	$\times 10^{-5}$	CL=90%	-			
$K_S^0 p K^-\bar{n} + c.c.$							
$\Theta(1540)K^-\bar{n} \rightarrow K_S^0 p K^-\bar{n}$	< 2.1	$\times 10^{-5}$	CL=90%	-			
$\Theta(1540)K_S^0\bar{p} \rightarrow K_S^0\bar{p}K^+n$	< 1.6	$\times 10^{-5}$	CL=90%	-			
$\bar{\Theta}(1540)K^+n \rightarrow K_S^0\bar{p}K^+n$	< 5.6	$\times 10^{-5}$	CL=90%	-			
$\bar{\Theta}(1540)K_S^0 p \rightarrow K_S^0 p K^-\bar{n}$	< 1.1	$\times 10^{-5}$	CL=90%	-			
<b>Decays into stable hadrons</b>							
$2(\pi^+\pi^-)\pi^0$	$(3.73 \pm 0.32) \%$		S=1.4 1496	$3\gamma$	$(1.16 \pm 0.22) \times 10^{-5}$		1548
$3(\pi^+\pi^-)\pi^0$	$(2.9 \pm 0.6) \%$		1433	$4\gamma$	< 9	$\times 10^{-6}$	CL=90% 1548
$\pi^+\pi^-\pi^0\pi^0\pi^0$	$(2.10 \pm 0.08) \%$		S=1.6 1533	$5\gamma$	< 1.5	$\times 10^{-5}$	CL=90% 1548
$\rho^\pm\pi^\mp\pi^0\pi^0$	$(2.71 \pm 0.29) \%$		1497	$\gamma\pi^0\pi^0$	$(1.15 \pm 0.05) \times 10^{-3}$		1543
$\rho^\pm\rho^-\pi^0$	$(1.41 \pm 0.22) \%$		1421	$\gamma\eta\pi^0$	$(2.14 \pm 0.31) \times 10^{-5}$		1497
$\pi^+\pi^-\pi^0 K^+K^-$	$(6.0 \pm 1.1) \times 10^{-3}$		1298	$\gamma a_0(980)^0 \rightarrow \gamma\eta\pi^0$	< 2.5	$\times 10^{-6}$	CL=95% -
$4(\pi^+\pi^-)\pi^0$	$(1.20 \pm 0.30) \%$		1368	$\gamma a_2(1320)^0 \rightarrow \gamma\eta\pi^0$	< 6.6	$\times 10^{-6}$	CL=95% -
$\pi^+\pi^-K^+K^-$	$(9.0 \pm 3.0) \times 10^{-3}$		1345	$\gamma K_S^0 K_S^0$	$(8.1 \pm 0.4) \times 10^{-4}$		1466
$\pi^+\pi^-K^0 K^0$	$(6.84 \pm 0.32) \times 10^{-3}$		1407	$\gamma\eta_c(1S)$	$(1.7 \pm 0.4) \%$	S=1.5	111
$\pi^+\pi^-K_S^0 K_L^0$	$(3.8 \pm 0.6) \times 10^{-3}$		1406	$\gamma\eta_c(1S) \rightarrow 3\gamma$	$(3.8 \pm 1.3)$	$\times 10^{-6}$	S=1.1 -
$\pi^\pm\pi^0 K_S^0 K_S^0$	$(1.68 \pm 0.19) \times 10^{-3}$		1406	$\gamma\pi^+\pi^-2\pi^0$	$(8.3 \pm 3.1) \times 10^{-3}$		1518
$\pi^\pm\pi^0 K^\pm K_S^0$	$(5.7 \pm 0.5) \times 10^{-3}$		1408	$\gamma\eta\pi\pi$	$(6.1 \pm 1.0) \times 10^{-3}$		1487
$K^+K^-K_S^0 K_S^0$	$(4.1 \pm 0.8) \times 10^{-4}$		1127	$\gamma\eta_2(1870) \rightarrow \gamma\eta\pi^+\pi^-$	$(6.2 \pm 2.4) \times 10^{-4}$		-
$\pi^+\pi^-K^+K^-\eta$	$(4.7 \pm 0.7) \times 10^{-3}$		1221	$\gamma\eta(1405/1475) \rightarrow \gamma K\bar{K}\pi$ [nnaa]	$(2.8 \pm 0.6) \times 10^{-3}$	S=1.6	1223
$\pi^0\pi^0 K^+K^-$	$(2.12 \pm 0.23) \times 10^{-3}$		1410	$\gamma\eta(1405/1475) \rightarrow \gamma\gamma\rho^0$	$(7.8 \pm 2.0) \times 10^{-5}$	S=1.8	1223
$\pi^0\pi^0 K_S^0 K_L^0$	$(1.9 \pm 0.4) \times 10^{-3}$		1408	$\gamma\eta(1405/1475) \rightarrow \gamma\eta\pi^+\pi^-$	$(3.0 \pm 0.5) \times 10^{-4}$		-
$K\bar{K}\pi$	$(6.1 \pm 1.0) \times 10^{-3}$		1442	$\gamma\eta(1405/1475) \rightarrow \gamma\gamma\phi$	< 8.2	$\times 10^{-5}$	CL=95% -
$K^+K^-\pi^0$	$(2.88 \pm 0.12) \times 10^{-3}$		1442	$\gamma\eta(1405) \rightarrow \gamma\gamma\gamma$	< 2.63	$\times 10^{-6}$	CL=90% -
$K_S^0 K^\pm\pi^\mp$	$(5.6 \pm 0.5) \times 10^{-3}$		1440	$\gamma\eta(1475) \rightarrow \gamma\gamma\gamma$	< 1.86	$\times 10^{-6}$	CL=90% -
$K_S^0 K_L^0\pi^0$	$(2.06 \pm 0.27) \times 10^{-3}$		1440	$\gamma\rho\rho$	$(4.5 \pm 0.8) \times 10^{-3}$		1340
$K^*(892)^0\bar{K}^0 + c.c. \rightarrow$	$(1.21 \pm 0.18) \times 10^{-3}$		-	$\gamma\rho\omega$	< 5.4	$\times 10^{-4}$	CL=90% 1338
$K_S^0 K_L^0\pi^0$				$\gamma\rho\phi$	< 8.8	$\times 10^{-5}$	CL=90% 1258
$K_2^*(1430)^0\bar{K}^0 + c.c. \rightarrow$				$\gamma\eta'(958)$	$(5.25 \pm 0.07) \times 10^{-3}$	S=1.3	1400
$K_S^0 K_L^0\pi^0$				$\gamma 2\pi^+2\pi^-$	$(2.8 \pm 0.5) \times 10^{-3}$	S=1.9	1517
$K_2^*(1430)^0\bar{K}^0 + c.c. \rightarrow$	$(4.3 \pm 1.3) \times 10^{-4}$		-	$\gamma f_2(1270) f_2(1270)$	$(9.5 \pm 1.7) \times 10^{-4}$		878
$K_S^0 K_L^0\pi^0$				$\gamma f_2(1270) f_2(1270)$ (non resonant)	$(8.2 \pm 1.9) \times 10^{-4}$		-
$K_S^0 K_L^0\eta$	$(1.44 \pm 0.34) \times 10^{-3}$		1328	$\gamma K^+K^-\pi^+\pi^-$	$(2.1 \pm 0.6) \times 10^{-3}$		1407
$2(\pi^+\pi^-)$	$(3.57 \pm 0.30) \times 10^{-3}$		1517	$\gamma f_4(2050)$	$(2.7 \pm 0.7) \times 10^{-3}$		891
$3(\pi^+\pi^-)$	$(4.3 \pm 0.4) \times 10^{-3}$		1466	$\gamma\omega\omega$	$(1.61 \pm 0.33) \times 10^{-3}$		1336
$2(\pi^+\pi^-\pi^0)$	$(1.61 \pm 0.21) \%$		1468	$\gamma\eta(1405/1475) \rightarrow \gamma\rho^0\rho^0$	$(1.7 \pm 0.4) \times 10^{-3}$	S=1.3	1223
$2(\pi^+\pi^-\eta)$	$(2.26 \pm 0.28) \times 10^{-3}$		1446	$\gamma f_2(1270)$	$(1.64 \pm 0.12) \times 10^{-3}$	S=1.3	1286
$3(\pi^+\pi^-\eta)$	$(7.2 \pm 1.5) \times 10^{-4}$		1379	$\gamma f_2(1270) \rightarrow \gamma K_S^0 K_S^0$	$(2.58 \pm 0.60)$	$\times 10^{-5}$	-
$\pi^+\pi^-\pi^0\pi^0\eta$	$(2.3 \pm 0.5) \times 10^{-3}$		1448	$\gamma f_0(1370) \rightarrow \gamma K\bar{K}$	$(4.2 \pm 1.5) \times 10^{-4}$		-
$\rho^\pm\pi^\mp\pi^0\eta$	$(1.9 \pm 0.8) \times 10^{-3}$		1326	$\gamma f_0(1370) \rightarrow \gamma K_S^0 K_S^0$	$(1.1 \pm 0.4) \times 10^{-5}$		-
$p\bar{p}$	$(2.121 \pm 0.029) \times 10^{-3}$		1232	$\gamma f_0(1500) \rightarrow \gamma K_S^0 K_S^0$	$(1.59 \pm 0.24)$	$\times 10^{-5}$	-
$p\bar{p}\pi^0$	$(1.19 \pm 0.08) \times 10^{-3}$		S=1.1 1176	$\gamma f_0(1710) \rightarrow \gamma K\bar{K}$	$(9.5 \pm 1.0)$	$\times 10^{-4}$	S=1.5 1075
$p\bar{p}\pi^+\pi^-$	$(6.0 \pm 0.5) \times 10^{-3}$		S=1.3 1107	$\gamma f_0(1710) \rightarrow \gamma\pi\pi$	$(3.8 \pm 0.5) \times 10^{-4}$		-
$p\bar{p}\pi^+\pi^-\pi^0$	[l/aa] $(2.3 \pm 0.9) \times 10^{-3}$		S=1.9 1033	$\gamma f_0(1710) \rightarrow \gamma\omega\omega$	$(3.1 \pm 1.0) \times 10^{-4}$		-
$p\bar{p}\eta$	$(2.00 \pm 0.12) \times 10^{-3}$		948	$\gamma f_0(1710) \rightarrow \gamma\eta\eta$	$(2.4 \pm 1.2)$	$\times 10^{-4}$	-
$p\bar{p}\rho$	< 3.1	$\times 10^{-4}$	CL=90% 774	$\gamma\eta$	$(1.108 \pm 0.027) \times 10^{-3}$		1500
				$\gamma f_1(1420) \rightarrow \gamma K\bar{K}\pi$	$(7.9 \pm 1.3) \times 10^{-4}$		1220
				$\gamma f_1(1285)$	$(6.1 \pm 0.8) \times 10^{-4}$		1283
				$\gamma f_1(1510) \rightarrow \gamma\eta\pi^+\pi^-$	$(4.5 \pm 1.2) \times 10^{-4}$		-

## Meson Summary Table

$\gamma f'_2(1525)$	$(5.7^{+0.8}_{-0.5}) \times 10^{-4}$	S=1.5	1177
$\gamma f'_2(1525) \rightarrow \gamma K_S^0 K_S^0$	$(8.0^{+0.7}_{-0.5}) \times 10^{-5}$		-
$\gamma f'_2(1525) \rightarrow \gamma \eta \eta$	$(3.4 \pm 1.4) \times 10^{-5}$		-
$\gamma f_2(1640) \rightarrow \gamma \omega \omega$	$(2.8 \pm 1.8) \times 10^{-4}$		-
$\gamma f_2(1910) \rightarrow \gamma \omega \omega$	$(2.0 \pm 1.4) \times 10^{-4}$		-
$\gamma f_0(1750) \rightarrow \gamma K_S^0 K_S^0$	$(1.11^{+0.20}_{-0.33}) \times 10^{-5}$		-
$\gamma f_0(1800) \rightarrow \gamma \omega \phi$	$(2.5 \pm 0.6) \times 10^{-4}$		-
$\gamma f_2(1810) \rightarrow \gamma \eta \eta$	$(5.4^{+3.5}_{-2.4}) \times 10^{-5}$		-
$\gamma f_2(1950) \rightarrow \gamma K^*(892) \bar{K}^*(892)$	$(7.0 \pm 2.2) \times 10^{-4}$		-
$\gamma K^*(892) \bar{K}^*(892)$	$(4.0 \pm 1.3) \times 10^{-3}$	S=2.1	1266
$\gamma \phi \phi$	$(4.0 \pm 1.2) \times 10^{-4}$		1166
$\gamma \rho \bar{\rho}$	$(3.8 \pm 1.0) \times 10^{-4}$		1232
$\gamma \eta(2225)$	$(3.14^{+0.50}_{-0.19}) \times 10^{-4}$		752
$\gamma \eta(1760) \rightarrow \gamma \rho^0 \rho^0$	$(1.3 \pm 0.9) \times 10^{-4}$		1048
$\gamma \eta(1760) \rightarrow \gamma \omega \omega$	$(1.98 \pm 0.33) \times 10^{-3}$		-
$\gamma \eta(1760) \rightarrow \gamma \gamma \gamma$	$< 4.80 \times 10^{-6}$	CL=90%	-
$\gamma X(1835) \rightarrow \gamma \pi^+ \pi^- \eta'$	$(2.77^{+0.34}_{-0.40}) \times 10^{-4}$	S=1.1	1006
$\gamma X(1835) \rightarrow \gamma \rho \bar{\rho}$	$(7.7^{+1.5}_{-0.9}) \times 10^{-5}$		-
$\gamma X(1835) \rightarrow \gamma K_S^0 K_S^0 \eta$	$(3.3^{+2.0}_{-1.3}) \times 10^{-5}$		-
$\gamma X(1835) \rightarrow \gamma \gamma \gamma$	$< 3.56 \times 10^{-6}$	CL=90%	-
$\gamma X(1840) \rightarrow \gamma 3(\pi^+ \pi^-)$	$(2.4^{+0.7}_{-0.8}) \times 10^{-5}$		-
$\gamma (K \bar{K} \pi) [J^{PC} = 0^{-+}]$	$(7 \pm 4) \times 10^{-4}$	S=2.1	1442
$\gamma \pi^0$	$(3.56 \pm 0.17) \times 10^{-5}$		1546
$\gamma \rho \bar{\rho} \pi^+ \pi^-$	$< 7.9 \times 10^{-4}$	CL=90%	1107
$\gamma A \bar{A}$	$< 1.3 \times 10^{-4}$	CL=90%	1074
$\gamma f_0(2100) \rightarrow \gamma \eta \eta$	$(1.13^{+0.60}_{-0.30}) \times 10^{-4}$		-
$\gamma f_0(2100) \rightarrow \gamma \pi \pi$	$(6.2 \pm 1.0) \times 10^{-4}$		-
$\gamma f_0(2200) \rightarrow \gamma K \bar{K}$	$(5.9 \pm 1.3) \times 10^{-4}$		-
$\gamma f_0(2200) \rightarrow \gamma K_S^0 K_S^0$	$(2.72^{+0.19}_{-0.50}) \times 10^{-4}$		-
$\gamma f_J(2220) \rightarrow \gamma \pi \pi$	$< 3.9 \times 10^{-5}$	CL=90%	-
$\gamma f_J(2220) \rightarrow \gamma K \bar{K}$	$< 4.1 \times 10^{-5}$	CL=90%	-
$\gamma f_J(2220) \rightarrow \gamma \rho \bar{\rho}$	$(1.5 \pm 0.8) \times 10^{-5}$		-
$\gamma f_0(2330) \rightarrow \gamma K_S^0 K_S^0$	$(4.9 \pm 0.7) \times 10^{-5}$		-
$\gamma f_2(2340) \rightarrow \gamma \eta \eta$	$(5.6^{+2.4}_{-2.2}) \times 10^{-5}$		-
$\gamma f_2(2340) \rightarrow \gamma K_S^0 K_S^0$	$(5.5^{+4.0}_{-1.5}) \times 10^{-5}$		-
$\gamma f_0(1500) \rightarrow \gamma \pi \pi$	$(1.09 \pm 0.24) \times 10^{-4}$		1183
$\gamma f_0(1500) \rightarrow \gamma \eta \eta$	$(1.7^{+0.6}_{-1.4}) \times 10^{-5}$		-
$\gamma A \rightarrow \gamma$ invisible	$[o\bar{o}\bar{o}\bar{a}] < 6.3 \times 10^{-6}$	CL=90%	-
$\gamma A^0 \rightarrow \gamma \mu^+ \mu^-$	$[p\bar{p}\bar{a}\bar{a}] < 5 \times 10^{-6}$	CL=90%	-

## Dalitz decays

$\pi^0 e^+ e^-$	$(7.6 \pm 1.4) \times 10^{-7}$		1546
$\eta e^+ e^-$	$(1.43 \pm 0.07) \times 10^{-5}$		1500
$\eta'(958) e^+ e^-$	$(6.59 \pm 0.18) \times 10^{-5}$		1400
$\eta U \rightarrow \eta e^+ e^-$	$< 9.11 \times 10^{-7}$	CL=90%	-
$\eta'(958) U \rightarrow \eta'(958) e^+ e^-$	$< 2.0 \times 10^{-7}$	CL=90%	-
$\phi e^+ e^-$	$< 1.2 \times 10^{-7}$	CL=90%	1381

## Weak decays

$D^- e^+ \nu_e$ + c.c.	$< 1.2 \times 10^{-5}$	CL=90%	984
$\bar{D}^0 e^+ e^-$ + c.c.	$< 8.5 \times 10^{-8}$	CL=90%	987
$D_s^- e^+ \nu_e$ + c.c.	$< 1.3 \times 10^{-6}$	CL=90%	923
$D_s^{*-} e^+ \nu_e$ + c.c.	$< 1.8 \times 10^{-6}$	CL=90%	828
$D^- \pi^+$ + c.c.	$< 7.5 \times 10^{-5}$	CL=90%	977
$\bar{D}^0 K^0$ + c.c.	$< 1.7 \times 10^{-4}$	CL=90%	898
$\bar{D}^0 \bar{K}^{*0}$ + c.c.	$< 2.5 \times 10^{-6}$	CL=90%	670
$D_s^- \pi^+$ + c.c.	$< 1.3 \times 10^{-4}$	CL=90%	915
$D_s^- \rho^+$ + c.c.	$< 1.3 \times 10^{-5}$	CL=90%	663

Charge conjugation (C), Parity (P),  
Lepton Family number (LF) violating modes

$\gamma \gamma$	C	$< 2.7 \times 10^{-7}$	CL=90%	1548
$\gamma \phi$	C	$< 1.4 \times 10^{-6}$	CL=90%	1381
$e^\pm \mu^\mp$	LF	$< 1.6 \times 10^{-7}$	CL=90%	1547
$e^\pm \tau^\mp$	LF	$< 8.3 \times 10^{-6}$	CL=90%	1039
$\mu^\pm \tau^\mp$	LF	$< 2.0 \times 10^{-6}$	CL=90%	1035
$A_c^+ e^-$ + c.c.		$< 6.9 \times 10^{-8}$	CL=90%	-

Other decays  
invisible  $< 7 \times 10^{-4}$  CL=90% -

$X_{c0}(1P)$

$$I^G(JPC) = 0^+(0^{++})$$

$$\text{Mass } m = 3414.71 \pm 0.30 \text{ MeV}$$

$$\text{Full width } \Gamma = 10.8 \pm 0.6 \text{ MeV}$$

$X_{c0}(1P)$ DECAY MODES	Fraction ( $\Gamma_i/\Gamma$ )	Scale factor/ Confidence level	$\rho$ (MeV/c)
<b>Hadronic decays</b>			
$2(\pi^+ \pi^-)$	$(2.34 \pm 0.18) \%$		1679
$\rho^0 \pi^+ \pi^-$	$(9.1 \pm 2.9) \times 10^{-3}$		1607
$f_0(980) f_0(980)$	$(6.6 \pm 2.1) \times 10^{-4}$		1391
$\pi^+ \pi^- \pi^0 \pi^0$	$(3.3 \pm 0.4) \%$		1680
$\rho^+ \pi^- \pi^0$ + c.c.	$(2.9 \pm 0.4) \%$		1607
$4\pi^0$	$(3.3 \pm 0.4) \times 10^{-3}$		1681
$\pi^+ \pi^- K^+ K^-$	$(1.81 \pm 0.14) \%$		1580
$K_0^*(1430)^0 \bar{K}_0^*(1430)^0 \rightarrow$ $\pi^+ \pi^- K^+ K^-$	$(9.8^{+4.0}_{-2.8}) \times 10^{-4}$		-
$K_0^*(1430)^0 \bar{K}_2^*(1430)^0$ + c.c. $\rightarrow$ $\pi^+ \pi^- K^+ K^-$	$(8.0^{+2.0}_{-2.4}) \times 10^{-4}$		-
$K_1(1270)^+ K^-$ + c.c. $\rightarrow$ $\pi^+ \pi^- K^+ K^-$	$(6.3 \pm 1.9) \times 10^{-3}$		-
$K_1(1400)^+ K^-$ + c.c. $\rightarrow$ $\pi^+ \pi^- K^+ K^-$	$< 2.7 \times 10^{-3}$	CL=90%	-
$f_0(980) f_0(980)$	$(1.6^{+1.0}_{-0.9}) \times 10^{-4}$		1391
$f_0(980) f_0(2200)$	$(7.9^{+2.0}_{-2.5}) \times 10^{-4}$		586
$f_0(1370) f_0(1370)$	$< 2.7 \times 10^{-4}$	CL=90%	1019
$f_0(1370) f_0(1500)$	$< 1.7 \times 10^{-4}$	CL=90%	920
$f_0(1370) f_0(1710)$	$(6.7^{+3.5}_{-2.3}) \times 10^{-4}$		740
$f_0(1500) f_0(1370)$	$< 1.3 \times 10^{-4}$	CL=90%	920
$f_0(1500) f_0(1500)$	$< 5 \times 10^{-5}$	CL=90%	804
$f_0(1500) f_0(1710)$	$< 7 \times 10^{-5}$	CL=90%	581
$K^+ K^- \pi^+ \pi^- \pi^0$	$(8.6 \pm 0.9) \times 10^{-3}$		1545
$K_S^0 K^\pm \pi^\mp \pi^+ \pi^-$	$(4.2 \pm 0.4) \times 10^{-3}$		1543
$K^+ K^- \pi^0 \pi^0$	$(5.6 \pm 0.9) \times 10^{-3}$		1582
$K^+ \pi^- \bar{K}^0 \pi^0$ + c.c.	$(2.49 \pm 0.33) \%$		1581
$\rho^+ K^- K^0$ + c.c.	$(1.21 \pm 0.21) \%$		1458
$K^*(892)^- K^+ \pi^0 \rightarrow$ $K^+ \pi^- \bar{K}^0 \pi^0$ + c.c.	$(4.6 \pm 1.2) \times 10^{-3}$		-
$K_S^0 K_S^0 \pi^+ \pi^-$	$(5.7 \pm 1.1) \times 10^{-3}$		1579
$K^+ K^- \eta \pi^0$	$(3.0 \pm 0.7) \times 10^{-3}$		1468
$3(\pi^+ \pi^-)$	$(1.20 \pm 0.18) \%$		1633
$K^+ \bar{K}^*(892)^0 \pi^-$ + c.c.	$(7.5 \pm 1.6) \times 10^{-3}$		1523
$K^*(892)^0 \bar{K}^*(892)^0$	$(1.7 \pm 0.6) \times 10^{-3}$		1456
$\pi \pi$	$(8.51 \pm 0.33) \times 10^{-3}$		1702
$\pi^0 \eta$	$< 1.8 \times 10^{-4}$		1661
$\pi^0 \eta'$	$< 1.1 \times 10^{-3}$		1570
$\pi^0 \eta_c$	$< 1.6 \times 10^{-3}$	CL=90%	383
$\eta \eta$	$(3.01 \pm 0.19) \times 10^{-3}$		1617
$\eta \eta'$	$(9.1 \pm 1.1) \times 10^{-5}$		1521
$\eta' \eta'$	$(2.17 \pm 0.12) \times 10^{-3}$		1413
$\omega \omega$	$(9.7 \pm 1.1) \times 10^{-4}$		1517
$\omega \phi$	$(1.41 \pm 0.13) \times 10^{-4}$		1447
$\omega K^+ K^-$	$(1.94 \pm 0.21) \times 10^{-3}$		1457
$K^+ K^-$	$(6.05 \pm 0.31) \times 10^{-3}$		1634
$K_S^0 K_S^0$	$(3.16 \pm 0.17) \times 10^{-3}$		1633
$\pi^+ \pi^- \eta$	$< 2.0 \times 10^{-4}$	CL=90%	1651
$\pi^+ \pi^- \eta'$	$< 4 \times 10^{-4}$	CL=90%	1560
$\bar{K}^0 K^+ \pi^-$ + c.c.	$< 9 \times 10^{-5}$	CL=90%	1610
$K^+ K^- \pi^0$	$< 6 \times 10^{-5}$	CL=90%	1611
$K^+ K^- \eta$	$< 2.3 \times 10^{-4}$	CL=90%	1512
$K^+ K^- K_S^0 K_S^0$	$(1.4 \pm 0.5) \times 10^{-3}$		1331
$K_S^0 K_S^0 K_S^0 K_S^0$	$(5.8 \pm 0.5) \times 10^{-4}$		1327
$K^+ K^- K^+ K^-$	$(2.82 \pm 0.29) \times 10^{-3}$		1333
$K^+ K^- \phi$	$(9.7 \pm 2.5) \times 10^{-4}$		1381
$\bar{K}^0 K^+ \pi^- \phi$ + c.c.	$(3.7 \pm 0.6) \times 10^{-3}$		1326
$K^+ K^- \pi^0 \phi$	$(1.90 \pm 0.35) \times 10^{-3}$		1329
$\phi \pi^+ \pi^- \pi^0$	$(1.18 \pm 0.15) \times 10^{-3}$		1525
$\phi \phi$	$(8.0 \pm 0.7) \times 10^{-4}$		1370
$\phi \phi \eta$	$(8.4 \pm 1.0) \times 10^{-4}$		1100
$\rho \bar{\rho}$	$(2.21 \pm 0.08) \times 10^{-4}$		1426
$\rho \bar{\rho} \pi^0$	$(7.0 \pm 0.7) \times 10^{-4}$		1379
$\rho \bar{\rho} \eta$	$(3.5 \pm 0.4) \times 10^{-4}$	S=1.3	1187

## Meson Summary Table

$\rho\bar{\rho}\omega$	$(5.2 \pm 0.6) \times 10^{-4}$		1043
$\rho\bar{\rho}\phi$	$(6.0 \pm 1.4) \times 10^{-5}$		876
$\rho\bar{\rho}\pi^+\pi^-$	$(2.1 \pm 0.7) \times 10^{-3}$	S=1.4	1320
$\rho\bar{\rho}\pi^0\pi^0$	$(1.04 \pm 0.28) \times 10^{-3}$		1324
$\rho\bar{\rho}K^+K^-$ (non-resonant)	$(1.22 \pm 0.26) \times 10^{-4}$		890
$\rho\bar{\rho}K_S^0K_S^0$	$< 8.8 \times 10^{-4}$	CL=90%	884
$\rho\bar{n}\pi^-$	$(1.27 \pm 0.11) \times 10^{-3}$		1376
$\bar{\rho}n\pi^+$	$(1.37 \pm 0.12) \times 10^{-3}$		1376
$\rho\bar{n}\pi^-\pi^0$	$(2.34 \pm 0.21) \times 10^{-3}$		1321
$\bar{\rho}n\pi^+\pi^0$	$(2.21 \pm 0.18) \times 10^{-3}$		1321
$\Lambda\bar{\Lambda}$	$(3.27 \pm 0.24) \times 10^{-4}$		1292
$\Lambda\bar{\Lambda}\pi^+\pi^-$	$(1.18 \pm 0.13) \times 10^{-3}$		1153
$\Lambda\bar{\Lambda}\pi^+\pi^-$ (non-resonant)	$< 5 \times 10^{-4}$	CL=90%	1153
$\Sigma(1385)^+\bar{\Lambda}\pi^- + c.c.$	$< 5 \times 10^{-4}$	CL=90%	1083
$\Sigma(1385)^-\bar{\Lambda}\pi^+ + c.c.$	$< 5 \times 10^{-4}$	CL=90%	1083
$K^+\bar{p}\Lambda + c.c.$	$(1.25 \pm 0.12) \times 10^{-3}$	S=1.3	1132
$K^*(892)^+\bar{p}\Lambda + c.c.$	$(4.8 \pm 0.9) \times 10^{-4}$		845
$K^+\bar{p}\Lambda(1520) + c.c.$	$(2.9 \pm 0.7) \times 10^{-4}$		859
$\Lambda(1520)\bar{\Lambda}(1520)$	$(3.1 \pm 1.2) \times 10^{-4}$		780
$\Sigma^0\bar{\Sigma}^0$	$(4.68 \pm 0.32) \times 10^{-4}$		1222
$\Sigma^+\bar{p}K_S^0 + c.c.$	$(3.52 \pm 0.27) \times 10^{-4}$		1089
$\Sigma^+\bar{\Sigma}^-$	$(4.6 \pm 0.8) \times 10^{-4}$	S=2.6	1225
$\Sigma(1385)^+\bar{\Sigma}(1385)^-$	$(1.6 \pm 0.6) \times 10^{-4}$		1001
$\Sigma(1385)^-\bar{\Sigma}(1385)^+$	$(2.3 \pm 0.7) \times 10^{-4}$		1001
$K^-\Lambda\bar{\Xi}^+ + c.c.$	$(1.94 \pm 0.35) \times 10^{-4}$		873
$\Xi^0\bar{\Xi}^0$	$(3.1 \pm 0.8) \times 10^{-4}$		1089
$\Xi^-\bar{\Xi}^+$	$(4.8 \pm 0.7) \times 10^{-4}$		1081
$\eta_c\pi^+\pi^-$	$< 7 \times 10^{-4}$	CL=90%	307
<b>Radiative decays</b>			
$\gamma J/\psi(1S)$	$(1.40 \pm 0.05) \%$		303
$\gamma\rho^0$	$< 9 \times 10^{-6}$	CL=90%	1619
$\gamma\omega$	$< 8 \times 10^{-6}$	CL=90%	1618
$\gamma\phi$	$< 6 \times 10^{-6}$	CL=90%	1555
$\gamma\gamma$	$(2.04 \pm 0.09) \times 10^{-4}$		1707
$e^+e^- J/\psi(1S)$	$(1.33 \pm 0.29) \times 10^{-4}$		303
$\mu^+\mu^- J/\psi(1S)$	$< 1.9 \times 10^{-5}$	CL=90%	226

 **$\chi_{c1}(1P)$** 

$$J^G(J^{PC}) = 0^+(1^{++})$$

Mass  $m = 3510.67 \pm 0.05$  MeV (S = 1.2)

Full width  $\Gamma = 0.84 \pm 0.04$  MeV

$\chi_{c1}(1P)$ DECAY MODES	Fraction ( $\Gamma_i/\Gamma$ )	Scale factor/ Confidence level	$\rho$ (MeV/c)
<b>Hadronic decays</b>			
$3(\pi^+\pi^-)$	$(5.8 \pm 1.4) \times 10^{-3}$	S=1.2	1683
$2(\pi^+\pi^-)$	$(7.6 \pm 2.6) \times 10^{-3}$		1728
$\pi^+\pi^-\pi^0\pi^0$	$(1.19 \pm 0.15) \%$		1729
$\rho^+\pi^-\pi^0 + c.c.$	$(1.45 \pm 0.24) \%$		1658
$\rho^0\pi^+\pi^-$	$(3.9 \pm 3.5) \times 10^{-3}$		1657
$4\pi^0$	$(5.4 \pm 0.8) \times 10^{-4}$		1729
$\pi^+\pi^-K^+K^-$	$(4.5 \pm 1.0) \times 10^{-3}$		1632
$K^+K^-\pi^0\pi^0$	$(1.12 \pm 0.27) \times 10^{-3}$		1634
$K^+K^-\pi^+\pi^-\pi^0$	$(1.15 \pm 0.13) \%$		1598
$K_S^0K^\pm\pi^\mp\pi^+\pi^-$	$(7.5 \pm 0.8) \times 10^{-3}$		1596
$K^\pm\pi^-\bar{K}^0\pi^0 + c.c.$	$(8.6 \pm 1.4) \times 10^{-3}$		1632
$\rho^-K^+\bar{K}^0 + c.c.$	$(5.0 \pm 1.2) \times 10^{-3}$		1514
$K^*(892)^0\bar{K}^0\pi^0 \rightarrow$ $K^+\pi^-\bar{K}^0\pi^0 + c.c.$	$(2.3 \pm 0.6) \times 10^{-3}$		-
$K^+K^-\eta\pi^0$	$(1.12 \pm 0.34) \times 10^{-3}$		1523
$\pi^+\pi^-K_S^0K_S^0$	$(6.9 \pm 2.9) \times 10^{-4}$		1630
$K^+K^-\eta$	$(3.2 \pm 1.0) \times 10^{-4}$		1566
$\bar{K}^0K^+\pi^- + c.c.$	$(7.0 \pm 0.6) \times 10^{-3}$		1661
$K^*(892)^0\bar{K}^0 + c.c.$	$(10 \pm 4) \times 10^{-4}$		1602
$K^*(892)^+K^- + c.c.$	$(1.4 \pm 0.6) \times 10^{-3}$		1602
$K_S^0(1430)^0\bar{K}^0 + c.c. \rightarrow$ $K_S^0K^+\pi^- + c.c.$	$< 8 \times 10^{-4}$	CL=90%	-
$K_S^0(1430)^+K^- + c.c. \rightarrow$ $K_S^0K^+\pi^- + c.c.$	$< 2.1 \times 10^{-3}$	CL=90%	-
$K^+K^-\pi^0$	$(1.81 \pm 0.24) \times 10^{-3}$		1662
$\eta\pi^+\pi^-$	$(4.62 \pm 0.23) \times 10^{-3}$		1701
$a_0(980)^+\pi^- + c.c. \rightarrow \eta\pi^+\pi^-$	$(3.2 \pm 0.4) \times 10^{-3}$	S=2.2	-
$a_2(1320)^+\pi^- + c.c. \rightarrow \eta\pi^+\pi^-$	$(1.76 \pm 0.24) \times 10^{-4}$		-
$a_2(1700)^+\pi^- + c.c. \rightarrow \eta\pi^+\pi^-$	$(4.6 \pm 0.7) \times 10^{-5}$		-
$f_2(1270)\eta \rightarrow \eta\pi^+\pi^-$	$(3.5 \pm 0.6) \times 10^{-4}$		-
$f_4(2050)\eta \rightarrow \eta\pi^+\pi^-$	$(2.5 \pm 0.9) \times 10^{-5}$		-

$\pi_1(1400)^+\pi^- + c.c. \rightarrow$ $\eta\pi^+\pi^-$	$< 5 \times 10^{-5}$	CL=90%	-
$\pi_1(1600)^+\pi^- + c.c. \rightarrow$ $\eta\pi^+\pi^-$	$< 1.5 \times 10^{-5}$	CL=90%	-
$\pi_1(2015)^+\pi^- + c.c. \rightarrow$ $\eta\pi^+\pi^-$	$< 8 \times 10^{-6}$	CL=90%	-
$f_2(1270)\eta$	$(6.7 \pm 1.1) \times 10^{-4}$		1467
$\pi^+\pi^-\eta'$	$(2.2 \pm 0.4) \times 10^{-3}$		1612
$K^+K^-\eta'(958)$	$(8.8 \pm 0.9) \times 10^{-4}$		1461
$K_0^*(1430)^+K^- + c.c.$	$(6.4 \pm 2.2 \pm 2.8) \times 10^{-4}$		-
$f_0(980)\eta'(958)$	$(1.6 \pm 1.4 \pm 0.7) \times 10^{-4}$		1460
$f_0(1710)\eta'(958)$	$(7 \pm 7) \times 10^{-5}$		1118
$f_2'(1525)\eta'(958)$	$(9 \pm 6) \times 10^{-5}$		1229
$\pi^0 f_0(980) \rightarrow \pi^0\pi^+\pi^-$	$(3.5 \pm 0.9) \times 10^{-7}$		-
$K^+K^*(892)^0\pi^- + c.c.$	$(3.2 \pm 2.1) \times 10^{-3}$		1577
$K^*(892)^0\bar{K}^*(892)^0$	$(1.4 \pm 0.4) \times 10^{-3}$		1512
$K^+K^-K_S^0K_S^0$	$< 4 \times 10^{-4}$	CL=90%	1390
$K_S^0K_S^0K_S^0K_S^0$	$(3.5 \pm 1.0) \times 10^{-5}$		1387
$K^+K^-K^+K^-$	$(5.4 \pm 1.1) \times 10^{-4}$		1393
$K^+K^-\phi$	$(4.1 \pm 1.5) \times 10^{-4}$		1440
$\bar{K}^0K^+\pi^-\phi + c.c.$	$(3.3 \pm 0.5) \times 10^{-3}$		1387
$K^+K^-\pi^0\phi$	$(1.62 \pm 0.30) \times 10^{-3}$		1390
$\phi\pi^+\pi^-\pi^0$	$(7.5 \pm 1.0) \times 10^{-4}$		1578
$\omega\omega$	$(5.7 \pm 0.7) \times 10^{-4}$		1571
$\omega K^+K^-$	$(7.8 \pm 0.9) \times 10^{-4}$		1513
$\omega\phi$	$(2.7 \pm 0.4) \times 10^{-5}$		1503
$\phi\phi$	$(4.2 \pm 0.5) \times 10^{-4}$		1429
$\phi\phi\eta$	$(3.0 \pm 0.5) \times 10^{-4}$		1172
$\rho\bar{\rho}$	$(7.60 \pm 0.34) \times 10^{-5}$		1484
$\rho\bar{\rho}\pi^0$	$(1.55 \pm 0.18) \times 10^{-4}$		1438
$\rho\bar{\rho}\eta$	$(1.45 \pm 0.25) \times 10^{-4}$		1254
$\rho\bar{\rho}\omega$	$(2.12 \pm 0.31) \times 10^{-4}$		1117
$\rho\bar{\rho}\phi$	$< 1.7 \times 10^{-5}$	CL=90%	962
$\rho\bar{\rho}\pi^+\pi^-$	$(5.0 \pm 1.9) \times 10^{-4}$		1381
$\rho\bar{\rho}\pi^0\pi^0$	$< 5 \times 10^{-4}$	CL=90%	1385
$\rho\bar{\rho}K^+K^-$ (non-resonant)	$(1.27 \pm 0.22) \times 10^{-4}$		974
$\rho\bar{\rho}K_S^0K_S^0$	$< 4.5 \times 10^{-4}$	CL=90%	968
$\rho\bar{n}\pi^-$	$(3.8 \pm 0.5) \times 10^{-4}$		1435
$\bar{\rho}n\pi^+$	$(3.9 \pm 0.5) \times 10^{-4}$		1435
$\rho\bar{n}\pi^-\pi^0$	$(1.03 \pm 0.12) \times 10^{-3}$		1383
$\bar{\rho}n\pi^+\pi^0$	$(1.01 \pm 0.12) \times 10^{-3}$		1383
$\Lambda\bar{\Lambda}$	$(1.14 \pm 0.11) \times 10^{-4}$		1355
$\Lambda\bar{\Lambda}\pi^+\pi^-$	$(2.9 \pm 0.5) \times 10^{-4}$		1223
$\Lambda\bar{\Lambda}\pi^+\pi^-$ (non-resonant)	$(2.5 \pm 0.6) \times 10^{-4}$		1223
$\Sigma(1385)^+\bar{\Lambda}\pi^- + c.c.$	$< 1.3 \times 10^{-4}$	CL=90%	1157
$\Sigma(1385)^-\bar{\Lambda}\pi^+ + c.c.$	$< 1.3 \times 10^{-4}$	CL=90%	1157
$K^+\bar{p}\Lambda + c.c.$	$(4.2 \pm 0.4) \times 10^{-4}$	S=1.2	1203
$K^*(892)^+\bar{p}\Lambda + c.c.$	$(4.9 \pm 0.7) \times 10^{-4}$		935
$K^+\bar{p}\Lambda(1520) + c.c.$	$(1.7 \pm 0.4) \times 10^{-4}$		951
$\Lambda(1520)\bar{\Lambda}(1520)$	$< 9 \times 10^{-5}$	CL=90%	880
$\Sigma^0\bar{\Sigma}^0$	$(4.2 \pm 0.6) \times 10^{-5}$		1288
$\Sigma^+\bar{p}K_S^0 + c.c.$	$(1.53 \pm 0.12) \times 10^{-4}$		1163
$\Sigma^+\bar{\Sigma}^-$	$(3.6 \pm 0.7) \times 10^{-5}$		1291
$\Sigma(1385)^+\bar{\Sigma}(1385)^-$	$< 9 \times 10^{-5}$	CL=90%	1081
$\Sigma(1385)^-\bar{\Sigma}(1385)^+$	$< 5 \times 10^{-5}$	CL=90%	1081
$K^-\Lambda\bar{\Xi}^+ + c.c.$	$(1.35 \pm 0.24) \times 10^{-4}$		963
$\Xi^0\bar{\Xi}^0$	$< 6 \times 10^{-5}$	CL=90%	1163
$\Xi^-\bar{\Xi}^+$	$(8.0 \pm 2.1) \times 10^{-5}$		1155
$\pi^+\pi^- + K^+K^-$	$< 2.1 \times 10^{-3}$		-
$K_S^0K_S^0$	$< 6 \times 10^{-5}$	CL=90%	1683
$\eta_c\pi^+\pi^-$	$< 3.2 \times 10^{-3}$	CL=90%	413

**Radiative decays**

$\gamma J/\psi(1S)$	$(34.3 \pm 1.0) \%$		389
$\gamma\rho^0$	$(2.16 \pm 0.17) \times 10^{-4}$		1670
$\gamma\omega$	$(6.8 \pm 0.8) \times 10^{-5}$		1668
$\gamma\phi$	$(2.4 \pm 0.5) \times 10^{-5}$		1607
$\gamma\gamma$	$< 6.3 \times 10^{-6}$	CL=90%	1755
$e^+e^- J/\psi(1S)$	$(3.46 \pm 0.22) \times 10^{-3}$		389
$\mu^+\mu^- J/\psi(1S)$	$(2.33 \pm 0.29) \times 10^{-4}$		335

 **$h_c(1P)$** 

$$J^G(J^{PC}) = 0^-(1^{+-})$$

Mass  $m = 3525.38 \pm 0.11$  MeV

Full width  $\Gamma = 0.7 \pm 0.4$  MeV

## Meson Summary Table

$h_c(1P)$ DECAY MODES	Fraction ( $\Gamma_i/\Gamma$ )	Confidence level	$p$ (MeV/c)
$J/\psi(1S)\pi\pi$	not seen		312
$J/\psi(1S)\pi^+\pi^-$	$< 2.3 \times 10^{-3}$	90%	305
$p\bar{p}$	$< 1.5 \times 10^{-4}$	90%	1492
$p\bar{p}\pi^+\pi^-$	$(2.9 \pm 0.6) \times 10^{-3}$		1390
$\pi^+\pi^-\pi^0$	$(1.6 \pm 0.5) \times 10^{-3}$		1749
$2\pi^+2\pi^-\pi^0$	$(8.1 \pm 1.8) \times 10^{-3}$		1716
$3\pi^+3\pi^-\pi^0$	$< 9 \times 10^{-3}$	90%	1661
$K^+K^-\pi^+\pi^-$	$< 6 \times 10^{-4}$	90%	1640
<b>Radiative decays</b>			
$\gamma\eta$	$(4.7 \pm 2.1) \times 10^{-4}$		1720
$\gamma\eta'(958)$	$(1.5 \pm 0.4) \times 10^{-3}$		1633
$\gamma\eta_c(1S)$	$(51 \pm 6) \%$		500

 **$\chi_{c2}(1P)$** 

$$I^G(J^{PC}) = 0^+(2^+ +)$$

Mass  $m = 3556.17 \pm 0.07$  MeV

Full width  $\Gamma = 1.97 \pm 0.09$  MeV

$\chi_{c2}(1P)$ DECAY MODES	Fraction ( $\Gamma_i/\Gamma$ )	Confidence level	$p$ (MeV/c)
<b>Hadronic decays</b>			
$2(\pi^+\pi^-)$	$(1.02 \pm 0.09) \%$		1751
$\pi^+\pi^-\pi^0\pi^0$	$(1.83 \pm 0.23) \%$		1752
$\rho^+\pi^-\pi^0 + c.c.$	$(2.19 \pm 0.34) \%$		1682
$4\pi^0$	$(1.11 \pm 0.15) \times 10^{-3}$		1752
$K^+K^-\pi^0\pi^0$	$(2.1 \pm 0.4) \times 10^{-3}$		1658
$K^+\pi^-\bar{K}^0\pi^0 + c.c.$	$(1.38 \pm 0.20) \%$		1657
$\rho^-K^+\bar{K}^0 + c.c.$	$(4.1 \pm 1.2) \times 10^{-3}$		1540
$K^*(892)^0K^-\pi^+ \rightarrow K^-\pi^+K^0\pi^0 + c.c.$	$(2.9 \pm 0.8) \times 10^{-3}$		-
$K^*(892)^0\bar{K}^0\pi^0 \rightarrow K^+\pi^-\bar{K}^0\pi^0 + c.c.$	$(3.8 \pm 0.9) \times 10^{-3}$		-
$K^*(892)^-K^+\pi^0 \rightarrow K^+\pi^-\bar{K}^0\pi^0 + c.c.$	$(3.7 \pm 0.8) \times 10^{-3}$		-
$K^*(892)^+\bar{K}^0\pi^- \rightarrow K^+\pi^-\bar{K}^0\pi^0 + c.c.$	$(2.9 \pm 0.8) \times 10^{-3}$		-
$K^+K^-\eta\pi^0$	$(1.3 \pm 0.4) \times 10^{-3}$		1549
$K^+K^-\pi^+\pi^-$	$(8.4 \pm 0.9) \times 10^{-3}$		1656
$K^+K^-\pi^+\pi^-\pi^0$	$(1.17 \pm 0.13) \%$		1623
$K_S^0K^\pm\pi^\mp\pi^\pm\pi^-$	$(7.3 \pm 0.8) \times 10^{-3}$		1621
$K^+\bar{K}^*(892)^0\pi^-\pi^0 + c.c.$	$(2.1 \pm 1.1) \times 10^{-3}$		1602
$K^*(892)^0\bar{K}^*(892)^0$	$(2.3 \pm 0.4) \times 10^{-3}$		1538
$3(\pi^+\pi^-)$	$(8.6 \pm 1.8) \times 10^{-3}$		1707
$\phi\phi$	$(1.06 \pm 0.09) \times 10^{-3}$		1457
$\phi\phi\eta$	$(5.3 \pm 0.6) \times 10^{-4}$		1206
$\omega\omega$	$(8.4 \pm 1.0) \times 10^{-4}$		1597
$\omega K^+K^-$	$(7.3 \pm 0.9) \times 10^{-4}$		1540
$\omega\phi$	$(9.6 \pm 2.7) \times 10^{-6}$		1529
$\pi\pi$	$(2.23 \pm 0.09) \times 10^{-3}$		1773
$\rho^0\pi^+\pi^-$	$(3.7 \pm 1.6) \times 10^{-3}$		1682
$\pi^+\pi^-\pi^0$ (non-resonant)	$(2.0 \pm 0.4) \times 10^{-5}$		1765
$\rho(770)^\pm\pi^\mp$	$(6 \pm 4) \times 10^{-6}$		-
$\pi^+\pi^-\eta$	$(4.8 \pm 1.3) \times 10^{-4}$		1724
$\pi^+\pi^-\eta'$	$(5.0 \pm 1.8) \times 10^{-4}$		1636
$\eta\eta$	$(5.4 \pm 0.4) \times 10^{-4}$		1692
$K^+K^-$	$(1.01 \pm 0.06) \times 10^{-3}$		1708
$K_S^0K_S^0$	$(5.2 \pm 0.4) \times 10^{-4}$		1707
$K^*(892)^\pm K^\mp$	$(1.44 \pm 0.21) \times 10^{-4}$		1627
$K^*(892)^0\bar{K}^0 + c.c.$	$(1.24 \pm 0.27) \times 10^{-4}$		1627
$K_2^*(1430)^\pm K^\mp$	$(1.48 \pm 0.12) \times 10^{-3}$		-
$K_2^*(1430)^0\bar{K}^0 + c.c.$	$(1.24 \pm 0.17) \times 10^{-3}$		1443
$K_3^*(1780)^\pm K^\mp$	$(5.2 \pm 0.8) \times 10^{-4}$		-
$K_3^*(1780)^0\bar{K}^0 + c.c.$	$(5.6 \pm 2.1) \times 10^{-4}$		1276
$a_2(1320)^0\pi^0$	$(1.29 \pm 0.34) \times 10^{-3}$		-
$a_2(1320)^\pm\pi^\mp$	$(1.8 \pm 0.6) \times 10^{-3}$		1531
$\bar{K}^0K^+\pi^- + c.c.$	$(1.28 \pm 0.18) \times 10^{-3}$		1685
$K^+K^-\pi^0$	$(3.0 \pm 0.8) \times 10^{-4}$		1686
$K^+K^-\eta$	$< 3.2 \times 10^{-4}$	90%	1592
$K^+K^-\eta'(958)$	$(1.94 \pm 0.34) \times 10^{-4}$		1488
$\eta\eta'$	$(2.2 \pm 0.5) \times 10^{-5}$		1600
$\eta'\eta'$	$(4.6 \pm 0.6) \times 10^{-5}$		1498
$\pi^+\pi^-K_S^0K_S^0$	$(2.2 \pm 0.5) \times 10^{-3}$		1655
$K^+K^-K_S^0K_S^0$	$< 4 \times 10^{-4}$	90%	1418
$K_S^0K_S^0K_S^0K_S^0$	$(1.13 \pm 0.18) \times 10^{-4}$		1415

$K^+K^-K^+K^-$	$(1.65 \pm 0.20) \times 10^{-3}$		1421
$K^+K^-\phi$	$(1.42 \pm 0.29) \times 10^{-3}$		1468
$\bar{K}^0K^+\pi^-\phi + c.c.$	$(4.8 \pm 0.7) \times 10^{-3}$		1416
$K^+K^-\pi^0\phi$	$(2.7 \pm 0.5) \times 10^{-3}$		1419
$\phi\pi^+\pi^-\pi^0$	$(9.3 \pm 1.2) \times 10^{-4}$		1603
$p\bar{p}$	$(7.33 \pm 0.33) \times 10^{-5}$		1510
$p\bar{p}\pi^0$	$(4.7 \pm 0.4) \times 10^{-4}$		1465
$p\bar{p}\eta$	$(1.74 \pm 0.25) \times 10^{-4}$		1285
$p\bar{p}\omega$	$(3.6 \pm 0.4) \times 10^{-4}$		1152
$p\bar{p}\phi$	$(2.8 \pm 0.9) \times 10^{-5}$		1002
$p\bar{p}\pi^+\pi^-$	$(1.32 \pm 0.34) \times 10^{-3}$		1410
$p\bar{p}\pi^0\pi^0$	$(7.8 \pm 2.3) \times 10^{-4}$		1414
$p\bar{p}K^+K^-$ (non-resonant)	$(1.91 \pm 0.32) \times 10^{-4}$		1013
$p\bar{p}K_S^0K_S^0$	$< 7.9 \times 10^{-4}$	90%	1007
$p\bar{n}\pi^-$	$(8.5 \pm 0.9) \times 10^{-4}$		1463
$\bar{p}n\pi^+$	$(8.9 \pm 0.8) \times 10^{-4}$		1463
$p\bar{n}\pi^-\pi^0$	$(2.17 \pm 0.18) \times 10^{-3}$		1411
$\bar{p}n\pi^+\pi^0$	$(2.11 \pm 0.18) \times 10^{-3}$		1411
$\Lambda\bar{\Lambda}$	$(1.84 \pm 0.15) \times 10^{-4}$		1384
$\Lambda\bar{\Lambda}\pi^+\pi^-$	$(1.25 \pm 0.15) \times 10^{-3}$		1255
$\Lambda\bar{\Lambda}\pi^+\pi^-$ (non-resonant)	$(6.6 \pm 1.5) \times 10^{-4}$		1255
$\Sigma(1385)^+\bar{\Lambda}\pi^- + c.c.$	$< 4 \times 10^{-4}$	90%	1192
$\Sigma(1385)^-\bar{\Lambda}\pi^+ + c.c.$	$< 6 \times 10^{-4}$	90%	1192
$K^+\bar{p}\Lambda + c.c.$	$(7.8 \pm 0.5) \times 10^{-4}$		1236
$K^*(892)^+\bar{p}\Lambda + c.c.$	$(8.2 \pm 1.1) \times 10^{-4}$		976
$K^+\bar{p}\Lambda(1520) + c.c.$	$(2.8 \pm 0.7) \times 10^{-4}$		992
$\Lambda(1520)\bar{\Lambda}(1520)$	$(4.6 \pm 1.5) \times 10^{-4}$		924
$\Sigma^0\bar{\Sigma}^0$	$(3.7 \pm 0.6) \times 10^{-5}$		1319
$\Sigma^+\bar{p}K_S^0 + c.c.$	$(8.2 \pm 0.9) \times 10^{-5}$		1197
$\Sigma^+\bar{\Sigma}^-$	$(3.4 \pm 0.7) \times 10^{-5}$		1322
$\Sigma(1385)^+\bar{\Sigma}(1385)^-$	$< 1.6 \times 10^{-4}$	90%	1118
$\Sigma(1385)^-\bar{\Sigma}(1385)^+$	$< 8 \times 10^{-5}$	90%	1118
$K^-\Lambda\Xi^+ + c.c.$	$(1.76 \pm 0.32) \times 10^{-4}$		1004
$\Xi^0\Xi^0$	$< 1.0 \times 10^{-4}$	90%	1197
$\Xi^-\Xi^+$	$(1.42 \pm 0.32) \times 10^{-4}$		1189
$J/\psi(1S)\pi^+\pi^-\pi^0$	$< 1.5 \%$		185
$\pi^0\eta_c$	$< 3.2 \times 10^{-3}$	90%	511
$\eta_c(1S)\pi^+\pi^-$	$< 5.4 \times 10^{-3}$	90%	459
<b>Radiative decays</b>			
$\gamma J/\psi(1S)$	$(19.0 \pm 0.5) \%$		430
$\gamma\rho^0$	$< 1.9 \times 10^{-5}$	90%	1694
$\gamma\omega$	$< 6 \times 10^{-6}$	90%	1692
$\gamma\phi$	$< 7 \times 10^{-6}$	90%	1632
$\gamma\gamma$	$(2.85 \pm 0.10) \times 10^{-4}$		1778
$e^+e^- J/\psi(1S)$	$(2.15 \pm 0.14) \times 10^{-3}$		430
$\mu^+\mu^- J/\psi(1S)$	$(2.02 \pm 0.33) \times 10^{-4}$		381

 **$\eta_c(2S)$** 

$$I^G(J^{PC}) = 0^+(0^- +)$$

Quantum numbers are quark model predictions.

Mass  $m = 3637.5 \pm 1.1$  MeV ( $S = 1.2$ )

Full width  $\Gamma = 11.3_{-2.9}^{+3.2}$  MeV

$\eta_c(2S)$ DECAY MODES	Fraction ( $\Gamma_i/\Gamma$ )	Confidence level	$p$ (MeV/c)
hadrons	not seen		-
$K\bar{K}\pi$	$(1.9 \pm 1.2) \%$		1729
$K\bar{K}\eta$	$(5 \pm 4) \times 10^{-3}$		1637
$2\pi^+2\pi^-$	not seen		1792
$\rho^0\rho^0$	not seen		1645
$3\pi^+3\pi^-$	not seen		1749
$K^+K^-\pi^+\pi^-$	not seen		1700
$K^*0\bar{K}^*0$	not seen		1585
$K^+K^-\pi^+\pi^-\pi^0$	$(1.4 \pm 1.0) \%$		1667
$K^+K^-\pi^+\pi^-\pi^0$	not seen		1627
$K_S^0K^-2\pi^+\pi^- + c.c.$	seen		1666
$2K^+2K^-$	not seen		1470
$\phi\phi$	not seen		1506
$p\bar{p}$	seen		1558
$p\bar{p}\pi^+\pi^-$	seen		1461
$\gamma\gamma$	$(1.9 \pm 1.3) \times 10^{-4}$		1819
$\gamma J/\psi(1S)$	$< 1.4 \%$	90%	500
$\pi^+\pi^-\eta$	not seen		1766
$\pi^+\pi^-\eta'$	not seen		1680
$\pi^+\pi^-\eta_c(1S)$	$< 25 \%$	90%	537

## Meson Summary Table

 **$\psi(2S)$** 

$$J^G(J^{PC}) = 0^-(1^{--})$$

Mass  $m = 3686.10 \pm 0.06$  MeV ( $S = 5.9$ )Full width  $\Gamma = 294 \pm 8$  keV $\Gamma_{ee} = 2.33 \pm 0.04$  keV

$\psi(2S)$ DECAY MODES	Fraction ( $\Gamma_i/\Gamma$ )	Scale factor/ Confidence level	$\rho$ (MeV/c)
hadrons	(97.85 ± 0.13) %	—	—
virtual $\gamma \rightarrow$ hadrons	(1.73 ± 0.14) %	$S=1.5$	—
$ggg$	(10.6 ± 1.6) %	—	—
$\gamma gg$	(1.03 ± 0.29) %	—	—
light hadrons	(15.4 ± 1.5) %	—	—
$e^+e^-$	(7.93 ± 0.17) $\times 10^{-3}$	—	1843
$\mu^+\mu^-$	(8.0 ± 0.6) $\times 10^{-3}$	—	1840
$\tau^+\tau^-$	(3.1 ± 0.4) $\times 10^{-3}$	—	489

Decays into  $J/\psi(1S)$  and anything

$J/\psi(1S)$ anything	(61.4 ± 0.6) %	—	—
$J/\psi(1S)$ neutrals	(25.38 ± 0.32) %	—	—
$J/\psi(1S)\pi^+\pi^-$	(34.68 ± 0.30) %	—	477
$J/\psi(1S)\pi^0\pi^0$	(18.24 ± 0.31) %	—	481
$J/\psi(1S)\eta$	(3.37 ± 0.05) %	—	199
$J/\psi(1S)\pi^0$	(1.268 ± 0.032) $\times 10^{-3}$	—	528

## Hadronic decays

$\pi^0 h_c(1P)$	(8.6 ± 1.3) $\times 10^{-4}$	—	85
$3(\pi^+\pi^-\pi^0)$	(3.5 ± 1.6) $\times 10^{-3}$	—	1746
$2(\pi^+\pi^-\pi^0)$	(2.9 ± 1.0) $\times 10^{-3}$	$S=4.7$	1799
$\rho a_2(1320)$	(2.6 ± 0.9) $\times 10^{-4}$	—	1501
$\pi^+\pi^-\pi^0\pi^0\pi^0$	(5.3 ± 0.9) $\times 10^{-3}$	—	1800
$\rho^\pm\pi^\mp\pi^0\pi^0$	< 2.7 $\times 10^{-3}$	CL=90%	1737
$p\bar{p}$	(2.94 ± 0.08) $\times 10^{-4}$	—	1586
$n\bar{n}$	(3.06 ± 0.15) $\times 10^{-4}$	—	1586
$\Delta^{++}\bar{\Delta}^{--}$	(1.28 ± 0.35) $\times 10^{-4}$	—	1371
$\Lambda\bar{\Lambda}\pi^0$	< 2.9 $\times 10^{-6}$	CL=90%	1412
$\Lambda\bar{\Lambda}\eta$	(2.5 ± 0.4) $\times 10^{-5}$	—	1197
$\Lambda\bar{\Lambda}K^+$	(1.00 ± 0.14) $\times 10^{-4}$	—	1327
$K^*(892)^+\bar{p}\Lambda + c.c.$	(6.3 ± 0.7) $\times 10^{-5}$	—	1087
$\Lambda\bar{\Lambda}K^+\pi^+\pi^-$	(1.8 ± 0.4) $\times 10^{-4}$	—	1167
$\Lambda\bar{\Lambda}\pi^+\pi^-$	(2.8 ± 0.6) $\times 10^{-4}$	—	1346
$\Lambda\bar{\Lambda}$	(3.81 ± 0.13) $\times 10^{-4}$	$S=1.4$	1467
$\Lambda\bar{\Sigma}^+\pi^- + c.c.$	(1.40 ± 0.13) $\times 10^{-4}$	—	1376
$\Lambda\bar{\Sigma}^-\pi^+ + c.c.$	(1.54 ± 0.14) $\times 10^{-4}$	—	1379
$\Lambda\bar{\Sigma}^0$	(1.23 ± 0.24) $\times 10^{-5}$	—	1437
$\Sigma^0\bar{p}K^+ + c.c.$	(1.67 ± 0.18) $\times 10^{-5}$	—	1291
$\Sigma^+\bar{\Sigma}^-$	(2.32 ± 0.12) $\times 10^{-4}$	—	1408
$\Sigma^0\bar{\Sigma}^0$	(2.35 ± 0.09) $\times 10^{-4}$	$S=1.1$	1405
$\Sigma(1385)^+\bar{\Sigma}(1385)^-$	(8.5 ± 0.7) $\times 10^{-5}$	—	1218
$\Sigma(1385)^-\bar{\Sigma}(1385)^+$	(8.5 ± 0.8) $\times 10^{-5}$	—	1218
$\Sigma(1385)^0\bar{\Sigma}(1385)^0$	(6.9 ± 0.7) $\times 10^{-5}$	—	1218
$\Xi^-\bar{\Xi}^+$	(2.87 ± 0.11) $\times 10^{-4}$	$S=1.1$	1284
$\Xi^0\bar{\Xi}^0$	(2.3 ± 0.4) $\times 10^{-4}$	$S=4.2$	1291
$\Xi(1530)^0\bar{\Xi}(1530)^0$	(5.2 $\pm_{-1.2}^{+3.2}$ ) $\times 10^{-5}$	—	1025
$K^-\Lambda\bar{\Xi}^+ + c.c.$	(3.9 ± 0.4) $\times 10^{-5}$	—	1114
$\Xi(1530)^-\bar{\Xi}(1530)^+$	(1.15 ± 0.07) $\times 10^{-4}$	—	1025
$\Xi(1530)^-\bar{\Xi}^+$	(7.0 ± 1.2) $\times 10^{-6}$	—	1165
$\Xi(1690)^-\bar{\Xi}^+ \rightarrow K^-\Lambda\bar{\Xi}^+ + c.c.$	(5.2 ± 1.6) $\times 10^{-6}$	—	—
$\Xi(1820)^-\bar{\Xi}^+ \rightarrow K^-\Lambda\bar{\Xi}^+ + c.c.$	(1.20 ± 0.32) $\times 10^{-5}$	—	—
$K^-\bar{\Sigma}^0\bar{\Xi}^+ + c.c.$	(3.7 ± 0.4) $\times 10^{-5}$	—	1060
$\Omega^-\bar{\Omega}^+$	(5.2 ± 0.4) $\times 10^{-5}$	—	774
$\pi^0 p\bar{p}$	(1.53 ± 0.07) $\times 10^{-4}$	—	1543
$N(940)\bar{p} + c.c. \rightarrow \pi^0 p\bar{p}$	(6.4 $\pm_{-1.3}^{+1.8}$ ) $\times 10^{-5}$	—	—
$N(1440)\bar{p} + c.c. \rightarrow \pi^0 p\bar{p}$	(7.3 $\pm_{-1.5}^{+1.7}$ ) $\times 10^{-5}$	$S=2.5$	—
$N(1520)\bar{p} + c.c. \rightarrow \pi^0 p\bar{p}$	(6.4 $\pm_{-1.8}^{+2.3}$ ) $\times 10^{-6}$	—	—
$N(1535)\bar{p} + c.c. \rightarrow \pi^0 p\bar{p}$	(2.5 ± 1.0) $\times 10^{-5}$	—	—
$N(1650)\bar{p} + c.c. \rightarrow \pi^0 p\bar{p}$	(3.8 $\pm_{-1.7}^{+1.4}$ ) $\times 10^{-5}$	—	—
$N(1720)\bar{p} + c.c. \rightarrow \pi^0 p\bar{p}$	(1.79 $\pm_{-0.70}^{+0.26}$ ) $\times 10^{-5}$	—	—
$N(2300)\bar{p} + c.c. \rightarrow \pi^0 p\bar{p}$	(2.6 $\pm_{-0.7}^{+1.2}$ ) $\times 10^{-5}$	—	—
$N(2570)\bar{p} + c.c. \rightarrow \pi^0 p\bar{p}$	(2.13 $\pm_{-0.31}^{+0.40}$ ) $\times 10^{-5}$	—	—
$\pi^0 f_0(2100) \rightarrow \pi^0 p\bar{p}$	(1.1 ± 0.4) $\times 10^{-5}$	—	—
$\eta p\bar{p}$	(6.0 ± 0.4) $\times 10^{-5}$	—	1373

$\eta f_0(2100) \rightarrow \eta p\bar{p}$	(1.2 ± 0.4) $\times 10^{-5}$	—	—
$N(1535)\bar{p} \rightarrow \eta p\bar{p}$	(4.4 ± 0.7) $\times 10^{-5}$	—	—
$\omega p\bar{p}$	(6.9 ± 2.1) $\times 10^{-5}$	—	1247
$\eta' p\bar{p}$	(1.10 ± 0.13) $\times 10^{-5}$	—	1141
$\phi p\bar{p}$	(6.1 ± 0.6) $\times 10^{-6}$	—	1109
$\phi X(1835) \rightarrow \phi p\bar{p}$	< 1.82 $\times 10^{-7}$	CL=90%	—
$\pi^+\pi^-\rho\bar{p}$	(6.0 ± 0.4) $\times 10^{-4}$	—	1491
$\rho\bar{n}\pi^-$ or c.c.	(2.48 ± 0.17) $\times 10^{-4}$	—	—
$\rho\bar{n}\pi^-\pi^0$	(3.2 ± 0.7) $\times 10^{-4}$	—	1492
$2(\pi^+\pi^-\pi^0)$	(4.8 ± 1.5) $\times 10^{-3}$	—	1776
$\eta\pi^+\pi^-$	< 1.6 $\times 10^{-4}$	CL=90%	1791
$\eta\pi^+\pi^-\pi^0$	(9.5 ± 1.7) $\times 10^{-4}$	—	1778
$2(\pi^+\pi^-\eta)$	(1.2 ± 0.6) $\times 10^{-3}$	—	1758
$\pi^+\pi^-\pi^0\pi^0\eta$	< 4 $\times 10^{-4}$	CL=90%	1760
$\eta'\pi^+\pi^-\pi^0$	(4.5 ± 2.1) $\times 10^{-4}$	—	1692
$\omega\pi^+\pi^-$	(7.3 ± 1.2) $\times 10^{-4}$	$S=2.1$	1748
$b_1^\pm\pi^\mp$	(4.0 ± 0.6) $\times 10^{-4}$	$S=1.1$	1635
$b_1^0\pi^0$	(2.4 ± 0.6) $\times 10^{-4}$	—	—
$\omega f_2(1270)$	(2.2 ± 0.4) $\times 10^{-4}$	—	1515
$\omega\pi^0\pi^0$	(1.11 ± 0.35) $\times 10^{-3}$	—	1749
$\pi^0\pi^0 K^+K^-$	(2.6 ± 1.3) $\times 10^{-4}$	—	1728
$\pi^+\pi^- K^+K^-$	(7.3 ± 0.5) $\times 10^{-4}$	—	1726
$\pi^0\pi^0 K_S^0 K_L^0$	(1.3 ± 0.6) $\times 10^{-3}$	—	1726
$\rho^0 K^+K^-$	(2.2 ± 0.4) $\times 10^{-4}$	—	1616
$K^*(892)^0 \bar{K}_2^*(1430)^0$	(1.9 ± 0.5) $\times 10^{-4}$	—	1417
$K^+K^-\pi^+\pi^-\eta$	(1.3 ± 0.7) $\times 10^{-3}$	—	1574
$K^+K^- 2(\pi^+\pi^-\pi^0)$	(1.00 ± 0.31) $\times 10^{-3}$	—	1611
$K^+K^- 2(\pi^+\pi^-)$	(1.9 ± 0.9) $\times 10^{-3}$	—	1654
$K_1^+(1270)^\pm K^\mp$	(1.00 ± 0.28) $\times 10^{-3}$	—	1588
$K_S^0 K_S^0 \pi^+\pi^-$	(2.2 ± 0.4) $\times 10^{-4}$	—	1724
$\rho^0 p\bar{p}$	(5.0 ± 2.2) $\times 10^{-5}$	—	1252
$K^+K^*(892)^0\pi^- + c.c.$	(6.7 ± 2.5) $\times 10^{-4}$	—	1674
$2(\pi^+\pi^-)$	(2.4 ± 0.6) $\times 10^{-4}$	$S=2.2$	1817
$\rho^0\pi^+\pi^-$	(2.2 ± 0.6) $\times 10^{-4}$	$S=1.4$	1750
$K^+K^-\pi^+\pi^-\pi^0$	(1.26 ± 0.09) $\times 10^{-3}$	—	1694
$\omega f_0(1710) \rightarrow \omega K^+K^-$	(5.9 ± 2.2) $\times 10^{-5}$	—	—
$K^*(892)^0 K^-\pi^+\pi^0 + c.c.$	(8.6 ± 2.2) $\times 10^{-4}$	—	—
$K^*(892)^+ K^-\pi^+\pi^- + c.c.$	(9.6 ± 2.8) $\times 10^{-4}$	—	—
$K^*(892)^+ K^-\rho^0 + c.c.$	(7.3 ± 2.6) $\times 10^{-4}$	—	—
$K^*(892)^0 K^-\rho^+ + c.c.$	(6.1 ± 1.8) $\times 10^{-4}$	—	—
$\eta K^+K^-, \text{ no } \eta\phi$	(3.1 ± 0.4) $\times 10^{-5}$	—	1664
$\omega K^+K^-$	(1.62 ± 0.11) $\times 10^{-4}$	$S=1.1$	1614
$\omega K^*(892)^+ K^- + c.c.$	(2.07 ± 0.26) $\times 10^{-4}$	—	1482
$\omega K_2^*(1430)^+ K^0 + c.c.$	(6.1 ± 1.2) $\times 10^{-5}$	—	1252
$\omega \bar{K}_2^*(892)^0 K^0$	(1.68 ± 0.30) $\times 10^{-4}$	—	1481
$\omega \bar{K}_2^*(1430)^0 K^0$	(5.8 ± 2.2) $\times 10^{-5}$	—	1250
$\omega X(1440) \rightarrow \omega K_S^0 K^-\pi^+ + c.c.$	(1.6 ± 0.4) $\times 10^{-5}$	—	—
$\omega X(1440) \rightarrow \omega K^+ K^-\pi^0$	(1.09 ± 0.26) $\times 10^{-5}$	—	—
$\omega f_1(1285) \rightarrow \omega K_S^0 K^-\pi^+ + c.c.$	(3.0 ± 1.0) $\times 10^{-6}$	—	—
$\omega f_1(1285) \rightarrow \omega K^+ K^-\pi^0$	(1.2 ± 0.7) $\times 10^{-6}$	—	—
$3(\pi^+\pi^-)$	(3.5 ± 2.0) $\times 10^{-4}$	$S=2.8$	1774
$p\bar{p}\pi^+\pi^-\pi^0$	(7.3 ± 0.7) $\times 10^{-4}$	—	1435
$K^+K^-$	(7.5 ± 0.5) $\times 10^{-5}$	—	1776
$K_S^0 K_L^0$	(5.34 ± 0.33) $\times 10^{-5}$	—	1775
$\pi^+\pi^-\pi^0$	(2.01 ± 0.17) $\times 10^{-4}$	$S=1.7$	1830
$\rho(2150)\pi \rightarrow \pi^+\pi^-\pi^0$	(1.9 $\pm_{-0.4}^{+1.2}$ ) $\times 10^{-4}$	—	—
$\rho(770)\pi \rightarrow \pi^+\pi^-\pi^0$	(3.2 ± 1.2) $\times 10^{-5}$	$S=1.8$	—
$\pi^+\pi^-$	(7.8 ± 2.6) $\times 10^{-6}$	—	1838
$K_1^+(1400)^\pm K^\mp$	< 3.1 $\times 10^{-4}$	CL=90%	1532
$K_2^*(1430)^\pm K^\mp$	(7.1 $\pm_{-0.9}^{+1.3}$ ) $\times 10^{-5}$	—	—
$K^+K^-\pi^0$	(4.07 ± 0.31) $\times 10^{-5}$	—	1754
$K_S^0 K_L^0 \pi^0$	< 3.0 $\times 10^{-4}$	CL=90%	1753
$K_S^0 K_L^0 \eta$	(1.3 ± 0.5) $\times 10^{-3}$	—	1661
$K^+K^*(892)^- + c.c.$	(2.9 ± 0.4) $\times 10^{-5}$	$S=1.2$	1698
$K^*(892)^0 \bar{K}^0 + c.c.$	(1.09 ± 0.20) $\times 10^{-4}$	—	1697
$\phi\pi^+\pi^-$	(1.18 ± 0.26) $\times 10^{-4}$	$S=1.5$	1690
$\phi f_0(980) \rightarrow \pi^+\pi^-$	(7.5 ± 3.3) $\times 10^{-5}$	$S=1.6$	—
$2(K^+K^-)$	(6.3 ± 1.3) $\times 10^{-5}$	—	1499
$\phi K^+K^-$	(7.0 ± 1.6) $\times 10^{-5}$	—	1546
$2(K^+K^-)\pi^0$	(1.10 ± 0.28) $\times 10^{-4}$	—	1440
$\phi\eta$	(3.10 ± 0.31) $\times 10^{-5}$	—	1654
$\eta\phi(2170), \phi(2170) \rightarrow$	< 2.2 $\times 10^{-6}$	CL=90%	—
$\phi f_0(980), f_0 \rightarrow \pi^+\pi^-$	(1.54 ± 0.20) $\times 10^{-5}$	—	1555

## Meson Summary Table

$\phi f_1(1285)$	$(3.0 \pm 1.3) \times 10^{-5}$	1436
$\phi\eta(1405) \rightarrow \phi\pi^+\pi^-\eta$	$(8.5 \pm 1.7) \times 10^{-6}$	-
$\omega\eta'$	$(3.2 \pm_{-2.1}^{2.5}) \times 10^{-5}$	1623
$\omega\pi^0$	$(2.1 \pm 0.6) \times 10^{-5}$	1757
$\rho\eta'$	$(1.9 \pm_{-1.2}^{1.7}) \times 10^{-5}$	1625
$\rho\eta$	$(2.2 \pm 0.6) \times 10^{-5}$	S=1.1 1717
$\omega\eta$	$< 1.1 \times 10^{-5}$	CL=90% 1715
$\phi\pi^0$	$< 4 \times 10^{-7}$	CL=90% 1699
$\eta_c\pi^+\pi^-\pi^0$	$< 1.0 \times 10^{-3}$	CL=90% 512
$\rho\bar{\rho}K^+K^-$	$(2.7 \pm 0.7) \times 10^{-5}$	1118
$\bar{\Lambda}nK_S^0$ + c.c.	$(8.1 \pm 1.8) \times 10^{-5}$	1324
$\phi f_2'(1525)$	$(4.4 \pm 1.6) \times 10^{-5}$	1325
$\Theta(1540)\bar{\Theta}(1540) \rightarrow K_S^0\rho K^-\bar{\pi}^+$ + c.c.	$< 8.8 \times 10^{-6}$	CL=90% -
$\Theta(1540)K^-\bar{\pi}^+ \rightarrow K_S^0\rho K^-\bar{\pi}^+$	$< 1.0 \times 10^{-5}$	CL=90% -
$\Theta(1540)K_S^0\bar{\rho} \rightarrow K_S^0\bar{\rho}K^+n$	$< 7.0 \times 10^{-6}$	CL=90% -
$\bar{\Theta}(1540)K^+n \rightarrow K_S^0\bar{\rho}K^+n$	$< 2.6 \times 10^{-5}$	CL=90% -
$\bar{\Theta}(1540)K_S^0\rho \rightarrow K_S^0\rho K^-\bar{\pi}^+$	$< 6.0 \times 10^{-6}$	CL=90% -
$K_S^0 K_S^0$	$< 4.6 \times 10^{-6}$	1775
$\Lambda_c^+\bar{\rho}e^+e^-$ + c.c.	$< 1.7 \times 10^{-6}$	CL=90% 830
<b>Radiative decays</b>		
$\gamma\chi_{c0}(1P)$	$(9.79 \pm 0.20) \%$	261
$\gamma\chi_{c1}(1P)$	$(9.75 \pm 0.24) \%$	171
$\gamma\chi_{c2}(1P)$	$(9.52 \pm 0.20) \%$	128
$\gamma\eta_c(1S)$	$(3.4 \pm 0.5) \times 10^{-3}$	S=1.3 635
$\gamma\eta_c(2S)$	$(7 \pm 5) \times 10^{-4}$	48
$\gamma\pi^0$	$(1.04 \pm 0.22) \times 10^{-6}$	S=1.4 1841
$\gamma\eta'(958)$	$(1.24 \pm 0.04) \times 10^{-4}$	1719
$\gamma f_2(1270)$	$(2.73 \pm_{-0.25}^{0.29}) \times 10^{-4}$	S=1.8 1622
$\gamma f_0(1370) \rightarrow \gamma K\bar{K}$	$(3.1 \pm 1.7) \times 10^{-5}$	1588
$\gamma f_0(1500)$	$(9.3 \pm 1.9) \times 10^{-5}$	1535
$\gamma f_2'(1525)$	$(3.3 \pm 0.8) \times 10^{-5}$	1531
$\gamma f_0(1710) \rightarrow \gamma\pi\pi$	$(3.5 \pm 0.6) \times 10^{-5}$	-
$\gamma f_0(1710) \rightarrow \gamma K\bar{K}$	$(6.6 \pm 0.7) \times 10^{-5}$	-
$\gamma f_0(2100) \rightarrow \gamma\pi\pi$	$(4.8 \pm 1.0) \times 10^{-6}$	1244
$\gamma f_0(2200) \rightarrow \gamma K\bar{K}$	$(3.2 \pm 1.0) \times 10^{-6}$	1193
$\gamma f_1(2220) \rightarrow \gamma\pi\pi$	$< 5.8 \times 10^{-6}$	CL=90% 1168
$\gamma f_2(2220) \rightarrow \gamma\pi\pi$	$< 9.5 \times 10^{-6}$	CL=90% 1168
$\gamma f_2(2220) \rightarrow \gamma K\bar{K}$	$< 1.5 \times 10^{-4}$	CL=90% 1843
$\gamma\gamma$	$(9.2 \pm 1.8) \times 10^{-7}$	1802
$\gamma\eta\pi^+\pi^-$	$(8.7 \pm 2.1) \times 10^{-4}$	1791
$\gamma\eta(1405) \rightarrow \gamma K\bar{K}\pi$	$< 9 \times 10^{-5}$	CL=90% 1569
$\gamma\eta(1405) \rightarrow \eta\pi^+\pi^-$	$(3.6 \pm 2.5) \times 10^{-5}$	-
$\gamma\eta(1405) \rightarrow \gamma f_0(980)\pi^0 \rightarrow \gamma\pi^+\pi^-\pi^0$	$< 5.0 \times 10^{-7}$	CL=90% -
$\gamma\eta(1475) \rightarrow K\bar{K}\pi$	$< 1.4 \times 10^{-4}$	CL=90% -
$\gamma\eta(1475) \rightarrow \eta\pi^+\pi^-$	$< 8.8 \times 10^{-5}$	CL=90% -
$\gamma 2(\pi^+\pi^-)$	$(4.0 \pm 0.6) \times 10^{-4}$	1817
$\gamma K^{*0}K^+\pi^-$ + c.c.	$(3.7 \pm 0.9) \times 10^{-4}$	1674
$\gamma K^{*0}\bar{K}^{*0}$	$(2.4 \pm 0.7) \times 10^{-4}$	1613
$\gamma K_S^0K^+\pi^-$ + c.c.	$(2.6 \pm 0.5) \times 10^{-4}$	1753
$\gamma K^+K^-\pi^+\pi^-$	$(1.9 \pm 0.5) \times 10^{-4}$	1726
$\gamma\rho\bar{\rho}$	$(3.9 \pm 0.5) \times 10^{-5}$	S=2.0 1586
$\gamma f_2(1950) \rightarrow \gamma\rho\bar{\rho}$	$(1.20 \pm 0.22) \times 10^{-5}$	-
$\gamma f_2(2150) \rightarrow \gamma\rho\bar{\rho}$	$(7.2 \pm 1.8) \times 10^{-6}$	-
$\gamma X(1835) \rightarrow \gamma\rho\bar{\rho}$	$(4.6 \pm_{-4.0}^{1.8}) \times 10^{-6}$	-
$\gamma X \rightarrow \gamma\rho\bar{\rho}$	$[qqaa] < 2 \times 10^{-6}$	CL=90% -
$\gamma\pi^+\pi^-\rho\bar{\rho}$	$(2.8 \pm 1.4) \times 10^{-5}$	1491
$\gamma 2(\pi^+\pi^-)K^+K^-$	$< 2.2 \times 10^{-4}$	CL=90% 1654
$\gamma 3(\pi^+\pi^-)$	$< 1.7 \times 10^{-4}$	CL=90% 1774
$\gamma K^+K^-K^+K^-$	$< 4 \times 10^{-5}$	CL=90% 1499
$\gamma\gamma J/\psi$	$(3.1 \pm_{-1.2}^{1.0}) \times 10^{-4}$	542
$e^+e^-\eta'$	$(1.90 \pm 0.26) \times 10^{-6}$	1719
$e^+e^-\chi_{c0}(1P)$	$(1.06 \pm 0.24) \times 10^{-3}$	261
$e^+e^-\chi_{c1}(1P)$	$(8.5 \pm 0.6) \times 10^{-4}$	171
$e^+e^-\chi_{c2}(1P)$	$(7.0 \pm 0.8) \times 10^{-4}$	128
<b>Weak decays</b>		
$D^0e^+e^-$ + c.c.	$< 1.4 \times 10^{-7}$	CL=90% 1371
<b>Other decays</b>		
invisible	$< 1.6 \%$	CL=90% -

 **$\psi(3770)$** 

$$J^G(J^{PC}) = 0^-(1^{--})$$

Mass  $m = 3773.7 \pm 0.4$  MeV (S = 1.4)Full width  $\Gamma = 27.2 \pm 1.0$  MeV $\Gamma_{ee} = 0.262 \pm 0.018$  keV (S = 1.4)

In addition to the dominant decay mode to  $D\bar{D}$ ,  $\psi(3770)$  was found to decay into the final states containing the  $J/\psi$  (BAI 05, ADAM 06). ADAMS 06 and HUANG 06A searched for various decay modes with light hadrons and found a statistically significant signal for the decay to  $\phi\eta$  only (ADAMS 06).

$\psi(3770)$ DECAY MODES	Fraction ( $\Gamma_i/\Gamma$ )	Scale factor/ Confidence level	$\rho$ (MeV/c)
$D\bar{D}$	$(93 \pm_{-9}^{+8}) \%$	S=2.0	287
$D^0\bar{D}^0$	$(52 \pm_{-5}^{+4}) \%$	S=2.0	287
$D^+D^-$	$(41 \pm 4) \%$	S=2.0	254
$J/\psi\pi^+\pi^-$	$(1.93 \pm 0.28) \times 10^{-3}$		561
$J/\psi\pi^0\pi^0$	$(8.0 \pm 3.0) \times 10^{-4}$		565
$J/\psi\eta$	$(9 \pm 4) \times 10^{-4}$		361
$J/\psi\pi^0$	$< 2.8 \times 10^{-4}$	CL=90%	604
$e^+e^-$	$(9.6 \pm 0.7) \times 10^{-6}$	S=1.3	1887
<b>Decays to light hadrons</b>			
$b_1(1235)\pi$	$< 1.4 \times 10^{-5}$	CL=90%	1684
$\phi\eta'$	$< 7 \times 10^{-4}$	CL=90%	1607
$\omega\eta'$	$< 4 \times 10^{-4}$	CL=90%	1672
$\rho^0\eta'$	$< 6 \times 10^{-4}$	CL=90%	1674
$\phi\eta$	$(3.1 \pm 0.7) \times 10^{-4}$		1703
$\omega\eta$	$< 1.4 \times 10^{-5}$	CL=90%	1762
$\rho^0\eta$	$< 5 \times 10^{-4}$	CL=90%	1764
$\phi\pi^0$	$< 3 \times 10^{-5}$	CL=90%	1746
$\omega\pi^0$	$< 6 \times 10^{-4}$	CL=90%	1803
$\pi^+\pi^-\pi^0$	$< 5 \times 10^{-6}$	CL=90%	1874
$\rho\pi$	$< 5 \times 10^{-6}$	CL=90%	1805
$K^*(892)^+K^-$ + c.c.	$< 1.4 \times 10^{-5}$	CL=90%	1745
$K^*(892)^0\bar{K}^0$ + c.c.	$< 1.2 \times 10^{-3}$	CL=90%	1745
$K_S^0 K_L^0$	$< 1.2 \times 10^{-5}$	CL=90%	1820
$2(\pi^+\pi^-)$	$< 1.12 \times 10^{-3}$	CL=90%	1861
$2(\pi^+\pi^-)\pi^0$	$< 1.06 \times 10^{-3}$	CL=90%	1844
$2(\pi^+\pi^-\pi^0)$	$< 5.85 \%$	CL=90%	1821
$\omega\pi^+\pi^-$	$< 6.0 \times 10^{-4}$	CL=90%	1794
$3(\pi^+\pi^-)$	$< 9.1 \times 10^{-3}$	CL=90%	1820
$3(\pi^+\pi^-)\pi^0$	$< 1.37 \%$	CL=90%	1792
$3(\pi^+\pi^-)2\pi^0$	$< 11.74 \%$	CL=90%	1760
$\eta\pi^+\pi^-$	$< 1.24 \times 10^{-3}$	CL=90%	1836
$\pi^+\pi^-2\pi^0$	$< 8.9 \times 10^{-3}$	CL=90%	1862
$\rho^0\pi^+\pi^-$	$< 6.9 \times 10^{-3}$	CL=90%	1796
$\eta 3\pi$	$< 1.34 \times 10^{-3}$	CL=90%	1824
$\eta 2(\pi^+\pi^-)$	$< 2.43 \%$	CL=90%	1804
$\eta\rho^0\pi^+\pi^-$	$< 1.45 \%$	CL=90%	1708
$\eta' 3\pi$	$< 2.44 \times 10^{-3}$	CL=90%	1741
$K^+K^-\pi^+\pi^-$	$< 9.0 \times 10^{-4}$	CL=90%	1773
$\phi\pi^+\pi^-$	$< 4.1 \times 10^{-4}$	CL=90%	1737
$K^+K^-2\pi^0$	$< 4.2 \times 10^{-3}$	CL=90%	1774
$4(\pi^+\pi^-)$	$< 1.67 \%$	CL=90%	1757
$4(\pi^+\pi^-)\pi^0$	$< 3.06 \%$	CL=90%	1720
$\phi f_0(980)$	$< 4.5 \times 10^{-4}$	CL=90%	1597
$K^+K^-\pi^+\pi^-\pi^0$	$< 2.36 \times 10^{-3}$	CL=90%	1741
$K^+K^-\rho^0\pi^0$	$< 8 \times 10^{-4}$	CL=90%	1624
$K^+K^-\rho^+\pi^-$	$< 1.46 \%$	CL=90%	1623
$\omega K^+K^-$	$< 3.4 \times 10^{-4}$	CL=90%	1664
$\phi\pi^+\pi^-\pi^0$	$< 3.8 \times 10^{-3}$	CL=90%	1723
$K^{*0}K^-\pi^+\pi^0$ + c.c.	$< 1.62 \%$	CL=90%	1694
$K^{*+}K^-\pi^+\pi^-$ + c.c.	$< 3.23 \%$	CL=90%	1693
$K^+K^-\pi^+\pi^-2\pi^0$	$< 2.67 \%$	CL=90%	1705
$K^+K^-2(\pi^+\pi^-)$	$< 1.03 \%$	CL=90%	1702
$K^+K^-2(\pi^+\pi^-)\pi^0$	$< 3.60 \%$	CL=90%	1661
$\eta K^+K^-$	$< 4.1 \times 10^{-4}$	CL=90%	1712
$\eta K^+K^-\pi^+\pi^-$	$< 1.24 \%$	CL=90%	1624
$\rho^0 K^+K^-$	$< 5.0 \times 10^{-3}$	CL=90%	1666
$2(K^+K^-)$	$< 6.0 \times 10^{-4}$	CL=90%	1552
$\phi K^+K^-$	$< 7.5 \times 10^{-4}$	CL=90%	1598
$2(K^+K^-)\pi^0$	$< 2.9 \times 10^{-4}$	CL=90%	1494
$2(K^+K^-)\pi^+\pi^-$	$< 3.2 \times 10^{-3}$	CL=90%	1426
$K_S^0 K^-\pi^+$	$< 3.2 \times 10^{-3}$	CL=90%	1799
$K_S^0 K^-\pi^+\pi^0$	$< 1.33 \%$	CL=90%	1773
$K_S^0 K^-\rho^+$	$< 6.6 \times 10^{-3}$	CL=90%	1665



## Meson Summary Table

$K_S^0 K^- 2\pi^+ \pi^-$	< 8.7	$\times 10^{-3}$	CL=90%	1740
$K_S^0 K^- \pi^+ \rho^0$	< 1.6	%	CL=90%	1621
$K_S^0 K^- \pi^+ \eta$	< 1.3	%	CL=90%	1670
$K_S^0 K^- 2\pi^+ \pi^- \pi^0$	< 4.18	%	CL=90%	1703
$K_S^0 K^- 2\pi^+ \pi^- \eta$	< 4.8	%	CL=90%	1570
$K_S^0 K^- \pi^+ 2(\pi^+ \pi^-)$	< 1.22	%	CL=90%	1658
$K_S^0 K^- \pi^+ 2\pi^0$	< 2.65	%	CL=90%	1742
$K_S^0 K^- K^+ K^- \pi^+$	< 4.9	$\times 10^{-3}$	CL=90%	1491
$K_S^0 K^- K^+ K^- \pi^+ \pi^0$	< 3.0	%	CL=90%	1427
$K_S^0 K^- K^+ K^- \pi^+ \eta$	< 2.2	%	CL=90%	1214
$K^{*0} K^- \pi^+ + c.c.$	< 9.7	$\times 10^{-3}$	CL=90%	1722
$\rho \bar{\rho} \pi^0$	< 4	$\times 10^{-5}$	CL=90%	1595
$\rho \bar{\rho} \pi^+ \pi^-$	< 5.8	$\times 10^{-4}$	CL=90%	1544
$\Lambda \bar{\Lambda}$	< 1.2	$\times 10^{-4}$	CL=90%	1522
$\rho \bar{\rho} \pi^+ \pi^- \pi^0$	< 1.85	$\times 10^{-3}$	CL=90%	1490
$\omega \rho \bar{\rho}$	< 2.9	$\times 10^{-4}$	CL=90%	1310
$\Lambda \bar{\Lambda} \pi^0$	< 7	$\times 10^{-5}$	CL=90%	1469
$\rho \bar{\rho} 2(\pi^+ \pi^-)$	< 2.6	$\times 10^{-3}$	CL=90%	1426
$\eta \rho \bar{\rho}$	< 5.4	$\times 10^{-4}$	CL=90%	1431
$\eta \rho \bar{\rho} \pi^+ \pi^-$	< 3.3	$\times 10^{-3}$	CL=90%	1284
$\rho^0 \rho \bar{\rho}$	< 1.7	$\times 10^{-3}$	CL=90%	1314
$\rho \bar{\rho} K^+ K^-$	< 3.2	$\times 10^{-4}$	CL=90%	1186
$\eta \rho \bar{\rho} K^+ K^-$	< 6.9	$\times 10^{-3}$	CL=90%	737
$\pi^0 \rho \bar{\rho} K^+ K^-$	< 1.2	$\times 10^{-3}$	CL=90%	1094
$\phi \rho \bar{\rho}$	< 1.3	$\times 10^{-4}$	CL=90%	1178
$\Lambda \bar{\Lambda} \pi^+ \pi^-$	< 2.5	$\times 10^{-4}$	CL=90%	1405
$\Lambda \bar{\rho} K^+$	< 2.8	$\times 10^{-4}$	CL=90%	1387
$\Lambda \bar{\rho} K^+ \pi^+ \pi^-$	< 6.3	$\times 10^{-4}$	CL=90%	1234
$\Lambda \bar{\Lambda} \eta$	< 1.9	$\times 10^{-4}$	CL=90%	1263
$\Sigma^+ \bar{\Sigma}^-$	< 1.0	$\times 10^{-4}$	CL=90%	1465
$\Sigma^0 \bar{\Sigma}^0$	< 4	$\times 10^{-5}$	CL=90%	1462
$\Xi^+ \bar{\Xi}^-$	< 1.5	$\times 10^{-4}$	CL=90%	1347
$\Xi^0 \bar{\Xi}^0$	< 1.4	$\times 10^{-4}$	CL=90%	1353

## Radiative decays

$\gamma \chi_{c2}$	< 6.4	$\times 10^{-4}$	CL=90%	211
$\gamma \chi_{c1}$	( 2.49 ± 0.23 ) $\times 10^{-3}$			254
$\gamma \chi_{c0}$	( 6.9 ± 0.6 ) $\times 10^{-3}$			342
$\gamma \eta_c$	< 7	$\times 10^{-4}$	CL=90%	707
$\gamma \eta_c(2S)$	< 9	$\times 10^{-4}$	CL=90%	134
$\gamma \eta'$	< 1.8	$\times 10^{-4}$	CL=90%	1765
$\gamma \eta$	< 1.5	$\times 10^{-4}$	CL=90%	1847
$\gamma \pi^0$	< 2	$\times 10^{-4}$	CL=90%	1884

 $\psi_2(3823)$ 

$$J^G(J^{PC}) = 0^-(2^- -)$$

$I, J, P$  need confirmation.

was  $\psi(3823)$ ,  $X(3823)$ Mass  $m = 3822.2 \pm 1.2$  MeVFull width  $\Gamma < 16$  MeV, CL = 90%

$\psi_2(3823)$ DECAY MODES	Fraction ( $\Gamma_i/\Gamma$ )	$\rho$ (MeV/c)
$\chi_{c1} \gamma$	seen	299
$\chi_{c2} \gamma$	not seen	257

 $\psi_3(3842)$ 

$$J^G(J^{PC}) = 0^-(3^- -)$$

$J, P$  need confirmation.

Mass  $m = 3842.71 \pm 0.20$  MeVFull width  $\Gamma = 2.8 \pm 0.6$  MeV

$\psi_3(3842)$ DECAY MODES	Fraction ( $\Gamma_i/\Gamma$ )	$\rho$ (MeV/c)
$D^+ D^-$	seen	443
$D^0 \bar{D}^0$	seen	463

 $\chi_{c1}(3872)$ 

$$J^G(J^{PC}) = 0^+(1^+ +)$$

also known as  $X(3872)$ Mass  $m = 3871.69 \pm 0.17$  MeV $m_{\chi_{c1}(3872)} - m_{J/\psi} = 775 \pm 4$  MeVFull width  $\Gamma < 1.2$  MeV, CL = 90%

$\chi_{c1}(3872)$ DECAY MODES	Fraction ( $\Gamma_i/\Gamma$ )	$\rho$ (MeV/c)
$\pi^+ \pi^- J/\psi(1S)$	> 3.2 %	650

$\omega J/\psi(1S)$	> 2.3 %	†
$D^0 \bar{D}^0 \pi^0$	>40 %	117
$\bar{D}^{*0} D^0$	>30 %	4
$\pi^0 \chi_{c1}$	> 2.8 %	319
$\gamma J/\psi$	> 7 $\times 10^{-3}$	697
$\gamma \psi(2S)$	> 4 %	181
$\pi^+ \pi^- \eta_c(1S)$	not seen	745
$\pi^+ \pi^- \chi_{c1}$	not seen	218
$\rho \bar{\rho}$	not seen	1693

 $Z_c(3900)$ 

$$J^G(J^{PC}) = 1^+(1^+ -)$$

was  $X(3900)$ Mass  $m = 3888.4 \pm 2.5$  MeV ( $S = 1.7$ )Full width  $\Gamma = 28.3 \pm 2.5$  MeV

$Z_c(3900)$ DECAY MODES	Fraction ( $\Gamma_i/\Gamma$ )	$\rho$ (MeV/c)
$J/\psi \pi$	seen	700
$h_c \pi^\pm$	not seen	319
$\eta_c \pi^\pm \pi^\mp$	not seen	760
$(D \bar{D}^*)^\pm$	seen	-
$D^0 D^{*-} + c.c.$	seen	160
$D^- D^{*0} + c.c.$	seen	152
$\omega \pi^\pm$	not seen	1863
$J/\psi \eta$	not seen	511
$D^+ D^{*-} + c.c.$	seen	-
$D^0 \bar{D}^{*0} + c.c.$	seen	-

 $X(3915)$ 

$$J^G(J^{PC}) = 0^+(0 \text{ or } 2^+ +)$$

was  $\chi_{c0}(3915)$ Mass  $m = 3918.4 \pm 1.9$  MeVFull width  $\Gamma = 20 \pm 5$  MeV ( $S = 1.1$ )

$X(3915)$ DECAY MODES	Fraction ( $\Gamma_i/\Gamma$ )	$\rho$ (MeV/c)
$\omega J/\psi$	seen	222
$\pi^+ \pi^- \eta_c(1S)$	not seen	785
$\eta_c \eta$	not seen	665
$\eta_c \pi^0$	not seen	814
$K \bar{K}$	not seen	1896
$\gamma \gamma$	seen	1959

 $\chi_{c2}(3930)$ 

$$J^G(J^{PC}) = 0^+(2^+ +)$$

Mass  $m = 3922.2 \pm 1.0$  MeV ( $S = 1.6$ )Full width  $\Gamma = 35.3 \pm 2.8$  MeV ( $S = 1.4$ )

$\chi_{c2}(3930)$ DECAY MODES	Fraction ( $\Gamma_i/\Gamma$ )	$\rho$ (MeV/c)
$\gamma \gamma$	seen	1961
$D \bar{D}$	seen	607
$D^+ D^-$	seen	592
$D^0 \bar{D}^0$	seen	607
$\pi^+ \pi^- \eta_c(1S)$	not seen	788
$K \bar{K}$	not seen	1898

 $X(4020)^\pm$ 

$$J^G(J^{PC}) = 1^+(?^- -)$$

Mass  $m = 4024.1 \pm 1.9$  MeVFull width  $\Gamma = 13 \pm 5$  MeV ( $S = 1.7$ )

$X(4020)^\pm$ DECAY MODES	Fraction ( $\Gamma_i/\Gamma$ )	$\rho$ (MeV/c)
$h_c(1P) \pi$	seen	450
$D^* \bar{D}^*$	seen	85
$D \bar{D}^* + c.c.$	not seen	542
$\eta_c \pi^+ \pi^-$	not seen	872
$J/\psi(1S) \pi^\pm$	not seen	811

 $\psi(4040)$  [rraa]

$$J^G(J^{PC}) = 0^-(1^- -)$$

Mass  $m = 4039 \pm 1$  MeVFull width  $\Gamma = 80 \pm 10$  MeV $\Gamma_{ee} = 0.86 \pm 0.07$  keV

## Meson Summary Table

Due to the complexity of the  $c\bar{c}$  threshold region, in this listing, "seen" ("not seen") means that a cross section for the mode in question has been measured at effective  $\sqrt{s}$  near this particle's central mass value, more (less) than  $2\sigma$  above zero, without regard to any peaking behavior in  $\sqrt{s}$  or absence thereof. See mode listing(s) for details and references.

$\psi(4040)$ DECAY MODES	Fraction ( $\Gamma_i/\Gamma$ )	Confidence level	$\rho$ (MeV/c)
$e^+e^-$	$(1.07 \pm 0.16) \times 10^{-5}$		2019
$D\bar{D}$	seen		775
$D^0\bar{D}^0$	seen		775
$D^+D^-$	seen		763
$D^*\bar{D}^+$ c.c.	seen		569
$D^*(2007)^0\bar{D}^0$ + c.c.	seen		575
$D^*(2010)^+D^-$ + c.c.	seen		561
$D^*\bar{D}^*$	seen		193
$D^*(2007)^0\bar{D}^*(2007)^0$	seen		226
$D^*(2010)^+D^*(2010)^-$	seen		193
$D^0D^-\pi^+$ + c.c. (excl. $D^*(2007)^0\bar{D}^0$ + c.c., $D^*(2010)^+D^-$ + c.c.)	not seen		-
$D\bar{D}^*\pi$ (excl. $D^*\bar{D}^*$ )	not seen		-
$D^0\bar{D}^{*-}\pi^+$ + c.c. (excl. $D^*(2010)^+D^*(2010)^-$ )	seen		-
$D_s^+D_s^-$	seen		452
$J/\psi\pi^+\pi^-$	$< 4 \times 10^{-3}$	90%	794
$J/\psi\pi^0\pi^0$	$< 2 \times 10^{-3}$	90%	797
$J/\psi\eta$	$(5.2 \pm 0.7) \times 10^{-3}$		675
$J/\psi\pi^0$	$< 2.8 \times 10^{-4}$	90%	823
$J/\psi\pi^+\pi^-\pi^0$	$< 2 \times 10^{-3}$	90%	746
$\chi_{c1}\gamma$	$< 3.4 \times 10^{-3}$	90%	494
$\chi_{c2}\gamma$	$< 5 \times 10^{-3}$	90%	454
$\chi_{c1}\pi^+\pi^-\pi^0$	$< 1.1 \%$	90%	306
$\chi_{c2}\pi^+\pi^-\pi^0$	$< 3.2 \%$	90%	233
$h_c(1P)\pi^+\pi^-$	$< 3 \times 10^{-3}$	90%	403
$\phi\pi^+\pi^-$	$< 3 \times 10^{-3}$	90%	1880
$\Lambda\bar{\Lambda}\pi^+\pi^-$	$< 2.9 \times 10^{-4}$	90%	1578
$\Lambda\bar{\Lambda}\pi^0$	$< 9 \times 10^{-5}$	90%	1636
$\Lambda\bar{\Lambda}\eta$	$< 3.0 \times 10^{-4}$	90%	1452
$\Sigma^+\bar{\Sigma}^-$	$< 1.3 \times 10^{-4}$	90%	1632
$\Sigma^0\bar{\Sigma}^0$	$< 7 \times 10^{-5}$	90%	1630
$\Xi^+\bar{\Xi}^-$	$< 1.6 \times 10^{-4}$	90%	1527
$\Xi^0\bar{\Xi}^0$	$< 1.8 \times 10^{-4}$	90%	1533

 **$\chi_{c1}(4140)$** 

$$I^G(J^{PC}) = 0^+(1^{++})$$

was  $X(4140)$ Mass  $m = 4146.8 \pm 2.4$  MeV ( $S = 1.1$ )Full width  $\Gamma = 22 \pm 7$  MeV ( $S = 1.3$ )

$\chi_{c1}(4140)$ DECAY MODES	Fraction ( $\Gamma_i/\Gamma$ )	$\rho$ (MeV/c)
$J/\psi\phi$	seen	217
$\gamma\gamma$	not seen	2073

 **$\psi(4160)$  [rraa]**

$$I^G(J^{PC}) = 0^-(1^{--})$$

Mass  $m = 4191 \pm 5$  MeVFull width  $\Gamma = 70 \pm 10$  MeV $\Gamma_{ee} = 0.48 \pm 0.22$  keV

Due to the complexity of the  $c\bar{c}$  threshold region, in this listing, "seen" ("not seen") means that a cross section for the mode in question has been measured at effective  $\sqrt{s}$  near this particle's central mass value, more (less) than  $2\sigma$  above zero, without regard to any peaking behavior in  $\sqrt{s}$  or absence thereof. See mode listing(s) for details and references.

$\psi(4160)$ DECAY MODES	Fraction ( $\Gamma_i/\Gamma$ )	Confidence level	$\rho$ (MeV/c)
$e^+e^-$	$(6.9 \pm 3.3) \times 10^{-6}$		2096
$\mu^+\mu^-$	seen		2093
$D\bar{D}$	seen		956
$D^0\bar{D}^0$	seen		956
$D^+D^-$	seen		947
$D^*\bar{D}^+$ c.c.	seen		798
$D^*(2007)^0\bar{D}^0$ + c.c.	seen		802
$D^*(2010)^+D^-$ + c.c.	seen		792
$D^*\bar{D}^*$	seen		592

$D^*(2007)^0\bar{D}^*(2007)^0$	seen		604
$D^*(2010)^+D^*(2010)^-$	seen		592
$D^0D^-\pi^+$ + c.c. (excl. $D^*(2007)^0\bar{D}^0$ + c.c., $D^*(2010)^+D^-$ + c.c.)	not seen		-
$D\bar{D}^*\pi$ + c.c. (excl. $D^*\bar{D}^*$ )	seen		-
$D^0D^{*-}\pi^+$ + c.c. (excl. $D^*(2010)^+D^*(2010)^-$ )	not seen		-
$D_s^+D_s^-$	not seen		719
$D_s^{*+}D_s^-$ + c.c.	seen		385
$J/\psi\pi^+\pi^-$	$< 3 \times 10^{-3}$	90%	919
$J/\psi\pi^0\pi^0$	$< 3 \times 10^{-3}$	90%	922
$J/\psi K^+K^-$	$< 2 \times 10^{-3}$	90%	407
$J/\psi\eta$	$< 8 \times 10^{-3}$	90%	822
$J/\psi\pi^0$	$< 1 \times 10^{-3}$	90%	944
$J/\psi\eta'$	$< 5 \times 10^{-3}$	90%	457
$J/\psi\pi^+\pi^-\pi^0$	$< 1 \times 10^{-3}$	90%	879
$\psi(2S)\pi^+\pi^-$	$< 4 \times 10^{-3}$	90%	396
$\chi_{c1}\gamma$	$< 5 \times 10^{-3}$	90%	625
$\chi_{c2}\gamma$	$< 1.3 \%$	90%	587
$\chi_{c1}\pi^+\pi^-\pi^0$	$< 2 \times 10^{-3}$	90%	496
$\chi_{c2}\pi^+\pi^-\pi^0$	$< 8 \times 10^{-3}$	90%	445
$h_c(1P)\pi^+\pi^-$	$< 5 \times 10^{-3}$	90%	556
$h_c(1P)\pi^0\pi^0$	$< 2 \times 10^{-3}$	90%	560
$h_c(1P)\eta$	$< 2 \times 10^{-3}$	90%	348
$h_c(1P)\pi^0$	$< 4 \times 10^{-4}$	90%	600
$\phi\pi^+\pi^-$	$< 2 \times 10^{-3}$	90%	1961
$\gamma\chi_{c1}(3872) \rightarrow \gamma J/\psi\pi^+\pi^-$	$< 6.8 \times 10^{-5}$	90%	-
$\gamma X(3915) \rightarrow \gamma J/\psi\pi^+\pi^-$	$< 1.36 \times 10^{-4}$	90%	-
$\gamma X(3930) \rightarrow \gamma J/\psi\pi^+\pi^-$	$< 1.18 \times 10^{-4}$	90%	-
$\gamma X(3940) \rightarrow \gamma J/\psi\pi^+\pi^-$	$< 1.47 \times 10^{-4}$	90%	-
$\gamma\chi_{c1}(3872) \rightarrow \gamma\gamma J/\psi$	$< 1.05 \times 10^{-4}$	90%	-
$\gamma X(3915) \rightarrow \gamma\gamma J/\psi$	$< 1.26 \times 10^{-4}$	90%	-
$\gamma X(3930) \rightarrow \gamma\gamma J/\psi$	$< 8.8 \times 10^{-5}$	90%	-
$\gamma X(3940) \rightarrow \gamma\gamma J/\psi$	$< 1.79 \times 10^{-4}$	90%	-

 **$\psi(4230)$** 

$$I^G(J^{PC}) = 0^-(1^{--})$$

also known as  $Y(4230)$ ; was  $X(4230)$ See also  $\psi(4260)$  entry in Particle Listings.Mass  $m = 4220 \pm 15$  MeVFull width  $\Gamma = 20$  to  $100$  MeV

$\psi(4230)$ DECAY MODES	Fraction ( $\Gamma_i/\Gamma$ )	$\rho$ (MeV/c)
$\omega\chi_{c0}$	seen	171
$\pi^+\pi^-h_c$	seen	583
$\pi^+\pi^-J/\psi$	seen	942
$\pi^+\pi^-\psi(2S)$	seen	426
$\pi^+D^0D^{*-}$ + c.c.	seen	650
$\gamma\chi_{c1}(3872)$	seen	334

 **$\chi_{c1}(4274)$** 

$$I^G(J^{PC}) = 0^+(1^{++})$$

was  $X(4274)$ Mass  $m = 4274 \pm 8$  MeVFull width  $\Gamma = 49 \pm 12$  MeV

$\chi_{c1}(4274)$ DECAY MODES	Fraction ( $\Gamma_i/\Gamma$ )	$\rho$ (MeV/c)
$J/\psi\phi$	seen	503

 **$\psi(4360)$** 

$$I^G(J^{PC}) = 0^-(1^{--})$$

also known as  $Y(4360)$ ; was  $X(4360)$ Mass  $m = 4368 \pm 13$  MeV ( $S = 3.7$ )Width  $\Gamma = 96 \pm 7$  MeV

$\psi(4360)$ DECAY MODES	Fraction ( $\Gamma_i/\Gamma$ )	$\rho$ (MeV/c)
$\psi(2S)\pi^+\pi^-$	seen	573
$\psi_2(3823)\pi^+\pi^-$	possibly seen	440
$D_1(2420)\bar{D}^+$ + c.c.	possibly seen	419

## Meson Summary Table

$\psi(4415)$ [rraa]	$J^{PC} = 0^-(1^{--})$			$\rho$ (MeV/c)
Mass $m = 4421 \pm 4$ MeV				
Full width $\Gamma = 62 \pm 20$ MeV				
$\Gamma_{ee} = 0.58 \pm 0.07$ keV				
Due to the complexity of the $c\bar{c}$ threshold region, in this listing, "seen" ("not seen") means that a cross section for the mode in question has been measured at effective $\sqrt{s}$ near this particle's central mass value, more (less) than $2\sigma$ above zero, without regard to any peaking behavior in $\sqrt{s}$ or absence thereof. See mode listing(s) for details and references.				
$\psi(4415)$ DECAY MODES	Fraction ( $\Gamma_i/\Gamma$ )	Confidence level		$\rho$ (MeV/c)
$D\bar{D}$	seen			1187
$D^0\bar{D}^0$	seen			1187
$D^+D^-$	seen			1179
$D^*\bar{D}^+$ c.c.	seen			1063
$D^*(2007)^0\bar{D}^0$ + c.c.	seen			1067
$D^*(2010)^+D^-$ + c.c.	seen			1059
$D^*\bar{D}^*$	seen			919
$D^*(2007)^0\bar{D}^*(2007)^0$ + c.c.	seen			927
$D^*(2010)^+D^*(2010)^-$ + c.c.	seen			919
$D^0D^-\pi^+$ (excl. $D^*(2007)^0\bar{D}^0$ )	< 2.3 %	90%		-
+c.c., $D^*(2010)^+D^-$ + c.c.				
$D\bar{D}_2^*(2460) \rightarrow D^0D^-\pi^+$ + c.c.	(10 $\pm$ 4) %			-
$D^0\bar{D}^*\pi^+$ + c.c.	< 11 %	90%		926
$D_1(2420)\bar{D}$ + c.c.	possibly seen			538
$D_s^+D_s^-$	not seen			1006
$\omega\chi_{c2}$	possibly seen			330
$D_s^{*+}D_s^-$ + c.c.	seen			-
$D_s^+D_s^{*-}$	not seen			652
$\psi_2(3823)\pi^+\pi^-$	possibly seen			494
$\psi(3770)\pi^+\pi^-$	possibly seen			541
$J/\psi\eta$	< 6 $\times 10^{-3}$	90%		1022
$\chi_{c1}\gamma$	< 8 $\times 10^{-4}$	90%		817
$\chi_{c2}\gamma$	< 4 $\times 10^{-3}$	90%		780
$e^+e^-$	(9.4 $\pm$ 3.2) $\times 10^{-6}$			2210

$Z_c(4430)$	$J^{PC} = 1^+(1^{+-})$			
was $X(4430)^\pm$	$G, C$ need confirmation.			
Quantum numbers not established.				
Mass $m = 4478^{+15}_{-18}$ MeV				
Full width $\Gamma = 181 \pm 31$ MeV				
$Z_c(4430)$ DECAY MODES	Fraction ( $\Gamma_i/\Gamma$ )			$\rho$ (MeV/c)
$\pi^+\psi(2S)$	seen			711
$\pi^+J/\psi$	seen			1162

$\psi(4660)$	$J^{PC} = 0^-(1^{--})$			
also known as $Y(4660)$ ; was $X(4660)$				
$\psi(4660)$ MASS = $4633 \pm 7$ MeV ( $S = 1.4$ )				
$\psi(4660)$ WIDTH = $64 \pm 9$ MeV				
$\psi(4660)$ DECAY MODES	Fraction ( $\Gamma_i/\Gamma$ )			$\rho$ (MeV/c)
$e^+e^-$	not seen			2316
$\psi(2S)\pi^+\pi^-$	seen			812
$J/\psi\eta$	not seen			1194
$D^0D^*\pi^+$	not seen			1156
$\chi_{c1}\gamma$	not seen			986
$\chi_{c2}\gamma$	not seen			952
$\Lambda_c^+\Lambda_c^-$	seen			371
$D_s^+D_{s1}(2536)^-$	seen			539

## $b\bar{b}$ MESONS

(including possibly non- $q\bar{q}$  states)

$\eta_b(1S)$	$J^{PC} = 0^+(0^{-+})$			
Mass $m = 9398.7 \pm 2.0$ MeV ( $S = 1.5$ )				
Full width $\Gamma = 10^{+5}_{-4}$ MeV				

$\eta_b(1S)$ DECAY MODES	Fraction ( $\Gamma_i/\Gamma$ )	Confidence level	$\rho$ (MeV/c)
hadrons	seen		-
$3h^+3h^-$	not seen		4672
$2h^+2h^-$	not seen		4689
$4h^+4h^-$	not seen		4648
$\gamma\gamma$	not seen		4699
$\mu^+\mu^-$	< $9 \times 10^{-3}$	90%	4698
$\tau^+\tau^-$	< 8 %	90%	4350

$T(1S)$	$J^{PC} = 0^-(1^{--})$			
Mass $m = 9460.30 \pm 0.26$ MeV ( $S = 3.3$ )				
Full width $\Gamma = 54.02 \pm 1.25$ keV				
$\Gamma_{ee} = 1.340 \pm 0.018$ keV				
$T(1S)$ DECAY MODES	Fraction ( $\Gamma_i/\Gamma$ )	Scale factor/Confidence level	$\rho$ (MeV/c)	
$\tau^+\tau^-$	(2.60 $\pm$ 0.10) %		4384	
$e^+e^-$	(2.38 $\pm$ 0.11) %		4730	
$\mu^+\mu^-$	(2.48 $\pm$ 0.05) %		4729	
<b>Hadronic decays</b>				
$ggg$	(81.7 $\pm$ 0.7) %		-	
$\gamma gg$	(2.2 $\pm$ 0.6) %		-	
$\eta'(958)$ anything	(2.94 $\pm$ 0.24) %		-	
$J/\psi(1S)$ anything	(5.4 $\pm$ 0.4) $\times 10^{-4}$	$S=1.4$	4223	
$J/\psi(1S)\eta_c$	< 2.2 $\times 10^{-6}$	CL=90%	3623	
$J/\psi(1S)\chi_{c0}$	< 3.4 $\times 10^{-6}$	CL=90%	3429	
$J/\psi(1S)\chi_{c1}$	(3.9 $\pm$ 1.2) $\times 10^{-6}$		3382	
$J/\psi(1S)\chi_{c2}$	< 1.4 $\times 10^{-6}$	CL=90%	3359	
$J/\psi(1S)\eta_c(2S)$	< 2.2 $\times 10^{-6}$	CL=90%	3317	
$J/\psi(1S)X(3940)$	< 5.4 $\times 10^{-6}$	CL=90%	3148	
$J/\psi(1S)X(4160)$	< 5.4 $\times 10^{-6}$	CL=90%	3018	
$X(4350)$ anything, $X \rightarrow J/\psi(1S)\phi$	< 8.1 $\times 10^{-6}$	CL=90%	-	
$Z_c(3900)^\pm$ anything, $Z_c \rightarrow J/\psi(1S)\pi^\pm$	< 1.3 $\times 10^{-5}$	CL=90%	-	
$Z_c(4200)^\pm$ anything, $Z_c \rightarrow J/\psi(1S)\pi^\pm$	< 6.0 $\times 10^{-5}$	CL=90%	-	
$Z_c(4430)^\pm$ anything, $Z_c \rightarrow J/\psi(1S)\pi^\pm$	< 4.9 $\times 10^{-5}$	CL=90%	-	
$X_{cs}^\pm$ anything, $X \rightarrow J/\psi K^\pm$	< 5.7 $\times 10^{-6}$	CL=90%	-	
$\chi_{c1}(3872)$ anything, $\chi_{c1} \rightarrow J/\psi(1S)\pi^+\pi^-$	< 9.5 $\times 10^{-6}$	CL=90%	-	
$\psi(4260)$ anything, $\psi \rightarrow J/\psi(1S)\pi^+\pi^-$	< 3.8 $\times 10^{-5}$	CL=90%	-	
$\psi(4260)$ anything, $\psi \rightarrow J/\psi(1S)K^+K^-$	< 7.5 $\times 10^{-6}$	CL=90%	-	
$\chi_{c1}(4140)$ anything, $\chi_{c1} \rightarrow J/\psi(1S)\phi$	< 5.2 $\times 10^{-6}$	CL=90%	-	
$\chi_{c0}$ anything	< 4 $\times 10^{-3}$	CL=90%	-	
$\chi_{c1}$ anything	(1.90 $\pm$ 0.35) $\times 10^{-4}$		-	
$\chi_{c1}(1P)X_{tetra}$	< 3.78 $\times 10^{-5}$	CL=90%	-	
$\chi_{c2}$ anything	(2.8 $\pm$ 0.8) $\times 10^{-4}$		-	
$\psi(2S)$ anything	(1.23 $\pm$ 0.20) $\times 10^{-4}$		-	
$\psi(2S)\eta_c$	< 3.6 $\times 10^{-6}$	CL=90%	3345	
$\psi(2S)\chi_{c0}$	< 6.5 $\times 10^{-6}$	CL=90%	3124	
$\psi(2S)\chi_{c1}$	< 4.5 $\times 10^{-6}$	CL=90%	3070	
$\psi(2S)\chi_{c2}$	< 2.1 $\times 10^{-6}$	CL=90%	3043	
$\psi(2S)\eta_c(2S)$	< 3.2 $\times 10^{-6}$	CL=90%	2994	
$\psi(2S)X(3940)$	< 2.9 $\times 10^{-6}$	CL=90%	2797	
$\psi(2S)X(4160)$	< 2.9 $\times 10^{-6}$	CL=90%	2642	
$\psi(4260)$ anything, $\psi \rightarrow \psi(2S)\pi^+\pi^-$	< 7.9 $\times 10^{-5}$	CL=90%	-	
$\psi(4360)$ anything, $\psi \rightarrow \psi(2S)\pi^+\pi^-$	< 5.2 $\times 10^{-5}$	CL=90%	-	
$\psi(4660)$ anything, $\psi \rightarrow \psi(2S)\pi^+\pi^-$	< 2.2 $\times 10^{-5}$	CL=90%	-	
$X(4050)^\pm$ anything, $X \rightarrow \psi(2S)\pi^\pm$	< 8.8 $\times 10^{-5}$	CL=90%	-	
$Z_c(4430)^\pm$ anything, $Z_c \rightarrow \psi(2S)\pi^\pm$	< 6.7 $\times 10^{-5}$	CL=90%	-	
$Z_c(4200)^+Z_c(4200)^-$	< 2.23 $\times 10^{-5}$	CL=90%	-	
$Z_c(3900)^+Z_c(4200)^-$	< 8.1 $\times 10^{-6}$	CL=90%	-	
$Z_c(3900)^+Z_c(3900)^-$	< 1.8 $\times 10^{-6}$	CL=90%	-	

# Meson Summary Table

$X(4050)^+X(4050)^-$	$< 1.58$	$\times 10^{-5}$	CL=90%	-
$X(4250)^+X(4250)^-$	$< 2.66$	$\times 10^{-5}$	CL=90%	-
$X(4050)^\pm X(4250)^\mp$	$< 4.42$	$\times 10^{-5}$	CL=90%	-
$Z_c(4430)^+Z_c(4430)^-$	$< 2.03$	$\times 10^{-5}$	CL=90%	-
$X(4055)^\pm X(4055)^\mp$	$< 2.33$	$\times 10^{-5}$	CL=90%	-
$X(4055)^\pm Z_c(4430)^\mp$	$< 4.55$	$\times 10^{-5}$	CL=90%	-
$\rho\pi$	$< 3.68$	$\times 10^{-6}$	CL=90%	4697
$\omega\pi^0$	$< 3.90$	$\times 10^{-6}$	CL=90%	4697
$\pi^+\pi^-$	$< 5$	$\times 10^{-4}$	CL=90%	4728
$K^+K^-$	$< 5$	$\times 10^{-4}$	CL=90%	4704
$p\bar{p}$	$< 5$	$\times 10^{-4}$	CL=90%	4636
$\pi^+\pi^-\pi^0$	( 2.1 $\pm$ 0.8 )	$\times 10^{-6}$		4725
$\phi K^+K^-$	( 2.4 $\pm$ 0.5 )	$\times 10^{-6}$		4622
$\omega\pi^+\pi^-$	( 4.5 $\pm$ 1.0 )	$\times 10^{-6}$		4694
$K^*(892)^0 K^-\pi^+$ + c.c.	( 4.4 $\pm$ 0.8 )	$\times 10^{-6}$		4667
$\phi f_2'(1525)$	$< 1.63$	$\times 10^{-6}$	CL=90%	4551
$\omega f_2'(1270)$	$< 1.79$	$\times 10^{-6}$	CL=90%	4611
$\rho(770)a_2(1320)$	$< 2.24$	$\times 10^{-6}$	CL=90%	4605
$K^*(892)^0 K_2^*(1430)^0$ + c.c.	( 3.0 $\pm$ 0.8 )	$\times 10^{-6}$		4578
$K_1(1270)^\pm K^\mp$	$< 2.41$	$\times 10^{-6}$	CL=90%	4634
$K_1(1400)^\pm K^\mp$	( 1.0 $\pm$ 0.4 )	$\times 10^{-6}$		4613
$b_1(1235)^\pm\pi^\mp$	$< 1.25$	$\times 10^{-6}$	CL=90%	4649
$\pi^+\pi^-\pi^0\pi^0$	( 1.28 $\pm$ 0.30 )	$\times 10^{-5}$		4720
$K_S^0 K^+\pi^-$ + c.c.	( 1.6 $\pm$ 0.4 )	$\times 10^{-6}$		4696
$K^*(892)^0 \bar{K}^0$ + c.c.	( 2.9 $\pm$ 0.9 )	$\times 10^{-6}$		4675
$K^*(892)^- K^+$ + c.c.	$< 1.11$	$\times 10^{-6}$	CL=90%	4675
$f_1(1285)$ anything	( 4.6 $\pm$ 3.1 )	$\times 10^{-3}$		-
$D^*(2010)^\pm$ anything	( 2.52 $\pm$ 0.20 )	%		-
$f_1(1285)X_{tetra}$	$< 6.24$	$\times 10^{-5}$	CL=90%	-
${}^2H$ anything	( 2.85 $\pm$ 0.25 )	$\times 10^{-5}$		-
Sum of 100 exclusive modes	( 1.200 $\pm$ 0.017 )	%		-
<b>Radiative decays</b>				
$\gamma\pi^+\pi^-$	( 6.3 $\pm$ 1.8 )	$\times 10^{-5}$		4728
$\gamma\pi^0\pi^0$	( 1.7 $\pm$ 0.7 )	$\times 10^{-5}$		4728
$\gamma\pi\pi$ (S-wave)	( 4.6 $\pm$ 0.7 )	$\times 10^{-5}$		4728
$\gamma\pi^0\eta$	$< 2.4$	$\times 10^{-6}$	CL=90%	4713
$\gamma K^+K^-$	[ssaa] ( 1.14 $\pm$ 0.13 )	$\times 10^{-5}$		4704
$\gamma p\bar{p}$	[ttaa] $< 6$	$\times 10^{-6}$	CL=90%	4636
$\gamma 2h^+ 2h^-$	( 7.0 $\pm$ 1.5 )	$\times 10^{-4}$		4720
$\gamma 3h^+ 3h^-$	( 5.4 $\pm$ 2.0 )	$\times 10^{-4}$		4703
$\gamma 4h^+ 4h^-$	( 7.4 $\pm$ 3.5 )	$\times 10^{-4}$		4679
$\gamma\pi^+\pi^-K^+K^-$	( 2.9 $\pm$ 0.9 )	$\times 10^{-4}$		4686
$\gamma 2\pi^+ 2\pi^-$	( 2.5 $\pm$ 0.9 )	$\times 10^{-4}$		4720
$\gamma 3\pi^+ 3\pi^-$	( 2.5 $\pm$ 1.2 )	$\times 10^{-4}$		4703
$\gamma 2\pi^+ 2\pi^- K^+K^-$	( 2.4 $\pm$ 1.2 )	$\times 10^{-4}$		4658
$\gamma\pi^+\pi^-p\bar{p}$	( 1.5 $\pm$ 0.6 )	$\times 10^{-4}$		4604
$\gamma 2\pi^+ 2\pi^- p\bar{p}$	( 4 $\pm$ 6 )	$\times 10^{-5}$		4563
$\gamma 2K^+ 2K^-$	( 2.0 $\pm$ 2.0 )	$\times 10^{-5}$		4601
$\gamma\eta'(958)$	$< 1.9$	$\times 10^{-6}$	CL=90%	4682
$\gamma\eta$	$< 1.0$	$\times 10^{-6}$	CL=90%	4714
$\gamma f_0(980)$	$< 3$	$\times 10^{-5}$	CL=90%	4678
$\gamma f_2'(1525)$	( 2.9 $\pm$ 0.6 )	$\times 10^{-5}$		4608
$\gamma f_2'(1270)$	( 1.01 $\pm$ 0.06 )	$\times 10^{-4}$		4644
$\gamma\eta(1405)$	$< 8.2$	$\times 10^{-5}$	CL=90%	4625
$\gamma f_0(1500)$	$< 1.5$	$\times 10^{-5}$	CL=90%	4610
$\gamma f_0(1500) \rightarrow \gamma K^+ K^-$	( 1.0 $\pm$ 0.4 )	$\times 10^{-5}$		-
$\gamma f_0(1710)$	$< 2.6$	$\times 10^{-4}$	CL=90%	4577
$\gamma f_0(1710) \rightarrow \gamma K^+ K^-$	( 1.01 $\pm$ 0.32 )	$\times 10^{-5}$		-
$\gamma f_0(1710) \rightarrow \gamma\pi^+\pi^-$	( 5.3 $\pm$ 2.0 )	$\times 10^{-6}$		-
$\gamma f_0(1710) \rightarrow \gamma\pi^0\pi^0$	$< 1.4$	$\times 10^{-6}$	CL=90%	-
$\gamma f_0(1710) \rightarrow \gamma\eta\eta$	$< 1.8$	$\times 10^{-6}$	CL=90%	-
$\gamma f_4(2050)$	$< 5.3$	$\times 10^{-5}$	CL=90%	4515
$\gamma f_0(2200) \rightarrow \gamma K^+ K^-$	$< 2$	$\times 10^{-4}$	CL=90%	4475
$\gamma f_J(2220) \rightarrow \gamma K^+ K^-$	$< 8$	$\times 10^{-7}$	CL=90%	4469
$\gamma f_J(2220) \rightarrow \gamma\pi^+\pi^-$	$< 6$	$\times 10^{-7}$	CL=90%	-
$\gamma f_J(2220) \rightarrow \gamma p\bar{p}$	$< 1.1$	$\times 10^{-6}$	CL=90%	-
$\gamma\eta(2225) \rightarrow \gamma\phi\phi$	$< 3$	$\times 10^{-3}$	CL=90%	4469
$\gamma\eta_c(1S)$	$< 5.7$	$\times 10^{-5}$	CL=90%	4260
$\gamma\chi_{c0}$	$< 6.5$	$\times 10^{-4}$	CL=90%	4114
$\gamma\chi_{c1}$	$< 2.3$	$\times 10^{-5}$	CL=90%	4079
$\gamma\chi_{c2}$	$< 7.6$	$\times 10^{-6}$	CL=90%	4062
$\gamma\chi_{c1}(3872) \rightarrow \pi^+\pi^-J/\psi$	$< 1.6$	$\times 10^{-6}$	CL=90%	-
$\gamma\chi_{c1}(3872) \rightarrow \pi^+\pi^-\pi^0J/\psi$	$< 2.8$	$\times 10^{-6}$	CL=90%	-
$\gamma X(3915) \rightarrow \omega J/\psi$	$< 3.0$	$\times 10^{-6}$	CL=90%	-
$\gamma\chi_{c1}(4140) \rightarrow \phi J/\psi$	$< 2.2$	$\times 10^{-6}$	CL=90%	-
$\gamma X$	[uuaa] $< 4.5$	$\times 10^{-6}$	CL=90%	-

$\gamma X\bar{X}$ ( $m_X < 3.1$ GeV)	[waa] $< 1$	$\times 10^{-3}$	CL=90%	-
$\gamma X\bar{X}$ ( $m_X < 4.5$ GeV)	[xaa] $< 2.4$	$\times 10^{-4}$	CL=90%	-
$\gamma X \rightarrow \gamma + \geq 4$ prongs	[yaa] $< 1.78$	$\times 10^{-4}$	CL=95%	-
$\gamma a_1^0 \rightarrow \gamma\mu^+\mu^-$	[zzaa] $< 9$	$\times 10^{-6}$	CL=90%	-
$\gamma a_1^0 \rightarrow \gamma\tau^+\tau^-$	[ssaa] $< 1.30$	$\times 10^{-4}$	CL=90%	-
$\gamma a_1^0 \rightarrow \gamma gg$	[aabb] $< 1$	%	CL=90%	-
$\gamma a_1^0 \rightarrow \gamma s\bar{s}$	[aabb] $< 1$	$\times 10^{-3}$	CL=90%	-
<b>Lepton Family number (LF) violating modes</b>				
$\mu^\pm\tau^\mp$	LF $< 6.0$	$\times 10^{-6}$	CL=95%	4563
<b>Other decays</b>				
invisible	$< 3.0$	$\times 10^{-4}$	CL=90%	-

**$\chi_{b0}(1P)$**  <sup>[bbbb]</sup>  $I^G(J^{PC}) = 0^+(0^{++})$   
*J* needs confirmation.  
 Mass  $m = 9859.44 \pm 0.42 \pm 0.31$  MeV

$\chi_{b0}(1P)$ DECAY MODES	Fraction ( $\Gamma_i/\Gamma$ )	Confidence level	$\rho$ (MeV/c)
$\gamma T(1S)$	( 1.94 $\pm$ 0.27 ) %		391
$D^0 X$	$< 10.4$	%	90%
$\pi^+\pi^-K^+K^-\pi^0$	$< 1.6$	$\times 10^{-4}$	90%
$2\pi^+\pi^-K^-K_S^0$	$< 5$	$\times 10^{-5}$	90%
$2\pi^+\pi^-K^-K_S^0 2\pi^0$	$< 5$	$\times 10^{-4}$	90%
$2\pi^+ 2\pi^- 2\pi^0$	$< 2.1$	$\times 10^{-4}$	90%
$2\pi^+ 2\pi^- K^+K^-$	( 1.1 $\pm$ 0.6 )	$\times 10^{-4}$	4861
$2\pi^+ 2\pi^- K^+K^-\pi^0$	$< 2.7$	$\times 10^{-4}$	90%
$2\pi^+ 2\pi^- K^+K^- 2\pi^0$	$< 5$	$\times 10^{-4}$	90%
$3\pi^+ 2\pi^- K^-K_S^0\pi^0$	$< 1.6$	$\times 10^{-4}$	90%
$3\pi^+ 3\pi^-$	$< 8$	$\times 10^{-5}$	90%
$3\pi^+ 3\pi^- 2\pi^0$	$< 6$	$\times 10^{-4}$	90%
$3\pi^+ 3\pi^- K^+K^-$	( 2.4 $\pm$ 1.2 )	$\times 10^{-4}$	4827
$3\pi^+ 3\pi^- K^+K^-\pi^0$	$< 1.0$	$\times 10^{-3}$	90%
$4\pi^+ 4\pi^-$	$< 8$	$\times 10^{-5}$	90%
$4\pi^+ 4\pi^- 2\pi^0$	$< 2.1$	$\times 10^{-3}$	90%
$J/\psi J/\psi$	$< 7$	$\times 10^{-5}$	90%
$J/\psi\psi(2S)$	$< 1.2$	$\times 10^{-4}$	90%
$\psi(2S)\psi(2S)$	$< 3.1$	$\times 10^{-5}$	90%
$J/\psi(1S)$ anything	$< 2.3$	$\times 10^{-3}$	90%

**$\chi_{b1}(1P)$**  <sup>[bbbb]</sup>  $I^G(J^{PC}) = 0^+(1^{++})$   
*J* needs confirmation.  
 Mass  $m = 9892.78 \pm 0.26 \pm 0.31$  MeV

$\chi_{b1}(1P)$ DECAY MODES	Fraction ( $\Gamma_i/\Gamma$ )	Confidence level	$\rho$ (MeV/c)
$\gamma T(1S)$	( 35.2 $\pm$ 2.0 ) %		423
$D^0 X$	( 12.6 $\pm$ 2.2 ) %		-
$\pi^+\pi^-K^+K^-\pi^0$	( 2.0 $\pm$ 0.6 )	$\times 10^{-4}$	4892
$2\pi^+\pi^-K^-K_S^0$	( 1.3 $\pm$ 0.5 )	$\times 10^{-4}$	4892
$2\pi^+\pi^-K^-K_S^0 2\pi^0$	$< 6$	$\times 10^{-4}$	90%
$2\pi^+ 2\pi^- 2\pi^0$	( 8.0 $\pm$ 2.5 )	$\times 10^{-4}$	4921
$2\pi^+ 2\pi^- K^+K^-$	( 1.5 $\pm$ 0.5 )	$\times 10^{-4}$	4878
$2\pi^+ 2\pi^- K^+K^-\pi^0$	( 3.5 $\pm$ 1.2 )	$\times 10^{-4}$	4863
$2\pi^+ 2\pi^- K^+K^- 2\pi^0$	( 8.6 $\pm$ 3.2 )	$\times 10^{-4}$	4845
$3\pi^+ 2\pi^- K^-K_S^0\pi^0$	( 9.3 $\pm$ 3.3 )	$\times 10^{-4}$	4844
$3\pi^+ 3\pi^-$	( 1.9 $\pm$ 0.6 )	$\times 10^{-4}$	4921
$3\pi^+ 3\pi^- 2\pi^0$	( 1.7 $\pm$ 0.5 )	$\times 10^{-3}$	4898
$3\pi^+ 3\pi^- K^+K^-$	( 2.6 $\pm$ 0.8 )	$\times 10^{-4}$	4844
$3\pi^+ 3\pi^- K^+K^-\pi^0$	( 7.5 $\pm$ 2.6 )	$\times 10^{-4}$	4825
$4\pi^+ 4\pi^-$	( 2.6 $\pm$ 0.9 )	$\times 10^{-4}$	4897
$4\pi^+ 4\pi^- 2\pi^0$	( 1.4 $\pm$ 0.6 )	$\times 10^{-3}$	4867
$\omega$ anything	( 4.9 $\pm$ 1.4 ) %		-
$\omega X_{tetra}$	$< 4.44$	$\times 10^{-4}$	90%
$J/\psi J/\psi$	$< 2.7$	$\times 10^{-5}$	90%
$J/\psi\psi(2S)$	$< 1.7$	$\times 10^{-5}$	90%
$\psi(2S)\psi(2S)$	$< 6$	$\times 10^{-5}$	90%
$J/\psi(1S)$ anything	$< 1.1$	$\times 10^{-3}$	90%
$J/\psi(1S)X_{tetra}$	$< 2.27$	$\times 10^{-4}$	90%

**$h_b(1P)$**   $I^G(J^{PC}) = 0^-(1^{+-})$   
 Mass  $m = 9899.3 \pm 0.8$  MeV

## Meson Summary Table

$h_b(1P)$ DECAY MODES	Fraction ( $\Gamma_i/\Gamma$ )	$\rho$ (MeV/c)
$\eta_b(1S)\gamma$	$(52^{+6}_{-5})\%$	488

**$\chi_{b2}(1P)$  <sup>[bbbb]</sup>**  $I^G(J^{PC}) = 0^+(2^+ +)$   
 $J$  needs confirmation.

Mass  $m = 9912.21 \pm 0.26 \pm 0.31$  MeV

$\chi_{b2}(1P)$ DECAY MODES	Fraction ( $\Gamma_i/\Gamma$ )	Confidence level	$\rho$ (MeV/c)
$\gamma T(1S)$	$(18.0 \pm 1.0)\%$		442
$D^0 X$	$< 7.9\%$	90%	–
$\pi^+ \pi^- K^+ K^- \pi^0$	$(8 \pm 5) \times 10^{-5}$		4902
$2\pi^+ \pi^- K^- K^0_S \pi^0$	$< 1.0 \times 10^{-4}$	90%	4901
$2\pi^+ \pi^- K^- K^0_S 2\pi^0$	$(5.3 \pm 2.4) \times 10^{-4}$		4873
$2\pi^+ 2\pi^- 2\pi^0$	$(3.5 \pm 1.4) \times 10^{-4}$		4931
$2\pi^+ 2\pi^- K^+ K^-$	$(1.1 \pm 0.4) \times 10^{-4}$		4888
$2\pi^+ 2\pi^- K^+ K^- \pi^0$	$(2.1 \pm 0.9) \times 10^{-4}$		4872
$2\pi^+ 2\pi^- K^+ K^- 2\pi^0$	$(3.9 \pm 1.8) \times 10^{-4}$		4855
$3\pi^+ 2\pi^- K^- K^0_S \pi^0$	$< 5 \times 10^{-4}$	90%	4854
$3\pi^+ 3\pi^-$	$(7.0 \pm 3.1) \times 10^{-5}$		4931
$3\pi^+ 3\pi^- 2\pi^0$	$(1.0 \pm 0.4) \times 10^{-3}$		4908
$3\pi^+ 3\pi^- K^+ K^-$	$< 8 \times 10^{-5}$	90%	4854
$3\pi^+ 3\pi^- K^+ K^- \pi^0$	$(3.6 \pm 1.5) \times 10^{-4}$		4835
$4\pi^+ 4\pi^-$	$(8 \pm 4) \times 10^{-5}$		4907
$4\pi^+ 4\pi^- 2\pi^0$	$(1.8 \pm 0.7) \times 10^{-3}$		4877
$J/\psi J/\psi$	$< 4 \times 10^{-5}$	90%	3869
$J/\psi \psi(2S)$	$< 5 \times 10^{-5}$	90%	3608
$\psi(2S)\psi(2S)$	$< 1.6 \times 10^{-5}$	90%	3313
$J/\psi(1S)$ anything	$(1.5 \pm 0.4) \times 10^{-3}$		–

**$T(2S)$**   $I^G(J^{PC}) = 0^-(1^- -)$

Mass  $m = 10023.26 \pm 0.31$  MeV

$m_{T(3S)} - m_{T(2S)} = 331.50 \pm 0.13$  MeV

Full width  $\Gamma = 31.98 \pm 2.63$  keV

$\Gamma_{ee} = 0.612 \pm 0.011$  keV

$T(2S)$ DECAY MODES	Fraction ( $\Gamma_i/\Gamma$ )	Scale factor/ Confidence level	$\rho$ (MeV/c)
$T(1S)\pi^+\pi^-$	$(17.85 \pm 0.26)\%$		475
$T(1S)\pi^0\pi^0$	$(8.6 \pm 0.4)\%$		480
$\tau^+\tau^-$	$(2.00 \pm 0.21)\%$		4686
$\mu^+\mu^-$	$(1.93 \pm 0.17)\%$	S=2.2	5011
$e^+e^-$	$(1.91 \pm 0.16)\%$		5012
$T(1S)\pi^0$	$< 4 \times 10^{-5}$	CL=90%	531
$T(1S)\eta$	$(2.9 \pm 0.4) \times 10^{-4}$	S=2.0	126
$J/\psi(1S)$ anything	$< 6 \times 10^{-3}$	CL=90%	4533
$J/\psi(1S)\eta_c$	$< 5.4 \times 10^{-6}$	CL=90%	3984
$J/\psi(1S)\chi_{c0}$	$< 3.4 \times 10^{-6}$	CL=90%	3808
$J/\psi(1S)\chi_{c1}$	$< 1.2 \times 10^{-6}$	CL=90%	3765
$J/\psi(1S)\chi_{c2}$	$< 2.0 \times 10^{-6}$	CL=90%	3744
$J/\psi(1S)\eta_c(2S)$	$< 2.5 \times 10^{-6}$	CL=90%	3707
$J/\psi(1S)X(3940)$	$< 2.0 \times 10^{-6}$	CL=90%	3555
$J/\psi(1S)X(4160)$	$< 2.0 \times 10^{-6}$	CL=90%	3440
$\chi_{c1}$ anything	$(2.2 \pm 0.5) \times 10^{-4}$		–
$\chi_{c1}(1P)^0 X_{tetra}$	$< 3.67 \times 10^{-5}$	CL=90%	–
$\chi_{c2}$ anything	$(2.3 \pm 0.8) \times 10^{-4}$		–
$\psi(2S)\eta_c$	$< 5.1 \times 10^{-6}$	CL=90%	3732
$\psi(2S)\chi_{c0}$	$< 4.7 \times 10^{-6}$	CL=90%	3536
$\psi(2S)\chi_{c1}$	$< 2.5 \times 10^{-6}$	CL=90%	3488
$\psi(2S)\chi_{c2}$	$< 1.9 \times 10^{-6}$	CL=90%	3464
$\psi(2S)\eta_c(2S)$	$< 3.3 \times 10^{-6}$	CL=90%	3422
$\psi(2S)X(3940)$	$< 3.9 \times 10^{-6}$	CL=90%	3250
$\psi(2S)X(4160)$	$< 3.9 \times 10^{-6}$	CL=90%	3118
$Z_c(3900)^+ Z_c(3900)^-$	$< 1.0 \times 10^{-6}$	CL=90%	–
$Z_c(4200)^+ Z_c(4200)^-$	$< 1.67 \times 10^{-5}$	CL=90%	–
$Z_c(3900)^\pm Z_c(4200)^\mp$	$< 7.3 \times 10^{-6}$	CL=90%	–
$X(4050)^+ X(4050)^-$	$< 1.35 \times 10^{-5}$	CL=90%	–
$X(4250)^+ X(4250)^-$	$< 2.67 \times 10^{-5}$	CL=90%	–
$X(4050)^\pm X(4250)^\mp$	$< 2.72 \times 10^{-5}$	CL=90%	–
$Z_c(4430)^+ Z_c(4430)^-$	$< 2.03 \times 10^{-5}$	CL=90%	–
$X(4055)^\pm X(4055)^\mp$	$< 1.11 \times 10^{-5}$	CL=90%	–
$X(4055)^\pm Z_c(4430)^\mp$	$< 2.11 \times 10^{-5}$	CL=90%	–
${}^2H$ anything	$(2.78^{+0.30}_{-0.26}) \times 10^{-5}$	S=1.2	–

hadrons	$(94 \pm 11)\%$	–
$ggg$	$(58.8 \pm 1.2)\%$	–
$\gamma gg$	$(1.87 \pm 0.28)\%$	–
$\phi K^+ K^-$	$(1.6 \pm 0.4) \times 10^{-6}$	4910
$\omega \pi^+ \pi^-$	$< 2.58 \times 10^{-6}$	CL=90% 4977
$K^*(892)^0 K^- \pi^+ + c.c.$	$(2.3 \pm 0.7) \times 10^{-6}$	4952
$\phi f_2'(1525)$	$< 1.33 \times 10^{-6}$	CL=90% 4842
$\omega f_2'(1270)$	$< 5.7 \times 10^{-7}$	CL=90% 4899
$\rho(770) a_2(1320)$	$< 8.8 \times 10^{-7}$	CL=90% 4894
$K^*(892)^0 \bar{K}_2^*(1430)^0 + c.c.$	$(1.5 \pm 0.6) \times 10^{-6}$	4869
$K_1(1270)^\pm K^\mp$	$< 3.22 \times 10^{-6}$	CL=90% 4921
$K_1(1400)^\pm K^\mp$	$< 8.3 \times 10^{-7}$	CL=90% 4901
$b_1(1235)^\pm \pi^\mp$	$< 4.0 \times 10^{-7}$	CL=90% 4935
$\rho \pi$	$< 1.16 \times 10^{-6}$	CL=90% 4981
$\pi^+ \pi^- \pi^0$	$< 8.0 \times 10^{-7}$	CL=90% 5007
$\omega \pi^0$	$< 1.63 \times 10^{-6}$	CL=90% 4980
$\pi^+ \pi^- \pi^0 \pi^0$	$(1.30 \pm 0.28) \times 10^{-5}$	5002
$K_S^0 K^+ \pi^- + c.c.$	$(1.14 \pm 0.33) \times 10^{-6}$	4979
$K^*(892)^0 \bar{K}^0 + c.c.$	$< 4.22 \times 10^{-6}$	CL=90% 4959
$K^*(892)^- K^+ + c.c.$	$< 1.45 \times 10^{-6}$	CL=90% 4960
$f_1(1285)$ anything	$(2.2 \pm 1.6) \times 10^{-3}$	–
$f_1(1285) X_{tetra}$	$< 6.47 \times 10^{-5}$	CL=90% –
Sum of 100 exclusive modes	$(2.90 \pm 0.30) \times 10^{-3}$	–

## Radiative decays

$\gamma \chi_{b1}(1P)$	$(6.9 \pm 0.4)\%$	130
$\gamma \chi_{b2}(1P)$	$(7.15 \pm 0.35)\%$	110
$\gamma \chi_{b0}(1P)$	$(3.8 \pm 0.4)\%$	162
$\gamma f_0(1710)$	$< 5.9 \times 10^{-4}$	CL=90% 4867
$\gamma f_2'(1525)$	$< 5.3 \times 10^{-4}$	CL=90% 4897
$\gamma f_2'(1270)$	$< 2.41 \times 10^{-4}$	CL=90% 4930
$\gamma \eta_c(1S)$	$< 2.7 \times 10^{-5}$	CL=90% 4567
$\gamma \chi_{c0}$	$< 1.0 \times 10^{-4}$	CL=90% 4430
$\gamma \chi_{c1}$	$< 3.6 \times 10^{-6}$	CL=90% 4397
$\gamma \chi_{c2}$	$< 1.5 \times 10^{-5}$	CL=90% 4381
$\gamma \chi_{c1}(3872) \rightarrow \pi^+ \pi^- J/\psi$	$< 8 \times 10^{-7}$	CL=90% –
$\gamma \chi_{c1}(3872) \rightarrow \pi^+ \pi^- \pi^0 J/\psi$	$< 2.4 \times 10^{-6}$	CL=90% –
$\gamma X(3915) \rightarrow \omega J/\psi$	$< 2.8 \times 10^{-6}$	CL=90% –
$\gamma \chi_{c1}(4140) \rightarrow \phi J/\psi$	$< 1.2 \times 10^{-6}$	CL=90% –
$\gamma X(4350) \rightarrow \phi J/\psi$	$< 1.3 \times 10^{-6}$	CL=90% –
$\gamma \eta_b(1S)$	$(5.5^{+1.1}_{-0.9}) \times 10^{-4}$	S=1.2 605
$\gamma \eta_b(1S) \rightarrow \gamma$ Sum of 26 exclusive modes	$< 3.7 \times 10^{-6}$	CL=90% –
$\gamma X_{b\bar{b}} \rightarrow \gamma$ Sum of 26 exclusive modes	$< 4.9 \times 10^{-6}$	CL=90% –
$\gamma X \rightarrow \gamma + \geq 4$ prongs [ccbb]	$< 1.95 \times 10^{-4}$	CL=95% –
$\gamma A^0 \rightarrow \gamma$ hadrons	$< 8 \times 10^{-5}$	CL=90% –
$\gamma a_1^0 \rightarrow \gamma \mu^+ \mu^-$	$< 8.3 \times 10^{-6}$	CL=90% –

## Lepton Family number (LF) violating modes

$e^\pm \tau^\mp$	LF	$< 3.2 \times 10^{-6}$	CL=90% 4854
$\mu^\pm \tau^\mp$	LF	$< 3.3 \times 10^{-6}$	CL=90% 4854

**$T_2(1D)$**   $I^G(J^{PC}) = 0^-(2^- -)$

was  $T(1D)$

Mass  $m = 10163.7 \pm 1.4$  MeV (S = 1.7)

$T_2(1D)$ DECAY MODES	Fraction ( $\Gamma_i/\Gamma$ )	$\rho$ (MeV/c)
$\gamma \gamma T(1S)$	seen	679
$\gamma \chi_{bJ}(1P)$	seen	300
$\eta T(1S)$	not seen	426
$\pi^+ \pi^- T(1S)$	$(6.6 \pm 1.6) \times 10^{-3}$	623

**$\chi_{b0}(2P)$  <sup>[bbbb]</sup>**  $I^G(J^{PC}) = 0^+(0^+ +)$   
 $J$  needs confirmation.

Mass  $m = 10232.5 \pm 0.4 \pm 0.5$  MeV

$\chi_{b0}(2P)$ DECAY MODES	Fraction ( $\Gamma_i/\Gamma$ )	Confidence level	$\rho$ (MeV/c)
$\gamma T(2S)$	$(1.38 \pm 0.30)\%$		207
$\gamma T(1S)$	$(3.8 \pm 1.7) \times 10^{-3}$		743
$D^0 X$	$< 8.2\%$	90%	–
$\pi^+ \pi^- K^+ K^- \pi^0$	$< 3.4 \times 10^{-5}$	90%	5064
$2\pi^+ \pi^- K^- K^0_S \pi^0$	$< 5 \times 10^{-5}$	90%	5063
$2\pi^+ \pi^- K^- K^0_S 2\pi^0$	$< 2.2 \times 10^{-4}$	90%	5036

## Meson Summary Table

$2\pi^+ 2\pi^- 2\pi^0$	< 2.4	$\times 10^{-4}$	90%	5092
$2\pi^+ 2\pi^- K^+ K^-$	< 1.5	$\times 10^{-4}$	90%	5050
$2\pi^+ 2\pi^- K^+ K^- \pi^0$	< 2.2	$\times 10^{-4}$	90%	5035
$2\pi^+ 2\pi^- K^+ K^- 2\pi^0$	< 1.1	$\times 10^{-3}$	90%	5019
$3\pi^+ 2\pi^- K^- K_S^0 \pi^0$	< 7	$\times 10^{-4}$	90%	5018
$3\pi^+ 3\pi^-$	< 7	$\times 10^{-5}$	90%	5091
$3\pi^+ 3\pi^- 2\pi^0$	< 1.2	$\times 10^{-3}$	90%	5070
$3\pi^+ 3\pi^- K^+ K^-$	< 1.5	$\times 10^{-4}$	90%	5017
$3\pi^+ 3\pi^- K^+ K^- \pi^0$	< 7	$\times 10^{-4}$	90%	4999
$4\pi^+ 4\pi^-$	< 1.7	$\times 10^{-4}$	90%	5069
$4\pi^+ 4\pi^- 2\pi^0$	< 6	$\times 10^{-4}$	90%	5039

 **$\chi_{b1}(2P)$  <sup>[bbbb]</sup>**

$$J^G(J^{PC}) = 0^+(1^{++})$$

*J* needs confirmation.

$$\text{Mass } m = 10255.46 \pm 0.22 \pm 0.50 \text{ MeV}$$

$$m_{\chi_{b1}(2P)} - m_{\chi_{b0}(2P)} = 23.5 \pm 1.0 \text{ MeV}$$

$\chi_{b1}(2P)$ DECAY MODES	Fraction ( $\Gamma_i/\Gamma$ )	$\rho$ (MeV/c)
$\omega \mathcal{T}(1S)$	$(1.63^{+0.40}_{-0.34})\%$	135
$\gamma \mathcal{T}(2S)$	$(18.1 \pm 1.9)\%$	230
$\gamma \mathcal{T}(1S)$	$(9.9 \pm 1.0)\%$	764
$\pi\pi \chi_{b1}(1P)$	$(9.1 \pm 1.3) \times 10^{-3}$	238
$D^0 X$	$(8.8 \pm 1.7)\%$	—
$\pi^+ \pi^- K^+ K^- \pi^0$	$(3.1 \pm 1.0) \times 10^{-4}$	5075
$2\pi^+ \pi^- K^- K_S^0$	$(1.1 \pm 0.5) \times 10^{-4}$	5075
$2\pi^+ \pi^- K^- K_S^0 2\pi^0$	$(7.7 \pm 3.2) \times 10^{-4}$	5047
$2\pi^+ 2\pi^- 2\pi^0$	$(5.9 \pm 2.0) \times 10^{-4}$	5104
$2\pi^+ 2\pi^- K^+ K^-$	$(1.0 \pm 0.4) \times 10^{-5}$	5062
$2\pi^+ 2\pi^- K^+ K^- \pi^0$	$(5.5 \pm 1.8) \times 10^{-4}$	5047
$2\pi^+ 2\pi^- K^+ K^- 2\pi^0$	$(1.0 \pm 0.4) \times 10^{-4}$	5030
$3\pi^+ 2\pi^- K^- K_S^0 \pi^0$	$(6.7 \pm 2.6) \times 10^{-4}$	5029
$3\pi^+ 3\pi^-$	$(1.2 \pm 0.4) \times 10^{-4}$	5103
$3\pi^+ 3\pi^- 2\pi^0$	$(1.2 \pm 0.4) \times 10^{-3}$	5081
$3\pi^+ 3\pi^- K^+ K^-$	$(2.0 \pm 0.8) \times 10^{-4}$	5029
$3\pi^+ 3\pi^- K^+ K^- \pi^0$	$(6.1 \pm 2.2) \times 10^{-4}$	5011
$4\pi^+ 4\pi^-$	$(1.7 \pm 0.6) \times 10^{-4}$	5080
$4\pi^+ 4\pi^- 2\pi^0$	$(1.9 \pm 0.7) \times 10^{-3}$	5051

 **$\chi_{b2}(2P)$  <sup>[bbbb]</sup>**

$$J^G(J^{PC}) = 0^+(2^{++})$$

*J* needs confirmation.

$$\text{Mass } m = 10268.65 \pm 0.22 \pm 0.50 \text{ MeV}$$

$$m_{\chi_{b2}(2P)} - m_{\chi_{b1}(2P)} = 13.10 \pm 0.24 \text{ MeV}$$

$\chi_{b2}(2P)$ DECAY MODES	Fraction ( $\Gamma_i/\Gamma$ )	Confidence level	$\rho$ (MeV/c)	
$\omega \mathcal{T}(1S)$	$(1.10^{+0.34}_{-0.30})\%$		194	
$\gamma \mathcal{T}(2S)$	$(8.9 \pm 1.2)\%$		242	
$\gamma \mathcal{T}(1S)$	$(6.6 \pm 0.8)\%$		777	
$\pi\pi \chi_{b2}(1P)$	$(5.1 \pm 0.9) \times 10^{-3}$		229	
$D^0 X$	< 2.4	90%	—	
$\pi^+ \pi^- K^+ K^- \pi^0$	< 1.1	$\times 10^{-4}$	90%	5082
$2\pi^+ \pi^- K^- K_S^0$	< 9	$\times 10^{-5}$	90%	5082
$2\pi^+ \pi^- K^- K_S^0 2\pi^0$	< 7	$\times 10^{-4}$	90%	5054
$2\pi^+ 2\pi^- 2\pi^0$	$(3.9 \pm 1.6) \times 10^{-4}$		5110	
$2\pi^+ 2\pi^- K^+ K^-$	$(9 \pm 4) \times 10^{-5}$		5068	
$2\pi^+ 2\pi^- K^+ K^- \pi^0$	$(2.4 \pm 1.1) \times 10^{-4}$		5054	
$2\pi^+ 2\pi^- K^+ K^- 2\pi^0$	$(4.7 \pm 2.3) \times 10^{-4}$		5037	
$3\pi^+ 2\pi^- K^- K_S^0 \pi^0$	< 4	$\times 10^{-4}$	90%	5036
$3\pi^+ 3\pi^-$	$(9 \pm 4) \times 10^{-5}$		5110	
$3\pi^+ 3\pi^- 2\pi^0$	$(1.2 \pm 0.4) \times 10^{-3}$		5088	
$3\pi^+ 3\pi^- K^+ K^-$	$(1.4 \pm 0.7) \times 10^{-4}$		5036	
$3\pi^+ 3\pi^- K^+ K^- \pi^0$	$(4.2 \pm 1.7) \times 10^{-4}$		5017	
$4\pi^+ 4\pi^-$	$(9 \pm 5) \times 10^{-5}$		5087	
$4\pi^+ 4\pi^- 2\pi^0$	$(1.3 \pm 0.5) \times 10^{-3}$		5058	

 **$\Upsilon(3S)$** 

$$J^G(J^{PC}) = 0^-(1^{--})$$

$$\text{Mass } m = 10355.2 \pm 0.5 \text{ MeV}$$

$$m_{\Upsilon(3S)} - m_{\Upsilon(2S)} = 331.50 \pm 0.13 \text{ MeV}$$

$$\text{Full width } \Gamma = 20.32 \pm 1.85 \text{ keV}$$

$$\Gamma_{ee} = 0.443 \pm 0.008 \text{ keV}$$

 **$\Upsilon(3S)$  DECAY MODES**

	Fraction ( $\Gamma_i/\Gamma$ )	Scale factor/ Confidence level	$\rho$ (MeV/c)
$\Upsilon(2S)$ anything	$(10.6 \pm 0.8)\%$		296
$\Upsilon(2S) \pi^+ \pi^-$	$(2.82 \pm 0.18)\%$	S=1.6	177
$\Upsilon(2S) \pi^0 \pi^0$	$(1.85 \pm 0.14)\%$		190
$\Upsilon(2S) \gamma \gamma$	$(5.0 \pm 0.7)\%$		327
$\Upsilon(2S) \pi^0$	< 5.1	$\times 10^{-4}$ CL=90%	298
$\Upsilon(1S) \pi^+ \pi^-$	$(4.37 \pm 0.08)\%$		813
$\Upsilon(1S) \pi^0 \pi^0$	$(2.20 \pm 0.13)\%$		816
$\Upsilon(1S) \eta$	< 1	$\times 10^{-4}$ CL=90%	677
$\Upsilon(1S) \pi^0$	< 7	$\times 10^{-5}$ CL=90%	846
$h_b(1P) \pi^0$	< 1.2	$\times 10^{-3}$ CL=90%	426
$h_b(1P) \pi^0 \rightarrow \gamma \eta_b(1S) \pi^0$	$(4.3 \pm 1.4) \times 10^{-4}$		—
$h_b(1P) \pi^+ \pi^-$	< 1.2	$\times 10^{-4}$ CL=90%	353
$\tau^+ \tau^-$	$(2.29 \pm 0.30)\%$		4863
$\mu^+ \mu^-$	$(2.18 \pm 0.21)\%$	S=2.1	5177
$e^+ e^-$	$(2.18 \pm 0.20)\%$		5178
hadrons	$(93 \pm 12)\%$		—
$g\bar{g}g$	$(35.7 \pm 2.6)\%$		—
$\gamma\bar{g}g$	$(9.7 \pm 1.8) \times 10^{-3}$		—
${}^2H$ anything	$(2.33 \pm 0.33) \times 10^{-5}$		—

**Radiative decays**

$\gamma \chi_{b2}(2P)$	$(13.1 \pm 1.6)\%$	S=3.4	86
$\gamma \chi_{b1}(2P)$	$(12.6 \pm 1.2)\%$	S=2.4	99
$\gamma \chi_{b0}(2P)$	$(5.9 \pm 0.6)\%$	S=1.4	122
$\gamma \chi_{b2}(1P)$	$(10.0 \pm 1.0) \times 10^{-3}$	S=1.7	434
$\gamma \chi_{b1}(1P)$	$(9 \pm 5) \times 10^{-4}$	S=1.8	452
$\gamma \chi_{b0}(1P)$	$(2.7 \pm 0.4) \times 10^{-3}$		484
$\gamma \eta_b(2S)$	< 6.2	$\times 10^{-4}$ CL=90%	350
$\gamma \eta_b(1S)$	$(5.1 \pm 0.7) \times 10^{-4}$		912
$\gamma A^0 \rightarrow \gamma$ hadrons	< 8	$\times 10^{-5}$ CL=90%	—
$\gamma X \rightarrow \gamma + \geq 4$ prongs	[ <i>d</i> dbb] < 2.2	$\times 10^{-4}$ CL=95%	—
$\gamma a_1^0 \rightarrow \gamma \mu^+ \mu^-$	< 5.5	$\times 10^{-6}$ CL=90%	—
$\gamma a_1^0 \rightarrow \gamma \tau^+ \tau^-$	[ <i>e</i> ebb] < 1.6	$\times 10^{-4}$ CL=90%	—

**Lepton Family number (LF) violating modes**

$e^\pm \tau^\mp$	LF	< 4.2	$\times 10^{-6}$ CL=90%	5025
$\mu^\pm \tau^\mp$	LF	< 3.1	$\times 10^{-6}$ CL=90%	5025

 **$\chi_{b1}(3P)$** 

$$J^G(J^{PC}) = 0^+(1^{++})$$

$$\text{Mass } m = 10513.4 \pm 0.7 \text{ MeV}$$

$\chi_{b1}(3P)$ DECAY MODES	Fraction ( $\Gamma_i/\Gamma$ )	$\rho$ (MeV/c)
$\Upsilon(1S) \gamma$	seen	1000
$\Upsilon(2S) \gamma$	seen	479
$\Upsilon(3S) \gamma$	seen	157

 **$\chi_{b2}(3P)$** 

$$J^G(J^{PC}) = 0^+(2^{++})$$

$$\text{Mass } m = 10524.0 \pm 0.8 \text{ MeV}$$

$\chi_{b2}(3P)$ DECAY MODES	Fraction ( $\Gamma_i/\Gamma$ )	$\rho$ (MeV/c)
$\Upsilon(3S) \gamma$	seen	167

 **$\Upsilon(4S)$** 

$$J^G(J^{PC}) = 0^-(1^{--})$$

also known as  $\Upsilon(10580)$

$$\text{Mass } m = 10579.4 \pm 1.2 \text{ MeV}$$

$$\text{Full width } \Gamma = 20.5 \pm 2.5 \text{ MeV}$$

$$\Gamma_{ee} = 0.272 \pm 0.029 \text{ keV} \quad (S = 1.5)$$

$\Upsilon(4S)$ DECAY MODES	Fraction ( $\Gamma_i/\Gamma$ )	Confidence level	$\rho$ (MeV/c)	
$B^+ \bar{B}^-$	> 96	%	95%	326
$B^+ B^-$	$(51.4 \pm 0.6)\%$		331	
$D^+ \text{ anything} + \text{ c.c.}$	$(17.8 \pm 2.6)\%$		—	
$B^0 \bar{B}^0$	$(48.6 \pm 0.6)\%$		326	
$J/\psi K_S^0 + (J/\psi, \eta_c) K_S^0$	< 4	$\times 10^{-7}$	90%	—
non- $B\bar{B}$	< 4	%	95%	—
$e^+ e^-$	$(1.57 \pm 0.08) \times 10^{-5}$		5290	
$\rho^+ \rho^-$	< 5.7	$\times 10^{-6}$	90%	5233

## Meson Summary Table

$K^*(892)^0 \bar{K}^0$	$< 2.0 \times 10^{-6}$	90%	5240
$J/\psi(1S)$ anything	$< 1.9 \times 10^{-4}$	95%	–
$D^{*+}$ anything + c.c.	$< 7.4$ %	90%	5099
$\phi$ anything	( 7.1 $\pm$ 0.6 ) %		5240
$\phi \eta$	$< 1.8 \times 10^{-6}$	90%	5226
$\phi \eta'$	$< 4.3 \times 10^{-6}$	90%	5196
$\rho \eta$	$< 1.3 \times 10^{-6}$	90%	5247
$\rho \eta'$	$< 2.5 \times 10^{-6}$	90%	5217
$\Upsilon(1S)$ anything	$< 4 \times 10^{-3}$	90%	1053
$\Upsilon(1S) \pi^+ \pi^-$	( 8.2 $\pm$ 0.4 ) $\times 10^{-5}$		1026
$\Upsilon(1S) \eta$	( 1.81 $\pm$ 0.18 ) $\times 10^{-4}$		924
$\Upsilon(1S) \eta'$	( 3.4 $\pm$ 0.9 ) $\times 10^{-5}$		–
$\Upsilon(2S) \pi^+ \pi^-$	( 8.2 $\pm$ 0.8 ) $\times 10^{-5}$		468
$h_b(1P) \pi^+ \pi^-$	not seen		600
$h_b(1P) \eta$	( 2.18 $\pm$ 0.21 ) $\times 10^{-3}$		390
${}^2H$ anything	$< 1.3 \times 10^{-5}$	90%	–

## Double Radiative Decays

$\gamma \gamma \Upsilon(D) \rightarrow \gamma \gamma \eta \Upsilon(1S)$	$< 2.3 \times 10^{-5}$	90%	–
---	------------------------	-----	---

**Z<sub>b</sub>(10610)**

$$I^G(J^{PC}) = 1^+(1^+ -)$$

was X(10610)

Mass  $m = 10607.2 \pm 2.0$  MeV  
 Full width  $\Gamma = 18.4 \pm 2.4$  MeV

<b>Z<sub>b</sub>(10610) DECAY MODES</b>	Fraction ( $\Gamma_i/\Gamma$ )	$p$ (MeV/c)
$\Upsilon(1S) \pi^+$	( 5.4 $\pm$ 1.9 $\pm$ 1.5 ) $\times 10^{-3}$	1077
$\Upsilon(1S) \pi^0$	not seen	1077
$\Upsilon(2S) \pi^+$	( 3.6 $\pm$ 1.1 $\pm$ 0.8 ) %	551
$\Upsilon(2S) \pi^0$	seen	552
$\Upsilon(3S) \pi^+$	( 2.1 $\pm$ 0.8 $\pm$ 0.6 ) %	207
$\Upsilon(3S) \pi^0$	seen	210
$h_b(1P) \pi^+$	( 3.5 $\pm$ 1.2 $\pm$ 0.9 ) %	671
$h_b(2P) \pi^+$	( 4.7 $\pm$ 1.7 $\pm$ 1.3 ) %	313
$B^+ \bar{B}^0$	not seen	505
$B^+ \bar{B}^{*0} + B^{*+} \bar{B}^0$	( 85.6 $\pm$ 2.1 $\pm$ 2.9 ) %	–

**Z<sub>b</sub>(10650)**

$$I^G(J^{PC}) = 1^+(1^+ -)$$

 $I, G, C$  need confirmation.was X(10650) $^\pm$ 

Mass  $m = 10652.2 \pm 1.5$  MeV  
 Full width  $\Gamma = 11.5 \pm 2.2$  MeV

 $Z_b(10650)^-$  decay modes are charge conjugates of the modes below.

<b>Z<sub>b</sub>(10650)<sup>+</sup> DECAY MODES</b>	Fraction ( $\Gamma_i/\Gamma$ )	$p$ (MeV/c)
$\Upsilon(1S) \pi^+$	( 1.7 $\pm$ 0.8 $\pm$ 0.6 ) $\times 10^{-3}$	1117
$\Upsilon(2S) \pi^+$	( 1.4 $\pm$ 0.6 $\pm$ 0.4 ) %	595
$\Upsilon(3S) \pi^+$	( 1.6 $\pm$ 0.7 $\pm$ 0.5 ) %	259
$h_b(1P) \pi^+$	( 8.4 $\pm$ 2.9 $\pm$ 2.4 ) %	714
$h_b(2P) \pi^+$	( 15 $\pm$ 4 ) %	360
$B^+ \bar{B}^0$	not seen	703
$B^+ \bar{B}^{*0} + B^{*+} \bar{B}^0$	not seen	–
$B^{*+} \bar{B}^{*0}$	( 74 $\pm$ 4 $\pm$ 6 ) %	122

 **$\Upsilon(10860)$** 

$$I^G(J^{PC}) = 0^-(1^- -)$$

Mass  $m = 10885.2 \pm 2.6 \pm 1.6$  MeV  
 Full width  $\Gamma = 37 \pm 4$  MeV  
 $\Gamma_{ee} = 0.31 \pm 0.07$  keV ( $S = 1.3$ )

<b><math>\Upsilon(10860)</math> DECAY MODES</b>	Fraction ( $\Gamma_i/\Gamma$ )	Confidence level	$p$ (MeV/c)
$B \bar{B} X$	( 76.2 $\pm$ 2.7 $\pm$ 4.0 ) %	–	–
$B \bar{B}$	( 5.5 $\pm$ 1.0 ) %	1322	–
$B \bar{B}^* +$ c.c.	( 13.7 $\pm$ 1.6 ) %	–	–
$B^* \bar{B}^*$	( 38.1 $\pm$ 3.4 ) %	1127	–

$B \bar{B}^{(*)} \pi$	$< 19.7$ %	90%	1015
$B \bar{B} \pi$	( 0.0 $\pm$ 1.2 ) %		1015
$B^* \bar{B} \pi + B \bar{B}^* \pi$	( 7.3 $\pm$ 2.3 ) %		–
$B^* \bar{B}^* \pi$	( 1.0 $\pm$ 1.4 ) %		739
$B \bar{B} \pi \pi$	$< 8.9$ %	90%	551
$B_s^{(*)} \bar{B}_s^{(*)}$	( 20.1 $\pm$ 3.1 ) %		905
$B_s \bar{B}_s$	( 5 $\pm$ 5 ) $\times 10^{-3}$		905
$B_s \bar{B}_s^* +$ c.c.	( 1.35 $\pm$ 0.32 ) %		–
$B_s^* \bar{B}_s^*$	( 17.6 $\pm$ 2.7 ) %		543
no open-bottom	( 3.8 $\pm$ 5.0 $\pm$ 0.5 ) %		–
$e^+ e^-$	( 8.3 $\pm$ 2.1 ) $\times 10^{-6}$		5443
$K^*(892)^0 \bar{K}^0$	$< 1.0 \times 10^{-5}$	90%	5395
$\Upsilon(1S) \pi^+ \pi^-$	( 5.3 $\pm$ 0.6 ) $\times 10^{-3}$		1306
$\Upsilon(2S) \pi^+ \pi^-$	( 7.8 $\pm$ 1.3 ) $\times 10^{-3}$		783
$\Upsilon(3S) \pi^+ \pi^-$	( 4.8 $\pm$ 1.9 $\pm$ 1.7 ) $\times 10^{-3}$		440
$\Upsilon(1S) K^+ K^-$	( 6.1 $\pm$ 1.8 ) $\times 10^{-4}$		959
$\eta \Upsilon_J(1D)$	( 4.8 $\pm$ 1.1 ) $\times 10^{-3}$		–
$h_b(1P) \pi^+ \pi^-$	( 3.5 $\pm$ 1.0 $\pm$ 1.3 ) $\times 10^{-3}$		903
$h_b(2P) \pi^+ \pi^-$	( 5.7 $\pm$ 1.7 $\pm$ 2.1 ) $\times 10^{-3}$		544
$\chi_{bJ}(1P) \pi^+ \pi^- \pi^0$	( 2.5 $\pm$ 2.3 ) $\times 10^{-3}$		894
$\chi_{b0}(1P) \pi^+ \pi^- \pi^0$	$< 6.3 \times 10^{-3}$	90%	894
$\chi_{b0}(1P) \omega$	$< 3.9 \times 10^{-3}$	90%	631
$\chi_{b0}(1P) (\pi^+ \pi^- \pi^0)_{\text{non-}\omega}$	$< 4.8 \times 10^{-3}$	90%	–
$\chi_{b1}(1P) \pi^+ \pi^- \pi^0$	( 1.85 $\pm$ 0.33 ) $\times 10^{-3}$		861
$\chi_{b1}(1P) \omega$	( 1.57 $\pm$ 0.30 ) $\times 10^{-3}$		582
$\chi_{b1}(1P) (\pi^+ \pi^- \pi^0)_{\text{non-}\omega}$	( 5.2 $\pm$ 1.9 ) $\times 10^{-4}$		–
$\chi_{b2}(1P) \pi^+ \pi^- \pi^0$	( 1.17 $\pm$ 0.30 ) $\times 10^{-3}$		841
$\chi_{b2}(1P) \omega$	( 6.0 $\pm$ 2.7 ) $\times 10^{-4}$		552
$\chi_{b2}(1P) (\pi^+ \pi^- \pi^0)_{\text{non-}\omega}$	( 6 $\pm$ 4 ) $\times 10^{-4}$		–
$\gamma X_b \rightarrow \gamma \Upsilon(1S) \omega$	$< 3.8 \times 10^{-5}$	90%	–

## Inclusive Decays.

These decay modes are submodes of one or more of the decay modes above.

$\phi$ anything	( 13.8 $\pm$ 2.4 $\pm$ 1.7 ) %	–
$D^0$ anything + c.c.	( 108 $\pm$ 8 ) %	–
$D_s$ anything + c.c.	( 46 $\pm$ 6 ) %	–
$J/\psi$ anything	( 2.06 $\pm$ 0.21 ) %	–
$B^0$ anything + c.c.	( 77 $\pm$ 8 ) %	–
$B^+$ anything + c.c.	( 72 $\pm$ 6 ) %	–

 **$\Upsilon(11020)$** 

$$I^G(J^{PC}) = 0^-(1^- -)$$

Mass  $m = 11000 \pm 4$  MeV  
 Full width  $\Gamma = 24 \pm 8 \pm 6$  MeV  
 $\Gamma_{ee} = 0.130 \pm 0.030$  keV

<b><math>\Upsilon(11020)</math> DECAY MODES</b>	Fraction ( $\Gamma_i/\Gamma$ )	$p$ (MeV/c)
$e^+ e^-$	( 5.4 $\pm$ 1.9 $\pm$ 2.1 ) $\times 10^{-6}$	5500
$\chi_{bJ}(1P) \pi^+ \pi^- \pi^0$	( 9 $\pm$ 9 $\pm$ 8 ) $\times 10^{-3}$	1007
$\chi_{b1}(1P) \pi^+ \pi^- \pi^0$	seen	975
$\chi_{b2}(1P) \pi^+ \pi^- \pi^0$	seen	956

## NOTES

In this Summary Table:

When a quantity has “(S = ...)” to its right, the error on the quantity has been enlarged by the “scale factor” S, defined as  $S = \sqrt{\chi^2/(N-1)}$ , where N is the number of measurements used in calculating the quantity. We do this when  $S > 1$ , which often indicates that the measurements are inconsistent. When  $S > 1.25$ , we also show in the Particle Listings an ideogram of the measurements. For more about S, see the Introduction.

A decay momentum  $p$  is given for each decay mode. For a 2-body decay,  $p$  is the momentum of each decay product in the rest frame of the decaying particle. For a 3-or-more-body decay,  $p$  is the largest momentum any of the products can have in this frame.

- [a] See the review on “Form Factors for Radiative Pion and Kaon Decays” for definitions and details.
- [b] Measurements of  $\Gamma(e^+\nu_e)/\Gamma(\mu^+\nu_\mu)$  always include decays with  $\gamma$ 's, and measurements of  $\Gamma(e^+\nu_e\gamma)$  and  $\Gamma(\mu^+\nu_\mu\gamma)$  never include low-energy  $\gamma$ 's. Therefore, since no clean separation is possible, we consider the modes with  $\gamma$ 's to be subreactions of the modes without them, and let  $[\Gamma(e^+\nu_e) + \Gamma(\mu^+\nu_\mu)]/\Gamma_{\text{total}} = 100\%$ .
- [c] See the  $\pi^\pm$  Particle Listings for the energy limits used in this measurement; low-energy  $\gamma$ 's are not included.
- [d] Derived from an analysis of neutrino-oscillation experiments.
- [e] Astrophysical and cosmological arguments give limits of order  $10^{-13}$ .
- [f] Forbidden by angular momentum conservation.
- [g]  $C$  parity forbids this to occur as a single-photon process.
- [h] The  $\omega\rho$  interference is then due to  $\omega\rho$  mixing only, and is expected to be small. If  $e\mu$  universality holds,  $\Gamma(\rho^0 \rightarrow \mu^+\mu^-) = \Gamma(\rho^0 \rightarrow e^+e^-) \times 0.99785$ .
- [i] See the “Note on  $a_1(1260)$ ” in the  $a_1(1260)$  Particle Listings in PDG 06, Journal of Physics **G33** 1 (2006).
- [j] Our estimate. See the Particle Listings for details.
- [k] See the note on “Non- $q\bar{q}$  mesons” in the Particle Listings in PDG 06, Journal of Physics **G33** 1 (2006).
- [l] See also the  $\omega(1650)$ .
- [n] See also the  $\omega(1420)$ .
- [o] See the note in the  $K^\pm$  Particle Listings.
- [p] Neglecting photon channels. See, e.g., A. Pais and S.B. Treiman, Phys. Rev. **D12**, 2744 (1975).
- [q] The definition of the slope parameters of the  $K \rightarrow 3\pi$  Dalitz plot is as follows (see also “Note on Dalitz Plot Parameters for  $K \rightarrow 3\pi$  Decays” in the  $K^\pm$  Particle Listings):
- $$|M|^2 = 1 + g(s_3 - s_0)/m_{\pi^+}^2 + \dots$$
- [r] For more details and definitions of parameters see the Particle Listings.
- [s] See the  $K^\pm$  Particle Listings for the energy limits used in this measurement.
- [t] Most of this radiative mode, the low-momentum  $\gamma$  part, is also included in the parent mode listed without  $\gamma$ 's.
- [u] Structure-dependent part.
- [v] Direct-emission branching fraction.
- [x] Violates angular-momentum conservation.
- [y] Derived from measured values of  $\phi_{+-}$ ,  $|\eta|$ ,  $|m_{K_L^0} - m_{K_S^0}|$ , and  $\tau_{K_S^0}$ , as described in the introduction to “Tests of Conservation Laws.”
- [z] The  $CP$ -violation parameters are defined as follows (see also “Note on  $CP$  Violation in  $K_S \rightarrow 3\pi$ ” and “Note on  $CP$  Violation in  $K_L^0$  Decay” in the Particle Listings):
- $$\eta_{+-} = |\eta_{+-}|e^{i\phi_{+-}} = \frac{A(K_L^0 \rightarrow \pi^+\pi^-)}{A(K_S^0 \rightarrow \pi^+\pi^-)} = \epsilon + \epsilon'$$
- $$\eta_{00} = |\eta_{00}|e^{i\phi_{00}} = \frac{A(K_L^0 \rightarrow \pi^0\pi^0)}{A(K_S^0 \rightarrow \pi^0\pi^0)} = \epsilon - 2\epsilon'$$
- $$\delta = \frac{\Gamma(K_L^0 \rightarrow \pi^-\ell^+\nu) - \Gamma(K_L^0 \rightarrow \pi^+\ell^-\nu)}{\Gamma(K_L^0 \rightarrow \pi^-\ell^+\nu) + \Gamma(K_L^0 \rightarrow \pi^+\ell^-\nu)},$$
- $$\text{Im}(\eta_{+-0})^2 = \frac{\Gamma(K_S^0 \rightarrow \pi^+\pi^-\pi^0)^{CP \text{ viol.}}}{\Gamma(K_L^0 \rightarrow \pi^+\pi^-\pi^0)},$$
- $$\text{Im}(\eta_{000})^2 = \frac{\Gamma(K_S^0 \rightarrow \pi^0\pi^0\pi^0)}{\Gamma(K_L^0 \rightarrow \pi^0\pi^0\pi^0)}.$$
- where for the last two relations  $CPT$  is assumed valid, i.e.,  $\text{Re}(\eta_{+-0}) \simeq 0$  and  $\text{Re}(\eta_{000}) \simeq 0$ .
- [aa] See the  $K_S^0$  Particle Listings for the energy limits used in this measurement.
- [bb] The value is for the sum of the charge states or particle/antiparticle states indicated.
- [cc]  $\text{Re}(\epsilon'/\epsilon) = \epsilon'/\epsilon$  to a very good approximation provided the phases satisfy  $CPT$  invariance.
- [dd] This mode includes gammas from inner bremsstrahlung but not the direct emission mode  $K_L^0 \rightarrow \pi^+\pi^-\gamma(\text{DE})$ .
- [ee] See the  $K_L^0$  Particle Listings for the energy limits used in this measurement.
- [ff] Allowed by higher-order electroweak interactions.
- [gg] Violates  $CP$  in leading order. Test of direct  $CP$  violation since the indirect  $CP$ -violating and  $CP$ -conserving contributions are expected to be suppressed.
- [hh] See the “Note on  $f_0(1370)$ ” in the  $f_0(1370)$  Particle Listings and in the 1994 edition.
- [ii] See the note in the  $L(1770)$  Particle Listings in Reviews of Modern Physics **56** S1 (1984), p. S200. See also the “Note on  $K_2(1770)$  and the  $K_2(1820)$ ” in the  $K_2(1770)$  Particle Listings.
- [jj] See the “Note on  $K_2(1770)$  and the  $K_2(1820)$ ” in the  $K_2(1770)$  Particle Listings.
- [kk] This result applies to  $Z^0 \rightarrow c\bar{c}$  decays only. Here  $\ell^+$  is an average (not a sum) of  $e^+$  and  $\mu^+$  decays.
- [ll] See the Particle Listings for the (complicated) definition of this quantity.
- [nn] The branching fraction for this mode may differ from the sum of the submodes that contribute to it, due to interference effects. See the relevant papers in the Particle Listings.
- [oo] These subfractions of the  $K^-2\pi^+$  mode are uncertain: see the Particle Listings.
- [pp] Submodes of the  $D^+ \rightarrow K^-2\pi^+\pi^0$  and  $K_S^0 2\pi^+\pi^-$  modes were studied by ANJOS 92C and COFFMAN 92B, but with at most 142 events for the first mode and 229 for the second – not enough for precise results. With nothing new for 18 years, we refer to our 2008 edition, Physics Letters **B667** 1 (2008), for those results.
- [qq] The unseen decay modes of the resonances are included.
- [rr] This is *not* a test for the  $\Delta C=1$  weak neutral current, but leads to the  $\pi^+\ell^+\ell^-$  final state.
- [ss] This mode is not a useful test for a  $\Delta C=1$  weak neutral current because both quarks must change flavor in this decay.
- [tt] In the 2010 *Review*, the values for these quantities were given using a measure of the asymmetry that was inconsistent with the usual definition.
- [uu] This value is obtained by subtracting the branching fractions for 2-, 4- and 6-prongs from unity.
- [vv] This is the sum of our  $K^-2\pi^+\pi^-$ ,  $K^-2\pi^+\pi^-\pi^0$ ,  $\bar{K}^0 2\pi^+2\pi^-$ ,  $K^+2K^-\pi^+$ ,  $2\pi^+2\pi^-$ ,  $2\pi^+2\pi^-\pi^0$ ,  $K^+K^-\pi^+\pi^-$ , and  $K^+K^-\pi^+\pi^-\pi^0$ , branching fractions.
- [xx] This is the sum of our  $K^-3\pi^+2\pi^-$  and  $3\pi^+3\pi^-$  branching fractions.
- [yy] The branching fractions for the  $K^-e^+\nu_e$ ,  $K^*(892)^-e^+\nu_e$ ,  $\pi^-e^+\nu_e$ , and  $\rho^-e^+\nu_e$  modes add up to  $6.17 \pm 0.17\%$ .
- [zz] This is a doubly Cabibbo-suppressed mode.
- [aaa] Submodes of the  $D^0 \rightarrow K_S^0\pi^+\pi^-\pi^0$  mode with a  $K^*$  and/or  $\rho$  were studied by COFFMAN 92B, but with only 140 events. With nothing new for 18 years, we refer to our 2008 edition, Physics Letters **B667** 1 (2008), for those results.
- [bbb] This branching fraction includes all the decay modes of the resonance in the final state.
- [ccc] This limit is for either  $D^0$  or  $\bar{D}^0$  to  $p e^-$ .
- [ddd] This limit is for either  $D^0$  or  $\bar{D}^0$  to  $\bar{p} e^+$ .
- [eee] This is the purely  $e^+$  semileptonic branching fraction: the  $e^+$  fraction from  $\tau^+$  decays has been subtracted off. The sum of our (non- $\tau$ )  $e^+$  exclusive fractions — an  $e^+\nu_e$  with an  $\eta$ ,  $\eta'$ ,  $\phi$ ,  $K^0$ , or  $K^{*0}$  — is  $5.99 \pm 0.31\%$ .
- [fff] This fraction includes  $\eta$  from  $\eta'$  decays.
- [ggg] The sum of our exclusive  $\eta'$  fractions —  $\eta'e^+\nu_e$ ,  $\eta'\mu^+\nu_\mu$ ,  $\eta'\pi^+$ ,  $\eta'\rho^+$ , and  $\eta'K^+$  — is  $11.8 \pm 1.6\%$ .
- [hhh] This branching fraction includes all the decay modes of the final-state resonance.
- [iii] A test for  $u\bar{u}$  or  $d\bar{d}$  content in the  $D_s^+$ . Neither Cabibbo-favored nor Cabibbo-suppressed decays can contribute, and  $\omega - \phi$  mixing is an unlikely explanation for any fraction above about  $2 \times 10^{-4}$ .
- [jjj] We decouple the  $D_s^+ \rightarrow \phi\pi^+$  branching fraction obtained from mass projections (and used to get some of the other branching fractions) from the  $D_s^+ \rightarrow \phi\pi^+$ ,  $\phi \rightarrow K^+K^-$  branching fraction obtained from the Dalitz-plot analysis of  $D_s^+ \rightarrow K^+K^-\pi^+$ . That is, the ratio of these two branching fractions is not exactly the  $\phi \rightarrow K^+K^-$  branching fraction 0.491.



# Meson Summary Table

- [kkk] This is the average of a model-independent and a  $K$ -matrix parametrization of the  $\pi^+\pi^-$   $S$ -wave and is a sum over several  $f_0$  mesons.
- [lll] An  $\ell$  indicates an  $e$  or a  $\mu$  mode, not a sum over these modes.
- [nnn] An  $CP(\pm 1)$  indicates the  $CP=+1$  and  $CP=-1$  eigenstates of the  $D^0$ - $\bar{D}^0$  system.
- [ooo]  $D$  denotes  $D^0$  or  $\bar{D}^0$ .
- [ppp]  $D_{CP+}^{*0}$  decays into  $D^0\pi^0$  with the  $D^0$  reconstructed in  $CP$ -even eigenstates  $K^+K^-$  and  $\pi^+\pi^-$ .
- [qqq]  $\bar{D}^{**}$  represents an excited state with mass  $2.2 < M < 2.8$  GeV/ $c^2$ .
- [rrr]  $\chi_{c1}(3872)^+$  is a hypothetical charged partner of the  $\chi_{c1}(3872)$ .
- [sss]  $\Theta(1710)^{++}$  is a possible narrow pentaquark state and  $G(2220)$  is a possible glueball resonance.
- [ttt]  $(\bar{\Lambda}_c^- p)_s$  denotes a low-mass enhancement near 3.35 GeV/ $c^2$ .
- [uuu] Stands for the possible candidates of  $K^*(1410)$ ,  $K_0^*(1430)$  and  $K_2^*(1430)$ .
- [vvv]  $B^0$  and  $B_s^0$  contributions not separated. Limit is on weighted average of the two decay rates.
- [xxx] This decay refers to the coherent sum of resonant and nonresonant  $J^P = 0^+$   $K\pi$  components with  $1.60 < m_{K\pi} < 2.15$  GeV/ $c^2$ .
- [yyy]  $X(214)$  is a hypothetical particle of mass 214 MeV/ $c^2$  reported by the HyperCP experiment, Physical Review Letters **94** 021801 (2005)
- [zzz]  $\Theta(1540)^+$  denotes a possible narrow pentaquark state.
- [aaa] Here  $S$  and  $P$  are the hypothetical scalar and pseudoscalar particles with masses of 2.5 GeV/ $c^2$  and 214.3 MeV/ $c^2$ , respectively.
- [bbaa] These values are model dependent.
- [ccaa] Here “anything” means at least one particle observed.
- [ddaa] This is a  $B(B^0 \rightarrow D^{*-} \ell^+ \nu_\ell)$  value.
- [eeaa]  $D^{**}$  stands for the sum of the  $D(1^1P_1)$ ,  $D(1^3P_0)$ ,  $D(1^3P_1)$ ,  $D(1^3P_2)$ ,  $D(2^1S_0)$ , and  $D(2^1S_1)$  resonances.
- [ffaa]  $D^{(*)}\bar{D}^{(*)}$  stands for the sum of  $D^*\bar{D}^*$ ,  $D^*\bar{D}$ ,  $D\bar{D}^*$ , and  $D\bar{D}$ .
- [ggaa]  $X(3915)$  denotes a near-threshold enhancement in the  $\omega J/\psi$  mass spectrum.
- [hhaa] Inclusive branching fractions have a multiplicity definition and can be greater than 100%.
- [iiaa]  $D_j$  represents an unresolved mixture of pseudoscalar and tensor  $D^{**}$  ( $P$ -wave) states.
- [jja] Not a pure measurement. See note at head of  $B_s^0$  Decay Modes.
- [kkaa] For  $E_\gamma > 100$  MeV.
- [laa] Includes  $p\bar{p}\pi^+\pi^-\gamma$  and excludes  $p\bar{p}\eta$ ,  $p\bar{p}\omega$ ,  $p\bar{p}\eta'$ .
- [naa] See the “Note on the  $\eta(1405)$ ” in the  $\eta(1405)$  Particle Listings.
- [oaa] For a narrow state  $A$  with mass less than 960 MeV.
- [ppa] For a narrow scalar or pseudoscalar  $A^0$  with mass 0.21–3.0 GeV.
- [qqa] For a narrow resonance in the range  $2.2 < M(X) < 2.8$  GeV.
- [raa]  $J^{PC}$  known by production in  $e^+e^-$  via single photon annihilation.  $I^G$  is not known; interpretation of this state as a single resonance is unclear because of the expectation of substantial threshold effects in this energy region.
- [ssa]  $2m_\tau < M(\tau^+\tau^-) < 9.2$  GeV
- [taa]  $2 \text{ GeV} < m_{K^+K^-} < 3$  GeV
- [uaa]  $X = \text{scalar with } m < 8.0$  GeV
- [vaa]  $X\bar{X} = \text{vectors with } m < 3.1$  GeV
- [xaa]  $X \text{ and } \bar{X} = \text{zero spin with } m < 4.5$  GeV
- [yaa]  $1.5 \text{ GeV} < m_X < 5.0$  GeV
- [zaa]  $201 \text{ MeV} < M(\mu^+\mu^-) < 3565$  MeV
- [aabb]  $0.5 \text{ GeV} < m_X < 9.0$  GeV, where  $m_X$  is the invariant mass of the hadronic final state.
- [bbbb] Spectroscopic labeling for these states is theoretical, pending experimental information.
- [ccb]  $1.5 \text{ GeV} < m_X < 5.0$  GeV
- [ddb]  $1.5 \text{ GeV} < m_X < 5.0$  GeV
- [eeb] For  $m_{\tau^+\tau^-}$  in the ranges 4.03–9.52 and 9.61–10.10 GeV.

Meson Summary Table

See also the table of suggested q-qbar quark-model assignments in the Quark Model section.

• Indicates particles that appear in the preceding Meson Summary Table. We do not regard the other entries as being established.

Table with 5 columns: LIGHT UNFLAVORED, STRANGE, CHARMED, STRANGE, and c-cbar continued. Each column lists various mesons with their quantum numbers (JPC) and specific mass values in parentheses. Includes sub-sections for BOTTOM, BOTTOM, STRANGE, and BOTTOM, CHARMED.

## Baryon Summary Table

This short table gives the name, the quantum numbers (where known), and the status of baryons in the Review. Only the baryons with 3- or 4-star status are included in the Baryon Summary Table. Due to insufficient data or uncertain interpretation, the other entries in the table are not established baryons. The names with masses are of baryons that decay strongly. The spin-parity  $J^P$  (when known) is given with each particle. For the strongly decaying particles, the  $J^P$  values are considered to be part of the names.

$p$	$1/2^+$	****	$\Delta(1232)$	$3/2^+$	****	$\Sigma^+$	$1/2^+$	****	$\Xi^0$	$1/2^+$	****	$\Xi_{cc}^{++}$	***	
$n$	$1/2^+$	****	$\Delta(1600)$	$3/2^+$	****	$\Sigma^0$	$1/2^+$	****	$\Xi^-$	$1/2^+$	****			
$N(1440)$	$1/2^+$	****	$\Delta(1620)$	$1/2^-$	****	$\Sigma^-$	$1/2^+$	****	$\Xi(1530)$	$3/2^+$	****	$\Lambda_b^0$	$1/2^+$	***
$N(1520)$	$3/2^-$	****	$\Delta(1700)$	$3/2^-$	****	$\Sigma(1385)$	$3/2^+$	****	$\Xi(1620)$	*		$\Lambda_b(5912)^0$	$1/2^-$	***
$N(1535)$	$1/2^-$	****	$\Delta(1750)$	$1/2^+$	*	$\Sigma(1580)$	$3/2^-$	*	$\Xi(1690)$	***		$\Lambda_b(5920)^0$	$3/2^-$	***
$N(1650)$	$1/2^-$	****	$\Delta(1900)$	$1/2^-$	***	$\Sigma(1620)$	$1/2^-$	*	$\Xi(1820)$	$3/2^-$	***	$\Lambda_b(6146)^0$	$3/2^+$	***
$N(1675)$	$5/2^-$	****	$\Delta(1905)$	$5/2^+$	****	$\Sigma(1660)$	$1/2^+$	***	$\Xi(1950)$	***		$\Lambda_b(6152)^0$	$5/2^+$	***
$N(1680)$	$5/2^+$	****	$\Delta(1910)$	$1/2^+$	****	$\Sigma(1670)$	$3/2^-$	****	$\Xi(2030)$	$\geq \frac{5}{2}?$	***	$\Sigma_b$	$1/2^+$	***
$N(1700)$	$3/2^-$	***	$\Delta(1920)$	$3/2^+$	***	$\Sigma(1750)$	$1/2^-$	***	$\Xi(2120)$	*		$\Sigma_b^*$	$3/2^+$	***
$N(1710)$	$1/2^+$	****	$\Delta(1930)$	$5/2^-$	***	$\Sigma(1775)$	$5/2^-$	****	$\Xi(2250)$	**		$\Sigma_b(6097)^+$	***	
$N(1720)$	$3/2^+$	****	$\Delta(1940)$	$3/2^-$	**	$\Sigma(1780)$	$3/2^+$	*	$\Xi(2370)$	**		$\Sigma_b(6097)^-$	***	
$N(1860)$	$5/2^+$	**	$\Delta(1950)$	$7/2^+$	****	$\Sigma(1880)$	$1/2^+$	**	$\Xi(2500)$	*		$\Xi_b^0, \Xi_b^-$	$1/2^+$	***
$N(1875)$	$3/2^-$	***	$\Delta(2000)$	$5/2^+$	**	$\Sigma(1900)$	$1/2^-$	**				$\Xi_b'(5935)^-$	$1/2^+$	***
$N(1880)$	$1/2^+$	***	$\Delta(2150)$	$1/2^-$	*	$\Sigma(1910)$	$3/2^-$	***	$\Omega^-$	$3/2^+$	****	$\Xi_b(5945)^0$	$3/2^+$	***
$N(1895)$	$1/2^-$	****	$\Delta(2200)$	$7/2^-$	***	$\Sigma(1915)$	$5/2^+$	****	$\Omega(2012)^-$	? <sup>-</sup>	***	$\Xi_b(5955)^-$	$3/2^+$	***
$N(1900)$	$3/2^+$	****	$\Delta(2300)$	$9/2^+$	**	$\Sigma(1940)$	$3/2^+$	*	$\Omega(2250)^-$	***		$\Xi_b(6227)$	***	
$N(1990)$	$7/2^+$	**	$\Delta(2350)$	$5/2^-$	*	$\Sigma(2010)$	$3/2^-$	*	$\Omega(2380)^-$	**		$\Omega_b^-$	$1/2^+$	***
$N(2000)$	$5/2^+$	**	$\Delta(2390)$	$7/2^+$	*	$\Sigma(2030)$	$7/2^+$	****	$\Omega(2470)^-$	**				
$N(2040)$	$3/2^+$	*	$\Delta(2400)$	$9/2^-$	**	$\Sigma(2070)$	$5/2^+$	*				$P_c(4312)^+$	*	
$N(2060)$	$5/2^-$	***	$\Delta(2420)$	$11/2^+$	****	$\Sigma(2080)$	$3/2^+$	*	$\Lambda_c^+$	$1/2^+$	****	$P_c(4380)^+$	*	
$N(2100)$	$1/2^+$	***	$\Delta(2750)$	$13/2^-$	**	$\Sigma(2100)$	$7/2^-$	*	$\Lambda_c(2595)^+$	$1/2^-$	***	$P_c(4440)^+$	*	
$N(2120)$	$3/2^-$	***	$\Delta(2950)$	$15/2^+$	**	$\Sigma(2160)$	$1/2^-$	*	$\Lambda_c(2625)^+$	$3/2^-$	***	$P_c(4457)^+$	*	
$N(2190)$	$7/2^-$	****				$\Sigma(2230)$	$3/2^+$	*	$\Lambda_c(2765)^+$	*				
$N(2220)$	$9/2^+$	****	$\Lambda$	$1/2^+$	****	$\Sigma(2250)$	***		$\Lambda_c(2860)^+$	$3/2^+$	***			
$N(2250)$	$9/2^-$	****	$\Lambda$	$1/2^-$	**	$\Sigma(2455)$	**		$\Lambda_c(2880)^+$	$5/2^+$	***			
$N(2300)$	$1/2^+$	**	$\Lambda(1405)$	$1/2^-$	****	$\Sigma(2620)$	**		$\Lambda_c(2940)^+$	$3/2^-$	***			
$N(2570)$	$5/2^-$	**	$\Lambda(1520)$	$3/2^-$	****	$\Sigma(3000)$	*		$\Sigma_c(2455)$	$1/2^+$	****			
$N(2600)$	$11/2^-$	***	$\Lambda(1600)$	$1/2^+$	****	$\Sigma(3170)$	*		$\Sigma_c(2520)$	$3/2^+$	***			
$N(2700)$	$13/2^+$	**	$\Lambda(1670)$	$1/2^-$	****				$\Sigma_c(2800)$	***				
			$\Lambda(1690)$	$3/2^-$	****				$\Xi_c^+$	$1/2^+$	***			
			$\Lambda(1710)$	$1/2^+$	*				$\Xi_c^0$	$1/2^+$	****			
			$\Lambda(1800)$	$1/2^-$	***				$\Xi_c^{'+}$	$1/2^+$	***			
			$\Lambda(1810)$	$1/2^+$	***				$\Xi_c^{'+0}$	$1/2^+$	***			
			$\Lambda(1820)$	$5/2^+$	****				$\Xi_c(2645)$	$3/2^+$	***			
			$\Lambda(1830)$	$5/2^-$	****				$\Xi_c(2790)$	$1/2^-$	***			
			$\Lambda(1890)$	$3/2^+$	****				$\Xi_c(2815)$	$3/2^-$	***			
			$\Lambda(2000)$	$1/2^-$	*				$\Xi_c(2930)$	**				
			$\Lambda(2050)$	$3/2^-$	*				$\Xi_c(2970)$	***				
			$\Lambda(2070)$	$3/2^+$	*				$\Xi_c(3055)$	***				
			$\Lambda(2080)$	$5/2^-$	*				$\Xi_c(3080)$	***				
			$\Lambda(2085)$	$7/2^+$	**				$\Xi_c(3123)$	*				
			$\Lambda(2100)$	$7/2^-$	****				$\Omega_c^0$	$1/2^+$	***			
			$\Lambda(2110)$	$5/2^+$	***				$\Omega_c(2770)^0$	$3/2^+$	***			
			$\Lambda(2325)$	$3/2^-$	*				$\Omega_c(3000)^0$	***				
			$\Lambda(2350)$	$9/2^+$	***				$\Omega_c(3050)^0$	***				
			$\Lambda(2585)$	**					$\Omega_c(3065)^0$	***				
									$\Omega_c(3090)^0$	***				
									$\Omega_c(3120)^0$	***				

\*\*\*\* Existence is certain, and properties are at least fairly well explored.

\*\*\* Existence ranges from very likely to certain, but further confirmation is desirable and/or quantum numbers, branching fractions, etc. are not well determined.

\*\* Evidence of existence is only fair.

\* Evidence of existence is poor.

# Baryon Summary Table

**N BARYONS**  
**(S = 0, I = 1/2)**  
*p, N<sup>+</sup> = uud; n, N<sup>0</sup> = udd*

**p**  $I(J^P) = \frac{1}{2}(\frac{1}{2}^+)$

Mass  $m = 1.00727646662 \pm 0.00000000009$  u (S = 3.1)  
 Mass  $m = 938.272081 \pm 0.000006$  MeV [a]  
 $|m_p - m_{\bar{p}}|/m_p < 7 \times 10^{-10}$ , CL = 90% [b]  
 $|\frac{q_{\bar{p}}}{m_{\bar{p}}}|/(\frac{q_p}{m_p}) = 1.00000000000 \pm 0.00000000007$   
 $|q_p + q_{\bar{p}}|/e < 7 \times 10^{-10}$ , CL = 90% [b]  
 $|q_p + q_e|/e < 1 \times 10^{-21}$  [c]  
 Magnetic moment  $\mu = 2.7928473446 \pm 0.0000000008$   $\mu_N$   
 $(\mu_p + \mu_{\bar{p}}) / \mu_p = (0.002 \pm 0.004) \times 10^{-6}$   
 Electric dipole moment  $d < 0.021 \times 10^{-23}$  e cm  
 Electric polarizability  $\alpha = (11.2 \pm 0.4) \times 10^{-4}$  fm<sup>3</sup>  
 Magnetic polarizability  $\beta = (2.5 \pm 0.4) \times 10^{-4}$  fm<sup>3</sup> (S = 1.2)  
 Charge radius,  $\mu p$  Lamb shift =  $0.84087 \pm 0.00039$  fm [d]  
 Charge radius =  $0.8409 \pm 0.0004$  fm [d]  
 Magnetic radius =  $0.851 \pm 0.026$  fm [e]  
 Mean life  $\tau > 3.6 \times 10^{29}$  years, CL = 90% [f] ( $p \rightarrow$  invisible mode)  
 Mean life  $\tau > 10^{31}$  to  $10^{33}$  years [f] (mode dependent)

See the "Note on Nucleon Decay" in our 1994 edition (Phys. Rev. **D50**, 1173) for a short review.

The "partial mean life" limits tabulated here are the limits on  $\tau/B_j$ , where  $\tau$  is the total mean life and  $B_j$  is the branching fraction for the mode in question. For  $N$  decays,  $p$  and  $n$  indicate proton and neutron partial lifetimes.

<b>p</b> DECAY MODES	Partial mean life (10 <sup>30</sup> years)	Confidence level	$\rho$ (MeV/c)
<b>Antilepton + meson</b>			
$N \rightarrow e^+ \pi$	> 5300 (n), > 16000 (p)	90%	459
$N \rightarrow \mu^+ \pi$	> 3500 (n), > 7700 (p)	90%	453
$N \rightarrow \nu \pi$	> 1100 (n), > 390 (p)	90%	459
$p \rightarrow e^+ \eta$	> 10000	90%	309
$p \rightarrow \mu^+ \eta$	> 4700	90%	297
$n \rightarrow \nu \eta$	> 158	90%	310
$N \rightarrow e^+ \rho$	> 217 (n), > 720 (p)	90%	149
$N \rightarrow \mu^+ \rho$	> 228 (n), > 570 (p)	90%	113
$N \rightarrow \nu \rho$	> 19 (n), > 162 (p)	90%	149
$p \rightarrow e^+ \omega$	> 1600	90%	143
$p \rightarrow \mu^+ \omega$	> 2800	90%	105
$n \rightarrow \nu \omega$	> 108	90%	144
$N \rightarrow e^+ K$	> 17 (n), > 1000 (p)	90%	339
$N \rightarrow \mu^+ K$	> 26 (n), > 1600 (p)	90%	329
$N \rightarrow \nu K$	> 86 (n), > 5900 (p)	90%	339
$n \rightarrow \nu K_S^0$	> 260	90%	338
$p \rightarrow e^+ K^*(892)^0$	> 84	90%	45
$N \rightarrow \nu K^*(892)$	> 78 (n), > 51 (p)	90%	45
<b>Antilepton + mesons</b>			
$p \rightarrow e^+ \pi^+ \pi^-$	> 82	90%	448
$p \rightarrow e^+ \pi^0 \pi^0$	> 147	90%	449
$n \rightarrow e^+ \pi^+ \pi^0$	> 52	90%	449
$p \rightarrow \mu^+ \pi^+ \pi^-$	> 133	90%	425
$p \rightarrow \mu^+ \pi^0 \pi^0$	> 101	90%	427
$n \rightarrow \mu^+ \pi^+ \pi^0$	> 74	90%	427
$n \rightarrow e^+ K^0 \pi^-$	> 18	90%	319
<b>Lepton + meson</b>			
$n \rightarrow e^- \pi^+$	> 65	90%	459
$n \rightarrow \mu^- \pi^+$	> 49	90%	453
$n \rightarrow e^- \rho^+$	> 62	90%	150
$n \rightarrow \mu^- \rho^+$	> 7	90%	115
$n \rightarrow e^- K^+$	> 32	90%	340
$n \rightarrow \mu^- K^+$	> 57	90%	330
<b>Lepton + mesons</b>			
$p \rightarrow e^- \pi^+ \pi^+$	> 30	90%	448
$n \rightarrow e^- \pi^+ \pi^0$	> 29	90%	449
$p \rightarrow \mu^- \pi^+ \pi^+$	> 17	90%	425
$n \rightarrow \mu^- \pi^+ \pi^0$	> 34	90%	427
$p \rightarrow e^- \pi^+ K^+$	> 75	90%	320
$p \rightarrow \mu^- \pi^+ K^+$	> 245	90%	279

<b>Antilepton + photon(s)</b>			
$p \rightarrow e^+ \gamma$	> 670	90%	469
$p \rightarrow \mu^+ \gamma$	> 478	90%	463
$n \rightarrow \nu \gamma$	> 550	90%	470
$p \rightarrow e^+ \gamma \gamma$	> 100	90%	469
$n \rightarrow \nu \gamma \gamma$	> 219	90%	470
<b>Antilepton + single massless</b>			
$p \rightarrow e^+ X$	> 790	90%	—
$p \rightarrow \mu^+ X$	> 410	90%	—
<b>Three (or more) leptons</b>			
$p \rightarrow e^+ e^+ e^-$	> 793	90%	469
$p \rightarrow e^+ \mu^+ \mu^-$	> 359	90%	457
$p \rightarrow e^+ \nu \nu$	> 170	90%	469
$n \rightarrow e^+ e^- \nu$	> 257	90%	470
$n \rightarrow \mu^+ e^- \nu$	> 83	90%	464
$n \rightarrow \mu^+ \mu^- \nu$	> 79	90%	458
$p \rightarrow \mu^+ e^+ e^-$	> 529	90%	463
$p \rightarrow \mu^+ \mu^+ \mu^-$	> 675	90%	439
$p \rightarrow \mu^+ \nu \nu$	> 220	90%	463
$p \rightarrow e^- \mu^+ \mu^+$	> 6	90%	457
$n \rightarrow 3\nu$	> $5 \times 10^{-4}$	90%	470
<b>Inclusive modes</b>			
$N \rightarrow e^+$ anything	> 0.6 (n, p)	90%	—
$N \rightarrow \mu^+$ anything	> 12 (n, p)	90%	—
$N \rightarrow e^+ \pi^0$ anything	> 0.6 (n, p)	90%	—

**$\Delta B = 2$  dinucleon modes**

The following are lifetime limits per iron nucleus.

$pp \rightarrow \pi^+ \pi^+$	> 72.2	90%	—
$pn \rightarrow \pi^+ \pi^0$	> 170	90%	—
$nn \rightarrow \pi^+ \pi^-$	> 0.7	90%	—
$nn \rightarrow \pi^0 \pi^0$	> 404	90%	—
$pp \rightarrow K^+ K^+$	> 170	90%	—
$pp \rightarrow e^+ e^+$	> 5.8	90%	—
$pp \rightarrow e^+ \mu^+$	> 3.6	90%	—
$pp \rightarrow \mu^+ \mu^+$	> 1.7	90%	—
$pn \rightarrow e^+ \bar{\nu}$	> 260	90%	—
$pn \rightarrow \mu^+ \bar{\nu}$	> 200	90%	—
$pn \rightarrow \tau^+ \bar{\nu}_\tau$	> 29	90%	—
$nn \rightarrow \nu_e \bar{\nu}_e$	> 1.4	90%	—
$nn \rightarrow \nu_\mu \bar{\nu}_\mu$	> 1.4	90%	—
$pn \rightarrow$ invisible	> $2.1 \times 10^{-5}$	90%	—
$pp \rightarrow$ invisible	> $5 \times 10^{-5}$	90%	—

**$\bar{p}$  DECAY MODES**

$\bar{p}$ DECAY MODES	Partial mean life (years)	Confidence level	$\rho$ (MeV/c)
$\bar{p} \rightarrow e^- \gamma$	> $7 \times 10^5$	90%	469
$\bar{p} \rightarrow \mu^- \gamma$	> $5 \times 10^4$	90%	463
$\bar{p} \rightarrow e^- \pi^0$	> $4 \times 10^5$	90%	459
$\bar{p} \rightarrow \mu^- \pi^0$	> $5 \times 10^4$	90%	453
$\bar{p} \rightarrow e^- \eta$	> $2 \times 10^4$	90%	309
$\bar{p} \rightarrow \mu^- \eta$	> $8 \times 10^3$	90%	297
$\bar{p} \rightarrow e^- K_S^0$	> 900	90%	337
$\bar{p} \rightarrow \mu^- K_S^0$	> $4 \times 10^3$	90%	326
$\bar{p} \rightarrow e^- K_L^0$	> $9 \times 10^3$	90%	337
$\bar{p} \rightarrow \mu^- K_L^0$	> $7 \times 10^3$	90%	326
$\bar{p} \rightarrow e^- \gamma \gamma$	> $2 \times 10^4$	90%	469
$\bar{p} \rightarrow \mu^- \gamma \gamma$	> $2 \times 10^4$	90%	463
$\bar{p} \rightarrow e^- \omega$	> 200	90%	143

**n**

$I(J^P) = \frac{1}{2}(\frac{1}{2}^+)$

Mass  $m = 1.0086649159 \pm 0.0000000005$  u  
 Mass  $m = 939.565413 \pm 0.000006$  MeV [a]  
 $(m_n - m_{\bar{n}}) / m_n = (9 \pm 6) \times 10^{-5}$   
 $m_n - m_p = 1.2933321 \pm 0.0000005$  MeV  
 =  $0.00138844919(45)$  u  
 Mean life  $\tau = 879.4 \pm 0.6$  s (S = 1.6)  
 $c\tau = 2.6362 \times 10^8$  km  
 Magnetic moment  $\mu = -1.9130427 \pm 0.0000005$   $\mu_N$   
 Electric dipole moment  $d < 0.18 \times 10^{-25}$  e cm, CL = 90%  
 Mean-square charge radius  $\langle r_n^2 \rangle = -0.1161 \pm 0.0022$  fm<sup>2</sup> (S = 1.3)

## Baryon Summary Table

Magnetic radius  $\sqrt{\langle r_M^2 \rangle} = 0.864^{+0.009}_{-0.008}$  fm  
 Electric polarizability  $\alpha = (11.8 \pm 1.1) \times 10^{-4}$  fm<sup>3</sup>  
 Magnetic polarizability  $\beta = (3.7 \pm 1.2) \times 10^{-4}$  fm<sup>3</sup>  
 Charge  $q = (-0.2 \pm 0.8) \times 10^{-21} e$   
 Mean  $n\bar{n}$ -oscillation time  $> 8.6 \times 10^7$  s, CL = 90% (free  $n$ )  
 Mean  $n\bar{n}$ -oscillation time  $> 2.7 \times 10^8$  s, CL = 90% [g] (bound  $n$ )  
 Mean  $n n'$ -oscillation time  $> 448$  s, CL = 90% [h]

 **$p e^- \nu_e$  decay parameters [i]**

$\lambda \equiv g_A / g_V = -1.2756 \pm 0.0013$  (S = 2.6)  
 $A = -0.11958 \pm 0.00021$  (S = 1.2)  
 $B = 0.9807 \pm 0.0030$   
 $C = -0.2377 \pm 0.0026$   
 $a = -0.1059 \pm 0.0028$   
 $\phi_{AV} = (180.017 \pm 0.026)^\circ$  [j]  
 $D = (-1.2 \pm 2.0) \times 10^{-4}$  [k]  
 $R = 0.004 \pm 0.013$  [k]

$n$ DECAY MODES	Fraction ( $\Gamma_i/\Gamma$ )	Confidence level	$\rho$ (MeV/c)
$p e^- \bar{\nu}_e$	100 %		1
$p e^- \bar{\nu}_e \gamma$	[j] $(9.2 \pm 0.7) \times 10^{-3}$		1
hydrogen-atom $\bar{\nu}_e$	$< 2.7 \times 10^{-3}$	95%	1.19

**Charge conservation (Q) violating mode**

$p \nu_e \bar{\nu}_e$	Q $< 8 \times 10^{-27}$	68%	1
-----------------------	-------------------------	-----	---

 **$N(1440) 1/2^+$** 

$$I(J^P) = \frac{1}{2}(1^+)$$

Re(pole position) = 1360 to 1380 ( $\approx 1370$ ) MeV  
 $-2\text{Im}(\text{pole position}) = 160$  to  $190$  ( $\approx 175$ ) MeV  
 Breit-Wigner mass = 1410 to 1470 ( $\approx 1440$ ) MeV  
 Breit-Wigner full width = 250 to 450 ( $\approx 350$ ) MeV

$N(1440)$ DECAY MODES	Fraction ( $\Gamma_i/\Gamma$ )	$\rho$ (MeV/c)
$N\pi$	55–75 %	398
$N\eta$	$< 1$ %	†
$N\pi\pi$	17–50 %	347
$\Delta(1232)\pi$ , P-wave	6–27 %	147
$N\sigma$	11–23 %	–
$p\gamma$ , helicity=1/2	0.035–0.048 %	414
$n\gamma$ , helicity=1/2	0.02–0.04 %	413

 **$N(1520) 3/2^-$** 

$$I(J^P) = \frac{1}{2}(3^-)$$

Re(pole position) = 1505 to 1515 ( $\approx 1510$ ) MeV  
 $-2\text{Im}(\text{pole position}) = 105$  to  $120$  ( $\approx 110$ ) MeV  
 Breit-Wigner mass = 1510 to 1520 ( $\approx 1515$ ) MeV  
 Breit-Wigner full width = 100 to 120 ( $\approx 110$ ) MeV

$N(1520)$ DECAY MODES	Fraction ( $\Gamma_i/\Gamma$ )	$\rho$ (MeV/c)
$N\pi$	55–65 %	453
$N\eta$	0.07–0.09 %	142
$N\pi\pi$	25–35 %	410
$\Delta(1232)\pi$	22–34 %	225
$\Delta(1232)\pi$ , S-wave	15–23 %	225
$\Delta(1232)\pi$ , D-wave	7–11 %	225
$N\sigma$	$< 2$ %	–
$p\gamma$	0.31–0.52 %	467
$p\gamma$ , helicity=1/2	0.01–0.02 %	467
$p\gamma$ , helicity=3/2	0.30–0.50 %	467
$n\gamma$	0.30–0.53 %	466
$n\gamma$ , helicity=1/2	0.04–0.10 %	466
$n\gamma$ , helicity=3/2	0.25–0.45 %	466

 **$N(1535) 1/2^-$** 

$$I(J^P) = \frac{1}{2}(1^-)$$

Re(pole position) = 1500 to 1520 ( $\approx 1510$ ) MeV  
 $-2\text{Im}(\text{pole position}) = 110$  to  $150$  ( $\approx 130$ ) MeV  
 Breit-Wigner mass = 1515 to 1545 ( $\approx 1530$ ) MeV  
 Breit-Wigner full width = 125 to 175 ( $\approx 150$ ) MeV

$N(1535)$ DECAY MODES	Fraction ( $\Gamma_i/\Gamma$ )	$\rho$ (MeV/c)
$N\pi$	32–52 %	464
$N\eta$	30–55 %	176
$N\pi\pi$	3–14 %	422
$\Delta(1232)\pi$ , D-wave	1–4 %	240
$N\sigma$	2–10 %	–
$N(1440)\pi$	5–12 %	†
$p\gamma$ , helicity=1/2	0.15–0.30 %	477
$n\gamma$ , helicity=1/2	0.01–0.25 %	477

 **$N(1650) 1/2^-$** 

$$I(J^P) = \frac{1}{2}(1^-)$$

Re(pole position) = 1640 to 1670 ( $\approx 1655$ ) MeV  
 $-2\text{Im}(\text{pole position}) = 100$  to  $170$  ( $\approx 135$ ) MeV  
 Breit-Wigner mass = 1635 to 1665 ( $\approx 1650$ ) MeV  
 Breit-Wigner full width = 100 to 150 ( $\approx 125$ ) MeV

$N(1650)$ DECAY MODES	Fraction ( $\Gamma_i/\Gamma$ )	$\rho$ (MeV/c)
$N\pi$	50–70 %	547
$N\eta$	15–35 %	348
$\Lambda K$	5–15 %	169
$N\pi\pi$	8–36 %	514
$\Delta(1232)\pi$ , D-wave	6–18 %	345
$N\sigma$	2–18 %	–
$N(1440)\pi$	6–26 %	150
$p\gamma$ , helicity=1/2	0.04–0.20 %	558
$n\gamma$ , helicity=1/2	0.003–0.17 %	557

 **$N(1675) 5/2^-$** 

$$I(J^P) = \frac{1}{2}(5^-)$$

Re(pole position) = 1655 to 1665 ( $\approx 1660$ ) MeV  
 $-2\text{Im}(\text{pole position}) = 125$  to  $150$  ( $\approx 135$ ) MeV  
 Breit-Wigner mass = 1665 to 1680 ( $\approx 1675$ ) MeV  
 Breit-Wigner full width = 130 to 160 ( $\approx 145$ ) MeV

$N(1675)$ DECAY MODES	Fraction ( $\Gamma_i/\Gamma$ )	$\rho$ (MeV/c)
$N\pi$	38–42 %	564
$N\eta$	$< 1$ %	376
$N\pi\pi$	25–45 %	532
$\Delta(1232)\pi$ , D-wave	23–37 %	366
$N\sigma$	3–7 %	–
$p\gamma$	0–0.02 %	575
$p\gamma$ , helicity=1/2	0–0.01 %	575
$p\gamma$ , helicity=3/2	0–0.01 %	575
$n\gamma$	0–0.15 %	574
$n\gamma$ , helicity=1/2	0–0.05 %	574
$n\gamma$ , helicity=3/2	0–0.10 %	574

 **$N(1680) 5/2^+$** 

$$I(J^P) = \frac{1}{2}(5^+)$$

Re(pole position) = 1665 to 1680 ( $\approx 1675$ ) MeV  
 $-2\text{Im}(\text{pole position}) = 110$  to  $135$  ( $\approx 120$ ) MeV  
 Breit-Wigner mass = 1680 to 1690 ( $\approx 1685$ ) MeV  
 Breit-Wigner full width = 115 to 130 ( $\approx 120$ ) MeV

$N(1680)$ DECAY MODES	Fraction ( $\Gamma_i/\Gamma$ )	$\rho$ (MeV/c)
$N\pi$	60–70 %	571
$N\eta$	$< 1$ %	386
$N\pi\pi$	20–40 %	539
$\Delta(1232)\pi$	11–23 %	374
$\Delta(1232)\pi$ , P-wave	4–10 %	374
$\Delta(1232)\pi$ , F-wave	1–13 %	374
$N\sigma$	9–19 %	–
$p\gamma$	0.21–0.32 %	581
$p\gamma$ , helicity=1/2	0.001–0.011 %	581
$p\gamma$ , helicity=3/2	0.20–0.32 %	581
$n\gamma$	0.021–0.046 %	581
$n\gamma$ , helicity=1/2	0.004–0.029 %	581
$n\gamma$ , helicity=3/2	0.01–0.024 %	581

## Baryon Summary Table

 **$N(1700) 3/2^-$** 

$$I(J^P) = \frac{1}{2}(\frac{3}{2}^-)$$

Re(pole position) = 1650 to 1750 ( $\approx 1700$ ) MeV  
 $-2\text{Im}(\text{pole position}) = 100$  to  $300$  ( $\approx 200$ ) MeV  
 Breit-Wigner mass = 1650 to 1800 ( $\approx 1720$ ) MeV  
 Breit-Wigner full width = 100 to 300 ( $\approx 200$ ) MeV

<b><math>N(1700)</math> DECAY MODES</b>	Fraction ( $\Gamma_i/\Gamma$ )	$\rho$ (MeV/c)
$N\pi$	7–17 %	594
$N\eta$	seen	422
$N\omega$	10–34 %	†
$N\pi\pi$	60–90 %	564
$\Delta(1232)\pi$	55–85 %	402
$\Delta(1232)\pi$ , S-wave	50–80 %	402
$\Delta(1232)\pi$ , D-wave	4–14 %	402
$N(1440)\pi$	3–11 %	225
$N(1520)\pi$	<4 %	145
$N\rho$ , S=3/2, S-wave	32–44 %	74
$N\sigma$	2–14 %	–
$\rho\gamma$	0.01–0.05 %	604
$\rho\gamma$ , helicity=1/2	0.0–0.024 %	604
$\rho\gamma$ , helicity=3/2	0.002–0.026 %	604
$n\gamma$	0.01–0.13 %	603
$n\gamma$ , helicity=1/2	0.0–0.09 %	603
$n\gamma$ , helicity=3/2	0.01–0.05 %	603

 **$N(1710) 1/2^+$** 

$$I(J^P) = \frac{1}{2}(\frac{1}{2}^+)$$

Re(pole position) = 1680 to 1720 ( $\approx 1700$ ) MeV  
 $-2\text{Im}(\text{pole position}) = 80$  to  $160$  ( $\approx 120$ ) MeV  
 Breit-Wigner mass = 1680 to 1740 ( $\approx 1710$ ) MeV  
 Breit-Wigner full width = 80 to 200 ( $\approx 140$ ) MeV

<b><math>N(1710)</math> DECAY MODES</b>	Fraction ( $\Gamma_i/\Gamma$ )	$\rho$ (MeV/c)
$N\pi$	5–20 %	588
$N\eta$	10–50 %	412
$N\omega$	1–5 %	†
$\Lambda K$	5–25 %	269
$\Sigma K$	seen	138
$N\pi\pi$	seen	557
$\Delta(1232)\pi$ , P-wave	3–9 %	394
$N(1535)\pi$	9–21 %	113
$N\rho$ , S=1/2, P-wave	11–23 %	†
$\rho\gamma$ , helicity=1/2	0.002–0.08 %	598
$n\gamma$ , helicity=1/2	0.0–0.02%	597

 **$N(1720) 3/2^+$** 

$$I(J^P) = \frac{1}{2}(\frac{3}{2}^+)$$

Re(pole position) = 1660 to 1690 ( $\approx 1675$ ) MeV  
 $-2\text{Im}(\text{pole position}) = 150$  to  $400$  ( $\approx 250$ ) MeV  
 Breit-Wigner mass = 1680 to 1750 ( $\approx 1720$ ) MeV  
 Breit-Wigner full width = 150 to 400 ( $\approx 250$ ) MeV

<b><math>N(1720)</math> DECAY MODES</b>	Fraction ( $\Gamma_i/\Gamma$ )	$\rho$ (MeV/c)
$N\pi$	8–14 %	594
$N\eta$	1–5 %	422
$N\omega$	12–40 %	†
$\Lambda K$	4–5 %	283
$N\pi\pi$	50–90 %	564
$\Delta(1232)\pi$	47–89 %	402
$\Delta(1232)\pi$ , P-wave	47–77 %	402
$\Delta(1232)\pi$ , F-wave	<12 %	402
$N\rho$ , S=1/2, P-wave	1–2 %	74
$N\sigma$	2–14 %	–
$N(1440)\pi$	<2 %	225
$N(1520)\pi$ , S-wave	1–5 %	145
$\rho\gamma$	0.05–0.25 %	604
$\rho\gamma$ , helicity=1/2	0.05–0.15 %	604
$\rho\gamma$ , helicity=3/2	0.002–0.16 %	604
$n\gamma$	0.0–0.016 %	603
$n\gamma$ , helicity=1/2	0.0–0.01 %	603
$n\gamma$ , helicity=3/2	0.0–0.015 %	603

 **$N(1875) 3/2^-$** 

$$I(J^P) = \frac{1}{2}(\frac{3}{2}^-)$$

Re(pole position) = 1850 to 1950 ( $\approx 1900$ ) MeV  
 $-2\text{Im}(\text{pole position}) = 100$  to  $220$  ( $\approx 160$ ) MeV  
 Breit-Wigner mass = 1850 to 1920 ( $\approx 1875$ ) MeV  
 Breit-Wigner full width = 120 to 250 ( $\approx 200$ ) MeV

<b><math>N(1875)</math> DECAY MODES</b>	Fraction ( $\Gamma_i/\Gamma$ )	$\rho$ (MeV/c)
$N\pi$	3–11 %	695
$N\eta$	<1 %	559
$N\omega$	15–25 %	371
$\Lambda K$	seen	454
$\Sigma K$	seen	384
$N\pi\pi$		670
$\Delta(1232)\pi$	10–35 %	520
$\Delta(1232)\pi$ , S-wave	7–21 %	520
$\Delta(1232)\pi$ , D-wave	2–12 %	520
$N\rho$ , S=3/2, S-wave	seen	379
$N\sigma$	30–60 %	–
$N(1440)\pi$	2–8 %	365
$N(1520)\pi$	<2 %	301
$\rho\gamma$	0.001–0.025 %	703
$\rho\gamma$ , helicity=1/2	0.001–0.021 %	703
$\rho\gamma$ , helicity=3/2	<0.003 %	703
$n\gamma$	<0.040 %	702
$n\gamma$ , helicity=1/2	<0.007 %	702
$n\gamma$ , helicity=3/2	<0.033 %	702

 **$N(1880) 1/2^+$** 

$$I(J^P) = \frac{1}{2}(\frac{1}{2}^+)$$

Re(pole position) = 1820 to 1900 ( $\approx 1860$ ) MeV  
 $-2\text{Im}(\text{pole position}) = 180$  to  $280$  ( $\approx 230$ ) MeV  
 Breit-Wigner mass = 1830 to 1930 ( $\approx 1880$ ) MeV  
 Breit-Wigner full width = 200 to 400 ( $\approx 300$ ) MeV

<b><math>N(1880)</math> DECAY MODES</b>	Fraction ( $\Gamma_i/\Gamma$ )	$\rho$ (MeV/c)
$N\pi$	3–9 %	698
$N\eta$	5–55 %	563
$N\omega$	12–28 %	377
$\Lambda K$	12–28 %	459
$\Sigma K$	10–24 %	389
$N\pi\pi$	30–80 %	673
$\Delta(1232)\pi$	18–42 %	524
$N\sigma$	10–40 %	539
$N(1535)\pi$	4–12 %	293
$N a_0(980)$	1–5 %	†
$\Lambda K^*(892)$	0.5–1 %	†
$\rho\gamma$ , helicity=1/2	seen	706
$n\gamma$ , helicity=1/2	0.002–0.63 %	705

 **$N(1895) 1/2^-$** 

$$I(J^P) = \frac{1}{2}(\frac{1}{2}^-)$$

Re(pole position) = 1890 to 1930 ( $\approx 1910$ ) MeV  
 $-2\text{Im}(\text{pole position}) = 80$  to  $140$  ( $\approx 110$ ) MeV  
 Breit-Wigner mass = 1870 to 1920 ( $\approx 1895$ ) MeV  
 Breit-Wigner full width = 80 to 200 ( $\approx 120$ ) MeV

<b><math>N(1895)</math> DECAY MODES</b>	Fraction ( $\Gamma_i/\Gamma$ )	$\rho$ (MeV/c)
$N\pi$	2–18 %	707
$N\eta$	15–40 %	575
$N\eta'$	10–40 %	†
$N\omega$	16–40 %	395
$\Lambda K$	13–23 %	473
$\Sigma K$	6–20 %	405
$\Delta(1232)\pi$ , D-wave	3–11 %	535
$N\rho$ , S=1/2, S-wave	seen	403
$N\rho$ , S=3/2, D-wave	3–12 %	403
$\Lambda K^*(892)$	4–9 %	†
$N\sigma$	seen	–
$N(1440)\pi$	1–4 %	382
$\rho\gamma$ , helicity=1/2	0.01–0.06 %	715
$n\gamma$ , helicity=1/2	0.003–0.05 %	715

## Baryon Summary Table

<b><math>N(1900) 3/2^+</math></b>	$I(J^P) = \frac{1}{2}(\frac{3}{2}^+)$
Re(pole position) = 1900 to 1940 ( $\approx 1920$ ) MeV	
$-2\text{Im}(\text{pole position}) = 100$ to $200$ ( $\approx 150$ ) MeV	
Breit-Wigner mass = 1890 to 1950 ( $\approx 1920$ ) MeV	
Breit-Wigner full width = 100 to 320 ( $\approx 200$ ) MeV	

<b><math>N(1900)</math> DECAY MODES</b>	Fraction ( $\Gamma_i/\Gamma$ )	$\rho$ (MeV/c)
$N\pi$	1–20 %	723
$N\eta$	2–14 %	595
$N\eta'$	4–8 %	151
$N\omega$	7–13 %	424
$\Lambda K$	2–20 %	495
$\Sigma K$	3–7 %	431
$N\pi\pi$	40–80 %	699
$\Delta(1232)\pi$	30–70 %	553
$\Delta(1232)\pi, P\text{-wave}$	9–25 %	553
$\Delta(1232)\pi, F\text{-wave}$	21–45 %	553
$\Lambda K^*(892)$	< 0.2 %	†
$N\sigma$	1–7 %	–
$N(1520)\pi$	7–23 %	341
$N(1535)\pi$	4–10 %	328
$p\gamma$	0.001–0.025 %	731
$p\gamma, \text{helicity}=1/2$	0.001–0.021 %	731
$p\gamma, \text{helicity}=3/2$	< 0.003 %	731
$n\gamma$	< 0.040 %	730
$n\gamma, \text{helicity}=1/2$	< 0.007 %	730
$n\gamma, \text{helicity}=3/2$	< 0.033 %	730

<b><math>N(2060) 5/2^-</math></b>	$I(J^P) = \frac{1}{2}(\frac{5}{2}^-)$
Re(pole position) = 2020 to 2130 ( $\approx 2070$ ) MeV	
$-2\text{Im}(\text{pole position}) = 350$ to $430$ ( $\approx 400$ ) MeV	
Breit-Wigner mass = 2030 to 2200 ( $\approx 2100$ ) MeV	
Breit-Wigner full width = 300 to 450 ( $\approx 400$ ) MeV	

<b><math>N(2060)</math> DECAY MODES</b>	Fraction ( $\Gamma_i/\Gamma$ )	$\rho$ (MeV/c)
$N\pi$	7–12 %	834
$N\eta$	2–6 %	729
$N\omega$	1–7 %	600
$\Lambda K$	seen	644
$\Sigma K$	1–5 %	593
$N\pi\pi$	7–19 %	814
$\Delta(1232)\pi, D\text{-wave}$	4–10 %	680
$N\rho, S=1/2, P\text{-wave}$	seen	605
$\Lambda K^*(892)$	0.3–1.3 %	307
$N\sigma$	3–9 %	–
$N(1440)\pi$	4–14 %	544
$N(1520)\pi, P\text{-wave}$	9–21 %	490
$N(1680)\pi, S\text{-wave}$	8–22 %	353
$p\gamma$	0.03–0.19 %	840
$p\gamma, \text{helicity}=1/2$	0.02–0.08 %	840
$p\gamma, \text{helicity}=3/2$	0.01–0.10 %	840
$n\gamma$	0.003–0.07 %	840
$n\gamma, \text{helicity}=1/2$	0.001–0.02 %	840
$n\gamma, \text{helicity}=3/2$	0.002–0.05 %	840

<b><math>N(2100) 1/2^+</math></b>	$I(J^P) = \frac{1}{2}(\frac{1}{2}^+)$
Re(pole position) = 2050 to 2150 ( $\approx 2100$ ) MeV	
$-2\text{Im}(\text{pole position}) = 240$ to $340$ ( $\approx 300$ ) MeV	
Breit-Wigner mass = 2050 to 2150 ( $\approx 2100$ ) MeV	
Breit-Wigner full width = 200 to 320 ( $\approx 260$ ) MeV	

<b><math>N(2100)</math> DECAY MODES</b>	Fraction ( $\Gamma_i/\Gamma$ )	$\rho$ (MeV/c)
$N\pi$	8–18 %	834
$N\eta$	seen	729
$N\eta'$	5–11 %	451
$N\omega$	10–25 %	600
$\Lambda K$	seen	644
$N\pi\pi$	20–40 %	814

$\Delta(1232)\pi, P\text{-wave}$	6–14 %	680
$N\rho, S=1/2, P\text{-wave}$	seen	605
$\Lambda K^*(892)$	3–11 %	307
$N\sigma$	14–26 %	–
$N(1535)\pi$	26–34 %	478
$N\gamma, \text{helicity}=1/2$	0.001–0.012 %	840

<b><math>N(2120) 3/2^-</math></b>	$I(J^P) = \frac{1}{2}(\frac{3}{2}^-)$
Re(pole position) = 2050 to 2150 ( $\approx 2100$ ) MeV	
$-2\text{Im}(\text{pole position}) = 200$ to $360$ ( $\approx 280$ ) MeV	
Breit-Wigner mass = 2060 to 2160 ( $\approx 2120$ ) MeV	
Breit-Wigner full width = 260 to 360 ( $\approx 300$ ) MeV	

<b><math>N(2120)</math> DECAY MODES</b>	Fraction ( $\Gamma_i/\Gamma$ )	$\rho$ (MeV/c)
$N\pi$	5–15 %	846
$N\eta'$	2–6 %	474
$N\omega$	4–20 %	617
$N\pi\pi$	50–95 %	827
$\Delta(1232)\pi$	40–90 %	693
$\Delta(1232)\pi, S\text{-wave}$	30–70 %	693
$\Delta(1232)\pi, D\text{-wave}$	8–32 %	693
$\Lambda K^*(892)$	< 0.2 %	339
$N\sigma$	7–15 %	–
$N(1535)\pi$	7–23 %	494
$p\gamma$	0.16–2.1 %	852
$p\gamma, \text{helicity}=1/2$	0.07–0.80 %	852
$p\gamma, \text{helicity}=3/2$	0.09–1.3 %	852
$n\gamma$	0.04–0.72 %	852
$n\gamma, \text{helicity}=1/2$	0.04–0.60 %	852
$n\gamma, \text{helicity}=3/2$	0.001–0.12 %	852

<b><math>N(2190) 7/2^-</math></b>	$I(J^P) = \frac{1}{2}(\frac{7}{2}^-)$
Re(pole position) = 2050 to 2150 ( $\approx 2100$ ) MeV	
$-2\text{Im}(\text{pole position}) = 300$ to $500$ ( $\approx 400$ ) MeV	
Breit-Wigner mass = 2140 to 2220 ( $\approx 2180$ ) MeV	
Breit-Wigner full width = 300 to 500 ( $\approx 400$ ) MeV	

<b><math>N(2190)</math> DECAY MODES</b>	Fraction ( $\Gamma_i/\Gamma$ )	$\rho$ (MeV/c)
$N\pi$	10–20 %	882
$N\eta$	1–3 %	785
$N\omega$	8–20 %	667
$\Delta(1232)\pi, D\text{-wave}$	19–31 %	734
$N\rho, S=3/2, D\text{-wave}$	seen	672
$\Lambda K^*(892)$	0.2–0.8 %	423
$N\sigma$	3–9 %	–
$p\gamma$	0.014–0.077 %	888
$n\gamma$	< 0.04 %	888
$n\gamma, \text{helicity}=3/2$	< 0.03 %	888

<b><math>N(2220) 9/2^+</math></b>	$I(J^P) = \frac{1}{2}(\frac{9}{2}^+)$
Re(pole position) = 2130 to 2200 ( $\approx 2170$ ) MeV	
$-2\text{Im}(\text{pole position}) = 360$ to $480$ ( $\approx 400$ ) MeV	
Breit-Wigner mass = 2200 to 2300 ( $\approx 2250$ ) MeV	
Breit-Wigner full width = 350 to 500 ( $\approx 400$ ) MeV	

<b><math>N(2220)</math> DECAY MODES</b>	Fraction ( $\Gamma_i/\Gamma$ )	$\rho$ (MeV/c)
$N\pi$	15–30 %	924

<b><math>N(2250) 9/2^-</math></b>	$I(J^P) = \frac{1}{2}(\frac{9}{2}^-)$
Re(pole position) = 2150 to 2250 ( $\approx 2200$ ) MeV	
$-2\text{Im}(\text{pole position}) = 350$ to $500$ ( $\approx 420$ ) MeV	
Breit-Wigner mass = 2250 to 2320 ( $\approx 2280$ ) MeV	
Breit-Wigner full width = 300 to 600 ( $\approx 500$ ) MeV	

<b><math>N(2250)</math> DECAY MODES</b>	Fraction ( $\Gamma_i/\Gamma$ )	$\rho$ (MeV/c)
$N\pi$	0.05 to 0.15 ( $\approx 0.10$ )	941

## Baryon Summary Table

 **$N(2600) 11/2^-$** 

$$I(J^P) = \frac{1}{2}(\frac{11}{2}^-)$$

Breit-Wigner mass = 2550 to 2750 ( $\approx$  2600) MeV  
 Breit-Wigner full width = 500 to 800 ( $\approx$  650) MeV

<b><math>N(2600)</math> DECAY MODES</b>	Fraction ( $\Gamma_i/\Gamma$ )	$\rho$ (MeV/c)
$N\pi$	3-8 %	1126

## $\Delta$ BARYONS ( $S=0, I=3/2$ )

$$\Delta^{++} = uuu, \quad \Delta^+ = uud, \quad \Delta^0 = udd, \quad \Delta^- = ddd$$

 **$\Delta(1232) 3/2^+$** 

$$I(J^P) = \frac{3}{2}(\frac{3}{2}^+)$$

Re(pole position) = 1209 to 1211 ( $\approx$  1210) MeV  
 $-2\text{Im}(\text{pole position}) = 98$  to  $102$  ( $\approx$  100) MeV  
 Breit-Wigner mass (mixed charges) = 1230 to 1234 ( $\approx$  1232) MeV  
 Breit-Wigner full width (mixed charges) = 114 to 120 ( $\approx$  117) MeV

<b><math>\Delta(1232)</math> DECAY MODES</b>	Fraction ( $\Gamma_i/\Gamma$ )	$\rho$ (MeV/c)
$N\pi$	99.4 %	229
$N\gamma$	0.55-0.65 %	259
$N\gamma$ , helicity=1/2	0.11-0.13 %	259
$N\gamma$ , helicity=3/2	0.44-0.52 %	259
$p e^+ e^-$	( $4.2 \pm 0.7$ ) $\times 10^{-5}$	259

 **$\Delta(1600) 3/2^+$** 

$$I(J^P) = \frac{3}{2}(\frac{3}{2}^+)$$

Re(pole position) = 1460 to 1560 ( $\approx$  1510) MeV  
 $-2\text{Im}(\text{pole position}) = 200$  to  $340$  ( $\approx$  270) MeV  
 Breit-Wigner mass = 1500 to 1640 ( $\approx$  1570) MeV  
 Breit-Wigner full width = 200 to 300 ( $\approx$  250) MeV

<b><math>\Delta(1600)</math> DECAY MODES</b>	Fraction ( $\Gamma_i/\Gamma$ )	$\rho$ (MeV/c)
$N\pi$	8-24 %	492
$N\pi\pi$	75-90 %	454
$\Delta(1232)\pi$	73-83 %	276
$\Delta(1232)\pi$ , $P$ -wave	72-82 %	276
$\Delta(1232)\pi$ , $F$ -wave	<2 %	276
$N(1440)\pi$ , $P$ -wave	15-25 %	†
$N\gamma$	0.001-0.035 %	505
$N\gamma$ , helicity=1/2	0.0-0.02 %	505
$N\gamma$ , helicity=3/2	0.001-0.015 %	505

 **$\Delta(1620) 1/2^-$** 

$$I(J^P) = \frac{3}{2}(\frac{1}{2}^-)$$

Re(pole position) = 1590 to 1610 ( $\approx$  1600) MeV  
 $-2\text{Im}(\text{pole position}) = 100$  to  $140$  ( $\approx$  120) MeV  
 Breit-Wigner mass = 1590 to 1630 ( $\approx$  1610) MeV  
 Breit-Wigner full width = 110 to 150 ( $\approx$  130) MeV

<b><math>\Delta(1620)</math> DECAY MODES</b>	Fraction ( $\Gamma_i/\Gamma$ )	$\rho$ (MeV/c)
$N\pi$	25-35 %	520
$N\pi\pi$	55-80 %	484
$\Delta(1232)\pi$ , $D$ -wave	52-72 %	311
$N\rho$ , $S=1/2$ , $S$ -wave	seen	†
$N\rho$ , $S=3/2$ , $D$ -wave	seen	†
$N(1440)\pi$	3-9 %	98
$N\gamma$ , helicity=1/2	0.03-0.10 %	532

 **$\Delta(1700) 3/2^-$** 

$$I(J^P) = \frac{3}{2}(\frac{3}{2}^-)$$

Re(pole position) = 1640 to 1690 ( $\approx$  1665) MeV  
 $-2\text{Im}(\text{pole position}) = 200$  to  $300$  ( $\approx$  250) MeV  
 Breit-Wigner mass = 1690 to 1730 ( $\approx$  1710) MeV  
 Breit-Wigner full width = 220 to 380 ( $\approx$  300) MeV

 **$\Delta(1700)$  DECAY MODES**

	Fraction ( $\Gamma_i/\Gamma$ )	$\rho$ (MeV/c)
$N\pi$	10-20 %	588
$N\pi\pi$	10-55 %	557
$\Delta(1232)\pi$	10-50 %	394
$\Delta(1232)\pi$ , $S$ -wave	5-35 %	394
$\Delta(1232)\pi$ , $D$ -wave	4-16 %	394
$N\rho$ , $S=3/2$ , $S$ -wave	seen	†
$N(1520)\pi$ , $P$ -wave	1-5 %	133
$N(1535)\pi$	0.5-1.5 %	113
$\Delta(1232)\eta$	3-7 %	†
$N\gamma$	0.22-0.60 %	598
$N\gamma$ , helicity=1/2	0.12-0.30 %	598
$N\gamma$ , helicity=3/2	0.10-0.30 %	598

 **$\Delta(1900) 1/2^-$** 

$$I(J^P) = \frac{3}{2}(\frac{1}{2}^-)$$

Re(pole position) = 1830 to 1900 ( $\approx$  1865) MeV  
 $-2\text{Im}(\text{pole position}) = 180$  to  $300$  ( $\approx$  240) MeV  
 Breit-Wigner mass = 1840 to 1920 ( $\approx$  1860) MeV  
 Breit-Wigner full width = 180 to 320 ( $\approx$  250) MeV

 **$\Delta(1900)$  DECAY MODES**

	Fraction ( $\Gamma_i/\Gamma$ )	$\rho$ (MeV/c)
$N\pi$	4-12 %	685
$\Sigma K$	seen	367
$N\pi\pi$	45-85 %	660
$\Delta(1232)\pi$ , $D$ -wave	30-70 %	509
$N\rho$ , $S=1/2$ , $S$ -wave	8-16 %	360
$N\rho$ , $S=3/2$ , $D$ -wave	18-28 %	360
$N(1440)\pi$	8-32 %	353
$N(1520)\pi$	2-10 %	288
$\Delta(1232)\eta$	0-2 %	251
$N\gamma$ , helicity=1/2	0.06-0.43 %	693

 **$\Delta(1905) 5/2^+$** 

$$I(J^P) = \frac{3}{2}(\frac{5}{2}^+)$$

Re(pole position) = 1770 to 1830 ( $\approx$  1800) MeV  
 $-2\text{Im}(\text{pole position}) = 260$  to  $340$  ( $\approx$  300) MeV  
 Breit-Wigner mass = 1855 to 1910 ( $\approx$  1880) MeV  
 Breit-Wigner full width = 270 to 400 ( $\approx$  330) MeV

 **$\Delta(1905)$  DECAY MODES**

	Fraction ( $\Gamma_i/\Gamma$ )	$\rho$ (MeV/c)
$N\pi$	9-15 %	698
$N\pi\pi$		673
$\Delta(1232)\pi$	80-100 %	524
$\Delta(1232)\pi$ , $P$ -wave	23-43 %	524
$\Delta(1232)\pi$ , $F$ -wave	56-72 %	524
$N\rho$ , $S=3/2$ , $P$ -wave	seen	385
$N(1535)\pi$	<1 %	293
$N(1680)\pi$ , $P$ -wave	5-15 %	133
$\Delta(1232)\eta$	2-6 %	282
$N\gamma$	0.012-0.036 %	706
$N\gamma$ , helicity=1/2	0.002-0.006 %	706
$N\gamma$ , helicity=3/2	0.01-0.03 %	706

 **$\Delta(1910) 1/2^+$** 

$$I(J^P) = \frac{3}{2}(\frac{1}{2}^+)$$

Re(pole position) = 1830 to 1890 ( $\approx$  1860) MeV  
 $-2\text{Im}(\text{pole position}) = 200$  to  $400$  ( $\approx$  300) MeV  
 Breit-Wigner mass = 1850 to 1950 ( $\approx$  1900) MeV  
 Breit-Wigner full width = 200 to 400 ( $\approx$  300) MeV

 **$\Delta(1910)$  DECAY MODES**

	Fraction ( $\Gamma_i/\Gamma$ )	$\rho$ (MeV/c)
$N\pi$	15-30 %	710
$\Sigma K$	4-14 %	410
$N\pi\pi$		686
$\Delta(1232)\pi$	34-66 %	539
$N(1440)\pi$	3-9 %	386
$\Delta(1232)\eta$	5-13 %	310
$N\gamma$ , helicity=1/2	0.0-0.02 %	718



## Baryon Summary Table

 **$\Delta(1920) 3/2^+$** 

$$I(J^P) = \frac{3}{2}(\frac{3}{2}^+)$$

Re(pole position) = 1850 to 1950 ( $\approx 1900$ ) MeV  
 $-2\text{Im}(\text{pole position}) = 200$  to  $400$  ( $\approx 300$ ) MeV  
 Breit-Wigner mass = 1870 to 1970 ( $\approx 1920$ ) MeV  
 Breit-Wigner full width = 240 to 360 ( $\approx 300$ ) MeV

$\Delta(1920)$ DECAY MODES	Fraction ( $\Gamma_i/\Gamma$ )	$\rho$ (MeV/c)
$N\pi$	5–20 %	723
$\Sigma K$	2–6 %	431
$N\pi\pi$		699
$\Delta(1232)\pi$	50–90 %	553
$\Delta(1232)\pi$ , <i>P</i> -wave	8–28 %	553
$\Delta(1232)\pi$ , <i>F</i> -wave	44–72 %	553
$N(1440)\pi$ , <i>P</i> -wave	<4 %	403
$N(1520)\pi$ , <i>S</i> -wave	<5 %	341
$N(1535)\pi$	<2 %	328
$N_{\Delta 0}(980)$	seen	41
$\Delta(1232)\eta$	5–17 %	336

 **$\Delta(1930) 5/2^-$** 

$$I(J^P) = \frac{3}{2}(\frac{5}{2}^-)$$

Re(pole position) = 1840 to 1920 ( $\approx 1880$ ) MeV  
 $-2\text{Im}(\text{pole position}) = 230$  to  $330$  ( $\approx 280$ ) MeV  
 Breit-Wigner mass = 1900 to 2000 ( $\approx 1950$ ) MeV  
 Breit-Wigner full width = 200 to 400 ( $\approx 300$ ) MeV

$\Delta(1930)$ DECAY MODES	Fraction ( $\Gamma_i/\Gamma$ )	$\rho$ (MeV/c)
$N\pi$	5–15 %	742
$N\gamma$	0.0–0.01 %	749
$N\gamma$ , helicity=1/2	0.0–0.005 %	749
$N\gamma$ , helicity=3/2	0.0–0.004 %	749

 **$\Delta(1950) 7/2^+$** 

$$I(J^P) = \frac{3}{2}(\frac{7}{2}^+)$$

Re(pole position) = 1870 to 1890 ( $\approx 1880$ ) MeV  
 $-2\text{Im}(\text{pole position}) = 220$  to  $260$  ( $\approx 240$ ) MeV  
 Breit-Wigner mass = 1915 to 1950 ( $\approx 1930$ ) MeV  
 Breit-Wigner full width = 235 to 335 ( $\approx 285$ ) MeV

$\Delta(1950)$ DECAY MODES	Fraction ( $\Gamma_i/\Gamma$ )	$\rho$ (MeV/c)
$N\pi$	35–45 %	729
$\Sigma K$	0.3–0.5 %	441
$N\pi\pi$		706
$\Delta(1232)\pi$ , <i>F</i> -wave	1–9 %	560
$N(1680)\pi$ , <i>P</i> -wave	3–9 %	191
$\Delta(1232)\eta$	< 0.6 %	349

 **$\Delta(2200) 7/2^-$** 

$$I(J^P) = \frac{3}{2}(\frac{7}{2}^-)$$

Re(pole position) = 2050 to 2150 ( $\approx 2100$ ) MeV  
 $-2\text{Im}(\text{pole position}) = 260$  to  $420$  ( $\approx 340$ ) MeV  
 Breit-Wigner mass = 2150 to 2250 ( $\approx 2200$ ) MeV  
 Breit-Wigner full width = 200 to 500 ( $\approx 350$ ) MeV

$\Delta(2200)$ DECAY MODES	Fraction ( $\Gamma_i/\Gamma$ )	$\rho$ (MeV/c)
$N\pi$	2–8 %	894
$\Sigma K$	1–7 %	672
$\Delta\pi$ , <i>D</i> -wave	40–100 %	747
$\Delta\pi$ , <i>G</i> -wave	5–25 %	747
$\Delta\eta$ , <i>D</i> -wave	seen	614

 **$\Delta(2420) 11/2^+$** 

$$I(J^P) = \frac{3}{2}(\frac{11}{2}^+)$$

Re(pole position) = 2300 to 2500 ( $\approx 2400$ ) MeV  
 $-2\text{Im}(\text{pole position}) = 350$  to  $550$  ( $\approx 450$ ) MeV  
 Breit-Wigner mass = 2300 to 2600 ( $\approx 2450$ ) MeV  
 Breit-Wigner full width = 300 to 700 ( $\approx 500$ ) MeV

 **$\Delta(2420)$  DECAY MODES**Fraction ( $\Gamma_i/\Gamma$ ) $\rho$  (MeV/c)

$N\pi$	5–10 %	1040
--------	--------	------

 **$\Lambda$  BARYONS**  
**( $S = -1, I = 0$ )**

$$\Lambda^0 = uds$$

 **$\Lambda$** 

$$I(J^P) = 0(\frac{1}{2}^+)$$

Mass  $m = 1115.683 \pm 0.006$  MeV

$$(m_\Lambda - m_{\bar{\Lambda}}) / m_\Lambda = (-0.1 \pm 1.1) \times 10^{-5} \quad (S = 1.6)$$

$$\text{Mean life } \tau = (2.632 \pm 0.020) \times 10^{-10} \text{ s} \quad (S = 1.6)$$

$$(\tau_\Lambda - \tau_{\bar{\Lambda}}) / \tau_\Lambda = -0.001 \pm 0.009$$

$$c\tau = 7.89 \text{ cm}$$

$$\text{Magnetic moment } \mu = -0.613 \pm 0.004 \mu_N$$

$$\text{Electric dipole moment } d < 1.5 \times 10^{-16} \text{ e cm, CL} = 95\%$$

**Decay parameters**

$$p\pi^- \quad \alpha_- = 0.732 \pm 0.014 \quad (S = 2.3)$$

$$\bar{p}\pi^+ \quad \alpha_+ = -0.758 \pm 0.012$$

$$\bar{\alpha}_0 \text{ FOR } \bar{\Lambda} \rightarrow \bar{n}\pi^0 = -0.692 \pm 0.017$$

$$p\pi^- \quad \phi_- = (-6.5 \pm 3.5)^\circ$$

$$" \quad \gamma_- = 0.76 [n]$$

$$" \quad \Delta_- = (8 \pm 4)^\circ [n]$$

$$\bar{\alpha}_0 / \alpha_+ \text{ in } \bar{\Lambda} \rightarrow \bar{n}\pi^0, \bar{\Lambda} \rightarrow \bar{p}\pi^+ = 0.913 \pm 0.030$$

$$R = |G_E/G_M| \text{ in } \Lambda \rightarrow p\pi^-, \bar{\Lambda} \rightarrow \bar{p}\pi^+ = 0.96 \pm 0.14$$

$$\Delta\Phi = \Phi_E - \Phi_M \text{ in } \Lambda \rightarrow p\pi^-, \bar{\Lambda} \rightarrow \bar{p}\pi^+ = 37 \pm 13 \text{ degrees}$$

$$n\pi^0 \quad \alpha_0 = 0.74 \pm 0.05$$

$$p e^- \bar{\nu}_e \quad g_A/g_V = -0.718 \pm 0.015 [l]$$

 **$\Lambda$  DECAY MODES**Fraction ( $\Gamma_i/\Gamma$ )

Confidence level

 $\rho$  (MeV/c)

$p\pi^-$	(63.9 $\pm$ 0.5) %		101
$n\pi^0$	(35.8 $\pm$ 0.5) %		104
$n\gamma$	(1.75 $\pm$ 0.15) $\times 10^{-3}$		162
$p\pi^-\gamma$	[o] (8.4 $\pm$ 1.4) $\times 10^{-4}$		101
$p e^- \bar{\nu}_e$	(8.32 $\pm$ 0.14) $\times 10^{-4}$		163
$p\mu^- \bar{\nu}_\mu$	(1.57 $\pm$ 0.35) $\times 10^{-4}$		131

**Lepton (L) and/or Baryon (B) number violating decay modes**

$\pi^+ e^-$	<i>L, B</i>	< 6	$\times 10^{-7}$	90%	549
$\pi^+ \mu^-$	<i>L, B</i>	< 6	$\times 10^{-7}$	90%	544
$\pi^- e^+$	<i>L, B</i>	< 4	$\times 10^{-7}$	90%	549
$\pi^- \mu^+$	<i>L, B</i>	< 6	$\times 10^{-7}$	90%	544
$K^+ e^-$	<i>L, B</i>	< 2	$\times 10^{-6}$	90%	449
$K^+ \mu^-$	<i>L, B</i>	< 3	$\times 10^{-6}$	90%	441
$K^- e^+$	<i>L, B</i>	< 2	$\times 10^{-6}$	90%	449
$K^- \mu^+$	<i>L, B</i>	< 3	$\times 10^{-6}$	90%	441
$K_S^0 \nu$	<i>L, B</i>	< 2	$\times 10^{-5}$	90%	447
$\bar{p}\pi^+$	<i>B</i>	< 9	$\times 10^{-7}$	90%	101

 **$\Lambda(1405) 1/2^-$** 

$$I(J^P) = 0(\frac{1}{2}^-)$$

Mass  $m = 1405.1^{+1.3}_{-1.0}$  MeVFull width  $\Gamma = 50.5 \pm 2.0$  MeVBelow  $\bar{K}N$  threshold **$\Lambda(1405)$  DECAY MODES**Fraction ( $\Gamma_i/\Gamma$ ) $\rho$  (MeV/c)

$\Sigma\pi$	100 %	155
-------------	-------	-----

 **$\Lambda(1520) 3/2^-$** 

$$I(J^P) = 0(\frac{3}{2}^-)$$

Mass  $m = 1518$  to  $1520$  ( $\approx 1519$ ) MeV [p]Full width  $\Gamma = 15$  to  $17$  ( $\approx 16$ ) MeV [p] **$\Lambda(1520)$  DECAY MODES**Fraction ( $\Gamma_i/\Gamma$ ) $\rho$  (MeV/c)

$N\bar{K}$	(45 $\pm 1$ ) %	242
$\Sigma\pi$	(42 $\pm 1$ ) %	268
$\Lambda\pi\pi$	(10 $\pm 1$ ) %	259

## Baryon Summary Table

$\Sigma \pi \pi$	( 0.9 ± 0.1 ) %	168
$\Lambda \gamma$	( 0.85 ± 0.15 ) %	350

 **$\Lambda(1600) 1/2^+$** 

$$I(J^P) = 0(\frac{1}{2}^+)$$

Mass  $m = 1570$  to  $1630$  ( $\approx 1600$ ) MeV  
Full width  $\Gamma = 150$  to  $250$  ( $\approx 200$ ) MeV

$\Lambda(1600)$ DECAY MODES	Fraction ( $\Gamma_i/\Gamma$ )	$\rho$ (MeV/c)
$N\bar{K}$	15–30 %	343
$\Sigma \pi$	10–60 %	338
$\Lambda \sigma$	(19 ± 4) %	–
$\Sigma(1385)\pi$	( 9 ± 4 ) %	158

 **$\Lambda(1670) 1/2^-$** 

$$I(J^P) = 0(\frac{1}{2}^-)$$

Mass  $m = 1670$  to  $1678$  ( $\approx 1674$ ) MeV  
Full width  $\Gamma = 25$  to  $35$  ( $\approx 30$ ) MeV

$\Lambda(1670)$ DECAY MODES	Fraction ( $\Gamma_i/\Gamma$ )	$\rho$ (MeV/c)
$N\bar{K}$	20–30 %	418
$\Sigma \pi$	25–55 %	398
$\Lambda \eta$	10–25 %	88
$\Sigma(1385)\pi, D$ -wave	( 6.0 ± 2.0 ) %	235
$N\bar{K}^*(892), S=3/2, D$ -wave	( 5 ± 4 ) %	†
$\Lambda \sigma$	(20 ± 8 ) %	–

 **$\Lambda(1690) 3/2^-$** 

$$I(J^P) = 0(\frac{3}{2}^-)$$

Mass  $m = 1685$  to  $1695$  ( $\approx 1690$ ) MeV  
Full width  $\Gamma = 60$  to  $80$  ( $\approx 70$ ) MeV

$\Lambda(1690)$ DECAY MODES	Fraction ( $\Gamma_i/\Gamma$ )	$\rho$ (MeV/c)
$N\bar{K}$	20–30 %	433
$\Sigma \pi$	20–40 %	410
$\Lambda \sigma$	(5.0 ± 2.0) %	–
$\Lambda \pi \pi$	~ 25 %	419
$\Sigma \pi \pi$	~ 20 %	358
$\Sigma(1385)\pi, S$ -wave	(9 ± 5 ) %	251
$\Sigma(1385)\pi, D$ -wave	(3.0 ± 2.0) %	251

 **$\Lambda(1800) 1/2^-$** 

$$I(J^P) = 0(\frac{1}{2}^-)$$

Mass  $m = 1750$  to  $1850$  ( $\approx 1800$ ) MeV  
Full width  $\Gamma = 150$  to  $250$  ( $\approx 200$ ) MeV

$\Lambda(1800)$ DECAY MODES	Fraction ( $\Gamma_i/\Gamma$ )	$\rho$ (MeV/c)
$N\bar{K}$	25–40 %	528
$\Sigma \pi$	seen	494
$\Lambda \sigma$	(15 ± 4) %	–
$\Sigma(1385)\pi$	seen	349
$\Lambda \eta$	0.01 to 0.10	326
$N\bar{K}^*(892)$	seen	†

 **$\Lambda(1810) 1/2^+$** 

$$I(J^P) = 0(\frac{1}{2}^+)$$

Mass  $m = 1740$  to  $1840$  ( $\approx 1790$ ) MeV  
Full width  $\Gamma = 50$  to  $170$  ( $\approx 110$ ) MeV

$\Lambda(1810)$ DECAY MODES	Fraction ( $\Gamma_i/\Gamma$ )	$\rho$ (MeV/c)
$N\bar{K}$	0.05 to 0.35	520
$\Sigma \pi$	(16 ± 5) %	487
$\Sigma(1385)\pi$	(40 ± 15) %	340
$N\bar{K}^*(892)$	30–60 %	†

 **$\Lambda(1820) 5/2^+$** 

$$I(J^P) = 0(\frac{5}{2}^+)$$

Mass  $m = 1815$  to  $1825$  ( $\approx 1820$ ) MeV  
Full width  $\Gamma = 70$  to  $90$  ( $\approx 80$ ) MeV

$\Lambda(1820)$ DECAY MODES	Fraction ( $\Gamma_i/\Gamma$ )	$\rho$ (MeV/c)
$N\bar{K}$	55–65 %	545
$\Sigma \pi$	8–14 %	509
$\Sigma(1385)\pi$	5–10 %	366
$N\bar{K}^*(892), S=3/2, P$ -wave	(3.0 ± 1.0) %	†

 **$\Lambda(1830) 5/2^-$** 

$$I(J^P) = 0(\frac{5}{2}^-)$$

Mass  $m = 1820$  to  $1830$  ( $\approx 1825$ ) MeV  
Full width  $\Gamma = 60$  to  $120$  ( $\approx 90$ ) MeV

$\Lambda(1830)$ DECAY MODES	Fraction ( $\Gamma_i/\Gamma$ )	Scale factor ( $\rho$ (MeV/c))
$N\bar{K}$	0.04 to 0.08	549
$\Sigma \pi$	35–75 %	512
$\Sigma(1385)\pi$	>15 %	370
$\Sigma(1385)\pi, D$ -wave	(40 ± 15) %	3.2

 **$\Lambda(1890) 3/2^+$** 

$$I(J^P) = 0(\frac{3}{2}^+)$$

Mass  $m = 1870$  to  $1910$  ( $\approx 1890$ ) MeV  
Full width  $\Gamma = 80$  to  $160$  ( $\approx 120$ ) MeV

$\Lambda(1890)$ DECAY MODES	Fraction ( $\Gamma_i/\Gamma$ )	$\rho$ (MeV/c)
$N\bar{K}$	0.24 to 0.36	599
$\Sigma \pi$	3–10 %	560
$\Sigma(1385)\pi$	seen	423
$\Sigma(1385)\pi, P$ -wave	(6.0 ± 3.0) %	423
$\Sigma(1385)\pi, F$ -wave	(4.0 ± 2.0) %	423
$N\bar{K}^*(892)$	seen	236

 **$\Lambda(2100) 7/2^-$** 

$$I(J^P) = 0(\frac{7}{2}^-)$$

Mass  $m = 2090$  to  $2110$  ( $\approx 2100$ ) MeV  
Full width  $\Gamma = 100$  to  $250$  ( $\approx 200$ ) MeV

$\Lambda(2100)$ DECAY MODES	Fraction ( $\Gamma_i/\Gamma$ )	$\rho$ (MeV/c)
$N\bar{K}$	25–35 %	751
$\Sigma \pi$	~ 5 %	705
$\Lambda \eta$	< 3 %	617
$\Xi K$	< 3 %	491
$\Lambda \omega$	< 8 %	443
$N\bar{K}^*(892)$	10–20 %	515
$\Sigma(1385)\pi, G$ -wave	(1.0 ± 1.0) %	584
$N\bar{K}^*(892), S=3/2, D$ -wave	(4.0 ± 2.0) %	515

 **$\Lambda(2110) 5/2^+$** 

$$I(J^P) = 0(\frac{5}{2}^+)$$

Mass  $m = 2050$  to  $2130$  ( $\approx 2090$ ) MeV  
Full width  $\Gamma = 200$  to  $300$  ( $\approx 250$ ) MeV

$\Lambda(2110)$ DECAY MODES	Fraction ( $\Gamma_i/\Gamma$ )	$\rho$ (MeV/c)
$N\bar{K}$	5–25 %	744
$\Sigma \pi$	10–40 %	698
$\Lambda \omega$	seen	432
$\Lambda \omega, S=3/2, P$ -wave	(5.0 ± 2.0) %	432
$\Sigma(1385)\pi$	seen	576
$N\bar{K}^*(892)$	10–60 %	505

 **$\Lambda(2350) 9/2^+$** 

$$I(J^P) = 0(\frac{9}{2}^+)$$

Mass  $m = 2340$  to  $2370$  ( $\approx 2350$ ) MeV  
Full width  $\Gamma = 100$  to  $250$  ( $\approx 150$ ) MeV

$\Lambda(2350)$ DECAY MODES	Fraction ( $\Gamma_i/\Gamma$ )	$\rho$ (MeV/c)
$N\bar{K}$	~ 12 %	915
$\Sigma \pi$	~ 10 %	867

# Baryon Summary Table

## Σ BARYONS

### (S = -1, I = 1)

$\Sigma^+ = uus, \Sigma^0 = uds, \Sigma^- = dds$

**Σ<sup>+</sup>**  $I(J^P) = 1(\frac{1}{2}^+)$

Mass  $m = 1189.37 \pm 0.07$  MeV (S = 2.2)  
 Mean life  $\tau = (0.8018 \pm 0.0026) \times 10^{-10}$  s  
 $c\tau = 2.404$  cm  
 $(\tau_{\Sigma^+} - \tau_{\Sigma^-}) / \tau_{\Sigma^+} = -0.0006 \pm 0.0012$   
 Magnetic moment  $\mu = 2.458 \pm 0.010 \mu_N$  (S = 2.1)  
 $(\mu_{\Sigma^+} + \mu_{\Sigma^-}) / \mu_{\Sigma^+} = 0.014 \pm 0.015$   
 $\Gamma(\Sigma^+ \rightarrow n\ell^+\nu) / \Gamma(\Sigma^- \rightarrow n\ell^-\bar{\nu}) < 0.043$

**Decay parameters**

$\rho\pi^0$   $\alpha_0 = -0.980^{+0.017}_{-0.015}$   
 "  $\phi_0 = (36 \pm 34)^\circ$   
 "  $\gamma_0 = 0.16 [n]$   
 "  $\Delta_0 = (187 \pm 6)^\circ [n]$   
 $n\pi^+$   $\alpha_+ = 0.068 \pm 0.013$   
 "  $\phi_+ = (167 \pm 20)^\circ$  (S = 1.1)  
 "  $\gamma_+ = -0.97 [n]$   
 "  $\Delta_+ = (-73^{+133}_{-10})^\circ [n]$   
 $\rho\gamma$   $\alpha_\gamma = -0.76 \pm 0.08$

Σ <sup>+</sup> DECAY MODES	Fraction (Γ <sub>i</sub> /Γ)	Confidence level	ρ (MeV/c)
$\rho\pi^0$	(51.57 ± 0.30) %		189
$n\pi^+$	(48.31 ± 0.30) %		185
$\rho\gamma$	( 1.23 ± 0.05 ) × 10 <sup>-3</sup>		225
$n\pi^+\gamma$	[a] ( 4.5 ± 0.5 ) × 10 <sup>-4</sup>		185
$\Lambda e^+\nu_e$	( 2.0 ± 0.5 ) × 10 <sup>-5</sup>		71

**ΔS = ΔQ (SQ) violating modes or  
ΔS = 1 weak neutral current (SI) modes**

$n e^+\nu_e$	SQ < 5	× 10 <sup>-6</sup>	90%	224
$n\mu^+\nu_\mu$	SQ < 3.0	× 10 <sup>-5</sup>	90%	202
$\rho e^+e^-$	SI < 7	× 10 <sup>-6</sup>		225
$\rho\mu^+\mu^-$	SI ( 2.4 <sup>+1.7</sup> <sub>-1.3</sub> ) × 10 <sup>-8</sup>			121

**Σ<sup>0</sup>**  $I(J^P) = 1(\frac{1}{2}^+)$

Mass  $m = 1192.642 \pm 0.024$  MeV  
 $m_{\Sigma^-} - m_{\Sigma^0} = 4.807 \pm 0.035$  MeV (S = 1.1)  
 $m_{\Sigma^0} - m_\Lambda = 76.959 \pm 0.023$  MeV  
 Mean life  $\tau = (7.4 \pm 0.7) \times 10^{-20}$  s  
 $c\tau = 2.22 \times 10^{-11}$  m  
 Transition magnetic moment  $|\mu_{\Sigma\Lambda}| = 1.61 \pm 0.08 \mu_N$

Σ <sup>0</sup> DECAY MODES	Fraction (Γ <sub>i</sub> /Γ)	Confidence level	ρ (MeV/c)
$\Lambda\gamma$	100 %		74
$\Lambda\gamma\gamma$	< 3 %	90%	74
$\Lambda e^+e^-$	[a] 5 × 10 <sup>-3</sup>		74

**Σ<sup>-</sup>**  $I(J^P) = 1(\frac{1}{2}^+)$

Mass  $m = 1197.449 \pm 0.030$  MeV (S = 1.2)  
 $m_{\Sigma^-} - m_{\Sigma^+} = 8.08 \pm 0.08$  MeV (S = 1.9)  
 $m_{\Sigma^-} - m_\Lambda = 81.766 \pm 0.030$  MeV (S = 1.2)  
 Mean life  $\tau = (1.479 \pm 0.011) \times 10^{-10}$  s (S = 1.3)  
 $c\tau = 4.434$  cm  
 Magnetic moment  $\mu = -1.160 \pm 0.025 \mu_N$  (S = 1.7)  
 $\Sigma^-$  charge radius = 0.78 ± 0.10 fm

**Decay parameters**

$n\pi^-$   $\alpha_- = -0.068 \pm 0.008$   
 "  $\phi_- = (10 \pm 15)^\circ$   
 "  $\gamma_- = 0.98 [n]$   
 "  $\Delta_- = (249^{+12}_{-120})^\circ [n]$   
 $n e^-\bar{\nu}_e$   $g_A/g_V = 0.340 \pm 0.017 [i]$   
 "  $f_2(0)/f_1(0) = 0.97 \pm 0.14$   
 "  $D = 0.11 \pm 0.10$   
 $\Lambda e^-\bar{\nu}_e$   $g_V/g_A = 0.01 \pm 0.10 [i]$  (S = 1.5)  
 "  $g_{WM}/g_A = 2.4 \pm 1.7 [i]$

Σ <sup>-</sup> DECAY MODES	Fraction (Γ <sub>i</sub> /Γ)	ρ (MeV/c)
$n\pi^-$	(99.848 ± 0.005) %	193
$n\pi^-\gamma$	[a] ( 4.6 ± 0.6 ) × 10 <sup>-4</sup>	193
$n e^-\bar{\nu}_e$	( 1.017 ± 0.034 ) × 10 <sup>-3</sup>	230
$n\mu^-\bar{\nu}_\mu$	( 4.5 ± 0.4 ) × 10 <sup>-4</sup>	210
$\Lambda e^-\bar{\nu}_e$	( 5.73 ± 0.27 ) × 10 <sup>-5</sup>	79

**Σ(1385) 3/2<sup>+</sup>**  $I(J^P) = 1(\frac{3}{2}^+)$

$\Sigma(1385)^+$  mass  $m = 1382.80 \pm 0.35$  MeV (S = 1.9)  
 $\Sigma(1385)^0$  mass  $m = 1383.7 \pm 1.0$  MeV (S = 1.4)  
 $\Sigma(1385)^-$  mass  $m = 1387.2 \pm 0.5$  MeV (S = 2.2)  
 $\Sigma(1385)^+$  full width  $\Gamma = 36.0 \pm 0.7$  MeV  
 $\Sigma(1385)^0$  full width  $\Gamma = 36 \pm 5$  MeV  
 $\Sigma(1385)^-$  full width  $\Gamma = 39.4 \pm 2.1$  MeV (S = 1.7)  
 Below  $\bar{K}N$  threshold

Σ(1385) DECAY MODES	Fraction (Γ <sub>i</sub> /Γ)	Confidence level	ρ (MeV/c)
$\Lambda\pi$	(87.0 ± 1.5) %		208
$\Sigma\pi$	(11.7 ± 1.5) %		129
$\Lambda\gamma$	( 1.25 <sup>+0.13</sup> <sub>-0.12</sub> ) %		241
$\Sigma^+\gamma$	( 7.0 ± 1.7 ) × 10 <sup>-3</sup>		180
$\Sigma^-\gamma$	< 2.4 × 10 <sup>-4</sup>	90%	173

**Σ(1660) 1/2<sup>+</sup>**  $I(J^P) = 1(\frac{1}{2}^+)$

Re(pole position) = 1585 ± 20 MeV  
 $-2\text{Im}(\text{pole position}) = 290^{+140}_{-40}$  MeV  
 Mass  $m = 1640$  to 1680 (≈ 1660) MeV  
 Full width  $\Gamma = 100$  to 300 (≈ 200) MeV

Σ(1660) DECAY MODES	Fraction (Γ <sub>i</sub> /Γ)	ρ (MeV/c)
$N\bar{K}$	0.05 to 0.15 (≈ 0.10)	405
$\Lambda\pi$	(35 ± 12) %	440
$\Sigma\pi$	(37 ± 10) %	387
$\Sigma\sigma$	(20 ± 8) %	-
$\Lambda(1405)\pi$	( 4.0 ± 2.0 ) %	199

**Σ(1670) 3/2<sup>-</sup>**  $I(J^P) = 1(\frac{3}{2}^-)$

Mass  $m = 1665$  to 1685 (≈ 1675) MeV  
 Full width  $\Gamma = 40$  to 100 (≈ 70) MeV

Σ(1670) DECAY MODES	Fraction (Γ <sub>i</sub> /Γ)	ρ (MeV/c)
$N\bar{K}$	0.06 to 0.12	419
$\Lambda\pi$	5-15 %	452
$\Sigma\pi$	30-60 %	398
$\Sigma\sigma$	(7.0 ± 3.0) %	-

**Σ(1750) 1/2<sup>-</sup>**  $I(J^P) = 1(\frac{1}{2}^-)$

Mass  $m = 1700$  to 1800 (≈ 1750) MeV  
 Full width  $\Gamma = 100$  to 200 (≈ 150) MeV

Σ(1750) DECAY MODES	Fraction (Γ <sub>i</sub> /Γ)	ρ (MeV/c)
$N\bar{K}$	0.06 to 0.12	486
$\Lambda\pi$	(14 ± 5) %	507
$\Sigma\pi$	(16 ± 4) %	456
$\Sigma\eta$	15-55 %	98
$\Sigma(1385)\pi, D\text{-wave}$	< 1 %	305
$\Lambda(1520)\pi$	( 2.0 ± 1.0 ) %	175
$NK^*(892), S=1/2$	( 8 ± 4 ) %	†

**Σ(1775) 5/2<sup>-</sup>**  $I(J^P) = 1(\frac{5}{2}^-)$

Mass  $m = 1770$  to 1780 (≈ 1775) MeV  
 Full width  $\Gamma = 105$  to 135 (≈ 120) MeV

## Baryon Summary Table

$\Sigma(1775)$ DECAY MODES	Fraction ( $\Gamma_i/\Gamma$ )	$\rho$ (MeV/c)
$N\bar{K}$	37–43%	508
$\Lambda\pi$	14–20%	525
$\Sigma\pi$	2–5%	475
$\Sigma(1385)\pi$	8–12%	327
$\Lambda(1520)\pi$ , $P$ -wave	17–23%	202

 $\Sigma(1910) 3/2^-$ 

$$I(J^P) = 1(\frac{3}{2}^-)$$

was  $\Sigma(1940)$ 

Full width  $\Gamma = 0.03 \pm 0.02$   
 Full width  $\Gamma = 0.16 \pm 0.04$   
 Full width  $\Gamma = 0.04 \pm 0.03$   
 Full width  $\Gamma = 0.01 \pm 0.01$   
 Full width  $\Gamma = 0.01 \pm 0.01$   
 Full width  $\Gamma = 0.03 \pm 0.01$   
 Full width  $\Gamma = 0.03 \pm 0.02$   
 Full width  $\Gamma = 0.02 \pm 0.01$   
 Full width  $\Gamma = 0.01 \pm 0.01$   
 Mass  $m = 1870$  to  $1950$  ( $\approx 1910$ ) MeV  
 Full width  $\Gamma = 150$  to  $300$  ( $\approx 220$ ) MeV

$\Sigma(1910)$ DECAY MODES	Fraction ( $\Gamma_i/\Gamma$ )	$\rho$ (MeV/c)
$N\bar{K}$	0.01 to 0.05 ( $\approx 0.02$ )	615
$\Lambda\pi$	( 6 $\pm$ 4 ) %	619
$\Sigma\pi$	(86 $\pm$ 21 ) %	574
$\Sigma(1385)\pi$	seen	439
$\Lambda(1520)\pi$	seen	329
$\Delta(1232)\bar{K}$	( 3.0 $\pm$ 1.0 ) %	377
$N\bar{K}^*(892)$	seen	274
$N\bar{K}^*(892)$ , $S=1/2$ , $D$ -wave	( 1.0 $\pm$ 1.0 ) %	274

 $\Sigma(1915) 5/2^+$ 

$$I(J^P) = 1(\frac{5}{2}^+)$$

Mass  $m = 1900$  to  $1935$  ( $\approx 1915$ ) MeV  
 Full width  $\Gamma = 80$  to  $160$  ( $\approx 120$ ) MeV

$\Sigma(1915)$ DECAY MODES	Fraction ( $\Gamma_i/\Gamma$ )	$\rho$ (MeV/c)
$N\bar{K}$	0.05 to 0.15	618
$\Lambda\pi$	( 6.0 $\pm$ 2.0 ) %	623
$\Sigma\pi$	(10.0 $\pm$ 2.0) %	577
$\Sigma(1385)\pi$ , $P$ -wave	( 2.0 $\pm$ 2.0 ) %	443
$\Sigma(1385)\pi$ , $F$ -wave	( 4.0 $\pm$ 2.0 ) %	443
$\Sigma(1385)\pi$	<5 %	443
$\Lambda(1520)\pi$ , $D$ -wave	( 8.0 $\pm$ 2.0 ) %	334
$N\bar{K}^*(892)$ , $S=1/2$ , $F$ -wave	( 5.0 $\pm$ 3.0 ) %	282
$N\bar{K}^*(892)$ , $S=3/2$ , $F$ -wave	( 5.0 $\pm$ 2.0 ) %	282
$\Delta\bar{K}$ , $P$ -wave	(16 $\pm$ 5 ) %	383
$\Delta\bar{K}$ , $F$ -wave	( 5.0 $\pm$ 3.0 ) %	383

 $\Sigma(2030) 7/2^+$ 

$$I(J^P) = 1(\frac{7}{2}^+)$$

Mass  $m = 2025$  to  $2040$  ( $\approx 2030$ ) MeV  
 Full width  $\Gamma = 150$  to  $200$  ( $\approx 180$ ) MeV

$\Sigma(2030)$ DECAY MODES	Fraction ( $\Gamma_i/\Gamma$ )	$\rho$ (MeV/c)
$N\bar{K}$	17–23 %	702
$\Lambda\pi$	17–23 %	700
$\Sigma\pi$	5–10 %	657
$\Xi K$	<2 %	422
$\Sigma(1385)\pi$	5–15 %	532
$\Sigma(1385)\pi$ , $F$ -wave	( 1.0 $\pm$ 1.0 ) %	532
$\Lambda(1520)\pi$	10–20 %	431
$\Delta(1232)\bar{K}$	10–20 %	498
$\Delta(1232)\bar{K}$ , $F$ -wave	(15 $\pm$ 5 ) %	498
$\Delta(1232)\bar{K}$ , $H$ -wave	( 1.0 $\pm$ 1.0 ) %	498
$N\bar{K}^*(892)$	<5 %	439
$N\bar{K}^*(892)$ , $S=3/2$ , $F$ -wave	(14 $\pm$ 8 ) %	439

 $\Sigma(2250)$ 

$$I(J^P) = 1(?^?)$$

Mass  $m = 2210$  to  $2280$  ( $\approx 2250$ ) MeV  
 Full width  $\Gamma = 60$  to  $150$  ( $\approx 100$ ) MeV

$\Sigma(2250)$ DECAY MODES	Fraction ( $\Gamma_i/\Gamma$ )	$\rho$ (MeV/c)
$N\bar{K}$	<10 %	851
$\Lambda\pi$	seen	842
$\Sigma\pi$	seen	803

 $\Xi$  BARYONS  
( $S = -2$ ,  $I = 1/2$ )

$$\Xi^0 = uss, \Xi^- = dss$$

 $\Xi^0$ 

$$I(J^P) = \frac{1}{2}(\frac{1}{2}^+)$$

 $P$  is not yet measured; + is the quark model prediction.

Mass  $m = 1314.86 \pm 0.20$  MeV  
 $m_{\Xi^-} - m_{\Xi^0} = 6.85 \pm 0.21$  MeV  
 Mean life  $\tau = (2.90 \pm 0.09) \times 10^{-10}$  s  
 $c\tau = 8.71$  cm  
 Magnetic moment  $\mu = -1.250 \pm 0.014 \mu_N$

## Decay parameters

$\Lambda\pi^0$   $\alpha = -0.356 \pm 0.011$   
 "  $\phi = (21 \pm 12)^\circ$   
 "  $\gamma = 0.85$  [n]  
 "  $\Delta = (218^{+12}_{-19})^\circ$  [n]  
 $\Lambda\gamma$   $\alpha = -0.70 \pm 0.07$   
 $\Lambda e^+ e^-$   $\alpha = -0.8 \pm 0.2$   
 $\Sigma^0 \gamma$   $\alpha = -0.69 \pm 0.06$   
 $\Sigma^+ e^- \bar{\nu}_e$   $g_1(0)/f_1(0) = 1.22 \pm 0.05$   
 $\Sigma^+ e^- \bar{\nu}_e$   $f_2(0)/f_1(0) = 2.0 \pm 0.9$

$\Xi^0$ DECAY MODES	Fraction ( $\Gamma_i/\Gamma$ )	Confidence level	$\rho$ (MeV/c)
$\Lambda\pi^0$	(99.524 $\pm$ 0.012) %		135
$\Lambda\gamma$	( 1.17 $\pm$ 0.07 ) $\times 10^{-3}$		184
$\Lambda e^+ e^-$	( 7.6 $\pm$ 0.6 ) $\times 10^{-6}$		184
$\Sigma^0 \gamma$	( 3.33 $\pm$ 0.10 ) $\times 10^{-3}$		117
$\Sigma^+ e^- \bar{\nu}_e$	( 2.52 $\pm$ 0.08 ) $\times 10^{-4}$		120
$\Sigma^+ \mu^- \bar{\nu}_\mu$	( 2.33 $\pm$ 0.35 ) $\times 10^{-6}$		64

 $\Delta S = \Delta Q$  (SQ) violating modes or  
 $\Delta S = 2$  forbidden ( $S_2$ ) modes

$\Sigma^- e^+ \nu_e$	$SQ < 9$	$\times 10^{-4}$	90%	112
$\Sigma^- \mu^+ \nu_\mu$	$SQ < 9$	$\times 10^{-4}$	90%	49
$p\pi^-$	$S_2 < 8$	$\times 10^{-6}$	90%	299
$p e^- \bar{\nu}_e$	$S_2 < 1.3$	$\times 10^{-3}$		323
$p \mu^- \bar{\nu}_\mu$	$S_2 < 1.3$	$\times 10^{-3}$		309

 $\Xi^-$ 

$$I(J^P) = \frac{1}{2}(\frac{1}{2}^+)$$

 $P$  is not yet measured; + is the quark model prediction.

Mass  $m = 1321.71 \pm 0.07$  MeV  
 $(m_{\Xi^-} - m_{\Xi^0}) / m_{\Xi^-} = (-3 \pm 9) \times 10^{-5}$   
 Mean life  $\tau = (1.639 \pm 0.015) \times 10^{-10}$  s  
 $c\tau = 4.91$  cm  
 $(\tau_{\Xi^-} - \tau_{\Xi^0}) / \tau_{\Xi^-} = -0.01 \pm 0.07$   
 Magnetic moment  $\mu = -0.6507 \pm 0.0025 \mu_N$   
 $(\mu_{\Xi^-} + \mu_{\Xi^0}) / |\mu_{\Xi^-}| = +0.01 \pm 0.05$

## Decay parameters

$\Lambda\pi^-$   $\alpha = -0.401 \pm 0.010$   
 $[\alpha(\Xi^-)\alpha_-(\Lambda) - \alpha(\Xi^0)\alpha_+(\bar{K})] / [\text{sum}] = (0 \pm 7) \times 10^{-4}$   
 "  $\phi = (-2.1 \pm 0.8)^\circ$   
 "  $\gamma = 0.89$  [n]  
 "  $\Delta = (175.9 \pm 1.5)^\circ$  [n]  
 $\Lambda e^- \bar{\nu}_e$   $g_A/g_V = -0.25 \pm 0.05$  [l]

## Baryon Summary Table

$\Xi^-$ DECAY MODES	Fraction ( $\Gamma_i/\Gamma$ )	Confidence level	$\rho$ (MeV/c)
$\Lambda\pi^-$	(99.887 ± 0.035) %		140
$\Sigma^- \gamma$	(1.27 ± 0.23) × 10 <sup>-4</sup>		118
$\Lambda e^- \bar{\nu}_e$	(5.63 ± 0.31) × 10 <sup>-4</sup>		190
$\Lambda \mu^- \bar{\nu}_\mu$	(3.5 <sup>+3.5</sup> / <sub>-2.2</sub> ) × 10 <sup>-4</sup>		163
$\Sigma^0 e^- \bar{\nu}_e$	(8.7 ± 1.7) × 10 <sup>-5</sup>		123
$\Sigma^0 \mu^- \bar{\nu}_\mu$	< 8 × 10 <sup>-4</sup>	90%	70
$\Xi^0 e^- \bar{\nu}_e$	< 2.3 × 10 <sup>-3</sup>	90%	7
<b><math>\Delta S = 2</math> forbidden (<math>S_2</math>) modes</b>			
$n\pi^-$	$S_2$ < 1.9 × 10 <sup>-5</sup>	90%	304
$n e^- \bar{\nu}_e$	$S_2$ < 3.2 × 10 <sup>-3</sup>	90%	327
$n \mu^- \bar{\nu}_\mu$	$S_2$ < 1.5 %	90%	314
$p\pi^- \pi^-$	$S_2$ < 4 × 10 <sup>-4</sup>	90%	223
$p\pi^- e^- \bar{\nu}_e$	$S_2$ < 4 × 10 <sup>-4</sup>	90%	305
$p\pi^- \mu^- \bar{\nu}_\mu$	$S_2$ < 4 × 10 <sup>-4</sup>	90%	251
$\rho\mu^- \mu^-$	$L$ < 4 × 10 <sup>-8</sup>	90%	272

 **$\Xi(1530) 3/2^+$** 

$$I(J^P) = \frac{1}{2}(\frac{3}{2}^+)$$

$\Xi(1530)^0$  mass  $m = 1531.80 \pm 0.32$  MeV ( $S = 1.3$ )  
 $\Xi(1530)^-$  mass  $m = 1535.0 \pm 0.6$  MeV  
 $\Xi(1530)^0$  full width  $\Gamma = 9.1 \pm 0.5$  MeV  
 $\Xi(1530)^-$  full width  $\Gamma = 9.9^{+1.7}_{-1.9}$  MeV

$\Xi(1530)$ DECAY MODES	Fraction ( $\Gamma_i/\Gamma$ )	Confidence level	$\rho$ (MeV/c)
$\Xi\pi$	100 %		158
$\Xi\gamma$	< 3.7 %	90%	202

 **$\Xi(1690)$** 

$$I(J^P) = \frac{1}{2}(?^?)$$

Mass  $m = 1690 \pm 10$  MeV [ $\rho$ ]  
 Full width  $\Gamma < 30$  MeV

$\Xi(1690)$ DECAY MODES	Fraction ( $\Gamma_i/\Gamma$ )	$\rho$ (MeV/c)
$\Lambda\bar{K}$	seen	240
$\Sigma\bar{K}$	seen	70
$\Xi\pi$	seen	311
$\Xi^- \pi^+ \pi^-$	possibly seen	213

 **$\Xi(1820) 3/2^-$** 

$$I(J^P) = \frac{1}{2}(\frac{3}{2}^-)$$

Mass  $m = 1823 \pm 5$  MeV [ $\rho$ ]  
 Full width  $\Gamma = 24^{+15}_{-10}$  MeV [ $\rho$ ]

$\Xi(1820)$ DECAY MODES	Fraction ( $\Gamma_i/\Gamma$ )	$\rho$ (MeV/c)
$\Lambda\bar{K}$	large	402
$\Sigma\bar{K}$	small	324
$\Xi\pi$	small	421
$\Xi(1530)\pi$	small	237

 **$\Xi(1950)$** 

$$I(J^P) = \frac{1}{2}(?^?)$$

Mass  $m = 1950 \pm 15$  MeV [ $\rho$ ]  
 Full width  $\Gamma = 60 \pm 20$  MeV [ $\rho$ ]

$\Xi(1950)$ DECAY MODES	Fraction ( $\Gamma_i/\Gamma$ )	$\rho$ (MeV/c)
$\Lambda\bar{K}$	seen	522
$\Sigma\bar{K}$	possibly seen	460
$\Xi\pi$	seen	519

 **$\Xi(2030)$** 

$$I(J^P) = \frac{1}{2}(\geq \frac{5}{2}^?)$$

Mass  $m = 2025 \pm 5$  MeV [ $\rho$ ]  
 Full width  $\Gamma = 20^{+15}_{-5}$  MeV [ $\rho$ ]

$\Xi(2030)$ DECAY MODES	Fraction ( $\Gamma_i/\Gamma$ )	$\rho$ (MeV/c)
$\Lambda\bar{K}$	~ 20 %	585
$\Sigma\bar{K}$	~ 80 %	529
$\Xi\pi$	small	574
$\Xi(1530)\pi$	small	416
$\Lambda\bar{K}\pi$	small	499
$\Sigma\bar{K}\pi$	small	428

 **$\Omega$  BARYONS**  
**( $S = -3, I = 0$ )**

$$\Omega^- = sss$$

 **$\Omega^-$** 

$$I(J^P) = 0(\frac{3}{2}^+)$$

$J^P = \frac{3}{2}^+$  is the quark-model prediction; and  $J = 3/2$  is fairly well established.

Mass  $m = 1672.45 \pm 0.29$  MeV  
 $(m_{\Omega^-} - m_{\bar{\Omega}^+}) / m_{\Omega^-} = (-1 \pm 8) \times 10^{-5}$   
 Mean life  $\tau = (0.821 \pm 0.011) \times 10^{-10}$  s  
 $c\tau = 2.461$  cm  
 $(\tau_{\Omega^-} - \tau_{\bar{\Omega}^+}) / \tau_{\Omega^-} = 0.00 \pm 0.05$   
 Magnetic moment  $\mu = -2.02 \pm 0.05 \mu_N$

**Decay parameters**

$\alpha(\Omega^-) \alpha_-(\Lambda)$  FOR  $\Omega^- \rightarrow \Lambda K^- = 0.0115 \pm 0.0015$   
 $\Lambda K^- \quad \alpha = 0.0157 \pm 0.0021$   
 $\Lambda K^-, \bar{\Lambda} K^+ \quad (\alpha + \bar{\alpha}) / (\alpha - \bar{\alpha}) = -0.02 \pm 0.13$   
 $\Xi^0 \pi^- \quad \alpha = 0.09 \pm 0.14$   
 $\Xi^- \pi^0 \quad \alpha = 0.05 \pm 0.21$

$\Omega^-$ DECAY MODES	Fraction ( $\Gamma_i/\Gamma$ )	Confidence level	$\rho$ (MeV/c)
$\Lambda K^-$	(67.8 ± 0.7) %		211
$\Xi^0 \pi^-$	(23.6 ± 0.7) %		294
$\Xi^- \pi^0$	(8.6 ± 0.4) %		289
$\Xi^- \pi^+ \pi^-$	(3.7 <sup>+0.7</sup> / <sub>-0.6</sub> ) × 10 <sup>-4</sup>		189
$\Xi(1530)^0 \pi^-$	< 7 × 10 <sup>-5</sup>	90%	17
$\Xi^0 e^- \bar{\nu}_e$	(5.6 ± 2.8) × 10 <sup>-3</sup>		319
$\Xi^- \gamma$	< 4.6 × 10 <sup>-4</sup>	90%	314

 **$\Delta S = 2$  forbidden ( $S_2$ ) modes**

$\Lambda\pi^-$	$S_2$ < 2.9 × 10 <sup>-6</sup>	90%	449
----------------	--------------------------------	-----	-----

 **$\Omega(2012)^-$** 

$$I(J^P) = 0(?^-)$$

Mass  $m = 2012.4 \pm 0.9$  MeV  
 Full width  $\Gamma = 6.4^{+3.0}_{-2.6}$  MeV

$\Omega(2012)^-$ DECAY MODES	Fraction ( $\Gamma_i/\Gamma$ )	Confidence level	$\rho$ (MeV/c)
$\Xi^0 K^-$	<b>DEFINED AS 1</b>		403
$\Xi^- K^0$	0.83 ± 0.21		392
$\Xi^0 \pi^0 K^-$	< 0.30	90%	245
$\Xi^0 \pi^- K^0$	< 0.21	90%	230
$\Xi^- \pi^+ K^-$	< 0.08	90%	224

 **$\Omega(2250)^-$** 

$$I(J^P) = 0(?^?)$$

Mass  $m = 2252 \pm 9$  MeV  
 Full width  $\Gamma = 55 \pm 18$  MeV

$\Omega(2250)^-$ DECAY MODES	Fraction ( $\Gamma_i/\Gamma$ )	$\rho$ (MeV/c)
$\Xi^- \pi^+ K^-$	seen	532
$\Xi(1530)^0 K^-$	seen	437

## CHARMED BARYONS (C = +1)

$$\Lambda_c^+ = udc, \quad \Sigma_c^{++} = uuc, \quad \Sigma_c^+ = udc, \quad \Sigma_c^0 = ddc, \\ \Xi_c^+ = usc, \quad \Xi_c^0 = dsc, \quad \Omega_c^0 = ssc$$

 $\Lambda_c^+$ 

$$I(J^P) = 0(\frac{1}{2}^+)$$

$$\text{Mass } m = 2286.46 \pm 0.14 \text{ MeV}$$

$$\text{Mean life } \tau = (202.4 \pm 3.1) \times 10^{-15} \text{ s} \quad (S = 1.7)$$

$$c\tau = 60.7 \mu\text{m}$$

### Decay asymmetry parameters

$$\Lambda\pi^+ \quad \alpha = -0.84 \pm 0.09$$

$$\Sigma^+\pi^0 \quad \alpha = -0.55 \pm 0.11$$

$$\alpha \text{ FOR } \Lambda_c^+ \rightarrow \Sigma^0\pi^+ = -0.73 \pm 0.18$$

$$\Lambda\ell^+\nu_\ell \quad \alpha = -0.86 \pm 0.04$$

$$\alpha \text{ FOR } \Lambda_c^+ \rightarrow pK_S^0 = 0.2 \pm 0.5$$

$$(\alpha + \bar{\alpha})/(\alpha - \bar{\alpha}) \text{ in } \Lambda_c^+ \rightarrow \Lambda\pi^+, \bar{\Lambda}_c^- \rightarrow \bar{\Lambda}\pi^- = -0.07 \pm 0.31$$

$$(\alpha + \bar{\alpha})/(\alpha - \bar{\alpha}) \text{ in } \Lambda_c^+ \rightarrow \Lambda e^+\nu_e, \bar{\Lambda}_c^- \rightarrow \bar{\Lambda} e^-\bar{\nu}_e = 0.00 \pm 0.04$$

$$A_{CP}(\Lambda X) \text{ in } \Lambda_c \rightarrow \Lambda X, \bar{\Lambda}_c \rightarrow \bar{\Lambda} X = (2 \pm 7)\%$$

$$\Delta A_{CP} = A_{CP}(\Lambda_c^+ \rightarrow pK^+K^-) - A_{CP}(\Lambda_c^+ \rightarrow p\pi^+\pi^-) = \\ (0.3 \pm 1.1)\%$$

Branching fractions marked with a footnote, e.g. [a], have been corrected for decay modes not observed in the experiments. For example, the sub-mode fraction  $\Lambda_c^+ \rightarrow p\bar{K}^*(892)^0$  seen in  $\Lambda_c^+ \rightarrow pK^-\pi^+$  has been multiplied up to include  $\bar{K}^*(892)^0 \rightarrow \bar{K}^0\pi^0$  decays.

$\Lambda_c^+$ DECAY MODES	Fraction ( $\Gamma_i/\Gamma$ )	Scale factor/ Confidence level	$p$ (MeV/c)
---------------------------	--------------------------------	-----------------------------------	----------------

### Hadronic modes with a $p$ or $n$ : $S = -1$ final states

$pK_S^0$	(1.59 ± 0.08) %	S=1.1	873
$pK_S^-\pi^+$	(6.28 ± 0.32) %	S=1.4	823
$p\bar{K}^*(892)^0$	[1] (1.96 ± 0.27) %		685
$\Delta(1232)^{++}K^-$	(1.08 ± 0.25) %		710
$\Lambda(1520)\pi^+$	[1] (2.2 ± 0.5) %		628
$pK^-\pi^+$ nonresonant	(3.5 ± 0.4) %		823
$pK_S^0\pi^0$	(1.97 ± 0.13) %	S=1.1	823
$nK_S^0\pi^+$	(1.82 ± 0.25) %		821
$p\bar{K}^0\eta$	(1.6 ± 0.4) %		568
$pK_S^0\pi^+\pi^-$	(1.60 ± 0.12) %	S=1.1	754
$pK^-\pi^+\pi^0$	(4.46 ± 0.30) %	S=1.5	759
$pK^*(892)^-\pi^+$	[1] (1.4 ± 0.5) %		580
$p(K^-\pi^+)_{\text{nonresonant}}\pi^0$	(4.6 ± 0.8) %		759
$\Delta(1232)\bar{K}^*(892)$	seen		419
$pK^-2\pi^+\pi^-$	(1.4 ± 0.9) × 10 <sup>-3</sup>		671
$pK^-\pi^+2\pi^0$	(1.0 ± 0.5) %		678

### Hadronic modes with a $p$ : $S = 0$ final states

$p\pi^0$	< 2.7 × 10 <sup>-4</sup>	CL=90%	945
$p\eta$	(1.24 ± 0.30) × 10 <sup>-3</sup>		856
$p\omega(782)^0$	(9 ± 4) × 10 <sup>-4</sup>		751
$p\pi^+\pi^-$	(4.61 ± 0.28) × 10 <sup>-3</sup>		927
$p f_0(980)$	[1] (3.5 ± 2.3) × 10 <sup>-3</sup>		614
$p2\pi^+2\pi^-$	(2.3 ± 1.4) × 10 <sup>-3</sup>		852
$pK^+K^-$	(1.06 ± 0.06) × 10 <sup>-3</sup>		616
$p\phi$	[1] (1.06 ± 0.14) × 10 <sup>-3</sup>		590
$pK^+K^-$ non- $\phi$	(5.3 ± 1.2) × 10 <sup>-4</sup>		616
$p\phi\pi^0$	(10 ± 4) × 10 <sup>-5</sup>		460
$pK^+K^-\pi^0$ nonresonant	< 6.3 × 10 <sup>-5</sup>	CL=90%	494

### Hadronic modes with a hyperon: $S = -1$ final states

$\Lambda\pi^+$	(1.30 ± 0.07) %	S=1.1	864
$\Lambda\pi^+\pi^0$	(7.1 ± 0.4) %	S=1.1	844
$\Lambda\rho^+$	< 6 %	CL=95%	636
$\Lambda\pi^-2\pi^+$	(3.64 ± 0.29) %	S=1.4	807
$\Sigma(1385)^+\pi^+\pi^-, \Sigma^{*+} \rightarrow$	(1.0 ± 0.5) %		688
$\Lambda\pi^+$			
$\Sigma(1385)^-2\pi^+, \Sigma^{*-} \rightarrow$	(7.6 ± 1.4) × 10 <sup>-3</sup>		688
$\Lambda\pi^-$			
$\Lambda\pi^+\rho^0$	(1.5 ± 0.6) %		524
$\Sigma(1385)^+\rho^0, \Sigma^{*+} \rightarrow \Lambda\pi^+$	(5 ± 4) × 10 <sup>-3</sup>		363
$\Lambda\pi^-2\pi^+$ nonresonant	< 1.1 %	CL=90%	807
$\Lambda\pi^-\pi^02\pi^+$ total	(2.3 ± 0.8) %		757
$\Lambda\pi^+\eta$	[1] (1.84 ± 0.26) %		691

$\Sigma(1385)^+\eta$	[1] (9.1 ± 2.0) × 10 <sup>-3</sup>		570
$\Lambda\pi^+\omega$	[1] (1.5 ± 0.5) %		517
$\Lambda\pi^-\pi^02\pi^+, \text{ no } \eta \text{ or } \omega$	< 8 × 10 <sup>-3</sup>	CL=90%	757
$\Lambda K^+\bar{K}^0$	(5.7 ± 1.1) × 10 <sup>-3</sup>	S=1.9	443
$\Xi(1690)^0K^+, \Xi^{*0} \rightarrow \Lambda\bar{K}^0$	(1.6 ± 0.5) × 10 <sup>-3</sup>		286
$\Sigma^0\pi^+$	(1.29 ± 0.07) %	S=1.1	825
$\Sigma^+\pi^0$	(1.25 ± 0.10) %		827
$\Sigma^+\eta$	(4.4 ± 2.0) × 10 <sup>-3</sup>		713
$\Sigma^+\eta'$	(1.5 ± 0.6) %		391
$\Sigma^+\pi^+\pi^-$	(4.50 ± 0.25) %	S=1.3	804
$\Sigma^+\rho^0$	< 1.7 %	CL=95%	575
$\Sigma^-2\pi^+$	(1.87 ± 0.18) %		799
$\Sigma^0\pi^+\pi^0$	(3.5 ± 0.4) %		803
$\Sigma^+\pi^0\pi^0$	(1.55 ± 0.15) %		806
$\Sigma^0\pi^-2\pi^+$	(1.11 ± 0.30) %		763
$\Sigma^+\pi^+\pi^-\pi^0$	—		767
$\Sigma^+\omega$	[1] (1.70 ± 0.21) %		569
$\Sigma^-02\pi^+$	(2.1 ± 0.4) %		762
$\Sigma^+K^+K^-$	(3.5 ± 0.4) × 10 <sup>-3</sup>	S=1.1	349
$\Sigma^+\phi$	[1] (3.9 ± 0.6) × 10 <sup>-3</sup>	S=1.1	295
$\Xi(1690)^0K^+, \Xi^{*0} \rightarrow$	(1.02 ± 0.25) × 10 <sup>-3</sup>		286
$\Sigma^+K^-$			
$\Sigma^+K^+K^-$ nonresonant	< 8 × 10 <sup>-4</sup>	CL=90%	349
$\Xi^0K^+$	(5.5 ± 0.7) × 10 <sup>-3</sup>		653
$\Xi^-K^+\pi^+$	(6.2 ± 0.6) × 10 <sup>-3</sup>	S=1.1	565
$\Xi(1530)^0K^+$	(4.3 ± 0.9) × 10 <sup>-3</sup>	S=1.1	473

### Hadronic modes with a hyperon: $S = 0$ final states

$\Lambda K^+$	(6.1 ± 1.2) × 10 <sup>-4</sup>		781
$\Lambda K^+\pi^+\pi^-$	< 5 × 10 <sup>-4</sup>	CL=90%	637
$\Sigma^0K^+$	(5.2 ± 0.8) × 10 <sup>-4</sup>		735
$\Sigma^0K^+\pi^+\pi^-$	< 2.6 × 10 <sup>-4</sup>	CL=90%	574
$\Sigma^+K^+\pi^-$	(2.1 ± 0.6) × 10 <sup>-3</sup>		670
$\Sigma^+K^*(892)^0$	[1] (3.5 ± 1.0) × 10 <sup>-3</sup>		470
$\Sigma^-K^+\pi^+$	< 1.2 × 10 <sup>-3</sup>	CL=90%	664

### Doubly Cabibbo-suppressed modes

$pK^+\pi^-$	(1.11 ± 0.18) × 10 <sup>-4</sup>		823
-------------	----------------------------------	--	-----

### Semileptonic modes

$\Lambda e^+\nu_e$	(3.6 ± 0.4) %		871
$\Lambda\mu^+\nu_\mu$	(3.5 ± 0.5) %		867

### Inclusive modes

$e^+$ anything	(3.95 ± 0.35) %		—
$p$ anything	(50 ± 16) %		—
$n$ anything	(50 ± 16) %		—
$\Lambda$ anything	(38.2 ± 2.9) %		—
3prongs	(24 ± 8) %		—

### $\Delta C = 1$ weak neutral current ( $CI$ ) modes, or Lepton Family number ( $LF$ ), or Lepton number ( $L$ ), or Baryon number ( $B$ ) violating modes

$p e^+ e^-$	$CI$	< 5.5 × 10 <sup>-6</sup>	CL=90%	951
$p\mu^+\mu^-$ non-resonant	$CI$	< 7.7 × 10 <sup>-8</sup>	CL=90%	937
$p e^+\mu^-$	$LF$	< 9.9 × 10 <sup>-6</sup>	CL=90%	947
$p e^-\mu^+$	$LF$	< 1.9 × 10 <sup>-5</sup>	CL=90%	947
$\bar{p}2e^+$	$L, B$	< 2.7 × 10 <sup>-6</sup>	CL=90%	951
$\bar{p}2\mu^+$	$L, B$	< 9.4 × 10 <sup>-6</sup>	CL=90%	937
$\bar{p}e^+\mu^+$	$L, B$	< 1.6 × 10 <sup>-5</sup>	CL=90%	947
$\Sigma^-\mu^+\mu^+$	$L$	< 7.0 × 10 <sup>-4</sup>	CL=90%	812

 $\Lambda_c(2955)^+$ 

$$I(J^P) = 0(\frac{1}{2}^-)$$

The spin-parity follows from the fact that  $\Sigma_c(2455)\pi$  decays, with little available phase space, are dominant. This assumes that  $J^P = 1/2^+$  for the  $\Sigma_c(2455)$ .

$$\text{Mass } m = 2592.25 \pm 0.28 \text{ MeV}$$

$$m - m_{\Lambda_c^+} = 305.79 \pm 0.24 \text{ MeV}$$

$$\text{Full width } \Gamma = 2.6 \pm 0.6 \text{ MeV}$$

$\Lambda_c^+\pi\pi$  and its submode  $\Sigma_c(2455)\pi$  — the latter just barely — are the only strong decays allowed to an excited  $\Lambda_c^+$  having this mass; and the submode seems to dominate.

## Baryon Summary Table

$\Lambda_c(2595)^+$ DECAY MODES	Fraction ( $\Gamma_i/\Gamma$ )	$\rho$ (MeV/c)
$\Lambda_c^+ \pi^+ \pi^-$	[s] —	117
$\Sigma_c(2455)^{++} \pi^-$	$24 \pm 7\%$	†
$\Sigma_c(2455)^0 \pi^+$	$24 \pm 7\%$	†
$\Lambda_c^+ \pi^+ \pi^-$ 3-body	$18 \pm 10\%$	117
$\Lambda_c^+ \pi^0$	[t] not seen	258
$\Lambda_c^+ \gamma$	not seen	288

$$\Lambda_c(2625)^+ \quad I(J^P) = 0(\frac{3}{2}^-)$$

$J^P$  has not been measured;  $\frac{3}{2}^-$  is the quark-model prediction.

$$\begin{aligned} \text{Mass } m &= 2628.11 \pm 0.19 \text{ MeV} \quad (S = 1.1) \\ m - m_{\Lambda_c^+} &= 341.65 \pm 0.13 \text{ MeV} \quad (S = 1.1) \\ \text{Full width } \Gamma &< 0.97 \text{ MeV, CL} = 90\% \end{aligned}$$

$\Lambda_c^+ \pi \pi$  and its submode  $\Sigma(2455)\pi$  are the only strong decays allowed to an excited  $\Lambda_c^+$  having this mass.

$\Lambda_c(2625)^+$ DECAY MODES	Fraction ( $\Gamma_i/\Gamma$ )	Confidence level	$\rho$ (MeV/c)
$\Lambda_c^+ \pi^+ \pi^-$	$\approx 67\%$		184
$\Sigma_c(2455)^{++} \pi^-$	$< 5$	90%	102
$\Sigma_c(2455)^0 \pi^+$	$< 5$	90%	102
$\Lambda_c^+ \pi^+ \pi^-$ 3-body	large		184
$\Lambda_c^+ \pi^0$	[i] not seen		293
$\Lambda_c^+ \gamma$	not seen		319

$$\Lambda_c(2860)^+ \quad I(J^P) = 0(\frac{3}{2}^+)$$

$$\begin{aligned} \text{Mass } m &= 2856.1_{-6.0}^{+2.3} \text{ MeV} \\ \text{Full width } \Gamma &= 68_{-22}^{+12} \text{ MeV} \end{aligned}$$

$\Lambda_c(2860)^+$ DECAY MODES	Fraction ( $\Gamma_i/\Gamma$ )	$\rho$ (MeV/c)
$D^0 p$	seen	259

$$\Lambda_c(2880)^+ \quad I(J^P) = 0(\frac{5}{2}^+)$$

$$\begin{aligned} \text{Mass } m &= 2881.63 \pm 0.24 \text{ MeV} \\ m - m_{\Lambda_c^+} &= 595.17 \pm 0.28 \text{ MeV} \\ \text{Full width } \Gamma &= 5.6_{-0.6}^{+0.8} \text{ MeV} \end{aligned}$$

$\Lambda_c(2880)^+$ DECAY MODES	Fraction ( $\Gamma_i/\Gamma$ )	$\rho$ (MeV/c)
$\Lambda_c^+ \pi^+ \pi^-$	seen	471
$\Sigma_c(2455)^0, ++ \pi^\pm$	seen	376
$\Sigma_c(2520)^0, ++ \pi^\pm$	seen	317
$p D^0$	seen	316

$$\Lambda_c(2940)^+ \quad I(J^P) = 0(\frac{3}{2}^-)$$

$J^P = 3/2^-$  is favored, but is not certain

$$\begin{aligned} \text{Mass } m &= 2939.6_{-1.5}^{+1.3} \text{ MeV} \\ \text{Full width } \Gamma &= 20_{-9}^{+6} \text{ MeV} \end{aligned}$$

$\Lambda_c(2940)^+$ DECAY MODES	Fraction ( $\Gamma_i/\Gamma$ )	$\rho$ (MeV/c)
$p D^0$	seen	420
$\Sigma_c(2455)^0, ++ \pi^\pm$	seen	—

$$\Sigma_c(2455) \quad I(J^P) = 1(\frac{1}{2}^+)$$

$$\begin{aligned} \Sigma_c(2455)^{++} \text{ mass } m &= 2453.97 \pm 0.14 \text{ MeV} \\ \Sigma_c(2455)^+ \text{ mass } m &= 2452.9 \pm 0.4 \text{ MeV} \\ \Sigma_c(2455)^0 \text{ mass } m &= 2453.75 \pm 0.14 \text{ MeV} \end{aligned}$$

$$m_{\Sigma_c^{++}} - m_{\Lambda_c^+} = 167.510 \pm 0.017 \text{ MeV}$$

$$m_{\Sigma_c^+} - m_{\Lambda_c^+} = 166.4 \pm 0.4 \text{ MeV}$$

$$m_{\Sigma_c^0} - m_{\Lambda_c^+} = 167.290 \pm 0.017 \text{ MeV}$$

$$m_{\Sigma_c^{++}} - m_{\Sigma_c^0} = 0.220 \pm 0.013 \text{ MeV}$$

$$m_{\Sigma_c^+} - m_{\Sigma_c^0} = -0.9 \pm 0.4 \text{ MeV}$$

$$\Sigma_c(2455)^{++} \text{ full width } \Gamma = 1.89_{-0.18}^{+0.09} \text{ MeV} \quad (S = 1.1)$$

$$\Sigma_c(2455)^+ \text{ full width } \Gamma < 4.6 \text{ MeV, CL} = 90\%$$

$$\Sigma_c(2455)^0 \text{ full width } \Gamma = 1.83_{-0.19}^{+0.11} \text{ MeV} \quad (S = 1.2)$$

$\Lambda_c^+ \pi$  is the only strong decay allowed to a  $\Sigma_c$  having this mass.

$\Sigma_c(2455)$ DECAY MODES	Fraction ( $\Gamma_i/\Gamma$ )	$\rho$ (MeV/c)
$\Lambda_c^+ \pi$	$\approx 100\%$	94

$$\Sigma_c(2520) \quad I(J^P) = 1(\frac{3}{2}^+)$$

$J^P$  has not been measured;  $\frac{3}{2}^+$  is the quark-model prediction.

$$\Sigma_c(2520)^{++} \text{ mass } m = 2518.41_{-0.19}^{+0.21} \text{ MeV} \quad (S = 1.1)$$

$$\Sigma_c(2520)^+ \text{ mass } m = 2517.5 \pm 2.3 \text{ MeV}$$

$$\Sigma_c(2520)^0 \text{ mass } m = 2518.48 \pm 0.20 \text{ MeV} \quad (S = 1.1)$$

$$m_{\Sigma_c(2520)^{++}} - m_{\Lambda_c^+} = 231.95_{-0.12}^{+0.17} \text{ MeV} \quad (S = 1.3)$$

$$m_{\Sigma_c(2520)^+} - m_{\Lambda_c^+} = 231.0 \pm 2.3 \text{ MeV}$$

$$m_{\Sigma_c(2520)^0} - m_{\Lambda_c^+} = 232.02_{-0.14}^{+0.15} \text{ MeV} \quad (S = 1.3)$$

$$m_{\Sigma_c(2520)^{++}} - m_{\Sigma_c(2520)^0} = 0.01 \pm 0.15 \text{ MeV}$$

$$\Sigma_c(2520)^{++} \text{ full width } \Gamma = 14.78_{-0.40}^{+0.30} \text{ MeV}$$

$$\Sigma_c(2520)^+ \text{ full width } \Gamma < 17 \text{ MeV, CL} = 90\%$$

$$\Sigma_c(2520)^0 \text{ full width } \Gamma = 15.3_{-0.5}^{+0.4} \text{ MeV}$$

$\Lambda_c^+ \pi$  is the only strong decay allowed to a  $\Sigma_c$  having this mass.

$\Sigma_c(2520)$ DECAY MODES	Fraction ( $\Gamma_i/\Gamma$ )	$\rho$ (MeV/c)
$\Lambda_c^+ \pi$	$\approx 100\%$	179

$$\Sigma_c(2800) \quad I(J^P) = 1(2^?)$$

$$\Sigma_c(2800)^{++} \text{ mass } m = 2801_{-6}^{+4} \text{ MeV}$$

$$\Sigma_c(2800)^+ \text{ mass } m = 2792_{-5}^{+14} \text{ MeV}$$

$$\Sigma_c(2800)^0 \text{ mass } m = 2806_{-7}^{+5} \text{ MeV} \quad (S = 1.3)$$

$$m_{\Sigma_c(2800)^{++}} - m_{\Lambda_c^+} = 514_{-6}^{+4} \text{ MeV}$$

$$m_{\Sigma_c(2800)^+} - m_{\Lambda_c^+} = 505_{-5}^{+14} \text{ MeV}$$

$$m_{\Sigma_c(2800)^0} - m_{\Lambda_c^+} = 519_{-7}^{+5} \text{ MeV} \quad (S = 1.3)$$

$$\Sigma_c(2800)^{++} \text{ full width } \Gamma = 75_{-17}^{+22} \text{ MeV}$$

$$\Sigma_c(2800)^+ \text{ full width } \Gamma = 62_{-40}^{+60} \text{ MeV}$$

$$\Sigma_c(2800)^0 \text{ full width } \Gamma = 72_{-15}^{+22} \text{ MeV}$$

$\Sigma_c(2800)$ DECAY MODES	Fraction ( $\Gamma_i/\Gamma$ )	$\rho$ (MeV/c)
$\Lambda_c^+ \pi$	seen	443

$$\Xi_c^+ \quad I(J^P) = \frac{1}{2}(\frac{1}{2}^+)$$

$J^P$  has not been measured;  $\frac{1}{2}^+$  is the quark-model prediction.

$$\text{Mass } m = 2467.94_{-0.20}^{+0.17} \text{ MeV}$$

$$\text{Mean life } \tau = (456 \pm 5) \times 10^{-15} \text{ s}$$

$$c\tau = 136.6 \mu\text{m}$$

Branching fractions marked with a footnote, e.g. [a], have been corrected for decay modes not observed in the experiments. For example, the submode fraction  $\Xi_c^+ \rightarrow \Sigma^+ \bar{K}^*(892)^0$  seen in  $\Xi_c^+ \rightarrow \Sigma^+ K^- \pi^+$  has been multiplied up to include  $\bar{K}^*(892)^0 \rightarrow \bar{K}^0 \pi^0$  decays.

## Baryon Summary Table

$\Xi_c^{\pm}$ DECAY MODES	Fraction ( $\Gamma_i/\Gamma$ )	Confidence level	$\rho$ (MeV/c)
---------------------------	--------------------------------	------------------	----------------

No absolute branching fractions have been measured.  
The following are branching ratios relative to  $\Xi^- 2\pi^+$ .

Cabibbo-favored ( $S = -2$ ) decays — relative to  $\Xi^- 2\pi^+$ 

$p 2K_S^0$		0.087 ± 0.021	767
$\Lambda \bar{K}^0 \pi^+$		—	852
$\Sigma(1385)^+ \bar{K}^0$	[r]	1.0 ± 0.5	746
$\Lambda K^- 2\pi^+$		0.323 ± 0.033	787
$\Lambda \bar{K}^*(892)^0 \pi^+$	[r]	< 0.16	90%
$\Sigma(1385)^+ K^- \pi^+$	[r]	< 0.23	90%
$\Sigma^+ K^- \pi^+$		0.94 ± 0.10	811
$\Sigma^+ \bar{K}^*(892)^0$	[r]	0.81 ± 0.15	658
$\Sigma^0 K^- 2\pi^+$		0.27 ± 0.12	735
$\Xi^0 \pi^+$		0.55 ± 0.16	877
$\Xi^- 2\pi^+$		<b>DEFINED AS 1</b>	851
$\Xi(1530)^0 \pi^+$	[r]	< 0.10	90%
$\Xi(1620)^0 \pi^+$		seen	—
$\Xi(1690)^0 \pi^+$		seen	644
$\Xi^0 \pi^+ \pi^0$		2.3 ± 0.7	856
$\Xi^0 \pi^- 2\pi^+$		1.7 ± 0.5	818
$\Xi^0 e^+ \nu_e$		2.3 $\begin{smallmatrix} +0.7 \\ -0.8 \end{smallmatrix}$	884
$\Omega^- K^+ \pi^+$		0.07 ± 0.04	399

Cabibbo-suppressed decays — relative to  $\Xi^- 2\pi^+$ 

$p K^- \pi^+$		0.0045 ± 0.0022	944
$p \bar{K}^*(892)^0$	[r]	0.0024 ± 0.0013	828
$\Sigma^+ \pi^+ \pi^-$		0.48 ± 0.20	922
$\Sigma^- 2\pi^+$		0.18 ± 0.09	918
$\Sigma^+ K^+ K^-$		0.15 ± 0.06	580
$\Sigma^+ \phi$	[r]	< 0.11	90%
$\Xi(1690)^0 K^+, \Xi^0 \rightarrow \Sigma^+ K^-$		< 0.05	90%
$p \phi(1020)$	(9 ± 4)	$\times 10^{-5}$	751

$\Xi_c^0$

$$I(J^P) = \frac{1}{2}(\frac{1}{2}^+)$$

$J^P$  has not been measured;  $\frac{1}{2}^+$  is the quark-model prediction.

$$\text{Mass } m = 2470.90 \pm_{-0.29}^{+0.22} \text{ MeV}$$

$$m_{\Xi_c^0} - m_{\Xi_c^+} = 2.96 \pm 0.22 \text{ MeV}$$

$$\text{Mean life } \tau = (153 \pm 6) \times 10^{-15} \text{ s } (S = 2.4)$$

$$c\tau = 45.8 \mu\text{m}$$

## Decay asymmetry parameters

$$\Xi^- \pi^+ \quad \alpha = -0.6 \pm 0.4$$

$\Xi_c^0$ DECAY MODES	Fraction ( $\Gamma_i/\Gamma$ )	Scale factor	$\rho$ (MeV/c)
-----------------------	--------------------------------	--------------	----------------

Cabibbo-favored ( $S = -2$ ) decays

$p K^- K^- \pi^+$	(4.8 ± 1.2) × 10 <sup>-3</sup>	1.1	676
$p K^- \bar{K}^*(892)^0, \bar{K}^{*0} \rightarrow K^- \pi^+$	(2.0 ± 0.6) × 10 <sup>-3</sup>		413
$p K^- K^- \pi^+$ (no $\bar{K}^{*0}$ )	(3.0 ± 0.9) × 10 <sup>-3</sup>		676
$\Lambda K_S^0$	(3.0 ± 0.8) × 10 <sup>-3</sup>		906
$\Lambda K^- \pi^+$	(1.45 ± 0.33) %	1.1	856
$\Lambda \bar{K}^0 \pi^+ \pi^-$	seen		787
$\Lambda K^- \pi^+ \pi^+ \pi^-$	seen		703
$\Xi^- \pi^+$	(1.43 ± 0.32) %	1.1	875
$\Xi^- \pi^+ \pi^+ \pi^-$	(4.8 ± 2.3) %		816
$\Omega^- K^+$	(4.2 ± 1.0) × 10 <sup>-3</sup>		522
$\Xi^- e^+ \nu_e$	(1.8 ± 1.2) %		882

## Cabibbo-suppressed decays

$\Xi^- K^+$	(3.9 ± 1.2) × 10 <sup>-4</sup>		790
$\Lambda K^+ K^-$ (no $\phi$ )	(4.1 ± 1.4) × 10 <sup>-4</sup>		648
$\Lambda \phi$	(4.9 ± 1.5) × 10 <sup>-4</sup>		621

$\Xi_c^{\pm}$

$$I(J^P) = \frac{1}{2}(\frac{1}{2}^+)$$

$J^P$  has not been measured;  $\frac{1}{2}^+$  is the quark-model prediction.

$$\text{Mass } m = 2578.4 \pm 0.5 \text{ MeV}$$

$$m_{\Xi_c^{\pm}} - m_{\Xi_c^{\mp}} = 110.5 \pm 0.4 \text{ MeV}$$

$$m_{\Xi_c^{\pm}} - m_{\Xi_c^0} = -0.8 \pm 0.6 \text{ MeV}$$

The  $\Xi_c^{\pm} - \Xi_c^0$  mass difference is too small for any strong decay to occur.

$\Xi_c^{\pm}$ DECAY MODES	Fraction ( $\Gamma_i/\Gamma$ )	$\rho$ (MeV/c)
$\Xi_c^{\pm} \gamma$	seen	108

$\Xi_c^0$

$$I(J^P) = \frac{1}{2}(\frac{1}{2}^+)$$

$J^P$  has not been measured;  $\frac{1}{2}^+$  is the quark-model prediction.

$$\text{Mass } m = 2579.2 \pm 0.5 \text{ MeV}$$

$$m_{\Xi_c^0} - m_{\Xi_c^+} = 108.3 \pm 0.4 \text{ MeV}$$

The  $\Xi_c^0 - \Xi_c^+$  mass difference is too small for any strong decay to occur.

$\Xi_c^0$ DECAY MODES	Fraction ( $\Gamma_i/\Gamma$ )	$\rho$ (MeV/c)
$\Xi_c^0 \gamma$	seen	106

$\Xi_c(2645)$

$$I(J^P) = \frac{1}{2}(\frac{3}{2}^+)$$

$J^P$  has not been measured;  $\frac{3}{2}^+$  is the quark-model prediction.

$$\Xi_c(2645)^+ \text{ mass } m = 2645.56 \pm_{-0.30}^{+0.24} \text{ MeV}$$

$$\Xi_c(2645)^0 \text{ mass } m = 2646.38 \pm_{-0.23}^{+0.20} \text{ MeV } (S = 1.1)$$

$$m_{\Xi_c(2645)^+} - m_{\Xi_c^0} = 174.66 \pm 0.09 \text{ MeV}$$

$$m_{\Xi_c(2645)^0} - m_{\Xi_c^+} = 178.44 \pm 0.10 \text{ MeV}$$

$$m_{\Xi_c(2645)^+} - m_{\Xi_c(2645)^0} = -0.82 \pm 0.26 \text{ MeV}$$

$$\Xi_c(2645)^+ \text{ full width } \Gamma = 2.14 \pm 0.19 \text{ MeV } (S = 1.1)$$

$$\Xi_c(2645)^0 \text{ full width } \Gamma = 2.35 \pm 0.22 \text{ MeV}$$

$\Xi_c \pi$  is the only strong decay allowed to a  $\Xi_c$  resonance having this mass.

$\Xi_c(2645)$ DECAY MODES	Fraction ( $\Gamma_i/\Gamma$ )	$\rho$ (MeV/c)
$\Xi_c^0 \pi^+$	seen	102
$\Xi_c^+ \pi^-$	seen	106

$\Xi_c(2790)$

$$I(J^P) = \frac{1}{2}(\frac{1}{2}^-)$$

$J^P$  has not been measured;  $\frac{1}{2}^-$  is the quark-model prediction.

$$\Xi_c(2790)^+ \text{ mass } = 2792.4 \pm 0.5 \text{ MeV}$$

$$\Xi_c(2790)^0 \text{ mass } = 2794.1 \pm 0.5 \text{ MeV}$$

$$m_{\Xi_c(2790)^+} - m_{\Xi_c^0} = 213.20 \pm 0.22 \text{ MeV}$$

$$m_{\Xi_c(2790)^0} - m_{\Xi_c^+} = 215.70 \pm 0.22 \text{ MeV}$$

$$m_{\Xi_c(2790)^+} - m_{\Xi_c(2790)^0} = -1.7 \pm 0.7 \text{ MeV}$$

$$\Xi_c(2790)^+ \text{ width } = 8.9 \pm 1.0 \text{ MeV}$$

$$\Xi_c(2790)^0 \text{ width } = 10.0 \pm 1.1 \text{ MeV}$$

$\Xi_c(2790)$ DECAY MODES	Fraction ( $\Gamma_i/\Gamma$ )	$\rho$ (MeV/c)
$\Xi_c^- \pi$	seen	160

$\Xi_c(2815)$

$$I(J^P) = \frac{1}{2}(\frac{3}{2}^-)$$

$J^P$  has not been measured;  $\frac{3}{2}^-$  is the quark-model prediction.

$$\Xi_c(2815)^+ \text{ mass } m = 2816.74 \pm_{-0.23}^{+0.20} \text{ MeV}$$

$$\Xi_c(2815)^0 \text{ mass } m = 2820.25 \pm_{-0.31}^{+0.29} \text{ MeV}$$

$$m_{\Xi_c(2815)^+} - m_{\Xi_c^+} = 348.80 \pm 0.10 \text{ MeV}$$

$$m_{\Xi_c(2815)^0} - m_{\Xi_c^0} = 349.35 \pm 0.11 \text{ MeV}$$

$$m_{\Xi_c(2815)^+} - m_{\Xi_c(2815)^0} = -3.51 \pm 0.26 \text{ MeV}$$

$$\Xi_c(2815)^+ \text{ full width } \Gamma = 2.43 \pm 0.26 \text{ MeV}$$

$$\Xi_c(2815)^0 \text{ full width } \Gamma = 2.54 \pm 0.25 \text{ MeV}$$

The  $\Xi_c \pi \pi$  modes are consistent with being entirely via  $\Xi_c(2645) \pi$ .

$\Xi_c(2815)$ DECAY MODES	Fraction ( $\Gamma_i/\Gamma$ )	$\rho$ (MeV/c)
$\Xi_c^- \pi$	seen	188
$\Xi_c(2645) \pi$	seen	102



## Baryon Summary Table

$$\Xi_c(2970) \quad I(J^P) = \frac{1}{2}(??)$$

was  $\Xi_c(2980)$ 

$$\Xi_c(2970)^+ m = 2966.34^{+0.17}_{-1.00} \text{ MeV}$$

$$\Xi_c(2970)^0 m = 2970.9^{+0.4}_{-0.6} \text{ MeV}$$

$$\quad m_{\Xi_c(2970)^+} - m_{\Xi_c^+} = 498.40^{+0.27}_{-0.90} \text{ MeV}$$

$$\quad m_{\Xi_c(2970)^0} - m_{\Xi_c^0} = 500.0^{+0.4}_{-0.6} \text{ MeV}$$

$$m_{\Xi_c(2970)^+} - m_{\Xi_c(2970)^0} = -4.6^{+0.4}_{-0.6} \text{ MeV}$$

$$\Xi_c(2970)^+ \text{ width } \Gamma = 20.9^{+2.4}_{-3.5} \text{ MeV} \quad (S = 1.2)$$

$$\Xi_c(2970)^0 \text{ width } \Gamma = 28.1^{+3.4}_{-4.0} \text{ MeV} \quad (S = 1.5)$$

$\Xi_c(2970)$ DECAY MODES	Fraction ( $\Gamma_i/\Gamma$ )	$\rho$ (MeV/c)
$\Lambda_c^+ \bar{K} \pi$	seen	228
$\Sigma_c(2455) \bar{K}$	seen	128
$\Lambda_c^+ \bar{K}$	not seen	412
$\Xi_c 2\pi$	seen	383
$\Xi_c' \pi$	seen	—
$\Xi_c(2645) \pi$	seen	275

$$\Xi_c(3055) \quad I(J^P) = ??(??)$$

$$\text{Mass } m = 3055.9 \pm 0.4 \text{ MeV}$$

$$\text{Full width } \Gamma = 7.8 \pm 1.9 \text{ MeV}$$

$\Xi_c(3055)$ DECAY MODES	Fraction ( $\Gamma_i/\Gamma$ )	$\rho$ (MeV/c)
$\Sigma^{++} K^-$	seen	—
$\Lambda D^+$	seen	316

$$\Xi_c(3080) \quad I(J^P) = \frac{1}{2}(??)$$

$$\Xi_c(3080)^+ m = 3077.2 \pm 0.4 \text{ MeV}$$

$$\Xi_c(3080)^0 m = 3079.9 \pm 1.4 \text{ MeV} \quad (S = 1.3)$$

$$\Xi_c(3080)^+ \text{ width } \Gamma = 3.6 \pm 1.1 \text{ MeV} \quad (S = 1.5)$$

$$\Xi_c(3080)^0 \text{ width } \Gamma = 5.6 \pm 2.2 \text{ MeV}$$

$\Xi_c(3080)$ DECAY MODES	Fraction ( $\Gamma_i/\Gamma$ )	$\rho$ (MeV/c)
$\Lambda_c^+ \bar{K} \pi$	seen	415
$\Sigma_c(2455) \bar{K}$	seen	342
$\Sigma_c(2455)^{++} K^-$	seen	342
$\Sigma_c(2520)^{++} K^-$	seen	239
$\Sigma_c(2455) \bar{K} + \Sigma_c(2520) \bar{K}$	seen	—
$\Lambda_c^+ \bar{K}$	not seen	536
$\Lambda_c^+ \bar{K} \pi^+ \pi^-$	not seen	144
$\Lambda D^+$	seen	362

$$\Omega_c^0 \quad I(J^P) = 0(\frac{1}{2}^+)$$

$J^P$  has not been measured;  $\frac{1}{2}^+$  is the quark-model prediction.

$$\text{Mass } m = 2695.2 \pm 1.7 \text{ MeV} \quad (S = 1.3)$$

$$\text{Mean life } \tau = (268 \pm 26) \times 10^{-15} \text{ s}$$

$$c\tau = 80 \mu\text{m}$$

$\Omega_c^0$ DECAY MODES	Fraction ( $\Gamma_i/\Gamma$ )	Confidence level	$\rho$ (MeV/c)
--------------------------	--------------------------------	------------------	----------------

No absolute branching fractions have been measured.  
The following are branching ratios relative to  $\Omega^- \pi^+$ .

Cabibbo-favored ( $S = -3$ ) decays — relative to  $\Omega^- \pi^+$

	DEFINED AS 1		
$\Omega^- \pi^+$	1.80 ± 0.33		821
$\Omega^- \pi^+ \pi^0$	>1.3	90%	797
$\Omega^- \rho^+$	0.31 ± 0.05		753
$\Omega^- \pi^- 2\pi^+$	2.4 ± 1.2		829
$\Omega^- e^+ \nu_e$	1.64 ± 0.29		950
$\Xi^0 \bar{K}^0$	1.20 ± 0.18		901
$\Xi^0 K^- \pi^+$	0.68 ± 0.16		764
$\Xi^0 \bar{K}^{*0}, \bar{K}^{*0} \rightarrow K^- \pi^+$	2.12 ± 0.28		895

$\Xi^- K^- 2\pi^+$	0.63 ± 0.09	830
$\Xi(1530)^0 K^- \pi^+, \Xi^{*0} \rightarrow$	0.21 ± 0.06	757
$\Xi^- \bar{K}^{*0} \pi^+$	0.34 ± 0.11	653
$\Sigma^+ K^- K^- \pi^+$	<0.32	90% 689
$\Lambda \bar{K}^0 \bar{K}^0$	1.72 ± 0.35	837

$$\Omega_c(2770)^0 \quad I(J^P) = 0(\frac{3}{2}^+)$$

$J^P$  has not been measured;  $\frac{3}{2}^+$  is the quark-model prediction.

$$\text{Mass } m = 2765.9 \pm 2.0 \text{ MeV} \quad (S = 1.2)$$

$$m_{\Omega_c(2770)^0} - m_{\Omega_c^0} = 70.7^{+0.8}_{-0.9} \text{ MeV}$$

The  $\Omega_c(2770)^0 - \Omega_c^0$  mass difference is too small for any strong decay to occur.

$\Omega_c(2770)^0$ DECAY MODES	Fraction ( $\Gamma_i/\Gamma$ )	$\rho$ (MeV/c)
$\Omega_c^0 \gamma$	presumably 100%	70

$$\Omega_c(3000)^0 \quad I(J^P) = ??(??)$$

$$\text{Mass } m = 3000.41 \pm 0.22 \text{ MeV}$$

$$\text{Full width } \Gamma = 4.5 \pm 0.7 \text{ MeV}$$

$\Omega_c(3000)^0$ DECAY MODES	Fraction ( $\Gamma_i/\Gamma$ )	$\rho$ (MeV/c)
$\Xi_c^+ K^-$	seen	181

$$\Omega_c(3050)^0 \quad I(J^P) = ??(??)$$

$$\text{Mass } m = 3050.20 \pm 0.13 \text{ MeV}$$

$$\text{Full width } \Gamma < 1.2 \text{ MeV, CL} = 95\%$$

$\Omega_c(3050)^0$ DECAY MODES	Fraction ( $\Gamma_i/\Gamma$ )	$\rho$ (MeV/c)
$\Xi_c^+ K^-$	seen	278

$$\Omega_c(3065)^0 \quad I(J^P) = ??(??)$$

$$\text{Mass } m = 3065.46 \pm 0.28 \text{ MeV}$$

$$\text{Full width } \Gamma = 3.5 \pm 0.4 \text{ MeV}$$

$\Omega_c(3065)^0$ DECAY MODES	Fraction ( $\Gamma_i/\Gamma$ )	$\rho$ (MeV/c)
$\Xi_c^+ K^-$	seen	303

$$\Omega_c(3090)^0 \quad I(J^P) = ??(??)$$

$$\text{Mass } m = 3090.0 \pm 0.5 \text{ MeV}$$

$$\text{Full width } \Gamma = 8.7 \pm 1.3 \text{ MeV}$$

$\Omega_c(3090)^0$ DECAY MODES	Fraction ( $\Gamma_i/\Gamma$ )	$\rho$ (MeV/c)
$\Xi_c^+ K^-$	seen	339

$$\Omega_c(3120)^0 \quad I(J^P) = ??(??)$$

$$\text{Mass } m = 3119.1 \pm 1.0 \text{ MeV}$$

$$\text{Full width } \Gamma < 2.6 \text{ MeV, CL} = 95\%$$

$\Omega_c(3120)^0$ DECAY MODES	Fraction ( $\Gamma_i/\Gamma$ )	$\rho$ (MeV/c)
$\Xi_c^+ K^-$	seen	379

## DOUBLY CHARMED BARYONS ( $C = +2$ )

$$\Xi_{cc}^{++} = ucc, \Xi_{cc}^+ = dcc, \Omega_{cc}^+ = scc$$

$$\Xi_{cc}^{++} \quad I(J^P) = ??(??)$$

$$\text{Mass } m = 3621.2 \pm 0.7 \text{ MeV}$$

$$\text{Mean life } \tau = (256 \pm 27) \times 10^{-15} \text{ s}$$

## Baryon Summary Table

$\Xi_{cc}^{++}$ DECAY MODES	Fraction ( $\Gamma_i/\Gamma$ )	$\rho$ (MeV/c)
$\Lambda_c^+ K^- \pi^+ \pi^+$	seen	880
$\Xi_c^+ \pi^+, \Xi_c^+ \rightarrow p K^- \pi^+$	seen	-

## BOTTOM BARYONS ( $B = -1$ )

$$\Lambda_b^0 = udb, \Xi_b^0 = usb, \Xi_b^- = dsb, \Omega_b^- = ssb$$

$\Lambda_b^0$

$$I(J^P) = 0(\frac{1}{2}^+)$$

$I(J^P)$  not yet measured;  $0(\frac{1}{2}^+)$  is the quark model prediction.

Mass  $m = 5619.60 \pm 0.17$  MeV

$$m_{\Lambda_b^0} - m_{B^0} = 339.2 \pm 1.4 \text{ MeV}$$

$$m_{\Lambda_b^0} - m_{B^+} = 339.72 \pm 0.28 \text{ MeV}$$

$$\text{Mean life } \tau = (1.471 \pm 0.009) \times 10^{-12} \text{ s}$$

$$c\tau = 441.0 \text{ } \mu\text{m}$$

$$A_{CP}(\Lambda_b \rightarrow p\pi^-) = -0.025 \pm 0.029 \quad (S = 1.2)$$

$$A_{CP}(\Lambda_b \rightarrow pK^-) = -0.025 \pm 0.022$$

$$\Delta A_{CP}(pK^-/\pi^-) = 0.014 \pm 0.024$$

$$A_{CP}(\Lambda_b \rightarrow p\bar{K}^0\pi^-) = 0.22 \pm 0.13$$

$$\Delta A_{CP}(J/\psi p\pi^-/K^-) = (5.7 \pm 2.7) \times 10^{-2}$$

$$A_{CP}(\Lambda_b \rightarrow \Lambda K^+\pi^-) = -0.53 \pm 0.25$$

$$A_{CP}(\Lambda_b \rightarrow \Lambda K^+K^-) = -0.28 \pm 0.12$$

$$\Delta A_{CP}(\Lambda_b^0 \rightarrow pK^- \mu^+ \mu^-) = (-4 \pm 5) \times 10^{-2}$$

$$\Delta A_{CP}(\Lambda_b^0 \rightarrow p\pi^- \pi^+ \pi^-) = (1.1 \pm 2.6) \times 10^{-2}$$

$$\Delta A_{CP}(\Lambda_b^0 \rightarrow (p\pi^- \pi^+ \pi^-)_{LBM}) = (4 \pm 4) \times 10^{-2}$$

$$\Delta A_{CP}(\Lambda_b^0 \rightarrow p a_1(1260)^- ) = (-1 \pm 4) \times 10^{-2}$$

$$\Delta A_{CP}(\Lambda_b^0 \rightarrow N(1520)^0 \rho(770)^0 ) = (2 \pm 5) \times 10^{-2}$$

$$\Delta A_{CP}(\Lambda_b^0 \rightarrow \Delta(1232)^{++} \pi^- \pi^-) = (0.1 \pm 3.3) \times 10^{-2}$$

$$\Delta A_{CP}(\Lambda_b^0 \rightarrow pK^- \pi^+ \pi^-) = (3.2 \pm 1.3) \times 10^{-2}$$

$$\Delta A_{CP}(\Lambda_b^0 \rightarrow (pK^- \pi^+ \pi^-)_{LBM}) = (3.5 \pm 1.6) \times 10^{-2}$$

$$\Delta A_{CP}(\Lambda_b^0 \rightarrow N(1520)^0 K^*(892)^0 ) = (5.5 \pm 2.5) \times 10^{-2}$$

$$\Delta A_{CP}(\Lambda_b^0 \rightarrow \Lambda(1520) \rho(770)^0 ) = (1 \pm 6) \times 10^{-2}$$

$$\Delta A_{CP}(\Lambda_b^0 \rightarrow \Delta(1232)^{++} K^- \pi^-) = (4.4 \pm 2.7) \times 10^{-2}$$

$$\Delta A_{CP}(\Lambda_b^0 \rightarrow pK_1(1410)^-) = (5 \pm 4) \times 10^{-2}$$

$$\Delta A_{CP}(\Lambda_b^0 \rightarrow pK^- K^+ \pi^-) = (-7 \pm 5) \times 10^{-2}$$

$$\Delta A_{CP}(\Lambda_b^0 \rightarrow pK^- K^+ K^-) = (0.2 \pm 1.9) \times 10^{-2}$$

$$\Delta A_{CP}(\Lambda_b^0 \rightarrow \Lambda(1520) \phi(1020)) = (4 \pm 6) \times 10^{-2}$$

$$\Delta A_{CP}(\Lambda_b^0 \rightarrow (pK^-)_{\text{highmass}} \phi(1020)) = (-0.7 \pm 3.4) \times 10^{-2}$$

$$\Delta A_{CP}(\Lambda_b^0 \rightarrow (pK^- K^+ K^-)_{LBM}) = (2.7 \pm 2.4) \times 10^{-2}$$

$$A_{FB}^{\ell}(\mu\mu) \text{ in } \Lambda_b \rightarrow \Lambda \mu^+ \mu^- = -0.39 \pm 0.04$$

$$\Delta(A_{FB}^{\ell}(\mu\mu)) \text{ in } \Lambda_b \rightarrow \Lambda \mu^+ \mu^- = -0.05 \pm 0.09$$

$$A_{FB}^{\ell}(p\pi) \text{ in } \Lambda_b \rightarrow \Lambda(p\pi) \mu^+ \mu^- = -0.30 \pm 0.05$$

$$A_{FB}^{\text{th}} \text{ in } \Lambda_b \rightarrow \Lambda \mu^+ \mu^- = 0.25 \pm 0.04$$

The branching fractions  $B(b\text{-baryon} \rightarrow \Lambda_c \ell^- \bar{\nu}_\ell \text{ anything})$  and  $B(\Lambda_b^0 \rightarrow \Lambda_c^+ \ell^- \bar{\nu}_\ell \text{ anything})$  are not pure measurements because the underlying measured products of these with  $B(b \rightarrow b\text{-baryon})$  were used to determine  $B(b \rightarrow b\text{-baryon})$ , as described in the note "Production and Decay of  $b$ -Flavored Hadrons."

For inclusive branching fractions, e.g.,  $\Lambda_b \rightarrow \bar{\Lambda}_c \text{ anything}$ , the values usually are multiplicities, not branching fractions. They can be greater than one.

$\Lambda_b^0$ DECAY MODES	Fraction ( $\Gamma_i/\Gamma$ )	Scale factor/ Confidence level	$\rho$ (MeV/c)
$J/\psi(1S) \Lambda \times B(b \rightarrow \Lambda_b^0)$	$(5.8 \pm 0.8) \times 10^{-5}$		1740
$pD^0 \pi^-$	$(6.3 \pm 0.7) \times 10^{-4}$		2370
$pD^0 K^-$	$(4.6 \pm 0.8) \times 10^{-5}$		2269
$pJ/\psi \pi^-$	$(2.6 \pm 0.5) \times 10^{-5}$		1755
$p\pi^- J/\psi, J/\psi \rightarrow \mu^+ \mu^-$	$(1.6 \pm 0.8) \times 10^{-6}$		-
$pJ/\psi K^-$	$(3.2 \pm 0.6) \times 10^{-4}$		1589
$P_c(4380)^+ K^-, P_c \rightarrow pJ/\psi$	[u] $(2.7 \pm 1.4) \times 10^{-5}$		-
$P_c(4450)^+ K^-, P_c \rightarrow pJ/\psi$	[u] $(1.3 \pm 0.4) \times 10^{-5}$		-
$\chi_{c1}(1P) pK^-$	$(7.6 \pm 1.5) \times 10^{-5}$		1242
$\chi_{c2}(1P) pK^-$	$(7.9 \pm 1.6) \times 10^{-5}$		1198

$pJ/\psi(1S) \pi^+ \pi^- K^-$	$(6.6 \pm 1.3) \times 10^{-5}$		1410
$p\psi(2S) K^-$	$(6.6 \pm 1.2) \times 10^{-5}$		1063
$\chi_{c1}(3872) pK^-, \chi_{c1}(3872) \rightarrow J/\psi \pi^+ \pi^-$	$(1.23 \pm 0.33) \times 10^{-6}$		-
$\psi(2S) p\pi^-$	$(7.5 \pm 1.6) \times 10^{-6}$		1320
$p\bar{K}^0 \pi^-$	$(1.3 \pm 0.4) \times 10^{-5}$		2693
$pK^0 K^-$	$< 3.5 \times 10^{-6}$	CL=90%	2639
$\Lambda_c^+ \pi^-$	$(4.9 \pm 0.4) \times 10^{-3}$	S=1.2	2342
$\Lambda_c^+ K^-$	$(3.59 \pm 0.30) \times 10^{-4}$	S=1.2	2314
$\Lambda_c^+ a_1(1260)^-$	seen		2153
$\Lambda_c^+ D^-$	$(4.6 \pm 0.6) \times 10^{-4}$		1886
$\Lambda_c^+ D_s^-$	$(1.10 \pm 0.10) \%$		1833
$\Lambda_c^+ \pi^+ \pi^- \pi^-$	$(7.7 \pm 1.1) \times 10^{-3}$	S=1.1	2323
$\Lambda_c(2595)^+ \pi^-$	$(3.4 \pm 1.5) \times 10^{-4}$		2210
$\Lambda_c(2595)^+ \rightarrow \Lambda_c^+ \pi^+ \pi^-$			
$\Lambda_c(2625)^+ \pi^-$	$(3.3 \pm 1.3) \times 10^{-4}$		2193
$\Lambda_c(2625)^+ \rightarrow \Lambda_c^+ \pi^+ \pi^-$			
$\Sigma_c(2455)^0 \pi^+ \pi^-, \Sigma_c^0 \rightarrow \Lambda_c^+ \pi^-$	$(5.7 \pm 2.2) \times 10^{-4}$		2265
$\Sigma_c(2455)^{++} \pi^- \pi^-, \Sigma_c^{++} \rightarrow \Lambda_c^+ \pi^+$	$(3.2 \pm 1.6) \times 10^{-4}$		2265
$\Lambda_c^+ p \bar{p} \pi^-$	$(2.65 \pm 0.29) \times 10^{-4}$		1805
$\Sigma_c(2455)^0 p \bar{p}, \Sigma_c(2455)^0 \rightarrow \Lambda_c^+ \pi^-$	$(2.4 \pm 0.5) \times 10^{-5}$		-
$\Sigma_c(2520)^0 p \bar{p}, \Sigma_c(2520)^0 \rightarrow \Lambda_c^+ \pi^-$	$(3.2 \pm 0.7) \times 10^{-5}$		-
$\Lambda_c^+ \ell^- \bar{\nu}_\ell \text{ anything}$	[v] $(10.9 \pm 2.2) \%$		-
$\Lambda_c^+ \ell^- \bar{\nu}_\ell$	$(6.2 \pm 1.4) \%$		2345
$\Lambda_c^+ \pi^+ \pi^- \ell^- \bar{\nu}_\ell$	$(5.6 \pm 3.1) \%$		2335
$\Lambda_c(2595)^+ \ell^- \bar{\nu}_\ell$	$(7.9 \pm 4.0) \times 10^{-3}$		2212
$\Lambda_c(2625)^+ \ell^- \bar{\nu}_\ell$	$(1.3 \pm 0.6) \%$		2195
$p h^-$	[x] $< 2.3 \times 10^{-5}$	CL=90%	2730
$p\pi^-$	$(4.5 \pm 0.8) \times 10^{-6}$		2730
$pK^-$	$(5.4 \pm 1.0) \times 10^{-6}$		2709
$pD_s^-$	$< 4.8 \times 10^{-4}$	CL=90%	2364
$p\mu^- \bar{\nu}_\mu$	$(4.1 \pm 1.0) \times 10^{-4}$		2730
$\Lambda \mu^+ \mu^-$	$(1.08 \pm 0.28) \times 10^{-6}$		2695
$p\pi^- \mu^+ \mu^-$	$(6.9 \pm 2.5) \times 10^{-8}$		2720
$\Lambda \gamma$	$(7.1 \pm 1.7) \times 10^{-6}$		2699
$\Lambda \eta$	$(9 \pm 7) \times 10^{-6}$		2670
$\Lambda \eta'(958)$	$< 3.1 \times 10^{-6}$	CL=90%	2611
$\Lambda \pi^+ \pi^-$	$(4.7 \pm 1.9) \times 10^{-6}$		2692
$\Lambda K^+ \pi^-$	$(5.7 \pm 1.3) \times 10^{-6}$		2660
$\Lambda K^+ K^-$	$(1.62 \pm 0.23) \times 10^{-5}$		2605
$\Lambda \phi$	$(9.8 \pm 2.6) \times 10^{-6}$		2599
$p\pi^- \pi^+ \pi^-$	$(2.11 \pm 0.23) \times 10^{-5}$		2715
$pK^- K^+ \pi^-$	$(4.1 \pm 0.6) \times 10^{-6}$		2612
$pK^- \pi^+ \pi^-$	$(5.1 \pm 0.5) \times 10^{-5}$		2675
$pK^- K^+ K^-$	$(1.27 \pm 0.14) \times 10^{-5}$		2524

$\Lambda_b(5912)^0$

$$J^P = \frac{1}{2}^-$$

Mass  $m = 5912.20 \pm 0.21$  MeV

Full width  $\Gamma < 0.66$  MeV, CL = 90%

$\Lambda_b(5912)^0$ DECAY MODES	Fraction ( $\Gamma_i/\Gamma$ )	$\rho$ (MeV/c)
$\Lambda_b^0 \pi^+ \pi^-$	seen	86

$\Lambda_b(5920)^0$

$$J^P = \frac{3}{2}^-$$

Mass  $m = 5919.92 \pm 0.19$  MeV (S = 1.1)

Full width  $\Gamma < 0.63$  MeV, CL = 90%

$\Lambda_b(5920)^0$ DECAY MODES	Fraction ( $\Gamma_i/\Gamma$ )	$\rho$ (MeV/c)
$\Lambda_b^0 \pi^+ \pi^-$	seen	108

## Baryon Summary Table

 **$\Lambda_b(6146)^0$** 

$$J^P = \frac{3}{2}^+$$

Mass  $m = 6146.2 \pm 0.4$  MeV  
 Full width  $\Gamma = 2.9 \pm 1.3$  MeV  
 Full width  $\Gamma = 526.55 \pm 0.34$  MeV

 **$\Lambda_b(6152)^0$** 

$$J^P = \frac{5}{2}^+$$

Mass  $m = 6152.5 \pm 0.4$  MeV  
 Full width  $\Gamma = 2.1 \pm 0.9$  MeV  
 Full width  $\Gamma = 532.89 \pm 0.28$  MeV  
 Full width  $\Gamma = 6.34 \pm 0.32$  MeV

 **$\Sigma_b$** 

$$I(J^P) = 1(\frac{1}{2}^+)$$

 $I, J, P$  need confirmation.

Mass  $m(\Sigma_b^+) = 5810.56 \pm 0.25$  MeV  
 Mass  $m(\Sigma_b^-) = 5815.64 \pm 0.27$  MeV  
 $m_{\Sigma_b^+} - m_{\Sigma_b^-} = -5.06 \pm 0.18$  MeV  
 $\Gamma(\Sigma_b^+) = 5.0 \pm 0.5$  MeV  
 $\Gamma(\Sigma_b^-) = 5.3 \pm 0.5$  MeV

 **$\Sigma_b$  DECAY MODES**Fraction ( $\Gamma_i/\Gamma$ ) $\rho$  (MeV/c)

$\Lambda_b^0 \pi$	dominant	133
-------------------	----------	-----

 **$\Sigma_b^*$** 

$$I(J^P) = 1(\frac{3}{2}^+)$$

 $I, J, P$  need confirmation.

Mass  $m(\Sigma_b^{*+}) = 5830.32 \pm 0.27$  MeV  
 Mass  $m(\Sigma_b^{*-}) = 5834.74 \pm 0.30$  MeV  
 $m_{\Sigma_b^{*+}} - m_{\Sigma_b^{*-}} = -4.37 \pm 0.33$  MeV ( $S = 1.6$ )  
 $m_{\Sigma_b^{*+}} - m_{\Sigma_b^+} = 19.73 \pm 0.18$   
 $m_{\Sigma_b^{*-}} - m_{\Sigma_b^-} = 19.09 \pm 0.22$   
 $\Gamma(\Sigma_b^{*+}) = 9.4 \pm 0.5$  MeV  
 $\Gamma(\Sigma_b^{*-}) = 10.4 \pm 0.8$  MeV ( $S = 1.3$ )  
 $m_{\Sigma_b^{*+}} - m_{\Sigma_b^+} = 21.2 \pm 2.0$  MeV

 **$\Sigma_b^*$  DECAY MODES**Fraction ( $\Gamma_i/\Gamma$ ) $\rho$  (MeV/c)

$\Lambda_b^0 \pi$	dominant	159
-------------------	----------	-----

 **$\Sigma_b(6097)^+$** 

$$J^P = ?^?$$

Mass  $m = 6095.8 \pm 1.7$  MeV  
 Full width  $\Gamma = 31 \pm 6$  MeV

 **$\Sigma_b(6097)^+$  DECAY MODES**Fraction ( $\Gamma_i/\Gamma$ ) $\rho$  (MeV/c)

$\Lambda_b \pi^+ \times B(b \rightarrow \Sigma_b(6097)^+)$	seen	-
--	------	---

 **$\Sigma_b(6097)^-$** 

$$J^P = ?^?$$

Mass  $m = 6098.0 \pm 1.8$  MeV  
 Full width  $\Gamma = 29 \pm 4$  MeV

 **$\Sigma_b(6097)^-$  DECAY MODES**Fraction ( $\Gamma_i/\Gamma$ ) $\rho$  (MeV/c)

$\Lambda_b \pi^- \times B(b \rightarrow \Sigma_b(6097)^-)$	seen	-
--	------	---

 **$\Xi_b^0, \Xi_b^-$** 

$$I(J^P) = \frac{1}{2}(\frac{1}{2}^+)$$

 $I, J, P$  need confirmation.

$m(\Xi_b^-) = 5797.0 \pm 0.6$  MeV ( $S = 1.7$ )  
 $m(\Xi_b^0) = 5791.9 \pm 0.5$  MeV  
 $m_{\Xi_b^-} - m_{\Lambda_b^0} = 177.5 \pm 0.5$  MeV ( $S = 1.6$ )  
 $m_{\Xi_b^0} - m_{\Lambda_b^0} = 172.5 \pm 0.4$  MeV  
 $m_{\Xi_b^-} - m_{\Xi_b^0} = 5.9 \pm 0.6$  MeV  
 Mean life  $\tau_{\Xi_b^-} = (1.572 \pm 0.040) \times 10^{-12}$  s  
 Mean life  $\tau_{\Xi_b^0} = (1.480 \pm 0.030) \times 10^{-12}$  s

 **$\Xi_b$  DECAY MODES**Fraction ( $\Gamma_i/\Gamma$ )Scale factor/  
Confidence level $\rho$   
(MeV/c)

$\Xi^- \ell^- \bar{\nu}_\ell X \times B(\bar{b} \rightarrow \Xi_b^-)$	$(3.9 \pm 1.2) \times 10^{-4}$	$S=1.4$	-
$J/\psi \Xi^- \times B(b \rightarrow \Xi_b^-)$	$(1.02^{+0.26}_{-0.21}) \times 10^{-5}$		1782
$J/\psi \Lambda K^- \times B(b \rightarrow \Xi_b^-)$	$(2.5 \pm 0.4) \times 10^{-6}$		1631
$\rho D^0 K^- \times B(\bar{b} \rightarrow \Xi_b^-)$	$(1.7 \pm 0.6) \times 10^{-6}$		2374
$\rho \bar{K}^0 \pi^- \times B(\bar{b} \rightarrow \Xi_b^-)/B(\bar{b} \rightarrow B^0)$	$< 1.6 \times 10^{-6}$	CL=90%	2783
$\rho K^0 K^- \times B(\bar{b} \rightarrow \Xi_b^-)/B(\bar{b} \rightarrow B^0)$	$< 1.1 \times 10^{-6}$	CL=90%	2730
$\rho K^- K^- \times B(\bar{b} \rightarrow \Xi_b^-)$	$(3.7 \pm 0.8) \times 10^{-8}$		2731
$\Lambda \pi^+ \pi^- \times B(b \rightarrow \Xi_b^0)/B(b \rightarrow \Lambda_b^0)$	$< 1.7 \times 10^{-6}$	CL=90%	2781
$\Lambda K^- \pi^+ \times B(b \rightarrow \Xi_b^0)/B(b \rightarrow \Lambda_b^0)$	$< 8 \times 10^{-7}$	CL=90%	2751
$\Lambda K^+ K^- \times B(b \rightarrow \Xi_b^0)/B(b \rightarrow \Lambda_b^0)$	$< 3 \times 10^{-7}$	CL=90%	2698
$\Lambda_c^+ K^- \times B(\bar{b} \rightarrow \Xi_b^-)$	$(6 \pm 4) \times 10^{-7}$		2416
$\Lambda_b^0 \pi^- \times B(b \rightarrow \Xi_b^-)/B(b \rightarrow \Lambda_b^0)$	$(5.7 \pm 2.0) \times 10^{-4}$		99
$\rho K^- \pi^+ \pi^- \times B(b \rightarrow \Xi_b^0)/B(b \rightarrow \Lambda_b^0)$	$(1.9 \pm 0.4) \times 10^{-6}$		2766
$\rho K^- K^- \pi^+ \times B(b \rightarrow \Xi_b^0)/B(b \rightarrow \Lambda_b^0)$	$(1.73 \pm 0.32) \times 10^{-6}$		2704
$\rho K^- K^+ K^- \times B(b \rightarrow \Xi_b^0)/B(b \rightarrow \Lambda_b^0)$	$(1.8 \pm 1.0) \times 10^{-7}$		2620

 **$\Xi_b'(5935)^-$** 

$$J^P = \frac{1}{2}^+$$

Mass  $m = 5935.02 \pm 0.05$  MeV  
 $m_{\Xi_b'(5935)^-} - m_{\Xi_b^0} - m_{\pi^-} = 3.653 \pm 0.019$  MeV  
 Full width  $\Gamma < 0.08$  MeV, CL = 95%

 **$\Xi_b'(5935)^-$  DECAY MODES**Fraction ( $\Gamma_i/\Gamma$ ) $\rho$  (MeV/c)

$\Xi_b^0 \pi^- \times B(\bar{b} \rightarrow \Xi_b'(5935)^-)/B(\bar{b} \rightarrow \Xi_b^0)$	$(11.8 \pm 1.8) \%$	31
---	---------------------	----

 **$\Xi_b(5945)^0$** 

$$J^P = \frac{3}{2}^+$$

Mass  $m = 5952.3 \pm 0.6$  MeV  
 Full width  $\Gamma = 0.90 \pm 0.18$  MeV

 **$\Xi_b(5945)^0$  DECAY MODES**Fraction ( $\Gamma_i/\Gamma$ ) $\rho$  (MeV/c)

$\Xi_b^- \pi^+$	seen	78
-----------------	------	----

 **$\Xi_b(5955)^-$** 

$$J^P = \frac{3}{2}^+$$

Mass  $m = 5955.33 \pm 0.13$  MeV  
 $m_{\Xi_b(5955)^-} - m_{\Xi_b^0} - m_{\pi^-} = 23.96 \pm 0.13$  MeV  
 Full width  $\Gamma = 1.65 \pm 0.33$  MeV

 **$\Xi_b(5955)^-$  DECAY MODES**Fraction ( $\Gamma_i/\Gamma$ ) $\rho$  (MeV/c)

$\Xi_b^0 \pi^- \times B(\bar{b} \rightarrow \Xi_b(5955)^-)/B(\bar{b} \rightarrow \Xi_b^0)$	$(20.7 \pm 3.5) \%$	84
--	---------------------	----

 **$\Xi_b(6227)$** 

$$J^P = ?^?$$

Mass  $m = 6226.9 \pm 2.0$  MeV  
 Full width  $\Gamma = 18 \pm 6$  MeV

 **$\Xi_b(6227)$  DECAY MODES**Fraction ( $\Gamma_i/\Gamma$ )Scale factor  
(MeV/c)

$\Lambda_b^0 K^- \times B(b \rightarrow \Xi_b(6227))/B(b \rightarrow \Lambda_b^0)$	$(3.20 \pm 0.35) \times 10^{-3}$	336
$\Xi_b^0 \pi^- \times B(b \rightarrow \Xi_b(6227))/B(b \rightarrow \Xi_b^0)$	$(2.8 \pm 1.1) \%$	1.8 398

## Baryon Summary Table

 $\Omega_b^-$ 

$$I(J^P) = 0(\frac{1}{2}^+)$$

$I, J, P$  need confirmation.

Mass  $m = 6046.1 \pm 1.7$  MeV  
 $m_{\Omega_b^-} - m_{\Lambda_b^0} = 426.4 \pm 2.2$  MeV  
 $m_{\Omega_b^-} - m_{\Xi_b^-} = 247.3 \pm 3.2$  MeV  
Mean life  $\tau = (1.64^{+0.18}_{-0.17}) \times 10^{-12}$  s  
 $\tau(\Omega_b^-)/\tau(\Xi_b^-)$  mean life ratio =  $1.11 \pm 0.16$

$\Omega_b^-$ DECAY MODES	Fraction ( $\Gamma_i/\Gamma$ )	Confidence level	$p$ (MeV/c)
$J/\psi \Omega_b^- \times B(b \rightarrow \Omega_b)$	$(2.9^{+1.1}_{-0.8}) \times 10^{-6}$		1806
$p K^- K^- \times B(\bar{b} \rightarrow \Omega_b)$	$< 2.5$	$\times 10^{-9}$	90% 2866
$p \pi^- \pi^- \times B(\bar{b} \rightarrow \Omega_b)$	$< 1.5$	$\times 10^{-8}$	90% 2943
$p K^- \pi^- \times B(\bar{b} \rightarrow \Omega_b)$	$< 7$	$\times 10^{-9}$	90% 2915

**b-baryon ADMIXTURE ( $\Lambda_b, \Xi_b, \Omega_b$ )**

These branching fractions are actually an average over weakly decaying  $b$ -baryons weighted by their production rates at the LHC, LEP, and Tevatron, branching ratios, and detection efficiencies. They scale with the  $b$ -baryon production fraction  $B(b \rightarrow b\text{-baryon})$ .

The branching fractions  $B(b\text{-baryon} \rightarrow \Lambda \ell^- \bar{\nu}_\ell \text{ anything})$  and  $B(\Lambda_b^0 \rightarrow \Lambda_c^+ \ell^- \bar{\nu}_\ell \text{ anything})$  are not pure measurements because the underlying measured products of these with  $B(b \rightarrow b\text{-baryon})$  were used to determine  $B(b \rightarrow b\text{-baryon})$ , as described in the note "Production and Decay of  $b$ -Flavored Hadrons."

For inclusive branching fractions, e.g.,  $B \rightarrow D^\pm \text{ anything}$ , the values usually are multiplicities, not branching fractions. They can be greater than one.

<b>b-baryon ADMIXTURE DECAY MODES</b> ( $\Lambda_b, \Xi_b, \Omega_b$ )	Fraction ( $\Gamma_i/\Gamma$ )	$p$ (MeV/c)
$p \mu^- \bar{\nu}$ anything	$(5.8^{+2.3}_{-2.0})\%$	—
$p \ell \bar{\nu}_\ell$ anything	$(5.6 \pm 1.2)\%$	—
$p$ anything	$(70 \pm 22)\%$	—
$\Lambda \ell^- \bar{\nu}_\ell$ anything	$(3.8 \pm 0.6)\%$	—
$\Lambda \ell^+ \nu_\ell$ anything	$(3.2 \pm 0.8)\%$	—
$\Lambda$ anything	$(39 \pm 7)\%$	—
$\Xi^- \ell^- \bar{\nu}_\ell$ anything	$(6.6 \pm 1.6) \times 10^{-3}$	—

**EXOTIC BARYONS** $P_c(4312)^+$ 

Mass  $m = 4311.9^{+7.0}_{-0.9}$  MeV  
Full width  $\Gamma = 10 \pm 5$  MeV

$P_c(4312)^+$ DECAY MODES	Fraction ( $\Gamma_i/\Gamma$ )	$p$ (MeV/c)
$J/\psi p$	seen	658

 $P_c(4380)^+$ 

Mass  $m = 4380 \pm 30$  MeV  
Full width  $\Gamma = 205 \pm 90$  MeV

$P_c(4380)^+$ DECAY MODES	Fraction ( $\Gamma_i/\Gamma$ )	$p$ (MeV/c)
$J/\psi p$	seen	741

 $P_c(4440)^+$ 

Mass  $m = 4440^{+4}_{-5}$  MeV  
Full width  $\Gamma = 21^{+10}_{-11}$  MeV

$P_c(4440)^+$ DECAY MODES	Fraction ( $\Gamma_i/\Gamma$ )	$p$ (MeV/c)
$J/\psi p$	seen	810

 $P_c(4457)^+$ was  $P_c(4457)$ 

Mass  $m = 4457.3^{+4.0}_{-1.8}$  MeV  
Full width  $\Gamma = 6.4^{+6.0}_{-2.8}$  MeV

$P_c(4457)^+$ DECAY MODES	Fraction ( $\Gamma_i/\Gamma$ )	$p$ (MeV/c)
$J/\psi p$	seen	828

## NOTES

This Summary Table only includes established baryons. The Particle Listings include evidence for other baryons. The masses, widths, and branching fractions for the resonances in this Table are Breit-Wigner parameters, but pole positions are also given for most of the  $N$  and  $\Delta$  resonances.

For most of the resonances, the parameters come from various partial-wave analyses of more or less the same sets of data, and it is not appropriate to treat the results of the analyses as independent or to average them together. Furthermore, the systematic errors on the results are not well understood. Thus, we usually only give ranges for the parameters. We then also give a best guess for the mass (as part of the name of the resonance) and for the width. The *Note on  $N$  and  $\Delta$  Resonances* and the *Note on  $\Lambda$  and  $\Sigma$  Resonances* in the Particle Listings review the partial-wave analyses.

When a quantity has "( $S = \dots$ )" to its right, the error on the quantity has been enlarged by the "scale factor"  $S$ , defined as  $S = \sqrt{\chi^2/(N-1)}$ , where  $N$  is the number of measurements used in calculating the quantity. We do this when  $S > 1$ , which often indicates that the measurements are inconsistent. When  $S > 1.25$ , we also show in the Particle Listings an ideogram of the measurements. For more about  $S$ , see the Introduction.

A decay momentum  $p$  is given for each decay mode. For a 2-body decay,  $p$  is the momentum of each decay product in the rest frame of the decaying particle. For a 3-or-more-body decay,  $p$  is the largest momentum any of the products can have in this frame. For any resonance, the *nominal* mass is used in calculating  $p$ . A dagger ("†") in this column indicates that the mode is forbidden when the nominal masses of resonances are used, but is in fact allowed due to the nonzero widths of the resonances.

- [a] The masses of the  $p$  and  $n$  are most precisely known in  $u$  (unified atomic mass units). The conversion factor to MeV,  $1 u = 931.494061(21)$  MeV, is less well known than are the masses in  $u$ .
- [b] The  $|m_p - m_{\bar{p}}|/m_p$  and  $|q_p + q_{\bar{p}}|/e$  are not independent, and both use the more precise measurement of  $|q_{\bar{p}}/m_{\bar{p}}|/(q_p/m_p)$ .
- [c] The limit is from neutrality-of-matter experiments; it assumes  $q_n = q_p + q_e$ . See also the charge of the neutron.
- [d] The  $\mu p$  and  $e p$  values for the charge radius are much too different to average them. The disagreement is not yet understood.
- [e] There is a lot of disagreement about the value of the proton magnetic charge radius. See the Listings.
- [f] The first limit is for  $p \rightarrow$  anything or "disappearance" modes of a bound proton. The second entry, a rough range of limits, assumes the dominant decay modes are among those investigated. For antiprotons the best limit, inferred from the observation of cosmic ray  $\bar{p}$ 's is  $\tau_{\bar{p}} > 10^7$  yr, the cosmic-ray storage time, but this limit depends on a number of assumptions. The best direct observation of stored antiprotons gives  $\tau_{\bar{p}}/B(\bar{p} \rightarrow e^- \gamma) > 7 \times 10^5$  yr.
- [g] There is some controversy about whether nuclear physics and model dependence complicate the analysis for bound neutrons (from which the best limit comes). The first limit here is from reactor experiments with free neutrons.
- [h] Lee and Yang in 1956 proposed the existence of a mirror world in an attempt to restore global parity symmetry—thus a search for oscillations between the two worlds. Oscillations between the worlds would be maximal when the magnetic fields  $B$  and  $B'$  were equal. The limit for any  $B'$  in the range 0 to 12.5  $\mu$ T is  $>12$  s (95% CL).
- [i] The parameters  $g_A, g_V$ , and  $g_{WM}$  for semileptonic modes are defined by  $\bar{B}_f[\gamma_\lambda(g_V + g_A\gamma_5) + i(g_{WM}/m_{B_i})\sigma_{\lambda\nu}q^\nu]B_i$ , and  $\phi_{AV}$  is defined by  $g_A/g_V = |g_A/g_V|e^{i\phi_{AV}}$ . See the "Note on Baryon Decay Parameters" in the neutron Particle Listings.
- [j] Time-reversal invariance requires this to be  $0^\circ$  or  $180^\circ$ .
- [k] This coefficient is zero if time invariance is not violated.
- [l] This limit is for  $\gamma$  energies between 0.4 and 782 keV.

## Baryon Summary Table

---

[n] The decay parameters  $\gamma$  and  $\Delta$  are calculated from  $\alpha$  and  $\phi$  using

$$\gamma = \sqrt{1-\alpha^2} \cos\phi, \quad \tan\Delta = -\frac{1}{\alpha} \sqrt{1-\alpha^2} \sin\phi.$$

See the "Note on Baryon Decay Parameters" in the neutron Particle Listings.

[o] See the Listings for the pion momentum range used in this measurement.

[p] Our estimate. See the Particle Listings for details.

[q] A theoretical value using QED.

[r] This branching fraction includes all the decay modes of the final-state resonance.

[s] See AALTONEN 11H, Fig. 8, for the calculated ratio of  $\Lambda_c^+ \pi^0 \pi^0$  and  $\Lambda_c^+ \pi^+ \pi^-$  partial widths as a function of the  $\Lambda_c(2595)^+ - \Lambda_c^+$  mass difference. At our value of the mass difference, the ratio is about 4.

[t] A test that the isospin is indeed 0, so that the particle is indeed a  $\Lambda_c^+$ .

[u]  $P_c^+$  is a pentaquark-charmonium state.

[v] Not a pure measurement. See note at head of  $\Lambda_b^0$  Decay Modes.

[x] Here  $h^-$  means  $\pi^-$  or  $K^-$ .

## SEARCHES not in other sections

### Magnetic Monopole Searches

The most sensitive experiments obtain negative results.  
Best cosmic-ray supermassive monopole flux limit:  
 $< 1.4 \times 10^{-16} \text{ cm}^{-2} \text{sr}^{-1} \text{s}^{-1}$  for  $1.1 \times 10^{-4} < \beta < 1$

### Supersymmetric Particle Searches

All supersymmetric mass bounds here are model dependent.  
The limits assume:

1)  $\tilde{\chi}_1^0$  is the lightest supersymmetric particle; 2)  $R$ -parity is conserved, unless stated otherwise;

See the Particle Listings for a Note giving details of supersymmetry.

$\tilde{\chi}_i^0$  — neutralinos (mixtures of  $\tilde{\gamma}$ ,  $\tilde{Z}^0$ , and  $\tilde{H}_i^0$ )

Mass  $m_{\tilde{\chi}_1^0} > 0 \text{ GeV}$ , CL = 95%  
[general MSSM, non-universal gaugino masses]

Mass  $m_{\tilde{\chi}_1^0} > 46 \text{ GeV}$ , CL = 95%

[all  $\tan\beta$ , all  $m_0$ , all  $m_{\tilde{\chi}_2^0} - m_{\tilde{\chi}_1^0}$ ]

Mass  $m_{\tilde{\chi}_2^0} > 62.4 \text{ GeV}$ , CL = 95%

[ $1 < \tan\beta < 40$ , all  $m_0$ , all  $m_{\tilde{\chi}_2^0} - m_{\tilde{\chi}_1^0}$ ]

Mass  $m_{\tilde{\chi}_3^0} > 99.9 \text{ GeV}$ , CL = 95%

[ $1 < \tan\beta < 40$ , all  $m_0$ , all  $m_{\tilde{\chi}_2^0} - m_{\tilde{\chi}_1^0}$ ]

Mass  $m_{\tilde{\chi}_4^0} > 116 \text{ GeV}$ , CL = 95%

[ $1 < \tan\beta < 40$ , all  $m_0$ , all  $m_{\tilde{\chi}_2^0} - m_{\tilde{\chi}_1^0}$ ]

$\tilde{\chi}_i^\pm$  — charginos (mixtures of  $\tilde{W}^\pm$  and  $\tilde{H}_i^\pm$ )

Mass  $m_{\tilde{\chi}_1^\pm} > 94 \text{ GeV}$ , CL = 95%

[ $\tan\beta < 40$ ,  $m_{\tilde{\chi}_1^\pm} - m_{\tilde{\chi}_1^0} > 3 \text{ GeV}$ , all  $m_0$ ]

Mass  $m_{\tilde{\chi}_2^\pm} > 810 \text{ GeV}$ , CL = 95%

[ $\ell^\pm \ell^\mp$ , Tchi1chi1C,  $m_{\tilde{\chi}_1^0} = 0 \text{ GeV}$ ]

$\tilde{\chi}^\pm$  — long-lived chargino

Mass  $m_{\tilde{\chi}^\pm} > 620 \text{ GeV}$ , CL = 95% [stable  $\tilde{\chi}^\pm$ ]

$\tilde{\nu}$  — sneutrino

Mass  $m > 41 \text{ GeV}$ , CL = 95% [model independent]

Mass  $m > 94 \text{ GeV}$ , CL = 95%

[CMSSM,  $1 \leq \tan\beta \leq 40$ ,  $m_{\tilde{\nu}_R} - m_{\tilde{\chi}_1^0} > 10 \text{ GeV}$ ]

Mass  $m > 3400 \text{ GeV}$ , CL = 95% [R-Parity Violating]

[ $\tilde{\nu}_\tau \rightarrow e\mu$ ,  $\lambda_{312} = \lambda_{321} = 0.07$ ,  $\lambda'_{311} = 0.11$ ]

$\tilde{e}$  — scalar electron (selectron)

Mass  $m(\tilde{e}_L) > 107 \text{ GeV}$ , CL = 95% [all  $m_{\tilde{e}_L} - m_{\tilde{\chi}_1^0}$ ]

Mass  $m > 410 \text{ GeV}$ , CL = 95% [R-Parity Violating]

[ $\geq 4\ell^\pm$ ,  $\tilde{\ell} \rightarrow l\tilde{\chi}_1^0$ ,  $\tilde{\chi}_1^0 \rightarrow \ell^\pm \ell^\mp \nu$ ]

$\tilde{\mu}$  — scalar muon (smuon)

Mass  $m > 94 \text{ GeV}$ , CL = 95%

[CMSSM,  $1 \leq \tan\beta \leq 40$ ,  $m_{\tilde{\mu}_R} - m_{\tilde{\chi}_1^0} > 10 \text{ GeV}$ ]

Mass  $m > 410 \text{ GeV}$ , CL = 95% [R-Parity Violating]

[ $\geq 4\ell^\pm$ ,  $\tilde{\ell} \rightarrow l\tilde{\chi}_1^0$ ,  $\tilde{\chi}_1^0 \rightarrow \ell^\pm \ell^\mp \nu$ ]

$\tilde{\tau}$  — scalar tau (stau)

Mass  $m > 81.9 \text{ GeV}$ , CL = 95%

[ $m_{\tilde{\tau}_R} - m_{\tilde{\chi}_1^0} > 15 \text{ GeV}$ , all  $\theta_\tau$ ,  $B(\tilde{\tau} \rightarrow \tau\tilde{\chi}_1^0) = 100\%$ ]

Mass  $m > 286 \text{ GeV}$ , CL = 95% [long-lived  $\tilde{\tau}$ ]

$\tilde{q}$  — squarks of the first two quark generations

Mass  $m > 1.450 \times 10^3 \text{ GeV}$ , CL = 95%

[CMSSM,  $\tan\beta = 30$ ,  $A_0 = -2\max(m_0, m_{1/2})$ ,  $\mu > 0$ ]

Mass  $m > 1630 \text{ GeV}$ , CL = 95%

[mass degenerate squarks]

Mass  $m > 1130 \text{ GeV}$ , CL = 95%

[single light squark bounds]

Mass  $m > 1.600 \times 10^3 \text{ GeV}$ , CL = 95% [R-Parity Violating]

[ $\tilde{q} \rightarrow q\tilde{\chi}_1^0$ ,  $\tilde{\chi}_1^0 \rightarrow \ell\ell\nu$ ,  $\lambda_{121}, \lambda_{122} \neq 0$ ,  $m_{\tilde{g}} = 2400 \text{ GeV}$ ]

$\tilde{q}$  — long-lived squark

Mass  $m > 1340$ , CL = 95% [ $\tilde{t}$  R-hadrons]

Mass  $m > 1250$ , CL = 95% [ $\tilde{b}$  R-hadrons]

$\tilde{b}$  — scalar bottom (sbottom)

Mass  $m > 1230 \text{ GeV}$ , CL = 95%

[jets+ $\cancel{E}_T$ , Tstop1,  $m_{\tilde{\chi}_1^0} = 0 \text{ GeV}$ ]

Mass  $m > 307 \text{ GeV}$ , CL = 95% [R-Parity Violating]

[ $\tilde{b} \rightarrow td$  or  $ts$ ,  $\lambda''_{332}$  or  $\lambda''_{331}$  coupling]

$\tilde{t}$  — scalar top (stop)

Mass  $m > 1190 \text{ GeV}$ , CL = 95%

[jets+ $\cancel{E}_T$ , Tstop1,  $m_{\tilde{\chi}_1^0} = 0 \text{ GeV}$ ]

Mass  $m > 1100 \text{ GeV}$ , CL = 95% [R-Parity Violating]

[ $\tilde{t} \rightarrow be$ , Tstop2RPV, prompt]

$\tilde{g}$  — gluino

Mass  $m > 2.000 \times 10^3 \text{ GeV}$ , CL = 95%

[jets +  $\cancel{E}_T$ , Tglu1A,  $m_{\tilde{\chi}_1^0} = 0 \text{ GeV}$ ]

Mass  $m > 2.260 \times 10^3 \text{ GeV}$ , CL = 95% [R-Parity Violating]

[ $\geq 4\ell$ ,  $\lambda_{12k} \neq 0$ ,  $m_{\tilde{\chi}_1^0} > 1000 \text{ GeV}$ ]

### Technicolor

The limits for technicolor (and top-color) particles are quite varied depending on assumptions. See the Technicolor section of the full *Review* (the data listings).

### Quark and Lepton Compositeness, Searches for

#### Scale Limits $\Lambda$ for Contact Interactions (the lowest dimensional interactions with four fermions)

If the Lagrangian has the form

$$\pm \frac{g^2}{2\Lambda^2} \bar{\psi}_L \gamma_\mu \psi_L \bar{\psi}_L \gamma^\mu \psi_L$$

(with  $g^2/4\pi$  set equal to 1), then we define  $\Lambda \equiv \Lambda_{LL}^\pm$ . For the full definitions and for other forms, see the Note in the Listings on Searches for Quark and Lepton Compositeness in the full *Review* and the original literature.

$$\Lambda_{LL}^+(eeee) > 8.3 \text{ TeV, CL} = 95\%$$

$$\Lambda_{LL}^-(eeee) > 10.3 \text{ TeV, CL} = 95\%$$

$$\Lambda_{LL}^+(ee\mu\mu) > 8.5 \text{ TeV, CL} = 95\%$$

$$\Lambda_{LL}^-(ee\mu\mu) > 9.5 \text{ TeV, CL} = 95\%$$

$$\Lambda_{LL}^+(ee\tau\tau) > 7.9 \text{ TeV, CL} = 95\%$$

$$\Lambda_{LL}^-(ee\tau\tau) > 7.2 \text{ TeV, CL} = 95\%$$

$$\Lambda_{LL}^+(ell\ell\ell) > 9.1 \text{ TeV, CL} = 95\%$$

$$\Lambda_{LL}^-(ell\ell\ell) > 10.3 \text{ TeV, CL} = 95\%$$

$$\Lambda_{LL}^+(eeqq) > 24 \text{ TeV, CL} = 95\%$$

$$\Lambda_{LL}^-(eeqq) > 37 \text{ TeV, CL} = 95\%$$

$$\Lambda_{LL}^+(eeuu) > 23.3 \text{ TeV, CL} = 95\%$$

$$\Lambda_{LL}^-(eeuu) > 12.5 \text{ TeV, CL} = 95\%$$

$$\Lambda_{LL}^+(eedd) > 11.1 \text{ TeV, CL} = 95\%$$

$$\Lambda_{LL}^-(eedd) > 26.4 \text{ TeV, CL} = 95\%$$

$$\Lambda_{LL}^+(eccc) > 9.4 \text{ TeV, CL} = 95\%$$

$$\Lambda_{LL}^-(eccc) > 5.6 \text{ TeV, CL} = 95\%$$

$$\Lambda_{LL}^+(ebbb) > 9.4 \text{ TeV, CL} = 95\%$$

$$\Lambda_{LL}^-(ebbb) > 10.2 \text{ TeV, CL} = 95\%$$

$$\Lambda_{LL}^+(\mu\mu qq) > 20 \text{ TeV, CL} = 95\%$$

$$\Lambda_{LL}^-(\mu\mu qq) > 30 \text{ TeV, CL} = 95\%$$

$$\Lambda(\ell\nu\ell\nu) > 3.10 \text{ TeV, CL} = 90\%$$

$$\Lambda(e\nu qq) > 2.81 \text{ TeV, CL} = 95\%$$

$$\Lambda_{LL}^+(qqqq) > 13.1 \text{ none } 17.4\text{--}29.5 \text{ TeV, CL} = 95\%$$

$$\Lambda_{LL}^-(qqqq) > 21.8 \text{ TeV, CL} = 95\%$$

$$\Lambda_{LL}^+(\nu\nu qq) > 5.0 \text{ TeV, CL} = 95\%$$

$$\Lambda_{LL}^-(\nu\nu qq) > 5.4 \text{ TeV, CL} = 95\%$$

# Searches Summary Table

## Excited Leptons

The limits from  $\ell^{*+} \ell^{*-}$  do not depend on  $\lambda$  (where  $\lambda$  is the  $\ell \ell^*$  transition coupling). The  $\lambda$ -dependent limits assume chiral coupling.

$e^{*\pm}$  — excited electron

- Mass  $m > 103.2$  GeV, CL = 95% (from  $e^* e^*$ )
- Mass  $m > 4.800 \times 10^3$  GeV, CL = 95% (from  $ee^*$ )
- Mass  $m > 356$  GeV, CL = 95% (if  $\lambda_\gamma = 1$ )

$\mu^{*\pm}$  — excited muon

- Mass  $m > 103.2$  GeV, CL = 95% (from  $\mu^* \mu^*$ )
- Mass  $m > 3.800 \times 10^3$  GeV, CL = 95% (from  $\mu\mu^*$ )

$\tau^{*\pm}$  — excited tau

- Mass  $m > 103.2$  GeV, CL = 95% (from  $\tau^* \tau^*$ )
- Mass  $m > 2.500 \times 10^3$  GeV, CL = 95% (from  $\tau\tau^*$ )

$\nu^*$  — excited neutrino

- Mass  $m > 1.600 \times 10^3$  GeV, CL = 95% (from  $\nu^* \nu^*$ )
- Mass  $m > 213$  GeV, CL = 95% (from  $\nu^* X$ )

$q^*$  — excited quark

- Mass  $m > 338$  GeV, CL = 95% (from  $q^* q^*$ )
- Mass  $m > 6.000 \times 10^3$  GeV, CL = 95% (from  $q^* X$ )

## Color Sextet and Octet Particles

Color Sextet Quarks ( $q_6$ )

- Mass  $m > 84$  GeV, CL = 95% (Stable  $q_6$ )

Color Octet Charged Leptons ( $\ell_8$ )

- Mass  $m > 86$  GeV, CL = 95% (Stable  $\ell_8$ )

Color Octet Neutrinos ( $\nu_8$ )

- Mass  $m > 110$  GeV, CL = 90% ( $\nu_8 \rightarrow \nu g$ )

## Extra Dimensions

Please refer to the Extra Dimensions section of the full *Review* for a discussion of the model-dependence of these bounds, and further constraints.

### Constraints on the radius of the extra dimensions, for the case of two-flat dimensions of equal radii

- $R < 30 \mu\text{m}$ , CL = 95% (direct tests of Newton's law)
- $R < 4.8 \mu\text{m}$ , CL = 95% ( $pp \rightarrow j\bar{G}$ )
- $R < 0.16\text{--}916$  nm (astrophysics; limits depend on technique and assumptions)

### Constraints on the fundamental gravity scale

- $M_{TT} > 9.02$  TeV, CL = 95% ( $pp \rightarrow$  dijet, angular distribution)
- $M_c > 4.16$  TeV, CL = 95% ( $pp \rightarrow \ell\bar{\ell}$ )

### Constraints on the Kaluza-Klein graviton in warped extra dimensions

- $M_G > 4.25$  TeV, CL = 95% ( $pp \rightarrow \gamma\gamma$ )

### Constraints on the Kaluza-Klein gluon in warped extra dimensions

- $M_{g_{KK}} > 3.8$  TeV, CL = 95% ( $g_{KK} \rightarrow t\bar{t}$ )

## WIMP and Dark Matter Searches

No confirmed evidence found for galactic WIMPs from the GeV to the TeV mass scales and down to  $1 \times 10^{-10}$  pb spin independent cross section at  $M = 100$  GeV.

## Tests of Conservation Laws

Written August 2019 by A. Pich (IFIC, Valencia) and M. Ramsey-Musolf (Tsung-Dao Lee Inst.; SJTU; U. Massachusetts).

In keeping with the current interest in tests of conservation laws, we collect together a Table of experimental limits on all weak and electromagnetic decays, mass differences, and moments, and on a few reactions, whose observation would violate conservation laws. The Table is given only in the full Review of Particle Physics (RPP), not in the Particle Physics Booklet, and organizes the data in two main sections: “Discrete Space-Time Symmetries”, *i.e.*,  $C$ ,  $P$ ,  $T$ ,  $CP$  and  $CPT$ ; and “Number Conservation Laws”, *i.e.*, lepton, baryon, flavor and charge conservation. The references for these data can be found in the Particle Listings. The following text discusses the best limits among those included in the Table and gives a brief overview of the current status. For some topics, a more extensive discussion of the framework for theoretical interpretation is provided, particularly where the analogous discussion does not appear elsewhere in the RPP. References to more extensive review articles are also included where appropriate. Unless otherwise specified, all limits quoted in this review are given at a C.L. of 90%.

### DISCRETE SPACE-TIME SYMMETRIES

Charge conjugation ( $C$ ), parity ( $P$ ) and time reversal ( $T$ ) are empirically exact symmetries of the electromagnetic (QED) and strong (QCD) interactions, but they are violated by the weak forces. Owing to the left-handed nature of the  $SU(2)_L \otimes U(1)_Y$  electroweak theory,  $C$  and  $P$  are maximally violated in the fermionic couplings of the  $W^\pm$  and (up to  $\sin^2 \theta_W$  corrections) the  $Z$ . However, their product  $CP$  is still an exact symmetry when only one or two fermion families are considered. With three generations of fermions,  $CP$  is violated through the single complex phase present in the Cabibbo-Kobayashi-Maskawa (CKM) quark mixing matrix. An analogous  $CP$ -violating (CPV) phase appears in the lepton sector when non-vanishing neutrino masses are taken into account (plus two additional phases if neutrinos are Majorana particles). The product of the three discrete symmetries,  $CPT$ , is an exact symmetry of any local and Lorentz-invariant quantum field theory with a positive-definite hermitian Hamiltonian that preserves micro-causality [1, 2]. Therefore, the breaking of  $CP$  implies a corresponding violation of  $T$ .

Violations of charge-conjugation symmetry have never been observed in electromagnetic and strong phenomena. The most stringent limits are extracted from  $C$ -violating transitions of neutral (self-conjugate) particles such as  $\text{Br}(\pi^0 \rightarrow 3\gamma) < 3.1 \times 10^{-8}$  [3] and  $\text{Br}(J/\psi \rightarrow 2\gamma) < 2.7 \times 10^{-7}$  [4].  $P$  (and  $CP$ ) conservation has been also precisely tested through forbidden decays such as  $\text{Br}(\eta \rightarrow 4\pi^0) < 6.9 \times 10^{-7}$  [5], but the best limits on  $P$  and  $T$  are set by the non-observation of electric dipole moments (see section 2). Obviously, the interplay of the weak interaction puts a lower bound in sensitivity for this type of tests, beyond which violations of the corresponding conservation laws should be detected.

### 1 Violations of $CP$ and $T$

The first evidence of  $CP$  non-invariance in particle physics was the observation in 1964 of  $K_L^0 \rightarrow \pi^+\pi^-$  decays [6]. For many years afterwards, the non-zero ratio

$$\begin{aligned} |\eta_{+-}| &\equiv |\mathcal{M}(K_L^0 \rightarrow \pi^+\pi^-)/\mathcal{M}(K_S^0 \rightarrow \pi^+\pi^-)| \\ &= (2.232 \pm 0.011) \times 10^{-3} \end{aligned} \quad (1)$$

could be explained as a  $K^0\text{-}\bar{K}^0$  mixing effect,  $\eta_{+-} = \epsilon$  (superweak  $CP$  violation), which would imply an identical ratio  $\eta_{00} \equiv \mathcal{M}(K_L^0 \rightarrow \pi^0\pi^0)/\mathcal{M}(K_S^0 \rightarrow \pi^0\pi^0)$  in the neutral decay mode and successfully predicts the observed CPV semileptonic asymmetry ( $A_L(e) \approx 2 \text{Re } \epsilon$ )

$$\begin{aligned} A_L(e) &\equiv \frac{\Gamma(K_L^0 \rightarrow \pi^- e^+ \nu_e) - \Gamma(K_L^0 \rightarrow \pi^+ e^- \bar{\nu}_e)}{\Gamma(K_L^0 \rightarrow \pi^- e^+ \nu_e) + \Gamma(K_L^0 \rightarrow \pi^+ e^- \bar{\nu}_e)} \\ &= (3.34 \pm 0.07) \times 10^{-3}. \end{aligned} \quad (2)$$

A tiny difference between  $\eta_{+-}$  and  $\eta_{00}$  was reported for the first time in 1988 by the CERN NA31 collaboration [7], and later es-

tablished at the  $7.2\sigma$  level with the full data samples from the NA31 [8], E731 [9], NA48 [10] and KTeV [11] experiments:

$$\text{Re}(\epsilon'/\epsilon) = \frac{1}{3} (1 - |\eta_{00}/\eta_{+-}|) = (1.66 \pm 0.23) \times 10^{-3}. \quad (3)$$

This important measurement confirmed that  $CP$  violation is associated with a  $\Delta S = 1$  transition, as predicted by the CKM mechanism. The Standard Model (SM) prediction,  $\text{Re}(\epsilon'/\epsilon) = (1.4 \pm 0.5) \times 10^{-3}$  [12, 13], is in good agreement with the measured ratio, although the theoretical uncertainty is unfortunately large.

Much larger  $CP$  asymmetries have been later measured in  $B$  meson decays, many of them involving the interference between  $B^0\text{-}\bar{B}^0$  mixing and the decay amplitude. They provide many successful tests of the CKM unitarity structure, validating the SM mechanism of CP violation (see the review on  $CP$  violation in the quark sector). Prominent signals of direct  $CP$  violation have been also clearly established in several  $B^\pm$ ,  $B_d^0$  and  $B_s^0$  decays, and, very recently, in charm decays [14]:

$$\begin{aligned} \Delta a_{CP}^{\text{dir}} &\equiv a_{CP}^{\text{dir}}(D^0 \rightarrow K^+K^-) - a_{CP}^{\text{dir}}(D^0 \rightarrow \pi^+\pi^-) \\ &= (-15.7 \pm 2.9) \times 10^{-4}. \end{aligned} \quad (4)$$

These direct  $CP$  asymmetries necessarily involve the presence of a strong phase-shift difference between (at least) two interfering amplitudes, which makes very challenging to perform reliable SM predictions for heavy-flavored mesons.

Global fits to neutrino oscillation data provide some hints of a non-zero mixing phase [15, 16]. Although the statistical significance is not yet compelling, they suggest that  $CP$ -violation effects in neutrino oscillations could be large (see the review on neutrino masses, mixings and oscillations). The future DUNE and Hyper-Kamiokande experiments are expected to confirm the presence of  $CP$  violation in the lepton sector or constrain the phase in the leptonic mixing matrix to be smaller than  $O(10^\circ)$ .

While  $CP$  violation implies a breaking of time-reversal symmetry, direct tests of  $T$  violation are much more difficult. The CPLEAR experiment observed longtime ago a non-zero difference between the oscillation probabilities of  $K^0 \rightarrow \bar{K}^0$  and  $\bar{K}^0 \rightarrow K^0$  [17]. Initial neutral kaons with defined strangeness were produced from proton-antiproton annihilations at rest,  $p\bar{p} \rightarrow K^-\pi^+K^0, K^+\pi^-K^0$ , and tagged by the accompanying charged kaon, while the strangeness of the final neutral kaon was identified through its semileptonic decay:  $K^0 \rightarrow e^+\pi^-\nu_e, \bar{K}^0 \rightarrow e^-\pi^+\bar{\nu}_e$ . The average asymmetry over the time interval from 1 to 20  $K_S^0$  lifetimes was found to be different from zero at  $4\sigma$  [17]:

$$\begin{aligned} \frac{R[\bar{K}^0(t=0) \rightarrow e^+\pi^-\nu_e(t)] - R[K^0(t=0) \rightarrow e^-\pi^+\bar{\nu}_e(t)]}{R[\bar{K}^0(t=0) \rightarrow e^+\pi^-\nu_e(t)] + R[K^0(t=0) \rightarrow e^-\pi^+\bar{\nu}_e(t)]} &= \\ = (6.6 \pm 1.3 \pm 1.0) \times 10^{-3}. \end{aligned} \quad (5)$$

Since this asymmetry violates also  $CP$ , its interpretation as direct evidence of  $T$  violation requires a detailed analysis of the underlying  $K^0\text{-}\bar{K}^0$  mixing process [18–20].

More recently, the exchange of initial and final states has been made possible in  $B$  decays, taking advantage of the entanglement of the two daughter mesons produced in the decay  $\Upsilon(4S) \rightarrow B\bar{B}$  which allows for both flavor ( $B^0 \rightarrow \ell^+X, \bar{B}^0 \rightarrow \ell^-X$ ) and  $CP$  ( $B_+ \rightarrow J/\psi K_L^0, B_- \rightarrow J/\psi K_S^0$ ) tagging. Selecting events where one  $B$  candidate is reconstructed in a  $CP$  eigenstate and the flavor of the other  $B$  is identified, one can compare the rates of the  $\bar{B}^0 \rightarrow B_\pm$  and  $B^0 \rightarrow B_\pm$  transitions with their  $T$ -reversed  $B_\pm \rightarrow \bar{B}^0$  and  $B_\pm \rightarrow B^0$  processes, as a function of the time difference  $\Delta t$  between the two  $B$  decays [21–23]. Neglecting the small width difference between the two  $B_d^0$  mass eigenstates, each of these eight transitions has a time-dependent decay rate of the form  $e^{-\Gamma_d \Delta t} \{1 + S_{\alpha,\beta}^\pm \sin(\Delta m_d \Delta t) + C_{\alpha,\beta}^\pm \cos(\Delta m_d \Delta t)\}$ , where  $\Gamma_d$  is the average decay width,  $\Delta m_d$  the  $B_d^0$  mass difference, the subindices  $\alpha = \ell^+, \ell^-$  and  $\beta = K_S^0, K_L^0$  stand for the reconstructed final states of the two  $B$  mesons and the superindex  $\pm$



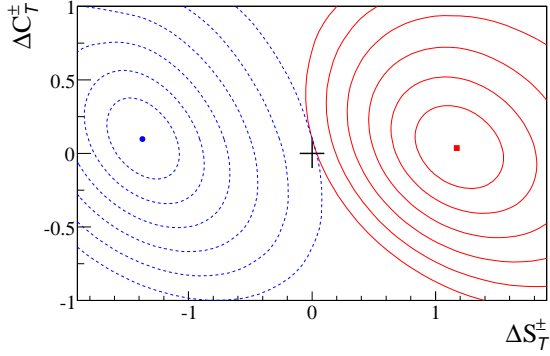


Figure 1: Measured values of  $\Delta S_T^+$ ,  $\Delta C_T^+$  (blue point, dashed lines) and  $\Delta S_T^-$ ,  $\Delta C_T^-$  (red square, solid lines) [24]. The two-dimensional contours correspond to  $1 - \text{CL} = 0.317, 4.55 \times 10^{-2}, 2.70 \times 10^{-3}, 6.33 \times 10^{-5}, 5.73 \times 10^{-7},$  and  $1.97 \times 10^{-9}$ . The + sign indicates the  $T$ -invariant point.

or  $-$  indicates whether the decay to the flavor final state  $\alpha$  occurs before or after the decay to the  $CP$  final state  $\beta$ . Figure 1 shows confidence-level contours for the  $T$ -asymmetry parameters  $\Delta S_T^\pm \equiv S_{\ell^-, K_L^0}^\mp - S_{\ell^+, K_S^0}^\pm$  and  $\Delta C_T^\pm \equiv C_{\ell^-, K_L^0}^\mp - C_{\ell^+, K_S^0}^\pm$ , reported by the BABAR experiment [24], which clearly demonstrate a violation of  $T$  in  $\Delta S_T^\pm$ , with a significance of  $14\sigma$ .

## 2 Electric dipole moments

Among the most powerful tests of  $CP$  invariance is the search for a permanent electric dipole moment (EDM) of an elementary fermion or non-degenerate quantum system. The EDM of an elementary spin-1/2 fermion  $f$  is defined by the effective, non-renormalizable interaction

$$\mathcal{L}_{\text{EDM}} = -\frac{i}{2} d_f \bar{f} \sigma_{\mu\nu} \gamma_5 f F^{\mu\nu} \quad (6)$$

where  $F^{\mu\nu}$  is the QED field strength tensor. The values for  $d_f$  are conventionally expressed in units of  $e \text{ cm}$ . The interaction (6) is separately odd under  $T$  and  $P$ . In the non-relativistic limit, Eq. (6) reduces to

$$\mathcal{L}_{\text{EDM}} \rightarrow d_f \chi_f^\dagger \vec{\sigma} \chi \cdot \vec{E} \quad (7)$$

where  $\chi$  is a two-component Pauli spinor and  $\vec{E}$  is the electric field. Note the interaction (7) is manifestly  $T$ -odd and carries no direct information on  $CP$ . The observation of a non-zero EDM of a non-relativistic (and non-degenerate) quantum system, such as the mercury atom (see below) would imply  $CP$  violation under the assumption of  $CPT$  invariance.

To date, no experimental observation of an EDM of an elementary particle or non-degenerate bound quantum system has been observed. The most stringent limits have been obtained for the EDMs of the electron, mercury atom, and neutron. A selection of the representative, most stringent limits is given in Table 1. The limits on the electron EDM are inferred from experiments involving polar molecules, paramagnetic systems with an unpaired electron spin. In contrast, the neutron and  $^{199}\text{Hg}$  atom are diamagnetic. A variety of experimental efforts aimed at improved sensitivities are underway. For reviews of the experimental and theoretical situation, see, *e.g.* [25–28].

### EDMs in the Standard Model

The SM provides two sources of  $d_f$ : the CPV phase in the CKM matrix and the  $P$ - and  $T$ -odd ‘ $\theta$  term’ in the QCD Lagrangian. The former is characterized by the Jarlskog invariant [35]

$$\mathcal{J} = \text{Im}(V_{us} V_{cs}^* V_{cb} V_{ub}^*) \sim A^2 \lambda^6 \eta < 10^{-4}, \quad (8)$$

while the latter is given by

$$\mathcal{L}_{\bar{\theta}} = -\frac{g_3^2}{16\pi^2} \bar{\theta} \text{Tr} (G^{\mu\nu} \tilde{G}_{\mu\nu}), \quad (9)$$

**Table 1:** Most stringent limits on electric dipole moments.

EDM	Limit ( $e \text{ cm}$ )	Source
Electron	$1.1 \times 10^{-29}$ (90% C.L.)	ThO [29]
	$1.3 \times 10^{-28}$ (90% C.L.)	HfF <sup>+</sup> [30]
Muon	$1.8 \times 10^{-19}$ (95% C.L.)	[31]
Neutron	$1.8 \times 10^{-26}$ (90% C.L.)	[32]
$^{199}\text{Hg}$ Atom	$7.4 \times 10^{-30}$ (95% C.L.)	[33]
$^{129}\text{Xe}$ Atom	$1.5 \times 10^{-27}$ (95% C.L.)	[34]

where  $G_{\mu\nu}$  ( $\tilde{G}_{\mu\nu} = \epsilon_{\mu\nu\alpha\beta} G^{\alpha\beta}/2$ ) is the QCD field strength tensor (dual).

The CKM-induced EDMs of quarks and charged leptons arise at three- and four-loop orders, respectively [36–39]. The resulting numerical impact for the experimental observables (see below) falls well below present and prospective experimental sensitivities. The most important impact of  $\mathcal{J}$  for the EDMs of the neutron and diamagnetic atoms arise via induced hadronic interactions. The resulting theoretical expectations for the electron, neutron and  $^{199}\text{Hg}$  EDMs are

$$|d_e|_{\text{CKM}} \approx 10^{-44} e \text{ cm} \quad [39], \quad (10a)$$

$$|d_n|_{\text{CKM}} \approx (1 - 6) \times 10^{-32} e \text{ cm} \quad [40], \quad (10b)$$

$$|d_A(^{199}\text{Hg})|_{\text{CKM}} \lesssim 4 \times 10^{-34} e \text{ cm} \quad [25]. \quad (10c)$$

For  $d_n$  and  $d_A(^{199}\text{Hg})$ , the dominant CKM contributions arise from four-quark operators (generated after integrating out the electroweak gauge bosons) rather than from the EDMs of the individual quarks. The corresponding sensitivities to the QCD  $\bar{\theta}$  parameter are given by

$$|d_n|_{\bar{\theta}} \approx (0.9 - 1.2) \times 10^{-16} \bar{\theta} e \text{ cm} \quad [40], \quad (11a)$$

$$|d_A(^{199}\text{Hg})|_{\bar{\theta}} \approx (0.07 - 8) \times 10^{-20} \bar{\theta} e \text{ cm} \quad [25, 26], \quad (11b)$$

where the ranges quoted include the impacts of hadronic, nuclear, and atomic theory uncertainties. The neutron EDM puts then a stringent limit on ‘strong’  $CP$  violation:  $\bar{\theta} \lesssim 2 \times 10^{-10}$ . The corresponding limit from  $d_A(^{199}\text{Hg})$  is weaker due to the large theoretical uncertainty.

### EDMs Beyond the Standard Model

It is possible that the next generation of EDM searches will yield a non-zero result, arising from the  $\bar{\theta}$ -term interaction and/or physics beyond the SM (BSM). Most of the considered BSM scenarios involve new particles with masses well above the electroweak scale. At energies much lower than the BSM mass scale  $\Lambda$ , the dynamics can be described through an effective field theory (SMEFT) involving an infinite set of non-renormalizable operators  $\mathcal{O}_k^{(d)}$ , with dimensions  $d > 4$ , that are invariant under the SM gauge group:

$$\mathcal{L}_{\text{SMEFT}} = \mathcal{L}_{\text{SM}} + \sum_{k,d} \alpha_k^{(d)} \left(\frac{1}{\Lambda}\right)^{d-4} \mathcal{O}_k^{(d)}. \quad (12)$$

The operators contain only SM fields, while all short-distance information on the BSM physics is encoded in their Wilson coefficients  $\alpha_k^{(d)}$ . The  $d = 4$  term corresponds to the SM Lagrangian.

For the systems of Table 1 and for many BSM scenarios of recent interest, it suffices to consider the leading contributions from  $d = 6$  operators. Considering only the first-generation SM fermions, there exist 12 independent CPV pertinent operators. For a complete listing, see *e.g.*, Refs. [26, 41]. For a given elementary fermion  $f$ , two of these operators reduce to the EDM interaction in Eq. (6). Of the remaining, the most relevant include the chromo-electric dipole moments (cEDMs) of the quarks; a  $CP$ -odd three gluon operator; three semileptonic, four-fermion operators; two four-quark operators; and a CPV interaction involving two Higgs fields and a right-handed quark current. For the dipole operators, it is useful to define a rescaled Wilson coefficient  $\alpha_{fV_j}^{(6)} \equiv g_j C_{fV_j}$ , where  $V_j$  ( $j = 1, 2, 3$ ) denote the gauge bosons for

**Table 2:** Pertinent dimension-six EDM and cEDM sources (first generation fermions only).

System	$d = 6$ Source	Wilson Coefficient
Paramagnetic	Electron EDM	$\text{Im } C_{e\gamma}$
	Electron-quark	$C_{e\bar{q}}^{(\pm)}$
Diamagnetic	Quark EDM	$\text{Im } C_{q\gamma}$
	Quark cEDM	$\text{Im } C_{qG}$
	Three gluon	$C_{\bar{G}}$
	Four quark	$\text{Im } C_{quqd}^{(1,8)}$
	Quark-Higgs	$\text{Im } C_{\varphi ud}$
	Electron-quark tensor*	$\text{Im } C_{\ell equ}^{(3)}$

\*Applicable only to atoms.

the three SM gauge groups with corresponding couplings  $g_j$ ; for all other  $d = 6$  operators we correspondingly identify  $\alpha_k^{(6)} \equiv C_k$ . In this case, one has for the EDM ( $d_f$ ) and cEDM ( $\tilde{d}_q$ )

$$d_f = -(1.13 \times 10^{-16} \text{ e cm}) \left(\frac{v}{\Lambda}\right)^2 \text{Im } C_{f\gamma}, \quad (13a)$$

$$\tilde{d}_q = -(1.13 \times 10^{-16} \text{ cm}) \left(\frac{v}{\Lambda}\right)^2 \text{Im } C_{qG}, \quad (13b)$$

with  $\text{Im } C_{f\gamma} = \text{Im } C_{fB} + 3I_3^f \text{Im } C_{fW}$ . As the expressions (13a,13b) illustrate, the magnitude of the BSM contributions scales with two inverse powers of the scale  $\Lambda$ . A similar conclusion holds for the contributions from the other  $d = 6$  operators to the EDMs of Table 1.

It is important to emphasize that if the BSM mediators are light, with masses below the weak scale, the effective field theory description of Eq. (12) does not apply. For recent studies along these lines, see, *e.g.* [42,43].

#### EDM Interpretation: From Short Distances to the Atomic Scale

The EDM limits in Table 1 are obtained using composite quantum systems, wherein the relevant dynamics involve physics at the hadronic, nuclear, atomic and molecular scales. The manifestation of a given CPV source (CKM,  $\theta$  term, BSM) involves an interplay of these dynamics. In all cases, one must first evolve the Wilson coefficients from the weak scale to the hadronic scale, then match onto the relevant low-energy degrees of freedom (electrons, nucleons, pions, *etc.*). At this level, the most straightforward interpretation involves the paramagnetic systems, for which two sources dominate: the electron EDM and the electron spin-dependent semileptonic interaction  $\bar{e}\gamma_5 e \bar{q}q$ . The latter gives rise to a spin-independent Hamiltonian, for an atom with  $Z$  electrons/protons and  $N$  neutrons,

$$\hat{H}_S = \frac{iG_F}{\sqrt{2}} \delta(\vec{r}) \left[ (Z + N) C_S^{(0)} + (Z - N) C_S^{(1)} \right] \gamma_0 \gamma_5, \quad (14)$$

where  $C_S^{(0)}$  ( $C_S^{(1)}$ ) is proportional to  $C_{e\bar{q}}^{(+)}$  ( $C_{e\bar{q}}^{(-)}$ ). The computation of  $C_S^{(0,1)}$  is relatively free from theoretical uncertainty since the operator  $\bar{q}q$  essentially counts the number of quarks of flavor  $q$  in the nucleus. Experimental results for paramagnetic systems, thus, often quote bounds on

$$C_S \equiv C_S^{(0)} + \left( \frac{Z - N}{Z + N} \right) C_S^{(1)} \quad (15)$$

as well as on  $d_e$ , assuming only one of these two sources is non-vanishing. Combining results from ThO and HfF<sup>+</sup> (see Figure 2) allows one to obtain the global, 90% C.L. bounds

$$|d_e| < 1.8 \times 10^{-28} \text{ e cm}, \quad |C_S| < 9.8 \times 10^{-9}. \quad (16)$$

Note that the limits on  $d_e$  given in Table 1 have been obtained assuming  $C_S = 0$ .

For the diamagnetic systems, the situation is considerably more involved. For the neutron, a variety of approaches – including

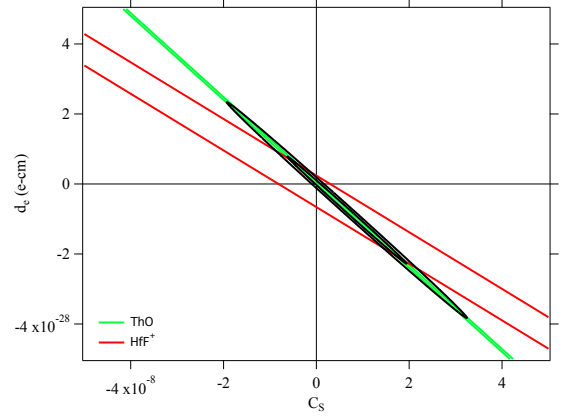


Figure 2: Constraints on  $d_e$  and  $C_S$  from EDM searches using polar molecules (updated by [44] from Ref. [25]).

lattice QCD, chiral perturbation theory, QCD sum rules, and the quark model – have been employed to compute the relevant hadronic matrix elements of the CPV sources (see, *e.g.*, [26,27,45,46]). For diamagnetic atoms, the non-leptonic sources of Table 2 give rise to the EDM of the nucleus as well as other  $P$ - and  $T$ -odd nuclear moments, as allowed by the nuclear spin. However, according to a theorem by Schiff [47], the nuclear EDM generates no contribution to the neutral-atom EDM due to screening by atomic electrons. The leading contribution from these sources, instead, arises via the nuclear Schiff moment,  $\vec{S}$ , an  $r^3$ -weighted moment of the  $T$ - and  $P$ -odd component of the nuclear charge density. The resulting effective atomic Hamiltonian is

$$\hat{H}_{\text{Schiff}} = -4\pi \vec{\nabla} \rho_e(0) \cdot \vec{S}, \quad (17)$$

where  $\vec{\nabla} \rho_e(0)$  is the gradient of the electron density at the nucleus. To date, computations of the nuclear Schiff moment have assumed that the leading contribution arises from a pion-exchange induced nuclear force, with the  $P$ - and  $T$ -odd  $\pi N$  interaction given by

$$\mathcal{L}_{\pi N}^{T,P} = \bar{N} \left[ \bar{g}_\pi^{(0)} \vec{\tau} \cdot \vec{\pi} + \bar{g}_\pi^{(1)} \pi^0 + \bar{g}_\pi^{(2)} (3\tau_3 \pi^0 - \vec{\tau} \cdot \vec{\pi}) \right] N. \quad (18)$$

Chiral effective field theory power counting implies that in general the magnitude of  $\bar{g}_\pi^{(2)}$  is suppressed with respect to the isoscalar and isovector couplings. The CPV sources then generate a diamagnetic atom EDM  $d_A$  via the sequence

$$\text{CPV source} \rightarrow \bar{g}_\pi^{(i)} \rightarrow \vec{S} \rightarrow d_A. \quad (19)$$

The steps in this sequence involve dynamics at the hadronic, nuclear, and atomic scales, respectively. In addition,  $d_A$  may receive contributions from the nuclear spin-dependent interaction generated by the semileptonic tensor interaction listed in Table 2, with the corresponding atomic Hamiltonian

$$\hat{H}_T = \frac{2iG_F}{\sqrt{2}} \delta(\vec{r}) \sum_N \left[ C_T^{(0)} + C_T^{(1)} \tau_3 \right] \vec{\sigma}_N \cdot \vec{\gamma}, \quad (20)$$

where  $\sigma_N$  is the nucleon spin Pauli matrix and  $C_T^{(0,1)} \propto \text{Im } C_{\ell equ}^{(3)}$ .

Given the large number of CPV sources and existing diamagnetic EDM limits, it is not possible to obtain a set of global constraints on the former. One may, however, do so for the low-energy effective parameters  $\bar{g}_\pi^{(0,1)}$ ,  $C_T^{(0,1)}$  and  $\bar{d}_n^{\text{sr}}$ , where the latter denotes a ‘short-range’ contribution to the neutron EDM [25,48]. In this context, the dominant source of theoretical uncertainty involves computations of the nuclear Schiff moment. From the bounds on the low-energy parameters, one may then derive constraints on the CPV sources by utilizing computations of the hadronic matrix elements. Reducing the degree of theoretical hadronic and nuclear physics uncertainty is an area of active effort.

### 3 Tests of $CPT$

$CPT$  symmetry implies the equality of the masses and widths of a particle and its antiparticle. The most constraining limits are extracted from the neutral kaons [49, 50]:

$$2 \frac{|m_{K^0} - m_{\bar{K}^0}|}{(m_{K^0} + m_{\bar{K}^0})} < 6 \times 10^{-19}, \quad (21)$$

$$2 \frac{|\Gamma_{K^0} - \Gamma_{\bar{K}^0}|}{(\Gamma_{K^0} + \Gamma_{\bar{K}^0})} = (8 \pm 8) \times 10^{-18}.$$

The limit on the  $K^0 - \bar{K}^0$  mass difference assumes that there is no other source of  $CPT$  violation. An upper bound on  $CPT$  breaking in  $K_L^0 \rightarrow 2\pi$  has been also set through the measured phase difference of the CPV ratios  $\eta_{00}$  and  $\eta_{+-}$ ,  $\phi_{00} - \phi_{+-} = (0.34 \pm 0.32)^\circ$ , thanks to the small value of  $(1 - |\eta_{00}/\eta_{+-}|)$  (see the review on  $CP$  violation in  $K_L^0$  decays).

The measured masses and electric charges of the electron, the proton and their antiparticles provide also strong limits on  $CPT$  violation [51–53]:

$$2 \frac{|m_{e^+} - m_{e^-}|}{m_{e^+} + m_{e^-}} < 8 \times 10^{-9}, \quad \frac{|q_{e^+} + q_{e^-}|}{e} < 4 \times 10^{-8},$$

$$\left| \frac{q_{\bar{p}}/m_{\bar{p}}}{q_p/m_p} - 1 \right| = (0.1 \pm 6.9) \times 10^{-11}. \quad (22)$$

Worth mentioning are also the tight constraints derived from the lepton and antilepton magnetic moments [54, 55],

$$2 \frac{g_{e^+} - g_{e^-}}{g_{e^+} + g_{e^-}} = (-0.5 \pm 2.1) \times 10^{-12},$$

$$2 \frac{g_{\mu^+} - g_{\mu^-}}{g_{\mu^+} + g_{\mu^-}} = (-0.11 \pm 0.12) \times 10^{-8}, \quad (23)$$

those of the proton and antiproton [56],

$$(\mu_p + \mu_{\bar{p}})/\mu_p = (2 \pm 4) \times 10^{-9}, \quad (24)$$

and the recent measurement of the 1S-2S atomic transition in anti-hydrogen which agrees with the corresponding frequency spectral line in hydrogen at a relative precision of  $2 \times 10^{-12}$  [57].

A violation of  $CPT$  in an interacting local quantum field theory would imply that Lorentz symmetry is also violated [58]. Signatures of Lorentz-invariance violation have been searched for with atomic clocks, penning traps, matter and antimatter spectroscopy, colliders and astroparticle experiments, with so far negative results [59]. A compilation of experimental bounds is given in Ref. [60], parametrized through the coefficients of the so-called Standard Model Extension (SME) Lagrangian which contains all possible Lorentz- and  $CPT$ -violating operators preserving gauge invariance, renormalizability, locality and observer causality [61].

### QUANTUM-NUMBER CONSERVATION LAWS

Conservation laws of several quantum numbers have been empirically established with a very high degree of confidence. They are usually associated with some global phase symmetry. However, while some of them are deeply rooted in basic principles such as gauge invariance (charge conservation; local symmetry implies global symmetry) or Lorentz symmetry (fermion number conservation), others appear to be accidental symmetries of the SM Lagrangian and could be broken by new physics interactions.

In fact, if one only assumes the SM gauge symmetries and particle content, the most general dynamics at energies below the BSM mass scale is described by the SMEFT Lagrangian in Eq. (12). All  $d = 4$  operators (*i.e.*, the SM) happen to preserve the  $B$  and  $L$  quantum numbers, but this is no-longer true for the gauge-invariant structures of higher dimensionality. There is only one operator with  $d = 5$  (up to hermitian conjugation and flavor assignments), and it violates lepton number by two units [62], giving rise to Majorana neutrino masses after the electroweak spontaneous symmetry breaking. With  $d = 6$ , there are five operators

that violate  $B$  and  $L$  [63, 64]. Thus, violations of these quantum numbers can be generically expected, unless there is an explicit symmetry protecting them.

### 4 Electric charge

The conservation of electric charges is associated with the QED gauge symmetry. The most precise tests are the non-observation of the decays  $e \rightarrow \nu_e \gamma$  (lifetime larger than  $6.6 \times 10^{28}$  yr [65]) and  $n \rightarrow p \nu_e \bar{\nu}_e$  ( $\text{Br} < 8 \times 10^{-27}$ , 68% C.L. [66]). The neutrality of matter can be also interpreted as a test of electric charge conservation. Worth mentioning are the experimental limits on the electric charge of the neutron,  $q_n/e = (-0.2 \pm 0.8) \times 10^{-21}$ , and on the sum of the proton and electron charges,  $|q_p + q_e|/e < 1 \times 10^{-21}$  (68% CL) [67].

The isotropy of the cosmic microwave background has been used to set stringent limits on a possible charge asymmetry of the Universe [68]. Assuming that charge asymmetries produced by different particles are not anticorrelated, this implies upper bounds on the photon ( $|q_\gamma|/e < 1 \times 10^{-35}$ ) and neutrino ( $|q_\nu|/e < 4 \times 10^{-35}$ ) electric charges. A much stronger upper bound on the photon charge ( $|q_\gamma|/e < 1 \times 10^{-46}$ ) has been derived from the non-observation of Aharonov-Bohm phase differences in interferometric experiments with photons that have traversed cosmological distances, under the assumption that both positive and negative charged photons exist [69].

### 5 Lepton family numbers

In the SM with massless left-handed neutrinos there is a separate conservation number for each lepton family. However, neutrino oscillations show that neutrinos have tiny masses and there are sizable mixings among the different lepton flavors. Compelling evidence from solar, atmospheric, accelerator and reactor neutrino experiments has established a quite solid pattern of neutrino mass differences and mixing angles [15, 16] (see the review on neutrino masses, mixings and oscillations). Nevertheless, flavor mixing among the different charged leptons has never been observed.

If neutrino masses and mixings among the three active neutrinos were the only sources of lepton-flavor violation (LFV), neutrinoless transitions from one charged lepton flavor to another would be heavily suppressed by powers of  $m_{\nu_i}$  (GIM mechanism), leading to un-observably small rates; for instance [72–77],

$$\text{Br}(\mu \rightarrow e\gamma) = \frac{3\alpha}{32\pi} \left| \sum_i U_{\mu i}^* U_{ei} \frac{m_{\nu_i}^2 - m_{\nu_1}^2}{M_W^2} \right|^2 < 10^{-54}, \quad (25)$$

where  $U_{ia}$  are the relevant elements of the PMNS mixing matrix. This contribution is clearly too small to be observed in any realistic experiment, so any experimentally accessible effect would arise from BSM physics with sources of LFV not related to  $m_{\nu_i}$ . The search for charged LFV (CLFV) remains an area of active interest, which has the potential to probe physics at scales much higher than the TeV.

Among the most sensitive probes are searches for the CLFV decays of the muon,  $\mu \rightarrow e\gamma$  and  $\mu \rightarrow 3e$ , as well as the conversion process  $\mu^- + A(N, Z) \rightarrow e^- + A(N, Z)$ , where  $A(N, Z)$  denotes a nucleus with  $N$  neutrons and  $Z$  protons. Searches for rare  $\tau$  decays such as  $\tau \rightarrow \ell\gamma$  ( $\ell = e, \mu$ ) also provide interesting probes of CLFV. A variety of BSM scenarios predict that rates for these CLFV processes could be sufficiently large to be observed in the present or planned searches. To date, no observation has been reported, and the resulting null results place strong constraints on BSM scenarios. For extensive reviews of the experimental and theoretical status and prospects, see Refs. [71, 78, 79].

A detailed set of upper bounds on CLFV branching ratios is given in the listings for the muon and tau leptons. Here we emphasize those with the strongest limits:

$$\text{Br}(\mu \rightarrow e\gamma) < 4.2 \times 10^{-13} \quad [80],$$

$$\text{Br}(\mu \rightarrow 3e) < 1.0 \times 10^{-12} \quad [81] \quad (26)$$

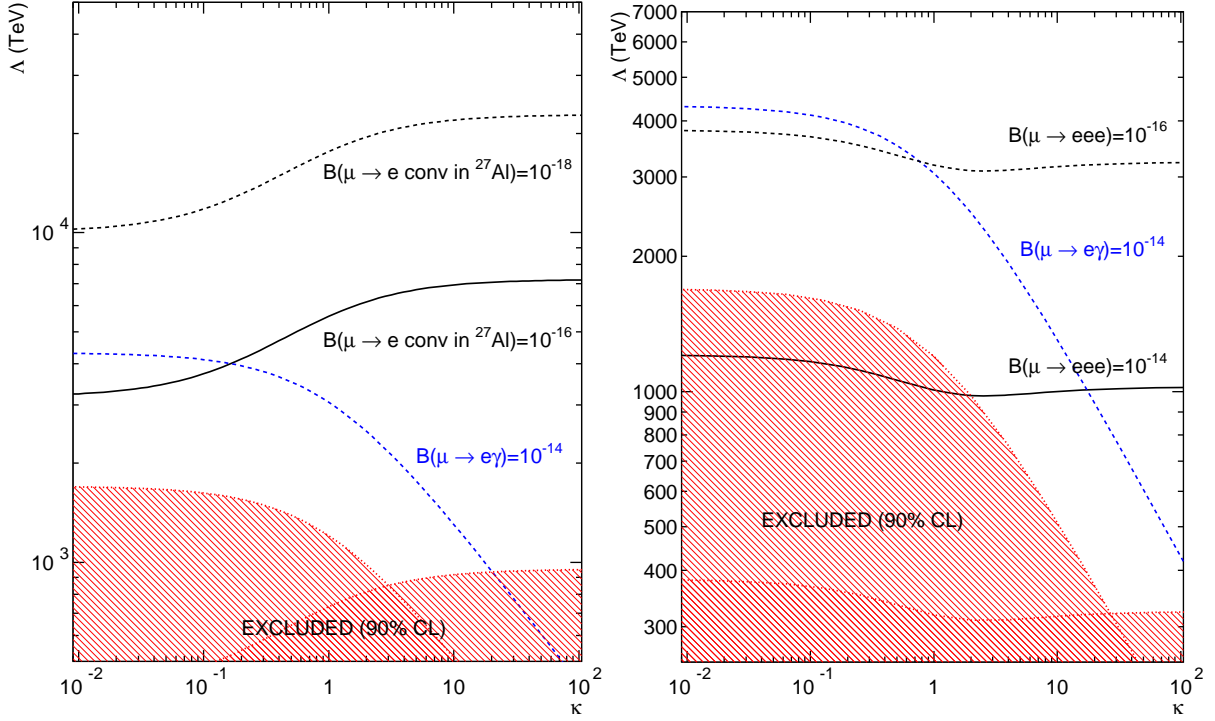


Figure 3: Model-independent CLFV sensitivities based on Eq (31). Left panel shows the comparison of present constraints with prospective future sensitivities for  $\mu \rightarrow e\gamma$  and  $\mu \rightarrow e$  conversion. Right panel gives analogous comparison for  $\mu \rightarrow e\gamma$  and  $\mu \rightarrow 3e$ . Updated by [70] from Ref. [71].

and

$$B_{\mu \rightarrow e} \equiv \frac{\Gamma(\mu^- + A(N, Z) \rightarrow e^- + A(N, Z))}{\Gamma(\mu^- + A(N, Z) \rightarrow \nu + A(N+1, Z-1))} \quad (27)$$

with the best limit so far,  $B_{\mu \rightarrow e} < 7 \times 10^{-13}$  [82], obtained with gold. Several proposed experiments aim to improve these limits by several orders of magnitude with different atoms.

One may interpret both  $\mu \rightarrow e\gamma$  and  $\mu \rightarrow e$  conversion in terms of the amplitudes to emit a real or virtual photon:

$$\begin{aligned} \mathcal{M}_{\mu \rightarrow e\gamma(*)} = & eG_\mu \varepsilon^{\alpha*} \bar{e}(p-q) \left[ (q^2 \gamma_\alpha - \not{q} q_\alpha) (\tilde{A}_1^R P_R + \tilde{A}_1^L P_L) \right. \\ & \left. + im_\mu \sigma_{\alpha\beta} q^\beta (\tilde{A}_2^R P_R + \tilde{A}_2^L P_L) \right] \mu(p), \end{aligned} \quad (28)$$

where it is conventional to normalize the amplitude to the Fermi constant. One then has

$$\text{Br}(\mu \rightarrow e\gamma) = 48\pi^3 \alpha (|\tilde{A}_2^R|^2 + |\tilde{A}_2^L|^2). \quad (29)$$

For the conversion process, the virtual photon is absorbed by the quarks in the nucleus, yielding an effective four-fermion operator. In general, the exchange of other particles could lead to similar or alternate Lorentz structures, and it is not possible to distinguish between the exchange of a virtual photon or other particle. It is conventional to write the most general four-fermion amplitude, valid for energies below the electroweak scale as (adapted from Ref. [88])

$$\mathcal{M}_{\mu \rightarrow e} = G_\mu \sum_{n,a,q} a_{a,q}^{(n)} \bar{e} \Gamma^n P_a \mu \bar{q} \Gamma_n q, \quad (30)$$

where  $P_a$  ( $a = L, R$ ) denote the left and right-handed projectors and  $\Gamma^n$  denotes  $1, \gamma_5, \gamma^\mu, \gamma^\mu \gamma_5$ , and  $\sigma_{\mu\nu}$ . If any of the coefficients  $a_{a,q}^{(n)}$  are generated by physics at a scale  $\Lambda > v$ , then their effects would be encoded in the SMEFT Lagrangian (12). For scenarios in which the leading CLFV operators occur at  $d = 6$ ,

the  $a_{a,q}^{(n)}$  will scale as  $(v/\Lambda)^2$ . The corresponding decay and conversion rates will then scale as  $(v/\Lambda)^4$ . Note that the scalar and time component of the vector interactions are coherent over the nucleus, essentially counting the number of quarks. Consequently, these interactions typically yield the greatest sensitivities to high BSM mass scales.

It is sometimes convenient to compare the relative sensitivities of the decay and conversion processes using the following simplified effective Lagrangian [71]:

$$\begin{aligned} \mathcal{L}_{\text{eff}}^{\text{CLFV}} = & \frac{m_\mu}{(\kappa+1)\Lambda^2} \bar{\mu}_R \sigma_{\mu\nu} e_L F^{\mu\nu} \\ & + \frac{\kappa}{(\kappa+1)\Lambda^2} \bar{\mu} \gamma_\mu e \sum_q \bar{q} \gamma^\mu q + \text{h.c.} \end{aligned} \quad (31)$$

Note that one may replace the second term in Eq. (31) by any one of the other four-fermion interactions given in Eq. (30). An analogous expression applies to the process  $\mu \rightarrow 3e$  when replacing the sum over quarks by the corresponding electron bilinear. A comparison of the present and prospective sensitivities for various muon CLFV searches in this framework is shown in Figure 3.

Stringent limits have been also set on the LFV decay modes of the  $\tau$  lepton [89]. As shown in Figure 4, the large  $\tau$  data samples collected at the  $B$  factories have made possible to reach a  $10^{-8}$  sensitivity for many of its leptonic ( $\tau \rightarrow \ell\gamma, \tau \rightarrow \ell'\ell^+\ell^-$ ) and semileptonic ( $\tau \rightarrow \ell P^0, \tau \rightarrow \ell V^0, \tau \rightarrow \ell P^0 P^0, \tau \rightarrow \ell P^+ P'^-$ ) neutrinoless LFV decays, and BELLE-II is expected to push these limits beyond the  $10^{-9}$  level [84]. Being a third generation lepton, the  $\tau$  could be more sensitive to heavier new-physics scales, which makes his LFV decays particularly interesting. Compared to the muon, the  $\tau$  decay amplitudes could be enhanced by a chirality ratio  $(m_\tau/m_\mu)^2 \sim 280$  and/or by lepton-mixing factors such as  $|U_{\tau 3}/U_{e 3}|^2 \sim 20$ , but the exact relation is model dependent. In any case, the  $\tau$  LFV decays provide a rich data set that is very complementary to the  $\mu$  bounds. If LFV is finally observed, the correlations between  $\mu$  and  $\tau$  data, and among different LFV  $\tau$  decays will allow to probe the underlying mechanism of lepton flavor breaking.

Interesting limits on LFV are also obtained in meson decays.

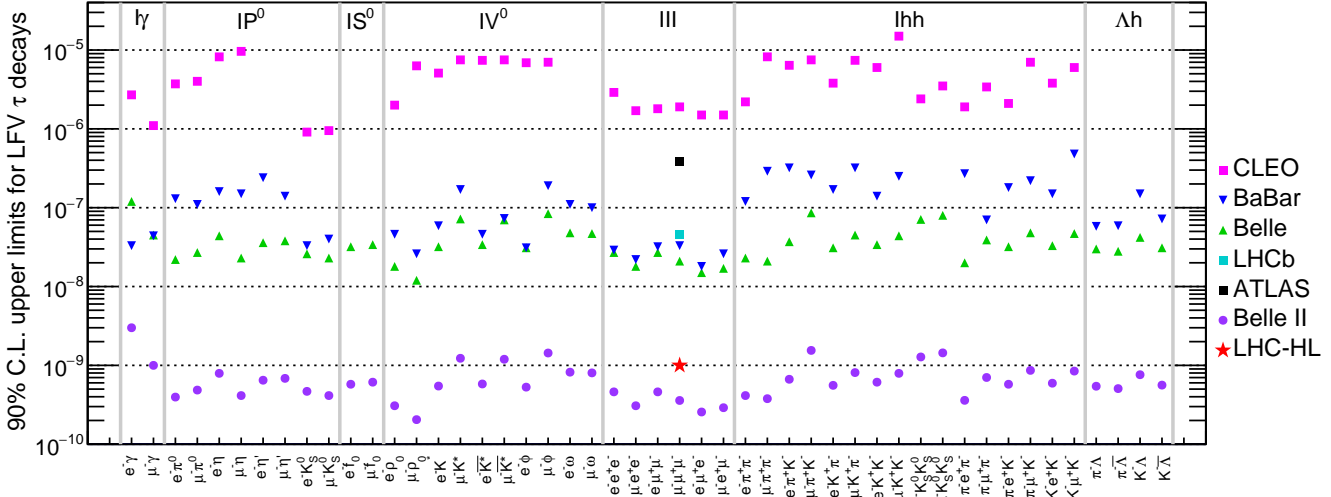


Figure 4: Current experimental limits on neutrinoless LFV  $\tau$  decays [83]. Also shown are the future projections at Belle-II [84] and at the HL-LHC [85].

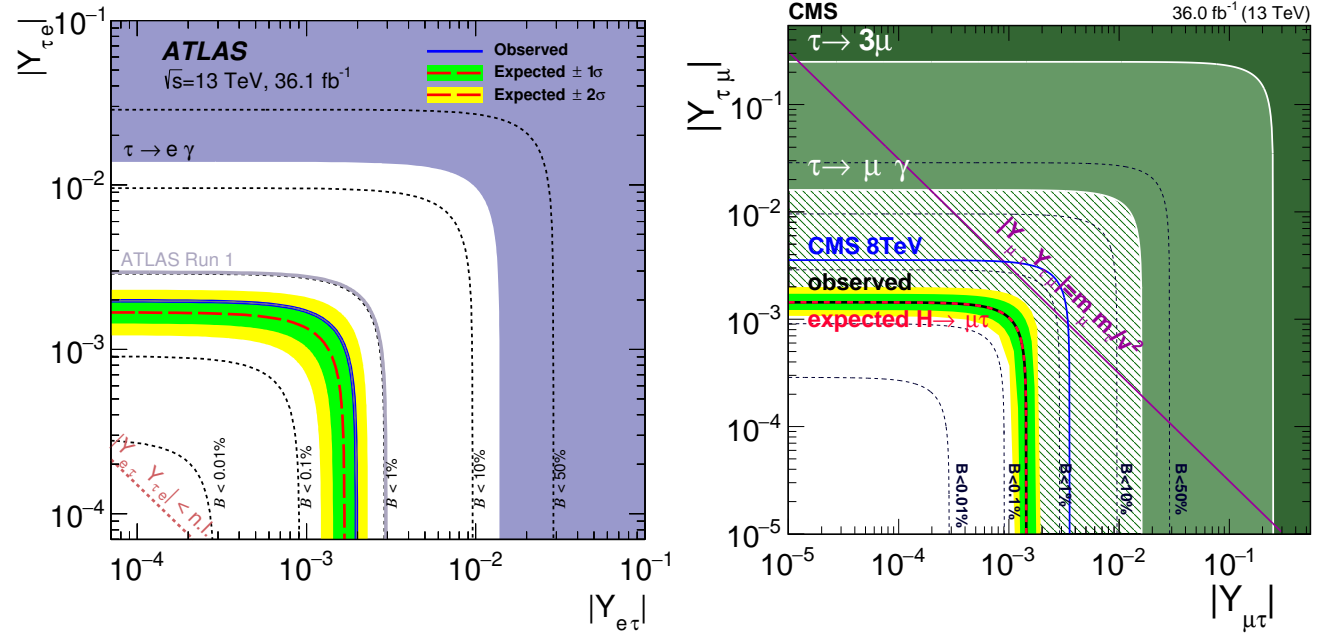


Figure 5: Current limits on the Higgs LFV  $\tau$  Yukawas from direct  $H^0 \rightarrow \ell^\pm \tau^\mp$  decays ( $\ell = e, \mu$ ), and indirect constraints from  $\tau$  decays [86, 87].

The best bounds come from kaon experiments, e.g.,  $\text{Br}(K_L^0 \rightarrow e^\pm \mu^\mp) < 4.7 \times 10^{-12}$  [90],  $\text{Br}(K^+ \rightarrow \pi^+ \mu^+ e^-) < 1.3 \times 10^{-11}$  [91]. Quite strong limits have also been set in decays of  $B$  and  $D$  mesons, the best upper bounds being  $\text{Br}(B^0 \rightarrow e^\pm \mu^\mp) < 1.0 \times 10^{-9}$  [92] and  $\text{Br}(D^0 \rightarrow e^\pm \mu^\mp) < 1.3 \times 10^{-8}$  [93].

The LFV decays of the  $Z$  boson were probed at LEP at the  $10^{-5}$  to  $10^{-6}$  level. The LHC ATLAS collaboration has put recently a stronger bound on the  $Z \rightarrow e^\pm \mu^\mp$  decay mode [94]. Currently, the best (95% C.L.) limits are [94–96]:

$$\begin{aligned} \text{Br}(Z \rightarrow e^\pm \mu^\mp) &< 7.5 \times 10^{-7}, & \text{Br}(Z \rightarrow e^\pm \tau^\mp) &< 9.8 \times 10^{-6}, \\ \text{Br}(Z \rightarrow \mu^\pm \tau^\mp) &< 1.2 \times 10^{-5}. \end{aligned} \quad (32)$$

LHC is now starting to test LFV in Higgs decays, within the available statistics. From the current (95% C.L.) experimental

upper bounds [86, 87, 97],

$$\begin{aligned} \text{Br}(H^0 \rightarrow e^\pm \mu^\mp) &< 6.1 \times 10^{-5}, & \text{Br}(H^0 \rightarrow e^\pm \tau^\mp) &< 0.47\%, \\ \text{Br}(H^0 \rightarrow \mu^\pm \tau^\mp) &< 0.25\%, \end{aligned} \quad (33)$$

one can derive direct limits on the LFV Yukawa couplings of the Higgs boson,

$$\mathcal{L}_Y = -H^0 \sum_{i \neq j} (Y_{\ell_i \ell_j} \bar{\ell}_i^j \ell_R^j + \text{h.c.}). \quad (34)$$

From  $H^0 \rightarrow e^\pm \mu^\mp$ , one obtains  $\sqrt{Y_{\mu e}^2 + Y_{e\mu}^2} < 2.2 \times 10^{-4}$ , which is not yet competitive with the indirect limit set by  $\mu \rightarrow e\gamma$  through a (one-loop) virtual Higgs exchange:

$$\sqrt{Y_{\mu e}^2 + Y_{e\mu}^2} < 3.6 \times 10^{-6}. \quad (35)$$

However, the LHC data provides at present the strongest bounds

on the LFV  $\tau$  Yukawas [86, 87]:

$$\sqrt{Y_{e\tau}^2 + Y_{\tau e}^2} < 2.0 \times 10^{-3}, \quad \sqrt{Y_{\mu\tau}^2 + Y_{\tau\mu}^2} < 1.4 \times 10^{-3}. \quad (36)$$

Figure 5 compares the Higgs exclusion limits on the  $\tau$  Yukawas with the current indirect constraints from LFV  $\tau$  decays.

## 6 Baryon and Lepton Number

The transitions discussed in the previous section preserve the total lepton number  $L = L_e + L_\mu + L_\tau$ . In the SM, conservation of  $B - L$  is an accidental symmetry of the Lagrangian. At the classical level,  $B + L$  is also conserved, though it is violated at the loop level by the anomaly. The latter is a topological effect that is highly suppressed at zero temperature and, moreover, does not contribute to the processes discussed in the review. Going beyond renormalizable interactions, there exists a tower of operators in the SMEFT Lagrangian (12), containing only SM fields, that break one or both of these symmetries. We briefly review these possibilities in turn.

### Lepton Number

The lowest-dimension operator containing only SM fields that breaks baryon or lepton number is the  $d = 5$ , lepton-number-violating (LNV) ‘Weinberg’ neutrino-mass operator [62]:

$$\mathcal{L}^{\text{LNV}} = \frac{y}{\Lambda} \bar{L}^C H H^T L. \quad (37)$$

When the neutral component of the Higgs field obtains its vacuum expectation value, this  $\Delta L = 2$  interaction yields a Majorana mass for the light, active neutrinos. The most comprehensive approach for probing this effect is the search for neutrinoless double-beta decay ( $0\nu\beta\beta$ ) of atomic nuclei,  $(Z, A) \rightarrow (Z + 2, A) + e^- + e^-$  [98, 99] (see the review on neutrinoless double- $\beta$  decay). The detection of a non-zero  $0\nu\beta\beta$  signal could represent a spectacular evidence of Majorana neutrinos. The current best limit,  $\tau_{1/2} > 1.07 \times 10^{26}$  yr, was obtained by the KamLAND-Zen experiment with  $^{136}\text{Xe}$  [100].

Theoretically, the interaction (37) can arise from BSM interactions in the well-known see-saw mechanism for neutrino mass (for a review, see [101]). In this context, the conventional choice for the scale  $\Lambda$  is of order the GUT scale, yielding light neutrino masses of order  $eV$  and below when the couplings  $y$  are of order the charged elementary fermion Yukawa couplings. BSM theories may also give rise to LNV observables in other contexts. In these scenarios, if the LNV scale is of order 1 TeV, one may observe signatures of LNV not only in  $0\nu\beta\beta$  but also in collider searches for final states containing same sign dileptons. Searches for same sign dileptons plus a di-jet pair at the LHC have placed constraints on TeV-scale LNV [102, 103] that in some cases complement those obtained from  $0\nu\beta\beta$ .

Stringent constraints on violations of  $L$  have been also set in  $\mu^- \rightarrow e^+$  conversion in muonic atoms, the best limit being  $\sigma(\mu^- \text{Ti} \rightarrow e^+ \text{Ca}) / \sigma(\mu^- \text{Ti} \rightarrow \text{all}) < 3.6 \times 10^{-11}$  [104], and at the flavor factories through  $L$ -violating decays of the  $\tau$  lepton and  $K$ ,  $D$  and  $B$  mesons. Some representative examples are  $\text{Br}(\tau^- \rightarrow e^+ \pi^- \pi^-) < 2.0 \times 10^{-8}$  [105],  $\text{Br}(K^+ \rightarrow \pi^- \mu^+ \mu^+) < 4.2 \times 10^{-11}$  [106],  $\text{Br}(D^+ \rightarrow \pi^- \mu^+ \mu^+) < 2.2 \times 10^{-8}$  [107] and  $\text{Br}(B^+ \rightarrow K^- e^+ e^+) < 3.0 \times 10^{-8}$  [108]. All these  $|\Delta L| = 2$  processes could be mediated by a massive Majorana neutrino. They provide useful bounds on the effective Majorana neutrino mass matrix  $m_{\ell\ell'} \sim \sum_i U_{\ell i} U_{\ell' i} m_{\nu_i}$  [109], although not as strong as the  $0\nu\beta\beta$  constraint on  $m_{ee}$ .

### Baryon Number

Grand Unified Theories (GUTs) combine leptons and quarks in the same symmetry multiplets and, therefore, predict the violation of the baryon and lepton quantum numbers. Many experiments have searched for  $B$ -violating transitions, but no positive signal has been identified so far. Proton decay would be the most relevant violation of  $B$ , as it would imply the instability of matter. The current lower bound on the proton lifetime is  $3.6 \times 10^{29}$  yr [110]. Stronger limits have been set for particular decay modes, such as  $\tau(p \rightarrow e^+ \pi^0) > 1.6 \times 10^{34}$  yr [111]. For a discussion of proton decay in the context of GUTs, see the review on Grand Unified Theories.

Another spectacular signal would be neutron-antineutron oscillations. Searches have been performed for quasi-free  $n-\bar{n}$  oscillations and for  $n\bar{n}$  annihilation products in a nucleus. The latter would arise when the  $\bar{n}$  produced through oscillations annihilates with another neutron in the nuclear medium. The corresponding best limits, expressed in terms of the free and bound oscillation times,  $\tau_{n\bar{n}}$  and  $\tau_m$ , respectively, are:

$$\tau_{n\bar{n}} > 0.86 \times 10^8 \text{ s} \quad [112], \quad (38a)$$

$$\tau_m > 1.9 \times 10^{32} \text{ yr} \quad [113]. \quad (38b)$$

From the latter, one may infer a bound  $\tau_{n\bar{n}} > 2.7 \times 10^8$  s, as discussed below. See Ref. [114] for a recent review.

The theoretical interpretation of these bounds starts with an assumed, effective Hamiltonian for the free (anti-)neutron,  $\mathcal{H}_{\text{eff}}$  that contains a  $B$ -violating part, yielding matrix elements

$$\langle n | \mathcal{H}_{\text{eff}} | n \rangle = \langle \bar{n} | \mathcal{H}_{\text{eff}} | \bar{n} \rangle = m - i \frac{\lambda}{2}, \quad (39a)$$

$$\langle n | \mathcal{H}_{\text{eff}} | \bar{n} \rangle = \langle \bar{n} | \mathcal{H}_{\text{eff}} | n \rangle \equiv \delta m, \quad (39b)$$

where  $CPT$  is assumed to be conserved, the neutron lifetime  $\tau_n = 1/\lambda$  and  $\tau_{n\bar{n}} = 1/|\delta m|$ . The rate for a neutron to oscillate into an antineutron after a time  $t$  is given by

$$\mathcal{P}_{n\bar{n}}(t) = \sin^2 \left( \frac{t}{\tau_{n\bar{n}}} \right) e^{-\lambda t}. \quad (40)$$

For  $t \ll \tau_n \ll \tau_{n\bar{n}}$ , one has

$$\mathcal{P}_{n\bar{n}}(t) \rightarrow (t/\tau_{n\bar{n}})^2. \quad (41)$$

In realistic experiments, there exist effects, such as background magnetic fields, that split the energies of the neutron and antineutron. One must ensure that the observation time is sufficiently short so that these effects do not overwhelm the small  $B$ -violating term  $\delta m$  and that Eq. (40) applies.

In nuclei, the interactions of neutrons and antineutrons with the surrounding medium are sufficiently distinct that one must take the corresponding matter potentials into account. In particular, the matrix elements in Eq. (39a) become

$$\langle n | \mathcal{H}_{\text{eff}} | n \rangle = m + V_n, \quad \langle \bar{n} | \mathcal{H}_{\text{eff}} | \bar{n} \rangle = m + V_{\bar{n}}, \quad (42)$$

with  $V_n$  being essentially real ( $V_n \equiv V_{nR}$ ) and  $V_{\bar{n}} = V_{\bar{n}R} - iV_{\bar{n}I}$ . The imaginary part  $V_{\bar{n}I}$  characterizes the annihilation of the antineutron with bound nucleons into secondary hadrons. The rate for a bound neutron to disappear is given by

$$\Gamma_m = \frac{2(\delta m)^2 |V_{\bar{n}I}|}{(V_{nR} - V_{\bar{n}R})^2 + V_{\bar{n}I}^2} \equiv (R\tau_{n\bar{n}}^2)^{-1}. \quad (43)$$

For the nuclei of experimental interest, nuclear theory computations yield  $R \sim 10^{23} \text{ s}^{-1}$ . Null results of bound  $n-\bar{n}$  oscillation searches thus allow one to infer a bound on  $\tau_{n\bar{n}}$  via Eq. (43).

From an elementary particle standpoint,  $n-\bar{n}$  oscillations involve the conversion of three quarks into three antiquarks (and vice-versa). The lowest-dimension operators mediating such process arise at dimension nine in the SMEFT:

$$\mathcal{L}_{n-\bar{n}} = \frac{1}{\Lambda^5} \sum_j \alpha_j^{(9)} \mathcal{O}_j^{\text{BNV}}. \quad (44)$$

Consequently, one expects

$$\delta m \sim \alpha_j^{(9)} \frac{\Lambda_{\text{HAD}}^6}{\Lambda^5}, \quad (45)$$

where  $\Lambda_{\text{HAD}}$  is a hadronic scale set by the  $n-\bar{n}$  matrix elements in Eq. (39b). Taking  $\Lambda_{\text{HAD}}$  to be of order the QCD scale and using the present bounds on  $\tau_{n\bar{n}}$  yields a lower bound on the  $B$ -violating mass scale of  $\sim 100$  TeV.

The search for  $B$ -violating decays of short-lived particles such as  $Z$  bosons,  $\tau$  leptons and  $B$  mesons provides also relevant constraints. The best limits are  $\text{Br}(Z \rightarrow pe, p\mu) < 1.8 \times 10^{-6}$  (95% C.L.) [115],  $\text{Br}(\tau^- \rightarrow A\pi^-) < 7.2 \times 10^{-8}$  [116] and  $\text{Br}(B^+ \rightarrow Ae^+) < 3.2 \times 10^{-8}$  [117].



## 7 Quark flavors

While strong and electromagnetic forces preserve the quark flavor, the charged-current weak interactions generate transitions among the different quark species (see the review on the CKM quark-mixing matrix). Since the SM flavor-changing mechanism is associated with the  $W^\pm$  fermionic vertices, the tree-level transitions satisfy a  $\Delta F = \Delta Q$  rule where  $\Delta Q$  denotes the change in charge of the relevant hadrons. Remember that the flavor quantum number  $F$  is defined to be +1 for positively charged quarks ( $F = U, C, T$ ) and -1 for quarks with negative charges ( $F = D, S, B$ ). The strongest tests on this conservation law have been obtained in kaon decays such as  $\text{Br}(K^+ \rightarrow \pi^+ \pi^+ e^- \bar{\nu}_e) < 1.3 \times 10^{-8}$  [118], and  $(\text{Re } x, \text{Im } x) = (-0.002 \pm 0.006, 0.0012 \pm 0.0021)$  [119, 120] where  $x \equiv \mathcal{M}(K^0 \rightarrow \pi^- \ell^+ \nu) / \mathcal{M}(K^0 \rightarrow \pi^- \ell^+ \nu)$ .

The  $\Delta F = \Delta Q$  rule can be violated through quantum loop contributions giving rise to flavor-changing neutral-current transitions (FCNCs). Owing to the GIM mechanism, processes of this type are very suppressed in the SM, which makes them a superb tool in the search for new physics associated with the flavor dynamics. Within the SM itself, these transitions are also sensitive to the heavy-quark mass scales and have played a crucial role identifying the size of the charm ( $K^0$ - $\bar{K}^0$  mixing) and top ( $B^0$ - $\bar{B}^0$  mixing) masses before the discovery of those quarks. In addition to the well-established  $\Delta F = 2$  mixings in neutral  $K$  and  $B$  mesons,  $\Delta M_{K^0} \equiv M_{K_L^0} - M_{K_S^0} = (0.5293 \pm 0.0009) \times 10^{10} \text{ s}^{-1}$ ,  $\Delta M_{B^0} \equiv M_{B_H^0} - M_{B_L^0} = (0.5065 \pm 0.0019) \times 10^{12} \text{ s}^{-1}$  and  $\Delta M_{B_s^0} \equiv M_{B_{sH}^0} - M_{B_{sL}^0} = (17.757 \pm 0.0021) \times 10^{12} \text{ s}^{-1}$ , there is now strong evidence for the mixing of the  $D^0$  meson and its antiparticle [121],

$$x_D \equiv (M_{D_H^0} - M_{D_L^0}) / \Gamma_{D^0} = (3.9^{+1.1}_{-1.2}) \times 10^{-3}, \quad (46)$$

showing that there is a nonzero mass difference between the two neutral charm-meson eigenstates, of the expected size. The SM prediction for  $x_D$  is dominated by long-distance physics, because it involves virtual loops with down-type light quarks, and has unfortunately quite large uncertainties [122].

The FCNC kaon decays into lepton-antilepton pairs put stringent constraints on new flavor-changing interactions. The measured  $K_L^0 \rightarrow \mu^+ \mu^-$  rate,  $\text{Br}(K_L^0 \rightarrow \mu^+ \mu^-) = (6.84 \pm 0.11) \times 10^{-9}$ , is completely dominated by the known  $2\gamma$  absorptive contribution, leaving very little room for new-physics, and  $\text{Br}(K_L^0 \rightarrow e^+ e^-) = (9^{+6}_{-4}) \times 10^{-12}$  [123] (the tiniest branching ratio ever measured) also agrees with the SM expectation [124]. The experimental  $K_S^0$  upper bounds on the electron,  $\text{Br}(K_S^0 \rightarrow e^+ e^-) < 9 \times 10^{-9}$  [125], and muon,  $\text{Br}(K_S^0 \rightarrow \mu^+ \mu^-) < 2.1 \times 10^{-10}$  [126], modes are still five and two orders of magnitude, respectively, larger than their SM predictions [124]. Another very clean test of FCNCs will be soon provided by the decay  $K^+ \rightarrow \pi^+ \nu \bar{\nu}$ . With a predicted SM branching fraction of  $(7.8 \pm 0.8) \times 10^{-11}$  [127], the CERN NA62 experiment is aiming to collect around one hundred events. Even more interesting is the  $CP$ -violating neutral mode  $K_L^0 \rightarrow \pi^0 \nu \bar{\nu}$ , expected at a rate of  $(2.4 \pm 0.4) \times 10^{-11}$  [127] that is still far away from the current upper bound of  $3.0 \times 10^{-9}$  [128]. The KOTO experiment at KEK is expected to substantially increase the sensitivity to this mode.

The strongest bound on FCNC transitions in charm decays is  $\text{Br}(D^0 \rightarrow \mu^+ \mu^-) < 6.2 \times 10^{-9}$  [129], while in  $B$  decays the LHC experiments have recently reached the SM sensitivity:  $\text{Br}(B_d^0 \rightarrow \mu^+ \mu^-) = (0.14^{+0.16}_{-0.14}) \times 10^{-9}$  and  $\text{Br}(B_s^0 \rightarrow \mu^+ \mu^-) = (3.0 \pm 0.4) \times 10^{-9}$ . At present, there is a lot of interest on the decays  $B \rightarrow K^{(*)} \ell^+ \ell^-$  where sizable discrepancies between the measured data and the SM predictions have been reported [130]. In particular, the LHCb experiment has found the ratios of produced muons versus electrons to be around  $2.5\sigma$  below the SM predictions, both in  $B \rightarrow K^* \ell^+ \ell^-$  [131] and in  $B^+ \rightarrow K^+ \ell^+ \ell^-$  [132] (for dilepton invariant-masses squared in the range  $q^2 \leq 6 \text{ GeV}^2$ ), suggesting a significant violation of lepton universality. The current Belle-II measurements of these ratios [133, 134] are consistent with the SM, but they are also compatible with the LHCb results. Future analyses from LHCb and Belle-II are expected to clarify the situation.

## References

- [1] G. Luders, Kong. Dan. Vid. Sel. Mat. Fys. Med. **28N5**, 5, 1 (1954).
- [2] W. Pauli, in L. Rosenfeld and V. Weisskopf, editors, “Niels Bohr and the Development of Physics,” 30–51, McGraw-Hill, New York (1955).
- [3] J. McDonough *et al.*, Phys. Rev. **D38**, 2121 (1988).
- [4] M. Ablikim *et al.* (BESIII), Phys. Rev. **D90**, 9, 092002 (2014), [arXiv:1409.4040].
- [5] S. Prakhov *et al.* (Crystal Ball), Phys. Rev. Lett. **84**, 4802 (2000).
- [6] J. H. Christenson *et al.*, Phys. Rev. Lett. **13**, 138 (1964).
- [7] H. Burkhardt *et al.* (NA31), Phys. Lett. **B206**, 169 (1988).
- [8] G. D. Barr *et al.* (NA31), Phys. Lett. **B317**, 233 (1993).
- [9] L. K. Gibbons *et al.*, Phys. Rev. Lett. **70**, 1203 (1993).
- [10] J. R. Batley *et al.* (NA48), Phys. Lett. **B544**, 97 (2002), [hep-ex/0208009].
- [11] E. Abouzaid *et al.* (KTeV), Phys. Rev. **D83**, 092001 (2011), [arXiv:1011.0127].
- [12] H. Gisbert and A. Pich, Rept. Prog. Phys. **81**, 7, 076201 (2018), [arXiv:1712.06147].
- [13] V. Cirigliano *et al.*, JHEP **02**, 032 (2020), [arXiv:1911.01359].
- [14] R. Aaij *et al.* (LHCb), Phys. Rev. Lett. **122**, 21, 211803 (2019), [arXiv:1903.08726].
- [15] P. F. de Salas *et al.*, Phys. Lett. **B782**, 633 (2018), [arXiv:1708.01186].
- [16] I. Esteban *et al.*, JHEP **01**, 106 (2019), [arXiv:1811.05487].
- [17] A. Angelopoulos *et al.* (CLEAR), Phys. Lett. **B444**, 43 (1998).
- [18] L. Wolfenstein, Phys. Rev. Lett. **83**, 911 (1999).
- [19] L. Alvarez-Gaume *et al.*, Phys. Lett. **B458**, 347 (1999), [hep-ph/9812326].
- [20] H. J. Gerber, Eur. Phys. J. **C35**, 195 (2004).
- [21] M. C. Bañuls and J. Bernabeu, Phys. Lett. **B464**, 117 (1999), [hep-ph/9908353].
- [22] M. C. Bañuls and J. Bernabeu, Nucl. Phys. **B590**, 19 (2000), [hep-ph/0005323].
- [23] J. Bernabeu, F. Martinez-Vidal and P. Villanueva-Perez, JHEP **08**, 064 (2012), [arXiv:1203.0171].
- [24] J. P. Lees *et al.* (BaBar), Phys. Rev. Lett. **109**, 211801 (2012), [arXiv:1207.5832].
- [25] T. Chupp *et al.*, Rev. Mod. Phys. **91**, 1, 015001 (2019), [arXiv:1710.02504].
- [26] J. Engel, M. J. Ramsey-Musolf and U. van Kolck, Prog. Part. Nucl. Phys. **71**, 21 (2013), [arXiv:1303.2371].
- [27] M. Pospelov and A. Ritz, Annals Phys. **318**, 119 (2005), [hep-ph/0504231].
- [28] J. S. M. Ginges and V. V. Flambaum, Phys. Rept. **397**, 63 (2004), [arXiv:physics/0309054].
- [29] V. Andreev *et al.* (ACME), Nature **562**, 7727, 355 (2018).
- [30] W. B. Cairncross *et al.*, Phys. Rev. Lett. **119**, 15, 153001 (2017), [arXiv:1704.07928].
- [31] G. W. Bennett *et al.* (Muon (g-2)), Phys. Rev. **D80**, 052008 (2009), [arXiv:0811.1207].
- [32] C. Abel *et al.* (nEDM), Phys. Rev. Lett. **124**, 8, 081803 (2020), [arXiv:2001.11966].
- [33] B. Graner *et al.*, Phys. Rev. Lett. **116**, 16, 161601 (2016), [Erratum: Phys. Rev. Lett. 119, no.11, 119901 (2017)], [arXiv:1601.04339].
- [34] F. Allmendinger *et al.*, Phys. Rev. **A100**, 2, 022505 (2019), [arXiv:1904.12295].

- [35] C. Jarlskog, Phys. Rev. Lett. **55**, 1039 (1985); C. Jarlskog, Z. Phys. **C29**, 491 (1985).
- [36] E. P. Shabalin, Sov. J. Nucl. Phys. **28**, 75 (1978), [Yad. Fiz.28,151(1978)].
- [37] E. P. Shabalin, Sov. Phys. Usp. **26**, 297 (1983), [Usp. Fiz. Nauk139,561(1983)].
- [38] W. Bernreuther and M. Suzuki, Rev. Mod. Phys. **63**, 313 (1991), [Erratum: Rev. Mod. Phys.64,633(1992)].
- [39] M. Pospelov and A. Ritz, Phys. Rev. **D89**, 5, 056006 (2014), [arXiv:1311.5537].
- [40] C.-Y. Seng, Phys. Rev. **C91**, 2, 025502 (2015), [arXiv:1411.1476].
- [41] B. Grzadkowski *et al.*, JHEP **10**, 085 (2010), [arXiv:1008.4884].
- [42] S. Mantry, M. Pitschmann and M. J. Ramsey-Musolf, Phys. Rev. **D90**, 5, 054016 (2014), [arXiv:1401.7339].
- [43] B. K. Sahoo, Phys. Rev. **D95**, 1, 013002 (2017), [arXiv:1612.09371].
- [44] T. Chupp, Private Communication (2019).
- [45] J. Bsaisou *et al.*, Annals Phys. **359**, 317 (2015), [arXiv:1412.5471].
- [46] J. de Vries *et al.*, Annals Phys. **338**, 50 (2013), [arXiv:1212.0990].
- [47] L. I. Schiff, Phys. Rev. **132**, 2194 (1963).
- [48] T. Chupp and M. Ramsey-Musolf, Phys. Rev. **C91**, 3, 035502 (2015), [arXiv:1407.1064].
- [49] J. Beringer *et al.* (Particle Data Group), Phys. Rev. **D86**, 010001 (2012).
- [50] A. Angelopoulos *et al.* (CPLEAR), Phys. Lett. **B471**, 332 (1999).
- [51] M. S. Fee *et al.*, Phys. Rev. **A48**, 192 (1993).
- [52] R. J. Hughes and B. I. Deutch, Phys. Rev. Lett. **69**, 578 (1992).
- [53] S. Ulmer *et al.* (BASE), Nature **524**, 7564, 196 (2015).
- [54] R. S. Van Dyck, P. B. Schwinberg and H. G. Dehmelt, Phys. Rev. Lett. **59**, 26 (1987).
- [55] G. W. Bennett *et al.* (Muon g-2), Phys. Rev. Lett. **92**, 161802 (2004), [hep-ex/0401008].
- [56] C. Smorra *et al.* (BASE), Nature **550**, 7676, 371 (2017).
- [57] M. Ahmadi *et al.*, Nature **557**, 7703, 71 (2018).
- [58] O. W. Greenberg, Phys. Rev. Lett. **89**, 231602 (2002), [hep-ph/0201258].
- [59] S. Liberati, Class. Quant. Grav. **30**, 133001 (2013), [arXiv:1304.5795].
- [60] V. A. Kostelecky and N. Russell, Rev. Mod. Phys. **83**, 11 (2011), [arXiv:0801.0287].
- [61] D. Colladay and V. A. Kostelecky, Phys. Rev. **D58**, 116002 (1998), [hep-ph/9809521].
- [62] S. Weinberg, Phys. Rev. Lett. **43**, 1566 (1979).
- [63] F. Wilczek and A. Zee, Phys. Rev. Lett. **43**, 1571 (1979).
- [64] L. F. Abbott and M. B. Wise, Phys. Rev. **D22**, 2208 (1980).
- [65] M. Agostini *et al.* (Borexino), Phys. Rev. Lett. **115**, 231802 (2015), [arXiv:1509.01223].
- [66] E. B. Norman, J. N. Bahcall and M. Goldhaber, Phys. Rev. **D53**, 4086 (1996).
- [67] G. Bressi *et al.*, Phys. Rev. **A83**, 5, 052101 (2011), [arXiv:1102.2766].
- [68] C. Caprini, S. Biller and P. G. Ferreira, JCAP **0502**, 006 (2005), [hep-ph/0310066].
- [69] B. Altschul, Phys. Rev. Lett. **98**, 261801 (2007), [hep-ph/0703126].
- [70] A. de Gouvea, Private Communication (2019).
- [71] A. de Gouvea and P. Vogel, Prog. Part. Nucl. Phys. **71**, 75 (2013), [arXiv:1303.4097].
- [72] S. T. Petcov, Sov. J. Nucl. Phys. **25**, 340 (1977), [Erratum: Yad. Fiz.25,1336(1977)].
- [73] W. J. Marciano and A. I. Sanda, Phys. Lett. **67B**, 303 (1977).
- [74] S. M. Bilenky, S. T. Petcov and B. Pontecorvo, Phys. Lett. **67B**, 309 (1977).
- [75] T.-P. Cheng and L.-F. Li, Phys. Rev. **D16**, 1425 (1977).
- [76] B. W. Lee and R. E. Shrock, Phys. Rev. **D16**, 1444 (1977).
- [77] B. W. Lee *et al.*, Phys. Rev. Lett. **38**, 937 (1977), [Erratum: Phys. Rev. Lett.38,1230(1977)].
- [78] R. H. Bernstein and P. S. Cooper, Phys. Rept. **532**, 27 (2013), [arXiv:1307.5787].
- [79] L. Calibbi and G. Signorelli, Riv. Nuovo Cim. **41**, 2, 71 (2018), [arXiv:1709.00294].
- [80] A. M. Baldini *et al.* (MEG), Eur. Phys. J. **C76**, 8, 434 (2016), [arXiv:1605.05081].
- [81] U. Bellgardt *et al.* (SINDRUM), Nucl. Phys. **B299**, 1 (1988).
- [82] W. H. Bertl *et al.* (SINDRUM II), Eur. Phys. J. **C47**, 337 (2006).
- [83] Y. S. Amhis *et al.* (HFLAV) (2019), [arXiv:1909.12524].
- [84] W. Altmannshofer *et al.* (Belle-II), PTEP **2019**, 12, 123C01 (2019), [arXiv:1808.10567].
- [85] A. Cerri *et al.*, CERN Yellow Rep. Monogr. **7**, 867 (2019), [arXiv:1812.07638].
- [86] G. Aad *et al.* (ATLAS), Phys. Lett. **B800**, 135069 (2020), [arXiv:1907.06131].
- [87] A. M. Sirunyan *et al.* (CMS), JHEP **06**, 001 (2018), [arXiv:1712.07173].
- [88] R. Kitano, M. Koike and Y. Okada, Phys. Rev. **D66**, 096002 (2002), [Erratum: Phys. Rev.D76,059902(2007)], [hep-ph/0203110].
- [89] A. Pich, Prog. Part. Nucl. Phys. **75**, 41 (2014), [arXiv:1310.7922].
- [90] D. Ambrose *et al.* (BNL), Phys. Rev. Lett. **81**, 5734 (1998), [hep-ex/9811038].
- [91] A. Sher *et al.*, Phys. Rev. **D72**, 012005 (2005), [hep-ex/0502020].
- [92] R. Aaij *et al.* (LHCb), JHEP **03**, 078 (2018), [arXiv:1710.04111].
- [93] R. Aaij *et al.* (LHCb), Phys. Lett. **B754**, 167 (2016), [arXiv:1512.00322].
- [94] G. Aad *et al.* (ATLAS), Phys. Rev. **D90**, 7, 072010 (2014), [arXiv:1408.5774].
- [95] R. Akers *et al.* (OPAL), Z. Phys. **C67**, 555 (1995).
- [96] P. Abreu *et al.* (DELPHI), Z. Phys. **C73**, 243 (1997).
- [97] G. Aad *et al.* (ATLAS), Phys. Lett. **B801**, 135148 (2020), [arXiv:1909.10235].
- [98] S. Dell’Oro *et al.*, Adv. High Energy Phys. **2016**, 2162659 (2016), [arXiv:1601.07512].
- [99] J. Engel and J. Menéndez, Rept. Prog. Phys. **80**, 4, 046301 (2017), [arXiv:1610.06548].
- [100] A. Gando *et al.* (KamLAND-Zen), Phys. Rev. Lett. **117**, 8, 082503 (2016), [Addendum: Phys. Rev. Lett.117,no.10,109903(2016)], [arXiv:1605.02889].
- [101] P. Fileviez Perez, Phys. Rept. **597**, 1 (2015), [arXiv:1501.01886].
- [102] M. Aaboud *et al.* (ATLAS), JHEP **01**, 016 (2019), [arXiv:1809.11105].
- [103] A. M. Sirunyan *et al.* (CMS), JHEP **05**, 05, 148 (2018), [arXiv:1803.11116].



- [104] J. Kaulard *et al.* (SINDRUM II), Phys. Lett. **B422**, 334 (1998).
- [105] Y. Miyazaki *et al.* (Belle), Phys. Lett. **B719**, 346 (2013), [arXiv:1206.5595].
- [106] E. Cortina Gil *et al.* (NA62), Phys. Lett. **B797**, 134794 (2019), [arXiv:1905.07770].
- [107] R. Aaij *et al.* (LHCb), Phys. Lett. **B724**, 203 (2013), [arXiv:1304.6365].
- [108] J. P. Lees *et al.* (BaBar), Phys. Rev. **D85**, 071103 (2012), [arXiv:1202.3650].
- [109] A. Abada *et al.*, JHEP **02**, 169 (2018), [arXiv:1712.03984].
- [110] M. Anderson *et al.* (SNO+), Phys. Rev. D **99**, 3, 032008 (2019), [arXiv:1812.05552].
- [111] K. Abe *et al.* (Super-Kamiokande), Phys. Rev. **D95**, 1, 012004 (2017), [arXiv:1610.03597].
- [112] M. Baldo-Ceolin *et al.*, Z. Phys. **C63**, 409 (1994).
- [113] K. Abe *et al.* (Super-Kamiokande), Phys. Rev. **D91**, 072006 (2015), [arXiv:1109.4227].
- [114] D. G. Phillips, II *et al.*, Phys. Rept. **612**, 1 (2016), [arXiv:1410.1100].
- [115] G. Abbiendi *et al.* (OPAL), Phys. Lett. **B447**, 157 (1999), [hep-ex/9901011].
- [116] Y. Miyazaki *et al.* (Belle), Phys. Lett. **B632**, 51 (2006), [hep-ex/0508044].
- [117] P. del Amo Sanchez *et al.* (BaBar), Phys. Rev. **D83**, 091101 (2011), [arXiv:1101.3830].
- [118] P. Bloch *et al.* (Geneva-Saclay), Phys. Lett. **60B**, 393 (1976).
- [119] A. Angelopoulos *et al.* (CPLEAR), Phys. Lett. **B444**, 38 (1998).
- [120] A. Angelopoulos *et al.* (CPLEAR), Eur. Phys. J. **C22**, 55 (2001).
- [121] R. Aaij *et al.* (LHCb), Phys. Rev. Lett. **122**, 23, 231802 (2019), [arXiv:1903.03074].
- [122] A. A. Petrov, Int. J. Mod. Phys. **A21**, 5686 (2006), [hep-ph/0611361].
- [123] D. Ambrose *et al.* (BNL E871), Phys. Rev. Lett. **81**, 4309 (1998), [hep-ex/9810007].
- [124] V. Cirigliano *et al.*, Rev. Mod. Phys. **84**, 399 (2012), [arXiv:1107.6001].
- [125] F. Ambrosino *et al.* (KLOE), Phys. Lett. **B672**, 203 (2009), [arXiv:0811.1007].
- [126] R. Aaij *et al.* (LHCb) (2020), [arXiv:2001.10354].
- [127] J. Brod, M. Gorbahn and E. Stamou, Phys. Rev. **D83**, 034030 (2011), [arXiv:1009.0947].
- [128] J. K. Ahn *et al.* (KOTO), Phys. Rev. Lett. **122**, 2, 021802 (2019), [arXiv:1810.09655].
- [129] R. Aaij *et al.* (LHCb), Phys. Lett. **B725**, 15 (2013), [arXiv:1305.5059].
- [130] S. Bifani *et al.*, J. Phys. **G46**, 2, 023001 (2019), [arXiv:1809.06229].
- [131] R. Aaij *et al.* (LHCb), JHEP **08**, 055 (2017), [arXiv:1705.05802].
- [132] R. Aaij *et al.* (LHCb), Phys. Rev. Lett. **122**, 19, 191801 (2019), [arXiv:1903.09252].
- [133] A. Abdesselam *et al.* (Belle) (2019), [arXiv:1904.02440].
- [134] A. Abdesselam *et al.* (2019), [arXiv:1908.01848].

## TESTS OF DISCRETE SPACE-TIME SYMMETRIES

## CHARGE CONJUGATION (C) INVARIANCE

$\Gamma(\pi^0 \rightarrow 3\gamma)/\Gamma_{\text{total}}$	$<3.1 \times 10^{-8}$ , CL = 90%
$\eta$ C-nonconserving decay parameters	
$\pi^+ \pi^- \pi^0$ left-right asymmetry	$(0.09 \pm 0.11) \times 10^{-2}$
$\pi^+ \pi^- \pi^0$ sextant asymmetry	$(0.12 \pm 0.10) \times 10^{-2}$
$\pi^+ \pi^- \pi^0$ quadrant asymmetry	$(-0.09 \pm 0.09) \times 10^{-2}$
$\pi^+ \pi^- \gamma$ left-right asymmetry	$(0.9 \pm 0.4) \times 10^{-2}$
$\pi^+ \pi^- \gamma$ parameter $\beta$ ( $D$ -wave)	$-0.02 \pm 0.07$ ( $S = 1.3$ )
$\Gamma(\eta \rightarrow \pi^0 \gamma)/\Gamma_{\text{total}}$	[a] $<9 \times 10^{-5}$ , CL = 90%
$\Gamma(\eta \rightarrow 2\pi^0 \gamma)/\Gamma_{\text{total}}$	$<5 \times 10^{-4}$ , CL = 90%
$\Gamma(\eta \rightarrow 3\pi^0 \gamma)/\Gamma_{\text{total}}$	$<6 \times 10^{-5}$ , CL = 90%
$\Gamma(\eta \rightarrow 3\gamma)/\Gamma_{\text{total}}$	$<1.6 \times 10^{-5}$ , CL = 90%
$\Gamma(\eta \rightarrow \pi^0 e^+ e^-)/\Gamma_{\text{total}}$	[b] $<8 \times 10^{-6}$ , CL = 90%
$\Gamma(\eta \rightarrow \pi^0 \mu^+ \mu^-)/\Gamma_{\text{total}}$	[b] $<5 \times 10^{-6}$ , CL = 90%
$\Gamma(\omega(782) \rightarrow \eta \pi^0)/\Gamma_{\text{total}}$	$<2.2 \times 10^{-4}$ , CL = 90%
$\Gamma(\omega(782) \rightarrow 2\pi^0)/\Gamma_{\text{total}}$	$<2.2 \times 10^{-4}$ , CL = 90%
$\Gamma(\omega(782) \rightarrow 3\pi^0)/\Gamma_{\text{total}}$	$<2.3 \times 10^{-4}$ , CL = 90%
asymmetry parameter for $\eta'(958) \rightarrow \pi^+ \pi^- \gamma$ decay	$-0.03 \pm 0.04$
$\Gamma(\eta'(958) \rightarrow \pi^0 e^+ e^-)/\Gamma_{\text{total}}$	[b] $<1.4 \times 10^{-3}$ , CL = 90%
$\Gamma(\eta'(958) \rightarrow \eta e^+ e^-)/\Gamma_{\text{total}}$	[b] $<2.4 \times 10^{-3}$ , CL = 90%
$\Gamma(\eta'(958) \rightarrow 3\gamma)/\Gamma_{\text{total}}$	$<1.0 \times 10^{-4}$ , CL = 90%
$\Gamma(\eta'(958) \rightarrow \mu^+ \mu^- \pi^0)/\Gamma_{\text{total}}$	[b] $<6.0 \times 10^{-5}$ , CL = 90%
$\Gamma(\eta'(958) \rightarrow \mu^+ \mu^- \eta)/\Gamma_{\text{total}}$	[b] $<1.5 \times 10^{-5}$ , CL = 90%
$\Gamma(J/\psi(1S) \rightarrow \gamma \gamma)/\Gamma_{\text{total}}$	$<2.7 \times 10^{-7}$ , CL = 90%
$\Gamma(J/\psi(1S) \rightarrow \gamma \phi)/\Gamma_{\text{total}}$	$<1.4 \times 10^{-6}$ , CL = 90%

## PARITY (P) INVARIANCE

$e$ electric dipole moment	$<0.11 \times 10^{-28}$ e cm, CL = 90%
$\mu$ electric dipole moment [d]	$<1.8 \times 10^{-19}$ e cm, CL = 95%
Re( $d_\tau = \tau$ electric dipole moment)	$-0.220$ to $0.45 \times 10^{-16}$ e cm, CL = 95%
$\Gamma(\eta \rightarrow \pi^+ \pi^-)/\Gamma_{\text{total}}$	$<1.3 \times 10^{-5}$ , CL = 90%
$\Gamma(\eta \rightarrow 2\pi^0)/\Gamma_{\text{total}}$	$<3.5 \times 10^{-4}$ , CL = 90%
$\Gamma(\eta \rightarrow 4\pi^0)/\Gamma_{\text{total}}$	$<6.9 \times 10^{-7}$ , CL = 90%
$\Gamma(\eta'(958) \rightarrow \pi^+ \pi^-)/\Gamma_{\text{total}}$	$<1.8 \times 10^{-5}$ , CL = 90%
$\Gamma(\eta'(958) \rightarrow \pi^0 \pi^0)/\Gamma_{\text{total}}$	$<4 \times 10^{-4}$ , CL = 90%
$\Gamma(\eta_c(1S) \rightarrow \pi^+ \pi^-)/\Gamma_{\text{total}}$	$<1.1 \times 10^{-4}$ , CL = 90%
$\Gamma(\eta_c(1S) \rightarrow \pi^0 \pi^0)/\Gamma_{\text{total}}$	$<4 \times 10^{-5}$ , CL = 90%
$\Gamma(\eta_c(1S) \rightarrow K^+ K^-)/\Gamma_{\text{total}}$	$<6 \times 10^{-4}$ , CL = 90%
$\Gamma(\eta_c(1S) \rightarrow K_S^0 K_S^0)/\Gamma_{\text{total}}$	$<3.1 \times 10^{-4}$ , CL = 90%
$p$ electric dipole moment	$<0.021 \times 10^{-23}$ e cm
$n$ electric dipole moment	$<0.18 \times 10^{-25}$ e cm, CL = 90%
$\Lambda$ electric dipole moment	$<1.5 \times 10^{-16}$ e cm, CL = 95%
$a_P(\Lambda_b^0 \rightarrow p \pi^- \pi^+ \pi^-)$	$(-3.7 \pm 1.5)\%$
$a_P(\Lambda_b^0 \rightarrow p K^- \pi^+ \pi^-)$	$(-0.6 \pm 0.9)\%$
$a_P(\Lambda_b^0 \rightarrow p K^- K^+ \pi^-)$	$(4 \pm 5)\%$
$a_P(\Lambda_b^0 \rightarrow p K^- K^+ K^-)$	$(-1.6 \pm 1.5)\%$
$a_P(\Lambda_b^0 \rightarrow p K^- \mu^+ \mu^-)$	$(-5 \pm 5)\%$
$a_P(\Xi_b^0 \rightarrow p K^- K^- \pi^+)$	$(-3 \pm 5)\%$

## TIME REVERSAL (T) INVARIANCE

$e$ electric dipole moment	$<0.11 \times 10^{-28}$ e cm, CL = 90%
$\mu$ electric dipole moment [d]	$<1.8 \times 10^{-19}$ e cm, CL = 95%
$\mu$ decay parameters	
transverse $e^+$ polarization normal to plane of $\mu$ spin, $e^+$ momentum	$(-2 \pm 8) \times 10^{-3}$
$\alpha'/A$	$(-10 \pm 20) \times 10^{-3}$
$\beta'/A$	$(2 \pm 7) \times 10^{-3}$
Re( $d_\tau = \tau$ electric dipole moment)	$-0.220$ to $0.45 \times 10^{-16}$ e cm, CL = 95%
$P_T$ in $K^+ \rightarrow \pi^0 \mu^+ \nu_\mu$	$(-1.7 \pm 2.5) \times 10^{-3}$
$P_T$ in $K^+ \rightarrow \mu^+ \nu_\mu \gamma$	$(-0.6 \pm 1.9) \times 10^{-2}$
Im( $\xi$ ) in $K^+ \rightarrow \pi^0 \mu^+ \nu_\mu$ decay (from transverse $\mu$ pol.)	$-0.006 \pm 0.008$
asymmetry $A_T$ in $K^0$ - $\bar{K}^0$ mixing	$(6.6 \pm 1.6) \times 10^{-3}$

Im( $\xi$ ) in $K_{\mu 3}^0$ decay (from transverse $\mu$ pol.)	$-0.007 \pm 0.026$
$A_T(D^\pm \rightarrow K_S^0 K^\pm \pi^+ \pi^-)$	[c] $(-12 \pm 11) \times 10^{-3}$
$A_T(D^0 \rightarrow K^+ K^- \pi^+ \pi^-)$	[c] $(2.9 \pm 2.2) \times 10^{-3}$
$A_T(D_S^\pm \rightarrow K_S^0 K^\pm \pi^+ \pi^-)$	[c] $(-14 \pm 8) \times 10^{-3}$
$\Delta S_T^+(S_{\ell^-, K_S^0}^- - S_{\ell^+, K_S^0}^+)$	$-1.37 \pm 0.15$
$\Delta S_T^-(S_{\ell^-, K_S^0}^+ - S_{\ell^+, K_S^0}^-)$	$1.17 \pm 0.21$
$\Delta C_T^+(C_{\ell^-, K_S^0}^- - C_{\ell^+, K_S^0}^+)$	$0.10 \pm 0.16$
$\Delta C_T^-(C_{\ell^-, K_S^0}^+ - C_{\ell^+, K_S^0}^-)$	$0.04 \pm 0.16$
$p$ electric dipole moment	$<0.021 \times 10^{-23}$ e cm
$n$ electric dipole moment	$<0.18 \times 10^{-25}$ e cm, CL = 90%
$n \rightarrow p e^- \bar{\nu}_e$ decay parameters	
$\phi_{AV}$ , phase of $g_A$ relative to $g_V$	[d] $(180.017 \pm 0.026)^\circ$
triple correlation coefficient $D$	[e] $(-1.2 \pm 2.0) \times 10^{-4}$
triple correlation coefficient $R$	[e] $0.004 \pm 0.013$
$\Lambda$ electric dipole moment	$<1.5 \times 10^{-16}$ e cm, CL = 95%
triple correlation coefficient $D$ for $\Sigma^- \rightarrow n e^- \bar{\nu}_e$	$0.11 \pm 0.10$

## CP INVARIANCE

Re( $d_T^W$ )	$<0.50 \times 10^{-17}$ e cm, CL = 95%
Im( $d_T^W$ )	$<1.1 \times 10^{-17}$ e cm, CL = 95%
$\delta$ ( $CP$ violating phase in neutrino mixing)	$1.36 \pm 0.17$ $\pi$ rad
$\eta \rightarrow \pi^+ \pi^- e^+ e^-$ decay-plane asymmetry	$(-0.6 \pm 3.1) \times 10^{-2}$
$\Gamma(\eta \rightarrow \pi^+ \pi^-)/\Gamma_{\text{total}}$	$<1.3 \times 10^{-5}$ , CL = 90%
$\Gamma(\eta \rightarrow 2\pi^0)/\Gamma_{\text{total}}$	$<3.5 \times 10^{-4}$ , CL = 90%
$\Gamma(\eta \rightarrow 4\pi^0)/\Gamma_{\text{total}}$	$<6.9 \times 10^{-7}$ , CL = 90%
$\Gamma(\eta'(958) \rightarrow \pi^+ \pi^-)/\Gamma_{\text{total}}$	$<1.8 \times 10^{-5}$ , CL = 90%
$\Gamma(\eta'(958) \rightarrow \pi^0 \pi^0)/\Gamma_{\text{total}}$	$<4 \times 10^{-4}$ , CL = 90%
$K^\pm \rightarrow \pi^\pm e^+ e^-$ rate difference/sum	$(-2.2 \pm 1.6) \times 10^{-2}$
$K^\pm \rightarrow \pi^\pm \mu^+ \mu^-$ rate difference/sum	$0.010 \pm 0.023$
$K^\pm \rightarrow \pi^\pm \pi^0 \gamma$ rate difference/sum	$(0.0 \pm 1.2) \times 10^{-3}$
$K^\pm \rightarrow \pi^\pm \pi^+ \pi^-$ rate difference/sum	$(0.04 \pm 0.06)\%$
$K^\pm \rightarrow \pi^\pm \pi^0 \pi^0$ rate difference/sum	$(-0.02 \pm 0.28)\%$
$K^\pm \rightarrow \pi^\pm \pi^+ \pi^- (g_+ - g_-) / (g_+ + g_-)$	$(-1.5 \pm 2.2) \times 10^{-4}$
$K^\pm \rightarrow \pi^\pm \pi^0 \pi^0 (g_+ - g_-) / (g_+ + g_-)$	$(1.8 \pm 1.8) \times 10^{-4}$
$A_S = [\Gamma(K_S^0 \rightarrow \pi^- e^+ \nu_e) - \Gamma(K_S^0 \rightarrow \pi^+ e^- \bar{\nu}_e)] / \text{SUM}$	$(-4 \pm 6) \times 10^{-3}$
Im( $\eta_{+-0}$ ) = Im( $A(K_S^0 \rightarrow \pi^+ \pi^- \pi^0)$ , $CP$ -violating) / $A(K_L^0 \rightarrow \pi^+ \pi^- \pi^0)$	$-0.002 \pm 0.009$
Im( $\eta_{000}$ ) = Im( $A(K_L^0 \rightarrow \pi^0 \pi^0 \pi^0)$ ) / $A(K_L^0 \rightarrow \pi^0 \pi^0 \pi^0)$	$-0.001 \pm 0.016$
$ \eta_{000}  =  A(K_S^0 \rightarrow 3\pi^0)/A(K_L^0 \rightarrow 3\pi^0) $	$<0.0088$ , CL = 90%
$CP$ asymmetry $A$ in $K_S^0 \rightarrow \pi^+ \pi^- e^+ e^-$	$(-0.4 \pm 0.8)\%$
$\Gamma(K_S^0 \rightarrow 3\pi^0)/\Gamma_{\text{total}}$	$<2.6 \times 10^{-8}$ , CL = 90%
linear coefficient $j$ for $K_L^0 \rightarrow \pi^+ \pi^- \pi^0$	$0.0012 \pm 0.0008$
quadratic coefficient $f$ for $K_L^0 \rightarrow \pi^+ \pi^- \pi^0$	$0.004 \pm 0.006$
$ \epsilon'_{+-\gamma} /\epsilon$ for $K_L^0 \rightarrow \pi^+ \pi^- \gamma$	$<0.3$ , CL = 90%
$ \delta_{E1} $ for $K_L^0 \rightarrow \pi^+ \pi^- \gamma$	$<0.21$ , CL = 90%
$\Gamma(K_L^0 \rightarrow \pi^0 \mu^+ \mu^-)/\Gamma_{\text{total}}$	[f] $<3.8 \times 10^{-10}$ , CL = 90%
$\Gamma(K_L^0 \rightarrow \pi^0 e^+ e^-)/\Gamma_{\text{total}}$	[f] $<2.8 \times 10^{-10}$ , CL = 90%
$\Gamma(K_L^0 \rightarrow \pi^0 \nu \bar{\nu})/\Gamma_{\text{total}}$	[g] $<3.0 \times 10^{-9}$ , CL = 90%
$A_{CP}(D^\pm \rightarrow \mu^\pm \nu)$	$(8 \pm 8)\%$
$A_{CP}(D^\pm \rightarrow K_L^0 e^\pm \nu)$	$(-0.6 \pm 1.6)\%$
$A_{CP}(D^\pm \rightarrow K_S^0 \pi^\pm)$	$(-0.41 \pm 0.09)\%$
$A_{CP}(D^\pm \rightarrow K^\mp 2\pi^\pm)$	$(-0.18 \pm 0.16)\%$
$A_{CP}(D^\pm \rightarrow K^\mp \pi^\pm \pi^\pm \pi^0)$	$(-0.3 \pm 0.7)\%$
$A_{CP}(D^\pm \rightarrow K_S^0 \pi^\pm \pi^0)$	$(-0.1 \pm 0.7)\%$
$A_{CP}(D^\pm \rightarrow K_S^0 \pi^\pm \pi^+ \pi^-)$	$(0.0 \pm 1.2)\%$
$A_{CP}(D^\pm \rightarrow \pi^\pm \pi^0)$	$(2.4 \pm 1.2)\%$
$A_{CP}(D^\pm \rightarrow \pi^\pm \eta)$	$(1.0 \pm 1.5)\%$ ( $S = 1.4$ )
$A_{CP}(D^\pm \rightarrow \pi^\pm \eta'(958))$	$(-0.6 \pm 0.7)\%$
$A_{CP}(D^\pm \rightarrow \bar{K}^0/K^0 K^\pm)$	$(0.11 \pm 0.17)\%$
$A_{CP}(D^\pm \rightarrow K_S^0 K^\pm)$	$(-0.01 \pm 0.07)\%$
$A_{CP}(D^\pm \rightarrow K^+ K^- \pi^\pm)$	$(0.37 \pm 0.29)\%$
$A_{CP}(D^\pm \rightarrow K^\pm K^*0)$	$(-0.3 \pm 0.4)\%$
$A_{CP}(D^\pm \rightarrow \phi \pi^\pm)$	$(0.01 \pm 0.09)\%$ ( $S = 1.8$ )
$A_{CP}(D^\pm \rightarrow K^\pm K_S^0(1430)^0)$	$(8 \pm 6)\%$

# Tests of Conservation Laws

$A_{CP}(D^\pm \rightarrow K^\pm K_2^*(1430)^0)$	$(43 \pm 20)\%$	$A_{CP}(D^0 \rightarrow K^- \pi^+ \pi^0)$	$(0.1 \pm 0.5)\%$
$A_{CP}(D^\pm \rightarrow K^\pm K_0^*(700))$	$(-12 \pm 18)\%$	$A_{CP}(D^0 \rightarrow K^+ \pi^- \pi^0)$	$(0 \pm 5)\%$
$A_{CP}(D^\pm \rightarrow a_0(1450)^0 \pi^\pm)$	$(-19 \pm 16)\%$	$A_{CP}(D^0 \rightarrow K_S^0 \pi^+ \pi^-)$	$(-0.1 \pm 0.8)\%$
$A_{CP}(D^\pm \rightarrow \phi(1680) \pi^\pm)$	$(-9 \pm 26)\%$	$A_{CP}(D^0 \rightarrow K^*(892)^- \pi^+ \rightarrow K_S^0 \pi^+ \pi^-)$	$(0.4 \pm 0.5)\%$
$A_{CP}(D^\pm \rightarrow \pi^+ \pi^- \pi^\pm)$	$(-2 \pm 4)\%$	$A_{CP}(D^0 \rightarrow K^*(892)^+ \pi^- \rightarrow K_S^0 \pi^+ \pi^-)$	$(1 \pm 6)\%$
$A_{CP}(D^\pm \rightarrow K_S^0 K^\pm \pi^+ \pi^-)$	$(-4 \pm 7)\%$	$A_{CP}(D^0 \rightarrow K_S^0 \rho^0 \rightarrow K_S^0 \pi^+ \pi^-)$	$(-0.1 \pm 0.5)\%$
$A_{CP}(D^\pm \rightarrow K^\pm \pi^0)$	$(-4 \pm 11)\%$	$A_{CP}(D^0 \rightarrow K_S^0 \omega \rightarrow K_S^0 \pi^+ \pi^-)$	$(-13 \pm 7)\%$
Local CPV in $D^\pm \rightarrow \pi^+ \pi^- \pi^\pm$	78.1%	$A_{CP}(D^0 \rightarrow K_S^0 f_0(980) \rightarrow K_S^0 \pi^+ \pi^-)$	$(-0.4 \pm 2.7)\%$
Local CPV in $D^\pm \rightarrow K^+ K^- \pi^\pm$	31%	$A_{CP}(D^0 \rightarrow K_S^0 f_2(1270) \rightarrow K_S^0 \pi^+ \pi^-)$	$(-4 \pm 5)\%$
$ q/p $ of $D^0$ - $\bar{D}^0$ mixing	$0.92 \pm 0.12$	$A_{CP}(D^0 \rightarrow K_S^0 f_0(1370) \rightarrow K_S^0 \pi^+ \pi^-)$	$(-1 \pm 9)\%$
$A_\Gamma$ of $D^0$ - $\bar{D}^0$ mixing	$(-0.125 \pm 0.526) \times 10^{-3}$	$A_{CP}(D^0 \rightarrow \bar{K}^0 \rho^0(1450) \rightarrow K_S^0 \pi^+ \pi^-)$	$(-4 \pm 10)\%$
Where there is ambiguity, the CP test is labelled by the $D^0$ decay mode.		$A_{CP}(D^0 \rightarrow \bar{K}^0 f_0(600) \rightarrow K_S^0 \pi^+ \pi^-)$	$(-3 \pm 5)\%$
$A_{CP}(D^0 \rightarrow K^+ K^-)$	$(-0.07 \pm 0.11)\%$	$A_{CP}(D^0 \rightarrow K^*(1410)^- \pi^+ \rightarrow K_S^0 \pi^+ \pi^-)$	$(-2 \pm 9)\%$
$A_{CP}(D^0 \rightarrow K_S^0 K_S^0)$	$(0.4 \pm 1.4)\%$	$A_{CP}(D^0 \rightarrow K_0^*(1430)^- \pi^+ \rightarrow K_S^0 \pi^+ \pi^-)$	$(4 \pm 4)\%$
$A_{CP}(D^0 \rightarrow \pi^+ \pi^-)$	$(0.13 \pm 0.14)\%$	$A_{CP}(D^0 \rightarrow K_0^*(1430)^- \pi^+ \rightarrow K_S^0 \pi^+ \pi^-)$	$(12 \pm 15)\%$
$A_{CP}(D^0 \rightarrow \pi^0 \pi^0)$	$(0.0 \pm 0.6)\%$	$A_{CP}(D^0 \rightarrow K_2^*(1430)^- \pi^+ \rightarrow K_S^0 \pi^+ \pi^-)$	$(3 \pm 6)\%$
$A_{CP}(D^0 \rightarrow \rho \gamma)$	$(6 \pm 15) \times 10^{-2}$	$A_{CP}(D^0 \rightarrow K_2^*(1430)^+ \pi^- \rightarrow K_S^0 \pi^+ \pi^-)$	$(-10 \pm 32)\%$
$A_{CP}(D^0 \rightarrow \phi \gamma)$	$(-9 \pm 7) \times 10^{-2}$	$A_{CP}(D^0 \rightarrow K^- \pi^+ \pi^+ \pi^-)$	$(0.2 \pm 0.5)\%$
$A_{CP}(D^0 \rightarrow \bar{K}^*(892)^0 \gamma)$	$(-0.3 \pm 2.0) \times 10^{-2}$	$A_{CP}(D^0 \rightarrow K^+ \pi^- \pi^+ \pi^-)$	$(-2 \pm 4)\%$
$A_{CP}(D^0 \rightarrow \pi^+ \pi^- \pi^0)$	$(0.3 \pm 0.4)\%$	$A_{CP}(D^0 \rightarrow K^+ K^- \pi^+ \pi^-)$	$(1.3 \pm 1.7)\%$
$A_{CP}(D^0 \rightarrow \rho(770)^+ \pi^- \rightarrow \pi^+ \pi^- \pi^0)$	[h] $(1.2 \pm 0.9)\%$	$A_{CP}(D^0 \rightarrow K_1^*(1270)^+ K^- \rightarrow K^+ K^- \pi^+ \pi^-)$	$(-2.3 \pm 1.7)\%$
$A_{CP}(D^0 \rightarrow \rho(770)^0 \pi^0 \rightarrow \pi^+ \pi^- \pi^0)$	[h] $(-3.1 \pm 3.0)\%$	$A_{CP}(D^0 \rightarrow K_1^*(1270)^+ K^- \rightarrow K^*0 \pi^+ K^-)$	$(-1 \pm 10)\%$
$A_{CP}(D^0 \rightarrow \rho(770)^- \pi^+ \rightarrow \pi^+ \pi^- \pi^0)$	[h] $(-1.0 \pm 1.7)\%$	$A_{CP}(D^0 \rightarrow K_1^*(1270)^- K^+ \rightarrow K^*0 \pi^- K^+)$	$(-10 \pm 32)\%$
$A_{CP}(D^0 \rightarrow \rho(1450)^+ \pi^- \rightarrow \pi^+ \pi^- \pi^0)$	[h] $(0 \pm 70)\%$	$A_{CP}(D^0 \rightarrow K_1^*(1270)^- K^+ \rightarrow K^+ K^- \pi^+ \pi^-)$	$(1.7 \pm 3.5)\%$
$A_{CP}(D^0 \rightarrow \rho(1450)^0 \pi^0 \rightarrow \pi^+ \pi^- \pi^0)$	[h] $(-20 \pm 40)\%$	$A_{CP}(D^0 \rightarrow K_1^*(1270)^+ K^- \rightarrow K^+ K^- \pi^+ \pi^-)$	$(-7 \pm 17)\%$
$A_{CP}(D^0 \rightarrow \rho(1450)^- \pi^+ \rightarrow \pi^+ \pi^- \pi^0)$	[h] $(6 \pm 9)\%$	$A_{CP}(D^0 \rightarrow K_1^*(1270)^+ K^- \rightarrow \rho^0 K^+ K^-)$	$(10 \pm 13)\%$
$A_{CP}(D^0 \rightarrow \rho(1700)^+ \pi^- \rightarrow \pi^+ \pi^- \pi^0)$	[h] $(-5 \pm 14)\%$	$A_{CP}(D^0 \rightarrow K_1^*(1270)^- K^+ \rightarrow \rho^0 K^- K^+)$	$(-4.4 \pm 2.1)\%$
$A_{CP}(D^0 \rightarrow \rho(1700)^0 \pi^0 \rightarrow \pi^+ \pi^- \pi^0)$	[h] $(13 \pm 9)\%$	$A_{CP}(D^0 \rightarrow K^*(1410)^+ K^- \rightarrow K^+ K^- \pi^+ \pi^-)$	$(-20 \pm 17)\%$
$A_{CP}(D^0 \rightarrow \rho(1700)^- \pi^+ \rightarrow \pi^+ \pi^- \pi^0)$	[h] $(8 \pm 11)\%$	$A_{CP}(D^0 \rightarrow K^*(1410)^- K^+ \rightarrow \bar{K}^*0 \pi^- K^+)$	$(-1 \pm 14)\%$
$A_{CP}(D^0 \rightarrow f_0(980) \pi^0 \rightarrow \pi^+ \pi^- \pi^0)$	[h] $(0 \pm 35)\%$	$A_{CP}(D^0 \rightarrow K^*(1680)^+ K^- \rightarrow K^+ K^- \pi^+ \pi^-)$	$(-17 \pm 29)\%$
$A_{CP}(D^0 \rightarrow f_0(1370) \pi^0 \rightarrow \pi^+ \pi^- \pi^0)$	[h] $(25 \pm 18)\%$	$A_{CP}(K^*0 \bar{K}^*0)$ in $D^0, \bar{D}^0 \rightarrow K^*0 \bar{K}^*0$	$(-5 \pm 14)\%$
$A_{CP}(D^0 \rightarrow f_0(1500) \pi^0 \rightarrow \pi^+ \pi^- \pi^0)$	[h] $(0 \pm 18)\%$	$A_{CP}(D^0 \rightarrow K^*0 \bar{K}^*0 S\text{-wave})$	$(-3.9 \pm 2.2)\%$
$A_{CP}(D^0 \rightarrow f_0(1710) \pi^0 \rightarrow \pi^+ \pi^- \pi^0)$	[h] $(0 \pm 24)\%$	$A_{CP}(\phi \rho^0)$ in $D^0, \bar{D}^0 \rightarrow \phi \rho^0$	$(1 \pm 9)\%$
$A_{CP}(D^0 \rightarrow f_2(1270) \pi^0 \rightarrow \pi^+ \pi^- \pi^0)$	[h] $(-4 \pm 6)\%$	$A_{CP}(D^0 \rightarrow \phi \rho^0 S\text{-wave})$	$(-3 \pm 5)\%$
$A_{CP}(D^0 \rightarrow \sigma(400) \pi^0 \rightarrow \pi^+ \pi^- \pi^0)$	[h] $(6 \pm 8)\%$	$A_{CP}(D^0 \rightarrow \phi \rho^0 D\text{-wave})$	$(-37 \pm 19)\%$
$A_{CP}(\text{nonresonant } D^0 \rightarrow \pi^+ \pi^- \pi^0)$	[h] $(-13 \pm 23)\%$	$A_{CP}(D^0 \rightarrow \phi(\pi^+ \pi^-) S\text{-wave})$	$(6 \pm 6)\%$
$A_{CP}(D^0, \bar{D}^0 \rightarrow 2\pi^+ 2\pi^-)$	$(0.5 \pm 1.2)\%$	$A_{CP}(D^0 \rightarrow K^*(892)^0 (K^- \pi^+) S\text{-wave})$	$(-10 \pm 40)\%$
$A_{CP}(D^0 \rightarrow a_1(1260)^+ \pi^- \rightarrow 2\pi^+ 2\pi^-)$	$(5 \pm 6)\%$	$A_{CP}(D^0 \rightarrow K^+ K^- \pi^+ \pi^- \text{non-resonant})$	$(8 \pm 20)\%$
$A_{CP}(D^0 \rightarrow a_1(1260)^- \pi^+ \rightarrow 2\pi^+ 2\pi^-)$	$(14 \pm 18)\%$	$A_{CP}((K^- \pi^+) P\text{-wave } (K^+ \pi^-) S\text{-wave})$	$(3 \pm 11)\%$
$A_{CP}(D^0 \rightarrow \pi(1300)^+ \pi^- \rightarrow 2\pi^+ 2\pi^-)$	$(-2 \pm 15)\%$	CP-even fraction in $D^0 \rightarrow \pi^+ \pi^- \pi^0$ decays	$(97.3 \pm 1.7)\%$
$A_{CP}(D^0 \rightarrow \pi(1300)^- \pi^+ \rightarrow 2\pi^+ 2\pi^-)$	$(-6 \pm 30)\%$	CP-even fraction in $D^0 \rightarrow K^+ K^- \pi^0$ decays	$(73 \pm 6)\%$
$A_{CP}(D^0 \rightarrow a_1(1640)^+ \pi^- \rightarrow 2\pi^+ 2\pi^-)$	$(9 \pm 26)\%$	CP-even fraction in $D^0 \rightarrow \pi^+ \pi^- \pi^+ \pi^-$ decays	$(76.9 \pm 2.3)\%$
$A_{CP}(D^0 \rightarrow \pi_2(1670)^+ \pi^- \rightarrow 2\pi^+ 2\pi^-)$	$(7 \pm 18)\%$	Local CPV p-value in $D^0, \bar{D}^0 \rightarrow \pi^+ \pi^- \pi^0$	4.9%
$A_{CP}(D^0 \rightarrow \sigma f_0(1370) \rightarrow 2\pi^+ 2\pi^-)$	$(-15 \pm 19)\%$	Local CPV p-value in $D^0, \bar{D}^0 \rightarrow \pi^+ \pi^- \pi^+ \pi^-$	$(0.6 \pm 0.2)\%$
$A_{CP}(D^0 \rightarrow \sigma \rho(770)^0 \rightarrow 2\pi^+ 2\pi^-)$	$(3 \pm 27)\%$	Local CPV p-value in $D^0, \bar{D}^0 \rightarrow K_S^0 \pi^+ \pi^-$	96%
$A_{CP}(D^0 \rightarrow 2\rho(770)^0 \rightarrow 2\pi^+ 2\pi^-)$	$(-6 \pm 6)\%$	Local CPV p-value in $D^0, \bar{D}^0 \rightarrow K^+ K^- \pi^0$	16.6%
$A_{CP}(D^0 \rightarrow 2f_2(1270) \rightarrow 2\pi^+ 2\pi^-)$	$(-28 \pm 24)\%$	Local CPV p-value in $D^0, \bar{D}^0 \rightarrow K^+ K^- \pi^+ \pi^-$	9.1%
$A_{CP}(D^0 \rightarrow K^+ K^- \pi^0)$	$(-1.0 \pm 1.7)\%$	$A_{CP}(D^\pm \rightarrow \mu^\pm \nu)$	$(5 \pm 6)\%$
$A_{CP}(D^0 \rightarrow K^*(892)^+ K^- \rightarrow K^+ K^- \pi^0)$	[h] $(-0.9 \pm 1.3)\%$	$A_{CP}(D^\pm \rightarrow K^\pm K_S^0)$	$(0.09 \pm 0.26)\%$
$A_{CP}(D^0 \rightarrow K^*(1410)^+ K^- \rightarrow K^+ K^- \pi^0)$	[h] $(-21 \pm 24)\%$	$A_{CP}(D^\pm \rightarrow K^+ K^- \pi^\pm)$	$(-0.5 \pm 0.9)\%$
$A_{CP}(D^0 \rightarrow (K^+ \pi^0)_S K^- \rightarrow K^+ K^- \pi^0)$	[h] $(7 \pm 15)\%$		
$A_{CP}(D^0 \rightarrow \phi(1020) \pi^0 \rightarrow K^+ K^- \pi^0)$	[h] $(1.1 \pm 2.2)\%$		
$A_{CP}(D^0 \rightarrow f_0(980) \pi^0 \rightarrow K^+ K^- \pi^0)$	[h] $(-3 \pm 19)\%$		
$A_{CP}(D^0 \rightarrow a_0(980)^0 \pi^0 \rightarrow K^+ K^- \pi^0)$	[h] $(-5 \pm 16)\%$		
$A_{CP}(D^0 \rightarrow f_2'(1525) \pi^0 \rightarrow K^+ K^- \pi^0)$	[h] $(0 \pm 160)\%$		
$A_{CP}(D^0 \rightarrow K^*(892)^- K^+ \rightarrow K^+ K^- \pi^0)$	[h] $(-5 \pm 4)\%$		
$A_{CP}(D^0 \rightarrow K^*(1410)^- K^+ \rightarrow K^+ K^- \pi^0)$	[h] $(-17 \pm 29)\%$		
$A_{CP}(D^0 \rightarrow (K^- \pi^0)_S\text{-wave } K^+ \rightarrow K^+ K^- \pi^0)$	[h] $(-10 \pm 40)\%$		
$A_{CP}(D^0 \rightarrow K_S^0 \pi^0)$	$(-0.20 \pm 0.17)\%$		
$A_{CP}(D^0 \rightarrow K_S^0 \eta)$	$(0.5 \pm 0.5)\%$		
$A_{CP}(D^0 \rightarrow K_S^0 \eta')$	$(1.0 \pm 0.7)\%$		
$A_{CP}(D^0 \rightarrow K_S^0 \phi)$	$(-3 \pm 9)\%$		
$A_{CP}(D^0 \rightarrow K^- \pi^+)$	$(0.2 \pm 0.5)\%$		
$A_{CP}(D^0 \rightarrow K^+ \pi^-)$	$(-0.9 \pm 1.4)\%$		
$A_{CP}(D_{CP}(\pm 1) \rightarrow K^\mp \pi^\pm)$	$(12.7 \pm 1.5)\%$		

Unless otherwise stated, limits are given at the 90% confidence level, while errors are given as  $\pm 1$  standard deviation.

## Tests of Conservation Laws

$A_{CP}(D_S^{\pm} \rightarrow \phi \pi^{\pm})$	$(-0.38 \pm 0.27)\%$	$A_{CP}(B^+ \rightarrow [K^+ K^-]_D \pi^+ \pi^- \pi^+)$	$-0.019 \pm 0.015$
$A_{CP}(D_S^{\pm} \rightarrow K^{\pm} K_S^0 \pi^0)$	$(-2 \pm 6)\%$	$A_{CP}(B^+ \rightarrow [\pi^+ \pi^-]_D \pi^+ \pi^- \pi^+)$	$-0.013 \pm 0.019$
$A_{CP}(D_S^{\pm} \rightarrow 2K_S^0 \pi^{\pm})$	$(3 \pm 5)\%$	$A_{CP}(B^+ \rightarrow [K^- \pi^+]_D \pi^+ \pi^- \pi^+)$	$-0.002 \pm 0.011$
$A_{CP}(D_S^{\pm} \rightarrow K^+ K^- \pi^{\pm} \pi^0)$	$(0.0 \pm 3.0)\%$	$A_{CP}(B^+ \rightarrow \overline{D}^{*0} \pi^+)$	$0.0010 \pm 0.0028$
$A_{CP}(D_S^{\pm} \rightarrow K^{\pm} K_S^0 \pi^+ \pi^-)$	$(-6 \pm 5)\%$	$A_{CP}(B^+ \rightarrow (D_{CP(+1)}^*)^0 \pi^+)$	$0.016 \pm 0.010$ ( $S = 1.2$ )
$A_{CP}(D_S^{\pm} \rightarrow K_S^0 K^{\mp} 2\pi^{\pm})$	$(4.1 \pm 2.8)\%$	$A_{CP}(B^+ \rightarrow (D_{CP(-1)}^*)^0 \pi^+)$	$-0.09 \pm 0.05$
$A_{CP}(D_S^{\pm} \rightarrow \pi^+ \pi^- \pi^{\pm})$	$(-0.7 \pm 3.1)\%$	$A_{CP}(B^+ \rightarrow D^{*0} K^+)$	$-0.001 \pm 0.011$ ( $S = 1.1$ )
$A_{CP}(D_S^{\pm} \rightarrow \pi^{\pm} \eta)$	$(1.1 \pm 3.1)\%$	$A_{CP}(B^+ \rightarrow D_{CP(+1)}^{*0} K^+)$	$-0.11 \pm 0.08$ ( $S = 2.7$ )
$A_{CP}(D_S^{\pm} \rightarrow \pi^{\pm} \eta')$	$(-0.9 \pm 0.5)\%$	$A_{CP}(B^+ \rightarrow D_{CP(-1)}^{*0} K^+)$	$0.07 \pm 0.10$
$A_{CP}(D_S^{\pm} \rightarrow \eta \pi^{\pm} \pi^0)$	$(-1 \pm 4)\%$	$A_{CP}(B^+ \rightarrow D_{CP(+1)} K^*(892)^+)$	$0.08 \pm 0.06$
$A_{CP}(D_S^{\pm} \rightarrow \eta' \pi^{\pm} \pi^0)$	$(0 \pm 8)\%$	$A_{CP}(B^+ \rightarrow D_{CP(-1)} K^*(892)^+)$	$-0.23 \pm 0.22$
$A_{CP}(D_S^{\pm} \rightarrow K^{\pm} \pi^0)$	$(-27 \pm 24)\%$	$A_{CP}(B^+ \rightarrow D_S^+ \phi)$	$0.0 \pm 0.4$
$A_{CP}(D_S^{\pm} \rightarrow \overline{K}^0 / K^0 \pi^{\pm})$	$(0.4 \pm 0.5)\%$	$A_{CP}(B^+ \rightarrow D_S^+ \overline{D}^0)$	$(-0.4 \pm 0.7)\%$
$A_{CP}(D_S^{\pm} \rightarrow K_S^0 \pi^{\pm})$	$(0.20 \pm 0.18)\%$	$A_{CP}(B^+ \rightarrow D^{*+} \overline{D}^{*0})$	$-0.15 \pm 0.11$
$A_{CP}(D_S^{\pm} \rightarrow K^{\pm} \pi^+ \pi^-)$	$(4 \pm 5)\%$	$A_{CP}(B^+ \rightarrow D^{*+} \overline{D}^0)$	$-0.06 \pm 0.13$
$A_{CP}(D_S^{\pm} \rightarrow K^{\pm} \eta)$	$(9 \pm 15)\%$	$A_{CP}(B^+ \rightarrow D^+ \overline{D}^{*0})$	$0.13 \pm 0.18$
$A_{CP}(D_S^{\pm} \rightarrow K^{\pm} \eta' (958))$	$(6 \pm 19)\%$	$A_{CP}(B^+ \rightarrow D^+ \overline{D}^0)$	$0.016 \pm 0.025$
$A_{CP}(B^+ \rightarrow J/\psi(1S) K^+)$	$(1.8 \pm 3.0) \times 10^{-3}$ ( $S = 1.5$ )	$A_{CP}(B^+ \rightarrow K_S^0 \pi^+)$	$-0.017 \pm 0.016$
$A_{CP}(B^+ \rightarrow J/\psi(1S) \pi^+)$	$(1.8 \pm 1.2) \times 10^{-2}$ ( $S = 1.3$ )	$A_{CP}(B^+ \rightarrow K^+ \pi^0)$	$0.037 \pm 0.021$
$A_{CP}(B^+ \rightarrow J/\psi \rho^+)$	$-0.05 \pm 0.05$	$A_{CP}(B^+ \rightarrow \eta' K^+)$	$0.004 \pm 0.011$
$A_{CP}(B^+ \rightarrow J/\psi K^*(892)^+)$	$-0.048 \pm 0.033$	$A_{CP}(B^+ \rightarrow \eta' K^*(892)^+)$	$-0.26 \pm 0.27$
$A_{CP}(B^+ \rightarrow \eta_c K^+)$	$0.01 \pm 0.07$ ( $S = 2.2$ )	$A_{CP}(B^+ \rightarrow \eta' K_S^0(1430)^+)$	$0.06 \pm 0.20$
$A_{CP}(B^+ \rightarrow \psi(2S) \pi^+)$	$0.03 \pm 0.06$	$A_{CP}(B^+ \rightarrow \eta' K_2^*(1430)^+)$	$0.15 \pm 0.13$
$A_{CP}(B^+ \rightarrow \psi(2S) K^+)$	$0.012 \pm 0.020$ ( $S = 1.5$ )	$A_{CP}(B^+ \rightarrow \eta K^*(892)^+)$	$0.02 \pm 0.06$
$A_{CP}(B^+ \rightarrow \psi(2S) K^*(892)^+)$	$0.08 \pm 0.21$	$A_{CP}(B^+ \rightarrow \eta K_0^*(1430)^+)$	$0.05 \pm 0.13$
$A_{CP}(B^+ \rightarrow \chi_{c1}(1P) \pi^+)$	$0.07 \pm 0.18$	$A_{CP}(B^+ \rightarrow \eta K_2^*(1430)^+)$	$-0.45 \pm 0.30$
$A_{CP}(B^+ \rightarrow \chi_{c0} K^+)$	$-0.20 \pm 0.18$ ( $S = 1.5$ )	$A_{CP}(B^+ \rightarrow \omega K^+)$	$-0.02 \pm 0.04$
$A_{CP}(B^+ \rightarrow \chi_{c1} K^+)$	$-0.009 \pm 0.033$	$A_{CP}(B^+ \rightarrow \omega K^{*+})$	$0.29 \pm 0.35$
$A_{CP}(B^+ \rightarrow \chi_{c1} K^*(892)^+)$	$0.5 \pm 0.5$	$A_{CP}(B^+ \rightarrow \omega(K\pi)_0^{*+})$	$-0.10 \pm 0.09$
$A_{CP}(B^+ \rightarrow \overline{D}^0 \pi^+)$	$-0.007 \pm 0.007$	$A_{CP}(B^+ \rightarrow \omega K_2^*(1430)^+)$	$0.14 \pm 0.15$
$A_{CP}(B^+ \rightarrow D_{CP(+1)} \pi^+)$	$-0.0080 \pm 0.0026$	$A_{CP}(B^+ \rightarrow K^{*0} \pi^+)$	$-0.04 \pm 0.09$ ( $S = 2.1$ )
$A_{CP}(B^+ \rightarrow D_{CP(-1)} \pi^+)$	$0.017 \pm 0.026$	$A_{CP}(B^+ \rightarrow K^*(892)^+ \pi^0)$	$-0.39 \pm 0.21$ ( $S = 1.6$ )
$A_{CP}([K^{\mp} \pi^{\pm} \pi^+ \pi^-]_D \pi^+)$	$0.02 \pm 0.05$	$A_{CP}(B^+ \rightarrow K^+ \pi^- \pi^+)$	$0.027 \pm 0.008$
$A_{CP}(B^+ \rightarrow [\pi^+ \pi^+ \pi^- \pi^-]_D K^+)$	$0.10 \pm 0.04$	$A_{CP}(B^+ \rightarrow K^+ K^- K^+ \text{ nonresonant})$	$0.06 \pm 0.05$
$A_{CP}(B^+ \rightarrow [\pi^+ \pi^- \pi^+ \pi^-]_D K^*(892)^+)$	$0.02 \pm 0.11$	$A_{CP}(B^+ \rightarrow f(980)^0 K^+)$	$-0.08 \pm 0.09$
$A_{CP}(B^+ \rightarrow \overline{D}^0 K^+)$	$-0.017 \pm 0.005$	$A_{CP}(B^+ \rightarrow f_0(1500) K^+)$	$0.28 \pm 0.30$
$A_{CP}([K^{\mp} \pi^{\pm} \pi^+ \pi^-]_D K^+)$	$-0.31 \pm 0.11$	$A_{CP}(B^+ \rightarrow f'_2(1525)^0 K^+)$	$-0.08^{+0.05}_{-0.04}$
$A_{CP}(B^+ \rightarrow [\pi^+ \pi^+ \pi^- \pi^-]_D \pi^+)$	$(-4 \pm 8) \times 10^{-3}$	$A_{CP}(B^+ \rightarrow K_0^*(1430)^0 \pi^+)$	$0.061 \pm 0.032$
$A_{CP}(B^+ \rightarrow [K^- \pi^+]_D K^+)$	$-0.58 \pm 0.21$	$A_{CP}(B^+ \rightarrow K_0^*(1430)^+ \pi^0)$	$0.26^{+0.18}_{-0.14}$
$A_{CP}(B^+ \rightarrow [K^- \pi^+ \pi^0]_D K^+)$	$0.07 \pm 0.30$ ( $S = 1.5$ )	$A_{CP}(B^+ \rightarrow K_2^*(1430)^0 \pi^+)$	$0.05^{+0.29}_{-0.24}$
$A_{CP}(B^+ \rightarrow [K^+ K^- \pi^0]_D K^+)$	$0.30 \pm 0.20$	$A_{CP}(B^+ \rightarrow K^+ \pi^0 \pi^0)$	$-0.06 \pm 0.07$
$A_{CP}(B^+ \rightarrow [\pi^+ \pi^- \pi^0]_D K^+)$	$0.05 \pm 0.09$	$A_{CP}(B^+ \rightarrow K^0 \rho^+)$	$-0.03 \pm 0.15$
$A_{CP}(B^+ \rightarrow \overline{D}^0 K^*(892)^+)$	$-0.007 \pm 0.019$	$A_{CP}(B^+ \rightarrow K^+ \pi^+ \pi^-)$	$0.07 \pm 0.08$
$A_{CP}(B^+ \rightarrow [K^- \pi^+ \pi^- \pi^+]_D K^*(892)^+)$	$-0.45 \pm 0.25$	$A_{CP}(B^+ \rightarrow \rho^0 K^*(892)^+)$	$0.31 \pm 0.13$
$A_{CP}(B^+ \rightarrow [K^- \pi^+]_D \pi^+)$	$0.00 \pm 0.09$	$A_{CP}(B^+ \rightarrow K^*(892)^+ f_0(980))$	$-0.15 \pm 0.12$
$A_{CP}(B^+ \rightarrow [K^- \pi^+ \pi^0]_D \pi^+)$	$0.35 \pm 0.16$	$A_{CP}(B^+ \rightarrow a_1^+ K^0)$	$0.12 \pm 0.11$
$A_{CP}(B^+ \rightarrow [K^+ K^- \pi^0]_D \pi^+)$	$-0.03 \pm 0.04$	$A_{CP}(B^+ \rightarrow b_1^+ K^0)$	$-0.03 \pm 0.15$
$A_{CP}(B^+ \rightarrow [\pi^+ \pi^- \pi^0]_D \pi^+)$	$-0.016 \pm 0.020$	$A_{CP}(B^+ \rightarrow K^*(892)^0 \rho^+)$	$-0.01 \pm 0.16$
$A_{CP}(B^+ \rightarrow [K^- \pi^+]_D \pi^+)$	$-0.09 \pm 0.27$	$A_{CP}(B^+ \rightarrow b_0^0 K^+)$	$-0.46 \pm 0.20$
$A_{CP}(B^+ \rightarrow [K^- \pi^+]_D \gamma \pi^+)$	$-0.7 \pm 0.6$	$A_{CP}(B^+ \rightarrow K^0 K^+)$	$0.04 \pm 0.14$
$A_{CP}(B^+ \rightarrow [K^- \pi^+]_D \pi) K^+)$	$0.8 \pm 0.4$	$A_{CP}(B^+ \rightarrow K^+ K_S^0 K_S^0)$	$0.025 \pm 0.031$
$A_{CP}(B^+ \rightarrow [K^- \pi^+]_D \gamma) K^+)$	$0.4 \pm 1.0$	$A_{CP}(B^+ \rightarrow \phi K^+)$	$0.024 \pm 0.028$ ( $S = 2.3$ )
$A_{CP}(B^+ \rightarrow [\pi^+ \pi^- \pi^0]_D K^+)$	$-0.02 \pm 0.15$	$A_{CP}(B^+ \rightarrow X_0(1550) K^+)$	$-0.04 \pm 0.07$
$A_{CP}(B^+ \rightarrow [K_S^0 K^+ \pi^-]_D K^+)$	$0.04 \pm 0.09$	$A_{CP}(B^+ \rightarrow K^+ K^+ K^-)$	$0.11 \pm 0.09$
$A_{CP}(B^+ \rightarrow [K_S^0 K^- \pi^+]_D K^+)$	$0.23 \pm 0.13$	$A_{CP}(B^+ \rightarrow \phi K^*(892)^+)$	$-0.01 \pm 0.08$
$A_{CP}(B^+ \rightarrow [K_S^0 K^- \pi^+]_D \pi^+)$	$-0.052 \pm 0.034$	$A_{CP}(B^+ \rightarrow \phi(K\pi)_0^{*+})$	$0.04 \pm 0.16$
$A_{CP}(B^+ \rightarrow [K_S^0 K^+ \pi^-]_D \pi^+)$	$-0.025 \pm 0.026$	$A_{CP}(B^+ \rightarrow \phi K_1(1270)^+)$	$0.15 \pm 0.20$
$A_{CP}(B^+ \rightarrow [K^*(892)^- K^+]_D K^+)$	$0.03 \pm 0.11$	$A_{CP}(B^+ \rightarrow \phi K_2^*(1430)^+)$	$-0.23 \pm 0.20$
$A_{CP}(B^+ \rightarrow [K^*(892)^+ K^-]_D K^+)$	$0.34 \pm 0.21$	$A_{CP}(B^+ \rightarrow K^+ \phi \phi)$	$-0.10 \pm 0.08$
$A_{CP}(B^+ \rightarrow [K^*(892)^+ K^-]_D \pi^+)$	$-0.05 \pm 0.05$	$A_{CP}(B^+ \rightarrow K^+ [\phi \phi]_{\eta_c})$	$0.09 \pm 0.10$
$A_{CP}(B^+ \rightarrow [K^*(892)^- K^+]_D \pi^+)$	$-0.012 \pm 0.030$	$A_{CP}(B^+ \rightarrow K^*(892)^+ \gamma)$	$0.014 \pm 0.018$
$A_{ADS}(B^+ \rightarrow D \pi^+)$	$0.100 \pm 0.032$	$A_{CP}(B^+ \rightarrow X_S \gamma)$	$0.028 \pm 0.019$
$A_{ADS}(B^+ \rightarrow [K^- \pi^+]_D K^+ \pi^- \pi^+)$	$-0.33 \pm 0.35$	$A_{CP}(B^+ \rightarrow \eta K^+ \gamma)$	$-0.12 \pm 0.07$
$A_{ADS}(B^+ \rightarrow [K^- \pi^+]_D \pi^+ \pi^- \pi^+)$	$-0.01 \pm 0.09$	$A_{CP}(B^+ \rightarrow \phi K^+ \gamma)$	$-0.13 \pm 0.11$ ( $S = 1.1$ )
$A_{CP}(B^+ \rightarrow D_{CP(-1)} K^+)$	$-0.10 \pm 0.07$	$A_{CP}(B^+ \rightarrow \rho^+ \gamma)$	$-0.11 \pm 0.33$
$A_{CP}(B^+ \rightarrow [K^+ K^-]_D K^+ \pi^- \pi^+)$	$-0.04 \pm 0.06$	$A_{CP}(B^+ \rightarrow \pi^+ \pi^0)$	$0.03 \pm 0.04$
$A_{CP}(B^+ \rightarrow [\pi^+ \pi^-]_D K^+ \pi^- \pi^+)$	$-0.05 \pm 0.10$	$A_{CP}(B^+ \rightarrow \rho^0 \pi^+)$	$0.009 \pm 0.019$
$A_{CP}(B^+ \rightarrow [K^- \pi^+]_D K^+ \pi^- \pi^+)$	$0.013 \pm 0.023$		

Unless otherwise stated, limits are given at the 90% confidence level, while errors are given as  $\pm 1$  standard deviation.

## Tests of Conservation Laws

$A_{CP}(B^+ \rightarrow \rho^0(1450)\pi^+)$	$-0.11 \pm 0.05$	$A_{CP}(B^0 \rightarrow K^{*0}\ell^+\ell^-)$	$-0.05 \pm 0.10$
$A_{CP}(B^+ \rightarrow \pi^+\pi^-\pi^+ \text{ nonresonant})$	$-0.14^{+0.23}_{-0.16}$	$A_{CP}(B^0 \rightarrow K^{*0}e^+e^-)$	$-0.21 \pm 0.19$
$A_{CP}(B^+ \rightarrow \rho^+\pi^0)$	$0.02 \pm 0.11$	$A_{CP}(B^0 \rightarrow K^{*0}\mu^+\mu^-)$	$-0.034 \pm 0.024$
$A_{CP}(B^+ \rightarrow \rho^+\rho^0)$	$-0.05 \pm 0.05$	$C_{D^*(2010)^-D^+}(B^0 \rightarrow D^{*(2010)^-}D^+)$	$-0.01 \pm 0.11$
$A_{CP}(B^+ \rightarrow \omega\pi^+)$	$-0.04 \pm 0.05$	$C_{D^*(2010)^+D^-}(B^0 \rightarrow D^{*(2010)^+}D^-)$	$0.00 \pm 0.13$ (S = 1.3)
$A_{CP}(B^+ \rightarrow \omega\rho^+)$	$-0.20 \pm 0.09$	$C_{D^{*+}D^{*-}}(B^0 \rightarrow D^{*+}D^{*-})$	$0.01 \pm 0.09$ (S = 1.6)
$A_{CP}(B^+ \rightarrow \eta\pi^+)$	$-0.14 \pm 0.07$ (S = 1.4)	$C_+(B^0 \rightarrow D^{*+}D^{*-})$	$0.00 \pm 0.10$ (S = 1.6)
$A_{CP}(B^+ \rightarrow \eta\rho^+)$	$0.11 \pm 0.11$	$C_-(B^0 \rightarrow D^{*+}D^{*-})$	$0.19 \pm 0.31$
$A_{CP}(B^+ \rightarrow \eta'\pi^+)$	$0.06 \pm 0.16$	$S_-(B^0 \rightarrow D^{*+}D^{*-})$	$0.1 \pm 1.6$ (S = 3.5)
$A_{CP}(B^+ \rightarrow \eta'\rho^+)$	$0.26 \pm 0.17$	$C(B^0 \rightarrow D^*(2010)^+D^*(2010)^-K_S^0)$	$0.01 \pm 0.29$
$A_{CP}(B^+ \rightarrow b_1^0\pi^+)$	$0.05 \pm 0.16$	$S(B^0 \rightarrow D^*(2010)^+D^*(2010)^-K_S^0)$	$0.1 \pm 0.4$
$A_{CP}(B^+ \rightarrow p\bar{p}\pi^+)$	$0.00 \pm 0.04$	$C_{D^+D^-}(B^0 \rightarrow D^+D^-)$	$-0.22 \pm 0.24$ (S = 2.5)
$A_{CP}(B^+ \rightarrow p\bar{p}K^+)$	$0.00 \pm 0.04$ (S = 2.2)	$C_{J/\psi(1S)\pi^0}(B^0 \rightarrow J/\psi(1S)\pi^0)$	$0.03 \pm 0.17$ (S = 1.5)
$A_{CP}(B^+ \rightarrow p\bar{p}K^*(892)^+)$	$0.21 \pm 0.16$ (S = 1.4)	$C(B^0 \rightarrow J/\psi(1S)\rho^0)$	$-0.06 \pm 0.06$
$A_{CP}(B^+ \rightarrow p\bar{p}\gamma)$	$0.17 \pm 0.17$	$C_{D_{CP}^{(*)}h^0}(B^0 \rightarrow D_{CP}^{(*)}h^0)$	$-0.02 \pm 0.08$
$A_{CP}(B^+ \rightarrow p\bar{p}\pi^0)$	$0.01 \pm 0.17$	$S_{D_{CP}^{(*)}h^0}(B^0 \rightarrow D_{CP}^{(*)}h^0)$	$-0.66 \pm 0.12$
$A_{CP}(B^+ \rightarrow K^+\ell^+\ell^-)$	$-0.02 \pm 0.08$	$C_{K^0\pi^0}(B^0 \rightarrow K^0\pi^0)$	$0.00 \pm 0.13$ (S = 1.4)
$A_{CP}(B^+ \rightarrow K^+e^+e^-)$	$0.14 \pm 0.14$	$C_{\eta'(958)K_S^0}(B^0 \rightarrow \eta'(958)K_S^0)$	$-0.04 \pm 0.20$ (S = 2.5)
$A_{CP}(B^+ \rightarrow K^+\mu^+\mu^-)$	$0.011 \pm 0.017$	$S_{\eta'(958)K_S^0}(B^0 \rightarrow \eta'(958)K_S^0)$	$0.43 \pm 0.17$ (S = 1.5)
$A_{CP}(B^+ \rightarrow K^*+\ell^+\ell^-)$	$-0.09 \pm 0.14$	$C_{\eta'K^0}(B^0 \rightarrow \eta'K^0)$	$-0.06 \pm 0.04$
$A_{CP}(B^+ \rightarrow K^*e^+e^-)$	$-0.14 \pm 0.23$	$C_{\omega K_S^0}(B^0 \rightarrow \omega K_S^0)$	$0.0 \pm 0.4$ (S = 3.0)
$A_{CP}(B^+ \rightarrow K^*\mu^+\mu^-)$	$-0.12 \pm 0.24$	$S_{\omega K_S^0}(B^0 \rightarrow \omega K_S^0)$	$0.70 \pm 0.21$
$\text{Re}(\epsilon_{B^0})/(1+ \epsilon_{B^0} ^2)$	$(-0.5 \pm 0.4) \times 10^{-3}$	$C(B^0 \rightarrow K_S^0\pi^0\pi^0)$	$-0.21 \pm 0.20$
$A_{T/CP}(B^0 \leftrightarrow \bar{B}^0)$	$0.005 \pm 0.018$	$S(B^0 \rightarrow K_S^0\pi^0\pi^0)$	$0.89^{+0.27}_{-0.30}$
$A_{CP}(B^0 \rightarrow D^*(2010)^+D^-)$	$0.037 \pm 0.034$	$C_{\rho^0 K_S^0}(B^0 \rightarrow \rho^0 K_S^0)$	$-0.04 \pm 0.20$
$A_{CP}(B^0 \rightarrow [K^+K^-]_D K^*(892)^0)$	$-0.05 \pm 0.10$	$S_{\rho^0 K_S^0}(B^0 \rightarrow \rho^0 K_S^0)$	$0.50^{+0.17}_{-0.21}$
$A_{CP}(B^0 \rightarrow [K^+\pi^-]_D K^*(892)^0)$	$0.047 \pm 0.029$	$C_{f_0(980)K_S^0}(B^0 \rightarrow f_0(980)K_S^0)$	$0.29 \pm 0.20$
$A_{CP}(B^0 \rightarrow [\pi^+\pi^-]_D K^*(892)^0)$	$-0.18 \pm 0.14$	$S_{f_0(980)K_S^0}(B^0 \rightarrow f_0(980)K_S^0)$	$-0.50 \pm 0.16$
$A_{CP}(B^0 \rightarrow \eta'K^*(892)^0)$	$-0.07 \pm 0.18$	$S_{f_2(1270)K_S^0}(B^0 \rightarrow f_2(1270)K_S^0)$	$-0.5 \pm 0.5$
$A_{CP}(B^0 \rightarrow \eta'K_0^*(1430)^0)$	$-0.19 \pm 0.17$	$C_{f_2(1270)K_S^0}(B^0 \rightarrow f_2(1270)K_S^0)$	$0.3 \pm 0.4$
$A_{CP}(B^0 \rightarrow \eta'K_2^*(1430)^0)$	$0.14 \pm 0.18$	$S_{f_x(1300)K_S^0}(B^0 \rightarrow f_x(1300)K_S^0)$	$-0.2 \pm 0.5$
$A_{CP}(B^0 \rightarrow \eta K_0^*(1430)^0)$	$0.06 \pm 0.13$	$C_{f_x(1300)K_S^0}(B^0 \rightarrow f_x(1300)K_S^0)$	$0.13 \pm 0.35$
$A_{CP}(B^0 \rightarrow \eta K_2^*(1430)^0)$	$-0.07 \pm 0.19$	$S_{K^0\pi^+\pi^-}(B^0 \rightarrow K^0\pi^+\pi^- \text{ nonresonant})$	$-0.01 \pm 0.33$
$A_{CP}(B^0 \rightarrow b_1 K^+)$	$-0.07 \pm 0.12$	$C_{K^0\pi^+\pi^-}(B^0 \rightarrow K^0\pi^+\pi^- \text{ nonresonant})$	$0.01 \pm 0.26$
$A_{CP}(B^0 \rightarrow \omega K^{*0})$	$0.45 \pm 0.25$	$C_{K_S^0 K_S^0}(B^0 \rightarrow K_S^0 K_S^0)$	$0.0 \pm 0.4$ (S = 1.4)
$A_{CP}(B^0 \rightarrow \omega(K\pi)_0^{*0})$	$-0.07 \pm 0.09$	$S_{K_S^0 K_S^0}(B^0 \rightarrow K_S^0 K_S^0)$	$-0.8 \pm 0.5$
$A_{CP}(B^0 \rightarrow \omega K_2^*(1430)^0)$	$-0.37 \pm 0.17$	$C_{K^+K^-K_S^0}(B^0 \rightarrow K^+K^-K_S^0)$	$0.06 \pm 0.08$
$A_{CP}(B^0 \rightarrow K^+\pi^-\pi^0)$	$(0 \pm 6) \times 10^{-2}$	$C_{K^+K^-K_S^0}(B^0 \rightarrow K^+K^-K_S^0 \text{ inclusive})$	$0.01 \pm 0.09$
$A_{CP}(B^0 \rightarrow \rho^-K^+)$	$0.20 \pm 0.11$	$C_{\phi K_S^0}(B^0 \rightarrow \phi K_S^0)$	$0.01 \pm 0.14$
$A_{CP}(B^0 \rightarrow \rho(1450)^-K^+)$	$-0.10 \pm 0.33$	$S_{\phi K_S^0}(B^0 \rightarrow \phi K_S^0)$	$0.59 \pm 0.14$
$A_{CP}(B^0 \rightarrow \rho(1700)^-K^+)$	$-0.4 \pm 0.6$	$C_{K_S K_S K_S}(B^0 \rightarrow K_S K_S K_S)$	$-0.23 \pm 0.14$
$A_{CP}(B^0 \rightarrow K^+\pi^-\pi^0 \text{ nonresonant})$	$0.10 \pm 0.18$	$S_{K_S K_S K_S}(B^0 \rightarrow K_S K_S K_S)$	$-0.5 \pm 0.6$ (S = 3.0)
$A_{CP}(B^0 \rightarrow K^0\pi^+\pi^-)$	$-0.01 \pm 0.05$	$C_{K_S^0\pi^0\gamma}(B^0 \rightarrow K_S^0\pi^0\gamma)$	$0.36 \pm 0.33$
$A_{CP}(B^0 \rightarrow (K\pi)_0^{*+}\pi^-)$	$0.02 \pm 0.04$	$S_{K_S^0\pi^0\gamma}(B^0 \rightarrow K_S^0\pi^0\gamma)$	$-0.8 \pm 0.6$
$A_{CP}(B^0 \rightarrow K_2^*(1430)^+\pi^-)$	$-0.29 \pm 0.24$	$C_{K^*(892)^0\gamma}(B^0 \rightarrow K^*(892)^0\gamma)$	$-0.04 \pm 0.16$ (S = 1.2)
$A_{CP}(B^0 \rightarrow K^*(1680)^+\pi^-)$	$-0.07 \pm 0.14$	$S_{K^*(892)^0\gamma}(B^0 \rightarrow K^*(892)^0\gamma)$	$-0.15 \pm 0.22$
$A_{CP}(B^0 \rightarrow f_0(980)K_S^0)$	$0.28 \pm 0.31$	$C_{\eta K^0\gamma}(B^0 \rightarrow \eta K^0\gamma)$	$0.1 \pm 0.4$ (S = 1.4)
$A_{CP}(B^0 \rightarrow (K\pi)_0^{*0}\pi^0)$	$-0.15 \pm 0.11$	$S_{\eta K^0\gamma}(B^0 \rightarrow \eta K^0\gamma)$	$-0.5 \pm 0.5$ (S = 1.2)
$A_{CP}(B^0 \rightarrow K^*0\pi^0)$	$-0.15 \pm 0.13$	$C_{K^0\phi\gamma}(B^0 \rightarrow K^0\phi\gamma)$	$-0.3 \pm 0.6$
$A_{CP}(B^0 \rightarrow K^*(892)^0\pi^+\pi^-)$	$0.07 \pm 0.05$	$S_{K^0\phi\gamma}(B^0 \rightarrow K^0\phi\gamma)$	$0.7^{+0.7}_{-1.1}$
$A_{CP}(B^0 \rightarrow K^*(892)^0\rho^0)$	$-0.06 \pm 0.09$	$C(B^0 \rightarrow K_S^0\rho^0\gamma)$	$-0.05 \pm 0.19$
$A_{CP}(B^0 \rightarrow K^*0 f_0(980))$	$0.07 \pm 0.10$	$S(B^0 \rightarrow K_S^0\rho^0\gamma)$	$-0.04 \pm 0.23$
$A_{CP}(B^0 \rightarrow K^*+\rho^-)$	$0.21 \pm 0.15$	$C(B^0 \rightarrow \rho^0\gamma)$	$0.4 \pm 0.5$
$A_{CP}(B^0 \rightarrow K^*(892)^0 K^+K^-)$	$0.01 \pm 0.05$	$S(B^0 \rightarrow \rho^0\gamma)$	$-0.8 \pm 0.7$
$A_{CP}(B^0 \rightarrow a_1^- K^+)$	$-0.16 \pm 0.12$	$C_{\pi^0\pi^0}(B^0 \rightarrow \pi^0\pi^0)$	$-0.33 \pm 0.22$
$A_{CP}(B^0 \rightarrow K^0 K^0)$	$-0.6 \pm 0.7$	$C_{\rho\pi}(B^0 \rightarrow \rho^+\pi^-)$	$-0.03 \pm 0.07$ (S = 1.2)
$A_{CP}(B^0 \rightarrow K^*(892)^0\phi)$	$0.00 \pm 0.04$		
$A_{CP}(B^0 \rightarrow K^*(892)^0 K^-\pi^+)$	$0.2 \pm 0.4$		
$A_{CP}(B^0 \rightarrow \phi(K\pi)_0^{*0})$	$0.12 \pm 0.08$		
$A_{CP}(B^0 \rightarrow \phi K_2^*(1430)^0)$	$-0.11 \pm 0.10$		
$A_{CP}(B^0 \rightarrow K^*(892)^0\gamma)$	$-0.006 \pm 0.011$		
$A_{CP}(B^0 \rightarrow K_2^*(1430)^0\gamma)$	$-0.08 \pm 0.15$		
$A_{CP}(B^0 \rightarrow X_S\gamma)$	$-0.009 \pm 0.018$		
$A_{CP}(B^0 \rightarrow \rho^+\pi^-)$	$0.13 \pm 0.06$ (S = 1.1)		
$A_{CP}(B^0 \rightarrow \rho^-\pi^+)$	$-0.08 \pm 0.08$		
$A_{CP}(B^0 \rightarrow a_1(1260)\pi^+\pi^-)$	$-0.07 \pm 0.06$		
$A_{CP}(B^0 \rightarrow b_1^-\pi^+)$	$-0.05 \pm 0.10$		
$A_{CP}(B^0 \rightarrow p\bar{p}K^*(892)^0)$	$0.05 \pm 0.12$		
$A_{CP}(B^0 \rightarrow p\bar{p}\pi^-)$	$0.04 \pm 0.07$		

## Tests of Conservation Laws

$S_{\rho\pi}(B^0 \rightarrow \rho^+\pi^-)$	$0.05 \pm 0.07$	$A_{CP}^1(B_S \rightarrow J/\psi \bar{K}^*(892)^0)$	$-0.05 \pm 0.10$
$\Delta S_{\rho\pi}(B^0 \rightarrow \rho^+\pi^-)$	$0.01 \pm 0.08$	$A_{CP}(B_S^0 \rightarrow [K^+K^-]_D \bar{K}^*(892)^0)$	$-0.04 \pm 0.07$
$C_{\rho^0\pi^0}(B^0 \rightarrow \rho^0\pi^0)$	$0.27 \pm 0.24$	$A_{CP}(B_S^0 \rightarrow [\pi^+K^-]_D K^*(892)^0)$	$-0.01 \pm 0.04$
$S_{\rho^0\pi^0}(B^0 \rightarrow \rho^0\pi^0)$	$-0.23 \pm 0.34$	$A_{CP}(B_S^0 \rightarrow [\pi^+\pi^-]_D K^*(892)^0)$	$0.06 \pm 0.13$
$C_{a_1\pi}(B^0 \rightarrow a_1(1260)^+\pi^-)$	$-0.05 \pm 0.11$	$\Gamma(\eta_C(1S) \rightarrow \pi^+\pi^-)/\Gamma_{\text{total}}$	$<1.1 \times 10^{-4}$ , CL = 90%
$S_{a_1\pi}(B^0 \rightarrow a_1(1260)^+\pi^-)$	$-0.2 \pm 0.4$ (S = 3.2)	$\Gamma(\eta_C(1S) \rightarrow \pi^0\pi^0)/\Gamma_{\text{total}}$	$<4 \times 10^{-5}$ , CL = 90%
$\Delta C_{a_1\pi}(B^0 \rightarrow a_1(1260)^+\pi^-)$	$0.43 \pm 0.14$ (S = 1.3)	$\Gamma(\eta_C(1S) \rightarrow K^+K^-)/\Gamma_{\text{total}}$	$<6 \times 10^{-4}$ , CL = 90%
$\Delta S_{a_1\pi}(B^0 \rightarrow a_1(1260)^+\pi^-)$	$-0.11 \pm 0.12$	$\Gamma(\eta_C(1S) \rightarrow K_S^0 K_S^0)/\Gamma_{\text{total}}$	$<3.1 \times 10^{-4}$ , CL = 90%
$C(B^0 \rightarrow b_1^- K^+)$	$-0.22 \pm 0.24$	$n$ electric dipole moment	$<0.18 \times 10^{-25}$ ecm, CL = 90%
$\Delta C(B^0 \rightarrow b_1^- \pi^+)$	$-1.04 \pm 0.24$	$(\alpha + \bar{\alpha})/(\alpha - \bar{\alpha})$ in $\Lambda \rightarrow p\pi^-, \bar{\Lambda} \rightarrow \bar{p}\pi^+$	$-0.002 \pm 0.012$
$C_{\rho^0\rho^0}(B^0 \rightarrow \rho^0\rho^0)$	$0.2 \pm 0.9$	$[\alpha(\Xi^-)\alpha_-(\Lambda) - \alpha(\Xi^+)\alpha_+(\Lambda)]$	$(0 \pm 7) \times 10^{-4}$
$S_{\rho^0\rho^0}(B^0 \rightarrow \rho^0\rho^0)$	$0.3 \pm 0.7$	$[\alpha(\Xi^-)\alpha_-(\Lambda) + \alpha(\Xi^+)\alpha_+(\Lambda)]$	
$C_{\rho\rho}(B^0 \rightarrow \rho^+\rho^-)$	$0.00 \pm 0.09$	$(\alpha + \bar{\alpha})/(\alpha - \bar{\alpha})$ in $\Omega^- \rightarrow \Lambda K^-, \bar{\Omega}^+ \rightarrow \bar{\Lambda} K^+$	$-0.02 \pm 0.13$
$S_{\rho\rho}(B^0 \rightarrow \rho^+\rho^-)$	$-0.14 \pm 0.13$	$(\alpha + \bar{\alpha})/(\alpha - \bar{\alpha})$ in $\Lambda_C^+ \rightarrow \Lambda\pi^+, \bar{\Lambda}_C^- \rightarrow \bar{\Lambda}\pi^-$	$-0.07 \pm 0.31$
$ \lambda (B^0 \rightarrow J/\psi K^*(892)^0)$	$<0.25$ , CL = 95%	$(\alpha + \bar{\alpha})/(\alpha - \bar{\alpha})$ in $\Lambda_C^+ \rightarrow \Lambda e^+ \nu_e, \bar{\Lambda}_C^- \rightarrow \bar{\Lambda} e^- \bar{\nu}_e$	$0.00 \pm 0.04$
$\cos 2\beta(B^0 \rightarrow J/\psi K^*(892)^0)$	$1.7_{-0.9}^{+0.7}$ (S = 1.6)	$A_{CP}(\Lambda_b \rightarrow p\pi^-)$	$-0.025 \pm 0.029$ (S = 1.2)
$\cos 2\beta(B^0 \rightarrow [K_S^0 \pi^+ \pi^-]_{D^{(*)}} h^0)$	$0.91 \pm 0.25$	$A_{CP}(\Lambda_b \rightarrow pK^-)$	$-0.025 \pm 0.022$
$(S_+ + S_-)/2(B^0 \rightarrow D^{*-}\pi^+)$	$-0.039 \pm 0.011$	$\Delta A_{CP}(pK^-/\pi^-)$	$0.014 \pm 0.024$
$(S_- - S_+)/2(B^0 \rightarrow D^{*-}\pi^+)$	$-0.009 \pm 0.015$	$A_{CP}(\Lambda_b \rightarrow p\bar{K}^0\pi^-)$	$0.22 \pm 0.13$
$(S_+ + S_-)/2(B^0 \rightarrow D^-\pi^+)$	$-0.046 \pm 0.023$	$\Delta A_{CP}(J/\psi p\pi^-/K^-)$	$(5.7 \pm 2.7) \times 10^{-2}$
$(S_- - S_+)/2(B^0 \rightarrow D^-\pi^+)$	$-0.022 \pm 0.021$	$A_{CP}(\Lambda_b \rightarrow \Lambda K^+\pi^-)$	$-0.53 \pm 0.25$
$S_+(B^0 \rightarrow D^-\pi^+)$	$0.058 \pm 0.023$	$A_{CP}(\Lambda_b \rightarrow \Lambda K^+K^-)$	$-0.28 \pm 0.12$
$S_-(B^0 \rightarrow D^+\pi^-)$	$0.038 \pm 0.021$	$\Delta A_{CP}(\Lambda_b^0 \rightarrow pK^-\mu^+\mu^-)$	$(-4 \pm 5) \times 10^{-2}$
$(S_+ + S_-)/2(B^0 \rightarrow D^-\rho^+)$	$-0.024 \pm 0.032$	$A_c(\Lambda)$	$-0.22 \pm 0.13$
$(S_- - S_+)/2(B^0 \rightarrow D^-\rho^+)$	$-0.10 \pm 0.06$	$A_s(\Lambda)$	$0.13 \pm 0.13$
$C_{\eta_C K_S^0}(B^0 \rightarrow \eta_C K_S^0)$	$0.08 \pm 0.13$	$A_c(\phi)$	$-0.01 \pm 0.12$
$C_{c\bar{c}K^{(*)0}}(B^0 \rightarrow c\bar{c}K^{(*)0})$	$(0.5 \pm 1.7) \times 10^{-2}$	$A_s(\phi)$	$-0.07 \pm 0.12$
$C_{J/\psi(nS)K^0}(B^0 \rightarrow J/\psi(nS)K^0)$	$(0.5 \pm 2.0) \times 10^{-2}$	$a_{CP}(\Lambda_b^0 \rightarrow p\pi^-\pi^+\pi^-)$	$(1.1 \pm 1.5)\%$
$C_{J/\psi K^{*0}}(B^0 \rightarrow J/\psi K^{*0})$	$0.03 \pm 0.10$	$a_{CP}(\Lambda_b^0 \rightarrow pK^-\pi^+\pi^-)$	$(-0.8 \pm 0.9)\%$
$S_{J/\psi K^{*0}}(B^0 \rightarrow J/\psi K^{*0})$	$0.60 \pm 0.25$	$a_{CP}(\Lambda_b^0 \rightarrow pK^-K^+\pi^-)$	$(-1 \pm 5)\%$
$C_{\chi_{c0} K_S^0}(B^0 \rightarrow \chi_{c0} K_S^0)$	$-0.3_{-0.4}^{+0.5}$	$a_{CP}(\Lambda_b^0 \rightarrow pK^-K^+K^-)$	$(1.1 \pm 1.5)\%$
$S_{\chi_{c0} K_S^0}(B^0 \rightarrow \chi_{c0} K_S^0)$	$-0.7 \pm 0.5$	$a_{CP}(\Lambda_b^0 \rightarrow pK^-\mu^+\mu^-)$	$(1 \pm 5)\%$
$C_{\chi_{c1} K_S^0}(B^0 \rightarrow \chi_{c1} K_S^0)$	$0.06 \pm 0.07$	$a_{CP}(\Xi_b^0 \rightarrow pK^-K^-\pi^+)$	$(-4 \pm 5)\%$
$\sin(2\beta_{\text{eff}})(B^0 \rightarrow \phi K^0)$	$0.22 \pm 0.30$	<b>CP VIOLATION OBSERVED</b>	
$\sin(2\beta_{\text{eff}})(B^0 \rightarrow \phi K_0^*(1430)^0)$	$0.97_{-0.52}^{+0.03}$	$\text{Re}(\epsilon)$	$(1.596 \pm 0.013) \times 10^{-3}$
$\sin(2\beta_{\text{eff}})(B^0 \rightarrow [K_S^0 \pi^+ \pi^-]_{D^{(*)}} h^0)$	$0.80 \pm 0.16$	charge asymmetry in $K_{L3}^0$ decays	
$ \lambda (B^0 \rightarrow [K_S^0 \pi^+ \pi^-]_{D^{(*)}} h^0)$	$1.01 \pm 0.08$	$A_L(\mu) = \text{weighted average of } A_L(\mu) \text{ and } A_L(e)$	$(0.332 \pm 0.006)\%$
$ \sin(2\beta + \gamma) $	$>0.40$ , CL = 90%	$A_L(\mu) = [\Gamma(\pi^-\mu^+\nu_\mu) - \Gamma(\pi^+\mu^-\bar{\nu}_\mu)]/\text{sum}$	$(0.304 \pm 0.025)\%$
$2\beta + \gamma$	$(83 \pm 60)^\circ$	$A_L(e) = [\Gamma(\pi^-e^+\nu_e) - \Gamma(\pi^+e^-\bar{\nu}_e)]/\text{sum}$	$(0.334 \pm 0.007)\%$
$x_+(B^0 \rightarrow D K^{*0})$	$0.04 \pm 0.17$	parameters for $K_L^0 \rightarrow 2\pi$ decay	
$x_-(B^0 \rightarrow D K^{*0})$	$-0.16 \pm 0.14$	$ \eta_{00}  =  A(K_L^0 \rightarrow 2\pi^0) / A(K_S^0 \rightarrow 2\pi^0) $	$(2.220 \pm 0.011) \times 10^{-3}$ (S = 1.8)
$y_-(B^0 \rightarrow D K^{*0})$	$0.20 \pm 0.25$ (S = 1.2)	$ \eta_{+-}  =  A(K_L^0 \rightarrow \pi^+\pi^-) / A(K_S^0 \rightarrow \pi^+\pi^-) $	$(2.232 \pm 0.011) \times 10^{-3}$ (S = 1.8)
$A_{CP}(B \rightarrow K^*(892)\gamma)$	$-0.003 \pm 0.011$	$ \epsilon  = (2 \eta_{+-}  +  \eta_{00} )/3$	$(2.228 \pm 0.011) \times 10^{-3}$ (S = 1.8)
$A_{CP}(B \rightarrow s\gamma)$	$0.015 \pm 0.011$	$ \eta_{00}/\eta_{+-} $	[i] $0.9950 \pm 0.0007$ (S = 1.6)
$A_{CP}(B \rightarrow (s+d)\gamma)$	$0.010 \pm 0.031$	$\text{Re}(\epsilon'/\epsilon) = (1 -  \eta_{00}/\eta_{+-} )/3$	[j] $(1.66 \pm 0.23) \times 10^{-3}$ (S = 1.6)
$A_{CP}(B \rightarrow X_S \ell^+ \ell^-)$	$0.04 \pm 0.11$	Assuming <i>CPT</i>	
$A_{CP}(B \rightarrow K^* e^+ e^-)$	$-0.18 \pm 0.15$	$\phi_{+-}$ , phase of $\eta_{+-}$	$(43.51 \pm 0.05)^\circ$ (S = 1.2)
$A_{CP}(B \rightarrow K^* \mu^+ \mu^-)$	$-0.03 \pm 0.13$	$\phi_{00}$ , phase of $\eta_{00}$	$(43.52 \pm 0.05)^\circ$ (S = 1.3)
$A_{CP}(B \rightarrow K^* \ell^+ \ell^-)$	$-0.04 \pm 0.07$	$\phi_\epsilon = (2\phi_{+-} + \phi_{00})/3$	$(43.52 \pm 0.05)^\circ$ (S = 1.2)
$A_{CP}(B \rightarrow \eta \text{ anything})$	$-0.13_{-0.05}^{+0.04}$	Not assuming <i>CPT</i>	
$\Delta A_{CP}(X_S \gamma) = A_{CP}(B^\pm \rightarrow X_S \gamma) - A_{CP}(B^0 \rightarrow X_S \gamma)$	$0.041 \pm 0.023$	$\phi_{+-}$ , phase of $\eta_{+-}$	$(43.4 \pm 0.5)^\circ$ (S = 1.2)
$\bar{A}_{CP}(B \rightarrow X_S \gamma) = (A_{CP}(B^+ \rightarrow X_S \gamma) + A_{CP}(B^0 \rightarrow X_S \gamma))/2$	$0.009 \pm 0.012$	$\phi_{00}$ , phase of $\eta_{00}$	$(43.7 \pm 0.6)^\circ$ (S = 1.2)
$\bar{A}_{CP}(B \rightarrow K^* \gamma) = (A_{CP}(B^+ \rightarrow K^* \gamma) + A_{CP}(B^0 \rightarrow K^* \gamma))/2$	$-0.001 \pm 0.014$	$\phi_\epsilon = (2\phi_{+-} + \phi_{00})/3$	$(43.5 \pm 0.5)^\circ$ (S = 1.3)
$\text{Re}(\epsilon_{B_S^0}) / (1 +  \epsilon_{B_S^0} ^2)$	$(-0.15 \pm 0.70) \times 10^{-3}$	$CP$ asymmetry $A$ in $K_L^0 \rightarrow \pi^+\pi^-e^+e^-$	$(13.7 \pm 1.5)\%$
$C_{KK}(B_S^0 \rightarrow K^+K^-)$	$0.14 \pm 0.11$	$\beta_{CP}$ from $K_L^0 \rightarrow e^+e^-e^+e^-$	$-0.19 \pm 0.07$
$S_{KK}(B_S^0 \rightarrow K^+K^-)$	$0.30 \pm 0.13$	$\gamma_{CP}$ from $K_L^0 \rightarrow e^+e^-e^+e^-$	$0.01 \pm 0.11$ (S = 1.6)
$r_B(B_S^0 \rightarrow D_S^\mp K^\pm)$	$0.37_{-0.09}^{+0.10}$	parameters for $K_L^0 \rightarrow \pi^+\pi^-\gamma$ decay	
$\delta_B(B_S^0 \rightarrow D_S^\pm K^\mp)$	$(358 \pm 14)^\circ$	$ \eta_{+-\gamma}  =  A(K_L^0 \rightarrow \pi^+\pi^-\gamma, CP \text{ violating}) / A(K_S^0 \rightarrow \pi^+\pi^-\gamma) $	$(2.35 \pm 0.07) \times 10^{-3}$
$CP$ Violation phase $\beta_s$	$(2.55 \pm 1.15) \times 10^{-2}$ rad	$\phi_{+-\gamma} = \text{phase of } \eta_{+-\gamma}$	$(44 \pm 4)^\circ$
$A_{CP}^1(B_S \rightarrow J/\psi \bar{K}^*(892)^0)$	$-0.05 \pm 0.06$		
$A_{CP}^1(B_S \rightarrow J/\psi \bar{K}^*(892)^0)$	$0.17 \pm 0.15$		

Unless otherwise stated, limits are given at the 90% confidence level, while errors are given as  $\pm 1$  standard deviation.

# Tests of Conservation Laws

$\Gamma(K_L^0 \rightarrow \pi^+ \pi^-) / \Gamma_{\text{total}}$	[j] $(1.967 \pm 0.010) \times 10^{-3}$ (S = 1.5)	$(m_{K^+} - m_{K^-}) / m_{\text{average}}$	$(-0.6 \pm 1.8) \times 10^{-4}$
$\Gamma(K_L^0 \rightarrow \pi^0 \pi^0) / \Gamma_{\text{total}}$	$(8.64 \pm 0.06) \times 10^{-4}$ (S = 1.8)	$(\tau_{K^+} - \tau_{K^-}) / \tau_{\text{average}}$	$(0.10 \pm 0.09)\%$ (S = 1.2)
$\Delta A_{CP}^{D^0} = A_{CP}(K^+ K^-) - A_{CP}(\pi^+ \pi^-)$	$(-0.154 \pm 0.029)\%$	$K^{\pm} \rightarrow \mu^{\pm} \nu_{\mu}$ rate difference/sum	$(-0.27 \pm 0.21)\%$
$A_{CP}(B^+ \rightarrow [K^- \pi^+] \overline{D}^0 K^*(892)^+)$	$-0.75 \pm 0.16$	$K^{\pm} \rightarrow \pi^{\pm} \pi^0$ rate difference/sum	[k] $(0.4 \pm 0.6)\%$
$A_{CP}(B^+ \rightarrow D_{CP}^{(+1)} K^+)$	$0.120 \pm 0.014$ (S = 1.4)	$\delta$ in $K^0 - \overline{K}^0$ mixing	
$A_{ADS}(B^+ \rightarrow D K^+)$	$-0.40 \pm 0.06$	real part of $\delta$	$(2.5 \pm 2.3) \times 10^{-4}$
$A_{CP}(B^+ \rightarrow \eta K^+)$	$-0.37 \pm 0.08$	imaginary part of $\delta$	$(-1.5 \pm 1.6) \times 10^{-5}$
$A_{CP}(B^+ \rightarrow f_2(1270) K^+)$	$-0.68^{+0.19}_{-0.17}$	Re(y), $K_{e3}$ parameter	$(0.4 \pm 2.5) \times 10^{-3}$
$A_{CP}(B^+ \rightarrow \rho^0 K^+)$	$0.37 \pm 0.10$	Re(x <sub>-</sub> ), $K_{e3}$ parameter	$(-2.9 \pm 2.0) \times 10^{-3}$
$A_{CP}(B^+ \rightarrow K^+ K^- \pi^+)$	$-0.122 \pm 0.021$	$ m_{K^0} - m_{\overline{K}^0}  / m_{\text{average}}$	[l] $< 6 \times 10^{-19}$ , CL = 90%
$A_{CP}(B^+ \rightarrow K^+ K^- K^+)$	$-0.033 \pm 0.008$	$(\Gamma_{K^0} - \Gamma_{\overline{K}^0}) / m_{\text{average}}$	$(8 \pm 8) \times 10^{-18}$
$A_{CP}(B^+ \rightarrow \pi^+ \pi^- \pi^+)$	$0.057 \pm 0.013$	phase difference $\phi_{00} - \phi_{+-}$	$(0.34 \pm 0.32)^\circ$
$A_{CP}(B^+ \rightarrow f_2(1270) \pi^+)$	$0.40 \pm 0.06$	$\text{Re}(\frac{2}{3}\eta_{+-} + \frac{1}{3}\eta_{00}) - \frac{A_{\mu}}{A_{\pi}}$	$(-3 \pm 35) \times 10^{-6}$
$A_{CP}(B^+ \rightarrow f_0(1370) \pi^+)$	$0.72 \pm 0.22$	$A_{CPT}(D^0 \rightarrow K^- \pi^+)$	$0.008 \pm 0.008$
$\gamma$	$(71.1^{+4.6}_{-5.3})^\circ$	$\Delta S_{CPT}^+(S_{\ell^+, K_S^0}^- - S_{\ell^+, K_S^0}^+)$	$0.16 \pm 0.23$
$r_B(B^+ \rightarrow D^0 K^+)$	$0.0993 \pm 0.0046$	$\Delta S_{CPT}^-(S_{\ell^+, K_S^0}^+ - S_{\ell^+, K_S^0}^-)$	$-0.03 \pm 0.14$
$\delta_B(B^+ \rightarrow D^0 K^+)$	$(129.6^{+5.0}_{-6.0})^\circ$	$\Delta C_{CPT}^+(C_{\ell^+, K_S^0}^- - C_{\ell^+, K_S^0}^+)$	$0.14 \pm 0.17$
$r_B(B^+ \rightarrow D^0 K^{*+})$	$0.076 \pm 0.020$	$\Delta C_{CPT}^-(C_{\ell^+, K_S^0}^+ - C_{\ell^+, K_S^0}^-)$	$0.03 \pm 0.14$
$\delta_B(B^+ \rightarrow D^0 K^{*+})$	$(98^{+18}_{-37})^\circ$		
$r_B(B^+ \rightarrow D^{*0} K^+)$	$0.140 \pm 0.019$	$ m_{\rho^-} - m_{\overline{\rho}^-}  / m_{\rho}$	[n] $< 7 \times 10^{-10}$ , CL = 90%
$\delta_B(B^+ \rightarrow D^{*0} K^+)$	$(319.2^{+7.7}_{-8.1})^\circ$	$(\frac{q_{\overline{\rho}^-}}{m_{\overline{\rho}^-}} - \frac{q_{\rho^-}}{m_{\rho^-}}) / \frac{q_{\rho^-}}{m_{\rho^-}}$	$(0.1 \pm 6.9) \times 10^{-11}$
$A_{CP}(B^0 \rightarrow K^+ \pi^-)$	$-0.083 \pm 0.004$	$ q_{\rho^-} + q_{\overline{\rho}^-}  / e$	[n] $< 7 \times 10^{-10}$ , CL = 90%
$A_{CP}(B^0 \rightarrow \eta K^*(892)^0)$	$0.19 \pm 0.05$	$(\mu_{\rho^-} + \mu_{\overline{\rho}^-}) / \mu_{\rho}$	$(0.002 \pm 0.004) \times 10^{-6}$
$A_{CP}(B^0 \rightarrow K^*(892)^+ \pi^-)$	$-0.27 \pm 0.04$	$(m_{\eta^-} - m_{\overline{\eta}^-}) / m_{\eta}$	$(9 \pm 6) \times 10^{-5}$
$S_{D^*(2010)-D^+}(B^0 \rightarrow D^*(2010)^- D^+)$	$-0.72 \pm 0.15$	$(m_{\Lambda^-} - m_{\overline{\Lambda}^-}) / m_{\Lambda}$	$(-0.1 \pm 1.1) \times 10^{-5}$ (S = 1.6)
$S_{D^*(2010)+D^-}(B^0 \rightarrow D^*(2010)^+ D^-)$	$-0.73 \pm 0.14$	$(\tau_{\Lambda^-} - \tau_{\overline{\Lambda}^-}) / \tau_{\Lambda}$	$-0.001 \pm 0.009$
$S_{D^{*+}D^{*-}}(B^0 \rightarrow D^{*+} D^{*-})$	$-0.59 \pm 0.14$ (S = 1.8)	$(\tau_{\Sigma^+} - \tau_{\overline{\Sigma}^-}) / \tau_{\Sigma^+}$	$-0.0006 \pm 0.0012$
$S_{+}(B^0 \rightarrow D^{*+} D^{*-})$	$-0.73 \pm 0.09$	$(\mu_{\Sigma^+} + \mu_{\overline{\Sigma}^-}) / \mu_{\Sigma^+}$	$0.014 \pm 0.015$
$S_{D^+D^-}(B^0 \rightarrow D^+ D^-)$	$-0.76^{+0.15}_{-0.13}$ (S = 1.2)	$(m_{\Xi^-} - m_{\overline{\Xi}^+}) / m_{\Xi^-}$	$(-3 \pm 9) \times 10^{-5}$
$S_{J/\psi(1S)\pi^0}(B^0 \rightarrow J/\psi(1S)\pi^0)$	$-0.88 \pm 0.32$ (S = 2.2)	$(\tau_{\Xi^-} - \tau_{\overline{\Xi}^+}) / \tau_{\Xi^-}$	$-0.01 \pm 0.07$
$S(B^0 \rightarrow J/\psi(1S)\rho^0)$	$-0.66^{+0.16}_{-0.12}$	$(\mu_{\Xi^-} + \mu_{\overline{\Xi}^+}) /  \mu_{\Xi^-} $	$+0.01 \pm 0.05$
$S_{K^0\pi^0}(B^0 \rightarrow K^0\pi^0)$	$0.58 \pm 0.17$	$(m_{\Omega^-} - m_{\overline{\Omega}^+}) / m_{\Omega^-}$	$(-1 \pm 8) \times 10^{-5}$
$S_{\eta'K^0}(B^0 \rightarrow \eta'K^0)$	$0.63 \pm 0.06$	$(\tau_{\Omega^-} - \tau_{\overline{\Omega}^+}) / \tau_{\Omega^-}$	$0.00 \pm 0.05$
$S_{K^+K^-K_S^0}(B^0 \rightarrow K^+K^-K_S^0)$ nonresonant)	$-0.66 \pm 0.11$		
$S_{K^+K^-K_S^0}(B^0 \rightarrow K^+K^-K_S^0)$ inclusive)	$-0.65 \pm 0.12$		
$C_{\pi\pi}(B^0 \rightarrow \pi^+\pi^-)$	$-0.32 \pm 0.04$		
$S_{\pi\pi}(B^0 \rightarrow \pi^+\pi^-)$	$-0.65 \pm 0.04$		
$\Delta C_{\rho\pi}(B^0 \rightarrow \rho^+\pi^-)$	$0.27 \pm 0.06$		
$S_{\eta_c K_S^0}(B^0 \rightarrow \eta_c K_S^0)$	$0.93 \pm 0.17$		
$\sin(2\beta)(B^0 \rightarrow J/\psi K_S^0)$	$0.695 \pm 0.019$		
$S_{J/\psi(nS)K^0}(B^0 \rightarrow J/\psi(nS)K^0)$	$0.701 \pm 0.017$		
$S_{\chi_{c1} K_S^0}(B^0 \rightarrow \chi_{c1} K_S^0)$	$0.63 \pm 0.10$		
$\sin(2\beta_{\text{eff}})(B^0 \rightarrow K^+K^-K_S^0)$	$0.77^{+0.13}_{-0.12}$		
$\alpha$	$(84.9^{+5.1}_{-4.5})^\circ$		
$r_{B^0}(B^0 \rightarrow D K^{*0})$	$0.220^{+0.041}_{-0.047}$		
$\delta_{B^0}(B^0 \rightarrow D K^{*0})$	$(194^{+30}_{-22})^\circ$		
$A_{CP}(B_S \rightarrow \pi^+ K^-)$	$0.221 \pm 0.015$		

## CPT INVARIANCE

$(m_{W^+} - m_{W^-}) / m_{\text{average}}$	$(-3.7 \pm 3.5) \times 10^{-4}$
$(m_{e^+} - m_{e^-}) / m_{\text{average}}$	$< 8 \times 10^{-9}$ , CL = 90%
$ q_{e^+} + q_{e^-}  / e$	$< 4 \times 10^{-8}$
$(g_{e^+} - g_{e^-}) / g_{\text{average}}$	$(-0.5 \pm 2.1) \times 10^{-12}$
$(\tau_{\mu^+} - \tau_{\mu^-}) / \tau_{\text{average}}$	$(2 \pm 8) \times 10^{-5}$
$(g_{\mu^+} - g_{\mu^-}) / g_{\text{average}}$	$(-0.11 \pm 0.12) \times 10^{-8}$
$(m_{\tau^+} - m_{\tau^-}) / m_{\text{average}}$	$< 2.8 \times 10^{-4}$ , CL = 90%
$\langle \Delta m_{21}^2 - \Delta \overline{m}_{21}^2 \rangle$ in neutrino mixing	$< 1.1 \times 10^{-4}$ eV <sup>2</sup> , CL = 99.7%
$\langle \Delta m_{32}^2 - \Delta \overline{m}_{32}^2 \rangle$ in neutrino mixing	$(-0.12 \pm 0.25) \times 10^{-3}$ eV <sup>2</sup>
$m_t - m_{\overline{t}}$	$-0.16 \pm 0.19$ GeV
$(m_{\pi^+} - m_{\pi^-}) / m_{\text{average}}$	$(2 \pm 5) \times 10^{-4}$
$(\tau_{\pi^+} - \tau_{\pi^-}) / \tau_{\text{average}}$	$(6 \pm 7) \times 10^{-4}$

## TESTS OF NUMBER CONSERVATION LAWS

### LEPTON FAMILY NUMBER

Lepton family number conservation means separate conservation of each of  $L_e, L_\mu, L_\tau$ .

$\Gamma(Z \rightarrow e^\pm \mu^\mp) / \Gamma_{\text{total}}$	[o] $< 7.5 \times 10^{-7}$ , CL = 95%
$\Gamma(Z \rightarrow e^\pm \tau^\mp) / \Gamma_{\text{total}}$	[o] $< 9.8 \times 10^{-6}$ , CL = 95%
$\Gamma(Z \rightarrow \mu^\pm \tau^\mp) / \Gamma_{\text{total}}$	[o] $< 1.2 \times 10^{-5}$ , CL = 95%
$\Gamma(H^0 \rightarrow e\mu) / \Gamma_{\text{total}}$	$< 6.1 \times 10^{-5}$ , CL = 95%
$\Gamma(H^0 \rightarrow e\tau) / \Gamma_{\text{total}}$	$< 4.7 \times 10^{-3}$ , CL = 95%
$\Gamma(H^0 \rightarrow \mu\tau) / \Gamma_{\text{total}}$	$< 2.5 \times 10^{-3}$ , CL = 95%
$\sigma(e^+e^- \rightarrow e^\pm \tau^\mp) / \sigma(e^+e^- \rightarrow \mu^+ \mu^-)$	$< 8.9 \times 10^{-6}$ , CL = 95%
$\sigma(e^+e^- \rightarrow \mu^\pm \tau^\mp) / \sigma(e^+e^- \rightarrow \mu^+ \mu^-)$	$< 4.0 \times 10^{-6}$ , CL = 95%
limit on $\mu^- \rightarrow e^-$ conversion	
$\sigma(\mu^- 32S \rightarrow e^- 32S) / \sigma(\mu^- 32S \rightarrow \nu_\mu 32P^*)$	$< 7 \times 10^{-11}$ , CL = 90%
$\sigma(\mu^- \text{Ti} \rightarrow e^- \text{Ti}) / \sigma(\mu^- \text{Ti} \rightarrow \text{capture})$	$< 4.3 \times 10^{-12}$ , CL = 90%
$\sigma(\mu^- \text{Pb} \rightarrow e^- \text{Pb}) / \sigma(\mu^- \text{Pb} \rightarrow \text{capture})$	$< 4.6 \times 10^{-11}$ , CL = 90%
$\sigma(\mu^- \text{Au} \rightarrow e^- \text{Au}) / \sigma(\mu^- \text{Au} \rightarrow \text{capture})$	$< 7 \times 10^{-13}$ , CL = 90%
limit on muonium $\rightarrow$ antimuonium conversion $R_g = G_C / G_F$	$< 0.0030$ , CL = 90%
$\Gamma(\mu^- \rightarrow e^- \nu_e \overline{\nu}_\mu) / \Gamma_{\text{total}}$	[p] $< 1.2 \times 10^{-2}$ , CL = 90%
$\Gamma(\mu^- \rightarrow e^- \gamma) / \Gamma_{\text{total}}$	$< 4.2 \times 10^{-13}$ , CL = 90%
$\Gamma(\mu^- \rightarrow e^- e^+ e^-) / \Gamma_{\text{total}}$	$< 1.0 \times 10^{-12}$ , CL = 90%
$\Gamma(\mu^- \rightarrow e^- 2\gamma) / \Gamma_{\text{total}}$	$< 7.2 \times 10^{-11}$ , CL = 90%

# Tests of Conservation Laws

$\Gamma(\tau^- \rightarrow e^- \gamma)/\Gamma_{\text{total}}$	$<3.3 \times 10^{-8}$ , CL = 90%	$\Gamma(D^+ \rightarrow \pi^+ e^- \mu^+)/\Gamma_{\text{total}}$	$<3.6 \times 10^{-6}$ , CL = 90%
$\Gamma(\tau^- \rightarrow \mu^- \gamma)/\Gamma_{\text{total}}$	$<4.4 \times 10^{-8}$ , CL = 90%	$\Gamma(D^+ \rightarrow K^+ e^+ \mu^-)/\Gamma_{\text{total}}$	$<1.2 \times 10^{-6}$ , CL = 90%
$\Gamma(\tau^- \rightarrow e^- \pi^0)/\Gamma_{\text{total}}$	$<8.0 \times 10^{-8}$ , CL = 90%	$\Gamma(D^+ \rightarrow K^+ e^- \mu^+)/\Gamma_{\text{total}}$	$<2.8 \times 10^{-6}$ , CL = 90%
$\Gamma(\tau^- \rightarrow \mu^- \pi^0)/\Gamma_{\text{total}}$	$<1.1 \times 10^{-7}$ , CL = 90%	$\Gamma(D^0 \rightarrow \mu^\pm e^\mp)/\Gamma_{\text{total}}$	[o] $<1.3 \times 10^{-8}$ , CL = 90%
$\Gamma(\tau^- \rightarrow e^- K_S^0)/\Gamma_{\text{total}}$	$<2.6 \times 10^{-8}$ , CL = 90%	$\Gamma(D^0 \rightarrow \pi^0 e^\pm \mu^\mp)/\Gamma_{\text{total}}$	[o] $<8.6 \times 10^{-5}$ , CL = 90%
$\Gamma(\tau^- \rightarrow \mu^- K_S^0)/\Gamma_{\text{total}}$	$<2.3 \times 10^{-8}$ , CL = 90%	$\Gamma(D^0 \rightarrow \eta e^\pm \mu^\mp)/\Gamma_{\text{total}}$	[o] $<1.0 \times 10^{-4}$ , CL = 90%
$\Gamma(\tau^- \rightarrow e^- \eta)/\Gamma_{\text{total}}$	$<9.2 \times 10^{-8}$ , CL = 90%	$\Gamma(D^0 \rightarrow \pi^+ \pi^- e^\pm \mu^\mp)/\Gamma_{\text{total}}$	[o] $<1.5 \times 10^{-5}$ , CL = 90%
$\Gamma(\tau^- \rightarrow \mu^- \eta)/\Gamma_{\text{total}}$	$<6.5 \times 10^{-8}$ , CL = 90%	$\Gamma(D^0 \rightarrow \rho^0 e^\pm \mu^\mp)/\Gamma_{\text{total}}$	[o] $<4.9 \times 10^{-5}$ , CL = 90%
$\Gamma(\tau^- \rightarrow e^- \rho^0)/\Gamma_{\text{total}}$	$<1.8 \times 10^{-8}$ , CL = 90%	$\Gamma(D^0 \rightarrow \omega e^\pm \mu^\mp)/\Gamma_{\text{total}}$	[o] $<1.2 \times 10^{-4}$ , CL = 90%
$\Gamma(\tau^- \rightarrow \mu^- \rho^0)/\Gamma_{\text{total}}$	$<1.2 \times 10^{-8}$ , CL = 90%	$\Gamma(D^0 \rightarrow K^- K^+ e^\pm \mu^\mp)/\Gamma_{\text{total}}$	[o] $<1.8 \times 10^{-4}$ , CL = 90%
$\Gamma(\tau^- \rightarrow e^- \omega)/\Gamma_{\text{total}}$	$<4.8 \times 10^{-8}$ , CL = 90%	$\Gamma(D^0 \rightarrow \phi e^\pm \mu^\mp)/\Gamma_{\text{total}}$	[o] $<3.4 \times 10^{-5}$ , CL = 90%
$\Gamma(\tau^- \rightarrow \mu^- \omega)/\Gamma_{\text{total}}$	$<4.7 \times 10^{-8}$ , CL = 90%	$\Gamma(D^0 \rightarrow \bar{K}^0 e^\pm \mu^\mp)/\Gamma_{\text{total}}$	[o] $<1.0 \times 10^{-4}$ , CL = 90%
$\Gamma(\tau^- \rightarrow e^- K^*(892)^0)/\Gamma_{\text{total}}$	$<3.2 \times 10^{-8}$ , CL = 90%	$\Gamma(D^0 \rightarrow K^- \pi^+ e^\pm \mu^\mp)/\Gamma_{\text{total}}$	[o] $<5.53 \times 10^{-4}$ , CL = 90%
$\Gamma(\tau^- \rightarrow \mu^- K^*(892)^0)/\Gamma_{\text{total}}$	$<5.9 \times 10^{-8}$ , CL = 90%	$\Gamma(D^0 \rightarrow \bar{K}^*(892)^0 e^\pm \mu^\mp)/\Gamma_{\text{total}}$	[o] $<8.3 \times 10^{-5}$ , CL = 90%
$\Gamma(\tau^- \rightarrow e^- \bar{K}^*(892)^0)/\Gamma_{\text{total}}$	$<3.4 \times 10^{-8}$ , CL = 90%	$\Gamma(D_S^+ \rightarrow \pi^+ e^+ \mu^-)/\Gamma_{\text{total}}$	$<1.2 \times 10^{-5}$ , CL = 90%
$\Gamma(\tau^- \rightarrow \mu^- \bar{K}^*(892)^0)/\Gamma_{\text{total}}$	$<7.0 \times 10^{-8}$ , CL = 90%	$\Gamma(D_S^+ \rightarrow \pi^+ e^- \mu^+)/\Gamma_{\text{total}}$	$<2.0 \times 10^{-5}$ , CL = 90%
$\Gamma(\tau^- \rightarrow e^- \eta'(958))/\Gamma_{\text{total}}$	$<1.6 \times 10^{-7}$ , CL = 90%	$\Gamma(D_S^+ \rightarrow K^+ e^+ \mu^-)/\Gamma_{\text{total}}$	$<1.4 \times 10^{-5}$ , CL = 90%
$\Gamma(\tau^- \rightarrow \mu^- \eta'(958))/\Gamma_{\text{total}}$	$<1.3 \times 10^{-7}$ , CL = 90%	$\Gamma(D_S^+ \rightarrow K^+ e^- \mu^+)/\Gamma_{\text{total}}$	$<9.7 \times 10^{-6}$ , CL = 90%
$\Gamma(\tau^- \rightarrow e^- f_0(980) \rightarrow e^- \pi^+ \pi^-)/\Gamma_{\text{total}}$	$<3.2 \times 10^{-8}$ , CL = 90%	$\Gamma(B^+ \rightarrow \pi^+ e^+ \mu^-)/\Gamma_{\text{total}}$	$<6.4 \times 10^{-3}$ , CL = 90%
$\Gamma(\tau^- \rightarrow \mu^- f_0(980) \rightarrow \mu^- \pi^+ \pi^-)/\Gamma_{\text{total}}$	$<3.4 \times 10^{-8}$ , CL = 90%	$\Gamma(B^+ \rightarrow \pi^+ e^- \mu^+)/\Gamma_{\text{total}}$	$<6.4 \times 10^{-3}$ , CL = 90%
$\Gamma(\tau^- \rightarrow e^- \phi)/\Gamma_{\text{total}}$	$<3.1 \times 10^{-8}$ , CL = 90%	$\Gamma(B^+ \rightarrow \pi^+ e^\pm \mu^\mp)/\Gamma_{\text{total}}$	$<1.7 \times 10^{-7}$ , CL = 90%
$\Gamma(\tau^- \rightarrow \mu^- \phi)/\Gamma_{\text{total}}$	$<8.4 \times 10^{-8}$ , CL = 90%	$\Gamma(B^+ \rightarrow \pi^+ e^\pm \tau^\mp)/\Gamma_{\text{total}}$	$<7.4 \times 10^{-5}$ , CL = 90%
$\Gamma(\tau^- \rightarrow e^- e^+ e^-)/\Gamma_{\text{total}}$	$<2.7 \times 10^{-8}$ , CL = 90%	$\Gamma(B^+ \rightarrow \pi^+ e^- \tau^+)/\Gamma_{\text{total}}$	$<2.0 \times 10^{-5}$ , CL = 90%
$\Gamma(\tau^- \rightarrow e^- \mu^+ \mu^-)/\Gamma_{\text{total}}$	$<2.7 \times 10^{-8}$ , CL = 90%	$\Gamma(B^+ \rightarrow \pi^+ e^\pm \tau^\mp)/\Gamma_{\text{total}}$	$<7.5 \times 10^{-5}$ , CL = 90%
$\Gamma(\tau^- \rightarrow e^+ \mu^- \mu^-)/\Gamma_{\text{total}}$	$<1.7 \times 10^{-8}$ , CL = 90%	$\Gamma(B^+ \rightarrow \pi^+ \mu^+ \tau^-)/\Gamma_{\text{total}}$	$<6.2 \times 10^{-5}$ , CL = 90%
$\Gamma(\tau^- \rightarrow \mu^- e^+ e^-)/\Gamma_{\text{total}}$	$<1.8 \times 10^{-8}$ , CL = 90%	$\Gamma(B^+ \rightarrow \pi^+ \mu^- \tau^+)/\Gamma_{\text{total}}$	$<4.5 \times 10^{-5}$ , CL = 90%
$\Gamma(\tau^- \rightarrow \mu^+ e^- e^-)/\Gamma_{\text{total}}$	$<1.5 \times 10^{-8}$ , CL = 90%	$\Gamma(B^+ \rightarrow \pi^+ \mu^\pm \tau^\mp)/\Gamma_{\text{total}}$	$<7.2 \times 10^{-5}$ , CL = 90%
$\Gamma(\tau^- \rightarrow \mu^- \mu^+ \mu^-)/\Gamma_{\text{total}}$	$<2.1 \times 10^{-8}$ , CL = 90%	$\Gamma(B^+ \rightarrow K^+ e^+ \mu^-)/\Gamma_{\text{total}}$	$<7.0 \times 10^{-9}$ , CL = 90%
$\Gamma(\tau^- \rightarrow e^- \pi^+ \pi^-)/\Gamma_{\text{total}}$	$<2.3 \times 10^{-8}$ , CL = 90%	$\Gamma(B^+ \rightarrow K^+ e^- \mu^+)/\Gamma_{\text{total}}$	$<6.4 \times 10^{-9}$ , CL = 90%
$\Gamma(\tau^- \rightarrow \mu^- \pi^+ \pi^-)/\Gamma_{\text{total}}$	$<2.1 \times 10^{-8}$ , CL = 90%	$\Gamma(B^+ \rightarrow K^+ e^\pm \mu^\mp)/\Gamma_{\text{total}}$	$<9.1 \times 10^{-8}$ , CL = 90%
$\Gamma(\tau^- \rightarrow e^- \pi^+ K^-)/\Gamma_{\text{total}}$	$<3.7 \times 10^{-8}$ , CL = 90%	$\Gamma(B^+ \rightarrow K^+ e^+ \tau^-)/\Gamma_{\text{total}}$	$<4.3 \times 10^{-5}$ , CL = 90%
$\Gamma(\tau^- \rightarrow e^- \pi^- K^+)/\Gamma_{\text{total}}$	$<3.1 \times 10^{-8}$ , CL = 90%	$\Gamma(B^+ \rightarrow K^+ e^- \tau^+)/\Gamma_{\text{total}}$	$<1.5 \times 10^{-5}$ , CL = 90%
$\Gamma(\tau^- \rightarrow e^- K_S^0 K_S^0)/\Gamma_{\text{total}}$	$<7.1 \times 10^{-8}$ , CL = 90%	$\Gamma(B^+ \rightarrow K^+ e^\pm \tau^\mp)/\Gamma_{\text{total}}$	$<3.0 \times 10^{-5}$ , CL = 90%
$\Gamma(\tau^- \rightarrow e^- K^+ K^-)/\Gamma_{\text{total}}$	$<3.4 \times 10^{-8}$ , CL = 90%	$\Gamma(B^+ \rightarrow K^+ \mu^+ \tau^-)/\Gamma_{\text{total}}$	$<4.5 \times 10^{-5}$ , CL = 90%
$\Gamma(\tau^- \rightarrow \mu^- \pi^+ K^-)/\Gamma_{\text{total}}$	$<8.6 \times 10^{-8}$ , CL = 90%	$\Gamma(B^+ \rightarrow K^+ \mu^- \tau^+)/\Gamma_{\text{total}}$	$<2.8 \times 10^{-5}$ , CL = 90%
$\Gamma(\tau^- \rightarrow \mu^- \pi^- K^+)/\Gamma_{\text{total}}$	$<4.5 \times 10^{-8}$ , CL = 90%	$\Gamma(B^+ \rightarrow K^+ \mu^\pm \tau^\mp)/\Gamma_{\text{total}}$	$<4.8 \times 10^{-5}$ , CL = 90%
$\Gamma(\tau^- \rightarrow \mu^- K_S^0 K_S^0)/\Gamma_{\text{total}}$	$<8.0 \times 10^{-8}$ , CL = 90%	$\Gamma(B^+ \rightarrow K^*(892)^+ e^+ \mu^-)/\Gamma_{\text{total}}$	$<1.3 \times 10^{-6}$ , CL = 90%
$\Gamma(\tau^- \rightarrow \mu^- K^+ K^-)/\Gamma_{\text{total}}$	$<4.4 \times 10^{-8}$ , CL = 90%	$\Gamma(B^+ \rightarrow K^*(892)^+ e^- \mu^+)/\Gamma_{\text{total}}$	$<9.9 \times 10^{-7}$ , CL = 90%
$\Gamma(\tau^- \rightarrow e^- \pi^0 \pi^0)/\Gamma_{\text{total}}$	$<6.5 \times 10^{-6}$ , CL = 90%	$\Gamma(B^+ \rightarrow K^*(892)^+ e^\pm \mu^\mp)/\Gamma_{\text{total}}$	$<1.4 \times 10^{-6}$ , CL = 90%
$\Gamma(\tau^- \rightarrow \mu^- \pi^0 \pi^0)/\Gamma_{\text{total}}$	$<1.4 \times 10^{-5}$ , CL = 90%	$\Gamma(B^0 \rightarrow e^\pm \mu^\mp)/\Gamma_{\text{total}}$	[o] $<1.0 \times 10^{-9}$ , CL = 90%
$\Gamma(\tau^- \rightarrow e^- \eta \eta)/\Gamma_{\text{total}}$	$<3.5 \times 10^{-5}$ , CL = 90%	$\Gamma(B^0 \rightarrow \pi^0 e^\pm \mu^\mp)/\Gamma_{\text{total}}$	$<1.4 \times 10^{-7}$ , CL = 90%
$\Gamma(\tau^- \rightarrow \mu^- \eta \eta)/\Gamma_{\text{total}}$	$<6.0 \times 10^{-5}$ , CL = 90%	$\Gamma(B^0 \rightarrow K^0 e^\pm \mu^\mp)/\Gamma_{\text{total}}$	$<2.7 \times 10^{-7}$ , CL = 90%
$\Gamma(\tau^- \rightarrow e^- \pi^0 \eta)/\Gamma_{\text{total}}$	$<2.4 \times 10^{-5}$ , CL = 90%	$\Gamma(B^0 \rightarrow K^*(892)^0 e^+ \mu^-)/\Gamma_{\text{total}}$	$<1.6 \times 10^{-7}$ , CL = 90%
$\Gamma(\tau^- \rightarrow \mu^- \pi^0 \eta)/\Gamma_{\text{total}}$	$<2.2 \times 10^{-5}$ , CL = 90%	$\Gamma(B^0 \rightarrow K^*(892)^0 e^- \mu^+)/\Gamma_{\text{total}}$	$<1.2 \times 10^{-7}$ , CL = 90%
$\Gamma(\tau^- \rightarrow e^- \text{light boson})/\Gamma_{\text{total}}$	$<2.7 \times 10^{-3}$ , CL = 95%	$\Gamma(B^0 \rightarrow K^*(892)^0 e^\pm \mu^\mp)/\Gamma_{\text{total}}$	$<1.8 \times 10^{-7}$ , CL = 90%
$\Gamma(\tau^- \rightarrow \mu^- \text{light boson})/\Gamma_{\text{total}}$	$<5 \times 10^{-3}$ , CL = 95%	$\Gamma(B^0 \rightarrow e^\pm \tau^\mp)/\Gamma_{\text{total}}$	[o] $<2.8 \times 10^{-5}$ , CL = 90%
<b>LEPTON FAMILY NUMBER VIOLATION IN NEUTRINOS</b>			
$\sin^2(\theta_{12})$	$0.307 \pm 0.013$	$\Gamma(B^0 \rightarrow \mu^\pm \tau^\mp)/\Gamma_{\text{total}}$	[o] $<1.4 \times 10^{-5}$ , CL = 95%
$\Delta m_{21}^2$	$(7.53 \pm 0.18) \times 10^{-5} \text{ eV}^2$	$\Gamma(B \rightarrow s e^\pm \mu^\mp)/\Gamma_{\text{total}}$	[o] $<2.2 \times 10^{-5}$ , CL = 90%
$\sin^2(\theta_{23})$ (Normal order)	$0.545 \pm 0.021$	$\Gamma(B \rightarrow \pi e^\pm \mu^\mp)/\Gamma_{\text{total}}$	$<9.2 \times 10^{-8}$ , CL = 90%
$\Delta m_{32}^2$ (Inverted order)	$(-2.546 \pm 0.034 \text{ } -0.040) \times 10^{-3} \text{ eV}^2$	$\Gamma(B \rightarrow \rho e^\pm \mu^\mp)/\Gamma_{\text{total}}$	$<3.2 \times 10^{-6}$ , CL = 90%
$\Delta m_{32}^2$ (Normal order)	$(2.453 \pm 0.034) \times 10^{-3} \text{ eV}^2$	$\Gamma(B \rightarrow K e^\pm \mu^\mp)/\Gamma_{\text{total}}$	$<3.8 \times 10^{-8}$ , CL = 90%
$\sin^2(\theta_{13})$	$(2.18 \pm 0.07) \times 10^{-2}$	$\Gamma(B \rightarrow K^*(892) e^\pm \mu^\mp)/\Gamma_{\text{total}}$	$<5.1 \times 10^{-7}$ , CL = 90%
$\Gamma(\pi^+ \rightarrow \mu^+ \nu_e)/\Gamma_{\text{total}}$	[q] $<8.0 \times 10^{-3}$ , CL = 90%	$\Gamma(B_S^0 \rightarrow e^\pm \mu^\mp)/\Gamma_{\text{total}}$	[o] $<5.4 \times 10^{-9}$ , CL = 90%
$\Gamma(\pi^+ \rightarrow \mu^- e^+ e^+ \nu)/\Gamma_{\text{total}}$	$<1.6 \times 10^{-6}$ , CL = 90%	$\Gamma(J/\psi(1S) \rightarrow e^\pm \mu^\mp)/\Gamma_{\text{total}}$	$<1.6 \times 10^{-7}$ , CL = 90%
$\Gamma(\pi^0 \rightarrow \mu^+ e^-)/\Gamma_{\text{total}}$	$<3.8 \times 10^{-10}$ , CL = 90%	$\Gamma(J/\psi(1S) \rightarrow e^\pm \tau^\mp)/\Gamma_{\text{total}}$	$<8.3 \times 10^{-6}$ , CL = 90%
$\Gamma(\pi^0 \rightarrow \mu^- e^+)/\Gamma_{\text{total}}$	$<3.4 \times 10^{-9}$ , CL = 90%	$\Gamma(J/\psi(1S) \rightarrow \mu^\pm \tau^\mp)/\Gamma_{\text{total}}$	$<2.0 \times 10^{-6}$ , CL = 90%
$\Gamma(\pi^0 \rightarrow \mu^+ e^- + \mu^- e^+)/\Gamma_{\text{total}}$	$<3.6 \times 10^{-10}$ , CL = 90%	$\Gamma(\Upsilon(1S) \rightarrow \mu^\pm \tau^\mp)/\Gamma_{\text{total}}$	$<6.0 \times 10^{-6}$ , CL = 95%
$\Gamma(\eta \rightarrow \mu^+ e^- + \mu^- e^+)/\Gamma_{\text{total}}$	$<6 \times 10^{-6}$ , CL = 90%	$\Gamma(\Upsilon(2S) \rightarrow e^\pm \tau^\mp)/\Gamma_{\text{total}}$	$<3.2 \times 10^{-6}$ , CL = 90%
$\Gamma(\eta'(958) \rightarrow e \mu)/\Gamma_{\text{total}}$	$<4.7 \times 10^{-4}$ , CL = 90%	$\Gamma(\Upsilon(2S) \rightarrow \mu^\pm \tau^\mp)/\Gamma_{\text{total}}$	$<3.3 \times 10^{-6}$ , CL = 90%
$\Gamma(\phi(1020) \rightarrow e^\pm \mu^\mp)/\Gamma_{\text{total}}$	$<2 \times 10^{-6}$ , CL = 90%	$\Gamma(\Upsilon(3S) \rightarrow e^\pm \tau^\mp)/\Gamma_{\text{total}}$	$<4.2 \times 10^{-6}$ , CL = 90%
$\Gamma(K^+ \rightarrow \mu^- \nu e^+ e^+)/\Gamma_{\text{total}}$	$<2.1 \times 10^{-8}$ , CL = 90%	$\Gamma(\Upsilon(3S) \rightarrow \mu^\pm \tau^\mp)/\Gamma_{\text{total}}$	$<3.1 \times 10^{-6}$ , CL = 90%
$\Gamma(K^+ \rightarrow \mu^+ \nu_e)/\Gamma_{\text{total}}$	[q] $<4 \times 10^{-3}$ , CL = 90%	$\Gamma(\Lambda_c^+ \rightarrow p e^+ \mu^-)/\Gamma_{\text{total}}$	$<9.9 \times 10^{-6}$ , CL = 90%
$\Gamma(K^+ \rightarrow \pi^+ \mu^+ e^-)/\Gamma_{\text{total}}$	$<1.3 \times 10^{-11}$ , CL = 90%	$\Gamma(\Lambda_c^+ \rightarrow p e^- \mu^+)/\Gamma_{\text{total}}$	$<1.9 \times 10^{-5}$ , CL = 90%
$\Gamma(K^+ \rightarrow \pi^+ \mu^- e^+)/\Gamma_{\text{total}}$	$<5.2 \times 10^{-10}$ , CL = 90%		
$\Gamma(K_L^0 \rightarrow e^\pm \mu^\mp)/\Gamma_{\text{total}}$	[o] $<4.7 \times 10^{-12}$ , CL = 90%		
$\Gamma(K_L^0 \rightarrow e^\pm e^\pm \mu^\mp \mu^\mp)/\Gamma_{\text{total}}$	[o] $<4.12 \times 10^{-11}$ , CL = 90%		
$\Gamma(K_L^0 \rightarrow \pi^0 \mu^\pm e^\mp)/\Gamma_{\text{total}}$	[o] $<7.6 \times 10^{-11}$ , CL = 90%		
$\Gamma(K_L^0 \rightarrow \pi^0 \pi^0 \mu^\pm e^\mp)/\Gamma_{\text{total}}$	$<1.7 \times 10^{-10}$ , CL = 90%		
$\Gamma(D^+ \rightarrow \pi^+ e^+ \mu^-)/\Gamma_{\text{total}}$	$<2.9 \times 10^{-6}$ , CL = 90%		

Unless otherwise stated, limits are given at the 90% confidence level, while errors are given as  $\pm 1$  standard deviation.



# Tests of Conservation Laws

## TOTAL LEPTON NUMBER

Violation of total lepton number conservation also implies violation of lepton family number conservation.

$\Gamma(Z \rightarrow \rho e)/\Gamma_{\text{total}}$	$<1.8 \times 10^{-6}$ , CL = 95%
$\Gamma(Z \rightarrow \rho \mu)/\Gamma_{\text{total}}$	$<1.8 \times 10^{-6}$ , CL = 95%
limit on $\mu^- \rightarrow e^+$ conversion	
$\sigma(\mu^- 32\text{S} \rightarrow e^+ 32\text{Si}^*) / \sigma(\mu^- 32\text{S} \rightarrow \nu_\mu 32\text{P}^*)$	$<9 \times 10^{-10}$ , CL = 90%
$\sigma(\mu^- 127\text{I} \rightarrow e^+ 127\text{Sb}^*) / \sigma(\mu^- 127\text{I} \rightarrow \text{anything})$	$<3 \times 10^{-10}$ , CL = 90%
$\sigma(\mu^- \text{Ti} \rightarrow e^+ \text{Ca}) / \sigma(\mu^- \text{Ti} \rightarrow \text{capture})$	$<3.6 \times 10^{-11}$ , CL = 90%
$\Gamma(\tau^- \rightarrow e^+ \pi^- \pi^-)/\Gamma_{\text{total}}$	$<2.0 \times 10^{-8}$ , CL = 90%
$\Gamma(\tau^- \rightarrow \mu^+ \pi^- \pi^-)/\Gamma_{\text{total}}$	$<3.9 \times 10^{-8}$ , CL = 90%
$\Gamma(\tau^- \rightarrow e^+ \pi^- K^-)/\Gamma_{\text{total}}$	$<3.2 \times 10^{-8}$ , CL = 90%
$\Gamma(\tau^- \rightarrow e^+ K^- K^-)/\Gamma_{\text{total}}$	$<3.3 \times 10^{-8}$ , CL = 90%
$\Gamma(\tau^- \rightarrow \mu^+ \pi^- K^-)/\Gamma_{\text{total}}$	$<4.8 \times 10^{-8}$ , CL = 90%
$\Gamma(\tau^- \rightarrow \mu^+ K^- K^-)/\Gamma_{\text{total}}$	$<4.7 \times 10^{-8}$ , CL = 90%
$\Gamma(\tau^- \rightarrow \rho \mu^- \mu^-)/\Gamma_{\text{total}}$	$<4.4 \times 10^{-7}$ , CL = 90%
$\Gamma(\tau^- \rightarrow \bar{p} \mu^+ \mu^-)/\Gamma_{\text{total}}$	$<3.3 \times 10^{-7}$ , CL = 90%
$\Gamma(\tau^- \rightarrow \bar{p} \gamma)/\Gamma_{\text{total}}$	$<3.5 \times 10^{-6}$ , CL = 90%
$\Gamma(\tau^- \rightarrow \bar{p} \pi^0)/\Gamma_{\text{total}}$	$<1.5 \times 10^{-5}$ , CL = 90%
$\Gamma(\tau^- \rightarrow \bar{p} 2\pi^0)/\Gamma_{\text{total}}$	$<3.3 \times 10^{-5}$ , CL = 90%
$\Gamma(\tau^- \rightarrow \bar{p} \eta)/\Gamma_{\text{total}}$	$<8.9 \times 10^{-6}$ , CL = 90%
$\Gamma(\tau^- \rightarrow \bar{p} \pi^0 \eta)/\Gamma_{\text{total}}$	$<2.7 \times 10^{-5}$ , CL = 90%
$\Gamma(\tau^- \rightarrow \Lambda \pi^-)/\Gamma_{\text{total}}$	$<7.2 \times 10^{-8}$ , CL = 90%
$\Gamma(\tau^- \rightarrow \bar{\Lambda} \pi^-)/\Gamma_{\text{total}}$	$<1.4 \times 10^{-7}$ , CL = 90%
$t_{1/2}(^{76}\text{Ge} \rightarrow ^{76}\text{Se} + 2 e^-)$	$>9.0 \times 10^{25}$ yr, CL = 90%
$t_{1/2}(^{136}\text{Xe} \rightarrow ^{136}\text{Ba} + 2 e^-)$	$>10.7 \times 10^{25}$ yr, CL = 90%
$t_{1/2}(^{130}\text{Te} \rightarrow ^{130}\text{Xe} + 2 e^-)$	$>1.5 \times 10^{25}$ yr, CL = 90%
$\Gamma(\pi^+ \rightarrow \mu^+ \bar{\nu}_e)/\Gamma_{\text{total}}$	[q] $<1.5 \times 10^{-3}$ , CL = 90%
$\Gamma(K^+ \rightarrow \pi^- \mu^+ e^+)/\Gamma_{\text{total}}$	$<5.0 \times 10^{-10}$ , CL = 90%
$\Gamma(K^+ \rightarrow \pi^- e^+ e^+)/\Gamma_{\text{total}}$	$<2.2 \times 10^{-10}$ , CL = 90%
$\Gamma(K^+ \rightarrow \pi^- \mu^+ \mu^+)/\Gamma_{\text{total}}$	[q] $<4.2 \times 10^{-11}$ , CL = 90%
$\Gamma(K^+ \rightarrow \mu^+ \bar{\nu}_e)/\Gamma_{\text{total}}$	[q] $<3.3 \times 10^{-3}$ , CL = 90%
$\Gamma(K^+ \rightarrow \pi^0 e^+ \bar{\nu}_e)/\Gamma_{\text{total}}$	$<3 \times 10^{-3}$ , CL = 90%
$\Gamma(D^+ \rightarrow \pi^- 2e^+)/\Gamma_{\text{total}}$	$<1.1 \times 10^{-6}$ , CL = 90%
$\Gamma(D^+ \rightarrow \pi^- 2\mu^+)/\Gamma_{\text{total}}$	$<2.2 \times 10^{-8}$ , CL = 90%
$\Gamma(D^+ \rightarrow \pi^- e^+ \mu^+)/\Gamma_{\text{total}}$	$<2.0 \times 10^{-6}$ , CL = 90%
$\Gamma(D^+ \rightarrow \rho^- 2\mu^+)/\Gamma_{\text{total}}$	$<5.6 \times 10^{-4}$ , CL = 90%
$\Gamma(D^+ \rightarrow K^- 2e^+)/\Gamma_{\text{total}}$	$<9 \times 10^{-7}$ , CL = 90%
$\Gamma(D^+ \rightarrow K^- 2\mu^+)/\Gamma_{\text{total}}$	$<1.0 \times 10^{-5}$ , CL = 90%
$\Gamma(D^+ \rightarrow K^- e^+ \mu^+)/\Gamma_{\text{total}}$	$<1.9 \times 10^{-6}$ , CL = 90%
$\Gamma(D^+ \rightarrow K^*(892)^- 2\mu^+)/\Gamma_{\text{total}}$	$<8.5 \times 10^{-4}$ , CL = 90%
$\Gamma(D^0 \rightarrow 2\pi^- 2e^+ + \text{c.c.})/\Gamma_{\text{total}}$	$<1.12 \times 10^{-4}$ , CL = 90%
$\Gamma(D^0 \rightarrow 2\pi^- 2\mu^+ + \text{c.c.})/\Gamma_{\text{total}}$	$<2.9 \times 10^{-5}$ , CL = 90%
$\Gamma(D^0 \rightarrow K^- \pi^- 2\mu^+ + \text{c.c.})/\Gamma_{\text{total}}$	$<3.9 \times 10^{-4}$ , CL = 90%
$\Gamma(D^0 \rightarrow 2K^- 2e^+ + \text{c.c.})/\Gamma_{\text{total}}$	$<1.52 \times 10^{-4}$ , CL = 90%
$\Gamma(D^0 \rightarrow 2K^- 2\mu^+ + \text{c.c.})/\Gamma_{\text{total}}$	$<9.4 \times 10^{-5}$ , CL = 90%
$\Gamma(D^0 \rightarrow \pi^- \pi^- e^+ \mu^+ + \text{c.c.})/\Gamma_{\text{total}}$	$<7.9 \times 10^{-5}$ , CL = 90%
$\Gamma(D^0 \rightarrow K^- \pi^- e^+ \mu^+ + \text{c.c.})/\Gamma_{\text{total}}$	$<2.18 \times 10^{-4}$ , CL = 90%
$\Gamma(D^0 \rightarrow 2K^- e^+ \mu^+ + \text{c.c.})/\Gamma_{\text{total}}$	$<5.7 \times 10^{-5}$ , CL = 90%
$\Gamma(D^0 \rightarrow \rho e^-)/\Gamma_{\text{total}}$	[r] $<1.0 \times 10^{-5}$ , CL = 90%
$\Gamma(D^0 \rightarrow \bar{p} e^+)/\Gamma_{\text{total}}$	[s] $<1.1 \times 10^{-5}$ , CL = 90%
$\Gamma(D_S^+ \rightarrow \pi^- 2e^+)/\Gamma_{\text{total}}$	$<4.1 \times 10^{-6}$ , CL = 90%
$\Gamma(D_S^+ \rightarrow \pi^- 2\mu^+)/\Gamma_{\text{total}}$	$<1.2 \times 10^{-7}$ , CL = 90%
$\Gamma(D_S^+ \rightarrow \pi^- e^+ \mu^+)/\Gamma_{\text{total}}$	$<8.4 \times 10^{-6}$ , CL = 90%
$\Gamma(D_S^+ \rightarrow K^- 2e^+)/\Gamma_{\text{total}}$	$<5.2 \times 10^{-6}$ , CL = 90%
$\Gamma(D_S^+ \rightarrow K^- 2\mu^+)/\Gamma_{\text{total}}$	$<1.3 \times 10^{-5}$ , CL = 90%
$\Gamma(D_S^+ \rightarrow K^- e^+ \mu^+)/\Gamma_{\text{total}}$	$<6.1 \times 10^{-6}$ , CL = 90%
$\Gamma(D_S^+ \rightarrow K^*(892)^- 2\mu^+)/\Gamma_{\text{total}}$	$<1.4 \times 10^{-3}$ , CL = 90%
$\Gamma(B^+ \rightarrow \pi^- e^+ e^+)/\Gamma_{\text{total}}$	$<2.3 \times 10^{-8}$ , CL = 90%
$\Gamma(B^+ \rightarrow \pi^- \mu^+ \mu^+)/\Gamma_{\text{total}}$	$<4.0 \times 10^{-9}$ , CL = 95%
$\Gamma(B^+ \rightarrow \pi^- e^+ \mu^+)/\Gamma_{\text{total}}$	$<1.5 \times 10^{-7}$ , CL = 90%
$\Gamma(B^+ \rightarrow \rho^- e^+ e^+)/\Gamma_{\text{total}}$	$<1.7 \times 10^{-7}$ , CL = 90%
$\Gamma(B^+ \rightarrow \rho^- \mu^+ \mu^+)/\Gamma_{\text{total}}$	$<4.2 \times 10^{-7}$ , CL = 90%
$\Gamma(B^+ \rightarrow \rho^- e^+ \mu^+)/\Gamma_{\text{total}}$	$<4.7 \times 10^{-7}$ , CL = 90%
$\Gamma(B^+ \rightarrow K^- e^+ e^+)/\Gamma_{\text{total}}$	$<3.0 \times 10^{-8}$ , CL = 90%
$\Gamma(B^+ \rightarrow K^- \mu^+ \mu^+)/\Gamma_{\text{total}}$	$<4.1 \times 10^{-8}$ , CL = 90%

$\Gamma(B^+ \rightarrow K^- e^+ \mu^+)/\Gamma_{\text{total}}$	$<1.6 \times 10^{-7}$ , CL = 90%
$\Gamma(B^+ \rightarrow K^*(892)^- e^+ e^+)/\Gamma_{\text{total}}$	$<4.0 \times 10^{-7}$ , CL = 90%
$\Gamma(B^+ \rightarrow K^*(892)^- \mu^+ \mu^+)/\Gamma_{\text{total}}$	$<5.9 \times 10^{-7}$ , CL = 90%
$\Gamma(B^+ \rightarrow K^*(892)^- e^+ \mu^+)/\Gamma_{\text{total}}$	$<3.0 \times 10^{-7}$ , CL = 90%
$\Gamma(B^+ \rightarrow D^- e^+ e^+)/\Gamma_{\text{total}}$	$<2.6 \times 10^{-6}$ , CL = 90%
$\Gamma(B^+ \rightarrow D^- e^+ \mu^+)/\Gamma_{\text{total}}$	$<1.8 \times 10^{-6}$ , CL = 90%
$\Gamma(B^+ \rightarrow D^- \mu^+ \mu^+)/\Gamma_{\text{total}}$	$<6.9 \times 10^{-7}$ , CL = 95%
$\Gamma(B^+ \rightarrow D^{*-} \mu^+ \mu^+)/\Gamma_{\text{total}}$	$<2.4 \times 10^{-6}$ , CL = 95%
$\Gamma(B^+ \rightarrow D_S^- \mu^+ \mu^+)/\Gamma_{\text{total}}$	$<5.8 \times 10^{-7}$ , CL = 95%
$\Gamma(B^+ \rightarrow \bar{D}^0 \pi^- \mu^+ \mu^+)/\Gamma_{\text{total}}$	$<1.5 \times 10^{-6}$ , CL = 95%
$\Gamma(B^+ \rightarrow \Lambda^0 \mu^+)/\Gamma_{\text{total}}$	$<6 \times 10^{-8}$ , CL = 90%
$\Gamma(B^+ \rightarrow \Lambda^0 e^+)/\Gamma_{\text{total}}$	$<3.2 \times 10^{-8}$ , CL = 90%
$\Gamma(B^+ \rightarrow \bar{\Lambda}^0 \mu^+)/\Gamma_{\text{total}}$	$<6 \times 10^{-8}$ , CL = 90%
$\Gamma(B^+ \rightarrow \bar{\Lambda}^0 e^+)/\Gamma_{\text{total}}$	$<8 \times 10^{-8}$ , CL = 90%
$\Gamma(B^0 \rightarrow \Lambda_C^+ \mu^-)/\Gamma_{\text{total}}$	$<1.4 \times 10^{-6}$ , CL = 90%
$\Gamma(B^0 \rightarrow \Lambda_C^+ e^-)/\Gamma_{\text{total}}$	$<4 \times 10^{-6}$ , CL = 90%
$\Gamma(\Lambda \rightarrow \pi^+ e^-)/\Gamma_{\text{total}}$	$<6 \times 10^{-7}$ , CL = 90%
$\Gamma(\Lambda \rightarrow \pi^+ \mu^-)/\Gamma_{\text{total}}$	$<6 \times 10^{-7}$ , CL = 90%
$\Gamma(\Lambda \rightarrow \pi^- e^+)/\Gamma_{\text{total}}$	$<4 \times 10^{-7}$ , CL = 90%
$\Gamma(\Lambda \rightarrow \pi^- \mu^+)/\Gamma_{\text{total}}$	$<6 \times 10^{-7}$ , CL = 90%
$\Gamma(\Lambda \rightarrow K^+ e^-)/\Gamma_{\text{total}}$	$<2 \times 10^{-6}$ , CL = 90%
$\Gamma(\Lambda \rightarrow K^+ \mu^-)/\Gamma_{\text{total}}$	$<3 \times 10^{-6}$ , CL = 90%
$\Gamma(\Lambda \rightarrow K^- e^+)/\Gamma_{\text{total}}$	$<2 \times 10^{-6}$ , CL = 90%
$\Gamma(\Lambda \rightarrow K^- \mu^+)/\Gamma_{\text{total}}$	$<3 \times 10^{-6}$ , CL = 90%
$\Gamma(\Lambda \rightarrow K_S^0 \nu)/\Gamma_{\text{total}}$	$<2 \times 10^{-5}$ , CL = 90%
$\Gamma(\Xi^- \rightarrow p \mu^- \mu^-)/\Gamma_{\text{total}}$	$<4 \times 10^{-8}$ , CL = 90%
$\Gamma(\Lambda_C^+ \rightarrow \bar{p} 2e^+)/\Gamma_{\text{total}}$	$<2.7 \times 10^{-6}$ , CL = 90%
$\Gamma(\Lambda_C^+ \rightarrow \bar{p} 2\mu^+)/\Gamma_{\text{total}}$	$<9.4 \times 10^{-6}$ , CL = 90%
$\Gamma(\Lambda_C^+ \rightarrow \bar{p} e^+ \mu^+)/\Gamma_{\text{total}}$	$<1.6 \times 10^{-5}$ , CL = 90%
$\Gamma(\Lambda_C^+ \rightarrow \Sigma^- \mu^+ \mu^+)/\Gamma_{\text{total}}$	$<7.0 \times 10^{-4}$ , CL = 90%

## BARYON NUMBER

$\Gamma(Z \rightarrow \rho e)/\Gamma_{\text{total}}$	$<1.8 \times 10^{-6}$ , CL = 95%
$\Gamma(Z \rightarrow \rho \mu)/\Gamma_{\text{total}}$	$<1.8 \times 10^{-6}$ , CL = 95%
$\Gamma(\tau^- \rightarrow \rho \mu^- \mu^-)/\Gamma_{\text{total}}$	$<4.4 \times 10^{-7}$ , CL = 90%
$\Gamma(\tau^- \rightarrow \bar{p} \mu^+ \mu^-)/\Gamma_{\text{total}}$	$<3.3 \times 10^{-7}$ , CL = 90%
$\Gamma(\tau^- \rightarrow \bar{p} \gamma)/\Gamma_{\text{total}}$	$<3.5 \times 10^{-6}$ , CL = 90%
$\Gamma(\tau^- \rightarrow \bar{p} \pi^0)/\Gamma_{\text{total}}$	$<1.5 \times 10^{-5}$ , CL = 90%
$\Gamma(\tau^- \rightarrow \bar{p} 2\pi^0)/\Gamma_{\text{total}}$	$<3.3 \times 10^{-5}$ , CL = 90%
$\Gamma(\tau^- \rightarrow \bar{p} \eta)/\Gamma_{\text{total}}$	$<8.9 \times 10^{-6}$ , CL = 90%
$\Gamma(\tau^- \rightarrow \bar{p} \pi^0 \eta)/\Gamma_{\text{total}}$	$<2.7 \times 10^{-5}$ , CL = 90%
$\Gamma(\tau^- \rightarrow \Lambda \pi^-)/\Gamma_{\text{total}}$	$<7.2 \times 10^{-8}$ , CL = 90%
$\Gamma(\tau^- \rightarrow \bar{\Lambda} \pi^-)/\Gamma_{\text{total}}$	$<1.4 \times 10^{-7}$ , CL = 90%
$\Gamma(D^0 \rightarrow \rho e^-)/\Gamma_{\text{total}}$	[r] $<1.0 \times 10^{-5}$ , CL = 90%
$\Gamma(D^0 \rightarrow \bar{p} e^+)/\Gamma_{\text{total}}$	[s] $<1.1 \times 10^{-5}$ , CL = 90%
$\Gamma(B^+ \rightarrow \Lambda^0 \mu^+)/\Gamma_{\text{total}}$	$<6 \times 10^{-8}$ , CL = 90%
$\Gamma(B^+ \rightarrow \Lambda^0 e^+)/\Gamma_{\text{total}}$	$<3.2 \times 10^{-8}$ , CL = 90%
$\Gamma(B^+ \rightarrow \bar{\Lambda}^0 \mu^+)/\Gamma_{\text{total}}$	$<6 \times 10^{-8}$ , CL = 90%
$\Gamma(B^+ \rightarrow \bar{\Lambda}^0 e^+)/\Gamma_{\text{total}}$	$<8 \times 10^{-8}$ , CL = 90%
$\Gamma(B^0 \rightarrow \Lambda_C^+ \mu^-)/\Gamma_{\text{total}}$	$<1.4 \times 10^{-6}$ , CL = 90%
$\Gamma(B^0 \rightarrow \Lambda_C^+ e^-)/\Gamma_{\text{total}}$	$<4 \times 10^{-6}$ , CL = 90%
$\rho$ mean life	[t] $>3.6 \times 10^{29}$ years, CL = 90%
A few examples of proton or bound neutron decay follow. For limits on many other nucleon decay channels, see the Baryon Summary Table.	
$\tau(N \rightarrow e^+ \pi)$	$> 5300 (n), > 16000 (p) \times 10^{30}$ years, CL = 90%
$\tau(N \rightarrow \mu^+ \pi)$	$> 3500 (n), > 7700 (p) \times 10^{30}$ years, CL = 90%
$\tau(N \rightarrow e^+ K)$	$> 17 (n), > 1000 (p) \times 10^{30}$ years, CL = 90%
$\tau(N \rightarrow \mu^+ K)$	$> 26 (n), > 16000 (p) \times 10^{30}$ years, CL = 90%
limit on $n\bar{n}$ oscillations (free $n$ )	$>0.86 \times 10^8$ s, CL = 90%
limit on $n\bar{n}$ oscillations (bound $n$ )	[u] $>2.7 \times 10^8$ s, CL = 90%
$\Gamma(\Lambda \rightarrow \pi^+ e^-)/\Gamma_{\text{total}}$	$<6 \times 10^{-7}$ , CL = 90%
$\Gamma(\Lambda \rightarrow \pi^+ \mu^-)/\Gamma_{\text{total}}$	$<6 \times 10^{-7}$ , CL = 90%
$\Gamma(\Lambda \rightarrow \pi^- e^+)/\Gamma_{\text{total}}$	$<4 \times 10^{-7}$ , CL = 90%
$\Gamma(\Lambda \rightarrow \pi^- \mu^+)/\Gamma_{\text{total}}$	$<6 \times 10^{-7}$ , CL = 90%
$\Gamma(\Lambda \rightarrow K^+ e^-)/\Gamma_{\text{total}}$	$<2 \times 10^{-6}$ , CL = 90%
$\Gamma(\Lambda \rightarrow K^+ \mu^-)/\Gamma_{\text{total}}$	$<3 \times 10^{-6}$ , CL = 90%
$\Gamma(\Lambda \rightarrow K^- e^+)/\Gamma_{\text{total}}$	$<2 \times 10^{-6}$ , CL = 90%

$\Gamma(\Lambda \rightarrow K^- \mu^+)/\Gamma_{\text{total}}$	$< 3 \times 10^{-6}$ , CL = 90%
$\Gamma(\Lambda \rightarrow K_S^0 \nu)/\Gamma_{\text{total}}$	$< 2 \times 10^{-5}$ , CL = 90%
$\Gamma(\Lambda \rightarrow \bar{p} \pi^+)/\Gamma_{\text{total}}$	$< 9 \times 10^{-7}$ , CL = 90%
$\Gamma(\Lambda_C^+ \rightarrow \bar{p} 2e^+)/\Gamma_{\text{total}}$	$< 2.7 \times 10^{-6}$ , CL = 90%
$\Gamma(\Lambda_C^+ \rightarrow \bar{p} 2\mu^+)/\Gamma_{\text{total}}$	$< 9.4 \times 10^{-6}$ , CL = 90%
$\Gamma(\Lambda_C^+ \rightarrow \bar{p} e^+ \mu^+)/\Gamma_{\text{total}}$	$< 1.6 \times 10^{-5}$ , CL = 90%

**ELECTRIC CHARGE (Q)**

$\gamma$ charge (mixed)	$< 1 \times 10^{-46} e$
$\gamma$ charge (single)	$< 1 \times 10^{-35} e$
$e \rightarrow \nu_e \gamma$ and astrophysical limits	[V] $> 6.6 \times 10^{28}$ yr, CL = 90%
$\nu$ charge	$< 4 \times 10^{-35} e$ , CL = 95%
$ q_p + q_e /e$	[X] $< 1 \times 10^{-21}$
$n$ charge	$(-0.2 \pm 0.8) \times 10^{-21} e$
$\Gamma(n \rightarrow p \nu_e \bar{\nu}_e)/\Gamma_{\text{total}}$	$< 8 \times 10^{-27}$ , CL = 68%

 **$\Delta S = \Delta Q$  RULE**

Violations allowed in second-order weak interactions.

$\Gamma(K^+ \rightarrow \pi^+ \pi^+ e^- \bar{\nu}_e)/\Gamma_{\text{total}}$	$< 1.3 \times 10^{-8}$ , CL = 90%
$\Gamma(K^+ \rightarrow \pi^+ \pi^+ \mu^- \bar{\nu}_\mu)/\Gamma_{\text{total}}$	$< 3.0 \times 10^{-6}$ , CL = 95%
Re( $\chi_+$ ), $K_{e3}$ parameter	$(-0.9 \pm 3.0) \times 10^{-3}$
$x = A(\bar{K}^0 \rightarrow \pi^- \ell^+ \nu)/A(K^0 \rightarrow \pi^- \ell^+ \nu) = A(\Delta S = -\Delta Q)/A(\Delta S = \Delta Q)$	
real part of $x$	$-0.002 \pm 0.006$
imaginary part of $x$	$0.0012 \pm 0.0021$
$\Gamma(\Sigma^+ \rightarrow n \ell^+ \nu)/\Gamma(\Sigma^- \rightarrow n \ell^- \bar{\nu})$	$< 0.043$
$\Gamma(\Sigma^+ \rightarrow n e^+ \nu_e)/\Gamma_{\text{total}}$	$< 5 \times 10^{-6}$ , CL = 90%
$\Gamma(\Sigma^+ \rightarrow n \mu^+ \nu_\mu)/\Gamma_{\text{total}}$	$< 3.0 \times 10^{-5}$ , CL = 90%
$\Gamma(\Xi^0 \rightarrow \Sigma^- e^+ \nu_e)/\Gamma_{\text{total}}$	$< 9 \times 10^{-4}$ , CL = 90%
$\Gamma(\Xi^0 \rightarrow \Sigma^- \mu^+ \nu_\mu)/\Gamma_{\text{total}}$	$< 9 \times 10^{-4}$ , CL = 90%

 **$\Delta S = 2$  FORBIDDEN**

Allowed in second-order weak interactions.

$\Gamma(\Xi^0 \rightarrow p \pi^-)/\Gamma_{\text{total}}$	$< 8 \times 10^{-6}$ , CL = 90%
$\Gamma(\Xi^0 \rightarrow p e^- \bar{\nu}_e)/\Gamma_{\text{total}}$	$< 1.3 \times 10^{-3}$
$\Gamma(\Xi^0 \rightarrow p \mu^- \bar{\nu}_\mu)/\Gamma_{\text{total}}$	$< 1.3 \times 10^{-3}$
$\Gamma(\Xi^- \rightarrow n \pi^-)/\Gamma_{\text{total}}$	$< 1.9 \times 10^{-5}$ , CL = 90%
$\Gamma(\Xi^- \rightarrow n e^- \bar{\nu}_e)/\Gamma_{\text{total}}$	$< 3.2 \times 10^{-3}$ , CL = 90%
$\Gamma(\Xi^- \rightarrow n \mu^- \bar{\nu}_\mu)/\Gamma_{\text{total}}$	$< 1.5 \times 10^{-2}$ , CL = 90%
$\Gamma(\Xi^- \rightarrow p \pi^- \pi^-)/\Gamma_{\text{total}}$	$< 4 \times 10^{-4}$ , CL = 90%
$\Gamma(\Xi^- \rightarrow p \pi^- e^- \bar{\nu}_e)/\Gamma_{\text{total}}$	$< 4 \times 10^{-4}$ , CL = 90%
$\Gamma(\Xi^- \rightarrow p \pi^- \mu^- \bar{\nu}_\mu)/\Gamma_{\text{total}}$	$< 4 \times 10^{-4}$ , CL = 90%
$\Gamma(\Omega^- \rightarrow \Lambda \pi^-)/\Gamma_{\text{total}}$	$< 2.9 \times 10^{-6}$ , CL = 90%

 **$\Delta S = 2$  VIA MIXING**

Allowed in second-order weak interactions, e.g. mixing.

$m_{K_L^0} - m_{K_S^0}$	$(0.5293 \pm 0.0009) \times 10^{10} \hbar s^{-1}$ (S = 1.3)
$m_{K_L^0} - m_{K_S^0}$	$(3.484 \pm 0.006) \times 10^{-12} \text{ MeV}$

 **$\Delta C = 2$  VIA MIXING**

Allowed in second-order weak interactions, e.g. mixing.

$ m_{D_1^0} - m_{D_2^0}  = x\Gamma$	$(0.95 \pm_{-0.44}^{0.41}) \times 10^{10} \hbar s^{-1}$
$(\Gamma_{D_1^0} - \Gamma_{D_2^0})/\Gamma = 2y$	$(1.29 \pm_{0.18}^{0.14}) \times 10^{-2}$

 **$\Delta B = 2$  VIA MIXING**

Allowed in second-order weak interactions, e.g. mixing.

$x_d$	$0.1858 \pm 0.0011$
$\Delta m_{B^0} = m_{B_H^0} - m_{B_L^0}$	$(0.5065 \pm 0.0019) \times 10^{12} \hbar s^{-1}$
$x_d = \Delta m_{B^0}/\Gamma_{B^0}$	$0.769 \pm 0.004$
$\Delta m_{B_s^0} = m_{B_{sH}^0} - m_{B_{sL}^0}$	$(17.749 \pm 0.020) \times 10^{12} \hbar s^{-1}$
$x_s = \Delta m_{B_s^0}/\Gamma_{B_s^0}$	$26.89 \pm 0.07$
$x_s$	$0.499312 \pm 0.000004$

 **$\Delta S = 1$  WEAK NEUTRAL CURRENT FORBIDDEN**

Allowed by higher-order electroweak interactions.

$\Gamma(K^+ \rightarrow \pi^+ e^+ e^-)/\Gamma_{\text{total}}$	$(3.00 \pm 0.09) \times 10^{-7}$
$\Gamma(K^+ \rightarrow \pi^+ \mu^+ \mu^-)/\Gamma_{\text{total}}$	$(9.4 \pm 0.6) \times 10^{-8}$ (S = 2.6)
$\Gamma(K^+ \rightarrow \pi^+ \nu \bar{\nu})/\Gamma_{\text{total}}$	$(1.7 \pm 1.1) \times 10^{-10}$
$\Gamma(K^+ \rightarrow \pi^+ \pi^0 \nu \bar{\nu})/\Gamma_{\text{total}}$	$< 4.3 \times 10^{-5}$ , CL = 90%
$\Gamma(K_S^0 \rightarrow \mu^+ \mu^-)/\Gamma_{\text{total}}$	$< 8 \times 10^{-10}$ , CL = 90%
$\Gamma(K_S^0 \rightarrow e^+ e^-)/\Gamma_{\text{total}}$	$< 9 \times 10^{-9}$ , CL = 90%
$\Gamma(K_S^0 \rightarrow \pi^0 e^+ e^-)/\Gamma_{\text{total}}$	[Y] $(3.0 \pm_{-1.2}^{1.5}) \times 10^{-9}$
$\Gamma(K_S^0 \rightarrow \pi^0 \mu^+ \mu^-)/\Gamma_{\text{total}}$	$(2.9 \pm_{-1.2}^{1.5}) \times 10^{-9}$
$\Gamma(K_L^0 \rightarrow \mu^+ \mu^-)/\Gamma_{\text{total}}$	$(6.84 \pm 0.11) \times 10^{-9}$
$\Gamma(K_L^0 \rightarrow e^+ e^-)/\Gamma_{\text{total}}$	$(9 \pm_{-4}^6) \times 10^{-12}$
$\Gamma(K_L^0 \rightarrow \pi^+ \pi^- e^+ e^-)/\Gamma_{\text{total}}$	[Z] $(3.11 \pm 0.19) \times 10^{-7}$
$\Gamma(K_L^0 \rightarrow \pi^0 \pi^0 e^+ e^-)/\Gamma_{\text{total}}$	$< 6.6 \times 10^{-9}$ , CL = 90%
$\Gamma(K_L^0 \rightarrow \pi^0 \pi^0 \mu^+ \mu^-)/\Gamma_{\text{total}}$	$< 9.2 \times 10^{-11}$ , CL = 90%
$\Gamma(K_L^0 \rightarrow \mu^+ \mu^- e^+ e^-)/\Gamma_{\text{total}}$	$(2.69 \pm 0.27) \times 10^{-9}$
$\Gamma(K_L^0 \rightarrow e^+ e^- e^+ e^-)/\Gamma_{\text{total}}$	$(3.56 \pm 0.21) \times 10^{-8}$
$\Gamma(K_L^0 \rightarrow \pi^0 \mu^+ \mu^-)/\Gamma_{\text{total}}$	$< 3.8 \times 10^{-10}$ , CL = 90%
$\Gamma(K_L^0 \rightarrow \pi^0 e^+ e^-)/\Gamma_{\text{total}}$	$< 2.8 \times 10^{-10}$ , CL = 90%
$\Gamma(K_L^0 \rightarrow \pi^0 \nu \bar{\nu})/\Gamma_{\text{total}}$	$< 3.0 \times 10^{-9}$ , CL = 90%
$\Gamma(K_L^0 \rightarrow \pi^0 \pi^0 \nu \bar{\nu})/\Gamma_{\text{total}}$	$< 8.1 \times 10^{-7}$ , CL = 90%
$\Gamma(\Sigma^+ \rightarrow p e^+ e^-)/\Gamma_{\text{total}}$	$< 7 \times 10^{-6}$
$\Gamma(\Sigma^+ \rightarrow p \mu^+ \mu^-)/\Gamma_{\text{total}}$	$(2.4 \pm_{-1.3}^{1.7}) \times 10^{-8}$

 **$\Delta C = 1$  WEAK NEUTRAL CURRENT FORBIDDEN**

Allowed by higher-order electroweak interactions.

$\Gamma(D^+ \rightarrow \pi^+ e^+ e^-)/\Gamma_{\text{total}}$	$< 1.1 \times 10^{-6}$ , CL = 90%
$\Gamma(D^+ \rightarrow \pi^+ \mu^+ \mu^-)/\Gamma_{\text{total}}$	$< 7.3 \times 10^{-8}$ , CL = 90%
$\Gamma(D^+ \rightarrow \rho^+ \mu^+ \mu^-)/\Gamma_{\text{total}}$	$< 5.6 \times 10^{-4}$ , CL = 90%
$\Gamma(D^0 \rightarrow \gamma \gamma)/\Gamma_{\text{total}}$	$< 8.5 \times 10^{-7}$ , CL = 90%
$\Gamma(D^0 \rightarrow e^+ e^-)/\Gamma_{\text{total}}$	$< 7.9 \times 10^{-8}$ , CL = 90%
$\Gamma(D^0 \rightarrow \mu^+ \mu^-)/\Gamma_{\text{total}}$	$< 6.2 \times 10^{-9}$ , CL = 90%
$\Gamma(D^0 \rightarrow \pi^0 e^+ e^-)/\Gamma_{\text{total}}$	$< 4 \times 10^{-6}$ , CL = 90%
$\Gamma(D^0 \rightarrow \pi^0 \mu^+ \mu^-)/\Gamma_{\text{total}}$	$< 1.8 \times 10^{-4}$ , CL = 90%
$\Gamma(D^0 \rightarrow \eta e^+ e^-)/\Gamma_{\text{total}}$	$< 3 \times 10^{-6}$ , CL = 90%
$\Gamma(D^0 \rightarrow \eta \mu^+ \mu^-)/\Gamma_{\text{total}}$	$< 5.3 \times 10^{-4}$ , CL = 90%
$\Gamma(D^0 \rightarrow \pi^+ \pi^- e^+ e^-)/\Gamma_{\text{total}}$	$< 7 \times 10^{-6}$ , CL = 90%
$\Gamma(D^0 \rightarrow \rho^0 e^+ e^-)/\Gamma_{\text{total}}$	$< 1.0 \times 10^{-4}$ , CL = 90%
$\Gamma(D^0 \rightarrow \pi^+ \pi^- \mu^+ \mu^-)/\Gamma_{\text{total}}$	$(9.6 \pm 1.2) \times 10^{-7}$
$\Gamma(D^0 \rightarrow \rho^0 \mu^+ \mu^-)/\Gamma_{\text{total}}$	$< 2.2 \times 10^{-5}$ , CL = 90%
$\Gamma(D^0 \rightarrow \omega e^+ e^-)/\Gamma_{\text{total}}$	$< 6 \times 10^{-6}$ , CL = 90%
$\Gamma(D^0 \rightarrow \omega \mu^+ \mu^-)/\Gamma_{\text{total}}$	$< 8.3 \times 10^{-4}$ , CL = 90%
$\Gamma(D^0 \rightarrow K^- K^+ e^+ e^-)/\Gamma_{\text{total}}$	$< 1.1 \times 10^{-5}$ , CL = 90%
$\Gamma(D^0 \rightarrow \phi e^+ e^-)/\Gamma_{\text{total}}$	$< 5.2 \times 10^{-5}$ , CL = 90%
$\Gamma(D^0 \rightarrow K^- K^+ \mu^+ \mu^-)/\Gamma_{\text{total}}$	$(1.54 \pm 0.32) \times 10^{-7}$
$\Gamma(D^0 \rightarrow \phi \mu^+ \mu^-)/\Gamma_{\text{total}}$	$< 3.1 \times 10^{-5}$ , CL = 90%
$\Gamma(D^0 \rightarrow K^- \pi^+ \mu^+ \mu^-)/\Gamma_{\text{total}}$	$< 3.59 \times 10^{-4}$ , CL = 90%
$\Gamma(D^0 \rightarrow \pi^+ \pi^- \pi^0 \mu^+ \mu^-)/\Gamma_{\text{total}}$	$< 8.1 \times 10^{-4}$ , CL = 90%
$\Gamma(D_s^+ \rightarrow K^+ e^+ e^-)/\Gamma_{\text{total}}$	$< 3.7 \times 10^{-6}$ , CL = 90%
$\Gamma(D_s^+ \rightarrow K^+ \mu^+ \mu^-)/\Gamma_{\text{total}}$	$< 2.1 \times 10^{-5}$ , CL = 90%
$\Gamma(D_s^+ \rightarrow K^*(892)^+ \mu^+ \mu^-)/\Gamma_{\text{total}}$	$< 1.4 \times 10^{-3}$ , CL = 90%
$\Gamma(\Lambda_C^+ \rightarrow p e^+ e^-)/\Gamma_{\text{total}}$	$< 5.5 \times 10^{-6}$ , CL = 90%

# Tests of Conservation Laws

$$\Gamma(\Lambda_c^+ \rightarrow p \mu^+ \mu^- \text{ non-resonant})/\Gamma_{\text{total}} < 7.7 \times 10^{-8}, \text{ CL} = 90\%$$

## $\Delta B = 1$ WEAK NEUTRAL CURRENT FORBIDDEN

Allowed by higher-order electroweak interactions.

$\Gamma(B^+ \rightarrow \pi^+ \ell^+ \ell^-)/\Gamma_{\text{total}}$	$< 4.9 \times 10^{-8}, \text{ CL} = 90\%$
$\Gamma(B^+ \rightarrow \pi^+ e^+ e^-)/\Gamma_{\text{total}}$	$< 8.0 \times 10^{-8}, \text{ CL} = 90\%$
$\Gamma(B^+ \rightarrow \pi^+ \mu^+ \mu^-)/\Gamma_{\text{total}}$	$(1.75 \pm 0.22) \times 10^{-8}$
$\Gamma(B^+ \rightarrow \pi^+ \nu \bar{\nu})/\Gamma_{\text{total}}$	$< 1.4 \times 10^{-5}, \text{ CL} = 90\%$
$\Gamma(B^+ \rightarrow K^+ \ell^+ \ell^-)/\Gamma_{\text{total}}$	[ <i>a</i> ] $(4.51 \pm 0.23) \times 10^{-7} (S = 1.1)$
$\Gamma(B^+ \rightarrow K^+ e^+ e^-)/\Gamma_{\text{total}}$	$(5.5 \pm 0.7) \times 10^{-7}$
$\Gamma(B^+ \rightarrow K^+ \mu^+ \mu^-)/\Gamma_{\text{total}}$	$(4.41 \pm 0.22) \times 10^{-7} (S = 1.2)$
$\Gamma(B^+ \rightarrow K^+ \mu^+ \mu^- \text{ nonresonant})/\Gamma_{\text{total}}$	$(4.37 \pm 0.27) \times 10^{-7}$
$\Gamma(B^+ \rightarrow K^+ \tau^+ \tau^-)/\Gamma_{\text{total}}$	$< 2.25 \times 10^{-3}, \text{ CL} = 90\%$
$\Gamma(B^+ \rightarrow K^+ \nu \bar{\nu})/\Gamma_{\text{total}}$	$< 1.6 \times 10^{-5}, \text{ CL} = 90\%$
$\Gamma(B^+ \rightarrow \rho^+ \nu \bar{\nu})/\Gamma_{\text{total}}$	$< 3.0 \times 10^{-5}, \text{ CL} = 90\%$
$\Gamma(B^+ \rightarrow K^*(892)^+ \ell^+ \ell^-)/\Gamma_{\text{total}}$	[ <i>a</i> ] $(1.01 \pm 0.11) \times 10^{-6} (S = 1.1)$
$\Gamma(B^+ \rightarrow K^*(892)^+ e^+ e^-)/\Gamma_{\text{total}}$	$(1.55 \pm_{-0.31}^{0.40}) \times 10^{-6}$
$\Gamma(B^+ \rightarrow K^*(892)^+ \mu^+ \mu^-)/\Gamma_{\text{total}}$	$(9.6 \pm 1.0) \times 10^{-7}$
$\Gamma(B^+ \rightarrow K^*(892)^+ \nu \bar{\nu})/\Gamma_{\text{total}}$	$< 4.0 \times 10^{-5}, \text{ CL} = 90\%$
$\Gamma(B^+ \rightarrow K^+ \pi^+ \pi^- \mu^+ \mu^-)/\Gamma_{\text{total}}$	$(4.3 \pm 0.4) \times 10^{-7}$
$\Gamma(B^+ \rightarrow \phi K^+ \mu^+ \mu^-)/\Gamma_{\text{total}}$	$(7.9 \pm_{-1.7}^{2.1}) \times 10^{-8}$
$\Gamma(B^0 \rightarrow \gamma \gamma)/\Gamma_{\text{total}}$	$< 3.2 \times 10^{-7}, \text{ CL} = 90\%$
$\Gamma(B^0 \rightarrow e^+ e^-)/\Gamma_{\text{total}}$	$< 8.3 \times 10^{-8}, \text{ CL} = 90\%$
$\Gamma(B^0 \rightarrow e^+ e^- \gamma)/\Gamma_{\text{total}}$	$< 1.2 \times 10^{-7}, \text{ CL} = 90\%$
$\Gamma(B^0 \rightarrow \mu^+ \mu^-)/\Gamma_{\text{total}}$	$(1.1 \pm_{-1.3}^{1.4}) \times 10^{-10} (S = 1.6)$
$\Gamma(B^0 \rightarrow \mu^+ \mu^- \gamma)/\Gamma_{\text{total}}$	$< 1.6 \times 10^{-7}, \text{ CL} = 90\%$
$\Gamma(B^0 \rightarrow \mu^+ \mu^- \mu^+ \mu^-)/\Gamma_{\text{total}}$	$< 6.9 \times 10^{-10}, \text{ CL} = 95\%$
$\Gamma(B^0 \rightarrow SP, S \rightarrow \mu^+ \mu^-, P \rightarrow \mu^+ \mu^-)/\Gamma_{\text{total}}$	[ <i>b</i> ] $< 6.0 \times 10^{-10}, \text{ CL} = 95\%$
$\Gamma(B^0 \rightarrow \tau^+ \tau^-)/\Gamma_{\text{total}}$	$< 2.1 \times 10^{-3}, \text{ CL} = 95\%$
$\Gamma(B^0 \rightarrow \pi^0 \ell^+ \ell^-)/\Gamma_{\text{total}}$	$< 5.3 \times 10^{-8}, \text{ CL} = 90\%$
$\Gamma(B^0 \rightarrow \pi^0 e^+ e^-)/\Gamma_{\text{total}}$	$< 8.4 \times 10^{-8}, \text{ CL} = 90\%$
$\Gamma(B^0 \rightarrow \pi^0 \mu^+ \mu^-)/\Gamma_{\text{total}}$	$< 6.9 \times 10^{-8}, \text{ CL} = 90\%$
$\Gamma(B^0 \rightarrow \eta \ell^+ \ell^-)/\Gamma_{\text{total}}$	$< 6.4 \times 10^{-8}, \text{ CL} = 90\%$
$\Gamma(B^0 \rightarrow \eta e^+ e^-)/\Gamma_{\text{total}}$	$< 1.08 \times 10^{-7}, \text{ CL} = 90\%$
$\Gamma(B^0 \rightarrow \eta \mu^+ \mu^-)/\Gamma_{\text{total}}$	$< 1.12 \times 10^{-7}, \text{ CL} = 90\%$
$\Gamma(B^0 \rightarrow \pi^0 \nu \bar{\nu})/\Gamma_{\text{total}}$	$< 9 \times 10^{-6}, \text{ CL} = 90\%$
$\Gamma(B^0 \rightarrow K^0 \ell^+ \ell^-)/\Gamma_{\text{total}}$	[ <i>a</i> ] $(3.1 \pm_{-0.7}^{0.8}) \times 10^{-7}$
$\Gamma(B^0 \rightarrow K^0 e^+ e^-)/\Gamma_{\text{total}}$	$(1.6 \pm_{-0.8}^{1.0}) \times 10^{-7}$
$\Gamma(B^0 \rightarrow K^0 \mu^+ \mu^-)/\Gamma_{\text{total}}$	$(3.39 \pm 0.34) \times 10^{-7}$
$\Gamma(B^0 \rightarrow K^0 \nu \bar{\nu})/\Gamma_{\text{total}}$	$< 2.6 \times 10^{-5}, \text{ CL} = 90\%$
$\Gamma(B^0 \rightarrow \rho^0 \nu \bar{\nu})/\Gamma_{\text{total}}$	$< 4.0 \times 10^{-5}, \text{ CL} = 90\%$
$\Gamma(B^0 \rightarrow K^*(892)^0 \ell^+ \ell^-)/\Gamma_{\text{total}}$	[ <i>a</i> ] $(9.9 \pm_{-1.1}^{1.2}) \times 10^{-7}$
$\Gamma(B^0 \rightarrow K^*(892)^0 e^+ e^-)/\Gamma_{\text{total}}$	$(1.03 \pm_{-0.17}^{0.19}) \times 10^{-6}$
$\Gamma(B^0 \rightarrow K^*(892)^0 \mu^+ \mu^-)/\Gamma_{\text{total}}$	$(9.4 \pm 0.5) \times 10^{-7}$
$\Gamma(B^0 \rightarrow \pi^+ \pi^- \mu^+ \mu^-)/\Gamma_{\text{total}}$	$(2.1 \pm 0.5) \times 10^{-8}$
$\Gamma(B^0 \rightarrow K^*(892)^0 \nu \bar{\nu})/\Gamma_{\text{total}}$	$< 1.8 \times 10^{-5}, \text{ CL} = 90\%$
$\Gamma(B^0 \rightarrow \text{invisible})/\Gamma_{\text{total}}$	$< 2.4 \times 10^{-5}, \text{ CL} = 90\%$
$\Gamma(B^0 \rightarrow \nu \bar{\nu} \gamma)/\Gamma_{\text{total}}$	$< 1.7 \times 10^{-5}, \text{ CL} = 90\%$
$\Gamma(B^0 \rightarrow \phi \nu \bar{\nu})/\Gamma_{\text{total}}$	$< 1.27 \times 10^{-4}, \text{ CL} = 90\%$
$\Gamma(B \rightarrow s e^+ e^-)/\Gamma_{\text{total}}$	$(6.7 \pm 1.7) \times 10^{-6} (S = 2.0)$
$\Gamma(B \rightarrow s \mu^+ \mu^-)/\Gamma_{\text{total}}$	$(4.3 \pm 1.0) \times 10^{-6}$
$\Gamma(B \rightarrow s \ell^+ \ell^-)/\Gamma_{\text{total}}$	[ <i>a</i> ] $(5.8 \pm 1.3) \times 10^{-6} (S = 1.8)$
$\Gamma(B \rightarrow \pi \ell^+ \ell^-)/\Gamma_{\text{total}}$	$< 5.9 \times 10^{-8}, \text{ CL} = 90\%$
$\Gamma(B \rightarrow \pi e^+ e^-)/\Gamma_{\text{total}}$	$< 1.10 \times 10^{-7}, \text{ CL} = 90\%$
$\Gamma(B \rightarrow \pi \mu^+ \mu^-)/\Gamma_{\text{total}}$	$< 5.0 \times 10^{-8}, \text{ CL} = 90\%$
$\Gamma(B \rightarrow K e^+ e^-)/\Gamma_{\text{total}}$	$(4.4 \pm 0.6) \times 10^{-7}$
$\Gamma(B \rightarrow K^*(892) e^+ e^-)/\Gamma_{\text{total}}$	$(1.19 \pm 0.20) \times 10^{-6} (S = 1.2)$
$\Gamma(B \rightarrow K \mu^+ \mu^-)/\Gamma_{\text{total}}$	$(4.4 \pm 0.4) \times 10^{-7}$
$\Gamma(B \rightarrow K^*(892) \mu^+ \mu^-)/\Gamma_{\text{total}}$	$(1.06 \pm 0.09) \times 10^{-6}$
$\Gamma(B \rightarrow K \ell^+ \ell^-)/\Gamma_{\text{total}}$	$(4.8 \pm 0.4) \times 10^{-7}$
$\Gamma(B \rightarrow K^*(892) \ell^+ \ell^-)/\Gamma_{\text{total}}$	$(1.05 \pm 0.10) \times 10^{-6}$
$\Gamma(B \rightarrow K \nu \bar{\nu})/\Gamma_{\text{total}}$	$< 1.6 \times 10^{-5}, \text{ CL} = 90\%$
$\Gamma(B \rightarrow K^* \nu \bar{\nu})/\Gamma_{\text{total}}$	$< 2.7 \times 10^{-5}, \text{ CL} = 90\%$
$\Gamma(B \rightarrow \pi \nu \bar{\nu})/\Gamma_{\text{total}}$	$< 8 \times 10^{-6}, \text{ CL} = 90\%$
$\Gamma(B \rightarrow \rho \nu \bar{\nu})/\Gamma_{\text{total}}$	$< 2.8 \times 10^{-5}, \text{ CL} = 90\%$
$\Gamma(\bar{B} \rightarrow \bar{s} \nu \bar{\nu})/\Gamma_{\text{total}}$	$< 6.4 \times 10^{-4}, \text{ CL} = 90\%$
$\Gamma(\bar{B} \rightarrow \mu^+ \mu^- \text{ anything})/\Gamma_{\text{total}}$	$< 3.2 \times 10^{-4}, \text{ CL} = 90\%$

Unless otherwise stated, limits are given at the 90% confidence level, while errors are given as  $\pm 1$  standard deviation.

$\Gamma(B_S^0 \rightarrow \gamma \gamma)/\Gamma_{\text{total}}$	$< 3.1 \times 10^{-6}, \text{ CL} = 90\%$
$\Gamma(B_S^0 \rightarrow \phi \gamma)/\Gamma_{\text{total}}$	$(3.4 \pm 0.4) \times 10^{-5}$
$\Gamma(B_S^0 \rightarrow \mu^+ \mu^-)/\Gamma_{\text{total}}$	$(3.0 \pm 0.4) \times 10^{-9}$
$\Gamma(B_S^0 \rightarrow e^+ e^-)/\Gamma_{\text{total}}$	$< 2.8 \times 10^{-7}, \text{ CL} = 90\%$
$\Gamma(B_S^0 \rightarrow \tau^+ \tau^-)/\Gamma_{\text{total}}$	$< 6.8 \times 10^{-3}, \text{ CL} = 95\%$
$\Gamma(B_S^0 \rightarrow \mu^+ \mu^- \mu^+ \mu^-)/\Gamma_{\text{total}}$	$< 2.5 \times 10^{-9}, \text{ CL} = 95\%$
$\Gamma(B_S^0 \rightarrow SP, S \rightarrow \mu^+ \mu^-, P \rightarrow \mu^+ \mu^-)/\Gamma_{\text{total}}$	[ <i>b</i> ] $< 2.2 \times 10^{-9}, \text{ CL} = 95\%$
$\Gamma(B_S^0 \rightarrow \phi(1020) \mu^+ \mu^-)/\Gamma_{\text{total}}$	$(8.2 \pm 1.2) \times 10^{-7}$
$\Gamma(B_S^0 \rightarrow \pi^+ \pi^- \mu^+ \mu^-)/\Gamma_{\text{total}}$	$(8.4 \pm 1.7) \times 10^{-8}$
$\Gamma(B_S^0 \rightarrow \phi \nu \bar{\nu})/\Gamma_{\text{total}}$	$< 5.4 \times 10^{-3}, \text{ CL} = 90\%$

## $\Delta T = 1$ WEAK NEUTRAL CURRENT FORBIDDEN

Allowed by higher-order electroweak interactions.

$\Gamma(t \rightarrow Zq(q=u,c))/\Gamma_{\text{total}}$	[ <i>cc</i> ] $< 5 \times 10^{-4}, \text{ CL} = 95\%$
$\Gamma(t \rightarrow Hu)/\Gamma_{\text{total}}$	$< 1.2 \times 10^{-3}, \text{ CL} = 95\%$
$\Gamma(t \rightarrow Hc)/\Gamma_{\text{total}}$	$< 1.1 \times 10^{-3}, \text{ CL} = 95\%$
$\Gamma(t \rightarrow \ell^+ \bar{q} q' (q=d,s,b; q'=u,c))/\Gamma_{\text{total}}$	$< 1.6 \times 10^{-3}, \text{ CL} = 95\%$

### NOTES

In this Summary Table:

When a quantity has “(S = ...)” to its right, the error on the quantity has been enlarged by the “scale factor” S, defined as  $S = \sqrt{\chi^2/(N-1)}$ , where N is the number of measurements used in calculating the quantity. We do this when  $S > 1$ , which often indicates that the measurements are inconsistent. When  $S > 1.25$ , we also show in the Particle Listings an ideogram of the measurements. For more about S, see the Introduction.

- [a] Forbidden by angular momentum conservation.
- [b] C parity forbids this to occur as a single-photon process.
- [c] See the Particle Listings for the (complicated) definition of this quantity.
- [d] Time-reversal invariance requires this to be  $0^\circ$  or  $180^\circ$ .
- [e] This coefficient is zero if time invariance is not violated.
- [f] Allowed by higher-order electroweak interactions.
- [g] Violates CP in leading order. Test of direct CP violation since the indirect CP-violating and CP-conserving contributions are expected to be suppressed.
- [h] In the 2010 Review, the values for these quantities were given using a measure of the asymmetry that was inconsistent with the usual definition.
- [i]  $\text{Re}(\epsilon'/\epsilon) = \epsilon'/\epsilon$  to a very good approximation provided the phases satisfy CPT invariance.
- [j] This mode includes gammas from inner bremsstrahlung but not the direct emission mode  $K_L^0 \rightarrow \pi^+ \pi^- \gamma$  (DE).
- [k] Neglecting photon channels. See, e.g., A. Pais and S.B. Treiman, Phys. Rev. **D12**, 2744 (1975).
- [l] Derived from measured values of  $\phi_{+-}, \phi_{00}, |\eta|, |m_{K_L^0} - m_{K_S^0}|$ , and  $\tau_{K_S^0}$ , as described in the introduction to “Tests of Conservation Laws.”
- [n] The  $|m_p - m_{\bar{p}}|/m_p$  and  $|q_p + q_{\bar{p}}|/e$  are not independent, and both use the more precise measurement of  $|q_{\bar{p}}/m_{\bar{p}}|/(q_p/m_p)$ .
- [o] The value is for the sum of the charge states or particle/antiparticle states indicated.
- [p] A test of additive vs. multiplicative lepton family number conservation.
- [q] Derived from an analysis of neutrino-oscillation experiments.
- [r] This limit is for either  $D^0$  or  $\bar{D}^0$  to  $p e^-$ .
- [s] This limit is for either  $D^0$  or  $\bar{D}^0$  to  $\bar{p} e^+$ .
- [t] The first limit is for  $p \rightarrow$  anything or “disappearance” modes of a bound proton. The second entry, a rough range of limits, assumes the dominant decay modes are among those investigated. For antiprotons the best limit, inferred from the observation of cosmic ray  $\bar{p}$ 's is  $\tau_{\bar{p}} > 10^7$  yr, the cosmic-ray storage time, but this limit depends on a number of assumptions. The best direct observation of stored antiprotons gives  $\tau_{\bar{p}}/B(\bar{p} \rightarrow e^- \gamma) > 7 \times 10^5$  yr.
- [u] There is some controversy about whether nuclear physics and model dependence complicate the analysis for bound neutrons (from which the

best limit comes). The first limit here is from reactor experiments with free neutrons.

[v] This is the best limit for the mode  $e^- \rightarrow \nu\gamma$ . The best limit for Nuclear de-excitation experiments is  $6.4 \times 10^{24}$  yr.

[x] The limit is from neutrality-of-matter experiments; it assumes  $q_n = q_p + q_e$ . See also the charge of the neutron.

[y] See the  $K_S^0$  Particle Listings for the energy limits used in this measurement.

[z] See the  $K_L^0$  Particle Listings for the energy limits used in this measurement.

[aa] An  $\ell$  indicates an  $e$  or a  $\mu$  mode, not a sum over these modes.

[bb] Here  $S$  and  $P$  are the hypothetical scalar and pseudoscalar particles with masses of  $2.5 \text{ GeV}/c^2$  and  $214.3 \text{ MeV}/c^2$ , respectively.

[cc] This limit is for  $\Gamma(t \rightarrow Zq)/\Gamma(t \rightarrow Wb)$ .



## REVIEWS, TABLES, AND PLOTS

### Constants, Units, Atomic and Nuclear Properties

1. Physical constants (rev.) . . . . .	137
2. Astrophysical constants (rev.) . . . . .	138
3. International system of units (SI) . . . . .	140
4. Periodic table of the elements (rev.) . . . . .	141
5. Electronic structure of the elements . . . . .	142
6. Atomic and nuclear properties of materials . . . . .	144
7. Electromagnetic relations . . . . .	146
8. Naming scheme for hadrons (rev.) . . . . .	148



## 1. Physical Constants (a major revision)

**Table 1.1.** Revised 2019 by C.G. Wohl (LBNL). Reviewed by P.J. Mohr and D.B. Newell (NIST). Mainly from “CODATA Recommended Values of the Fundamental Physical Constants: 2018,” E. Tiesinga, D.B. Newell, P.J. Mohr, and B.N. Taylor, NIST SP961 (May 2019). The electron charge magnitude  $e$ , and the Planck, Boltzmann, and Avogadro constants  $h$ ,  $k$ , and  $N_A$ , now join  $c$  as having defined values; the free-space permittivity and permeability constants  $\epsilon_0$  and  $\mu_0$  are no longer exact. These changes affect practically everything else in the Table. Figures in parentheses after the values are the 1-standard-deviation uncertainties in the last digits; the fractional uncertainties in parts per  $10^9$  (ppb) are in the last column. The full 2018 CODATA Committee on Data for Science and Technology set of constants are found at <https://physics.nist.gov/constants>. The last set of constants (beginning with the Fermi coupling constant) comes from the Particle Data Group. See also “The International System of Units (SI),” 9th ed. (2019) of the International Bureau of Weights and Measures (BIPM), <https://www.bipm.org/utis/common/pdf/si-brochure/SI-Brochure-9-EN.pdf>.

Quantity	Symbol, equation	Value	Uncertainty (ppb)
speed of light in vacuum	$c$	299 792 458 m s <sup>-1</sup>	exact
Planck constant	$h$	6.626 070 15×10 <sup>-34</sup> J s (or J/Hz) <sup>‡</sup>	exact
Planck constant, reduced	$\hbar \equiv h/2\pi$	1.054 571 817... × 10 <sup>-34</sup> J s = 6.582 119 569... × 10 <sup>-22</sup> MeV s	exact* exact*
electron charge magnitude	$e$	1.602 176 634×10 <sup>-19</sup> C	exact
conversion constant	$\hbar c$	197.326 980 4... MeV fm	exact*
conversion constant	$(\hbar c)^2$	0.389 379 372 1... GeV <sup>2</sup> mbarn	exact*
electron mass	$m_e$	0.510 998 950 00(15) MeV/c <sup>2</sup> = 9.109 383 7015(28)×10 <sup>-31</sup> kg	0.30
proton mass	$m_p$	938.272 088 16(29) MeV/c <sup>2</sup> = 1.672 621 923 69(51)×10 <sup>-27</sup> kg = 1.007 276 466 621(53) u = 1836.152 673 43(11) $m_e$	0.053, 0.060
neutron mass	$m_n$	939.565 420 52(54) MeV/c <sup>2</sup> = 1.008 664 915 95(49) u	0.57, 0.48
deuteron mass	$m_d$	1875.612 942 57(57) MeV/c <sup>2</sup>	0.30
unified atomic mass unit**	$u = (\text{mass } ^{12}\text{C atom})/12$	931.494 102 42(28) MeV/c <sup>2</sup> = 1.660 539 066 60(50)×10 <sup>-27</sup> kg	0.30
permittivity of free space	$\epsilon_0 = 1/\mu_0 c^2$	8.854 187 8128(13) × 10 <sup>-12</sup> F m <sup>-1</sup>	0.15
permeability of free space	$\mu_0/(4\pi \times 10^{-7})$	1.000 000 000 55(15) N A <sup>-2</sup>	0.15
fine-structure constant	$\alpha = e^2/4\pi\epsilon_0\hbar c$	7.297 352 5693(11)×10 <sup>-3</sup> = 1/137.035 999 084(21) <sup>†</sup>	0.15
classical electron radius	$r_e = e^2/4\pi\epsilon_0 m_e c^2$	2.817 940 3262(13)×10 <sup>-15</sup> m	0.45
( $e^-$ Compton wavelength)/2 $\pi$	$\lambda_e = \hbar/m_e c = r_e \alpha^{-1}$	3.861 592 6796(12)×10 <sup>-13</sup> m	0.30
Bohr radius ( $m_{\text{nucleus}} = \infty$ )	$a_\infty = 4\pi\epsilon_0\hbar^2/m_e e^2 = r_e \alpha^{-2}$	0.529 177 210 903(80)×10 <sup>-10</sup> m	0.15
wavelength of 1 eV/c particle	$\hbar c/(1 \text{ eV})$	1.239 841 984... × 10 <sup>-6</sup> m	exact*
Rydberg energy	$\hbar c R_\infty = m_e e^4/2(4\pi\epsilon_0)^2 \hbar^2 = m_e c^2 \alpha^2/2$	13.605 693 122 994(26) eV	1.9×10 <sup>-3</sup>
Thomson cross section	$\sigma_T = 8\pi r_e^2/3$	0.665 245 873 21(60) barn	0.91
Bohr magneton	$\mu_B = e\hbar/2m_e$	5.788 381 8060(17)×10 <sup>-11</sup> MeV T <sup>-1</sup>	0.3
nuclear magneton	$\mu_N = e\hbar/2m_p$	3.152 451 258 44(96)×10 <sup>-14</sup> MeV T <sup>-1</sup>	0.31
electron cyclotron freq./field	$\omega_{\text{cycl}}^e/B = e/m_e$	1.758 820 010 76(53)×10 <sup>11</sup> rad s <sup>-1</sup> T <sup>-1</sup>	0.30
proton cyclotron freq./field	$\omega_{\text{cycl}}^p/B = e/m_p$	9.578 833 1560(29)×10 <sup>7</sup> rad s <sup>-1</sup> T <sup>-1</sup>	0.31
gravitational constant <sup>‡</sup>	$G_N$	6.674 30(15)×10 <sup>-11</sup> m <sup>3</sup> kg <sup>-1</sup> s <sup>-2</sup> = 6.708 83(15)×10 <sup>-39</sup> $\hbar c$ (GeV/c <sup>2</sup> ) <sup>-2</sup>	2.2 × 10 <sup>4</sup> 2.2 × 10 <sup>4</sup>
standard gravitational accel.	$g_N$	9.806 65 m s <sup>-2</sup>	exact
Avogadro constant	$N_A$	6.022 140 76×10 <sup>23</sup> mol <sup>-1</sup>	exact
Boltzmann constant	$k$	1.380 649×10 <sup>-23</sup> J K <sup>-1</sup> = 8.617 333 262... × 10 <sup>-5</sup> eV K <sup>-1</sup>	exact* exact*
molar volume, ideal gas at STP	$N_A k$ (273.15 K)/(101 325 Pa)	22.413 969 54... × 10 <sup>-3</sup> m <sup>3</sup> mol <sup>-1</sup>	exact*
Wien displacement law constant	$b = \lambda_{\text{max}} T$	2.897 771 955... × 10 <sup>-3</sup> m K	exact*
Stefan-Boltzmann constant	$\sigma = \pi^2 k^4/60\hbar^3 c^2$	5.670 374 419... × 10 <sup>-8</sup> W m <sup>-2</sup> K <sup>-4</sup>	exact*
Fermi coupling constant <sup>‡‡</sup>	$G_F/(\hbar c)^3$	1.166 378 7(6)×10 <sup>-5</sup> GeV <sup>-2</sup>	510
weak-mixing angle	$\sin^2 \hat{\theta}(M_Z) (\overline{\text{MS}})$	0.231 21(4) <sup>††</sup>	1.7 × 10 <sup>5</sup>
$W^\pm$ boson mass	$m_W$	80.379(12) GeV/c <sup>2</sup>	1.5 × 10 <sup>5</sup>
$Z^0$ boson mass	$m_Z$	91.1876(21) GeV/c <sup>2</sup>	2.3 × 10 <sup>4</sup>
strong coupling constant	$\alpha_s(m_Z)$	0.1179(10)	8.5 × 10 <sup>6</sup>
$\pi = 3.141 592 653 589 793 238...$		$e = 2.718 281 828 459 045 235...$	$\gamma = 0.577 215 664 901 532 860...$
1 in $\equiv$ 0.0254 m	1 G $\equiv$ 10 <sup>-4</sup> T	1 eV = 1.602 176 634 × 10 <sup>-19</sup> J (exact)	$kT$ at 300 K = [38.681 740(22)] <sup>-1</sup> eV
1 Å $\equiv$ 0.1 nm	1 dyne $\equiv$ 10 <sup>-5</sup> N	(1 kg)c <sup>2</sup> = 5.609 588 603... × 10 <sup>35</sup> eV (exact*)	0 °C $\equiv$ 273.15 K
1 barn $\equiv$ 10 <sup>-28</sup> m <sup>2</sup>	1 erg $\equiv$ 10 <sup>-7</sup> J	1 C = 2.997 924 58 × 10 <sup>9</sup> esu	1 atmosphere $\equiv$ 760 Torr $\equiv$ 101 325 Pa

<sup>‡</sup> CODATA recommends that the unit be J/Hz to stress that in  $h = E/\nu$  the frequency  $\nu$  is in cycles/sec (Hz), not radians/sec.

\* These are calculated from exact values and are exact to the number of places given (*i.e.* no rounding).

\*\* The molar mass of <sup>12</sup>C is 11.999 999 9958(36) g.

<sup>†</sup> At  $Q^2 = 0$ . At  $Q^2 \approx m_W^2$  the value is  $\sim 1/128$ .

<sup>‡</sup> Absolute laboratory measurements of  $G_N$  have been made only on scales of about 1 cm to 1 m.

<sup>‡‡</sup> See the discussion in Sec. 10, “Electroweak model and constraints on new physics.”

<sup>††</sup> The corresponding  $\sin^2 \theta$  for the effective angle is 0.23153(4).



## 2. Astrophysical Constants and Parameters

**Table 2.1:** Revised August 2019 by D.E. Groom (LBNL) and D. Scott (U. of British Columbia). The figures in parentheses after some values give the  $1\text{-}\sigma$  uncertainties in the last digit(s). Physical constants are from Ref. [1]. While every effort has been made to obtain the most accurate current values of the listed quantities, the table does not represent a critical review or adjustment of the constants, and is not intended as a primary reference. The values and uncertainties for the cosmological parameters depend on the exact data sets, priors, and basis parameters used in the fit. Many of the derived parameters reported in this table have non-Gaussian likelihoods. Parameters may be highly correlated, so care must be taken in propagating errors. Unless otherwise specified, cosmological parameters are derived from a 6-parameter  $\Lambda$ CDM cosmology fit to *Planck* cosmic microwave background 2018 temperature (TT) + polarization (TE,EE+lowE) + lensing data [2]. For more information see Ref. [3] and the original papers.

Quantity	Symbol, equation.	Value	Reference, footnote
Newtonian constant of gravitation	$G_N$	$6.674\,30(15) \times 10^{-11} \text{ m}^3 \text{ kg}^{-1} \text{ s}^{-2}$	[1]
Planck mass	$M_P = \sqrt{\hbar c/G_N}$	$1.220\,890(14) \times 10^{19} \text{ GeV}/c^2 = 2.176\,434(24) \times 10^{-8} \text{ kg}$	[1]
Planck length	$l_P = \sqrt{\hbar G_N/c^3}$	$1.616\,255(18) \times 10^{-35} \text{ m}$	[1]
tropical year (equinox to equinox, 2020)	yr	$31\,556\,925.1 \text{ s} = 365.242\,189 \text{ days}$	[4]
sidereal year (period of Earth around Sun relative to stars)		$31\,558\,149.8 \text{ s} \approx \pi \times 10^7 \text{ s}$	[4]
mean sidereal day (Earth rotation period relative to stars)		$23^{\text{h}}\,56^{\text{m}}\,04^{\text{s}}.090\,53$	[4]
astronomical unit	au	$149\,597\,870\,700 \text{ m}$	exact [5]
parsec (1 au/1 arc sec)	pc	$3.085\,677\,581\,49 \times 10^{16} \text{ m} = 3.261\,56 \dots \text{ ly}$	exact [6]
light year (deprecated unit)	ly	$0.306\,601 \dots \text{ pc} = 0.946\,073 \dots \times 10^{16} \text{ m}$	[7]
solid angle	$\text{deg}^2$	$(\pi/180)^2 \text{ sr} = 3.046\,17 \dots \times 10^{-4} \text{ sr}$	[8]
Schwarzschild radius of the Sun	$2G_N M_\odot/c^2$	$2.953\,250\,076\,100\,25 \text{ km}$	[9]
Solar mass	$M_\odot$	$1.988\,41(4) \times 10^{30} \text{ kg}$	[10]
nominal Solar equatorial radius	$R_\odot$	$6.957 \times 10^8 \text{ m}$	exact [11]
nominal Solar constant	$S_\odot$	$1361 \text{ W m}^{-2}$	exact [11, 12]
nominal Solar photosphere temperature	$T_\odot$	$5772 \text{ K}$	exact [11]
nominal Solar luminosity	$L_\odot$	$3.828 \times 10^{26} \text{ W}$	exact [11, 13]
Schwarzschild radius of the Earth	$2G_N M_\oplus/c^2$	$8.870\,055\,940 \text{ mm}$	[9]
Earth mass	$M_\oplus$	$5.972\,17(13) \times 10^{24} \text{ kg}$	[10]
nominal Earth equatorial radius	$R_\oplus$	$6.3781 \times 10^6 \text{ m}$	exact [11]
Chandrasekhar mass	$M_{\text{Ch}}$	$3.097\,972 \mu^{-2} M_P^3/m_H^2 = 1.433\,77(6) (\mu/2)^{-2} M_\odot$	[14, 15]
Eddington luminosity	$L_{\text{Ed}}$	$1.257\,065\,179\,8(12) \times 10^{31} (M/M_\odot) \text{ W}$ $= 3.283\,869\,330\,8(31) \times 10^4 (M/M_\odot) L_\odot$	[16, 17]
jansky (flux density)	Jy	$10^{-26} \text{ W m}^{-2} \text{ Hz}^{-1}$	definition
luminosity conversion	$f_0$	$3.0128 \times 10^{28} \times 10^{-0.4 M_{\text{Bol}}} \text{ W}$ ( $M_{\text{Bol}}$ = absolute bolometric magnitude = bolometric magnitude at 10 pc)	exact [18]
flux conversion	$\mathcal{F}$	$2.518\,021\,002 \times 10^{-8} \times 10^{-0.4 m_{\text{Bol}}} \text{ W m}^{-2}$ ( $m_{\text{Bol}}$ = apparent bolometric magnitude)	exact [18]
ABsolute monochromatic magnitude	AB	$-2.5 \log_{10} f_\nu - 56.10$ (for $f_\nu$ in $\text{W m}^{-2} \text{ Hz}^{-1}$ ) $= -2.5 \log_{10} f_\nu + 8.90$ (for $f_\nu$ in Jy)	[19]
Solar angular velocity around Galactic center	$\Theta_0/R_0$	$27.1(5) \text{ km s}^{-1} \text{ kpc}^{-1}$	[20]
Solar distance from Galactic center	$R_0$	$8.178 \pm 0.013(\text{stat.}) \pm 0.022(\text{sys.}) \text{ kpc}$	[21, 22]
circular velocity at $R_0$	$v_0$ or $\Theta_0$	$240(8) \text{ km s}^{-1}$	[22, 23]
escape velocity from the Galaxy	$v_{\text{esc}}$	$492 \text{ km s}^{-1} < v_{\text{esc}} < 587 \text{ km s}^{-1}$ (90%)	[24]
local disk density	$\rho_{\text{disk}}$	$6.6(9) \times 10^{-24} \text{ g cm}^{-3} = 3.7(5) \text{ GeV}/c^2 \text{ cm}^{-3}$	[25]
local dark matter density	$\rho_\chi$	canonical value $0.3 \text{ GeV}/c^2 \text{ cm}^{-3}$ within factor 2–3	[26]
present-day CMB temperature	$T_0$	$2.7255(6) \text{ K}$	[27, 28]
present-day CMB dipole amplitude	$d$	$3.3621(10) \text{ mK}$	[27, 29]
Solar velocity with respect to CMB	$v_\odot$	$369.82(11) \text{ km s}^{-1}$ towards $(l, b) = (264.021(11)^\circ, 48.253(5)^\circ)$	[29]
Local Group velocity with respect to CMB	$v_{\text{LG}}$	$620(15) \text{ km s}^{-1}$ towards $(l, b) = (271.9(20)^\circ, 29.6(14)^\circ)$	[29]
number density of CMB photons	$n_\gamma$	$410.7(3) (T/2.7255)^3 \text{ cm}^{-3}$	[30]
density of CMB photons	$\rho_\gamma$	$4.645(4) (T/2.7255)^4 \times 10^{-34} \text{ g cm}^{-3} \approx 0.260 \text{ eV cm}^{-3}$	[30]
entropy density/Boltzmann constant	$s/k$	$2.891.2 (T/2.7255)^3 \text{ cm}^{-3}$	[30]
present-day Hubble expansion rate	$H_0$	$100 h \text{ km s}^{-1} \text{ Mpc}^{-1} = h \times (9.777\,752 \text{ Gyr})^{-1}$	[31]
scaling factor for Hubble expansion rate	$h$	$0.674(5)$	[2, 32]
Hubble length	$c/H_0$	$0.925\,0629 \times 10^{26} h^{-1} \text{ m} = 1.372(10) \times 10^{26} \text{ m}$	
scaling for cosmological constant	$c^2/3H_0^2$	$2.85247 \times 10^{51} h^{-2} \text{ m}^2 = 6.21(9) \times 10^{51} \text{ m}^2$	
critical density of the Universe	$\rho_{\text{crit}} = 3H_0^2/8\pi G_N$	$1.878\,34(4) \times 10^{-29} h^2 \text{ g cm}^{-3}$ $= 1.053\,672(24) \times 10^{-5} h^2 (\text{GeV}/c^2) \text{ cm}^{-3}$ $= 2.77536627 \times 10^{11} h^2 M_\odot \text{ Mpc}^{-3}$	
baryon-to-photon ratio (from BBN)	$\eta = n_b/n_\gamma$	$5.8 \times 10^{-10} \leq \eta \leq 6.5 \times 10^{-10}$ (95% CL)	[33]
number density of baryons	$n_b$	$2.515(17) \times 10^{-7} \text{ cm}^{-3}$ $(2.4 \times 10^{-7} < n_b < 2.7 \times 10^{-7}) \text{ cm}^{-3}$ (95% CL, $\eta \times n_\gamma$ )	[2, 3, 34, 35]
CMB radiation density of the Universe	$\Omega_\gamma = \rho_\gamma/\rho_{\text{crit}}$	$2.473 \times 10^{-5} (T/2.7255)^4 h^{-2} = 5.38(15) \times 10^{-5}$	[30]
--- <i>Planck</i> 2018 6-parameter fit to flat $\Lambda$ CDM cosmology ---			
baryon density of the Universe	$\Omega_b = \rho_b/\rho_{\text{crit}}$	$\ddagger 0.02237(15) h^{-2} = \dagger 0.0493(6)$	[2, 3, 27]
cold dark matter density of the Universe	$\Omega_c = \rho_c/\rho_{\text{crit}}$	$\ddagger 0.1200(12) h^{-2} = \dagger 0.265(7)$	[2, 3, 27]
100 $\times$ approx to $r_*/D_A$	$100 \times \theta_{\text{MC}}$	$\ddagger 1.04092(31)$	[2, 3, 27]
reionization optical depth	$\tau$	$\ddagger 0.054(7)$	[2, 3, 27]
ln(power prim. curv. pert.) ( $k_0 = 0.05 \text{ Mpc}^{-1}$ )	$\ln(10^{10} \Delta_{\mathcal{R}}^2)$	$\ddagger 3.044(14)$	[2, 3, 27]
scalar spectral index	$n_s$	$\ddagger 0.965(4)$	[2, 3, 27]
pressureless matter parameter	$\Omega_m = \Omega_c + \Omega_b$	$\dagger 0.315(7)$	[2, 3]
dark energy density parameter	$\Omega_\Lambda$	$\dagger 0.685(7)$	[2, 3]
energy density of dark energy	$\rho_\Lambda$	$\dagger 5.83(16) \times 10^{-30} \text{ g cm}^{-3}$	[2]
cosmological constant	$\Lambda$	$\dagger 1.088(30) \times 10^{-56} \text{ cm}^{-2}$	[2]
fluctuation amplitude at $8 h^{-1} \text{ Mpc}$ scale	$\sigma_8$	$\dagger 0.811(6)$	[2, 3]

Quantity	Symbol, equation.	Value	Reference, footnote
redshift of matter-radiation equality	$z_{\text{eq}}$	$\dagger 3402(26)$	[2, 36]
age at matter-radiation equality	$t_{\text{eq}}$	$\dagger 51.1(8)$ kyr	[2, 37]
redshift at which optical depth equals unity	$z_*$	$\dagger 1089.92(25)$	[2]
comoving size of sound horizon at $z_*$	$r_*$	$\dagger 144.43(26)$ Mpc	[2, 38]
age when optical depth equals unity	$t_*$	$\dagger 372.9(10)$ kyr	[2, 37]
redshift at half reionization	$z_i$	$\dagger 7.7(7)$	[2, 39]
age at half reionization	$t_i$	$\dagger 690(90)$ Myr	[2]
redshift when acceleration was zero	$z_q$	$\dagger 0.636(18)$	[2, 37]
age when acceleration was zero	$t_q$	$\dagger 7.70(10)$ Gyr	[2]
age of the Universe today	$t_0$	$\dagger 13.797(23)$ Gyr	[2]
effective number of neutrinos	$N_{\text{eff}}$	$\# 2.99(17)$	[2, 40, 41]
sum of neutrino masses	$\Sigma m_\nu$	$\# < 0.12$ eV (95%, CMB + BAO); $\geq 0.06$ eV (mixing)	[2, 41–43]
neutrino density of the Universe	$\Omega_\nu = h^{-2} \Sigma m_{\nu_j} / 93.14$ eV	$\# < 0.003$ (95%, CMB + BAO); $\geq 0.0012$ (mixing)	[2, 42, 43]
curvature	$\Omega_K$	$\# 0.0007(19)$	[2]
running spectral index, $k_0 = 0.05$ Mpc $^{-1}$	$dn_s/d \ln k$	$\# -0.004(7)$	[2]
tensor-to-scalar field perturbations ratio,	$r_{0.002} = T/S$	$\# < 0.058$ (95% CL, $k_0 = 0.002$ Mpc $^{-1}$ , no running)	[2, 44, 45]
dark energy equation of state parameter	$w$	$-1.028(31)$	[2, 46]
primordial helium fraction	$Y_p$	$0.245(4)$	[47]

$\dagger$  Parameter in 6-parameter  $\Lambda$ CDM fit;  $\ddagger$  Derived parameter in 6-parameter  $\Lambda$ CDM fit;  $\#$  Extended model parameter, *Planck* + BAO data [2].

## References

- [1] CODATA recommended 2018 values of the fundamental physical constants: <https://physics.nist.gov/cuu/Constants/index.html>.
- [2] Planck Collab. 2018 Results VI (2018), [arXiv:1807.06209].
- [3] O. Lahav & A.R. Liddle, “The Cosmological Parameters,” Sec. 25.1 in this *Review*.
- [4] *The Astronomical Almanac for the year 2020*.
- [5] The astronomical unit of length (au) in meters is re-defined (IAU XXVIII General Assembly 2012, Resolution B2) to be a conventional unit of length in agreement with the value adopted in IAU XXVII 2009 Resolution B2. It is to be used with all time scales.
- [6] The distance at which 1 au subtends 1 arc sec: 1 au divided by  $\pi/648000$ .
- [7] IAU XVI GA 1976, Recommendations.
- [8] The number of square degrees on a sphere is  $360^2/\pi = 41\,259.9\dots$
- [9] Observationally determined mass parameter  $G_N M \times 2/c^2$  [1] for either the Sun or the Earth, where  $\mathcal{G}M_\odot = 1.327\,124\,4 \times 10^{20}$  m $^3$  s $^{-2}$  and  $\mathcal{G}M_\oplus = 3.986\,004 \times 10^{14}$  m $^3$  s $^{-2}$  [48].
- [10]  $G_N M \div G_N$  [1].
- [11] IAU XXIX GA, 2015, Resolution B3, “on recommended nominal conversion constants ...” Calligraphic symbol indicates recommended nominal value.
- [12] See also G. Kopp & J.L. Lean, *Geophys. Res. Lett.* **38**, L01706 (2011), who give  $(1360.8 \pm 0.6)$  W m $^{-2}$ ; see paper for caveats and other measurements.
- [13]  $4\pi(1\text{ au})^2 \times S_\odot$ , assuming isotropic irradiance.
- [14] S. Chandrasekhar, *Astrophys. J.* **74**, 81 (1931).
- [15] This value assumes an ideal Fermi gas, using a numerical constant from the Lane-Emden equation [49], and with  $\mu$  the average molecular weight per electron, defined relative to the mass of the single-proton hydrogen atom.
- [16] A. S. Eddington, *Mon. Not. R. Astron. Soc.* **77**, 16 (1916).
- [17] The maximum luminosity assuming pure electron scattering for the outward force arising from radiation pressure:  $4\pi G_N M m_p c / \sigma_T$ .
- [18] IAU XXIX GA, 2015, Resolution B2, “on recommended zero points for the absolute and apparent bolometric magnitude scales”.
- [19] J. Oke and J. Gunn, *Astrophys. J.* **266**, 713 (1983).
- [20] J. Bovy, *Mon. Not. R. Astron. Soc.* **468**, 1, L63 (2017).
- [21] R. Abuter *et al.* (2019), [arXiv:1904.05721].
- [22] IAU XIX GA (1985) suggested that “in cases where standardization on a common set of galactic parameters is desirable” that the values  $R_0 = (8.5 \pm 1.0)$  kpc and  $\theta_0 = (220 \pm 20)$  km s $^{-1}$  should be used.
- [23] M. Reid *et al.*, *Astrophys. J.* **783**, 2, 130 (2014).
- [24] T. Piffl *et al.*, *Astron. Astrophys.* **562**, A91 (2014), [arXiv:1309.4293].
- [25] C. F. McKee, A. Parravano and D. J. Hollenbach, *Astrophys. J.* **814**, 1, 13 (2015); This is representative of other published estimates.
- [26] J. Read, *J. Phys.* **G41**, 063101 (2014); A. M. Green, *J. Phys.* **G44**, 8, 084001 (2017); The conclusion is  $\rho_{\text{DM}}^{\text{local}} = 0.39 \pm 0.03$  GeV cm $^{-3}$ .
- [27] D. Scott & G.F. Smoot, “Cosmic Microwave Background,” Sec. 29 in this *Review*.
- [28] D. J. Fixsen, *Astrophys. J.* **707**, 916 (2009).
- [29] Planck Collab. 2018 Results I (2018), [arXiv:1807.06205].
- [30]  $n_\gamma = \frac{2c(3)}{\pi^2} \left(\frac{kT}{hc}\right)^3$ ;  $\rho_\gamma = \frac{\pi^2 kT}{15 c^2} \left(\frac{kT}{hc}\right)^3$ ;  $s/k = \frac{2.43 \cdot \pi^2}{11.45} \left(\frac{kT}{hc}\right)^3$ ;  $kT/hc = 11.90\,235(T/2.7255)/\text{cm}$ .
- [31] Conversion using length of sidereal year.
- [32] Distance-ladder estimates of  $H_0$  tend to give higher values than derived from the CMB, *e.g.* Riess *et al.*, *Astrophys. J.* **826**, 56 (2016) give  $h = 0.732 \pm 0.017$ ; for discussion see O. Lahav & A.R. Liddle, “The Cosmological Parameters,” Sec. 25.1 in this *Review*.
- [33] B.D. Fields, P. Molaro, & S. Sarkar, “Big-Bang Nucleosynthesis,” Sec. 24 in this *Review*.
- [34]  $n_b$  depends only upon the measured  $\Omega_b h^2$ , the average baryon mass at the present epoch [35], and  $G_N$ :  $n_b = (\Omega_b h^2)(h^{-2} \rho_{\text{crit}})/(0.93711 \text{ GeV}/c^2 \text{ per baryon})$ .
- [35] G. Steigman, *JCAP* **0610**, 016 (2006).
- [36] Here ‘radiation’ includes three species of light neutrinos as well as photons.
- [37] D. Scott, A. Narimani and D. N. Page, *Phys. Canada* **70**, 258 (2014).
- [38] D.H. Weinberg, M. White, “Dark Energy,” Sec. 28 in this *Review*.
- [39] Planck Collab. Intern. Results XLVI, *Astron. & Astrophys.* **596**, A108 (2016) extend the range by  $\Delta z \approx 1$ , depending on the reionization model.
- [40] Summary Tables in this *Review* list  $N_\nu = 2.984(8)$  (Standard Model fits to LEP-SLC data). Because neutrinos are not completely decoupled at  $e^\pm$  annihilation, the effective number of massless neutrino species is 3.045, rather than 3.
- [41] J. Lesgourgues & L. Verde, “Neutrinos in Cosmology,” Sec. 26 in this *Review*.
- [42] The sum is over all neutrino mass eigenstates, the lower limit following from neutrino mixing results reported in this *Review* combined with the assumptions that there are three light neutrinos and that the lightest neutrino is substantially less massive than the others.
- [43] Astrophysical determinations of  $\sum m_{\nu_j}$ , reported in the Full Listings of this *Review* under “Sum of the neutrino masses,” range from  $< 0.17$  eV to  $< 2.3$  eV in papers published since 2003.
- [44] P. A. R. Ade *et al.* (BICEP2, Keck Array), *Phys. Rev. Lett.* **121**, 221301 (2018).
- [45] *Planck* data alone give  $r < 0.10$ ; adding the BICEP/Keck data tightens the constraint.
- [46] This constraint uses BAO and SNe data, as described in Ref. [2]; see discussion in D.H. Weinberg, M. White, “Dark Energy,” Sec. 28 in this *Review*.
- [47] E. Aver, K. A. Olive and E. D. Skillman, *JCAP* **1507**, 07, 011 (2015).
- [48] IAU XXIX GA 2015, Resolution B2.
- [49] G. P. Horedt, *Astrophys. Space Sci.* **126**, 2, 357 (1986).

### 3. International System of Units (SI)

See “The International System of Units (SI),” NIST Special Publication **330**, B.N. Taylor, ed. (USGPO, Washington, DC, 1991); and “Guide for the Use of the International System of Units (SI),” NIST Special Publication **811**, 1995 edition, B.N. Taylor (USGPO, Washington, DC, 1995).

Physical quantity	Name of unit	Symbol
<i>Base units</i>		
length	meter	m
mass	kilogram	kg
time	second	s
electric current	ampere	A
thermodynamic temperature	kelvin	K
amount of substance	mole	mol
luminous intensity	candela	cd
<i>Derived units with special names</i>		
plane angle	radian	rad
solid angle	steradian	sr
frequency	hertz	Hz
energy	joule	J
force	newton	N
pressure	pascal	Pa
power	watt	W
electric charge	coulomb	C
electric potential	volt	V
electric resistance	ohm	$\Omega$
electric conductance	siemens	S
electric capacitance	farad	F
magnetic flux	weber	Wb
inductance	henry	H
magnetic flux density	tesla	T
luminous flux	lumen	lm
illuminance	lux	lx
celsius temperature	degree celsius	$^{\circ}\text{C}$
activity (of a radioactive source)*	becquerel	Bq
absorbed dose (of ionizing radiation)*	gray	Gy
dose equivalent*	sievert	Sv

#### SI prefixes

$10^{24}$	yotta	(Y)
$10^{21}$	zetta	(Z)
$10^{18}$	exa	(E)
$10^{15}$	peta	(P)
$10^{12}$	tera	(T)
$10^9$	giga	(G)
$10^6$	mega	(M)
$10^3$	kilo	(k)
$10^2$	hecto	(h)
10	deca	(da)
$10^{-1}$	deci	(d)
$10^{-2}$	centi	(c)
$10^{-3}$	milli	(m)
$10^{-6}$	micro	( $\mu$ )
$10^{-9}$	nano	(n)
$10^{-12}$	pico	(p)
$10^{-15}$	femto	(f)
$10^{-18}$	atto	(a)
$10^{-21}$	zepto	(z)
$10^{-24}$	yocto	(y)

\*See our section 37, on “Radioactivity and radiation protection.”

4. Periodic Table of the Elements

**Table 4.1.** Revised June 2019 by D.E. Groom (LBNL). The atomic number (top left) is the number of protons in the nucleus. The atomic masses (bottom) of stable elements are weighted by isotopic abundances in the Earth's surface. Atomic masses are relative to the mass of <sup>12</sup>C, defined to be exactly 12 unified atomic mass units (u) (1 u ≈ 1 g/mole). The exceptions are Th, Pa, and U, which have no stable isotopes but do have characteristic terrestrial compositions. Relative isotopic abundances often vary considerably, both in natural and commercial samples; this is reflected in the number of significant figures given for the mass. Masses may be found at <https://www.nist.gov/pml/atomic-weights-and-isotopic-compositions-relative-atomic-masses>. If there is no stable isotope, the atomic mass of the most stable isotope known as of June 2019 is given in parentheses.

IUPAC announced verification of the discoveries of elements 113, 115, 117, and 118 in December 2015. The names were approved November 2016. The 7th period of the periodic table is now complete.

		PERIODIC TABLE OF THE ELEMENTS																																																																															
		VIIA										VIA						VA		IVA		IIIA		IIA		IA																																																							
		17										16						15		14		13		12		11		10		9		8		7		6		5		4		3		2																																					
		VIIA										VIA						VA		IVA		IIIA		IIA		IA		VIII		VIIA		VIA		VA		IVA		IIIA		IIA		IA																																							
		F										O						N		C		B		5		4		3		2		1		18		17		16		15		14		13		12		11		10		9		8		7		6		5		4		3		2															
		fluorine										oxygen						nitrogen		carbon		boron		5		4		3		2		18		17		16		15		14		13		12		11		10		9		8		7		6		5		4		3		2																	
		18										S						P		Si		Al		13		12		11		10		9		8		7		6		5		4		3		2																																			
		argon										sulfur						phosphorus		silicon		aluminum		13		12		11		10		9		8		7		6		5		4		3		2																																			
		35.45										32.06						30.973761998		28.085		26.9815385		20.1797		18.998403163		15.999		14.007		12.0107		10.81		9.012182		7.94		6.94		4.002602		2.016																																					
1	H	1.008	2	He	4.002602																	18	Ar	39.948																	18	Ar	39.948																	VIIIA	He	4.002602																			
3	Li	6.94	4	Be	9.012182																	10	Ne	20.1797																	10	Ne	20.1797																	VIIIA	Ne	20.1797																			
11	Na	22.98976928	12	Mg	24.305																	11	IB																		11	IB																		11	IB																		VIIIA	Ne	20.1797
19	K	39.0983	20	Ca	40.078																	19	IIA																		19	IIA																		19	IIA																		VIIIA	Ne	20.1797
37	Rb	85.4678	38	Sr	87.62																	37	IIIB																		37	IIIB																		37	IIIB																		VIIIA	Ne	20.1797
55	Cs	132.90545196	56	Ba	137.327																	55	IIIB																		55	IIIB																		55	IIIB																		VIIIA	Ne	20.1797
87	Fr	(223.01974)	88	Ra	(226.02541)																	87	IIIB																		87	IIIB																		87	IIIB																		VIIIA	Ne	20.1797
Lanthanide series		57	La	138.90547	58	Ce	140.116	59	Pr	140.90766	60	Nd	144.242	61	Pm	(144.91276)	62	Sm	150.36	63	Eu	151.964	64	Gd	157.25	65	Tb	158.92535	66	Dy	162.500	67	Ho	164.93033	68	Er	167.259	69	Tm	168.93422	70	Yb	173.054	71	Lu	174.9668																																			
Actinide series		89	Ac	(227.02775)	90	Th	232.0377	91	Pa	231.03588	92	U	238.02891	93	Np	(237.04817)	94	Pu	(244.06420)	95	Am	(243.06138)	96	Cm	(247.07035)	97	Bk	(247.07031)	98	Cf	(251.07959)	99	Es	(252.08298)	100	Fm	(257.09511)	101	Md	(258.109844)	102	No	(259.10103)	103	Lr	(262.10961)																																			

## 5. Electronic Structure of the Elements

**Table 5.1.** Reviewed 2011 by J.E. Sansonetti (NIST). The electronic configurations and the ionization energies are from the NIST database, “Ground Levels and Ionization Energies for the Neutral Atoms,” W.C. Martin, A. Musgrove, S. Kotochigova, and J.E. Sansonetti, [http://www.nist.gov/pml/data/ion\\_energy.cfm](http://www.nist.gov/pml/data/ion_energy.cfm). The electron configuration for, say, iron indicates an argon electronic core (see argon) plus six 3*d* electrons and two 4*s* electrons.

Element	Electron configuration (3 <i>d</i> <sup>5</sup> = five 3 <i>d</i> electrons, <i>etc.</i> )	Ground state $2S+1L_J$	Ionization energy (eV)
1 H Hydrogen	1 <i>s</i>	$^2S_{1/2}$	13.5984
2 He Helium	1 <i>s</i> <sup>2</sup>	$^1S_0$	24.5874
3 Li Lithium	(He) 2 <i>s</i>	$^2S_{1/2}$	5.3917
4 Be Beryllium	(He) 2 <i>s</i> <sup>2</sup>	$^1S_0$	9.3227
5 B Boron	(He) 2 <i>s</i> <sup>2</sup> 2 <i>p</i>	$^2P_{1/2}$	8.2980
6 C Carbon	(He) 2 <i>s</i> <sup>2</sup> 2 <i>p</i> <sup>2</sup>	$^3P_0$	11.2603
7 N Nitrogen	(He) 2 <i>s</i> <sup>2</sup> 2 <i>p</i> <sup>3</sup>	$^4S_{3/2}$	14.5341
8 O Oxygen	(He) 2 <i>s</i> <sup>2</sup> 2 <i>p</i> <sup>4</sup>	$^3P_2$	13.6181
9 F Fluorine	(He) 2 <i>s</i> <sup>2</sup> 2 <i>p</i> <sup>5</sup>	$^2P_{3/2}$	17.4228
10 Ne Neon	(He) 2 <i>s</i> <sup>2</sup> 2 <i>p</i> <sup>6</sup>	$^1S_0$	21.5645
11 Na Sodium	(Ne) 3 <i>s</i>	$^2S_{1/2}$	5.1391
12 Mg Magnesium	(Ne) 3 <i>s</i> <sup>2</sup>	$^1S_0$	7.6462
13 Al Aluminum	(Ne) 3 <i>s</i> <sup>2</sup> 3 <i>p</i>	$^2P_{1/2}$	5.9858
14 Si Silicon	(Ne) 3 <i>s</i> <sup>2</sup> 3 <i>p</i> <sup>2</sup>	$^3P_0$	8.1517
15 P Phosphorus	(Ne) 3 <i>s</i> <sup>2</sup> 3 <i>p</i> <sup>3</sup>	$^4S_{3/2}$	10.4867
16 S Sulfur	(Ne) 3 <i>s</i> <sup>2</sup> 3 <i>p</i> <sup>4</sup>	$^3P_2$	10.3600
17 Cl Chlorine	(Ne) 3 <i>s</i> <sup>2</sup> 3 <i>p</i> <sup>5</sup>	$^2P_{3/2}$	12.9676
18 Ar Argon	(Ne) 3 <i>s</i> <sup>2</sup> 3 <i>p</i> <sup>6</sup>	$^1S_0$	15.7596
19 K Potassium	(Ar) 4 <i>s</i>	$^2S_{1/2}$	4.3407
20 Ca Calcium	(Ar) 4 <i>s</i> <sup>2</sup>	$^1S_0$	6.1132
21 Sc Scandium	(Ar) 3 <i>d</i> 4 <i>s</i> <sup>2</sup>	$^2D_{3/2}$	6.5615
22 Ti Titanium	(Ar) 3 <i>d</i> <sup>2</sup> 4 <i>s</i> <sup>2</sup>	$^3F_2$	6.8281
23 V Vanadium	(Ar) 3 <i>d</i> <sup>3</sup> 4 <i>s</i> <sup>2</sup>	$^4F_{3/2}$	6.7462
24 Cr Chromium	(Ar) 3 <i>d</i> <sup>5</sup> 4 <i>s</i>	$^7S_3$	6.7665
25 Mn Manganese	(Ar) 3 <i>d</i> <sup>5</sup> 4 <i>s</i> <sup>2</sup>	$^6S_{5/2}$	7.4340
26 Fe Iron	(Ar) 3 <i>d</i> <sup>6</sup> 4 <i>s</i> <sup>2</sup>	$^5D_4$	7.9024
27 Co Cobalt	(Ar) 3 <i>d</i> <sup>7</sup> 4 <i>s</i> <sup>2</sup>	$^4F_{9/2}$	7.8810
28 Ni Nickel	(Ar) 3 <i>d</i> <sup>8</sup> 4 <i>s</i> <sup>2</sup>	$^3F_4$	7.6399
29 Cu Copper	(Ar) 3 <i>d</i> <sup>10</sup> 4 <i>s</i>	$^2S_{1/2}$	7.7264
30 Zn Zinc	(Ar) 3 <i>d</i> <sup>10</sup> 4 <i>s</i> <sup>2</sup>	$^1S_0$	9.3942
31 Ga Gallium	(Ar) 3 <i>d</i> <sup>10</sup> 4 <i>s</i> <sup>2</sup> 4 <i>p</i>	$^2P_{1/2}$	5.9993
32 Ge Germanium	(Ar) 3 <i>d</i> <sup>10</sup> 4 <i>s</i> <sup>2</sup> 4 <i>p</i> <sup>2</sup>	$^3P_0$	7.8994
33 As Arsenic	(Ar) 3 <i>d</i> <sup>10</sup> 4 <i>s</i> <sup>2</sup> 4 <i>p</i> <sup>3</sup>	$^4S_{3/2}$	9.7886
34 Se Selenium	(Ar) 3 <i>d</i> <sup>10</sup> 4 <i>s</i> <sup>2</sup> 4 <i>p</i> <sup>4</sup>	$^3P_2$	9.7524
35 Br Bromine	(Ar) 3 <i>d</i> <sup>10</sup> 4 <i>s</i> <sup>2</sup> 4 <i>p</i> <sup>5</sup>	$^2P_{3/2}$	11.8138
36 Kr Krypton	(Ar) 3 <i>d</i> <sup>10</sup> 4 <i>s</i> <sup>2</sup> 4 <i>p</i> <sup>6</sup>	$^1S_0$	13.9996
37 Rb Rubidium	(Kr) 5 <i>s</i>	$^2S_{1/2}$	4.1771
38 Sr Strontium	(Kr) 5 <i>s</i> <sup>2</sup>	$^1S_0$	5.6949
39 Y Yttrium	(Kr) 4 <i>d</i> 5 <i>s</i> <sup>2</sup>	$^2D_{3/2}$	6.2173
40 Zr Zirconium	(Kr) 4 <i>d</i> <sup>2</sup> 5 <i>s</i> <sup>2</sup>	$^3F_2$	6.6339
41 Nb Niobium	(Kr) 4 <i>d</i> <sup>4</sup> 5 <i>s</i>	$^6D_{1/2}$	6.7589
42 Mo Molybdenum	(Kr) 4 <i>d</i> <sup>5</sup> 5 <i>s</i>	$^7S_3$	7.0924
43 Tc Technetium	(Kr) 4 <i>d</i> <sup>5</sup> 5 <i>s</i> <sup>2</sup>	$^6S_{5/2}$	7.28
44 Ru Ruthenium	(Kr) 4 <i>d</i> <sup>7</sup> 5 <i>s</i>	$^5F_5$	7.3605
45 Rh Rhodium	(Kr) 4 <i>d</i> <sup>8</sup> 5 <i>s</i>	$^4F_{9/2}$	7.4589
46 Pd Palladium	(Kr) 4 <i>d</i> <sup>10</sup>	$^1S_0$	8.3369
47 Ag Silver	(Kr) 4 <i>d</i> <sup>10</sup> 5 <i>s</i>	$^2S_{1/2}$	7.5762
48 Cd Cadmium	(Kr) 4 <i>d</i> <sup>10</sup> 5 <i>s</i> <sup>2</sup>	$^1S_0$	8.9938

49	In	Indium	(Kr)4d <sup>10</sup> 5s <sup>2</sup> 5p		<sup>2</sup> P <sub>1/2</sub>	5.7864
50	Sn	Tin	(Kr)4d <sup>10</sup> 5s <sup>2</sup> 5p <sup>2</sup>		<sup>3</sup> P <sub>0</sub>	7.3439
51	Sb	Antimony	(Kr)4d <sup>10</sup> 5s <sup>2</sup> 5p <sup>3</sup>		<sup>4</sup> S <sub>3/2</sub>	8.6084
52	Te	Tellurium	(Kr)4d <sup>10</sup> 5s <sup>2</sup> 5p <sup>4</sup>		<sup>3</sup> P <sub>2</sub>	9.0096
53	I	Iodine	(Kr)4d <sup>10</sup> 5s <sup>2</sup> 5p <sup>5</sup>		<sup>2</sup> P <sub>3/2</sub>	10.4513
54	Xe	Xenon	(Kr)4d <sup>10</sup> 5s <sup>2</sup> 5p <sup>6</sup>		<sup>1</sup> S <sub>0</sub>	12.1298
55	Cs	Cesium	(Xe) 6s		<sup>2</sup> S <sub>1/2</sub>	3.8939
56	Ba	Barium	(Xe) 6s <sup>2</sup>		<sup>1</sup> S <sub>0</sub>	5.2117
57	La	Lanthanum	(Xe) 5d 6s <sup>2</sup>		<sup>2</sup> D <sub>3/2</sub>	5.5769
58	Ce	Cerium	(Xe)4f 5d 6s <sup>2</sup>		<sup>1</sup> G <sub>4</sub>	5.5387
59	Pr	Praseodymium	(Xe)4f <sup>3</sup> 6s <sup>2</sup>	L	<sup>4</sup> I <sub>9/2</sub>	5.473
60	Nd	Neodymium	(Xe)4f <sup>4</sup> 6s <sup>2</sup>	a	<sup>5</sup> I <sub>4</sub>	5.5250
61	Pm	Promethium	(Xe)4f <sup>5</sup> 6s <sup>2</sup>	n	<sup>6</sup> H <sub>5/2</sub>	5.582
62	Sm	Samarium	(Xe)4f <sup>6</sup> 6s <sup>2</sup>	t	<sup>7</sup> F <sub>0</sub>	5.6437
63	Eu	Europium	(Xe)4f <sup>7</sup> 6s <sup>2</sup>	h	<sup>8</sup> S <sub>7/2</sub>	5.6704
64	Gd	Gadolinium	(Xe)4f <sup>7</sup> 5d 6s <sup>2</sup>	a	<sup>9</sup> D <sub>2</sub>	6.1498
65	Tb	Terbium	(Xe)4f <sup>9</sup> 6s <sup>2</sup>	n	<sup>6</sup> H <sub>15/2</sub>	5.8638
66	Dy	Dysprosium	(Xe)4f <sup>10</sup> 6s <sup>2</sup>	i	<sup>5</sup> I <sub>8</sub>	5.9389
67	Ho	Holmium	(Xe)4f <sup>11</sup> 6s <sup>2</sup>	d	<sup>4</sup> I <sub>15/2</sub>	6.0215
68	Er	Erbium	(Xe)4f <sup>12</sup> 6s <sup>2</sup>	e	<sup>3</sup> H <sub>6</sub>	6.1077
69	Tm	Thulium	(Xe)4f <sup>13</sup> 6s <sup>2</sup>	s	<sup>2</sup> F <sub>7/2</sub>	6.1843
70	Yb	Ytterbium	(Xe)4f <sup>14</sup> 6s <sup>2</sup>		<sup>1</sup> S <sub>0</sub>	6.2542
71	Lu	Lutetium	(Xe)4f <sup>14</sup> 5d 6s <sup>2</sup>		<sup>2</sup> D <sub>3/2</sub>	5.4259
72	Hf	Hafnium	(Xe)4f <sup>14</sup> 5d <sup>2</sup> 6s <sup>2</sup>	T	<sup>3</sup> F <sub>2</sub>	6.8251
73	Ta	Tantalum	(Xe)4f <sup>14</sup> 5d <sup>3</sup> 6s <sup>2</sup>	r	<sup>4</sup> F <sub>3/2</sub>	7.5496
74	W	Tungsten	(Xe)4f <sup>14</sup> 5d <sup>4</sup> 6s <sup>2</sup>	a	<sup>5</sup> D <sub>0</sub>	7.8640
75	Re	Rhenium	(Xe)4f <sup>14</sup> 5d <sup>5</sup> 6s <sup>2</sup>	n	<sup>6</sup> S <sub>5/2</sub>	7.8335
76	Os	Osmium	(Xe)4f <sup>14</sup> 5d <sup>6</sup> 6s <sup>2</sup>	s	<sup>5</sup> D <sub>4</sub>	8.4382
77	Ir	Iridium	(Xe)4f <sup>14</sup> 5d <sup>7</sup> 6s <sup>2</sup>	i	<sup>4</sup> F <sub>9/2</sub>	8.9670
78	Pt	Platinum	(Xe)4f <sup>14</sup> 5d <sup>9</sup> 6s	t	<sup>3</sup> D <sub>3</sub>	8.9588
79	Au	Gold	(Xe)4f <sup>14</sup> 5d <sup>10</sup> 6s	i	<sup>2</sup> S <sub>1/2</sub>	9.2255
80	Hg	Mercury	(Xe)4f <sup>14</sup> 5d <sup>10</sup> 6s <sup>2</sup>	n	<sup>1</sup> S <sub>0</sub>	10.4375
81	Tl	Thallium	(Xe)4f <sup>14</sup> 5d <sup>10</sup> 6s <sup>2</sup> 6p		<sup>2</sup> P <sub>1/2</sub>	6.1082
82	Pb	Lead	(Xe)4f <sup>14</sup> 5d <sup>10</sup> 6s <sup>2</sup> 6p <sup>2</sup>		<sup>3</sup> P <sub>0</sub>	7.4167
83	Bi	Bismuth	(Xe)4f <sup>14</sup> 5d <sup>10</sup> 6s <sup>2</sup> 6p <sup>3</sup>		<sup>4</sup> S <sub>3/2</sub>	7.2855
84	Po	Polonium	(Xe)4f <sup>14</sup> 5d <sup>10</sup> 6s <sup>2</sup> 6p <sup>4</sup>		<sup>3</sup> P <sub>2</sub>	8.414
85	At	Astatine	(Xe)4f <sup>14</sup> 5d <sup>10</sup> 6s <sup>2</sup> 6p <sup>5</sup>		<sup>2</sup> P <sub>3/2</sub>	
86	Rn	Radon	(Xe)4f <sup>14</sup> 5d <sup>10</sup> 6s <sup>2</sup> 6p <sup>6</sup>		<sup>1</sup> S <sub>0</sub>	10.7485
87	Fr	Francium	(Rn) 7s		<sup>2</sup> S <sub>1/2</sub>	4.0727
88	Ra	Radium	(Rn) 7s <sup>2</sup>		<sup>1</sup> S <sub>0</sub>	5.2784
89	Ac	Actinium	(Rn) 6d 7s <sup>2</sup>		<sup>2</sup> D <sub>3/2</sub>	5.3807
90	Th	Thorium	(Rn) 6d <sup>2</sup> 7s <sup>2</sup>		<sup>3</sup> F <sub>2</sub>	6.3067
91	Pa	Protactinium	(Rn)5f <sup>2</sup> 6d 7s <sup>2</sup>	A	<sup>4</sup> K <sub>11/2</sub> *	5.89
92	U	Uranium	(Rn)5f <sup>3</sup> 6d 7s <sup>2</sup>	c	<sup>5</sup> L <sub>6</sub> *	6.1939
93	Np	Neptunium	(Rn)5f <sup>4</sup> 6d 7s <sup>2</sup>	t	<sup>6</sup> L <sub>11/2</sub> *	6.2657
94	Pu	Plutonium	(Rn)5f <sup>6</sup> 7s <sup>2</sup>	i	<sup>7</sup> F <sub>0</sub>	6.0260
95	Am	Americium	(Rn)5f <sup>7</sup> 7s <sup>2</sup>	n	<sup>8</sup> S <sub>7/2</sub>	5.9738
96	Cm	Curium	(Rn)5f <sup>7</sup> 6d 7s <sup>2</sup>	d	<sup>9</sup> D <sub>2</sub>	5.9914
97	Bk	Berkelium	(Rn)5f <sup>9</sup> 7s <sup>2</sup>	e	<sup>6</sup> H <sub>15/2</sub>	6.1979
98	Cf	Californium	(Rn)5f <sup>10</sup> 7s <sup>2</sup>	s	<sup>5</sup> I <sub>8</sub>	6.2817
99	Es	Einsteinium	(Rn)5f <sup>11</sup> 7s <sup>2</sup>		<sup>4</sup> I <sub>15/2</sub>	6.3676
100	Fm	Fermium	(Rn)5f <sup>12</sup> 7s <sup>2</sup>		<sup>3</sup> H <sub>6</sub>	6.50
101	Md	Mendelevium	(Rn)5f <sup>13</sup> 7s <sup>2</sup>		<sup>2</sup> F <sub>7/2</sub>	6.58
102	No	Nobelium	(Rn)5f <sup>14</sup> 7s <sup>2</sup>		<sup>1</sup> S <sub>0</sub>	6.65
103	Lr	Lawrencium	(Rn)5f <sup>14</sup> 7s <sup>2</sup> 7p?		<sup>2</sup> P <sub>1/2</sub> ?	4.9?
104	Rf	Rutherfordium	(Rn)5f <sup>14</sup> 6d <sup>2</sup> 7s <sup>2</sup> ?		<sup>3</sup> F <sub>2</sub> ?	6.0?

\* The usual *LS* coupling scheme does not apply for these three elements. See the introductory note to the NIST table from which this table is taken.

## 6. Atomic and Nuclear Properties of Materials

**Table 6.1** Abridged from [pdg.lbl.gov/AtomicNuclearProperties](http://pdg.lbl.gov/AtomicNuclearProperties) by D.E. Groom (2017). See web pages for more detail about entries in this table and for several hundred others. Parentheses in the  $dE/dx$  and density columns indicate gases at 20° C and 1 atm. Boiling points are at 1 atm. Refractive indices  $n$  are evaluated at the sodium D line blend (589.2 nm); values  $\gg 1$  in brackets indicate  $(n - 1) \times 10^6$  for gases at 0° C and 1 atm.

Material	$Z$	$A$	$\langle Z/A \rangle$	Nucl.coll. length $\lambda_T$ {g cm <sup>-2</sup> }	Nucl.inter. length $\lambda_I$ {g cm <sup>-2</sup> }	Rad.len. $X_0$ {g cm <sup>-2</sup> }	$dE/dx _{\min}$ { MeV g <sup>-1</sup> cm <sup>2</sup> }	Density {g cm <sup>-3</sup> } ({g ℓ <sup>-1</sup> })	Melting point (K)	Boiling point (K)	Refract. index @ Na D
H <sub>2</sub>	1	1.008(7)	0.99212	42.8	52.0	63.05	(4.103)	0.071(0.084)	13.81	20.28	1.11[132.]
D <sub>2</sub>	1	2.014101764(8)	0.49650	51.3	71.8	125.97	(2.053)	0.169(0.168)	18.7	23.65	1.11[138.]
He	2	4.002602(2)	0.49967	51.8	71.0	94.32	(1.937)	0.125(0.166)		4.220	1.02[35.0]
Li	3	6.94(2)	0.43221	52.2	71.3	82.78	1.639	0.534	453.6	1615.	
Be	4	9.0121831(5)	0.44384	55.3	77.8	65.19	1.595	1.848	1560.	2744.	
C diamond	6	12.0107(8)	0.49955	59.2	85.8	42.70	1.725	3.520			2.419
C graphite	6	12.0107(8)	0.49955	59.2	85.8	42.70	1.742	2.210	Sublimes at 4098. K		
N <sub>2</sub>	7	14.007(2)	0.49976	61.1	89.7	37.99	(1.825)	0.807(1.165)	63.15	77.29	1.20[298.]
O <sub>2</sub>	8	15.999(3)	0.50002	61.3	90.2	34.24	(1.801)	1.141(1.332)	54.36	90.20	1.22[271.]
F <sub>2</sub>	9	18.998403163(6)	0.47372	65.0	97.4	32.93	(1.676)	1.507(1.580)	53.53	85.03	[195.]
Ne	10	20.1797(6)	0.49555	65.7	99.0	28.93	(1.724)	1.204(0.839)	24.56	27.07	1.09[67.1]
Al	13	26.9815385(7)	0.48181	69.7	107.2	24.01	1.615	2.699	933.5	2792.	
Si	14	28.0855(3)	0.49848	70.2	108.4	21.82	1.664	2.329	1687.	3538.	3.95
Cl <sub>2</sub>	17	35.453(2)	0.47951	73.8	115.7	19.28	(1.630)	1.574(2.980)	171.6	239.1	[773.]
Ar	18	39.948(1)	0.45059	75.7	119.7	19.55	(1.519)	1.396(1.662)	83.81	87.26	1.23[281.]
Ti	22	47.867(1)	0.45961	78.8	126.2	16.16	1.477	4.540	1941.	3560.	
Fe	26	55.845(2)	0.46557	81.7	132.1	13.84	1.451	7.874	1811.	3134.	
Cu	29	63.546(3)	0.45636	84.2	137.3	12.86	1.403	8.960	1358.	2835.	
Ge	32	72.630(1)	0.44053	86.9	143.0	12.25	1.370	5.323	1211.	3106.	
Sn	50	118.710(7)	0.42119	98.2	166.7	8.82	1.263	7.310	505.1	2875.	
Xe	54	131.293(6)	0.41129	100.8	172.1	8.48	(1.255)	2.953(5.483)	161.4	165.1	1.39[701.]
W	74	183.84(1)	0.40252	110.4	191.9	6.76	1.145	19.300	3695.	5828.	
Pt	78	195.084(9)	0.39983	112.2	195.7	6.54	1.128	21.450	2042.	4098.	
Au	79	196.966569(5)	0.40108	112.5	196.3	6.46	1.134	19.320	1337.	3129.	
Pb	82	207.2(1)	0.39575	114.1	199.6	6.37	1.122	11.350	600.6	2022.	
U	92	[238.02891(3)]	0.38651	118.6	209.0	6.00	1.081	18.950	1408.	4404.	
Air (dry, 1 atm)			0.49919	61.3	90.1	36.62	(1.815)	(1.205)		78.80	[289]
Shielding concrete			0.50274	65.1	97.5	26.57	1.711	2.300			
Borosilicate glass (Pyrex)			0.49707	64.6	96.5	28.17	1.696	2.230			
Lead glass			0.42101	95.9	158.0	7.87	1.255	6.220			
Standard rock			0.50000	66.8	101.3	26.54	1.688	2.650			
Methane (CH <sub>4</sub> )			0.62334	54.0	73.8	46.47	(2.417)	(0.667)	90.68	111.7	[444.]
Ethane (C <sub>2</sub> H <sub>6</sub> )			0.59861	55.0	75.9	45.66	(2.304)	(1.263)	90.36	184.5	
Propane (C <sub>3</sub> H <sub>8</sub> )			0.58962	55.3	76.7	45.37	(2.262)	0.493(1.868)	85.52	231.0	
Butane (C <sub>4</sub> H <sub>10</sub> )			0.59497	55.5	77.1	45.23	(2.278)	(2.489)	134.9	272.6	
Octane (C <sub>8</sub> H <sub>18</sub> )			0.57778	55.8	77.8	45.00	2.123	0.703	214.4	398.8	
Paraffin (CH <sub>3</sub> (CH <sub>2</sub> ) <sub>n≈23</sub> CH <sub>3</sub> )			0.57275	56.0	78.3	44.85	2.088	0.930			
Nylon (type 6, 6/6)			0.54790	57.5	81.6	41.92	1.973	1.18			
Polycarbonate (Lexan)			0.52697	58.3	83.6	41.50	1.886	1.20			
Polyethylene ([CH <sub>2</sub> CH <sub>2</sub> ] <sub>n</sub> )			0.57034	56.1	78.5	44.77	2.079	0.89			
Polyethylene terephthalate (Mylar)			0.52037	58.9	84.9	39.95	1.848	1.40			
Polyimide film (Kapton)			0.51264	59.2	85.5	40.58	1.820	1.42			
Polymethylmethacrylate (acrylic)			0.53937	58.1	82.8	40.55	1.929	1.19			1.49
Polypropylene			0.55998	56.1	78.5	44.77	2.041	0.90			
Polystyrene ([C <sub>6</sub> H <sub>5</sub> CHCH <sub>2</sub> ] <sub>n</sub> )			0.53768	57.5	81.7	43.79	1.936	1.06			1.59
Polytetrafluoroethylene (Teflon)			0.47992	63.5	94.4	34.84	1.671	2.20			
Polyvinyltoluene			0.54141	57.3	81.3	43.90	1.956	1.03			1.58
Aluminum oxide (sapphire)			0.49038	65.5	98.4	27.94	1.647	3.970	2327.	3273.	1.77
Barium fluoride (BaF <sub>2</sub> )			0.42207	90.8	149.0	9.91	1.303	4.893	1641.	2533.	1.47
Bismuth germanate (BGO)			0.42065	96.2	159.1	7.97	1.251	7.130	1317.		2.15
Carbon dioxide gas (CO <sub>2</sub> )			0.49989	60.7	88.9	36.20	1.819	(1.842)			[449.]
Solid carbon dioxide (dry ice)			0.49989	60.7	88.9	36.20	1.787	1.563	Sublimes at 194.7 K		
Cesium iodide (CsI)			0.41569	100.6	171.5	8.39	1.243	4.510	894.2	1553.	1.79
Lithium fluoride (LiF)			0.46262	61.0	88.7	39.26	1.614	2.635	1121.	1946.	1.39
Lithium hydride (LiH)			0.50321	50.8	68.1	79.62	1.897	0.820	965.		
Lead tungstate (PbWO <sub>4</sub> )			0.41315	100.6	168.3	7.39	1.229	8.300	1403.		2.20
Silicon dioxide (SiO <sub>2</sub> , fused quartz)			0.49930	65.2	97.8	27.05	1.699	2.200	1986.	3223.	1.46
Sodium chloride (NaCl)			0.47910	71.2	110.1	21.91	1.847	2.170	1075.	1738.	1.54
Sodium iodide (NaI)			0.42697	93.1	154.6	9.49	1.305	3.667	933.2	1577.	1.77
Water (H <sub>2</sub> O)			0.55509	58.5	83.3	36.08	1.992	1.000	273.1	373.1	1.33
Silica aerogel			0.50093	65.0	97.3	27.25	1.740	0.200	(0.03 H <sub>2</sub> O, 0.97 SiO <sub>2</sub> )		

Material	Dielectric constant ( $\kappa = \epsilon/\epsilon_0$ ) ( ) is $(\kappa-1)\times 10^6$ for gas	Young's modulus [ $10^6$ psi]	Coeff. of thermal expansion [ $10^{-6}$ cm/cm- $^{\circ}$ C]	Specific heat [cal/g- $^{\circ}$ C]	Electrical resistivity [ $\mu\Omega$ cm(@ $^{\circ}$ C)]	Thermal conductivity [cal/cm- $^{\circ}$ C-sec]
H <sub>2</sub>	(253.9)	—	—	—	—	—
He	(64)	—	—	—	—	—
Li	—	—	56	0.86	8.55(0 $^{\circ}$ )	0.17
Be	—	37	12.4	0.436	5.885(0 $^{\circ}$ )	0.38
C	—	0.7	0.6–4.3	0.165	1375(0 $^{\circ}$ )	0.057
N <sub>2</sub>	(548.5)	—	—	—	—	—
O <sub>2</sub>	(495)	—	—	—	—	—
Ne	(127)	—	—	—	—	—
Al	—	10	23.9	0.215	2.65(20 $^{\circ}$ )	0.53
Si	11.9	16	2.8–7.3	0.162	—	0.20
Ar	(517)	—	—	—	—	—
Ti	—	16.8	8.5	0.126	50(0 $^{\circ}$ )	—
Fe	—	28.5	11.7	0.11	9.71(20 $^{\circ}$ )	0.18
Cu	—	16	16.5	0.092	1.67(20 $^{\circ}$ )	0.94
Ge	16.0	—	5.75	0.073	—	0.14
Sn	—	6	20	0.052	11.5(20 $^{\circ}$ )	0.16
Xe	—	—	—	—	—	—
W	—	50	4.4	0.032	5.5(20 $^{\circ}$ )	0.48
Pt	—	21	8.9	0.032	9.83(0 $^{\circ}$ )	0.17
Pb	—	2.6	29.3	0.038	20.65(20 $^{\circ}$ )	0.083
U	—	—	36.1	0.028	29(20 $^{\circ}$ )	0.064



## 7. Electromagnetic Relations

Revised September 2005 by H.G. Spieler (LBNL).

Quantity	Gaussian CGS	SI
Conversion factors:		
Charge:	$2.997\,924\,58 \times 10^9$ esu	$= 1\text{ C} = 1\text{ A s}$
Potential:	$(1/299.792\,458)$ statvolt (ergs/esu)	$= 1\text{ V} = 1\text{ J C}^{-1}$
Magnetic field:	$10^4$ gauss = $10^4$ dyne/esu	$= 1\text{ T} = 1\text{ N A}^{-1}\text{m}^{-1}$
	$\mathbf{F} = q(\mathbf{E} + \frac{\mathbf{v}}{c} \times \mathbf{B})$	$\mathbf{F} = q(\mathbf{E} + \mathbf{v} \times \mathbf{B})$
	$\nabla \cdot \mathbf{D} = 4\pi\rho$ $\nabla \times \mathbf{H} - \frac{1}{c} \frac{\partial \mathbf{D}}{\partial t} = \frac{4\pi}{c} \mathbf{J}$ $\nabla \cdot \mathbf{B} = 0$ $\nabla \times \mathbf{E} + \frac{1}{c} \frac{\partial \mathbf{B}}{\partial t} = 0$	$\nabla \cdot \mathbf{D} = \rho$ $\nabla \times \mathbf{H} - \frac{\partial \mathbf{D}}{\partial t} = \mathbf{J}$ $\nabla \cdot \mathbf{B} = 0$ $\nabla \times \mathbf{E} + \frac{\partial \mathbf{B}}{\partial t} = 0$
Constitutive relations:	$\mathbf{D} = \mathbf{E} + 4\pi\mathbf{P}$ , $\mathbf{H} = \mathbf{B} - 4\pi\mathbf{M}$	$\mathbf{D} = \epsilon_0\mathbf{E} + \mathbf{P}$ , $\mathbf{H} = \mathbf{B}/\mu_0 - \mathbf{M}$
Linear media:	$\mathbf{D} = \epsilon\mathbf{E}$ , $\mathbf{H} = \mathbf{B}/\mu$ 1 1	$\mathbf{D} = \epsilon\mathbf{E}$ , $\mathbf{H} = \mathbf{B}/\mu$ $\epsilon_0 = 8.854\,187 \dots \times 10^{-12}$ F m <sup>-1</sup> $\mu_0 = 4\pi \times 10^{-7}$ N A <sup>-2</sup>
	$\mathbf{E} = -\nabla V - \frac{1}{c} \frac{\partial \mathbf{A}}{\partial t}$ $\mathbf{B} = \nabla \times \mathbf{A}$	$\mathbf{E} = -\nabla V - \frac{\partial \mathbf{A}}{\partial t}$ $\mathbf{B} = \nabla \times \mathbf{A}$
	$V = \sum_{\text{charges}} \frac{q_i}{r_i} = \int \frac{\rho(\mathbf{r}')}{ \mathbf{r} - \mathbf{r}' } d^3x'$ $\mathbf{A} = \frac{1}{c} \oint \frac{I d\boldsymbol{\ell}}{ \mathbf{r} - \mathbf{r}' } = \frac{1}{c} \int \frac{\mathbf{J}(\mathbf{r}')}{ \mathbf{r} - \mathbf{r}' } d^3x'$	$V = \frac{1}{4\pi\epsilon_0} \sum_{\text{charges}} \frac{q_i}{r_i} = \frac{1}{4\pi\epsilon_0} \int \frac{\rho(\mathbf{r}')}{ \mathbf{r} - \mathbf{r}' } d^3x'$ $\mathbf{A} = \frac{\mu_0}{4\pi} \oint \frac{I d\boldsymbol{\ell}}{ \mathbf{r} - \mathbf{r}' } = \frac{\mu_0}{4\pi} \int \frac{\mathbf{J}(\mathbf{r}')}{ \mathbf{r} - \mathbf{r}' } d^3x'$
	$\mathbf{E}'_{\parallel} = \mathbf{E}_{\parallel}$ $\mathbf{E}'_{\perp} = \gamma(\mathbf{E}_{\perp} + \frac{1}{c} \mathbf{v} \times \mathbf{B})$ $\mathbf{B}'_{\parallel} = \mathbf{B}_{\parallel}$ $\mathbf{B}'_{\perp} = \gamma(\mathbf{B}_{\perp} - \frac{1}{c} \mathbf{v} \times \mathbf{E})$	$\mathbf{E}'_{\parallel} = \mathbf{E}_{\parallel}$ $\mathbf{E}'_{\perp} = \gamma(\mathbf{E}_{\perp} + \mathbf{v} \times \mathbf{B})$ $\mathbf{B}'_{\parallel} = \mathbf{B}_{\parallel}$ $\mathbf{B}'_{\perp} = \gamma(\mathbf{B}_{\perp} - \frac{1}{c^2} \mathbf{v} \times \mathbf{E})$
	$\frac{1}{4\pi\epsilon_0} = c^2 \times 10^{-7} \text{ N A}^{-2} = 8.987\,55 \dots \times 10^9 \text{ m F}^{-1}$ ; $\frac{\mu_0}{4\pi} = 10^{-7} \text{ N A}^{-2}$ ; $c = \frac{1}{\sqrt{\mu_0\epsilon_0}} = 2.997\,924\,58 \times 10^8 \text{ m s}^{-1}$	

### 7.1. Impedances (SI units)

$\rho$  = resistivity at room temperature in  $10^{-8} \Omega \text{ m}$ :  
 $\sim 1.7$  for Cu  $\sim 5.5$  for W  
 $\sim 2.4$  for Au  $\sim 73$  for SS 304  
 $\sim 2.8$  for Al  $\sim 100$  for Nichrome  
 (Al alloys may have double the Al value.)

For alternating currents, instantaneous current  $I$ , voltage  $V$ , angular frequency  $\omega$ :

$$V = V_0 e^{j\omega t} = ZI. \quad (7.1)$$

Impedance of self-inductance  $L$ :  $Z = j\omega L$ .

Impedance of capacitance  $C$ :  $Z = 1/j\omega C$ .

Impedance of free space:  $Z = \sqrt{\mu_0/\epsilon_0} = 376.7 \Omega$ .

High-frequency surface impedance of a good conductor:

$$Z = \frac{(1+j)\rho}{\delta}, \quad \text{where } \delta = \text{skin depth}; \quad (7.2)$$

$$\delta = \sqrt{\frac{\rho}{\pi\nu\mu}} \approx \frac{6.6 \text{ cm}}{\sqrt{\nu \text{ (Hz)}}} \quad \text{for Cu}. \quad (7.3)$$

### 7.2. Capacitors, inductors, and transmission Lines

The capacitance between two parallel plates of area  $A$  spaced by the distance  $d$  and enclosing a medium with the dielectric constant  $\epsilon$  is

$$C = K\epsilon A/d, \quad (7.4)$$

where the correction factor  $K$  depends on the extent of the fringing field. If the dielectric fills the capacitor volume without extending beyond the electrodes, the correction factor  $K \approx 0.8$  for capacitors of typical geometry.

The inductance at high frequencies of a straight wire whose length  $\ell$  is much greater than the wire diameter  $d$  is

$$L \approx 2.0 \left[ \frac{\text{nH}}{\text{cm}} \right] \cdot \ell \left( \ln \left( \frac{4\ell}{d} \right) - 1 \right). \quad (7.5)$$

For very short wires, representative of vias in a printed circuit board, the inductance is

$$L(\text{in nH}) \approx \ell/d. \quad (7.6)$$

A transmission line is a pair of conductors with inductance  $L$  and capacitance  $C$ . The characteristic impedance  $Z = \sqrt{L/C}$  and the phase velocity  $v_p = 1/\sqrt{LC} = 1/\sqrt{\mu\epsilon}$ , which decreases with the inverse square root of the dielectric constant of the medium. Typical coaxial and ribbon cables have a propagation delay of about 5 ns/cm. The impedance of a coaxial cable with outer diameter  $D$  and inner diameter  $d$  is

$$Z = 60 \Omega \cdot \frac{1}{\sqrt{\epsilon_r}} \ln \frac{D}{d}, \quad (7.7)$$

where the relative dielectric constant  $\epsilon_r = \epsilon/\epsilon_0$ . A pair of parallel wires of diameter  $d$  and spacing  $a > 2.5d$  has the impedance

$$Z = 120 \Omega \cdot \frac{1}{\sqrt{\epsilon_r}} \ln \frac{2a}{d}. \quad (7.8)$$

This yields the impedance of a wire at a spacing  $h$  above a ground plane,

$$Z = 60 \Omega \cdot \frac{1}{\sqrt{\epsilon_r}} \ln \frac{4h}{d}. \quad (7.9)$$

A common configuration utilizes a thin rectangular conductor above a ground plane with an intermediate dielectric (microstrip). Detailed calculations for this and other transmission line configurations are given by Gunston.\*

### 7.3. Synchrotron radiation (CGS units)

For a particle of charge  $e$ , velocity  $v = \beta c$ , and energy  $E = \gamma mc^2$ , traveling in a circular orbit of radius  $R$ , the classical energy loss per revolution  $\delta E$  is

$$\delta E = \frac{4\pi}{3} \frac{e^2}{R} \beta^3 \gamma^4. \quad (7.10)$$

For high-energy electrons or positrons ( $\beta \approx 1$ ), this becomes

$$\delta E \text{ (in MeV)} \approx 0.0885 [E(\text{in GeV})]^4/R(\text{in m}). \quad (7.11)$$

For  $\gamma \gg 1$ , the energy radiated per revolution into the photon energy interval  $d(\hbar\omega)$  is

$$dI = \frac{8\pi}{9} \alpha \gamma F(\omega/\omega_c) d(\hbar\omega), \quad (7.12)$$

where  $\alpha = e^2/\hbar c$  is the fine-structure constant and

$$\omega_c = \frac{3\gamma^3 c}{2R} \quad (7.13)$$

is the critical frequency. The normalized function  $F(y)$  is

$$F(y) = \frac{9}{8\pi} \sqrt{3} y \int_y^\infty K_{5/3}(x) dx, \quad (7.14)$$

where  $K_{5/3}(x)$  is a modified Bessel function of the third kind. For electrons or positrons,

$$\hbar\omega_c \text{ (in keV)} \approx 2.22 [E(\text{in GeV})]^3/R(\text{in m}). \quad (7.15)$$

Fig. 7.1 shows  $F(y)$  over the important range of  $y$ .

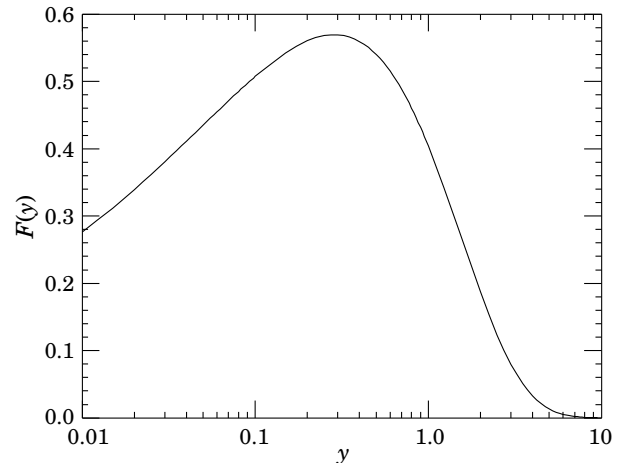


Figure 7.1: The normalized synchrotron radiation spectrum  $F(y)$ .

For  $\gamma \gg 1$  and  $\omega \ll \omega_c$ ,

$$\frac{dI}{d(\hbar\omega)} \approx 3.3\alpha (\omega R/c)^{1/3}, \quad (7.16)$$

whereas for

$$\gamma \gg 1 \text{ and } \omega \gtrsim 3\omega_c,$$

$$\frac{dI}{d(\hbar\omega)} \approx \sqrt{\frac{3\pi}{2}} \alpha \gamma \left( \frac{\omega}{\omega_c} \right)^{1/2} e^{-\omega/\omega_c} \left[ 1 + \frac{55}{72} \frac{\omega_c}{\omega} + \dots \right]. \quad (7.17)$$

The radiation is confined to angles  $\lesssim 1/\gamma$  relative to the instantaneous direction of motion. For  $\gamma \gg 1$ , where Eq. (7.12) applies, the mean number of photons emitted per revolution is

$$N_\gamma = \frac{5\pi}{\sqrt{3}} \alpha \gamma, \quad (7.18)$$

and the mean energy per photon is

$$\langle \hbar\omega \rangle = \frac{8}{15\sqrt{3}} \hbar\omega_c. \quad (7.19)$$

When  $\langle \hbar\omega \rangle \gtrsim O(E)$ , quantum corrections are important.

\* M.A.R. Gunston. Microwave Transmission Line Data, Noble Publishing Corp., Atlanta (1997) ISBN 1-884932-57-6, TK6565.T73G85.

See J.D. Jackson, *Classical Electrodynamics*, 3<sup>rd</sup> edition (John Wiley & Sons, New York, 1998) for more formulae and details. (Note that earlier editions had  $\omega_c$  twice as large as Eq. (7.13).

## 8. Naming Scheme for Hadrons

Revised August 2019 by V. Burkert (Jefferson Lab), S. Eidelman (Budker Inst., Novosibirsk; Novosibirsk U.), C. Hanhart (Jülich), E. Klempt (Bonn U.), R.E. Mitchell (Indiana U.), U. Thoma (Bonn U.), L. Tiator (KPH, JGU Mainz) and R.L. Workman (George Washington U.).

In the 1986 edition [1], the Particle Data Group extended and systematized the naming scheme for mesons and baryons. The extensions were necessary in order to name the new particles containing *c* or *b* quarks that were rapidly being discovered. With the discoveries of particles that are candidates for states with more complicated structures than just  $q\bar{q}$  or  $qqq$ , it is necessary to extend the naming scheme again.

### 8.1 “Neutral-flavor” mesons

The naming of mesons is based on their quantum numbers. Although we use names established within the naive quark model, the name does *not* necessarily designate a (predominantly)  $q\bar{q}$  state. In other words, the name provides information on the quantum numbers of a given state and not about its dominant component, which might well be  $q\bar{q}$  (if allowed) or tetraquark, molecule, etc. In many cases, exotic states will be difficult to distinguish from  $q\bar{q}$  states and will likely mix with them, and we make no attempt to, e.g., distinguish those that are “mostly gluonium” from those that are “mostly  $q\bar{q}$ .”

**Table 8.1:** Symbols for mesons with strangeness and heavy-flavor quantum numbers equal to zero. States that do not yet appear in the RPP are listed in parentheses.

$J^{PC} = \left\{ \begin{array}{cccc} 0^{-+} & 1^{+-} & 1^{--} & 0^{++} \\ 2^{-+} & 3^{+-} & 2^{--} & 1^{++} \\ \vdots & \vdots & \vdots & \vdots \end{array} \right.$				
Minimal quark content				
$u\bar{d}, u\bar{u} - d\bar{d}, d\bar{u} (I = 1)$	$\pi$	$b$	$\rho$	$a$
$d\bar{d} + u\bar{u}$ and/or $s\bar{s} (I = 0)$	$\eta, \eta'$	$h, h'$	$\omega, \phi$	$f, f'$
$c\bar{c}$	$\eta_c$	$h_c$	$\psi^*$	$\chi_c$
$b\bar{b}$	$\eta_b$	$h_b$	$\Upsilon$	$\chi_b$
$I = 1$ with $c\bar{c}$	$(\Pi_c)$	$Z_c$	$R_c$	$(W_c)$
$I = 1$ with $b\bar{b}$	$(\Pi_b)$	$Z_b$	$(R_b)$	$(W_b)$

\*The  $J/\psi$  remains the  $J/\psi$ .

Table 8.1 shows the names for mesons having strangeness and all heavy-flavor quantum numbers equal to zero. The rows of Table 8.1 give the minimal  $q\bar{q}$  content. The columns give the possible parity/charge-conjugation states,

$$PC = --, +-, --, \text{ and } ++ .$$

Within the naive quark model, these combinations correspond one-to-one to the angular-momentum state  $^{2S+1}L_J$  of the  $q\bar{q}$  system being

$$^1(L \text{ even})_J, ^1(L \text{ odd})_J, ^3(L \text{ even})_J, \text{ or } ^3(L \text{ odd})_J ,$$

respectively. Here  $S$ ,  $L$ , and  $J$  are the spin, orbital, and total angular momenta of the  $q\bar{q}$  system. Within the naive quark model, the quantum numbers are related by  $P = (-1)^{L+1}$ ,  $C = (-1)^{L+S}$ , and  $G$  parity  $= (-1)^{L+S+I}$ , where the quantum number  $C$  is only relevant to neutral mesons with neutral-flavor quantum numbers and  $G$  extends to isovector mesons; see the review on the quark model. These expressions impose restrictions on the quantum numbers that are allowed for  $q\bar{q}$  states. However, they do not apply to more complicated structures such as tetraquarks.

The spin  $J$  is added as a subscript in the name except for pseudoscalar and vector mesons, and the mass is added in parentheses for mesons that decay strongly. However, for some of the familiar mesons (e.g.  $\eta', \phi, \omega$ ), we omit the mass.

Measurements of the mass, quark content (where relevant), and quantum numbers  $I$ ,  $J$ ,  $P$ , and  $C$  (or  $G$ ) of a meson thus deter-

mine its symbol. Conversely, these properties may be inferred unambiguously from the symbol. The name  $X$  is used for states with still unknown quantum numbers.

The mass label used in particle names is chosen using the best information available when a name is assigned. A more accurate value of a particle mass may become available at a later time. PDG will decide on a case-by-case basis whether to revise the mass label, taking into account the updated information.

With  $u$ ,  $d$ , and  $s$  quarks, there are two isospin-0 mesons. A prime is used to distinguish one from the other (e.g.  $\eta$  and  $\eta'$ ). Vector mesons decoupling to  $u\bar{u} + d\bar{d}$  and  $s\bar{s}$  (ideal mixing) are labeled  $\omega$  and  $\phi$ , respectively. As usual, we assign the spectroscopic name (e.g.  $\Upsilon(1S)$ ) as the primary name to most of those  $\psi$ ,  $\Upsilon$ , and  $\chi$  states whose spectroscopic identity is known. We use the form  $\Upsilon(9460)$  as an alternative, and as the primary name when the spectroscopic identity is not known.

Since the top quark is so heavy that it decays too rapidly to form bound states, no name is assigned to structures like  $t\bar{t}$ .

Mesons with quantum numbers  $J^{PC} = 0^{-+}, 0^{+-}, 1^{-+}, 2^{+-}, 3^{-+}$ , etc. cannot be  $q\bar{q}$ . For such a “manifestly exotic” meson, we use the same symbol as for a  $q\bar{q}$  meson; the exotic nature of the meson can be inferred from the values of the  $P$  and  $C$  quantum numbers (given by the symbol), and the spin  $J$  (given by the subscript). For example, an isospin-0  $1^{-+}$  meson containing only  $u$ ,  $d$ , and  $s$  quarks and antiquarks would be denoted  $\eta_1$  and an isospin-1  $0^{--}$  meson containing only  $u$ ,  $d$ , and  $s$  quarks and antiquarks would be denoted  $\rho_0$ .

The last two lines of Table 8.1 list isospin-1 states that also contain hidden heavy flavor, i.e. whose minimal quark content includes  $c\bar{c}$  or  $b\bar{b}$ . We have assigned new names to these states, in keeping with the practice in the light-quark sector, where the  $I = 0$  and  $I = 1$  states have distinct names. The currently established  $I = 1$  states in the heavy-quark sector have quantum numbers  $J^{PC} = 1^{+-}$  and the proposed scheme keeps their original names  $Z$ .

### 8.2 Remarks on “neutral-flavor” mesons with hidden charm or bottom not classified as $q\bar{q}$

In the heavy-quark sector, there are several states with properties – such as masses, decay patterns, and widths – that are in disagreement with predictions from the naive quark model. For example, the vector state at 4260 MeV does not decay into  $D\bar{D}$ , although within the naive quark model its quantum numbers would call for this decay channel to be dominant. In recent literature, these states have been called  $X$ ,  $Y$ , or  $Z$ , with their masses added in parentheses. This nomenclature conflicts with the rules outlined in the previous section, since the meson names are not related to their quantum numbers. However, these states have properties in conflict with the naive quark model and therefore deserve some special labeling.

Therefore in the Review of Particle Physics we will keep two names, one that carries the quantum number information and the other the original name. However, the former name will be given priority. In particular, it will be used when the particle appears as a decay product. Thus, in the Listings as well as Summary Tables from the 2018 edition onwards (listed are only some examples of the particles that appear in the Summary Tables),

- $X(3872)$  will appear as ‘ $\chi_{c1}(3872)$  also known as  $X(3872)$ ’;
- $X(3900)^\pm$  will appear as ‘ $Z_c(3900)^\pm$ ’;
- $X(4260)$  will appear as ‘ $\psi(4260)$  also known as  $Y(4260)$ ’;

In addition, states with quantum numbers allowed by the naive quark model but showing some peculiarities, such as an unusual decay pattern, will have the following information in the header:

This state shows properties different from a conventional  $q\bar{q}$  state. A candidate for an exotic structure. See the minireview on non- $q\bar{q}$  states.

The states that cannot be classified as  $q\bar{q}$  states (such as charged states with strong decays to heavy quarkonia) will have in the header:

Properties incompatible with a  $q\bar{q}$  structure (exotic state). See the minireview on non- $q\bar{q}$  states.

The names  $Z_c$  and  $Z_b$  used in the literature for isovector states in the  $c\bar{c}$  and  $b\bar{b}$  sector, respectively, will now also be the official PDG names. No heavy isovector  $PC = -+, --, \text{ or } ++$  states have yet been confirmed, but provisional names for such states –  $H$ ,  $R$ , and  $W$ , respectively – are listed in Table 8.1. Note that the heavy isovector  $PC = ++$  states were predicted to exist as spin partners of the  $Z$  states in [2], where the name  $W$  was also introduced.

By analogy to the light-quark sector, states with quantum numbers that are in conflict with the naive quark model are labeled according to their  $I$ ,  $P$ ,  $C$ , and spin  $J$ . The exotic nature can be inferred from the quantum numbers.

### 8.3 Mesons with nonzero $S$ , $C$ and/or $B$

Mesons with nonzero strangeness  $S$  or heavy flavor  $C$  and/or  $B$  are not eigenstates of charge conjugation, and in each of them one of the quarks is heavier than the other (as above, states containing top quarks are not considered). The rules have been and remain:

1. The main symbol is an upper-case italic letter indicating the heavier quark as follows:

$$s \rightarrow \bar{K} \quad c \rightarrow D \quad b \rightarrow \bar{B},$$

We use the convention that *the flavor quantum number and the charge of a quark have the same sign*. Thus the strangeness of the  $s$  quark is negative, the charm of the  $c$  quark is positive, and the bottomness of the  $b$  quark is negative. The effect of this convention is as follows: *any flavor carried by a charged meson has the same sign as its charge*. Thus the  $K^+$ ,  $D^+$ , and  $B^+$  have positive strangeness, charm, and bottomness, respectively, and all have positive  $I_3$ . The  $D_s^+$  has positive charm and strangeness. Furthermore, the  $\Delta(\text{flavor}) = \Delta Q$  rule, best known for the strange kaons, applies to every flavor.

2. If the lighter quark is not a  $u$  or a  $d$  quark, its identity is given by a subscript. The  $D_s^+$  is an example.
3. When the spin-parity is in the natural series,  $J^P = 0^+, 1^-, 2^+, \dots$ , a superscript “\*” is added.
4. The spin is added as a subscript except for pseudoscalar or vector mesons.

### 8.4 Ordinary (3-quark) baryons

All baryons having quantum numbers consistent with a minimal quark content of three quarks are denoted by the symbols  $N$ ,  $\Delta$ ,  $\Lambda$ ,  $\Sigma$ ,  $\Xi$ , and  $\Omega$  introduced more than 50 years ago. These symbols are followed by  $J^P$  signifying their spin  $J$  and parity  $P$ . For those where the minimal content involves one or more heavier quarks than the light ( $u$ ,  $d$ , and  $s$ ) quarks, subscripts are added to their symbols, ( $c$  and  $b$ ) as appropriate. The rules are:

1. Baryons with minimal content of *three*  $u$  and/or  $d$  quarks are  $N$ 's (isospin 1/2) or  $\Delta$ 's (isospin 3/2).
2. Baryons with *two*  $u$  and/or  $d$  quarks are  $\Lambda$ 's (isospin 0) or  $\Sigma$ 's (isospin 1). If the third quark is a  $c$  or  $b$  quark, its identity is given by a subscript.
3. Baryons with *one*  $u$  or  $d$  quark are  $\Xi$ 's (isospin 1/2). One or two subscripts are used if one or both of the remaining quarks are heavy: thus  $\Xi_c$ ,  $\Xi_{cc}$ ,  $\Xi_b$ , etc.\*
4. Baryons with *no*  $u$  or  $d$  quarks are  $\Omega$ 's (isospin 0), and subscripts indicate any heavy-quark content.
5. A baryon that decays strongly has its mass in parentheses. Examples are the  $\Delta(1232)$   $3/2^+$ ,  $\Sigma(1385)$   $3/2^+$ ,  $N(1440)$   $1/2^+$ ,  $\Xi_c(2645)$   $3/2^+$ .

In short, the minimal number of  $u$  plus  $d$  quarks together with the isospin determine the main symbol, and subscripts indicate any content of heavy quarks. A  $\Sigma$  always has isospin 1, an  $\Omega$  always has isospin 0, etc.

### 8.5 Exotic baryons

In 2003, several experiments reported finding a strangeness  $S = +1$ , charge  $Q = +1$  baryon, and one experiment reported finding an  $S = -2$ ,  $Q = -2$  baryon. Baryons with such quantum numbers cannot be made from three quarks, and thus they are exotic with respect to the naive quark model. However, these “discoveries” were then ruled out by many experiments with far larger statistics: See our 2008 *Review* [3].

More recently, the LHCb collaboration found a series of candidates for pentaquark states in the  $J/\psi p$  system extracted from data on  $\Lambda_b^0 \rightarrow J/\psi K^- p$  [4,5].\*\* These have the quantum numbers of excited nucleons, but have a minimal quark content of  $c\bar{c}uud$ . Following the name established by the LHCb collaboration, we label these  $P_c^+(\text{mass})J^P$ , with the mass given in parentheses.

### 8.6 Change of meson names

For the recently discovered particles above open-flavor threshold in the charmonium and bottomonium systems (previously the “XYZ” mesons), there are a number of differences between the names newly adopted by the PDG and those that have commonly appeared in the literature. Table 8.2 maps the names now used in the PDG to former commonly used names.

#### Footnotes and References:

\* See the “Note on Charmed Baryons” in the Charmed Baryon Listings.

\*\* See our review “Pentaquarks” in the 2016 Edition.

**Table 8.2:** A comparison of current PDG names to former names commonly used in the literature.

Mesons with complete $I^G J^{PC}$ assignment	
PDG Name	Former Common Name(s)
$\psi_2(3823)^*$	$X(3823)$
$\chi_{c1}(3872)$	$X(3872)$
$Z_c(3900)$	$Z_c(3900)$
$\chi_{c2}(3930)^\dagger$	$\chi_{c2}(2P)$ , $Z(3930)$
$\chi_{c1}(4140)$	$Y(4140)$
$Z_c(4200)$	$Z_c(4200)$
$\psi(4230)$	$Y(4230)$
$R_{c0}(4240)$	$Z_c(4240)$
$\psi(4260)$	$Y(4260)$
$\chi_{c1}(4274)$	$Y(4274)$
$\psi(4360)$	$Y(4360)$
$Z_c(4430)$	$Z_c(4430)$
$\chi_{c0}(4500)$	$X(4500)$
$\psi(4660)$	$X(4630)$ , $Y(4660)$
$\chi_{c0}(4700)$	$X(4700)$
$Z_b(10610)$	$Z_b(10610)$
$Z_b(10650)$	$Z_b^{(1)}(10650)$
Mesons with incomplete $I^G J^{PC}$ assignment	
PDG Name	Former Common Name(s)
$X(3915)^\ddagger$	$\chi_{c0}(3915)$ , $X(3915)$ , $Y(3940)$
$X(3940)$	$X(3940)$
$X(4020)$	$Z_c^{(1)}(4020)$
$X(4050)^\pm$	$Z_1(4050)$
$X(4055)^\pm$	$Z_c(4055)$
$X(4160)$	$X(4160)$
$X(4250)^\pm$	$Z_2(4250)$
$X(4350)$	$X(4350)$

\*The 2016 edition used  $\psi(3823)$ .

†The 2016 edition used  $\chi_{c2}(2P)$ . The mass is now used in the name following the current prescription.

‡The 2016 edition used  $\chi_{c0}(3915)$ . The  $J^{PC}$  have since been questioned.

#### References

- [1] M. Aguilar-Benitez *et al.* (Particle Data Group), *Phys. Lett.* **170B**, 1 (1986).
- [2] M. B. Voloshin, *Phys. Rev.* **D84**, 031502 (2011), [arXiv:1105.5829].

- [3] C. Amsler *et al.* (Particle Data Group), Phys. Lett. **B667**, 1 (2008). [arXiv:1507.03414].
- [4] R. Aaij *et al.* (LHCb), Phys. Rev. Lett. **115**, 072001 (2015), [arXiv:1507.03414].
- [5] R. Aaij *et al.* (LHCb), Phys. Rev. Lett. **122**, 22, 222001 (2019), [arXiv:1904.03947].

## Standard Model and Related Topics

9. Quantum chromodynamics (rev.) . . . . .	153
10. Electroweak model and constraints on new physics (rev.) . . . . .	180
11. Higgs boson physics, status of (rev.) . . . . .	203
12. CKM quark-mixing matrix (rev.) . . . . .	261
13. $CP$ violation in the quark sector (rev.) . . . . .	271
14. Neutrino mass, mixing, and oscillations (new) . . . . .	285
15. Quark model (rev.) . . . . .	312
16. Heavy-quark & soft-collinear effective theory (rev.) . . . . .	325
17. Lattice quantum chromodynamics (rev.) . . . . .	333
18. Structure functions (rev.) . . . . .	347
19. Fragmentation functions in $e^+e^-$ , $ep$ and $pp$ collisions (rev.) . . . . .	368
20. High Energy Soft QCD and Diffraction (new) . . . . .	385



## 9. Quantum Chromodynamics

Revised August 2019 by J. Huston (Michigan State U.), K. Rabertz (KIT) and G. Zanderighi (MPI Munich).

### 9.1 Basics

Quantum Chromodynamics (QCD), the gauge field theory that describes the strong interactions of colored quarks and gluons, is the SU(3) component of the SU(3)×SU(2)×U(1) Standard Model of Particle Physics. The Lagrangian of QCD is given by

$$\mathcal{L} = \sum_q \bar{\psi}_{q,a} (i\gamma^\mu \partial_\mu \delta_{ab} - g_s \gamma^\mu t_{ab}^C \mathcal{A}_\mu^C - m_q \delta_{ab}) \psi_{q,b} - \frac{1}{4} F_{\mu\nu}^A F^{A\mu\nu}, \quad (9.1)$$

where repeated indices are summed over. The  $\gamma^\mu$  are the Dirac  $\gamma$ -matrices. The  $\psi_{q,a}$  are quark-field spinors for a quark of flavor  $q$  and mass  $m_q$ , with a color-index  $a$  that runs from  $a = 1$  to  $N_c = 3$ , *i.e.* quarks come in three “colors.” Quarks are said to be in the fundamental representation of the SU(3) color group.

The  $\mathcal{A}_\mu^C$  correspond to the gluon fields, with  $C$  running from 1 to  $N_c^2 - 1 = 8$ , *i.e.* there are eight kinds of gluon. Gluons transform under the adjoint representation of the SU(3) color group. The  $t_{ab}^C$  correspond to eight  $3 \times 3$  matrices and are the generators of the SU(3) group (*cf.* the section on “SU(3) isoscalar factors and representation matrices” in this *Review*, with  $t_{ab}^C \equiv \lambda_{ab}^C/2$ ). They encode the fact that a gluon’s interaction with a quark rotates the quark’s color in SU(3) space. The quantity  $g_s$  (or  $\alpha_s = \frac{g_s^2}{4\pi}$ ) is the QCD coupling constant. Besides quark masses, who have electroweak origin, it is the only fundamental parameter of QCD. Finally, the field tensor  $F_{\mu\nu}^A$  is given by

$$F_{\mu\nu}^A = \partial_\mu \mathcal{A}_\nu^A - \partial_\nu \mathcal{A}_\mu^A - g_s f_{ABC} \mathcal{A}_\mu^B \mathcal{A}_\nu^C, \quad (9.2)$$

$$[t^A, t^B] = i f_{ABC} t^C,$$

where the  $f_{ABC}$  are the structure constants of the SU(3) group.

Neither quarks nor gluons are observed as free particles. Hadrons are color-singlet (*i.e.* color-neutral) combinations of quarks, anti-quarks, and gluons.

Ab-initio predictive methods for QCD include lattice gauge theory and perturbative expansions in the coupling. The Feynman rules of QCD involve a quark-antiquark-gluon ( $q\bar{q}g$ ) vertex, a 3-gluon vertex (both proportional to  $g_s$ ), and a 4-gluon vertex (proportional to  $g_s^2$ ). A full set of Feynman rules is to be found for example in Refs. [1, 2].

Useful color-algebra relations include:  $t_{ab}^A t_{bc}^A = C_F \delta_{ac}$ , where  $C_F \equiv (N_c^2 - 1)/(2N_c) = 4/3$  is the color-factor (“Casimir”) associated with gluon emission from a quark;  $f_{ACD} f_{BCD} = C_A \delta_{AB}$ , where  $C_A \equiv N_c = 3$  is the color-factor associated with gluon emission from a gluon;  $t_{ab}^A t_{ab}^B = T_R \delta_{AB}$ , where  $T_R = 1/2$  is the color-factor for a gluon to split to a  $q\bar{q}$  pair.

There is freedom for an additional CP-violating term to be present in the QCD Lagrangian,  $\theta \frac{\alpha_s}{8\pi} F_{\mu\nu}^A \tilde{F}^{A\mu\nu}$ , where  $\tilde{F}^{A\mu\nu}$  is the dual of the gluon field tensor,  $\frac{1}{2} \epsilon_{\mu\nu\sigma\rho} F^{A\sigma\rho}$ , where  $\epsilon_{\mu\nu\sigma\rho}$  is the fully antisymmetric Levi-Civita symbol. Experimental limits on ultracold neutrons [3, 4] and atomic mercury [5] constrain the QCD vacuum angle to satisfy  $|\theta| \lesssim 10^{-10}$ . Further discussion is to be found in Ref. [6] and in the Axions section in the Listings of this *Review*.

This section will concentrate mainly on perturbative aspects of QCD as they relate to collider physics. Related textbooks and lecture notes include Refs. [1, 2, 7–9]. Aspects specific to Monte Carlo event generators are reviewed in the dedicated section 41. Lattice QCD is also reviewed in a section of its own, Sec. 17, with further discussion of perturbative and non-perturbative aspects to be found in the sections on “Quark Masses”, “The CKM quark-mixing matrix”, “Structure Functions”, “Fragmentation Functions”, “Passage of Particles Through Matter” and “Heavy-Quark and Soft-Collinear Effective Theory” in this *Review*.

#### 9.1.1 Running coupling

In the framework of perturbative QCD (pQCD), predictions for observables are expressed in terms of the renormalized coupling  $\alpha_s(\mu_R^2)$ , a function of an (unphysical) renormalization scale  $\mu_R$ . When one takes  $\mu_R$  close to the scale of the momentum transfer  $Q$

in a given process, then  $\alpha_s(\mu_R^2 \simeq Q^2)$  is indicative of the effective strength of the strong interaction in that process.

The coupling satisfies the following renormalization group equation (RGE):

$$\mu_R^2 \frac{d\alpha_s}{d\mu_R^2} = \beta(\alpha_s) = -(b_0 \alpha_s^2 + b_1 \alpha_s^3 + b_2 \alpha_s^4 + \dots), \quad (9.3)$$

where  $b_0 = (11C_A - 4n_f T_R)/(12\pi) = (33 - 2n_f)/(12\pi)$  is referred to as the 1-loop  $\beta$ -function coefficient, the 2-loop coefficient is  $b_1 = (17C_A^2 - n_f T_R(10C_A + 6C_F))/(24\pi^2) = (153 - 19n_f)/(24\pi^2)$ , and the 3-loop coefficient is  $b_2 = (2857 - \frac{5033}{9} n_f + \frac{325}{27} n_f^2)/(128\pi^3)$  for the SU(3) values of  $C_A$  and  $C_F$ . Here  $n_f$  is the number of quark flavours. The 4-loop coefficient,  $b_3$ , is to be found in Refs. [10, 11], while the 5-loop coefficient,  $b_4$ , is in Refs. [12–16]. The coefficients  $b_2$  and  $b_3$  (and beyond) are renormalization-scheme-dependent and given here in the modified minimal subtraction ( $\overline{\text{MS}}$ ) scheme [17], by far the most widely used scheme in QCD and the one adopted in the following.

The minus sign in Eq. (9.3) is the origin of Asymptotic Freedom [18, 19], *i.e.* the fact that the strong coupling becomes weak for processes involving large momentum transfers (“hard processes”). For momentum transfers in the 0.1–1 TeV range,  $\alpha_s \sim 0.1$ , while the theory is strongly interacting for scales around and below 1 GeV.

The  $\beta$ -function coefficients, the  $b_i$ , are given for the coupling of an *effective theory* in which  $n_f$  of the quark flavors are considered light ( $m_q \ll \mu_R$ ), and in which the remaining heavier quark flavors decouple from the theory. One may relate the coupling for the theory with  $n_f + 1$  light flavors to that with  $n_f$  flavors through an equation of the form

$$\alpha_s^{(n_f+1)}(\mu_R^2) = \alpha_s^{(n_f)}(\mu_R^2) \times \left( 1 + \sum_{n=1}^{\infty} \sum_{\ell=0}^n c_{n\ell} [\alpha_s^{(n_f)}(\mu_R^2)]^n \ln^\ell \frac{\mu_R^2}{m_h^2} \right), \quad (9.4)$$

where  $m_h$  is the mass of the  $(n_f + 1)^{\text{th}}$  flavor, and the first few  $c_{n\ell}$  coefficients are  $c_{11} = \frac{1}{6\pi}$ ,  $c_{10} = 0$ ,  $c_{22} = c_{11}^2$ ,  $c_{21} = \frac{11}{24\pi^2}$ , and  $c_{20} = -\frac{11}{72\pi^2}$  when  $m_h$  is the  $\overline{\text{MS}}$  mass at scale  $m_h$ , while  $c_{20} = \frac{7}{24\pi^2}$  when  $m_h$  is the pole mass (mass definitions are discussed below in Sec. (9.1.2) and in the review on “Quark Masses”). Terms up to  $c_{4\ell}$  are to be found in Refs. [20, 21]. Numerically, when one chooses  $\mu_R = m_h$ , the matching is a modest effect, owing to the zero value for the  $c_{10}$  coefficient. Relations between  $n_f$  and  $(n_f + 2)$  flavors where the two heavy flavors are close in mass are given to three loops in Ref. [22].

Working in an energy range where the number of flavors is taken constant, a simple exact analytic solution exists for Eq. (9.3) only if one neglects all but the  $b_0$  term, giving  $\alpha_s(\mu_R^2) = (b_0 \ln(\mu_R^2/\Lambda^2))^{-1}$ . Here  $\Lambda$  is a constant of integration, which corresponds to the scale where the perturbatively-defined coupling would diverge. Its value is indicative of the energy range where non-perturbative dynamics dominates. A convenient approximate analytic solution to the RGE that includes terms up to  $b_4$  is given by solving iteratively Eq. (9.3)

$$\alpha_s(\mu_R^2) \simeq \frac{1}{b_0 t} \left( 1 - \frac{b_1 \ell}{b_0^2 t} + \frac{b_1^2 (\ell^2 - \ell - 1) + b_0 b_2}{b_0^4 t^2} + \frac{b_1^3 (-2\ell^3 + 5\ell^2 + 4\ell - 1) - 6b_0 b_2 b_1 \ell + b_0^2 b_3}{2b_0^6 t^3} + \frac{18b_0 b_2 b_1^2 (2\ell^2 - \ell - 1) + b_1^4 (6\ell^4 - 26\ell^3 - 9\ell^2 + 24\ell + 7)}{6b_0^8 t^4} + \frac{-b_0^2 b_3 b_1 (12\ell + 1) + 2b_0^2 (5b_2^2 + b_0 b_4)}{6b_0^8 t^4} \right), \quad (9.5)$$



with  $t \equiv \ln \frac{\mu_R^2}{\Lambda^2}$  and  $\ell = \ln t$ , again parametrized in terms of a constant  $\Lambda$ . Note that Eq. (9.5) is one of several possible approximate 4-loop solutions for  $\alpha_s(\mu_R^2)$ , and that a value for  $\Lambda$  only defines  $\alpha_s(\mu_R^2)$  once one knows which particular approximation is being used. An alternative to the use of formulas such as Eq. (9.5) is to solve the RGE exactly, numerically (including the discontinuities, Eq. (9.4), at flavor thresholds). In such cases the quantity  $\Lambda$  does not directly arise (though it can be defined, *cf.* Eqs. (1–3) of Ref. [23]). For these reasons, in determinations of the coupling, it has become standard practice to quote the value of  $\alpha_s$  at a given scale (typically the mass of the  $Z$  boson,  $M_Z$ ) rather than to quote a value for  $\Lambda$ .

A discussion of determinations of the coupling and a graph illustrating its scale dependence (“running”) are to be found in Section 9.4. The RunDec package [24–26] is often used to calculate the evolution of the coupling. For a discussion of electroweak effects in the evolution of the QCD coupling, see Ref. [27] and references therein.

### 9.1.2 Quark masses

Free quarks have never been observed, which is understood as a result of a long-distance, confining property of the strong QCD force: up, down, strange, charm, and bottom quarks all *hadronize*, *i.e.* become part of a meson or baryon, on a timescale  $\sim 1/\Lambda$ ; the top quark instead decays before it has time to hadronize. This means that the question of what one means by the quark mass is a complex one, which requires one to adopt a specific prescription. A perturbatively defined prescription is the pole mass,  $m_q$ , which corresponds to the position of the divergence of the propagator. This is close to one’s physical picture of mass. However, when relating it to observable quantities, it suffers from substantial non-perturbative ambiguities (see *e.g.* Ref. [28–30]). An alternative is the  $\overline{\text{MS}}$  mass,  $\overline{m}_q(\mu_R^2)$ , which depends on the renormalization scale  $\mu_R$ .

Results for the masses of heavier quarks are often quoted either as the pole mass or as the  $\overline{\text{MS}}$  mass evaluated at a scale equal to the mass,  $\overline{m}_q(\overline{m}_q^2)$ ; light quark masses are often quoted in the  $\overline{\text{MS}}$  scheme at a scale  $\mu_R \sim 2 \text{ GeV}$ . The pole and  $\overline{\text{MS}}$  masses are related by a series that starts as  $m_q = \overline{m}_q(\overline{m}_q^2)(1 + \frac{4\alpha_s(\overline{m}_q^2)}{3\pi} + \mathcal{O}(\alpha_s^2))$ , while the scale-dependence of  $\overline{\text{MS}}$  masses is given at lowest order by

$$\mu_R^2 \frac{d\overline{m}_q(\mu_R^2)}{d\mu_R^2} = \left[ -\frac{\alpha_s(\mu_R^2)}{\pi} + \mathcal{O}(\alpha_s^2) \right] \overline{m}_q(\mu_R^2). \quad (9.6)$$

A more detailed discussion is to be found in a dedicated section of the *Review*, “Quark Masses”, with detailed formulas also in Ref. [31] and references therein.

In perturbative QCD calculations of scattering processes, it is common to work in an approximation in which one neglects (*i.e.* sets to zero) the masses of all quarks, whose mass is significantly smaller than the momentum transfer in the process.

## 9.2 Structure of QCD predictions

### 9.2.1 Fully inclusive cross sections

The simplest observables in perturbative QCD are those that do not involve initial-state hadrons and that are fully inclusive with respect to details of the final state. One example is the total cross section for  $e^+e^- \rightarrow \text{hadrons}$  at center-of-mass energy  $Q$ , for which one can write

$$\frac{\sigma(e^+e^- \rightarrow \text{hadrons}, Q)}{\sigma(e^+e^- \rightarrow \mu^+\mu^-, Q)} \equiv R(Q) = R_{\text{EW}}(Q)(1 + \delta_{\text{QCD}}(Q)), \quad (9.7)$$

where  $R_{\text{EW}}(Q)$  is the purely electroweak prediction for the ratio and  $\delta_{\text{QCD}}(Q)$  is the correction due to QCD effects. To keep the discussion simple, we can restrict our attention to energies  $Q \ll M_Z$ , where the process is dominated by photon exchange (neglecting electroweak and finite-quark-mass corrections  $R_{\text{EW}} = N_c \sum_q e_q^2$ , where the  $e_q$  are the electric charges of the quarks) and

$$\delta_{\text{QCD}}(Q) = \sum_{n=1}^{\infty} c_n \cdot \left( \frac{\alpha_s(Q^2)}{\pi} \right)^n + \mathcal{O} \left( \frac{\Lambda^4}{Q^4} \right). \quad (9.8)$$

The first four terms in the  $\alpha_s$  series expansion are then to be found in Ref. [32],

$$c_1 = 1, \quad c_2 = 1.9857 - 0.1152n_f, \quad (9.9a)$$

$$c_3 = -6.63694 - 1.20013n_f - 0.00518n_f^2 - 1.240\eta, \quad (9.9b)$$

$$c_4 = -156.61 + 18.775n_f - 0.7974n_f^2 + 0.0215n_f^3 - (17.828 - 0.575n_f)\eta, \quad (9.9c)$$

with  $\eta = (\sum e_q)^2 / (3 \sum e_q^2)$ . For corresponding expressions including also  $Z$  exchange and finite-quark-mass effects, see Refs. [33–35].

A related series holds also for the QCD corrections to the hadronic decay width of the  $\tau$  lepton, which essentially involves an integral of  $R(Q)$  over the allowed range of invariant masses of the hadronic part of the  $\tau$  decay (see *e.g.* Ref. [36]). The series expansions for QCD corrections to Higgs-boson hadronic (partial) decay widths in the limit of heavy top quark and massless light flavours at N<sup>4</sup>LO are given in Ref. [37].

One characteristic feature of Eqs. (9.8) and (9.9) is that the coefficients of  $\alpha_s^n$  increase order by order: calculations in perturbative QCD tend to converge more slowly than would be expected based just on the size of  $\alpha_s$ . The situation is significantly worse near thresholds or in the presence of tight kinematic cuts. Another feature is the existence of an extra “power-correction” term  $\mathcal{O}(\Lambda^4/Q^4)$  in Eq. (9.8), which accounts for contributions that are fundamentally non-perturbative. All high-energy QCD predictions involve power corrections  $(\Lambda/Q)^p$ , although typically the suppression of these corrections with  $Q$  is smaller than given in Eq. (9.8) where  $p = 4$ . The exact power  $p$  depends on the observable and, for many processes and observables, it is possible to introduce an operator product expansion and associate power suppressed terms with specific higher-dimension (non-perturbative) operators [38].

**Scale dependence.** In Eq. (9.8) the renormalization scale for  $\alpha_s$  has been chosen equal to  $Q$ . The result can also be expressed in terms of the coupling at an arbitrary renormalization scale  $\mu_R$ ,

$$\delta_{\text{QCD}}(Q) = \sum_{n=1}^{\infty} \bar{c}_n \left( \frac{\mu_R^2}{Q^2} \right) \cdot \left( \frac{\alpha_s(\mu_R^2)}{\pi} \right)^n + \mathcal{O} \left( \frac{\Lambda^4}{Q^4} \right), \quad (9.10)$$

where  $\bar{c}_1(\mu_R^2/Q^2) \equiv c_1$ ,  $\bar{c}_2(\mu_R^2/Q^2) = c_2 + \pi b_0 c_1 \ln(\mu_R^2/Q^2)$ ,  $\bar{c}_3(\mu_R^2/Q^2) = c_3 + (2b_0 c_2 \pi + b_1 c_1 \pi^2) \times \ln(\mu_R^2/Q^2) + b_0^2 c_1 \pi^2 \ln^2(\mu_R^2/Q^2)$ , *etc.* Given an infinite number of terms in the  $\alpha_s$  expansion, the  $\mu_R$  dependence of the  $\bar{c}_n(\mu_R^2/Q^2)$  coefficients will exactly cancel that of  $\alpha_s(\mu_R^2)$ , and the final result will be independent of the choice of  $\mu_R$ : physical observables do not depend on unphysical scales.<sup>1</sup>

With just terms up to some finite  $n = N$ , a residual  $\mu_R$  dependence will remain, which implies an uncertainty on the prediction of  $R(Q)$  due to the arbitrariness of the scale choice. This uncertainty will be  $\mathcal{O}(\alpha_s^{N+1})$ , *i.e.* of the same order as the neglected higher-order terms. For this reason it is customary to use QCD predictions’ scale dependence as an estimate of the uncertainties due to neglected terms. One usually takes a central value for  $\mu_R \sim Q$ , in order to avoid the poor convergence of the perturbative series that results from the large  $\ln^{n-1}(\mu_R^2/Q^2)$  terms in the  $\bar{c}_n$  coefficients when  $\mu_R \ll Q$  or  $\mu_R \gg Q$ . Uncertainties are then

<sup>1</sup> With respect to pQCD there is an important caveat to this statement: at sufficiently high orders, perturbative series generally suffer from “renormalon” divergences  $\alpha_s^n n!$  (reviewed in Ref. [28]). This phenomenon is not usually visible with the limited number of perturbative terms available today. However it is closely connected with non-perturbative contributions and sets a limit on the possible precision of perturbative predictions. The cancellation of scale dependence will also ultimately be affected by this renormalon-induced breakdown of perturbation theory.

commonly determined by varying  $\mu_R$  by a factor of two up and down around the central scale choice. A more detailed discussion on the accuracy of theoretical predictions and on ways to estimate the theoretical uncertainties can be found in Section 9.2.4.

### 9.2.2 Processes with initial-state hadrons

**Deep-Inelastic Scattering.** To illustrate the key features of QCD cross sections in processes with initial-state hadrons, let us consider deep-inelastic scattering (DIS),  $ep \rightarrow e + X$ , where an electron  $e$  with four-momentum  $k$  emits a highly off-shell photon (momentum  $q$ ) that interacts with the proton (momentum  $p$ ). For photon virtualities  $Q^2 \equiv -q^2$  far above the squared proton mass (but far below the  $Z$  mass), the differential cross section in terms of the kinematic variables  $Q^2$ ,  $x = Q^2/(2p \cdot q)$  and  $y = (q \cdot p)/(k \cdot p)$  is

$$\frac{d^2\sigma}{dx dQ^2} = \frac{4\pi\alpha^2}{2xQ^4} \left[ (1 + (1-y)^2)F_2(x, Q^2) - y^2 F_L(x, Q^2) \right], \quad (9.11)$$

where  $\alpha$  is the electromagnetic coupling and  $F_2(x, Q^2)$  and  $F_L(x, Q^2)$  are proton structure functions, which encode the interaction between the photon (in given polarization states) and the proton. In the presence of parity-violating interactions (e.g.  $\nu p$  scattering) an additional  $F_3$  structure function is present. For an extended review, including equations for the full electroweak and polarized cases, see Sec. 18 of this *Review*.

Structure functions are not calculable in perturbative QCD, nor is any other cross section that involves QCD interactions and initial-state hadrons. To zeroth order in  $\alpha_s$ , the structure functions are given directly in terms of non-perturbative parton (quark or gluon) distribution functions (PDFs),

$$F_2(x, Q^2) = x \sum_q e_q^2 f_{q/p}(x), \quad F_L(x, Q^2) = 0, \quad (9.12)$$

where  $f_{q/p}(x)$  is the non-perturbative PDF for quarks of type  $q$  inside the proton, i.e. the number density of quarks of type  $q$  inside a fast-moving proton that carry a fraction  $x$  of its longitudinal momentum (the quark flavor index  $q$ , here, is not to be confused with the photon momentum  $q$  in the lines preceding Eq. (9.11)). Recently, some first determinations on lattice started to appear [39–43] but there is also some debate about the underlying methods [44]. Accordingly, for all practical uses, PDFs are currently determined from data (cf. Sec. 18 of this *Review* and also Refs. [45, 46])<sup>2</sup>.

The above result, with PDFs  $f_{q/p}(x)$  that are independent of the scale  $Q$ , corresponds to the “quark-parton model” picture in which the photon interacts with point-like free quarks, or equivalently, one has incoherent elastic scattering between the electron and individual constituents of the proton. As a consequence, in this picture also  $F_2$  and  $F_L$  are independent of  $Q$  [50]. When including higher orders in pQCD,

$$F_2(x, Q^2) = x \sum_{n=0}^{\infty} \frac{\alpha_s^n(\mu_R^2)}{(2\pi)^n} \times \sum_{i=q,g} \int_x^1 \frac{dz}{z} C_{2,i}^{(n)}(z, Q^2, \mu_R^2, \mu_F^2) f_{i/p}\left(\frac{x}{z}, \mu_F^2\right) + \mathcal{O}\left(\frac{\Lambda^2}{Q^2}\right). \quad (9.13)$$

<sup>2</sup>PDFs can be determined from data in a global fit at LO, NLO and NNLO, depending on the order of the matrix elements used to describe the data. In modern global PDF fits, data are included from DIS, DY, jets and  $t\bar{t}$  processes, and more LHC collider data, with the global PDF fits using 3000–4000 data points. There is a large change in the PDFs from LO to NLO, with a much smaller change from NLO to NNLO. LO PDFs can be unreliable for collider predictions, especially at low and high  $x$ . The uncertainties of the resulting PDFs are determined from the experimental uncertainties of the data that serves as input to the global PDF fits. The PDF uncertainties can either be determined through a Hessian approach or through the use of Monte Carlo replicas. It is now relatively straightforward to convert results from one approach to the other. The PDF4LHC15 PDF set is formed by combining replicas of the CT14, MMHT2014 and NNPDF3.0 PDF sets, at NLO and at NNLO [47]. Recently, theoretical uncertainties related to missing higher orders have been included in global PDF determinations but so far only at NLO [48, 49].

Just as in Eq. (9.10), we have a series in powers of  $\alpha_s(\mu_R^2)$ , each term involving a coefficient  $C_{2,i}^{(n)}$  that can be calculated using Feynman graphs. At variance with the parton model, the PDFs in pQCD depend on an additional scale, the factorization scale  $\mu_F$ , whose significance will be discussed in the following. Another important difference is the additional integral over  $z$ . The parton that comes from the proton can undergo a splitting before it interacts with the photon. As a result, the  $C_{2,i}^{(n)}$  coefficients are functions that depend on the ratio,  $z$ , of the parton’s momentum before and after radiation, and one must integrate over that ratio. For the electromagnetic component of DIS with light quarks and gluons, the zeroth order coefficient functions are  $C_{2,q}^{(0)} = e_q^2 \delta(1-z)$  and  $C_{2,g}^{(0)} = 0$ . Corrections are known up to  $\mathcal{O}(\alpha_s^3)$  (next-to-next-to-next-to-leading order, N<sup>3</sup>LO) for both electromagnetic [51] and weak currents [52, 53]. For heavy-quark production they are known to  $\mathcal{O}(\alpha_s^2)$  [54, 55] (next-to-leading order, NLO, insofar as the series starts at  $\mathcal{O}(\alpha_s)$ ). For precise comparisons of LHC cross sections with theoretical predictions, the photon PDF of the proton is also needed. It has been computed precisely in Ref. [56] and has now been implemented in most global PDF fits.

The majority of the emissions that modify a parton’s momentum are collinear (parallel) to that parton, and do not depend on the fact that the parton is destined to interact with a photon. It is natural to view these emissions as modifying the proton’s structure rather than being part of the coefficient function for the parton’s interaction with the photon. Technically, one uses a procedure known as *collinear factorization* to give a well-defined meaning to this distinction, most commonly through the  $\overline{\text{MS}}$  factorization scheme, defined in the context of dimensional regularization. The  $\overline{\text{MS}}$  factorization scheme involves an arbitrary choice of *factorization scale*,  $\mu_F$ , whose meaning can be understood roughly as follows: emissions with transverse momenta above  $\mu_F$  are included in the  $C_{2,q}^{(n)}(z, Q^2, \mu_R^2, \mu_F^2)$ ; emissions with transverse momenta below  $\mu_F$  are accounted for within the PDFs,  $f_{i/p}(x, \mu_F^2)$ . While collinear factorization is generally believed to be valid for suitable (sufficiently inclusive) observables in processes with hard scales, Ref. [57], which reviews the factorization proofs in detail, is cautious in the statements it makes about their exhaustivity, notably for the hadron-collider processes which we shall discuss below. Further discussion is to be found in Refs. [58, 59].

The PDFs’ resulting dependence on  $\mu_F$  is described by the Dokshitzer-Gribov-Lipatov-Altarelli-Parisi (DGLAP) equations [60], which to leading order (LO) read<sup>3</sup>

$$\mu_F^2 \frac{\partial f_{i/p}(x, \mu_F^2)}{\partial \mu_F^2} = \sum_j \frac{\alpha_s(\mu_F^2)}{2\pi} \int_x^1 \frac{dz}{z} P_{i \leftarrow j}^{(1)}(z) f_{j/p}\left(\frac{x}{z}, \mu_F^2\right), \quad (9.14)$$

with, for example,  $P_{q \leftarrow g}^{(1)}(z) = T_R(z^2 + (1-z)^2)$ . The other LO splitting functions are listed in Sec. 18 of this *Review*, while results up to NLO,  $\alpha_s^2$ , and NNLO,  $\alpha_s^3$ , are given in Refs. [61] and [62] respectively. At N<sup>3</sup>LO accuracy, only partial results are currently available Ref. [63–65].

Splitting functions for polarized PDFs are given in Ref. [66]. Beyond LO, the coefficient functions are also  $\mu_F$  dependent, for example  $C_{2,i}^{(1)}(x, Q^2, \mu_R^2, \mu_F^2) = C_{2,i}^{(1)}(x, Q^2, \mu_R^2, Q^2) - \ln\left(\frac{\mu_F^2}{Q^2}\right) \sum_j \int_x^1 \frac{dz}{z} \times C_{2,j}^{(0)}\left(\frac{x}{z}\right) P_{j \leftarrow i}^{(1)}(z)$ . In certain contexts, higher-order QED and mixed QED-QCD corrections to the splitting functions are also needed [67].

As with the renormalization scale, the choice of factorization scale is arbitrary, but if one has an infinite number of terms in the perturbative series, the  $\mu_F$ -dependencies of the coefficient functions and PDFs will compensate each other fully. Given only  $N$  terms of the series, a residual  $\mathcal{O}(\alpha_s^{N+1})$  uncertainty is associated with the ambiguity in the choice of  $\mu_F$ . As with  $\mu_R$ , varying  $\mu_F$  provides an input in estimating uncertainties on predictions. In inclusive DIS predictions, the default choice for the scales is

<sup>3</sup> LO is generally taken to mean the lowest order at which a quantity is non-zero.

usually  $\mu_R = \mu_F = Q$ .

As is the case for the running coupling, in DGLAP evolution one can introduce flavor thresholds near the heavy quark masses: below a given heavy quark's mass, that quark is not considered to be part of the proton's structure, while above it is considered to be part of the proton's structure and evolves with massless DGLAP splitting kernels. With appropriate parton distribution matching terms at threshold, such a variable flavor number scheme (VFNS), when used with massless coefficient functions, gives the full heavy-quark contributions at high  $Q^2$  scales. For scales near the threshold, it is instead necessary to appropriately adapt the standard massive coefficient functions to account for the heavy-quark contribution already included in the PDFs [68–70].

At sufficiently small  $x$  and  $Q^2$  in inclusive DIS, resummation of small  $x$  logarithms may be necessary [71, 72]. This may in fact have been observed in Refs. [73] based on HERA data [74], in a kinematic region where useful information for PDFs for collider predictions is present. A better description of the data in this region can be gained by small  $x$  resummation matched to NNLO [73, 75], or by the inclusion of power-suppressed contributions [76] or by using an  $x$ -dependent factorization scale in the NNLO DIS predictions [77].

**Hadron-hadron collisions.** The extension to processes with two initial-state hadrons can be illustrated with the example of the total (inclusive) cross section for  $W$  boson production in collisions of hadrons  $h_1$  and  $h_2$ , which can be written as

$$\begin{aligned} \sigma(h_1 h_2 \rightarrow W + X) &= \sum_{n=0}^{\infty} \alpha_s^n(\mu_R^2) \\ &\times \sum_{i,j} \int dx_1 dx_2 f_{i/h_1}(x_1, \mu_F^2) f_{j/h_2}(x_2, \mu_F^2) \\ &\times \hat{\sigma}_{ij \rightarrow W+X}^{(n)}(x_1 x_2 s, \mu_R^2, \mu_F^2) + \mathcal{O}\left(\frac{\Lambda^2}{M_W^4}\right), \end{aligned} \quad (9.15)$$

where  $s$  is the squared center-of-mass energy of the collision. At LO,  $n = 0$ , the hard (partonic) cross section  $\hat{\sigma}_{ij \rightarrow W+X}^{(0)}(x_1 x_2 s, \mu_R^2, \mu_F^2)$  is simply proportional to  $\delta(x_1 x_2 s - M_W^2)$ , in the narrow  $W$ -boson width approximation (see Sec. 5.0 of this *Review* for detailed expressions for this and other hard scattering cross sections). It is non-zero only for choices of  $i, j$  that can directly give a  $W$ , such as  $i = u, j = \bar{d}$ . At higher orders,  $n \geq 1$ , new partonic channels contribute, such as  $gg$ , and  $x_1 x_2 s \geq M_W^2$  in the narrow  $W$ -boson width approximation.

Eq. (9.15) involves a collinear factorization between the hard cross section and the PDFs, just like Eq. (9.13). As long as the same factorization scheme is used in DIS and  $pp$  or  $p\bar{p}$  (usually the  $\overline{\text{MS}}$  scheme), then PDFs extracted in DIS can be directly used in  $pp$  and  $p\bar{p}$  predictions [57, 78] (with the anti-quark distributions in an anti-proton being the same as the quark distributions in a proton).

Fully inclusive hard cross sections are known to NNLO, *i.e.* corrections up to relative order  $\alpha_s^2$ , for Drell-Yan (DY) lepton-pair and vector-boson production [79, 80], Higgs-boson production in association with a vector boson [81], Higgs-boson production via vector-boson fusion [82] (in an approximation that factorizes the production of the two vector bosons), Higgs-pair production with full  $m_t$  dependence [83], top-antitop production [84] and vector-boson pair production [85–87].<sup>4</sup> Inclusive Higgs production through gluon fusion in the large  $m_t$  limit was calculated at N<sup>3</sup>LO [88, 89]. A calculation at this order, differential in the Higgs rapidity has also been presented recently [90]. Vector-boson fusion Higgs production is also known to N<sup>3</sup>LO [91] in the factorized approximation. A discussion of many other calculations for Higgs production processes is to be found in Ref. [92].

**Photoproduction.**  $\gamma p$  (and  $\gamma\gamma$ ) collisions are similar to  $pp$  collisions, with the subtlety that the photon can behave in two ways:

there is “direct” photoproduction, in which the photon behaves as a point-like particle and takes part directly in the hard collision, with hard subprocesses such as  $\gamma g \rightarrow q\bar{q}$ ; there is also resolved photoproduction, in which the photon behaves like a hadron, with non-perturbative partonic substructure and a corresponding PDF for its quark and gluon content,  $f_{i/\gamma}(x, Q^2)$ . While useful to understand the general structure of  $\gamma p$  collisions, the distinction between direct and resolved photoproduction is not well defined beyond leading order, as discussed for example in Ref. [93].

**The high-energy (BFKL) limit.** In situations in which the total center-of-mass energy  $\sqrt{s}$  is much larger than all other momentum-transfer scales in the problem (*e.g.*  $Q$  in DIS,  $m_b$  for  $b\bar{b}$  production in  $pp$  collisions, *etc.*), each power of  $\alpha_s$  beyond LO can be accompanied by a power of  $\ln(s/Q^2)$  (or  $\ln(s/m_b^2)$ , *etc.*). This is variously referred to as the high-energy, small- $x$  or Balitsky-Fadin-Kuraev-Lipatov (BFKL) limit [72, 94, 95]. Currently it is possible to account for the dominant and first sub-dominant [96, 97] power of  $\ln s$  at each order of  $\alpha_s$ , and also to estimate further sub-dominant contributions that are numerically large (see Refs. [98–101] and references therein). Progress towards NNLO is discussed in Ref. [102].

Physically, the summation of all orders in  $\alpha_s$  can be understood as leading to a growth with  $s$  of the gluon density in the proton. At sufficiently high energies this implies non-linear effects (commonly referred to as parton saturation), whose treatment has been the subject of intense study (see for example Refs. [103, 104] and references thereto).

### 9.2.3 Cross sections with phase-space restrictions

QCD final states always consist of hadrons, while perturbative QCD calculations deal with partons. Physically, an energetic parton fragments (“showers”) into many further partons, which then, on later timescales, undergo a transition to hadrons (“hadronization”). Fixed-order perturbation theory captures only a small part of these dynamics. This does not matter for the fully inclusive cross sections discussed above: the showering and hadronization stages are approximately unitary, *i.e.* they do not substantially change the overall probability of hard scattering, because they occur long after it has taken place (they introduce at most a correction proportional to a power of the ratio of timescales involved, *i.e.* a power of  $\Lambda/Q$ , where  $Q$  is the hard scattering scale).

Less inclusive measurements, in contrast, may be affected by the extra dynamics. For those sensitive just to the main directions of energy flow (jet rates, event shapes, *cf.* Sec. 9.3.1) fixed-order perturbation theory is often still adequate, because showering and hadronization do not substantially change the overall energy flow. This means that one can make a prediction using just a small number of partons, which should correspond well to a measurement of the same observable carried out on hadrons. For observables that instead depend on distributions of individual hadrons (which, *e.g.*, are the inputs to detector simulations), it is mandatory to account for showering and hadronization. The range of predictive techniques available for QCD final states reflects this diversity of needs of different measurements.

While illustrating the different methods, we shall for simplicity mainly use expressions that hold for  $e^+e^-$  scattering. The extension to cases with initial-state partons will be mostly straightforward (space constraints unfortunately prevent us from addressing diffraction and exclusive hadron-production processes; extensive discussion is to be found in Refs. [105, 106]).

#### 9.2.3.1 Soft and collinear limits

Before examining specific predictive methods, it is useful to be aware of a general property of QCD matrix elements in the soft and collinear limits. Consider a squared tree-level matrix element  $|M_n^2(p_1, \dots, p_n)|$  for the process  $e^+e^- \rightarrow n$  partons with momenta  $p_1, \dots, p_n$ , and a corresponding phase-space integration measure  $d\Phi_n$ . If particle  $n$  is a gluon, which becomes collinear (parallel) to another particle  $i$  and additionally its momentum tends to zero

<sup>4</sup> Processes with jets or photons in the final state have divergent cross sections unless one places a cut on the jet or photon momentum. Accordingly, they are discussed below in Section 9.2.3.2.

(is “soft”), the matrix element simplifies as follows,

$$\lim_{\theta_{in} \rightarrow 0, E_n \rightarrow 0} d\Phi_n |M_n^2(p_1, \dots, p_n)| = d\Phi_{n-1} |M_{n-1}^2(p_1, \dots, p_{n-1})| \frac{\alpha_s C_i}{\pi} \frac{d\theta_{in}^2}{\theta_{in}^2} \frac{dE_n}{E_n}, \quad (9.16)$$

where  $C_i = C_F$  ( $C_A$ ) if  $i$  is a quark (gluon). This formula has non-integrable divergences both for the inter-parton angle  $\theta_{in} \rightarrow 0$  and for the gluon energy  $E_n \rightarrow 0$ , which are mirrored also in the structure of divergences in loop diagrams. These divergences are important for at least two reasons: firstly, they govern the typical structure of events (inducing many emissions either with low energy or at small angle with respect to hard partons); secondly, they will determine which observables can be calculated within perturbative QCD.

### 9.2.3.2 Fixed-order predictions

Let us consider an observable  $\mathcal{O}$  that is a function  $\mathcal{O}_n(p_1, \dots, p_n)$  of the four-momenta of the  $n$  final-state particles in an event (either partons or hadrons). In what follows, we shall consider the cross section for events weighted with the value of the observable,  $\sigma_{\mathcal{O}}$ . As examples, if  $\mathcal{O}_n \equiv 1$  for all  $n$ , then  $\sigma_{\mathcal{O}}$  is just the total cross section; if  $\mathcal{O}_n \equiv \hat{\tau}(p_1, \dots, p_n)$  where  $\hat{\tau}$  is the value of the Thrust for that event (see Sec. 9.3.1.2), then the average value of the Thrust is  $\langle \tau \rangle = \sigma_{\mathcal{O}} / \sigma_{\text{tot}}$ ; if  $\mathcal{O}_n \equiv \delta(\tau - \hat{\tau}(p_1, \dots, p_n))$  then one gets the differential cross section as a function of the Thrust,  $\sigma_{\mathcal{O}} \equiv d\sigma/d\tau$ .

In the expressions below, we shall omit to write the non-perturbative power correction term, which for most common observables is proportional to a single power of  $\Lambda/Q$ .

**Leading Order.** If the observable  $\mathcal{O}$  is non-zero only for events with at least  $n$  final-state particles, then the LO QCD prediction for the weighted cross section in  $e^+e^-$  annihilation is

$$\sigma_{\mathcal{O}, LO} = \alpha_s^{n-2} (\mu_R^2) \int d\Phi_n |M_n^2(p_1, \dots, p_n)| \mathcal{O}_n(p_1, \dots, p_n), \quad (9.17)$$

where the squared tree-level matrix element,  $|M_n^2(p_1, \dots, p_n)|$ , including relevant symmetry factors, has been summed over all subprocesses (e.g.  $e^+e^- \rightarrow q\bar{q}q\bar{q}$ ,  $e^+e^- \rightarrow q\bar{q}gg$ ) and has had all factors of  $\alpha_s$  extracted in front. In processes other than  $e^+e^-$  collisions, the center-of-mass energy of the LO process is generally not fixed, and so the powers of the coupling are often brought inside the integrals, with the scale  $\mu_R$  chosen event by event, as a function of the event kinematics.

Other than in the simplest cases (see the review on Cross Sections in this *Review*), the matrix elements in Eq. (9.17) are usually calculated automatically with programs such as CompHEP [107], MadGraph [108], Alpgen [109], Comix/Sherpa [110], and Helac/Phegas [111]. Some of these (CompHEP, MadGraph) use formulas obtained from direct evaluations of Feynman diagrams. Others (Alpgen, Helac/Phegas and Comix/Sherpa) use methods designed to be particularly efficient at high multiplicities, such as Berends-Giele recursion [112], which builds up amplitudes for complex processes from simpler ones (see also Refs. [113–116] for reviews on the topic and for other tree-level calculational methods).

The phase-space integration is usually carried out by Monte Carlo sampling, in order to deal with the possibly involved kinematic cuts that are used in the corresponding experimental measurements. Because of the divergences in the matrix element, Eq. (9.16), the integral converges only if the observable vanishes for kinematic configurations in which one of the  $n$  particles is arbitrarily soft or it is collinear to another particle. As an example, the cross section for producing any configuration of  $n$  partons will lead to an infinite integral, whereas a finite result will be obtained for the cross section for producing  $n$  deposits of energy (or jets, see Sec. 9.3.1.1), each above some energy threshold and well separated from each other in angle.

At a practical level, LO calculations can be carried out for  $2 \rightarrow n$  processes with  $n \lesssim 6 - 10$ . The exact upper limit depends on the process, the method used to evaluate the matrix elements (recursive methods are more efficient), and the extent to which

the phase-space integration can be optimized to work around the large variations in the values of the matrix elements.

**NLO.** Given an observable that is non-zero starting from  $n$  final-state particles, its prediction at NLO involves supplementing the LO result, Eq. (9.17), with the  $2 \rightarrow (n+1)$ -particle squared tree-level matrix element ( $|M_{n+1}^2|$ ), and the interference of a  $2 \rightarrow n$  tree-level and  $2 \rightarrow n$  1-loop amplitude ( $2\text{Re}(M_n M_{n,1\text{-loop}}^*)$ ),

$$\begin{aligned} \sigma_{\mathcal{O}}^{NLO} &= \sigma_{\mathcal{O}}^{LO} + \alpha_s^{n-1} (\mu_R^2) \int d\Phi_{n+1} |M_{n+1}^2(p_1, \dots, p_{n+1})| \\ &\quad \times \mathcal{O}_{n+1}(p_1, \dots, p_{n+1}) + \alpha_s^{n-1} (\mu_R^2) \\ &\quad \times \int d\Phi_n 2\text{Re} [ M_n(p_1, \dots, p_n) M_{n,1\text{-loop}}^*(p_1, \dots, p_n) ] \\ &\quad \times \mathcal{O}_n(p_1, \dots, p_n). \end{aligned} \quad (9.18)$$

Relative to LO calculations, two important issues appear in the NLO calculations. Firstly, the extra complexity of loop-calculations relative to tree-level calculations means that automated calculations started to appear only about fifteen years ago (see below). Secondly, loop amplitudes are infinite in 4 dimensions, while tree-level amplitudes are finite, but their *integrals* are infinite, due to the divergences of Eq. (9.16). These two sources of infinities have the same soft and collinear origins and cancel after the integration only if the observable  $\mathcal{O}$  satisfies the property of infrared and collinear safety, which means that the observable is non-sensitive to soft emissions or to collinear splittings, *i.e.*

$$\begin{aligned} \mathcal{O}_{n+1}(p_1, \dots, p_s, \dots, p_n) &\rightarrow \mathcal{O}_n(p_1, \dots, p_{s-1}, p_{s+1}, \dots, p_n) \\ &\quad \text{if } p_s \rightarrow 0 \\ \mathcal{O}_{n+1}(p_1, \dots, p_a, p_b, \dots, p_n) &\rightarrow \mathcal{O}_n(p_1, \dots, p_a + p_b, \dots, p_n) \\ &\quad \text{if } p_a \parallel p_b. \end{aligned} \quad (9.19)$$

Examples of infrared-safe quantities include event-shape distributions and jet cross sections (with appropriate jet algorithms, see below). Unsafe quantities include the distribution of the momentum of the hardest QCD particle (which is not conserved under collinear splitting), observables that require the complete absence of radiation in some region of phase space (e.g. rapidity gaps or 100% isolation cuts, which are affected by soft emissions), or the particle multiplicity (affected by both soft and collinear emissions). The non-cancellation of divergences at NLO due to infrared or collinear unsafety compromises the usefulness not only of the NLO calculation, but also that of a LO calculation, since LO is only an acceptable approximation if one can prove that higher-order terms are smaller. Infrared and collinear unsafety usually also imply large non-perturbative effects.

As with LO calculations, the phase-space integrals in Eq. (9.18) are usually carried out by Monte Carlo integration, so as to facilitate the study of arbitrary observables. Various methods exist to obtain numerically efficient cancellation among the different infinities. These include notably dipole [117], FKS [118] and antenna [119] subtraction.

Thanks to new ideas like the OPP method [120], generalised [121] and  $D$ -dimensional [122] unitarity, onshell methods [123], and on the fly reduction algorithms [124], recent years have seen a breakthrough in the calculation of one-loop matrix elements (for reviews on unitarity based method see Ref. [125, 126]). Thanks to these innovative methods, automated NLO calculations tools have been developed and a number of programs are available publicly: Madgraph5\_aMC@NLO [108] and Helac-NLO [127] provide full frameworks for NLO calculations; GoSam [128], Njet [129], OpenLoops [130] and Recola [131] calculate just the 1-loop part and are typically interfaced with an external tool such as Sherpa [132] for a combination with the appropriate tree-level amplitudes. Other tools such as NLOJet++ [133], MCFM [134], VBFNLO [135], the Phox family [136] or BlackHat [137] implement analytic calculations for a selected class of processes. Given that NLO computation for high-multiplicity final states is numerically demanding,

procedures [138–141] have been developed for *a posteriori* PDF and scale change. These methods represent NLO (or NNLO) results, for a given set of cuts and binning, as an effective coefficient function on a grid in parton momentum fractions and factorization scales.

Recently, a lot of attention has also been paid to the calculation of NLO electroweak corrections. Electroweak corrections are especially important for transverse momenta significantly above the  $W$  and  $Z$  masses, because they are enhanced by two powers of  $\ln p_t/M_W$  for each power of the electroweak coupling, and close to Sudakov peaks, where most of the data lie and the best experimental precision can be achieved. In some cases the above programs (or development versions of them) can be used to calculate also NLO electroweak or beyond-standard-model corrections [142–148].

Given the progress in QCD and EW fixed-order computations, the largest unknown from fixed-order corrections is often given by the mixed QCD-electroweak corrections of  $\mathcal{O}(\alpha_s\alpha)$ . These mixed two-loop corrections are often available only in an approximate form [149–154] and first three-loop results  $\mathcal{O}(\alpha_s^3\alpha)$  in the case of Higgs productions started to appear recently [155].

**NNLO.** Conceptually, NNLO and NLO calculations are similar, except that one must add a further order in  $\alpha_s$ , consisting of: the squared  $(n+2)$ -parton tree-level amplitude, the interference of the  $(n+1)$ -parton tree-level and 1-loop amplitudes, the interference of the  $n$ -parton tree-level and 2-loop amplitudes, and the squared  $n$ -parton 1-loop amplitude.

Each of these elements involves large numbers of soft and collinear divergences, satisfying relations analogous to Eq. (9.16) which now involve multiple collinear or soft particles and higher loop orders (see *e.g.* Refs. [156–158]). Arranging for the cancellation of the divergences after numerical Monte Carlo integration has been one of the significant challenges of NNLO calculations, as has been the determination of the relevant 2-loop amplitudes. For the cancellations of divergences a wide range of methods has been developed. Some of them [159–163] retain the approach, inherent in NLO methods, of directly combining the separate loop and tree-level amplitudes. Others combine a suitably chosen, partially inclusive  $2 \rightarrow n$  NNLO calculation with a fully differential  $2 \rightarrow n+1$  NLO calculation [164–167].

Quite a number of processes have been calculated differentially at NNLO so far. The state of the art for  $e^+e^-$  collisions is  $e^+e^- \rightarrow 3$  jets [168–170]. For DIS, dijet production is known at NNLO [171] and the description jet production has been recently pushed even to  $N^3$ LO using the Projection-to-Born method [172,173]. For hadron colliders, all  $2 \rightarrow 1$  processes are known, specifically vector boson [174,175] and Higgs boson production [164,176]. For most of the above calculations there exist public codes (EERAD3 for  $e^+e^-$ , DYNLO, FEWZ and MATRIX for  $W$  and  $Z$  production, Fehipro and HNNLO for Higgs production), links to which are to be found among the above references. Substantial progress has been made in the past couple of years for hadron-collider  $2 \rightarrow 2$  processes, with calculations having been performed for nearly all relevant processes:  $ZZ$  [86]  $WW$  [85] and  $WZ$  [177],  $\gamma\gamma$  [178,179],  $Z\gamma$  [180] and  $W\gamma$  [181] (many of these colour singlet processes are available also in MCFM [182] or MATRIX [87]), inclusive photon [183,184],  $\gamma$ +jet [184,185],  $W$ +jet [165],  $Z$ +jet [185–187]  $H$ +jet [188–191],  $WH$  [192] and  $ZH$  [193],  $t$ -channel single-top [194,195],  $t\bar{t}$  production [196], dijet production [197], and  $HH$  [198] (in large-top-mass approximation, see also the exact (two-loop) NLO result [83]). One  $2 \rightarrow 3$  process is known at NNLO, Higgs production through vector-boson fusion, using an approximation in which the two underlying DIS-like  $q \rightarrow qV$  scatterings are factorised, the so-called structure function approximation [167,199]. Corrections beyond the structure function approximation are expected to be small, on the order of a percent or less [200].

The Les Houches precision wishlist compiles predictions needed to fully exploit the data that will be taken at the High Luminosity LHC [201]. Most of the needed calculations require accuracy of at least NNLO QCD and NLO EW, and many require the prediction of  $2 \rightarrow 3$  processes, such as  $W/Z+ \geq 2$  jets,  $H+ \geq 2$  jets, and  $t\bar{t}H$  to NNLO.

As discussed in this section, calculations at NLO can now be

relatively easily generated by non-experts using the programs described. However, many NNLO calculations can be too complex and CPU-intensive to allow such an approach. In these cases, the relevant matrix element information can be stored in a grid format (or in ROOT ntuples) allowing predictions to be generated on-the-fly, similar to what has been available at NLO.

### 9.2.3.3 Resummation

Many experimental measurements place tight constraints on emissions in the final state. For example, in  $e^+e^-$  events, that (one minus) the Thrust should be less than some value  $\tau \ll 1$ , or, in  $pp \rightarrow Z$ , events that the  $Z$ -boson transverse momentum or the transverse momentum of the accompanying jet should be much smaller than the  $Z$ -boson mass. A further example is the production of heavy particles or jets near threshold (so that little energy is left over for real emissions) in DIS and  $pp$  collisions.

In such cases, the constraint vetoes a significant part of the integral over the soft and collinear divergence of Eq. (9.16). As a result, there is only a partial cancellation between real emission terms (subject to the constraint) and loop (virtual) contributions (not subject to the constraint), causing each order of  $\alpha_s$  to be accompanied by a large coefficient  $\sim L^2$ , where *e.g.*  $L = \ln \tau$  or  $L = \ln(M_Z/p_t^Z)$ . One ends up with a perturbative series, whose terms go as  $\sim (\alpha_s L^2)^n$ . It is not uncommon that  $\alpha_s L^2 \gg 1$ , so that the perturbative series converges very poorly if at all.<sup>5</sup> In such cases one may carry out a “resummation”, which accounts for the dominant logarithmically enhanced terms to all orders in  $\alpha_s$ , by making use of known properties of matrix elements for multiple soft and collinear emissions, and of the all-orders properties of the divergent parts of virtual corrections, following original works such as Refs. [202–211] and also through soft-collinear effective theory [212,213] (*cf.* also the section on “Heavy-Quark and Soft-Collinear Effective Theory” in this *Review*, as well as Ref. [214]).

For cases with double logarithmic enhancements (two powers of logarithm per power of  $\alpha_s$ ), there are two classification schemes for resummation accuracy. Writing the cross section including the constraint as  $\sigma(L)$  and the unconstrained (total) cross section as  $\sigma_{\text{tot}}$ , the series expansion takes the form

$$\sigma(L) \simeq \sigma_{\text{tot}} \sum_{n=0}^{\infty} \sum_{k=0}^{2n} R_{nk} \alpha_s^n (\mu_R^2/L)^k, \quad L \gg 1, \quad (9.20)$$

and leading log (LL) resummation means that one accounts for all terms with  $k = 2n$ , next-to-leading-log (NLL) includes additionally all terms with  $k = 2n - 1$ , *etc.* Often  $\sigma(L)$  (or its Fourier or Mellin transform) *exponentiates*<sup>6</sup>,

$$\sigma(L) \simeq \sigma_{\text{tot}} \exp \left[ \sum_{n=1}^{\infty} \sum_{k=0}^{n+1} G_{nk} \alpha_s^n (\mu_R^2/L)^k \right], \quad L \gg 1, \quad (9.21)$$

where one notes the different upper limit on  $k$  ( $\leq n+1$ ) compared to Eq. (9.20). This is a more powerful form of resummation: the  $G_{12}$  term alone reproduces the full LL series in Eq. (9.20). With the form Eq. (9.21) one still uses the nomenclature LL, but this now means that all terms with  $k = n+1$  are included, and NLL implies all terms with  $k = n$ , *etc.*

For a large number of observables, NLL resummations are available in the sense of Eq. (9.21) (see Refs. [218–220] and references therein). NNLL has been achieved for the DY and Higgs-boson  $p_t$  distributions [221–224] (also available in the CuTe [225], HRes [226] and ResBos [227] families of programs and also differentially in vector-boson decay products [228]) and related variables [229], for the  $p_t$  of vector-boson pairs [230], for the back-to-back energy-energy correlation in  $e^+e^-$  [231], the jet broadening

<sup>5</sup> To be precise one should be aware of two causes of the divergence of perturbative series. That which interests us here is associated with the presence of a new large parameter (*e.g.* ratio of scales). It is distinct from the “renormalon” induced factorial divergences of perturbation theory which were discussed above.

<sup>6</sup> Whether or not this happens depends on the quantity being resummed. A classic example involves two-jet rate in  $e^+e^-$  collisions as a function of a jet-resolution parameter  $y_{\text{cut}}$ . The logarithms of  $1/y_{\text{cut}}$  exponentiate for the  $k_t$  (Durham) jet algorithm [215], but not [216] for the JADE algorithm [217] (both are discussed below in Sec. 9.3.1.1).

in  $e^+e^-$  collisions [232], the jet-veto survival probability in Higgs and  $Z$  boson production in  $pp$  collisions [233, 234]<sup>7</sup>, an event-shape type observable known as the beam Thrust [235], hadron-collider jet masses in specific limits [236] (see also Ref. [237]), the production of top anti-top pairs near threshold [238–240] (and references therein), and high- $p_t$   $W$  and  $Z$  production [241]. Automation of NNLL jet-veto resummations for different processes has been achieved in Ref. [242] (*cf.* also the NLL automation in Ref. [243]), while automation for a certain class of  $e^+e^-$  observables has been achieved in Ref. [244]. N<sup>3</sup>LL resummations are available for the Thrust variable,  $C$ -parameter and heavy-jet mass in  $e^+e^-$  annihilations [245–247] (confirmed for Thrust at NNLL in Ref. [248]), for  $p_t$  distribution of the Higgs boson [249] and weak gauge bosons [250] and for Higgs- and vector-boson production near threshold [251]. An extensive discussion of jet masses for heavy-quark induced jets has been given in Ref. [252] (see also Ref. [253]). In order to make better contact with experimental measurements, recent years have seen an increasing interest in resummations in exclusive phase-space regions and joint resummations [254–260]. Finally, there has also been considerable progress in resummed calculations for jet substructure, whose observables involve more complicated definitions than is the case for standard resummations [261–267], see also Refs. [268, 269]. The inputs and methods involved in these various calculations are somewhat too diverse to discuss in detail here, so we recommend that the interested reader consult the original references for further details.

#### 9.2.3.4 Fragmentation functions

Since the parton-hadron transition is non-perturbative, it is not possible to perturbatively calculate quantities such as the energy-spectra of specific hadrons in high-energy collisions. However, one can factorize perturbative and non-perturbative contributions via the concept of fragmentation functions. These are the final-state analogue of the parton distribution functions which are used for initial-state hadrons. Like parton distribution functions, they depend on a (fragmentation) factorization scale and satisfy a DGLAP evolution equation.

It should be added that if one ignores the non-perturbative difficulties and just calculates the energy and angular spectrum of partons in perturbative QCD with some low cutoff scale  $\sim \Lambda$  (using resummation to sum large logarithms of  $\sqrt{s}/\Lambda$ ), then this reproduces many features of the corresponding hadron spectra [270]. This is often taken to suggest that hadronization is “local”, in this sense it mainly involves partons that are close both in position and in momentum.

Section 19 of this *Review* provides further information (and references) on these topics, including also the question of heavy-quark fragmentation.

#### 9.2.3.5 Parton-shower Monte Carlo generators

Parton-shower Monte Carlo (MC) event generators like PYTHIA [271–273], HERWIG [274–276] and SHERPA [132] provide fully exclusive simulations of QCD events.<sup>8</sup> Because they provide access to “hadron-level” events, they are a crucial tool for all applications that involve simulating the response of detectors to QCD events. Here we give only a brief outline of how they work and refer the reader to Sec. 41 and Ref. [278] for a full overview.

The MC generation of an event involves several stages. It starts with the random generation of the kinematics and partonic channels of whatever *hard scattering process* the user has requested at some high scale  $Q_0$  (for complex processes, this may be carried out by an external program). This is followed by a *parton shower*, usually based on the successive random generation of gluon emissions (or  $g \rightarrow q\bar{q}$  splittings). Emissions are ordered according to some ordering variable. Common choices of scale for the ordering of emissions are virtuality, transverse momentum or angle. Each emission is generated at a scale lower than the previous

emission, following a (soft and collinear resummed) perturbative QCD distribution, which depends on the momenta of all previous emissions. Parton showering stops at a scale of order 1 GeV, at which point a *hadronization model* is used to convert the resulting partons into hadrons. One widely-used model involves stretching a color “string” across quarks and gluons, and breaking it up into hadrons [279, 280]. Another breaks each gluon into a  $q\bar{q}$  pair and then groups quarks and anti-quarks into colorless “clusters”, which then give the hadrons [274]. As both models are tuned primarily to LEP data, the cluster and string models provide similar results for most observables [281]. For  $pp$  and  $\gamma p$  processes, modeling is also needed to treat the collision between the two hadron remnants, which generates an *underlying event* (UE), usually implemented via additional  $2 \rightarrow 2$  scatterings (“multiple parton interactions”) at a scale of a few GeV, following Ref. [282]. The parameter values for the multiple parton interaction models must be determined from fits to the underlying event levels from LHC collision data. As the different Monte Carlo programs fit to essentially the same data, there should be similar results for each program. One complication, however, is the non-universality of the underlying event for different physics processes.

A deficiency of the soft and collinear approximations that underlie parton showers is that they may fail to reproduce the full pattern of hard wide-angle emissions, important, for example, in many new physics searches. It is therefore common to use LO multi-parton matrix elements to generate hard high-multiplicity partonic configurations as additional starting points for the showering, supplemented with some prescription (CKKW [283], MLM [284]) for consistently merging samples with different initial multiplicities. Monte Carlo generators, as described above, compute cross sections for the requested hard process that are correct at LO.

A wide variety of processes are available in MC implementations that are correct also to NLO, using the MC@NLO [285] or POWHEG [286] prescriptions, notably through the Madgraph5\_aMC@NLO [108], POWHEGBox [287] and Sherpa [110] programs. Techniques have also been developed to combine NLO plus shower accuracy for different multiplicities of final-state jets [288]. Building in part on some of that work, several groups have also obtained NNLO plus shower accuracy for Drell-Yan and Higgs production [289], as well as for a handful of  $2 \rightarrow 2$  processes [290–292].

In general, we expect parton-shower matched predictions to differ from the underlying fixed-order results in regions where (1) there is a large sensitivity to jet shapes (for instance small  $R$  jets), (2) there is a restriction in phase space such that soft gluon resummation effects become important, (3) the observable contains multiple disparate scales, (4) there are perturbative instabilities at fixed order, *e.g.* related to kinematical cuts, and (5) the observable is sensitive to higher multiplicity states than those described by the fixed-order calculation [281].

#### 9.2.4 Accuracy of predictions

Estimating the accuracy of perturbative QCD predictions is not an exact science. It is often said that LO calculations are accurate to within a factor of two. This is based on experience with NLO corrections in the cases where these are available. In processes involving new partonic scattering channels at NLO and/or large ratios of scales (such as jet observables in processes with vector bosons, or the production of high- $p_t$  jets containing  $B$ -hadrons), the ratio of the NLO to LO predictions, commonly called the “ $K$ -factor”, can be substantially larger than two. NLO corrections tend to be large for processes for which there is a great deal of color annihilation in the interaction. In addition, NLO corrections tend to decrease as more final state legs are added.

For calculations beyond LO, a conservative approach to estimate the perturbative uncertainty is to take it to be the last known perturbative correction; a more widely used method is to estimate it from the change in the prediction when varying the renormalization and factorization scales around a central value  $Q$  that is taken close to the physical scale of the process. A conventional range of variation is  $Q/2 < \mu_R, \mu_F < 2Q$ , varying the two scales independently with the restriction  $\frac{1}{2}\mu_R < \mu_F < 2\mu_R$  [293]. This constraint limits the risk of misleadingly small uncertainties due

<sup>7</sup>A veto on the jet phase space can be severe, for example by requiring exactly zero jets above a given transverse momentum cut accompanying a Higgs boson, or relatively mild, for example by placing a transverse momentum cut of 30 GeV on the measurement of the production of a Higgs boson with one or more jets. In general, inclusive cross sections are preferable, as uncertainties on both the theoretical and experimental sides are smaller.

<sup>8</sup>The program ARIADNE [277] has also been widely used for simulating  $e^+e^-$  and DIS collisions.

to fortuitous cancellations between the  $\mu_F$  and  $\mu_R$  dependence when both are varied together, while avoiding the appearance of large logarithms of  $\mu_R^2/\mu_F^2$  when both are varied completely independently. Where possible, it can be instructive to examine the two-dimensional scale distributions ( $\mu_R$  vs.  $\mu_F$ ) to obtain a better understanding of the interplay between  $\mu_R$  and  $\mu_F$ . This procedure should not be assumed to always estimate the full uncertainty from missing higher orders, but it does indicate the size of one important known source of higher-order ambiguity.<sup>9</sup>

For processes involving jets in the final state, estimates of the uncertainties at NNLO, along the lines described above, can be misleading for jets of smaller radii, due to accidental cancellations. Procedures are available to provide more reasonable estimates of the uncertainties in those cases [281, 302]. In addition, care must be taken as to the form of the central scale [303].

Calculations that involve resummations usually have an additional source of uncertainty associated with the choice of argument of the logarithms being resummed, *e.g.*  $\ln(2 \frac{p_t^Z}{M_Z})$  as opposed to  $\ln(\frac{1}{2} \frac{p_t^Z}{M_Z})$ . In addition to varying renormalization and factorization scales, it is therefore also advisable to vary the argument of the logarithm by a suitable factor in either direction with respect to the “natural” argument.

The accuracy of QCD predictions is limited also by non-perturbative corrections, which typically scale as a power of  $A/Q$ .<sup>10</sup> For measurements that are directly sensitive to the structure of the hadronic final state, the corrections are usually linear in  $A/Q$ . The non-perturbative corrections are further enhanced in processes with a significant underlying event (*i.e.* in  $pp$  and  $p\bar{p}$  collisions) and in cases where the perturbative cross sections fall steeply as a function of  $p_t$  or some other kinematic variable, for example in inclusive jet spectra or dijet mass spectra. In general, the underlying event for a hard scattering process, such as dijet production, is of a similar order, but somewhat harder, than the average energy density in a minimum-bias event. Under high-luminosity running conditions, such as 13 TeV at the LHC, there can be on the order of 50 minimum-bias interactions occurring at each beam-beam crossing. This additional energy needs to be corrected for, and is typically removed by subtracting a rapidity-dependent transverse energy density determined on an event-by-event basis [304]. This subtraction, of necessity, also removes the underlying event, which must be added back in to restore the measured event to the hadron level.

Non-perturbative corrections are commonly estimated from the difference between Monte Carlo events at the parton level and after hadronization. An issue to be aware of with this procedure is that “parton level” is not a uniquely defined concept. For example, in an event generator it depends on a (somewhat arbitrary and tunable) internal cutoff scale that separates the parton showering from the hadronization. In contrast, no such cutoff scale exists in an NLO or NNLO partonic calculation. There exist alternative methods for estimating hadronization corrections, that attempt to analytically deduce non-perturbative effects in one observable based on measurements of other observables (see the reviews [28, 305]). While they directly address the problem of different possible definitions of parton level, it should also be said that they are far less flexible than Monte Carlo programs and not always able to provide equally good descriptions of the data.

One of the main issues is whether the fixed partonic final state of a NLO or NNLO prediction can match the parton shower in its ability to describe the experimental jet shape (minus any underlying event). NNLO calculations provide a better match to the parton shower predictions than do NLO ones, as might be expected from the additional gluon available to describe the jet shape. The hadronization predictions appear to work for both orders, but at an unknown accuracy. The impact of any error should fall as a power correction.

<sup>9</sup> A number of prescriptions also exist for setting the scale automatically, *e.g.* Refs. [294–298], eliminating uncertainties from scale variation, though not from the truncation of the perturbative series itself. Recently, there have also been studies of how to estimate uncertainties from missing higher orders that go beyond scale variations [299–301].

<sup>10</sup> In some circumstances, the scale in the denominator could be a smaller kinematic or physical scale that depends on the observable.

## 9.3 Experimental studies of QCD

Since we are not able to directly measure partons (quarks or gluons), but only hadrons and their decay products, a central issue for every experimental study of perturbative QCD is establishing a correspondence between observables obtained at the partonic and the hadronic level. The only theoretically sound correspondence is achieved by means of *infrared and collinear safe* quantities, which allow one to obtain finite predictions at any order of perturbative QCD.

As stated above, the simplest case of infrared- and collinear-safe observables are total cross sections. More generally, when measuring fully inclusive observables, the final state is not analyzed at all regarding its (topological, kinematical) structure or its composition. Basically the relevant information consists in the rate of a process ending up in a partonic or hadronic final state. In  $e^+e^-$  annihilation, widely used examples are the ratios of partial widths or branching ratios for the electroweak decay of particles into hadrons or leptons, such as  $Z$  or  $\tau$  decays, (*cf.* Sec. 9.2.1). Such ratios are often favored over absolute cross sections or partial widths because of large cancellations of experimental and theoretical systematic uncertainties. The strong suppression of non-perturbative effects,  $\mathcal{O}(A^4/Q^4)$ , is one of the attractive features of such observables, however, at the same time, the sensitivity to radiative QCD corrections is small, which for example affects the statistical uncertainty when using them for the determination of the strong coupling constant. In the case of  $\tau$  decays not only the hadronic branching ratio is of interest, but also moments of the spectral functions of hadronic tau decays, which sample different parts of the decay spectrum and thus provide additional information. Other examples of fully inclusive observables are structure functions (and related sum rules) in DIS. These are extensively discussed in Sec. 18 of this *Review*.

On the other hand, often the structure or composition of the final state are analyzed and cross sections differential in one or more variables characterizing this structure are of interest. Examples are jet rates, jet substructure, event shapes or transverse momentum distributions of jets or vector bosons in hadron collisions. The case of fragmentation functions, *i.e.* the measurement of hadron production as a function of the hadron momentum relative to some hard scattering scale, is discussed in Sec. 19 of this *Review*.

It is worth mentioning that, besides the correspondence between the parton and hadron level, also a correspondence between the hadron level and the actually measured quantities in the detector has to be established. The simplest examples are corrections for finite experimental acceptance and efficiencies. Whereas acceptance corrections essentially are of theoretical nature, since they involve extrapolations from the measurable (partial) to the full phase space, other corrections such as for efficiency, resolution and response are of experimental nature. For example, measurements of differential cross sections such as jet rates require corrections in order to relate, *e.g.*, the energy deposits in a calorimeter to the jets at the hadron level. Typically detector simulations and/or data-driven methods are used in order to obtain these corrections. Care should be taken here in order to have a clear separation between the parton-to-hadron level and hadron-to-detector level corrections. Finally, for the sake of an easy comparison to the results of other experiments and/or theoretical calculations, it is suggested to provide, whenever possible, measurements corrected for detector effects and/or all necessary information related to the detector response (*e.g.*, the detector response matrix).

### 9.3.1 Hadronic final-state observables

#### 9.3.1.1 Jets

In hard interactions, final-state partons and hadrons appear predominantly in collimated bunches, which are generically called *jets*. To a first approximation, a jet can be thought of as a hard parton that has undergone soft and collinear showering and then hadronization. Jets are used both for testing our understanding and predictions of high-energy QCD processes, and also for identifying the hard partonic structure of decays of massive particles such as top quarks and W, Z and Higgs bosons.

In order to map observed hadrons onto a set of jets, one uses a *jet definition*. The mapping involves explicit choices: for example when a gluon is radiated from a quark, for what range of kinematics should the gluon be part of the quark jet, or instead form a separate jet? Good jet definitions are infrared and collinear safe, simple to use in theoretical and experimental contexts, applicable to any type of inputs (parton or hadron momenta, charged particle tracks, and/or energy deposits in the detectors) and lead to jets that are not too sensitive to non-perturbative effects.

An extensive treatment of the topic of jet definitions is given in Ref. [306] (for  $e^+e^-$  collisions) and Refs. [307–309]. Here we briefly review the two main classes: cone algorithms, extensively used at older hadron colliders, and sequential recombination algorithms, more widespread in  $e^+e^-$  and  $ep$  colliders and at the LHC.

Very generically, most (iterative) cone algorithms start with some seed particle  $i$ , sum the momenta of all particles  $j$  within a cone of opening-angle  $R$ , typically defined in terms of rapidity and azimuthal angle. They then take the direction of this sum as a new seed and repeat until the direction of the cone is stable, and call the contents of the resulting stable cone a jet if its transverse momentum is above some threshold  $p_{t,\min}$ . The parameters  $R$  and  $p_{t,\min}$  should be chosen according to the needs of a given analysis.

There are many variants of the cone algorithm, and they differ in the set of seeds they use and the manner in which they ensure a one-to-one mapping of particles to jets, given that two stable cones may share particles (“overlap”). The use of seed particles is a problem w.r.t. infrared and collinear safety. Seeded algorithms are generally not compatible with higher-order (or sometimes even leading-order) QCD calculations, especially in multi-jet contexts, as well as potentially subject to large non-perturbative corrections and instabilities. Seeded algorithms (JetCLU, MidPoint, and various other experiment-specific iterative cone algorithms) are therefore to be deprecated. Such algorithms are not used at the LHC, but were at the Fermilab Tevatron, where data still provide useful information, for example for global PDF fits. A modern alternative is to use a seedless variant, SIScone [310].

Sequential recombination algorithms at hadron colliders (and in DIS) are characterized by a distance  $d_{ij} = \min(k_{t,i}^{2p}, k_{t,j}^{2p}) \Delta_{ij}^2 / R^2$  between all pairs of particles  $i, j$ , where  $\Delta_{ij}$  is their separation in the rapidity-azimuthal plane,  $k_{t,i}$  is the transverse momentum w.r.t. the incoming beams, and  $R$  is a free parameter. At the LHC,  $R$  is typically in the range from 0.4 to 0.7. They also involve a “beam” distance  $d_{iB} = k_{t,i}^{2p}$ . One identifies the smallest of all the  $d_{ij}$  and  $d_{iB}$ , and if it is a  $d_{ij}$ , then  $i$  and  $j$  are merged into a new pseudo-particle (with some prescription, a recombination scheme, for the definition of the merged four-momentum). If the smallest distance is a  $d_{iB}$ , then  $i$  is removed from the list of particles and called a jet. As with cone algorithms, one usually considers only jets above some transverse-momentum threshold  $p_{t,\min}$ . The parameter  $p$  determines the kind of algorithm:  $p = 1$  corresponds to the (*inclusive*-) $k_t$  algorithm [215, 311, 312],  $p = 0$  defines the *Cambridge-Aachen* algorithm [313, 314], while for the *anti- $k_t$*  algorithm  $p = -1$  [315]. All these variants are infrared and collinear safe. Whereas the former two lead to irregularly shaped jet boundaries, the latter results in cone-like boundaries. The *anti- $k_t$*  algorithm has become the de-facto standard for the LHC experiments.

In  $e^+e^-$  annihilation the  $k_t$  algorithm [215] uses  $y_{ij} = 2 \min(E_i^2, E_j^2) (1 - \cos \theta_{ij}) / Q^2$  as distance measure between two particles/partons  $i$  and  $j$  and repeatedly merges the pair with smallest  $y_{ij}$ , until all  $y_{ij}$  distances are above some threshold  $y_{\text{cut}}$ , the jet resolution parameter.  $Q$  is a measure of the overall hardness of the event. The (pseudo)-particles that remain at this point are called the jets. Here it is  $y_{\text{cut}}$  (rather than  $R$  and  $p_{t,\min}$ ) that should be chosen according to the needs of the analysis. The two-jet rate in the  $k_t$  algorithm has the property that logarithms  $\ln(1/y_{\text{cut}})$  exponentiate. This is one reason why it is preferred over the earlier JADE algorithm [217], which uses the distance measure  $y_{ij} = 2 E_i E_j (1 - \cos \theta_{ij}) / Q^2$ . Note that other variants of sequential recombination algorithms for  $e^+e^-$  annihilations, using different definitions of the resolution measure  $y_{ij}$ , exhibit

much larger sensitivities to fragmentation and hadronization effects than the  $k_t$  and JADE algorithms [316]. Efficient implementations of the above algorithms are available through the *FastJet* package [317].

### 9.3.1.2 Event Shapes

Event-shape variables are functions of the four momenta of the particles in the final state and characterize the topology of an event’s energy flow. They are sensitive to QCD radiation (and correspondingly to the strong coupling) insofar as gluon emission changes the shape of the energy flow.

The classic example of an event shape is the *Thrust* [318, 319] in  $e^+e^-$  annihilations, defined as

$$\hat{\tau} = \max_{\vec{n}_\tau} \frac{\sum_i |\vec{p}_i \cdot \vec{n}_\tau|}{\sum_i |\vec{p}_i|}, \quad (9.22)$$

where  $\vec{p}_i$  are the momenta of the particles or the jets in the final state and the maximum is obtained for the Thrust axis  $\vec{n}_\tau$ . In the Born limit of the production of a perfect back-to-back  $q\bar{q}$  pair, the limit  $\hat{\tau} \rightarrow 1$  is obtained, whereas a perfectly spherical many-particle configuration leads to  $\hat{\tau} \rightarrow 1/2$ . Further event shapes of similar nature have been extensively measured at LEP and at HERA, and for their definitions and reviews we refer to Refs. [1, 7, 305, 320, 321]. The energy-energy correlation function [322], namely the energy-weighted angular distribution of produced hadron pairs, and its associated asymmetry are further shape variables which have been studied in detail at  $e^+e^-$  colliders. For hadron colliders the appropriate modification consists in only taking the transverse momentum component [323]. More recently, the event shape  *$N$ -jettiness* has been proposed [324], that measures the degree to which the hadrons in the final state are aligned along  $N$  jet axes or the beam direction. It vanishes in the limit of exactly  $N$  infinitely narrow jets.

Phenomenological discussions of event shapes at hadron colliders can be found in Refs. [324–328]. Measurements of hadronic event-shape distributions have been published by CDF [329], ATLAS [330–335] and CMS [336–339].

Event shapes are used for many purposes. These include measuring the strong coupling, tuning the parameters of Monte Carlo programs, investigating analytical models of hadronization and distinguishing QCD events from events that might involve decays of new particles (giving event-shape values closer to the spherical limit).

### 9.3.1.3 Jet substructure, quark vs. gluon jets

Jet substructure, which can be resolved by finding subjets or by measuring jet shapes, is sensitive to the details of QCD radiation in the shower development inside a jet and has been extensively used to study differences in the properties of quark and gluon induced jets, strongly related to their different color charges. In general, there is clear experimental evidence that gluon jets have a softer particle spectrum and are “broader” than (light-) quark jets (as expected from perturbative QCD) when looking at observables such as the jet shape  $\Psi(r/R)$ . This is the fractional transverse momentum contained within a sub-cone of cone-size  $r$  for jets of cone-size  $R$ . It is sensitive to the relative fractions of quark and gluon jets in an inclusive jet sample and receives contributions from soft-gluon initial-state radiation and the underlying event. Therefore, it has been widely employed for validation and tuning of Monte Carlo parton-shower models. Furthermore, this quantity turns out to be sensitive to the modification of the gluon radiation pattern in heavy ion collisions (see *e.g.* Ref. [340]).

The most recent jet shape measurements using proton-proton collision data have been presented for inclusive jet samples [341–343] and for top-quark production [344]. Further discussions, references and summaries can be found in Refs. [321, 345, 346] and Sec. 4 of Ref. [347].

The use of jet substructure has also been investigated in order to distinguish QCD jets from jets that originate from hadronic decays of boosted massive particles (high- $p_t$  electroweak bosons, top quarks and hypothesized new particles). A considerable number of experimental studies have been carried out with Tevatron and LHC data, in order to investigate on the performance of the



proposed algorithms for resolving jet substructure and to apply them to searches for new physics, as well as to the reconstruction of boosted top quarks, vector bosons and the Higgs boson. For reviews of this rapidly growing field, see sec. 5.3 of Ref. [307], Ref. [348] and Refs. [347, 349–352]. Perhaps no other sub-field has benefited as much from machine learning techniques as the study of jet substructure. As a jet can have  $O(100)$  constituents each with kinematic and other information, jet substructure analysis is naturally a highly multivariate problem. Deep learning techniques can use all of the available information to study jets in their natural high dimensionality. Such techniques have not only improved discrimination between different final states/types of jets, but have also improved our understanding of perturbative QCD. See for example the review in Ref. [268].

### 9.3.2 QCD measurements at colliders

There exists a wealth of data on QCD-related measurements in  $e^+e^-$ ,  $ep$ ,  $pp$ , and  $p\bar{p}$  collisions, to which a short overview like this would not be able to do any justice. Extensive reviews of the subject have been published in Refs. [320, 321] for  $e^+e^-$  colliders and in Ref. [353] for  $ep$  scattering, whereas for hadron colliders comprehensive overviews are given in, *e.g.*, Refs. [308, 346] and Refs. [2, 354–356].

Below we concentrate our discussion on measurements that are most sensitive to hard QCD processes with focus on jet production.

#### 9.3.2.1 $e^+e^-$ colliders

Analyses of jet production in  $e^+e^-$  collisions are mostly based on data from the JADE experiment at center-of-mass energies between 14 and 44 GeV, as well as on LEP collider data at the  $Z$  resonance and up to 209 GeV. The analyses cover the measurements of (differential or exclusive) jet rates (with multiplicities typically up to 4, 5 or 6 jets), the study of 3-jet events and particle production between the jets, as well as 4-jet production and angular correlations in 4-jet events.

Event-shape distributions from  $e^+e^-$  data have been an important input to the tuning of parton shower MC models, typically matched to matrix elements for 3-jet production. In general these models provide good descriptions of the available, highly precise data. Especially for the large LEP data sample at the  $Z$  peak, the statistical uncertainties are mostly negligible and the experimental systematic uncertainties are at the percent level or even below. These are usually dominated by the uncertainties related to the MC model dependence of the efficiency and acceptance corrections (often referred to as “detector corrections”).

Observables measured in  $e^+e^-$  collisions have been used for determinations of the strong coupling constant (*cf.* Section 9.4 below) and for putting constraints on the QCD color factors (*cf.* Sec. 9.1 for their definitions), thus probing the non-Abelian nature of QCD. Typically, cross sections can be expressed as functions of these color factors, for example  $\sigma = f(\alpha_s C_F, C_A/C_F, n_f T_R/C_F)$ . Angular correlations in 4-jet events give sensitivity at leading order. Some sensitivity to these color factors, although only at NLO, is also obtained from event-shape distributions. Scaling violations of fragmentation functions and the different substructure in quark and gluon induced jets also give access to these color factors. In order to extract absolute values, *e.g.* for  $C_F$  and  $C_A$ , certain assumptions have to be made for other parameters, such as  $T_R, n_f$  or  $\alpha_s$ , since typically only combinations (ratios, products) of all the relevant parameters appear in the perturbative predictions. A compilation of results [321] quotes world average values of  $C_A = 2.89 \pm 0.03(\text{stat}) \pm 0.21(\text{syst})$  and  $C_F = 1.30 \pm 0.01(\text{stat}) \pm 0.09(\text{syst})$ , with a correlation coefficient of 82%. These results are in perfect agreement with the expectations from  $SU(3)$  of  $C_A = 3$  and  $C_F = 4/3$ .

#### 9.3.2.2 DIS and photoproduction

Jet measurements in  $ep$  collisions, both in the DIS and photoproduction regimes, allow for tests of QCD factorization (as they involve only one initial state proton and thus one PDF function), and provide sensitivity to both the gluon distribution and to the strong coupling constant. Calculations are available at NNLO in both regimes [357, 358]. Experimental uncertainties of the order of 5–10% have been achieved, mostly dominated by the jet energy

scale, whereas statistical uncertainties are negligible to a large extent. For comparison to theoretical predictions, at large jet  $p_t$  the PDF uncertainty dominates the theoretical uncertainty (typically of order 5–10%, in some regions of phase space up to 20%), therefore jet observables become useful inputs for PDF fits.

In general, the data are well described by the NLO and NNLO matrix-element calculations, combined with DGLAP evolution equations, in particular at large  $Q^2$  and central values of jet pseudo-rapidity. At low values of  $Q^2$  and  $x$ , in particular for large jet pseudo-rapidities, certain features of the data have been interpreted as requiring BFKL-type evolution, though the predictions for such schemes are still limited. It is worth noting that there is lack of consensus throughout the community regarding this need of BFKL-evolution at currently probed  $x, Q^2$  values, and an alternative approach [359], which implements the merging of LO matrix-element based event generation with a parton shower (using the SHERPA framework), successfully describes the data in all kinematical regions, including the low  $Q^2$ , low  $x$  domain. At moderately small  $x$  values, it should perhaps not be surprising that the BFKL approach and fixed-order matrix-element merging with parton showers may both provide adequate descriptions of the data, because some part of the multi-parton phase space that they model is common to both approaches.

In the case of photoproduction, a wealth of measurements with low  $p_t$  jets were performed in order to constrain the photon content of the proton. The uncertainties related to such photon PDFs play a minor role at high jet  $p_t$ , which has allowed for precise tests of pQCD calculations.

A few examples of recent measurements can be found in Refs. [360–364] for photoproduction and in Refs. [365–374] for DIS.

#### 9.3.2.3 Hadron-hadron colliders

The spectrum of observables and the number of measurements performed at hadron colliders is enormous, probing many regions of phase space and covering a huge range of cross sections, as illustrated in Fig. 9.1 for the case of the ATLAS and CMS experiments at the LHC. In general, the theory agreement with data is excellent for a wide variety of processes, indicating the success of perturbative QCD with the PDF and strong coupling inputs. For the sake of brevity, in the following only certain classes of those measurements will be discussed, which allow addressing particular aspects of the various QCD studies performed. Most of our discussion will focus on LHC results, which are available for center-of-mass energies of 2.76, 5, 7, 8 and 13 TeV with integrated luminosities of up to  $140 \text{ fb}^{-1}$ . Generally speaking, besides representing a general test of the standard model and QCD in particular, these measurements serve several purposes, such as: (i) probing pQCD and its various approximations and implementations in MC models, in order to quantify the order of magnitude of not yet calculated contributions and to gauge their precision when used as background predictions, or (ii) extracting/constraining model parameters such as the strong coupling constant or PDFs. Indeed, data from the LHC is becoming increasingly important for the determination of both, PDFs and the strong coupling constant.

The final states measured at the LHC include single, double and triple gauge boson production, top production (single top, top pair and four top production), Higgs boson production, alone and in conjunction with a W or Z boson, and with a top quark pair. Many/most of these events are accompanied by additional jets. So far only relatively loose limits have been placed on double Higgs production. The volume of LHC results prohibits a comprehensive description in this *Review*; hence, only a few highlights will be presented.

Among the most important cross sections measured, and the one with the largest dynamic range, is the inclusive jet spectrum as a function of the jet transverse momentum ( $p_t$ ), for several rapidity regions and for  $p_t$  up to 700 GeV at the Tevatron and  $\sim 3.5$  TeV at the LHC. It is worth noting that this upper limit in  $p_t$  corresponds to a distance scale of  $\sim 10^{-19}$  m: no other experiment so far is able to directly probe smaller distance scales of nature than this measurement. The Tevatron inclusive jet measurements in Run 2 (Refs. [377–380]) were carried out with the MidPoint jet clustering algorithm (or its equivalent) and with the  $k_t$  jet

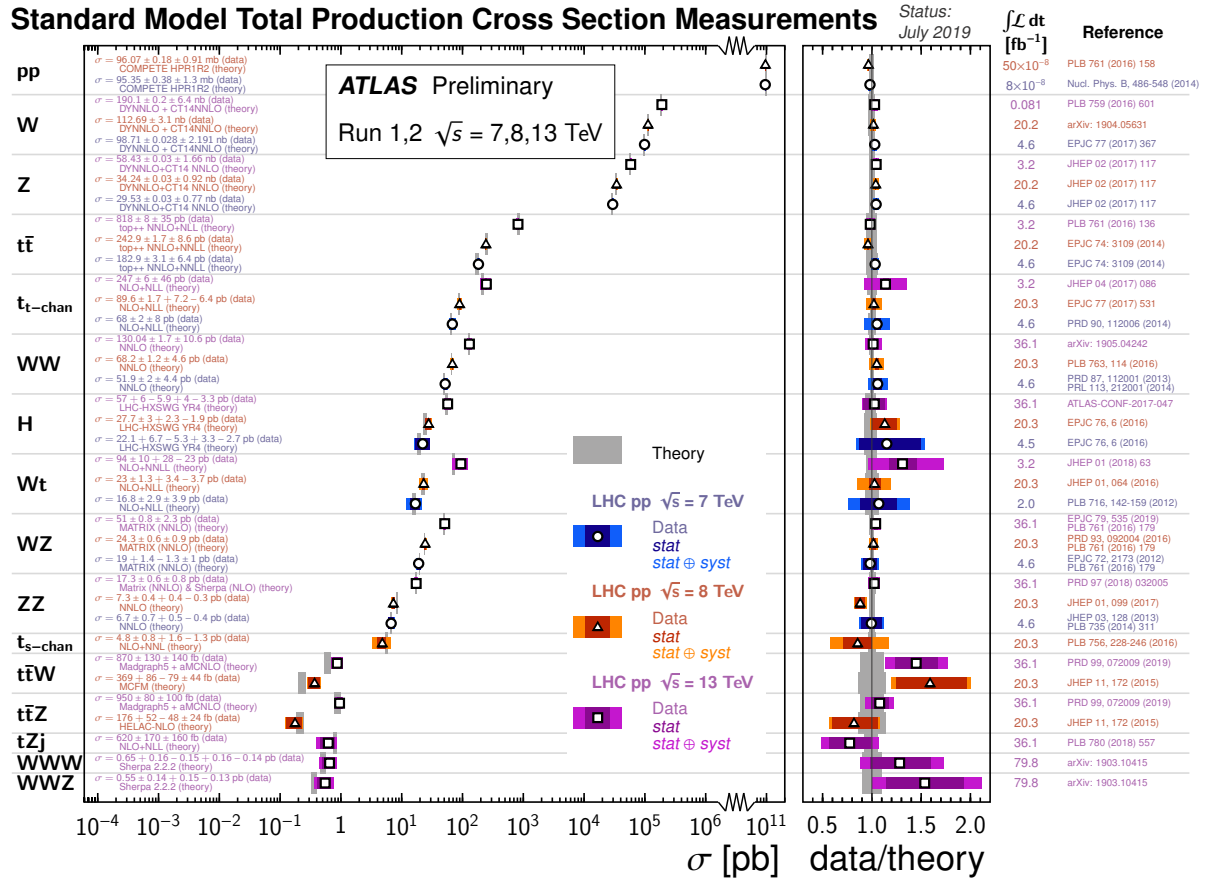
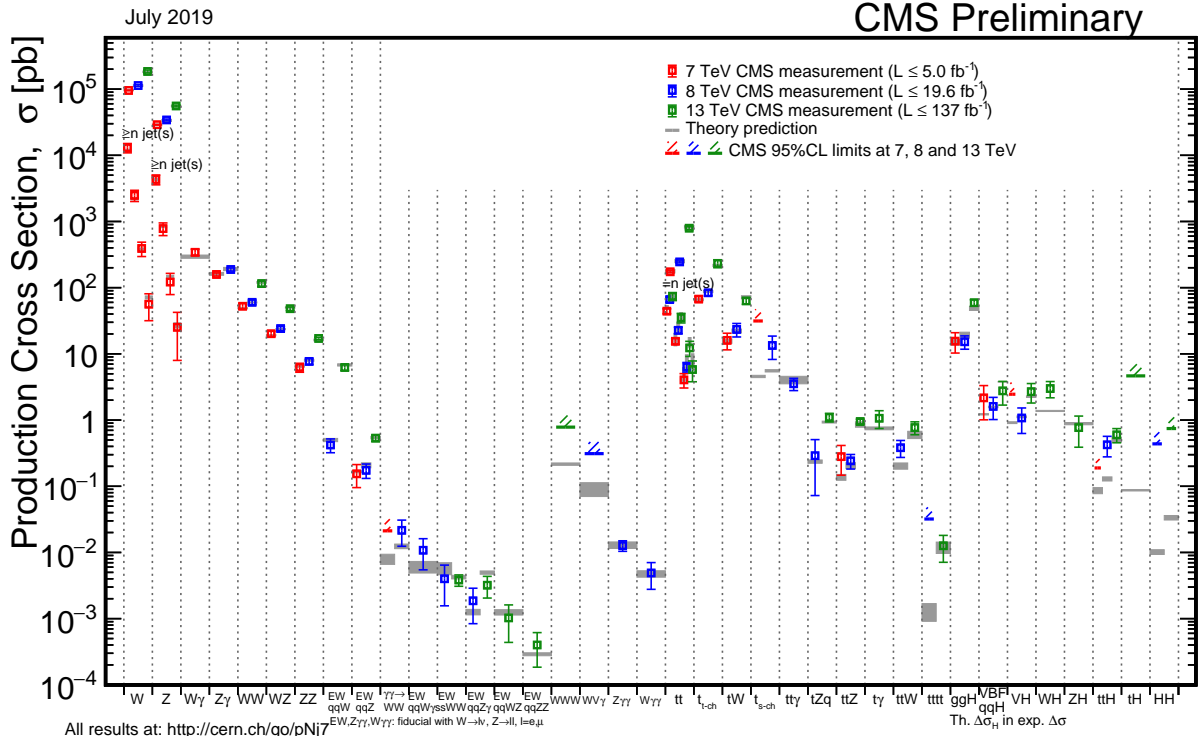


Figure 9.1: Overview of cross section measurements for a wide class of processes and observables, as obtained by the CMS [375] and ATLAS [376] experiments at the LHC, for centre-of-mass energies of 7, 8 and 13 TeV. Also shown are the theoretical predictions and their uncertainties.

clustering algorithm. Most of the LHC measurements use the *anti- $k_t$*  algorithm, with a variety of jet radii. The use of multiple jet radii in the same analysis allows a better understanding of the underlying QCD dynamics. Measurements by ALICE, ATLAS

and CMS have been published in Refs. [381–389].

In general, we observe a good description of the data by the NLO and NNLO QCD predictions over about 11 orders of magnitude in cross section, as long as care is taken for the form of

the central scale choice [303]. The experimental systematic uncertainties are dominated by the jet energy scale uncertainty, quoted to be in the range of a few percent (see for instance the review in Ref. [390]), leading to uncertainties of  $\sim 5 - 30\%$  on the cross section, increasing with  $p_t$  and rapidity. The PDF uncertainties dominate the theoretical uncertainty at large  $p_t$  and rapidity. In fact, inclusive jet data are one of the most important inputs to global PDF fits, in particular for constraining the high- $x$  gluon PDF [77, 391]. Constraints on the PDFs can also be obtained from ratios of inclusive cross sections at different center-of-mass energies [382, 387]. In general, ratios of jet cross sections are a means to (at least partially) cancel the jet energy scale uncertainties and thus provide jet observables with significantly improved precision.

Dijet events are analyzed in terms of their invariant mass or average dijet  $p_t$  and angular distributions, which allows for tests of NLO and NNLO QCD predictions (see *e.g.* Refs. [386, 392, 393] for recent LHC results), and for setting stringent limits on deviations from the Standard Model, such as quark compositeness or contact interactions (some examples can be found in Refs. [389, 394–400]). Furthermore, dijet azimuthal correlations between the two leading jets, normalized to the total dijet cross section, are an extremely valuable tool for studying the spectrum of gluon radiation in the event. The azimuthal separation of the two leading jets is sensitive to multi-jet production, avoiding at the same time large systematic uncertainties from the jet energy calibration. For example, results from the Tevatron [401, 402] and the LHC [335, 403–407] show that the LO (non-trivial) prediction for this observable, with at most three partons in the final state, is not able to describe the data for an azimuthal separation below  $2\pi/3$ , where NLO contributions (with 4 partons) restore the agreement with data. In addition, this observable can be employed to tune Monte Carlo predictions of soft gluon radiation. Further examples of dijet observables that probe special corners of phase space are those that involve forward (large rapidity) jets and where a large rapidity separation, possibly also a rapidity gap, is required between the two jets. Reviews of such measurements can be found in Ref. [346], showing that no single prediction is capable of describing the data in all phase-space regions. In particular, no conclusive evidence for BFKL effects in these observables has been established so far.

Beyond dijet final states, measurements of the production of three or more jets, including cross section ratios, have been performed (see Refs. [346, 408] for recent reviews), as a means of testing perturbative QCD predictions, determining the strong coupling constant (at NLO precision so far), and probing/tuning MC models, in particular those combining multi-parton matrix elements with parton showers.

$W$  and  $Z$  production serve as benchmark cross sections at the LHC. The large boson mass provides a stability for the perturbative predictions which results in better theoretical precision. In terms of experimental precision, measurements of inclusive vector boson ( $W, Z$ ) production provide the most precisely determined observables at hadron colliders so far. This is because the experimental signatures are based on leptons which are measured much more accurately than jets or photons. At the LHC [409–416], the dominant uncertainty stems from the luminosity determination ( $\leq 2-4\%$ ), while other uncertainties (*e.g.* statistics, lepton efficiencies) are controlled at the  $\sim 0.5-3\%$  level. The uncertainty from the acceptance correction of about  $\sim 1-2\%$  can be reduced by measuring so-called fiducial cross sections, *ie.* by applying kinematic cuts also to the particle level of the theoretical predictions. A further reduction or even complete elimination of particular uncertainties (*e.g.* luminosity) is achieved by measuring cross section ratios ( $W/Z$  or  $W^+/W^-$ ) or differential distributions that are normalised to the inclusive cross section. On the theory side, as discussed earlier in this *Review*, the production of these color-singlet states has been calculated up to NNLO accuracy, with some progress towards N<sup>3</sup>LO. Since the dominant theoretical uncertainty is related to the choice of PDFs, these high-precision data provide useful handles for PDF determinations.

Further insights are obtained from measurements of differential vector boson production, as a function of the invariant dilepton mass, the boson's rapidity or its transverse momentum. For

example, the dilepton invariant mass distribution has been measured [417–422] for masses between 15 and 3000 GeV, covering more than 8 orders of magnitude in cross section. NNLO QCD predictions, together with modern PDF sets and including higher-order electroweak and QED final-state radiation corrections, describe the data to within 5–10% over this large range, whereas NLO predictions show larger deviations, unless matched to a parton shower.

Similar conclusions can be drawn from the observed rapidity distribution of the dilepton system (see *e.g.* Refs. [409, 418, 423]) or, in the case of  $W$  production, from the observed charged lepton rapidity distribution and its charge asymmetry. The latter is particularly sensitive to differences among PDF sets [409, 424–426], also thanks to the high precision achieved by the ATLAS and CMS experiments for central rapidity ranges. These measurements are nicely extended to the very forward region, up to 4.5 in lepton rapidity, by the LHCb experiment.

An overview of this kind of measurements can be found in Ref. [346]. There one can also find a discussion of and references to LHC results from studies of the vector boson's transverse momentum distribution,  $p_t^V$  (see also Refs. [427–429]). This observable covers a wide kinematic range and probes different aspects of higher-order QCD effects. It is sensitive to jet production in association with the vector boson, without suffering from the large jet energy scale uncertainties. In the  $p_t^V$  region of several tens of GeV to over 1 TeV, the NNLO predictions for V+jet<sup>11</sup> can be used to predict the high  $p_t$  boson transverse cross section. The NNLO predictions agree with the data to within about 10%, and agree somewhat better at high transverse momentum than do the NLO predictions [430]. At transverse momenta below  $\sim 20$  GeV, the fixed-order predictions fail and soft-gluon resummation is needed to restore the agreement with data. The soft gluon resummation can either be performed analytically, or effectively using parton showering implemented in Monte Carlo programs.

The addition of jets to the final state extends the kinematic range as well as increasing the complexity of the calculation/measurements.<sup>12</sup> The number of results obtained both at the Tevatron and at the LHC is extensive. Recent summaries can be found in Refs. [346, 432]. Some more recent results can be found in Refs. [430, 433–436].

The measurements cover a very large phase space, *e.g.* with jet transverse momenta between 30 GeV and  $\sim 1.5$  TeV and jet rapidities up to  $|y| < 4.4$  [430]. Jet multiplicities as high as seven jets accompanying the vector boson have already been probed at the LHC, together with a substantial number of other kinematical observables, such as angular correlations among the various jets or among the jets and the vector boson, or the sum of jet transverse momenta,  $H_T$ . Whereas the jet  $p_t$  and  $H_T$  distributions are dominated by jet energy scale uncertainties at levels similar to those discussed above for inclusive jet production, angular correlations and jet multiplicity ratios have been measured with a precision of  $\sim 10\%$ , see *e.g.* Refs. [337, 437].

NLO calculations for up to five jets [438] in addition to the vector boson are in good agreement with the data over that phase space, where the calculations are applicable; that is, one can not expect such predictions to work for *e.g.* the  $p_t$  distribution of the  $n + 1$ st jet with  $V + n$  jets calculated at NLO. However, with the higher kinematic reach achieved by the LHC experiments, some more detailed observations can be made. NLO fixed-order predictions describe the  $W$  boson  $p_t$  distribution and the lead jet  $p_t$  distribution reasonably well at transverse momenta below around 500 GeV, but predict smaller cross sections than the data at higher transverse momenta. Predictions for V+jet at NNLO improve the description of the data. MC models that implement parton shower matching to matrix elements (either at LO or NLO) have mixed results.

The challenges get even more severe in the case of vector boson plus heavy quark ( $b, c$ ) production, both because of theoretical

<sup>11</sup>For these calculations, there is a requirement of the presence of a jet, but the  $p_t$  cut is typically small (30 GeV) compared to the high  $p_t$  region being discussed here.

<sup>12</sup>For reliable predictions, the scale used in the higher order calculations should be proportional to the sum of the transverse momenta of all of the objects in the final state [431].

issues (an additional scale is introduced by the heavy quark mass and different schemes exist for the handling of heavy quarks and their mass effects in the initial and/or final state) and because of additional experimental uncertainties related to the heavy-flavour tagging. A review of heavy quark production at the LHC can be found in Ref. [439]. There it is stated that studies of  $b$ -jet production with or without associated  $W$  and  $Z$  bosons reveal the di- $b$ -jet  $p_t$  and mass spectra to be well modelled, within experimental and theoretical uncertainties, by most generators on the market. However, sizable differences between data and predictions are seen in the modelling of events with single  $b$  jets, particularly at large  $b$ -jet  $p_t$ , where gluon splitting processes become dominant, as also confirmed by studies of  $b$ -hadron and  $b$ -jet angular correlations.

The precision reached in photon measurements is in between that for lepton and jet measurements. The photon 4-vectors can be measured at about the same precision as the lepton 4-vectors in Drell-Yan production, but there are greater challenges encountered in photon reconstruction (for example isolation) and in purity determination. Note, though, that the photon purity approaches unity as the photon  $p_t$  increases. At high  $p_t$ , it becomes increasingly difficult for a jet to fragment into an isolated neutral electromagnetic cluster which mimics the photon signature. The inclusive photon cross section can be measured [392, 440–443], as well as the production of a photon accompanied by one or more jets [443–445, 445–448]. The kinematic range for photon production is less than that for jet production because of the presence of the electromagnetic coupling, but still reaches about 2 TeV. Better agreement is obtained with NNLO predictions for photon production than for NLO predictions, except when the latter are matched to matrix element plus parton shower predictions. Photon production in association with a heavy-flavor jet is a useful input for the determination of the  $b$  and  $c$  quark PDFs [449].

Electroweak corrections are expected to become more and more relevant now that the TeV energy range starts to be explored. For example, such corrections were found [450] to be sizable (tens of percent) when studying the ratio  $(d\sigma^\gamma/dp_t)/(d\sigma^Z/dp_t)$  in  $\gamma(Z)$ -jet production,  $p_t$  being the boson's transverse momentum, and might account for (some of) the differences observed in a CMS measurement [451] of this quantity.

A number of interesting developments, in terms of probing higher-order QCD effects, have occurred in the sector of diboson production, in particular for the  $WW$  and  $\gamma\gamma$  cases. Regarding the former, an early disagreement of about 10% between the LHC measurements and the NLO predictions had led to a number of speculations of possible new physics effects in this channel. However, more recent ATLAS and CMS measurements [452–455] are in agreement with the NNLO prediction [85]. The statistical reach of the LHC has resulted in evidence for triple massive gauge boson production [456].

In the case of diphoton production, ATLAS [457, 458] and CMS [459] have provided accurate measurements, in particular for phase-space regions that are sensitive to radiative QCD corrections (multi-jet production), such as small azimuthal photon separation. While there are large deviations between data and NLO predictions in this region, a calculation [178] at NNLO accuracy manages to mostly fill this gap. This is an interesting example where scale variations can not provide a reliable estimate of missing contributions beyond NLO, since at NNLO new channels appear in the initial state (gluon fusion in this case). These missing channels can be included in a matrix element plus parton shower calculation in which two additional jets are included at NLO. The result is a similar level of agreement as that obtained at NNLO. Three photon production has also been measured [460].

In terms of heaviest particle involved, top-quark production at the LHC has become an important tool for probing higher-order QCD calculations, thanks to very impressive achievements both on the experimental and theoretical side, as extensively summarised in Ref. [461]. Regarding  $t\bar{t}$  production, the most precise inclusive cross section measurements are achieved using the dilepton ( $e\mu$ ) final state, with a total uncertainty of 4% [462–465]. This is of about the same size as the uncertainty on the most advanced theoretical predictions [84, 466–468], obtained at NNLO with additional soft-gluon resummation at NNLL accuracy [469]. There

is excellent agreement between data and the QCD predictions.

The  $t\bar{t}$  final state allows multiple observables to be measured. A large number of differential cross section measurements have been performed at 7, 8 and 13 TeV centre-of-mass energy, studying distributions such as the top-quark  $p_t$  and rapidity, the transverse momentum and invariant mass of the  $t\bar{t}$  system (probing scales up to the TeV range), or the number of additional jets. These measurements have been compared to a wide range of predictions, at fixed order up to NNLO as well as using LO or NLO matrix elements matched to parton showers. Each of the observables provides information on the high  $x$  gluon and have been used in global PDF fits. While in general there is reasonable agreement observed with data, most MC simulations predict a somewhat harder top-quark  $p_t$  distribution than seen in data.

Thanks to both the precise measurements of, and predictions for, the inclusive top-pair cross section, which is sensitive to the strong coupling constant and the top-quark mass, this observable has been used to measure the strong coupling constant at NNLO accuracy from hadron collider data [470, 471] (*cf.* Section 9.4 below), as well as to obtain a measurement of the top-quark's pole mass without employing direct reconstruction methods [470, 472, 473].

The Higgs boson lends itself to being a tool for QCD studies, especially as the dominant production mechanism is  $gg$  fusion, which is subject to very large QCD corrections. Higgs boson production has been measured in the  $ZZ, \gamma\gamma, WW$  and  $\tau\tau$  decay channels. The experimental cross section is now known with a precision approaching 10% [474, 475], similar to the size of the theoretical uncertainty [92], of which the PDF+ $\alpha_s$  uncertainty is the largest component. The experimental precision has allowed detailed fiducial and differential cross section measurements. For example, with the diphoton final state, the transverse momentum of the Higgs boson can be measured out to 350–400 GeV [476, 477], where top quark mass effects become important. The production of a Higgs boson with up to 4 jets has been measured [476, 478]. The experimental cross sections have been compared to NNLO predictions (for  $H + \geq 1$  jet), NLO for 2 and 3 jets, and NNLO+NNLL for the transverse momentum distribution. In addition, finite top quark mass effects have been taken into account at NLO. The use of the boosted  $H \rightarrow b\bar{b}$  topology allows probes of Higgs boson transverse momenta on the order of 600 GeV [478]. So far the agreement with the perturbative QCD corrections is good.

#### 9.4 Determinations of the strong coupling constant

Beside the quark masses, the only free parameter in the QCD Lagrangian is the strong coupling constant  $\alpha_s$ . The coupling constant in itself is not a physical observable, but rather a quantity defined in the context of perturbation theory, which enters predictions for experimentally measurable observables, such as  $R$  in Eq. (9.7). The value of the strong coupling constant must be inferred from such measurements and is subject to experimental and theoretical uncertainties. The incomplete knowledge of  $\alpha_s$  propagates into uncertainties in numerous precision tests of the Standard Model. Here we present an update of the 2016 PDG average value of  $\alpha_s(M_Z^2)$  and its uncertainty [479], which were retained in the 2018 edition of this *Review* [480].<sup>13</sup>

Many experimental observables are used to determine  $\alpha_s$ . A number of recent determinations are collected in Ref. [484]. Further discussions and considerations on determinations of  $\alpha_s$  can also be found in Refs. [485, 486]. Such considerations include:

- The observable's sensitivity to  $\alpha_s$  as compared to the experimental precision. For example, for the  $e^+e^-$  cross section to hadrons (*cf.*  $R$  in Sec. 9.2.1), QCD effects are only a small correction, since the perturbative series starts at order  $\alpha_s^0$ ; 3-jet production or event shapes in  $e^+e^-$  annihilations are directly sensitive to  $\alpha_s$  since they start at order  $\alpha_s$ ; the hadronic decay width of heavy quarkonia,  $\Gamma(\Upsilon \rightarrow \text{hadrons})$ , is very sensitive to  $\alpha_s$  since its leading order term is  $\propto \alpha_s^3$ .

<sup>13</sup> The time evolution of  $\alpha_s$  combinations can be followed by consulting Refs. [481–483] as well as earlier editions of this *Review*.

- The accuracy of the perturbative prediction, or equivalently of the relation between  $\alpha_s$  and the value of the observable. The minimal requirement is generally considered to be an NLO prediction. Some observables (many inclusive ones as well as 3-jet rates and event shapes in  $e^+e^-$  collisions) are known to NNLO since quite some time. Recent additions to the list of processes calculated up to NNLO comprise inclusive jet and dijet production in DIS and  $pp$  or  $p\bar{p}$  collisions. Likewise,  $t\bar{t}$  and  $W/Z$ +jet production cross sections have been computed up to NNLO for  $pp$  and  $p\bar{p}$  scattering. The  $e^+e^-$  hadronic cross section and  $\tau$  branching fraction to hadrons are even known to N<sup>3</sup>LO, where one denotes the LO as the first non-trivial term. In certain cases, fixed-order predictions are supplemented with resummation. The precise magnitude of the associated theory uncertainties usually is estimated as discussed in Sec. 9.2.4.
- The size of non-perturbative effects. Sufficiently inclusive quantities, like the  $e^+e^-$  cross section to hadrons, have small non-perturbative contributions  $\sim \Lambda^4/Q^4$ . Others, such as event-shape distributions, have typically contributions  $\sim \Lambda/Q$ .
- The scale at which the measurement is performed. An uncertainty  $\delta$  on a measurement of  $\alpha_s(Q^2)$ , at a scale  $Q$ , translates to an uncertainty  $\delta' = (\alpha_s^2(M_Z^2)/\alpha_s^2(Q^2)) \cdot \delta$  on  $\alpha_s(M_Z^2)$ . For example, this enhances the already important impact of precise low- $Q$  measurements, such as from  $\tau$  decays, in combinations performed at the  $M_Z$  scale.

The selection of results from which to determine the world average value of  $\alpha_s(M_Z^2)$  is restricted to those that are

- published in a peer-reviewed journal at the time of writing this report,
- based on the most complete perturbative QCD predictions of at least NNLO accuracy,
- accompanied by reliable estimates of all experimental and theoretical uncertainties.

We note that all determinations of  $\alpha_s(M_Z^2)$  entering the average of the lattice gauge community as summarised comprehensively in the FLAG2019 report [487] are published in peer-reviewed journals, although the FLAG report itself that only describes the averaging procedure is not.

We also note that a prediction in perturbative QCD for the determination of  $\alpha_s(M_Z^2)$  at NNLO accuracy requires the calculation of at least three consecutive terms in powers  $p > 0$  of  $\alpha_s^p$ . Although this condition is fulfilled, measurements from jet production in DIS and at hadron colliders (with one exception) are still excluded, because the determination of  $\alpha_s(M_Z^2)$  has not yet been upgraded to NNLO. Nevertheless, the NLO analyses will be discussed in this *Review*, as they are important ingredients for the experimental evidence of the energy dependence of  $\alpha_s$ , *i.e.* for Asymptotic Freedom, one of the key features of QCD.

In order to calculate the world average value of  $\alpha_s(M_Z^2)$ , as in earlier editions we apply an intermediate step of pre-averaging results within the sub-fields now labelled “Hadronic  $\tau$  decays and low  $Q^2$  continuum” ( $\tau$  decays and low  $Q^2$ ), “Heavy quarkonia decays” ( $Q\bar{Q}$  bound states), “Deep-inelastic scattering and global PDF fits” (DIS & PDF fits), “Hadronic final states of  $e^+e^-$  annihilations” ( $e^+e^-$  jets & shapes), “Hadron collider results” (hadron collider), and “Electroweak precision fit” (electroweak) as explained in the following sections. For each sub-field, the *unweighted average* of all selected results is taken as the pre-average value of  $\alpha_s(M_Z^2)$ , and the unweighted average of the quoted uncertainties is assigned to be the respective overall error of this pre-average.<sup>14</sup> At variance with previous reviews, for the “Lattice QCD” (lattice) sub-field we do not perform a pre-averaging;

<sup>14</sup>In the previous review, if this error appeared to be smaller than the unweighted standard deviation - *i.e.* the *spread* - of the results, the standard deviation was taken as the overall uncertainty instead. This was done in order to arrive at an unbiased estimator of the average value of  $\alpha_s(M_Z^2)$  from a given sub-field, and to avoid that singular, optimistic estimates of systematic uncertainties unduly bias the uncertainty of the sub-field average. Here we find that, for all six sub-fields, the quoted error is larger than the standard deviation.

instead, we adopt for this sub-field the FLAG2019 average value and uncertainty derived in Ref. [487].

Assuming that the six sub-fields (excluding lattice) are largely independent of each other, we determine a non-lattice world average value using a ‘ $\chi^2$  averaging’ method. In a last step we perform an unweighted average of the values and uncertainties of  $\alpha_s(M_Z^2)$  from our non-lattice result and the lattice result presented in the FLAG 2019 report [487].

#### 9.4.1 Hadronic $\tau$ decays and low $Q^2$ continuum:

Based on complete N<sup>3</sup>LO predictions [36], analyses of the  $\tau$  hadronic decay width and spectral functions have been performed, *e.g.* in Refs. [36, 488–493], and lead to precise determinations of  $\alpha_s$  at the energy scale of  $M_\tau^2$ . They are based on different approaches to treat perturbative and non-perturbative contributions, the impacts of which have been a matter of intense discussions since a long time, see *e.g.* Refs. [492–495]. In particular, in  $\tau$  decays there is a significant difference between results obtained using fixed-order (FOPT) or contour improved perturbation theory (CIPT), such that analyses based on CIPT generally arrive at larger values of  $\alpha_s(M_\tau^2)$  than those based on FOPT. In addition, some results show differences in  $\alpha_s(M_\tau^2)$  between different groups using the same data sets and perturbative calculations, most likely due to different treatments of the non-perturbative contributions, *cf.* Ref. [493] with Refs. [492, 496].

Here, we largely keep the same input calculations as in the previous review, with only the following changes. The result of Ref. [492] has been replaced by the one of Ref. [495]. From Ref. [493] we use the values resulting from a combination of ALEPH and OPAL data instead of ALEPH data alone. Moreover, we include the new  $\alpha_s$  determination obtained from  $R(s)$  below the charm threshold [497]. Here, the average from the FOPT and CIPT results gives  $\alpha_s(M_\tau^2) = 0.301 \pm 0.019$ , where the difference between the two amounts to 2% at  $m_\tau$ . This corresponds to  $\alpha_s(M_Z^2) = 0.1162 \pm 0.0025$ .

In summary, we determine the pre-average value of  $\alpha_s(M_Z^2)$  for this sub-field from studies that employ both FOPT and CIPT expansions, and that account for the difference among these in the quoted overall uncertainty:  $\alpha_s(M_Z^2) = 0.1202 \pm 0.0019$  [36],  $\alpha_s(M_Z^2) = 0.1199 \pm 0.0015$  [496],  $\alpha_s(M_Z^2) = 0.1175 \pm 0.0017$  [493],  $\alpha_s(M_Z^2) = 0.1197 \pm 0.0015$  [495], and  $\alpha_s(M_Z^2) = 0.1162 \pm 0.0025$  [497]. Additionally, we include the result from  $\tau$  decay and lifetime measurements, obtained in Sec. *Electroweak Model and constraints on New Physics* of the 2018 edition of this *Review*,  $\alpha_s(M_Z^2) = 0.1184 \pm 0.0019$ . The latter result, being a global fit of  $\tau$  data, involve some correlations with the other extractions of this category. However, since we perform an unweighted average of the central value and uncertainty, we do not need to worry about double counting.

All these results are summarised in Fig. 9.2. Determining the unweighted average of the central values and their overall uncertainties, we arrive at  $\alpha_s(M_Z^2) = 0.1187 \pm 0.0018$ , which we will use as the first input for determining the world average value of  $\alpha_s(M_Z^2)$ . This corresponds to  $\alpha_s(M_\tau^2) = 0.325 \pm 0.016$ .

#### 9.4.2 Heavy quarkonia decays:

For a long time, the best determination of the strong coupling constant from radiative  $\Upsilon$  decays was the one of Ref. [498], which resulted in  $\alpha_s(M_Z^2) = 0.119_{-0.005}^{+0.006}$ . This determination is based on QCD at NLO only, so it will not be considered for the final extraction of the world average value of  $\alpha_s$ ; it is, however, an important ingredient for the demonstration of Asymptotic Freedom as given in Fig. 9.3. More recently, two determinations have been performed [499, 500] that are based on N<sup>3</sup>LO accurate predictions. Reference [499] performs a simultaneous fit of the strong coupling and the bottom mass  $\overline{m}_b$ , including states with principal quantum number up to  $n \leq 2$  in order to break the degeneracy between  $\alpha_s$  and  $\overline{m}_b$ , finding  $\alpha_s(M_Z^2) = 0.1178 \pm 0.0051$ . Reference [500] instead uses as input of the fit the renormalon-free energy combination of  $B_c$  and bottomonium  $\eta_b$  and charmonium  $\eta_c$ ,  $M_{B_c} - M_{\eta_b}/2 - M_{\eta_c}/2$ , which is weakly dependent on the heavy quark masses, but shows a good dependence on  $\alpha_s$ . Using this observable, they obtain  $\alpha_s(M_Z^2) = 0.1178 \pm 0.0051$ . These two determinations satisfy our criteria to be included in the world

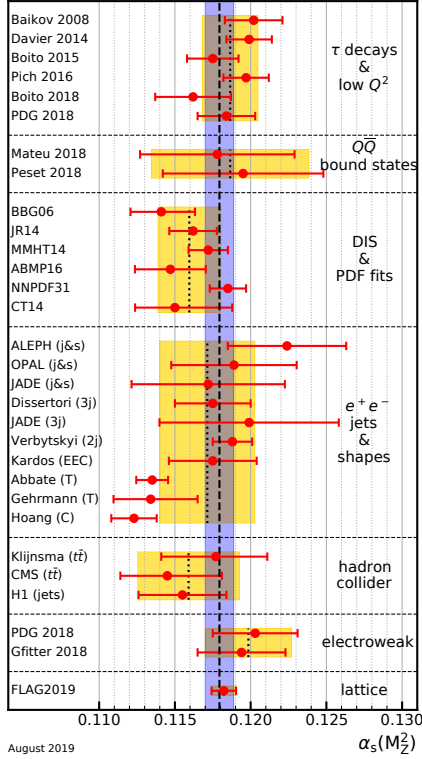


Figure 9.2: Summary of determinations of  $\alpha_s(M_Z^2)$  from the seven sub-fields discussed in the text. The yellow (light shaded) bands and dotted lines indicate the pre-average values of each sub-field. The dashed line and blue (dark shaded) band represent the final world average value of  $\alpha_s(M_Z^2)$ .

average and are at the moment the only input values in the Heavy-quarkonia category. Their unweighted combination leads to the pre-average for this category of  $\alpha_s(M_Z^2) = 0.1187 \pm 0.0052$ . We note that, while we include this result in our final average, because of the large uncertainty of the two determinations in this category, removing this pre-average would not change the final result within the quoted uncertainty.

#### 9.4.3 Deep-inelastic scattering and global PDF fits:

Studies of DIS final states have led to a number of precise determinations of  $\alpha_s$ : a combination [501] of precision measurements at HERA, based on NLO fits to inclusive jet cross sections in neutral current DIS at high  $Q^2$ , provides combined values of  $\alpha_s$  at different energy scales  $Q$ , as shown in Fig. 9.3, and quotes a combined result of  $\alpha_s(M_Z^2) = 0.1198 \pm 0.0032$ . A more recent study of multijet production [373], based on improved reconstruction and data calibration, confirms the general picture, albeit with a somewhat smaller value of  $\alpha_s(M_Z^2) = 0.1165 \pm 0.0039$ , still at NLO. An evaluation of inclusive jet production, including *approximate* NNLO contributions [502], reduces the theoretical prediction for jet production in DIS, improves the description of the final HERA data in particular at high photon virtuality  $Q^2$  and increases the central fit value of the strong coupling constant.

Another class of studies, analyzing structure functions at NNLO QCD (and partly beyond), provide results that serve as relevant inputs for the world average of  $\alpha_s$ . Most of these studies do *not*, however, explicitly include estimates of theoretical uncertainties when quoting fit results of  $\alpha_s$ . In such cases we add, in quadrature, half of the difference between the results obtained in NNLO and NLO to the quoted errors: a combined analysis of non-singlet structure functions from DIS [503], based on QCD predictions up to N<sup>3</sup>LO in some of its parts, results in  $\alpha_s(M_Z^2) = 0.1141 \pm 0.0022$  (BBG). Studies of singlet and non-singlet structure functions, based on NNLO predictions, result in  $\alpha_s(M_Z^2) = 0.1162 \pm 0.0017$  [504] (JR14). The AMBP group [505, 506] determined a set of parton distribution functions using data from HERA, NOMAD,

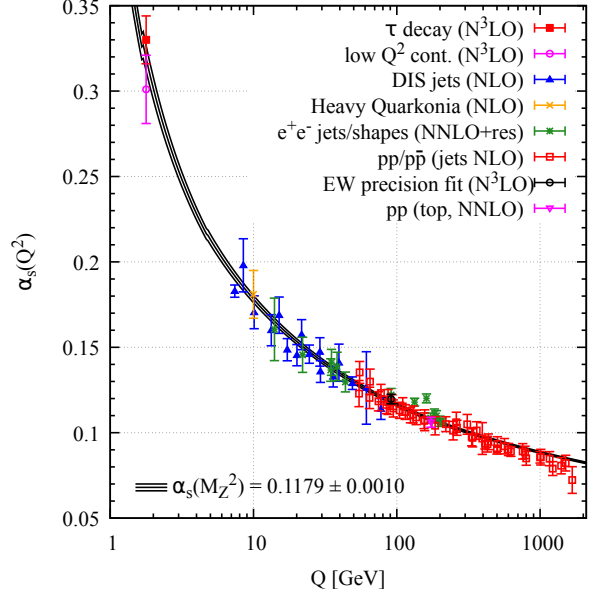


Figure 9.3: Summary of measurements of  $\alpha_s$  as a function of the energy scale  $Q$ . The respective degree of QCD perturbation theory used in the extraction of  $\alpha_s$  is indicated in brackets (NLO: next-to-leading order; NNLO: next-to-next-to-leading order; NNLO+res.: NNLO matched to a resummed calculation; N<sup>3</sup>LO: next-to-NNLO).

CHORUS, from Tevatron and the LHC for the Drell-Yan process and the hadro-production of single-top and top-quark pairs and determined  $\alpha_s(M_Z^2) = 0.1147 \pm 0.0024$  [505]. The MMHT group [507], also including hadron collider data, determined a new set of parton density functions (MMHT2014) together with  $\alpha_s(M_Z^2) = 0.1172 \pm 0.0013$ . Similarly, the CT group [508] determined the CT14 parton density set together with  $\alpha_s(M_Z^2) = 0.1150^{+0.0036}_{-0.0024}$ . The NNPDF group [509] presented NNPDF3.1 parton distribution functions together with  $\alpha_s(M_Z^2) = 0.1185 \pm 0.0012$ .

We note that criticism has been expressed on some of the above extractions. Among the issues raised, we mention the neglect of singlet contributions at  $x \geq 0.3$  in pure non-singlet fits [510], the impact and detailed treatment of particular classes of data in the fits [510, 511], possible biases due to insufficiently flexible parametrizations of the PDFs [512] and the use of a fixed-flavor number scheme [513, 514].

Summarizing the results from world data on structure functions, taking the *unweighted average* of the central values and errors of all selected results, leads to a pre-average value of  $\alpha_s(M_Z^2) = 0.1161 \pm 0.0018$ , see Fig. 9.2.

#### 9.4.4 Hadronic final states of $e^+e^-$ annihilations:

Re-analyses of event shapes in  $e^+e^-$  annihilation (j&s), measured around the  $Z$  peak and at LEP2 center-of-mass energies up to 209 GeV, using NNLO predictions matched to NLL resummation and Monte Carlo models to correct for hadronization effects, resulted in  $\alpha_s(M_Z^2) = 0.1224 \pm 0.0039$  (ALEPH) [515], with a dominant theoretical uncertainty of 0.0035, and in  $\alpha_s(M_Z^2) = 0.1189 \pm 0.0043$  (OPAL) [516]. Similarly, an analysis of JADE data [517] at center-of-mass energies between 14 and 46 GeV gives  $\alpha_s(M_Z^2) = 0.1172 \pm 0.0051$ , with contributions from the hadronization model and from perturbative QCD uncertainties of 0.0035 and 0.0030, respectively. Precise determinations of  $\alpha_s$  from 3-jet production alone (3j), at NNLO, resulted in  $\alpha_s(M_Z^2) = 0.1175 \pm 0.0025$  [518] from ALEPH data and in  $\alpha_s(M_Z^2) = 0.1199 \pm 0.0059$  [519] from JADE. A recent determination is based on an NNLO+NNLL accurate calculation that allows to fit the region of lower 3-jet rate (2j) using data collected at LEP and PETRA at different energies. This fit gives  $\alpha_s(M_Z^2) = 0.1188 \pm 0.0013$  [520], where the dominant uncertainty is the hadronization uncertainty, which is estimated



from Monte Carlo simulations. A fit of energy-energy-correlation (EEC) also based on an NNLO+NNLL calculation together with a Monte Carlo based modelling of hadronization corrections gives  $\alpha_s(M_Z^2) = 0.1175 \pm 0.0029$  [521]. These results are summarized in the upper seven rows of the  $e^+e^-$  sector of Fig. 9.2.

Another class of  $\alpha_s$  determinations is based on analytic modelling of non-perturbative and hadronization effects, rather than on Monte Carlo models [522–525], using methods like power corrections, factorization of soft-collinear effective field theory, dispersive models and low scale QCD effective couplings. In these studies, the world data on Thrust distributions (T), or - most recently - C-parameter distributions (C), are analysed and fitted to perturbative QCD predictions at NNLO matched with resummation of leading logs up to N<sup>3</sup>LL accuracy, see Sec. 9.2.3.3. The results are  $\alpha_s(M_Z^2) = 0.1135 \pm 0.0011$  [523] and  $\alpha_s(M_Z^2) = 0.1134^{+0.0031}_{-0.0025}$  [524] from Thrust, and  $\alpha_s(M_Z^2) = 0.1123 \pm 0.0015$  [525] from C-parameter. They are displayed in the lower three rows of the  $e^+e^-$  sector of Fig. 9.2.

The determination of Ref. [522],  $\alpha_s(M_Z^2) = 0.1164^{+0.0028}_{-0.0024}$ , is no longer included in the average as it is superseded by other determinations that use the same Thrust data but rely on more accurate theoretical predictions. Not included in the computation of the world average but worth mentioning are a computation of the NLO corrections to 5-jet production and comparison to the measured 5-jet rates at LEP [526], giving  $\alpha_s(M_Z^2) = 0.1156^{+0.0041}_{-0.0034}$ , and a computation of non-perturbative and perturbative QCD contributions to the scale evolution of quark and gluon jet multiplicities, including resummation, resulting in  $\alpha_s(M_Z^2) = 0.1199 \pm 0.0026$  [527].

We note that there is criticism on both classes of  $\alpha_s$  extractions described above: those based on corrections of non-perturbative hadronization effects using QCD-inspired Monte Carlo generators (since the parton level of a Monte Carlo simulation is not defined in a manner equivalent to that of a fixed-order calculation), as well as studies based on non-perturbative analytic modelling, as their systematics have not yet been fully verified. For the latter case, Refs. [523, 525] quote surprisingly small overall experimental, hadronization, and theoretical uncertainties of only 2, 5, and 9 per-mille, respectively, which calls for an independent confirmation.

In view of these open questions, the determination of the *unweighted average* and uncertainties is intended to provide the most appropriate and unbiased estimate of the average value of  $\alpha_s(M_Z^2)$  for this sub-field, which results in  $\alpha_s(M_Z^2) = 0.1171 \pm 0.0031$ .

#### 9.4.5 Hadron collider results:

Until recently, determinations of  $\alpha_s$  using hadron collider data, mostly from jet or  $t\bar{t}$  production processes, could be performed at NLO only. In the meantime, NNLO calculations have become available for  $t\bar{t}$  [84, 466, 468] and for inclusive jet and dijet production [197, 528, 529]. Both can be supplemented by electroweak corrections [530–532], which become important for high- $p_T$  collisions at the LHC; for  $t\bar{t}$  logarithms have been resummed [469].  $Z$ +jet production, studied with respect to an  $\alpha_s$  determination at NLO from multi-jet events in Ref. [533], is also known at NNLO for the 1-jet case [187, 534].

The first determination of  $\alpha_s$  at NNLO accuracy in QCD has been reported by CMS [470] from the  $t\bar{t}$  production cross section at  $\sqrt{s} = 7$  TeV:  $\alpha_s(M_Z^2) = 0.1151^{+0.0028}_{-0.0027}$ , whereby the dominating contributions to the overall uncertainty are experimental ( $^{+0.0017}_{-0.0018}$ ), from parton density functions ( $^{+0.0013}_{-0.0011}$ ) and the value of the top quark pole mass ( $\pm 0.0013$ ). In the last *Review* this opened up a new sub-field on its own. In the meantime, multiple datasets on  $t\bar{t}$  production from Tevatron at  $\sqrt{s} = 1.96$  TeV and from LHC at  $\sqrt{s} = 7, 8,$  and  $13$  TeV have been analyzed simultaneously to determine  $\alpha_s$  [471] to

$$\alpha_s(M_Z^2) = 0.1177^{+0.0034}_{-0.0036},$$

where the largest uncertainties are associated with missing higher orders and with PDFs. Since this combined analysis contains among other things an updated measurement as compared to the dataset used by CMS, the latter is replaced in the averaging by

the new combined result. A second entry into this sub-field is given by an analysis of new  $t\bar{t}$  production data at  $\sqrt{s} = 13$  TeV from the CMS collaboration [464]. From the four values presented for the chosen PDF sets, the unweighted average is taken:

$$\alpha_s(M_Z^2) = 0.1145^{+0.0036}_{-0.0031}.$$

From jet production only one  $\alpha_s$  determination has been performed yet at NNLO using DIS data of the H1 Collaboration [374]. Two strategies are pursued for the extraction of  $\alpha_s$ , one using pre-determined PDFs as input and a second strategy fitting the proton PDFs together with the strong coupling constant. From the first approach we choose the result with the smallest total uncertainty,  $\alpha_s(M_Z^2) = 0.1168 \pm 0.0030$ , where the analysis is restricted to the phase space with the most precise theoretical prediction at the cost of excluding numerous data points at lower scale values. The second approach gives  $\alpha_s(M_Z^2) = 0.1142 \pm 0.0028$ , which we combine with the first result to our unweighted input average:

$$\alpha_s(M_Z^2) = 0.1155 \pm 0.0029.$$

As unweighted pre-average for this sub-field we obtain:  $\alpha_s(M_Z^2) = 0.1159 \pm 0.0034$ . Also worth mentioning is a recent still unpublished extraction of  $\alpha_s(M_Z^2) = 0.1170 \pm 0.0030$  [535] using HERA jet data and relying on fast interpolation grid techniques.

Many further  $\alpha_s$  determinations from jet measurements either could not yet be advanced to NNLO accuracy or the NNLO predictions are not yet available as is the case for observables requiring three or more jets in the final state. A selection of results from inclusive jet [373, 387, 536–541] and multi-jet measurements [332, 334, 335, 373, 542–546] is presented in Fig. 9.4, where the uncertainty in most cases is dominated by the impact of missing higher orders estimated through scale variations. The multi-jet  $\alpha_s$  determinations are based on 3-jet cross sections (m3j), 3- to 2-jet cross-section ratios (R32), dijet angular decorrelations (RdR, RdPhi), and transverse energy-energy-correlations and their asymmetry (TEEC, ATEEC). The H1 result is extracted from a fit to inclusive 1-, 2-, and 3-jet cross sections (nj) simultaneously.

The CMS Collaboration has also derived an  $\alpha_s$  value at NLO from dijet production at  $\sqrt{s} = 8$  TeV [393], but only in combination with a PDF fit. The last point of the inclusive jet sub-field from Ref. [541] is derived from a simultaneous fit to six datasets from different experiments and partially includes data used already for the other data points, *e.g.* the CMS result at 7 TeV.

All NLO results are within their large uncertainties in agreement with the world average and the associated analyses provide valuable new values for the scale dependence of  $\alpha_s$  at energy scales now extending up to almost 2.0 TeV as shown in Fig. 9.3.

#### 9.4.6 Electroweak precision fit:

For this category, we update the global electroweak fit result of Ref. [547] to the one of Ref. [548], which now includes kinematic top quark and  $W$  boson mass measurements from the LHC, new determinations of the effective leptonic electroweak mixing angles from the Tevatron, a Higgs mass measurement from ATLAS and CMS, and a new evaluation of the hadronic contribution to the running of the electromagnetic coupling at the  $Z$ -boson mass. In addition, we use the newer results of the electroweak fit at the  $Z$  mass pole from LEP and SLC data presented in Sec. *Electroweak Model and constraints on New Physics* of the 2018 edition of this *Review*. Both very similar results,  $\alpha_s(M_Z^2) = 0.1203 \pm 0.0028$  [480],  $\alpha_s(M_Z^2) = 0.1194 \pm 0.0029$  [548], are also in perfect agreement with the original result obtained from LEP and SLD data [549]. Our pre-averaging gives  $\alpha_s(M_Z^2) = 0.1199 \pm 0.0029$ .

We note, however, that results from electroweak precision data strongly depend on the strict validity of Standard Model predictions and the existence of the minimal Higgs mechanism to implement electroweak symmetry breaking. Any - even small - deviation of nature from this model could strongly influence this extraction of  $\alpha_s$ .

#### 9.4.7 Lattice QCD:

Several methods exist to extract the strong coupling constant from lattice QCD, as reviewed also in Sec. *Lattice QCD* of this *Review*.

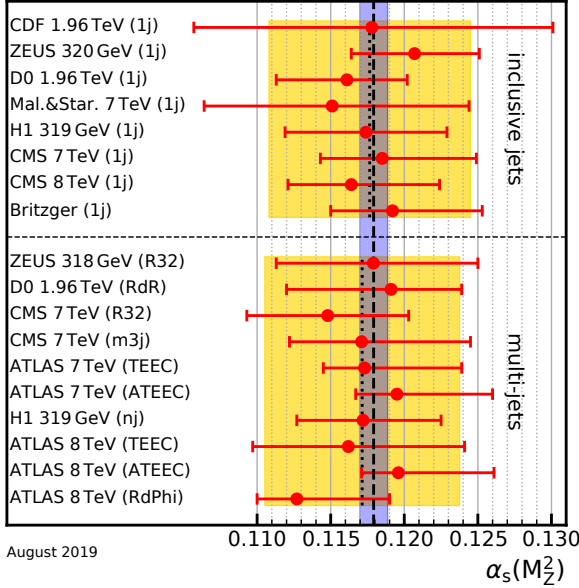


Figure 9.4: Summary of determinations of  $\alpha_s(M_Z^2)$  at NLO from inclusive and multi-jet measurements at hadron colliders. The uncertainty is dominated by estimates of the impact of missing higher orders. The yellow (light shaded) bands and dotted lines indicate average values for the two sub-fields. The dashed line and blue (dark shaded) band represent the final world average value of  $\alpha_s(M_Z^2)$ .

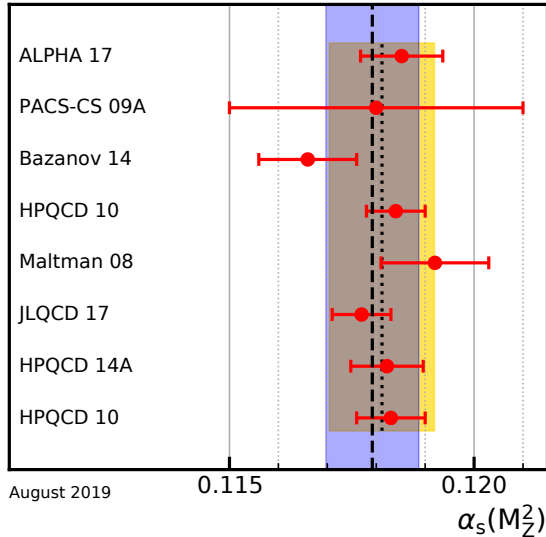


Figure 9.5: Lattice determinations that enter the FLAG2019 average. The yellow (light shaded) band and dotted line indicates the average value for this sub-field. The dashed line and blue (dark shaded) band represent the final world average value of  $\alpha_s(M_Z^2)$ .

The Flavour Lattice Averaging Group (FLAG) has recently considered the most up-to-date determinations and combined them to produce an update of their average  $\alpha_s$  [487]. Their final result is obtained by considering seventeen possible input calculations [550–567] and by retaining in their final average only those eight [551–553, 556, 559–561, 563] that fulfill their predefined quality criteria. These determinations, together with their uncertainties, are displayed in Fig. 9.5. The yellow (light shaded) band and dotted line indicate the FLAG 2018 average, while the dashed line and blue (dark shaded) band represent the world average (see later). The level of agreement of individual results to the world average, or to the non-lattice world average is very similar. The criteria applied are detailed in the Sec. 9.2.1 of Ref. [487]. We

note that, as in our case, the calculation must be published in a peer-reviewed journal for it to be eligible to be included in the FLAG average. We also note that the criteria applied now are considered relatively loose by the FLAG collaboration and they have already formulated more stringent criteria. It is likely that in future FLAG averages only results satisfying these stricter criteria will be included in their averaging.

Similarly to what is done here, the FLAG collaboration built pre-averages of results that belong to different classes. The categories that currently contribute to the average are: step-scaling methods ( $\alpha_s(M_Z^2) = 0.11848^{+0.00081}_{-0.00081}$ ), the potential at short distances ( $\alpha_s(M_Z^2) = 0.11660^{+0.00160}_{-0.00160}$ ), Wilson loops ( $\alpha_s(M_Z^2) = 0.11858^{+0.00120}_{-0.00120}$ ), and heavy-quark current two-point functions ( $\alpha_s(M_Z^2) = 0.11824^{+0.00150}_{-0.00150}$ ).

Other categories like the vacuum polarization at short distances, the calculation of QCD vertices, or of the eigenvalue spectrum of the Dirac operator have not yet published results that fulfill all requirements to be included in the average. Ref. [568] has been completed after the publication of Ref. [487], hence these results have not been considered in the last FLAG average.

The final value is obtained by performing an unweighted average of the pre-averages. In order to be conservative, the final uncertainty is not the combined uncertainty of the pre-averages, rather it is taken to be the smallest uncertainty of the pre-averages, which is the uncertainty of the step-scaling category and is dominated by the ALPHA 17 result [563]. The final FLAG average (rounded to four digits) is

$$\alpha_s(M_Z^2) = 0.1182 \pm 0.0008, \quad (\text{lattice}). \quad (9.23)$$

We believe that this result expresses to a large extent the consensus of the lattice community and that the imposed criteria and the rigorous assessment of systematic uncertainties qualify for a direct inclusion of this FLAG average here. In contrast to the previous review, we therefore decided to adopt the FLAG average with its uncertainty as our value of  $\alpha_s$  for the lattice category. Moreover, this lattice result will not be directly combined with any other sub-field average, but with our non-lattice average to give our final world average value for  $\alpha_s$ .

**9.4.8 Determination of the world average value of  $\alpha_s(M_Z^2)$ :** Obtaining a world average value for  $\alpha_s(M_Z^2)$  is a non-trivial exercise. A certain arbitrariness and subjective component is inevitable because of the choice of measurements to be included in the average, the treatment of (non-Gaussian) systematic uncertainties of mostly theoretical nature, as well as the treatment of correlations among the various inputs, of theoretical as well as experimental origin.

We have chosen to determine pre-averages for sub-fields of measurements that are considered to exhibit a maximum of independence among each other, considering experimental as well as theoretical issues. The seven pre-averages are summarized in Fig. 9.2. We recall that these are exclusively obtained from extractions that are based on (at least) full NNLO QCD predictions, and are published in peer-reviewed journals at the time of completing this Review. To obtain our final world average, we first combine six pre-averages, excluding the lattice result, using a  $\chi^2$  averaging method. This gives

$$\alpha_s(M_Z^2) = 0.1176 \pm 0.0011, \quad (\text{without lattice}). \quad (9.24)$$

This result is fully compatible with the lattice pre-average Eq. (9.23) and has a comparable error. In order to be conservative, we combine these two numbers using an unweighted average and take as an uncertainty the average between these two uncertainties. This gives our final world average value

$$\alpha_s(M_Z^2) = 0.1179 \pm 0.0010. \quad (9.25)$$

This world average value is in very good agreement with the last version of this Review, which was  $\alpha_s(M_Z^2) = 0.1181 \pm 0.0011$ , with only a slightly lower central value and decreased overall uncertainty. Performing a weighted average of all seven categories



gives  $\alpha_s(M_Z^2) = 0.1180 \pm 0.0007$ . Our uncertainty instead is about 50% larger.

Notwithstanding the many open issues still present within each of the sub-fields summarised in this *Review*, the wealth of available results provides a rather precise and reasonably stable world average value of  $\alpha_s(M_Z^2)$ , as well as a clear signature and proof of the energy dependence of  $\alpha_s$ , in full agreement with the QCD prediction of Asymptotic Freedom. This is demonstrated in Fig. 9.3, where results of  $\alpha_s(Q^2)$  obtained at discrete energy scales  $Q$ , now also including those based just on NLO QCD, are summarised. Thanks to the results from the Tevatron and from the LHC, the energy scales, at which  $\alpha_s$  is determined, now extend up to almost 2 TeV.<sup>15</sup>

## 9.5 Acknowledgments

We are grateful to S. Bethke, G. Dissertori, D. d'Enterría, C. Glasman, A. Hoang, D. Lombardi, G.P. Salam, and B. Webber for discussions and for their comments on the manuscript, and to J. Andersen, A. Bazavov, H.-L. Win, and J. Smillie for useful discussions.

## References

- [1] R. K. Ellis, W. J. Stirling and B. R. Webber, *Camb. Monogr. Part. Phys. Nucl. Phys. Cosmol.* **8**, 1 (1996).
- [2] J. Campbell, J. Huston, F. Krauss “*The Black Book of Quantum Chromodynamics, a Primer for the QCD Era*,” Oxford University Press, UK (2017).
- [3] C. A. Baker *et al.*, *Phys. Rev. Lett.* **97**, 131801 (2006), [hep-ex/0602020].
- [4] J. M. Pendlebury *et al.*, *Phys. Rev.* **D92**, 9, 092003 (2015), [arXiv:1509.04411].
- [5] B. Graner *et al.*, *Phys. Rev. Lett.* **116**, 16, 161601 (2016), [Erratum: *Phys. Rev. Lett.* 119, no.11, 119901 (2017)], [arXiv:1601.04339].
- [6] J. E. Kim and G. Carosi, *Rev. Mod. Phys.* **82**, 557 (2010), [arXiv:0807.3125].
- [7] G. Dissertori, I. G. Knowles and M. Schmelling, *High energy experiments and theory*, Oxford, UK: Clarendon (2003).
- [8] R. Brock *et al.* (CTEQ), *Rev. Mod. Phys.* **67**, 157 (1995); see also <http://www.phys.psu.edu/~cteq/handbook/v1.1/handbook.pdf>.
- [9] K. Melnikov, *CERN Yellow Rep. School Proc.* **3**, 37 (2018).
- [10] T. van Ritbergen, J. A. M. Vermaseren and S. A. Larin, *Phys. Lett.* **B400**, 379 (1997), [hep-ph/9701390].
- [11] M. Czakon, *Nucl. Phys.* **B710**, 485 (2005), [hep-ph/0411261].
- [12] P. A. Baikov, K. G. Chetyrkin and J. H. Kühn, *Phys. Rev. Lett.* **118**, 8, 082002 (2017), [arXiv:1606.08659].
- [13] T. Luthe *et al.*, *JHEP* **07**, 127 (2016), [arXiv:1606.08662].
- [14] F. Herzog *et al.*, *JHEP* **02**, 090 (2017), [arXiv:1701.01404].
- [15] T. Luthe *et al.*, *JHEP* **10**, 166 (2017), [arXiv:1709.07718].
- [16] K. G. Chetyrkin *et al.*, *JHEP* **10**, 179 (2017), [Addendum: *JHEP* 12, 006 (2017)], [arXiv:1709.08541].
- [17] W. A. Bardeen *et al.*, *Phys. Rev.* **D18**, 3998 (1978).
- [18] D. J. Gross and F. Wilczek, *Phys. Rev. Lett.* **30**, 1343 (1973), [,271(1973)].
- [19] H. D. Politzer, *Phys. Rev. Lett.* **30**, 1346 (1973), [,274(1973)].
- [20] Y. Schroder and M. Steinhauser, *JHEP* **01**, 051 (2006), [hep-ph/0512058].
- [21] K. G. Chetyrkin, J. H. Kuhn and C. Sturm, *Nucl. Phys.* **B744**, 121 (2006), [hep-ph/0512060].
- [22] A. G. Grozin *et al.*, *JHEP* **09**, 066 (2011), [arXiv:1107.5970].
- [23] M. Dalla Brida *et al.* (ALPHA), *Phys. Rev. Lett.* **117**, 18, 182001 (2016), [arXiv:1604.06193].
- [24] K. G. Chetyrkin, J. H. Kuhn and M. Steinhauser, *Comput. Phys. Commun.* **133**, 43 (2000), [hep-ph/0004189].
- [25] B. Schmidt and M. Steinhauser, *Comput. Phys. Commun.* **183**, 1845 (2012), [arXiv:1201.6149].
- [26] F. Herren and M. Steinhauser, *Comput. Phys. Commun.* **224**, 333 (2018), [arXiv:1703.03751].
- [27] A. V. Bednyakov, *Phys. Lett.* **B741**, 262 (2015), [arXiv:1410.7603].
- [28] M. Beneke, *Phys. Rept.* **317**, 1 (1999), [hep-ph/9807443].
- [29] M. Beneke *et al.*, *Phys. Lett.* **B775**, 63 (2017), [arXiv:1605.03609].
- [30] A. H. Hoang, C. Lepenik and M. Preisser, *JHEP* **09**, 099 (2017), [arXiv:1706.08526].
- [31] P. Marquard *et al.*, *Phys. Rev. Lett.* **114**, 14, 142002 (2015), [arXiv:1502.01030].
- [32] P. A. Baikov *et al.*, *Phys. Lett.* **B714**, 62 (2012), [arXiv:1206.1288].
- [33] K. G. Chetyrkin, J. H. Kuhn and A. Kwiatkowski (1996), [Phys. Rept. 277, 189 (1996)], [hep-ph/9503396].
- [34] Y. Kiyo *et al.*, *Nucl. Phys.* **B823**, 269 (2009), [arXiv:0907.2120].
- [35] P. A. Baikov *et al.*, *Phys. Rev. Lett.* **108**, 222003 (2012), [arXiv:1201.5804].
- [36] P. A. Baikov, K. G. Chetyrkin and J. H. Kuhn, *Phys. Rev. Lett.* **101**, 012002 (2008), [arXiv:0801.1821].
- [37] F. Herzog *et al.*, *JHEP* **08**, 113 (2017), [arXiv:1707.01044].
- [38] V. A. Novikov *et al.*, *Nucl. Phys.* **B174**, 378 (1980).
- [39] H.-W. Lin *et al.*, *Phys. Rev.* **D91**, 054510 (2015), [arXiv:1402.1462]; C. Alexandrou *et al.*, *Phys. Rev.* **D92**, 014502 (2015), [arXiv:1504.07455].
- [40] H.-W. Lin *et al.*, *Prog. Part. Nucl. Phys.* **100**, 107 (2018), [arXiv:1711.07916].
- [41] C. Alexandrou *et al.*, *Phys. Rev. Lett.* **121**, 11, 112001 (2018), [arXiv:1803.02685].
- [42] J.-W. Chen *et al.* (2018), [arXiv:1803.04393].
- [43] K. Cichy, L. Del Debbio and T. Giani (2019), [arXiv:1907.06037].
- [44] G. C. Rossi and M. Testa, *Phys. Rev.* **D96**, 1, 014507 (2017), [arXiv:1706.04428].
- [45] J. Gao, L. Harland-Lang and J. Rojo, *Phys. Rept.* **742**, 1 (2018), [arXiv:1709.04922].
- [46] K. Kovařík, P. M. Nadolsky and D. E. Soper (2019), [arXiv:1905.06957].
- [47] J. Butterworth *et al.*, *J. Phys.* **G43**, 023001 (2016), [arXiv:1510.03865].
- [48] R. Abdul Khalek *et al.* (NNPDF) (2019), [arXiv:1905.04311].
- [49] R. Abdul Khalek *et al.* (NNPDF) (2019), [arXiv:1906.10698].
- [50] J. D. Bjorken and E. A. Paschos, *Phys. Rev.* **185**, 1975 (1969).
- [51] J. A. M. Vermaseren, A. Vogt and S. Moch, *Nucl. Phys.* **B724**, 3 (2005), [hep-ph/0504242].
- [52] S. Moch, J. A. M. Vermaseren and A. Vogt, *Nucl. Phys.* **B813**, 220 (2009), [arXiv:0812.4168].
- [53] J. Davies *et al.*, *PoS DIS2016*, 059 (2016), [arXiv:1606.08907].
- [54] E. Laenen *et al.*, *Nucl. Phys.* **B392**, 162 (1993); S. Riemersma, J. Smith and W. L. van Neerven, *Phys. Lett.* **B347**, 143 (1995), [hep-ph/9411431].

<sup>15</sup>We note, however, that in many such studies, like those based on exclusive states of jet multiplicities, the relevant energy scale of the measurement is not uniquely defined. For instance, in studies of the ratio of 3- to 2-jet cross sections at the LHC, the relevant scale was taken to be the average of the transverse momenta of the two leading jets [543], but could alternatively have been chosen to be the transverse momentum of the 3<sup>rd</sup> jet.

- [55] J. Blümlein *et al.* (2019), [arXiv:1903.06155].
- [56] A. Manohar *et al.*, Phys. Rev. Lett. **117**, 24, 242002 (2016), [arXiv:1607.04266].
- [57] J. C. Collins, D. E. Soper and G. F. Sterman, Adv. Ser. Direct. High Energy Phys. **5**, 1 (1989), [hep-ph/0409313].
- [58] J.C. Collins, *Foundations of Perturbative QCD*, Cambridge University Press, 2011.
- [59] G. C. Nayak, J.-W. Qiu and G. F. Sterman, Phys. Rev. **D72**, 114012 (2005), [hep-ph/0509021].
- [60] V. N. Gribov and L. N. Lipatov, Sov. J. Nucl. Phys. **15**, 438 (1972), [Yad. Fiz.15,781(1972)]; L. N. Lipatov, Sov. J. Nucl. Phys. **20**, 94 (1975), [Yad. Fiz.20,181(1974)]; G. Altarelli and G. Parisi, Nucl. Phys. **B126**, 298 (1977); Y. L. Dokshitzer, Sov. Phys. JETP **46**, 641 (1977), [Zh. Eksp. Teor. Fiz.73,1216(1977)].
- [61] G. Curci, W. Furmanski and R. Petronzio, Nucl. Phys. **B175**, 27 (1980); W. Furmanski and R. Petronzio, Phys. Lett. **97B**, 437 (1980).
- [62] A. Vogt, S. Moch and J. A. M. Vermaseren, Nucl. Phys. **B691**, 129 (2004), [hep-ph/0404111]; S. Moch, J. A. M. Vermaseren and A. Vogt, Nucl. Phys. **B688**, 101 (2004), [hep-ph/0403192].
- [63] S. Moch *et al.*, JHEP **10**, 041 (2017), [arXiv:1707.08315].
- [64] A. Vogt *et al.*, PoS **RADCOR2017**, 046 (2018), [arXiv:1801.06085].
- [65] A. Vogt *et al.*, PoS **LL2018**, 050 (2018), [arXiv:1808.08981].
- [66] S. Moch, J. A. M. Vermaseren and A. Vogt, Nucl. Phys. **B889**, 351 (2014), [arXiv:1409.5131].
- [67] D. de Florian, G. F. R. Sborlini and G. Rodrigo, Eur. Phys. J. **C76**, 5, 282 (2016), [arXiv:1512.00612]; D. de Florian, G. F. R. Sborlini and G. Rodrigo, JHEP **10**, 056 (2016), [arXiv:1606.02887].
- [68] R. S. Thorne, Phys. Rev. **D73**, 054019 (2006), [hep-ph/0601245].
- [69] S. Forte *et al.*, Nucl. Phys. **B834**, 116 (2010), [arXiv:1001.2312].
- [70] M. Guzzi *et al.*, Phys. Rev. **D86**, 053005 (2012), [arXiv:1108.5112].
- [71] V. S. Fadin, E. A. Kuraev and L. N. Lipatov, Phys. Lett. **60B**, 50 (1975).
- [72] I. I. Balitsky and L. N. Lipatov, Sov. J. Nucl. Phys. **28**, 822 (1978), [Yad. Fiz.28,1597(1978)].
- [73] R. D. Ball *et al.*, Eur. Phys. J. **C78**, 4, 321 (2018), [arXiv:1710.05935].
- [74] H. Abramowicz *et al.* (H1, ZEUS), Eur. Phys. J. **C75**, 12, 580 (2015), [arXiv:1506.06042].
- [75] H. Abdolmaleki *et al.* (xFitter Developers' Team), Eur. Phys. J. **C78**, 8, 621 (2018), [arXiv:1802.00064].
- [76] L. A. Harland-Lang *et al.*, Eur. Phys. J. **C76**, 4, 186 (2016), [arXiv:1601.03413].
- [77] T.-J. Hou *et al.* (2019), [arXiv:1908.11238].
- [78] J. C. Collins, D. E. Soper and G. F. Sterman, Nucl. Phys. **B261**, 104 (1985).
- [79] R. Hamberg, W. L. van Neerven and T. Matsuura, Nucl. Phys. **B359**, 343 (1991), [Erratum: Nucl. Phys. **B644**, 403(2002)].
- [80] R. V. Harlander and W. B. Kilgore, Phys. Rev. Lett. **88**, 201801 (2002), [hep-ph/0201206].
- [81] O. Brein, A. Djouadi and R. Harlander, Phys. Lett. **B579**, 149 (2004), [hep-ph/0307206].
- [82] P. Bolzoni *et al.*, Phys. Rev. Lett. **105**, 011801 (2010), [arXiv:1003.4451].
- [83] S. Borowka *et al.*, Phys. Rev. Lett. **117**, 1, 012001 (2016), [Erratum: Phys. Rev. Lett. **117**, no.7, 079901(2016)], [arXiv:1604.06447].
- [84] M. Czakon, P. Fiedler and A. Mitov, Phys. Rev. Lett. **110**, 252004 (2013), [arXiv:1303.6254].
- [85] T. Gehrmann *et al.*, Phys. Rev. Lett. **113**, 21, 212001 (2014), [arXiv:1408.5243].
- [86] F. Cascioli *et al.*, Phys. Lett. **B735**, 311 (2014), [arXiv:1405.2219].
- [87] M. Grazzini, S. Kallweit and M. Wiesemann, Eur. Phys. J. **C78**, 7, 537 (2018), [arXiv:1711.06631].
- [88] C. Anastasiou *et al.*, Phys. Rev. Lett. **114**, 212001 (2015), [arXiv:1503.06056]; C. Anastasiou *et al.*, JHEP **05**, 058 (2016), [arXiv:1602.00695].
- [89] B. Mistlberger, JHEP **05**, 028 (2018), [arXiv:1802.00833].
- [90] F. Dulat, B. Mistlberger and A. Pelloni, Phys. Rev. **D99**, 3, 034004 (2019), [arXiv:1810.09462].
- [91] F. A. Dreyer and A. Karlberg, Phys. Rev. Lett. **117**, 7, 072001 (2016), [arXiv:1606.00840].
- [92] D. de Florian *et al.* (LHC Higgs Cross Section Working Group) (2016), [arXiv:1610.07922].
- [93] M. Greco and A. Vicini, Nucl. Phys. **B415**, 386 (1994).
- [94] L. N. Lipatov, Sov. J. Nucl. Phys. **23**, 338 (1976), [Yad. Fiz.23,642(1976)].
- [95] E. A. Kuraev, L. N. Lipatov and V. S. Fadin, Sov. Phys. JETP **45**, 199 (1977), [Zh. Eksp. Teor. Fiz.72,377(1977)].
- [96] V. S. Fadin and L. N. Lipatov, Phys. Lett. **B429**, 127 (1998), [hep-ph/9802290].
- [97] M. Ciafaloni and G. Camici, Phys. Lett. **B430**, 349 (1998), [hep-ph/9803389].
- [98] G. Altarelli, R. D. Ball and S. Forte, Nucl. Phys. **B799**, 199 (2008), [arXiv:0802.0032].
- [99] M. Ciafaloni *et al.*, JHEP **08**, 046 (2007), [arXiv:0707.1453].
- [100] C. D. White and R. S. Thorne, Phys. Rev. **D75**, 034005 (2007), [hep-ph/0611204].
- [101] E. Iancu *et al.*, Phys. Lett. **B744**, 293 (2015), [arXiv:1502.05642].
- [102] N. Gromov, F. Levkovich-Maslyuk and G. Sizov, Phys. Rev. Lett. **115**, 25, 251601 (2015), [arXiv:1507.04010]; V. N. Velizhanin (2015), [arXiv:1508.02857]; S. Caron-Huot and M. Herranen, JHEP **02**, 058 (2018), [arXiv:1604.07417].
- [103] I. Balitsky, Nucl. Phys. **B463**, 99 (1996), [hep-ph/9509348].
- [104] Y. V. Kovchegov, Phys. Rev. **D60**, 034008 (1999), [hep-ph/9901281].
- [105] A. Hebecker, Phys. Rept. **331**, 1 (2000), [hep-ph/9905226].
- [106] A. V. Belitsky and A. V. Radyushkin, Phys. Rept. **418**, 1 (2005), [hep-ph/0504030].
- [107] E. Boos *et al.* (CompHEP), Nucl. Instrum. Meth. **A534**, 250 (2004), [hep-ph/0403113]; <http://compep.sinp.su.ru/>.
- [108] J. Alwall *et al.*, JHEP **07**, 079 (2014), [arXiv:1405.0301]; <https://launchpad.net/mg5amcnlo>.
- [109] M. L. Mangano *et al.*, JHEP **07**, 001 (2003), [hep-ph/0206293]; <http://cern.ch/mlm/alpgen/>.
- [110] T. Gleisberg and S. Hoeche, JHEP **12**, 039 (2008), [arXiv:0808.3674]; <https://sherpa.hepforge.org/trac/wiki>.
- [111] A. Cafarella, C. G. Papadopoulos and M. Worek, Comput. Phys. Commun. **180**, 1941 (2009), [arXiv:0710.2427]; <http://cern.ch/helac-phegas/>.
- [112] F. A. Berends and W. T. Giele, Nucl. Phys. **B306**, 759 (1988).
- [113] L. J. Dixon, in "QCD and beyond. Proceedings, Theoretical Advanced Study Institute in Elementary Particle Physics, TASI-95, Boulder, USA, June 4-30, 1995," 539-584 (1996), [hep-ph/9601359], URL <http://www-public.slac.stanford.edu/sciDoc/docMeta.aspx?slacPubNumber=SLAC-PUB-7106>.

- [114] R. Britto, F. Cachazo and B. Feng, Nucl. Phys. **B715**, 499 (2005), [hep-th/0412308].
- [115] F. Cachazo, P. Svrcek and E. Witten, JHEP **09**, 006 (2004), [hep-th/0403047].
- [116] S. Badger *et al.*, Phys. Rev. **D87**, 3, 034011 (2013), [arXiv:1206.2381].
- [117] S. Catani and M. H. Seymour, Nucl. Phys. **B485**, 291 (1997), [Erratum: Nucl. Phys.B510,503(1998)], [hep-ph/9605323].
- [118] S. Frixione, Z. Kunszt and A. Signer, Nucl. Phys. **B467**, 399 (1996), [hep-ph/9512328].
- [119] D. A. Kosower, Phys. Rev. **D57**, 5410 (1998), [hep-ph/9710213]; J. M. Campbell, M. A. Cullen and E. W. N. Glover, Eur. Phys. J. **C9**, 245 (1999), [hep-ph/9809429]; D. A. Kosower, Phys. Rev. **D71**, 045016 (2005), [hep-ph/0311272].
- [120] G. Ossola, C. G. Papadopoulos and R. Pittau, Nucl. Phys. **B763**, 147 (2007), [hep-ph/0609007].
- [121] R. Britto, F. Cachazo and B. Feng, Nucl. Phys. **B725**, 275 (2005), [hep-th/0412103].
- [122] R. K. Ellis *et al.*, Nucl. Phys. **B822**, 270 (2009), [arXiv:0806.3467].
- [123] C. F. Berger and D. Forde, Ann. Rev. Nucl. Part. Sci. **60**, 181 (2010), [arXiv:0912.3534].
- [124] F. Cascioli, P. Maierhofer and S. Pozzorini, Phys. Rev. Lett. **108**, 111601 (2012), [arXiv:1111.5206].
- [125] Z. Bern, L. J. Dixon and D. A. Kosower, Annals Phys. **322**, 1587 (2007), [arXiv:0704.2798].
- [126] R. K. Ellis *et al.*, Phys. Rept. **518**, 141 (2012), [arXiv:1105.4319].
- [127] G. Bevilacqua *et al.*, Comput. Phys. Commun. **184**, 986 (2013), [arXiv:1110.1499]; <http://cern.ch/helax-pegas/>.
- [128] G. Cullen *et al.*, Eur. Phys. J. **C74**, 8, 3001 (2014), [arXiv:1404.7096]; <http://gosam.hepforge.org/>.
- [129] S. Badger *et al.*, Comput. Phys. Commun. **184**, 1981 (2013), [arXiv:1209.0100]; <https://bitbucket.org/njet/wiki/Home/>.
- [130] F. Buccioni, S. Pozzorini and M. Zoller, Eur. Phys. J. **C78**, 1, 70 (2018), [arXiv:1710.11452]; <https://openloops.hepforge.org/>.
- [131] S. Actis *et al.*, Comput. Phys. Commun. **214**, 140 (2017), [arXiv:1605.01090].
- [132] T. Gleisberg *et al.*, JHEP **02**, 007 (2009), [arXiv:0811.4622]; <http://projects.hepforge.org/sherpa>.
- [133] Z. Nagy, Phys. Rev. **D68**, 094002 (2003), [hep-ph/0307268]; <http://www.desy.de/~znagy/Site/NLOJet++.html>.
- [134] J. M. Campbell and R. K. Ellis, Phys. Rev. **D62**, 114012 (2000), [hep-ph/0006304].
- [135] J. Baglio *et al.* (2011), [arXiv:1107.4038]; <http://www-itp.particle.uni-karlsruhe.de/~vbfnlweb>.
- [136] T. Binoth *et al.*, Eur. Phys. J. **C16**, 311 (2000), [hep-ph/9911340]; [http://lapth.in2p3.fr/PHOX\\_FAMILY/](http://lapth.in2p3.fr/PHOX_FAMILY/).
- [137] Z. Bern *et al.*, PoS **LL2012**, 018 (2012), [arXiv:1210.6684].
- [138] T. Kluge, K. Rabbertz and M. Wobisch, *FastNLO: Fast pQCD calculations for PDF fits* (2006), [hep-ph/0609285], URL [http://lss.fnal.gov/cgi-bin/find\\_paper.pl?conf-06-352](http://lss.fnal.gov/cgi-bin/find_paper.pl?conf-06-352); <http://fastnlo.hepforge.org/>.
- [139] T. Carli *et al.*, Eur. Phys. J. **C66**, 503 (2010), [arXiv:0911.2985]; <https://apllgrid.hepforge.org/>.
- [140] L. Del Debbio, N. P. Hartland and S. Schumann, Comput. Phys. Commun. **185**, 2115 (2014), [arXiv:1312.4460]; <http://mcgrid.hepforge.org/>.
- [141] V. Bertone *et al.*, JHEP **08**, 166 (2014), [arXiv:1406.7693]; <https://amcfast.hepforge.org/>.
- [142] G. Cullen, N. Greiner and G. Heinrich, Eur. Phys. J. **C73**, 4, 2388 (2013), [arXiv:1212.5154].
- [143] S. Kallweit *et al.*, JHEP **04**, 012 (2015), [arXiv:1412.5157].
- [144] A. Denner *et al.*, JHEP **04**, 018 (2015), [arXiv:1412.7421].
- [145] M. Chiesa, N. Greiner and F. Tramontano, J. Phys. **G43**, 1, 013002 (2016), [arXiv:1507.08579].
- [146] S. Frixione *et al.*, JHEP **06**, 184 (2015), [arXiv:1504.03446].
- [147] B. Biedermann *et al.*, Eur. Phys. J. **C77**, 492 (2017), [arXiv:1704.05783].
- [148] R. Frederix *et al.*, JHEP **07**, 185 (2018), [arXiv:1804.10017].
- [149] C. Anastasiou, R. Boughezal and F. Petriello, JHEP **04**, 003 (2009), [arXiv:0811.3458].
- [150] S. Dittmaier, A. Huss and C. Schwinn, Nucl. Phys. **B885**, 318 (2014), [arXiv:1403.3216].
- [151] S. Dittmaier, A. Huss and C. Schwinn, Nucl. Phys. **B904**, 216 (2016), [arXiv:1511.08016].
- [152] D. de Florian, M. Der and I. Fabre, Phys. Rev. **D98**, 9, 094008 (2018), [arXiv:1805.12214].
- [153] M. Bonetti, K. Melnikov and L. Tancredi, Phys. Rev. **D97**, 5, 056017 (2018), [Erratum: Phys. Rev. **D97**, no.9, 099906(2018)], [arXiv:1801.10403].
- [154] C. Anastasiou *et al.*, JHEP **03**, 162 (2019), [arXiv:1811.11211].
- [155] M. Bonetti, K. Melnikov and L. Tancredi, Phys. Rev. **D97**, 3, 034004 (2018), [arXiv:1711.11113].
- [156] Z. Bern *et al.*, Nucl. Phys. **B425**, 217 (1994), [hep-ph/9403226].
- [157] J. M. Campbell and E. W. N. Glover, Nucl. Phys. **B527**, 264 (1998), [hep-ph/9710255].
- [158] S. Catani and M. Grazzini, Phys. Lett. **B446**, 143 (1999), [hep-ph/9810389].
- [159] T. Binoth and G. Heinrich, Nucl. Phys. **B585**, 741 (2000), [hep-ph/0004013].
- [160] C. Anastasiou, K. Melnikov and F. Petriello, Phys. Rev. **D69**, 076010 (2004), [hep-ph/0311311].
- [161] A. Gehrmann-De Ridder, T. Gehrmann and E. W. N. Glover, JHEP **09**, 056 (2005), [hep-ph/0505111].
- [162] G. Somogyi, Z. Trocsanyi and V. Del Duca, JHEP **01**, 070 (2007), [hep-ph/0609042].
- [163] M. Czakon, Phys. Lett. **B693**, 259 (2010), [arXiv:1005.0274].
- [164] S. Catani and M. Grazzini, Phys. Rev. Lett. **98**, 222002 (2007), [hep-ph/0703012]; <http://theory.fi.infn.it/grazzini/codes.html>.
- [165] R. Boughezal *et al.*, Phys. Rev. Lett. **115**, 6, 062002 (2015), [arXiv:1504.02131].
- [166] J. Gaunt *et al.*, JHEP **09**, 058 (2015), [arXiv:1505.04794].
- [167] M. Cacciari *et al.*, Phys. Rev. Lett. **115**, 8, 082002 (2015), [Erratum: Phys. Rev. Lett. **120**, no.13, 139901(2018)], [arXiv:1506.02660].
- [168] A. Gehrmann-De Ridder *et al.*, Phys. Rev. Lett. **99**, 132002 (2007), [arXiv:0707.1285]; A. Gehrmann-De Ridder *et al.*, JHEP **12**, 094 (2007), [arXiv:0711.4711]; A. Gehrmann-De Ridder *et al.*, Phys. Rev. Lett. **100**, 172001 (2008), [arXiv:0802.0813].
- [169] A. Gehrmann-De Ridder *et al.*, Comput. Phys. Commun. **185**, 3331 (2014), [arXiv:1402.4140]; <https://eerad3.epforge.org/>.
- [170] S. Weinzierl, Phys. Rev. Lett. **101**, 162001 (2008), [arXiv:0807.3241]; S. Weinzierl, JHEP **06**, 041 (2009), [arXiv:0904.1077].
- [171] J. Currie, T. Gehrmann and J. Niehues, Phys. Rev. Lett. **117**, 4, 042001 (2016), [arXiv:1606.03991].
- [172] J. Currie *et al.*, JHEP **05**, 209 (2018), [arXiv:1803.09973].

- [173] T. Gehrmann *et al.*, Phys. Lett. **B792**, 182 (2019), [arXiv:1812.06104].
- [174] K. Melnikov and F. Petriello, Phys. Rev. **D74**, 114017 (2006), [hep-ph/0609070]; <http://gate.hep.anl.gov/fpetriello/FEWZ.html>.
- [175] S. Catani *et al.*, Phys. Rev. Lett. **103**, 082001 (2009), [arXiv:0903.2120]; <http://theory.fi.infn.it/gazzani/dy.html>.
- [176] C. Anastasiou, K. Melnikov and F. Petriello, Nucl. Phys. **B724**, 197 (2005), [hep-ph/0501130]; <http://www.phys.ethz.ch/~pheno/fehipro/>.
- [177] M. Grazzini *et al.*, JHEP **05**, 139 (2017), [arXiv:1703.09065].
- [178] S. Catani *et al.*, Phys. Rev. Lett. **108**, 072001 (2012), [Erratum: Phys. Rev. Lett.117,no.8,089901(2016)], [arXiv:1110.2375].
- [179] J. M. Campbell *et al.*, JHEP **07**, 148 (2016), [arXiv:1603.02663].
- [180] M. Grazzini *et al.*, Phys. Lett. **B731**, 204 (2014), [arXiv:1309.7000].
- [181] M. Grazzini, S. Kallweit and D. Rathlev, JHEP **07**, 085 (2015), [arXiv:1504.01330].
- [182] R. Boughezal *et al.*, Eur. Phys. J. **C77**, 1, 7 (2017), [arXiv:1605.08011].
- [183] J. M. Campbell, R. K. Ellis and C. Williams, Phys. Rev. Lett. **118**, 22, 222001 (2017), [arXiv:1612.04333].
- [184] X. Chen *et al.*, Submitted to: J. High Energy Phys. (2019), [arXiv:1904.01044].
- [185] J. M. Campbell, R. K. Ellis and C. Williams, Phys. Rev. **D96**, 1, 014037 (2017), [arXiv:1703.10109].
- [186] A. Gehrmann-De Ridder *et al.*, Phys. Rev. Lett. **117**, 2, 022001 (2016), [arXiv:1507.02850].
- [187] R. Boughezal *et al.*, Phys. Rev. Lett. **116**, 15, 152001 (2016), [arXiv:1512.01291].
- [188] R. Boughezal *et al.*, Phys. Rev. Lett. **115**, 8, 082003 (2015), [arXiv:1504.07922].
- [189] R. Boughezal *et al.*, Phys. Lett. **B748**, 5 (2015), [arXiv:1505.03893].
- [190] F. Caola, K. Melnikov and M. Schulze, Phys. Rev. **D92**, 7, 074032 (2015), [arXiv:1508.02684].
- [191] X. Chen *et al.*, JHEP **10**, 066 (2016), [arXiv:1607.08817].
- [192] G. Ferrera, M. Grazzini and F. Tramontano, Phys. Rev. Lett. **107**, 152003 (2011), [arXiv:1107.1164].
- [193] G. Ferrera, M. Grazzini and F. Tramontano, Phys. Lett. **B740**, 51 (2015), [arXiv:1407.4747].
- [194] M. Brucherseifer, F. Caola and K. Melnikov, Phys. Lett. **B736**, 58 (2014), [arXiv:1404.7116].
- [195] E. L. Berger *et al.*, Phys. Rev. **D94**, 7, 071501 (2016), [arXiv:1606.08463].
- [196] M. Czakon, P. Fiedler and A. Mitov, Phys. Rev. Lett. **115**, 5, 052001 (2015), [arXiv:1411.3007].
- [197] J. Currie, E. W. N. Glover and J. Pires, Phys. Rev. Lett. **118**, 7, 072002 (2017), [arXiv:1611.01460].
- [198] D. de Florian and J. Mazzitelli, Phys. Rev. Lett. **111**, 201801 (2013), [arXiv:1309.6594].
- [199] J. Cruz-Martinez *et al.*, Phys. Lett. **B781**, 672 (2018), [arXiv:1802.02445].
- [200] T. Liu, K. Melnikov and A. A. Penin (2019), [arXiv:1906.10899].
- [201] *Les Houches 2017: Physics at TeV Colliders Standard Model Working Group Report* (2018), [arXiv:1803.07977], URL <http://lss.fnal.gov/archive/2018/conf/fermilab-conf-18-122-cd-t.pdf>.
- [202] Y. L. Dokshitzer, D. Diakonov and S. I. Troian, Phys. Rept. **58**, 269 (1980).
- [203] G. Parisi and R. Petronzio, Nucl. Phys. **B154**, 427 (1979).
- [204] G. Curci, M. Greco and Y. Srivastava, Nucl. Phys. **B159**, 451 (1979).
- [205] A. Bassetto, M. Ciafaloni and G. Marchesini, Nucl. Phys. **B163**, 477 (1980).
- [206] J. C. Collins and D. E. Soper, Nucl. Phys. **B193**, 381 (1981), [Erratum: Nucl. Phys.B213,545(1983)].
- [207] J. C. Collins and D. E. Soper, Nucl. Phys. **B197**, 446 (1982).
- [208] J. Kodaira and L. Trentadue, Phys. Lett. **112B**, 66 (1982).
- [209] J. Kodaira and L. Trentadue, Phys. Lett. **123B**, 335 (1983).
- [210] J. C. Collins, D. E. Soper and G. F. Sterman, Nucl. Phys. **B250**, 199 (1985).
- [211] S. Catani *et al.*, Nucl. Phys. **B407**, 3 (1993).
- [212] C. W. Bauer *et al.*, Phys. Rev. **D63**, 114020 (2001), [hep-ph/0011336].
- [213] C. W. Bauer, D. Pirjol and I. W. Stewart, Phys. Rev. **D65**, 054022 (2002), [hep-ph/0109045].
- [214] T. Becher, A. Broggio and A. Ferroglia, Lect. Notes Phys. **896**, pp.1 (2015), [arXiv:1410.1892].
- [215] S. Catani *et al.*, Phys. Lett. **B269**, 432 (1991).
- [216] N. Brown and W. J. Stirling, Phys. Lett. **B252**, 657 (1990).
- [217] W. Bartel *et al.* (JADE), Z. Phys. **C33**, 23 (1986), [53(1986)].
- [218] N. Kidonakis, G. Oderda and G. F. Sterman, Nucl. Phys. **B531**, 365 (1998), [hep-ph/9803241].
- [219] R. Bonciani *et al.*, Phys. Lett. **B575**, 268 (2003), [hep-ph/0307035].
- [220] A. Banfi, G. P. Salam and G. Zanderighi, JHEP **03**, 073 (2005), [hep-ph/0407286].
- [221] D. de Florian and M. Grazzini, Phys. Rev. Lett. **85**, 4678 (2000), [hep-ph/0008152].
- [222] G. Bozzi *et al.*, Nucl. Phys. **B737**, 73 (2006), [hep-ph/0508068]; <http://theory.fi.infn.it/grazzini/codes.html>.
- [223] G. Bozzi *et al.*, Phys. Lett. **B696**, 207 (2011), [arXiv:1007.2351].
- [224] T. Becher and M. Neubert, Eur. Phys. J. **C71**, 1665 (2011), [arXiv:1007.4005].
- [225] T. Becher, M. Neubert, and D. Wilhelm, <http://cute.hepforge.org/>.
- [226] D. de Florian *et al.*, JHEP **06**, 132 (2012), [arXiv:1203.6321]; <http://theory.fi.infn.it/grazzini/codes.html>.
- [227] C. Balazs and C. P. Yuan, Phys. Rev. **D56**, 5558 (1997), [hep-ph/9704258].
- [228] S. Catani *et al.*, JHEP **12**, 047 (2015), [arXiv:1507.06937].
- [229] A. Banfi *et al.*, Phys. Lett. **B715**, 152 (2012), [arXiv:1205.4760].
- [230] M. Grazzini *et al.*, JHEP **08**, 154 (2015), [arXiv:1507.02565].
- [231] D. de Florian and M. Grazzini, Nucl. Phys. **B704**, 387 (2005), [hep-ph/0407241].
- [232] T. Becher and G. Bell, JHEP **11**, 126 (2012), [arXiv:1210.0580].
- [233] A. Banfi *et al.*, Phys. Rev. Lett. **109**, 202001 (2012), [arXiv:1206.4998]; T. Becher, M. Neubert and L. Rothen, JHEP **10**, 125 (2013), [arXiv:1307.0025].
- [234] I. W. Stewart *et al.*, Phys. Rev. **D89**, 5, 054001 (2014), [arXiv:1307.1808].
- [235] I. W. Stewart, F. J. Tackmann and W. J. Waalewijn, Phys. Rev. Lett. **106**, 032001 (2011), [arXiv:1005.4060].
- [236] Y.-T. Chien *et al.*, Phys. Rev. **D87**, 1, 014010 (2013), [arXiv:1208.0010]; T. T. Jouttenus *et al.*, Phys. Rev. **D88**, 5, 054031 (2013), [arXiv:1302.0846].

- [237] M. Dasgupta *et al.*, JHEP **10**, 126 (2012), [arXiv:1207.1640].
- [238] V. Ahrens *et al.*, JHEP **09**, 097 (2010), [arXiv:1003.5827].
- [239] M. Aliev *et al.*, Comput. Phys. Commun. **182**, 1034 (2011), [arXiv:1007.1327].
- [240] N. Kidonakis, Phys. Rev. **D82**, 114030 (2010), [arXiv:1009.4935].
- [241] T. Becher, C. Lorentzen and M. D. Schwartz, Phys. Rev. Lett. **108**, 012001 (2012), [arXiv:1106.4310].
- [242] T. Becher *et al.*, Eur. Phys. J. **C75**, 4, 154 (2015), [arXiv:1412.8408].
- [243] E. Gerwick *et al.*, JHEP **02**, 106 (2015), [arXiv:1411.7325].
- [244] A. Banfi *et al.*, JHEP **05**, 102 (2015), [arXiv:1412.2126].
- [245] T. Becher and M. D. Schwartz, JHEP **07**, 034 (2008), [arXiv:0803.0342].
- [246] A. H. Hoang *et al.*, Phys. Rev. **D91**, 9, 094017 (2015), [arXiv:1411.6633].
- [247] Y.-T. Chien and M. D. Schwartz, JHEP **08**, 058 (2010), [arXiv:1005.1644].
- [248] P. F. Monni, T. Gehrmann and G. Luisoni, JHEP **08**, 010 (2011), [arXiv:1105.4560].
- [249] W. Bizon *et al.*, JHEP **02**, 108 (2018), [arXiv:1705.09127].
- [250] W. Bizon *et al.* (2019), [arXiv:1905.05171].
- [251] S. Catani *et al.*, Nucl. Phys. **B888**, 75 (2014), [arXiv:1405.4827].
- [252] S. Fleming *et al.*, Phys. Rev. **D77**, 074010 (2008), [hep-ph/0703207].
- [253] A. H. Hoang, P. Pietrulewicz and D. Samitz, Phys. Rev. **D93**, 3, 034034 (2016), [arXiv:1508.04323].
- [254] A. Banfi *et al.*, JHEP **04**, 049 (2016), [arXiv:1511.02886].
- [255] A. J. Larkoski and I. Moult, Phys. Rev. **D93**, 014017 (2016), [arXiv:1510.08459].
- [256] G. Lustermsans, W. J. Waalewijn and L. Zeune, Phys. Lett. **B762**, 447 (2016), [arXiv:1605.02740].
- [257] C. Muselli, S. Forte and G. Ridolfi, JHEP **03**, 106 (2017), [arXiv:1701.01464].
- [258] M. Bonvini and S. Marzani, Phys. Rev. Lett. **120**, 202003 (2018), [arXiv:1802.07758].
- [259] M. Procura, W. J. Waalewijn and L. Zeune, JHEP **10**, 098 (2018), [arXiv:1806.10622].
- [260] G. Lustermsans *et al.*, JHEP **03**, 124 (2019), [arXiv:1901.03331].
- [261] I. Feige *et al.*, Phys. Rev. Lett. **109**, 092001 (2012), [arXiv:1204.3898].
- [262] M. Dasgupta *et al.*, JHEP **09**, 029 (2013), [arXiv:1307.0007].
- [263] A. J. Larkoski *et al.*, JHEP **05**, 146 (2014), [arXiv:1402.2657].
- [264] M. Dasgupta, A. Powling and A. Siodmok, JHEP **08**, 079 (2015), [arXiv:1503.01088].
- [265] A. J. Larkoski, I. Moult and D. Neill, JHEP **05**, 117 (2016), [arXiv:1507.03018].
- [266] C. Frye *et al.*, JHEP **07**, 064 (2016), [arXiv:1603.09338].
- [267] A. J. Larkoski, I. Moult and D. Neill, JHEP **02**, 144 (2018), [arXiv:1710.00014].
- [268] A. J. Larkoski, I. Moult and B. Nachman (2017), [arXiv:1709.04464].
- [269] S. Marzani, G. Soyez and M. Spannowsky (2019), [Lect. Notes Phys.958,pp.(2019)], [arXiv:1901.10342].
- [270] Yu.L. Dokshitzer *et al.*, "Basics of perturbative QCD," Gif-sur-Yvette, France: Éditions frontières (1991), see also <http://www.lpthe.jussieu.fr/~yuri/BPQCD/cover.html>.
- [271] T. Sjostrand *et al.*, Comput. Phys. Commun. **135**, 238 (2001), [hep-ph/0010017].
- [272] T. Sjostrand, S. Mrenna and P. Z. Skands, JHEP **05**, 026 (2006), [hep-ph/0603175]; <http://projects.hepforge.org/pythia6/>.
- [273] T. Sjostrand *et al.*, Comput. Phys. Commun. **191**, 159 (2015), [arXiv:1410.3012]; <http://home.thep.lu.se/~torbjorn/Pythia.html>.
- [274] B. R. Webber, Nucl. Phys. **B238**, 492 (1984).
- [275] G. Corcella *et al.*, JHEP **01**, 010 (2001), [hep-ph/0011363]; <http://www.hep.phy.cam.ac.uk/theory/webber/Herwig/>.
- [276] M. Bahr *et al.*, Eur. Phys. J. **C58**, 639 (2008), [arXiv:0803.0883]; <http://projects.hepforge.org/herwig/>.
- [277] L. Lonnblad, Comput. Phys. Commun. **71**, 15 (1992).
- [278] A. Buckley *et al.*, Phys. Rept. **504**, 145 (2011), [arXiv:1101.2599].
- [279] B. Andersson *et al.*, Phys. Rept. **97**, 31 (1983).
- [280] T. Sjostrand, Nucl. Phys. **B248**, 469 (1984).
- [281] J. Bellm *et al.* (2019), [arXiv:1903.12563].
- [282] T. Sjostrand and M. van Zijl, Phys. Rev. **D36**, 2019 (1987).
- [283] S. Catani *et al.*, JHEP **11**, 063 (2001), [hep-ph/0109231].
- [284] J. Alwall *et al.*, Eur. Phys. J. **C53**, 473 (2008), [arXiv:0706.2569].
- [285] S. Frixione and B. R. Webber, JHEP **06**, 029 (2002), [hep-ph/0204244].
- [286] P. Nason, JHEP **11**, 040 (2004), [hep-ph/0409146].
- [287] S. Alioli *et al.*, JHEP **06**, 043 (2010), [arXiv:1002.2581]; <http://powhegbox.mib.infn.it/>.
- [288] S. Plätzer, JHEP **08**, 114 (2013), [arXiv:1211.5467]; R. Frederix and S. Frixione, JHEP **12**, 061 (2012), [arXiv:1209.6215]; K. Hamilton *et al.*, JHEP **05**, 082 (2013), [arXiv:1212.4504].
- [289] K. Hamilton *et al.*, JHEP **10**, 222 (2013), [arXiv:1309.0017]; A. Karlberg, E. Re and G. Zanderighi, JHEP **09**, 134 (2014), [arXiv:1407.2940]; S. Höche, Y. Li and S. Prestel, Phys. Rev. **D91**, 7, 074015 (2015), [arXiv:1405.3607]; S. Höche, Y. Li and S. Prestel, Phys. Rev. **D90**, 5, 054011 (2014), [arXiv:1407.3773]; S. Alioli *et al.*, Phys. Rev. **D92**, 9, 094020 (2015), [arXiv:1508.01475]; P. F. Monni *et al.* (2019), [arXiv:1908.06987].
- [290] W. Astill *et al.*, JHEP **06**, 154 (2016), [arXiv:1603.01620].
- [291] W. Astill *et al.*, JHEP **11**, 157 (2018), [arXiv:1804.08141].
- [292] E. Re, M. Wiesemann and G. Zanderighi, JHEP **12**, 121 (2018), [arXiv:1805.09857].
- [293] M. Cacciari *et al.*, JHEP **04**, 068 (2004), [hep-ph/0303085].
- [294] P. M. Stevenson, Phys. Lett. **100B**, 61 (1981).
- [295] P. M. Stevenson, Phys. Rev. **D23**, 2916 (1981).
- [296] G. Grunberg, Phys. Rev. **D29**, 2315 (1984).
- [297] S. J. Brodsky, G. P. Lepage and P. B. Mackenzie, Phys. Rev. **D28**, 228 (1983).
- [298] S.-Q. Wang *et al.* (2019), [arXiv:1908.00060].
- [299] M. Cacciari and N. Houdeau, JHEP **09**, 039 (2011), [arXiv:1105.5152].
- [300] A. David and G. Passarino, Phys. Lett. **B726**, 266 (2013), [arXiv:1307.1843].
- [301] E. Bagnaschi *et al.*, JHEP **02**, 133 (2015), [arXiv:1409.5036].
- [302] M. Dasgupta *et al.*, JHEP **06**, 057 (2016), [arXiv:1602.01110].
- [303] J. Currie *et al.*, JHEP **10**, 155 (2018), [arXiv:1807.03692].
- [304] G. Soyez *et al.*, Phys. Rev. Lett. **110**, 16, 162001 (2013), [arXiv:1211.2811].

- [305] M. Dasgupta and G. P. Salam, *J. Phys.* **G30**, R143 (2004), [hep-ph/0312283].
- [306] S. Moretti, L. Lonnblad and T. Sjostrand, *JHEP* **08**, 001 (1998), [hep-ph/9804296].
- [307] G. P. Salam, *Eur. Phys. J.* **C67**, 637 (2010), [arXiv:0906.1833].
- [308] S. D. Ellis *et al.*, *Prog. Part. Nucl. Phys.* **60**, 484 (2008), [arXiv:0712.2447].
- [309] M. Cacciari, *Int. J. Mod. Phys.* **A30**, 31, 1546001 (2015), [arXiv:1509.02272].
- [310] G. P. Salam and G. Soyez, *JHEP* **05**, 086 (2007), [arXiv:0704.0292].
- [311] S. Catani *et al.*, *Nucl. Phys.* **B406**, 187 (1993).
- [312] S. D. Ellis and D. E. Soper, *Phys. Rev.* **D48**, 3160 (1993), [hep-ph/9305266].
- [313] Y. L. Dokshitzer *et al.*, *JHEP* **08**, 001 (1997), [hep-ph/9707323].
- [314] M. Wobisch and T. Wengler, in “Monte Carlo generators for HERA physics. Proceedings, Workshop, Hamburg, Germany, 1998-1999,” 270–279 (1998), [hep-ph/9907280].
- [315] M. Cacciari, G. P. Salam and G. Soyez, *JHEP* **04**, 063 (2008), [arXiv:0802.1189].
- [316] S. Bethke *et al.*, *Nucl. Phys.* **B370**, 310 (1992), [Erratum: *Nucl. Phys.* B523,681(1998)].
- [317] M. Cacciari and G. P. Salam, *Phys. Lett.* **B641**, 57 (2006), [hep-ph/0512210]; M. Cacciari, G. P. Salam and G. Soyez, *Eur. Phys. J.* **C72**, 1896 (2012), [arXiv:1111.6097].
- [318] S. Brandt *et al.*, *Phys. Lett.* **12**, 57 (1964).
- [319] E. Farhi, *Phys. Rev. Lett.* **39**, 1587 (1977).
- [320] O. Biebel, *Phys. Rept.* **340**, 165 (2001).
- [321] S. Kluth, *Rept. Prog. Phys.* **69**, 1771 (2006), [hep-ex/0603011].
- [322] C. L. Basham *et al.*, *Phys. Rev. Lett.* **41**, 1585 (1978).
- [323] A. Ali, E. Pietarinen and W. J. Stirling, *Phys. Lett.* **141B**, 447 (1984).
- [324] I. W. Stewart, F. J. Tackmann and W. J. Waalewijn, *Phys. Rev. Lett.* **105**, 092002 (2010), [arXiv:1004.2489].
- [325] A. Banfi, G. P. Salam and G. Zanderighi, *JHEP* **08**, 062 (2004), [hep-ph/0407287].
- [326] A. Banfi, G. P. Salam and G. Zanderighi, *JHEP* **06**, 038 (2010), [arXiv:1001.4082].
- [327] T. Becher, X. Garcia i Tormo and J. Piclum, *Phys. Rev.* **D93**, 5, 054038 (2016), [Erratum: *Phys. Rev.* D93,no.7,079905(2016)], [arXiv:1512.00022].
- [328] A. Gao *et al.*, *Phys. Rev. Lett.* **123**, 6, 062001 (2019), [arXiv:1901.04497].
- [329] T. Aaltonen *et al.* (CDF), *Phys. Rev.* **D83**, 112007 (2011), [arXiv:1103.5143].
- [330] G. Aad *et al.* (ATLAS), *Eur. Phys. J.* **C72**, 2211 (2012), [arXiv:1206.2135].
- [331] G. Aad *et al.* (ATLAS), *Phys. Rev.* **D88**, 3, 032004 (2013), [arXiv:1207.6915].
- [332] G. Aad *et al.* (ATLAS), *Phys. Lett.* **B750**, 427 (2015), [arXiv:1508.01579].
- [333] G. Aad *et al.* (ATLAS), *Eur. Phys. J.* **C76**, 7, 375 (2016), [arXiv:1602.08980].
- [334] M. Aaboud *et al.* (ATLAS), *Eur. Phys. J.* **C77**, 12, 872 (2017), [arXiv:1707.02562].
- [335] M. Aaboud *et al.* (ATLAS), *Phys. Rev.* **D98**, 9, 092004 (2018), [arXiv:1805.04691].
- [336] V. Khachatryan *et al.* (CMS), *Phys. Lett.* **B699**, 48 (2011), [arXiv:1102.0068].
- [337] S. Chatrchyan *et al.* (CMS), *Phys. Lett.* **B722**, 238 (2013), [arXiv:1301.1646].
- [338] V. Khachatryan *et al.* (CMS), *JHEP* **10**, 87 (2014), [arXiv:1407.2856].
- [339] A. M. Sirunyan *et al.* (CMS), *JHEP* **12**, 117 (2018), [arXiv:1811.00588].
- [340] S. Chatrchyan *et al.* (CMS), *Phys. Lett.* **B730**, 243 (2014), [arXiv:1310.0878].
- [341] G. Aad *et al.* (ATLAS), *Phys. Rev.* **D83**, 052003 (2011), [arXiv:1101.0070].
- [342] S. Chatrchyan *et al.* (CMS), *JHEP* **06**, 160 (2012), [arXiv:1204.3170].
- [343] B. B. Abelev *et al.* (ALICE), *Phys. Rev.* **D91**, 11, 112012 (2015), [arXiv:1411.4969].
- [344] G. Aad *et al.* (ATLAS), *Eur. Phys. J.* **C73**, 12, 2676 (2013), [arXiv:1201.5749].
- [345] C. Glasman (H1, ZEUS), *Nucl. Phys. Proc. Suppl.* **191**, 121 (2009), [arXiv:0812.0757].
- [346] T. Carli, K. Rabbertz and S. Schumann, in T. Schörner-Sadenius, editor, “The Large Hadron Collider: Harvest of Run 1,” 139–194 (2015), [arXiv:1506.03239].
- [347] A. Abdesselam *et al.*, *Eur. Phys. J.* **C71**, 1661 (2011), [arXiv:1012.5412].
- [348] D. Krohn, J. Thaler and L.-T. Wang, *JHEP* **02**, 084 (2010), [arXiv:0912.1342].
- [349] A. Altheimer *et al.*, *J. Phys.* **G39**, 063001 (2012), [arXiv:1201.0008].
- [350] A. Altheimer *et al.*, *Eur. Phys. J.* **C74**, 3, 2792 (2014), [arXiv:1311.2708].
- [351] P. C. Stichel and W. J. Zakrzewski, *Eur. Phys. J.* **C75**, 1, 9 (2015), [arXiv:1409.1363].
- [352] D. Adams *et al.*, *Eur. Phys. J.* **C75**, 9, 409 (2015), [arXiv:1504.00679].
- [353] T. Schorner-Sadenius, *Eur. Phys. J.* **C72**, 2060 (2012), [Erratum: *Eur. Phys. J.* C72,2133(2012)].
- [354] J. M. Campbell, J. W. Huston and W. J. Stirling, *Rept. Prog. Phys.* **70**, 89 (2007), [hep-ph/0611148].
- [355] M. L. Mangano, *Phys. Usp.* **53**, 109 (2010), [*Usp. Fiz. Nauk*180,113(2010)].
- [356] J. M. Butterworth, G. Dissertori and G. P. Salam, *Ann. Rev. Nucl. Part. Sci.* **62**, 387 (2012), [arXiv:1202.0583].
- [357] J. Currie *et al.*, *JHEP* **07**, 018 (2017), [arXiv:1703.05977].
- [358] M. Klasen, G. Kramer and M. Michael, *Phys. Rev.* **D89**, 7, 074032 (2014), [arXiv:1310.1724].
- [359] T. Carli, T. Gehrman and S. Hoeche, *Eur. Phys. J.* **C67**, 73 (2010), [arXiv:0912.3715].
- [360] S. Chekanov *et al.* (ZEUS), *Nucl. Phys.* **B792**, 1 (2008), [arXiv:0707.3749].
- [361] S. Chekanov *et al.* (ZEUS), *Phys. Rev.* **D76**, 072011 (2007), [arXiv:0706.3809].
- [362] A. Aktas *et al.* (H1), *Phys. Lett.* **B639**, 21 (2006), [hep-ex/0603014].
- [363] H. Abramowicz *et al.* (ZEUS), *Eur. Phys. J.* **C71**, 1659 (2011), [arXiv:1104.5444].
- [364] H. Abramowicz *et al.* (ZEUS), *Nucl. Phys.* **B864**, 1 (2012), [arXiv:1205.6153].
- [365] F. D. Aaron *et al.* (H1), *Eur. Phys. J.* **C65**, 363 (2010), [arXiv:0904.3870].
- [366] F. D. Aaron *et al.* (H1), *Eur. Phys. J.* **C54**, 389 (2008), [arXiv:0711.2606].
- [367] S. Chekanov *et al.* (ZEUS), *Eur. Phys. J.* **C52**, 515 (2007), [arXiv:0707.3093].
- [368] S. Chekanov *et al.* (ZEUS), *Phys. Rev.* **D78**, 032004 (2008), [arXiv:0802.3955].
- [369] H. Abramowicz *et al.* (ZEUS), *Eur. Phys. J.* **C70**, 965 (2010), [arXiv:1010.6167].

- [370] H. Abramowicz *et al.* (ZEUS), Phys. Lett. **B691**, 127 (2010), [arXiv:1003.2923].
- [371] S. Chekanov *et al.* (ZEUS), Phys. Rev. **D85**, 052008 (2012), [arXiv:0808.3783].
- [372] F. D. Aaron *et al.* (H1), Eur. Phys. J. **C67**, 1 (2010), [arXiv:0911.5678].
- [373] V. Andreev *et al.* (H1), Eur. Phys. J. **C75**, 2, 65 (2015), [arXiv:1406.4709].
- [374] V. Andreev *et al.* (H1), Eur. Phys. J. **C77**, 11, 791 (2017), [arXiv:1709.07251].
- [375] <http://twiki.cern.ch/twiki/bin/view/CMSPublic/PhysicsResultsCombined>.
- [376] <http://atlas.web.cern.ch/Atlas/GROUPS/PHYSICS/CombinedSummaryPlots/SM>.
- [377] A. Abulencia *et al.* (CDF), Phys. Rev. **D75**, 092006 (2007), [Erratum: Phys. Rev. **D75**, 119901(2007)], [hep-ex/0701051].
- [378] T. Aaltonen *et al.* (CDF), Phys. Rev. **D78**, 052006 (2008), [Erratum: Phys. Rev. **D79**, 119902(2009)], [arXiv:0807.2204].
- [379] V. M. Abazov *et al.* (D0), Phys. Rev. Lett. **101**, 062001 (2008), [arXiv:0802.2400].
- [380] V. M. Abazov *et al.* (D0), Phys. Rev. **D85**, 052006 (2012), [arXiv:1110.3771].
- [381] B. Abelev *et al.* (ALICE), Phys. Lett. **B722**, 262 (2013), [arXiv:1301.3475].
- [382] G. Aad *et al.* (ATLAS), Eur. Phys. J. **C73**, 8, 2509 (2013), [arXiv:1304.4739].
- [383] G. Aad *et al.* (ATLAS), JHEP **02**, 153 (2015), [Erratum: JHEP09,141(2015)], [arXiv:1410.8857].
- [384] M. Aaboud *et al.* (ATLAS), JHEP **09**, 020 (2017), [arXiv:1706.03192].
- [385] V. Khachatryan *et al.* (CMS), Eur. Phys. J. **C76**, 5, 265 (2016), [arXiv:1512.06212].
- [386] S. Chatrchyan *et al.* (CMS), Phys. Rev. **D87**, 11, 112002 (2013), [Erratum: Phys. Rev. **D87**, no.11, 119902(2013)], [arXiv:1212.6660].
- [387] V. Khachatryan *et al.* (CMS), JHEP **03**, 156 (2017), [arXiv:1609.05331].
- [388] V. Khachatryan *et al.* (CMS), Eur. Phys. J. **C76**, 8, 451 (2016), [arXiv:1605.04436].
- [389] M. Aaboud *et al.* (ATLAS), JHEP **05**, 195 (2018), [arXiv:1711.02692].
- [390] A. Schwartzman, Int. J. Mod. Phys. **A30**, 31, 1546002 (2015), [arXiv:1509.05459].
- [391] J. Rojo, Int. J. Mod. Phys. **A30**, 1546005 (2015), [arXiv:1410.7728].
- [392] G. Aad *et al.* (ATLAS), JHEP **05**, 059 (2014), [arXiv:1312.3524].
- [393] A. M. Sirunyan *et al.* (CMS), Eur. Phys. J. **C77**, 11, 746 (2017), [arXiv:1705.02628].
- [394] T. Aaltonen *et al.* (CDF), Phys. Rev. **D79**, 112002 (2009), [arXiv:0812.4036].
- [395] V. M. Abazov *et al.* (D0), Phys. Rev. Lett. **103**, 191803 (2009), [arXiv:0906.4819].
- [396] S. Chatrchyan *et al.* (CMS), JHEP **05**, 055 (2012), [arXiv:1202.5535].
- [397] V. Khachatryan *et al.* (CMS), Phys. Lett. **B746**, 79 (2015), [arXiv:1411.2646].
- [398] A. M. Sirunyan *et al.* (CMS), JHEP **07**, 013 (2017), [arXiv:1703.09986].
- [399] G. Aad *et al.* (ATLAS), JHEP **01**, 029 (2013), [arXiv:1210.1718].
- [400] M. Aaboud *et al.* (ATLAS), Phys. Rev. **D96**, 5, 052004 (2017), [arXiv:1703.09127].
- [401] V. M. Abazov *et al.* (D0), Phys. Rev. Lett. **94**, 221801 (2005), [hep-ex/0409040].
- [402] V. M. Abazov *et al.* (D0), Phys. Lett. **B721**, 212 (2013), [arXiv:1212.1842].
- [403] G. Aad *et al.* (ATLAS), Phys. Rev. Lett. **106**, 172002 (2011), [arXiv:1102.2696].
- [404] V. Khachatryan *et al.* (CMS), Phys. Rev. Lett. **106**, 122003 (2011), [arXiv:1101.5029].
- [405] V. Khachatryan *et al.* (CMS), Eur. Phys. J. **C76**, 10, 536 (2016), [arXiv:1602.04384].
- [406] A. M. Sirunyan *et al.* (CMS), Eur. Phys. J. **C78**, 7, 566 (2018), [arXiv:1712.05471].
- [407] A. M. Sirunyan *et al.* (CMS) (2019), [arXiv:1902.04374].
- [408] P. Kokkas, Int. J. Mod. Phys. **A30**, 31, 1546004 (2015), [arXiv:1509.02144].
- [409] M. Aaboud *et al.* (ATLAS), Eur. Phys. J. **C77**, 6, 367 (2017), [arXiv:1612.03016].
- [410] G. Aad *et al.* (ATLAS), Phys. Lett. **B759**, 601 (2016), [arXiv:1603.09222].
- [411] R. Aaij *et al.* (LHCb), JHEP **08**, 039 (2015), [arXiv:1505.07024].
- [412] S. Chatrchyan *et al.* (CMS), JHEP **10**, 132 (2011), [arXiv:1107.4789].
- [413] S. Chatrchyan *et al.* (CMS), Phys. Rev. Lett. **112**, 191802 (2014), [arXiv:1402.0923].
- [414] R. Aaij *et al.* (LHCb), JHEP **06**, 058 (2012), [arXiv:1204.1620].
- [415] R. Aaij *et al.* (LHCb), JHEP **01**, 155 (2016), [arXiv:1511.08039].
- [416] R. Aaij *et al.* (LHCb), JHEP **09**, 136 (2016), [arXiv:1607.06495].
- [417] S. Chatrchyan *et al.* (CMS), JHEP **10**, 007 (2011), [arXiv:1108.0566].
- [418] V. Khachatryan *et al.* (CMS), Eur. Phys. J. **C75**, 4, 147 (2015), [arXiv:1412.1115].
- [419] G. Aad *et al.* (ATLAS), Phys. Lett. **B725**, 223 (2013), [arXiv:1305.4192].
- [420] G. Aad *et al.* (ATLAS), JHEP **06**, 112 (2014), [arXiv:1404.1212].
- [421] G. Aad *et al.* (ATLAS), JHEP **08**, 009 (2016), [arXiv:1606.01736].
- [422] A. M. Sirunyan *et al.* (CMS), Submitted to: JHEP (2018), [arXiv:1812.10529].
- [423] M. Aaboud *et al.* (ATLAS), JHEP **12**, 059 (2017), [arXiv:1710.05167].
- [424] S. Chatrchyan *et al.* (CMS), Phys. Rev. **D90**, 3, 032004 (2014), [arXiv:1312.6283].
- [425] V. Khachatryan *et al.* (CMS), Eur. Phys. J. **C76**, 8, 469 (2016), [arXiv:1603.01803].
- [426] G. Aad *et al.* (ATLAS), Submitted to: Eur. Phys. J. (2019), [arXiv:1904.05631].
- [427] G. Aad *et al.* (ATLAS), Eur. Phys. J. **C76**, 5, 291 (2016), [arXiv:1512.02192].
- [428] V. Khachatryan *et al.* (CMS), JHEP **02**, 096 (2017), [arXiv:1606.05864].
- [429] A. M. Sirunyan *et al.* (CMS), JHEP **03**, 172 (2018), [arXiv:1710.07955].
- [430] M. Aaboud *et al.* (ATLAS), JHEP **05**, 077 (2018), [arXiv:1711.03296].
- [431] C. F. Berger *et al.*, Phys. Rev. **D80**, 074036 (2009), [arXiv:0907.1984].
- [432] U. Blumenschein, Int. J. Mod. Phys. **A30**, 31, 1546007 (2015), [arXiv:1509.04885].
- [433] G. Aad *et al.* (ATLAS) (2019), [arXiv:1907.06728].

- [434] V. Khachatryan *et al.* (CMS), Phys. Rev. **D95**, 052002 (2017), [arXiv:1610.04222].
- [435] A. M. Sirunyan *et al.* (CMS), Phys. Rev. **D96**, 7, 072005 (2017), [arXiv:1707.05979].
- [436] A. M. Sirunyan *et al.* (CMS), Eur. Phys. J. **C78**, 11, 965 (2018), [arXiv:1804.05252].
- [437] G. Aad *et al.* (ATLAS), JHEP **07**, 032 (2013), [arXiv:1304.7098].
- [438] Z. Bern *et al.*, Phys. Rev. **D88**, 1, 014025 (2013), [arXiv:1304.1253].
- [439] M. Voutilainen, Int. J. Mod. Phys. **A30**, 31, 1546008 (2015), [arXiv:1509.05026].
- [440] G. Aad *et al.* (ATLAS), JHEP **08**, 005 (2016), [arXiv:1605.03495].
- [441] G. Aad *et al.* (ATLAS) (2019), [arXiv:1908.02746].
- [442] S. Chatrchyan *et al.* (CMS), Phys. Rev. **D84**, 052011 (2011), [arXiv:1108.2044].
- [443] S. Chatrchyan *et al.* (CMS), JHEP **06**, 009 (2014), [arXiv:1311.6141].
- [444] G. Aad *et al.* (ATLAS), Phys. Rev. **D89**, 5, 052004 (2014), [arXiv:1311.1440].
- [445] M. Aaboud *et al.* (ATLAS), Phys. Lett. **B780**, 578 (2018), [arXiv:1801.00112].
- [446] M. Aaboud *et al.* (ATLAS), Nucl. Phys. **B918**, 257 (2017), [arXiv:1611.06586].
- [447] A. M. Sirunyan *et al.* (CMS), Eur. Phys. J. **C79**, 1, 20 (2019), [arXiv:1807.00782].
- [448] A. M. Sirunyan *et al.* (CMS) (2019), [arXiv:1907.08155].
- [449] M. Aaboud *et al.* (ATLAS), Phys. Lett. **B776**, 295 (2018), [arXiv:1710.09560].
- [450] J. H. Kuhn *et al.*, JHEP **03**, 059 (2006), [hep-ph/0508253].
- [451] V. Khachatryan *et al.* (CMS), JHEP **10**, 128 (2015), [Erratum: JHEP04,010(2016)], [arXiv:1505.06520].
- [452] G. Aad *et al.* (ATLAS), JHEP **09**, 029 (2016), [arXiv:1603.01702].
- [453] M. Aaboud *et al.* (ATLAS), Phys. Lett. **B773**, 354 (2017), [arXiv:1702.04519].
- [454] M. Aaboud *et al.* (ATLAS) (2019), [arXiv:1905.04242].
- [455] V. Khachatryan *et al.* (CMS), Eur. Phys. J. **C76**, 7, 401 (2016), [arXiv:1507.03268].
- [456] G. Aad *et al.* (ATLAS) (2019), [arXiv:1903.10415].
- [457] G. Aad *et al.* (ATLAS), JHEP **01**, 086 (2013), [arXiv:1211.1913].
- [458] M. Aaboud *et al.* (ATLAS), Phys. Rev. **D95**, 11, 112005 (2017), [arXiv:1704.03839].
- [459] S. Chatrchyan *et al.* (CMS), Eur. Phys. J. **C74**, 11, 3129 (2014), [arXiv:1405.7225].
- [460] M. Aaboud *et al.* (ATLAS), Phys. Lett. **B781**, 55 (2018), [arXiv:1712.07291].
- [461] K. Kröninger, A. B. Meyer and P. Uwer, in T. Schörner-Sadenius, editor, “The Large Hadron Collider: Harvest of Run 1,” 259–300 (2015), [arXiv:1506.02800].
- [462] M. Aaboud *et al.* (ATLAS), Phys. Rev. **D94**, 9, 092003 (2016), [arXiv:1607.07281].
- [463] M. Aaboud *et al.* (ATLAS), Eur. Phys. J. **C77**, 5, 292 (2017), [arXiv:1612.05220].
- [464] A. M. Sirunyan *et al.* (CMS), Eur. Phys. J. **C79**, 5, 368 (2019), [arXiv:1812.10505].
- [465] A. M. Sirunyan *et al.* (CMS), Submitted to: Eur. Phys. J. (2019), [arXiv:1904.05237].
- [466] M. Czakon, D. Heymes and A. Mitov, Phys. Rev. Lett. **116**, 8, 082003 (2016), [arXiv:1511.00549].
- [467] S. Catani *et al.*, Phys. Rev. **D99**, 5, 051501 (2019), [arXiv:1901.04005].
- [468] S. Catani *et al.*, JHEP **07**, 100 (2019), [arXiv:1906.06535].
- [469] M. Czakon *et al.*, JHEP **05**, 149 (2018), [arXiv:1803.07623].
- [470] S. Chatrchyan *et al.* (CMS), Phys. Lett. **B728**, 496 (2014), [Erratum: Phys. Lett. B738,526(2014)], [arXiv:1307.1907].
- [471] T. Klijnsma *et al.*, Eur. Phys. J. **C77**, 11, 778 (2017), [arXiv:1708.07495].
- [472] G. Aad *et al.* (ATLAS), Eur. Phys. J. **C74**, 10, 3109 (2014), [Addendum: Eur. Phys. J. C76,no.11,642(2016)], [arXiv:1406.5375].
- [473] A. M. Sirunyan *et al.* (CMS), JHEP **09**, 051 (2017), [arXiv:1701.06228].
- [474] M. Aaboud *et al.* (ATLAS), Phys. Lett. **B786**, 114 (2018), [arXiv:1805.10197].
- [475] A. M. Sirunyan *et al.* (CMS), Phys. Lett. **B792**, 369 (2019), [arXiv:1812.06504].
- [476] M. Aaboud *et al.* (ATLAS), Phys. Rev. **D98**, 052005 (2018), [arXiv:1802.04146].
- [477] A. M. Sirunyan *et al.* (CMS), JHEP **01**, 183 (2019), [arXiv:1807.03825].
- [478] A. M. Sirunyan *et al.* (CMS Collaboration), Phys. Lett. B **792**, arXiv:1812.06504. CMS-HIG-17-028-003, 369. 28 p (2018), submitted to Phys.Lett., URL <http://cds.cern.ch/record/2651932>.
- [479] C. Patrignani *et al.* (Particle Data Group), Chin. Phys. **C40**, 10, 100001 (2016).
- [480] M. Tanabashi *et al.* (Particle Data Group), Phys. Rev. **D98**, 3, 030001 (2018).
- [481] S. Bethke, Prog. Part. Nucl. Phys. **58**, 351 (2007), [hep-ex/0606035].
- [482] S. Bethke, Eur. Phys. J. **C64**, 689 (2009), [111(2009)], [arXiv:0908.1135].
- [483] S. Bethke, J. Phys. **G26**, R27 (2000), [hep-ex/0004021].
- [484] D. d’Enterria *et al.*, in “Workshop on precision measurements of the QCD coupling constant (alphas-2019) Trento, Trentino, Italy, February 11-15, 2019,” (2019), [arXiv:1907.01435].
- [485] G. P. Salam, in A. Levy, S. Forte and G. Ridolfi, editors, “From My Vast Repertoire ...: Guido Altarelli’s Legacy,” 101–121 (2019), [arXiv:1712.05165].
- [486] A. Pich *et al.*, in “13th Conference on Quark Confinement and the Hadron Spectrum (Confinement XIII) Maynooth, Ireland, July 31-August 6, 2018,” (2018), [arXiv:1811.11801].
- [487] S. Aoki *et al.* (Flavour Lattice Averaging Group) (2019), [arXiv:1902.08191].
- [488] M. Beneke and M. Jamin, JHEP **09**, 044 (2008), [arXiv:0806.3156].
- [489] K. Maltman and T. Yavin, Phys. Rev. **D78**, 094020 (2008), [arXiv:0807.0650].
- [490] S. Narison, Phys. Lett. **B673**, 30 (2009), [arXiv:0901.3823].
- [491] I. Caprini and J. Fischer, Eur. Phys. J. **C64**, 35 (2009), [arXiv:0906.5211].
- [492] A. Pich, Prog. Part. Nucl. Phys. **75**, 41 (2014), [arXiv:1310.7922].
- [493] D. Boito *et al.*, Phys. Rev. **D91**, 3, 034003 (2015), [arXiv:1410.3528].
- [494] G. Altarelli, PoS **Corfu2012**, 002 (2013), [arXiv:1303.6065].
- [495] A. Pich and A. Rodríguez-Sánchez, Phys. Rev. **D94**, 3, 034027 (2016), [arXiv:1605.06830].
- [496] M. Davier *et al.*, Eur. Phys. J. **C74**, 3, 2803 (2014), [arXiv:1312.1501].
- [497] D. Boito *et al.*, Phys. Rev. **D98**, 7, 074030 (2018), [arXiv:1805.08176].



- [498] N. Brambilla *et al.*, Phys. Rev. **D75**, 074014 (2007), [hep-ph/0702079].
- [499] V. Mateu and P. G. Ortega, JHEP **01**, 122 (2018), [arXiv:1711.05755].
- [500] C. Peset, A. Pineda and J. Segovia, JHEP **09**, 167 (2018), [arXiv:1806.05197].
- [501] C. Glasman (H1, ZEUS), J. Phys. Conf. Ser. **110**, 022013 (2008), [arXiv:0709.4426].
- [502] T. Biekötter, M. Klasen and G. Kramer, Phys. Rev. **D92**, 7, 074037 (2015), [arXiv:1508.07153].
- [503] J. Blumlein, H. Bottcher and A. Guffanti, Nucl. Phys. **B774**, 182 (2007), [hep-ph/0607200].
- [504] P. Jimenez-Delgado and E. Reya, Phys. Rev. **D89**, 7, 074049 (2014), [arXiv:1403.1852].
- [505] S. Alekhin *et al.*, Phys. Rev. **D96**, 1, 014011 (2017), [arXiv:1701.05838].
- [506] S. Alekhin, J. Blümlein and S. Moch, Eur. Phys. J. **C78**, 6, 477 (2018), [arXiv:1803.07537].
- [507] L. A. Harland-Lang *et al.*, Eur. Phys. J. **C75**, 9, 435 (2015), [arXiv:1506.05682].
- [508] S. Dulat *et al.*, Phys. Rev. **D93**, 3, 033006 (2016), [arXiv:1506.07443].
- [509] R. D. Ball *et al.* (NNPDF), Eur. Phys. J. **C78**, 5, 408 (2018), [arXiv:1802.03398].
- [510] R. S. Thorne and G. Watt, JHEP **08**, 100 (2011), [arXiv:1106.5789].
- [511] S. Alekhin, J. Blumlein and S. Moch, Eur. Phys. J. **C71**, 1723 (2011), [arXiv:1101.5261].
- [512] R. D. Ball *et al.* (NNPDF), Phys. Lett. **B704**, 36 (2011), [arXiv:1102.3182].
- [513] R. D. Ball *et al.* (NNPDF), Phys. Lett. **B723**, 330 (2013), [arXiv:1303.1189].
- [514] R. S. Thorne, PoS **DIS2013**, 042 (2013), [arXiv:1306.3907].
- [515] G. Dissertori *et al.*, JHEP **08**, 036 (2009), [arXiv:0906.3436].
- [516] G. Abbiendi *et al.* (OPAL), Eur. Phys. J. **C71**, 1733 (2011), [arXiv:1101.1470].
- [517] S. Bethke *et al.* (JADE), Eur. Phys. J. **C64**, 351 (2009), [arXiv:0810.1389].
- [518] G. Dissertori *et al.*, Phys. Rev. Lett. **104**, 072002 (2010), [arXiv:0910.4283].
- [519] J. Schieck *et al.* (JADE), Eur. Phys. J. **C73**, 3, 2332 (2013), [arXiv:1205.3714].
- [520] A. Verbitsky *et al.*, JHEP **08**, 129 (2019), [arXiv:1902.08158].
- [521] A. Kardos *et al.*, Eur. Phys. J. **C78**, 6, 498 (2018), [arXiv:1804.09146].
- [522] R. A. Davison and B. R. Webber, Eur. Phys. J. **C59**, 13 (2009), [arXiv:0809.3326].
- [523] R. Abbate *et al.*, Phys. Rev. **D83**, 074021 (2011), [arXiv:1006.3080].
- [524] T. Gehrmann, G. Luisoni and P. F. Monni, Eur. Phys. J. **C73**, 1, 2265 (2013), [arXiv:1210.6945].
- [525] A. H. Hoang *et al.*, Phys. Rev. **D91**, 9, 094018 (2015), [arXiv:1501.04111].
- [526] R. Frederix *et al.*, JHEP **11**, 050 (2010), [arXiv:1008.5313].
- [527] P. Bolzoni, B. A. Kniehl and A. V. Kotikov, Nucl. Phys. **B875**, 18 (2013), [arXiv:1305.6017].
- [528] J. Currie *et al.*, Phys. Rev. Lett. **119**, 15, 152001 (2017), [arXiv:1705.10271].
- [529] M. Czakon *et al.* (2019), [arXiv:1907.12911].
- [530] S. Dittmaier, A. Huss and C. Speckner, JHEP **11**, 095 (2012), [arXiv:1210.0438].
- [531] R. Frederix *et al.*, JHEP **04**, 076 (2017), [arXiv:1612.06548].
- [532] M. Czakon *et al.*, JHEP **10**, 186 (2017), [arXiv:1705.04105].
- [533] M. Johnson and D. Maître, Phys. Rev. **D97**, 5, 054013 (2018), [arXiv:1711.01408].
- [534] A. Gehrmann-De Ridder *et al.*, JHEP **07**, 133 (2016), [arXiv:1605.04295].
- [535] D. Britzger *et al.* (2019), [arXiv:1906.05303].
- [536] T. Affolder *et al.* (CDF), Phys. Rev. Lett. **88**, 042001 (2002), [hep-ex/0108034].
- [537] S. Chekanov *et al.* (ZEUS), Phys. Lett. B **649**, 12 (2007), [hep-ex/0701039].
- [538] V. M. Abazov *et al.* (D0), Phys. Rev. **D80**, 111107 (2009), [arXiv:0911.2710].
- [539] B. Malaescu and P. Starovoitov, Eur. Phys. J. **C72**, 2041 (2012), [arXiv:1203.5416].
- [540] V. Khachatryan *et al.* (CMS), Eur. Phys. J. **C75**, 6, 288 (2015), [arXiv:1410.6765].
- [541] D. Britzger *et al.*, Eur. Phys. J. **C79**, 1, 68 (2019), [arXiv:1712.00480].
- [542] S. Chekanov *et al.* (ZEUS), Eur. Phys. J. **C44**, 183 (2005), [hep-ex/0502007].
- [543] S. Chatrchyan *et al.* (CMS), Eur. Phys. J. **C73**, 10, 2604 (2013), [arXiv:1304.7498].
- [544] V. M. Abazov *et al.* (D0), Phys. Lett. **B718**, 56 (2012), [arXiv:1207.4957].
- [545] V. Khachatryan *et al.* (CMS), Eur. Phys. J. **C75**, 5, 186 (2015), [arXiv:1412.1633].
- [546] V. Andreev *et al.* (H1), Eur. Phys. J. C **77**, 4, 215 (2017), [arXiv:1611.03421].
- [547] M. Baak *et al.* (Gfitter Group), Eur. Phys. J. **C74**, 3046 (2014), [arXiv:1407.3792].
- [548] J. Haller *et al.*, Eur. Phys. J. **C78**, 8, 675 (2018), [arXiv:1803.01853].
- [549] S. Schael *et al.* (ALEPH, DELPHI, L3, OPAL, SLD, LEP Electroweak Working Group, SLD Electroweak Group, SLD Heavy Flavour Group), Phys. Rept. **427**, 257 (2006), [hep-ex/0509008].
- [550] I. Allison *et al.* (HPQCD), Phys. Rev. **D78**, 054513 (2008), [arXiv:0805.2999].
- [551] K. Maltman *et al.*, Phys. Rev. **D78**, 114504 (2008), [arXiv:0807.2020].
- [552] S. Aoki *et al.* (PACS-CS), JHEP **10**, 053 (2009), [arXiv:0906.3906].
- [553] C. McNeile *et al.*, Phys. Rev. **D82**, 034512 (2010), [arXiv:1004.4285].
- [554] E. Shintani *et al.*, Phys. Rev. **D82**, 7, 074505 (2010), [Erratum: Phys. Rev. D89, no.9, 099903(2014)], [arXiv:1002.0371].
- [555] B. Blossier *et al.*, Phys. Rev. **D85**, 034503 (2012), [arXiv:1110.5829].
- [556] A. Bazavov *et al.*, Phys. Rev. **D86**, 114031 (2012), [arXiv:1205.6155].
- [557] B. Blossier *et al.*, Phys. Rev. Lett. **108**, 262002 (2012), [arXiv:1201.5770].
- [558] B. Blossier *et al.* (ETM), Phys. Rev. **D89**, 1, 014507 (2014), [arXiv:1310.3763].
- [559] B. Chakraborty *et al.*, Phys. Rev. **D91**, 5, 054508 (2015), [arXiv:1408.4169].
- [560] A. Bazavov *et al.*, Phys. Rev. **D90**, 7, 074038 (2014), [arXiv:1407.8437].
- [561] K. Nakayama, B. Fahy and S. Hashimoto, Phys. Rev. **D94**, 5, 054507 (2016), [arXiv:1606.01002].
- [562] Y. Maezawa and P. Petreczky, Phys. Rev. **D94**, 3, 034507 (2016), [arXiv:1606.08798].
- [563] M. Bruno *et al.* (ALPHA), Phys. Rev. Lett. **119**, 10, 102001 (2017), [arXiv:1706.03821].

- [564] R. J. Hudspith *et al.* (2018), [arXiv:1804.10286].
- [565] H. Takaura *et al.*, Phys. Lett. **B789**, 598 (2019), [arXiv:1808.01632].
- [566] H. Takaura *et al.*, JHEP **04**, 155 (2019), [arXiv:1808.01643].
- [567] K. Nakayama, H. Fukaya and S. Hashimoto, Phys. Rev. **D98**, 1, 014501 (2018), [arXiv:1804.06695].
- [568] A. Bazavov *et al.* (2019), [arXiv:1907.11747].

## 10. Electroweak Model and Constraints on New Physics

Revised March 2020 by J. Erler (IF-UNAM; U. of Mainz) and A. Freitas (Pittsburg U.).

10.1	Introduction . . . . .	180
10.2	Renormalization and radiative corrections . . . . .	180
10.2.1	The Fermi constant . . . . .	181
10.2.2	The electromagnetic coupling . . . . .	181
10.2.3	Quark masses . . . . .	182
10.2.4	The weak mixing angle . . . . .	182
10.2.5	Radiative corrections . . . . .	183
10.3	Low energy electroweak observables . . . . .	184
10.3.1	Neutrino scattering . . . . .	184
10.3.2	Parity violating lepton scattering . . . . .	185
10.3.3	Atomic parity violation . . . . .	186
10.4	Precision flavor physics . . . . .	187
10.4.1	The $\tau$ lifetime . . . . .	187
10.4.2	The muon anomalous magnetic moment . . . . .	187
10.5	Physics of the massive electroweak bosons . . . . .	188
10.5.1	Electroweak physics off the $Z$ pole . . . . .	189
10.5.2	$Z$ pole physics . . . . .	189
10.5.3	$W$ and $Z$ decays . . . . .	190
10.6	Global fit results . . . . .	192
10.7	Constraints on new physics . . . . .	194

### 10.1 Introduction

The standard model of the electroweak interactions (SM) [1–4] is based on the gauge group  $SU(2) \times U(1)$ , with gauge bosons  $W_\mu^i$ ,  $i = 1, 2, 3$ , and  $B_\mu$  for the  $SU(2)$  and  $U(1)$  factors, respectively, and the corresponding gauge coupling constants  $g$  and  $g'$ . The left-handed fermion fields of the  $i^{\text{th}}$  fermion family transform as doublets  $\Psi_i = \begin{pmatrix} \nu_i \\ d_i' \end{pmatrix}$  and  $\begin{pmatrix} u_i \\ d_i' \end{pmatrix}$  under  $SU(2)$ , where  $d_i' \equiv \sum_j V_{ij} d_j$ , and  $V$  is the Cabibbo-Kobayashi-Maskawa mixing [5, 6] matrix<sup>1</sup>. The right-handed fields are  $SU(2)$  singlets. From Higgs and electroweak precision data it is known that there are precisely three sequential fermion families.

A complex scalar Higgs doublet,  $\phi$ , is added to the model for mass generation through spontaneous symmetry breaking with potential<sup>2</sup> given by,

$$V(\phi) = \mu^2 \phi^\dagger \phi + \frac{\lambda^2}{2} (\phi^\dagger \phi)^2, \quad \phi \equiv \begin{pmatrix} \phi^+ \\ \phi^0 \end{pmatrix}. \quad (10.1)$$

For  $\mu^2$  negative,  $\phi$  develops a vacuum expectation value,  $v/\sqrt{2} = |\mu|/\lambda$ , where  $v = 246.22$  GeV, breaking part of the electroweak (EW) gauge symmetry, after which only one neutral Higgs scalar,  $H$ , remains in the physical particle spectrum. In non-minimal models there are additional charged and neutral scalar Higgs particles. Higgs boson physics is reviewed in the Section on the ‘‘Status of Higgs Boson Physics’’ in this *Review*.

After symmetry breaking the Lagrangian for the fermion fields,

$\psi_i$ , is

$$\begin{aligned} \mathcal{L}_F = & \sum_i \bar{\psi}_i \left( i \not{\partial} - m_i - \frac{m_i H}{v} \right) \psi_i \\ & - \frac{g}{2\sqrt{2}} \sum_i \bar{\Psi}_i \gamma^\mu (1 - \gamma^5) (T^+ W_\mu^+ + T^- W_\mu^-) \Psi_i \\ & - e \sum_i Q_i \bar{\psi}_i \gamma^\mu \psi_i A_\mu \\ & - \frac{g}{2 \cos \theta_W} \sum_i \bar{\psi}_i \gamma^\mu (g_V^i - g_A^i \gamma^5) \psi_i Z_\mu. \end{aligned} \quad (10.2)$$

Here  $\theta_W \equiv \tan^{-1}(g'/g)$  is the weak mixing angle and  $e = g \sin \theta_W$  is the positron electric charge. Furthermore,

$$A_\mu \equiv B_\mu \cos \theta_W + W_\mu^3 \sin \theta_W, \quad (10.3a)$$

$$W_\mu^\pm \equiv \frac{W_\mu^1 \mp i W_\mu^2}{\sqrt{2}}, \quad (10.3b)$$

$$Z_\mu \equiv -B_\mu \sin \theta_W + W_\mu^3 \cos \theta_W, \quad (10.3c)$$

are the photon field ( $\gamma$ ) and the charged ( $W^\pm$ ) and neutral ( $Z$ ) weak boson fields, respectively.

The Yukawa coupling of  $H$  to  $\psi_i$  in the first term in  $\mathcal{L}_F$ , which is flavor diagonal in the minimal model, is  $gm_i/2M_W$ . The boson masses in the EW sector are given (at tree level, *i.e.*, to lowest order in perturbation theory) by,

$$M_H = \lambda v, \quad (10.4a)$$

$$M_W = \frac{gv}{2} = \frac{ev}{2 \sin \theta_W}, \quad (10.4b)$$

$$M_Z = \sqrt{g^2 + g'^2} \frac{v}{2} = \frac{ev}{2 \sin \theta_W \cos \theta_W}, \quad (10.4c)$$

$$M_\gamma = 0. \quad (10.4d)$$

The second term in  $\mathcal{L}_F$  represents the charged-current weak interaction [8–10], where  $T^+$  and  $T^-$  are the weak isospin raising and lowering operators. For example, the coupling of a  $W$  to an electron and a neutrino is

$$-\frac{e}{2\sqrt{2} \sin \theta_W} \left[ W_\mu^- \bar{e} \gamma^\mu (1 - \gamma^5) \nu + W_\mu^+ \bar{\nu} \gamma^\mu (1 - \gamma^5) e \right]. \quad (10.5)$$

For momenta small compared to  $M_W$ , this term gives rise to the effective four-fermion interaction with the Fermi constant given by  $G_F/\sqrt{2} = 1/2v^2 = g^2/8M_W^2$ . CP violation is incorporated into the EW model by a single observable phase in  $V_{ij}$ .

The third term in  $\mathcal{L}_F$  describes electromagnetic interactions (QED) [11, 12], and the last is the weak neutral-current interaction [9, 10, 13]. The vector and axial-vector couplings are

$$g_V^i \equiv t_{3L}(i) - 2Q_i \sin^2 \theta_W, \quad (10.6a)$$

$$g_A^i \equiv t_{3L}(i), \quad (10.6b)$$

where  $t_{3L}(i)$  is the weak isospin of fermion  $i$  ( $+1/2$  for  $u_i$  and  $\nu_i$ ;  $-1/2$  for  $d_i$  and  $e_i$ ) and  $Q_i$  is the charge of  $\psi_i$  in units of  $e$ .

The first term in Eq. (10.2) also gives rise to fermion masses, and in the presence of right-handed neutrinos to Dirac neutrino masses. The possibility of Majorana masses is discussed in the Section on ‘‘Neutrino Mass, Mixing, and Oscillations’’ in this *Review*.

### 10.2 Renormalization and radiative corrections

In addition to the Higgs boson mass,  $M_H$ , the fermion masses and mixings, and the strong coupling constant,  $\alpha_s$ , the SM has three parameters. The set with the smallest experimental errors contains the  $Z$  mass<sup>3</sup>, the Fermi constant, and the fine structure

<sup>3</sup>We emphasize that in the fits described in Sec. 10.6 and Sec. 10.7 the values of the SM parameters are affected by all observables that depend on

<sup>1</sup>Constraints on  $V$  and tests of universality are discussed in Ref. [7] and in the Section on the ‘‘CKM Quark-Mixing Matrix’’ in this *Review*. The extension of the formalism to allow an analogous leptonic mixing matrix is discussed in the Section on ‘‘Neutrino Masses, Mixing, and Oscillations’’ in this *Review*.

<sup>2</sup>There is no generally accepted convention to write the quartic term. Our numerical coefficient simplifies Eq. (10.4a) below and the squared coupling preserves the relation between the number of external legs and the power counting of couplings at a given loop order. This structure also naturally emerges from physics beyond the SM, such as Supersymmetry.

constant, to be discussed in turn (the numerical values quoted in Sections 10.2–10.4 correspond to the main fit result in Table 10.7).

The  $Z$  boson mass,  $M_Z = 91.1876 \pm 0.0021$  GeV, has been determined from the  $Z$  lineshape scan at LEP 1 [14]. This value of  $M_Z$  corresponds to a definition based on a Breit-Wigner shape with an energy-dependent width<sup>4</sup> (see the Section on the “ $Z$  Boson” in this *Review*).

### 10.2.1 The Fermi constant

The Fermi constant,  $G_F = 1.1663787(6) \times 10^{-5}$  GeV<sup>-2</sup>, is derived from the  $\mu$  lifetime formula<sup>5</sup>,

$$\frac{\hbar}{\tau_\mu} = \frac{G_F^2 m_\mu^5}{192\pi^3} F(\rho) \left[ 1 + H_1(\rho) \frac{\hat{\alpha}(m_\mu)}{\pi} + H_2(\rho) \frac{\hat{\alpha}^2(m_\mu)}{\pi^2} \right], \quad (10.7)$$

where  $\rho = m_e^2/m_\mu^2$ , and where

$$F(\rho) = 1 - 8\rho + 8\rho^3 - \rho^4 - 12\rho^2 \ln \rho = 0.99981295, \quad (10.8a)$$

$$\begin{aligned} H_1(\rho) &= \frac{25}{8} - \frac{\pi^2}{2} - (9 + 4\pi^2 + 12 \ln \rho) \rho + 16\pi^2 \rho^{3/2} + \mathcal{O}(\rho^2) \\ &= -1.80793, \end{aligned} \quad (10.8b)$$

$$\begin{aligned} H_2(\rho) &= \frac{156815}{5184} - \frac{518}{81} \pi^2 - \frac{895}{36} \zeta(3) + \frac{67}{720} \pi^4 + \frac{53}{6} \pi^2 \ln 2 \\ &\quad - (0.042 \pm 0.002)_{\text{had}} - \frac{5}{4} \pi^2 \sqrt{\rho} + \mathcal{O}(\rho) = 6.64, \end{aligned} \quad (10.8c)$$

$$\hat{\alpha}(m_\mu)^{-1} = \alpha^{-1} + \frac{1}{3\pi} \ln \rho + \mathcal{O}(\alpha) = 135.901. \quad (10.8d)$$

$H_1$  and  $H_2$  capture the QED corrections within the Fermi model. The results for  $\rho = 0$  have been obtained in Refs. [16] and [17, 18] for  $H_1$  and  $H_2$ , respectively, where the term in parentheses is from the hadronic vacuum polarization [17]. The mass corrections to  $H_1$  have been known for some time [19], while those to  $H_2$  are more recent [20]. Notice the term linear in  $m_e$  whose appearance was unforeseen and can be traced to the use of the muon pole mass in the prefactor [20]. The remaining uncertainty in  $G_F$  is mostly experimental and has been reduced by an order of magnitude by the MuLan collaboration [15] at the PSI.

### 10.2.2 The electromagnetic coupling

The fine structure constant,  $\alpha$ , can be extracted from the  $e^\pm$  anomalous magnetic moment [21],  $a_e = (1159652180.91 \pm 0.26) \times 10^{-12}$  [22], which gives the value  $\alpha^{-1} = 137.035999150(33)$ . Another approach combines measurements of the Rydberg constant and atomic masses with interferometry of atomic recoil kinematics. Applied to  $^{87}\text{Rb}$  [23] and  $^{133}\text{Cs}$  [24], this method implies the results  $\alpha^{-1} = 137.035998997(85)$  and  $\alpha^{-1} = 137.035999047(28)$ , respectively, which can be combined to give  $\alpha^{-1} = 137.035999042(26)$ . Finally, combining the anomalous magnetic moment and atomic interferometry methods leads to the world average of  $\alpha^{-1} = 137.035999084(21)$ , but notice that they also show a  $2.6 \sigma$  discrepancy. If this is interpreted as due to physics beyond the SM (BSM), the new physics would contribute to  $a_e$  with opposite sign compared to the  $\mu^\pm$  anomalous magnetic moment,  $a_\mu$ , to be discussed in Section 10.4.2.

In most EW renormalization schemes, it is convenient to define a running  $\alpha$  dependent on the energy scale of the process, with

them. This is of no practical consequence for  $\alpha$  and  $G_F$ , however, since they are very precisely known.

<sup>4</sup>The theoretically consistent and gauge-invariant definition of the  $Z$ -boson mass through the complex pole of the propagator would instead lead to a Breit-Wigner with a constant width. The two definitions differ numerically, and this difference has to be accounted for in theoretical calculations.

<sup>5</sup>In the spirit of the Fermi theory, we incorporated the small propagator correction,  $3/5 m_\mu^2/M_W^2$ , into  $\Delta r$  (see below). This is also the convention adopted by the MuLan collaboration [15]. While this breaks with historical consistency, the numerical difference was negligible in the past.

$\alpha^{-1} \approx 137.036$  appropriate at very low energy, *i.e.* close to the Thomson limit. The OPAL [25] and L3 [26] collaborations at LEP could also observe the running directly in small and large angle Bhabha scattering, respectively. For scales above a few hundred MeV the low energy hadronic contribution to vacuum polarization introduces a theoretical uncertainty in  $\alpha$ . In the modified minimal subtraction ( $\overline{\text{MS}}$ ) scheme<sup>6</sup> [27] (used for this *Review*), and with  $\alpha_s(M_Z) = 0.1185 \pm 0.0016$  we have  $\hat{\alpha}^{(4)}(m_\tau)^{-1} = 133.472 \pm 0.007$  and  $\hat{\alpha}^{(5)}(M_Z)^{-1} = 127.952 \pm 0.009$ . The latter corresponds to a quark sector contribution (without the top) to the conventional (on-shell) QED coupling,

$$\alpha(M_Z) = \frac{\alpha}{1 - \Delta\alpha(M_Z)}, \quad (10.9)$$

of  $\Delta\alpha_{\text{had}}^{(5)}(M_Z) = 0.02766 \pm 0.00007$ . These values are updated from Ref. [28] with  $\Delta\alpha_{\text{had}}^{(5)}(M_Z)$  moved downwards and its uncertainty reduced (partly due to a more precise charm quark mass). Its correlation with  $a_\mu$ , as well as the non-linear  $\alpha_s$  dependence of  $\hat{\alpha}(M_Z)$  and the resulting correlation with the input variable  $\alpha_s$ , are fully taken into account in the fits. This is done by using as actual input (fit constraint) instead of  $\Delta\alpha_{\text{had}}^{(5)}(M_Z)$  the low energy contribution by the three light quarks,  $\Delta\alpha_{\text{had}}^{(3)}(2.0 \text{ GeV}) = (58.84 \pm 0.51) \times 10^{-4}$  [29], and by calculating the perturbative and heavy quark contributions to  $\hat{\alpha}(M_Z)$  in each call of the fits according to [28]. Part of the error ( $\pm 0.37 \times 10^{-4}$ ) is from  $e^+e^-$  annihilation data below 2 GeV, as well as isospin rotated data from  $\tau$  decays into two- and four-pion final states [30] (including uncertainties from isospin breaking effects [31]), but uncalculated higher order perturbative ( $\pm 0.21 \times 10^{-4}$ ) and non-perturbative ( $\pm 0.28 \times 10^{-4}$  [29]) QCD corrections and the  $\overline{\text{MS}}$  quark mass values (see below) also contribute. Various evaluations of  $\Delta\alpha_{\text{had}}^{(5)}(M_Z)$  are summarized in Table 10.1, where the relation<sup>7</sup> between the  $\overline{\text{MS}}$  and on-shell definitions (obtained using Ref [34]) is given by,

$$\begin{aligned} \Delta\hat{\alpha}(M_Z) &= \Delta\alpha(M_Z) + \frac{\alpha}{\pi} \left[ \frac{100}{27} - \frac{1}{6} - \frac{7}{4} \ln \frac{M_Z^2}{M_W^2} \right. \\ &\quad \left. + \frac{\alpha_s(M_Z)}{\pi} \left( \frac{605}{108} - \frac{44}{9} \zeta(3) \right) \right. \\ &\quad \left. + \frac{\alpha_s^2}{\pi^2} \left( \frac{976481}{23328} - \frac{253}{36} \zeta(2) - \frac{781}{18} \zeta(3) + \frac{275}{27} \zeta(5) \right) \right] \\ &= 0.007127(2), \end{aligned} \quad (10.10)$$

and where the first entry of the lowest order term is from fermions and the other two are from  $W^\pm$  loops, which are usually excluded from the on-shell definition. Fermion mass effects and corrections of  $\mathcal{O}(\alpha\alpha_s^3)$  and  $\mathcal{O}(\alpha^2)$  contributing to Eq. (10.10) are small, partly cancel each other and are not included here. The most recent results on  $\Delta\alpha_{\text{had}}^{(5)}(M_Z)$  [29, 35–37] typically assume the validity of perturbative QCD (PQCD) at scales of  $\sim 2$  GeV or above and are in good agreement with each other. In regions where PQCD is not trusted, one can use  $e^+e^- \rightarrow$  hadrons cross-section data and  $\tau$  decay spectral functions [38], where the latter derive from OPAL [39], CLEO [40], ALEPH [41], and Belle [42]. Recently, new data for various  $e^+e^- \rightarrow$  hadrons channels was obtained from BaBar, BES III, CLEO, the SND and CMD-3 experiments at VEPP-2000, and the KEDR experiments at VEPP-4M (for a list of references see, *e.g.*, Ref. [29]). While VEPP-2000 and VEPP-4M scanned center-of-mass (CM) energies up to 2 GeV and between about 3 and 4 GeV, respectively, the BaBar collaboration studied multi-hadron events radiatively returned from the  $\Upsilon(4S)$ ,

<sup>6</sup>In this Section we denote quantities defined in the  $\overline{\text{MS}}$  scheme by a caret; the exception is the strong coupling constant,  $\alpha_s$ , which will always correspond to the  $\overline{\text{MS}}$  definition and where the caret will be dropped.

<sup>7</sup>In practice,  $\alpha(M_Z)$  is directly evaluated in the  $\overline{\text{MS}}$  scheme using the FORTRAN package GAPP [32], including the QED contributions of both leptons and quarks. The leptonic three-loop contribution in the on-shell scheme has been obtained in Ref. [33].

reconstructing the radiated photon and normalizing to  $\mu^\pm\gamma$  final states. The precision of these results generally exceeds those from  $\tau$  decays. There are significant discrepancies between the older (CMD-2) and newer (CMD-3) measurements of  $e^+e^- \rightarrow K^+K^-$ , which could be due to difficulties in determining the detection efficiency of low-momentum kaons. The radiative return data from BaBar is expected to be more reliable for this channel owing to an additional boost of the final-state hadrons.

### 10.2.3 Quark masses

Further free parameters entering into Eq. (10.2) are the quark and lepton masses, where  $m_i$  is the mass of the  $i^{\text{th}}$  fermion  $\psi_i$ . For the light quarks, as described in the Section on “Quark Masses” in this Review,  $\widehat{m}_u = 2.16_{-0.26}^{+0.49}$  MeV,  $\widehat{m}_d = 4.67_{-0.17}^{+0.48}$  MeV, and  $\widehat{m}_s = 93_{-5}^{+11}$  MeV. These are running  $\overline{\text{MS}}$  masses evaluated at the scale  $\mu = 2$  GeV. For the charm mass we use the constraint [51],

$$\widehat{m}_c(\widehat{m}_c) = 1274 \pm 8 + 2616[\alpha_s(M_Z) - 0.1182] \text{ MeV}, \quad (10.11)$$

which is based on QCD sum rules [52, 53], and recalculate  $\widehat{m}_c$  in each call of our fits to account for its  $\alpha_s$  dependence. Similarly, for the bottom quark mass we use,

$$\widehat{m}_b(\widehat{m}_b) = 4180 \pm 8 + 108[\alpha_s(M_Z) - 0.1182] \text{ MeV}, \quad (10.12)$$

with a theoretical correlation of about 60% arising mostly from the PQCD truncation uncertainty which is similar for  $\widehat{m}_c(\widehat{m}_c)$  and  $\widehat{m}_b(\widehat{m}_b)$ . To improve the precisions in  $\widehat{m}_c(\widehat{m}_c)$  and  $\widehat{m}_b(\widehat{m}_b)$  in the future it would help to remeasure the threshold regions of the heavy quarks, as well as the electronic decay widths of the narrow  $c\bar{c}$  and  $b\bar{b}$  resonances.

The top quark “pole” mass (the quotation marks are a reminder that the experiments do not strictly measure the pole mass and that quarks do not form asymptotic states), has been kinematically reconstructed by the Tevatron collaborations, CDF and DØ, in leptonic, hadronic, and mixed channels with the result  $m_t = 174.30 \pm 0.35_{\text{stat.}} \pm 0.54_{\text{syst.}}$  GeV [54]. Likewise, using data from CM energies  $\sqrt{s} = 7$  and 8 TeV (Run 1), ATLAS and CMS (including alternative technique measurements) at the LHC obtained  $m_t = 172.69 \pm 0.25_{\text{stat.}} \pm 0.41_{\text{syst.}}$  GeV [55] and  $m_t = 172.43 \pm 0.13_{\text{stat.}} \pm 0.46_{\text{syst.}}$  GeV [56], respectively. In addition, there are first results with  $\sqrt{s} = 13$  TeV data (Run 2). CMS obtained  $m_t = 172.26 \pm 0.07_{\text{mostly stat.}} \pm 0.61_{\text{syst.}}$  GeV [57] in the lepton + jets and all-jets channels, and  $m_t = 172.33 \pm 0.14_{\text{stat.}} \pm 0.69_{\text{syst.}}$  GeV [58] in the di-lepton channel. Using a leptonic invariant mass and thus featuring reduced correlation with the more traditional analysis approaches, ATLAS quotes  $m_t = 174.48 \pm 0.40_{\text{stat.}} \pm 0.67_{\text{syst.}}$  GeV [59] from the lepton + jets channel. While there seems to be generally good agreement between all these measurements, we observe a  $2.8\sigma$  discrepancy (or more in case of correlated systematics) between the two most precise determinations,  $174.98 \pm 0.76$  GeV [60] (by the DØ collaboration) and  $172.25 \pm 0.63$  GeV [61] (by the CMS collaboration), both from the lepton + jets channels. In addition, the latter is also  $2.2\sigma$  lower than the preliminary result of Ref. [59]. Assuming a systematic error component of 0.17 GeV (the QCD, PDF and Monte Carlo type errors at ATLAS at Run 1) is common to all six results, we arrive at the combination,

$$m_t = 172.89 \pm 0.28_{\text{exp.}} \text{ GeV} + \Delta m_{\text{MC}}, \quad (10.13)$$

where  $\Delta m_{\text{MC}}$  is defined to account for any difference between the top pole mass,  $m_t$ , and the mass parameter implemented in the Monte Carlo event generators employed by the experimental groups.  $\Delta m_{\text{MC}}$  is expected to be of order  $\alpha_s(Q_0)Q_0$  with a low scale  $Q_0 \sim \mathcal{O}(1 \text{ GeV})$  [62], but its value is unknown in hadron collider environments so that we will treat it as an uncertainty instead, and choose for definiteness  $Q_0 = \Gamma_t = 1.42$  GeV to arrive at  $\Delta m_{\text{MC}} = 0 \pm 0.52$  GeV. We further assume that an uncertainty [63] of  $\pm 0.32$  GeV in the relation [64] between  $m_t$  and the  $\overline{\text{MS}}$  definition,  $\widehat{m}_t(\widehat{m}_t)$ , entering electroweak radiative correction libraries, including the renormalon ambiguity [65], is already included in  $\Delta m_{\text{MC}}$ , as  $m_t$  merely serves as an intermediate book-keeping device in Ref. [62]. A promising future direction to arrive

at a competitive independent constraint on  $m_t$  is to analyze differential top quark pair production cross-sections at next-to-next-to-leading order (NNLO) [66], as  $m_t$  extraction based on them are easier to interpret, and experimentally they have become much more precise recently [67, 68]. The combination in Eq. (10.13) differs slightly from the average,  $m_t = 172.9 \pm 0.4_{\text{exp.}}$  GeV, which appears in the Top Quark Listings in this Review, as its uncertainty has been scaled up by a factor of 1.3. For more details and references, see the Section on the “Top Quark” and the Quarks Listings in this Review.

### 10.2.4 The weak mixing angle

The observables  $\sin^2\theta_W$  and  $M_W$  can be calculated from  $M_Z$ ,  $\widehat{\alpha}(M_Z)$ , and  $G_F$ , when values for  $m_t$  and  $M_H$  are given, or conversely,  $M_H$  can be constrained by  $\sin^2\theta_W$  and  $M_W$ . The value of  $\sin^2\theta_W$  is extracted from neutral-current processes (see Sec. 10.3) and  $Z$  pole observables (see Sec. 10.5.3) and depends on the renormalization prescription. There are a number of popular schemes [9] leading to values which differ by small factors depending on  $m_t$  and  $M_H$ . The notation for these schemes is shown in Table 10.2.

- (i) The on-shell scheme [70] promotes the tree-level formula  $\sin^2\theta_W = 1 - M_W^2/M_Z^2$  to a definition of the renormalized  $\sin^2\theta_W$  to all orders in perturbation theory, *i.e.*,

$$\sin^2\theta_W \rightarrow s_W^2 \equiv 1 - \frac{M_W^2}{M_Z^2}, \quad (10.14a)$$

$$M_W = \frac{A_0}{s_W(1 - \Delta r)^{1/2}}, \quad M_Z = \frac{M_W}{c_W}, \quad (10.14b)$$

where  $c_W \equiv \cos\theta_W$ ,  $A_0 = (\pi\alpha/\sqrt{2}G_F)^{1/2} = 37.28038(1)$  GeV, and  $\Delta r$  includes the radiative corrections relating  $\alpha$ ,  $\alpha(M_Z)$ ,  $G_F$ ,  $M_W$ , and  $M_Z$ . One finds  $\Delta r \sim \Delta r_0 - \rho_t \tan^{-2}\theta_W$ , where  $\Delta r_0 = 1 - \alpha/\widehat{\alpha}(M_Z) = 0.06629(7)$  is due to the running of  $\alpha$ , and

$$\rho_t = \frac{3G_F m_t^2}{8\sqrt{2}\pi^2} = 0.00937 \times \frac{m_t^2}{(172.89 \text{ GeV})^2}, \quad (10.15)$$

represents the dominant (quadratic)  $m_t$  dependence. There are additional contributions to  $\Delta r$  from bosonic loops, including those which depend logarithmically on  $M_H$  and higher-order corrections<sup>8</sup>. One has  $\Delta r = 0.03652 \mp 0.00021 \pm 0.00007$ , where the first uncertainty is from  $m_t$  and the second is from  $\alpha(M_Z)$ . Thus the value of  $s_W^2$  extracted from  $M_Z$  includes an uncertainty ( $\mp 0.00007$ ) from the currently allowed range of  $m_t$ . This scheme is simple conceptually. However, the relatively large ( $\sim 3\%$ ) correction from  $\rho_t$  causes large spurious contributions in higher orders.  $s_W^2$  depends not only on the gauge couplings but also on the spontaneous-symmetry breaking, and it is awkward in the presence of any extension of the SM which perturbs the value of  $M_Z$  (or  $M_W$ ). Other definitions are motivated by the tree-level coupling constant definition  $\theta_W = \tan^{-1}(g'/g)$ :

- (ii) In particular, the  $\overline{\text{MS}}$  scheme introduces the quantity,

$$\sin^2\widehat{\theta}_W(\mu) \equiv \frac{\widehat{g}'^2(\mu)}{\widehat{g}^2(\mu) + \widehat{g}'^2(\mu)}, \quad (10.16)$$

where the couplings  $\widehat{g}$  and  $\widehat{g}'$  are defined by modified minimal subtraction and the scale  $\mu$  is conveniently chosen to be  $M_Z$  for many EW processes. The value of  $\widehat{s}_Z^2 \equiv \sin^2\widehat{\theta}_W(M_Z)$  extracted from  $M_Z$  is less sensitive than  $s_W^2$  to  $m_t$  (by a factor of  $\tan^2\theta_W$ ), and is less sensitive to most types of new physics. It is also very useful for comparing with the predictions of grand unification. There are actually several variant definitions of  $\sin^2\widehat{\theta}_W(M_Z)$ , differing according

<sup>8</sup>All explicit numbers quoted here and below include the two- and three-loop corrections described near the end of Sec. 10.2.

**Table 10.1:** Evaluations of the on-shell  $\Delta\alpha_{\text{had}}^{(5)}(M_Z)$  by different groups (for a more complete list of evaluations see the 2012 edition of this *Review*). For better comparison we adjusted central values and errors to correspond to a common and fixed value of  $\alpha_s(M_Z) = 0.120$ . References quoting results without the top quark decoupled are converted to the five flavor definition. Ref. [43] uses  $\Lambda_{\text{QCD}} = 380 \pm 60$  MeV; for the conversion we assumed  $\alpha_s(M_Z) = 0.118 \pm 0.003$ .

Reference	Result	Comment
Geshkenbein, Morgunov [44]	$0.02780 \pm 0.00006$	$\mathcal{O}(\alpha_s)$ resonance model
Swartz [45]	$0.02754 \pm 0.00046$	use of fitting function
Krasnikov, Rodenberg [46]	$0.02737 \pm 0.00039$	PQCD for $\sqrt{s} > 2.3$ GeV
Kühn & Steinhauser [47]	$0.02778 \pm 0.00016$	full $\mathcal{O}(\alpha_s^2)$ for $\sqrt{s} > 1.8$ GeV
Groote <i>et al.</i> [43]	$0.02787 \pm 0.00032$	use of QCD sum rules
Martin <i>et al.</i> [48]	$0.02741 \pm 0.00019$	incl. new BES data
de Troconiz, Yndurain [49]	$0.02754 \pm 0.00010$	PQCD for $s > 2$ GeV <sup>2</sup>
Burkhardt, Pietrzyk [50]	$0.02750 \pm 0.00033$	PQCD for $\sqrt{s} > 12$ GeV
Erlar, Ferro-Hernández [35]	$0.02761 \pm 0.00010$	conv. from $\overline{\text{MS}}$ scheme
Jegerlehner [36]	$0.02755 \pm 0.00013$	Euclidean split technique
Davier <i>et al.</i> [29]	$0.02760 \pm 0.00010$	PQCD for $\sqrt{s} = 1.8\text{--}3.7$ & $> 5$ GeV
Keshavarzi <i>et al.</i> [37]	$0.02761 \pm 0.00011$	PQCD for $\sqrt{s} > 11.2$ GeV

**Table 10.2:** Notations used to indicate the various schemes discussed in the text. Each definition of  $\sin^2\theta_W$  leads to values that differ by small factors depending on  $m_t$  and  $M_H$ . Numerical values and the uncertainties induced by the imperfectly known SM parameters and unknown higher orders [69] are also given for illustration.

Scheme	Notation	Value	Uncertainty
On-shell	$s_W^2$	0.22337	$\pm 0.00010$
$\overline{\text{MS}}$	$\widehat{s}_Z^2$	0.23121	$\pm 0.00004$
$\overline{\text{MS}}_{\text{ND}}$	$\widehat{s}_{\text{ND}}^2$	0.23141	$\pm 0.00004$
$\overline{\text{MS}}$	$\widehat{s}_0^2$	0.23857	$\pm 0.00005$
Effective angle	$\widehat{s}_\ell^2$	0.23153	$\pm 0.00004$

to whether or how finite  $\alpha \ln(m_t/M_Z)$  terms are decoupled (subtracted from the couplings). One cannot entirely decouple the  $\alpha \ln(m_t/M_Z)$  terms from all EW quantities because  $m_t \gg m_b$  breaks SU(2) symmetry. The scheme that will be adopted here decouples the  $\alpha \ln(m_t/M_Z)$  terms from the  $\gamma$ - $Z$  mixing [27, 71], essentially eliminating any  $\ln(m_t/M_Z)$  dependence in the formulae for asymmetries at the  $Z$  pole when written in terms of  $\widehat{s}_Z^2$ . (A similar definition is used for  $\widehat{\alpha}$ .) The on-shell and  $\overline{\text{MS}}$  definitions are related by

$$\widehat{s}_Z^2 = c(m_t, M_H) s_W^2 = (1.0351 \pm 0.0003) s_W^2. \quad (10.17)$$

The quadratic  $m_t$  dependence is given by  $c \sim 1 + \rho_t / \tan^2\theta_W$ . The expressions for  $M_W$  and  $M_Z$  in the  $\overline{\text{MS}}$  scheme are

$$M_W = \frac{A_0}{\widehat{s}_Z(1 - \Delta\widehat{r}_W)^{1/2}}, \quad M_Z = \frac{M_W}{\widehat{\rho}^{1/2} \widehat{c}_Z}, \quad (10.18)$$

and one predicts  $\Delta\widehat{r}_W = 0.06918 \pm 0.00007$ .  $\Delta\widehat{r}_W$  has no quadratic  $m_t$  dependence, because shifts in  $M_W$  are absorbed into the observed  $G_F$ , so that the error in  $\Delta\widehat{r}_W$  is almost entirely due to  $\Delta r_0 = 1 - \alpha/\widehat{\alpha}(M_Z)$ . The quadratic  $m_t$  dependence has been shifted into  $\widehat{\rho} \sim 1 + \rho_t$ , where including bosonic loops,  $\widehat{\rho} = 1.01019 \pm 0.00009$ .

- (iii) A variant  $\overline{\text{MS}}$  quantity  $\widehat{s}_{\text{ND}}^2$  (used in the 1992 edition of this *Review*) does not decouple the  $\alpha \ln(m_t/M_Z)$  terms [72]. It is related to  $\widehat{s}_Z^2$  by

$$\widehat{s}_Z^2 = \frac{\widehat{s}_{\text{ND}}^2}{1 + \frac{\alpha}{\pi} d}, \quad (10.19)$$

$$d = \frac{1}{3} \left( \frac{1}{\widehat{s}^2} - \frac{8}{3} \right) \left[ \left( 1 + \frac{\alpha_s}{\pi} \right) \ln \frac{m_t}{M_Z} - \frac{15\alpha_s}{8\pi} \right].$$

Thus,  $\widehat{s}_Z^2 - \widehat{s}_{\text{ND}}^2 = -0.0002$ .

- (iv) Some of the low-energy experiments discussed in the next section are sensitive to the weak mixing angle at almost vanishing momentum transfer [35, 73–75]. Thus, Table 10.2 also includes  $\widehat{s}_0^2 \equiv \sin^2\widehat{\theta}_W(0)$ .

- (v) Yet another definition, the effective angle [76, 77],  $\widehat{s}_f^2 \equiv \sin^2\theta_{\text{eff}}^f$ , for the  $Z$  vector coupling to fermion  $f$ , is based on  $Z$  pole observables and described in Sec. 10.5.

### 10.2.5 Radiative corrections

Experiments are at such level of precision [69] that complete one-loop, dominant two-loop, and partial three and four-loop radiative corrections must be applied. For neutral-current and  $Z$  pole processes, these corrections are conveniently divided into two classes:

1. QED diagrams involving the emission of real photons or the exchange of virtual photons in loops, but not including vacuum polarization diagrams. These graphs often yield finite and gauge-invariant contributions to observable processes. However, they are dependent on energies, experimental cuts, *etc.*, and must be calculated individually for each experiment.
2. EW corrections, including  $\gamma\gamma$ ,  $\gamma Z$ ,  $ZZ$ , and  $WW$  vacuum polarization diagrams, as well as vertex corrections, box graphs, *etc.*, involving virtual  $W$  and  $Z$  bosons. One-loop corrections [78] are included for all processes, and many two-loop corrections are also important. In particular, two-loop corrections involving the top quark modify  $\rho_t$  in  $\widehat{\rho}$ ,  $\Delta r$ , and elsewhere by

$$\rho_t \rightarrow \rho_t \left[ 1 + R(M_H, m_t) \frac{\rho_t}{3} \right]. \quad (10.20)$$

$R(M_H, m_t)$  can be described as an expansion in  $M_Z^2/m_t^2$ , for which the leading  $m_t^4/M_Z^4$  [79, 80] and next-to-leading  $m_t^2/M_Z^2$  [81, 82] terms are known. The complete two-loop calculation of  $\Delta r$  (without further approximation) has been performed in Refs. [83–87]. More recently, Ref. [88] obtained

the  $\overline{\text{MS}}$  quantities  $\Delta\widehat{\nu}_W$  and  $\widehat{\rho}$  to two-loop accuracy, confirming the prediction of  $M_W$  in the on-shell scheme from Refs. [85, 89] within about 4 MeV. Similarly, the EW two-loop corrections for the relation between  $\widehat{s}_{\ell,b}^2$  and  $s_W^2$  are known [90–95], as well as for the partial decay and total decay widths and the effective couplings of the  $Z$  boson [96–99]. For  $\widehat{s}_{s,c}$  only two-loop corrections from diagrams with closed fermion loops are available [100], but given the experimental precision this is more than adequate.

The mixed QCD-EW contributions to gauge boson self-energies of order  $\alpha\alpha_s m_t^2$  [101, 102],  $\alpha\alpha_s^2 m_t^2$  [103, 104], and  $\alpha\alpha_s^3 m_t^2$  [105–107] increase the predicted value of  $m_t$  by 6%. This is, however, almost entirely an artifact of using the pole mass definition for  $m_t$ . The equivalent corrections when using the  $\overline{\text{MS}}$  definition  $\widehat{m}_t$  increase  $m_t$  by less than 0.5%. The sub-leading  $\alpha\alpha_s$  corrections [108–111] are also included. Further three-loop corrections of order  $\alpha\alpha_s^2$  [112, 113],  $\alpha^3 m_t^6$ , and  $\alpha^2\alpha_s m_t^4$  [114, 115], are rather small. The same is true for  $\alpha^3 M_H^4$  [116] corrections unless  $M_H$  approaches 1 TeV. The theoretical uncertainty from unknown higher-order corrections [69] is estimated to amount to 4 MeV for the prediction of  $M_W$  [89] and  $4.5 \times 10^{-5}$  for  $\widehat{s}_\ell^2$  [100].

Throughout this *Review* we utilize EW radiative corrections from the program GAPP [32], which works entirely in the  $\overline{\text{MS}}$  scheme, and which is independent of the package ZFITTER [117].

### 10.3 Low energy electroweak observables

In the following we discuss EW precision observables obtained at low momentum transfers [118], *i.e.*,  $Q^2 \ll M_Z^2$ . It is convenient to write the four-fermion interactions relevant to  $\nu$ -hadron,  $\nu$ - $e$ , as well as parity violating  $e$ -hadron and  $e$ - $e$  neutral-current processes, in a form that is valid in an arbitrary gauge theory (assuming massless left-handed neutrinos). One has<sup>9</sup>,

$$-\mathcal{L}^{\nu e} = \frac{G_F}{\sqrt{2}} \bar{\nu}\gamma_\mu(1-\gamma^5)\nu \bar{e}\gamma^\mu(g_{LV}^{\nu e} - g_{LA}^{\nu e}\gamma^5)e, \quad (10.21a)$$

$$-\mathcal{L}^{\nu h} = \frac{G_F}{\sqrt{2}} \bar{\nu}\gamma_\mu(1-\gamma^5)\nu \sum_q \left[ g_{LL}^{\nu q} \bar{q}\gamma^\mu(1-\gamma^5)q + g_{LR}^{\nu q} \bar{q}\gamma^\mu(1+\gamma^5)q \right] \quad (10.21b)$$

$$-\mathcal{L}^{ee} = -\frac{G_F}{\sqrt{2}} g_{AV}^{ee} \bar{e}\gamma_\mu\gamma^5 e \bar{e}\gamma^\mu e, \quad (10.21c)$$

$$-\mathcal{L}^{eh} = -\frac{G_F}{\sqrt{2}} \sum_q \left[ g_{AV}^{eq} \bar{e}\gamma_\mu\gamma^5 e \bar{q}\gamma^\mu q + g_{VA}^{eq} \bar{e}\gamma_\mu e \bar{q}\gamma^\mu\gamma^5 q \right], \quad (10.21d)$$

where one must include the charged-current contribution for  $\nu_e$ - $e$  and  $\bar{\nu}_e$ - $e$  and the parity conserving QED contribution for electron scattering. The SM tree level expressions for the four-Fermi couplings are given in Table 10.3. Note that they differ from the respective products of the gauge couplings in (10.6) in the radiative corrections and in the presence of possible physics beyond the SM.

#### 10.3.1 Neutrino scattering

The cross-section in the laboratory system for  $\nu_\mu e \rightarrow \nu_\mu e$  or  $\bar{\nu}_\mu e \rightarrow \bar{\nu}_\mu e$  elastic scattering [9, 119] is (in this subsection we drop

<sup>9</sup>We use here slightly different definitions (and to avoid confusion also a different notation) for the coefficients of these four-Fermi operators than we did in previous editions of this *Review*. The new couplings [13] are defined in the static limit,  $Q^2 \rightarrow 0$ , with specific radiative corrections included, while others (more experiment specific ones) are assumed to be removed by the experimentalist. They are convenient in that their determinations from very different types of processes can be straightforwardly combined.

the redundant index  $L$  in the effective neutrino couplings),

$$\frac{d\sigma_{\nu,\bar{\nu}}}{dy} = \frac{G_F^2 m_e E_\nu}{2\pi} \left[ (g_V^{\nu e} \pm g_A^{\nu e})^2 + (g_V^{\nu e} \mp g_A^{\nu e})^2 (1-y)^2 - (g_V^{\nu e 2} - g_A^{\nu e 2}) \frac{y m_e}{E_\nu} \right], \quad (10.22)$$

where the upper (lower) sign refers to  $\nu_\mu$  ( $\bar{\nu}_\mu$ ), and  $y \equiv T_e/E_\nu$  (which runs from 0 to  $(1+m_e/2E_\nu)^{-1}$ ) is the ratio of the kinetic energy of the recoil electron to the incident  $\nu$  or  $\bar{\nu}$  energy. For  $E_\nu \gg m_e$  this yields a total cross-section

$$\sigma = \frac{G_F^2 m_e E_\nu}{2\pi} \left[ (g_V^{\nu e} \pm g_A^{\nu e})^2 + \frac{1}{3} (g_V^{\nu e} \mp g_A^{\nu e})^2 \right]. \quad (10.23)$$

The most accurate measurements of  $\sin^2 \theta_W$  from  $\nu$ -lepton scattering (see Sec. 10.6) are from the ratio  $R \equiv \sigma_{\nu_\mu e}/\sigma_{\bar{\nu}_\mu e}$ , in which many of the systematic uncertainties cancel. The results are  $\sin^2 \theta_W = 0.211 \pm 0.037$  [120],  $\sin^2 \theta_W = 0.195 \pm 0.022$  [121], and  $\sin^2 \theta_W = 0.2324 \pm 0.0083$  [122], where radiative corrections (other than  $m_t$  effects) are small compared to the precision of present experiments and have negligible effect. As shown in Fig. 10.1, one can determine  $g_{V,A}^{\nu e}$  from the experimental data as well. The cross-sections for  $\nu_e$ - $e$  and  $\bar{\nu}_e$ - $e$  may be obtained from Eq. (10.22) by replacing  $g_{V,A}^{\nu e}$  by  $g_{V,A}^{\nu e} + 1$ , where the 1 is due to the charged-current contribution.

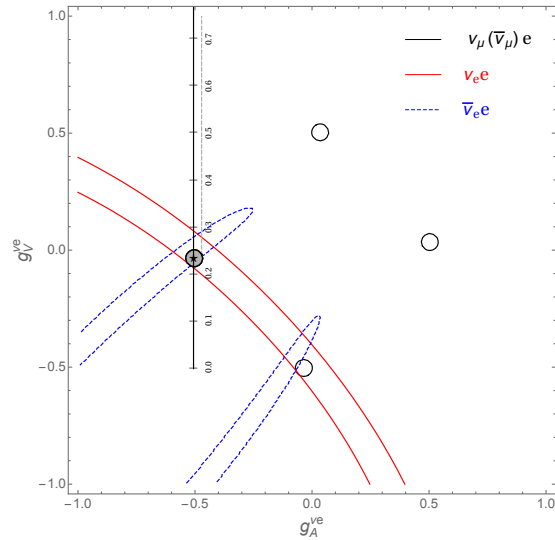


Figure 10.1: Allowed contours in  $g_A^{\nu e}$  vs.  $g_V^{\nu e}$  from neutrino-electron scattering and the SM prediction as a function of  $\widehat{s}_Z^2$ . (The SM best fit value,  $\widehat{s}_Z^2 = 0.23121$ , is also indicated.) The  $\nu_e$ - $e$  [123, 124] and  $\bar{\nu}_e$ - $e$  [125] constraints are at  $1\sigma$ , while each of the four equivalent  $\nu_\mu$  ( $\bar{\nu}_\mu$ )- $e$  [120–122] solutions ( $g_{V,A} \rightarrow -g_{V,A}$  and  $g_{V,A} \rightarrow g_{A,V}$ ) are at the 90% CL. The global best fit region (shaded) almost exactly coincides with the corresponding  $\nu_\mu$  ( $\bar{\nu}_\mu$ )- $e$  region. The solution near  $g_A = 0$  and  $g_V = -0.5$  is eliminated by  $e^+e^- \rightarrow \ell^+\ell^-$  data under the weak additional assumption that the neutral current is dominated by the exchange of a single  $Z$  boson.

A precise determination of the on-shell  $s_W^2$ , which depends only very weakly on  $m_t$  and  $M_H$ , is obtained from deep inelastic scattering (DIS) of neutrinos [119, 126] from (approximately) isoscalar targets. The ratio  $R_\nu \equiv \sigma_{\nu N}^{NC}/\sigma_{\nu N}^{CC}$  of neutral-to-charged-current cross-sections has been measured to 1% accuracy by CDHS [127] and CHARM [128] at CERN. CCFR [129] at Fermilab has obtained an even more precise result, so it is important to obtain theoretical expressions for  $R_\nu$  and  $R_{\bar{\nu}} \equiv \sigma_{\bar{\nu} N}^{NC}/\sigma_{\bar{\nu} N}^{CC}$  to comparable accuracy. Fortunately, many of the uncertainties from the strong interactions and neutrino spectra cancel in the ratio. A large theoretical uncertainty is associated with the  $c$ -threshold,

**Table 10.3:** SM tree level expressions for the neutral-current parameters for  $\nu$ -hadron,  $\nu$ - $e$ , and  $e^-$  scattering processes. To obtain the SM values in the last column, the tree level expressions have to be multiplied by the low-energy neutral-current  $\rho$  parameter,  $\rho_{NC} = 1.00063$ , and further vertex and box corrections need to be added as detailed in Ref. [13]. The dominant  $m_t$  dependence is again given by  $\rho_{NC} \sim 1 + \rho_t$ .

Quantity	SM tree level	SM value
$g_{LV}^{\nu\mu e}$	$-\frac{1}{2} + 2\widehat{s}_0^2$	-0.0398
$g_{LA}^{\nu\mu e}$	$-\frac{1}{2}$	-0.5064
$g_{LL}^{\nu\mu u}$	$\frac{1}{2} - \frac{2}{3}\widehat{s}_0^2$	0.3458
$g_{LL}^{\nu\mu d}$	$-\frac{1}{2} + \frac{1}{3}\widehat{s}_0^2$	-0.4288
$g_{LR}^{\nu\mu u}$	$-\frac{2}{3}\widehat{s}_0^2$	-0.1552
$g_{LR}^{\nu\mu d}$	$\frac{1}{3}\widehat{s}_0^2$	0.0777
$g_{AV}^{ee}$	$\frac{1}{2} - 2\widehat{s}_0^2$	0.0227
$g_{AV}^{eu}$	$-\frac{1}{2} + \frac{4}{3}\widehat{s}_0^2$	-0.1888
$g_{AV}^{ed}$	$\frac{1}{2} - \frac{2}{3}\widehat{s}_0^2$	0.3419
$g_{VA}^{eu}$	$-\frac{1}{2} + 2\widehat{s}_0^2$	-0.0352
$g_{VA}^{ed}$	$\frac{1}{2} - 2\widehat{s}_0^2$	0.0249

which mainly affects  $\sigma^{CC}$ . Using the slow rescaling prescription [130, 131] the central value of  $\sin^2 \theta_W$  from CCFR varies as  $0.0111(m_c/\text{GeV}-1.31)$ , where  $m_c$  is the effective mass which is numerically close to the  $\overline{\text{MS}}$  mass  $\widehat{m}_c(\widehat{m}_c)$ , but their exact relation is unknown at higher orders. For  $m_c = 1.31 \pm 0.24$  GeV, which was determined from  $\nu$ -induced di-muon production [132], this contributes  $\pm 0.003$  to the total uncertainty of  $\Delta \sin^2 \theta_W = \pm 0.004$ , where the experimental uncertainty was also  $\pm 0.003$ . This uncertainty largely cancels, however, in the Paschos-Wolfenstein ratio [133],

$$R^- = \frac{\sigma_{\nu N}^{NC} - \sigma_{\bar{\nu} N}^{NC}}{\sigma_{\nu N}^{CC} - \sigma_{\bar{\nu} N}^{CC}}. \quad (10.24)$$

It was measured by Fermilab's NuTeV collaboration [134] for the first time, and required a high-intensity and high-energy anti-neutrino beam.

A simple zero<sup>th</sup>-order approximation is,

$$R_\nu = g_L^2 + g_R^2 r, \quad R_{\bar{\nu}} = g_L^2 + \frac{g_R^2}{r}, \quad (10.25a)$$

$$R^- = g_L^2 - g_R^2, \quad r \equiv \frac{\sigma_{\bar{\nu} N}^{CC}}{\sigma_{\nu N}^{CC}}, \quad (10.25b)$$

where  $r$  is the ratio of  $\bar{\nu}$  to  $\nu$  charged-current cross-sections which can be measured directly<sup>10</sup>, and

$$g_L^2 \equiv (g_{LL}^{\nu\mu u})^2 + (g_{LL}^{\nu\mu d})^2 \approx \frac{1}{2} - \sin^2 \theta_W + \frac{5}{9} \sin^4 \theta_W, \quad (10.26a)$$

$$g_R^2 \equiv (g_{LR}^{\nu\mu u})^2 + (g_{LR}^{\nu\mu d})^2 \approx \frac{5}{9} \sin^4 \theta_W. \quad (10.26b)$$

In practice, Eq. (10.25b) must be corrected for quark mixing, quark sea effects,  $c$  quark threshold effects, non-isoscalarity,  $W$ - $Z$  propagator differences, the finite muon mass, QED and EW radiative corrections. Details of the neutrino spectra, experimental cuts,  $x$  and  $Q^2$  dependence of structure functions, and longitudinal structure functions, enter only at the level of these corrections and therefore lead to very small uncertainties. CCFR quotes  $s_W^2 = 0.2236 \pm 0.0041$  for the reference values  $(m_t, M_H) = (175, 150)$  GeV with very little sensitivity to  $(m_t, M_H)$ .

The NuTeV collaboration found  $s_W^2 = 0.2277 \pm 0.0016$  (for the same reference values), which was  $3.0 \sigma$  higher than the SM prediction [134]. However, since then several groups have raised concerns about the interpretation of the NuTeV result, which could

affect the extracted  $g_{L,R}^2$  (and thus  $s_W^2$ ) including their uncertainties and correlation. These include the assumption of symmetric strange and anti-strange sea quark distributions, the electron neutrino contamination from  $K_{e3}$  decays, isospin symmetry violation in the parton distribution functions and from QED splitting effects, nuclear shadowing effects, and a more complete treatment of EW and QCD radiative corrections. A more detailed discussion and a list of references can be found in the 2016 edition of this *Review*. The precise impact of these effects would need to be evaluated carefully by the collaboration, but in the absence of such an effort we do not include the  $\nu$ DIS constraints in our default set of fits.

Very recently, the COHERENT collaboration was the first to observe the coherent elastic neutrino nucleus scattering (CE $\nu$ NS) process [135] on a target consisting mostly of  $^{133}\text{Cs}$  and  $^{127}\text{I}$ , and at the opposite end of the kinematic scale where the momentum transfer is significantly smaller than the inverse of the nuclear radius. The coherence enhances the process roughly proportional to the square of the number of neutrons in the nuclei, but the process is difficult to observe as the experimental signature is a mere keV scale nuclear recoil.

### 10.3.2 Parity violating lepton scattering

Reviews on weak polarized electron scattering may be found in Refs. [9, 136]. The SLAC polarized electron-deuteron DIS (eDIS) experiment [137] measured the parity violating right-left asymmetry,

$$A_{RL} \equiv \frac{\sigma_R - \sigma_L}{\sigma_R + \sigma_L}, \quad (10.27)$$

where  $\sigma_{R,L}$  is the cross-section for the deep-inelastic scattering of a right- or left-handed electron,  $e_{R,L}N \rightarrow eX$ . In the quark parton model,

$$\frac{A_{RL}}{Q^2} = a_1 + a_2 \frac{1 - (1-y)^2}{1 + (1-y)^2}, \quad (10.28)$$

where  $Q^2 > 0$  is the momentum transfer and  $y$  is the fractional energy transfer from the electron to the hadrons. For the deuteron or other isoscalar targets, one has, neglecting the  $s$  quark and anti-quarks,

$$a_1 = \frac{3G_F}{5\sqrt{2}\pi\alpha} \left( g_{AV}^{eu} - \frac{1}{2}g_{AV}^{ed} \right) \approx \frac{3G_F}{5\sqrt{2}\pi\alpha} \left( -\frac{3}{4} + \frac{5}{3}\widehat{s}_0^2 \right), \quad (10.29a)$$

$$a_2 = \frac{3G_F}{5\sqrt{2}\pi\alpha} \left( g_{VA}^{eu} - \frac{1}{2}g_{VA}^{ed} \right) \approx \frac{9G_F}{5\sqrt{2}\pi\alpha} \left( \widehat{s}_0^2 - \frac{1}{4} \right). \quad (10.29b)$$

The Jefferson Lab Hall A collaboration [138, 139] improved on the SLAC result by measuring  $A_{RL}$  at  $Q^2 = 1.085$  GeV<sup>2</sup> and

<sup>10</sup>In the simple parton model, ignoring hadron energy cuts,  $r \approx (1 + 3\epsilon)/(3 + \epsilon)$ , where  $\epsilon \sim 0.125$  is the ratio of the fraction of the nucleon's momentum carried by anti-quarks to that carried by quarks.



1.901 GeV<sup>2</sup>, and determined the weak mixing angle to 2% precision,  $\hat{s}^2(161 \text{ MeV}) = 0.2403 \pm 0.0043$ . In another polarized electron scattering experiment on deuterons, but in the quasi-elastic kinematic regime, the SAMPLE experiment [140, 141] at MIT-Bates extracted the combination  $g_{V_A}^{eu} - g_{V_A}^{ed}$  at  $Q^2$  values of 0.038 GeV<sup>2</sup> and 0.091 GeV<sup>2</sup>. What was actually determined were nucleon form factors from which the quoted results were obtained by the removal of a multi-quark radiative correction [142]. Other linear combinations of the effective couplings have been determined in polarized lepton scattering at CERN in  $\mu$ -<sup>12</sup>C DIS [143] (the observable was the double charge-helicity cross-section asymmetry), at Mainz in  $e$ -<sup>9</sup>Be (quasi-elastic) [144], and at Bates in  $e$ -<sup>12</sup>C (elastic) [145]. More recent polarized electron scattering experiments, *i.e.*, SAMPLE, the PVA4 experiment at Mainz, and the HAPPEX and GØ experiments at Jefferson Lab, have focussed on the strange quark content of the nucleon [146].

$A_{RL}$  can also be measured in fixed target polarized Møller scattering,  $e^-e^- \rightarrow e^-e^-$ , and reads [147],

$$\frac{A_{RL}}{Q^2} = -2g_{AV}^{ee} \frac{G_F}{\sqrt{2}\pi\alpha} \frac{1-y}{1+y^4+(1-y)^4}. \quad (10.30)$$

It has been determined at low  $Q^2 = 0.026 \text{ GeV}^2$  in the SLAC E158 experiment [148], with the result,  $A_{RL} = (-1.31 \pm 0.14_{\text{stat.}} \pm$

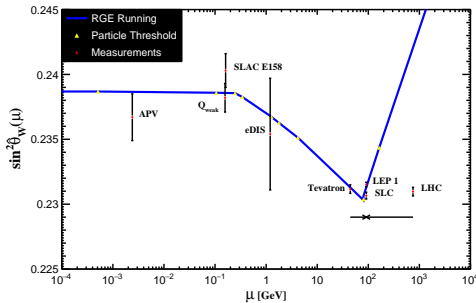


Figure 10.2: Scale dependence of the weak mixing angle defined in the  $\overline{\text{MS}}$  scheme [35, 74] (for the scale dependence in a mass-dependent renormalization scheme, see Ref. [73]). The minimum of the curve corresponds to  $\mu = M_W$ , below which we switch to an effective theory with the  $W^\pm$  bosons integrated out, and where the  $\beta$ -function for  $\hat{s}^2(\mu)$  changes sign. At  $M_W$  and each fermion mass there are also discontinuities arising from scheme dependent matching terms, which are necessary to ensure that the various effective field theories within a given loop order describe the same physics. However, in the  $\overline{\text{MS}}$  scheme these are very small numerically and barely visible in the figure provided one decouples quarks at  $\mu = \hat{m}_q(\bar{m}_q)$ . The width of the curve exceeds the theory uncertainty from strong interaction effects which at low energies is at the level of  $\pm 2 \times 10^{-5}$  [35]. The Tevatron and LHC measurements are strongly dominated by invariant masses of the final-state di-lepton pair of  $\mathcal{O}(M_Z)$  and can thus be considered as additional  $Z$  pole data points. For clarity we displayed the Tevatron and LHC points horizontally to the left and right, respectively.

$0.10_{\text{sys.}}) \times 10^{-7}$ . Expressed in terms of the weak mixing angle in the  $\overline{\text{MS}}$  scheme this yields  $\hat{s}^2(161 \text{ MeV}) = 0.2403 \pm 0.0013$ , and as shown in Fig. 10.2 established the scale dependence of the weak mixing angle at the level of  $6.4 \sigma$ . One also extracts the model-independent effective coupling,  $g_{AV}^{ee} = 0.0190 \pm 0.0027$  [13]. One-loop radiative corrections and implications are discussed in Ref. [73].

In a similar experiment and at about the same  $Q^2 = 0.0248 \text{ GeV}^2$ , the  $Q_{\text{weak}}$  collaboration at Jefferson Lab obtained  $A_{RL} = (-2.265 \pm 0.073_{\text{stat.}} \pm 0.058_{\text{sys.}}) \times 10^{-7}$  [149, 150] in elastic  $e^-p \rightarrow e^-p$  scattering. To extract the physical quantity of interest, the weak charge of the proton [151], a large ( $\approx 30\%$ ) correction had to be applied to  $A_{RL}$  arising from electromagnetic, strange, and axial form factors. This was achieved by

performing a global fit [152] including a large number of  $A_{RL}$  data points at larger  $Q^2$ , dominated by the HAPPEX result at  $Q^2 = 0.109 \text{ GeV}^2$  [153]. Finally, the constraint,  $2g_{AV}^{eu} + g_{AV}^{ed} = 0.0356 \pm 0.0023$ , which translates into a weak mixing angle measurement of  $\hat{s}^2(157 \text{ MeV}) = 0.2382 \pm 0.0011$ , could be deduced, after correcting for a relatively large and uncertain contribution from the  $\gamma Z$  box diagram [154–157].

### 10.3.3 Atomic parity violation

There are precise measurements of atomic parity violation (APV) [9, 158, 159] in <sup>133</sup>Cs [160, 161] (at the 0.4% level [160]), <sup>205</sup>Tl [162, 163], <sup>208</sup>Pb [164], and <sup>209</sup>Bi [165]. The EW physics is contained in the nuclear weak charges  $Q_W(Z, N)$ , where  $Z$  and  $N$  are the numbers of protons and neutrons in the nucleus. In terms of the nucleon vector couplings,

$$g_{AV}^{ep} \equiv 2g_{AV}^{eu} + g_{AV}^{ed} \approx -\frac{1}{2} + 2\hat{s}_0^2, \quad (10.31a)$$

$$g_{AV}^{en} \equiv g_{AV}^{eu} + 2g_{AV}^{ed} \approx +\frac{1}{2}, \quad (10.31b)$$

one has,

$$Q_W(Z, N) \equiv -2 \left[ Z(g_{AV}^{ep} + 0.00005) + N(g_{AV}^{en} + 0.00006) \right] \times \left( 1 - \frac{\alpha}{2\pi} \right), \quad (10.32)$$

where the numerically small adjustments are discussed in Ref. [13] and include the result of the  $\gamma Z$ -box correction from Ref. [166].

*E.g.*,  $Q_W(^{133}\text{Cs})$  is extracted by measuring experimentally the ratio of the parity violating amplitude,  $E_{\text{PNC}}$ , to the Stark vector transition polarizability,  $\beta$ , and by calculating theoretically  $E_{\text{PNC}}$  in terms of  $Q_W$ . One can then write,

$$Q_W(^{133}\text{Cs}) = N \left( \frac{\text{Im } E_{\text{PNC}}}{\beta} \right)_{\text{exp.}} \left( \frac{|e| a_B Q_W}{\text{Im } E_{\text{PNC}} N} \right)_{\text{th.}} \times \left( \frac{\beta}{a_B^3} \right)_{\text{exp.+th.}} \left( \frac{a_B^2}{|e|} \right), \quad (10.33)$$

where  $a_B$  is the Bohr radius. There are currently two semi-empirical approaches to  $\beta$  of similar precision. The ratio of the off-diagonal hyperfine amplitude to the vector polarizability was measured directly by the Boulder group [167]. Combined with the hyperfine amplitude, computed precisely in Ref. [168], one finds  $\beta = (26.957 \pm 0.044_{\text{exp.}} \pm 0.027_{\text{th.}}) a_B^3$ . Alternatively, one can combine [169] the measurement of the ratio of scalar to vector transition polarizabilities [170] with the recent calculation of the scalar polarizability [171] to obtain  $\beta = (27.139 \pm 0.030_{\text{exp.}} \pm 0.030_{\text{th.}}) a_B^3$ , in agreement with earlier results [172, 173] based on this approach. The two determinations average to  $\beta = (27.064 \pm 0.025_{\text{exp.}} \pm 0.021_{\text{th.}}) a_B^3$ , while they differ by  $2.7 \sigma$ .

The uncertainties associated with the atomic wave function calculations are relatively small for cesium [9, 174–176]. State-of-the-art many-body atomic structure computations of the parity non-conserving amplitude,  $\text{Im } E_{\text{PNC}} = (0.8977 \pm 0.0040) \times 10^{-11} |e| a_B Q_W/N$  [177–182], together with the measurements [160, 161] which can be combined to give  $\text{Im } E_{\text{PNC}}/\beta = -1.5924 \pm 0.0055 \text{ mV/cm}$ , imply,

$$Q_W(^{133}\text{Cs}) = -72.82 \pm 0.26_{\text{exp.}} \pm 0.33_{\text{th.}}, \quad (10.34)$$

or equivalently the constraint,  $55g_{AV}^{ep} + 78g_{AV}^{en} = 36.46 \pm 0.21$ . Within the SM this can also be translated into a determination of the weak mixing angle,  $\hat{s}^2(2.4 \text{ MeV}) = 0.2367 \pm 0.0018$ , where the scale setting follows the estimate in Ref. [183] for the typical momentum transfer for parity violation experiments in Cs (the corresponding estimate for Tl amounts to 8 MeV). By comparing different hyperfine transitions, the Boulder experiment in cesium also observed the parity violating weak corrections to the nuclear electromagnetic vertex, called the nuclear anapole moment [184–186].

The theoretical atomic structure uncertainties are 3% for thallium [187] and even larger for the other atoms. However, they mostly cancel if one takes ratios of parity violation in different isotopes [188]. The first result of this type of experiment was announced very recently by the Mainz group [189], who studied APV in  $^{100}\text{Yb}$ ,  $^{102}\text{Yb}$ ,  $^{104}\text{Yb}$ , and  $^{106}\text{Yb}$ , at the 0.5% level. The resulting three ratios can be interpreted as a measurement of  $\widehat{s}_0^2 = 0.258 \pm 0.052$ , and represent a very complementary approach to search for BSM physics [190]. If the precision increases in the future, one would ultimately face uncertainties from differences in the neutron charge radii [191, 192]. These can be constrained experimentally [193], *e.g.*, by measuring  $A_{RL}$  in heavier nuclei as done by the PREX collaboration at Jefferson Lab on  $^{208}\text{Pb}$  [194].

## 10.4 Precision flavor physics

In addition to cross-sections, asymmetries, parity violation,  $W$ ,  $Z$ , Higgs and other collider physics, there is a large number of experiments and observables testing the flavor structure of the SM. These are addressed elsewhere in this *Review*, and are generally not included in this Section. However, we identify three precision observables with sensitivity to similar types of new physics as the other processes discussed here. The branching fraction of the flavor changing transition  $b \rightarrow s\gamma$  is of comparatively low precision, but since it is a loop-level process (in the SM) its sensitivity to new physics (and SM parameters, such as heavy quark masses) is enhanced. A discussion can be found in the 2010 edition of this *Review*.

The  $\tau$  lepton lifetime and leptonic branching ratios are primarily sensitive to  $\alpha_s$  and not affected significantly by many types of new physics. However, having an independent and reliable low energy measurement of  $\alpha_s$  in a global analysis allows the comparison with the  $Z$  lineshape determination of  $\alpha_s$  which shifts easily in the presence of new physics contributions. By far the most precise observable discussed here is the anomalous magnetic moment of the muon. Its combined experimental and theoretical uncertainty is smaller than typical electroweak scale contributions. The electron magnetic moment is measured to even greater precision, and as discussed in Sec. 10.2.2 can be used to determine  $\alpha$ . Its new physics sensitivity, however, is suppressed by an additional factor of  $m_e^2/m_\mu^2$ , unless there is a new light degree of freedom such as a dark  $Z$  [195] boson.

### 10.4.1 The $\tau$ lifetime

The extraction of  $\alpha_s$  from the  $\tau$  lifetime  $\tau_\tau$  [196, 197] is standing out from other determinations because of a variety of independent reasons:

- (i) The  $\tau$ -scale is low, so that upon extrapolation to the  $Z$  scale (where it can be compared to the theoretically clean  $Z$  lineshape determinations) the  $\alpha_s$  error shrinks by about an order of magnitude.
- (ii) Yet, this scale is high enough that perturbation theory and the operator product expansion (OPE) can be applied.
- (iii) These observables are fully inclusive and thus free of fragmentation and hadronization effects that would have to be modeled or measured.
- (iv) Duality violation (DV) effects are most problematic near the branch cut but there they are suppressed by a double zero at  $s = m_\tau^2$ .
- (v) There are data [39, 41, 198] to constrain non-perturbative effects both within and breaking the OPE.
- (vi) A complete four-loop order QCD calculation is available [199–203] in the massless limit.
- (vii) Large effects associated with the QCD  $\beta$ -function can be re-summed [204] in what has become known as contour improved perturbation theory (CIPT).

However, while CIPT certainly shows faster convergence in the lower (calculable) orders, doubts have been cast on the method by the observation that at least in a specific model [205], which includes the exactly known coefficients and theoretical constraints on the large-order behavior, ordinary fixed order perturbation theory (FOPT) may nevertheless give a better approximation to the

full result. We therefore use the expressions [53, 203, 206],

$$\tau_\tau = \hbar \frac{1 - \mathcal{B}_\tau^s}{\Gamma_\tau^e + \Gamma_\tau^\mu + \Gamma_\tau^{ud}} = 290.75 \pm 0.36 \text{ fs}, \quad (10.35)$$

and

$$\Gamma_\tau^{ud} = \frac{G_F^2 m_\tau^5 |V_{ud}|^2}{64\pi^3} S(m_\tau, M_Z) \left( 1 + \frac{3}{5} \frac{m_\tau^2 - m_\mu^2}{M_W^2} \right) \times \left[ 1 + \frac{\alpha_s(m_\tau)}{\pi} + 5.202 \frac{\alpha_s^2}{\pi^2} + 26.37 \frac{\alpha_s^3}{\pi^3} + 127.1 \frac{\alpha_s^4}{\pi^4} + \widehat{\alpha} \left( \frac{85}{24} - \frac{\pi^2}{2} \right) + \delta_{\text{NP}} \right], \quad (10.36)$$

where  $\Gamma_\tau^e$  and  $\Gamma_\tau^\mu$  can be taken from Eq. (10.7) with obvious replacements. The relative fraction of strangeness changing ( $\Delta S = -1$ ) decays,  $\mathcal{B}_\tau^s = 0.0292 \pm 0.0004$ , is based on experimental data since the value for the strange quark mass,  $\widehat{m}_s(m_\tau)$ , is not well known and the QCD expansion proportional to  $\widehat{m}_s^2$  converges poorly and cannot be trusted.  $S(m_\tau, M_Z) = 1.01907 \pm 0.0003$  is a logarithmically enhanced EW correction factor [207] with higher orders re-summed [208].

$\delta_{\text{NP}}$  collects non-perturbative and quark-mass suppressed contributions, including the dimension four, six and eight terms in the OPE, as well as DV effects. We use the average  $\delta_{\text{NP}} = 0.0141 \pm 0.0072$  derived from the  $\tau$  decay spectral functions provided by OPAL [39] and ALEPH [41, 198], which give  $\delta_{\text{NP}} = 0.000 \pm 0.012$  and  $\delta_{\text{NP}} = 0.022 \pm 0.009$ , respectively. These numbers are based on the original analyses in Refs. [209, 210], but are modified to correspond to a strict FOPT analysis as is appropriate for our purpose<sup>11</sup> (for alternative analyses, see Refs. [197, 198, 211]).

The dominant uncertainty arises from the truncation of the FOPT series and is conservatively taken as the  $\alpha_s^4$  term (this is re-calculated in each call of the fits, leading to an  $\alpha_s$ -dependent and thus asymmetric error) until a better understanding of the numerical differences between FOPT and CIPT has been gained. Our perturbative error covers almost the entire range from using CIPT to assuming that the nearly geometric series in Eq. (10.36) continues to higher orders. The experimental uncertainty in Eq. (10.35) is from the combination of the two leptonic branching ratios with the direct  $\tau_\tau$ . Included are also various smaller uncertainties ( $\pm 0.15$  fs) from other sources. Based on the method of Refs. [53, 212], we obtain in total

$$\alpha_s^{(4)}(m_\tau) = 0.312_{-0.013}^{+0.016}, \quad \alpha_s^{(5)}(M_Z) = 0.1170_{-0.0017}^{+0.0019}, \quad (10.37)$$

which represents a 1.5% determination of  $\alpha_s(M_Z)$ . For more details, see Refs. [209, 210] where the  $\tau$  spectral functions themselves and an estimate of the unknown  $\alpha_s^5$  term were used as additional inputs.

### 10.4.2 The muon anomalous magnetic moment

The world average of the muon anomalous magnetic moment<sup>12</sup>,

$$a_\mu^{\text{exp}} = \frac{g_\mu - 2}{2} = (1165920.91 \pm 0.63) \times 10^{-9}, \quad (10.38)$$

is dominated by the final result of the BNL E821 collaboration [213]. The QED contribution has been calculated to five loops [214–216] (fully analytic to three loops [217–221] and semi-analytic to four loops [222]). The estimated SM EW contribution [223–228],  $a_\mu^{\text{EW}} = (1.54 \pm 0.01) \times 10^{-9}$ , includes two

<sup>11</sup>We are indebted to Diogo Boito, Maarten Golterman, Kim Maltman and Santiago Peris for privately communicating these results to us.

<sup>12</sup>In what follows, we summarize the most important aspects of  $a_\mu$  and give some details on the evaluation in our fits. For more details and references, see the Section on the ‘‘Muon Anomalous Magnetic Moment’’ in this *Review*. There are some numerical differences, which are well understood and arise because internal consistency of the fits requires the calculation of all observables from analytical expressions and common inputs and fit parameters, so that an independent evaluation is necessary for this Section. Note, that in the spirit of a global analysis based on all available information we have chosen here to also include  $\tau$  decay data [30], corrected for isospin breaking effects [31].

loop [229–233] and leading three-loop [234, 235] corrections and is at the level of twice the current uncertainty.

The limiting factor in the interpretation of the result are the uncertainties from hadronic effects. The most recent evaluations of the leading-order (two-loop) hadronic vacuum polarization contribution obtained  $a_\mu^{\text{had,VP}}(\alpha^2) = (68.81 \pm 0.41) \times 10^{-9}$  [236],  $a_\mu^{\text{had,VP}}(\alpha^2) = (69.39 \pm 0.40) \times 10^{-9}$  [29], and  $a_\mu^{\text{had,VP}}(\alpha^2) = (69.28 \pm 0.24) \times 10^{-9}$  [37]. These are mainly based on data from  $e^+e^- \rightarrow \text{hadrons}$  (see, *e.g.*, Ref. [29] for references). Our analysis combines the  $e^+e^-$  [29] and  $\tau$ -decay data [30, 31] for contributions up to  $\sqrt{s} = 2$  GeV,  $a_\mu^{\text{had,VP}}(\alpha^2, 2 \text{ GeV}) = (64.49 \pm 0.33) \times 10^{-9}$ , with analytical PQCD expressions for energies beyond 2 GeV and for the  $c$  and  $b$  quark contributions [221]. By now there are also precise results for the determination of  $a_\mu^{\text{had,VP}}(\alpha^2)$  from lattice QCD calculations [237] at the 2–3% level [238–242], while the most recent one has a 0.6% quoted uncertainty [243] (for a comparative appraisal and further references, see Ref. [244]). The result of Ref. [243],  $(71.24 \pm 0.45) \times 10^{-9}$ , has a more than  $3\sigma$  conflict with the data-driven evaluations, while there is very good statistical agreement among the different lattice results, assuming them to be uncorrelated ( $\chi^2/\text{d.o.f.} = 5.1/5$ ). If confirmed, the recent lattice determinations for  $a_\mu^{\text{had,VP}}(\alpha^2)$  may point to a problem with the data-driven approach to this quantity.

The other hadronic uncertainty is induced by the three-loop light-by-light scattering amplitude, where a number of independent model calculations yield results which are in reasonable agreement with each other,  $a_\mu^{\text{had,\gamma}\times\gamma}(\alpha^3) = (1.36 \pm 0.25) \times 10^{-9}$  [245],  $a_\mu^{\text{had,\gamma}\times\gamma}(\alpha^3) = 1.37^{+0.15}_{-0.27} \times 10^{-9}$  [246],  $a_\mu^{\text{had,\gamma}\times\gamma}(\alpha^3) = (1.05 \pm 0.26) \times 10^{-9}$  [247], and  $a_\mu^{\text{had,\gamma}\times\gamma}(\alpha^3) = (1.03 \pm 0.29) \times 10^{-9}$  [236], but the sign of this effect is opposite [248] to the one quoted in the 2002 edition of this *Review*. There is also an upper bound given by  $a_\mu^{\text{had,\gamma}\times\gamma}(\alpha^3) < 1.59 \times 10^{-9}$  [246] but this requires an *ad hoc* assumption, too. An effort to improve the evaluation of the light-by-light contribution by using experimental input where available yields a slightly lower value,  $a_\mu^{\text{had,\gamma}\times\gamma}(\alpha^3) = (0.87 \pm 0.13) \times 10^{-9}$  [249]. A first complete result from lattice simulations,  $a_\mu^{\text{had,\gamma}\times\gamma}(\alpha^3) = (0.79 \pm 0.35) \times 10^{-9}$  [250], accounting for all systematic errors, is consistent with the model and data-driven calculations. For the fits, we take the result from Ref. [236], shifted by  $2 \times 10^{-11}$  to account for the more accurate charm quark treatment of Ref. [246], and with increased error to cover all recent evaluations, resulting in  $a_\mu^{\text{had,\gamma}\times\gamma}(\alpha^3) = (1.05 \pm 0.33) \times 10^{-9}$ .

Sub-leading hadronic vacuum polarization effects at three-loop [251] and four-loop order [252] contribute  $a_\mu^{\text{had,VP}}(\alpha^3) = (-0.983 \pm 0.004) \times 10^{-9}$  [37] and  $a_\mu^{\text{had,VP}}(\alpha^4) = (0.124 \pm 0.001) \times 10^{-9}$  [252], respectively. The correlations with the two-loop hadronic contribution and with  $\Delta\alpha(M_Z)$  (see Sec. 10.2) were considered in Ref. [221]. The contributions with a hadronic light-by-light scattering subgraph have been estimated in Ref. [253], with the result,  $a_\mu^{\text{had,\gamma}\times\gamma}(\alpha^4) = (0.03 \pm 0.02) \times 10^{-9}$ .

Altogether, the SM prediction is

$$a_\mu^{\text{theory}} = (1165918.46 \pm 0.47) \times 10^{-9}, \quad (10.39)$$

where the error is from the hadronic uncertainties excluding parametric ones such as from  $\alpha_s$  and the heavy quark masses. We evaluate the correlation of the total (experimental plus theoretical) uncertainty in  $a_\mu$  with  $\Delta\alpha(M_Z)$  to amount to roughly 30%. The overall  $3.1\sigma$  discrepancy between  $a_\mu^{\text{theory}}$  and  $a_\mu^{\text{exp}}$  could be due to fluctuations (the E821 result is statistics dominated) or underestimates of the theoretical uncertainties. On the other hand, the deviation could also arise from physics beyond the SM, such as supersymmetric models with large  $\tan\beta$  and moderately light superparticle masses [254], or a dark  $Z$  boson [195].

## 10.5 Physics of the massive electroweak bosons

If the CM energy  $\sqrt{s}$  is large compared to the fermion mass  $m_f$ , the unpolarized Born cross-section for  $e^+e^- \rightarrow f\bar{f}$  [255] can

be written as,

$$\frac{d\sigma}{d\cos\theta} = \frac{\pi\alpha^2(s)}{2s} [F_1(1 + \cos^2\theta) + 2F_2\cos\theta] + B, \quad (10.40a)$$

$$F_1 = Q_e^2 Q_f^2 - 2\chi Q_e Q_f \bar{g}_V^e \bar{g}_V^f \cos\delta_R + \chi^2 (\bar{g}_V^e{}^2 + \bar{g}_A^e{}^2) (\bar{g}_V^f{}^2 + \bar{g}_A^f{}^2), \quad (10.40b)$$

$$F_2 = -2\chi Q_e Q_f \bar{g}_A^e \bar{g}_A^f \cos\delta_R + 4\chi^2 \bar{g}_V^e \bar{g}_A^e \bar{g}_V^f \bar{g}_A^f, \quad (10.40c)$$

where,

$$\tan\delta_R = \frac{\bar{M}_Z \bar{\Gamma}_Z}{\bar{M}_Z^2 - s}, \quad \chi = \frac{G_F}{2\sqrt{2}\pi\alpha(s)} \frac{s\bar{M}_Z^2}{\left[(\bar{M}_Z^2 - s)^2 + \bar{M}_Z^2 \bar{\Gamma}_Z^2\right]^{1/2}}. \quad (10.41)$$

$B$  accounts for box graphs involving virtual  $Z$  and  $W$  bosons, and the  $\bar{g}_{V,A}^f$  are defined in Eq. (10.42) below.  $\bar{M}_Z$  and  $\bar{\Gamma}_Z$  correspond to mass and width definitions based on a Breit-Wigner shape with an energy-independent width (see the Section on the “ $Z$  Boson” in this *Review*). The differential cross-section receives important corrections from QED effects in the initial and final state, and interference between the two [256]. For  $q\bar{q}$  production, there are additional final-state QCD corrections, which are relatively large. Note also that the equations above are written in the CM frame of the incident  $e^+e^-$  system, which may be boosted due to the initial-state QED radiation.

Some of the leading virtual EW corrections are captured by the running QED coupling  $\alpha(s)$  and the Fermi constant  $G_F$ . The remaining corrections to the  $Zf\bar{f}$  interactions are absorbed by replacing the tree-level couplings in Eq. (10.6) with the  $s$ -dependent *effective couplings* [14],

$$\bar{g}_V^f = \sqrt{\rho_f} (t_{3L}^f - 2Q_f \kappa_f \sin^2\theta_W), \quad (10.42a)$$

$$\bar{g}_A^f = \sqrt{\rho_f} t_{3L}^f. \quad (10.42b)$$

In these equations, the effective couplings are to be taken at the scale  $\sqrt{s}$ , but for notational simplicity we do not show this explicitly. At tree-level,  $\rho_f = \kappa_f = 1$ , but inclusion of EW radiative corrections leads to  $\rho_f \neq 1$  and  $\kappa_f \neq 1$ , which depend on the fermion  $f$  and on the renormalization scheme. In the on-shell scheme, the quadratic  $m_t$  dependence is given by,

$$\rho_f \sim 1 + \rho_t, \quad \kappa_f \sim 1 + \frac{\rho_t}{\tan^2\theta_W}, \quad (10.43)$$

while in  $\overline{\text{MS}}$ ,  $\hat{\rho}_f \sim \hat{\kappa}_f \sim 1$ , for  $f \neq b$ , and

$$\hat{\rho}_b \sim 1 - \frac{4}{3}\rho_t, \quad \hat{\kappa}_b \sim 1 + \frac{2}{3}\rho_t. \quad (10.44)$$

In the  $\overline{\text{MS}}$  scheme the normalization is changed according to  $G_F M_Z^2 / 2\sqrt{2}\pi \rightarrow \hat{\alpha} / 4\hat{s}_Z^2 \hat{c}_Z^2$  in the second Eq. (10.41).

As reviewed in Sec. 10.2.5, for the high precision  $Z$  pole observables discussed below, many additional bosonic and fermionic loop effects, vertex corrections, and higher order contributions, *etc.*, must be included. For example, in the  $\overline{\text{MS}}$  scheme one has  $\hat{\rho}_\ell = 0.9977$ ,  $\hat{\kappa}_\ell = 1.0014$ ,  $\hat{\rho}_b = 0.9866$ , and  $\hat{\kappa}_b = 1.0068$ .

To connect to measured quantities, it is convenient to define an effective angle

$$\bar{s}_f^2 \equiv \sin^2\bar{\theta}_{Wf} \equiv \hat{\kappa}_f \hat{s}_Z^2 = \kappa_f s_W^2, \quad (10.45)$$

in terms of which  $\bar{g}_V^f$  and  $\bar{g}_A^f$  are given by  $\sqrt{\rho_f}$  times their tree-level formulae. One finds that the  $\hat{\kappa}_f$  ( $f \neq b$ ) are almost independent of  $m_t$  and  $M_H$ , and thus one can write,

$$\bar{s}_\ell^2 = \hat{s}_Z^2 + 0.00032, \quad (10.46)$$

while the  $\kappa_f$  for the on-shell scheme are  $m_t$  dependent.

### 10.5.1 Electroweak physics off the $Z$ pole

Experiments at PEP, PETRA and TRISTAN have measured the unpolarized forward-backward asymmetry,  $A_{FB}$ , and the total cross-section relative to pure QED,  $R$ , for  $e^+e^- \rightarrow \ell^+\ell^-$ ,  $\ell = \mu$  or  $\tau$  at CM energies  $\sqrt{s} < M_Z$ . They are defined as

$$A_{FB} \equiv \frac{\sigma_F - \sigma_B}{\sigma_F + \sigma_B}, \quad R = \frac{\sigma}{\mathcal{R}_{\text{ini}} \otimes 4\pi\alpha^2/3s}, \quad (10.47)$$

where  $\sigma_F$  ( $\sigma_B$ ) is the cross-section for  $\ell^-$  to travel forward (backward) with respect to the  $e^-$  direction, and  $\mathcal{R}_{\text{ini}} \otimes$  denotes convolution with initial-state QED corrections. Neglecting box graph contributions, they are given by,

$$A_{FB} = \frac{3}{4} \frac{F_2}{F_1}, \quad R = F_1. \quad (10.48)$$

For the available data, it is sufficient to approximate the EW corrections through the leading running  $\alpha(s)$  and quadratic  $m_t$  contributions [257], as described above. Reviews and formulae for  $e^+e^- \rightarrow$  hadrons may be found in [9, 258, 259].

LEP 2 [260] ran at several energies above the  $Z$  pole up to  $\sim 209$  GeV. Measurements were made of a number of observables, including the total production cross-sections of  $f\bar{f}$  pairs for  $f = \mu, \tau$ , and  $q$  (hadrons), of four-fermion final states, of  $\gamma\gamma$ ,  $ZZ$ ,  $WW$ ,  $WW\gamma$ , and  $WWZ$ , as well as of single resonant  $W$  and  $Z$  bosons. The differential cross-sections for all three lepton flavors, and the leptonic and hadronic  $W$  branching ratios were also extracted.

Among the most important LEP 2 results were the measurements [260] of the  $W$  boson mass,

$$M_W = 80.376 \pm 0.025_{\text{stat.}} \pm 0.022_{\text{syst.}} \text{ GeV (LEP 2)}, \quad (10.49)$$

which were dominated by kinematic reconstruction, but included the complementary albeit statistics limited and thus much less precise determination from a  $WW$  threshold cross section scan. The kinematic method was also employed at the Tevatron [261] and by ATLAS [263]. They quote,

$$M_W = 80.387 \pm 0.016 \text{ GeV (Tevatron)}, \quad (10.50a)$$

$$M_W = 80.3695 \pm 0.0068_{\text{stat.}} \pm 0.0106_{\text{syst.}} \pm 0.0136_{\text{th.}} \text{ GeV (ATLAS)}. \quad (10.50b)$$

We assume an error component of 7 MeV to be common between the two hadron collider determinations. This is smaller than the 10 MeV PDF uncertainty quoted by CDF, because the larger CM energy at the LHC enhances the sensitivity to second generation quark PDFs, in addition to the greater sea quark PDF dependence of the Drell-Yan process in the  $pp$  environment. There may also be some correlation due to other production modeling uncertainties. This implies for the average,

$$M_W = 80.379 \pm 0.012 \text{ GeV (world average)}. \quad (10.51)$$

For details and references, see the Section on the ‘‘Mass and Width of the  $W$  Boson’’ in this *Review*.

Strong constraints on anomalous triple and quartic gauge couplings have been obtained at LEP 2, the Tevatron, and the LHC. These are described in detail in the three Sections on the ‘‘Extraction of Triple Gauge Couplings (TGCs)’’, ‘‘Anomalous  $W/Z$  Quartic Couplings (QGCs)’’, and ‘‘Anomalous  $ZZ\gamma$ ,  $Z\gamma\gamma$ , and  $ZZV$  Couplings’’ in this *Review*.

After their discovery of the Higgs boson [264, 265], the LHC experiments are now performing high precision measurements of its mass. We average the results,  $M_H = 124.97 \pm 0.16_{\text{stat.}} \pm 0.18_{\text{syst.}} \text{ GeV}$  from ATLAS [266], and  $M_H = 125.38 \pm 0.11_{\text{stat.}} \pm 0.09_{\text{syst.}} \text{ GeV}$  from CMS [267], by conservatively treating the smaller systematic error as common among the two determinations, and arrive at,

$$M_H = 125.30 \pm 0.09_{\text{stat.}} \pm 0.09_{\text{syst.}} \text{ GeV (LHC)}. \quad (10.52)$$

For further references and many more details on Higgs boson properties, see the Section on the ‘‘Status of Higgs Boson Physics’’ in this *Review*. The principal non- $Z$  pole observables discussed here and in Sections 10.2–10.4 are summarized in Table 10.4.

### 10.5.2 $Z$ pole physics

High precision measurements of various  $Z$  pole ( $\sqrt{s} \approx M_Z$ ) observables [9, 276, 277] have been performed at LEP 1 and SLC [14, 273, 274, 278, 279], as summarized in Table 10.5. These include the  $Z$  mass and total width,  $\Gamma_Z$ , and partial widths  $\Gamma_{f\bar{f}}$  for  $Z \rightarrow f\bar{f}$ , where  $f = e, \mu, \tau$ , light hadrons,  $b$ , and  $c$ . It is convenient to use the variables  $M_Z, \Gamma_Z$ ,

$$\sigma_{\text{had}} \equiv \frac{12\pi\Gamma_{e^+e^-}\Gamma_{\text{had}}}{M_Z^2\Gamma_Z^2}, \quad R_\ell \equiv \frac{\Gamma_{\text{had}}}{\Gamma_{\ell^+\ell^-}}, \quad R_q \equiv \frac{\Gamma_{q\bar{q}}}{\Gamma_{\text{had}}}, \quad (10.53)$$

for  $\ell = e, \mu$  or  $\tau$ , and  $q = b$  or  $c$ , where  $\Gamma_{\text{had}}$  is the partial width into hadrons. Most of these are weakly correlated experimentally. The three values for  $R_\ell$  are consistent with lepton universality (although  $R_\tau$  is somewhat low compared to  $R_e$  and  $R_\mu$ ), but we use the general analysis in which the three observables are treated as independent. Similar remarks apply to  $A_{FB}^{0,\ell}$  defined through Eq. (10.54) with  $P_e = 0$ , where  $A_{FB}^{0,\tau}$  is somewhat high. Initial-state radiation reduces the peak cross section by more than 25%, where  $\mathcal{O}(\alpha^3)$  QED effects induce a large anti-correlation ( $-30\%$ ) between  $\Gamma_Z$  and  $\sigma_{\text{had}}$ . The anti-correlation between  $R_b$  and  $R_c$  amounts to  $-18\%$  [14]. The  $R_\ell$  are insensitive to  $m_t$  except for the  $Z \rightarrow b\bar{b}$  vertex, final-state corrections, and the implicit dependence through  $\sin^2\theta_W$ . Thus, they are especially useful for constraining  $\alpha_s$ .

Very important constraints follow from measurements of various  $Z$  pole asymmetries. These include the forward-backward asymmetry,  $A_{FB}$ , and the polarization or left-right asymmetry,  $A_{LR}$ , defined analogously to Eq. (10.27). The latter was measured precisely by the SLD collaboration at the SLC [273], and has the advantages of being very sensitive to  $\bar{s}_\ell^2$  and that systematic uncertainties largely cancel. After removing initial-state QED corrections and contributions from photon exchange,  $\gamma$ - $Z$  interference, as well as the EW boxes in Eq. (10.40a), one can use the effective tree-level expressions,

$$A_{LR} = A_e P_e, \quad A_{FB} = \frac{3}{4} A_f \frac{A_e + P_e}{1 + P_e A_e}, \quad (10.54)$$

where,

$$A_f \equiv \frac{2\bar{g}_V^f \bar{g}_A^f}{\bar{g}_V^{f2} + \bar{g}_A^{f2}} = \frac{1 - 4|Q_f|\bar{s}_f^2}{1 - 4|Q_f|\bar{s}_f^2 + 8(|Q_f|\bar{s}_f^2)^2}. \quad (10.55)$$

$P_e$  is the initial  $e^-$  polarization, so that the second equality in Eq. (10.56) is reproduced for  $P_e = 1$ , and the  $Z$  pole forward-backward asymmetries at LEP 1 ( $P_e = 0$ ) are given by  $A_{FB}^{(0,f)} = \frac{3}{4} A_e A_f$  for  $f = e, \mu, \tau, b, c, s$  [14], and  $q$ , and where  $A_{FB}^{(0,q)}$  refers to the hadronic charge asymmetry. Corrections for  $t$ -channel exchange and  $s/t$ -channel interference cause  $A_{FB}^{(0,e)}$  to be strongly anti-correlated with  $R_e$  ( $-37\%$ ). Very recently, the  $m_b$ -dependence [280] of the  $\mathcal{O}(\alpha_s^2)$  QCD correction [281], affecting the reference axis of the  $b$  quark asymmetry [282], increased the extracted<sup>13</sup>  $A_{FB}^{(0,b)}$  by about  $0.2\sigma$ . The correlation between  $A_{FB}^{(0,b)}$  and  $A_{FB}^{(0,c)}$  amounts to 15%.

In addition, SLD extracted the final-state couplings  $A_b, A_c$  [14],  $A_s$  [278],  $A_\tau$ , and  $A_\mu$  [274], from left-right forward-backward asymmetries, using

$$A_{LR}^{FB}(f) = \frac{\sigma_{LF}^f - \sigma_{LB}^f - \sigma_{RF}^f + \sigma_{RB}^f}{\sigma_{LF}^f + \sigma_{LB}^f + \sigma_{RF}^f + \sigma_{RB}^f} = \frac{3}{4} A_f, \quad (10.56)$$

where, for example,  $\sigma_{LF}^f$  is the cross-section for a left-handed incident electron to produce a fermion  $f$  traveling in the forward hemisphere. Similarly,  $A_\tau$  and  $A_e$  were measured at LEP 1 [14] through the  $\tau$  polarization,  $\mathcal{P}_\tau$ , as a function of the scattering

<sup>13</sup>We are grateful to Werner Bernreuther and Long Chen for the recalculation of their result employing the more appropriate  $\overline{\text{MS}}$  mixing angle,  $\bar{s}_Z^2$ , instead of the on-shell quantity,  $s_W^2$ .

**Table 10.4:** Non- $Z$  pole observables, compared with the SM best fit predictions. The first  $M_W$  and  $\Gamma_W$  values are from the Tevatron [261, 262], the second ones from LEP 2 [260], while the third  $M_W$  is from ATLAS [263]. The entry of  $m_t$  differs from the one in the Particle Listings as it includes an additional theory error. The world averages for  $g_{V,A}^{\nu e}$  are dominated by the CHARM II [122] results,  $g_V^{\nu e} = -0.035 \pm 0.017$  and  $g_A^{\nu e} = -0.503 \pm 0.017$ . The  $\tau_\tau$  value is the  $\tau$  lifetime world average computed by combining the direct measurements with values derived from the leptonic branching ratios [53]; in this case, the theory error is included in the SM prediction. In all other SM predictions, the uncertainty is parametric from  $M_Z$ ,  $M_H$ ,  $m_t$ ,  $m_b$ ,  $m_c$ ,  $\hat{\alpha}(M_Z)$ , and  $\alpha_s$ , and theoretical from unknown higher orders [69], where correlations due to both types have been accounted for. The column denoted by Pull gives the standard deviations.

Quantity	Value	Standard Model	Pull
$m_t$ [GeV]	$172.89 \pm 0.59$	$173.19 \pm 0.55$	-0.5
$M_H$ [GeV]	$125.30 \pm 0.13$	$125.30 \pm 0.13$	0.0
$M_W$ [GeV]	$80.387 \pm 0.016$	$80.361 \pm 0.006$	1.6
	$80.376 \pm 0.033$		0.5
	$80.370 \pm 0.019$		0.5
$\Gamma_W$ [GeV]	$2.046 \pm 0.049$	$2.090 \pm 0.001$	-0.9
	$2.195 \pm 0.083$		1.3
$g_V^{\nu e}$	$-0.040 \pm 0.015$	$-0.0398 \pm 0.0001$	0.0
$g_A^{\nu e}$	$-0.507 \pm 0.014$	$-0.5064$	0.0
$Q_W(e)$	$-0.0403 \pm 0.0053$	$-0.0476 \pm 0.0002$	1.4
$Q_W(p)$	$0.0719 \pm 0.0045$	$0.0711 \pm 0.0002$	0.2
$Q_W(Cs)$	$-72.82 \pm 0.42$	$-73.23 \pm 0.01$	1.0
$Q_W(Tl)$	$-116.4 \pm 3.6$	$-116.88 \pm 0.02$	0.1
$\hat{s}_Z^2(\text{eDIS})$	$0.2299 \pm 0.0043$	$0.23121 \pm 0.00004$	-0.3
$\tau_\tau$ [fs]	$290.75 \pm 0.36$	$288.90 \pm 2.24$	0.8
$\frac{1}{2}(g_\mu - 2 - \frac{\alpha}{\pi})$	$(4511.18 \pm 0.78) \times 10^{-9}$	$(4508.74 \pm 0.03) \times 10^{-9}$	3.1

angle  $\theta$ , which can be written as,

$$\mathcal{P}_\tau = -\frac{A_\tau(1 + \cos^2 \theta) + 2A_e \cos \theta}{(1 + \cos^2 \theta) + 2A_\tau A_e \cos \theta}. \quad (10.57)$$

The average polarization,  $\langle \mathcal{P}_\tau \rangle$ , obtained by integrating over  $\cos \theta$  in the numerator and denominator of Eq. (10.57), yields  $\langle \mathcal{P}_\tau \rangle = -A_\tau$ , and  $A_e$  can be extracted from the  $\mathcal{P}_\tau$  angular distribution. The initial-state coupling,  $A_e$ , was also determined through the left-right charge asymmetry [279] and in polarized Bhabba scattering [274] at the SLC. Because  $\hat{g}_V^f$  is very small, not only  $A_{LR}^0 = A_e$ ,  $A_{FB}^{(0,\ell)}$ , and  $\mathcal{P}_\tau$ , but also  $A_{FB}^{(0,q)}$  for  $q = b, c$ , and  $s$ , as well as the hadronic asymmetries are mainly sensitive to  $\hat{s}_\ell^2$ .

As an example of the precision of the  $Z$  pole observables, the values of  $\hat{g}_A^f$  and  $\hat{g}_V^f$  for  $f = e, \mu, \tau$ , and  $\ell$ , extracted from the LEP and SLC lineshape and asymmetry data, are shown in Fig. 10.3. It may be compared with Fig. 10.1 as the two sets of parameters coincide at the SM at tree-level.

As for hadron colliders, the forward-backward asymmetry,  $A_{FB}$ , for  $e^+e^-$  and  $\mu^+\mu^-$  final states (with invariant masses restricted to or dominated by values around  $M_Z$ ) in  $p\bar{p}$  collisions has been measured by the CDF [283] and DØ [284] collaborations, and the values  $\hat{s}_\ell^2 = 0.23221 \pm 0.00046$  and  $\hat{s}_\ell^2 = 0.23095 \pm 0.00040$  were extracted, respectively. The combination of these measurements (which differ by more than  $2\sigma$ ) yields [268],

$$\hat{s}_\ell^2 = 0.23148 \pm 0.00033 \text{ (Tevatron)}. \quad (10.58)$$

By varying the invariant mass and the scattering angle (and assuming the electron couplings), information on the effective  $Z$  couplings to light quarks,  $\hat{g}_{V,A}^{u,d}$ , could also be obtained [285, 286], but with large uncertainties, mutual correlations, and not independently of  $\hat{s}_\ell^2$  above. Similar analyses have also been reported by the H1 [287] and ZEUS [288] collaborations at HERA and by the LEP collaborations [14]. This kind of measurement is harder in the  $pp$  environment due to the difficulty to assign the initial quark and antiquark in the underlying Drell-Yan process to the protons, thus requiring excellent control of uncertainties from parton distribution functions. ATLAS obtained  $\hat{s}_\ell^2 = 0.2308 \pm 0.0012$  using 7 TeV data [269] and  $\hat{s}_\ell^2 = 0.23140 \pm 0.00036$  at 8 TeV [270],

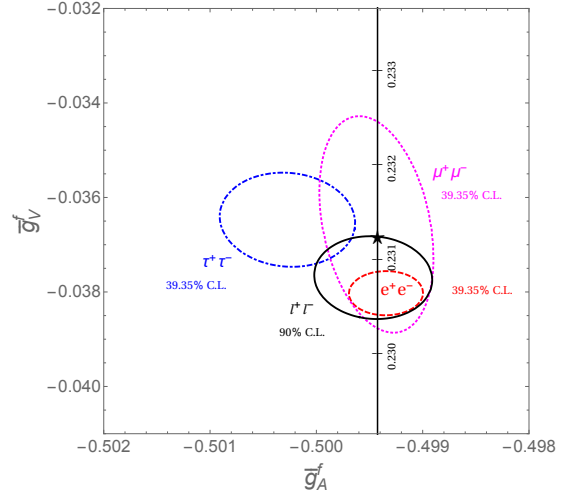


Figure 10.3:  $1\sigma$  (39.35% CL) contours of the effective couplings  $\hat{g}_A^f$  and  $\hat{g}_V^f$  for  $f = e, \mu$  and  $\tau$  from LEP and SLC, compared to the SM expectation as a function of  $\hat{s}_Z^2$ . (The SM best fit value  $\hat{s}_Z^2 = 0.23121$  is also indicated.) Also shown is the 90% CL allowed region in  $\hat{g}_{A,V}^f$  obtained assuming lepton universality.

while CMS measured  $\hat{s}_\ell^2 = 0.23101 \pm 0.00053$  (8 TeV) [271] and LHCb reported  $\hat{s}_\ell^2 = 0.23142 \pm 0.00106$  (from both 7 and 8 TeV data, but only analyzing  $\mu^+\mu^-$  final state) [272]. Assuming that the smallest theoretical and PDF uncertainty ( $\pm 0.00024$  from ATLAS [270]) is fully correlated among the four determinations, they combine to

$$\hat{s}_\ell^2 = 0.23129 \pm 0.00033 \text{ (LHC)}. \quad (10.59)$$

### 10.5.3 $W$ and $Z$ decays

The partial decay widths for gauge bosons to decay into massless fermions  $f_1\bar{f}_2$  (the numerical values include the small EW

**Table 10.5:** Principal  $Z$  pole observables and their SM predictions (*cf.* Table 10.4). The first  $\bar{s}_\ell^2$  is the effective weak mixing angle extracted from the hadronic charge asymmetry at LEP 1 [14], the second is the combined value from the Tevatron [268], and the third is from the LHC [269–272]. The values of  $A_e$  are (i) from  $A_{LR}$  for hadronic final states [273]; (ii) from  $A_{LR}$  for leptonic final states and from polarized Bhabba scattering [274]; and (iii) from the angular distribution of the  $\tau$  polarization at LEP 1 [14]. The  $A_\tau$  values are from SLD [274] and the total  $\tau$  polarization, respectively. Note that the SM errors in  $\Gamma_Z$ , the  $R_\ell$ , and  $\sigma_{\text{had}}$  are largely dominated by the uncertainty in  $\alpha_s$ .

Quantity	Value	Standard Model	Pull
$M_Z$ [GeV]	$91.1876 \pm 0.0021$	$91.1882 \pm 0.0020$	−0.3
$\Gamma_Z$ [GeV]	$2.4955 \pm 0.0023$	$2.4942 \pm 0.0009$	0.6
$\sigma_{\text{had}}$ [nb]	$41.481 \pm 0.033$	$41.482 \pm 0.008$	0.0
$R_e$	$20.804 \pm 0.050$	$20.736 \pm 0.010$	1.4
$R_\mu$	$20.784 \pm 0.034$	$20.735 \pm 0.010$	1.4
$R_\tau$	$20.764 \pm 0.045$	$20.781 \pm 0.010$	−0.4
$R_b$	$0.21629 \pm 0.00066$	$0.21581 \pm 0.00002$	0.7
$R_c$	$0.1721 \pm 0.0030$	$0.17221 \pm 0.00003$	0.0
$A_{FB}^{(0,e)}$	$0.0145 \pm 0.0025$	$0.01619 \pm 0.00007$	−0.7
$A_{FB}^{(0,\mu)}$	$0.0169 \pm 0.0013$		0.5
$A_{FB}^{(0,\tau)}$	$0.0188 \pm 0.0017$		1.5
$A_{FB}^{(0,b)}$	$0.0996 \pm 0.0016$	$0.1030 \pm 0.0002$	−2.1
$A_{FB}^{(0,c)}$	$0.0707 \pm 0.0035$	$0.0736 \pm 0.0002$	−0.8
$A_{FB}^{(0,s)}$	$0.0976 \pm 0.0114$	$0.1031 \pm 0.0002$	−0.5
$\bar{s}_\ell^2$	$0.2324 \pm 0.0012$	$0.23153 \pm 0.00004$	0.7
	$0.23148 \pm 0.00033$		−0.2
	$0.23129 \pm 0.00033$		−0.7
$A_e$	$0.15138 \pm 0.00216$	$0.1469 \pm 0.0003$	2.1
	$0.1544 \pm 0.0060$		1.2
	$0.1498 \pm 0.0049$		0.6
$A_\mu$	$0.142 \pm 0.015$		−0.3
$A_\tau$	$0.136 \pm 0.015$		−0.7
	$0.1439 \pm 0.0043$		−0.7
$A_b$	$0.923 \pm 0.020$	0.9347	−0.6
$A_c$	$0.670 \pm 0.027$	$0.6677 \pm 0.0001$	0.1
$A_s$	$0.895 \pm 0.091$	0.9356	−0.4

**Table 10.6:** Results derived from Table 10.5 and the corresponding covariance matrices [14, 275], and the SM predictions for the partial and total  $Z$  decay widths [in MeV]. In the (second) third column lepton universality is (not) assumed.

Quantity	Value	Value (universal)	Standard Model
$\Gamma_{e^+e^-}$	$83.87 \pm 0.12$	$83.942 \pm 0.085$	$83.964 \pm 0.009$
$\Gamma_{\mu^+\mu^-}$	$83.95 \pm 0.18$	$83.941 \pm 0.085$	$83.963 \pm 0.009$
$\Gamma_{\tau^+\tau^-}$	$84.03 \pm 0.21$	$83.759 \pm 0.085$	$83.780 \pm 0.009$
$\Gamma_{\text{inv}}$	$498.9 \pm 2.5$	$500.5 \pm 1.5$	$501.464 \pm 0.047$
$\Gamma_{u\bar{u}}$	—	—	$299.91 \pm 0.20$
$\Gamma_{c\bar{c}}$	$300.3 \pm 5.3$	$300.0 \pm 5.2$	$299.83 \pm 0.20$
$\Gamma_{d\bar{d}}, \Gamma_{s\bar{s}}$	—	—	$382.79 \pm 0.14$
$\Gamma_{b\bar{b}}$	$377.4 \pm 1.3$	$377.0 \pm 1.2$	$375.75 \pm 0.18$
$\Gamma_{\text{had}}$	$1744.8 \pm 2.6$	$1743.2 \pm 1.9$	$1741.06 \pm 0.85$
$\Gamma_Z$	$2495.5 \pm 2.3$	$2495.5 \pm 2.3$	$2494.23 \pm 0.86$

radiative corrections and final-state mass effects) are given by,

$$\Gamma(W^+ \rightarrow e^+\nu_e) = \frac{M_W^3}{12\pi v^2} = 226.35 \pm 0.05 \text{ MeV}, \quad (10.60a)$$

$$\Gamma(W^+ \rightarrow u_i\bar{d}_j) = \frac{M_W^3}{12\pi v^2} |V_{ij}|^2 \mathcal{R}_V^q = (705.4 \pm 0.4 \text{ MeV}) |V_{ij}|^2, \quad (10.60b)$$

$$\Gamma(Z \rightarrow f\bar{f}) = \frac{M_Z^3}{12\pi v^2} [\mathcal{R}_V^f \bar{g}_V^{f2} + \mathcal{R}_A^f \bar{g}_A^{f2}], \quad (10.60c)$$

where the result for the latter are shown in Table 10.6. Final-state QED and QCD corrections [289] to the vector and axial-vector form factors are given by,

$$\mathcal{R}_{V,A}^f = N_C \left[ 1 + \frac{3}{4} \left( Q_f^2 \frac{\alpha(s)}{\pi} + \frac{N_C^2 - 1}{2N_C} \frac{\alpha_s(s)}{\pi} \right) + \dots \right], \quad (10.61)$$

where  $N_C = 3$  (1) is the color factor for quarks (leptons) and the dots indicate finite fermion mass effects proportional to  $m_f^2/s$  which are different for  $\mathcal{R}_V^f$  and  $\mathcal{R}_A^f$ , as well as higher-order QCD corrections [290], which are known to  $\mathcal{O}(\alpha_s^4)$  [203]. These include

singlet contributions starting from two-loop order which are large, strongly top quark mass dependent, family universal, and flavor non-universal [291–295]. The  $\mathcal{O}(\alpha^2)$  self-energy corrections from Ref. [296] are also taken into account.

For the  $W$  decay into quarks, Eq. (10.60b), only the universal massless part (non-singlet and  $m_q = 0$ ) of the final-state QCD radiator function in  $\mathcal{R}_V$  from Eq. (10.61) is used, and the QED corrections are modified. Expressing the widths in terms of  $G_F M_W^3$ ,  $Z$  incorporates the largest radiative corrections from the running QED coupling. EW corrections to the  $Z$  widths are then taken into account through the effective couplings  $\bar{g}_{V,A}^i$ . Hence, in the on-shell scheme the  $Z$  widths are proportional to  $\rho_i \sim 1 + \rho_t$ . There is additional (negative) quadratic  $m_t$  dependence in the  $Z \rightarrow b\bar{b}$  vertex corrections [297, 298] which causes  $\Gamma_{b\bar{b}}$  to decrease with  $m_t$ . The dominant effect is to multiply  $\Gamma_{b\bar{b}}$  by the vertex correction  $1 + \delta\rho_{b\bar{b}}$ , where  $\delta\rho_{b\bar{b}} \sim 10^{-2}(-\frac{1}{2}m_t^2/M_Z^2 + \frac{1}{5})$ . In practice, the corrections are included in  $\hat{\rho}_b$  and  $\hat{\kappa}_b$ , as discussed in Sec. 10.5.

Starting at  $\mathcal{O}(\alpha\alpha_s)$ , the factorized form indicated in Eq. (10.60) is violated and corrections need to be included [299–301]. They add coherently, resulting in a sizable effect, and shift  $\alpha_s(M_Z)$  when extracted from  $Z$  lineshape observables by about  $+0.0007$ . Similar non-factorizable corrections are also known for mixed QED-EW corrections [97, 98, 100, 302].

For three fermion families the total widths of the  $Z$  [303–307] and  $W$  [308, 309] bosons are predicted to be,

$$\Gamma_Z = 2.4942 \pm 0.0009 \text{ GeV}, \quad \Gamma_W = 2.0896 \pm 0.0008 \text{ GeV}. \quad (10.62)$$

The uncertainties in these predictions are almost entirely induced by the parametric error in  $\alpha_s(M_Z) = 0.1185 \pm 0.0016$  from the global fit. These predictions can be compared with the experimental results,  $\Gamma_Z = 2.4955 \pm 0.0023 \text{ GeV}$  [14, 275] and  $\Gamma_W = 2.085 \pm 0.042 \text{ GeV}$  [260, 262] (see the Gauge & Higgs Bosons Particle Listings). The measurements of the total and partial widths are generally in good agreement with the SM. The exception is the branching ratio  $W \rightarrow \tau + \nu_\tau$  from LEP 2, which is  $2.6 \sigma$  larger than the electron-muon average [260].

The invisible decay width,  $\Gamma_{\text{inv}} = \Gamma_Z - \Gamma_{e^+e^-} - \Gamma_{\mu^+\mu^-} - \Gamma_{\tau^+\tau^-} - \Gamma_{\text{had}}$ , can be used to determine the number of neutrino flavors,  $N_\nu$ , much lighter than  $M_Z/2$ . The hadronic peak cross section, and therefore the extracted  $\Gamma_{\text{had}}$ , depends strongly on the knowledge of the LEP 1 luminosity derived from small-angle Bhabha scattering. However, the prediction for the Bhabha cross-section was very recently found to be overestimated, and consequently the luminosity underestimated [275]. The updated analysis involved an improved  $Z$  lineshape fit, significantly reducing  $\sigma_{\text{had}}$ , while slightly increasing  $\Gamma_Z$ , with the result,  $N_\nu = 2.9963 \pm 0.0074$  [275]. In practice, we determine  $N_\nu$  by allowing it as an additional fit parameter and obtain,

$$N_\nu = 3.0026 \pm 0.0061, \quad (10.63)$$

which is now in perfect agreement with the observed number of fermion generations and  $N_\nu = 3$  (a  $1.3 \sigma$  deviation was observed in the 2018 edition of this *Review* before including the correction in the luminosity determination).

## 10.6 Global fit results

In this section, we present the results of global fits, subject to the experimental data and theoretical constraints discussed in Section 10.2–10.4. For earlier analyses, see Refs. [14, 69, 310–313] and previous editions of this *Review*. The values for  $m_t$ ,  $M_W$  [260, 261, 263],  $\Gamma_W$  [260, 262], the weak charges of the electron [148], the proton [149], cesium [160, 161] and thallium [162, 163], the weak mixing angle extracted from eDIS [138],  $\nu_\mu(\bar{\nu}_\mu)$ - $e$  scattering [120–122], the  $\tau$  lifetime, and the  $\mu$  anomalous magnetic moment [213] are listed in Table 10.4. Likewise, Table 10.5 summarizes the principal  $Z$  pole observables, where the LEP 1 averages of the ALEPH, DELPHI, L3, and OPAL results include common systematic uncertainties and correlations [14, 275]. The heavy flavor results [14, 280] of LEP 1 and SLD are based on common inputs, and are thus correlated, as well.

Also shown in both tables are the SM predictions for the values of  $M_Z$ ,  $M_H$ ,  $\alpha_s(M_Z)$ ,  $\Delta\alpha_{\text{had}}^{(3)}$  and the heavy quark masses shown in Table 10.7. The predictions result from a global least-square ( $\chi^2$ ) fit to all data using the minimization package MINUIT [314] and the EW library GAPP [32]. In most cases, we treat all input errors (the uncertainties of the values) as Gaussian. The reason is not that we assume that theoretical and systematic errors are intrinsically bell-shaped (which they are not) but because in most cases the input errors are either dominated by the statistical components or they are combinations of many different (including statistical) error sources, which should yield approximately Gaussian combined errors by the large number theorem. An exception is the theory dominated error on the  $\tau$  lifetime, which we recalculate in each  $\chi^2$ -function call since it depends itself on  $\alpha_s$ . Sizes and shapes of the output errors (the uncertainties of the predictions and the SM fit parameters) are fully determined by the fit, and  $1 \sigma$  errors are defined to correspond to  $\Delta\chi^2 = \chi^2 - \chi_{\text{min}}^2 = 1$ , and do not necessarily correspond to the 68.3% probability range or the 39.3% probability contour (for 2 parameters).

The agreement is generally very good. Despite the few discrepancies addressed in the following, the global electroweak fit describes the data very well, with an excellent  $\chi^2/\text{d.o.f.} = 40.8/41$ . The probability of a larger  $\chi^2$  is 48%, and only  $g_\mu - 2$  is currently showing a larger ( $3.1 \sigma$ ) conflict. In addition,  $A_{LR}^0$  (SLD) from hadronic final states and  $A_{FB}^{(0,b)}$  (LEP 1) deviate at the  $2 \sigma$  level.  $g_L^2$  from NuTeV is nominally in conflict with the SM, as well, but the precise status is unresolved (see Sec. 10.3.1). We also emphasize that there are a number of discrepancies among individual measurements of certain quantities, as discussed in previous sections, but that they are not reflected in the overall  $\chi^2$  of the fit as only the corresponding combinations are used as constraints.

$A_b$  can be extracted from  $A_{FB}^{(0,b)}$  when  $A_e = 0.1501 \pm 0.0016$  is taken from a fit to leptonic asymmetries (using lepton universality). The result,  $A_b = 0.885 \pm 0.017$ , is  $2.9 \sigma$  below the SM prediction<sup>14</sup> and also  $1.4 \sigma$  below  $A_b = 0.923 \pm 0.020$  obtained from  $A_{LR}^{FB}(b)$  at SLD. Thus, it appears that at least some of the problem in  $A_b$  is due to a statistical fluctuation or other experimental effect in one of the asymmetries. Note, however, that the uncertainty in  $A_{FB}^{(0,b)}$  is strongly statistics dominated. The combined value,  $A_b = 0.901 \pm 0.013$  deviates by  $2.6 \sigma$ .

The left-right asymmetry,  $A_{LR}^0 = 0.15138 \pm 0.00216$  [273], from hadronic decays at SLD, differs by  $2.1 \sigma$  from the SM expectation of  $0.1469 \pm 0.0003$ . The combined value of  $A_\ell = 0.1513 \pm 0.0021$  from SLD (using lepton-family universality and including correlations) is also  $2.1 \sigma$  above the SM prediction; but there is experimental agreement between this SLD value and the LEP 1 value,  $A_\ell = 0.1481 \pm 0.0027$ , obtained from a fit to  $A_{FB}^{(0,\ell)}$ ,  $A_e(\mathcal{P}_\tau)$ , and  $A_\tau(\mathcal{P}_\tau)$ , again assuming universality.

The observables in Table 10.4 and Table 10.5, as well as some other less precise observables, are used in the global fits described below. In all fits, the errors include full statistical, systematic, and theoretical uncertainties. The correlations from the LEP 1 lineshape and  $\tau$  polarization measurements, the LEP/SLD heavy flavor observables, the SLD lepton asymmetries, and the  $\nu$ - $e$  scattering observables, are included. The theoretical correlations between  $\Delta\alpha_{\text{had}}^{(5)}$ ,  $\hat{s}_0^2$ , and  $g_\mu - 2$ , and between the  $M_W$  extractions from ATLAS and the Tevatron, are also accounted for.

The electroweak data allow a simultaneous determination of  $M_Z$ ,  $m_t$ , and  $\alpha_s(M_Z)$ . The direct measurements of  $M_H$  at the LHC [266, 267] have reached a precision that the global fit result for  $M_H$  coincides with the constraint in Eq. (10.52) with negligible correlations with the other fit parameters.  $\hat{m}_c$ ,  $\hat{m}_b$ , and  $\Delta\alpha_{\text{had}}^{(3)}$  are also allowed to float in the fits, subject to the theoretical constraints [28, 51] described in Sec. 10.2, and are correlated with  $\alpha_s$ , which in turn is determined mainly through  $R_\ell$ ,  $\Gamma_Z$ ,  $\sigma_{\text{had}}$ , and  $\tau_\tau$ . The global fit to all data, including the hadron collider  $m_t$  average in Eq. (10.13), yields the results in Table 10.7, while those

<sup>14</sup>Alternatively, one can use  $A_\ell = 0.1481 \pm 0.0027$ , which is from LEP 1 alone and in excellent agreement with the SM, and obtain  $A_b = 0.897 \pm 0.022$  which is  $1.7 \sigma$  low. This illustrates that some of the discrepancy is related to the one in  $A_{LR}$ .



**Table 10.7:** Principal SM fit result including mutual correlations.

$M_Z$ [GeV]	$91.1882 \pm 0.0020$	1.00	-0.07	0.00	0.00	0.02	0.02
$\widehat{m}_t(\widehat{m}_t)$ [GeV]	$163.51 \pm 0.55$	-0.07	1.00	0.00	-0.11	-0.22	0.04
$\widehat{m}_b(\widehat{m}_b)$ [GeV]	$4.180 \pm 0.008$	0.00	0.00	1.00	0.20	-0.02	0.00
$\widehat{m}_c(\widehat{m}_c)$ [GeV]	$1.275 \pm 0.009$	0.00	-0.11	0.20	1.00	0.47	0.00
$\alpha_s(M_Z)$	$0.1185 \pm 0.0016$	0.02	-0.22	-0.02	0.47	1.00	-0.03
$\Delta\alpha_{\text{had}}^{(3)}(2 \text{ GeV})$	$0.00592 \pm 0.00005$	0.02	0.04	0.00	0.00	-0.03	1.00

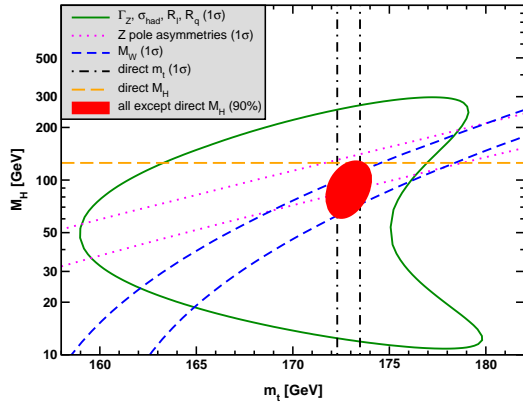


Figure 10.4: Fit result and one-standard-deviation (39.35% for the closed contours and 68% for the others) uncertainties in  $M_H$  as a function of  $m_t$  for various inputs, and the 90% CL region ( $\Delta\chi^2 = 4.605$ ) allowed by all data.  $\alpha_s(M_Z) = 0.1185$  is assumed except for the fits including the  $Z$  lineshape. The width of the horizontal dashed band is not visible on the scale of the plot.

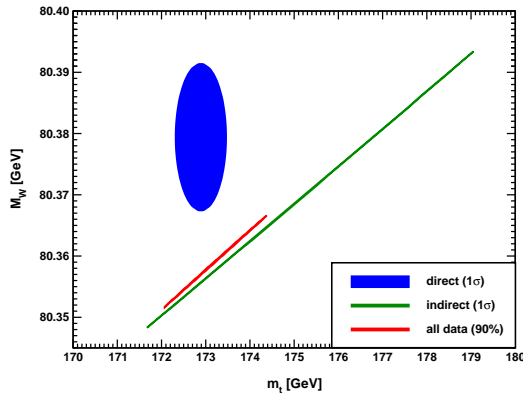


Figure 10.5: One-standard-deviation (39.35%) regions in  $M_W$  as a function of  $m_t$  for the direct and indirect data, and the 90% CL region ( $\Delta\chi^2 = 4.605$ ) allowed by all data.

for the weak mixing angle in various schemes are summarized in Table 10.2.

Removing the kinematic constraint on  $M_H$  from LHC gives the loop-level determination from the precision data,

$$M_H = 90_{-16}^{+18} \text{ GeV}, \quad (10.64)$$

which is  $1.8 \sigma$  below the value in Eq. (10.52). The latter is also slightly outside the 90% central confidence range,

$$64 \text{ GeV} < M_H < 122 \text{ GeV}. \quad (10.65)$$

This is mostly a reflection of the Tevatron determination of  $M_W$ , which is  $1.6 \sigma$  higher than the SM best fit value in Table 10.4. This is shown in Fig. 10.4 where one sees that the precision data

together with  $M_H$  from the LHC prefer  $m_t$  to be closer to the upper end of its  $1 \sigma$  allowed range.

Conversely, one can remove the explicit  $M_W$  and  $\Gamma_W$  constraints from the global fit and use  $M_H = 125.30 \pm 0.13$  GeV to obtain  $M_W = 80.357 \pm 0.006$  GeV, which is  $1.7 \sigma$  below the world average in Eq. (10.51). Finally, one can carry out a fit without including the direct constraint,  $m_t = 172.89 \pm 0.59$  GeV, from the hadron colliders. One obtains  $m_t = 176.3 \pm 1.9$  GeV, which is  $1.7 \sigma$  higher than the collider average. (The indirect prediction is for the  $\overline{\text{MS}}$  mass definition,  $\widehat{m}_t(\widehat{m}_t) = 166.4 \pm 1.8$  GeV, which is in the end converted to the pole mass.) The situation is summarized in Fig. 10.5 showing the  $1 \sigma$  contours in the  $M_W$ - $m_t$  plane from the direct and indirect determinations, as well as the combined 90% CL region.

In view of these tensions it is instructive to study the effect of doubling the uncertainty in  $\Delta\alpha_{\text{had}}^{(3)}(2 \text{ GeV}) = (58.84 \pm 0.51) \times 10^{-4}$  (see Sec. 10.2) on the loop-level determination of the Higgs boson mass. The result,  $M_H = 88_{-17}^{+18}$  GeV, deviates even slightly *more* ( $1.9 \sigma$ ) than Eq. (10.64), and demonstrates that the uncertainty in  $\Delta\alpha_{\text{had}}$  is currently of only secondary importance. Note also that a shift of  $\pm 10^{-4}$  in  $\Delta\alpha_{\text{had}}^{(3)}(2 \text{ GeV})$  corresponds to a shift of  $\mp 4.4$  GeV in  $M_H$ . The hadronic contribution to  $\alpha(M_Z)$  is correlated with  $g_\mu - 2$  (see Sec. 10.4). The measurement of the latter is higher than the SM prediction, and its inclusion in the fit favors a larger  $\alpha(M_Z)$  and a lower  $M_H$  from the precision data (currently by  $2.3 \text{ GeV}$ ).

The weak mixing angle can be determined from  $Z$  pole observables,  $M_W$ , and a variety of neutral-current processes spanning a very wide  $Q^2$  range. The results (for older low energy neutral-current data see Refs. [310–313], as well as earlier editions of this *Review*) shown in Table 10.8 are in reasonable agreement with each other, indicating the quantitative success of the SM. One of the largest discrepancies is the value  $\widehat{s}_Z^2 = 0.23176 \pm 0.00027$  from  $A_{FB}^{(0,b)}$  and  $A_{FB}^{(0,c)}$ , which is  $2.0 \sigma$  above the value  $0.23121 \pm 0.00004$  from the global fit to all data. Similarly,  $\widehat{s}_Z^2 = 0.23064 \pm 0.00028$  from the SLD asymmetries (in both cases when combined with  $M_Z$ ,  $\Gamma_Z$ , and  $m_t$ ) is  $2.0 \sigma$  low.

The extracted  $Z$  pole value of  $\alpha_s(M_Z)$  is based on a formula with negligible theoretical uncertainty if one assumes the exact validity of the SM. One should keep in mind, however, that this value,  $\alpha_s(M_Z) = 0.1221 \pm 0.0027$ , which increased after the updated analysis in Ref. [275], is very sensitive to certain types of new physics such as non-universal vertex corrections. In contrast, the value derived from  $\tau$  decays,  $\alpha_s(M_Z) = 0.1170_{-0.0017}^{+0.0019}$ , is theory dominated but less sensitive to new physics. The agreement between the two values is only marginal, but the latter does agree well with the averages deduced from DIS and global PDF fits ( $0.1161 \pm 0.0018$ ), hadronic final states of  $e^+e^-$  annihilations ( $0.1171 \pm 0.0031$ ), hadron colliders ( $0.1159 \pm 0.0034$ ), as well as lattice QCD simulations ( $0.1182 \pm 0.0008$ ). For more details, other determinations, and references, see the Section on “Quantum Chromodynamics” in this *Review*.

Using  $\alpha(M_Z)$  and  $\widehat{s}_Z^2$  as inputs, one can predict  $\alpha_s(M_Z)$  assuming grand unification. One finds  $\alpha_s(M_Z) = 0.13 \pm 0.01$  [317, 318] for the simplest theories based on the minimal supersymmetric extension of the SM, where the uncertainty is from the unknown particle thresholds. This is slightly larger, but consistent with  $\alpha_s(M_Z) = 0.1185 \pm 0.0016$  from our fit and most other determinations, while minimal non-supersymmetric theories predict much lower and excluded values (see the Section on “Grand Unified The-



**Table 10.8:** Values of  $\widehat{s}_Z^2$ ,  $s_W^2$ ,  $\alpha_s$ ,  $m_t$  and  $M_H$  for various data sets. In the fit to the LHC data, the  $\alpha_s$  constraint is from a combined NNLO analysis of inclusive electroweak boson production cross-sections at the LHC [315]. Likewise, for the Tevatron fit we use the  $\alpha_s$  result from the inclusive jet cross-section at DØ [316].

data set	$\widehat{s}_Z^2$	$s_W^2$	$\alpha_s(M_Z)$	$m_t$ [GeV]	$M_H$ [GeV]
all data	0.23121(4)	0.22337(10)	0.1185(16)	$173.2 \pm 0.6$	125
all data except $M_H$	0.23107(9)	0.22309(19)	0.1189(17)	$172.9 \pm 0.6$	$90_{-16}^{+18}$
all data except $M_Z$	0.23111(6)	0.22334(10)	0.1185(16)	$172.9 \pm 0.6$	125
all data except $M_W$	0.23123(4)	0.22345(11)	0.1189(17)	$172.9 \pm 0.6$	125
all data except $m_t$	0.23113(6)	0.22305(21)	0.1190(17)	$176.3 \pm 1.9$	125
$M_{H,Z} + \Gamma_Z + m_t$	0.23126(8)	0.22351(17)	0.1215(47)	$172.9 \pm 0.6$	125
LHC	0.23113(10)	0.22337(13)	0.1188(16)	$172.7 \pm 0.6$	125
Tevatron + $M_Z$	0.23102(13)	0.22295(30)	0.1160(44)	$174.3 \pm 0.8$	$99_{-26}^{+32}$
LEP 1 + LEP 2	0.23137(18)	0.22353(46)	0.1235(29)	$178 \pm 11$	$201_{-113}^{+279}$
LEP 1 + SLD	0.23116(17)	0.22348(58)	0.1221(27)	$169 \pm 10$	$80_{-39}^{+101}$
SLD + $M_Z + \Gamma_Z + m_t$	0.23064(28)	0.22227(54)	0.1188(48)	$172.9 \pm 0.6$	$37_{-21}^{+30}$
$A_{FB}^{(b,c)} + M_Z + \Gamma_Z + m_t$	0.23176(27)	0.22467(66)	0.1266(46)	$172.9 \pm 0.6$	$280_{-100}^{+145}$
$M_{W,Z} + \Gamma_{W,Z} + m_t$	0.23103(12)	0.22302(25)	0.1198(44)	$172.9 \pm 0.6$	$84_{-20}^{+24}$
low energy + $M_{H,Z}$	0.23176(94)	0.2254(35)	0.1171(18)	$156 \pm 29$	125

**Table 10.9:** Values of model-independent neutral-current parameters, compared with the SM predictions, where the uncertainties in the latter are  $\lesssim 0.0001$ , throughout.

Quantity	Experimental Value	Standard Model	Correlation
$g_{LV}^{\nu e}$	$-0.040 \pm 0.015$	-0.0398	-0.05
$g_{LA}^{\nu e}$	$-0.507 \pm 0.014$	-0.5064	
$g_{AV}^{eu} + 2g_{AV}^{ed}$	$0.4927 \pm 0.0031$	0.4950	-0.88 0.20
$2g_{AV}^{eu} - g_{AV}^{ed}$	$-0.7165 \pm 0.0068$	-0.7195	-0.22
$2g_{VA}^{eu} - g_{VA}^{ed}$	$-0.13 \pm 0.06$	-0.0954	
$g_{VA}^{ee}$	$0.0190 \pm 0.0027$	0.0227	

ories” in this *Review*).

Most of the parameters relevant to  $\nu$ -hadron,  $\nu$ - $e$ ,  $e$ -hadron, and  $e$ - $e$  processes are determined uniquely and precisely from the data in “model-independent” fits, *i.e.*, fits allowing for an arbitrary EW gauge theory. The values for the parameters defined in Eq. (10.21) are given in Table 10.9 along with the predictions of the SM. The agreement is very good. (The  $\nu$ -hadron results including NuTeV [134] and other  $\nu$ -DIS data can be found in the 2006 edition of this *Review*, and fits with modified NuTeV constraints in the 2008 and 2010 editions.)

### 10.7 Constraints on new physics

The masses and decay properties of the electroweak bosons and low energy data can be used to search for and set limits on deviations from the SM. We will mainly discuss the effects of exotic particles (with heavy masses  $M_{\text{new}} \gg M_Z$  in an expansion in  $M_Z/M_{\text{new}}$ ) on the gauge boson self-energies. (Brief remarks are made on new physics which is not of this type.) Most of the effects on precision measurements can be described by three gauge self-energy parameters  $S$ ,  $T$ , and  $U$ . We will define these, as well as the related parameters  $\rho_0$ ,  $\epsilon_i$ , and  $\widehat{\epsilon}_i$ , to arise from new physics only. In other words, they are equal to zero ( $\rho_0 = 1$ ) exactly in the SM, and do not include any (loop induced) contributions that depend on  $m_t$  or  $M_H$ , which are treated separately. Our treatment differs from most of the original papers.

The dominant effect of many extensions of the SM can be described by the  $\rho_0$  parameter,

$$\rho_0 \equiv \frac{M_W^2}{M_Z^2 \widehat{c}_Z^2 \widehat{\rho}}, \quad (10.66)$$

which describes new sources of SU(2) breaking that cannot be accounted for by the SM Higgs doublet or by  $m_t$  effects.  $\widehat{\rho}$  is calculated as in Eq. (10.18) assuming the validity of the SM. In the

presence of  $\rho_0 \neq 1$ , Eq. (10.66) generalizes the second Eq. (10.18) while the first remains unchanged. Provided that the new physics which yields  $\rho_0 \neq 1$  is a small perturbation which does not significantly affect other radiative corrections,  $\rho_0$  can be regarded as a phenomenological parameter which multiplies  $G_F$  in Eqs. (10.21) and (10.41), as well as  $\Gamma_Z$  in Eq. (10.60c). There are enough data to determine  $\rho_0$ ,  $M_H$ ,  $m_t$ , and  $\alpha_s$ , simultaneously. From the global fit,

$$\rho_0 = 1.00038 \pm 0.00020, \quad (10.67a)$$

$$\alpha_s(M_Z) = 0.1188 \pm 0.0017, \quad (10.67b)$$

where as before the uncertainty is from the experimental inputs and includes an estimate of the error from unknown higher-order electroweak corrections. The result in Eq. (10.67a) is 1.9  $\sigma$  above the SM expectation,  $\rho_0 = 1$ . It can be used to constrain higher-dimensional Higgs representations to have vacuum expectation values of less than a few percent of those of the doublets. Indeed, the relation between  $M_W$  and  $M_Z$  is modified if there are Higgs multiplets with weak isospin  $> 1/2$  and significant vacuum expectation values. For a general (charge-conserving) Higgs structure,

$$\rho_0 = \frac{\sum_i [t_i(t_i + 1) - t_{3i}^2] |v_i|^2}{2 \sum_i t_{3i}^2 |v_i|^2}, \quad (10.68)$$

where  $v_i$  is the expectation value of the neutral component of a Higgs multiplet with weak isospin  $t_i$  and third component  $t_{3i}$ . In order to calculate to higher orders in such theories one must define a set of four fundamental renormalized parameters which one may conveniently choose to be  $\alpha$ ,  $G_F$ ,  $M_Z$ , and  $M_W$ , since  $M_W$  and  $M_Z$  are directly measurable. Then  $\widehat{s}_Z^2$  and  $\rho_0$  can be considered dependent parameters.

Eq. (10.67a) can also be used to constrain other types of new physics. For example, non-degenerate multiplets of heavy

fermions or scalars break the vector part of weak SU(2) and lead to a decrease in the value of  $M_Z/M_W$ . Each non-degenerate SU(2) doublet  $\begin{pmatrix} f_1 \\ f_2 \end{pmatrix}$  yields a positive contribution to  $\rho_0$  [319–321] of

$$\frac{N_C G_F}{8\sqrt{2}\pi^2} \Delta m^2, \quad (10.69)$$

where

$$\Delta m^2 \equiv m_1^2 + m_2^2 - \frac{4m_1^2 m_2^2}{m_1^2 - m_2^2} \ln \frac{m_1}{m_2} \geq (m_1 - m_2)^2, \quad (10.70)$$

and  $N_C = 1$  (3) for color singlets (triplets). Eq. (10.67a) taken together with Eq. (10.69) implies the following constraint on the mass splitting at the 90% CL,

$$(14 \text{ GeV})^2 < \sum_i \frac{N_C^i}{3} \Delta m_i^2 < (48 \text{ GeV})^2, \quad (10.71)$$

where the sum runs over all new-physics doublets, for example fourth-family quarks or leptons,  $\begin{pmatrix} t' \\ b' \end{pmatrix}$  or  $\begin{pmatrix} \nu' \\ e' \end{pmatrix}$ , vector-like fermion doublets (which contribute to the sum in Eq. (10.71) with an extra factor of 2), and scalar doublets such as  $\begin{pmatrix} \xi \\ \eta \end{pmatrix}$  in Supersymmetry (in the absence of  $L$ - $R$  mixing).

Non-degenerate multiplets usually imply  $\rho_0 > 1$ . Similarly, heavy  $Z'$  bosons decrease the prediction for  $M_Z$  due to mixing and generally lead to  $\rho_0 > 1$  [322]. On the other hand, extra Higgs doublets participating in spontaneous symmetry breaking [323–325] or heavy lepton doublets involving Majorana neutrinos [326], both of which have more complicated expressions, and the  $\nu_i$  of higher-dimensional Higgs representations can contribute to  $\rho_0$  with either sign.

A number of authors [327–329] have considered the general effects on neutral-current,  $Z$  and  $W$  boson observables of various types of heavy (*i.e.*,  $M_{\text{new}} \gg M_Z$ ) physics which contribute to the  $W$  and  $Z$  self-energies but which do not have any direct coupling to the ordinary fermions (an alternative formulation is given by Ref. [330]). In addition to non-degenerate multiplets, which break the vector part of weak SU(2), these include heavy degenerate multiplets of chiral fermions which break the axial generators.

Such effects can be described by just three parameters,  $S$ ,  $T$ , and  $U$  [331], at the (EW) one-loop level<sup>15</sup>.  $T$  is proportional to the difference between the  $W$  and  $Z$  self-energies at  $Q^2 = 0$  (*i.e.*, vector SU(2)-breaking), while  $S$  ( $S + U$ ) is associated with the difference between the  $Z$  ( $W$ ) self-energy at  $Q^2 = M_{Z,W}^2$  and  $Q^2 = 0$  (axial SU(2)-breaking). Denoting the contributions of new physics to the various self-energies by  $\Pi_{ij}^{\text{new}}$ , we have

$$\widehat{\alpha}(M_Z)T \equiv \frac{\Pi_{WW}^{\text{new}}(0)}{M_W^2} - \frac{\Pi_{ZZ}^{\text{new}}(0)}{M_Z^2}, \quad (10.72a)$$

$$\begin{aligned} \frac{\widehat{\alpha}(M_Z)}{4\widehat{s}_Z^2\widehat{c}_Z^2} S \equiv & \frac{\Pi_{ZZ}^{\text{new}}(M_Z^2) - \Pi_{ZZ}^{\text{new}}(0)}{M_Z^2} - \frac{\widehat{c}_Z^2 - \widehat{s}_Z^2}{\widehat{c}_Z\widehat{s}_Z} \frac{\Pi_{Z\gamma}^{\text{new}}(M_Z^2)}{M_Z^2} \\ & - \frac{\Pi_{\gamma\gamma}^{\text{new}}(M_Z^2)}{M_Z^2}, \end{aligned} \quad (10.72b)$$

$$\begin{aligned} \frac{\widehat{\alpha}(M_Z)}{4\widehat{s}_Z^2} (S + U) \equiv & \frac{\Pi_{WW}^{\text{new}}(M_W^2) - \Pi_{WW}^{\text{new}}(0)}{M_W^2} - \frac{\widehat{c}_Z}{\widehat{s}_Z} \frac{\Pi_{Z\gamma}^{\text{new}}(M_Z^2)}{M_Z^2} \\ & - \frac{\Pi_{\gamma\gamma}^{\text{new}}(M_Z^2)}{M_Z^2}. \end{aligned} \quad (10.72c)$$

$S$ ,  $T$ , and  $U$  are defined with a factor proportional to  $\widehat{\alpha}$  removed, so that they are expected to be of order unity in the presence of new physics. In the  $\overline{\text{MS}}$  scheme as defined in Ref. [71], the last

<sup>15</sup>Three additional parameters are needed if the new physics scale is comparable to  $M_Z$  [332]. Further generalizations, including effects relevant to LEP 2 and Drell-Yan production at the LHC, are described in Refs. [333] and [334], respectively.

two terms in Eqs. (10.72b) and (10.72c) can be omitted, as was done in some earlier editions of this *Review*. These parameters are related to other parameter sets,  $S_i$  [71],  $\widehat{\epsilon}_i$  [335], and  $h_i$  [336], by

$$T = h_V = \frac{\widehat{\epsilon}_1}{\widehat{\alpha}(M_Z)}, \quad (10.73a)$$

$$S = h_{AZ} = S_Z = 4\widehat{s}_Z^2 \frac{\widehat{\epsilon}_3}{\widehat{\alpha}(M_Z)}, \quad (10.73b)$$

$$U = h_{AW} - h_{AZ} = S_W - S_Z = -4\widehat{s}_Z^2 \frac{\widehat{\epsilon}_2}{\widehat{\alpha}(M_Z)}. \quad (10.73c)$$

A heavy non-degenerate multiplet of fermions or scalars contributes positively to  $T$  as

$$\rho_0 - 1 = \frac{1}{1 - \widehat{\alpha}(M_Z)T} - 1 \approx \widehat{\alpha}(M_Z)T, \quad (10.74)$$

where  $\rho_0 - 1$  is given in Eq. (10.69). The effects of non-standard Higgs representations cannot be separated from heavy non-degenerate multiplets unless the new physics has other consequences, such as vertex corrections. Most of the original papers defined  $T$  to include the effects of loops only. However, we will redefine  $T$  to include all new sources of SU(2) breaking, including non-standard Higgs, so that  $T$  and  $\rho_0$  are equivalent by Eq. (10.74).

A multiplet of heavy degenerate chiral fermions yields

$$S = \frac{N_C}{3\pi} \sum_i (t_{3i}^L - t_{3i}^R)^2, \quad (10.75)$$

where  $t_{3i}^{L,R}$  is the 3<sup>rd</sup> component of weak isospin of the left-(right)-handed component of fermion  $i$ . For example, a heavy degenerate ordinary or mirror family would contribute  $2/3\pi$  to  $S$ . In models with warped extra dimensions [337], sizeable corrections to the  $S$  parameter are generated through mixing between the SM gauge bosons and their Kaluza-Klein (KK) excitations, and one finds  $S \approx 30 v^2 M_{KK}^{-2}$  [338], where  $M_{KK}$  is the mass scale of the KK gauge bosons. Large positive values of  $S$  can also be generated in models with dynamical electroweak symmetry breaking, where the Higgs boson is composite. In simple composite Higgs models, the dominant contribution stems from heavy spin-1 resonances of the strong dynamics leading to  $S \approx 4\pi v^2 (M_V^{-2} + M_A^{-2})$ , where  $M_{V,A}$  are the masses of the lightest vector and axial-vector resonances, respectively [339].

Negative values of  $S$  are possible, for example, in models of walking Technicolor [340–347], or from loops involving scalars or Majorana particles [348, 349]. The simplest origin of  $S < 0$  would probably be an additional heavy  $Z'$  boson [322]. Supersymmetric extensions of the SM [350, 351] generally give very small effects. For more details and references, see Refs. [352–361] and the Sections on “Supersymmetry” in this *Review*. Most simple types of new physics yield  $U = 0$ , although there are counter-examples, such as the effects of anomalous triple gauge vertices [335].

The SM expressions for observables are replaced by,

$$M_Z^2 = M_{Z0}^2 \frac{1 - \widehat{\alpha}(M_Z)T}{1 - G_F M_{Z0}^2 S / 2\sqrt{2}\pi}, \quad (10.76a)$$

$$M_W^2 = M_{W0}^2 \frac{1}{1 - G_F M_{W0}^2 (S + U) / 2\sqrt{2}\pi}, \quad (10.76b)$$

where  $M_{Z0}$  and  $M_{W0}$  are the SM expressions (as functions of  $m_t$  and  $M_H$ ) in the  $\overline{\text{MS}}$  scheme. Furthermore,

$$\Gamma_Z = \frac{M_Z^3 \beta_Z}{1 - \widehat{\alpha}(M_Z)T}, \quad (10.77a)$$

$$\Gamma_W = M_W^3 \beta_W, \quad (10.77b)$$

$$A_i = \frac{A_{i0}}{1 - \widehat{\alpha}(M_Z)T}, \quad (10.77c)$$

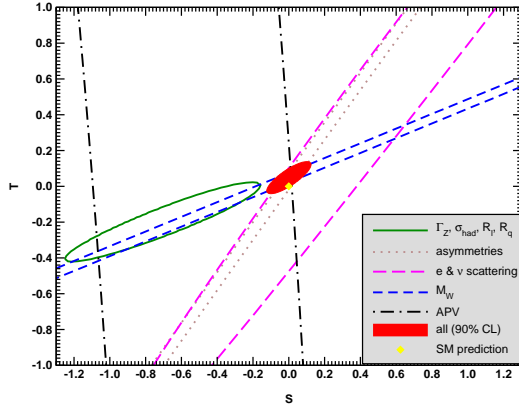


Figure 10.6:  $1\sigma$  constraints (39.35% for the closed contours and 68% for the others) on  $S$  and  $T$  (for  $U = 0$ ) from various inputs combined with  $M_Z$ .  $S$  and  $T$  represent the contributions of new physics only. Data sets not involving  $M_W$  or  $\Gamma_W$  are insensitive to  $U$ . With the exception of the fit to all data, we fix  $\alpha_s = 0.1185$ . The black dot indicates the Standard Model values  $S = T = 0$ .

where  $\beta_{Z,W}$  are the SM expressions for the reduced widths  $\Gamma_{Z0}/M_{Z0}^3$  and  $\Gamma_{W0}/M_{W0}^3$ ,  $M_Z$  and  $M_W$  are the physical masses, and  $A_i$  ( $A_{i0}$ ) is a neutral-current amplitude (in the SM).

The data allows for a simultaneous determination of  $M_H$  and  $m_t$  (from the hadron colliders),  $S$  (from  $M_Z$ ),  $T$  (mainly from  $\Gamma_Z$ ),  $U$  (from  $M_W$ ),  $\hat{s}_Z^2 = 0.23112 \pm 0.00013$  (from the  $Z$  pole asymmetries), and  $\alpha_s(M_Z) = 0.1189 \pm 0.0018$  (from  $R_\ell$ ,  $\sigma_{\text{had}}$ , and  $\tau_\tau$ ), giving,

$$S = -0.01 \pm 0.10, \quad (10.78a)$$

$$T = 0.03 \pm 0.12, \quad (10.78b)$$

$$U = 0.02 \pm 0.11, \quad (10.78c)$$

with little correlation among the SM parameters, where the uncertainties are from unknown higher orders in the SM predictions and the inputs. The parameters in Eq. (10.78), which by definition are due to new physics only, are in excellent agreement with the SM values of zero. Fixing  $U = 0$ , which is motivated by the fact that  $U$  is suppressed by an additional factor  $M_{\text{new}}^2/M_Z^2$  compared to  $S$  and  $T$  [362], greatly improves the precision on  $S$  and particularly  $T$ ,

$$S = 0.00 \pm 0.07, \quad (10.79a)$$

$$T = 0.05 \pm 0.06. \quad (10.79b)$$

If only any one of the three parameters is allowed, then this parameter would deviate at the 1.6 to 1.9  $\sigma$  level, reflecting the deviation in  $M_W$ . Using Eq. (10.74), the value of  $\rho_0$  corresponding to  $T$  in Eqs. (10.78) is  $1.0002 \pm 0.0009$ , while the one corresponding to Eqs. (10.79) is  $1.0004 \pm 0.0005$ . Thus, the multi-parameter fits are consistent with  $\rho_0 = 1$ , in contrast to the fit with  $S = U = 0$  in Eq. (10.67a). There is a strong correlation (92%) between the  $S$  and  $T$  parameters. The  $U$  parameter is  $-80\%$  ( $-93\%$ ) anticorrelated with  $S$  ( $T$ ). The allowed regions in  $S$ - $T$  (for  $U = 0$ ) are shown in Fig. 10.6. From Eq. (10.78) one obtains  $S < 0.14$  and  $T < 0.22$  at 95% CL, where the former puts the constraint  $M_{KK} \gtrsim 3.6$  TeV on the masses of KK gauge bosons in warped extra dimensions. In minimal composite Higgs models, the bound on  $S$  requires  $M_V \gtrsim 4$  TeV [363], but this constraint can be relaxed, *e.g.*, if the fermionic sector is also allowed to be partially composite [364, 365].

The  $S$  parameter can also be used to constrain the number of fermion families, *under the assumption* that there are no new contributions to  $T$  or  $U$  and therefore that any new families are degenerate; then an extra generation of SM fermions is excluded at the  $8\sigma$  level corresponding to  $N_F = 2.75 \pm 0.15$ . This can be compared to the fit to the number of light neutrinos given in Eq. (10.63),

$N_\nu = 3.0026 \pm 0.0061$ , but the  $S$  parameter fits are valid even for a very heavy fourth family neutrino. Allowing  $T$  to vary as well, the constraint on a fourth family is weaker [366]. However, a heavy fourth family would increase the Higgs production cross-section through gluon fusion by a factor of about 9 [367], which is in considerable tension with the observed Higgs signal at the LHC [368]. Combining the limits from electroweak precision data with the measured Higgs production rate and limits from direct searches for heavy quarks [369], a fourth family of chiral fermions is now excluded by more than five standard deviations [370, 371]. Similar remarks apply to a heavy mirror family [372] involving right-handed SU(2) doublets and left-handed singlets. In contrast, new doublets that receive most of their mass from a different source than the Higgs vacuum expectation value, such as vector-like fermion doublets or scalar doublets in Supersymmetry, give small or no contribution to  $S$ ,  $T$ ,  $U$ , and the Higgs production cross-section and are therefore still allowed. Partial or complete vector-like fermion families are predicted in many Grand Unified Theories [373] (see the Section on “Grand Unified Theories” in this *Review*), and many other models including supersymmetric and superstring inspired ones [374–377].

As discussed in Sec. 10.6, there is a 3.6% deviation in the asymmetry parameter  $A_b$ . Assuming that this is due to new physics affecting preferentially the third generation, we can perform a fit allowing additional  $Z \rightarrow b\bar{b}$  vertex corrections  $\rho_b$  and  $\kappa_b$  as in Eq. (10.42) (here defined to be due to new physics only with the SM contributions removed), as well as  $S$ ,  $T$ ,  $U$ , and the SM parameters, with the result,

$$\rho_b = 0.058 \pm 0.020, \quad (10.80a)$$

$$\kappa_b = 0.185 \pm 0.067, \quad (10.80b)$$

with an almost perfect correlation of 99% (because  $R_b$  is much better determined than  $A_b$ ). The central values of the oblique parameters are consistent with their SM values of zero, and there is little change in the SM parameters, except that the value of  $\alpha_s(M_Z)$  is lower by 0.0008 compared to the SM fit. Given that an  $\mathcal{O}(20\%)$  correction to  $\kappa_b$  would be necessary, it would be difficult to account for the deviation in  $A_b$  by new physics that enters only at the level of radiative corrections. Thus, if it is due to new physics, it is most likely of tree-level type affecting preferentially the third generation. Examples include the decay of a scalar neutrino resonance [378], mixing of the  $b$  quark with heavy exotics [379], and a heavy  $Z'$  with family non-universal couplings [380, 381]. It is difficult, however, to simultaneously account for  $R_b$  without tuning, which has been measured on the  $Z$  peak and off-peak [382] at LEP 1.

There is no simple parametrization to describe the effects of every type of new physics on every possible observable. The  $S$ ,  $T$ , and  $U$  formalism describes many types of heavy physics which affect only the gauge self-energies, and it can be applied to all precision observables. However, new physics which couples directly to ordinary fermions cannot be fully parametrized in the  $S$ ,  $T$ , and  $U$  framework. Examples include heavy  $Z'$  bosons [322], mixing with exotic fermions [9, 383, 384], leptoquark exchange [260, 385, 386], supersymmetric models, strong EW dynamics [364], Little Higgs models [387, 388], and TeV-scale extra spatial dimensions [389–392] (for more details and references, see the Section on “Extra Dimensions” in this *Review*). These types of new physics can be parametrized in a model-independent way by using an effective field theory description [393–396]. Here the SM is extended by a set of higher-dimensional operators, denoted  $\mathcal{O}_i$ ,

$$\mathcal{L} = \mathcal{L}_{\text{SM}} + \sum_{d>4} \sum_i \frac{C_i}{\Lambda^{d-4}} \mathcal{O}_i, \quad (10.81)$$

where  $\Lambda$  is the characteristic scale of the new physics sector, which is assumed to satisfy  $\Lambda \gg v$ . For EW precision observables, the leading new operators enter at dimension  $d = 6$ . Note that  $S$  and  $T$  can be identified with two of these operators (or linear combinations thereof, depending on the chosen operator basis), while  $U$  corresponds to a dimension-8 operator [362, 397]. With current data on  $M_W$  and  $Z$  pole observables,  $\Lambda$  is constrained to

be larger than  $\mathcal{O}(\text{TeV})$  if the Wilson coefficients  $C_i$  are of order unity [398–402].

An alternate formalism [403] defines parameters,  $\epsilon_1, \epsilon_2, \epsilon_3$ , and  $\epsilon_b$  in terms of the specific observables  $M_W/M_Z, \Gamma_{\ell\ell}, A_{FB}^{(0,\ell)}$ , and  $R_b$ . The definitions coincide with those for  $\hat{\epsilon}_i$  in Eqs. (10.72) and (10.73c) for physics which affects gauge self-energies only, but the  $\epsilon$ 's now parametrize arbitrary types of new physics. However, the  $\epsilon_i$  are not related to other observables unless additional model-dependent assumptions are made.

Limits on new four-Fermi operators and on leptoquarks using LEP 2 and lower energy data are given in Refs. [260, 404–406], while constraints on various types of new physics are addressed in Refs. [9, 151, 277, 407, 408]. For a particularly well motivated and explored type of physics beyond the SM, see the Section on “ $Z'$ -Boson Searches” in this *Review*.

#### Acknowledgments

It is a pleasure to thank Rodolfo Ferro-Hernández for discussions, for performing some of the calculations and checks, and for producing the plot in Fig. 10.2. J.E. is supported by the German–Mexican research collaboration grant SP 778/4–1 (DFG) and 278017 (CONACyT). A.F. is supported in part by the National Science Foundation under grant no. PHY–1820760.

#### References

- [1] S. Glashow, Nucl. Phys. **22**, 579 (1961).
- [2] S. Weinberg, Phys. Rev. Lett. **19**, 1264 (1967).
- [3] A. Salam, Conf. Proc. C **680519**, 367 (1968).
- [4] S. Glashow, J. Iliopoulos and L. Maiani, Phys. Rev. D **2**, 1285 (1970).
- [5] N. Cabibbo, Phys. Rev. Lett. **10**, 531 (1963).
- [6] M. Kobayashi and T. Maskawa, Prog. Theor. Phys. **49**, 652 (1973).
- [7] S. Descotes-Genon and P. Koppenburg, Ann. Rev. Nucl. Part. Sci. **67**, 97 (2017), [arXiv:1702.08834].
- [8] E. Commins and P. Bucksbaum, *Weak Interactions of Leptons and Quarks*, Cambridge Univ. Pr., Cambridge, USA (1983), ISBN 978-0-521-27370-1.
- [9] P. Langacker, editor, *Precision tests of the standard electroweak model*, volume 14, WSP, Singapore (1996).
- [10] P. Langacker, *The standard model and beyond*, CRC Pr., Boca Raton, USA (2010), ISBN 978-1-4200-7906-7.
- [11] T. Kinoshita, editor, *Quantum electrodynamics*, volume 7, WSP, Singapore (1990).
- [12] S. G. Karshenboim, Phys. Rept. **422**, 1 (2005), [hep-ph/0509010].
- [13] J. Erler and S. Su, Prog. Part. Nucl. Phys. **71**, 119 (2013), [arXiv:1303.5522].
- [14] S. Schael *et al.* (ALEPH, DELPHI, L3, OPAL, SLD, LEP Electroweak Working Group, SLD Electroweak Group, SLD Heavy Flavour Group), Phys. Rept. **427**, 257 (2006), [hep-ex/0509008].
- [15] D. Webber *et al.* (MuLan), Phys. Rev. Lett. **106**, 041803 (2011), [arXiv:1010.0991].
- [16] T. Kinoshita and A. Sirlin, Phys. Rev. **113**, 1652 (1959).
- [17] T. van Ritbergen and R. G. Stuart, Nucl. Phys. B **564**, 343 (2000), [hep-ph/9904240].
- [18] M. Steinhauser and T. Seidensticker, Phys. Lett. B **467**, 271 (1999), [hep-ph/9909436].
- [19] Y. Nir, Phys. Lett. B **221**, 184 (1989).
- [20] A. Pak and A. Czarnecki, Phys. Rev. Lett. **100**, 241807 (2008), [arXiv:0803.0960].
- [21] T. Aoyama, T. Kinoshita and M. Nio, Atoms **7**, 1, 28 (2019).
- [22] P. J. Mohr, D. B. Newell and B. N. Taylor, Rev. Mod. Phys. **88**, 3, 035009 (2016), [arXiv:1507.07956].
- [23] R. Bouchendira *et al.*, Phys. Rev. Lett. **106**, 080801 (2011), [arXiv:1012.3627].
- [24] R. H. Parker *et al.*, Science **360**, 191 (2018), [arXiv:1812.04130].
- [25] G. Abbiendi *et al.* (OPAL), Eur. Phys. J. C **45**, 1 (2006), [hep-ex/0505072].
- [26] P. Achard *et al.* (L3), Phys. Lett. B **623**, 26 (2005), [hep-ex/0507078].
- [27] S. Fanchiotti, B. A. Kniehl and A. Sirlin, Phys. Rev. D **48**, 307 (1993), [hep-ph/9212285].
- [28] J. Erler, Phys. Rev. D **59**, 054008 (1999), [hep-ph/9803453].
- [29] M. Davier *et al.*, Eur. Phys. J. C **80**, 3, 241 (2020), [arXiv:1908.00921].
- [30] F. Jegerlehner, EPJ Web Conf. **118**, 01016 (2016), [arXiv:1511.04473].
- [31] F. Jegerlehner and R. Szafron, Eur. Phys. J. C **71**, 1632 (2011), [arXiv:1101.2872].
- [32] J. Erler (1999), [hep-ph/0005084].
- [33] M. Steinhauser, Phys. Lett. B **429**, 158 (1998), [hep-ph/9803313].
- [34] K. Chetyrkin, J. H. Kuhn and M. Steinhauser, Nucl. Phys. B **482**, 213 (1996), [hep-ph/9606230].
- [35] J. Erler and R. Ferro-Hernández, JHEP **03**, 196 (2018), [arXiv:1712.09146].
- [36] *Theory report on the 11th FCC-ee workshop* (2019), [arXiv:1905.05078].
- [37] A. Keshavarzi, D. Nomura and T. Teubner, Phys. Rev. D **101**, 1, 014029 (2020), [arXiv:1911.00367].
- [38] M. Davier *et al.*, Eur. Phys. J. C **71**, 1515 (2011), [Erratum: Eur.Phys.J.C **72**, 1874 (2012)], [arXiv:1010.4180].
- [39] K. Ackerstaff *et al.* (OPAL), Eur. Phys. J. C **7**, 571 (1999), [hep-ex/9808019].
- [40] S. Anderson *et al.* (CLEO), Phys. Rev. D **61**, 112002 (2000), [hep-ex/9910046].
- [41] S. Schael *et al.* (ALEPH), Phys. Rept. **421**, 191 (2005), [hep-ex/0506072].
- [42] M. Fujikawa *et al.* (Belle), Phys. Rev. D **78**, 072006 (2008), [arXiv:0805.3773].
- [43] S. Groote *et al.*, Phys. Lett. B **440**, 375 (1998), [hep-ph/9802374].
- [44] B. Geshkenbein and V. Morgunov, Phys. Lett. B **352**, 456 (1995).
- [45] M. L. Swartz, Phys. Rev. D **53**, 5268 (1996), [hep-ph/9509248].
- [46] N. Krasnikov and R. Rodenberg, Nuovo Cim. A **111**, 217 (1998), [hep-ph/9711367].
- [47] J. H. Kuhn and M. Steinhauser, Phys. Lett. B **437**, 425 (1998), [hep-ph/9802241].
- [48] A. D. Martin, J. Outhwaite and M. Ryskin, Phys. Lett. B **492**, 69 (2000), [hep-ph/0008078].
- [49] J. de Troconiz and F. Yndurain, Phys. Rev. D **65**, 093002 (2002), [hep-ph/0107318].
- [50] H. Burkhardt and B. Pietrzyk, Phys. Rev. D **84**, 037502 (2011), [arXiv:1106.2991].
- [51] J. Erler, P. Masjuan and H. Spiesberger, Eur. Phys. J. C **77**, 2, 99 (2017), [arXiv:1610.08531].
- [52] V. Novikov *et al.*, Phys. Rept. **41**, 1 (1978).
- [53] J. Erler and M. Luo, Phys. Lett. B **558**, 125 (2003), [hep-ph/0207114].
- [54] T. Aaltonen *et al.* (CDF, DØ, Tevatron Electroweak Working Group) (2016), [arXiv:1608.01881].
- [55] M. Aaboud *et al.* (ATLAS), Eur. Phys. J. C **79**, 4, 290 (2019), [arXiv:1810.01772].
- [56] Technical Report CMS-PAS-TOP-15-012, CERN, Geneva (2016), URL <https://cds.cern.ch/record/2235162>.

- [57] A. M. Sirunyan *et al.* (CMS), *Eur. Phys. J. C* **79**, 4, 313 (2019), [arXiv:1812.10534].
- [58] A. M. Sirunyan *et al.* (CMS), *Eur. Phys. J. C* **79**, 5, 368 (2019), [arXiv:1812.10505].
- [59] Technical Report ATLAS-CONF-2019-046, CERN, Geneva (2019), URL <https://cds.cern.ch/record/2693954>.
- [60] V. M. Abazov *et al.* (DØ), *Phys. Rev. Lett.* **113**, 032002 (2014), [arXiv:1405.1756].
- [61] A. M. Sirunyan *et al.* (CMS), *Eur. Phys. J. C* **78**, 11, 891 (2018), [arXiv:1805.01428].
- [62] A. H. Hoang, S. Plätzer and D. Samitz, *JHEP* **10**, 200 (2018), [arXiv:1807.06617].
- [63] M. Beneke *et al.*, *Phys. Lett. B* **775**, 63 (2017), [arXiv:1605.03609].
- [64] P. Marquard *et al.*, *Phys. Rev. Lett.* **114**, 14, 142002 (2015), [arXiv:1502.01030].
- [65] M. Beneke, *Phys. Rept.* **317**, 1 (1999), [hep-ph/9807443].
- [66] S. Catani *et al.*, *JHEP* **07**, 100 (2019), [arXiv:1906.06535].
- [67] Technical Report CMS-PAS-TOP-18-004, CERN, Geneva (2018), URL <https://cds.cern.ch/record/2647989>.
- [68] G. Aad *et al.* (ATLAS), *JHEP* **11**, 150 (2019), [arXiv:1905.02302].
- [69] J. Erler and M. Schott, *Prog. Part. Nucl. Phys.* **106**, 68 (2019), [arXiv:1902.05142].
- [70] A. Sirlin, *Phys. Rev. D* **22**, 971 (1980).
- [71] W. J. Marciano and J. L. Rosner, *Phys. Rev. Lett.* **65**, 2963 (1990), [Erratum: *Phys.Rev.Lett.* 68, 898 (1992)].
- [72] G. Degrassi, S. Fanchiotti and A. Sirlin, *Nucl. Phys. B* **351**, 49 (1991).
- [73] A. Czarnecki and W. J. Marciano, *Int. J. Mod. Phys. A* **15**, 2365 (2000), [hep-ph/0003049].
- [74] J. Erler and M. J. Ramsey-Musolf, *Phys. Rev. D* **72**, 073003 (2005), [hep-ph/0409169].
- [75] K. Kumar *et al.*, *Ann. Rev. Nucl. Part. Sci.* **63**, 237 (2013), [arXiv:1302.6263].
- [76] G. Degrassi and A. Sirlin, *Nucl. Phys. B* **352**, 342 (1991).
- [77] P. Gambino and A. Sirlin, *Phys. Rev. D* **49**, 1160 (1994), [hep-ph/9309326].
- [78] W. Hollik, *Fortsch. Phys.* **38**, 165 (1990).
- [79] R. Barbieri *et al.*, *Nucl. Phys. B* **409**, 105 (1993).
- [80] J. Fleischer, O. Tarasov and F. Jegerlehner, *Phys. Lett. B* **319**, 249 (1993).
- [81] G. Degrassi, P. Gambino and A. Vicini, *Phys. Lett. B* **383**, 219 (1996), [hep-ph/9603374].
- [82] G. Degrassi, P. Gambino and A. Sirlin, *Phys. Lett. B* **394**, 188 (1997), [hep-ph/9611363].
- [83] A. Freitas *et al.*, *Phys. Lett. B* **495**, 338 (2000), [Erratum: *Phys.Lett.B* 570, 265 (2003)], [hep-ph/0007091].
- [84] M. Awramik and M. Czakon, *Phys. Lett. B* **568**, 48 (2003), [hep-ph/0305248].
- [85] A. Freitas *et al.*, *Nucl. Phys. B* **632**, 189 (2002), [Erratum: *Nucl.Phys.B* 666, 305–307 (2003)], [hep-ph/0202131].
- [86] M. Awramik and M. Czakon, *Phys. Rev. Lett.* **89**, 241801 (2002), [hep-ph/0208113].
- [87] A. Onishchenko and O. Veretin, *Phys. Lett. B* **551**, 111 (2003), [hep-ph/0209010].
- [88] G. Degrassi, P. Gambino and P. P. Giardino, *JHEP* **05**, 154 (2015), [arXiv:1411.7040].
- [89] M. Awramik *et al.*, *Phys. Rev. D* **69**, 053006 (2004), [hep-ph/0311148].
- [90] M. Awramik *et al.*, *Phys. Rev. Lett.* **93**, 201805 (2004), [hep-ph/0407317].
- [91] W. Hollik, U. Meier and S. Uccirati, *Nucl. Phys. B* **731**, 213 (2005), [hep-ph/0507158].
- [92] M. Awramik, M. Czakon and A. Freitas, *Phys. Lett. B* **642**, 563 (2006), [hep-ph/0605339].
- [93] W. Hollik, U. Meier and S. Uccirati, *Nucl. Phys. B* **765**, 154 (2007), [hep-ph/0610312].
- [94] M. Awramik *et al.*, *Nucl. Phys. B* **813**, 174 (2009), [arXiv:0811.1364].
- [95] I. Dubovyk *et al.*, *Phys. Lett. B* **762**, 184 (2016), [arXiv:1607.08375].
- [96] A. Freitas, *Phys. Lett. B* **730**, 50 (2014), [arXiv:1310.2256].
- [97] A. Freitas, *JHEP* **04**, 070 (2014), [arXiv:1401.2447].
- [98] I. Dubovyk *et al.*, *Phys. Lett. B* **783**, 86 (2018), [arXiv:1804.10236].
- [99] I. Dubovyk *et al.*, *JHEP* **08**, 113 (2019), [arXiv:1906.08815].
- [100] M. Awramik, M. Czakon and A. Freitas, *JHEP* **11**, 048 (2006), [hep-ph/0608099].
- [101] A. Djouadi and C. Verzegnassi, *Phys. Lett. B* **195**, 265 (1987).
- [102] A. Djouadi, *Nuovo Cim. A* **100**, 357 (1988).
- [103] K. Chetyrkin, J. H. Kuhn and M. Steinhauser, *Phys. Lett. B* **351**, 331 (1995), [hep-ph/9502291].
- [104] L. Avdeev *et al.*, *Phys. Lett. B* **336**, 560 (1994), [Erratum: *Phys.Lett.B* 349, 597–598 (1995)], [hep-ph/9406363].
- [105] Y. Schroder and M. Steinhauser, *Phys. Lett. B* **622**, 124 (2005), [hep-ph/0504055].
- [106] K. Chetyrkin *et al.*, *Phys. Rev. Lett.* **97**, 102003 (2006), [hep-ph/0605201].
- [107] R. Boughezal and M. Czakon, *Nucl. Phys. B* **755**, 221 (2006), [hep-ph/0606232].
- [108] B. A. Kniehl, J. H. Kuhn and R. Stuart, *Phys. Lett. B* **214**, 621 (1988).
- [109] B. A. Kniehl, *Nucl. Phys. B* **347**, 86 (1990).
- [110] F. Halzen and B. A. Kniehl, *Nucl. Phys. B* **353**, 567 (1991).
- [111] A. Djouadi and P. Gambino, *Phys. Rev. D* **49**, 3499 (1994), [Erratum: *Phys.Rev.D* 53, 4111 (1996)], [hep-ph/9309298].
- [112] A. Anselm, N. Dombey and E. Leader, *Phys. Lett. B* **312**, 232 (1993).
- [113] K. Chetyrkin, J. H. Kuhn and M. Steinhauser, *Phys. Rev. Lett.* **75**, 3394 (1995), [hep-ph/9504413].
- [114] J. van der Bij *et al.*, *Phys. Lett. B* **498**, 156 (2001), [hep-ph/0011373].
- [115] M. Faisst *et al.*, *Nucl. Phys. B* **665**, 649 (2003), [hep-ph/0302275].
- [116] R. Boughezal, J. Tausk and J. van der Bij, *Nucl. Phys. B* **725**, 3 (2005), [hep-ph/0504092].
- [117] A. Arbuzov *et al.*, *Comput. Phys. Commun.* **174**, 728 (2006), [hep-ph/0507146].
- [118] J. Erler and M. J. Ramsey-Musolf, *Prog. Part. Nucl. Phys.* **54**, 351 (2005), [hep-ph/0404291].
- [119] J. Formaggio and G. Zeller, *Rev. Mod. Phys.* **84**, 1307 (2012), [arXiv:1305.7513].
- [120] J. Dorenbosch *et al.* (CHARM), *Z. Phys. C* **41**, 567 (1989), [Erratum: *Z.Phys.C* 51, 142 (1991)].
- [121] L. Ahrens *et al.*, *Phys. Rev. D* **41**, 3297 (1990).
- [122] P. Vilain *et al.* (CHARM-II), *Phys. Lett. B* **335**, 246 (1994).
- [123] R. Allen *et al.*, *Phys. Rev. D* **47**, 11 (1993).
- [124] L. Auerbach *et al.* (LSND), *Phys. Rev. D* **63**, 112001 (2001), [hep-ex/0101039].
- [125] M. Deniz *et al.* (TEXONO), *Phys. Rev. D* **81**, 072001 (2010), [arXiv:0911.1597].
- [126] J. M. Conrad, M. H. Shaevitz and T. Bolton, *Rev. Mod. Phys.* **70**, 1341 (1998), [hep-ex/9707015].

- [127] A. Blondel *et al.*, *Z. Phys. C* **45**, 361 (1990).
- [128] J. Allaby *et al.* (CHARM), *Z. Phys. C* **36**, 611 (1987).
- [129] K. S. McFarland *et al.* (CCFR, E744, E770), *Eur. Phys. J. C* **1**, 509 (1998), [hep-ex/9701010].
- [130] R. Barnett, *Phys. Rev. D* **14**, 70 (1976).
- [131] H. Georgi and H. Politzer, *Phys. Rev. D* **14**, 1829 (1976).
- [132] S. Rabinowitz *et al.*, *Phys. Rev. Lett.* **70**, 134 (1993).
- [133] E. Paschos and L. Wolfenstein, *Phys. Rev. D* **7**, 91 (1973).
- [134] G. Zeller *et al.* (NuTeV), *Phys. Rev. Lett.* **88**, 091802 (2002), [Erratum: *Phys.Rev.Lett.* 90, 239902 (2003)], [hep-ex/0110059].
- [135] D. Akimov *et al.* (COHERENT), *Science* **357**, 6356, 1123 (2017), [arXiv:1708.01294].
- [136] J. Erler *et al.*, *Ann. Rev. Nucl. Part. Sci.* **64**, 269 (2014), [arXiv:1401.6199].
- [137] C. Prescott *et al.*, *Phys. Lett. B* **84**, 524 (1979).
- [138] D. Wang *et al.* (PVDIS), *Nature* **506**, 7486, 67 (2014).
- [139] D. Wang *et al.*, *Phys. Rev. C* **91**, 4, 045506 (2015), [arXiv:1411.3200].
- [140] R. Hasty *et al.* (SAMPLE), *Science* **290**, 2117 (2000), [arXiv:nucl-ex/0102001].
- [141] E. Beise, M. Pitt and D. Spayde, *Prog. Part. Nucl. Phys.* **54**, 289 (2005), [arXiv:nucl-ex/0412054].
- [142] S.-L. Zhu *et al.*, *Phys. Rev. D* **62**, 033008 (2000), [hep-ph/0002252].
- [143] A. Argento *et al.*, *Phys. Lett. B* **120**, 245 (1983).
- [144] W. Heil *et al.*, *Nucl. Phys. B* **327**, 1 (1989).
- [145] P. Souder *et al.*, *Phys. Rev. Lett.* **65**, 694 (1990).
- [146] D. Armstrong and R. McKeown, *Ann. Rev. Nucl. Part. Sci.* **62**, 337 (2012), [arXiv:1207.5238].
- [147] E. Derman and W. J. Marciano, *Annals Phys.* **121**, 147 (1979).
- [148] P. Anthony *et al.* (SLAC E158), *Phys. Rev. Lett.* **95**, 081601 (2005), [hep-ex/0504049].
- [149] D. Androić *et al.* (Qweak), *Nature* **557**, 7704, 207 (2018), [arXiv:1905.08283].
- [150] R. D. Carlini *et al.*, *Ann. Rev. Nucl. Part. Sci.* **69**, 191 (2019).
- [151] J. Erler, A. Kurylov and M. J. Ramsey-Musolf, *Phys. Rev. D* **68**, 016006 (2003), [hep-ph/0302149].
- [152] R. D. Young *et al.*, *Phys. Rev. Lett.* **99**, 122003 (2007), [arXiv:0704.2618].
- [153] A. Acha *et al.* (HAPPEX), *Phys. Rev. Lett.* **98**, 032301 (2007), [arXiv:nucl-ex/0609002].
- [154] M. Gorchtein and C. Horowitz, *Phys. Rev. Lett.* **102**, 091806 (2009), [arXiv:0811.0614].
- [155] M. Gorchtein, C. Horowitz and M. J. Ramsey-Musolf, *Phys. Rev. C* **84**, 015502 (2011), [arXiv:1102.3910].
- [156] N. Hall *et al.*, *Phys. Lett. B* **753**, 221 (2016), [arXiv:1504.03973].
- [157] J. Erler *et al.*, *Phys. Rev. D* **100**, 5, 053007 (2019), [arXiv:1907.07928].
- [158] M. Bouchiat and C. Bouchiat, *Phys. Lett. B* **48**, 111 (1974).
- [159] M. Safronova *et al.*, *Rev. Mod. Phys.* **90**, 2, 025008 (2018), [arXiv:1710.01833].
- [160] C. Wood *et al.*, *Science* **275**, 1759 (1997).
- [161] J. Guena, M. Lintz and M. Bouchiat, *Phys. Rev. A* **71**, 042108 (2005), [arXiv:physics/0412017].
- [162] N. Edwards *et al.*, *Phys. Rev. Lett.* **74**, 2654 (1995).
- [163] P. Vetter *et al.*, *Phys. Rev. Lett.* **74**, 2658 (1995).
- [164] D. Meekhof *et al.*, *Phys. Rev. Lett.* **71**, 3442 (1993).
- [165] M. Macpherson *et al.*, *Phys. Rev. Lett.* **67**, 20, 2784 (1991).
- [166] P. Blunden, W. Melnitchouk and A. Thomas, *Phys. Rev. Lett.* **109**, 262301 (2012), [arXiv:1208.4310].
- [167] S. Bennett and C. E. Wieman, *Phys. Rev. Lett.* **82**, 2484 (1999), [Erratum: *Phys.Rev.Lett.* 82, 4153 (1999), Erratum: *Phys.Rev.Lett.* 83, 889 (1999)], [hep-ex/9903022].
- [168] V. Dzuba and V. Flambaum., *Phys. Rev. A* **62**, 052101 (2000), [arXiv:physics/0005038].
- [169] V. Dzuba, V. Flambaum and O. Sushkov, *Phys. Rev. A* **56**, 4357 (1997), [hep-ph/9709251].
- [170] D. Cho *et al.*, *Phys. Rev. A* **55**, 1007 (1997).
- [171] G. Toh *et al.*, *Phys. Rev. Lett.* **123**, 7, 073002 (2019), [arXiv:1905.02768].
- [172] A. A. Vasilyev *et al.*, *Phys. Rev. A* **66**, 020101 (2002).
- [173] V. Dzuba, V. Flambaum and J. Ginges, *Phys. Rev. D* **66**, 076013 (2002), [hep-ph/0204134].
- [174] J. Ginges and V. Flambaum, *Phys. Rept.* **397**, 63 (2004), [arXiv:physics/0309054].
- [175] A. Derevianko and S. G. Porsev, *Eur. Phys. J. A* **32**, 4, 517 (2007), [hep-ph/0608178].
- [176] B. Roberts, V. Dzuba and V. Flambaum, *Ann. Rev. Nucl. Part. Sci.* **65**, 63 (2015), [arXiv:1412.6644].
- [177] A. Derevianko, *Phys. Rev. Lett.* **85**, 1618 (2000), [hep-ph/0005274].
- [178] W. Johnson, I. Bednyakov and G. Soff, *Phys. Rev. Lett.* **87**, 233001 (2001), [Erratum: *Phys.Rev.Lett.* 88, 079903 (2002)], [hep-ph/0110262].
- [179] M. Kuchiev and V. Flambaum, *Phys. Rev. Lett.* **89**, 283002 (2002), [hep-ph/0206124].
- [180] A. Milstein, O. Sushkov and I. Terekhov, *Phys. Rev. Lett.* **89**, 283003 (2002), [hep-ph/0208227].
- [181] S. Porsev, K. Beloy and A. Derevianko, *Phys. Rev. Lett.* **102**, 181601 (2009), [arXiv:0902.0335].
- [182] V. Dzuba *et al.*, *Phys. Rev. Lett.* **109**, 203003 (2012), [arXiv:1207.5864].
- [183] C. Bouchiat and C. Pickety, *Phys. Lett. B* **128**, 73 (1983).
- [184] I. Zel'dovich, *J. Exp. Theor. Phys.* **6**, 1184 (1958).
- [185] V. Flambaum and D. Murray, *Phys. Rev. C* **56**, 1641 (1997), [arXiv:nucl-th/9703050].
- [186] W. Haxton and C. E. Wieman, *Ann. Rev. Nucl. Part. Sci.* **51**, 261 (2001), [arXiv:nucl-th/0104026].
- [187] V. Dzuba *et al.*, *J. Phys. B* **20**, 3297 (1987).
- [188] J. L. Rosner, *Phys. Rev. D* **53**, 2724 (1996), [hep-ph/9507375].
- [189] D. Antypas *et al.*, *Nature Phys.* **15**, 2, 120 (2019), [arXiv:1804.05747].
- [190] M. Ramsey-Musolf, *Phys. Rev. C* **60**, 015501 (1999), [hep-ph/9903264].
- [191] S. Pollock, E. Fortson and L. Wilets, *Phys. Rev. C* **46**, 2587 (1992), [arXiv:nucl-th/9211004].
- [192] B. Chen and P. Vogel, *Phys. Rev. C* **48**, 1392 (1993), [arXiv:nucl-th/9303003].
- [193] C. Horowitz *et al.*, *Phys. Rev. C* **63**, 025501 (2001), [arXiv:nucl-th/9912038].
- [194] S. Abrahamyan *et al.*, *Phys. Rev. Lett.* **108**, 112502 (2012), [arXiv:1201.2568].
- [195] H. Davoudiasl, H.-S. Lee and W. J. Marciano, *Phys. Rev. D* **86**, 095009 (2012), [arXiv:1208.2973].
- [196] E. Braaten, S. Narison and A. Pich, *Nucl. Phys. B* **373**, 581 (1992).
- [197] A. Pich, *Prog. Part. Nucl. Phys.* **75**, 41 (2014), [arXiv:1310.7922].
- [198] M. Davier *et al.*, *Eur. Phys. J. C* **74**, 3, 2803 (2014), [arXiv:1312.1501].

- [199] K. Chetyrkin, A. Kataev and F. Tkachov, *Phys. Lett. B* **85**, 277 (1979).
- [200] M. Dine and J. Sapirstein, *Phys. Rev. Lett.* **43**, 668 (1979).
- [201] S. Gorishnii, A. Kataev and S. Larin, *Phys. Lett. B* **259**, 144 (1991).
- [202] L. R. Surguladze and M. A. Samuel, *Phys. Rev. Lett.* **66**, 560 (1991), [Erratum: *Phys.Rev.Lett.* 66, 2416 (1991)].
- [203] P. Baikov, K. Chetyrkin and J. H. Kuhn, *Phys. Rev. Lett.* **101**, 012002 (2008), [arXiv:0801.1821].
- [204] F. Le Diberder and A. Pich, *Phys. Lett. B* **286**, 147 (1992).
- [205] M. Beneke and M. Jamin, *JHEP* **09**, 044 (2008), [arXiv:0806.3156].
- [206] E. Braaten and C.-S. Li, *Phys. Rev. D* **42**, 3888 (1990).
- [207] W. Marciano and A. Sirlin, *Phys. Rev. Lett.* **61**, 1815 (1988).
- [208] J. Erler, *Rev. Mex. Fis.* **50**, 200 (2004), [hep-ph/0211345].
- [209] D. Boito *et al.*, *Phys. Rev. D* **85**, 093015 (2012), [arXiv:1203.3146].
- [210] D. Boito *et al.*, *Phys. Rev. D* **91**, 3, 034003 (2015), [arXiv:1410.3528].
- [211] A. Pich and A. Rodríguez-Sánchez, *Phys. Rev. D* **94**, 3, 034027 (2016), [arXiv:1605.06830].
- [212] J. Erler (2011), [arXiv:1102.5520].
- [213] G. Bennett *et al.* (Muon g-2), *Phys. Rev. Lett.* **92**, 161802 (2004), [hep-ex/0401008].
- [214] T. Aoyama *et al.*, *Phys. Rev. Lett.* **109**, 111808 (2012), [arXiv:1205.5370].
- [215] T. Aoyama *et al.*, *PTEP* **2012**, 01A107 (2012).
- [216] P. Baikov, A. Maier and P. Marquard, *Nucl. Phys. B* **877**, 647 (2013), [arXiv:1307.6105].
- [217] G. Li, R. Mendel and M. A. Samuel, *Phys. Rev. D* **47**, 1723 (1993).
- [218] S. Laporta and E. Remiddi, *Phys. Lett. B* **301**, 440 (1993).
- [219] S. Laporta and E. Remiddi, *Phys. Lett. B* **379**, 283 (1996), [hep-ph/9602417].
- [220] A. Czarnecki and M. Skrzypek, *Phys. Lett. B* **449**, 354 (1999), [hep-ph/9812394].
- [221] J. Erler and M. Luo, *Phys. Rev. Lett.* **87**, 071804 (2001), [hep-ph/0101010].
- [222] S. Laporta, *Phys. Lett. B* **772**, 232 (2017), [arXiv:1704.06996].
- [223] S. J. Brodsky and J. D. Sullivan, *Phys. Rev.* **156**, 1644 (1967).
- [224] T. Burnett and M. Levine, *Phys. Lett. B* **24**, 467 (1967).
- [225] R. Jackiw and S. Weinberg, *Phys. Rev. D* **5**, 2396 (1972).
- [226] I. Bars and M. Yoshimura, *Phys. Rev. D* **6**, 374 (1972).
- [227] K. Fujikawa, B. Lee and A. Sanda, *Phys. Rev. D* **6**, 2923 (1972).
- [228] W. A. Bardeen, R. Gastmans and B. Lautrup, *Nucl. Phys. B* **46**, 319 (1972).
- [229] T. Kukhto *et al.*, *Nucl. Phys. B* **371**, 567 (1992).
- [230] S. Peris, M. Perrottet and E. de Rafael, *Phys. Lett. B* **355**, 523 (1995), [hep-ph/9505405].
- [231] A. Czarnecki, B. Krause and W. J. Marciano, *Phys. Rev. D* **52**, 2619 (1995), [hep-ph/9506256].
- [232] A. Czarnecki, B. Krause and W. J. Marciano, *Phys. Rev. Lett.* **76**, 3267 (1996), [hep-ph/9512369].
- [233] C. Gnendiger, D. Stöckinger and H. Stöckinger-Kim, *Phys. Rev. D* **88**, 053005 (2013), [arXiv:1306.5546].
- [234] G. Degrossi and G. Giudice, *Phys. Rev. D* **58**, 053007 (1998), [hep-ph/9803384].
- [235] A. Czarnecki, W. J. Marciano and A. Vainshtein, *Phys. Rev. D* **67**, 073006 (2003), [Erratum: *Phys.Rev.D* 73, 119901 (2006)], [hep-ph/0212229].
- [236] F. Jegerlehner, *EPJ Web Conf.* **166**, 00022 (2018), [arXiv:1705.00263].
- [237] H. B. Meyer and H. Wittig, *Prog. Part. Nucl. Phys.* **104**, 46 (2019), [arXiv:1807.09370].
- [238] T. Blum *et al.* (RBC, UKQCD), *Phys. Rev. Lett.* **121**, 2, 022003 (2018), [arXiv:1801.07224].
- [239] D. Giusti *et al.*, *Phys. Rev. D* **99**, 11, 114502 (2019), [arXiv:1901.10462].
- [240] E. Shintani and Y. Kuramashi (PACS), *Phys. Rev. D* **100**, 3, 034517 (2019), [arXiv:1902.00885].
- [241] C. Davies *et al.* (Fermilab Lattice, LATTICE-HPQCD, MILC), *Phys. Rev. D* **101**, 3, 034512 (2020), [arXiv:1902.04223].
- [242] A. Gérardin *et al.*, *Phys. Rev. D* **100**, 1, 014510 (2019), [arXiv:1904.03120].
- [243] S. Borsanyi *et al.* (2020), [arXiv:2002.12347].
- [244] C. Lehner and A. S. Meyer (2020), [arXiv:2003.04177].
- [245] K. Melnikov and A. Vainshtein, *Phys. Rev. D* **70**, 113006 (2004), [hep-ph/0312226].
- [246] J. Erler and G. Toledo Sanchez, *Phys. Rev. Lett.* **97**, 161801 (2006), [hep-ph/0605052].
- [247] J. Prades, E. de Rafael and A. Vainshtein **20**, 303 (2009), [arXiv:0901.0306].
- [248] M. Knecht and A. Nyffeler, *Phys. Rev. D* **65**, 073034 (2002), [hep-ph/0111058].
- [249] I. Danilkin, C. F. Redmer and M. Vanderhaeghen, *Prog. Part. Nucl. Phys.* **107**, 20 (2019), [arXiv:1901.10346].
- [250] T. Blum *et al.* (2019), [arXiv:1911.08123].
- [251] B. Krause, *Phys. Lett. B* **390**, 392 (1997), [hep-ph/9607259].
- [252] A. Kurz *et al.*, *Phys. Lett. B* **734**, 144 (2014), [arXiv:1403.6400].
- [253] G. Colangelo *et al.*, *Phys. Lett. B* **735**, 90 (2014), [arXiv:1403.7512].
- [254] J. L. Lopez, D. V. Nanopoulos and X. Wang, *Phys. Rev. D* **49**, 366 (1994), [hep-ph/9308336].
- [255] G. Passarino and M. Veltman, *Nucl. Phys. B* **160**, 151 (1979).
- [256] W. Hollik and G. Duckeck, *Springer Tracts Mod. Phys.* **162**, 1 (2000).
- [257] B. Lynn and R. Stuart, *Nucl. Phys. B* **253**, 216 (1985).
- [258] S. L. Wu, *Phys. Rept.* **107**, 59 (1984).
- [259] R. Marshall, *Z. Phys. C* **43**, 607 (1989).
- [260] S. Schael *et al.* (ALEPH, DELPHI, L3, OPAL, LEP Electroweak), *Phys. Rept.* **532**, 119 (2013), [arXiv:1302.3415].
- [261] T. A. Aaltonen *et al.* (CDF, DØ), *Phys. Rev. D* **88**, 5, 052018 (2013), [arXiv:1307.7627].
- [262] Technical Report TEVEWWG/WZ 2010/01, FERMILAB, Batavia (2010), [arXiv:1003.2826], URL <https://www-d0.fnal.gov/Run2Physics/WWW/results/prelim/EW/E34>.
- [263] M. Aaboud *et al.* (ATLAS), *Eur. Phys. J. C* **78**, 2, 110 (2018), [Erratum: *Eur.Phys.J.C* 78, 898 (2018)], [arXiv:1701.07240].
- [264] G. Aad *et al.* (ATLAS), *Phys. Lett. B* **716**, 1 (2012), [arXiv:1207.7214].
- [265] S. Chatrchyan *et al.* (CMS), *Phys. Lett. B* **716**, 30 (2012), [arXiv:1207.7235].
- [266] M. Aaboud *et al.* (ATLAS), *Phys. Lett. B* **784**, 345 (2018), [arXiv:1806.00242].
- [267] A. M. Sirunyan *et al.* (CMS) (2020), [arXiv:2002.06398].
- [268] T. A. Aaltonen *et al.* (CDF, DØ), *Phys. Rev. D* **97**, 11, 112007 (2018), [arXiv:1801.06283].



- [269] G. Aad *et al.* (ATLAS), JHEP **09**, 049 (2015), [arXiv:1503.03709].
- [270] Technical Report ATLAS-CONF-2018-037, CERN, Geneva (2018), URL <https://cds.cern.ch/record/2630340>.
- [271] A. M. Sirunyan *et al.* (CMS), Eur. Phys. J. C **78**, 9, 701 (2018), [arXiv:1806.00863].
- [272] R. Aaij *et al.* (LHCb), JHEP **11**, 190 (2015), [arXiv:1509.07645].
- [273] K. Abe *et al.* (SLD), Phys. Rev. Lett. **84**, 5945 (2000), [hep-ex/0004026].
- [274] K. Abe *et al.* (SLD), Phys. Rev. Lett. **86**, 1162 (2001), [hep-ex/0010015].
- [275] P. Janot and S. Jadach, Phys. Lett. B **803**, 135319 (2020), [arXiv:1912.02067].
- [276] D. Kennedy *et al.*, Nucl. Phys. B **321**, 83 (1989).
- [277] S. Riemann, Rept. Prog. Phys. **73**, 126201 (2010).
- [278] K. Abe *et al.* (SLD), Phys. Rev. Lett. **85**, 5059 (2000), [hep-ex/0006019].
- [279] K. Abe *et al.* (SLD), Phys. Rev. Lett. **78**, 17 (1997), [hep-ex/9609019].
- [280] W. Bernreuther *et al.*, JHEP **01**, 053 (2017), [arXiv:1611.07942].
- [281] S. Catani and M. H. Seymour, JHEP **07**, 023 (1999), [hep-ph/9905424].
- [282] A. Djouadi, J. H. Kuhn and P. Zerwas, Z. Phys. C **46**, 411 (1990).
- [283] T. A. Aaltonen *et al.* (CDF), Phys. Rev. D **93**, 11, 112016 (2016), [Addendum: Phys.Rev.D 95, 119901 (2017)], [arXiv:1605.02719].
- [284] V. M. Abazov *et al.* (DØ), Phys. Rev. Lett. **120**, 24, 241802 (2018), [arXiv:1710.03951].
- [285] V. Abazov *et al.* (DØ), Phys. Rev. D **84**, 012007 (2011), [arXiv:1104.4590].
- [286] D. Acosta *et al.* (CDF), Phys. Rev. D **71**, 052002 (2005), [hep-ex/0411059].
- [287] A. Aktas *et al.* (H1), Phys. Lett. B **632**, 35 (2006), [hep-ex/0507080].
- [288] H. Abramowicz *et al.* (ZEUS), Phys. Rev. D **93**, 9, 092002 (2016), [arXiv:1603.09628].
- [289] D. Albert *et al.*, Nucl. Phys. B **166**, 460 (1980).
- [290] K. Chetyrkin, J. H. Kuhn and A. Kwiatkowski, Phys. Rept. **277**, 189 (1996), [hep-ph/9503396].
- [291] B. A. Kniehl and J. H. Kuhn, Nucl. Phys. B **329**, 547 (1990).
- [292] K. Chetyrkin and A. Kwiatkowski, Phys. Lett. B **319**, 307 (1993), [hep-ph/9310229].
- [293] S. Larin, T. van Ritbergen and J. Vermaseren, Phys. Lett. B **320**, 159 (1994), [hep-ph/9310378].
- [294] K. Chetyrkin and O. Tarasov, Phys. Lett. B **327**, 114 (1994), [hep-ph/9312323].
- [295] P. Baikov *et al.*, Phys. Rev. Lett. **108**, 222003 (2012), [arXiv:1201.5804].
- [296] A. Kataev, Phys. Lett. B **287**, 209 (1992).
- [297] B. W. Lynn and R. G. Stuart, Phys. Lett. B **252**, 676 (1990).
- [298] J. Bernabeu, A. Pich and A. Santamaria, Nucl. Phys. B **363**, 326 (1991).
- [299] A. Czarnecki and J. H. Kuhn, Phys. Rev. Lett. **77**, 3955 (1996), [hep-ph/9608366].
- [300] R. Harlander, T. Seidensticker and M. Steinhauser, Phys. Lett. B **426**, 125 (1998), [hep-ph/9712228].
- [301] J. Fleischer *et al.*, Phys. Lett. B **459**, 625 (1999), [hep-ph/9904256].
- [302] P. A. Grassi, B. A. Kniehl and A. Sirlin, Phys. Rev. Lett. **86**, 389 (2001), [hep-th/0005149].
- [303] A. Akhundov, D. Bardin and T. Riemann, Nucl. Phys. B **276**, 1 (1986).
- [304] F. Jegerlehner, Z. Phys. C **32**, 425 (1986), [Erratum: Z.Phys.C 38, 519 (1988)].
- [305] W. Beenakker and W. Hollik, Z. Phys. C **40**, 141 (1988).
- [306] D. Bardin *et al.*, Z. Phys. C **44**, 493 (1989).
- [307] A. Borrelli *et al.*, Nucl. Phys. B **333**, 357 (1990).
- [308] A. Denner and T. Sack, Z. Phys. C **46**, 653 (1990).
- [309] A. Denner, Fortsch. Phys. **41**, 307 (1993), [arXiv:0709.1075].
- [310] U. Amaldi *et al.*, Phys. Rev. D **36**, 1385 (1987).
- [311] G. Costa *et al.*, Nucl. Phys. B **297**, 244 (1988).
- [312] P. Langacker and M. Luo, Phys. Rev. D **44**, 817 (1991).
- [313] J. Erler and P. Langacker, Phys. Rev. D **52**, 441 (1995), [hep-ph/9411203].
- [314] F. James and M. Roos, Comput. Phys. Commun. **10**, 343 (1975).
- [315] D. d'Enterria and A. Poldaru (2019), [arXiv:1912.11733].
- [316] V. Abazov *et al.* (DØ), Phys. Rev. D **80**, 111107 (2009), [arXiv:0911.2710].
- [317] J. Bagger, K. T. Matchev and D. Pierce, Phys. Lett. B **348**, 443 (1995), [hep-ph/9501277].
- [318] P. Langacker and N. Polonsky, Phys. Rev. D **52**, 3081 (1995), [hep-ph/9503214].
- [319] M. Veltman, Nucl. Phys. B **123**, 89 (1977).
- [320] M. S. Chanowitz, M. Furman and I. Hinchliffe, Phys. Lett. B **78**, 285 (1978).
- [321] J. van der Bij and F. Hoogeveen, Nucl. Phys. B **283**, 477 (1987).
- [322] P. Langacker and M. Luo, Phys. Rev. D **45**, 278 (1992).
- [323] A. Denner, R. Guth and J. H. Kuhn, Phys. Lett. B **240**, 438 (1990).
- [324] W. Grimus *et al.*, J. Phys. G **35**, 075001 (2008), [arXiv:0711.4022].
- [325] H. E. Haber and D. O'Neil, Phys. Rev. D **83**, 055017 (2011), [arXiv:1011.6188].
- [326] S. Bertolini and A. Sirlin, Phys. Lett. B **257**, 179 (1991).
- [327] M. Golden and L. Randall, Nucl. Phys. B **361**, 3 (1991).
- [328] B. Holdom and J. Terning, Phys. Lett. B **247**, 88 (1990).
- [329] M. E. Peskin and T. Takeuchi, Phys. Rev. Lett. **65**, 964 (1990).
- [330] K. Hagiwara *et al.*, Z. Phys. C **64**, 559 (1994), [Erratum: Z.Phys.C 68, 352 (1995)], [hep-ph/9409380].
- [331] M. E. Peskin and T. Takeuchi, Phys. Rev. D **46**, 381 (1992).
- [332] I. Maksymyk, C. Burgess and D. London, Phys. Rev. D **50**, 529 (1994), [hep-ph/9306267].
- [333] R. Barbieri *et al.*, Nucl. Phys. B **703**, 127 (2004), [hep-ph/0405040].
- [334] M. Farina *et al.*, Phys. Lett. B **772**, 210 (2017), [arXiv:1609.08157].
- [335] G. Altarelli and R. Barbieri, Phys. Lett. B **253**, 161 (1991).
- [336] D. Kennedy and P. Langacker, Phys. Rev. D **44**, 1591 (1991).
- [337] L. Randall and R. Sundrum, Phys. Rev. Lett. **83**, 3370 (1999), [hep-ph/9905221].
- [338] M. Carena *et al.*, Nucl. Phys. B **759**, 202 (2006), [hep-ph/0607106].
- [339] R. Contino (2011), [arXiv:1005.4269].
- [340] E. Gates and J. Terning, Phys. Rev. Lett. **67**, 1840 (1991).
- [341] R. Sundrum, Nucl. Phys. B **395**, 60 (1993), [hep-ph/9205203].
- [342] R. Sundrum and S. D. Hsu, Nucl. Phys. B **391**, 127 (1993), [hep-ph/9206225].



- [343] M. A. Luty and R. Sundrum, *Phys. Rev. Lett.* **70**, 529 (1993), [hep-ph/9209255].
- [344] T. Appelquist and J. Terning, *Phys. Lett. B* **315**, 139 (1993), [hep-ph/9305258].
- [345] D. D. Dietrich, F. Sannino and K. Tuominen, *Phys. Rev. D* **72**, 055001 (2005), [hep-ph/0505059].
- [346] N. D. Christensen and R. Shrock, *Phys. Lett. B* **632**, 92 (2006), [hep-ph/0509109].
- [347] M. Harada, M. Kurachi and K. Yamawaki, *Prog. Theor. Phys.* **115**, 765 (2006), [hep-ph/0509193].
- [348] H. Georgi, *Nucl. Phys. B* **363**, 301 (1991).
- [349] M. J. Dugan and L. Randall, *Phys. Lett. B* **264**, 154 (1991).
- [350] H. E. Haber and G. L. Kane, *Phys. Rept.* **117**, 75 (1985).
- [351] A. Djouadi, *Phys. Rept.* **459**, 1 (2008), [hep-ph/0503173].
- [352] R. Barbieri *et al.*, *Nucl. Phys. B* **341**, 309 (1990).
- [353] R. Barbieri, M. Frigeni and F. Caravaglios, *Phys. Lett. B* **279**, 169 (1992).
- [354] J. Erler and D. M. Pierce, *Nucl. Phys. B* **526**, 53 (1998), [hep-ph/9801238].
- [355] G.-C. Cho and K. Hagiwara, *Nucl. Phys. B* **574**, 623 (2000), [hep-ph/9912260].
- [356] G. Altarelli *et al.*, *JHEP* **06**, 018 (2001), [hep-ph/0106029].
- [357] S. Heinemeyer, W. Hollik and G. Weiglein, *Phys. Rept.* **425**, 265 (2006), [hep-ph/0412214].
- [358] S. P. Martin, K. Tobe and J. D. Wells, *Phys. Rev. D* **71**, 073014 (2005), [hep-ph/0412424].
- [359] M. Ramsey-Musolf and S. Su, *Phys. Rept.* **456**, 1 (2008), [hep-ph/0612057].
- [360] S. Heinemeyer *et al.*, *JHEP* **04**, 039 (2008), [arXiv:0710.2972].
- [361] O. Buchmuller *et al.*, *Eur. Phys. J. C* **72**, 2020 (2012), [arXiv:1112.3564].
- [362] B. Grinstein and M. B. Wise, *Phys. Lett. B* **265**, 326 (1991).
- [363] A. Pich, I. Rosell and J. Sanz-Cillero, *JHEP* **01**, 157 (2014), [arXiv:1310.3121].
- [364] C. T. Hill and E. H. Simmons, *Phys. Rept.* **381**, 235 (2003), [Erratum: *Phys.Rept.* 390, 553–554 (2004)], [hep-ph/0203079].
- [365] G. Panico and A. Wulzer **913** (2016), [arXiv:1506.01961].
- [366] J. Erler and P. Langacker, *Phys. Rev. Lett.* **105**, 031801 (2010), [arXiv:1003.3211].
- [367] J. Gunion, D. W. McKay and H. Pois, *Phys. Rev. D* **53**, 1616 (1996), [hep-ph/9507323].
- [368] A. Lenz, *Adv. High Energy Phys.* **2013**, 910275 (2013).
- [369] S. Chatrchyan *et al.* (CMS), *Phys. Rev. D* **86**, 112003 (2012), [arXiv:1209.1062].
- [370] A. Djouadi and A. Lenz, *Phys. Lett. B* **715**, 310 (2012), [arXiv:1204.1252].
- [371] O. Eberhardt *et al.*, *Phys. Rev. Lett.* **109**, 241802 (2012), [arXiv:1209.1101].
- [372] J. Maalampi and M. Roos, *Phys. Rept.* **186**, 53 (1990).
- [373] P. Langacker, *Phys. Rept.* **72**, 185 (1981).
- [374] J. L. Hewett and T. G. Rizzo, *Phys. Rept.* **183**, 193 (1989).
- [375] J. Kang, P. Langacker and B. D. Nelson, *Phys. Rev. D* **77**, 035003 (2008), [arXiv:0708.2701].
- [376] S. P. Martin, *Phys. Rev. D* **81**, 035004 (2010), [arXiv:0910.2732].
- [377] P. W. Graham *et al.*, *Phys. Rev. D* **81**, 055016 (2010), [arXiv:0910.3020].
- [378] J. Erler, J. L. Feng and N. Polonsky, *Phys. Rev. Lett.* **78**, 3063 (1997), [hep-ph/9612397].
- [379] D. Choudhury, T. M. Tait and C. Wagner, *Phys. Rev. D* **65**, 053002 (2002), [hep-ph/0109097].
- [380] J. Erler and P. Langacker, *Phys. Rev. Lett.* **84**, 212 (2000), [hep-ph/9910315].
- [381] P. Langacker and M. Plumacher, *Phys. Rev. D* **62**, 013006 (2000), [hep-ph/0001204].
- [382] P. Abreu *et al.* (DELPHI), *Eur. Phys. J. C* **10**, 415 (1999).
- [383] P. Langacker and D. London, *Phys. Rev. D* **38**, 886 (1988).
- [384] F. del Aguila, J. de Blas and M. Perez-Victoria, *Phys. Rev. D* **78**, 013010 (2008), [arXiv:0803.4008].
- [385] M. Chemtob, *Prog. Part. Nucl. Phys.* **54**, 71 (2005), [hep-ph/0406029].
- [386] R. Barbieri *et al.*, *Phys. Rept.* **420**, 1 (2005), [hep-ph/0406039].
- [387] T. Han, H. E. Logan and L.-T. Wang, *JHEP* **01**, 099 (2006), [hep-ph/0506313].
- [388] M. Perelstein, *Prog. Part. Nucl. Phys.* **58**, 247 (2007), [hep-ph/0512128].
- [389] I. Antoniadis (2001), [hep-th/0102202].
- [390] M. Carena *et al.*, *Phys. Rev. D* **68**, 035010 (2003), [hep-ph/0305188].
- [391] K. Agashe *et al.*, *JHEP* **08**, 050 (2003), [hep-ph/0308036].
- [392] I. Gogoladze and C. Macesanu, *Phys. Rev. D* **74**, 093012 (2006), [hep-ph/0605207].
- [393] S. Weinberg, *Phys. Rev. Lett.* **43**, 1566 (1979).
- [394] W. Buchmuller and D. Wyler, *Nucl. Phys. B* **268**, 621 (1986).
- [395] B. Grzadkowski *et al.*, *JHEP* **10**, 085 (2010), [arXiv:1008.4884].
- [396] R. Contino *et al.*, *JHEP* **07**, 035 (2013), [arXiv:1303.3876].
- [397] K. Hagiwara *et al.*, *Phys. Rev. D* **48**, 2182 (1993).
- [398] A. Falkowski, F. Riva and A. Urbano, *JHEP* **11**, 111 (2013), [arXiv:1303.1812].
- [399] A. Pomarol and F. Riva, *JHEP* **01**, 151 (2014), [arXiv:1308.2803].
- [400] J. Ellis, V. Sanz and T. You, *JHEP* **03**, 157 (2015), [arXiv:1410.7703].
- [401] A. Efrati, A. Falkowski and Y. Soreq, *JHEP* **07**, 018 (2015), [arXiv:1503.07872].
- [402] J. de Blas *et al.*, *PoS EPS-HEP2017*, 467 (2017), [arXiv:1710.05402].
- [403] G. Altarelli, R. Barbieri and S. Jadach, *Nucl. Phys. B* **369**, 3 (1992), [Erratum: *Nucl.Phys.B* 376, 444 (1992)].
- [404] G.-C. Cho, K. Hagiwara and S. Matsumoto, *Eur. Phys. J. C* **5**, 155 (1998), [hep-ph/9707334].
- [405] K. Cheung, *Phys. Lett. B* **517**, 167 (2001), [hep-ph/0106251].
- [406] Z. Han and W. Skiba, *Phys. Rev. D* **71**, 075009 (2005), [hep-ph/0412166].
- [407] P. Langacker, M. Luo and A. K. Mann, *Rev. Mod. Phys.* **64**, 87 (1992).
- [408] P. Langacker, *Rev. Mod. Phys.* **81**, 1199 (2009), [arXiv:0801.1345].

## 11. Status of Higgs Boson Physics

Revised August 2019 by M. Carena (FNAL; Chicago U.; Chicago U., Kavli Inst.), C. Grojean (Theoriegruppe, DESY, Hamburg; Physik, Humboldt U.), M. Kado (Rome U. Sapienza; INFN, Rome; U. Paris-Saclay, IJCLab) and V. Sharma (UC San Diego).

11.1	Introduction . . . . .	203
11.2	The Standard Model and the mechanism of electroweak symmetry breaking . . . . .	204
11.2.1	The SM Higgs boson mass, couplings and quantum numbers . . . . .	204
11.2.2	The SM custodial symmetry . . . . .	205
11.2.3	Stability of the Higgs potential . . . . .	205
11.2.4	Higgs boson production and decay mechanisms . . . . .	205
11.3	The experimental profile of the Higgs boson . . . . .	209
11.3.1	The principal decay channels to vector bosons . . . . .	209
11.3.2	Decays to third generation fermions ( $b\bar{b}$ and $\tau^+\tau^-$ ) . . . . .	212
11.3.3	Higgs boson production in association with top quarks or in top decays . . . . .	214
11.3.4	Higgs boson pair production . . . . .	215
11.3.5	Searches for rare decays of the Higgs boson . . . . .	216
11.3.6	Searches for non-SM decay channels . . . . .	218
11.4	Combining the main channels . . . . .	220
11.4.1	Principles of the combination . . . . .	220
11.4.2	Main decay modes . . . . .	221
11.4.3	Main production modes . . . . .	222
11.5	Main quantum numbers and width of the Higgs boson . . . . .	222
11.5.1	Main quantum numbers $J^{PC}$ . . . . .	222
11.5.2	Off-shell couplings of the Higgs boson . . . . .	225
11.5.3	The Higgs boson width . . . . .	226
11.6	Probing the coupling properties of the Higgs boson . . . . .	227
11.6.1	Effective Lagrangian framework . . . . .	228
11.6.2	Probing coupling properties . . . . .	228
11.7	New physics models of EWSB in the light of the Higgs boson discovery . . . . .	234
11.7.1	Higgs bosons in the minimal supersymmetric standard model (MSSM) . . . . .	235
11.7.2	Supersymmetry with singlet extensions . . . . .	238
11.7.3	Supersymmetry with extended gauge sectors . . . . .	238
11.7.4	Effects of $CP$ violation . . . . .	239
11.7.5	Non-supersymmetric extensions of the Higgs sector . . . . .	240
11.7.6	Composite Higgs models . . . . .	242
11.7.7	Searches for signatures of extended Higgs sectors . . . . .	245
11.8	Summary and outlook . . . . .	250

### 11.1 Introduction

Understanding the mechanism that breaks the electroweak symmetry and generates the masses of the known elementary particles has been one of the fundamental endeavours in particle physics for several decades. The discovery in 2012 by the ATLAS [1] and the CMS [2] collaborations of a new resonance with a mass of approximately 125 GeV and the subsequent studies of its properties with the full data set from Run 1, from 2009 to 2012, with a centre-of-mass energy of 7 TeV and 8 TeV, conclusively provided a first portrait of the Electroweak Symmetry Breaking (EWSB) mechanism. The data collected during the LHC Run 2, from 2015 to 2018, with a higher centre-of-mass energy of 13 TeV and more conspicuous dataset, put in solid grounds the compatibility of the measured resonance with the Higgs boson of the Standard Model (SM) [3].

In the SM, the electroweak interactions are described by a gauge field theory invariant under the  $SU(2)_L \times U(1)_Y$  symmetry group. The mechanism of EWSB [4] provides a general framework to keep untouched the structure of these gauge interactions at high energies and still generate the observed masses of the  $W$  and  $Z$  gauge bosons. The EWSB mechanism posits a self-interacting complex

EW doublet scalar field, whose  $CP$ -even neutral component acquires a vacuum expectation value (VEV)  $v \approx 246$  GeV, which sets the scale of the symmetry breaking. Three massless Goldstone bosons are generated and are absorbed to give masses to the  $W$  and  $Z$  gauge bosons. The remaining component of the complex doublet becomes the Higgs boson – a new, and so far unique, fundamental scalar particle. The masses of all fermions are also a consequence of EWSB since the Higgs doublet is postulated to couple to the fermions through Yukawa interactions

The initial measurements during the LHC Run 1 were accessible mainly through production and decay channels related to the couplings of the Higgs boson to the vector gauge bosons (the mediators of the electroweak interactions,  $W^\pm$ ,  $Z$  and  $\gamma$ , as well as the gluons,  $g$ , mediators of the strong interactions).

The outstanding performance of the LHC Run 2, made it possible for the ATLAS and CMS experiments to independently and unambiguously establish the couplings of the Higgs boson to the charged fermions of the third generation (the top quark, the bottom quark, and the tau). These observations of fundamental importance were made with partial Run 2 datasets.

In all observed production and decay modes measured so far, the rates and differential measurements are found to be consistent, within experimental and theoretical uncertainties, with the SM predictions. In high resolution decay channels, such as the ones with four leptons (electrons or muons) or diphoton final states, the mass of the Higgs boson has been measured at the permill precision level.

Nevertheless, several channels are still out of reach experimentally and the couplings of the Higgs boson to light fermions are yet to be proven. Moreover, within the current precision, a more complex sector with additional states is not ruled out, nor has it been established whether the Higgs boson is an elementary particle or whether it has an internal structure like any other scalar particles observed before it.

Without the Higgs boson, the calculability of the SM would have been spoiled. In particular, perturbative unitarity [5] would be lost at high energies since the longitudinal  $W/Z$  boson scattering amplitude would grow with the centre-of-mass energy. In addition, the radiative corrections to the gauge boson self-energies would exhibit dangerous logarithmic divergences that would be difficult to reconcile with EW precision data. With the discovery of the Higgs boson, the SM is a spontaneously broken gauge theory and, as such, it could a priori be consistently extrapolated well above the masses of the  $W$  and  $Z$  bosons. Hence, formally there is no need for new physics at the EW scale. However, as the SM Higgs boson is a scalar particle, at the quantum level it has sensitivity to possible new physics scales. Quite generally, the Higgs boson mass is affected by the presence of heavy particles and receives quantum corrections which destabilise the weak scale barring a large fine tuning of unrelated parameters. This is known as the Higgs naturalness or hierarchy problem [6]. It has been the prime argument for expecting new physics right at the TeV scale. New theoretical paradigms have been imagined, such as a new fermion-boson symmetry called supersymmetry (SUSY) [7] (for recent reviews, see Refs. [8, 9]), or the existence of strong interactions at a scale of the order of a TeV from which the Higgs boson would emerge as a composite state [10] (see Refs. [11, 12] for recent reviews). Alternatively, new agents stabilising the weak scale could also be light but elusive, like in models of neutral naturalness [13, 14]. Other more recent scenarios [15], instead, rely on the cosmological evolution of the Universe to drive the Higgs boson mass to a value much smaller than the cutoff of the theory and aim at alleviating the hierarchy problem without the need for TeV scale new physics, even though there might still be interesting and spectacular signatures [15, 16]. Beyond the naturalness problem, extensions of the SM Higgs sector without other low-energy particles have been proposed, for example, to provide explanations for the fermion mass hierarchies, see e.g. Ref. [17], to account for the Dark Matter abundance, see e.g. Ref. [18], or to modify the properties of the electroweak phase transition [19]. Such models with additional scalars provide grounds to explore new Higgs boson signals in concrete and complete scenarios, with different types of coupling structure to fermions and gauge bosons.

The Higgs boson is anyway special and, in the eight years since its discovery, it became a powerful tool to explore the manifestations of the SM and to probe the physics landscape beyond it. It might offer direct insights on what comes beyond the weak scale through possible sizeable effects on the Higgs boson properties. The Higgs boson couplings, however, are observed to be in good agreement with their SM predictions. This, together with the strong bounds from precision electroweak and flavour data, leaves open the possibility that the Higgs boson may well be elementary, weakly coupled and solitary up to the Planck scale, rendering the EW vacuum potentially metastable [20].

After completion of the first two runs, the LHC has only gathered approximately 5% of its projected full dataset. During the second long shut down currently underway, the LHC is undergoing important upgrades in order to prepare for its high luminosity phase. The foreseen larger datasets to be collected during Run 3 and ultimately during the High Luminosity LHC (HL-LHC), will enable yet more fundamental and challenging measurements to explore new physics.

This review is organised as follows. Section 11.2 is a theoretical review of the SM Higgs boson, its properties, production mechanisms and decay rates. In Section 11.3, the experimental measurements are described. In Section 11.4, the combination of the main Higgs boson production and decay channels is presented. In Section 11.5, measurements of the main quantum numbers and  $CP$  properties of the Higgs boson are reported and the bounds on its total width are discussed. In Section 11.6, a general theoretical framework to describe the deviations of the Higgs boson couplings from the SM predictions is introduced and the experimental measurements of these Higgs couplings is reviewed. Measurements of differential cross sections are outlined. Section 11.7 presents, in detail, some interesting models proposed for extensions of the SM Higgs sector, addressing the hierarchy problem or not, and considers their experimental signatures. Section 11.8 provides a short summary and a brief outlook.

## 11.2 The Standard Model and the mechanism of electroweak symmetry breaking

In the SM [3], electroweak symmetry breaking [4] is responsible for generating mass for the  $W$  and  $Z$  gauge bosons rendering the weak interactions short ranged. The SM scalar potential reads:

$$V(\Phi) = m^2 \Phi^\dagger \Phi + \lambda (\Phi^\dagger \Phi)^2 \quad (11.1)$$

with the Higgs field  $\Phi$  being a self-interacting  $SU(2)_L$  complex doublet (four real degrees of freedom) with weak hypercharge  $Y=1$  (the hypercharge is normalised such that  $Q = T_{3L} + Y/2$ ,  $Q$  being the electric charge and  $T_{3L}$  the eigenvalue of the diagonal generator of  $SU(2)_L$ ):

$$\Phi = \frac{1}{\sqrt{2}} \begin{pmatrix} \sqrt{2}\phi^+ \\ \phi^0 + ia^0 \end{pmatrix}, \quad (11.2)$$

where  $\phi^0$  and  $a^0$  are the  $CP$ -even and  $CP$ -odd neutral components, and  $\phi^+$  is the complex charged component of the Higgs doublet, respectively.  $V(\Phi)$  is the most general renormalisable scalar potential. If the quadratic term is negative, the neutral component of the scalar doublet acquires a non-zero vacuum expectation value (VEV)

$$\langle \Phi \rangle = \frac{1}{\sqrt{2}} \begin{pmatrix} 0 \\ v \end{pmatrix}, \quad (11.3)$$

with  $\phi^0 = H + \langle \phi^0 \rangle$  and  $\langle \phi^0 \rangle \equiv v$ , inducing the spontaneous breaking of the SM gauge symmetry  $SU(3)_C \times SU(2)_L \times U(1)_Y$  into  $SU(3)_C \times U(1)_{em}$ . The global minimum of the theory defines the ground state, and spontaneous symmetry breaking implies that there is a (global and/or local) symmetry of the system that is not respected by the ground state. From the four generators of the  $SU(2)_L \times U(1)_Y$  SM gauge group, three are spontaneously broken, implying that they lead to non-trivial transformations of the ground state and indicate the existence of three massless Goldstone bosons identified with three of the four Higgs field degrees of freedom. The Higgs field couples to the  $W_\mu$  and  $B_\mu$  gauge fields associated with the  $SU(2)_L \times U(1)_Y$  local symmetry through the

covariant derivative appearing in the kinetic term of the Higgs Lagrangian,

$$\mathcal{L}_{\text{Higgs}} = (D_\mu \Phi)^\dagger (D^\mu \Phi) - V(\Phi), \quad (11.4)$$

where  $D_\mu \Phi = (\partial_\mu + ig\sigma^a W_\mu^a/2 + ig'YB_\mu/2)\Phi$ ,  $g$  and  $g'$  are the  $SU(2)_L$  and  $U(1)_Y$  gauge couplings, respectively, and  $\sigma^a, a = 1, 2, 3$  are the usual Pauli matrices. As a result, the neutral and the two charged massless Goldstone degrees of freedom mix with the gauge fields corresponding to the broken generators of  $SU(2)_L \times U(1)_Y$  and become, in the unitarity gauge, the longitudinal components of the  $Z$  and  $W$  physical gauge bosons, respectively. The  $Z$  and  $W$  gauge bosons acquire masses,

$$m_W^2 = \frac{g^2 v^2}{4}, \quad m_Z^2 = \frac{(g^2 + g'^2)v^2}{4}. \quad (11.5)$$

The fourth generator remains unbroken since it is the one associated to the conserved  $U(1)_{em}$  gauge symmetry, and its corresponding gauge field, the photon, remains massless. Similarly the eight color gauge bosons, the gluons, corresponding to the conserved  $SU(3)_C$  gauge symmetry with 8 unbroken generators, also remain massless (though confined inside hadrons and mesons as the result of the asymptotic freedom behaviour of QCD). Hence, from the initial four degrees of freedom of the Higgs field, two are absorbed by the  $W^\pm$  gauge bosons, one by the  $Z$  gauge boson, and there is one remaining degree of freedom,  $H$ , that is the physical Higgs boson — a new scalar particle first imagined by P. Higgs [4]. The Higgs boson is neutral under the electromagnetic interactions and transforms as a singlet under  $SU(3)_C$  and hence does not couple at tree level to the massless photons and gluons.

The fermions of the SM acquire mass through renormalisable interactions between the Higgs field and the fermions: the Yukawa interactions,

$$\mathcal{L}_{\text{Yukawa}} = -\hat{h}_{d_{ij}} \bar{q}_{L_i} \Phi d_{R_j} - \hat{h}_{u_{ij}} \bar{q}_{L_i} \tilde{\Phi} u_{R_j} - \hat{h}_{l_{ij}} \bar{l}_{L_i} \Phi e_{R_j} + h.c., \quad (11.6)$$

which respect the symmetries of the SM but generate fermion masses once EWSB occurs. In the Lagrangian above,  $\tilde{\Phi} = i\sigma_2 \Phi^*$  and  $q_L$  ( $l_L$ ) and  $u_R$ ,  $d_R$  ( $e_R$ ) are the quark (lepton)  $SU(2)_L$  doublets and singlets, respectively, while in each term,  $\hat{h}_{X_{ij}}$  is parametrised by a  $3 \times 3$  matrix in family space. The mass term for neutrinos is omitted, but could be added in an analogous manner to the up-type quarks when right-handed neutrinos are supplementing the SM particle content (neutrinos can also acquire Majorana masses via non-renormalisable dimension-5 interactions with the Higgs field [21]). Once the Higgs field acquires a VEV, and after rotation to the fermion mass eigenstate basis that also diagonalises the Higgs-fermion interactions,  $\hat{h}_{f_{ij}} \rightarrow h_{f_i} \delta_{ij}$ , all fermions acquire a mass given by  $m_{f_i} = h_{f_i} v / \sqrt{2}$ . The indices  $i, j = 1, 2, 3$  refer to the three families in the up-quark, down-quark or charged lepton sectors. It should be noted that the EWSB mechanism provides no additional insight on possible underlying reasons for the large variety of masses of the fermions, often referred to as the flavour hierarchy. The fermion masses, accounting for a large number of the free parameters of the SM, are simply translated into Yukawa couplings.

### 11.2.1 The SM Higgs boson mass, couplings and quantum numbers

The SM Higgs boson is a  $CP$ -even scalar of spin 0. Its mass is given by  $m_H = \sqrt{2\lambda} v$ , where  $\lambda$  is the self coupling parameter in  $V(\Phi)$ . The expectation value of the Higgs field,  $v = (\sqrt{2}G_F)^{-1/2} \approx 246 \text{ GeV}$ , is fixed by the Fermi coupling  $G_F$ , which is determined with a precision of 0.6 ppm from muon decay measurements [22]. The quartic coupling  $\lambda$  is a free parameter in the SM, and hence, there is no a priori prediction for the Higgs mass. Moreover the sign of the mass parameter  $m^2 = -\lambda v^2$  has to be negative for the EW symmetry breaking to take place, but there is no a priori understanding of what decides of this sign. The experimentally measured Higgs boson mass,  $m_H = 125.10 \pm 0.14 \text{ GeV}$  [22], implies that  $\lambda \simeq 0.13$  and  $|m| \simeq 88.4 \text{ GeV}$ .

The Higgs boson couplings to the fundamental particles are set by their masses. This is a new type of interaction; very weak for light particles, such as up and down quarks, and electrons, but strong for heavy particles such as the  $W$  and  $Z$  bosons and the top quark. More precisely, the SM Higgs couplings to fundamental fermions are linearly proportional to the fermion masses, whereas the couplings to bosons are proportional to the square of the boson masses. The SM Higgs boson couplings to gauge bosons and fermions, as well as the Higgs boson self coupling, are summarised in the following Lagrangian:

$$\mathcal{L} = -g_{Hf\bar{f}}\bar{f}fH + \frac{g_{HHH}}{6}H^3 + \frac{g_{HHHH}}{24}H^4 + \delta_V V_\mu V^\mu \left( g_{HVV}H + \frac{g_{HHVV}}{2}H^2 \right) \quad (11.7)$$

with

$$g_{Hf\bar{f}} = \frac{m_f}{v}, \quad g_{HVV} = \frac{2m_V^2}{v}, \quad g_{HHVV} = \frac{2m_V^2}{v^2}, \quad (11.8)$$

$$g_{HHH} = \frac{3m_H^2}{v}, \quad g_{HHHH} = \frac{3m_H^2}{v^2},$$

where  $V = W^\pm$  or  $Z$  and  $\delta_W = 1, \delta_Z = 1/2$ . As a result, the dominant mechanisms for Higgs boson production and decay involve the coupling of  $H$  to  $W, Z$  and/or the third generation quarks and leptons. The Higgs boson coupling to gluons [23, 24] is induced at leading order by a one-loop process in which  $H$  couples to a virtual  $t\bar{t}$  pair (with minor contributions from the other lighter quarks). Likewise, the Higgs boson coupling to photons is also generated via loops, although in this case the one-loop graph with a virtual  $W^+W^-$  pair provides the dominant contribution [25] and it is interfering with the smaller contribution involving a virtual  $t\bar{t}$  pair (as such, the Higgs coupling to photons is sensitive to the relative phase of the interactions between bosons and fermions).

### 11.2.2 The SM custodial symmetry

The SM Higgs Lagrangian,  $\mathcal{L}_{\text{Higgs}} + \mathcal{L}_{\text{Yukawa}}$  of Eq. (11.4) and Eq. (11.6), is, by construction,  $SU(2)_L \times U(1)_Y$  gauge invariant, but it also has an approximate global symmetry. In the limit  $g' \rightarrow 0$  and  $h_f \rightarrow 0$ , the Higgs sector has a global  $SU(2)_R$  symmetry, and hence it is invariant under a global  $SU(2)_L \times SU(2)_R$  symmetry, with  $SU(2)_L$  just being the global variant of the SM chiral gauge symmetry. This symmetry is preserved for non-vanishing Yukawa couplings, provided  $h_u = h_d$ . Once the Higgs acquires a VEV, both the  $SU(2)_L$  and  $SU(2)_R$  symmetry groups are broken but the diagonal subgroup  $SU(2)_{L+R}$  remains unbroken and it is the subgroup that defines the custodial symmetry of the SM [26].

In the limit  $g' \rightarrow 0$ , the  $W$  and  $Z$  gauge bosons have equal mass and form a triplet of the  $SU(2)_{L+R}$  unbroken global symmetry. Using the expressions for the  $W$  and  $Z$  gauge boson masses in term of the gauge couplings, one obtains at tree level

$$\frac{m_W^2}{m_Z^2} = \frac{g^2}{g'^2 + g^2} = \cos^2 \theta_W \quad \text{or} \quad \rho \equiv \frac{m_W^2}{m_Z^2 \cos^2 \theta_W} = 1. \quad (11.9)$$

The custodial symmetry protects the above relation from large radiative corrections. All corrections to the  $\rho$  parameter are therefore proportional to terms that break the custodial symmetry. For instance, radiative corrections involving the Higgs boson are proportional to  $\sin^2 \theta_W$ ,  $\delta\rho = -11G_F m_Z^2 \sin^2 \theta_W \log(m_H^2/m_Z^2)/(24\sqrt{2}\pi^2)$ , and vanish in the limit  $g' \rightarrow 0$ . Since  $m_t \neq m_b$ , there are also relevant radiative corrections generated by massive fermions. They are proportional to  $m_t^2 + m_b^2 - 2(m_t^2 m_b^2) \log(m_t^2/m_b^2)/(m_t^2 - m_b^2)$  and would indeed vanish for  $m_t = m_b$  [27].

### 11.2.3 Stability of the Higgs potential

The discovery of the Higgs boson with  $m_H \approx 125$  GeV has far reaching consequences within the SM framework. In particular, the precise value of  $m_H$  determines the value of the quartic coupling  $\lambda$  at the electroweak scale and makes it possible to study its behavior up to high energy scales. A larger value of  $m_H$  would have implied that the self coupling  $\lambda$  would become non-perturbative at some scale  $\Lambda$  that could be well below the Planck scale [28].

However, for the value of Higgs boson mass experimentally measured, the EW vacuum of the Higgs potential is most likely metastable [20]. The high energy evolution of  $\lambda$  shows that it becomes negative at energies  $\Lambda = \mathcal{O}(10^{11})$  GeV (even though  $\lambda$  could remain positive till higher energy, maybe all the way to the Planck scale, if the top quark mass exceeds its current measured value by  $3\sigma$ ). When this occurs, the SM Higgs potential develops an instability and the long term existence of the EW vacuum is challenged. This behaviour may call for new physics at an intermediate scale before the instability develops, i.e., below  $M_{\text{Planck}}$ , even though new physics at  $M_{\text{Planck}}$  could influence the stability of the EW vacuum and possibly modify this conclusion [29]. The consequences of the instability of the EW vacuum on high-scale inflation have been discussed in Ref. [30]. It was also noticed that Higgs field fluctuations during inflation could seed the formation of primordial black holes, possibly making up the Dark Matter relic abundance [31] or they could produce a stochastic background of gravitational waves with characteristic structures [32], offering a probe of the EW vacuum near criticality.

The lifetime of the EW metastable vacuum is determined by the rate of quantum tunnelling from this vacuum into the true vacuum of the theory (for the most recent computation of the EW vacuum lifetime within the SM, see Ref. [33]). Within the SM, the running of the Higgs self coupling slows down at high energies with a cancellation of its  $\beta$ -function at energies just one to two orders of magnitude below the Planck scale [34]. This slow evolution of the quartic coupling is responsible for saving the EW vacuum from premature collapse. It might also help the Higgs boson to play the role of an inflaton [35] (see, however, Ref. [36] for potential issues with this Higgs-boson-as-an-inflaton idea).

### 11.2.4 Higgs boson production and decay mechanisms

Reviews of the SM Higgs boson's properties and phenomenology, with an emphasis on the impact of loop corrections to the Higgs boson decay rates and cross sections, can be found in Refs. [37–44].

#### 11.2.4.1 Production mechanisms at hadron colliders

The main production mechanisms at the Tevatron collider and the LHC are gluon fusion (ggF), weak-boson fusion (VBF), associated production with a gauge boson ( $VH$ ), and associated production with a pair of  $t\bar{t}$  quarks ( $t\bar{t}H$ ) or with a single top quark ( $tHq$ ). Figure 11.1 depicts representative diagrams for these dominant Higgs boson production processes.

The state-of-the-art of the theoretical calculations in the main different production channels is summarized in Table 11.1.

The cross sections for the production of a SM Higgs boson as a function of  $\sqrt{s}$ , the center of mass energy, for  $pp$  collisions, including bands indicating the theoretical uncertainties, are summarised in Fig. 11.2 (left) [45]. A detailed discussion, including uncertainties in the theoretical calculations due to missing higher-order effects and experimental uncertainties on the determination of SM parameters involved in the calculations, can be found in Refs. [41–44]. These references also contain state-of-the-art discussions on the impact of PDF uncertainties, QCD scale uncertainties and uncertainties due to different procedures for including higher-order corrections matched to parton shower simulations, as well as uncertainties due to hadronisation and parton-shower events.

Table 11.2 summarises the Higgs boson production cross sections and relative uncertainties for a Higgs boson mass of 125 GeV, for  $\sqrt{s} = 7, 8, 13$  and 14 TeV. The Higgs boson production cross sections in  $pp$  collisions at  $\sqrt{s} = 1.96$  TeV for the Tevatron are obtained from Ref. [46].

#### i. Gluon fusion production mechanism

At high-energy hadron colliders, the Higgs boson production mechanism with the largest cross section is the gluon-fusion process,  $gg \rightarrow H + X$ , mediated by the exchange of a virtual, heavy top quark [47]. Contributions from lighter quarks propagating in the loop are suppressed proportionally to  $m_q^2$ . QCD radiative corrections to the gluon-fusion process are very important and have been studied in detail. Including the full dependence on the

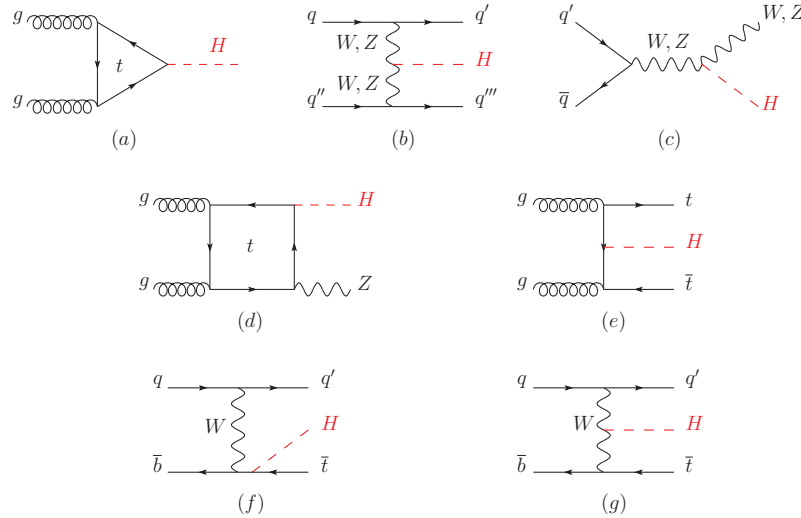


Figure 11.1: Main leading order Feynman diagrams contributing to the Higgs boson production in (a) gluon fusion, (b) Vector-boson fusion, (c) Higgs-strahlung (or associated production with a gauge boson at tree level from a quark-quark interaction), (d) associated production with a gauge boson (at loop level from a gluon-gluon interaction), (e) associated production with a pair of top quarks (there is a similar diagram for the associated production with a pair of bottom quarks), (f-g) production in association with a single top quark

Table 11.1: State-of-the-art of the theoretical calculations in the main Higgs boson production channels in the SM, and the major MC tools used in the simulations

ggF	VBF	VH	ttH
Fixed order: N3LO QCD + NLO EW (HIGLU, iHixs, FeHiPro, HNNLO)	Fixed order: NNLO QCD (VBF@NNLO)	Fixed order: NLO QCD+EW (V2HV and HAWK)	Fixed order: NLO QCD+EW (Powheg)
Resummed: NNLO + NNLL QCD (HRes)	Fixed order: NLO QCD + NLO EW (HAWK)	Fixed order: NNLO QCD (VH@NNLO)	(MG5_aMC@NLO)
Higgs $p_T$ : NNLO+NNLL (HqT, HRes)			
Jet Veto: N3LO+NNLL			

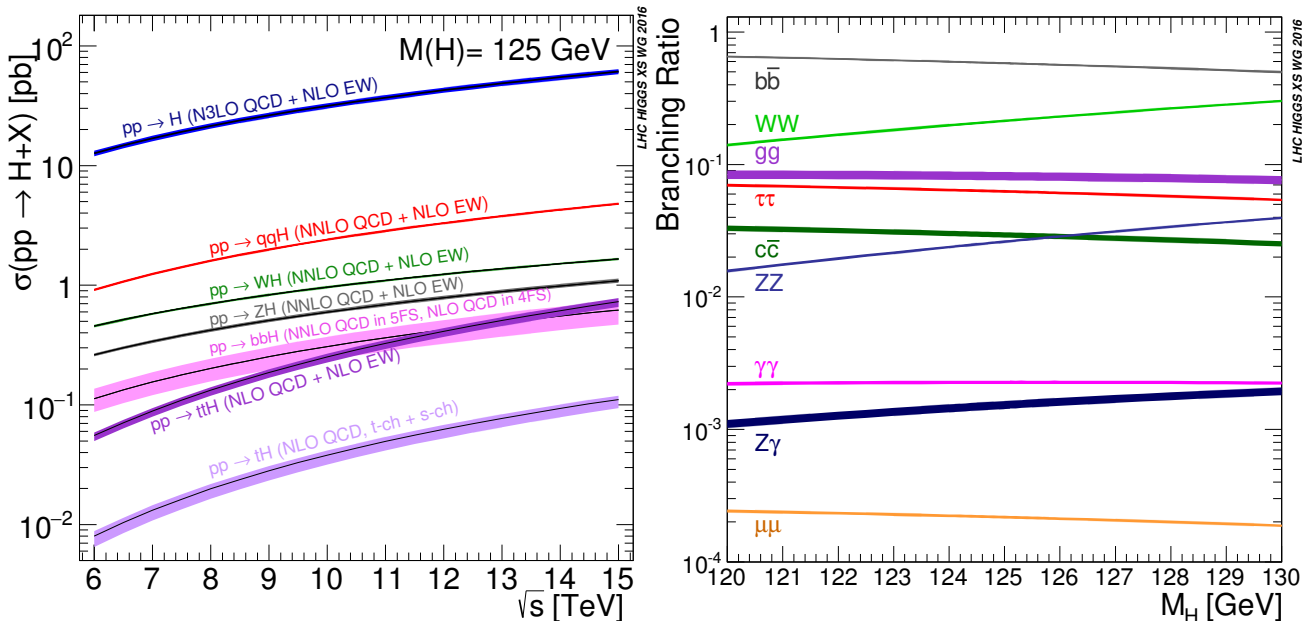


Figure 11.2: (Left) The SM Higgs boson production cross sections as a function of the center of mass energy,  $\sqrt{s}$ , for  $pp$  collisions [45]. The VBF process is indicated here as  $qqH$ . The theoretical uncertainties are indicated as bands. (Right) The branching ratios for the main decays of the SM Higgs boson near  $m_H = 125$  GeV [43, 44]. The theoretical uncertainties are indicated as bands.

(top, bottom, charm) quark and Higgs boson masses, the cross section has been calculated at the next-to-leading order (NLO)

**Table 11.2:** The SM Higgs boson production cross sections for  $m_H = 125$  GeV in  $pp$  collisions ( $p\bar{p}$  collisions at  $\sqrt{s} = 1.96$  TeV for the Tevatron), as a function of the center of mass energy,  $\sqrt{s}$ . The predictions for the LHC energies are taken from Refs. [41–44], the ones for the Tevatron energy are from Ref. [46]. The predictions for the ggF channel at the LHC include the latest N3LO results leading to reduced theoretical uncertainties by a factor around 2 compared to the NNLO+NLL results. The total uncertainties are estimated assuming no correlations between  $\alpha_s$  and PDF uncertainties.

$\sqrt{s}$ (TeV)	Production cross section (in pb) for $m_H = 125$ GeV					
	ggF	VBF	$WH$	$ZH$	$t\bar{t}H$	total
1.96	$0.95^{+17\%}_{-17\%}$	$0.065^{+8\%}_{-7\%}$	$0.13^{+8\%}_{-8\%}$	$0.079^{+8\%}_{-8\%}$	$0.004^{+10\%}_{-10\%}$	1.23
7	$16.9^{+4.4\%}_{-7.0\%}$	$1.24^{+2.1\%}_{-2.1\%}$	$0.58^{+2.2\%}_{-2.3\%}$	$0.34^{+3.1\%}_{-3.0\%}$	$0.09^{+5.6\%}_{-10.2\%}$	19.1
8	$21.4^{+4.4\%}_{-6.9\%}$	$1.60^{+2.3\%}_{-2.1\%}$	$0.70^{+2.1\%}_{-2.2\%}$	$0.42^{+3.4\%}_{-2.9\%}$	$0.13^{+5.9\%}_{-10.1\%}$	24.2
13	$48.6^{+4.6\%}_{-6.7\%}$	$3.78^{+2.2\%}_{-2.2\%}$	$1.37^{+2.6\%}_{-2.6\%}$	$0.88^{+4.1\%}_{-3.5\%}$	$0.50^{+6.8\%}_{-9.9\%}$	55.1
14	$54.7^{+4.6\%}_{-6.7\%}$	$4.28^{+2.2\%}_{-2.2\%}$	$1.51^{+1.9\%}_{-2.0\%}$	$0.99^{+4.1\%}_{-3.7\%}$	$0.60^{+6.9\%}_{-9.8\%}$	62.1

in  $\alpha_s$  [48, 49]. To a very good approximation, the leading top-quark contribution can be evaluated in the limit  $m_t \rightarrow \infty$  by matching the SM to an effective theory. The gluon-fusion amplitude is then evaluated from an effective Lagrangian containing a local  $HG_{\mu\nu}^a G^{a\mu\nu}$  operator [23, 24]. In this approximation, the cross section is known at next-to-next-to-next-to-leading order (N3LO) [50]. The validity of the effective theory with infinite  $m_t$  is greatly enhanced by rescaling the result by the exact LO result:  $\sigma = (\sigma_{m_t}^{\text{LO}}/\sigma_{m_t=\infty}^{\text{LO}}) \times \sigma_{m_t=\infty}$  [44]. The large top-quark mass approximation, after this rescaling of the cross section, yields a NNLO result that has been established to be at the percent level accuracy [51]. Further progress is made to include full top mass dependence at NNLO [52].

The LO and NLO QCD corrections [53] amount to about 80% of the total N3LO cross section. The NNLO corrections [54] further enhance the cross section by approximately 30% of the LO plus NLO result (at  $\mu_f = \mu_r = m_H/2$ ). Electroweak radiative corrections have been computed at NLO and increase the LO cross section by about 5% for  $m_H \simeq 125$  GeV [55]. Mixed QCD-EW corrections are now being investigated with encouraging results on the computation of the exact 3-loop amplitude [56] complementing the results obtained in either limit of heavy [57] or massless [58] gauge bosons.

At N3LO, the perturbation series is rather stable with a mere enhancement of 3% of the total cross section, with a central value quite insensitive to threshold resummation effects with the scale choice mentioned above [44, 50, 59]. At the LHC with a center-of-mass energy of 13 TeV, the most up-to-date value for the production cross section of a 125 GeV Higgs boson amounts to [44]

$$\sigma_{\text{ggF}}^{\text{N3LO}} = 48.6 \text{ pb}^{+2.2 \text{ pb} (+4.6\%)}_{-3.3 \text{ pb} (-6.7\%)} \text{ (theory)} \pm 1.6 \text{ pb} (3.2\%) \text{ (PDF} + \alpha_s \text{)}. \quad (11.10)$$

Besides considering the inclusive Higgs boson production cross section at the LHC, it is important to study differential distributions in order to probe the properties of the Higgs boson in a detailed way. A more exclusive account of Higgs boson production is also required because experimental analyses often impose cuts on the final states in order to improve the signal-to-background ratio. To this end, it is useful to define benchmark cuts and compare the differential distributions obtained at various levels of theoretical accuracy (i.e., at NLO or NNLO) with Monte-Carlo generators. In the infinite top mass limit, the Higgs

boson  $p_T$  distribution is known at NNLO [60, 61] (see Ref. [62] for a recent reappraisal) and heavy quark mass effects, including top-bottom interferences, have been computed at NLO [63], revealing a non-trivial logarithmic structure that will make resummation difficult [64]. A programmatic approach for a fixed-order/resummation matching of the top-bottom interferences has been proposed [65]. Many search modes for the Higgs boson are carried out by separating the events according to the number of jets or the transverse momentum and rapidity of the Higgs boson. For  $p_T < 35$  GeV, predictions for the transverse-momentum distribution can only be trusted after large logarithms of the form  $\alpha_s^n \ln^k(m_H/p_T^{\text{veto}})$ ,  $k \leq 2n - 1$ , and (non-Sudakov) double logarithms of the form  $g_{Hq\bar{q}} m_q/m_H [\ln^2(m_H/m_q), \ln^2(p_T/m_q)]$  have been resummed. This has been accomplished with N3LL accuracy [66] and the results have been matched onto the fixed-order prediction at NNLO [67]. In addition, impressive progress is made to improve the calculation of the Higgs boson production cross section with a jet veto (the “0-jet bin” or in the presence of a veto bounding the transverse momentum of the hardest accompanying jet) [68], reaching N2LL accuracy matched to N3LO. These accurate predictions for the jet-veto cross section are required, e.g., to suppress the  $t\bar{t}$  background in the  $H \rightarrow WW$  channel [69]. Electroweak corrections have been studied in Ref. [70]. Note that in the boosted regime, at  $p_T \sim 1$  TeV,  $VH$  takes over ggF as the dominant channel [71].

### ii. Vector boson fusion production mechanism

The SM Higgs boson production mode with the second-largest cross section at the LHC is vector boson fusion. At the Tevatron collider, VBF also occurred, but for  $m_H = 125$  GeV had a smaller cross section than Higgs boson production in association with a  $W$  or  $Z$  boson. Higgs boson production via VBF,  $qq \rightarrow qqH$ , proceeds by the scattering of two (anti-)quarks, mediated by  $t$ - or  $u$ -channel exchange of a  $W$  or  $Z$  boson, with the Higgs boson radiated off the weak-boson propagator. The scattered quarks give rise to two back-to-back hard jets in the forward and backward regions of the detector [72]. Because of the color-singlet nature of the weak-gauge boson exchange, gluon radiation from the central-rapidity regions is strongly suppressed. These characteristic features of VBF processes can be exploited to distinguish them from overwhelming QCD backgrounds, including gluon-fusion induced Higgs boson + 2 jet production, and from  $s$ -channel  $WH$  or  $ZH$  production with a hadronically decaying weak gauge boson. After the application of specific selection cuts, the VBF channel provides a clean environment, not only for the Higgs boson searches originally performed, but also for the subsequent determination of Higgs boson couplings at the LHC.

At the inclusive level, the cross-section is known at N3LO [73], with a residual uncertainty of the order of few permill. However, this result is obtained in the DIS/factorised approximation [74] where the fusing gauge bosons are emitted from the two quark legs independently. While, the exact NNLO VBF calculation will remain out-of-reach in the near future, the leading non-factorisable contributions with two forward jets have been estimated [75]. They give some corrections, also of the order of few permill, to inclusive quantities, but they are an order of magnitude larger for differential observables. Full NNLO QCD and NLO EW results in the DIS approximation are known [76] and the residual uncertainty is of the order of a few percent but is quite sensitive to the tagging jet cuts and jet radius modelling [77].

### iii. $WH$ and $ZH$ associated production mechanism

The next most relevant Higgs boson production mechanisms after ggF and VBF at the LHC, and the most relevant ones after ggF at the Tevatron collider, are associated production with  $W$  and  $Z$  gauge bosons. The cross sections for the associated production processes,  $pp \rightarrow VH + X$ , with  $V = W^\pm, Z$  receive contributions at NLO given by NLO QCD corrections to the Drell–Yan cross section [78, 79] and from NLO EW corrections. The latter, unlike the QCD corrections, do not respect the factorisation into Drell–Yan production since there are irreducible box contributions already at one loop [80]. At NNLO, the Drell–Yan-like corrections

to  $WH$  production also give the bulk of the corrections to  $ZH$  production [81]. For  $ZH$  production there are, however, gluon-gluon induced contributions that do not involve a virtual  $Z$  gauge boson but are such that the  $Z$  gauge boson and  $H$  boson couple to gluons via top-quark loops [82], see diagram (d) in Fig. 11.1. In addition,  $WH$  and  $ZH$  production receive non Drell–Yan-like corrections in the  $q\bar{q}'$  and  $q\bar{q}$  initiated channels, respectively, at the NNLO level, where the Higgs boson is radiated off top-quark loops [83]. The full QCD corrections up to NNLO order, the NLO EW corrections and the NLO corrections to the gluon-gluon channel are available in  $\overline{\text{VH@NNLO}}$  [84].

As neither the Higgs boson nor the weak gauge bosons are stable particles, their decays also have to be taken into account. Providing full kinematical information for the decay products can furthermore help in the suppression of large QCD backgrounds. Differential distributions for the processes  $pp \rightarrow WH \rightarrow \bar{\nu}_\ell \ell H$  and  $pp \rightarrow ZH \rightarrow \ell^+ \ell^- H / \nu_\ell \bar{\nu}_\ell H$ , including NLO QCD and EW corrections, have been presented in Ref. [85]. The NNLO QCD corrections to differential observables for  $WH$  production at the LHC, including the leptonic decays of the  $W$  boson and the decay of the Higgs boson into a  $b\bar{b}$  pair, are presented in Ref. [86]. Calculations at the same level, including also the  $ZH$  process have been performed [87]. The  $WH$  production mode has also been matched to a parton shower at NNLO accuracy [88]. Full NNLO results for both the production and decay are available [89] and show a large impact of radiation from the final-state bottoms. The  $WH$  and  $ZH$  production modes, especially in the boosted regime, provide a relatively clean environment for studying the decay of the Higgs boson into bottom quarks [90].

#### iv. Higgs boson production in association with $t\bar{t}$

Higgs boson radiation off top quarks,  $pp \rightarrow t\bar{t}H$ , provides a direct probe of the top-Higgs Yukawa coupling. The LO cross section for this production process was computed in Ref. [91]. Later, the NLO(+NNLL) QCD [92] and NLO EW corrections [93] were evaluated yielding a moderate increase in the total cross section of at most 20%, but significantly reducing the scale dependence of the inclusive cross section. The EW corrections can be enhanced by large electroweak Sudakov logarithms in particular in the boosted regime often used in the phenomenological analyses [94]. The total theoretical errors, estimated by combining the uncertainties from factorisation and renormalisation scales, strong gauge coupling, and parton distributions, amount to 10–15% of the corresponding inclusive cross section. Interfaces between NLO QCD calculations for  $t\bar{t}H$  production with parton-shower Monte-Carlo programs have been provided in Ref. [95]. These programs provide the most flexible tools to date for the computation of differential distributions, including experimental selection cuts and vetoes on the final-state particles and their decay products. The fixed-order NLO QCD calculation have been interfaced with the standard Parton Shower Monte-Carlo generators, allowing an accurate description of the  $t\bar{t}H$  signal, from the energy scale of the hard scattering to the hadronisation energy scale. The exploitation of this channel requires, however, a proper description of the background, in particular  $t\bar{t}b\bar{b}$ , which exhibits a huge k-factor<sup>1</sup> enhancement from shower effects, see Ref. [44] for a detailed discussion.

#### v. Other single Higgs boson production mechanisms at the LHC

The Higgs boson production in association with a single top quark, though subdominant, can bring valuable information, in particular regarding the sign of the top Yukawa coupling. This is due to an almost totally destructive interference between two large contributions, one where the Higgs boson couples to a space-like  $W$  boson and the other where it couples to the top quark. This process has been computed at NLO in a five-flavour scheme [96] and amounts to about 90 fb at  $\sqrt{s} = 14$  TeV (with the opposite sign of the top Yukawa coupling, the cross section increases by one or

der of magnitude while the cross section for associated production with a pair of top quarks is unaffected).

The Higgs boson production in association with a pair of bottom quarks ( $b\bar{b}H$ ) is known at NNLO in the case of five quark flavours [97–99]. The coupling of the Higgs boson to a  $b$ -quark is suppressed in the SM by the bottom-quark mass over the Higgs VEV,  $m_b/v$ , implying that associated production of a SM Higgs boson with  $b$ -quarks is small at the LHC. Yet, at high energy, large logarithms are present and need to be resummed, leading to an enhancement of the inclusive cross section. At  $\sqrt{s} = 14$  TeV, the  $b\bar{b}H$  cross section can be as large as 550 fb, still two orders of magnitude below the ggF production cross section. In a two Higgs doublet model or a SUSY model, which will be discussed in Section 11.7, this coupling is proportional to the ratio of neutral Higgs boson vacuum expectation values,  $\tan \beta$ , and can be significantly enhanced for large values of this ratio. Consequently, the  $b\bar{b}H$  mode can even become the dominant production process for the Higgs boson, unlike in the SM.

The Higgs boson production in association with charm quarks is also known at NNLO and its cross section is approximately 85 fb at  $\sqrt{s} = 13$  TeV [44].

#### vi. Double Higgs boson production at the LHC

The main interest in the double Higgs boson production is that it can provide invaluable information on the Higgs potential. In particular, it gives access to the Higgs trilinear self coupling. The dominant production is via gluon fusion  $gg \rightarrow HH$ . It accounts for more than 90% of the total inclusive cross-section, the sub-leading production mechanisms are VBF  $HHjj$  (around 1.7 fb at 13 TeV),  $HHW$  (0.50 fb),  $HHZ$  (0.36 fb) and  $t\bar{t}HH$  (0.8 fb). The fixed order QCD corrections, computed in the infinite top mass limit, are large, typically doubling the cross section from LO to NLO [100] and further enhancing it by 20% from NLO to NNLO [101] to reach at 13 TeV [45]

$$\begin{aligned} \sigma(gg \rightarrow HH)_{\text{ggF}}^{\text{NNLO, FTa}} &= 31.05 \text{ fb}_{-5.0\%}^{+2.2\%} \text{ (theory)} \\ &\pm 3\% \text{ (PDF} + \alpha_s) \pm 2.6\% (m_t). \end{aligned} \quad (11.11)$$

Recently, the complete NLO corrections with all top quark mass effects also became available numerically [102, 103], intriguingly revealing a k-factor much less flat than predicted in the large top mass approximations. The non-trivial dependence of the results on the renormalisation scheme and scale for the top quark mass [103] questions the assessment of the scale uncertainty and would warrant a proper NNLO computation that will however remain out of reach for quite some time. At the differential level, the destructive interference between the box and the triangle contributions complicates the predictions made in the infinite top mass limit for both the  $HH$  invariant mass and the leading Higgs boson  $p_T$  distributions. With an inclusive cross section of about 35 fb at  $\sqrt{s} = 13$  TeV and a difficult signal vs background discrimination, the double Higgs boson production remains a challenging channel to probe and will greatly benefit from the high-luminosity run of the LHC [104].

#### 11.2.4.2 Production mechanisms at $e^+e^-$ colliders

The dominant Higgs boson production cross sections at an  $e^+e^-$  collider are from the Higgs-strahlung process [23, 105],  $e^+e^- \rightarrow ZH$ , and the  $WW$  fusion process [106],  $e^+e^- \rightarrow \bar{\nu}_e \nu_e W^* W^* \rightarrow \bar{\nu}_e \nu_e H$ . The cross-section for the Higgs-strahlung process scales as  $s^{-1}$  and is predominant at low energies, while the cross-section for the  $WW$  fusion process scales as  $\ln(s/m_H^2)$  and dominates at high energies [107]. The  $ZZ$  fusion mechanism,  $e^+e^- \rightarrow e^+e^- Z^* Z^* \rightarrow e^+e^- H$ , also contributes to the Higgs boson production, with a cross-section suppressed by an order of magnitude with respect to that of  $WW$  fusion. The process  $e^+e^- \rightarrow t\bar{t}H$  [108] becomes important for  $\sqrt{s} \geq 500$  GeV. For a more detailed discussion of Higgs boson production properties at lepton colliders, see for example Ref. [109].

<sup>1</sup>the k-factor is defined as the ratio of a physical quantity with and without radiative corrections included.

### 11.2.4.3 SM Higgs boson branching ratios and total width

For the understanding and interpretation of the experimental results, the computation of all relevant Higgs boson decay widths is essential, including an estimate of their uncertainties and, when appropriate, the effects of Higgs boson decays into off-shell particles with successive decays into lighter SM ones. A Higgs boson mass of about 125 GeV allows to explore the Higgs boson couplings to many SM particles. In particular the dominant decay modes are  $H \rightarrow b\bar{b}$  and  $H \rightarrow WW^*$ , followed by  $H \rightarrow gg$ ,  $H \rightarrow \tau^+\tau^-$ ,  $H \rightarrow c\bar{c}$  and  $H \rightarrow ZZ^*$ . With much smaller rates follow the Higgs boson decays into  $H \rightarrow \gamma\gamma$ ,  $H \rightarrow \gamma Z$  and  $H \rightarrow \mu^+\mu^-$ . Since the decays into gluons, diphotons and  $Z\gamma$  are loop induced, they provide indirect information on the Higgs boson couplings to  $WW$ ,  $ZZ$  and  $t\bar{t}$  in different combinations. The uncertainties in the branching ratios include the missing higher-order corrections in the theoretical calculations as well as the errors in the SM input parameters, in particular fermion masses and the QCD gauge coupling, involved in the decay. In the following the state-of-the-art of the theoretical calculations will be discussed and the reader is referred to Refs. [41–44, 110] for detail.

The evaluation of the radiative corrections to the fermionic decays of the SM Higgs boson are implemented in HDECAY [111] at different levels of accuracy. The computations of the  $H \rightarrow b\bar{b}$  and  $H \rightarrow c\bar{c}$  decays include the complete massless QCD corrections up to N4LO, with a corresponding scale dependence of about 0.1% [112]. Both the electroweak corrections to  $H \rightarrow b\bar{b}$ ,  $c\bar{c}$  as well as  $H \rightarrow \tau^+\tau^-$  are known at NLO [113] providing predictions with an overall accuracy of about 1–2% for  $m_H \simeq 125$  GeV.

The loop induced decays of the SM Higgs boson are known fully at NLO and partially beyond that approximation. For  $H \rightarrow gg$ , the QCD corrections are known up to N3LO in the limit of heavy top quarks [49, 114] and the uncertainty from the scale dependence is about 3%. For the  $H \rightarrow \gamma\gamma$ , the full NLO QCD corrections are available [49, 115] and the three-loop QCD corrections have also been evaluated [116]. The NLO electroweak corrections to  $H \rightarrow gg$  and  $H \rightarrow \gamma\gamma$  have been computed in Ref. [117]. All these corrections are implemented in HDECAY [111]. For  $m_H \simeq 125$  GeV, the overall impact of known QCD and EW radiative effects turns out to be well below 1%. In addition, the contribution of the  $H \rightarrow \gamma e^+e^-$  decay via virtual photon conversion has been computed in Ref. [118]. The partial decay width  $H \rightarrow Z\gamma$  is only implemented at LO in HDECAY, including the virtual  $W$ , top-, bottom-, and  $\tau$ -loop contributions. The QCD corrections have been calculated and are at the percent level [119]. The theoretical uncertainty due to unknown electroweak corrections is estimated to be less than 5%, an accuracy that will be hard to achieve in the measurement of this process at the LHC.

**Table 11.3:** The branching ratios and the relative uncertainty [43, 44] for a SM Higgs boson with  $m_H = 125$  GeV.

Decay channel	Branching ratio	Rel. uncertainty
$H \rightarrow \gamma\gamma$	$2.27 \times 10^{-3}$	2.1%
$H \rightarrow ZZ$	$2.62 \times 10^{-2}$	$\pm 1.5\%$
$H \rightarrow W^+W^-$	$2.14 \times 10^{-1}$	$\pm 1.5\%$
$H \rightarrow \tau^+\tau^-$	$6.27 \times 10^{-2}$	$\pm 1.6\%$
$H \rightarrow b\bar{b}$	$5.82 \times 10^{-1}$	+1.2% –1.3%
$H \rightarrow c\bar{c}$	$2.89 \times 10^{-2}$	+5.5% –2.0%
$H \rightarrow Z\gamma$	$1.53 \times 10^{-3}$	$\pm 5.8\%$
$H \rightarrow \mu^+\mu^-$	$2.18 \times 10^{-4}$	$\pm 1.7\%$

The decays  $H \rightarrow WW/ZZ \rightarrow 4f$  can be simulated with the

Prophecy4f Monte-Carlo generator [120] that includes complete NLO QCD and EW corrections for Higgs decays into any possible four-fermion final state. All calculations are consistently performed with off-shell gauge bosons, without any on-shell approximation. For the SM Higgs boson, the missing higher-order corrections are estimated to be roughly 0.5%. Such uncertainties will have to be combined with the parametric uncertainties, in particular those associated to the bottom-quark mass and the strong gauge coupling, to arrive at the full theory uncertainty. A detailed treatment of the differential distributions for a Higgs boson decay into four charged leptons in the final state is discussed in Refs. [43, 121].

The total width of a 125 GeV SM Higgs boson is  $\Gamma_H = 4.07 \times 10^{-3}$  GeV, with a relative uncertainty of  $^{+4.0\%}_{-3.9\%}$ . The branching ratios for the most relevant decay modes of the SM Higgs boson as a function of  $m_H$ , including the most recent theoretical uncertainties, are shown in Fig. 11.2 (right) and listed for  $m_H = 125$  GeV in Table 11.3. Further details of these calculations can be found in the reviews [41–44] and references therein.

### 11.3 The experimental profile of the Higgs boson

The observation [1, 2] at the LHC of a narrow resonance with a mass of about 125 GeV was an important landmark in the decades-long direct search [46, 122] for the SM Higgs boson. This was followed by a detailed exploration of properties of the Higgs boson at the different runs of the LHC at  $\sqrt{s} = 7, 8$  and 13 TeV.

The dataset at  $\sqrt{s} = 13$  TeV in the Run 2 phase of the LHC operation corresponds to an integrated luminosity of about  $156 \text{ fb}^{-1}$  see Table 11.4. The datasets effectively useful for analysis need to take into account the data-taking efficiency with fully operational detectors and the data quality efficiency. The typical total inefficiency for both ATLAS and CMS is approximately 10%, where approximately half is due to the data taking inefficiency and half from data quality.

In this section, most of the references for the Run 1 measurements that have been updated at the Run 2 are given in the previous version of this review [123] and are not repeated herein.

**Table 11.4:** The LHC  $pp$  collision centre-of-mass energies and delivered data samples.

Year	$\sqrt{s}$ (TeV)	$\int \text{L.d.t}$ ( $\text{fb}^{-1}$ )	Period
2010	7	0.04	Run 1
2011	7	6.1	Run 1
2012	8	23.3	Run 1
2015	13	4.2	Run 2
2016	13	40.8	Run 2
2017	13	50.2	Run 2
2018	13	60.6	Run 2

#### 11.3.1 The principal decay channels to vector bosons

For a given  $m_H$ , the sensitivity of a channel depends on the production cross section of the Higgs boson, its decay branching fraction, the reconstructed mass resolution, the selection efficiency and the level of background in the final state. For a low-mass Higgs boson ( $110 \text{ GeV} < m_H < 150 \text{ GeV}$ ) for which the SM width would be only a few MeV, five decay channels play an important role at the LHC. In the  $H \rightarrow \gamma\gamma$  and  $H \rightarrow ZZ^* \rightarrow 4\ell$  channels, all final state particles can be very precisely measured and the reconstructed  $m_H$  resolution is excellent (typically 1–2%). While the  $H \rightarrow W^+W^- \rightarrow \ell^+\nu_\ell\ell'^-\bar{\nu}_{\ell'}$  channel has relatively large branching fraction, however, due to the presence of neutrinos which are not reconstructed in the final state, the  $m_H$  resolution, obtained through observables sensitive to the Higgs boson mass such as the transverse mass, is poor (approximately 20%). The  $H \rightarrow b\bar{b}$  and the  $H \rightarrow \tau^+\tau^-$  channels suffer from large backgrounds and lead to an intermediate mass resolution of about 10% and 15% respectively.

With the increase in the size of datasets, measurements in the most sensitive channels are now carried out differentially or in exclusive modes depending on specific production characteristics. These measurements are discussed in Section 11.6.2.4.



The candidate events in each Higgs boson decay channel are split into several mutually exclusive categories (or event tags) based on the specific topological, kinematic or other features present in the event. The categorization of events increases the sensitivity of the overall analysis and allows a separation of different Higgs boson production processes. Most categories are dominated by signal from one Higgs boson decay mode but contain an admixture of various Higgs boson production processes. For example, a typical VBF selection requires Higgs boson candidates to be accompanied by two energetic jets ( $\geq 30$  GeV) with a large dijet mass ( $\geq 400$  GeV) and separated by a large pseudo-rapidity ( $\Delta\eta_{jj} \geq 3.5$ ) [124]. While such a category is enriched in Higgs bosons produced via VBF, the contamination from the ggF production mechanism can be significant. Hence, a measurement of the signal rate in the VBF category does not imply a measurement of VBF production cross section since one cannot resolve the contamination from ggF. Simulations are used to determine the relative contributions of the various Higgs boson production modes in each specific categories.

An important difference between the Run 1 and Run 2 results, in particular when comparing signal strengths, and therefore in the measurement of the couplings of the Higgs boson as discussed in Section 11.4, is that values and errors of the predicted cross sections have been improved (mostly the scale and PDF uncertainties). The theoretical predictions are however compatible and therefore, the signal strengths can be compared on a sound basis.

#### 11.3.1.1 $H \rightarrow \gamma\gamma$

In the  $H \rightarrow \gamma\gamma$  channel, a search is performed for a narrow peak over a smoothly falling background in the invariant mass distribution of two high  $p_T$  photons. The background in this channel is conspicuous and stems from prompt  $\gamma\gamma$  processes for the irreducible backgrounds, and the  $\gamma$ +jet and dijet processes for the reducible backgrounds where one jet fragments typically into a leading  $\pi^0$ . In order to optimise search sensitivity and also to separate the various Higgs boson production modes, ATLAS and CMS split events into several mutually exclusive categories. Diphoton events containing a high  $p_T$  muon or electron, or missing energy ( $E_T^{\text{miss}}$ ) consistent with the decay of a  $W$  or  $Z$  boson, are tagged in the  $VH$  production category. Diphoton events containing energetic dijets with a large mass and pseudo-rapidity difference are assigned to the VBF production category, and the remaining events are considered either in the  $VH$  category when the two jets are compatible with the hadronic decay of a  $W$  or a  $Z$ , or in the ggF production category. While the leptonic  $VH$  category is relatively pure, the VBF category has significant contamination from the gluon fusion process. Events which are not picked by any of the above selections are further categorised according to their expected  $m_{\gamma\gamma}$  resolution and signal-to-background ratio. Categories with good  $m_H$  resolution and larger signal-to-background ratio contribute most to the sensitivity of the search.

Both ATLAS and CMS have studied in detail the calibration of the energy response of photons, in particular using  $Z \rightarrow e^+e^-$ ,  $Z \rightarrow \mu^+\mu^-$  and the response of muons in the calorimeter (for ATLAS) from  $Z \rightarrow \mu^+\mu^-$  events. This information is used to correct the simulated signal mass line-shapes. In each category, parametric signal models are adjusted to these line-shapes to provide a functional form for the signal. Simple monotonic functional forms of the backgrounds are determined by a fit to the  $m_{\gamma\gamma}$  distribution in each category (typically exponential, Bernstein polynomials, Laurent series or power laws). All categories are fitted simultaneously to determine the signal yield at the measured combined Run 1 mass of  $125.09 \pm 0.27$  GeV [127] discussed in Section 11.3.2. The  $m_{\gamma\gamma}$  distribution after combining all categories is shown in Fig. 11.3, using the full ATLAS Run 2 dataset.

The signal strength,  $\mu = (\sigma \cdot \text{BR})_{\text{obs}} / (\sigma \cdot \text{BR})_{\text{SM}}$ , which is the observed product of the Higgs boson production cross section ( $\sigma$ ) and its branching ratio (BR) normalised to the corresponding SM values, is  $1.17 \pm 0.27$  for ATLAS in Run 1 and  $1.02 \pm 0.14$  in Run 2 [128] (where this signal strength measurement is estimated from the measured fiducial cross sections and thus neglects acceptance systematic uncertainties, which are not expected to be dominant in particular given that the measurement is inclusive).

The signal strengths  $^2$  measured in Run 1 and Run 2 by the CMS collaboration are  $1.18_{-0.23}^{+0.26}$  and  $1.18_{-0.14}^{+0.17}$  [129] respectively.

#### 11.3.1.2 $H \rightarrow ZZ^* \rightarrow \ell^+\ell^-\ell^+\ell^-$

In the  $H \rightarrow ZZ^* \rightarrow \ell^+\ell^-\ell^+\ell^-$  channel, a search is performed for a narrow mass peak over a small continuous background dominated by non-resonant  $ZZ^*$  production from  $q\bar{q}$  annihilation and  $gg$  fusion processes. The contribution and the shape of this irreducible background is taken from simulation. The subdominant and reducible backgrounds stem from  $Z+b\bar{b}$ ,  $t\bar{t}$  and  $Z$ +jets events. Their contribution is suppressed by requirements on lepton isolation and lepton impact parameter and their yield is estimated from control samples in data.

To help to distinguish the Higgs boson signal from the dominant non-resonant  $ZZ^*$  background, both ATLAS and CMS [130] use a matrix element likelihood approach to construct a kinematic discriminant built for each  $4\ell$  event based on the ratio of complete leading-order matrix elements  $|\mathcal{M}_{\text{sig}}|^2 / |\mathcal{M}_{\text{bkg}}|^2$  for the signal ( $gg \rightarrow H \rightarrow 4\ell$ ) and background ( $q\bar{q} \rightarrow ZZ \rightarrow 4\ell$ ) hypotheses. To further enhance the sensitivity, experiments also use multivariate techniques.

To improve the sensitivity to more exclusive production processes such as VBF,  $VH$  and  $t\bar{t}H$ , the experiments divide  $4\ell$  events into mutually exclusive categories. Events are categorised in terms of the number of reconstructed jets, the number of additional leptons (from the decay of a vector boson in the associated production mode), number of jet tagged as containing a  $b$ -hadron, the transverse momentum of the Higgs boson (or e.g. its associated vector boson) and missing transverse momentum. The exclusive processes are also further separated in different kinematic regions in a framework referred to as Simplified Template Cross Sections (see Section 11.6.2.4). Dijets with a large mass and pseudo-rapidity difference populate the VBF category. ATLAS requires the presence of an additional lepton in the  $VH$  category. In events with less than two jets, CMS uses the  $p_T^{4\ell}$  to distinguish between production via the gluon fusion and the  $VH$ /VBF processes.

Since the  $m_{4\ell}$  resolutions and the reducible background levels are different in the  $4\mu$ ,  $4e$  and  $2e2\mu$  sub-channels, they are analysed separately and the results are then combined. The distribution of the reconstructed invariant mass of the four leptons for CMS [126] is given in Fig. 11.3 (right), showing a clear excess at a mass of approximately  $m_H = 125$  GeV. Both experiments also observe a clear peak at  $m_{4\ell} = 91$  GeV from the production of a  $Z$  boson on-mass-shell and decaying to four leptons due typically to the emission of an off-shell photon from one of the primary leptons from the  $Z$  boson decay.

The signal strengths  $\mu$  for the inclusive  $H \rightarrow 4\ell$  production measured by ATLAS and CMS are  $1.44_{-0.33}^{+0.40}$  at  $m_H = 125.36$  GeV and  $0.93_{-0.25}^{+0.29}$  at  $m_H = 125.6$  GeV respectively, in Run 1. The signal strengths measured by ATLAS and CMS in Run 2 are  $1.04 \pm 0.10$  [131] and  $0.94 \pm 0.10$  [126] respectively (the ATLAS measurement is made at the combined Run 1 Higgs boson mass of  $m_H = 125.09$  GeV while the  $m_H$  is profiled in the CMS analysis). The dominant uncertainty in these measurements remains the statistical uncertainty.

#### 11.3.1.3 Measurement of the Higgs boson mass

To measure the mass of the Higgs boson, ATLAS and CMS collaborations rely on the two high mass-resolution and sensitive channels,  $\gamma\gamma$  and  $ZZ^*/4\ell$ . The ATLAS and CMS approaches are very similar in these two analyses with small differences on the usage of categories, additional discriminating variables and per-event errors. In these two channels, the mass resolutions range from 1.4 GeV to 2 GeV for ATLAS and from 1.0 GeV to 2.8 GeV for CMS (see Ref. [127] and the reconstruction-performance references therein). The best mass resolution is obtained for both experiments in the diphoton channel for central diphoton pairs (typically for events where both photons are not converted). The signal strengths in the  $\gamma\gamma$  and  $ZZ$  channels are assumed to be

<sup>2</sup>The Run 1 results for ATLAS and CMS are at fixed values of  $m_H = 125.4$  GeV and 124.7 GeV, respectively.

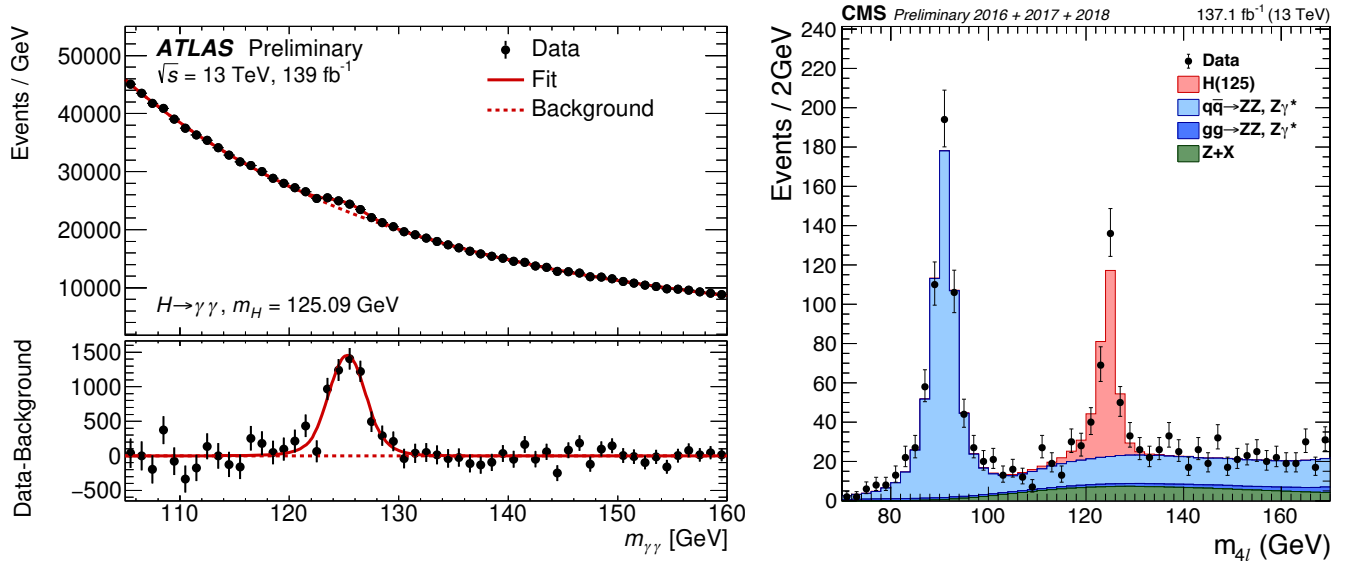


Figure 11.3: (Left) The invariant mass distribution of diphoton candidates, with each event weighted by the ratio of signal-to-background in each event category, observed by ATLAS [125] at Run 2. The residuals of the data with respect to the fitted background are displayed in the lower panel. (Right) The  $m_{4\ell}$  distribution from CMS [126] Run 2 data.

independent and not constrained to the expected rate ( $\mu = 1$ ) for the SM Higgs boson.

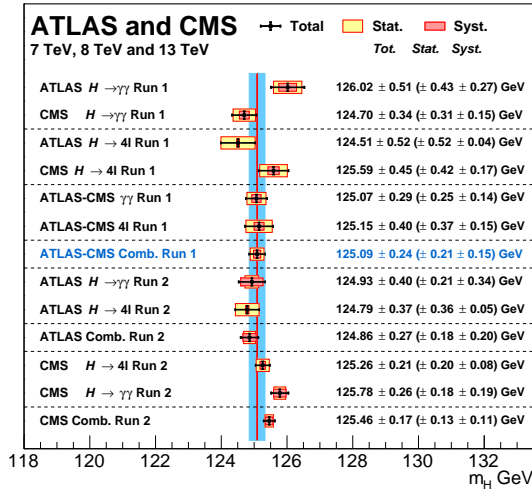


Figure 11.4: Summary of the CMS and ATLAS mass measurements in the  $\gamma\gamma$  and  $ZZ$  channels in Run 1 and Run 2.

Figure 11.4 summarizes all measurements of the Higgs boson mass, including the individual and combined Run 1 measurements [127] and the Run 2 measurement by ATLAS [132] and CMS [130, 133] for both the diphoton and the  $4\ell$  channels.

In the diphoton channel, as discussed in Section 11.5.3.2, a mass shift is expected to be induced by the deformation of the mass line-shape of the signal in presence of background, from the interference between the Higgs boson production and the continuum irreducible background. It is a small but non negligible effect of approximately 35 MeV [134] for a Higgs boson width close to that of the SM. This effect could be larger if the width of the Higgs boson were to be substantially larger. This effect estimated by ATLAS with a full simulation is still relatively small with respect to the total uncertainty on the mass and is therefore neglected.

#### 11.3.1.4 $H \rightarrow W^+W^- \rightarrow \ell^+\nu\ell^-\bar{\nu}$

In this intricate channel, experiments search for an excess of events with two leptons of opposite charge accompanied by missing energy and/or jets. A typical event selection is described below in order to give an idea of the main challenges. Specific se-

lections vary between experiments and between Run 1 and Run 2 analyses. Events are divided into several categories depending on the lepton flavour combination ( $e^+e^-$ ,  $\mu^+\mu^-$  and  $e^\pm\mu^\mp$ ) and the number of accompanying jets ( $N_{\text{jet}} = 0, 1, \geq 2$ ). In the ATLAS analysis, the  $N_{\text{jet}} \geq 2$  category is optimised for the VBF production process by selecting two leading jets with a large pseudorapidity difference and with a large mass ( $m_{jj} > 500$  GeV).

Backgrounds contributing to this channel are numerous and depend on the category of selected events. Reducing them and accurately estimating the remainder is a major challenge in this analysis. For events with opposite-flavour leptons and no accompanying high  $p_T$  jets, the dominant background stems from non-resonant  $WW$  production. Events with same-flavour leptons suffer from large Drell–Yan contamination (note that also the opposite-flavour leptons analysis has Drell–Yan  $\tau\tau$  background in 0-jet category). The  $t\bar{t}$ ,  $tW$  and  $W$ +jets (with the jet misidentified as a lepton) events contaminate all categories. Non-resonant  $WZ$ ,  $ZZ$  and  $W\gamma$  processes also contribute to the background at a sub-leading level.

A requirement of large missing transverse energy ( $E_T^{\text{miss}}$ ) is used to reduce the Drell–Yan and multijet backgrounds. In the  $e^+e^-$  and  $\mu^+\mu^-$  categories, events with  $m_{\ell\ell}$  consistent with the  $Z$  mass are vetoed. The  $t\bar{t}$  background is suppressed by a veto against identified  $b$ -jets or low  $p_T$  muons assumed to be coming from semi-leptonic  $b$ -hadron decays within jets (this soft muon veto was not applied anymore in Run 2 analysis) and tight isolation requirements diminish the  $W$ +jets background. The scalar nature of the Higgs boson and the  $V-A$  nature of the  $W$  boson decay implies that the two charged leptons in the final state are preferentially emitted at small angles with respect to each other. Therefore the dilepton invariant mass ( $m_{\ell\ell}$ ) and the azimuthal angle difference between the leptons ( $\Delta\phi_{\ell\ell}$ ) are used to discriminate between the signal and non-resonant  $WW$  events [135]. The transverse mass, constructed from the dilepton  $p_T$  ( $p_T^{\ell\ell}$ ),  $E_T^{\text{miss}}$  and the azimuthal angle between  $E_T^{\text{miss}}$  and  $p_T^{\ell\ell}$ , is defined as

$$m_T = \sqrt{2p_T^{\ell\ell}E_T^{\text{miss}}(1 - \cos\Delta\phi_{E_T^{\text{miss}}\ell\ell})}$$

and serves as an effective discriminant against backgrounds. The transverse mass variable also tracks the Higgs boson mass but with a poor mass resolution. Background rates except for the small contributions typically from non-resonant  $WZ$ ,  $ZZ$  and  $W\gamma$  are evaluated from data control samples with floating normalisation.

ATLAS fitted the  $m_T$  distributions and observed an excess at  $m_H = 125.36$  GeV with a local significance of  $6.1\sigma$  similar to that expected from a 125 GeV SM Higgs boson. The measured inclusive

signal strength is  $\mu = 1.09_{-0.21}^{+0.23}$ . In the VBF category, an excess with a significance of  $3.2\sigma$  corresponding to a signal strength of  $\mu = 1.27_{-0.45}^{+0.53}$  is observed. The CMS analysis of 0- and 1-jet categories, using all lepton flavour combinations, shows an excess with an observed significance of  $4.3\sigma$ , lower than the expected sensitivity of  $5.8\sigma$  for a 125.6 GeV SM Higgs boson. CMS observes no significant excess in the VBF production mode and sets a 95% CL limit on the signal strength of  $\mu_{\text{VBF}} < 1.7$  for  $m_H = 125.6$  GeV.

ATLAS and CMS have also searched for the associated Higgs boson production in this channel. The signal consists of up to three ( $WH$ ) or four ( $ZH$ ) high  $p_T$  isolated leptons with missing transverse energy and low hadronic activity. The major backgrounds stem from triboson and diboson production where each boson decays leptonically. ATLAS observes [136] an excess at  $m_H = 125.36$  GeV with a local significance of  $2.5\sigma$  corresponding to a  $\mu_{\text{VH}} = 3.0_{-1.0}^{+1.6}$ . CMS instead sets a 95% CL limit of  $\mu_{\text{VH}} < 4.7$ .

In this difficult channel, the full Run 2 dataset has not yet been analysed by ATLAS nor CMS. There have been partial analyses made with Run 2 data at 13 TeV by both ATLAS and CMS. ATLAS has analysed the  $WW \rightarrow e\nu\mu\nu$  decay mode in the gluon fusion, the VBF and  $VH$  production modes with 2015 and 2016 datasets [137, 138]. With this limited dataset the measured gluon fusion signal strength yielded [138]  $\mu_{\text{ggF}} = 1.10 \pm 0.20$ , with the largest uncertainties being the experimental systematic uncertainties.

CMS has performed a more complete analysis with the full 2016 dataset, with most production channels covering both the opposite- and same-flavour final states of opposite charge leptons (electrons or muons), obtaining a combined signal strength of  $\mu_{\text{WW}} = 1.28 \pm 0.18$  [139]. This analysis aims at several production modes (ggF, VBF and VH – with the vector boson reconstructed both in jet and leptonic decay modes).

### 11.3.2 Decays to third generation fermions ( $b\bar{b}$ and $\tau^+\tau^-$ )

In the SM, fermions acquire a mass through gauge invariant interactions with the Higgs field which is also responsible for the electroweak symmetry breaking and thus for generating the masses of gauge bosons (see Section 11.2 for more details). While this minimal solution is very elegant, there is no fundamental reason for it to be the case, and probing the couplings of the Higgs boson to fermions is therefore of fundamental importance, in particular since BSM physics can largely change the SM predictions.

The discovery of the Higgs boson was made essentially through bosonic final states. These decays probed mostly the couplings of the Higgs boson to vector bosons (the decay of the Higgs boson to photons occurring only through loops is also dominated in the SM by the coupling of the Higgs boson to  $W$  bosons). However, the predominant Higgs boson production mode is the gluon fusion, occurring only through loops dominated by the coupling of the Higgs boson to fermions. The observation of the Higgs boson in the two photons or two gluons decay modes is also an indirect evidence for the coupling of the Higgs boson to fermions (and in particular to the top quark). Nevertheless, the observation of either decays to fermions or production modes which unambiguously proceed through fermion couplings provide direct probes of the coupling of the Higgs boson to fermions and is thus of fundamental importance.

At hadron colliders, the most promising channel for probing the coupling of the Higgs field to the quarks and leptons are  $H \rightarrow b\bar{b}$  and  $H \rightarrow \tau^+\tau^-$ , respectively. For a Higgs boson with  $m_H \approx 125$  GeV, the branching fraction to  $b\bar{b}$  is about 58% and to  $\tau^+\tau^-$  is about 6%. Nevertheless, the presence of very large backgrounds makes the isolation of a Higgs boson signal in these channels quite challenging.

One of the most prominent goals of the LHC Run 2 for ATLAS and CMS was the direct observation of the Yukawa coupling of the Higgs boson to fermions of the third generation (bottom quarks, tau leptons and top quarks). This goal has been reached independently by both ATLAS and CMS and with only partial Run 2 datasets.

#### 11.3.2.1 $H \rightarrow \tau^+\tau^-$

In the  $H \rightarrow \tau^+\tau^-$  search,  $\tau$  leptons decaying to electrons ( $\tau_e$ ), muons ( $\tau_\mu$ ) and hadrons ( $\tau_{had}$ ) are considered. The  $\tau^+\tau^-$  invariant mass ( $m_{\tau\tau}$ ) is reconstructed from a kinematic fit of the visible products from the two  $\tau$  leptons and the missing energy observed in the event. Due to the presence of missing neutrinos, the  $m_{\tau\tau}$  resolution is poor ( $\approx 15\%$ ). As a result, a broad excess over the expected background in the  $m_{\tau\tau}$  distribution is searched for. The major sources of background stem from Drell–Yan  $Z \rightarrow \tau^+\tau^-$  and  $Z \rightarrow e^+e^-$ ,  $W$ +jets,  $t\bar{t}$  and multijet production. Events in all sub-channels are divided into categories based on the number and kinematic properties of additional energetic jets in the event and the transverse momentum of the reconstructed Higgs boson and the distance  $\Delta R$  distance between the two  $\tau$ 's. The sensitivity of the search is generally higher for categories with one or more additional jets. The VBF category, consisting of a  $\tau$  pair with two energetic jets separated by a large pseudo-rapidity, has the best signal-to-background ratio and search sensitivity, followed by the  $\tau^+\tau^-+1$  jet category. The signal to background discrimination relies in part on the  $m_{\tau\tau}$  resolution, which improves with the boost of the Higgs boson. The non-VBF categories are further subdivided according to the observed boost of the  $\tau^+\tau^-$  system. CMS primarily uses the reconstructed  $m_{\tau\tau}$  as the final discriminating variable while ATLAS combines various kinematic properties of each event categories with multivariate techniques to build the final discriminant [140].

Searches for  $H \rightarrow \tau^+\tau^-$  decays in the  $VH$  production mode are also performed in final states where the  $W$  or  $Z$  boson decays into leptons or jets. The irreducible background in this search arises from non-resonant  $WZ$  and  $ZZ$  diboson production. The reducible backgrounds originate from  $W$ ,  $Z$ , and  $t\bar{t}$  events that contain at least one fake lepton in the final state due to a misidentified jet. The shape and yield of the major backgrounds in each category are estimated from control samples in data. Contributions from non-resonant  $WZ$  and  $ZZ$  diboson production are estimated from simulations but corrected for reconstruction efficiency using control samples formed from observed data.

For CMS, the significance of the observed excess at  $m_H = 125$  GeV in Run 1 is  $3.2\sigma$ , close to the expected  $3.7\sigma$  sensitivity, and corresponds to a signal strength of  $\mu = 0.86 \pm 0.29$ . The observed (expected) deviation from the background-only hypothesis in ATLAS corresponds to a local significance of  $4.5\sigma$  ( $3.4\sigma$ ) and the best fit value of the signal strength is  $\mu = 1.43_{-0.37}^{+0.43}$  [140].

When the ATLAS and CMS  $H \rightarrow \tau\tau$  Run 1 measurements are combined [141], the significance of the observed excess corresponding to  $m_H = 125.09$  GeV is  $5.5\sigma$  and the combined signal strength is  $\mu = 1.11_{-0.22}^{+0.24}$ , consistent with the SM expectation.

The Run 1 evidence was strong only through the combination of the two experiments. The Run 2 larger dataset at a greater centre-of-mass energy is essential to further confirm this observation and perform first precision measurements in this important channel.

ATLAS has analysed its 2015 and 2016 dataset so far, providing further evidence at the  $4.4\sigma$  level with an expected significance of  $4.1\sigma$ . When combined with the Run 1 data the single experiment observation significance is  $6.4\sigma$  ( $5.4\sigma$  expected) [142].

In the CMS analysis of the 2016 data [143], the strategy was improved using additional categories aiming at the inclusive production of the Higgs boson and binned in transverse momentum of the  $\tau^+\tau^-$  system, and for the VBF production, the analysis is binned as a function of the dijet mass. This analysis reached a sensitivity of  $4.7\sigma$  with a dataset corresponding to an integrated luminosity of  $35.9 \text{ fb}^{-1}$ . CMS observes an excess with a significance of  $4.9\sigma$ . In combination with the Run 1 results, this provides an unambiguous observation of the direct coupling of the Higgs boson to taus, in the VBF production mode.

CMS has then also extended to additional production modes via the associated production with a vector boson [144] and analysed a larger dataset corresponding to an integrated luminosity of almost  $80 \text{ fb}^{-1}$  of data collected in 2016 and 2017, providing results which complete the Run 1 search for an unambiguous observation of the direct decay of the Higgs bosons to a pair of taus (and measurements of cross sections times branching-fractions) [145].

11.3.2.2  $H \rightarrow b\bar{b}$ 

In the search for the decay of the Higgs boson to a pair of  $b$ -quarks, the most sensitive production modes are the associated  $WH$  and  $ZH$  processes allowing use of the leptonic  $W$  and  $Z$  decays for triggering, and to purify the signal and reject QCD backgrounds. The  $W$  bosons are reconstructed via their leptonic decay  $W \rightarrow \ell\bar{\nu}_\ell$  where  $\ell = e, \mu$  or  $\tau$ . The  $Z$  bosons are reconstructed via their decay into  $e^+e^-, \mu^+\mu^-$  or  $\nu\bar{\nu}$ . The Higgs boson candidate mass is reconstructed from two  $b$ -tagged jets in the event. Backgrounds arise from production of  $W$  and  $Z$  bosons in association with gluon, light and heavy-flavoured jets ( $V$ +jets),  $t\bar{t}$ , diboson ( $ZZ$  and  $WZ$  with  $Z \rightarrow b\bar{b}$ ) and QCD multi-jet processes. Due to the limited  $m_{b\bar{b}}$  mass resolution, a SM Higgs boson signal is expected to appear as a broad enhancement in the reconstructed dijet mass distribution. The crucial elements in this search are  $b$ -jet tagging with high efficiency and low fake rate, accurate estimate of  $b$ -jet momentum and estimate of backgrounds from various signal depleted control samples constructed from data.

At the Tevatron, the  $H \rightarrow b\bar{b}$  channel contributes the majority of the Higgs boson search sensitivity below  $m_H = 130$  GeV. To separate signal from background, CDF and D0 use multivariate analysis (MVA) techniques that combine several discriminating variables into a single final discriminant. Each channel is divided into exclusive sub-channels according to various lepton, jet multiplicity, and  $b$ -tagging characteristics in order to group events with similar signal-to-background ratio and thus optimise the overall search sensitivity. The combined CDF and D0 data show [46, 146] an excess of events with respect to the predicted background in the 115–140 GeV mass range in the most sensitive bins of the discriminant distributions suggesting the potential presence of a signal. At  $m_H = 125$  GeV, the observed signal strength is  $\mu = 1.59^{+0.69}_{-0.72}$ .

At the LHC, in order to reduce the dominant  $V$ +jets background, following Ref. [90], experiments select a region in the  $VH$  production phase space where the vector boson is significantly boosted and recoils from the  $H \rightarrow b\bar{b}$  candidate with a large azimuthal angle  $\Delta\phi_{VH}$ . For each channel, events are categorised into different  $p_T(V)$  regions with varying signal/background ratios. Events with higher  $p_T(V)$  have smaller backgrounds and better  $m_{b\bar{b}}$  resolution. CMS uses MVA classifiers based on kinematic, topological and quality of  $b$ -jet tagging and trained on different values of  $m_H$  to separate Higgs boson signal in each category from backgrounds. The MVA outputs for all categories are then fit simultaneously.

The nominal results from ATLAS are also based on a combination of (i) a multivariate analysis of their 8 TeV data, incorporating various kinematic variables in addition to  $m_{b\bar{b}}$  and  $b$ -tagging information and (ii) a statistical analysis of their 7 TeV data centred on  $m_{b\bar{b}}$  as the main discriminant. In both cases, customised control samples devised from data are used to constrain the contributions of the dominant background processes.

The direct observation of the Higgs boson decaying to a pair of  $b$ -quarks, a major result of Run 2, was obtained by both ATLAS and CMS independently after the update of their search with similar analyses as those performed at Run 1 but with a larger dataset of approximately  $80 \text{ fb}^{-1}$  of data collected in 2015, 2016 and 2017. The increase in signal cross sections of nearly a factor of 3 at the centre-of-mass energy of 13 TeV with respect to 7 TeV, has also been instrumental in bringing the two experiments to the required sensitivity to claim an evidence for this decay mode in the  $VH$  production mode (in the high transverse momentum of the vector boson fiducial region of interest for this channel). The expected significance for a SM Higgs boson is  $4.3\sigma$  for ATLAS [147] and  $4.9\sigma$  for CMS [148]. Both ATLAS and CMS observe significant excesses corresponding to  $4.9\sigma$  and  $4.8\sigma$  respectively with Run 2 data only. When combined with results obtained in Run 1, the observed (expected) significance of the excesses are  $5.4\sigma$  ( $5.5\sigma$ ) and  $5.6\sigma$  ( $5.5\sigma$ ) respectively. These results provide direct evidence for the Higgs boson decay to a  $b\bar{b}$  through the  $VH$  production mode. All these results are summarised in Table 11.5. It should be noted that the sensitivity of these analyses are already limited by systematic uncertainties.

This channel has also been exploited by ATLAS to produce a

measurement at higher transverse momentum of the vector boson in the framework of Simplified Template Cross Sections (STXS) discussed in Section 11.6.2.4 [149]. In this case, at higher transverse momentum, the statistical uncertainty still dominates.

Also, the LHCb collaboration has performed a search for the  $VH$  production with subsequent decay of the Higgs boson to a pair of  $b$ -quarks [150] with  $1.98 \text{ fb}^{-1}$  of data taken at a centre-of-mass energy of 8 TeV. The final state is required to have two reconstructed  $b$  quarks and one lepton in the LHCb acceptance of  $2 < \eta < 5$ . The sensitivity of this search is an expected 95% CL exclusion of 84 times the SM production rate. This analysis is also used to set a limit on the  $VH$  production with the subsequent decay of the Higgs boson in a pair of  $c$  quarks with a 95% CL limit at  $6.4 \times 10^3$  times the SM production rate, while the expected sensitivity corresponds to an exclusion of  $7.9 \times 10^3$  times the SM production rate.

ATLAS and CMS have also searched for  $H \rightarrow b\bar{b}$  in the VBF production mode. The event topology consists of two VBF-tagging energetic light-quark jets in the forward and backward direction relative to the beam direction and two  $b$ -tagged jets in the central region of the detector. Due to the electroweak nature of the process, for the signal events, no additional energetic jet activity (excluding that from the Higgs boson) is expected in the rapidity gap between the two VBF-tagging jets. The dominant background in this search stems from QCD production of multi-jet events and the hadronic decays of vector bosons accompanied by additional jets. A contribution of Higgs boson events produced in the  $ggF$  process but with two or more associated jets is expected in the signal sample. The signal is expected as a broad enhancement in the  $m_{b\bar{b}}$  distribution over the smoothly falling contribution from the SM background processes. Both ATLAS [151] and CMS [152] have produced results in this channel with Run 1 data, but with limited sensitivity. Both experiments performed a similar analysis with Run 2 data [153]. The results are summarised in Table 11.5.

Two of the main difficulties for the VBF production mode are the large QCD background and the difficulty in triggering events fully hadronic events. Both difficulties are addressed, by the proposal made in Ref. [154], where the requirement of an additional photon in the final state reduces the background through an interference effect and enhances the possibilities for triggering. This analysis has been carried out by ATLAS at Run 2 [153] (see Table 11.5).

The sensitivity in the inclusive search for the Higgs boson in the  $ggF$  production mode with  $H \rightarrow b\bar{b}$  is limited by the overwhelming background from the inclusive production of  $pp \rightarrow b\bar{b} + X$  via the strong interaction. For this reason, no meaningful results exist with the Run 1 dataset for this production mode. With the increase in centre-of-mass energy to 13 TeV, and by taking advantage of the harder transverse momentum spectrum of the  $gg \rightarrow H$  production mode with respect to the QCD background, a search for high  $p_T$  Higgs boson decaying to a pair of  $b$  quarks in association with an energetic Initial State Radiation (ISR) jet, has been performed by ATLAS [155] and CMS [156]. For this analysis with the Run 2 data, ATLAS and CMS require jets clustered with the anti- $k_T$  algorithm [157] with a distance parameter of 1.0 and 0.8 respectively, with a transverse momentum in excess of 480 GeV and 450 GeV respectively. As in the case of  $VH$  production mode, this analysis is sensitive also to the  $VZ, Z \rightarrow b\bar{b}$  production, which is an important step in the validation of the analysis chain. The  $Z \rightarrow b\bar{b}$  decay is observed with a significance of  $5.8\sigma$ , in good agreement with the expected sensitivity of  $5.1\sigma$ . CMS provides an expected sensitivity to the observation of a Higgs boson of  $0.7\sigma$ . This estimate has a non negligible uncertainty from the precise estimate of the fiducial signal cross section in the specific acceptance of this analysis. Both ATLAS and CMS observe small and non significant excesses at  $m_H = 125$  GeV of  $1.6\sigma$  and  $1.5\sigma$  respectively. These results are reported in Table 11.5.

Another important production mode sensitive to the decay of the Higgs boson to bottom quarks, is the associated production with a pair of top quarks. The results of the searches for this process have been combined with the channels described above, to provide an additional constraint on the Yukawa coupling of

**Table 11.5:** Summary of the results of measurements for a Higgs boson decaying to a pair of  $b$ -quarks by ATLAS and CMS. The results are given in terms of measured signal strength. When available, the statistical and systematic contributions to the total uncertainty are reported separately and in this order.

$H \rightarrow b\bar{b}$	Tevatron	ATLAS Run 1	CMS Run 1	ATLAS Run 2	CMS Run 2
$VH$	$1.6 \pm 0.7$	$0.52 \pm 0.32 \pm 0.24$	$1.0 \pm 0.5$	$1.16 \pm 0.16^{+0.21}_{-0.19}$	$1.01 \pm 0.22$
VBF ( $\gamma$ )	—	$-0.8 \pm 2.3$	$2.8 \pm 1.4 \pm 0.8$	$2.5 \pm 1.3$	$1.3 \pm 1.2$
$t\bar{t}H$	—	$1.4 \pm 0.6 \pm 0.8$	$0.7 \pm 1.9$	$0.79 \pm 0.29 \pm 0.53$	$1.49 \pm 0.21 \pm 0.39$
Inclusive	—	—	—	$5.8 \pm 3.1 \pm 2.5$	$2.3 \pm 1.7$

the Higgs boson to bottom quarks. The channels corresponding to this production mode are described in Section 11.3.3. The results are, however, also reported in Table 11.5.

### 11.3.3 Higgs boson production in association with top quarks or in top decays

#### 11.3.3.1 The associated production with top quark pairs

As discussed in Section 11.2, the coupling of the Higgs boson to top quarks plays a special role in the electroweak symmetry breaking mechanism in the SM, as well as in its possible extensions. Substantial indirect evidence of this coupling is provided by the compatibility of observed rates of the Higgs boson in the principal discovery channels, given that the main production process – the gluon fusion – is dominated by a top quark loop. Direct evidence of this coupling at the LHC and the future  $e^+e^-$  colliders will be mainly available through the  $t\bar{t}H$  final state and will permit a clean measurement of the top quark-Higgs boson Yukawa coupling. The  $t\bar{t}H$  production cross section at the LHC is small in comparison with the ggF or even  $VH$  production modes. The production cross section for a 125 GeV Higgs boson in  $pp$  collisions at  $\sqrt{s} = 8$  TeV of about 130 fb made it challenging to measure the  $t\bar{t}H$  process with the LHC Run 1 dataset. However, in Run 2, the increase in cross section at  $\sqrt{s} = 13$  TeV is substantial, reaching approximately 500 fb. For a sensitive search, at Run 1, it was important to target as many accessible experimental signatures as possible. The analysis channels for such complex final states can be separated in four classes according to the decays of the Higgs boson. In each of these classes, most of the decay final states of the top quarks are considered (fully hadronic, semi-leptonic and dilepton decay final states).

The first analysis in this ensemble is the search for  $t\bar{t}H$  production in the  $H \rightarrow \gamma\gamma$  channel. This analysis relies on the search for a narrow mass peak in the  $m_{\gamma\gamma}$  distribution. The background is estimated from the  $m_{\gamma\gamma}$  sidebands. The sensitivity in this channel is mostly limited by the available statistics. The second analysis is the search for the Higgs boson decaying to  $ZZ^*$  and subsequently to four leptons (electrons and/or muons). This channel is currently limited by the low statistics due to the small branching fraction of the  $Z$  decays to leptons. The third analysis is the search in the  $H \rightarrow b\bar{b}$  channel. This search is intricate due to the large backgrounds, both physical and combinatorial in resolving the  $b\bar{b}$  system from the Higgs boson decay, in events with six jets and four  $b$ -tagged jets. Already with the Run 1 dataset, the sensitivity of this analysis was strongly impacted by the systematic uncertainties on the background predictions. The fourth analysis channel is a specific search for  $\tau^+\tau^-$  where the two tau leptons decay to hadrons. Finally, the  $W^+W^-$ ,  $\tau^+\tau^-$  and  $ZZ^*$  final states can be searched for inclusively in multilepton event topologies (not including the resonant  $H \rightarrow 4\ell$  channel that is covered in a more specific analysis). The corresponding  $t\bar{t}H$  modes can be decomposed in terms of the decays of the Higgs boson and those of the top quarks as having two  $b$ -quarks and four  $W$  bosons (or two  $W$  and two taus, or two  $W$  and two  $Z$ ) in the final state.

ATLAS and CMS have provided a complete set of results in these channels and their combination with the Run 1 data [158, 159]. Results for most of these channels have been updated with Run 2 data.

With the large increase in production cross section for the  $t\bar{t}H$  associated production process of a factor of 3.9 from 7 TeV to 13 TeV, an outstanding goal of the Run 2 physics program was the direct observation of the top Yukawa coupling through this production mode. As could be seen in the Run 1 results, the  $H \rightarrow b\bar{b}$  channel sensitivity was already dominated by systematic uncertainties and the multilepton channel had already large systematic uncertainties, while channels such as the  $H \rightarrow \gamma\gamma$  had very limited sensitivity due to the low statistics. With a conspicuous amount of data, the hierarchy of channels was therefore bound to change.

ATLAS and CMS have analysed Run 2 data in all the sensitive decay channels for this production mode, with datasets of variable size of up to the full Run 2 dataset in the case where it matters the most, i.e., the  $t\bar{t}(H \rightarrow \gamma\gamma)$  channel. With this partial analysis of the Run 2 data, ATLAS and CMS were able to independently observe the production of the Higgs boson in association with a pair of top quarks, and therefore the Yukawa coupling of the Higgs boson to the top quark [160]. This observation is particularly important in comparison to the indirect evidence through the gluon fusion production process dominated by the top quark loop.

The observation made independently by the two experiments was based on all the channels that were studied at the Run 1. ATLAS used up to  $79.8 \text{ fb}^{-1}$  of Run 2 data and CMS has used its 2016 dataset of  $35.9 \text{ fb}^{-1}$ . ATLAS reached an expected sensitivity of  $4.9\sigma$  and an observed significance of  $5.8\sigma$  with the Run 2 partial dataset alone, and  $6.3\sigma$  (with  $5.1\sigma$  expected) in combination with the Run 1 results. CMS reached a sensitivity of  $4.2\sigma$  and observed an excess with respect to the background-only hypothesis of  $5.2\sigma$ , combining the Run 1 and Run 2 results.

With the larger Run 2 dataset, the dominant mode is the  $t\bar{t}(H \rightarrow \gamma\gamma)$  channel, where a narrow peak over a continuous background is searched for. At Run 2, this channel has reached a signal-to-background ratio in excess of 1 in the most signal-like categories. This is in contrast with the inclusive diphoton channel Higgs channels where the signal-to-background ratios are of the order of a few percent. ATLAS has analysed the entire Run 2 dataset reaching an observed (expected) sensitivity of  $4.9\sigma$  ( $4.2\sigma$ ) [161] and CMS has utilised  $77.4 \text{ fb}^{-1}$  of Run 2 data for this channel with an observed (expected) sensitivity of  $4.1\sigma$  ( $2.7\sigma$ ) [162], providing nearly unambiguous observations in this channel alone. These results are largely dominated by statistical uncertainty and are therefore expected to improve significantly with more data. These results with the full dataset from ATLAS [161] and with a larger Run 2 dataset for CMS [162] are not part of the ATLAS and CMS combinations and therefore provide substantially more evidence for the direct coupling of the Higgs boson to the top quark.

The resonant search for the resonant Higgs boson decay to four leptons in the associated production with a pair of top quarks has also been updated in ATLAS [131] with the full Run 2 dataset and reported in Table 11.6, but it is also not included in the combination.

An update of the  $H \rightarrow b\bar{b}$  channel made by CMS with a partial Run 2 dataset of  $41.5 \text{ fb}^{-1}$  [163], using in particular the fully hadronic channel, is not in combination either. It is nevertheless reported in Table 11.5.

For the so-called “multi-lepton” channels which cover mostly



the  $WW$ ,  $ZZ$  and  $\tau\tau$  decay modes, ATLAS and CMS have analysed only part of the Run 2 datasets [164].

All results are summarized in Table 11.6.

### 11.3.3.2 The associated production with a single top quark

An additional production mode of the Higgs boson in association with a top quark is the single top associated production mode. There is an interesting similarity between this production mode and the  $H \rightarrow \gamma\gamma$  decay mode. Both processes proceed through either the top Yukawa coupling or the interaction of the Higgs boson with the  $W$  boson, with a negative interference between the two. Representative Feynman diagrams for this production process are shown in Fig. 11.1. Contrary to the diphoton decay channel, in this production mode the interference occurs at the tree level and is dominant. This process can therefore be used to further discriminate a negative relative sign between the couplings of the Higgs boson to fermions and its couplings to gauge bosons [165].

ATLAS and CMS have produced specific searches for the  $tH$  production mode with the Run 1 and Run 2 data exploiting a variety of Higgs boson decay modes resulting in final states with photons, bottom quarks, and multiple charged leptons, including tau leptons. In particular, with the Run 2 data, CMS has searched for multi-lepton decay signatures from the  $H \rightarrow WW^*$ ,  $H \rightarrow \tau^+\tau^-$  and  $H \rightarrow ZZ^*$  modes [166]. This analysis restricts values of  $\kappa_t$ , the top-Higgs coupling normalized to its SM value, to  $[-1.25, 1.60]$  at 95% CL. CMS has also performed an analysis of the 2015 dataset to search for the  $H \rightarrow b\bar{b}$  mode [167], yielding much less stringent constraints.

The diphoton channel has also been used to search specifically for this production mode by ATLAS using Run 1 data, yielding the restricted range of allowed values of  $\kappa_t$  at the 95% CL to  $[-1.3, 8]$ .

The strongest constraint on the negative (relative) sign of  $\kappa_t$  was obtained by CMS with a recent analysis of the 2016 dataset [168] in the multilepton ( $H \rightarrow WW$ ,  $H \rightarrow ZZ$ ,  $H \rightarrow \tau\tau$ ) and  $H \rightarrow b\bar{b}$  channels, all combined with a reinterpretation of the  $H \rightarrow \gamma\gamma$  analysis channel aiming at measuring the  $pp \rightarrow t\bar{t}H$  production mode. Negative values of  $\kappa_t$  are disfavoured at approximately  $1.5\sigma$  and values of  $\kappa_t$  below  $-0.9$  are excluded at 95% CL.

### 11.3.3.3 Flavour changing neutral current decays of the top quark

The discovery of the Higgs boson at a mass smaller than the top quark mass opened a new decay channel for the top quark. The decays of the top quark to a Higgs boson and a charm or an up quark proceed through a Flavour Changing Neutral Current (FCNC) which are forbidden at tree level and suppressed at higher orders through the Glashow–Iliopoulos–Maiani (GIM) mechanism [3]. The SM prediction for these branching fractions is  $\text{BR}(t \rightarrow Hc) = 10^{-15}$  and two orders of magnitude less for the  $Hu$  final state. These decay channels of the top quark are, therefore, very interesting to probe possible FCNC interactions in the Yukawa couplings to the quark sector, see Section 11.7.

ATLAS has searched for FCNC top decays specifically in channels involving a Higgs boson with subsequent decays to two photons and a pair of  $b$ -quarks [169]. It has also reinterpreted a search for the  $t\bar{t}H$  production in the multilepton final state (discussed in Section 11.3.6.1) [159]. The latter channel covers Higgs boson decays to a pair of  $W$  bosons and a pair of taus. No significant excess was observed in any of the specific channels (as discussed in Section 11.3.6.1, a slight excess is observed in the  $t\bar{t}H$  multilepton channel) and 95% CL upper limits are set on  $\text{BR}(t \rightarrow Hc) < 0.46\%$  with an expected sensitivity of 0.25% and  $\text{BR}(t \rightarrow Hu) < 0.45\%$  with an expected sensitivity of 0.29%. CMS has performed a search for these FCNC top decays in the diphoton and multi-lepton channels [170], placing a 95% CL upper limit on  $\text{BR}(t \rightarrow Hc) < 0.40\%$  with an expected sensitivity of 0.43%.

From these limits on branching fractions, constraints on non-flavour-diagonal Yukawa couplings of a FCNC Lagrangian of the form:

$$\mathcal{L}_{\text{FCNC}} = \lambda_{tc}H\bar{t}Hc + \lambda_{tu}H\bar{t}Hu + h.c. \quad (11.12)$$

can be derived. The 95% CL observed (expected) upper limits from ATLAS on the  $|\lambda_{tc}|$  and  $|\lambda_{tu}|$  couplings are 0.13 (0.10)

and 0.13 (0.10), respectively.

The results above are derived from the combination of several channels for searches performed with Run 1 data. Both ATLAS and CMS have produced updates of individual channels with Run 2 data. ATLAS has searched for FCNC top decays with subsequent decays of the Higgs boson to a pair of photons [171], yielding a 95% CL upper limit on  $\text{BR}(t \rightarrow Hc) < 0.22\%$  with an expected sensitivity of 0.16%. CMS has searched for FCNC top decays with subsequent decays of the Higgs boson to a pair of  $b$ -quarks [172], yielding a 95% CL upper limit on  $\text{BR}(t \rightarrow Hc) < 0.47\%$  with an expected sensitivity of 0.44%.

### 11.3.4 Higgs boson pair production

Higgs boson pair production in the SM is a rare but very important mode to measure and search for. The measurement of Higgs boson pair production is essential to directly constrain the trilinear Higgs boson self coupling and the search for Higgs boson pair resonances is key in a variety of BSM models. The latter searches are discussed in Section 11.7.7.

In the SM, the main non-resonant production mode of two Higgs bosons proceeds through a loop, mainly of top quarks, see Fig. 11.5(a). Another production mode is via the trilinear coupling of the Higgs boson, see Fig. 11.5(b), whose amplitude is not negligible compared to the former. These diagrams interfere negatively, making the overall production rate smaller than what would be expected in the absence of a trilinear coupling.

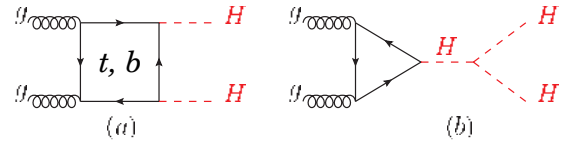


Figure 11.5: Feynman diagrams contributing at leading order to Higgs boson pair production through (a) a top- and bottom-quark loop and (b) through the self coupling of the Higgs boson.

#### 11.3.4.1 Searches for Higgs boson pair production

The searches for Higgs boson pair production both resonant and non-resonant are very interesting probes for a variety of BSM theories, and they can be done in a large number of Higgs boson decay channels. At Run 1, ATLAS and CMS have searched for both resonant and non resonant Higgs boson pair production in the following channels: (i)  $HH \rightarrow b\bar{b}\gamma\gamma$ ; (ii)  $HH \rightarrow b\bar{b}\tau^+\tau^-$ ; (iii)  $HH \rightarrow b\bar{b}b\bar{b}$ ; (iv)  $HH \rightarrow WW^*\gamma\gamma$ ; (v) in final states containing multiple leptons (electrons or muons) covering the  $WW^*WW^*$ ,  $WW^*ZZ^*$ ,  $ZZ^*ZZ^*$ ,  $ZZ^*\tau^+\tau^-$ ,  $WW^*\tau^+\tau^-$ ,  $ZZ^*b\bar{b}$ ,  $\tau^+\tau^-\tau^+\tau^-$  channels; and (vi)  $\gamma\gamma\tau^+\tau^-$  channels.

At Run 2, similarly to the  $t\bar{t}H$  production process, the di-Higgs production gains a substantial increase in production cross section of a factor in excess of 3 from 8 TeV to 13 TeV, and most of these channels have been updated both by ATLAS [173] and CMS [174] using the 2016 datasets with the addition of the (vii)  $HH \rightarrow b\bar{b}b\bar{b}$  channels. The detailed description of the analyses can be found in references within the combination results published by the collaborations [173, 174]. All the results and their combinations are summarised in Table 11.7.

#### 11.3.4.2 The Higgs boson self coupling

The Higgs boson self coupling is an extremely important direct probe of the Higgs potential with implications on our understanding of the electroweak phase transition. Constraints on the trilinear self coupling from  $HH$  processes is an outstanding long term goal of the LHC and the reach in sensitivity has been reappraised in the light of the recent  $HH$  analyses from ATLAS and CMS, shedding a different light on the achievable sensitivity [104]. Constraints from the  $HHH$  final state on the quartic Higgs boson self coupling are out of reach at the LHC due mostly to the very small production rates and intricate final states.

In the SM, the Higgs boson pair production through the trilinear Higgs boson self coupling has an on-shell component and a large off-shell component. The on-shell  $H \rightarrow H^*H^*$  is strongly disfavoured, requiring two off-shell Higgs bosons in the final state.

**Table 11.6:** Summary of the results of searches for a Higgs boson in association with a top quark pair by ATLAS and CMS. The results are given in terms of a measured signal strength. When available, the statistical and systematic contributions to the total uncertainty are reported separately and in this order. The ATLAS [161] and CMS [162] diphoton results indicated by (\*) are not included in the overall combinations which include versions of the diphoton analyses with smaller Run2 datasets. The combination includes the  $t\bar{t}(H \rightarrow b\bar{b})$  channels reported in Table 11.5.

$t\bar{t}H$	ATLAS Run 1	CMS Run 1	ATLAS Run 2	CMS Run 2
$H \rightarrow \gamma\gamma$	$1.3^{+2.6}_{-1.7}{}^{+2.5}_{-1.7}$	$1.2^{+2.5}_{-1.7}{}^{+2.6}_{-1.8}$	$1.38^{+0.33}_{-0.31}{}^{+0.26}_{-0.18}$ (*)	$2.27^{+0.86}_{-0.74}$ (*)
$H \rightarrow 4\ell$	—	—	$1.2^{+1.4}_{-0.8}$ (*)	$0.0 \pm 1.2$ (*)
$WW/\tau\tau/ZZ$	$1.4 \pm 0.6 \pm 1.0$	$3.3 \pm 1.4$	$1.56^{+0.30}_{-0.29}{}^{+0.30}_{-0.27}$	$0.96^{+0.34}_{-0.31}$
Comb.	$1.7 \pm 0.5 \pm 0.8$	$2.6^{+1.0}_{-0.9}$	$1.32 \pm 0.18^{+0.21}_{-0.19}$	$1.49 \pm 0.16^{+0.27}_{-0.21}$

**Table 11.7:** Summary of the final states investigated in the search for Higgs boson pair production by ATLAS and CMS, most analyses make use of the 2016 Run2 dataset corresponding to integrated luminosities of up to  $36 \text{ fb}^{-1}$ . For ATLAS, the result indicated by (\*) uses mostly the  $b\bar{b}W^+W^-$  channel. Results are 95% CL upper limits on the observed (expected) SM signal strengths.

Channel	ATLAS	CMS
$b\bar{b}\gamma\gamma$	20.3 (26)	23.6 (18.8)
$b\bar{b}b\bar{b}$	12.9 (21)	74.6 (36.9)
$b\bar{b}\tau^+\tau^-$	12.5 (15)	31.4 (25.1)
$W^+W^-W^+W^-$	160 (120)	—
$W^+W^-\gamma\gamma$	230 (170)	—
$b\bar{b}VV$	305 (305)*	79 (89)
Combination	6.9 (10)	22.2 (12.8)

The sensitivity region to the trilinear coupling production as in Fig. 11.5(b), is mainly in the kinematic region where the two Higgs boson in the final state are on-shell and the Higgs boson acts as a propagator (off-shell). As discussed in the introduction to this section, this process interferes negatively with the background Higgs boson pair production (Fig. 11.5(a)).

The measurement of the trilinear coupling requires separating the contributions of the diagram of Fig. 11.5(b) from the box diagram of Fig. 11.5(b), and therefore a precise knowledge of the top-Yukawa coupling is needed. Each diagram alone would produce rather distinct  $m_{HH}$  distribution. And, for values of the trilinear coupling close to the SM value, an additional discriminating feature of the signal with respect to one obtained with the box contribution alone is a deficit in the number of events. With large variations of the trilinear coupling, an excess of events over the SM prediction would be observed (for a value of the trilinear coupling about 6 times larger than its SM value, the number of events is equal to the SM expectation). Additional sensitivity to the trilinear coupling is also obtained from the kinematical distributions of the signal taking in particular into account the effect of the  $HH$  mass distribution which discriminates the main contributions of Fig. 11.5. This further discrimination is instrumental in resolving the degeneracy in the total cross section mentioned above. The bounds obtained by ATLAS [173] and CMS [174] are

the following:

$$\begin{aligned}
 (\text{ATLAS}) & - 5.0 < \kappa_\lambda < 12.0 \text{ (observed)}, \\
 & - 5.8 < \kappa_\lambda < 12.0 \text{ (expected)}, \\
 (\text{CMS}) & - 11.8 < \kappa_\lambda < 18.8 \text{ (observed)}, \\
 & - 7.1 < \kappa_\lambda < 13.6 \text{ (expected)},
 \end{aligned} \tag{11.13}$$

where  $\kappa_\lambda$  is the ratio between the trilinear coupling value left free in the fit and its expected value in the SM ( $\kappa_\lambda = 1$  corresponds to the SM). These results are also illustrated in Fig. 11.6.

The analyses performed at Run2 bring substantial improvements from those of Run1, and they were used to reappraise the sensitivity of the LHC in the High Luminosity regime in the framework of the update of the European Strategy for Particle Physics [104]. The result in terms of bounds on the trilinear coupling are shown in Fig. 11.6, indicating that the significance of the observation of the  $HH$  process reaches  $4\sigma$ . It is also apparent that the degeneracy of secondary minimum at intermediate values of  $\kappa_\lambda$  is resolved by the use of the kinematic discriminants. Indeed, this secondary minimum is expected to be excluded at 99.4% CL. This is very important to allow the measurement in the vicinity of the SM value at one standard deviation and to provide a meaningful confidence interval. At HL-LHC, the foreseen precision on  $\kappa_\lambda$  is approximately 50%.

Significantly higher precisions can be reached at  $pp$  colliders (and  $e^+e^-$  colliders) at higher centre-of-mass energies. The foreseen precision for a High-Energy (HE) LHC at a centre-of-mass energy of 27 TeV is expected to be within 10% to 20% [104]. At a very large hadron collider at a centre-of-mass energy of 100 TeV, a 5% sensitivity is expected to be reached, provided that the theoretical and parametric uncertainties are kept at the 1% level.

Indirect constraints on the Higgs boson trilinear coupling from single Higgs boson production processes will be discussed in Section 11.6.2.5.

### 11.3.5 Searches for rare decays of the Higgs boson

#### 11.3.5.1 $H \rightarrow Z\gamma$ and the Dalitz $H \rightarrow \ell^+\ell^-\gamma$ decay

The search for  $H \rightarrow Z\gamma$  is performed in the final states where the  $Z$  boson decays into opposite sign and same flavour leptons ( $\ell^+\ell^-$ ),  $\ell$  here refers to  $e$  or  $\mu$ . While the branching fraction for  $H \rightarrow Z\gamma$  is comparable to  $H \rightarrow \gamma\gamma$  (about  $10^{-3}$ ) at  $m_H = 125 \text{ GeV}$ , the observable signal yield is brought down by the small branching ratio of  $Z \rightarrow (e^+e^- + \mu^+\mu^-) = 6.7 \times 10^{-2}$ . In these channels, the  $m_{\ell\ell\gamma}$  mass resolution is excellent (1–3%), therefore the analyses search for a narrow mass peak over a continuous background. The major backgrounds arise from the  $Z + \gamma$  final state radiation in Drell–Yan decays and from the  $Z + \text{jets}$  processes where a jet is misidentified as a photon. The ratio of signal over background in this channel is typically of the order of 0.5%. In a narrow window of a few GeV around 125 GeV, several hundreds of events are expected in a Run 2 dataset corresponding to approximately  $36 \text{ fb}^{-1}$ .

Events are divided into mutually exclusive categories on the basis of the expected  $m_{Z\gamma}$  resolution and the signal-to-background ratio. A VBF category is formed for  $H \rightarrow Z\gamma$  candidates which

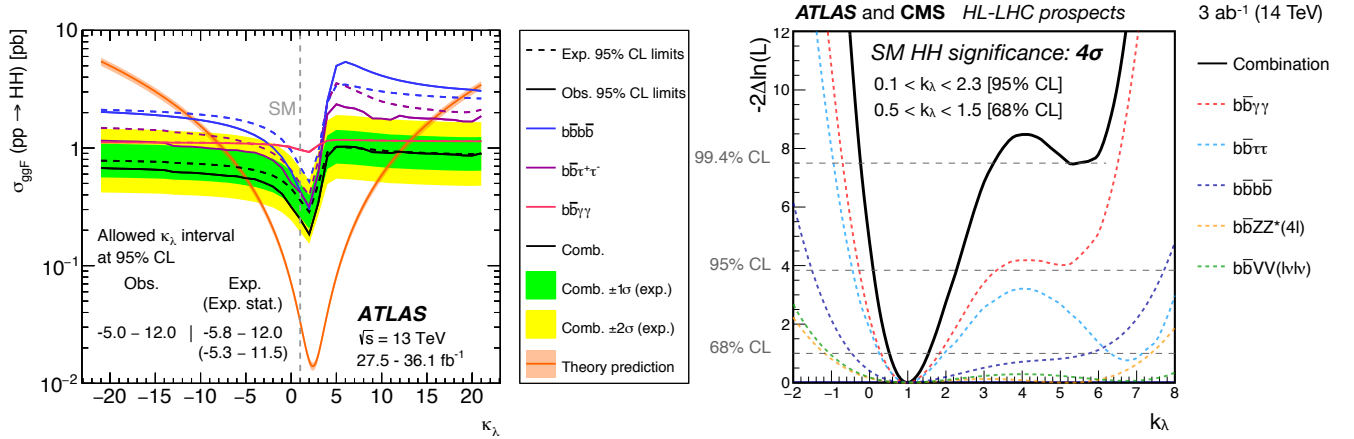


Figure 11.6: (Left) Upper limit obtained by ATLAS on the total  $pp \rightarrow HH$  production cross section as a function of the trilinear coupling modifier  $\kappa_\lambda$ . The variation of the limit corresponds to variations in the signal acceptance. The expected total production cross section is also illustrated (red). (Right) Expected combined ATLAS and CMS likelihood for the searches for the  $pp \rightarrow HH$  production at the High Luminosity LHC. The channels used in the combination are indicated in the figure.

are accompanied by two energetic jets separated by a large pseudorapidity. While this category contains only about 2% of the total event count, the signal-to-noise ratio is about an order of magnitude higher. The search for a Higgs boson is conducted independently in each category and the results from all categories are then combined.

No excess of events is observed in either ATLAS or CMS in the Run 1 data. The CMS expected and observed 95% CL upper limits for  $m_H = 125$  GeV on the signal strength  $\mu$  are 10.0 and 9.5 respectively. The ATLAS expected and observed upper limits on the signal strength  $\mu$  are 9.0 and 11.0 respectively, for  $m_H = 125.5$  GeV.

The CMS analysis also extended the search for the so-called Dalitz Higgs boson decays  $H \rightarrow \gamma^* \gamma \rightarrow \ell^+ \ell^- \gamma$  in the low mass  $\gamma^*$  range of  $m_{\ell\ell} < 20$  GeV. This decay mode has a substantially larger branching fraction compared to the  $Z\gamma$  decay, as  $\Gamma(H \rightarrow \gamma^* \gamma \rightarrow e^+ e^- \gamma) \sim 3.5\% \times \Gamma(H \rightarrow \gamma\gamma)$  and  $\Gamma(H \rightarrow \gamma^* \gamma \rightarrow \mu^+ \mu^- \gamma) \sim 1.7\% \times \Gamma(H \rightarrow \gamma\gamma)$ , while  $\Gamma(H \rightarrow Z\gamma) = 2.3\% \times \Gamma(H \rightarrow \gamma\gamma)$  (which does not account for the subsequent decay of the Z boson to electrons or muons). The limits in this channel are therefore stronger and CMS has observed an upper limit of 6.7 times the SM branching ratio [175].

ATLAS has performed an analysis of the full 2015 and 2016 Run 2 data to search for the  $Z\gamma$  decay mode [176]. No significant excess was observed and 95% CL observed (expected) upper limits on the signal strength are 6.6 (5.2).

CMS has repeated its  $Z\gamma$  and  $\gamma^* \gamma$  analyses with the 2016 dataset and obtained much more stringent observed limits on cross section times the corresponding branching fractions of 1.4 and 4.0 (6.1 and 11.4) times the SM cross section for  $H \rightarrow \gamma^* \gamma$  ( $H \rightarrow Z\gamma$ ) [177]. CMS also performed a combination of the two modes, obtaining a combined observed (expected) limit of 3.9 (2.0) times the SM branching fractions.

### 11.3.5.2 $H \rightarrow \mu^+ \mu^-$

The branching fraction in the  $H \rightarrow \mu^+ \mu^-$  channel for a 125 GeV SM Higgs boson is  $2.2 \times 10^{-4}$ , about ten times smaller than that for  $H \rightarrow \gamma\gamma$ . The dominant and irreducible background arises from the  $Z/\gamma^* \rightarrow \mu^+ \mu^-$  process which has a rate several orders of magnitude larger than that from the SM Higgs boson signal. Due to the precise muon momentum measurement achieved by ATLAS and CMS, the  $m_{\mu^+ \mu^-}$  mass resolution is very good ( $\approx 2-3\%$  for ATLAS and  $\approx 1-3\%$  for CMS depending on the selected categories; a better resolution is expected for CMS due to its higher field in the inner detector). A search is performed for a narrow peak over a large but smoothly falling background. For optimal search sensitivity, events are divided into several categories. Either taking advantage of the superior muon momentum measurement in the central region, events can be subdivided by the pseudo-rapidity of the muons, or designing selections aiming

at specific production processes such in particular as the vector boson fusion.

No excess in the  $m_{\mu^+ \mu^-}$  spectrum is observed near 125 GeV. From an analysis of the Run 1 data, ATLAS sets an observed (expected) 95% CL upper limit on the signal strength  $\mu < 7.0$  (7.2). The CMS analysis of its 7 and 8 TeV data sets an observed (expected) limit of  $\mu < 7.4$  (6.5).

ATLAS performed a reoptimised analysis using the full Run 2 dataset and categorising events in number of jets including VBF-topology specific categories [178]. The data showed a non-significance excess with a best-fit value of the signal strength for Higgs boson with a mass of 125 GeV,  $\mu = 0.5 \pm 0.7$ . The data subsequently yielded an observed (expected) 95% CL upper limit on the signal strength of 1.7 (1.3), assuming  $\text{BR}(H \rightarrow \mu\mu) = 0$ , (while the expected limit assuming the SM value for  $\text{BR}(H \rightarrow \mu\mu)$  is 2.2).

CMS, having analysed its 2016 dataset of Run 2, has obtained an observed (expected) limit on the production cross section times the branching fraction to a pair of muons of 3.0 (2.5) times the SM expectation [179]. In combination with the Run 1 data, the limit improves to 2.2 times the SM expectation. A non significant excess is also observed (with a significance of approximately  $1\sigma$ ) and the best fit signal strength is  $1.0 \pm 1.0$  (stat)  $\pm 0.1$  (syst).

### 11.3.5.3 $H \rightarrow e^+ e^-$

A search similar to the  $H \rightarrow \mu^+ \mu^-$  is performed by CMS in the di-electron channel. In this search channel, the contribution from the peaking background from Higgs boson decays to diphotons mis-identified as di-electrons (when mostly converted photons are faking electrons) needs to be assessed. The sensitivity to the SM Higgs decays is negligible given the extremely small branching fraction to  $e^+ e^-$ , approximately 40'000 times smaller than the branching fraction to dimuons. It is nevertheless interesting to probe this decay channel to search for potential large anomalous couplings. Assuming a SM Higgs boson production cross section, the observed limit on the branching fraction at the 95% CL is 0.0019, five orders of magnitude larger than the expected SM prediction. It is also important to note that processes not depending on the electron Yukawa coupling such as the  $H \rightarrow e^+ e^- \gamma$  (where the photon is soft), are sizeably larger than the direct Yukawa coupling process, but also much smaller than the current constraints, making any interpretation in terms of constraint on the electron Yukawa couplings far from straightforward.

At Run 2, ATLAS has also performed a search for the  $H \rightarrow e^+ e^-$  decay mode with the full dataset, improving the current limit by a factor of approximately 5, with a limit of  $3.6 \times 10^{-4}$  on the branching fraction [180].



### 11.3.5.4 Lepton flavour violating (LFV) Higgs boson decays

Given the Yukawa suppression of the couplings of the Higgs boson to quarks and leptons of the first two generations and the small total width of the Higgs boson, new physics contributions could easily have sizable branching fractions. One very interesting possibility is the Lepton Flavour Violating (LFV) decays of the Higgs boson, in particular in the  $\tau\mu$  and  $\tau e$  modes. These decays are suppressed in the SM but they could easily be enhanced in theories such as two-Higgs-doublet models (discussed in Section 11.7).

There are already constraints on LFV Yukawa couplings  $|Y_{\tau\mu}|$  from channels such as the  $\tau \rightarrow 3\mu$  or  $\tau \rightarrow \mu\gamma$ , or a re-interpretation of the search for Higgs boson decays to  $\tau^+\tau^-$ . A direct search at the LHC, however, complements these indirect limits. The search for LFV decays in the  $\tau\mu$  channel have been done with the Run 1 dataset in several channels according to the subsequent decay of the  $\tau$ . The results from CMS [181] and from ATLAS for the hadronic [182], the leptonic [183] decays of the tau, and their combination [183] are reported in Table 11.8. It is interesting to note that the analysis strategies at Run 1 for the di-lepton  $\tau_{\text{lep}}\mu$  channel are very different between ATLAS [183] and CMS [181].

As shown in Table 11.8, an excess was observed in this channel by CMS with a significance of  $2.5\sigma$ , while in ATLAS analysis, the excess is smaller, about  $1\sigma$  at Run 1. CMS has performed the search again with the full 2016 Run 2 dataset [184], relying on a multivariate analysis. The observed best fit branching fraction is  $(0.00 \pm 0.12)\%$ . These limits are reported in Table 11.8.

ATLAS and CMS have also performed a search for the LFV Higgs boson decays in the  $\tau e$  and  $\mu e$  channels [183–185]. No significant excess was observed and 95% CL limits are reported in Table 11.8, for the  $\tau e$  channel only. For the  $\mu e$  channel, the constraints from the  $\mu \rightarrow e\gamma$  experiments [186] are much stronger than those from the direct LFV Higgs boson decay search. However these indirect constraints can be relaxed by the cancellation of LFV effects from new physics.

At Run 2, ATLAS has performed searches for LFV decays of the Higgs boson in the  $e\tau$  and  $\mu\tau$  channels [187] as well as in the  $e\mu$  channel [180]. The searches for the  $H \rightarrow e\tau$  and  $H \rightarrow \mu\tau$  decays where done with the 2016 data only and yielded upper limits on the LFV decay branching fraction of 0.47% (0.34%) and 0.28% (0.37%), respectively.

CMS has also searched for LFV decays with the 2016 dataset at Run 2 and obtained observed (expected) limits on the LFV branching fraction of  $\text{BR}(H \rightarrow \mu\tau) < 0.25\%$  (0.25%) and  $\text{BR}(H \rightarrow e\tau) < 0.61\%$  (0.37%), at the 95% CL [188]. These limits were also interpreted in terms of constraints on the corresponding off-diagonal Yukawa couplings.

The results obtained by ATLAS and CMS at Run 2 do not confirm the excesses observed at Run 1.

### 11.3.5.5 Probing charm- and light-quark-Yukawa couplings

Probing the Yukawa couplings to quarks of the second or even the first generation is extremely challenging given the overwhelming backgrounds and very small rates.

The possibility of probing the Yukawa coupling to the charm has been discussed in Ref. [189] where indirect bounds are estimated from a combined fit to the Higgs data and the importance of using charm tagging is emphasised. Searches in the  $VH$  production mode have then been carried out, in the channels very similarly to those aiming at the  $b$ -quark Yukawa coupling, by both ATLAS [190] and CMS [191] with Run 2 data. The upper limits obtained (expected) on the  $VH$  production cross section times the charm quark decay branching fraction of the Higgs boson are:

$$\text{(ATLAS)} \quad \sigma(ZH) \times \text{BR}(H \rightarrow c\bar{c}) < 2.7 \quad (3.9^{+2.1}_{-1.1}) \text{ pb}, \quad (11.14)$$

$$\text{(CMS)} \quad \frac{\sigma(VH) \times \text{BR}(H \rightarrow c\bar{c})}{\sigma(VH)_{SM} \times \text{BR}(H \rightarrow c\bar{c})_{SM}} < 70 \quad (37^{+16}_{-10}). \quad (11.15)$$

The ATLAS search [190] was done in the  $ZH$  channel where the  $Z$  boson decays to a pair of leptons (electrons or muons) only. The expected cross section times branching fraction  $\sigma(ZH) \times \text{BR}(H \rightarrow c\bar{c})$  is  $26 \text{ fb}^{-1}$ .

Another possibility to access the charm Yukawa coupling has been discussed in Ref. [192]. It relies on the decays of the Higgs boson to a final state with charmonium:  $H \rightarrow J/\Psi\gamma$ . Higgs boson decays in this final state have been searched for by ATLAS [193]. The sensitivity of this analysis is, however, several orders of magnitude above the branching fraction estimated in the SM:  $\text{BR}(H \rightarrow J/\Psi\gamma) = (2.8 \pm 0.2) \times 10^{-6}$ . ATLAS [193] has also searched for Higgs boson decays to  $\Upsilon(nS)\gamma$  where ( $n = 1, 2, 3$ ), a channel with much lower sensitivity than the  $H \rightarrow b\bar{b}$  to the Yukawa coupling to  $b$ -quarks.

More recently, ATLAS has searched, , with a specific trigger, for another quarkonia final state where the Higgs boson decays to  $\phi\gamma$  [194] at the LHC Run 2 and a center-of-mass energy of 13 TeV. This channel could probe deviations from the strange-quark Yukawa coupling. Its sensitivity is several orders of magnitude above the SM expectation. Other quarkonia final states, such as the  $\rho\gamma$ , which could potentially probe the Yukawa coupling to light quarks, can also be searched for.

CMS has also performed a search of the decays of the Higgs boson in the  $J/\Psi J/\Psi$  and  $\Upsilon\Upsilon$  decay to cover the cases where the photon in the  $J/\Psi\gamma$  decay is virtual and transforms into a  $J/\Psi$  meson. These decays provide an additional channel potentially sensitive to BSM phenomena [195].

### 11.3.5.6 Rare decays outlook

Rare decays such as those described in the above sections have clearly a limited sensitivity. However, they already deliver interesting messages. For example, if the coupling of the Higgs boson to muons was as strong as it is to top quarks, this mode should have been observed. Therefore, it can be concluded that the observed couplings of the Higgs boson are manifestly non-universal. Further developing these rare decay modes is an important component of the High Luminosity program of the LHC in order to directly probe the couplings of the Higgs boson, and to potentially measure the Yukawa coupling to the fermions of the second generation, in particular to muons. It is also an integral part of the physics program of the discussed potential future Higgs boson factories.

### 11.3.6 Searches for non-SM decay channels

The main decay and production properties of the observed Higgs boson are consistent with the SM predictions. The Higgs boson may, however, have other decay channels beyond those anticipated in the SM. Among these, and of great interest, are the invisible decays into stable particles, such as DM particle candidates, that interact very weakly with the detector, and that remain undetected. Other non standard decay channels that have been investigated are the decays of the Higgs particle to hidden valley or dark particles.

#### 11.3.6.1 Invisible decays of the Higgs boson

The discovery of the Higgs boson immediately raised the question of its couplings to DM and how it could be used to reveal at colliders the existence of a dark sector coupled to the SM via the Higgs boson portal, see Ref. [196] and references therein. If kinematically accessible and with a sufficiently large coupling to the Higgs boson, DM particles, such as, e.g., neutralinos in SUSY models, graviscalars in models with extra dimensions or heavy neutrinos in the context of four-generation fermion models, would manifest themselves as invisible decays of the Higgs boson, thus strongly motivating searches for the invisible decays of the Higgs boson.

To identify an invisibly decaying Higgs boson at the LHC, it must be produced in association with other particles. Searches for invisible decays of the Higgs particle at the LHC have been carried out in the three associated production modes of the Higgs boson with the highest SM cross sections and target events with large missing energy.

The  $ggF$  production mode has the largest SM cross section but it usually results in the Higgs boson being created alone and hence leaving no characteristic signature in the detector of its invisible decay. One way to search for invisible decays in  $ggF$  production mode is to look for events with the monojet topology arising from initial state gluon radiation and containing missing energy. The major irreducible background in such searches stems from  $Z + \text{jets}$

**Table 11.8:** Summary of the results of searches for lepton flavour violating decays of the Higgs boson in the  $\tau\mu$  and  $\tau e$  channels from ATLAS and CMS. For the result with \*, the expected sensitivity was not reported but appears consistent with the observed one.

	ATLAS (Run 1)	CMS (Run 1)	CMS (Run 2)
$\text{BR}(H \rightarrow \tau\mu)$	$(0.53 \pm 0.51)\%$	$(0.84^{+0.39}_{-0.37})\%$	$(0.00 \pm 0.12)\%$
95% CL Obs. (Exp.)	1.43% (1.01%)	1.51% (0.75%)	0.25% (0.25%)
$H \rightarrow \tau e$ 95% CL Obs. (Exp.)	1.02% (1.21%)	0.69%*	0.61% (0.37%)

events where the  $Z$  boson decays into a pair of neutrinos [197]. The analysis with the best sensitivity targets the VBF production topology but it suffers from large backgrounds arising from events with two jets and large missing energy. The  $VH$  mode has much smaller cross section but the presence of a  $W$  or  $Z$  boson allows a variety of final states that can be tagged with relatively low background.

ATLAS and CMS have searched for such final states at Run 1 and have observed no significant excess over the predicted backgrounds (for references, see the previous edition of this review [123]). Table 11.9 summarizes the 95% CL limits on the invisible decays of the Higgs boson assuming a SM Higgs boson production cross section and the corresponding detector acceptances.

ATLAS has performed the search for invisible decays of the Higgs boson at Run 2 with the 2015 and 2016 datasets, corresponding to an integrated luminosity of approximately  $36 \text{ fb}^{-1}$ , in the VBF production [198], the  $ZH$  associated production where the  $Z$  boson subsequently decays to a pair of leptons [199], and the  $VH$  associated production where the vector boson (a  $W$  or a  $Z$ ) subsequently decays hadronically [200]. The most stringent constraint is obtained through the VBF channel. All results and their combination [201] are reported in Table 11.9. Combined with the Run 1 results, the ATLAS limit on the invisible branching fraction reaches 26%, with an expected sensitivity of 17% [201].

CMS has updated the search for invisible decays of the Higgs boson in the vector boson fusion and the associated production with a vector boson channels (both with subsequent leptonic [202] and hadronic decays [203]) using Run 2 data collected in 2016 [204]. It has produced a combination with Run 1 channels, yielding a limit on the invisible branching fraction of 19%, with an expected sensitivity of 15% [204].

CMS has also reinterpreted a search for scalar top quarks in the all-hadronic, semi-leptonic and fully leptonic final state with the 2016 data of Run 2 to set limits on the invisible Higgs decays through the  $pp \rightarrow t\bar{t}H$  production mode [205]. The results of the search are reported in Table 11.9.

This constraint can then be further used to probe Higgs portal models to DM [196], where an additional weakly interacting particle  $\chi$  with mass lower than  $m_H/2$  is introduced as DM candidate and where the Higgs boson is considered as the only mediator between the SM particles and DM. In this model, it is interesting to express the limit on the invisible branching fraction in terms of strength of interaction of DM with standard matter, i.e., in terms of its interaction cross section with nucleons  $\sigma_{\chi-N}$ . In this model, the couplings of the Higgs boson to SM particles are assumed to be those of the SM and the interaction of the Higgs boson with the nucleon is parametrised in a Higgs-Nucleon form factor estimated using lattice QCD calculations [196]. The exclusion limits from the constraints on invisible Higgs boson decays, both direct and indirect from the measurement of the coupling properties of the Higgs boson can be compared to direct detection experiments. For comparison, the limit at 90% CL on the invisible branching fraction of  $\text{BR}_{\text{inv}} < 0.16$  [204] is used and converted into limits on  $\sigma_{\chi-N}$  under several hypotheses on the nature of DM particles depending mainly on their spin (scalar- or fermion-like). The vector DM hypothesis is not included since (renormalisable) models of vectorial DM require an extended dark sector that could imply modifications of the signal. The results are shown in Fig. 11.7.

### 11.3.6.2 Exotic Higgs boson decays

The 125 GeV Higgs boson serves not only as a probe for potential DM candidates, but also to search for other exotic particles arising from fields associated with a low-mass hidden sector. Such

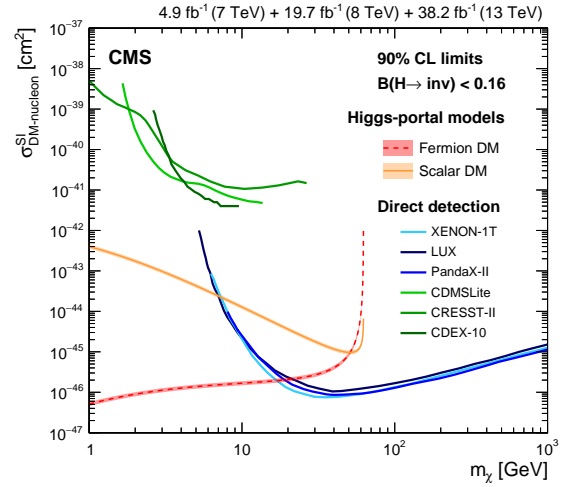


Figure 11.7: 90% CL upper limits on the WIMP-nucleon scattering cross section as a function of the DM particle mass. Spin-independent results excluded and favored regions from direct detection experiments are also shown.

hidden sectors are composed of fields that are singlet under the SM gauge group  $SU(3) \times SU(2) \times U(1)$ . These models are referred to as hidden valley models [206]. Since a light Higgs boson is a particle with a narrow width, even modest couplings to new states can give rise to a significant modification of the Higgs boson phenomenology through exotic decays. Simple hidden valley models exist in which the Higgs boson decays to an invisible fundamental particle, which has a long lifetime to decay back to SM particles through a small mixing with the SM Higgs boson, see Ref. [206] for a concrete example. The Higgs boson may also decay to a pair of hidden valley “ $v$ -quarks,” which subsequently hadronise in the hidden sector, forming “ $v$ -mesons.” These mesons often prefer to decay to the heaviest state kinematically available, so that a possible signature is  $H \rightarrow 4b$ . Some of the  $v$ -mesons may be stable, implying a mixed missing energy plus heavy flavour final state. In other cases, the  $v$ -mesons may decay to leptons, implying the presence of low mass lepton resonances in high- $H_T$  events [207]. Other scenarios have been studied [208] in which the Higgs boson decays predominantly into light hidden sector particles, either directly, or through light SUSY states, and with subsequent cascades that increase the multiplicity of hidden sector particles. In such scenarios, the high-multiplicity hidden-sector particles, after decaying back into the SM, appear in the detector as clusters of collimated leptons known as “lepton jets”.

A variety of models have been investigated searching for final states involving dark photons and hidden valley scalars. The resulting topologies typically have leptons or light hadrons which in some cases can be prompt (i.e., originating from the hard process interaction point) or not and are in some cases collimated and reconstructed as jets [209, 210], and long lived weakly interacting particles. The latter occur not only in hidden valley scenarios, but also in gauge-mediated extensions of the minimal SUSY standard model (MSSM), the MSSM with R-parity violation, and inelastic DM scenarios [211]. Finally, CMS has performed a search for pair production of light bosons [212]. Such a scenario can occur in SUSY models with additional hidden (or dark) valleys.

**Table 11.9:** Summary of the channels searched for and the corresponding 95% CL limits from ATLAS and CMS on the branching fraction for the Higgs boson decay to invisible particles assuming a SM Higgs boson production cross section. The results in parentheses are the expected exclusions.

	ATLAS (Run 1)	ATLAS (Run 2)	CMS (Run 1)	CMS (Run 2)
ggF (monojet); $H \rightarrow \text{inv.}$	–	–	67 (71) %	66 (59) %
VBF; $H \rightarrow \text{inv.}$	28 (31) %	37 (28) %	57 (40) %	33 (25) %
ZH; $Z \rightarrow \ell^+ \ell^-$ ; $H \rightarrow \text{inv.}$	75 (62) %	67 (39) %	75 (91) %	40 (42) %
VH; $Z, W \rightarrow jj$ ; $H \rightarrow \text{inv.}$	78 (86) %	83 (58) %	–	50 (48) %
ZH; $Z \rightarrow b\bar{b}$ ; $H \rightarrow \text{inv.}$	–	–	182 (189) %	–
Combination	25 (27) %	38 (21) %	–	26 (20) %
Run 1 & 2 Combination	–	26 (17) %	19 (15) %	–
$t\bar{t}H$ ; $H \rightarrow \text{inv.}$	–	–	–	46 (48) %

## 11.4 Combining the main channels

The analysis strategy used by the LHC experiments to perform the searches for the Higgs boson has been based on the Higgs boson decay modes. It is a natural choice given that it focusses on the decay products of the object searched for. However, for each channel, exclusive sub-channels have been defined according to the Higgs boson production processes and, in the results presented, these sub-channels have been combined. The natural extension of this approach in order to probe further the production and decay modes of the Higgs boson is to combine the analysis channels together. Such a combination is also used in Section 11.6 to further measure the coupling properties of the Higgs boson.

At the LHC, the total cross section cannot be measured in any of the production modes. As a consequence, neither the absolute branching fractions nor the total width of the Higgs boson can be directly measured, at least if the width is of the SM size. However, a combined measurement of the large variety of categories described in Section 11.3, with different sensitivities to various production and decay modes, permits a wide variety of measurements of the production, decay and coupling properties. These measurements require, in general, a limited but nevertheless restrictive number of assumptions.

In this section, three sets of results will be given. The first one is the ATLAS and CMS Run 1 combination [141]. The other two are the individual combinations of ATLAS and CMS independently with partial Run 2 dataset. It is important to note that, between the Run 1 and the Run 2 results, the signal theoretical systematic uncertainties have improved significantly.

The Run 1 full combination results were derived by the two collaborations, taking rigorously into account all correlations in the systematic uncertainties and in the large number of channels and their categories.

At Run 2, ATLAS [213] and CMS [214] have already produced combined measurements of the coupling properties of the Higgs boson with partial datasets, of up to  $80 \text{ fb}^{-1}$  and up to  $36 \text{ fb}^{-1}$  respectively.

In this section, only the results on the main Higgs boson production and decay modes will be discussed. Only a brief presentation of the combination framework is given here (a more detailed description is given in Ref. [215]). This framework will also be used in Section 11.6 to discuss the measurements of the coupling properties of the Higgs boson.

### 11.4.1 Principles of the combination

The combination of the Higgs boson analysis channels in each experiment and for the two experiments together was done using a fit of a signal and background model to the data. As described above, the data was made of a large number of categories, aiming at reconstructing exclusive production and decay modes. In the combination of ATLAS and CMS [141], there were approximately 600 categories. The combination was a simultaneous fit to all these categories, using a reduced number of parameters of interest and a Higgs boson mass fixed at its measured value (see Section 11.3.2). The much larger number of categories present in the ATLAS and CMS combination [141] is due to additional separation in terms of finer exclusive production regions, decay channels of the  $Z$  and the  $W$  bosons, and taus, control regions where

little-to-no signal is present, and different center-of-mass energies. It should be noted that the individual combination performed by ATLAS [216] included two additional decay channels: the  $\mu^+ \mu^-$  and  $Z\gamma$ . For the sake of simplicity these channels were omitted in the ATLAS–CMS combination. In addition, a  $H \rightarrow b\bar{b}$  analysis performed by CMS, see the reference in Ref [123], and included in its own combination, has been omitted from the ATLAS–CMS combination.

In their Run 2 individual combinations, ATLAS and CMS have not considered the  $Z\gamma$  channel. The CMS experiment has included the  $\mu\mu$  channel.

The key to understand how the combination of channels works relies on the combination master formula, which expresses for each category, indexed by  $c$ , of a given channel (typically a category covers mostly one decay mode, but possibly various production modes), the measured number of signal events  $n_s^c$  as a function of a limited number of parameters as follows:

$$n_s^c = \left( \sum_{i,f} \mu_i \sigma_i^{\text{SM}} \times A_{if}^c \times \varepsilon_{if}^c \times \mu_f \text{BR}_f^{\text{SM}} \right) \times \mathcal{L}^c. \quad (11.16)$$

The production index is defined as  $i \in \{\text{ggF}, \text{VBF}, \text{VH}, \text{t}\bar{t}H\}$  and the decay index is defined as  $f \in \{\gamma\gamma, WW, ZZ, b\bar{b}, \tau\tau\}$ , while  $\sigma_i^{\text{SM}}$  and  $\text{BR}_f^{\text{SM}}$  are the corresponding production cross sections and decay branching fractions, estimated as described in Section 11.2, assuming that the Higgs boson is that of the SM.  $A_{if}^c$  and  $\varepsilon_{if}^c$  are the signal acceptance and the reconstruction efficiency for the given production and decay modes in the category  $c$ .  $\mathcal{L}^c$  is the integrated luminosity used for that specific category. For the purpose of this review, these parameters can be considered as fixed<sup>3</sup>.

The parameters of interest in the master formula are the signal strength parameters  $\mu_i$  and  $\mu_f$ . It is important to note that the formula relies on the factorisation of the production cross section and decay branching fraction, which assumes the narrow width approximation. The width of the Higgs boson will be discussed in Section 11.5, however, for the precision needed here, the fact that the Higgs boson has been observed in decay channels with high mass resolution as a resonance is sufficient to validate this hypothesis. It is also manifest in the above equation that the ten parameters for the production modes ( $\mu_i$ ) and decay modes ( $\mu_f$ ) cannot be determined simultaneously. This illustrates that total cross sections or branching fractions cannot be measured without further assumptions in this fit.

The master formula also illustrates an important caveat to the measurement of signal strength parameters. In case these are interpreted as scale factors of the production cross sections or branching fractions, then all the other quantities such as the acceptances and efficiencies,  $A_{if}^c$  and  $\varepsilon_{if}^c$ , need to be assumed as independent and fixed to their estimated values for the SM Higgs boson. An additional important caveat to note concerning these combined results is that only the normalisation is varied, while the discriminating variables for the signal are not modified and

<sup>3</sup>In the combination performed by ATLAS and CMS, the systematic uncertainties on these parameters are taken into account by allowing these parameters to vary in the fit.

**Table 11.10:** Summary of the observation significances (with respect to the background only hypothesis) for the main production and decay processes at the LHC. Measured signal strengths are reported when the observation has been established unambiguously. Measured signal strengths are reported with the uncertainty of statistical nature first and systematic last, ATLAS has not reported these results in its Run 2 combination (NR). \*The Run 2  $VH$  significances reported in this table are obtained from the observation of the Higgs boson decays to  $b$  quarks, while the Run 1 combination corresponds to combination of all channels.

	Decay modes			
	ATLAS (Run 1)	CMS (Run 1)	ATLAS (Run 2)	CMS (Run 2)
$\gamma\gamma$	4.6 $\sigma$ (5.3 $\sigma$ )	5.2 $\sigma$ (4.6 $\sigma$ )	NR	1.20 $^{+0.13}_{-0.11}$ $^{+0.12}_{-0.09}$
$ZZ$	6.2 $\sigma$ (6.3 $\sigma$ )	8.1 $\sigma$ (6.5 $\sigma$ )	NR	1.06 $^{+0.16}_{-0.15}$ $^{+0.11}_{-0.08}$
$WW$	5.9 $\sigma$ (5.4 $\sigma$ )	6.5 $\sigma$ (4.7 $\sigma$ )	NR	1.28 $^{+0.09}_{-0.09}$ $^{+0.14}_{-0.13}$
$\tau^+\tau^-$	3.4 $\sigma$ (3.9 $\sigma$ )	4.5 $\sigma$ (3.8 $\sigma$ )	6.4 $\sigma$ (5.4 $\sigma$ )	5.9 $\sigma$ (5.9 $\sigma$ )
	Comb. 5.0 $\sigma$ (5.5 $\sigma$ )			
$b\bar{b}$	2.6 $\sigma$ (2.5 $\sigma$ )	1.4 $\sigma$ (2.1 $\sigma$ )	5.4 $\sigma$ (5.5 $\sigma$ )	5.5 $\sigma$ (5.6 $\sigma$ )
	Comb. 3.7 $\sigma$ (2.6 $\sigma$ )			
	Production modes			
	ATLAS and CMS (Run 1)		ATLAS (Run 2)	CMS (Run 2)
$qq \rightarrow qqH$ (VBF)	Comb. 5.4 $\sigma$ (4.6 $\sigma$ )		1.21 $^{+0.18}_{-0.17}$ $^{+0.16}_{-0.13}$	0.73 $^{+0.24}_{-0.23}$ $^{+0.17}_{-0.15}$
$pp \rightarrow VH$	Comb. 3.5 $\sigma$ (4.2 $\sigma$ )		5.3 $\sigma$ (4.8 $\sigma$ )*	4.8 $\sigma$ (4.9 $\sigma$ )*
$pp \rightarrow t\bar{t}H$	Comb. 4.4 $\sigma$ (2.2 $\sigma$ )		5.8 $\sigma$ (4.9 $\sigma$ )	5.2 $\sigma$ (4.2 $\sigma$ )

are still used in the fit. These caveats are of particular importance in the use of the combination to measure the coupling properties of the Higgs boson, as discussed in Section 11.6. For relatively small perturbations of the couplings of the Higgs boson from the SM values, this hypothesis is valid.

However, the products  $\mu_i \times \mu_f$  can be considered as free parameters and in principle measurable (if there is sufficient sensitivity from specific categories). Measuring the products of signal strengths can be viewed as measuring the cross sections times the branching fraction,  $\sigma \cdot \text{BR}$ . An illustration of the results for the Run 2 combinations of ATLAS and CMS is presented in Fig. 11.8 for the combination of ATLAS and CMS.

A coherent picture emerges (including the Run 1 results, see Ref. [123]) where an excellent consistency between the observation in each channel and the SM expectation. This multi-parameter fit quantifies the current experimental knowledge of the main production and decays modes. Run 2 results are also available [213, 214]. These are not included in the figure for the sake of simplicity. The Run 2 results are already competitive with the Run 1 results. In Fig. 11.8, the Run 1 results are kept for illustration purposes. The theoretical uncertainty in the aforementioned fit is not included in the measured values of the signal strengths but is illustrated on the unit value corresponding to the SM expectation.

Other fits involving ratios of cross sections, which are less sensitive to theory uncertainties, are performed and reported in Ref. [215].

The most constrained fit in the combination allows for only one single parameter to vary, i.e.,  $\forall(i, f), \mu_i = \mu_f = \mu$ . This global-signal-strength model provides the simplest probe of the compatibility of the signal with the SM Higgs boson. Indeed, it is sensitive to any deviation from the SM Higgs boson couplings provided that these deviations do not cancel overall. The full Run 1 combination determines the global signal strength to be

$$\mu = 1.09 \pm 0.11 = 1.09 \pm 0.07 \text{ (stat.)} \pm 0.04 \text{ (expt.)} \pm 0.03 \text{ (th. bkg.)} \pm 0.07 \text{ (th. sig.)}, \quad (11.17)$$

where the statistical, experimental uncertainties as well as the theoretical uncertainties on the background and on the signal are reported separately. The ATLAS Run 2 combination of the global

signal strength yields [213]:

$$\mu = 1.11^{+0.09}_{-0.08} = 1.11 \pm 0.05 \text{ (stat.)}^{+0.05}_{-0.04} \text{ (expt.)} \pm 0.03 \text{ (th. bkg.)}^{+0.05}_{-0.04} \text{ (th. sig.)}, \quad (11.18)$$

while the CMS Run 2 combination yields [214]:

$$\mu = 1.17 \pm 0.10 = 1.17 \pm 0.06 \text{ (stat.)}^{+0.06}_{-0.05} \text{ (th. sig.)} \pm 0.06 \text{ (other. syst.)}. \quad (11.19)$$

These overall signal strengths are fully compatible with the SM expectation,  $\mu = 1$ , with a precision of 10%. It is interesting to note that the main uncertainty in these measurements arises from the limited precision in the theoretical predictions for the signal production processes. The precision reached with the individual experiments combinations using partial Run 2 data sets have already exceeded the full Run 1 ATLAS and CMS combination precision.

#### 11.4.2 Main decay modes

Despite the large number of decay channels, since the cross sections cannot be independently measured, from the measurements described in this section it is impossible to measure the decay branching fractions without a loss of generality. The simplest assumption that can be made is that the production cross sections are those of the SM, which is equivalent to assume that, for all  $i$  indices,  $\mu_i = 1$ . All branching fractions  $\mu_f$  can then be measured in a simple 5 parameter fit. The results of these fits are reported in Table 11.10 in terms of significances to highlight their unambiguous observations: all the measured branching fractions are compatible with the SM values.

For the  $\tau^+\tau^-$  channel, ATLAS and CMS were both only mildly sensitive at the Run 1 and have observed excesses in their data. The individual results were not sufficiently significant to claim an observation, however, in combination the evidence was very strong. It is really with the addition of the Run 2 data that the decay of the Higgs boson to tau pairs has been established by the two experiments independently and unambiguously (see Table 11.10 and Section 11.3.2).

As illustrated in Table 11.10, ATLAS and CMS were both less sensitive in the  $H \rightarrow b\bar{b}$  decay mode. The available sensitivity

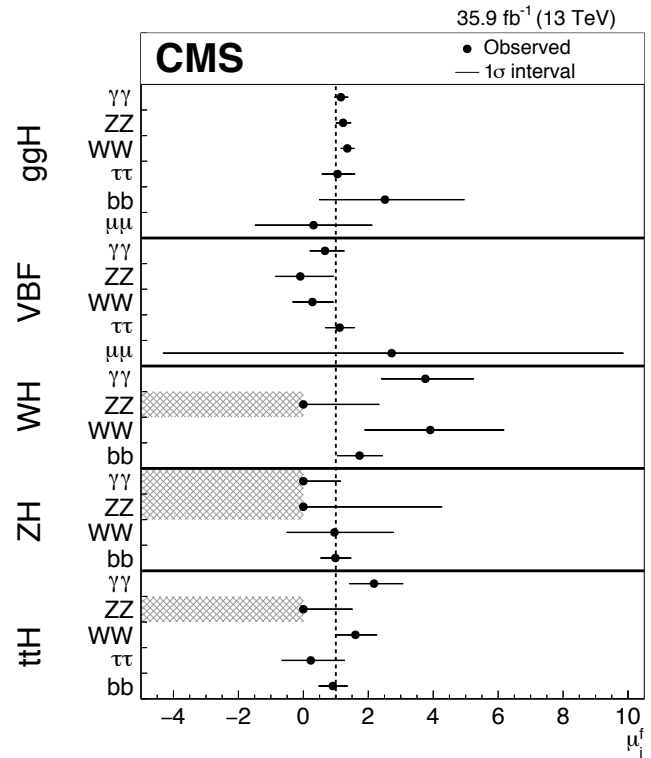
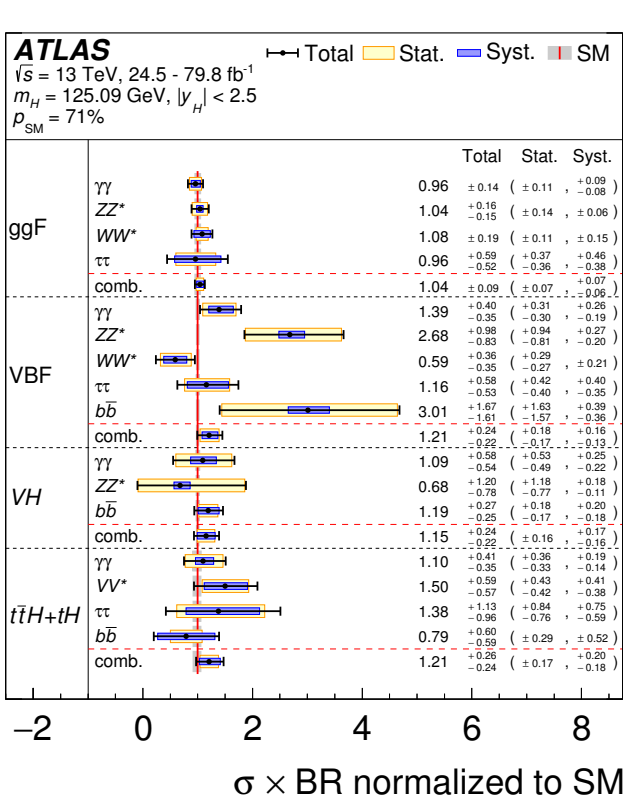


Figure 11.8: Combined measurements of the products  $\sigma \cdot \text{BR}$ , normalised to the SM predictions, for the five main production and five main decay modes. The hatched combinations require more data for a meaningful confidence interval to be provided.

came mostly from the  $VH$  process. The combined significance of  $3.7\sigma$  at Run 1 was sufficient to suggest evidence, however ATLAS and CMS observations were both low with respect to the rate expected in the SM. At Run 2, this channel benefited largely from the increased production cross sections at 13 TeV and the much larger dataset. In this case as well, it is with the addition of the Run 2 data that both experiments were able to establish a measurement in this channel (as discussed in Section 11.3.2).

These are major milestones of the LHC physics program.

#### 11.4.3 Main production modes

Most analysis channels are divided into exclusive categories allowing for an increased overall sensitivity and permitting to access the various Higgs boson production modes. The cross sections of the main production modes can be measured assuming that the branching fractions are those of the SM, i.e., for all  $f$  indices  $\mu_f = 1$ . These assumptions lead to a 5 parameter combination. The results are reported in terms of significances of observation of the production modes in Table 11.10.

The gluon fusion production process is the dominant production mode. Although no numerical estimate of combined significance of observation for this process has been given by the experiments, it is considered as established due to the overwhelming evidence from the three main discovery channels. None of the other production modes have been firmly established by the experiments individually. However, the table shows that, for the VBF production mode, the combination had a large sensitivity and produced a combined observation of  $5.4\sigma$ , therefore establishing this process with a rate compatible with that expected in the SM.

The  $VH$  production mode has only very recently been unambiguously observed by ATLAS and CMS independently (as discussed in Section 11.3.2) through the  $V(H \rightarrow b\bar{b})$  channel. This is illustrated in the relative contributions of all channels to the  $VH$  process shown in Figure 11.8.

With the Run 2 data, all production processes have been established, and in particular the  $pp \rightarrow t\bar{t}H$  process, which provides direct evidence of the coupling of the Higgs boson to top quarks. This is another milestone in the LHC physics program.

## 11.5 Main quantum numbers and width of the Higgs boson

### 11.5.1 Main quantum numbers $J^{PC}$

Probing the Higgs boson quantum numbers is essential to further unveiling its coupling properties. The measurements of the signal event yields in all the channels discussed in Sections 11.3 and 11.4, and their compatibility with the SM Higgs boson predictions, give a qualitative but, nonetheless, compelling indication of its nature. This qualitative picture is further complemented by the implications of the observation of the particle in the diphoton channel. According to the Landau–Yang theorem [217], the observation made in the diphoton channel excludes the spin-1 hypothesis and restricts possibilities for the spin to 0 or 2.

The Landau–Yang theorem does not apply if the observed state is not decaying to a pair of photons but to a pair of scalars subsequently decaying to two very collimated pairs of photons (as for example in the case of  $H \rightarrow a_1 a_1 \rightarrow 4\gamma$ ). This possibility has not been rigorously excluded but is not experimentally favoured since tight selection criteria are applied on the electromagnetic shower shapes of the reconstructed photons. A more systematic analysis of shower shapes and the fraction of conversions could be performed to further discriminate between the single prompt photon and the two overlapping photons hypotheses. There are also potential theoretical loopholes concerning the applicability of the Landau–Yang theorem, such as off-shell vector boson decays. However, for the observed particle not to be of spin 0 and +1 parity would require an improbable conspiracy of effects. It is nevertheless important to test this hypothesis independently, in particular since the measurements of coupling properties of the Higgs boson assume that it is a  $CP$ -even state.

#### 11.5.1.1 Charge conjugation

The charge conjugation quantum number is multiplicative, therefore given that the Higgs-like particle is observed in the  $H \rightarrow \gamma\gamma$  channel, and given that photons are  $C$ -odd eigenstates, assuming  $C$  conservation, the observed neutral particle should be  $C$ -even.

## 11.5.1.2 Spin and parity

To probe the spin and parity quantum numbers of the discovered particle, a systematic analysis of its production and decay processes is performed in several analyses. These analyses are designed to be independent of the measured event yields and they rely instead on the production and the decay angles, and on the threshold distributions as long as a significant signal is observed, i.e., in situations when an excess over the expected background can be used to further discriminate between signal hypotheses. These analyses are based on probing various alternative models of spin and parity [218]. These models can be expressed in terms of an effective Lagrangian [219] or in terms of helicity amplitudes [220]. The two approaches are equivalent. In the following, the effective Lagrangian formalism is chosen to describe the models considered and a restricted number of models are discussed [219]. In the analysis performed by CMS [220], a larger number of models have been investigated, however, the main channels studied by both experiments are essentially the same and the main conclusions are similar and fully consistent.

## i. Spin-0 model

The interaction Lagrangian relevant for the analysis of spin-0 particle interaction with a pair of  $W$  or  $Z$  bosons with either fixed or mixed SM and BSM  $CP$ -even couplings or  $CP$ -odd couplings, is the following [221]:

$$\begin{aligned} \mathcal{L}_0^{W,Z} \supset & \left\{ \cos(\alpha)\kappa_{SM} \left[ \frac{1}{2}g_{HZZ}Z_\mu Z^\mu + g_{HWW}W_\mu^+ W^{-\mu} \right] \right. \\ & - \frac{1}{4\Lambda} \left[ \cos(\alpha)\kappa_{HZZ}Z_{\mu\nu}Z^{\mu\nu} + \sin(\alpha)\kappa_{AZZ}Z_{\mu\nu}\tilde{Z}^{\mu\nu} \right] \\ & \left. - \frac{1}{2\Lambda} \left[ \cos(\alpha)\kappa_{HWW}W_{\mu\nu}^+ W^{-\mu\nu} + \sin(\alpha)\kappa_{AWW}W_{\mu\nu}^+\tilde{W}^{-\mu\nu} \right] \right\} H, \end{aligned} \quad (11.20)$$

where  $V^\mu = Z^\mu, W^{+\mu}$  are the vector boson fields,  $V^{\pm\mu\nu}$  are the reduced field tensors and  $\tilde{V}^{\pm\mu\nu} = 1/2 \varepsilon^{\mu\nu\rho\sigma} V_{\rho\sigma}$  are the dual tensor fields. And  $\Lambda$  defines an effective theory energy scale. The factors  $\kappa_{SM}, \kappa_{HZZ}, \kappa_{HWW}, \kappa_{AZZ}, \kappa_{AWW}$  denote the coupling constants corresponding of the coupling of the SM and BSM  $CP$ -even and  $CP$ -odd components of the Higgs boson to the  $W$  and  $Z$  fields. The mixing angle  $\alpha$  allows for the production of a  $CP$ -mixed state and the  $CP$ -symmetry is broken when  $\alpha \neq 0, \pi$ .

This formalism can be used to probe both  $CP$ -mixing for a spin-0 state, as discussed in Section 11.5.1.4 or specific alternative hypotheses, as discussed below in Section 11.5.1.3, such as a pure  $CP$ -odd state ( $J^P = 0^-$ ) corresponding to  $\alpha = \pi/2$ ,  $\kappa_{SM} = \kappa_{HVV} = 0$  and  $\kappa_{AVV} = 1$ . A BSM  $CP$ -even state  $J^P = 0^+$  corresponds to  $\alpha = 0$ ,  $\kappa_{AVV} = 0$ ,  $\kappa_{HVV} = 1$  and  $\kappa_{SM}$  arbitrary. These hypotheses are compared to the SM Higgs boson hypothesis corresponding to  $\alpha = 0$  and  $\kappa_{HVV} = \kappa_{AVV} = 0$  and  $\kappa_{SM} = 1$ . This formalism has been adopted by the ATLAS experiment. The analysis of these benchmarks are illustrated in Fig. 11.9.

A different parametrisation of anomalous couplings of a spin-zero boson with two gauge bosons  $VV$  can also be expressed in the general form of the scattering amplitude  $A$ :

$$\begin{aligned} A \sim & \left[ a_1^{VV} - \frac{\kappa_1^{VV} q_1^2 + \kappa_2^{VV} q_2^2}{(A_1^{VV})^2} - \frac{\kappa_3^{VV} (q_1 + q_2)^2}{(A_Q^{VV})^2} \right] m_{V_1}^2 \varepsilon_{V_1}^* \varepsilon_{V_2}^* \\ & + a_2^{VV} f_{\mu\nu}^{*(1)} f^{*(2)\mu\nu} + a_3^{VV} f_{\mu\nu}^{*(1)} \tilde{f}^{*(2)\mu\nu} \end{aligned} \quad (11.21)$$

where  $\varepsilon_i$  is the polarization vector of the boson  $V_i$ ,  $f_{\mu\nu}^{*(i)} = \varepsilon_i^\mu q^\nu - \varepsilon_i^\nu q^\mu$  is a scalar tensor constructed from the vector boson  $V_i$  polarization and four momentum,  $\tilde{f}_{\mu\nu}^{*(i)} = \frac{1}{2} \varepsilon_{\mu\nu\rho\sigma} f^{*(i)\rho\sigma}$  is the corresponding pseudo-scalar tensor.  $A_1$  and  $A_Q$  are new physics scales,  $a_{1,2,3}$  are coupling strength modifiers and  $|\kappa_{(1,2,3)}^{VV}| = 0$  or 1. The custodial symmetry would require that  $a^{WW} = a^{ZZ}$  and, at tree-level, the only non-zero contributions would come from the  $a_1$  term. This parametrisation is used by CMS. It is fully equivalent to the interaction Lagrangian approach described above.

## ii. Spin-2 model

The graviton-inspired interaction Lagrangian for a spin-2 boson  $X^{\mu\nu}$  that does not carry any color, weak and electromagnetic charge and that uniquely interacts with the energy momentum tensor  $\mathcal{T}^{V,f}$  of vector bosons  $V$  or fermions  $f$ , can be written as follows [221]:

$$\mathcal{L}_2 \supset \frac{1}{\Lambda} \left[ \sum_V \xi_V \mathcal{T}_{\mu\nu}^V X^{\mu\nu} + \sum_f \xi_f \mathcal{T}_{\mu\nu}^f X^{\mu\nu} \right], \quad (11.22)$$

where the strength of the interaction is determined by the couplings  $\xi_V$  and  $\xi_f$ . The simplest scenarios, referred to as universal couplings (UC), correspond to  $\xi_V = \xi_f$ . They predict a large branching ratio to photons (of approximately 5%) and negligible couplings to massive gauge bosons ( $W$  and  $Z$ ). They are therefore disfavoured, and other models are investigated where the couplings of the  $W$ ,  $Z$  and  $\gamma$  are assumed to be independent. Universality of the couplings refers to  $\xi_g = \xi_q$ . Two other scenarios are considered:  $\xi_q = 0$  and  $\xi_q = 2\xi_g$ . In these scenarios, a large enhancement of the tail of the transverse momentum of the spin-2 state is expected and requires a further selection requirement in order to probe the models within the range of validity of the effective field theory. Two requirements are considered,  $p_T^X < 300$  GeV and  $p_T^X < 125$  GeV [219]. The analysis of these benchmarks are discussed below and results are illustrated in Fig. 11.9.

11.5.1.3 Probing fixed  $J^P$  scenarios

At the LHC, the determination of the spin and  $CP$  properties of the Higgs boson is done independently from the total rates measurement, it uses a global angular helicity analysis and, when applicable, the study of threshold effects. The channels used for this analysis,  $H \rightarrow \gamma\gamma$ ,  $H \rightarrow WW^{(*)} \rightarrow \ell\nu\ell\nu$  and  $H \rightarrow ZZ^{(*)} \rightarrow 4\ell$ , are those where the observation of a signal is unambiguous.

At the Tevatron, an analysis using the threshold distribution in the associated production mode  $VH$  with subsequent decay to a pair of  $b$  quarks was performed by the D0 collaboration.

i. The  $VH$  production at D0

The mass of the  $VH$  system is a powerful discriminant to distinguish a  $J^P = 0^+$ , with a threshold behaviour in  $d\sigma/dM^2 \sim \beta, \beta^3, \beta^5$  from a  $0^+, 0^-$  and  $2^+$  state, respectively [222]. The  $VH$  mass observable not only discriminates signal hypotheses, but also has an increased separation between the  $0^-$  and  $2^+$  hypotheses with respect to the backgrounds, thus allowing, with a small and not yet significant signal yield, to exclude that the observed state is  $0^-$  at 98% CL [223] and  $2^+$  at the 99.9% CL [224], assuming a signal produced with their best fit signal strength (which was  $\mu = 1.23$ ).

ii. The  $\gamma\gamma$  channel at the LHC

In the  $H \rightarrow \gamma\gamma$  channel, the analysis is performed inclusively using the production angle  $\cos\theta_{CS}^*$  and the transverse momentum of the diphoton pair [219]. The polar angle in the rest frame is defined with respect to the bisector axis of the momenta of the incoming protons and is referred to as the polar angle in the Collins-Soper frame [225]. The SM Higgs boson signal distribution is expected to be uniform with a cutoff due to the selection requirements on the photons transverse momentum. The  $H \rightarrow \gamma\gamma$  channel is mostly sensitive to the gluon-initiated spin-2 production scenarios, which yield a  $\cos\theta_{CS}^*$  distribution peaking at values close to 1. The ATLAS limits are derived from a fit of the signal in bins of  $\cos\theta_{CS}^*$  and diphoton transverse momentum and are summarised in Fig. 11.9 (right) (only combined results are shown). The data shows a good compatibility with the SM  $0^+$  hypothesis and contributes strongly to the exclusion of several spin-2 scenarios. The conclusions are the same from CMS results [220].

iii. The  $H \rightarrow WW^{(*)} \rightarrow \ell\nu\ell\nu$  channel at the LHC

In the  $H \rightarrow WW^{(*)} \rightarrow \ell\nu\ell\nu$  channel, the production and decay angles cannot be easily reconstructed due to the presence of neu-



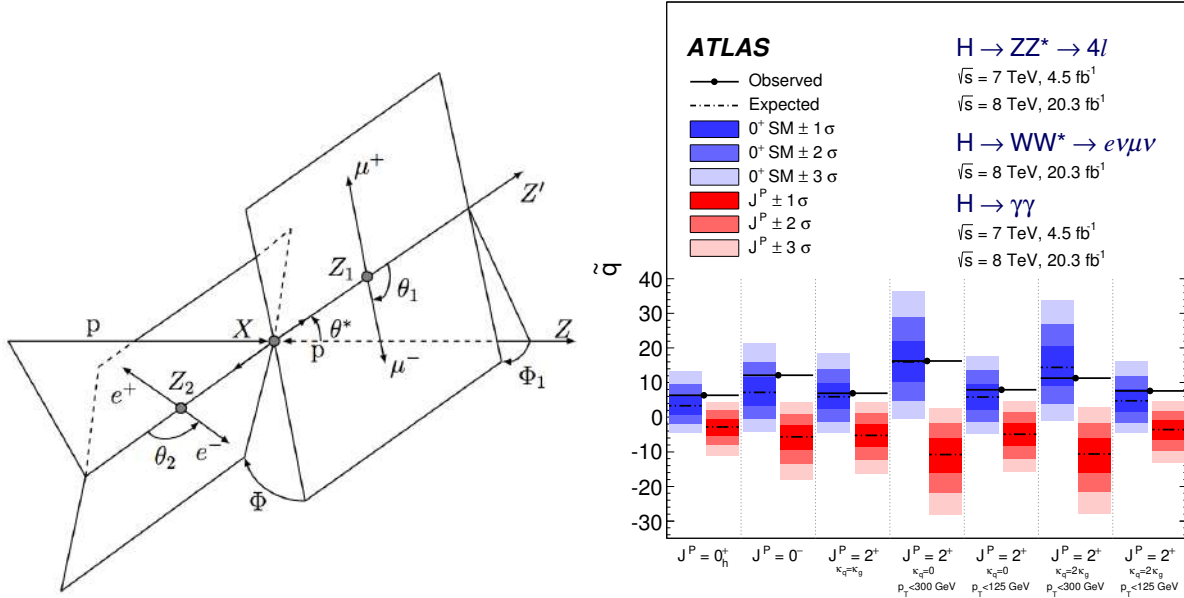


Figure 11.9: (Left) Definition of the production and decay angles defined for the  $H \rightarrow ZZ^{(*)} \rightarrow 4\ell$  final state [220]. (Right) Expected distributions of the test statistic for the SM hypothesis (in blue) and several alternative spin and parity hypotheses (in red).

trinos in the final state, however, sensitivity arises from the  $V-A$  structure of the decay of the  $W$  bosons. A scalar state thus yields a clear spin correlation pattern that implies that the charged leptons  $e$  or  $\mu$  from the decays of the  $W$  bosons are produced close to one another in the transverse plane. This feature impacts observables such as the azimuthal angle between the two leptons  $\Delta\Phi_{\ell\ell}$  or their invariant mass  $m_{\ell\ell}$  in addition to the threshold behaviour of the decay. It can be used to discriminate between various spin and parity hypotheses. The approach adopted by ATLAS uses a multivariate discriminant, whereas CMS uses a 2D-fit of the dilepton mass and the transverse mass. Figure 11.9 (right) summarises the ATLAS results of the  $H \rightarrow WW^{(*)} \rightarrow \ell\nu\ell\nu$  analyses alone and in combination with other channels. Spin-1 hypotheses ( $1^+$  and  $1^-$ ) have also been tested in this channel by ATLAS and CMS. ATLAS and CMS exclude the  $1^+$  and  $1^-$  hypotheses at more than 95% CL.

#### iv. The $H \rightarrow ZZ^{(*)} \rightarrow 4\ell$ channel at the LHC

The  $H \rightarrow ZZ^{(*)} \rightarrow 4\ell$  coupling analysis, as described in Section 11.3, also uses a discriminant based on the  $0^+$  nature of the Higgs boson to further separate signal and background. In this analysis, this feature is used to discriminate between signal hypotheses. The observables sensitive to the spin and parity are [226] the masses of the two  $Z$  bosons (due to the threshold dependence of the mass of the off-shell  $Z$  boson), two production angle  $\theta^*$  and  $\Phi_1$ , and three decay angles,  $\Phi$ ,  $\theta_1$  and  $\theta_2$ . The production and decay angles are defined as:

- $\theta_1$  and  $\theta_2$ , the angles between the negative final state lepton and the direction of flight of  $Z_1$  and  $Z_2$  in the rest frame.
- $\Phi$ , the angle between the decay planes of the four final state leptons expressed in the four lepton rest frame.
- $\Phi_1$ , the angle defined between the decay plane of the leading lepton pair and a plane defined by the vector of the  $Z_1$  in the four lepton rest frame and the positive direction of the proton axis.
- $\theta^*$ , the production angle of the  $Z_1$  defined in the four lepton rest frame with respect to the proton axis.

These angles are illustrated in Fig. 11.9 (left). There are two approaches to this analysis. The first, used by CMS, is a matrix element likelihood approach where a kinematic discriminant is defined based on the ratio of the signal and background probabilities. These probabilities are defined using the leading-order matrix elements. A similar approach is also performed by ATLAS as a cross check of their main result. The main approach adopted by ATLAS is the combination of sensitive observables

with a Boosted Decision Tree. These analyses are sensitive to various  $J^P$  hypotheses and in particular discriminate the  $0^+$  hypothesis from the  $0^-$ . In all scenarios investigated, and for both ATLAS and CMS, the data is compatible with the  $0^+$  hypothesis. ATLAS and CMS exclude a pure pseudo-scalar nature of the observed boson at  $CL_S$  levels of 98% and 99.8% [220].

#### 11.5.1.4 Probing $CP$ -mixing and anomalous $HVV$ couplings

The careful study of the kinematic properties of the events observed in the  $H \rightarrow ZZ^{(*)} \rightarrow 4\ell$  and  $H \rightarrow WW^{(*)} \rightarrow \ell\nu\ell\nu$  channel, and in particular the angular distributions described above, allows one to further probe the  $HVV$  coupling beyond testing fixed hypotheses. Assuming that the observed particle is a spin-0 state, and using several discriminating observables in the  $H \rightarrow ZZ^{(*)} \rightarrow 4\ell$  and  $H \rightarrow WW^{(*)} \rightarrow \ell\nu\ell\nu$  channels, the anomalous terms in the formalism of Eq. (11.20) can be probed. In the approach of helicity amplitudes used by CMS [220], all terms are essentially equivalent, except for one additional phase which is neglected in Eq. (11.20).

Results are derived in terms of the parameters  $\tilde{\kappa}_{HVV} = v\kappa_{HVV}/\Lambda$  and  $\tilde{\kappa}_{AVV} = v\kappa_{AVV}/\Lambda$ , and, more precisely, as measurements of  $\tilde{\kappa}_{HVV}/\kappa_{SM}$  and  $\tan\alpha \cdot \tilde{\kappa}_{AVV}/\kappa_{SM}$ , as shown in Fig. 11.10. These parameters can be interpreted as mixing parameters of a tensor anomalous  $CP$ -even coupling and a  $CP$ -odd component. The measurements are made in the  $H \rightarrow ZZ^{(*)} \rightarrow 4\ell$  and  $H \rightarrow WW^{(*)} \rightarrow \ell\nu\ell\nu$  channels independently and then combined assuming that the  $\tilde{\kappa}_{HVV}/\kappa_{SM}$  and  $\tan\alpha \cdot \tilde{\kappa}_{AVV}/\kappa_{SM}$  are the same for the  $W$  and  $Z$  vector bosons. Only the combination of the  $WW$  and  $ZZ$  channels is shown in Fig. 11.10. The asymmetric shape of the likelihood as a function of  $\tilde{\kappa}_{HWW}, HZZ/\kappa_{SM}$  is mainly due to the interference between the BSM and the SM contributions that gives a maximal deviation from the SM predictions for negative relative values of the BSM couplings. In Fig. 11.10, the expected likelihood profiles for a SM Higgs boson are also displayed. While no significant deviation from the SM expectation is observed, the precision of the measurements of the mixing parameters is fairly low. The results and conclusions from the CMS measurements [220] are very similar.

An individual  $ZZ^*$  channel measurement has also been carried out with a partial Run2 dataset by ATLAS [227]. CMS has performed a  $CP$ -mixing analysis of a partial Run2 dataset of  $36\text{ pb}^{-1}$  combined with the full Run1 data using the  $ZZ^*$  channel [228]. In this analysis the CMS experiment sets constraints on the following parameters defined in the scattering amplitude

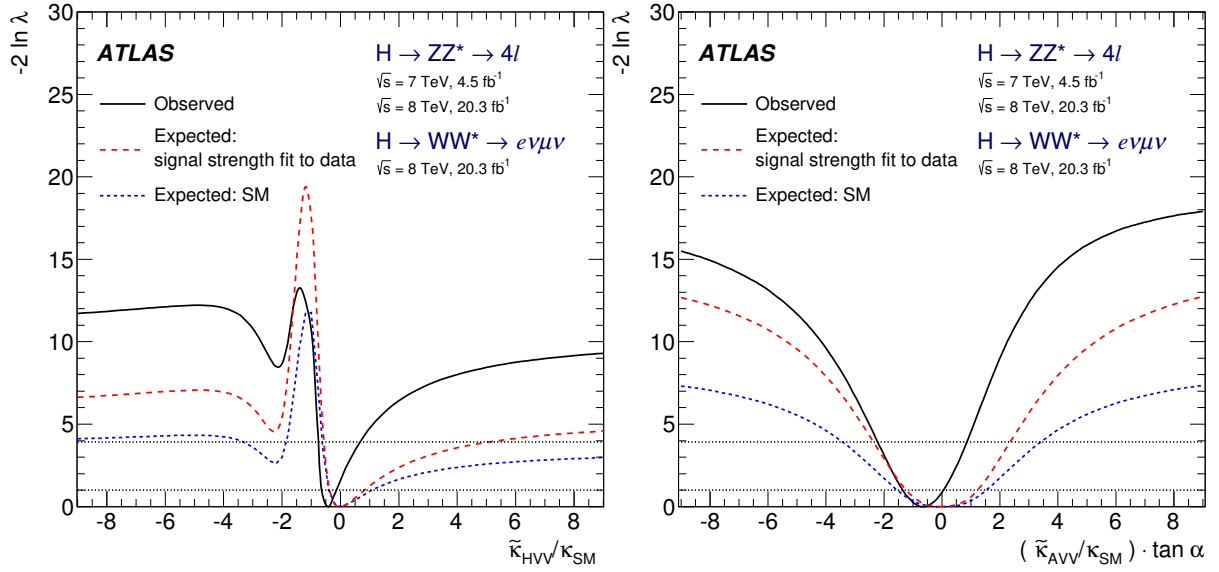


Figure 11.10: Likelihood profiles for the  $\tilde{\kappa}_{HV V}$  and  $\tilde{\kappa}_{AVV} \cdot \tan \alpha$  parameters, representing respectively  $CP$ -even and  $CP$ -odd anomalous couplings of the Higgs boson.

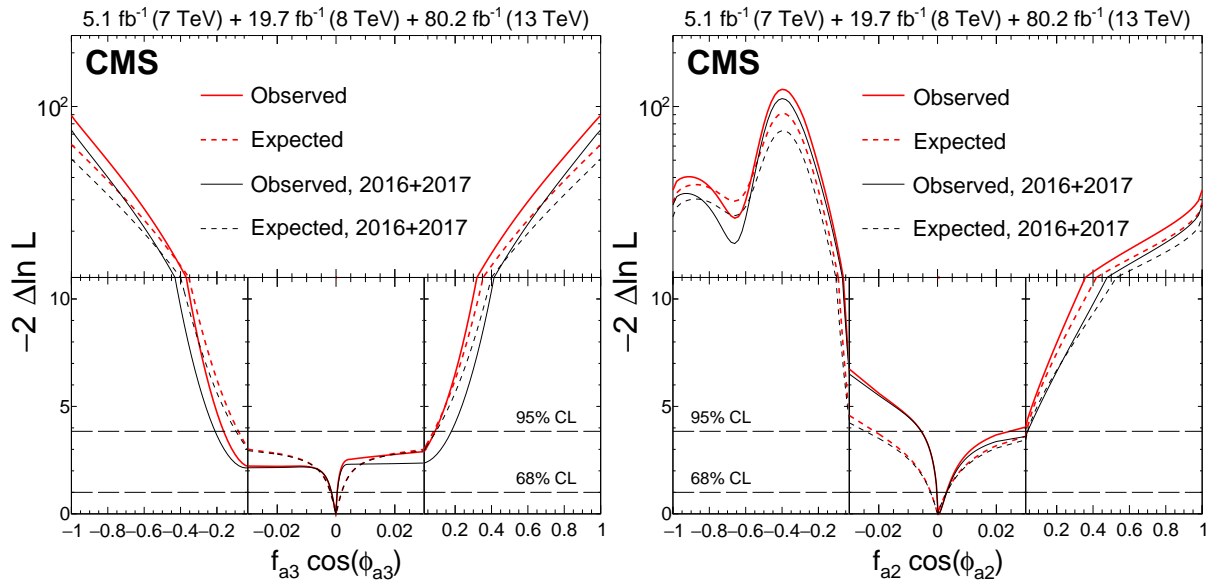


Figure 11.11: Observed (solid) and expected (dashed) likelihoods as a function of  $f_{a_3} \cos(\phi_{a_3})$  (left),  $f_{a_2} \cos(\phi_{a_2})$  (right) for the Run 1 and Run 2 datasets separately and combined.

parametrisation (11.21):

$$f_{a_i} = \frac{|a_i|^2 \sigma_i}{\sum_{j=1,2,3} |a_j|^2 \sigma_j}, \quad \phi_{a_i} = \arg\left(\frac{a_i}{a_1}\right), \quad (11.23)$$

where  $\sigma_i$  is the cross section for process with  $a_i = 1$  and  $a_{j \neq i} = 0$ . The constraints on these parameters are shown in Fig. 11.11.

$CP$  invariance in the  $HVV$  coupling can also be probed with the VBF production process in the  $H \rightarrow \tau^+ \tau^-$  channel. CMS has performed an analysis in this channel and has combined its results with the aforementioned  $ZZ^*$  channel using the same dataset [229].

ATLAS has also performed an analysis using optimal observables [230], defined as the ratio of the interference between the  $CP$ -odd and the SM contributions normalised to the SM matrix element squared, using the Run1 data. In this study, the  $CP$ -mixing contributions are described in the framework of an effective field theory governed by a single parameter  $\tilde{d}$ , found to be consistent with its SM value of  $\tilde{d} = 0$  and constrained to the interval  $[-0.11, 0.05]$  at the 68% CL.

### 11.5.2 Off-shell couplings of the Higgs boson

In the dominant ggF production mode with a subsequent decay of the Higgs boson into a pair of  $Z$  bosons, the production cross section of an off-shell Higgs boson is known to be sizeable. This follows as a consequence of the enhanced couplings of the Higgs boson to the longitudinal polarisation of the massive vector bosons at high energy.

The off-shell to on-shell cross section ratio is approximately 8% in the SM [231]. Still the Higgs contribution to  $VV$  production at large invariant mass remains small compared to the background. It is nevertheless interesting to probe Higgs production in this regime as it is sensitive to new physics beyond the SM.

The difficulty in the off-shell  $VV$  analysis, beyond the small signal-to-background ratio, is due to a large negative interference between the signal and the  $gg \rightarrow VV$  background.

The resulting presence of a SM Higgs boson signal in the far off-shell domain results in a deficit of events with respect to the expectation from background only events. It is only when the off-shell couplings of the Higgs boson are larger than expected in



the SM that the presence of a signal appears as an excess over the background expectation. One additional intricacy arises from the precision in the prediction of the rate for  $gg \rightarrow VV$ , a loop process at lowest order, and its interference with the signal. At the time of the publication of the original ATLAS and CMS results, a full NLO prediction had not been computed.

It is interesting to note that, in this regime, the Higgs boson is studied as a propagator and not as a particle. The measurement of its off-shell couplings is therefore absolute and does not rely on the knowledge of the total Higgs boson width. The off-shell coupling constraints can then be used to indirectly constrain the width of the Higgs boson, under specific assumptions detailed in Section 11.5.3.3.

This measurement has been carried out in the  $H \rightarrow ZZ \rightarrow 4\ell$ ,  $H \rightarrow ZZ \rightarrow \ell\nu\nu$  and  $H \rightarrow WW \rightarrow \ell\nu\nu$  channels. To enhance the sensitivity of the analysis, the knowledge of the full kinematics of the events is important. In particular the signal and the background can be further distinguished by the invariant mass of the  $VV$  system, which is more accurately accessible in the  $H \rightarrow ZZ \rightarrow 4\ell$  channel. Angular distributions also play an important role in this analysis. For these reasons, the  $H \rightarrow ZZ^{(*)} \rightarrow 4\ell$  channel is significantly more sensitive than  $H \rightarrow WW^{(*)} \rightarrow \ell\nu\nu$ . The CMS results in Refs. [232] include the VBF and  $VH$  processes through the selection of two additional jets in the final state. The ATLAS results do not have a specific selection for the VBF or  $VH$  production processes, but their contributions are taken into account.

Limits on the off-shell rates have been reported for the two channels by ATLAS [233] and CMS [232]. The combined results, assuming that the off-shell rates in the  $ZZ$  and  $WW$  channels scale equally, are given for two different hypotheses on the VBF production rate: fixing it to its SM value or scaling it as the gluon fusion rate. The observed (expected) limits on the off-shell rate fraction with respect to its SM expectation is 6.7 (9.1) for ATLAS [233] with the VBF rate fixed to its SM value and 2.4 (6.2) for CMS [232] where no assumption is made on the relative production rates of gluon-fusion and VBF. In both cases, the custodial symmetry is assumed and the ratio of the rates in the  $ZZ$  and  $WW$  decays are fixed to those of the SM. Results without this assumption have also been reported in Ref. [232].

Both ATLAS [234] and CMS [228] have performed off-shell Higgs boson analyses to constrain the off-shell Higgs boson production rates with partial Run 2 datasets, corresponding respectively to luminosities of  $36.1 \text{ fb}^{-1}$  and  $80.2 \text{ fb}^{-1}$ . With the increase in centre-of-mass energy and luminosities, significantly better sensitivities are achieved. The ATLAS analysis is based on two decay channels,  $H \rightarrow 4\ell$  and  $H \rightarrow 2\ell 2\nu$ , and the two main ggF and VBF production modes, while the CMS analysis is based on the  $H \rightarrow 4\ell$  channel exclusively, but uses the exclusive  $VH$  categories. The results obtained have already reached an impressive sensitivity, with 95% CL upper limits on the off shell signal strength  $\mu_{\text{off-shell}}$ :

$$\begin{aligned} (\text{ATLAS}) \quad \mu_{\text{off-shell}} &< 3.8 \text{ (obs)} \quad [3.4 \text{ (exp)}], \\ (\text{CMS}) \quad \mu_{\text{off-shell}} &< 2.28 \text{ (obs)} \quad [3.2 \text{ (exp)}]. \end{aligned} \quad (11.24)$$

### 11.5.3 The Higgs boson width

In the SM, the Higgs boson width is very precisely predicted once the Higgs boson mass is known. For a mass of 125 GeV, the Higgs boson has a very narrow width of 4.1 MeV [44]. It is dominated by the fermionic decays partial width at approximately 75%, while the vector boson modes are suppressed and contribute 25% only.

At the LHC or the Tevatron, in all production modes, only the cross sections times branching fractions can be measured. As a consequence, the total width of the Higgs boson cannot be inferred from measurements of Higgs boson rates. Direct constraints on the Higgs boson width are much larger than the expected width of the SM Higgs boson.

#### 11.5.3.1 Direct constraints

Analyses of the reconstructed mass line-shape in the two channels with a good mass resolution, the  $H \rightarrow \gamma\gamma$  and  $H \rightarrow ZZ^{(*)} \rightarrow 4\ell$  channels, allow for a direct measurement of the

width of the SM Higgs boson. The intrinsic mass resolution in these channels is about 1–2 GeV, much larger than the expected width of the SM Higgs boson. As a result, only upper limits on the Higgs boson width have been set by ATLAS [235] and CMS [236]. The two main challenges of direct constraints on the width through the measurement of the line-shape are: (i) the modelling of resolution uncertainties and (ii) the modelling of the interference between the signal and the continuum background which can be sizeable for large widths, in particular in the range where direct constraints are set. Given that these interference effects are small with respect to the individual channels sensitivity, they are neglected in deriving constraints on the total width. The combined constraints, however, being more precise, could be affected by the interference. ATLAS [235] has therefore not combined the constraints on the width from the two channels. The results are reported in Table 11.11. These constraints are still three orders of magnitude larger than the expected SM width and are fully compatible with the SM hypothesis.

Another direct constraint on the Higgs boson width can be obtained, in the  $H \rightarrow ZZ^{(*)} \rightarrow 4\ell$  channel, from the measurement of the average lifetime of the Higgs boson calculated from the displacement of the four-lepton vertex from the beam spot. This analysis has been carried out by CMS (see references in Ref. [123]), using the measured decay length. The measured  $c\tau_H$  is  $2_{-2}^{+25} \mu\text{m}$ , yielding an observed (and expected) limit at the 95% CL of  $c\tau_H < 57(56) \mu\text{m}$ . From this upper limit on the lifetime of the Higgs boson, the 95% CL lower limit on its width is  $\Gamma_H > 3.5 \times 10^{-12} \text{ GeV}$ .

#### 11.5.3.2 Indirect constraints from mass shift in the diphoton channel

In the diphoton channel, it was noticed in Ref. [237], that the effect of the interference between the main signal  $gg \rightarrow H \rightarrow \gamma\gamma$  and the continuum irreducible background  $gg \rightarrow \gamma\gamma$ , taking into account detector resolution effects, is responsible for a non negligible mass shift. The size of the mass shift depends on the total width of the Higgs boson and it was suggested that measuring this mass shift could provide a constraint on the width [237]. It was further noticed that the mass shift has a dependence also on the diphoton transverse momentum. The total width of the Higgs boson could therefore be constrained using the diphoton channel alone.

Further studies were performed by ATLAS to estimate the size of the expected mass shift [134]. The expected shift in mass in the diphoton channel is  $35 \pm 9 \text{ MeV}$  for the SM Higgs boson. Very preliminary studies of the sensitivity of this method to estimate the width of the Higgs boson in the High-Luminosity regime have been made by ATLAS [238] and yield an expected 95% CL upper limit on the total width of approximately 200 MeV from  $3 \text{ ab}^{-1}$  of 14 TeV data.

#### 11.5.3.3 Indirect constraints from on-shell rate in the diphoton channel

In the diphoton channel, it was noticed in Ref. [239], that the interference between the main signal  $gg \rightarrow H \rightarrow \gamma\gamma$  amplitude and the continuum irreducible background  $gg \rightarrow \gamma\gamma$  amplitude generates non-negligible change in the on-shell cross sections, as a result of the existence of a relative phase between these amplitudes. The size of this on-shell interference effect depends on the total width of the Higgs boson and it was suggested that measuring this on-shell cross section precisely could provide a constraint on the Higgs total width. This interference effect yields around 2% reduction for the  $gg \rightarrow H \rightarrow \gamma\gamma$  cross section measurement. The current evaluation of this interference effect is performed at NLO and has a  $^{+50\%}_{-30\%}$  uncertainty, due to the fact that the large relative phase is driven by the two-loop  $gg \rightarrow \gamma\gamma$  background amplitude [237, 239]. This on-shell interference effect has a dependence on the  $p_T$  of the diphoton system and the photon polar angle in the diphoton rest frame, which can be further exploited to improve the measurement to constrain the Higgs total width.

Taking the ratios of the on-shell cross section of Higgs boson to diphoton channel and the cross section of Higgs boson to four-leptons channel where the interference effect is negligible could put bound on the Higgs boson total width. This ratio is free

**Table 11.11:** Run 1 observed (expected) direct 95% CL constraints on the width of the 125 GeV resonance from fits to the  $\gamma\gamma$  and  $ZZ$  mass spectra and to the  $4\ell$  vertex lifetime. \*The CMS measurement from the  $4\ell$  mass line-shape was performed using Run 2 data.

Exp.	$M_{\gamma\gamma}$ mass spectrum	$M_{4\ell}$ spectrum	$4\ell$ vertex lifetime
ATLAS	$< 5.0$ (6.2) GeV	$< 2.6$ (6.2) GeV	—
CMS	$< 2.4$ (3.1) GeV	$< 1.1$ (1.6) GeV*	$> 3.5 \times 10^{-12}$ GeV

from many dominant sources of systematic uncertainties for cross section measurements, i.e., PDF uncertainty and luminosity uncertainty, and can be further improved by the accumulation of the LHC data. From this cross section ratio measurement alone, a preliminary estimation of the current limit from this interference effect with current 30% precision puts an upper bound of 800 MeV on the Higgs boson total width and the limit improves to 60 MeV with  $3 \text{ ab}^{-1}$  of 14 TeV data [239,240].

### 11.5.3.4 Indirect constraints from off-shell couplings

Using simultaneously on-shell and off-shell measurements in the  $VV$  channels, it was noticed [231,241] that the total width of the Higgs boson could be constrained. This can be illustrated from the parametrisation of the signal strength measurements both on-shell ( $\mu_{\text{on-shell}}$ ) and off-shell ( $\mu_{\text{off-shell}}$ ) as a function of the couplings modifiers  $\kappa_g$  and  $\kappa_V$  parameterising the main process  $gg \rightarrow H \rightarrow VV$  (see Section 11.6.2 for the definition of these coupling modifiers). The on-shell and off-shell signal strengths can be written as:

$$\begin{aligned}\mu_{\text{on-shell}} &= \frac{\kappa_{g,\text{on-shell}}^2 \kappa_{V,\text{on-shell}}^2}{\Gamma_H/\Gamma_{\text{SM}}}, \\ \mu_{\text{off-shell}} &= \kappa_{g,\text{off-shell}}^2 \kappa_{V,\text{off-shell}}^2.\end{aligned}\quad (11.25)$$

A bound on the Higgs boson width can then be obtained from the measurements of the on-shell and off-shell signal strengths. This assumes that no new physics alters the Higgs boson couplings in the off-shell regime, i.e., that the running of its couplings is negligible in the off-shell regime [242,243]. Both ATLAS [233] and CMS [232] have used their off-shell production limits to constrain the width of the Higgs boson.

Both ATLAS and CMS analyses use the kinematic event characteristics to further gain in sensitivity to discriminate between the signal and background. The ATLAS analysis assumed that there are no anomalous couplings of the Higgs boson to vector bosons, and obtains 95% CL observed (expected) upper limit on the total width of  $5.7 \times \Gamma_{\text{SM}}$  ( $9.0 \times \Gamma_{\text{SM}}$ ) with the Run 1 dataset. In the CMS analysis, the observed (expected) limit on the total width is  $6.2 \times \Gamma_{\text{SM}}$  ( $9.8 \times \Gamma_{\text{SM}}$ ) for the  $ZZ$  channel only at Run 1.

In addition, in the CMS analysis, results are also derived allowing for anomalous couplings of the Higgs boson, therefore reducing the discriminating power of the kinematic variables used in the analysis but reducing the model dependence. The observed (expected) limit on the total width is  $10.9 \times \Gamma_{\text{SM}}$  ( $17.4 \times \Gamma_{\text{SM}}$ ).

CMS has also combined the  $ZZ$  and  $W^+W^-$  channels while keeping the gluon-fusion and VBF production processes separate. For the gluon fusion mode, the observed (expected) combined upper limit at the 95% CL on the total width of the Higgs boson is  $2.4 \times \Gamma_{\text{SM}}$  ( $6.2 \times \Gamma_{\text{SM}}$ ) [232], while for the VBF production mode the exclusion limits are  $19.3 \times \Gamma_{\text{SM}}$  ( $34.4 \times \Gamma_{\text{SM}}$ ) [232].

At Run 2, using the ATLAS [234] and CMS [228] analyses described in Section 11.5.2, the following bounds were obtained:

$$(\text{ATLAS}) \quad \Gamma_H/\Gamma_H^{\text{SM}} < 3.5 \quad [3.7 \text{ (exp)}], \quad (11.26)$$

$$\begin{aligned}(\text{CMS}) \quad \Gamma_H &< 9.16 \quad [13.7 \text{ (exp)}] \text{ MeV} \\ \text{or } \Gamma_H \Gamma_H^{\text{SM}} &= 3.2_{-2.2}^{+2.8} \quad [4.1_{-4.0}^{+5.0} \text{ (exp)}].\end{aligned}\quad (11.27)$$

CMS has also performed this analysis considering possible anomalous  $HZZ$  couplings as discussed in Section 11.5.1.4. Neither the results nor the sensitivities are significantly affected by allowing specific anomalous coupling parameters to float in the fits.

ATLAS and CMS have also performed a study of the prospects for measuring the Higgs boson width mainly in the four lepton channel. Projecting to a luminosity of  $3 \text{ ab}^{-1}$ , it was concluded that, within assumptions similar to the ones mentioned above and assuming the SM central value, the observed (expected) combined

upper limit at the 95% CL on the total width of the Higgs boson would be  $3.8 \times \Gamma_{\text{SM}}$  ( $3.4 \times \Gamma_{\text{SM}}$ ), i.e., the width of the Higgs boson could be constrained with the following precision [104]:

$$\Gamma_H = 4.1_{-0.8}^{+0.7} \text{ MeV}. \quad (11.28)$$

## 11.6 Probing the coupling properties of the Higgs boson

As discussed in Section 11.2, within the SM, all the Higgs boson couplings are fixed unambiguously once all the particle masses are known. Any deviation in the measurement of the couplings of the Higgs boson could therefore signal BSM physics.

Measuring the Higgs boson couplings without relying on the SM assumption requires a general framework treating deviations from the SM coherently at the quantum level in order to provide theoretical predictions for relevant observables to be confronted with experimental data. An attempt in that direction has been formalised in the so-called  $\kappa$ -formalism [244], following earlier attempts [245] and initial phenomenological studies of the first hints of the existence of the Higgs boson [246]. In this LO-inspired approach, the SM Higgs boson couplings are rescaled by arbitrary factors,  $\kappa$ 's, keeping the same Lorentz structure of the interactions. This formalism allows for simple interpretation of the signal strengths measured in the various Higgs channels. It has been utilised to test various physics scenarios, like the existence of additional new particles contributing to the radiative Higgs boson production and decays, or to probe various symmetries of the SM itself, as for example the custodial symmetry. It only compares the experimental measurements to their best SM predictions and does not require any new BSM computations per se. And, from a more theoretical perspective, its relevance arises from the fact that it actually fully captures the leading effects in single Higgs processes of well motivated scenarios. Still, the  $\kappa$ -formalism has obvious limitations and certainly does not capture the most general deformations of the SM, even under the assumptions of heavy and decoupling new physics. A particularly acute shortcoming at the time Higgs physics is entering a precision era is the lack of proficiency to assert the richness of kinematical distributions beyond simple signal strength measurements. Several extensions and alternative approaches are being developed as part of the activities of the LHC Higgs Cross Section Working Group [45].

The Higgs Pseudo-Observable (HPO) approach [247] allows one to report the data in terms of a finite set of on-shell form factors parameterising amplitudes of physical processes subject to constraints from Lorentz invariance and other general requirements like analyticity, unitarity, and crossing symmetry. These form factors are expanded in powers of kinematical invariants of the process around the known poles of SM particles, assuming that poles from BSM particles are absent in the relevant energy regime. A set of HPOs have been proposed to characterise both the Higgs boson decays and the EW Higgs boson production channels, thus exploring different kinematical regimes. Prospective studies concluded that these HPOs can be measured/bounded at the percent level at the HL-LHC and could therefore be used to constrain some explicit models of new physics.

Another systematic approach to characterise the possible Higgs boson coupling deviations induced by BSM physics is the use of Effective Field Theories (EFT) [248,249]. This approach assumes again that the new physics degrees of freedom are sufficiently heavy to be integrated out and they give rise to effective interactions among the light SM particles. By construction, the effective Lagrangians cannot account for deviations in Higgs physics induced by light degrees of freedom, unless they are added themselves as extra fields in the effective Lagrangians. In Section 11.7, several examples of models with light degrees of freedom affect-

ing Higgs boson production and decay rates will be presented. The main advantage of EFTs is their prowess to relate different observables in different sectors and at different energies to constrain a finite set of effective interactions among the SM degrees of freedom. In an EFT, the SM Lagrangian is extended by a set of higher-dimensional operators, and it reproduces the low-energy limit of a more fundamental UV description. It will be assumed that the Higgs boson is part of a  $CP$ -even EW doublet,  $\Phi$ , and that the Lagrangian is an analytic function of the gauge invariant  $\Phi^\dagger\Phi$ . This scenario is commonly referred to as SMEFT. Even though it is not fully established experimentally, this set-up is motivated by the measurements of the Higgs couplings to the different SM particles that show an alignment with their masses, such an alignment naturally follows under this assumption of a linear realisation of the  $SU(2)_L \times U(1)_Y$  symmetry of the SM but would require an ad-hoc tuning otherwise. General Lagrangians bypassing this linear assumption have been explicitly written down, see for instance Ref. [250]. They rely on a chiral expansion with a specific power-counting, effectively resumming the expansion in powers of the Higgs field, usually referred to as HEFT as opposed to SMEFT.

### 11.6.1 Effective Lagrangian framework

The SMEFT has the same field content and it respects the same linearly-realised  $SU(3)_C \times SU(2)_L \times U(1)_Y$  local symmetry as the SM. The difference is the presence of operators with canonical mass-dimension  $d$  larger than 4. These are organised in a systematic expansion in  $d$ , where each consecutive term is suppressed by a larger power of a high mass scale. Assuming baryon and lepton number conservation, the most general Lagrangian takes the form

$$\mathcal{L}_{\text{eff}} = \mathcal{L}_{\text{SM}} + \sum_i c_i^{(6)} \mathcal{O}_i^{(6)} + \sum_j c_j^{(8)} \mathcal{O}_j^{(8)} + \dots \quad (11.29)$$

The contribution of the higher order operators of dimension  $d$  to physical amplitudes is suppressed by  $(E/\Lambda)^{d-4}$ , where  $E$  is the relevant energy scale of the process and  $\Lambda$  is the energy scale suppressing the higher-dimensional operators. The Wilson coefficients  $c_i^{(d)}$  encode the virtual effects of the heavy new physics in low-energy observables. Their precise forms in terms of masses and couplings of the new particles can be obtained via matching with the ultraviolet (UV) completion of the SM, see, e.g., Ref. [251], or inferred using specific power-counting rules [248, 252].

The list of dimension-6 operators was first classified in a systematic way in Ref. [253] after the works of Ref. [254]. Subsequent analyses pointed out the presence of redundant operators, and a minimal and complete list of operators was finally provided in Ref. [255]<sup>4</sup>. For a single family of fermions, there are 76 real ways to deform the SM generated by 59 independent operators. With the 3 families of fermions of the SM, flavour indices can be added to these 59 operators, and furthermore, new operator structures, that have been dismissed by means of Fierz transformations in the single family case, have to be considered, for a total of 2499 real deformations [258]. When considering Higgs data, one can reasonably focus on a relatively small subset of the 2499 operators of dimension 6. In particular the vast subset of 4-fermion operators, whether flavour and  $CP$  preserving or not, can be more strongly constrained by other processes. Thus, it makes sense to neglect this whole class, with the exception of one particular four-fermion interaction that contributes to the muon decay and thus directly affects the Fermi constant. The dipole operators, instead do directly affect Higgs boson production, however, under very general and plausible assumptions on the flavour structure of new physics, the coefficients of these operators display the same structure and the same chiral suppression of the Yukawa couplings. The consequence is that, with the possible exception of processes involving the top quark, their effect in Higgs boson production is expected to be negligible. Furthermore, as far as Higgs boson decays

are concerned, the dipole operators only contribute to three (or more)-body final states (for instance  $H \rightarrow b\bar{b}\gamma$ ) and as such they can easily be neglected too. Eliminating these two classes, there remain three other classes: 1) purely bosonic operators, 2) generalised Yukawas, 3) Higgs-fermion current operators. Operators in class 2 and 3, per se, can still contain  $CP$ - or flavour-violating terms, on which experimental constraints are rather strong. Under the assumption of flavour universality (respectively diagonality), one is left with 12 (14) parameters affecting EW precision measurements, diboson processes and single- and double-Higgs data and 7 (17) other parameters modifying the EW gauge boson couplings to fermions, see Ref. [44] for further technical details. Working in the unitary gauge and performing suitable redefinition of fields and input parameters the effective Lagrangian can be conveniently expressed in the parameterisation of Ref. [259], the so-called *Higgs basis* that conveniently single out these special less constrained parameters. Such a classification reflects the current experimental situation and the hierarchy in the sensitivity of the experimental measurements in the various sectors of the SM. As the sensitivity of the measurements in the Higgs sector improves, another and more general parametrisation of the SM deformation will have to be retained, in particular a parametrisation more suited for a treatment at the quantum level. In other bases of operators, in particular the so-called Warsaw basis [255] used in some experimental EFT analyses [128, 260, 261], one finds strong correlations among the operators affecting the EW gauge couplings to fermions, leaving 12 (14) linear combinations of operators with weaker constraints.

Section 11.6.2 illustrates how the Higgs data accumulated at the LHC can (partially) constrain the SM deformations, i.e., the dimension-6 operators of the SEMFT Lagrangian. Automatic tools are being developed to analyse the experimental data within an EFT framework, see the report [262] and references therein.

### 11.6.2 Probing coupling properties

As described in Section 11.3, a framework was developed by ATLAS and CMS [141], individually and together, to combine the very large number of exclusive categories aimed at reconstructing the five main decay modes and the five main production modes of the Higgs boson. The general conclusion of this combination, illustrating the compatibility of the observation with the SM expectations, is given in Section 11.3. The same framework with its master formula, Eq. (11.16), can be used to further measure coupling properties of the Higgs boson under specific additional assumptions.

#### 11.6.2.1 Combined measurements of the Higgs boson coupling properties

##### i. From effective Lagrangians to Higgs observables

The  $\kappa$  framework, described in detail in Ref. [43, 244], facilitates the characterisation of Higgs coupling properties in terms of a series of Higgs coupling strength modifier parameters  $\kappa_i$ , which are defined as the ratios of the couplings of the Higgs bosons to particles  $i$  to their corresponding SM values. The  $\kappa$  framework assumes a single narrow resonance so that the zero-width approximation can be used to decompose the cross section as a product of two factors characterising the production and the decay of the Higgs boson. The  $\kappa$  parameters are introduced by expressing each of these factors as their SM expectation multiplied by the square of a coupling strength modifier for the corresponding process at leading order:

$$\begin{aligned} (\sigma \cdot \text{BR})(i \rightarrow H \rightarrow f) &= \frac{\sigma_i^{\text{SM}} \kappa_i^2 \cdot \Gamma_f^{\text{SM}} \kappa_f^2}{\Gamma_H^{\text{SM}} \kappa_H^2} \rightarrow \\ &\rightarrow \mu_i^f \equiv \frac{\sigma \cdot \text{BR}}{\sigma_{\text{SM}} \cdot \text{BR}_{\text{SM}}} = \frac{\kappa_i^2 \cdot \kappa_f^2}{\kappa_H^2}, \end{aligned} \quad (11.30)$$

where  $\mu_i^f$  is the rate relative to the SM expectation and  $\kappa_H^2$  is an expression that adjusts the SM Higgs width to take into account the modifications induced by the deformed Higgs boson couplings. When all  $\kappa_i$  are set to 1, the SM is reproduced. For loop-induced processes, e.g.  $H \rightarrow \gamma\gamma$ , there is a choice of either resolving the coupling strength modification in its SM expectation,

<sup>4</sup>Complete enumerations of  $d=8$  operators have been obtained [256] and some preliminary constraints on peculiar subsets of these operators have been derived from experimental measurements [257]. Still, in this review, the EFT Lagrangians will be truncated at the level of dimension-6 operators.

i.e.,  $\kappa_\gamma(\kappa_t, \kappa_W)$  or keeping  $\kappa_\gamma$  as an effective coupling strength parameter.

The  $\kappa$ -framework is the simplest parametrisation directly related to experimental measurements of the Higgs boson production and decay modes. For this reason, it has been widely used by the community. It can also be connected to the SMEFT formalism as follows. Restricting to the EFT directions not probed outside Higgs physics [263], the Higgs boson couplings are written in the unitary gauge as:

$$\begin{aligned} \mathcal{L} = & \kappa_Z \frac{m_Z^2}{v} Z_\mu Z^\mu H + \kappa_W \frac{2m_W^2}{v} W_\mu^+ W^{-\mu} H \\ & + \kappa_{VV} \frac{\alpha}{2\pi v} \left( \cos^2 \theta_W Z_{\mu\nu} Z^{\mu\nu} + 2W_{\mu\nu}^+ W^{-\mu\nu} \right) H \\ & + \kappa_g \frac{\alpha_s}{12\pi v} G_{\mu\nu}^a G^{a\mu\nu} H + \kappa_\gamma \frac{\alpha}{2\pi v} A_{\mu\nu} A^{\mu\nu} H + \kappa_{Z\gamma} \frac{\alpha}{\pi v} A_{\mu\nu} Z^{\mu\nu} H \\ & + \kappa_3 \frac{m_H^2}{2v} H^3 \\ & - \left( \kappa_t \sum_{f=u,c,t} \frac{m_f}{v} + \kappa_b \sum_{f=d,s,b} \frac{m_f}{v} + \kappa_\tau \sum_{f=e,\mu,\tau} \frac{m_f}{v} \right) f\bar{f}H. \end{aligned} \quad (11.31)$$

The exact correspondence between the effective coefficients of the dimension-6 operators and the  $\kappa$ 's can be found for instance in Ref. [44]. In the SM, the Higgs boson does not couple to massless gauge bosons at tree level, hence  $\kappa_g = \kappa_\gamma = \kappa_{Z\gamma} = 0$ . Nonetheless, the contact operators are generated radiatively by SM particles loops. In particular, the top quark gives a contribution to the 3 coefficients  $\kappa_g, \kappa_\gamma, \kappa_{Z\gamma}$  that does not decouple in the infinite top mass limit. For instance, in that limit  $\kappa_\gamma = \kappa_g = 1$  [23, 24, 264].

The coefficient for the contact interactions of the Higgs boson to the  $W$  and  $Z$  field strengths is not independent but obeys the relation

$$(1 - \cos^4 \theta_W) \kappa_{VV} = \sin 2\theta_W \kappa_{Z\gamma} + \sin^2 \theta_W \kappa_{\gamma\gamma}. \quad (11.32)$$

This relation is a general consequence of the custodial symmetry [265], which also imposes  $\kappa_Z = \kappa_W$  at leading order ( $\kappa_Z/\kappa_W - 1$  is a measure of custodial symmetry breaking and, as such, is already constrained by electroweak precision data and the bounds on anomalous gauge couplings). When the Higgs boson is part of a  $SU(2)_L$  doublet, the custodial symmetry in the bosonic sector could only be broken by the  $\mathcal{O}_T = \frac{1}{2} (\Phi^\dagger \overleftrightarrow{D}^\mu \Phi)^2$  operator at the level of dimension-6 operators and it is accidentally realised among the interactions with four derivatives, like the contact interactions considered.

The coefficient  $\kappa_3$  can be accessed directly only through double Higgs boson production processes, hence it will remain largely unconstrained at the LHC. Before the associated production of a Higgs boson with a pair of top quarks was observed, the Higgs boson coupling to the top quark was only probed indirectly via the one-loop gluon fusion production or the radiative decay into two photons. However, these two processes are only sensitive to the combinations of couplings ( $\kappa_t + \kappa_g$ ) and ( $\kappa_t + \kappa_\gamma$ ) and not to the individual couplings. Therefore a deviation in the Higgs boson coupling to the top quark can in principle always be masked by new contact interactions to photons and gluons (and this is precisely what is happening in minimal incarnations of composite Higgs models [266]). The current and still limited sensitivity, of the order of 20%, in the  $t\bar{t}H$  channel leaves elongated ellipses in the direction  $\kappa_g = \kappa_\gamma = 1 - \kappa_t$ .

The operators already bounded by EW precision data and the limits on anomalous gauge couplings modify in general the Lorentz structure of the Higgs couplings and hence induce some modifications of the kinematical differential distributions [267]. A promising way to have a direct access to the effective coefficients of these operators in Higgs physics is to study the  $VH$  associated production with a  $W$  or a  $Z$  at large invariant mass of the  $VH$  system [268]. These differential distributions could also be a way to test the hypothesis that the Higgs boson belongs to a  $SU(2)_L$  doublet together with the longitudinal components of the massive electroweak gauge bosons.

## ii. Interpretations of the experimental data

The measurements of the coupling properties of the Higgs boson are entirely based on the formalism of the effective Lagrangian described above. Measurements of coupling properties in this framework implies assessing the parameters of the model Eq. (11.31) or combinations of these parameters with different sets of assumptions.

These measurements are carried out with the combination framework described in Section 11.4, where the  $\mu_i$  and  $\mu_f$  signal strength parameters are further interpreted in terms of modifiers of the SM couplings  $\kappa_k$  where  $k \in \{Z, W, f, g, \gamma, Z\gamma\}$  as in Eq. (11.31). The number of signal events per category for the various production modes are typically estimated at higher orders in the analyses but are scaled by these single LO-inspired factors, thus not taking into account possible intricacies and correlations of these parameters through the higher-order corrections. This approximation is valid within the level of precision of current results and their compatibility with the SM expectation.

In this formalism, further assumptions are explicitly made: (i) the signals observed in the different search channels originate from a single narrow resonance with a mass of 125 GeV; (ii) similarly to the combination described in Section 11.4, the narrow width approximation is assumed (to allow the decomposition of signal yields into products of production and decay signal strengths); (iii) the tensor structure of the couplings is assumed to be the same as that of a SM Higgs boson. This means in particular that the observed state is assumed to be a  $CP$ -even scalar as in the SM.

Loop-level couplings such as the  $gg \rightarrow H$ ,  $H \rightarrow \gamma\gamma$  and  $H \rightarrow Z\gamma$  can either be treated effectively, with  $\kappa_g, \kappa_\gamma$  and  $\kappa_{Z\gamma}$  as free parameters in the fit or these parameters can be expressed in terms of the know SM field content and as a function of the SM coupling modifiers, in the following way [269]:

$$\begin{aligned} \kappa_g^2(\kappa_t, \kappa_b, \kappa_c) = & 1.042 \kappa_t^2 - 0.040 \kappa_t \kappa_b + 0.002 \kappa_b^2 \\ & - 0.005 \kappa_t \kappa_c + 0.0005 \kappa_b \kappa_c + 0.00002 \kappa_c^2, \\ \kappa_\gamma^2(\kappa_F, \kappa_V) = & 1.59 \kappa_V^2 - 0.66 \kappa_V \kappa_F + 0.07 \kappa_F^2, \\ \kappa_{Z\gamma}^2(\kappa_F, \kappa_V) = & 1.12 \kappa_V^2 - 0.15 \kappa_V \kappa_F + 0.03 \kappa_F^2. \end{aligned} \quad (11.33)$$

The  $\kappa_{Z\gamma}$  parametrisation has been used only in the ATLAS Run 1 combined measurements of the coupling properties of the Higgs boson. The  $\mu^+\mu^-$  channels is included neither in the CMS and ATLAS-CMS Run 1 combinations, nor in the ATLAS [213] Run 2 individual combination, while it is included in the CMS [214] Run 2 combination.

The parametrisations are given for a Higgs boson mass hypothesis of 125.09 GeV (and in the last two expressions, all the Higgs-fermion couplings are assumed to be rescaled by an universal multiplicative factor  $\kappa_F$ ). It can be noted from the expression of  $\kappa_\gamma$  that the coupling of the Higgs boson to photons is dominated by the loop of  $W$  bosons, and it is affected by the top quark loop mostly through its interference with the  $W$  loop. The sensitivity of the current measurements to the relative sign of the fermion and vector boson couplings to the Higgs boson is due to this large negative interference term. The  $\kappa_g$  parameter is expressed in terms of the scaling of production cross sections and therefore also depends on the  $pp$  collisions centre-of-mass energy. The parametrisations of  $\kappa_\gamma$  and  $\kappa_{Z\gamma}$  are obtained from the scaling of partial widths and are only dependent on the Higgs boson mass hypothesis. Experiments use a more complete parametrisation with the contributions from the  $b$ -quarks,  $\tau$ -leptons in the loops [43, 244].

The global fit is then performed expressing the  $\mu_i$  and  $\mu_f$  parameters in terms of a limited number of  $\kappa_k$  parameters or their ratios, under various assumptions. The parametrisation for the main production modes are: (i)  $\mu_{\text{ggF}} = \kappa_g^2$  for the gluon fusion and an effective coupling of the Higgs boson to the gluons; (ii)  $\mu_{\text{VBF}, VH} = \kappa_V^2$  for the VBF and  $VH$  processes when the  $W$  and  $Z$  couplings are assumed to scale equally, and  $\mu_{\text{VBF}}^2(\kappa_W, \kappa_Z) = (\kappa_W^2 \sigma_{WWH} + \kappa_Z^2 \sigma_{ZZH}) / (\sigma_{WWH} + \sigma_{ZZH})$ , when the couplings to the  $W$  and  $Z$  bosons are varied independently ( $\sigma_{WWH}$  and

$\sigma_{ZZH}$  denote the VBF cross sections via the fusion of a  $W$  and a  $Z$  boson respectively, the small interference term is neglected); (iii)  $\mu_{t\bar{t}H} = \kappa_t^2$  for the  $t\bar{t}H$  production mode. Numerically the production modes signal strengths as a function of the coupling modifiers to the SM fields are:

$$\begin{aligned}\mu_{\text{ggF}} &= 1.06\kappa_t^2 + 0.01\kappa_b^2 - 0.07\kappa_t\kappa_b, \quad \text{and} \\ \mu_{\text{VBF}} &= 0.74\kappa_W^2 + 0.26\kappa_Z^2.\end{aligned}\quad (11.34)$$

The decay mode signal strengths are parametrised as  $\mu_k = \kappa_k^2/\kappa_H^2$  where  $k \in \{Z, W, f, g, \gamma, Z\gamma\}$  denotes the decay mode and  $\kappa_H$ , the overall modifier of the total width that affects all the signal yields.  $\kappa_H$  is a priori an independent parameter. However, when it is assumed that the Higgs boson cannot decay to new particles beyond those of the SM,  $\kappa_H$  can also be treated as an effective parameter and expressed in terms of the coupling modifiers to the SM field content. Its general expression is:

$$\begin{aligned}\kappa_H^2 &= 0.57\kappa_b^2 + 0.06\kappa_\tau^2 + 0.03\kappa_c^2 + 0.22\kappa_W^2 + 0.03\kappa_Z^2 + 0.09\kappa_g^2 \\ &\quad + 0.0023\kappa_\gamma^2.\end{aligned}\quad (11.35)$$

The general expression of the total width of the Higgs boson can be written as follows:

$$\Gamma_H = \frac{\kappa_H^2 \Gamma_H^{\text{SM}}}{1 - \text{BR}_{\text{BSM}}}\quad (11.36)$$

where  $\Gamma_H^{\text{SM}}$  is the total width of the SM Higgs boson and  $\text{BR}_{\text{BSM}}$  is the branching fraction of the Higgs boson to new particles beyond the SM.

Specific parametrisations will be made in order to address the following aspects of the coupling properties of the Higgs boson under different assumptions: (i) the relative couplings of the Higgs boson to fermions and bosons; (ii) the potential impact of the presence of new particles beyond the SM either in the loops or both in the loops and the decay of the  $H$ ; and (iii) also, more general models either of coupling modifiers or their ratios, under different assumptions.

### iii. Couplings to bosons and fermions

As it will be discussed in Section 11.7.6.3, it is interesting to probe a model where no additional field content is considered in the decay width of the Higgs boson and where the relative couplings of the Higgs boson to  $W$ - and  $Z$ -bosons is fixed to its SM value, i.e.,  $\kappa_W = \kappa_Z$ , and where all Yukawa couplings scale with one coupling modifier. In this model, only the SM particles are assumed to contribute to the gluon fusion and the diphoton loops, and all fermion couplings modifiers are required to scale simultaneously with a unique factor  $\kappa_F$  while all vector boson couplings modifiers also scale with a common factor  $\kappa_V$ . It is a two-parameter fit with  $\kappa_V$  and  $\kappa_F$  as free variables of interest. The ATLAS-CMS combined results for each channel independently, the combinations of all channels for the two experiments separately and the results of the overall combination are all shown in Fig. 11.12.

The global fit is only sensitive to the relative sign of  $\kappa_V$  and  $\kappa_F$ . By convention, either  $\kappa_F$  or  $\kappa_V$  can be considered positive and negative values of  $\kappa_V$  or  $\kappa_F$  respectively can be considered. Such values are not excluded a priori, but would imply the existence of new physics at a light scale and would also raise questions about the validity of the perturbative treatment of the SM deformations and also about the stability of the vacuum [271]. Among the five main Higgs boson decay channels, only the  $\gamma\gamma$  is sensitive to the sign of  $\kappa_F$  (or  $\kappa_V$ ) through the interference of the  $W$  and  $t$  loops as shown in Eq. (11.33). The current global fit disfavors a negative value of  $\kappa_F$  at more than five standard deviations. A specific analysis for the Higgs boson production in association with a single top quark has been proposed in order to more directly probe the sign of  $\kappa_F$  (see references in Ref. [123]). All available experimental data show a fair agreement of the SM prediction of the couplings of the Higgs boson to fermions and gauge bosons. The results shown in Fig. 11.12 assume that  $\kappa_F \geq 0$ , however, in Ref. [141], a similar combination is done without this assumption.

The observed exclusion is fully compatible with the SM expectation. The ATLAS and CMS combined measurements with the Run 1 dataset lead to

$$\kappa_V = 1.04 \pm 0.05 \quad \text{and} \quad \kappa_F = 0.98_{-0.10}^{+0.11}, \quad (11.37)$$

and were already at an impressive 5% level of accuracy for the  $\kappa_V$  parameter. The ATLAS Run 2 combination yielded:

$$\kappa_V = 1.05 \pm 0.04 \quad \text{and} \quad \kappa_F = 1.05 \pm 0.09. \quad (11.38)$$

And the results for the CMS Run 2 are reported as likelihood contours shown in Fig. 11.12.

### iv. Probing new physics in the loops (and the decay)

A more constrained model fully focussing on BSM scenarios with new heavy particles contributing to the loops and where all couplings to the SM particles are assumed to be the same as in the SM ( $\kappa_W = \kappa_Z = \kappa_t = \kappa_b = \kappa_\tau = 1$ ) is also used to constrain the  $\kappa_g$  and  $\kappa_\gamma$  parameters only. In this model, it can be assumed that the new physics affecting the loops are either introducing new decay channels (i.e.,  $\text{BR}_{\text{BSM}}$  allowed to vary in the fit) or not (i.e.,  $\text{BR}_{\text{BSM}} = 0$ ). In the two cases, the results on the couplings through loops (to gluons and photons) do not change significantly. The constraints on  $\text{BR}_{\text{BSM}}$  will be discussed in the next section, while here the focus will be on the effective couplings of the Higgs boson to gluons and photons. The contours of the combined likelihood in the  $(\kappa_\gamma, \kappa_g)$  plane for the ATLAS and CMS experiments and their combination are shown in Fig. 11.13. The measured values of these parameters for the ATLAS and CMS Run 1 combination are:

$$\kappa_g = 0.78_{-0.10}^{+0.13} \quad \text{and} \quad \kappa_\gamma = 0.87_{-0.09}^{+0.14}. \quad (11.39)$$

At Run 2, the ATLAS combination yielded:

$$\kappa_g = 1.03_{-0.06}^{+0.07} \quad \text{and} \quad \kappa_\gamma = 1.00 \pm 0.06. \quad (11.40)$$

The CMS results are reported as likelihood contours in the  $(\kappa_g, \kappa_\gamma)$  plane only, as shown in Fig. 11.13.

In this model as well, all results are fully compatible with the SM expectations.

### v. Coupling measurements and probing BSM physics in loops and in the decay

In the models described above, it was either assumed that no new latent BSM degree of freedom distorts neither the loop-induced Higgs boson couplings to gluons and photons nor the total Higgs boson width, or that all tree level couplings to SM particles are SM-like. These assumptions can be relaxed.

In order to probe simultaneously the Higgs boson couplings to massive and massless particles, only the assumption  $\text{BR}_{\text{BSM}} = 0$  is kept. The couplings to photons and gluons are then parametrised by independent effective couplings,  $\kappa_g$  and  $\kappa_\gamma$ , and  $\kappa_Z$ ,  $\kappa_W$ ,  $\kappa_t$ ,  $|\kappa_\tau|$ , and  $|\kappa_b|$  are measured simultaneously. The absolute values of certain coupling modifiers only indicate the degeneracy of combined likelihood for the two signs. It can be noted that when the coupling to gluons is not considered effective, there is some sensitivity to the sign of  $\kappa_b$  through the interference between the top- and bottom-quark loops in the gluon fusion process. In this analysis, the constraint on the top quark Yukawa coupling comes from the  $t\bar{t}H$  direct search channels only. The complete set of results from this model is given in Table 11.12 for the ATLAS-CMS combination using the full Run 1 dataset [270] and for the ATLAS [213] and CMS [214] individual combinations using partial Run 2 datasets. Figure 11.14 also displays the results of the individual ATLAS and CMS combinations. A negative relative sign is allowed for the  $\kappa_W$  and  $\kappa_Z$  parameters without loss of generality. This convention is used in the ATLAS and CMS Run 1 combination and in the CMS Run 2 combination. Neglecting the very small interference between the  $W$  and  $Z$  exchanges in the VBF production and when treating the photon and gluon couplings as effective, the sensitivity to the negative signs of the

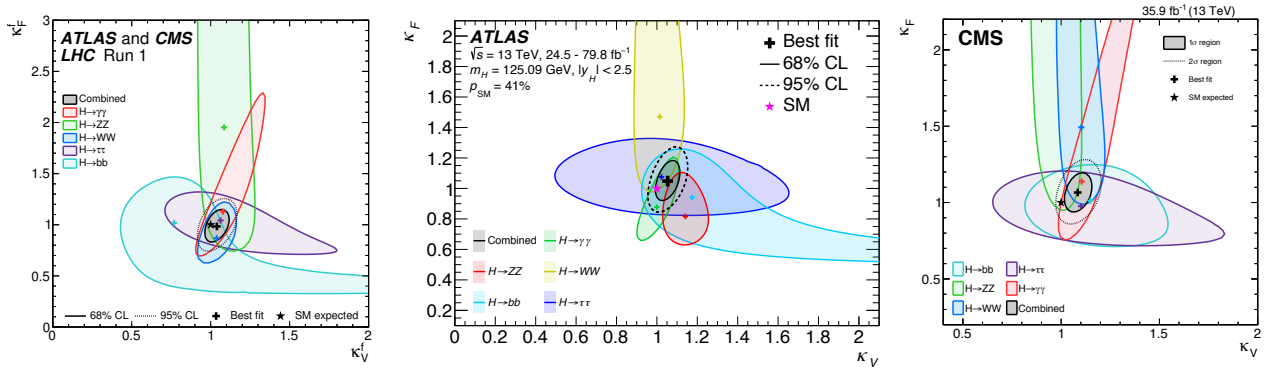


Figure 11.12: Likelihood contours in the  $(\kappa_F, \kappa_V)$  plane for the ATLAS-CMS Run 1 combination [270] (left) and the ATLAS [213] (center) and CMS [214] (right) individual Run 2 combinations.

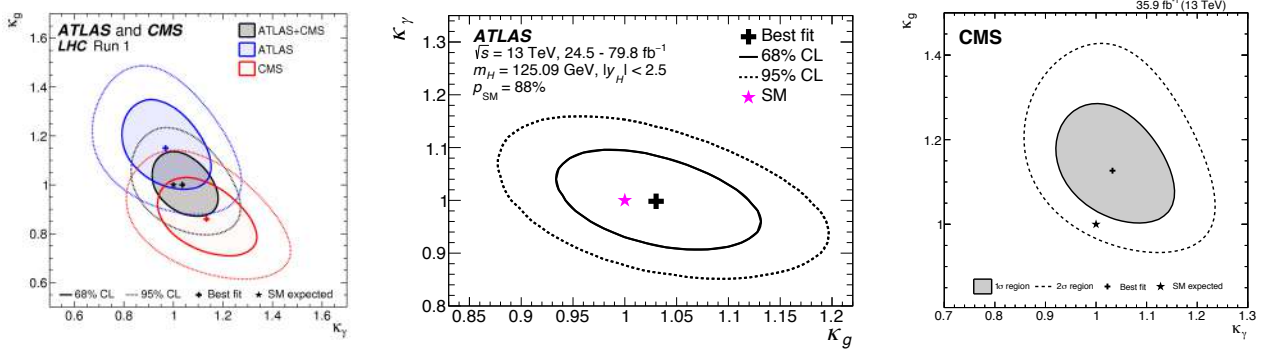


Figure 11.13: Likelihood contours in the  $(\kappa_g, \kappa_\gamma)$  plane for the ATLAS-CMS [270] combination (left) and for the ATLAS [213] (center) and CMS [214] (right) individual Run 2 combinations.

couplings of the Higgs boson to the  $W$  and the top quark and that of the  $Z$  to the gluon come respectively from the  $tH$  and the  $ggHZ$  production processes. In the case of the ATLAS Run 2 combination, only a relative negative sign of the coupling of the Higgs boson to the top quark is allowed. The cases reported in Table 11.12 of negative values of the couplings correspond to *quasi*-degenerate cases and the choice of sign is therefore not significant. For instance, the negative value of  $\kappa_W$  obtained by CMS in its Run 2 combination is due to  $tH$  contribution to the  $t\bar{t}H$  channels as the specific  $tH$  analyses described in Section 11.3.3 are not included in the combination.

It is interesting to note that, with a partial Run 2 dataset, the sensitivity of individual experiments is already better than the one obtained at Run 1. This is in large part due to the improved systematic uncertainties related to the predictions of the Higgs boson production and decay that have been discussed in Section 11.2.

The results above are obtained under the assumption that the Higgs boson decays only to SM particles. This assumption is necessary since the signal rates cannot resolve separately  $\kappa_H$  and the absolute couplings of the Higgs boson to the SM particles. This degeneracy can, however, be resolved using an independent constraint on the Higgs boson width as the one derived from off-shell couplings measurements. This approach was used by the ATLAS experiment (see references in Ref. [123]), thus yielding a priori an absolute measurement of the couplings of the Higgs boson. The validity of the results obtained still relies on assumptions that have been discussed in Section 11.5.2. Another well-motivated assumption to resolve the aforementioned degeneracy preventing the determination of  $\kappa_H$  is inspired by unitarity conditions. Requiring that  $\kappa_V \leq 1$  allows to free the  $\text{BR}_{\text{BSM}}$  parameter and further probe new physics in the decay of the Higgs boson. An intuitive understanding of how this constraint works can be given by a simple example. In the VBF  $H \rightarrow W^+W^-$  channel, the number of signal events compared to the SM prediction is rescaled by  $(1 - \text{BR}_{\text{BSM}})\kappa_W^4/\kappa_H^2$ , and, an observed signal close to the SM expectation cannot accommodate a large value of

$\text{BR}_{\text{BSM}}$  since the depletion factor  $(1 - \text{BR}_{\text{BSM}})$  cannot be compensated by an enhanced value  $\kappa_W > 1$ . Or, in other terms, if  $\kappa_W \sim 1$  is preferred from other channels, a low signal in the VBF  $H \rightarrow W^+W^-$  channel would be a sign of the presence of BSM physics in the Higgs boson decays. Within this framework, all the Higgs boson couplings to massive and massless SM particles can be measured in addition to  $\text{BR}_{\text{BSM}}$ . The results of this combination are shown in Fig. 11.14 (left). The results for all parameters do not change significantly with respect to the previous fit that assumed  $\text{BR}_{\text{BSM}} = 0$ . But a 95% CL bound on this parameter can now be obtained:

$$\text{BR}_{\text{BSM}} < 34\% \text{ (ATLAS)}, \quad \text{BR}_{\text{BSM}} < 38\% \text{ (CMS)}. \quad (11.41)$$

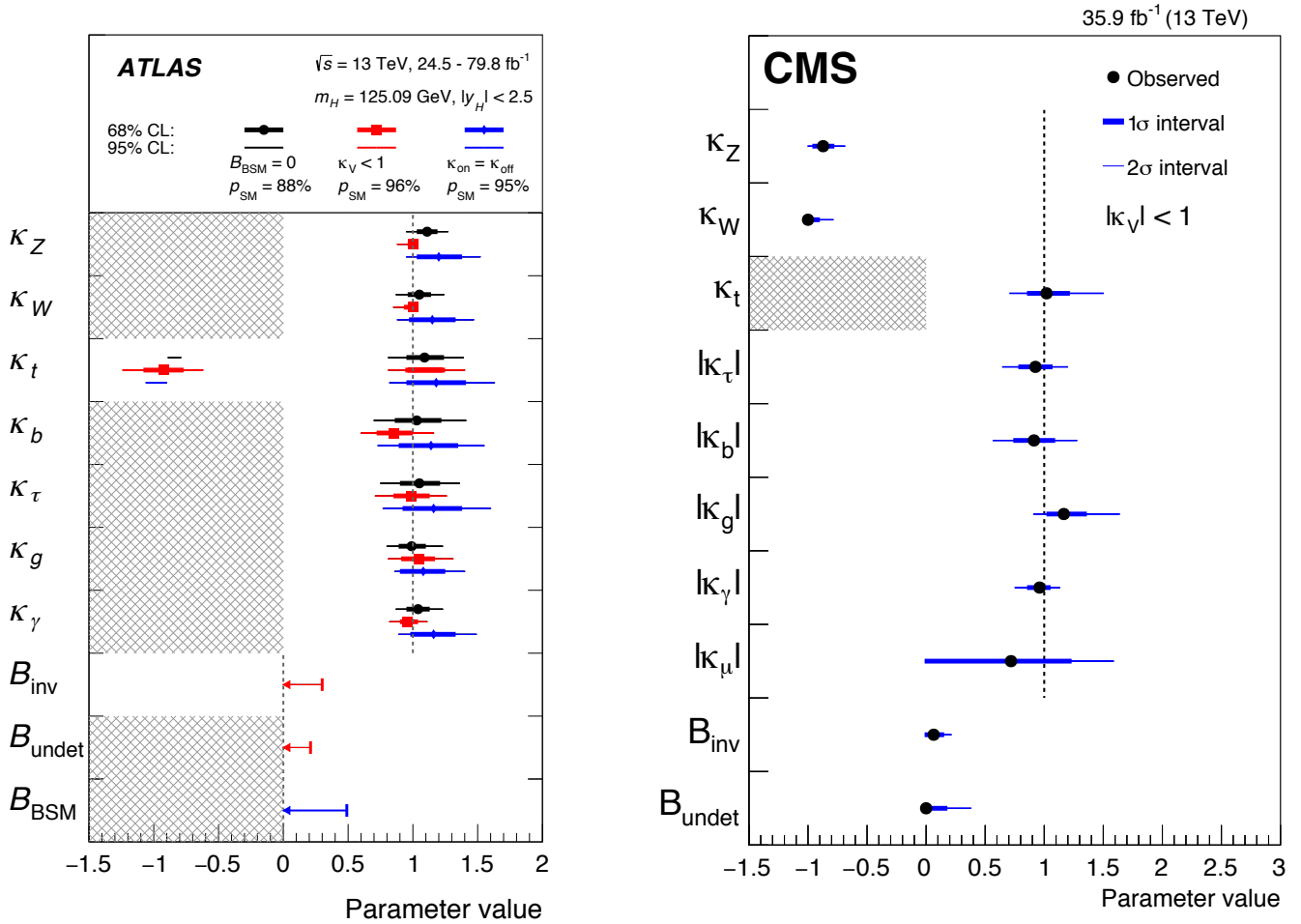
Both ATLAS and CMS in their Run 2 combinations have included the search for invisible decays of the Higgs boson [213,214], described in Section 11.3. This allows for a coherent interpretation of the constraints on invisible decays and the measurements in the visible channels as well as simultaneously constraining  $\text{BR}_{\text{inv}}$  and the overall branching fraction to potentially “visible” particles but to which none of the considered measurements are sensitive, as for example Higgs boson decays to light quarks or BSM particles decaying subsequently mainly to light quarks ( $\text{BR}_{\text{und}}$  referred to as branching fraction to undetected particles). The limits obtained on the invisible branching fractions are:

$$\text{BR}_{\text{inv}} < 30\% \text{ (ATLAS)}, \quad \text{BR}_{\text{inv}} < 22\% \text{ (CMS)}. \quad (11.42)$$

Models which are less sensitive to modelling systematic uncertainties and requiring no constraints on the natural width of the Higgs bosons have been considered, either through the ratio of cross section and branching ratios (see results in Ref. [123]) or through a more generic approach to avoid the degeneracy in the measurement of the coupling modifiers, probing the coupling properties of the Higgs boson through ratio of couplings. In the latter model, the cross section times branching fraction of the  $gg \rightarrow H \rightarrow ZZ$  process is parametrised as a function of a single

**Table 11.12:** Coupling modifier combined measurements assuming the absence of perceptible new physics in the decay of the Higgs boson. No assumption is made for the loop level couplings of the Higgs boson to gluons and photons which are considered as effective.

	LHC Run 1	ATLAS Run 2	CMS Run 2	HL-LHC (expected)
$\kappa_\gamma$	$0.87^{+0.14}_{-0.09}$	$1.05 \pm 0.09$	$1.07^{+0.10+0.09}_{-0.14-0.05}$	1.8%
$\kappa_W$	$0.87^{+0.13}_{-0.09}$	$1.05 \pm 0.09$	$-1.13^{+0.15+0.06}_{-0.10-0.08}$	1.7%
$\kappa_Z$	$-0.98 \pm 0.10$	$1.11 \pm 0.08$	$1.00^{+0.09+0.06}_{-0.09-0.07}$	1.5%
$\kappa_g$	$0.78^{+0.13}_{-0.10}$	$0.99^{+0.11}_{-0.10}$	$1.18^{+0.10+0.12}_{-0.09-0.10}$	2.5%
$\kappa_t$	$1.40^{+0.24}_{-0.21}$	$1.09^{+0.15}_{-0.14}$	$0.98^{+0.08+0.12}_{-0.08-0.11}$	3.4%
$\kappa_b$	$0.49^{+0.27}_{-0.15}$	$1.03^{+0.19}_{-0.18}$	$1.17^{+0.18+0.20}_{-0.29-0.10}$	3.7%
$\kappa_\tau$	$0.84^{+0.15}_{-0.11}$	$1.05^{+0.16}_{-0.15}$	$0.80^{+0.56+0.17}_{-0.81-0.00}$	1.9%

Figure 11.14: ATLAS [213] (left) and CMS [214] (right) combined measurements of coupling modifiers in the  $\kappa_V < 1$  scenario, and in the case of the ATLAS measurements with the assumption  $\text{BR}_{\text{BSM}} = 0$  and using the off-shell Higgs measurements.

coupling modifier:

$$\kappa_{gZ} = \kappa_g \times \frac{\kappa_Z}{\kappa_H} \quad (11.43)$$

Then all combination signals can be parametrised with the following ratios of coupling modifiers: (i) the  $\lambda_{Zg} = \kappa_Z/\kappa_g$  ratio which is mainly probed by the measurements of the VBF and  $ZH$  production; (ii) the  $\lambda_{tg} = \kappa_t/\kappa_g$  ratio constrained by the  $t\bar{t}H$  production process; (iii) the  $\lambda_{WZ} = \kappa_W/\kappa_Z$  ratio mainly probed by the  $WW$  and  $ZZ$  decay modes; (iv) the  $\lambda_{\tau Z} = \kappa_\tau/\kappa_Z$  ratio constrained by the  $\tau^+\tau^-$  channel; (v) the  $\lambda_{bZ} = \kappa_b/\kappa_Z$  ratio probed mainly by the  $VH(b\bar{b})$  channels; and (vi) the  $\lambda_{\gamma Z} = \kappa_\gamma/\kappa_Z$  ratio constrained by the diphoton channel. In this parametrisation, the

$ZZ$  channel plays an important normalisation role (the results are discussed in detail in the previous edition of this review [123]).

#### 11.6.2.2 Differential cross sections

To further characterise the production and decay properties of the Higgs boson, with the increase in size of the LHC datasets, measurements of fiducial and differential cross sections are being carried out by ATLAS and CMS both at Run 1 (the references can be found in the previous edition of this review [123]) and Run 2 [260, 272] and in several channels: (i) the diphoton, (ii) the four leptons, and (iii) the  $WW$  channels.

The definition of a fiducial volume as close as possible to the reconstruction level selection criteria is very important as it will



minimise the model dependence from possible variations in the signal reconstruction efficiencies. Minimising model dependence of unfolded fiducial differential cross section measurements is also key to ensure their usefulness to further probe and tune more accurate models in the future.

As an example in the diphoton channel for the ATLAS Run 1 analysis (similar criteria are used at Run 2 and by CMS), the selection criteria defining the fiducial volume are the following: the two highest transverse momentum ( $E_T$ ), isolated final state photons, within  $|\eta| < 2.37$  and with  $105 \text{ GeV} < M_{\gamma\gamma} < 160 \text{ GeV}$  are selected (the transition region between the barrel and end-cap calorimeters is not removed); after the pair is selected, the same cut on  $E_T/M_{\gamma\gamma}$  as in the event selection, i.e., in excess of 0.35 (0.25) for the two photons is applied. The requirement of the isolation of the photon to define the fiducial volume is particularly important to avoid potentially large variations of the reconstruction efficiency within this volume for production processes as different as the gluon fusion and  $t\bar{t}H$ .

While strict fiducial requirements are key to minimise model dependence, these make combinations of decay channels impossible. To gain precision in the measurement of the production properties of the Higgs boson, the fiducial volume defined on the decay products of the Higgs boson can be removed and channels can be combined relying on the extrapolation from the reconstruction acceptance using Monte Carlo simulations. This has been used to combine differential cross section for instance in the transverse momentum of the Higgs boson. Such hybrid approaches are also discussed in Section 11.6.2.4.

A large number of observables have been studied aiming at probing the accuracy of the modelling of the Higgs boson production simulations. Some examples include (i) the transverse momentum and pseudo rapidity of the objects, such as jets or leptons, produced in association with the Higgs boson in several modes, the principal distributions of the Higgs boson decay products such for instance in the diphoton channel; (ii) the production angle in the Collins–Soper frame [225] in the diphoton channel; (iii) the overall distribution of the Higgs boson transverse momentum.

The measured differential cross section in the Higgs boson transverse momentum by ATLAS and CMS using the full Run 2 datasets are illustrated in Fig. 11.15.

### 11.6.2.3 Constraints on non-SM Higgs boson interactions in an effective Lagrangian

An example of the possible use of differential cross sections in constraining non-SM Higgs boson couplings in an EFT is given by ATLAS [273]. In this analysis, differential cross section measured in the diphoton channel are used to constrain an effective Lagrangian where the SM is supplemented by dimension six  $CP$ -even operators of the Strongly Interacting Light Higgs (SILH) formulation [248] and corresponding  $CP$ -odd operators. The diphoton differential cross sections are mainly sensitive to the operators that affect the Higgs boson interactions with gauge bosons. CMS has also recently analysed [260] the Higgs boson transverse momentum distribution to constrain the Higgs boson couplings to top, bottom, and charm quarks as well as the effective coupling to gluons. This analysis is, however, not performed in an EFT framework.

The differential distributions used in this combination are: (i) the transverse momentum of the Higgs boson, (ii) the number of reconstructed jets produced in association with the diphoton pair, (iii) the invariant mass of the diphoton system and (iv) the difference in azimuthal angle of the leading and sub-leading jets in events with two or more jets. This analysis shows how differential information significantly improves the sensitivity to dimension-6 operators.

### 11.6.2.4 Simplified Template Cross Sections (STXS)

An overarching subject of discussion between the theory and experimental communities in the field of Higgs physics has been how experimentalists could best communicate their results for them to be most efficiently used by others for further interpretation.

In the field of precision SM measurements, the commonly used practise is that results are given at particle level within a well

defined fiducial volume of phase space. The fiducial volume is usually defined close enough to the experimental reconstruction to minimise the possible variations of the reconstruction efficiency within the particle level fiducial volume. In this way, results minimise their dependence on theoretical uncertainties.

ATLAS and CMS have produced fiducial and unfolded cross sections based on all objects reconstructed in the events. These measurements could be used for further interpretation. However, performing a proper combination of channels taking into account all experimental systematic uncertainties is non trivial. A proposal [44, 274] was made by the LHC Higgs Cross Section Working Group to produce results in each decay channel with a well defined fiducial phase space of the Higgs boson (and not its decay products) and for other associated objects pertaining to all channels, such as jets and missing transverse momentum (MET). The definition of the fiducial regions is motivated by maximising the experimental sensitivity, isolating possible BSM effects, and minimising the dependence on theoretical uncertainties. The number of regions is also minimised to avoid the loss of experimental sensitivity. The observables that are measured in this approach are still the standard production cross sections (the gluon fusion, the vector boson fusion, the  $VH$  and  $t\bar{t}H$  associated production modes) within the defined fiducial volumes.

In summary, this approach is hybrid. It is fiducial on specific objects to reduce the theory dependence and inclusive in the Higgs kinematics in order to allow for a more straightforward combination. This approach also allows the use of multivariate techniques to enhance the sensitivity within given fiducial regions, at the expense of a greater extrapolation and therefore increased model dependence.

The currently used Simplified Template Cross Sections (STXS) scheme covers, with a limited number of bins, the  $ggF$  process in four categories in number of jets (0, 1, 2 and 2 VBF-like jets, where VBF-like means a selection of two high invariant mass jets with large pseudo rapidity difference) further subdivided in four transverse momentum categories covering the full spectrum with the last bin being inclusive for  $p_T > 200 \text{ GeV}$ . The  $VH$  process is subdivided two categories depending on the number of reconstructed charged leptons corresponding to the decays of either a  $W$  boson or a  $Z$  boson, and two bins in transverse momentum. VBF and hadronic  $VH$  categories are defined using jet cuts and two bins in transverse momentum.

Measurements in this framework have been made in various decay channels. The first measurements have been performed in the main Higgs boson discovery channels. ATLAS has produced measurements of the diphoton and the  $4\ell$  channels with Run 2 data [125, 227, 236, 275, 276]. And full Run 2 results are available for the  $H \rightarrow 4\ell$  channel from ATLAS [131] and CMS [277].

CMS has carried out a measurement of the STXS in the  $H \rightarrow \tau^+\tau^-$  decay channel targeting the high transverse momentum of the Higgs boson [145], in particular in the channel where the Higgs boson is produced with one jet of transverse energy in excess of 200 GeV.

ATLAS [149] has made a measurement of the STXS aiming at the  $VH$  production mode in the  $H \rightarrow b\bar{b}$  decay mode at high transverse momentum of the vector boson above 250 GeV, where the discrimination of the background further increases.

A combination of STXS across decay channels has also been carried out by ATLAS with a dataset corresponding to an integrated luminosity of up to  $80 \text{ fb}^{-1}$  [213].

### 11.6.2.5 Indirect constraints on the Higgs boson couplings

The direct measurements at the LHC provide direct probes of the Higgs boson couplings to the vector bosons (photons,  $W$ ,  $Z$  and gluons) and to a limited number of Yukawa couplings to fermions. Currently these include essentially the third generation fermions – tau leptons, bottom and top quarks. For the High-Luminosity run, prospective studies [104] have shown that a good precision will be reached in the measurement of the coupling of the Higgs boson to muons and an evidence of the Higgs boson trilinear self-coupling with a precision of the order of 50% can be achieved. For the couplings of the Higgs boson to the other light SM fermions, direct evidences will be hard to reach at the LHC. However, from the measurements of the main observed Higgs final



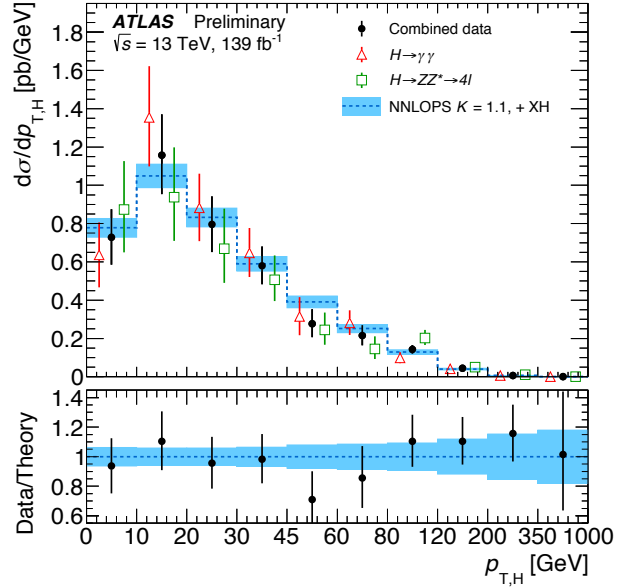
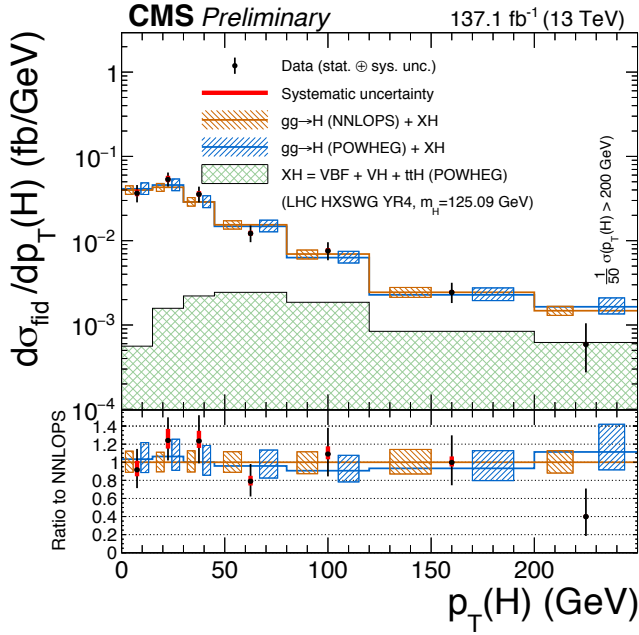


Figure 11.15: (Left) Fiducial differential, closely matching the reconstruction level selections, cross sections in Higgs boson transverse momentum in the  $H \rightarrow 4\ell$  channel from the CMS experiment [126]. (Right) Partially fiducial combined cross sections using the  $H \rightarrow \gamma\gamma$  and  $H \rightarrow 4\ell$  channels from the ATLAS experiment [272].

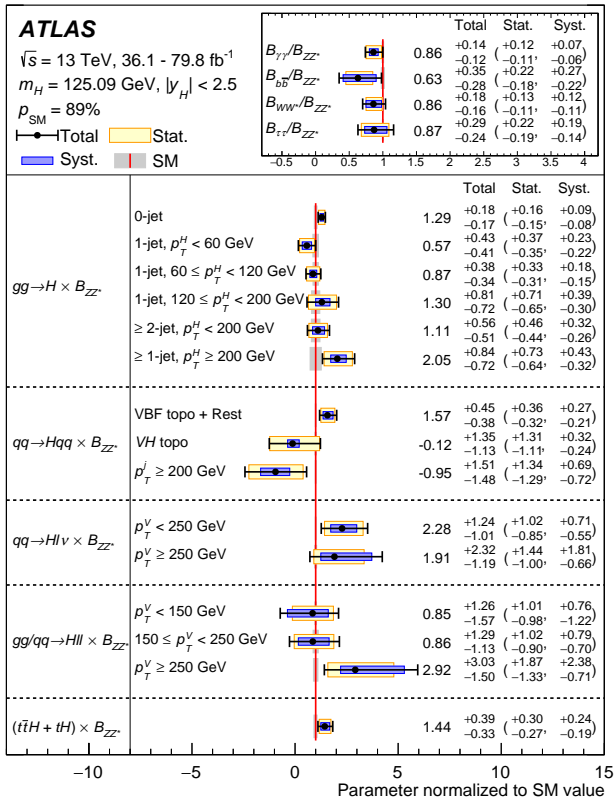


Figure 11.16: Simultaneous measurement of the simplified template cross sections times the branching fraction  $\text{BR}(H \rightarrow ZZ)$  (normalised to their Standard Model expectations) and the ratios of branching fractions  $\text{BR}(f)/\text{BR}(ZZ)$  [213].

states, it is possible to constrain specific couplings through their radiative corrections to dominant processes. Two prime examples are: (i) the trilinear self-coupling can be constrained through loop corrections to the single Higgs boson production [278–280], see the interpretation carried out by ATLAS of the combination of

the main decay channels [281]; (ii) the charm Yukawa coupling can be constrained from the differential cross section in Higgs boson transverse momentum [282], see the ATLAS [283] and CMS [260] analyses in the diphoton channel. These indirect constraints, however, require assumptions on the possible variations of all the other couplings.

ATLAS has also performed a preliminary combination of the single Higgs boson production measurements [284], using the approach and parametrisations of Ref. [279], which yield the following constraint:

$$-3.2 < \kappa_\lambda < 11.9. \quad (11.44)$$

When combined with results of the double Higgs boson production searches, the following combined constraint on the Higgs boson trilinear coupling yields:

$$-2.3 < \kappa_\lambda < 10.3 \text{ (obs)} \quad [-5.1 < \kappa_\lambda < 11.2 \text{ (exp)}]. \quad (11.45)$$

The *direct* and *indirect* constraints on the Higgs boson trilinear self-coupling are currently of similar strength. The double Higgs boson measurements are dominated by statistical uncertainties and are expected to improve much more rapidly than the precision on single Higgs boson measurements. Furthermore, it should be stressed that the constraints on the trilinear self-coupling obtained via the NLO fit of single Higgs boson data are less robust and more model-dependent since the NLO effects induced by a shift of the trilinear self-coupling compete with possible LO effects sourced by the deviations of the Higgs boson couplings to the other SM particles. The different effects can be disentangled by the measurements of various kinematical differential distributions in addition to the study of the inclusive rates [285], but the expected sensitivity in such global fits is not as promising as the one obtained when only the Higgs boson self-coupling is allowed to deviate from its SM value [286].

## 11.7 New physics models of EWSB in the light of the Higgs boson discovery

The discovery of a light scalar with couplings to gauge bosons and fermions that are consistent with SM predictions, together with the slow running of the Higgs boson self-coupling at high energies allow one to consider the SM as a valid perturbative description of nature all the way to the Planck scale. This picture is admittedly very attractive, but it posits that the Higgs boson

is an elementary scalar field, whose mass has quantum sensitivity to possible new physics scales. This EW/Higgs naturalness problem [6] has become much more definite after the Higgs boson discovery.

There are two broad classes of models addressing the naturalness problem<sup>5</sup>. One is based on SUSY [7] (for recent reviews, see Refs. [8, 9]). This is a weakly coupled approach to EWSB, maintaining the perturbativity of the SM, and, the Higgs boson remains elementary and the corrections to its mass are screened at the scale at which SUSY is broken so the value of the weak scale remains insensitive to the details of the physics at higher scales. These theories predict at least three neutral Higgs particles and a pair of charged Higgs particles [25]. One of the neutral Higgs bosons, most often the lightest  $CP$ -even one, has properties that could resemble those of the SM Higgs boson (at least in some regions of the parameter space). It is referred to as a SM-like Higgs boson, meaning that its couplings are close to the ones predicted in the SM. The other approach invokes the existence of strong interactions at a scale of the order of one TeV or above and these new interactions induce the breaking of the electroweak symmetry [288]. In the original incarnation, dubbed technicolor, the strong interactions themselves trigger EWSB without the need of a Higgs boson. Another possibility, more compatible with the ATLAS and CMS discovery, is that the strong interactions produce four light resonances identified with the Higgs doublet and EWSB proceeds through vacuum misalignment [10] (see Refs. [11, 12] for recent reviews). In that case, the Higgs boson itself has a finite size and thus never feels the UV degrees of freedom that would otherwise have dragged its mass to much higher scales. The Higgs boson could also correspond to the Goldstone boson associated with the spontaneous breaking of scale invariance, see Ref. [289] and references therein. However, this dilaton/radion scenario now requires a jumbled model-building to be consistent with the constraints from the coupling measurements. All these BSM scenarios can have important effects on the phenomenology of the Higgs boson. Also, in each case, the role of the Higgs boson in the unitarisation of scattering amplitudes is shared by other particles which remain targets of experimental searches.

The realisation of SUSY at low energies has many good qualities that render it attractive as a model of new physics. First of all since, for every SM degree of freedom, there is a superpartner of different spin but of equal mass and effective coupling to the SM-like Higgs boson, in the case of exact SUSY, an automatic cancellation of quantum corrections to the Higgs mass parameter holds. In practice, it is known that SUSY must be broken since no superpartners of the SM particles have been observed so far. The mass difference between the precise value of the mass of any particle and that of its corresponding superpartner is proportional to the correlated soft SUSY breaking parameter, generically called  $M_{\text{SUSY}}$ . The quantum corrections to the Higgs boson mass parameter are proportional to  $M_{\text{SUSY}}^2$ , and provided  $M_{\text{SUSY}}$  is of order of a few TeV, the low energy mass parameters of the Higgs sector become insensitive to physics at the GUT or Planck scale. Another interesting feature of SUSY theories is related to the dynamical generation of EWSB [290]. In the SM, a negative Higgs mass parameter,  $m^2$ , needs to be inserted by hand to induce EWSB, see Eq. (11.1). In SUSY, instead, even if the relevant Higgs mass parameter is positive in the ultraviolet, it may become negative and induce EWSB radiatively through the strong effect of the top quark-Higgs boson coupling in its renormalisation group evolution [290].

In the following, the Higgs sector will be explored in specific SUSY models. In all of them, it is often possible to find regions of the parameter space that accommodate one neutral Higgs boson with properties that resemble those of the SM Higgs boson, whereas additional neutral and charged Higgs bosons are also predicted and are intensively being sought for at the LHC (see Section 11.7.7). In the simplest SUSY model, accommodating a SM-like Higgs boson mass of about 125 GeV results in constraints on the stop sector, with at least one stop mass in the few TeV

mass range. In non-minimal SUSY extensions of the SM (details and related references can be found in the previous edition of this review [123]), a SM-like Higgs boson with mass of 125 GeV can be accommodated with less restrictions on the stop sector. While naturalness dictates relatively light stops and - at the two loop level - also gluinos, the first and second generation of squarks and sleptons couple weakly to the Higgs sector and may be heavy. Moreover, small values of the  $\mu$  parameter and therefore light Higgsinos, the fermionic superpartners of the Higgs bosons, would be a signature of a natural realization of electroweak symmetry breaking [291]. Such SUSY spectra, consisting of TeV range stop masses and light Higgsinos, continue to be under intense scrutiny by the experimental collaborations [292] in order to understand if such natural SUSY scenarios endure and can explain why the Higgs boson remains light.

In the context of weakly coupled models of EWSB, one can also consider multiple Higgs  $SU(2)_L$  doublets as well as additional Higgs singlets, triplets or even more complicated multiplet structures, with or without low energy SUSY. In general, for such models, one needs to take into account experimental constraints from precision measurements and flavour changing neutral currents. The LHC signatures of such extended Higgs sectors are largely shaped by the role of the exotic scalar fields in EWSB.

The idea that the Higgs boson itself could be a composite bound state emerging from a new strongly-coupled sector has been reconsidered thanks to the insights gained from the AdS/CFT duality. The composite Higgs boson idea is an incarnation of EWSB via strong dynamics that smoothly interpolates between the standard technicolor approach and the true SM limit. To avoid the usual conflict with EW data, it is sufficient, if not necessary, that a mass gap separates the Higgs resonance from the other resonances of the strong sector. Such a mass gap can naturally follow from dynamics if the strongly-interacting sector exhibits a global symmetry,  $G$ , broken dynamically to a subgroup  $H$  at the scale  $f$ , such that, in addition to the three Nambu-Goldstone bosons of  $SO(4)/SO(3)$  that describe the longitudinal components of the massive  $W$  and  $Z$ , the coset  $G/H$  contains a fourth Nambu-Goldstone boson that can be identified with the physical Higgs boson. Simple examples of such a coset are  $SU(3)/SU(2)$  or  $SO(5)/SO(4)$ , the latter being favoured since it is invariant under the custodial symmetry. It is also possible to have non-minimal custodial cosets with extra Goldstone bosons leading to additional Higgs bosons in the spectrum, see for instance Ref. [293]. Modern incarnations of composite Higgs models have been recently investigated in the framework of 5D warped models where, according to the principles of the AdS/CFT correspondence, the holographic composite Higgs boson then originates from a component of a gauge field along the 5th dimension with appropriate boundary conditions.

A last crucial ingredient in the construction of viable composite Higgs boson models is the concept of partial compositeness [294], i.e., the idea that there are only linear mass mixings between elementary fields and composite states. After diagonalisation of the mass matrices, the SM particles, fermions and gauge bosons, are admixtures of elementary and composite states and thus they interact with the strong sector, and in particular with the Higgs boson, through their composite component. This setup has important consequences on the flavour properties, chiefly the suppression of large flavour changing neutral currents involving light fermions. It also plays an important role in dynamically generating a potential for the would-be Goldstone bosons. Partial compositeness also links the properties of the Higgs boson to the spectrum of the fermionic resonances, i.e., the partners of the top quark. As in the MSSM, these top partners are really the agents that trigger the EWSB and also generate the mass of the Higgs boson that otherwise would remain an exact Goldstone boson and hence massless. The bounds from the direct searches for the top partners, in addition to the usual constraints from EW precision data, force the minimal composite Higgs models into some unnatural corners of their parameter spaces [295].

### 11.7.1 Higgs bosons in the minimal supersymmetric standard model (MSSM)

The particle masses and interactions in a SUSY theory are uniquely defined as a function of the superpotential and the Kähler

<sup>5</sup>Another solution to the naturalness problem is to lower the fundamental scale of quantum gravity, like for instance in models with large extra-dimensions, see Ref. [287].

ler potential [9]. A fundamental theory of SUSY breaking, however, is unknown at this time. Nevertheless, one can parametrise the low-energy theory in terms of the most general set of soft SUSY-breaking operators [9]. The simplest realistic model of low-energy SUSY is the minimal SUSY extension of the SM (MSSM) [9, 296], that associates a SUSY partner to each gauge boson and chiral fermion of the SM, and provides a realistic model of physics at the weak scale. However, even in this minimal model with the most general set of soft SUSY-breaking terms, more than 100 new parameters are introduced. Fortunately, only a subset of these parameters impact the Higgs boson phenomenology either directly at tree-level or through quantum effects.

The MSSM contains the particle spectrum of a two-Higgs-doublet model (2HDM) extension of the SM and the corresponding SUSY partners. Two Higgs doublets,  $\Phi_1$  and  $\Phi_2$ , with hypercharge  $Y = -1$  and  $Y = 1$ , respectively, are required to ensure an anomaly-free SUSY extension of the SM and to generate mass for down-type quarks/charged leptons ( $\Phi_1$ ) and up-type quarks ( $\Phi_2$ ) [25]. The Higgs potential reads

$$\begin{aligned} V = & m_1^2 \Phi_1^\dagger \Phi_1 + m_2^2 \Phi_2^\dagger \Phi_2 - m_3^2 (\Phi_1^T i \sigma_2 \Phi_2 + \text{h.c.}) \\ & + \frac{1}{2} \lambda_1 (\Phi_1^\dagger \Phi_1)^2 + \frac{1}{2} \lambda_2 (\Phi_2^\dagger \Phi_2)^2 + \lambda_3 (\Phi_1^\dagger \Phi_1) (\Phi_2^\dagger \Phi_2) \\ & + \lambda_4 |\Phi_1^T i \sigma_2 \Phi_2|^2 + \frac{1}{2} \lambda_5 [(\Phi_1^T i \sigma_2 \Phi_2)^2 + \text{h.c.}] \\ & + [[\lambda_6 (\Phi_1^\dagger \Phi_1) + \lambda_7 (\Phi_2^\dagger \Phi_2)] \Phi_1^T i \sigma_2 \Phi_2 + \text{h.c.}], \end{aligned} \quad (11.46)$$

where  $m_i^2 = \mu^2 + m_{H_i}^2$  ( $i = 1, 2$ ), with  $\mu$  being the supersymmetric Higgsino mass parameter and  $m_i$  the soft supersymmetric breaking mass parameters of the two Higgs doublets;  $m_3^2 \equiv B\mu$  is associated to the B-term soft SUSY breaking parameter; and  $\lambda_i$ , for  $i = 1$  to  $7$ , are all the Higgs quartic couplings.

After the spontaneous breaking of the electroweak symmetry, five physical Higgs particles are left in the MSSM spectrum: one charged Higgs pair,  $H^\pm$ , one  $CP$ -odd neutral scalar,  $A$ , and two  $CP$ -even neutral states,  $H$  and  $h$ , with  $h$  being the lightest.<sup>6</sup> The Higgs sector at tree level depends on the electroweak gauge coupling constants and the vacuum expectation value  $v$  – or equivalently the  $Z$  gauge boson mass – and is determined by only two free parameters:  $\tan \beta$  – the ratio of the two Higgs doublets' vacuum expectation values  $v_2/v_1$  – and one Higgs boson mass, conventionally chosen to be the  $CP$ -odd Higgs boson mass,  $m_A$ . The other tree-level Higgs boson masses are then given in terms of these parameters. The tree level value of  $m_h$  is maximised not only for  $m_A \gg m_Z$  but also for  $\tan \beta \gg 1$ . For  $m_A \gg m_Z$  it acquires a maximum value  $m_h = m_Z \cos 2\beta$ .

Radiative corrections have a significant impact on the values of Higgs boson masses and couplings in the MSSM. The dominant radiative effects to the SM-like Higgs boson mass arise from the incomplete cancellation between top and scalar-top (stop) loops and at large  $\tan \beta$  also from sbottom and stau loops. The stop, sbottom and stau masses and mixing angles depend on the SUSY Higgsino mass parameter  $\mu$  and on the soft-SUSY-breaking parameters [9, 296]:  $M_Q$ ,  $M_U$ ,  $M_D$ ,  $M_L$ ,  $M_E$ , and  $A_t$ ,  $A_b$ ,  $A_\tau$ . The first three of these are the left-chiral and the right-chiral top and bottom scalar quark mass parameters. The next two are the left-chiral stau/sneutrino and the right-chiral stau mass parameters, and the last three are the trilinear parameters that enter in the off-diagonal squark/slepton mixing elements:  $X_t \equiv A_t - \mu \cot \beta$  and  $X_{b,\tau} \equiv A_{b,\tau} - \mu \tan \beta$ . At one-loop, the electroweak gauginos yield a small contribution to the Higgs boson mass, and at the two-loop level, the masses of the gluinos also enter in the calculations. Radiative corrections to the Higgs boson masses have been computed using a number of techniques, with a variety of approximations; for a discussion see for example Refs. [39, 297, 298]

<sup>6</sup>Observe that in the SM sections of this review,  $H$  denotes the SM Higgs boson, whereas in the sections about SUSY, or extensions of the SM with two Higgs doublets,  $H$  is used for the heaviest  $CP$ -even Higgs boson, since this is the standard notation in the literature, and the 125 GeV SM-like light Higgs boson will be denoted by  $h$ . Generically, in the MSSM, the lightest  $CP$ -even Higgs boson is indeed SM-like and thus it is naturally identified with the 125 GeV Higgs boson discovered by ATLAS and CMS, while in 2HDM extensions, with or without SUSY, there could still be lighter scalar states below 125 GeV.

and the corresponding section of the previous edition of this review [123].

The discovered SM-like Higgs boson, if interpreted as the lightest MSSM Higgs boson with a mass of about 125 GeV, provides information on the possible MSSM parameter space, see Fig. 11.17.

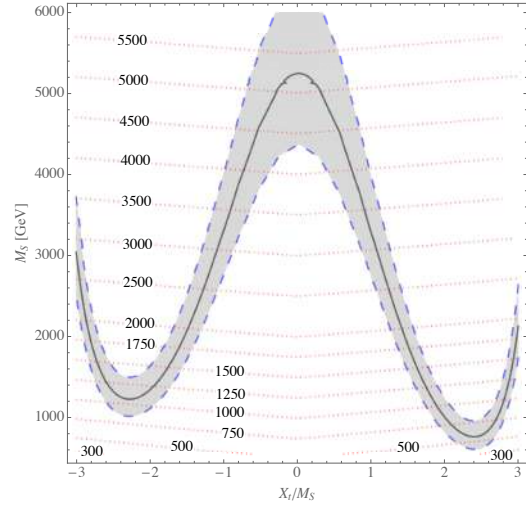


Figure 11.17: Values of the SUSY mass scale  $M_{\text{SUSY}} = M_S$  versus the stop mixing parameter normalised by the SUSY mass scale  $X_t/M_{\text{SUSY}}$ , for fixed  $\tan \beta = 20$ ,  $\mu = 200$  GeV and  $M_A = A_t = A_b = A_\tau = M_{\text{SUSY}}$ . The solid black line corresponds to  $m_h = 125$  GeV while in the grey band  $m_h$  varies by  $\pm 1$  GeV. The red dotted lines are iso-values of the stop mass. This figure is based on Ref. [299].

The phenomenology of the Higgs sector depends on the couplings of the Higgs bosons to gauge bosons and fermions. At tree-level, the couplings of the two  $CP$ -even Higgs bosons to  $W$  and  $Z$  bosons are given in terms of the angles  $\alpha$ , that diagonalises the  $CP$ -even Higgs boson squared-mass matrix, and  $\beta$

$$g_{hVV} = g_V m_V \sin(\beta - \alpha), \quad g_{HVV} = g_V m_V \cos(\beta - \alpha), \quad (11.47)$$

where  $g_V \equiv 2m_V/v$ , for  $V = W$  or  $Z$  ( $g_V m_V$  is the SM  $hVV$  coupling). Observe that in the limit  $\cos(\beta - \alpha) \rightarrow 0$ , the lightest  $CP$ -even Higgs boson  $h$  behaves as the SM Higgs boson. This situation is called alignment and is achieved in specific regions of parameter space for  $m_A \geq m_Z$  [300] or in the large  $m_A \gg m_Z$  limit, in which alignment is achieved through decoupling [300, 301]. There are no tree-level couplings of  $A$  or  $H^\pm$  to  $VV$ . The couplings of the  $Z$  boson to two neutral Higgs bosons are given by  $g_{\phi AZ}(p_\phi - p_A)$ , where  $\phi = H$  or  $h$ , the momenta  $p_\phi$  and  $p_A$  point into the vertex, and

$$g_{hAZ} = g_Z \cos(\beta - \alpha)/2, \quad g_{HAZ} = -g_Z \sin(\beta - \alpha)/2. \quad (11.48)$$

The expressions of the couplings between a charged Higgs boson, a neutral Higgs boson and the  $W$  boson as well as the expressions of the four-point couplings of vector bosons and Higgs bosons can be found in Ref. [25].

The tree-level Higgs boson couplings to fermions obey the following property: the neutral components of one Higgs doublet,  $\Phi_1$ , couple exclusively to down-type fermion pairs while the neutral components of the other doublet,  $\Phi_2$ , couple exclusively to up-type fermion pairs [25]. This Higgs-fermion coupling structure defines the Type-II 2HDM. In the MSSM, fermion masses are generated when both neutral Higgs components acquire a vacuum expectation value, and the relations between Yukawa couplings and fermion masses are (in third-generation notation)

$$h_{b,\tau} = \sqrt{2} m_{b,\tau} / (v \cos \beta), \quad h_t = \sqrt{2} m_t / (v \sin \beta). \quad (11.49)$$

The couplings of the neutral Higgs bosons to  $f\bar{f}$ , relative to their

SM values,  $g m_f / (2m_W)$ , are given by

$$\begin{aligned} h\bar{b}b &: -\sin\alpha/\cos\beta, & ht\bar{t} &: \cos\alpha/\sin\beta, \\ H\bar{b}b &: \cos\alpha/\cos\beta, & Ht\bar{t} &: \sin\alpha/\sin\beta, \\ A\bar{b}b &: \gamma_5 \tan\beta, & At\bar{t} &: \gamma_5 \cot\beta. \end{aligned} \quad (11.50)$$

In each relation above, the factor listed for  $b\bar{b}$  also pertains to  $\tau^+\tau^-$ . The charged Higgs boson couplings to fermion pairs, normalised to  $g/(\sqrt{2}m_W)$ , are given by

$$\begin{aligned} g_{H-t\bar{b}} &: m_t \cot\beta \frac{1+\gamma_5}{2} + m_b \tan\beta \frac{1-\gamma_5}{2}, \\ g_{H-\tau+\nu} &: m_\tau \tan\beta \frac{1-\gamma_5}{2}. \end{aligned} \quad (11.51)$$

The non-standard neutral Higgs bosons have significantly enhanced couplings to down-type fermions at sizeable  $\tan\beta$ . Radiative corrections can modify significantly the values of the Higgs boson couplings to fermion pairs and to vector boson pairs, through a radiatively-corrected value for  $\cos(\beta-\alpha)$  as well as from the one-loop vertex corrections to tree-level Higgs-fermion Yukawa couplings, see Ref. [9] and references therein, for a detailed discussion.

#### 11.7.1.1 MSSM Higgs boson phenomenology

The MSSM parameters have to be arranged such that the mass, the  $CP$  properties, the decay and production properties of one of the neutral Higgs bosons agree with the LHC Higgs data. Given that present data allows only for moderate departures from the SM predictions, it implies that some degree of alignment is necessary.

The SM-like branching ratios of  $h$  can be modified if decays into SUSY particles are kinematically allowed, and, in particular, decays into a pair of the lightest SUSY particles – i.e., the lightest neutralinos,  $\tilde{\chi}_1^0$  – can become dominant and would be invisible if  $R$ -parity is conserved [302]. Moreover, if light superpartners exist and couple to photons and/or gluons, the  $h$  loop-induced coupling to  $gg$  and  $\gamma\gamma$  could deviate sizeably from the corresponding SM predictions (see for instance the review [297]), and would be in conflict with present data (see Section 11.3). For the heavier Higgs states, there are two possibilities to be considered<sup>7</sup>:

- i) Alignment triggered by decoupling, hence  $m_A \geq$  several hundred GeV: The  $HWW$  and  $HZZ$  couplings are very small. The dominant  $H, A$  decay branching ratios strongly depend on  $\tan\beta$ . The decay modes  $H, A \rightarrow b\bar{b}, \tau^+\tau^-$  dominate when  $\tan\beta$  is large (this holds even away from decoupling). For small  $\tan\beta$ , the  $t\bar{t}$  decay mode dominates above its kinematic threshold. For the charged Higgs boson,  $H^\pm \rightarrow t\bar{b}$  dominates.
- ii) Some degree of alignment without decoupling, hence  $m_A \leq$  a few hundred GeV: The main difference with the previous case is that, in the low  $\tan\beta$  regime ( $\tan\beta \leq 5$ ), additional decay channels may be allowed which involve decays into the lightest SM-like Higgs boson;  $A \rightarrow Zh, H \rightarrow hh$  as well as  $H \rightarrow WW/ZZ$  decay modes are available (they are suppressed in the strict alignment limit). When kinematically open, the decays  $A/H \rightarrow t\bar{t}$  become relevant or even dominant for sufficiently small  $\tan\beta$ . For the charged Higgs boson,  $H^\pm \rightarrow \tau^+\nu_\tau$  dominates below the  $t\bar{b}$  threshold, and also  $H^\pm \rightarrow W^\pm h$  may be searched for.

In both cases i) and ii), the heavier Higgs states,  $H, A$  and  $H^\pm$ , are roughly mass degenerate (with masses  $\pm 20$  GeV or less apart). If kinematically allowed, the heavy Higgs boson decays into charginos, neutralinos and third-generation squarks and sleptons can be important [305].

At hadron colliders, the dominant neutral Higgs boson production mechanism at moderate values of  $\tan\beta$  is gluon fusion, mediated by loops containing heavy top and bottom quarks and the corresponding SUSY partners. The effect of light stops that may

contribute to the gluon fusion production can be partially cancelled by mixing effects. Higgs boson radiation off bottom quarks becomes important for large  $\tan\beta$ , where at least two of the three neutral Higgs bosons have enhanced couplings to bottom-type fermions [306, 307]. Detailed discussions of the impact of radiative corrections in these search modes are presented for instance in Ref. [308]. The vector boson fusion and Higgs-strahlung production of the  $CP$ -even Higgs bosons as well as the associated production of neutral Higgs bosons with top quark pairs have lower production cross sections by at least an order of magnitude with respect to the dominant ones, depending on the precise region of MSSM parameter space [41–44]. Higgs boson pair production of non-standard MSSM Higgs bosons has been studied in Ref. [309]. For a discussion of charged Higgs boson production at LHC, see Refs. [42, 43, 310].

Strong production of a heavy neutral Higgs boson followed by its decay into top-quark pairs is a challenging channel, only most recently being searched for by ATLAS and CMS. Interference effects between the signal and the SM  $t\bar{t}$  background need to be carefully taken into account [311].

Summarising, the additional Higgs bosons are sought for mainly via the channels:

$$\begin{aligned} pp &\rightarrow A/H \rightarrow \tau^+\tau^- \text{ (inclusive)}, \\ \bar{b}b A/H, A/H &\rightarrow \tau^+\tau^- \text{ (with } b\text{-tag)}, \\ \bar{b}b A/H, A/H &\rightarrow b\bar{b} \text{ (with } b\text{-tag)}, \\ pp &\rightarrow t\bar{t} \rightarrow H^\pm W^\mp b\bar{b}, H^\pm \rightarrow \tau\nu_\tau, \\ gb &\rightarrow H^- t \text{ or } g\bar{b} \rightarrow H^+ \bar{t}, H^\pm \rightarrow \tau\nu_\tau. \end{aligned} \quad (11.52)$$

After the Higgs boson discovery, updated MSSM benchmark scenarios have been defined to highlight interesting conditions for the MSSM Higgs boson searches [43, 304, 312]. The latest benchmark scenarios update [304], partly based in MSSM parameter space discussions in Ref. [312], considers six benchmarks to illustrate different aspects of Higgs phenomenology in the MSSM. They include one case with complex parameters, but they all assume  $R$ -parity conservation and no flavour mixing. Each scenario contains one  $CP$ -even scalar with mass around 125 GeV and SM-like couplings. These scenarios include a  $M_h^{125}$  scenario with relatively heavy superparticles, so the Higgs phenomenology at the LHC resembles that of a 2HDM with MSSM-inspired Higgs boson couplings. Other two scenarios are characterised by some of the superparticles – staus or electroweakinos – being relatively light, that in turn is of relevance for heavy neutral Higgs boson searches. In particular, the traditional  $A/H \rightarrow \tau^+\tau^-$  search channel varies depending on the values of  $\mu$  and  $M_2$ , that may enable the  $A/H$  decays into electroweakinos. Another two scenarios are characterised by the phenomenon of alignment without decoupling, in which one of the two neutral  $CP$ -even scalars has SM-like couplings independently of the mass spectrum of the remaining Higgs bosons, hence allowing for all the Higgs bosons to have relatively low mass values (about few hundred GeV). Finally there is one scenario which incorporates  $CP$  violation in the Higgs sector and gives rise to a strong admixture of the two heavier neutral states. All the above scenarios assume all parameters in the mass range from 1 to a few TeV, hence they are not applicable for values of  $\tan\beta$  of order a few, for which a Higgs boson mass value of 125 GeV is out of reach. An additional study, EFTMSSM [313], proposes two scenarios specifically designed for the low  $\tan\beta$  region and ensures a 125 GeV Higgs boson mass in almost the entire parameter space by employing a flexible supersymmetric mass scale, reaching values of up to  $10^{16}$  GeV.

An alternative approach to reduce the large number of parameters relevant to the Higgs sector is to consider that, in the Higgs basis, the only important radiative corrections are those affecting the Higgs boson mass [314]. This approximation is called hMSSM and works well in large regions of parameter space but it breaks down for sizeable values of  $\mu$  and  $A_t$ , and moderate values of  $\tan\beta$ , for which the radiative corrections to the mixing between the two  $CP$  even eigenstates become relevant. The effect of such radiative corrections is to allow for alignment for small to intermediate values of  $\tan\beta$ , independent of the specific value of  $m_A$  [315]. In

<sup>7</sup>In very special regions of the parameter space, there is still the possibility that the heavier  $CP$ -even Higgs state is identified with the 125 GeV Higgs boson discovered by ATLAS and CMS, see for instance the discussion in Ref. [303] and the benchmark  $M_H^{125}$  defined in Ref. [304].

addition, the hMSSM assumption that the right value of the Higgs boson mass may be obtained for all values of  $m_A$  and  $\tan\beta$  is in conflict with the MSSM predictions for the Higgs boson mass for small values of  $m_A$  and  $\tan\beta \simeq \mathcal{O}(1)$ . The recent  $M_h^{125}$  [304] and EFTMSSM benchmarks [313], are designed to address the limitations of the hMSSM, in particular the low  $\tan\beta$  region for the EFTMSSM.

The  $M_h^{125}$  scenarios are aiming at treating more rigorously all radiative correction to the observed Higgs boson mass as well as specifically taking into possibly intermediate to light MSSM colorless states as electroweakinos or staus [304]. The main  $M_h^{125}$  benchmark, however, assumes that super partners are heavy, so that the phenomenology of the observed Higgs boson is not altered except in its couplings due to the existence of another doublet. Another important example scenario, referred to as  $M_h^{125}(\tilde{\chi})$ , considers light electroweakinos and therefore the heavy Higgs bosons  $H$  and  $A$  can have sizeable decay rates to charginos and neutralinos, consequently suppressing the  $\tau^+\tau^-$  decay rate. It is interesting to note that in this scenario the branching fraction of the Higgs boson to photons is enhanced for small values of  $\tan\beta$  due to the presence of electroweakinos in the loop. These two scenarios are illustrated in Fig. 11.18.

The compatibility between the predicted and measured Higgs boson mass is an important constraint in these scenarios. The predictions are illustrated in Fig. 11.18. To use the predicted Higgs boson mass as a constraint (exclusion at nearly constant  $\tan\beta$  at high  $M_A$  in the  $(M_A, \tan\beta)$  plane), it is important to account for the theoretical uncertainty on the prediction which is in excess of an order of magnitude larger than the experimental uncertainty on the measured mass of the Higgs boson. The theoretical uncertainty depends itself on the specific SUSY spectrum for a given MSSM parameter set and should be estimated accordingly, however, a more generic estimate of  $\pm 3$  GeV is made and found to be a conservative choice.

Reviews of the properties and phenomenology of the Higgs bosons of the MSSM can be found for example in Refs. [9, 39, 297]. Future precision measurements of the Higgs boson couplings to fermions and gauge bosons together with information on heavy Higgs boson searches will provide powerful information on the SUSY parameter space [315, 316].

Improvements in our understanding of  $B$ -physics observables put indirect constraints on additional Higgs bosons in mass ranges that would be accessible in direct LHC searches. In particular,  $\text{BR}(B_s \rightarrow \mu^+\mu^-)$ ,  $\text{BR}(b \rightarrow s\gamma)$ , and  $\text{BR}(B_u \rightarrow \tau\nu)$  play an important role within minimal flavour-violating (MFV) models [317], in which flavor effects proportional to the CKM matrix elements are induced as in the SM.

### 11.7.2 Supersymmetry with singlet extensions

The Higgs mass parameter  $\mu$  is a SUSY parameter, and as such, it should naturally be of order  $M_{GUT}$  or  $M_{Planck}$ . The fact that phenomenologically it is required that  $\mu$  be at the electroweak/TeV scale is known as the  $\mu$  problem [318]. SUSY models with additional singlets can provide a solution to the  $\mu$  problem, by promoting the  $\mu$  parameter to a dynamical singlet superfield  $S$  that only interacts with the MSSM Higgs doublets through a coupling  $\lambda_S$  at the level of the superpotential. An effective  $\mu$  is generated when the real scalar component of  $S$  acquires a vacuum expectation value  $v_S$ , yielding  $\mu_{\text{eff}} = \lambda_S v_S$ . After the minimization of the Higgs potential, the vacuum state relates the vacuum expectation values of the three  $CP$ -even neutral scalars,  $v_1$ ,  $v_2$  and  $v_S$ , to the scalar doublet and singlet soft SUSY breaking masses, hence, one expects that these VEVs should all be of order  $M_{\text{SUSY}}$  and therefore the  $\mu$  problem is solved.

The addition of a singlet superfield to the MSSM may come along with additional symmetries imposed to the theory. Depending on such symmetries, different models with singlet extensions of the MSSM (xMSSM) have been proposed, see Ref. [319] for a general review. Among the most studied examples are the NMSSM with an additional discrete  $Z_3$  symmetry (first introduced in Ref. [320]), the Nearly-Minimal SUSY SM (nMSSM), with additional discrete  $Z_5^R$ , and  $Z_7^R$  symmetries [321], and the  $U(1)'$ -extended MSSM (UMSSM) [322]. A Secluded  $U(1)'$ -extended MSSM (sMSSM) [323] contains three singlets in addition to the

standard UMSSM Higgs boson singlet; this model is equivalent to the nMSSM in the limit that the additional singlet VEV's are large, and the trilinear singlet coupling,  $\lambda_S$ , is small [324].

A singlet extended SUSY Higgs sector opens new avenues for discovery. Since the singlet pseudoscalar particle may be identified as the pseudo-Goldstone boson of a spontaneously broken Peccei–Quinn symmetry, it may become naturally light [325]. Generally, there is mixing of the singlet sector with the MSSM Higgs sector, and for a sufficiently light, singlet-dominated scalar or pseudoscalar,  $h_S$  or  $A_S$ , respectively, the SM-like Higgs boson  $h$  may decay to pairs of  $h_S$  or  $A_S$ . The light scalar and/or pseudoscalar may subsequently decay to  $\tau\tau$  or  $b\bar{b}$  pairs. Such cascade decays are more difficult to detect than in standard searches due to the potentially soft decay products. There is also a rich phenomenology for the decays of the heavy  $CP$ -even and  $CP$ -odd doublets,  $H$  and  $A$  into two lighter Higgs bosons such as  $H \rightarrow hh_S$ ,  $hh$ ,  $h_S h_S$  or  $A \rightarrow A_S h_S$ ,  $A_S h$  as well as into a light Higgs boson and a gauge boson:  $H \rightarrow A_S Z$ ;  $A \rightarrow h_S Z$ ,  $hZ$ . If kinematically allowed, the heavy Higgs bosons decay into  $t\bar{t}$ . If the singlet-dominated scalar or pseudoscalar are somewhat heavier, the decays  $h_S \rightarrow WW$  or  $A_S \rightarrow h_S Z$  will be allowed.

In addition, the light singlet scenario in the NMSSM or nMSSM is typically associated with a light singlino-dominated neutralino. The recently discovered SM-like Higgs boson can then decay to pairs of this neutralino [326], opening an invisible decay mode that is not excluded by present data. All of the Higgs bosons can decay into electroweakinos depending on kinematics and on the singlino or Higgsino composition of the electroweakinos.

In models with extended singlets, at low  $\tan\beta$ , it is possible to trade the requirement of a large stop mixing by a sizeable trilinear Higgs-singlet Higgs coupling  $\lambda_S$ , rendering more freedom on the requirements for gluon fusion production. As in the MSSM, mixing in the Higgs sector – additionally triggered by the extra new parameter  $\lambda_S$  – can produce variations in the Higgs– $b\bar{b}$  and Higgs– $\tau^-\tau^+$  couplings that can alter the Higgs to  $ZZ$ / $WW$  and to diphoton rates. Light charginos at low  $\tan\beta$  can independently contribute to enhance the di-photon rate, without altering any other of the Higgs boson decay rates, see for instance Ref. [327].

There is much activity in exploring the NMSSM phenomenology in the light of the 125 GeV Higgs boson as well as in defining benchmark scenarios with new topologies including Higgs decay chains, see Refs. [44, 328] and references therein. An analytic understanding of the alignment condition in the NMSSM is presented in Ref. [329]. The NMSSM with a Higgs boson of mass 125 GeV can be compatible with stop masses of order of the electroweak/TeV scale, thereby reducing the degree of fine tuning necessary to achieve electroweak symmetry breaking. Interestingly, the alignment conditions point toward a more natural region of parameter space for electroweak symmetry breaking, while allowing for perturbativity of the theory up to the Planck scale and yielding a rich and interesting Higgs boson phenomenology at the LHC.

### 11.7.3 Supersymmetry with extended gauge sectors

In the MSSM, the tree-level value of the lightest  $CP$ -even Higgs boson mass originates from the D-term dependence of the scalar potential that comes from the SUSY kinetic terms in the Kähler potential. The D-terms lead to tree-level quartic couplings which are governed by the squares of the gauge couplings of the weak interactions, under which the Higgs boson has non-trivial charges. Hence, the lightest Higgs mass is bounded to be smaller than  $M_Z$ . In the presence of new gauge interactions at the TeV scale, and if the Higgs fields had non-trivial charges under them, new D-term contributions would lead to an enhancement of the tree-level Higgs boson mass value. Since the low energy gauge interactions reduce to the known  $SU(3)_c \times SU(2)_L \times U(1)_Y$  ones, in order for this mechanism to work, the extended gauge and Higgs sectors should be integrated out in a non-SUSY way. This means that there must be SUSY breaking terms that are of the order of, or larger than, the new gauge boson masses. The tree-level quartic couplings would then be enhanced through their dependence on the square of the gauge couplings of the extended Higgs sector. This effect will be suppressed when the heavy gauge boson masses are larger than the SUSY breaking scale and will acquire its full



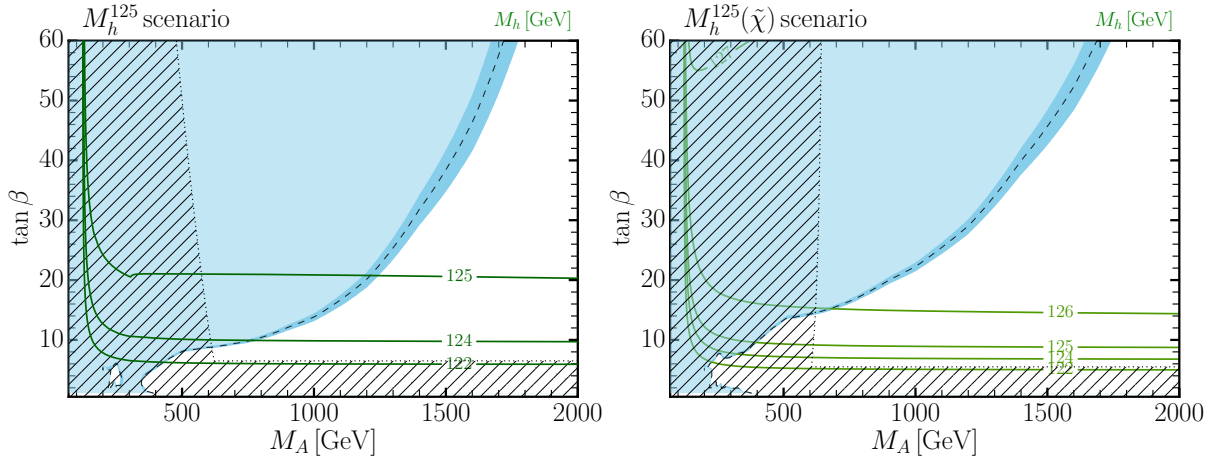


Figure 11.18: The 95% CL exclusion contours in the  $(M_A, \tan\beta)$  parameter space for the  $M_h^{125}$  (right) and  $M_h^{125}(\tilde{\chi})$  (left) benchmark scenarios. The nearly vertical dotted line illustrated the lower limit on the mass of the  $A$  boson and the close-to horizontal dotted line represents the limit on  $\tan\beta$  from the compatibility of the measured mass of the observed Higgs boson and the prediction using radiative corrections (mostly from the stop sector).

potential only for large values of this scale.

One of the simplest possibilities is to extend the weak interactions to a  $SU(2)_1 \times SU(2)_2$  sector, such that the known weak interactions are obtained after the spontaneous breaking of these groups to  $SU(2)_L$  [330]. This example is briefly summarized in the previous editions of this review [123]. Assuming SUSY breaking terms of the order of the new gauge boson masses, enhancements of order 50% of the MSSM D-term contribution to the Higgs boson mass may be obtained. Such enhancements are sufficient to obtain the measured Higgs mass without the need for very heavy stops or large stop mixing parameters. This gauge extension leads to new, heavy gauge and Higgs bosons, as well as new neutralinos and charginos, that depending on the region of parameter space can induce novel phenomenology at the LHC. Gauge extensions including new abelian gauge groups have also been considered.

Gauge extensions of the MSSM can also lead to an enhancement of the Higgs boson mass value by modifying the renormalisation group evolution of the Higgs quartic coupling to low energies. In the MSSM, the evolution of the quartic coupling is governed by the top-quark Yukawa interactions and depends on the fourth power of the top-quark Yukawa coupling. The neutralino and chargino contributions, which depend on the fourth power of the weak gauge couplings, are small due to the smallness of these couplings. Depending on the values of the soft SUSY breaking parameters in the gaugino and Higgsino sectors, the  $SU(2)_1$  gauginos may become light, with masses of the order of the weak scale. Since the  $SU(2)_1$  coupling may be significantly larger than the  $SU(2)_L$  one, for small values of the Higgsino mass parameter  $\mu$ , the associated charginos and neutralinos may modify the evolution of the quartic coupling in a significant way [331]. This may lead to a significant increase of the lightest  $CP$ -even Higgs boson mass, even for small values of  $\tan\beta \simeq 1$  for which the D-term contributions become small. Radiative corrections should be properly taken into account in this scenario as they might modify the tree-level result.

#### 11.7.4 Effects of $CP$ violation

SUSY scenarios with  $CP$ -violation ( $CPV$ ) phases are theoretically appealing, since additional  $CPV$  beyond that observed in the  $K$ ,  $D$ , and  $B$  meson systems is required to explain the observed cosmic matter-antimatter asymmetry. In the MSSM,  $CP$ -violation effects in the Higgs sector appear at the quantum level, while in singlet extensions of the MSSM  $CP$ -violation effects can already be effective at tree level. In general,  $CP$ -violation effects in the Higgs sector have significant constraints from electric dipole moments data [332].

In the MSSM, the gaugino mass parameters  $(M_{1,2,3})$ , the Higgsino mass parameter,  $\mu$ , the bilinear Higgs squared-mass parameter,  $m_{12}^2$ , and the trilinear couplings of the squark and

slepton fields to the Higgs fields,  $A_f$ , may carry non-trivial phases. The two parameter combinations  $\arg[\mu A_f (m_{12}^2)^*]$  and  $\arg[\mu M_i (m_{12}^2)^*]$  are invariant under phase redefinitions of the MSSM fields [333, 334]. Therefore, if one of these quantities is non-zero, there would be new sources of  $CP$ -violation affecting the Higgs sector through radiative corrections, see Ref. [335] and references therein. The mixing of the neutral  $CP$ -odd and  $CP$ -even Higgs boson states is no longer forbidden. Hence,  $m_A$  is no longer a physical parameter. However, the charged Higgs boson mass  $m_{H^\pm}$  is still physical and can be used as an input for the computation of the neutral Higgs boson spectrum of the theory. For large values of  $m_{H^\pm}$ , corresponding to the decoupling limit, the properties of the lightest neutral Higgs boson state approach those of the SM Higgs boson. In particular, the upper bound on the lightest neutral Higgs boson mass takes the same value as in the  $CP$ -conserving case [334]. Nevertheless, there still can be significant mixing between the two heavier neutral mass eigenstates. For a detailed study of the Higgs boson mass spectrum and parametric dependence of the associated radiative corrections, see Ref. [335] and references therein.

Major variations to the Higgs boson phenomenology occur in the presence of explicit  $CPV$  phases. In the  $CPV$  case, vector boson pairs couple to all three neutral Higgs boson mass eigenstates,  $H_i$  ( $i = 1, 2, 3$ ), with couplings

$$\begin{aligned} g_{H_i V V} &= \cos\beta \mathcal{O}_{1i} + \sin\beta \mathcal{O}_{2i}, \\ g_{H_i H_j Z} &= \mathcal{O}_{3i} (\cos\beta \mathcal{O}_{2j} - \sin\beta \mathcal{O}_{1j}) \\ &\quad - \mathcal{O}_{3j} (\cos\beta \mathcal{O}_{2i} - \sin\beta \mathcal{O}_{1i}), \end{aligned} \quad (11.53)$$

where the  $g_{H_i V V}$  couplings are normalised to the analogous SM coupling and the  $g_{H_i H_j Z}$  have been normalised to  $g_Z^{\text{SM}}/2$ . The orthogonal matrix  $\mathcal{O}_{ij}$ , only defined in the  $p^2 \rightarrow 0$  limit, is relating the weak eigenstates to the mass eigenstates. It has non-zero off-diagonal entries mixing the  $CP$ -even and  $CP$ -odd components of the weak eigenstates. Moreover,  $CPV$  phases imply that all neutral Higgs bosons can couple to both scalar and pseudoscalar fermion bilinear densities. The couplings of the mass eigenstates  $H_i$  to fermions depend on the loop-corrected fermion Yukawa couplings (similarly to the  $CP$  conserving ( $CPC$ ) case), on  $\tan\beta$  and on  $\mathcal{O}_{ji}$  [336].

The production processes of neutral MSSM Higgs bosons in the  $CPV$  scenario are similar to those in the  $CPC$  scenario. Regarding the decay properties, the lightest mass eigenstate,  $H_1$ , predominantly decays to  $b\bar{b}$  if kinematically allowed, with a smaller fraction decaying to  $\tau^+\tau^-$ . If kinematically allowed, a SM-like neutral Higgs boson,  $H_2$  or  $H_3$  can decay predominantly to  $H_1 H_1$  leading to many new interesting signals both at lepton and hadron colliders; otherwise it will decay preferentially to  $b\bar{b}$ .

The discovery of a 125 GeV Higgs boson has put strong constraints on the realisation of the  $CPV$  scenario within the MSSM. This is partly due to the fact that the observed Higgs boson rates are close to the SM values, and a large  $CP$ -violating component would necessarily induce a large variation in the rate of the SM-like Higgs boson decays into the weak gauge bosons  $W^\pm$  and  $Z$ . The measured Higgs mass imposes additional constraints on the realisation of this scenario. Once all effects are considered, the  $CP$ -odd Higgs boson  $A$  component of the lightest Higgs boson tends to be smaller than about 10% [337]. This restriction can be alleviated in the NMSSM or more general two Higgs doublet models.  $CP$ -violating effects can still be significant in the heavy Higgs sector. For instance, the Higgs bosons  $H_2$  and  $H_3$  may be admixtures of  $CP$ -even and  $CP$ -odd scalars, and therefore both may be able to decay into pairs of weak gauge bosons. The observation of such decays would be a clear signal of  $CP$ -violation. In the MSSM, the proximity of the masses of  $H_2$  and  $H_3$  makes the measurement of such effect quite challenging, but in generic two Higgs doublet models, the mass splitting between the two heavy mass eigenstates may become larger, facilitating the detection of  $CP$ -violating effects at collider experiments [338].

### 11.7.5 Non-supersymmetric extensions of the Higgs sector

There are many ways to extend the minimal Higgs sector of the SM. In the preceding sections the phenomenology of SUSY Higgs sectors is considered, which at tree level implies a constrained type-II 2HDM (with restrictions on the Higgs boson masses and couplings). In the following discussion, more generic 2HDM's are presented (for some comprehensive reviews, see Ref. [339]). These models are theoretically less compelling since they do not provide an explanation for the SM Higgs naturalness problem, but can lead to different patterns of Higgs-fermion couplings, hence, to different phenomenology. It is also possible to consider models with a SM Higgs boson and one or more additional scalar  $SU(2)$  doublets that acquire no VEV and hence play no role in the EWSB mechanism. Such models are dubbed Inert Higgs Doublet Models (IHD) [340]. Without a VEV associated to it, a Higgs boson from an inert doublet has no tree-level coupling to gauge bosons and hence cannot decay into a pair of them. Moreover, imposing a  $Z_2$  symmetry that prevents them from coupling to the fermions, it follows that, if the lightest inert Higgs boson is neutral, it becomes a good DM candidate with interesting associated collider signals. Various studies of IHD models in the light of a 125 GeV Higgs boson have been performed, see for instance Ref. [341], showing an interesting interplay between collider and direct DM detection signals.

An interesting type of 2HDMs are those in which an abelian flavour symmetry broken at the electroweak scales creates the fermion mass hierarchies and mixing angles [17]. This idea is based on the Froggatt–Nielsen model [342], where a flavon field couples differently to the SM fermions of different flavour charges. Such flavon acquires a vacuum expectation value, breaking the flavour symmetry but leaving both the flavour breaking and the new physics scales undetermined. In Refs. [343], it was proposed to relate the flavour breaking scale to the electroweak scale by identifying the flavon with the modulus square of the Higgs field. A 2HDM, however, provides a more compelling realisation of the electroweak scale flavour breaking idea. In the most ambitious constructions of two Higgs doublet flavour models (2HDFM), the textures of the Yukawa couplings are a result of an abelian flavour symmetry that only allows renormalisable Yukawa couplings of the top quark to the Higgs bosons. All other Yukawa couplings are generated by higher dimensional operators that produce hierarchical entries of the Yukawa matrices, explaining the observed quark masses and mixing angles. Flavour observables, LHC Higgs signal strength measurements, electroweak precision measurements, unitarity and perturbativity bounds, as well as collider searches for new scalar resonances result in precise predictions for the parameters of these 2HDFMs. In particular, correlated departures from SM Higgs boson couplings, as well as additional Higgs bosons with masses  $< 700$  GeV must be observed at the LHC. Other incarnations of 2HDFMs can aim at only partially explaining the fermion mass hierarchies but are therefore less restrictive.

Other extensions of the Higgs sector can include multiple copies

of  $SU(2)_L$  doublets [344], additional Higgs singlets [345], triplets or more complicated combinations of Higgs multiplets. It is also possible to enlarge the gauge symmetry beyond  $SU(2)_L \times U(1)_Y$  along with the necessary Higgs field structure to generate gauge boson and fermion masses. There are two main experimental constraints on these extensions: (i) precision measurements which constrain  $\rho = m_W^2/(m_Z^2 \cos^2 \theta_W)$  to be very close to 1 and (ii) flavour changing neutral current (FCNC) effects. In electroweak models based on the SM gauge group, the tree-level value of  $\rho$  is determined by the Higgs multiplet structure. By suitable choices for the hypercharges, and in some cases the mass splitting between the charged and neutral Higgs sector or the vacuum expectation values of the Higgs fields, it is possible to obtain a richer combination of singlets, doublets, triplets and higher multiplets compatible with precision measurements. Concerning the constraints coming from FCNC effects, the Glashow–Weinberg (GW) criterion [346] states that, in the presence of multiple Higgs doublets, the tree-level FCNC's mediated by neutral Higgs bosons will be absent if all fermions of a given electric charge couple to no more than one Higgs doublet. An alternative way of suppressing FCNC in a two Higgs doublet model has been considered in Ref. [347], where it is shown that it is possible to have tree level FCNC completely fixed by the CKM matrix, as a result of an abelian symmetry.

#### 11.7.5.1 Two-Higgs-doublet models

General two Higgs doublet models [339] can have a more diverse Higgs-fermion coupling structure than in SUSY, and can be viewed as a simple extension of the SM to realise the spontaneous breakdown of  $SU(2)_L \times U(1)_Y$  to  $U(1)_{em}$ . Quite generally, if the two Higgs doublets contain opposite hypercharges, the scalar potential will contain mixing mass parameters of the kind  $m_{12}^2 \Phi_1^T i\sigma_2 \Phi_2 + h.c.$ . In the presence of such terms, both Higgs doublets will acquire vacuum expectation values,  $v_1/\sqrt{2}$  and  $v_2/\sqrt{2}$ , respectively, and the gauge boson masses will keep their SM expressions with the Higgs VEV  $v$  replaced by  $\sqrt{v_1^2 + v_2^2}$ . Apart from the mass terms, the most generic renormalisable and gauge invariant scalar potential for two Higgs doublets with opposite hypercharges contains seven quartic couplings, as presented in Eq. (11.46).

Just as in the MSSM case, after electroweak symmetry breaking and in the absence of  $CP$ -violation, the physical spectrum contains a pair of charged Higgs bosons  $H^\pm$ , a  $CP$ -odd Higgs boson  $A$  and two neutral  $CP$ -even Higgs bosons,  $h$  and  $H$ . The angles  $\alpha$  and  $\beta$  diagonalise the  $CP$ -even, and the  $CP$ -odd and charged Higgs sectors, respectively. The complete 2HDM is defined only after considering the interactions of the Higgs fields to fermions. Yukawa couplings of the generic form

$$-h_{ij}^a \bar{\Psi}_L^i H_a \Psi_R^j + h.c. \quad (11.54)$$

may be added to the renormalisable Lagrangian of the theory. Contrary to the SM, the two Higgs doublet structure does not ensure the alignment of the fermion mass terms  $m_{ij} = h_{ij}^a v_a/\sqrt{2}$  with the Yukawa couplings  $h_{ij}^a$ . This implies that quite generally the neutral Higgs boson will mediate flavour changing interactions between the different mass eigenstates of the fermion fields. Such flavour changing interactions should be suppressed in order to describe properly the Kaon,  $D$  and  $B$  meson phenomenology. Based on the Glashow–Weinberg criterion, it is clear that the simplest way of avoiding such transitions is to assume the existence of a symmetry that ensures the couplings of the fermions of each given quantum number (up-type and down-type quarks, charged and neutral leptons) to only one of the two Higgs doublets. Different models may be defined depending on which of these fermion fields couple to a given Higgs boson, see Table 11.13. Models of type-I are those in which all SM fermions couple to a single Higgs field. In type-II models, down-type quarks and charged leptons couple to a common Higgs field, while the up-type quarks and neutral leptons couple to the other. In models of type-III (lepton-specific), quarks couple to one of the Higgs bosons, while leptons couple to the other. Finally, in models of type-IV (flipped), up-type quarks and charged leptons couple to one of the Higgs fields while down-quarks and neutral leptons couple to the other.

**Table 11.13:** Higgs boson couplings to up, down and charged lepton-type  $SU(2)_L$  singlet fermions in the four discrete types of 2HDM models that satisfy the Glashow–Weinberg criterion.

Model	2HDM I	2HDM II	2HDM III	2HDM IV
$u$	$\Phi_2$	$\Phi_2$	$\Phi_2$	$\Phi_2$
$d$	$\Phi_2$	$\Phi_1$	$\Phi_2$	$\Phi_1$
$e$	$\Phi_2$	$\Phi_1$	$\Phi_1$	$\Phi_2$

The two Higgs doublet model phenomenology depends strongly on the size of the mixing angle  $\alpha$  and therefore on the quartic couplings. For large values of  $m_A$ ,  $\sin \alpha \rightarrow -\cos \beta$ ,  $\cos \alpha \rightarrow \sin \beta$ ,  $\cos(\beta - \alpha) \rightarrow 0$ , and the lightest  $CP$ -even Higgs boson  $h$  behaves as the SM Higgs boson. The same behaviour is obtained if the quartic couplings are such that  $\mathcal{M}_{12}^2 \sin \beta = -(\mathcal{M}_{11}^2 - m_h^2) \cos \beta$ . The latter condition represents a situation in which the couplings of  $h$  to fermions and weak gauge bosons become the same as in the SM, without decoupling the rest of the non-standard scalars and it is of particular interest due to the fact that the discovered Higgs boson has SM-like properties. This situation will be referred to as alignment, as in the MSSM case.

In analogy to the effects of  $CP$  violation in the SUSY 2HDM, some parameters of the Higgs potential can be complex and one has a model that is explicitly  $CP$  violating. The three neutral mass eigenstates mixed with each other and the Higgs phenomenology is analogous to the one described for the SUSY case above, with the caveat that when considering the neutral Higgs boson couplings to the scalar and pseudoscalar fermion bilinear densities, the proper weight should be considered for the respective 2HDM's.

In type-II Higgs doublet models, at large values of  $\tan \beta$  and moderate values of  $m_A$ , the non-standard Higgs bosons  $H$ ,  $A$  and  $H^\pm$  couple strongly to bottom quarks and  $\tau$  leptons. Hence the decay modes of the non-standard Higgs bosons tend to be dominated by the  $b$ -quark and  $\tau$ -lepton modes, including top quarks or neutrinos in the case of the charged Higgs boson. However, for large and negative values of  $\lambda_4$ , the charged Higgs boson mass may be sufficiently heavy to allow on-shell decays  $H^\pm \rightarrow W^\pm + (H, A)$ , via a trilinear coupling

$$g_{H^\pm W^\mp H, A} \simeq \frac{M_W}{v} \sin(\beta - \alpha)(p_{H^\pm} - p_{H, A}), \quad (11.55)$$

where  $p_{H^\pm}$  and  $p_{H, A}$  are the charged and neutral scalar Higgs boson momenta pointing into the vertex. On the other hand, for large and positive values of  $\lambda_5$ , the above charged Higgs boson decay into a  $W^\pm$  and the  $CP$ -odd Higgs boson may be allowed, but the heavy Higgs boson  $H$  may be sufficiently heavy to decay into a  $CP$ -odd Higgs boson and an on-shell  $Z$ ,  $H \rightarrow Z + A$ , via

$$g_{HZA} \simeq \frac{M_Z}{v} \sin(\beta - \alpha)(p_H - p_A). \quad (11.56)$$

The decay  $H^\pm \rightarrow W^\pm + H$ , on the other hand may be allowed only if  $\lambda_4 < -\lambda_5$ . The couplings controlling all the above decay modes are proportional to  $\sin(\beta - \alpha)$  and therefore they are unsuppressed in the alignment limit. Moreover, these could still be the dominant decay modes at moderate values of  $\tan \beta$ , offering a way to evade the current bounds obtained assuming a dominant decay into  $b$ -quarks or  $\tau$ -leptons.

The quartic couplings are restricted by the condition of stability of the effective potential as well as by the restriction of obtaining the proper value of the lightest  $CP$ -even Higgs boson mass. Close to the alignment limit, the lightest  $CP$ -even Higgs boson mass becomes approximately independent of  $m_A$  and is given by

$$m_h^2 \simeq v^2(\lambda_1 \cos^4 \beta + \lambda_2 \sin^4 \beta + 2\tilde{\lambda}_3 v^2 \cos^2 \beta \sin^2 \beta + 4\lambda_6 \cos^3 \beta \sin \beta + 4\lambda_7 \sin^3 \beta \cos \beta), \quad (11.57)$$

where  $\tilde{\lambda}_3 = \lambda_3 + \lambda_4 + \lambda_5$ .

The stability conditions imply the positiveness of all masses, as well as the avoidance of run-away solutions to large negative

values of the fields in the scalar potential. These conditions imply

$$\begin{aligned} \lambda_1 \geq 0, \quad \lambda_2 \geq 0, \quad \lambda_3 + \lambda_4 - |\lambda_5| &\geq -\sqrt{\lambda_1 \lambda_2}, \quad \lambda_3 \geq -\sqrt{\lambda_1 \lambda_2}, \\ 2|\lambda_6 + \lambda_7| &< \frac{\lambda_1 + \lambda_2}{2} + \tilde{\lambda}_3, \end{aligned} \quad (11.58)$$

where the first four conditions are necessary and sufficient conditions in the case of  $\lambda_6 = \lambda_7 = 0$ , while the last one is a necessary condition in the case all couplings are non-zero. Therefore, to obtain the conditions that allow the decays  $H^\pm \rightarrow W^\pm H$ ,  $A$  and  $H \rightarrow ZA$ ,  $\lambda_3$  should take large positive values in order to compensate for the effects of  $\lambda_4$  and  $\lambda_5$ . For more detailed discussions about 2HDM phenomenology, see for example Refs. [44, 339].

### 11.7.5.2 Higgs triplets

Electroweak triplet scalars are the simplest non-doublet extension of the SM that can participate in the spontaneous breakdown of  $SU(2)_L \times U(1)_Y$  to  $U(1)_{\text{em}}$ . Two types of model have been developed in enough detail to make a meaningful comparison to LHC data: the Higgs triplet model (HTM) [348] and the Georgi–Machacek model (GM) [349].

The Higgs triplet model extends the SM by the addition of a complex  $SU(2)_L$  triplet scalar field  $\Delta$  with hypercharge  $Y = 2$ , and a general gauge-invariant renormalisable potential  $V(\Phi, \Delta)$  for  $\Delta$  and the SM Higgs doublet  $\Phi$ . The components of the triplet field can be parameterised as

$$\Delta = \frac{1}{\sqrt{2}} \begin{pmatrix} \Delta^+ & \sqrt{2}\Delta^{++} \\ v_\Delta + \delta + i\xi & -\Delta^+ \end{pmatrix}. \quad (11.59)$$

where  $\Delta^+$  is a singly-charged field,  $\Delta^{++}$  is a doubly-charged field,  $\delta$  is a neutral  $CP$ -even scalar,  $\xi$  is a neutral  $CP$ -odd scalar, and  $v_\Delta$  is the triplet VEV. The general scalar potential mixes the doublet and triplet components. After electroweak symmetry breaking there are seven physical mass eigenstates, denoted  $H^{\pm\pm}$ ,  $H^\pm$ ,  $A$ ,  $H$ , and  $h$ .

A distinguishing feature of the HTM is that it violates the custodial symmetry of the SM; thus the  $\rho$  parameter deviates from 1 even at tree level. Letting  $x$  denote the ratio of triplet and doublet VEVs, the tree level expression is

$$\rho = \frac{1 + 2x^2}{1 + 4x^2}. \quad (11.60)$$

The measured value of the  $\rho$  parameter then limits the triplet VEV to be quite small,  $x \lesssim 0.03$ , or  $v_\Delta < 8$  GeV. This constraint severely limits the role of the triplet scalar in the EWSB mechanism.

The small VEV of the Higgs triplet in the HTM is a virtue from the point of view of generating neutrino masses without the necessity for introducing right-handed neutrino fields. The gauge invariant dimension four interaction

$$h_{\nu_{ij}} \ell_i^T C^{-1} i\sigma_2 \Delta \ell_j, \quad (11.61)$$

where  $\ell_i$  are the lepton doublets,  $C$  is the charge conjugation matrix, and  $h_{\nu_{ij}}$  is a complex symmetric coupling matrix, generates a Majorana mass matrix for the neutrinos:

$$m_{\nu_{ij}} = \sqrt{2} h_{\nu_{ij}} v_\Delta. \quad (11.62)$$

This can be combined with the usual neutrino seesaw to produce what is known as the type-II seesaw [350].

The HTM suggests the exciting possibility of measuring parameters of the neutrino mass matrix at the LHC. If the doubly-charged Higgs boson is light enough and/or its couplings to  $W^+W^+$  are sufficiently suppressed, then its primary decay is into same-sign lepton pairs:  $H^{++} \rightarrow \ell_i^+ \ell_j^+$ ; from Eq. (11.61) and Eq. (11.62), it is apparent that these decays are in general lepton-flavor violating with branchings proportional to elements of the neutrino mass matrix [351].

Precision electroweak data constrain the mass spectrum as well as the triplet VEV of the HTM [352]. These constraints favour a spectrum where  $H^{++}$  is the lightest of the exotic bosons, and



where the mass difference between  $H^+$  and  $H^{++}$  is a few hundred GeV. The favoured triplet VEV is a few GeV, which also favours  $H^{++}$  decays into  $W^+W^+$  over same-sign dileptons.

The GM model addresses the  $\rho$  parameter constraint directly by building in custodial symmetry. Writing the complex scalar doublet of the SM as a  $(2, 2)$  under  $SU(2)_L \times SU(2)_R$ , it is obvious that the next simplest construction respecting custodial symmetry is a scalar transforming like a  $(3, 3)$  [353]. These nine real degrees of freedom correspond to a complex electroweak triplet combined with a real triplet, with the scalar potential required to be invariant under  $SU(2)_R$ . Under the custodial  $SU(2)_{L+R}$ , they transform as  $1 \oplus 3 \oplus 5$ , with a  $CP$ -even neutral scalar as the custodial singlet (thus matching the SM Higgs boson), a  $CP$ -odd neutral scalar in the custodial triplet, and another  $CP$ -even neutral scalar in the custodial 5-plet.

The scalar components can be decomposed as

$$\Xi = \begin{pmatrix} \chi_3^* & \xi_1 & \chi_1 \\ -\chi_2^* & \xi_2 & \chi_2 \\ \chi_1^* & -\xi_1^* & \chi_3 \end{pmatrix}, \quad (11.63)$$

where  $\xi_2$  is a real scalar and the others are complex scalars. Linear combinations of these scalars account for the neutral custodial singlet, a neutral and singly-charged field making up the custodial triplet, and neutral, singly-charged, and doubly-charged fields making up the custodial 5-plet.

When combined with the usual SM doublet field  $\Phi$ , the electroweak scale  $v$  is now related to the doublet and triplet VEVs by

$$v^2 = v_\Phi^2 + 8v_\Xi^2. \quad (11.64)$$

Note that the GM triplets by themselves are sufficient to explain electroweak symmetry breaking and the existence of a 125 GeV neutral boson along with a custodial triplet of Goldstone bosons; the complex doublet field in the GM model is required to generate fermion masses via the usual dimension four Yukawa couplings. This raises the question of whether one can rule out the possibility that the 125 GeV boson is the neutral member of a custodial 5-plet rather than a custodial singlet, without invoking decays to fermions. A conclusive answer is given by observing that the ratio of the branching fractions to  $W$  versus  $Z$  bosons is completely determined by the custodial symmetry properties of the boson. For a custodial 5-plet, the ratio of the signal strength to  $WW$  over that to  $ZZ$  is predicted to be  $1/4$  that of a SM Higgs boson [353], and thus already ruled out by the experimental results presented in Section 11.6.

Another interesting general feature of Higgs triplet models is that, after mixing, the SM-like neutral boson can have stronger couplings to  $WW$  and  $ZZ$  than predicted by the SM [354]; this is in contrast to mixing with additional doublets and singlet, which can only reduce the  $WW$  and  $ZZ$  couplings versus the SM. This emphasises that LHC Higgs data cannot extract model independent coupling strengths for the Higgs boson [244].

Because of the built-in custodial symmetry, the triplet VEV in the GM model can be large compared to the doublet VEV. The custodial singlet neutral boson from the triplets mixes with the neutral boson from the doublet. Two interesting special cases are (i) the triplet VEV is small and the 125 GeV boson is SM-like except for small deviations, and (ii) the 125 GeV boson is mostly the custodial singlet neutral boson from the electroweak triplets. The phenomenology of the doubly-charged and singly-charged bosons is similar to that of the HTM. The constraints on the GM model from precision electroweak data, LEP data, and current LHC data are summarised in Ref. [44].

### 11.7.6 Composite Higgs models

Within the SM, EWSB is posited but has no dynamical origin. Furthermore, the Higgs boson appears to be unnaturally light. A scenario that remedies these two catches is to consider the Higgs boson as a bound state of new dynamics becoming strong around the weak scale. The Higgs boson can be made significantly lighter than the other resonances of the strong sector if it appears as a pseudo-Nambu-Goldstone boson, see Refs. [11] for reviews.

#### 11.7.6.1 Little Higgs models

The idea behind the Little Higgs boson models [355] is to identify the Higgs doublet as a (pseudo) Nambu-Goldstone boson while keeping some sizeable non-derivative interactions, in particular a largish Higgs quartic interaction. By analogy with QCD where the pions  $\pi^{\pm,0}$  appear as Nambu-Goldstone bosons associated to the breaking of the chiral symmetry  $SU(2)_L \times SU(2)_R/SU(2)$ , switching on some interactions that break explicitly the global symmetry will generate masses for the would-be massless Nambu-Goldstone bosons of the order of  $g\Lambda_{G/H}/(4\pi)$ , where  $g$  is the coupling of the symmetry breaking interaction and  $\Lambda_{G/H} = 4\pi f_{G/H}$  is the dynamical scale of the global symmetry breaking  $G/H$ . In the case of the Higgs boson, the top Yukawa interaction or the gauge interactions themselves will certainly break explicitly (part of) the global symmetry since they act non-linearly on the Higgs boson. Therefore, obtaining a Higgs boson mass around 125 GeV would demand a dynamical scale  $\Lambda_{G/H}$  of the order of 1 TeV, which is known to lead to too large oblique corrections. Raising the strong dynamical scale by at least one order of magnitude requires an additional selection rule to ensure that a Higgs boson mass is generated at the 2-loop level only

$$m_H^2 = \frac{g^2}{16\pi^2} \Lambda_{G/H}^2 \rightarrow m_H^2 = \frac{g^2 g_2^2}{(16\pi^2)^2} \Lambda_{G/H}^2. \quad (11.65)$$

The way to enforce this selection rule is through a ‘‘collective breaking’’ of the global symmetry:

$$\mathcal{L} = \mathcal{L}_{G/H} + g_1 \mathcal{L}_1 + g_2 \mathcal{L}_2. \quad (11.66)$$

Each interaction  $\mathcal{L}_1$  or  $\mathcal{L}_2$  individually preserves a subset of the global symmetry such that the Higgs boson remains an exact Nambu-Goldstone boson whenever either  $g_1$  or  $g_2$  is vanishing. A mass term for the Higgs boson can be generated only by diagrams involving simultaneously both interactions. At one-loop, such diagrams are not quadratically divergent, so the Higgs boson mass is not UV sensitive. Explicitly, the cancellation of the SM quadratic divergences is achieved by a set of new particles around the Fermi scale: gauge bosons, vector-like quarks, and extra massive scalars, which are related, by the original global symmetry, to the SM particles with the same spin. Contrary to SUSY, the cancellation of the quadratic divergences is achieved by same-spin particles. These new particles, with definite couplings to SM particles as dictated by the global symmetries of the theory, are perfect goals for the LHC.

The simplest incarnation of the collective breaking idea, the so-called littlest Higgs boson model, is based on a non-linear  $\sigma$ -model describing the spontaneous breaking  $SU(5)$  down to  $SO(5)$ . A subgroup  $SU(2)_1 \times U(1)_1 \times SU(2)_2 \times U(1)_2$  is weakly gauged. This model contains a weak doublet, that is identified with the Higgs doublet, and a complex weak triplet whose mass is not protected by collective breaking. Other popular little Higgs models are based on different coset spaces: minimal moose ( $SU(3)^2/SU(3)$ ), the simplest little Higgs ( $SU(3)^2/SU(2)^2$ ), the bestest little Higgs ( $SO(6)^2/SO(6)$ ). For comprehensive reviews, see Ref. [356].

Generically, oblique corrections in Little Higgs models are reduced either by increasing the coupling of one of the gauge groups (in the case of product group models) or by increasing the masses of the  $W$  and  $Z$  partners, leading ultimately to a fine-tuning of the order of a few percents (see for instance Ref. [357] and references therein). The compatibility of Little Higgs models with experimental data is significantly improved when the global symmetry involves a custodial symmetry as well as a  $T$ -parity [358] under which, in analogy with  $R$ -parity in SUSY models, the SM particles are even and their partners are odd. Such Little Higgs models would therefore appear in colliders as jet(s) with missing transverse energy [359] and the ATLAS and CMS searches for squarks and gluinos (see ‘‘Supersymmetry, Part II’’ in this review) can be recast to obtain limits on the masses of the heavy vector-like quarks. The  $T$ -even top partner, with an expected mass below 1 TeV to cancel the top loop quadratic divergence without too much fine-tuning, would decay dominantly into a  $t + Z$  pair or into a  $b + W$  pair or even into  $t + H$ . The latest CMS and ATLAS direct searches [360] for vector-like top partners put a lower bound

around 1.1–1.3 TeV (for various branching fraction combinations), excluding the most natural region of the parameter space of these models, i.e., imposing a fine-tuning below the percent level.

The motivation for Little Higgs models is to solve the little hierarchy problem, i.e., to push the need for new physics (responsible for the stability of the weak scale) up to around 10 TeV. Per se, Little Higgs models are effective theories valid up to their cut-off scale  $\Lambda_{G/H}$ . Their UV completions could either be weakly or strongly coupled.

11.7.6.2 Models of partial compositeness

Even in composite models, the Higgs boson cannot appear as a regular resonance of the strong sector without endangering the viability of the setup when confronted to data. The way out is that the Higgs boson appears as a pseudo Nambu–Goldstone boson: the new strongly coupled sector is supposed to be invariant under a global symmetry  $G$  spontaneously broken to a subgroup  $H$  at the scale  $f$  (the typical mass scale of the resonances of the strong sector is  $m_\rho \sim g_\rho f$  with  $g_\rho$  the characteristic coupling of the strong sector). To avoid conflict with EW precision measurements, the strong interactions themselves should better not break the EW symmetry. Hence the SM gauge symmetry itself should be contained in  $H$ . See Table 11.14 for a few examples of coset spaces.

**Table 11.14:** Global symmetry breaking patterns and the corresponding Goldstone boson contents of the SM, the minimal composite Higgs model, the next to minimal composite Higgs model, and the minimal composite two Higgs doublet model. Note that the SU(3) model does not have a custodial invariance.  $a$  denotes a CP-odd scalar while  $h$  and  $H$  are CP-even scalars.

Model	Symmetry Pattern	Goldstones
SM	SO(4)/SO(3)	$W_L, Z_L$
–	SU(3)/SU(2)×U(1)	$W_L, Z_L, H$
MCHM	SO(5)/SO(4)	$W_L, Z_L, H$
NMCHM	SO(6)/SO(5)	$W_L, Z_L, H, a$
MC2HM	SO(6)/SO(4)×SO(2)	$W_L, Z_L, h, H, H^\pm, a$

The SM (light) fermions and gauge bosons cannot be part of the strong sector itself since LEP data have already put stringent bounds on the compositeness scale of these particles far above the TeV scale. The gauge bosons couple to the strong sector by a weak gauging of a SU(2)×U(1) subgroup of the global symmetry  $G$ . Inspiration for the construction of such models comes from the AdS/CFT correspondence: the components of a gauge field along an extra warped space dimension can be interpreted as the Goldstone bosons resulting from the breaking of global symmetry of the strong sector. The couplings of the SM fermions to the strong sector could a priori take two different forms:

- (i) a bilinear coupling of two SM fermions to a composite scalar operator,  $\mathcal{O}$ , of the form  $\mathcal{L} = y \bar{q}_L u_R \mathcal{O} + h.c.$ , in simple analogy with the SM Yukawa interactions. This is the way fermion masses were introduced in technicolor theories and it generically comes with severe flavour problems and calls for extended model-building gymnastics [12] to circumvent them;
- (ii) a linear mass mixing with fermionic vector-like operators:  $\mathcal{L} = \lambda_L \bar{q}_L \mathcal{Q}_R + \lambda_R \bar{U}_L u_R$ .  $\mathcal{Q}$  and  $\mathcal{U}$  are two fermionic composite operators of mass  $M_Q$  and  $M_U$ .

Being part of the composite sector, the composite fermionic operators can have a direct coupling of generic order  $Y_*$  to the Higgs boson. In analogy with the photon- $\rho$  mixing in QCD, once the linear mixings are diagonalised, the physical states are a linear combination of elementary and composite fields. Effective Yukawa couplings are generated and read for instance for the up-type quark

$$y = Y_* \sin \theta_L \sin \theta_R \tag{11.67}$$

where  $\sin \theta_i = \lambda_i / \sqrt{M_{Q,U}^2 + \lambda_i^2}$ ,  $i = L, R$ , measure the amount of compositeness of the SM left- and right-handed up-type quark.

If the strong sector is flavour-anarchic, i.e., if the couplings of the Higgs boson to the composite fermions does not exhibit any particular flavour structure, the relation Eq. (11.67) implies that the light fermions are mostly elementary states ( $\sin \theta_i \ll 1$ ), while the third generation quarks need to have a sizable degree of compositeness. The partial compositeness paradigm offers an appealing dynamical explanation of the hierarchies in the fermion masses. In fact, assuming the strong sector to be almost conformal above the confinement scale, the low-energy values of the mass-mixing parameters  $\lambda_{L,R}$  are determined by the (constant) anomalous dimension of the composite operator they mix with. If the UV scale at which the linear mixings are generated is large, then  $\mathcal{O}(1)$  differences in the anomalous dimensions can generate naturally large hierarchies in the fermion masses via renormalisation group running [361]. While the introduction of partial compositeness greatly ameliorated the flavor problem of the original composite Higgs models, nevertheless, it did not solve the issue completely, at least in the case where the strong sector is assumed to be flavour-anarchic [362]. While the partial compositeness set-up naturally emerges in models built in space-times with extra dimensions, no fully realistic microscopic realisation of partial compositeness has been proposed in the literature.

Another nice aspect of the partial compositeness structure is the dynamical generation of the Higgs potential that is not arbitrary like in the SM. The Higgs boson being a pseudo-Nambu–Goldstone boson, its mass does not receive any contribution from the strong sector itself but it is generated at the one-loop level via the couplings of the SM particles to the strong sector since these interactions are breaking the global symmetries under which the Higgs doublet transforms non-linearly. Obtaining  $v \ll f$ , as required phenomenologically, requires some degree of tuning, which scales like  $\xi \equiv v^2/f^2$ . A mild tuning of the order of 10% ( $\xi \approx 0.1$ ) is typically enough to comply with electroweak precision constraints. This is an important point: in partial compositeness models, the entire Higgs potential is generated at one loop, therefore the separation between  $v$  and  $f$  can only be obtained at a price of a tuning. This marks a difference with respect to the Little Higgs models which realise a parametric hierarchy between the quartic and mass terms through the collective symmetry breaking mechanism. In fact in Little Higgs models, the quartic coupling is a tree-level effect, leading to a potential

$$V(H) \approx \frac{g_{SM}^2}{16\pi^2} m_\rho^2 H^2 + g_{SM}^2 H^4, \tag{11.68}$$

where  $g_{SM}$  generically denotes the SM couplings. The minimisation condition reads  $v^2/f^2 \sim g_\rho^2/(16\pi^2)$ , therefore  $v$  is formally loop suppressed with respect to  $f$ . This is the major achievement of the Little Higgs constructions, which however comes at the price of the presence of sub-TeV vectors carrying EW quantum numbers and therefore giving rise generically to large oblique corrections to the propagators of the  $W$  and the  $Z$  gauge bosons.

After minimisation, the dynamically generated potential leads to an estimate of the Higgs boson mass as

$$m_H^2 \approx g_\rho^3 y_t^2 \pi^2 v^2. \tag{11.69}$$

It follows that the limit  $f \rightarrow \infty$ , i.e.,  $\xi \rightarrow 0$ , is a true decoupling limit: all the resonances of the strong sector become heavy but the Higgs boson whose mass is protected by the symmetries of the coset  $G/H$ . When compared to the experimentally measured Higgs boson mass, this estimate puts an upper bound on the strength of the strong interactions:  $g_\rho \lesssim 2$ . In this limit of not so large coupling, the Higgs potential receives additional contributions. In particular, the fermionic resonances in the top sector which follow from the global symmetry structure of the new physics sector can help raising the Higgs boson mass. Using some dispersion relation techniques, the mass of the Higgs is connected to the resonance masses. In the minimal SO(5)/SO(4) model, it was shown [363] that a 125 GeV mass can be obtained if at least one of the fermionic resonances is lighter than  $\sim 1.4 f$ . As in SUSY scenarios, the top sector is playing a crucial role in the dynamics of EWSB and can provide the first direct signs of new physics. The direct searches for these top partners, in particular

the ones with exotic electric charges 5/3, are already exploring the natural parameter spaces of these models [364].

The main physics properties of a pseudo Nambu–Goldstone Higgs boson can be captured in a model-independent way by a small number of higher-dimensional operators. Indeed, the strong dynamics at the origin of the composite Higgs boson singles out a few operators among the complete list discussed earlier in Section 11.6: these are the operators that involve extra powers of the Higgs doublets and they are therefore generically suppressed by a factor  $1/f^2$  as opposed to the operators that involve extra derivatives or gauge bosons that are suppressed by a factor  $1/(g_\rho^2 f^2)$ . The relevant effective Lagrangian describing a strongly interacting light Higgs boson is:

$$\begin{aligned} \mathcal{L}_{\text{SILH}} = & \frac{c_H}{2f^2} (\partial_\mu (\Phi^\dagger \Phi))^2 + \frac{c_T}{2f^2} (\Phi^\dagger \overleftrightarrow{D}^\mu \Phi)^2 - \frac{c_6 \lambda}{f^2} (\Phi^\dagger \Phi)^3 \\ & + \left( \sum_f \frac{c_f y_f}{f^2} \Phi^\dagger \Phi \bar{f}_L \Phi f_R + \text{h.c.} \right). \end{aligned} \quad (11.70)$$

Typically, these new interactions induce deviations in the Higgs boson couplings that scale like  $\mathcal{O}(v^2/f^2)$ . Hence the measurements of the Higgs boson couplings can be translated into some constraints on the compositeness scale,  $4\pi f$ , of the Higgs boson. The peculiarity of these composite models is that, due to the Goldstone nature of the Higgs boson, the direct couplings to photons and gluons are further suppressed and generically the coupling modifiers scale like

$$\begin{aligned} \kappa_{W,Z,f} & \sim 1 + \mathcal{O}\left(\frac{v^2}{f^2}\right), \quad \kappa_{Z\gamma} \sim \mathcal{O}\left(\frac{v^2}{f^2}\right), \\ \kappa_{\gamma,g} & \sim \mathcal{O}\left(\frac{v^2}{f^2} \times \frac{y_t^2}{g_\rho^2}\right), \end{aligned} \quad (11.71)$$

where  $g_\rho$  denotes the typical coupling strength among the states of the strongly coupled sector and  $y_t$  is the top Yukawa coupling, the largest interaction that breaks the Goldstone symmetry. The  $\kappa_{Z\gamma,\gamma,g}$  coupling modifiers are not generated by the strong coupling operators of Eq. (11.70) but by some subleading form-factor operator generated by loops of heavy resonances of the strong sector. The coupling modifiers also receive additional contributions from the other resonances of the strong sector, in particular the fermionic resonances of the top sector that are required to be light to generate a 125 GeV Higgs boson mass. Some indirect information on the resonance spectrum could thus be inferred by a precise measurement of the Higgs boson coupling deviations. However, it was realised, see in particular Ref. [266], that the task is actually complicated by the fact that, in the minimal models, these top partners give a contribution to both  $\kappa_t$  (resulting from a modification of the top Yukawa coupling) and  $\kappa_\gamma$  and  $\kappa_g$  (resulting from new heavy particles running into the loops) and the structure of interactions is such that the net effect vanishes for inclusive quantities like  $\sigma(gg \rightarrow H)$  or  $\Gamma(H \rightarrow \gamma\gamma)$  as a consequence of the Higgs low energy theorem [23, 24, 264]. So, one would need to rely on differential distribution, like the Higgs boson  $p_T$  distribution discussed in Section 11.2.4.1, to see the top partner effects in Higgs data [365]. The off-shell channel  $gg \rightarrow H^* \rightarrow 4\ell$  [243] and the double Higgs boson production  $gg \rightarrow HH$  [366] can also help to resolve the gluon loop and separate the top and top-partner contributions.

### 11.7.6.3 Minimal composite Higgs models

The minimal composite Higgs models (MCHM) are concrete examples of the partial compositeness paradigm. The Higgs doublet is described by the coset space  $\text{SO}(5)/\text{SO}(4)$  where a subgroup  $\text{SU}(2)_L \times \text{U}(1)_Y$  is weakly gauged and under which the four Goldstone bosons transform as a doublet of hypercharge 1. There is some freedom on how the global symmetry is acting on the SM fermions: in MCHM4 the quarks and leptons are embedded into spinorial representations of  $\text{SO}(5)$ , while in MCHM5 they are part of fundamental representations (it might also be interesting phenomenologically to consider larger representations

like MCHM14 [367] with the SM fermions inside a representation of dimension 14). It is also possible to consider that fermions of different chirality and flavour are in different representations of  $\text{SO}(5)$ , leading to a more varied phenomenology [368]. The non-linearly realised symmetry acting on the Goldstone bosons leads to general predictions of the coupling of the Higgs boson to the EW gauge bosons. For instance, it can be shown that the quadratic terms in the  $W$  and  $Z$  bosons read

$$m_W^2(H) \left( W_\mu W^\mu + \frac{1}{2 \cos^2 \theta_W} Z_\mu Z^\mu \right), \quad (11.72)$$

with  $m_W(H) = \frac{gf}{2} \sin \frac{H}{f}$ . Expanding around the EW vacuum, the expression of the weak scale is  $v = f \sin(\langle H \rangle / f)$ . And the values of the modified Higgs boson couplings to the  $W$  and  $Z$  become:

$$g_{HVV} = \frac{2m_V^2}{v} \sqrt{1 - v^2/f^2}, \quad g_{HHVV} = \frac{2m_V^2}{v^2} (1 - 2v^2/f^2). \quad (11.73)$$

Note that the Higgs boson couplings to gauge bosons is always suppressed compared to the SM prediction. This is a general result [369] that holds as long as the coset space is compact.

The Higgs boson couplings to the fermions depend on the representation which the SM fermions are embedded into. The most commonly used embeddings consider all fermion doublets and singlets in the same representations. While, in MCHM4 and MCHM5, the modifications of the couplings depend only on the Higgs boson compositeness scale, in MCHM14 the leading corrections depend also on the mass spectrum of the resonances [367]. This is due to the fact that more than one  $\text{SO}(5)$  invariant gives rise to SM fermion masses. The  $(\kappa_V, \kappa_f)$  experimental fit of the Higgs boson couplings can be used to derive a lower bound on the Higgs boson compositeness scale  $4\pi f \gtrsim 9 \text{ TeV}$ , which is less stringent than the indirect bound obtained from EW precision data,  $4\pi f \gtrsim 15 \text{ TeV}$  [370] but more robust and less subject on assumptions [371].

### 11.7.6.4 Twin Higgs models

In all composite models presented above, the particles responsible for canceling the quadratic divergences in the Higgs boson mass are charged under the SM gauge symmetries. In particular, the top partner carries color charge, implying a reasonably large minimal production cross section at the LHC. An alternative scenario, which is experimentally quite challenging and might explain the null result in various new physics searches, is the case nowadays referred to as “neutral naturalness” [13, 14], where the particles canceling the 1-loop quadratic divergences are neutral under the SM. The canonical example for such theories is the Twin Higgs model of Ref. [13]. This is an example of a pseudo-Goldstone boson model with an approximate global  $\text{SU}(4)$  symmetry broken to  $\text{SU}(3)$ . The Twin Higgs model is obtained by gauging the  $\text{SU}(2)_A \times \text{SU}(2)_B$  subgroup of  $\text{SU}(4)$ , where  $\text{SU}(2)_A$  is identified with the SM  $\text{SU}(2)_L$ , while  $\text{SU}(2)_B$  is the twin  $\text{SU}(2)$  group. Gauging this subgroup breaks the  $\text{SU}(4)$  symmetry explicitly, but quadratically divergent corrections do not involve the Higgs boson when the gauge couplings of the two  $\text{SU}(2)$  subgroups are equal,  $g_A = g_B$ . The  $\text{SU}(4) \rightarrow \text{SU}(3)$  breaking will also result in the breaking of the twin  $\text{SU}(2)_B$  group and, as a result, three of the seven Goldstone bosons will be eaten, leaving 4 Goldstone bosons corresponding to the SM Higgs doublet. In fact, imposing the  $Z_2$  symmetry on the full model will ensure the cancellation of all 1-loop quadratic divergences to the Higgs boson mass. Logarithmically divergent terms can, however, arise for example from gauge loops, leading to a Higgs boson mass of order  $g^2 f / 4\pi$ , which is of the order of the physical Higgs boson mass for  $f \sim 1 \text{ TeV}$ . The quadratic divergences from the top sector can be eliminated if the  $Z_2$  protecting the Higgs boson mass remains unbroken by the couplings that result in the top Yukawa coupling. This can be achieved by introducing top partners charged under a twin  $\text{SU}(3)_C$ . In this case, the quadratic divergences are cancelled by top partners that are neutral under the SM gauge symmetries.

Twin Higgs models are low-energy effective theories valid up to a cutoff scale of order  $\Lambda \sim 4\pi f \sim 5\text{--}10 \text{ TeV}$ , beyond which a UV

completion has to be specified. The simplest such possibility is to also make the Higgs boson composite, and to UV complete the twin Higgs model via gauge and top partners at masses of the order of a few TeV. A concrete implementation is the holographic twin Higgs model [372], which also incorporates a custodial symmetry to protect the  $T$ -parameter from large corrections. It is based on a warped extra dimensional theory with a bulk  $SO(8)$  gauge group, which incorporates the  $SU(4)$  global symmetry discussed above enlarged to contain the  $SU(2)_L \times SU(2)_R$  custodial symmetry. In addition the bulk contains either a full  $SU(7)$  group or an  $SU(3) \times SU(3) \times U(1) \times U(1) \times Z_2$  subgroup of it to incorporate the QCD, its twin, and the hypercharge local symmetries. The breaking on the UV brane is to the SM symmetries and their twin symmetries, while on the IR brane  $SO(8) \rightarrow SO(7)$ , giving rise to the 7 Goldstone bosons, three of which will be again eaten by the twin  $W, Z$ . The main difference compared to ordinary composite Higgs models is that, in composite twin Higgs models, the cancellation of the one-loop quadratic divergences is achieved by the twin partners. They have a mass of order  $700 \text{ GeV} - 1 \text{ TeV}$  and they are uncharged under the SM gauge group. This allows the IR scale of the warped extra dimension to be raised to the multi-TeV range without reintroducing the hierarchy problem. The role of the composite partners is to UV complete the theory, rather than to cancel the one-loop quadratic divergences. For more details about the composite twin Higgs models, see Refs. [373].

### 11.7.7 Searches for signatures of extended Higgs sectors

The measurements described in Sections 11.3 to 11.6 have established the existence of one state of the electroweak symmetry breaking sector, compatible with a SM Higgs boson, but not that it is the only one. As was discussed above, several classes of models beyond the SM require extended Higgs sectors. The searches are typically designed to be as model-independent as possible<sup>8</sup> and can be categorised in the classes summarised as follows:

- (i) the search for an additional  $CP$ -even state mostly in the high mass domain decaying to vector bosons, which would correspond either to the heavy  $CP$ -even state in a generic 2HDM where the light state would be the discovered Higgs boson at  $125 \text{ GeV}$  or to a generic additional singlet;
- (ii) the search for a state in the high mass domain decaying to pairs of fermions, which would correspond to the  $CP$ -odd  $A$  or the heavy  $CP$ -even state  $H$  in a generic 2HDM;
- (iii) the search for charged Higgs bosons, which also appear in generic 2HDMs;
- (iv) the search for a  $CP$ -odd state  $a$  in the low mass region which appears in the NMSSM in a variety of final states, e.g., with one or two  $a$  bosons decaying to pairs of photons, muons, taus, and  $b$ -quarks;
- (v) the search for doubly charged Higgs bosons which are expected in extensions of the Higgs sector with triplets.

Below is a concise description of the most recent searches performed at the LHC and elsewhere. A summary of these searches in terms of final states is given in Table 11.15 where the corresponding references are given for more details.

#### 11.7.7.1 Searches for an additional $CP$ -even state

##### (a) Exclusion limits from LEP

The searches for the SM Higgs boson at LEP provided an absolute lower limit of  $114 \text{ GeV}$  on its mass. These searches are also relevant for non-SM Higgs bosons. These searches were interpreted as 95% CL upper bounds on the ratio of the coupling  $g_{HZZ}$  to its SM prediction as a function of the Higgs boson mass [122, 436]. These results have an impact on MSSM benchmarks such as the low- $m_H$  scenario, which is also nearly ruled out by current direct constraints and charged Higgs boson limits from LHC. These results also impact scenarios of light  $CP$ -even Higgs boson of the NMSSM which are constrained to project predominantly onto the

<sup>8</sup>Still, most non-SUSY models are likely to include further states and dynamics above the weak scale to stabilise the scalar sector and this new and unknown physics may influence the searches described in this section in a way difficult to estimate.

EW singlet component. Additional interest for these scenarios is due to the slight excess observed at LEP [122] at a Higgs boson mass hypothesis of approximately  $98 \text{ GeV}$ .

##### (b) Searches at the LHC

At the LHC, the searches for the SM Higgs boson before the 2012 discovery covered a wide range of mass hypotheses up to approximately  $1 \text{ TeV}$ . After the discovery, the SM Higgs boson searches have been reappraised to search for a heavy  $CP$ -even state, extending progressively the search mass range beyond  $1 \text{ TeV}$ . This state could be the heavy  $CP$ -even Higgs boson of a 2HDM, or a generic additional singlet. In both cases, the natural width of the additional  $H$  state can be very different from that of the SM Higgs boson. To preserve unitarity of the longitudinal vector boson scattering and the longitudinal vector boson scattering into fermion pairs, the couplings of the additional  $CP$ -even Higgs boson to gauge bosons and fermions should not be too large and should constrain the natural width to be smaller than that of a unique Higgs boson at high mass with couplings to fermions and gauge bosons as predicted by the SM (and provided that trilinear and quartic couplings are not too large and that no new state affects the heavy state total width). It is therefore reasonable to consider total widths for the high mass  $CP$ -even state smaller than the equivalent SM width. Two specific cases have been considered: (i) the SM width using the complex pole scheme (CPS), and (ii) the narrow width approximation. For the sake of generality, these searches are now done as a function of the Higgs boson mass and total width.

Searches for the Higgs boson in the channels  $H \rightarrow \gamma\gamma$ ,  $H \rightarrow Z\gamma$ ,  $H \rightarrow WW^{(*)}$  leptonic and semi-leptonic, and in the  $H \rightarrow ZZ^{(*)}$  searches in the  $4\ell$ ,  $\ell\ell q\bar{q}$  and  $\ell\ell\nu\nu$  channels have also been done, but some of them are simple reinterpretations of the SM Higgs boson search in the CPS scheme. References for these searches are summarised in Table 11.15.

##### (c) Searches for an additional resonance decaying to a pair of Higgs bosons

In addition to the rare and expected Higgs boson pair production mode, high mass  $CP$ -even Higgs bosons can be searched for in the resonant double Higgs boson mode. Searches for such processes, where the Higgs boson is used as a tool for searches for BSM phenomena, have been carried out in a variety of distinct modes depending on the subsequent decays of each Higgs bosons. ATLAS and CMS have searched for the  $H \rightarrow hh \rightarrow b\bar{b}\tau\tau$ ,  $b\bar{b}\gamma\gamma$ ,  $H \rightarrow hh \rightarrow 4b$ ,  $H \rightarrow hh \rightarrow \gamma\gamma WW^*$ ,  $H \rightarrow hh \rightarrow b\bar{b}WW^*$ ,  $H \rightarrow hh \rightarrow WW^* WW^*$  and  $H \rightarrow hh \rightarrow b\bar{b}ZZ^*$  final states. For mass hypotheses of an additional Higgs boson below  $500 \text{ GeV}$ , the two dominant search channels are the  $b\bar{b}\gamma\gamma$  and the  $b\bar{b}\tau\tau$  channels. For masses above  $500 \text{ GeV}$ , the most powerful search is with the  $4b$  final state. As illustrated in Figure 11.19, these searches provide useful limits in the low  $\tan\beta$  and high mass domain. The list of references for these searches is given in Table 11.15.

##### (d) Searches for an additional state with the presence of the Higgs boson

In the post-discovery era, analyses searching for additional Higgs bosons need to take into account the presence of the  $125 \text{ GeV}$  Higgs boson. For searches with sufficiently high mass resolution to disentangle the additional states which are not degenerate in mass, the strength of the observed state and limits on the signal strength of a potential additional state can be set independently, as discussed in the next section. However, in some cases where channels do not have a sufficiently fine mass resolution to resolve states nearly degenerate in mass, specific analyses need to be designed. There are two examples of such analyses: (i) the search for an additional state in the  $H \rightarrow WW^{(*)} \rightarrow \nu\ell\nu$  channel in ATLAS, and (ii) the search for nearly degenerate states in the  $H \rightarrow \gamma\gamma$  channel with the CMS detector.

In the  $H \rightarrow WW^{(*)} \rightarrow \nu\ell\nu$  channel, the search for an additional state is done using a boosted decision tree combining several discriminating kinematic characteristics to separate both the signal from the background and a high mass signal  $H$  from the lower mass state  $h$  [437]. A simultaneous fit of the two states  $h$

**Table 11.15:** Summary of references to the searches for additional states from extended Higgs sectors. (BBr) denotes the BaBar experiment and (TeV), the Tevatron experiments. Results using the full Run 2 dataset are indicated by (\*).  $V$  denotes either the  $W$  or the  $Z$  boson. Only Run 2 searches references are indicated except when searches have been carried out using Run 1 data only. References for Run 1 searches are available in Ref. [123].

	ATLAS	CMS	Other experiments
<i>CP-even H</i>			
$H \rightarrow \gamma\gamma$	[374]	[375]	—
$H \rightarrow \gamma\gamma$ (low mass)	[374]	[376]	—
$H \rightarrow Z\gamma$	[176]	[377]	—
$H \rightarrow ZZ \rightarrow 4\ell$	[378]	[379]	—
$H \rightarrow ZZ \rightarrow \ell\nu\nu$	[378]	[380]	—
$H \rightarrow ZZ \rightarrow \ell\ell q\bar{q}$	[381]	[382]	—
$H \rightarrow ZZ \rightarrow \nu\nu q\bar{q}$	[381]	—	—
$H \rightarrow WW \rightarrow \ell\nu\ell\nu$	[383]	* [384]	—
$H \rightarrow WW \rightarrow \ell\nu q\bar{q}$	[385]	[384]	—
$H \rightarrow VV \rightarrow q\bar{q}'q\bar{q}'(JJ)$	[386, 387]	—	—
$H \rightarrow VV$ combination	[388]	—	—
$H \rightarrow hh \rightarrow b\bar{b}\tau\tau, b\bar{b}\gamma\gamma, 4b,$ $\gamma\gamma WW^*, bbWW^*, WW^*WW^*, bbZZ^*$	* [389, 390]	[391–393]	—
<i>CP-odd A (and/or CP-even H)</i>			
$H, A \rightarrow \tau^+\tau^-$	* [394]	* [395]	[396, 397] (TeV) [398] (LHCb)
$A \rightarrow \tau^+\tau^-$ (low mass)	—	[399]	—
$H, A \rightarrow \mu^+\mu^-$	[400]	[401]	—
$H \rightarrow \mu\tau, e\tau$ LFV	—	[402]	—
$bj\mu^+\mu^-$ (low $\mu^+\mu^-$ mass)	* [403]	[404]	—
$H, A \rightarrow t\bar{t}$	* [387, 405]	[406]	—
$H, A \rightarrow b\bar{b}$	[407]	[408]	[409, 410] (TeV)
$A \rightarrow hV \rightarrow b\bar{b}q\bar{q}', b\bar{b}\ell\nu, b\bar{b}\ell\ell, \ell\ell\tau\tau, \nu\bar{\nu}b\bar{b}$	* [411]	[392, 412]	—
$H \rightarrow ZA \rightarrow b\bar{b}\ell^+\ell^-$	—	[413]	—
<i>Charged <math>H^\pm</math></i>			
$H^\pm \rightarrow \tau^\pm\nu$	* [414, 415]	* [416]	—
$H^\pm \rightarrow cs$	[417]	[418]	—
$H^\pm \rightarrow tb$	* [419]	[420]	—
$H^\pm \rightarrow W^\pm Z$	[421]	* [422]	—
$H^\pm \rightarrow W^\pm A$	—	* [423]	—
$H^\pm \rightarrow cb$	—	* [424]	—
<i>CP-odd NMSSM <math>a</math></i>			
$a \rightarrow \mu^+\mu^-$	[425]	* [426]	—
$h \rightarrow aa \rightarrow 4\mu, 4\tau, 2\mu 2\tau, 4\gamma,$ $aa \rightarrow \mu^+\mu^-\mu^+\mu^-$	[427]	* [428] [430]	[429] (TeV)
$bb\mu\mu, bb\tau\tau$	—	—	[431] (LEP)
$\Upsilon_{1s,3s} \rightarrow a\gamma$	—	—	[432, 433] (BBr)
Doubly charged $H^{\pm\pm}$	* [434]	* [435]	—

and  $H$  is then made to test the presence of an additional state. In this case, the usual null hypothesis of background includes the SM signal.

The CMS search for nearly degenerate mass states decaying to a pair of photons [438] is more generic and could for instance apply to  $CP$ -odd Higgs bosons as well. It consists of a fit to the diphoton mass spectrum using two nearly degenerate mass templates.

(e) *Type I 2HDM and fermiophobia*

The measurements of coupling properties of the 125 GeV Higgs boson directly establish its couplings to fermions. However, the presence of an additional fermiophobic state, as predicted by Type I 2HDMs, is not excluded. Prior to the discovery, ATLAS and CMS have performed searches for a fermiophobic Higgs boson, i.e., produced through couplings with vector bosons only (VBF and  $VH$ ) and decaying in two photons. CMS has further combined these results with searches in the  $W^+W^-$  and  $ZZ$  channels, assuming fermiophobic production and decay. This way, CMS excluded a fermiophobic Higgs boson in the range  $110 \text{ GeV} < m_H < 188 \text{ GeV}$  at the 95% CL. References for these Run 1 measurements can be found in Ref. [123]

11.7.7.2 *Searches for additional neutral states ( $\phi \equiv h, H, A$ ) decaying to fermions*

(a) *Exclusion limits from LEP*

In  $e^+e^-$  collisions, around the centre-of-mass energies reached by LEP, the main production mechanisms of the neutral MSSM Higgs bosons were the Higgs-strahlung processes  $e^+e^- \rightarrow hZ$ ,  $HZ$  and the pair production processes  $e^+e^- \rightarrow hA$ ,  $HA$ , while the vector boson fusion processes played a marginal role. Higgs boson decays to  $b\bar{b}$  and  $\tau^+\tau^-$  were used in these searches.

The searches and limits from the four LEP experiments are described in Refs. [439]. The combined LEP data did not contain any excess of events which would imply the production of a Higgs boson. Combined limits were derived [436]. For  $m_A \gg M_Z$ , the limit on  $m_h$  is nearly that of the SM searches, as  $\sin^2(\beta - \alpha) \approx 1$ . For high values of  $\tan\beta$  and low  $m_A$  ( $m_A \leq m_h^{max}$ ), the  $e^+e^- \rightarrow hA$  searches become the most important, and the lightest Higgs boson  $h$  is non SM-like. In this region, the 95% CL mass bounds are  $m_h > 92.8 \text{ GeV}$  and  $m_A > 93.4 \text{ GeV}$ . In the  $m_h^{max}$  scenario [440], values of  $\tan\beta$  from 0.7 to 2.0 are excluded taking  $m_t = 174.3 \text{ GeV}$ , while a much larger  $\tan\beta$  region is excluded for other benchmark scenarios such as the no-mixing one.

A flavour-independent limit for Higgs bosons in the Higgs-strahlung process at LEP has also been set at 112 GeV [441].

Neutral Higgs bosons may also be produced by Yukawa processes  $e^+e^- \rightarrow f\bar{f}\phi$ , where the Higgs particle  $\phi \equiv h, H, A$ , is radiated off a massive fermion ( $f \equiv b$  or  $\tau^\pm$ ). These processes can be dominant at low masses, and whenever the  $e^+e^- \rightarrow hZ$  and  $hA$  processes are suppressed. The corresponding ratios of

the  $f\bar{f}h$  and  $f\bar{f}A$  couplings to the SM coupling are  $-\sin\alpha/\cos\beta$  and  $\tan\beta$ , respectively. The LEP data have been used to search for  $b\bar{b}b\bar{b}$ ,  $b\bar{b}\tau^+\tau^-$ , and  $\tau^+\tau^-\tau^+\tau^-$  final states [442]. Regions of low mass and high enhancement factors are excluded by these searches.

The searches for the Higgs boson at LEP also included the case where it does not predominantly decay to a pair of  $b$  quarks. All four collaborations conducted dedicated searches for the Higgs boson with reduced model dependence, assuming it is produced via the Higgs-strahlung process, and not addressing its flavour of decay, a lower limit on the Higgs boson mass of 112.9 GeV is set by combining the data of all four experiments [441].

Using an effective Lagrangian approach and combining results sensitive to the  $h\gamma\gamma$ ,  $hZ\gamma$  and  $hZZ$  couplings, an interpretation of several searches for the Higgs boson was made and set a lower limit of 106.7 GeV on the mass of a Higgs boson that can couple anomalously to photons [441].

(b) *Searches at the Tevatron and the LHC*

The best sensitivity is in the regime with low to moderate  $m_A$  and with large  $\tan\beta$  which enhances the couplings of the Higgs bosons to down-type fermions. The corresponding limits on the Higgs boson production cross section times the branching ratio of the Higgs boson into down-type fermions can be interpreted in MSSM benchmark scenarios [443]. If  $\phi = A, H$  for  $m_A > m_h^{\max}$ , and  $\phi = A, h$  for  $m_A < m_h^{\max}$ , the most promising channels at the Tevatron are the inclusive  $p\bar{p} \rightarrow \phi \rightarrow \tau^+\tau^-$  process, with contributions from both  $gg \rightarrow \phi$  and  $b\bar{b}\phi$  production, and  $b\bar{b}\phi, \phi \rightarrow \tau^+\tau^-$  or  $\phi \rightarrow b\bar{b}$ , with  $b\tau\tau$  or three tagged  $b$ -jets in the final state, respectively. Although the Higgs boson production via gluon fusion has a higher cross section in general than via associated production, it cannot be used to study the  $\phi \rightarrow b\bar{b}$  decay mode since the signal is overwhelmed by the QCD background.

CDF and D0 have searched for neutral Higgs bosons produced in association with bottom quarks and which decay into  $b\bar{b}$  [409, 410], or into  $\tau^+\tau^-$  [396, 397]. The most recent searches in the  $b\bar{b}\phi$  channel with  $\phi \rightarrow b\bar{b}$  analyse approximately  $2.6\text{ fb}^{-1}$  (CDF) and  $5.2\text{ fb}^{-1}$  (D0) of data, seeking events with at least three  $b$ -tagged jets. The cross section is defined such that at least one  $b$  quark not from  $\phi$  decay is required to have  $p_T > 20\text{ GeV}$  and  $|\eta| < 5$ . The invariant mass of the two leading jets as well as  $b$ -tagging variables are used to discriminate the signal from the backgrounds. The QCD background rates and shapes are inferred from data control samples, in particular, the sample with two  $b$ -tagged jets and a third, untagged jet. Separate-signal hypotheses are tested and limits are placed on  $\sigma(p\bar{p} \rightarrow b\bar{b}\phi) \times \text{BR}(\phi \rightarrow b\bar{b})$ . A local excess of approximately  $2.5\sigma$  significance has been observed in the mass range of 130–160 GeV, but D0's search is more sensitive and sets stronger limits. The D0 result had a  $\mathcal{O}(2\sigma)$  local upward fluctuation in the 110 to 125 GeV mass range. These results have been superseded by the LHC searches and the excess seen by D0 has not been confirmed elsewhere.

A substantially larger sensitivity in the search for the  $\phi \rightarrow \tau^+\tau^-$  is obtained with the ATLAS and CMS analyses. The higher centre-of-mass energy reached at the Run 2 brings a substantial, though not excessively large, increase in sensitivity due to the intermediate masses probed. Both ATLAS and CMS have reported the result of their searches in this important channel with the full 2016 dataset. The searches are performed in categories of the decays of the two tau leptons:  $e\tau_{\text{had}}, \mu\tau_{\text{had}}, e\mu$ , and  $\mu\mu$ , where  $\tau_{\text{had}}$  denotes a tau lepton which decays to one or more hadrons plus a tau neutrino,  $e$  denotes  $\tau \rightarrow e\nu\nu$ , and  $\mu$  denotes  $\tau \rightarrow \mu\nu\nu$ . The dominant background comes from  $Z \rightarrow \tau^+\tau^-$  decays, although  $t\bar{t}$ ,  $W$ +jets and  $Z$ +jets events contribute as well. Separating events into categories based on the number of  $b$ -tagged jets improves the sensitivity in the MSSM. The  $b\bar{b}$  annihilation process and radiation of a Higgs boson from a  $b$  quark gives rise to events in which the Higgs boson is accompanied by a  $b\bar{b}$  pair in the final state. Requiring the presence of one or more  $b$ -jets reduces the background from  $Z$ +jets. Data control samples are used to constrain background rates. The rates for jets to be identified as a hadronically decaying tau lepton are measured in dijet samples, and  $W$ +jets samples provide a measurement of the rate of

events that, with a fake hadronic tau, can pass the signal selection requirements. Lepton fake rates are measured using samples of isolated lepton candidates and same-sign lepton candidates. Constraints from the ATLAS searches are shown in Fig. 11.19 (left) in the hMSSM approximation defined in Ref. [314]. The neutral Higgs boson searches consider the contributions of both the  $CP$ -odd and  $CP$ -even neutral Higgs bosons with enhanced couplings to bottom quarks, similarly to was done for the Tevatron results. In Fig. 11.19, decays of the charged Higgs boson into  $\tau\nu$  and decays of the heavy Higgs boson into a pair of SM-like Higgs bosons or gauge bosons, or decays of  $A$  into  $hZ$  are also being constrained. In addition, decays of the neutral Higgs bosons into muon pairs are also being explored. In the  $m_h$ -mod+ scenario the region of  $\tan\beta$  lower than 5 does not allow for a Higgs boson mass  $m_h$  close to 125 GeV. For the hMSSM scenario, instead, the SM-like Higgs boson mass is fixed as an input and hence the requirement that it is close to 125 GeV is always fulfilled, although this may imply other limitations as discussed in Section 11.7.1.1.

A search for  $\phi \rightarrow \mu^+\mu^-$  has also been performed by ATLAS [400] and CMS [401].

Finally searches for a resonance decaying to a top quark pair were done by ATLAS [405, 444] and CMS [406, 445]. These searches were interpreted as searches for scalar resonances by ATLAS [405], however, an important component of these searches is an accurate treatment of the interference effects between the signal and the continuum background. These effects can yield a dip and peak structure instead of a simple peak [311]. ATLAS has performed a search for a high mass state decaying to a pair of top quarks taking into account the deformation in mass shape of the signal in the presence of the continuum background [446].

The LHC has the potential to explore a broad range of SUSY parameter space through the search for non-SM-like Higgs bosons. As illustrated in Fig. 11.19, the parameter space corresponding to large  $\tan\beta$  values and large masses of the  $A$  boson are covered mostly by the searches in the  $A, H \rightarrow \tau^+\tau^-$  channel. A projection of the combined sensitivity of ATLAS and CMS at the HL-LHC has been performed in Ref. [104], showing that, compared to the current sensitivity, the full HL-LHC luminosity can expand the exclusion domain by nearly 1 TeV. In the low  $\tan\beta$  limit, the parameter space spanning large  $A$  boson masses is best excluded indirectly from the observed Higgs boson measurements. This is illustrated in the Mh125 scenario by the nearly horizontal exclusion which is due to the compatibility of the Higgs boson mass measurement with its prediction from radiative corrections (mostly from the stop sector). Nevertheless, Fig. 11.19 (right) shows a broad region with intermediate  $\tan\beta$  and large values of  $m_A$  that is not accessed by current searches, and in which the most promising channel is the very difficult search for  $t\bar{t}$  decays with its aforementioned intricacies. In this region of parameter space, it is possible that only the SM-like Higgs boson can be within the LHC's reach. If no other state of the EWSB sector than the 125 GeV state is discovered, it may be challenging to determine only from the Higgs sector whether there is a SUSY extension of the SM in nature.

11.7.7.3 *Searches for a CP-odd state decaying to hZ*

Similarly to the search for a  $CP$ -even high mass Higgs boson decaying to a pair of Higgs bosons, the search for a  $CP$ -odd states decaying to  $hZ$  was carried out at the LHC by ATLAS and CMS in various channels:

- (i)  $(Z \rightarrow \ell\ell)(h \rightarrow b\bar{b})$ ,
- (ii)  $(Z \rightarrow \nu\nu)(h \rightarrow b\bar{b})$ ,
- (iii)  $(Z \rightarrow \ell\ell)(h \rightarrow \tau\tau)$ ,
- (iv) and  $(Z \rightarrow \ell\ell)(h \rightarrow \tau\tau)$ .

The searches where the  $A$  boson decays to a pair of  $b$  quarks have been performed both in the regime where both  $b$ -jets are resolved and in the boosted regime where the two  $b$ -jets are merged in a single larger radius jet. These searches have been used to constrain the parameter space of 2HDMS. In the MSSM, these searches place limits on small values of  $\tan\beta$  for masses of  $A$  between 220 GeV and 360 GeV.

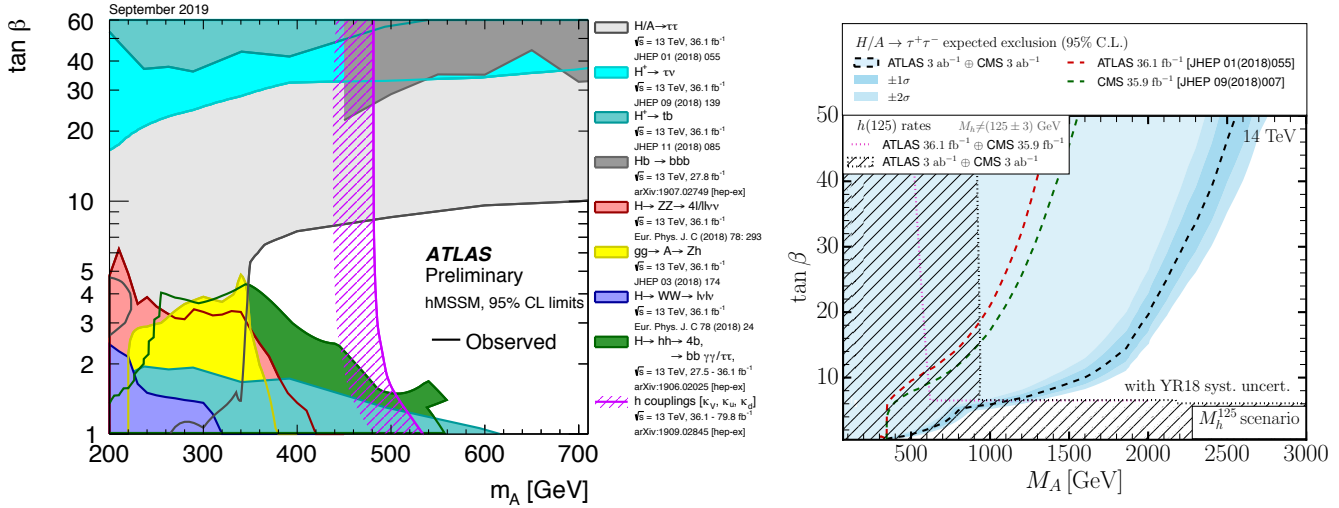


Figure 11.19: The 95% CL exclusion contours in the  $(M_A, \tan \beta)$  parameter space for: (left) a summary of ATLAS Run 2 searches in the hMSSM and (right) the projected sensitivity for the combination of ATLAS and CMS searches in the  $A, H \rightarrow \tau^+\tau^-$  channel at HL-LHC and the interpretation of the constraints from the measurements of the Higgs boson couplings in the  $M_{h125}$  benchmark (the projected ATLAS sensitivity in the  $A, H \rightarrow \tau^+\tau^-$  channel used for this projection was not optimised for high masses, when re-optimised similar sensitivities are obtained between ATLAS and CMS).

#### 11.7.7.4 Searches for low mass states

Searches for pseudo-scalar Higgs boson at intermediate to low masses, below the  $Z$  mass (in the 25 GeV to 80 GeV mass range) have been performed by CMS both in the  $\tau^+\tau^-$  [447] and the  $\mu^+\mu^-$  [448] decay channels. A light pseudo-scalar in this mass range is excluded by current direct constraints in the MSSM but not in general 2HDMs [449]. These searches are done in the decay channels where the pseudo-scalar Higgs boson is produced in association with a pair of  $b$ -quarks and decays into a pair of taus or muons.

CMS has also reported an anomaly observed in the search for  $\mu^+\mu^-$  resonances produced with one jet tagged as containing a  $b$ -hadron and a forward jet in the Run 1 data. A mild excess appeared in the di-muon mass distribution at approximately 28 GeV. Another very mild excess was then also found in the 2016 Run 2 data [404]. ATLAS then performed a similar analysis with the full Run 2 dataset corresponding to an integrated luminosity of approximately  $139 \text{ fb}^{-1}$ , and no significant excess was found [403].

Searches for low mass Higgs bosons were also performed in the diphoton channel by both ATLAS and CMS [450, 451] at Run 1. CMS has updated the results of this search with the full 2016 dataset [452]. A modest excess has been observed by CMS at a mass of 95.3 GeV with a local significance of  $2.8\sigma$  (the corresponding global significance is  $1.3\sigma$ ). A slight excess was also seen by CMS in the 8 TeV data at a slightly higher mass of 97.6 GeV with a local significance of  $2.0\sigma$  ( $1.47\sigma$  global). No significant excess has been observed in this region by ATLAS neither in the Run 1 nor Run 2 [374] data. It should, however, be noted that the ATLAS search does not reach the level of sensitivity to exclude at the 95% CL the excess seen in CMS. This mildly significant excess also coincides in mass with the excess observed at LEP and discussed in Section 11.7.7.1. It has therefore raised interest and speculations on its possible nature, see for instance Ref. [453] and references therein.

#### 11.7.7.5 Searches for charged Higgs bosons $H^\pm$

At  $e^+e^-$  colliders, charged Higgs bosons can be pair produced in the  $s$ -channel via  $\gamma$  or  $Z$  boson exchange. This process is dominant in the LEP centre-of-mass energies range, i.e., up to 209 GeV. At higher centre-of-mass energies, other processes can play an important role such as the production in top quark decays via  $t \rightarrow b + H^+$  if  $m_{H^\pm} < m_t - m_b$  or via the one-loop process  $e^+e^- \rightarrow W^\pm H^\mp$  [454, 455], which allows the production of a charged Higgs boson with  $m_{H^\pm} > \sqrt{s}/2$ , even when  $H^+H^-$  production is kinematically forbidden. Other single charged Higgs boson production mechanisms include  $t\bar{b}H^-/\bar{t}bH^+$

production [108],  $\tau^+\nu H^-/\tau^-\bar{\nu}H^+$  production [456], and a variety of processes in which  $H^\pm$  is produced in association with a one or two other gauge and/or Higgs bosons [457].

At hadron colliders, charged Higgs bosons can be produced in several different modes depending on the value of its mass with respect to the top-quark mass. For light values of the charged Higgs boson mass, defined by Higgs boson masses smaller than the mass of the top quark (with experimental analyses typically considering masses up to  $m_{H^\pm} \leq 160 \text{ GeV}$ ), the top-quark decay  $t \rightarrow Hb$  is allowed and the charged Higgs boson is light enough so that top-quark off-shell effects can be neglected. The cross section for the production of a light charged Higgs boson is simply given by the product of the top-pair production cross section and the branching ratio of a top quark into a charged Higgs boson. The top-pair production cross section is known up to NNLO in perturbative QCD [458], and relevant QCD and SUSY-QCD including NLO corrections to the branching ratio for  $t \rightarrow H^+b$  have been computed in the literature, see Refs. [459–461] and references therein. At present, the theoretical accuracy for the production of a light charged Higgs boson is at the few percent level. For the intermediate mass range, values of  $m_{H^\pm}$  near  $m_t$ , the finite top-width effects as well as the interplay between top-quark resonant and non-resonant diagrams cannot be neglected. Hence, the full process  $pp \rightarrow H^\pm W^\mp b\bar{b}$  (with massive  $b$ -quarks) must be considered to perform a reliable perturbative calculation of the charged Higgs boson production cross section [461]. For heavy charged Higgs boson scenarios, with charged Higgs boson masses larger than the top-quark mass (typically above 180 GeV), the dominant charged Higgs boson production channel is the associated production with a top quark/antiquark and a (possibly low transverse momentum) bottom antiquark/quark. Theoretical calculation at NLO have been computed both at the inclusive and fully-differential level in the five-flavour scheme and in the four-flavour scheme, see Ref. [44] and references therein. Charged Higgs bosons can also be produced via associated production with  $W^\pm$  bosons through  $b\bar{b}$  annihilation and  $gg$ -fusion annihilation [462].

For charged Higgs boson production cross section predictions for the Tevatron and the LHC, see Refs. [42, 43, 310].

##### (a) Exclusion limits from LEP

Charged Higgs bosons have been searched for at LEP, where the combined data of the four experiments, ALEPH, DELPHI, L3, and OPAL, were sensitive to masses of up to about 90 GeV [436] in two decay channels,  $\tau\nu$  and  $c\bar{s}$ . The combined LEP data exclude, at 95% CL, charged Higgs bosons with mass below 80 GeV (Type II scenario) or 72.5 GeV (Type I scenario) [463].



## (b) Exclusion limits from Tevatron

Compared to the mass domain covered by LEP searches, the Tevatron covered a complementary range of charged Higgs boson masses. CDF and D0 have also searched for charged Higgs bosons in top quark decays with subsequent decays to  $\tau\nu$  or to  $c\bar{s}$  [464]. For the  $H^+ \rightarrow c\bar{s}$  channel, the limits on  $\text{BR}(t \rightarrow H^+b)$  from CDF and D0 are  $\approx 20\%$  in the mass range  $90 \text{ GeV} < m_{H^+} < 160 \text{ GeV}$  and assuming a branching fraction of 100% in this specific final state.  $H^+ \rightarrow \tau^+\nu_\tau$  channel, D0's limits on  $\text{BR}(t \rightarrow H^+b)$  are also  $\approx 20\%$  in the same mass range and assuming a branching fraction of 100% in this final state. These limits are valid in general 2HDMs, and they have also been interpreted in terms of the MSSM [464].

## (c) Exclusion limits from LHC

Similarly to the Tevatron, at the LHC, light charged Higgs bosons can be searched for in the decays of top quarks. The main initial production mode for light charged Higgs bosons ( $m_{H^\pm} < m_t - m_b$ ) is top pair production. The subsequent decay modes of the charged Higgs boson for these searches are  $\tau\nu$  and  $c\bar{s}$ . More recently, ATLAS and CMS have also searched for higher mass charged Higgs bosons ( $m_{H^\pm} > m_t + m_b$ ) in  $H^+ \rightarrow t\bar{b}$ . The main production modes are the associated production of a charged Higgs boson in association with a top and a bottom quark or in association with a top quark only.

The decay  $H^+ \rightarrow \tau^+\nu_\tau$  is searched typically in three final state topologies:

- (i) lepton+jets: with  $t\bar{t} \rightarrow \bar{b}WH^+ \rightarrow \bar{b}\bar{b}(q\bar{q}')(\tau_{\text{lep}}\nu)$ , i.e., the  $W$  boson decays hadronically and the tau decays into an electron or a muon, with two neutrinos;
- (ii)  $\tau$  +lepton: with  $t\bar{t} \rightarrow \bar{b}WH^+ \rightarrow \bar{b}\bar{b}(\ell\nu)(\tau_{\text{had}}\nu)$ , i.e., the  $W$  boson decays leptonically (with  $\ell = e, \mu$ ) and the tau decays hadronically;
- (iii)  $\tau$ +jets:  $t\bar{t} \rightarrow \bar{b}WH^+ \rightarrow \bar{b}\bar{b}(q\bar{q}')(\tau_{\text{had}}\nu)$ , i.e., both the  $W$  boson and the  $\tau$  decay hadronically.

CMS has also searched for the charged Higgs boson in the decay products of top quark pairs:  $t\bar{t} \rightarrow H^\pm W^\mp b\bar{b}$  and  $t\bar{t} \rightarrow H^+ H^- b\bar{b}$  as well. Three types of final states with large missing transverse energy and jets originating from  $b$ -quark hadronisation have been analysed: the fully-hadronic channel with a hadronically decaying tau in association with jets, the dilepton channel with a hadronically decaying tau in association with an electron or muon and the dilepton channel with an electron-muon pair. The results of the searches at the LHC are illustrated in Figure 11.19.

Both ATLAS and CMS have also searched for high mass charged Higgs bosons decaying to a top and bottom quarks. The main production mode for this search is the associated production with one top quark (5-flavour scheme) or a top quark and a bottom quark (4-flavour scheme) in the final state. The  $s$ -channel production mode where the charged Higgs boson is produced alone in the final state at tree level is also considered. This search is particularly intricate and it is sensitive to the modelling of the top pair production background produced in association with additional partons and in particular  $b$ -quarks. No excess was found and the results are expressed in terms of exclusion limits of cross section times branching fractions.

ATLAS and CMS have also searched for charged Higgs bosons in top quark decays assuming  $\text{BR}(H^+ \rightarrow c\bar{s}) = 100\%$  [417, 418], and sets limits of  $\approx 20\%$  on  $\text{BR}(t \rightarrow H^+b)$  in the  $90 \text{ GeV} < m_{H^+} < 160 \text{ GeV}$  mass range.

In 2HDMs, the decay of the charged Higgs boson to a  $W$  and a  $Z$  boson is allowed only at loop level and is therefore suppressed. However the  $H^\pm \rightarrow W^\pm Z$  decay channel is allowed in Higgs triplet models. ATLAS [421] has searched for such decays, requiring that the charged Higgs boson is produced through the fusion of vector bosons. No excess with respect to the SM backgrounds has been observed in this channel, and the results are interpreted in the Georgi–Machacek model [349] discussed in Section 11.7.5.2.

At the LHC, various other channels still remain to be explored, in particular searches involving additional neutral scalars in particular in the  $WH$ ,  $WA$  channels ( $A$  is the pseudo-scalar MSSM

Higgs boson), and in the  $Wa$  channel ( $a$  is the light  $CP$ -odd scalars of the NMSSM).

## 11.7.7.6 Interpretation of the measurements of the coupling properties of the Higgs boson

The 125 GeV Higgs boson being part of any hypothetically extended EWSB sector, it can be used through the compatibility of its measured couplings and mass with those predicted in specific models to provide constraints on these specific models parameters.

As discussed in Section 11.7.1.1, the mass of the Higgs boson limits drastically the MSSM parameter space and can be used to set limits on specific MSSM benchmarks. This is the case for the Mh125 scenario as illustrated in Figure 11.18 and in Figure 11.19, corresponding approximately to a lower limit on  $\tan\beta$  in this model [104].

The measurements of the Higgs boson couplings, discussed in Section 11.6, can be interpreted in the framework of a constrained model where the couplings of the Higgs boson to vector bosons, up-type quarks, down-type quarks and leptons, are varied. In 2HDMs, these couplings are functions of the mixing angle  $\alpha$  between the observed Higgs boson and the heavy  $CP$ -even neutral scalar, and of the ratio of the vacuum expectation values of the two doublets,  $\tan\beta$ . In the case of the MSSM, the two parameters are the  $A$  boson mass and  $\tan\beta$  (the sole two parameters needed to describe the MSSM Higgs sector at tree level). The coupling measurements have been interpreted both by ATLAS [213] and CMS [214] in specific MSSM benchmarks and in 2HDMs. The exclusion contour in the hMSSM for the ATLAS combination [213] is illustrated in Figure 11.19.

11.7.7.7 Searches for a light  $CP$ -odd Higgs boson

A light pseudo-scalar boson  $a$  is present in any two Higgs doublet model enhanced with an additional singlet field. A prominent example is the NMSSM. The theoretical motivations for singlet extensions of the MSSM are discussed in Section 11.7.2. There is also a variety of other models with light additional spin-0 bosons such as two Higgs doublet models with a scalar, Little Higgs models or light scalar mediator to a dark sector.

In the framework of the NMSSM, the searches now focus on the low  $a$  mass region for several reasons:

- (i) in the NMSSM, the light pseudo-scalar  $a$  boson can, as a pseudo-Goldstone boson, be a natural candidate for an axion;
- (ii) scenarios where  $m_a > 2m_b$  and a  $CP$ -even state  $h$  decaying to a pair of  $a$  ( $m_h > 2m_a$ ) are excluded by direct searches at LEP in the four  $b$ 's channel [429, 436, 465];
- (iii) in the pre-discovery era, LEP limits on a  $CP$ -even Higgs boson resulted in fine tuning MSSM constraints [466] which could be evaded through non standard decays of the Higgs boson to  $aa$ ;
- (iv) in the NMSSM, a  $CP$ -odd  $a$  boson with a mass in the range 9.2–12 GeV can also account for the difference observed between the measured anomalous muon magnetic moment and its prediction [467].

The benchmark scenarios have also changed in the light of the Higgs boson discovery. The 125 GeV state could be the lightest or the next-to-lightest of the three  $CP$ -even states of the NMSSM. Light pseudo-scalar scenarios are still very interesting in particular for the potential axion candidate. There are three main types of direct searches for the light  $a$  boson:

- (i) for masses below the  $\Upsilon$  resonance, the search is for radiative decays  $\Upsilon \rightarrow a\gamma$  at B-factories;
- (ii) the inclusive search in high energy  $pp$  collisions at the LHC;
- (iii) the search for decays of the observed  $CP$ -even Higgs  $h$  boson into a pair of  $a$  bosons.

Radiative decays  $\Upsilon \rightarrow a\gamma$  have been searched for in various colliders, the most recent results are searches for radiative decays of the  $\Upsilon(1s)$  to  $a\gamma$  with a subsequent decay of the  $a$  boson to a pair of taus at CLEO [468], and the radiative decays of the  $\Upsilon(1s, 2s, 3s)$  to  $a\gamma$  with subsequent decays to a pair of muons or taus by BaBar [432, 433].



Direct inclusive searches for the light pseudo scalar  $a$  boson were performed in the  $a \rightarrow \mu\mu$  channel at the Tevatron by D0 [429] and by ATLAS [425], CMS [426], and LHCb [151] at the LHC.

Finally, searches for the decays of the Higgs boson to a pair of  $a$  bosons were performed with subsequent decays to four photons, in the four muons final state, in the two muons and two taus final state, and in the four taus final state.

No significant excess in the searches for a light  $CP$ -odd  $a$  boson was found and limits on the production times branching fractions of the  $a$  boson have been set.

References for all these searches are summarised in Table 11.15.

#### 11.7.7.8 Searches for doubly charged Higgs bosons $H^{\pm\pm}$

As discussed in Section 11.7.5, the generation of small neutrino masses via the standard EWSB mechanism described in Section 11.2 requires unnaturally small Yukawa couplings, provided that neutrinos are Dirac-type fermions. A Majorana mass term with a see-saw mechanism for neutrinos, would allow for naturally small masses and would also yield a framework for the appealing scenario of leptogenesis. However, within the SM, Majorana mass terms correspond to (non-renormalizable) dimension-5 operators. Such effective interactions can be generated via renormalisable interactions with an electroweak triplet of complex scalar fields (corresponding to a type-II see-saw mechanism). Other models such as the Zee–Babu model, with the introduction of two  $SU(2)_L$  singlets, also generate Majorana mass terms. The signature of such models would be the presence of doubly charged Higgs bosons  $H^{\pm\pm}$ .

The main production mechanisms of  $H^{\pm\pm}$  bosons at hadron colliders are the pair production in the  $s$ -channel through the exchange of a  $Z$  boson or a photon and the associated production with a charged Higgs boson through the exchange of a  $W$  boson. Various searches for doubly charged Higgs bosons have been performed by ATLAS and CMS at Run 1 [469] and Run 2 [434, 435]. Typically, these searches aim at low values of the Higgs triplet vacuum expectation for which the doubly charged Higgs boson will decay mostly to leptons (for high values, the decay to  $W$  bosons will become predominant). These searches assume that the coupling to  $W$  bosons is negligible and that the main production mode is through the Drell–Yan process.

#### 11.7.7.9 Searches for non-standard production processes of the Higgs boson

The discovery of the Higgs boson has also allowed for searches of BSM processes involving standard decays of the Higgs boson. One example directly pertaining to the search for additional states of the EWSB sector is the search for Higgs bosons in the cascade decay of a heavy  $CP$ -even Higgs boson decaying to charged Higgs boson and a  $W$  boson, and the charged Higgs boson subsequently decaying to  $H$  and another  $W$  boson. This search has been performed by ATLAS in  $b\bar{b}$  decays of the 125 GeV Higgs boson [470].

#### 11.7.7.10 Outlook on searches for additional states

The LHC program of searches for additional states covers a large variety of decay and production channels. Since the Higgs boson discovery, many new channels have been explored at the LHC, e.g., the searches for additional states decaying into  $hh$  or  $Vh$  or  $ZA$ . The search for charged Higgs bosons has been extended to include the  $WZ$ ,  $WA$  and the very difficult  $t\bar{b}$  decay channel.

## 11.8 Summary and outlook

*Summary*– The discovery of the Higgs boson is a major milestone in the history of particle physics as well as an extraordinary achievement of the LHC machine and the ATLAS and CMS experiments. Seven years after the discovery, substantial progress in the field of Higgs boson physics has been accomplished and a significant number of measurements probing the nature of this unique particle have been made. They are revealing an increasingly precise profile of the Higgs boson.

The LHC has now concluded its Run 2, delivering a dataset of 13 TeV  $pp$  collisions corresponding to an integrated luminosity of approximately  $140 \text{ fb}^{-1}$  of data collected by ATLAS and CMS. With the substantial increase in production rates at the higher

center-of-mass energy and the larger datasets, new landmark results in Higgs physics have been achieved.

Three new results of fundamental importance have been achieved with partial Run 2 datasets by ATLAS and CMS independently: (i) the clear and unambiguous observation of the Higgs boson decay to taus; (ii) the clear and unambiguous observation of the Higgs boson decay to a pair of  $b$  quarks; (iii) the clear and unambiguous observation of the production of the Higgs boson through the  $t\bar{t}H$  process. These results provide direct evidence for the Yukawa coupling of the Higgs boson to fermions of the third generation: taus, bottom quarks and top quarks, at rates compatible with those expected in the SM. These, and all other experimental measurements, are consistent with the EWSB mechanism of the SM.

New theoretical calculations and developments in Monte-Carlo simulation pertaining to Higgs physics are still occurring at a rapid pace. For example, the theoretical prediction for the dominant gluon fusion production mode now includes the latest N3LO result, which is twice as precise as previous N2LO calculations. With these improvements in the state-of-the-art theory predictions and the increase in luminosity and center-of-mass energy, Higgs physics has definitively entered a precision era. Its impact can already be seen on the latest Run 2 combined measurements of the Higgs boson couplings (see Section 11.6).

Since the discovery of the Higgs boson, new ideas have emerged to probe its rare decays and production modes, as well as to indirectly measure the Higgs boson width through the study of its off-shell couplings, or via on-shell interference effects. The Higgs boson has now become part of the standard toolkit in searches for new physics.

Many extensions of the SM at higher energies call for an enlargement of the EWSB sector. Hence, direct searches for additional scalar states can provide valuable insights on the dynamics of the EWSB mechanism. The ATLAS and CMS experiments have searched for additional Higgs bosons in the Run 2 data, and have imposed constraints in broad ranges of mass and couplings for various scenarios with an extended Higgs sector.

The landscape of Higgs physics has been extended extraordinarily since its discovery. The current dataset is approximately only five percent of the total dataset foreseen for the High Luminosity phase of the LHC project. The current precisions on the measurements of the couplings of the Higgs boson to gauge bosons and third generation fermions are typically of the order of 10–20%. The uncertainty on the Higgs boson coupling to the muon is approximately 100%, and the upper limits on the branching fraction to new invisible or undetected particles are approximately 20%. The sensitivity to the Higgs boson self-coupling has not reached the SM value yet and there is no information on how the Higgs field acquired its VEV in the early times of the Universe. This situation allows for new challenges to ultimately increase further the reach in precision and it also widens the possibilities of unveiling the true nature and the dynamics of the electroweak symmetry breaking.

*Outlook*– The unitarisation of the vector boson scattering (VBS) amplitudes, dominated at high energies by their longitudinal polarisation, has been the basis of the *no lose* theorem at the LHC, and was a determining consideration in the building of the accelerator and detectors. It motivated the existence of a Higgs boson or the observability of manifestations of strong dynamics at the TeV scale. Now that a Higgs boson has been found and its couplings to gauge bosons are consistent with the SM predictions, perturbative unitarity is preserved to a large extent with the sole exchange of the Higgs boson, and without the need for any additional states. VBS is, however, still an important channel to further investigate in order to better understand the nature of the Higgs sector and the possible completion of the SM at the TeV scale. In association with the double Higgs boson production channel by vector boson fusion, VBS could, for instance, confirm that the Higgs boson is part of a weak doublet and also establish whether it is an elementary object or a composite state that could emerge as a pseudo-Nambu–Goldstone boson from a new underlying broken symmetry.

The fermion-Higgs boson couplings are not governed by local

gauge symmetry. Thus, in addition to a new particle, the LHC has also discovered a new force, different in nature from the other fundamental interactions since it is non-universal and distinguishes between the three families of quarks and leptons. The existence of the Higgs boson embodies the problem of an unnatural cancellation among the quantum corrections to its mass if new physics is present at scales significantly higher than the EW scale. The non-observation of additional states which could stabilise the Higgs boson mass is a challenge for natural scenarios like SUSY or models with a new strong interaction in which the Higgs boson is not a fundamental particle. This increasingly pressing paradox starts questioning the principle of naturalness.

The search for the Higgs boson has occupied the particle physics community for the last 50 years. Its discovery has shaped and sharpened the physics programs of the LHC and of prospective future accelerators [471]. With the HL-LHC, the precision will improve by a factor 5–10 on all observables with respect to current data. Table 11.12 displays the expected sensitivities in the characterization of the Higgs boson at HL-LHC: in this table, the parameters  $\kappa_i$  specify by how much the coupling of the Higgs boson to a given particle  $i$  deviates from the SM expectation. The only channels which are expected to be limited by data statistics are the rare decays to muons and  $Z\gamma$ . In all other cases, the experimental systematic uncertainties are similar to the statistical uncertainties, but the dominant source of uncertainty arises from theory, and this remains the case even after assuming that, by the end of the HL-LHC run, the theory uncertainties can be reduced by a factor two compared to the current uncertainties, a hypothesis that appears realistic but still requires dedicated and concerted work [104]. For both hadron and lepton colliders, some theoretical progress is crucial to fully exploit and capitalise on the experimental data. In particular, the expected HL-LHC data together with rapid ongoing progress in theoretical calculations are defining a new era of precision Higgs boson measurements.

### Acknowledgements

We would like to thank many of our colleagues for proofreading this review, for useful criticism and for their input in general: W. Altmannshofer, J. de Blas, G. Branco, J. Campbell, F. Caola, F. Cerutti, C. Csáki, R. Contino, J. Conway, N. Craig, A. David, S. Dawson, J.B. De Vivie, J. D’Hondt, G. Durieux, C. Englert, J.R. Espinosa, A. Falkowski, L. Fayard, W. Fischer, S. Forte, M. Grazzini, J. Gu, H. Haber, B. Heinemann, S. Heinemeyer, J. Hubisz, A. Korytov, B. Jäger, H. Ji, T. Junk, P. Langacker, J. Lykken, F. Maltoni, M.L. Mangano, B. Mansoulié, M. McCullough, R. Mishra, M. Mühlleitner, B. Murray, M. Neubert, A. Nisati, Y. Paul, G. Perez, G. Petruccianni, A. Pomarol, E. Pontón, R. Rattazzi, D. Rebutti, F. Riva, R. Salerno, E. Salvioni, N. Shah, G. Shaughnessy, M. Spira, O. Stål, A. Strumia, K. Tackmann, R. Tanaka, J. Terning, A. Vartak, C. Wagner, A. Weiler, A. Wulzer, and G. Zanderighi. We are also most grateful to the ATLAS, CDF, CMS and D0 collaborations for their help with this review.

M.C. is supported by Fermilab, that is operated by Fermi Research Alliance, LLC under Contract No. DE-AC02-07CH11359 with the United States Department of Energy. C.G. is supported by the Helmholtz Association and by the Deutsche Forschungsgemeinschaft under Germany’s Excellence Strategy – EXC 2121 “Quantum Universe” – 390833306. V.S. is supported by the grant DE-SC0009919 of the United States Department of Energy.

### References

- [1] G. Aad *et al.* (ATLAS), Phys. Lett. **B716**, 1 (2012), [arXiv:1207.7214].
- [2] S. Chatrchyan *et al.* (CMS), Phys. Lett. **B716**, 30 (2012), [arXiv:1207.7235].
- [3] S.L. Glashow, Nucl. Phys. **20**, 579 (1961); S. Weinberg, Phys. Rev. Lett. **19**, 1264 (1967); A. Salam, *Elementary Particle Theory*, eds.: Svartholm, Almqvist and Wiksells, Stockholm, 1968; S. L. Glashow, J. Iliopoulos and L. Maiani, Phys. Rev. **D2**, 1285 (1970).
- [4] F. Englert and R. Brout, Phys. Rev. Lett. **13**, 321 (1964), [157(1964)]; P. W. Higgs, Phys. Rev. **145**, 1156 (1966); G. S. Guralnik, C. R. Hagen and T. W. B. Kibble, Phys. Rev. Lett. **13**, 585 (1964), [162(1964)].
- [5] J. M. Cornwall, D. N. Levin and G. Tiktopoulos, Phys. Rev. Lett. **30**, 1268 (1973), [Erratum: Phys. Rev. Lett. **31**, 572 (1973)]; J. M. Cornwall, D. N. Levin and G. Tiktopoulos, Phys. Rev. **D10**, 1145 (1974), [Erratum: Phys. Rev. **D11**, 972 (1975)]; C. H. Llewellyn Smith, Phys. Lett. **46B**, 233 (1973); B. W. Lee, C. Quigg and H. B. Thacker, Phys. Rev. **D16**, 1519 (1977).
- [6] K. G. Wilson, Phys. Rev. **D3**, 1818 (1971); G. ’t Hooft, in *Proc. of 1979 Cargèse Institute on Recent Developments in Gauge Theories*, p. 135 Press, New York 1980; For a recent review, see G.F. Giudice, PoS EPS-HEP2013, 163 (2013).
- [7] J. Wess and B. Zumino, Phys. Lett. **49B**, 52 (1974).
- [8] S. P. Martin, Adv. Ser. Direct. High Energy Phys. 1–98 (1998), [hep-ph/9709356].
- [9] B.C. Allanach and H.E. Haber, *Supersymmetry, Part I (Theory)*, in this volume.
- [10] D. B. Kaplan and H. Georgi, Phys. Lett. **136B**, 183 (1984).
- [11] B. Bellazzini, C. Csaki and J. Serra, Eur. Phys. J. **C74**, 5, 2766 (2014), [arXiv:1401.2457]; G. Panico and A. Wulzer, Lect. Notes Phys. **913**, pp.1 (2016), [arXiv:1506.01961]; C. Csaki, C. Grojean and J. Terning, Rev. Mod. Phys. **88**, 4, 045001 (2016), [arXiv:1512.00468].
- [12] K.M. Black, R.S. Chivukula and M. Narain, *Dynamical Electroweak Symmetry Breaking: Implications of the H0*, in this volume.
- [13] Z. Chacko, H.-S. Goh and R. Harnik, Phys. Rev. Lett. **96**, 231802 (2006), [hep-ph/0506256]; Z. Chacko, H.-S. Goh and R. Harnik, JHEP **01**, 108 (2006), [hep-ph/0512088].
- [14] N. Craig *et al.*, JHEP **07**, 105 (2015), [arXiv:1501.05310]; N. Craig, S. Knapen and P. Longhi, Phys. Rev. Lett. **114**, 6, 061803 (2015), [arXiv:1410.6808].
- [15] P. W. Graham, D. E. Kaplan and S. Rajendran, Phys. Rev. Lett. **115**, 22, 221801 (2015), [arXiv:1504.07551]; J. R. Espinosa *et al.*, Phys. Rev. Lett. **115**, 25, 251803 (2015), [arXiv:1506.09217]; G. Dvali (2019), [arXiv:1908.05984].
- [16] T. Flacke *et al.*, JHEP **06**, 050 (2017), [arXiv:1610.02025].
- [17] M. Bauer, M. Carena and K. Gemmler, JHEP **11**, 016 (2015), [arXiv:1506.01719]; M. Bauer, M. Carena and K. Gemmler, Phys. Rev. **D94**, 11, 115030 (2016), [arXiv:1512.03458].
- [18] R. Barbieri, L. J. Hall and V. S. Rychkov, Phys. Rev. **D74**, 015007 (2006), [hep-ph/0603188].
- [19] D. E. Morrissey and M. J. Ramsey-Musolf, New J. Phys. **14**, 125003 (2012), [arXiv:1206.2942].
- [20] G. Degrandi *et al.*, JHEP **08**, 098 (2012), [arXiv:1205.6497]; S. Alekhin, A. Djouadi and S. Moch, Phys. Lett. **B716**, 214 (2012), [arXiv:1207.0980]; D. Buttazzo *et al.*, JHEP **12**, 089 (2013), [arXiv:1307.3536].
- [21] S. Weinberg, Phys. Rev. Lett. **43**, 1566 (1979).
- [22] See the particle listing section at <http://pdg.lbl.gov>.
- [23] J. R. Ellis, M. K. Gaillard and D. V. Nanopoulos, Nucl. Phys. **B106**, 292 (1976).
- [24] M. A. Shifman *et al.*, Sov. J. Nucl. Phys. **30**, 711 (1979), [Yad. Fiz.30,1368(1979)].
- [25] J. F. Gunion *et al.*, *The Higgs Hunter’s Guide*, Addison-Wesley (1990).
- [26] P. Sikivie *et al.*, Nucl. Phys. **B173**, 189 (1980); H. Georgi, Ann. Rev. Nucl. Part. Sci. **43**, 209 (1993).
- [27] M. J. G. Veltman, Nucl. Phys. **B123**, 89 (1977).
- [28] M. Luscher and P. Weisz, Nucl. Phys. **B290**, 25 (1987); M. Luscher and P. Weisz, Nucl. Phys. **B295**, 65 (1988).
- [29] V. Branchina, E. Messina and M. Sher, Phys. Rev. **D91**, 013003 (2015), [arXiv:1408.5302].

- [30] A. Hook *et al.*, JHEP **01**, 061 (2015), [arXiv:1404.5953]; J. Kearney, H. Yoo and K. M. Zurek, Phys. Rev. **D91**, 12, 123537 (2015), [arXiv:1503.05193].
- [31] J. R. Espinosa, D. Racco and A. Riotto, Phys. Rev. Lett. **120**, 12, 121301 (2018), [arXiv:1710.11196].
- [32] J. R. Espinosa, D. Racco and A. Riotto, JCAP **1809**, 09, 012 (2018), [arXiv:1804.07732].
- [33] A. Andreassen, W. Frost and M. D. Schwartz, Phys. Rev. **D97**, 5, 056006 (2018), [arXiv:1707.08124]; S. Chigusa, T. Moroi and Y. Shoji, Phys. Rev. Lett. **119**, 21, 211801 (2017), [arXiv:1707.09301].
- [34] M. Shaposhnikov and C. Wetterich, Phys. Lett. **B683**, 196 (2010), [arXiv:0912.0208]; M. Holthausen, K. S. Lim and M. Lindner, JHEP **02**, 037 (2012), [arXiv:1112.2415].
- [35] F. L. Bezrukov and M. Shaposhnikov, Phys. Lett. **B659**, 703 (2008), [arXiv:0710.3755]; F. L. Bezrukov, A. Magnin and M. Shaposhnikov, Phys. Lett. **B675**, 88 (2009), [arXiv:0812.4950].
- [36] C. P. Burgess, H. M. Lee and M. Trott, JHEP **09**, 103 (2009), [arXiv:0902.4465]; J. L. F. Barbon and J. R. Espinosa, Phys. Rev. **D79**, 081302 (2009), [arXiv:0903.0355]; M. P. Hertzberg, JHEP **11**, 023 (2010), [arXiv:1002.2995].
- [37] B. A. Kniehl, Phys. Rept. **240**, 211 (1994).
- [38] M. Spira, Fortsch. Phys. **46**, 203 (1998), [hep-ph/9705337].
- [39] M. Carena and H. E. Haber, Prog. Part. Nucl. Phys. **50**, 63 (2003), [hep-ph/0208209].
- [40] A. Djouadi, Phys. Rept. **457**, 1 (2008), [hep-ph/0503172].
- [41] S. Dittmaier *et al.* (LHC Higgs Cross Section Working Group), CERN Report **2011-002** (2011), [arXiv:1101.0593].
- [42] S. Dittmaier *et al.* (LHC Higgs Cross Section Working Group), CERN Report **2012-002** (2012), [arXiv:1201.3084].
- [43] S. Heinemeyer *et al.* (LHC Higgs Cross Section Working Group), CERN Report **2013-004** (2013), [arXiv:1307.1347].
- [44] D. de Florian *et al.* (LHC Higgs Cross Section Working Group), CERN Report **2017-002** (2016), [arXiv:1610.07922].
- [45] LHC Higgs Cross Section Working Group, <https://twiki.cern.ch/twiki/bin/view/LHCPhysics/LHCHXSWG>.
- [46] T. Aaltonen *et al.* (CDF, D0), Phys. Rev. **D88**, 5, 052014 (2013), [arXiv:1303.6346].
- [47] H. M. Georgi *et al.*, Phys. Rev. Lett. **40**, 692 (1978).
- [48] D. Graudenz, M. Spira and P. M. Zerwas, Phys. Rev. Lett. **70**, 1372 (1993).
- [49] M. Spira *et al.*, Nucl. Phys. **B453**, 17 (1995), [hep-ph/9504378].
- [50] C. Anastasiou *et al.*, Phys. Rev. Lett. **114**, 212001 (2015), [arXiv:1503.06056]; C. Anastasiou *et al.*, JHEP **05**, 058 (2016), [arXiv:1602.00695].
- [51] R. V. Harlander and K. J. Ozeren, JHEP **11**, 088 (2009), [arXiv:0909.3420]; A. Pak, M. Rogal and M. Steinhauser, JHEP **02**, 025 (2010), [arXiv:0911.4662].
- [52] J. Davies *et al.*, Phys. Rev. **D100**, 3, 034017 (2019), [arXiv:1906.00982].
- [53] S. Dawson, Nucl. Phys. **B359**, 283 (1991); A. Djouadi, M. Spira and P. M. Zerwas, Phys. Lett. **B264**, 440 (1991).
- [54] R. V. Harlander and W. B. Kilgore, Phys. Rev. Lett. **88**, 201801 (2002), [hep-ph/0201206]; C. Anastasiou and K. Melnikov, Nucl. Phys. **B646**, 220 (2002), [hep-ph/0207004]; V. Ravindran, J. Smith and W. L. van Neerven, Nucl. Phys. **B665**, 325 (2003), [hep-ph/0302135].
- [55] A. Djouadi and P. Gambino, Phys. Rev. Lett. **73**, 2528 (1994), [hep-ph/9406432]; S. Actis *et al.*, Phys. Lett. **B670**, 12 (2008), [arXiv:0809.1301]; U. Aglietti *et al.*, Phys. Lett. **B595**, 432 (2004), [hep-ph/0404071]; G. Degrandi and F. Maltoni, Phys. Lett. **B600**, 255 (2004), [hep-ph/0407249].
- [56] M. Bonetti, K. Melnikov and L. Tancredi, Phys. Rev. **D97**, 5, 056017 (2018), [Erratum: Phys. Rev. **D97**, 9, 099906 (2018)], [arXiv:1801.10403].
- [57] C. Anastasiou, R. Boughezal and F. Petriello, JHEP **04**, 003 (2009), [arXiv:0811.3458].
- [58] C. Anastasiou *et al.*, JHEP **03**, 162 (2019), [arXiv:1811.11211].
- [59] M. Bonvini *et al.*, JHEP **08**, 105 (2016), [arXiv:1603.08000]; B. Mistlberger, JHEP **05**, 028 (2018), [arXiv:1802.00833].
- [60] R. Boughezal *et al.*, Phys. Rev. Lett. **115**, 8, 082003 (2015), [arXiv:1504.07922].
- [61] X. Chen *et al.*, Phys. Lett. **B740**, 147 (2015), [arXiv:1408.5325].
- [62] J. M. Campbell, R. K. Ellis and S. Seth (2019), [arXiv:1906.01020].
- [63] J. M. Lindert *et al.*, Phys. Rev. Lett. **118**, 25, 252002 (2017), [arXiv:1703.03886]; J. M. Lindert *et al.*, Phys. Lett. **B782**, 210 (2018), [arXiv:1801.08226]; S. P. Jones, M. Kerner and G. Luisoni, Phys. Rev. Lett. **120**, 16, 162001 (2018), [arXiv:1802.00349]; T. Neumann, J. Phys. Comm. **2**, 9, 095017 (2018), [arXiv:1802.02981].
- [64] S. Forte and C. Muselli, JHEP **03**, 122 (2016), [arXiv:1511.05561]; K. Melnikov and A. Penin, JHEP **05**, 172 (2016), [arXiv:1602.09020]; T. Liu and A. Penin, JHEP **11**, 158 (2018), [arXiv:1809.04950].
- [65] F. Caola *et al.*, JHEP **09**, 035 (2018), [arXiv:1804.07632].
- [66] W. Bizon *et al.*, JHEP **02**, 108 (2018), [arXiv:1705.09127]; X. Chen *et al.*, Phys. Lett. **B788**, 425 (2019), [arXiv:1805.00736].
- [67] S. Catani and M. Grazzini, Eur. Phys. J. **C72**, 2013 (2012), [Erratum: Eur. Phys. J. **C72**, 2132 (2012)], [arXiv:1106.4652].
- [68] A. Banfi, G. P. Salam and G. Zanderighi, JHEP **06**, 159 (2012), [arXiv:1203.5773]; T. Becher, M. Neubert and D. Wilhelm, JHEP **05**, 110 (2013), [arXiv:1212.2621]; A. Banfi *et al.*, JHEP **04**, 049 (2016), [arXiv:1511.02886]; J. K. L. Michel, P. Pietrulewicz and F. J. Tackmann, JHEP **04**, 142 (2019), [arXiv:1810.12911]; P. F. Monni, L. Rottoli and P. Torrielli (2019), [arXiv:1909.04704].
- [69] I. Moulton and I. W. Stewart, JHEP **09**, 129 (2014), [arXiv:1405.5534].
- [70] W.-Y. Keung and F. J. Petriello, Phys. Rev. **D80**, 013007 (2009), [arXiv:0905.2775]; S. Bühler *et al.*, JHEP **07**, 115 (2012), [arXiv:1204.4415].
- [71] LHC Higgs Cross Section Working Group, "Recommended predictions for the boosted-Higgs cross section", Note LHCHXSWG-2019-002, <https://cds.cern.ch/record/2669113>.
- [72] V. D. Barger *et al.*, Phys. Rev. **D44**, 1426 (1991).
- [73] F. A. Dreyer and A. Karlberg, Phys. Rev. Lett. **117**, 7, 072001 (2016), [arXiv:1606.00840].
- [74] T. Han, G. Valencia and S. Willenbrock, Phys. Rev. Lett. **69**, 3274 (1992), [hep-ph/9206246].
- [75] T. Liu, K. Melnikov and A. A. Penin (2019), [arXiv:1906.10899].
- [76] M. Cacciari *et al.*, Phys. Rev. Lett. **115**, 8, 082002 (2015), [Erratum: Phys. Rev. Lett. **120**, 13, 139901 (2018)], [arXiv:1506.02660]; J. Cruz-Martinez *et al.*, Phys. Lett. **B781**, 672 (2018), [arXiv:1802.02445].
- [77] M. Rauch and D. Zeppenfeld, Phys. Rev. **D95**, 11, 114015 (2017), [arXiv:1703.05676].

- [78] S. L. Glashow, D. V. Nanopoulos and A. Yildiz, *Phys. Rev.* **D18**, 1724 (1978); T. Han and S. Willenbrock, *Phys. Lett.* **B273**, 167 (1991); T. Han, G. Valencia, and S. Willenbrock, *Phys. Rev. Lett.* **69**, 3274 (1992); H. Baer, B. Bailey and J. F. Owens, *Phys. Rev.* **D47**, 2730 (1993); J. Ohnemus and W. J. Stirling, *Phys. Rev.* **D47**, 2722 (1993).
- [79] A. Stange, W. J. Marciano and S. Willenbrock, *Phys. Rev.* **D49**, 1354 (1994), [hep-ph/9309294]; A. Stange, W. J. Marciano and S. Willenbrock, *Phys. Rev.* **D50**, 4491 (1994), [hep-ph/9404247].
- [80] M. L. Ciccolini, S. Dittmaier and M. Kramer, *Phys. Rev.* **D68**, 073003 (2003), [hep-ph/0306234]; A. Denner *et al.*, *JHEP* **03**, 075 (2012), [arXiv:1112.5142].
- [81] R. Hamberg, W. L. van Neerven and T. Matsuura, *Nucl. Phys.* **B359**, 343 (1991), [Erratum: *Nucl. Phys.* **B644**, 403 (2002)].
- [82] O. Brein, A. Djouadi and R. Harlander, *Phys. Lett.* **B579**, 149 (2004), [hep-ph/0307206]; L. Altenkamp *et al.*, *JHEP* **02**, 078 (2013), [arXiv:1211.5015].
- [83] O. Brein *et al.*, *Eur. Phys. J.* **C72**, 1868 (2012), [arXiv:1111.0761].
- [84] O. Brein, R.V. Harlander, and T.J. Zirke, *Comp. Phys. Comm.* **184**, 998 (2013).
- [85] A. Denner *et al.*, *JHEP* **03**, 075 (2012), [arXiv:1112.5142].
- [86] G. Ferrera, M. Grazzini, and F. Tramontano, *Phys. Rev. Lett.* **107**, 152003 (2011).
- [87] G. Ferrera, M. Grazzini and F. Tramontano, *Phys. Lett.* **B740**, 51 (2015), [arXiv:1407.4747]; J. M. Campbell, R. K. Ellis and C. Williams, *JHEP* **06**, 179 (2016), [arXiv:1601.00658].
- [88] W. Astill *et al.*, *JHEP* **06**, 154 (2016), [arXiv:1603.01620].
- [89] F. Caola *et al.*, *Phys. Rev.* **D97**, 7, 074022 (2018), [arXiv:1712.06954]; R. Gauld *et al.* (2019), [arXiv:1907.05836].
- [90] J. M. Butterworth *et al.*, *Phys. Rev. Lett.* **100**, 242001 (2008), [arXiv:0802.2470].
- [91] R. Raitio and W. W. Wada, *Phys. Rev.* **D19**, 941 (1979); Z. Kunszt, *Nucl. Phys.* **B247**, 339 (1984); J. F. Gunion, *Phys. Lett.* **B261**, 510 (1991); W. J. Marciano and F. E. Paige, *Phys. Rev. Lett.* **66**, 2433 (1991).
- [92] W. Beenakker *et al.*, *Phys. Rev. Lett.* **87**, 201805 (2001), [hep-ph/0107081]; L. Reina and S. Dawson, *Phys. Rev. Lett.* **87**, 201804 (2001), [hep-ph/0107101]; S. Dawson *et al.*, *Phys. Rev.* **D67**, 071503 (2003), [hep-ph/0211438]; W. Beenakker *et al.*, *Nucl. Phys.* **B653**, 151 (2003), [hep-ph/0211352]; S. Dawson *et al.*, *Phys. Rev.* **D68**, 034022 (2003), [hep-ph/0305087].
- [93] Y. Zhang *et al.*, *Phys. Lett.* **B738**, 1 (2014), [arXiv:1407.1110]; S. Frixione *et al.*, *JHEP* **09**, 065 (2014), [arXiv:1407.0823].
- [94] T. Plehn, G. P. Salam and M. Spannowsky, *Phys. Rev. Lett.* **104**, 111801 (2010), [arXiv:0910.5472].
- [95] R. Frederix *et al.*, *Phys. Lett.* **B701**, 427 (2011), [arXiv:1104.5613]; M. V. Garzelli *et al.*, *EPL* **96**, 1, 11001 (2011), [arXiv:1108.0387].
- [96] F. Demartin *et al.*, *Eur. Phys. J.* **C75**, 6, 267 (2015), [arXiv:1504.00611].
- [97] K.A. Assamagan *et al.*, [Higgs Working Group, “Physics at TeV Colliders” workshop, Les Houches, 2003], arXiv:hep-ph/0406152 (2004).
- [98] R. V. Harlander and W. B. Kilgore, *Phys. Rev.* **D68**, 013001 (2003), [hep-ph/0304035]; J. M. Campbell *et al.*, *Phys. Rev.* **D67**, 095002 (2003), [hep-ph/0204093]; S. Dawson *et al.*, *Phys. Rev. Lett.* **94**, 031802 (2005), [hep-ph/0408077]; S. Dittmaier, M. Krämer and M. Spira, *Phys. Rev.* **D70**, 074010 (2004), [hep-ph/0309204]; S. Dawson *et al.*, *Phys. Rev.* **D69**, 074027 (2004), [hep-ph/0311067].
- [99] W. J. Stirling and D. J. Summers, *Phys. Lett.* **B283**, 411 (1992); F. Maltoni *et al.*, *Phys. Rev.* **D64**, 094023 (2001), [hep-ph/0106293].
- [100] S. Dawson, S. Dittmaier and M. Spira, *Phys. Rev.* **D58**, 115012 (1998), [hep-ph/9805244].
- [101] D. de Florian and J. Mazzitelli, *Phys. Rev. Lett.* **111**, 201801 (2013), [arXiv:1309.6594].
- [102] S. Borowka *et al.*, *Phys. Rev. Lett.* **117**, 1, 012001 (2016), [Erratum: *Phys. Rev. Lett.* **117**, 7, 079901 (2016)], [arXiv:1604.06447].
- [103] J. Baglio *et al.*, *Eur. Phys. J.* **C79**, 6, 459 (2019), [arXiv:1811.05692].
- [104] M. Cepeda *et al.* (HL/HE WG2 group) (2019), [arXiv:1902.00134].
- [105] B.L. Ioffe and V.A. Khoze, *Sov. J. Nucl. Phys.* **9**, 50 (1978).
- [106] D. R. T. Jones and S. T. Petcov, *Phys. Lett.* **84B**, 440 (1979); R. N. Cahn and S. Dawson, *Phys. Lett.* **136B**, 196 (1984), [Erratum: *Phys. Lett.* **138B**, 464 (1984)]; G. L. Kane, W. W. Repko and W. B. Rolnick, *Phys. Lett.* **148B**, 367 (1984); G. Altarelli, B. Mele and F. Pitolli, *Nucl. Phys.* **B287**, 205 (1987); W. Kilian, M. Kramer and P. M. Zerwas, *Phys. Lett.* **B373**, 135 (1996), [hep-ph/9512355].
- [107] B. A. Kniehl, *Z. Phys.* **C55**, 605 (1992); J. Fleischer and F. Jegerlehner, *Nucl. Phys.* **B216**, 469 (1983); A. Denner *et al.*, *Z. Phys.* **C56**, 261 (1992); B. A. Kniehl, *Int. J. Mod. Phys.* **A17**, 1457 (2002), [hep-ph/0112023].
- [108] K. J. F. Gaemers and G. J. Gounaris, *Phys. Lett.* **77B**, 379 (1978); A. Djouadi, J. Kalinowski and P. M. Zerwas, *Z. Phys.* **C54**, 255 (1992); B. A. Kniehl, F. Madricardo and M. Steinhauser, *Phys. Rev.* **D66**, 054016 (2002), [hep-ph/0205312]; S. Dittmaier *et al.*, *Phys. Lett.* **B441**, 383 (1998), [hep-ph/9808433]; S. Dittmaier *et al.*, *Phys. Lett.* **B478**, 247 (2000), [hep-ph/0002035]; S. Dawson and L. Reina, *Phys. Rev.* **D59**, 054012 (1999), [hep-ph/9808443].
- [109] A. Arbey *et al.*, *Eur. Phys. J.* **C75**, 8, 371 (2015), [arXiv:1504.01726].
- [110] A. Denner *et al.*, *Eur. Phys. J.* **C71**, 1753 (2011), [arXiv:1107.5909].
- [111] A. Djouadi, J. Kalinowski, and M. Spira, *Comp. Phys. Comm.* **108**, 56 (1998); A. Djouadi *et al.*, arXiv:1003.1643 [hep-ph] (2010).
- [112] S. G. Gorishnii *et al.*, *Mod. Phys. Lett.* **A5**, 2703 (1990); S. G. Gorishnii *et al.*, *Phys. Rev.* **D43**, 1633 (1991); A. L. Kataev and V. T. Kim, *Mod. Phys. Lett.* **A9**, 1309 (1994); L. R. Surguladze, *Phys. Lett.* **B341**, 60 (1994), [hep-ph/9405325]; S. A. Larin, T. van Ritbergen and J. A. M. Vermaseren, *Phys. Lett.* **B362**, 134 (1995), [hep-ph/9506465]; K. G. Chetyrkin and A. Kwiatkowski, *Nucl. Phys.* **B461**, 3 (1996), [hep-ph/9505358]; K. G. Chetyrkin, *Phys. Lett.* **B390**, 309 (1997), [hep-ph/9608318]; P. A. Baikov, K. G. Chetyrkin and J. H. Kuhn, *Phys. Rev. Lett.* **96**, 012003 (2006), [hep-ph/0511063].
- [113] J. Fleischer and F. Jegerlehner, *Phys. Rev.* **D23**, 2001 (1981); D. Yu. Bardin, B. M. Vilensky and P. K. Khristova, *Sov. J. Nucl. Phys.* **53**, 152 (1991), [Yad. Fiz.53,240(1991)]; A. Dabelstein and W. Hollik, *Z. Phys.* **C53**, 507 (1992); B. A. Kniehl, *Nucl. Phys.* **B376**, 3 (1992); A. Djouadi *et al.*, in “In \*Munich/Annecy/Hamburg 1991, Proceedings, e+ e- collisions at 500-GeV, pt. A\* 11-30,” (1991).
- [114] T. Inami, T. Kubota and Y. Okada, *Z. Phys.* **C18**, 69 (1983); K. G. Chetyrkin, B. A. Kniehl and M. Steinhauser, *Phys. Rev. Lett.* **79**, 353 (1997), [hep-ph/9705240]; P. A. Baikov and K. G. Chetyrkin, *Phys. Rev. Lett.* **97**, 061803 (2006), [hep-ph/0604194].
- [115] H.-Q. Zheng and D.-D. Wu, *Phys. Rev.* **D42**, 3760 (1990); A. Djouadi *et al.*, *Phys. Lett.* **B257**, 187 (1991); S. Dawson and R. P. Kauffman, *Phys. Rev.* **D47**, 1264 (1993); A. Djouadi, M. Spira and P. M. Zerwas, *Phys. Lett.*

- B311**, 255 (1993), [hep-ph/9305335]; K. Melnikov and O. I. Yakovlev, Phys. Lett. **B312**, 179 (1993), [hep-ph/9302281]; M. Inoue *et al.*, Mod. Phys. Lett. **A9**, 1189 (1994).
- [116] P. Maierhöfer and P. Marquard, Phys. Lett. **B721**, 131 (2013), [arXiv:1212.6233].
- [117] U. Aglietti *et al.*, Phys. Lett. **B595**, 432 (2004), [hep-ph/0404071]; G. Degrossi and F. Maltoni, Phys. Lett. **B600**, 255 (2004), [hep-ph/0407249]; S. Actis *et al.*, Phys. Lett. **B670**, 12 (2008), [arXiv:0809.1301]; U. Aglietti *et al.*, Phys. Lett. **B600**, 57 (2004), [hep-ph/0407162]; G. Degrossi and F. Maltoni, Nucl. Phys. **B724**, 183 (2005), [hep-ph/0504137]; U. Aglietti *et al.*, FERMI LAB-CONF (2006), [hep-ph/0612172].
- [118] A. Abbasabadi *et al.*, Phys. Rev. **D55**, 5647 (1997), [hep-ph/9611209]; A. Abbasabadi and W. W. Repko, Phys. Rev. **D71**, 017304 (2005), [hep-ph/0411152]; A. Abbasabadi and W. W. Repko, JHEP **08**, 048 (2006), [hep-ph/0602087]; D. A. Dicus and W. W. Repko, Phys. Rev. **D87**, 7, 077301 (2013), [arXiv:1302.2159]; L.-B. Chen, C.-F. Qiao and R.-L. Zhu, Phys. Lett. **B726**, 306 (2013), [arXiv:1211.6058]; Y. Sun, H.-R. Chang and D.-N. Gao, JHEP **05**, 061 (2013), [arXiv:1303.2230]; G. Passarino, Phys. Lett. **B727**, 424 (2013), [arXiv:1308.0422].
- [119] M. Spira, A. Djouadi and P. M. Zerwas, Phys. Lett. **B276**, 350 (1992).
- [120] A. Bredenstein *et al.*, Phys. Rev. **D74**, 013004 (2006), [hep-ph/0604011]; A. Bredenstein *et al.*, JHEP **02**, 080 (2007), [hep-ph/0611234]; A. Bredenstein *et al.*, Prophecy4f: A Monte Carlo generator for a proper description of the Higgs decay into 4 fermions, <http://omnibus.uni-freiburg.de/~sd565/programs/prophecy4f/prophecy4f.html>.
- [121] A. Ghinculov, Phys. Lett. **B337**, 137 (1994), [Erratum: Phys. Lett. **B346**, 426 (1995)], [hep-ph/9405394]; L. Durand, B. A. Kniehl and K. Riesselmann, Phys. Rev. **D51**, 5007 (1995), [hep-ph/9412311]; L. Durand, K. Riesselmann and B. A. Kniehl, Phys. Rev. Lett. **72**, 2534 (1994), [Erratum: Phys. Rev. Lett. **74**, 1699 (1995)].
- [122] R. Barate *et al.* (LEP Working Group for Higgs boson searches, ALEPH, DELPHI, L3, OPAL), Phys. Lett. **B565**, 61 (2003), [hep-ex/0306033].
- [123] M. Tanabashi *et al.* (Particle Data Group), Phys. Rev. **D98**, 3, 030001 (2018).
- [124] Y. L. Dokshitzer, S. I. Troian and V. A. Khoze, Sov. J. Nucl. Phys. **46**, 712 (1987), [Yad. Fiz. **46**, 1220(1987)].
- [125] ATLAS Collaboration, ATLAS-CONF-2017-045 (2017).
- [126] CMS Collaboration, CMS-PAS-HIG-19-001 (2019).
- [127] G. Aad *et al.* (ATLAS, CMS), Phys. Rev. Lett. **114**, 191803 (2015), [arXiv:1503.07589].
- [128] ATLAS Collaboration, ATLAS-CONF-2019-029 (2019).
- [129] A. M. Sirunyan *et al.* (CMS), JHEP **11**, 185 (2018), [arXiv:1804.02716].
- [130] A. M. Sirunyan *et al.* (CMS), JHEP **11**, 047 (2017), [arXiv:1706.09936].
- [131] ATLAS Collaboration, ATLAS-CONF-2019-025 (2019).
- [132] M. Aaboud *et al.* (ATLAS), Phys. Lett. **B784**, 345 (2018), [arXiv:1806.00242].
- [133] CMS Collaboration, CMS-PAS-HIG-18-029 (2019).
- [134] ATLAS Collaboration, ATLAS-CONF-2016-009 (2016).
- [135] M. Dittmar and H. K. Dreiner, Phys. Rev. **D55**, 167 (1997), [hep-ph/9608317].
- [136] G. Aad *et al.* (ATLAS), JHEP **08**, 137 (2015), [arXiv:1506.06641].
- [137] ATLAS Collaboration, ATLAS-CONF-2016-112 (2016).
- [138] M. Aaboud *et al.* (ATLAS), Phys. Lett. **B789**, 508 (2019), [arXiv:1808.09054].
- [139] A. M. Sirunyan *et al.* (CMS), Phys. Lett. **B791**, 96 (2019), [arXiv:1806.05246].
- [140] G. Aad *et al.* (ATLAS), JHEP **04**, 117 (2015), [arXiv:1501.04943].
- [141] ATLAS and CMS Collaboration, ATLAS-CONF-2015-044 and CMS-PAS-HIG-15-002 (2015).
- [142] M. Aaboud *et al.* (ATLAS), Phys. Rev. **D99**, 072001 (2019), [arXiv:1811.08856].
- [143] A. M. Sirunyan *et al.* (CMS), Phys. Lett. **B779**, 283 (2018), [arXiv:1708.00373].
- [144] A. M. Sirunyan *et al.* (CMS), JHEP **06**, 093 (2019), [arXiv:1809.03590].
- [145] CMS Collaboration, CMS-PAS-HIG-18-032 (2019).
- [146] T. Aaltonen *et al.* (CDF, D0), Phys. Rev. Lett. **109**, 071804 (2012), [arXiv:1207.6436].
- [147] M. Aaboud *et al.* (ATLAS), Phys. Lett. **B786**, 59 (2018), [arXiv:1808.08238].
- [148] A. M. Sirunyan *et al.* (CMS), Phys. Rev. Lett. **121**, 12, 121801 (2018), [arXiv:1808.08242].
- [149] M. Aaboud *et al.* (ATLAS), JHEP **05**, 141 (2019), [arXiv:1903.04618].
- [150] LHCb Collaboration, LHCb-CONF-2016-006, CERN-LHCb-CONF-2016-006 (2016).
- [151] M. Aaboud *et al.* (ATLAS), JHEP **11**, 112 (2016), [arXiv:1606.02181].
- [152] V. Khachatryan *et al.* (CMS), Phys. Rev. **D92**, 3, 032008 (2015), [arXiv:1506.01010].
- [153] M. Aaboud *et al.* (ATLAS), Phys. Rev. **D98**, 5, 052003 (2018), [arXiv:1807.08639]; CMS Collaboration, CMS-PAS-HIG-16-003 (2019).
- [154] E. Gabrielli *et al.*, Nucl. Phys. **B781**, 64 (2007), [hep-ph/0702119].
- [155] ATLAS Collaboration, ATLAS-CONF-2018-052 (2018).
- [156] A. M. Sirunyan *et al.* (CMS), Phys. Rev. Lett. **120**, 7, 071802 (2018), [arXiv:1709.05543].
- [157] M. Cacciari, G. P. Salam and G. Soyez, JHEP **04**, 063 (2008), [arXiv:0802.1189].
- [158] V. Khachatryan *et al.* (CMS), Eur. Phys. J. **C75**, 6, 251 (2015), [arXiv:1502.02485].
- [159] G. Aad *et al.* (ATLAS), Phys. Lett. **B749**, 519 (2015), [arXiv:1506.05988].
- [160] M. Aaboud *et al.* (ATLAS), Phys. Lett. **B784**, 173 (2018), [arXiv:1806.00425]; A. M. Sirunyan *et al.* (CMS), Phys. Rev. Lett. **120**, 23, 231801 (2018), [arXiv:1804.02610].
- [161] ATLAS Collaboration, ATLAS-CONF-2019-004 (2019).
- [162] CMS Collaboration, CMS-PAS-HIG-18-018 (2019).
- [163] CMS Collaboration, CMS-PAS-HIG-18-030 (2019).
- [164] ATLAS Collaboration, ATLAS-CONF-2017-077 (2017); A. M. Sirunyan *et al.* (CMS), JHEP **08**, 066 (2018), [arXiv:1803.05485]; CMS Collaboration, CMS-PAS-HIG-18-019 (2018); ATLAS Collaboration, ATLAS-CONF-2019-045 (2019).
- [165] M. Farina *et al.*, JHEP **05**, 022 (2013), [arXiv:1211.3736].
- [166] CMS Collaboration, CMS-PAS-HIG-17-005 (2017).
- [167] CMS Collaboration, CMS-PAS-HIG-16-019 (2016).
- [168] A. M. Sirunyan *et al.* (CMS), Phys. Rev. **D99**, 9, 092005 (2019), [arXiv:1811.09696].
- [169] G. Aad *et al.* (ATLAS), JHEP **12**, 061 (2015), [arXiv:1509.06047].
- [170] V. Khachatryan *et al.* (CMS), JHEP **02**, 079 (2017), [arXiv:1610.04857].
- [171] ATLAS Collaboration, JHEP **129**, 010 (2017).
- [172] CMS Collaboration, CMS-PAS-TOP-2017-003 (2017).
- [173] G. Aad *et al.* (ATLAS) (2019), [arXiv:1906.02025].

- [174] A. M. Sirunyan *et al.* (CMS), Phys. Rev. Lett. **122**, 12, 121803 (2019), [arXiv:1811.09689].
- [175] V. Khachatryan *et al.* (CMS), Phys. Lett. **B753**, 341 (2016), [arXiv:1507.03031].
- [176] M. Aaboud *et al.* (ATLAS), JHEP **10**, 112 (2017), [arXiv:1708.00212].
- [177] A. M. Sirunyan *et al.* (CMS), JHEP **11**, 152 (2018), [arXiv:1806.05996].
- [178] ATLAS Collaboration, ATLAS-CONF-2019-028 (2019).
- [179] A. M. Sirunyan *et al.* (CMS), Phys. Rev. Lett. **122**, 2, 021801 (2019), [arXiv:1807.06325].
- [180] ATLAS Collaboration, ATLAS-CONF-2019-037 (2019).
- [181] V. Khachatryan *et al.* (CMS), Phys. Lett. **B749**, 337 (2015), [arXiv:1502.07400].
- [182] G. Aad *et al.* (ATLAS), JHEP **11**, 211 (2015), [arXiv:1508.03372].
- [183] G. Aad *et al.* (ATLAS), Eur. Phys. J. **C77**, 2, 70 (2017), [arXiv:1604.07730].
- [184] CMS Collaboration, CMS-PAS-HIG-17-001 (2017).
- [185] V. Khachatryan *et al.* (CMS), Phys. Lett. **B763**, 472 (2016), [arXiv:1607.03561].
- [186] R. Harnik, J. Kopp and J. Zupan, JHEP **03**, 026 (2013), [arXiv:1209.1397].
- [187] G. Aad *et al.* (ATLAS) (2019), [arXiv:1907.06131].
- [188] A. M. Sirunyan *et al.* (CMS), JHEP **06**, 001 (2018), [arXiv:1712.07173].
- [189] C. Delaunay *et al.*, Phys. Rev. **D89**, 3, 033014 (2014), [arXiv:1310.7029].
- [190] M. Aaboud *et al.* (ATLAS), Phys. Rev. Lett. **120**, 21, 211802 (2018), [arXiv:1802.04329].
- [191] CMS Collaboration, CMS-PAS-HIG-18-031 (2019).
- [192] G. Isidori, A. V. Manohar and M. Trott, Phys. Lett. **B728**, 131 (2014), [arXiv:1305.0663]; G. T. Bodwin *et al.*, Phys. Rev. **D88**, 5, 053003 (2013), [arXiv:1306.5770]; M. König and M. Neubert, JHEP **08**, 012 (2015), [arXiv:1505.03870].
- [193] G. Aad *et al.* (ATLAS), Phys. Rev. Lett. **114**, 12, 121801 (2015), [arXiv:1501.03276].
- [194] M. Aaboud *et al.* (ATLAS), Phys. Rev. Lett. **117**, 11, 111802 (2016), [arXiv:1607.03400].
- [195] A. M. Sirunyan *et al.* (CMS), Phys. Lett. **B797**, 134811 (2019), [arXiv:1905.10408].
- [196] A. Djouadi *et al.*, Eur. Phys. J. **C73**, 6, 2455 (2013), [arXiv:1205.3169].
- [197] O. J. P. Eboli and D. Zeppenfeld, Phys. Lett. **B495**, 147 (2000), [hep-ph/0009158].
- [198] M. Aaboud *et al.* (ATLAS), Phys. Lett. **B793**, 499 (2019), [arXiv:1809.06682].
- [199] M. Aaboud *et al.* (ATLAS), Phys. Lett. **B776**, 318 (2018), [arXiv:1708.09624].
- [200] M. Aaboud *et al.* (ATLAS), JHEP **10**, 180 (2018), [arXiv:1807.11471].
- [201] M. Aaboud *et al.* (ATLAS), Phys. Rev. Lett. **122**, 23, 231801 (2019), [arXiv:1904.05105].
- [202] A. M. Sirunyan *et al.* (CMS), Eur. Phys. J. **C78**, 4, 291 (2018), [arXiv:1711.00431].
- [203] A. M. Sirunyan *et al.* (CMS), Phys. Rev. **D97**, 9, 092005 (2018), [arXiv:1712.02345].
- [204] A. M. Sirunyan *et al.* (CMS), Phys. Lett. **B793**, 520 (2019), [arXiv:1809.05937].
- [205] CMS Collaboration, CMS-PAS-HIG-18-008 (2019).
- [206] M. J. Strassler and K. M. Zurek, Phys. Lett. **B651**, 374 (2007), [hep-ph/0604261]; M. J. Strassler and K. M. Zurek, Phys. Lett. **B661**, 263 (2008), [hep-ph/0605193].
- [207] T. Han *et al.*, JHEP **07**, 008 (2008), [arXiv:0712.2041].
- [208] A. Falkowski *et al.*, Phys. Rev. Lett. **105**, 241801 (2010), [arXiv:1007.3496].
- [209] G. Aad *et al.* (ATLAS) (2019), [arXiv:1909.01246].
- [210] CMS Collaboration, CMS-PAS-EXO-19-007 (2019).
- [211] D. Tucker-Smith and N. Weiner, Phys. Rev. **D64**, 043502 (2001), [hep-ph/0101138].
- [212] S. Chatrchyan *et al.* (CMS), Phys. Lett. **B726**, 564 (2013), [arXiv:1210.7619].
- [213] G. Aad *et al.* (ATLAS) (2019), [arXiv:1909.02845].
- [214] A. M. Sirunyan *et al.* (CMS), Eur. Phys. J. **C79**, 5, 421 (2019), [arXiv:1809.10733].
- [215] C. Patrignani *et al.* (Particle Data Group), Chin. Phys. **C40**, 10, 100001 (2016).
- [216] G. Aad *et al.* (ATLAS), Eur. Phys. J. **C76**, 1, 6 (2016), [arXiv:1507.04548].
- [217] L. D. Landau, Dokl. Akad. Nauk Ser. Fiz. **60**, 2, 207 (1948); C.-N. Yang, Phys. Rev. **77**, 242 (1950).
- [218] S. Bolognesi *et al.*, Phys. Rev. **D86**, 095031 (2012), [arXiv:1208.4018].
- [219] G. Aad *et al.* (ATLAS), Eur. Phys. J. **C75**, 10, 476 (2015), [Erratum: Eur. Phys. J. **C76**, 3, 152 (2016)], [arXiv:1506.05669].
- [220] V. Khachatryan *et al.* (CMS), Phys. Rev. **D92**, 1, 012004 (2015), [arXiv:1411.3441]; G. Aad *et al.* (ATLAS), Phys. Lett. **B726**, 120 (2013), [arXiv:1307.1432].
- [221] P. Artoisenet *et al.*, JHEP **11**, 043 (2013), [arXiv:1306.6464].
- [222] J. Ellis *et al.*, JHEP **11**, 134 (2012), [arXiv:1208.6002].
- [223] D0 Collaboration, Note 6387-CONF (2013).
- [224] D0 Collaboration, Note 6406-CONF (2013).
- [225] J. C. Collins and D. E. Soper, Phys. Rev. **D16**, 2219 (1977).
- [226] A. De Rijula *et al.*, Phys. Rev. **D82**, 013003 (2010), [arXiv:1001.5300].
- [227] ATLAS Collaboration, ATLAS-CONF-2017-043 (2017).
- [228] A. M. Sirunyan *et al.* (CMS), Phys. Rev. **D99**, 11, 112003 (2019), [arXiv:1901.00174].
- [229] A. M. Sirunyan *et al.* (CMS), Submitted to: Phys. Rev. (2019), [arXiv:1903.06973].
- [230] G. Aad *et al.* (ATLAS), Eur. Phys. J. **C76**, 12, 658 (2016), [arXiv:1602.04516].
- [231] N. Kauer and G. Passarino, JHEP **08**, 116 (2012), [arXiv:1206.4803].
- [232] V. Khachatryan *et al.* (CMS), JHEP **09**, 051 (2016), [arXiv:1605.02329].
- [233] G. Aad *et al.* (ATLAS), Eur. Phys. J. **C75**, 7, 335 (2015), [arXiv:1503.01060].
- [234] M. Aaboud *et al.* (ATLAS), Phys. Lett. **B786**, 223 (2018), [arXiv:1808.01191].
- [235] G. Aad *et al.* (ATLAS), Phys. Rev. **D90**, 5, 052004 (2014), [arXiv:1406.3827].
- [236] CMS Collaboration, CMS-PAS-HIG-16-041 (2017).
- [237] L. J. Dixon and M. S. Siu, Phys. Rev. Lett. **90**, 252001 (2003), [hep-ph/0302233]; S. P. Martin, Phys. Rev. **D86**, 073016 (2012), [arXiv:1208.1533]; L. J. Dixon and Y. Li, Phys. Rev. Lett. **111**, 111802 (2013), [arXiv:1305.3854].
- [238] ATLAS Collaboration, ATL-PHYS-PUB-2013-014 (2013).
- [239] J. Campbell *et al.*, Phys. Rev. Lett. **119**, 18, 181801 (2017), [Addendum: Phys. Rev. Lett. **119**, 19, 199901 (2017)], [arXiv:1704.08259].
- [240] ATLAS Collaboration, ATL-PHYS-PUB-2014-016 (2014).

- [241] F. Caola and K. Melnikov, *Phys. Rev.* **D88**, 054024 (2013), [arXiv:1307.4935]; J. M. Campbell, R. K. Ellis and C. Williams, *JHEP* **04**, 060 (2014), [arXiv:1311.3589]; J. M. Campbell, R. K. Ellis and C. Williams, *Phys. Rev.* **D89**, 5, 053011 (2014), [arXiv:1312.1628].
- [242] C. Englert and M. Spannowsky, *Phys. Rev.* **D90**, 053003 (2014), [arXiv:1405.0285].
- [243] A. Azatov *et al.*, *Zh. Eksp. Teor. Fiz.* **147**, 410 (2015), [*J. Exp. Theor. Phys.* 120,354(2015)], [arXiv:1406.6338]; A. Azatov *et al.*, *JHEP* **09**, 123 (2016), [arXiv:1608.00977].
- [244] A. David *et al.* (LHC Higgs Cross Section Working Group), “LHC HXSWG interim recommendations to explore the coupling structure of a Higgs-like particle,” (2012), [arXiv:1209.0040].
- [245] M. Dührssen, “Prospects for the measurement of Higgs boson coupling parameters in the mass range from 110–190 GeV,” (2003); M. Dührssen *et al.*, *Phys. Rev.* **D70**, 113009 (2004), [hep-ph/0406323]; R. Lafaye *et al.*, *JHEP* **08**, 009 (2009), [arXiv:0904.3866].
- [246] J. R. Espinosa *et al.*, *JHEP* **05**, 097 (2012), [arXiv:1202.3697]; A. Azatov, R. Contino and J. Galloway, *JHEP* **04**, 127 (2012), [Erratum: *JHEP* **04**, 140 (2013)], [arXiv:1202.3415]; D. Carmi *et al.*, *JHEP* **07**, 136 (2012), [arXiv:1202.3144]; J. R. Espinosa *et al.*, *JHEP* **12**, 045 (2012), [arXiv:1207.1717].
- [247] M. Gonzalez-Alonso *et al.*, *Eur. Phys. J.* **C75**, 128 (2015), [arXiv:1412.6038]; A. Greljo *et al.*, *Eur. Phys. J.* **C76**, 3, 158 (2016), [arXiv:1512.06135].
- [248] G. F. Giudice *et al.*, *JHEP* **06**, 045 (2007), [hep-ph/0703164].
- [249] S. Willenbrock and C. Zhang, *Ann. Rev. Nucl. Part. Sci.* **64**, 83 (2014), [arXiv:1401.0470]; I. Brivio and M. Trott, *Phys. Rept.* **793**, 1 (2019), [arXiv:1706.08945]; S. Dawson, C. Englert and T. Plehn, *Phys. Rept.* **816**, 1 (2019), [arXiv:1808.01324]; T. Cohen, *PoS TASI2018*, 011 (2019), [arXiv:1903.03622].
- [250] F. Feruglio, *Int. J. Mod. Phys.* **A8**, 4937 (1993), [hep-ph/9301281]; G. Buchalla, O. Catà and C. Krause, *Nucl. Phys.* **B880**, 552 (2014), [Erratum: *Nucl. Phys.* **B913**, 475 (2016)], [arXiv:1307.5017]; R. Alonso *et al.*, *Phys. Lett.* **B722**, 330 (2013), [Erratum: *Phys. Lett.* **B726**, 926 (2013)], [arXiv:1212.3305]; A. V. Manohar, in “Les Houches summer school: EFT in Particle Physics and Cosmology Les Houches, Chamonix Valley, France, July 3-28, 2017,” (2018), [arXiv:1804.05863]; I. Brivio *et al.*, *JHEP* **03**, 024 (2014), [arXiv:1311.1823].
- [251] J. de Blas *et al.*, *JHEP* **03**, 109 (2018), [arXiv:1711.10391].
- [252] A. Manohar and H. Georgi, *Nucl. Phys.* **B234**, 189 (1984); M. A. Luty, *Phys. Rev.* **D57**, 1531 (1998), [hep-ph/9706235]; D. Liu *et al.*, *JHEP* **11**, 141 (2016), [arXiv:1603.03064].
- [253] W. Buchmuller and D. Wyler, *Nucl. Phys.* **B268**, 621 (1986).
- [254] C. J. C. Burges and H. J. Schnitzer, *Nucl. Phys.* **B228**, 464 (1983); C. N. Leung, S. T. Love and S. Rao, *Z. Phys.* **C31**, 433 (1986).
- [255] B. Grzadkowski *et al.*, *JHEP* **10**, 085 (2010), [arXiv:1008.4884].
- [256] L. Lehman and A. Martin, *JHEP* **02**, 081 (2016), [arXiv:1510.00372]; B. Henning *et al.*, *JHEP* **08**, 016 (2017), [arXiv:1512.03433].
- [257] C. Hays *et al.*, *JHEP* **02**, 123 (2019), [arXiv:1808.00442].
- [258] R. Alonso *et al.*, *JHEP* **04**, 159 (2014), [arXiv:1312.2014].
- [259] A. Falkowski, LHCHSWG-INT-2015-001 (2015); A. Falkowski, *Pramana* **87**, 3, 39 (2016), [arXiv:1505.00046].
- [260] A. M. Sirunyan *et al.* (CMS), *Phys. Lett.* **B792**, 369 (2019), [arXiv:1812.06504].
- [261] M. Aaboud *et al.* (ATLAS), *Phys. Rev.* **D98**, 052005 (2018), [arXiv:1802.04146].
- [262] F. Maltoni *et al.* (2019), [arXiv:1906.12310].
- [263] R. S. Gupta, A. Pomarol and F. Riva, *Phys. Rev.* **D91**, 3, 035001 (2015), [arXiv:1405.0181].
- [264] B. A. Kniehl and M. Spira, *Z. Phys.* **C69**, 77 (1995), [hep-ph/9505225].
- [265] R. Contino *et al.*, *JHEP* **07**, 035 (2013), [arXiv:1303.3876].
- [266] A. Azatov and J. Galloway, *Phys. Rev.* **D85**, 055013 (2012), [arXiv:1110.5646].
- [267] G. Isidori and M. Trott, *JHEP* **02**, 082 (2014), [arXiv:1307.4051]; A. Pomarol and F. Riva, *JHEP* **01**, 151 (2014), [arXiv:1308.2803].
- [268] J. Ellis, V. Sanz and T. You, *JHEP* **07**, 036 (2014), [arXiv:1404.3667]; A. Biekötter *et al.*, *Phys. Rev.* **D91**, 055029 (2015), [arXiv:1406.7320].
- [269] LHC Higgs Cross Section Working Group, <https://twiki.cern.ch/twiki/bin/view/LHCPhysics/LHCHSWG2KAPPA>.
- [270] ATLAS and C. Collaboration (CMS) (2015).
- [271] M. Reece, *New J. Phys.* **15**, 043003 (2013), [arXiv:1208.1765].
- [272] ATLAS Collaboration, ATLAS-CONF-2019-032 (2019).
- [273] G. Aad *et al.* (ATLAS), *Phys. Lett.* **B753**, 69 (2016), [arXiv:1508.02507].
- [274] N. Berger *et al.* (2019), [arXiv:1906.02754].
- [275] CMS Collaboration, CMS-PAS-HIG-16-040 (2017).
- [276] ATLAS Collaboration, ATLAS-CONF-2018-028 (2018).
- [277] ATLAS Collaboration, CMS-PAS-HIG-19-001 (2019).
- [278] M. McCullough, *Phys. Rev.* **D90**, 1, 015001 (2014), [Erratum: *Phys. Rev.* **D92**, 3, 039903 (2015)], [arXiv:1312.3322].
- [279] G. Degrossi *et al.*, *JHEP* **12**, 080 (2016), [arXiv:1607.04251].
- [280] M. Gorbahn and U. Haisch, *JHEP* **10**, 094 (2016), [arXiv:1607.03773].
- [281] ATLAS Collaboration, ATLAS-PHYS-PUB-2019-009 (2019).
- [282] F. Bishara *et al.*, *Phys. Rev. Lett.* **118**, 12, 121801 (2017), [arXiv:1606.09253].
- [283] T. A. collaboration (ATLAS) (2019).
- [284] ATLAS Collaboration, ATLAS-CONF-2019-049 (2019).
- [285] S. Di Vita *et al.*, *JHEP* **09**, 069 (2017), [arXiv:1704.01953]; F. Maltoni *et al.*, *Eur. Phys. J.* **C77**, 12, 887 (2017), [arXiv:1709.08649].
- [286] B. Di Micco *et al.* (2019), [arXiv:1910.00012].
- [287] J. Parsons, and A. Pomarol, *Extra Dimensions*, in this volume.
- [288] S. Weinberg, *Phys. Rev.* **D13**, 974 (1976), [Addendum: *Phys. Rev.* D19,1277(1979)]; L. Susskind, *Phys. Rev.* **D20**, 2619 (1979); For a review, see C. T. Hill and E. H. Simmons, *Phys. Reports* **381**, 235 (2003) [Erratum: 390, 553 (2004)], [arXiv:hep-ph/0203079].
- [289] Z. Chacko, R. Franceschini and R. K. Mishra, *JHEP* **04**, 015 (2013), [arXiv:1209.3259].
- [290] L. E. Ibanez and G. G. Ross, *Phys. Lett.* **110B**, 215 (1982); L. E. Ibanez, *Phys. Lett.* **118B**, 73 (1982); J. R. Ellis, D. V. Nanopoulos and K. Tamvakis, *Phys. Lett.* **121B**, 123 (1983); L. Alvarez-Gaume, J. Polchinski and M. B. Wise, *Nucl. Phys.* **B221**, 495 (1983).
- [291] S. Dimopoulos and G. F. Giudice, *Phys. Lett.* **B357**, 573 (1995), [hep-ph/9507282]; M. Papucci, J. T. Ruderman and A. Weiler, *JHEP* **09**, 035 (2012), [arXiv:1110.6926].
- [292] ATLAS Collaboration, <https://twiki.cern.ch/twiki/bin/view/AtlasPublic/Publications>; CMS Collaboration, <http://cms-results.web.cern.ch/cms-results/public-results/publications/SUS/STOP.html>.

- [293] J. Mrazek *et al.*, Nucl. Phys. **B853**, 1 (2011), [arXiv:1105.5403].
- [294] D. B. Kaplan, Nucl. Phys. **B365**, 259 (1991).
- [295] G. Panico *et al.*, JHEP **03**, 051 (2013), [arXiv:1210.7114].
- [296] H. E. Haber and G. L. Kane, Phys. Rept. **117**, 75 (1985).
- [297] A. Djouadi, Phys. Rept. **459**, 1 (2008), [hep-ph/0503173].
- [298] S. Heinemeyer, W. Hollik and G. Weiglein, Phys. Rept. **425**, 265 (2006), [hep-ph/0412214].
- [299] P. Draper, G. Lee and C. E. M. Wagner, Phys. Rev. **D89**, 5, 055023 (2014), [arXiv:1312.5743].
- [300] J. F. Gunion and H. E. Haber, Phys. Rev. **D67**, 075019 (2003), [hep-ph/0207010].
- [301] H. E. Haber and Y. Nir, Nucl. Phys. **B335**, 363 (1990).
- [302] E. L. Berger *et al.*, Phys. Rev. **D66**, 095001 (2002), [hep-ph/0205342].
- [303] P. Bechtle *et al.*, Eur. Phys. J. **C77**, 2, 67 (2017), [arXiv:1608.00638].
- [304] E. Bagnaschi *et al.*, Eur. Phys. J. **C79**, 7, 617 (2019), [arXiv:1808.07542].
- [305] A. Djouadi, J. Kalinowski and P. M. Zerwas, Z. Phys. **C57**, 569 (1993).
- [306] G. Lee and C. E. M. Wagner, Phys. Rev. **D92**, 7, 075032 (2015), [arXiv:1508.00576].
- [307] D. Dicus *et al.*, Phys. Rev. **D59**, 094016 (1999), [hep-ph/9811492].
- [308] M. Carena *et al.*, JHEP **07**, 091 (2012), [arXiv:1203.1041].
- [309] A. A. Barrientos Bendezu and B. A. Kniehl, Phys. Rev. **D64**, 035006 (2001), [hep-ph/0103018].
- [310] LHC Higgs Cross Section Working Group, <https://twiki.cern.ch/twiki/bin/view/LHCPhysics/LHCHXSWGSMSSMCharged>.
- [311] A. Djouadi, J. Ellis and J. Quevillon, JHEP **07**, 105 (2016), [arXiv:1605.00542]; M. Carena and Z. Liu, JHEP **11**, 159 (2016), [arXiv:1608.07282].
- [312] M. Carena *et al.*, Eur. Phys. J. **C26**, 601 (2003), [hep-ph/0202167]; M. Carena *et al.*, Eur. Phys. J. **C73**, 9, 2552 (2013), [arXiv:1302.7033].
- [313] H. Bahl, S. Liebler and T. Stefaniak, Eur. Phys. J. **C79**, 3, 279 (2019), [arXiv:1901.05933].
- [314] L. Maiani, A. D. Polosa and V. Riquer, Phys. Lett. **B718**, 465 (2012), [arXiv:1209.4816]; A. Djouadi and J. Quevillon, JHEP **10**, 028 (2013), [arXiv:1304.1787]; A. Djouadi *et al.*, Eur. Phys. J. **C73**, 2650 (2013), [arXiv:1307.5205].
- [315] M. Carena *et al.*, Phys. Rev. **D91**, 3, 035003 (2015), [arXiv:1410.4969].
- [316] M. Carena *et al.*, JHEP **04**, 015 (2014), [arXiv:1310.2248]; K. Blum, R. T. D'Agnolo and J. Fan, JHEP **01**, 057 (2013), [arXiv:1206.5303]; A. Djouadi *et al.*, JHEP **06**, 168 (2015), [arXiv:1502.05653].
- [317] R. S. Chivukula and H. Georgi, Phys. Lett. **B188**, 99 (1987); L. J. Hall and L. Randall, Phys. Rev. Lett. **65**, 2939 (1990); A. J. Buras *et al.*, Phys. Lett. **B500**, 161 (2001), [hep-ph/0007085]; G. D'Ambrosio *et al.*, Nucl. Phys. **B645**, 155 (2002), [hep-ph/0207036].
- [318] L. J. Hall, J. D. Lykken and S. Weinberg, Phys. Rev. **D27**, 2359 (1983); J. E. Kim and H. P. Nilles, Phys. Lett. **138B**, 150 (1984); G. F. Giudice and A. Masiero, Phys. Lett. **B206**, 480 (1988).
- [319] U. Ellwanger, C. Hugonie and A. M. Teixeira, Phys. Rept. **496**, 1 (2010), [arXiv:0910.1785].
- [320] P. Fayet, Nucl. Phys. **B90**, 104 (1975).
- [321] C. Panagiotakopoulos and K. Tamvakis, Phys. Lett. **B469**, 145 (1999), [hep-ph/9908351]; A. Dedes *et al.*, Phys. Rev. **D63**, 055009 (2001), [hep-ph/0009125]; A. Menon, D. E. Morrissey and C. E. M. Wagner, Phys. Rev. **D70**, 035005 (2004), [hep-ph/0404184].
- [322] M. Cvetič *et al.*, Phys. Rev. **D56**, 2861 (1997), [Erratum: Phys. Rev. **D58**, 119905 (1998)], [hep-ph/9703317]; P. Langacker and J. Wang, Phys. Rev. **D58**, 115010 (1998), [hep-ph/9804428].
- [323] J. Erler, P. Langacker and T.-j. Li, Phys. Rev. **D66**, 015002 (2002), [hep-ph/0205001]; T. Han, P. Langacker and B. McElrath, Phys. Rev. **D70**, 115006 (2004), [hep-ph/0405244]; V. Barger *et al.*, Phys. Rev. **D73**, 115010 (2006), [hep-ph/0603247].
- [324] V. Barger, P. Langacker and G. Shaughnessy, Phys. Rev. **D75**, 055013 (2007), [hep-ph/0611239].
- [325] B. A. Dobrescu, G. L. Landsberg and K. T. Matchev, Phys. Rev. **D63**, 075003 (2001), [hep-ph/0005308]; R. Dermisek and J. F. Gunion, Phys. Rev. Lett. **95**, 041801 (2005), [hep-ph/0502105].
- [326] O. J. P. Eboli and D. Zeppenfeld, Phys. Lett. **B495**, 147 (2000), [hep-ph/0009158]; H. Davoudiasl, T. Han and H. E. Logan, Phys. Rev. **D71**, 115007 (2005), [hep-ph/0412269].
- [327] J.-J. Cao *et al.*, JHEP **03**, 086 (2012), [arXiv:1202.5821].
- [328] LHC Higgs Cross Section Working Group, Beyond the Standard Model Higgs – NMSSM, <https://twiki.cern.ch/twiki/bin/view/LHCPhysics/LHCHXSWGSMSSM>.
- [329] M. Carena *et al.*, Phys. Rev. **D93**, 3, 035013 (2016), [arXiv:1510.09137].
- [330] P. Batra *et al.*, JHEP **02**, 043 (2004), [hep-ph/0309149].
- [331] R. Huo *et al.*, Phys. Rev. **D87**, 5, 055011 (2013), [arXiv:1212.0560].
- [332] J. Engel, M. J. Ramsey-Musolf and U. van Kolck, Prog. Part. Nucl. Phys. **71**, 21 (2013), [arXiv:1303.2371].
- [333] S. Dimopoulos and S. D. Thomas, Nucl. Phys. **B465**, 23 (1996), [hep-ph/9510220]; S. D. Thomas, Int. J. Mod. Phys. **A13**, 2307 (1998), [hep-ph/9803420].
- [334] A. Pilaftsis and C. E. M. Wagner, Nucl. Phys. **B553**, 3 (1999), [hep-ph/9902371].
- [335] M. Frank *et al.*, JHEP **02**, 047 (2007), [hep-ph/0611326].
- [336] M. Carena *et al.*, Nucl. Phys. **B586**, 92 (2000), [hep-ph/0003180].
- [337] B. Li and C. E. M. Wagner, Phys. Rev. **D91**, 095019 (2015), [arXiv:1502.02210].
- [338] M. D. Goodsell and F. Staub, Eur. Phys. J. **C77**, 1, 46 (2017), [arXiv:1604.05335]; A. Chakraborty *et al.*, Phys. Rev. **D90**, 5, 055005 (2014), [arXiv:1301.2745]; M. Carena *et al.*, JHEP **02**, 123 (2016), [arXiv:1512.00437].
- [339] J. F. Gunion and H. E. Haber, Phys. Rev. **D67**, 075019 (2003), [hep-ph/0207010]; G. C. Branco *et al.*, Phys. Rept. **516**, 1 (2012), [arXiv:1106.0034].
- [340] N. G. Deshpande and E. Ma, Phys. Rev. **D18**, 2574 (1978).
- [341] A. Goudelis, B. Herrmann and O. Stål, JHEP **09**, 106 (2013), [arXiv:1303.3010].
- [342] C. D. Froggatt and H. B. Nielsen, Nucl. Phys. **B147**, 277 (1979).
- [343] K. S. Babu and S. Nandi, Phys. Rev. **D62**, 033002 (2000), [hep-ph/9907213]; G. F. Giudice and O. Lebedev, Phys. Lett. **B665**, 79 (2008), [arXiv:0804.1753].
- [344] E. Accomando *et al.*, CERN Report **2006-009** (2006), [hep-ph/0608079].
- [345] T. Robens and T. Stefaniak, Eur. Phys. J. **C75**, 104 (2015), [arXiv:1501.02234].
- [346] S. L. Glashow and S. Weinberg, Phys. Rev. **D15**, 1958 (1977); E. A. Paschos, Phys. Rev. **D15**, 1966 (1977).
- [347] G. C. Branco, W. Grimus and L. Lavoura, Phys. Lett. **B380**, 119 (1996), [hep-ph/9601383]; F. J. Botella, G. C. Branco and M. N. Rebelo, Phys. Lett. **B687**, 194 (2010), [arXiv:0911.1753].



- [348] J. Schechter and J. W. F. Valle, Phys. Rev. **D22**, 2227 (1980); T. P. Cheng and L.-F. Li, Phys. Rev. **D22**, 2860 (1980).
- [349] H. Georgi and M. Machacek, Nucl. Phys. **B262**, 463 (1985); M. S. Chanowitz and M. Golden, Phys. Lett. **165B**, 105 (1985); J. F. Gunion, R. Vega and J. Wudka, Phys. Rev. **D42**, 1673 (1990).
- [350] P. Nath *et al.*, Nucl. Phys. Proc. Suppl. **200-202**, 185 (2010), [arXiv:1001.2693].
- [351] J. Garayoa and T. Schwetz, JHEP **03**, 009 (2008), [arXiv:0712.1453].
- [352] H. E. Haber and H. E. Logan, Phys. Rev. **D62**, 015011 (2000), [hep-ph/9909335]; J. F. Gunion, R. Vega and J. Wudka, Phys. Rev. **D43**, 2322 (1991); S. Kanemura and K. Yagyu, Phys. Rev. **D85**, 115009 (2012), [arXiv:1201.6287].
- [353] I. Low and J. Lykken, JHEP **10**, 053 (2010), [arXiv:1005.0872]; I. Low, J. Lykken and G. Shaughnessy, Phys. Rev. **D86**, 093012 (2012), [arXiv:1207.1093].
- [354] H. E. Logan and M.-A. Roy, Phys. Rev. **D82**, 115011 (2010), [arXiv:1008.4869]; A. Falkowski, S. Rychkov and A. Urbano, JHEP **04**, 073 (2012), [arXiv:1202.1532].
- [355] N. Arkani-Hamed *et al.*, JHEP **07**, 034 (2002), [hep-ph/0206021]; N. Arkani-Hamed, A. G. Cohen and H. Georgi, Phys. Lett. **B513**, 232 (2001), [hep-ph/0105239].
- [356] M. Perelstein, Prog. Part. Nucl. Phys. **58**, 247 (2007), [hep-ph/0512128]; M. Schmaltz and D. Tucker-Smith, Ann. Rev. Nucl. Part. Sci. **55**, 229 (2005), [hep-ph/0502182].
- [357] J. A. Casas, J. R. Espinosa and I. Hidalgo, JHEP **03**, 038 (2005), [hep-ph/0502066].
- [358] H.-C. Cheng and I. Low, JHEP **09**, 051 (2003), [hep-ph/0308199].
- [359] M. Carena *et al.*, Phys. Rev. **D75**, 091701 (2007), [hep-ph/0610156].
- [360] M. Aaboud *et al.* (ATLAS), Phys. Rev. Lett. **121**, 21, 211801 (2018), [arXiv:1808.02343]; A. M. Sirunyan *et al.* (CMS), Eur. Phys. J. **C79**, 4, 364 (2019), [arXiv:1812.09768].
- [361] H. Georgi, A. E. Nelson and A. Manohar, Phys. Lett. **126B**, 169 (1983); A. E. Nelson and M. J. Strassler, JHEP **09**, 030 (2000), [hep-ph/0006251]; S. Davidson, G. Isidori and S. Uhlig, Phys. Lett. **B663**, 73 (2008), [arXiv:0711.3376].
- [362] C. Csaki, A. Falkowski and A. Weiler, JHEP **09**, 008 (2008), [arXiv:0804.1954]; B. Keren-Zur *et al.*, Nucl. Phys. **B867**, 394 (2013), [arXiv:1205.5803].
- [363] O. Matsedonskyi, G. Panico and A. Wulzer, JHEP **01**, 164 (2013), [arXiv:1204.6333]; M. Redi and A. Tesi, JHEP **10**, 166 (2012), [arXiv:1205.0232]; D. Marzocca, M. Serone and J. Shu, JHEP **08**, 013 (2012), [arXiv:1205.0770]; A. Pomarol and F. Riva, JHEP **08**, 135 (2012), [arXiv:1205.6434].
- [364] R. Contino and G. Servant, JHEP **06**, 026 (2008), [arXiv:0801.1679]; J. Mrazek and A. Wulzer, Phys. Rev. **D81**, 075006 (2010), [arXiv:0909.3977]; A. De Simone *et al.*, JHEP **04**, 004 (2013), [arXiv:1211.5663]; A. Azatov *et al.*, Phys. Rev. **D89**, 7, 075001 (2014), [arXiv:1308.6601].
- [365] A. Banfi, A. Martin and V. Sanz, JHEP **08**, 053 (2014), [arXiv:1308.4771]; A. Azatov and A. Paul, JHEP **01**, 014 (2014), [arXiv:1309.5273]; C. Grojean *et al.*, JHEP **05**, 022 (2014), [arXiv:1312.3317].
- [366] A. Azatov *et al.*, Phys. Rev. **D92**, 3, 035001 (2015), [arXiv:1502.00539].
- [367] K. Agashe, R. Contino and A. Pomarol, Nucl. Phys. **B719**, 165 (2005), [hep-ph/0412089]; R. Contino, L. Da Rold and A. Pomarol, Phys. Rev. **D75**, 055014 (2007), [hep-ph/0612048]; D. Pappadopulo, A. Thamm and R. Torre, JHEP **07**, 058 (2013), [arXiv:1303.3062]; M. Montull *et al.*, Phys. Rev. **D88**, 095006 (2013), [arXiv:1308.0559].
- [368] M. Carena, L. Da Rold and E. Pontón, JHEP **06**, 159 (2014), [arXiv:1402.2987]; D. Liu, I. Low and C. E. M. Wagner, Phys. Rev. **D96**, 3, 035013 (2017), [arXiv:1703.07791].
- [369] I. Low, R. Rattazzi and A. Vichi, JHEP **04**, 126 (2010), [arXiv:0907.5413].
- [370] M. Ciuchini *et al.*, JHEP **08**, 106 (2013), [arXiv:1306.4644].
- [371] C. Grojean, O. Matsedonskyi and G. Panico, JHEP **10**, 160 (2013), [arXiv:1306.4655].
- [372] M. Geller and O. Telem, Phys. Rev. Lett. **114**, 191801 (2015), [arXiv:1411.2974].
- [373] P. Batra and Z. Chacko, Phys. Rev. **D79**, 095012 (2009), [arXiv:0811.0394]; R. Barbieri *et al.*, JHEP **08**, 161 (2015), [arXiv:1501.07803]; M. Low, A. Tesi and L.-T. Wang, Phys. Rev. **D91**, 095012 (2015), [arXiv:1501.07890].
- [374] M. Aaboud *et al.* (ATLAS), Phys. Lett. **B775**, 105 (2017), [arXiv:1707.04147].
- [375] CMS Collaboration, CMS-PAS-HIG-17-13 (2017); V. Khachatryan *et al.* (CMS), Phys. Lett. **B767**, 147 (2017), [arXiv:1609.02507].
- [376] A. M. Sirunyan *et al.* (CMS), Phys. Lett. **B793**, 320 (2019), [arXiv:1811.08459].
- [377] CMS Collaboration, CMS-PAS-HIG-16-014 (2016).
- [378] ATLAS Collaboration, ATLAS-CONF-2017-058 (2017).
- [379] CMS Collaboration, CMS-PAS-HIG-16-033 (2016).
- [380] CMS Collaboration, CMS-PAS-HIG-16-023 (2016).
- [381] ATLAS Collaboration, ATLAS-CONF-2016-082 (2016).
- [382] CMS Collaboration, CMS-PAS-HIG-16-034 (2017).
- [383] ATLAS Collaboration, ATLAS-CONF-2013-067 (2013).
- [384] CMS Collaboration, CMS-PAS-HIG-17-033 (2019).
- [385] ATLAS Collaboration, ATLAS-CONF-2012-018 (2012).
- [386] M. Aaboud *et al.* (ATLAS), Phys. Lett. **B777**, 91 (2018), [arXiv:1708.04445].
- [387] G. Aad *et al.* (ATLAS), JHEP **09**, 091 (2019), [arXiv:1906.08589].
- [388] M. Aaboud *et al.* (ATLAS), Phys. Rev. **D98**, 5, 052008 (2018), [arXiv:1808.02380].
- [389] ATLAS Collaboration, ATLAS-CONF-2016-004 (2016); M. Aaboud *et al.* (ATLAS), JHEP **05**, 124 (2019), [arXiv:1811.11028]; M. Aaboud *et al.* (ATLAS), Eur. Phys. J. **C78**, 12, 1007 (2018), [arXiv:1807.08567].
- [390] ATLAS Collaboration, ATLAS-CONF-2019-030 (2019); M. Aaboud *et al.* (ATLAS), Phys. Rev. Lett. **121**, 19, 191801 (2018), [Erratum: Phys. Rev. Lett. **122**, 089901 (2019)], [arXiv:1808.00336]; G. Aad *et al.* (ATLAS) (2019), [arXiv:1908.06765].
- [391] CMS Collaboration, CMS-PAS-HIG-2017-008 (2016).
- [392] V. Khachatryan *et al.* (CMS), Phys. Lett. **B755**, 217 (2016), [arXiv:1510.01181].
- [393] CMS Collaboration, CMS-PAS-HIG-18-013 (2019).
- [394] M. Aaboud *et al.* (ATLAS), JHEP **01**, 055 (2018), [arXiv:1709.07242].
- [395] A. M. Sirunyan *et al.* (CMS), JHEP **09**, 007 (2018), [arXiv:1803.06553].
- [396] V. M. Abazov *et al.* (D0), Phys. Rev. Lett. **104**, 151801 (2010), [arXiv:0912.0968].
- [397] D0 Collaboration, D0Note 5974-CONF (2011).
- [398] R. Aaij *et al.* (LHCb), JHEP **05**, 132 (2013), [arXiv:1304.2591].
- [399] A. M. Sirunyan *et al.* (CMS), JHEP **05**, 210 (2019), [arXiv:1903.10228].
- [400] M. Aaboud *et al.* (ATLAS), JHEP **07**, 117 (2019), [arXiv:1901.08144].
- [401] A. M. Sirunyan *et al.* (CMS) (2019), [arXiv:1907.03152].

- [402] CMS Collaboration, CMS-PAS-HIG-18-017 (2019).
- [403] ATLAS Collaboration, ATLAS-CONF-2019-036 (2019).
- [404] A. M. Sirunyan *et al.* (CMS), JHEP **11**, 161 (2018), [arXiv:1808.01890].
- [405] G. Aad *et al.* (ATLAS), JHEP **08**, 148 (2015), [arXiv:1505.07018].
- [406] A. M. Sirunyan *et al.* (CMS) (2019), [arXiv:1908.01115].
- [407] G. Aad *et al.* (ATLAS) (2019), [arXiv:1907.02749].
- [408] S. Chatrchyan *et al.* (CMS), Phys. Lett. **B722**, 207 (2013), [arXiv:1302.2892]; CMS Collaboration, CMS-PAS-HIG-16-025 (2016); A. M. Sirunyan *et al.* (CMS), JHEP **08**, 113 (2018), [arXiv:1805.12191].
- [409] V. M. Abazov *et al.* (D0), Phys. Lett. **B698**, 97 (2011), [arXiv:1011.1931].
- [410] T. Aaltonen *et al.* (CDF), Phys. Rev. **D85**, 032005 (2012), [arXiv:1106.4782].
- [411] ATLAS Collaboration, ATLAS-CONF-2017-055 (2017); G. Aad *et al.* (ATLAS), Phys. Lett. **B744**, 163 (2015), [arXiv:1502.04478].
- [412] A. M. Sirunyan *et al.* (CMS), Eur. Phys. J. **C79**, 7, 564 (2019), [arXiv:1903.00941].
- [413] CMS Collaboration, CMS-PAS-HIG-18-012 (2019).
- [414] M. Aaboud *et al.* (ATLAS), Phys. Lett. **B759**, 555 (2016), [arXiv:1603.09203].
- [415] M. Aaboud *et al.* (ATLAS), JHEP **09**, 139 (2018), [arXiv:1807.07915].
- [416] CMS Collaboration, CMS-PAS-HIG-16-031 (2016); A. M. Sirunyan *et al.* (CMS), JHEP **07**, 142 (2019), [arXiv:1903.04560].
- [417] ATLAS Collaboration, ATLAS-CONF-2012-010 (2012).
- [418] V. Khachatryan *et al.* (CMS), JHEP **12**, 178 (2015), [arXiv:1510.04252].
- [419] ATLAS Collaboration, ATLAS-CONF-2016-089 (2016); M. Aaboud *et al.* (ATLAS), JHEP **11**, 085 (2018), [arXiv:1808.03599].
- [420] V. Khachatryan *et al.* (CMS), JHEP **11**, 018 (2015), [arXiv:1508.07774]; A. M. Sirunyan *et al.* (CMS) (2019), [arXiv:1908.09206].
- [421] G. Aad *et al.* (ATLAS), Phys. Rev. Lett. **114**, 23, 231801 (2015), [arXiv:1503.04233].
- [422] A. M. Sirunyan *et al.* (CMS), Phys. Rev. Lett. **119**, 14, 141802 (2017), [arXiv:1705.02942].
- [423] A. M. Sirunyan *et al.* (CMS), Phys. Rev. Lett. **123**, 13, 131802 (2019), [arXiv:1905.07453].
- [424] CMS Collaboration, CMS-PAS-HIG-16-030 (2016).
- [425] ATLAS Collaboration, ATLAS-CONF-2011-020 (2011).
- [426] CMS Collaboration, CMS-PAS-HIG-15-009 (2016).
- [427] G. Aad *et al.* (ATLAS), Phys. Rev. **D92**, 5, 052002 (2015), [arXiv:1505.01609]; ATLAS Collaboration, ATLAS-CONF-2012-079 (2012).
- [428] CMS Collaboration, CMS-PAS-HIG-16-055 (2016); V. Khachatryan *et al.* (CMS), JHEP **10**, 076 (2017), [arXiv:1701.02032]; A. M. Sirunyan *et al.* (CMS), Phys. Lett. **B795**, 398 (2019), [arXiv:1812.06359]; A. M. Sirunyan *et al.* (CMS) (2019), [arXiv:1907.07235]; A. M. Sirunyan *et al.* (CMS), Phys. Lett. **B785**, 462 (2018), [arXiv:1805.10191]; A. M. Sirunyan *et al.* (CMS), JHEP **11**, 018 (2018), [arXiv:1805.04865]; CMS Collaboration, CMS-PAS-HIG-18-015 (2019).
- [429] V. M. Abazov *et al.* (D0), Phys. Rev. Lett. **103**, 061801 (2009), [arXiv:0905.3381].
- [430] A. M. Sirunyan *et al.* (CMS), Phys. Lett. **B796**, 131 (2019), [arXiv:1812.00380].
- [431] S. Schael *et al.* (ALEPH), JHEP **05**, 049 (2010), [arXiv:1003.0705].
- [432] B. Aubert *et al.* (BaBar), Phys. Rev. Lett. **103**, 081803 (2009), [arXiv:0905.4539].
- [433] B. Aubert *et al.* (BaBar), Phys. Rev. Lett. **103**, 181801 (2009), [arXiv:0906.2219].
- [434] ATLAS Collaboration, ATLAS-CONF-2016-051 (2016); ATLAS Collaboration, ATLAS-CONF-2017-053 (2017); M. Aaboud *et al.* (ATLAS), Eur. Phys. J. **C79**, 1, 58 (2019), [arXiv:1808.01899].
- [435] CMS Collaboration, CMS-PAS-HIG-16-036 (2017).
- [436] S. Schael *et al.* (ALEPH, DELPHI, L3, OPAL, LEP Working Group for Higgs Boson Searches), Eur. Phys. J. **C47**, 547 (2006), [hep-ex/0602042].
- [437] ATLAS Collaboration, ATLAS-CONF-2013-027 (2013).
- [438] CMS Collaboration, CMS-PAS-HIG-13-016 (2013).
- [439] A. Heister *et al.* (ALEPH), Phys. Lett. **B526**, 191 (2002), [hep-ex/0201014]; P. Achard *et al.* (L3), Phys. Lett. **B545**, 30 (2002), [hep-ex/0208042].
- [440] M. Carena *et al.* (1999), [hep-ph/9912223].
- [441] M. M. Kado and C. G. Tully, Ann. Rev. Nucl. Part. Sci. **52**, 65 (2002).
- [442] G. Abbiendi *et al.* (OPAL), Eur. Phys. J. **C23**, 397 (2002), [hep-ex/0111010]; J. Abdallah *et al.* (DELPHI), Eur. Phys. J. **C38**, 1 (2004), [hep-ex/0410017].
- [443] M. Carena *et al.*, Eur. Phys. J. **C45**, 797 (2006), [hep-ph/0511023].
- [444] ATLAS Collaboration, ATLAS-CONF-2016-104 (2016).
- [445] S. Chatrchyan *et al.* (CMS), JHEP **09**, 029 (2012), [Erratum: JHEP **03**, 132 (2014)], [arXiv:1204.2488].
- [446] M. Aaboud *et al.* (ATLAS), Phys. Rev. Lett. **119**, 19, 191803 (2017), [arXiv:1707.06025].
- [447] V. Khachatryan *et al.* (CMS), Phys. Lett. **B758**, 296 (2016), [arXiv:1511.03610].
- [448] A. M. Sirunyan *et al.* (CMS), JHEP **11**, 010 (2017), [arXiv:1707.07283].
- [449] J. Bernon *et al.*, Phys. Rev. **D91**, 7, 075019 (2015), [arXiv:1412.3385].
- [450] G. Aad *et al.* (ATLAS), Phys. Rev. Lett. **113**, 17, 171801 (2014), [arXiv:1407.6583].
- [451] CMS Collaboration, CMS-PAS-HIG-14-037 (2015).
- [452] CMS Collaboration, CMS-PAS-HIG-17-013 (2017).
- [453] S. Heinemeyer, Int. J. Mod. Phys. **A33**, 31, 1844006 (2018).
- [454] S. H. Zhu, arXiv preprint (1999), [hep-ph/9901221].
- [455] H. E. Logan and S.-f. Su, Phys. Rev. **D66**, 035001 (2002), [hep-ph/0203270].
- [456] A. Gutierrez-Rodriguez and O. A. Sampayo, Phys. Rev. **D62**, 055004 (2000).
- [457] S. Kanemura, S. Moretti and K. Odagiri, JHEP **02**, 011 (2001), [hep-ph/0012030].
- [458] M. Czakon, P. Fiedler and A. Mitov, Phys. Rev. Lett. **110**, 252004 (2013), [arXiv:1303.6254].
- [459] M. Carena *et al.*, Nucl. Phys. **B577**, 88 (2000), [hep-ph/9912516].
- [460] J. M. Campbell, R. K. Ellis and F. Tramontano, Phys. Rev. **D70**, 094012 (2004), [hep-ph/0408158].
- [461] C. Degrande *et al.*, Phys. Lett. **B772**, 87 (2017), [arXiv:1607.05291].
- [462] A. A. Barrientos Bendezu and B. A. Kniehl, Phys. Rev. **D63**, 015009 (2001), [hep-ph/0007336]; A. A. Barrientos Bendezu and B. A. Kniehl, Nucl. Phys. **B568**, 305 (2000), [hep-ph/9908385].
- [463] G. Abbiendi *et al.* (ALEPH, DELPHI, L3, OPAL, LEP), Eur. Phys. J. **C73**, 2463 (2013), [arXiv:1301.6065].

- [464] B. Abbott *et al.* (D0), Phys. Rev. Lett. **82**, 4975 (1999), [hep-ex/9902028]; A. Abulencia *et al.* (CDF), Phys. Rev. Lett. **96**, 042003 (2006), [hep-ex/0510065]; V. M. Abazov *et al.* (D0), Phys. Lett. **B682**, 278 (2009), [arXiv:0908.1811].
- [465] J. Abdallah *et al.* (DELPHI), Eur. Phys. J. **C54**, 1 (2008), [Erratum: Eur. Phys. J. **C56**, 165 (2008)], [arXiv:0801.3586].
- [466] R. Dermisek, Mod. Phys. Lett. **A24**, 1631 (2009), [arXiv:0907.0297].
- [467] J. F. Gunion, JHEP **08**, 032 (2009), [arXiv:0808.2509].
- [468] W. Love *et al.* (CLEO), Phys. Rev. Lett. **101**, 151802 (2008), [arXiv:0807.1427].
- [469] G. Aad *et al.* (ATLAS), Eur. Phys. J. **C72**, 2244 (2012), [arXiv:1210.5070]; S. Chatrchyan *et al.* (CMS), Eur. Phys. J. **C72**, 2189 (2012), [arXiv:1207.2666].
- [470] G. Aad *et al.* (ATLAS), Phys. Rev. **D89**, 3, 032002 (2014), [arXiv:1312.1956].
- [471] J. de Blas *et al.*, JHEP **01**, 139 (2020), [arXiv:1905.03764].

## 12. CKM Quark-Mixing Matrix

Revised March 2020 by A. Ceccucci (CERN), Z. Ligeti (LBNL) and Y. Sakai (KEK).

### 12.1 Introduction

The masses and mixings of quarks have a common origin in the Standard Model (SM). They arise from the Yukawa interactions with the Higgs condensate,

$$\mathcal{L}_Y = -Y_{ij}^d \overline{Q_{Li}^I} \phi d_{Rj}^I - Y_{ij}^u \overline{Q_{Li}^I} \epsilon \phi^* u_{Rj}^I + \text{h.c.}, \quad (12.1)$$

where  $Y^{u,d}$  are  $3 \times 3$  complex matrices,  $\phi$  is the Higgs field,  $i, j$  are generation labels, and  $\epsilon$  is the  $2 \times 2$  antisymmetric tensor.  $Q_L^I$  are left-handed quark doublets, and  $d_R^I$  and  $u_R^I$  are right-handed down- and up-type quark singlets, respectively, in the weak-eigenstate basis. When  $\phi$  acquires a vacuum expectation value,  $\langle \phi \rangle = (0, v/\sqrt{2})$ , Eq. (12.1) yields mass terms for the quarks. The physical states are obtained by diagonalizing  $Y^{u,d}$

by four unitary matrices,  $V_{L,R}^{u,d}$ , as  $M_{\text{diag}}^f = V_L^f Y^f V_R^{f\dagger} (v/\sqrt{2})$ ,  $f = u, d$ . As a result, the charged-current  $W^\pm$  interactions couple to the physical  $u_{Lj}$  and  $d_{Lk}$  quarks with couplings given by

$$\frac{-g}{\sqrt{2}} (\overline{u_L}, \overline{c_L}, \overline{t_L}) \gamma^\mu W_\mu^+ V_{\text{CKM}} \begin{pmatrix} d_L \\ s_L \\ b_L \end{pmatrix} + \text{h.c.}, \quad (12.2)$$

$$V_{\text{CKM}} \equiv V_L^u V_L^{d\dagger} = \begin{pmatrix} V_{ud} & V_{us} & V_{ub} \\ V_{cd} & V_{cs} & V_{cb} \\ V_{td} & V_{ts} & V_{tb} \end{pmatrix}.$$

This Cabibbo-Kobayashi-Maskawa (CKM) matrix [1,2] is a  $3 \times 3$  unitary matrix. It can be parameterized by three mixing angles and the  $CP$ -violating KM phase [2]. Of the many possible conventions, a standard choice has become [3]

$$V_{\text{CKM}} = \begin{pmatrix} 1 & 0 & 0 \\ 0 & c_{23} & s_{23} \\ 0 & -s_{23} & c_{23} \end{pmatrix} \begin{pmatrix} c_{13} & 0 & s_{13} e^{-i\delta} \\ 0 & 1 & 0 \\ -s_{13} e^{i\delta} & 0 & c_{13} \end{pmatrix} \begin{pmatrix} c_{12} & s_{12} & 0 \\ -s_{12} & c_{12} & 0 \\ 0 & 0 & 1 \end{pmatrix} \quad (12.3)$$

$$= \begin{pmatrix} c_{12} c_{13} & s_{12} c_{13} & s_{13} e^{-i\delta} \\ -s_{12} c_{23} - c_{12} s_{23} s_{13} e^{i\delta} & c_{12} c_{23} - s_{12} s_{23} s_{13} e^{i\delta} & s_{23} c_{13} \\ s_{12} s_{23} - c_{12} c_{23} s_{13} e^{i\delta} & -s_{12} s_{23} - c_{12} c_{23} s_{13} e^{i\delta} & c_{23} c_{13} \end{pmatrix},$$

where  $s_{ij} = \sin \theta_{ij}$ ,  $c_{ij} = \cos \theta_{ij}$ , and  $\delta$  is the phase responsible for all  $CP$ -violating phenomena in flavor-changing processes in the SM. The angles  $\theta_{ij}$  can be chosen to lie in the first quadrant, so  $s_{ij}, c_{ij} \geq 0$ .

It is known experimentally that  $s_{13} \ll s_{23} \ll s_{12} \ll 1$ , and it is convenient to exhibit this hierarchy using the Wolfenstein parameterization. We define [4–6]

$$s_{12} = \lambda = \frac{|V_{us}|}{\sqrt{|V_{ud}|^2 + |V_{us}|^2}}, \quad s_{23} = A\lambda^2 = \lambda \left| \frac{V_{cb}}{V_{us}} \right|,$$

$$s_{13} e^{i\delta} = V_{ub}^* = A\lambda^3 (\rho + i\eta) = \frac{A\lambda^3 (\bar{\rho} + i\bar{\eta}) \sqrt{1 - A^2 \lambda^4}}{\sqrt{1 - \lambda^2} [1 - A^2 \lambda^4 (\bar{\rho} + i\bar{\eta})]}. \quad (12.4)$$

These relations ensure that  $\bar{\rho} + i\bar{\eta} = -(V_{ud} V_{ub}^*) / (V_{cd} V_{cb}^*)$  is phase convention independent, and the CKM matrix written in terms of  $\lambda, A, \bar{\rho}$ , and  $\bar{\eta}$  is unitary to all orders in  $\lambda$ . The definitions of  $\bar{\rho}, \bar{\eta}$  reproduce all approximate results in the literature; *i.e.*,  $\bar{\rho} = \rho(1 - \lambda^2/2 + \dots)$  and  $\bar{\eta} = \eta(1 - \lambda^2/2 + \dots)$ , and one can write  $V_{\text{CKM}}$  to  $\mathcal{O}(\lambda^4)$  either in terms of  $\bar{\rho}, \bar{\eta}$  or, traditionally,

$$V_{\text{CKM}} = \begin{pmatrix} 1 - \lambda^2/2 & \lambda & A\lambda^3(\rho - i\eta) \\ -\lambda & 1 - \lambda^2/2 & A\lambda^2 \\ A\lambda^3(1 - \rho - i\eta) & -A\lambda^2 & 1 \end{pmatrix} + \mathcal{O}(\lambda^4). \quad (12.5)$$

The CKM matrix elements are fundamental parameters of the SM, so their precise determination is important. The unitarity of the CKM matrix imposes  $\sum_i V_{ij} V_{ik}^* = \delta_{jk}$  and  $\sum_j V_{ij} V_{kj}^* = \delta_{ik}$ . The six vanishing combinations can be represented as triangles in a complex plane, of which those obtained by taking scalar products of neighboring rows or columns are nearly degenerate. The areas of all triangles are the same, half of the Jarlskog invariant,  $J$  [7], which is a phase-convention-independent measure of  $CP$  violation, defined by  $\text{Im} [V_{ij} V_{kl} V_{il}^* V_{kj}^*] = J \sum_{m,n} \epsilon_{ikm} \epsilon_{jln}$ .

The most commonly used unitarity triangle arises from

$$V_{ud} V_{ub}^* + V_{cd} V_{cb}^* + V_{td} V_{tb}^* = 0, \quad (12.6)$$

by dividing each side by the best-known one,  $V_{cd} V_{cb}^*$  (see Fig. 12.1). Its vertices are exactly  $(0, 0)$ ,  $(1, 0)$ , and, due to the definition in Eq. (12.4),  $(\bar{\rho}, \bar{\eta})$ . An important goal of flavor physics is to overconstrain the CKM elements, and many measurements can be conveniently displayed and compared in the  $\bar{\rho}, \bar{\eta}$  plane. While

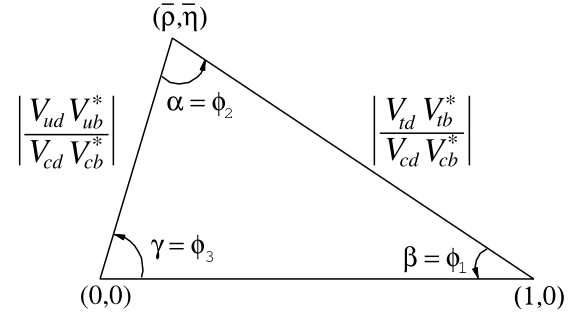


Figure 12.1: Sketch of the unitarity triangle.

the Lagrangian in Eq. (12.1) is normalized, and the CKM matrix has a well known scale dependence above the weak scale [8], below  $\mu = m_W$  the CKM elements can be treated as constants, with all  $\mu$ -dependence contained in the running of quark masses and higher-dimension operators.

Unless explicitly stated otherwise, we describe all measurements assuming the SM, to extract magnitudes and phases of CKM elements in Sec. 12.2 and 12.3. Processes dominated by loop-level contributions in the SM are particularly sensitive to new physics beyond the SM (BSM). We give the global fit results for the CKM elements in Sec. 12.4, and discuss some implications for beyond standard model physics in Sec. 12.5.

### 12.2 Magnitudes of CKM elements

#### 12.2.1 $|V_{ud}|$

The most precise determination of  $|V_{ud}|$  comes from the study of superallowed  $0^+ \rightarrow 0^+$  nuclear beta decays, which are pure vector transitions. Taking the average of the fourteen most precise determinations [9] yields [10]

$$|V_{ud}| = 0.97370 \pm 0.00014. \quad (12.7)$$

This value is about  $2\sigma$  smaller than in the review two years ago, mainly due to adopting a recent calculation of electroweak corrections based on dispersion relations [11]. The dominant and comparable uncertainties are the experimental ones, and from the estimates of the radiative corrections. A less precise determination of  $|V_{ud}|$  can be obtained from the measurement of the neutron lifetime. The theoretical uncertainties are very small, but the determination is limited by the knowledge of the ratio of the axial-

vector and vector couplings,  $g_A = G_A/G_V$  [10]. The PIBETA experiment [12] has improved the measurement of the  $\pi^+ \rightarrow \pi^0 e^+ \nu$  branching ratio to 0.6%, and quotes  $|V_{ud}| = 0.9739 \pm 0.0029$ , in agreement with the more precise result listed above. The interest in this measurement is that the determination of  $|V_{ud}|$  is very clean theoretically, because it is a pure vector transition and is free from nuclear-structure uncertainties.

### 12.2.2 $|V_{us}|$

The product of  $|V_{us}|$  and the form factor at  $q^2 = 0$ ,  $|V_{us}| f_+(0)$ , has been extracted traditionally from  $K_L^0 \rightarrow \pi e \nu$  decays in order to avoid isospin-breaking corrections ( $\pi^0 - \eta$  mixing) that affect  $K^\pm$  semileptonic decay, and the complications induced by a second (scalar) form factor present in the muonic decays. The last round of measurements has led to enough experimental constraints to justify the comparison between different decay modes. Systematic errors related to the experimental quantities, *e.g.*, the lifetime of neutral or charged kaons, and the form factor determinations for electron and muonic decays, differ among decay modes, and the consistency between different determinations enhances the confidence in the final result. For this reason, we follow the prescription [13] to average  $K_L^0 \rightarrow \pi e \nu$ ,  $K_L^0 \rightarrow \pi \mu \nu$ ,  $K^\pm \rightarrow \pi^0 e^\pm \nu$ ,  $K^\pm \rightarrow \pi^0 \mu^\pm \nu$  and  $K_S^0 \rightarrow \pi e \nu$ . The average of these five decay modes yields  $|V_{us}| f_+(0) = 0.2165 \pm 0.0004$ . Results obtained from each decay mode, and exhaustive references to the experimental data, are listed for instance in Ref. [10]. The form factor average  $f_+(0) = 0.9706 \pm 0.0027$  [14] from  $N_f = 2 + 1 + 1$  lattice QCD calculations gives  $|V_{us}| = 0.2231 \pm 0.0007$  [10].<sup>1</sup> The broadly used classic calculation of  $f_+(0)$  [16] is in good agreement with this value, while other calculations [18] differ by as much as 2%.

The calculation of the ratio of the kaon and pion decay constants enables one to extract  $|V_{us}/V_{ud}|$  from  $K \rightarrow \mu \nu(\gamma)$  and  $\pi \rightarrow \mu \nu(\gamma)$ , where  $(\gamma)$  indicates that radiative decays are included [19]. The value of  $\Gamma(K \rightarrow \mu \nu(\gamma))$  [10] derived from the KLOE measurement of the corresponding branching ratio [20], combined with the lattice QCD result,  $f_K/f_\pi = 1.1932 \pm 0.0019$  [14], leads to  $|V_{us}| = 0.2252 \pm 0.0005$ , where the accuracy is limited by the knowledge of the ratio of the decay constants. The average of these two determinations, with the error scaled according to the PDG prescription [21] by  $\sqrt{\chi^2} = 2.0$ , is quoted as [10]

$$|V_{us}| = 0.2245 \pm 0.0008. \quad (12.8)$$

It is important to include both QED and QCD isospin violations in the lattice QCD calculations.

The latest determination from hyperon decays can be found in Ref. [22]. The authors focus on the analysis of the vector form factor, protected from first order  $SU(3)$  breaking effects by the Ademollo-Gatto theorem [23], and treat the ratio between the axial and vector form factors  $g_1/f_1$  as experimental input, thus avoiding first order  $SU(3)$  breaking effects in the axial-vector contribution. They find  $|V_{us}| = 0.2250 \pm 0.0027$ , although this does not include an estimate of the theoretical uncertainty due to second-order  $SU(3)$  breaking, contrary to Eq. (12.8). Concerning hadronic  $\tau$  decays to strange particles, averaging the inclusive decay and the exclusive  $\tau \rightarrow h \nu$  ( $h = \pi, K$ ) measurements yields  $|V_{us}| = 0.2221 \pm 0.0013$  [24].

### 12.2.3 $|V_{cd}|$

The magnitude of  $V_{cd}$  can be extracted from semileptonic charm decays, using theoretical knowledge of the form factors. In semileptonic  $D$  decays, lattice QCD calculations have predicted the normalization of the  $D \rightarrow \pi \ell \nu$  and  $D \rightarrow K \ell \nu$  form factors [14]. The dependence on the invariant mass of the lepton pair,  $q^2$ , is determined from lattice QCD and theoretical constraints from analyticity [15]. Using  $N_f = 2 + 1 + 1$  lattice QCD calculations for  $D \rightarrow \pi \ell \nu$ ,  $f_+^{D\pi}(0) = 0.612 \pm 0.035$  [14], and the average [24] of the measurements of  $D \rightarrow \pi \ell \nu$  decays by

<sup>1</sup>For lattice QCD inputs, we use the averages from Ref. [14], unless the minireviews [10,15] choose different values. We only use unquenched results, and if both  $N_f = 2 + 1 + 1$  and  $2 + 1$  calculations are available, we use the former.

*BABAR* [25], *BESIII* [26,27], *CLEO-c* [28], and *Belle* [29], one obtains  $|V_{cd}| = 0.2330 \pm 0.0029 \pm 0.0133$ , where the first uncertainty is experimental, and the second is from the theoretical uncertainty of the form factor.

The determination of  $|V_{cd}|$  is also possible from the leptonic decay  $D^+ \rightarrow \mu^+ \nu$ . The experimental uncertainties have not decreased significantly recently. Averaging the *BESIII* [30] and earlier *CLEO* [31] measurements, and using the  $N_f = 2 + 1 + 1$  lattice QCD result,  $f_D = 212.0 \pm 0.7$  MeV [14], yields  $|V_{cd}| = 0.2173 \pm 0.0051 \pm 0.0007$  [24].<sup>2</sup>

Earlier determinations of  $|V_{cd}|$  came from neutrino scattering data. The difference of the ratio of double-muon to single-muon production by neutrino and antineutrino beams is proportional to the charm cross section off valence  $d$  quarks, and therefore to  $|V_{cd}|^2$  times the average semileptonic branching ratio of charm mesons,  $\mathcal{B}_\mu$ . The method was used first by CDHS [32] and then by CCFR [33,34] and CHARM II [35]. Averaging these results is complicated, because it requires assumptions about the scale of the QCD corrections, and because  $\mathcal{B}_\mu$  is an effective quantity, which depends on the specific neutrino beam characteristics. With no recent experimental input available, we quote the average from a past review,  $\mathcal{B}_\mu |V_{cd}|^2 = (0.463 \pm 0.034) \times 10^{-2}$  [36]. Analysis cuts make these experiments insensitive to neutrino energies smaller than 30 GeV. Thus,  $\mathcal{B}_\mu$  should be computed using only neutrino interactions with visible energy larger than 30 GeV. An appraisal [37] based on charm-production fractions measured in neutrino interactions [38,39] gives  $\mathcal{B}_\mu = 0.088 \pm 0.006$ . Data from the CHORUS experiment [40] are sufficiently precise to extract  $\mathcal{B}_\mu$  directly, by comparing the number of charm decays with a muon to the total number of charmed hadrons found in the nuclear emulsions. Requiring the visible energy to be larger than 30 GeV, CHORUS found  $\mathcal{B}_\mu = 0.085 \pm 0.009 \pm 0.006$ . We use the average of these two determinations,  $\mathcal{B}_\mu = 0.087 \pm 0.005$ , and obtain  $|V_{cd}| = 0.230 \pm 0.011$ . Averaging the three determinations above, we find

$$|V_{cd}| = 0.221 \pm 0.004. \quad (12.9)$$

### 12.2.4 $|V_{cs}|$

The direct determination of  $|V_{cs}|$  is possible from semileptonic  $D$  or leptonic  $D_s$  decays, using lattice QCD calculations of the semileptonic  $D$  form factor or the  $D_s$  decay constant. For muonic decays, the average of *Belle* [41], *CLEO-c* [42], *BABAR* [43], and *BESIII* [44,45] is  $\mathcal{B}(D_s^+ \rightarrow \mu^+ \nu) = (5.51 \pm 0.16) \times 10^{-3}$  [24]. For decays to  $\tau$  leptons, the average of *CLEO-c* [42,46,47], *BABAR* [43], *Belle* [41], and *BESIII* [44] gives  $\mathcal{B}(D_s^+ \rightarrow \tau^+ \nu) = (5.52 \pm 0.24) \times 10^{-2}$  [24]. From each of these values, determinations of  $|V_{cs}|$  can be obtained using the PDG values for the mass and lifetime of the  $D_s$ , the masses of the leptons, and  $f_{D_s} = (249.9 \pm 0.5)$  MeV [14]. The average of these determinations gives  $|V_{cs}| = 0.992 \pm 0.012$ , where the error is dominated by the experimental uncertainty. In semileptonic  $D$  decays, lattice QCD calculations of the  $D \rightarrow K \ell \nu$  form factor are available [14]. Using  $f_+^{DK}(0) = 0.765 \pm 0.031$  and the average [24] of *CLEO-c* [28], *Belle* [29], *BABAR* [48], and recent *BESIII* [26,49] measurements of  $D \rightarrow K \ell \nu$  decays, one obtains  $|V_{cs}| = 0.939 \pm 0.038$ , where the dominant uncertainty is from the theoretical calculation of the form factor. Averaging the determinations from leptonic and semileptonic decays, we find

$$|V_{cs}| = 0.987 \pm 0.011. \quad (12.10)$$

Measurements of on-shell  $W^\pm$  decays sensitive to  $|V_{cs}|$  were made by LEP-2. The  $W$  branching ratios depend on the six CKM elements involving quarks lighter than  $m_W$ . The  $W$  branching ratio to each lepton flavor is  $1/\mathcal{B}(W \rightarrow \ell \bar{\nu}_\ell) = 3[1 + \sum_{u,c,d,s,b} |V_{ij}|^2 (1 + \alpha_s(m_W)/\pi) + \dots]$ . Assuming lepton universality, the measurement  $\mathcal{B}(W \rightarrow \ell \bar{\nu}_\ell) = (10.83 \pm 0.07 \pm 0.07)\%$  [50] implies  $\sum_{u,c,d,s,b} |V_{ij}|^2 = 2.002 \pm 0.027$ . This is a precise test of unitarity; however, only flavor-tagged  $W$ -decays determine  $|V_{cs}|$

<sup>2</sup>Hereafter the first error is statistical and the second is systematic, unless mentioned otherwise.

directly, such as DELPHI's tagged  $W^+ \rightarrow c\bar{s}$  analysis, yielding  $|V_{cs}| = 0.94_{-0.26}^{+0.32} \pm 0.13$  [51].

### 12.2.5 $|V_{cb}|$

This matrix element can be determined from exclusive and inclusive semileptonic decays of  $B$  mesons to charm. The inclusive determinations use the semileptonic decay rate measurement, together with (certain moments of) the lepton energy and the hadronic invariant-mass spectra. The theoretical basis is the operator product expansion [52, 53], which allows calculation of the decay rate and various spectra as expansions in  $\alpha_s$  and inverse powers of the heavy-quark mass. The dependence on  $m_b$ ,  $m_c$ , and the parameters that occur at subleading order is different for different moments, and a large number of measured moments overconstrain all the parameters, and tests the consistency of the determination. The precise extraction of  $|V_{cb}|$  requires using a "threshold" quark mass definition [54, 55]. Inclusive measurements have been performed using  $B$  mesons from  $Z^0$  decays at LEP, and at  $e^+e^-$  machines operated at the  $\Upsilon(4S)$ . At LEP, the large boost of  $B$  mesons from the  $Z^0$  decay allows the determination of the moments throughout phase space, which is not possible otherwise, but the large statistics available at the  $B$  factories lead to more precise determinations. An average of the measurements and a compilation of the references are provided in Ref. [15]:  $|V_{cb}| = (42.2 \pm 0.8) \times 10^{-3}$ .

Complementary determinations are based on exclusive semileptonic  $B$  decays to  $D$  and  $D^*$ . In the  $m_{b,c} \gg \Lambda_{\text{QCD}}$  limit, all form factors are given by a single Isgur-Wise function [56], which depends on the product of the four-velocities of the  $B$  and  $D^{(*)}$  mesons,  $w = v \cdot v'$ . Heavy-quark symmetry determines the rate at  $w = 1$ , the maximum momentum transfer to the  $\ell\bar{\nu}$  pair, and  $|V_{cb}|$  is obtained from an extrapolation to  $w = 1$ . The current update of the  $V_{cb}$  and  $V_{ub}$  minireview quotes from exclusive decays  $|V_{cb}| = (39.5 \pm 0.9) \times 10^{-3}$  [15], based on the only unfolded measurement of  $B \rightarrow D^*$  semileptonic decay distributions [57], and using a more general fit [58] than in earlier  $B$  factory measurements. With the uncertainty scaled by  $\sqrt{\chi^2} = 2.4$ , this yields the combination [15],

$$|V_{cb}| = (41.0 \pm 1.4) \times 10^{-3}. \quad (12.11)$$

Less precise measurements of  $|V_{cb}|$ , not included in this average, can be obtained from  $\mathcal{B}(B \rightarrow D^{(*)}\tau\bar{\nu})$ . The most precise data involving  $\tau$  leptons are the  $|V_{cb}|$ -independent ratios,  $\mathcal{B}(B \rightarrow D^{(*)}\tau\bar{\nu})/\mathcal{B}(B \rightarrow D^{(*)}\ell\bar{\nu})$  measured by BaBar, Belle, and LHCb. If the current, approximately  $3\sigma$  [24], hint of lepton non-universality prevails, the determination of  $|V_{cb}|$  becomes more complicated.

### 12.2.6 $|V_{ub}|$

The determination of  $|V_{ub}|$  from inclusive  $B \rightarrow X_u\ell\bar{\nu}$  decay is complicated due to large  $B \rightarrow X_c\ell\bar{\nu}$  backgrounds. In most regions of phase space where the charm background is kinematically forbidden, the hadronic physics enters via unknown nonperturbative functions, so-called shape functions. (In contrast, the nonperturbative physics for  $|V_{cb}|$  is encoded in a few parameters.) At leading order in  $\Lambda_{\text{QCD}}/m_b$ , there is only one shape function, which can be extracted from the photon energy spectrum in  $B \rightarrow X_s\gamma$  [59, 60], and applied to several spectra in  $B \rightarrow X_u\ell\bar{\nu}$ . The subleading shape functions are modeled in the current determinations. Phase space cuts for which the rate has only subleading dependence on the shape function are also possible [61]. The measurements of both the hadronic and the leptonic systems are important for an optimal choice of phase space. A different approach is to make the measurements more inclusive by extending them deeper into the  $B \rightarrow X_c\ell\bar{\nu}$  region, and thus reduce the theoretical uncertainties. Analyses of the electron-energy endpoint from CLEO [62], BABAR [63], and Belle [64] quote  $B \rightarrow X_u e\bar{\nu}$  partial rates for  $|\vec{p}_e| \geq 2.0 \text{ GeV}$  and  $1.9 \text{ GeV}$ , which are well below the charm endpoint. The large and pure  $B\bar{B}$  samples at the  $B$  factories permit the selection of  $B \rightarrow X_u\ell\bar{\nu}$  decays in events where the other  $B$  is fully reconstructed [65]. With this full-reconstruction tag method, the four-momenta of both the leptonic and the hadronic final states can be measured. It also gives access to a wider kinematic region, because of improved signal purity. Ref. [15] quotes the inclusive average,  $|V_{ub}| = (4.25 \pm 0.12_{-0.14}^{+0.15} \pm 0.23) \times 10^{-3}$ , where the first error is experimental, the second arises from the model dependence quoted by the individual measurements, and the third is an additional one estimated in Ref. [15].

To extract  $|V_{ub}|$  from exclusive decays, the form factors have to be known. Experimentally, better signal-to-background ratios are offset by smaller yields. The  $B \rightarrow \pi\ell\bar{\nu}$  branching ratio is now known to 5%. Lattice QCD calculations of the  $B \rightarrow \pi\ell\bar{\nu}$  form factor are available [66] for the high  $q^2$  region ( $q^2 > 16$  or  $18 \text{ GeV}^2$ ). A fit to the experimental partial rates and lattice QCD results versus  $q^2$  yields  $|V_{ub}| = (3.70 \pm 0.10 \pm 0.12) \times 10^{-3}$  [24]. Light-cone QCD sum rules are supposed to be applicable for  $q^2 < 12 \text{ GeV}^2$  [67], yielding a combination,  $|V_{ub}| = (3.67 \pm 0.09 \pm 0.12) \times 10^{-3}$  [15, 24].

The uncertainties in extracting  $|V_{ub}|$  from inclusive and exclusive decays are different to a large extent. An average of these determinations, with the uncertainty scaled by  $\sqrt{\chi^2} = 1.6$ , is [15]

$$|V_{ub}| = (3.82 \pm 0.24) \times 10^{-3}. \quad (12.12)$$

A determination of  $|V_{ub}|$  not included in this average can be obtained from  $\mathcal{B}(B \rightarrow \tau\bar{\nu}) = (1.06 \pm 0.19) \times 10^{-4}$  [24]. Using  $f_B = (190.0 \pm 1.3) \text{ MeV}$  [14] and  $\tau_{B^\pm} = (1.638 \pm 0.004) \text{ ps}$  [68], we find the remarkably consistent result,  $|V_{ub}| = (4.05 \pm 0.36) \times 10^{-3}$ . This decay is sensitive, for example, to tree-level charged Higgs contributions, and the measured rate is consistent with the SM expectation. The LHCb measurement  $|V_{ub}/V_{cb}| = 0.079 \pm 0.006$  [69] from the ratio of  $\Lambda_b \rightarrow p^+\mu^-\bar{\nu}$  and  $\Lambda_b \rightarrow \Lambda_c^+\mu^-\bar{\nu}$  in different regions of  $q^2$ , provides another complementary determination.

### 12.2.7 $|V_{td}|$ and $|V_{ts}|$

The CKM elements  $|V_{td}|$  and  $|V_{ts}|$  are not likely to be precisely measurable in tree-level processes involving top quarks, so one has to rely on determinations from  $B-\bar{B}$  oscillations dominated by box diagrams with top quarks, or loop-mediated rare  $K$  and  $B$  decays. Theoretical uncertainties in hadronic effects limit the accuracy of the current determinations. These can be reduced by taking ratios of processes that are equal in the flavor  $SU(3)$  limit to determine  $|V_{td}/V_{ts}|$ .

The mixing of the two  $B^0$  mesons was discovered by ARGUS [70], and the mass difference is now precisely measured as  $\Delta m_d = (0.5065 \pm 0.0019) \text{ ps}^{-1}$  [71]. In the  $B_s^0$  system,  $\Delta m_s$  was first measured significantly by CDF [72] and the world average, dominated by an LHCb measurement [73], is  $\Delta m_s = (17.749 \pm 0.020) \text{ ps}^{-1}$  [71]. Neglecting corrections suppressed by  $|V_{tb}| - 1$ , and using the lattice QCD results  $f_{B_d}\sqrt{\widehat{B}_{B_d}} = (225 \pm 9) \text{ MeV}$  and  $f_{B_s}\sqrt{\widehat{B}_{B_s}} = (274 \pm 8) \text{ MeV}$  [14],

$$|V_{td}| = (8.0 \pm 0.3) \times 10^{-3}, \quad |V_{ts}| = (38.8 \pm 1.1) \times 10^{-3}. \quad (12.13)$$

The uncertainties are dominated by lattice QCD. Several uncertainties are reduced in the calculation of the ratio  $\xi = (f_{B_s}\sqrt{\widehat{B}_{B_s}})/(f_{B_d}\sqrt{\widehat{B}_{B_d}}) = 1.206 \pm 0.038$  [14] and therefore the constraint on  $|V_{td}/V_{ts}|$  from  $\Delta m_d/\Delta m_s$  is more reliable theoretically. These provide a theoretically clean and significantly improved determination,

$$|V_{td}/V_{ts}| = 0.205 \pm 0.001 \pm 0.006. \quad (12.14)$$

The inclusive branching ratio  $\mathcal{B}(B \rightarrow X_s\gamma) = (3.32 \pm 0.15) \times 10^{-4}$  extrapolated to  $E_\gamma > E_0 = 1.6 \text{ GeV}$  [24] is also sensitive to  $|V_{tb}V_{ts}|$ . In addition to  $t$ -quark penguins, a substantial part of the rate comes from charm contributions proportional to  $V_{cb}V_{cs}^*$  via the application of  $3 \times 3$  CKM unitarity (which is used here). With the NNLO calculation of  $\mathcal{B}(B \rightarrow X_s\gamma)_{E_\gamma > E_0}/\mathcal{B}(B \rightarrow X_c e\bar{\nu})$  [74], we obtain  $|V_{ts}/V_{cb}| = 0.98 \pm 0.04$ . The  $B_s \rightarrow \mu^+\mu^-$  rate is also proportional to  $|V_{tb}V_{ts}|^2$  in the SM, and the world average,  $\mathcal{B}(B_s \rightarrow \mu^+\mu^-) = (3.1 \pm 0.6) \times 10^{-9}$  [24], is consistent with the SM, with sizable uncertainties.

A complementary determination of  $|V_{td}/V_{ts}|$  is possible from the ratio of  $B \rightarrow \rho\gamma$  and  $K^*\gamma$  rates. The ratio of the neutral modes

is theoretically cleaner than that of the charged ones, because the poorly known spectator-interaction contribution is expected to be smaller ( $W$ -exchange vs. weak annihilation). For now, because of low statistics, we average the charged and neutral rates assuming the isospin symmetry and heavy-quark limit motivated relation,  $|V_{td}/V_{ts}|^2/\xi_\gamma^2 = [\Gamma(B^+ \rightarrow \rho^+\gamma) + 2\Gamma(B^0 \rightarrow \rho^0\gamma)]/[\Gamma(B^+ \rightarrow K^{*+}\gamma) + \Gamma(B^0 \rightarrow K^{*0}\gamma)] = (3.37 \pm 0.49)\%$  [24]. Here  $\xi_\gamma$  contains the poorly known hadronic physics. Using  $\xi_\gamma = 1.2 \pm 0.2$  [75] gives  $|V_{td}/V_{ts}| = 0.220 \pm 0.016 \pm 0.037$ , where the first uncertainty is experimental and the second is theoretical.

A theoretically clean determination of  $|V_{td}V_{ts}^*|$  is possible from  $K^+ \rightarrow \pi^+\nu\bar{\nu}$  decay [76]. Experimentally, only a handful of events have been observed [77, 78] and the rate is consistent with the SM with large uncertainties. Much more data are needed for a precision measurement.

### 12.2.8 $|V_{tb}|$

The determination of  $|V_{tb}|$  from top decays uses the ratio of branching fractions  $R = \mathcal{B}(t \rightarrow Wb)/\mathcal{B}(t \rightarrow Wq) = |V_{tb}|^2/(\sum_q |V_{tq}|^2) = |V_{tb}|^2$ , where  $q = b, s, d$ . The CDF and DØ measurements performed on data collected during Run II of the Tevatron give  $|V_{tb}| > 0.78$  [79] and  $0.99 > |V_{tb}| > 0.90$  [80], respectively, at 95% CL. CMS measured the same quantity at 8 TeV and obtained  $|V_{tb}| > 0.975$  [81] at 95% CL.

The direct determination of  $|V_{tb}|$ , without assuming unitarity, is possible from the single top quark production cross section. The  $(3.30^{+0.52}_{-0.40})$  pb combined cross section [82] of DØ and CDF measurements implies  $|V_{tb}| = 1.02^{+0.06}_{-0.05}$ . The LHC experiments, ATLAS and CMS, have measured single top quark production cross sections (and extracted  $|V_{tb}|$ ) in  $t$ -channel,  $Wt$ -channel, and  $s$ -channel at 7 TeV, 8 TeV, and 13 TeV [83]. The average of these  $|V_{tb}|$  values is calculated to be  $|V_{tb}| = 1.010 \pm 0.036$ , where all systematic errors and theoretical errors are treated to be fully correlated. The average of Tevatron and LHC values gives

$$|V_{tb}| = 1.013 \pm 0.030. \quad (12.15)$$

The experimental systematic uncertainties dominate, and a dedicated combination would be welcome.

A weak constraint on  $|V_{tb}|$  can be obtained from precision electroweak data, where top quarks enter in loops. The sensitivity is best in  $\Gamma(Z \rightarrow b\bar{b})$  and yields  $|V_{tb}| = 0.77^{+0.18}_{-0.24}$  [84].

## 12.3 Phases of CKM elements

As can be seen from Fig. 12.1, the angles of the unitarity triangle are

$$\begin{aligned} \beta &= \phi_1 = \arg\left(-\frac{V_{cd}V_{cb}^*}{V_{td}V_{tb}^*}\right), \\ \alpha &= \phi_2 = \arg\left(-\frac{V_{td}V_{tb}^*}{V_{ud}V_{ub}^*}\right), \\ \gamma &= \phi_3 = \arg\left(-\frac{V_{ud}V_{ub}^*}{V_{cd}V_{cb}^*}\right). \end{aligned} \quad (12.16)$$

Since  $CP$  violation involves phases of CKM elements, many measurements of  $CP$ -violating observables can be used to constrain these angles and the  $\bar{\rho}, \bar{\eta}$  parameters.

### 12.3.1 $\epsilon$ and $\epsilon'$

The measurement of  $CP$  violation in  $K^0-\bar{K}^0$  mixing,  $|\epsilon| = (2.228 \pm 0.011) \times 10^{-3}$  [85], provides important information about the CKM matrix. The phase of  $\epsilon$  is determined by long-distance physics,  $\epsilon = \frac{1}{2} e^{i\phi_\epsilon} \sin\phi_\epsilon \arg(-M_{12}/\Gamma_{12})$ , where  $\phi_\epsilon = \arctan[2\Delta m_K/\Delta\Gamma_K] \simeq 43.5^\circ$ . The SM prediction can be written as

$$\begin{aligned} \epsilon &= \kappa_\epsilon e^{i\phi_\epsilon} \frac{G_F^2 m_W^2 m_K}{12\sqrt{2}\pi^2 \Delta m_K} f_K^2 \hat{B}_K \left\{ \eta_{tt} S(x_t) \text{Im}[(V_{ts}V_{td}^*)^2] \right. \\ &\quad \left. + 2\eta_{ct} S(x_c, x_t) \text{Im}(V_{cs}V_{cd}^*V_{ts}V_{td}^*) + \eta_{cc} x_c \text{Im}[(V_{cs}V_{cd}^*)^2] \right\}, \end{aligned} \quad (12.17)$$

where  $\kappa_\epsilon \simeq 0.94 \pm 0.02$  [86] includes the effects of strangeness changing  $\Delta s = 1$  operators and additional dependence on  $\phi_\epsilon \neq$

$\pi/4$  (see also Ref. [87]). The displayed terms are the short-distance  $\Delta s = 2$  contribution to  $\text{Im}M_{12}$  in the usual phase convention,  $S$  is an Inami-Lim function [88],  $x_q = m_q^2/m_W^2$ , and  $\eta_{ij}$  are perturbative QCD corrections. The constraint from  $\epsilon$  in the  $\bar{\rho}, \bar{\eta}$  plane is bounded by approximate hyperbolas. Lattice QCD determined the bag parameter  $\hat{B}_K = 0.717 \pm 0.024$  [14], and the main uncertainties are from  $(V_{ts}V_{td}^*)^2$  (approximately given by that of  $|V_{cb}|^4$  or  $A^4$ ), the  $\eta_{ij}$  coefficients, and estimates of  $\kappa_\epsilon$ .

The measurement of  $6 \text{Re}(\epsilon'/\epsilon) = 1 - |\eta_{00}/\eta_{+-}|^2$ , where each  $\eta_{ij} = \langle \pi^i \pi^j | \mathcal{H}(K_L) \rangle / \langle \pi^i \pi^j | \mathcal{H}(K_S) \rangle$  violates  $CP$ , provides a qualitative test of the CKM mechanism, and strong constraints on many BSM scenarios. Its nonzero value,  $\text{Re}(\epsilon'/\epsilon) = (1.67 \pm 0.23) \times 10^{-3}$  [85], demonstrated the existence of direct  $CP$  violation, a prediction of the KM ansatz. While  $\text{Re}(\epsilon'/\epsilon) \propto \text{Im}(V_{td}V_{ts}^*)$ , this quantity cannot easily be used to extract CKM parameters, because cancellations between the electromagnetic and gluonic penguin contributions for large  $m_t$  [89] enhance the hadronic uncertainties. Most SM estimates [90] agree with the observed value, indicating that  $\bar{\eta}$  is positive. Progress in lattice QCD [91] may yield a precise SM prediction in the future, and trigger new work on assessing the consistency of the SM with the measured value [92, 93].

### 12.3.2 $\beta / \phi_1$

#### 12.3.2.1 Charmonium modes

$CP$ -violation measurements in  $B$ -meson decays provide direct information on the angles of the unitarity triangle, shown in Fig. 12.1. These overconstraining measurements serve to improve the determination of the CKM elements, and to reveal possible effects beyond the SM.

The time-dependent  $CP$  asymmetry of neutral  $B$  decays to a final state  $f$  common to  $B^0$  and  $\bar{B}^0$  is given by [94–96]

$$\begin{aligned} \mathcal{A}_f &= \frac{\Gamma(\bar{B}^0(t) \rightarrow f) - \Gamma(B^0(t) \rightarrow f)}{\Gamma(\bar{B}^0(t) \rightarrow f) + \Gamma(B^0(t) \rightarrow f)}, \\ &= S_f \sin(\Delta m_d t) - C_f \cos(\Delta m_d t), \end{aligned} \quad (12.18)$$

where

$$S_f = \frac{2 \text{Im}\lambda_f}{1 + |\lambda_f|^2}, \quad C_f = \frac{1 - |\lambda_f|^2}{1 + |\lambda_f|^2}, \quad \lambda_f = \frac{q}{p} \frac{\bar{A}_f}{A_f}. \quad (12.19)$$

Here,  $q/p$  describes  $B^0-\bar{B}^0$  mixing and, to a good approximation in the SM,  $q/p = V_{tb}^*V_{td}/V_{tb}V_{td}^* = e^{-2i\beta + \mathcal{O}(\lambda^4)}$  in the usual phase convention.  $A_f$  ( $\bar{A}_f$ ) is the amplitude of the  $B^0 \rightarrow f$  ( $\bar{B}^0 \rightarrow f$ ) decay. If  $f$  is a  $CP$  eigenstate, and amplitudes with one CKM phase dominate the decay, then  $|A_f| = |\bar{A}_f|$ ,  $C_f = 0$ , and  $S_f = \sin(\arg\lambda_f) = \eta_f \sin 2\phi$ , where  $\eta_f$  is the  $CP$  eigenvalue of  $f$  and  $2\phi$  is the phase difference between the  $B^0 \rightarrow f$  and  $B^0 \rightarrow \bar{B}^0 \rightarrow f$  decay paths. A contribution of another amplitude to the decay with a different CKM phase makes the value of  $S_f$  sensitive to relative strong-interaction phases between the decay amplitudes (it also makes  $C_f \neq 0$  possible).

The  $b \rightarrow c\bar{c}s$  decays to  $CP$  eigenstates ( $B^0 \rightarrow$  charmonium  $K_{S,L}^0$ ) are the theoretically cleanest examples, measuring  $S_f = -\eta_f \sin 2\beta$ . The  $b \rightarrow s$  penguin amplitudes have dominantly the same weak phase as the  $b \rightarrow c\bar{c}s$  tree amplitude. Since only  $\lambda^2$ -suppressed penguin amplitudes introduce a different  $CP$ -violating phase, amplitudes with a single weak phase dominate, and we expect  $|\bar{A}_\psi K/A_\psi K| - 1| < 0.01$ . The  $e^+e^-$  asymmetric-energy  $B$ -factory experiments, BABAR [97] and Belle [98], and LHCb [99] provided precise measurements. The world average, including some other measurements, is [24]

$$\sin 2\beta = 0.699 \pm 0.017. \quad (12.20)$$

This measurement has a four-fold ambiguity in  $\beta$ , which can be resolved by a global fit as mentioned in Sec. 12.4. Experimentally, the two-fold ambiguity  $\beta \rightarrow \pi/2 - \beta$  (but not  $\beta \rightarrow \pi + \beta$ ) can be resolved by a time-dependent angular analysis of  $B^0 \rightarrow J/\psi K^{*0}$  [100, 101], or a time-dependent Dalitz plot analysis of  $B^0 \rightarrow \bar{D}^0 h^0$ . The time-dependent Dalitz plot analysis of  $B^0 \rightarrow \bar{D}^0 h^0$  ( $h^0 = \pi^0, \eta, \omega$ ) with  $\bar{D}^0 \rightarrow K_S^0 \pi^+ \pi^-$ , jointly performed by Belle and BABAR, excludes the  $\pi/2 - \beta$  solution with  $7.3\sigma$  confidence level

[102]. These results indicate that negative  $\cos 2\beta$  solutions are very unlikely, in agreement with the global CKM fit result.

The  $b \rightarrow c\bar{c}d$  mediated transitions, such as  $B^0 \rightarrow J/\psi\pi^0$  and  $B^0 \rightarrow D^{(*)+}D^{(*)-}$ , also measure approximately  $\sin 2\beta$ . However, the dominant component of the  $b \rightarrow d$  penguin amplitude has a different CKM phase ( $V_{tb}^*V_{td}$ ) than the tree amplitude ( $V_{cb}^*V_{cd}$ ), and their magnitudes are of the same order in  $\lambda$ . Therefore, the effect of penguins could be large, resulting in  $S_f \neq -\eta_f \sin 2\beta$  and  $C_f \neq 0$ . Such decay modes have been measured by *BABAR*, Belle, and LHCb. The world averages [24],  $S_{J/\psi\pi^0} = -0.86 \pm 0.14$ ,  $S_{J/\psi\rho^0} = -0.66^{+0.16}_{-0.12}$ ,  $S_{D^+D^-} = -0.84 \pm 0.12$ , and  $S_{D^{*+}D^{*-}} = -0.71 \pm 0.09$  (where  $\eta_f = +1$  for the  $J/\psi\pi^0$  and  $D^+D^-$  modes, while  $J/\psi\rho^0$  and  $D^{*+}D^{*-}$  are mixtures of  $CP$  even and odd states), are consistent with  $\sin 2\beta$  obtained from  $B^0 \rightarrow$  charmonium  $K^0$  decays, and the  $C_f$ 's are consistent with zero, although the uncertainties are sizable.

The  $b \rightarrow c\bar{u}d$  decays  $B^0 \rightarrow \bar{D}^0(*)h^0$ , with  $\bar{D}^0 \rightarrow CP$  eigenstates and  $\bar{D}^0 \rightarrow K_S^0\pi^+\pi^-$  with Dalitz plot analysis, have no penguin contributions, and provide theoretically clean  $\sin 2\beta$  measurements. The average of joint analyses of *BABAR* and Belle data [102, 103] give  $\sin 2\beta = 0.71 \pm 0.09$  [24, 104].

### 12.3.2.2 Penguin-dominated modes

The  $b \rightarrow s\bar{q}q$  penguin-dominated decays have the same CKM phase as the  $b \rightarrow c\bar{c}s$  tree level decays, up to corrections suppressed by  $\lambda^2$ , since  $V_{tb}^*V_{ts} = -V_{cb}^*V_{cs}[1 + \mathcal{O}(\lambda^2)]$ . Therefore, decays such as  $B^0 \rightarrow \phi K^0$  and  $\eta' K^0$  provide  $\sin 2\beta$  measurements in the SM. Any BSM contribution to the amplitude with a different weak phase would give rise to  $S_f \neq -\eta_f \sin 2\beta$ , and possibly  $C_f \neq 0$ . Therefore, the main interest in these modes is not simply to measure  $\sin 2\beta$ , but to search for new physics. Measurements of many other decay modes in this category, such as  $B \rightarrow \pi^0 K_S^0$ ,  $K_S^0 K_S^0 K_S^0$ , etc., have also been performed by *BABAR* and Belle. The results and their uncertainties are summarized in Fig. 12.3 and Table 12.1 of Ref. [95]. The comparison of  $CP$  violation measurements between tree-dominated and penguin-dominated modes in  $B_s^0$  decays provides similar sensitivity to new physics.

### 12.3.3 $\alpha / \phi_2$

Since  $\alpha$  is the phase between  $V_{tb}^*V_{td}$  and  $V_{ub}^*V_{ud}$ , only time-dependent  $CP$  asymmetries in decay modes dominated by  $b \rightarrow u\bar{u}d$  transition can directly measure  $\sin 2\alpha$ , in contrast to  $\sin 2\beta$ , where several different quark-level transitions can be used. Since  $b \rightarrow d$  penguin amplitudes have a different CKM phase than  $b \rightarrow u\bar{u}d$  tree amplitudes, and their magnitudes are of the same order in  $\lambda$ , the penguin contribution can be sizable, which makes the determination of  $\alpha$  complicated. To date,  $\alpha$  has been measured in  $B \rightarrow \pi\pi$ ,  $\rho\pi$  and  $\rho\rho$  decay modes.

#### 12.3.3.1 $B \rightarrow \pi\pi$

It is well established from the data that there is a sizable contribution of  $b \rightarrow d$  penguin amplitudes in  $B \rightarrow \pi\pi$  decays. Thus,  $S_{\pi^+\pi^-}$  in the time-dependent  $B^0 \rightarrow \pi^+\pi^-$  analysis does not measure  $\sin 2\alpha$ , but

$$S_{\pi^+\pi^-} = \sqrt{1 - C_{\pi^+\pi^-}^2} \sin(2\alpha + 2\Delta\alpha), \quad (12.21)$$

where  $2\Delta\alpha$  is the phase difference between  $e^{2i\gamma}\bar{A}_{\pi^+\pi^-}$  and  $A_{\pi^+\pi^-}$ . The value of  $\Delta\alpha$ , and hence  $\alpha$ , can be extracted using the isospin relation among the amplitudes of  $B^0 \rightarrow \pi^+\pi^-$ ,  $B^0 \rightarrow \pi^0\pi^0$ , and  $B^+ \rightarrow \pi^+\pi^0$  decays [105],

$$\frac{1}{\sqrt{2}} A_{\pi^+\pi^-} + A_{\pi^0\pi^0} - A_{\pi^+\pi^0} = 0, \quad (12.22)$$

and a similar expression for the  $\bar{A}_{\pi\pi}$ 's. This method utilizes the fact that a pair of pions from  $B \rightarrow \pi\pi$  decay must be in a zero angular momentum state, and, because of Bose statistics, they must have even isospin. Consequently,  $\pi^\pm\pi^0$  is in a pure isospin-2 state, while the penguin amplitudes only contribute to the isospin-0 final state. The latter does not hold for the electroweak penguin amplitudes, but their effect is expected to be small. The isospin

analysis uses the world averages of *BABAR*, Belle, and LHCb measurements,  $S_{\pi^+\pi^-} = -0.63 \pm 0.04$ ,  $C_{\pi^+\pi^-} = -0.32 \pm 0.04$ , the decay widths of all three modes, and the direct  $CP$  asymmetry  $C_{\pi^0\pi^0} = -0.33 \pm 0.22$  [24]. This analysis leads to 16 mirror solutions for  $0 \leq \alpha < 2\pi$ . Because of this, and due to the experimental uncertainties, some of these solutions are not well separated [96].

#### 12.3.3.2 $B \rightarrow \rho\rho$

The decay  $B^0 \rightarrow \rho^+\rho^-$  contains two vector mesons in the final state, and so in general is a mixture of  $CP$ -even and  $CP$ -odd components. Therefore, it was thought that extracting  $\alpha$  from this mode would be complicated.

However, the longitudinal polarization fractions in  $B^+ \rightarrow \rho^+\rho^0$  and  $B^0 \rightarrow \rho^+\rho^-$  decays were measured to be close to unity [106], which implies that the final states are almost purely  $CP$ -even. Furthermore,  $\mathcal{B}(B^0 \rightarrow \rho^0\rho^0) = (0.95 \pm 0.16) \times 10^{-6}$  is much smaller than  $\mathcal{B}(B^0 \rightarrow \rho^+\rho^-) = (27.7 \pm 1.9) \times 10^{-6}$  and  $\mathcal{B}(B^+ \rightarrow \rho^+\rho^0) = (24.0_{-2.0}^{+1.9}) \times 10^{-6}$  [24], which implies that the effect of the penguin contributions is small. The isospin analysis using the world averages,  $S_{\rho^+\rho^-} = -0.14 \pm 0.13$  and  $C_{\rho^+\rho^-} = 0.00 \pm 0.09$  [24], together with the time-dependent  $CP$  asymmetry,  $S_{\rho^0\rho^0} = -0.3 \pm 0.7$  and  $C_{\rho^0\rho^0} = -0.2 \pm 0.9$  [107], and the above mentioned branching fractions and longitudinal polarization fractions, gives two solutions (with mirror solutions at  $3\pi/2 - \alpha$ ) [96]. A possible small violation of Eq. (12.22) due to the finite width of the  $\rho$  [108] is so far neglected.

#### 12.3.3.3 $B \rightarrow \rho\pi$

The final state in  $B^0 \rightarrow \rho^+\pi^-$  decay is not a  $CP$  eigenstate, but this decay proceeds via the same quark-level diagrams as  $B^0 \rightarrow \pi^+\pi^-$ , and both  $B^0$  and  $\bar{B}^0$  can decay to  $\rho^+\pi^-$ , while the final state in  $B^0 \rightarrow \rho^0\pi^0$  is a  $CP$  eigenstate. Consequently, mixing-induced  $CP$  violation can occur in  $B^0$  and  $\bar{B}^0$  decays to  $\rho^\pm\pi^\mp$  and  $\rho^0\pi^0$ . The time-dependent Dalitz plot analysis of  $B^0 \rightarrow \pi^+\pi^-\pi^0$  decays permits the extraction of  $\alpha$  with a single discrete ambiguity,  $\alpha \rightarrow \alpha + \pi$ , since one knows the variation of the strong phases in the interference regions of the  $\rho^+\pi^-$ ,  $\rho^-\pi^+$ , and  $\rho^0\pi^0$  amplitudes in the Dalitz plot [109]. The combination of Belle [110] and *BABAR* [111] measurements gives only moderate constraints [96].

Combining the  $B \rightarrow \pi\pi$ ,  $\rho\pi$ , and  $\rho\rho$  decay modes [24, 96],  $\alpha$  is constrained as

$$\alpha = (84.9_{-4.5}^{+5.1})^\circ. \quad (12.23)$$

Similar results can be found in Refs. [112, 113].

### 12.3.4 $\gamma / \phi_3$

By virtue of Eq. (12.16),  $\gamma$  does not depend on CKM elements involving the top quark, so it can be measured in tree-level  $B$  decays. This is an important distinction from the measurements of  $\alpha$  and  $\beta$ , and implies that measurements of  $\gamma$  are unlikely to be affected by physics beyond the SM.

#### 12.3.4.1 $B_{(s)} \rightarrow D_{(s)}K^{(*)}$

The interference of  $B^- \rightarrow D^0K^-$  ( $b \rightarrow c\bar{u}s$ ) and  $B^- \rightarrow \bar{D}^0K^-$  ( $b \rightarrow u\bar{c}s$ ) transitions can be studied in final states accessible in both  $D^0$  and  $\bar{D}^0$  decays [94]. In principle, it is possible to extract the  $B$  and  $D$  decay amplitudes, the relative strong phases, and the weak phase  $\gamma$  from the data [96].

A practical complication is that the precision depends sensitively on the ratio of the interfering amplitudes

$$r_B = \left| A(B^- \rightarrow \bar{D}^0K^-) / A(B^- \rightarrow D^0K^-) \right|, \quad (12.24)$$

which is around 0.1. The original GLW method [114, 115] considers  $D$  decays to  $CP$  eigenstates, such as  $B^\pm \rightarrow D_{CP}^{(*)}(\rightarrow \pi^+\pi^-)K^{(*)\pm}$ . To alleviate the smallness of  $r_B$  and make the interfering amplitudes (which are products of the  $B$  and  $D$  decay amplitudes) comparable in magnitude, the ADS method [116] considers final states where Cabibbo-allowed  $\bar{D}^0$  and doubly-Cabibbo-suppressed  $D^0$  decays interfere. Measurements have been made by the  $B$  factories, CDF, and LHCb, using both methods [24]. The GLW method currently gives only a loose constraint on  $\gamma$ ,  $14.9^\circ < \gamma < 30.8^\circ$ ,  $69.9^\circ < \gamma < 87.9^\circ$ ,  $92.1^\circ < \gamma < 110.1^\circ$ ,



and  $149.2^\circ < \gamma < 165.1^\circ$  at 68% CL; while the ADS method provides  $\gamma = (72^{+12}_{-14})^\circ$  [24, 104].

The BPGGSZ method [117, 118] utilizes that both  $D^0$  and  $\bar{D}^0$  can have large branching fractions to  $CP$  self-conjugate three-body final states, such as  $K_S^0 \pi^+ \pi^-$ , and the analysis can be optimized by studying the Dalitz plot dependence of the interferences. The best present determination of  $\gamma$  comes from this method. Combining the measurements by Belle [119], *BABAR* [120] and LHCb [121],  $\gamma = (73.8^{+6.8}_{-7.0})^\circ$  is obtained [24, 104]. The error is sensitive to the central value of the amplitude ratio  $r_B$  (and  $r_B^*$  for the  $D^* K$  mode), for which Belle found somewhat larger central values than *BABAR* and LHCb. The same values of  $r_B^{(*)}$  enter the ADS analyses, and the data can be combined to fit for  $r_B^{(*)}$  and  $\gamma$ . The effect of  $D^0$ - $\bar{D}^0$  mixing on  $\gamma$  is far below the present experimental accuracy [122], unless  $D^0$ - $\bar{D}^0$  mixing is due to  $CP$ -violating new physics, in which case it can be included in the analysis [123].

The amplitude ratio is much larger in the analogous  $B_s^0 \rightarrow D_s^\pm K^\mp$  decays, which allows a model-independent extraction of  $\gamma - 2\beta_s$  [124] (here  $\beta_s = \arg(-V_{ts} V_{tb}^* / V_{cs} V_{cb}^*)$  is related to the phase of  $B_s$  mixing). A recent measurement by LHCb [125] gives  $\gamma = (127^{+17}_{-22})^\circ$  using a constraint on  $2\beta_s$  (see Sec. 12.5).

Combining all the above measurements [24, 96],  $\gamma$  is constrained as

$$\gamma = (72.1^{+4.1}_{-4.5})^\circ. \quad (12.25)$$

Similar results can be found in Refs. [112, 113].

#### 12.3.4.2 $B^0 \rightarrow D^{(*)\pm} \pi^\mp$

The interference of  $b \rightarrow u$  and  $b \rightarrow c$  transitions can be studied in  $\bar{B}^0 \rightarrow D^{(*)+} \pi^-$  ( $b \rightarrow c\bar{u}d$ ) and  $\bar{B}^0 \rightarrow B^0 \rightarrow D^{(*)+} \pi^-$  ( $\bar{b} \rightarrow \bar{u}c\bar{d}$ ) decays and their  $CP$  conjugates, since both  $B^0$  and  $\bar{B}^0$  decay to  $D^{(*)\pm} \pi^\mp$  (or  $D^\pm \rho^\mp$ , etc.). Since there are only tree and no penguin contributions to these decays, in principle, it is possible to extract from the four time-dependent rates the magnitudes of the two hadronic amplitudes, their relative strong phase, and the weak phase between the two decay paths, which is  $2\beta + \gamma$ .

A complication is that the ratio of the interfering amplitudes is very small,  $r_{D\pi} = A(B^0 \rightarrow D^+ \pi^-) / A(\bar{B}^0 \rightarrow D^+ \pi^-) = \mathcal{O}(0.01)$  (and similarly for  $r_{D^* \pi}$  and  $r_{D\rho}$ ), and therefore it has not been possible to measure it. To obtain  $2\beta + \gamma$ ,  $SU(3)$  flavor symmetry and dynamical assumptions have been used to relate  $A(\bar{B}^0 \rightarrow D^- \pi^+)$  to  $A(\bar{B}^0 \rightarrow D_s^- \pi^+)$ , so this measurement is not model independent at present. Combining the  $D^\pm \pi^\mp$ ,  $D^{*\pm} \pi^\mp$  and  $D^\pm \rho^\mp$  measurements [126] gives  $\sin(2\beta + \gamma) > 0.68$  at 68% CL [112], consistent with the previously discussed results for  $\beta$  and  $\gamma$ .

## 12.4 Global fit in the Standard Model

Using the independently measured CKM elements mentioned in the previous sections, the unitarity of the CKM matrix can be checked. We obtain  $|V_{ud}|^2 + |V_{us}|^2 + |V_{ub}|^2 = 0.9985 \pm 0.0005$  (1st row),  $|V_{cd}|^2 + |V_{cs}|^2 + |V_{cb}|^2 = 1.025 \pm 0.022$  (2nd row),  $|V_{ud}|^2 + |V_{cd}|^2 + |V_{td}|^2 = 0.9970 \pm 0.0018$  (1st column), and  $|V_{us}|^2 + |V_{cs}|^2 + |V_{ts}|^2 = 1.026 \pm 0.022$  (2nd column), respectively. Due to the recent reduction of the value of  $|V_{ud}|$ , there is a  $3\sigma$  tension with unitarity in the 1st row, leading also to poor consistency of the SM fit below. The uncertainties in the second row and column are dominated by that of  $|V_{cs}|$ . For the second row, another check is obtained from the measurement of  $\sum_{u,c,d,s,b} |V_{ij}|^2$  in Sec. 12.2.4, minus the sum in the first row above:  $|V_{cd}|^2 + |V_{cs}|^2 + |V_{cb}|^2 = 1.002 \pm 0.027$ . These provide strong tests of the unitarity of the CKM matrix. With the significantly improved direct determination of  $|V_{tb}|$ , the unitarity checks for the third row and column have also become fairly precise, leaving decreasing room for mixing with other states. The sum of the three angles of the unitarity triangle,  $\alpha + \beta + \gamma = (179^{+7}_{-6})^\circ$ , is also consistent with the SM expectation.

The CKM matrix elements can be most precisely determined using a global fit to all available measurements and imposing the SM constraints (i.e., three generation unitarity). The fit must also use theory predictions for hadronic matrix elements, which

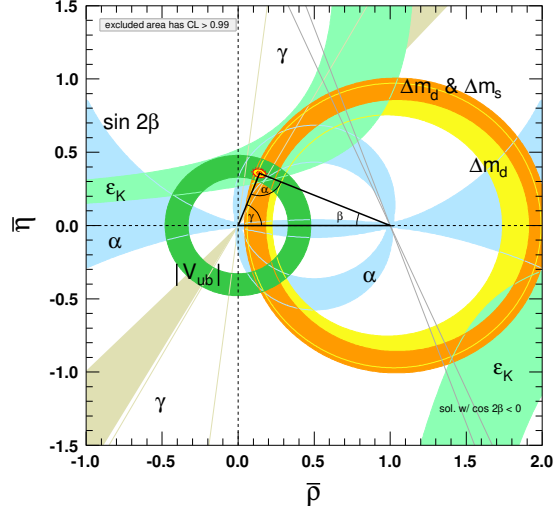


Figure 12.2: Constraints on the  $\bar{\rho}, \bar{\eta}$  plane. The shaded areas have 99% CL.

sometimes have significant uncertainties. There are several approaches to combining the experimental data. CKMfitter [6, 112] and Ref. [127] (which develops [128, 129] further) use frequentist statistics, while UFit [113, 130] uses a Bayesian approach. These approaches provide similar results.

The constraints implied by the unitarity of the three generation CKM matrix significantly reduce the allowed range of some of the CKM elements. The fit for the Wolfenstein parameters defined in Eq. (12.4) gives

$$\begin{aligned} \lambda &= 0.22650 \pm 0.00048, & A &= 0.790^{+0.017}_{-0.012}, \\ \bar{\rho} &= 0.141^{+0.016}_{-0.017}, & \bar{\eta} &= 0.357 \pm 0.011. \end{aligned} \quad (12.26)$$

These values are obtained using the method of Refs. [6, 112]. Using the prescription of Refs. [113, 130] gives  $\lambda = 0.22658 \pm 0.00044$ ,  $A = 0.818 \pm 0.012$ ,  $\bar{\rho} = 0.139 \pm 0.014$ ,  $\bar{\eta} = 0.356 \pm 0.010$  [131]. The fit results for the magnitudes of all nine CKM elements are

$$V_{\text{CKM}} = \begin{pmatrix} 0.97401 \pm 0.00011 & 0.22650 \pm 0.00048 & 0.00361^{+0.00011}_{-0.00009} \\ 0.22636 \pm 0.00048 & 0.97320 \pm 0.00011 & 0.04053^{+0.00083}_{-0.00061} \\ 0.00854^{+0.00023}_{-0.00016} & 0.03978^{+0.00082}_{-0.00060} & 0.999172^{+0.00024}_{-0.00035} \end{pmatrix}, \quad (12.27)$$

and the Jarlskog invariant is  $J = (3.00^{+0.15}_{-0.09}) \times 10^{-5}$ . The parameters in Eq. (12.3) are

$$\begin{aligned} \sin \theta_{12} &= 0.22650 \pm 0.00048, & \sin \theta_{13} &= 0.00361^{+0.00011}_{-0.00009}, \\ \sin \theta_{23} &= 0.04053^{+0.00083}_{-0.00061}, & \delta &= 1.196^{+0.045}_{-0.043}. \end{aligned} \quad (12.28)$$

Fig. 12.2 illustrates the constraints on the  $\bar{\rho}, \bar{\eta}$  plane from various measurements, and the global fit result. The CL of each of the shaded regions was increased from 95% to 99% for this edition, because the reduction in  $|V_{ud}|$  discussed above leads to poor consistency between the fit result (for  $\bar{\rho}$  and  $\bar{\eta}$ ) and the individual constraints shown in the plot. The shaded 99% CL regions all overlap consistently around the global fit region.

If one uses only tree-level inputs (magnitudes of CKM elements not coupling to the top quark and the angle  $\gamma$ ), the resulting fit is almost identical for  $\lambda$  in Eq. (12.26), while the other parameters' central values can change by about a sigma and their uncertainties double, yielding  $\lambda = 0.22653 \pm 0.00048$ ,  $A = 0.799^{+0.027}_{-0.028}$ ,  $\bar{\rho} = 0.123^{+0.032}_{-0.028}$ , and  $\bar{\eta} = 0.382^{+0.029}_{-0.028}$ . This illustrates how the constraints can be less tight in the presence of BSM physics.

## 12.5 Implications beyond the SM

The effects in  $B$ ,  $B_s$ ,  $K$ , and  $D$  decays and mixings due to high-scale physics ( $W$ ,  $Z$ ,  $t$ ,  $H$  in the SM, and unknown heavier particles) can be parameterized by operators composed of SM fields, obeying the  $SU(3) \times SU(2) \times U(1)$  gauge symmetry. Flavor-changing neutral currents, suppressed in the SM, are especially sensitive to beyond SM contributions. Processes studied in great detail, both experimentally and theoretically, include neutral meson mixings,  $B_{(s)} \rightarrow X\gamma$ ,  $X\ell^+\ell^-$ ,  $\ell^+\ell^-$ ,  $K \rightarrow \pi\nu\bar{\nu}$ , etc. The BSM contributions to these operators are suppressed by powers of the scale at which they are generated. Already at lowest order, there are many dimension-6 operators, and the observable effects of BSM interactions are encoded in their coefficients. In the SM, these coefficients are determined by just the four CKM parameters, and the  $W$ ,  $Z$ , and quark masses. For example,  $\Delta m_d$ ,  $\Gamma(B \rightarrow \rho\gamma)$ ,  $\Gamma(B \rightarrow \pi\ell^+\ell^-)$ , and  $\Gamma(B \rightarrow \ell^+\ell^-)$  are all proportional to  $|V_{td}V_{tb}|^2$  in the SM, however, they may receive unrelated BSM contributions. These BSM contributions may or may not obey the SM relations. (For example, the flavor sector of the MSSM contains 69  $CP$ -conserving parameters and 41  $CP$ -violating phases, *i.e.*, 40 new ones [132]). Thus, similar to the measurements of  $\sin 2\beta$  in tree- and loop-dominated decay modes, overconstraining measurements of the magnitudes and phases of flavor-changing neutral-current amplitudes gives good sensitivity to BSM.

To illustrate the level of suppression required for BSM contributions, consider a class of models in which the unitarity of the CKM matrix is maintained, and the dominant BSM effects modify the neutral meson mixing amplitudes [133] by  $(z_{ij}/\Lambda^2)(\bar{q}_i\gamma^\mu P_L q_j)^2$ , where  $z_{ij}$  is an unknown coefficient and  $\Lambda$  is the scale suppressing this BSM contribution (see, [134, 135]). It is only known since the measurements of  $\gamma$  and  $\alpha$  that the SM gives the leading contribution to  $B^0 - \bar{B}^0$  mixing [6, 136]. Nevertheless, new physics with a generic weak phase may still contribute to neutral meson mixings at a significant fraction of the SM [130, 137, 138]. The existing data imply that  $\Lambda/|z_{ij}|^{1/2}$  has to exceed about  $10^4$  TeV for  $K^0 - \bar{K}^0$  mixing,  $10^3$  TeV for  $D^0 - \bar{D}^0$  mixing, 500 TeV for  $B^0 - \bar{B}^0$  mixing, and 100 TeV for  $B_s^0 - \bar{B}_s^0$  mixing [130, 135]. (Some other operators are even better constrained [130].) The constraints are the strongest in the kaon sector, because the CKM suppression is the most severe. Thus, if there is new physics at the TeV scale,  $|z_{ij}| \ll 1$  is required. Even if  $|z_{ij}|$  are suppressed by a loop factor and  $|V_{ti}^*V_{tj}|^2$  (in the down quark sector), similar to the SM, one expects percent-level effects, which may be observable in forthcoming flavor physics experiments. To constrain such extensions of the SM, many measurements irrelevant for the SM-CKM fit, such as the  $CP$  asymmetry in semileptonic  $B_{d,s}^0$  decays,  $A_{SL}^{d,s}$ , are important [139]. The current world averages [24] are consistent with the SM, with experimental uncertainties far greater than those of the theory predictions.

There are many key measurements sensitive to BSM physics, which do not constrain the unitarity triangle in Fig. 12.1. For example, a key quantity in the  $B_s$  system is  $\beta_s = \arg(-V_{ts}V_{tb}^*/V_{cs}V_{cb}^*)$ , which is the small,  $\lambda^2$ -suppressed, angle of a “squashed” unitarity triangle, obtained by taking the scalar product of the second and third columns of the CKM matrix. This angle can be measured via time-dependent  $CP$  violation in  $B_s^0 \rightarrow J/\psi\phi$ , similar to  $\beta$  in  $B^0 \rightarrow J/\psi K^0$ . Since the  $J/\psi\phi$  final state is not a  $CP$  eigenstate, an angular analysis of the decay products is needed to separate the  $CP$ -even and  $CP$ -odd components, which give opposite asymmetries. In the SM, the asymmetry for the  $CP$ -even part is  $2\beta_s$ , when one neglects subdominant amplitudes with a weak phase  $V_{ub}$ . (Sometimes the notation  $\phi_s = -2\beta_s$  plus a possible BSM contribution to the  $B_s$  mixing phase is used.) Testing if the data agree with the SM prediction,  $2\beta_s = 0.0383_{-0.0011}^{+0.0012}$  [112], is another sensitive probe of the SM. The current world average, dominated by LHC measurements [140] including the  $B_s \rightarrow J/\psi K^+ K^-$  and  $J/\psi \pi^+ \pi^-$  decay modes, is  $2\beta_s = 0.051 \pm 0.023$  [71]. Since the uncertainty is much larger than that in the SM, a lot will be learned from more precise future measurements. Searches for  $CP$  violation in the charm sector, in particular in  $D^0 - \bar{D}^0$  mixing, provide complementary sensitivity to BSM.

In the kaon sector, the  $CP$ -violating observables,  $\epsilon$  and  $\epsilon'$ , are tiny, so models in which all sources of  $CP$  violation are small were viable before the  $B$ -factory measurements. Since the measurement of  $\sin 2\beta$ , we know that  $CP$  violation can be an  $\mathcal{O}(1)$  effect, and only flavor mixing is suppressed between the three quark generations. Thus, many models with spontaneous  $CP$  violation were excluded. In the kaon sector, clean tests of the SM can come from measurements of  $K^+ \rightarrow \pi^+ \nu\bar{\nu}$  [78] and  $K_L^0 \rightarrow \pi^0 \nu\bar{\nu}$  [141]. These loop-induced rare decays are sensitive to BSM, and will allow precise tests [142] of the CKM paradigm, independent of  $B$  decays.

The CKM elements are fundamental parameters, so they should be measured as precisely as possible. The overconstraining measurements of  $CP$  asymmetries, mixing, semileptonic, and rare decays severely constrain the magnitudes and phases of possible BSM contributions to flavor-changing interactions. If new particles are observed at the LHC, it will be important to explore their flavor parameters as precisely as possible to understand the underlying physics.

### References

- [1] N. Cabibbo, Phys. Rev. Lett. **10**, 531 (1963).
- [2] M. Kobayashi and T. Maskawa, Prog. Theor. Phys. **49**, 652 (1973).
- [3] L.-L. Chau and W.-Y. Keung, Phys. Rev. Lett. **53**, 1802 (1984).
- [4] L. Wolfenstein, Phys. Rev. Lett. **51**, 1945 (1983).
- [5] A. J. Buras, M. E. Lautenbacher and G. Ostermaier, Phys. Rev. **D50**, 3433 (1994), [hep-ph/9403384].
- [6] J. Charles *et al.* (CKMfitter Group), Eur. Phys. J. **C41**, 1, 1 (2005), [hep-ph/0406184].
- [7] C. Jarlskog, Phys. Rev. Lett. **55**, 1039 (1985).
- [8] W. J. Marciano and A. Sirlin, Nucl. Phys. **B93**, 303 (1975); K. S. Babu, Z. Phys. **C35**, 69 (1987).
- [9] J. Hardy and I. S. Towner, PoS **CKM2016**, 028 (2016).
- [10] E. Blucher and W.J. Marciano, “ $V_{ud}$ ,  $V_{us}$ , the Cabibbo Angle and CKM Unitarity,” in this *Review*.
- [11] C.-Y. Seng *et al.*, Phys. Rev. Lett. **121**, 24, 241804 (2018), [arXiv:1807.10197].
- [12] D. Poganic *et al.*, Phys. Rev. Lett. **93**, 181803 (2004), [hep-ex/0312030].
- [13] M. Antonelli *et al.* (FlaviaNet Working Group on Kaon Decays), Eur. Phys. J. **C69**, 399 (2010), [arXiv:1005.2323]; see also <http://www.lnf.infn.it/wg/vus>.
- [14] S. Aoki *et al.* (Flavour Lattice Averaging Group), Eur. Phys. J. **C80**, 2, 113 (2020), [arXiv:1902.08191]; The original papers that led to the quoted averages are cited in this reference or on the web page <http://flag.unibe.ch/>.
- [15] T. Mannel and P. Urquijo, “Semileptonic  $b$ -Hadron Decays, Determination of  $V_{cb}$  and  $V_{ub}$ ,” in this *Review*.
- [16] H. Leutwyler and M. Roos, Z. Phys. **C25**, 91 (1984); For earlier fits for  $|V_{ud}|$  and  $|V_{us}|$  in the 3-generation SM, see Ref. [17].
- [17] R. E. Shrock and L.-L. Wang, Phys. Rev. Lett. **41**, 1692 (1978).
- [18] J. Bijnens and P. Talavera, Nucl. Phys. **B669**, 341 (2003), [hep-ph/0303103]; M. Jamin, J. A. Oller and A. Pich, JHEP **02**, 047 (2004), [hep-ph/0401080]; V. Cirigliano *et al.*, JHEP **04**, 006 (2005), [hep-ph/0503108]; C. Dawson *et al.*, PoS **LAT2005**, 337 (2006), [hep-lat/0510018]; N. Tsutsui *et al.* (JLQCD), PoS **LAT2005**, 357 (2006), [hep-lat/0510068]; M. Okamoto (Fermilab Lattice, MILC, HPQCD), in “3rd Conference on Flavor Physics and CP Violation (FPCP 2004) Daegu, Korea, October 4-9, 2004,” (2004), [hep-lat/0412044].
- [19] W. J. Marciano, Phys. Rev. Lett. **93**, 231803 (2004), [hep-ph/0402299].
- [20] F. Ambrosino *et al.* (KLOE), Phys. Lett. **B632**, 76 (2006), [hep-ex/0509045].

- [21] See Sec. 5.2, “Averages and fits,” in the Introduction to this *Review*, <http://pdg.lbl.gov/2019/reviews/rpp2019-rev-rpp-intro.pdf>.
- [22] N. Cabibbo, E. C. Swallow and R. Winston, *Ann. Rev. Nucl. Part. Sci.* **53**, 39 (2003), [hep-ph/0307298]; N. Cabibbo, E. C. Swallow and R. Winston, *Phys. Rev. Lett.* **92**, 251803 (2004), [hep-ph/0307214].
- [23] M. Ademollo and R. Gatto, *Phys. Rev. Lett.* **13**, 264 (1964).
- [24] Y. S. Amhis *et al.* (HFLAV) (2019), [arXiv:1909.12524]; and updates at <https://hflav.web.cern.ch/>.
- [25] J. P. Lees *et al.* (BaBar), *Phys. Rev.* **D91**, 5, 052022 (2015), [arXiv:1412.5502].
- [26] M. Ablikim *et al.* (BESIII), *Phys. Rev.* **D92**, 7, 072012 (2015), [arXiv:1508.07560].
- [27] M. Ablikim *et al.* (BESIII), *Phys. Rev.* **D96**, 1, 012002 (2017), [arXiv:1703.09084].
- [28] D. Besson *et al.* (CLEO), *Phys. Rev.* **D80**, 032005 (2009), [arXiv:0906.2983].
- [29] L. Widhalm *et al.* (Belle), *Phys. Rev. Lett.* **97**, 061804 (2006), [hep-ex/0604049].
- [30] M. Ablikim *et al.* (BESIII), *Phys. Rev.* **D89**, 5, 051104 (2014), [arXiv:1312.0374].
- [31] B. I. Eisenstein *et al.* (CLEO), *Phys. Rev.* **D78**, 052003 (2008), [arXiv:0806.2112].
- [32] H. Abramowicz *et al.*, *Z. Phys.* **C15**, 19 (1982).
- [33] S. A. Rabinowitz *et al.*, *Phys. Rev. Lett.* **70**, 134 (1993).
- [34] A. O. Bazarko *et al.* (CCFR), *Z. Phys.* **C65**, 189 (1995), [hep-ex/9406007].
- [35] P. Vilain *et al.* (CHARM II), *Eur. Phys. J.* **C11**, 19 (1999).
- [36] F. J. Gilman, K. Kleinknecht and B. Renk (2004).
- [37] G. De Lellis, P. Migliozi and P. Santorelli, *Phys. Rept.* **399**, 227 (2004), [Erratum: *Phys. Rept.* 411,323(2005)].
- [38] N. Ushida *et al.* (Fermilab E531), *Phys. Lett.* **B206**, 380 (1988).
- [39] T. Bolton (1997), [hep-ex/9708014].
- [40] A. Kayis-Topaksu *et al.* (CHORUS), *Phys. Lett.* **B626**, 24 (2005).
- [41] A. Zupanc *et al.* (Belle), *JHEP* **09**, 139 (2013), [arXiv:1307.6240].
- [42] J. P. Alexander *et al.* (CLEO), *Phys. Rev.* **D79**, 052001 (2009), [arXiv:0901.1216].
- [43] P. del Amo Sanchez *et al.* (BaBar), *Phys. Rev.* **D82**, 091103 (2010), [Erratum: *Phys. Rev.* D91,no.1,019901(2015)], [arXiv:1008.4080].
- [44] M. Ablikim *et al.* (BESIII), *Phys. Rev.* **D94**, 7, 072004 (2016), [arXiv:1608.06732].
- [45] M. Ablikim *et al.* (BESIII), *Phys. Rev. Lett.* **122**, 7, 071802 (2019), [arXiv:1811.10890].
- [46] P. U. E. Onyisi *et al.* (CLEO), *Phys. Rev.* **D79**, 052002 (2009), [arXiv:0901.1147].
- [47] P. Naik *et al.* (CLEO), *Phys. Rev.* **D80**, 112004 (2009), [arXiv:0910.3602].
- [48] B. Aubert *et al.* (BaBar), *Phys. Rev.* **D76**, 052005 (2007), [arXiv:0704.0020].
- [49] M. Ablikim *et al.* (BESIII), *Phys. Rev. Lett.* **122**, 1, 011804 (2019), [arXiv:1810.03127].
- [50] LEP *W* branching fraction results for this Review of Particle Physics, LEPEWWG/XSEC/2005-01, <http://lepewwg.web.cern.ch/LEPEWWG/lepww/4f/Winter05>.
- [51] P. Abreu *et al.* (DELPHI), *Phys. Lett.* **B439**, 209 (1998).
- [52] I. I. Y. Bigi *et al.*, *Phys. Rev. Lett.* **71**, 496 (1993), [hep-ph/9304225].
- [53] A. V. Manohar and M. B. Wise, *Phys. Rev.* **D49**, 1310 (1994), [hep-ph/9308246].
- [54] I. I. Y. Bigi *et al.*, *Phys. Rev.* **D56**, 4017 (1997), [hep-ph/9704245].
- [55] A. H. Hoang, Z. Ligeti and A. V. Manohar, *Phys. Rev.* **D59**, 074017 (1999), [hep-ph/9811239]; A. H. Hoang, Z. Ligeti and A. V. Manohar, *Phys. Rev. Lett.* **82**, 277 (1999), [hep-ph/9809423]; A. H. Hoang and T. Teubner, *Phys. Rev.* **D60**, 114027 (1999), [hep-ph/9904468].
- [56] N. Isgur and M. B. Wise, *Phys. Lett.* **B237**, 527 (1990); N. Isgur and M. B. Wise, *Phys. Lett.* **B232**, 113 (1989).
- [57] A. Abdesselam *et al.* (Belle) (2017), [arXiv:1702.01521].
- [58] C. G. Boyd, B. Grinstein and R. F. Lebed, *Phys. Rev.* **D56**, 6895 (1997), [hep-ph/9705252]; C. G. Boyd, B. Grinstein and R. F. Lebed, *Nucl. Phys.* **B461**, 493 (1996), [hep-ph/9508211].
- [59] M. Neubert, *Phys. Rev.* **D49**, 3392 (1994), [hep-ph/9311325]; M. Neubert, *Phys. Rev.* **D49**, 4623 (1994), [hep-ph/9312311].
- [60] I. I. Y. Bigi *et al.*, *Int. J. Mod. Phys.* **A9**, 2467 (1994), [hep-ph/9312359].
- [61] C. W. Bauer, Z. Ligeti and M. E. Luke, *Phys. Lett.* **B479**, 395 (2000), [hep-ph/0002161]; C. W. Bauer, Z. Ligeti and M. E. Luke, *Phys. Rev.* **D64**, 113004 (2001), [hep-ph/0107074].
- [62] A. Bornheim *et al.* (CLEO), *Phys. Rev. Lett.* **88**, 231803 (2002), [hep-ex/0202019].
- [63] B. Aubert *et al.* (BaBar), *Phys. Rev.* **D73**, 012006 (2006), [hep-ex/0509040].
- [64] A. Limosani *et al.* (Belle), *Phys. Lett.* **B621**, 28 (2005), [hep-ex/0504046].
- [65] P. Urquijo *et al.* (Belle), *Phys. Rev. Lett.* **104**, 021801 (2010), [arXiv:0907.0379]; J. P. Lees *et al.* (BaBar), *Phys. Rev.* **D86**, 032004 (2012), [arXiv:1112.0702].
- [66] J. A. Bailey *et al.* (Fermilab Lattice, MILC), *Phys. Rev.* **D92**, 1, 014024 (2015), [arXiv:1503.07839]; J. M. Flynn *et al.*, *Phys. Rev.* **D91**, 7, 074510 (2015), [arXiv:1501.05373]; B. Colquhoun *et al.*, *Phys. Rev.* **D93**, 3, 034502 (2016), [arXiv:1510.07446].
- [67] P. Ball and R. Zwicky, *Phys. Rev.* **D71**, 014015 (2005), [hep-ph/0406232]; A. Khodjamirian *et al.*, *Phys. Rev.* **D83**, 094031 (2011), [arXiv:1103.2655].
- [68] Particle listing, in this *Review*.
- [69] R. Aaij *et al.* (LHCb), *Nature Phys.* **11**, 743 (2015), [arXiv:1504.01568].
- [70] H. Albrecht *et al.* (ARGUS), *Phys. Lett.* **B192**, 245 (1987).
- [71] O. Schneider, “ $B^0-\bar{B}^0$  mixing,” in this *Review*.
- [72] A. Abulencia *et al.* (CDF), *Phys. Rev. Lett.* **97**, 242003 (2006), [hep-ex/0609040].
- [73] R. Aaij *et al.* (LHCb), *New J. Phys.* **15**, 053021 (2013), [arXiv:1304.4741].
- [74] M. Misiak *et al.*, *Phys. Rev. Lett.* **114**, 22, 221801 (2015), [arXiv:1503.01789]; M. Czakon *et al.*, *JHEP* **04**, 168 (2015), [arXiv:1503.01791].
- [75] B. Grinstein and D. Pirjol, *Phys. Rev.* **D62**, 093002 (2000), [hep-ph/0002216]; A. Ali, E. Lunghi and A. Ya. Parkhomenko, *Phys. Lett.* **B595**, 323 (2004), [hep-ph/0405075]; M. Beneke, T. Feldmann and D. Seidel, *Nucl. Phys.* **B612**, 25 (2001), [hep-ph/0106067]; S. W. Bosch and G. Buchalla, *Nucl. Phys.* **B621**, 459 (2002), [hep-ph/0106081]; Z. Ligeti and M. B. Wise, *Phys. Rev.* **D60**, 117506 (1999), [hep-ph/9905277]; D. Becirevic *et al.*, *JHEP* **05**, 007 (2003), [hep-lat/0301020]; P. Ball, G. W. Jones and R. Zwicky, *Phys. Rev.* **D75**, 054004 (2007), [hep-ph/0612081]; W. Wang, R.-H. Li and C.-D. Lu (2007), [arXiv:0711.0432]; C.-D. Lu, W. Wang and Z.-T. Wei, *Phys. Rev.* **D76**, 014013 (2007), [hep-ph/0701265].
- [76] A. J. Buras *et al.*, *Phys. Rev. Lett.* **95**, 261805 (2005), [hep-ph/0508165].

- [77] A. V. Artamonov *et al.* (E949), Phys. Rev. Lett. **101**, 191802 (2008), [arXiv:0808.2459]; A. V. Artamonov *et al.* (BNL-E949), Phys. Rev. **D79**, 092004 (2009), [arXiv:0903.0030].
- [78] E. Cortina Gil *et al.* (NA62), Phys. Lett. **B791**, 156 (2019), [arXiv:1811.08508].
- [79] D. Acosta *et al.* (CDF), Phys. Rev. Lett. **95**, 102002 (2005), [hep-ex/0505091].
- [80] V. M. Abazov *et al.* (D0), Phys. Rev. Lett. **107**, 121802 (2011), [arXiv:1106.5436].
- [81] V. Khachatryan *et al.* (CMS), Phys. Lett. **B736**, 33 (2014), [arXiv:1404.2292].
- [82] T. A. Aaltonen *et al.* (CDF, D0), Phys. Rev. Lett. **115**, 15, 152003 (2015), [arXiv:1503.05027].
- [83] LHC Top Working Group summary plots, single top quark production, Nov. 2017, <https://twiki.cern.ch/twiki/bin/view/LHCPhysics/LHCtopWGSummaryPlots>.
- [84] J. Swain and L. Taylor, Phys. Rev. **D58**, 093006 (1998), [hep-ph/9712420].
- [85] “ $K_L^0$  meson” particle listing, in this *Review*.
- [86] A. J. Buras, D. Guadagnoli and G. Isidori, Phys. Lett. **B688**, 309 (2010), [arXiv:1002.3612]; For earlier discussions, see Ref. [87].
- [87] E. A. Andriyash, G. G. Ovanesyan and M. I. Vysotsky, Phys. Lett. **B599**, 253 (2004), [hep-ph/0310314]; K. Anikeev *et al.*, in “Workshop on  $B$  Physics at the Tevatron: Run II and Beyond Batavia, Illinois, September 23-25, 1999,” (2001), [hep-ph/0201071]; A. J. Buras and D. Guadagnoli, Phys. Rev. **D78**, 033005 (2008), [arXiv:0805.3887].
- [88] T. Inami and C. S. Lim, Prog. Theor. Phys. **65**, 297 (1981), [Erratum: Prog. Theor. Phys. **65**, 1772 (1981)].
- [89] J. M. Flynn and L. Randall, Phys. Lett. **B224**, 221 (1989), [Erratum: Phys. Lett. **B235**, 412 (1990)]; G. Buchalla, A. J. Buras and M. K. Harlander, Nucl. Phys. **B337**, 313 (1990).
- [90] M. Ciuchini *et al.*, Phys. Lett. **B301**, 263 (1993), [hep-ph/9212203]; A. J. Buras, M. Jamin and M. E. Lautenbacher, Nucl. Phys. **B408**, 209 (1993), [hep-ph/9303284]; T. Hambye *et al.*, Nucl. Phys. **B564**, 391 (2000), [hep-ph/9906434]; S. Bertolini, J. O. Eeg and M. Fabbrichesi, Phys. Rev. **D63**, 056009 (2001), [hep-ph/0002234]; V. Cirigliano *et al.*, Phys. Rev. Lett. **91**, 162001 (2003), [hep-ph/0307030].
- [91] Z. Bai *et al.* (RBC, UKQCD), Phys. Rev. Lett. **115**, 21, 212001 (2015), [arXiv:1505.07863].
- [92] A. J. Buras *et al.*, JHEP **11**, 202 (2015), [arXiv:1507.06345].
- [93] V. Cirigliano *et al.*, JHEP **02**, 032 (2020), [arXiv:1911.01359].
- [94] A. B. Carter and A. I. Sanda, Phys. Rev. Lett. **45**, 952 (1980); A. B. Carter and A. I. Sanda, Phys. Rev. **D23**, 1567 (1981).
- [95] A more detailed discussion and references can be found in: T. Gershon and Y. Nir, “ $CP$  violation in meson decays,” in this *Review*.
- [96] T. Gershon, M. Kenzie and K. Trabelsi, “Determination of CKM angles from  $B$  hadrons,” in this *Review*.
- [97] B. Aubert *et al.* (BaBar), Phys. Rev. **D79**, 072009 (2009), [arXiv:0902.1708].
- [98] I. Adachi *et al.* (Belle), Phys. Rev. Lett. **108**, 171802 (2012), [arXiv:1201.4643].
- [99] R. Aaij *et al.* (LHCb), Phys. Rev. Lett. **115**, 3, 031601 (2015), [arXiv:1503.07089].
- [100] B. Aubert *et al.* (BaBar), Phys. Rev. **D71**, 032005 (2005), [hep-ex/0411016].
- [101] R. Itoh *et al.* (Belle), Phys. Rev. Lett. **95**, 091601 (2005), [hep-ex/0504030].
- [102] I. Adachi *et al.* (BaBar, Belle), Phys. Rev. Lett. **121**, 26, 261801 (2018), [arXiv:1804.06152]; I. Adachi *et al.* (BaBar, Belle), Phys. Rev. **D98**, 11, 112012 (2018), [arXiv:1804.06153].
- [103] A. Abdesselam *et al.* (BaBar, Belle), Phys. Rev. Lett. **115**, 12, 121604 (2015), [arXiv:1505.04147].
- [104] Heavy Flavor Averaging Group [24], Moriond 2020 updates for Unitarity Triangle Parameters: <https://hflav-eos.web.cern.ch/hflav-eos/triangle/PDG2020/>.
- [105] M. Gronau and D. London, Phys. Rev. Lett. **65**, 3381 (1990).
- [106] J. Zhang *et al.* (Belle), Phys. Rev. Lett. **91**, 221801 (2003), [hep-ex/0306007]; A. Somov *et al.* (Belle), Phys. Rev. Lett. **96**, 171801 (2006), [hep-ex/0601024]; B. Aubert *et al.* (BaBar), Phys. Rev. Lett. **97**, 261801 (2006), [hep-ex/0607092]; B. Aubert *et al.* (BaBar), Phys. Rev. **D76**, 052007 (2007), [arXiv:0705.2157].
- [107] B. Aubert *et al.* (BaBar), Phys. Rev. **D78**, 071104 (2008), [arXiv:0807.4977].
- [108] A. F. Falk *et al.*, Phys. Rev. **D69**, 011502 (2004), [hep-ph/0310242].
- [109] A. E. Snyder and H. R. Quinn, Phys. Rev. **D48**, 2139 (1993).
- [110] A. Kusaka *et al.* (Belle), Phys. Rev. Lett. **98**, 221602 (2007), [hep-ex/0701015].
- [111] J. P. Lees *et al.* (BaBar), Phys. Rev. **D88**, 1, 012003 (2013), [arXiv:1304.3503].
- [112] A. Hocker *et al.*, Eur. Phys. J. **C21**, 225 (2001), [hep-ph/0104062]; and updates at <http://ckmfitter.in2p3.fr/>.
- [113] M. Bona *et al.* (UTfit), JHEP **07**, 028 (2005), [hep-ph/0501199]; and updates at <http://www.utfit.org>.
- [114] M. Gronau and D. London, Phys. Lett. **B253**, 483 (1991).
- [115] M. Gronau and D. Wyler, Phys. Lett. **B265**, 172 (1991).
- [116] D. Atwood, I. Dunietz and A. Soni, Phys. Rev. Lett. **78**, 3257 (1997), [hep-ph/9612433]; D. Atwood, I. Dunietz and A. Soni, Phys. Rev. **D63**, 036005 (2001), [hep-ph/0008090].
- [117] A. Bondar, talk at the Belle analysis workshop, Novosibirsk, September 2002; A. Poluektov *et al.* (Belle), Phys. Rev. **D70**, 072003 (2004), [hep-ex/0406067].
- [118] A. Giri *et al.*, Phys. Rev. **D68**, 054018 (2003), [hep-ph/0303187].
- [119] A. Poluektov *et al.* (Belle), Phys. Rev. **D81**, 112002 (2010), [arXiv:1003.3360].
- [120] P. del Amo Sanchez *et al.* (BaBar), Phys. Rev. Lett. **105**, 121801 (2010), [arXiv:1005.1096].
- [121] R. Aaij *et al.* (LHCb), JHEP **10**, 097 (2014), [arXiv:1408.2748].
- [122] Y. Grossman, A. Soffer and J. Zupan, Phys. Rev. **D72**, 031501 (2005), [hep-ph/0505270].
- [123] A. Amorim, M. G. Santos and J. P. Silva, Phys. Rev. **D59**, 056001 (1999), [hep-ph/9807364].
- [124] R. Aleksan, I. Dunietz and B. Kayser, Z. Phys. **C54**, 653 (1992).
- [125] R. Aaij *et al.* (LHCb), JHEP **03**, 059 (2018), [arXiv:1712.07428].
- [126] B. Aubert *et al.* (BaBar), Phys. Rev. **D71**, 112003 (2005), [hep-ex/0504035]; B. Aubert *et al.* (BaBar), Phys. Rev. **D73**, 111101 (2006), [hep-ex/0602049]; F. J. Ronga *et al.* (Belle), Phys. Rev. **D73**, 092003 (2006), [hep-ex/0604013]; S. Bahinipati *et al.* (Belle), Phys. Rev. **D84**, 021101 (2011), [arXiv:1102.0888]; R. Aaij *et al.* (LHCb), JHEP **06**, 084 (2018), [arXiv:1805.03448].
- [127] G. P. Dubois-Felsmann *et al.*, *Sensitivity of CKM fits to theoretical uncertainties and their representation* (2003), [hep-ph/0308262]; G. Eigen *et al.*, Phys. Rev. **D89**, 3, 033004 (2014), [arXiv:1301.5867].

- [128] D. Boutigny *et al.* (BaBar), in “Workshop on Physics at an Asymmetric B Factory (BaBar Collaboration Meeting) Pasadena, California, September 22-24, 1997,” (1998), URL <http://www-public.slac.stanford.edu/sciDoc/docMeta.aspx?slacPubNumber=SLAC-R-504>.
- [129] S. Plaszczynski and M.-H. Schune hf8/019 (1999), [PoShf8,019(1999)], [hep-ph/9911280].
- [130] M. Bona *et al.* (UTfit), JHEP **03**, 049 (2008), [arXiv:0707.0636].
- [131] We thank the CKMfitter and UTfit groups for performing fits and preparing plots using input values from this *Review*.
- [132] H. E. Haber, Nucl. Phys. Proc. Suppl. **62**, 469 (1998), [hep-ph/9709450]; Y. Nir, *CP violation: A New era* (2001), [hep-ph/0109090].
- [133] J. M. Soares and L. Wolfenstein, Phys. Rev. **D47**, 1021 (1993); T. Goto *et al.*, Phys. Rev. **D53**, 6662 (1996), [hep-ph/9506311]; J. P. Silva and L. Wolfenstein, Phys. Rev. **D55**, 5331 (1997), [hep-ph/9610208].
- [134] Y. Grossman, Z. Ligeti and Y. Nir, Prog. Theor. Phys. **122**, 125 (2009), [arXiv:0904.4262].
- [135] G. Isidori, Y. Nir and G. Perez, Ann. Rev. Nucl. Part. Sci. **60**, 355 (2010), [arXiv:1002.0900]; G. Isidori, in “Proceedings, 2012 European School of High-Energy Physics (ES-HEP 2012): La Pommeraye, Anjou, France, June 06-19, 2012,” 69–105 (2014), [arXiv:1302.0661].
- [136] Z. Ligeti, Int. J. Mod. Phys. **A20**, 5105 (2005), [hep-ph/0408267].
- [137] J. Charles *et al.*, Phys. Rev. **D89**, 3, 033016 (2014), [arXiv:1309.2293].
- [138] K. Agashe *et al.* (2005), [hep-ph/0509117].
- [139] S. Laplace *et al.*, Phys. Rev. **D65**, 094040 (2002), [hep-ph/0202010].
- [140] R. Aaij *et al.* (LHCb), JHEP **08**, 037 (2017), [arXiv:1704.08217]; G. Aad *et al.* (ATLAS) (2020), [arXiv:2001.07115]; V. Khachatryan *et al.* (CMS), Phys. Lett. **B757**, 97 (2016), [arXiv:1507.07527].
- [141] J. K. Ahn *et al.* (KOTO), Phys. Rev. Lett. **122**, 2, 021802 (2019), [arXiv:1810.09655].
- [142] A. J. Buras *et al.*, JHEP **11**, 033 (2015), [arXiv:1503.02693].

### 13. CP Violation in the Quark Sector

Revised August 2019 by T. Gershon (Warwick U.) and Y. Nir (Weizmann Inst.).

The  $CP$  transformation combines charge conjugation  $C$  with parity  $P$ . Under  $C$ , particles and antiparticles are interchanged, by conjugating all internal quantum numbers, *e.g.*,  $Q \rightarrow -Q$  for electromagnetic charge. Under  $P$ , the handedness of space is reversed,  $\vec{x} \rightarrow -\vec{x}$ . Thus, for example, a left-handed electron  $e_L^-$  is transformed under  $CP$  into a right-handed positron,  $e_R^+$ .

If  $CP$  were an exact symmetry, the laws of Nature would be the same for matter and for antimatter. We observe that most phenomena are  $C$ - and  $P$ -symmetric, and therefore, also  $CP$ -symmetric. In particular, these symmetries are respected by the gravitational, electromagnetic, and strong interactions. The weak interactions, on the other hand, violate  $C$  and  $P$  in the strongest possible way. For example, the charged  $W$  bosons couple to left-handed electrons,  $e_L^-$ , and to their  $CP$ -conjugate right-handed positrons,  $e_R^+$ , but to neither their  $C$ -conjugate left-handed positrons,  $e_L^+$ , nor their  $P$ -conjugate right-handed electrons,  $e_R^-$ . While weak interactions violate  $C$  and  $P$  separately,  $CP$  is still preserved in most weak interaction processes. The  $CP$  symmetry is, however, violated in certain rare processes, as discovered in neutral  $K$  decays in 1964 [1], and established later in  $B$  (2001) and  $D$  (2019) decays. A  $K_L$  meson decays more often to  $\pi^- e^+ \nu_e$  than to  $\pi^+ e^- \bar{\nu}_e$ , thus allowing electrons and positrons to be unambiguously distinguished, but the decay-rate asymmetry is only at the 0.003 level. The  $CP$ -violating effects observed in the  $B$  system are larger: the parameter describing the  $CP$  asymmetry in the decay time distribution of  $B^0/\bar{B}^0$  meson transitions to  $CP$  eigenstates like  $J/\psi K_S$  is about 0.7 [2, 3]. These effects are related to  $K^0-\bar{K}^0$  and  $B^0-\bar{B}^0$  mixing, but  $CP$  violation arising solely from decay amplitudes has also been observed, first in  $K \rightarrow \pi\pi$  decays [4–6], subsequently in  $B^0$  [7, 8],  $B^+$  [9–11], and  $B_s^0$  [12] decays, and most recently in charm decays [13]. Similar effects could also occur in decays of baryons, but have not yet been observed. Moreover,  $CP$  violation has not yet been observed in processes involving the top quark, nor in flavor-conserving processes such as electric dipole moments, nor in the lepton sector; for all of these any significant observation would be a clear indication of physics beyond the Standard Model.

In addition to parity and to continuous Lorentz transformations, there is one other spacetime operation that could be a symmetry of the interactions: time reversal  $T$ ,  $t \rightarrow -t$ . Violations of  $T$  symmetry have been observed in neutral  $K$  decays [14]. More recently, exploiting the fact that for neutral  $B$  mesons both flavor tagging and  $CP$  tagging can be used [15],  $T$  violation has been observed between states that are not  $CP$ -conjugate [16]. Moreover,  $T$  violation is expected as a corollary of  $CP$  violation if the combined  $CPT$  transformation is a fundamental symmetry of Nature [17]. All observations indicate that  $CPT$  is indeed a symmetry of Nature. Furthermore, one cannot build a locally Lorentz-invariant quantum field theory with a Hermitian Hamiltonian that violates  $CPT$ . (At several points in our discussion, we avoid assumptions about  $CPT$ , in order to identify cases where evidence for  $CP$  violation relies on assumptions about  $CPT$ .)

Within the Standard Model,  $CP$  symmetry is broken by complex phases in the Yukawa couplings (that is, the couplings of the Higgs scalar to quarks). When all manipulations to remove unphysical phases in this model are exhausted, one finds that there is a single  $CP$ -violating parameter [18]. In the basis of mass eigenstates, this single phase appears in the  $3 \times 3$  unitary matrix that gives the  $W$ -boson couplings to an up-type antiquark and a down-type quark. (If the Standard Model is supplemented with Majorana mass terms for the neutrinos, the analogous mixing matrix for leptons has three  $CP$ -violating phases.) The beautifully consistent and economical Standard-Model description of  $CP$  violation in terms of Yukawa couplings, known as the Kobayashi-Maskawa (KM) mechanism [18], agrees with all measurements to date. (Some measurements are in tension with the predictions, and are discussed in more detail below. Pending verification, the results are not considered to change the overall picture of agreement with the Standard Model.) Furthermore, one can fit

the data allowing new physics contributions to loop processes to compete with, or even dominate over, the Standard Model amplitudes [19, 20]. Such an analysis provides model-independent proof that the KM phase is different from zero, and that the matrix of three-generation quark mixing is the dominant source of  $CP$  violation in meson decays.

The current level of experimental accuracy and the theoretical uncertainties involved in the interpretation of the various observations leave room, however, for additional subdominant sources of  $CP$  violation from new physics. Indeed, almost all extensions of the Standard Model imply that there are such additional sources. Moreover,  $CP$  violation is a necessary condition for baryogenesis, the process of dynamically generating the matter-antimatter asymmetry of the Universe [21]. Despite the phenomenological success of the KM mechanism, it fails (by several orders of magnitude) to accommodate the observed asymmetry [22]. This discrepancy strongly suggests that Nature provides additional sources of  $CP$  violation beyond the KM mechanism. The evidence for neutrino masses implies that  $CP$  can be violated also in the lepton sector. This situation makes leptogenesis [23, 24], a scenario where  $CP$ -violating phases in the Yukawa couplings of the neutrinos play a crucial role in the generation of the baryon asymmetry, a very attractive possibility. The expectation of new sources motivates the large ongoing experimental effort to find deviations from the predictions of the KM mechanism.

$CP$  violation can be experimentally searched for in a variety of processes, such as hadron decays, electric dipole moments of neutrons, electrons and nuclei, and neutrino oscillations. Hadron decays via the weak interaction probe flavor-changing  $CP$  violation. The search for electric dipole moments may find (or constrain) sources of  $CP$  violation that, unlike the KM phase, are not related to flavor-changing couplings. Following the discovery of the Higgs boson [25, 26], searches for  $CP$  violation in the Higgs sector are becoming feasible. Future searches for  $CP$  violation in neutrino oscillations might provide further input on leptogenesis.

The present measurements of  $CP$  asymmetries provide some of the strongest constraints on the weak couplings of quarks. Future measurements of  $CP$  violation in  $K$ ,  $D$ ,  $B$ , and  $B_s^0$  meson decays will provide additional constraints on the flavor parameters of the Standard Model, and can probe new physics. In this review, we give the formalism and basic physics that are relevant to present and near future measurements of  $CP$  violation in the quark sector.

Before going into details, we list here the observables where  $CP$  violation has been observed at a level above  $5\sigma$  [27–29]:

- Indirect  $CP$  violation in  $K \rightarrow \pi\pi$  and  $K \rightarrow \pi\ell\nu$  decays, and in the  $K_L \rightarrow \pi^+ \pi^- e^+ e^-$  decay, is given by

$$|\epsilon| = (2.228 \pm 0.011) \times 10^{-3}. \quad (13.1)$$

- Direct  $CP$  violation in  $K \rightarrow \pi\pi$  decays is given by

$$\mathcal{R}e(\epsilon'/\epsilon) = (1.65 \pm 0.26) \times 10^{-3}. \quad (13.2)$$

- $CP$  violation in the interference of mixing and decay in the tree-dominated  $b \rightarrow c\bar{c}s$  transitions, such as  $B^0 \rightarrow \psi K^0$ , is given by (we use  $K^0$  throughout to denote results that combine  $K_S$  and  $K_L$  modes, but use the sign appropriate to  $K_S$ ):

$$S_{\psi K^0} = +0.699 \pm 0.017. \quad (13.3)$$

- $CP$  violation in the interference of mixing and decay in modes governed by the tree-dominated  $b \rightarrow c\bar{u}d$  transitions is given by

$$S_{D^{(*)}h^0} = +0.71 \pm 0.09, \quad (13.4)$$

- $CP$  violation in the interference of mixing and decay in various modes related to  $b \rightarrow c\bar{c}d$  transitions is given by

$$\begin{aligned} S_{\psi\pi^0} &= -0.86 \pm 0.14, \\ S_{D^+D^-} &= -0.84 \pm 0.12, \\ S_{D^{*+}D^{*-}} &= -0.71 \pm 0.09. \end{aligned} \quad (13.5)$$

- CP violation in the interference of mixing and decay in various modes related to  $b \rightarrow q\bar{q}s$  (penguin) transitions is given by

$$\begin{aligned} S_{\phi K^0} &= +0.74^{+0.11}_{-0.13}, \\ S_{\eta' K^0} &= +0.63 \pm 0.06, \\ S_{f_0 K^0} &= +0.69^{+0.10}_{-0.12}, \\ S_{K^+ K^- K_S} &= +0.68^{+0.09}_{-0.10}. \end{aligned} \quad (13.6)$$

- CP violation in the interference of mixing and decay in the  $B^0 \rightarrow \pi^+ \pi^-$  mode is given by

$$S_{\pi^+ \pi^-} = -0.63 \pm 0.04. \quad (13.7)$$

- Direct CP violation in the  $B^0 \rightarrow \pi^+ \pi^-$  mode is given by

$$C_{\pi^+ \pi^-} = -0.32 \pm 0.04. \quad (13.8)$$

- Direct CP violation in  $B^+ \rightarrow D_+ K^+$  decays ( $D_+$  is the CP-even neutral  $D$  state) is given by

$$\mathcal{A}_{B^+ \rightarrow D_+ K^+} = +0.129 \pm 0.012, \quad (13.9)$$

while the corresponding quantity in the case that the neutral  $D$  meson is reconstructed in the suppressed  $K^- \pi^+$  final state is

$$\mathcal{A}_{B^+ \rightarrow D K^- \pi^+} = -0.41 \pm 0.06, \quad (13.10)$$

- Direct CP violation has also been observed in  $B^+ \rightarrow DK^+$  decays through differences between the Dalitz plot distributions of subsequent  $D \rightarrow K_S \pi^+ \pi^-$  decays.
- Direct CP violation in the  $\bar{B}^0 \rightarrow K^- \pi^+$  mode is given by

$$\mathcal{A}_{\bar{B}^0 \rightarrow K^- \pi^+} = -0.084 \pm 0.004. \quad (13.11)$$

- Direct CP violation in the  $\bar{B}_s^0 \rightarrow K^+ \pi^-$  mode is given by

$$\mathcal{A}_{\bar{B}_s^0 \rightarrow K^+ \pi^-} = +0.213 \pm 0.017. \quad (13.12)$$

- Direct CP violation in  $B^+ \rightarrow K^+ K^- \pi^+$  decays is given by

$$\mathcal{A}_{B^+ \rightarrow K^+ K^- \pi^+} = -0.118 \pm 0.022. \quad (13.13)$$

An amplitude analysis has established a large CP violation effect associated with  $\pi\pi \leftrightarrow KK$  S-wave rescattering in  $B^+ \rightarrow K^+ K^- \pi^+$  decays.

- Large CP violation effects have also been observed in certain regions of the phase space of  $B^+ \rightarrow K^+ K^- K^+$ ,  $\pi^+ \pi^- K^+$  and  $\pi^+ \pi^- \pi^+$  decays.
- Direct CP violation has been established in the difference of asymmetries for  $D^0 \rightarrow K^+ K^-$  and  $D^0 \rightarrow \pi^+ \pi^-$  decays

$$\Delta a_{CP} = (-0.164 \pm 0.028) \times 10^{-3}. \quad (13.14)$$

### 13.1 Formalism

The phenomenology of CP violation for neutral flavored mesons is particularly interesting, since many of the observables can be cleanly interpreted. Although the phenomenology is superficially different for  $K^0$ ,  $D^0$ ,  $B^0$ , and  $B_s^0$  decays, this is primarily because each of these systems is governed by a different balance between decay rates, oscillations, and lifetime splitting. However, the general considerations presented in this section are identical for all flavored neutral pseudoscalar mesons. The phenomenology of CP violation for neutral mesons that do not carry flavor quantum numbers (such as the  $\eta^{(l)}$  state) is quite different: such states are their own antiparticles and have definite CP eigenvalues, so the signature of CP violation is simply the decay to a final state with the opposite CP. Such decays are mediated by the electromagnetic or (OZI-suppressed) strong interaction, where CP violation is not expected and has not yet been observed. In the remainder of this review, we restrict ourselves to considerations of weakly decaying hadrons.

In this section, we present a general formalism for, and classification of, CP violation in the decay of a weakly decaying hadron,

denoted  $M$ . We pay particular attention to the case that  $M$  is a  $K^0$ ,  $D^0$ ,  $B^0$ , or  $B_s^0$  meson. Subsequent sections describe the CP-violating phenomenology, approximations, and alternative formalisms that are specific to each system.

#### 13.1.1 Charged- and neutral-hadron decays

We define decay amplitudes of  $M$  (which could be charged or neutral) and its CP conjugate  $\bar{M}$  to a multi-particle final state  $f$  and its CP conjugate  $\bar{f}$  as

$$A_f = \langle f | \mathcal{H} | M \rangle, \quad \bar{A}_f = \langle f | \mathcal{H} | \bar{M} \rangle, \quad (13.15a)$$

$$\bar{A}_{\bar{f}} = \langle \bar{f} | \mathcal{H} | M \rangle, \quad \bar{A}_{\bar{f}} = \langle \bar{f} | \mathcal{H} | \bar{M} \rangle, \quad (13.15b)$$

where  $\mathcal{H}$  is the Hamiltonian governing weak interactions. The action of CP on these states introduces phases  $\xi_M$  and  $\xi_f$  that depend on their flavor content, according to

$$CP|M\rangle = e^{+i\xi_M} |\bar{M}\rangle, \quad CP|f\rangle = e^{+i\xi_f} |\bar{f}\rangle, \quad (13.16a)$$

$$CP|\bar{M}\rangle = e^{-i\xi_M} |M\rangle, \quad CP|\bar{f}\rangle = e^{-i\xi_f} |f\rangle, \quad (13.16b)$$

so that  $(CP)^2 = 1$ . The phases  $\xi_M$  and  $\xi_f$  are arbitrary and unobservable because of the flavor symmetry of the strong interaction. If CP is conserved by the dynamics,  $[CP, \mathcal{H}] = 0$ , then  $A_f$  and  $\bar{A}_{\bar{f}}$  have the same magnitude and an arbitrary unphysical relative phase

$$\bar{A}_{\bar{f}} = e^{i(\xi_f - \xi_M)} A_f. \quad (13.17)$$

#### 13.1.2 Neutral-meson mixing

A state that is initially a superposition of  $M^0$  and  $\bar{M}^0$ , say

$$|\psi(0)\rangle = a(0)|M^0\rangle + b(0)|\bar{M}^0\rangle, \quad (13.18)$$

will evolve in time acquiring components that describe all possible decay final states  $\{f_1, f_2, \dots\}$ , that is,

$$|\psi(t)\rangle = a(t)|M^0\rangle + b(t)|\bar{M}^0\rangle + c_1(t)|f_1\rangle + c_2(t)|f_2\rangle + \dots \quad (13.19)$$

If we are interested in computing only the values of  $a(t)$  and  $b(t)$  (and not the values of all  $c_i(t)$ ), and if the times  $t$  in which we are interested are much larger than the typical strong interaction scale, then we can use a much simplified formalism [30]. The simplified time evolution is determined by a  $2 \times 2$  effective Hamiltonian  $\mathbf{H}$  that is not Hermitian, since otherwise the mesons would only oscillate and not decay. Any complex matrix, such as  $\mathbf{H}$ , can be written in terms of Hermitian matrices  $\mathbf{M}$  and  $\mathbf{\Gamma}$  as

$$\mathbf{H} = \mathbf{M} - \frac{i}{2} \mathbf{\Gamma}. \quad (13.20)$$

$\mathbf{M}$  and  $\mathbf{\Gamma}$  are associated with  $(M^0, \bar{M}^0) \leftrightarrow (M^0, \bar{M}^0)$  transitions via off-shell (dispersive), and on-shell (absorptive) intermediate states, respectively. Diagonal elements of  $\mathbf{M}$  and  $\mathbf{\Gamma}$  are associated with the flavor-conserving transitions  $M^0 \rightarrow M^0$  and  $\bar{M}^0 \rightarrow \bar{M}^0$ , while off-diagonal elements are associated with flavor-changing transitions  $M^0 \leftrightarrow \bar{M}^0$ .

The eigenvectors of  $\mathbf{H}$  have well-defined masses and decay widths. To specify the components of the strong interaction eigenstates,  $M^0$  and  $\bar{M}^0$ , in the light ( $M_L$ ) and heavy ( $M_H$ ) mass eigenstates, we introduce three complex parameters:  $p$ ,  $q$ , and, for the case that both CP and CPT are violated in mixing,  $z$ :

$$|M_L\rangle \propto p\sqrt{1-z}|M^0\rangle + q\sqrt{1+z}|\bar{M}^0\rangle, \quad (13.21a)$$

$$|M_H\rangle \propto p\sqrt{1+z}|M^0\rangle - q\sqrt{1-z}|\bar{M}^0\rangle, \quad (13.21b)$$

with the normalization  $|q|^2 + |p|^2 = 1$  when  $z = 0$ . (Another possible choice of labelling, which is in standard usage for  $K$  mesons, defines the mass eigenstates according to their lifetimes:  $K_S$  for the short-lived and  $K_L$  for the long-lived state. The  $K_L$  is experimentally found to be the heavier state. Yet another choice is often used for the  $D$  mesons [31]: the eigenstates are labelled according to their dominant CP content.)

The real and imaginary parts of the eigenvalues  $\omega_{L,H}$  corresponding to  $|M_{L,H}\rangle$  represent their masses and decay widths, respectively. The mass and width splittings are

$$\Delta m \equiv m_H - m_L = \mathcal{R}e(\omega_H - \omega_L), \quad (13.22a)$$

$$\Delta\Gamma \equiv \Gamma_H - \Gamma_L = -2\mathcal{I}m(\omega_H - \omega_L). \quad (13.22b)$$

Note that here  $\Delta m$  is positive by definition, while the sign of  $\Delta\Gamma$  must be experimentally determined. The sign of  $\Delta\Gamma$  has not yet been established for  $B^0$  mesons, while  $\Delta\Gamma < 0$  is established for  $K$  and  $B_s^0$  mesons. The Standard Model predicts  $\Delta\Gamma < 0$  for  $B_{(s)}^0$  mesons; for this reason,  $\Delta\Gamma = \Gamma_L - \Gamma_H$ , which is still a signed quantity, is often used in the  $B_{(s)}^0$  literature and is the convention used in the PDG experimental summaries.

Solving the eigenvalue problem for  $\mathbf{H}$  yields

$$\left(\frac{q}{p}\right)^2 = \frac{\mathbf{M}_{12}^* - (i/2)\mathbf{\Gamma}_{12}^*}{\mathbf{M}_{12} - (i/2)\mathbf{\Gamma}_{12}} \quad (13.23)$$

and

$$z \equiv \frac{\delta m - (i/2)\delta\Gamma}{\Delta m - (i/2)\Delta\Gamma}, \quad (13.24)$$

where

$$\delta m \equiv \mathbf{M}_{11} - \mathbf{M}_{22}, \quad \delta\Gamma \equiv \mathbf{\Gamma}_{11} - \mathbf{\Gamma}_{22} \quad (13.25)$$

are the differences in effective mass and decay-rate expectation values for the strong interaction states  $M^0$  and  $\bar{M}^0$ .

If either  $CP$  or  $CPT$  is a symmetry of  $\mathbf{H}$  (independently of whether  $T$  is conserved or violated), then the values of  $\delta m$  and  $\delta\Gamma$  are both zero, and hence  $z = 0$ . We also find that

$$\omega_H - \omega_L = 2\sqrt{\left(\mathbf{M}_{12} - \frac{i}{2}\mathbf{\Gamma}_{12}\right)\left(\mathbf{M}_{12}^* - \frac{i}{2}\mathbf{\Gamma}_{12}^*\right)}. \quad (13.26)$$

If either  $CP$  or  $T$  is a symmetry of  $\mathbf{H}$  (independently of whether  $CPT$  is conserved or violated), then  $\mathbf{\Gamma}_{12}/\mathbf{M}_{12}$  is real, leading to

$$\left(\frac{q}{p}\right)^2 = e^{2i\xi_M} \Rightarrow \left|\frac{q}{p}\right| = 1, \quad (13.27)$$

where  $\xi_M$  is the arbitrary unphysical phase introduced in Eq. (13.16). If, and only if,  $CP$  is a symmetry of  $\mathbf{H}$  (independently of  $CPT$  and  $T$ ), then both of the above conditions hold, with the result that the mass eigenstates are orthogonal

$$\langle M_H | M_L \rangle = |p|^2 - |q|^2 = 0. \quad (13.28)$$

### 13.1.3 CP-violating observables

All  $CP$ -violating observables in  $M$  and  $\bar{M}$  decays to final states  $f$  and  $\bar{f}$  can be expressed in terms of phase-convention-independent combinations of  $A_f$ ,  $\bar{A}_f$ ,  $A_{\bar{f}}$ , and  $\bar{A}_{\bar{f}}$ , together with, for neutral meson decays only,  $q/p$ .  $CP$  violation in charged meson and all baryon decays depends only on the combination  $|\bar{A}_{\bar{f}}/A_f|$ , while  $CP$  violation in flavored neutral meson decays is complicated by  $M^0 \leftrightarrow \bar{M}^0$  oscillations, and depends, additionally, on  $|q/p|$  and on  $\lambda_f \equiv (q/p)(\bar{A}_{\bar{f}}/A_f)$ .

The decay rates of the two neutral kaon mass eigenstates,  $K_S$  and  $K_L$ , are different enough ( $\Gamma_S/\Gamma_L \sim 500$ ) that one can, in most cases, actually study their decays independently. For  $D^0$ ,  $B^0$ , and  $B_s^0$  mesons, however, values of  $\Delta\Gamma/\Gamma$  (where  $\Gamma \equiv (\Gamma_H + \Gamma_L)/2$ ) are relatively small, and so both mass eigenstates must be considered in their evolution. We denote the state of an initially pure  $|M^0\rangle$  or  $|\bar{M}^0\rangle$  after an elapsed proper time  $t$  as  $|M_{\text{phys}}^0(t)\rangle$  or  $|\bar{M}_{\text{phys}}^0(t)\rangle$ , respectively. Using the effective Hamiltonian approximation, but not assuming  $CPT$  to be a good symmetry, we obtain

$$|M_{\text{phys}}^0(t)\rangle = (g_+(t) + z g_-(t)) |M^0\rangle - \sqrt{1 - z^2} \frac{q}{p} g_-(t) |\bar{M}^0\rangle, \quad (13.29a)$$

$$|\bar{M}_{\text{phys}}^0(t)\rangle = (g_+(t) - z g_-(t)) |\bar{M}^0\rangle - \sqrt{1 - z^2} \frac{p}{q} g_-(t) |M^0\rangle, \quad (13.29b)$$

where

$$g_{\pm}(t) \equiv \frac{1}{2} \left[ \exp\left(-im_H t - \frac{1}{2}\Gamma_H t\right) \pm \exp\left(-im_L t - \frac{1}{2}\Gamma_L t\right) \right] \quad (13.30)$$

and  $z = 0$  if either  $CPT$  or  $CP$  is conserved.

Defining  $x \equiv \Delta m/\Gamma$  and  $y \equiv \Delta\Gamma/(2\Gamma)$ , and assuming  $z = 0$ , one obtains the following time-dependent decay rates:

$$\begin{aligned} \frac{d\Gamma[M_{\text{phys}}^0(t) \rightarrow f]/dt}{e^{-\Gamma t} \mathcal{N}_f} &= (|A_f|^2 + |(q/p)\bar{A}_f|^2) \cosh(y\Gamma t) \\ &+ (|A_f|^2 - |(q/p)\bar{A}_f|^2) \cos(x\Gamma t) \\ &+ 2\mathcal{R}e((q/p)A_f^* \bar{A}_f) \sinh(y\Gamma t) \\ &- 2\mathcal{I}m((q/p)A_f^* \bar{A}_f) \sin(x\Gamma t), \end{aligned} \quad (13.31a)$$

$$\begin{aligned} \frac{d\Gamma[\bar{M}_{\text{phys}}^0(t) \rightarrow \bar{f}]/dt}{e^{-\Gamma t} \mathcal{N}_{\bar{f}}} &= (|(p/q)A_f|^2 + |\bar{A}_f|^2) \cosh(y\Gamma t) \\ &- (|(p/q)A_f|^2 - |\bar{A}_f|^2) \cos(x\Gamma t) \\ &+ 2\mathcal{R}e((p/q)A_f \bar{A}_f^*) \sinh(y\Gamma t) \\ &- 2\mathcal{I}m((p/q)A_f \bar{A}_f^*) \sin(x\Gamma t), \end{aligned} \quad (13.31b)$$

where  $\mathcal{N}_f$  is a common, time-independent, normalization factor that can be determined bearing in mind that the range of  $t$  is  $0 < t < \infty$ . Decay rates to the  $CP$ -conjugate final state  $\bar{f}$  are obtained analogously, with  $\mathcal{N}_f = \mathcal{N}_{\bar{f}}$  and the substitutions  $A_f \rightarrow A_{\bar{f}}$  and  $\bar{A}_f \rightarrow \bar{A}_{\bar{f}}$  in Eqs. (13.31a) and (13.31b). Terms proportional to  $|A_f|^2$  or  $|\bar{A}_f|^2$  are associated with decays that occur without any net  $M^0 \leftrightarrow \bar{M}^0$  oscillation, while terms proportional to  $|(q/p)\bar{A}_f|^2$  or  $|(p/q)A_f|^2$  are associated with decays following a net oscillation. The  $\sinh(y\Gamma t)$  and  $\sin(x\Gamma t)$  terms of Eqs. (13.31a) and (13.31b) are associated with the interference between these two cases. Note that, in multi-body decays, amplitudes are functions of variables that describe the phase-space of the final state. Interference may be present in some regions but not others, and is strongly influenced by resonant substructure.

When neutral pseudoscalar mesons are produced coherently in pairs from the decay of a vector resonance,  $V \rightarrow M^0 \bar{M}^0$  (for example,  $\Upsilon(4S) \rightarrow B^0 \bar{B}^0$ ,  $\psi(3770) \rightarrow D^0 \bar{D}^0$  or  $\phi \rightarrow K^0 \bar{K}^0$ ), the time-dependence of their subsequent decays to final states  $f_1$  and  $f_2$  has a similar form to Eqs. (13.31a) and (13.31b):

$$\begin{aligned} \frac{d\Gamma[V_{\text{phys}}(t_1, t_2) \rightarrow f_1 f_2]/d(\Delta t)}{e^{-\Gamma|\Delta t|} \mathcal{N}_{f_1 f_2}} &= (|a_+|^2 + |a_-|^2) \cosh(y\Gamma \Delta t) \\ &+ (|a_+|^2 - |a_-|^2) \cos(x\Gamma \Delta t) \\ &- 2\mathcal{R}e(a_+^* a_-) \sinh(y\Gamma \Delta t) \\ &+ 2\mathcal{I}m(a_+^* a_-) \sin(x\Gamma \Delta t), \end{aligned} \quad (13.32)$$

where  $\Delta t \equiv t_2 - t_1$  is the difference in the production times,  $t_1$  and  $t_2$ , of  $f_1$  and  $f_2$ , respectively, and the dependence on the average decay time and on decay angles has been integrated out. The normalisation factor  $\mathcal{N}_{f_1 f_2}$  can be evaluated, noting that the range of  $\Delta t$  is  $-\infty < \Delta t < \infty$ . The coefficients in Eq. (13.32) are determined by the amplitudes for no net oscillation from  $t_1 \rightarrow t_2$ ,  $\bar{A}_{f_1} A_{f_2}$ , and  $A_{f_1} \bar{A}_{f_2}$ , and for a net oscillation,  $(q/p)\bar{A}_{f_1} \bar{A}_{f_2}$  and  $(p/q)A_{f_1} A_{f_2}$ , via

$$a_+ \equiv \bar{A}_{f_1} A_{f_2} - A_{f_1} \bar{A}_{f_2}, \quad (13.33a)$$

$$\begin{aligned} a_- \equiv & -\sqrt{1 - z^2} \left( \frac{q}{p} \bar{A}_{f_1} \bar{A}_{f_2} - \frac{p}{q} A_{f_1} A_{f_2} \right) \\ & + z \left( \bar{A}_{f_1} A_{f_2} + A_{f_1} \bar{A}_{f_2} \right). \end{aligned} \quad (13.33b)$$

Assuming  $CPT$  conservation,  $z = 0$ , and identifying  $\Delta t \rightarrow t$  and  $f_2 \rightarrow f$ , we find that Eqs. (13.32) and (13.33) reduce to



Eq. (13.31a) with  $A_{f_1} = 0$ ,  $\bar{A}_{f_1} = 1$ , or to Eq. (13.31b) with  $\bar{A}_{f_1} = 0$ ,  $A_{f_1} = 1$ . Indeed, such a situation plays an important role in experiments that exploit the coherence of  $V \rightarrow M^0 \bar{M}^0$  production. Final states  $f_1$  with  $A_{f_1} = 0$  or  $\bar{A}_{f_1} = 0$  are called tagging states, because they identify the decaying pseudoscalar meson as, respectively,  $\bar{M}^0$  or  $M^0$ . Before one of  $M^0$  or  $\bar{M}^0$  decays, they evolve in phase, so that there is always one  $M^0$  and one  $\bar{M}^0$  present. A tagging decay of one meson sets the clock for the time evolution of the other: it starts at  $t_1$  as purely  $M^0$  or  $\bar{M}^0$ , with time evolution that depends only on  $t_2 - t_1$ .

When  $f_1$  is a state that both  $M^0$  and  $\bar{M}^0$  can decay into, then Eq. (13.32) contains interference terms proportional to  $A_{f_1} \bar{A}_{f_1} \neq 0$  that are not present in Eqs. (13.31a) and (13.31b). Even when  $f_1$  is dominantly produced by  $M^0$  decays rather than  $\bar{M}^0$  decays, or vice versa,  $A_{f_1} \bar{A}_{f_1}$  can be non-zero owing to doubly-CKM-suppressed decays (with amplitudes suppressed by at least two powers of  $\lambda$  relative to the dominant amplitude, in the language of Section 13.3), and these terms should be considered for precision studies of  $CP$  violation in coherent  $V \rightarrow M^0 \bar{M}^0$  decays [32]. The correlations in  $V \rightarrow M^0 \bar{M}^0$  decays can also be exploited to determine strong phase differences between favored and suppressed decay amplitudes [33].

### 13.1.4 Classification of CP-violating effects

We distinguish three types of  $CP$ -violating effects that can occur in the quark sector:

- I.  $CP$  violation in decay is defined by

$$|\bar{A}_{\bar{f}}/A_f| \neq 1. \quad (13.34)$$

In charged meson (and all baryon) decays, where mixing effects are absent, this is the only possible source of  $CP$  asymmetries:

$$\mathcal{A}_{f\pm} \equiv \frac{\Gamma(M^- \rightarrow f^-) - \Gamma(M^+ \rightarrow f^+)}{\Gamma(M^- \rightarrow f^-) + \Gamma(M^+ \rightarrow f^+)} = \frac{|\bar{A}_{f-}/A_{f+}|^2 - 1}{|\bar{A}_{f-}/A_{f+}|^2 + 1}. \quad (13.35)$$

Note that the usual sign convention for  $CP$  asymmetries of hadrons is for the difference between the rate involving the particle that contains a heavy quark and that which contains an antiquark. Hence Eq. (13.35) corresponds to the definition for  $B^\pm$  mesons, but the opposite sign is used for  $D_{(s)}^\pm$  decays.

- II.  $CP$  (and  $T$ ) violation in mixing is defined by

$$|q/p| \neq 1. \quad (13.36)$$

In charged-current semileptonic neutral meson decays  $M, \bar{M} \rightarrow \ell^\pm X$  (taking  $|A_{\ell^+ X}| = |\bar{A}_{\ell^- X}|$  and  $A_{\ell^- X} = \bar{A}_{\ell^+ X} = 0$ , as is the case in the Standard Model, to lowest order in  $G_F$ , and in most of its reasonable extensions), this is the only source of  $CP$  violation, and can be measured via the asymmetry of “wrong-sign” decays induced by oscillations:

$$\begin{aligned} \mathcal{A}_{\text{SL}}(t) & \equiv \frac{d\Gamma/dt[\bar{M}_{\text{phys}}^0(t) \rightarrow \ell^+ X] - d\Gamma/dt[M_{\text{phys}}^0(t) \rightarrow \ell^- X]}{d\Gamma/dt[\bar{M}_{\text{phys}}^0(t) \rightarrow \ell^+ X] + d\Gamma/dt[M_{\text{phys}}^0(t) \rightarrow \ell^- X]}, \\ & \quad (13.37a) \end{aligned}$$

$$= \frac{1 - |q/p|^4}{1 + |q/p|^4}. \quad (13.37b)$$

Note that this asymmetry of time-dependent decay rates is actually time-independent.

- III.  $CP$  violation in interference between a decay without mixing,  $M^0 \rightarrow f$ , and a decay with mixing,  $M^0 \rightarrow \bar{M}^0 \rightarrow f$  (such an effect occurs only in decays to final states that are common to  $M^0$  and  $\bar{M}^0$ , including all  $CP$  eigenstates), is defined by

$$\arg(\lambda_f) + \arg(\lambda_{\bar{f}}) \neq 0, \quad \text{with} \quad \lambda_f \equiv \frac{q \bar{A}_f}{p A_f}. \quad (13.38)$$

For final  $CP$  eigenstates,  $f_{CP}$ , the condition Eq. (13.38) simplifies to

$$\text{Im}(\lambda_{f_{CP}}) \neq 0, \quad (13.39)$$

This form of  $CP$  violation can be observed, for example, using the asymmetry of neutral meson decays into  $CP$  eigenstates

$$\begin{aligned} \mathcal{A}_{f_{CP}}(t) & \equiv \\ & \equiv \frac{d\Gamma/dt[\bar{M}_{\text{phys}}^0(t) \rightarrow f_{CP}] - d\Gamma/dt[M_{\text{phys}}^0(t) \rightarrow f_{CP}]}{d\Gamma/dt[\bar{M}_{\text{phys}}^0(t) \rightarrow f_{CP}] + d\Gamma/dt[M_{\text{phys}}^0(t) \rightarrow f_{CP}]}. \end{aligned} \quad (13.40)$$

If  $\Delta\Gamma = 0$ , as expected to a good approximation for  $B^0$  mesons but not for  $K^0$  and  $B_s^0$  mesons, and  $|q/p| = 1$ , then  $\mathcal{A}_{f_{CP}}$  has a particularly simple form (see Eq. (13.89), below). If, in addition, the decay amplitudes fulfill  $|\bar{A}_{f_{CP}}| = |A_{f_{CP}}|$ , the interference between decays with and without mixing is the only source of asymmetry and  $\mathcal{A}_{f_{CP}}(t) = \text{Im}(\lambda_{f_{CP}}) \sin(x\Gamma t)$ .

Examples of these three types of  $CP$  violation will be given in Sections 13.4, 13.5, and 13.6.

## 13.2 Theoretical Interpretation: General Considerations

Consider the  $M \rightarrow f$  decay amplitude  $A_f$ , and the  $CP$  conjugate process,  $\bar{M} \rightarrow \bar{f}$ , with decay amplitude  $\bar{A}_{\bar{f}}$ . There are two types of phases that may appear in these decay amplitudes. Complex parameters in any Lagrangian term that contributes to the amplitude will appear in complex conjugate form in the  $CP$ -conjugate amplitude. Thus, their phases appear in  $A_f$  and  $\bar{A}_{\bar{f}}$  with opposite signs. In the Standard Model, these phases occur only in the couplings of the  $W^\pm$  bosons, and hence, are often called “weak phases.” The weak phase of any single term is convention-dependent. However, the difference between the weak phases in two different terms in  $A_f$  is convention-independent. A second type of phase can appear in scattering or decay amplitudes, even when the Lagrangian is real. This phase originates from the possible contribution from intermediate on-shell states in the decay process. Since such phases are generated by  $CP$ -invariant interactions, they are the same in  $A_f$  and  $\bar{A}_{\bar{f}}$ . Usually the dominant rescattering is due to strong interactions; hence the designation “strong phases” for the phase shifts so induced. Again, only the relative strong phases between different terms in the amplitude are physically meaningful.

The “weak” and “strong” phases discussed here appear in addition to the spurious  $CP$ -transformation phases of Eq. (13.17). Those spurious phases are due to an arbitrary choice of phase convention, and do not originate from any dynamics or induce any  $CP$  violation. For simplicity, we set them to zero from here on.

It is useful to write each contribution  $a_i$  to  $A_f$  in three parts: its magnitude  $|a_i|$ , its weak phase  $\phi_i$ , and its strong phase  $\delta_i$ . If, for example, there are two such contributions,  $A_f = a_1 + a_2$ , we have

$$A_f = |a_1|e^{i(\delta_1 + \phi_1)} + |a_2|e^{i(\delta_2 + \phi_2)}, \quad (13.41a)$$

$$\bar{A}_{\bar{f}} = |a_1|e^{i(\delta_1 - \phi_1)} + |a_2|e^{i(\delta_2 - \phi_2)}. \quad (13.41b)$$

Similarly, for neutral mesons, it is useful to write

$$\mathbf{M}_{12} = |\mathbf{M}_{12}|e^{i\phi_M}, \quad \mathbf{\Gamma}_{12} = |\mathbf{\Gamma}_{12}|e^{i\phi_\Gamma}. \quad (13.42)$$

Each of the phases appearing in Eqs. (13.41) and (13.42) is convention-dependent, but combinations such as  $\delta_1 - \delta_2$ ,  $\phi_1 - \phi_2$ ,  $\phi_M - \phi_\Gamma$ , and  $\phi_M + \phi_1 - \bar{\phi}_1$  (where  $\bar{\phi}_1$  is a weak phase contributing to  $\bar{A}_{\bar{f}}$ ) are physical.

It is now straightforward to evaluate the various asymmetries in terms of the theoretical parameters introduced here. We will do so with approximations that are often relevant to the most interesting measured asymmetries.

1. The  $CP$  asymmetry in charged meson and all baryon decays [Eq. (13.35)] is given by

$$\mathcal{A}_f = - \frac{2|a_1 a_2| \sin(\delta_2 - \delta_1) \sin(\phi_2 - \phi_1)}{|a_1|^2 + |a_2|^2 + 2|a_1 a_2| \cos(\delta_2 - \delta_1) \cos(\phi_2 - \phi_1)}. \quad (13.43)$$

The quantity of most interest to theory is the weak phase difference  $\phi_2 - \phi_1$ . Its extraction from the asymmetry requires, however, that the amplitude ratio  $|a_2/a_1|$  and the strong phase difference  $\delta_2 - \delta_1$  are known. Both quantities depend on non-perturbative hadronic parameters that are difficult to calculate, but in some cases can be obtained from experiment.

2. In the approximation that  $|\Gamma_{12}/\mathbf{M}_{12}| \ll 1$  (valid for  $B^0$  and  $B_s^0$  mesons), the  $CP$  asymmetry in semileptonic neutral-meson decays [Eq. (13.37)] is given by

$$A_{\text{SL}} = - \left| \frac{\Gamma_{12}}{\mathbf{M}_{12}} \right| \sin(\phi_M - \phi_\Gamma). \quad (13.44)$$

The quantity of most interest to theory is the weak phase  $\phi_M - \phi_\Gamma$ . Its extraction from the asymmetry requires, however, that  $|\Gamma_{12}/\mathbf{M}_{12}|$  is known. State of the art calculations of this quantity for the  $B^0$  and  $B_s^0$  mesons have uncertainties of around 15–20% [34].

3. In the approximations that only a single weak phase contributes to decay,  $A_f = |a_f|e^{i(\delta_f + \phi_f)}$ , and that  $|\Gamma_{12}/\mathbf{M}_{12}| = 0$ , we obtain  $|\lambda_f| = 1$ , and the  $CP$  asymmetries in decays to a final  $CP$  eigenstate  $f$  [Eq. (13.40)] with eigenvalue  $\eta_f = \pm 1$  are given by

$$A_{fCP}(t) = \mathcal{I}m(\lambda_f) \sin(\Delta mt) \quad \text{with} \quad \mathcal{I}m(\lambda_f) = \eta_f \sin(\phi_M + 2\phi_f). \quad (13.45)$$

Note that the phase measured is purely a weak phase, and no hadronic parameters are involved in the extraction of its value from  $\mathcal{I}m(\lambda_f)$ .

The discussion above allows us to introduce another classification of  $CP$ -violating effects:

1. *Indirect CP violation* is consistent with taking  $\phi_M \neq 0$  and setting all other  $CP$  violating phases to zero.  $CP$  violation in mixing (type II) belongs to this class.
2. *Direct CP violation* cannot be accounted for by just  $\phi_M \neq 0$ .  $CP$  violation in decay (type I) belongs to this class.

The historical significance of this classification is related to theory. In superweak models [35],  $CP$  violation appears only in diagrams that contribute to  $\mathbf{M}_{12}$ , hence they predict that there is no direct  $CP$  violation. In most models and, in particular, in the Standard Model,  $CP$  violation is both direct and indirect. As concerns type III  $CP$  violation, a single observation of such an

effect would be consistent with indirect  $CP$  violation, but observing  $\eta_{f_1} \mathcal{I}m(\lambda_{f_1}) \neq \eta_{f_2} \mathcal{I}m(\lambda_{f_2})$  (for the same decaying meson and two different final  $CP$  eigenstates  $f_1$  and  $f_2$ ) would establish direct  $CP$  violation. The experimental observation of  $\epsilon' \neq 0$ , which was achieved by establishing that  $\mathcal{I}m(\lambda_{\pi^+\pi^-}) \neq \mathcal{I}m(\lambda_{\pi^0\pi^0})$  (see Section 13.4), excluded the superweak scenario.

### 13.3 Theoretical Interpretation: The KM Mechanism

Of all the Standard Model quark parameters, only the Kobayashi-Maskawa (KM) phase is  $CP$ -violating. Having a single source of  $CP$  violation, the Standard Model is very predictive for  $CP$  asymmetries: some vanish, and those that do not are correlated.

To be precise,  $CP$  could be violated also by strong interactions. The experimental upper bound on the electric-dipole moment of the neutron implies, however, that  $\theta_{\text{QCD}}$ , the non-perturbative parameter that determines the strength of this type of  $CP$  violation, is tiny, if not zero. (The smallness of  $\theta_{\text{QCD}}$  constitutes a theoretical puzzle, known as “the strong  $CP$  problem.”) In particular, it is irrelevant to our discussion of hadron decays.

The charged current interactions (that is, the  $W^\pm$  interactions) for quarks are given by

$$-\mathcal{L}_{W^\pm} = \frac{g}{\sqrt{2}} \bar{u}_L^i \gamma^\mu (V_{\text{CKM}})_{ij} d_{Lj} W_\mu^\pm + \text{h.c.} \quad (13.46)$$

Here  $i, j = 1, 2, 3$  are generation numbers. The Cabibbo-Kobayashi-Maskawa (CKM) mixing matrix for quarks is a  $3 \times 3$  unitary matrix [36]. Ordering the quarks by their masses, *i.e.*,  $(u_1, u_2, u_3) \rightarrow (u, c, t)$  and  $(d_1, d_2, d_3) \rightarrow (d, s, b)$ , the elements of  $V_{\text{CKM}}$  are written as follows:

$$V_{\text{CKM}} = \begin{pmatrix} V_{ud} & V_{us} & V_{ub} \\ V_{cd} & V_{cs} & V_{cb} \\ V_{td} & V_{ts} & V_{tb} \end{pmatrix}. \quad (13.47)$$

While a general  $3 \times 3$  unitary matrix depends on three real angles and six phases, the freedom to redefine the phases of the quark mass eigenstates can be used to remove five of the phases, leaving a single physical phase, the Kobayashi-Maskawa phase, that is responsible for all  $CP$  violation in the Standard Model.

The fact that one can parametrize  $V_{\text{CKM}}$  by three real and only one imaginary physical parameters can be made manifest by choosing an explicit parametrization. The Wolfenstein parametrization [37, 38] is particularly useful:

$$V_{\text{CKM}} = \begin{pmatrix} 1 - \frac{1}{2}\lambda^2 - \frac{1}{8}\lambda^4 & \lambda & A\lambda^3(\rho - i\eta) \\ -\lambda + \frac{1}{2}A^2\lambda^5[1 - 2(\rho + i\eta)] & 1 - \frac{1}{2}\lambda^2 - \frac{1}{8}\lambda^4(1 + 4A^2) & A\lambda^2 \\ A\lambda^3[1 - (1 - \frac{1}{2}\lambda^2)(\rho + i\eta)] & -A\lambda^2 + \frac{1}{2}A\lambda^4[1 - 2(\rho + i\eta)] & 1 - \frac{1}{2}A^2\lambda^4 \end{pmatrix}. \quad (13.48)$$

Here  $\lambda \approx 0.23$  (not to be confused with  $\lambda_f$ ), the sine of the Cabibbo angle, plays the role of an expansion parameter, and  $\eta$  represents the  $CP$ -violating phase. Terms of  $\mathcal{O}(\lambda^6)$  have been neglected.

The unitarity of the CKM matrix,  $(VV^\dagger)_{ij} = (V^\dagger V)_{ij} = \delta_{ij}$ , leads to twelve distinct complex relations among the matrix elements. The six relations with  $i \neq j$  can be represented geometrically as triangles in the complex plane. Two of these,

$$V_{ud}V_{ub}^* + V_{cd}V_{cb}^* + V_{td}V_{tb}^* = 0, \quad (13.49a)$$

$$V_{td}V_{ud}^* + V_{ts}V_{us}^* + V_{tb}V_{ub}^* = 0, \quad (13.49b)$$

have terms of equal order,  $\mathcal{O}(A\lambda^3)$ , and so have corresponding triangles whose interior angles are all  $\mathcal{O}(1)$  physical quantities that can be independently measured. The angles of the first triangle

(see Fig. 13.1) are given by

$$\alpha \equiv \varphi_2 \equiv \arg \left( -\frac{V_{td}V_{tb}^*}{V_{ud}V_{ub}^*} \right) \simeq \arg \left( -\frac{1 - \rho - i\eta}{\rho + i\eta} \right), \quad (13.50a)$$

$$\beta \equiv \varphi_1 \equiv \arg \left( -\frac{V_{cd}V_{cb}^*}{V_{td}V_{tb}^*} \right) \simeq \arg \left( \frac{1}{1 - \rho - i\eta} \right), \quad (13.50b)$$

$$\gamma \equiv \varphi_3 \equiv \arg \left( -\frac{V_{ud}V_{ub}^*}{V_{cd}V_{cb}^*} \right) \simeq \arg(\rho + i\eta). \quad (13.50c)$$

The angles of the second triangle are equal to  $(\alpha, \beta, \gamma)$  up to corrections of  $\mathcal{O}(\lambda^2)$ . The notations  $(\alpha, \beta, \gamma)$  and  $(\varphi_1, \varphi_2, \varphi_3)$  are both in common usage but, for convenience, we only use the first convention in the following.

Another relation that can be represented as a triangle,

$$V_{us}V_{ub}^* + V_{cs}V_{cb}^* + V_{ts}V_{tb}^* = 0, \quad (13.51)$$

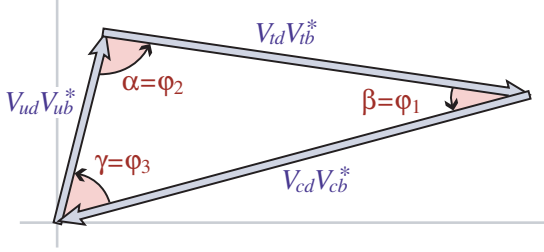


Figure 13.1: Graphical representation of the unitarity constraint  $V_{ud}V_{ub}^* + V_{cd}V_{cb}^* + V_{td}V_{tb}^* = 0$  as a triangle in the complex plane.

and, in particular, its small angle, of  $\mathcal{O}(\lambda^2)$ ,

$$\beta_s \equiv \arg\left(-\frac{V_{ts}V_{tb}^*}{V_{cs}V_{cb}^*}\right), \quad (13.52)$$

is convenient for analyzing  $CP$  violation in the  $B_s^0$  sector.

All unitarity triangles have the same area, commonly denoted by  $J/2$  [39]. If  $CP$  is violated,  $J$  is different from zero and can be taken as the single  $CP$ -violating parameter. In the Wolfenstein parametrization of Eq. (13.48),  $J \simeq \lambda^6 A^2 \eta$ .

### 13.4 Kaons

$CP$  violation was discovered in  $K \rightarrow \pi\pi$  decays in 1964 [1]. The same mode provided the first observation of direct  $CP$  violation [4–6].

The decay amplitudes actually measured in neutral  $K$  decays refer to the mass eigenstates  $K_L$  and  $K_S$ , rather than to the  $K$  and  $\bar{K}$  states referred to in Eq. (13.15). The final  $\pi^+\pi^-$  and  $\pi^0\pi^0$  states are  $CP$ -even. In the  $CP$  conservation limit,  $K_S$  ( $K_L$ ) would be  $CP$ -even (odd), and therefore would (would not) decay to two pions. We define  $CP$ -violating amplitude ratios for two-pion final states,

$$\eta_{00} \equiv \frac{\langle \pi^0\pi^0 | \mathcal{H} | K_L \rangle}{\langle \pi^0\pi^0 | \mathcal{H} | K_S \rangle}, \quad \eta_{+-} \equiv \frac{\langle \pi^+\pi^- | \mathcal{H} | K_L \rangle}{\langle \pi^+\pi^- | \mathcal{H} | K_S \rangle}. \quad (13.53)$$

Another important observable is the asymmetry of time-integrated semileptonic decay rates:

$$\delta_L \equiv \frac{\Gamma(K_L \rightarrow \ell^+\nu_\ell\pi^-) - \Gamma(K_L \rightarrow \ell^-\bar{\nu}_\ell\pi^+)}{\Gamma(K_L \rightarrow \ell^+\nu_\ell\pi^-) + \Gamma(K_L \rightarrow \ell^-\bar{\nu}_\ell\pi^+)}. \quad (13.54)$$

$CP$  violation has been observed as an appearance of  $K_L$  decays to two-pion final states [27],

$$|\eta_{00}| = (2.220 \pm 0.011) \times 10^{-3}, \quad (13.55a)$$

$$|\eta_{+-}| = (2.232 \pm 0.011) \times 10^{-3}, \quad (13.55b)$$

$$|\eta_{00}/\eta_{+-}| = 0.9950 \pm 0.0007, \quad (13.55c)$$

where the phase  $\phi_{ij}$  of the amplitude ratio  $\eta_{ij}$  has been determined both assuming  $CPT$  invariance:

$$\phi_{00} = (43.52 \pm 0.05)^\circ, \quad \phi_{+-} = (43.51 \pm 0.05)^\circ, \quad (13.56)$$

and without assuming  $CPT$  invariance:

$$\phi_{00} = (43.7 \pm 0.6)^\circ, \quad \phi_{+-} = (43.4 \pm 0.5)^\circ. \quad (13.57)$$

$CP$  violation has also been observed in semileptonic  $K_L$  decays [27]

$$\delta_L = (3.32 \pm 0.06) \times 10^{-3}, \quad (13.58)$$

where  $\delta_L$  is a weighted average of muon and electron measurements, as well as in  $K_L$  decays to  $\pi^+\pi^-\gamma$  and  $\pi^+\pi^-e^+e^-$  [27].  $CP$  violation in  $K \rightarrow 3\pi$  decays has not yet been observed [27,40].

Historically,  $CP$  violation in neutral  $K$  decays has been described in terms of the complex parameters  $\epsilon$  and  $\epsilon'$ . The observables  $\eta_{00}$ ,  $\eta_{+-}$ , and  $\delta_L$  are related to these parameters, and to

those of Section 13.1, by

$$\eta_{00} = \frac{1 - \lambda_{\pi^0\pi^0}}{1 + \lambda_{\pi^0\pi^0}} = \epsilon - 2\epsilon', \quad (13.59a)$$

$$\eta_{+-} = \frac{1 - \lambda_{\pi^+\pi^-}}{1 + \lambda_{\pi^+\pi^-}} = \epsilon + \epsilon', \quad (13.59b)$$

$$\delta_L = \frac{1 - |q/p|^2}{1 + |q/p|^2} = \frac{2\mathcal{R}e(\epsilon)}{1 + |\epsilon|^2}, \quad (13.59c)$$

where, in the last line, we have assumed that  $|A_{\ell^+\nu_\ell\pi^-}| = |\bar{A}_{\ell^-\bar{\nu}_\ell\pi^+}|$  and  $|A_{\ell^-\bar{\nu}_\ell\pi^+}| = |\bar{A}_{\ell^+\nu_\ell\pi^-}| = 0$ . (The convention-dependent parameter  $\tilde{\epsilon} \equiv (1 - q/p)/(1 + q/p)$ , sometimes used in the literature, is, in general, different from  $\epsilon$  but yields a similar expression,  $\delta_L = 2\mathcal{R}e(\tilde{\epsilon})/(1 + |\tilde{\epsilon}|^2)$ .) A fit to the  $K \rightarrow \pi\pi$  data yields [27]

$$|\epsilon| = (2.228 \pm 0.011) \times 10^{-3}, \quad (13.60a)$$

$$\mathcal{R}e(\epsilon'/\epsilon) = (1.66 \pm 0.23) \times 10^{-3}. \quad (13.60b)$$

In discussing two-pion final states, it is useful to express the amplitudes  $A_{\pi^0\pi^0}$  and  $A_{\pi^+\pi^-}$  in terms of their isospin components via

$$A_{\pi^0\pi^0} = \sqrt{\frac{1}{3}} |A_0| e^{i(\delta_0 + \phi_0)} - \sqrt{\frac{2}{3}} |A_2| e^{i(\delta_2 + \phi_2)}, \quad (13.61a)$$

$$A_{\pi^+\pi^-} = \sqrt{\frac{2}{3}} |A_0| e^{i(\delta_0 + \phi_0)} + \sqrt{\frac{1}{3}} |A_2| e^{i(\delta_2 + \phi_2)}, \quad (13.61b)$$

where we parameterize the amplitude  $A_I(\bar{A}_I)$  for  $K^0(\bar{K}^0)$  decay into two pions with total isospin  $I = 0$  or  $2$  as

$$A_I \equiv \langle (\pi\pi)_I | \mathcal{H} | K^0 \rangle = |A_I| e^{i(\delta_I + \phi_I)}, \quad (13.62a)$$

$$\bar{A}_I \equiv \langle (\pi\pi)_I | \mathcal{H} | \bar{K}^0 \rangle = |\bar{A}_I| e^{i(\delta_I - \phi_I)}. \quad (13.62b)$$

The smallness of  $|\eta_{00}|$  and  $|\eta_{+-}|$  allows us to approximate

$$\epsilon \simeq \frac{1}{2}(1 - \lambda_{(\pi\pi)_{I=0}}), \quad \epsilon' \simeq \frac{1}{6}(\lambda_{\pi^0\pi^0} - \lambda_{\pi^+\pi^-}). \quad (13.63)$$

The parameter  $\epsilon$  represents indirect  $CP$  violation, while  $\epsilon'$  parameterizes direct  $CP$  violation:  $\mathcal{R}e(\epsilon')$  measures  $CP$  violation in decay (type I),  $\mathcal{R}e(\epsilon)$  measures  $CP$  violation in mixing (type II), and  $\mathcal{I}m(\epsilon)$  and  $\mathcal{I}m(\epsilon')$  measure the interference between decays with and without mixing (type III).

The following expressions for  $\epsilon$  and  $\epsilon'$  are useful for theoretical evaluations:

$$\epsilon \simeq \frac{e^{i\pi/4} \mathcal{I}m(\mathbf{M}_{12})}{\sqrt{2} \Delta m}, \quad \epsilon' = \frac{i}{\sqrt{2}} \left| \frac{A_2}{A_0} \right| e^{i(\delta_2 - \delta_0)} \sin(\phi_2 - \phi_0). \quad (13.64)$$

The expression for  $\epsilon$  is only valid in a phase convention where  $\phi_2 = 0$ , corresponding to a real  $V_{ud}V_{us}^*$ , and in the approximation that also  $\phi_0 = 0$ . The phase of  $\epsilon$ ,  $\arg(\epsilon) \approx \arctan(-2\Delta m/\Delta\Gamma)$ , is determined by non-perturbative QCD dynamics and is experimentally determined to be about  $\pi/4$ . The calculation of  $\epsilon$  benefits from the fact that  $\mathcal{I}m(\mathbf{M}_{12})$  is dominated by short distance physics. Consequently, the main sources of uncertainty in theoretical interpretations of  $\epsilon$  are the values of matrix elements, such as  $\langle K^0 | (\bar{s}d)_{V-A}(\bar{s}d)_{V-A} | \bar{K}^0 \rangle$ . The expression for  $\epsilon'$  is valid to first order in  $|A_2/A_0| \sim 1/20$ . The phase of  $\epsilon'$  is experimentally determined,  $\pi/2 + \delta_2 - \delta_0 \approx \pi/4$ , and is independent of the electroweak model. Note that, accidentally,  $\epsilon'/\epsilon$  is real to a good approximation. Determination of weak phase information from the measurement of  $\mathcal{R}e(\epsilon'/\epsilon)$  given in Eq. (13.60) has until now been precluded by uncertainties in the hadronic parameters, but recent advances in lattice QCD calculations [41, 42] suggest that it may become possible [43].

A future measurement of much interest is that of  $CP$  violation in the rare  $K \rightarrow \pi\nu\bar{\nu}$  decays. The signal for  $CP$  violation is simply observing the  $K_L \rightarrow \pi^0\nu\bar{\nu}$  decay. The effect here is that

of interference between decays with and without mixing (type III) [44]:

$$\frac{\Gamma(K_L \rightarrow \pi^0 \nu \bar{\nu})}{\Gamma(K^+ \rightarrow \pi^+ \nu \bar{\nu})} = \frac{1}{2} [1 + |\lambda_{\pi \nu \bar{\nu}}|^2 - 2 \mathcal{R}e(\lambda_{\pi \nu \bar{\nu}})] \quad (13.65)$$

$$\simeq 1 - \mathcal{R}e(\lambda_{\pi \nu \bar{\nu}}),$$

where in the last equation we neglect  $CP$  violation in decay and in mixing (expected, model-independently, to be of order  $10^{-5}$  and  $10^{-3}$ , respectively). Such a measurement is experimentally very challenging but would be theoretically very rewarding [45]. Similar to the  $CP$  asymmetry in  $B^0 \rightarrow J/\psi K_S$ , the  $CP$  violation in  $K \rightarrow \pi \nu \bar{\nu}$  decay is predicted to be large (that is, the ratio in Eq. (13.65) is neither CKM- nor loop-suppressed) and can be very cleanly interpreted.

Within the Standard Model, the  $K_L \rightarrow \pi^0 \nu \bar{\nu}$  decay is dominated by an intermediate top quark contribution and, consequently, can be interpreted in terms of CKM parameters [46]. (For the charged mode,  $K^+ \rightarrow \pi^+ \nu \bar{\nu}$ , the contribution from an intermediate charm quark is not negligible, and constitutes a source of hadronic uncertainty.) In particular,  $\mathcal{B}(K_L \rightarrow \pi^0 \nu \bar{\nu})$  provides a theoretically clean way to determine the Wolfenstein parameter  $\eta$  [47]:

$$\mathcal{B}(K_L \rightarrow \pi^0 \nu \bar{\nu}) = \kappa_L [X(m_t^2/m_W^2)]^2 A^4 \eta^2, \quad (13.66)$$

where the hadronic parameter  $\kappa_L \sim 2 \times 10^{-10}$  incorporates the value of the four-fermion matrix element which is deduced, using isospin relations, from  $\mathcal{B}(K^+ \rightarrow \pi^0 e^+ \nu_e)$ , and  $X(m_t^2/m_W^2)$  is a known function of the top mass. An explicit calculation gives  $\mathcal{B}(K_L \rightarrow \pi^0 \nu \bar{\nu}) = (3.00 \pm 0.30) \times 10^{-11}$  [48].

The currently tightest experimental limit is  $\mathcal{B}(K_L \rightarrow \pi^0 \nu \bar{\nu}) < 3.0 \times 10^{-9}$  [49], which does not yet reach the bound that can be derived from Eq. (13.65),  $\mathcal{B}(K_L \rightarrow \pi^0 \nu \bar{\nu}) < 4.4 \times \mathcal{B}(K^+ \rightarrow \pi^+ \nu \bar{\nu})$  [44]. Significant further progress is anticipated from experiments searching for  $K \rightarrow \pi \nu \bar{\nu}$  decays in the next few years [50,51].

### 13.5 Charm

The existence of  $D^0-\bar{D}^0$  mixing is well established [52–55], with the latest experimental constraints giving [29, 56]  $x \equiv \Delta m/\Gamma = (0.39_{-0.12}^{+0.11}) \times 10^{-2}$  and  $y \equiv \Delta\Gamma/(2\Gamma) = (0.65_{-0.07}^{+0.06}) \times 10^{-2}$ . Thus, the data clearly show that  $y \neq 0$ , but improved measurements are needed to be sure of the size of  $x$ . Long-distance contributions make it difficult to calculate Standard Model predictions for the  $D^0-\bar{D}^0$  mixing parameters. Therefore, the goal of the search for  $D^0-\bar{D}^0$  mixing is not to constrain the CKM parameters, but rather to probe new physics. Here  $CP$  violation plays an important role. Within the Standard Model, the  $CP$ -violating effects are predicted to be small, since the mixing and the relevant decays are described, to an excellent approximation, by the physics of the first two generations only. The expectation is that the Standard Model size of  $CP$  violation in  $D$  decays is  $\mathcal{O}(10^{-3})$  or less. At present, the most sensitive searches involve the  $D^0 \rightarrow K^+ K^-$ ,  $D^0 \rightarrow \pi^+ \pi^-$  and  $D^0 \rightarrow K^\pm \pi^\mp$  modes.

The neutral  $D$  mesons decay via a singly-Cabibbo-suppressed transition to the  $CP$  eigenstates  $K^+ K^-$  and  $\pi^+ \pi^-$ . These decays are dominated by Standard-Model tree diagrams. Thus, we can write, for  $f = K^+ K^-$  or  $\pi^+ \pi^-$ ,

$$A_f = A_f^T e^{+i\phi_f^T} [1 + r_f e^{i(\delta_f + \phi_f)}], \quad (13.67a)$$

$$\bar{A}_f = A_f^T e^{-i\phi_f^T} [1 + r_f e^{i(\delta_f - \phi_f)}], \quad (13.67b)$$

where  $A_f^T e^{\pm i\phi_f^T}$  is the Standard Model tree-level contribution,  $\phi_f^T$  and  $\phi_f$  are weak,  $CP$  violating phases,  $\delta_f$  is a strong phase difference, and  $r_f$  is the ratio between a subleading ( $r_f \ll 1$ ) contribution with a weak phase different from  $\phi_f^T$  and the Standard Model tree-level contribution. Neglecting  $r_f$ ,  $\lambda_f$  is universal, and we can define an observable phase  $\phi_D$  via

$$\lambda_f \equiv -|q/p| e^{i\phi_D}. \quad (13.68)$$

(In the limit of  $CP$  conservation, choosing  $\phi_D = 0$  is equivalent to defining the mass eigenstates by their  $CP$  eigenvalue:  $|D_\mp\rangle =$

$p|D^0\rangle \pm q|\bar{D}^0\rangle$ , with  $D_-$  ( $D_+$ ) being the  $CP$ -odd ( $CP$ -even) state; that is, the state that does not (does) decay into  $K^+ K^-$ .)

We define the time integrated  $CP$  asymmetry for a final  $CP$  eigenstate  $f$  as follows:

$$a_f \equiv \frac{\int_0^\infty \Gamma(D_{\text{phys}}^0(t) \rightarrow f) dt - \int_0^\infty \Gamma(\bar{D}_{\text{phys}}^0(t) \rightarrow f) dt}{\int_0^\infty \Gamma(D_{\text{phys}}^0(t) \rightarrow f) dt + \int_0^\infty \Gamma(\bar{D}_{\text{phys}}^0(t) \rightarrow f) dt}. \quad (13.69)$$

(This expression corresponds to the  $D$  meson being tagged at production, hence the integration goes from 0 to  $+\infty$ ; measurements are also possible with  $\psi(3770) \rightarrow D^0 \bar{D}^0$ , in which case the integration goes from  $-\infty$  to  $+\infty$  giving slightly different results; see the discussion in Section 13.1.3.) We take  $x, y, r_f \ll 1$  and expand to leading order in these parameters. We can then separate the contribution to  $a_f$  into three parts [57],

$$a_f = a_f^d + a_f^m + a_f^i, \quad (13.70)$$

with the following underlying mechanisms:

1.  $a_f^d$  signals  $CP$  violation in decay (similar to Eq. (13.35)):

$$a_f^d = 2r_f \sin \phi_f \sin \delta_f. \quad (13.71)$$

2.  $a_f^m$  signals  $CP$  violation in mixing (similar to Eq. (13.44)).

With our approximations, it is universal:

$$a^m = -\frac{y}{2} \left( \left| \frac{q}{p} \right| - \left| \frac{p}{q} \right| \right) \cos \phi_D. \quad (13.72)$$

3.  $a_f^i$  signals  $CP$  violation in the interference of mixing and decay (similar to Eq. (13.45)). With our approximations, it is universal:

$$a^i = \frac{x}{2} \left( \left| \frac{q}{p} \right| + \left| \frac{p}{q} \right| \right) \sin \phi_D. \quad (13.73)$$

One can isolate the effects of direct  $CP$  violation by taking the difference between the  $CP$  asymmetries in the  $K^+ K^-$  and  $\pi^+ \pi^-$  modes:

$$\Delta a_{CP} \equiv a_{K^+ K^-} - a_{\pi^+ \pi^-} = a_{K^+ K^-}^d - a_{\pi^+ \pi^-}^d, \quad (13.74)$$

where we neglected a residual, experiment-dependent, contribution from indirect  $CP$  violation due to the fact that there may be a decay time-dependent acceptance function that can be different for the  $K^+ K^-$  and  $\pi^+ \pi^-$  channels. The current average gives [29]:

$$a_{K^+ K^-}^d - a_{\pi^+ \pi^-}^d = (-0.164 \pm 0.028) \times 10^{-3}, \quad (13.75)$$

demonstrating  $CP$  violation in charm decay.

One can also isolate the effects of indirect  $CP$  violation in the following way. Consider the time-dependent decay rates in Eq. (13.31a) and Eq. (13.31b). The mixing processes modify the time dependence from a pure exponential. However, given the small values of  $x$  and  $y$ , the time dependences can be recast, to a good approximation, into purely exponential form, but with modified decay-rate parameters [58,59] (given here for the  $K^+ K^-$  final state):

$$\Gamma_{D^0 \rightarrow K^+ K^-} = \Gamma \times [1 + |q/p| (y \cos \phi_D - x \sin \phi_D)], \quad (13.76a)$$

$$\Gamma_{\bar{D}^0 \rightarrow K^+ K^-} = \Gamma \times [1 + |p/q| (y \cos \phi_D + x \sin \phi_D)]. \quad (13.76b)$$

One can define  $CP$ -conserving and  $CP$ -violating combinations of these two observables (normalized to the true width  $\Gamma$ ):

$$y_{CP} \equiv \frac{\Gamma_{\bar{D}^0 \rightarrow K^+ K^-} + \Gamma_{D^0 \rightarrow K^+ K^-}}{2\Gamma} - 1$$

$$= (y/2) (|q/p| + |p/q|) \cos \phi_D - (x/2) (|q/p| - |p/q|) \sin \phi_D, \quad (13.77a)$$

$$A_\Gamma \equiv \frac{\Gamma_{D^0 \rightarrow K^+ K^-} - \Gamma_{\bar{D}^0 \rightarrow K^+ K^-}}{2\Gamma}$$

$$= -(a^m + a^i). \quad (13.77b)$$

In the limit of  $CP$  conservation (and, in particular, within the Standard Model),  $y_{CP} = (\Gamma_+ - \Gamma_-)/2\Gamma = y$  (where  $\Gamma_+(\Gamma_-)$  is the decay width of the  $CP$ -even (-odd) mass eigenstate) and  $A_\Gamma = 0$ . Indeed, present measurements imply that  $CP$  violation is small [29],

$$y_{CP} = (+0.72 \pm 0.11) \times 10^{-2}, \quad (13.78a)$$

$$A_\Gamma = (-0.032 \pm 0.026) \times 10^{-2}. \quad (13.78b)$$

The  $K^\pm\pi^\mp$  states are not  $CP$  eigenstates, but they are still common final states for  $D^0$  and  $\bar{D}^0$  decays. Since  $D^0(\bar{D}^0) \rightarrow K^-\pi^+$  is a Cabibbo-favored (doubly-Cabibbo-suppressed) process, these processes are particularly sensitive to  $x$  and/or  $y = \mathcal{O}(\lambda^2)$ . Taking into account that  $|\lambda_{K^-\pi^+}|, |\lambda_{K^+\pi^-}^{-1}| \ll 1$  and  $x, y \ll 1$ , assuming that there is no direct  $CP$  violation (these are Standard Model tree-level decays dominated by a single weak phase, and there is no contribution from penguin-like and chromomagnetic operators), and expanding the time-dependent rates for  $xt, yt \lesssim \Gamma^{-1}$ , one obtains

$$\begin{aligned} \Gamma[D_{\text{phys}}^0(t) \rightarrow K^+\pi^-] &= e^{-\Gamma t} |\bar{A}_{K^-\pi^+}|^2 \\ &\times \left[ r_d^2 + r_d \left| \frac{q}{p} \right| (y' \cos \phi_D - x' \sin \phi_D) \Gamma t + \left| \frac{q}{p} \right|^2 \frac{y^2 + x^2}{4} (\Gamma t)^2 \right], \end{aligned} \quad (13.79a)$$

$$\begin{aligned} \Gamma[\bar{D}_{\text{phys}}^0(t) \rightarrow K^-\pi^+] &= e^{-\Gamma t} |\bar{A}_{K^-\pi^+}|^2 \\ &\times \left[ r_d^2 + r_d \left| \frac{p}{q} \right| (y' \cos \phi_D + x' \sin \phi_D) \Gamma t + \left| \frac{p}{q} \right|^2 \frac{y^2 + x^2}{4} (\Gamma t)^2 \right], \end{aligned} \quad (13.79b)$$

where

$$y' \equiv y \cos \delta - x \sin \delta \quad \text{and} \quad x' \equiv x \cos \delta + y \sin \delta. \quad (13.80)$$

The weak phase  $\phi_D$  is the same as that of Eq. (13.68) (a consequence of neglecting direct  $CP$  violation) and  $r_d = \mathcal{O}(\tan^2 \theta_c)$  is the amplitude ratio,  $r_d = |\bar{A}_{K^-\pi^+}/A_{K^-\pi^+}| = |A_{K^+\pi^-}/\bar{A}_{K^+\pi^-}|$ , that is,  $\lambda_{K^-\pi^+} = r_d |q/p| e^{-i(\delta - \phi_D)}$  and  $\lambda_{K^+\pi^-}^{-1} = r_d |p/q| e^{-i(\delta + \phi_D)}$ . The parameter  $\delta$  is a strong-phase difference for these processes, that can be obtained from measurements of quantum correlated  $\psi(3770) \rightarrow D^0 \bar{D}^0$  decays [60,61]. By fitting to the six coefficients of the various time-dependences, one can determine  $r_d, |q/p|, (x^2 + y^2), y' \cos \phi_D$ , and  $x' \sin \phi_D$ . In particular, finding  $CP$  violation ( $|q/p| \neq 1$  and/or  $\sin \phi_D \neq 0$ ) at a level much higher than  $10^{-3}$  would constitute evidence for new physics. The most stringent constraints to date on  $CP$  violation in charm mixing have been obtained with this method [62] and from the  $A_\Gamma$  measurement [63].

A fit to all data [29], including also results from time-dependent analyses of  $D^0 \rightarrow K_S \pi^+ \pi^-$  decays, from which  $x, y, |q/p|$  and  $\phi_D$  can be determined directly, yields no evidence for indirect  $CP$  violation:

$$1 - |q/p| = +0.031_{-0.050}^{+0.045}, \quad (13.81a)$$

$$\phi_D = (-3.9_{-4.6}^{+4.5})^\circ. \quad (13.81b)$$

With the additional assumption of no direct  $CP$  violation in doubly-Cabibbo-suppressed  $D$  decays [64–66], tighter constraints are obtained:

$$1 - |q/p| = +0.002 \pm 0.008, \quad (13.82a)$$

$$\phi_D = (+0.08 \pm 0.31)^\circ. \quad (13.82b)$$

More details on various theoretical and experimental aspects of  $D^0\text{--}\bar{D}^0$  mixing can be found in Ref. [31].

Searches for  $CP$  violation in charged  $D_{(s)}$  decays have been performed in many modes. Searches in decays mediated by Cabibbo-suppressed amplitudes are particularly interesting, since in other channels effects are likely to be too small to be observable in current experiments. Examples of relevant two-body modes are  $D^+ \rightarrow \pi^+\pi^0, K_S K^+, \phi\pi^+$  and  $D_s^+ \rightarrow K^+\pi^0, K_S \pi^+, \phi K^+$ . The

most precise results are  $\mathcal{A}_{D^+ \rightarrow K_S K^+} = +0.0011 \pm 0.0017$  and  $\mathcal{A}_{D_s^+ \rightarrow K_S \pi^+} = +0.0038 \pm 0.0048$  [29]. The precision of experiments is now sufficient that the effect from  $CP$  violation in the neutral kaon system can be seen in  $D^+ \rightarrow K_S \pi^+$  decays [67,68].

Three- and four-body final states provide additional possibilities to search for  $CP$  violation, since effects may vary over the phase-space [69]. A number of methods have been proposed to exploit this feature and search for  $CP$  violation in ways that do not require modelling of the decay distribution [70–73]. Such methods are useful for analysis of charm decays since they are less sensitive to biases from production asymmetries, and are well suited to address the issue of whether or not  $CP$  violation effects are present. They can also be applied to tagged neutral  $D$  meson as well as to charged  $D_{(s)}$  decays (flavor tagging is typically achieved from the charge of the pion produced in  $D^{*+} \rightarrow D^0 \pi^+$  decays). The results of all searches to date are consistent with the absence of  $CP$  violation, with the most significant hint at the level of  $2.7\sigma$  [74].

## 13.6 Beauty

### 13.6.1 CP violation in mixing of $B^0$ and $B_s^0$ mesons

The upper bound on the  $CP$  asymmetry in semileptonic  $B$  decays [28] implies that  $CP$  violation in  $B^0\text{--}\bar{B}^0$  mixing is a small effect (we use  $\mathcal{A}_{\text{SL}}/2 \approx 1 - |q/p|$ , see Eq. (13.37)):

$$\mathcal{A}_{\text{SL}}^d = (-2.1 \pm 1.7) \times 10^{-3} \implies |q/p| = 1.0010 \pm 0.0008. \quad (13.83)$$

The Standard Model prediction is

$$\mathcal{A}_{\text{SL}}^d = \mathcal{O}[(m_c^2/m_t^2) \sin \beta] \lesssim 0.001. \quad (13.84)$$

An explicit calculation gives  $(-4.7 \pm 0.6) \times 10^{-4}$  [34].

The experimental constraint on  $CP$  violation in  $B_s^0\text{--}\bar{B}_s^0$  mixing is somewhat weaker than that in the  $B^0\text{--}\bar{B}^0$  system [28]

$$\mathcal{A}_{\text{SL}}^s = (-0.6 \pm 2.8) \times 10^{-3} \implies |q/p| = 1.0003 \pm 0.0014. \quad (13.85)$$

The Standard Model prediction is  $\mathcal{A}_{\text{SL}}^s = \mathcal{O}[(m_c^2/m_t^2) \sin \beta_s] \lesssim 10^{-4}$ , with an explicit calculation giving  $(2.22 \pm 0.27) \times 10^{-5}$  [34].

The fit to experimental data that results in the averages quoted above has a  $\chi^2$  probability of 4.5% indicating some tension between the different measurements [29]. This originates in part from a result from the D0 collaboration for the inclusive same-sign dimuon asymmetry that deviates from the Standard Model prediction by  $3.6\sigma$  [75]. As yet, this has not been confirmed by independent studies.

In models where  $\Gamma_{12}/\mathbf{M}_{12}$  is approximately real, such as the Standard Model, an upper bound on  $\Delta\Gamma/\Delta m \approx \mathcal{R}e(\Gamma_{12}/\mathbf{M}_{12})$  provides yet another upper bound on the deviation of  $|q/p|$  from one. This constraint does not hold if  $\Gamma_{12}/\mathbf{M}_{12}$  is approximately imaginary. (An alternative parameterization uses  $q/p = (1 - \bar{\epsilon}_B)/(1 + \bar{\epsilon}_B)$ , leading to  $\mathcal{A}_{\text{SL}} \simeq 4\mathcal{R}e(\bar{\epsilon}_B)$ .)

### 13.6.2 CP violation in interference of $B^0$ decays with and without mixing

The small deviation (less than one percent) of  $|q/p|$  from 1 implies that, at the present level of experimental precision,  $CP$  violation in  $B^0$  mixing is a negligible effect. Thus, for the purpose of analyzing  $CP$  asymmetries in hadronic  $B^0$  decays, we can use

$$\lambda_f = e^{-i\phi_{M(B^0)}} (\bar{A}_f/A_f), \quad (13.86)$$

where  $\phi_{M(B^0)}$  refers to the phase of  $\mathbf{M}_{12}$  appearing in Eq. (13.42) that is appropriate for  $B^0\text{--}\bar{B}^0$  oscillations. Within the Standard Model, the corresponding phase factor is given by

$$e^{-i\phi_{M(B^0)}} = (V_{tb}^* V_{td}) / (V_{tb} V_{td}^*). \quad (13.87)$$

The class of  $CP$  violation effects in interference between mixing and decay is studied with final states that are common to  $B^0$  and  $\bar{B}^0$  decays [76–78]. It is convenient to rewrite Eq. (13.40) for  $B^0$  decays as [79–81]

$$\mathcal{A}_f(t) = S_f \sin(\Delta m t) - C_f \cos(\Delta m t), \quad (13.88)$$

$$S_f \equiv \frac{2\text{Im}(\lambda_f)}{1 + |\lambda_f|^2}, \quad C_f \equiv \frac{1 - |\lambda_f|^2}{1 + |\lambda_f|^2}, \quad (13.89)$$

where we assume that  $\Delta\Gamma = 0$  and  $|q/p| = 1$ . An alternative notation in use is  $A_f \equiv -C_f$  – this  $A_f$  should not be confused with the  $A_f$  of Eq. (13.15), but in the limit that  $|q/p| = 1$  is equivalent with the  $A_f$  of Eq. (13.35).

A large class of interesting processes proceed via quark transitions of the form  $\bar{b} \rightarrow \bar{q}q\bar{q}'$  with  $q' = s$  or  $d$ . For  $q = c$  or  $u$ , there are contributions from both tree ( $t$ ) and penguin ( $p^{qu}$ , where  $q_u = u, c, t$  is the quark in the loop) diagrams (see Fig. 13.2) which carry different weak phases:

$$A_f = (V_{qb}^* V_{qq'}) t_f + \sum_{q_u=u,c,t} (V_{q_u b}^* V_{q_u q'}) p_f^{q_u}. \quad (13.90)$$

(The distinction between tree and penguin contributions is a heuristic one; the separation by the operator that enters is more precise. A more detailed discussion of the operator product expansion approach, which also includes higher order QCD corrections, can be found in Ref. [82] for example.) Using CKM unitarity, these decay amplitudes can always be written in terms of just two CKM combinations. For example, for  $f = \pi\pi$ , which proceeds via a  $\bar{b} \rightarrow \bar{u}u\bar{d}$  transition, we can write

$$A_{\pi\pi} = (V_{ub}^* V_{ud}) T_{\pi\pi} + (V_{tb}^* V_{td}) P_{\pi\pi}^t, \quad (13.91)$$

where  $T_{\pi\pi} = t_{\pi\pi} + p_{\pi\pi}^u - p_{\pi\pi}^c$  and  $P_{\pi\pi}^t = p_{\pi\pi}^t - p_{\pi\pi}^c$ .  $CP$ -violating phases in Eq. (13.91) appear only in the CKM elements, so that

$$\frac{\bar{A}_{\pi\pi}}{A_{\pi\pi}} = \frac{(V_{ub} V_{ud}^*) T_{\pi\pi} + (V_{tb} V_{td}^*) P_{\pi\pi}^t}{(V_{ub}^* V_{ud}) T_{\pi\pi} + (V_{tb}^* V_{td}) P_{\pi\pi}^t}. \quad (13.92)$$

For  $f = J/\psi K$ , which proceeds via a  $\bar{b} \rightarrow \bar{c}c\bar{s}$  transition, we can write

$$A_{\psi K} = (V_{cb}^* V_{cs}) T_{\psi K} + (V_{ub}^* V_{us}) P_{\psi K}^u, \quad (13.93)$$

where  $T_{\psi K} = t_{\psi K} + p_{\psi K}^c - p_{\psi K}^t$  and  $P_{\psi K}^u = p_{\psi K}^u - p_{\psi K}^t$ . A subtlety arises in this decay that is related to the fact that  $B^0$  decays into a final  $J/\psi K^0$  state while  $\bar{B}^0$  decays into a final  $J/\psi \bar{K}^0$  state. A common final state, *e.g.*,  $J/\psi K_S$ , is reached only via  $K^0$ – $\bar{K}^0$  mixing. Consequently, the phase factor (defined in Eq. (13.42)) corresponding to neutral  $K$  mixing,  $e^{-i\phi_M(K)} = (V_{cd}^* V_{cs}) / (V_{cd} V_{cs}^*)$ , plays a role:

$$\frac{\bar{A}_{\psi K_S}}{A_{\psi K_S}} = - \frac{(V_{cb} V_{cs}^*) T_{\psi K} + (V_{ub} V_{us}^*) P_{\psi K}^u}{(V_{cb}^* V_{cs}) T_{\psi K} + (V_{ub}^* V_{us}) P_{\psi K}^u} \times \frac{V_{cd}^* V_{cs}}{V_{cd} V_{cs}^*}. \quad (13.94)$$

For  $q = s$  or  $d$ , there are only penguin contributions to  $A_f$ , that is,  $t_f = 0$  in Eq. (13.90). (The tree  $\bar{b} \rightarrow \bar{u}u\bar{q}'$  transition followed by  $\bar{u}u \rightarrow \bar{q}q$  rescattering is included below in the  $P^u$  terms.) Again, CKM unitarity allows us to write  $A_f$  in terms of two CKM combinations. For example, for  $f = \phi K_S$ , which proceeds via a  $\bar{b} \rightarrow \bar{s}s\bar{s}$  transition, we can write

$$\frac{\bar{A}_{\phi K_S}}{A_{\phi K_S}} = - \frac{(V_{cb} V_{cs}^*) P_{\phi K}^c + (V_{ub} V_{us}^*) P_{\phi K}^u}{(V_{cb}^* V_{cs}) P_{\phi K}^c + (V_{ub}^* V_{us}) P_{\phi K}^u} \times \frac{V_{cd}^* V_{cs}}{V_{cd} V_{cs}^*}, \quad (13.95)$$

where  $P_{\phi K}^c = p_{\phi K}^c - p_{\phi K}^t$  and  $P_{\phi K}^u = p_{\phi K}^u - p_{\phi K}^t$ .

Since in general the amplitude  $A_f$  involves two different weak phases, the corresponding decays can exhibit both  $CP$  violation in the interference of decays with and without mixing,  $S_f \neq 0$ , and  $CP$  violation in decay,  $C_f \neq 0$ . (At the present level of experimental precision, the contribution to  $C_f$  from  $CP$  violation in mixing is negligible, see Eq. (13.83).) If the contribution from a second weak phase is suppressed, then the interpretation of  $S_f$  in terms of Lagrangian  $CP$ -violating parameters is clean, while  $C_f$  is small. If such a second contribution is not suppressed,  $S_f$  depends on hadronic parameters and, if the relevant strong phase difference is large,  $C_f$  is large.

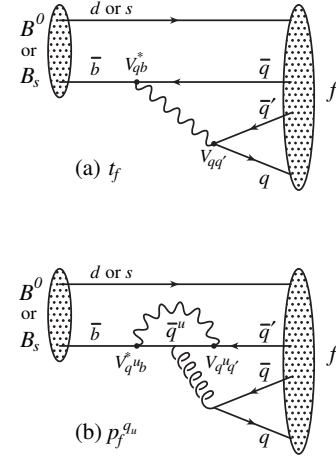


Figure 13.2: Feynman diagrams for (a) tree and (b) penguin amplitudes contributing to  $B^0 \rightarrow f$  or  $B_s^0 \rightarrow f$  via a  $\bar{b} \rightarrow \bar{q}q\bar{q}'$  quark-level process.

A summary of  $\bar{b} \rightarrow \bar{q}q\bar{q}'$  modes with  $q' = s$  or  $d$  is given in Table 13.1. The  $\bar{b} \rightarrow \bar{d}d\bar{q}$  transitions lead to final states that are similar to those from  $\bar{b} \rightarrow \bar{u}u\bar{q}$  transitions and have similar phase dependence. Final states that consist of two vector mesons ( $\psi\phi$  and  $\phi\phi$ ) are not  $CP$  eigenstates, and angular analysis is needed to separate the  $CP$ -even from the  $CP$ -odd contributions.

The cleanliness of the theoretical interpretation of  $S_f$  can be assessed from the information in the last column of Table 13.1. In case of small uncertainties, the expression for  $S_f$  in terms of CKM phases can be deduced from the fourth column of Table 13.1 in combination with Eq. (13.87) (and, for  $b \rightarrow q\bar{q}s$  decays, the example in Eq. (13.94)). Here we consider several interesting examples.

For  $B^0 \rightarrow J/\psi K_S$  and other  $\bar{b} \rightarrow \bar{c}c\bar{s}$  processes, we can neglect the  $P^u$  contribution to  $A_f$ , in the Standard Model, to an approximation that is better than one percent, giving:

$$\lambda_{\psi K_S} = -e^{-2i\beta} \Rightarrow S_{\psi K_S} = \sin 2\beta, \quad C_{\psi K_S} = 0. \quad (13.96)$$

It is important to verify experimentally the level of suppression of the penguin contribution. Methods based on flavor symmetries [83–86] allow limits to be obtained. All are currently consistent with the  $P^u$  term being negligible. Explicit calculations [86–89] also support this conclusion.

In the presence of new physics,  $A_f$  is still likely to be dominated by the  $T$  term, but the mixing amplitude might be modified. We learn that, model-independently,  $C_f \approx 0$  while  $S_f$  cleanly determines the mixing phase ( $\phi_M - 2\arg(V_{cb} V_{cd}^*)$ ). The experimental measurement [29],  $S_{\psi K} = +0.699 \pm 0.017$ , gave the first precision test of the Kobayashi-Maskawa mechanism, and its consistency with the predictions for  $\sin 2\beta$  makes it very likely that this mechanism is indeed the dominant source of  $CP$  violation in the quark sector.

For  $B^0 \rightarrow \phi K_S$  and other  $\bar{b} \rightarrow \bar{s}s\bar{s}$  processes (as well as some  $\bar{b} \rightarrow \bar{u}u\bar{s}$  processes), we can neglect the subdominant contributions, in the Standard Model, to an approximation that is good to the order of a few percent:

$$\lambda_{\phi K_S} = -e^{-2i\beta} \Rightarrow S_{\phi K_S} = \sin 2\beta, \quad C_{\phi K_S} = 0. \quad (13.97)$$

A review of explicit calculations of the effects of subleading amplitudes can be found in Ref. [90]. In the presence of new physics, both  $A_f$  and  $M_{12}$  can have contributions that are comparable in size to those of the Standard Model and carry new weak phases. Such a situation gives several interesting consequences for penguin-dominated  $\bar{b} \rightarrow \bar{q}q\bar{s}$  decays ( $q = u, d, s$ ) to a final state  $f$ :

1. The value of  $-\eta_f S_f$  may be different from  $S_{\psi K_S}$  by more than a few percent, where  $\eta_f$  is the  $CP$  eigenvalue of the final state.



**Table 13.1:** Summary of  $\bar{b} \rightarrow \bar{q}q\bar{q}'$  modes with  $q' = s$  or  $d$ . The second and third columns give examples of hadronic final states (usually those which are experimentally most convenient to study). The fourth column gives the CKM dependence of the amplitude  $A_f$ , using the notation of Eqs. ((13.91), (13.93), (13.95)), with the dominant term first and the subdominant second. The suppression factor of the second term compared to the first is given in the last column. “Loop” refers to a penguin versus tree-suppression factor (it is mode-dependent and roughly  $\mathcal{O}(0.2 - 0.3)$ ) and  $\lambda \simeq 0.23$  is the expansion parameter of Eq. (13.48).

$\bar{b} \rightarrow \bar{q}q\bar{q}'$	$B^0 \rightarrow f$	$B_s^0 \rightarrow f$	CKM dependence of $A_f$	Suppression
$\bar{b} \rightarrow \bar{c}c\bar{s}$	$\psi K_S$	$\psi\phi$	$(V_{cb}^* V_{cs})T + (V_{ub}^* V_{us})P^u$	loop $\times \lambda^2$
$\bar{b} \rightarrow \bar{s}s\bar{s}$	$\phi K_S$	$\phi\phi$	$(V_{cb}^* V_{cs})P^c + (V_{ub}^* V_{us})P^u$	$\lambda^2$
$\bar{b} \rightarrow \bar{u}u\bar{s}$	$\pi^0 K_S$	$K^+ K^-$	$(V_{cb}^* V_{cs})P^c + (V_{ub}^* V_{us})T$	$\lambda^2/\text{loop}$
$\bar{b} \rightarrow \bar{c}c\bar{d}$	$D^+ D^-$	$\psi K_S$	$(V_{cb}^* V_{cd})T + (V_{tb}^* V_{td})P^t$	loop
$\bar{b} \rightarrow \bar{s}s\bar{d}$	$K_S K_S$	$\phi K_S$	$(V_{tb}^* V_{td})P^t + (V_{cb}^* V_{cd})P^c$	$\lesssim 1$
$\bar{b} \rightarrow \bar{u}u\bar{d}$	$\pi^+ \pi^-$	$\rho^0 K_S$	$(V_{ub}^* V_{ud})T + (V_{tb}^* V_{td})P^t$	loop
$\bar{b} \rightarrow \bar{c}c\bar{u}$	$D_{CP}\pi^0$	$D_{CP}K_S$	$(V_{cb}^* V_{ud})T + (V_{ub}^* V_{cd})T'$	$\lambda^2$
$\bar{b} \rightarrow \bar{c}c\bar{s}$	$D_{CP}K_S$	$D_{CP}\phi$	$(V_{cb}^* V_{us})T + (V_{ub}^* V_{cs})T'$	$\lesssim 1$

- The values of  $\eta_f S_f$  for different final states  $f$  may be different from each other by more than a few percent (for example,  $S_{\phi K_S} \neq S_{\eta' K_S}$ ).
- The value of  $C_f$  may be different from zero by more than a few percent.

While a clear interpretation of such signals in terms of Lagrangian parameters will be difficult because, under these circumstances, hadronic parameters play a role, any of the above three options will clearly signal new physics. In addition flavor symmetry relations, such as those which relate observables in  $B \rightarrow K\pi$  decays [91,92] can be used to provide further tests of the Standard Model. Fig. 13.3 summarizes the present experimental results: none of the possible signatures listed above is unambiguously established, but there is definitely still room for new physics.

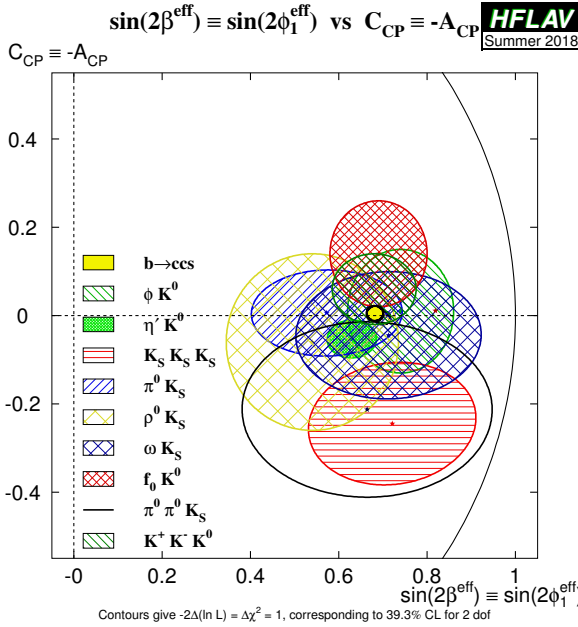


**Figure 13.3:** Summary of the results [29] of time-dependent analyses of  $b \rightarrow \bar{q}q\bar{s}$  decays, which are potentially sensitive to new physics.

For the  $\bar{b} \rightarrow \bar{u}u\bar{d}$  process  $B \rightarrow \pi\pi$  and other related channels, the penguin-to-tree ratio can be estimated using SU(3) relations and experimental data on related  $B \rightarrow K\pi$  decays. The result (for  $\pi\pi$ ) is that the suppression is at the level of 0.2 – 0.3 and so cannot be neglected. The expressions for  $S_{\pi\pi}$  and  $C_{\pi\pi}$  to leading order in  $R_{PT} \equiv (|V_{tb}V_{td}|P_{\pi\pi}^t)/(|V_{ub}V_{ud}|T_{\pi\pi})$  are:

$$\lambda_{\pi\pi} = e^{2i\alpha} \left[ (1 - R_{PT}e^{-i\alpha}) / (1 - R_{PT}e^{+i\alpha}) \right] \Rightarrow \quad (13.98)$$

$$S_{\pi\pi} \approx \sin 2\alpha + 2 \operatorname{Re}(R_{PT}) \cos 2\alpha \sin \alpha, \quad C_{\pi\pi} \approx 2 \operatorname{Im}(R_{PT}) \sin \alpha. \quad (13.99)$$

Note that  $R_{PT}$  is mode-dependent and, in particular, could be different for  $\pi^+\pi^-$  and  $\pi^0\pi^0$ . If strong phases can be neglected, then  $R_{PT}$  is real, resulting in  $C_{\pi\pi} = 0$ . The size of  $C_{\pi\pi}$  is an indicator of how large the strong phase is. The present experimental average is  $C_{\pi^+\pi^-} = -0.32 \pm 0.04$  [29]. As concerns  $S_{\pi\pi}$ , it is clear from Eq. (13.99) that the relative size or strong phase of the penguin contribution must be known to extract  $\alpha$ . This is the problem of penguin pollution.

The cleanest solution involves isospin relations among the  $B \rightarrow \pi\pi$  amplitudes [93]:

$$\frac{1}{\sqrt{2}} A_{\pi^+\pi^-} + A_{\pi^0\pi^0} = A_{\pi^+\pi^0}. \quad (13.100)$$

The method exploits the fact that the penguin contribution to  $P_{\pi\pi}^t$  is pure  $\Delta I = 1/2$  (this is not true for the electroweak penguins which, however, are expected to be small), while the tree contribution to  $T_{\pi\pi}$  contains pieces that are both  $\Delta I = 1/2$  and  $\Delta I = 3/2$ . A simple geometric construction then allows one to find  $R_{PT}$  and extract  $\alpha$  cleanly from  $S_{\pi^+\pi^-}$ . The key experimental difficulty is that one must measure accurately the separate rates for  $B^0$  and  $\bar{B}^0 \rightarrow \pi^0\pi^0$ .

$CP$  asymmetries in  $B \rightarrow \rho\pi$  and  $B \rightarrow \rho\rho$  can also be used to determine  $\alpha$ . In particular, the  $B \rightarrow \rho\rho$  measurements are presently very significant in constraining  $\alpha$ . The extraction proceeds via isospin analysis similar to that of  $B \rightarrow \pi\pi$ . There are, however, several important differences. First, due to the finite width of the  $\rho$  mesons, a final  $(\rho\rho)_{I=1}$  state is possible [94]. The effect is, however, of the order of  $(\Gamma_\rho/m_\rho)^2 \sim 0.04$ . Second, due to the presence of three helicity states for the two vector mesons, angular analysis is needed to separate the  $CP$ -even and  $CP$ -odd components. The theoretical expectation is that the  $CP$ -odd component is small, which is supported by experiments which find that the  $\rho^+\rho^-$  and  $\rho^\pm\rho^0$  modes are dominantly longitudinally polarized. Third, an important advantage of the  $\rho\rho$  modes is that the penguin contribution is expected to be small due to different hadronic dynamics. This expectation is confirmed by the smallness of  $\mathcal{B}(B^0 \rightarrow \rho^0\rho^0) = (0.95 \pm 0.16) \times 10^{-6}$  [29,95] compared to  $\mathcal{B}(B^0 \rightarrow \rho^+\rho^-) = (24.2 \pm 3.1) \times 10^{-6}$  [29]. Thus,  $S_{\rho^+\rho^-}$  is far from  $\sin 2\alpha$ . Finally, both  $S_{\rho^0\rho^0}$  and  $C_{\rho^0\rho^0}$  are experimentally accessible, which may allow a precision determination of  $\alpha$ . However, a full isospin analysis should allow that the fractions of longitudinal polarisation in  $B$  and  $\bar{B}$  decays may differ, which has not yet been done by the experiments.

Detailed discussion of the determination of  $\alpha$  with these methods, and the latest world average, can be found in Refs. [36,96]. The consistency between the range of  $\alpha$  determined by the  $B \rightarrow \pi\pi$ ,  $\rho\pi$  and  $\rho\rho$  measurements and the range allowed by CKM fits (excluding these direct determinations) provides further support to the Kobayashi-Maskawa mechanism.

All modes discussed in this Section so far have possible contributions from penguin amplitudes. As shown in Table 13.1,  $CP$  violation can also be studied with final states, typically containing charmed mesons, where no such contribution is possible. The neutral charmed meson must be reconstructed in a final state, such as a  $CP$  eigenstate, common to  $D^0$  and  $\bar{D}^0$  so that the am-

plitudes for the  $B$  and  $\bar{B}$  meson decays interfere. Although there is a second tree amplitude with a different weak phase, the contributions of the different diagrams can in many cases be separated experimentally (for example by exploiting different decays of the neutral  $D$  mesons) making these channels very clean theoretically. The first determination of  $\sin(2\beta)$ , with significance of  $CP$  violation over  $5\sigma$ , with this method has recently been reported [97]. Moreover, the interference between the two tree diagrams gives sensitivity to  $\gamma$ , as will be discussed in Section 13.6.4.

### 13.6.3 CP violation in interference of $B_s^0$ decays with and without mixing

As discussed in Section 13.6.1, the world average for  $|q/p|$  in the  $B_s^0$  system currently deviates from the Standard Model expectation due to an anomalous value of the dimuon asymmetry. Attributing the dimuon asymmetry result to a fluctuation, we again neglect the deviation of  $|q/p|$  from 1, and use

$$\lambda_f = e^{-i\phi_M(B_s^0)} (\bar{A}_f/A_f). \quad (13.101)$$

Within the Standard Model,

$$e^{-i\phi_M(B_s^0)} = (V_{tb}^* V_{ts}) / (V_{tb} V_{ts}^*). \quad (13.102)$$

Note that  $\Delta\Gamma/\Gamma = 0.132 \pm 0.008$  [29] and therefore  $y$  should not be put to zero in Eqs. (13.31a) and (13.31b). However,  $|q/p| = 1$  is expected to hold to an even better approximation than for  $B^0$  mesons. One therefore obtains

$$\mathcal{A}_f(t) = \frac{S_f \sin(\Delta mt) - C_f \cos(\Delta mt)}{\cosh(\Delta\Gamma t/2) - A_f^{\Delta\Gamma} \sinh(\Delta\Gamma t/2)}, \quad (13.103)$$

$$A_f^{\Delta\Gamma} \equiv \frac{-2\mathcal{R}e(\lambda_f)}{1 + |\lambda_f|^2}. \quad (13.104)$$

The presence of the  $A_f^{\Delta\Gamma}$  term implies that information on  $\lambda_f$  can be obtained from analyses that do not use tagging of the initial flavor, through so-called effective lifetime measurements [98].

The  $B_s^0 \rightarrow J/\psi\phi$  decay proceeds via the  $\bar{b} \rightarrow \bar{c}\bar{c}\bar{s}$  transition. The  $CP$  asymmetry in this mode thus determines (with angular analysis to disentangle the  $CP$ -even and  $CP$ -odd components of the final state)  $\sin 2\beta_s$ , where  $\beta_s$  is defined in Eq. (13.52) [99]. The  $B_s^0 \rightarrow J/\psi\pi^+\pi^-$  decay, which has a large contribution from  $J/\psi f_0(980)$  and is assumed to also proceed dominantly via the  $\bar{b} \rightarrow \bar{c}\bar{c}\bar{s}$  transition, has also been used to determine  $\beta_s$ . In this case no angular analysis is necessary, since the final state has been shown to be dominated by the  $CP$ -odd component [100]. The combination of measurements yields [29]

$$-2\beta_s = -0.021 \pm 0.031, \quad (13.105)$$

consistent with the Standard Model prediction,  $\beta_s = 0.0184 \pm 0.0004$  [19].

The experimental investigation of  $CP$  violation in the  $B_s^0$  sector is still at a relatively early stage, and far fewer modes have been studied than in the  $B^0$  system. First results on the  $\bar{b} \rightarrow \bar{q}q\bar{s}$  decays  $B_s^0 \rightarrow \phi\phi$ ,  $K^+K^-$  and  $K^{*0}\bar{K}^{*0}$  have been reported. More channels are expected to be studied in the near future.

### 13.6.4 Direct CP violation in the B system

An interesting class of decay modes is that of the tree-level decays  $B^\pm \rightarrow D^{(*)}K^\pm$ . These decays provide golden methods for a clean determination of the angle  $\gamma$  [101–106]. The method uses the decays  $B^+ \rightarrow D^0K^+$ , which proceeds via the quark transition  $\bar{b} \rightarrow \bar{u}\bar{c}\bar{s}$ , and  $B^+ \rightarrow \bar{D}^0K^+$ , which proceeds via the quark transition  $\bar{b} \rightarrow \bar{c}\bar{u}\bar{s}$ , with the  $D^0$  and  $\bar{D}^0$  decaying into a common final state. The decays into common final states, such  $(\pi^0 K_S)DK^+$ , involve interference effects between the two amplitudes, with sensitivity to the relative phase,  $\delta + \gamma$  ( $\delta$  is the relevant strong phase difference). The  $CP$ -conjugate processes are sensitive to  $\delta - \gamma$ . Measurements of branching ratios and  $CP$  asymmetries allow the determination of  $\gamma$  and  $\delta$  from amplitude triangle relations. The method suffers from discrete ambiguities but, since all hadronic parameters can be determined from the data, has negligible theoretical uncertainty [107].

Unfortunately, the smallness of the CKM-suppressed  $b \rightarrow u$  transitions makes it difficult to use the simplest methods alone [101–103] to determine  $\gamma$ . These difficulties are overcome (and the discrete ambiguities are removed) by performing a Dalitz plot analysis for multi-body  $D$  decays [104–106]. Detailed discussion of the determination of  $\gamma$  with these methods can be found in Ref. [36].

Constraints on  $\gamma$  from combinations of results on various  $B \rightarrow D^{(*)}K^{(*)}$  processes have been obtained by experiments [108, 109]. The latest world average is [29]:

$$\gamma = (71.1_{-5.3}^{+4.6})^\circ. \quad (13.106)$$

The consistency between the range of  $\gamma$  determined by the  $B \rightarrow DK$  measurements and the range allowed by CKM fits (excluding these direct determinations) provides further support to the Kobayashi-Maskawa mechanism. As more data become available, determinations of  $\gamma$  from  $B_s^0 \rightarrow D_s^\mp K^\pm$  [110, 111] and  $B^0 \rightarrow DK^{*0}$  [112–115] are expected to also give competitive measurements.

Decays to the final state  $K^\mp\pi^\pm$  provided the first observations of direct  $CP$  violation in both  $B^0$  and  $B_s^0$  systems. The asymmetry arises due to interference between tree and penguin diagrams [116], similar to the effect discussed in Section 13.6.2. In principle, measurements of  $\mathcal{A}_{\bar{B}^0 \rightarrow K^-\pi^+}$  and  $\mathcal{A}_{B^0 \rightarrow K^+\pi^-}$  could be used to determine the weak phase difference  $\gamma$ , but lack of knowledge of the relative magnitude and strong phase of the contributing amplitudes limits the achievable precision. The uncertainties on these hadronic parameters can be reduced by exploiting flavor symmetries, which predict a number of relations between asymmetries in different modes. One such relation is that the partial rate differences for  $B^0$  and  $B_s^0$  decays to  $K^\mp\pi^\pm$  are expected to be approximately equal and opposite [117], which is consistent with current data. It is also expected that the partial rate asymmetries for  $\bar{B}^0 \rightarrow K^-\pi^+$  and  $B^- \rightarrow K^-\pi^0$  should be approximately equal; however, the experimental results currently show a significant discrepancy [29]:

$$\mathcal{A}_{\bar{B}^0 \rightarrow K^-\pi^+} = -0.084 \pm 0.004, \quad \mathcal{A}_{B^- \rightarrow K^-\pi^0} = +0.040 \pm 0.021. \quad (13.107)$$

It is therefore of great interest to understand whether this originates from Standard Model QCD corrections, or whether it is a signature of new dynamics. Improved tests of a more precise relation between the partial rate differences of all four  $K\pi$  final states [118–121], currently limited by knowledge of the  $CP$  asymmetry in  $\bar{B}^0 \rightarrow K_S\pi^0$  decays, may help to resolve the situation.

It is also of interest to investigate whether similar patterns appear among the  $CP$  violating asymmetries in  $B$  meson decays to final states containing one pseudoscalar and one vector meson. Since the vector resonance decays to two particles, such channels can be studied through Dalitz plot analysis of the three-body final state. Model-independent analyses of  $B^+ \rightarrow K^+K^-K^+$ ,  $\pi^+\pi^-K^+$ ,  $\pi^+\pi^-K^+$  and  $K^+K^-\pi^+$  decays have revealed large  $CP$  violation effects in certain regions of phase space [122]. For the  $B^+ \rightarrow K^+K^-\pi^+$  decay, an amplitude analysis has established a large  $CP$  violation effect associated with  $\pi\pi \leftrightarrow KK$  S-wave rescattering [123]. For the other channels it remains to be seen whether the  $CP$  violation effects are associated to particular resonances or to interference effects, which will be necessary to understand the underlying dynamics.

## 13.7 Summary and Outlook

$CP$  violation has been experimentally established in  $K$ ,  $D$  and  $B$  meson decays. A full list of  $CP$  asymmetries that have been measured at a level higher than  $5\sigma$  is given in the introduction to this review. In Section 13.1.4 we introduced three types of  $CP$ -violating effects. Examples of these three types include the following:

1. All three types of  $CP$  violation have been observed in  $K \rightarrow \pi\pi$



decays:

$$\begin{aligned} \mathcal{R}e(\epsilon') &= \frac{1}{6} \left( \left| \frac{\bar{A}_{\pi^0\pi^0}}{A_{\pi^0\pi^0}} \right| - \left| \frac{\bar{A}_{\pi^+\pi^-}}{A_{\pi^+\pi^-}} \right| \right) \\ &= (2.5 \pm 0.4) \times 10^{-6}, \end{aligned} \quad (\text{I}) \quad (13.108a)$$

$$\begin{aligned} \mathcal{R}e(\epsilon) &= \frac{1}{2} \left( 1 - \left| \frac{q}{p} \right| \right) \\ &= (1.66 \pm 0.02) \times 10^{-3}, \end{aligned} \quad (\text{II}) \quad (13.108b)$$

$$\begin{aligned} \mathcal{I}m(\epsilon) &= -\frac{1}{2} \mathcal{I}m(\lambda_{(\pi\pi)_{I=0}}) \\ &= (1.57 \pm 0.02) \times 10^{-3}. \end{aligned} \quad (\text{III}) \quad (13.108c)$$

2. For  $D$  mesons,  $CP$  violation in decay has been established in the difference of asymmetries for  $D^0 \rightarrow K^+K^-$  and  $D^0 \rightarrow \pi^+\pi^-$  decays.

$$\begin{aligned} \Delta a_{CP} &= \frac{|\bar{A}_{K^+K^-}/A_{K^+K^-}|^2 - 1}{|\bar{A}_{K^+K^-}/A_{K^+K^-}|^2 + 1} - \frac{|\bar{A}_{\pi^+\pi^-}/A_{\pi^+\pi^-}|^2 - 1}{|\bar{A}_{\pi^+\pi^-}/A_{\pi^+\pi^-}|^2 + 1} \\ &= (-0.164 \pm 0.028) \times 10^{-3}, \end{aligned} \quad (\text{I}) \quad (13.109)$$

3. In the  $B$  meson system,  $CP$  violation in decay has been observed in, for example,  $B^0 \rightarrow K^+\pi^-$  transitions, while  $CP$  violation in interference of decays with and without mixing has been observed in, for example, the  $B^0 \rightarrow J/\psi K_S$  channel:

$$\begin{aligned} A_{K^+\pi^-} &= \frac{|\bar{A}_{K^-\pi^+}/A_{K^+\pi^-}|^2 - 1}{|\bar{A}_{K^-\pi^+}/A_{K^+\pi^-}|^2 + 1} \\ &= -0.084 \pm 0.004, \end{aligned} \quad (\text{I}) \quad (13.110a)$$

$$\begin{aligned} S_{\psi K} &= \mathcal{I}m(\lambda_{\psi K}) \\ &= +0.699 \pm 0.017. \end{aligned} \quad (\text{III}) \quad (13.110b)$$

Based on Standard Model predictions, further observations of  $CP$  violation in  $B^0$ ,  $B^+$  and  $B_s^0$  decays seem likely in the near future, at both LHCb and its upgrades [124–126] as well as the Belle II experiment [127]. The first observation of  $CP$  violation in  $b$  baryons is also likely to be within reach of LHCb. Further improvements in the sensitivity to  $CP$  violation effects in the charm sector can also be anticipated, though uncertainty in the Standard Model predictions makes it difficult to forecast whether or not additional discoveries will be forthcoming. A number of upcoming experiments have potential to make significant progress on rare kaon decays. Observables that are subject to clean theoretical interpretation, such as  $\beta$  from  $S_{\psi K_S}$ ,  $\beta_s$  from  $B_s^0 \rightarrow J/\psi\phi$ ,  $\mathcal{B}(K_L \rightarrow \pi^0\nu\bar{\nu})$  and  $\gamma$  from  $CP$  violation in  $B \rightarrow DK$  decays, are of particular value for constraining the values of the CKM parameters and probing the flavor sector of extensions to the Standard Model. Progress in lattice QCD calculations is also needed to complement the anticipated experimental results. Other probes of  $CP$  violation now being pursued experimentally include the electric dipole moments of the neutron and electron, and the decays of tau leptons. Additional processes that are likely to play an important role in future  $CP$  studies include top-quark production and decay, Higgs boson decays and neutrino oscillations.

All measurements of  $CP$  violation to date are consistent with the predictions of the Kobayashi-Maskawa mechanism of the Standard Model. In fact, it is now established that the KM mechanism plays a major role in the  $CP$  violation measured in the quark sector. However, a dynamically-generated matter-antimatter asymmetry of the universe requires additional sources of  $CP$  violation, and such sources are naturally generated by extensions to the Standard Model. New sources might eventually reveal themselves as small deviations from the predictions of the KM mechanism, or else might not be observable in the quark sector at all, but observable with future probes such as neutrino oscillations or electric dipole moments. The fundamental nature of  $CP$  violation demands a vigorous search.

A number of excellent reviews of  $CP$  violation are available [128–135], where the interested reader may find a detailed discussion of the various topics that are briefly reviewed here.

We thank David Kirkby for significant contributions to earlier versions of this review.

### References

- [1] J. H. Christenson *et al.*, Phys. Rev. Lett. **13**, 138 (1964).
- [2] B. Aubert *et al.* (BaBar), Phys. Rev. Lett. **87**, 091801 (2001), [hep-ex/0107013].
- [3] K. Abe *et al.* (Belle), Phys. Rev. Lett. **87**, 091802 (2001), [hep-ex/0107061].
- [4] H. Burkhardt *et al.* (NA31), Phys. Lett. **B206**, 169 (1988).
- [5] V. Fanti *et al.* (NA48), Phys. Lett. **B465**, 335 (1999), [hep-ex/9909022].
- [6] A. Alavi-Harati *et al.* (KTeV), Phys. Rev. Lett. **83**, 22 (1999), [hep-ex/9905060].
- [7] B. Aubert *et al.* (BaBar), Phys. Rev. Lett. **93**, 131801 (2004), [hep-ex/0407057].
- [8] Y. Chao *et al.* (Belle), Phys. Rev. Lett. **93**, 191802 (2004), [hep-ex/0408100].
- [9] A. Poluektov *et al.* (Belle), Phys. Rev. **D81**, 112002 (2010), [arXiv:1003.3360].
- [10] P. del Amo Sanchez *et al.* (BaBar), Phys. Rev. **D82**, 072004 (2010), [arXiv:1007.0504].
- [11] R. Aaij *et al.* (LHCb), Phys. Lett. **B712**, 203 (2012), [Erratum: Phys. Lett. **B713**, 351 (2012)], [arXiv:1203.3662].
- [12] R. Aaij *et al.* (LHCb), Phys. Rev. Lett. **110**, 22, 221601 (2013), [arXiv:1304.6173].
- [13] R. Aaij *et al.* (LHCb), Phys. Rev. Lett. **122**, 21, 211803 (2019), [arXiv:1903.08726].
- [14] See results on the “Time reversal invariance,” within the review on “Tests of Conservation Laws,” in this *Review*.
- [15] J. Bernabeu, F. Martinez-Vidal and P. Villanueva-Perez, JHEP **08**, 064 (2012), [arXiv:1203.0171].
- [16] J. P. Lees *et al.* (BaBar), Phys. Rev. Lett. **109**, 211801 (2012), [arXiv:1207.5832].
- [17] See, for example, R. F. Streater and A. S. Wightman, *CPT, Spin and Statistics, and All That*, reprinted by Addison-Wesley, New York (1989).
- [18] M. Kobayashi and T. Maskawa, Prog. Theor. Phys. **49**, 652 (1973).
- [19] J. Charles *et al.* (CKMfitter Group), Eur. Phys. J. **C41**, 1, 1 (2005), updated results and plots available at: <http://ckmfitter.in2p3.fr>, [hep-ph/0406184].
- [20] M. Bona *et al.* (UTfit), JHEP **10**, 081 (2006), updated results and plots available at: <http://www.utfit.org/UTfit>, [hep-ph/0606167].
- [21] A. D. Sakharov, Pisma Zh. Eksp. Teor. Fiz. **5**, 32 (1967), [Usp. Fiz. Nauk **161**, no.5, 61 (1991)].
- [22] A. Riotto, in “Proceedings, Summer School in High-energy physics and cosmology: Trieste, Italy, June 29-July 17, 1998,” 326–436 (1998), [hep-ph/9807454].
- [23] M. Fukugita and T. Yanagida, Phys. Lett. **B174**, 45 (1986).
- [24] S. Davidson, E. Nardi and Y. Nir, Phys. Rept. **466**, 105 (2008), [arXiv:0802.2962].
- [25] G. Aad *et al.* (ATLAS), Phys. Lett. **B716**, 1 (2012), [arXiv:1207.7214].
- [26] S. Chatrchyan *et al.* (CMS), Phys. Lett. **B716**, 30 (2012), [arXiv:1207.7235].
- [27] See the  $K$ -meson Listings in this *Review*.
- [28] See the  $B$ -meson Listings in this *Review*.
- [29] Y. Amhis *et al.* (HFLAV), Eur. Phys. J. **C77**, 12, 895 (2017), [arXiv:1612.07233].
- [30] V. Weisskopf and E. P. Wigner, Z. Phys. **63**, 54 (1930).
- [31] See the review on “ $D^0 - \bar{D}^0$  Mixing” in this *Review*.
- [32] O. Long *et al.*, Phys. Rev. **D68**, 034010 (2003), [hep-ex/0303030].

- [33] M. Gronau, Y. Grossman and J. L. Rosner, Phys. Lett. **B508**, 37 (2001), [hep-ph/0103110].
- [34] M. Artuso, G. Borissov and A. Lenz, Rev. Mod. Phys. **88**, 4, 045002 (2016), [arXiv:1511.09466].
- [35] L. Wolfenstein, Phys. Rev. Lett. **13**, 562 (1964).
- [36] See the review on “Cabibbo-Kobayashi-Maskawa Mixing Matrix,” in this *Review*.
- [37] L. Wolfenstein, Phys. Rev. Lett. **51**, 1945 (1983).
- [38] A. J. Buras, M. E. Lautenbacher and G. Ostermaier, Phys. Rev. **D50**, 3433 (1994), [hep-ph/9403384].
- [39] C. Jarlskog, Phys. Rev. Lett. **55**, 1039 (1985).
- [40] See the review on “CP violation in  $K_S \rightarrow 3\pi$ ,” in this *Review*.
- [41] T. Blum *et al.*, Phys. Rev. **D91**, 7, 074502 (2015), [arXiv:1502.00263].
- [42] Z. Bai *et al.* (RBC, UKQCD), Phys. Rev. Lett. **115**, 21, 212001 (2015), [arXiv:1505.07863].
- [43] A. J. Buras *et al.*, JHEP **11**, 202 (2015), [arXiv:1507.06345].
- [44] Y. Grossman and Y. Nir, Phys. Lett. **B398**, 163 (1997), [hep-ph/97011313].
- [45] L. S. Littenberg, Phys. Rev. **D39**, 3322 (1989).
- [46] A. J. Buras, Phys. Lett. **B333**, 476 (1994), [hep-ph/9405368].
- [47] G. Buchalla and A. J. Buras, Nucl. Phys. **B400**, 225 (1993).
- [48] A. J. Buras *et al.*, JHEP **11**, 033 (2015), [arXiv:1503.02693].
- [49] J. K. Ahn *et al.* (KOTO), Phys. Rev. Lett. **122**, 2, 021802 (2019), [arXiv:1810.09655].
- [50] T. Yamanaka (KOTO), PTEP **2012**, 02B006 (2012).
- [51] M. Mirra [NA62 Collab.], Nuovo Cimento **C038**, 13 (2015).
- [52] B. Aubert *et al.* (BaBar), Phys. Rev. Lett. **98**, 211802 (2007), [hep-ex/0703020].
- [53] M. Staric *et al.* (BELLE), Phys. Rev. Lett. **98**, 211803 (2007), [65(2007)], [hep-ex/0703036].
- [54] T. Aaltonen *et al.* (CDF), Phys. Rev. Lett. **100**, 121802 (2008), [arXiv:0712.1567].
- [55] R. Aaij *et al.* (LHCb), Phys. Rev. Lett. **110**, 10, 101802 (2013), [arXiv:1211.1230].
- [56] See the *D*-meson Listings in this *Review*.
- [57] Y. Grossman, A. L. Kagan and Y. Nir, Phys. Rev. **D75**, 036008 (2007), [hep-ph/0609178].
- [58] S. Bergmann *et al.*, Phys. Lett. **B486**, 418 (2000), [hep-ph/0005181].
- [59] M. Gersabeck *et al.*, J. Phys. **G39**, 045005 (2012), [arXiv:1111.6515].
- [60] D. M. Asner *et al.* (CLEO), Phys. Rev. **D78**, 012001 (2008), [arXiv:0802.2268].
- [61] M. Ablikim *et al.* (BESIII), Phys. Lett. **B734**, 227 (2014), [arXiv:1404.4691].
- [62] R. Aaij *et al.* (LHCb), Phys. Rev. Lett. **111**, 25, 251801 (2013), [arXiv:1309.6534].
- [63] R. Aaij *et al.* (LHCb), Phys. Rev. Lett. **118**, 26, 261803 (2017), [arXiv:1702.06490].
- [64] M. Ciuchini *et al.*, Phys. Lett. **B655**, 162 (2007), [hep-ph/0703204].
- [65] Y. Grossman, Y. Nir and G. Perez, Phys. Rev. Lett. **103**, 071602 (2009), [arXiv:0904.0305].
- [66] A. L. Kagan and M. D. Sokoloff, Phys. Rev. **D80**, 076008 (2009), [arXiv:0907.3917].
- [67] Y. Grossman and Y. Nir, JHEP **04**, 002 (2012), [arXiv:1110.3790].
- [68] B. R. Ko *et al.* (Belle), Phys. Rev. Lett. **109**, 021601 (2012), [Erratum: Phys. Rev. Lett.109,119903(2012)], [arXiv:1203.6409].
- [69] See the “Review of Multibody Charm Analyses” in this *Review*.
- [70] B. Aubert *et al.* (BaBar), Phys. Rev. **D78**, 051102 (2008), [arXiv:0802.4035].
- [71] I. Bediaga *et al.*, Phys. Rev. **D80**, 096006 (2009), [arXiv:0905.4233].
- [72] I. Bediaga *et al.*, Phys. Rev. **D86**, 036005 (2012), [arXiv:1205.3036].
- [73] M. Williams, Phys. Rev. **D84**, 054015 (2011), [arXiv:1105.5338].
- [74] R. Aaij *et al.* (LHCb), Phys. Lett. **B769**, 345 (2017), [arXiv:1612.03207].
- [75] V. M. Abazov *et al.* (D0), Phys. Rev. **D82**, 032001 (2010), [arXiv:1005.2757].
- [76] A. B. Carter and A. I. Sanda, Phys. Rev. Lett. **45**, 952 (1980).
- [77] A. B. Carter and A. I. Sanda, Phys. Rev. **D23**, 1567 (1981).
- [78] I. I. Y. Bigi and A. I. Sanda, Nucl. Phys. **B193**, 85 (1981).
- [79] I. Dunietz and J. L. Rosner, Phys. Rev. **D34**, 1404 (1986).
- [80] Y. I. Azimov, N. G. Uraltsev and V. A. Khoze, Sov. J. Nucl. Phys. **45**, 878 (1987), [Yad. Fiz.45,1412(1987)].
- [81] I. I. Y. Bigi and A. I. Sanda, Nucl. Phys. **B281**, 41 (1987).
- [82] G. Buchalla, A. J. Buras and M. E. Lautenbacher, Rev. Mod. Phys. **68**, 1125 (1996), [hep-ph/9512380].
- [83] R. Fleischer, Eur. Phys. J. **C10**, 299 (1999), [hep-ph/9903455].
- [84] M. Ciuchini, M. Pierini and L. Silvestrini, Phys. Rev. Lett. **95**, 221804 (2005), [hep-ph/0507290].
- [85] S. Faller *et al.*, Phys. Rev. **D79**, 014030 (2009), [arXiv:0809.0842].
- [86] M. Jung, Phys. Rev. **D86**, 053008 (2012), [arXiv:1206.2050].
- [87] H.-n. Li and S. Mishima, JHEP **03**, 009 (2007), [hep-ph/0610120].
- [88] K. De Bruyn and R. Fleischer, JHEP **03**, 145 (2015), [arXiv:1412.6834].
- [89] P. Frings, U. Nierste and M. Wiebusch, Phys. Rev. Lett. **115**, 6, 061802 (2015), [arXiv:1503.00859].
- [90] L. Silvestrini, Ann. Rev. Nucl. Part. Sci. **57**, 405 (2007), [arXiv:0705.1624].
- [91] R. Fleischer *et al.*, Phys. Rev. **D78**, 111501 (2008), [arXiv:0806.2900].
- [92] R. Fleischer *et al.*, Eur. Phys. J. **C78**, 11, 943 (2018), [arXiv:1806.08783].
- [93] M. Gronau and D. London, Phys. Rev. Lett. **65**, 3381 (1990).
- [94] A. F. Falk *et al.*, Phys. Rev. **D69**, 011502 (2004), [hep-ph/0310242].
- [95] R. Aaij *et al.* (LHCb), Phys. Lett. **B747**, 468 (2015), [arXiv:1503.07770].
- [96] J. Charles *et al.*, Eur. Phys. J. **C77**, 8, 574 (2017), [arXiv:1705.02981].
- [97] A. Abdesselam *et al.* (BaBar, Belle), Phys. Rev. Lett. **115**, 12, 121604 (2015), [arXiv:1505.04147].
- [98] R. Fleischer and R. Knegjens, Eur. Phys. J. **C71**, 1789 (2011), [arXiv:1109.5115].
- [99] A. S. Dighe, I. Dunietz and R. Fleischer, Eur. Phys. J. **C6**, 647 (1999), [hep-ph/9804253].
- [100] R. Aaij *et al.* (LHCb), Phys. Rev. **D89**, 9, 092006 (2014), [arXiv:1402.6248].
- [101] M. Gronau and D. London, Phys. Lett. **B253**, 483 (1991).
- [102] M. Gronau and D. Wyler, Phys. Lett. **B265**, 172 (1991).
- [103] D. Atwood, I. Dunietz and A. Soni, Phys. Rev. Lett. **78**, 3257 (1997), [hep-ph/9612433].

- [104] D. Atwood, I. Dunietz and A. Soni, Phys. Rev. **D63**, 036005 (2001), [hep-ph/0008090].
- [105] A. Giri *et al.*, Phys. Rev. **D68**, 054018 (2003), [hep-ph/0303187].
- [106] A. Bondar, *Proceedings of BINP special analysis meeting on Dalitz analysis*, 24-26 Sep. 2002, unpublished.
- [107] J. Brod and J. Zupan, JHEP **01**, 051 (2014), [arXiv:1308.5663].
- [108] J. P. Lees *et al.* (BaBar), Phys. Rev. **D87**, 5, 052015 (2013), [arXiv:1301.1029].
- [109] R. Aaij *et al.* (LHCb), JHEP **12**, 087 (2016), [arXiv:1611.03076].
- [110] R. Aleksan, I. Dunietz and B. Kayser, Z. Phys. **C54**, 653 (1992).
- [111] R. Fleischer, Nucl. Phys. **B671**, 459 (2003), [hep-ph/0304027].
- [112] I. Dunietz, Phys. Lett. **B270**, 75 (1991).
- [113] M. Gronau, Phys. Lett. **B557**, 198 (2003), [hep-ph/0211282].
- [114] T. Gershon, Phys. Rev. **D79**, 051301 (2009), [arXiv:0810.2706].
- [115] T. Gershon and M. Williams, Phys. Rev. **D80**, 092002 (2009), [arXiv:0909.1495].
- [116] M. Bander, D. Silverman and A. Soni, Phys. Rev. Lett. **43**, 242 (1979).
- [117] X.-G. He, Eur. Phys. J. **C9**, 443 (1999), [hep-ph/9810397].
- [118] D. Atwood and A. Soni, Phys. Rev. **D58**, 036005 (1998), [hep-ph/9712287].
- [119] M. Gronau and J. L. Rosner, Phys. Rev. **D59**, 113002 (1999), [hep-ph/9809384].
- [120] H. J. Lipkin, Phys. Lett. **B445**, 403 (1999), [hep-ph/9810351].
- [121] M. Gronau, Phys. Lett. **B627**, 82 (2005), [hep-ph/0508047].
- [122] R. Aaij *et al.* (LHCb), Phys. Rev. **D90**, 11, 112004 (2014), [arXiv:1408.5373].
- [123] R. Aaij *et al.* (LHCb) (2019), [arXiv:1905.09244].
- [124] A. A. Alves, Jr. *et al.* (LHCb), JINST **3**, S08005 (2008).
- [125] I. Bediaga *et al.* (LHCb) (2012).
- [126] R. Aaij *et al.* [LHCb Collab.], CERN-LHCC-2017-003.
- [127] T. Aushev *et al.* (2010), [arXiv:1002.5012].
- [128] G. C. Branco, L. Lavoura and J. P. Silva, Int. Ser. Monogr. Phys. **103**, 1 (1999).
- [129] I. I. Bigi and A. I. Sanda (2000), [Camb. Monogr. Part. Phys. Nucl. Phys. Cosmol.9,1(2009)].
- [130] A. J. Bevan *et al.* (BaBar, Belle), Eur. Phys. J. **C74**, 3026 (2014), [arXiv:1406.6311].
- [131] H.R. Quinn and Y. Nir, “*The Mystery of the Missing Antimatter*,” Princeton University Press, Princeton (2008).
- [132] T. E. Browder *et al.*, Rev. Mod. Phys. **81**, 1887 (2009), [arXiv:0802.3201].
- [133] M. Ciuchini and A. Stocchi, Ann. Rev. Nucl. Part. Sci. **61**, 491 (2011), [arXiv:1110.3920].
- [134] R. Aaij *et al.* (LHCb), Eur. Phys. J. **C73**, 4, 2373 (2013), [arXiv:1208.3355].
- [135] T. Gershon and V. V. Gligorov, Rept. Prog. Phys. **80**, 4, 046201 (2017), [arXiv:1607.06746].

## 14. Neutrino Masses, Mixing, and Oscillations

Written August 2019 by M.C. Gonzalez-Garcia (YITP, Stony Brook; ICREA, Barcelona; ICC, U. of Barcelona) and M. Yokoyama (Tokyo U.; Kavli IPMU (WPI), U. Tokyo).

14.1	Neutrinos in the Standard Model: Massless Neutrinos . . . . .	285
14.2	Extending the Standard Model to Introduce Massive Neutrinos . . . . .	285
14.2.1	Dirac Neutrinos . . . . .	286
14.2.2	The See-saw Mechanism . . . . .	286
14.2.3	Light Sterile Neutrinos . . . . .	287
14.2.4	Neutrino Masses from Generic New Physics . . . . .	287
14.3	Lepton Mixing . . . . .	287
14.4	Mass-Induced Flavour Oscillations in Vacuum . . . . .	288
14.5	Propagation of Massive Neutrinos in Matter . . . . .	289
14.5.1	The Mhhheev-Smirnov-Wolfenstein Effect for Solar Neutrinos . . . . .	291
14.6	Experimental Study of Neutrino Oscillations . . . . .	291
14.6.1	Solar Neutrinos . . . . .	291
14.6.2	Atmospheric Neutrinos . . . . .	293
14.6.3	Accelerator Neutrinos . . . . .	294
14.6.4	Reactor Antineutrinos . . . . .	297
14.7	Combined Analysis of Experimental Results: The $3\nu$ Paradigm . . . . .	300
14.7.1	$3\nu$ Oscillation Probabilities . . . . .	301
14.7.2	$3\nu$ Oscillation Analysis . . . . .	302
14.7.3	Convention-independent Measures of Leptonic CP Violation in $3\nu$ Mixing . . . . .	302
14.8	Beyond $3\nu$ : Additional Neutrinos at the eV Scale . . . . .	304
14.9	Laboratory Probes of $\nu$ Mass Scale and its Nature . . . . .	305
14.9.1	Constraints from Kinematics of Weak Decays . . . . .	305
14.9.2	Dirac vs Majorana: Neutrinoless Double-beta Decay . . . . .	306
14.9.3	Experimental Search for Neutrinoless Double-beta Decay . . . . .	307

### 14.1 Neutrinos in the Standard Model: Massless Neutrinos

The gauge symmetry principle is one of the pillars of the great success of modern particle physics as it establishes an unambiguous connection between local (gauge) symmetries and forces mediated by spin-1 particles. In the Standard Model (SM) of particle physics the strong, weak, and electromagnetic interactions are connected to gauge symmetry under  $SU(3)_C \times SU(2)_L \times U(1)_Y$  where  $C$  stands for colour,  $L$  for left-handedness, and  $Y$  for hypercharge. The SM gauge symmetry is spontaneously broken to  $SU(3)_C \times U(1)_{EM}$  where  $U(1)_{EM}$  couples to the electromagnetic charge  $Q_{EM} = T_{L3} + Y$  ( $T_{L3}$  is the weak isospin which is the third generator of  $SU(2)_L$ ). The model explains all the interactions of the known fermions once they are assigned to well defined representation of the gauge group. The construction and tests of the Standard Model as a gauge theory are covered in the review sections on “Quantum chromodynamics” and “Electroweak model and constraints on new physics” respectively. In here we emphasize that the gauge invariance principle requires that all terms in the Lagrangian, including the mass terms, respect the local symmetry. This has important implications for the neutrino and in particular for the question of the neutrino mass <sup>1</sup>.

In the SM, neutrinos are fermions that do not have strong nor electromagnetic interactions. Consequently they are singlets of the subgroup  $SU(3)_C \times U(1)_{EM}$ . They are part of the lepton doublets  $L_{L\ell} = \begin{pmatrix} \nu_\ell \\ \ell \end{pmatrix}_L$  where  $f_L$  is the left-handed component of the fermion  $f$ ,  $f_L = P_L f \equiv \frac{1-\gamma_5}{2} f$ . In what follows we will refer as *active* neutrinos to neutrinos that are part of these lepton doublets. In the SM there is one active neutrino for each charged

leptons,  $\ell = e, \mu, \tau$ .  $SU(2)_L$  gauge invariance dictates the form of weak charged current (CC) interactions between the neutrinos and their corresponding charged leptons and neutral current (NC) among themselves to be:

$$-\mathcal{L}_{CC} = \frac{g}{\sqrt{2}} \sum_{\ell} \bar{\nu}_{L\ell} \gamma^\mu \ell_L^- W_\mu^+ + \text{h.c.}, \quad (14.1)$$

$$-\mathcal{L}_{NC} = \frac{g}{2 \cos \theta_W} \sum_{\ell} \bar{\nu}_{L\ell} \gamma^\mu \nu_{L\ell} Z_\mu^0. \quad (14.2)$$

In the above equations  $g$  is the coupling constant associated to  $SU(2)$  and  $\theta_W$  is the Weinberg angle.

Equations(14.1) and (14.2) describe all the neutrino interactions in the SM. In particular, Eq.(14.2) determines the decay width of the  $Z^0$  boson into light ( $m_\nu \leq m_{Z^0}/2$ ) left-handed neutrinos states. Thus from the measurement of the total decay width of the  $Z^0$  one can infer the number of such states. At present the measurement implies  $N_\nu = 2.984 \pm 0.008$  (see Particle Listing). As a result any extension of the SM should contain three, and only three, light active neutrinos.

*Sterile* neutrinos are defined as having no SM gauge interactions, that is, they are singlets of the complete SM gauge group. Thus the SM, as the gauge theory able to describe all known particle interactions, contains no sterile neutrinos.

The SM with its gauge symmetry and the particle content required for the gauge interactions, that is, in the absence of SM singlets, respects an accidental global symmetry which is not imposed but appears as consequence of the gauge symmetry and the representation of the matter fields:

$$G_{SM}^{\text{global}} = U(1)_B \times U(1)_{L_e} \times U(1)_{L_\mu} \times U(1)_{L_\tau}, \quad (14.3)$$

where  $U(1)_B$  is the baryon number symmetry, and  $U(1)_{L_e, L_\mu, L_\tau}$  are the three lepton flavour symmetries. The total lepton number,  $L_e + L_\mu + L_\tau$ , is then also an accidental symmetry since is a subgroup of  $G_{SM}^{\text{global}}$ . This fact has consequences which are relevant to the question of the neutrino mass as we argue next.

In the SM, the masses of the fermions are generated via a Yukawa coupling of the scalar Higgs doublet  $\phi$  with a fermion right-handed and left-handed component. The former is an  $SU(2)_L$  singlet, the latter is part of a doublet. For leptons, we can one can build such term coupling the left-handed lepton doublets  $L_L$  with the right-handed charged lepton fields  $E_R$ :

$$-\mathcal{L}_{\text{Yukawa,lep}} = Y_{ij}^\ell \bar{L}_{Li} \phi E_{Rj} + \text{h.c.} \quad (14.4)$$

After spontaneous symmetry breaking these terms lead to charged lepton masses

$$m_{ij}^\ell = Y_{ij}^\ell \frac{v}{\sqrt{2}}, \quad (14.5)$$

where  $v$  is the vacuum expectation value of the Higgs field. However, since the model does not contain right-handed neutrinos, no such Yukawa interaction can be built for the neutrinos, which are consequently massless at the Lagrangian level.

In principle, a neutrino mass term could be generated at loop level. With the particle content of the SM the only possible neutrino mass term that could be constructed is the bilinear  $\bar{L}_L L_L^c$ , where  $L_L^c$  is the charge conjugated field,  $L_L^c = C \bar{L}_L^T$  and  $C$  is the charge conjugation matrix. However this term is forbidden in the SM because it violates the total lepton symmetry by two units and therefore it cannot be induced by loop corrections because it breaks the accidental symmetry of the model. Also, because  $U(1)_{B-L}$  is a non-anomalous subgroup of  $G_{SM}^{\text{global}}$ , the bilinear  $\bar{L}_L L_L^c$ , cannot be induced by nonperturbative corrections either since it breaks  $B - L$ .

We conclude that within the SM neutrinos are precisely massless. Consequently one must go beyond the SM in order to add a mass to the neutrino.

### 14.2 Extending the Standard Model to Introduce Massive Neutrinos

From the above discussion we conclude that it is not possible to construct a renormalizable mass term for the neutrinos with the

<sup>1</sup>The physics of massive neutrinos has been the subject of excellent books such as [1–5] and multiple review articles. The contents of the present review is built upon the structure and the contents of the review articles [6, 7].

fermionic content and gauge symmetry of the SM. The obvious consequence is that in order to introduce a neutrino mass in the theory one must extend the particle content of the model, depart from gauge invariance and/or renormalizability, or do both.

As a matter of fact, neutrino mass terms can be constructed in different ways. In the following we shall assume to maintain the gauge symmetry and explore the different possibilities to introduce a neutrino mass term adding to the SM an arbitrary number of sterile neutrinos  $\nu_{si}$  ( $i = 1, \dots, m$ ).

In the SM extended with the addition of  $m$  number of sterile neutrinos one can construct two gauge invariant renormalizable operators leading to two type of mass terms

$$-\mathcal{L}_{M_\nu} = M_{Dij} \bar{\nu}_{si} \nu_{Lj} + \frac{1}{2} M_{Nij} \bar{\nu}_{si} \nu_{sj}^c + \text{h.c.}, \quad (14.6)$$

where  $\nu^c$  is the neutrino charge conjugated field (defined in section 14.1).  $M_D$  is a complex matrix of dimension  $m \times 3$  and  $M_N$  is a symmetric  $m \times m$  matrix.

The first term is generated after spontaneous electroweak symmetry breaking from Yukawa interactions,

$$Y_{ij}^\nu \bar{\nu}_{si} \tilde{\phi}^\dagger L_{Lj} \Rightarrow M_{Dij} = Y_{ij}^\nu \frac{v}{\sqrt{2}}, \quad (14.7)$$

in similarity to Eqs.(14.4) and (14.5) for the charged fermion masses. It is correspondingly called a Dirac mass term. It conserves total lepton number but it can break the lepton flavour number symmetries.

The second term in Eq.(14.6) is a Majorana mass term and it differs from the Dirac mass terms in several relevant aspects. First, it is a singlet of the SM gauge group and, as such, it can appear as a bare mass term in the Lagrangian. Second, since it involves two neutrino fields (right-handed in this case), it breaks lepton number by two units. In general such a term is not allowed if the neutrinos carry any additive conserved charge.

It is possible to rewrite Eq.(14.6) as:

$$-\mathcal{L}_{M_\nu} = \frac{1}{2} (\bar{\nu}_L^c, \bar{\nu}_s^c) \begin{pmatrix} 0 & M_D^T \\ M_D & M_N \end{pmatrix} \begin{pmatrix} \bar{\nu}_L \\ \bar{\nu}_s^c \end{pmatrix} + \text{h.c.} \equiv \bar{\nu}^c M_\nu \bar{\nu} + \text{h.c.}, \quad (14.8)$$

where  $\bar{\nu} = (\bar{\nu}_L, \bar{\nu}_s^c)^T$  is a  $(3+m)$ -dimensional vector. The matrix  $M_\nu$  is complex and symmetric<sup>2</sup>. Thus it can be diagonalized by a unitary matrix  $V^\nu$  of dimension  $(3+m)$ , so

$$(V^\nu)^T M_\nu V^\nu = \text{diag}(m_1, m_2, \dots, m_{3+m}). \quad (14.9)$$

One can express the original weak eigenstates in terms of the resulting  $3+m$  mass eigenstates

$$\bar{\nu}_{\text{mass}} = (V^\nu)^\dagger \bar{\nu}, \quad (14.10)$$

and in terms of the mass eigenstates Eq.(14.8) takes the form:

$$\begin{aligned} -\mathcal{L}_{M_\nu} &= \frac{1}{2} \sum_{k=1}^{3+m} m_k (\bar{\nu}_{\text{mass},k}^c \nu_{\text{mass},k} + \bar{\nu}_{\text{mass},k} \nu_{\text{mass},k}^c) \\ &= \frac{1}{2} \sum_{k=1}^{3+m} m_k \bar{\nu}_{Mk} \nu_{Mk}, \end{aligned} \quad (14.11)$$

where

$$\nu_{Mk} = \nu_{\text{mass},k} + \nu_{\text{mass},k}^c = (V^\nu)^\dagger \bar{\nu}_k + (V^\nu)^\dagger \bar{\nu}_k^c. \quad (14.12)$$

So these states obey the Majorana condition

$$\nu_M = \nu_M^c, \quad (14.13)$$

and are referred to as Majorana neutrinos. The Majorana condition implies that only one field describes both neutrino and antineutrino states, unlike in the case of a charge for which particle

<sup>2</sup>Notice that Eq.(14.8) corresponds to the tree-level neutrino mass matrix. Corrections are induced at the loop level, which in particular lead to non-vanishing  $\bar{\nu}_L^c \nu_L$  entry [8].

and antiparticle are described by two different fields. So a Majorana neutrino can be described by a two-component spinor unlike the charged fermions, which are Dirac particles, and are represented by four-component spinors.

Inverting Eq.(14.12) we can write the weak-doublet components of the neutrino fields as:

$$\nu_{Li} = P_L \sum_{j=1}^{3+m} V_{ij}^\nu \nu_{Mj} \quad i = 1, 2, 3, \quad (14.14)$$

where  $P_L$  is the left projector.

In what follows we will discuss some interesting particular cases of this general framework: light Dirac neutrinos in Sec.14.2.1, and light Majorana neutrinos and the see-saw mechanism in Sec.14.2.2. A special case of the second one is the possibility of light-sterile neutrinos discussed in Sec.14.2.3. In Sec.14.2.4 we shall discuss the effective generation of neutrino masses from non-renormalizable operators (of which the see-saw mechanism is a particular realization).

#### 14.2.1 Dirac Neutrinos

Imposing  $M_N = 0$  is equivalent to imposing lepton number symmetry on the model. Doing so only the first term in Eq.(14.6), the Dirac mass term, is allowed. If sterile neutrinos are three ( $m = 3$ ), we can identify them with the right-handed component of a four-spinor neutrino field. In this case the Dirac mass term can be diagonalized with two  $3 \times 3$  unitary matrices,  $V^\nu$  and  $V_R^\nu$  as:

$$V_R^{\nu\dagger} M_D V^\nu = \text{diag}(m_1, m_2, m_3). \quad (14.15)$$

The neutrino mass term can be written as:

$$-\mathcal{L}_{M_\nu} = \sum_{k=1}^3 m_k \bar{\nu}_{Dk} \nu_{Dk}, \quad (14.16)$$

where

$$\nu_{Dk} = (V^\nu)^\dagger \bar{\nu}_L)_k + (V_R^{\nu\dagger} \bar{\nu}_s)_k, \quad (14.17)$$

so the weak-doublet components of the neutrino fields are

$$\nu_{Li} = P_L \sum_{j=1}^3 V_{ij}^\nu \nu_{Dj}. \quad i = 1, 2, 3. \quad (14.18)$$

Let's stress that in this case both the low energy matter content and the assumed symmetries are different from those of the SM. Consequently the SM is not even a good low-energy effective theory. Furthermore, this scenario does not explain the fact that neutrinos are much lighter than the corresponding charged fermions, because all acquire their mass via the same mechanism.

#### 14.2.2 The See-saw Mechanism

If the mass eigenvalues of  $M_N$  are much higher than the scale of electroweak symmetry breaking  $v$ , the diagonalization of  $M_\nu$  leads to three light neutrinos,  $\nu_l$ , and  $m$  heavy neutrinos,  $N$ :

$$-\mathcal{L}_{M_\nu} = \frac{1}{2} \bar{\nu}_l M^l \nu_l + \frac{1}{2} \bar{N} M^h N, \quad (14.19)$$

with

$$M^l \simeq -V_l^T M_D^T M_N^{-1} M_D V_l, \quad M^h \simeq V_h^T M_N V_h, \quad (14.20)$$

and

$$V^\nu \simeq \begin{bmatrix} \left(1 - \frac{1}{2} M_D^\dagger M_N^* - 1 M_N^{-1} M_D\right) V_l & M_D^\dagger M_N^* V_h \\ -M_N^{-1} M_D V_l & \left(1 - \frac{1}{2} M_N^{-1} M_D M_D^\dagger M_N^* - 1\right) V_h \end{bmatrix}, \quad (14.21)$$

where  $V_l$  and  $V_h$  are  $3 \times 3$  and  $m \times m$  unitary matrices respectively. From Eq.(14.20) we see that the masses of the heavier states are proportional to  $M_N$  while those of the lighter ones to  $M_N^{-1}$ , hence the name of *see-saw mechanism* [9–13]. Also, as seen from Eq.(14.21), the heavy states are mostly right-handed while the light ones are mostly left-handed. Both the light and the heavy neutrinos are Majorana particles. Two well-known examples of extensions of the SM leading to a see-saw mechanism for neutrino masses are SO(10) Grand Unified Theories [10, 11] and left-right symmetry [13].

In this case the SM is a good effective low energy theory. Indeed the see-saw mechanism is a particular example of a full theory whose low energy effective realization is the SM with three light Majorana neutrinos which we describe in Sec.14.2.4.

#### 14.2.3 Light Sterile Neutrinos

If the scale of some  $n_s \leq m$  eigenvalues of  $M_N$  are not higher than the electroweak scale, the low energy spectrum contains  $n_s$  additional light states with large admixture of sterile component. As in the case with Dirac Neutrinos, the SM is not a good low energy effective theory: there are more than three ( $3+n_s$ ) light neutrinos, and they are admixtures of doublet and singlet fields. As in the general case, both light and heavy neutrinos are Majorana particles.

#### 14.2.4 Neutrino Masses from Generic New Physics

Under the generic hypothesis that new physics (NP) beyond the SM only manifests itself directly above some scale  $\Lambda_{\text{NP}}$ , we can consider that the SM is an effective low energy theory which is valid to describe the physical world at energies well below  $\Lambda_{\text{NP}}$  with the same gauge group, fermionic spectrum, and the pattern of spontaneous symmetry breaking of the SM. However, this is an effective theory, holding only till energy below  $\Lambda_{\text{NP}}$ , and consequently does not need to be renormalizable. In this case the low energy Lagrangian can contain non-renormalizable higher dimensional terms whose effect will be suppressed by powers  $1/\Lambda_{\text{NP}}^{\text{dim}-4}$ .

In this approach, the least suppressed NP effects at low energy are expected to come from  $\text{dim}=5$  operators. With the SM fields an gauge symmetry one can only construct the following set of dimension-five terms

$$\mathcal{O}_5 = \frac{Z_{ij}^\nu}{\Lambda_{\text{NP}}} (\bar{L}_{Li} \tilde{\phi}) (\tilde{\phi}^T L_{Lj}^C) + \text{h.c.} \quad (14.22)$$

This set violates (14.3) which poses no problem since in general there is no reason for the NP to respect the accidental symmetries of the SM. In particular it violates total lepton number by two units and after spontaneous symmetry breaking it generates a bilinear neutrino field term:

$$-\mathcal{L}_{M_\nu} = \frac{Z_{ij}^\nu}{2} \frac{v^2}{\Lambda_{\text{NP}}} \bar{\nu}_{Li} \nu_{Lj}^c + \text{h.c.} \quad (14.23)$$

This is a Majorana mass term (see Eq.(14.8)). It is built with the left-handed neutrino fields and with mass matrix:

$$(M_\nu)_{ij} = Z_{ij}^\nu \frac{v^2}{\Lambda_{\text{NP}}}. \quad (14.24)$$

We conclude that Eq.(14.24) would arise in a generic extension of the SM and that neutrino masses are very likely to appear if there is NP. Comparing Eq.(14.24) and Eq.(14.5), we also find that the scale of neutrino masses is suppressed by  $v/\Lambda_{\text{NP}}$  when compared to the scale of charged fermion masses providing an explanation for their smallness. Furthermore, both total lepton number and the lepton flavour symmetry  $U(1)_e \times U(1)_\mu \times U(1)_\tau$  are broken by Eq.(14.24) which means that, generically, in the absence of additional symmetries on the coefficients  $Z_{ij}$ , we can expect lepton flavour mixing and CP violation as we discuss in next section.

Finally, we notice that, as mentioned in Sec.14.2.2, a theory where the NP is composed of  $m$  heavy sterile neutrinos, provides an specific example of a theory which at low energy theory contains three light mass eigenstates with an effective dim-5 interaction of the form (14.22) with  $\Lambda_{\text{NP}} = M_N$ . This is, in this case the NP scale is the characteristic mass scale of the heavy sterile neutrinos.

### 14.3 Lepton Mixing

Let us start by considering  $n = 3 + m$  massive neutrino states and denote the neutrino mass eigenstates by  $(\nu_1, \nu_2, \nu_3, \dots, \nu_n)$ . The neutrino interaction eigenstates are denoted by  $\tilde{\nu} = (\nu_{Le}, \nu_{L\mu}, \nu_{L\tau}, \nu_{s1}, \dots, \nu_{sm})$ . We label the corresponding mass and interaction eigenstates for the charged leptons as  $(e, \mu, \tau)$  and  $(e^I, \mu^I, \tau^I)$  respectively. The Lagrangian for the leptonic charged current interactions in the mass basis takes the form:

$$-\mathcal{L}_{\text{CC}} = \frac{g}{\sqrt{2}} (\bar{e}_L, \bar{\mu}_L, \bar{\tau}_L) \gamma^\mu U \begin{pmatrix} \nu_1 \\ \nu_2 \\ \nu_3 \\ \vdots \\ \nu_n \end{pmatrix} W_\mu^+ + \text{h.c.}, \quad (14.25)$$

where  $U$  is a  $3 \times n$  matrix [14–16]. It satisfies the unitary condition

$$UU^\dagger = I_{3 \times 3}. \quad (14.26)$$

However, in general  $U^\dagger U \neq I_{n \times n}$ .

In the interaction basis, the mass terms for the leptons are:

$$-\mathcal{L}_M = [(\bar{e}_L^I, \bar{\mu}_L^I, \bar{\tau}_L^I) M_\ell \begin{pmatrix} e_R^I \\ \mu_R^I \\ \tau_R^I \end{pmatrix} + \text{h.c.}] - \mathcal{L}_{M_\nu}, \quad (14.27)$$

with  $\mathcal{L}_{M_\nu}$  given in Eq.(14.8).  $M_\ell$  can be diagonalize with two  $3 \times 3$  unitary matrices  $V^\ell$  and  $V_R^\ell$  which satisfy

$$V^{\ell\dagger} M_\ell V_R^\ell = \text{diag}(m_e, m_\mu, m_\tau). \quad (14.28)$$

Then for the charged leptons we have

$$-\mathcal{L}_{M_\ell} = \sum_{k=1}^3 m_{\ell k} \bar{\ell}_k \ell_k, \quad (14.29)$$

with

$$\ell_k = (V^{\ell\dagger} \ell_L^I)_k + (V_R^\ell \ell_R^I)_k. \quad (14.30)$$

Inverting the equation above we find that the weak-doublet components of the charged lepton fields are

$$\ell_{Li}^I = P_L \sum_{j=1}^3 V_{ij}^\ell \ell_{Lj}. \quad i = 1, 2, 3 \quad (14.31)$$

From Eqs.(14.14), (14.18) and (14.31) we find that the mixing matrix  $U$  can be expressed as:

$$U_{ij} = \mathcal{P}_{\ell,ii} V_{ik}^{\ell\dagger} V_{kj}^\nu (\mathcal{P}_{\nu,jj}). \quad (14.32)$$

The matrix  $V^{\ell\dagger} V^\nu$  contains a number of phases that are not physical. Three of them are eliminated by the diagonal  $3 \times 3$  phase matrix  $\mathcal{P}_\ell$  that absorbs them in the charged lepton mass eigenstates. If neutrinos are Dirac states, further  $n - 1$  are similarly eliminated by absorbing them in the neutrino mass eigenstates with the diagonal  $n \times n$  phase matrix  $\mathcal{P}_\nu$ . For Majorana neutrinos,  $\mathcal{P}_\nu = I_{n \times n}$  because one cannot rotate by an arbitrary phase a Majorana field without physical effects. If one rotates a Majorana neutrino by a phase, this phase will appear in its mass term which will no longer be real. Consequently the number of phases

that can be absorbed by redefining the mass eigenstates depends on whether the neutrinos are Dirac or Majorana particles. Altogether for  $n \geq 3$  Majorana [Dirac] neutrinos the  $U$  matrix contains a total of  $6(n-2)$  [ $5n-11$ ] real parameters, of which  $3(n-2)$  are angles and  $3(n-2)$  [ $2n-5$ ] can be interpreted as physical phases.

The possibility of arbitrary mixing between massive neutrino states was first discussed in the context of two neutrinos introduced in Ref. [17] (the possibility of two mixed massless flavour neutrino states had been previously considered in the literature [18], and even before the possibility of mixing between neutrino

and antineutrino states in the seminal paper of Pontecorvo [19]). For that case, in which only mixing between two generations is considered with  $n = 2$  distinct neutrino masses, the  $U$  matrix is  $2 \times 2$  and contains one mixing angle if the neutrinos are Dirac and an additional physical phase if they are Majorana.

If there are only  $n = 3$  Majorana neutrinos,  $U$  is a  $3 \times 3$  matrix analogous to the CKM matrix for the quarks [20,21] but due to the Majorana nature of the neutrinos it depends on six independent parameters: three mixing angles and three phases. In this case the mixing matrix can be conveniently parametrized as:

$$U = \begin{pmatrix} 1 & 0 & 0 \\ 0 & c_{23} & s_{23} \\ 0 & -s_{23} & c_{23} \end{pmatrix} \cdot \begin{pmatrix} c_{13} & 0 & s_{13}e^{-i\delta_{CP}} \\ 0 & 1 & 0 \\ -s_{13}e^{i\delta_{CP}} & 0 & c_{13} \end{pmatrix} \cdot \begin{pmatrix} c_{21} & s_{12} & 0 \\ -s_{12} & c_{12} & 0 \\ 0 & 0 & 1 \end{pmatrix} \cdot \begin{pmatrix} e^{i\eta_1} & 0 & 0 \\ 0 & e^{i\eta_2} & 0 \\ 0 & 0 & 1 \end{pmatrix}, \quad (14.33)$$

where  $c_{ij} \equiv \cos \theta_{ij}$  and  $s_{ij} \equiv \sin \theta_{ij}$ . The angles  $\theta_{ij}$  can be taken without loss of generality to lie in the first quadrant,  $\theta_{ij} \in [0, \pi/2]$  and the phases  $\delta_{CP}, \eta_i \in [0, 2\pi]$ . This is to be compared to the case of three Dirac neutrinos. In this case the Majorana phases,

$\eta_1$  and  $\eta_2$ , can be absorbed in the neutrino states so number of physical phases is one (similar to the CKM matrix). Thus we can write  $U$  as:

$$U = \begin{pmatrix} c_{12} c_{13} & s_{12} c_{13} & s_{13} e^{-i\delta_{CP}} \\ -s_{12} c_{23} - c_{12} s_{13} s_{23} e^{i\delta_{CP}} & c_{12} c_{23} - s_{12} s_{13} s_{23} e^{i\delta_{CP}} & c_{13} s_{23} \\ s_{12} s_{23} - c_{12} s_{13} c_{23} e^{i\delta_{CP}} & -c_{12} s_{23} - s_{12} s_{13} c_{23} e^{i\delta_{CP}} & c_{13} c_{23} \end{pmatrix}. \quad (14.34)$$

This matrix is often called the Pontecorvo-Maki-Nakagawa-Sakata (PMNS) mixing matrix.

Notice that when the charged leptons have no other interactions than the SM ones, one can identify their interaction eigenstates with the corresponding mass eigenstates up to phase redefinition. This implies that, in this case,  $U$  is just a  $3 \times n$  sub-matrix of the unitary neutrino mass diagonalizing matrix  $V^\nu$ .

Finally, let us point out that for the case of 3 light Dirac neutrinos the procedure above leads to a unitary  $U$  matrix for the light states. But for three light Majorana neutrinos this is not the case when the full spectrum contains states which are heavy and are not in the low energy spectrum as seen, for example, in Eq.(14.21). This implies that, strictly speaking, the parametrization in Eq.(14.33) is not valid to describe the flavour mixing of the three light Majorana neutrinos in the see-saw mechanism. The violation of unitarity, however, is rather small, of the order  $\mathcal{O}(M_D/M_N)$  as seen in Eq.(14.21). It is also severely constrained experimentally [22,23]. For all these reasons, for all practical purposes, we will consider the  $U$  matrix for the  $3\nu$  mixing case to be unitary independently of whether neutrinos are Dirac or Majorana particles.

### 14.4 Mass-Induced Flavour Oscillations in Vacuum

If neutrinos have masses and lepton flavours are mixed in the weak CC interactions, lepton flavour is not conserved in neutrino propagation [19,24]. This phenomenon is usually referred to as *neutrino oscillations*. In brief, a weak eigenstates,  $\nu_\alpha$ , which by default is the state produced in the weak CC interaction of a charged lepton  $\ell_\alpha$ , is the linear combination determined by the mixing matrix  $U$

$$|\nu_\alpha\rangle = \sum_{i=1}^n U_{\alpha i}^* |\nu_i\rangle, \quad (14.35)$$

where  $\nu_i$  are the mass eigenstates and here  $n$  is the number of light neutrino species (implicit in our definition of the state  $|\nu\rangle$  is its energy-momentum and space-time dependence). After travelling a distance  $L$  ( $L \simeq ct$  for relativistic neutrinos), that state evolves as:

$$|\nu_\alpha(t)\rangle = \sum_{i=1}^n U_{\alpha i}^* |\nu_i(t)\rangle. \quad (14.36)$$

This neutrino can then undergo a charged-current (CC) interaction producing a charge lepton  $\ell_\beta$ ,  $\nu_\alpha(t)N' \rightarrow \ell_\beta N$ , with a

probability

$$P_{\alpha\beta} = |\langle \nu_\beta | \nu_\alpha(t) \rangle|^2 = \left| \sum_{i=1}^n \sum_{j=1}^n U_{\alpha i}^* U_{\beta j} \langle \nu_j | \nu_i(t) \rangle \right|^2. \quad (14.37)$$

Assuming that  $|\nu\rangle$  is a plane wave,  $|\nu_i(t)\rangle = e^{-i E_i t} |\nu_i(0)\rangle$ ,<sup>3</sup> with  $E_i = \sqrt{p_i^2 + m_i^2}$  and  $m_i$  being, respectively, the energy and the mass of the neutrino mass eigenstate  $\nu_i$ . In all practical cases neutrinos are very relativistic, so  $p_i \simeq p_j \equiv p \simeq E$ . We can then write

$$E_i = \sqrt{p_i^2 + m_i^2} \simeq p + \frac{m_i^2}{2E}, \quad (14.38)$$

and use the orthogonality of the mass eigenstates,  $\langle \nu_j | \nu_i \rangle = \delta_{ij}$ , to arrive to the following form for  $P_{\alpha\beta}$ :

$$P_{\alpha\beta} = \delta_{\alpha\beta} - 4 \sum_{i<j} \text{Re}[U_{\alpha i} U_{\beta i}^* U_{\alpha j}^* U_{\beta j}] \sin^2 X_{ij} + 2 \sum_{i<j} \text{Im}[U_{\alpha i} U_{\beta i}^* U_{\alpha j}^* U_{\beta j}] \sin 2X_{ij}, \quad (14.39)$$

where

$$X_{ij} = \frac{(m_i^2 - m_j^2)L}{4E} = 1.267 \frac{\Delta m_{ij}^2}{\text{eV}^2} \frac{L/E}{\text{m/MeV}}. \quad (14.40)$$

If we had made the same derivation for antineutrino states we would have ended with a similar expression but with the exchange  $U \rightarrow U^*$ . Consequently we conclude that the first term in the right-hand-side of Eq.(14.39) is CP conserving since it is the same for neutrinos and antineutrinos, while the last one is CP violating because it has opposite sign for neutrinos and antineutrinos.

Equation (14.39) oscillatory in distance with oscillation lengths

$$L_{0,ij}^{\text{osc}} = \frac{4\pi E}{|\Delta m_{ij}^2|}, \quad (14.41)$$

and with amplitudes proportional to products of elements in the mixing matrix. Thus, neutrinos must have different masses

<sup>3</sup> For a pedagogical discussion of the quantum mechanical description of flavour oscillations in the wave package approach see for example Ref. [3]. A recent review of the quantum mechanical aspects and subtleties on neutrino oscillations can be found in Ref. [25].

( $\Delta m_{ij}^2 \neq 0$ ) and they must have not vanishing mixing ( $U_{\alpha_i} U_{\beta_i} \neq 0$ ) in order to undergo flavour oscillations. Also, from Eq.(14.39) we see that the Majorana phases cancel out in the oscillation probability. This is expected because flavour oscillation is a total lepton number conserving process.

Ideally, a neutrino oscillation experiment would like to measure an oscillation probability over a distance  $L$  between the source and the detector, for neutrinos of a definite energy  $E$ . In practice, neutrino beams, both from natural or artificial sources, are never monoenergetic, but have an energy spectrum  $\Phi(E)$ . In addition each detector has a finite energy resolution. Under these circumstances what is measured is an average probability

$$\begin{aligned} \langle P_{\alpha\beta} \rangle &= \frac{\int dE \frac{d\Phi}{dE} \sigma(E) P_{\alpha\beta}(E) \epsilon(E)}{\int dE \frac{d\Phi}{dE} \sigma_{CC}(E) \epsilon(E)} \\ &= \delta_{\alpha\beta} - 4 \sum_{i < j}^n \text{Re}[U_{\alpha i} U_{\beta i}^* U_{\alpha j}^* U_{\beta j}] \langle \sin^2 X_{ij} \rangle \\ &\quad + 2 \sum_{i < j}^n \text{Im}[U_{\alpha i} U_{\beta i}^* U_{\alpha j}^* U_{\beta j}] \langle \sin 2X_{ij} \rangle. \end{aligned} \quad (14.42)$$

$\sigma$  is the cross section for the process in which the neutrino flavour is detected, and  $\epsilon(E)$  is the detection efficiency. The minimal range of the energy integral is determined by the energy resolution of the experiment.

It is clear from the above expression that if  $(E/L) \gg |\Delta m_{ij}^2|$  ( $L \ll L_{0,ij}^{\text{osc}}$ ) so  $\sin^2 X_{ij} \ll 1$ , the oscillation phase does not give any appreciable effect. Conversely if  $L \gg L_{0,ij}^{\text{osc}}$ , many oscillation cycles occur between production and detection so the oscillating term is averaged to  $\langle \sin^2 X_{ij} \rangle = 1/2$ .

We summarize in Table 14.1. the typical values of  $L/E$  for different types of neutrino sources and experiments and the corresponding ranges of  $\Delta m^2$  to which they can be most sensitive.

**Table 14.1:** Characteristic values of  $L$  and  $E$  for experiments performed using various neutrino sources and the corresponding ranges of  $|\Delta m^2|$  to which they can be most sensitive to flavour oscillations in vacuum. SBL stands for Short Baseline and LBL for Long Baseline.

Experiment	$L$ (m)	$E$ (MeV)	$ \Delta m^2 $ (eV <sup>2</sup> )
Solar	$10^{10}$	1	$10^{-10}$
Atmospheric	$10^4 - 10^7$	$10^2 - 10^5$	$10^{-1} - 10^{-4}$
Reactor	SBL $10^2 - 10^3$	1	$10^{-2} - 10^{-3}$
	LBL $10^4 - 10^5$		$10^{-4} - 10^{-5}$
Accelerator	SBL $10^2$	$10^3 - 10^4$	$> 0.1$
	LBL $10^5 - 10^6$	$10^3 - 10^4$	$10^{-2} - 10^{-3}$

Historically, the results of neutrino oscillation experiments were interpreted assuming two-neutrino states so there is only one oscillating phase, the mixing matrix depends on a single mixing angle  $\theta$  and no CP violation effect in oscillations is possible. At present, as we will discuss in Sec.14.7, we need at least the mixing among three-neutrino states to fully describe the bulk of experimental results. However, in many cases, the observed results can be understood in terms of oscillations dominantly driven by one  $\Delta m^2$ . In this limit  $P_{\alpha\beta}$  of Eq.(14.39) takes the form [24]

$$P_{\alpha\beta} = \delta_{\alpha\beta} - (2\delta_{\alpha\beta} - 1) \sin^2 2\theta \sin^2 X. \quad (14.43)$$

In this effective  $2 - \nu$  limit, changing the sign of the mass difference,  $\Delta m^2 \rightarrow -\Delta m^2$ , and changing the octant of the mixing angle,  $\theta \rightarrow \frac{\pi}{2} - \theta$ , is just redefining the mass eigenstates,  $\nu_1 \leftrightarrow \nu_2$ :

$P_{\alpha\beta}$  must be invariant under such transformation. So the physical parameter space can be covered with either  $\Delta m^2 \geq 0$  with  $0 \leq \theta \leq \frac{\pi}{2}$ , or, alternatively,  $0 \leq \theta \leq \frac{\pi}{4}$  with either sign for  $\Delta m^2$ .

However, from Eq.(14.43) we see that  $P_{\alpha\beta}$  is actually invariant under the change of sign of the mass splitting and the change of octant of the mixing angle separately. This implies that there is a two-fold discrete ambiguity since the two different sets of physical parameters,  $(\Delta m^2, \theta)$  and  $(\Delta m^2, \frac{\pi}{2} - \theta)$ , give the same transition probability in vacuum. In other words, one could not tell from a measurement of, say,  $P_{e\mu}$  in vacuum whether the larger component of  $\nu_e$  resides in the heavier or in the lighter neutrino mass eigenstate. This symmetry is broken when one considers mixing of three or more neutrinos in the flavour evolution and/or when the neutrinos traverse regions of dense matter as we describe in Sec.14.7.1 and Sec.14.5 respectively.

## 14.5 Propagation of Massive Neutrinos in Matter

Neutrinos propagating in a dense medium can interact with the particles in the medium. The probability of an incoherent inelastic scattering is very small. For example the characteristic cross section for  $\nu$ -proton scattering is of the order

$$\sigma \sim \frac{G_F^2 s}{\pi} \sim 10^{-43} \text{ cm}^2 \left( \frac{E}{\text{MeV}} \right)^2, \quad (14.44)$$

where  $G_F$  is the Fermi constant and  $s$  is the square of the center of mass energy of the collision.

But when neutrinos propagate in dense matter, they can also interact coherently with the particles in the medium. By definition, in coherent interactions, the medium remains unchanged so it is possible to have interference of the forward scattered and the unscattered neutrino waves which enhances the effect of matter in the neutrino propagation. In this case the effect of the medium is not on the intensity of the propagating neutrino beam, which remains unchanged, but on the phase velocity of the neutrino wave, and for this reason the effect is proportional to  $G_F$ , instead of the  $G_F^2$  dependence of the incoherent scattering. Coherence also allows decoupling the evolution equation of the neutrinos from those of the medium. In this limit the effect of the medium is introduced in the evolution equation for the neutrinos in the form of an effective potential which depends on the density and composition of the matter [26].

As an example, let us consider the evolution of  $\nu_e$  in a medium with electrons, protons and neutrons with corresponding  $n_e$ ,  $n_p$  and  $n_n$  number densities. The effective low-energy Hamiltonian describing the relevant neutrino interactions at point  $x$  is given by

$$H_W = \frac{G_F}{\sqrt{2}} \left[ J^{(+)\alpha}(x) J_{\alpha}^{(-)}(x) + \frac{1}{4} J^{(N)\alpha}(x) J_{\alpha}^{(N)}(x) \right], \quad (14.45)$$

where the  $J_{\alpha}$ 's are the standard fermionic currents

$$J_{\alpha}^{(+)}(x) = \bar{\nu}_e(x) \gamma_{\alpha} (1 - \gamma_5) e(x), \quad (14.46)$$

$$J_{\alpha}^{(-)}(x) = \bar{e}(x) \gamma_{\alpha} (1 - \gamma_5) \nu_e(x), \quad (14.47)$$

$$\begin{aligned} J_{\alpha}^{(N)}(x) &= \bar{\nu}_e(x) \gamma_{\alpha} (1 - \gamma_5) \nu_e(x) \\ &\quad - \bar{e}(x) [\gamma_{\alpha} (1 - \gamma_5) - 4 \sin^2 \theta_W \gamma_{\alpha}] e(x) \\ &\quad + \bar{p}(x) [\gamma_{\alpha} (1 - g_A^{(p)} \gamma_5) - 4 \sin^2 \theta_W \gamma_{\alpha}] p(x) \\ &\quad - \bar{n}(x) \gamma_{\alpha} (1 - g_A^{(n)} \gamma_5) n(x), \end{aligned} \quad (14.48)$$

and  $g_A^{(n,p)}$  are the axial couplings for neutrons and protons, respectively.

Let us focus first on the the effect of the charged current interactions. The effective CC Hamiltonian due to electrons in the medium is



$$\begin{aligned}
 H_C^{(e)} &= \frac{G_F}{\sqrt{2}} \int d^3 p_e f(E_e, T) \times \left\langle \langle e(s, p_e) | \bar{e}(x) \gamma^\alpha (1 - \gamma_5) \nu_e(x) \bar{\nu}_e(x) \gamma_\alpha (1 - \gamma_5) e(x) | e(s, p_e) \rangle \right\rangle \\
 &= \frac{G_F}{\sqrt{2}} \bar{\nu}_e(x) \gamma_\alpha (1 - \gamma_5) \nu_e(x) \int d^3 p_e f(E_e, T) \left\langle \langle e(s, p_e) | \bar{e}(x) \gamma_\alpha (1 - \gamma_5) e(x) | e(s, p_e) \rangle \right\rangle.
 \end{aligned} \tag{14.49}$$

In the above equation we denote by  $s$  the electron spin, and by  $p_e$  its momentum and  $f(E_e, T)$ , is the energy distribution function of the electrons in the medium which is assumed to be homogeneous and isotropic and is normalized as

$$\int d^3 p_e f(E_e, T) = 1. \tag{14.50}$$

We denote by  $\langle \dots \rangle$  the averaging over electron spinors and summing over all electrons in the medium. Coherence dictates that  $s, p_e$  are the same for initial and final electrons. The axial current reduces to the spin in the non-relativistic limit and therefore averages to zero for a background of non-relativistic electrons. The spatial components of the vector current cancel because of isotropy. Therefore the only non trivial average is

$$\int d^3 p_e f(E_e, T) \left\langle \langle e(s, p_e) | \bar{e}(x) \gamma_0 e(x) | e(s, p_e) \rangle \right\rangle = n_e(x), \tag{14.51}$$

which gives a contribution to the effective Hamiltonian

$$H_C^{(e)} = \sqrt{2} G_F n_e \bar{\nu}_{eL}(x) \gamma_0 \nu_{eL}(x). \tag{14.52}$$

This can be interpreted as a contribution to the  $\nu_{eL}$  potential energy

$$V_C = \sqrt{2} G_F n_e. \tag{14.53}$$

Should we have considered antineutrino states we would have ended up with  $V_C = -\sqrt{2} G_F n_e$ . For a more detailed derivation of the matter potentials see, for example, Ref. [3].

With an equivalent derivation we find that for  $\nu_\mu$  and  $\nu_\tau$ , the potential due to its CC interactions is zero for most media since neither  $\mu$ 's nor  $\tau$ 's are present, while the effective potential for any active neutrino due to the neutral current interactions is found to be

$$V_{NC} = \frac{\sqrt{2}}{2} G_F \left[ -n_e (1 - 4 \sin^2 \theta_w) + n_p (1 - 4 \sin^2 \theta_w) - n_n \right]. \tag{14.54}$$

In neutral matter  $n_e = n_p$  and the contribution from electrons and protons cancel each other. So we are left only with the neutron contribution

$$V_{NC} = -1/\sqrt{2} G_F n_n. \tag{14.55}$$

After including these effects, the evolution equation for  $n$  ultrarelativistic neutrinos propagating in matter written in the mass basis is (see for instance Ref. [27–29] for the derivation):

$$i \frac{d\vec{\nu}}{dx} = H \vec{\nu}, \quad H = H_m + U^{\nu\dagger} V U^\nu. \tag{14.56}$$

Here  $\vec{\nu} \equiv (\nu_1, \nu_2, \dots, \nu_n)^T$ ,  $H_m$  is the kinetic Hamiltonian,

$$H_m = \frac{1}{2E} \text{diag}(m_1^2, m_2^2, \dots, m_n^2), \tag{14.57}$$

and  $V$  is the effective neutrino potential in the interaction basis.  $U^\nu$  is the  $n \times n$  submatrix of the unitary  $V^\nu$  matrix corresponding to the  $n$  ultrarelativistic neutrino states. For the three SM active neutrinos with purely SM interactions crossing a neutral medium with electrons, protons and neutrons, the evolution equation takes the form (14.56) with  $U^\nu \equiv U$ , and the effective potential:

$$V = \text{diag}(\pm\sqrt{2} G_F n_e(x), 0, 0) \equiv \text{diag}(V_e, 0, 0). \tag{14.58}$$

The sign  $+$  ( $-$ ) in Eq.(14.58) applies to neutrinos (antineutrinos), and  $n_e(x)$  is the electron number density in the medium, which

in general is not constant along the neutrino trajectory so the potential is not constant. Characteristic value of the potential at the Earth core is  $V_e \sim 10^{-13}$  eV while at the solar core  $V_e \sim 10^{-12}$  eV. Since the neutral current potential Eq.(14.55) is flavour diagonal, it can be eliminated from the evolution equation as it only contributes to an overall unobservable phase.

The instantaneous mass eigenstates in matter,  $\nu_i^m$ , are the eigenstates of the Hamiltonian  $H$  in (14.56) for a fixed value of  $x$ , and they are related to the interaction basis by

$$\vec{\nu} = \tilde{U}(x) \nu^{\vec{m}}. \tag{14.59}$$

The corresponding instantaneous eigenvalues of  $H$  are  $\mu_i(x)^2/(2E)$  with  $\mu_i(x)$  being the instantaneous effective neutrino masses.

Let us take for simplicity a neutrino state which is an admixture of only two neutrino species  $|\nu_\alpha\rangle$  and  $|\nu_\beta\rangle$ , so the two instantaneous mass eigenstates in matter  $\nu_1^m$  and  $\nu_2^m$  have instantaneous effective neutrino masses

$$\mu_{1,2}^2(x) = \frac{m_1^2 + m_2^2}{2} + E[V_\alpha + V_\beta] \tag{14.60}$$

$$\mp \frac{1}{2} \sqrt{[\Delta m^2 \cos 2\theta - A]^2 + [\Delta m^2 \sin 2\theta]^2},$$

and  $\tilde{U}(x)$  is a 2x2 rotation matrix with the instantaneous mixing angle in matter given by

$$\tan 2\theta_m = \frac{\Delta m^2 \sin 2\theta}{\Delta m^2 \cos 2\theta - A}. \tag{14.61}$$

In the Eqs.(14.60) and (14.61)  $A$  is

$$A \equiv 2E(V_\alpha - V_\beta), \tag{14.62}$$

and its sign depends on depends on the composition of the medium and on the flavour composition of the neutrino state considered. From the expressions above we see that for a given sign of  $A$  the mixing angle in matter is larger(smaller) than in vacuum if this last one is in the first (second) octant. We see that the symmetry about 45 degrees which existing in vacuum oscillations between two neutrino states is broken by the matter potential in propagation in a medium. The expressions above show that very important effects are present when  $A$ , is close to  $\Delta m^2 \cos 2\theta$ . In particular, as seen in Eq.(14.61), the tangent of the mixing angle changes sign if, along its path, the neutrino passes by some matter density region satisfying, for its energy, the *resonance condition*

$$A_R = \Delta m^2 \cos 2\theta. \tag{14.63}$$

This implies that if the neutrino is created in a region where the relevant potential satisfies  $A_0 > A_R$  ( $A_0$  here is the value of the relevant potential at the production point), then the effective mixing angle in matter at the production point is such that  $\text{sgn}(\cos 2\theta_{m,0}) = -\text{sgn}(\cos 2\theta)$ . So the flavour component of the mass eigenstates is inverted as compared to their composition in vacuum. In particular, if at production point we have  $A_0 = 2A_R$ , then  $\theta_{m,0} = \frac{\pi}{2} - \theta$ . Asymptotically, for  $A_0 \gg A_R$ ,  $\theta_{m,0} \rightarrow \frac{\pi}{2}$ . In other words, if in vacuum the lightest (heaviest) mass eigenstate has a larger projection on the flavour  $\alpha$  ( $\beta$ ), inside a matter with density and composition such that  $A > A_R$ , the opposite holds. So if the neutrino system is travelling across a monotonically varying matter potential, the dominant flavour component of a given mass eigenstate changes when crossing the region with  $A = A_R$ . This phenomenon is known as *level crossing*.

Taking the derivative of Eq.(14.59) with respect to  $x$  and using Eq.(14.56), we find that in the instantaneous mass basis the evolution equation reads:

$$i \frac{d\vec{\nu}^m}{dx} = \left[ \frac{1}{2E} \text{diag} (\mu_1^2(x), \mu_2^2(x), \dots, \mu_n^2(x)) - i \tilde{U}^\dagger(x) \frac{d\tilde{U}(x)}{dx} \right] \vec{\nu}^m. \quad (14.64)$$

The presence of the last term, Eq.(14.64) implies that this is a system of coupled equations. So in general, the instantaneous mass eigenstates,  $\nu_i^m$  are not energy eigenstates. For constant or slowly enough varying matter potential this last term can be neglected and the instantaneous mass eigenstates,  $\nu_i^m$ , behave approximately as energy eigenstates and they do not mix in the evolution. This is the *adiabatic* transition approximation. On the contrary, when the last term in Eq.(14.64) cannot be neglected, the instantaneous mass eigenstates mix along the neutrino path. This implies there can be *level-jumping* [30–33] and the evolution is *non-adiabatic*.

For adiabatic evolution in matter the oscillation probability take a form very similar to the vacuum oscillation expression, Eq.(14.39). For example, neglecting CP violation:

$$P_{\alpha\beta} = \left| \sum_i \tilde{U}_{\alpha i}(0) \tilde{U}_{\beta i}(L) \exp \left( -\frac{i}{2E} \int_0^L \mu_i^2(x') dx' \right) \right|^2. \quad (14.65)$$

To compute  $P_{\alpha\beta}$  in a varying potential one can always solve the evolution equation numerically. Also several analytic approximations for specific profiles of the matter potential can be found in the literature [34].

#### 14.5.1 The Mikheev-Smirnov-Wolfenstein Effect for Solar Neutrinos

The matter effects discussed in the previous section are of special relevance for solar neutrinos. As the Sun produces  $\nu_e$ 's in its core, here we shall consider the propagation of a  $\nu_e - \nu_X$  neutrino system ( $X$  is some superposition of  $\mu$  and  $\tau$ , which is arbitrary because  $\nu_\mu$  and  $\nu_\tau$  have only and equal neutral current interactions) in the matter density of the Sun.

The density of solar matter is a monotonically decreasing function of the distance  $R$  from the center of the Sun, and it can be approximated by an exponential for  $R < 0.9R_\odot$

$$n_e(R) = n_e(0) \exp(-R/r_0), \quad (14.66)$$

with  $r_0 = R_\odot/10.54 = 6.6 \times 10^7 \text{ m} = 3.3 \times 10^{14} \text{ eV}^{-1}$ .

As mentioned above, the nuclear reactions in the Sun produce electron neutrinos. After crossing the Sun, the composition of the neutrino state exiting the Sun will depend on the relative size of  $\Delta m^2 \cos 2\theta$  versus  $A_0 = 2E G_F n_{e,0}$  (here 0 refers to the neutrino production point which is near but not exactly at the center of the Sun,  $R = 0$ ).

If the relevant matter potential at production is well below the resonant value,  $A_R = \Delta m^2 \cos 2\theta \gg A_0$ , matter effects are negligible. With the characteristic matter density and energy of the solar neutrinos, this condition is fulfilled for values of  $\Delta m^2$  such that  $\Delta m^2/E \gg L_{\text{Sun-Earth}}$ . So the propagation occurs as in vacuum with the oscillating phase averaged to  $1/2$  and the survival probability at the exposed surface of the Earth is

$$P_{ee}(\Delta m^2 \cos 2\theta \gg A_0) = 1 - \frac{1}{2} \sin^2 2\theta > \frac{1}{2}. \quad (14.67)$$

If the relevant matter potential at production is only slightly below the resonant value,  $A_R = \Delta m^2 \cos 2\theta \gtrsim A_0$ , the neutrino does not cross a region with resonant density, but matter effects are sizable enough to modify the mixing. The oscillating phase is averaged in the propagation between the Sun and the Earth. This regime is well described by an adiabatic propagation, Eq.(14.65). Using that  $\tilde{U}(0)$  is a  $2 \times 2$  rotation of angle  $\theta_{m,0}$  – the mixing

angle in matter at the neutrino production point–, and  $\tilde{U}(L)$  is the corresponding rotation with vacuum mixing angle  $\theta$ , we get

$$P_{ee}(\Delta m^2 \cos 2\theta \geq A_0) = \cos^2 \theta_{m,0} \cos^2 \theta + \sin^2 \theta_{m,0} \sin^2 \theta = \frac{1}{2} [1 + \cos 2\theta_{m,0} \cos 2\theta]. \quad (14.68)$$

This expression reflects that an electron neutrino produced at  $A_0$  is an admixture of  $\nu_1$  with fraction  $P_{e1,0} = \cos^2 \theta_{m,0}$  and  $\nu_2$  with fraction  $P_{e2,0} = \sin^2 \theta_{m,0}$ . On exiting the Sun,  $\nu_1$  consists of  $\nu_e$  with fraction  $P_{1e} = \cos^2 \theta$ , and  $\nu_2$  consists of  $\nu_e$  with fraction  $P_{2e} = \sin^2 \theta$  so  $P_{ee} = P_{e1,0}P_{1e} + P_{e2,0}P_{2e} = \cos^2 \theta_{m,0} \cos^2 \theta + \sin^2 \theta_{m,0} \sin^2 \theta$  [35–37], exactly as given in Eq.(14.68). Since  $A_0 < A_R$  the resonance is not crossed so  $\cos 2\theta_{m,0}$  has the same sign as  $\cos 2\theta$  and still  $P_{ee} \geq 1/2$ .

Finally, in the case that  $A_R = \Delta m^2 \cos 2\theta < A_0$ , the neutrino can cross the resonance on its way out. In the convention of  $\Delta m^2 > 0$  this occurs if  $\cos 2\theta > 0$  ( $\theta < \pi/4$ ). which means that in vacuum  $\nu_e$  is a combination of  $\nu_1$  and  $\nu_2$  with larger  $\nu_1$  component, while at the production point  $\nu_e$  is a combination of  $\nu_1^m$  and  $\nu_2^m$  with larger  $\nu_2^m$  component. In particular, if the density at the production point is much higher than the resonant density,  $\Delta m^2 \cos 2\theta \ll A_0$ ,

$$\theta_{m,0} = \frac{\pi}{2} \Rightarrow \cos 2\theta_{m,0} = -1, \quad (14.69)$$

and the produced  $\nu_e$  is purely  $\nu_2^m$ .

In this regime, the evolution of the neutrino ensemble can be adiabatic or non-adiabatic depending on the particular values of  $\Delta m^2$  and the mixing angle. The oscillation parameters (see Secs.14.6.1 and 14.7) happen to be such that the transition is adiabatic in all ranges of solar neutrino energies. Thus the survival probability at the exposed surface of the Earth is given by Eq.(14.68) but now with mixing angle (14.69) so

$$P_{ee}(\Delta m^2 \cos 2\theta < A_0) = \frac{1}{2} [1 + \cos 2\theta_{m,0} \cos 2\theta] = \sin^2 \theta. \quad (14.70)$$

So in this case  $P_{ee}$  can be much smaller than  $1/2$  because  $\cos 2\theta_{m,0}$  and  $\cos 2\theta$  have opposite signs. This is referred to as the Mikheev-Smirnov-Wolfenstein (MSW) effect [26, 38] which plays a fundamental role in the interpretation of the solar neutrino data.

The resulting energy dependence of the survival probability of solar neutrinos is shown in Fig.14.3 (together with a compilation of data from solar experiments). The plotted curve corresponds to  $\Delta m^2 \sim 7.5 \times 10^{-5} \text{ eV}^2$  and  $\sin^2 \theta \sim 0.3$  (the so-called large mixing angle, LMA, solution). The figure illustrates the regimes described above. For these values of the oscillation parameters, neutrinos with  $E \ll 1 \text{ MeV}$  are in the regime with  $\Delta m^2 \cos 2\theta \gg A_0$  so the curve represents the value of vacuum averaged survival probability, Eq.(14.67), and therefore  $P_{ee} > 0.5$ . For  $E > 10 \text{ MeV}$ , on the contrary,  $\Delta m^2 \cos 2\theta \ll A_0$  and the survival probability is given by Eq.(14.70), so  $P_{ee} = \sin^2 \theta \sim 0.3$ . In between, the survival probability is given by Eq.(14.68) with  $\theta_0$  changing rapidly from its vacuum value to the asymptotic matter value (14.69),  $90^\circ$ .

## 14.6 Experimental Study of Neutrino Oscillations

Neutrino flavour transitions, or neutrino oscillations, have been experimentally studied using various neutrino sources and detection techniques. Intense sources and large detectors are mandatory because of a large distance necessary for observable oscillation effects in addition to the small cross sections. Also, the relevant neutrino flux before oscillations should be known with sufficient precision for a definitive measurement. Here, the experimental status of neutrino oscillations with the different neutrino sources, the Sun, Earth's atmosphere, accelerators and nuclear reactors, are reviewed.

### 14.6.1 Solar Neutrinos

#### 14.6.1.1 Solar neutrino flux

In the Sun, electron neutrinos are produced in the thermonuclear reactions which generate the solar energy. These reac-

tions occur via two main chains, the  $pp$  chain and the CNO cycle. The  $pp$  chain includes reactions  $p + p \rightarrow d + e^+ + \nu$  ( $pp$ ),  $p + e^- + p \rightarrow d + \nu$  ( $pep$ ),  ${}^3\text{He} + p \rightarrow {}^4\text{He} + e^+ + \nu$  ( $hep$ ),  ${}^7\text{Be} + e^- \rightarrow {}^7\text{Li} + \nu$  ( ${}^7\text{Be}$ ), and  ${}^8\text{B} \rightarrow {}^8\text{Be}^* + e^+ + \nu$  ( ${}^8\text{B}$ ). The CNO cycle involves  ${}^{13}\text{N} \rightarrow {}^{13}\text{C} + e^+ + \nu$  ( ${}^{13}\text{N}$ ),  ${}^{15}\text{O} \rightarrow {}^{15}\text{N} + e^+ + \nu$  ( ${}^{15}\text{O}$ ), and  ${}^{17}\text{F} \rightarrow {}^{17}\text{O} + e^+ + \nu$  ( ${}^{17}\text{F}$ ). Those reactions result in the overall fusion of protons into  ${}^4\text{He}$ ,  $4p \rightarrow {}^4\text{He} + 2e^+ + 2\nu_e$ , where the energy released in the reaction,  $Q = 4m_p - m_{{}^4\text{He}} - 2m_e \sim 26$  MeV, is mostly radiated through the photons and only a small fraction is carried by the neutrinos,  $\langle E_{2\nu_e} \rangle = 0.59$  MeV. In addition, electron capture on  ${}^{13}\text{N}$ ,  ${}^{15}\text{O}$ , and  ${}^{17}\text{F}$  produces line spectra of neutrinos called ecCNO neutrinos. Dividing the solar luminosity by the energy released per neutrino production, the total neutrino flux can be estimated. At the Earth, the  $pp$  solar neutrino flux is about  $6 \times 10^{10} \text{ cm}^{-2}\text{s}^{-1}$ .

The detailed calculation of the solar neutrino fluxes has been done based on the Standard Solar Model (SSM). The SSM describes the structure and evolution of the Sun based on a variety of inputs such as the mass, luminosity, radius, surface temperature, age, and surface elemental abundances. In addition, the knowledge of the absolute nuclear reaction cross sections for the relevant fusion reactions and the radiative opacities are necessary. John Bahcall and his collaborators continuously updated the SSM calculations over several decades [39, 40]. Figure 14.1 shows the solar neutrino fluxes predicted by the SSM calculation in [41] and ecCNO neutrinos in [42].

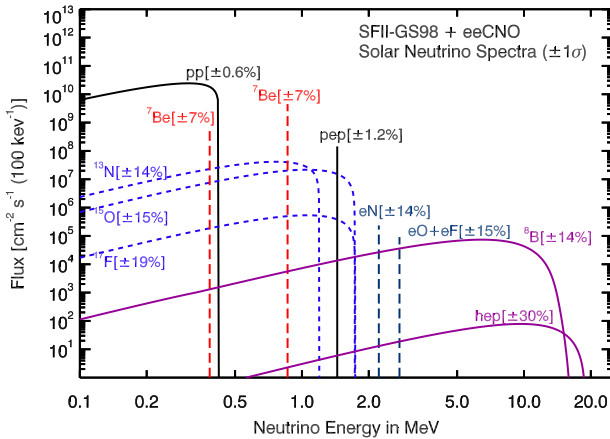


Figure 14.1: Spectrum of solar neutrino fluxes predicted by SSM calculation in [41]. In addition to standard fluxes, ecCNO neutrinos have been added based on [42]. Electron capture fluxes are given in  $\text{cm}^{-2}\text{s}^{-1}$ . Taken from [43]

#### 14.6.1.2 Detection of solar neutrinos and the solar neutrino problem

Experiments which observed solar neutrinos are summarized in Table 14.2.

A pioneering solar neutrino experiment was carried out by R. Davis, Jr. and collaborators at Homestake starting in the late 1960s [44]. The Davis' experiment utilizes the reaction  $\nu_e + {}^{37}\text{Cl} \rightarrow e^- + {}^{37}\text{Ar}$ . Because this process has an energy threshold of 814 keV, the most relevant fluxes are the  ${}^7\text{Be}$  and  ${}^8\text{B}$  neutrinos. The detector contained  $\sim 615$  t of  $\text{C}_2\text{Cl}_4$ . The produced  ${}^{37}\text{Ar}$ , which has a half life of 34.8 d, was chemically extracted and introduced into a low-background proportional chamber every few months. The Auger electrons from electron capture of  ${}^{37}\text{Ar}$  were counted to determine the reaction rate.

From the beginning, the observed number of neutrinos in the Homestake mine experiment was significantly smaller than the prediction by SSM — it was almost one third. After thorough check of both experimental and theoretical work, the discrepancy remained. This became to be known as the solar neutrino problem. The final result from Homestake experiment is  $2.56 \pm 0.16 \pm 0.16$  SNU [45], where SNU (solar neutrino unit) is a unit of event rate,  $1 \text{ SNU} = 10^{-36}$  captures/(s atom). On the other hand, prediction based on SSM is  $8.46^{+0.87}_{-0.88}$  SNU [46].

The detection of neutrinos from other production processes was recognized as an important input to investigate the origin of the solar neutrino problem. In particular, the  $pp$  neutrino is most abundant, and its flux prediction has the smallest uncertainty. Using the radiochemical technique with gallium, the reaction  $\nu_e + {}^{71}\text{Ga} \rightarrow e^- + {}^{71}\text{Ge}$  has an energy threshold of 233 keV and can be used for the  $pp$  neutrino detection. According to the SSM, more than a half of the events on  ${}^{71}\text{Ga}$  are due to the  $pp$  neutrinos, with the second dominant contribution coming from the  ${}^7\text{Be}$  neutrinos.  ${}^{71}\text{Ge}$  decays via electron capture with a half life of 11.4 d. The SAGE experiment in Baksan [47] used about 50 t of liquid metallic gallium as a target. The GALLEX experiment in LNGS [48] used 101 t of  $\text{GaCl}_3$ , containing 30.3 t of gallium. Both experiments used natural gallium, containing 39.9% of  ${}^{71}\text{Ga}$  isotope. GALLEX was followed by its successor GNO experiment. The measured capture rate is  $69.3 \pm 4.1 \pm 3.6$  SNU for GALLEX+GNO [49] and  $65.4^{+3.1+2.6}_{-3.0-2.8}$  SNU for SAGE [50]. A SSM prediction is  $127.9^{+8.1}_{-8.2}$  SNU [46].

The radiochemical detectors measure the reaction rate integrated between extractions. The real time measurement of solar neutrino was realized by the Kamiokande experiment [51]. The Kamiokande detector was a 3,000-t water-Cherenkov detector in the Kamioka mine. An array of 50 cm diameter PMTs were attached onto the inner wall of the detector to detect Cherenkov light. Although the original purpose of the Kamiokande detector was search for nucleon decays, with an upgrade of detector Kamiokande-II achieved an energy threshold sufficiently low to allow for the observation of solar neutrinos using  $\nu_e$ - $e$  elastic scattering (ES),  $\nu_x + e^- \rightarrow \nu_x + e^-$ . The signal and background from radioactivity can be statistically separated by using the directional correlation between the incoming neutrino and the recoil electron. The Super-Kamiokande, the successor of Kamiokande, started operation in April 1996. It is a large upright cylindrical water Cherenkov detector containing 50 kt of pure water. An inner detector volume corresponding to 32 kt water mass is viewed by more than 11,000 inward-facing 50 cm diameter PMTs.

The ES reaction occurs via both charged and neutral current interactions. Consequently, it is sensitive to all active neutrino flavours, although the cross section for  $\nu_e$ , which is the only flavour to interact via charged current, is about six times larger than that for  $\nu_\mu$  or  $\nu_\tau$ . Because the energy threshold is 6.5 MeV for Kamiokande and 3.5 MeV for the present Super-Kamiokande (for the kinetic energy of recoil electron), these experiments are sensitive to primarily to  ${}^8\text{B}$  neutrinos.

The results from Kamiokande [52, 53] and Super-Kamiokande [54, 55] showed significantly smaller numbers of observed solar neutrinos compared to the prediction. The latest  ${}^8\text{B}$  neutrino flux measured by Super-Kamiokande is  $(2.345 \pm 0.014 \pm 0.036) \times 10^6 \text{ cm}^{-2}\text{s}^{-1}$  [56], while a prediction based on the SSM is  $(5.46 \pm 0.66) \times 10^6 \text{ cm}^{-2}\text{s}^{-1}$  [57]. In addition, no significant zenith angle variation nor spectrum distortion were observed in the initial phase of Super-Kamiokande, which placed strong constraints on the solution of the solar neutrino problem [58, 59].

#### 14.6.1.3 Solution of the solar neutrino problem

SNO experiment in Canada used 1,000 t of heavy water ( $\text{D}_2\text{O}$ ) contained in a spherical acrylic vessel which was surrounded by an  $\text{H}_2\text{O}$  shield. An array of PMTs installed on a stainless steel structure detected Cherenkov radiation produced in both the  $\text{D}_2\text{O}$  and  $\text{H}_2\text{O}$ . The SNO detector observed  ${}^8\text{B}$  neutrinos via three different reactions. In addition to the ES scattering with an electron, with  $\text{D}_2\text{O}$  target the charged current (CC)  $\nu_e + d \rightarrow e^- + p + p$  and the neutral current (NC)  $\nu_x + d \rightarrow \nu_x + p + n$  interactions are possible. The CC reaction is sensitive to only  $\nu_e$ , while NC reaction is sensitive to all active flavours of neutrinos with equal cross sections. Therefore, by comparing the measurements of different reactions, SNO could provide a model independent test of the neutrino flavour change.

In 2001, SNO reported the initial result of CC measurement [62]. Combined with the high statistics measurement of  $\nu_e$ - $e$  elastic scattering from Super-Kamiokande [58], it provided a direct evidence for existence of non- $\nu_e$  component in solar neutrino flux. The result of NC measurement in 2002 [63] established it

**Table 14.2:** List of solar neutrino experiments

Name	Target material	Energy threshold (MeV)	Mass (ton)	Years
Homestake	C <sub>2</sub> Cl <sub>4</sub>	0.814	615	1970–1994
SAGE	Ga	0.233	50	1989–
GALEX	GaCl <sub>3</sub>	0.233	100 [30.3 for Ga]	1991–1997
GNO	GaCl <sub>3</sub>	0.233	100 [30.3 for Ga]	1998–2003
Kamiokande	H <sub>2</sub> O	6.5	3,000	1987–1995
Super-Kamiokande	H <sub>2</sub> O	3.5	50,000	1996–
SNO	D <sub>2</sub> O	3.5	1,000	1999–2006
KamLAND	Liquid scintillator	0.5/5.5	1,000	2001–2007
Borexino	Liquid scintillator	0.19	300	2007–

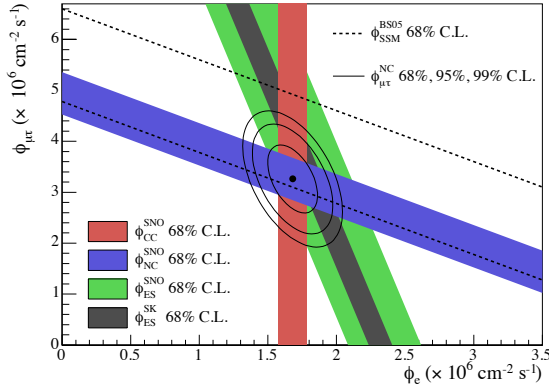


Figure 14.2: Fluxes of  $^8\text{B}$  solar neutrinos,  $\phi(\nu_e)$ , and  $\phi(\nu_{\mu,\tau})$ , deduced from the SNO's CC, ES, and NC results [60]. The Super-Kamiokande ES flux is from [61]. The BS05(OP) standard solar model prediction [40] is also shown. The bands represent the  $1\sigma$  error. The contours show the 68%, 95%, and 99% joint probability for  $\phi(\nu_e)$  and  $\phi(\nu_{\mu,\tau})$ . The figure is from [60].

with  $5.3\sigma$  of statistical significance. Figure 14.2 shows the fluxes of electron neutrinos ( $\phi(\nu_e)$ ) and muon and tau neutrinos ( $\phi(\nu_{\mu,\tau})$ ) with the 68%, 95%, and 99% joint probability contours, obtained with the SNO data. Finally, together with the reactor neutrino experiment KamLAND (see Sec.14.6.4), the solution of solar neutrino problem was found to be the MSW adiabatic flavour transitions in the solar matter, the so-called large mixing angle (LMA) solution, with parameters  $\Delta m^2 \sim 7.5 \times 10^{-5} \text{ eV}^2$  and  $\sin^2 \theta \sim 0.3$ .

From a combined result of three phases of SNO [64], the total flux of  $^8\text{B}$  solar neutrino is found to be  $(5.25 \pm 0.16^{+0.11}_{-0.13}) \text{ cm}^{-2}\text{s}^{-1}$ , consistent with the SSM prediction. This consistency is one of major accomplishments of SSM.

In order to understand the SSM as well as to study the MSW effect for the solar neutrino, measurements of solar neutrinos other than  $^8\text{B}$  are important. The Borexino experiment at Gran Sasso, Italy, detects solar neutrino via  $\nu$ -e scattering in real time with a low energy threshold. The Borexino detector consists of 300 t of ultra-pure liquid scintillator, which achieved 0.19 MeV of energy threshold and 5% energy resolution at 1 MeV. Borexino reported the first real time detection of  $^7\text{Be}$  solar neutrinos [66]. They also measured the fluxes of  $pep$  [67] and  $pp$  neutrino [68] for the first time. Together with  $^8\text{B}$  [69] neutrino measurement, Borexino provides important data to study the MSW effect. The KamLAND experiment also measured  $^8\text{B}$  [70] and  $^7\text{Be}$  [71] solar neutrinos. Figure 14.3 shows the survival probability of solar  $\nu_e$  as a function of neutrino energy. The data points are from the Borexino results [72, 73] except the SNO+SK  $^8\text{B}$  data. The theoretical curve shows the prediction of the MSW-LMA solution. All the data shown in this plot are consistent with the theoretically calculated curve. This indicates that these solar neutrino measurements are consistent with the MSW-LMA solution of the solar neutrino problem.

The matter effects can also be relevant to the propagation of solar neutrinos through the Earth. Because solar neutrinos go through the Earth before interaction in the detector during the

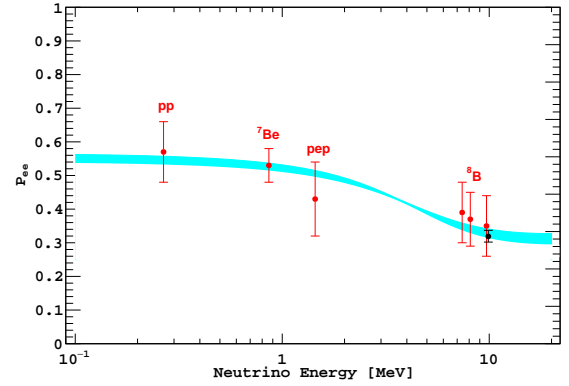


Figure 14.3: Electron neutrino survival probability as a function of neutrino energy. The points represent, from left to right, the Borexino  $pp$ ,  $^7\text{Be}$ ,  $pep$ , and  $^8\text{B}$  data (red points) and the SNO+SK  $^8\text{B}$  data (black point). The three Borexino  $^8\text{B}$  data points correspond, from left to right, to the low-energy (LE) range, LE+HE range, and the high-energy (HE) range. The electron neutrino survival probabilities from experimental points are determined using a high metallicity SSM from Ref. [57]. The error bars represent the  $\pm 1\sigma$  experimental + theoretical uncertainties. The curve corresponds to the  $\pm 1\sigma$  prediction of the MSW-LMA solution using the parameter values given in [65]. This figure is provided by A. Ianni.

nighttime, a comparison of measured event rate between daytime and nighttime provides a clean and direct test of matter effects on neutrino oscillations. Super-Kamiokande reported the first indication of the day/night asymmetry in  $^8\text{B}$  solar neutrinos [74]. The measured asymmetry, defined as the difference of the average day rate and average night rate divided by the average of those two rates, is  $(-3.2 \pm 1.1 \pm 0.5)\%$ , corresponding to a statistical significance of  $2.7\sigma$ . The measured value of the asymmetry is consistent with the LMA solution.

#### 14.6.2 Atmospheric Neutrinos

##### 14.6.2.1 Atmospheric neutrino flux

Atmospheric neutrinos are produced by the decays of pions and kaons generated in the interaction of cosmic rays and nucleons in the Earth's atmosphere. They have a broad range of energy ( $\sim 0.1 \text{ GeV}$  to  $> \text{TeV}$ ) and long travel distances before detection ( $\sim 10$  to  $1.3 \times 10^4 \text{ km}$ ). As shown in Table 14.1, atmospheric neutrino oscillation experiments are most sensitive to flavour oscillations with  $\Delta m^2 \sim 10^{-1}$  to  $10^{-4} \text{ eV}^2$ .

Considering their dominant production modes, some generic relations for flux ratios of different flavour of neutrinos can be derived without detailed calculations. From the decay chain of a charged pion  $\pi^+ \rightarrow \mu^+ \nu_\mu$  followed by  $\mu^+ \rightarrow e^+ \nu_e \bar{\nu}_\mu$  (and the charge conjugate for  $\pi^-$ ), the ratio  $(\nu_\mu + \bar{\nu}_\mu)/(\nu_e + \bar{\nu}_e)$  is expected to be around 2 at low energies ( $\sim 1 \text{ GeV}$ ) where most muons decay in the atmosphere. For higher energies, some of muons reach the Earth before they decay and the ratio increases. One can also expect that the zenith angle distributions of atmospheric neutrinos are symmetric between upward-going and downward-going

neutrinos. It is true for the energy above 1 GeV, but at lower energies, the Earth's geomagnetic field induces up-down asymmetries in the primary cosmic ray. The zenith angle corresponds to the flight length of atmospheric neutrinos. Vertically upward-going neutrinos come from the other side of the Earth with flight lengths of  $\sim 10^4$  km, while downward-going neutrinos produced just above the experimental site travel  $\sim 10$  km before detection.

The atmospheric neutrino fluxes are calculated in detail based on the energy spectrum and composition of primary cosmic rays and their hadronic interactions in the atmosphere. The effects of solar activity and geomagnetic field should be also taken into account. Results of calculations by several groups are available [75–78]. A typical uncertainty of the absolute flux is 10–20%, while the ratio of fluxes between different flavour has much smaller uncertainty ( $< 5\%$ ).

#### 14.6.2.2 Observation of atmospheric neutrino oscillations

The first detection of atmospheric neutrinos was reported in the 1960's by the underground experiments in the Kolar Gold Field experiment in India [79] and in South Africa [80]. In the 1980's, experiments searching for nucleon decays started operation. They used large underground detectors which could also observe atmospheric neutrinos. In these experiments, atmospheric neutrinos were studied as backgrounds to nucleon decays. Among the early experiments were Kamiokande [81] and IMB [82] using water Cherenkov detectors, and Frejus [83] and NUSEX [84] using iron tracking calorimeters.

The flavour of atmospheric neutrino can be identified in charged current interaction with nuclei, which produces the corresponding charged lepton. In order to study the neutrino oscillations, the identification of charged lepton is essential. Those detectors originally designed for nucleon decay search had capability to distinguish muons and electrons. For example, a water Cherenkov detector can utilize the information from Cherenkov ring patterns for particle identification;  $e$ -like particles ( $e^\pm$ ,  $\gamma$ ) produce more diffuse ring than  $\mu$ -like particles ( $\mu^\pm$ ,  $\pi^\pm$ ) because of electromagnetic cascades and multiple Coulomb scattering effects.

To reduce the uncertainty, in early results the flux ratio  $\nu_\mu/\nu_e \equiv (\nu_\mu + \bar{\nu}_\mu)/(\nu_e + \bar{\nu}_e)$  was measured, and the double ratio between observation and expectation  $(\nu_\mu/\nu_e)_{\text{obs}}/(\nu_\mu/\nu_e)_{\text{exp}}$  was reported. The Kamiokande experiment reported an indication of a deficit of  $(\nu_\mu + \bar{\nu}_\mu)$  flux [81]. IMB also observed similar deficit [82], but measurements by Frejus [83] and NUSEX [84] were consistent with the expectations. This was the original formulation of the atmospheric neutrino anomaly. Kamiokande reported studies with an increased data set of the sub-GeV ( $< 1.33$  GeV) [85] as well as the multi-GeV ( $> 1.33$  GeV) [86] samples. In the latter, they reported an analysis of zenith angle distributions, which showed an indication that the muon disappearance probability is dependent on the zenith angle, hence the travel length of neutrinos. However, the statistical significance was not sufficient to provide a conclusive interpretation.

The solution to the atmospheric neutrino anomaly was brought by Super-Kamiokande, which reported compelling evidence for neutrino oscillations in atmospheric neutrinos in 1998 [87]. The zenith angle ( $\theta_z$ , with  $\theta_z = 0$  for vertically downward-going) distributions of  $\mu$ -like events showed a clear deficit of upward-going events, while no significant asymmetry was observed for  $e$ -like events. The asymmetry is defined as  $A = (U - D)/(U + D)$ , where  $U$  is the number of upward-going ( $-1 < \cos \theta_z < -0.2$ ) events and  $D$  is the number of downward-going ( $0.2 < \cos \theta_z < 1.0$ ) events. With multi-GeV (visible energy  $> 1.33$  GeV)  $\mu$ -like events alone, the measured asymmetry was  $A = -0.296 \pm 0.048 \pm 0.001$ , deviating from zero by more than  $6\sigma$ . The sub-GeV ( $< 1.33$  GeV)  $\mu$ -like, upward through going, and upward stopping  $\mu$  samples, which correspond to different energy range of neutrino, show the consistent behaviour, strengthening the credibility of the observation. The corresponding oscillation parameters were found to be  $\Delta m^2 \sim 2.5 \times 10^{-3} \text{ eV}^2$  and  $\theta \sim 45^\circ$ . Super-Kamiokande's results were confirmed by other atmospheric neutrino observations MACRO [88] and Soudan2 [89].

Although the energy and zenith-angle dependent muon neutrino disappearance observed with atmospheric neutrinos could be consistently explained by the neutrino oscillations between  $\nu_\mu$

and  $\nu_\tau$ , other exotic explanations such as neutrino decay or de-coherence were not initially ruled out. By using a selected sample from Super-Kamiokande's atmospheric data with good  $L/E$  resolution, the  $L/E$  dependence of the survival probability was measured [90]. The observed dip in the  $L/E$  distribution was consistent with the expectation from neutrino oscillation, while alternative models were strongly disfavored.

As an experimental proof of  $\nu_\mu$ - $\nu_\tau$  oscillation, appearance signal of  $\nu_\tau$  was searched for in the atmospheric neutrino data. Because of the high energy threshold ( $> 3.5$  GeV) of  $\nu_\tau$  CC interaction and the short lifetime of  $\tau$  lepton (0.3 ps), the identification of  $\nu_\tau$  appearance is experimentally very difficult. Super-Kamiokande reported evidence of tau neutrino appearance using atmospheric neutrino data with  $4.6\sigma$  significance [91]. The definitive observation of  $\nu_\tau$  appearance was made by the long-baseline experiment, OPERA [92] (See Sec.14.6.3.3), and recently IceCube also reported the  $\nu_\tau$  appearance analysis [93] using atmospheric neutrinos.

#### 14.6.2.3 Neutrino oscillation measurements using atmospheric neutrinos

Figure 14.4 shows the zenith angle distributions of atmospheric neutrino data from Super-Kamiokande. For wide range of neutrino energy and path length, the observed distributions are consistent with the expectation from neutrino oscillation. Atmospheric neutrinos in the energy region of a few to  $\sim 10$  GeV provide information for the determination of the neutrino mass ordering [94].

The neutrino telescopes primarily built for the high energy neutrino astronomy such as ANTARES [95] and IceCube [96] can also measure neutrino oscillations with atmospheric neutrinos. ANTARES consists of a sparse array of PMTs deployed under the Mediterranean Sea at a depth of about 2.5 km to instrument a  $10^5 \text{ m}^3$  volume. IceCube is a detector deployed in ice in Antarctica at the South Pole, at depth between 1.45 and 2.45 km. In the bottom center of IceCube there is a region of  $\sim 10^7 \text{ m}^3$  volume with denser PMT spacing called DeepCore to extend the observable energies to lower energy region. By observing the charged current interaction of up-going  $\nu_\mu$ , they measure the  $\nu_\mu$  disappearance. ANTARES reported a measurement of  $\nu_\mu$  disappearance with 20 GeV threshold [97]. With analysis of events with 6–56 GeV energy range, the results on  $\nu_\mu$  disappearance measurements from IceCube DeepCore [98] provided a precision comparable to the measurements by Super-Kamiokande and long-baseline experiments.

There are several projects for atmospheric neutrino observations either proposed or under preparation. The atmospheric neutrino observation program is included in the plans for future neutrino telescopes, ORCA in the second phase of KM3NeT project [99] in the Mediterranean Sea, and PINGU in the upgrade of IceCube [100]. In India, a 50 kt magnetized iron tracking calorimeter ICAL is planned at the INO [101]. Future large underground detectors, Hyper-Kamiokande in Japan [102] and DUNE in US [103] can also study the atmospheric neutrinos.

### 14.6.3 Accelerator Neutrinos

#### 14.6.3.1 Accelerator neutrino beams

A comprehensive description of the accelerator neutrino beams is found in [104]. Conventional neutrino beams from accelerators are produced by colliding high energy protons onto a target, producing  $\pi$  and  $K$  which then decay into neutrinos, and stopping undecayed mesons and muons in the beam dump and soil. Because pions are the most abundant product in the high energy collisions, a conventional neutrino beam contains dominantly muon-type neutrinos (or antineutrinos).

Focusing devices called magnetic horns are used to concentrate the neutrino beam flux towards the desired direction. A magnetic horn is a pulsed electromagnet with toroidal magnetic fields to focus charged particles that are parents of neutrinos. One can choose the dominant component of the beam to be either neutrinos or antineutrinos by selecting the direction of current in the magnetic horns. Even with the focusing with horns, *wrong sign* neutrinos contaminate in the beam. Also, there is small amount of contamination of  $\nu_e$  and  $\bar{\nu}_e$  coming primarily from kaon and

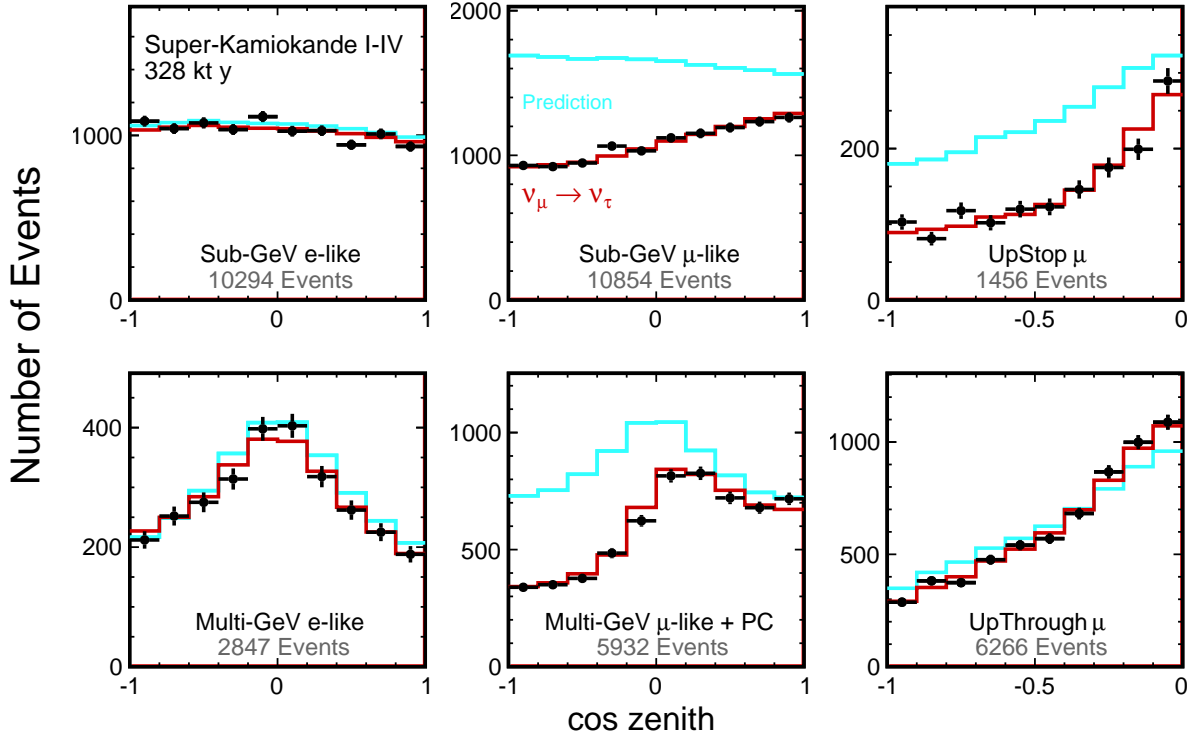


Figure 14.4: The zenith angle distributions of Super-Kamiokande atmospheric neutrino events. Fully contained 1-ring  $e$ -like and  $\mu$ -like events with visible energy  $< 1.33$  GeV (sub-GeV) and  $> 1.33$  GeV (multi-GeV), as well as upward stopping and upward stopping  $\mu$  samples are shown. Partially contained (PC) events are combined with multi-GeV  $\mu$ -like events. The blue histograms show the non-oscillated Monte Carlo events, and the red histograms show the best-fit expectations for  $\nu_\mu$ - $\nu_\tau$  oscillations. (This figure is provided by the Super-Kamiokande Collaboration)

Table 14.3: List of long-baseline neutrino oscillation experiments

Name	Beamline	Far Detector	L (km)	$E_\nu$ (GeV)	Year
K2K	KEK-PS	Water Cherenkov	250	1.3	1999–2004
MINOS	NuMI	Iron-scintillator	735	3	2005–2013
MINOS+	NuMI	Iron-scintillator	735	7	2013–2016
OPERA	CNGS	Emulsion	730	17	2008–2012
ICARUS	CNGS	Liquid argon TPC	730	17	2010–2012
T2K	J-PARC	Water Cherenkov	295	0.6	2010–
NOvA	NuMI	Liquid scint. tracking calorimeter	810	2	2014–

muon decays.

In order to maximize the sensitivity of the experiment, the ratio of baseline and neutrino energy ( $L/E$ ) should be chosen to match the oscillation effects to be studied. In addition to maximizing the flux of neutrinos with relevant energy, neutrinos with irrelevant energy that result in unwanted background process should be suppressed. The energy of neutrino from a pion decay is

$$E_\nu = \frac{[1 - (m_\mu/m_\pi)^2]E_\pi}{1 + \gamma^2\theta^2}, \quad (14.71)$$

where  $E_\nu$  and  $E_\pi$  are the energy of neutrino and pion, respectively,  $\theta$  is the angle between the pion and neutrino direction, and  $\gamma = E_\pi/m_\pi$ . For  $\theta = 0$ , the energy of neutrino is linearly proportional to the energy of pion. In this case, a narrow band beam can be made by selecting the momentum of pions. On the other hand, for  $\theta \neq 0$ , the energy of neutrino is not strongly dependent on the parent energy for a wide range of pion energy, but dependent on the off-axis angle  $\theta$ . Using this relation, a neutrino beam with narrow energy spectrum, around the energy determined by  $\theta$ , can be produced. This off-axis beam method was first introduced for BNL E889 proposal [105] and adopted in T2K and NOvA experiments. For a list of neutrino beamlines, see also the review 32. Neutrino Beam Lines at High-Energy Proton Synchrotrons.

As indicated in Table 14.1, there are two different scales of base-

lines for accelerator-based experiments to study different ranges of  $\Delta m^2$ . The atmospheric mass splitting  $\Delta m^2 \sim 2.5 \times 10^{-3} \text{ eV}^2$  gives rise to the first oscillation maximum at  $L/E \sim 500 \text{ GeV/km}$ . In order to study this parameter region with  $\sim 1$  GeV accelerator neutrino beam, a long baseline of a few hundreds to thousand km is necessary. On the other hand, there have been reports of possible neutrino oscillations at  $\sim 1 \text{ eV}$  scale, which can be studied at  $\sim 1 \text{ km}$  baseline with neutrinos from accelerators. These experiments are called short-baseline oscillation experiments.

The flux of a neutrino beam is calculated using Monte Carlo simulation based on the configuration of the beamline. An important ingredient of the neutrino flux prediction is the hadron production cross section. Data from dedicated hadron production experiments [106–108] are used to tune the beam simulation and constrain the uncertainty. The uncertainty of predicted neutrino flux for the most relevant energy region is  $\sim 5$ – $10\%$  with the latest hadron production data.

#### 14.6.3.2 Near detectors and neutrino interaction cross sections

Many long-baseline experiments use two detectors to reduce the systematic uncertainties arising from neutrino flux and neutrino-nucleus interactions. The near detectors either use the same technology as the far detector or consist of sub-detectors with complementary functions to obtain detailed information of the neutrino beam and interactions. The near detectors provide information



for the neutrino flux, energy spectrum, and the interaction cross sections, which is used as an input to make predictions of observables at the far detector. However, even with the two-detector configuration, one should note that the neutrino flux is inevitably different between the near and the far detectors. In addition to the fact that the neutrino source looks like a line source for the near detector while it looks as a point source for the far detector, the neutrino oscillations alter the flavour composition of the neutrino beam quite significantly, as the design of a neutrino oscillation experiment requires.

For the precision measurements of neutrino oscillations with long-baseline experiments, the understanding of the neutrino-nucleus interaction becomes crucial. Because heavy nuclei are used as the interaction target, the nuclear effects complicate the understanding of the neutrino-nucleus interaction. For more information on the neutrino cross sections, see also the review 50. Neutrino Cross Section Measurements.

#### 14.6.3.3 Long-baseline experiments

The first long-baseline experiment was the K2K experiment which used a neutrino beam from the KEK 12 GeV proton synchrotron directed towards Super-Kamiokande with a baseline of 250 km [109]. The beam had an average energy of 1.3 GeV. The K2K near detectors, located 300 m downstream of the production target, consisted of a combination of a 1 kt water Cherenkov detector and a set of fine grained detectors. K2K reported the confirmation of muon neutrino disappearance originally reported by Super-Kamiokande atmospheric neutrino observation [110].

The MINOS experiment used a beam from Fermilab and a detector in Soudan mine 735 km away [111]. The neutrino beam is produced in NuMI beamline [112] with 120 GeV proton beam from the Main Injector. The MINOS detectors are both iron-scintillator tracking calorimeters with toroidal magnetic fields. The far detector was 5.4 kt, while the near detector had a total mass of 0.98 kt and was located 1 km downstream of the production target. The NuMI beamline can vary the neutrino energy spectrum by changing the relative position of target and horns. Most of MINOS data were taken with the “low energy” configuration with the peak energy of around 3 GeV. MINOS combined accelerator and atmospheric neutrino data in both disappearance and appearance modes to measure oscillation parameters [113, 114]. Utilizing the separation of  $\mu^-$  and  $\mu^+$  with the magnetic field in the far detector, MINOS also reported separate measurements of atmospheric neutrinos and antineutrinos [115].

When the NuMI beamline started operation for the NOvA experiment in 2013, it was set to the “medium energy” configuration which provided a beam with the peak neutrino energy of around 7 GeV to the MINOS+ experiment, which used the same MINOS near and far detectors. MINOS+ verified the energy dependence of  $\nu_\mu$  disappearance at energies above the first oscillation maximum. Utilizing the wide neutrino energy spectrum and high intensity in the medium energy configuration, limits on sterile neutrinos is reported [116].

In Europe, the CNGS neutrino beamline provided a beam with mean energy of 17 GeV from CERN to LNGS for long-baseline experiments with 732 km of baseline. The beam energy was chosen so that charged current (CC) interaction of  $\nu_\tau$  can occur for direct confirmation of  $\nu_\tau$  appearance. There was no near detector in CNGS because it was not necessary for the  $\nu_\tau$  appearance search. The OPERA experiment used a detector consisted of an emulsion/lead target with about 1.25 kt total mass complemented by electronic detectors. The excellent spatial resolution of emulsion enabled the event-by-event identification of  $\tau$  leptons. OPERA observed ten  $\nu_\tau$  CC candidate events with  $2.0 \pm 0.4$  expected background [92] and confirmed  $\nu_\mu \rightarrow \nu_\tau$  oscillation in appearance mode with a statistical significance of  $6.1\sigma$ . Another neutrino experiment, ICARUS [117], which used 600 t liquid argon time projection chambers, was operated in Gran Sasso from 2010 to 2012.

The first generation of long-baseline experiments confirmed the existence of neutrino oscillation. The major initial goal of second generation experiments was the observation of  $\nu_\mu \rightarrow \nu_e$  oscillation. Using this appearance mode, by comparison of neutrino and antineutrino oscillation probabilities, search for CP violation

in the neutrino mixing becomes possible.

The T2K experiment started in 2010 using a newly constructed high-intensity proton synchrotron J-PARC and the Super-Kamiokande detector. It is the first long-baseline experiment to employ the off-axis neutrino beam. The off-axis angle of  $2.5^\circ$  was chosen to set the peak of neutrino energy spectrum at 0.6 GeV, matching the first maximum of oscillation probability at the 295 km baseline for  $\Delta m^2 \sim 2.5 \times 10^{-3} \text{ eV}^2$ . T2K employs a set of near detectors at about 280 m from the production target. The on-axis detector, called INGRID, is an array of iron-scintillator sandwich trackers to monitor the beam intensity, direction and profile. The off-axis detector ND280, consisting of several sub-detectors inside a magnet, is placed in the direction of far detector to measure the neutrino beam properties and to study neutrino interactions.

In 2011, T2K reported the first indication of  $\nu_\mu \rightarrow \nu_e$  oscillation with a statistical significance of  $2.5\sigma$  [118]. In the framework of  $3\nu$  mixing, it corresponds to detecting non-zero amplitude generated by the mixing angle  $\theta_{13}$  (see Eq.14.33). Later  $\nu_\mu \rightarrow \nu_e$  oscillation was established by T2K with more than  $7\sigma$  in 2014 [119]. Figure 14.5 shows the reconstructed energy distributions from T2K, for neutrino and anti-neutrino beam mode and also for muon and electron candidates. The muon type events show clear deficit in both neutrino and antineutrino mode, consistent with the energy-dependent disappearance probability expected from neutrino oscillations. By a combined analysis of the neutrino and antineutrino data, T2K reported a hint of CP violation with more than  $2\sigma$  [120, 121].

The NOvA experiment uses the NuMI beamline with an off-axis configuration. The 14 kt NOvA far detector is located near Ash River, Minnesota, 810 km away from the source. At 14.6 mrad off-axis from the central axis of the NuMI beam, the neutrino energy spectrum at the far detector has a peak around 2 GeV, corresponding to the first oscillation maximum at 810 km baseline. The near detector, located around 1 km from the source, has a functionally identical design to the far detector with a total active mass of 193 t. Both detectors are tracking calorimeters consisting of planes of polyvinyl chloride cells alternating in vertical and horizontal orientation filled with liquid scintillator.

The physics run of NOvA was started in 2014. Although the initial data indicated non-maximal mixing [122], later analysis with increased data and improved analysis resulted in the allowed region consistent with maximal mixing [123]. After confirmation of  $\nu_e$  appearance from  $\nu_\mu$  beam [124, 125], NOvA started data taking with antineutrino beam in 2016. Using the antineutrino beam data, NOvA has reported the observation of  $\bar{\nu}_e$  appearance from  $\bar{\nu}_\mu$  beam with  $4.4\sigma$  significance [126]. Figure 14.6 shows the reconstructed neutrino energy distributions from NOvA. Some values of the CP-violating phase  $\delta_{\text{CP}}$  (see Eq.14.33) have been excluded for the inverted mass ordering ( $m_3 < m_2 < m_1$ , see Sec.14.7 for definitions), while no significant limit has been set for the case of normal mass ordering ( $m_1 < m_2 < m_3$ , see Sec.14.7 for definitions).

Two large-scale long-baseline experiments are under preparation or proposed in future. DUNE [103] will be a 1,300 km long-baseline experiment based in US. The DUNE far detector will consist of four modules of at least 10 kt fiducial mass liquid argon time projection chambers, located 1.5 km underground at the Sanford Underground Research Facility in South Dakota. The beamline for DUNE, 1.2 MW at start and upgradable to 2.4 MW, as well as the facility for near detectors will be newly constructed at Fermilab. In Japan, Hyper-Kamiokande [102] is proposed as the successor of the Super-Kamiokande detector. It will be a water Cherenkov detector with 260 (190) kt total (fiducial) mass. With upgrade of existing accelerator and beamline, J-PARC will provide a 1.3 MW neutrino beam to Hyper-Kamiokande. Both DUNE and Hyper-Kamiokande will have a rich physics program besides the long-baseline experiment, such as searches for nucleon decays and study of supernova neutrinos.

#### 14.6.3.4 Short-baseline experiments

The LSND experiment searched for neutrino oscillation using neutrinos from stopped pions at Los Alamos. A 800 MeV linac was used to produce pions which stopped in the target. Most of

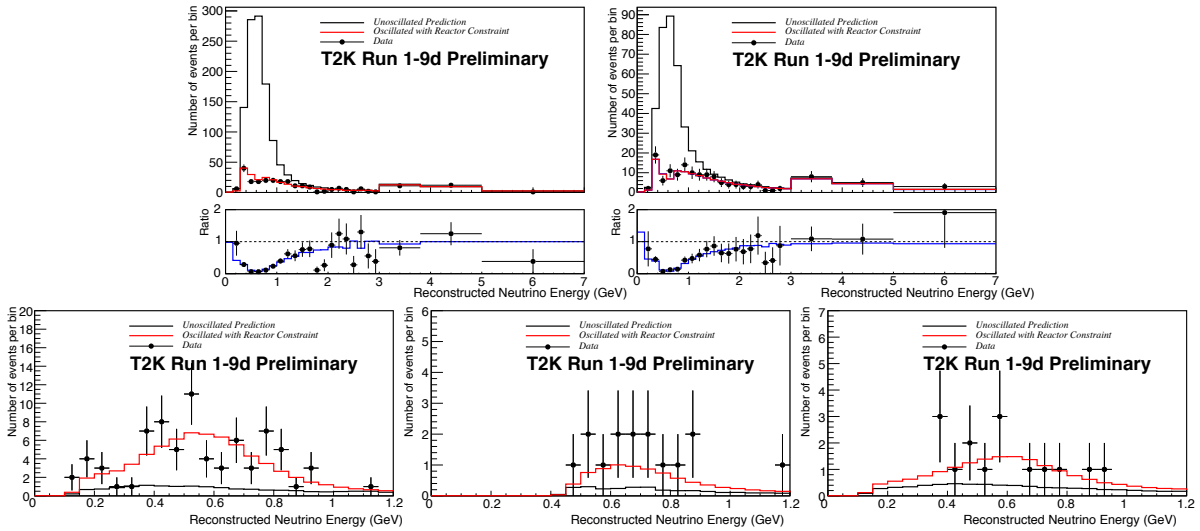


Figure 14.5: Reconstructed neutrino energy distributions from T2K. Data points with statistical error bars are shown together with the prediction without (black line) and including (red line) neutrino oscillation. Top: Single ring  $\mu$ -like events. The left and right plot is for neutrino and antineutrino beam mode, respectively. Below each plot, the ratio to the prediction without oscillation is also shown. Bottom: Single ring  $e$ -like events. From left to right, 0 decay electron sample for neutrino beam, 1 decay electron sample for neutrino beam, and 0 decay electron sample for antineutrino beam. (This figure is provided by the T2K Collaboration)

$\pi^-$ s are absorbed by the nuclei inside the target, while  $\pi^+$ s and their daughter  $\mu^+$ s decay and produce neutrinos. Therefore, the produced neutrinos are mostly  $\nu_\mu$ ,  $\bar{\nu}_\mu$ , and  $\nu_e$  with very small contamination of  $\bar{\nu}_e$ . The detector was a tank filled with 167 t of diluted liquid scintillator, located about 30 m from the neutrino source. LSND searched for  $\bar{\nu}_\mu \rightarrow \bar{\nu}_e$  appearance using the inverse beta decay process,  $\bar{\nu}_e + p \rightarrow e^+ + n$ , and found an excess of  $87.9 \pm 22.4 \pm 6.0$  events over the expected background [127].

The KARMEN experiment was performed at the neutron spallation facility ISIS of the Rutherford Appleton Laboratory. The KARMEN 2 detector was a segmented liquid scintillation calorimeter with total volume of  $65 \text{ m}^3$  located at a mean distance of 17.7 m from the ISIS target. KARMEN found a number of events consistent with the total background expectation, showing no signal for  $\bar{\nu}_\mu \rightarrow \bar{\nu}_e$  oscillations [128]. The resulting limits exclude large regions of the parameter area favored by LSND.

The MiniBooNE experiment at Fermilab used a conventional neutrino beam to search for  $\nu_e$  and  $\bar{\nu}_e$  appearance in the same parameter region as LSND. The booster neutrino beamline (BNB) with a single magnetic horn uses a 8 GeV proton beam from the Fermilab booster to produce a neutrino (antineutrino) beam with energy spectrum peak of 600 (400) MeV. The MiniBooNE detector consists of a 12.2 m diameter sphere filled with 818 t of mineral and oil located 541 m from the target. MiniBooNE reported  $\nu_e$  and  $\bar{\nu}_e$  event excess in both neutrino and antineutrino running modes. In total,  $460.5 \pm 99.0$  excess events are observed over the expected backgrounds, corresponding to  $4.7\sigma$  significance [129].

Both LSND and MiniBooNE are single detector experiments. The reported excess will be further investigated with the multi-detector short-baseline neutrino (SBN) program at Fermilab BNB [130]. The SBN program comprises three liquid argon time projection chambers at different baselines in the same neutrino beamline. The 112 t Short-Baseline Near Detector will be located at 110 m from the target. The 85 t MicroBooNE detector has been operated at 470 m from the target. The ICARUS detector has been transported from Europe after refurbishment at CERN and is located at a baseline of 600 m.

JSNS<sup>2</sup> experiment at J-PARC will search for neutrino oscillations with  $\Delta m^2 \sim 1 \text{ eV}^2$  [131]. 1MW proton beam from the 3 GeV Rapid Cycling Synchrotron of J-PARC will produce neutrinos from muon decay at rest. With a detector filled with gadolinium loaded liquid scintillator of 17 t fiducial mass at 24 m from the target, JSNS<sup>2</sup> is aiming to provide a direct test of the LSND anomaly.

#### 14.6.4 Reactor Antineutrinos

##### 14.6.4.1 Reactor antineutrino flux

Nuclear reactors are very intense sources of  $\bar{\nu}_e$ 's in the MeV energy region, which are generated in nuclear fission of heavy isotopes (mainly  $^{235}\text{U}$ ,  $^{238}\text{U}$ ,  $^{239}\text{Pu}$ , and  $^{241}\text{Pu}$ ). The  $\bar{\nu}_e$  flux from a reactor can be estimated based on the thermal power output and fuel composition as a function of time. On average, about six  $\bar{\nu}_e$ 's are emitted and about 200 MeV of energy is released per fission. Therefore, a 1 GW<sub>th</sub> (thermal power) reactor produces about  $2 \times 10^{20}$   $\bar{\nu}_e$ 's per second.

The detailed estimate of  $\bar{\nu}_e$  flux and energy spectrum can be obtained by either summing up the spectra of beta decays involved using available nuclear data information of each fission fragment and its decays, or using measurements of cumulative electron spectra associated with the beta decays of fission fragments. Because the fission of four main fuel isotopes involves thousands of beta-decay branches, a completely *ab initio* calculation is challenging. The cumulative electron spectra for  $^{235}\text{U}$ ,  $^{239}\text{Pu}$ , and  $^{241}\text{Pu}$  were measured at the Institut Laue-Langevin (ILL) reactor in Grenoble, France in the 1980s [132–134]. For the prediction of  $\bar{\nu}_e$  flux from  $^{238}\text{U}$ , a summation calculation in [135] was often used together with the ILL results.

A recent calculation of the reactor  $\bar{\nu}_e$  flux [136] uses an improved *ab initio* approach for  $^{238}\text{U}$  and combined information from nuclear databases and electron spectra measured at ILL for  $^{235}\text{U}$ ,  $^{239}\text{Pu}$ , and  $^{241}\text{Pu}$ . Another calculation [137] is provided for  $^{235}\text{U}$ ,  $^{239}\text{Pu}$ , and  $^{241}\text{Pu}$  based on the ILL measurement of electron spectra, taking into account higher order corrections and minimizing the use of nuclear databases. Both calculations predict about 3% higher normalization for the energy-averaged antineutrino fluxes of  $^{235}\text{U}$ ,  $^{239}\text{Pu}$ , and  $^{241}\text{Pu}$  compared to the original analyses of ILL data. However, the reactor antineutrino flux measurement at Daya Bay [138] is consistent with the old flux predictions and the flux measurement results. Also, an excess of  $\bar{\nu}_e$  flux around 5 MeV, compared to the prediction, has been observed by recent reactor experiments [139–142]. Measurements of a fuel-dependent reactor  $\bar{\nu}_e$  rate by Daya Bay [143] and RENO [144], and individual antineutrino spectra from  $^{235}\text{U}$  and  $^{239}\text{Pu}$  by Daya Bay [145] showed a discrepancy between the observed and predicted rate and spectrum from  $^{235}\text{U}$ .

##### 14.6.4.2 Reactor antineutrino oscillation experiments

Charged current interaction cannot happen if a reactor  $\bar{\nu}_e$  changes its flavour to  $\bar{\nu}_\mu$  or  $\bar{\nu}_\tau$ , because its energy is not sufficient to produce heavier charged leptons. Thus,  $\bar{\nu}_e$  disappearance is the



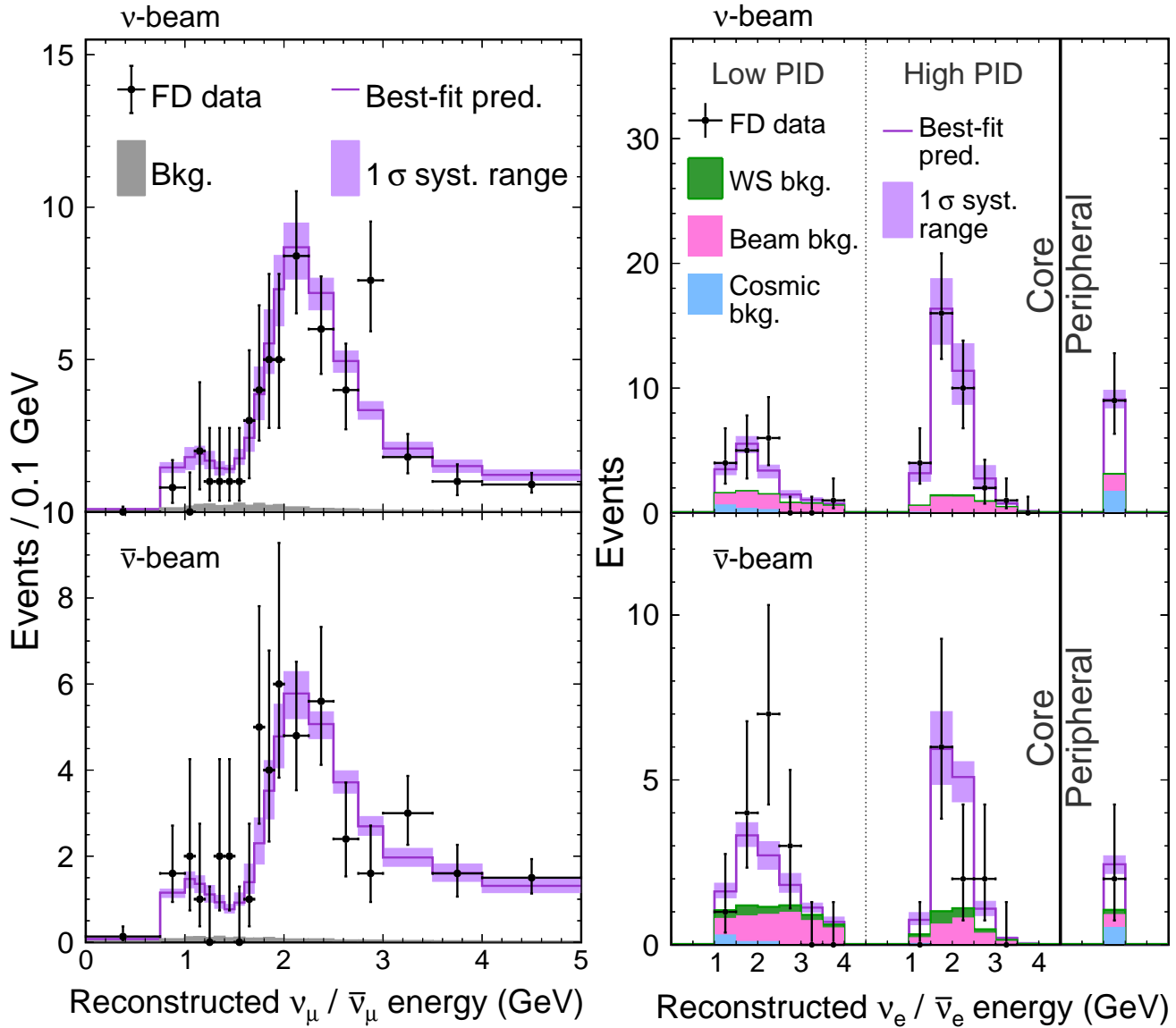


Figure 14.6: Reconstructed neutrino energy distributions from the NOvA far detector [126]. Top plots are for neutrino beam mode and bottom plots are for antineutrino beam mode. Left: muon-type candidates. Right: electron-type candidates, split into a low and high purity sample as well as the event counts in the peripheral sample which occurred near the edge of the detector.

**Table 14.4:** List of reactor antineutrino oscillation experiments

Name	Reactor power (GW <sub>th</sub> )	Baseline (km)	Detector mass (t)	Year
KamLAND	various	180 (ave.)	1,000	2001–
Double Chooz	4.25×2	1.05	8.3	2011–2018
Daya Bay	2.9×6	1.65	20×4	2011–
RENO	2.8×6	1.38	16	2011–
JUNO	26.6 (total)	53	20,000	

only channel to study neutrino flavour change with reactor experiments. The inverse beta decay  $\bar{\nu}_e + p \rightarrow e^+ + n$  provides a way to detect  $\bar{\nu}_e$  in the relevant energy region. The energy of prompt signal from  $e^+$ ,  $E_p$ , is related to the energy of  $\bar{\nu}_e$ ,  $E_{\bar{\nu}_e} \sim E_p + 0.8$  MeV. The delayed coincidence with the signal from  $\gamma$  ray emitted by neutron capture on nucleus after thermalization very efficiently suppresses the backgrounds. Liquid scintillator is often used to realize large detectors containing hydrogen as the target of inverse beta decay. In order to increase the neutron detection efficiency, liquid scintillator is sometimes loaded with gadolinium because of large neutron capture cross section and higher energy of emitted  $\gamma$  rays, the total energy of about 8 MeV, by gadolinium, in contrast

to 2.2 MeV for the capture by hydrogen.

Early reactor experiments that searched for neutrino oscillations at short or intermediate baselines reported negative results. The CHOOZ [146] and Palo Verde [147] experiments in 1990's searched for neutrino oscillations in the  $\Delta m^2 \sim 10^{-2}$ – $10^{-3}$  eV<sup>2</sup> range and set a limit on the corresponding mixing angle  $\sin^2 2\theta < 0.1$  at 90% CL.

Table 14.4 shows a list of reactor antineutrino experiments measuring neutrino oscillation. As was also shown in Table 14.1, experiments are designed with different baselines because of the different scale of mass splittings found by solar and atmospheric neutrino experiments. Experiments with O(100) km baseline are

sensitive to  $\Delta m^2$  of  $10^{-4}$ – $10^{-5}$  eV<sup>2</sup>, while  $\sim 1$  km of baseline results in a sensitivity in a range of  $10^{-2}$ – $10^{-3}$  eV<sup>2</sup>.

The KamLAND detector consists of 1,000 t of ultra-pure liquid scintillator contained in a 13-m diameter spherical balloon [148]. The detector is located in the original Kamiokande cavern, where the  $\bar{\nu}_e$  flux was dominated by a few reactors at an average distance of  $\sim 180$  km until 2011. KamLAND reported the first results in 2002 showing that the ratio of the observed number of  $\bar{\nu}_e$  events and expectation without disappearance is  $0.611 \pm 0.085 \pm 0.041$ , evidence for reactor  $\bar{\nu}_e$  disappearance at the 99.95% confidence level [148]. It confirmed a large value of the mixing angle corresponding to the LMA solution, which was reported by solar neutrino experiments. It is noted that there is a  $\sim 2\sigma$  level tension between the global solar neutrino data and KamLAND reactor data regarding the best-fit value of  $\Delta m^2$ , while the mixing angle is consistent. KamLAND also showed the evidence of  $\bar{\nu}_e$  spectrum distortion consistent with the expectation from neutrino oscillations [149]. Figure 14.7 shows the ratio of observed  $\bar{\nu}_e$  spectrum to the expectation for no-oscillation as a function of  $L_0/E$  ( $L_0 = 180$  km) for the KamLAND data. A clear oscillatory signature can be seen.

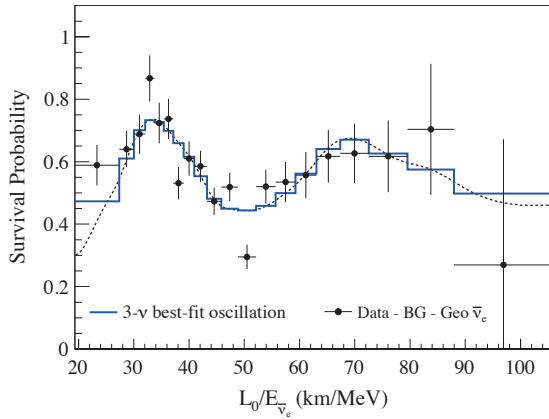


Figure 14.7: Ratio of the observed  $\bar{\nu}_e$  spectrum to the expectation for no-oscillation versus  $L_0/E$  for the KamLAND data.  $L_0 = 180$  km is the flux-weighted average reactor baseline. The 3- $\nu$  histogram is the best-fit survival probability curve from the three-flavour unbinned maximum-likelihood analysis using only the KamLAND data. This figure is taken from [150].

Following the establishment of neutrino oscillations with atmospheric, solar, accelerator, and reactor experiments, the measurement of the remaining mixing angle  $\theta_{13}$  was recognized as the next major milestone. A reactor neutrino experiment with a baseline of  $\sim 1$  km can make an almost pure measurement of  $\sin^2 2\theta_{13}$  from disappearance of  $\bar{\nu}_e$ . To be sensitive to a small value below the limit set by CHOOZ and Palo Verde, experiments with two detectors were proposed. Among several proposals, three experiments have been realized: Double Chooz in France [151], Daya Bay in China [152], and RENO in Korea [153].

These three experiments employ similar detector design optimized for the precise measurement of reactor antineutrino. An antineutrino detector consists of a cylindrical stainless steel vessel that houses two nested acrylic cylindrical vessels. The innermost vessel is filled with gadolinium-doped liquid scintillator as the primary antineutrino target. It is surrounded by a liquid scintillator layer to contain  $\gamma$  rays from the target volume. A buffer layer of mineral oil is placed an outside to shield inner volumes from radioactivity of PMTs and surrounding rock. The light from liquid scintillator is detected by an array of PMTs mounted on the stainless steel vessel. Optically separated by the stainless steel vessel, outside region is instrumented as a veto detector with either liquid scintillator (Double Chooz) or water Cherenkov (Daya Bay and RENO) detector.

The Double Chooz detector has gadolinium-doped liquid scintillator with mass of 8.3 t. The far detector at a baseline of  $\sim 1050$  m from the two 4.25 GW<sub>th</sub> reactors started physics data taking in

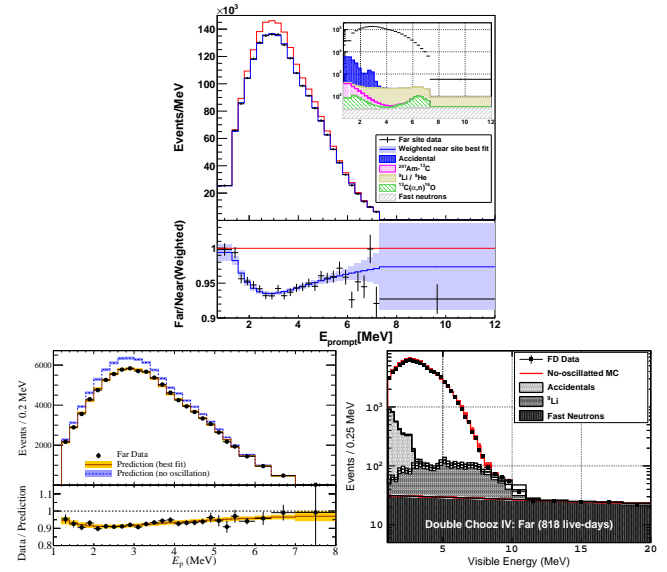


Figure 14.8: Energy spectra for prompt events at the far detectors for Daya Bay [139], RENO [140], and Double Chooz [141].

2011. The near detector, located at  $\sim 400$  m from the reactors, was completed in the end of 2014. Double Chooz finished data taking in early 2018. Daya Bay has two near (flux-weighted baseline 470 m and 576 m) and one far (1648 m) underground experimental halls near six reactors with 2.9 GW<sub>th</sub> each. Daya Bay has eight antineutrino detectors in total; two detectors in each of the near detector halls, and four detectors in the far detector hall. Each detector contains 20 t of gadolinium-loaded liquid scintillator. RENO has two identical detectors located at 294 m and 1383 m from the center of an array of six 2.8 GW<sub>th</sub> reactors. The mass of gadolinium-loaded liquid scintillator is 16 t per detector. RENO started data taking with both near and far detectors from August 2011.

All the three reactor neutrino experiments published first results in 2012. First, Double Chooz reported an indication of reactor electron antineutrino disappearance with the ratio of observed to expected events of  $R = 0.944 \pm 0.016 \pm 0.04$ , ruling out the no-oscillation hypothesis at the 94.6% CL [154]. Daya Bay observed  $R = 0.940 \pm 0.011 \pm 0.004$ , corresponding to 5.2 $\sigma$  significance of non-zero value of  $\theta_{13}$  [155]. RENO also reported  $R = 0.920 \pm 0.009 \pm 0.014$ , indicating a non-zero value of  $\theta_{13}$  with a significance of 4.9 $\sigma$  [156]. These results established non-zero value of  $\theta_{13}$ .

In the latest analysis, both Daya Bay [139] and RENO [140] report results constraining mass-squared difference as well as the mixing angle by using both relative  $\bar{\nu}_e$  rate and energy spectra information. Double Chooz has reported the first analysis based on both far and near detectors [141] for the mixing angle, using neutron capture on any elements (primarily gadolinium and hydrogen) to increase the effective target mass. Figure 14.8 shows the energy spectra of the prompt signals observed in the far detector of three experiments.

In all three experiments as well as in the NEOS experiment [142], an excess of  $\bar{\nu}_e$  events over expected energy spectrum have been observed around 5 MeV as mentioned earlier. This excess is observed in both near and far detectors and scales with the reactor power. Thanks to the cancellation between the near and far detectors, the neutrino oscillation measurements are not affected in multi-detector setup.

With a baseline of  $\sim 50$  km and an excellent energy measurement, reactor antineutrino experiments have significant sensitivity to the mass ordering. The JUNO experiment [157] aims to determine the mass ordering with this technique as its primary goal. It can also provide precision measurements of neutrino mixing parameters as well as a broad non-oscillation program. The JUNO detector, which is under construction, will consist of 20 kt

**Table 14.5:** List of reactor antineutrino experiments for  $O(eV^2)$  oscillations

Name	Reactor power (MW <sub>th</sub> )	Baseline (m)	Detector mass (t)	Detector technology	S/B
NEOS	2,800	24	1	Gd-LS	22
DANSS	3,100	10–12	0.9	Gd-PS	~30
STEREO	57	9–11	1.7	Gd-LS	0.9
PROSPECT	85	7–9	4	<sup>6</sup> Li-LS	1.3
NEUTRINO-4	100	6–12	1.5	Gd-LS	0.5
SoLid	80	6–9	1.6	<sup>6</sup> Li-PS	

liquid scintillator and be located at 53 km from two nuclear power plants in China.

#### 14.6.4.3 New reactor experiments sensitive to $O(1)$ $eV^2$ oscillations

Possible hints of neutrino oscillation at a scale of  $\Delta m^2 \sim 1 eV^2$  (see Sec.14.8) have motivated reactor experiments at a distance of  $\sim 10$  m from the core. Recent experiments searching for  $\sim 1 eV^2$  oscillation at reactors are summarized in Table 14.5.

As the antineutrino source, some use industrial reactors which can provide a large flux leading to a high statistical precision. On the other hand, though the flux is orders of magnitude smaller, a research reactor could have favorable conditions, such as relatively easier access to a short baseline, simpler fuel composition, and compact size of the core.

The detectors are based on organic scintillators, either liquid scintillator (LS) or solid plastic scintillator (PS), which contain hydrogen as the target for inverse beta decay ( $\bar{\nu}_e + p \rightarrow e^+ + n$ ). To identify the signal, neutron capture on either gadolinium (Gd) or <sup>6</sup>Li is detected with delayed coincidence. When a neutron is captured by Gd,  $\gamma$  rays with a total energy of 8 MeV are emitted. After neutron capture, <sup>6</sup>Li decays into triton and  $\alpha$ . The effect of neutrino oscillation appears as a distortion of energy spectrum. To be independent from the reactor neutrino spectrum uncertainties, some experiments compare the spectra at different baselines by using a segmented detector or moving the detector.

The NEOS [142] uses about 1 t of gadolinium-loaded liquid scintillator in an unsegmented detector. It is located at 23.7 m from the center of a commercial reactor and covered by an overburden of about 20 meters of water equivalent. Thanks to the high power reactor, NEOS observes antineutrino events at a rate of 1976 per day, with a signal to background ratio of about 22. The energy resolution is 5% at 1 MeV.

DANSS [158] is another experiment using a commercial reactor. The detector is highly segmented, consisting of 2,500 plastic scintillator strips, each with the size of  $1 \times 4 \times 100$  cm<sup>3</sup> and coated with a thin gadolinium-loaded reflective layer. The detector is placed on a movable platform below the reactor core. The overburden of 50 m water-equivalent reduces the cosmic muon flux by a factor of six. Data are taken with three baselines, 10.7, 11.7, and 12.7 m for a comparison between different baselines. The energy resolution of  $\sigma_E/E \sim 34\%$  at 1 MeV and the large size of the reactor core, 3.7 m in height and 3.2 m in diameter, somewhat smear the oscillation pattern. However it is compensated by high statistics due to the high power reactor. The observed event rate is 4899 events per day, with less than 3% cosmic background contamination, at 10.7 m position.

The STEREO detector [159] has six identical target cells of 37 cm length,  $\sim 2m^3$  of volume in total, filled with gadolinium-loaded liquid scintillator. They are placed from 9.4 to 11.1 m from the compact (80 cm high, 40 cm diameter) core of the ILL research reactor. The reconstructed energy resolution ( $\sigma_E/E$ ) is about 9% at 0.835 MeV. The antineutrino event rate is 396 events per day with a signal to background ratio of about 0.9.

The PROSPECT detector [160] consists of a segmented 4 t <sup>6</sup>Li-doped liquid scintillator detector covering a baseline range of 7–9 m from the reactor core. Thin reflecting panels divide the LS volume into an  $11 \times 14$  two-dimensional array of 154 optically isolated rectangular segments ( $14.5 \times 14.5 \times 117.6$  cm<sup>3</sup>). The energy resolution is 4.5% at 1 MeV. The detector is placed on the ground floor with an overburden of less than 1 m water-equivalent. With

efficient background suppression by using pulse shape discrimination and 3D position reconstruction, a signal to background ratio of 1.3 is achieved. The antineutrino rate is 771 events per day.

NEUTRINO-4 [161] uses a gadolinium-loaded liquid scintillator detector segmented in  $10 \times 5$  sections with a total volume of 1.8 m<sup>3</sup>. The detector is installed on a movable platform and moved to various positions with baselines of 6–12 m. With the detector location close to the surface and no pulse shape discrimination capability, the signal to background ratio is about 0.5. The energy resolution is 16% at 1 MeV.

The SoLid detector [162] is a finely segmented detector made of  $5 \times 5 \times 5$  cm<sup>3</sup> plastic scintillator cubes and <sup>6</sup>LiF:ZnS sheets. A detector with 1.6 t of active volume is installed at a distance of 6–9 m from the research reactor core with an overburden of 10 m water-equivalent. The triton and  $\alpha$  from neutron capture by <sup>6</sup>Li are detected by scintillation of ZnS. A high  $n$ - $\gamma$  separation capability is achieved using the difference of time constant of scintillation between ZnS and plastic scintillator. Very fine segmentation of the detector allows 3D reconstruction of events, which also provide effective background discrimination. The energy resolution ( $\sigma_E/E$ ) is expected to be  $\sim 14\%$  at 1 MeV.

## 14.7 Combined Analysis of Experimental Results: The $3\nu$ Paradigm

From the experimental situation described in Sec.14.6 we conclude that

- Atmospheric  $\nu_\mu$  and  $\bar{\nu}_\mu$  disappear most likely converting to  $\nu_\tau$  and  $\bar{\nu}_\tau$ . The results show an energy and distance dependence perfectly described by mass-induced oscillations.
- Accelerator  $\nu_\mu$  and  $\bar{\nu}_\mu$  disappear over distances of  $\sim 200$  to 800 km. The energy spectrum of the results show a clear oscillatory behaviour also in accordance with mass-induced oscillations with wavelength in agreement with the effect observed in atmospheric neutrinos.
- Accelerator  $\nu_\mu$  and  $\bar{\nu}_\mu$  appear as  $\nu_e$  and  $\bar{\nu}_e$  at distances  $\sim 200$  to 800 km.
- Solar  $\nu_e$  convert to  $\nu_\mu$  and/or  $\nu_\tau$ . The observed energy dependence of the effect is well described by massive neutrino conversion in the Sun matter according to the MSW effect
- Reactor  $\bar{\nu}_e$  disappear over distances of  $\sim 200$  km and  $\sim 1.5$  km with different probabilities. The observed energy spectra show two different mass-induced oscillation wavelengths: at short distances in agreement with the one observed in accelerator  $\nu_\mu$  disappearance, and a long distance compatible with the required parameters for MSW conversion in the Sun.

The minimum scenario to describe these results requires the mixing between the three flavour neutrinos of the standard model in three distinct mass eigenstates. In this case  $U$  in Eq. (14.32) is a  $3 \times 3$  matrix analogous to the CKM matrix for the quarks [21] but due to the possible Majorana nature of the neutrinos it can depend on six independent parameters: three mixing angles and three phases. There are several possible conventions for the ranges of the angles and ordering of the states. The community finally agreed to a parametrization of the leptonic mixing matrix as in Eq. (14.33). The angles  $\theta_{ij}$  can be taken without loss of generality to lie in the first quadrant,  $\theta_{ij} \in [0, \pi/2]$ , and the phase  $\delta_{CP} \in [0, 2\pi]$ . Values of  $\delta_{CP}$  different from 0 and  $\pi$  imply CP violation in neutrino oscillations in vacuum [163–165]. The Majorana phases  $\eta_1$  and  $\eta_2$  play no role in neutrino oscillations [164, 166].

Hence for the study of neutrino oscillations in the  $3\nu$  mixing scenario one can use the parametrization in Eq. (14.34) irrespective of whether neutrinos are Dirac or Majorana particles. Indeed, Majorana phases are very hard to measure since they are only physical if neutrino mass is non-zero and therefore the amplitude of any process involving them is suppressed a factor  $m_\nu/E$  to some power where  $E$  is the energy involved in the process which is typically much larger than the neutrino mass. The most sensitive experimental probe of Majorana phases is the rate of neutrinoless  $\beta\beta$  decay as discussed in Secs. 14.9.3 and 14.9.2.

In this convention there are two non-equivalent orderings for the spectrum of neutrino masses:

- Spectrum with Normal Ordering (NO) with  $m_1 < m_2 < m_3$
- Spectrum Inverted ordering (IO) with  $m_3 < m_1 < m_2$ .

Furthermore the data show a hierarchy between the mass splittings,  $\Delta m_{21}^2 \ll |\Delta m_{31}^2| \simeq |\Delta m_{32}^2|$  with  $\Delta m_{ij}^2 \equiv m_i^2 - m_j^2$ .

In this section we follow the convention used in the listing section of the PDG and discuss the results for both, NO and IO, using  $\Delta m_{21}^2$ , which is always the smallest mass splitting, and  $\Delta m_{32}^2$  which, up to a sign, is the largest mass splitting for IO, while for NO the largest mass splitting is  $\Delta m_{31}^2 = \Delta m_{32}^2 + \Delta m_{21}^2$ .

With what we know of the mass differences (see table 14.7) and the neutrino mass scale (see Sec. 14.9), depending on the value of the lightest neutrino mass, the neutrino mass spectrum can be further classified in:

- Normal Hierarchical Spectrum (NH):  $m_1 \ll m_2 < m_3$ ,  
 $\Rightarrow m_2 \simeq \sqrt{\Delta m_{21}^2} \sim 8.6 \times 10^{-3} \text{eV}$ ,  $m_3 \simeq \sqrt{\Delta m_{32}^2 + \Delta m_{21}^2} \sim 0.05 \text{eV}$ ,
- Inverted Hierarchical Spectrum (IH):  $m_3 \ll m_1 < m_2$ ,  
 $\Rightarrow m_1 \simeq \sqrt{|\Delta m_{32}^2 + \Delta m_{21}^2|} \sim 0.0492 \text{eV}$ ,  $m_2 \simeq \sqrt{|\Delta m_{32}^2|} \sim 0.05 \text{eV}$ ,
- Quasidegenerate Spectrum (QD):  $m_1 \simeq m_2 \simeq m_3 \gg \sqrt{|\Delta m_{32}^2|}$ .

Sometimes in the literature the determination of the neutrino mass spectrum is referred to as determination of the neutrino hierarchy. However, as described above, with what we know so far of the neutrino mass scale, the neutrino spectrum may or may not be hierarchical. Therefore determination of neutrino mass ordering is a more precise expression and it is the one used in this review.

In total the  $3\nu$  oscillation analysis of the existing data involves six parameters: 2 mass differences (one of which can be positive or negative), 3 mixing angles, and the CP phase. The different experiments described in Sec.14.6 provide information on different subsets of these parameters. The precise statistical analysis of the data requires the numerical evaluation of the corresponding oscillation probabilities by solving the evolution equation of the neutrino ensemble from their source to the experiment. Nevertheless the dominant effects in the different experiments can be qualitatively understood in terms of approximate expressions for the oscillation probabilities which, for convenience, we briefly summarize here.

#### 14.7.1 $3\nu$ Oscillation Probabilities

The relevant survival probabilities for solar and KamLAND experiments in the framework of three neutrino oscillations can be written as:

$$P_{ee}^{3\nu} = \sin^4 \theta_{13} + \cos^4 \theta_{13} P_{ee}^{2\nu}(\Delta m_{21}^2, \theta_{12}), \quad (14.72)$$

where we have used the fact that  $L_{0,32}^{\text{osc}} = 4\pi E_\nu / \Delta m_{32}^2$  is much shorter than the distance travelled by both solar and KamLAND neutrinos, so that the oscillations related to  $L_{0,32}^{\text{osc}}$  are averaged. In presence of matter effects  $P_{ee}^{2\nu}(\Delta m_{21}^2, \theta_{12})$  should be calculated taking into account the evolution in an effective matter density  $n_e^{\text{eff}} = n_e \cos^2 \theta_{13}$ . For  $10^{-5} \lesssim \Delta m^2 / \text{eV}^2 \lesssim$

$10^{-4}$ ,  $P_{ee}^{2\nu}(\Delta m_{21}^2, \theta_{12})$  presents the following asymptotic behaviours [167]:

$$P_{ee}^{2\nu, \text{sun}} \simeq 1 - \frac{1}{2} \sin^2(2\theta_{12}) \quad \text{for } E_\nu \lesssim \text{few} \times 100 \text{ keV}, \quad (14.73)$$

$$P_{ee}^{2\nu, \text{sun}} \simeq \sin^2(\theta_{12}) \quad \text{for } E_\nu \gtrsim \text{few} \times 1 \text{ MeV}, \quad (14.74)$$

$$P_{ee}^{2\nu, \text{kam}} = 1 - \frac{1}{2} \sin^2(2\theta_{12}) \sin^2 \frac{\Delta m_{21}^2 L}{2E_\nu}. \quad (14.75)$$

At present most of the precision of the solar analysis is provided by SNO and SK for which the relevant MSW survival probability provides a direct measurement of  $\sin^2 \theta_{12}$ , as seen in Eq. (14.74). In the MSW regime the determination of  $\Delta m_{21}^2$  in solar experiments comes dominantly from the ratio between the solar potential and the  $\Delta m_{21}^2$  term required to simultaneously describe the CC/NC data at SNO and the undistorted spectra of  $^8\text{B}$  neutrinos as measured in both SK and SNO. Conversely, KamLAND  $\bar{\nu}_e$  survival probability proceeds dominantly as vacuum oscillations and provides a most precise determination of  $\Delta m_{21}^2$  via the strong effect of the oscillating phase in the distortion of the reactor energy spectrum. On the contrary it yields a weaker constraint on  $\theta_{12}$  as the vacuum oscillation probability depends on the double-valued and “flatter” function  $\sin^2(2\theta_{12})$ .

In what respects the interpretation of  $\nu_\mu$  disappearance data at LBL experiments, the  $\nu_\mu$  survival probability can be expanded in the small parameters  $\sin \theta_{13}$  and  $\alpha \equiv \Delta m_{21}^2 / \Delta m_{31}^2$  to good accuracy as [168, 169]

$$\begin{aligned} P_{\nu_\mu \rightarrow \nu_\mu} &\approx 1 - \sin^2 2\theta_{\mu\mu} \sin^2 \frac{\Delta m_{\mu\mu}^2 L}{4E_\nu} \\ &\approx 1 - \cos^2 \theta_{13} \sin^2(2\theta_{23}) \sin^2 \frac{\Delta m_{32}^2 L}{4E_\nu} + \mathcal{O}(\alpha, s_{13}^2), \end{aligned} \quad (14.76)$$

with

$$\begin{aligned} \sin^2 \theta_{\mu\mu} &= \cos^2 \theta_{13} \sin^2 \theta_{23}, \\ \Delta m_{\mu\mu}^2 &= \sin^2 \theta_{12} \Delta m_{31}^2 + \cos^2 \theta_{12} \Delta m_{32}^2 \\ &\quad + \cos \delta_{\text{CP}} \sin \theta_{13} \sin 2\theta_{12} \tan \theta_{23} \Delta m_{21}^2. \end{aligned}$$

At present  $\nu_\mu$  disappearance results at LBL provide the best determination of  $|\Delta m_{32}^2|$  and  $\theta_{23}$  but as seen above, the probability is symmetric with respect to the octant of  $\theta_{\mu\mu}$  which implies symmetry around  $s_{23}^2 = 0.5/c_{13}^2$ .

The relevant oscillation probability for  $\nu_e$  appearance at LBL experiments can be expanded at the second order in the small parameters  $\sin \theta_{13}$  and  $\alpha$ , and assuming a constant matter density it takes the form [170–172]:

$$\begin{aligned} P_{\nu_\mu \rightarrow \nu_e, (\bar{\nu}_\mu \rightarrow \bar{\nu}_e)} &\approx 4 \sin^2 \theta_{13} \sin^2 \theta_{23} \frac{\sin^2 \Delta}{(1-A)^2} \\ &\quad + \alpha^2 \sin^2 2\theta_{12} \cos^2 \theta_{23} \frac{\sin^2 A \Delta}{A^2} \\ &\quad + 8\alpha J_{\text{CP}}^{\text{max}} \cos(\Delta \pm \delta_{\text{CP}}) \frac{\sin \Delta A}{A} \frac{\sin \Delta(1-A)}{1-A}, \end{aligned} \quad (14.77)$$

with

$$J_{\text{CP}}^{\text{max}} = \cos \theta_{12} \sin \theta_{12} \cos \theta_{23} \sin \theta_{23} \cos^2 \theta_{13} \sin \theta_{13}, \quad (14.78)$$

and

$$\Delta \equiv \frac{\Delta m_{31}^2 L}{4E_\nu}, \quad A \equiv \frac{2E_\nu V}{\Delta m_{31}^2}, \quad (14.79)$$

where  $V$  is the effective matter potential in the Earth crust. Results on  $\nu_e$  appearance at LBL provide us with the dominant information on leptonic CP violation. Furthermore  $\alpha$ ,  $\Delta$ , and  $A$  are sensitive to the sign of  $\Delta m_{32}^2$  (*i.e.*, the type of the neutrino mass ordering). The plus (minus) sign in Eq. (14.77) applies for

neutrinos (antineutrinos), and for antineutrinos  $V \rightarrow -V$ , which implies  $A \rightarrow -A$ . Numerically one finds for a typical Earth crust matter density of  $3 \text{ g/cm}^3$  that at T2K with  $E \sim 0.7 \text{ GeV}$ , matter effects are of order few percent, whereas in NOvA with  $E \sim 2 \text{ GeV}$  we can have  $|A| \sim 0.2$ . Also  $\alpha^2 \approx 10^{-3}$ , which implies that the second term in the first line of Eq. (14.77) gives a very small contribution compared to the other terms. Also, the first term in Eq. (14.77) (which dominates for large  $\theta_{13}$ ) depends on  $\sin^2 \theta_{23}$  and therefore is sensitive to the octant.

The  $\nu_e$  survival probability relevant for reactor experiments with medium baseline (MBL),  $L \sim 1 \text{ km}$ , can be approximated as [169, 173]:

$$P_{\nu_e \rightarrow \nu_e} = 1 - \sin^2 2\theta_{13} \sin^2 \frac{\Delta m_{ee}^2 L}{4E\nu} + \mathcal{O}(\alpha^2), \quad (14.80)$$

where

$$\Delta m_{ee}^2 = \cos^2 \theta_{12} \Delta m_{31}^2 + \sin^2 \theta_{12} \Delta m_{32}^2. \quad (14.81)$$

These MBL reactor experiments provide the most precise determination of  $\theta_{13}$ . Furthermore there is an additional effect sensitive to the mass ordering when comparing the disappearance of  $\nu_\mu$  at LBL experiments – which is symmetric with respect to the sign of  $\Delta m_{\mu\mu}^2$  given in Eq.(14.7.1)–, with that of  $\nu_e$  disappearance at MBL reactors which is symmetric with respect to the slightly different effective mass-squared difference  $\Delta m_{ee}^2$  given in Eq. (14.81)

Finally for atmospheric neutrinos the fluxes contain  $\nu_e$ ,  $\nu_\mu$ ,  $\bar{\nu}_e$  and  $\bar{\nu}_\mu$  and for a good fraction of the events, neutrinos travel through the Earth matter. In the context of  $3\nu$  mixing, the dominant oscillation channel of atmospheric neutrinos is  $\nu_\mu \rightarrow \nu_\tau$  driven by  $|\Delta m_{32}^2|$  with an amplitude controlled by  $\theta_{23}$  with sub-leading oscillation modes, triggered by  $\Delta m_{21}^2$  and/or  $\theta_{13}$ , which depend on the octant of  $\theta_{23}$ , on the mass ordering and on  $\delta_{\text{CP}}$ . In that respect an interesting observable is the deviation of  $e$ -like events relative to the no-oscillation prediction  $N_e^0$ , since in the two-flavour limit one expects  $N_e = N_e^0$ . Such deviation can be written in the following way (see, e.g., [174]):

$$\begin{aligned} \frac{N_e}{N_e^0} - 1 &\approx (r \sin^2 \theta_{23} - 1) P_{2\nu}(\Delta m_{32}^2, \theta_{13}) \\ &+ (r \cos^2 \theta_{23} - 1) P_{2\nu}(\Delta m_{21}^2, \theta_{12}) \\ &- \sin \theta_{13} \sin 2\theta_{23} r \Re(A_{ee}^* A_{\mu e}). \end{aligned} \quad (14.82)$$

Here  $r \equiv \Phi_\mu/\Phi_e$  is the flux ratio with  $r \approx 2$  in the sub-GeV range and  $r \approx 2.6 \rightarrow 4.5$  in the multi-GeV range.  $P_{2\nu}(\Delta m^2, \theta)$  is an effective two-flavour oscillation probability and  $A_{ee}, A_{\mu e}$  are elements of a transition amplitude matrix. The three terms appearing in Eq. (14.82) have a well defined physical interpretation. The first term is important in the multi-GeV range and is controlled by the mixing angle  $\theta_{13}$  in  $P_{2\nu}(\Delta m_{32}^2, \theta_{13})$ . This probability can be strongly affected by resonant matter effects [175–180]. Depending on the mass ordering the resonance will occur either for neutrinos or antineutrinos. The second term is important for sub-GeV events and it takes into account the effect of oscillations due to  $\Delta m_{21}^2$  and  $\theta_{12}$  [181–184]. Via the pre-factor containing the flux ratio  $r$  both, the first and second terms in Eq. (14.82) depend on the octant of  $\theta_{23}$ , though in opposite directions: the multi-GeV (sub-GeV) excess is suppressed (enhanced) for  $\theta_{23} < 45^\circ$ . Finally, the last term in Eq. (14.82) is an interference term between  $\theta_{13}$  and  $\Delta m_{21}^2$  amplitudes and this term shows also dependence on the CP phase  $\delta_{\text{CP}}$  [174, 184].

Subdominant three neutrino effects can also affect  $\mu$ -like events. For example for multi-GeV muon events one can write the excess in  $\mu$ -like events as [185, 186]

$$\begin{aligned} \frac{N_\mu}{N_\mu^0} - 1 &\approx \sin^2 \theta_{23} \left( \frac{1}{r} - \sin^2 \theta_{23} \right) P_{2\nu}(\Delta m_{32}^2, \theta_{13}) \\ &- \frac{1}{2} \sin^2 2\theta_{23} [1 - \Re(A_{33})]. \end{aligned} \quad (14.83)$$

The first term is controlled by  $\theta_{13}$  and is subject to resonant matter effects, similar to the first term in Eq. (14.82), though with a different dependence on  $\theta_{23}$  and the flux ratio. In the second term,

$A_{33}$  is a probability amplitude satisfying  $P_{2\nu}(\Delta m_{32}^2, \theta_{13}) = 1 - |A_{33}|^2$ . In the limit  $\theta_{13} = 0$  we have  $\Re(A_{33}) = \cos(\Delta m_{32}^2 L/2E)$ , such that the second term in Eq. (14.83) just describes two-flavour  $\nu_\mu \rightarrow \nu_\mu$  vacuum oscillations.

#### 14.7.2 $3\nu$ Oscillation Analysis

We summarize in Table 14.6 the different experiments which dominantly contribute to the present determination of the different parameters in the chosen convention.

The table illustrates that the determination of the leptonic parameters requires global analysis of the data from the different experiments. Over the years these analyses have been in the hands of a few phenomenological groups. We show in Table 14.7 the results from the latest analyses in Refs. [187–190]. For the sake of comparison all results are presented in the convention of the listing section as described above.

The table illustrates the dependence of the present determination of the parameters on variations of the statistical analysis performed by the different groups and on the data samples included. In that last respect the main difference resides on the results from Super-Kamiokande atmospheric data [94] which, at present, can only be included in these analysis by directly adding the  $\chi^2$  tabulated  $\chi^2$  map provided by the experiment.

Altogether the different analysis find consistent results, in particular on the better known parameters,  $\theta_{12}$ ,  $\theta_{13}$  and  $\Delta m_{21}^2$  and  $|\Delta m_{32}^2|$ . The issues which still require clarification are: the mass ordering discrimination, the determination of  $\theta_{23}$  and the leptonic CP phase  $\delta_{\text{CP}}$ :

- In all analyses the best fit is for the normal mass ordering. Inverted ordering is disfavoured with a  $\Delta\chi^2$  which ranges from slightly above  $2\sigma$  – driven by the interplay of long-baseline accelerator and short-baseline reactor data – to  $3\sigma$  when adding the atmospheric  $\chi^2$  table from Ref. [94].
- All analyses find some preference for the second octant of  $\theta_{23}$  but with statistical significance still well below  $3\sigma$ .
- The best fit for the complex phase in NO is at  $\delta_{\text{CP}} \sim 120^\circ$  but CP conservation (for  $\delta_{\text{CP}} \sim 180^\circ$ ) is still allowed at a confidence level (CL) of  $1-2\sigma$ . We notice that, at present, the significance of CP violation in the global analysis is reduced with respect to that reported by T2K [191] because NOvA data does not show a significant indication of CP violation.

#### 14.7.3 Convention-independent Measures of Leptonic CP Violation in $3\nu$ Mixing

In the framework of  $3\nu$  mixing leptonic CP violation can also be quantified in terms of the leptonic Jarlskog invariant [192], defined by:

$$\begin{aligned} \Im[U_{\alpha i} U_{\alpha j}^* U_{\beta i} U_{\beta j}] &\equiv \sum_{\gamma=e,\mu,\tau} \sum_{k=1,2,3} J_{\text{CP}} \epsilon_{\alpha\beta\gamma} \epsilon_{ijk} \\ &\equiv J_{\text{CP}}^{\text{max}} \sin \delta_{\text{CP}}. \end{aligned} \quad (14.84)$$

With the convention in Eq. (14.33)  $J_{\text{CP}}^{\text{max}}$  is the combination of mixing angles in Eq. (14.78). For example from the analysis in Ref. [187, 188]

$$J_{\text{CP}}^{\text{max}} = 0.03359 \pm 0.0006 (\pm 0.0019), \quad (14.85)$$

at  $1\sigma$  ( $3\sigma$ ) for both orderings, and the preference of the present data for non-zero  $\delta_{\text{CP}}$  implies a non-zero best fit value  $J_{\text{CP}}^{\text{best}} = -0.019$ .

The status of the determination of leptonic CP violation can also be graphically displayed by projecting the results of the global analysis in terms of leptonic unitarity triangles [193–195]. Since in the analysis  $U$  is unitary by construction, any given pair of rows or columns can be used to define a triangle in the complex plane. There a total of six possible triangles corresponding to the unitary conditions

$$\sum_{i=1,2,3} U_{\alpha i} U_{\beta i}^* = 0 \text{ with } \alpha \neq \beta, \quad \sum_{\alpha=e,\mu,\tau} U_{\alpha i} U_{\alpha j}^* = 0 \text{ with } i \neq j. \quad (14.86)$$

**Table 14.6:** Experiments contributing to the present determination of the oscillation parameters.

Experiment	Dominant	Important
Solar Experiments	$\theta_{12}$	$\Delta m_{21}^2, \theta_{13}$
Reactor LBL (KamLAND)	$\Delta m_{21}^2$	$\theta_{12}, \theta_{13}$
Reactor MBL (Daya-Bay, Reno, D-Chooz)	$\theta_{13},  \Delta m_{31,32}^2 $	
Atmospheric Experiments (SK, IC-DC)		$\theta_{23},  \Delta m_{31,32}^2 , \theta_{13}, \delta_{CP}$
Accel LBL $\nu_\mu, \bar{\nu}_\mu$ , Disapp (K2K, MINOS, T2K, NO $\nu$ A)	$ \Delta m_{31,32}^2 , \theta_{23}$	
Accel LBL $\nu_e, \bar{\nu}_e$ App (MINOS, T2K, NO $\nu$ A)	$\delta_{CP}$	$\theta_{13}, \theta_{23}$

**Table 14.7:**  $3\nu$  oscillation parameters obtained from different global analysis of neutrino data. In all cases the numbers labeled as NO (IO) are obtained assuming NO (IO), *i.e.*, relative to the respective local minimum. SK-ATM makes reference to the tabulated  $\chi^2$  map from the Super-Kamiokande analysis of their data in Ref. [94].

Param	Ref. [188] w/o SK-ATM		Ref. [188] w SK-ATM		Ref. [189] w SK-ATM		Ref. [190] w SK-ATM	
	Best Fit Ordering		Best Fit Ordering		Best Fit Ordering		Best Fit Ordering	
	bfp $\pm 1\sigma$	$3\sigma$ range	bfp $\pm 1\sigma$	$3\sigma$ range	bfp $\pm 1\sigma$	$3\sigma$ range	bfp $\pm 1\sigma$	$3\sigma$ range
$\sin^2 \theta_{12}$	$3.10^{+0.13}_{-0.12}$	2.75 $\rightarrow$ 3.50	$3.10^{+0.13}_{-0.12}$	2.75 $\rightarrow$ 3.50	$3.04^{+0.14}_{-0.13}$	2.65 $\rightarrow$ 3.46	$3.20^{+0.20}_{-0.16}$	2.73 $\rightarrow$ 3.79
$\theta_{12}/^\circ$	$33.82^{+0.78}_{-0.76}$	31.61 $\rightarrow$ 36.27	$33.82^{+0.78}_{-0.76}$	31.61 $\rightarrow$ 36.27	$33.46^{+0.87}_{-0.88}$	30.98 $\rightarrow$ 36.03	$34.5^{+1.2}_{-1.0}$	31.5 $\rightarrow$ 38.0
$\sin^2 \theta_{23}$	$5.58^{+0.20}_{-0.33}$	4.27 $\rightarrow$ 6.09	$5.63^{+0.18}_{-0.24}$	4.33 $\rightarrow$ 6.09	$5.51^{+0.19}_{-0.80}$	4.30 $\rightarrow$ 6.02	$5.47^{+0.20}_{-0.30}$	4.45 $\rightarrow$ 5.99
$\theta_{23}/^\circ$	$48.3^{+1.2}_{-1.9}$	40.8 $\rightarrow$ 51.3	$48.6^{+1.0}_{-1.4}$	41.1 $\rightarrow$ 51.3	$47.9^{+1.1}_{-4.0}$	41.0 $\rightarrow$ 50.9	$47.7^{+1.2}_{-1.7}$	41.8 $\rightarrow$ 50.7
$\sin^2 \theta_{13}$	$2.241^{+0.066}_{-0.065}$	2.046 $\rightarrow$ 2.440	$2.237^{+0.066}_{-0.065}$	2.044 $\rightarrow$ 2.435	$2.14^{+0.09}_{-0.07}$	1.90 $\rightarrow$ 2.39	$2.160^{+0.083}_{-0.069}$	1.96 $\rightarrow$ 2.41
$\theta_{13}/^\circ$	$8.61^{+0.13}_{-0.13}$	8.22 $\rightarrow$ 8.99	$8.60^{+0.13}_{-0.13}$	8.22 $\rightarrow$ 8.98	$8.41^{+0.18}_{-0.14}$	7.9 $\rightarrow$ 8.9	$8.45^{+0.16}_{-0.14}$	8.0 $\rightarrow$ 8.9
$\delta_{CP}/^\circ$	$222^{+38}_{-28}$	141 $\rightarrow$ 370	$221^{+39}_{-28}$	144 $\rightarrow$ 357	$238^{+41}_{-33}$	149 $\rightarrow$ 358	$218^{+38}_{-27}$	157 $\rightarrow$ 349
$\Delta m_{21}^2$	$7.39^{+0.21}_{-0.20}$	6.79 $\rightarrow$ 8.01	$7.39^{+0.21}_{-0.20}$	6.79 $\rightarrow$ 8.01	$7.34^{+0.17}_{-0.14}$	6.92 $\rightarrow$ 7.91	$7.55^{+0.20}_{-0.16}$	7.05 $\rightarrow$ 8.24
$\Delta m_{32}^2$	$2.449^{+0.032}_{-0.030}$	2.358 $\rightarrow$ 2.544	$2.454^{+0.029}_{-0.031}$	2.362 $\rightarrow$ 2.544	$2.419^{+0.035}_{-0.032}$	2.319 $\rightarrow$ 2.521	$2.424 \pm 0.03$	2.334 $\rightarrow$ 2.524
IO	$\Delta\chi^2 = 6.2$		$\Delta\chi^2 = 10.4$		$\Delta\chi^2 = 9.5$		$\Delta\chi^2 = 11.7$	
$\sin^2 \theta_{12}$	$3.10^{+0.13}_{-0.12}$	2.75 $\rightarrow$ 3.50	$3.10^{+0.13}_{-0.12}$	2.75 $\rightarrow$ 3.50	$3.03^{+0.14}_{-0.13}$	2.64 $\rightarrow$ 3.45	$3.20^{+0.20}_{-0.16}$	2.73 $\rightarrow$ 3.79
$\theta_{12}/^\circ$	$33.82^{+0.78}_{-0.76}$	31.61 $\rightarrow$ 36.27	$33.82^{+0.78}_{-0.75}$	31.62 $\rightarrow$ 36.27	$33.40^{+0.87}_{-0.81}$	30.92 $\rightarrow$ 35.97	$34.5^{+1.2}_{-1.0}$	31.5 $\rightarrow$ 38.0
$\sin^2 \theta_{23}$	$5.63^{+0.19}_{-0.26}$	4.30 $\rightarrow$ 6.12	$5.65^{+0.17}_{-0.22}$	4.36 $\rightarrow$ 6.10	$5.57^{+0.17}_{-0.24}$	4.44 $\rightarrow$ 6.03	$5.51^{+0.18}_{-0.30}$	4.53 $\rightarrow$ 5.98
$\theta_{23}/^\circ$	$48.6^{+1.1}_{-1.5}$	41.0 $\rightarrow$ 51.5	$48.8^{+1.0}_{-1.2}$	41.4 $\rightarrow$ 51.3	$48.2^{+1.0}_{-1.4}$	41.8 $\rightarrow$ 50.9	$47.9^{+1.0}_{-1.7}$	42.3 $\rightarrow$ 50.7
$\sin^2 \theta_{13}$	$2.261^{+0.067}_{-0.064}$	2.066 $\rightarrow$ 2.461	$2.259^{+0.065}_{-0.065}$	2.064 $\rightarrow$ 2.457	$2.18^{+0.08}_{-0.07}$	1.95 $\rightarrow$ 2.43	$2.220^{+0.074}_{-0.076}$	1.99 $\rightarrow$ 2.44
$\theta_{13}/^\circ$	$8.65^{+0.13}_{-0.12}$	8.26 $\rightarrow$ 9.02	$8.64^{+0.12}_{-0.13}$	8.26 $\rightarrow$ 9.02	$8.49^{+0.15}_{-0.14}$	8.0 $\rightarrow$ 9.0	$8.53^{+0.14}_{-0.15}$	8.1 $\rightarrow$ 9.0
$\delta_{CP}/^\circ$	$285^{+24}_{-26}$	205 $\rightarrow$ 354	$282^{+23}_{-25}$	205 $\rightarrow$ 348	$247^{+26}_{-27}$	193 $\rightarrow$ 346	$281^{+23}_{-27}$	202 $\rightarrow$ 349
$\Delta m_{21}^2$	$7.39^{+0.21}_{-0.20}$	6.79 $\rightarrow$ 8.01	$7.39^{+0.21}_{-0.20}$	6.79 $\rightarrow$ 8.01	$7.34^{+0.17}_{-0.14}$	6.92 $\rightarrow$ 7.91	$7.55^{+0.20}_{-0.16}$	7.05 $\rightarrow$ 8.24
$\Delta m_{32}^2$	$-2.509^{+0.032}_{-0.032}$	-2.603 $\rightarrow$ -2.416	$-2.510^{+0.030}_{-0.031}$	-2.601 $\rightarrow$ -2.419	$-2.478^{+0.035}_{-0.033}$	-2.577 $\rightarrow$ -2.375	$-2.50 \pm 0.04$	-2.59 $\rightarrow$ -2.39

As illustration we show in Fig. 14.9 the recasting of the allowed regions of the analysis in Ref. [187, 188] in terms of one leptonic unitarity triangle. We show the triangle corresponding to the unitarity conditions on the first and third columns (after the shown rescaling) which is the equivalent to the one usually shown for the quark sector. In this figure the absence of CP violation would imply a flat triangle, *i.e.*,  $\Im(z) = 0$ . So the CL at which leptonic CP violation is being observed would be given by the CL at which the region crosses the horizontal axis. Notice however, that this representation is made *under the assumption of a unitary U matrix* and therefore does not provide any test of unitarity in the leptonic sector.

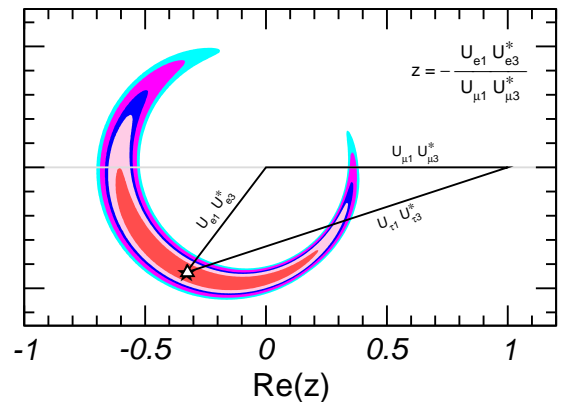


Figure 14.9: Leptonic unitarity triangle for the first and third columns of the mixing matrix. After scaling and rotating the triangle so that two of its vertices always coincide with (0, 0) and (1, 0) the figure shows the  $1\sigma$ , 90%,  $2\sigma$ , 99%,  $3\sigma$  CL (2 dof) allowed regions of the third vertex for the NO from the analysis in Ref. [187, 188].

### 14.8 Beyond $3\nu$ : Additional Neutrinos at the eV Scale

Besides the huge success of three-flavour oscillations described in Sec.14.7, as mentioned in Secs.14.6.3 and 14.6.4, there are some anomalies which cannot be explained within the  $3\nu$  framework and which might point towards the existence of additional neutrino states with masses at the eV scale. In brief:

- the LSND experiment [127] reports evidence for  $\bar{\nu}_\mu \rightarrow \bar{\nu}_e$  transitions with  $E/L \sim 1 \text{ eV}^2$ , where  $E$  and  $L$  are the neutrino energy and the distance between source and detector, respectively (see *Short Baseline Experiments* subsection of Sec.14.6.3).
- this effect has also been searched for by the MiniBooNE experiment [196], which reports a yet unexplained event excess in the low-energy region of the electron neutrino and anti-neutrino event spectra. No significant excess is found at higher neutrino energies. Interpreting the data in terms of oscillations, parameter values consistent with the ones from LSND are obtained, but the test is not definitive;
- radioactive source experiments at the Gallium solar neutrino experiments both in SAGE and GALLEX/GNO have obtained an event rate which is somewhat lower than expected. If not due to uncertainties in the interaction cross section, this effect can be explained by the hypothesis of  $\nu_e$  disappearance due to oscillations with  $\Delta m^2 \gtrsim 1 \text{ eV}^2$  (“Gallium anomaly”) [197, 198];
- new calculations of the neutrino flux emitted by nuclear reactors [136, 137] predict a neutrino rate which is a few percent higher than observed in short-baseline ( $L \lesssim 100 \text{ m}$ ) reactor experiments<sup>4</sup>. If not due to systematic or theoretical uncertainties, a decrease rate at those distances can be explained by assuming  $\bar{\nu}_e$  disappearance due to oscillations with  $\Delta m^2 \sim 1 \text{ eV}^2$  (“reactor anomaly”) [200]. This reactor anomaly is under study both by the experimental community – with a set of follow-up measurements performed at SBL both at reactors and accelerators (see the corresponding subsections in Sec.14.6.4 and Sec.14.6.3)–, and by the theory community for improvements of the reactor flux calculations.

As mentioned in Sec.14.1 whatever the extension of the SM we want to consider it must contain only three light active neutrinos. Therefore if we need more than three light massive neutrinos we must add sterile neutrinos to the particle content of the model.

The most immediate question as these anomalies were reported was whether they could all be consistently described in combination with the rest of the neutrino data – in particular with the negative results on disappearance of  $\nu_\mu$  at short distances – if one adds those additional sterile states. Quantitatively one can start by adding a fourth massive neutrino state to the spectrum, and perform a global data analysis to answer this question. Although the answer is always the same the physical reason behind it depends on ordering assumed for the states. In brief, there are six possible four-neutrino schemes which can in principle accommodate the results of solar+KamLAND and atmospheric+LBL neutrino experiments as well as the SBL result. They can be divided in two classes: (2+2) and (3+1). In the (3+1) schemes, there is a group of three close-by neutrino masses (as on the  $3\nu$  schemes described in the previous section) that is separated from the fourth one by a gap of the order of 1 eV, which is responsible for the SBL oscillations. In (2+2) schemes, there are two pairs of close masses (one pair responsible for solar results and the other for atmospheric [201]) separated by the  $\mathcal{O}(\text{eV})$  gap. The main difference between these two classes is the following: if a (2+2)-spectrum is realized in nature, the transition into the sterile neutrino is a solution of either the solar or the atmospheric neutrino problem, or the sterile neutrino takes part in both. Consequently a (2+2)-spectrum is easier to test because the required mixing of sterile neutrinos in either solar and/or atmospheric oscillations would modify their effective matter potential in the Sun

<sup>4</sup>However, as discussed in Sec.14.6.4, the reactor antineutrino flux measurement at Daya Bay [143, 199] is consistent with the old flux predictions and the flux measurement results in the previous short-baseline reactor neutrino oscillation experiments.

and in the Earth and giving distinctive effects in the solar and/or atmospheric neutrino observables. Those distinctive effects were not observed so oscillations into sterile neutrinos did not describe well either solar or atmospheric data. Consequently as soon as the early 2000’s 2+2 spectra could be ruled out already beyond  $3\text{--}4 \sigma$  as seen in the left panel in Fig.14.10 taken from Ref. [202].

On the contrary, for a (3+1)-spectrum (and more generally for a  $3+N$ -spectrum with an arbitrary  $N$  number of sterile states), the sterile neutrino(s) could be only slightly mixed with the active ones and mainly provide a description of the SBL results. In this case the oscillation probabilities for experiments working at  $E/L \sim 1 \text{ eV}^2$  take a simple form:

$$P_{\alpha\alpha} = 1 - \sin^2 2\theta_{\alpha\alpha} \sin^2 \Delta, \quad P_{\mu e} = \sin^2 2\theta_{\mu e} \sin^2 \Delta, \quad (14.87)$$

where  $\Delta \equiv \Delta m_{41}^2 L/4E$  and one can define effective mixing angles

$$\sin^2 2\theta_{\alpha\alpha} \equiv 4|U_{\alpha 4}|^2(1 - |U_{\alpha 4}|^2), \quad \sin^2 2\theta_{\mu e} \equiv 4|U_{\mu 4}|^2|U_{e 4}|^2. \quad (14.88)$$

In here  $\alpha = e, \mu$  and  $U_{\alpha 4}$  are the elements of the lepton mixing matrix describing the mixing of the 4th neutrino mass state with the electron and muon flavour. In this scenario there is no sensitivity to CP violation in the  $\Delta$  driven oscillations, so the relations above are valid for both neutrinos and antineutrinos. At linear order in the mixing elements one can derive a relation between the amplitudes of appearance and disappearance probabilities:

$$4 \sin^2 2\theta_{\mu e} \approx \sin^2 2\theta_{ee} \sin^2 2\theta_{\mu\mu}. \quad (14.89)$$

This relation implies a constraint between the possible results in disappearance and appearance experiments. Consequently it is not trivial to find a consistent description to all the SBL anomalies. Over the years, different groups have performed a variety of such global analysis leading to quantitative different conclusions on the statistical quality of the global fit (see for example [203–208], see also Refs. [209, 210] for recent reviews on the subject). Generically the results of the global analysis show that there is significant tension between groups of different data sets – in particular between appearance and disappearance results – and Eq.(14.89) makes it difficult to obtain a good global fit as illustrated in the right panel in Fig.14.10 taken from Ref. [203] which concluded that 3+1 scenario is excluded at  $4.7\sigma$  level.

A straightforward question to ask is whether the situation improves if more neutrino states at the eV scale are introduced. Simplest extension is the introduction of 2 states with eV scale mass splittings,  $\nu_4$  and  $\nu_5$ . The ordering of the states can be such that  $\Delta m_{41}^2$  and  $\Delta m_{51}^2$  are both positive (“3+2”) or one of them is negative (“1+3+1”). From the point of view of the description of the data the most important new qualitative feature is that now non-zero CP violation at  $E/L \sim \text{eV}^2$  is possibly observable [206, 211–213]. This allows some additional freedom in fitting neutrino versus anti-neutrino data from LSND and MiniBooNE together. However, it still holds that a non-zero  $\nu_\mu \rightarrow \nu_e$  appearance at SBL necessarily predicts SBL disappearance for both  $\nu_e$  and  $\nu_\mu$ . So, generically, the tension between appearance and disappearance results remains, thought differences in the methodology of statistical quantification of the degree of agreement/disagreement in these scenarios can lead to different conclusions on whether they can provide a successful description of all the data [203, 209, 210]. Cosmological observations can provide complementary information on the number of relativistic neutrino states in thermal equilibrium in the early Universe and on the sum of their masses which sets further constraints on light sterile neutrino scenarios (see Section 26, Neutrinos in cosmology).



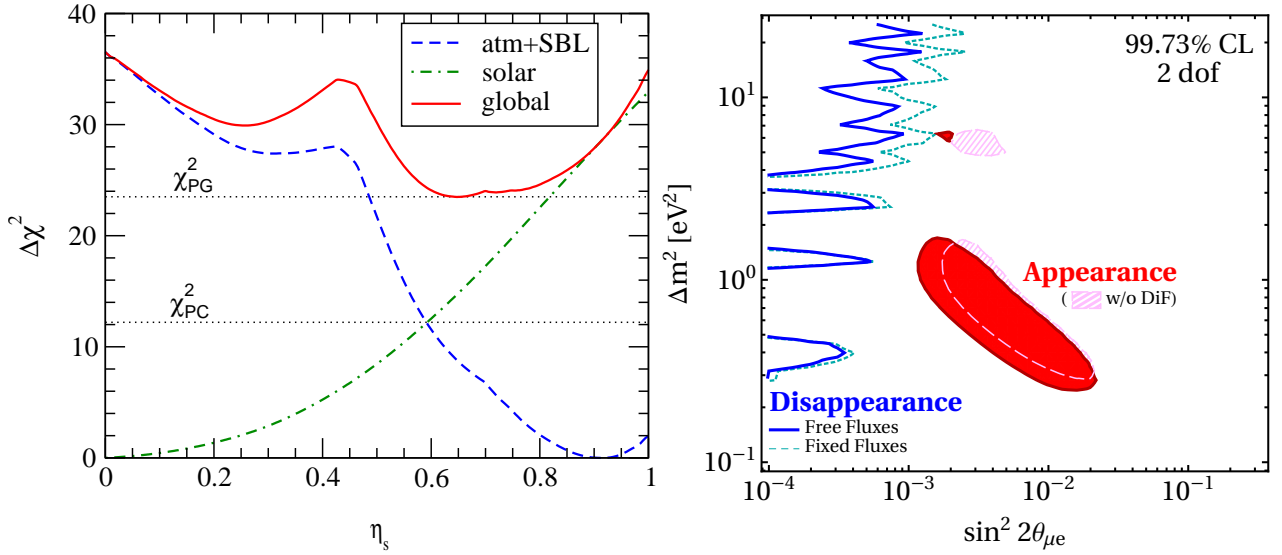


Figure 14.10: *Left*: Status of the 2+2 oscillation scenarios from Ref. [202] ( $\eta_S = \sum_i |U_{is}|^2$  where  $i$  runs over the two massive states mostly relevant for solar neutrino oscillations). In the figure also shown are the values of  $\chi_{PC}^2$  and  $\chi_{PG}^2$  relevant for parameter consistency test and parameter goodness of fit respectively. *Right*: Present status of 3+1 oscillation scenarios from Ref. [203].

## 14.9 Laboratory Probes of $\nu$ Mass Scale and its Nature

As described in Secs.14.4 and 14.5 neutrino flavour oscillations in vacuum and flavour transitions in matter only depend on the differences between the neutrino masses-squared,  $\Delta m_{ij}^2$ , and on the mixing matrix elements,  $U_{ij}$ . But they are insensitive to the absolute mass scale for the neutrinos,  $m_i$ . They also give us no information on whether they are Dirac or Majorana particles.

Clearly the observation of flavour oscillations imply a lower bound on the mass of the heavier neutrino in  $\Delta m_{ij}^2$ ,  $|m_i| \geq \sqrt{\Delta m_{ij}^2}$  for  $\Delta m_{ij}^2 > 0$ . But there is no upper bound on  $m_i$ . In particular, oscillation results allow neutrino spectrum to be approximately degenerate at a mass scale that is much higher than the  $\sqrt{\Delta m_{ij}^2}$  that they determine. Information of the mass scale of the neutrino is provided by other type of experiments. In here we briefly summarize the most sensitive laboratory probes of the neutrino mass scale and on whether they are Dirac or Majorana particles. Cosmological observations provide, albeit indirectly, complementary information on the neutrino mass scale as it is reviewed in Section 26, Neutrinos in cosmology.

### 14.9.1 Constraints from Kinematics of Weak Decays

The only model independent information on the neutrino masses, rather than mass differences, can be extracted from energy-momentum conservation relation in reactions in which a neutrino or an anti-neutrino is involved.

Historically these bounds were labeled as limits on the mass of the flavour neutrino states corresponding to the charged flavour involved in the decay. Fermi proposed in 1933 such a kinematic search for the  $\nu_e$  neutrino mass (which we will label here as  $m_{\nu_e}^{\text{eff}}$ ) in the end part of the beta spectra in  ${}^3\text{H}$  beta decay  ${}^3\text{H} \rightarrow {}^3\text{He} + e^- + \bar{\nu}_e$ .

Because  ${}^3\text{H}$  beta decay is a superallowed transition, the nuclear matrix elements are energy independent so the electron spectrum is determined exclusively by the phase space

$$\begin{aligned} \frac{dN}{dE} &= C p E (Q - T) \sqrt{(Q - T)^2 - (m_{\nu_e}^{\text{eff}})^2} F(E) \\ &\equiv R(E) \sqrt{(E_0 - E)^2 - (m_{\nu_e}^{\text{eff}})^2}. \end{aligned} \quad (14.90)$$

$E_0$  is the mass difference between the initial and final nucleus,  $E = T + m_e$  is the total electron energy,  $p$  its momentum,  $Q \equiv E_0 - m_e$  is the maximum kinetic energy of the electron and Final state Coulomb interactions are contained in the Fermi

function  $F(E)$ .  $R(E)$  in the second equality contains all the  $m_{\nu}$ -independent factors.

The Kurie function is defined as  $K(T) \equiv \sqrt{\frac{dN}{dE} \frac{1}{pEF(E)}}$ . From Eq.(14.90) we see that if  $m_{\nu_e}^{\text{eff}}=0$   $K(T)$  would depend linearly on  $T$ . A non-vanishing neutrino mass then provokes a distortion from the straight-line  $T$ -dependence at the end point, So for  $m_{\nu_e}^{\text{eff}} = 0$ ,  $T_{\text{max}} = Q$ , while for  $m_{\nu_e}^{\text{eff}} \neq 0$ ,  $T_{\text{max}} = Q - m_{\nu_e}^{\text{eff}}$ . In  ${}^3\text{H}$  beta decay  $Q = 18.6$  KeV is very small and therefore this decay is more sensitive to this  $m_{\nu_e}^{\text{eff}}$ -induced distortion.

The most recent result on the kinematic search for neutrino mass in tritium decay is from KATRIN [214], experiment which has found so far no indication of  $m_{\nu_e} \neq 0$  and sets an upper limit

$$m_{\nu_e}^{\text{eff}} < 1.1 \text{ eV}, \quad (14.91)$$

at 90% CL improving over the previous bound from the Mainz [215] and Troitsk [216] experiments which constrained  $m_{\nu_e}^{\text{eff}} < 2.2$  eV at 95% CL. KATRIN continues running with an estimated sensitivity limit of  $m_{\nu_e}^{\text{eff}} \sim 0.2$  eV. Project 8 is exploring a new technique for  $\beta$ -spectrometry based on cyclotron radiation [217].

An alternative isotope to Tritium is  ${}^{163}\text{Ho}$  [218] which presents the advantage of a smaller  $Q = 2.8$  KeV. It decays via electron-capture to  ${}^{163}\text{Dy}$ . Currently, there are three experiments exploring this decay to probe the neutrino mass: ECHO [219], HOLMES [220], and NuMECS [221]. These experiments are complementary to tritium-based searches from a technical point-of-view. Also the decay of  ${}^{163}\text{Ho}$  determines the effective electron neutrino mass as opposed to anti-neutrino in Tritium.

For the other flavours the present limits compiled in the listing section of the PDG read

$$m_{\nu_\mu}^{\text{eff}} < 190 \text{ keV (90\% CL)} \quad \text{from} \quad \pi^- \rightarrow \mu^- + \bar{\nu}_\mu, \quad (14.92)$$

$$m_{\nu_\tau}^{\text{eff}} < 18.2 \text{ MeV (95\% CL)} \quad \text{from} \quad \tau^- \rightarrow n\pi + \nu_\tau. \quad (14.93)$$

In the presence of mixing and for neutrinos with small mass differences the distortion of the beta spectrum is given by the sum of the individual spectra generated incoherently by each neutrino massive state weighted with the relevant mixing matrix element squared [222]:

$$\frac{dN}{dE} = R(E) \sum_i |U_{ei}|^2 \sqrt{(E_0 - E)^2 - m_i^2} \Theta(E_0 - E - m_i). \quad (14.94)$$



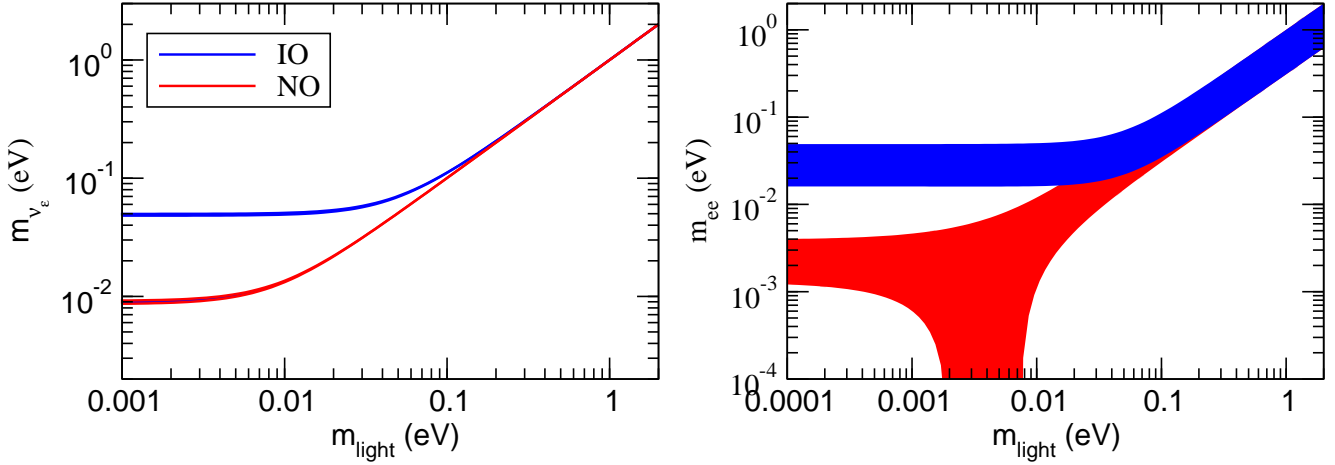


Figure 14.11: Allowed 95% CL ranges (1 dof) for the neutrino mass observable determined in  ${}^3\text{H}$  beta decay (left panel) and in  $0\nu\beta\beta$  (right panel) in the framework of  $3\nu$  mixing as a function of the lightest neutrino mass. The ranges are obtained by projecting the results of the global analysis of oscillation data (w/o SK-atm) in Ref. [187]. The region for each ordering is defined with respect to its local minimum.

The step function,  $\Theta(E_0 - E - m_i)$  arises because a neutrino with a given mass  $m_i$  can only be produced if the available energy is larger than its mass. Equation (14.94) shows the two main effects of the neutrino masses and mixings on the electron energy spectrum: First kinks appear at the electron energies  $E_e^{(i)} = E \sim E_0 - m_i$  with sizes that are determined by  $|U_{ei}|^2$ . Second the end point shifts to  $E_{ep} = E_0 - m_0$ , where  $m_0$  is the lightest neutrino mass. Corrections are induced once the the energy resolution of the experiment is considered [223,224]

In the  $3\nu$  mixing scenario the distortion of the spectrum can still be effectively described by a single parameter – which we will still denote as  $m_{\nu_e}$  – if for all neutrino states  $E_0 - E = Q - T \gg m_i$ . In this case one can expand Eq.(14.94) as:

$$\frac{dN}{dE} \simeq R(E) \sum_i |U_{ei}|^2 \sqrt{(E_0 - E)^2 - (m_{\nu_e}^{\text{eff}})^2}, \quad (14.95)$$

with

$$(m_{\nu_e}^{\text{eff}})^2 = \frac{\sum_i m_i^2 |U_{ei}|^2}{\sum_i |U_{ei}|^2} = \sum_i m_i^2 |U_{ei}|^2, \quad (14.96)$$

where unitarity is assumed in the second equality. In this approximation the distortion of the end point of the spectrum is described by a single parameter, and with the present results from KATRIN it is bounded to be

$$1.1 \text{ eV} \geq m_{\nu_e}^{\text{eff}} = \sqrt{\sum_i m_i^2 |U_{ei}|^2} = \begin{cases} \sqrt{m_0^2 + \Delta m_{21}^2 (1 - c_{13}^2 c_{12}^2) + \Delta m_{32}^2 s_{13}^2} & \text{in NO,} \\ \sqrt{m_0^2 + \Delta m_{21}^2 c_{13}^2 c_{12}^2 - \Delta m_{32}^2 c_{13}^2} & \text{in IO,} \end{cases} \quad (14.97)$$

where  $m_0 = m_1$  ( $m_3$ ) is the lightest neutrino mass in NO (IO) spectrum. Correspondingly the bounds in Eqs.(14.92) and (14.93) apply to the combinations  $\sum_i m_i^2 |U_{\alpha i}|^2$  for  $\alpha = \mu$  and  $\tau$  respectively. So with the values known of the mixing matrix elements the strongest constraint on the absolute value of the neutrino mass comes from Tritium beta decay.

From Eq.(14.97) we see that, given the present knowledge of the neutrino mass differences and their mixing from oscillation experiments, it is possible to translate the experimental information of  $m_{\nu_e}$  on a corresponding range for the lightest neutrino mass and that such relation depends on the ordering of the states. We plot in Fig.14.11 the recasting of the allowed regions of the analysis

in Ref. [187] in terms of the allowed range  $m_{\nu_e}$  as a function of  $m_{\text{light}} \equiv m_0$ . In particular one finds that the results of oscillation experiments imply a lower bound on  $m_{\nu_e} > 0.048$  (0.0085) eV for IO (NO) at 95% CL.

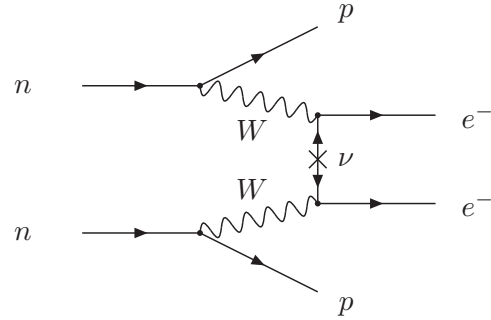


Figure 14.12: Feynman diagram for neutrinoless double-beta decay.

#### 14.9.2 Dirac vs Majorana: Neutrinoless Double-beta Decay

The most sensitive probe to whether neutrinos are Dirac or Majorana states is the neutrinoless double beta decay ( $0\nu\beta\beta$ ):

$$(A, Z) \rightarrow (A, Z + 2) + e^- + e^-. \quad (14.98)$$

In the presence of neutrino masses and mixing the process in Eq.(14.98) can be generated at lower order in perturbation theory by the term represented in Fig.14.12. The corresponding amplitude is proportional to the product of the two leptonic currents

$$M_{\alpha\beta} \propto [\bar{e}\gamma_\alpha(1 - \gamma_5)\nu_e] [\bar{e}\gamma_\beta(1 - \gamma_5)\nu_e] \propto \sum_i (U_{ei})^2 [\bar{e}\gamma_\alpha(1 - \gamma_5)\nu_i] [\bar{e}\gamma_\beta(1 - \gamma_5)\nu_i]. \quad (14.99)$$

The neutrino propagator in Fig.14.12 can only arise from the contraction  $\langle 0 | \nu_i(x) \nu_i(y)^T | 0 \rangle$ . But if the neutrino is a Dirac particle  $\nu_i$  field annihilates a neutrino states and creates an antineutrino state which are different, so the contraction  $\langle 0 | \nu_i(x) \nu_i(y)^T | 0 \rangle = 0$  and  $M_{\alpha\beta} = 0$ . On the other hand, if  $\nu_i$  is a Majorana particle, neutrino and antineutrino are described by the same field and  $\langle 0 | \nu_i(x) \nu_i(y)^T | 0 \rangle \neq 0$ .

The conclusion is that in order to induce the  $0\nu\beta\beta$  decay, neutrinos must be Majorana particles. This is consistent with the fact that the process (14.98) violates total lepton number by two

units. Conversely, if  $0\nu\beta\beta$  decay is observed, massive neutrinos cannot be Dirac states [225].

It is important to stress that neutrinoless double beta decay could be dominantly induced by other new physics effects beyond that of Majorana neutrino masses. Consequently the connection between the observation or limitation of the neutrinoless double beta decay and the neutrino mass can only be made under some assumption about the source of total lepton number violation in the model.

The observable determined by the experiments is the half-life of

$$m_{ee} = \left| \sum_i m_i U_{ei}^2 \right| = \begin{cases} \left| m_0 c_{12}^2 c_{13}^2 + \sqrt{\Delta m_{21}^2 + m_0^2} s_{12}^2 c_{13}^2 e^{2i(\eta_2 - \eta_1)} + \sqrt{\Delta m_{32}^2 + \Delta m_{21}^2 + m_0^2} s_{13}^2 e^{-2i(\delta_{CP} + \eta_1)} \right| & \text{in NO,} \\ \left| m_0 s_{13}^2 + \sqrt{m_0^2 - \Delta m_{32}^2} s_{12}^2 c_{13}^2 e^{2i(\eta_2 + \delta_{CP})} + \sqrt{m_0^2 - \Delta m_{32}^2 - \Delta m_{21}^2} c_{12}^2 c_{13}^2 e^{2i(\eta_1 + \delta_{CP})} \right| & \text{in IO,} \end{cases}$$

which, in addition to the masses and mixing parameters that affect the tritium beta decay spectrum, depends also on the leptonic CP violating phases. We plot in Fig.14.11 the the recasting of the allowed regions of the analysis in Ref. [187] in terms of the allowed range  $m_{ee}$  as a function of  $m_{\text{light}} \equiv m_0$  for the two orderings. As a consequence of the dependence on the unknown Majorana phases, the allowed range of  $m_{ee}$  for a given value of  $m_{\text{light}}$  and ordering is substantially broader than that of  $m_{\nu_e}$ . Nevertheless, the results of oscillation experiments imply a lower bound on the effective Majorana mass for the IO, which at 95%CL reads  $m_{ee} > 0.016$  eV.

From Eq.(14.100) we see that nuclear structure details enter relation between the decay rate (or lifetime) and the effective Majorana mass. As a consequence uncertainties in the nuclear structure calculations result in a spread of  $m_{ee}$  values for a given  $T_{1/2}^{0\nu}$  by a factor of 2–3 [226].

We present in Sec.14.9.3 a brief description of the experimental searches for neutrinoless double-beta decay. At the time of writing of this review the strongest bound on  $0\nu\beta\beta$  decay lifetime comes from the search in KamLAND-Zen experiment [227] (see Sec.14.9.3) which uses 13 Tons of Xe-loaded liquid scintillator to search for the decay  $0\nu\beta\beta$  of  $^{136}\text{Xe}$  and has set a bound on the half-life of  $T_{1/2}^{0\nu} > 1.07 \times 10^{26}$  yr at 90% CL. Using a variety of nuclear matrix element calculations, the corresponding upper bound on the effective Majorana mass is

$$m_{ee} < 61 - 165 \text{ meV}. \quad (14.101)$$

### 14.9.3 Experimental Search for Neutrinoless Double-beta Decay

The signature of  $0\nu\beta\beta$  is that the sum of energy of two electrons is equal to the  $Q$ -value of the nuclear transition. Various requirements must be met to achieve high sensitivity such as a large source mass with isotopic enrichment, underground location to shield cosmic-ray induced background, and ultra-low background techniques to reduce radioactive background. The sensitivity to the half-life is proportional to  $\varepsilon Mt$  in the case of a background-free measurement and  $\varepsilon \sqrt{\frac{Mt}{b\Delta E}}$  for the case background exists, where  $\varepsilon$  is the detection efficiency of the signal,  $M$  is the source mass,  $t$  is the measurement time,  $b$  is the background rate, and  $\Delta E$  is the energy resolution.

There are 35 candidate nuclei for double-beta decay. Currently, experiments using  $^{136}\text{Xe}$  and  $^{76}\text{Ge}$  have reported the most sensitive results of  $0\nu\beta\beta$  search. Because of the uncertainties related to the nuclear matrix element, complementarity of technologies, different background, and the investigation of the mechanism behind the  $0\nu\beta\beta$  in case of a positive signal, it is important to pursue the searches with various isotopes.

The energy from electrons is measured with either ionization, scintillation, or through phonons. In some experiments a combination of two techniques is used. Among those using

the decay. Under the assumption that the Majorana neutrino mass is the only source of lepton number violation at low energies, the decay half-life is given by:

$$(T_{1/2}^{0\nu})^{-1} = G^{0\nu} |M^{0\nu}|^2 \left( \frac{m_{ee}}{m_e} \right)^2, \quad (14.100)$$

where  $G^{0\nu}$  is the phase space integral taking into account the final atomic state,  $|M^{0\nu}|$  is the nuclear matrix element of the transition, and  $m_{ee}$  is the *effective Majorana mass* of  $\nu_e$ ,

ionization detection, ultra-high-purity germanium detector provides the best sensitivity thanks to high energy resolution and low background. GERDA uses total 20.0 kg of broad energy germanium (BEGe) and 15.6 kg of coaxial detectors, both enriched in  $^{76}\text{Ge}$ , for the second phase. Background levels of  $(5.6^{+3.4}_{-2.4}) \times 10^{-4}$  counts/(keV·kg·year) for BEGe detectors and  $(5.7^{+4.1}_{-2.6}) \times 10^{-4}$  counts/(keV·kg·year) for coaxial detectors have been achieved [228], which enable a background-free search. The Majorana-Demonstrator [229] consists of 44.1 kg of Ge (29.7 kg enriched to 88% in  $^{76}\text{Ge}$ ) detectors split between two modules. It has achieved energy resolution of 2.5 keV FWHM at the  $Q$ -value (2.039 MeV).

Liquid scintillator detectors have simple structure and can utilize existing large detectors with low background environments. By adding an inner balloon to contain xenon-loaded liquid scintillator to the KamLAND detector, KamLAND-Zen used 380 kg of xenon with 90.1% enrichment in  $^{136}\text{Xe}$ . Reducing the background level by purification of scintillator, KamLAND-Zen reported the half-life limit above  $10^{26}$  years at 90% CL [227]. The SNO detector has been also upgraded to be filled with liquid scintillator in SNO+ experiment [230]. The SNO+ detector will be loaded with 0.5% natural tellurium, corresponding to approximately 1330 kg of  $^{130}\text{Te}$  to search for  $0\nu\beta\beta$ .

With a time projection chamber, one can utilize both ionization and scintillation. EXO-200 uses a liquid xenon time projection chamber with enrichment to 80.6%, corresponding to 74.7 kg of  $^{136}\text{Xe}$  in the fiducial mass [231]. An energy resolution of 1.15% ( $\sigma/E$ ) is achieved at the  $Q$ -value of  $^{136}\text{Xe}$   $0\nu\beta\beta$ . The NEXT collaboration has been developing a high-pressure xenon gas time projection chamber with electroluminescent amplification and optical readouts. An energy resolution of 1% FWHM at the  $Q$ -value of  $^{136}\text{Xe}$   $0\nu\beta\beta$  is demonstrated with NEXT-White detector [232].

CUORE uses cryogenic bolometer to measure the energy in a calorimetric way. The detector is located in Gran Sasso and composed of 988  $\text{TeO}_2$  bolometers for a total mass of 742 kg, corresponding to 206 kg of  $^{130}\text{Te}$ . An effective energy resolution of  $(7.7 \pm 0.5)$  keV FWHM is achieved for the first result [233]. For further reduction of background towards future search based on the CUORE technology, CUPID proposes to simultaneously measure the calorimetric signal and the scintillation light. Using the prototype CUPID-0, the technology is demonstrated and also  $0\nu\beta\beta$  is searched for with  $^{82}\text{Se}$  [234].

AMoRE also uses the simultaneous detection of heat and scintillation. Six  $^{100}\text{Mo}$ -enriched and  $^{48}\text{Ca}$ -depleted  $\text{CaMoO}_4$  crystals with a total mass of 1.9 kg (AMoRE-Pilot) are operated in Yangyang underground laboratory located in South Korea, searching for  $0\nu\beta\beta$  of  $^{100}\text{Mo}$  [235].

A tracker-calorimeter technique is employed in NEMO. Source isotopes are hosted in thin foils surrounded by a tracking detector, which in turn is surrounded by a calorimeter. Full topological event reconstruction with this configuration enables background rejection and gives additional information after discovery. The

NEMO-3 experiment used 7 isotopes, with the largest mass comprised of  $^{100}\text{Mo}$  (7 kg) [236]. NEMO-3 also reported a first search for neutrinoless quadruple- $\beta$  decay of  $^{150}\text{Nd}$  [237].

### References

- [1] J. N. Bahcall, *NEUTRINO ASTROPHYSICS* (1989), ISBN 9780521379755.
- [2] R. N. Mohapatra and P. B. Pal, World Sci. Lect. Notes Phys. **60**, 1 (1998), [World Sci. Lect. Notes Phys.72,1(2004)].
- [3] C. W. Kim and A. Pevsner, Contemp. Concepts Phys. **8**, 1 (1993).
- [4] B. Kayser, F. Gibrat-Debu and F. Perrier, World Sci. Lect. Notes Phys. **25**, 1 (1989).
- [5] C. Giunti and C. W. Kim, *Fundamentals of Neutrino Physics and Astrophysics* (2007), ISBN 9780198508717.
- [6] M. C. Gonzalez-Garcia and Y. Nir, Rev. Mod. Phys. **75**, 345 (2003), [hep-ph/0202058].
- [7] M. C. Gonzalez-Garcia and M. Maltoni, Phys. Rept. **460**, 1 (2008), [arXiv:0704.1800].
- [8] A. Pilaftsis, Z. Phys. **C55**, 275 (1992), [hep-ph/9901206].
- [9] P. Minkowski, Phys. Lett. **67B**, 421 (1977).
- [10] P. Ramond, in “International Symposium on Fundamentals of Quantum Theory and Quantum Field Theory Palm Coast, Florida, February 25-March 2, 1979,” 265–280 (1979), [hep-ph/9809459].
- [11] M. Gell-Mann, P. Ramond and R. Slansky, Conf. Proc. **C790927**, 315 (1979), [arXiv:1306.4669].
- [12] T. Yanagida, Conf. Proc. **C7902131**, 95 (1979).
- [13] R. N. Mohapatra and G. Senjanovic, Phys. Rev. Lett. **44**, 912 (1980), [231(1979)].
- [14] J. Schechter and J. W. F. Valle, Phys. Rev. **D21**, 309 (1980).
- [15] J. Schechter and J. W. F. Valle, Phys. Rev. **D22**, 2227 (1980).
- [16] J. Schechter and J. W. F. Valle, Phys. Rev. **D24**, 1883 (1981), [Erratum: Phys. Rev. D25,283(1982)].
- [17] Z. Maki, M. Nakagawa and S. Sakata, Prog. Theor. Phys. **28**, 870 (1962), [34(1962)].
- [18] Y. Katayama *et al.*, Prog. Theor. Phys. **28**, 675 (1962).
- [19] B. Pontecorvo, Sov. Phys. JETP **26**, 984 (1968), [Zh. Eksp. Teor. Fiz.53,1717(1967)].
- [20] N. Cabibbo, Phys. Rev. Lett. **10**, 531 (1963), [648(1963)].
- [21] M. Kobayashi and T. Maskawa, Prog. Theor. Phys. **49**, 652 (1973).
- [22] S. Antusch *et al.*, JHEP **10**, 084 (2006), [hep-ph/0607020].
- [23] S. Antusch and O. Fischer, JHEP **10**, 094 (2014), [arXiv:1407.6607].
- [24] V. N. Gribov and B. Pontecorvo, Phys. Lett. **28B**, 493 (1969).
- [25] E. Akhmedov, in “International Conference on History of the Neutrino: 1930-2018 Paris, France, September 5-7, 2018,” (2019), [arXiv:1901.05232].
- [26] L. Wolfenstein, Phys. Rev. **D17**, 2369 (1978), [294(1977)].
- [27] A. Halprin, Phys. Rev. **D34**, 3462 (1986).
- [28] A. J. Baltz and J. Weneser, Phys. Rev. **D37**, 3364 (1988).
- [29] P. D. Mannheim, Phys. Rev. **D37**, 1935 (1988).
- [30] L. Landau, Phys. Z. Sov. **2**, 46 (1932).
- [31] C. Zener, Proc. Roy. Soc. Lond. **A137**, 696 (1932).
- [32] E. Majorana, Nuovo Cim. **9**, 43 (1932).
- [33] E. C. G. Stueckelberg, Helv. Phys. Acta **5**, 369 (1932).
- [34] T.-K. Kuo and J. T. Pantaleone, Rev. Mod. Phys. **61**, 937 (1989).
- [35] S. J. Parke, Phys. Rev. Lett. **57**, 1275 (1986), [328(1986)].
- [36] W. C. Haxton, Phys. Rev. Lett. **57**, 1271 (1986), [332(1986)].
- [37] S. T. Petcov, Phys. Lett. **B191**, 299 (1987), [427(1987)].
- [38] S. P. Mikheyev and A. Yu. Smirnov, Sov. J. Nucl. Phys. **42**, 913 (1985), [305(1986)].
- [39] J. N. Bahcall *et al.*, Rev. Mod. Phys. **54**, 767 (1982).
- [40] J. N. Bahcall, A. M. Serenelli and S. Basu, Astrophys. J. **621**, L85 (2005), [arXiv:astro-ph/0412440].
- [41] A. M. Serenelli, W. C. Haxton and C. Pena-Garay, Astrophys. J. **743**, 24 (2011), [arXiv:1104.1639].
- [42] F. L. Villante, Phys. Lett. **B742**, 279 (2015), [arXiv:1410.2796].
- [43] A. Serenelli, Eur. Phys. J. **A52**, 4, 78 (2016), [arXiv:1601.07179].
- [44] R. Davis, Jr., D. S. Harmer and K. C. Hoffman, Phys. Rev. Lett. **20**, 1205 (1968).
- [45] B. T. Cleveland *et al.*, Astrophys. J. **496**, 505 (1998).
- [46] C. Pena-Garay and A. Serenelli (2008), [arXiv:0811.2424].
- [47] J. N. Abdurashitov *et al.* (SAGE), J. Exp. Theor. Phys. **95**, 181 (2002), [Zh. Eksp. Teor. Fiz.122,211(2002)], [arXiv:astro-ph/0204245].
- [48] W. Hampel *et al.* (GALLEX), Phys. Lett. **B447**, 127 (1999).
- [49] M. Altmann *et al.* (GNO), Phys. Lett. **B616**, 174 (2005), [hep-ex/0504037].
- [50] J. N. Abdurashitov *et al.* (SAGE), Phys. Rev. **C80**, 015807 (2009), [arXiv:0901.2200].
- [51] K. S. Hirata *et al.* (Kamiokande-II), Phys. Rev. Lett. **63**, 16 (1989).
- [52] K. S. Hirata *et al.* (Kamiokande-II), Phys. Rev. **D44**, 2241 (1991), [Erratum: Phys. Rev. D45,2170(1992)].
- [53] Y. Fukuda *et al.* (Kamiokande), Phys. Rev. Lett. **77**, 1683 (1996).
- [54] Y. Fukuda *et al.* (Super-Kamiokande), Phys. Rev. Lett. **81**, 1158 (1998), [Erratum: Phys. Rev. Lett.81,4279(1998)], [hep-ex/9805021].
- [55] Y. Fukuda *et al.* (Super-Kamiokande), Phys. Rev. Lett. **82**, 2430 (1999), [hep-ex/9812011].
- [56] K. Abe *et al.* (Super-Kamiokande), Phys. Rev. **D94**, 5, 052010 (2016), [arXiv:1606.07538].
- [57] N. Vinyoles *et al.*, Astrophys. J. **835**, 2, 202 (2017), [arXiv:1611.09867].
- [58] S. Fukuda *et al.* (Super-Kamiokande), Phys. Rev. Lett. **86**, 5651 (2001), [hep-ex/0103032].
- [59] S. Fukuda *et al.* (Super-Kamiokande), Phys. Rev. Lett. **86**, 5656 (2001), [hep-ex/0103033].
- [60] B. Aharmim *et al.* (SNO), Phys. Rev. **C72**, 055502 (2005), [arXiv:nucl-ex/0502021].
- [61] S. Fukuda *et al.* (Super-Kamiokande), Phys. Lett. **B539**, 179 (2002), [hep-ex/0205075].
- [62] Q. R. Ahmad *et al.* (SNO), Phys. Rev. Lett. **87**, 071301 (2001), [arXiv:nucl-ex/0106015].
- [63] Q. R. Ahmad *et al.* (SNO), Phys. Rev. Lett. **89**, 011301 (2002), [arXiv:nucl-ex/0204008].
- [64] B. Aharmim *et al.* (SNO), Phys. Rev. **C88**, 025501 (2013), [arXiv:1109.0763].
- [65] J. Bergstrom *et al.*, JHEP **03**, 132 (2016), [arXiv:1601.00972].
- [66] C. Arpesella *et al.* (Borexino), Phys. Lett. **B658**, 101 (2008), [arXiv:0708.2251].
- [67] G. Bellini *et al.* (Borexino), Phys. Rev. Lett. **108**, 051302 (2012), [arXiv:1110.3230].
- [68] M. Agostini *et al.* (BOREXINO), Nature **562**, 7728, 505 (2018).
- [69] G. Bellini *et al.* (Borexino), Phys. Rev. **D82**, 033006 (2010), [arXiv:0808.2868].

- [70] S. Abe *et al.* (KamLAND), Phys. Rev. **C84**, 035804 (2011), [arXiv:1106.0861].
- [71] A. Gando *et al.* (KamLAND), Phys. Rev. **C92**, 5, 055808 (2015), [arXiv:1405.6190].
- [72] M. Agostini *et al.* (Borexino) (2017), [arXiv:1707.09279].
- [73] M. Agostini *et al.* (Borexino) (2017), [arXiv:1709.00756].
- [74] A. Renshaw *et al.* (Super-Kamiokande), Phys. Rev. Lett. **112**, 9, 091805 (2014), [arXiv:1312.5176].
- [75] M. Honda *et al.*, Phys. Rev. **D92**, 2, 023004 (2015), [arXiv:1502.03916].
- [76] G. D. Barr *et al.*, Phys. Rev. **D74**, 094009 (2006), [arXiv:astro-ph/0611266].
- [77] G. Battistoni *et al.*, Astropart. Phys. **19**, 269 (2003), [Erratum: Astropart. Phys.19,291(2003)], [hep-ph/0207035].
- [78] J. Evans *et al.*, Phys. Rev. **D95**, 2, 023012 (2017), [arXiv:1612.03219].
- [79] C. V. Achar *et al.*, Phys. Lett. **18**, 196 (1965).
- [80] F. Reines *et al.*, Phys. Rev. Lett. **15**, 429 (1965).
- [81] K. S. Hirata *et al.* (Kamiokande-II), Phys. Lett. **B205**, 416 (1988), [447(1988)].
- [82] D. Casper *et al.*, Phys. Rev. Lett. **66**, 2561 (1991).
- [83] K. Daum *et al.* (Frejus), Z. Phys. **C66**, 417 (1995).
- [84] M. Aglietta *et al.* (NUSEX), Europhys. Lett. **8**, 611 (1989).
- [85] K. S. Hirata *et al.* (Kamiokande-II), Phys. Lett. **B280**, 146 (1992).
- [86] Y. Fukuda *et al.* (Kamiokande), Phys. Lett. **B335**, 237 (1994).
- [87] Y. Fukuda *et al.* (Super-Kamiokande), Phys. Rev. Lett. **81**, 1562 (1998), [hep-ex/9807003].
- [88] M. Ambrosio *et al.* (MACRO), Phys. Lett. **B517**, 59 (2001), [hep-ex/0106049].
- [89] M. C. Sanchez *et al.* (Soudan 2), Phys. Rev. **D68**, 113004 (2003), [hep-ex/0307069].
- [90] Y. Ashie *et al.* (Super-Kamiokande), Phys. Rev. Lett. **93**, 101801 (2004), [hep-ex/0404034].
- [91] Z. Li *et al.* (Super-Kamiokande), Phys. Rev. **D98**, 5, 052006 (2018), [arXiv:1711.09436].
- [92] N. Agafonova *et al.* (OPERA), Phys. Rev. Lett. **120**, 21, 211801 (2018), [Erratum: Phys. Rev. Lett.121,no.13,139901(2018)], [arXiv:1804.04912].
- [93] M. G. Aartsen *et al.* (IceCube), Phys. Rev. **D99**, 3, 032007 (2019), [arXiv:1901.05366].
- [94] K. Abe *et al.* (Super-Kamiokande), Phys. Rev. **D97**, 7, 072001 (2018), [arXiv:1710.09126].
- [95] M. Ageron *et al.* (ANTARES), Nucl. Instrum. Meth. **A656**, 11 (2011), [arXiv:1104.1607].
- [96] M. G. Aartsen *et al.* (IceCube), JINST **12**, 03, P03012 (2017), [arXiv:1612.05093].
- [97] A. Albert *et al.* (ANTARES), JHEP **06**, 113 (2019), [arXiv:1812.08650].
- [98] M. G. Aartsen *et al.* (IceCube), Phys. Rev. Lett. **120**, 7, 071801 (2018), [arXiv:1707.07081].
- [99] S. Adrian-Martinez *et al.* (KM3Net), J. Phys. **G43**, 8, 084001 (2016), [arXiv:1601.07459].
- [100] M. G. Aartsen *et al.* (IceCube), J. Phys. **G44**, 5, 054006 (2017), [arXiv:1607.02671].
- [101] S. Ahmed *et al.* (ICAL), Pramana **88**, 5, 79 (2017), [arXiv:1505.07380].
- [102] K. Abe *et al.* (Hyper-Kamiokande) (2018), [arXiv:1805.04163].
- [103] B. Abi *et al.* (DUNE) (2018), [arXiv:1807.10334].
- [104] S. E. Kopp, Phys. Rept. **439**, 101 (2007), [arXiv:physics/0609129].
- [105] D. Beavis *et al.* (E899) (1995).
- [106] M. G. Catanesi *et al.* (HARP), Nucl. Instrum. Meth. **A571**, 527 (2007).
- [107] J. M. Paley *et al.* (MIPP), Phys. Rev. **D90**, 3, 032001 (2014), [arXiv:1404.5882].
- [108] N. Abgrall *et al.* (NA61), JINST **9**, P06005 (2014), [arXiv:1401.4699].
- [109] S. H. Ahn *et al.* (K2K), Phys. Lett. **B511**, 178 (2001), [hep-ex/0103001].
- [110] M. H. Ahn *et al.* (K2K), Phys. Rev. **D74**, 072003 (2006), [hep-ex/0606032].
- [111] D. G. Michael *et al.* (MINOS), Nucl. Instrum. Meth. **A596**, 190 (2008), [arXiv:0805.3170].
- [112] P. Adamson *et al.*, Nucl. Instrum. Meth. **A806**, 279 (2016), [arXiv:1507.06690].
- [113] P. Adamson *et al.* (MINOS), Phys. Rev. Lett. **110**, 25, 251801 (2013), [arXiv:1304.6335].
- [114] P. Adamson *et al.* (MINOS), Phys. Rev. Lett. **112**, 191801 (2014), [arXiv:1403.0867].
- [115] P. Adamson *et al.* (MINOS), Phys. Rev. **D86**, 052007 (2012), [arXiv:1208.2915].
- [116] P. Adamson *et al.* (MINOS+), Phys. Rev. Lett. **122**, 9, 091803 (2019), [arXiv:1710.06488].
- [117] C. Rubbia *et al.*, JINST **6**, P07011 (2011), [arXiv:1106.0975].
- [118] K. Abe *et al.* (T2K), Phys. Rev. Lett. **107**, 041801 (2011), [arXiv:1106.2822].
- [119] K. Abe *et al.* (T2K), Phys. Rev. Lett. **112**, 061802 (2014), [arXiv:1311.4750].
- [120] K. Abe *et al.* (T2K), Phys. Rev. Lett. **121**, 17, 171802 (2018), [arXiv:1807.07891].
- [121] K. Abe *et al.* (T2K) (2019), [arXiv:1910.03887].
- [122] P. Adamson *et al.* (NOvA), Phys. Rev. Lett. **118**, 15, 151802 (2017), [arXiv:1701.05891].
- [123] M. A. Acero *et al.* (NOvA), Phys. Rev. **D98**, 032012 (2018), [arXiv:1806.00096].
- [124] P. Adamson *et al.* (NOvA), Phys. Rev. Lett. **116**, 15, 151806 (2016), [arXiv:1601.05022].
- [125] P. Adamson *et al.* (NOvA), Phys. Rev. Lett. **118**, 23, 231801 (2017), [arXiv:1703.03328].
- [126] M. A. Acero *et al.* (NOvA), Phys. Rev. Lett. **123**, 151803 (2019), [arXiv:1906.04907].
- [127] A. Aguilar-Arevalo *et al.* (LSND), Phys. Rev. **D64**, 112007 (2001), [hep-ex/0104049].
- [128] B. Armbruster *et al.* (KARMEN), Phys. Rev. **D65**, 112001 (2002), [hep-ex/0203021].
- [129] A. A. Aguilar-Arevalo *et al.* (MiniBooNE), Phys. Rev. Lett. **121**, 22, 221801 (2018), [arXiv:1805.12028].
- [130] M. Antonello *et al.* (MicroBooNE, LAr1-ND, ICARUS-WA104) (2015), [arXiv:1503.01520].
- [131] S. Ajimura *et al.* (2017), [arXiv:1705.08629].
- [132] F. Von Feilitzsch, A. A. Hahn and K. Schreckenbach, Phys. Lett. **118B**, 162 (1982).
- [133] K. Schreckenbach *et al.*, Phys. Lett. **160B**, 325 (1985).
- [134] A. A. Hahn *et al.*, Phys. Lett. **B218**, 365 (1989).
- [135] P. Vogel *et al.*, Phys. Rev. **C24**, 1543 (1981).
- [136] T. A. Mueller *et al.*, Phys. Rev. **C83**, 054615 (2011), [arXiv:1101.2663].
- [137] P. Huber, Phys. Rev. **C84**, 024617 (2011), [Erratum: Phys. Rev. C85,029901(2012)], [arXiv:1106.0687].
- [138] D. Adey *et al.* (Daya Bay), Phys. Rev. **D100**, 5, 052004 (2019), [arXiv:1808.10836].

- [139] D. Adey *et al.* (Daya Bay), Phys. Rev. Lett. **121**, 24, 241805 (2018), [arXiv:1809.02261].
- [140] G. Bak *et al.* (RENO), Phys. Rev. Lett. **121**, 20, 201801 (2018), [arXiv:1806.00248].
- [141] H. de Kerret *et al.* (Double Chooz) (2019), [arXiv:1901.09445].
- [142] Y. J. Ko *et al.* (NEOS), Phys. Rev. Lett. **118**, 12, 121802 (2017), [arXiv:1610.05134].
- [143] F. P. An *et al.* (Daya Bay), Phys. Rev. Lett. **118**, 25, 251801 (2017), [arXiv:1704.01082].
- [144] G. Bak *et al.* (RENO), Phys. Rev. Lett. **122**, 23, 232501 (2019), [arXiv:1806.00574].
- [145] D. Adey *et al.* (Daya Bay), Phys. Rev. Lett. **123**, 11, 111801 (2019), [arXiv:1904.07812].
- [146] M. Apollonio *et al.* (CHOOZ), Eur.Phys.J. **C27**, 331 (2003), [hep-ex/0301017].
- [147] F. Boehm *et al.*, Phys. Rev. **D64**, 112001 (2001), [hep-ex/0107009].
- [148] K. Eguchi *et al.* (KamLAND), Phys. Rev. Lett. **90**, 021802 (2003), [hep-ex/0212021].
- [149] T. Araki *et al.* (KamLAND), Phys. Rev. Lett. **94**, 081801 (2005), [hep-ex/0406035].
- [150] A. Gando *et al.* (KamLAND), Phys. Rev. **D88**, 3, 033001 (2013), [arXiv:1303.4667].
- [151] F. Ardellier *et al.* (Double Chooz) (2006), [hep-ex/0606025].
- [152] X. Guo *et al.* (Daya Bay) (2007), [hep-ex/0701029].
- [153] J. K. Ahn *et al.* (RENO) (2010), [arXiv:1003.1391].
- [154] Y. Abe *et al.* (Double Chooz), Phys. Rev. Lett. **108**, 131801 (2012), [arXiv:1112.6353].
- [155] F. P. An *et al.* (Daya Bay), Phys. Rev. Lett. **108**, 171803 (2012), [arXiv:1203.1669].
- [156] J. K. Ahn *et al.* (RENO), Phys. Rev. Lett. **108**, 191802 (2012), [arXiv:1204.0626].
- [157] F. An *et al.* (JUNO), J. Phys. **G43**, 3, 030401 (2016), [arXiv:1507.05613].
- [158] I. Alekseev *et al.* (DANSS), Phys. Lett. **B787**, 56 (2018), [arXiv:1804.04046].
- [159] H. Almazán *et al.* (STEREO), Phys. Rev. Lett. **121**, 16, 161801 (2018), [arXiv:1806.02096].
- [160] J. Ashenfelter *et al.* (PROSPECT), Phys. Rev. Lett. **121**, 25, 251802 (2018), [arXiv:1806.02784].
- [161] A. P. Serebrov *et al.* (NEUTRINO-4), Pisma Zh. Eksp. Teor. Fiz. **109**, 4, 209 (2019), [JETP Lett.109,no.4,213(2019)], [arXiv:1809.10561].
- [162] Y. Abreu *et al.* (SoLid), JINST **12**, 04, P04024 (2017), [arXiv:1703.01683].
- [163] N. Cabibbo, Phys. Lett. **72B**, 333 (1978).
- [164] S. M. Bilenky, J. Hosek and S. T. Petcov, Phys. Lett. **94B**, 495 (1980).
- [165] V. D. Barger, K. Whisnant and R. J. N. Phillips, Phys. Rev. Lett. **45**, 2084 (1980).
- [166] P. Langacker *et al.*, Nucl. Phys. **B282**, 589 (1987).
- [167] S. Goswami and A. Yu. Smirnov, Phys. Rev. **D72**, 053011 (2005), [hep-ph/0411359].
- [168] N. Okamura, Prog. Theor. Phys. **114**, 1045 (2006), [hep-ph/0411388].
- [169] H. Nunokawa, S. J. Parke and R. Zukanovich Funchal, Phys. Rev. **D72**, 013009 (2005), [hep-ph/0503283].
- [170] A. Cervera *et al.*, Nucl. Phys. **B579**, 17 (2000), [Erratum: Nucl. Phys. B593,731(2001)], [hep-ph/0002108].
- [171] M. Freund, Phys. Rev. **D64**, 053003 (2001), [hep-ph/0103300].
- [172] E. K. Akhmedov *et al.*, JHEP **04**, 078 (2004), [hep-ph/0402175].
- [173] H. Minakata *et al.*, Phys. Rev. **D74**, 053008 (2006), [hep-ph/0607284].
- [174] O. L. G. Peres and A. Yu. Smirnov, Nucl. Phys. **B680**, 479 (2004), [hep-ph/0309312].
- [175] S. Petcov, Phys.Lett. **B434**, 321 (1998), [hep-ph/9805262].
- [176] E. K. Akhmedov *et al.*, Nucl.Phys. **B542**, 3 (1999), [hep-ph/9808270].
- [177] E. K. Akhmedov, Nucl.Phys. **B538**, 25 (1999), [hep-ph/9805272].
- [178] M. Chizhov, M. Maris and S. Petcov (1998), [hep-ph/9810501].
- [179] M. Chizhov and S. Petcov, Phys.Rev.Lett. **83**, 1096 (1999), [hep-ph/9903399].
- [180] E. K. Akhmedov, M. Maltoni and A. Y. Smirnov, JHEP **0705**, 077 (2007), [hep-ph/0612285].
- [181] C. Kim and U. Lee, Phys.Lett. **B444**, 204 (1998), [hep-ph/9809491].
- [182] O. Peres and A. Y. Smirnov, Phys.Lett. **B456**, 204 (1999), [hep-ph/9902312].
- [183] M. Gonzalez-Garcia, M. Maltoni and A. Y. Smirnov, Phys.Rev. **D70**, 093005 (2004), [hep-ph/0408170].
- [184] E. K. Akhmedov, M. Maltoni and A. Y. Smirnov, JHEP **0806**, 072 (2008), [arXiv:0804.1466].
- [185] J. Bernabeu, S. Palomares Ruiz and S. Petcov, Nucl.Phys. **B669**, 255 (2003), [hep-ph/0305152].
- [186] S. Petcov and T. Schwetz, Nucl.Phys. **B740**, 1 (2006), [hep-ph/0511277].
- [187] I. Esteban *et al.*, JHEP **01**, 106 (2019), [arXiv:1811.05487].
- [188] I. Esteban *et al.*, “Nufit4.1 at nufit webpage,” <http://www.nu-fit.org>.
- [189] F. Capozzi *et al.*, Prog. Part. Nucl. Phys. **102**, 48 (2018), [arXiv:1804.09678].
- [190] P. F. de Salas *et al.*, Phys. Lett. **B782**, 633 (2018), [arXiv:1708.01186].
- [191] M. Friend, “Updated Results from the T2K Experiment with  $3.13 \times 10^{21}$  Protons on Target,” (2019), KEK/J-PARC Physics seminar, January 10, 2019, URL <https://t2k.org/docs/talk/335/2019kekseminar>.
- [192] C. Jarlskog, Phys. Rev. Lett. **55**, 1039 (1985).
- [193] M. C. Gonzalez-Garcia, M. Maltoni and T. Schwetz, JHEP **11**, 052 (2014), [arXiv:1409.5439].
- [194] Y. Farzan and A. Yu. Smirnov, Phys. Rev. **D65**, 113001 (2002), [hep-ph/0201105].
- [195] A. Dueck, S. Petcov and W. Rodejohann, Phys. Rev. **D82**, 013005 (2010), [arXiv:1006.0227].
- [196] A. Aguilar-Arevalo *et al.* (MiniBooNE) (2012), [arXiv:1207.4809].
- [197] M. A. Acero, C. Giunti and M. Laveder, Phys. Rev. **D78**, 073009 (2008), [arXiv:0711.4222].
- [198] C. Giunti and M. Laveder, Phys. Rev. **C83**, 065504 (2011), [arXiv:1006.3244].
- [199] F. P. An *et al.* (Daya Bay), Phys. Rev. Lett. **116**, 6, 061801 (2016), [Erratum: Phys. Rev. Lett.118,no.9,099902(2017)], [arXiv:1508.04233].
- [200] G. Mention *et al.*, Phys. Rev. **D83**, 073006 (2011), [arXiv:1101.2755].
- [201] J. J. Gomez-Cadenas and M. C. Gonzalez-Garcia, Z. Phys. **C71**, 443 (1996), [hep-ph/9504246].
- [202] M. Maltoni *et al.*, Nucl. Phys. **B643**, 321 (2002), [hep-ph/0207157].
- [203] M. Dentler *et al.*, JHEP **08**, 010 (2018), [arXiv:1803.10661].
- [204] C. Giunti and M. Laveder, Phys. Rev. **D84**, 093006 (2011), [arXiv:1109.4033].

- [205] J. M. Conrad *et al.*, Adv. High Energy Phys. **2013**, 163897 (2013), [arXiv:1207.4765].
- [206] J. Kopp *et al.*, JHEP **05**, 050 (2013), [arXiv:1303.3011].
- [207] G. H. Collin *et al.*, Phys. Rev. Lett. **117**, 22, 221801 (2016), [arXiv:1607.00011].
- [208] S. Gariazzo *et al.*, JHEP **06**, 135 (2017), [arXiv:1703.00860].
- [209] A. Diaz *et al.* (2019), [arXiv:1906.00045].
- [210] S. Böser *et al.* (2019), [arXiv:1906.01739].
- [211] G. Karagiorgi *et al.*, Phys. Rev. **D75**, 013011 (2007), [Erratum: Phys. Rev.D80,099902(2009)], [hep-ph/0609177].
- [212] M. Maltoni and T. Schwetz, Phys. Rev. **D76**, 093005 (2007), [arXiv:0705.0107].
- [213] C. Giunti and M. Laveder, Phys. Rev. **D84**, 073008 (2011), [arXiv:1107.1452].
- [214] M. Aker *et al.* (KATRIN) (2019), [arXiv:1909.06048].
- [215] J. Bonn *et al.*, Nucl. Phys. Proc. Suppl. **91**, 273 (2001), [PoShep2001,192(2001)].
- [216] V. M. Lobashev *et al.*, Nucl. Phys. Proc. Suppl. **91**, 280 (2001), [280(2001)].
- [217] B. Monreal and J. A. Formaggio, Phys. Rev. **D80**, 051301 (2009), [arXiv:0904.2860].
- [218] A. De Rujula and M. Lusignoli, Phys. Lett. **118B**, 429 (1982).
- [219] L. Gastaldo *et al.*, J. Low Temp. Phys. **176**, 5-6, 876 (2014), [arXiv:1309.5214].
- [220] B. Alpert *et al.*, Eur. Phys. J. **C75**, 3, 112 (2015), [arXiv:1412.5060].
- [221] M. P. Croce *et al.*, J. Low. Temp. Phys. **184**, 3-4, 958 (2016), [arXiv:1510.03874].
- [222] R. E. Shrock, Phys. Lett. **96B**, 159 (1980).
- [223] F. Vissani, Nucl. Phys. Proc. Suppl. **100**, 273 (2001), [273(2000)], [hep-ph/0012018].
- [224] Y. Farzan, O. L. G. Peres and A. Yu. Smirnov, Nucl. Phys. **B612**, 59 (2001), [hep-ph/0105105].
- [225] J. Schechter and J. W. F. Valle, Phys. Rev. **D25**, 2951 (1982), [289(1981)].
- [226] J. Engel and J. Menendez, Rept. Prog. Phys. **80**, 4, 046301 (2017), [arXiv:1610.06548].
- [227] A. Gando *et al.* (KamLAND-Zen), Phys. Rev. Lett. **117**, 8, 082503 (2016), [Addendum: Phys. Rev. Lett.117,no.10,109903(2016)], [arXiv:1605.02889].
- [228] M. Agostini *et al.* (GERDA), Science **365**, 1445 (2019), [arXiv:1909.02726].
- [229] S. I. Alvis *et al.* (Majorana) (2019), [arXiv:1902.02299].
- [230] S. Andringa *et al.* (SNO+), Adv. High Energy Phys. **2016**, 6194250 (2016), [arXiv:1508.05759].
- [231] G. Anton *et al.* (EXO-200) (2019), [arXiv:1906.02723].
- [232] J. Renner *et al.* (NEXT), JINST **13**, 10, P10020 (2018), [arXiv:1808.01804].
- [233] C. Alduino *et al.* (CUORE), Phys. Rev. Lett. **120**, 13, 132501 (2018), [arXiv:1710.07988].
- [234] O. Azzolini *et al.* (CUPID), Phys. Rev. Lett. **123**, 3, 032501 (2019), [arXiv:1906.05001].
- [235] V. Alenkov *et al.*, Eur. Phys. J. **C79**, 9, 791 (2019), [arXiv:1903.09483].
- [236] R. Arnold *et al.* (NEMO-3), Phys. Rev. **D92**, 7, 072011 (2015), [arXiv:1506.05825].
- [237] R. Arnold *et al.* (NEMO-3), Phys. Rev. Lett. **119**, 4, 041801 (2017), [arXiv:1705.08847].

## 15. Quark Model

Revised August 2019 by C. Amsler (Stefan Meyer Inst.), T. De-Grand (Colorado U., Boulder) and B. Krusche (Basel U.).

### 15.1 Quantum numbers of the quarks

Quantum chromodynamics (QCD) is the theory of strong interactions. QCD is a quantum field theory and its constituents are a set of fermions, the quarks, and gauge bosons, the gluons. Strongly interacting particles, the hadrons, are bound states of quark and gluon fields. As gluons carry no intrinsic quantum numbers beyond color charge, and because color is believed to be permanently confined, most of the quantum numbers of strongly interacting particles are given by the quantum numbers of their constituent quarks and antiquarks. The description of hadronic properties which strongly emphasizes the role of the minimum-quark-content part of the wave function of a hadron is generically called the quark model. It exists on many levels: from the simple, almost dynamics-free picture of strongly interacting particles as bound states of quarks and antiquarks, to more detailed descriptions of dynamics, either through models or directly from QCD itself. The different sections of this review survey the many approaches to the spectroscopy of strongly interacting particles which fall under the umbrella of the quark model.

Quarks are strongly interacting fermions with spin 1/2 and, by convention, positive parity. Antiquarks have negative parity. Quarks have the additive baryon number 1/3, antiquarks -1/3. Table 15.1 gives the other additive quantum numbers (flavors) for the three generations of quarks. They are related to the charge  $Q$  (in units of the elementary charge  $e$ ) through the generalized Gell-Mann-Nishijima formula

$$Q = I_z + \frac{B + S + C + B + T}{2}, \quad (15.1)$$

where  $B$  is the baryon number. The convention is that the quark flavor ( $I_z$ ,  $S$ ,  $C$ ,  $B$ , or  $T$ ) has the same sign as its charge  $Q$ . With this convention, any flavor carried by a charged meson has

Table 15.1

	$d$	$u$	$s$	$c$	$b$	$t$
$Q$ - electric charge	$-\frac{1}{3}$	$+\frac{2}{3}$	$-\frac{1}{3}$	$+\frac{2}{3}$	$-\frac{1}{3}$	$+\frac{2}{3}$
$I$ - isospin	$\frac{1}{2}$	$\frac{1}{2}$	0	0	0	0
$I_z$ - isospin $z$ -component	$-\frac{1}{2}$	$+\frac{1}{2}$	0	0	0	0
$S$ - strangeness	0	0	-1	0	0	0
$C$ - charm	0	0	0	+1	0	0
$B$ - bottomness	0	0	0	0	-1	0
$T$ - topness	0	0	0	0	0	+1

the same sign as its charge, e.g., the strangeness of the  $K^+$  is +1, the bottomness of the  $B^+$  is +1, and the charm and strangeness of the  $D_s^-$  are each -1. Antiquarks have the opposite flavor signs. The hypercharge is defined as

$$Y = B + S - \frac{C - B + T}{3}. \quad (15.2)$$

Thus  $Y$  is equal to  $\frac{1}{3}$  for the  $u$  and  $d$  quarks,  $-\frac{2}{3}$  for the  $s$  quark, and 0 for all other quarks. More details and derivations on the quark structure of mesons and baryons can be found in Ref. [1].

### 15.2 Mesons

Mesons have baryon number  $B = 0$ . In the quark model, they are  $q\bar{q}'$  bound states of quarks  $q$  and antiquarks  $\bar{q}'$  (the flavors of  $q$  and  $q'$  may be different). If the orbital angular momentum of the  $q\bar{q}'$  state is  $\ell$ , then the parity  $P$  is  $(-1)^{\ell+1}$ . The meson spin  $J$  is given by the usual relation  $|\ell - s| \leq J \leq |\ell + s|$ , where  $s$  is 0 (antiparallel quark spins) or 1 (parallel quark spins). The charge conjugation, or  $C$ -parity  $C = (-1)^{\ell+s}$ , is defined only for the  $q\bar{q}$  states made of quarks and their own antiquarks. The  $C$ -parity can be generalized to the  $G$ -parity  $G = (-1)^{I+\ell+s}$  for mesons made of quarks and their own antiquarks (isospin  $I_z = 0$ ), and for the charged  $u\bar{d}$  and  $d\bar{u}$  states (isospin  $I = 1$ ).

The mesons are classified in  $J^{PC}$  multiplets. The  $\ell = 0$  states are the pseudoscalars ( $0^{-+}$ ) and the vectors ( $1^{--}$ ). The orbital

excitations  $\ell = 1$  are the scalars ( $0^{++}$ ), the axial vectors ( $1^{+-}$ ) and ( $1^{+}$ ), and the tensors ( $2^{++}$ ). Assignments for many of the known mesons are given in Tables 15.2, 15.3 and 15.4. Radial excitations are denoted by the principal quantum number  $n$ . The very short lifetime of the  $t$  quark makes it likely that bound-state hadrons containing  $t$  quarks and/or antiquarks do not exist.

States in the natural spin-parity series  $P = (-1)^J$  must, according to the above, have  $s = 1$  and hence,  $CP = +1$ . Thus, mesons with natural spin-parity and  $CP = -1$  ( $0^{+-}$ ,  $1^{+-}$ ,  $2^{+-}$ ,  $3^{-+}$ , etc.) are forbidden in the  $q\bar{q}'$  model. The  $J^{PC} = 0^{-}$  state is forbidden as well. Mesons with such exotic quantum numbers may exist, but would lie outside the  $q\bar{q}'$  model (see section below on exotic mesons).

Following SU(3), the nine possible  $q\bar{q}'$  combinations containing the light  $u$ ,  $d$ , and  $s$  quarks are grouped into an octet and a singlet of light quark mesons:

$$3 \otimes \bar{3} = 8 \oplus 1. \quad (15.3)$$

A fourth quark such as charm  $c$  can be included by extending SU(3) to SU(4). However, SU(4) is badly broken owing to the much heavier  $c$  quark. Nevertheless, in an SU(4) classification, the sixteen mesons are grouped into a 15-plet and a singlet:

$$4 \otimes \bar{4} = 15 \oplus 1. \quad (15.4)$$

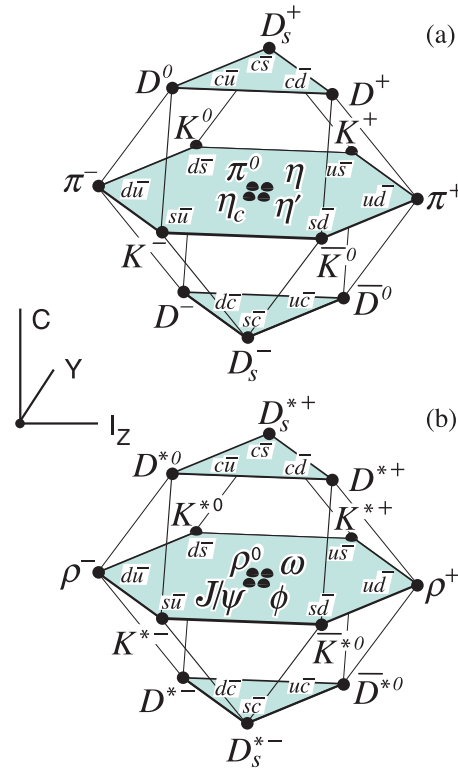


Figure 15.1: SU(4) weight diagram showing the 16-plets for the pseudoscalar (a) and vector mesons (b) made of the  $u$ ,  $d$ ,  $s$ , and  $c$  quarks as a function of isospin  $I_z$ , charm  $C$ , and hypercharge  $Y = B + S - \frac{C}{3}$ . The nonets of light mesons occupy the central planes to which the  $c\bar{c}$  states have been added.

The weight diagrams for the ground-state pseudoscalar ( $0^{-+}$ ) and vector ( $1^{--}$ ) mesons are depicted in Fig. 15.1. The light quark mesons are members of nonets building the middle plane in Fig. 15.1(a) and (b).

Isoscalar states with the same  $J^{PC}$  mix, but mixing between the two light quark isoscalar mesons, and the much heavier charmonium or bottomonium states, are generally assumed to be negligible. In the following, we shall use the generic names  $a$  for the  $I = 1$ ,  $K$  for the  $I = 1/2$ , and  $f$  and  $f'$  for the  $I = 0$  members of

**Table 15.2:** Suggested  $q\bar{q}$  quark-model assignments for some of the observed light mesons. Mesons in bold face are included in the Meson Summary Table. The wave functions  $f$  and  $f'$  are given in the text (Eqn. 15.9). The singlet-octet mixing angles from the linear mass formula (15.12) and its quadratic version (in which the masses are squared) are also given for the well established nonets. The classification of the  $0^{++}$  mesons is tentative: the light scalars  $a_0(980)$ ,  $f_0(980)$ ,  $f_0(500)$  and  $K_0^*(700)$  are often considered to be four-quark states, and are omitted from the table, see Eqn. (15.26) below. The isoscalar  $0^{++}$  mesons  $f_0(1370)$ ,  $f_0(1500)$  (not shown) and  $f_0(1710)$  are expected to mix, see the “Note on Non- $q\bar{q}$  mesons” and the “Note on Scalar Mesons below 2 GeV” in the Meson Listings for details. The isoscalar assignments in the  $2^1S_0$  ( $0^{-+}$ ) nonet are also tentative. The  $\eta(1405)$  (not shown) and  $\eta(1475)$  may be manifestations of the same state, see the “Note on Pseudoscalar and Pseudovector Mesons in the 1400 MeV Region” in the Meson Listings.  
<sup>†</sup> The  $1^{+\pm}$  and  $2^{-\pm}$  isospin  $\frac{1}{2}$  states mix. In particular, the  $K_{1A}$  and  $K_{1B}$  are nearly equal ( $45^\circ$ ) mixtures of the  $K_1(1270)$  and  $K_1(1400)$  (see [2] and references therein).  
<sup>‡</sup> The physical vector mesons may be mixtures of  $1^3D_1$  and  $2^3S_1$  [3].

$n^{2s+1}\ell_J$	$J^{PC}$	$l = 1$	$l = \frac{1}{2}$	$l = 0$	$l = 0$	$\theta_{\text{quad}}$ [ $^\circ$ ]	$\theta_{\text{lin}}$ [ $^\circ$ ]
		$u\bar{d}, \bar{u}d,$ $\frac{1}{\sqrt{2}}(d\bar{d} - u\bar{u})$	$u\bar{s}, d\bar{s};$ $\bar{d}s, \bar{u}s$	$f'$	$f$		
$1^1S_0$	$0^{-+}$	$\pi$	$K$	$\eta$	$\eta'(958)$	-11.3	-24.5
$1^3S_1$	$1^{--}$	$\rho(770)$	$K^*(892)$	$\phi(1020)$	$\omega(782)$	39.2	36.5
$1^1P_1$	$1^{+-}$	$b_1(1235)$	$K_{1B}^\dagger$	$h_1(1415)$	$h_1(1170)$		
$1^3P_0$	$0^{++}$	$a_0(1450)$	$K_0^*(1430)$	$f_0(1710)$	$f_0(1370)$		
$1^3P_1$	$1^{++}$	$a_1(1260)$	$K_{1A}^\dagger$	$f_1(1420)$	$f_1(1285)$		
$1^3P_2$	$2^{++}$	$a_2(1320)$	$K_2^*(1430)$	$f_2'(1525)$	$f_2(1270)$	29.6	28.0
$1^1D_2$	$2^{-+}$	$\pi_2(1670)$	$K_2(1770)^\dagger$	$\eta_2(1870)$	$\eta_2(1645)$		
$1^3D_1$	$1^{--}$	$\rho(1700)$	$K^*(1680)^\ddagger$		$\omega(1650)$		
$1^3D_2$	$2^{--}$		$K_2(1820)^\dagger$				
$1^3D_3$	$3^{--}$	$\rho_3(1690)$	$K_3^*(1780)$	$\phi_3(1850)$	$\omega_3(1670)$	31.8	30.8
$1^3F_4$	$4^{++}$	$a_4(1970)$	$K_4^*(2045)$	$f_4(2300)$	$f_4(2050)$		
$1^3G_5$	$5^{--}$	$\rho_5(2350)$	$K_5^*(2380)$				
$2^1S_0$	$0^{-+}$	$\pi(1300)$	$K(1460)$	$\eta(1475)$	$\eta(1295)$		
$2^3S_1$	$1^{--}$	$\rho(1450)$	$K^*(1410)^\ddagger$	$\phi(1680)$	$\omega(1420)$		
$2^3P_1$	$1^{++}$	$a_1(1640)$					
$2^3P_2$	$2^{++}$	$a_2(1700)$	$K_2^*(1980)$	$f_2(1950)$	$f_2(1640)$		

**Table 15.3:**  $c\bar{c}$  quark-model assignments for the charmonium and open charm mesons with established  $J^{PC}$ . Mesons in bold face are included in the Meson Summary Table. The open flavor states in the  $1^{+-}$  and  $1^{++}$  rows are mixtures of the  $1^{+\pm}$  states.  
<sup>†</sup> The masses are considerably smaller than most theoretical predictions.  
These states have also been considered as four-quark states.  
<sup>‡</sup> Mixtures of the  $1^3D_1$  and  $2^3S_1$  states.

$n^{2s+1}\ell_J$	$J^{PC}$	$l = 0$	$l = \frac{1}{2}$	$l = 0$
		$c\bar{c}$	$c\bar{u}, c\bar{d};$ $\bar{c}u, \bar{c}d$	$c\bar{s};$ $\bar{c}s$
$1^1S_0$	$0^{-+}$	$\eta_c(1S)$	$D$	$D_s^\pm$
$1^3S_1$	$1^{--}$	$J/\psi(1S)$	$D^*$	$D_s^{*\pm}$
$1^3P_0$	$0^{++}$	$\chi_{c0}(1P)$	$D_0^*(2300)$	$D_{s0}^*(2317)^\pm$
$1^3P_1$	$1^{++}$	$\chi_{c1}(1P)$	$D_1(2430)$	$D_{s1}(2460)^\pm$
$1^1P_1$	$1^{+-}$	$h_c(1P)$	$D_1(2420)$	$D_{s1}(2536)^\pm$
$1^3P_2$	$2^{++}$	$\chi_{c2}(1P)$	$D_2^*(2460)$	$D_{s2}^*(2573)$
$2^1S_0$	$0^{-+}$	$\eta_c(2S)$		
$2^3S_1$	$1^{--}$	$\psi(2S)$		$D_{s1}^*(2700)^\pm$
$1^3D_1$	$1^{--}$	$\psi(3770)$		$D_{s1}^*(2860)^\pm$
$1^3D_2$	$2^{--}$	$\psi_2(3823)$		
$2^3P_J$	$0, 1^{++}$	$\chi_{c0}(3860)$		
	$2^{++}$	$\chi_{c2}(3930)$		
$3^3S_1$	$1^{--}$	$\psi(4040)$		
$2^3D_1$	$1^{--}$	$\psi(4160)$		
$4^3S_1$	$1^{--}$	$\psi(4415)$		
$1^3D_3$	$3^{--}$		$D_3^*(2750)$	$D_{s3}^*(2860)^\pm$



**Table 15.4:**  $b\bar{b}$  quark-model assignments for the bottomonium and  $B$  mesons with established  $J^{PC}$ .

$n^{2s+1}\ell_J$	$J^{PC}$	$l = 0$ $b\bar{b}$	$l = \frac{1}{2}$ $b\bar{u}, b\bar{d};$ $\bar{b}u, \bar{b}d$	$l = 0$ $b\bar{s};$ $\bar{b}s$	$l = 0$ $b\bar{c};$ $\bar{b}c$
$1^1S_0$	$0^{-+}$	$\eta_b(1S)$	$B$	$B_s^0$	$B_c^\pm$
$1^3S_1$	$1^{--}$	$\Upsilon(1S)$	$B^*$	$B_s^*$	
$1^3P_0$	$0^{++}$	$\chi_{b0}(1P)$			
$1^3P_1$	$1^{++}$	$\chi_{b1}(1P)$			
$1^1P_1$	$1^{+-}$	$h_b(1P)$	$B_1(5721)$	$B_{s1}(5830)^0$	
$1^3P_2$	$2^{++}$	$\chi_{b2}(1P)$	$B_2^*(5747)$	$B_{s2}^*(5840)^0$	
$2^1S_0$	$0^{-+}$	$\eta_b(2S)$			$B_c(2S)^\pm$
$2^3S_1$	$1^{--}$	$\Upsilon(2S)$			$B_c^*(2S)^\pm$
$1^3D_2$	$2^{--}$	$\Upsilon_2(1D)$			
$2^3P_J$	$0, 1, 2^{++}$	$\chi_{b0,1,2}(2P)$			
$2^1P_1$	$1^{+-}$	$h_b(2P)$			
$3^3S_1$	$1^{--}$	$\Upsilon(3S)$			
$3^3P_J$	$0, 1, 2^{++}$	$\chi_{b1,2}(3P)$			
$4^3S_1$	$1^{--}$	$\Upsilon(4S)$			

the light quark nonets. Thus, the physical isoscalars are mixtures of the SU(3) wave function  $\psi_8$  and  $\psi_1$ :

$$f' = \psi_8 \cos \theta - \psi_1 \sin \theta, \quad (15.5)$$

$$f = \psi_8 \sin \theta + \psi_1 \cos \theta, \quad (15.6)$$

where  $\theta$  is the nonet mixing angle and

$$\psi_8 = \frac{1}{\sqrt{6}}(u\bar{u} + d\bar{d} - 2s\bar{s}), \quad (15.7)$$

$$\psi_1 = \frac{1}{\sqrt{3}}(u\bar{u} + d\bar{d} + s\bar{s}). \quad (15.8)$$

These mixing relations are often rewritten to exhibit the  $u\bar{u} + d\bar{d}$  and  $s\bar{s}$  components which decouple for the ‘‘ideal’’ mixing angle  $\theta_i$ , such that  $\tan \theta_i = 1/\sqrt{2}$  (or  $\theta_i = 35.3^\circ$ ). Defining  $\alpha = \theta + 54.7^\circ$ , one obtains the physical isoscalar in the flavor basis

$$f' = \frac{1}{\sqrt{2}}(u\bar{u} + d\bar{d}) \cos \alpha - s\bar{s} \sin \alpha, \quad (15.9)$$

and its orthogonal partner  $f$  (replace  $\alpha$  by  $\alpha - 90^\circ$ ). Thus for ideal mixing ( $\alpha_i = 90^\circ$ ), the  $f'$  becomes pure  $s\bar{s}$  and the  $f$  pure  $u\bar{u} + d\bar{d}$ . The mixing angle  $\theta$  can be derived by diagonalizing the mass matrix

$$\begin{pmatrix} m_8 & m_{81} \\ m_{18} & m_1 \end{pmatrix} \quad (15.10)$$

The mass eigenvalues are  $m_{f'}$  and  $m_f$ . The mixing angle is given by

$$\tan \theta = \frac{m_8 - m_{f'}}{m_{81}}. \quad (15.11)$$

Calculating  $m_8$  and  $m_{81}$  from the wave functions Eq. 15.7 and Eq. 15.8, and expressing the quark masses as a function of the  $l = 1/2$  and  $l = 1$  meson masses, one obtains

$$\tan \theta = \frac{4m_K - m_a - 3m_{f'}}{2\sqrt{2}(m_a - m_K)}, \quad (15.12)$$

which also determines the sign of  $\theta$ . Alternatively, one can express the mixing angle as a function of all nonet masses. The octet mass is given by

$$m_8 = m_{f'} \cos^2 \theta + m_f \sin^2 \theta \quad (15.13)$$

whence

$$\tan^2 \theta = \frac{4m_K - m_a - 3m_{f'}}{-4m_K + m_a + 3m_f}. \quad (15.14)$$

Eliminating  $\theta$  from Eq. (15.12) and Eq. (15.14) leads to the sum rule [4]

$$(m_f + m_{f'})(4m_K - m_a) - 3m_f m_{f'} = 8m_K^2 - 8m_K m_a + 3m_a^2. \quad (15.15)$$

This relation is verified for the ground-state vector mesons. We identify the  $\phi(1020)$  with the  $f'$  and the  $\omega(783)$  with the  $f$ . Thus

$$\begin{aligned} \phi(1020) &= \psi_8 \cos \theta_V - \psi_1 \sin \theta_V, \\ \omega(782) &= \psi_8 \sin \theta_V + \psi_1 \cos \theta_V, \end{aligned} \quad (15.16)$$

with the vector mixing angle  $\theta_V = 36.4^\circ$  from Eq. (15.14), very close to ideal mixing. Thus  $\phi(1020)$  is nearly pure  $s\bar{s}$ . For ideal mixing, Eq. (15.12) and Eq. (15.14) lead to the relations

$$m_K = \frac{m_f + m_{f'}}{2}, \quad m_a = m_f, \quad (15.17)$$

which are satisfied for the vector mesons.

The situation for the pseudoscalar and scalar mesons is not so clear cut, either theoretically or experimentally. For the pseudoscalars, the mixing angle is small. This can be understood qualitatively via gluon-line counting of the mixing process. The size of the mixing process between the nonstrange and strange mass bases scales as  $\alpha_s^2$ , not  $\alpha_s^3$ , because of two rather than three gluon exchange as it does for the vector mesons. It may also be that the lightest isoscalar pseudoscalars mix more strongly with excited states or with states of substantial non- $\bar{q}q$  content, as will be discussed below.

A variety of analysis methods lead to similar results: First, for these states, Eqn. 15.15 is satisfied only approximately. Then Eqn. 15.12 and Eqn. 15.14 lead to somewhat different values for the mixing angle. Identifying the  $\eta$  with the  $f'$  one gets

$$\eta = \psi_8 \cos \theta_P - \psi_1 \sin \theta_P, \quad (15.18)$$

$$\eta' = \psi_8 \sin \theta_P + \psi_1 \cos \theta_P. \quad (15.19)$$

Following chiral perturbation theory, the meson masses in the mass formulae (Eq. (15.12) and Eq. (15.14)) might be replaced by their squares. Table 15.5 lists the mixing angle  $\theta_{\text{lin}}$  from Eqn. 15.14 (using the neutral members of the nonets) and the corresponding  $\theta_{\text{quad}}$  obtained by replacing the meson masses by their squares throughout.

**Table 15.5:** Singlet-octet mixing angles for the well established nonets from the linear mass formula (15.12) and its quadratic version in which the masses are squared.

$n^{2s+1}\ell_J$	$J^{PC}$	$\theta_{\text{quad}}$ [ $^\circ$ ]	$\theta_{\text{lin}}$ [ $^\circ$ ]
$1^1S_0$	$0^{-+}$	-11.3	-24.5
$1^3S_1$	$1^{--}$	39.2	36.5
$1^3P_2$	$2^{++}$	29.6	28.0
$1^3D_3$	$3^{--}$	31.8	30.8

The pseudoscalar mixing angle  $\theta_P$  can also be measured by comparing the partial widths for radiative  $J/\psi$  decay into a vector and a pseudoscalar [5], radiative  $\phi(1020)$  decay into  $\eta$  and  $\eta'$  [6], radiative decays between pseudoscalar and vector mesons [7], or  $p\bar{p}$  annihilation at rest into a pair of vector and pseudoscalar or into two pseudoscalars [8,9]. One obtains a mixing angle between  $-10^\circ$  and  $-20^\circ$ . More recently, a lattice QCD simulation, Ref. [10], has successfully reproduced the masses of the  $\eta$  and  $\eta'$ , and as a byproduct find a mixing angle  $\theta_{lin} = -14.1(2.8)^\circ$ . We return to this point in Sec. 15.6.

The nonet mixing angles can be measured in  $\gamma\gamma$  collisions, *e.g.*, for the  $0^{-+}$ ,  $0^{++}$ , and  $2^{++}$  nonets. In the quark model, the amplitude for the coupling of neutral mesons to two photons is proportional to  $\sum_i Q_i^2$ , where  $Q_i$  is the charge of the  $i$ -th quark. The  $2\gamma$  partial width of an isoscalar meson with mass  $m$  is then given in terms of the mixing angle  $\alpha$  by

$$\Gamma_{2\gamma} = C(5 \cos \alpha - \sqrt{2} \sin \alpha)^2 m^3, \quad (15.20)$$

- for  $f'$  and  $f$  ( $\alpha \rightarrow \alpha - 90^\circ$ ). The coupling  $C$  may depend on the meson mass. It is often assumed to be a constant in the nonet. For the isovector  $a$ , one then finds  $\Gamma_{2\gamma} = 9 C m^3$ . Thus the members of an ideally mixed nonet couple to  $2\gamma$  with partial widths in the ratios  $f : f' : a = 25 : 2 : 9$ . For tensor mesons, one finds from the ratios of the measured  $2\gamma$  partial widths for the  $f_2(1270)$  and  $f'_2(1525)$  mesons a mixing angle  $\alpha_T$  of  $(81 \pm 1)^\circ$ , or  $\theta_T = (27 \pm 1)^\circ$ , in accord with the linear mass formula. For the pseudoscalars, one finds from the ratios of partial widths  $\Gamma(\eta' \rightarrow 2\gamma)/\Gamma(\eta \rightarrow 2\gamma)$  a mixing angle  $\theta_P = (-18 \pm 2)^\circ$ , while the ratio  $\Gamma(\eta' \rightarrow 2\gamma)/\Gamma(\pi^0 \rightarrow 2\gamma)$  leads to  $\sim -24^\circ$ . SU(3) breaking effects for pseudoscalars are discussed in [11].

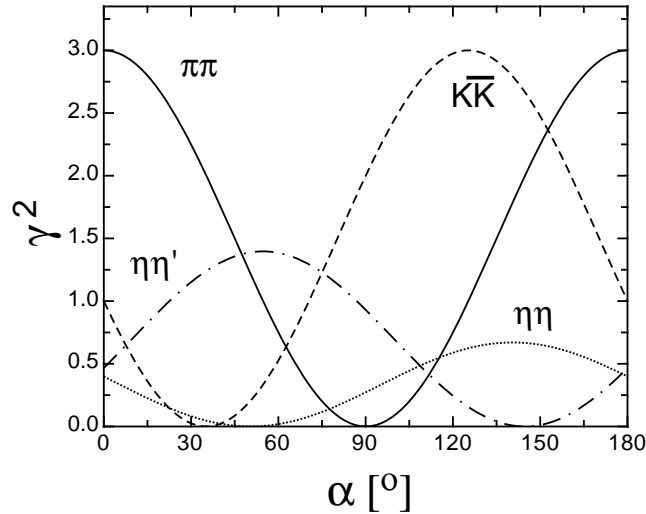


Figure 15.2: SU(3) couplings as a function of mixing angle  $\alpha$  for isoscalar decays, up to a common multiplicative factor  $C$  and for  $\theta_P = -17.3^\circ$ .

The partial width for the decay of a scalar or a tensor meson into a pair of pseudoscalar mesons is model-dependent. Following Ref. [13],

$$\Gamma = C \times \gamma^2 \times |F(q)|^2 \times q. \quad (15.21)$$

$C$  is a nonet constant,  $q$  the momentum of the decay products,  $F(q)$  a form factor, and  $\gamma^2$  the SU(3) coupling. The model-dependent form factor may be written as

$$|F(q)|^2 = q^{2\ell} \times \exp\left(-\frac{q^2}{8\beta^2}\right), \quad (15.22)$$

where  $\ell$  is the relative angular momentum between the decay products. The decay of a  $q\bar{q}$  meson into a pair of mesons involves the creation of a  $q\bar{q}$  pair from the vacuum, and SU(3) symmetry assumes that the matrix elements for the creation of  $s\bar{s}$ ,  $u\bar{u}$ , and  $d\bar{d}$  pairs are equal. The couplings  $\gamma^2$  are given in Table 15.6, and

**Table 15.6:** SU(3) couplings  $\gamma^2$  for quarkonium decays as a function of nonet mixing angle  $\alpha$ , up to a common multiplicative factor  $C$  ( $\phi = 54.7^\circ + \theta_P$ ).

Isospin	Decay channel	$\gamma^2$
0	$\pi\pi$	$3 \cos^2 \alpha$
	$K\bar{K}$	$(\cos \alpha - \sqrt{2} \sin \alpha)^2$
	$\eta\eta$	$(\cos \alpha \cos^2 \phi - \sqrt{2} \sin \alpha \sin^2 \phi)^2$
	$\eta\eta'$	$\frac{1}{2} \sin^2 2\phi (\cos \alpha + \sqrt{2} \sin \alpha)^2$
1	$\eta\pi$	$2 \cos^2 \phi$
	$\eta'\pi$	$2 \sin^2 \phi$
	$K\bar{K}$	1
$\frac{1}{2}$	$K\pi$	$\frac{3}{2}$
	$K\eta$	$(\sin \phi - \frac{\cos \phi}{\sqrt{2}})^2$
	$K\eta'$	$(\cos \phi + \frac{\sin \phi}{\sqrt{2}})^2$

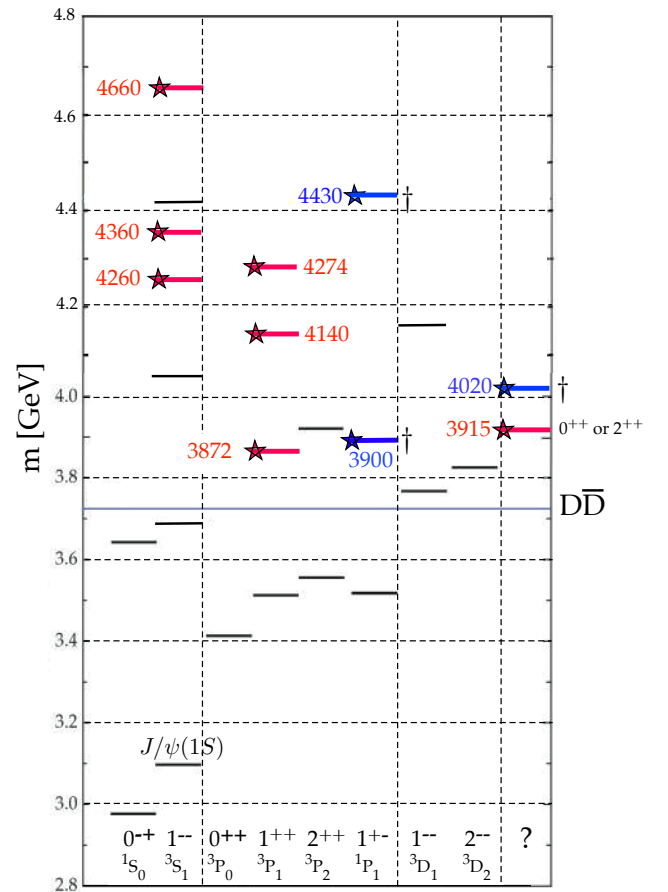


Figure 15.3: Established states populating the charmonium spectrum that are listed in the Summary Tables. The  $c\bar{c}$  states are shown in black, the exotic ones are tagged by stars (red for the isoscalars, blue for the isovectors). The quantum numbers of the two states in the right column are not firmly established.

their dependence upon the mixing angle  $\alpha$  is shown in Fig. 15.2 for isoscalar decays. The generalization to unequal  $s\bar{s}$ ,  $u\bar{u}$ , and  $d\bar{d}$  couplings is given in Ref. [13]. An excellent fit to the tensor meson decay widths is obtained assuming SU(3) symmetry, with  $\beta \simeq 0.5$  GeV/c,  $\theta_V \simeq 26^\circ$  and  $\theta_P \simeq -17^\circ$  [13].

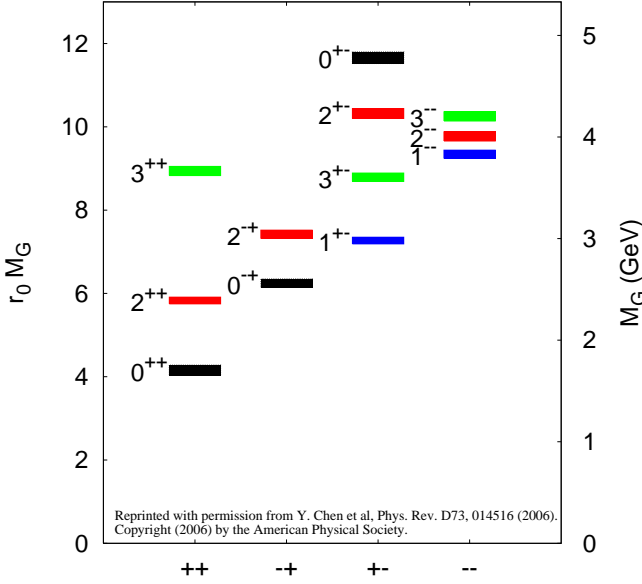


Figure 15.4: Predicted glueball mass spectrum from the lattice in quenched approximation (from [12]).

### 15.3 Exotic mesons

The existence of a light nonet composed of four quarks (tetraquarks) with masses below 1 GeV was suggested a long time ago [14] [15]. Coupling two triplets of light quarks  $u$ ,  $d$ , and  $s$ , one obtains nine states, of which the six symmetric ( $uu$ ,  $dd$ ,  $ss$ ,  $ud + du$ ,  $us + su$ ,  $ds + sd$ ) form the six dimensional representation  $\mathbf{6}$ , while the three antisymmetric ( $ud - du$ ,  $us - su$ ,  $ds - sd$ ) form the three dimensional representation  $\bar{\mathbf{3}}$  of SU(3):

$$\mathbf{3} \otimes \mathbf{3} = \mathbf{6} \oplus \bar{\mathbf{3}}. \quad (15.23)$$

Hence for tetraquarks one gets the reduction

$$\begin{aligned} \mathbf{3} \otimes \mathbf{3} \otimes \bar{\mathbf{3}} \otimes \bar{\mathbf{3}} \\ &= \mathbf{6} \oplus \bar{\mathbf{3}} \otimes \bar{\mathbf{6}} \otimes \bar{\mathbf{3}} \\ &= \bar{\mathbf{3}} \otimes \mathbf{3} \oplus \mathbf{6} \otimes \bar{\mathbf{6}} \oplus \mathbf{6} \otimes \mathbf{3} \oplus \bar{\mathbf{3}} \otimes \bar{\mathbf{6}} \\ &= \mathbf{9} \oplus \mathbf{36} \oplus \mathbf{18} \oplus \bar{\mathbf{18}}. \end{aligned} \quad (15.24)$$

$$(15.25)$$

Combining with spin and color and requiring antisymmetry for diquarks and antidiquarks, one finds for ground states (zero angular momenta) that the most deeply bound tetraquarks (and hence the lightest ones) lie in the nonet and are scalar mesons (see also [1]). The average mass is estimated to be around 900 MeV from the mass differences between the  $\rho$  and  $\pi$  masses. Letting the strange quark determine the mass splittings one obtains a mass inverted spectrum with a light isosinglet, a medium heavy isodoublet and a heavy isotriplet + isosinglet. It is then tempting to identify these mesons as the lightest scalars

$$\begin{aligned} f_0(500) &= \bar{u}\bar{d}ud, \quad K_0^*(700) = (\bar{s}\bar{d}ud, \bar{s}\bar{u}ud) \quad \text{and} \quad (\bar{u}\bar{d}us, \bar{u}\bar{d}ds), \\ a_0(980) &= (us\bar{d}\bar{s}, \frac{1}{\sqrt{2}}[u\bar{u} - d\bar{d}]s\bar{s}, \bar{u}\bar{s}ds), \\ f_0(980) &= \frac{1}{\sqrt{2}}[u\bar{u} + d\bar{d}]s\bar{s}. \end{aligned} \quad (15.26)$$

A plethora of new states have been reported in the charmonium and bottomonium spectra. The most prominent one is the  $\chi_{c1}(3872)$  (formerly  $X(3872)$ ), first observed in 2003 in  $B$ -decays in the final state  $J/\psi \pi^+ \pi^-$  (see Fig. 15.3). Even more remarkable is the observation of isovector (charged) mesons decaying into  $c\bar{c}$  plus a charged pion, such as the  $Z^\pm(4430)$  decaying into  $\psi(2S)\pi^\pm$ , which a priori excludes an interpretation as true  $c\bar{c}$  (charmonium) state. Similar states are also observed in the bottomonium spectrum. Some of these states may be tetraquarks (e.g.  $cq\bar{c}\bar{q}$ ), molecular structures (e.g.  $c\bar{q}c\bar{q}$ ) made of pairs of

mesons such as  $D$ ,  $D_s$  and  $D^*$ ,  $D_s^*$  excitations, or their  $B$  and  $B^*$  counterparts. They could also be mimicked by kinematical effects. Details and references can be found in recent reviews [16], [17] and in the “Note on Non- $q\bar{q}$  Mesons” in the Meson Listings.

QCD predicts the existence of extra isoscalar mesons. In the pure gauge theory they contain only gluons, and are called glueballs. The ground state glueball is predicted by lattice gauge theories to be  $0^{++}$ , the first excited state  $2^{++}$ . Errors on the mass predictions are large. From Ref. [18] one obtains 1750 (50) (80) MeV for the mass of the lightest  $0^{++}$  glueball from quenched QCD. As an example for the glueball mass spectrum, we show in Fig. 15.4 a calculation from Ref. [12]. A mass of 1710 MeV is predicted for the ground state, also with an error of about 100 MeV. Earlier work by other groups produced masses at 1650 MeV [19] and 1550 MeV [20] (see also [21]). The first excited state has a mass of about 2.4 GeV, and the lightest glueball with exotic quantum numbers ( $2^{+-}$ ) has a mass of about 4 GeV.

These calculations are made in the so-called “quenched approximation” which neglects  $q\bar{q}$  loops. However, both glue and  $q\bar{q}$  states couple to singlet scalar mesons. Therefore glueballs will mix with nearby  $q\bar{q}$  states of the same quantum numbers. For example, the two isoscalar  $0^{++}$  mesons around 1500 MeV will mix with the pure ground state glueball to generate the observed physical states  $f_0(1370)$ ,  $f_0(1500)$ , and  $f_0(1710)$  [13, 22]. The first results from lattice calculations, which include these effects, indicate that the mass shifts are small. We return to a discussion of this point in Sec. 15.6.

The existence of three singlet scalar mesons around 1.5 GeV suggests additional degrees of freedom such as glue, since only two mesons are predicted in this mass range. The  $f_0(1500)$  [13, 22] or, alternatively, the  $f_0(1710)$  [19], have been proposed as candidates for the scalar glueball, both states having considerable mixing also with the  $f_0(1370)$ . Other mixing schemes, in particular with the  $f_0(500)$  and the  $f_0(980)$ , have also been proposed [23]. According to a holographic model of low-energy QCD scalar glueballs decay strongly into kaons and  $\eta$  mesons, in good agreement with data on the  $f_0(1710)$  [24]. Details can be found in the “Note on Non- $q\bar{q}$  Mesons” in the Meson Listings and in Ref. [25]. See also the “Note on Scalar Mesons below 2 GeV”.

Mesons made of  $q\bar{q}$  pairs bound by excited gluons  $g$ , the hybrid states  $q\bar{q}g$ , are also predicted. They should lie in the 1.9 GeV mass region, according to gluon flux tube models [26]. Lattice QCD also predicts the lightest hybrid, an exotic  $1^{-+}$ , at a mass of 1.8 to 1.9 GeV [27]. However, the bag model predicts four nonets, among them an exotic  $1^{-+}$  around or above 1.4 GeV [28, 29]. There are so far two candidates for exotic states with quantum numbers  $1^{-+}$ , the  $\pi_1(1400)$  and  $\pi_1(1600)$ , which could be hybrids or four-quark states (see the “Note on Non- $q\bar{q}$  Mesons” in the Meson Listings and in [25]).

### 15.4 Baryons: $qqq$ states

Baryons are fermions with baryon number  $B = 1$ , *i.e.*, in the most general case, they are composed of three quarks plus any number of quark - antiquark pairs. Until recently, all established baryons were 3-quark ( $qqq$ ) configurations, which we mainly discuss in this section. However, in 2015 the LHCb collaboration published first evidence for charmed ‘pentaquark’ states of minimal quark content  $c\bar{c}uud$  at invariant masses close to 4.4 GeV [30]. More refined LHCb experiments have revealed evidence for three such states called  $P_c(4312)^+$ ,  $P_c(4440)^+$ , and  $P_c(4457)^+$  [31]. These states are located close to the thresholds of the production of ordinary baryon-meson pairs like  $\Sigma_c^+ \bar{D}^0$  and  $\Sigma_c^+ \bar{D}^{*0}$  and are discussed in terms of molecular-like states. A nice overview on the discussion of pentaquark and tetraquark states is given in Ref. [32].

The color part of baryon state functions is an SU(3) singlet, a completely antisymmetric state of the three colors. Since the quarks are fermions, the state function must be antisymmetric under interchange of any two equal-mass quarks (up and down quarks in the limit of isospin symmetry). Thus it can be written as

$$|qqq\rangle_A = |\text{color}\rangle_A \times |\text{space, spin, flavor}\rangle_S, \quad (15.27)$$

where the subscripts  $S$  and  $A$  indicate symmetry or antisymme-

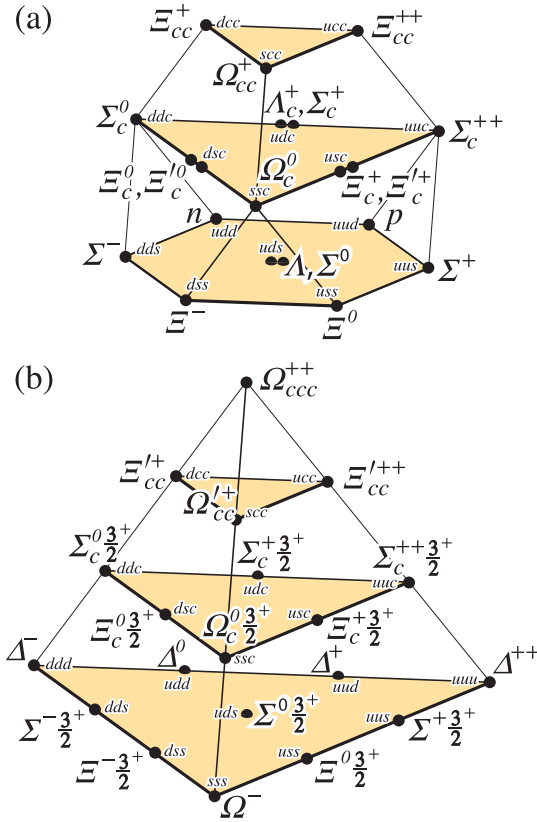


Figure 15.5: SU(4) multiplets of baryons made of  $u$ ,  $d$ ,  $s$ , and  $c$  quarks. (a) The spin 1/2 20-plet with an SU(3) octet. (b) The spin 3/2 20-plet with an SU(3) decuplet.

try under interchange of any two equal-mass quarks. Note the contrast with the state function for the three nucleons in  ${}^3\text{H}$  or  ${}^3\text{He}$ :

$$|NNN\rangle_A = |\text{space, spin, isospin}\rangle_A. \quad (15.28)$$

This difference has major implications for internal structure, magnetic moments, etc. (For a nice discussion, see Ref. [33])

The “ordinary” baryons are made up of  $u$ ,  $d$ , and  $s$  quarks. The three flavors imply an approximate flavor SU(3), which requires that baryons made of these quarks belong to the multiplets on the right side of

$$\mathbf{3} \otimes \mathbf{3} \otimes \mathbf{3} = \mathbf{10}_S \oplus \mathbf{8}_M \oplus \mathbf{8}_M \oplus \mathbf{1}_A \quad (15.29)$$

(see the section on “SU( $n$ ) Multiplets and Young Diagrams”). Here the subscripts indicate symmetric, mixed-symmetry, or antisymmetric states under interchange of any two quarks. The  $\mathbf{1}$  is a  $uds$  state ( $A_1$ ), and the octet contains a similar state ( $A_8$ ). If these have the same spin and parity, they can mix. The mechanism is the same as for the mesons (see above). In the ground state multiplet, the SU(3) flavor singlet  $A_1$  is forbidden by Fermi statistics. The section on “SU(3) Isoscalar Factors and Representation Matrices,” shows how relative decay rates in, say,  $\mathbf{10} \rightarrow \mathbf{8} \otimes \mathbf{8}$  decays may be calculated.

The addition of the  $c$  quark to the light quarks extends the flavor symmetry to SU(4). However, due to the large mass of the  $c$  quark, this symmetry is much more strongly broken than the SU(3) of the three light quarks. Figures 15.5(a) and 15.5(b) show the SU(4) baryon multiplets that have as their bottom levels an SU(3) octet, such as the octet that includes the nucleon, or an SU(3) decuplet, such as the decuplet that includes the  $\Delta(1232)$ . All particles in a given SU(4) multiplet have the same spin and parity. The charmed baryons are discussed in more detail in the “Note on Charmed Baryons” in the Particle Listings. The same multiplets as shown in Fig. 15.5 can be constructed when the  $c$  quark is replaced by the  $b$  quark, or they can be embedded in

a larger SU(5) group that accounts for all baryons that can be constructed from the five quark flavors. The existence of baryons with  $t$ -quarks is very unlikely due to the short lifetime of the  $t$ -quark. The heavy quark baryons have recently gained a lot of interest [34]. Their relatively narrow widths allow to isolate the states much easier than the light quark baryon resonances which require intricate partial wave analyses. The only problem on the experimental side are the small production cross sections, but the recent measurements at the  $e^+e^-$  colliding  $B$  factories, at the  $p\bar{p}$  Tevatron collider, and at LHCb at CERN have boosted this field. The LHCb collaboration has published evidence for five new narrow  $\Omega_c^0$  states ( $css$ ) [35] and for a doubly charmed  $\Xi_{cc}^{++}$  ( $ccu$ ) [36] baryon. Doubly charmed baryons have a much different structure from light baryons, more resembling a heavy ‘double-star’ system with an attached light ‘planet’ and open a new window for QCD properties. Another candidate for a doubly charmed baryon ( $\Xi_{cc}^+$ , ( $ccd$ )) had been earlier reported by the SELEX experiment [37, 38] but could so far not be confirmed by other experiments and the difference in mass between the LHCb  $\Xi_{cc}^{++}$  and the SELEX  $\Xi_{cc}^+$  would be much larger than predicted. Quark model predictions for baryons with two heavy quarks are given in Ref. [39] and lattice results for doubly and triply charmed states are discussed in Sec. 15.6 of this review.

For the “ordinary” baryons (no  $c$  or  $b$  quark), flavor and spin may be combined in an approximate flavor-spin SU(6), in which the six basic states are  $d \uparrow$ ,  $d \downarrow$ ,  $\dots$ ,  $s \downarrow$  ( $\uparrow$ ,  $\downarrow$  = spin up, down). Then the baryons belong to the multiplets on the right side of

$$\mathbf{6} \otimes \mathbf{6} \otimes \mathbf{6} = \mathbf{56}_S \oplus \mathbf{70}_M \oplus \mathbf{70}_M \oplus \mathbf{20}_A.$$

These SU(6) multiplets decompose into flavor SU(3) multiplets as follows:

$$\mathbf{56} = \mathbf{4} \mathbf{10} \oplus \mathbf{2} \mathbf{8} \quad (15.30)$$

$$\mathbf{70} = \mathbf{2} \mathbf{10} \oplus \mathbf{4} \mathbf{8} \oplus \mathbf{2} \mathbf{8} \oplus \mathbf{2} \mathbf{1} \quad (15.31)$$

$$\mathbf{20} = \mathbf{2} \mathbf{8} \oplus \mathbf{4} \mathbf{1}, \quad (15.32)$$

where the superscript ( $2S+1$ ) gives the net spin  $S$  of the quarks for each particle in the SU(3) multiplet. The  $J^P = 1/2^+$  octet containing the nucleon and the  $J^P = 3/2^+$  decuplet containing the  $\Delta(1232)$  together make up the “ground-state” 56-plet, in which the orbital angular momenta between the quark pairs are zero (so that the spatial part of the state function is trivially symmetric). The  $\mathbf{70}$  and  $\mathbf{20}$  require some excitation of the spatial part of the state function in order to make the overall state function symmetric. States with nonzero orbital angular momenta are classified in SU(6) $\otimes$ O(3) supermultiplets.

It is useful to classify the baryons into bands that have the same number  $N$  of quanta of excitation. Each band consists of a number of supermultiplets, specified by  $(D, L_N^P)$ , where  $D$  is the dimensionality of the SU(6) representation,  $L$  is the total quark orbital angular momentum, and  $P$  is the total parity. Supermultiplets contained in bands up to  $N = 12$  are given in Ref. [40]. The  $N = 0$  band, which contains the nucleon and  $\Delta(1232)$ , consists only of the  $(56, 0_0^+)$  supermultiplet. The  $N = 1$  band consists only of the  $(70, 1_1^-)$  multiplet and contains the negative-parity baryons with masses below about 1.9 GeV. The  $N = 2$  band contains five supermultiplets:  $(56, 0_2^+)$ ,  $(70, 0_2^+)$ ,  $(56, 2_2^+)$ ,  $(70, 2_2^+)$ , and  $(20, 1_2^+)$ .

The wave functions of the non-strange baryons in the harmonic oscillator basis are often labeled by  $|X^{2S+1} L_\pi J^P\rangle$ , where  $S, L, J, P$  are as above,  $X = N$  or  $\Delta$ , and  $\pi = S, M$  or  $A$  denotes the symmetry of the spatial wave function. The possible model states for the bands with  $N=0,1,2$  are given in Table 15.8. The assignment of experimentally observed states is only complete and well established up to the  $N=1$  band. Some more tentative assignments for higher multiplets are suggested in [41].

In Table 15.7, quark-model assignments are given for many of the established baryons whose SU(6) $\otimes$ O(3) compositions are relatively unmixed. One must, however, keep in mind that apart from the mixing of the  $A$  singlet and octet states, states with same  $J^P$  but different  $L, S$  combinations can also mix. In the quark model with one-gluon exchange motivated interactions, the size of the mixing is determined by the relative strength of the tensor term with respect to the contact term (see below). The

**Table 15.7:** Quark-model assignments for some of the known baryons in terms of a flavor-spin SU(6) basis. Only the dominant representation is listed. Assignments for several states, especially for the  $\Lambda(1810)$ ,  $\Lambda(2350)$ ,  $\Xi(1820)$ , and  $\Xi(2030)$ , are merely educated guesses. <sup>†</sup> suggestions for assignments and re-assignments from Ref. [42]. For assignments of the charmed baryons, see the “Note on Charmed Baryons” in the Particle Listings.

$J^P$	$(D, L_N^P)$	$S$	Octet members				Singlets
1/2 <sup>+</sup>	(56, 0 <sub>0</sub> <sup>+</sup> )	1/2	$N(939)$	$\Lambda(1116)$	$\Sigma(1193)$	$\Xi(1318)$	
1/2 <sup>+</sup>	(56, 0 <sub>2</sub> <sup>+</sup> )	1/2	$N(1440)$	$\Lambda(1600)$	$\Sigma(1660)$	$\Xi(1690)$ <sup>†</sup>	
1/2 <sup>-</sup>	(70, 1 <sub>1</sub> <sup>-</sup> )	1/2	$N(1535)$	$\Lambda(1670)$	$\Sigma(1620)$	$\Xi(?)$	$\Lambda(1405)$
					$\Sigma(1560)$ <sup>†</sup>		
3/2 <sup>-</sup>	(70, 1 <sub>1</sub> <sup>-</sup> )	1/2	$N(1520)$	$\Lambda(1690)$	$\Sigma(1670)$	$\Xi(1820)$	$\Lambda(1520)$
1/2 <sup>-</sup>	(70, 1 <sub>1</sub> <sup>-</sup> )	3/2	$N(1650)$	$\Lambda(1800)$	$\Sigma(1750)$	$\Xi(?)$	
					$\Sigma(1620)$ <sup>†</sup>		
3/2 <sup>-</sup>	(70, 1 <sub>1</sub> <sup>-</sup> )	3/2	$N(1700)$	$\Lambda(?)$	$\Sigma(1940)$ <sup>†</sup>	$\Xi(?)$	
5/2 <sup>-</sup>	(70, 1 <sub>1</sub> <sup>-</sup> )	3/2	$N(1675)$	$\Lambda(1830)$	$\Sigma(1775)$	$\Xi(1950)$ <sup>†</sup>	
1/2 <sup>+</sup>	(70, 0 <sub>2</sub> <sup>+</sup> )	1/2	$N(1710)$	$\Lambda(1810)$	$\Sigma(1880)$	$\Xi(?)$	$\Lambda(1810)$ <sup>†</sup>
3/2 <sup>+</sup>	(56, 2 <sub>2</sub> <sup>+</sup> )	1/2	$N(1720)$	$\Lambda(1890)$	$\Sigma(?)$	$\Xi(?)$	
5/2 <sup>+</sup>	(56, 2 <sub>2</sub> <sup>+</sup> )	1/2	$N(1680)$	$\Lambda(1820)$	$\Sigma(1915)$	$\Xi(2030)$	
7/2 <sup>-</sup>	(70, 3 <sub>3</sub> <sup>-</sup> )	1/2	$N(2190)$	$\Lambda(?)$	$\Sigma(?)$	$\Xi(?)$	$\Lambda(2100)$
9/2 <sup>-</sup>	(70, 3 <sub>3</sub> <sup>-</sup> )	3/2	$N(2250)$	$\Lambda(?)$	$\Sigma(?)$	$\Xi(?)$	
9/2 <sup>+</sup>	(56, 4 <sub>4</sub> <sup>+</sup> )	1/2	$N(2220)$	$\Lambda(2350)$	$\Sigma(?)$	$\Xi(?)$	

Decuplet members						
3/2 <sup>+</sup>	(56, 0 <sub>0</sub> <sup>+</sup> )	3/2	$\Delta(1232)$	$\Sigma(1385)$	$\Xi(1530)$	$\Omega(1672)$
3/2 <sup>+</sup>	(56, 0 <sub>2</sub> <sup>+</sup> )	3/2	$\Delta(1600)$	$\Sigma(1690)$ <sup>†</sup>	$\Xi(?)$	$\Omega(?)$
1/2 <sup>-</sup>	(70, 1 <sub>1</sub> <sup>-</sup> )	1/2	$\Delta(1620)$	$\Sigma(1750)$ <sup>†</sup>	$\Xi(?)$	$\Omega(?)$
3/2 <sup>-</sup>	(70, 1 <sub>1</sub> <sup>-</sup> )	1/2	$\Delta(1700)$	$\Sigma(?)$	$\Xi(?)$	$\Omega(?)$
5/2 <sup>+</sup>	(56, 2 <sub>2</sub> <sup>+</sup> )	3/2	$\Delta(1905)$	$\Sigma(?)$	$\Xi(?)$	$\Omega(?)$
7/2 <sup>+</sup>	(56, 2 <sub>2</sub> <sup>+</sup> )	3/2	$\Delta(1950)$	$\Sigma(2030)$	$\Xi(?)$	$\Omega(?)$
11/2 <sup>+</sup>	(56, 4 <sub>4</sub> <sup>+</sup> )	3/2	$\Delta(2420)$	$\Sigma(?)$	$\Xi(?)$	$\Omega(?)$

**Table 15.8:**  $N$  and  $\Delta$  states in the  $N=0,1,2$  harmonic oscillator bands.  $L^P$  denotes angular momentum and parity,  $S$  the three-quark spin and ‘sym’=A,S,M the symmetry of the spatial wave function. Listed are all possible spin/parity combinations and assignments of experimentally observed states. Only dominant components are indicated. Assignments in the  $N=2$  band are partly tentative.

N	sym	$L^P$	$S$	$N(I = 1/2)$			
2	A	1 <sup>+</sup>	1/2	1/2 <sup>+</sup>	3/2 <sup>+</sup>	-	-
2	M	2 <sup>+</sup>	3/2	1/2 <sup>+</sup>	3/2 <sup>+</sup>	5/2 <sup>+</sup>	7/2 <sup>+</sup>
2	M	2 <sup>+</sup>	1/2	-	3/2 <sup>+</sup>	5/2 <sup>+</sup>	-
2	M	0 <sup>+</sup>	3/2	-	3/2 <sup>+</sup>	-	-
2	M	0 <sup>+</sup>	1/2	1/2 <sup>+</sup> $N(1710)$	-	-	-
2	S	2 <sup>+</sup>	3/2	-	-	-	-
2	S	2 <sup>+</sup>	1/2	-	3/2 <sup>+</sup> $N(1720)$	5/2 <sup>+</sup> $N(1680)$	-
2	S	0 <sup>+</sup>	3/2	-	-	-	-
2	S	0 <sup>+</sup>	1/2	1/2 <sup>+</sup> $N(1440)$	-	-	-
1	M	1 <sup>-</sup>	3/2	1/2 <sup>-</sup> $N(1650)$	3/2 <sup>-</sup> $N(1700)$	5/2 <sup>-</sup> $N(1675)$	-
1	M	1 <sup>-</sup>	1/2	1/2 <sup>-</sup> $N(1535)$	3/2 <sup>-</sup> $N(1520)$	-	-
0	S	0 <sup>+</sup>	3/2	-	-	-	-
0	S	0 <sup>+</sup>	1/2	1/2 <sup>+</sup> $N(938)$	-	-	-

N	sym	$L^P$	$S$	$\Delta(I = 3/2)$			
2	A	1 <sup>+</sup>	1/2	-	-	-	-
2	M	2 <sup>+</sup>	3/2	-	-	-	-
2	M	2 <sup>+</sup>	1/2	-	3/2 <sup>+</sup>	5/2 <sup>+</sup>	-
2	M	0 <sup>+</sup>	3/2	-	-	-	-
2	M	0 <sup>+</sup>	1/2	1/2 <sup>+</sup> $\Delta(1750)$	-	-	-
2	S	2 <sup>+</sup>	3/2	1/2 <sup>+</sup> $\Delta(1910)$	3/2 <sup>+</sup> $\Delta(1920)$	5/2 <sup>+</sup> $\Delta(1905)$	7/2 <sup>+</sup> $\Delta(1950)$
2	S	2 <sup>+</sup>	1/2	-	-	-	-
2	S	0 <sup>+</sup>	3/2	-	3/2 <sup>+</sup> $\Delta(1600)$	-	-
2	S	0 <sup>+</sup>	1/2	-	-	-	-
1	M	1 <sup>-</sup>	3/2	-	-	-	-
1	M	1 <sup>-</sup>	1/2	1/2 <sup>-</sup> $\Delta(1620)$	3/2 <sup>-</sup> $\Delta(1700)$	-	-
0	S	0 <sup>+</sup>	3/2	-	3/2 <sup>+</sup> $\Delta(1232)$	-	-
0	S	0 <sup>+</sup>	1/2	-	-	-	-

mixing is more important for the decay patterns of the states than for their positions. An example are the lowest lying  $(70, 1_1^-)$  states with  $J^P=1/2^-$  and  $3/2^-$ . The physical states are:

$$|N(1535)1/2^- \rangle = \cos(\Theta_S)|N^2P_M1/2^- \rangle - \sin(\Theta_S)|N^4P_M1/2^- \rangle \quad (15.33)$$

$$|N(1520)3/2^- \rangle = \cos(\Theta_D)|N^2P_M3/2^- \rangle - \sin(\Theta_D)|N^4P_M3/2^- \rangle \quad (15.34)$$

and the orthogonal combinations for  $N(1650)1/2^-$  and  $N(1700)3/2^-$ . The mixing is large for the  $J^P=1/2^-$  states ( $\Theta_S \approx -32^\circ$ ), but small for the  $J^P=3/2^-$  states ( $\Theta_D \approx +6^\circ$ ) [43–45].

All baryons of the ground state multiplets are known. Many of their properties, in particular their masses, are in good agreement even with the most basic versions of the quark model, including harmonic (or linear) confinement and a spin-spin interaction, which is responsible for the octet - decuplet mass shifts. A consistent description of the ground-state electroweak properties, however, requires refined relativistic constituent quark models.

The situation for the excited states is much less clear. The assignment of some experimentally observed states with strange quarks to model configurations is only tentative and in many cases candidates are completely missing. Melde, Plessas and Sengl [42] have calculated baryon properties in relativistic constituent quark models, using one-gluon exchange and Goldstone-boson exchange for the modeling of the hyperfine interactions (see Sec. 15.5 on Dynamics). Both types of models give qualitatively comparable results, and underestimate in general experimentally observed decay widths. Nevertheless, in particular on the basis of the observed decay patterns, the authors have assigned some additional states with strangeness to the SU(3) multiplets and suggest re-assignments for a few others. Among the new assignments are states with weak experimental evidence (two or three star ratings) and partly without firm spin/parity assignments, so that further experimental efforts are necessary before final conclusions can be drawn. We have added their suggestions in Table 15.7.

In the non-strange sector there are two main problems which are illustrated in Fig. 15.6, where the experimentally observed excitation spectrum of the nucleon ( $N$  and  $\Delta$  resonances) is compared to the results of a typical quark model calculation [46]. The lowest states from the N=2 band, the  $N(1440)1/2^+$ , and the  $\Delta(1600)3/2^+$ , appear lower than the negative parity states from the N=1 band (see Table 15.8) and much lower than predicted by most models. Also negative parity  $\Delta$  states from the N=3 band ( $\Delta(1900)1/2^-$ ,  $\Delta(1940)3/2^-$ , and  $\Delta(1930)5/2^-$ ) are too low in energy. Part of the problem could be experimental. Among the negative parity  $\Delta$  states, only the  $\Delta(1930)5/2^-$  has three stars and the uncertainty in the position of the  $\Delta(1600)3/2^+$  is large (1550 - 1700 MeV).

Furthermore, many more states are predicted than observed. This has been known for a long time as the ‘missing resonance’ problem [43]. Up to an excitation energy of 2.4 GeV, about 45  $N$  states are predicted, but only 20 are established (four- or three-star; see Note on  $N$  and  $\Delta$  Resonances for the rating of the status of resonances) and 5 are tentative (two- or one-star). Even for the N=2 band, up to now only half of the predicted states have been observed. However, there is some recent progress. The total number of states has not much changed but the number of states with four- or three-star rating has increased from 14 to 20 compared to the 2018 PDG particle listings. Most of this progress is due to the programs concentrating on the study of meson photoproduction reactions, while the most recent partial wave analysis of elastic pion scattering and charge exchange data by Arndt and collaborators [47] found no evidence for almost half of the states listed in this review (and included in Fig. 15.6). Such analyses are of course biased against resonances which couple only weakly to the  $N\pi$  channel. Quark model predictions for the couplings to other hadronic channels and to photons are given in Ref. [46]. The large experimental effort ongoing at several electron accelerators to study the baryon resonance spectrum with real and virtual photon-induced meson production reactions includes the search for as-yet-unobserved states, as well as detailed studies of the properties of the low lying states (decay patterns, electromagnetic couplings, magnetic moments, etc.) (see Ref. [48] for

reviews). There are two major new aspects of this program. The investigation of single and double polarization observables allows via the study of interference terms access to small partial waves that do not leave a footprint in unpolarized cross sections. An example for the impact of such data is given by a comparison of results from different multipole analyses of pion photoproduction [49]. It shows clearly that with the inclusion of polarization observables the reaction model results start to converge. This will in the near future much improve the data basis for excited baryons in the light quark sector.

The other aspect is the study of final states with meson pairs, in particular  $\pi\pi$  and  $\pi\eta$  pairs, which made large progress during the last few years. This is important for higher lying states, which in the quark model may have both possible oscillations excited. Such states can be expected to decay in sequential processes de-exciting the two oscillations step-by-step so that they couple strongly to multiple-meson final states but not to single-meson production. Detailed analyses of such data are for example given in [50, 51] and had already significant impact on partial wave analyses.

In quark models, the number of excited states is determined by the effective degrees of freedom, while their ordering and decay properties are related to the residual quark - quark interaction. An overview of quark models for baryons is given in [52], recent discussions of baryon spectroscopy are given in [34, 41]. The effective degrees of freedom in the standard nonrelativistic quark model are three equivalent valence quarks with one-gluon exchange-motivated, flavor-independent color-magnetic interactions. The QCD aspect of gluon-gluon interactions is emphasized by the hypercentral quark model [53, 54], which includes in a natural way three-body forces between the quarks. A different class of models uses interactions which give rise to a quark - diquark clustering of the baryons: for a review see [55]. If there is a tightly bound diquark, only two degrees of freedom are available at low energies, and thus fewer states are predicted. Furthermore, selection rules in the decay pattern may arise from the quantum numbers of the diquark. More states are predicted by collective models of the baryon like the algebraic approach in [56]. In this approach, the quantum numbers of the valence quarks are distributed over a Y-shaped string-like configuration, and additional states arise *e.g.*, from vibrations of the strings. More states are also predicted in the framework of flux-tube models, see [57], which are motivated by lattice QCD. In addition to the quark degrees of freedom, flux-tubes responsible for the confinement of the quarks are considered as degrees of freedom. These models include hybrid baryons containing explicit excitations of the gluon fields. However, since all half integral  $J^P$  quantum numbers are possible for ordinary baryons, such ‘exotics’ will be very hard to identify, and probably always mix with ordinary states. So far, the experimentally observed number of states is still far lower even than predicted by the quark-diquark models.

The influence of chiral symmetry on the excitation spectrum of the nucleon has been debated from a somewhat different perspective. Chiral symmetry, the fundamental symmetry of QCD, is strongly broken for the low lying states, resulting in large mass differences of parity partners like the  $J^P=1/2^+$   $N(938)1/2^+$  ground state and the  $J^P=1/2^-$   $N(1535)1/2^-$  excitation. However, at higher excitation energies there is some evidence for parity doublets and even some very tentative suggestions for full chiral multiplets of  $N^*$  and  $\Delta$  resonances. An effective restoration of chiral symmetry at high excitation energies due to a decoupling from the quark condensate of the vacuum has been discussed (see Ref. [58] for recent reviews) as a possible cause. In this case, the mass generating mechanisms for low and high lying states would be essentially different. As a further consequence, the parity doublets would decouple from pions, so that experimental bias would be worse. However, parity doublets might also arise from the spin-orbital dynamics of the 3-quark system. Presently, the status of data does not allow final conclusions.

The most recent developments on the theory side are the first unquenched lattice calculations for the excitation spectrum discussed in Sec15.6. The results are basically consistent with the level counting of  $SU(6)\otimes O(3)$  in the standard non-relativistic quark model and show no indication for quark-diquark structures



or parity doubling. Consequently, there is as yet no indication from lattice that the mis-match between the excitation spectrum predicted by the standard quark model and experimental observations is due to inappropriate degrees of freedom in the quark model.

## 15.5 Dynamics

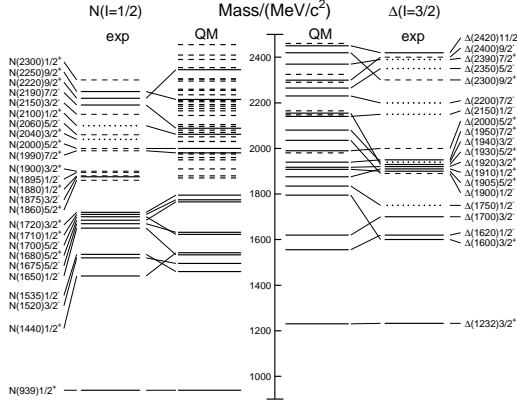


Figure 15.6: Excitation spectrum of the nucleon. Compared are the positions of the excited states identified in experiment, to those predicted by a relativized quark model calculation. Left hand side: isospin  $I = 1/2$   $N$ -states, right hand side: isospin  $I = 3/2$   $\Delta$ -states. Experimental: (columns labeled 'exp'), three- and four-star states are indicated by full lines (two-star dashed lines, one-star dotted lines). At the very left and right of the figure, the spectroscopic notation of these states is given. Quark model [46, 59]: (columns labeled 'QM'), all states for the  $N=1,2$  bands, low-lying states for the  $N=3,4,5$  bands. Full lines: at least tentative assignment to observed states, dashed lines: so far no observed counterparts. Many of the assignments between predicted and observed states are highly tentative.

Quantum chromodynamics (QCD) is well-established as the theory for the strong interactions. As such, one of the goals of QCD is to predict the spectrum of strongly-interacting particles. To date, the only first-principles calculations of spectroscopy from QCD use lattice methods. These are the subject of Sec. 15.6. These calculations are difficult and unwieldy, and many interesting questions do not have a good lattice-based method of solution. Therefore, it is natural to build models, whose ingredients are abstracted from QCD, or from the low-energy limit of QCD (such as chiral Lagrangians) or from the data itself. The words “quark model” are a shorthand for such phenomenological models. Many specific quark models exist, but most contain a similar basic set of dynamical ingredients. These include:

1. A confining interaction, which is generally spin-independent (*e.g.*, harmonic oscillator or linear confinement);
2. Different types of spin-dependent interactions:

a) commonly used is a color-magnetic flavor-independent interaction modeled after the effects of gluon exchange in QCD (see *e.g.*, Ref. [60]). For example, in the  $S$ -wave states, there is a spin-spin hyperfine interaction of the form

$$H_{HF} = -\alpha_S M \sum_{i>j} (\vec{\sigma}\lambda_a)_i (\vec{\sigma}\lambda_a)_j, \quad (15.35)$$

where  $M$  is a constant with units of energy,  $\lambda_a$  ( $a = 1, \dots, 8$ ) is the set of SU(3) unitary spin matrices, defined in the review “SU(3) Isoscalar Factors and Representation Matrices,” and the sum runs over constituent quarks or antiquarks. Spin-orbit interactions, although allowed, seem to be small in general, but a tensor term is responsible for the mixing of states with the same  $J^P$  but different  $L, S$  combinations.

b) other approaches include flavor-dependent short-range quark forces from instanton effects (see *e.g.*, [61, 62]). This interaction acts only on scalar, isoscalar pairs of quarks in a relative  $S$ -wave state:

$$\langle q^2; S, L, T | W | q^2; S, L, T \rangle = -4g\delta_{S,0}\delta_{L,0}\delta_{T,0}W \quad (15.36)$$

where  $W$  is the radial matrix element of the contact interaction.

c) a rather different and controversially discussed approach is based on flavor-dependent spin-spin forces arising from one-boson exchange. The interaction term is of the form:

$$H_{HF} \propto \sum_{i<j} V(\vec{r}_{ij}) \lambda_i^F \cdot \lambda_j^F \vec{\sigma}_i \cdot \vec{\sigma}_j \quad (15.37)$$

where the  $\lambda_i^F$  are in flavor space (see *e.g.*, Ref. [63]).

3. A strange quark mass somewhat larger than the up and down quark masses, in order to split the SU(3) multiplets;
4. In the case of spin-spin interactions (iia,c), a flavor-symmetric interaction for mixing  $q\bar{q}$  configurations of different flavors (*e.g.*,  $u\bar{u} \leftrightarrow d\bar{d} \leftrightarrow s\bar{s}$ ), in isoscalar channels, so as to reproduce *e.g.*, the  $\eta - \eta'$  and  $\omega - \phi$  mesons.

These ingredients provide the basic mechanisms that determine the hadron spectrum in the standard quark model.

## 15.6 Lattice Calculations of Hadronic Spectroscopy

Lattice calculations are a major source of information about QCD masses and matrix elements. The necessary theoretical background is given in Sec. 17 of this *Review*. Here we confine ourselves to some general comments and illustrations of lattice calculations for spectroscopy.

In general, the cleanest lattice results come from computations of processes in which there is only one particle in the simulation volume. These quantities include masses of hadrons, simple decay constants, like pseudoscalar meson decay constants, and semileptonic form factors (such as the ones appropriate to  $B \rightarrow D\nu, K\nu, \pi\nu$ ). The cleanest predictions for masses are for states which have narrow decay widths and are far below any thresholds to open channels, since the effects of final state interactions are not yet under complete control on the lattice. As a simple corollary, the lightest state in a channel is easier to study than the heavier ones. “Difficult” states for the quark model (such as exotics) are also difficult for the lattice because of the lack of simple operators which couple well to them.

Good-quality modern lattice calculations will present multi-part error budgets with their predictions. A small part of the uncertainty is statistical, from sample size. Typically, the quoted statistical uncertainty includes uncertainty from a fit: it is rare that a simulation computes one global quantity which is the desired observable. Simulations which include virtual quark-antiquark pairs (also known as “dynamical quarks” or “sea quarks”) are often done at up and down quark mass values heavier than the experimental ones, and it is then necessary to extrapolate in these quark masses. Simulations can work at the physical values of the heavier quarks’ masses. They are always done at nonzero lattice spacing, and so it is necessary to extrapolate to zero lattice spacing. Some theoretical input is needed to do this. Much of the uncertainty in these extrapolations is systematic, from the choice of fitting function. Other systematics include the effect of finite simulation volume, the number of flavors of dynamical quarks actually simulated, and technical issues with how these dynamical quarks are included. The particular choice of a fiducial mass (to normalize other predictions) is not standardized; there are many possible choices, each with its own set of strengths and weaknesses, and determining it usually requires a second lattice simulation from that used to calculate the quantity under consideration.

A systematic error of major historical interest is the “quenched approximation,” in which dynamical quarks are simply left out of the simulation. This was done because the addition of these

virtual pairs presented an expensive computational problem. No generally-accepted methodology has ever allowed one to correct for quenching effects, short of redoing all calculations with dynamical quarks. Recent advances in algorithms and computer hardware have rendered it obsolete.

With these brief remarks, we turn to examples. The field of lattice QCD simulations is vast, and so it is not possible to give a comprehensive review of them in a small space. The history of lattice QCD simulations is a story of thirty years of incremental improvements in physical understanding, algorithm development, and ever faster computers, which have combined to bring the field to a present state where it is possible to carry out very high quality calculations. We present a few representative illustrations, to show the current state of the art.

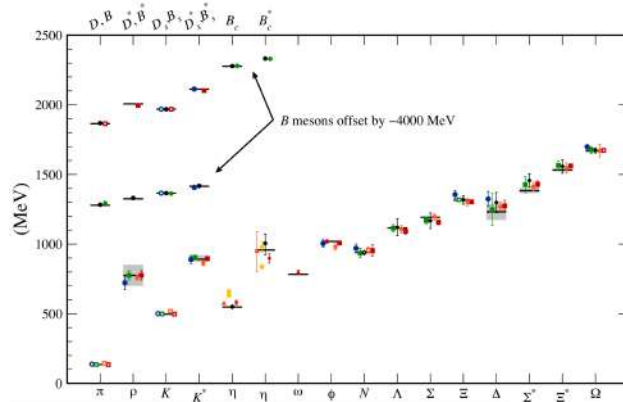


Figure 15.7: Hadron spectrum from lattice QCD. Comprehensive results for mesons and baryons are from MILC [64, 65], PACS-CS [66], BMW [67], QCDSF [68], and ETM [69]. Results for  $\eta$  and  $\eta'$  are from RBC & UKQCD [10], Hadron Spectrum [70] (also the only  $\omega$  mass), UKQCD [71], and Michael, Otnad, and Urbach [72]. Results for heavy-light hadrons from Fermilab-MILC [73], HPQCD [74, 75], and Mohler and Woloshyn [76]. Circles, squares, diamonds, and triangles stand for staggered, Wilson, twisted-mass Wilson, and chiral sea quarks, respectively. Asterisks represent anisotropic lattices. Open symbols denote the masses used to fix parameters. Filled symbols (and asterisks) denote results. Red, orange, yellow, green, and blue stand for increasing numbers of ensembles (i.e., lattice spacing and sea quark mass) Black symbols stand for results with 2+1+1 flavors of sea quarks. Horizontal bars (gray boxes) denote experimentally measured masses (widths).  $b$ -flavored meson masses are offset by  $-4000$  MeV.

By far, the major part of all lattice spectroscopy is concerned with that of the light hadrons, and so we illustrate results in Fig. 15.7, a comprehensive summary provided by A. Kronfeld (private communication; see also [77]).

Flavor singlet mesons are at the frontier of lattice QCD calculations, because one must include the effects of “annihilation graphs,” for the valence  $q$  and  $\bar{q}$ . Recently, several groups, Refs. [10, 71, 78], have reported calculations of the  $\eta$  and  $\eta'$  mesons. The numbers of [10] are typical, finding masses of 573(6) and 947(142) MeV for the  $\eta$  and  $\eta'$ . The singlet-octet mixing angle (in the conventions of Table 15.2) is  $\theta_{lin} = -14.1(2.8)^\circ$ .

The spectroscopy of mesons containing heavy quarks has become a truly high-precision endeavor. These simulations use Non-Relativistic QCD (NRQCD) or Heavy Quark Effective Theory (HQET), systematic expansions of the QCD Lagrangian in powers of the heavy quark velocity, or the heavy quark mass. Terms in the Lagrangian have obvious quark model analogs, but are derived directly from QCD. For example, the heavy quark potential is a derived quantity, extracted from simulations. Fig. 15.8 shows the mass spectrum for mesons containing at least one heavy ( $b$  or  $c$ ) quark from Ref. [75]. It also contains results from Ref. [79, 80]. The calculations use a discretization of nonrelativistic QCD for bottom quarks with charm and lighter quarks being handled with an improved relativistic action. Four flavors ( $u, d, s, c$ ) of dynam-

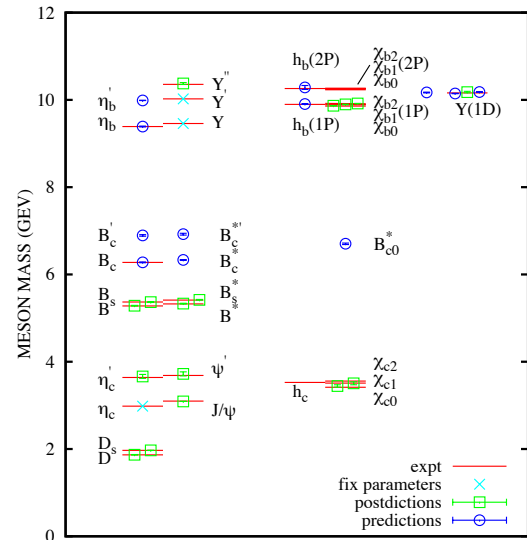


Figure 15.8: Spectroscopy for mesonic systems containing one or more heavy quarks (adapted from Ref. [75]). Particles whose masses are used to fix lattice parameters are shown with crosses; the authors distinguish between “predictions” and “postdictions” of their calculation. Lines represent experiment.

ical quarks are included.

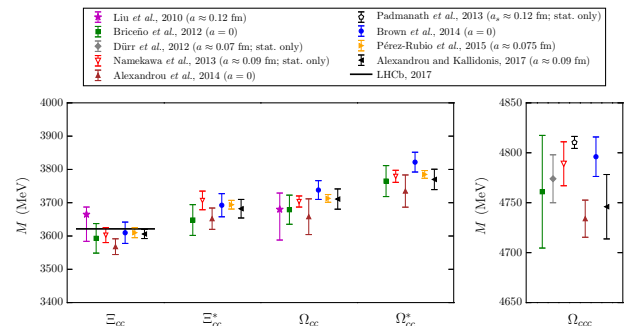


Figure 15.9: Comparison of lattice QCD results for the doubly and triply charmed baryon masses. Labels are Liu, *et al.*, [81]; Briceno, *et al.*, [82]; Namekawa, *et al.*, [83]; Padmanath, *et al.*, [84]; Alexandrou, *et al.*, [69]; Brown, *et al.*, [85]; Perez-Rubio *et al.*, [86]; Alexandrou and Kallidonis 2017, [87]. Only calculations with dynamical light quarks are included; for the doubly charmed baryons, only calculations were performed at or extrapolated to the physical pion mass are shown. Results without estimates of systematic uncertainties are labeled “stat. only”. The lattice spacing values used in the calculations are also given;  $a = 0$  indicates that the results have been extrapolated to the continuum limit. In the plot of the doubly charmed baryons, the recently announced experimental result for the  $\Xi_{cc}^+$  mass from LHCb [36] is shown with a horizontal line.

Fig. 15.9 shows a compilation of recent lattice results for doubly and triply charmed baryons, provided by S. Meinel [88]. The state recently announced by LHCb [36] is also shown. Note that the lattice calculations for the mass of this state were predictions, not postdictions.

Recall that lattice calculations take operators which are interpolating fields with quantum numbers appropriate to the desired states, compute correlation functions of these operators, and fit the correlation functions to functional forms parametrized by a set of masses and matrix elements. As we move away from hadrons which can be created by the simplest quark model operators (appropriate to the lightest meson and baryon multiplets) we encounter a host of new problems: either no good interpolating fields, or too many possible interpolating fields, and many states



with the same quantum numbers. Techniques for dealing with these interrelated problems vary from collaboration to collaboration, but all share common features: typically, correlation functions from many different interpolating fields are used, and the signal is extracted in what amounts to a variational calculation using the chosen operator basis. In addition to mass spectra, wave function information can be garnered from the form of the best variational wave function. Of course, the same problems which are present in the spectroscopy of the lightest hadrons (the need to extrapolate to infinite volume, physical values of the light quark masses, and zero lattice spacing) are also present. We briefly touch on three different kinds of hadrons: excited states of mesons (including hybrids), excited states of baryons, and glueballs. The quality of the data is not as good as for the ground states, and so the results continue to evolve.

Modern calculations use a large bases of trial states, which allow them to probe many quantum number channels simultaneously. This is vital for studying “difficult sectors” of QCD, such as the isoscalar mesons. A recent example of meson spectroscopy where this is done, by [89], is shown in Fig. 15.10. The quark masses are still heavier than their physical values, so the pion is at 392 MeV. The authors can assign a relative composition of nonstrange and strange quark content to their states, observing, for example, a nonstrange  $\omega$  and a strange  $\phi$ . Some states also have a substantial component of gluonic excitation. Note especially the three exotic channels  $J^{PC} = 1^{-+}, 0^{+-},$  and  $2^{+-}$ , with states around 2 GeV. These calculations will continue to improve as the quark masses are carried lower.

The interesting physics questions of excited baryon spectroscopy to be addressed are precisely those enumerated in the last section. An example of a recent calculation, due to Ref. [90] is shown in Fig. 15.11. Notice that the pion is not yet at its physical value. The lightest positive parity state is the nucleon, and the Roper resonance has not yet appeared as a light state.

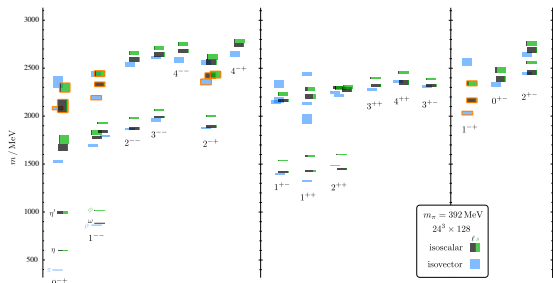


Figure 15.10: Isoscalar (green and black) and isovector (blue) spectrum from Ref. [89]. States are labeled  $J^{PC}$ . The quark mass is heavier than its physical value;  $m_\pi = 392$  MeV. The vertical height of each box indicates the statistical uncertainty in the mass. Black and green indicate relative nonstrange and strange composition. Orange outlines show states with a large chromomagnetic component to their wave function, which the authors argue are hybrid states. Note the exotic states in the three right-most columns.

Most hadrons are resonances, and lattice calculations will have to deal with this fact as the quark masses are taken ever smaller. The actual calculation is of the combined mass of two (or more) hadrons in a box of finite size. The combined mass is shifted from being the sum of the individual masses because the finite box forces the hadrons to interact with each other. The volume-dependent mass shift yields the phase shift for the continuum scattering amplitude, which in turn can be used to extract the resonance mass and width, with some degree of modeling. So far only two-body resonances, the rho meson and a few others, have been well studied. This is an active research area. A recent review, [91], summarizes the situation, and example of a calculation of the rho meson decay width is [92]. The mass and decay width of the  $f_0(500)$  have recently been computed in [93]. Ref. [94] studies the decay width of the  $\Delta(1238)$ . Lattice calculations relevant to the extra states observed in the charmonium spectrum (Sec. 15.3)

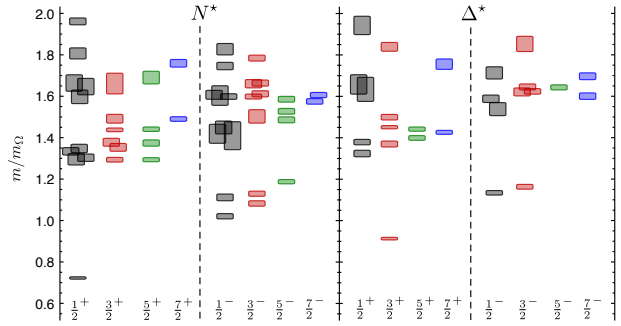


Figure 15.11: Spin-identified spectrum of nucleons and deltas, from lattices where  $m_\pi = 396$  MeV, in units of the calculated  $\Omega$  mass, from Ref. [90]. The colors just correspond to the different  $J$  assignments: grey for  $J = 1/2$ , red for  $J = 3/2$ , green for  $5/2$ , blue for  $J = 7/2$ .

are difficult, because the states sit high in the spectrum of most channels and due to the number of nearby multiparticle states.

In Fig. 15.4 we showed a figure from [12] presenting a lattice prediction for the glueball mass spectrum in quenched approximation. A true QCD prediction of the glueball spectrum requires dynamical light quarks and (because glueball operators are intrinsically noisy) high statistics. Only recently have the first useful such calculations appeared, in [95, 96]. Fig. 15.12 shows results from [95], done with dynamical  $u, d$  and  $s$  quarks at two lattice spacings, 0.123 and 0.092 fm, along with comparisons to the quenched lattice calculation of [18] and to experimental isosinglet mesons. The dynamical simulation is, of course, not the last word on this subject, but it shows that the effects of quenching seem to be small.

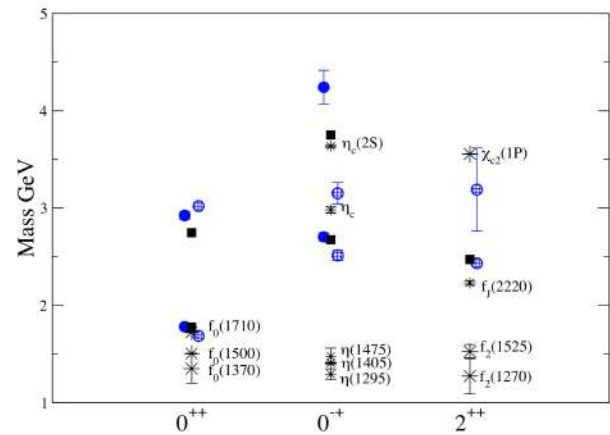


Figure 15.12: Lattice QCD predictions for glueball masses. The open and closed circles are the larger and smaller lattice spacing data of the full QCD calculation of glueball masses of Ref. [95]. Squares are the quenched data for glueball masses of Ref. [18]. The bursts labeled by particle names are experimental states with the appropriate quantum numbers.

As a final part of spectroscopy we mention electromagnetic mass splittings (such as the neutron - proton mass difference). They are interesting but difficult. These calculations are important for determining the values of the quark masses (for a discussion see the review in the PDG). Knowing that the neutron is heavier than the proton tells us that these splittings have a complicated origin. One part of the shift is because the up and down quarks have slightly different masses. The second is that the quarks have (different) charges. Phenomenologists (compare Ref. [97]) combine Coulomb forces and spin-dependent electromagnetic hyperfine interactions to model their charge effects. In order to compute hadronic mass differences on the lattice, electromagnetic interactions must be included in the simulations. This creates a host of technical is-

sues. An important one is that electromagnetic interactions are long range, but lattice simulations are done in finite volumes. The theoretical situation is summarized in the recent review [98]. A recent calculation, Ref. [99], has presented the first results for electromagnetic mass splittings in the baryon octet, with good agreement with observation. Ref. [100] has calculations for meson splittings.

### References

- [1] C. Amsler in the Quark Structure of Hadrons, Lecture Notes in Physics **949** (2018), ed. Springer.
- [2] K.-C. Yang, Nucl. Phys. **B776**, 187 (2007), [arXiv:0705.0692].
- [3] L. Burakovsky and J. T. Goldman, Nucl. Phys. **A625**, 220 (1997), [hep-ph/9703272].
- [4] J. Schwinger, Phys. Rev. **135**, B816 (1964).
- [5] A. Bramon, R. Escribano and M. D. Scadron, Phys. Lett. **B403**, 339 (1997), [hep-ph/9703313].
- [6] A. Aloisio *et al.* (KLOE), Phys. Lett. **B541**, 45 (2002), [hep-ex/0206010].
- [7] F. Ambrosino *et al.*, JHEP **07**, 105 (2009), [arXiv:0906.3819].
- [8] C. Amsler *et al.* (Crystal Barrel), Phys. Lett. **B294**, 451 (1992).
- [9] C. Amsler, Rev. Mod. Phys. **70**, 1293 (1998), [hep-ex/9708025].
- [10] N. H. Christ *et al.*, Phys. Rev. Lett. **105**, 241601 (2010), [arXiv:1002.2999].
- [11] T. Feldmann, Int. J. Mod. Phys. **A915**, 159 (2000).
- [12] Y. Chen *et al.*, Phys. Rev. **D73**, 014516 (2006), [hep-lat/0510074].
- [13] C. Amsler and F. E. Close, Phys. Rev. **D53**, 295 (1996), [hep-ph/9507326].
- [14] R. L. Jaffe, Phys. Rev. **D15**, 267 (1977).
- [15] R. L. Jaffe, Phys. Rev. **D15**, 281 (1977).
- [16] S.L. Olsen, Front. Phys. **10**, 121 (2015).
- [17] S. L. Olsen, T. Skwarnicki and D. Zieminska, Rev. Mod. Phys. **90**, 1, 015003 (2018), [arXiv:1708.04012].
- [18] C. J. Morningstar and M. J. Peardon, Phys. Rev. **D60**, 034509 (1999), [hep-lat/9901004].
- [19] W.-J. Lee and D. Weingarten, Phys. Rev. **D61**, 014015 (2000), [hep-lat/9910008].
- [20] G. S. Bali *et al.* (UKQCD), Phys. Lett. **B309**, 378 (1993), [hep-lat/9304012].
- [21] C. Michael, AIP Conf. Proc. **432**, 1, 657 (1998), [hep-ph/9710502].
- [22] F. E. Close and A. Kirk, Eur. Phys. J. **C21**, 531 (2001), [hep-ph/0103173].
- [23] W. Ochs, J. Phys. **G40**, 043001 (2013), [arXiv:1301.5183].
- [24] F. Brünner and A. Rebhan, Phys. Rev. Lett. **115**, 13, 131601 (2015), [arXiv:1504.05815].
- [25] C. Amsler and N. A. Tornqvist, Phys. Rept. **389**, 61 (2004).
- [26] N. Isgur and J. E. Paton, Phys. Rev. **D31**, 2910 (1985).
- [27] P. Lacock *et al.* (UKQCD), Phys. Lett. **B401**, 308 (1997), [hep-lat/9611011].
- [28] M. S. Chanowitz and S. R. Sharpe, Nucl. Phys. **B222**, 211 (1983), [Erratum: Nucl. Phys. **B228**, 588 (1983)].
- [29] T. Barnes *et al.*, Nucl. Phys. **B224**, 241 (1983).
- [30] R. Aaij *et al.* (LHCb), Phys. Rev. Lett. **115**, 072001 (2015), [arXiv:1507.03414].
- [31] R. Aaij *et al.* (LHCb), Phys. Rev. Lett. **122**, 22, 222001 (2019), [arXiv:1904.03947].
- [32] Y.-R. Liu *et al.*, Prog. Part. Nucl. Phys. **107**, 237 (2019), [arXiv:1903.11976].
- [33] F.E. Close, in *Quarks and Nuclear Forces* (Springer-Verlag, 1982), p. 56.
- [34] V. Crede and W. Roberts, Rept. on Prog. in Phys. **76**, 076301 (2013).
- [35] R. Aaij *et al.* (LHCb), Phys. Rev. Lett. **118**, 18, 182001 (2017), [arXiv:1703.04639].
- [36] R. Aaij *et al.* (LHCb), Phys. Rev. Lett. **119**, 11, 112001 (2017), [arXiv:1707.01621].
- [37] M. Mattson *et al.* (SELEX), Phys. Rev. Lett. **89**, 112001 (2002), [hep-ex/0208014].
- [38] A. Ocherashvili *et al.* (SELEX), Phys. Lett. **B628**, 18 (2005), [hep-ex/0406033].
- [39] M. Karliner and J. L. Rosner, Phys. Rev. **D90**, 9, 094007 (2014), [arXiv:1408.5877].
- [40] R.H. Dalitz and L.J. Reinders, in “Hadron Structure as Known from Electromagnetic and Strong Interactions,” *Proceedings of the Hadron ’77 Conference* (Veda, 1979), p. 11.
- [41] E. Klempt and J.-M. Richard, Rev. Mod. Phys. **82**, 1095 (2010), [arXiv:0901.2055].
- [42] T. Melde, W. Plessas and B. Sengl, Phys. Rev. **D77**, 114002 (2008), [arXiv:0806.1454].
- [43] N. Isgur and G. Karl, Phys. Rev. **D18**, 4187 (1978).
- [44] N. Isgur and G. Karl, Phys. Rev. **D19**, 2653 (1979), [Erratum: Phys. Rev. **D23**, 817 (1981)].
- [45] S. Capstick and W. Roberts, Prog. Part. Nucl. Phys. **45**, S241 (2000), [arXiv:nucl-th/0008028].
- [46] S. Capstick and W. Roberts, Phys. Rev. **D58**, 074011 (1998), [arXiv:nucl-th/9804070].
- [47] R. A. Arndt *et al.*, Phys. Rev. **C74**, 045205 (2006), [arXiv:nucl-th/0605082].
- [48] B. Krusche and S. Schadmand, Prog. Part. Nucl. Phys. **51**, 399 (2003), [arXiv:nucl-ex/0306023].
- [49] A. V. Anisovich *et al.*, Eur. Phys. J. **A52**, 9, 284 (2016), [arXiv:1604.05704].
- [50] E. Gutz *et al.* (CBELSA/TAPS), Eur. Phys. J. **A50**, 74 (2014), [arXiv:1402.4125].
- [51] V. Sokhoyan *et al.* (CBELSA/TAPS), Eur. Phys. J. **A51**, 8, 95 (2015), [Erratum: Eur. Phys. J. **A51**, no.12, 187 (2015)], [arXiv:1507.02488].
- [52] S. Capstick and W. Roberts, Prog. in Part. Nucl. Phys. **45**, 241 (2000).
- [53] M. Ferraris *et al.*, Phys. Lett. **B364**, 231 (1995).
- [54] M. M. Giannini and E. Santopinto, Chin. J. Phys. **53**, 020301 (2015), [arXiv:1501.03722].
- [55] M. Anselmino *et al.*, Rev. Mod. Phys. **65**, 1199 (1993).
- [56] R. Bijker, F. Iachello and A. Leviatan, Annals Phys. **236**, 69 (1994), [arXiv:nucl-th/9402012].
- [57] S. Capstick and P. R. Page, Phys. Rev. **C66**, 065204 (2002), [arXiv:nucl-th/0207027].
- [58] R. L. Jaffe, D. Pirjol and A. Scardicchio, Phys. Rept. **435**, 157 (2006), [hep-ph/0602010].
- [59] S. Capstick, Phys. Rev. **D46**, 2864 (1992).
- [60] A. De Rujula, H. Georgi and S. L. Glashow, Phys. Rev. **D12**, 147 (1975).
- [61] W. H. Blask *et al.*, Z. Phys. **A337**, 327 (1990).
- [62] U. Loring *et al.*, Eur. Phys. J. **A10**, 309 (2001), [hep-ph/0103287].
- [63] L. Ya. Glozman and D. O. Riska, Phys. Rept. **268**, 263 (1996), [hep-ph/9505422].
- [64] C. Aubin *et al.*, Phys. Rev. **D70**, 094505 (2004), [hep-lat/0402030].
- [65] A. Bazavov *et al.* (MILC), Rev. Mod. Phys. **82**, 1349 (2010), [arXiv:0903.3598].

- [66] S. Aoki *et al.* (PACS-CS), Phys. Rev. **D79**, 034503 (2009), [arXiv:0807.1661].
- [67] S. Durr *et al.*, Science **322**, 1224 (2008), [arXiv:0906.3599].
- [68] W. Bietenholz *et al.*, Phys. Rev. **D84**, 054509 (2011), [arXiv:1102.5300].
- [69] C. Alexandrou *et al.*, Phys. Rev. **D90**, 7, 074501 (2014), [arXiv:1406.4310].
- [70] J. J. Dudek *et al.*, Phys. Rev. **D83**, 111502 (2011), [arXiv:1102.4299].
- [71] E. B. Gregory *et al.* (UKQCD), Phys. Rev. **D86**, 014504 (2012), [arXiv:1112.4384].
- [72] C. Michael, K. Ottnad and C. Urbach (ETM), Phys. Rev. Lett. **111**, 18, 181602 (2013), [arXiv:1310.1207].
- [73] C. Bernard *et al.* (Fermilab Lattice, MILC), Phys. Rev. **D83**, 034503 (2011), [arXiv:1003.1937].
- [74] E. B. Gregory *et al.*, Phys. Rev. **D83**, 014506 (2011), [arXiv:1010.3848].
- [75] R. J. Dowdall *et al.*, Phys. Rev. **D86**, 094510 (2012), [arXiv:1207.5149].
- [76] D. Mohler and R. M. Woloshyn, Phys. Rev. **D84**, 054505 (2011), [arXiv:1103.5506].
- [77] A. S. Kronfeld, Ann. Rev. Nucl. Part. Sci. **62**, 265 (2012), [arXiv:1203.1204].
- [78] K. Ottnad, C. Urbach and F. Zimmermann (OTM), Nucl. Phys. **B896**, 470 (2015), [arXiv:1501.02645].
- [79] J. O. Daldrop, C. T. H. Davies and R. J. Dowdall (HPQCD), Phys. Rev. Lett. **108**, 102003 (2012), [arXiv:1112.2590].
- [80] G. C. Donald *et al.*, Phys. Rev. **D86**, 094501 (2012), [arXiv:1208.2855].
- [81] L. Liu *et al.*, Phys. Rev. **D81**, 094505 (2010), [arXiv:0909.3294].
- [82] R. A. Briceno, H.-W. Lin and D. R. Bolton, Phys. Rev. **D86**, 094504 (2012), [arXiv:1207.3536].
- [83] Y. Namekawa *et al.* (PACS-CS), Phys. Rev. **D87**, 9, 094512 (2013), [arXiv:1301.4743].
- [84] M. Padmanath *et al.*, Phys. Rev. **D90**, 7, 074504 (2014), [arXiv:1307.7022].
- [85] Z. S. Brown *et al.*, Phys. Rev. **D90**, 9, 094507 (2014), [arXiv:1409.0497].
- [86] P. Pérez-Rubio, S. Collins and G. S. Bali, Phys. Rev. **D92**, 3, 034504 (2015), [arXiv:1503.08440].
- [87] C. Alexandrou and C. Kallidonis, Phys. Rev. **D96**, 3, 034511 (2017), [arXiv:1704.02647].
- [88] S. Meinel, private communication .
- [89] J. J. Dudek *et al.* (Hadron Spectrum), Phys. Rev. **D88**, 9, 094505 (2013), [arXiv:1309.2608].
- [90] R. G. Edwards *et al.*, Phys. Rev. **D84**, 074508 (2011), [arXiv:1104.5152].
- [91] R. A. Briceno, J. J. Dudek and R. D. Young, Rev. Mod. Phys. **90**, 2, 025001 (2018), [arXiv:1706.06223].
- [92] J. Bulava *et al.*, Nucl. Phys. **B910**, 842 (2016), [arXiv:1604.05593].
- [93] R. A. Briceno *et al.*, Phys. Rev. Lett. **118**, 2, 022002 (2017), [arXiv:1607.05900].
- [94] C. W. Andersen *et al.*, Phys. Rev. **D97**, 1, 014506 (2018), [arXiv:1710.01557].
- [95] C. M. Richards *et al.* (UKQCD), Phys. Rev. **D82**, 034501 (2010), [arXiv:1005.2473].
- [96] E. Gregory *et al.*, JHEP **10**, 170 (2012), [arXiv:1208.1858].
- [97] M. Karliner and J. L. Rosner (2019), [arXiv:1906.07799].
- [98] A. Patella, PoS **LATTICE2016**, 020 (2017), [arXiv:1702.03857].
- [99] S. Borsanyi *et al.*, Science **347**, 1452 (2015), [arXiv:1406.4088].
- [100] D. Giusti *et al.*, Phys. Rev. **D95**, 11, 114504 (2017), [arXiv:1704.06561].

## 16. Heavy-Quark and Soft-Collinear Effective Theory

Revised August 2019 by C.W. Bauer (LBNL) and M. Neubert (PRISMA, Mainz Inst. for Theor. Physics, JG U.).

### 16.1 Effective Field Theories

Quantum field theories provide the most precise computational tools for describing physics at the highest energies. One of their characteristic features is that they almost inevitably involve multiple length scales. When trying to determine the value of an observable, quantum field theory demands that all possible virtual states and hence all particles be included in the calculation. Since these particles have widely different masses, the final prediction is sensitive to many scales. This fact represents a formidable challenge from a practical point of view. No realistic quantum field theories can be solved exactly, so that one needs to resort to approximation schemes; these, however, are typically most straightforward when only a single scale is involved at a time.

Effective field theories (EFTs) provide a general theoretical framework to deal with the multi-scale problems of realistic quantum field theories. This framework aims at reducing such problems to a combination of separate and simpler single-scale problems; simultaneously, however, it provides an organization scheme whereby the other scales are not omitted but allowed to play their role in a separate step of the computation. The philosophy and basic principles of this approach are very generic, and correspondingly EFTs represent a widely used method in many different areas of high-energy physics, from the low-energy scales of atomic and nuclear physics to the high-energy scales of (partly yet unknown) elementary-particle physics, see [1–3] for some early references. EFTs can play a role both within analytic perturbative computations and in the context of non-perturbative numerical simulations; One of the simplest applications of EFTs to particle physics concerns the description of an underlying theory that is only probed at energy scales  $E < \Lambda$ . Any particle with mass  $m > \Lambda$  cannot be produced as a real state and therefore only leads to short-distance virtual effects. Thus, one can construct an effective theory in which the quantum fluctuations of such heavy particles are “integrated out” from the generating functional for Green functions. This results in a simpler theory containing only those degrees of freedom that are relevant to the energy scales under consideration. In fact, the standard model of particle physics itself is widely viewed as an EFT of some yet unknown, more fundamental theory.

The development of any effective theory starts by identifying the degrees of freedom that are relevant to describe the physics at a given energy (or length) scale and constructing the Lagrangian describing the interactions among these fields. Short-distance quantum fluctuations associated with much smaller length scales are absorbed into the coefficients of the various operators in the effective theory. These coefficients are determined in a matching procedure, by requiring that the EFT reproduces the matrix elements of the full theory up to power corrections. In many cases the effective Lagrangian exhibits enhanced symmetries compared with the fundamental theory, allowing for simple and sometimes striking predictions relating different observables.

### 16.2 Heavy-Quark Effective Theory

Heavy-quark systems provide prime examples for applications of the EFT technology, because the hierarchy  $m_Q \gg \Lambda_{\text{QCD}}$  (with  $Q = b, c$ ) provides a natural separation of scales. Physics at the scale  $m_Q$  is of a short-distance nature and can be treated perturbatively, while for heavy-quark systems there is always also some hadronic physics governed by the confinement scale  $\Lambda_{\text{QCD}}$  of the strong interaction. Being able to separate the short-distance and long-distance effects associated with these two scales is crucial for any quantitative description. For instance, if the long-distance hadronic matrix elements are obtained from lattice QCD, then it is necessary to analytically compute the effects of short-wavelength modes that do not fit on the lattice. In many other instances, the long-distance physics can be encoded in a small number of hadronic parameters.

#### 16.2.1 General idea and derivation of the effective Lagrangian

The simplest effective theory for heavy-quark systems is the heavy-quark effective theory (HQET) [4–7] (see [8, 9] for detailed discussions). It provides a simplified description of the soft interactions of a single heavy quark with light partons. This includes the interactions that bind the heavy quark with other light partons inside heavy mesons and baryons.

A softly interacting heavy quark is nearly on-shell. Its momentum may be decomposed as  $p_Q = m_Q v + k$ , where  $v$  is the 4-velocity of the hadron containing the heavy quark. The “residual momentum”  $k$  results from the soft interactions of the heavy quark with its environment and satisfies  $v \cdot k \sim \Lambda_{\text{QCD}}$  and  $k^2 \sim \Lambda_{\text{QCD}}^2$ , which in the rest frame of the heavy hadron reduces to  $k^\mu \sim \Lambda_{\text{QCD}}$ . In the limit  $m_Q \gg \Lambda_{\text{QCD}}$ , the soft interactions do not change the 4-velocity of the heavy quark, which is therefore a conserved quantum number that is often used as a label on the effective heavy-quark fields. A nearly on-shell Dirac spinor has two large and two small components. We define

$$Q(x) = e^{-im_Q v \cdot x} [h_v(x) + H_v(x)], \quad (16.1)$$

where

$$h_v(x) = e^{im_Q v \cdot x} \frac{1 + \not{v}}{2} Q(x), \quad H_v(x) = e^{im_Q v \cdot x} \frac{1 - \not{v}}{2} Q(x) \quad (16.2)$$

are the large (“upper”) and small (“lower”) components of the spinor field, respectively. The extraction of the phase factor in (16.1) implies that the fields  $h_v$  and  $H_v$  carry the residual momentum  $k$ . The field  $H_v$  is  $1/m_Q$  suppressed relative to  $h_v$  and describes quantum fluctuations far off the mass shell. Integrating it out using its equations of motion yields the HQET Lagrangian

$$\begin{aligned} \mathcal{L}_{\text{HQET}} = & \bar{h}_v i v \cdot D_s h_v \\ & + \frac{1}{2m_Q} \left[ \bar{h}_v (iD_s)^2 h_v + C_{\text{mag}}(\mu) \frac{g}{2} \bar{h}_v \sigma_{\mu\nu} G_s^{\mu\nu} h_v \right] + \dots \end{aligned} \quad (16.3)$$

The covariant derivative  $iD_s^\mu = i\partial^\mu + gA_s^\mu$  and the field strength  $G_s^{\mu\nu}$  contain only the soft gluon field. Hard gluons have been integrated out, and their effects are contained in the Wilson coefficients of the operators in the effective Lagrangian. From the leading operator one derives the Feynman rules of HQET. The new operators entering at subleading order are referred to as the “kinetic energy” and “chromo-magnetic interaction”. The kinetic-energy operator corresponds to the first correction term in the Taylor expansion of the relativistic energy  $E = m_Q + \vec{p}^2/2m_Q + \dots$ . Lorentz invariance, which is encoded as a reparametrization invariance of the effective Lagrangian [10], ensures that its Wilson coefficient is not renormalized ( $C_{\text{kin}} \equiv 1$ ). The coefficient  $C_{\text{mag}}$  of the chromo-magnetic operator receives corrections starting at one-loop order.

#### 16.2.2 Spin-flavor symmetry

The leading term in the HQET Lagrangian exhibits a global spin-flavor symmetry. Its physical meaning is that, in the infinite mass limit, the properties of hadronic systems containing a single heavy quark are insensitive to the spin and flavor of the heavy quark [11, 12]. The spin symmetry results from the fact that there are no Dirac matrices in the leading term of the effective Lagrangian in (16.3), implying that the interactions of the heavy quark with soft gluons leave its spin unchanged. The flavor symmetry arises since the mass of the heavy quark does not appear at leading order. For  $n_Q$  heavy quarks moving at the same velocity, one can simply extend (16.3) by summing over  $n_Q$  identical terms for heavy-quark fields  $h_v^i$ . The result is invariant under rotations in flavor space. When combined with the spin symmetry, the symmetry group becomes promoted to  $SU(2n_Q)$ . These symmetries are broken by the operators at subleading power in the  $1/m_Q$  expansion.

The spin-flavor symmetry leads to many interesting relations between the properties of hadrons containing a heavy quark. The most direct consequences concern the spectroscopy of such states

[13]. In the heavy-quark limit, the spin of the heavy quark and the total angular momentum  $j$  of the light degrees of freedom are separately conserved by the strong interactions. Because of heavy-quark symmetry, the dynamics is independent of the spin and mass of the heavy quark. Hadronic states can thus be classified by the quantum numbers (flavor, spin, parity, etc.) of the light degrees of freedom. The spin symmetry predicts that, for fixed  $j \neq 0$ , there is a doublet of degenerate states with total spin  $J = j \pm \frac{1}{2}$ . The flavor symmetry relates the properties of states with different heavy-quark flavor.

### 16.2.3 Weak decay form factors

Of particular interest are the relations between the weak decay form factors of heavy mesons, which parametrize hadronic matrix elements of currents between two mesons containing a heavy quark. These relations have been derived by Isgur and Wise [12], generalizing ideas developed by Nussinov and Wetzel [14] and Voloshin and Shifman [15]. For the purpose of this discussion, it is convenient to work with a mass-independent normalization of meson states and use velocity rather than momentum variables.

Consider the elastic scattering of a pseudoscalar meson,  $P(v) \rightarrow P(v')$ , induced by an external vector current coupled to the heavy quark contained in  $P$ , which acts as a color source moving with the meson's velocity  $v$ . The action of the current is to replace instantaneously the color source by one moving at velocity  $v'$ . Soft gluons need to be exchanged in order to rearrange the light degrees of freedom and build up the final state meson moving at velocity  $v'$ . This rearrangement leads to a form-factor suppression. The important observation is that, in the  $m_Q \rightarrow \infty$  limit, the form factor can only depend on the Lorentz boost  $\gamma = v \cdot v'$  connecting the rest frames of the initial and final-state mesons (as long as  $\gamma = \mathcal{O}(1)$ ). In the effective theory the hadronic matrix element describing the scattering process can therefore be written as

$$\langle P(v') | \bar{h}_{v'} \gamma^\mu h_v | P(v) \rangle = \xi(v \cdot v') (v + v')^\mu, \quad (16.4)$$

with a form factor  $\xi(v \cdot v')$  that is real and independent of  $m_Q$ . By flavor symmetry, the form factor remains identical when one replaces the heavy quark  $Q$  in one of the meson states by a heavy quark  $Q'$  of a different flavor, thereby turning  $P$  into another pseudoscalar meson  $P'$ . At the same time, the current becomes a flavor-changing vector current. This universal form factor is called the Isgur-Wise function [12]. For equal velocities the vector current  $J^\mu = \bar{h}_v \gamma^\mu h_v$  is conserved in the effective theory, irrespective of the flavor of the heavy quarks. The corresponding conserved charges are the generators of the flavor symmetry. It follows that the Isgur-Wise function is normalized at the point of equal velocities:  $\xi(1) = 1$ . Since the recoil energy of the daughter meson  $P'$  in the rest frame of the parent meson  $P$  is  $E_{\text{recoil}} = m_{P'}(v \cdot v' - 1)$ , the point  $v \cdot v' = 1$  is referred to as the zero-recoil limit. The heavy-quark spin symmetry leads to additional relations among weak decay form factors. It can be used to relate matrix elements involving vector mesons to those involving pseudoscalar mesons, which once again can be described completely in terms of the universal Isgur-Wise function.

The form factor relations imposed by heavy-quark symmetry describe the semileptonic decay processes  $\bar{B} \rightarrow D \ell \bar{\nu}$  and  $\bar{B} \rightarrow D^* \ell \bar{\nu}$  in the limit of infinite heavy-quark masses. They are model-independent consequences of QCD. The known normalization of the Isgur-Wise function at zero recoil can be used to obtain a model-independent measurement of the element  $|V_{cb}|$  of the Cabibbo-Kobayashi-Maskawa (CKM) matrix. The semileptonic decay  $\bar{B} \rightarrow D^* \ell \bar{\nu}$  is particularly well suited for this purpose [16]. Experimentally this is a very clean mode, since the reconstruction of the  $D^*$  meson mass provides a powerful rejection against background. From the theoretical point of view, it is ideal since the decay rate at zero recoil is protected by Luke's theorem against first-order power corrections in  $1/m_Q$  [17]. This is described in more detail in Section 12. Corrections to the heavy-quark symmetry relations for the  $\bar{B} \rightarrow D^{(*)}$  form factors near zero recoil can also be constrained using sum rules derived in the small-velocity limit [18, 19].

### 16.2.4 Decoupling transformation

At leading order in  $1/m_Q$ , the couplings of soft gluons to heavy quarks in the effective Lagrangian (16.3) can be removed by the field redefinition  $h_v(x) = Y_v(x) \bar{h}_v^{(0)}(x)$ , where  $Y_v(x)$  is a soft Wilson line along the direction of  $v$ , extending from minus infinity to the point  $x$ . In terms of the new fields the leading-order HQET Lagrangian becomes  $\mathcal{L}_{\text{HQET}} = \bar{h}_v^{(0)} i v \cdot \partial h_v^{(0)}$ . It describes a free theory as far as the strong interactions of heavy quarks are concerned. However, the theory is nevertheless non-trivial in the presence of external sources. Consider, e.g., the case of a weak-interaction heavy-quark current

$$\bar{h}_{v'} \gamma^\mu (1 - \gamma_5) h_v = \bar{h}_{v'}^{(0)} \gamma^\mu (1 - \gamma_5) Y_{v'}^\dagger Y_v h_v^{(0)}, \quad (16.5)$$

where  $v$  and  $v'$  are the velocities of the heavy mesons containing the heavy quarks. Unless the two velocities are equal, corresponding to the zero-recoil limit discussed above, the object  $Y_{v'}^\dagger Y_v$  is non-trivial, and hence the soft gluons do not decouple from the heavy quarks inside the current operator. One may interpret  $Y_{v'}^\dagger Y_v$  as a Wilson loop with a cusp at the point  $x$ , where the two paths parallel to the different velocity vectors intersect. The presence of the cusp leads to non-trivial ultra-violet behavior (for  $v \neq v'$ ), which is described by a cusp anomalous dimension  $\Gamma_{\text{cusp}}(v \cdot v')$  that was calculated at two-loop order in [20]. It coincides with the velocity-dependent anomalous dimension of heavy-quark currents, which was introduced in the context of HQET in [21]. The interpretation of heavy quarks as Wilson lines is a useful tool, which was put forward in one of the very first papers on the subject [4]. This technology will be useful in the study of the interactions of heavy quarks with collinear degrees of freedom discussed later in this review.

### 16.2.5 Heavy-quark expansion for inclusive decays

The theoretical description of inclusive decays of hadrons containing a heavy quark exploits two observations [22–26]: bound-state effects related to the initial state can be calculated using the heavy-quark expansion, and the fact that the final state consists of a sum over many hadronic channels eliminates the sensitivity to the properties of individual final-state hadrons. The second feature rests on the hypothesis of quark-hadron duality, i.e. the assumption that decay rates are calculable in QCD after a smearing procedure has been applied [27]. In semileptonic decays, the integration over the lepton spectrum provides a smearing over the invariant hadronic mass of the final state (global duality). For nonleptonic decays, where the total hadronic mass is fixed, the summation over many hadronic final states provides an averaging (local duality). Since global duality is a much weaker assumption, the theoretical control of inclusive semileptonic decays is on firmer footing.

Using the optical theorem, the inclusive decay width of a hadron  $H_b$  containing a  $b$  quark can be written in the form

$$\Gamma(H_b) = \frac{1}{M_{H_b}} \text{Im} \langle H_b | i \int d^4x T \{ \mathcal{H}_{\text{eff}}(x), \mathcal{H}_{\text{eff}}(0) \} | H_b \rangle. \quad (16.6)$$

The effective weak Hamiltonian for  $b$ -quark decays consists of dimension-6 four-fermion operators and dipole operators [28]. Because of the large mass of the  $b$  quark, it follows that the separation of fields in the time-ordered product in (16.6) is small, of order  $x \sim 1/m_b$ . It is thus possible to construct an operator-product expansion (OPE) for the time-ordered product, in which it is represented as a series of local operators in HQET. The leading operator  $\bar{h}_v h_v$  has a trivial matrix element. The next contributions arise at  $\mathcal{O}(1/m_b^2)$  and give rise to two parameters  $\mu_\pi^2(H_b)$  and  $\mu_G^2(H_b)$ , which are defined as the matrix elements of the heavy-quark kinetic energy and chromo-magnetic interaction inside the hadron  $H_b$ , respectively [29]. For the ground-state heavy mesons and baryons, one has  $\mu_G^2(B) = 3(m_{B^*}^2 - m_B^2)/4 \simeq 0.36 \text{ GeV}^2$  and  $\mu_G^2(\Lambda_b) = 0$ . Thus, the total inclusive decay rate of a hadron  $H_b$

can be written as [23, 24]

$$\Gamma(H_b) = \frac{G_F^2 m_b^5 |V_{cb}|^2}{192\pi^3} \left[ c_1 + c_2 \frac{\mu_\pi^2(H_b)}{2m_b^2} + c_3 \frac{\mu_G^2(H_b)}{2m_b^2} + \mathcal{O}\left(\frac{1}{m_b^3}\right) + \dots \right], \quad (16.7)$$

where the prefactor arises from the loop integrations and is proportional to the fifth power of the  $b$ -quark mass. The coefficient functions  $c_i$  are calculable order by order in perturbation theory. While  $c_1$  corresponds to the decay rate of a free heavy quark, the higher-order coefficients systematically account for bound-state effects. The coefficients of the subleading operators and of the leading operator at third order in  $1/m_b$  have recently been calculated at NLO [30–34], and the heavy-quark expansion has been pushed to fifth order in  $1/m_b$  [35].

From the fully inclusive width in (16.7) one can obtain the lifetime of a heavy hadron via  $\tau(H_b) = 1/\Gamma(H_b)$ . Due to the universality of the leading term in the heavy-quark expansion, lifetime ratios such as  $\tau(B^-)/\tau(B^0)$ ,  $\tau(\bar{B}_s^0)/\tau(B^0)$  and  $\tau(A_b)/\tau(\bar{B}^0)$  are particularly sensitive to the hadronic parameters determining the power corrections in the expansion. In order to understand these ratios theoretically, it is necessary to include phase-space enhanced power corrections of order  $(\Lambda_{\text{QCD}}/m_b)^3$  [36, 37] as well as short-distance perturbative effects [38] in the calculation (see [39] for a recent discussion of the status of the corresponding calculations).

A formula analogous to (16.7) can be derived for differential distributions in specific inclusive decay processes, assuming that these distributions are integrated over a sufficiently large region of phase space to ensure quark-hadron duality. Important examples are the distributions in the lepton energy and the lepton invariant mass, as well as moments of the invariant hadronic mass distribution in the semileptonic processes  $\bar{B} \rightarrow X_u \ell \bar{\nu}$  and  $\bar{B} \rightarrow X_c \ell \bar{\nu}$ . A global fit of semileptonic decay distributions can be used to determine the CKM matrix elements  $|V_{ub}|$  and  $|V_{cb}|$  along with heavy-quark parameters such as the masses  $m_b$ ,  $m_c$  and the hadronic parameters  $\mu_\pi^2(B)$ ,  $\mu_G^2(B)$ . These determinations provide some of the most accurate values for these parameters (see e.g. [40–42]).

### 16.2.6 Shape functions and non-local power corrections

In certain regions of phase space, in which the hadronic final state in an inclusive heavy-hadron decay is made up of light energetic partons, the local OPE for inclusive decays must be replaced by a more complicated expansion involving hadronic matrix elements of non-local light-ray operators [43, 44]. Prominent examples are the radiative decay  $\bar{B} \rightarrow X_s \gamma$  for large photon energy  $E_\gamma$  near  $m_B/2$ , and the semileptonic decay  $\bar{B} \rightarrow X_u \ell \bar{\nu}$  at large lepton energy or small hadronic invariant mass. In these cases, the differential decay rates at leading order in the heavy-quark expansion can be written in the factorized form  $d\Gamma = H \otimes J \otimes S$  [45], where the hard function  $H$  and the jet function  $J$  are calculable in perturbation theory. The characteristic scales for these functions are set by  $m_b$  and  $(m_b \Lambda_{\text{QCD}})^{1/2}$ , respectively. The soft function

$$S(\omega) = \int \frac{dt}{4\pi} e^{-i\omega t} \langle \bar{B}(v) | \bar{h}_v(tn) Y_n(tn) Y_n^\dagger(0) h_v(0) | \bar{B}(v) \rangle \quad (16.8)$$

is a non-perturbative object called the shape function [43, 44]. Here  $Y_n$  are soft Wilson lines along a light-like direction  $n$  aligned with the momentum of the hadronic final-state jet. The jet function and the shape function share a common variable  $\omega \sim \Lambda_{\text{QCD}}$ , and the symbol  $\otimes$  denotes a convolution in this variable.

While the hard functions are different for the decays  $\bar{B} \rightarrow X_s \gamma$  and  $\bar{B} \rightarrow X_u \ell \bar{\nu}$ , the jet and soft functions are identical at leading order in  $\Lambda_{\text{QCD}}/m_Q$ . This is particularly important for the shape function, which introduces non-perturbative physics into the theoretical predictions for the decay rates in the regions of experimental interest. The fact that both processes depend on the same non-perturbative function makes it possible to use the measured shape of the  $\bar{B} \rightarrow X_s \gamma$  photon spectrum to reduce the theoretical uncertainties in the determination of the CKM element  $|V_{ub}|$  from semileptonic decays. In higher orders of the heavy-quark

expansion, an increasing number of subleading jet and soft functions are required to describe the decay distributions [46]. These have been analyzed in detail at order  $1/m_b$  [47–49]. In the case of  $\bar{B} \rightarrow X_s \gamma$  (and also in the related case of  $\bar{B} \rightarrow X_s \ell \bar{\ell}$ ), some of these non-local effects survive in the total decay rate and give rise to irreducible hadronic uncertainties [50]. The technology for deriving the corresponding factorization theorems relies on the soft-collinear effective theory, to which we now turn.

## 16.3 Soft-Collinear Effective Theory

As discussed in the previous section, soft gluons that bind a heavy quark inside a heavy meson cannot change the virtuality of that heavy quark by a significant amount. The ratio  $\Lambda_{\text{QCD}}/m_Q$  provides the expansion parameter in HQET, which is a small parameter since  $m_Q \gg \Lambda_{\text{QCD}}$ . This obviously does not work when considering light quarks. However, if the energy  $Q$  of the quarks is large, the ratio  $\Lambda_{\text{QCD}}/Q$  provides a small parameter, which can be used to construct an effective theory. One major difference to HQET is that light energetic quarks cannot only emit soft gluons, but they can also emit collinear gluons (an energetic gluon in the same direction as the original quark), without parametrically changing their virtuality. Thus, to fully reproduce the long-distance physics of energetic quarks requires that one includes their interactions with both soft and collinear particles. The resulting effective theory is therefore called soft-collinear effective theory (SCET) [51–53] (see [54] for a review).

A single energetic particle can always be boosted to a frame where all momentum components have similar size, in which case there is no small expansion parameter. Thus the presence of energetic particles must refer to a reference frame defined by external kinematics. SCET has a wide range of applications; some examples are the production of energetic, light states in the decay of a heavy particle in its rest frame, the production of energetic jets in collider environments, and the scattering of energetic particles off a target at rest. In this brief review we will outline the main features of this effective theory and mention a few selected applications.

### 16.3.1 General idea of the expansion

Consider a quark with virtuality much less than its energy  $Q$ , moving along the direction  $\vec{n}$ . It is convenient to parameterize the momentum  $p_n$  of this particle in terms of its light-cone components, defined by  $(p_n^-, p_n^+, p_n^\perp) = (\vec{n} \cdot p_n, n \cdot p_n, p_n^\perp)$ , where  $n^\mu = (1, \vec{n})$  and  $\bar{n}^\mu = (1, -\vec{n})$  are light-like vectors, and  $n \cdot p_n^\perp = \bar{n} \cdot p_n^\perp = 0$ . The subscript  $n$  on the momentum indicates the direction of the collinear particle. In terms of these light-cone components, the virtuality satisfies  $p_n^2 = p_n^+ p_n^- + p_n^{\perp 2}$ . The individual components of the momentum obey

$$(p_n^-, p_n^+, p_n^\perp) \sim Q(1, \lambda^2, \lambda), \quad (16.9)$$

where  $\lambda^2 = p^2/Q^2$  is the expansion parameter of SCET. The virtuality of such an energetic particle remains parametrically unchanged if it interacts with energetic particles in the same direction  $n$ , or with soft particles with momentum scaling as

$$(p_s^-, p_s^+, p_s^\perp) \sim Q(\lambda^2, \lambda^2, \lambda^2). \quad (16.10)$$

SCET is constructed in such a way as to reproduce the long-distance dynamics arising from the interactions of collinear and soft degrees of freedom.

In the above power counting the transverse momenta of soft degrees of freedom scale as  $p_s^\perp \sim Q\lambda^2$ , which is much smaller than the transverse momenta  $p_c^\perp \sim Q\lambda$  of collinear fields. This theory is usually called SCET<sub>I</sub>. If the external kinematics require that the transverse momenta of both soft and collinear fields are of the same size,  $p_c^\perp \sim p_s^\perp$ , then the appropriate degrees of freedom have the scaling  $p_c \sim Q(1, \lambda^2, \lambda)$  and  $p_s \sim Q(\lambda, \lambda, \lambda)$ . This theory is usually called SCET<sub>II</sub> and is required, e.g., for exclusive hadronic decays such as  $\bar{B} \rightarrow D\pi$ , where the virtuality of both collinear and soft degrees of freedom are set by  $\Lambda_{\text{QCD}}$ , or for the description of transverse-momentum distributions at colliders. SCET<sub>I</sub> power counting is assumed in the following sections, while SCET<sub>II</sub> is discussed in more detail in 16.3.6.

### 16.3.2 Leading-order Lagrangian

The derivation of the SCET Lagrangian follows similar steps as described for HQET in Section 16.2.1. One begins by deriving the Lagrangian for a theory containing only a single collinear sector. Similar to HQET, one separates the full QCD field into two components,  $q_n(x) = \psi_n(x) + \Xi_n(x)$ , where (with  $n \cdot \bar{n} = 2$ )

$$\psi_n(x) = \frac{\not{n}\not{\bar{n}}}{4} q_n(x), \quad \Xi_n(x) = \frac{\not{\bar{n}}\not{n}}{4} q_n(x). \quad (16.11)$$

The degrees of freedom described by the field  $\Xi_n$  are far off shell and can therefore be eliminated using its equation of motion. This gives

$$\mathcal{L}_n = \bar{\psi}_n(x) \left[ in \cdot D + i\mathcal{D}^\perp \frac{1}{i\bar{n} \cdot D} i\mathcal{D}^\perp \right] \frac{\not{n}}{2} \psi_n(x). \quad (16.12)$$

As a next step, one separates the large and residual momentum components by decomposing the collinear momentum into a “label” and a residual momentum,  $p^\mu = P^\mu + k^\mu$  with  $n \cdot P = 0$ . One then performs a phase redefinition on the collinear fields, such that  $\psi_n(x) = e^{iP \cdot x} \xi_n(x)$ . Derivatives acting on the fields  $\xi_n(x)$  now only pick out the residual momentum. Since unlike in HQET the label momentum in SCET is not conserved, one defines a label operator  $\mathcal{P}^\mu$  acting as  $\mathcal{P}^\mu \xi_n(x) = P^\mu \xi_n(x)$  [52], as well as a corresponding covariant label operator  $i\mathcal{D}_n^\mu = \mathcal{P}^\mu + gA_n^\mu(x)$ . Note that at leading order in power counting  $i\mathcal{D}_n^\mu$  does not contain the soft gluon field. This leads to the final SCET Lagrangian [52,53,55,56]

$$\mathcal{L}_n = \bar{\xi}_n(x) \left[ in \cdot D_n + gn \cdot A_s + i\mathcal{P}_n^\perp \frac{1}{i\bar{n} \cdot \mathcal{D}_n} i\mathcal{P}_n^\perp \right] \frac{\not{n}}{2} \xi_n(x) + \dots, \quad (16.13)$$

where we have split  $in \cdot D$  into a collinear piece  $in \cdot D_n = in \cdot \partial + gn \cdot A_n$  and a soft piece  $gn \cdot A_s$ . This latter term gives rise to the only interaction between a collinear quark and soft gluons at leading power in  $\lambda$ . The ellipses represent higher-order interactions between soft and collinear particles.

The Lagrangian describing collinear fields in different light-like directions is simply given by the sum of the Lagrangians for each direction  $n$ , i.e.  $\mathcal{L} = \sum_n \mathcal{L}_n$ . The soft gluons are the same in each individual Lagrangian. An alternative way to understand the separation between large and small momentum components is to derive the Lagrangian of SCET in position space [56]. In this case no label operators are required, and the dependence on short-distance effects is contained in non-localities at short distances. An important difference between SCET and HQET is that the SCET Lagrangian is not corrected by short distance fluctuations. The physical reason is that in the construction described above no high-momentum modes have been integrated out [56]. Such hard modes arise when different collinear sectors are coupled via some external current (e.g. in jet production at  $e^+e^-$  or hadron colliders), or when collinear particles are produced in the rest frame of a decaying heavy object (such as in  $B$  decays). Short-distance effects are then incorporated in the Wilson coefficients of the external source operators.

### 16.3.3 Collinear gauge invariance and Wilson lines

An important aspect of SCET is the implementation of local gauge invariance. Because the effective field operators describe modes with certain momentum scalings, the effective Lagrangian respects only residual gauge symmetries. One of them satisfies the collinear scaling

$$(\bar{n} \cdot \partial, n \cdot \partial, \partial^\perp) U_n(x) \sim Q(\lambda^2, \lambda) U_n(x), \quad (16.14)$$

and one the soft scaling

$$(\bar{n} \cdot \partial, n \cdot \partial, \partial^\perp) U_s(x) \sim Q(\lambda^2, \lambda^2, \lambda^2) U_s(x). \quad (16.15)$$

While the soft gauge transformation is common for all fields, collinear fields in different directions each transform under their own collinear gauge transformation, which means that each collinear sector, containing particles with large momenta along a certain direction, has to be separately gauge invariant under its

collinear gauge transformation. This requires the introduction of collinear Wilson lines [52]

$$W_n(x) = \text{P exp} \left[ -ig \int_{-\infty}^0 ds \bar{n} \cdot A_n(s\bar{n} + x) \right], \quad (16.16)$$

which transform under collinear gauge transformations according to  $W_n \rightarrow U_n W_n$ . Thus, the combination  $\chi_n \equiv W_n^\dagger \psi_n$  is gauge invariant. In a similar manner, one can define the gauge-invariant gluon field  $B_n^\mu = g^{-1} W_n^\dagger iD_n^\mu W_n$  [57, 58]. Collinear operators in SCET are typically constructed from such collinearly gauge-invariant building blocks.

### 16.3.4 Derivation of factorization theorems

One of the important applications of SCET is to understand how to factorize cross sections involving energetic particles moving in different directions into simpler pieces that can either be calculated perturbatively or determined from data. Factorization theorems have been around for much longer than SCET (see [59] for a review). However, the effective theory allows for a conceptually simpler understanding of certain classes of factorization theorems [57], since most simplifications happen already at the level of the Lagrangian. The discussion in this section is valid to leading order in the power counting of the effective theory.

As discussed in the previous section, the Lagrangian of SCET does not involve any couplings between collinear particles moving in different directions. Soft gluons couple to collinear quarks only through the term  $\xi_n gn \cdot A_s (\not{n}/2) \xi_n$  in the effective Lagrangian in (16.13). This coupling is similar to the coupling of soft gluons to heavy quarks in HQET, see Section 16.2.4. It can be removed by means of the field redefinition [53]

$$\psi_n(x) = Y_n(x) \psi_n^{(0)}(x), \quad A_n^a(x) = Y_n^{ab}(x) A_n^{b(0)}(x), \quad (16.17)$$

where  $Y_n$  and  $Y_n^{ab}$  live in the fundamental and adjoint representations of  $SU(3)$ , respectively. This fact greatly facilitates proofs of factorization theorems in SCET. A QCD operator  $O(x)$  describing the interactions of collinear partons moving in different directions can thus be written as (omitting color indices for simplicity)

$$\langle O(x) \rangle = C_O(\mu) \langle [C_{n_a}^{(0)} C_{n_b}^{(0)} C_{n_1}^{(0)} \dots C_{n_N}^{(0)}](x) [\mathcal{Y}_{n_a} \mathcal{Y}_{n_b} \mathcal{Y}_{n_1} \dots \mathcal{Y}_{n_N}](x) \rangle_\mu. \quad (16.18)$$

Here  $C_{n_i}^{(0)}(x)$  denotes a gauge-invariant combination of collinear fields (either quark or gluon fields) in the direction  $n_i$ . The hard matching coefficient  $C_O$  accounts for short-distance effects at the scale  $Q$ . The soft Wilson lines can either be in a color triplet or color octet representation, and are collectively denoted by  $\mathcal{Y}_{n_i}$ . Both the matrix elements and the coefficient  $C_O$  depend on the renormalization scale  $\mu$ .

Having defined the operator mediating a given process, one can calculate the cross section by squaring the operator, taking the forward matrix element and integrating over the phase space of all final-state particles. The absence of interactions between collinear degrees of freedom moving along different directions or soft degrees of freedom implies that the forward matrix element can be factorized as

$$\begin{aligned} \langle \text{in} | O(x) O^\dagger(0) | \text{in} \rangle &= |C_O(\mu)|^2 \langle \text{in}_a | C_{n_a}(x) C_{n_a}^\dagger(0) | \text{in}_a \rangle_\mu \\ &\times \langle \text{in}_b | C_{n_b}(x) C_{n_b}^\dagger(0) | \text{in}_b \rangle_\mu \\ &\times \langle 0 | C_{n_1}(x) C_{n_1}^\dagger(0) | 0 \rangle_\mu \dots \langle 0 | C_{n_N}(x) C_{n_N}^\dagger(0) | 0 \rangle_\mu \\ &\times \langle 0 | [\mathcal{Y}_{n_a} \dots \mathcal{Y}_{n_N}](x) [\mathcal{Y}_{n_a} \dots \mathcal{Y}_{n_N}]^\dagger(0) | 0 \rangle_\mu. \end{aligned} \quad (16.19)$$

Thus, the matrix element can be written as a product of simpler structures, each of which can be evaluated separately.

The vacuum matrix elements of the outgoing collinear fields are determined by jet functions  $J_i(\mu)$ . As long as the relevant scale (for example the jet mass) is sufficiently large, these functions can

be calculated perturbatively. The matrix elements of the incoming collinear fields are non-perturbative objects  $B_{p/N}(\mu)$  called beam functions for parton  $p$  in nucleon  $N$  [60]. For many applications they can be related perturbatively to the well-known parton distribution functions. Finally, the vacuum matrix element of the soft Wilson lines defines a so-called soft function  $S_{ab\dots N}(\mu)$ . The shared dependence on  $x$  in the above equation implies that in momentum space the various components of the factorization theorem are convoluted with one another. Deriving this convolution requires a careful treatment of the phase-space integration and the factorization of the measurement defining the cross section of interest, in particular treating the large and residual components of each momentum appropriately.

Putting all information together, the differential cross section for a proton-proton collision with  $N$  jet-like objects can schematically be written as

$$d\sigma \sim \sum_{ab} H_{ab}(\mu) [B_{a/P}(\mu) B_{b/P}(\mu)] \otimes [J_1(\mu) \dots J_N(\mu)] \otimes S_{ab\dots N}(\mu). \quad (16.20)$$

The hard function is equal to the square of the matching coefficient,  $H_{ab}(\mu) = |C_O(\mu)|^2$ , and the beam, jet, and soft functions and their convolution structure depend on the specific  $N$ -jet measurement. It should be mentioned that the most difficult part of traditional factorization proofs involves showing that so-called Glauber gluons do not spoil the above factorization theorem [61]. Significant progress toward the description of Glauber effects within SCET has been made in [62], where a closed form for the effective Lagrangian describing these interactions was derived. In this context, a proof of factorization requires demonstrating that this Lagrangian has no impact on a particular cross section, and such proofs have not yet been fully derived within SCET.

### 16.3.5 Resummation of large logarithms

SCET can be used to sum the large logarithms arising in perturbative calculations to all orders in the strong coupling constant  $\alpha_s$ . In general, perturbation theory will generate a logarithmic dependence on any ratio of scales  $r$  in a problem. For processes that involve initial or final states with energy much in excess of their mass, there are two powers of logarithms for every power of  $\alpha_s$ . These are referred to as Sudakov logarithms. For widely separated scales these large logarithms can spoil the convergence of fixed-order perturbation theory. One thus needs to reorganize the expansion in such a way that  $\alpha_s L = \mathcal{O}(1)$  is kept fixed, with  $L = \ln r$ . More precisely, a proper resummation requires summing logarithms of the form  $\alpha_s^n L^m$  with  $m \leq (n+1)$  in the logarithm of a cross section, by writing  $\ln \sigma \sim L g_0(\alpha_s L) + g_1(\alpha_s L) + \alpha_s g_2(\alpha_s L) + \dots$ , with functions  $g_n(x)$  that need to be determined.

The important ingredient in achieving this resummation is the fact that SCET factorizes a given cross section into simpler pieces, each of which depends on a single physical scale. The only dependence on that scale can arise through logarithms of its ratio with the renormalization scale  $\mu$ . Thus, for each of the components in the factorization theorem one can choose a renormalization scale  $\mu$  for which the large logarithmic terms are absent. Of course, the factorization formula requires a common renormalization scale  $\mu$  in all its components, and one therefore has to use the renormalization group (RG) to evolve the various component functions from their preferred scale to the common scale  $\mu$ . A novel feature of RG equations in SCET, as opposed to other EFTs, is that the anomalous dimensions entering the evolution equations of the hard, beam, jet and soft functions in a factorization formula such as (16.20) contain a single power of the logarithm of the relevant energy scale. For example, the anomalous dimension  $\gamma_H$  of the hard function has the form

$$\gamma_H(\mu) = c_H \Gamma_{\text{cusp}}(\alpha_s) \ln \frac{Q^2}{\mu^2} + \gamma(\alpha_s), \quad (16.21)$$

where  $c_H$  is a process-dependent coefficient and  $\Gamma_{\text{cusp}}$  denotes the

so-called cusp anomalous dimension [20, 63]. Collinear and soft functions have similar anomalous dimensions, which also involve a cusp and a non-cusp part. The non-cusp part  $\gamma$  of the anomalous dimensions is process (and observable) dependent. The presence of a logarithm in the anomalous dimension is characteristic of Sudakov problems and arises since the perturbative series contains double logarithms of scale ratios.

Solving the RG equations one can systematically resum all large logarithms of scale ratios in the factorized cross section and express the functions  $g_n(\alpha_s L)$  introduced above in terms of ratios of running coupling constants. In order to compute the first two terms  $L g_0(\alpha_s L) + g_1(\alpha_s L)$  in  $\ln \sigma$ , corresponding to the next-to-leading logarithmic (NLL) approximation, one needs two-loop expressions for the cusp anomalous dimension and  $\beta$  function, one-loop expressions for the non-cusp pieces in the anomalous dimensions, and tree-level matching conditions for all component functions at their characteristic scales. To calculate the next term  $\alpha_s g_2(\alpha_s L)$  in the expansion, corresponding to NNLL order, one needs to go one order higher in the loop expansion, and so on.

### 16.3.6 Factorization and resummation in SCET<sub>II</sub>

The effective theory SCET<sub>II</sub> contains collinear and soft particles with momenta scaling as  $(p_n^-, p_n^+, p_n^\perp) \sim Q(1, \lambda^2, \lambda)$  and  $(p_s^-, p_s^+, p_s^\perp) \sim Q(\lambda, \lambda, \lambda)$ . They have the same small virtuality ( $p_n^2 \sim p_s^2 \sim Q^2 \lambda^2$ ) but differ in their rapidities. An important class of observables, for which this scaling is relevant, contains cross sections for processes in which the transverse momenta of particles are constrained by external kinematics. The prime example are the transverse-momentum distributions of electroweak gauge bosons or Higgs bosons produced at hadron colliders. The parton transverse momenta are constrained by the fact that their vector sum must be equal and opposite to the transverse momentum  $q_T$  of the boson. Standard RG evolution in the effective theory controls the logarithms arising from the fact that the virtualities of the collinear and soft modes are much smaller than the hard scale  $Q$  in the process (the boson mass). However, additional large logarithms arise since the rapidities of collinear and soft modes are parametrically different, such that  $e^{|\ln \lambda - \ln \lambda|} \sim 1/\lambda$ . These logarithms can be traced to a new source of divergences and an unusual failure of dimensional regularization. They need to be factorized in the cross section and resummed by other means.

Two equivalent approaches exist for how to deal with the additional rapidity logarithms in SCET. In the approach of [64], they are interpreted as a consequence of a ‘‘collinear anomaly’’ of the effective theory SCET<sub>II</sub>, resulting from the fact that a classical rescaling symmetry of the effective Lagrangian is broken by quantum effects. The extra large logarithms can be resummed by means of simple differential equations, which typically state that to all orders in perturbation theory (and in an appropriate space) the logarithm of the cross section contains only a single extra logarithm of  $\lambda \sim q_T/Q$  not contained in the hard function. Another approach to resum the rapidity logarithms uses the ‘‘rapidity renormalization group’’ [65], in which the relevant differential equations are obtained by considering a new type of scale variation in a parameter  $\nu$ , which separates the phase space for collinear and soft particles along a hyperbola in the  $(p_-, p_+)$  plane. In contrast to the standard RG, there is no running coupling involved in the  $\nu$  evolution, since the different contributions live at the same virtuality.

SCET<sub>II</sub> also plays an important role in the study of factorization for a variety of exclusive  $B$  meson decays, such as  $\bar{B} \rightarrow \pi \ell \bar{\nu}$ ,  $\bar{B} \rightarrow K^* \gamma$  and  $\bar{B} \rightarrow \pi \pi$ , for which the virtualities of energetic (collinear) final-state particles are of order  $\Lambda_{\text{QCD}}$ , which is also the scale for the soft light degrees of freedom contained in the initial-state  $B$  meson.

### 16.3.7 Applications

Most of the applications of SCET are either in flavor physics, where the decay of a heavy  $B$  meson can give rise to energetic light partons, or in collider physics, where the presence of jets naturally leads to collimated sets of energetic particles. For some of these applications alternative approaches existed before the invention of SCET, but the effective theory has opened up alternative ways to understand the physics of these processes. For



many examples, however, SCET has allowed new insights and new applications. The investigation of heavy-to-light form factors has been instrumental for understanding factorization in exclusive semileptonic  $B$  decays [66]. SCET has also provided a field-theoretic basis for the QCD factorization approach to exclusive, non-leptonic decays of  $B$  mesons [67]. Using SCET methods, proofs of factorization were derived for the color-allowed decay  $\bar{B}^0 \rightarrow D^+\pi^-$  [68], the color-suppressed decay  $\bar{B}^0 \rightarrow D^0\pi^0$  [69], and the radiative decay  $\bar{B} \rightarrow K^*\gamma$  [70]. Further examples are factorization theorems and the resummation of endpoint logarithms for quarkonia production [71], the resummation of large logarithmic terms for the thrust [72] and jet broadening [73] distributions in  $e^+e^-$  annihilation beyond NLL order, the development of new factorizable observables to veto extra jets [60, 74], all-orders factorization theorems for processes containing electroweak Sudakov logarithms [75], and the resummation of threshold (soft gluon) logarithms in momentum space for several important processes at hadron colliders [76–78]. There has also been a lot of activity describing  $p_T$ -based resummation at hadron colliders. Prominent examples are the transverse-momentum distributions of electroweak bosons [64, 65, 79]. Finally, SCET has given new insights into the jet substructure methods (see [80] for a recent review). We now describe a few of these applications in more detail.

Event-shape distributions, in particular the thrust distribution, have been measured to high accuracy at LEP [81]. They can be used for a determination of the strong coupling constant  $\alpha_s$ . SCET has increased the theoretical accuracy in the calculations of the thrust and  $C$ -parameter distributions significantly. First, it has allowed to increase the perturbative accuracy of the thrust spectrum. The resummation of logarithms of  $\tau$ , which become important for  $\tau \ll 1$ , has been performed to  $N^3\text{LL}$  [72], two orders beyond what was previously available. Combining this resummation with the known two-loop spectrum [82, 83] gives precise perturbative predictions both at small and large values of  $\tau$ . Second, the factorization of the cross section in SCET has made it possible to include non-perturbative physics through a shape function, in analogy with the  $B$ -physics case discussed in Section 16.2.6. Comparing the theoretical predictions to the measured thrust and  $C$ -parameter distributions yields a precise value of the strong coupling constant  $\alpha_s(m_Z)$ , which however is lower than the average value cited in Section 9 by several standard deviations [84, 85]. For more discussions on this, see Section 9.

The Higgs-boson production cross section in gluon fusion at the LHC, defined with a jet veto stating that no jet in the final state has transverse momentum above a threshold  $p_T^{\text{veto}}$ , can be factorized in the form [86, 87] (see [88] for a corresponding calculation outside the SCET framework)

$$\begin{aligned} \sigma(p_T^{\text{veto}}) = & H(m_H, \mu) \left(\frac{\nu_B}{\nu_S}\right)^{-2F_{gg}(R, p_T^{\text{veto}}, \mu)} S_{gg}(R, p_T^{\text{veto}}, \mu, \frac{\nu_S}{p_T^{\text{veto}}}) \\ & \times \int_{\tau}^1 \frac{dz}{z} B_{g/P}\left(z, R, p_T^{\text{veto}}, \mu, \frac{\nu_B}{m_H}\right) B_{g/P}\left(\frac{\tau}{z}, R, p_T^{\text{veto}}, \mu, \frac{\nu_B}{m_H}\right), \end{aligned} \quad (16.22)$$

where  $\tau = m_H^2/s$ , and  $\mu \sim p_T^{\text{veto}}$  is a common factorization scale. The beam functions  $B_{g/P}$ , the soft function  $S_{gg}$  and the exponent  $F_{gg}$  all depend on the jet radius  $R$  as well as the jet clustering algorithm. The scale dependence of the hard function  $H$  is controlled by standard RG evolution in SCET. The beam functions can be factorized further into calculable collinear kernels convoluted with parton distribution functions. In addition to the renormalization scale  $\mu$ , the beam and soft functions depend on two rapidity scales  $\nu_B \sim m_H$  and  $\nu_S \sim p_T^{\text{veto}}$ , respectively. In [86] the default values  $\nu_B = m_H$  and  $\nu_S = p_T^{\text{veto}}$  are used for these scales, and the soft function  $S_{gg}$  is absorbed into the beam functions. In [87] the exponent  $F_{gg}$  is called  $-\gamma_g^g/2$ . The second factor on the right-hand side of the factorization formula (16.22), which resums large rapidity logarithms, implies that the logarithm of the jet-veto cross section contains a single large logarithm  $\ln \sigma = -2F_{gg}(R, p_T^{\text{veto}}, \mu) \ln(m_H/p_T^{\text{veto}}) + \dots$  not contained in the hard function. Its coefficient can be calculated in fixed-order per-

turbation theory.

Obtaining more precise fixed-order calculations has been an important goal for many years. A major difficulty in these calculations is the proper handling of the infrared singularities that arise in both virtual and real contributions. A method based on  $N$ -jettiness ( $\mathcal{T}_N$ ) slicing [89, 90] allows one to obtain the NNLO result from a much easier NLO calculation, combined with information about the singular dependence of the cross section on the  $\mathcal{T}_N$  resolution variable [74]. This has been used to compute various processes with final states containing up to one hard, colored particle [91–95]. While the NLO calculations can be performed using well established techniques, the singular dependence on  $\mathcal{T}_N$  can be calculated using SCET at NNLO. Calculations of the leading power corrections in  $\mathcal{T}_0/Q$  [96, 97] have helped to improve the numerical stability for several processes. The  $N$ -jettiness ( $\mathcal{T}_N$ ) slicing method has been used prior to the fixed-order application in the combination of higher order resummation with parton showers [98, 99].

More generally, there is currently a strong effort to push the applications of SCET toward factorization and resummation at subleading power in the expansion in  $\lambda$ . The subleading SCET Lagrangian [56, 100] and current operators arising in  $B$ -meson decays and their anomalous dimensions [55, 56, 101–103] have been studied a long time ago. More recently, the focus has shifted to subleading operators arising in important collider processes, such as Drell-Yan or Higgs production. The general set of operators for such processes have been identified [104–106], and several of their anomalous dimensions have been calculated [106, 107]. First resummed results at subleading power have been presented for event shapes [108] and the Drell-Yan process [109].

## 16.4 Open issues and perspectives

HQET has successfully passed many experimental tests, and there are not many open questions that still need to be addressed. One concept that has not been derived from first principles is the notion of quark-hadron duality, which underlies the application of HQET to the description of inclusive decays of  $B$  mesons. The validity of global duality (at energies even lower than those relevant in  $B$  decays) has been tested experimentally using high-precision data on semileptonic  $B$  decays and on hadronic  $\tau$  decays. However, assigning a theoretical uncertainty due to possible duality violations remains a difficult task. Another known issue is that the measured values of the CKM element  $|V_{ub}|$  extracted from exclusive or inclusive decays of  $B$  mesons differ from each other by several standard deviations (see Section 75). This measurement relies on the heavy-quark limit, and the uncertainty quoted includes a theoretical estimate of the effect of power corrections arising from the finite  $b$ -quark mass. It remains an open question whether the discrepancy is due to underestimated theoretical or experimental uncertainties, or whether it may hint to the existence of new physics.

SCET, on the other hand, is still an active field of research, and new results are being obtained regularly. An important example concerns the understanding of non-global logarithms arising in hadron-collider processes with jets [110, 111]. For a long time a fully factorized form of non-global jet cross sections has not been available, despite significant progress towards this goal [112, 113]. A consistent factorization formula for non-global jet observables was developed in [114, 115]. It requires the introduction of a collinear-soft mode in the SCET Lagrangian. The first application of this formalism was to the light jet mass distribution [116], and significant steps toward an extension to NLL accuracy have been taken in [117]. It is believed that the results obtained from the factorization theorem derived in [114, 115] are equivalent to those obtained using the approaches proposed in [112, 113]. The various methods differ in the way in which they organize the all-order expansion for the appearing complicated multi-Wilson-line structures.

Another active field concerns the study of Glauber gluons in SCET [118] and their relation to the BFKL equation familiar from small- $x$  physics [119]. A systematic account of the effects of Glauber gluons in the context of the SCET Lagrangian has been developed in [62]. The formalism has been extended to Glauber quarks in [120]. These developments set the basis for

a solid understanding of the impact of Glauber exchanges on factorization theorems. Glauber gluons also play an important role in SCET-based analysis of jet propagation in dense QCD media [121, 122], which gives rise to the jet-quenching phenomenon in heavy-ion collisions. An important open question facing some applications of SCET concerns factorized expressions containing endpoint-divergent convolution integrals.

We close this short review by mentioning a particularly nice application combining the methods of heavy-particle EFTs such as HQET and non-relativistic QCD with SCET in the context of describing the interactions of heavy dark matter (with mass  $M \gg v$ ) with SM particles. In [123] it was realized that the interactions of heavy, weakly interacting massive particles (WIMPs) with nuclear targets can be described in a model-independent way using heavy-particle EFTs. The WIMPs are charged under  $SU(2)_L$  and can interact with electroweak gauge bosons and the Higgs boson. The WIMP EFT was later extended by describing the produced, highly energetic electroweak gauge bosons in terms of soft or collinear fields in SCET [124–126]. This allows one to systematically separate all relevant mass scales, resum electroweak Sudakov logarithms and disentangle the so-called Sommerfeld enhancement from the short-distance hard annihilation process.

### References

- [1] E. Witten, Nucl. Phys. **B122**, 109 (1977).
- [2] S. Weinberg, Phys. Lett. **91B**, 51 (1980).
- [3] L. J. Hall, Nucl. Phys. **B178**, 75 (1981).
- [4] E. Eichten and B. R. Hill, Phys. Lett. **B234**, 511 (1990).
- [5] H. Georgi, Phys. Lett. **B240**, 447 (1990).
- [6] B. Grinstein, Nucl. Phys. **B339**, 253 (1990).
- [7] T. Mannel, W. Roberts and Z. Ryzak, Nucl. Phys. **B368**, 204 (1992).
- [8] M. Neubert, Phys. Rept. **245**, 259 (1994), [hep-ph/9306320].
- [9] A. V. Manohar and M. B. Wise, Camb. Monogr. Part. Phys. Nucl. Phys. Cosmol. **10**, 1 (2000).
- [10] M. E. Luke and A. V. Manohar, Phys. Lett. **B286**, 348 (1992), [hep-ph/9205228].
- [11] E. V. Shuryak, Phys. Lett. **93B**, 134 (1980).
- [12] N. Isgur and M. B. Wise, Phys. Lett. **B232**, 113 (1989).
- [13] N. Isgur and M. B. Wise, Phys. Rev. Lett. **66**, 1130 (1991).
- [14] S. Nussinov and W. Wetzel, Phys. Rev. **D36**, 130 (1987).
- [15] M. A. Shifman and M. B. Voloshin, Sov. J. Nucl. Phys. **45**, 292 (1987), [Yad. Fiz.45,463(1987)].
- [16] M. Neubert, Phys. Lett. **B264**, 455 (1991).
- [17] M. E. Luke, Phys. Lett. **B252**, 447 (1990).
- [18] I. I. Y. Bigi *et al.*, Phys. Rev. **D52**, 196 (1995), [hep-ph/9405410].
- [19] N. Uraltsev, Phys. Lett. **B501**, 86 (2001), [195(2000)], [hep-ph/0011124].
- [20] G. P. Korchemsky and A. V. Radyushkin, Nucl. Phys. **B283**, 342 (1987).
- [21] A. F. Falk *et al.*, Nucl. Phys. **B343**, 1 (1990).
- [22] J. Chay, H. Georgi and B. Grinstein, Phys. Lett. **B247**, 399 (1990).
- [23] I. I. Y. Bigi, N. G. Uraltsev and A. I. Vainshtein, Phys. Lett. **B293**, 430 (1992), [Erratum: Phys. Lett. B297,477(1992)], [hep-ph/9207214].
- [24] A. V. Manohar and M. B. Wise, Phys. Rev. **D49**, 1310 (1994), [hep-ph/9308246].
- [25] T. Mannel, Nucl. Phys. **B413**, 396 (1994), [hep-ph/9308262].
- [26] A. F. Falk, M. E. Luke and M. J. Savage, Phys. Rev. **D49**, 3367 (1994), [hep-ph/9308288].
- [27] E. C. Poggio, H. R. Quinn and S. Weinberg, Phys. Rev. **D13**, 1958 (1976).
- [28] G. Buchalla, A. J. Buras and M. E. Lautenbacher, Rev. Mod. Phys. **68**, 1125 (1996), [hep-ph/9512380].
- [29] A. F. Falk and M. Neubert, Phys. Rev. **D47**, 2965 (1993), [hep-ph/9209268].
- [30] T. Becher, H. Boos and E. Lunghi, JHEP **12**, 062 (2007), [arXiv:0708.0855].
- [31] A. Alberti, P. Gambino and S. Nandi, JHEP **01**, 147 (2014), [arXiv:1311.7381].
- [32] T. Mannel, A. A. Pivovarov and D. Rosenthal, Phys. Lett. **B741**, 290 (2015), [arXiv:1405.5072].
- [33] T. Mannel, A. A. Pivovarov and D. Rosenthal, Phys. Rev. **D92**, 5, 054025 (2015), [arXiv:1506.08167].
- [34] T. Mannel and A. A. Pivovarov, Phys. Rev. **D100**, 9, 093001 (2019), [arXiv:1907.09187].
- [35] T. Mannel, S. Turczyk and N. Uraltsev, JHEP **11**, 109 (2010), [arXiv:1009.4622].
- [36] M. Neubert and C. T. Sachrajda, Nucl. Phys. **B483**, 339 (1997), [hep-ph/9603202].
- [37] M. Beneke, G. Buchalla and I. Dumietz, Phys. Rev. **D54**, 4419 (1996), [Erratum: Phys. Rev. D83,119902(2011)], [hep-ph/9605259].
- [38] M. Beneke *et al.*, Phys. Lett. **B459**, 631 (1999), [hep-ph/9808385].
- [39] M. Kirk, A. Lenz and T. Rauh, JHEP **12**, 068 (2017), [arXiv:1711.02100].
- [40] P. Gambino and C. Schwanda, Phys. Rev. **D89**, 1, 014022 (2014), [arXiv:1307.4551].
- [41] Y. Amhis *et al.* (HFLAV), Eur. Phys. J. **C77**, 12, 895 (2017), [arXiv:1612.07233].
- [42] P. Gambino, M. Jung and S. Schacht, Phys. Lett. **B795**, 386 (2019), [arXiv:1905.08209].
- [43] M. Neubert, Phys. Rev. **D49**, 3392 (1994), [hep-ph/9311325].
- [44] I. I. Y. Bigi *et al.*, Int. J. Mod. Phys. **A9**, 2467 (1994), [hep-ph/9312359].
- [45] G. P. Korchemsky and G. F. Sterman, Phys. Lett. **B340**, 96 (1994), [hep-ph/9407344].
- [46] C. W. Bauer, M. E. Luke and T. Mannel, Phys. Rev. **D68**, 094001 (2003), [hep-ph/0102089].
- [47] K. S. M. Lee and I. W. Stewart, Nucl. Phys. **B721**, 325 (2005), [hep-ph/0409045].
- [48] S. W. Bosch, M. Neubert and G. Paz, JHEP **11**, 073 (2004), [hep-ph/0409115].
- [49] M. Beneke *et al.*, JHEP **06**, 071 (2005), [hep-ph/0411395].
- [50] M. Benzke *et al.*, JHEP **08**, 099 (2010), [arXiv:1003.5012].
- [51] C. W. Bauer, S. Fleming and M. E. Luke, Phys. Rev. **D63**, 014006 (2000), [hep-ph/0005275].
- [52] C. W. Bauer and I. W. Stewart, Phys. Lett. **B516**, 134 (2001), [hep-ph/0107001].
- [53] C. W. Bauer, D. Pirjol and I. W. Stewart, Phys. Rev. **D65**, 054022 (2002), [hep-ph/0109045].
- [54] T. Becher, A. Broggio and A. Ferroglia, Lect. Notes Phys. **896**, pp.1 (2015), [arXiv:1410.1892].
- [55] J. Chay and C. Kim, Phys. Rev. **D65**, 114016 (2002), [hep-ph/0201197].
- [56] M. Beneke *et al.*, Nucl. Phys. **B643**, 431 (2002), [hep-ph/0206152].
- [57] C. W. Bauer *et al.*, Phys. Rev. **D66**, 014017 (2002), [hep-ph/0202088].
- [58] R. J. Hill and M. Neubert, Nucl. Phys. **B657**, 229 (2003), [hep-ph/0211018].
- [59] J. C. Collins, D. E. Soper and G. F. Sterman, Adv. Ser. Direct. High Energy Phys. **5**, 1 (1989), [hep-ph/0409313].

- [60] I. W. Stewart, F. J. Tackmann and W. J. Waalewijn, *Phys. Rev.* **D81**, 094035 (2010), [arXiv:0910.0467].
- [61] J. C. Collins, D. E. Soper and G. F. Sterman, *Nucl. Phys.* **B261**, 104 (1985).
- [62] I. Z. Rothstein and I. W. Stewart, *JHEP* **08**, 025 (2016), [arXiv:1601.04695].
- [63] I. A. Korchemskaya and G. P. Korchemsky, *Phys. Lett.* **B287**, 169 (1992).
- [64] T. Becher and M. Neubert, *Eur. Phys. J.* **C71**, 1665 (2011), [arXiv:1007.4005].
- [65] J.-Y. Chiu *et al.*, *JHEP* **05**, 084 (2012), [arXiv:1202.0814].
- [66] M. Beneke and T. Feldmann, *Nucl. Phys.* **B685**, 249 (2004), [hep-ph/0311335].
- [67] M. Beneke *et al.*, *Phys. Rev. Lett.* **83**, 1914 (1999), [hep-ph/9905312].
- [68] C. W. Bauer, D. Pirjol and I. W. Stewart, *Phys. Rev. Lett.* **87**, 201806 (2001), [hep-ph/0107002].
- [69] S. Mantry, D. Pirjol and I. W. Stewart, *Phys. Rev.* **D68**, 114009 (2003), [hep-ph/0306254].
- [70] T. Becher, R. J. Hill and M. Neubert, *Phys. Rev.* **D72**, 094017 (2005), [hep-ph/0503263].
- [71] S. Fleming, A. K. Leibovich and T. Mehen, *Phys. Rev.* **D68**, 094011 (2003), [hep-ph/0306139].
- [72] T. Becher and M. D. Schwartz, *JHEP* **07**, 034 (2008), [arXiv:0803.0342].
- [73] T. Becher and G. Bell, *JHEP* **11**, 126 (2012), [arXiv:1210.0580].
- [74] I. W. Stewart, F. J. Tackmann and W. J. Waalewijn, *Phys. Rev. Lett.* **105**, 092002 (2010), [arXiv:1004.2489].
- [75] J.-y. Chiu, R. Kelley and A. V. Manohar, *Phys. Rev.* **D78**, 073006 (2008), [arXiv:0806.1240].
- [76] T. Becher, M. Neubert and G. Xu, *JHEP* **07**, 030 (2008), [arXiv:0710.0680].
- [77] V. Ahrens *et al.*, *Eur. Phys. J.* **C62**, 333 (2009), [arXiv:0809.4283].
- [78] X. Liu, S. Mantry and F. Petriello, *Phys. Rev.* **D86**, 074004 (2012), [arXiv:1205.4465].
- [79] M. G. Echevarria, A. Idilbi and I. Scimemi, *JHEP* **07**, 002 (2012), [arXiv:1111.4996].
- [80] A. J. Larkoski, I. Moulton and B. Nachman (2017), [arXiv:1709.04464].
- [81] S. Kluth, *Rept. Prog. Phys.* **69**, 1771 (2006), [hep-ex/0603011].
- [82] A. Gehrmann-De Ridder *et al.*, *Phys. Rev. Lett.* **99**, 132002 (2007), [arXiv:0707.1285].
- [83] S. Weinzierl, *Phys. Rev. Lett.* **101**, 162001 (2008), [arXiv:0807.3241].
- [84] R. Abbate *et al.*, *Phys. Rev.* **D83**, 074021 (2011), [arXiv:1006.3080].
- [85] A. H. Hoang *et al.*, *Phys. Rev.* **D91**, 9, 094018 (2015), [arXiv:1501.04111].
- [86] T. Becher and M. Neubert, *JHEP* **07**, 108 (2012), [arXiv:1205.3806].
- [87] I. W. Stewart *et al.*, *Phys. Rev.* **D89**, 5, 054001 (2014), [arXiv:1307.1808].
- [88] A. Banfi *et al.*, *Phys. Rev. Lett.* **109**, 202001 (2012), [arXiv:1206.4998].
- [89] R. Boughezal, X. Liu and F. Petriello, *Phys. Rev.* **D91**, 9, 094035 (2015), [arXiv:1504.02540].
- [90] J. Gaunt *et al.*, *JHEP* **09**, 058 (2015), [arXiv:1505.04794].
- [91] R. Boughezal *et al.*, *Phys. Lett.* **B748**, 5 (2015), [arXiv:1505.03893].
- [92] R. Boughezal *et al.*, *Phys. Rev. Lett.* **116**, 15, 152001 (2016), [arXiv:1512.01291].
- [93] J. M. Campbell, R. K. Ellis and C. Williams, *JHEP* **06**, 179 (2016), [arXiv:1601.00658].
- [94] J. M. Campbell *et al.*, *JHEP* **07**, 148 (2016), [arXiv:1603.02663].
- [95] G. Heinrich *et al.*, *JHEP* **03**, 142 (2018), [arXiv:1710.06294].
- [96] I. Moulton *et al.*, *Phys. Rev.* **D95**, 7, 074023 (2017), [arXiv:1612.00450].
- [97] R. Boughezal, X. Liu and F. Petriello, *JHEP* **03**, 160 (2017), [arXiv:1612.02911].
- [98] S. Alioli *et al.*, *JHEP* **09**, 120 (2013), [arXiv:1211.7049].
- [99] S. Alioli *et al.*, *Phys. Rev.* **D92**, 9, 094020 (2015), [arXiv:1508.01475].
- [100] C. W. Bauer, D. Pirjol and I. W. Stewart, *Phys. Rev.* **D68**, 034021 (2003), [hep-ph/0303156].
- [101] D. Pirjol and I. W. Stewart, *Phys. Rev.* **D67**, 094005 (2003), [Erratum: *Phys. Rev.* **D69**, 019903 (2004)], [hep-ph/0211251].
- [102] R. J. Hill *et al.*, *JHEP* **07**, 081 (2004), [hep-ph/0404217].
- [103] M. Beneke and D. Yang, *Nucl. Phys.* **B736**, 34 (2006), [hep-ph/0508250].
- [104] I. Moulton, I. W. Stewart and G. Vita, *JHEP* **07**, 067 (2017), [arXiv:1703.03408].
- [105] I. Feige *et al.*, *JHEP* **11**, 142 (2017), [arXiv:1703.03411].
- [106] M. Beneke *et al.*, *JHEP* **03**, 001 (2018), [arXiv:1712.04416].
- [107] S. Alte, M. König and M. Neubert, *JHEP* **08**, 095 (2018), [arXiv:1806.01278].
- [108] I. Moulton *et al.*, *JHEP* **08**, 013 (2018), [arXiv:1804.04665].
- [109] M. Beneke *et al.*, *JHEP* **03**, 043 (2019), [arXiv:1809.10631].
- [110] M. Dasgupta and G. P. Salam, *Phys. Lett.* **B512**, 323 (2001), [hep-ph/0104277].
- [111] R. B. Appleby and M. H. Seymour, *JHEP* **12**, 063 (2002), [hep-ph/0211426].
- [112] S. Caron-Huot, *JHEP* **03**, 036 (2018), [arXiv:1501.03754].
- [113] A. J. Larkoski, I. Moulton and D. Neill, *JHEP* **09**, 143 (2015), [arXiv:1501.04596].
- [114] T. Becher *et al.*, *Phys. Rev. Lett.* **116**, 19, 192001 (2016), [arXiv:1508.06645].
- [115] T. Becher *et al.*, *JHEP* **11**, 019 (2016), [Erratum: *JHEP* **05**, 154 (2017)], [arXiv:1605.02737].
- [116] T. Becher, B. D. Pecjak and D. Y. Shao, *JHEP* **12**, 018 (2016), [arXiv:1610.01608].
- [117] M. Balsiger, T. Becher and D. Y. Shao, *JHEP* **04**, 020 (2019), [arXiv:1901.09038].
- [118] C. W. Bauer, B. O. Lange and G. Ovanesyan, *JHEP* **07**, 077 (2011), [arXiv:1010.1027].
- [119] S. Fleming, *Phys. Lett.* **B735**, 266 (2014), [arXiv:1404.5672].
- [120] I. Moulton *et al.*, *JHEP* **02**, 134 (2018), [arXiv:1709.09174].
- [121] A. Idilbi and A. Majumder, *Phys. Rev.* **D80**, 054022 (2009), [arXiv:0808.1087].
- [122] G. Ovanesyan and I. Vitev, *JHEP* **06**, 080 (2011), [arXiv:1103.1074].
- [123] R. J. Hill and M. P. Solon, *Phys. Lett.* **B707**, 539 (2012), [arXiv:1111.0016].
- [124] M. Bauer *et al.*, *JHEP* **01**, 099 (2015), [arXiv:1409.7392].
- [125] M. Baumgart, I. Z. Rothstein and V. Vaidya, *Phys. Rev. Lett.* **114**, 211301 (2015), [arXiv:1409.4415].
- [126] G. Ovanesyan, T. R. Slatyer and I. W. Stewart, *Phys. Rev. Lett.* **114**, 21, 211302 (2015), [arXiv:1409.8294].

## 17. Lattice Quantum Chromodynamics

Revised August 2019 by S. Hashimoto (KEK), J. Laiho (Syracuse U.) and S.R. Sharpe (U. Washington).

17.1	Lattice regularization of QCD . . . . .	333
17.1.1	Gauge invariance, gluon fields and the gluon action . . . . .	333
17.1.2	Lattice fermions . . . . .	334
17.1.3	Heavy quarks on the lattice . . . . .	335
17.1.4	QED on the lattice . . . . .	336
17.1.5	Basic inputs for lattice calculations . . . . .	336
17.1.6	Sources of systematic error . . . . .	337
17.2	Methods and status . . . . .	337
17.2.1	Monte-Carlo method . . . . .	338
17.2.2	Two-point functions . . . . .	338
17.2.3	Three-point functions . . . . .	339
17.2.4	Scattering amplitudes and resonances . . . . .	339
17.2.5	Recent advances . . . . .	339
17.2.6	Status of LQCD simulations . . . . .	340
17.3	Physics applications . . . . .	340
17.3.1	Spectrum . . . . .	340
17.3.2	Decay constants and bag parameters . . . . .	340
17.3.3	Form factors ( $K \rightarrow \pi \ell \nu$ , $D \rightarrow K \ell \nu$ , $B \rightarrow \pi \ell \nu$ , $B \rightarrow D^{(*)} \ell \nu$ ) . . . . .	341
17.3.4	Strong coupling constant . . . . .	341
17.3.5	Quark masses . . . . .	342
17.3.6	Other applications . . . . .	342
17.4	Outlook . . . . .	342

Many physical processes considered in the Review of Particle Properties (RPP) involve hadrons. The properties of hadrons—which are composed of quarks and gluons—are governed primarily by Quantum Chromodynamics (QCD) (with small corrections from Quantum Electrodynamics [QED]). Theoretical calculations of these properties require non-perturbative methods, and Lattice Quantum Chromodynamics (LQCD) is a tool to carry out such calculations. It has been successfully applied to many properties of hadrons. Most important for the RPP are the calculation of electroweak form factors, which are needed to extract Cabbibo-Kobayashi-Maskawa (CKM) matrix elements when combined with the corresponding experimental measurements. LQCD has also been used to determine other fundamental parameters of the standard model, in particular the strong coupling constant and quark masses, as well as to predict hadronic contributions to the anomalous magnetic moment of the muon,  $g_\mu - 2$ .

This review describes the theoretical foundations of LQCD and sketches the methods used to calculate the quantities relevant for the RPP. It also describes the various sources of error that must be controlled in a LQCD calculation. Results for hadronic quantities are given in the corresponding dedicated reviews.

### 17.1 Lattice regularization of QCD

Gauge theories form the building blocks of the Standard Model. While the SU(2) and U(1) parts have weak couplings and can be studied accurately with perturbative methods, the SU(3) component—QCD—is only amenable to a perturbative treatment at high energies. The growth of the coupling constant in the infrared—the flip-side of asymptotic freedom—requires the use of non-perturbative methods to determine the low energy properties of QCD. Lattice gauge theory, proposed by K. Wilson in 1974 [1], provides such a method, for it gives a non-perturbative definition of vector-like gauge field theories like QCD. In lattice regularized QCD—commonly called lattice QCD or LQCD—Euclidean space-time is discretized, usually on a hypercubic lattice with lattice spacing  $a$ , with quark fields placed on sites and gauge fields on the links between sites. The lattice spacing plays the role of the ultraviolet regulator, rendering the quantum field theory finite. The continuum theory is recovered by taking the limit of vanishing lattice spacing, which can be reached by tuning the bare coupling constant to zero according to the renormalization group.

Unlike dimensional regularization, which is commonly used in continuum QCD calculations, the definition of LQCD does not

rely on the perturbative expansion. Indeed, LQCD allows non-perturbative calculations by numerical evaluation of the path integral that defines the theory.

Practical LQCD calculations are limited by the availability of computational resources and the efficiency of algorithms. Because of this, LQCD results come with both statistical and systematic errors, the former arising from the use of Monte-Carlo integration, the latter, for example, from the use of non-zero values of  $a$ . There are also different ways in which the QCD action can be discretized, and all must give consistent results in the continuum limit,  $a \rightarrow 0$ . It is the purpose of this review to provide an outline of the methods of LQCD, with particular focus on applications to particle physics, and an overview of the various sources of error. This should allow the reader to better understand the LQCD results that are presented in other reviews, primarily those on “Quark Masses,” “Quantum Chromodynamics,” “CKM quark-mixing matrix,” “ $V_{ud}$ ,  $V_{us}$ , Cabibbo angle and CKM Unitarity,” “Leptonic Decays of Charged Pseudoscalar Mesons,” “ $B^0 - \bar{B}^0$  Mixing,” and “Semileptonic  $b$ -Hadron Decays, Determination of  $V_{cb}$  and  $V_{ub}$ .” For more extensive explanations the reader should consult the available textbooks or lecture notes, the most up-to-date of which are Refs. [2–4].

#### 17.1.1 Gauge invariance, gluon fields and the gluon action

A key feature of the lattice formulation of QCD is that it preserves gauge invariance. This is in contrast to perturbative calculations, where gauge fixing is an essential step. The preservation of gauge invariance leads to considerable simplifications, e.g. restricting the form of operators that can mix under renormalization.

The gauge transformations of lattice quark fields are just as in the continuum:  $q(x) \rightarrow V(x)q(x)$  and  $\bar{q}(x) \rightarrow \bar{q}(x)V^\dagger(x)$ , with  $V(x)$  an arbitrary element of SU(3). The only difference is that the Euclidean space-time positions  $x$  are restricted to lie on the sites of the lattice, i.e.  $x = a(n_1, n_2, n_3, n_4)$  for a hypercubic lattice, with the  $n_j$  being integers. Quark bilinears involving different lattice points can be made gauge invariant by introducing the gluon field  $U_\mu(x)$ . For example, for adjacent points the bilinear is  $\bar{q}(x)U_\mu(x)q(x+a\hat{\mu})$ , with  $\hat{\mu}$  the unit vector in the  $\mu$ 'th direction. (This form is used in the construction of the lattice covariant derivative.) This is illustrated in Fig. 17.1. The gluon field (or “gauge link”) is an element of the group, SU(3), in contrast to the continuum field  $A_\mu$  which takes values in the Lie algebra. The bilinear is invariant if  $U_\mu$  transforms as  $U_\mu(x) \rightarrow V(x)U_\mu(x)V^\dagger(x+a\hat{\mu})$ . The lattice gluon field is naturally associated with the link joining  $x$  and  $x+a\hat{\mu}$ , and corresponds in the continuum to a Wilson line connecting these two points,  $P \exp(i \int_x^{x+a\hat{\mu}} dx_\mu A_\mu^{\text{cont}}(x))$  (where P indicates a path-ordered integral, and the superscript on  $A_\mu$  indicates that it is a continuum field). The trace of a product of the  $U_\mu(x)$  around any closed loop is easily seen to be gauge invariant and is the lattice version of a Wilson loop.

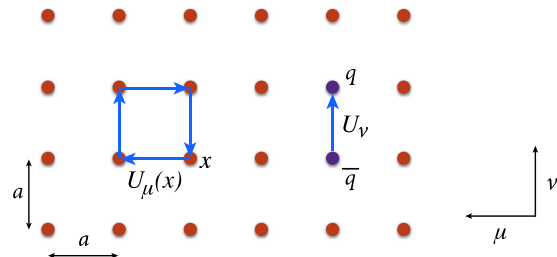


Figure 17.1: Sketch of a two-dimensional slice through the  $\mu - \nu$  plane of a lattice, showing gluon fields lying on links and forming either the plaquette product appearing in the gauge action or a component of the covariant derivative connecting quark and antiquark fields.

The simplest possible gauge action, usually called the Wilson gauge action, is given by the product of gauge links around elementary plaquettes:

$$S_g = \beta \sum_{x,\mu,\nu} \left[ 1 - \frac{1}{3} \text{ReTr}[U_\mu(x)U_\nu(x+a\hat{\mu})U_\mu^\dagger(x+a\hat{\nu})U_\nu^\dagger(x)] \right]. \quad (17.1)$$

This is illustrated in Fig. 17.1. For small  $a$ , assuming that the fields are slowly varying, one can expand the action in powers of  $a$  using  $U_\mu(x) = \exp(iaA_\mu(x))$ . Keeping only the leading non-vanishing term, and replacing the sum with an integral, one finds the continuum form,

$$S_g \longrightarrow \int d^4x \frac{1}{4g_{\text{lat}}^2} \text{Tr}[F_{\mu\nu}^2(x)], \quad (F_{\mu\nu} = \partial_\mu A_\nu - \partial_\nu A_\mu + i[A_\mu, A_\nu]) \quad (17.2)$$

as long as one chooses  $\beta = 6/g_{\text{lat}}^2$  for the lattice coupling. In this expression,  $g_{\text{lat}}$  is the bare coupling constant in the lattice scheme, which can be related (by combining continuum and lattice perturbation theory) to a more conventional coupling constant such as that in the  $\overline{\text{MS}}$  scheme (see Sec. 17.3.4 below).

In practice, the lattice spacing  $a$  is non-zero, leading to discretization errors. In particular, the lattice breaks Euclidean rotational invariance (which is the Euclidean version of Lorentz invariance) down to a discrete hypercubic subgroup. One wants to reduce discretization errors as much as possible. A very useful tool for understanding and then reducing discretization errors is the Symanzik effective action: the interactions of quarks and gluons with momenta low compared to the lattice cutoff ( $|p| \ll 1/a$ ) are described by a continuum action consisting of the standard continuum terms (e.g. the gauge action given in Eq. (17.2)) augmented by higher dimensional operators suppressed by powers of  $a$  [5]. For the Wilson lattice gauge action, the leading corrections come in at  $\mathcal{O}(a^2)$ . They take the form  $\sum_j a^2 c_j \mathcal{O}_6^{(j)}$ , with the sum running over all dimension-six operators  $\mathcal{O}_6^{(j)}$  allowed by the lattice symmetries, and  $c_j$  unknown coefficients. Some of these operators violate Euclidean rotational invariance, and all of them lead to discretization errors of the form  $a^2 \Lambda^2$ , where  $\Lambda$  is a typical momentum scale for the quantity being calculated. These errors can, however, be reduced by adding corresponding operators to the lattice action and tuning their coefficients to eliminate the dimension-six operators in the effective action to a given order in perturbation theory or even non-perturbatively. This is the idea of the Symanzik improvement program [5]. In the case of the gauge action, one adds Wilson loops involving six gauge links (as opposed to the four links needed for the original plaquette action, Eq. (17.1)) to define the  $\mathcal{O}(a^2)$  improved (or “Symanzik”) action [6]. In practical implementations, the improvement is either at tree-level (so that residual errors are proportional to  $\alpha_s a^2$ , where the coupling is evaluated at a scale  $\sim 1/a$ ), or at one loop order (errors proportional to  $\alpha_s^2 a^2$ ). Another popular choice is motivated by studies of renormalization group (RG) flow. It has the same terms as the  $\mathcal{O}(a^2)$  improved action but with different coefficients, and is called the RG-improved or “Iwasaki” action [7].

### 17.1.2 Lattice fermions

Discretizing the fermion action turns out to involve subtle issues, and the range of actions being used is more extensive than for gauge fields. Recall that the continuum fermion action is  $S_f = \int d^4x \bar{q}[iD_\mu \gamma_\mu + m_q]q$ , where  $D_\mu = \partial_\mu + iA_\mu$  is the gauge-covariant derivative. The simplest discretization replaces the derivative with a symmetric difference:

$$D_\mu q(x) \longrightarrow \frac{1}{2a} [U_\mu(x)q(x+a\hat{\mu}) - U_\mu(x-a\hat{\mu})^\dagger q(x-a\hat{\mu})]. \quad (17.3)$$

The factors of  $U_\mu$  ensure that  $D_\mu q(x)$  transforms under gauge transformations in the same way as  $q(x)$ , so that the discretized version of  $\bar{q}(x)D_\mu \gamma_\mu q(x)$  is gauge invariant. The choice in Eq. (17.3) leads to the so-called naive fermion action. This, however, suffers from the fermion doubling problem—in  $d$  dimensions it describes  $2^d$  equivalent fermion fields in the continuum limit. The appearance of the extra “doubler” fermions is related to the deeper theoretical problem of formulating chirally symmetric fermions on the lattice. This is encapsulated by the Nielsen-Ninomiya theorem [8]: one cannot define lattice fermions having

exact, continuum-like chiral symmetry without producing doublers. Naive lattice fermions do have chiral symmetry but at the cost of introducing 15 unwanted doublers (for  $d = 4$ ).

There are a number of different strategies for dealing with the doubling problem, each with their own theoretical and computational advantages and disadvantages. Wilson fermions [1] add a term proportional to  $a\bar{q}\Delta q$  to the fermion action (the “Wilson term”—in which  $\Delta$  is a covariant lattice Laplacian). This gives a mass of  $\mathcal{O}(1/a)$  to the doublers, so that they decouple in the continuum limit. The Wilson term, however, violates chiral symmetry, and also introduces discretization errors linear in  $a$ . A commonly used variant that eliminates the  $\mathcal{O}(a)$  discretization error is the  $\mathcal{O}(a)$ -improved Wilson (or “clover”) fermion [9]. In this application of Symanzik improvement, methods have been developed to remove  $\mathcal{O}(a)$  terms non-perturbatively using auxiliary simulations to tune parameters [10]. Such “non-perturbative improvement” is of great practical importance as it brings the discretization error from the fermion action down to the same level as that from the gauge action.

The advantages of Wilson fermions are their theoretical simplicity and relatively low computational cost. Their main disadvantage is the lack of chiral symmetry, which makes them difficult to use in cases where mixing with wrong chirality operators can occur, particularly if this involves divergences proportional to powers of  $1/a$ . A related problem is the presence of potential numerical instabilities due to spurious near-zero modes of the lattice Dirac operator. There are, however, studies that successfully ameliorate these problems and increase the range of quantities for which Wilson fermions can be used (see, e.g., Refs. [11–14]).

Twisted-mass fermions [15] are a variant of Wilson fermions in which two flavors are treated together with an isospin-breaking mass term (the “twisted mass” term). The main advantage of this approach is that all errors linear in  $a$  are automatically removed (without the need for tuning of parameters) by a clever choice of twisted mass and operators [16]. A disadvantage is the presence of isospin breaking effects (such as a splitting between charged and neutral pion masses even when up and down quarks are degenerate), which, however, vanish as  $a^2 \Lambda^2$  in the continuum limit. Strange and charm quarks can be added as a second pair, with a term added to split their masses [17, 18].

Staggered fermions are a reduced version of naive fermions in which there is only a single fermion Dirac component on each lattice site, with the full Dirac structure built up from neighboring sites [19]. They have the advantages of being somewhat faster to simulate than Wilson-like fermions, of preserving some chiral symmetry, and of having discretization errors of  $\mathcal{O}(a^2)$ . Their disadvantage is that they retain some of the doublers (3 for  $d = 4$ ). The action thus describes four degenerate fermions in the continuum limit. These are usually called “tastes”, to distinguish them from physical flavors, and the corresponding  $\text{SU}(4)$  symmetry is referred to as the “taste symmetry”. The preserved chiral symmetry in this formulation has non-singlet taste. Practical applications usually introduce one staggered fermion for each physical flavor, and remove contributions from the unwanted tastes by taking the fourth-root of the fermion determinant appearing in the path integral. The validity of this “rooting” procedure is not obvious because taste symmetry is violated for non-zero lattice spacing. Theoretical arguments, supported by numerical evidence, suggest that the procedure is valid as long as one takes the continuum limit before approaching the light quark mass region [20]. Additional issues arise for the valence quarks (those appearing in quark propagators, as described in Sec. 17.2 below), where rooting is not possible, and one must ignore the extra tastes, or account for them by dividing by appropriate factors of four [21].

Just as for Wilson fermions, the staggered action can be improved, so as to reduce discretization errors. The Asqtad ( $a$ -squared tadpole improved) action [22] was used until recently in many large scale simulations [23]. More recent calculations use the HISQ (highly improved staggered quark) action, introduced in Ref. [24]. At tree-level it removes both  $\mathcal{O}(a^2)$  errors and, to lowest order in the quark speed  $v/c$ ,  $\mathcal{O}([am]^4)$  errors. It also substantially reduces effects caused by taste-symmetry breaking. This makes it attractive not only for light quarks, but means that it is

also quite accurate for heavy quarks because it suppresses  $(am)^n$  errors. It is being used to directly simulate charm quarks and to approach direct simulations of bottom quarks (see, e.g. [25, 26]).

There is an important class of lattice fermions, “Ginsparg-Wilson fermions,” that possess a continuum-like chiral symmetry without introducing unwanted doublers. The lattice Dirac operator  $D$  for these fermions satisfies the Ginsparg-Wilson relation  $D\gamma_5 + \gamma_5 D = aD\gamma_5 D$  [27]. In the continuum, the right-hand-side vanishes, leading to chiral symmetry. On the lattice, it is non-vanishing, but with a particular form (with two factors of  $D$ ) that restricts the violations of chiral symmetry in Ward-Takahashi identities to short-distance terms that do not contribute to physical matrix elements [28]. In fact, one can define a modified chiral transformation on the lattice (by including dependence on the gauge fields) such that Ginsparg-Wilson fermions have an exact chiral symmetry for on-shell quantities [29]. The net result is that such fermions essentially have the same properties under chiral transformations as do continuum fermions, including the index theorem [28]. Their leading discretization errors are of  $\mathcal{O}(a^2)$ .

Two types of Ginsparg-Wilson fermions are currently being used in large-scale numerical simulations. The first is Domain-wall fermions (DWF). These are defined on a five-dimensional space, in which the fifth dimension is fictitious [30]. The action is chosen so that the low-lying modes are chiral, with left- and right-handed modes localized on opposite four-dimensional surfaces. For an infinite fifth dimension, these fermions satisfy the Ginsparg-Wilson relation. In practice, the fifth dimension is kept finite, and there remains a small, controllable violation of chiral symmetry. The second type is Overlap fermions. These appeared from a completely different context and have an explicit form that exactly satisfies the Ginsparg-Wilson relation [31]. Their numerical implementation requires an approximation of the matrix sign function of a Wilson-like fermion operator, and various approaches are being used. In fact, it is possible to rewrite these approximations in terms of a five-dimensional formulation, showing that the DWF and Overlap approaches are essentially equivalent [32, 33]. Numerically, the five-dimensional approach appears to be more computationally efficient.

The various lattice fermion formulations are often combined with the technique of link smearing. Here one couples the fermions to a smoother gauge link, defined by averaging with adjacent links in a gauge invariant manner. Several closely related implementations are being used. All reduce the coupling of fermions to the short-distance fluctuations in the gauge field, leading to an improvement in the numerical stability and speed of algorithms. One cannot perform this smearing too aggressively, however, since the smearing may distort short distance physics and enhance discretization errors.

As noted above, each fermion formulation has its own advantages and disadvantages. For instance, domain-wall and overlap fermions are theoretically preferred as they have chiral symmetry without doublers, but their computational cost is greater than for other choices. If the physics application of interest and the target precision do not require near-exact chiral symmetry, there is no strong motivation to use these expensive formulations. On the other hand, there is a class of applications (including the calculation of the  $\Delta I = 1/2$  amplitude for  $K \rightarrow \pi\pi$  decays and the S-parameter [34]) where chiral symmetry plays an essential role and for which the use of Ginsparg-Wilson fermions is strongly favored.

### 17.1.3 Heavy quarks on the lattice

The fermion formulations described in the previous subsection can be used straightforwardly only for quarks whose masses are small compared to the lattice cutoff,  $m_q \lesssim 1/a$ . This is because there are discretization errors proportional to powers of  $am_q$ , and if  $am_q \gtrsim 1$  these errors are large and uncontrolled. Present LQCD simulations typically have cutoffs in the range of  $1/a = 2 - 4$  GeV (corresponding to  $a \approx 0.1 - 0.05$  fm). Thus, while for the up, down and strange quarks one has  $am_q \ll 1$ , for bottom quarks (with  $m_b \approx 4.5$  GeV) one must use alternative approaches. Charm quarks ( $m_c \approx 1.5$  GeV) are an intermediate case, allowing simulations using both direct and alternative approaches.

For the charm quark, the straightforward approach is to simul-

aneously reduce the lattice spacing and to improve the fermion action so as to reduce the size of errors proportional to powers of  $am_c$ . This approach has been followed successfully using the HISQ, twisted-mass and domain-wall actions [24–26, 35, 36]. It is important to note, however, that reducing  $a$  increases the computational cost because an increased number of lattice points are needed for the same physical volume. One cannot reduce the spatial size below  $2 - 3$  fm without introducing finite volume errors. Present lattices have typical sizes of  $\sim 64^3 \times 128$  (with the long direction being Euclidean time), and thus allow a lattice cutoff up to  $1/a \sim 4$  GeV.

This approach can, to some extent, be extended to the bottom quark, by the use of simulations with small lattice spacings [37]. This has been pursued with the HISQ action, using lattices of size up to  $144^3 \times 288$  and lattice spacings down to  $a \approx 0.03$  fm ( $1/a \approx 6.6$  GeV) [38]. Extrapolation in  $m_b$  is still needed [39], however, and this makes use of the mass dependence predicted by Heavy Quark Effective Theory (HQET).

Alternative approaches for discretizing heavy quarks are motivated by effective field theories. For a bottom quark in heavy-light hadrons, one can use HQET to expand about the infinite quark-mass limit. In this limit, the bottom quark is a static color source, and one can straightforwardly write the corresponding lattice action [40]. Corrections, proportional to powers of  $1/m_b$ , can be introduced as operator insertions, with coefficients that can be determined non-perturbatively using existing techniques [41]. This method allows the continuum limit to be taken controlling all  $1/m_b$  corrections.

Another way of introducing the  $1/m_b$  corrections is to include the relevant terms in the effective action. This leads to a non-relativistic QCD (NRQCD) action, in which the heavy quark is described by a two-component spinor [42]. This approach has the advantage over HQET that it can also be used for heavy-heavy systems, such as the Upsilon states. Moreover, the bottom quark can be treated without any extrapolation in  $m_b$ . A disadvantage is that some of the parameters in this effective theory are determined perturbatively (originally at tree-level, but more recently at one-loop [43]), which limits the precision of the final results. Although discretization effects can be controlled with good numerical precision for a range of lattice spacings, these artifacts cannot be extrapolated away by taking the lattice spacing to zero. This is because NRQCD is a nonrelativistic effective field theory and so ceases to work when the cutoff  $\pi/a$  becomes much larger than the heavy-quark mass. In practice these effects are accounted for in the error budget.

This problem can be avoided if one uses HQET power counting to analyze and reduce discretization effects for heavy quarks while using conventional fermion actions [44]. For instance, one can tune the parameters of an improved Wilson quark action so that the leading HQET corrections to the static quark limit are correctly accounted for. As the lattice spacing becomes finer, the action smoothly goes over to that of a light Wilson quark action, where the continuum limit can be taken as usual. In principle, one can improve the action in the heavy quark regime up to arbitrarily high orders using HQET, but so far large-scale simulations have typically used clover improved Wilson quarks, where tuning the parameters of the action corresponds to including all corrections through next-to-leading order in HQET. Three different methods for tuning the parameters of the clover action are being used: the Fermilab [44], Tsukuba [45] and Columbia [46] approaches. An advantage of this HQET approach is that the  $c$  and  $b$  quarks can be treated on the same footing. Parameter tuning has typically been done perturbatively, as in NRQCD, but recent work using the Columbia approach has used non-perturbative tuning of some of the parameters [47, 48]. One can improve the effective theory including the terms beyond the next-to-leading order. The Oktay-Kronfeld action that includes dimension-six and -seven operators has been constructed [49] and recently used in large-scale numerical calculations [50].

Another approach is the “ratio method” introduced in Ref. [51]. Here one uses quarks with masses lying at, or slightly above, the charm mass  $m_c$ , which can be simulated with a relativistic action, and extrapolates to  $m_b$  incorporating the behavior predicted by

HQET. The particular implementation relies on the use of ratios. As an example, consider the  $B$  meson decay constant  $f_B$ . According to HQET, this scales as  $1/\sqrt{m_B}$  for  $m_B \gg \Lambda_{\text{QCD}}$ , up to a logarithmic dependence that is calculable in perturbative QCD (but will be suppressed in the following). Here  $m_B$  is the  $B$  meson mass, which differs from  $m_b$  by  $\sim \Lambda_{\text{QCD}}$ . One considers the ratio  $y(\lambda, m_{b'}) \equiv f_{B''} \sqrt{m_{B''}} / f_{B'} \sqrt{m_{B'}}$  for fictitious  $B$  mesons containing  $b$  quarks with unphysical masses  $m_{b'}$  and  $m_{b''} = \lambda m_{b'}$ . HQET implies that  $y(\lambda, m_{b'})$  approaches unity for large  $m_{b'}$  and any fixed  $\lambda > 1$ . The ratios are evaluated on the lattice for the sequence of masses  $m_{b'} = m_c, \lambda m_c, \lambda^2 m_c$ , all well below the physical  $m_b$ , and for each the continuum limit is taken. The form of the ratio for larger values of  $m_{b'}$  is obtained by fitting, incorporating the constraints implied by HQET. The result for  $f_B \sqrt{m_B}$  is then obtained as a product of  $y$ 's with  $f_D \sqrt{m_D}$ .

#### 17.1.4 QED on the lattice

Quarks in nature are electrically charged, and the resultant coupling to photons leads to shifts in the properties of hadrons that are generically of  $\mathcal{O}(\alpha_{\text{EM}})$ . Thus, for example, the proton mass is increased by  $\sim 1$  MeV relative to that of the neutron due to its overall charge although this effect is more than compensated for by the  $\sim 2.5$  MeV relative decrease due to the up quark being lighter than the down quark [52]. This example shows that once pure QCD, isospin-symmetric lattice calculations reach percent level accuracy, further improvement requires the inclusion of effects due to both electromagnetism and the up-down mass difference. This level of accuracy has in fact been obtained for various quantities, e.g. light hadron masses and decay constants (see Ref. [53]), and simulations including QED in addition to QCD are becoming more common.

The extension of lattice methods to include QED is straightforward, although some new subtleties arise. The essential change is that the quark must now propagate through a background field containing both gluons and photons. The gauge field  $U_\mu$  that appears in the covariant derivative of Eq. (17.3) is extended from an SU(3) matrix to one living in U(3):  $U_\mu \rightarrow U_\mu e^{iaq_e A_\mu^{\text{EM}}}$ . Here  $A_\mu^{\text{EM}}$  is the photon field,  $e$  the electromagnetic coupling, and  $q$  the charge of the quark, e.g.  $q = 2/3$  for up and  $-1/3$  for down and strange quarks. The lattice action for the photon that is typically used is a discretized version of the continuum action Eq. (17.2), rather than the form used for the gluons, Eq. (17.1). This “non-compact” action has the advantage that it is quadratic in  $A_\mu^{\text{EM}}$ , which simplifies the QED part of the generation of configurations.

One subtlety that arises is that Gauss’ law forbids a charged particle in a box with periodic boundary conditions. This finite volume effect can be overcome by including a uniform background charge, and this can be shown to be equivalent to removing the zero-momentum mode from the photon field. This is an example of the enhanced finite-volume effects that arise in the presence of the massless photon.

Simulations including QED have progressed over the last few years, and now a full inclusion of QED has been achieved with almost physical quark masses [52, 54]. Alternative approaches have also been used: reweighting the QCD fields *a posteriori* [55, 56], and keeping only the linear term in an expansion in  $\alpha_{\text{EM}}$  about the QCD only case [57]. In addition, some calculations have included QED effects for the valence quarks but not the sea quarks (the “electroquenched approximation”)—for a recent example see Ref. [58].

The QED corrections to processes including leptons, such as the leptonic and semileptonic decays of hadrons, involve additional diagrams in which a photon propagator bridges between a hadron and a lepton. Such diagrams induce infrared divergences that cancel against soft photon radiation (Bloch-Nordsieck theorem [59]). Methods have been developed to implement this cancellation in lattice calculations, treating the soft photon analytically [60], with first results reported recently for leptonic pion and kaon decays [61, 62].

#### 17.1.5 Basic inputs for lattice calculations

Since LQCD is nothing but a regularization of QCD, the renormalizability of QCD implies that the number of input parameters in LQCD is the same as for continuum QCD—the strong coupling

constant  $\alpha_s = g^2/(4\pi)$ , the quark masses for each flavor, and the CP violating phase  $\theta$ . The  $\theta$  parameter is usually assumed to be zero, while the other parameters must be determined using experimental inputs.

##### 17.1.5.1 Lattice spacing

In QCD, the coupling constant is a function of scale. With lattice regularization, this scale is the inverse lattice spacing  $1/a$ , and choosing the bare coupling constant is equivalent to fixing the lattice spacing.

In principle,  $a$  can be determined using any dimensionful quantity measured by experiments. For example, using the mass of hadron  $H$  one has  $a = (am_H)^{\text{lat}}/m_H^{\text{exp}}$ . One chooses quantities that can be calculated accurately on the lattice, and that are only weakly dependent on the light quark masses. The latter property minimizes errors from extrapolating or interpolating to the physical light quark masses or from mistuning of these masses.

Commonly used choices are the spin-averaged 1S-1P or 1S-2S splittings in the Upsilon system, the mass of the  $\Omega^-$  baryon, and the pion decay constant  $f_\pi$ . Ultimately, all choices must give consistent results for  $a$ , and that this is the case provides a highly non-trivial check of both the calculational method and of QCD.

##### 17.1.5.2 Light quark masses

In LQCD simulations, the up, down and strange quarks are usually referred to as the light quarks, in the sense that  $m_q < \Lambda_{\text{QCD}}$ . (The standard definition of  $\Lambda_{\text{QCD}}$  is given in the “Quantum Chromodynamics” review; in this review we are using it only to indicate the approximate non-perturbative scale of QCD.) This condition is stronger than that used above to distinguish quarks with small discretization errors,  $m_q < 1/a$ . Loop effects from light quarks must be included in the simulations to accurately represent QCD. At present, most simulations are done in the isospin symmetric limit  $m_u = m_d \equiv m_\ell < m_s$ , and are often referred to as “ $N_f = 2 + 1$ ” simulations. Increasingly, simulations also include loops of charm quarks (denoted  $N_f = 2 + 1 + 1$  simulations), although the effect of charmed sea quarks on low-energy physics is generically expected to be at the sub-percent level [63–66]. Precision is now reaching the point where isospin breaking effects must be included. To do so without approximation requires simulating with nondegenerate up and down quarks (leading to  $N_f = 1 + 1 + 1$  or  $1 + 1 + 1 + 1$  simulations) as well as including electromagnetism (as described above). This has been done in Ref. [52]. Alternatively, one can use a perturbative approach, expanding about the isospin symmetric theory and working to linear order in  $\alpha_{\text{EM}}$  and  $m_u - m_d$  [57, 67].

We now describe the tuning of  $m_\ell$ ,  $m_s$  and  $m_c$  to their physical values. (For brevity, we ignore isospin violation in the following discussion.) The most commonly used quantities for these tunings are, respectively,  $m_\pi$ ,  $m_K$  and  $m_{\eta_c}$ . If the scale is being set by  $m_\Omega$ , then one adjusts the lattice quark masses until the ratios  $m_\pi/m_\Omega$ ,  $m_K/m_\Omega$  and  $m_{\eta_c}/m_\Omega$  take their physical values. In the past, most calculations needed to extrapolate to the physical value of  $m_\ell$  (typically using forms based on chiral perturbation theory [ChPT]), while simulating directly at or near to the physical values of  $m_s$  and  $m_c$ . Present calculations are increasingly done with physical or near physical values of  $m_\ell$ , requiring at most only a short extrapolation.

##### 17.1.5.3 Heavy quark masses

The  $b$  quark is usually treated only as a valence quark, with no loop effects included. The errors introduced by this approximation can be estimated to be  $\sim \alpha_s(m_b) \Lambda_{\text{QCD}}^2/m_b^2$  and are likely to be very small. In the past, the same approximation has been made for the  $c$  quark, leading to errors  $\sim \alpha_s(m_c) \Lambda_{\text{QCD}}^2/m_c^2$ . (See Ref. [63] for a quantitative estimate of the effects of including the charm quark on some low energy physical quantities, and Ref. [68] for similar estimates for  $B$ -meson matrix elements.) For high precision, however, dynamical charm quarks are necessary, and some of the most recent simulations now include them.

The  $b$  quark mass can be tuned by setting heavy-heavy ( $\mathcal{Y}$ ) or heavy-light ( $B$ ) meson masses to their experimental values. Consistency between these two determinations provides an important check that the determination of parameters in the heavy quark lat-



tice formulations is being done correctly (see, e.g., Ref. [37,69,70])

### 17.1.6 Sources of systematic error

Lattice results have statistical and systematic errors that must be quantified for any calculation in order for the result to be a useful input to phenomenology. The statistical error is due to the use of Monte Carlo importance sampling to evaluate the path integral (a method discussed below). There are, in addition, a number of systematic errors that are always present to some degree in lattice calculations, although the size of any given error depends on the particular quantity under consideration and the parameters of the ensembles being used. The most common lattice errors are reviewed below.

Although not strictly a systematic error, it is important to note that the presence of long autocorrelations in the sequence of lattice configurations generated by the Monte Carlo method can lead to underestimates of statistical errors [71]. It is known that the global topological charge of the gauge fields decorrelates very slowly with certain algorithms [71,72]. The effect of poorly sampling topological charge is expected to be most significant for the pion mass and related quantities [73,74]. This issue becomes more relevant as the precision of the final results increases.

#### 17.1.6.1 Continuum limit

Physical results are obtained in the limit that the lattice spacing  $a$  goes to zero. The Symanzik effective theory determines the scaling of lattice artefacts with  $a$ . Most lattice calculations use improved actions with leading discretization errors of  $\mathcal{O}(a^2\Lambda^2)$ ,  $\mathcal{O}(\alpha_s a^2\Lambda^2)$ , or  $\mathcal{O}(\alpha_s a\Lambda)$ , where  $\Lambda$  is a typical momentum scale in the system. Knowledge of the scaling of the leading discretization errors allows controlled extrapolation to  $a = 0$  when multiple lattice spacings are available, as in current state-of-the-art calculations. Residual errors arise from the exclusion of subleading  $a$  dependence from the fits.

For many quantities the typical momentum scale in the system is  $\sim \Lambda_{\text{QCD}} \approx 300$  MeV. Discretization errors are expected to be larger for quantities involving larger scales, for example form factors or decays involving particles with momenta larger than  $\Lambda_{\text{QCD}}$ .

#### 17.1.6.2 Infinite volume limit

LQCD calculations are necessarily carried out in finite space-time boxes, leading to departures of physical quantities (masses, decay constants, etc.) from their measured, infinite volume values. These finite-volume shifts are an important systematic that must be estimated and minimized.

Typical lattices are asymmetric, with  $N_s$  points in the three spatial directions and  $N_t$  in the (Euclidean) temporal direction. The spatial and temporal sizes in physical units are thus  $L_s = aN_s$  and  $L_t = aN_t$ , respectively. (Anisotropic lattice spacings are also sometimes used, as discussed below in Sec. 17.2.2.) Typically,  $L_t \geq 2L_s$ , a longer temporal direction being used to allow excited-state contributions to correlators to decay. This means that the dominant impact of using finite volume is from the presence of a finite spatial box.

High-precision LQCD calculations are of quantities involving no more than a single particle in initial and final states (with the exception of the  $K \rightarrow \pi\pi$  decay amplitudes). For such quantities, once the volume exceeds about 2 fm (so that the particle is not “squeezed”), the dominant finite-volume effect comes from virtual pions wrapping around the lattice in the spatial directions. This effect is exponentially suppressed as the volume becomes large, roughly as  $\sim \exp(-m_\pi L_s)$ , and has been estimated using ChPT [75] or other methods [76]. The estimates suggest that finite volume shifts are sub-percent effects when  $m_\pi L_s \gtrsim 4$ , and most large-scale simulations use lattices satisfying this condition. This becomes challenging as one approaches the physical pion mass, for which  $L_s \gtrsim 5$  fm is required.

Finite volume errors are usually determined by repeating the simulations on two or more different volumes (with other parameters fixed). If different volumes are not available, the ChPT estimate can be used, often inflated to account for the fact that the ChPT calculation is truncated at some order.

In the future, LQCD calculations involving more than a single hadron will become increasingly precise. Examples include

the calculation of resonance parameters and the above-mentioned  $K \rightarrow \pi\pi$  amplitudes. Finite volume effects are much larger in these cases, with power-law terms (e.g.  $1/L_s^3$ ) in addition to exponential dependence. Indeed, as will be discussed in Sec. 17.2.4, one can use the volume dependence to indirectly extract infinite-volume quantities such as scattering lengths. Doing so, however, requires a set of lattice volumes satisfying  $m_\pi L_s \gtrsim 4$  and is thus more challenging than for single-particle quantities.

#### 17.1.6.3 Chiral extrapolation

Until recently, an important source of systematic error in LQCD calculations was the need to extrapolate in  $m_u$  and  $m_d$  (or, equivalently, in  $m_\pi$ ). This extrapolation was usually done using functional forms based on ChPT, or with analytic functions, with the difference between different fits used as an estimate of the systematic error, which was often substantial. Increasingly, however, calculations work directly at, or very close to, the physical quark masses. This either removes entirely, or greatly reduces, the uncertainties in the extrapolation, such that this error is subdominant.

#### 17.1.6.4 Operator matching

Many of the quantities that LQCD can precisely calculate involve hadronic matrix elements of operators from the electroweak Hamiltonian. Examples include the pion and kaon decay constants, semileptonic form factors and the kaon mixing parameter  $B_K$  (the latter defined in Eq. (17.13)). The operators in the lattice matrix elements are defined in the lattice regularization scheme. To be used in tests of the Standard Model, however, they must be matched to the continuum regularization scheme in which the corresponding Wilson coefficients have been calculated. The only case in which such matching is not needed is if the operator is a conserved or partially conserved current. Similar matching is also needed for the conversion of lattice bare quark masses to those in the continuum  $\overline{\text{MS}}$  scheme.

Several methods are used to calculate the matching factors: perturbation theory (usually to one- or two-loop order), non-perturbative renormalization (NPR) using Landau-gauge quark and gluon external states [77], NPR using gauge-invariant methods based on the Schrödinger functional [78], NPR using gauge-invariant short-distance hadron correlators [79], and NPR using gauge-invariant heavy-heavy correlators [26,80]. The NPR methods replace truncation errors (which can only be approximately estimated) by statistical and systematic errors that can be determined reliably and systematically reduced.

An issue that arises in some of such calculations (e.g. for quark masses and  $B_K$ ) is that, using NPR with Landau-gauge quark and gluon external states, one ends up with operators regularized in a MOM-like scheme (or a Schrödinger-functional scheme), rather than the  $\overline{\text{MS}}$  scheme mostly used for calculating the Wilson coefficients. To make contact with this scheme requires a purely continuum perturbative matching calculation. The resultant truncation error can, however, be minimized by pushing up the momentum scale at which the matching is done using step-scaling techniques as part of the NPR calculation [81]. It should also be noted that this final step in the conversion to the  $\overline{\text{MS}}$  scheme could be avoided if continuum calculations used a MOM-like scheme or if one imposes a renormalization condition for quantities that are calculable both in the  $\overline{\text{MS}}$  scheme and in LQCD, such as the hadron correlators at short distances (see, e.g., Ref. [82]).

## 17.2 Methods and status

Once the lattice action is chosen, it is straightforward to define the quantum theory using the path integral formulation. The Euclidean-space partition function is

$$Z = \int [dU] \prod_f [dq_f][d\bar{q}_f] e^{-S_g[U] - \sum_f \bar{q}_f (D[U] + m_f) q_f}, \quad (17.4)$$

where link variables are integrated over the SU(3) manifold,  $q_f$  and  $\bar{q}_f$  are Grassmann (anticommuting) quark and antiquark fields of flavor  $f$ , and  $D[U]$  is the chosen lattice Dirac operator with  $m_f$  the quark mass in lattice units. Integrating out the quark



and antiquark fields, one arrives at a form suitable for simulation:

$$Z = \int [dU] e^{-S_g[U]} \prod_f \det(D[U] + m_f). \quad (17.5)$$

$$\langle \mathcal{O}(U, q, \bar{q}) \rangle = (1/Z) \int [dU] \prod_f [dq_f][d\bar{q}_f] \mathcal{O}(U, q, \bar{q}) e^{-S_g[U] - \sum_f \bar{q}_f (D[U] + m_f) q_f}. \quad (17.6)$$

If the operators depend on the (anti-)quark fields  $q_f$  and  $\bar{q}_f$ , then integrating these fields out leads not only to the fermion determinant but also, through Wick's theorem, to a series of quark "propagators",  $(D[U] + m_f)^{-1}$ , connecting the positions of the fields.

This set-up allows one to choose, by hand, the masses of the quarks in the determinant (the sea quarks) differently from those in the propagators (valence quarks). This is called "partial quenching", and is used by some calculations as a way of obtaining more data points from which to extrapolate both sea and valence quarks to their physical values.

### 17.2.1 Monte-Carlo method

Since the number of integration variables  $U$  is huge ( $N_s^3 \times N_t \times 4 \times 9$ ), direct numerical integration is impractical and one has to use Monte-Carlo techniques. In this method, one generates a Markov chain of gauge configurations (a "configuration" being the set of  $U$ 's on all links) distributed according to the probability measure  $[dU] e^{-S_g[U]} \prod_f \det(D[U] + m_f)$ . Once the configurations are generated, expectation values  $\langle \mathcal{O}(U, q, \bar{q}) \rangle$  are calculated by averaging over those configurations. In this way the configurations can be used repeatedly for many different calculations, and there are several large collections of ensembles of configurations (with a range of values of  $a$ , lattice sizes and quark masses) that are publicly available through the International Lattice Data Grid (ILDG). As the number of the configurations,  $N$ , is increased, the error decreases as  $1/\sqrt{N}$ .

The most challenging part of the generation of gauge configurations is the need to include the fermion determinant. Direct evaluation of the determinant is not feasible, as it requires  $\mathcal{O}((N_s^3 \times N_t)^3)$  computations. Instead, one rewrites it in terms of "pseudofermion" fields  $\phi$  (auxiliary fermion fields with bosonic statistics). For example, for two degenerate quarks one has

$$\det(D[U] + m_f)^2 = \int [d\phi] e^{-\phi^\dagger (D[U] + m_f)^{-2} \phi}. \quad (17.7)$$

By treating the pseudofermions as additional integration variables in the path integral, one obtains a totally bosonic representation. The price one pays is that the pseudofermion effective action is highly non-local since it includes the inverse Dirac operator  $(D[U] + m_f)^{-1}$ . Thus, the large sparse matrix  $(D[U] + m)$  has to be inverted every time one needs an evaluation of the effective action.

Present simulations generate gauge configurations using the Hybrid Monte Carlo (HMC) algorithm [83], or variants thereof. This algorithm combines molecular dynamics (MD) evolution in a fictitious time (which is also discretized) with a Metropolis "accept-reject" step. It makes a global update of the configuration, and is made exact by the Metropolis step. In its original form it can be used only for two degenerate flavors, but extensions (particularly the rational HMC [84]) are available for single flavors. Considerable speed-up of the algorithms has been achieved over the last two decades using a variety of techniques.

All these algorithms spend the bulk of their computational time on the repeated inversion of  $(D[U] + m)$  acting on a source (which is required at every step of the MD evolution). Inversions are done using a variety of iterative algorithms, e.g. the conjugate gradient algorithm. In this class of algorithms, computational cost is proportional to the condition number of the matrix, which is the ratio of maximum and minimum eigenvalues. For  $(D[U] + m)$  the smallest eigenvalue is  $\approx m$ , so the condition number and cost are

The building blocks for calculations are expectation values of multi-local gauge-invariant operators, also known as "correlation functions",

inversely proportional to the quark mass. This is a major reason why simulations at the physical quark mass are challenging.

Recent algorithmic improvements have significantly reduced this problem. The main idea is to separate different length scales. Since the low eigenvalues of  $(D[U] + m)$  are associated with long wavelength quark modes, one may project the problem onto that of a coarse-grained lattice by averaging the field within a block of sublattices and carrying out the inversion on this coarse lattice. The result is then fed back to the original lattice as an efficient *preconditioner* for the iterative solver, and the whole procedure may be nested multiple times. Variants of such methods have been implemented, specifically domain-decomposition [11, 12], deflation [85–88] and multigrid [89, 90]. They are increasingly used in large-scale lattice simulations.

A practical concern is the inevitable presence of correlations between configurations in the Markov chain. These are characterized by an autocorrelation length in the fictitious MD time. One aims to use configurations separated in MD time by greater than this autocorrelation length. In practice, it is difficult to measure this length accurately, see, e.g., [91], and this leads to some uncertainty in the resulting statistical errors, as well as the possibility of insufficient equilibration.

For most of the applications of LQCD discussed in this review, the cost of generating gauge configurations is larger than or similar to that of performing the "measurements" on those configurations. The computational cost of gauge generation grows with the lattice volume,  $V_{\text{lat}} = N_s^3 N_t$ , as  $V_{\text{lat}}^{1+\delta}$ . Here  $\delta = 1/4$  for the HMC algorithm [92] and can be reduced slightly using modern variants. Such growth with  $V_{\text{lat}}$  provides a (time-dependent) limit on the largest lattice volumes that can be simulated. At present, the largest lattices being used have  $N_s = 144$  and  $N_t = 288$ . Typically one aims to create an ensemble of  $\sim 10^3$  statistically independent configurations at each choice of parameters ( $a$ ,  $m_q$  and  $V_{\text{lat}}$ ). For most physical quantities of interest, this is sufficient to make the resulting statistical errors smaller than or comparable to the systematic errors.

### 17.2.2 Two-point functions

One can extract properties of stable hadrons using two-point correlation functions,  $\langle O_X(x) O_Y^\dagger(0) \rangle$ . Here  $O_{X,Y}(x)$  are operators that have non-zero overlaps with the hadronic state of interest  $|H\rangle$ , i.e.  $\langle 0|O_{X,Y}(x)|H\rangle \neq 0$ . One usually Fourier transforms in the spatial directions and considers correlators as a function of Euclidean time:

$$C_{XY}(t; \vec{p}) = \sum_{\vec{x}} \langle O_X(t, \vec{x}) O_Y^\dagger(0) \rangle e^{-i\vec{p}\cdot\vec{x}}. \quad (17.8)$$

(Here and throughout this section all quantities are expressed in dimensionless lattice units, so that, for example,  $\vec{p} = a\vec{p}_{\text{phys}}$ .) By inserting a complete set of states having spatial momentum  $\vec{p}$ , the two-point function can be written as

$$C_{XY}(t; \vec{p}) = \sum_{i=0}^{\infty} \frac{1}{2E_i(\vec{p})} \langle 0|O_X(0)|H_i(\vec{p})\rangle \langle H_i(\vec{p})|O_Y^\dagger(0)|0\rangle e^{-E_i(\vec{p})t}, \quad (17.9)$$

where the energy of the  $i$ -th state  $E_i(\vec{p})$  appears as an eigenvalue of the time evolution operator  $e^{-Ht}$  in the Euclidean time direction. The factor of  $1/[2E_i(\vec{p})]$  is due to the relativistic normalization used for the states. For large enough  $t$ , the dominant contribution

is that of the lowest energy state  $|H_0(\vec{p})\rangle$ :

$$C_{XY}(t) \xrightarrow{t \rightarrow \infty} \frac{1}{2E_0(\vec{p})} \langle 0|O_X(0)|H_0(\vec{p})\rangle \langle H_0(\vec{p})|O_Y^\dagger(0)|0\rangle e^{-E_0(\vec{p})t}. \quad (17.10)$$

One can thus obtain the energy  $E_0(\vec{p})$ , which equals the hadron mass  $m_H$  when  $\vec{p} = 0$ , and the product of matrix elements  $\langle 0|O_X(0)|H_i(\vec{p})\rangle \langle H_i(\vec{p})|O_Y^\dagger(0)|0\rangle$ .

This method can be used to determine the masses of all the stable mesons and baryons by making appropriate choices of operators. For example, if one uses the axial current,  $O_X = O_Y = A_\mu = \bar{d}\gamma_\mu\gamma_5 u$ , then one can determine  $m_{\pi^+}$  from the rate of exponential fall-off, and in addition the decay constant  $f_\pi$  from the coefficient of the exponential. A complication arises for states with high spins ( $j \geq 4$  for bosons) because the spatial rotation group on the lattice is a discrete subgroup of the continuum group  $SO(3)$ . This implies that lattice operators, even when chosen to lie in irreducible representations of the lattice rotation group, have overlap with states that have a number of values of  $j$  in the continuum limit [93]. For example  $j = 0$  operators can also create mesons with  $j = 4$ . Methods to overcome this problem in practice are available [94, 95] and have been used successfully.

The expression given above for the correlator  $C_{XY}(t; \vec{p})$  shows how, in principle, one can determine the energies of the excited hadron states having the same quantum numbers as the operators  $O_{X,Y}$ , by fitting the correlation function to a sum of exponentials, which is also important to precisely determine the ground-state exponential. In practice, in order to reliably identify the excited state, one often needs to use a large basis of operators and to adopt the variational approach such as that of Ref. [96]. One can also use an anisotropic lattice in which  $a_t$ , the lattice spacing in the time direction, is smaller than its spatial counterpart  $a_s$ . Using a combination of these and other technical improvements extensive excited-state spectra have been obtained [95, 97–100].

### 17.2.3 Three-point functions

Hadronic matrix elements needed to calculate semileptonic form factors and neutral meson mixing amplitudes can be computed from three-point correlation functions. We discuss here, as a representative example, the  $D \rightarrow K$  amplitude. As in the case of two-point correlation functions one constructs operators  $O_D$  and  $O_K$  having overlap, respectively, with the  $D$  and  $K$  mesons. We are interested in calculating the matrix element  $\langle K|V_\mu|D\rangle$ , with  $V_\mu = \bar{c}\gamma_\mu s$  the vector current calculations of this contribution.

To obtain this, we use the three-point correlator

$$C_{KV_\mu D}(t_x, t_y; \vec{p}) = \sum_{\vec{x}, \vec{y}} \langle O_K(t_x, \vec{x}) V_\mu(0) O_D^\dagger(t_y, \vec{y}) \rangle e^{-i\vec{p}\cdot\vec{x}}, \quad (17.11)$$

and focus on the limit  $t_x \rightarrow \infty$ ,  $t_y \rightarrow -\infty$ . In this example we set the  $D$ -meson at rest while the kaon carries three-momentum  $\vec{p}$ . Momentum conservation then implies that the weak operator  $V_\mu$  inserts three-momentum  $-\vec{p}$ . Inserting a pair of complete sets of states between each pair of operators, we find

$$C_{KV_\mu D}(t_x, t_y; \vec{p}) = \sum_{i,j} \frac{1}{2m_{D_i} 2E_{K_j}(\vec{p})} e^{-m_{D_i} t_x - E_{K_j}(\vec{p}) |t_y|} \langle 0|O_K(0)|K_i(\vec{p})\rangle \langle K_i(\vec{p})|V_\mu(0)|D_j(\vec{0})\rangle \langle D_j(\vec{0})|O_D^\dagger(0)|0\rangle. \quad (17.12)$$

The matrix element  $\langle K_i(\vec{p})|V_\mu(0)|D_j(\vec{0})\rangle$  can then be extracted, since all other quantities in this expression can be obtained from two-point correlation functions. Typically one is interested in the weak matrix elements of ground states, such as the lightest pseudoscalar mesons. In the limit of large separation between the three operators in Euclidean time, the three-point correlation function yields the weak matrix element of the transition between ground states.

### 17.2.4 Scattering amplitudes and resonances

The methods described thus far yield matrix elements involving single, stable particles (where by stable we mean here absolutely stable to strong interaction decays). Most of the particles listed in the Review of Particle Properties are, however, unstable—they

are resonances decaying into final states consisting of multiple strongly interacting particles. LQCD simulations cannot directly calculate resonance properties, but methods have been developed to do so indirectly for resonances coupled to two-particle final states in the elastic regime, starting from the seminal work of Lüscher [101].

The difficulty faced by LQCD calculations is that, to obtain resonance properties, or, more generally, scattering phase-shifts, one must calculate multiparticle scattering amplitudes in momentum space and put the external particles on their mass-shells. This requires analytically continuing from Euclidean to Minkowski momenta. Although it is straightforward in LQCD to generalize the methods described above to calculate four- and higher-point correlation functions, one necessarily obtains them at a discrete and finite set of Euclidean momenta. Analytic continuation to  $p_E^2 = -m^2$  is then an ill-posed and numerically unstable problem. The same problem arises for single-particle states, but can be largely overcome by picking out the exponential fall-off of the Euclidean correlator, as described above. With a multi-particle state there is no corresponding trick, except for two particles at threshold [102], although recent ideas using smeared correlators and advanced spectral-reconstruction methods offer hope for future progress [103–105].

What LQCD can calculate are the energies of the eigenstates of the QCD Hamiltonian in a finite box. The energies of states containing two stable particles, e.g. two pions, clearly depend on the interactions between the particles. It is possible to invert this dependence and, with plausible assumptions, determine the scattering phase-shifts at a discrete set of momenta from a calculation of the two-particle energy levels for a variety of spatial volumes [101]. This is a challenging calculation, but it has recently been carried through in several channels with quark masses approaching physical values. Channels studied include  $\pi\pi$  (for  $I = 2, 1$  and  $0$ ),  $\bar{K}K$ ,  $K\pi$ ,  $\pi\omega$ ,  $\pi\phi$ ,  $KD$ ,  $DD^*$  and  $B\pi$ . For recent comprehensive reviews see [106, 107]. Extensions to nucleon interactions are also being actively studied [108]. The generalization of the formalism to the case of three particles is under active development [109–111]. For a recent review, see [112].

It is also possible to extend the methodology to calculate electroweak decay amplitudes to two particles below the inelastic threshold, e.g.  $\Gamma(K \rightarrow \pi\pi)$  [113]. Results for both the  $\Delta I = 3/2$  and  $1/2$  amplitudes with physical quark masses have been obtained [114, 115], the former now including a controlled continuum limit [116]. First results for the CP-violating quantity  $\epsilon'$  have been obtained [115].

Partial extensions of the formalism above the elastic threshold have been worked out, in particular for the case of multiple two-particle channels [117]. Another theoretical extension is to allow the calculation of form factors between a stable particle and a resonance [118], and between two resonances [119]. The former has been used to calculate the  $\gamma\pi \rightarrow \rho$  amplitude, albeit for unphysically large quark masses [120].

While a systematic extension to decays with many multiparticle channels, e.g. hadronic  $B$  decays, has, however, yet to be formulated, some interesting new ideas have been recently proposed [121, 122].

### 17.2.5 Recent advances

In some physics applications, one is interested in the two-point correlation function  $\langle O_X(x) O_Y^\dagger(0) \rangle$  for all values of the separation  $x$ , not just its asymptotic form for large separations (which is used to determine the hadron spectrum as sketched above). A topical example is the hadronic vacuum polarization function  $\Pi_{\mu\nu}(x) = \langle V_\mu(x) V_\nu(0) \rangle$  and its Fourier transform  $\Pi_{\mu\nu}(q^2)$ . Since the lattice is in Euclidean space-time, only space-like momenta,  $q^2 = -Q^2 < 0$ , are accessible. Nevertheless, this quantity is of significant interest. It is related by a dispersion relation to the cross section for  $e^+e^- \rightarrow$  hadrons, and is needed for a first-principles calculation of the “hadronic vacuum polarization” contribution to the muon anomalous magnetic moment  $a_\mu$ . This is the contribution with the largest theoretical uncertainty at present. There are a number of lattice calculations of this contribution (see, e.g., Refs. [123–138] following the pioneering work Ref. [139]). Since the relevant scale is set by the muon mass  $m_\mu$ , this quantity is

most sensitive to the low-energy region  $Q^2 \simeq m_\mu^2$  of  $\Pi_{\mu\nu}(-Q^2)$ , where the long-range contribution of multibody states become relevant. The lattice calculation is challenging because of this and also because the necessary precision is high (below 1%). Many systematic effects must be carefully studied and controlled in order to achieve this precision, including finite volume errors and QED corrections.

Calculations of the light-by-light scattering contribution to  $a_\mu$  are also underway. These involve the calculations of four-point correlation functions with various external momenta. Clever ways to sum over them to evaluate the contribution to  $a_\mu$  are developed and first results have been reported [140–144]. Another approach to the light-by-light scattering is to decompose the amplitude to components using ChPT or phenomenological models, and to calculate the components in LQCD. Calculations of the  $\pi \rightarrow \gamma^* \gamma^*$  amplitudes follow similar directions [145–147].

There are other processes for which lattice calculations can make a significant contribution to establishing a quantitative understanding. One example is the long-distance contribution to the neutral kaon mass splitting,  $\Delta M_K$ . This also requires the evaluation of a four-point function, constructed from the two-point functions described above by the insertion of two electroweak Hamiltonians [148]. Rare kaon decays  $K \rightarrow \pi \ell^+ \ell^-$  and  $K \rightarrow \pi \nu \bar{\nu}$  are also important processes for which first lattice studies have recently appeared [149–153].

### 17.2.6 Status of LQCD simulations

Until the 1990s, most large-scale lattice simulations were limited to the “quenched” approximation, wherein the fermion determinant is omitted from the path integral. While much of the basic methodology was developed in this era, the results obtained had uncontrolled systematic errors and were not suitable for use in placing precision constraints on the Standard Model. During the 1990s, more extensive simulations including the fermion determinant (also known as simulations with “dynamical” fermions) were begun, but with unphysically heavy quark masses ( $m_\ell \sim 50 - 100$  MeV), such that the extrapolation to the physical light quark masses was a source of large systematic errors [154]. During the 2000s, advances in both algorithms and computers allowed simulations to reach much smaller quark masses ( $m_\ell \sim 10 - 20$  MeV) such that LQCD calculations of selected quantities with all sources of error controlled and small became available. Their results played an important role in constraints on the CKM matrix and other phenomenological analyses. In the last few years, simulations directly at the physical isospin-symmetric light quark masses have become standard, removing the need for a chiral extrapolation and thus significantly reducing the overall error. The present frontier, as noted above, is the inclusion of isospin breaking. This will be needed to push the accuracy of calculations below the percent level.

On a more qualitative level, analytic and numerical results from LQCD have demonstrated that QCD confines color and spontaneously breaks chiral symmetry. Confinement can be seen as a linearly rising potential between heavy quark and anti-quark in the absence of quark loops. Analytically, this can be shown in the strong coupling limit  $g_{\text{lat}} \rightarrow \infty$  [1]. At weaker couplings there are precise numerical calculations of the potential that clearly show that this behavior persists in the continuum limit [155–157].

Chiral symmetry breaking was also demonstrated in the strong coupling limit on the lattice [19, 158], and there have been a number of numerical studies showing that this holds also in the continuum limit. The accumulation of low-lying modes of the Dirac operator, which is the analog of Cooper pair condensation in superconductors, has been observed, yielding a determination of the chiral condensate [159–164]. Many relations among physical quantities that can be derived under the assumption of broken chiral symmetry have been confirmed by a number of lattice groups [165].

## 17.3 Physics applications

In this section we describe the main applications of LQCD that are both computationally mature and relevant for the determination of particle properties.

A general feature to keep in mind is that, since there are many

different choices for lattice actions, all of which lead to the same continuum theory, a crucial test is that results for any given quantity are consistent. In many cases, different lattice calculations are completely independent and often have very different systematic errors. Thus final agreement, if found, is a highly non-trivial check, just as it is for different experimental measurements.

The number, variety and precision of the calculations has progressed to the point that an international “Flavour Lattice Averaging Group” (FLAG) has been formed. The main aims of FLAG include collecting all lattice results of relevance for a variety of phenomenologically interesting quantities and providing averages of those results which pass appropriate quality criteria. The averages attempt to account for possible correlations between results (which can arise, for example, if they use common gauge configurations). The quantities considered are those we discuss in this section, with the exception of the hadron spectrum. The most recent FLAG review is from 2019 [53] (see also an older edition, Ref. [165]). The interested reader can consult this review for very extensive discussions of the details of the calculations and of the sources of systematic errors.

We stress that the results we quote below are those obtained using the physical complement of light quarks (i.e.  $N_f = 2 + 1$  or  $2 + 1 + 1$  simulations).

### 17.3.1 Spectrum

The most basic prediction of LQCD is of the hadron spectrum. Once the input parameters are fixed as described in Sec. 17.1.5, the masses or resonance parameters of all other states can be predicted. This includes hadrons composed of light ( $u$ ,  $d$  and  $s$ ) quarks, as well as heavy-light and heavy-heavy hadrons. It also includes quark-model exotics (e.g.  $J^{PC} = 1^{-+}$  mesons) and glueballs. Thus, in principle, LQCD calculations should be able to reproduce many of the experimental results compiled in the Review of Particle Properties. Doing so would test both that the error budgets of LQCD calculations are accurate and that QCD indeed describes the strong interactions in the low-energy domain. The importance of the latter test can hardly be overstated.

What is the status of this fundamental test? As discussed in Sec. 1.2, LQCD calculations are most straightforward for stable, low-lying hadrons. Calculations of the properties of resonances that can decay into only two particles are more challenging, though substantial progress has been made. First theoretical work on decays to more than two particles has begun, but the methodology is not yet practical. It is also more technically challenging to calculate masses of flavor singlet states (which can annihilate into purely gluonic intermediate states) than those of flavor non-singlets, although again algorithmic and computational advances have begun to make such calculations accessible, although not yet for physical quark masses. The present status for light hadrons is that fully controlled results are available for the masses of the octet light baryons, while results with less than complete control are available for the decuplet baryon resonances, the vector meson resonances and the  $\eta$  and  $\eta'$ . In addition, it has been possible to calculate the isospin splitting in light mesons and baryons (due to the up-down mass difference and the incorporation of QED). There are also extensive results for heavy-light ( $D$  and  $B$  systems) and heavy-heavy ( $J/\psi$  and  $\Upsilon$  systems). All present results, which are discussed in the “Quark Model” review, are consistent with experimental values, and several predictions have been made. We refer the reader to that review for references to the relevant work.

### 17.3.2 Decay constants and bag parameters

The pseudoscalar decay constants can be determined from two-point correlation functions involving the axial-vector current, as discussed in Sec. 17.2.2. The decay constant  $f_P$  of a meson  $P$  is extracted from the weak matrix element involving the axial-vector current using the relation  $\langle 0 | A_\mu(x) | P(\vec{p}) \rangle = f_P p_\mu \exp(-ip \cdot x)$ , where  $p_\mu$  is the momentum of  $P$  and  $A_\mu(x)$  is the axial-vector current. Since they are among the simplest quantities to calculate, decay constants provide good benchmarks for lattice methods, in addition to being important inputs for flavor physics phenomenology in their own right. Results from many lattice groups for the pion and kaon decay constants now have errors at the percent level or better. The decay constants in the charm and bottom sectors,

$f_D$ ,  $f_{D_s}$ ,  $f_B$ , and  $f_{B_s}$ , have also been calculated to high precision. Lattice results for all of these decay constants are discussed in detail in the review “Leptonic Decays of Charged Pseudoscalar Mesons.”

Another important lattice quantity is the kaon bag parameter,  $B_K$ , which is needed to turn the precise measurement of CP-violation in kaon mixing into a constraint on the Standard Model. It is defined by

$$\frac{8}{3} m_K^2 f_K^2 B_K(\mu) = \langle \bar{K}^0 | Q_{\Delta S=2}(\mu) | K^0 \rangle, \quad (17.13)$$

where  $m_K$  is the kaon mass,  $f_K$  is the kaon decay constant,  $Q_{\Delta S=2} = \bar{s}\gamma_\mu(1-\gamma_5)d\bar{s}\gamma_\mu(1-\gamma_5)d$  is the four-quark operator of the effective electroweak Hamiltonian and  $\mu$  is the renormalization scale. The short distance contribution to the electroweak Hamiltonian can be calculated perturbatively, but the hadronic matrix element parameterized by  $B_K$  must be computed using non-perturbative methods. In order to be of use to phenomenology, the renormalization factor of the four-quark operator must be matched to a continuum renormalization scheme, e.g. to  $\overline{\text{MS}}$ , as described in Sec. 17.1.6.4. Determinations with percent-level precision using different fermion actions and  $N_f = 2+1$  light sea quarks are now available using DWF [166], staggered fermions [167], DWF valence on staggered sea quarks [168], and Wilson fermions [13]. The results are all consistent, and the present FLAG average is  $\hat{B}_K = 0.7625(97)$  [53].

The bag parameters for  $B$  and  $B_s$  meson mixing are defined analogously to that for kaon mixing. The  $B$  and  $B_s$  mesons contain a valence  $b$ -quark so that calculations of these quantities must use one of the methods for heavy quarks described above. Calculations with  $N_f = 2+1$  light fermions have been done using NRQCD [169], the Fermilab formalism [68], and static heavy quarks [170]. All results are consistent. The FLAG averages for the quantities relevant for  $B_s$  and  $B$  mixing are  $f_{B_s}\sqrt{B_{B_s}} = 274(8)$  MeV and  $f_B\sqrt{B_B} = 225(9)$  MeV, with their ratio (which is somewhat better determined) being  $\xi = 1.206(17)$  [53]. Note that the errors for quantities involving  $b$  quarks are larger than those for quantities involving only light quarks, although the difference has decreased over the last two years.

For the  $K$ ,  $D$  and  $B$  systems, one can also consider the matrix elements of four-fermion operators that arise in beyond-the-standard-model (BSM) theories, which can have a different chiral structure. Knowledge of these matrix elements allows one to constrain the parameters of the BSM theories, and is complementary to direct searches at the LHC. Reliable results are now available from lattice calculations, and are reviewed by FLAG in the case of kaon mixing [53]. Complete results for  $D$  and  $B$  mixing are presented in Ref. [171] and Ref. [68], respectively.

The results for mixing matrix elements are used in the reviews “The CKM Quark-Mixing Matrix,” and “ $B^0 - \bar{B}^0$  Mixing.”

### 17.3.3 Form factors ( $K \rightarrow \pi\ell\nu$ , $D \rightarrow K\ell\nu$ , $B \rightarrow \pi\ell\nu$ , $B \rightarrow D^{(*)}\ell\nu$ )

Semileptonic decay rates can be used to extract CKM matrix elements once the semileptonic form factors are known from lattice calculations. For example, the matrix element of a pseudoscalar meson  $P$  undergoing semileptonic decay to another pseudoscalar meson  $D$  is mediated by the vector current, and can be written in terms of form factors as

$$\langle D(p_D) | V_\mu | P(p_P) \rangle = f_+(q^2)(p_D + p_P - \Delta)_\mu + f_0(q^2)\Delta_\mu, \quad (17.14)$$

where  $q = p_D - p_P$ ,  $\Delta_\mu = (m_D^2 - m_P^2)q_\mu/q^2$  and  $V_\mu$  is the quark vector current. The shape of the form factor is typically well determined by experiment, and the value of  $f_+(q^2)$  at some reference value of  $q^2$  is needed from the lattice in order to extract CKM matrix elements. Typically  $f_+(q^2)$  dominates the decay rate, since the contribution from  $f_0(q^2)$  is suppressed when the final state lepton is light.

The form factor  $f_+(0)$  for  $K \rightarrow \pi\ell\nu$  decays is highly constrained by the Ademollo-Gatto theorem [172] and chiral symmetry. Old estimates using chiral perturbation theory combined with quark models quote sub-percent precision [173], though they suffer from

some model dependence. Utilizing the constraint from the vector current conservation that  $f_+(0)$  is normalized to unity in the limit of degenerate up and strange quark masses, the lattice calculation can be made very precise and has now matched the precision of the phenomenological estimates [174–181]. The present FLAG average (from  $N_f = 2+1$  simulations) is  $f_+(0) = 0.9677(27)$  [53].

Charm meson semileptonic decays have been calculated by different groups using methods similar to those used for charm decay constants, and results are steadily improving in precision [182–185]. For semileptonic decays involving a bottom quark, one uses HQET or NRQCD to control the discretization errors of the bottom quark. The form factors for the semileptonic decay  $B \rightarrow \pi\ell\nu$  have been calculated in unquenched lattice QCD by a number of groups [186–191]. These  $B$  semileptonic form factors are difficult to calculate at low  $q^2$ , *i.e.* when the mass of the  $B$ -meson must be balanced by a large pion momentum, in order to transfer a large momentum to the lepton pair. The low  $q^2$  region has large discretization errors and very large statistical errors, while the high  $q^2$  region is much more accessible to the lattice. For experiment, the opposite is true. To combine lattice and experimental results it has proved helpful to use the  $z$ -parameter expansion [192]. This provides a theoretically constrained parameterization of the entire  $q^2$  range, and allows one to obtain  $|V_{ub}|$  without model dependence [193, 194].

The semileptonic decays  $B \rightarrow D\ell\nu$  and  $B \rightarrow D^*\ell\nu$  can be used to extract  $|V_{cb}|$  once the corresponding form factors are known. The lattice calculation is most precise at zero recoil since the bulk of the systematic error cancels for appropriate ratios between  $B \rightarrow D^{(*)}$  and  $B \rightarrow B$  or  $D^{(*)} \rightarrow D^{(*)}$  [195, 196]. The unquenched calculation of the  $B \rightarrow D^{(*)}\ell\nu$  form factor at zero recoil has been performed with various formulations for the heavy quark [197–201]. Calculations at non-zero recoil have also been performed to constrain the functional form of the form factor, which can be used to extrapolate the experimental data to the zero-recoil point or to determine  $|V_{cb}|$  directly at the non-zero recoil points [202–205]. Semileptonic decays of the  $\Lambda_b$  baryon can also be used to constrain  $|V_{cb}|$  and  $|V_{ub}|$  using lattice calculations of the relevant form factors [206, 207].

The rare decays  $B \rightarrow K^{(*)}\ell^+\ell^-$  involve matrix elements similar to those needed for semileptonic decays, Eq. (17.14), except that the vector current  $V_\mu$  is replaced by the operators  $\bar{s}\gamma^\mu(1-\gamma_5)b$  or  $\bar{s}\sigma^{\mu\nu}(1+\gamma_5)b$ . Lattice calculations of the corresponding form factors involve similar techniques to those for the semileptonic form factors. The values of  $q^2$  for which lattice calculations can be done are limited as for  $B$  semileptonic decays, and, in addition, the region of  $c\bar{c}$  resonances has to be avoided. Recent lattice calculations [190, 208–210] have been used to constrain the standard model and new physics contributions.

The results discussed in this section are used in the reviews “The CKM Quark-Mixing Matrix,” “ $V_{ud}$ ,  $V_{us}$ , the Cabibbo Angle and CKM Unitarity,” and “ $V_{cb}$  and  $V_{ub}$  CKM Matrix Elements.”

### 17.3.4 Strong coupling constant

As explained in Sec. 17.1.5.1, for a given lattice action, the choice of bare lattice coupling constant,  $g_{\text{lat}}$ , determines the lattice spacing  $a$ . If one then calculates  $a$  as described in Sec. 17.1.5.1, one knows the strong coupling constant in the bare lattice scheme at the scale  $1/a$ ,  $\alpha_{\text{lat}} = g_{\text{lat}}^2/(4\pi)$ . This is not, however, useful for comparing to results for  $\alpha_s$  obtained from other inputs, such as deep inelastic scattering or jet shape variables. This is because the latter results give  $\alpha_s$  in the  $\overline{\text{MS}}$  scheme, which is commonly used in such analyses, and the conversion factor between these two schemes is known to converge extremely poorly in perturbation theory. Instead one must use a method which directly determines  $\alpha_s$  on the lattice in a scheme closer to  $\overline{\text{MS}}$ .

Several such methods have been used, all following a similar strategy. One calculates a short-distance quantity  $K$  both perturbatively ( $K^{\text{PT}}$ ) and non-perturbatively ( $K^{\text{NP}}$ ) on the lattice, and requires equality:  $K^{\text{NP}} = K^{\text{PT}} = \sum_{i=0}^n c_i \alpha_s^i$ . Solving this equation one obtains  $\alpha_s$  at a scale related to the quantity being used. Often,  $\alpha_s$  thus obtained is not defined in the conventional  $\overline{\text{MS}}$  scheme, and one has to convert among the different schemes using perturbation theory. Unlike for the bare lattice scheme, the required conversion factors are reasonably convergent. As a fi-

nal step, one uses the renormalization group to run the resulting coupling to a canonical scale (such as  $M_Z$ ).

In the work of the HPQCD collaboration [211, 212], the short-distance quantities are Wilson loops of several sizes and their ratios. These quantities are perturbatively calculated through  $\mathcal{O}(\alpha_s^3)$  using the  $V$ -scheme defined through the heavy quark potential. The coefficients of even higher orders are estimated using the data at various values of  $a$ . In addition, this work obtains a result for  $\alpha_s$  by matching with  $\alpha_{\text{lat}}$  in a tadpole-improved scheme that improves convergence.

Another choice of short-distance quantities is to use current-current correlators. Appropriate moments of these correlators are ultraviolet finite, and by matching lattice results to the *continuum* perturbative predictions, one can directly extract the  $\overline{\text{MS}}$  coupling. The method can be applied for light meson correlators [213, 214] as well as heavy meson correlators [36, 212, 215–217]. Yet another choice of short-distance quantity is the static-quark potential, where the lattice result for the potential is compared to perturbative calculations; this method was used to compute  $\alpha_s$  within 2+1 flavor QCD [218–222]. There is also a determination of  $\alpha_s$  from a comparison of lattice data for the ghost-gluon coupling with that of perturbation theory [223, 224].

With a definition of  $\alpha_s$  given using the Schrödinger functional, one can non-perturbatively control the evolution of  $\alpha_s$  to high-energy scales, such as 100 GeV, where the perturbative expansion converges very well. This method developed by the ALPHA collaboration [81] has been applied to 2+1-flavor QCD in [225–227].

The various lattice methods for calculating  $\alpha_s$  have significantly different sources of systematic error. The FLAG review [53] reported an estimate  $\alpha_{\overline{\text{MS}}}^{(5)}(M_Z) = 0.11823(81)$  based on these various lattice calculations. A comparison to other phenomenological determinations can be found in the “Quantum Chromodynamics” review.

### 17.3.5 Quark masses

Once the quark mass parameters are tuned in the lattice action, the remaining task is to convert them to those of the conventional definition. Since the quarks do not appear as asymptotic states due to confinement, the pole mass of the quark propagator is not a physical quantity. Instead, one defines the quark mass after subtracting the ultra-violet divergences in some particular way. The conventional choice is again the  $\overline{\text{MS}}$  scheme at a canonical scale such as 2 or 3 GeV. Ratios such as  $m_c/m_s$  and  $m_b/m_c$  are also useful as they are free from multiplicative renormalization (in a mass-independent scheme).

As discussed in Sec. 17.1.6.4, one must convert the lattice bare quark mass to that in the  $\overline{\text{MS}}$  scheme. Older calculations did so directly using perturbation theory; most recent calculations use an intermediate NPR method (e.g. RI/MOM or RI/SMOM) which is then converted to the  $\overline{\text{MS}}$  scheme using perturbation theory (see, e.g., [166, 228, 229]).

Alternatively, one can use a definition based on the Schrödinger functional, which allows one to evolve the quark mass to a high scale non-perturbatively [230]. In practice, one can reach scales as high as  $\sim 100$  GeV, at which matching to the  $\overline{\text{MS}}$  scheme can be reliably calculated in perturbation theory.

Another approach available for heavy quarks is to match current-current correlators at short distances calculated on the lattice to those obtained in continuum perturbation theory in the  $\overline{\text{MS}}$  scheme [36, 212, 215–217]. This has allowed an accurate determination of  $m_c$  and  $m_b$  [80, 212, 216].

The ratio method for heavy quarks (discussed earlier) can also be used to determine  $m_b$  [231].

Results are summarized in the review of “Quark Masses.”

### 17.3.6 Other applications

In this review we have concentrated on applications of LQCD that are relevant to the quantities discussed in the Review of Particle Properties. We have not discussed at all several other applications that are being actively pursued by simulations. Here we list the major such applications. The reader can consult the aforementioned texts [2–4] for further details, as well as the proceedings of recent lattice conferences [232], and several recent white

papers [233–239].

LQCD can be used, in principle, to simulate QCD at non-zero temperature and density, and in particular to study how confinement and chiral-symmetry breaking are lost as  $T$  and  $\mu$  (the chemical potential) are increased. This is of relevance to heavy-ion collisions, the early Universe and neutron-star structure. In practice, finite temperature simulations are computationally tractable and relatively mature, while simulations at finite  $\mu$  suffer from a “sign problem” and are at a rudimentary stage.

Another topic under active investigation is nucleon structure and inter-nucleon interactions. The simplest nucleon matrix elements are calculable with a precision that is now starting to rival that for some mesonic quantities. Of particular interest are those of the axial current (leading to  $g_A$ ) and of the scalar density (with  $\langle N|\bar{s}s|N\rangle$  needed for dark matter searches). Other such matrix elements provide information on the parton distribution functions (PDFs) including their low moments. More recently, methods to directly access PDFs are being developed (see, e.g., Ref. [233] for a recent summary).

Finally, we note that there is much recent interest in studying QCD-like theories with more fermions, possibly in other representations of the gauge group (see, e.g., [235]). The main interest is to find nearly conformal theories which might be candidates for “walking technicolor” models.

## 17.4 Outlook

While LQCD calculations have made major strides in the last decade, and are now playing an important role in constraining the Standard Model, there are many calculations that could be done in principle but are not yet mature due to limitations in computational resources. As we move to exascale resources ( $10^{18}$  floating point operations per second), the list of mature calculations will grow. Examples that we expect to mature in the next few years are results for  $B$  meson and  $\Lambda_b$  baryon form factors covering the full range of  $q^2$ ; results for excited hadrons, including quark-model exotics, at close to physical light-quark masses; results for moments of structure functions; results for the simplest nucleon matrix elements;  $K \rightarrow \pi\pi$  amplitudes (allowing a prediction of  $\epsilon'/\epsilon$  from the Standard Model); hadronic vacuum polarization contributions to  $g_\mu - 2$ , the running of  $\alpha_{\text{EM}}$  and  $\alpha_s$ ;  $\pi \rightarrow \gamma\gamma$  and related amplitudes; long-distance contributions to  $\overline{K} \leftrightarrow K$  mixing; the light-by-light contribution to  $g_\mu - 2$ ; and determinations of long distance contributions to rare kaon decays such as  $K \rightarrow \pi\nu\bar{\nu}$ . There will also be steady improvement in the precision attained for the mature quantities discussed above. As already noted, this will ultimately require simulations with  $m_u \neq m_d$  and including electromagnetic effects.

## References

- [1] K. G. Wilson, Phys. Rev. **D10**, 2445 (1974).
- [2] T. Degrand & C. DeTar, “Lattice Methods for Quantum Chromodynamics,” World Scientific (2006).
- [3] C. Gattringer & C.B. Lang, “Quantum Chromodynamics on the Lattice: An Introductory Presentation,” Springer (2009).
- [4] “Modern Perspectives in Lattice QCD: quantum field theory and high performance computing” (Lecture notes of the Les Houches Summer School, Vol. 93) eds. L. Lellouch *et al.*, Oxford Univ. Press. (Aug. 2011).
- [5] W. Zimmermann, in “Lectures on Elementary Particles and Quantum Field Theory”, ed. S. Deser *et al.*, MIT Press, Cambridge, MA (1971); K. Symanzik, Nucl. Phys. **B226**, 187 (1983); K. Symanzik, Nucl. Phys. **B226**, 205 (1983).
- [6] M. Luscher and P. Weisz, Commun. Math. Phys. **97**, 59 (1985), [Erratum: Commun. Math. Phys.98,433(1985)].
- [7] Y. Iwasaki, UT-HEP-118.
- [8] H. B. Nielsen and M. Ninomiya, Phys. Lett. **105B**, 219 (1981).
- [9] B. Sheikholeslami and R. Wohlert, Nucl. Phys. **B259**, 572 (1985).
- [10] K. Jansen *et al.*, Phys. Lett. **B372**, 275 (1996), [hep-lat/9512009].

- [11] M. Luscher, JHEP **05**, 052 (2003), [hep-lat/0304007].
- [12] M. Luscher, Comput. Phys. Commun. **156**, 209 (2004), [hep-lat/0310048]; M. Luscher, Comput. Phys. Commun. **165**, 199 (2005), [hep-lat/0409106]; M. Hasenbusch, Phys. Lett. **B519**, 177 (2001), [hep-lat/0107019]; C. Urbach *et al.*, Comput. Phys. Commun. **174**, 87 (2006), [hep-lat/0506011].
- [13] S. Durr *et al.*, Phys. Lett. **B705**, 477 (2011), [arXiv:1106.3230].
- [14] N. Ishizuka *et al.*, Phys. Rev. **D92**, 7, 074503 (2015), [arXiv:1505.05289].
- [15] R. Frezzotti *et al.* (Alpha), JHEP **08**, 058 (2001), [hep-lat/0101001].
- [16] R. Frezzotti and G. C. Rossi, JHEP **08**, 007 (2004), [hep-lat/0306014].
- [17] R. Frezzotti and G. C. Rossi, Nucl. Phys. Proc. Suppl. **128**, 193 (2004), [hep-lat/0311008].
- [18] R. Frezzotti and G. C. Rossi, JHEP **10**, 070 (2004), [hep-lat/0407002].
- [19] L. Susskind, Phys. Rev. **D16**, 3031 (1977).
- [20] M. Golterman, PoS **CONFINEMENT8**, 014 (2008).
- [21] C. Bernard, Phys. Rev. **D73**, 114503 (2006), [hep-lat/0603011]; S. R. Sharpe, PoS **LAT2006**, 022 (2006), [hep-lat/0610094].
- [22] G. P. Lepage, Phys. Rev. **D59**, 074502 (1999), [hep-lat/9809157].
- [23] A. Bazavov *et al.* (MILC), Rev. Mod. Phys. **82**, 1349 (2010), [arXiv:0903.3598].
- [24] E. Follana *et al.* (HPQCD, UKQCD), Phys. Rev. **D75**, 054502 (2007), [hep-lat/0610092].
- [25] C. T. H. Davies *et al.*, Phys. Rev. **D82**, 114504 (2010), [arXiv:1008.4018].
- [26] G. C. Donald *et al.*, Phys. Rev. **D86**, 094501 (2012), [arXiv:1208.2855].
- [27] P. H. Ginsparg and K. G. Wilson, Phys. Rev. **D25**, 2649 (1982).
- [28] P. Hasenfratz, V. Laliena and F. Niedermayer, Phys. Lett. **B427**, 125 (1998), [hep-lat/9801021].
- [29] M. Luscher, Phys. Lett. **B428**, 342 (1998), [hep-lat/9802011].
- [30] D. B. Kaplan, Phys. Lett. **B288**, 342 (1992), [hep-lat/9206013]; Y. Shamir, Nucl. Phys. **B406**, 90 (1993), [hep-lat/9303005]; Y. Shamir, Nucl. Phys. **B417**, 167 (1994), [hep-lat/9310006].
- [31] H. Neuberger, Phys. Lett. **B417**, 141 (1998), [hep-lat/9707022]; H. Neuberger, Phys. Lett. **B427**, 353 (1998), [hep-lat/9801031].
- [32] A. Borici, NATO Sci. Ser. C **553**, 41 (2000), [hep-lat/9912040].
- [33] A. D. Kennedy (2006), [hep-lat/0607038].
- [34] E. Shintani *et al.* (JLQCD), Phys. Rev. Lett. **101**, 242001 (2008), [arXiv:0806.4222].
- [35] P. A. Boyle *et al.*, JHEP **12**, 008 (2017), [arXiv:1701.02644].
- [36] K. Nakayama, B. Fahy and S. Hashimoto, Phys. Rev. **D94**, 5, 054507 (2016), [arXiv:1606.01002].
- [37] C. McNeile *et al.*, Phys. Rev. **D85**, 031503 (2012), [arXiv:1110.4510].
- [38] A. Bazavov *et al.*, Phys. Rev. **D98**, 7, 074512 (2018), [arXiv:1712.09262].
- [39] A. Bazavov *et al.* (Fermilab Lattice, MILC, TUMQCD), Phys. Rev. **D98**, 5, 054517 (2018), [arXiv:1802.04248].
- [40] E. Eichten and B. R. Hill, Phys. Lett. **B234**, 511 (1990).
- [41] J. Heitger and R. Sommer (ALPHA), JHEP **02**, 022 (2004), [hep-lat/0310035]; B. Blossier *et al.* (ALPHA), JHEP **12**, 039 (2010), [arXiv:1006.5816].
- [42] B. A. Thacker and G. P. Lepage, Phys. Rev. **D43**, 196 (1991); G. P. Lepage *et al.*, Phys. Rev. **D46**, 4052 (1992), [hep-lat/9205007].
- [43] R. J. Dowdall *et al.* (HPQCD), Phys. Rev. **D85**, 054509 (2012), [arXiv:1110.6887].
- [44] A. X. El-Khadra, A. S. Kronfeld and P. B. Mackenzie, Phys. Rev. **D55**, 3933 (1997), [hep-lat/9604004].
- [45] S. Aoki, Y. Kuramashi and S.-i. Tominaga, Prog. Theor. Phys. **109**, 383 (2003), [hep-lat/0107009].
- [46] N. H. Christ, M. Li and H.-W. Lin, Phys. Rev. **D76**, 074505 (2007), [hep-lat/0608006].
- [47] Y. Aoki *et al.* (RBC, UKQCD), Phys. Rev. **D86**, 116003 (2012), [arXiv:1206.2554].
- [48] N. H. Christ *et al.*, Phys. Rev. **D91**, 5, 054502 (2015), [arXiv:1404.4670].
- [49] M. B. Oktay and A. S. Kronfeld, Phys. Rev. **D78**, 014504 (2008), [arXiv:0803.0523].
- [50] J. A. Bailey *et al.*, Eur. Phys. J. **C77**, 11, 768 (2017), [arXiv:1701.00345].
- [51] B. Blossier *et al.* (ETM), JHEP **04**, 049 (2010), [arXiv:0909.3187].
- [52] S. Borsanyi *et al.*, Science **347**, 1452 (2015), [arXiv:1406.4088].
- [53] S. Aoki *et al.* (Flavour Lattice Averaging Group) (2019), [arXiv:1902.08191].
- [54] R. Horsley *et al.*, J. Phys. G **43**, no. 10, 10LT02 (2016).
- [55] S. Aoki *et al.* [PACS-CS Collab.], PTEP **2012**, 01A102 (2012).
- [56] T. Ishikawa *et al.*, Phys. Rev. Lett. **109**, 072002 (2012), [arXiv:1202.6018].
- [57] G. M. de Divitiis *et al.* (RM123), Phys. Rev. **D87**, 11, 114505 (2013), [arXiv:1303.4896].
- [58] P. Boyle *et al.*, JHEP **09**, 153 (2017), [arXiv:1706.05293].
- [59] F. Bloch and A. Nordsieck, Phys. Rev. **52**, 54 (1937).
- [60] N. Carrasco *et al.*, Phys. Rev. **D91**, 7, 074506 (2015), [arXiv:1502.00257].
- [61] D. Giusti *et al.*, Phys. Rev. Lett. **120**, 7, 072001 (2018), [arXiv:1711.06537].
- [62] M. Di Carlo *et al.* (2019), [arXiv:1904.08731].
- [63] M. Bruno *et al.* (ALPHA), Phys. Rev. Lett. **114**, 10, 102001 (2015), [arXiv:1410.8374].
- [64] F. Knechtli *et al.* (ALPHA), Phys. Lett. **B774**, 649 (2017), [arXiv:1706.04982].
- [65] A. Athenodorou *et al.* (ALPHA), Nucl. Phys. **B943**, 114612 (2019), [arXiv:1809.03383].
- [66] S. Cali, F. Knechtli and T. Korzec, Eur. Phys. J. **C79**, 7, 607 (2019), [arXiv:1905.12971].
- [67] D. Giusti *et al.*, Phys. Rev. **D95**, 11, 114504 (2017), [arXiv:1704.06561].
- [68] A. Bazavov *et al.* (Fermilab Lattice, MILC), Phys. Rev. **D93**, 11, 113016 (2016), [arXiv:1602.03560].
- [69] R. J. Dowdall *et al.*, Phys. Rev. **D86**, 094510 (2012), [arXiv:1207.5149].
- [70] C. McNeile *et al.*, Phys. Rev. **D86**, 074503 (2012), [arXiv:1207.0994].
- [71] S. Schaefer, R. Sommer and F. Virotta (ALPHA), Nucl. Phys. **B845**, 93 (2011), [arXiv:1009.5228].
- [72] M. Luscher, PoS **LATTICE2010**, 015 (2010), [arXiv:1009.5877].
- [73] R. Brower *et al.*, Phys. Lett. **B560**, 64 (2003), [hep-lat/0302005].
- [74] S. Aoki *et al.*, Phys. Rev. **D76**, 054508 (2007), [arXiv:0707.0396].

- [75] G. Colangelo, S. Durr and C. Haefeli, Nucl. Phys. **B721**, 136 (2005), [hep-lat/0503014].
- [76] M. Luscher, Commun. Math. Phys. **104**, 177 (1986).
- [77] G. Martinelli *et al.*, Nucl. Phys. **B445**, 81 (1995), [hep-lat/9411010].
- [78] M. Luscher *et al.*, Nucl. Phys. **B384**, 168 (1992), [hep-lat/9207009].
- [79] G. Martinelli *et al.*, Phys. Lett. **B411**, 141 (1997), [hep-lat/9705018].
- [80] B. Colquhoun *et al.*, Phys. Rev. **D91**, 7, 074514 (2015), [arXiv:1408.5768].
- [81] M. Luscher *et al.*, Nucl. Phys. **B413**, 481 (1994), [hep-lat/9309005]; M. Della Morte *et al.* (ALPHA), Nucl. Phys. **B713**, 378 (2005), [hep-lat/0411025].
- [82] M. Tomii *et al.* (JLQCD), Phys. Rev. **D94**, 5, 054504 (2016), [arXiv:1604.08702].
- [83] S. Duane *et al.*, Phys. Lett. **B195**, 216 (1987).
- [84] M. A. Clark and A. D. Kennedy, Phys. Rev. Lett. **98**, 051601 (2007), [hep-lat/0608015].
- [85] M. Luscher, JHEP **07**, 081 (2007), [arXiv:0706.2298].
- [86] M. Luscher, JHEP **12**, 011 (2007), [arXiv:0710.5417].
- [87] A. Stathopoulos and K. Orginos, SIAM J. Sci. Comput. **32**, 439 (2010), [arXiv:0707.0131].
- [88] P. A. Boyle (2014), [arXiv:1402.2585].
- [89] R. Babich *et al.*, Phys. Rev. Lett. **105**, 201602 (2010), [arXiv:1005.3043].
- [90] A. Frommer *et al.*, SIAM J. Sci. Comput. **36**, A1581 (2014), [arXiv:1303.1377].
- [91] M. Bruno, S. Schaefer and R. Sommer (ALPHA), JHEP **08**, 150 (2014), [arXiv:1406.5363].
- [92] M. Creutz, Phys. Rev. **D38**, 1228 (1988); R. Gupta, G. W. Kilcup and S. R. Sharpe, Phys. Rev. **D38**, 1278 (1988).
- [93] J. E. Mandula, G. Zweig and J. Govaerts, Nucl. Phys. **B228**, 91 (1983); J. E. Mandula and E. Shpiz, Nucl. Phys. **B232**, 180 (1984).
- [94] H. B. Meyer and M. J. Teper, Nucl. Phys. **B658**, 113 (2003), [hep-lat/0212026].
- [95] J. J. Dudek *et al.*, Phys. Rev. **D82**, 034508 (2010), [arXiv:1004.4930]; J. J. Dudek *et al.*, Phys. Rev. **D83**, 111502 (2011), [arXiv:1102.4299]; R. G. Edwards *et al.*, Phys. Rev. **D84**, 074508 (2011), [arXiv:1104.5152].
- [96] M. Luscher and U. Wolff, Nucl. Phys. **B339**, 222 (1990).
- [97] G. P. Engel *et al.* (BGR [Bern-Graz-Regensburg]), Phys. Rev. **D82**, 034505 (2010), [arXiv:1005.1748]; D. Mohler *et al.*, Phys. Rev. Lett. **111**, 22, 222001 (2013), [arXiv:1308.3175].
- [98] M. S. Mahbub *et al.*, Annals Phys. **342**, 270 (2014), [arXiv:1310.6803].
- [99] J. Bulava *et al.*, Nucl. Phys. **B910**, 842 (2016), [arXiv:1604.05593].
- [100] R. Brett *et al.*, Nucl. Phys. **B932**, 29 (2018), [arXiv:1802.03100].
- [101] M. Luscher, Commun. Math. Phys. **105**, 153 (1986); M. Luscher, Nucl. Phys. **B364**, 237 (1991).
- [102] L. Maiani and M. Testa, Phys. Lett. **B245**, 585 (1990).
- [103] M. T. Hansen, H. B. Meyer and D. Robaina, Phys. Rev. **D96**, 9, 094513 (2017), [arXiv:1704.08993].
- [104] M. Hansen, A. Lupo and N. Tantalo, Phys. Rev. **D99**, 9, 094508 (2019), [arXiv:1903.06476].
- [105] J. Bulava and M. T. Hansen (2019), [arXiv:1903.11735].
- [106] R. A. Briceño, J. J. Dudek and R. D. Young, Rev. Mod. Phys. **90**, 2, 025001 (2018), [arXiv:1706.06223].
- [107] N. Brambilla *et al.* (2019), [arXiv:1907.07583].
- [108] M. J. Savage, Prog. Part. Nucl. Phys. **67**, 140 (2012), [arXiv:1110.5943]; T. Inoue *et al.* (HAL QCD), Phys. Rev. **C91**, 1, 011001 (2015), [arXiv:1408.4892].
- [109] K. Polejaeva and A. Rusetsky, Eur. Phys. J. **A48**, 67 (2012), [arXiv:1203.1241]; R. A. Briceño and Z. Davoudi, Phys. Rev. **D87**, 9, 094507 (2013), [arXiv:1212.3398]; M. T. Hansen and S. R. Sharpe, Phys. Rev. **D90**, 11, 116003 (2014), [arXiv:1408.5933]; M. T. Hansen and S. R. Sharpe, Phys. Rev. **D92**, 11, 114509 (2015), [arXiv:1504.04248]; R. A. Briceño, M. T. Hansen and S. R. Sharpe, Phys. Rev. **D95**, 7, 074510 (2017), [arXiv:1701.07465]; H. W. Hammer, J. Y. Pang and A. Rusetsky, JHEP **10**, 115 (2017), [arXiv:1707.02176].
- [110] R. A. Briceño, M. T. Hansen and S. R. Sharpe, Phys. Rev. **D99**, 1, 014516 (2019), [arXiv:1810.01429].
- [111] M. Mai and M. Döring, Eur. Phys. J. **A53**, 12, 240 (2017), [arXiv:1709.08222].
- [112] M. T. Hansen and S. R. Sharpe (2019), [arXiv:1901.00483].
- [113] L. Lellouch and M. Luscher, Commun. Math. Phys. **219**, 31 (2001), [hep-lat/0003023].
- [114] T. Blum *et al.*, Phys. Rev. Lett. **108**, 141601 (2012), [arXiv:1111.1699]; T. Blum *et al.*, Phys. Rev. **D86**, 074513 (2012), [arXiv:1206.5142].
- [115] Z. Bai *et al.* (RBC, UKQCD), Phys. Rev. Lett. **115**, 21, 212001 (2015), [arXiv:1505.07863].
- [116] T. Blum *et al.*, Phys. Rev. **D91**, 7, 074502 (2015), [arXiv:1502.00263].
- [117] V. Bernard *et al.*, JHEP **01**, 019 (2011), [arXiv:1010.6018]; M. Doring *et al.*, Eur. Phys. J. **A47**, 139 (2011), [arXiv:1107.3988]; M. T. Hansen and S. R. Sharpe, Phys. Rev. **D86**, 016007 (2012), [arXiv:1204.0826]; R. A. Briceño and Z. Davoudi, Phys. Rev. **D88**, 9, 094507 (2013), [arXiv:1204.1110].
- [118] R. A. Briceño, M. T. Hansen and A. Walker-Loud, Phys. Rev. **D91**, 3, 034501 (2015), [arXiv:1406.5965].
- [119] R. A. Briceño and M. T. Hansen, Phys. Rev. **D94**, 1, 013008 (2016), [arXiv:1509.08507].
- [120] R. A. Briceño *et al.*, Phys. Rev. **D93**, 11, 114508 (2016), [arXiv:1604.03530].
- [121] D. Agadjanov *et al.*, JHEP **06**, 043 (2016), [arXiv:1603.07205].
- [122] S. Hashimoto, PTEP **2017**, 5, 053B03 (2017), [arXiv:1703.01881].
- [123] X. Feng *et al.*, Phys. Rev. Lett. **107**, 081802 (2011), [arXiv:1103.4818].
- [124] P. Boyle *et al.*, Phys. Rev. **D85**, 074504 (2012), [arXiv:1107.1497].
- [125] M. Della Morte *et al.*, JHEP **03**, 055 (2012), [arXiv:1112.2894].
- [126] F. Burger *et al.* (ETM), JHEP **02**, 099 (2014), [arXiv:1308.4327].
- [127] B. Chakraborty *et al.* (HPQCD), Phys. Rev. **D89**, 11, 114501 (2014), [arXiv:1403.1778].
- [128] F. Burger, K. Jansen, M. Petschlies and G. Pientka, Eur. Phys. J. **C76**, 464 (2016).
- [129] B. Chakraborty *et al.*, Phys. Rev. **D93**, 7, 074509 (2016), [arXiv:1512.03270].
- [130] B. Chakraborty *et al.*, Phys. Rev. **D96**, 3, 034516 (2017), [arXiv:1601.03071].
- [131] T. Blum *et al.* (RBC/UKQCD), JHEP **04**, 063 (2016), [Erratum: JHEP05,034(2017)], [arXiv:1602.01767].
- [132] S. Borsanyi *et al.*, Phys. Rev. **D96**, 7, 074507 (2017), [arXiv:1612.02364].
- [133] M. Della Morte *et al.*, JHEP **10**, 020 (2017), [arXiv:1705.01775].

- [134] S. Borsanyi *et al.* (Budapest-Marseille-Wuppertal), Phys. Rev. Lett. **121**, 2, 022002 (2018), [arXiv:1711.04980].
- [135] T. Blum *et al.* (RBC, UKQCD), Phys. Rev. Lett. **121**, 2, 022003 (2018), [arXiv:1801.07224].
- [136] B. Chakraborty *et al.*, Phys. Rev. **D98**, 9, 094503 (2018), [arXiv:1806.08190].
- [137] D. Giusti, F. Sanfilippo and S. Simula, Phys. Rev. **D98**, 11, 114504 (2018), [arXiv:1808.00887].
- [138] C. T. H. Davies *et al.* (Fermilab Lattice, LATTICE-HPQCD, MILC) (2019), [arXiv:1902.04223].
- [139] T. Blum, Phys. Rev. Lett. **91**, 052001 (2003), [hep-lat/0212018].
- [140] T. Blum *et al.*, Phys. Rev. Lett. **114**, 1, 012001 (2015), [arXiv:1407.2923].
- [141] T. Blum *et al.*, Phys. Rev. **D93**, 1, 014503 (2016), [arXiv:1510.07100].
- [142] J. Green *et al.*, Phys. Rev. Lett. **115**, 22, 222003 (2015), [arXiv:1507.01577].
- [143] T. Blum *et al.*, Phys. Rev. Lett. **118**, 2, 022005 (2017), [arXiv:1610.04603].
- [144] T. Blum *et al.*, Phys. Rev. **D96**, 3, 034515 (2017), [arXiv:1705.01067].
- [145] X. Feng *et al.*, Phys. Rev. Lett. **109**, 182001 (2012), [arXiv:1206.1375].
- [146] A. Gérardin, H. B. Meyer and A. Nyffeler, Phys. Rev. **D94**, 7, 074507 (2016), [arXiv:1607.08174].
- [147] A. Gérardin *et al.*, Phys. Rev. **D98**, 7, 074501 (2018), [arXiv:1712.00421].
- [148] Z. Bai *et al.*, Phys. Rev. Lett. **113**, 112003 (2014), [arXiv:1406.0916].
- [149] N. H. Christ *et al.* (RBC, UKQCD), Phys. Rev. **D92**, 9, 094512 (2015), [arXiv:1507.03094].
- [150] N. H. Christ *et al.* (RBC, UKQCD), Phys. Rev. **D93**, 11, 114517 (2016), [arXiv:1605.04442].
- [151] N. H. Christ *et al.*, Phys. Rev. **D94**, 11, 114516 (2016), [arXiv:1608.07585].
- [152] Z. Bai *et al.*, Phys. Rev. Lett. **118**, 25, 252001 (2017), [arXiv:1701.02858].
- [153] Z. Bai *et al.*, Phys. Rev. **D98**, 7, 074509 (2018), [arXiv:1806.11520].
- [154] C. Bernard *et al.*, Nucl. Phys. Proc. Suppl. **119**, 170 (2003), [hep-lat/0209086].
- [155] S. Perantoni and C. Michael, Nucl. Phys. **B347**, 854 (1990).
- [156] G. S. Bali and K. Schilling, Phys. Rev. **D46**, 2636 (1992).
- [157] S. Necco and R. Sommer, Nucl. Phys. **B622**, 328 (2002), [hep-lat/0108008].
- [158] J. M. Blairon *et al.*, Nucl. Phys. **B180**, 439 (1981).
- [159] H. Fukaya *et al.* (JLQCD), Phys. Rev. Lett. **104**, 122002 (2010), [Erratum: Phys. Rev. Lett.105,159901(2010)], [arXiv:0911.5555].
- [160] H. Fukaya *et al.* (JLQCD, TWQCD), Phys. Rev. **D83**, 074501 (2011), [arXiv:1012.4052].
- [161] L. Giusti and M. Luscher, JHEP **03**, 013 (2009), [arXiv:0812.3638].
- [162] K. Cichy, E. Garcia-Ramos and K. Jansen, JHEP **10**, 175 (2013), [arXiv:1303.1954].
- [163] G. P. Engel *et al.*, Phys. Rev. Lett. **114**, 11, 112001 (2015), [arXiv:1406.4987].
- [164] G. P. Engel *et al.*, Phys. Rev. **D91**, 5, 054505 (2015), [arXiv:1411.6386].
- [165] S. Aoki *et al.*, Eur. Phys. J. **C77**, 2, 112 (2017), [arXiv:1607.00299].
- [166] T. Blum *et al.* (RBC, UKQCD), Phys. Rev. **D93**, 7, 074505 (2016), [arXiv:1411.7017].
- [167] B. J. Choi *et al.* (SWME), Phys. Rev. **D93**, 1, 014511 (2016), [arXiv:1509.00592].
- [168] J. Laiho and R. S. Van de Water, PoS **LATTICE2011**, 293 (2011), [arXiv:1112.4861].
- [169] E. Gamiz *et al.* (HPQCD), Phys. Rev. **D80**, 014503 (2009), [arXiv:0902.1815].
- [170] Y. Aoki *et al.*, Phys. Rev. **D91**, 11, 114505 (2015), [arXiv:1406.6192].
- [171] A. Bazavov *et al.*, Phys. Rev. **D97**, 3, 034513 (2018), [arXiv:1706.04622].
- [172] M. Ademollo and R. Gatto, Phys. Rev. Lett. **13**, 264 (1964).
- [173] H. Leutwyler and M. Roos, Z. Phys. **C25**, 91 (1984).
- [174] P. A. Boyle *et al.*, Phys. Rev. Lett. **100**, 141601 (2008), [arXiv:0710.5136].
- [175] V. Lubicz *et al.* (ETM), Phys. Rev. **D80**, 111502 (2009), [arXiv:0906.4728]; V. Lubicz *et al.* (ETM), PoS **LATTICE2010**, 316 (2010), [arXiv:1012.3573].
- [176] P. A. Boyle *et al.* (RBC-UKQCD), Eur. Phys. J. **C69**, 159 (2010), [arXiv:1004.0886].
- [177] A. Bazavov *et al.*, Phys. Rev. **D87**, 073012 (2013), [arXiv:1212.4993].
- [178] T. Kaneko *et al.* (JLQCD), PoS **LATTICE2012**, 111 (2012), [arXiv:1211.6180].
- [179] P. A. Boyle *et al.*, JHEP **08**, 132 (2013), [arXiv:1305.7217].
- [180] P. A. Boyle *et al.* (RBC/UKQCD), JHEP **06**, 164 (2015), [arXiv:1504.01692].
- [181] N. Carrasco *et al.*, Phys. Rev. **D93**, 11, 114512 (2016), [arXiv:1602.04113].
- [182] H. Na *et al.*, Phys. Rev. **D82**, 114506 (2010), [arXiv:1008.4562].
- [183] H. Na *et al.*, Phys. Rev. **D84**, 114505 (2011), [arXiv:1109.1501].
- [184] V. Lubicz *et al.* (ETM), Phys. Rev. **D96**, 5, 054514 (2017), [Erratum: Phys. Rev.D99,no.9,099902(2019)], [arXiv:1706.03017].
- [185] T. Kaneko *et al.* (JLQCD), EPJ Web Conf. **175**, 13007 (2018), [arXiv:1711.11235].
- [186] E. Dalgic *et al.*, Phys. Rev. **D73**, 074502 (2006), [Erratum: Phys. Rev.D75,119906(2007)], [hep-lat/0601021].
- [187] J. M. Flynn *et al.*, Phys. Rev. **D91**, 7, 074510 (2015), [arXiv:1501.05373].
- [188] J. A. Bailey *et al.* (Fermilab Lattice, MILC), Phys. Rev. **D92**, 1, 014024 (2015), [arXiv:1503.07839].
- [189] B. Colquhoun *et al.*, Phys. Rev. **D93**, 3, 034502 (2016), [arXiv:1510.07446].
- [190] Z. Gelzer *et al.*, EPJ Web Conf. **175**, 13024 (2018), [arXiv:1710.09442].
- [191] B. Colquhoun, S. Hashimoto and T. Kaneko, PoS **LATTICE2018**, 274 (2018), [arXiv:1811.00227].
- [192] C. Bourrely, B. Machet and E. de Rafael, Nucl. Phys. **B189**, 157 (1981); C. G. Boyd, B. Grinstein and R. F. Lebed, Phys. Rev. Lett. **74**, 4603 (1995), [hep-ph/9412324]; T. Becher and R. J. Hill, Phys. Lett. **B633**, 61 (2006), [hep-ph/0509090]; C. Bourrely, I. Caprini and L. Lellouch, Phys. Rev. **D79**, 013008 (2009), [Erratum: Phys. Rev.D82,099902(2010)], [arXiv:0807.2722].
- [193] M. C. Arnesen *et al.*, Phys. Rev. Lett. **95**, 071802 (2005), [hep-ph/0504209].
- [194] J. A. Bailey *et al.*, Phys. Rev. **D79**, 054507 (2009), [arXiv:0811.3640].
- [195] S. Hashimoto *et al.*, Phys. Rev. **D61**, 014502 (1999), [hep-ph/9906376].



- [196] S. Hashimoto *et al.*, Phys. Rev. **D66**, 014503 (2002), [hep-ph/0110253].
- [197] C. Bernard *et al.*, Phys. Rev. **D79**, 014506 (2009), [arXiv:0808.2519].
- [198] J. A. Bailey *et al.* (Fermilab Lattice, MILC), Phys. Rev. **D89**, 11, 114504 (2014), [arXiv:1403.0635].
- [199] J. Harrison, C. Davies and M. Wingate (HPQCD), Phys. Rev. **D97**, 5, 054502 (2018), [arXiv:1711.11013].
- [200] E. McLean *et al.*, Phys. Rev. **D99**, 11, 114512 (2019), [arXiv:1904.02046].
- [201] T. Bhattacharya *et al.* (LANL/SWME), PoS **LATTICE2018**, 283 (2018).
- [202] J. A. Bailey *et al.* (MILC), Phys. Rev. **D92**, 3, 034506 (2015), [arXiv:1503.07237].
- [203] H. Na *et al.* (HPQCD), Phys. Rev. **D92**, 5, 054510 (2015), [Erratum: Phys. Rev.D93,no.11,119906(2016)], [arXiv:1505.03925].
- [204] A. V. Avilés-Casco *et al.* (Fermilab Lattice, MILC), PoS **LATTICE2018**, 282 (2019), [arXiv:1901.00216].
- [205] T. Kaneko *et al.* (JLQCD), PoS **LATTICE2018**, 311 (2018), [arXiv:1811.00794].
- [206] W. Detmold, C. Lehner and S. Meinel, Phys. Rev. **D92**, 3, 034503 (2015), [arXiv:1503.01421].
- [207] W. Detmold and S. Meinel, Phys. Rev. **D93**, 7, 074501 (2016), [arXiv:1602.01399].
- [208] R. R. Horgan *et al.*, Phys. Rev. **D89**, 9, 094501 (2014), [arXiv:1310.3722].
- [209] J. A. Bailey *et al.*, Phys. Rev. **D93**, 2, 025026 (2016), [arXiv:1509.06235].
- [210] D. Du *et al.*, Phys. Rev. **D93**, 3, 034005 (2016), [arXiv:1510.02349].
- [211] C. T. H. Davies *et al.* (HPQCD), Phys. Rev. **D78**, 114507 (2008), [arXiv:0807.1687].
- [212] C. McNeile *et al.*, Phys. Rev. **D82**, 034512 (2010), [arXiv:1004.4285].
- [213] E. Shintani *et al.*, Phys. Rev. **D82**, 7, 074505 (2010), [Erratum: Phys. Rev.D89,no.9,099903(2014)], [arXiv:1002.0371].
- [214] R. J. Hudspith *et al.*, Mod. Phys. Lett. **A31**, 32, 1630037 (2016).
- [215] I. Allison *et al.* (HPQCD), Phys. Rev. **D78**, 054513 (2008), [arXiv:0805.2999].
- [216] B. Chakraborty *et al.*, Phys. Rev. **D91**, 5, 054508 (2015), [arXiv:1408.4169].
- [217] Y. Maezawa and P. Petreczky, Phys. Rev. **D94**, 3, 034507 (2016), [arXiv:1606.08798].
- [218] Q. Mason *et al.* (HPQCD, UKQCD), Phys. Rev. Lett. **95**, 052002 (2005), [hep-lat/0503005].
- [219] A. Bazavov *et al.*, Phys. Rev. **D86**, 114031 (2012), [arXiv:1205.6155].
- [220] A. Bazavov *et al.*, Phys. Rev. **D90**, 7, 074038 (2014), [arXiv:1407.8437].
- [221] F. Karbstein, M. Wagner and M. Weber, Phys. Rev. **D98**, 11, 114506 (2018), [arXiv:1804.10909].
- [222] H. Takaura *et al.*, JHEP **04**, 155 (2019), [arXiv:1808.01643].
- [223] B. Blossier *et al.*, Phys. Rev. **D85**, 034503 (2012), [arXiv:1110.5829]; B. Blossier *et al.*, Phys. Rev. Lett. **108**, 262002 (2012), [arXiv:1201.5770].
- [224] S. Zafeiropoulos *et al.*, Phys. Rev. Lett. **122**, 16, 162002 (2019), [arXiv:1902.08148].
- [225] S. Aoki *et al.* (PACS-CS), JHEP **10**, 053 (2009), [arXiv:0906.3906].
- [226] P. Fritzsche *et al.*, PoS **LATTICE2014**, 291 (2014), [arXiv:1411.7648].
- [227] M. Bruno *et al.* (ALPHA), Phys. Rev. Lett. **119**, 10, 102001 (2017), [arXiv:1706.03821].
- [228] S. Durr *et al.*, Phys. Lett. **B701**, 265 (2011), [arXiv:1011.2403].
- [229] S. Durr *et al.*, JHEP **08**, 148 (2011), [arXiv:1011.2711].
- [230] S. Capitani *et al.*, Nucl. Phys. **B544**, 669 (1999), [Erratum: Nucl. Phys.B582,762(2000)], [hep-lat/9810063].
- [231] A. Bussone *et al.* (ETM), Phys. Rev. **D93**, 11, 114505 (2016), [arXiv:1603.04306].
- [232] SISSA, *Proceedings, 36th International Symposium on Lattice Field Theory (Lattice 2018)*, volume LATTICE2018, SISSA (2019), URL <https://pos.sissa.it/334/>.
- [233] W. Detmold *et al.* (USQCD) (2019), [arXiv:1904.09512].
- [234] A. S. Kronfeld *et al.* (USQCD) (2019), [arXiv:1904.09931].
- [235] R. C. Brower *et al.* (USQCD) (2019), [arXiv:1904.09964].
- [236] C. Lehner *et al.* (USQCD) (2019), [arXiv:1904.09479].
- [237] A. Bazavov *et al.* (USQCD) (2019), [arXiv:1904.09951].
- [238] V. Cirigliano *et al.* (USQCD) (2019), [arXiv:1904.09704].
- [239] B. Joó *et al.* (USQCD) (2019), [arXiv:1904.09725].

## 18. Structure Functions

Revised August 2019 by E.C. Aschenauer (BNL), R.S. Thorne (UCL) and R. Yoshida (Jefferson Lab).

### 18.1 Deep inelastic scattering

High-energy lepton-nucleon scattering plays a key role in determining the partonic structure of the proton. The process  $\ell N \rightarrow \ell' X$  is illustrated in Fig. 18.1. The filled circle in this figure represents the internal structure of the proton which can be expressed in terms of structure functions.

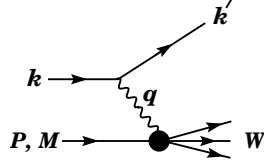


Figure 18.1: Kinematic quantities for the description of deep inelastic scattering. The quantities  $k$  and  $k'$  are the four-momenta of the incoming and outgoing leptons,  $P$  is the four-momentum of a nucleon with mass  $M$ , and  $W$  is the mass of the recoiling system  $X$ . The exchanged particle is a  $\gamma$ ,  $W^\pm$ , or  $Z$ ; it transfers four-momentum  $q = k - k'$  to the nucleon.

Invariant quantities:

$\nu = \frac{q \cdot P}{M} = E - E'$  is the lepton's energy loss in the nucleon rest frame (in earlier literature sometimes  $\nu = q \cdot P$ ). Here,  $E$  and  $E'$  are the initial and final lepton energies in the nucleon rest frame.

$Q^2 = -q^2 = 2(E E' - \vec{k} \cdot \vec{k}') - m_\ell^2 - m_{\ell'}^2$ , where  $m_\ell$  ( $m_{\ell'}$ ) is the initial (final) lepton mass. If  $E E' \sin^2(\theta/2) \gg m_\ell^2, m_{\ell'}^2$ , then

$\approx 4E E' \sin^2(\theta/2)$ , where  $\theta$  is the lepton's scattering angle with respect to the lepton beam direction.

$x = \frac{Q^2}{2M\nu}$  where, in the parton model,  $x$  is the fraction of the nucleon's momentum carried by the struck quark. Beyond leading order the equation remains the definition of  $x$ , but this is no longer identical to nucleon momentum fraction.

$y = \frac{q \cdot P}{k \cdot P} = \frac{\nu}{E}$  is the fraction of the lepton's energy lost in the nucleon rest frame.

$W^2 = (P + q)^2 = M^2 + 2M\nu - Q^2$  is the mass squared of the system  $X$  recoiling against the scattered lepton.

$s = (k + P)^2 = \frac{Q^2}{xy} + M^2 + m_\ell^2$  is the center-of-mass energy squared of the lepton-nucleon system.

The process in Fig. 18.1 is called deep ( $Q^2 \gg M^2$ ) inelastic ( $W^2 \gg M^2$ ) scattering (DIS). In what follows, the masses of the initial and scattered leptons,  $m_\ell$  and  $m_{\ell'}$ , are neglected.

#### 18.1.1 DIS cross sections

The double-differential cross section for deep inelastic scattering can be expressed in terms of kinematic variables in several ways.

$$\frac{d^2\sigma}{dx dy} = x(s - M^2) \frac{d^2\sigma}{dx dQ^2} = \frac{2\pi M\nu}{E'} \frac{d^2\sigma}{d\Omega_{N\text{rest}} dE'} \quad (18.1)$$

In lowest-order perturbation theory, the cross section for the scattering of polarized leptons on polarized nucleons can be expressed in terms of the products of leptonic and hadronic tensors associated with the coupling of the exchanged bosons at the upper and lower vertices in Fig. 18.1 (see Refs. [1–4])

$$\frac{d^2\sigma}{dx dy} = \frac{2\pi y \alpha^2}{Q^4} \sum_j \eta_j L_j^{\mu\nu} W_{\mu\nu}^j \quad (18.2)$$

For neutral-current processes, the summation is over  $j = \gamma, Z$  and  $\gamma Z$  representing photon and  $Z$  exchange and the interference

between them, whereas for charged-current interactions there is only  $W$  exchange,  $j = W$ . (For transverse nucleon polarization, there is a dependence on the azimuthal angle of the scattered lepton.) The lepton tensor  $L_{\mu\nu}$  is associated with the coupling of the exchange boson to the leptons. For incoming leptons of charge  $e = \pm 1$  and helicity  $\lambda = \pm 1$ ,

$$\begin{aligned} L_{\mu\nu}^\gamma &= 2(k_\mu k'_\nu + k'_\mu k_\nu - (k \cdot k' - m_\ell^2)g_{\mu\nu} - i\lambda \varepsilon_{\mu\nu\alpha\beta} k^\alpha k'^\beta), \\ L_{\mu\nu}^{\gamma Z} &= (g_V^e + e\lambda g_A^e) L_{\mu\nu}^\gamma, \quad L_{\mu\nu}^Z = (g_V^e + e\lambda g_A^e)^2 L_{\mu\nu}^\gamma, \\ L_{\mu\nu}^W &= (1 + e\lambda)^2 L_{\mu\nu}^\gamma, \end{aligned} \quad (18.3)$$

where  $g_V^e = -\frac{1}{2} + 2\sin^2\theta_W$ ,  $g_A^e = -\frac{1}{2}$ .

Although here the helicity formalism is adopted, an alternative approach is to express the tensors in Eq. (18.3) in terms of the polarization of the lepton.

The factors  $\eta_j$  in Eq. (18.2) denote the ratios of the corresponding propagators and couplings to the photon propagator and coupling squared

$$\begin{aligned} \eta_\gamma &= 1; \quad \eta_{\gamma Z} = \left( \frac{G_F M_Z^2}{2\sqrt{2}\pi\alpha} \right) \left( \frac{Q^2}{Q^2 + M_Z^2} \right); \\ \eta_Z &= \eta_{\gamma Z}^2; \quad \eta_W = \frac{1}{2} \left( \frac{G_F M_W^2}{4\pi\alpha} \frac{Q^2}{Q^2 + M_W^2} \right)^2. \end{aligned} \quad (18.4)$$

The hadronic tensor, which describes the interaction of the appropriate electroweak currents with the target nucleon, is given by

$$W_{\mu\nu} = \frac{1}{4\pi} \int d^4z e^{iq \cdot z} \langle P, S | [J_\mu^\dagger(z), J_\nu(0)] | P, S \rangle, \quad (18.5)$$

where  $J_\alpha$  is the hadronic contribution to the electromagnetic, or weak current and  $S$  denotes the nucleon-spin 4-vector, with  $S^2 = -M^2$  and  $S \cdot P = 0$ .

### 18.2 Structure functions of the proton

The structure functions are defined in terms of the hadronic tensor (see Refs. [1–3])

$$\begin{aligned} W_{\mu\nu} &= \left( -g_{\mu\nu} + \frac{q_\mu q_\nu}{q^2} \right) F_1(x, Q^2) + \frac{\hat{P}_\mu \hat{P}_\nu}{P \cdot q} F_2(x, Q^2) \\ &- i\varepsilon_{\mu\nu\alpha\beta} \frac{q^\alpha P^\beta}{2P \cdot q} F_3(x, Q^2) \\ &+ i\varepsilon_{\mu\nu\alpha\beta} \frac{q^\alpha}{P \cdot q} \left[ S^\beta g_1(x, Q^2) + \left( S^\beta - \frac{S \cdot q}{P \cdot q} P^\beta \right) g_2(x, Q^2) \right] \\ &+ \frac{1}{P \cdot q} \left[ \frac{1}{2} (\hat{P}_\mu \hat{S}_\nu + \hat{S}_\mu \hat{P}_\nu) - \frac{S \cdot q}{P \cdot q} \hat{P}_\mu \hat{P}_\nu \right] g_3(x, Q^2) \\ &+ \frac{S \cdot q}{P \cdot q} \left[ \frac{\hat{P}_\mu \hat{P}_\nu}{P \cdot q} g_4(x, Q^2) + \left( -g_{\mu\nu} + \frac{q_\mu q_\nu}{q^2} \right) g_5(x, Q^2) \right] \end{aligned} \quad (18.6)$$

where

$$\hat{P}_\mu = P_\mu - \frac{P \cdot q}{q^2} q_\mu, \quad \hat{S}_\mu = S_\mu - \frac{S \cdot q}{q^2} q_\mu \quad (18.7)$$

In [2], the definition of  $W_{\mu\nu}$  with  $\mu \leftrightarrow \nu$  is adopted, which changes the sign of the  $\varepsilon_{\mu\nu\alpha\beta}$  terms in Eq. (18.6), although the formulae given below are unchanged. Ref. [1] tabulates the relation between the structure functions defined in Eq. (18.6) and other choices available in the literature.

The cross sections for neutral- and charged-current deep inelastic scattering on unpolarized nucleons can be written in terms of

the structure functions in the generic form

$$\begin{aligned} \frac{d^2\sigma^i}{dx dy} &= \frac{4\pi\alpha^2}{xyQ^2} \eta^i \left\{ \left( 1 - y - \frac{x^2 y^2 M^2}{Q^2} \right) F_2^i \right. \\ &\quad \left. + y^2 x F_1^i \mp \left( y - \frac{y^2}{2} \right) x F_3^i \right\}, \end{aligned} \quad (18.8)$$

where  $i = \text{NC, CC}$  corresponds to neutral-current ( $eN \rightarrow eX$ ) or charged-current ( $eN \rightarrow \nu X$  or  $\nu N \rightarrow eX$ ) processes, respectively. For incoming neutrinos,  $L_{\mu\nu}^W$  of Eq. (18.3) is still true, but with  $e, \lambda$  corresponding to the outgoing charged lepton. In the last term of Eq. (18.8), the  $-$  sign is taken for an incoming  $e^+$  or  $\bar{\nu}$  and the  $+$  sign for an incoming  $e^-$  or  $\nu$ . The factor  $\eta^{\text{NC}} = 1$  for unpolarized  $e^\pm$  beams, whereas

$$\eta^{\text{CC}} = (1 \pm \lambda)^2 \eta_W \quad (18.9)$$

with  $\pm$  for  $\ell^\pm$ ; and where  $\lambda$  is the helicity of the incoming lepton and  $\eta_W$  is defined in Eq. (18.4); for incoming neutrinos  $\eta^{\text{CC}} = 4\eta_W$ . The CC structure functions, which derive exclusively from  $W$  exchange, are

$$F_1^{\text{CC}} = F_1^W, \quad F_2^{\text{CC}} = F_2^W, \quad xF_3^{\text{CC}} = xF_3^W. \quad (18.10)$$

The NC structure functions  $F_2^\gamma, F_2^{\gamma Z}, F_2^Z$  are, for  $e^\pm N \rightarrow e^\pm X$ , given by [5],

$$F_2^{\text{NC}} = F_2^\gamma - (g_V^e \pm \lambda g_A^e) \eta_{\gamma Z} F_2^{\gamma Z} + (g_V^e \mp \lambda g_A^e)^2 \pm 2\lambda g_V^e g_A^e \eta_Z F_2^Z \quad (18.11)$$

and similarly for  $F_1^{\text{NC}}$ , whereas

$$xF_3^{\text{NC}} = -(g_A^e \pm \lambda g_V^e) \eta_{\gamma Z} x F_3^{\gamma Z} + [2g_V^e g_A^e \pm \lambda (g_V^e \mp \lambda g_A^e)] \eta_Z x F_3^Z. \quad (18.12)$$

The polarized cross-section difference

$$\Delta\sigma = \sigma(\lambda_n = -1, \lambda_\ell) - \sigma(\lambda_n = 1, \lambda_\ell), \quad (18.13)$$

where  $\lambda_\ell, \lambda_n$  are the helicities ( $\pm 1$ ) of the incoming lepton and nucleon, respectively, may be expressed in terms of the five structure functions  $g_{1, \dots, 5}(x, Q^2)$  of Eq. (18.6). Explicitly,

$$\begin{aligned} \frac{d^2\Delta\sigma^i}{dx dy} &= \frac{8\pi\alpha^2}{xyQ^2} \eta^i \left\{ -\lambda_\ell y \left( 2 - y - 2x^2 y^2 \frac{M^2}{Q^2} \right) x g_1^i \right. \\ &\quad \left. + \lambda_\ell 4x^3 y^2 \frac{M^2}{Q^2} g_2^i + 2x^2 y \frac{M^2}{Q^2} \left( 1 - y - x^2 y^2 \frac{M^2}{Q^2} \right) g_3^i \right. \\ &\quad \left. - \left( 1 + 2x^2 y \frac{M^2}{Q^2} \right) \left[ \left( 1 - y - x^2 y^2 \frac{M^2}{Q^2} \right) g_4^i + x y^2 g_5^i \right] \right\} \end{aligned} \quad (18.14)$$

with  $i = \text{NC or CC}$  as before. The Eq. (18.13) corresponds to the difference of antiparallel minus parallel spins of the incoming particles for  $e^-$  or  $\nu$  initiated reactions, but the difference of parallel minus antiparallel for  $e^+$  or  $\bar{\nu}$  initiated processes. For longitudinal nucleon polarization, the contributions of  $g_2$  and  $g_3$  are suppressed by powers of  $M^2/Q^2$ . These structure functions give an unsuppressed contribution to the cross section for transverse polarization [1], but in this case the cross-section difference vanishes as  $M/Q \rightarrow 0$ .

Because the same tensor structure occurs in the spin-dependent and spin-independent parts of the hadronic tensor of Eq. (18.6) in the  $M^2/Q^2 \rightarrow 0$  limit, the differential cross-section difference of Eq. (18.14) may be obtained from the differential cross section Eq. (18.8) by replacing

$$F_1 \rightarrow -g_5, \quad F_2 \rightarrow -g_4, \quad F_3 \rightarrow 2g_1, \quad (18.15)$$

and multiplying by two, since the total cross section is the average over the initial-state polarizations. In this limit, Eq. (18.8) and Eq. (18.14) may be written in the form

$$\begin{aligned} \frac{d^2\sigma^i}{dx dy} &= \frac{2\pi\alpha^2}{xyQ^2} \eta^i \left[ Y_+ F_2^i \mp Y_- x F_3^i - y^2 F_L^i \right], \\ \frac{d^2\Delta\sigma^i}{dx dy} &= \frac{4\pi\alpha^2}{xyQ^2} \eta^i \left[ -Y_+ g_4^i \mp Y_- 2x g_1^i + y^2 g_L^i \right], \end{aligned} \quad (18.16)$$

with  $i = \text{NC or CC}$ , where  $Y_\pm = 1 \pm (1 - y)^2$  and

$$F_L^i = F_2^i - 2x F_1^i, \quad g_L^i = g_4^i - 2x g_5^i. \quad (18.17)$$

In the naive quark-parton model, the analogy with the Callan-Gross relations [6]  $F_L^i = 0$ , are the Dicus relations [7]  $g_L^i = 0$ . Therefore, there are only two independent polarized structure functions:  $g_1$  (parity conserving) and  $g_5$  (parity violating), in analogy with the unpolarized structure functions  $F_1$  and  $F_3$ .

### 18.2.1 Structure functions in the quark-parton model

In the naive quark-parton model [8, 9], contributions to the structure functions  $F^i$  and  $g^i$  can be expressed in terms of the quark distribution functions  $q(x, Q^2)$  of the proton, where  $q = u, \bar{u}, d, \bar{d}$  etc. The quantity  $q(x, Q^2) dx$  is the number of quarks (or antiquarks) of designated flavor that carry a momentum fraction between  $x$  and  $x + dx$  of the proton's momentum in a frame in which the proton momentum is large.

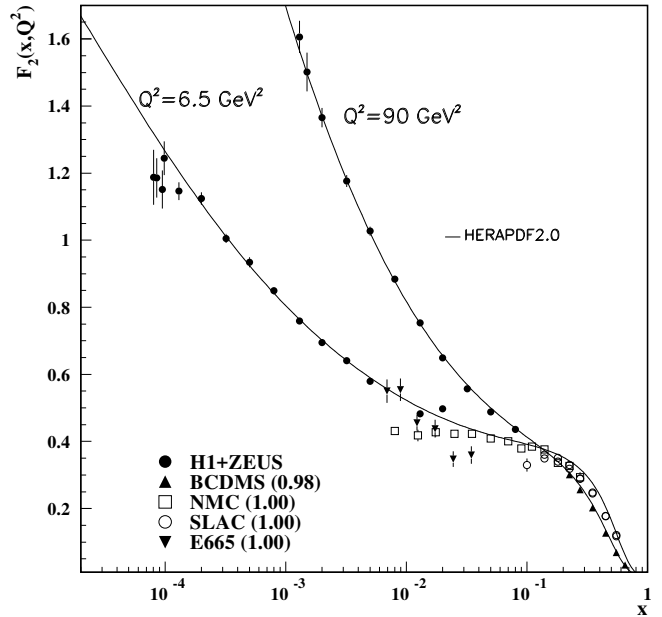


Figure 18.2: The proton structure function  $F_2^p$  given at two  $Q^2$  values ( $6.5 \text{ GeV}^2$  and  $90 \text{ GeV}^2$ ), which exhibit scaling at the ‘pivot’ point  $x \sim 0.14$ . See the captions in Fig. 18.8 and Fig. 18.10 for the references of the data. The various data sets have been renormalized by the factors shown in brackets in the key to the plot, which were globally determined in a previous HERAPDF analysis [10]. The curves were obtained using the PDFs from the HERAPDF analysis [11]. In practice, data for the reduced cross section,  $F_2(x, Q^2) - (y^2/Y_+)F_L(x, Q^2)$ , were fitted, rather than  $F_2$  and  $F_L$  separately. The agreement between data and theory at low  $Q^2$  and  $x$  can be improved by a positive higher-twist correction to  $F_L(x, Q^2)$  [12, 13] (see Fig. 8 of Ref. [13]), or small- $x$  resummation [14, 15].

For the neutral-current processes  $ep \rightarrow eX$ ,

$$\begin{aligned} [F_2^\gamma, F_2^{\gamma Z}, F_2^Z] &= x \sum_q [e_q^2, 2e_q g_V^q, g_V^{q^2} + g_A^{q^2}] (q + \bar{q}), \\ [F_3^\gamma, F_3^{\gamma Z}, F_3^Z] &= \sum_q [0, 2e_q g_A^q, 2g_V^q g_A^q] (q - \bar{q}), \\ [g_1^\gamma, g_1^{\gamma Z}, g_1^Z] &= \frac{1}{2} \sum_q [e_q^2, 2e_q g_V^q, g_V^{q^2} + g_A^{q^2}] (\Delta q + \Delta \bar{q}), \\ [g_5^\gamma, g_5^{\gamma Z}, g_5^Z] &= \sum_q [0, e_q g_A^q, g_V^q g_A^q] (\Delta \bar{q} - \Delta q), \end{aligned} \quad (18.18)$$

where  $g_V^q = \pm \frac{1}{2} - 2e_q \sin^2 \theta_W$  and  $g_A^q = \pm \frac{1}{2}$ , with  $\pm$  according to whether  $q$  is a  $u$ - or  $d$ -type quark respectively. The quantity  $\Delta q$  is the difference  $q \uparrow - q \downarrow$  of the distributions with the quark spin parallel and antiparallel to the proton spin.

For the charged-current processes  $e^- p \rightarrow \nu X$  and  $\bar{\nu} p \rightarrow e^+ X$ , the structure functions are:

$$\begin{aligned} F_2^{W^-} &= 2x(u + \bar{d} + \bar{s} + c \dots), \\ F_3^{W^-} &= 2(u - \bar{d} - \bar{s} + c \dots), \\ g_1^{W^-} &= (\Delta u + \Delta \bar{d} + \Delta \bar{s} + \Delta c \dots), \\ g_5^{W^-} &= (-\Delta u + \Delta \bar{d} + \Delta \bar{s} - \Delta c \dots), \end{aligned} \quad (18.19)$$

where only the active flavors have been kept and where CKM mixing has been neglected. For  $e^+ p \rightarrow \bar{\nu} X$  and  $\nu p \rightarrow e^- X$ , the structure functions  $F_i^{W^+}, g_i^{W^+}$  are obtained by the flavor interchanges  $d \leftrightarrow u, s \leftrightarrow c$  in the expressions for  $F_i^{W^-}, g_i^{W^-}$ . The structure functions for scattering on a neutron are obtained from those of the proton by the interchange  $u \leftrightarrow d$ . For both the neutral- and charged-current processes, the quark-parton model predicts  $2xF_1^i = F_2^i$  and  $g_4^i = 2xg_5^i$ .

Neglecting masses, the structure functions  $g_2$  and  $g_3$  contribute only to scattering from transversely polarized nucleons, and have no simple interpretation in terms of the quark-parton model. They arise from off-diagonal matrix elements  $\langle P, \lambda' | [J_\mu^\dagger(z), J_\nu(0)] | P, \lambda \rangle$ , where the proton helicities satisfy  $\lambda' \neq \lambda$ . In fact, the leading-twist contributions to both  $g_2$  and  $g_3$  are both twist-2 and twist-3, which contribute at the same order of  $Q^2$ . The Wandzura-Wilczek relation [16] expresses the twist-2 part of  $g_2$  in terms of  $g_1$  as

$$g_2^i(x) = -g_1^i(x) + \int_x^1 \frac{dy}{y} g_1^i(y). \quad (18.20)$$

However, the twist-3 component of  $g_2$  is unknown. Similarly, there is a relation expressing the twist-2 part of  $g_3$  in terms of  $g_4$ . A complete set of relations, including  $M^2/Q^2$  effects, can be found in [17].

### 18.2.2 Structure functions and QCD

One of the most striking predictions of the quark-parton model is that the structure functions  $F_i, g_i$  scale, i.e.,  $F_i(x, Q^2) \rightarrow F_i(x)$  in the Bjorken limit that  $Q^2$  and  $\nu \rightarrow \infty$  with  $x$  fixed [18]. This property is related to the assumption that the transverse momentum of the partons in the infinite-momentum frame of the proton is small. In QCD, however, the radiation of hard gluons from the quarks violates this assumption, leading to logarithmic scaling violations, which are particularly large at small  $x$ , see Fig. 18.2. The radiation of gluons produces the evolution of the structure functions. As  $Q^2$  increases, more and more gluons are radiated, which in turn split into  $q\bar{q}$  pairs. This process leads both to the softening of the initial quark momentum distributions and to the growth of the gluon density and the  $q\bar{q}$  sea as  $x$  decreases.

In QCD, the above processes are described in terms of scale-dependent parton distributions  $f_a(x, \mu^2)$ , where  $a = g$  or  $q$  and, typically,  $\mu$  is the scale of the probe  $Q$ . For parton distributions

$x$  always refers to the nucleon momentum fraction of the parton, whereas for structure functions it retains the definition in Sec. 18.1. For  $Q^2 \gg M^2$ , the structure functions are of the form

$$F_i = \sum_a C_i^a \otimes f_a + \mathcal{O}(M^2/Q^2), \quad (18.21)$$

where  $\otimes$  denotes the convolution integral

$$C \otimes f = \int_x^1 \frac{dy}{y} C(y) f\left(\frac{x}{y}\right), \quad (18.22)$$

and where the coefficient functions  $C_i^a$  are given as a power series in  $\alpha_s$ . The parton distribution  $f_a$  corresponds, at a given  $x$ , to the density of parton  $a$  in the proton integrated over transverse momentum  $k_t$  up to  $\mu$ . Its evolution in  $\mu$  is described in QCD by a DGLAP equation (see Refs. [19–22]) which has the schematic form

$$\frac{\partial f_a}{\partial \ln \mu^2} \sim \frac{\alpha_s(\mu^2)}{2\pi} \sum_b (P_{ab} \otimes f_b), \quad (18.23)$$

where the  $P_{ab}$ , which describe the parton splitting  $b \rightarrow a$ , are also given as a power series in  $\alpha_s$ . Although perturbative QCD can predict, via Eq. (18.23), the evolution of the parton distribution functions from a particular scale,  $\mu_0$ , these DGLAP equations cannot predict them *a priori* at any particular  $\mu_0$ . Thus they must be measured at a starting point  $\mu_0$  before the predictions of QCD can be compared to the data at other scales,  $\mu$ . In general, all observables involving a hard hadronic interaction (such as structure functions) can be expressed as a convolution of calculable, process-dependent coefficient functions and these universal parton distributions, e.g. Eq. (18.21).

It is often convenient to write the evolution equations in terms of the gluon, non-singlet ( $q^{NS}$ ) and singlet ( $q^S$ ) quark distributions, such that

$$q^{NS} = q_i - \bar{q}_i \quad (\text{or } q_i - q_j), \quad q^S = \sum_i (q_i + \bar{q}_i). \quad (18.24)$$

The non-singlet distributions have non-zero values of flavor quantum numbers, such as isospin and baryon number. The DGLAP evolution equations then take the form

$$\begin{aligned} \frac{\partial q^{NS}}{\partial \ln \mu^2} &= \frac{\alpha_s(\mu^2)}{2\pi} P_{qq} \otimes q^{NS}, \\ \frac{\partial}{\partial \ln \mu^2} \begin{pmatrix} q^S \\ g \end{pmatrix} &= \frac{\alpha_s(\mu^2)}{2\pi} \begin{pmatrix} P_{qq} & 2n_f P_{qg} \\ P_{gq} & P_{gg} \end{pmatrix} \otimes \begin{pmatrix} q^S \\ g \end{pmatrix}, \end{aligned} \quad (18.25)$$

where  $P$  are splitting functions that describe the probability of a given parton splitting into two others, and  $n_f$  is the number of (active) quark flavors. The leading-order Altarelli-Parisi [21]

**Table 18.1:** The main processes relevant to global PDF analyses, ordered in three groups: fixed-target experiments, HERA and the  $p\bar{p}$  Tevatron /  $pp$  LHC. For each process we give an indication of their dominant partonic subprocesses, the primary partons which are probed and the approximate range of  $x$  constrained by the data.

Process	Subprocess	Partons	$x$ range
$\ell^\pm \{p, n\} \rightarrow \ell^\pm X$	$\gamma^* q \rightarrow q$	$q, \bar{q}, g$	$x \gtrsim 0.01$
$\ell^\pm n/p \rightarrow \ell^\pm X$	$\gamma^* d/u \rightarrow d/u$	$d/u$	$x \gtrsim 0.01$
$pp \rightarrow \mu^+ \mu^- X$	$u\bar{u}, d\bar{d} \rightarrow \gamma^*$	$\bar{q}$	$0.015 \lesssim x \lesssim 0.35$
$pn/pp \rightarrow \mu^+ \mu^- X$	$(u\bar{d})/(u\bar{u}) \rightarrow \gamma^*$	$\bar{d}/\bar{u}$	$0.015 \lesssim x \lesssim 0.35$
$\nu(\bar{\nu}) N \rightarrow \mu^-(\mu^+) X$	$W^* q \rightarrow q'$	$q, \bar{q}$	$0.01 \lesssim x \lesssim 0.5$
$\nu N \rightarrow \mu^- \mu^+ X$	$W^* s \rightarrow c$	$s$	$0.01 \lesssim x \lesssim 0.2$
$\bar{\nu} N \rightarrow \mu^+ \mu^- X$	$W^* \bar{s} \rightarrow \bar{c}$	$\bar{s}$	$0.01 \lesssim x \lesssim 0.2$
$e^\pm p \rightarrow e^\pm X$	$\gamma^* q \rightarrow q$	$g, q, \bar{q}$	$10^{-4} \lesssim x \lesssim 0.1$
$e^+ p \rightarrow \bar{\nu} X$	$W^+ \{d, s\} \rightarrow \{u, c\}$	$d, s$	$x \gtrsim 0.01$
$e^\pm p \rightarrow e^\pm c\bar{c}X, e^\pm b\bar{b}X$	$\gamma^* c \rightarrow c, \gamma^* g \rightarrow c\bar{c}$	$c, b, g$	$10^{-4} \lesssim x \lesssim 0.01$
$e^\pm p \rightarrow \text{jet}+X$	$\gamma^* g \rightarrow q\bar{q}$	$g$	$0.01 \lesssim x \lesssim 0.1$
$p\bar{p}, pp \rightarrow \text{jet}+X$	$gg, qg, q\bar{q} \rightarrow 2j$	$g, q$	$0.00005 \lesssim x \lesssim 0.5$
$p\bar{p} \rightarrow (W^\pm \rightarrow \ell^\pm \nu) X$	$ud \rightarrow W^+, \bar{u}\bar{d} \rightarrow W^-$	$u, d, \bar{u}, \bar{d}$	$x \gtrsim 0.05$
$pp \rightarrow (W^\pm \rightarrow \ell^\pm \nu) X$	$u\bar{d} \rightarrow W^+, d\bar{u} \rightarrow W^-$	$u, d, \bar{u}, \bar{d}, g$	$x \gtrsim 0.001$
$p\bar{p}(pp) \rightarrow (Z \rightarrow \ell^+ \ell^-) X$	$uu, dd, ..(u\bar{u}, ..) \rightarrow Z$	$u, d, ..(g)$	$x \gtrsim 0.001$
$pp \rightarrow W^- c, W^+ \bar{c}$	$gs \rightarrow W^- c$	$s, \bar{s}$	$x \sim 0.01$
$pp \rightarrow (\gamma^* \rightarrow \ell^+ \ell^-) X$	$u\bar{u}, d\bar{d}, .. \rightarrow \gamma^*$	$\bar{q}, g$	$x \gtrsim 10^{-5}$
$pp \rightarrow (\gamma^* \rightarrow \ell^+ \ell^-) X$	$u\gamma, d\gamma, .. \rightarrow \gamma^*$	$\gamma$	$x \gtrsim 10^{-2}$
$pp \rightarrow b\bar{b} X, t\bar{t} X$	$gg \rightarrow b\bar{b}, t\bar{t}$	$g$	$x \gtrsim 10^{-5}, 10^{-2}$
$pp \rightarrow \text{exclusive } J/\psi, \Upsilon$	$\gamma^*(gg) \rightarrow J/\psi, \Upsilon$	$g$	$x \gtrsim 10^{-5}, 10^{-4}$
$pp \rightarrow \gamma X$	$gq \rightarrow \gamma q, g\bar{q} \rightarrow \gamma\bar{q}$	$g$	$x \gtrsim 0.005$

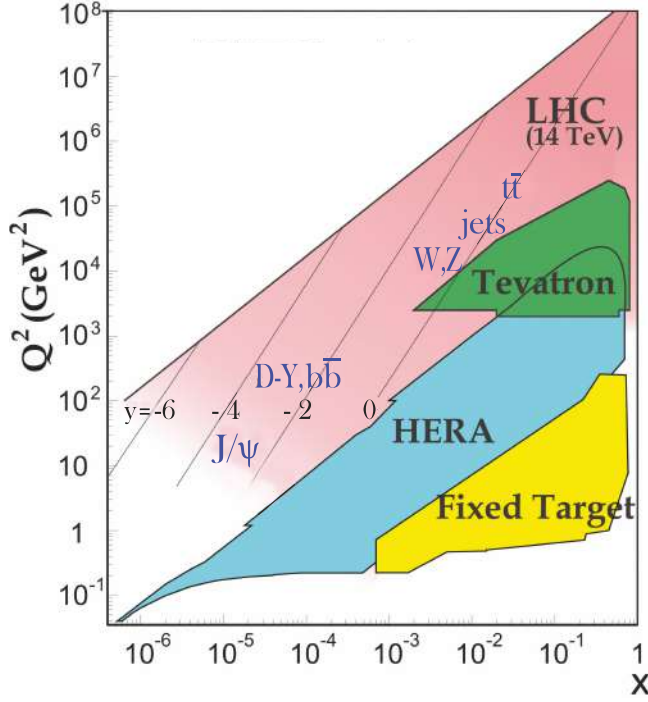


Figure 18.3: Kinematic domains in  $x$  and  $Q^2$  probed by fixed-target and collider experiments, where here  $Q^2$  can refer either the literal  $Q^2$  for deep inelastic scattering, or the hard scale of the process in hadron-hadron collisions, e.g. invariant mass or transverse momentum  $p_T^2$ . Some of the final states accessible at the LHC are indicated in the appropriate regions, where  $y$  is the rapidity. The incoming partons have  $x_{1,2} = (Q/14 \text{ TeV})e^{\pm y}$  where  $Q$  is the hard scale of the process shown in blue in the figure. For example, open charm production [23] and exclusive  $J/\psi$  and  $\Upsilon$  production [24] at high  $|y|$  at the LHC may probe the gluon PDF down to  $x \sim 10^{-5}$ .

splitting functions are

$$P_{qq} = \frac{4}{3} \left[ \frac{1+x^2}{(1-x)_+} \right] = \frac{4}{3} \left[ \frac{1+x^2}{(1-x)_+} \right] + 2\delta(1-x), \quad (18.26)$$

$$P_{gq} = \frac{1}{2} [x^2 + (1-x)^2], \quad P_{gq} = \frac{4}{3} \left[ \frac{1+(1-x)^2}{x} \right], \quad (18.27)$$

$$P_{gg} = 6 \left[ \frac{1-x}{x} + x(1-x) + \frac{x}{(1-x)_+} \right] + \left[ \frac{11}{2} - \frac{n_f}{3} \right] \delta(1-x), \quad (18.28)$$

where the notation  $[F(x)]_+$  defines a distribution such that for any sufficiently regular test function,  $f(x)$ ,

$$\int_0^1 dx f(x) [F(x)]_+ = \int_0^1 dx (f(x) - f(1)) F(x). \quad (18.29)$$

In general, the splitting functions can be expressed as a power series in  $\alpha_s$ . The series contains both terms proportional to  $\ln \mu^2$  and to  $\ln(1/x)$  and  $\ln(1-x)$ . The leading-order DGLAP evolution sums up the  $(\alpha_s \ln \mu^2)^n$  contributions, while at next-to-leading order (NLO) the sum over the  $\alpha_s (\alpha_s \ln \mu^2)^{n-1}$  terms is included [28, 29]. The NNLO contributions to the splitting functions and the DIS coefficient functions are also all known [30–32].

In the kinematic region of very small  $x$ , one may also sum leading terms in  $\ln(1/x)$ , independent of the value of  $\ln \mu^2$ . At leading order, LLx, this is done by the BFKL equation for the unintegrated distributions (see Refs. [33, 34]). The leading-order  $(\alpha_s \ln(1/x))^n$  terms result in a power-like growth,  $x^{-\omega}$  with

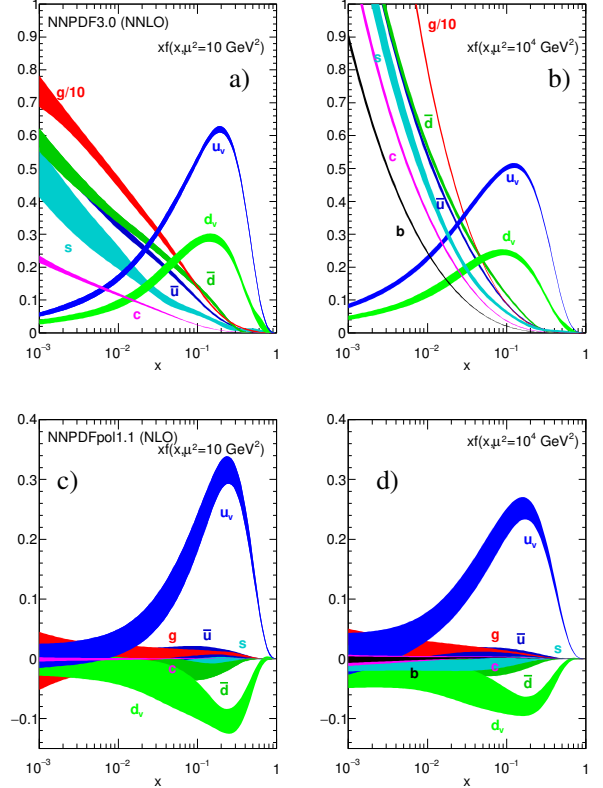


Figure 18.4: The bands are  $x$  times the unpolarized (a,b) parton distributions  $f(x)$  (where  $f = u_v, d_v, \bar{u}, \bar{d}, s \simeq \bar{s}, c = \bar{c}, b = \bar{b}, g$ ) obtained in NNLO NNPDF3.0 global analysis [25] at scales  $\mu^2 = 10 \text{ GeV}^2$  (left) and  $\mu^2 = 10^4 \text{ GeV}^2$  (right), with  $\alpha_s(M_Z^2) = 0.118$ . The analogous results obtained in the NNLO MMHT analysis can be found in Fig. 1 of Ref [26]. The corresponding polarized parton distributions are shown (c,d), obtained in NLO with NNPDFpol1.1 [27].

$\omega = (12\alpha_s \ln 2)/\pi$ , at asymptotic values of  $\ln 1/x$ . The next-to-leading  $\ln 1/x$  (NLLx) contributions are also available [35, 36]. They are so large (and negative) that the results initially appeared to be perturbatively unstable. Methods, based on a combination of collinear and small- $x$  resummations, have been developed which reorganize the perturbative series into a more stable hierarchy [37–40], and this has been used as the basis for a framework for including the corrections in phenomenological studies [41, 42]. There are some limited indications that small- $x$  resummations become necessary for sufficient precision for  $x \lesssim 10^{-3}$  at low scales [14, 15]. There is not yet any very convincing indication for a ‘non-linear’ regime, for  $Q^2 \gtrsim 2 \text{ GeV}^2$ , in which the gluon density would be so high that gluon-gluon recombination effects would become significant.

The precision of the experimental data demands that at least NLO, and preferably NNLO, DGLAP evolution be used in comparisons between QCD theory and experiment. Beyond the leading order, it is necessary to specify, and to use consistently, both a renormalization and a factorization scheme. The renormalization scheme used almost universally is the modified minimal subtraction ( $\overline{\text{MS}}$ ) scheme [43, 44]. The most popular choices for the factorization scheme is also  $\overline{\text{MS}}$  [45]. However, sometimes the DIS [46] scheme is adopted, in which there are no higher-order corrections to the  $F_2$  structure function. The two schemes differ in how the non-divergent pieces are assimilated in the parton distribution functions.

The discussion above relates to the  $Q^2$  behavior of leading-twist (twist-2) contributions to the structure functions. Higher-twist terms, which involve their own non-perturbative input, exist. These die off as powers of  $Q$ ; specifically twist- $n$  terms are damped by  $1/Q^{n-2}$ . Provided a cut, say  $W^2 > 15 \text{ GeV}^2$  is imposed, the

higher-twist terms appear to be numerically unimportant for  $Q^2$  above a few  $\text{GeV}^2$ , except possibly for very small  $x$  and more definitely for  $x$  close to 1 [47–49], though it is important to note that they are likely to be larger in  $xF_3(x, Q^2)$  than in  $F_2(x, Q^2)$  (see e.g. [50]) due to a lack of a constraining sum rule for  $xF_3(x, Q^2)$ .

### 18.3 Determination of parton distributions

The parton distribution functions (PDFs) can be determined from an analysis of data for deep inelastic lepton-nucleon scattering and for related hard-scattering processes initiated by nucleons; see Refs. [51–56] for reviews. Table 18.1 highlights some of the processes, where LHC data are playing an increasing role [57], and their primary sensitivity to PDFs. Fixed-target and collider experiments have complementary kinematic reach (as is shown in Fig. 18.3), which enables the determination of PDFs over a wide range in  $x$  and  $\mu^2$ . As more precise LHC data for  $W^\pm$ ,  $Z$ ,  $\gamma$ , jet,  $b\bar{b}$ ,  $t\bar{t}$  and  $J/\psi$  production become available, tighter constraints on the PDFs are expected in a wider kinematic range.

Recent determinations and releases of the unpolarized PDFs up to NNLO have been made by six groups: MMHT [26], NNPDF [58], CT(EQ) [59], HERAPDF [11], ABMP [60] and JR [61]. JR generate ‘dynamical’ PDFs from a valence-like input at a very low starting scale,  $Q_0^2 = 0.5 \text{ GeV}^2$ , whereas other groups start evolution at  $Q_0^2 = 1\text{--}4 \text{ GeV}^2$ . Most groups use input PDFs of the form  $xf = x^a(\dots)(1-x)^b$  with 14–28 free parameters in total. In these cases the PDF uncertainties are made available using the ‘‘Hessian’’ formulation. The free parameters are expanded around their best fit values, and orthogonal eigenvector sets of PDFs depending on linear combinations of the parameter variations are obtained. The uncertainty is then the quadratic sum of the uncertainties arising from each eigenvector. The NNPDF group combines a Monte Carlo representation of the probability measure in the space of PDFs with the use of neural networks. Fits are performed to a number of ‘‘replica’’ data sets obtained by allowing individual data points to fluctuate randomly by amounts determined by the size of the data uncertainties. This results in a set of replicas of unbiased PDF sets. In this case the best prediction is the average obtained using all PDF replicas and the uncertainty is the standard deviation over all replicas. It is now possible to convert the eigenvectors of Hessian-based PDFs to Monte Carlo replicas [62] and *vice versa* [63].

In these analyses, the  $u$ ,  $d$  and  $s$  quarks are taken to be massless, but the treatment of the heavy  $c$  and  $b$  quark masses,  $m_Q$ , differs, and has a long history, which may be traced from Refs. [64–75]. The MSTW, CT, NNPDF and HERAPDF analyses use different variants of the General-Mass Variable-Flavour-Number Scheme (GM-VFNS). This combines fixed-order contributions to the coefficient functions (or partonic cross sections) calculated with the full  $m_Q$  dependence, with the all-order resummation of contributions via DGLAP evolution in which the heavy quarks are treated as massless after starting evolution at some transition point. Transition matrix elements are computed, following [67], which provide the boundary conditions between  $n_f$  and  $n_f + 1$  PDFs. The ABMP and JR analyses use a FFNS where only the three light (massless) quarks enter the evolution, while the heavy quarks enter the partonic cross sections with their full  $m_Q$  dependence. The GM-VFNS and FFNS approaches yield different results: in particular  $\alpha_s(M_Z^2)$  and the large- $x$  gluon PDF at large  $Q^2$  are both significantly smaller in the FFNS. It has been argued [48, 49, 74] that the difference is due to the slow convergence of the  $\ln^n(Q^2/m_Q^2)$  terms in certain regions in a FFNS. The final HERA combination of heavy flavour structure function data has recently been published [76], and the evolution of these measurements and their interpretation may be traced in [77].

The most recent determinations of the groups fitting a variety of data and using a GM-VFNS (MMHT, NNPDF and CT) have converged, so that now a good agreement has been achieved between the resulting PDFs. Indeed, the CT14 [59], MMHT2014 [26], and NNPDF3.0 [25] PDF sets have been combined [78] using the Monte Carlo approach [62] mentioned above. The single combined set of PDFs is discussed in detail in Ref. [78].

For illustration, we show in Fig. 18.4 the PDFs obtained in the NNLO NNPDF analysis [25] at scales  $\mu^2 = 10$  and  $10^4 \text{ GeV}^2$ . The

values of  $\alpha_s$  found by MMHT [79] may be taken as representative of those resulting from the GM-VFNS analyses

$$\text{NLO} : \alpha_s(M_Z^2) = 0.1201 \pm 0.0015,$$

$$\text{NNLO} : \alpha_s(M_Z^2) = 0.1172 \pm 0.0012,$$

where the error (at 68% C.L.) corresponds to the uncertainties resulting from the data fitted (the uncertainty that might be expected from the neglect of higher orders is at least as large). A similar result is found by the NNPDF group [80], who find  $\alpha_s(M_Z^2) = 0.1185 \pm 0.0005$  at NNLO. The ABMP analysis [60], which uses a FFNS, finds  $\alpha_s(M_Z^2) = 0.1147 \pm 0.0011$  at NNLO.

As a first step towards the inclusion of higher order electroweak corrections a recent development has been a vastly increased understanding of the photon content of the proton. Sets of PDFs with a photon contribution were first considered in Ref. [81] and then in subsequent PDF sets [82, 83]. However, due to weak data constraints, the uncertainty was extremely large. Subsequently, there has been a much improved understanding of the separation into elastic and inelastic contributions [84–86]. This gives much more theoretical precision, since the elastic contribution, arising from coherent emission of a photon from the proton, can be directly related to the well-known proton electric and magnetic form factors; the model dependence of the inelastic (incoherent) contribution, related to the quark PDFs, is at the level of tens of percent. A final development directly relating the entire photon contribution to the proton structure function [87] resulted in a determination of the photon content of the proton as precise as that of the light quarks. The framework has been applied within global fits to PDFs via an iterative procedure in [88] and to provide the low-scale input photon PDF in [89].

**Nuclear PDFs:** The study of the parton distributions for nucleons within nuclei, so-called nuclear parton distribution functions (nPDFs), is now reaching a level of maturity and sophistication similar to nucleon PDFs. The PDFs are now also a function of the nucleon number of the nucleus,  $A$ . The nPDFs are obtained via fits to deep inelastic scattering data and dilepton (Drell-Yan) and pion production from proton-nucleus. There are a number of recent examples of NLO analyses, DSSZ [90], nCTEQ15 [91], EPPS16 [92], while an NNLO analysis with a smaller selection of data types now also exists [93]. Much of the heavy-nucleus data included are in the form of ratios to proton or deuteron measurements. And most nuclear PDFs are related to a particular proton PDF via a nuclear modification factor, i.e.

$$f_i^{p/A}(x, Q^2) = R_i^A(x, Q^2) f_i^p(x, Q^2). \quad (18.30)$$

An exception is the PDFs in [91] which parameterise the nuclear PDFs directly but are equal to proton PDFs in the limit  $A = 1$ . There is some variation in whether charged current neutrino DIS data is used as well as neutral current DIS data since there is no clear compatibility in the modification factors obtained [94, 95]. Recently, LHC data from vector boson production [96, 97] in proton-lead collisions has been studied [98] or used directly [92], and LHC jet data [99] has been included [92], giving extra constraint on the gluon within nuclei. Further information at smaller  $x$  values should soon be extracted from heavy meson production at LHCb [100] and pion production [101]. All the PDF extractions above are based on the Hessian formulation, but the first NNPDF study of nPDFs has appeared [102], so far based on neutral current DIS data only. As well as improved constraints from further LHC data, nPDFs would be significantly improved by data from a potential high-energy Electron-Ion Collider [103].

**Polarized PDFs:** For spin-dependent structure functions, data exists for a more restricted range of  $Q^2$  and has lower precision, so that the scaling violations are not seen so clearly. However, spin-dependent (or polarized) parton distributions have been extracted by comparison to data using NLO global analyses which include measurements of the  $g_1$  structure function in inclusive polarized



DIS, ‘flavour-tagged’ semi-inclusive DIS data, open-charm production in DIS and results from polarized  $pp$  scattering at RHIC. There are recent results on DIS from JLAB [104] (for  $g_1^n/F_1^n$ ), COMPASS [105,106] and CLAS [107]. NLO analyses are given in Refs. [108–111] and more recent extractions [112,113]. Improved parton-to-hadron fragmentation functions, needed to describe the semi-inclusive DIS (SIDIS) data, can be found in Refs. [114–117]. Only the DSSV collaboration includes in their NLO analysis to extract polarized PDFs all the world data, inclusive and semi-inclusive DIS, double spin asymmetries in jet, dijet and inclusive

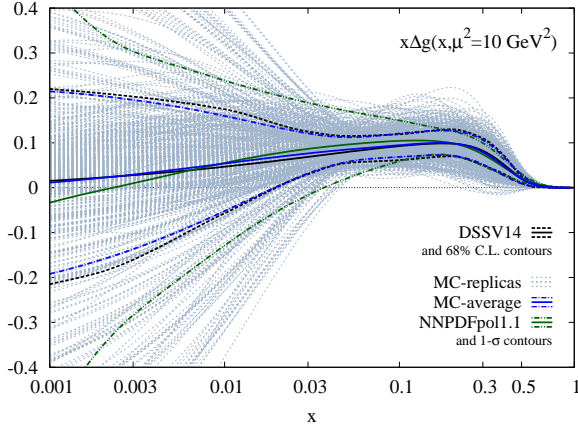


Figure 18.5: Ensemble of replicas (dotted blue lines) for the NLO gluon helicity density  $\Delta g(x, Q^2)$  at  $Q^2 = 10 \text{ GeV}^2$  shown along with its statistical average (solid blue line) and variance (dot-dashed blue lines). The corresponding results from the DSSV14 fit (black lines) [112] and the NNPDFpol1.1 analysis (green lines) [27] are shown for comparison. Figure taken from Ref. [118].

$\pi^0$ -production as well as the single spin asymmetries in  $W^\pm, Z^0$  production. A determination [119], using the NNPDF methodology, concentrates just on the inclusive polarized DIS data, and finds the uncertainties on the polarized gluon PDF have been underestimated in the earlier analyses. An update to this [27], where jet and  $W^\pm$  data from  $pp$  collisions and open-charm DIS data have been included via reweighting, reduces the uncertainty and suggests a positive polarized gluon PDF. The DSSV group has recently implemented a Monte Carlo sampling strategy to extract helicity parton densities and their uncertainties from a reference set of longitudinally polarized scattering data [118].

A comparison of the polarized gluon PDFs obtained in the NLO analyses of NNPDF [27] and DSSV [118] is shown in Fig. 18.5 at scale  $\mu^2 = 10 \text{ GeV}^2$ . The world data of the inclusive structure function  $g_1$  for proton and deuterium included in these analysis are shown in Fig. 18.14 and Fig. 18.15.

Comprehensive sets of PDFs are available from the LHAPDF library [120], which can be linked directly into a user’s programme to provide access to recent PDFs in a standard format.

#### 18.4 The hadronic structure of the photon

Besides the *direct* interactions of the photon, it is possible for it to fluctuate into a hadronic state via the process  $\gamma \rightarrow q\bar{q}$ . While in this state, the partonic content of the photon may be *resolved*, for example, through the process  $e^+e^- \rightarrow e^+e^-\gamma^* \rightarrow e^+e^-X$ , where the virtual photon emitted by the DIS lepton probes the hadronic structure of the quasi-real photon emitted by the other lepton. The perturbative LO QED contributions to this process with  $\gamma \rightarrow q\bar{q}$  in conjunction with  $\gamma^*q(\bar{q}) \rightarrow q(\bar{q})$ , are subject to QCD corrections due to the radiation of gluons from these quarks.

Often the equivalent-photon approximation is used to express the differential cross section for deep inelastic electron–photon scattering in terms of the structure functions of the transverse quasi-real photon times a flux factor  $N_\gamma^T$  (for these incoming

quasi-real photons of transverse polarization)

$$\frac{d^2\sigma}{dx dQ^2} = N_\gamma^T \frac{2\pi\alpha^2}{xQ^4} \left[ (1 + (1-y)^2) F_2^\gamma(x, Q^2) - y^2 F_L^\gamma(x, Q^2) \right], \quad (18.31)$$

where we have used  $F_2^\gamma = 2xF_T^\gamma + F_L^\gamma$  (where  $F_T$  is the transverse structure function), not to be confused with  $F_2^\gamma$  of Sec. 18.2. Complete formulae are given, for example, in the comprehensive review of [121].

The hadronic photon structure function,  $F_2^\gamma$ , evolves with increasing  $Q^2$  from the ‘hadron-like’ behavior, calculable via the vector-meson-dominance model, to the dominating ‘point-like’ behaviour, calculable in perturbative QCD. Due to the point-like coupling, the logarithmic evolution of  $F_2^\gamma$  with  $Q^2$  has a *positive* slope for all values of  $x$ , see Fig. 18.16. The ‘loss’ of quarks at large  $x$  due to gluon radiation is over-compensated by the ‘creation’ of quarks via the point-like  $\gamma \rightarrow q\bar{q}$  coupling. The logarithmic evolution was first predicted in the quark–parton model ( $\gamma^* \gamma \rightarrow q\bar{q}$ ) [122,123], and then an improved expression was obtained using QCD corrections in the limit of large  $Q^2$  [124]. The evolution is now known to NLO [125–127]. The NLO data analyses to determine the parton densities of the photon can be found in Refs. [128–130].

#### 18.5 Diffractive DIS (DDIS)

Some 10% of DIS events are diffractive,  $\gamma^*p \rightarrow X + p$ , in which the slightly deflected proton and the cluster  $X$  of outgoing hadrons are well-separated in rapidity [131]. Besides  $x$  and  $Q^2$ , two extra

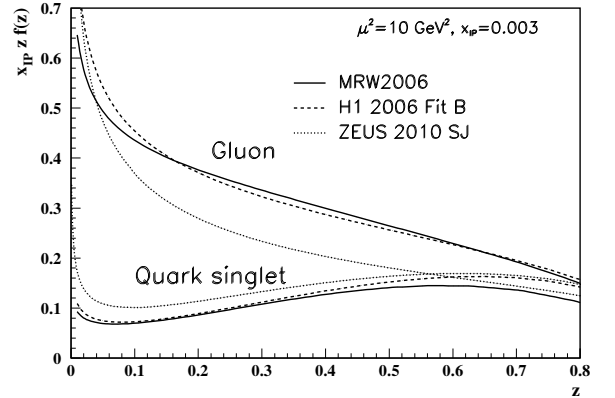


Figure 18.6: Diffractive parton distributions,  $x_{IP} z f_{a/p}^D$ , obtained from fitting to the ZEUS data with  $Q^2 > 5 \text{ GeV}^2$  [132], H1 data with  $Q^2 > 8.5 \text{ GeV}^2$  assuming Regge factorization [133], and from MRW2006 [134] using a more perturbative QCD approach [134]. Only the Pomeron contributions are shown and not the secondary Reggeon contributions, which are negligible at the value of  $x_{IP} = 0.003$  chosen here. The H1 2007 Jets distribution [135] is similar to H1 2006 Fit B.

variables are needed to describe a DDIS event: the fraction  $x_{IP}$  of the proton’s momentum transferred across the rapidity gap and  $t$ , the square of the 4-momentum transfer of the proton. The DDIS data [136,137] are usually analysed using two levels of factorization. First, the diffractive structure function  $F_2^D$  satisfies *collinear factorization*, and can be expressed as the convolution [138]

$$F_2^D = \sum_{a=q,g} C_2^a \otimes f_{a/p}^D, \quad (18.32)$$

with the same coefficient functions as in DIS (see Eq. (18.21)), and where the diffractive parton distributions  $f_{a/p}^D$  ( $a = q, g$ ) satisfy DGLAP evolution. Second, *Regge factorization* is assumed [139],

$$f_{a/p}^D(x_{IP}, t, z, \mu^2) = f_{IP/p}(x_{IP}, t) f_{a/IP}(z, \mu^2), \quad (18.33)$$

where  $f_{a/IP}$  are the parton densities of the Pomeron, which itself is treated like a hadron, and  $z \in [x/x_{IP}, 1]$  is the fraction of the Pomeron’s momentum carried by the parton entering the



hard subprocess. The Pomeron flux factor  $f_{\mathbb{P}/p}(x_{\mathbb{P}}, t)$  is taken from Regge phenomenology. There are also secondary Reggeon contributions to Eq. (18.33). A sample of the  $t$ -integrated diffractive parton densities, obtained in this way, is shown in Fig. 18.6. A more recent extraction of the parton densities may be found in [140].

Although collinear factorization holds as  $\mu^2 \rightarrow \infty$ , there are non-negligible corrections for finite  $\mu^2$  and small  $x_{\mathbb{P}}$ . Besides the *resolved* interactions of the Pomeron, the perturbative QCD Pomeron may also interact *directly* with the hard subprocess, giving rise to an inhomogeneous evolution equation for the diffractive parton densities analogous to the photon case. The results of the MRW analysis [134], which includes these contributions, are also shown in Fig. 18.6.

Unlike the inclusive case, the diffractive parton densities cannot be directly used to calculate diffractive hadron-hadron cross sections, since account must first be taken of “soft” rescattering effects.

### 18.6 Generalized parton distributions

The parton distributions of the proton of Sec. 18.3 are given by the diagonal matrix elements  $\langle P, \lambda | \hat{O} | P, \lambda \rangle$ , where  $P$  and  $\lambda$  are the 4-momentum and helicity of the proton, and  $\hat{O}$  is a twist-2 quark or gluon operator. However, there is new information in the so-called generalised parton distributions (GPDs) defined in terms of the off-diagonal matrix elements  $\langle P', \lambda' | \hat{O} | P, \lambda \rangle$ ; see Refs. [141–146] for reviews. Unlike the diagonal PDFs, the GPDs cannot be regarded as parton densities, but are to be interpreted as probability amplitudes.

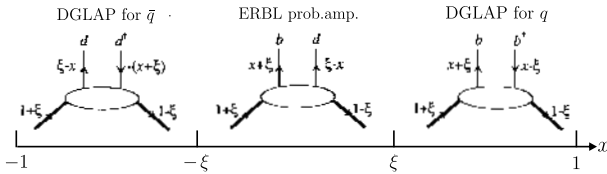


Figure 18.7: Schematic diagrams of the three distinct kinematic regions of the imaginary part of  $H_q$ . The proton and quark momentum fractions refer to  $\bar{P}^+$ , and  $x$  covers the interval  $(-1, 1)$ . In the ERBL domain the GPDs are generalisations of distribution amplitudes which occur in processes such as  $p\bar{p} \rightarrow J/\psi$ .

The physical significance of GPDs is best seen using light-cone coordinates,  $z^\pm = (z^0 \pm z^3)/\sqrt{2}$ , and in the light-cone gauge,  $A^+ = 0$ . It is conventional to define the generalised quark distributions in terms of quark operators at light-like separation

$$F_q(x, \xi, t) = \frac{1}{2} \int \frac{dz^-}{2\pi} e^{ix\bar{P}^+z^-} \langle P' | \bar{\psi}(-z/2) \gamma^+ \psi(z/2) | P \rangle \Big|_{z^+=z^1=z^2=0} = \frac{1}{2\bar{P}^+} \times \left( H_q(x, \xi, t) \bar{u}(P') \gamma^+ u(P) + E_q(x, \xi, t) \bar{u}(P') \frac{i\sigma^{+\alpha} \Delta_\alpha}{2m} u(P) \right) \quad (18.34)$$

with  $\bar{P} = (P + P')/2$  and  $\Delta = P' - P$ , and where we have suppressed the helicity labels of the protons and spinors. We now have two extra kinematic variables:

$$t = \Delta^2, \quad \xi = -\Delta^+ / (P + P')^+. \quad (18.35)$$

We see that  $-1 \leq \xi \leq 1$ . Similarly, we may define GPDs  $\tilde{H}_q$  and  $\tilde{E}_q$  with an additional  $\gamma_5$  between the quark operators in Eq. (18.34); and also an analogous set of gluon GPDs,  $H_g, E_g, \tilde{H}_g$  and  $\tilde{E}_g$ . After a Fourier transform with respect to the transverse components of  $\Delta$ , we are able to describe the spatial distribution of partons in the impact parameter plane in terms of GPDs [147, 148].

For  $P' = P, \lambda' = \lambda$  the matrix elements reduce to the ordinary PDFs of Sec. 18.2.1

$$H_q(x, 0, 0) = q(x), \quad H_q(-x, 0, 0) = -\bar{q}(x), \quad H_g(x, 0, 0) = xg(x), \quad (18.36)$$

$$\tilde{H}_q(x, 0, 0) = \Delta q(x), \quad \tilde{H}_q(-x, 0, 0) = \Delta \bar{q}(x), \quad \tilde{H}_g(x, 0, 0) = x\Delta g(x), \quad (18.37)$$

where  $\Delta q = q \uparrow - q \downarrow$  as in Eq. (18.18). No corresponding relations exist for  $E, \tilde{E}$  as they decouple in the forward limit,  $\Delta = 0$ .

The functions  $H_g, E_g$  are even in  $x$ , and  $\tilde{H}_g, \tilde{E}_g$  are odd functions of  $x$ . We can introduce valence and ‘singlet’ quark distributions which are even and odd functions of  $x$  respectively. For example

$$H_q^V(x, \xi, t) \equiv H_q(x, \xi, t) + H_q(-x, \xi, t) = H_q^V(-x, \xi, t), \quad (18.38)$$

$$H_q^S(x, \xi, t) \equiv H_q(x, \xi, t) - H_q(-x, \xi, t) = -H_q^S(-x, \xi, t). \quad (18.39)$$

All the GPDs satisfy relations of the form

$$H(x, -\xi, t) = H(x, \xi, t) \quad \text{and} \quad H(x, -\xi, t)^* = H(x, \xi, t), \quad (18.40)$$

and so are real-valued functions. Moreover, the moments of GPDs, that is the  $x$  integrals of  $x^n H_q$  etc., are *polynomials* in  $\xi$  of order  $n + 1$ . Another important property of GPDs are Ji’s sum rule [141]

$$\frac{1}{2} \int_{-1}^1 dx x (H_q(x, \xi, t) + E_q(x, \xi, t)) = J_q(t), \quad (18.41)$$

where  $J_q(0)$  is the total angular momentum carried by quarks and antiquarks of flavour  $q$ , with a similar relation for gluons.

To visualize the physical content of  $H_q$ , we Fourier expand  $\psi$  in terms of quark, antiquark creation ( $b, d$ ) and annihilation ( $b^\dagger, d^\dagger$ ) operators, and sketch the result in Fig. 18.7. There are two types of domain: (i) the time-like or ‘annihilation’ domain, with  $|x| < |\xi|$ , where the GPDs describe the wave functions of a  $t$ -channel  $q\bar{q}$  (or gluon) pair and evolve according to modified ERBL equations [149, 150]; (ii) the space-like or ‘scattering’ domain, with  $|x| > |\xi|$ , where the GPDs generalise the familiar  $\bar{q}, q$  (and gluon) PDFs and describe processes such as ‘deeply virtual Compton scattering’ ( $\gamma^* p \rightarrow \gamma p$ ),  $\gamma p \rightarrow J/\psi p$ , etc., and evolve according to modified DGLAP equations. The splitting functions for the evolution of GPDs are known to NLO [151–153].

GPDs describe new aspects of proton structure and must be determined from experiment. We can parametrise them in terms of ‘double distributions’ [154, 155], which reduce to diagonal PDFs as  $\xi \rightarrow 0$ . Alternatively, flexible  $SO(3)$ -based parametrisations have been used to determine GPDs from DVCS data [156, 157]; a more recent summary may be found in Ref. [158, 159].

### 18.7 Transverse momentum dependent distributions

Transverse momentum dependent distributions (TMDs) are complementary to GPDs. Together, they describe the three-dimensional structure of hadrons. In contrast to GPDs that encode the transverse position of a parton in a nucleon, TMDs encompassing both the parton distributions (TMD PDF) and fragmentation functions (TMD FF) encode the transverse momenta and lead to observable transverse momenta in the final state. Both TMDs and GPDs derive, via integration over the appropriate variable, from Wigner distributions [160–162] that depend on the average transverse momentum and position of partons.

For a proton, there are eight independent TMD PDFs, at leading twist, three of which correspond to the usual unpolarized, longitudinally polarized and transversely polarized quark parton distributions [163, 164]. The novel TMD PDFs have physical interpretations. For example, the Sivers function [165] represents the distribution of unpolarized partons inside a transversely polarized hadron. For (pseudo)scalar particles, such as kaon and pions, there are two independent leading-twist TMD FFs, one being the ordinary unpolarized fragmentation function and the other the Collins FF [166] which is related to the probability of a polarized quark fragmenting into an unpolarized hadron.

Factorization of TMDs have been shown for semi-inclusive DIS, for the Drell-Yan process as well as for electron-position annihilation into dihadrons [167–172]. Recently first TMD global fits have become available [173–180], although problems with consistent descriptions still remain [181, 182].

Because TMD PDFs encode nonperturbative information about transverse momentum and polarization degrees of freedom, they are important for descriptions of multi-scale, non-inclusive collider observables, for example, production of electroweak gauge bosons at LHC [183] and can have an effect on determination of the  $W$  boson mass [184]. The combination of TMD PDFs and FFs can give consistent global description of spin and azimuthal asymmetries and provide predictions. Some recent reviews of this rapidly developing field are given here [183, 185–187].

### References

- [1] J. Blumlein and N. Kochelev, Nucl. Phys. **B498**, 285 (1997), [hep-ph/9612318].
- [2] S. Forte, M. L. Mangano and G. Ridolfi, Nucl. Phys. **B602**, 585 (2001), [hep-ph/0101192].
- [3] M. Anselmino, P. Gambino and J. Kalinowski, Z. Phys. **C64**, 267 (1994), [hep-ph/9401264].
- [4] M. Anselmino, A. Efremov and E. Leader, Phys. Rept. **261**, 1 (1995), [Erratum: Phys. Rept.281,399(1997)], [hep-ph/9501369].
- [5] M. Klein and T. Riemann, Z. Phys. **C24**, 151 (1984).
- [6] C. G. Callan, Jr. and D. J. Gross, Phys. Rev. Lett. **22**, 156 (1969).
- [7] D. A. Dicus, Phys. Rev. **D5**, 1367 (1972).
- [8] J. D. Bjorken and E. A. Paschos, Phys. Rev. **185**, 1975 (1969).
- [9] R.P. Feynman, Photon Hadron Interactions (Benjamin, New York, 1972).
- [10] A.M. Cooper-Sarkar, private communication.
- [11] H. Abramowicz *et al.* (H1, ZEUS), Eur. Phys. J. **C75**, 12, 580 (2015), [arXiv:1506.06042].
- [12] L. A. Harland-Lang *et al.*, Eur. Phys. J. **C76**, 4, 186 (2016), [arXiv:1601.03413].
- [13] I. Abt *et al.*, Phys. Rev. **D94**, 3, 034032 (2016), [arXiv:1604.02299].
- [14] R. D. Ball *et al.*, Eur. Phys. J. **C78**, 4, 321 (2018), [arXiv:1710.05935].
- [15] H. Abdolmaleki *et al.* (xFitter Developers' Team), Eur. Phys. J. **C78**, 8, 621 (2018), [arXiv:1802.00064].
- [16] S. Wandzura and F. Wilczek, Phys. Lett. **72B**, 195 (1977).
- [17] J. Blumlein and A. Tkabladze, Nucl. Phys. **B553**, 427 (1999), [hep-ph/9812478].
- [18] J. D. Bjorken, Phys. Rev. **179**, 1547 (1969).
- [19] V. N. Gribov and L. N. Lipatov, Sov. J. Nucl. Phys. **15**, 438 (1972), [Yad. Fiz.15,781(1972)].
- [20] L.N. Lipatov, Sov. J. Nucl. Phys. **20**, 95 (1975).
- [21] G. Altarelli and G. Parisi, Nucl. Phys. **B126**, 298 (1977).
- [22] Y. L. Dokshitzer, Sov. Phys. JETP **46**, 641 (1977), [Zh. Eksp. Teor. Fiz.73,1216(1977)].
- [23] O. Zenaiev *et al.* (PROSA), Eur. Phys. J. **C75**, 8, 396 (2015), [arXiv:1503.04581].
- [24] R. Aaij *et al.* (LHCb), J. Phys. **G41**, 055002 (2014), [arXiv:1401.3288].
- [25] R. D. Ball *et al.* (NNPDF), JHEP **04**, 040 (2015), [arXiv:1410.8849].
- [26] L. A. Harland-Lang *et al.*, Eur. Phys. J. **C75**, 5, 204 (2015), [arXiv:1412.3989].
- [27] E. R. Nocera *et al.* (NNPDF), Nucl. Phys. **B887**, 276 (2014), [arXiv:1406.5539].
- [28] G. Curci, W. Furmanski and R. Petronzio, Nucl. Phys. **B175**, 27 (1980); W. Furmanski and R. Petronzio, Phys. Lett. **97B**, 437 (1980).
- [29] R.K. Ellis *et al.*, QCD and Collider Physics (Cambridge UP, 1996).
- [30] W. L. van Neerven and E. B. Zijlstra, Phys. Lett. **B272**, 127 (1991); E. B. Zijlstra and W. L. van Neerven, Phys. Lett. **B273**, 476 (1991); E. B. Zijlstra and W. L. van Neerven, Phys. Lett. **B297**, 377 (1992); E. B. Zijlstra and W. L. van Neerven, Nucl. Phys. **B383**, 525 (1992).
- [31] S. Moch and J. A. M. Vermaseren, Nucl. Phys. **B573**, 853 (2000), [hep-ph/9912355].
- [32] S. Moch, J. A. M. Vermaseren and A. Vogt, Nucl. Phys. **B688**, 101 (2004), [hep-ph/0403192]; A. Vogt, S. Moch and J. A. M. Vermaseren, Nucl. Phys. **B691**, 129 (2004), [hep-ph/0404111]; S. Moch, J. A. M. Vermaseren and A. Vogt, Phys. Lett. **B606**, 123 (2005), [hep-ph/0411112]; J. A. M. Vermaseren, A. Vogt and S. Moch, Nucl. Phys. **B724**, 3 (2005), [hep-ph/0504242].
- [33] V. S. Fadin, E. A. Kuraev and L. N. Lipatov, Phys. Lett. **60B**, 50 (1975); E. A. Kuraev, L. N. Lipatov and V. S. Fadin, Sov. Phys. JETP **44**, 443 (1976), [Zh. Eksp. Teor. Fiz.71,840(1976)]; E. A. Kuraev, L. N. Lipatov and V. S. Fadin, Sov. Phys. JETP **45**, 199 (1977), [Zh. Eksp. Teor. Fiz.72,377(1977)].
- [34] I. I. Balitsky and L. N. Lipatov, Sov. J. Nucl. Phys. **28**, 822 (1978), [Yad. Fiz.28,1597(1978)].
- [35] V. S. Fadin and L. N. Lipatov, Phys. Lett. **B429**, 127 (1998), [hep-ph/9802290].
- [36] G. Camici and M. Ciafaloni, Phys. Lett. **B412**, 396 (1997), [Erratum: Phys. Lett. B417,390(1998)], [hep-ph/9707390]; M. Ciafaloni and G. Camici, Phys. Lett. **B430**, 349 (1998), [hep-ph/9803389].
- [37] M. Ciafaloni, D. Colferai and G. P. Salam, Phys. Rev. **D60**, 114036 (1999), [hep-ph/9905566]; M. Ciafaloni, D. Colferai and G. P. Salam, JHEP **07**, 054 (2000), [hep-ph/0007240].
- [38] M. Ciafaloni *et al.*, Phys. Lett. **B576**, 143 (2003), [hep-ph/0305254]; M. Ciafaloni *et al.*, Phys. Rev. **D68**, 114003 (2003), [hep-ph/0307188].
- [39] G. Altarelli, R. D. Ball and S. Forte, Nucl. Phys. **B742**, 1 (2006), [hep-ph/0512237]; G. Altarelli, R. D. Ball and S. Forte, Nucl. Phys. **B799**, 199 (2008), [arXiv:0802.0032].
- [40] C. D. White and R. S. Thorne, Phys. Rev. **D75**, 034005 (2007), [hep-ph/0611204].
- [41] M. Bonvini, S. Marzani and T. Peraro, Eur. Phys. J. **C76**, 11, 597 (2016), [arXiv:1607.02153].
- [42] M. Bonvini, S. Marzani and C. Muselli, JHEP **12**, 117 (2017), [arXiv:1708.07510].
- [43] G. 't Hooft and M. J. G. Veltman, Nucl. Phys. **B44**, 189 (1972).
- [44] G. 't Hooft, Nucl. Phys. **B61**, 455 (1973).
- [45] W. A. Bardeen *et al.*, Phys. Rev. **D18**, 3998 (1978).
- [46] G. Altarelli, R. K. Ellis and G. Martinelli, Nucl. Phys. **B143**, 521 (1978), [Erratum: Nucl. Phys. B146,544(1978)].
- [47] A. D. Martin *et al.*, Eur. Phys. J. **C35**, 325 (2004), [hep-ph/0308087].
- [48] R. D. Ball *et al.* (NNPDF), Phys. Lett. **B723**, 330 (2013), [arXiv:1303.1189].
- [49] R. S. Thorne, Eur. Phys. J. **C74**, 7, 2958 (2014), [arXiv:1402.3536].
- [50] M. Dasgupta and B. R. Webber, Phys. Lett. **B382**, 273 (1996), [hep-ph/9604388].
- [51] A. De Roeck and R. S. Thorne, Prog. Part. Nucl. Phys. **66**, 727 (2011), [arXiv:1103.0555].
- [52] S. Forte and G. Watt, Ann. Rev. Nucl. Part. Sci. **63**, 291 (2013), [arXiv:1301.6754].

- [53] J. Blumlein, *Prog. Part. Nucl. Phys.* **69**, 28 (2013), [arXiv:1208.6087].
- [54] E. Perez and E. Rizvi, *Rept. Prog. Phys.* **76**, 046201 (2013), [arXiv:1208.1178].
- [55] R. D. Ball *et al.*, *JHEP* **04**, 125 (2013), [arXiv:1211.5142].
- [56] J. Gao, L. Harland-Lang and J. Rojo, *Phys. Rept.* **742**, 1 (2018), [arXiv:1709.04922].
- [57] J. Rojo *et al.*, *J. Phys.* **G42**, 103103 (2015), [arXiv:1507.00556].
- [58] R. D. Ball *et al.* (NNPDF), *Eur. Phys. J.* **C77**, 10, 663 (2017), [arXiv:1706.00428].
- [59] CT<sub>14</sub>, S. Dulat *et al.*, *Phys. Rev.* **D93**, 3, 033006 (2016), [arXiv:1506.07443].
- [60] S. Alekhin *et al.*, *Phys. Rev.* **D96**, 1, 014011 (2017), [arXiv:1701.05838].
- [61] P. Jimenez-Delgado and E. Reya, *Phys. Rev.* **D89**, 7, 074049 (2014), [arXiv:1403.1852].
- [62] G. Watt and R. S. Thorne, *JHEP* **08**, 052 (2012), [arXiv:1205.4024].
- [63] S. Carrazza *et al.*, *Eur. Phys. J.* **C75**, 8, 369 (2015), [arXiv:1505.06736].
- [64] J. C. Collins, F. Wilczek and A. Zee, *Phys. Rev.* **D18**, 242 (1978).
- [65] E. Laenen *et al.*, *Nucl. Phys.* **B392**, 162 (1993).
- [66] M. A. G. Aivazis *et al.*, *Phys. Rev.* **D50**, 3102 (1994), [hep-ph/9312319].
- [67] M. Buza *et al.*, *Eur. Phys. J.* **C1**, 301 (1998), [hep-ph/9612398].
- [68] J. C. Collins, *Phys. Rev.* **D58**, 094002 (1998), [hep-ph/9806259].
- [69] A. Chuvakin, J. Smith and W. L. van Neerven, *Phys. Rev.* **D61**, 096004 (2000), [hep-ph/9910250].
- [70] R. S. Thorne, *Phys. Rev.* **D73**, 054019 (2006), [hep-ph/0601245].
- [71] R. S. Thorne and W. K. Tung, in “Proceedings, HERA and the LHC Workshop Series on the implications of HERA for LHC physics: 2006-2008,” 332–351 (2008), [2(2008)], [arXiv:0809.0714].
- [72] S. Alekhin and S. Moch, *Phys. Lett.* **B699**, 345 (2011), [arXiv:1011.5790].
- [73] S. Forte *et al.*, *Nucl. Phys.* **B834**, 116 (2010), [arXiv:1001.2312].
- [74] R. S. Thorne, *Phys. Rev.* **D86**, 074017 (2012), [arXiv:1201.6180].
- [75] E. G. de Oliveira *et al.*, *Eur. Phys. J.* **C73**, 10, 2616 (2013), [arXiv:1307.3508].
- [76] H. Abramowicz *et al.* (H1, ZEUS), *Eur. Phys. J.* **C78**, 6, 473 (2018), [arXiv:1804.01019].
- [77] O. Behnke, A. Geiser and M. Lisovsky, *Prog. Part. Nucl. Phys.* **84**, 1 (2015), [arXiv:1506.07519].
- [78] J. Butterworth *et al.*, *J. Phys.* **G43**, 023001 (2016), [arXiv:1510.03865].
- [79] L. A. Harland-Lang *et al.*, *Eur. Phys. J.* **C75**, 9, 435 (2015), [arXiv:1506.05682].
- [80] R. D. Ball *et al.* (NNPDF), *Eur. Phys. J.* **C78**, 5, 408 (2018), [arXiv:1802.03398].
- [81] A. D. Martin *et al.*, *Eur. Phys. J.* **C39**, 155 (2005), [hep-ph/0411040].
- [82] R. D. Ball *et al.* (NNPDF), *Nucl. Phys.* **B877**, 290 (2013), [arXiv:1308.0598].
- [83] C. Schmidt *et al.*, *Phys. Rev.* **D93**, 11, 114015 (2016), [arXiv:1509.02905].
- [84] M. Gluck, C. Pisano and E. Reya, *Phys. Lett.* **B540**, 75 (2002), [hep-ph/0206126].
- [85] A. D. Martin and M. G. Ryskin, *Eur. Phys. J.* **C74**, 3040 (2014), [arXiv:1406.2118].
- [86] L. A. Harland-Lang, V. A. Khoze and M. G. Ryskin, *Phys. Rev.* **D94**, 7, 074008 (2016), [arXiv:1607.04635].
- [87] A. Manohar *et al.*, *Phys. Rev. Lett.* **117**, 24, 242002 (2016), [arXiv:1607.04266].
- [88] V. Bertone *et al.* (NNPDF), *SciPost Phys.* **5**, 1, 008 (2018), [arXiv:1712.07053].
- [89] L. A. Harland-Lang *et al.*, *Eur. Phys. J.* **C79**, 10, 811 (2019), [arXiv:1907.02750].
- [90] D. de Florian *et al.*, *Phys. Rev.* **D85**, 074028 (2012), [arXiv:1112.6324].
- [91] K. Kovarik *et al.*, *Phys. Rev.* **D93**, 8, 085037 (2016), [arXiv:1509.00792].
- [92] H. Paukkunen, *Nucl. Phys.* **A967**, 241 (2017), [arXiv:1704.04036].
- [93] H. Khanpour and S. Atashbar Tehrani, *Phys. Rev.* **D93**, 1, 014026 (2016), [arXiv:1601.00939].
- [94] K. Kovarik *et al.*, *Phys. Rev. Lett.* **106**, 122301 (2011), [arXiv:1012.0286].
- [95] H. Paukkunen and C. A. Salgado, *Phys. Rev. Lett.* **110**, 21, 212301 (2013), [arXiv:1302.2001].
- [96] G. Aad *et al.* (ATLAS), *Phys. Rev.* **C92**, 4, 044915 (2015), [arXiv:1507.06232].
- [97] V. Khachatryan *et al.* (CMS), *Phys. Lett.* **B750**, 565 (2015), [arXiv:1503.05825].
- [98] A. Kusina *et al.*, *Eur. Phys. J.* **C77**, 7, 488 (2017), [arXiv:1610.02925].
- [99] S. Chatrchyan *et al.* (CMS), *Eur. Phys. J.* **C74**, 7, 2951 (2014), [arXiv:1401.4433].
- [100] R. Aaij *et al.* (LHCb), *JHEP* **10**, 090 (2017), [arXiv:1707.02750].
- [101] S. Acharya *et al.* (ALICE), *Eur. Phys. J.* **C78**, 8, 624 (2018), [arXiv:1801.07051].
- [102] R. Abdul Khalek, J. J. Ethier and J. Rojo (NNPDF), *Eur. Phys. J.* **C79**, 6, 471 (2019), [arXiv:1904.00018].
- [103] E. C. Aschenauer *et al.*, *Phys. Rev.* **D96**, 11, 114005 (2017), [arXiv:1708.05654].
- [104] D. Flay *et al.* (Jefferson Lab Hall A), *Phys. Rev.* **D94**, 5, 052003 (2016), [arXiv:1603.03612].
- [105] C. Adolph *et al.* (COMPASS), *Phys. Lett.* **B753**, 18 (2016), [arXiv:1503.08935].
- [106] C. Adolph *et al.* (COMPASS), *Phys. Lett.* **B769**, 34 (2017), [arXiv:1612.00620].
- [107] R. Fersch *et al.* (CLAS), *Phys. Rev.* **C96**, 6, 065208 (2017), [arXiv:1706.10289].
- [108] M. Hirai and S. Kumano (Asymmetry Analysis), *Nucl. Phys.* **B813**, 106 (2009), [arXiv:0808.0413].
- [109] D. de Florian *et al.*, *Phys. Rev. Lett.* **101**, 072001 (2008), [arXiv:0804.0422]; D. de Florian *et al.*, *Phys. Rev.* **D80**, 034030 (2009), [arXiv:0904.3821].
- [110] E. Leader, A. V. Sidorov and D. B. Stamenov, *Phys. Rev.* **D82**, 114018 (2010), [arXiv:1010.0574].
- [111] J. Blumlein and H. Bottcher, *Nucl. Phys.* **B841**, 205 (2010), [arXiv:1005.3113].
- [112] D. de Florian *et al.*, *Phys. Rev. Lett.* **113**, 1, 012001 (2014), [arXiv:1404.4293].
- [113] N. Sato *et al.* (Jefferson Lab Angular Momentum), *Phys. Rev.* **D93**, 7, 074005 (2016), [arXiv:1601.07782].
- [114] D. de Florian *et al.*, *Phys. Rev.* **D91**, 1, 014035 (2015), [arXiv:1410.6027].
- [115] D. de Florian *et al.*, *Phys. Rev.* **D95**, 9, 094019 (2017), [arXiv:1702.06353].

- [116] V. Bertone *et al.* (NNPDF), *Eur. Phys. J.* **C77**, 8, 516 (2017), [arXiv:1706.07049].
- [117] V. Bertone *et al.* (NNPDF), *Eur. Phys. J.* **C78**, 8, 651 (2018), [arXiv:1807.03310].
- [118] D. De Florian *et al.* (2019), [arXiv:1902.10548].
- [119] R. D. Ball *et al.* (NNPDF), *Nucl. Phys.* **B874**, 36 (2013), [arXiv:1303.7236].
- [120] A. Buckley *et al.*, *Eur. Phys. J.* **C75**, 132 (2015), [arXiv:1412.7420].
- [121] R. Nisius, *Phys. Rept.* **332**, 165 (2000), [hep-ex/9912049].
- [122] T. F. Walsh and P. M. Zerwas, *Phys. Lett.* **44B**, 195 (1973).
- [123] R. L. Kingsley, *Nucl. Phys.* **B60**, 45 (1973).
- [124] E. Witten, *Nucl. Phys.* **B120**, 189 (1977).
- [125] W. A. Bardeen and A. J. Buras, *Phys. Rev.* **D20**, 166 (1979), [Erratum: *Phys. Rev.*D21,2041(1980)].
- [126] M. Fontannaz and E. Pilon, *Phys. Rev.* **D45**, 382 (1992).
- [127] M. Gluck, E. Reya and A. Vogt, *Phys. Rev.* **D45**, 3986 (1992).
- [128] F. Cornet, P. Jankowski and M. Krawczyk, *Phys. Rev.* **D70**, 093004 (2004), [hep-ph/0404063].
- [129] P. Aurenche, M. Fontannaz and J. P. Guillet, *Eur. Phys. J.* **C44**, 395 (2005), [hep-ph/0503259].
- [130] W. Slominski, H. Abramowicz and A. Levy, *Eur. Phys. J.* **C45**, 633 (2006), [hep-ph/0504003].
- [131] H. Abramowicz and A. Caldwell, *Rev. Mod. Phys.* **71**, 1275 (1999), [hep-ex/9903037].
- [132] S. Chekanov *et al.* (ZEUS), *Nucl. Phys.* **B831**, 1 (2010), [arXiv:0911.4119].
- [133] A. Aktas *et al.* (H1), *Eur. Phys. J.* **C48**, 715 (2006), [hep-ex/0606004].
- [134] A. D. Martin, M. G. Ryskin and G. Watt, *Phys. Lett.* **B644**, 131 (2007), [hep-ph/0609273].
- [135] A. Aktas *et al.* (H1), *JHEP* **10**, 042 (2007), [arXiv:0708.3217].
- [136] F. D. Aaron *et al.* (H1, ZEUS), *Eur. Phys. J.* **C72**, 2175 (2012), [arXiv:1207.4864].
- [137] F. D. Aaron *et al.* (H1), *Eur. Phys. J.* **C72**, 2074 (2012), [arXiv:1203.4495].
- [138] J. C. Collins, *Phys. Rev.* **D57**, 3051 (1998), [Erratum: *Phys. Rev.*D61,019902(2000)], [hep-ph/9709499].
- [139] G. Ingelman and P. E. Schlein, *Phys. Lett.* **152B**, 256 (1985).
- [140] M. Goharipour, H. Khanpour and V. Guzey, *Eur. Phys. J.* **C78**, 4, 309 (2018), [arXiv:1802.01363].
- [141] X.-D. Ji, *J. Phys.* **G24**, 1181 (1998), [hep-ph/9807358].
- [142] K. Goeke, M. V. Polyakov and M. Vanderhaeghen, *Prog. Part. Nucl. Phys.* **47**, 401 (2001), [hep-ph/0106012].
- [143] M. Diehl, *Phys. Rept.* **388**, 41 (2003), [hep-ph/0307382].
- [144] A. V. Belitsky and A. V. Radyushkin, *Phys. Rept.* **418**, 1 (2005), [hep-ph/0504030].
- [145] S. Boffi and B. Pasquini, *Riv. Nuovo Cim.* **30**, 387 (2007), [arXiv:0711.2625].
- [146] K. Kumericki, S. Liuti and H. Moutarde, *Eur. Phys. J.* **A52**, 6, 157 (2016), [arXiv:1602.02763].
- [147] M. Burkardt, *Int. J. Mod. Phys.* **A18**, 173 (2003), [hep-ph/0207047].
- [148] M. Diehl, *Eur. Phys. J.* **C25**, 223 (2002), [Erratum: *Eur. Phys. J.*C31,277(2003)], [hep-ph/0205208].
- [149] A. V. Efremov and A. V. Radyushkin, *Phys. Lett.* **94B**, 245 (1980).
- [150] G. P. Lepage and S. J. Brodsky, *Phys. Rev.* **D22**, 2157 (1980).
- [151] A. V. Belitsky, A. Freund and D. Mueller, *Phys. Lett.* **B493**, 341 (2000), [hep-ph/0008005].
- [152] A. V. Belitsky, A. Freund and D. Mueller, *Nucl. Phys.* **B574**, 347 (2000), [hep-ph/9912379].
- [153] V. M. Braun *et al.*, *JHEP* **06**, 037 (2017), [arXiv:1703.09532].
- [154] A. V. Radyushkin, *Phys. Rev.* **D59**, 014030 (1999), [hep-ph/9805342].
- [155] A. V. Radyushkin, *Phys. Lett.* **B449**, 81 (1999), [hep-ph/9810466].
- [156] K. Kumericki and D. Mueller, *Nucl. Phys.* **B841**, 1 (2010), [arXiv:0904.0458].
- [157] N. d'Hose, S. Niccolai and A. Rostomyan, *Eur. Phys. J.* **A52**, 6, 151 (2016).
- [158] M. Guidal, H. Moutarde and M. Vanderhaeghen, *Rept. Prog. Phys.* **76**, 066202 (2013), [arXiv:1303.6600].
- [159] M. Anselmino, M. Guidal and P. Rossi, *The European Physical Journal A* **52**, 6, 149 (2016), ISSN 1434-601X, URL <https://doi.org/10.1140/epja/i2016-16164-4>.
- [160] X. Ji, *Phys. Rev. Lett.* **91**, 062001 (2003), [hep-ph/0304037].
- [161] A. V. Belitsky, X. Ji and F. Yuan, *Phys. Rev.* **D69**, 074014 (2004), [hep-ph/0307383].
- [162] C. Lorce, B. Pasquini and M. Vanderhaeghen, *JHEP* **05**, 041 (2011), [arXiv:1102.4704].
- [163] P. J. Mulders and R. D. Tangerman, *Nucl. Phys.* **B461**, 197 (1996), [Erratum: *Nucl. Phys.*B484,538(1997)], [hep-ph/9510301].
- [164] D. Boer and P. J. Mulders, *Phys. Rev.* **D57**, 5780 (1998), [hep-ph/9711485].
- [165] D. W. Sivers, *Phys. Rev.* **D41**, 83 (1990).
- [166] J. C. Collins, *Nucl. Phys.* **B396**, 161 (1993), [hep-ph/9208213].
- [167] X. Ji, J. Ma and F. Yuan, *Phys. Rev.* **D71**, 034005 (2005), [hep-ph/0404183].
- [168] J. Collins, *Foundations of perturbative QCD Camb. Monogr. Part. Phys. Nucl. Phys. Cosmol.* **32** (2011) 1-624 and references therein.
- [169] S. M. Aybat and T. C. Rogers, *Phys. Rev.* **D83**, 114042 (2011), [arXiv:1101.5057].
- [170] M. G. Echevarria, A. Idilbi and I. Scimemi, *JHEP* **07**, 002 (2012), [arXiv:1111.4996].
- [171] M. G. A. Buffing, A. Mukherjee and P. J. Mulders, *Phys. Rev.* **D88**, 054027 (2013), [arXiv:1306.5897].
- [172] T. C. Rogers and P. J. Mulders, *Phys. Rev.* **D81**, 094006 (2010), [arXiv:1001.2977].
- [173] A. Signori *et al.*, *JHEP* **11**, 194 (2013), [arXiv:1309.3507].
- [174] M. Anselmino *et al.*, *JHEP* **04**, 005 (2014), [arXiv:1312.6261].
- [175] U. D'Alesio *et al.*, *JHEP* **11**, 098 (2014), [arXiv:1407.3311].
- [176] M. G. Echevarria *et al.*, *Phys. Rev.* **D89**, 074013 (2014), [arXiv:1401.5078].
- [177] P. Sun *et al.*, *Int. J. Mod. Phys.* **A33**, 11, 1841006 (2018), [arXiv:1406.3073].
- [178] A. Bacchetta *et al.*, *JHEP* **06**, 081 (2017), [Erratum: *JHEP*06,051(2019)], [arXiv:1703.10157].
- [179] I. Scimemi and A. Vladimirov, *Eur. Phys. J.* **C78**, 2, 89 (2018), [arXiv:1706.01473].
- [180] V. Bertone, I. Scimemi and A. Vladimirov, *JHEP* **06**, 028 (2019), [arXiv:1902.08474].
- [181] J. O. Gonzalez-Hernandez *et al.*, *Phys. Rev.* **D98**, 11, 114005 (2018), [arXiv:1808.04396].
- [182] A. Bacchetta *et al.*, *Phys. Rev.* **D100**, 1, 014018 (2019), [arXiv:1901.06916].

- [183] R. Angeles-Martinez *et al.*, *Acta Phys. Polon.* **B46**, 12, 2501 (2015), [arXiv:1507.05267].
- [184] A. Bacchetta *et al.*, *Phys. Lett.* **B788**, 542 (2019), [arXiv:1807.02101].
- [185] M. Diehl, *Eur. Phys. J.* **A52**, 6, 149 (2016), [arXiv:1512.01328].
- [186] A. Bacchetta, *Eur. Phys. J.* **A52**, 6, 163 (2016).
- [187] <http://hepdata.cedar.ac.uk/pdfs>.

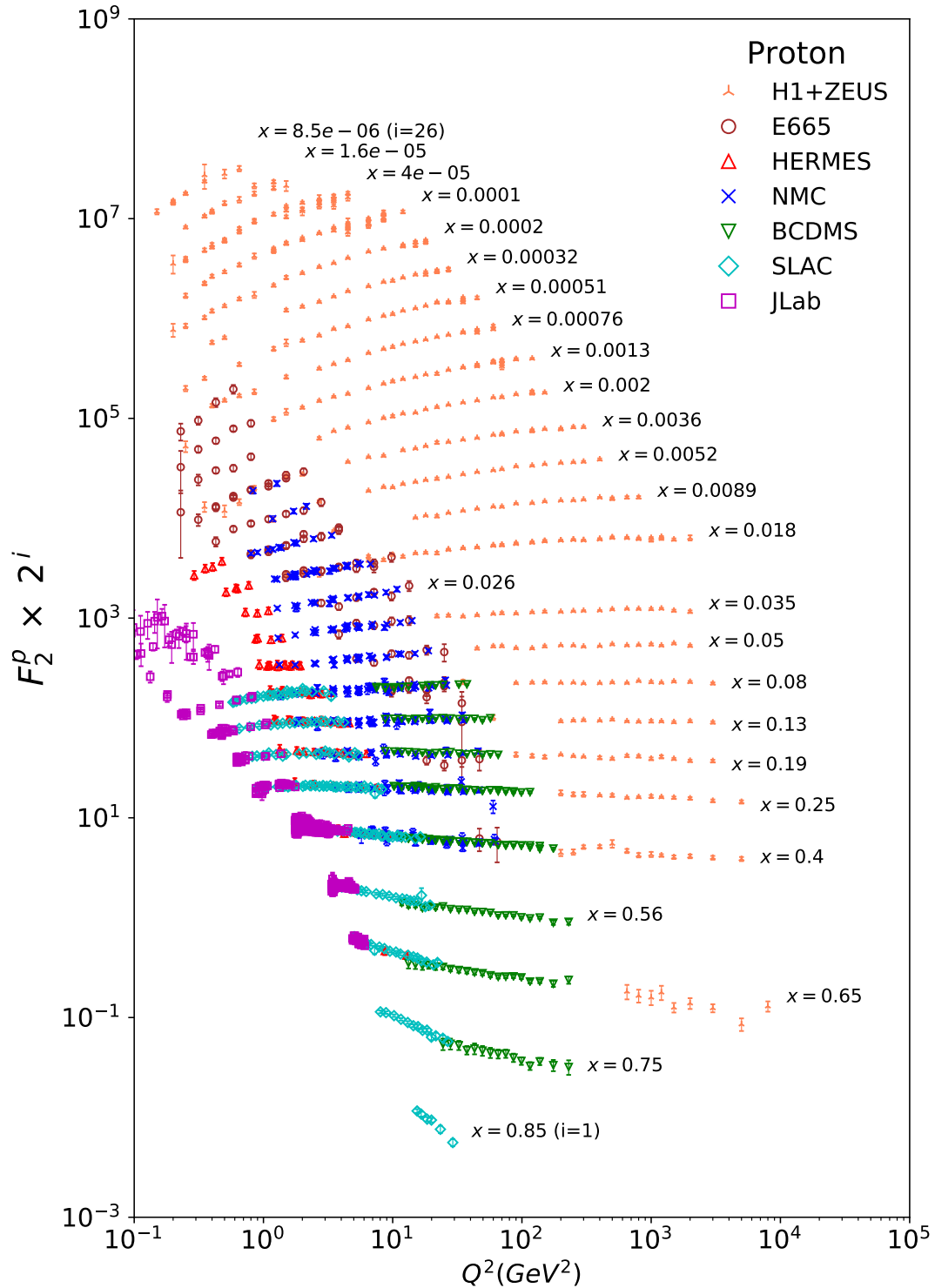


Figure 18.8: The proton structure function  $F_2^p$  measured in electromagnetic scattering of electrons and positrons on protons, and for electrons/positrons (SLAC, HERMES, JLAB) and muons (BCDMS, E665, NMC) on a fixed target. Statistical and systematic errors added in quadrature are shown. The H1+ZEUS combined values are obtained from the measured reduced cross section and converted to  $F_2^p$  with a HERAPDF NLO fit, for all measured points where the predicted ratio of  $F_2^p$  to reduced cross-section was within 10% of unity. The data are plotted as a function of  $Q^2$  in bins of fixed  $x$ . Some points have been slightly offset in  $Q^2$  for clarity. The H1+ZEUS combined binning in  $x$  is used in this plot; all other data are rebinned to the  $x$  values of these data. For the purpose of plotting,  $F_2^p$  has been multiplied by  $2^{i_x}$ , where  $i_x$  is the number of the  $x$  bin, ranging from  $i_x = 1$  ( $x = 0.85$ ) to  $i_x = 26$  ( $x = 0.0000085$ ). Only data with  $W^2 > 3.5 \text{ GeV}^2$  is included. Plot from CJ collaboration (Shujie Li – private communication). References: **H1 and ZEUS**—H. Abramowicz *et al.*, Eur. Phys. J. **C75**, 580 (2015) (for both data and HERAPDF parameterization); **BCDMS**—A.C. Benvenuti *et al.*, Phys. Lett. **B223**, 485 (1989) (as given in [187]); **E665**—M.R. Adams *et al.*, Phys. Rev. **D54**, 3006 (1996); **NMC**—M. Arneodo *et al.*, Nucl. Phys. **B483**, 3 (1997); **SLAC**—L.W. Whitlow *et al.*, Phys. Lett. **B282**, 475 (1992); **HERMES**—A. Airapetian *et al.*, JHEP **1105**, 126 (2011); **JLAB**—Y. Liang *et al.*, Jefferson Lab Hall C E94-110 collaboration, nucl-ex/0410027, M.E. Christy *et al.*, Jefferson Lab Hall C E94-110 Collaboration, Phys. Rev. **C70**, 015206 (2004), S. Malace *et al.*, Jefferson Lab Hall C E00-116 Collaboration, Phys. Rev. **C80**, 035207 (2009), V. Tvaskis *et al.*, Jefferson Lab Hall C E99-118 Collaboration, Phys. Rev. **C81**, 055207 (2010), M. Osipenko *et al.*, Jefferson Lab Hall B CLAS6 Collaboration, Phys. Rev. **D67**, 092001 (2003).

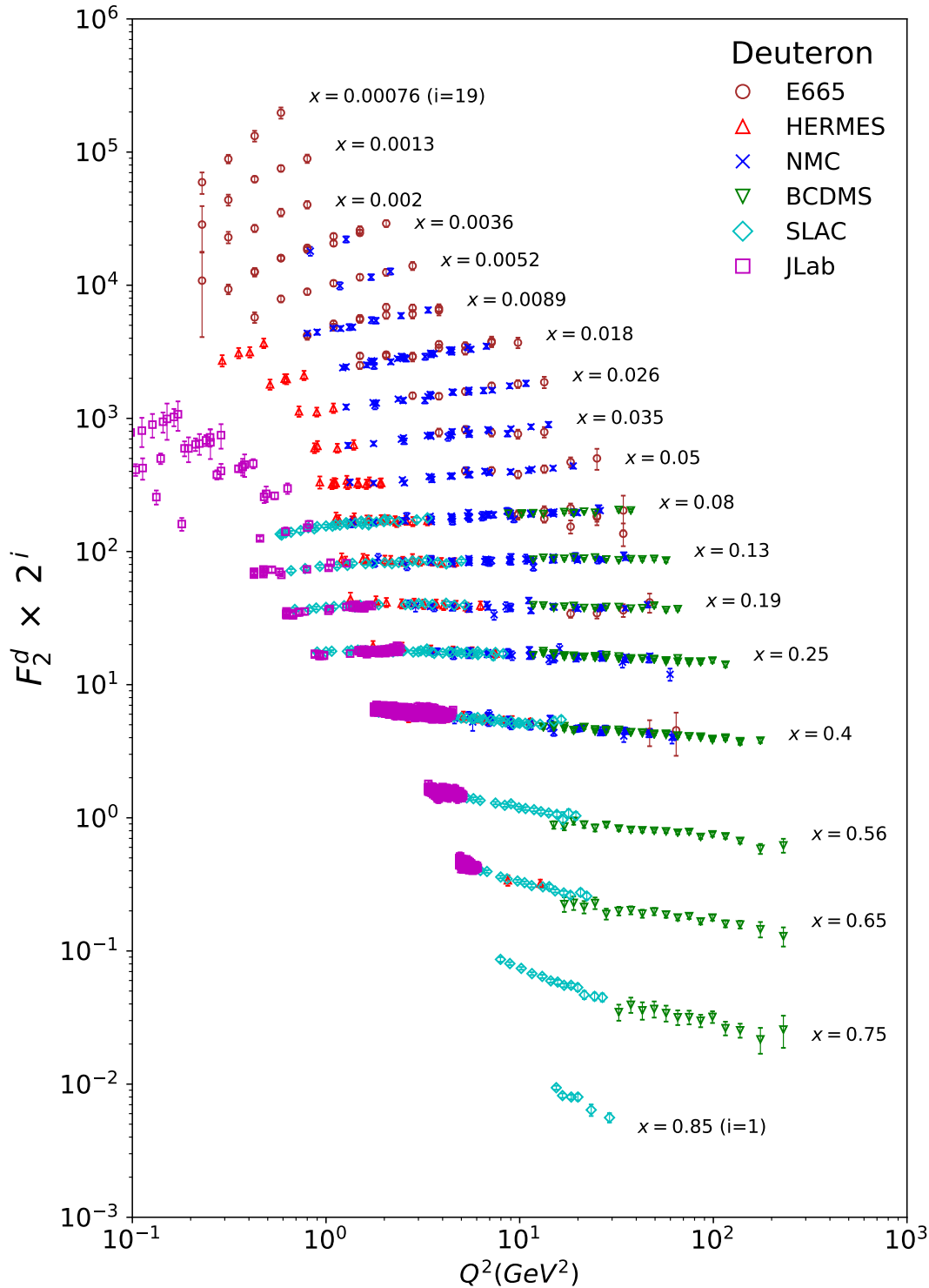


Figure 18.9: The deuteron structure function  $F_2^d$  measured in electromagnetic scattering of electrons/positrons (SLAC, HERMES, JLAB) and muons (BCDMS, E665, NMC) on a fixed target, shown as a function of  $Q^2$  for bins of fixed  $x$ . Statistical and systematic errors added in quadrature are shown. For the purpose of plotting,  $F_2^d$  has been multiplied by  $2^{i_x}$ , where  $i_x$  is the number of the  $x$  bin, ranging from 1 ( $x = 0.85$ ) to 29 ( $x = 0.00076$ ). Only data with  $W^2 > 3.5$  GeV<sup>2</sup> is included. Plot from CJ collaboration (Shujie Li – private communication) References: **BCDMS**—A.C. Benvenuti *et al.*, Phys. Lett. **B237**, 592 (1990). **E665**, **NMC**, **SLAC**, **HERMES**—same references as Fig. 18.8; **JLAB**—S. Malace *et al.*, Jefferson Lab Hall C E00-116 Collaboration, Phys. Rev. **C80**, 035207 (2009), V. Tvaskis *et al.*, Jefferson Lab Hall C E99-118 Collaboration, Phys. Rev. **C81**, 055207 (2010), J. Seely (MIT, LNS) *et al.*, Jefferson Lab Hall C E03-103 Collaboration, Phys. Rev. Lett. **103**, 202301 (2009), M. Osipenko *et al.*, Jefferson Lab Hall B CLAS6 Collaboration, Phys. Rev. **C73**, 045205 (2006).

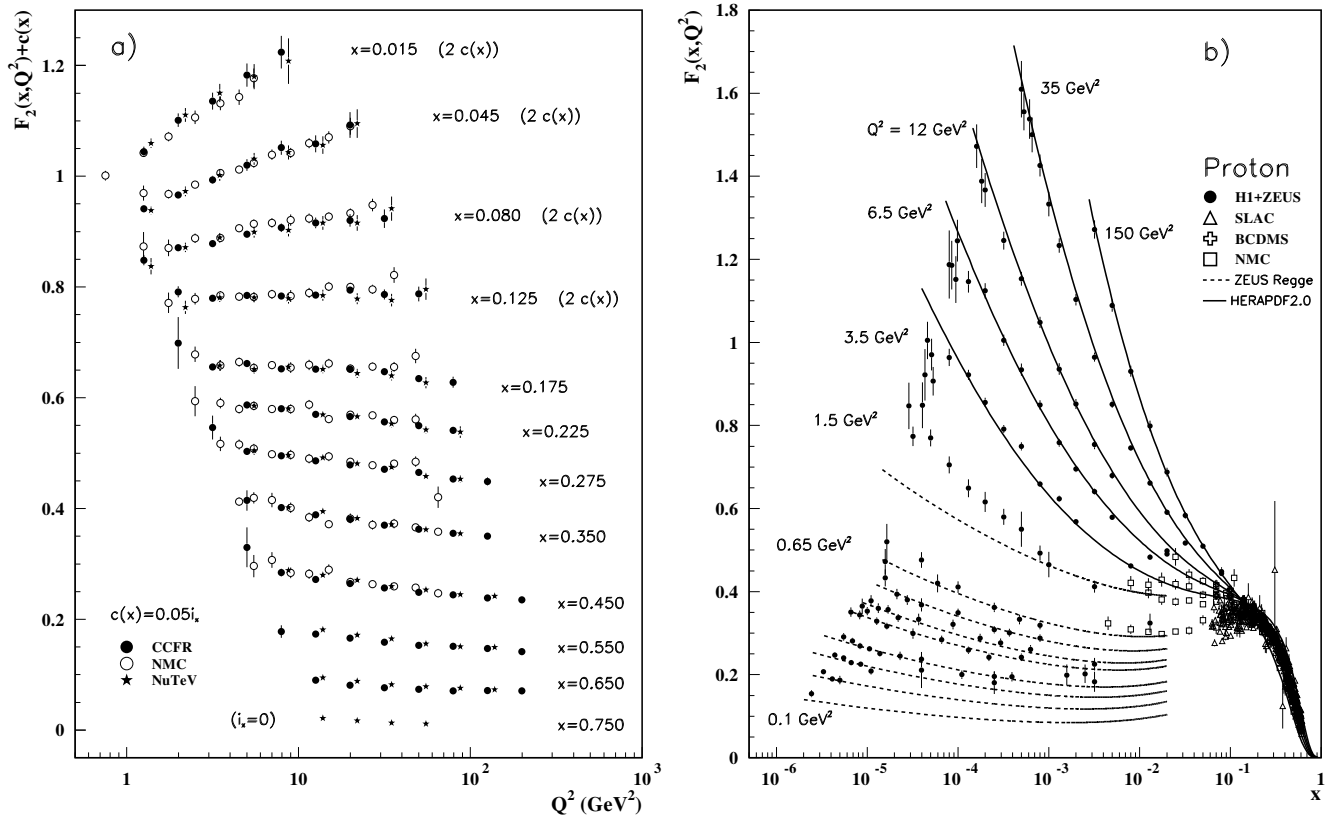


Figure 18.10: a) The deuteron structure function  $F_2$  measured in deep inelastic scattering of muons on a fixed target (NMC) is compared to the structure function  $F_2$  from neutrino-iron scattering (CCFR and NuTeV) using  $F_2^{\mu} = (5/18)F_2^{\nu} - x(s + \bar{s})/6$ , where heavy-target effects have been taken into account. The data are shown versus  $Q^2$ , for bins of fixed  $x$ . The NMC data have been rebinned to CCFR and NuTeV  $x$  values. For the purpose of plotting, a constant  $c(x) = 0.05i_x$  is added to  $F_2$ , where  $i_x$  is the number of the  $x$  bin, ranging from 0 ( $x = 0.75$ ) to 7 ( $x = 0.175$ ). For  $i_x = 8$  ( $x = 0.125$ ) to 11 ( $x = 0.015$ ),  $2c(x)$  has been added. References: **NMC**—M. Arneodo *et al.*, Nucl. Phys. **B483**, 3 (1997); **CCFR/NuTeV**—U.K. Yang *et al.*, Phys. Rev. Lett. **86**, 2741 (2001); **NuTeV**—M. Tzanov *et al.*, Phys. Rev. **D74**, 012008 (2006).

b) The proton structure function  $F_2^p$  mostly at small  $x$  and  $Q^2$ , measured in electromagnetic scattering of electrons and positrons (H1, ZEUS), electrons (SLAC), and muons (BCDMS, NMC) on protons. Lines are ZEUS Regge and HERAPDF parameterizations for lower and higher  $Q^2$ , respectively. The width of the bins can be up to 10% of the stated  $Q^2$ . Some points have been slightly offset in  $x$  for clarity. The H1+ZEUS combined values for  $Q^2 \geq 3.5$  GeV<sup>2</sup> are obtained from the measured reduced cross section and converted to  $F_2^p$  with a HERAPDF NLO fit, for all measured points where the predicted ratio of  $F_2^p$  to reduced cross-section was within 10% of unity. A turn-over is visible in the low- $x$  points at medium  $Q^2$  (3.5 GeV<sup>2</sup> and 6 GeV<sup>2</sup>) for the H1+ZEUS combined values. In order to obtain  $F_2^p$  from the measured reduced cross-section,  $F_L$  must be estimated; for the points shown, this estimate is obtained from HERAPDF2.0. No  $F_L$  value consistent with the HERA data can eliminate the turn-over. This may indicate that at low  $x$  and  $Q^2$  there are contributions to the structure functions that cannot be described in standard DGLAP evolution.

References: **H1 and ZEUS**—F.D. Aaron *et al.*, JHEP **1001**, 109 (2010) (data for  $Q^2 < 3.5$  GeV<sup>2</sup>), H. Abramowicz *et al.*, Eur. Phys. J. **C75**, 580 (2015) (data for  $Q^2 \geq 3.5$  GeV<sup>2</sup> and HERAPDF parameterization); **ZEUS**—J. Breitweg *et al.*, Phys. Lett. **B487**, 53 (2000) (ZEUS Regge parameterization); **BCDMS, NMC, SLAC**—same references as Fig. 18.8.

Statistical and systematic errors added in quadrature are shown for both plots.



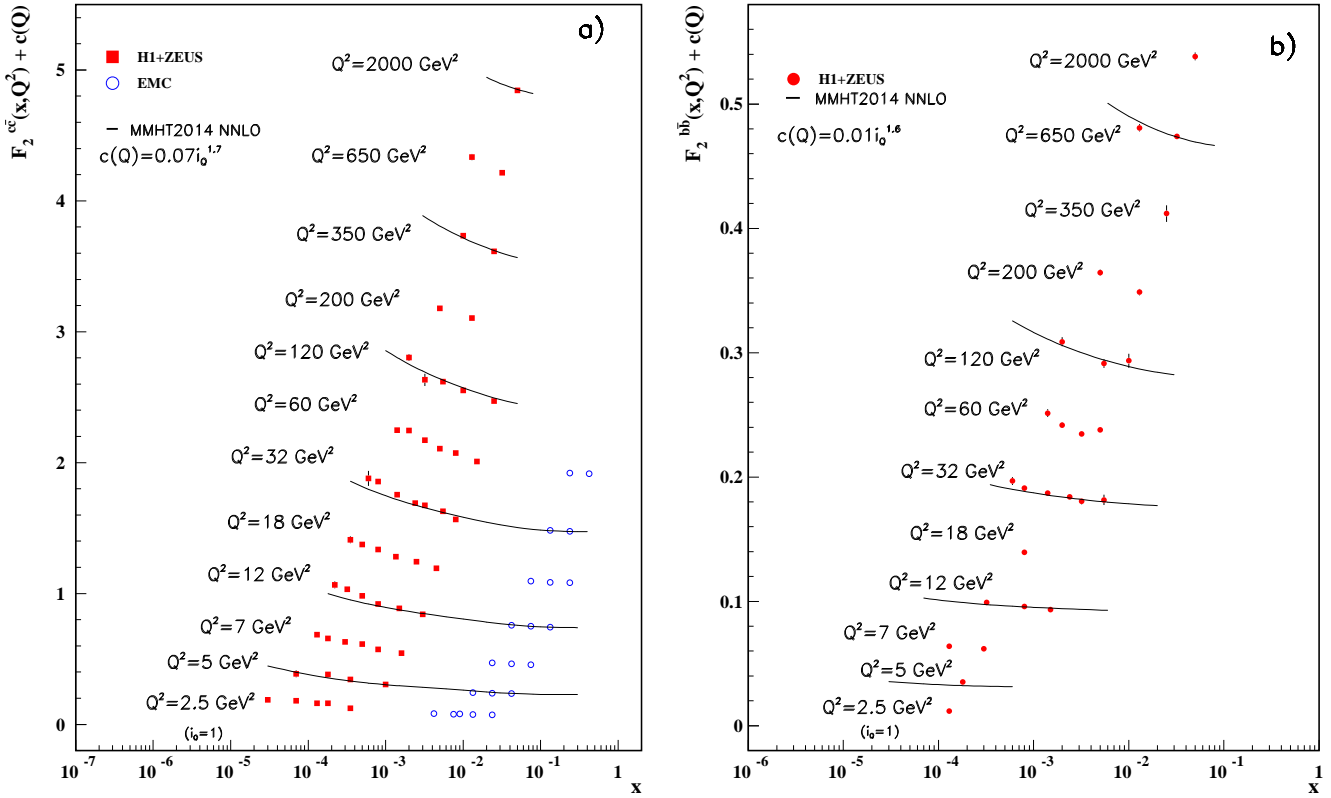


Figure 18.11: a) The charm-quark structure function  $F_2^{c\bar{c}}(x)$ , i.e. that part of the inclusive structure function  $F_2^P$  arising from the production of charm quarks, measured in electromagnetic scattering of positrons on protons (H1, ZEUS) (the values are obtained from the measured reduced cross section and converted to  $F_2^{c\bar{c}}$  using the PDFs from the MMHT NNLO fit) and muons on iron (EMC). For the purpose of plotting, a constant  $c(Q) = 0.07i_Q^{1.7}$  is added to  $F_2^{c\bar{c}}$  where  $i_Q$  is the number of the  $Q^2$  bin, ranging from 1 ( $Q^2 = 2.5 \text{ GeV}^2$ ) to 12 ( $Q^2 = 2000 \text{ GeV}^2$ ). References: **H1 and ZEUS run I +II combination**—H. Abramowicz *et al.*, *Eur. Phys. J. C* **78**, 473 (2018); **EMC**—J.J. Aubert *et al.*, *Nucl. Phys. B* **213**, 31 (1983).

b) The bottom-quark structure function  $F_2^{b\bar{b}}(x)$ . For the purpose of plotting, a constant  $c(Q) = 0.01i_Q^{1.6}$  is added to  $F_2^{b\bar{b}}$  where  $i_Q$  is the number of the  $Q^2$  bin, ranging from 1 ( $Q^2 = 2.5 \text{ GeV}^2$ ) to 12 ( $Q^2 = 2000 \text{ GeV}^2$ ). References: **H1 and ZEUS run I combination**—H. Abramowicz *et al.*, *Eur. Phys. J. C* **78**, 473 (2018).

For both plots, statistical and systematic errors added in quadrature are shown. The data are given as a function of  $x$  in bins of  $Q^2$ . Points may have been slightly offset in  $x$  for clarity. Some data have been rebinned to common  $Q^2$  values. Also shown is the MMHT2014 parameterization given at several  $Q^2$  values (L. A. Harland-Lang *et al.*, *Eur. Phys. J. C* **75**, 204 (2015)).

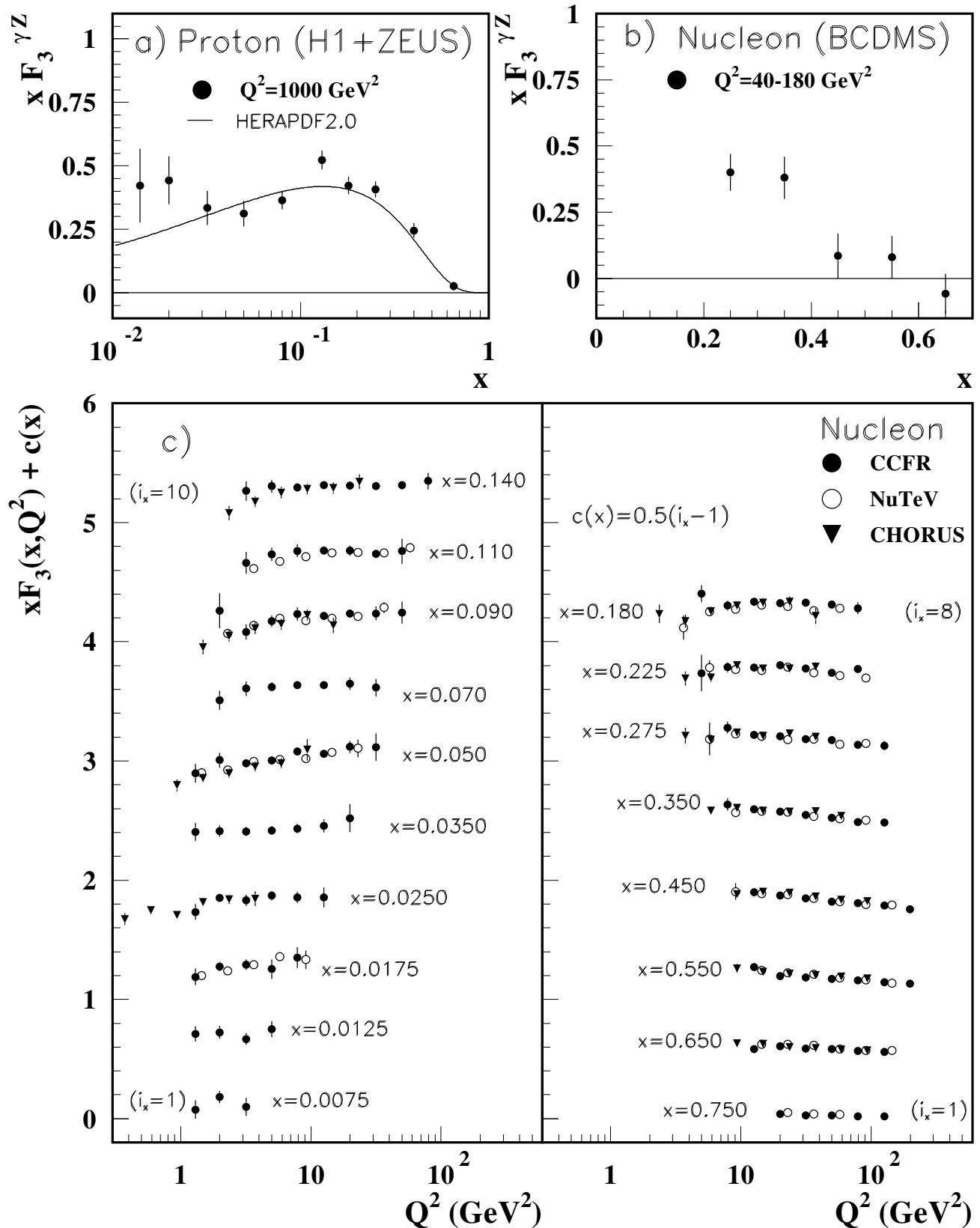


Figure 18.12: The structure function  $x F_3^{\gamma Z}$  measured in electroweak scattering of **a)** electrons on protons (H1 and ZEUS) and **b)** muons on carbon (BCDMS). The line in **a)** is the HERAPDF parameterization. References: **H1 and ZEUS**—H. Abramowicz *et al.*, Eur. Phys. J. **C75**, 580 (2015) (for both data and HERAPDF parameterization); **BCDMS**—A. Argento *et al.*, Phys. Lett. **B140**, 142 (1984). **c)** The structure function  $x F_3$  of the nucleon measured in  $\nu$ -Fe scattering. The data are plotted as a function of  $Q^2$  in bins of fixed  $x$ . For the purpose of plotting, a constant  $c(x) = 0.5(i_x - 1)$  is added to  $x F_3$ , where  $i_x$  is the number of the  $x$  bin as shown in the plot. The NuTeV and CHORUS points have been shifted to the nearest corresponding  $x$  bin as given in the plot and slightly offset in  $Q^2$  for clarity. References: **CCFR**—W.G. Seligman *et al.*, Phys. Rev. Lett. **79**, 1213 (1997); **NuTeV**—M. Tzanov *et al.*, Phys. Rev. **D74**, 012008 (2006); **CHORUS**—G. Öngüt *et al.*, Phys. Lett. **B632**, 65 (2006).

Statistical and systematic errors added in quadrature are shown for all plots.

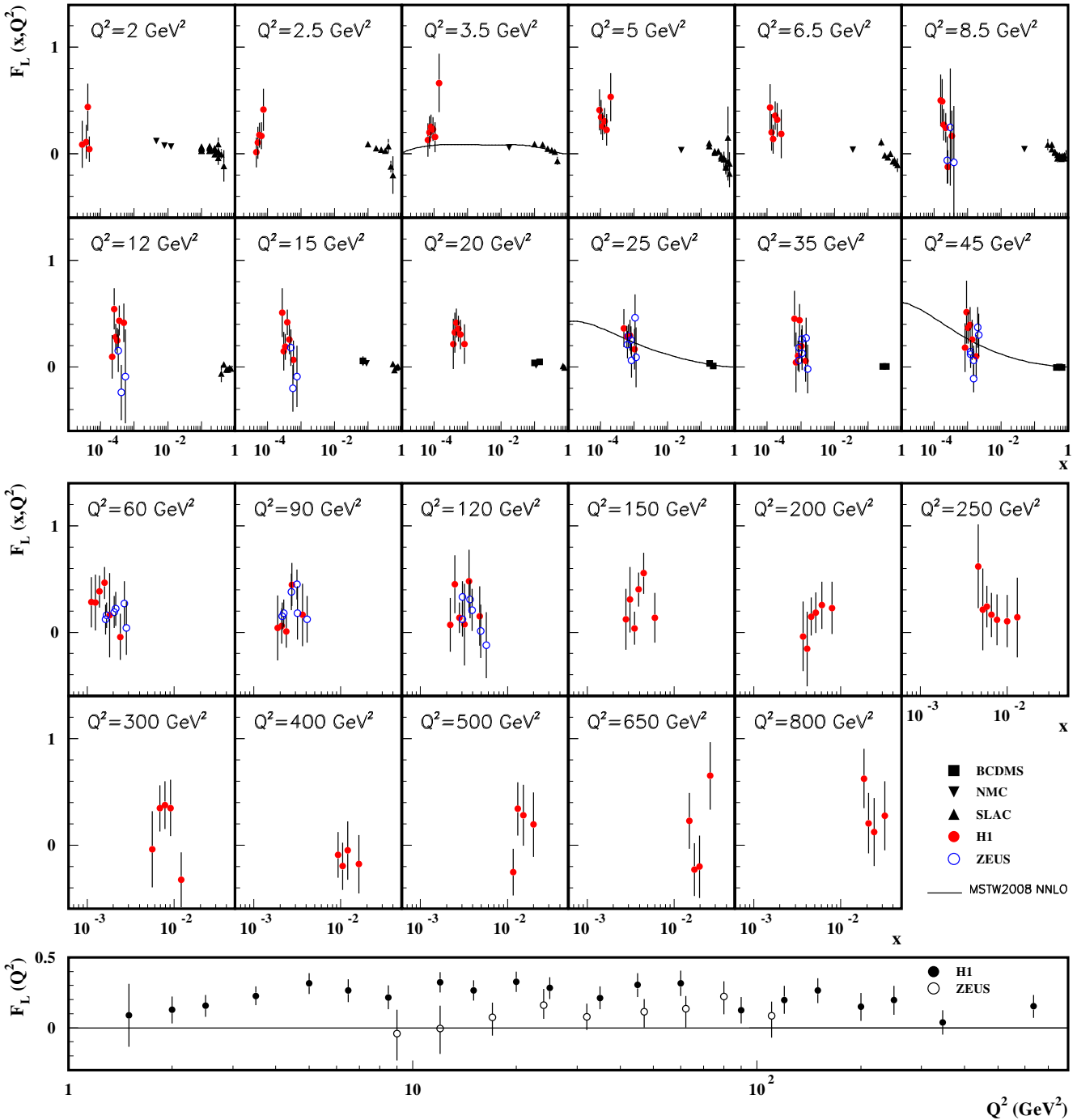


Figure 18.13: Top panels: The longitudinal structure function  $F_L$  as a function of  $x$  in bins of fixed  $Q^2$  measured on the proton (except for the SLAC data which also contain deuterium data). BCDMS, NMC, and SLAC results are from measurements of  $R$  (the ratio of longitudinal to transverse photon absorption cross sections) which are converted to  $F_L$  by using the BCDMS parameterization of  $F_2$  (A.C. Benvenuti *et al.*, Phys. Lett. **B223**, 485 (1989)). It is assumed that the  $Q^2$  dependence of the fixed-target data is small within a given  $Q^2$  bin. Some of the other data may have been rebinned to common  $Q^2$  values. Some points have been slightly offset in  $x$  for clarity. Also shown is the MSTW2008 parameterization given at three  $Q^2$  values (A.D. Martin *et al.*, Eur. Phys. J. **C63**, 189 (2009)). References: **H1**—V. Andreev *et al.*, Eur. Phys. J. **C74**, 2814 (2014); **ZEUS**—S. Chekanov *et al.*, Phys. Lett. **B682**, 8 (2009); H. Abramowicz *et al.*, Phys. Rev. **D90**, 072002 (2014); **BCDMS**—A. Benvenuti *et al.*, Phys. Lett. **B223**, 485 (1989); **NMC**—M. Arneodo *et al.*, Nucl. Phys. **B483**, 3 (1997); **SLAC**—L.W. Whitlow *et al.*, Phys. Lett. **B250**, 193 (1990) and numerical values from the thesis of L.W. Whitlow (SLAC-357). Bottom panel: The longitudinal structure function  $F_L$  as a function of  $Q^2$ . Some points have been slightly offset in  $Q^2$  for clarity. References: **H1**—V. Andreev *et al.*, Eur. Phys. J. **C74**, 2814 (2014); **ZEUS**—H. Abramowicz *et al.*, Phys. Rev. **D90**, 072002 (2014). The results shown in the bottom plot require the assumption of the validity of the QCD form for the  $F_2$  structure function in order to extract  $F_L$ . Statistical and systematic errors added in quadrature are shown for both plots.

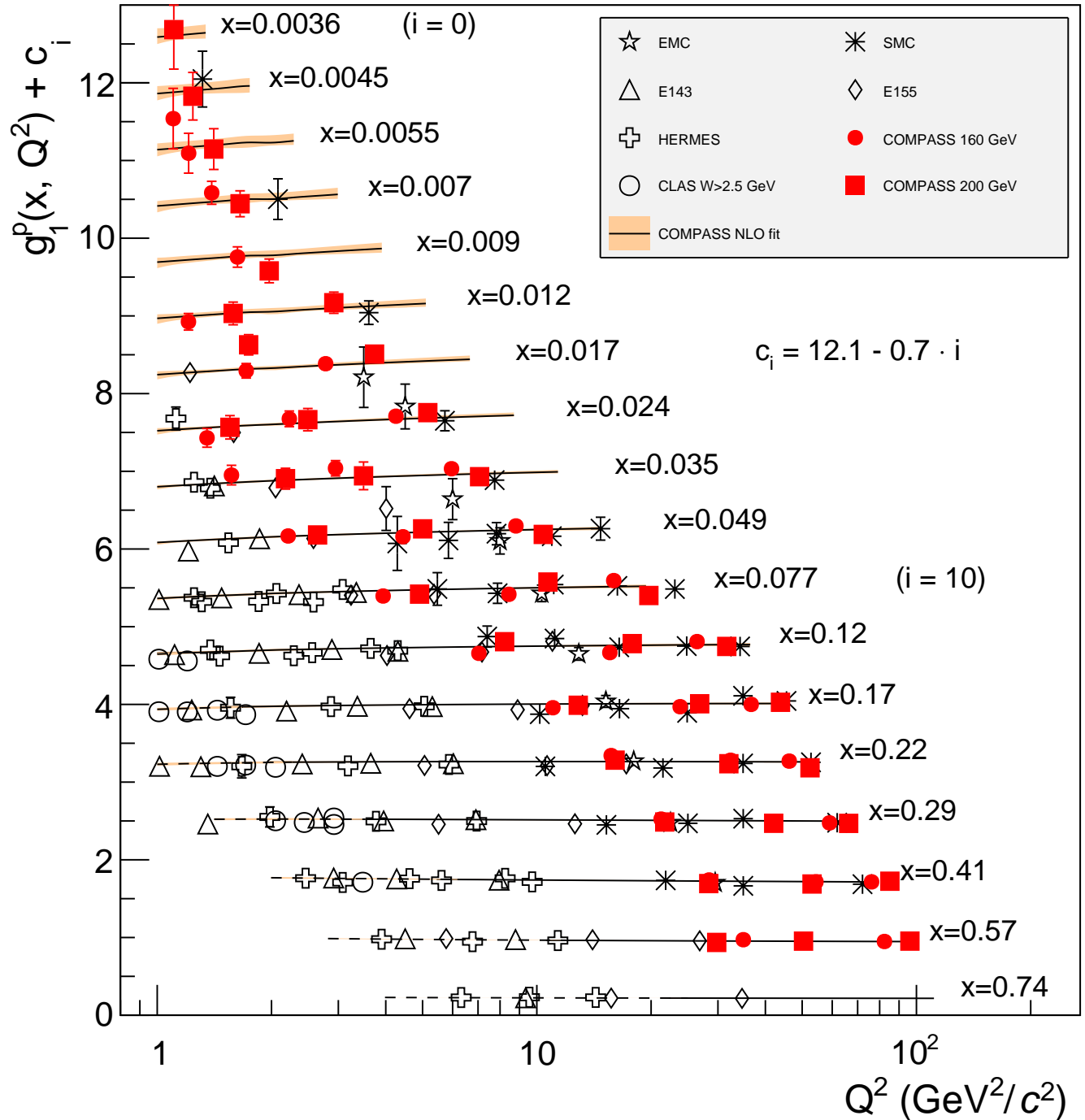


Figure 18.14: World data on the spin-dependent structure function  $g_1^p$  as a function of  $Q^2$  for various values of  $x$ . The lines represent the  $Q^2$  dependence for each value of  $x$ , as determined from a NLO QCD fit. The dashed ranges represent the region with  $W^2 < 10$  ( $\text{GeV}/c^2$ )<sup>2</sup>. References: **EMC**—J. Ashman *et al.*, Phys. Lett. **B206**, 363 (1988); Nucl. Phys. **B328**, 1 (1989); **E143**—K. Abe *et al.*, Phys. Rev. **D58**, 112003 (1998); **SMC**—B. Adeva *et al.*, Phys. Rev. **D58**, 112001 (1998); **HERMES**—A. Airapetian *et al.*, Phys. Rev. **D75**, 012007 (2007); **E155**—P.L. Anthony *et al.*, Phys. Lett. **B493**, 19 (2000); **COMPASS**—M.G. Alekseev *et al.*, Phys. Lett. **B690**, 466 (2010), C. Adolph, *et al.*, Phys. Lett. **B753**, 18 (2016); **CLAS**—K.V. Dharmawardane *et al.*, Phys. Lett. **B641**, 11 (2006) (which also includes resonance region data not shown on this plot — there is also low  $W^2$  CLAS data in Y. Prok *et al.*, Phys. Rev. **C90**, 025212 (2014) and N. Guler *et al.*, Phys. Rev. **C92**, 055201 (2015)).

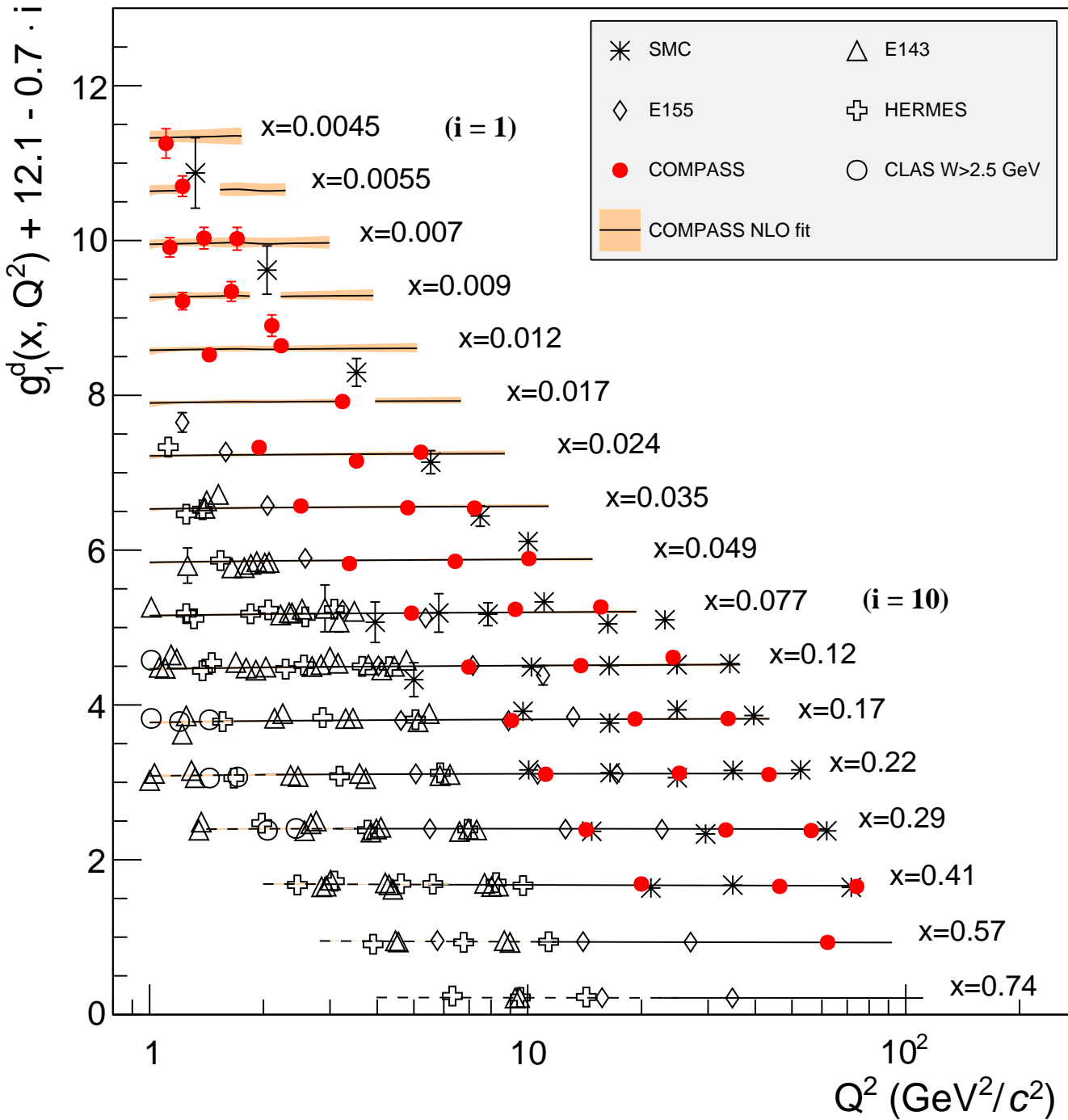


Figure 18.15: World data on the spin-dependent structure function  $g_1^d$  as a function of  $Q^2$  for various values of  $x$ . The lines represent the  $Q^2$  dependence for each value of  $x$ , as determined from a NLO QCD fit. The dashed ranges represent the region with  $W^2 < 10$   $(\text{GeV}/c^2)^2$ . CLAS—K.V. Dharmawardane *et al.*, Phys. Lett. **B641**, 11 (2006); HERMES—A. Airapetian *et al.*, Phys. Rev. **D75**, 012007 (2007); SMC—B. Adeva *et al.*, Phys. Rev. **D58**, 112001 (1998); E155—P.L. Anthony *et al.*, Phys. Lett. **B463**, 339 (1999); E143—K. Abe *et al.*, Phys. Rev. **D58**, 112003 (1998); COMPASS—C. Adolph, *et al.*, Phys. Lett. **B769**, 34 (2017);

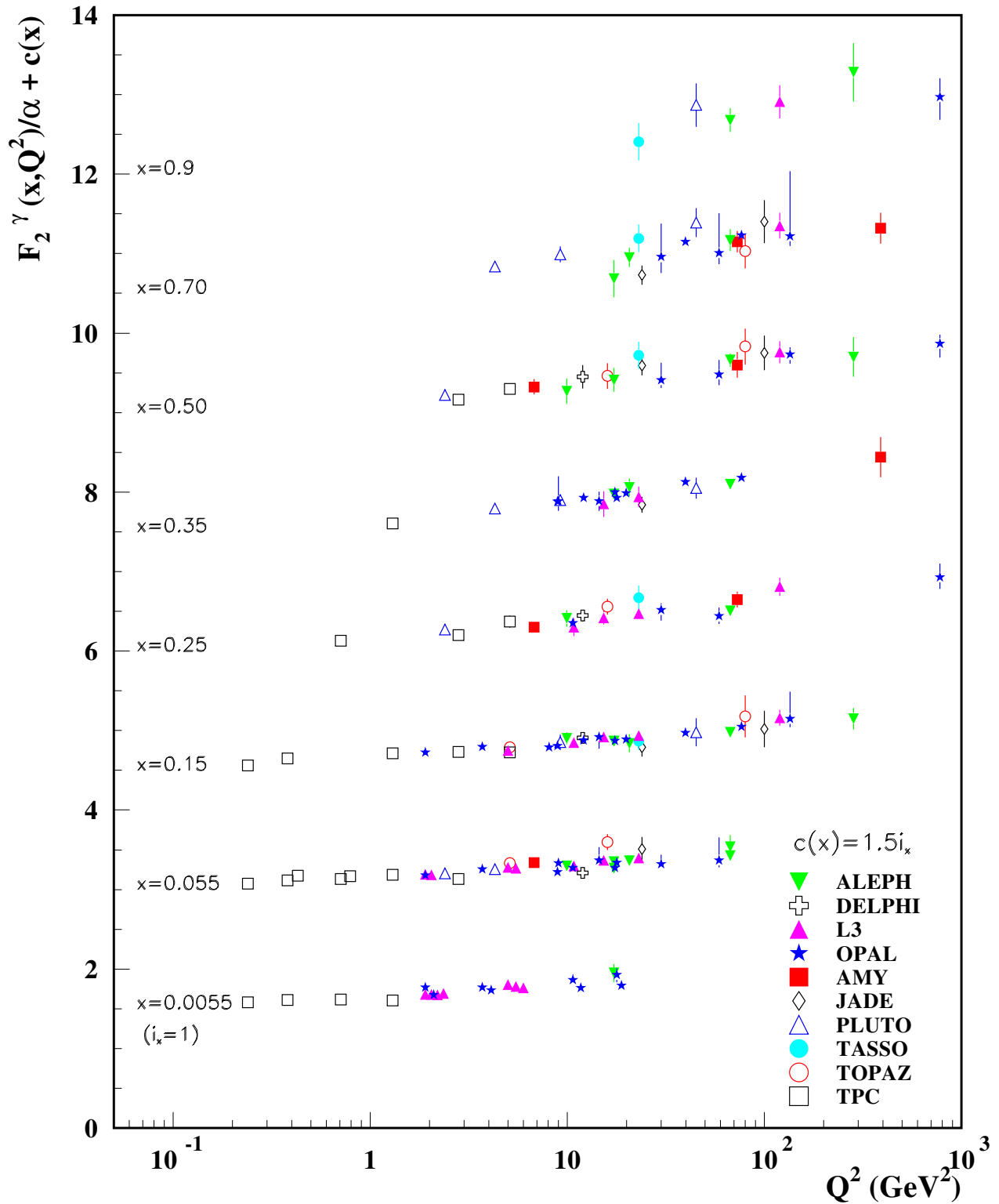


Figure 18.16: The hadronic structure function of the photon  $F_2^\gamma$  divided by the fine structure constant  $\alpha$  measured in  $e^+e^-$  scattering, shown as a function of  $Q^2$  for bins of  $x$ . Data points have been shifted to the nearest corresponding  $x$  bin as given in the plot. Some points have been offset in  $Q^2$  for clarity. Statistical and systematic errors added in quadrature are shown. For the purpose of plotting, a constant  $c(x) = 1.5i_x$  is added to  $F_2^\gamma/\alpha$  where  $i_x$  is the number of the  $x$  bin, ranging from 1 ( $x = 0.0055$ ) to 8 ( $x = 0.9$ ). References: **ALEPH**–R. Barate *et al.*, Phys. Lett. **B458**, 152 (1999); A. Heister *et al.*, Eur. Phys. J. **C30**, 145 (2003); **DELPHI**–P. Abreu *et al.*, Z. Phys. **C69**, 223 (1995); **L3**–M. Acciarri *et al.*, Phys. Lett. **B436**, 403 (1998); M. Acciarri *et al.*, Phys. Lett. **B447**, 147 (1999); M. Acciarri *et al.*, Phys. Lett. **B483**, 373 (2000); **OPAL**–A. Ackerstaff *et al.*, Phys. Lett. **B411**, 387 (1997); A. Ackerstaff *et al.*, Z. Phys. **C74**, 33 (1997); G. Abbiendi *et al.*, Eur. Phys. J. **C18**, 15 (2000); G. Abbiendi *et al.*, Phys. Lett. **B533**, 207 (2002) (note that there is overlap of the data samples in these last two papers); **AMY**–S.K. Sahu *et al.*, Phys. Lett. **B346**, 208 (1995); T. Kojima *et al.*, Phys. Lett. **B400**, 395 (1997); **JADE**–W. Bartel *et al.*, Z. Phys. **C24**, 231 (1984); **PLUTO**–C. Berger *et al.*, Phys. Lett. **142B**, 111 (1984); C. Berger *et al.*, Nucl. Phys. **B281**, 365 (1987); **TASSO**–M. Althoff *et al.*, Z. Phys. **C31**, 527 (1986); **TOPAZ**–K. Muramatsu *et al.*, Phys. Lett. **B332**, 477 (1994); **TPC/Two Gamma**–H. Aihara *et al.*, Z. Phys. **C34**, 1 (1987).

## 19. Fragmentation Functions in $e^+e^-$ , $ep$ , and $pp$ Collisions

Revised August 2019 by O. Biebel (Ludwig-Maximilians U.), D. de Florian (ICAS and ICIFI, UNSAM), D. Milstead (Stockholm U.) and W. Vogelsang (Tübingen U.).

### 19.1 Introduction to fragmentation

Quarks and gluons produced in hard-scattering reactions will ultimately give rise to the colorless hadronic bound states that may be observed in the detector. The associated hadronization process is described by fragmentation functions  $D_i^h(x, \mu^2)$  ( $i = q, \bar{q}, g$ ) which are universal functions representing, in the simplest picture, a measure of the probability density that an outgoing parton produces a hadron  $h$ . Here,  $x$  is the fraction of the parton's momentum transferred to the hadron, and  $\mu$  is a 'resolution' scale known as factorization scale. The  $D_i^h(x, \mu^2)$  may be viewed as the final-state analogs of the initial-state parton distribution functions (PDFs) addressed in Section 18 of this *Review*. They are also sometimes referred to as *timelike* distributions since they are primarily accessed in  $e^+e^-$  annihilation via a timelike intermediate boson. (See Refs. [1,2] for introductory reviews, and Refs. [3–5] for summaries of experimental and theoretical research in this field.)

The cleanest laboratory for the study of fragmentation functions is provided by semi-inclusive electron-positron annihilation,  $e^+e^- \rightarrow \gamma/Z \rightarrow h+X$ . The cross section for this reaction may be expressed in terms of 'fragmentation structure functions'  $F_{T,L,A}$  that are directly related to the fragmentation functions. At center-of-mass (CM) energy  $\sqrt{s} = q^2$  we have

$$\begin{aligned} \frac{1}{\sigma_0} \frac{d^2\sigma^h}{dx d\cos\theta} &= \frac{3}{8}(1 + \cos^2\theta)F_T^h(x, q^2) + \frac{3}{4}\sin^2\theta F_L^h(x, q^2) \\ &+ \frac{3}{4}\cos\theta F_A^h(x, q^2). \end{aligned} \quad (19.1)$$

Here,  $q$  is the four-momentum of the intermediate photon or  $Z$ -boson, with  $q^2 > 0$ , and  $x = 2P_h \cdot q/q^2$  with the hadron's four-momentum  $P_h$  is the fragmentation counterpart of the familiar DIS Bjorken variable. (Note that  $x = 2E_h/\sqrt{s} \leq 1$  in terms of the energy  $E_h$  of the produced hadron in the CM frame of the electron positron pair.) Furthermore, in the same frame,  $\theta$  is the hadron's angle relative to the electron beam direction. Eq. (19.1) is the most general form for unpolarized inclusive single-particle production via vector bosons [6]. The fragmentation structure functions  $F_T$  and  $F_L$  represent the contributions from  $\gamma/Z$  polarizations transverse or longitudinal with respect to the direction of motion of the hadron. The parity-violating term with the asymmetric fragmentation function  $F_A$  arises from the interference between vector and axial-vector contributions. Various normalization factors  $\sigma_0$  are used in the literature, ranging from the total cross section  $\sigma_{\text{tot}}$  for  $e^+e^- \rightarrow \text{hadrons}$ , including all weak and QCD contributions, to  $\sigma_0 = 4\pi\alpha^2 N_c/3s$  with  $N_c = 3$ , the lowest-order QED cross section for  $e^+e^- \rightarrow \mu^+\mu^-$  times the number of colors  $N_c$ . LEP1 measurements of the three fragmentation structure functions are shown in Fig. 19.1.

Integration of Eq. (19.1) over all  $\theta$  yields the total fragmentation structure function  $F^h = F_T^h + F_L^h$ :

$$\begin{aligned} \frac{1}{\sigma_0} \frac{d\sigma^h}{dx} &= F^h(x, q^2) \\ &= \sum_i \int_x^1 \frac{dz}{z} C_i \left( z, \alpha_s(\mu), \frac{q^2}{\mu^2} \right) D_i^h \left( \frac{x}{z}, \mu^2 \right). \end{aligned} \quad (19.2)$$

On the right we have written the factorized expression for the structure function in terms of a sum over convolutions of the fragmentation functions  $D_i^h$  for partons  $i = u, \bar{u}, d, \bar{d}, \dots, g$  with perturbative coefficient functions  $C_i$ . Since photons and  $Z$  bosons do not distinguish between quarks and antiquarks,  $e^+e^-$  annihilation primarily constrains the combinations  $D_q^h + D_{\bar{q}}^h$ . Gluon fragmentation contributes only at higher order in perturbation theory or by scaling violations. Corrections to the factorized expression in Eq. (19.2) are suppressed by inverse powers of  $q^2$ . They arise from quark and hadron mass terms and from non-perturbative effects.

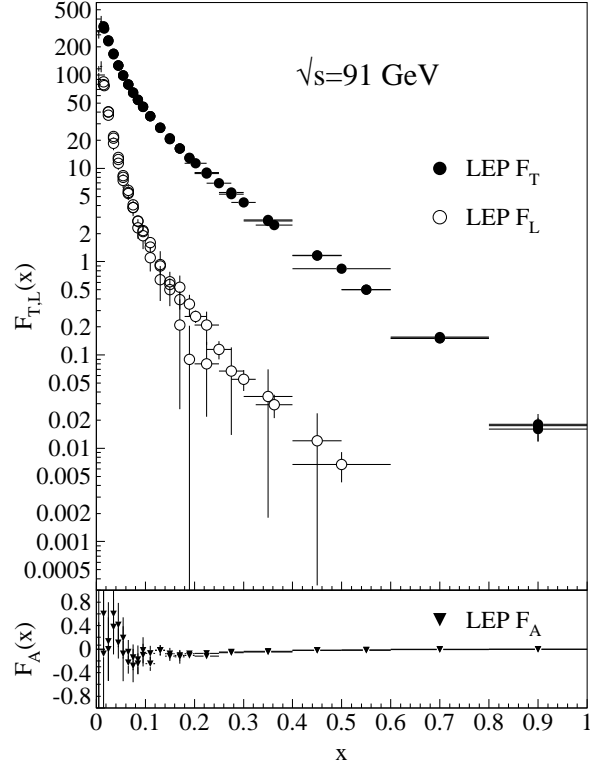


Figure 19.1: LEP1 measurements of total transverse ( $F_T$ ), longitudinal ( $F_L$ ), and asymmetric ( $F_A$ ) fragmentation structure functions [7]. Data points with relative errors greater than 100% are omitted.

Analogous factorized expressions as in Eq. (19.2) may be written for each of the structure functions  $F_{T,L,A}$  individually.

The fragmentation functions obey the momentum sum rule constraint

$$\sum_h \int_0^1 dx x D_i^h(x, \mu^2) = 1, \quad (19.3)$$

separately for each flavor  $i$ . Note that the sum rule involves a sum over all possible produced hadrons. The dependence of the functions  $D_i^h$  on the factorization scale  $\mu^2$  will be discussed in the next section.

Measurements of hadron production in deeply-inelastic lepton-proton scattering and hadron-hadron scattering are complementary to those in  $e^+e^-$  annihilation. The former process,  $\ell p \rightarrow \ell' + h + X$ , is known as *semi-inclusive deep-inelastic scattering (SIDIS)*. Here, in analogy with Eq. (19.2), the high virtuality of the photon in DIS also permits factorization of the cross section in terms of fragmentation functions, PDFs for the incoming proton, and perturbative hard-scattering cross sections. Likewise, factorization also occurs for  $pp \rightarrow h + X$  at large transverse momentum of the produced hadron, and for  $pp \rightarrow \text{jet}(h) + X$ , where the hadron is part of a fully reconstructed jet. The fragmentation functions contributing to  $e^+e^- \rightarrow h + X$ ,  $\ell p \rightarrow \ell' + h + X$ , and  $pp \rightarrow h + X$ ,  $pp \rightarrow \text{jet}(h) + X$  are universal in the sense that the same functions appear in the factorized expressions for the three reactions. Modern QCD analyses of fragmentation functions ‘globally’ take into account experimental data sets for all three types of processes in order to obtain optimal sets of fragmentation functions.

Electron-positron annihilation has the advantage that there is no hadronic initial state and hence no beam remnant. This is in contrast to  $\ell p \rightarrow \ell' + h + X$  or  $pp \rightarrow h + X$ , which are affected by hadron remnant contributions associated with the partons of the initial-state hadron(s) which are collaterally involved in the hard lepton-parton or parton-parton collision. On the other hand,

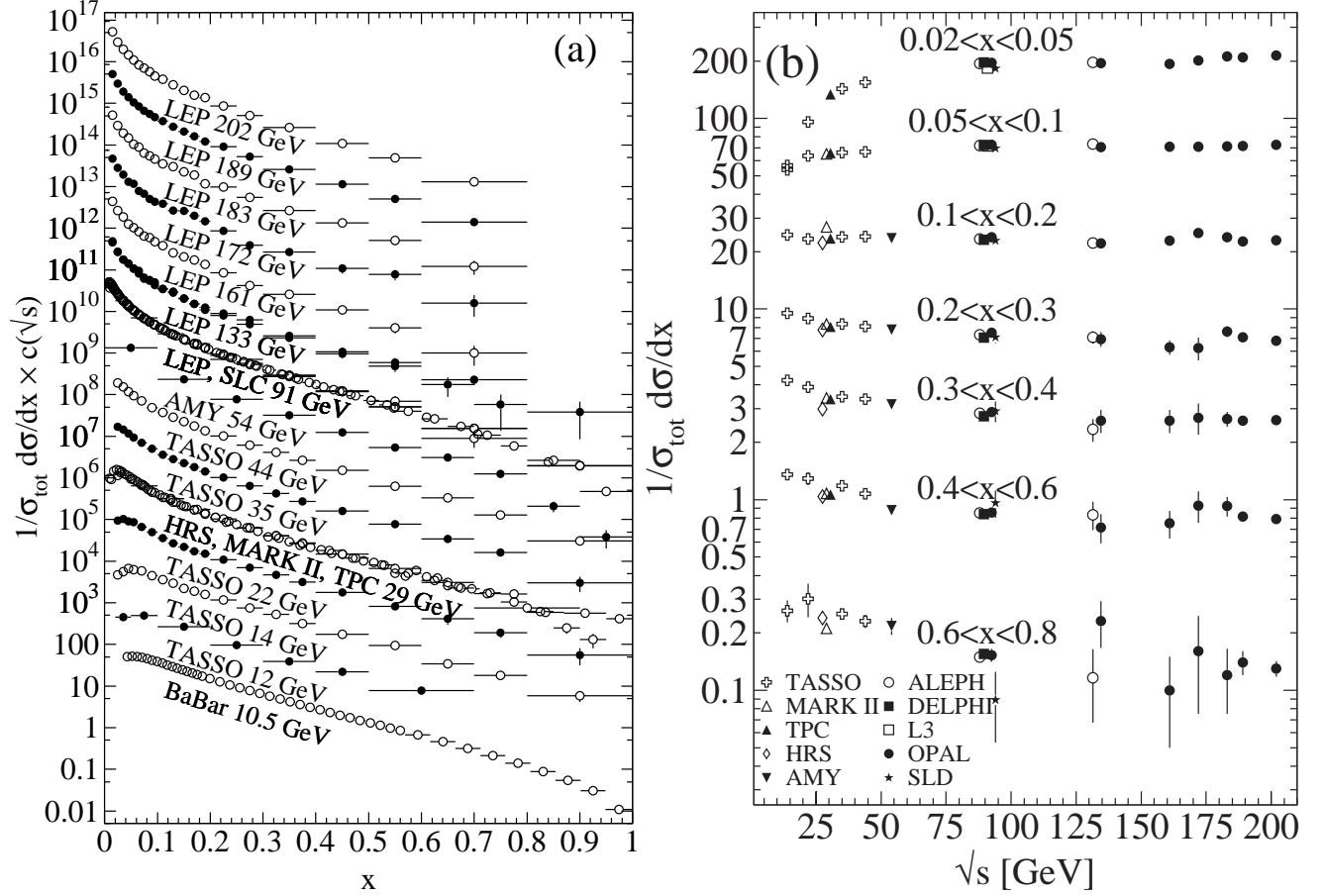


Figure 19.2: Cross section for  $e^+e^- \rightarrow h + X$  for all charged hadrons [8–26], (a) for different CM energies  $\sqrt{s}$  versus  $x$ , and (b) for various ranges of  $x$  versus  $\sqrt{s}$ . For (a) the distributions have been scaled by  $c(\sqrt{s}) = 10^i$  with  $i$  ranging from  $i = 0$  ( $\sqrt{s} = 12$  GeV) to  $i = 13$  ( $\sqrt{s} = 202$  GeV).

$e^+e^- \rightarrow h + X$  has little sensitivity to  $D_g^h$  and is insensitive to the charge asymmetries  $D_q^h - D_{\bar{q}}^h$ . These quantities are best constrained in proton-(anti-)proton and electron-proton scattering, respectively. Especially the latter provides an environment that allows the study of the influence of initial-state QCD radiation on the fragmentation process, of the partonic and spin structure of the hadron target, and of the target remnant system. (See Ref. [27] for a comprehensive review of the measurements and models of fragmentation in lepton-hadron scattering).

Moreover, unlike  $e^+e^-$  annihilation where  $q^2 = s$  is fixed by the collider energy, lepton-hadron scattering has two independent scales,  $Q^2 = -q^2$  and the invariant mass squared,  $W^2 \approx Q^2(1-x)/x$ , of the hadronic final state, which both can vary by several orders of magnitudes for a given CM energy, thus allowing the study of fragmentation in different environments by a single experiment. For example, in photoproduction the exchanged photon is quasi-real ( $Q^2 \approx 0$ ), leading to processes akin to hadron-hadron scattering. In DIS ( $Q^2 \gg 1$  GeV<sup>2</sup>), using factorization, the hadronic fragments of the struck quark can be directly compared with quark fragmentation in  $e^+e^-$  in a suitable frame. Results from lepton-hadron experiments quoted in this report primarily concern fragmentation in the DIS regime. Studies performed by lepton-hadron experiments of fragmentation with photoproduction data containing high transverse momentum jets or particles are also reported, when these are directly comparable to DIS and  $e^+e^-$  results.

Fragmentation studies in lepton-hadron collisions are usually performed in one of two frames in which the target hadron and the exchanged boson are collinear. The hadronic center-of-mass frame (HCMS) is defined as the rest system of the exchanged boson and incoming hadron, with the  $z^*$ -axis defined along the direction of the exchanged boson. The positive  $z^*$  direction de-

fines the so-called current fragmentation region. Fragmentation measurements performed in the HCMS often use the Feynman- $x$  variable  $x_F = 2p_z^*/W$ , where  $p_z^*$  is the longitudinal momentum of the particle in this frame. As  $W$  is the invariant mass of the hadronic final state,  $x_F$  ranges between  $-1$  and  $1$ .

The Breit system [28, 29] is related to the HCMS by a longitudinal boost such that the time component of  $q$  vanishes, i.e.,  $q = (0, 0, 0, -Q)$ . In the parton model, the struck parton then has the longitudinal momentum  $Q/2$  which becomes  $-Q/2$  after the collision. As compared with the HCMS, the current fragmentation region of the Breit frame is more closely matched to the partonic scattering process, and is thus appropriate for direct comparisons of fragmentation functions in DIS with those from  $e^+e^-$  annihilation. The variable  $x_p = 2p^*/Q$ , where  $p^*$  is the particle's momentum in the current region of the Breit frame, is used at HERA for measurements in the Breit frame, enabling rather direct comparisons of DIS and  $e^+e^-$  results.

## 19.2 Scaling violations and QCD corrections

As mentioned, the coefficient functions for the fragmentation structure functions in  $e^+e^- \rightarrow h + X$  are amenable to QCD perturbation theory. For each of the structure functions  $F_{T,L,A}(x, q^2)$  in Eq. (19.1) (and hence for the total structure function  $F^h$  in Eq. (19.2)) the coefficient function has an expansion of the form

$$C_{a,i} \left( z, \alpha_s(\mu), \frac{q^2}{\mu^2} \right) = (1 - \delta_{aL}) \delta_{iq} \delta(1-z) + \frac{\alpha_s(\mu)}{2\pi} c_{a,i}^{(1)} \left( z, \frac{q^2}{\mu^2} \right) + \left( \frac{\alpha_s(\mu)}{2\pi} \right)^2 c_{a,i}^{(2)} \left( z, \frac{q^2}{\mu^2} \right) + \dots (19.4)$$



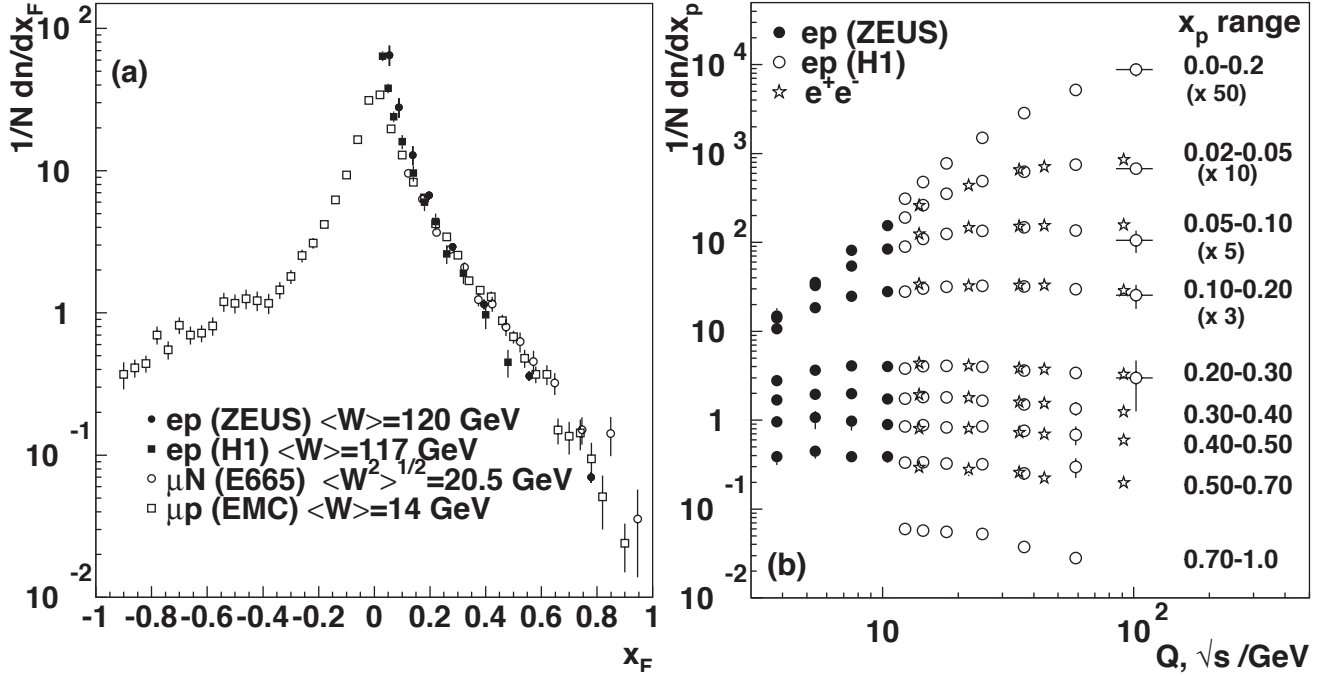


Figure 19.3: (a) The distribution  $1/N \cdot dn/dx_F$  for all charged particles in DIS lepton-hadron experiments at different values of  $W$ , measured in the HCMS [30–33]. (b) Scaling violations of the fragmentation structure function for all charged particles in the current region of the Breit frame of DIS [34, 35] and in  $e^+e^-$  interactions [19, 36]. The data are shown as a function of  $\sqrt{s}$  for  $e^+e^-$  results, and as a function of  $Q$  for the DIS results, each within the same indicated intervals of the scaled momentum  $x_p$ . The data for the four lowest intervals of  $x_p$  are multiplied by factors 50, 10, 5, and 3, respectively for better visibility.

where  $a = T, L, A$ . At the zeroth order in the strong coupling  $\alpha_s$  the coefficient functions  $C_g$  for gluons vanish, while for (anti-) quarks  $C_i = g_i(s) \delta(1-z)$  (except for  $F_L$  for which the leading contribution is of order  $\alpha_s$ , as indicated in Eq. (19.4)). Here  $g_i(s)$  is the appropriate electroweak coupling. In particular,  $g_i(s)$  is proportional to the squared charge of the quark  $i$  at  $s \ll M_Z^2$ , when weak effects can be neglected. The full electroweak prefactors  $g_i(s)$  can be found in Ref. [6]. The first-order QCD corrections to the coefficient functions have been calculated in Refs. [37, 38], and the second-order terms in [39–41]. Thus, the coefficient functions are known to NNLO, except for  $F_L$ . We note that beyond the leading order the coefficient functions, and hence the fragmentation functions, start to depend on the choice of factorization scheme. The standard choice in the literature is the  $\overline{\text{MS}}$  scheme.

The simplest parton-model approach would predict scale-independent (‘scaling’)  $x$ -distributions for both the structure function  $F^h$  and the parton fragmentation functions  $D_i^h$ . Perturbative QCD corrections lead to logarithmic scaling violations via the evolution equations [42]

$$\frac{\partial}{\partial \ln \mu^2} D_i^h(x, \mu^2) = \sum_j \int_x^1 \frac{dz}{z} P_{ji}(z, \alpha_s(\mu^2)) D_j^h\left(\frac{x}{z}, \mu^2\right), \quad (19.5)$$

where the functions  $P_{ij}(z, \alpha_s(\mu^2))$  describe the splitting process  $i \rightarrow j + X$ , where parton  $j$  carries the longitudinal momentum fraction  $z$  of parton  $i$ . Note that for fragmentation the relevant splitting functions are  $P_{ji}$  (rather than  $P_{ij}$  as for the PDFs) since  $D_j^h$  represents the fragmentation of the final parton. Usually the system of evolution equations is decomposed into a  $2 \times 2$  flavor-singlet sector comprising the gluon and the sum of all quark and antiquark fragmentation functions, and scalar (‘non-singlet’) equations for quark-antiquark and flavor differences.

The splitting functions in Eq. (19.5) have the perturbative expansion

$$P_{ji}(z, \alpha_s) = \frac{\alpha_s}{2\pi} P_{ji}^{(0)}(z) + \left(\frac{\alpha_s}{2\pi}\right)^2 P_{ji}^{(1)}(z) + \left(\frac{\alpha_s}{2\pi}\right)^3 P_{ji}^{(2)}(z) + \dots, \quad (19.6)$$

where the leading-order (LO) functions  $P^{(0)}(z)$  [42, 43] are the same as those for the initial-state parton distributions. The next-to-leading order (NLO) corrections  $P^{(1)}(z)$  have been calculated in Refs. [44–48] (there are well-known misprints in the journal version of Ref. [45]). Ref. [48] also includes the spin-dependent case. The timelike functions are different from, but related to, their spacelike counterparts, see also Ref. [49]. The connections between the two sets of functions has facilitated recent calculations of the next-to-next-to-leading order (NNLO) quantities  $P_{qq}^{(2)}(z)$  and  $P_{gg}^{(2)}(z)$  in Eq. (19.6) [40, 50]. In the same way, the corresponding off-diagonal quantities  $P_{qg}^{(2)}$  and  $P_{gq}^{(2)}$  were recently obtained in Ref. [51] with the help of constraints from the momentum sum rule Eq. (19.3) [50] and of the limit of  $C_A = C_F = n_f$  for which QCD becomes supersymmetric. An uncertainty still remains for the  $P_{gg}^{(2)}$  kernel, which however does not affect the logarithmic behavior at small and large momentum fractions. With the exception of Ref. [47], all these higher-order results refer to the standard  $\overline{\text{MS}}$  scheme with a fixed number  $n_f$  of light flavors. When the threshold for the production of a heavier quark flavor is crossed in the course of the scale evolution, fragmentation functions change. The NLO treatment of these flavor thresholds in the evolution has been addressed in Ref. [52].

The phenomenological effect of scale evolution is similar in the timelike and spacelike cases: As the scale increases, one observes a scaling violation in which the  $x$ -distribution is shifted towards lower values. This can be seen from Fig. 19.2 where a set of measurements of the total fragmentation structure function in  $e^+e^-$  annihilation are shown. In particular, the figure on the right exhibits the dependence on  $\sqrt{q^2} = \sqrt{s}$  at fixed values of  $x$ . QCD analyses of these data are discussed in Section 19.5 below.

The NLO coefficient functions for SIDIS,  $ep \rightarrow e + h + X$ , have been presented in Refs. [37, 38] Corresponding results have also been obtained for the case that a non-vanishing hadron transverse momentum is required in the HCMS frame [53, 54].

Scaling violations in DIS are shown in Fig. 19.3 for both the HCMS and the Breit frames. In Fig. 1.3(a) the distribution in terms of  $x_F = 2p_z^*/W$  shows a steeper slope in  $ep$  data than for the lower-energy  $\mu p$  data for  $x_F > 0.15$ , indicating the scaling

violations. At smaller values of  $x_F$  in the current jet region, the multiplicity of particles substantially increases with  $W$ , owing to the increased phase space available for the fragmentation process. The EMC data access both the current region and the region of the fragmenting target remnant system. At higher values of  $|x_F|$ , due to the extended nature of the remnant, the multiplicity in the target region far exceeds that in the current region. For acceptance reasons the remnant hemisphere of the HCMS is only accessible by the lower-energy fixed-target experiments.

Using hadrons from the current hemisphere in the Breit frame, measurements of fragmentation functions and the production properties of particles in  $ep$  scattering have been reported in Refs. [34, 35, 55–58]. Fig. 19.3(b) compares results from  $ep$  scattering and  $e^+e^-$  experiments; the latter results have been divided by two as they cover both event hemispheres. The agreement between the DIS and  $e^+e^-$  results is fairly good. However, processes in DIS which are not present in  $e^+e^-$  annihilation, such as boson-gluon fusion and initial-state QCD radiation, can depopulate the current region. These effects become most prominent at low values of  $Q$  and  $x_p$ . Hence, when compared with  $e^+e^-$  annihilation data at  $\sqrt{s} = 5.2, 6.5$  GeV [59] not shown here, the DIS particle rates tend to lie below those observed in  $e^+e^-$  annihilation. A ZEUS study [60] finds that the direct comparability of the  $ep$  data to  $e^+e^-$  results at low scales is improved if twice the energy in the current hemisphere of the Breit frame,  $2E_B^{\text{cr}}$ , is used instead of  $Q/2$  as the fragmentation scale. Choosing  $2E_B^{\text{cr}}$  for the fragmentation scale approximates QCD radiation effects relevant at low scales, as detailed in Ref. [29].

### 19.3 Fragmentation functions for small particle momenta

The higher-order timelike splitting functions in Eq. (19.6) are singular at small values of  $x$ . They show a double-logarithmic enhancement, with leading terms of the form  $\alpha_s^k (\ln^{2k-2} x)/x$  at the  $k$ th order of perturbation theory, corresponding to poles  $\alpha_s^k (N-1)^{1-2k}$  for the Mellin moments

$$P^{(k)}(N) = \int_0^1 dx x^{N-1} P^{(k)}(x). \quad (19.7)$$

Despite large cancellations between leading and non-leading logarithms at non-asymptotic values of  $x$ , the resulting small- $x$  rise in the timelike splitting functions dwarfs that of their spacelike counterparts for the evolution of the parton distributions in Section 18 of this *Review*, see Fig. 1 of Ref. [50]. Consequently, in fragmentation the fixed-order approximation to the evolution breaks down orders of magnitude earlier in  $x$  than in DIS.

The pattern of the known coefficients and other considerations suggest that the double-logarithmic terms sum to all-order expressions without any pole at  $N = 1$ , such as [61, 62]

$$P_{gg}^{\text{LL}}(N) = -\frac{1}{4} \left( N-1 - \sqrt{(N-1)^2 \cdot 24\alpha_s/\pi} \right) \quad (19.8)$$

for the gluon-to-gluon splitting function at leading logarithmic order. Keeping the first three terms in the resulting expansion of Eq. (19.5) around  $N = 1$  and taking the Mellin inverse yields a Gaussian in the variable  $\xi = \ln(1/x)$  for the small- $x$  fragmentation functions,

$$xD(x, q^2 = s) \propto \exp \left[ -\frac{1}{2\sigma^2} (\xi - \xi_p)^2 \right], \quad (19.9)$$

with the peak position and width varying with the energy as [63] (see also Ref. [2])

$$\xi_p \simeq \frac{1}{4} \ln \left( \frac{s}{\Lambda^2} \right), \quad \sigma \propto \left[ \ln \left( \frac{s}{\Lambda^2} \right) \right]^{3/4}. \quad (19.10)$$

Next-to-leading logarithmic corrections to the above predictions have been calculated [64]. In the method of Ref. [65], see also Refs. [66, 67], the corrections are included in an analytical form known as the ‘modified leading logarithmic approximation’ (MLLA). Alternatively they can be used to compute higher-moment correc-

tions to the shape in Eq. (19.9) [68]. The small- $x$  resummation of the coefficient functions for semi-inclusive  $e^+e^-$  annihilation and of the timelike splitting functions in the standard  $\overline{\text{MS}}$  scheme was extended in Refs. [69–73] and has reached full next-to-next-to-leading logarithmic accuracy. Applications of these results to gluon and quark jet multiplicities have been presented in Refs. [74].

Fig. 19.4 shows the  $\xi$  distribution for charged particles produced in the current region of the Breit frame in DIS and in  $e^+e^-$  annihilation. Consistently with Eq. (19.9) (the ‘hump backed plateau’) and Eq. (19.10) the distributions have a Gaussian shape, with the peak position and area increasing with CM energy ( $e^+e^-$ ) and  $Q^2$  (DIS).

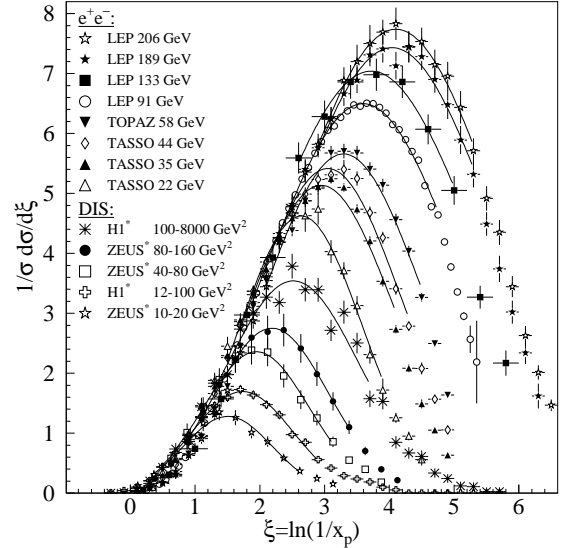


Figure 19.4: Distribution of the normalized fragmentation cross sections in  $\xi = \ln(1/x_p)$  at several CM energies ( $e^+e^-$ ) [10, 11, 16–19, 57, 58, 75–78] and for intervals of  $Q^2$  (DIS). At each energy only one representative measurement is displayed. For clarity some measurements at intermediate CM energies ( $e^+e^-$ ) or  $Q^2$  ranges (DIS) are not shown. The DIS measurements (\*) have been scaled by a factor of 2 for direct comparability with the  $e^+e^-$  results. Fits of simple Gaussian functions are overlaid for illustration.

The predicted energy dependence of the peak in the  $\xi$  distribution (see Eq. (19.10)) is explained by soft gluon coherence (angular ordering), *i.e.*, the destructive interference of the color wavefunction of low energy gluon radiation, which correctly predicts the suppression of hadron production at small  $x$ . Of course, a decrease at very small  $x$  is expected on purely kinematical grounds, but this would occur at particle energies proportional to their masses, *i.e.*, at  $x \propto m/\sqrt{s}$  and hence  $\xi \sim \frac{1}{2} \ln s$ . Thus, if the suppression were purely kinematic, the peak position  $\xi_p$  would vary twice as rapidly with the energy, which is ruled out by the data in Fig. 19.5. The  $e^+e^-$  and DIS data agree well with each other, demonstrating the universality of hadronization and the MLLA prediction. Measurements of the higher moments of the  $\xi$  distribution in  $e^+e^-$  [19, 78–80] and DIS [58] have also been performed and show consistency with each other.

The average charged-particle multiplicity is another observable sensitive to fragmentation functions for small particle momenta. Perturbative predictions using both NLO [89] and MLLA [90, 91] have been obtained by solving Eq. (19.5) yielding

$$\langle n_G(Q^2) \rangle \propto \alpha_s^b(Q^2) \exp \left[ \frac{c}{4\pi b_0 \sqrt{\alpha_s(Q^2)}} \cdot \left( 1 + 6a_2 \frac{\alpha_s(Q^2)}{\pi} \right) \right], \quad (19.11)$$

where  $b = \frac{1}{4} + \frac{10}{27} \frac{n_f}{4\pi b_0}$ ,  $c = \sqrt{96\pi}$ , with  $b_0 = (33 - 2n_f)/(12\pi)$ , *cf.* Section 9 of this *Review*, for  $n_f$  contributing quark flavors. Higher-order corrections to Eq. (19.11) are known up to next-to-next-to-next-to-leading order (N<sup>3</sup>LO), for details and references

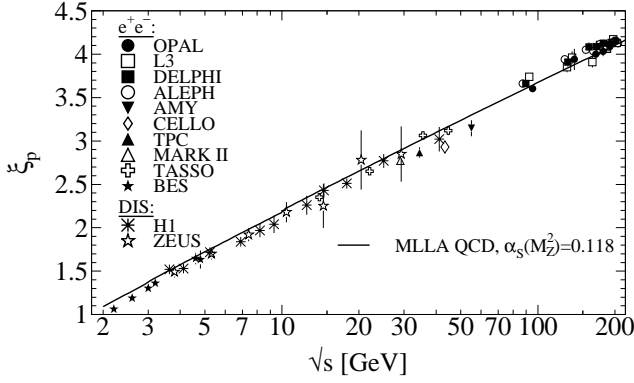


Figure 19.5: Evolution of the peak position,  $\xi_p$ , of the  $\xi$  distribution with the CM energy  $\sqrt{s}$ . The MLLA QCD prediction  $\alpha_s(s = M_Z^2) = 0.118$  is superimposed to the data of Refs. [10, 12, 15, 19, 56, 57, 76, 77, 80–88].

see [92]. The term proportional to  $a_2 \approx -0.502 + 0.0421 n_f - 0.00036 n_f^2$  in Eq. (19.11) is the contribution due to NNLO corrections [93]. The quantity  $\langle n_G(Q^2) \rangle$  refers to the average number of gluons, while for  $\langle n_q(Q^2) \rangle$  for quarks a correction factor  $1/r$  is required due to the different color factors in quark and gluon couplings, so that  $\langle n_q(Q^2) \rangle = \langle n_G(Q^2) \rangle / r$ . The correction factor depends only weakly on  $Q^2$ ; higher-order corrections up to N<sup>3</sup>LO on the asymptotic value  $r = C_A/C_F = 9/4$  [94] are quoted in [92].

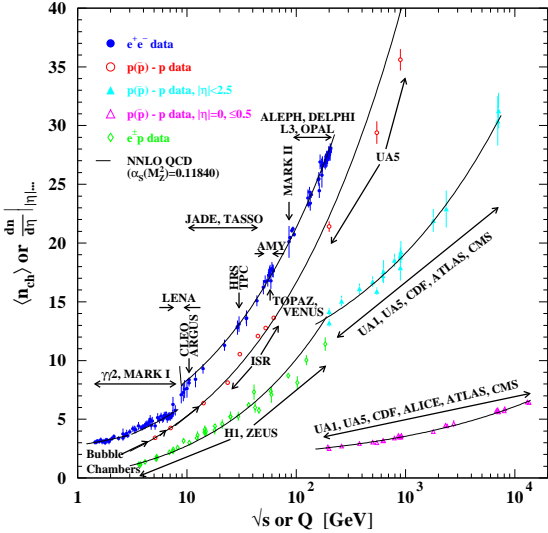


Figure 19.6: Average charged-particle multiplicity  $\langle n_{\text{ch}} \rangle$  as a function of  $\sqrt{s}$  or  $Q$  for  $e^+e^-$  and  $p\bar{p}$  annihilations, and  $pp$  and  $ep$  collisions. The indicated errors are statistical and systematic uncertainties added in quadrature, except when no systematic uncertainties are given. All NNLO QCD curves are from Eq. (19.11) with fitted normalization,  $K_{\text{LHPD}}$ , and offset,  $n_0$ , using a fixed  $\alpha_s(M_Z^2) = 0.1184$  [95] and for  $e^+e^-$  annihilation data  $n_f = 3, 4$ , or  $5$  depending on  $\sqrt{s}$ , else  $n_f = 3$ .  $e^+e^-$ : Contributions from  $K_S^0$  and  $\Lambda$  decays included. Data compiled from Refs. [8, 10, 16, 16, 22, 77, 83, 96–106];  $e^\pm p$ : Multiplicities have been measured in the current fragmentation region of the Breit frame. Data compiled from Refs. [35, 57, 58, 60, 107];  $p(\bar{p})$ : Measured values above 20 GeV refer to non-single diffractive (NSD) processes. Central pseudorapidity multiplicities  $(dn/d\eta)|_{|\eta| \dots}$  refer to either  $|\eta| < 2.5$  (CMS:  $|\eta| < 2.4$ ) or  $|\eta| = 0$  (UA5, CMS, ALICE:  $|\eta| < 0.5$ ). Data compiled from Refs. [108–123].

Employing the hypothesis of ‘Local Parton-Hadron Duality’ (LPHD) [90], *i.e.*, that the color charge of partons is balanced locally in phase space and, hence, their hadronization occurs locally such that (Mellin transformed) parton and hadron inclusive

distributions directly correspond, Eq. (19.11) can be applied to describe average charged particle multiplicities obtained in  $e^+e^-$  annihilation. The equation can also be applied to  $e^\pm p$  scattering if the current fragmentation region of the Breit frame is considered for measuring the average charged-particle multiplicity. Fig. 19.6 shows corresponding data and fits of Eq. (19.11) where apart from an LPHD normalization factor a constant offset has been allowed for, so that  $\langle n_{\text{ch}}(Q) \rangle = K_{\text{LHPD}} \cdot \langle n_G(Q) \rangle / r + n_0$ .

In hadron-hadron collisions beam remnants, *e.g.* from single-diffractive (SD) scattering where one colliding proton is negligibly deflected while hadrons related with the other colliding proton are well-separated in rapidity from the former proton, contribute to the measurement of the hadron multiplicity from a hard parton-parton scattering, making interpretation of the data more model dependent. Experimental results are usually given for inelastic processes or for non-single diffractive processes (NSD). Due to the large beam particle momenta at Tevatron and LHC, not all final state particles can be detected within the limited detector acceptance. Therefore, experiments at Tevatron and LHC quote particle multiplicities for limited ranges of pseudo-rapidity  $\eta = -\ln \tan(\vartheta/2)$  or at central rapidity, *i.e.*  $\eta = 0$ , as shown in Fig. 19.6.

A universality of the average particle multiplicities in  $e^+e^-$  and  $p(\bar{p})$  processes has been reported in Ref. [124] when considering an effective collision energy  $Q_{\text{eff}} = \sqrt{s}/k$  in  $p(\bar{p})$  reduced by a factor of  $k \approx 3$ , plus a constant offset of  $n_0 \approx 2$ . A more detailed review is available in Ref. [125]. According to the investigations presented in Ref. [126] the universality of the energy dependence of average particle multiplicities also applies to hadron-hadron and nucleus-nucleus collisions for both full and central rapidity multiplicities. Evidence for this universality is given by the good agreement for the energy dependence of Eq. (19.11) when fit to the  $p(\bar{p})$  data as shown in Fig. 19.6.

## 19.4 Fragmentation models

Although the scaling violations can be calculated perturbatively, the actual form of the parton fragmentation functions is non-perturbative. Perturbative evolution gives rise to a shower of quarks and gluons (partons). Multi-parton final states from leading and higher order matrix element calculations are linked to these parton showers using factorization prescriptions, also called matching schemes, see Ref. [127] for an overview.

Phenomenological schemes are then used to model the carry-over of parton momenta and flavor to the hadrons. Implemented in Monte Carlo event generators (see Section 42 of this Review), these schemes have been tuned using  $e^+e^-$  data and provide good description of hadron collisions as well, thus providing evidence of the universality of fragmentation. However,  $e^+e^-$  mainly fix the quark jet fragmentation while it provides less constraints for modelling the gluon jet fragmentation.

## 19.5 Phenomenology of quark and gluon fragmentation functions

The fragmentation functions are solutions to the evolution equations Eq. (19.5), but need to be specified at some initial scale  $\mu_0^2$  (usually around 1 GeV<sup>2</sup> for light quarks and gluons, and at  $m_Q^2$  for heavy quarks). A typical parameterization for a given light hadron is [128, 129, 131–137]

$$D_i^h(x, \mu_0^2) = N_i x^{\alpha_i} (1-x)^{\beta_i} (1 + \gamma_i(1-x)^{\delta_i}), \quad (19.12)$$

where as indicated the normalization  $N_i$ , and the parameters  $\alpha_i$ ,  $\beta_i$ ,  $\gamma_i$  and  $\delta_i$  depend on the type  $i$  of the fragmenting parton. Heavy flavor fragmentation into heavy mesons is discussed in Sec. 19.8 below. The parameters of Eq. (19.12) are obtained by performing global fits to data on various hadron types for different combinations of partons and hadrons in  $e^+e^-$ , lepton-hadron and hadron-hadron collisions. We note that the choice of parameterization of the fragmentation functions at the initial scale necessarily introduces a bias since it imposes a certain form of the functions. This bias is largely avoided in neural network approaches which offer a wide flexibility of the initial functions and have recently been applied to fragmentation functions as well [130]. Sets of fragmentation functions are now available for

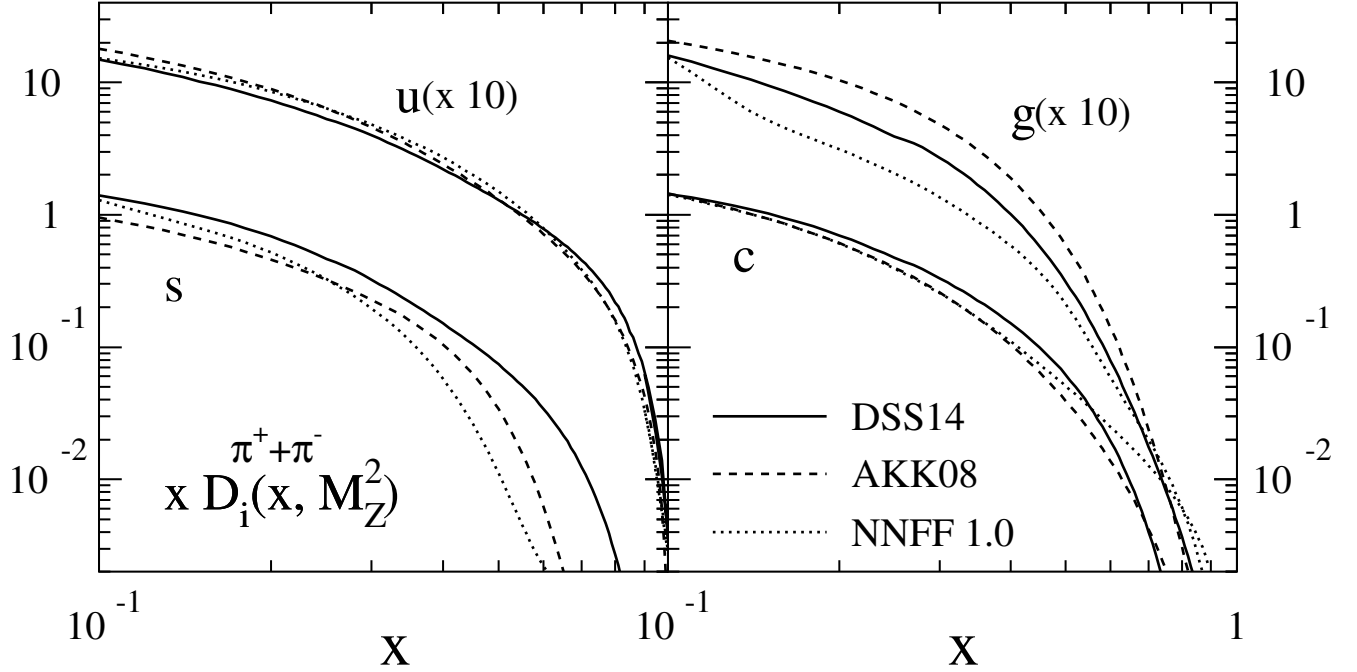


Figure 19.7: Comparison of up, strange, charm and gluon NLO fragmentation functions for  $\pi^+ + \pi^-$  at the mass of the  $Z$ . The different lines correspond to the results of the analyses performed in Refs. [128–130].

pions, kaons, protons, neutrons,  $\eta$  mesons,  $\Lambda$  baryons, and charged hadrons [128–130, 132–140]. They are all at NLO level, except for Refs. [130, 139] which have been performed at NNLO level. The latter sets are restricted to the analysis of  $e^+e^-$  annihilation data. Recently, data from hadron-hadron collisions have been added in the framework of the neural network approach at NLO accuracy for charged hadrons [141]. It is noteworthy that the NNLO effects lead to an improvement in the theoretical description of the data in  $e^+e^-$  annihilation.

Data from  $e^+e^-$  annihilation present the cleanest experimental source for the measurement of fragmentation functions, but cannot be used to disentangle quark from antiquark fragmentation. Since the bulk of the  $e^+e^-$  annihilation data is obtained at the mass of the  $Z$ -boson, where the electroweak couplings are roughly the same for the different partons, it provides the most precise determination of the flavor-singlet combination of quark and antiquark fragmentation functions. Flavor-tagged results [142], distinguishing between the light quark, charm and bottom contributions are of particular value for flavor decomposition, even though those measurements cannot be unambiguously interpreted in perturbative QCD.

The most relevant source for quark-antiquark (and also flavor) separation is provided by SIDIS data. Semi-inclusive measurements are usually performed at much lower scales than for  $e^+e^-$  annihilation. The inclusion of SIDIS data in global fits allows for a wider coverage in the evolution of the fragmentation functions, resulting at the same time in a stringent test of the universality of the distributions. Charged-hadron production data in hadronic collisions also have sensitivity to (anti-)quark fragmentation functions.

The gluon fragmentation function  $D_g^h(x)$  can be extracted, in principle, from the longitudinal fragmentation structure function  $F_L$  in Eq. (19.2), as the coefficient functions  $C_{L,i}$  for quarks and gluons are comparable at order  $\alpha_s$ . However at NLO, *i.e.*, including the  $\mathcal{O}(\alpha_s^2)$  coefficient functions  $C_{L,i}^{(2)}$  [39], quark fragmentation is dominant in  $F_L$  over a large part of the kinematic range, reducing the sensitivity to  $D_g^h$ . This distribution could be determined also by analyzing the scale evolution of the fragmentation functions. This possibility is limited by the lack of sufficiently precise data at energy scales away from the  $Z$ -resonance and the dominance of the quark contributions at medium and large values of  $x$ . In  $e^+e^-$  annihilation,  $D_g^h$  can also be deduced from the study

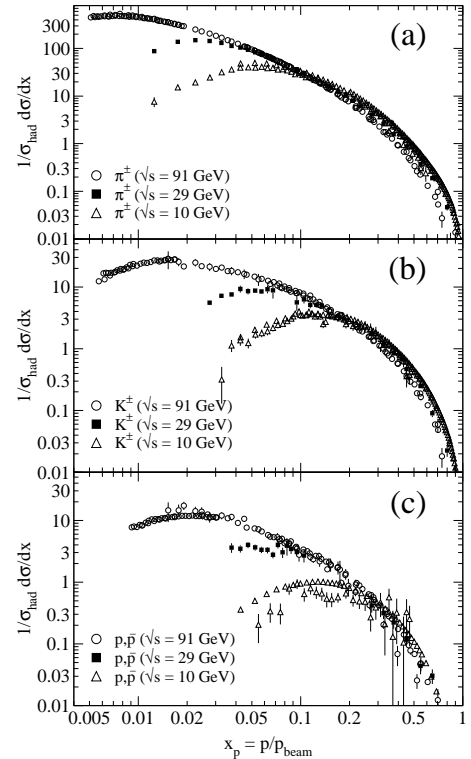


Figure 19.8: Scaled momentum spectra of (a)  $\pi^\pm$ , (b)  $K^\pm$ , and (c)  $p, \bar{p}$  at  $\sqrt{s} = 10, 29$ , and  $91$  GeV [24, 26, 85, 143, 144].

of three-jet events in which the gluon jet is identified, for example, by tagging the other two jets with heavy quark decays. To leading order, the measured distributions of  $x = E_{\text{had}}/E_{\text{jet}}$  for particles in gluon jets can be identified directly with the gluon fragmentation function  $D_g^h(x)$ .

Data for  $p(\bar{p}) \rightarrow h + X$  provide much more direct constraint on  $D_g^h$ . At variance with  $e^+e^-$  annihilation and SIDIS, here gluon

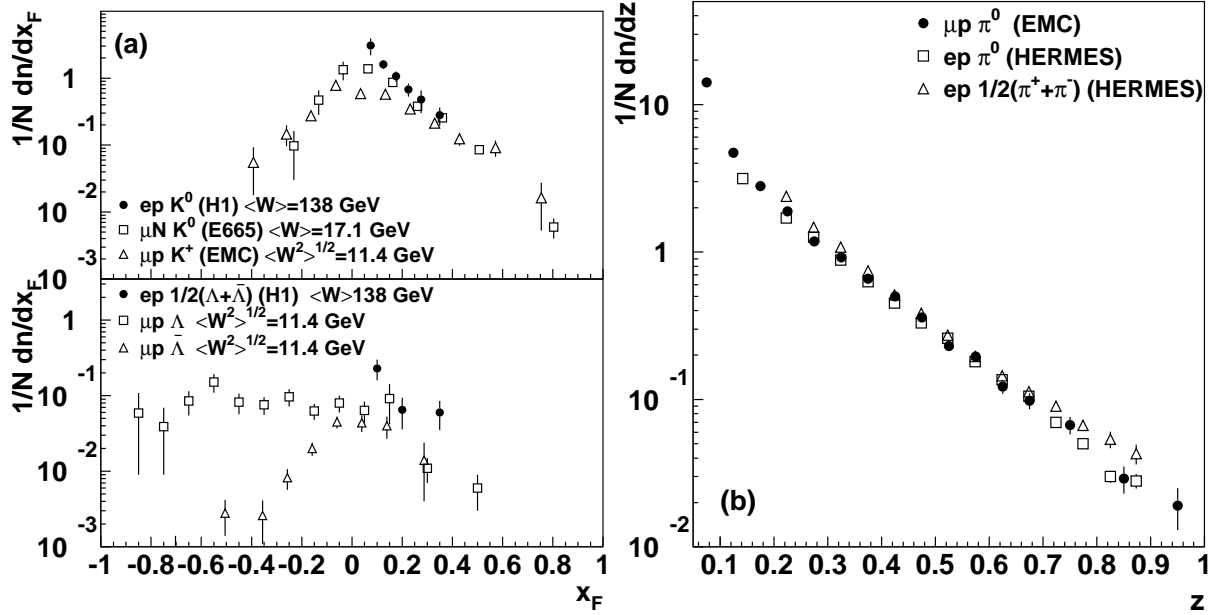


Figure 19.9: (a)  $1/N \cdot dn/dx_F$  for identified strange particles in DIS at various values of  $W$  [145–147]. (b)  $1/N \cdot dn/dz$  for measurements of pions in fixed-target DIS experiments [148–150].

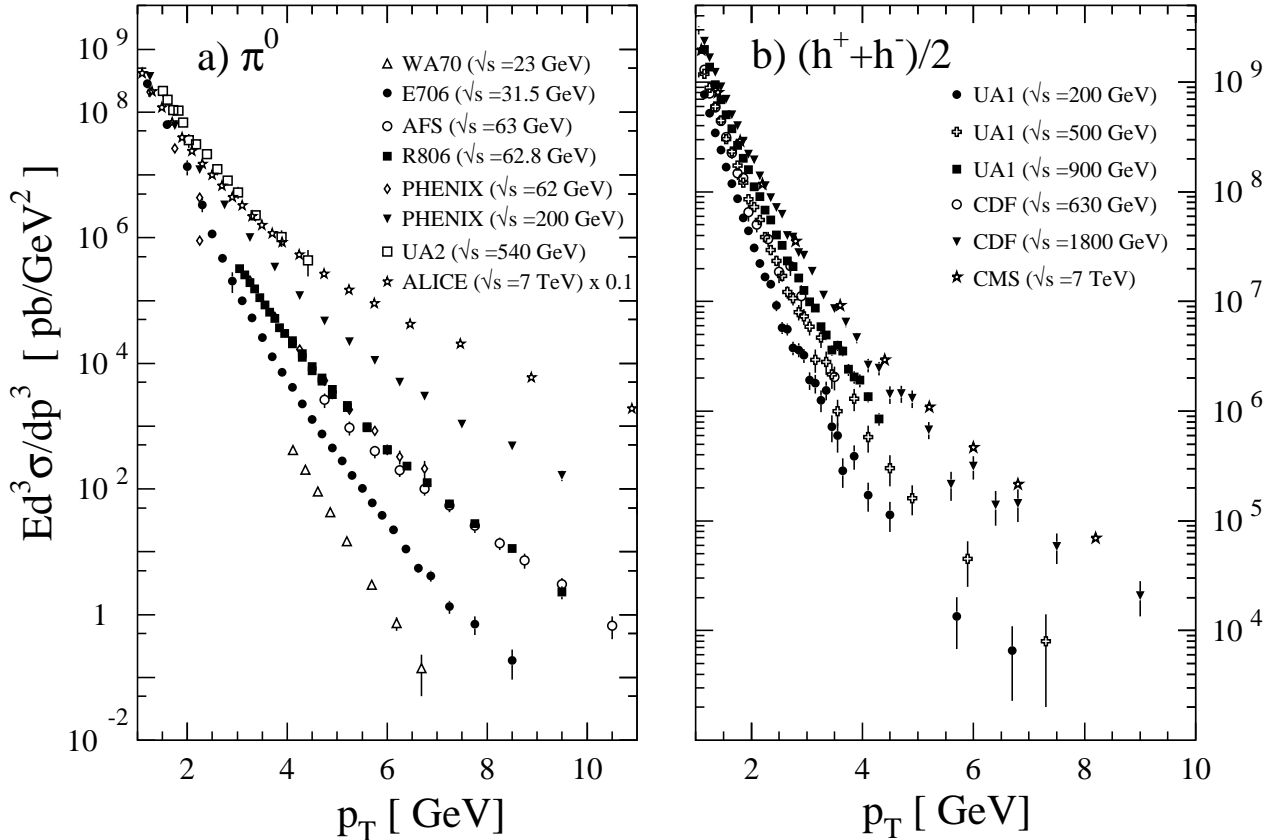


Figure 19.10: Selection of inclusive (a)  $\pi^0$  and (b) charged-hadron production data from  $pp$  [118, 151–156] and  $p\bar{p}$  [114, 157, 158] collisions.

fragmentation contributes already at the lowest order in the coupling constant. At large  $x \gtrsim 0.5$ , where information from  $e^+e^-$  is sparse, data from hadronic colliders significantly improve extractions of  $D_g^h$  [128, 129, 131, 138]. Recent LHC data has been included in the NLO analyses [129, 137] of pion-fragmentation functions; see Sec. (17.7) for more details. Note that these analyses are currently the only ones that ‘globally’ incorporate available data

from all sources,  $e^+e^- \rightarrow h + X$ ,  $ep \rightarrow e'h + X$  and  $pp \rightarrow h + X$ .

We note that recently a ‘hybrid’ type of high- $p_T$  jet/hadron observable has also been considered both theoretically [159–165] and experimentally [166–173]. It is defined by an identified specific hadron found inside a fully reconstructed jet. This gives rise to a *same-side* hadron-jet momentum correlation that may be addressed using perturbative methods. One of several rele-

**Table 19.1:** Classification of spin- and transverse-momentum dependent quark fragmentation functions. For simplicity we have left out the ubiquitous label for flavor  $i$  of the fragmenting quark and for hadron species  $h$ . Each of the functions carries the argument  $(x, x^2 k_T^2)$  (plus dependence on a factorization scale), where  $xk_T = p_T^h$  is the hadron's transverse momentum.  $\lambda$  and  $\Lambda$  are the quark's and hadron's helicities, respectively, and  $\vec{s}_T$  and  $\vec{S}_T$  are their transverse spin vectors. We have defined  $[\vec{a} \times \vec{b}] \equiv a^1 b^2 - a^2 b^1$ . Finally,  $m_h$  is the mass of the produced hadron.

hadron pol.	quark polarization		
	unpolarized	long. polarized	transv. polarized
unpol.	$D$	–	$\frac{[\vec{k}_T \times \vec{s}_T]}{m_h} H^\perp$
long. pol.	–	$\lambda \Lambda G_L$	$\frac{\vec{k}_T \cdot \vec{s}_T}{m_h} \Lambda H_L^\perp$
transv. pol.	$\frac{[\vec{k}_T \times \vec{s}_T]}{m_h} D_T^\perp$	$\frac{\vec{k}_T \cdot \vec{s}_T}{m_h} \lambda G_T^\perp$	$(\vec{s}_T \cdot \vec{S}_T) H_T + \frac{\vec{k}_T \cdot \vec{s}_T}{m_h} \frac{\vec{k}_T \cdot \vec{S}_T}{m_h} H_T^\perp$

variant kinematical variables (see [164] for an overview) is  $z_h \equiv (\vec{p}_T^h \cdot \vec{p}_T^{\text{jet}}) / (p_T^{\text{jet}})^2$ , where  $\vec{p}_T^h$  and  $\vec{p}_T^{\text{jet}}$  are the transverse momenta of the hadron and the jet, respectively. The observable provides an alternative window on fragmentation functions in a more exclusive setting, enabling novel tests of the universality of fragmentation functions. Varying  $z_h$  and/or the hadron species, one can map out the fragmentation functions ‘locally’ as functions of  $x$ . This is in contrast to the single-inclusive observable  $pp \rightarrow h + X$ , which inevitably samples over a broad range of  $x$ . Although hadron-in-jet data are not yet routinely included in analyses of fragmentation functions, a ‘proof-of-principle’ analysis does exist [174] that shows the potential of the observable in providing constraint on fragmentation functions.

A comparison of recent NLO fits of fragmentation functions for  $\pi^+ + \pi^-$  obtained by DSS14 [129], AKK08 [128] and NNPDF1.0 [130] is shown in Fig. 19.7. Differences among the functions for these sets are large, especially for the gluon fragmentation function over the full range of  $x$  and for the quark functions at large momentum fractions. The differences are even larger for other species of hadrons like kaons and protons [128, 131, 135, 138]. Recent analyses [129, 130, 135, 137, 175, 176] estimate the uncertainties involved in the extraction of fragmentation functions.

Photonic fragmentation functions play a relevant role in the theoretical understanding of inclusive photon production in (leptonic and hadronic) high energy processes. In the spirit of the analogy between parton fragmentation functions and parton distribution functions, also photonic fragmentation functions are analogous to the photon structure function  $F_2^\gamma$  and to the proton's photonic parton distributions (see review on structure functions in Section 18 of this *Review*). Since photons have a pointlike coupling to quarks [177], the corresponding fragmentation functions obey inhomogeneous evolution equations and are generally decomposed into a perturbative and a non-perturbative component [134, 178, 179]. The hadronic part, sometimes approximated by the Vector Meson Dominance Model, can in principle be obtained by performing a global analysis to the available prompt photon production data [7, 12, 15, 19–21, 85, 143, 180, 181], although in practice this has not been done. We note that also the cross section for photons produced in fully reconstructed jets has been proposed [182] as a new tool for obtaining access to photon fragmentation functions, in analogy to the hadron-in-jet cross section discussed above.

## 19.6 Identified particles in $e^+e^-$ and semi-inclusive DIS

There is a great wealth of measurements of  $e^+e^-$  fragmentation into identified particles. A collection of references for data on fragmentation into identified particles is provided in Table 52.1 of this *Review*. As a representative example, Figure 19.8 shows differential charged-hadron spectra as functions of the scaled hadron momentum at several CM energies.

Quantitative results of studies of scaling violations in  $e^+e^-$  fragmentation have been reported in [7, 21, 183, 184]. Scaling viola-

tions may be used to extract a value of  $\alpha_s$ ; the values obtained are consistent with the world average (see review on QCD in Section 9 of this *Review*).

Many studies have been made of production of identified particles in lepton-hadron scattering, although fewer particle species have been measured than in  $e^+e^-$  collisions. References [145, 146, 148–150, 185–187] and [147, 188–193] are representative of the data from fixed target and  $ep$  collider experiments, respectively. QCD calculations performed at NLO provide an overall good description of the HERA data [33, 34, 58, 193–195], both for SIDIS [196] and for the hadron transverse momentum distribution [53, 197] in the kinematic regions in which the calculations are predictive. A first step towards an NNLO calculation for SIDIS has been presented in [198].

Fig. 19.9(a) compares lower-energy fixed-target and HERA data on strangeness production, showing that the HERA spectra have substantially increased multiplicities, albeit with statistical precision that is insufficient to study scaling violations. The fixed-target data show that the  $\Lambda$  rate substantially exceeds the  $\bar{\Lambda}$  rate in the remnant region, owing to the conserved baryon number from the baryon target. Fig. 19.9(b) shows  $1/N \cdot dn/dz$  for neutral and charged pion production, where  $z$  is defined as the ratio of the pion energy to that of the exchanged boson, both measured in the laboratory frame. Results are shown from the HERMES and the EMC experiments, where the HERMES data have been evolved to  $\langle Q^2 \rangle = 25 \text{ GeV}^2$  at NLO QCD, in order to be comparable with the EMC data. Each of the experiments uses various kinematic cuts to ensure that the measured particles lie in the region that is expected to be associated with the struck quark. In the DIS kinematic regime accessed at these experiments, and over the range in  $z$  shown in Fig. 19.9, the  $z$  and  $x_F$  variables have similar values [30]. The precision data on identified particles can be used in the study of the quark flavor content of the proton [175, 214, 215].

Data on identified particle production can aid the investigation of the universality of jet fragmentation in  $e^+e^-$  and DIS. The strangeness suppression factor  $\gamma_s$ , as derived principally from tuning the Lund string model [216] within JETSET [217], is typically found to be around 0.3 in  $e^+e^-$  experiments [75], although values closer to 0.2 [218] have also been obtained. A number of measurements of so-called  $V^0$ -particles ( $K^0$ ,  $\Lambda^0$ ) and the relative rates of  $V^0$ 's and inclusively produced charged particles have been performed at HERA [147, 188, 219] and fixed target experiments [145]. These typically favour a stronger suppression ( $\gamma_s \approx 0.2$ ) than usually obtained from  $e^+e^-$  data, although values close to 0.3 have also been obtained [220, 221].

However, when comparing the description of QCD-based models for lepton-hadron interactions and  $e^+e^-$  collisions, it is important to note that the overall description by event generators of inclusively produced hadronic final states is more accurate in  $e^+e^-$  collisions than in lepton-hadron interactions [222]. Predictions of particle rates in lepton-hadron scattering are affected by uncertainties in the modelling of the parton composition of the

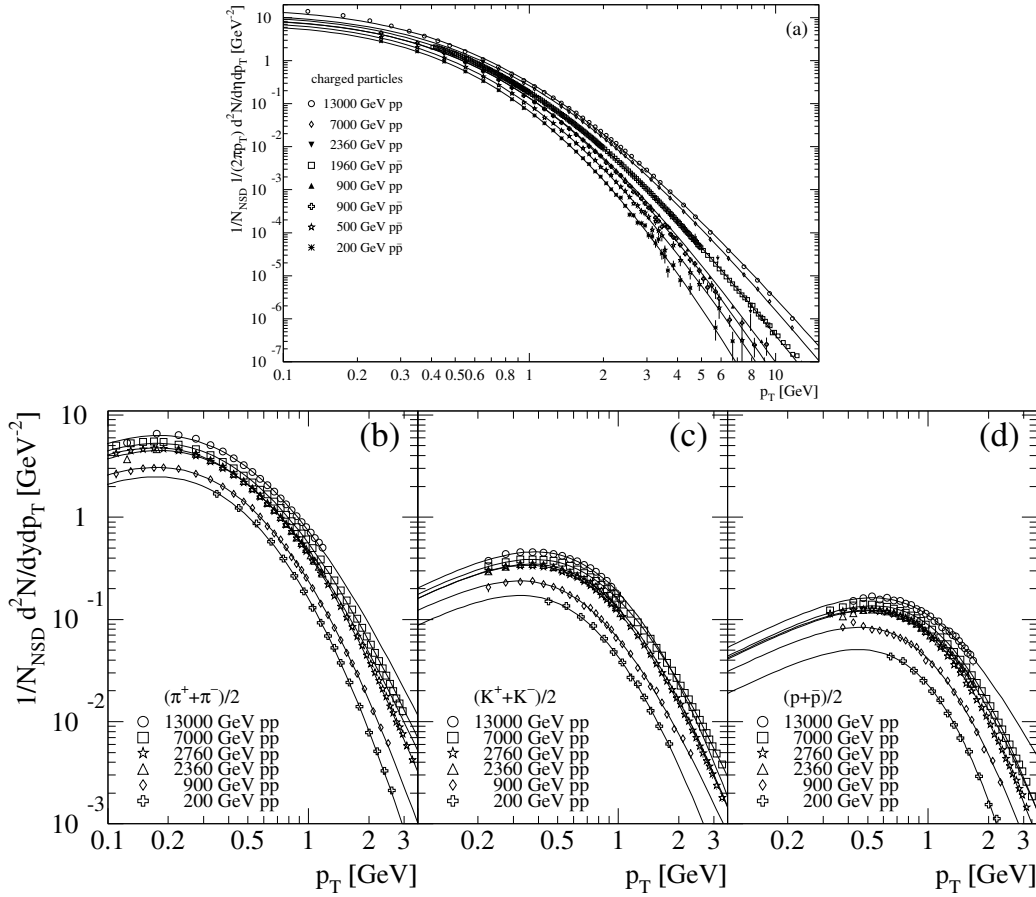


Figure 19.11: (a) Selection of inclusive charged-particle transverse momentum spectra [114, 117, 119, 121, 157, 199, 200], normalized to the non-single diffractive cross section (NSD). (b)–(d) Selection of identified charged-particle transverse momentum spectra [201–206] normalized to the NSD cross section. All spectra are scaled to the NSD cross-section using measurements of total, inelastic, elastic, single, or non-single diffractive cross sections from [207–211, 211–213]. The overall normalization uncertainty of about 3% is not shown. Superimposed are fits of the Tsallis distribution in Eq. (19.13).

proton and photon, the extended target remnant, and initial and final-state QCD radiation. Furthermore, the tuning of event generators for  $e^+e^-$  collisions is typically based on a larger set of parameters and uses more observables [75] than are used when optimizing models for lepton-hadron data [223].

### 19.7 Fragmentation in hadron-hadron collisions

An extensive set on high-transverse momentum ( $p_T$ ) single-inclusive hadron data has been collected in  $h_1 h_2 \rightarrow hX$  scattering processes, both at high energy colliders and fixed-target experiments [151–158, 181, 224–246]. Fig. 19.10 shows the invariant cross sections  $Ed^3\sigma/dp^3$  for a compilation of neutral-pion and charged-hadron production data for energies in the range  $\sqrt{s} \approx 23 - 7000$  GeV.

The differential cross section for high-transverse momentum hadron production has been computed to NLO accuracy in perturbative QCD [247]. The NLO corrections are typically large and can even double the prediction for the cross section at fixed-target energies. Nevertheless, the NLO calculations significantly under-predict the cross-section for several fixed-target energy data sets [242, 248, 249]. Different strategies have been developed to ameliorate the theoretical description at fixed-target energies. A possible phenomenological approach involves the introduction of a non-perturbative intrinsic partonic transverse momentum [156, 242, 250, 251]. Furthermore, the resummation of the dominant higher order corrections at threshold produces an enhancement of the theoretical calculation that significantly improves the description of the data [252, 253].

Data collected at high energy colliders are either included in global fit analyses or used as a test for the universality of fragmentation functions. A certain tension has been observed between

data sets from RHIC and the LHC [254]. The tension can be largely resolved [129] by excluding data with transverse momentum smaller than  $\sim 5$  GeV from the analysis, where fixed-order pQCD calculations are not expected to provide an accurate description of the process. Still, after removing these smaller  $p_T$  values where the data sets appear to be mutually exclusive in the global fit, the RHIC data show a preference towards harder gluon fragmentation at large  $x$  than the LHC data.

Transverse momentum distributions can usually be fit by power laws [255]. An approach to describe the low  $p_T$  particle spectra is the Tsallis distribution [256–258], which is based on a non-extensive generalization of the Boltzmann-Gibbs statistics. The functional form [259]

$$\frac{d^2N}{dp_T dy} = p_T \frac{dN}{dy} \frac{(n-1)(n-2)}{nT(nT + m_0(n-2))} \left[ 1 + \frac{m_T - m_0}{nT} \right]^{-n} \quad (19.13)$$

is frequently used to fit the transverse momentum spectra, where  $dN/dy$  is the particle's multiplicity,  $T$  and  $n$  are fit parameters of the Tsallis distribution,  $m_0$  is the either the mass of the most abundant particle, i.e. the pion for inclusive spectra, or the mass of an identified particle, and  $m_T = \sqrt{p_T^2 + m_0^2}$ . The parameter  $n$  is related to the non-extensive parameter  $q = n/(n-1)$  of the original Tsallis formula [260], and  $T$  is connected to the temperature in the Boltzmann-Gibbs statistics. The Tsallis distribution has been very successfully fit to measured transverse momentum distributions of both inclusive charged particles and identified particle spectra for hadron-hadron collisions, see for example [261–263], for collisions of heavy nuclei, see for example [264], and also for  $e^+e^-$  collisions, see for example [265]. The energy dependence of



the fitted Tsallis parameters has also been investigated in detail, see [259, 266]. Fig. 19.11 shows examples of hadron production data in  $pp$  and  $p\bar{p}$  collisions compared to Tsallis distributions.

Hadron production provides a critical observable for probing the high energy-density matter produced in heavy-ion collisions. Measurements at colliders show a suppression of inclusive hadron yields at high transverse momentum for  $AA$  collisions compared to  $pp$  scattering, indicating the formation of a dense medium opaque to quark and gluons, see e.g. [267].

### 19.8 Heavy quark fragmentation

It was recognized very early [268] that a heavy flavored meson should retain a large fraction of the momentum of the primordial heavy quark, and therefore its fragmentation function should be much harder than that of a light hadron. In the limit of a very heavy quark, one expects the fragmentation function for a heavy quark to go into any heavy hadron to be peaked near  $x = 1$ .

When the heavy quark is produced at a momentum much larger than its mass, one expects important perturbative effects, enhanced by powers of the logarithm of the transverse momentum over the heavy quark mass, to intervene and modify the shape of the fragmentation function. In leading logarithmic order (*i.e.*, including all powers of  $\alpha_s \log(m_Q/p_T)$ ), the total (*i.e.*, summed over all hadron types) perturbative fragmentation function is simply obtained by solving the leading evolution equation for fragmentation functions, Eq. (19.5), with the initial condition due to the finite mass of the heavy quark given by  $D_Q(x, \mu^2)|_{\mu^2=m_Q^2} = \delta(1-x)$  and  $D_i(x, \mu^2)|_{\mu^2=m_Q^2} = 0$  for  $i \neq Q$  (here  $D_i(x, \mu^2)$ , stands for the probability to produce a heavy quark  $Q$  from parton  $i$  with a fraction  $x$  of the parton momentum).

Several extensions of the leading logarithmic result have appeared in the literature. Next-to-leading-log (NLL) order results for the perturbative heavy quark fragmentation function have been obtained in [272]. The resummation of the dominant logarithmic contributions at large  $x$  was performed in [273] to next-to-leading-log accuracy. Fixed-order calculations of the fragmentation function at order  $\alpha_s^2$  in  $e^+e^-$  annihilation have appeared in [274] while the initial condition for the perturbative heavy quark fragmentation function has been extended to NNLO in [275].

Inclusion of non-perturbative effects in the calculation of the heavy-quark fragmentation function is done by convoluting the perturbative result with a phenomenological non-perturbative form. This form follows from the simple kinematical consideration that the formation of a hadron by attaching light quarks/anti-quarks to the heavy quark will slightly decelerate the heavy quark. Thus its shape will show a peak that becomes increasingly centered next to  $x = 1$  the higher the quark mass. Among the most popular parameterizations we have the following:

$$\text{Peterson } et al. [276]: D_{np}(x) \propto \frac{1}{x} \left(1 - \frac{1}{x} - \frac{\epsilon}{1-x}\right)^{-2}, \quad (19.14)$$

$$\text{Kartvelishvili } et al. [277]: D_{np}(x) \propto x^\alpha(1-x), \quad (19.15)$$

$$\begin{aligned} \text{Collins \& Spiller [278]: } D_{np}(x) \propto & \left(\frac{1-x}{x} + \frac{(2-x)\epsilon_C}{1-x}\right) \times \\ & (1+x^2) \times \left(1 - \frac{1}{x} - \frac{\epsilon_C}{1-x}\right)^{-2} \end{aligned} \quad (19.16)$$

$$\text{Colangelo \& Nason [279]: } D_{np}(x) \propto (1-x)^\alpha x^\beta \quad (19.17)$$

$$\begin{aligned} \text{Bowler [280]: } D_{np}(x) \propto & x^{-(1+bm_{h,\perp}^2)} \times \\ & (1-x)^a \exp\left(-\frac{bm_{h,\perp}^2}{x}\right) \end{aligned} \quad (19.18)$$

$$\text{Braaten } et al. [281]: \text{ (see Eqs. (31), (32) in [281])} \quad (19.19)$$

where  $\epsilon$ ,  $\epsilon_C$ ,  $a$ ,  $bm_{h,\perp}^2$ ,  $\alpha$ , and  $\beta$  are non-perturbative param-

eters that depend on the heavy hadron considered. The parameters entering the non-perturbative forms are fitted together with some model of hard radiation, which can be either a shower Monte Carlo, a leading-log or NLL calculation (which may or may not include Sudakov resummation), or a fixed order calculation. In [274], for example, the Peterson *et al.* [276]  $\epsilon$  parameter for charm and bottom production is fitted from the measured distributions of Refs. [282, 283] for charm, and of [284] for bottom. If the leading-logarithmic approximation (LLA) is used for the perturbative part, one finds  $\epsilon_c \approx 0.05$  and  $\epsilon_b \approx 0.006$ ; if a second order calculation is used one finds  $\epsilon_c \approx 0.035$  and  $\epsilon_b \approx 0.0033$ ; if a NLL improved fixed order  $\mathcal{O}(\alpha_s^2)$  calculation is used instead of NLO  $\mathcal{O}(\alpha_s)$  one finds  $\epsilon_c \approx 0.022$  and  $\epsilon_b \approx 0.0023$ . The larger values found in the LL approximation are consistent with what is obtained in the context of parton shower models [285], as expected. The  $\epsilon$  parameter for charm and bottom scales roughly with the inverse square of the heavy flavor mass. This behavior can be justified by several arguments [268, 286, 287]. It can be used to relate the non-perturbative parts of the fragmentation functions of charm and bottom quarks [274, 279, 288].

A more conventional approach [289] involves the introduction of a unique set of heavy quark fragmentation functions of non-perturbative nature that obey the usual massless evolution equations in Eq. (19.5). Finite mass terms of the form  $(m_Q/p_T)^n$  are kept in the corresponding short distance coefficient function for each scattering process. Within this approach, the initial condition for the perturbative fragmentation function provides the term needed to define the correct subtraction scheme to match the massless limit for the coefficient function (see e.g. [290]). Such an implementation is in line with the variable flavor number scheme introduced for parton distributions functions, as described in Section 18 of this *Review*.

High statistics data for charmed-meson production near the  $\Upsilon$  resonance (excluding decay products of  $B$  mesons) have been published [269, 270]. They include results for  $D$  and  $D^*$ ,  $D_s$  (see also [291, 292]) and  $\Lambda_c$ . Shown in Fig. 19.12(a) are the CLEO and BELLE inclusive cross-sections times branching ratio  $\mathcal{B}$ ,  $s\mathcal{B}d\sigma/dx_p$ , for the production of  $D^0$  and  $D^{*+}$ . The variable  $x_p$  approximates the light-cone momentum fraction  $x$ , but is not identical to it. The two measurements are consistent with each other.

The branching ratio  $\mathcal{B}$  represents  $D^0 \rightarrow K^-\pi^+$  for the  $D^0$  results and for the  $D^{*+}$  the product of the branching fractions for  $D^{*+} \rightarrow D^0\pi^+$  and  $D^0 \rightarrow K^-\pi^+$ . Given the high precision of CLEO's and BELLE's data, a superposition of different parametric forms for the non-perturbative contribution is needed to obtain a good fit [52]. Older studies are reported in Refs. [283, 293, 294]. Charmed meson spectra on the  $Z$  peak have been published by OPAL and ALEPH [295, 296].

Charm quark production has also been extensively studied at HERA by the H1 and ZEUS collaborations. Measurements have been made of  $D^{*\pm}$ ,  $D^\pm$ , and  $D_s^\pm$  mesons and the  $\Lambda_c$  baryon. See, for example, Refs. [297, 298].

Experimental studies of the fragmentation function for  $b$  quarks, shown in Fig. 19.12(b), have been performed at LEP and SLD [271, 284, 299]. Commonly used methods identify the  $B$  meson through its semileptonic decay or based upon tracks emerging from the  $B$  secondary vertex. Heavy flavor contributions from gluon splitting are usually explicitly removed before fitting the fragmentation functions. The studies in [271] fit the  $B$  spectrum using a Monte Carlo shower model supplemented with non-perturbative fragmentation functions yielding consistent results.

The experiments measure primarily the spectrum of  $B$  mesons. This defines a fragmentation function that includes the effect of the decay of higher mass excitations, like the  $B^*$  and  $B^{**}$ . In the literature (cf. details in Ref. [300]), there is sometimes ambiguity in what is defined to be the bottom fragmentation function. Instead of using what is directly measured (*i.e.*, the  $B$  meson spectrum), in some cases corrections are applied to account for  $B^*$  or  $B^{**}$  production.

Heavy-flavor production in  $e^+e^-$  collisions is the primary source of information for the role of fragmentation effects in heavy-flavor production in hadron-hadron and lepton-hadron collisions. The



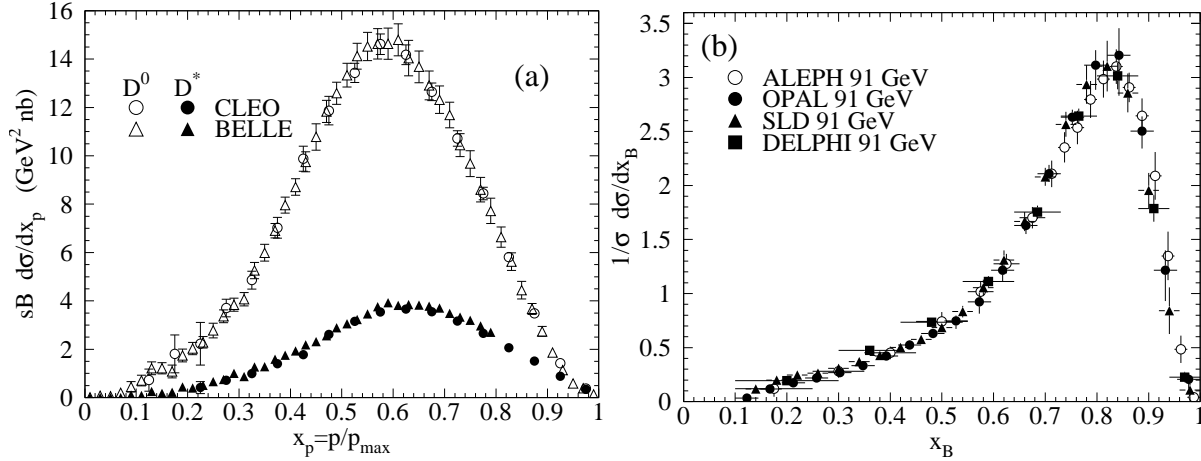


Figure 19.12: (a) Efficiency-corrected inclusive cross-section measurements for the production of  $D^0$  and  $D^{*+}$  in  $e^+e^-$  measurements at  $\sqrt{s} \approx 10.6$  GeV, excluding  $B$  decay products [269] [270]. (b) Measured  $e^+e^-$  fragmentation function of  $b$  quarks into  $B$  hadrons at  $\sqrt{s} \approx 91$  GeV [271].

QCD calculations tend to underestimate the data in certain regions of phase space. Some experimental results from LHC summarized in [301] show such deviations e.g. at high transverse jet momentum and also at low di-jet separation angles, see [302] for details, and were already theoretically investigated in [303].

Both bottomed- and charmed-meson spectra have been measured at the Tevatron with unprecedented accuracy [304]. The measured spectra are in good agreement with QCD calculations (including non-perturbative fragmentation effects inferred from  $e^+e^-$  data [305]).

The HERA collaborations have produced a number of measurements of beauty production; see, for example, Refs. [297, 306–309]. As for the Tevatron data, the HERA results are described well by QCD-based calculations using fragmentation models optimised with  $e^+e^-$  data.

Besides degrading the fragmentation function by gluon radiation, QCD evolution can also generate soft heavy quarks, increasing in the small  $x$  region as  $\sqrt{s}$  increases. Several theoretical studies are available on the issue of how often  $b\bar{b}$  or  $c\bar{c}$  pairs are produced indirectly via a gluon splitting mechanism [310–312]. Experimental results from studies on charm and bottom production via gluon splitting, given in [296, 313–317], yield weighted averages of  $\bar{n}_{g \rightarrow c\bar{c}} = 3.05 \pm 0.45\%$  and  $\bar{n}_{g \rightarrow b\bar{b}} = 0.277 \pm 0.072\%$ , respectively. The production of bottom-antibottom quark pairs via gluon splitting has also been investigated at hadron colliders, see for example [318–320].

### 19.9 Spin-dependent and transverse-momentum dependent fragmentation functions

The fragmentation functions we have considered so far apply to the spin-averaged case in which the polarization of the produced hadron is not observed, or the hadron has spin-0. We have also only considered ‘collinear’ fragmentation functions  $D_i^h(x, \mu^2)$  which carry only one kinematical variable, the momentum fraction  $x$ . New insights into fragmentation and hadronization become available when also the dependence of fragmentation functions on the spin of the produced hadron and/or its relative transverse momentum with respect to the fragmenting parton are considered. In the latter case, one refers to the fragmentation functions as ‘transverse-momentum dependent (TMD)’ fragmentation functions.

Staying first with collinear fragmentation functions, two types of spin-dependent fragmentation functions to spin-1/2 hadrons can be considered. The helicity-dependent fragmentation function measures the transfer of longitudinal spin from the fragmenting parton to the hadron [38, 321–324]. It is given by

$$\Delta D_i^h(x, \mu^2) \equiv D_{i+}^{h+}(x, \mu^2) - D_{i+}^{h-}(x, \mu^2), \quad (19.20)$$

where the superscripts  $\pm$  refer to the helicities of the parton and

hadron.  $\Lambda$  hyperons are ideally suited for measurements of the  $\Delta D_i^h$ , thanks to their self-analyzing weak decay  $\Lambda \rightarrow \pi p$ . Measurements of the longitudinal spin transfer to Lambda hyperons have been presented in  $e^+e^-$  (on the  $Z$  resonance),  $\ell p$ , and  $pp$  scattering in Refs. [325–331]. One may readily extend Eq. (19.20) to the case of transverse polarization of hadrons and quarks [332], where the corresponding fragmentation functions are known as ‘transversity’ fragmentation functions. There are also measurements constraining these fragmentation functions [326, 333, 334].

If the transverse-momentum ( $k_T$ ) dependence of fragmentation functions is considered, there are eight types of leading-twist functions, defined by the correlations among the hadronic and partonic spin vectors and transverse-momentum vectors they represent. (For review, see [5]). We note that the eight fragmentation functions given in the table below exist separately for each quark and antiquark flavor, and a similar set may be introduced for gluons. Upon integration over the transverse momentum  $k_T$  the collinear unpolarized, helicity, and transversity fragmentation functions are reproduced.

The various fragmentation functions may be obtained from spin asymmetries and angular distributions in hadron production processes. There is a large body of precision data by now on transverse-momentum distributions in  $e^+e^-$  annihilation [335] and SIDIS [186, 336] that provide constraints on the unpolarized TMD fragmentation functions  $D_i^h$ , which have been analyzed theoretically, partly also including TMD evolution effects and high orders of perturbation theory [337–342].

Besides the unpolarized functions  $D$  most of the attention in experiment and theory has been on the function  $H^\perp$  which describes the production of unpolarized (or spin-0) hadrons by transversely polarized quarks. This function is known as the ‘Collins function’ [343]. Its importance also derives from the fact that it may be used to probe the quark transversity PDF of the nucleon [344] which gives the probability of finding a transversely polarized quark with its spin aligned or anti-aligned with the spin of a transversely polarized nucleon. The transversity function is chiral-odd, and therefore not accessible through measurements of inclusive lepton-hadron scattering. The Collins effect in semi-inclusive DIS, on the other hand, provides an avenue for accessing transversity. The Collins fragmentation function is chiral-odd and T-odd, leading to a characteristic single-spin asymmetry in the azimuthal angular distribution of the produced hadron in the hadron scattering plane. A number of SIDIS [345–356] and  $e^+e^-$  experiments [357–361] have performed measurements of the Collins effect, for charged pions and kaons. These have been analyzed theoretically [362, 363], leading to an extraction of the nucleon’s transversity distributions [363]. The Collins effect has also been studied in  $pp$  scattering, where one considers azimuthal transverse single-spin asymmetries for distributions of hadrons inside

jets [173, 364, 365].

In the context of extractions of transversity PDFs also fragmentation functions for same-side pairs of hadrons with small invariant mass, *dihadrons*, have been introduced and studied [366–374]. Compared to the Collins effect, dihadron fragmentation functions have the advantage that they may be defined purely in collinear factorization. The relevant spin-dependent dihadron fragmentation function exploits a correlation between the transverse polarization of the fragmenting quark and the relative momentum of the two hadrons. In SIDIS with a transversely polarized hadron beam, the dihadron cross section then contains a specific modulation in the azimuthal orientation of the plane containing the momenta of the two hadrons. The coefficient of this modulation is a product of the spin-dependent dihadron fragmentation function and the target’s transversity PDF. The dihadron fragmentation functions may be separately extracted from measurements in  $e^+e^-$  annihilation, and the Belle experiment has presented data [375] that have been analyzed theoretically [376, 377]. In lepton scattering, HERMES [378] and COMPASS [379, 380] have reported data sensitive to the spin-dependent dihadron fragmentation functions, and recently the STAR experiment at RHIC has presented data in the azimuthal distribution of  $\pi^+\pi^-$  pairs produced in  $pp$  scattering with one transversely polarized proton [381]. The results have been successfully used for the extraction of transversity PDFs [377, 382–384].

### References

- [1] G. Altarelli, Phys. Rept. **81**, 1 (1982).
- [2] R.K. Ellis *et al.*, *QCD and Collider Physics*, Cambridge University Press (1996).
- [3] S. Albino *et al.* (2008), [arXiv:0804.2021].
- [4] F. Arleo, Eur. Phys. J. **C61**, 603 (2009), [arXiv:0810.1193].
- [5] A. Metz and A. Vossen, Prog. Part. Nucl. Phys. **91**, 136 (2016), [arXiv:1607.02521].
- [6] P. Nason and B. R. Webber, Nucl. Phys. **B421**, 473 (1994), [Erratum: Nucl. Phys. **B480**, 755 (1996)].
- [7] D. Buskulic *et al.* (ALEPH), Phys. Lett. **B357**, 487 (1995), [Erratum: Phys. Lett. **B364**, 247 (1995)].
- [8] P. Abreu *et al.* (DELPHI), Eur. Phys. J. **C6**, 19 (1999).
- [9] R. Barate *et al.* (ALEPH), Phys. Rept. **294**, 1 (1998).
- [10] D. Buskulic *et al.* (ALEPH), Z. Phys. **C73**, 409 (1997).
- [11] B. Adeva *et al.* (L3), Phys. Lett. **B259**, 199 (1991).
- [12] Y. K. Li *et al.* (AMY), Phys. Rev. **D41**, 2675 (1990).
- [13] D. Bender *et al.*, Phys. Rev. **D31**, 1 (1985).
- [14] G. S. Abrams *et al.*, Phys. Rev. Lett. **64**, 1334 (1990).
- [15] A. Petersen *et al.*, Phys. Rev. **D37**, 1 (1988).
- [16] G. Alexander *et al.* (OPAL), Z. Phys. **C72**, 191 (1996).
- [17] K. Ackerstaff *et al.* (OPAL), Z. Phys. **C75**, 193 (1997).
- [18] G. Abbiendi *et al.* (OPAL), Eur. Phys. J. **C16**, 185 (2000), [hep-ex/0002012].
- [19] W. Braunschweig *et al.* (TASSO), Z. Phys. **C47**, 187 (1990).
- [20] K. Ackerstaff *et al.* (OPAL), Eur. Phys. J. **C7**, 369 (1999), [hep-ex/9807004].
- [21] P. Abreu *et al.* (DELPHI), Phys. Lett. **B398**, 194 (1997).
- [22] G. Abbiendi *et al.* (OPAL), Eur. Phys. J. **C37**, 1, 25 (2004), [hep-ex/0404026].
- [23] R. Brandelik *et al.* (TASSO), Phys. Lett. **114B**, 65 (1982).
- [24] K. Abe *et al.* (SLD), Phys. Rev. **D69**, 072003 (2004), [hep-ex/0310017].
- [25] H. Aihara *et al.* (TPC/Two Gamma), Phys. Rev. Lett. **61**, 1263 (1988).
- [26] M. Leitgab *et al.* (Belle), Phys. Rev. Lett. **111**, 062002 (2013), [arXiv:1301.6183].
- [27] W. Kittel and E.A. De Wolf, *Soft Multihadron Dynamics*, World Scientific (2005).
- [28] H.F. Jones, Nuovo Cimento **40A**, 1018 (1965).
- [29] K. H. Streng, T. F. Walsh and P. M. Zerwas, Z. Phys. **C2**, 237 (1979).
- [30] M. R. Adams *et al.* (E-665), Phys. Lett. **B272**, 163 (1991).
- [31] M. Arneodo *et al.* (European Muon), Z. Phys. **C35**, 417 (1987).
- [32] I. Abt *et al.* (H1), Z. Phys. **C63**, 377 (1994).
- [33] M. Derrick *et al.* (ZEUS), Z. Phys. **C70**, 1 (1996), [hep-ex/9511010].
- [34] J. Breitweg *et al.* (ZEUS), Phys. Lett. **B414**, 428 (1997), [hep-ex/9710011].
- [35] F. D. Aaron *et al.* (H1), Phys. Lett. **B654**, 148 (2007), [arXiv:0706.2456].
- [36] P. Abreu *et al.* (DELPHI), Phys. Lett. **B311**, 408 (1993).
- [37] G. Altarelli *et al.*, Nucl. Phys. **B160**, 301 (1979); R. Baier and K. Fey, Z. Phys. **C2**, 339 (1979).
- [38] D. de Florian, M. Stratmann and W. Vogelsang, Phys. Rev. **D57**, 5811 (1998), [hep-ph/9711387].
- [39] P. J. Rijken and W. L. van Neerven, Phys. Lett. **B386**, 422 (1996), [hep-ph/9604436]; P. J. Rijken and W. L. van Neerven, Phys. Lett. **B392**, 207 (1997), [hep-ph/9609379]; P. J. Rijken and W. L. van Neerven, Nucl. Phys. **B487**, 233 (1997), [hep-ph/9609377].
- [40] A. Mitov, S. Moch and A. Vogt, Phys. Lett. **B638**, 61 (2006), [hep-ph/0604053].
- [41] A. Mitov and S.-O. Moch, Nucl. Phys. **B751**, 18 (2006), [hep-ph/0604160].
- [42] V. N. Gribov and L. N. Lipatov, Sov. J. Nucl. Phys. **15**, 438 (1972), [Yad. Fiz. **15**, 781 (1972)]; V. N. Gribov and L. N. Lipatov, Sov. J. Nucl. Phys. **15**, 675 (1972), [Yad. Fiz. **15**, 1218 (1972)]; L.N. Lipatov, Sov. J. Nucl. Phys. **20**, 95 (1975); Yu.L. Dokshitzer, Sov. Phys. JETP Lett. **46**, 641 (1977); G. Altarelli and G. Parisi, Nucl. Phys. **B126**, 298 (1977).
- [43] H. Georgi and H. D. Politzer, Nucl. Phys. **B136**, 445 (1978); J. F. Owens, Phys. Lett. **76B**, 85 (1978); T. Uematsu, Phys. Lett. **79B**, 97 (1978).
- [44] G. Curci, W. Furmanski and R. Petronzio, Nucl. Phys. **B175**, 27 (1980).
- [45] W. Furmanski and R. Petronzio, Phys. Lett. **97B**, 437 (1980).
- [46] E. G. Floratos, C. Kounnas and R. Lacaze, Nucl. Phys. **B192**, 417 (1981).
- [47] J. Kalinowski, K. Konishi and T. R. Taylor, Nucl. Phys. **B181**, 221 (1981).
- [48] M. Stratmann and W. Vogelsang, Nucl. Phys. **B496**, 41 (1997), [hep-ph/9612250].
- [49] Yu. L. Dokshitzer, G. Marchesini and G. P. Salam, Phys. Lett. **B634**, 504 (2006), [hep-ph/0511302].
- [50] S. Moch and A. Vogt, Phys. Lett. **B659**, 290 (2008), [arXiv:0709.3899].
- [51] A. A. Almasy, S. Moch and A. Vogt, Nucl. Phys. **B854**, 133 (2012), [arXiv:1107.2263].
- [52] M. Cacciari, P. Nason and C. Oleari, JHEP **04**, 006 (2006), [hep-ph/0510032]; M. Cacciari, P. Nason and C. Oleari, JHEP **10**, 034 (2005), [hep-ph/0504192].
- [53] P. Aurenche *et al.*, Eur. Phys. J. **C34**, 277 (2004), [hep-ph/0312359]; A. Daleo, D. de Florian and R. Sassot, Phys. Rev. **D71**, 034013 (2005), [hep-ph/0411212]; B. A. Kniehl, G. Kramer and M. Maniatis, Nucl. Phys. **B711**, 345 (2005), [Erratum: Nucl. Phys. **B720**, 231 (2005)], [hep-ph/0411300].
- [54] B. Wang *et al.*, Phys. Rev. **D99**, 9, 094029 (2019), [arXiv:1903.01529].
- [55] S. Aid *et al.* (H1), Nucl. Phys. **B445**, 3 (1995), [hep-ex/9505003].
- [56] M. Derrick *et al.* (ZEUS), Z. Phys. **C67**, 93 (1995), [hep-ex/9501012].

- [57] C. Adloff *et al.* (H1), Nucl. Phys. **B504**, 3 (1997), [hep-ex/9707005].
- [58] J. Breitweg *et al.* (ZEUS), Eur. Phys. J. **C11**, 251 (1999), [hep-ex/9903056].
- [59] J. F. Patrick *et al.*, Phys. Rev. Lett. **49**, 1232 (1982).
- [60] S. Chekanov *et al.* (ZEUS), JHEP **06**, 061 (2008), [arXiv:0803.3878].
- [61] A. H. Mueller, Phys. Lett. **104B**, 161 (1981).
- [62] A. Bassetto *et al.*, Nucl. Phys. **B207**, 189 (1982).
- [63] Yu.L. Dokshitzer *et al.*, Z. Phys. **C15**, 324 (1982).
- [64] A. H. Mueller, Nucl. Phys. **B213**, 85 (1983); A. H. Mueller, Nucl. Phys. **B241**, 141 (1984).
- [65] Y. L. Dokshitzer, V. A. Khoze and S. I. Troian, Int. J. Mod. Phys. **A7**, 1875 (1992).
- [66] Yu.L. Dokshitzer *et al.*, *Basics of Perturbative QCD*, Editions Frontières (1991).
- [67] V. A. Khoze and W. Ochs, Int. J. Mod. Phys. **A12**, 2949 (1997), [hep-ph/9701421].
- [68] C. P. Fong and B. R. Webber, Nucl. Phys. **B355**, 54 (1991).
- [69] S. Albino *et al.*, Phys. Rev. Lett. **95**, 232002 (2005), [hep-ph/0503170].
- [70] S. Albino *et al.*, Phys. Rev. **D73**, 054020 (2006), [hep-ph/0510319].
- [71] S. Albino *et al.*, Nucl. Phys. **B851**, 86 (2011), [arXiv:1104.3018]; S. Albino *et al.*, Nucl. Phys. **B855**, 801 (2012), [arXiv:1108.3948].
- [72] A. Vogt, JHEP **10**, 025 (2011), [arXiv:1108.2993]; C. H. Kom, A. Vogt and K. Yeats, JHEP **10**, 033 (2012), [arXiv:1207.5631].
- [73] D. P. Anderle *et al.*, Phys. Rev. **D95**, 5, 054003 (2017), [arXiv:1611.03371].
- [74] P. Bolzoni, B. A. Kniehl and A. V. Kotikov, Phys. Rev. Lett. **109**, 242002 (2012), [arXiv:1209.5914]; P. Bolzoni, B. A. Kniehl and A. V. Kotikov, Nucl. Phys. **B875**, 18 (2013), [arXiv:1305.6017].
- [75] P. Abreu *et al.* (DELPHI), Z. Phys. **C73**, 11 (1996).
- [76] P. Abreu *et al.* (DELPHI), Z. Phys. **C73**, 229 (1997).
- [77] P. Achard *et al.* (L3), Phys. Rept. **399**, 71 (2004), [hep-ex/0406049].
- [78] R. Itoh *et al.* (TOPAZ), Phys. Lett. **B345**, 335 (1995), [hep-ex/9412015].
- [79] M. Althoff *et al.* (TASSO), Z. Phys. **C22**, 307 (1984).
- [80] M. Z. Akrawy *et al.* (OPAL), Phys. Lett. **B247**, 617 (1990).
- [81] W. Dunwoodie *et al.* (BES), Phys. Rev. **D69**, 072002 (2004), [hep-ex/0306055].
- [82] D. Buskulic *et al.* (ALEPH), Z. Phys. **C55**, 209 (1992).
- [83] A. Heister *et al.* (ALEPH), Eur. Phys. J. **C35**, 457 (2004).
- [84] P. Abreu *et al.* (DELPHI), Phys. Lett. **B275**, 231 (1992).
- [85] P. Abreu *et al.* (DELPHI), Eur. Phys. J. **C5**, 585 (1998).
- [86] P. Abreu *et al.* (DELPHI), Phys. Lett. **B459**, 397 (1999).
- [87] M. Acciarri *et al.* (L3), Phys. Lett. **B444**, 569 (1998).
- [88] TPC/TWO-GAMMA Collab.: H. Aihara *et al.*, LBL 23737.
- [89] B. R. Webber, Phys. Lett. **143B**, 501 (1984).
- [90] Y. I. Azimov *et al.*, Z. Phys. **C27**, 65 (1985).
- [91] Y. I. Azimov *et al.*, Z. Phys. **C31**, 213 (1986).
- [92] I. M. Dremin and J. W. Gary, Phys. Rept. **349**, 301 (2001), [hep-ph/0004215].
- [93] I. M. Dremin and V. A. Nechitailo, Mod. Phys. Lett. **A9**, 1471 (1994), [hep-ex/9406002].
- [94] S. J. Brodsky and J. F. Gunion, Phys. Rev. Lett. **37**, 402 (1976).
- [95] J. Beringer *et al.* (Particle Data Group), Phys. Rev. **D86**, 010001 (2012).
- [96] R. Akers *et al.* (OPAL), Z. Phys. **C68**, 203 (1995).
- [97] P. D. Acton *et al.* (OPAL), Z. Phys. **C53**, 539 (1992).
- [98] D. Buskulic *et al.* (ALEPH), Z. Phys. **C69**, 15 (1995).
- [99] P. Abreu *et al.* (DELPHI), Phys. Lett. **B372**, 172 (1996).
- [100] P. Abreu *et al.* (DELPHI), Phys. Lett. **B416**, 233 (1998).
- [101] P. Abreu *et al.* (DELPHI), Eur. Phys. J. **C18**, 203 (2000), [Erratum: Eur. Phys. J. **C25**, 493(2002)], [hep-ex/0103031].
- [102] M. Acciarri *et al.* (L3), Phys. Lett. **B371**, 137 (1996).
- [103] M. Acciarri *et al.* (L3), Phys. Lett. **B404**, 390 (1997).
- [104] K. Nakabayashi *et al.* (TOPAZ), Phys. Lett. **B413**, 447 (1997).
- [105] K. Okabe *et al.* (VENUS), Phys. Lett. **B423**, 407 (1998).
- [106] H. Albrecht *et al.* (ARGUS), Z. Phys. **C54**, 13 (1992).
- [107] S. Chekanov *et al.* (ZEUS), Phys. Lett. **B510**, 36 (2001), [hep-ex/0104036].
- [108] J. Benecke *et al.* (Bonn-Hamburg-Munich), Nucl. Phys. **B76**, 29 (1974).
- [109] W. M. Morse *et al.*, Phys. Rev. **D15**, 66 (1977).
- [110] W. Thome *et al.* (Aachen-CERN-Heidelberg-Munich), Nucl. Phys. **B129**, 365 (1977).
- [111] A. Breakstone *et al.* (Ames-Bologna-CERN-Dortmund-Heidelberg-Warsaw), Phys. Rev. **D30**, 528 (1984).
- [112] G. J. Alner *et al.* (UA5), Phys. Rept. **154**, 247 (1987).
- [113] R. E. Ansorge *et al.* (UA5), Z. Phys. **C43**, 357 (1989).
- [114] C. Albajar *et al.* (UA1), Nucl. Phys. **B335**, 261 (1990).
- [115] F. Abe *et al.* (CDF), Phys. Rev. **D41**, 2330 (1990), [119(1989)].
- [116] K. Aamodt *et al.* (ALICE), Eur. Phys. J. **C68**, 89 (2010), [arXiv:1004.3034].
- [117] V. Khachatryan *et al.* (CMS), JHEP **02**, 041 (2010), [arXiv:1002.0621].
- [118] V. Khachatryan *et al.* (CMS), JHEP **01**, 079 (2011), [arXiv:1011.5531].
- [119] V. Khachatryan *et al.* (CMS), Phys. Rev. Lett. **105**, 022002 (2010), [arXiv:1005.3299].
- [120] G. Aad *et al.* (ATLAS), Eur. Phys. J. **C76**, 7, 403 (2016), [arXiv:1603.02439].
- [121] M. Aaboud *et al.* (ATLAS), Eur. Phys. J. **C76**, 9, 502 (2016), [arXiv:1606.01133].
- [122] J. Adam *et al.* (ALICE), Phys. Lett. **B753**, 319 (2016), [arXiv:1509.08734].
- [123] J. Adam *et al.* (ALICE), Eur. Phys. J. **C77**, 1, 33 (2017), [arXiv:1509.07541].
- [124] P. V. Chliapnikov and V. A. Uvarov, Phys. Lett. **B251**, 192 (1990).
- [125] J. F. Grosse-Oetringhaus and K. Reygers, J. Phys. **G37**, 083001 (2010), [arXiv:0912.0023].
- [126] E. K. G. Sarkisyan and A. S. Sakharov (2004), [hep-ph/0410324]; E. K. G. Sarkisyan and A. S. Sakharov, AIP Conf. Proc. **828**, 1, 35 (2006), [hep-ph/0510191]; E. K. G. Sarkisyan and A. S. Sakharov, Eur. Phys. J. **C70**, 533 (2010), [arXiv:1004.4390].
- [127] S. Hoeche *et al.*, in "HERA and the LHC: A Workshop on the implications of HERA for LHC physics: Proceedings Part A," 288–289 (2005), [hep-ph/0602031]; S. Mrenna and P. Richardson, JHEP **05**, 040 (2004), [hep-ph/0312274]; J. Alwall *et al.*, Eur. Phys. J. **C53**, 473 (2008), [arXiv:0706.2569].
- [128] S. Albino, B. A. Kniehl and G. Kramer, Nucl. Phys. **B803**, 42 (2008), [arXiv:0803.2768].

- [129] D. de Florian *et al.*, Phys. Rev. **D91**, 1, 014035 (2015), [arXiv:1410.6027].
- [130] V. Bertone *et al.* (NNPDF), Eur. Phys. J. **C77**, 8, 516 (2017), [arXiv:1706.07049].
- [131] D. de Florian, R. Sassot and M. Stratmann, Phys. Rev. **D76**, 074033 (2007), [arXiv:0707.1506].
- [132] S. Kretzer, E. Leader and E. Christova, Eur. Phys. J. **C22**, 269 (2001), [hep-ph/0108055].
- [133] S. Kretzer, Phys. Rev. **D62**, 054001 (2000), [hep-ph/0003177].
- [134] L. Bourhis *et al.*, Eur. Phys. J. **C19**, 89 (2001), [hep-ph/0009101].
- [135] M. Hirai *et al.*, Phys. Rev. **D75**, 094009 (2007), [hep-ph/0702250].
- [136] C. A. Aidala *et al.*, Phys. Rev. **D83**, 034002 (2011), [arXiv:1009.6145].
- [137] D. de Florian *et al.*, Phys. Rev. **D95**, 9, 094019 (2017), [arXiv:1702.06353].
- [138] D. de Florian, R. Sassot and M. Stratmann, Phys. Rev. **D75**, 114010 (2007), [hep-ph/0703242].
- [139] D. P. Anderle, F. Ringer and M. Stratmann, Phys. Rev. **D92**, 11, 114017 (2015), [arXiv:1510.05845].
- [140] E. Leader, A. V. Sidorov and D. B. Stamenov, Phys. Rev. **D93**, 7, 074026 (2016), [arXiv:1506.06381].
- [141] V. Bertone *et al.* (NNPDF), Eur. Phys. J. **C78**, 8, 651 (2018), [arXiv:1807.03310].
- [142] R. Barate *et al.* (ALEPH), Eur. Phys. J. **C17**, 1 (2000); R. Akers *et al.* (OPAL), Z. Phys. **C68**, 179 (1995); G. Abbiendi *et al.* (OPAL), Eur. Phys. J. **C11**, 217 (1999), [hep-ex/9903027].
- [143] K. Abe *et al.* (SLD), Phys. Rev. **D59**, 052001 (1999), [hep-ex/9805029].
- [144] D. Buskulic *et al.* (ALEPH), Z. Phys. **C66**, 355 (1995); H. Albrecht *et al.* (ARGUS), Z. Phys. **C44**, 547 (1989); R. Akers *et al.* (OPAL), Z. Phys. **C63**, 181 (1994).
- [145] M. R. Adams *et al.* (E665), Z. Phys. **C61**, 539 (1994).
- [146] M. Arneodo *et al.* (European Muon), Z. Phys. **C34**, 283 (1987).
- [147] S. Aid *et al.* (H1), Nucl. Phys. **B480**, 3 (1996), [hep-ex/9607010].
- [148] J. J. Aubert *et al.* (European Muon), Z. Phys. **C18**, 189 (1983).
- [149] A. Airapetian *et al.* (HERMES), Eur. Phys. J. **C21**, 599 (2001), [hep-ex/0104004].
- [150] T. P. McPharlin *et al.*, Phys. Lett. **90B**, 479 (1980).
- [151] S. S. Adler *et al.* (PHENIX), Phys. Rev. Lett. **91**, 241803 (2003), [hep-ex/0304038].
- [152] B. Abelev *et al.* (ALICE), Phys. Lett. **B717**, 162 (2012), [arXiv:1205.5724].
- [153] M. Bonesini *et al.* (WA70), Z. Phys. **C38**, 371 (1988).
- [154] T. Akeson *et al.* (Axial Field Spectrometer), Sov. J. Nucl. Phys. **51**, 836 (1990), [Yad. Fiz.51,1314(1990)].
- [155] C. Kourkoumelis *et al.*, Z. Phys. **C5**, 95 (1980).
- [156] L. Apanasevich *et al.* (Fermilab E706), Phys. Rev. **D68**, 052001 (2003), [hep-ex/0204031].
- [157] F. Abe *et al.* (CDF), Phys. Rev. Lett. **61**, 1819 (1988).
- [158] M. Banner *et al.* (UA2), Phys. Lett. **115B**, 59 (1982).
- [159] M. Procura and I. W. Stewart, Phys. Rev. **D81**, 074009 (2010), [Erratum: Phys. Rev.D83,039902(2011)], [arXiv:0911.4980].
- [160] A. Jain, M. Procura and W. J. Waalewijn, JHEP **05**, 035 (2011), [arXiv:1101.4953].
- [161] M. Procura and W. J. Waalewijn, Phys. Rev. **D85**, 114041 (2012), [arXiv:1111.6605].
- [162] F. Arleo *et al.*, JHEP **04**, 147 (2014), [arXiv:1311.7356].
- [163] M. Ritzmann and W. J. Waalewijn, Phys. Rev. **D90**, 5, 054029 (2014), [arXiv:1407.3272].
- [164] T. Kaufmann, A. Mukherjee and W. Vogelsang, Phys. Rev. **D92**, 5, 054015 (2015), [arXiv:1506.01415].
- [165] Y.-T. Chien *et al.*, JHEP **05**, 125 (2016), [arXiv:1512.06851].
- [166] F. Abe *et al.* (CDF), Phys. Rev. Lett. **65**, 968 (1990).
- [167] T. A. collaboration (ATLAS) (2015).
- [168] S. Chatrchyan *et al.* (CMS), JHEP **10**, 087 (2012), [arXiv:1205.5872].
- [169] X. Lu (ALICE), Nucl. Phys. **A931**, 428 (2014), [arXiv:1407.8385].
- [170] C. Bianchin (ALICE), J. Phys. Conf. Ser. **612**, 1, 012020 (2015).
- [171] F. Krizek (ALICE), J. Phys. Conf. Ser. **668**, 1, 012018 (2016), [arXiv:1509.02024].
- [172] M. Aaboud *et al.* (ATLAS), Nucl. Phys. **A978**, 65 (2018), [arXiv:1706.02859].
- [173] L. Adamczyk *et al.* (STAR), Phys. Rev. **D97**, 3, 032004 (2018), [arXiv:1708.07080].
- [174] D. P. Anderle *et al.*, Phys. Rev. **D96**, 3, 034028 (2017), [arXiv:1706.09857].
- [175] N. Sato *et al.* (JAM) (2019), [arXiv:1905.03788].
- [176] M. Epele *et al.*, Phys. Rev. **D86**, 074028 (2012), [arXiv:1209.3240].
- [177] E. Witten, Nucl. Phys. **210**, 189 (1977).
- [178] L. Bourhis, M. Fontannaz and J. P. Guillet, Eur. Phys. J. **C2**, 529 (1998), [hep-ph/9704447].
- [179] M. Gluck, E. Reya and A. Vogt, Phys. Rev. **D48**, 116 (1993), [Erratum: Phys. Rev.D51,1427(1995)]; Erratum *ibid.* **D51**, 1427 (1995).
- [180] G. Abbiendi *et al.* (OPAL), Eur. Phys. J. **C27**, 467 (2003), [hep-ex/0209048].
- [181] G. Bocquet *et al.*, Phys. Lett. **B366**, 434 (1996).
- [182] T. Kaufmann, A. Mukherjee and W. Vogelsang, Phys. Rev. **D93**, 11, 114021 (2016), [arXiv:1604.07175].
- [183] P. Abreu *et al.* (DELPHI), Eur. Phys. J. **C13**, 573 (2000).
- [184] B. A. Kniehl, G. Kramer and B. Potter, Phys. Rev. Lett. **85**, 5288 (2000), [hep-ph/0003297].
- [185] M. Arneodo *et al.* (European Muon), Z. Phys. **C33**, 167 (1986).
- [186] A. Airapetian *et al.* (HERMES), Phys. Rev. **D87**, 074029 (2013), [arXiv:1212.5407].
- [187] C. Adolph *et al.* (COMPASS), Phys. Lett. **B764**, 1 (2017), [arXiv:1604.02695].
- [188] F. D. Aaron *et al.* (H1), Phys. Lett. **B673**, 119 (2009), [arXiv:0901.0477].
- [189] M. Derrick *et al.* (ZEUS), Z. Phys. **C68**, 29 (1995), [hep-ex/9505011].
- [190] S. Chekanov *et al.* (ZEUS), Phys. Lett. **B553**, 141 (2003), [hep-ex/0211025].
- [191] S. Chekanov *et al.* (ZEUS), Nucl. Phys. **B786**, 181 (2007), [arXiv:0705.3770].
- [192] F. D. Aaron *et al.* (H1), Eur. Phys. J. **C61**, 185 (2009), [arXiv:0810.4036].
- [193] A. Aktas *et al.* (H1), Eur. Phys. J. **C36**, 413 (2004), [hep-ex/0403056].
- [194] P. Dixon, D. Kant and G. Thompson, J. Phys. **G25**, 1453 (1999).
- [195] C. Adloff *et al.* (H1), Phys. Lett. **B462**, 440 (1999), [hep-ex/9907030].

- [196] D. Graudenz, Fortsch. Phys. **45**, 629 (1997), [hep-ph/9701334].
- [197] P. M. Nadolsky, D. R. Stump and C. P. Yuan, Phys. Rev. **D61**, 014003 (2000), [Erratum: Phys. Rev. D64,059903(2001)], [hep-ph/9906280].
- [198] D. de Florian *et al.*, Phys. Rev. **D95**, 0334027 (2017).
- [199] T. Aaltonen *et al.* (CDF), Phys. Rev. **D79**, 112005 (2009), [Erratum: Phys. Rev. D82,119903(2010)], [arXiv:0904.1098].
- [200] G. Aad *et al.* (ATLAS), New J. Phys. **13**, 053033 (2011), [arXiv:1012.5104].
- [201] B. I. Abelev *et al.* (STAR), Phys. Rev. **C75**, 064901 (2007), [arXiv:nucl-ex/0607033].
- [202] K. Aamodt *et al.* (ALICE), Eur. Phys. J. **C71**, 1655 (2011), [arXiv:1101.4110].
- [203] B. B. Abelev *et al.* (ALICE), Phys. Lett. **B736**, 196 (2014), [arXiv:1401.1250].
- [204] J. Adam *et al.* (ALICE), Eur. Phys. J. **C75**, 5, 226 (2015), [arXiv:1504.00024].
- [205] S. Chatrchyan *et al.* (CMS), Eur. Phys. J. **C72**, 2164 (2012), [arXiv:1207.4724].
- [206] A. M. Sirunyan *et al.* (CMS), Phys. Rev. **D96**, 11, 112003 (2017), [arXiv:1706.10194].
- [207] G. J. Alner *et al.* (UA5), Z. Phys. **C32**, 153 (1986).
- [208] B. Abelev *et al.* (ALICE), Eur. Phys. J. **C73**, 6, 2456 (2013), [arXiv:1208.4968].
- [209] G. Antchev *et al.* (TOTEM), EPL **101**, 2, 21004 (2013).
- [210] A. M. Sirunyan *et al.* (CMS), JHEP **07**, 161 (2018), [arXiv:1802.02613].
- [211] F. Abe *et al.* (CDF), Phys. Rev. **D50**, 5550 (1994).
- [212] F. Abe *et al.* (CDF), Phys. Rev. **D50**, 5518 (1994).
- [213] S. S. Adler *et al.* (PHENIX), Phys. Rev. **C74**, 024904 (2006), [arXiv:nucl-ex/0603010].
- [214] S. Albino *et al.*, Phys. Rev. **D75**, 034018 (2007), [hep-ph/0611029].
- [215] I. Borsa, R. Sassot and M. Stratmann, Phys. Rev. **D96**, 9, 094020 (2017), [arXiv:1708.01630].
- [216] B. Andersson *et al.*, Phys. Rept. **97**, 31 (1983).
- [217] T. Sjostrand and M. Bengtsson, Comput. Phys. Commun. **43**, 367 (1987); T. Sjostrand, Comput. Phys. Commun. **82**, 74 (1994).
- [218] P. D. Acton *et al.* (OPAL), Phys. Lett. **B305**, 407 (1993).
- [219] J. Breitweg *et al.* (ZEUS), Eur. Phys. J. **C2**, 77 (1998), [hep-ex/9711018].
- [220] D. DeProspero *et al.* (E632), Phys. Rev. **D50**, 6691 (1994).
- [221] S. Chekanov *et al.* (ZEUS), Eur. Phys. J. **C51**, 1 (2007), [hep-ex/0612023].
- [222] G. Grindhammer *et al.*, in: *Proceedings of the Workshop on Monte Carlo Generators for HERA Physics*, Hamburg, Germany, 1998/1999.
- [223] N. Brook *et al.*, in: *Proceedings of the Workshop for Future HERA Physics at HERA*, Hamburg, Germany, 1996.
- [224] D. Acosta *et al.* (CDF), Phys. Rev. **D72**, 052001 (2005), [hep-ex/0504048].
- [225] G. Arnison *et al.* (UA1), Phys. Lett. **118B**, 167 (1982).
- [226] M. Banner *et al.* (UA2), Phys. Lett. **122B**, 322 (1983).
- [227] M. Banner *et al.* (UA2, Bern-CERN-Copenhagen-Osaka-Pavia-Saclay), Z. Phys. **C27**, 329 (1985).
- [228] A. Adare *et al.* (PHENIX), Phys. Rev. **D76**, 051106 (2007), [arXiv:0704.3599].
- [229] A. Adare *et al.* (PHENIX), Phys. Rev. **D83**, 032001 (2011), [arXiv:1009.6224].
- [230] A. Adare *et al.* (PHENIX), Phys. Rev. **D86**, 092006 (2012), [arXiv:1202.4020].
- [231] A. Adare *et al.* (PHENIX), Phys. Rev. **D88**, 3, 032006 (2013), [arXiv:1209.3283].
- [232] A. Adare *et al.* (PHENIX), Phys. Rev. **D91**, 3, 032001 (2015), [arXiv:1409.1907].
- [233] A. Adare *et al.* (PHENIX), Phys. Rev. **D90**, 7, 072008 (2014), [arXiv:1406.3541].
- [234] A. Adare *et al.* (PHENIX), Phys. Rev. **D93**, 1, 011501 (2016), [arXiv:1510.02317].
- [235] I. Arsene *et al.* (BRAHMS), Phys. Rev. Lett. **98**, 252001 (2007), [hep-ex/0701041].
- [236] J. Adams *et al.* (STAR), Phys. Rev. Lett. **97**, 152302 (2006), [arXiv:nucl-ex/0602011].
- [237] J. Adams *et al.* (STAR), Phys. Lett. **B637**, 161 (2006), [arXiv:nucl-ex/0601033].
- [238] B. I. Abelev *et al.* (STAR), Phys. Rev. **D80**, 111108 (2009), [arXiv:0911.2773].
- [239] G. Agakishiev *et al.* (STAR), Phys. Rev. Lett. **108**, 072302 (2012), [arXiv:1110.0579].
- [240] L. Adamczyk *et al.* (STAR), Phys. Rev. **D89**, 1, 012001 (2014), [arXiv:1309.1800].
- [241] B. B. Abelev *et al.* (ALICE), Eur. Phys. J. **C73**, 12, 2662 (2013), [arXiv:1307.1093].
- [242] L. Apanasevich *et al.* (Fermilab E706), Phys. Rev. Lett. **81**, 2642 (1998), [hep-ex/9711017].
- [243] G. Balocchi *et al.* (UA6), Phys. Lett. **B436**, 222 (1998).
- [244] K. Aamodt *et al.* (ALICE), Eur. Phys. J. **C71**, 1594 (2011), [arXiv:1012.3257].
- [245] R. Aaij *et al.* (LHCb), Phys. Lett. **B703**, 267 (2011), [arXiv:1107.3935].
- [246] G. Aad *et al.* (ATLAS), Phys. Lett. **B758**, 67 (2016), [arXiv:1602.01633].
- [247] F. Aversa *et al.*, Nucl. Phys. **B327**, 105 (1989); D. de Florian, Phys. Rev. **D67**, 054004 (2003), [hep-ph/0210442]; B. Jager *et al.*, Phys. Rev. **D67**, 054005 (2003), [hep-ph/0211007].
- [248] U. Baur *et al.*, in "QCD and weak boson physics in Run II. Proceedings, Batavia, USA, March 4-6, June 3-4, November 4-6, 1999," 115-164 (2000), [115(2000)], [hep-ph/0005226], URL <http://lss.fnal.gov/archive/preprint/fermilab-conf-00-411-ae.shtml>.
- [249] P. Aurenche *et al.*, Eur. Phys. J. **C13**, 347 (2000), [hep-ph/9910252].
- [250] L. Apanasevich *et al.*, Phys. Rev. **D59**, 074007 (1999), [hep-ph/9808467].
- [251] U. D'Alesio and F. Murgia, Phys. Rev. **D70**, 074009 (2004), [hep-ph/0408092].
- [252] D. de Florian and W. Vogelsang, Phys. Rev. **D71**, 114004 (2005), [hep-ph/0501258].
- [253] P. Hinderer *et al.*, Phys. Rev. **D99**, 5, 054019 (2019), [arXiv:1812.00915].
- [254] D. d'Enterria *et al.*, Nucl. Phys. **B883**, 615 (2014), [arXiv:1311.1415].
- [255] G. Wilk and Z. Wlodarczyk, Eur. Phys. J. **A40**, 299 (2009), [arXiv:0810.2939].
- [256] C. Tsallis, J. Statist. Phys. **52**, 479 (1988).
- [257] C. Tsallis, Braz. J. Phys. **29**, 1 (1999).
- [258] C. Tsallis, Eur. Phys. J. **A40**, 257 (2009), [arXiv:0812.4370].
- [259] M. D. Azmi and J. Cleymans, J. Phys. **G41**, 065001 (2014), [arXiv:1401.4835].
- [260] G. Wilk and Z. Wlodarczyk, Phys. Rev. Lett. **84**, 2770 (2000), [hep-ph/9908459].
- [261] T. Bhattacharyya *et al.*, J. Phys. **G45**, 5, 055001 (2018), [arXiv:1709.07376].

- [262] S. Grigoryan, Phys. Rev. **D95**, 5, 056021 (2017), [arXiv:1702.04110].
- [263] T. Wibig, Int. J. Mod. Phys. **A29**, 1450021 (2014).
- [264] K. Saraswat, P. Shukla and V. Singh, J. Phys. Comm. **2**, 3, 035003 (2018), [arXiv:1706.04860].
- [265] K. Urmossy, G. G. Barnafoldi and T. S. Biro, Phys. Lett. **B701**, 111 (2011), [arXiv:1101.3023].
- [266] A. S. Parvan, O. V. Teryaev and J. Cleymans, Eur. Phys. J. **A53**, 5, 102 (2017), [arXiv:1607.01956].
- [267] K. Adcox *et al.* (PHENIX), Phys. Rev. Lett. **88**, 022301 (2002), [arXiv:nucl-ex/0109003]; C. Adler *et al.* (STAR), Phys. Rev. Lett. **90**, 082302 (2003), [arXiv:nucl-ex/0210033].
- [268] V.A. Khoze *et al.*, *Proceedings, Conference on High-Energy Physics, Tbilisi 1976*; J. D. Bjorken, Phys. Rev. **D17**, 171 (1978).
- [269] M. Artuso *et al.* (CLEO), Phys. Rev. **D70**, 112001 (2004), [hep-ex/0402040].
- [270] R. Seuster *et al.* (Belle), Phys. Rev. **D73**, 032002 (2006), [hep-ex/0506068].
- [271] A. Heister *et al.* (ALEPH), Phys. Lett. **B512**, 30 (2001), [hep-ex/0106051]; J. Abdallah *et al.* (DELPHI), Eur. Phys. J. **C71**, 1557 (2011), [arXiv:1102.4748]; G. Abbiendi *et al.* (OPAL), Eur. Phys. J. **C29**, 463 (2003), [hep-ex/0210031]; K. Abe *et al.* (SLD), Phys. Rev. **D65**, 092006 (2002), [Erratum: Phys. Rev.D66,079905(2002)], [hep-ex/0202031].
- [272] B. Mele and P. Nason, Phys. Lett. **B245**, 635 (1990); B. Mele and P. Nason, Nucl. Phys. **B361**, 626 (1991), [Erratum: Nucl. Phys.B921,841(2017)].
- [273] M. Cacciari and S. Catani, Nucl. Phys. **B617**, 253 (2001), [hep-ph/0107138].
- [274] P. Nason and C. Oleari, Phys. Lett. **B418**, 199 (1998), [hep-ph/9709358]; P. Nason and C. Oleari, Phys. Lett. **B447**, 327 (1999), [hep-ph/9811206]; P. Nason and C. Oleari, Nucl. Phys. **B565**, 245 (2000), [hep-ph/9903541].
- [275] K. Melnikov and A. Mitov, Phys. Rev. **D70**, 034027 (2004), [hep-ph/0404143].
- [276] C. Peterson *et al.*, Phys. Rev. **D27**, 105 (1983).
- [277] V. G. Kartvelishvili, A. K. Likhoded and V. A. Petrov, Phys. Lett. **78B**, 615 (1978).
- [278] P. D. B. Collins and T. P. Spiller, J. Phys. **G11**, 1289 (1985).
- [279] G. Colangelo and P. Nason, Phys. Lett. **B285**, 167 (1992).
- [280] M. G. Bowler, Z. Phys. **C11**, 169 (1981).
- [281] E. Braaten *et al.*, Phys. Rev. **D51**, 4819 (1995), [hep-ph/9409316].
- [282] R. Akers *et al.* (OPAL), Z. Phys. **C67**, 27 (1995).
- [283] H. Albrecht *et al.* (ARGUS), Z. Phys. **C52**, 353 (1991).
- [284] D. Buskulic *et al.* (ALEPH), Phys. Lett. **B357**, 699 (1995).
- [285] J. Chrin, Z. Phys. **C36**, 163 (1987).
- [286] R. L. Jaffe and L. Randall, Nucl. Phys. **B412**, 79 (1994), [hep-ph/9306201].
- [287] M. Cacciari and E. Gardi, Nucl. Phys. **B664**, 299 (2003), [hep-ph/0301047].
- [288] L. Randall and N. Rius, Nucl. Phys. **B441**, 167 (1995), [hep-ph/9405217].
- [289] J. C. Collins, Phys. Rev. **D58**, 094002 (1998), [hep-ph/9806259].
- [290] B. A. Kniehl *et al.*, Eur. Phys. J. **C41**, 199 (2005), [hep-ph/0502194].
- [291] S. Ahmed *et al.* (CLEO), Phys. Rev. **D62**, 112003 (2000), [hep-ex/0008015].
- [292] B. Aubert *et al.* (BaBar), Phys. Rev. **D65**, 091104 (2002), [hep-ex/0201041].
- [293] D. Bortoletto *et al.* (CLEO), Phys. Rev. **D37**, 1719 (1988), [Erratum: Phys. Rev.D39,1471(1989)].
- [294] H. Albrecht *et al.* (ARGUS), Z. Phys. **C54**, 1 (1992).
- [295] G. Alexander *et al.* (OPAL), Z. Phys. **C69**, 543 (1996).
- [296] A. Heister *et al.* (ALEPH), Phys. Lett. **B561**, 213 (2003), [hep-ex/0302003].
- [297] F. D. Aaron *et al.* (H1), Eur. Phys. J. **C65**, 89 (2010), [arXiv:0907.2643].
- [298] S. Chekanov *et al.* (ZEUS), JHEP **07**, 074 (2007), [arXiv:0704.3562]; ZEUS Collab: H. Abramowicz *et al.*, JHEP, 1309 (2013); A. Aktas *et al.* (H1), Eur. Phys. J. **C51**, 271 (2007), [hep-ex/0701023]; F. D. Aaron *et al.* (H1), Eur. Phys. J. **C59**, 589 (2009), [arXiv:0808.1003].
- [299] B. Adeva *et al.* (L3), Phys. Lett. **B261**, 177 (1991).
- [300] O. Biebel, P. Nason and B. R. Webber (2001), [hep-ph/0109282].
- [301] H. Evans (ALICE, ATLAS, CMS, LHCb), in “Proceedings, 14th International Conference on Hadron spectroscopy (Hadron 2011): Munich, Germany, June 13-17, 2011,” (2011), [arXiv:1110.5294]; E. Aguilo, in “Proceedings, 47th Rencontres de Moriond on QCD and High Energy Interactions: La Thuile, France, March 10-17, 2012,” 115–120 (2012), [arXiv:1205.5678]; F. Simonetto, Journal of Physics: Conference Series **347**, 012014 (2012).
- [302] V. Khachatryan *et al.* (CMS), JHEP **03**, 136 (2011), [arXiv:1102.3194]; G. Aad *et al.* (ATLAS), Eur. Phys. J. **C71**, 1846 (2011), [arXiv:1109.6833]; S. Chatrchyan *et al.* (CMS), JHEP **04**, 084 (2012), [arXiv:1202.4617]; G. Aad *et al.* (ATLAS), Eur. Phys. J. **C73**, 2, 2301 (2013), [arXiv:1210.0441].
- [303] H. Jung *et al.*, Phys. Rev. **D85**, 034035 (2012), [arXiv:1111.1942].
- [304] D. Acosta *et al.* (CDF), Phys. Rev. Lett. **91**, 241804 (2003), [hep-ex/0307080]; D. Acosta *et al.* (CDF), Phys. Rev. **D71**, 032001 (2005), [hep-ex/0412071].
- [305] M. Cacciari and P. Nason, JHEP **09**, 006 (2003), [hep-ph/0306212]; M. Cacciari *et al.*, JHEP **07**, 033 (2004), [hep-ph/0312132]; B. A. Kniehl *et al.*, Phys. Rev. Lett. **96**, 012001 (2006), [hep-ph/0508129].
- [306] H. Abramowicz *et al.* (ZEUS), Eur. Phys. J. **C71**, 1573 (2011), [arXiv:1101.3692].
- [307] S. Chekanov *et al.* (ZEUS), Phys. Rev. **D78**, 072001 (2008), [arXiv:0805.4390].
- [308] S. Chekanov *et al.* (ZEUS), JHEP **02**, 032 (2009), [arXiv:0811.0894].
- [309] F. D. Aaron *et al.* (H1), Eur. Phys. J. **C72**, 2148 (2012), [arXiv:1206.4346].
- [310] M. L. Mangano and P. Nason, Phys. Lett. **B285**, 160 (1992).
- [311] M. H. Seymour, Nucl. Phys. **B436**, 163 (1995).
- [312] D. J. Miller and M. H. Seymour, Phys. Lett. **B435**, 213 (1998), [hep-ph/9805414].
- [313] R. Barate *et al.* (ALEPH), Phys. Lett. **B434**, 437 (1998).
- [314] P. Abreu *et al.* (DELPHI), Phys. Lett. **B405**, 202 (1997).
- [315] M. Acciarri *et al.* (L3), Phys. Lett. **B476**, 243 (2000), [hep-ex/9911016].
- [316] G. Abbiendi *et al.* (OPAL), Eur. Phys. J. **C13**, 1 (2000), [hep-ex/9908001].
- [317] K. Abe *et al.* (SLD) (1999), [hep-ex/9908028], URL <http://www-public.slac.stanford.edu/sciDoc/docMeta.aspx?slacPubNumber=SLAC-PUB-8157>.
- [318] C. Albajar *et al.* (UA1 Collaboration), Z. Phys. **C 61**, 41 (1993), URL <http://cds.cern.ch/record/253028>.
- [319] R. Aaij *et al.* (LHCb), JHEP **11**, 030 (2017), [arXiv:1708.05994].
- [320] M. Aaboud *et al.* (ATLAS), Phys. Rev. **D99**, 5, 052004 (2019), [arXiv:1812.09283].

- [321] M. Burkardt and R. L. Jaffe, Phys. Rev. Lett. **70**, 2537 (1993), [hep-ph/9302232].
- [322] P. J. Mulders and R. D. Tangerman, Nucl. Phys. **B461**, 197 (1996), [Erratum: Nucl. Phys. **B484**, 538 (1997)], [hep-ph/9510301].
- [323] R. Jakob, Nucl. Phys. **A711**, 35 (2002), [hep-ph/0206271].
- [324] D. de Florian, M. Stratmann and W. Vogelsang, Phys. Rev. Lett. **81**, 530 (1998), [hep-ph/9802432].
- [325] D. Buskulic *et al.* (ALEPH), Phys. Lett. **B374**, 319 (1996).
- [326] K. Ackerstaff *et al.* (OPAL), Eur. Phys. J. **C2**, 49 (1998), [hep-ex/9708027].
- [327] G. Abbiendi *et al.* (OPAL), Phys. Lett. **B444**, 539 (1998), [hep-ex/9808006].
- [328] M. Alekseev *et al.* (COMPASS), Eur. Phys. J. **C64**, 171 (2009), [arXiv:0907.0388].
- [329] A. Airapetian *et al.* (HERMES), Phys. Rev. **D74**, 072004 (2006), [hep-ex/0607004].
- [330] G. Karyan (HERMES), Int. J. Mod. Phys. Conf. Ser. **40**, 1660067 (2016).
- [331] J. Adam *et al.* (STAR), Phys. Rev. **D98**, 11, 112009 (2018), [arXiv:1808.07634].
- [332] R. L. Jaffe, Phys. Rev. **D54**, 11, R6581 (1996), [hep-ph/9605456].
- [333] A. Airapetian *et al.* (HERMES), Phys. Rev. **D76**, 092008 (2007), [arXiv:0704.3133].
- [334] A. Moretti (COMPASS), PoS **SPIN2018**, 138 (2018), [arXiv:1901.01735].
- [335] R. Seidl *et al.* (Belle), Phys. Rev. **D99**, 11, 112006 (2019), [arXiv:1902.01552].
- [336] C. Adolph *et al.* (COMPASS), Eur. Phys. J. **C73**, 8, 2531 (2013), [Erratum: Eur. Phys. J. **C75**, no.2, 94 (2015)], [arXiv:1305.7317].
- [337] A. Signori *et al.*, JHEP **11**, 194 (2013), [arXiv:1309.3507].
- [338] M. Anselmino *et al.*, JHEP **04**, 005 (2014), [arXiv:1312.6261].
- [339] M. G. Echevarria *et al.*, Phys. Rev. **D89**, 074013 (2014), [arXiv:1401.5078].
- [340] M. G. Echevarria, I. Scimemi and A. Vladimirov, Phys. Rev. **D93**, 1, 011502 (2016), [Erratum: Phys. Rev. **D94**, no.9, 099904 (2016)], [arXiv:1509.06392].
- [341] M. G. Echevarria, I. Scimemi and A. Vladimirov, JHEP **09**, 004 (2016), [arXiv:1604.07869].
- [342] A. Bacchetta *et al.*, JHEP **06**, 081 (2017), [Erratum: JHEP **06**, 051 (2019)], [arXiv:1703.10157].
- [343] J. C. Collins, Nucl. Phys. **B396**, 161 (1993), [hep-ph/9208213].
- [344] J. P. Ralston and D. E. Soper, Nucl. Phys. **B152**, 109 (1979).
- [345] H. Avakian *et al.* (CLAS), Phys. Rev. **D69**, 112004 (2004), [hep-ex/0301005].
- [346] A. Airapetian *et al.* (HERMES), Phys. Rev. Lett. **84**, 4047 (2000), [hep-ex/9910062].
- [347] A. Airapetian *et al.* (HERMES), Phys. Rev. **D64**, 097101 (2001), [hep-ex/0104005].
- [348] A. Airapetian *et al.* (HERMES), Phys. Rev. Lett. **94**, 012002 (2005), [hep-ex/0408013].
- [349] A. Airapetian *et al.* (HERMES), Phys. Lett. **B693**, 11 (2010), [arXiv:1006.4221].
- [350] V. Yu. Alexakhin *et al.* (COMPASS), Phys. Rev. Lett. **94**, 202002 (2005), [hep-ex/0503002].
- [351] E. S. Ageev *et al.* (COMPASS), Nucl. Phys. **B765**, 31 (2007), [hep-ex/0610068].
- [352] M. Alekseev *et al.* (COMPASS), Phys. Lett. **B673**, 127 (2009), [arXiv:0802.2160].
- [353] M. G. Alekseev *et al.* (COMPASS), Phys. Lett. **B692**, 240 (2010), [arXiv:1005.5609].
- [354] M. G. Alekseev *et al.* (COMPASS), Eur. Phys. J. **C70**, 39 (2010), [arXiv:1007.1562].
- [355] C. Adolph *et al.* (COMPASS), Phys. Lett. **B717**, 376 (2012), [arXiv:1205.5121].
- [356] C. Adolph *et al.* (COMPASS), Phys. Lett. **B744**, 250 (2015), [arXiv:1408.4405].
- [357] K. Abe *et al.* (Belle), Phys. Rev. Lett. **96**, 232002 (2006), [hep-ex/0507063].
- [358] R. Seidl *et al.* (Belle), Phys. Rev. **D78**, 032011 (2008), [Erratum: Phys. Rev. **D86**, 039905 (2012)], [arXiv:0805.2975].
- [359] J. P. Lees *et al.* (BaBar), Phys. Rev. **D90**, 5, 052003 (2014), [arXiv:1309.5278].
- [360] J. P. Lees *et al.* (BaBar), Phys. Rev. **D92**, 11, 111101 (2015), [arXiv:1506.05864].
- [361] M. Ablikim *et al.* (BESIII), Phys. Rev. Lett. **116**, 4, 042001 (2016), [arXiv:1507.06824].
- [362] M. Anselmino *et al.*, Phys. Rev. **D92**, 11, 114023 (2015), [arXiv:1510.05389].
- [363] Z.-B. Kang *et al.*, Phys. Rev. **D93**, 1, 014009 (2016), [arXiv:1505.05589].
- [364] F. Yuan, Phys. Rev. Lett. **100**, 032003 (2008), [arXiv:0709.3272].
- [365] Z.-B. Kang *et al.*, JHEP **11**, 068 (2017), [arXiv:1705.08443].
- [366] K. Konishi, A. Ukawa and G. Veneziano, Phys. Lett. **78B**, 243 (1978).
- [367] I. Vendramin, Nuovo Cim. **A66**, 339 (1981).
- [368] J. C. Collins, S. F. Heppelmann and G. A. Ladinsky, Nucl. Phys. **B420**, 565 (1994), [hep-ph/9305309].
- [369] R. L. Jaffe, X.-m. Jin and J. Tang, Phys. Rev. Lett. **80**, 1166 (1998), [hep-ph/9709322].
- [370] R. L. Jaffe, X.-m. Jin and J.-a. Tang, Phys. Rev. **D57**, 5920 (1998), [hep-ph/9710561].
- [371] A. Bianconi *et al.*, Phys. Rev. **D62**, 034008 (2000), [hep-ph/9907475].
- [372] M. Radici, R. Jakob and A. Bianconi, Phys. Rev. **D65**, 074031 (2002), [hep-ph/0110252].
- [373] D. de Florian and L. Vanni, Phys. Lett. **B578**, 139 (2004), [hep-ph/0310196].
- [374] A. Bacchetta and M. Radici, Phys. Rev. **D67**, 094002 (2003), [hep-ph/0212300].
- [375] A. Vossen *et al.* (Belle), Phys. Rev. Lett. **107**, 072004 (2011), [arXiv:1104.2425].
- [376] A. Courtoy *et al.*, Phys. Rev. **D85**, 114023 (2012), [arXiv:1202.0323].
- [377] M. Radici *et al.*, JHEP **05**, 123 (2015), [arXiv:1503.03495].
- [378] A. Airapetian *et al.* (HERMES), JHEP **06**, 017 (2008), [arXiv:0803.2367].
- [379] C. Adolph *et al.* (COMPASS), Phys. Lett. **B713**, 10 (2012), [arXiv:1202.6150].
- [380] C. Adolph *et al.* (COMPASS), Phys. Lett. **B736**, 124 (2014), [arXiv:1401.7873].
- [381] L. Adamczyk *et al.* (STAR), Phys. Rev. Lett. **115**, 242501 (2015), [arXiv:1504.00415].
- [382] A. Bacchetta, A. Courtoy and M. Radici, Phys. Rev. Lett. **107**, 012001 (2011), [arXiv:1104.3855].
- [383] A. Bacchetta, A. Courtoy and M. Radici, JHEP **03**, 119 (2013), [arXiv:1212.3568].
- [384] M. Radici and A. Bacchetta, Phys. Rev. Lett. **120**, 19, 192001 (2018), [arXiv:1802.05212].

## 20. High Energy Soft QCD and Diffraction

Written February 2020 by V.A. Khoze (Durham U.; Petersburg Nuclear Phys. Inst.), M. Ryskin (Petersburg Nuclear Phys. Inst.) and M. Taševský (Prague, Inst. Phys.).

### 20.1 Introduction

Despite the enormous successes of Quantum Chromodynamics (QCD) (see Section 9 in [1] and [2]) there remain a number of deep questions to be answered in the domain of strong interaction physics. These concern first of all small momentum transfer processes which are generically called soft interactions.

One of the most challenging problems is the high-energy behaviour of hadronic scattering processes. At high collision energies,  $\sqrt{s}$ , soft interactions play a dominant role. Unfortunately, soft interactions cannot be described in terms of perturbative QCD. These are non-perturbative phenomena related to confinement which are generally considered in the context of the analytic  $S$ -matrix, based on *first principles*, such as analyticity, crossing symmetry and unitarity of partial waves, see e.g. [3, 4]. At high energies the most self-consistent way to perform the calculations and to describe the data is the Regge approach (see for example [5–7]), which will be considered below. As discussed in Section 20.5, this formalism could be smoothly matched with perturbative QCD calculations at larger transverse momenta. Therefore, here we will concentrate on the properties of high energy soft interactions that can be expected from the extension of the perturbative QCD domain.

The main aim of this review is to present the well-established theoretical framework, based on Regge theory and QCD, used for describing high-energy collisions. A limited number of some new experimental results, mainly from the LHC, are shown in order to demonstrate that the gross features of the data are in agreement with this approach. We are not focussing on any particular phenomenological or Monte Carlo model, which are covered in the dedicated reviews and books, see e.g. Section 41 in [1], [2, 8–14] and Chapter 2 in [15].

Typically, in multiparticle production, the secondaries<sup>1</sup> fill the whole available rapidity interval.<sup>2</sup> However, there exists an important class of events in which a large interval of rapidity (typically at least 4 units) is devoid of any hadronic activity. Such an interval is called a Large Rapidity Gap (LRG). The most frequent case with a LRG is elastic scattering. There are also events in which one of the incoming protons (or both) is transformed (dissociates) into a set of two or more final state particles with the mass  $M \ll \sqrt{s}$  and proton quantum number. All these events have properties similar to those of the well-known from optics pattern of diffraction of a beam of light on an obstacle. By analogy, in high-energy physics, the corresponding processes are usually called diffractive. The classic example is the elastic scattering of hadrons on nuclei (see e.g. [16]), which manifests an angular distribution with a series of minima and maxima, analogous to the diffraction of light on a black disk. At LHC energies diffractive processes constitute up to 40% of the total ( $pp$ ) cross section,  $\sigma_{\text{tot}}$ . Therefore, we will pay special attention to the description of the elastic scattering amplitude and proton diffractive dissociation. Diffraction dissociation can be considered as a quantum mechanical process caused by the fact that different components of the incoming hadron wave function have different probabilities for interaction with a target [17]. This feature allows us to probe the transverse size of the interaction region.

Note that besides being of a fundamental interest in their own right for understanding the high energy behaviour of the QCD amplitude, there are several reasons why it is important to study soft and diffractive processes. Firstly, soft interactions unavoidably give an underlying component to rare ‘hard’ events, from which we hope to extract signals for New Physics. Secondly, we should be able to estimate the probability that rapidity gaps, which oc-

cur in ‘hard’ diffractive events, survive rescattering effects, that is, survive the population of the gaps by the secondary particles from the underlying event. Thirdly, an understanding of diffractive processes is very important for evaluation of pile-up backgrounds in high-luminosity  $pp$  collisions, which have a direct impact on various experimental measurements. Pile-up corresponds to soft independent interactions in the same bunch crossing whose number rises with increasing instantaneous luminosity. And, finally, studies of diffractive processes should help in the understanding of the structure of high-energy cosmic ray cascades, which requires a very detailed knowledge of the spectra of particles carrying a large fraction  $x$  of the incoming momentum in proton-air and nucleus-air interactions, see for instance [18].

Experimentally, diffractive processes are selected using two distinct features:

1. large regions (typically at least  $\Delta\eta > 4$ ) in the detector are devoid of hadronic activity (LRG) and/or
2. one or both incoming particles stay intact after collision and are registered by the dedicated forward detectors placed a few hundred meters from the interaction point. The momentum loss of the initial particle,  $\xi = 1 - x$ , is typically smaller than 0.15.

Thus, in the case of proton-proton collisions, diffractive events correspond to elastic  $pp \rightarrow pp$  scattering and to  $pp \rightarrow p + X$  (Single Dissociation, SD) and  $pp \rightarrow X + Y$  (Double Dissociation, DD) processes, where the  $+$  sign denotes a large rapidity gap. Note that strictly speaking in high energy physics it is impossible to define (and select) rigorously purely diffractive events. We can always have some admixture of events of different origin. As a rule we call ‘diffractive’ the events with sufficiently large gap (with say  $\Delta y > 4$ , see above) and the vacuum quantum numbers transferred across the gap. Typically at the LHC the integrated cross sections of diffractive dissociation,  $\sigma_{\text{SD}}$ ,  $\sigma_{\text{DD}}$ , are of the order of 5–10 mb depending on the gap size. Schematic diagrams of all discussed processes are shown in Fig. 20.1.

### 20.2 Regge pole approach

In pre-QCD times, in order to describe the behaviour of scattering amplitudes at high energy,  $\sqrt{s}$ , and small momentum-transfer squared,  $-t$ , Regge theory was developed and successfully applied in a wide range of energies. The Regge approach [5–7] is based on the singularities of amplitudes in the complex angular momentum,  $j$ , plane.

For instance, the measured  $\pi^- p \rightarrow \pi^0 n$  amplitude behaves as

$$T_{\pi p}(s, t) \propto s^{\alpha_\rho(t)}, \quad (20.1)$$

where the process is described by the exchange of the  $\rho$ -trajectory,  $j = \alpha_\rho(t) \simeq 0.5 + 0.9t$  (with  $t = (p_{\pi^-} - p_{\pi^0})^2$  in  $\text{GeV}^2$ ). This trajectory passes through the spin-1  $\rho$ -meson resonance in the ‘crossed’  $t$ -channel  $\pi^- \pi^0 \rightarrow \bar{p}n$ ; that is,  $\alpha_\rho(t = m_\rho^2) = 1$ . The corresponding cross section decreases with increasing  $s$ .

On the other hand, high-energy total and elastic  $pp$  cross sections are observed to grow slowly with energy (see e.g. Section 52 in [1]) and in terms of Regge theory are dominated by the exchange of a trajectory with vacuum quantum numbers,  $\sigma_{\text{tot}} \propto s^{j-1}$ . The simplest possibility is to assume that the rightmost singularity in the  $j$ -plane, which drives the high-energy behaviour of the cross section, is the leading (at  $t \leq 0$ ) Regge pole at  $j = \alpha(t)$ . Then the  $pp$  elastic amplitude reads

$$T_{\text{el}}(s, t) \propto s^{\alpha_P(t)}. \quad (20.2)$$

The total cross section can then be conveniently expressed using the so called optical theorem which states that

$$s\sigma_{\text{tot}} = \text{Im}T_{\text{el}}(s, t = 0), \quad (20.3)$$

as illustrated in the upper part of Fig. 20.2, and thus

$$\sigma_{\text{tot}} \propto s^{\alpha_P(0)-1}. \quad (20.4)$$

<sup>1</sup>Here and in what follows, we call secondaries the new particles produced in the course of the interaction.

<sup>2</sup>For definition of particle rapidity (pseudorapidity), see Section 48.5.2 in [1];  $y = \frac{1}{2} \ln \frac{E+p_z}{E-p_z}$  ( $\eta = -\ln(\tan(\theta/2))$ ); the correct variable is the rapidity  $y$ , however, experimentally it is simpler to use the pseudorapidity  $\eta$  which does not require identifying the particles, setting  $m = 0$ . For  $p_T \gg m$ ,  $\eta \simeq y$ .



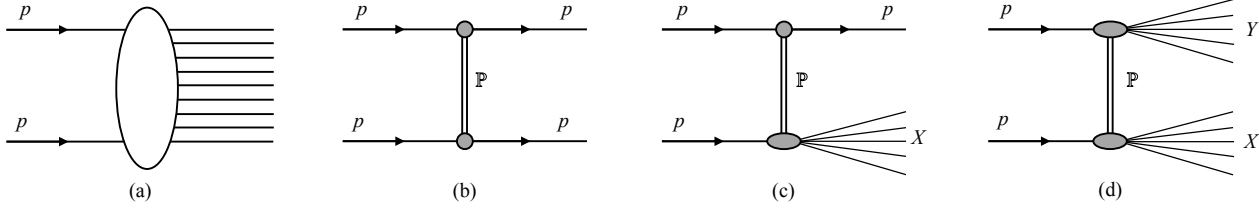


Figure 20.1: Schematic diagrams of soft  $pp$  processes. (a) non-diffractive processes, (b) elastic scattering, (c) single dissociation and (d) double dissociation. The double line corresponds to the Pomeron exchange.

$$\sigma_{\text{tot}} = \sum_X \left| \begin{array}{c} \text{Diagram: } p \text{ and } \bar{p} \text{ meeting at a circle with } X \text{ lines} \end{array} \right|^2 = \text{Im} \begin{array}{c} \text{Diagram: } p \text{ and } \bar{p} \text{ meeting at a circle with } X \text{ lines} \end{array} = \begin{array}{c} \text{Diagram: } p \text{ and } \bar{p} \text{ meeting at a circle with } X \text{ lines} \end{array} \alpha_{\mathbb{P}}(0) \sim g_N^2 \left( \frac{s}{s_0} \right)^{\alpha_{\mathbb{P}}(0)-1}$$

$$M^2 \frac{d\sigma}{dM^2} = \left| \begin{array}{c} \text{Diagram: } p \text{ and } \bar{p} \text{ meeting at a circle with } X \text{ lines, } t \text{ channel} \end{array} \right|^2 = \begin{array}{c} \text{Diagram: } p \text{ and } \bar{p} \text{ meeting at a circle with } X \text{ lines, } t \text{ channel} \end{array} = \begin{array}{c} \text{Diagram: } p \text{ and } \bar{p} \text{ meeting at a circle with } X \text{ lines, } t \text{ channel} \end{array} \alpha_{\mathbb{P}}(t) \alpha_{\mathbb{P}}(0)$$

$$\underbrace{\hspace{15em}}_{g_{3P} g_N^3 \left( \frac{M^2}{s_0} \right)^{\alpha_{\mathbb{P}}(0)-1} \left( \frac{s}{M^2} \right)^{2\alpha_{\mathbb{P}}(t)-2}}$$

Figure 20.2: Illustration of the optical theorem for the total cross section and for high-mass diffractive dissociation in the absence of absorptive corrections.

The pole with the largest intercept, originally assumed to be  $\alpha_{\mathbb{P}}(0) = 1$  since high-energy total cross sections were thought to have a constant asymptotic behaviour, is called the *Pomeron*<sup>3</sup>

Prior to the LHC, the energy behaviour of  $pp, p\bar{p}, \pi p, Kp$  cross sections was satisfactorily reproduced by the sum of the Pomeron and secondary Reggeons (the poles at lower values of  $j$ , typically with  $\alpha_{\rho}(0) \simeq 0.5$ , see [22, 23] and Section 51 in [24]). However, above Tevatron energies the secondary Reggeon contributions (which all have intercepts  $\alpha(0) \simeq 0.5$ ) are highly suppressed, which enables us to study the properties of the Pomeron only.

A popular parameterization of the elastic  $pp$ -scattering amplitude by Donnachie-Landshoff (DL) is the Regge form [25]

$$T_{\text{el}}(s, t) = \eta_P \sigma_0 F_1^2(t) s^{\alpha_{\mathbb{P}}(t)}, \quad (20.5)$$

where  $\sigma_0 = 21.7$  mb [26] and  $\eta_P$  is the signature factor

$$\eta_P = \frac{1 + \exp(-i\pi\alpha_{\mathbb{P}}(t))}{\sin(-\pi\alpha_{\mathbb{P}}(t))}, \quad (20.6)$$

$F_1$  is the Dirac electromagnetic form factor of the proton and the *effective* Pomeron trajectory

$$\alpha_{\mathbb{P}}(t) = 1 + \Delta + \alpha' t \simeq 1 + 0.0808 + 0.25t, \quad (20.7)$$

with  $t$  given in  $\text{GeV}^2$ . The intercept  $\alpha_{\mathbb{P}}(0)$  just above 1 reproduces the observed slow growth of the total hadron-hadron cross sections at high energies.

However, this simple parameterization is becoming increasingly deficient at higher energies. This is because due to unitarity we have to take into account not only Regge poles, but also the cuts in the  $j$ -plane [27, 28], which correspond to the multiple exchange of Regge poles in the  $t$ -channel, see for instance [29–31]. A powerful technique to evaluate Reggeon diagrams was developed by Gribov [7, 32] (Reggeon calculus or Reggeon Field Theory (RFT)), which allows us to calculate the multi-Pomeron contributions.

<sup>3</sup>Pomeron pole was named after I. Y. Pomeranchuk. The history of the Pomeron is discussed in [19–21].

## 20.3 Theoretical description of high-energy diffraction

Diffractive processes (see e.g. reviews [33–37]) represent a rich testing ground for the dynamics of soft interactions as well as Monte Carlo models for soft hadron-hadron physics (see for reviews e.g. [8], Section 41 in [1] and Chapter 2 in [15]).

There is no universally agreed definition of diffractive processes. Theoretically, diffraction is the effect caused by the absorption of the incoming plane-wave in some region of impact parameter,  $b$ . After a decomposition of the distorted plane-wave over the outgoing momentum,  $q$ , due to absorption we arrive at some set of plane-waves with non-zero transverse momentum,  $q_t \neq 0$ . Experimentally, we call diffractive the events with large rapidity gaps (LRG) in the distribution of the final state particles. However, this definition is appropriate only for the events with very large gap sizes ( $\Delta\eta > 4 - 5$ ); otherwise gaps can also be caused by fluctuations in the hadronization process [38].

In the case of proton-proton collisions, diffraction corresponds to elastic  $pp \rightarrow pp$  scattering and to the  $pp \rightarrow p + X$  and  $pp \rightarrow X_1 + X_2$  processes where one or both protons are allowed to dissociate into a system  $X$  with the quantum numbers of the proton. The  $p \rightarrow X$  dissociation is caused by the fact that the individual components of the incoming proton wave function interact differently with the target (see Section 20.3.1).

Theoretically, high-energy diffraction may be studied from either the  $s$ -channel or the  $t$ -channel viewpoint.

### 20.3.1 Diffraction from the $s$ -channel viewpoint

Unitarity plays a central role in diffractive processes. To discuss unitarity effects it is convenient to work in terms of impact parameter,  $b$ . The total cross section is closely related to the elastic scattering amplitude and the scattering into inelastic final states via the  $s$ -channel unitarity of the  $S$ -matrix (see Sections 49 and 52 in [1]),  $SS^\dagger = I$ , or

$$\text{disc } T \equiv T - T^\dagger = iT^\dagger T \quad (20.8)$$

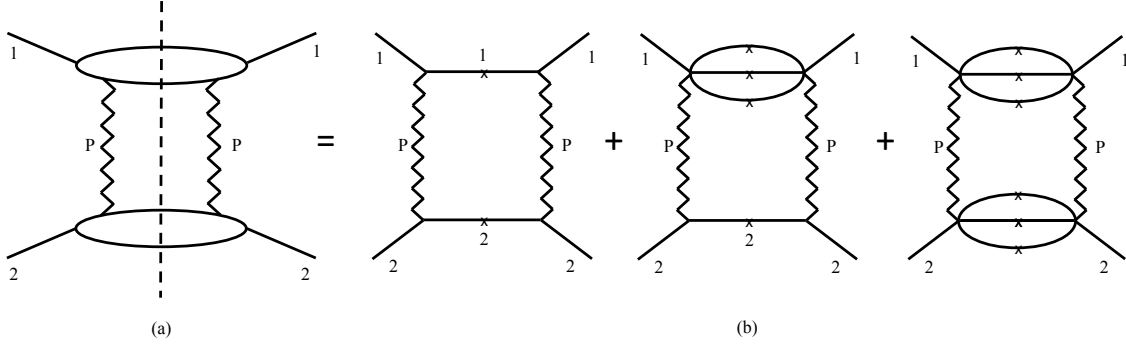


Figure 20.3: Two-Pomeron exchange in the  $t$  channel expressed as a sum over all diffractive intermediate states in the  $s$ -channel. The crosses indicate that the particles are on the mass shell.

with  $S = I + iT$ . If we were to focus, for example, on the unitarity for elastic and quasielastic processes, then *disc*  $T$  would simply denote a cut in  $s$ -channel between incoming and outgoing particles as visualized by crosses in Fig. 20.3.

At high energies, the  $s$ -channel unitarity relation is diagonal in the  $b$  basis such that

$$2\text{Im} T_{\text{el}}(s, b) = |T_{\text{el}}(s, b)|^2 + G_{\text{inel}}(s, b) \quad (20.9)$$

with

$$\sigma_{\text{tot}} = 2 \int d^2b \text{Im} T_{\text{el}}(s, b) \quad (20.10)$$

$$\sigma_{\text{el}} = \int d^2b |T_{\text{el}}(s, b)|^2 \quad (20.11)$$

$$\sigma_{\text{inel}} = \int d^2b [2\text{Im} T_{\text{el}}(s, b) - |T_{\text{el}}(s, b)|^2]. \quad (20.12)$$

The general solution of Eq. (20.9) is

$$T_{\text{el}}(b) = i(1 - e^{-\Omega(b)/2}) \quad (20.13)$$

and

$$G_{\text{inel}}(s, b) = 1 - e^{-\text{Re}\Omega(b)} = 1 - P_{\text{nointer}}(s, b), \quad (20.14)$$

where  $G_{\text{inel}}$  is the sum over all inelastic intermediate states and  $P_{\text{nointer}}$  is a probability to have no inelastic interactions.  $G_{\text{inel}}(s, b)$  describes the  $b$ -profile of inelastic particle collisions. It satisfies the condition  $0 \leq G_{\text{inel}} \leq 1$  and determines how absorptive the interaction region is at a given impact parameter (with  $G_{\text{inel}} = 1$  for full absorption and  $G_{\text{inel}} = 0$  for the complete dominance of elastic scattering). As seen from Eq. (20.14),  $\exp(-\text{Re}\Omega(s, b))$  is the probability that no inelastic interactions occur at impact parameter  $b$ .  $\Omega$  ( $\text{Re}\Omega \geq 0$ ) is called the opacity (optical density) or eikonal. The quantity

$$S^2(b) \equiv e^{-\text{Re}\Omega(b)} = P_{\text{nointer}}(b) \quad (20.15)$$

is the so-called survival factor, which enables us to calculate the probability that the LRG survives soft rescattering.

In terms of the opacity the elastic cross section takes the form

$$\begin{aligned} \frac{d\sigma_{\text{el}}}{dt} &= \frac{1}{16\pi s^2} |T_{\text{el}}(s, t)|^2 = \frac{1}{4\pi} \left| \int d^2b e^{i\vec{q}_t \cdot \vec{b}} (1 - e^{-\Omega(b)/2}) \right|^2 \\ &= \pi \left| \int b db J_0(q_t b) (1 - e^{-\Omega(b)/2}) \right|^2, \end{aligned} \quad (20.16)$$

where  $q_t = \sqrt{|t|}$  and  $J_0$  is the zeroth-order Bessel function.

To describe the elastic scattering at one fixed energy we can always find an appropriate parameterization for the opacity  $\Omega(b)$  and tune the parameters to reproduce the observed  $d\sigma_{\text{el}}/dt$  cross

section. Moreover, we can fix the form of the parameterization, but choose, at each particular energy, the corresponding values of parameters; see, e.g. [39]. Alternatively, we may simply take the Fourier-Bessel transform from the experimental data [33, 40, 41]

$$\text{Im} T_{\text{el}}(b) = \int \frac{q_t dq_t}{4\pi} \sqrt{\frac{d\sigma_{\text{el}}}{dt} \frac{16\pi}{1 + \rho^2}} J_0(q_t b), \quad (20.17)$$

where the square root represents  $\text{Im} T_{\text{el}}(q_t)$ , with  $\rho \equiv \text{Re} T_{\text{el}}/\text{Im} T_{\text{el}}$ . In this way, we first determine  $T_{\text{el}}$  from the data for  $d\sigma_{\text{el}}/dt$ , and then calculate  $\Omega(b)$  using Eq. (20.13), assuming in accordance with data that  $\rho$  is small (or  $\rho(t) = \text{constant}$ ).

At high energies  $\rho^2 \ll 1$ , which is usually well justified except in the diffractive dip region (see Section 20.3.3.1 for discussion of the dip region).

The value of  $\rho$  can be derived via the dispersion relation, see [3]:

$$\frac{1}{s} \text{Re} T_{\text{el}}(s) = \frac{1}{\pi} \int_{-\infty}^{+\infty} \frac{ds'}{s' - s} \sigma_{\text{tot}}(|s'|) = \frac{1}{\pi} \int_0^{\infty} \sigma_{\text{tot}}(s') \frac{2s ds'}{s'^2 - s^2}. \quad (20.18)$$

Since we consider just the charge-parity  $C$ -even amplitude, here for negative  $s'$  we put  $\sigma_{p\bar{p}} = \sigma_{pp}$ . That is, for negative  $s'$ , which corresponds to the interaction with an *antiparticle*, we use the same  $\sigma_{pp}(|s'|)$ . The major contribution comes from  $s' \simeq s$ . Thus, with a good accuracy we can evaluate  $\rho(t=0)$  as

$$\rho \simeq \frac{\pi}{2} \frac{\partial \ln \sigma_{\text{tot}}(s)}{\partial \ln s}. \quad (20.19)$$

### 20.3.2 Diffractive dissociation

The elastic cross section probes the optical density of the proton. The well known example of scattering on a black disk, with  $G_{\text{inel}} = 1$  for  $b < R$ , gives  $\sigma_{\text{el}} = \sigma_{\text{inel}} = \pi R^2$  and  $\sigma_{\text{tot}} = 2\pi R^2$ . In general, the absorption of the initial wave (due to inelastic channels) leads, via  $s$ -channel unitarity, to elastic scattering.

Inelastic diffraction (i.e. proton dissociation) is a consequence of the *internal structure* of hadrons. This can be conveniently described at high energies, where the lifetimes of each particular Fock component of the incoming hadron/proton wave function (the hadronic fluctuations) are large,  $\tau \sim E/m^2$ , and during these time intervals the corresponding Fock states can be considered as ‘frozen’. Each hadronic constituent can undergo a scattering with its own probability and thus destroys coherence of the fluctuations<sup>4</sup>. As a result, the outgoing superposition of states will be different from the incident particle, and will most likely contain multiparticle states, so we will have *inelastic*, as well as elastic scattering.

To calculate diffractive dissociation we can enlarge the set of intermediate states ( $p, N_a^*$ ), from just the single elastic channel, and introduce a multichannel eikonal. However, it is more convenient

<sup>4</sup>At high energies the configurations with different transverse separation,  $r$ , between the quarks (valence partons) can serve as an example of such Fock states. An interaction with the QCD Pomeron does not change the value of  $r$ , while the cross section  $\sigma \propto \alpha_s^2 r^2$  (see Section 20.4.2 and [42–44]).

to follow Good and Walker [45], and to introduce states  $\phi_k$  diagonalising the  $T$  matrix (which e.g. in the proton case describes different  $p \rightarrow N^*$ ,  $N_a^* \rightarrow N_b^*$  transitions). Such eigenstates only undergo elastic scattering. Since there are no off-diagonal transitions,

$$\langle \phi_i | T | \phi_k \rangle = 0 \quad \text{for } i \neq k, \quad (20.20)$$

a state  $k$  cannot diffractively dissociate into a state  $j \neq k$ . Working in terms of the Good-Walker eigenstates  $\phi_i$ , we have a simple one-channel eikonal for each state. We denote the orthogonal matrix which diagonalizes  $T$  by  $a$ , so that

$$T = a F a^T \quad \text{with} \quad \langle \phi_i | F | \phi_k \rangle = F_k \delta_{ik}, \quad (20.21)$$

where  $F_k$  is the probability amplitude of the hadronic process proceeding via the diffractive eigenstate  $\phi_k$ .

Now consider the diffractive dissociation of an incoming state  $|h\rangle$ . We can write

$$|h\rangle = \sum_k a_{hk} |\phi_k\rangle. \quad (20.22)$$

The elastic scattering amplitude satisfies

$$\langle h | T | h \rangle = \sum_k |a_{hk}|^2 F_k = \langle F \rangle, \quad (20.23)$$

where  $F_k \equiv \langle \phi_k | F | \phi_k \rangle$  and where the brackets of  $\langle F \rangle$  mean that we take the average of  $F$  over the initial probability distribution of diffractive eigenstates. After the diffractive scattering described by  $T_{fh}$ , the final state  $|f\rangle$  will, in general, be a different superposition of eigenstates from that of  $|h\rangle$ , which was shown in Eq. (20.22). Neglecting the real parts, for the cross sections at a given impact parameter  $b$ , we have

$$\begin{aligned} \frac{d\sigma_{\text{tot}}}{d^2b} &= 2 \text{Im} \langle h | T | h \rangle = 2 \sum_k |a_{hk}|^2 \text{Im} F_k = 2 \langle \text{Im} F \rangle \\ \frac{d\sigma_{\text{el}}}{d^2b} &= |\langle h | T | h \rangle|^2 = \left| \sum_k |a_{hk}|^2 F_k \right|^2 = \langle |F|^2 \rangle \\ \frac{d\sigma_{\text{el} + \text{SD}}}{d^2b} &= \sum_k |\langle \phi_k | T | h \rangle|^2 = \sum_k |a_{hk}|^2 |F_k|^2 = \langle |F^2| \rangle. \end{aligned} \quad (20.24)$$

It follows that the cross section for the single diffractive dissociation of a proton,

$$\frac{d\sigma_{\text{SD}}}{d^2b} = \langle |F^2| \rangle - \langle |F|^2 \rangle, \quad (20.25)$$

is given by the statistical dispersion in the absorption probabilities of the diffractive eigenstates. Here the average is taken over the components  $k$  of the incoming proton which dissociates. If the averages are taken over the components of both of the incoming particles, then Eq. (20.25) is the sum of the cross sections for single and double dissociation, see Fig. 20.3.

Note that if all the components  $\phi_k$  of the incoming proton  $|h\rangle$  were absorbed equally, then the diffracted superposition would be proportional to the incident one and the probability of the inelastic diffraction would be zero. Thus if, at very high energies, the amplitudes  $F_k$  at small impact parameters are equal to the black disk limit,  $F_k = i$ , then diffractive production will be equal to zero in this impact parameter domain, and so will only occur in the peripheral  $b$  region where the edge of the disk becomes not completely black. Hence the impact parameter structure of diffractive dissociation and elastic scattering is drastically different in the presence of absorptive  $s$ -channel unitarity effects (see the  $G_{\text{inel}}$  term in Eq. (20.9)). Under the assumption that amplitudes  $F_k$  at high energies cannot exceed the black disk limit,  $\text{Im} F_k \leq 1$ , equations 20.24 lead to the following bound

$$\frac{d\sigma_{\text{el} + \text{SD}_1 + \text{SD}_2 + \text{DD}}}{d^2b} \leq \frac{1}{2} \frac{d\sigma_{\text{tot}}}{d^2b}. \quad (20.26)$$

known as the Pumplin bound [46]<sup>5</sup>.

### 20.3.3 Diffraction from the $t$ -channel viewpoint

The  $t$ -channel approach is based on the Regge model (see Section 20.2), where high-energy diffractive processes are mediated by the exchange of a Pomeron ( $\mathbb{P}$ ). In the case of the elastic  $pp$ -scattering amplitude in the eikonal model (see Eq. (20.13)), the opacity corresponding to the exchange of one Pomeron is

$$\Omega(s, b) = \int \frac{d^2q_t}{4\pi^2} \Omega(s, q_t) e^{i\vec{q}_t \cdot \vec{b}} \quad (20.27)$$

with

$$\Omega(s, q_t) = \frac{1}{s} T'_{\text{el}} = -i\eta_P(t) g_N(t) g_N(t) \left( \frac{s}{s_0} \right)^{\alpha_{\mathbb{P}}(t)-1}, \quad (20.28)$$

where  $T'_{\text{el}}$  is the two-particle  $s$ -channel irreducible elastic amplitude, cf. Eq. (20.5), and  $g_N(t)$  is the proton-Pomeron coupling.

If we assume an exponential  $t$ -dependence of the coupling,  $g_N(t) = g_N(0) \exp(B_0 t)$ , and neglect the Pomeron phase, then the opacity is

$$\Omega(s, q_t) = g_N(0) g_N(0) \left( \frac{s}{s_0} \right)^{\alpha_{\mathbb{P}}(0)-1} e^{Bt}, \quad (20.29)$$

with the  $t$ -slope given by

$$B = 2B_0 + \alpha'_{\mathbb{P}} \ln \left( \frac{s}{s_0} \right). \quad (20.30)$$

At high energies the opacity has a Gaussian form in the  $b$ -space:

$$\Omega(s, b) = \frac{g_N^2(0)}{4\pi B} \left( \frac{s}{s_0} \right)^{\alpha_{\mathbb{P}}(0)-1} e^{-b^2/4B}. \quad (20.31)$$

In terms of opacity the effective radius of interaction increases at high energies as  $\sqrt{\alpha'_{\mathbb{P}} \ln(s/s_0)}$ . This means that with energy increasing the differential cross section becomes steeper (the so called *shrinkage* of the diffractive peak).

If we were to take for the Pomeron the DL parametrisation [25, 26], that is to keep just the first,  $T(b) = \Omega(b)/2$ , term in the elastic amplitude (Eq. (20.13)) then, at LHC energies, the Gaussian would exceed the black disk limit at small  $b$ . However, the eikonal unitarization reduces the power growth of the one-Pomeron exchange cross section. Thus, in Eq. (20.31)  $\Omega(s, b) \propto (s/s_0)^{\alpha_{\mathbb{P}}-1}$  gives an amplitude  $\text{Im} T_{\text{el}}(s, b) = 1 - e^{-\Omega/2} < 1$ . Hence the total cross section is limited by the size of the effective interaction area  $\sigma_{\text{tot}} < 2\pi R^2$ , where the interaction radius  $R$  can be estimated from Eq. (20.31) as the value of  $b$  where  $\text{Re}\Omega(b)$  becomes  $\sim 1$ .

For the parameterization of Eq. (20.31) the corresponding radius grows at very large energies as

$$b^2 = R^2 = 4B \ln \left[ \frac{g_N^2(0)}{4\pi B} \left( \frac{s}{s_0} \right)^{\alpha_{\mathbb{P}}(0)-1} \right] \simeq 4\Delta \alpha'_{\mathbb{P}} \ln^2(s/s_0). \quad (20.32)$$

That is for  $\Delta = 0.1$  and  $\alpha'_{\mathbb{P}} = 0.25 \text{ GeV}^{-2}$  we may expect that the cross section increases as

$$\sigma_{\text{tot}} = 2\pi R^2 \simeq c \cdot \ln^2 s, \quad (20.33)$$

with  $c = 8\pi\Delta\alpha'_{\mathbb{P}} = 0.24 \text{ mb}$ . This value is close to that obtained by the COMPETE parameterization ( $c = 0.27 \text{ mb}$  [22, 24]) but much smaller than the Froissart-Lukaszuk-Martin (FLM) bound [47–49]. With  $c^{\text{FLM}} = \pi/m_{\pi}^2 \simeq 60 \text{ mb}$ , see Section 20.7,

$$\sigma_{\text{tot}} \leq \frac{\pi}{m_{\pi}^2} \ln^2 \left( \frac{s}{s_0} \right). \quad (20.34)$$

<sup>5</sup>Strictly speaking the proof of the Pumplin bound is justified only for low mass dissociation. When the masses  $M_{1,2}$  become so large (say,  $M_i^2 > \sqrt{ss_0}$ ) that the Good-Walker states  $|\phi_i\rangle$ , corresponding to two incoming protons overlap, we may face double counting. Therefore, the high mass dissociation will be considered in the next Section, in terms of the multi-Pomeron diagram. Here and in what follows  $s_0$  is a constant which should be defined for a particular theoretical model or fitted from experiment.

The fact that  $c = (0.24-0.27) \text{ mb} \ll c^{\text{FLM}} = 60 \text{ mb}$  demonstrates that even at the LHC we are very far from true high-energy asymptotics<sup>6</sup>, and the observed growth of the cross section is driven by the interactions at relatively large transverse momenta  $k_t \gg m_\pi$  rather than the smallest hadron mass  $m_\pi$  in the denominator of Eq. (20.34).

### 20.3.3.1 The $t$ -slope and dip in the elastic cross section

We first start with a relatively small one-Pomeron amplitude and consider the two-Pomeron contribution corresponding to the  $\Omega^2$  term in the expansion of the eikonal  $1 - \exp(-\Omega/2)$ . In this term the momentum transferred,  $q_t = \sqrt{|t|}$ , is divided between the two Pomerons so that each Pomeron carries about a momentum  $q_t/2$ . Correspondingly, the  $t$  dependence of the whole ‘two-Pomeron’ amplitude will be  $\exp(2B(t/4)) = \exp(Bt/2)$ <sup>7</sup>.

Since the two-Pomeron contribution has an opposite sign in comparison with the one-Pomeron exchange, their interference will result in the appearance of the first diffractive minimum which moves to smaller  $|t|$  with energy increasing. Such interference effects are largely responsible for the zero in the imaginary part of the amplitude (with the minimum filled by the real part).

It is worth mentioning that the one-channel eikonal discussed so far is a rather oversimplified approximation. It provides some indications about the behaviour we may expect for the elastic cross section, but clearly it does not give the whole story. Moreover, even within the framework of the one-channel eikonal, the expectation for the elastic slope  $t$ -dependence could be masked by other effects. Firstly, there is no reason why the  $t$ -dependence of the proton-Pomeron coupling  $g_N(t)$  has to be a pure exponent. Next, there exists a two-pion singularity at  $t = 4m_\pi^2$  (close to the physical region) in the Pomeron trajectory which generates some curvature in the behaviour of  $d\sigma_{el}/dt$  [50–52]. So there may be some compensation between the effects caused by the eikonal (arising from the interference between the different multi-Pomeron contributions), and the curvatures coming from the form of the proton-Pomeron coupling and the two-pion singularity of the Pomeron trajectory. However, an exact compensation looks quite non-trivial and a *pure* exponential behaviour of  $d\sigma_{el}/dt$  looks highly unlikely.

Indeed, the measurements by the TOTEM collaboration at 8 TeV [53] and at 13 TeV [54] clearly demonstrate that the local slope of the elastic  $pp$  cross section,

$$B = d[\ln(d\sigma_{el}/dt)]/dt, \quad (20.35)$$

at  $-t \lesssim 0.3 \text{ GeV}^2$  varies with  $t$ .

### 20.3.3.2 High mass dissociation

Let us turn to inelastic diffractive processes that is, to single and double proton dissociations,  $pp \rightarrow X+p$  and  $pp \rightarrow X_1+X_2$ , where the  $+$  sign denotes the presence of a LRG in the distribution of final state particles. For example, for the diffractive dissociation of a proton into a system of mass  $M$ , the rapidity gap between the incoming proton and the remaining hadrons is

$$\Delta y = \ln\left(\frac{s}{M^2}\right) = \ln\left(\frac{1}{\xi}\right), \quad (20.36)$$

where  $\xi = 1-x$  and  $x$  is the initial momentum fraction (Feynman variable) carried by the outgoing proton. The masses,  $M$ , of the diffractively excited states, produced in high  $\sqrt{s}$  collisions, can be large. To separate dissociation from the common inelastic process, usually the condition  $M^2 \ll s$  is imposed.

The simplest multi-Pomeron diagram used to describe the diffractive dissociation is the so-called triple-Pomeron graph, shown at the end of Fig. 20.2.

In the Regge pole model, the cross section for the inclusive single diffractive (SD) dissociation process [55–57] can be written

in the form (see Fig. 20.2)

$$\begin{aligned} \xi d\sigma_{\text{SD}} &= \frac{M^2 d\sigma_{\text{SD}}}{dt d\xi} \\ &= \frac{g_{3\mathbb{P}}(t)g_N(0)g_N^2(t)}{16\pi^2} \left(\frac{s}{M^2}\right)^{2\alpha_{\mathbb{P}}(t)-2} \left(\frac{M^2}{s_0}\right)^{\alpha_{\mathbb{P}}(0)-1}, \end{aligned} \quad (20.37)$$

where  $g_{3\mathbb{P}}(t)$  is the triple-Pomeron coupling. The value of the coupling  $g_{3\mathbb{P}}$  is usually obtained from a triple-Regge analysis of lower energy data (see e.g. [34]).

In an analogous way the cross section for double dissociation reads

$$\begin{aligned} \xi_1 \xi_2 d\sigma_{\text{DD}} &= \frac{M_1^2 M_2^2 d\sigma_{\text{DD}}}{dt d\xi_1 d\xi_2} \\ &= \frac{g_{3\mathbb{P}}^2(t)g_N^2(0)}{16\pi^3} \left(\frac{ss_0}{M_1^2 M_2^2}\right)^{2\alpha_{\mathbb{P}}(t)-2} \left(\frac{M_1^2 M_2^2}{s_0^2}\right)^{\alpha_{\mathbb{P}}(0)-1}, \end{aligned} \quad (20.38)$$

where  $t$  is the momentum squared transferred through the LRG. As discussed in Section 20.5, from a microscopic point of view the

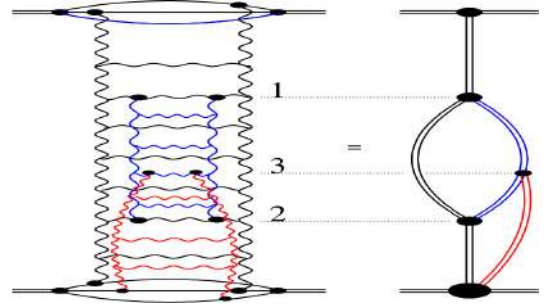


Figure 20.4: Pomeron exchange with schematic diagrams for the enhanced and semi-enhanced exchanges.

Pomeron exchange is described by a set of ladder-type diagrams (see [58–60]), which can lead to a rescattering of the intermediate partons (produced inside this ladder during the evolution), see Fig. 20.4. The left plot shows the Pomeron exchange complemented with the rescattering of partons 1 and 2 and the scattering of a parton 3 on the target. In terms of multi-Pomeron exchanges this corresponds to the diagram on the right hand side, where the Pomeron exchange is shown by the double line of a corresponding colour. The blue one is called ‘enhanced’ (its contribution is integrated over the rapidities of both upper and lower vertices, i.e. of partons 1 and 2). The loop formed by the Pomerons shown in red is called ‘semi-enhanced’ (it is integrated over the rapidity of one intermediate parton).

While the rescattering of the incoming hadron (proton) is already embedded in the eikonal formula (Eq. (20.13)), the rescattering of the intermediate partons in RFT is accounted for by the so-called enhanced diagrams<sup>8</sup> with multi-Pomeron vertices,  $g_m^n$ , which couple  $m$  to  $n$  Pomerons. It is quite a challenging task to resum all the enhanced diagrams, however this was successfully performed within the framework of the QGSJET Monte Carlo [61]. An elegant approach to sum up all enhanced diagrams in the case when each extra effective Pomeron contribution is very large was proposed in [62], assuming the analyticity of the  $g_m^n$  vertices in  $n$  and  $m$  in the right half of the complex  $n$ - and  $m$ -planes. The resulting amplitude becomes a black disk.

The simplest triple-Pomeron vertex  $g_3^1 = g_{3\mathbb{P}}$  produces the first multi-Pomeron graph considered above (see the end of Fig. 20.2). However, numerically the multi-Pomeron vertices are relatively small. Note also that the value of  $g_{3\mathbb{P}}$ , determined from the fit to

<sup>8</sup>This contribution is *enhanced* due to the large parton multiplicity.

<sup>6</sup>As usual, we assume  $s_0 = 1 \text{ GeV}^2$ , but the qualitative conclusion does not depend on any realistic choice of  $s_0$ .

<sup>7</sup>The two-Pomeron contribution has a factor of two smaller  $t$ -slope, and in terms of the impact parameter, the  $\Omega^2(b)$  term is concentrated in the domain of a smaller radius. In such a simplified picture, the impact parameters corresponding to an exchange of  $n$  Pomerons will rapidly decrease with  $n$  increasing.

experimental data (e.g. [63]), is actually an effective vertex with coupling

$$g_{\text{eff}} = g_{3\mathbb{P}} \langle S^2 \rangle, \quad (20.39)$$

which already includes the survival factor  $S^2(b)$ , see Eq. (20.15).

Since the opacity  $\Omega$  increases with energy, at large  $\Omega$  the number of multiple interactions grows as  $N \propto \Omega$ , leading to a smaller  $S^2$ . An explicit analysis [64] accounting for the survival effects gives a coupling  $g_{3\mathbb{P}}$  about a factor of 3 larger than  $g_{\text{eff}}$ , namely  $g_{3\mathbb{P}} \simeq 0.2g_N$ .

Recall that the Pomeron exchange simultaneously describes both the elastic scattering amplitude,  $T_{\text{el}}$ , and the multiparticle production cross section,  $G_{\text{inel}}$ . The discontinuity (*disc*  $T_{\text{el}}$ ) of the ladder diagram corresponds to the production of secondary particles, practically homogeneously distributed over the whole available rapidity interval covered by the Pomeron, as illustrated by the right-hand diagram in Fig. 20.5.

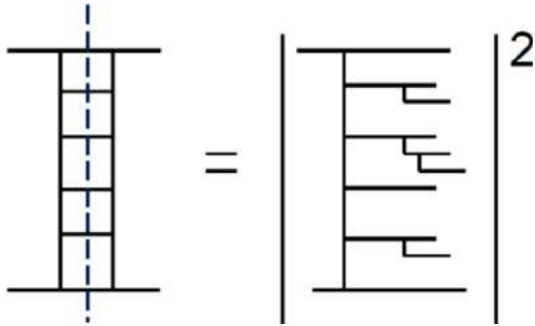


Figure 20.5: Cut Pomeron contribution to the inelastic cross section.

For the one-Pomeron case this discontinuity is called the “cut Pomeron”. Correspondingly each multi-Pomeron diagram describes a series of different processes. Cutting  $k$  Pomerons in the diagram with  $n$  Pomerons we get the inelastic interaction with the multiplicity (density of secondaries)  $k$  times larger than that,  $N_0$ , produced by one cut Pomeron,  $dN/dy = k \cdot N_0$ . The remaining  $n - k$  (elastic) Pomerons account for the absorptive corrections to the subprocess with  $k$  cut Pomerons. Indeed, the contribution of the diagram with  $n$  Pomerons includes also the processes with larger,  $(k + i) \cdot N_0$  multiplicities (cut Pomerons), where  $(i = 1, 2, \dots, n - k)$ . Absorptive corrections, described by the remaining elastic Pomerons, play a role of the survival factor  $S^2$  for the process with the fixed particle density  $k \cdot N_0$ . They ensure probability conservation (the sum of the probabilities of all possible different channels is equal to one) and restore unitarity. Note that the multi-Pomeron diagrams represent all possible interactions between partons from the protons and partons from the Pomerons. In the case of Monte Carlo generators, the non-enhanced multi-Pomeron contributions are included in terms of the multiple parton interaction (MPI) option, see [13, 65] and Section 7.2 in [2]. However, as a rule, this option accounts mainly for the multiple interactions between the partons from the protons (incoming hadrons). The energy-momentum sharing between the various inelastic rescattering processes (including the cut and uncut Pomerons) was performed at the amplitude level within the EPOS Monte Carlo [66].

### 20.3.3.3 AGK cutting rules

The relation between the cross sections of subprocesses with a different number of cut Pomerons within a given diagram with  $n$  Pomerons is given by the AGK (Abramovsky-Gribov-Kancheli [67]) cutting rules. These rules include also the cut *between* the Pomerons with  $k = 0$  which corresponds to the contribution of the particular diagram to the elastic cross section. By applying these rules, it is possible to show the self-consistency of the approach, which was lacking in the pure Regge-pole model.

Consider a diagram where the elastic scattering amplitude is mediated by an exchange of  $n$  Pomerons. The AGK cutting rules specify the coefficients  $c_n^k$  arising when  $k$  of these Pomerons are cut. Recall that the Pomeron cut discontinuities give the

corresponding inelastic contributions to  $\sigma_{\text{tot}}$ . The terms with  $k = 0$  correspond to the diffractive cutting of the diagram (that is, the cut is between the Pomeron exchanges, and not through the Pomerons themselves), while the terms with  $k = 1, 2, \dots$  describe the processes with  $k$  cut Pomerons. The coefficients  $c_n^k = \sigma_n^k / |\sigma_{\text{tot}}^{(n)}|$  are <sup>9</sup>

$$c_n^{k=0} = (-1)^n (2^{n-1} - 1), \quad c_n^{k \neq 0} = (-2)^{n-1} \frac{(-1)^{k-1} n!}{k!(n-k)!} \quad (20.40)$$

where  $\sigma_{\text{tot}}^{(n)}$  denotes the contribution of the  $n$ -Pomeron diagram to the total cross section. Note the alternating sign of  $\sigma_{\text{tot}}^{(n)}$  expressed as  $(-1)^{n-1}$ .

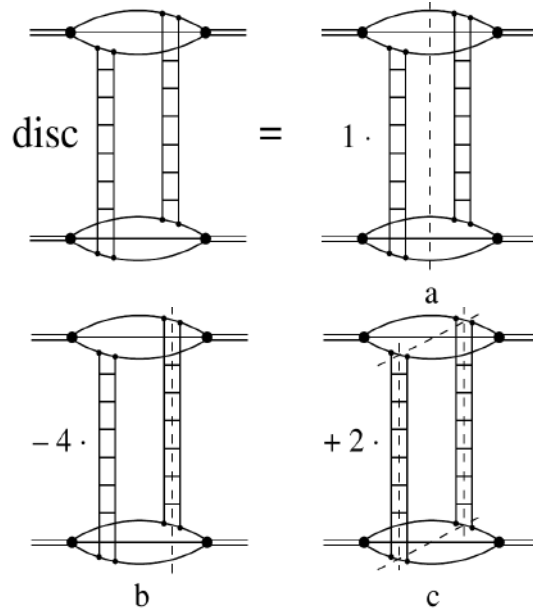


Figure 20.6: Two-Pomeron exchange diagram as a sum of different AGK cuts shown by the dashed lines.

For the two-Pomeron exchange,  $n = 2$ , the coefficients are  $+1$ ,  $-4$ , or  $+2$  according to whether  $k = 0, 1$  or  $2$  Pomerons are cut, respectively. As shown in Fig. 20.6, the amplitude of the two-Pomeron exchange corresponds to a sum of three processes: i) inelastic interaction with particle density twice that caused by one Pomeron (see Fig. 20.6(c)) which enters with the coefficient ‘2’, ii) shadowing (absorptive) correction to the one-Pomeron exchange contribution, which corresponds to events with a single Pomeron density (only one Pomeron is cut), see Fig. 20.6 (b), which enters with a factor ‘-4’, and iii) diffractive elastic scattering or proton dissociation (when different components of the proton wave function correspond to different interaction cross sections), caused by the distortion of the incoming plane wave, see Fig. 20.6(a).

Note that the inclusive cross section is not affected by the multi-Pomeron contribution:  $2 \times (2) + 1 \times (-4) = 0$ . This is a general property of the AGK rules valid for any number of Pomerons  $n$ . Thus in order to calculate the inclusive single-particle cross section, it is sufficient to consider just the *one*-Pomeron exchange diagram.

Let us emphasize that the AGK rules provide a framework to consistently work with multi-Pomeron diagrams, that is, with the Regge cuts, accounting for their contributions to different processes (elastic scattering and diffractive dissociation, inelastic events with different densities,  $dN/dy$ , of secondaries, etc.).

Measurements of diffractive dissociation cross sections have been made in a wide range of pre-LHC energies, see e.g. [68–73]. At the LHC, cross sections of events with a LRG were measured by the ATLAS, CMS and ALICE collaborations at 7 and 8 TeV,

<sup>9</sup>In their complete form the AGK cutting rules were implemented in the QGSJET Monte Carlo [61].

see [74–77]. ATLAS [78] and CMS and TOTEM [79] presented first measurements of SD cross sections at 8 TeV with a tagged forward proton. While ATLAS measured inclusive SD cross section, CMS and TOTEM studied SD dijet production. Note that in [78] the measured slope  $B = 7.65 \pm 0.34 \text{ GeV}^{-2}$  of the inclusive SD cross section as well as the differential distributions  $\frac{d\sigma_{\text{SD}}}{dt d\xi}$  for  $0.0001 \leq \xi \leq 0.025$  are (within the experimental uncertainties) in a good agreement with the theoretical expectations [29, 80]. Moreover a relatively small (in comparison with the  $d\sigma_{\text{el}}/dt$ ) slope  $B$  indicates that the size of the triple-Pomeron vertex is much smaller than the proton size.

### 20.3.4 Central Diffractive processes

Processes  $pp \rightarrow p + X + p$ , where an object  $X$ , produced in the central rapidity region, is separated from the outgoing protons by a LRG on each side, are called Central Exclusive Production (CEP). They are described by the double Pomeron exchange (DPE) diagrams. When the mass of the central system,  $M_X$ , is large and the interaction in the  $M_X$  region can be described by Pomeron exchange, the corresponding cross section reads

$$\frac{\xi_1 \xi_2 d\sigma^{\text{CEP}}}{d\xi_1 dt_1 d\xi_2 dt_2} = \frac{g_N^2(t_1) g_N^2(t_2)}{(16\pi^2)^2} \left(\frac{1}{\xi_1}\right)^{2\alpha_{\text{P}}(t_1)-2} \left(\frac{1}{\xi_2}\right)^{2\alpha_{\text{P}}(t_2)-2} \times g_{3\text{P}}^2(0) \left(\frac{M_X^2}{s_0}\right)^{\alpha_{\text{P}}(0)-1}. \quad (20.41)$$

If the mass  $M_X$  is not too large or for the cases (such as exclusive Higgs boson or dijet production) where the mass  $M_X$  is comparable with the corresponding hard scale, the last factor  $g_{3\text{P}}^2(0)(M_X^2/s_0)^{\alpha_{\text{P}}(0)-1}$  should be replaced by the corresponding ‘Pomeron-Pomeron cross section’, see for instance [81, 82].

Note that equations (20.37), (20.38) and (20.41) are written in a simplified way without accounting for absorptive corrections. That is, the cross sections in equations (20.37) (20.38) and (20.41) should be multiplied by the gap survival factor  $S^2$  (see Eq. (20.15)).

Since the QCD Pomeron is built mainly from gluons it is natural to search for glueballs in double Pomeron exchange processes, and in particular, in CEP.

Resonance production in the Pomeron-Pomeron fusion was extensively studied at the CERN ISR at  $\sqrt{s}$  from 22 GeV to 63 GeV (see for reviews [82–84]) and, after the ISR closure in 1983, in fixed target experiments at the CERN SPS [85] and E690 at the Tevatron [86, 87]. Glueballs were actively searched for and the properties of the  $f_0$  and  $f_2$  production studied in detail using multiparticle spectrometers, such as the Omega facility at the CERN SPS experiments (WA76, WA91 and WA102), see for a review [85].

An important property of CEP processes, which can be expected from matching with the perturbative QCD LO (leading order) calculation, is the  $J_z = 0$  dominance. Perturbatively, for the CEP of a heavy object, the leading contribution comes from a configuration with the projection of this object spin onto the beam axis  $J_z = 0$  [81]. Note that the CEP cross section is suppressed at large  $M_X$  by a strong bremsstrahlung off the incoming gluons (from the Pomeron) which would violate the ‘exclusivity’. The small probability of not having such radiation is described by the Sudakov suppression factor,  $T_{\text{Sud}}$ , [88], see [81] for details.

### 20.3.5 Diffractive parton distributions

Selecting in Deep Inelastic Scattering (DIS) events with a LRG (see e.g. [89, 90]) or detecting the leading proton (see Section V.C. in the review [91]) we can study the parton (quark and gluon) distributions of the Pomeron<sup>10</sup>. In other words, such events can be treated as DIS on the Pomeron target with the incoming Pomeron flux given by

$$f_{\mathbb{P}}(x_{\mathbb{P}}) = \int dt \frac{g_N^2(t)}{16\pi^2} x_{\mathbb{P}}^{2(1-\alpha_{\mathbb{P}}(t))}, \quad (20.42)$$

<sup>10</sup>see also Section 18.5 in [1]

where the proton momentum fraction transferred through the Pomeron  $x_{\mathbb{P}} = \xi = M^2/s$ .

These Pomeron PDFs were extracted from the HERA measurements of  $ep$  scattering with leading protons or a LRG and can be used to describe the inclusive production of high  $E_T$  dijets or another hard process based on the collinear factorization theorem in the same way as that in non-diffractive collisions (see [91]). The inclusive measurements of these PDFs are described in [92–94], with the combined H1 and ZEUS data using tagged protons analyzed in [95]. The impact of diffractive jet measurements is addressed e.g. in [96] and the measured charm contribution is presented in [97, 98]. As far as the parton distributions are known, we can calculate the corresponding inelastic cross section of the Pomeron-proton interaction using one of the ‘general purpose’ Monte Carlo generators (see e.g. [13]), multiply it by the Pomeron flux and compare the obtained result with the Regge formula in Eq. (20.37). This approach provides another way to evaluate the triple-Pomeron vertex  $g_{3\text{P}}$ . The corresponding analysis was performed in [99] and leads to practically the same (within the error bars) value of  $g_{3\text{P}} = 0.2g_N(0)$ .

It is worth mentioning that in DIS at large  $Q^2$  we are dealing with small-size objects and the rescattering effects are small. Therefore, the survival factor  $S^2 \simeq 1$  and does not affect the results.

## 20.4 Experimental data on diffraction at high energies

### 20.4.1 Total and elastic cross sections

The elastic scattering of protons is a process with a special and rather simple experimental signature: the central detector is empty while the incoming protons after the collisions are detected in the dedicated forward proton detectors (FPD) placed far from the interaction point (IP). Elastic scattering data are taken in special runs in order to be able to reach different ranges of  $t$ -values and thanks to the very large value of the cross section the data can be collected with a relatively low instantaneous luminosity and hence a negligible pile-up.<sup>11</sup>

These special runs usually have very few proton bunches and differ in the  $t$  range covered, which is governed roughly by the relation  $t_{\text{min}} \propto d^2/\beta^*$ . Here  $d$  is the distance, expressed in multiples of the beam size at the detector, from the centre of the LHC beam and  $\beta^*$  is defined as the distance from the IP to the point where the transverse area of the beam is twice as wide as that at the IP (see Section 31 in [1]). Note that if we work at large  $\beta^*$ , the incoming protons have very small angular divergence leading to small average transverse momentum, which allows us to measure very small  $|t|$  values. The lowest  $|t|$  values measured so far at the LHC are  $4 \times 10^{-4} \text{ GeV}^2$  (ALFA) and  $6 \times 10^{-4} \text{ GeV}^2$  (TOTEM) reached with the 8 TeV LHC beam configured with  $\beta^* = 1 \text{ km}$  optics. The largest  $t$  values of about  $4 \text{ GeV}^2$  were measured by TOTEM at 8 and 13 TeV with  $\beta^* = 90 \text{ m}$  thanks to special triggers. Other  $\beta^*$  values used in special runs are 3.5 m, 11 m and 2.5 km.

There are four ways to determine the  $\sigma_{\text{tot}}$  value:

1. **Elastic and Inelastic.** This method does not require the optical theorem and hence no extrapolation of  $d\sigma_{\text{el}}/dt$  to  $t = 0$  and no  $\rho$  (defined below Eq. (20.17)) but rather the luminosity and measuring rates  $N_{\text{el}}$  (elastic) and  $N_{\text{inel}}$  (inelastic). The total cross section is then simply:

$$\sigma_{\text{tot}} = \frac{1}{\mathcal{L}}(N_{\text{el}} + N_{\text{inel}}). \quad (20.43)$$

Of course, both  $N_{\text{el}}$  and  $N_{\text{inel}}$  should be corrected for the detector acceptance and efficiency. This is especially important for  $N_{\text{inel}}$  since the detectors never cover the whole rapidity region (i.e. the whole  $4\pi$ ).

2. **Elastic only.** This approach necessitates measuring  $d\sigma_{\text{el}}/dt$  and using the optical theorem with a known value of  $\rho$ . As explained in Section 20.2, the optical theorem states that

<sup>11</sup>The pile-up is formed by additional  $pp$  collisions which typically produce low- $p_T$  particles. These may affect the signal sample and worsen various reconstruction and identification efficiencies.



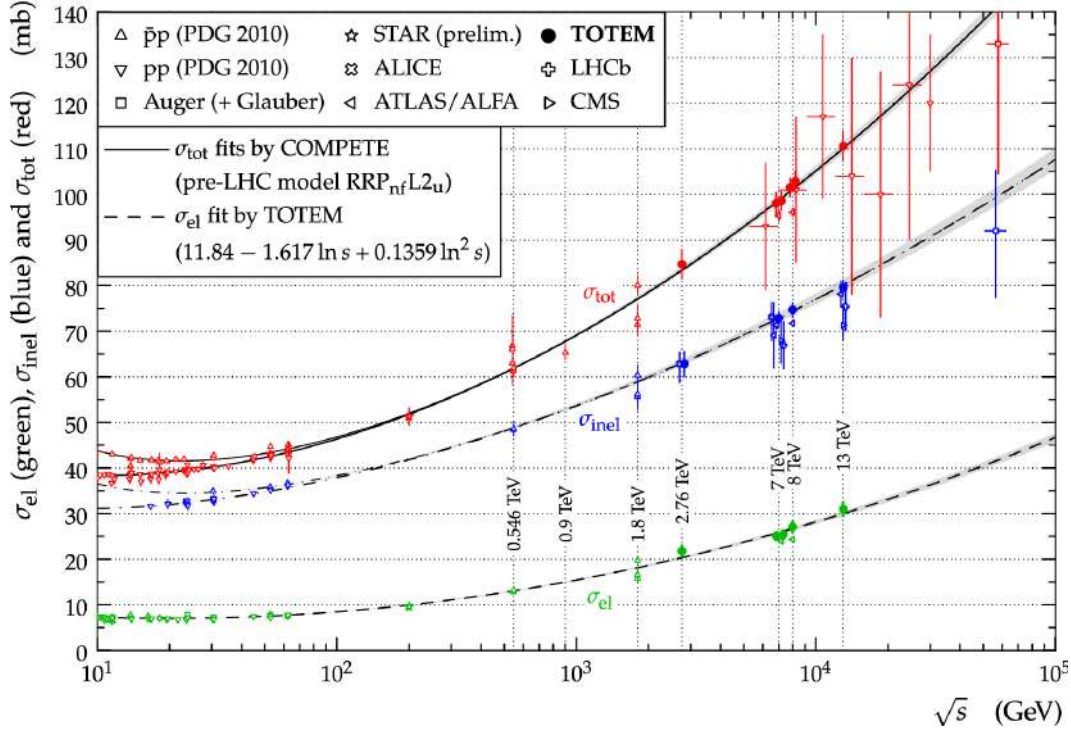


Figure 20.7: Overview of elastic ( $\sigma_{\text{el}}$ ), inelastic ( $\sigma_{\text{inel}}$ ) and total ( $\sigma_{\text{tot}}$ ) cross section data for  $pp$  and  $p\bar{p}$  collisions as a function of  $\sqrt{s}$ . The continuous black lines (lower for  $pp$ , upper for  $p\bar{p}$ ) represent the best fits of the total cross section data by the COMPETE collaboration [22]. The dashed line is a fit of the elastic cross section data. The dashed-dotted lines refer to the inelastic cross section and are obtained from the difference between the continuous and dashed lines. Figure from Ref. [100].

$\sigma_{\text{tot}} \propto \text{Im}[T_{\text{el}}(t \rightarrow 0)]$ , see Eq. (20.3). Since in practice it is not possible to measure down to  $t = 0$ , we need to extrapolate. To minimize the model dependence when extrapolating, it is vital to measure down to as low  $|t|$  values as possible (i.e. high  $\beta^*$ ). This method requires an independent luminosity measurement. Once the luminosity is known,  $d\sigma_{\text{el}}/dt$  can be normalized and used to extract  $\sigma_{\text{tot}}$  using the formula:

$$\sigma_{\text{tot}}^2 = \frac{16\pi}{1 + \rho^2} \left. \frac{d\sigma_{\text{el}}}{dt} \right|_{t \rightarrow 0}. \quad (20.44)$$

**3. Coulomb normalization.** Similarly to the previous method, this approach relies on the elastic observables only and requires a measurement of the elastic cross section at very low values of  $|t|$ , where it is sensitive to the theoretically well known Coulomb QED contribution  $4\pi\alpha_{\text{QED}}^2/t^2$ . The normalization of  $d\sigma_{\text{el}}/dt$  is then determined by fitting the experimental data at very low  $|t|$  using a formula including the Coulomb amplitude and its interference with the strongly interacting (the so-called nuclear) term. This method has been successfully used by UA4/2 [101] and TOTEM [102].

**4. Luminosity-independent.** This method does not rely on the knowledge of luminosity but rather on the knowledge of  $N_{\text{el}}$  and  $N_{\text{inel}}$  and on the optical theorem: combining equations (20.43) and (20.44) with  $\frac{d\sigma_{\text{el}}}{dt} = \frac{1}{L} \frac{dN_{\text{el}}}{dt}$  we get

$$\sigma_{\text{tot}} = \frac{16\pi}{1 + \rho^2} \frac{dN_{\text{el}}/dt|_{t=0}}{N_{\text{el}} + N_{\text{inel}}}, \quad (20.45)$$

where  $dN_{\text{el}}/dt|_{t=0}$  corresponds to the extrapolation to  $t = 0$  of the nuclear term only. By independently and simultaneously measuring  $N_{\text{el}}$  and  $N_{\text{inel}}$ , and applying the optical theorem, we can also determine the luminosity.

The TOTEM [100, 103–105] and ATLAS [106, 107] collaborations at CERN have covered an energy range from  $\sqrt{s}=2.76$  TeV to 13 TeV. A compilation of high energy total  $pp$  and  $p\bar{p}$  cross section measurements is shown in Fig. 20.7 (for discussion of the pre-LHC elastic scattering data see review [108]).

Despite some tension between the Tevatron CDF [109] and E811 [110] data<sup>12</sup> and to a lesser extent between the TOTEM [104, 105] and ATLAS [106, 107] measurements, the data clearly indicate that in the Tevatron – LHC energy interval the total cross section starts to grow *faster* than the power-law parametrization [26] describing the data below the Tevatron energy. In particular, while the DL fit [26] predicts  $\sigma_{\text{tot}} = 90.7$  mb at  $\sqrt{s} = 7$  TeV, the TOTEM experiment observes  $98.6 \pm 2.2$  mb [104].

A compilation of the high-energy data on the elastic slope is shown in Fig. 20.8. It is clearly seen that in the TeV energy range the slope increases with  $\sqrt{s}$  more rapidly than the logarithmic behaviour expected in the case of one-Pomeron exchange, see Eq. (20.30). Such an acceleration of the  $t$ -slope derivative,  $dB/d\ln s$ , is a clear manifestation of the increasing role of the multi-Pomeron exchanges, where asymptotically the slope should rise as  $\ln^2 s$ , see [117]. Finally, Fig. 20.9 illustrates the energy dependence of the differential elastic  $pp$  cross section. As expected (see Section 20.3.3.1), the diffractive dip moves to smaller  $|t|$  with increasing energy.

#### 20.4.2 Diffractive vector meson production

The exclusive production of vector mesons was studied in detail at HERA (see for a review [91]). It is well described within the ‘dipole model’ (see for review and references [120]), where the incoming photon first fluctuates into a quark-antiquark, which then interacts with the target proton and, finally, with the probability given by the overlap integral between the vector meson wave function and the outgoing  $q\bar{q}$ -pair, the vector meson is produced. The crucial quantity is the value of cross section,  $\sigma(q\bar{q} - p)$ , of elastic scattering of the  $q\bar{q}$ -pair on the proton. The energy behaviour of  $\sigma(q\bar{q} - p)$  is driven by the intercept,  $\alpha_{\text{eff}}(0)$ , of the effective Pomeron<sup>13</sup> (rightmost singularity in the  $j$ -plane), while

<sup>12</sup>The CDF 1.8 TeV point [109] is  $2.8 \sigma$  higher than the corresponding E811 result [110].

<sup>13</sup>Effective Pomeron means that this is not an original pole in the  $j$ -plane, but it includes the corrections (renormalizations) caused by the enhanced diagrams (see e.g. [121]).

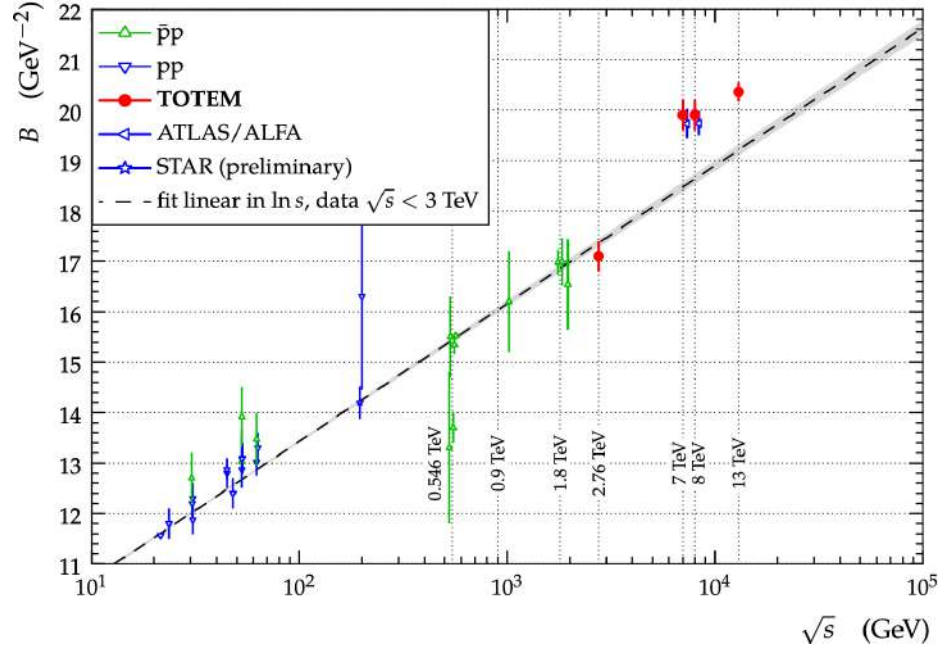


Figure 20.8: The diffractive slope  $B$  for  $pp$  and  $p\bar{p}$  elastic scattering as a function of  $\sqrt{s}$ . The experimental uncertainties represent the quadratic sum of statistical and systematic uncertainties. The dashed line is a result of a linear fit to data at  $\sqrt{s} < 3$  TeV. The data points come from [103–107, 111–113]. Figure from Ref. [100].

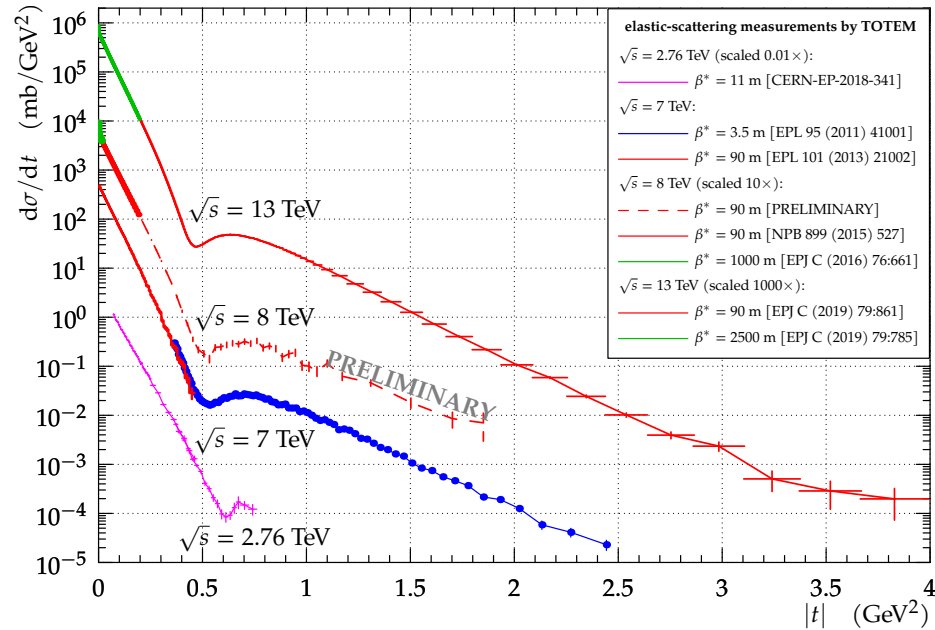


Figure 20.9: The  $t$ -dependence of the  $pp$  elastic cross section for collision energies  $\sqrt{s} = 2.76$  TeV [103], 7 TeV [104, 114], 8 TeV [53, 115, 116] and 13 TeV [54, 102]. The experimental uncertainties represent the quadratic sum of statistical and systematic uncertainties. Figure from Ref. [116].

the value of the cross section depends on the quark separation,  $r$ , in the transverse plane,  $\sigma(q\bar{q} - p) \propto \alpha_s^2 \langle r^2 \rangle$  [43, 44]. Thus different processes with the same  $\langle r^2 \rangle$  are driven by the same  $\sigma(q\bar{q} - p)$  cross section.

In the DIS case this separation in turn is controlled by the photon virtuality,  $Q^2$ , and the quark mass,  $m_q$ :  $\langle r^2 \rangle \simeq 1/(z(1-z)Q^2 + m_q^2)$  ( $z$  is the photon momentum fraction carried by the quark). Indeed, the cross section of the  $\rho$  meson diffractive production in DIS at  $Q^2 = M_{J/\psi}^2$  is close (up to the difference in the quark electric charges) to that for the  $J/\psi$  photoproduction, see Fig. 20.10 (Left).

The production cross section depends non-trivially on  $W$ , the

energy of the  $\gamma^*p$  center of mass system. It increases with  $W$  as  $W^n$ , where  $n = 0.2$  for  $\rho, \omega$  and  $\phi$  (light quark)-mesons but  $n = 0.8$  for  $J/\psi$ . Note that in the  $J/\psi$  case the energy dependence is close to that of the BFKL (Balitsky-Fadin-Kuraev-Lipatov) Pomeron [59, 122, 123], that is, the singularity calculated within the leading (and next-to-leading) approximation in perturbative QCD. But at lower scales the absorptive (multi-Pomeron) corrections tame the growth which leads to smaller values of  $n$  ([124–127]), see Fig. 20.10 (Right).

A similar situation reveals in the dependence of  $\alpha_{\text{eff}}$  on  $Q^2$ , as can be seen in Fig. 47 of [91]. At a large scale  $\mu^2 = (Q^2 + M_\rho^2)/4$  the value of  $\alpha_{\text{eff}} \simeq 1.3$  is close to the prediction for the QCD



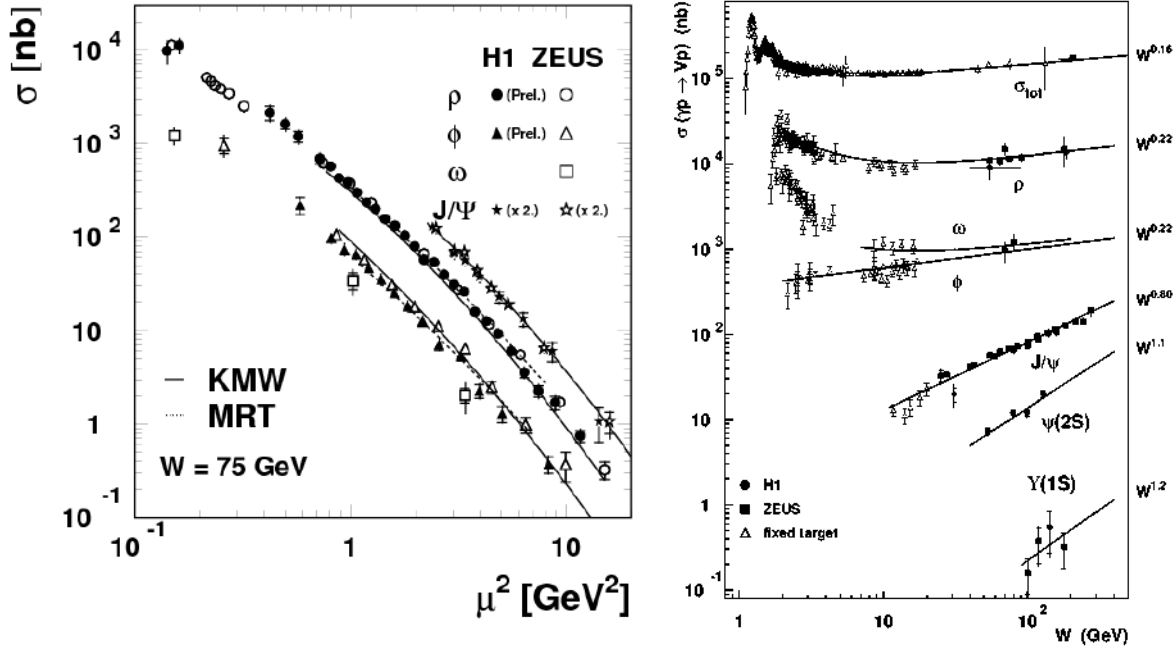


Figure 20.10: (Left) The  $\rho$ ,  $\omega$ ,  $\phi$  and  $J/\psi$  elastic production cross sections as a function of the scale  $\mu^2 = (Q^2 + M_V^2)/4$ . For readability of the figure, the  $J/\psi$  cross sections are multiplied by a factor 2. Figure from Ref. [118]. (Right) Compilation of photoproduction cross section measurements as a function of the  $\gamma p$  centre-of-mass energy,  $W$ . The total cross section and various vector meson production cross sections are included, with the approximate power law dependences  $\sigma \propto W^\delta$  indicated for each process. Figure from Ref. [119].

Pomeron, while for a smaller scale, the absorptive corrections described by the multi-Pomeron diagrams start to reduce the cross section, and  $\alpha_{\text{eff}}$  decreases.

## 20.5 Pomeron in QCD

All features described in the previous Sections were based on *first principles*, such as analyticity (based on causality), unitarity, crossing symmetry, etc. Since QCD theory satisfies all these principles it should reveal a corresponding ‘‘Regge’’ behaviour. Indeed, within perturbative QCD there is a Pomeron: an even-signature singularity in the  $j$ -plane with vacuum quantum numbers. While in the old Regge theory the Regge trajectories and their couplings were phenomenological numbers fitted from experiment, perturbative QCD allows one to calculate the positions of the singularities and the corresponding couplings with  $O(\alpha_s)$  and even with  $O(\alpha_s^2)$  accuracy [59, 122, 123, 128–131].

In terms of Feynman diagrams, the QCD Pomeron may be viewed as a sum of multi-particle ladders built by the exchange of two  $t$ -channel (reggeized<sup>14</sup>) gluons, see the left-hand side of Fig. 20.5.

The sum of ladder diagrams of the type of Fig. 20.5 is the simplest multiparticle structure which reproduces the power-like  $s^\alpha$  behaviour of the Pomeron pole. In other words it corresponds to a sum of completely inelastic  $2 \rightarrow n$  processes, that is, to the last term  $G_{\text{inel}} = 1 - \exp(-\Omega)$  in the unitarity equation (20.9). This set of diagrams was resummed in the limit of a small QCD coupling,  $\alpha_s \ll 1$ , but large energy, such that  $\alpha_s \ln(s/s_0) \sim O(1)$  [59]. The summation results in the right-most singularity at  $j = 1 + \omega_0 > 1$ . After accounting for the next-to-leading logarithmic (NLL) corrections, the position of the singularity (Pomeron intercept) corresponds to  $\omega_0 = 0.25\text{--}0.3$  depending only weakly on the scale [122, 123, 132–136], whose value is characterized by the transverse momentum,  $k_t$ , of gluons in the ladder.

It was demonstrated (see e.g. [137]) that the resummation of

the  $(\alpha_s \ln(1/x))^n$  terms based on the QCD Pomeron results essentially improves the description of low- $x$  inclusive HERA data within the framework of the NNLO DGLAP evolution.

At this stage the singularity is the cut in the  $j$ -plane. However we have to account for the boundary conditions at relatively small  $k_t$ . Imposing a reasonable boundary, we arrive at a series of Regge poles in the interval from  $j = 1$  to  $j = 1 + \omega_0$  instead of the cut [134]. Note that the first (corresponding to the rightmost pole in the  $j$ -plane, i.e. to the pole with the largest  $\text{Re } j$ ) eigenfunction consists of gluons with relatively small  $k_t$ , while for the next poles the  $k_t$  increases. DIS inclusive  $\gamma^* p$  cross sections were fitted in [135] using the QCD based approach in which Pomeron is represented by series of Regge poles obtained within the perturbative QCD BFKL approach. It was concluded that the first pole has a small coupling to the proton. It is possible that this small value of the coupling to the proton is related to the fact that the enhanced multi-Pomeron diagrams (i.e. the rescattering of intermediate partons) were neglected in the fit. The main effect of this enhanced contribution is the ‘‘renormalization’’ of the intercept which diminishes the effective value of  $\omega_0$ . Besides this, the enhanced diagrams provide a saturation by reducing the rise of the parton densities in the  $(b, k_t, y)$ -space (see e.g. [138, 139]).

Note that perturbative QCD allows us to understand why the values of the phenomenological multi-Pomeron vertices and the shift,  $\omega_0$ , of the intercept, are small (due to  $\alpha_s \ll 1$  and some numerical factors such as  $N_c$  and  $\pi$ ). Indeed, at the lowest  $\alpha_s$  orders we get for the  $\omega_0$  value and the simplest multi-Pomeron vertices (see e.g. [59, 139, 140]):

$$\omega_0 \propto \frac{N_c \alpha_s}{\pi}, \quad g_{3\mathbb{P}} \propto \frac{N_c \alpha_s^2}{(N_c^2 - 1)\pi^2} \quad \text{and} \quad g_2^2 \propto \frac{N_c \alpha_s}{(N_c^2 - 1)^2}, \quad (20.46)$$

where  $g_2^2$  is the coupling corresponding to the transition of 2 into 2 Pomerons.

### 20.5.1 BFKL evolution in the ‘dipole’ representation

It was shown in [141–144] that the LO BFKL Pomeron equation [59] can be written in terms of the evolution of the dipole

<sup>14</sup>That is, the virtual loop corrections to the one-gluon exchanges are included. These corrections are important in order to provide infrared stability of the results.

density,  $N(x_d, y_d; y)$ , in rapidity  $y$  (here  $x_d$  and  $y_d$  are the transverse coordinates of two  $t$ -channel gluons which form the colour singlet dipole). Indeed, after the emission of a new gluon at point  $z_d$ , the initial colour dipole with coordinates  $(x_d, y_d)$  turns into a pair of dipoles  $(x_d, z_d)$  and  $(z_d, y_d)$ . This can be considered as a development of a ‘dipole cascade’. Moreover in this formalism it is easy to include the non-linear absorptive corrections (last term in the square brackets in Eq. (20.47)), which accounts for the rescattering of the intermediate partons (gluons) on the target proton. The corresponding contribution is described by the so-called ‘fan’ diagrams and these are the most important corrections to the linear DGLAP (Dokshitzer-Gribov-Lipatov-Altarelli-Parisi) evolution [145] in the case of DIS at not large scales but at very small momentum fraction [139].

The resulting non-linear evolution (Balitsky-Kovchegov equation [146–148]) reads

$$\begin{aligned} \frac{d}{dy} N(x_d, y_d; y) &= \frac{\alpha_s N_c}{2\pi^2} \int d^2 z_d \frac{(x_d - y_d)^2}{(x_d - z_d)^2 (y_d - z_d)^2} \\ &\times [N(x_d, z_d; y) + N(y_d, z_d; y) - N(x_d, y_d; y) \\ &\quad - N(x_d, z_d; y) N(y_d, z_d; y)] . \end{aligned} \quad (20.47)$$

For a small density  $N$  the last term in the square brackets can be neglected, and the first three terms in Eq. (20.47) reproduce the conventional BFKL equation in the coordinate representation. However, for large  $N \rightarrow 1$  the right-hand side of Eq. (20.47) vanishes and we reach the saturation  $N = 1$ . It is worth mentioning that, as shown in [149], in terms of ‘dipole’ formalism, with the triple-Pomeron vertex generated by the ‘one dipole to two dipoles’ transition, it is possible to relate the Good-Walker approach to high mass diffraction with the triple-Pomeron diagram.

### 20.5.2 Distribution of secondaries: theory versus experiment

As already discussed, in terms of Feynman diagrams the cut Pomeron can be viewed as a set of ladder diagrams corresponding to a sum of completely inelastic  $2 \rightarrow n$  processes, that is, to the last term  $G_{\text{inel}} = 1 - \exp(-\Omega)$  in the unitarity equation (20.9). Here  $n > 2$  means the production of additional  $(n - 2)$  gluons which, after hadronization, form minijets.<sup>15</sup> Therefore, in the final state driven by one Pomeron we expect to observe gluon minijets with a flat rapidity distribution in the central (plateau) rapidity region. This would correspond to a flat pseudorapidity distribution of produced particles if they were massless. A typical pseudorapidity distribution of charged particles in inclusive events (up to  $|\eta| = 7$ ) is shown in Fig. 20.11 (left) [150] (see also Fig. 52.1 in [1]). The central part ( $|\eta| < 2.5$ ) was measured by CMS, while the forward region was covered by TOTEM. The dip observed at  $\eta = 0$  is explained by the presence of massive particles (the Jacobian  $J(p_T, m, \eta) = p_T/E \rightarrow p_T/\sqrt{p_T^2 + m^2}$  at  $\eta = 0$ ). A photon energy spectrum is shown in Fig. 20.11 (right) [151], measured by LHCf inclusively and in events with a diffraction topology, i.e. no charged particles with  $p_T > 100$  MeV and  $|\eta| < 2.5$  observed by ATLAS. As expected in diffractive events the energy flow decreases with  $E_\gamma$  more slowly than that in the inclusive case.

The energy dependence of the particle density  $dN_{\text{ch}}/d\eta$  at  $\eta = 0$  is shown in Fig. 20.12 (left). Neglecting absorptive corrections given by the enhanced diagrams (which mainly change (‘renormalize’) the effective Pomeron intercept  $\alpha_{\text{eff}}(0) = 1 + \Delta$  [121]), we conclude that according to the AGK rules the plateau height  $d\sigma/d\eta \propto s^\Delta$  is driven just by the one-Pomeron exchange with effective  $\Delta \sim 0.2$  (see Section 20.3.3.3). That is, the density of secondaries observed in the inclusive process increases with increasing energy faster than the total cross section, whose growth is tamed by the multi-Pomeron diagrams. Indeed, as is seen from Fig. 20.12 (left), in the interval of collider energies  $dN_{\text{ch}}/d\eta = (1/\sigma_{\text{inel}})d\sigma/d\eta \propto s^{0.115}$  (i.e.  $d\sigma/d\eta \propto s^{0.215}$ ), while  $\sigma_{\text{inel}} \propto s^{0.1}$ .

<sup>15</sup>Minijets result from hadronization of partons emitted from the cut QCD Pomeron. Typically these are groups of hadrons with comparatively low overall  $E_T \lesssim 5\text{--}10$  GeV.

Contrary to the ‘old’ Regge theory where it was *assumed* (based on the experimental data existing in the 1950s and 1960s) that all transverse momenta are limited, in QCD the  $k_t$  distributions of jets (charged particles) have a long  $k_t$  tail ( $d\sigma/dk_t^2 \propto \alpha_s^2(k_t^2)/k_t^4$  at large  $k_t$  and very large energy  $s \gg k_t^2$ ). An example of the  $p_T$  distribution of charged secondaries is shown in Fig. 20.12 (right).

Note that the mean transverse momentum of secondaries, produced via jet fragmentation, slowly increases with collision energy, see Fig. 20.13 (right). This is caused by the stronger absorption (at larger  $\sqrt{s}$ ) of the gluons with a smaller  $k_t$  ( $\sigma^{\text{abs}} \propto 1/k_t^2$ ). The growth of  $\langle p_T \rangle$  with multiplicity (see Fig. 20.13 (left)) can be explained by the fact that events with larger  $N_{\text{ch}}$  correspond to a smaller impact parameter,  $b$ , where the absorption of a low  $k_t$  component is stronger and, next, larger multiplicity can be originated by the events with jets/minijets with higher  $p_T$ . Since the mean  $p_T$  of secondaries grows with  $\sqrt{s}$ , the increase with  $\sqrt{s}$  of transverse energy flow is a bit faster than that of particle density.

The model [162] based on a modification of the classic RFT allows one to trace the smooth transition from the pure perturbative, large  $k_t$ , region into the *soft* domain. A strong absorption of the low  $k_t$  partons plays a crucial role here since it produces an effective infrared cutoff,  $k_{\text{sat}}$ , and provides the possibility of extending the parton approach, used for ‘hard’ processes, to also describe high-energy soft and semihard interactions. This approach combines a description of soft physics and diffraction with jet physics in a coherent self-consistent way.

Another way is to include the soft and hard components independently [37, 66, 163, 164]. In this approach the soft part is described in terms of RFT with the phenomenological ‘soft’ Pomeron pole while the hard part is calculated in terms of the parton model for minijet production with the energy dependent cutoff  $k_t > k_0(s)$ . A combined description of soft and hard processes in hadronic collisions is reached within the QGSJET Monte Carlo model (e.g. [61]) in the framework of the so-called ‘semihard Pomeron’ approach (see e.g. [165]).

In [166] a model was constructed, which incorporated the attractive features of the two successful theoretical approaches to high energy QCD: BFKL Pomeron calculus [59, 60] and the Colour Glass Condensate/saturation [167].

#### 20.5.2.1 Correlations

All LHC experiments routinely measure tracks with  $p_T > p_{\text{min}}$ , where  $p_{\text{min}}$  can vary in different studies. Typically,  $p_{\text{min}} = 200$  MeV, where tracking reconstruction efficiencies are larger than 70%. In order to identify particle species, each experiment has sophisticated identification procedures usually based on the ionization energy loss,  $dE/dx$ , or other techniques, with different regions of applicability for different particle species. Thanks to usually relatively large cross sections of soft QCD processes, most of the results below come from event samples with very low or negligible pile-up.

Following the notation in [168], symmetrized inclusive particle number densities for  $q$  points at  $y_1, \dots, y_q$  (where  $y_i$  represents the 4-momentum of the  $i$ th particle,  $\rho_q(y_1, \dots, y_q)$ , are related to the inclusive differential cross section by

$$\frac{1}{\sigma_{\text{inel}}} d\sigma = \rho_1(y) dy, \quad \frac{1}{\sigma_{\text{inel}}} d^2\sigma = \rho_2(y_1, y_2) dy_1 dy_2 \quad \text{etc.} \quad (20.48)$$

By integrating we get

$$\int \rho_1(y) dy = \langle n \rangle, \quad \int \int \rho_2(y_1, y_2) dy_1 dy_2 = \langle n(n-1) \rangle \quad \text{etc.}, \quad (20.49)$$

where the angular brackets denote averaging over the event sample and  $n$  is the particle multiplicity.

Since the inclusive  $q$ -particle densities in general contain trivial contributions from lower-order densities, it is convenient to consider quantities  $C_q$  which vanish when one of their arguments becomes statistically independent of (uncorrelated with) the others. These quantities  $C_q$ , called correlation functions (or cumulant

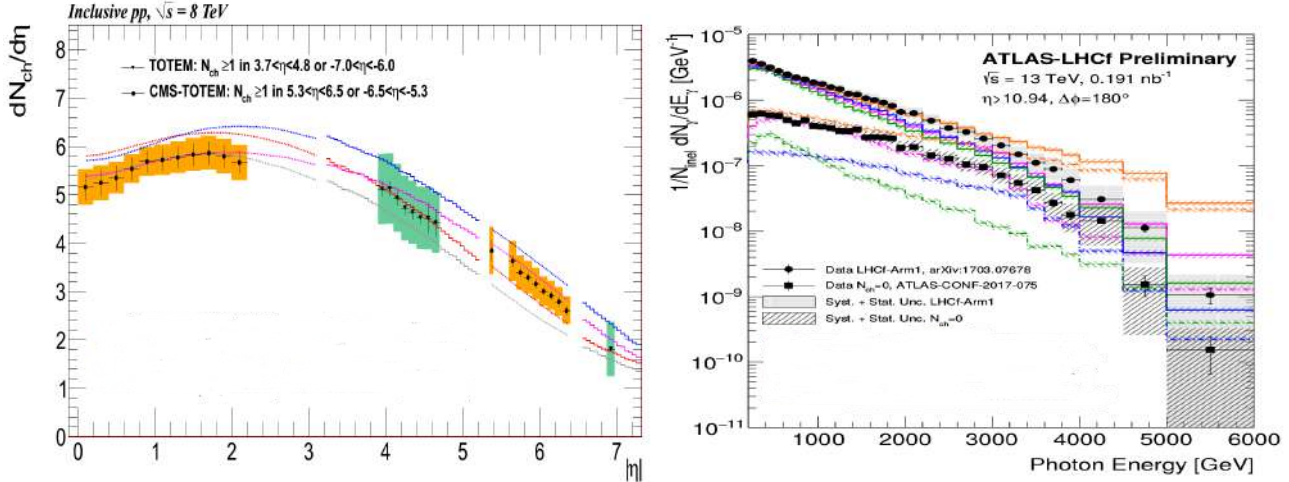


Figure 20.11: (Left) Charged-particle pseudorapidity distribution for inclusive events measured by CMS and TOTEM [150]. The error bars represent the statistical and uncorrelated systematic uncertainties between neighboring bins, while the shaded areas denote the combined statistical and full systematic uncertainties. The coloured lines indicate model predictions. (Right) Photon energy spectrum measured by LHCf at  $|\eta| > 10.94$ . The filled circles show the inclusive photon spectrum measured by LHCf [152] and filled squares the spectrum for  $N_{ch} = 0$  events where no charged particles with  $p_T > 100$  MeV and  $|\eta| < 2.5$  are observed by ATLAS [153]. The coloured lines indicate model predictions. The error bars correspond to the statistical uncertainties and the shaded areas denote the combined statistical and systematic uncertainties. Figure from Ref. [151].

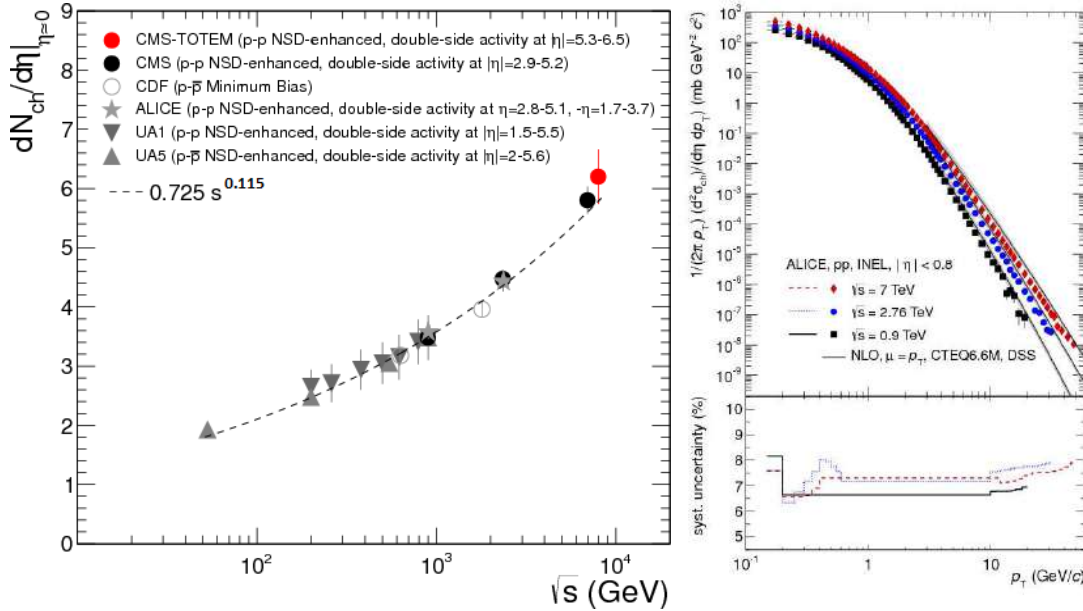


Figure 20.12: (Left) Energy dependence of the charged particle density  $dN_{ch}/d\eta$  at  $\eta \approx 0$  for  $pp$  and  $p\bar{p}$  collisions. Shown are measurements performed with different Non-SD event selections from UA1 [154], UA5 [155], CDF [156,157], ALICE [158] and CMS [159]. The dashed line is a power-law fit to the data. Figure from Ref. [150]. (Right) Differential cross section of charged particles with  $|\eta| < 0.8$  in inelastic  $pp$  collisions at  $\sqrt{s} = 0.9, 2.76$  and  $7$  TeV as a function of  $p_T$ . Only statistical uncertainties are shown. Figure from Ref. [160].

functions), are defined as:

$$\begin{aligned}
 C_2(1, 2) &= \rho_2(1, 2) - \rho_1(1)\rho_1(2), \quad C_3(1, 2, 3) \\
 &= \rho_3(1, 2, 3) - \sum_{(3)} \rho_1(1)\rho_2(2, 3) + 2\rho_1(1)\rho_1(2)\rho_1(3), \\
 C_4(1, 2, 3, 4) &= \rho_4(1, 2, 3, 4) - \sum_{(4)} \rho_1(1)\rho_3(1, 2, 3) \\
 &\quad - \sum_{(3)} \rho_2(1, 2)\rho_2(3, 4) + 2 \sum_{(6)} \rho_1(1)\rho_1(2)\rho_2(3, 4) \\
 &\quad - 6\rho_1(1)\rho_1(2)\rho_1(3)\rho_1(4).
 \end{aligned} \tag{20.50}$$

The 2D two-particle correlation function is defined as

$$C(\Delta\eta, \Delta\phi) = \frac{\rho_2(\Delta\eta, \Delta\phi)}{\rho_1(\eta_a, \phi_a)\rho_1(\eta_b, \phi_b)}. \tag{20.51}$$

The distribution  $\rho_2(\Delta\eta, \Delta\phi)$  is usually interpreted as a conditional probability to observe a particle  $a$  at the phase-space point  $(\eta_a, \phi_a)$  if a particle  $b$  at  $(\eta_b, \phi_b)$  is observed as well, and  $\Delta\eta = \eta_a - \eta_b$  and  $\Delta\phi = \phi_a - \phi_b$ . The distributions  $\rho_1(\eta_a, \phi_a)$  and  $\rho_1(\eta_b, \phi_b)$  are probabilities to observe a single particle at  $(\eta_a, \phi_a)$  and  $(\eta_b, \phi_b)$ , respectively. The denominator of Eq. (20.51) is constructed as a product of two single-particle distributions using an event mixing technique, where each particle in the pair comes from a different event. Experimentally, each reconstructed track

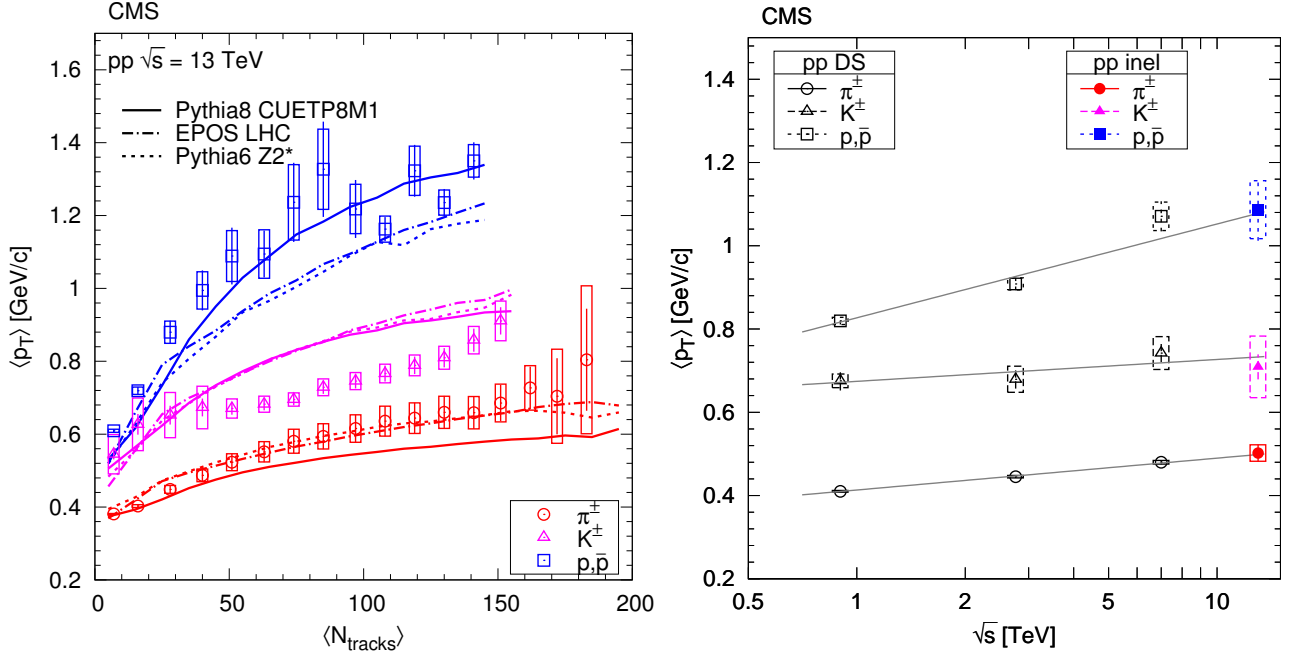


Figure 20.13: Average  $p_T$  of pions, kaons and protons in the range  $|\eta| < 1.0$  as a function of (left) track multiplicity at  $|\eta| < 2.4$  and (right) of center-of-mass energy where the curves show linear fits using lns. The error bars indicate the uncorrelated combined uncertainties, while the boxes show the uncorrelated systematic uncertainties. Figures from Ref. [161].

is weighted by the inverse of an efficiency factor which accounts for the detector acceptance, the reconstruction and particle identification efficiencies, the contamination by secondary particles and the fraction of misreconstructed tracks.

An example of two-particle correlation functions measured in  $pp$  collisions at 7 TeV is shown in Fig. 20.14 for identical-particle pairs (right panel) and for particle–anti-particle pairs (left panel) [169].

We observe two distinct features which can be explained by short-range (in rapidity) correlations: 1) a near-side peak at  $\Delta\phi \approx 0$  and 2) an away-side peak or rather a ridge at  $\Delta\phi \approx \pi$ . The near-side peak is considered to be caused by at least three effects:

- *fragmentation of partons scattered at a hard scale.* These relatively high  $p_T$  partons produce showers which after the hadronization form the mini-jets which create a broad structure extending over at least one unit in  $\Delta\eta$  and  $\Delta\phi$ .
- *resonance decays.* The decay of resonances contributes to the near-side peak at  $\Delta\eta \sim 0$  and extended in  $\Delta\phi$  [170–172], depending on the released kinetic energy of the given resonance. This effect is mostly visible for unlike-sign particle pairs.
- *femtoscopic correlations.* The term “femtoscopic” refers to a length scale of the order of  $10^{-15}$  m. These correlations are present at low relative momenta of the particles in a pair (representing a very small phase-space corner, so they are practically invisible in terms of  $(\Delta\eta, \Delta\phi)$ ) and give rise to an enhancement of the correlation function (due to Bose-Einstein quantum statistics for identical bosons) or its suppression (due to Fermi-Dirac quantum statistics for identical fermions). Besides this, at low relative momenta there are correlations caused by Coulomb and/or other final state interactions. The shape of all these effects in  $(\Delta\eta, \Delta\phi)$  space depend strongly on the mass of the particle type as well as on the size of the particle-emitting system. The latter is traditionally measured in Bose-Einstein correlation (BEC) analyses and is not part of this review.

The away-side peak originates from energy-momentum conservation which manifests itself by the quark and the anti-quark going back-to-back in  $\phi$ . In this case the rapidity width of the away-side peak is much larger than the near-side peak since in the original matrix element the quark and the antiquark can be separated by some  $\Delta\eta$  interval.

As discussed in Sections 20.3.3.2 and 20.3.3.3, there may be several cut Pomerons in the same event, each giving rise to particle sets which are, in general, independent of each other (except for small Bose-Einstein correlations). This leads to long-range (in rapidity) correlations. Since the density of secondaries,  $dN/dy$ , is proportional to the number of cut Pomerons,  $k$ , the probability to observe at least one particle is proportional to  $\langle k \rangle$ , while the probability to observe simultaneously two particles separated by some (rather large) rapidity interval is proportional to  $\langle k^2 \rangle$ . Thus the long-range correlations are predicted to be  $C_2 = \langle k^2 \rangle / \langle k \rangle^2 - 1 > 0$  which depends weakly on the separation  $\Delta\eta$  between the two particles [173, 174]. In the case of the pure eikonal approach, neglecting the enhanced diagrams and the conservation law effects in the proton fragmentation region, we expect that these long-range correlations,

$$C_2(\Delta y) = \frac{\sigma_{\text{inel}} d^2\sigma/dy_1 dy_2}{d\sigma/dy_1 d\sigma/dy_2} - 1 \sim \text{const}, \quad (20.52)$$

do not depend on the rapidity separation,  $\Delta y = |y_1 - y_2|$ , between the two particles. The contribution of the processes with more cut Pomerons also results in a much wider multiplicity distribution and in a larger density of soft particles coming from the ‘underlying event’.

#### 20.5.2.2 Color reconnection

In this context, we have to mention also the so-called ‘colour reconnection’ phenomenon. This is a pure ‘soft QCD’ effect. The point is that after a number of coloured secondary partons are produced, there are different possibilities to form the colour flow between these partons and to group the partons into colourless clusters. In the process of reconnection, one rearranges the colour flow in such a way as to minimize the size of the clusters. This is especially important when dealing with MPI contributions. The reconnection between the different cut Pomerons diminishes the final multiplicity and can change the form of the  $N_{\text{ch}}$  distributions (see e.g. Section 41.3.3 of [1] and [2, 13, 177, 178]).

#### 20.5.2.3 Double parton scattering

The probability of MPI depends on the spatial distribution of partons in the incoming protons. The effects of MPI are suppressed if the density of partons is low and the partons from the incoming beam particles are separated from each other by a large

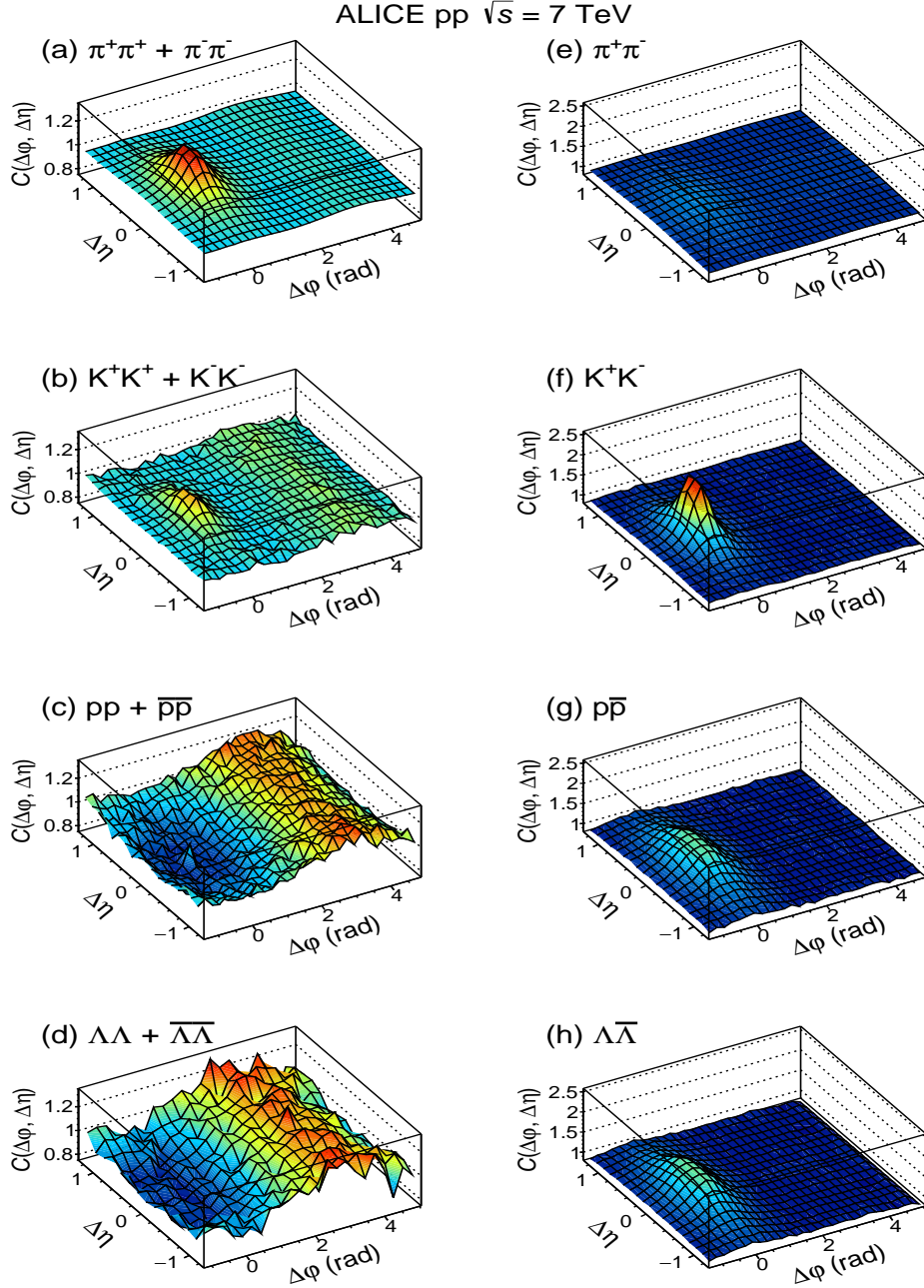


Figure 20.14: Two-particle correlation functions for identical-particle pairs:  $\pi^+\pi^+ + \pi^-\pi^-$ ,  $K^+K^+ + K^-K^-$ ,  $pp + \bar{p}\bar{p}$ , and  $\Lambda\Lambda + \bar{\Lambda}\bar{\Lambda}$  (left panel) and particle-anti-particle pairs:  $\pi^+\pi^-$ ,  $K^+K^-$ ,  $p\bar{p}$  and  $\Lambda\bar{\Lambda}$  (right panel). Figure from Ref. [169].

interval in transverse coordinate space  $\vec{x}_t$ . Events in which two hard subprocesses, caused by interactions of two different parton pairs (say,  $(a_1b_1)$  and  $(a_2b_2)$ ), take place simultaneously, are called Double Parton Scattering (DPS). The DPS cross section is driven by the ‘double parton distributions’,  $D(y_{a_1}, y_{a_2}, \dots)$ , where  $y_{a_1}$  and  $y_{a_2}$  are momentum fractions carried by the partons from the proton  $a$  and the dots denote all other coordinates. As a rule, experiments study DPS processes at relatively small momentum fractions  $y_i$ . Here, correlations due to momentum conservation (like  $y_{a_1} + y_{a_2} < 1$ ) are not so important, and with a reasonable accuracy we can assume a factorization

$$D(y_{a_1}, y_{a_2}, \dots) \propto F(y_{a_1}) \cdot F(y_{a_2}), \quad (20.53)$$

where  $F(y_{a_i})$  are the single parton distributions. In such a case the DPS cross section takes the form

$$\sigma^{\text{DPS}} = c \cdot \frac{\sigma_{a_1b_1} \sigma_{a_2b_2}}{\sigma_{\text{eff}}}, \quad (20.54)$$

where  $\sigma_{a_1b_1}$  and  $\sigma_{a_2b_2}$  are cross sections for the two *independent* hard processes, while  $\sigma_{\text{eff}}$  characterizes the mean area occupied by the partons  $a_1$  and  $b_1$ ; the constant factor  $c = 1/2$  if both hard processes  $(a_1b_1)$  and  $(a_2b_2)$  are identical, otherwise  $c = 1$ . Thus the DPS cross section is sensitive to the spatial separations between partons in the proton (see Section 7.2.3 in [2] and [179, 180] for more explanations and reviews).

One problem is that within this approach we *assume* that the partons  $a_1$  and  $a_2$  are produced by two independent parton showers (and similarly for the other incoming proton). On the other hand, there is a probability that from the beginning we start with the evolution of a single shower which further splits into two different branches. In this case the separation between the two partons (two shower branches) becomes very small – of the order of the inverse scale ( $\sim 1/\sqrt{q^2}$ ) at which the splitting occurs. The exact value of this ‘splitting’ scale  $q^2$  depends on the particular kinematics of the DPS process. So, different experiments (with



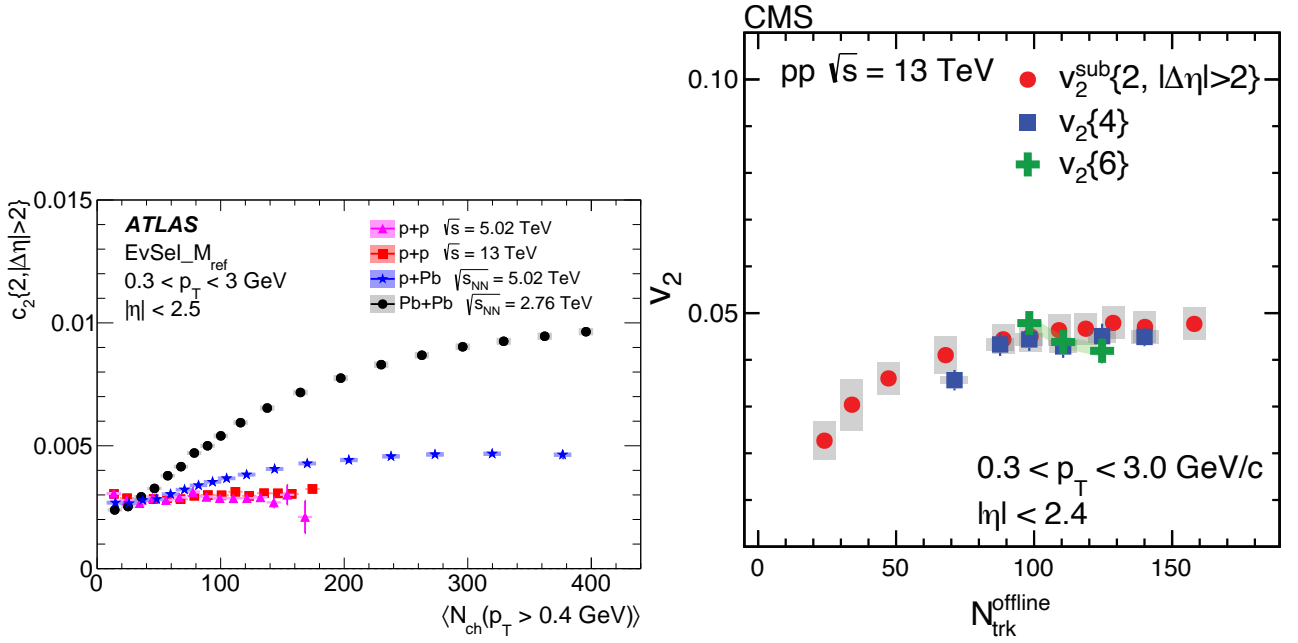


Figure 20.15: (Left) The two-particle cumulant,  $c_2\{2, |\Delta\eta| > 2\}$ , as a function of  $\langle N_{\text{ch}}(p_T > 0.4 \text{ GeV}) \rangle$  for  $pp$  collisions at  $\sqrt{s} = 5.02$  and 13 TeV,  $pPb$  collisions at  $\sqrt{s_{NN}} = 5.02$  TeV and low-multiplicity  $PbPb$  collisions at  $\sqrt{s_{NN}} = 2.76$  TeV. The data are constructed from particles with  $0.3 < p_T < 3.0$  GeV. Figure from Ref. [175]. (Right) The  $v_2\{2, |\Delta\eta| > 2\}$ ,  $v_2\{4\}$  and  $v_2\{6\}$  values as a function of charged particles, averaged over  $0.3 < p_T < 3.0$  GeV and  $|\eta| < 2.4$ , in  $pp$  collisions at  $\sqrt{s} = 13$  TeV. Figure from Ref. [176]. The error bars correspond to the statistical uncertainties, while the shaded areas denote the systematic uncertainties.

different kinematical conditions) can give somewhat different values of  $\sigma_{\text{eff}}$ . In general, the value of  $\sigma_{\text{eff}}$  depends on the following features: a) on the measured process since the spatial ( $b_t$ ) distributions of different incoming partons (light quarks, heavy quarks, gluons) can be different; b) on the splitting scale,  $\sqrt{q^2}$ , of one parton cascade into two branches. The typically high value of the splitting scale then explains the fact that the experimentally measured values of  $\sigma_{\text{eff}} \sim 7\text{--}25$  mb (see Fig. 4 of [181]) are smaller than  $\sigma_{\text{tot}}$  or mostly even lower than the proton area  $\pi R_p^2 \sim 22\text{--}24$  mb (see e.g. [182]); c) on the  $p_T$  balance,  $k_T$ , in the individual hard process (e.g. for two dijet productions  $k_T = |\vec{p}_{T1}| + |\vec{p}_{T2}|$  where  $p_{T1}$  and  $p_{T2}$  are jet  $p_T$ 's of the first hard process (similarly for the second hard process)). A small value of  $k_T$  indicates that there were no splittings or the splitting scale  $\sqrt{q^2}$  was small and, therefore, we expect larger  $\sigma_{\text{eff}}$ ; d) on the contribution of single parton scatterings misidentified as DPS. For a lower scale of the hard process this contribution is larger (see [183] for more detailed discussion).

#### 20.5.2.4 Final state interactions

The formalism of the RFT does not include ‘final state interactions’<sup>16</sup>. Therefore, besides the correlations considered in the previous Section 20.5.2.1 we have to expect the correlation caused by partons and hadrons rescattering in the final state. These effects are not crucial at lower energies, but become more important at high LHC energies, in particular in heavy-ion collisions where the particle density is large. For example, the final state interactions (FSI) lead to the formation of the collective flow of secondaries (see e.g. [185] for a review), especially in high-multiplicity events. To study the collective flow experimentally, one has to subtract correlations coming from few-particle sources such as resonance decays, mini-jets, multi-jets and BEC (so called ‘non-flow’). The non-flow can efficiently be suppressed using the sub-event method, that is by studying the azimuthal correlations between particles separated in  $\eta$  [186], or subtracted using the multi-particle correlation (or cumulant) techniques.

The cumulant method is based on calculating  $2k$ -particle

azimuthal correlations,  $\text{corr}_n\{2k\}$ , and cumulants  $c_n\{2k\}$  (where  $k = 1, 2, \dots$ ), for  $n$ th Fourier harmonics. The  $\text{corr}_n\{2k\}$  are defined as [187, 188]:

$$\begin{aligned} \langle\langle \text{corr}_n\{2\} \rangle\rangle &= \langle\langle e^{in(\phi_1 - \phi_2)} \rangle\rangle, & \langle\langle \text{corr}_n\{4\} \rangle\rangle &= \langle\langle e^{in(\phi_1 + \phi_2 - \phi_3 - \phi_4)} \rangle\rangle, \\ \langle\langle \text{corr}_n\{6\} \rangle\rangle &= \langle\langle e^{in(\phi_1 + \phi_2 + \phi_3 - \phi_4 - \phi_5 - \phi_6)} \rangle\rangle \end{aligned}$$

and similarly for higher numbers of correlated particles. The double-brackets  $\langle\langle \rangle\rangle$  denote averaging first over particles in an event and then over events within a given event class. For every event, the average is taken over all possible combinations of azimuthal angles  $\phi_l$  ( $l = 1, \dots, 2k$ ) of the  $2k$  particles. The cumulants are then obtained from multi-particle azimuthal correlations after subtracting correlations between  $2(k-1)$  particles according to the following formulae [187, 188]:

$$\begin{aligned} c_n\{2\} &= \langle\langle \text{corr}_n\{2\} \rangle\rangle, & c_n\{4\} &= \langle\langle \text{corr}_n\{4\} \rangle\rangle - 2\langle\langle \text{corr}_n\{2\} \rangle\rangle^2, \\ c_n\{6\} &= \langle\langle \text{corr}_n\{6\} \rangle\rangle - 9\langle\langle \text{corr}_n\{2\} \rangle\rangle \times \langle\langle \text{corr}_n\{4\} \rangle\rangle + 12\langle\langle \text{corr}_n\{2\} \rangle\rangle^3. \end{aligned}$$

The cumulants for higher particle multiplicities are calculated in [187, 188]. The cumulants then serve to estimate the Fourier harmonics  $v_n$  as follows [187]:

$$v_n\{2\} = \sqrt{c_n\{2\}}, \quad v_n\{4\} = \sqrt[4]{-c_n\{4\}}, \quad v_n\{6\} = \sqrt[6]{c_n\{6\}}/4.$$

Some of the long-range correlation ( $|\Delta\eta| > 2$ ) results obtained on a sample of charged particles with  $0.3 < p_T < 3.0$  GeV and  $|\eta| < 2.4$  are summarized in Fig. 20.15. The left plot shows the cumulant  $c_2$  measured for  $pp$ ,  $pPb$  and  $PbPb$  collisions [175], while the right plot shows the elliptical harmonics  $v_2$  measured for  $pp$  collisions [176], both as functions of multiplicities of charged particles. The two-particle correlations are observed to be strongest and rising with  $N_{\text{ch}}$  for  $PbPb$  collisions, and weakest and rather flat for  $pp$  collisions. The elliptical-flow harmonics for 4- and 6-particle correlations show again a rather flat multiplicity dependence (at least for large multiplicities). Within experimental uncertainties, the values of  $v_2\{2\}$ ,  $v_2\{4\}$  and  $v_2\{6\}$  measured in  $pp$  collisions at 13 TeV are consistent with each other. The similarity between  $v_2\{4\}$  and  $v_2\{6\}$  suggests that some collective effects are occurring in  $pp$  collisions at high multiplicity and the obser-

<sup>16</sup>In general, final state interactions can be included into the detailed structure of the multi-Pomeron vertices. However these vertices are phenomenological objects which are not well known experimentally.

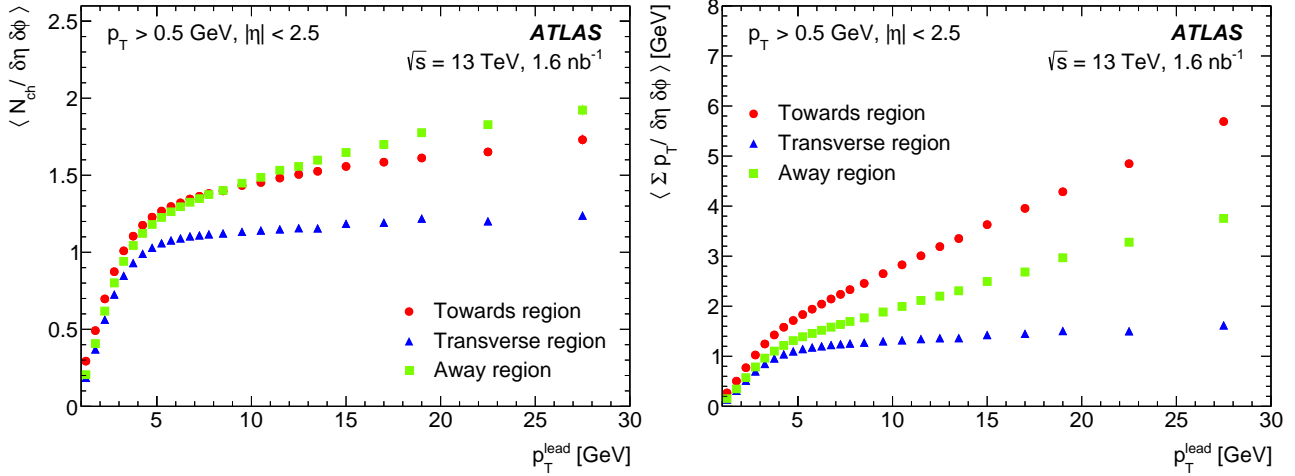


Figure 20.16: Mean charged particle density (left) and the sum of transverse momenta of secondaries (right) in events with the ‘leading’ high  $p_T$  particle as a function of  $p_T^{\text{lead}}$  in the transverse, towards and away azimuthal regions. Secondaries with  $p_T > 0.5$  GeV and  $|\eta| < 2.5$  are registered. The error bars (mostly hidden by the data markers) represent combined statistical and systematic uncertainties. Figures from [184].

vations are similar to those in  $PbPb$  collisions, where the  $v_2\{4\}$  values were measured to be close to  $v_2\{6\}$  but they are both lower than  $v_2\{2\}$  (not shown here).

Another example of long-range correlations is the so-called ‘ridge effect’. Here not only the ‘back-to-back’ jet correlations are registered, but also an excess of particles going in the same (in the azimuthal plane) direction as the leading (relatively high  $p_T$ ) hadron. Moreover, this excess is seen at the rapidities separated from the leading hadron by a rather large interval (see e.g. [189] for a review).

It is popular to describe such FSI effects within the hydrodynamic model [190], which operates with collective (thermodynamic) variables. In terms of microscopic interactions, the collective flow can be caused by the geometry of a particular collision (the absorption is smaller for the secondaries flying in the direction orthogonal to the impact parameter vector  $\vec{b}$  [191, 192]), or by the colour reconnection at the hadronization stage [193], or accounting for the rescattering of secondaries directly, as was done, for example, in the AMPT model [194].

### 20.5.3 The underlying event

Except for the exclusive case, any ‘hard’ subprocess is accompanied by soft secondaries coming from initial state radiation (ISR), final state radiation (FSR) and multiple parton interaction (MPI), see Subsection 7.2.2 in [2]. These extra particles distort the signal we are looking for. In particular, they affect the isolation criteria applied to photons and charged leptons and the vertex reconstruction efficiency. In general, also the effects of colour reconnection (discussed in Section 20.5.2.2) contribute to the underlying event.

The usual procedure of estimating the amount of underlying event (UE) is to spatially divide tracks in each event according to their azimuthal angle into the Toward region (where the highest  $p_T$  jet points), the Away region (opposite to the Toward region) and to two Transverse regions. The standard observables are the average track multiplicity per unit area and the average scalar sum of track  $p_T$  per unit area. Figure 20.16 shows the particle density and the sum of  $p_T$  for the UE in ATLAS events containing at least one charged particle with  $p_T > 0.5$  GeV and  $|\eta| < 2.5$  [184].

Note that by construction the largest values of  $\langle p_T \rangle$  are observed in the ‘Toward’ region, while in the ‘Away’ region we observe a slightly larger density than in the Toward region. These are results of the ‘leading’ and ‘backward’ jet fragmentation. In the transverse region, mostly filled by particles from the UE, the particle density and sum of  $p_T$  per unit  $(\Delta\eta, \Delta\phi)$  area practically do not depend on the  $p_T^{\text{lead}}$  since these secondaries come from the other cut Pomeron(s), that is, from other ‘multiple interactions’. For low  $p_T^{\text{lead}} < 2$  GeV the distributions in all three regions are close to each other. These events actually do not contain a ‘hard’

subprocess. Moreover, for a very small  $p_T^{\text{lead}} \rightarrow 1$  GeV we start to select soft events with abnormally low  $p_T < p_T^{\text{lead}}$  particles. Since only particles with  $p_T > 0.5$  GeV are registered, the signal drops fast for  $p_T^{\text{lead}} \rightarrow 1$  GeV. As a function of collision energy  $\sqrt{s}$ , the energy flow in the transverse region increases as  $\sum p_T \sim s^{0.2}$  (as follows from Fig. 7 (right) in [184]) due to the larger number of MPI collisions and larger  $\langle p_T \rangle$  in each collision<sup>17</sup>. As follows from this and other UE-dedicated LHC studies [195], from the comparisons of the data to the models with and without MPI, the necessity of MPI is convincingly demonstrated.

## 20.6 The Odderon

Apart from the even-signature singularity (Pomeron), in QCD with  $N_c = 3$  there exists its counterpart, the odd-signature singularity placed at  $j \simeq 1$  and formed by three t-channel reggeized gluons connected in colour space by the symmetric  $d^{abc}$  tensor of the colour  $SU(3)$  group [196, 197]. This object is called the Odderon. The Odderon exchange amplitude has opposite sign for  $pp$  and  $p\bar{p}$  scatterings. Its intercept is predicted to be very close to  $j = 1$  [198–200], while according to perturbative estimates the coupling to the nucleon is rather small [201, 202]. The corresponding amplitude is mainly real and is about 100 times smaller than the imaginary part of the Pomeron exchange amplitude. Calculating the elastic amplitude via the eikonal formula (20.13) we have to replace the opacity  $\Omega(b)$  by the sum  $\Omega = \Omega_{\text{even}} + \Omega_{\text{odd}}$ , where  $\Omega_{\text{even}}$  is mainly real and  $\Omega_{\text{odd}}$  is imaginary. Note that at  $t = 0$  this QCD Odderon does not couple to mesons, and the  $t$ -slope of the Odderon amplitude is expected to be smaller than that for the Pomeron; instead of the singularity at  $t = 4m_\pi^2$  in the Pomeron case, the nearest singularity in the Odderon channel is at  $t = 9m_\pi^2$ , see for instance [200]. Thus, in the impact parameter  $b$  space the QCD Odderon occupies an area of a smaller radius, see e.g. [203].

Experimentally an indication in favour of a manifestation of the high energy C-odd amplitude was observed by comparing the elastic  $pp$  and  $p\bar{p}$  cross sections in the dip region (where the contribution from the C-even amplitude has a minimum) at the CERN-ISR [205], see Fig. 20.17 (left)<sup>18</sup>.

To get a better understanding of the Odderon effects it would be very instructive to have the  $d\sigma_{el}/dt$  data for both  $pp$  and  $p\bar{p}$  reactions at the same but higher energy  $\sim 1$  TeV (ideally in the same apparatus) and, in the ideal case, to study the energy de-

<sup>17</sup>Recall the stronger absorption of the low  $k_t$  partons.

<sup>18</sup>Note that a qualitatively similar behaviour to the  $p\bar{p}$  ISR data, namely a filling in of the dip in the  $t$ -distribution, was observed by the UA4 collaboration at the CERN  $Spp\bar{S}$  collider at  $\sqrt{s}=546$  and 630 GeV (see [208, 209] and in particular Fig. 2 in [209]) and by the  $D0$  collaboration at the Tevatron at 1.96 TeV [207].

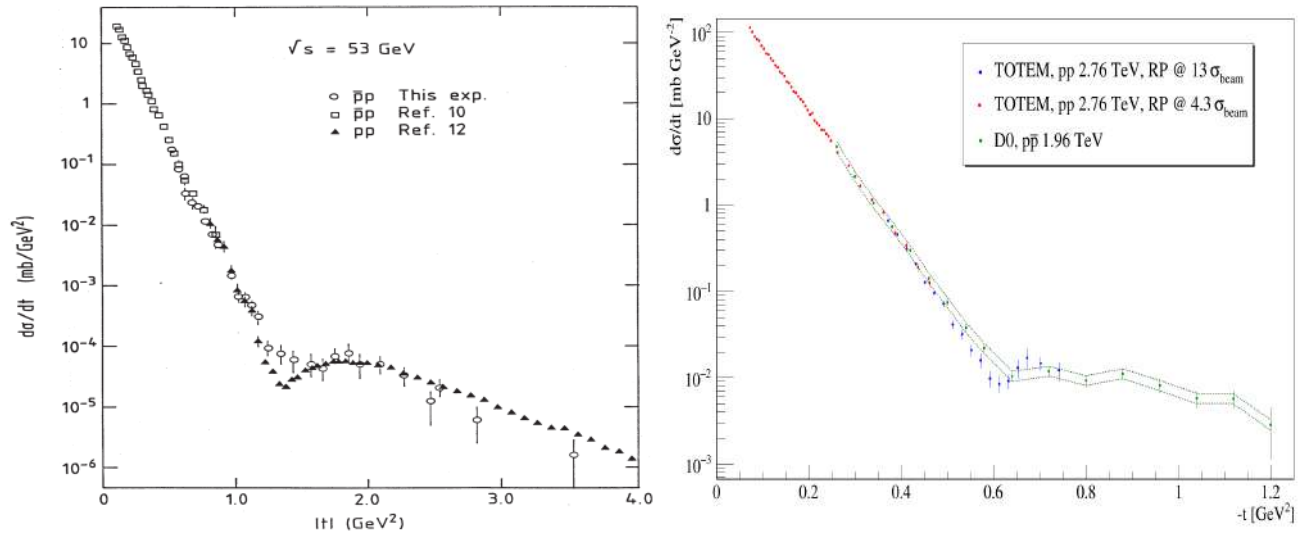


Figure 20.17: Comparison of the  $t$ -dependence of the elastic cross sections from  $pp$  and  $p\bar{p}$  collisions. (Left) Data from the ISR energy of 53 GeV are shown by closed triangles [204] for  $pp$  collisions and by open circles [205] and open squares [206] for  $p\bar{p}$  collisions. Only  $t$ -dependent uncertainties are shown and the systematic scale uncertainty is estimated to be  $\pm 30\%$ . Figure from Ref. [205]. (Right) Data from the D0 experiment at 1.96 TeV [207] are compared with data from the TOTEM experiment [103]. The green dashed line indicates the normalization uncertainty of the D0 measurement. Figure from Ref. [103].

pendence.

At the moment we can only compare the  $pp$  cross section measured by TOTEM at  $\sqrt{s} = 2.76$  TeV [103] with the  $d\sigma/dt$  values measured by the D0 collaboration at 1.96 TeV in  $p\bar{p}$  collisions [207], see Fig. 20.17 (right).

The situation looks quite intriguing, but needs further investigation. Note that in the TeV energy range the  $\omega, \rho$  and  $\omega P, \rho P$  exchange contributions, which may be responsible for the difference between the  $pp$  and  $p\bar{p}$  cross sections in the dip region at the ISR energies, are practically negligible.

Another way to search for the Odderon is to measure the real part of the elastic  $pp$  scattering amplitude via the interference with the pure QED one-photon exchange. Since the one-photon exchange amplitude contribution is sizeable only at very small  $|t|$ , this way we can study the Odderon at or near to  $t = 0$ . Indeed, the value of the ratio  $\rho \equiv \text{Re}T_{\text{el}}/\text{Im}T_{\text{el}}$ , obtained by TOTEM at 13 TeV ( $\rho = 0.10 \pm 0.01$  [102]), turns out to be smaller than that expected for the pure even-signature amplitude, see Fig. 20.18.

Based on dispersion relations and assuming the  $C$ -even contribution only, from the known total cross sections we would rather expect  $\rho \simeq 0.13$ – $0.14$ . The difference could indicate that the rise of the total cross section at energies above those of the LHC slows down (see the dispersion relation, Eq. (20.19)) or this could be attributed to an Odderon contribution (see e.g. [210]). However, the Odderon exchange amplitude extracted in this analysis has opposite sign to that for the lowest- $\alpha_s$ -order QCD Odderon, see e.g. [201, 202, 211, 212]. Besides this, the Odderon contribution to  $\rho$ , obtained in [210], grows with  $\sqrt{s}$  (for  $\sqrt{s} > 0.5$  TeV), while in QCD we expect that the Odderon contribution to  $\rho$  decreases with energy, since the QCD Odderon intercept is smaller than that of the QCD Pomeron.

It is worth mentioning also that the Odderon contribution is strongly screened by the multi-Pomeron diagrams, which facilitate the falling-off of  $\rho$  with energy increasing, see [213, 214]. On the other hand, analyzing the whole ensemble of high energy elastic  $pp$  ( $p\bar{p}$ ) low  $|t|$  data, a reasonable description can be obtained using the even-signature amplitude only, that is, without the Odderon. In particular, the RR(PL2)qc model/version of the COMPETE parameterization is consistent with the TOTEM 13 TeV data on  $\sigma_{\text{tot}}$  and  $\rho$  within  $1\sigma$ <sup>19</sup>. Another example is the recent analysis in [212] of the low  $|t| < 0.1$   $\text{GeV}^2$  elastic data. Fitting all the low- $t$   $pp$  and  $p\bar{p}$  data in the range of  $\sqrt{s}$  between 13 GeV and 13 TeV without Odderon, Donnachie and Landshoff [212] succeeded to

describe the TOTEM cross section with less than  $1\sigma$  deviation in each  $d\sigma_{\text{el}}/dt$  point (see Fig. 8 of [212]). Note that in this analysis, they get a larger value of  $\rho$  close to 0.14 at 13 TeV.

It was proposed also to search for the Odderon in exclusive  $C$ -even meson ( $\pi^0, \eta, f_2, \eta_c, \dots$ ) photoproduction (see e.g. [215, 216]). However the expected cross sections are small (e.g. for  $\eta_c$ ) and in each channel there is a large background caused either by Pomeron-Pomeron fusion (such as CEP of the  $f_2$  meson production in  $pp$  or  $pPb$  collisions) or due to the vector meson radiative decay (such as  $\omega \rightarrow \pi^0\gamma$  for the case of pion) [217]. Up to now, no definitive Odderon signal in the  $C$ -even meson production has been observed. At the moment there exist only upper limits on the photoproduction cross sections obtained in the measurements at HERA with  $\sqrt{s} \simeq 200$  GeV [218–220].

To conclude, let us emphasize that the existence of the  $C$ -odd singularity with intercept

$\alpha_{\text{odd}}(0) \simeq 1$  is a firm prediction of QCD. At least in the high  $k_t$  region there is a well established  $C$ -odd three-gluon contribution to the scattering amplitude. However the expected coupling of such an Odderon singularity is numerically very small. Therefore it is quite challenging to observe its manifestation experimentally. Currently it seems to be a bit premature to draw any definite conclusion about an experimental observation of the Odderon signal.

## 20.7 Asymptotics

The high-energy behaviour of total hadronic cross sections has been one of the oldest problems of strong interactions over many decades, beginning from Heisenberg [221]. The most important bound obtained based on general analytical properties of scattering amplitudes is the FLM bound [47–49]. It states that the growth of the total hadronic cross section with energy does not exceed  $\ln^2 s$ , see Eq. (20.34).

Recall that we neglected the photon contribution as well as the whole electro-weak sector, and that the parameter in Eq. (20.34)  $s_0$  is an *a priori* unknown scale. However, if we were to assume a reasonable hadronic scale,  $s_0 \simeq 1 \text{ GeV}^2$ , we would find that Eq. (20.34) implies an unrealistically high upper bound in comparison with the cross sections observed at present collider energies. Nevertheless there is a common trend in the literature (see for instance, reviews [222, 223] and references therein) to fit phenomenologically the total cross section with  $\ln^2 s$ , keeping in mind the saturation of the FLM bound. Such an asymptotic behaviour is assumed also by the COMPETE collaboration [22], which achieved a comprehensive description of all soft pre-LHC data measured at  $\sqrt{s} \geq 4$  GeV as well as total  $pp$  cross sections

<sup>19</sup>We thank Jean-Rene Cudell for clarifying this issue.



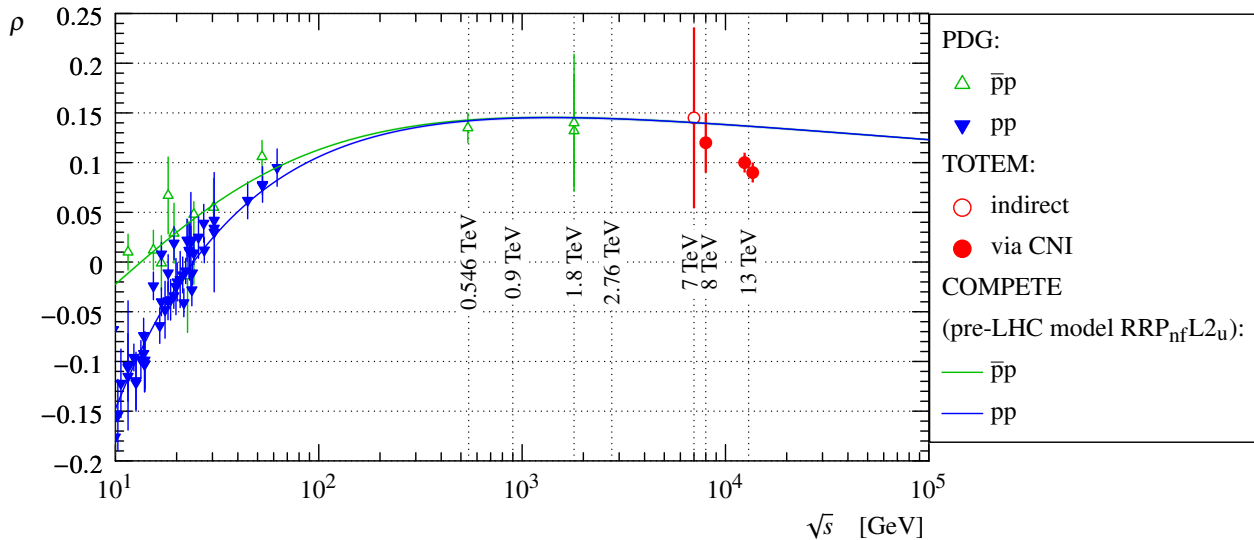


Figure 20.18: The dependence of the  $\rho$  parameter on the collision energy. The  $pp$  (blue) and  $p\bar{p}$  (green) data are taken from [1]. The TOTEM measurements are marked in red. The two points at 13 TeV correspond to two fit cases, discussed in [102], using the same data. The lines represent fits to the data using the COMPETE parameterization [22]. Figure from Ref. [102].

from the LHC available in the first half of 2015 (see Section 51 in [24]).

It is interesting that the Froissart-type  $\ln^2 s$  asymptotics of the  $pp$  total cross section are also supported by numerical results in lattice QCD [224]. Such a behaviour is also observed in the approach [225] based on Colour Glass Condensate saturation.

Finally, it is worth mentioning that the possibility that *asymptotically* the Pomeron intercept becomes smaller than 1,  $\alpha_{\mathbb{P}}(0) < 1$ , and at very high energies the total cross section starts to decrease with energy, though highly unlikely, is not yet completely rejected. For instance, such a behaviour is expected in a theory with only the triple-Pomeron coupling,  $g_{3\mathbb{P}}$ , and which neglects the more complicated multi-Pomeron vertices  $g_m^n$ , such as the  $2 \rightarrow 2$  Pomeron coupling [226, 227].

It was also argued that in the case of an increasing (with energy) cross section the only regime consistent asymptotically with both the  $s$ - and the  $t$ -channel unitarities is that of a *black disc* whose radius increases as  $R = c \cdot \ln s$  [228] (i.e.  $R \propto (\ln s)^\gamma$ , with  $\gamma = 1$  exactly).

## 20.8 Acknowledgements

It is a pleasure to thank Michael Albrow, Robert Cahn, Robert Ciesielski, Per Grafstrom, Frank Krauss, Paul Newman, Sergey Ostapchenko and Edward Sarkisyan-Grinbaum for discussions, suggestions and comments on this review. Special thanks to Graeme Watt who read the article through and helped to improve the presentation. MT is supported by MEYS of the Czech Republic within project LTT17018. VAK thanks the Institute of Physics of the Czech Academy of Sciences in Prague for hospitality.

## References

- [1] M. Tanabashi *et al.* (Particle Data Group), *Phys. Rev.* **D98**, 3, 030001 (2018).
- [2] J. Campbell, J. Huston and F. Krauss, *The Black Book of Quantum Chromodynamics*, Oxford University Press (2017), ISBN 9780199652747, URL <https://global.oup.com/academic/product/the-black-book-of-quantum-chromodynamics-9780199652747>.
- [3] R. J. Eden *et al.*, *The analytic S-matrix*, Cambridge Univ. Press, Cambridge (1966).
- [4] A. Martin, *Lect. Notes Phys.* **3**, 1 (1969).
- [5] P. D. B. Collins, *An Introduction to Regge Theory and High-Energy Physics*, Cambridge Monographs on Mathematical Physics, Cambridge Univ. Press, Cambridge, UK (2009), ISBN 9780521110358, URL <http://www-spires.fnal.gov/spires/find/books/www?cl=QC793.3.R4C695>.
- [6] S. Donnachie *et al.*, *Camb. Monogr. Part. Phys. Nucl. Phys. Cosmol.* **19**, 1 (2002).
- [7] V. N. Gribov, *The theory of complex angular momenta: Gribov lectures on theoretical physics*, Cambridge Monographs on Mathematical Physics, Cambridge University Press (2007), ISBN 9780521037037, 9780521818346, 9780511055041, URL <http://www.cambridge.org/uk/catalogue/catalogue.asp?isbn=0521307848>.
- [8] S. Ostapchenko, in “25th European Cosmic Ray Symposium (ECRS 2016) Turin, Italy, September 04-09, 2016,” (2016), [arXiv:1612.09461].
- [9] T. Sjostrand, *Int. J. Mod. Phys.* **A3**, 751 (1988).
- [10] B. Andersson, *Camb. Monogr. Part. Phys. Nucl. Phys. Cosmol.* **7**, 1 (1997).
- [11] W. Kittel and E. A. De Wolf, *Soft multihadron dynamics* (2005), ISBN 9789812562951.
- [12] I. M. Dremin and A. B. Kaidalov, *Phys. Usp.* **49**, 263 (2006), [*Usp. Fiz. Nauk*176,275(2006)].
- [13] A. Buckley *et al.*, *Phys. Rept.* **504**, 145 (2011), [arXiv:1101.2599].
- [14] R. Ciesielski and K. Goulios, *PoS ICHEP2012*, 301 (2013), [arXiv:1205.1446].
- [15] K. Akiba *et al.* (LHC Forward Physics Working Group), *J. Phys.* **G43**, 110201 (2016), [arXiv:1611.05079].
- [16] G. D. Alkhalov, S. L. Belostotsky and A. A. Vorobev, *Phys. Rept.* **42**, 89 (1978).
- [17] E. L. Feinberg and I. Y. Pomeranchuk, *Doklady Akad. Nauk SSSR* **93**, 439 (1953); E. L. Feinberg and I. Y. Pomeranchuk, *Suppl. Nuovo Cimento* **III**, serie X, 652 (1956).
- [18] R. Engel, D. Heck and T. Pierog, *Ann. Rev. Nucl. Part. Sci.* **61**, 467 (2011).
- [19] M. Gell-Mann, in “High-energy physics. Proceedings, 11th International Conference, ICHEP’62, Geneva, Switzerland, Jul 4-11, 1962,” 533–542 (1962).
- [20] S. Frautschi, M. Gell-Mann and F. Zachariasen, *Phys. Rev.* **126**, 6, 2204 (1962).
- [21] K. G. Borekov, A. B. Kaidalov and O. V. Kancheli, *Phys. Atom. Nucl.* **69**, 1765 (2006), [*Yad. Fiz.*69,1802(2006)].
- [22] J. R. Cudell *et al.* (COMPETE), *Phys. Rev. Lett.* **89**, 201801 (2002), [hep-ph/0206172].

- [23] C. Bourrely, J. Soffer and T. T. Wu, *Eur. Phys. J.* **C28**, 97 (2003), [hep-ph/0210264].
- [24] C. Patrignani *et al.* (Particle Data Group), *Chin. Phys.* **C40**, 10, 100001 (2016).
- [25] A. Donnachie and P. V. Landshoff, *Nucl. Phys.* **B231**, 189 (1984).
- [26] A. Donnachie and P. V. Landshoff, *Phys. Lett.* **B296**, 227 (1992), [hep-ph/9209205].
- [27] S. Mandelstam, *Nuovo Cim.* **30**, 1148 (1963).
- [28] V. N. Gribov, I. Ya. Pomeranchuk and K. A. Ter-Martirosian, *Phys. Lett.* **9**, 269 (1964).
- [29] V. A. Khoze, A. D. Martin and M. G. Ryskin, *Int. J. Mod. Phys.* **A30**, 08, 1542004 (2015), [arXiv:1402.2778].
- [30] E. Gotsman, E. Levin and U. Maor, *Int. J. Mod. Phys.* **A30**, 08, 1542005 (2015), [arXiv:1403.4531].
- [31] S. Ostapchenko, *Phys. Rev.* **D81**, 114028 (2010), [arXiv:1003.0196].
- [32] V. N. Gribov, *Sov. Phys. JETP* **26**, 414 (1968), [*Zh. Eksp. Teor. Fiz.* 53,654(1967)].
- [33] U. Amaldi, M. Jacob and G. Matthiae, *Ann. Rev. Nucl. Part. Sci.* **26**, 385 (1976).
- [34] A. B. Kaidalov, *Phys. Rept.* **50**, 157 (1979).
- [35] V. Barone and E. Predazzi, *High-Energy Particle Diffraction*, volume v.565 of *Texts and Monographs in Physics*, Springer-Verlag, Berlin Heidelberg (2002), ISBN 3540421076, URL <http://www-spires.fnal.gov/spires/find/books/www?cl=QC794.6.C6B37::2002>.
- [36] A. B. Kaidalov *et al.*, *Acta Phys. Polon.* **B34**, 3163 (2003), [hep-ph/0303111].
- [37] L. Frankfurt and M. Strikman, in E. M. Henley and S. D. Ellis, editors, "100 Years of Subatomic Physics," 363–423 (2013), [arXiv:1304.4308].
- [38] V. A. Khoze *et al.*, *Eur. Phys. J.* **C69**, 85 (2010), [arXiv:1005.4839].
- [39] D. A. Fagundes *et al.*, *Phys. Rev.* **D88**, 9, 094019 (2013), [arXiv:1306.0452].
- [40] R. Fiore *et al.*, *Int. J. Mod. Phys.* **A24**, 2551 (2009), [arXiv:0810.2902].
- [41] I. M. Dremin, *Phys. Usp.* **56**, 3 (2013), [*Usp. Fiz. Nauk* 183, 3 (2013)], [arXiv:1206.5474].
- [42] L. Frankfurt *et al.*, *Phys. Rev. Lett.* **101**, 202003 (2008), [arXiv:0808.0182].
- [43] G. Bertsch *et al.*, *Phys. Rev. Lett.* **47**, 297 (1981).
- [44] B. Z. Kopeliovich, L. I. Lapidus and A. B. Zamolodchikov, *JETP Lett.* **33**, 595 (1981), [*Pisma Zh. Eksp. Teor. Fiz.* 33, 612 (1981)].
- [45] M. L. Good and W. D. Walker, *Phys. Rev.* **120**, 1855 (1960).
- [46] J. Pumplin, *Phys. Rev.* **D8**, 2899 (1973).
- [47] M. Froissart, *Phys. Rev.* **123**, 1053 (1961).
- [48] A. Martin, *Nuovo Cim.* **A42**, 930 (1965).
- [49] L. Lukaszuk and A. Martin, *Nuovo Cim.* **A52**, 122 (1967).
- [50] A. A. Anselm and V. N. Gribov, *Phys. Lett.* **40B**, 487 (1972).
- [51] G. Cohen-Tannoudji, V. V. Ilyin and L. L. Jenkovszky, *Lett. Nuovo Cim.* **5S2**, 957 (1972), [*Lett. Nuovo Cim.* 5,957(1972)].
- [52] V. A. Khoze, A. D. Martin and M. G. Ryskin, *Eur. Phys. J.* **C18**, 167 (2000), [hep-ph/0007359].
- [53] G. Antchev *et al.* (TOTEM), *Nucl. Phys.* **B899**, 527 (2015), [arXiv:1503.08111].
- [54] G. Antchev *et al.* (TOTEM), *Eur. Phys. J.* **C79**, 10, 861 (2019), [arXiv:1812.08283].
- [55] L. Caneschi and A. Pignotti, *Phys. Rev. Lett.* **22**, 1219 (1969).
- [56] O. V. Kancheli, *JETP Lett.* **11**, 267 (1970), [*Pisma Zh. Eksp. Teor. Fiz.* 11, 397 (1970)].
- [57] A. H. Mueller, *Phys. Rev.* **D4**, 150 (1971).
- [58] D. Amati, A. Stanghellini and S. Fubini, *Nuovo Cim.* **26**, 896 (1962).
- [59] V. S. Fadin, E. A. Kuraev and L. N. Lipatov, *Phys. Lett.* **60B**, 50 (1975); E. A. Kuraev, L. N. Lipatov and V. S. Fadin, *Sov. Phys. JETP* **44**, 443 (1976), [*Zh. Eksp. Teor. Fiz.* 71,840(1976)]; E. A. Kuraev, L. N. Lipatov and V. S. Fadin, *Sov. Phys. JETP* **45**, 199 (1977), [*Zh. Eksp. Teor. Fiz.* 72,377(1977)]; I. I. Balitsky and L. N. Lipatov, *Sov. J. Nucl. Phys.* **28**, 822 (1978), [*Yad. Fiz.* 28,1597(1978)].
- [60] B. L. Ioffe, V. S. Fadin and L. N. Lipatov, *Quantum chromodynamics: Perturbative and nonperturbative aspects*, volume 30, Cambridge Univ. Press (2010), ISBN 9781107424753, 9780521631488, 9780511717444, URL <http://www.cambridge.org/de/knowledge/isbn/item2710695>.
- [61] S. Ostapchenko, *Phys. Rev.* **D83**, 014018 (2011), [arXiv:1010.1869].
- [62] J. L. Cardy, *Nucl. Phys.* **B75**, 413 (1974).
- [63] A. B. Kaidalov *et al.*, *Phys. Lett.* **45B**, 493 (1973).
- [64] E. G. S. Luna *et al.*, *Eur. Phys. J.* **C59**, 1 (2009), [arXiv:0807.4115].
- [65] T. Sjöstrand, *Adv. Ser. Direct. High Energy Phys.* **29**, 191 (2018), [arXiv:1706.02166].
- [66] K. Werner, F.-M. Liu and T. Pierog, *Phys. Rev.* **C74**, 044902 (2006), [hep-ph/0506232].
- [67] V. A. Abramovsky, V. N. Gribov and O. V. Kancheli, *Yad. Fiz.* **18**, 595 (1973), [*Sov. J. Nucl. Phys.* 18, 308 (1974)].
- [68] G. Alberi and G. Goggi, *Phys. Rept.* **74**, 1 (1981).
- [69] K. A. Goulianos, *Phys. Rept.* **101**, 169 (1983).
- [70] D. Bernard *et al.* (UA4), *Phys. Lett.* **B186**, 227 (1987).
- [71] R. E. Ansorge *et al.* (UA5), *Z. Phys.* **C33**, 175 (1986).
- [72] N. A. Amos *et al.* (E710), *Phys. Lett.* **B301**, 313 (1993).
- [73] F. Abe *et al.* (CDF), *Phys. Rev.* **D50**, 5535 (1994).
- [74] G. Aad *et al.* (ATLAS), *Eur. Phys. J.* **C72**, 1926 (2012), [arXiv:1201.2808].
- [75] V. Khachatryan *et al.* (CMS), *Phys. Rev.* **D92**, 1, 012003 (2015), [arXiv:1503.08689].
- [76] B. Abelev *et al.* (ALICE), *Eur. Phys. J.* **C73**, 6, 2456 (2013), [arXiv:1208.4968].
- [77] G. Aad *et al.* (ATLAS), *Phys. Lett.* **B754**, 214 (2016), [arXiv:1511.00502].
- [78] G. Aad *et al.* (ATLAS), *JHEP* **02**, 042 (2020), [arXiv:1911.00453].
- [79] A. M. Sirunyan *et al.* (CMS and TOTEM) (2020), [arXiv:2002.12146].
- [80] V. A. Khoze, A. D. Martin and M. G. Ryskin, *Eur. Phys. J.* **C73**, 2503 (2013), [arXiv:1306.2149].
- [81] V. A. Khoze, A. D. Martin and M. G. Ryskin, *Eur. Phys. J.* **C23**, 311 (2002), [hep-ph/0111078].
- [82] M. G. Albrow, T. D. Coughlin and J. R. Forshaw, *Prog. Part. Nucl. Phys.* **65**, 149 (2010), [arXiv:1006.1289].
- [83] M. Albrow, *Int. J. Mod. Phys.* **A29**, 1402006 (2014).
- [84] H. G. Fischer, W. Geist and M. Makariev, *Int. J. Mod. Phys.* **A29**, 28, 1446005 (2014).
- [85] A. Kirk, *Int. J. Mod. Phys.* **A29**, 28, 1446001 (2014), [arXiv:1408.1196].
- [86] M. A. Reyes *et al.* (E690), *Phys. Rev. Lett.* **81**, 4079 (1998).
- [87] G. Gutierrez and M. A. Reyes, *Int. J. Mod. Phys.* **A29**, 28, 1446008 (2014), [arXiv:1409.8243].
- [88] Y. L. Dokshitzer, D. Diakonov and S. I. Troian, *Phys. Rept.* **58**, 269 (1980).

- [89] M. Derrick *et al.* (ZEUS), Phys. Lett. **B315**, 481 (1993).
- [90] T. Ahmed *et al.* (H1), Nucl. Phys. **B429**, 477 (1994).
- [91] P. Newman and M. Wing, Rev. Mod. Phys. **86**, 3, 1037 (2014), [arXiv:1308.3368].
- [92] A. Aktas *et al.* (H1), Eur. Phys. J. **C48**, 715 (2006), [hep-ex/0606004].
- [93] S. Chekanov *et al.* (ZEUS), Nucl. Phys. **B816**, 1 (2009), [arXiv:0812.2003].
- [94] F. D. Aaron *et al.* (H1), Eur. Phys. J. **C72**, 2074 (2012), [arXiv:1203.4495].
- [95] F. D. Aaron *et al.* (H1, ZEUS), Eur. Phys. J. **C72**, 2175 (2012), [arXiv:1207.4864].
- [96] A. Aktas *et al.* (H1), JHEP **10**, 042 (2007), [arXiv:0708.3217].
- [97] A. Aktas *et al.* (H1), Eur. Phys. J. **C50**, 1 (2007), [hep-ex/0610076].
- [98] S. Chekanov *et al.* (ZEUS), Nucl. Phys. **B672**, 3 (2003), [hep-ex/0307068].
- [99] E. G. de Oliveira, A. D. Martin and M. G. Ryskin, Phys. Lett. **B695**, 162 (2011), [arXiv:1010.1366].
- [100] G. Antchev *et al.* (TOTEM), Eur. Phys. J. **C79**, 2, 103 (2019), [arXiv:1712.06153].
- [101] C. Augier *et al.* (UA4/2), Phys. Lett. **B316**, 448 (1993).
- [102] G. Antchev *et al.* (TOTEM), Eur. Phys. J. **C79**, 9, 785 (2019), [arXiv:1812.04732].
- [103] G. Antchev *et al.* (TOTEM), Eur. Phys. J. **C80**, 2, 91 (2020), [arXiv:1812.08610].
- [104] G. Antchev *et al.* (TOTEM), EPL **101**, 2, 21002 (2013).
- [105] G. Antchev *et al.* (TOTEM), Phys. Rev. Lett. **111**, 1, 012001 (2013).
- [106] G. Aad *et al.* (ATLAS), Nucl. Phys. **B889**, 486 (2014), [arXiv:1408.5778].
- [107] M. Aaboud *et al.* (ATLAS), Phys. Lett. **B761**, 158 (2016), [arXiv:1607.06605].
- [108] M. M. Block and R. N. Cahn, Rev. Mod. Phys. **57**, 563 (1985).
- [109] F. Abe *et al.* (CDF), Phys. Rev. **D50**, 5550 (1994).
- [110] C. Avila *et al.* (E811), Phys. Lett. **B445**, 419 (1999).
- [111] W. Guryn, “Invited talk at the Workshop on Diffraction and Low-x Physics, Reggio Calabria, Italy, August 26th–September 1st, 2018,” .
- [112] K. Nakamura *et al.* (Particle Data Group), J. Phys. **G37**, 075021 (2010).
- [113] F. J. Nemes, PoS **DIS2017**, 059 (2018).
- [114] G. Antchev *et al.* (TOTEM), EPL **95**, 4, 41001 (2011), [arXiv:1110.1385].
- [115] G. Antchev *et al.* (TOTEM), Eur. Phys. J. **C76**, 12, 661 (2016), [arXiv:1610.00603].
- [116] J. Kaspar, “Invited talk at the meeting of the LHC Working Group on Forward Physics and Diffraction, CERN, Switzerland, December 16-17th, 2019,” .
- [117] V. A. Schegelsky and M. G. Ryskin, Phys. Rev. **D85**, 094024 (2012), [arXiv:1112.3243].
- [118] A. Bruni, X. Janssen and P. Marage, in “Proceedings, HERA and the LHC Workshop Series on the implications of HERA for LHC physics: 2006-2008,” 427–439 (2008), [arXiv:0812.0539].
- [119] A. Levy, in “Proceedings, 17th International Workshop on Deep-Inelastic Scattering and Related Subjects (DIS 2009): Madrid, Spain, April 26-30, 2009,” 177 (2009), [arXiv:0907.2178].
- [120] J. R. Forshaw, R. Sandapen and G. Shaw, JHEP **11**, 025 (2006), [hep-ph/0608161].
- [121] A. Capella *et al.*, Nucl. Phys. **B593**, 336 (2001), [hep-ph/0005049].
- [122] V. S. Fadin and L. N. Lipatov, Phys. Lett. **B429**, 127 (1998), [hep-ph/9802290].
- [123] M. Ciafaloni and G. Camici, Phys. Lett. **B430**, 349 (1998), [hep-ph/9803389].
- [124] F. D. Aaron *et al.* (H1), JHEP **05**, 032 (2010), [arXiv:0910.5831].
- [125] C. Adloff *et al.* (H1), Eur. Phys. J. **C13**, 371 (2000), [hep-ex/9902019].
- [126] J. Breitweg *et al.* (ZEUS), Eur. Phys. J. **C6**, 603 (1999), [hep-ex/9808020].
- [127] S. Chekanov *et al.* (ZEUS), PMC Phys. **A1**, 6 (2007), [arXiv:0708.1478].
- [128] M. Ciafaloni, Nucl. Phys. **B296**, 49 (1988).
- [129] S. Catani, F. Fiorani and G. Marchesini, Phys. Lett. **B234**, 339 (1990).
- [130] S. Catani, F. Fiorani and G. Marchesini, Nucl. Phys. **B336**, 18 (1990).
- [131] G. Marchesini, Nucl. Phys. **B445**, 49 (1995), [hep-ph/9412327].
- [132] G. P. Salam, JHEP **07**, 019 (1998), [hep-ph/9806482].
- [133] M. Ciafaloni and D. Colferai, Phys. Lett. **B452**, 372 (1999), [hep-ph/9812366].
- [134] H. Kowalski, L. N. Lipatov and D. A. Ross, Eur. Phys. J. **C76**, 1, 23 (2016), [arXiv:1508.05744].
- [135] H. Kowalski *et al.*, Eur. Phys. J. **C77**, 11, 777 (2017), [arXiv:1707.01460].
- [136] S. J. Brodsky *et al.*, JETP Lett. **70**, 155 (1999), [hep-ph/9901229].
- [137] R. D. Ball *et al.*, Eur. Phys. J. **C78**, 4, 321 (2018), [arXiv:1710.05935].
- [138] E. M. Levin and M. G. Ryskin, Phys. Rept. **189**, 267 (1990).
- [139] L. V. Gribov, E. M. Levin and M. G. Ryskin, Phys. Rept. **100**, 1 (1983).
- [140] E. M. Levin, M. G. Ryskin and A. G. Shuvaev, Nucl. Phys. **B387**, 589 (1992).
- [141] A. H. Mueller, Phys. Rept. **73**, 237 (1981).
- [142] A. H. Mueller, Nucl. Phys. **B415**, 373 (1994).
- [143] A. H. Mueller and B. Patel, Nucl. Phys. **B425**, 471 (1994), [hep-ph/9403256].
- [144] N. N. Nikolaev, B. G. Zakharov and V. R. Zoller, JETP Lett. **59**, 6 (1994), [hep-ph/9312268].
- [145] V. N. Gribov and L. N. Lipatov, Sov. J. Nucl. Phys. **15**, 438 (1972), [Yad. Fiz.15,781(1972)]; G. Altarelli and G. Parisi, Nucl. Phys. **B126**, 298 (1977); Y. L. Dokshitzer, Sov. Phys. JETP **46**, 641 (1977), [Zh. Eksp. Teor. Fiz. 73, 1216 (1977)].
- [146] I. Balitsky, Nucl. Phys. **B463**, 99 (1996), [hep-ph/9509348].
- [147] I. Balitsky, Phys. Rev. **D60**, 014020 (1999), [hep-ph/9812311].
- [148] Y. V. Kovchegov, Phys. Rev. **D60**, 034008 (1999), [hep-ph/9901281].
- [149] G. Gustafson, Phys. Lett. **B718**, 1054 (2013), [arXiv:1206.1733].
- [150] S. Chatrchyan *et al.* (CMS, TOTEM), Eur. Phys. J. **C74**, 10, 3053 (2014), [arXiv:1405.0722].
- [151] Q.-D. Zhou (LHCF, ATLAS), EPJ Web Conf. **208**, 05008 (2019).
- [152] O. Adriani *et al.* (LHCf), Phys. Lett. **B780**, 233 (2018), [arXiv:1703.07678].
- [153] M. Aaboud *et al.* (ATLAS), ATLAS-CONF-2017-075.
- [154] C. Albajar *et al.* (UA1), Nucl. Phys. **B335**, 261 (1990).
- [155] G. J. Alner *et al.* (UA5), Z. Phys. **C33**, 1 (1986).

- [156] T. Aaltonen *et al.* (CDF), Phys. Rev. **D79**, 112005 (2009), [Erratum: Phys. Rev. **D82**, 119903(2010)], [arXiv:0904.1098].
- [157] F. Abe *et al.* (CDF), Phys. Rev. **D41**, 2330 (1990), [119(1989)].
- [158] K. Aamodt *et al.* (ALICE), Eur. Phys. J. **C68**, 89 (2010), [arXiv:1004.3034].
- [159] V. Khachatryan *et al.* (CMS), Phys. Rev. Lett. **105**, 022002 (2010), [arXiv:1005.3299].
- [160] B. B. Abelev *et al.* (ALICE), Eur. Phys. J. **C73**, 12, 2662 (2013), [arXiv:1307.1093].
- [161] A. M. Sirunyan *et al.* (CMS), Phys. Rev. **D96**, 11, 112003 (2017), [arXiv:1706.10194].
- [162] M. G. Ryskin, A. D. Martin and V. A. Khoze, Eur. Phys. J. **C71**, 1617 (2011), [arXiv:1102.2844].
- [163] X.-N. Wang, Phys. Rept. **280**, 287 (1997), [hep-ph/9605214].
- [164] S. Ostapchenko and M. Bleicher, Universe **5**, 5, 106 (2019).
- [165] F. M. Liu *et al.*, J. Phys. **G28**, 2597 (2002), [hep-ph/0109104].
- [166] E. Gotsman, E. Levin and U. Maor, Acta Phys. Polon. Supp. **8**, 777 (2015).
- [167] Y. V. Kovchegov and E. Levin, Camb. Monogr. Part. Phys. Nucl. Phys. Cosmol. **33**, 1 (2012).
- [168] E. A. De Wolf, I. M. Dremin and W. Kittel, Phys. Rept. **270**, 1 (1996), [hep-ph/9508325].
- [169] J. Adam *et al.* (ALICE), Eur. Phys. J. **C77**, 8, 569 (2017), [arXiv:1612.08975].
- [170] V. Khachatryan *et al.* (CMS), JHEP **09**, 091 (2010), [arXiv:1009.4122].
- [171] K. Eggert *et al.*, Nucl. Phys. **B86**, 201 (1975).
- [172] B. Alver *et al.* (PHOBOS), Phys. Rev. **C75**, 054913 (2007), [arXiv:0704.0966].
- [173] E. M. Levin and M. G. Ryskin, Sov. J. Nucl. Phys. **20**, 280 (1975), [Yad. Fiz. **20**, 519(1974)].
- [174] A. Capella and A. Krzywicki, Phys. Rev. **D18**, 4120 (1978).
- [175] M. Aaboud *et al.* (ATLAS), Eur. Phys. J. **C77**, 6, 428 (2017), [arXiv:1705.04176].
- [176] V. Khachatryan *et al.* (CMS), Phys. Lett. **B765**, 193 (2017), [arXiv:1606.06198].
- [177] S. Gieseke, "Invited talk at the Workshop on Multiple Partonic Interactions at the LHC, Prague, Czech Republic, November 18th–26th, 2019," .
- [178] S. Kundu, B. Mohanty and D. Mallick (2019), [arXiv:1912.05176].
- [179] M. Diehl, D. Ostermeier and A. Schafer, JHEP **03**, 089 (2012), [Erratum: JHEP **03**, 001(2016)], [arXiv:1111.0910].
- [180] T. Sjostrand and P. Z. Skands, JHEP **03**, 053 (2004), [hep-ph/0402078].
- [181] M. Aaboud *et al.* (ATLAS), Phys. Lett. **B790**, 595 (2019), [Phys. Lett. **790**, 595(2019)], [arXiv:1811.11094].
- [182] M. G. Ryskin and A. M. Snigirev, Phys. Rev. **D83**, 114047 (2011), [arXiv:1103.3495].
- [183] B. Blok *et al.*, Eur. Phys. J. **C74**, 2926 (2014), [arXiv:1306.3763].
- [184] M. Aaboud *et al.* (ATLAS), JHEP **03**, 157 (2017), [arXiv:1701.05390].
- [185] R. Snellings, New J. Phys. **13**, 055008 (2011), [arXiv:1102.3010].
- [186] M. Aaboud *et al.* (ATLAS), Phys. Rev. **C97**, 2, 024904 (2018), [arXiv:1708.03559].
- [187] N. Borghini, P. M. Dinh and J.-Y. Ollitrault, Phys. Rev. **C63**, 054906 (2001), [arXiv:nucl-th/0007063].
- [188] A. Bilandzic, R. Snellings and S. Voloshin, Phys. Rev. **C83**, 044913 (2011), [arXiv:1010.0233].
- [189] W. Li, Mod. Phys. Lett. **A27**, 1230018 (2012), [arXiv:1206.0148].
- [190] B. Schenke, J. Phys. **G38**, 124009 (2011), [arXiv:1106.6012].
- [191] K. G. Boreskov, A. B. Kaidalov and O. V. Kancheli, Eur. Phys. J. **C58**, 445 (2008), [arXiv:0809.0625].
- [192] K. G. Boreskov, A. B. Kaidalov and O. V. Kancheli, Phys. Atom. Nucl. **72**, 361 (2009), [Yad. Fiz. **72**, 390(2009)].
- [193] C. Bierlich and J. R. Christiansen, Phys. Rev. **D92**, 9, 094010 (2015), [arXiv:1507.02091].
- [194] Z.-W. Lin *et al.*, Phys. Rev. **C72**, 064901 (2005), [arXiv:nucl-th/0411110].
- [195] V. Khachatryan *et al.* (CMS), CMS-PAS-FSQ-16-008.
- [196] J. Bartels, Nucl. Phys. **B175**, 365 (1980).
- [197] J. Kwiecinski and M. Praszalowicz, Phys. Lett. **94B**, 413 (1980).
- [198] M. A. Braun (1998), [hep-ph/9805394].
- [199] J. Bartels, L. N. Lipatov and G. P. Vacca, Phys. Lett. **B477**, 178 (2000), [hep-ph/9912423].
- [200] C. Ewerz (2003), [hep-ph/0306137].
- [201] M. Fukugita and J. Kwiecinski, Phys. Lett. **83B**, 119 (1979), [625(1979)].
- [202] M. G. Ryskin, Sov. J. Nucl. Phys. **46**, 337 (1987), [Yad. Fiz. **46**, 611(1987)].
- [203] J. Bartels, C. Contreras and G. P. Vacca (2019), [arXiv:1910.04588].
- [204] E. Nagy *et al.*, Nucl. Phys. **B150**, 221 (1979).
- [205] A. Breakstone *et al.*, Phys. Rev. Lett. **54**, 2180 (1985).
- [206] A. Breakstone *et al.* (AMES-BOLOGNA-CERN-DORTMUND-HEIDELBERG-WARSAW), Nucl. Phys. **B248**, 253 (1984).
- [207] V. M. Abazov *et al.* (D0), Phys. Rev. **D86**, 012009 (2012), [arXiv:1206.0687].
- [208] M. Bozzo *et al.* (UA4), Phys. Lett. **155B**, 197 (1985).
- [209] D. Bernard *et al.* (UA4), Phys. Lett. **B171**, 142 (1986).
- [210] E. Martynov and B. Nicolescu, Eur. Phys. J. **C79**, 6, 461 (2019), [arXiv:1808.08580].
- [211] A. Donnachie and P. V. Landshoff, Phys. Lett. **123B**, 345 (1983).
- [212] A. Donnachie and P. V. Landshoff, Phys. Lett. **B798**, 135008 (2019), [arXiv:1904.11218].
- [213] J. Finkelstein *et al.*, Phys. Lett. **B232**, 257 (1989).
- [214] V. A. Khoze, A. D. Martin and M. G. Ryskin, Phys. Lett. **B780**, 352 (2018), [arXiv:1801.07065].
- [215] W. Kilian and O. Nachtmann, Eur. Phys. J. **C5**, 317 (1998), [hep-ph/9712371].
- [216] J. Bartels *et al.*, Eur. Phys. J. **C20**, 323 (2001), [hep-ph/0102221].
- [217] L. A. Harland-Lang *et al.*, Phys. Rev. **D99**, 3, 034011 (2019), [arXiv:1811.12705].
- [218] J. Olsson (H1), in "New trends in high-energy physics: Experiment, phenomenology, theory. Proceedings, International Conference, Yalta, Crimea, Ukraine, September 22-29, 2001," 79–87 (2001), [hep-ex/0112012].
- [219] C. Adloff *et al.* (H1), Phys. Lett. **B544**, 35 (2002), [hep-ex/0206073].
- [220] T. Berndt (H1), Acta Phys. Polon. **B33**, 3499 (2002), [182(2002)].
- [221] W. Heisenberg, Z. Phys. **133**, 65 (1952).
- [222] G. Pancheri and Y. N. Srivastava, Eur. Phys. J. **C77**, 3, 150 (2017), [arXiv:1610.10038].
- [223] M. M. Block, Phys. Rept. **436**, 71 (2006), [hep-ph/0606215].
- [224] M. Giordano, E. Meggiolaro and N. Moretti, JHEP **09**, 031 (2012), [arXiv:1203.0961].

- [225] E. Ferreiro *et al.*, Nucl. Phys. **A710**, 373 (2002), [hep-ph/0206241].
- [226] P. Grassberger and K. Sundermeyer, Phys. Lett. **77B**, 220 (1978).
- [227] K. G. Boreskov, in M. Olshanetsky and A. Vainshtein, editors, “Multiple facets of quantization and supersymmetry,” 322–351 (2001), [hep-ph/0112325].
- [228] V. A. Khoze, A. D. Martin and M. G. Ryskin, Phys. Lett. **B787**, 167 (2018), [arXiv:1809.10406].

## Astrophysics and Cosmology

21. Experimental tests of gravitational theory (rev.) . . . . .	409
22. Big-Bang cosmology (rev.) . . . . .	422
23. Inflation (rev.) . . . . .	435
24. Big-Bang nucleosynthesis (rev.) . . . . .	451
25. Cosmological parameters (rev.) . . . . .	458
26. Neutrinos in cosmology (new) . . . . .	467
27. Dark matter (new) . . . . .	474
28. Dark energy (rev.) . . . . .	490
29. Cosmic microwave background (rev.) . . . . .	499
30. Cosmic rays (rev.) . . . . .	510



## 21. Experimental Tests of Gravitational Theory

Revised August 2019 by T. Damour (IHES, Bures-sur-Yvette).

### 21.1 General Relativity

Einstein's theory of General Relativity (GR), the current “standard” theory of gravitation, describes gravity as a universal deformation of the Minkowski metric:

$$g_{\mu\nu}(x^\lambda) = \eta_{\mu\nu} + h_{\mu\nu}(x^\lambda), \text{ where } \eta_{\mu\nu} = \text{diag}(-1, +1, +1, +1). \quad (21.1)$$

GR is classically defined by two postulates, embodied in the total action defining the theory:

$$S_{\text{tot}}[g_{\mu\nu}, \psi, A_\mu, H] = c^{-1} \int d^4x (\mathcal{L}_{\text{Ein}} + \mathcal{L}_{\text{SM}}). \quad (21.2)$$

The first postulate states that the Lagrangian density describing the propagation and self-interaction of the gravitational field is

$$\mathcal{L}_{\text{Ein}}[g_{\alpha\beta}] = \frac{c^4}{16\pi G} \sqrt{g} g^{\mu\nu} R_{\mu\nu}(g_{\alpha\beta}), \quad (21.3)$$

where  $G$  denotes Newton's constant,  $g = -\det(g_{\mu\nu})$ ,  $g^{\mu\nu}$  is the matrix inverse of  $g_{\mu\nu}$ , and where the Ricci tensor  $R_{\mu\nu} \equiv R^\alpha{}_{\mu\alpha\nu}$  is the only independent trace of the curvature tensor

$$R^\alpha{}_{\mu\beta\nu} = \partial_\beta \Gamma_{\mu\nu}^\alpha - \partial_\nu \Gamma_{\mu\beta}^\alpha + \Gamma_{\sigma\beta}^\alpha \Gamma_{\mu\nu}^\sigma - \Gamma_{\sigma\nu}^\alpha \Gamma_{\mu\beta}^\sigma, \quad (21.4)$$

$$\Gamma_{\mu\nu}^\lambda = \frac{1}{2} g^{\lambda\sigma} (\partial_\mu g_{\nu\sigma} + \partial_\nu g_{\mu\sigma} - \partial_\sigma g_{\mu\nu}). \quad (21.5)$$

The second postulate states that  $g_{\mu\nu}$  (and its associated connection) couples universally, and minimally, to all the bosonic (respectively fermionic) fields of the Standard Model by replacing everywhere the Minkowski metric  $\eta_{\mu\nu}$  (respectively the flat Minkowski connection). Schematically (suppressing matrix indices and labels for the various gauge fields and fermions and for the Higgs doublet),

$$\begin{aligned} \mathcal{L}_{\text{SM}}[\psi, A_\mu, H, g_{\mu\nu}] = & \\ & - \frac{1}{4} \sum \sqrt{g} g^{\mu\alpha} g^{\nu\beta} F_{\mu\nu}^\alpha F_{\alpha\beta}^\nu - \sum \sqrt{g} \bar{\psi} \gamma^\mu (D_\mu + \frac{1}{4} \omega_{ij\mu} \gamma^{ij}) \psi \\ & - \frac{1}{2} \sqrt{g} g^{\mu\nu} \bar{D}_\mu \bar{H} D_\nu H - \sqrt{g} V(H) - \sum \lambda \sqrt{g} \bar{\psi} H \psi. \end{aligned} \quad (21.6)$$

Here  $F_{\mu\nu}^\alpha = \partial_\mu A_\nu^\alpha - \partial_\nu A_\mu^\alpha + g_A f_{bc}^a A_\mu^b A_\nu^c$  and the (representation-dependent) gauge-field covariant derivative  $D_\mu = \partial_\mu + g_A A_\mu^a T_a^{\text{rep}}$  are defined as in Special Relativity, while the derivative of spin- $\frac{1}{2}$  fermions also includes a coupling to the gravitational “spin-connection”  $\omega_{ij\mu} = -\omega_{ji\mu}$ , via its contraction with  $\gamma^{ij} = \frac{1}{2}(\gamma^i \gamma^j - \gamma^j \gamma^i)$ , where  $i, j = 0, 1, 2, 3$  and  $\gamma^i = e^\mu{}_{i\mu} \gamma^\mu$  are usual (numerical) Dirac matrices satisfying  $\gamma^i \gamma^j + \gamma^j \gamma^i = 2\eta^{ij}$ . The connection components  $\omega_{ij\mu}$  are defined in terms of the local orthonormal frame (vierbein)  $e^i{}_\mu$  (such that  $g_{\mu\nu} = \eta_{ij} e^i{}_\mu e^j{}_\nu$ ) used to describe the components of the various fermions  $\psi$ , and of its inverse  $e_i{}^\mu$  (such that  $e_i{}^\mu e^j{}_\mu = \delta_i^j$ ), by  $\omega_{ij\mu} = \frac{1}{2} (C_{i[jk]} + C_{j[ki]} - C_{k[ij]}) e_k{}^\mu$  where  $C_{i[jk]} = \eta_{is} C^s{}_{[jk]}$ , with  $C^i{}_{[jk]} \equiv (\partial_\mu e^i{}_\nu - \partial_\nu e^i{}_\mu) e_j{}^\mu e_k{}^\nu$ . From the total action follow Einstein's field equations,

$$R_{\mu\nu} - \frac{1}{2} R g_{\mu\nu} = \frac{8\pi G}{c^4} T_{\mu\nu}. \quad (21.7)$$

Here  $R = g^{\mu\nu} R_{\mu\nu}$  is the scalar curvature, and  $T_{\mu\nu} \equiv g_{\mu\alpha} g_{\nu\beta} T^{\alpha\beta}$  where  $T^{\mu\nu} = (2/\sqrt{g}) \delta \mathcal{L}_{\text{SM}} / \delta g_{\mu\nu}$  is the (symmetric) energy-momentum tensor of the Standard Model matter. The theory is invariant under arbitrary coordinate transformations:  $x^\mu = f^\mu(x^\nu)$  (as well as under arbitrary local  $\text{SO}(3,1)$  rotations of the vierbein,  $e^i{}_\mu = \Lambda^i{}_j(x) e'^j{}_\mu$ ). To solve the field equations Eq. (21.7), one needs to fix the coordinate gauge freedom, e.g., the “harmonic gauge” (which is the analogue of the Lorenz gauge,  $\partial_\mu A^\mu = 0$ , in electromagnetism) corresponds to imposing the condition  $\partial_\nu (\sqrt{g} g^{\mu\nu}) = 0$ .

In this *Review*, we only consider the classical limit of gravitation (i.e. classical matter and classical gravity). Quantum

gravitational effects are expected (when considered at low energy) to correct the classical action Eq. (21.2) by additional terms involving quadratic and higher powers of the curvature tensor. This suggests that the validity of classical gravity extends (at most) down to length scales of order the Planck length  $L_P = \sqrt{\hbar G/c^3} \simeq 1.62 \times 10^{-33}$  cm, i.e., up to energy scales of order the Planck energy  $E_P = \sqrt{\hbar c^5/G} \simeq 1.22 \times 10^{19}$  GeV. Considering quantum matter in a classical gravitational background also poses interesting challenges, notably the possibility that the zero-point fluctuations of the matter fields generate a nonvanishing vacuum energy density  $\rho_{\text{vac}}$ , corresponding to a term  $-\sqrt{g} \rho_{\text{vac}}$  in  $\mathcal{L}_{\text{SM}}$  [1]. This is equivalent to adding a “cosmological constant” term  $+\Lambda g_{\mu\nu}$  on the left-hand side of Einstein's equations, Eq. (21.7), with  $\Lambda = 8\pi G \rho_{\text{vac}}/c^4$ . Recent cosmological observations (see the following *Reviews*) suggest a positive value of  $\Lambda$  corresponding to  $\rho_{\text{vac}} \approx (2.3 \times 10^{-3} \text{eV})^4$ . Such a small value has a negligible effect on the non-cosmological tests discussed below.

### 21.2 Key features and predictions of GR

The definition of GR recalled above makes predictions both about the coupling of gravity to matter, and about the structure of the gravitational field beyond its previously known Newtonian aspects.

#### 21.2.1 Equivalence Principle

First, the universal nature of the coupling between  $g_{\mu\nu}$  and the Standard Model matter postulated in Eq. (21.6) entails many observable consequences that go under the generic name of “Equivalence Principle”.

A first aspect of the Equivalence Principle is that the outcome of a local non-gravitational experiment, referred to local standards, should not depend on where, when, and in which locally inertial frame, the experiment is performed. This means, for instance, that local experiments should neither feel the cosmological evolution of the Universe (constancy of the “constants”), nor exhibit preferred directions in spacetime (isotropy of space, local Lorentz invariance).

A second aspect of the Equivalence Principle is that the kinetic terms,  $g^{\mu\nu} \partial_\mu \phi \partial_\nu \phi$  or  $\bar{\psi} \gamma^i e_i{}^\mu \partial_\mu \psi$ , of all the fields of Nature (including the gravitational field itself) are universally coupled to the same curved spacetime metric  $g_{\mu\nu}(x) = \eta_{ij} e^i{}_\mu e^j{}_\nu$ . This implies in particular that all massless fields should propagate with the same speed.

A third aspect of the Equivalence Principle is that two (electrically neutral) test bodies dropped at the same location and with the same velocity in an external gravitational field should fall in the same way, independently of their masses and compositions (“universality of free fall” or “Weak Equivalence Principle”). In addition, the study (using the nonlinear structure of GR) of the motion, in an external gravitational field, of bodies having a non-negligible, or even strong, self-gravity (such as planets, neutron stars, or black holes) has shown that the latter property of free-fall universality holds equally well for self-gravitating bodies (“Strong Equivalence Principle”).

A last aspect of the Equivalence Principle concerns various universality features of the gravitational redshift of clock rates. GR predicts that, when intercomparing them by means of electromagnetic signals, two (non gravity-based) clocks located along two different spacetime worldlines should exhibit a universal difference in clock rate that depends on their worldlines, but that is independent of their nature and constitution. For instance, two clocks located at two different positions in a static external Newtonian potential  $U(\mathbf{x}) = \sum Gm/r$  should exhibit, when intercompared by electromagnetic signals, the difference in clock rate,  $\tau_1/\tau_2 = \nu_2/\nu_1 = 1 + [U(\mathbf{x}_1) - U(\mathbf{x}_2)]/c^2 + O(1/c^4)$ , (“universal gravitational redshift of clock rates”). Similarly, the comparison of atomic-transition frequencies when observing on Earth a transition that took place on a far-away galaxy should involve (at lowest order in cosmological perturbations) the universal cosmological redshift factor  $1+z = a(t_{\text{reception}})/a(t_{\text{emission}})$  between the Friedmann scale factors  $a(t)$  (see below).



### 21.2.2 Quasi-stationary, weak-field (post-Newtonian) gravity

When applied to quasi-stationary, weak-field gravitational fields, Einstein equations, Eq. (21.7), entail a spacetime structure which predicts deviations from Newtonian gravity of the first post-Newtonian (1PN) order, *i.e.*, fractionally smaller than Newtonian effects by a factor  $O(v^2/c^2) \sim O(GM/(c^2r))$ . The 1PN-accurate solution of Eq. (21.7) reads (in harmonic gauge)

$$\begin{aligned} g_{00} &= -1 + \frac{2}{c^2}V - \frac{2}{c^4}V^2 + O\left(\frac{1}{c^6}\right), \\ g_{0i} &= -\frac{4}{c^3}V_i + O\left(\frac{1}{c^5}\right), \\ g_{ij} &= \delta_{ij}\left[1 + \frac{2}{c^2}V\right] + O\left(\frac{1}{c^4}\right), \end{aligned} \quad (21.8)$$

where  $x^0 = ct$ ,  $i, j = 1, 2, 3$ , and where the scalar,  $V$ , and vector,  $V_i$ , (retarded) potentials are defined in terms of the sources  $\sigma = \frac{T^{00} + T^{ii}}{c^2}$ ,  $\sigma_i = \frac{T^{0i}}{c}$  by

$$V = \square_{\text{ret}}^{-1}[-4\pi G\sigma]; \quad V_i = \square_{\text{ret}}^{-1}[-4\pi G\sigma_i]. \quad (21.9)$$

In GR the gravitational interaction of  $N$  moving point masses (labelled by  $A = 1, \dots, N$ ) is described by a reduced (classical) action that admits a diagrammatic expansion:

$$S_{\text{reduced}} = S^{\text{free}} + S^{\text{tree-level}} + S^{\text{one-loop}} + \dots \quad (21.10)$$

where the free (special-relativistic) action reads

$$\begin{aligned} S^{\text{free}} &= -\sum_A \int m_A c \sqrt{-\eta_{\mu\nu} dx_A^\mu dx_A^\nu} \\ &= -\sum_A \int dt m_A c^2 \sqrt{1 - \mathbf{v}_A^2/c^2}, \end{aligned} \quad (21.11)$$

while the tree-level (one-graviton-exchange) interaction term reads

$$S^{\text{tree-level}} = -\frac{8\pi G}{c^4} \int d^4x T^{\mu\nu} \square^{-1}(T_{\mu\nu} - \frac{1}{2}T\eta_{\mu\nu}) = \int dt L^{(2)}. \quad (21.12)$$

Corresponding to the 1PN-accurate metric of Eq. (21.8), the 1PN-accurate expansion of the latter tree-level, two-body interaction Lagrangian  $L^{(2)}$  reads (with  $r_{AB} \equiv |\mathbf{x}_A - \mathbf{x}_B|$ ,  $\mathbf{n}_{AB} \equiv (\mathbf{x}_A - \mathbf{x}_B)/r_{AB}$ )

$$\begin{aligned} L^{(2)} &= \frac{1}{2} \sum_{A \neq B} \frac{G m_A m_B}{r_{AB}} \left[ 1 + \frac{3}{2c^2}(v_A^2 + v_B^2) - \frac{7}{2c^2}(\mathbf{v}_A \cdot \mathbf{v}_B) \right. \\ &\quad \left. - \frac{1}{2c^2}(\mathbf{n}_{AB} \cdot \mathbf{v}_A)(\mathbf{n}_{AB} \cdot \mathbf{v}_B) + O\left(\frac{1}{c^4}\right) \right] \end{aligned} \quad (21.13)$$

The two-body interactions, Eq. (21.13), exhibit  $v^2/c^2$  corrections to Newton's  $1/r$  potential induced by spin-2 exchange ("gravitomagnetism"). Consistency at the 1PN level,  $v^2/c^2 \sim Gm/rc^2$ , requires that one also considers the three-body interactions contained in the one-loop contribution  $S^{\text{one-loop}}$ , corresponding to terms induced by some of the three-graviton vertices and other non-linearities (terms  $O(h^2)$  and  $O(hT)$  in Eq. (21.15) below), *i.e.*, to the  $O(V^2)$  term in Eq. (21.8):

$$L^{(3)} = -\frac{1}{2} \sum_{B \neq A \neq C} \frac{G^2 m_A m_B m_C}{r_{AB} r_{AC} c^2} + O\left(\frac{1}{c^4}\right). \quad (21.14)$$

### 21.2.3 Gravitational Waves in GR

The linearized approximation to Einstein's field equations, Eq. (21.7), in harmonic gauge  $\partial^\nu(h_{\mu\nu} - \frac{1}{2}h\eta_{\mu\nu}) = 0$  (with  $h \equiv \eta^{\mu\nu}h_{\mu\nu}$ ), reads

$$\square h_{\mu\nu} = -\frac{16\pi G}{c^4}(T_{\mu\nu} - \frac{1}{2}T\eta_{\mu\nu}) + O(h^2) + O(hT). \quad (21.15)$$

Outside of any source (*i.e.*, when  $T_{\mu\nu} = 0$ ), this yields  $\square h_{\mu\nu} = 0$ , with  $\partial^\nu(h_{\mu\nu} - \frac{1}{2}h\eta_{\mu\nu}) = 0$ . The generic linearized solution (modulo the diffeomorphism freedom) of the latter vacuum Einstein equations can be written as (with  $k^2 = k \cdot k = \eta_{\mu\nu}k^\mu k^\nu$ ,  $k \cdot x = k_\mu x^\mu$ )

$$h_{\mu\nu}(x) = \int d^4k \delta(k^2) \epsilon_{\mu\nu}(k) e^{ik \cdot x}, \quad (21.16)$$

where the polarization tensor  $\epsilon_{\mu\nu}(k)$  must be transverse ( $\epsilon_{\mu\nu}k^\nu = 0$ ) and traceless ( $\eta^{\mu\nu}\epsilon_{\mu\nu} = 0$ ). In addition,  $\epsilon_{\mu\nu}(k)$  can be freely submitted to the gauge freedom  $\epsilon'_{\mu\nu} = \epsilon_{\mu\nu} + \xi_\mu k_\nu + \xi_\nu k_\mu$ . This implies that gravitational waves (GW) propagate with the speed of light, and (like electromagnetic waves) have only two independent polarizations. In a frame where, say,  $k^\mu = (ck, 0, 0, k)$ , the two independent linear polarization tensors can be taken to have components only in the transverse 1-2 plane, of the following form:  $\epsilon_{11}^+ = -\epsilon_{22}^+ = \epsilon^+$ , with  $\epsilon_{12}^+ = \epsilon_{21}^+ = 0$ ; or  $\epsilon_{11}^\times = +\epsilon_{22}^\times = \epsilon^\times$ , with  $\epsilon_{12}^\times = \epsilon_{21}^\times = 0$ . Under a little-group rotation of angle  $\theta$  in the 1-2 plane, the two circular polarization amplitudes  $\epsilon^{(\pm)} = \epsilon^+ \mp i\epsilon^\times$  vary as  $\epsilon'^{(\pm)} = e^{\pm 2i\theta} \epsilon^{(\pm)}$ , thereby characterizing the helicity-2 nature of GWs.

When solving the inhomogeneous equation Eq. (21.15), taking into account the nonlinear contributions  $O(h^2) + O(hT)$ , one finds that, to lowest order, the GW amplitude emitted at large distances by a matter distribution is given by the following "quadrupole formula"

$$h_{ij}^{\text{TT}}(T, \mathbf{X}) \approx \frac{2G}{c^4} P_{ijab}^{\text{TT}}(\mathbf{N}) \frac{\ddot{Q}_{ab}(T - R/c)}{R}, \quad (21.17)$$

where  $Q_{ij}(t) = \int d^3x \sigma(t, \mathbf{x})(x^i x^j - \frac{1}{3}\delta_{ij}x^2)$  ( $a, b, i, j = 1, 2, 3$ ) is the quadrupole moment of the source,  $R = |\mathbf{X}|$  the distance to the source,  $\mathbf{N} = \mathbf{X}/R$  the unit direction from the source to the observer, and  $P_{ijab}^{\text{TT}}(\mathbf{N}) = (\delta_{ia} - N_i N_a)(\delta_{jb} - N_j N_b) - \frac{1}{2}(\delta_{ij} - N_i N_j)(\delta_{ab} - N_a N_b)$  the transverse-traceless projector onto the 2-plane orthogonal to  $\mathbf{N}$ .

### 21.2.4 Strong gravitational fields: neutron stars and black holes

The nonlinear structure of Einstein's equations implies many predictions for strong gravitational fields that distinguish GR from Newtonian gravity. For instance, in Newtonian gravity, there is no upper limit to the dimensionless gravitational potential  $U/c^2$ , with  $U$  satisfying Poisson's equation  $\Delta U = -4\pi G\rho$ , where  $\rho$  denotes the Newtonian mass density. By contrast, in GR, the dimensionless surface gravitational potential  $GM/(c^2R)$  of a spherically symmetric (perfect fluid) body cannot exceed  $\frac{4}{9}[2]$ .

Given an equation of state  $p = f(\rho)$  modeling the interior of a (cold) spherically symmetric body (say a non-rotating neutron star), Einstein equations, Eq. (21.7), with  $T^{\mu\nu} = (\rho + p)u^\mu u^\nu + pg^{\mu\nu}$ , and

$$g_{\mu\nu} dx^\mu dx^\nu = -e^{2\Phi(r)} c^2 dt^2 + \frac{dr^2}{1 - \frac{2GM(r)}{c^2 r}} + r^2 (d\theta^2 + \sin^2 \theta d\phi^2), \quad (21.18)$$

yield the following Tolman-Oppenheimer-Volkoff radial equations:

$$p'(r) = -\frac{G(\rho + p/c^2)(M(r) + 4\pi r^3 p/c^2)}{r^2(1 - 2GM(r)/(c^2 r))}; \quad (21.19)$$

$$M'(r) = 4\pi r^2 \rho; \quad (21.20)$$

$$\Phi'(r) = \frac{G(M(r) + 4\pi r^3 p/c^2)}{r^2(1 - 2GM(r)/(c^2 r))}. \quad (21.21)$$

In the exterior of the star ( $r \geq R$ ), the metric takes the Schwarzschild form

$$\begin{aligned} g_{\mu\nu} dx^\mu dx^\nu &= -\left(1 - \frac{2GM}{c^2 r}\right) c^2 dt^2 + \frac{dr^2}{1 - \frac{2GM}{c^2 r}} \\ &\quad + r^2 (d\theta^2 + \sin^2 \theta d\phi^2), \end{aligned} \quad (21.22)$$

where  $M \equiv M(R)$  is the total gravitational mass of the star. GR predicts, for any given  $p = f(\rho)$ , several (in principle) observable

features of neutron stars, such as: (i) the maximum mass of a neutron star; (ii) the relation between the radius  $R$  and the total mass  $M$ ; (iii) the dimensionless surface gravitational potential  $GM/(c^2R)$  (linked to the surface redshift  $\sqrt{-g_{00}} = \sqrt{1 - \frac{2GM}{c^2R}}$  measured by an observer at infinity); (iv) the moment of inertia; and (v) the Love number (tidal polarizability). The current uncertainty on the equation of state of a neutron star yields the GR-predicted approximate range for the maximum mass of non-rotating neutron stars  $1.5 M_\odot \lesssim M_{\max} \lesssim 2.5 M_\odot$ , and the absolute upper bound  $M_{\max} < 3 M_\odot$  [3]. The surface gravitational potential of a typical neutron star is  $GM/c^2 R_{\text{NS}} \simeq 0.17$ , which is a factor  $\sim 10^8$  higher than the surface potential of the Earth, and a mere factor 3 below the black hole limit  $GM/c^2 R_{\text{BH}} = \frac{1}{2}$  to be discussed next.

The existence of a maximum mass for a neutron star led Oppenheimer and Snyder [4] to predict that the end point of stellar evolution for sufficiently heavy stars, after exhaustion of all thermonuclear sources of energy, will be what are now called “black holes.” The latter are solutions of Einstein’s equations whose past structure involves a gravitationally collapsing star, but whose presently observable structure is essentially described (for non-rotating black holes) by the vacuum Schwarzschild solution Eq. (21.22). It took many years for theoretical (and mathematical) physicists to understand that the apparent singularity of the Schwarzschild solution at  $r = \frac{2GM}{c^2}$  was a coordinate singularity and that the Schwarzschild spacetime was regular at the “black hole horizon”,  $R_{\text{BH}} \equiv \frac{2GM}{c^2}$ . The rotating analog of the Schwarzschild spacetime is the Kerr black hole [5].

Black holes are outstanding consequences of GR which enjoy many remarkable properties, notably: (i) presence of a one-way surface (the horizon) for all waves and particles; (ii) absence of “hair” (*i.e.*, barring a possible electric charge, their structure is fully described by only two parameters, total mass,  $M$ , and total angular momentum,  $J \leq GM^2/c$ ); (iii) existence of a spectrum of damped quasi-normal vibrational modes; and (iv) a behavior under external perturbations similar to ordinary physical objects satisfying the laws of (dissipative) thermodynamics. Moreover, though no classical waves or particles can get out of the horizon, black holes are predicted to slowly evaporate via quantum particle creation.

### 21.2.5 Cosmology

To complete our short tour of the main predictions of GR, let us mention that GR offers the current standard framework for describing the large-scale structure of the Cosmos, from the nearly homogeneous Big Bang (and its plausible inflationary beginning) to the current inhomogeneous Universe undergoing an accelerated expansion. The spacetime structure on large (temporal and spatial) scales is well described by a solution of Einstein’s equations of the form

$$ds^2 = -(1 + 2\Phi(t, \mathbf{x}))c^2 dt^2 + 2W_i(t, \mathbf{x})dt dx^i + a^2(t)((1 - 2\Psi(t, \mathbf{x}))\delta_{ij} + h_{ij}(t, \mathbf{x}))dx^i dx^j, \quad (21.23)$$

where, after a suitable gauge-fixing [6],  $W_i(t, \mathbf{x})$  is transverse, while  $h_{ij}(t, \mathbf{x})$  is transverse and traceless. The source  $T^{\mu\nu}$  must involve a certain number of postulated ingredients: an inflaton field; the matter of the Standard Model; a dark matter component; and a cosmological constant contribution  $T_\Lambda^{\mu\nu} = -\rho_{\text{vac}}g^{\mu\nu}$ , with  $\rho_{\text{vac}} \equiv c^4\Lambda/(8\pi G)$ . The scale factor  $a(t)$  of the Friedmann background metric  $ds_0^2 = -c^2 dt^2 + a^2(t)\delta_{ij}dx^i dx^j$  satisfies the GR-predicted Friedmann equations (with vanishing spatial curvature  $k = 0$ ),

$$H^2 \equiv \left(\frac{\dot{a}}{a}\right)^2 = \frac{8\pi G}{3}\rho_{\text{tot}}, \quad (21.24)$$

$$\frac{\ddot{a}}{a} = -\frac{4\pi G}{3}\left(\rho_{\text{tot}} + \frac{3}{c^2}p_{\text{tot}}\right), \quad (21.25)$$

while the scalar  $(\Phi(t, \mathbf{x}), \Psi(t, \mathbf{x}))$ , vector  $(W_i(t, \mathbf{x}))$ , and tensor  $(h_{ij}(t, \mathbf{x}))$  inhomogeneous perturbations satisfy some GR-predicted propagation equations (coupled to matter perturbations); see [6] and the following *Reviews*. When the cosmic fluid is

well approximated by a perfect fluid, Einstein’s equations predict the following link between the scalar perturbations

$$\Phi(t, \mathbf{x}) = \Psi(t, \mathbf{x}). \quad (21.26)$$

## 21.3 A roadmap of parametrizations of deviations from GR, and of modified gravity

As will be discussed below, all currently performed gravitational experiments are compatible with GR. However, similarly to what is done in discussions of precision electroweak experiments, it is useful to quantify the significance of precision gravitational experiments by parameterizing possible deviations from GR. One can distinguish two main approaches to considering, and parameterizing, deviations from GR: (i) theory-agnostic phenomenological approaches; or, (ii) the study of the predictions of specific classes of alternative theories of gravity. Both types have led to useful ways of discussing tests of gravity. Both types also have their limitations. Considering them together leads to cross-fertilization.

### 21.3.1 Theory-agnostic phenomenological approaches to parameterizing deviations from GR

The theory-agnostic phenomenological approach is the oldest, and, arguably, the most robust one. It essentially consists in starting from specific observable predictions within the considered standard theory, and of deforming them by introducing some free parameters measuring either deviations from effects already present within the standard theory, or new effects absent from the standard theory. A classic example is the periastron advance of Mercury (and the other planets). When working within Newtonian gravity as a standard theory of gravity, the rate of periastron advance of Mercury,  $\dot{\omega}$ , is (when neglecting the quadrupole moment of the Sun) a calculable function of the masses and semi-major axes of the other planets of the solar system, say  $\dot{\omega}^{\text{Newton}}(m_i, a_i)$ . However,  $\dot{\omega}$  is also a directly observable quantity, so that one can parameterize the periastron advance of Mercury by writing

$$\dot{\omega}^{\text{obs}} = \dot{\omega}^{\text{Newton}}(m_i, a_i) + \Delta\dot{\omega}. \quad (21.27)$$

Using other observable data to determine some “observed” values of the  $m_i$ ’s and  $a_i$ ’s, one can then measure the anomalous periastron precession  $\Delta\dot{\omega}$  and see whether it is compatible with zero, or not. As is well-known, Leverrier used such a methodology and, in 1859, measured an anomalous periastron precession of about  $\Delta\dot{\omega} \simeq 38$  arcsec/century (later re-estimated at 43 arcsec/century), which was explained in 1915 as a GR prediction. Let us discuss further examples of the use of such theory-agnostic approaches for discussing deviations from GR.

### 21.3.2 Parameterized post-Newtonian (PPN) formalism.

When considering the weak-field slow-motion limit appropriate to describing gravitational experiments in the solar system, it has been traditional to parameterize possible (long-range) deviations from the GR-predicted 1PN metric by introducing extra dimensionless coefficients in the various terms of the metric of Eq. (21.8). The minimal version of the parameterized post-Newtonian (PPN) formalism (essentially due to Eddington) involves only two parameters  $\beta$  and  $\gamma$ , namely

$$g_{00} = -1 + \frac{2}{c^2}V - \frac{2\beta}{c^4}V^2 + O\left(\frac{1}{c^6}\right), \quad (21.28)$$

$$g_{0i} = -\frac{2(\gamma+1)}{c^3}V_i + O\left(\frac{1}{c^5}\right), \quad (21.29)$$

$$g_{ij} = \delta_{ij}\left[1 + \frac{2\gamma}{c^2}V\right] + O\left(\frac{1}{c^4}\right), \quad (21.30)$$

with  $V$  and  $V_i$  defined by Eq. (21.9), with the same vectorial source  $\sigma_i = \frac{T^{0i}}{c}$ , but a modified scalar source

$$\sigma^{\text{PPN}} = \frac{1}{c^2}\left[\left(1 + (3\gamma - 2\beta - 1)\frac{V}{c^2}\right)T^{00} + \gamma T^{ii}\right]. \quad (21.31)$$

In GR,  $\beta^{\text{GR}} = 1$  and  $\gamma^{\text{GR}} = 1$ , so that deviations from GR are parameterized by  $\bar{\beta} \equiv \beta - 1$  and  $\bar{\gamma} \equiv \gamma - 1$ . Richer versions of the

PPN formalism (involving up to ten parameters) were developed in interaction with the study of classes of alternative theories of gravity [7, 8]. This led to parameterizing new types of contributions to the IPN metric that are absent in the GR framework.

When deriving the IPN-accurate dynamics of  $N$  point masses predicted by the PPN-modified metric, Eq. (21.28), one finds that the free Lagrangian is not modified (because we are considering here a Lorentz-invariant subclass of PPN metrics), while there are modifications of both the two-body Lagrangian,  $L^{(2)}$ , Eq. (21.13), and the three-body one,  $L^{(3)}$ , Eq. (21.14). More precisely, denoting  $\eta \equiv 4\bar{\beta} - \bar{\gamma}$ , the Newtonian interaction energy term in Eq. (21.13) is modified into  $G_{AB}m_A m_B/r_{AB}$ , with a body-dependent gravitational “constant”

$$G_{AB} = G[1 + \eta(E_A^{\text{grav}}/m_A c^2 + E_B^{\text{grav}}/m_B c^2) + O(1/c^4)], \quad (21.32)$$

where  $E_A^{\text{grav}}$  denotes the gravitational binding energy of body  $A$ . In addition, there is the additional contribution  $+\bar{\gamma}(\mathbf{v}_A - \mathbf{v}_B)^2/c^2$  in the brackets on the right-hand side of  $L^{(2)}$ , Eq. (21.13). As for the three-body interaction term  $L^{(3)}$ , Eq. (21.14), it is modified by the overall factor  $1 + 2\bar{\beta}$ .

These results show how the introduction of the two minimal PPN deviation parameters  $\bar{\beta} \equiv \beta - 1$  and  $\bar{\gamma} \equiv \gamma - 1$  suffices to introduce many different observable effects. Some of them (the ones linked with  $\bar{\gamma}$ ) concern deviations at the linearized (one-graviton-exchange) level (and affect, for instance, light deflection and time-delay effects), while the deviation parameter  $\bar{\beta}$  parameterizes effects linked to the cubic vertex of Einstein’s gravity (and affects, for instance, periastron precession). Of particular interest is the fact that Eq. (21.32) shows that the combination  $\eta \equiv 4\bar{\beta} - \bar{\gamma}$  parameterizes a violation of the Strong Equivalence Principle, because the gravitational interaction between self-gravitating bodies is seen to be influenced by the gravitational binding energy of each body [9]. As stated above, this effect is absent in GR (where  $\eta^{\text{GR}} = 0$ ). This is an example where the fact of contrasting GR with some deviations from it gives physical significance to a null effect in GR (namely the universality of free fall of self-gravitating bodies).

Finally, one can extend the PPN formalism by allowing for a slow, phenomenological time variation of Newton’s constant:

$$G(t) = G_0 \left[ 1 + \frac{\dot{G}_0}{G_0}(t - t_0) \right]. \quad (21.33)$$

Here, one assumes that there exist units in which the masses,  $m_i$ , of elementary particles stay constant, and that  $G$  is measured in such units. A possible time variation of  $G$  then corresponds to a possible common variation of the dimensionless couplings  $Gm_i^2/(\hbar c)$ .

### 21.3.3 Parameterized post-Keplerian (PPK) formalism.

The discovery of pulsars (*i.e.*, rotating neutron stars emitting a beam of radio noise) in gravitationally bound orbits [10, 11] has given us our first experimental handle on a regime of relativistic gravity going significantly beyond the uniformly weak-field, and quasi-stationary regime of solar-system gravity. Binary pulsars allow us to probe some radiative effects, and also some strong-gravitational-field effects. In these systems, the finite speed of propagation of the gravitational interaction between the pulsar and its companion generates damping-like terms at order  $(v/c)^5$  in the equations of motion [12]. These damping forces are the local counterparts of the gravitational radiation emitted at infinity by the system (“gravitational radiation reaction”). They cause the binary orbit to shrink and its orbital period  $P_b$  to decrease. The remarkable stability of pulsar clocks has allowed one to measure the corresponding very small orbital period decay  $\dot{P}_b \equiv dP_b/dt \sim -(v/c)^5 \sim -10^{-12} - 10^{-14}$  in several binary systems, thereby giving us a direct experimental handle on the propagation properties of the gravitational field. In addition, the large surface gravitational potential of a neutron star allows one to probe the quasi-static strong-gravitational-field regime, as is discussed below.

It is possible to extract phenomenological (theory-independent) tests of gravity from binary pulsar data by using the parameter-

ized post-Keplerian (PPK) formalism [13]. The basis of this formalism is the fact that, after correcting for the Earth’s motion around the Sun and for the dispersion due to propagation in the interstellar plasma, the time of arrival of the  $N$ th pulse  $t_N$  can be described by a generic, parameterized “timing formula” [13, 14], whose functional form is common to the whole class of tensor-scalar gravitation theories:

$$t_N - t_0 = F[T_N(\nu_p, \dot{\nu}_p, \ddot{\nu}_p); \{p^K\}; \{p^{PK}\}]. \quad (21.34)$$

Here,  $T_N$  is the pulsar proper time corresponding to the  $N$ th turn given by  $N/2\pi = \nu_p T_N + \frac{1}{2}\dot{\nu}_p T_N^2 + \frac{1}{6}\ddot{\nu}_p T_N^3$  (with  $\nu_p \equiv 1/P_p$  the spin frequency of the pulsar, *etc.*),  $\{p^K\} = \{P_b, T_0, e, \omega_0, x\}$  is the set of “Keplerian” parameters (notably, orbital period  $P_b$ , eccentricity  $e$ , periastron longitude  $\omega_0$  and projected semi-major axis  $x = a \sin i/c$ ), and  $\{p^{PK}\} = \{k, \gamma_{\text{timing}}, \dot{P}_b, r, s, \delta_\theta, \dot{e}, \dot{x}\}$  denotes the set of (separately measurable) “post-Keplerian” parameters. Most important among these are: the fractional periastron advance per orbit  $k \equiv \dot{\omega} P_b/2\pi$ ; a dimensionful time-dilation parameter  $\gamma_{\text{timing}}$ ; the orbital period derivative  $\dot{P}_b$ ; and the “range” and “shape” parameters of the gravitational time delay caused by the companion,  $r$  and  $s$ .

Without assuming any specific theory of gravity, one can phenomenologically analyze the data from any binary pulsar by least-squares fitting the observed sequence of pulse arrival times to the timing formula of Eq. (21.34). This fit yields the “measured” values of the parameters  $\{\nu_p, \dot{\nu}_p, \ddot{\nu}_p\}$ ,  $\{p^K\}$ ,  $\{p^{PK}\}$ . Now, each specific relativistic theory of gravity predicts that, for instance,  $k$ ,  $\gamma_{\text{timing}}$ ,  $\dot{P}_b$ ,  $r$ , and  $s$  (to quote parameters that have been successfully measured from some binary pulsar data) are some theory-dependent functions of the Keplerian parameters and of the (unknown) masses  $m_1, m_2$  of the pulsar and its companion. For instance, in GR, one finds (with  $M \equiv m_1 + m_2$ ,  $n \equiv 2\pi/P_b$ ),

$$\begin{aligned} k^{\text{GR}}(m_1, m_2) &= 3(1 - e^2)^{-1}(GMn/c^3)^{2/3}, \\ \gamma_{\text{timing}}^{\text{GR}}(m_1, m_2) &= en^{-1}(GMn/c^3)^{2/3}m_2(m_1 + 2m_2)/M^2, \\ \dot{P}_b^{\text{GR}}(m_1, m_2) &= -(192\pi/5)(1 - e^2)^{-7/2} \left( 1 + \frac{73}{24}e^2 + \frac{37}{96}e^4 \right) \\ &\quad \times (GMn/c^3)^{5/3}m_1m_2/M^2, \\ r^{\text{GR}}(m_1, m_2) &= Gm_2/c^3, \\ s^{\text{GR}}(m_1, m_2) &= nx(GMn/c^3)^{-1/3}M/m_2. \end{aligned} \quad (21.35)$$

In alternative gravity theories each of the functions  $k^{\text{theory}}(m_1, m_2)$ ,  $\gamma_{\text{timing}}^{\text{theory}}(m_1, m_2)$ ,  $\dot{P}_b^{\text{theory}}(m_1, m_2)$ , *etc.*, is modified by quasi-static strong field effects (associated with the self-gravities of the pulsar and its companion), while the particular function  $\dot{P}_b^{\text{theory}}(m_1, m_2)$  is further modified by radiative effects [15–18]. If one measures  $N > 2$  PPK parameters from the data of a specific binary pulsar, these  $N$  measurements determine, for each given theory,  $N$  curves (defined by the  $N$  equations  $k_i^{\text{theory}}(m_1, m_2) = k_i^{\text{obs}}$ ) in the two-dimensional mass plane  $(m_1, m_2)$ . This yields  $N - 2$  tests of the specified theory, according to whether the  $N$  curves (or strips) have one point in common, as they should.

### 21.3.4 Parameterized-post-Friedmannian (PPF) formalisms.

We have recalled above that, in GR, the two functions,  $\Phi(t, \mathbf{x})$ , and  $\Psi(t, \mathbf{x})$ , parameterizing (in the “longitudinal gauge”) the scalar perturbations of the background Friedmann metric are related (in absence of anisotropic stresses) by Eq. (21.26). Several authors [19–28] have defined various types of parameterized-post-Friedmannian (PPF) formalisms involving (generally space and time dependent) phenomenological parameters. The simplest versions of these formalisms involve two phenomenological parameters measuring: (i) the ratio between  $\Phi(t, \mathbf{x})$ , and  $\Psi(t, \mathbf{x})$ , say (using a parametrization which parallels the usual PPN parametrization)

$$\Psi(t, \mathbf{x}) = \gamma_{\text{cosmo}}(t, \mathbf{x})\Phi(t, \mathbf{x}); \quad (21.36)$$

and (ii) the effective gravitational constant entering the Poisson equation for  $\Phi(t, \mathbf{x})$ , say

$$\Delta\Phi(t, \mathbf{x}) = 4\pi G_{\Phi}(t, \mathbf{x})\delta\rho(t, \mathbf{x}). \quad (21.37)$$

However, the peculiarities of cosmological observables limit the domain of applicability of such phenomenological approaches [26] (notably because the strong dependence of cosmological probes on epochs and scales obliges one to rely on specific parameterizations of the functions  $\gamma_{\text{cosmo}}(t, \mathbf{x})$  and  $G_{\Phi}(t, \mathbf{x})$ , *e.g.*, [25, 28]). Approaches based on specific classes of modified-gravity theories allow for a more complete treatment involving, in principle, all existing cosmological observables: Big Bang nucleosynthesis, cosmic microwave background, large-scale structure, Hubble diagram, weak lensing, etc. Discussing the current cosmological tests using either such PPF formalisms, or comparisons with the predictions of modified-gravity theories, is beyond the scope of this review. See [29] for a comprehensive recent discussion. The bottom line is that all present cosmological data have been found to be compatible with GR (within the Friedmann-Lemaître-based  $\Lambda$ CDM model). Beyond the quantitative limits on various parameterized theoretical models [29], one should remember the striking (strong-field-type) qualitative verification of GR embodied in the fact that relativistic cosmological models give an accurate picture of the Universe over a period during which the spatial metric has been blown up by a gigantic factor, say  $(1+z)^2 \sim 10^{19}$  between Big Bang nucleosynthesis and now.

### 21.3.5 Various phenomenological tests of GR from gravitational wave (GW) data

The observation by the US-based Laser Interferometer Gravitational-wave Observatory (LIGO), later joined by the Europe-based Virgo detector, of gravitational-wave (GW) signals [30–34], has opened up a novel testing ground for relativistic gravity. The first two observing runs of the LIGO-Virgo Collaboration (LVC) have led to the detection of GW signals from ten binary black-hole coalescences, and one binary neutron-star merger [35].

Several approaches have been used to either test consistency with GR, or to look for special types of possible deviations. Making accurate predictions for GW signals from coalescing black holes within GR took years of both analytical [36, 37] and numerical [38] work. Some works have started (both analytically [15, 39–43] and numerically [44–46]) to derive the corresponding predictions within some modified-gravity theories. Phenomenological approaches are very useful for parameterizing general, conceivable deviations from GR when analyzing the GW signals emitted by coalescing black holes or neutron stars.

A first phenomenological, global consistency test simply consists of measuring the noise-weighted correlation  $\mathcal{C}$  between each detected strain signal and the corresponding best-fit GR-predicted waveform.  $\mathcal{C}^{\text{obs}}$  should be equal to 1, modulo statistical (and/or systematic) errors.

Various other phenomenological tests of the structure of the GR-predicted waveforms emitted by coalescing compact binaries have been suggested. One general idea [47–49] (dubbed “parameterized post-Einsteinian formalism” in [50]) is to deform the existing phenomenological representation [51] of the GR-predicted phase  $\psi(f)$  of the Fourier-space black-hole coalescence GW signals  $h(f) = A(f)e^{i\psi(f)}$  by introducing GR-deviation parameters, say

$$\psi(f) = \sum_i p_i^{\text{GR}}(m_1, m_2, S_1, S_2)(1 + \delta\hat{p}_i)u_i(f). \quad (21.38)$$

Here, the  $u_i(f)$ ’s define a basis of functions of the GW frequency  $f$  (*e.g.*  $u_0(f) = f^{-5/3}\theta[0.018 - G(m_1 + m_2)f/c^3]$ , where  $\theta$  denotes the step function, parameterizes the leading-order (LO) term in the phase evolution during the early inspiral) while the corresponding mass- and spin-dependent GR-predicted coefficients are denoted  $p_i^{\text{GR}}(m_1, m_2, S_1, S_2)$  (*e.g.*,  $p_0^{\text{GR}} = \frac{3(m_1+m_2)^2}{128m_1m_2}(\pi G(m_1+m_2)/c^3)^{-5/3}$ ). In GR the next-to-leading-order (NLO) term is a  $O(v^2/c^2)$  correction  $p_2^{\text{GR}}u_2(f)$  with  $u_2(f) = f^{-1}\theta[0.018 - G(m_1 + m_2)f/c^3]$ . Each dimensionless

parameter  $\delta\hat{p}_i$  introduces a fractional deviation from the corresponding individual phasing GR effect having the frequency dependence  $u_i(f)$ , and can, in principle, be extracted by fitting the inspiral part of the observed waveform to the deformed template of Eq. (21.38). However, one must also use this deformed template for simultaneously extracting the values of  $m_1, m_2, S_1$ , and  $S_2$ . Together with signal-to-noise ratio (SNR) considerations, and parameter-correlation issues, this limits the applicability of such a test to introducing only one deformation parameter  $\delta\hat{p}_i$  at a time. A particularly meaningful test [47] is to leave undeformed the LO and NLO terms  $p_0^{\text{GR}}u_0(f) + p_2^{\text{GR}}u_2(f)$  and to vary the third coefficient  $p_3$  parameterizing the next, “GW tail”-related  $O(v^3/c^3)$  correction, with  $u_3(f) = f^{-2/3}\theta[0.018 - G(m_1 + m_2)f/c^3]$ . Another well-motivated test [50] is to introduce a new coefficient  $\delta\hat{p}_{-2}$ , which is absent in GR, and which parameterizes an  $O((v/c)^{-2})$  fractional correction to the LO, quadrupolar term, thereby allowing for a possible dipolar GW flux (indeed, dipolar GW radiation generally exists in theories containing scalar excitations). As  $p_{-2}^{\text{GR}}$  vanishes,  $\delta\hat{p}_{-2}$  is added as an absolute deviation, scaled by the LO term  $p_0^{\text{GR}}$ .

The coalescence of two black holes, or of a black hole and a neutron star (or of two heavy-enough neutron stars) leads to the formation of a black hole that is initially formed in a perturbed state. The relaxation of the latter perturbed black hole into its stationary, equilibrium state leads to the emission of characteristic (rapidly decaying) ringing GW modes (a.k.a. quasi-normal modes) [52, 53], whose frequencies and decay times are functions of the mass ( $M_f$ ) and spin ( $S_f \equiv GM_f^2 a_f/c$ ) of the final black hole, say

$$\omega_a = (c^3/GM_f)[2\pi\hat{f}_a^{\text{QNM}}(a_f) - i/\hat{\tau}_a^{\text{QNM}}(a_f)], \quad (21.39)$$

where  $a = 1, 2, \dots$  labels the various ringing modes, starting from the least-damped one. In principle, if the SNR is large enough, one can directly test for the presence of one or several of these modes in the post-merger signal, and measure both  $\text{Re}(\omega_a)$  and  $\text{Im}(\omega_a)$  in a theory-independent way. These phenomenological measurements then lead to null tests of GR, from which one can extract theoretical information about eventual deviations from GR [54, 55].

As recalled above, GR predicts that GWs propagate (in vacuum) at exactly the same speed as light (*i.e.*, they have the same dispersion law  $g^{\mu\nu}k_\mu k_\nu = 0$  in curved spacetime). Deviations from such a universal, scale-free dispersion law can be phenomenologically parameterized in several ways. If one phenomenologically assumes that the graviton dispersion law includes a mass term, say  $g^{\mu\nu}k_\mu k_\nu + m_g^2/h^2 = 0$ , or some more general type of frequency-dependent modification, such changes affect the phasing of the inspiral GW signal and can be directly tested [56]. When one observes *both* GWs and electromagnetic waves emitted by the same system, one can also directly test whether both types of waves propagate in the same way.

Let us now present some examples of theory-dependent discussions of experimental tests based on considering specific classes of alternative theories. The most conservative deviations from Einstein’s pure spin-2 theory are defined by adding new, bosonic, light or massless, macroscopically coupled fields.

### 21.3.6 Gravity tests within classes of tensor-scalar theories of gravity

The possible existence of new gravitational-strength couplings leading to deviations from Einsteinian (and Newtonian) gravity has been suggested by many natural extensions of GR, starting with the classic Kaluza-Klein idea, and continuing up to now with the study of extended supergravity theories, and of (super)string theory. In particular, a recurrent suggestion of such theories (which dates back to pioneering work by Jordan, and by Fierz [57]) is the existence of a scalar field  $\varphi$  coupled both to the scalar curvature  $R$  and to the various  $F_{\mu\nu}^a$  gauge-field actions. Such fields (“dilaton” or “moduli”) generically appear in string theory and are massless at the tree-level, but could acquire a self-interaction potential  $V(\varphi)$  beyond the tree-level.

The exchange of such a dilaton-like field leads to several types of observational deviations from GR. For experimental limits on the

gravitational inverse-square-law (down to the micrometer range) see Refs. [58–60]. If the potential  $V(\varphi)$  is zero or negligible for the considered range, the coupling of  $\varphi$  to  $F_{\mu\nu}^a$  leads to apparent violations of the weak equivalence principle, with rather specific composition-dependence [61]. Next, when neglecting the fractionally small composition-dependent effects, such a field approximately couples to the trace of the energy-momentum tensor  $T = g_{\mu\nu}T^{\mu\nu}$ . The most general such theory contains (after suitable field redefinitions) two arbitrary functions of the scalar field, namely the self-interaction potential  $V(\varphi)$ , and a matter-coupling function  $a(\varphi)$ :

$$\mathcal{L}_{\text{tot}}[g_{\mu\nu}, \varphi, \psi, A_\mu, H] = \frac{c^4}{16\pi G_*} \sqrt{g}(R(g_{\mu\nu}) - 2g^{\mu\nu}\partial_\mu\varphi\partial_\nu\varphi) - \sqrt{g}V(\varphi) + \mathcal{L}_{\text{SM}}[\psi, A_\mu, H, \tilde{g}_{\mu\nu}]. \quad (21.40)$$

Here  $G_*$  is a “bare” Newton constant, and the Standard Model matter is coupled not to the “Einstein” (pure spin-2) metric  $g_{\mu\nu}$ , but to the conformally related (“Jordan-Fierz”) metric

$$\tilde{g}_{\mu\nu} = \exp(2a(\varphi))g_{\mu\nu}. \quad (21.41)$$

The scalar field equation

$$\square_g\varphi = \frac{4\pi G}{c^4} \left( -\alpha(\varphi)T + \frac{\partial V(\varphi)}{\partial\varphi} \right), \quad (21.42)$$

features

$$\alpha(\varphi) \equiv \partial a(\varphi)/\partial\varphi, \quad (21.43)$$

as the basic (field-dependent) coupling between  $\varphi$  and matter [15, 62]. The best-known, special case of these theories is the one-parameter ( $\omega$ ) Jordan-Fierz-Brans-Dicke theory [63], with  $V(\varphi) = 0$  and  $a(\varphi) = \alpha_0\varphi$ , leading to a field-independent coupling  $\alpha(\varphi) = \alpha_0$  (with  $\alpha_0^2 = 1/(2\omega + 3)$ ). More generally, if we consider the massless theories ( $V(\varphi) = 0$ ) with arbitrary (non-linear) coupling function  $a(\varphi)$ , they modify Einstein’s predictions in the weak-field slow-motion limit appropriate to describing gravitational experiments in the solar system (1PN approximation) only through the appearance of exactly the same two “post-Einstein” dimensionless parameters  $\bar{\gamma} = \gamma - 1$  and  $\bar{\beta} = \beta - 1$  that entered the minimal (Eddington) PPN formalism presented above. However, we now have the following theoretical expressions relating the latter phenomenological parameters to the coupling functions entering the tensor-scalar action Eq. (21.40):

$$\bar{\gamma} = -2\frac{\alpha_0^2}{1 + \alpha_0^2}; \quad (21.44)$$

$$\bar{\beta} = +\frac{1}{2}\frac{\beta_0\alpha_0^2}{(1 + \alpha_0^2)^2}. \quad (21.45)$$

Here  $\alpha_0 \equiv \alpha(\varphi_0)$ , and  $\beta_0 \equiv \partial\alpha(\varphi_0)/\partial\varphi_0$ , with  $\varphi_0$  denoting the vacuum expectation value (VEV) of  $\varphi$  around the solar system. In addition, the observable value  $G^{\text{obs}}$  of the gravitational constant is found to be field-dependent and given (at a place where  $\varphi = \varphi_0$ ) by

$$G^{\text{obs}} = G(\varphi_0) \equiv G_* \exp[2a(\varphi_0)](1 + \alpha_0^2). \quad (21.46)$$

This makes it clear that the parameter  $\bar{\gamma}$  is the basic post-Einstein parameter, which measures the admixture of an additional field (here a spin-0 field) to the pure spin-2 GR. One also sees how the parameter  $\bar{\beta}$  is linked to non-linear effects (here coupling terms  $\beta_0(\varphi - \varphi_0)^2 T$  in the action), and how the Nordtvedt parameter  $\eta \equiv 4\bar{\beta} - \bar{\gamma}$  is related to the field-dependence of  $G^{\text{obs}}$  ( $\eta = (\alpha_0/(1 + \alpha_0^2))\partial \ln G(\varphi_0)/\partial\varphi_0$ ).

The advantage of a theory-dependent approach, such as Eq. (21.40), over the phenomenological minimal PPN approach of Eq. (21.28), is that it allows one to consistently predict the observational deviations from GR in all possible gravity regimes: the quasi-stationary weak-field regime; the wavelike weak-field regime; the strong-field regime; the cosmological regime, etc. All such observational deviations can be consistently worked out once one

chooses specific forms of the coupling function  $a(\varphi)$ , and of  $V(\varphi)$ . The simple choice of a two-parameter quadratic coupling function, say  $a(\varphi) = \alpha_0(\varphi - \varphi_0) + \frac{1}{2}\beta_0(\varphi - \varphi_0)^2$ , has been found useful for describing many possible observable deviations from GR.

The observable consequences for binary pulsar observations of the strong-field and radiative effects linked to the coupling to  $\varphi$  have been explicitly worked out in Refs. [15, 42] in the case where  $\varphi$  is massless (see Ref. [64] for the case where  $\varphi$  is massive). In particular, the strong-field nature of the pulsar tests is demonstrated by the fact that some tensor-scalar theories can be as close as desired to GR in the weak-field regime of the solar-system (*i.e.*,  $\bar{\gamma}$  and  $\bar{\beta}$  can be as small as desired, or even exactly zero), while developing (via a “spontaneous scalarization” mechanism) differences of order unity with GR in binary pulsar experiments [17, 18].

### 21.3.7 Attractor and screening mechanisms in modified gravity

As will follow from the discussion of experimental data below, the comparison between the predictions of general massless tensor-scalar theories and current data shows that the basic coupling parameter  $\alpha_0$  must be tuned to a small value (especially when allowing for composition-dependent effects). This raises the issue of the naturalness of such small coupling parameters. It has been shown in this respect that, in many tensor-scalar theories, there is an *attractor mechanism* by which the cosmological evolution naturally drives the VEV  $\varphi_0(t)$  towards a value for which the coupling parameter  $\alpha_0 = \alpha(\varphi_0)$  vanishes, thereby making it natural to expect only small deviations from GR (at least for the weak-field regime) at our current cosmological epoch [65, 66].

There are other theoretical mechanisms (generally called “screening mechanisms”) that could explain why a theory of gravity whose theoretical content significantly differs from that of GR could naturally pass all the stringent, GR-compatible experimental limits that will be discussed below. In particular, when considering a self-interacting scalar field ( $V(\varphi) \neq 0$ ), the interplay between the two terms on the right-hand side of Eq. (21.42) tends to drive the local VEV  $\varphi_0$  of  $\varphi$  to a density-dependent value. In turn, this leads to a corresponding density-dependent effective mass  $m_0(\varphi_0) = \sqrt{4\pi G\partial^2 V(\varphi_0)/\partial\varphi_0^2}$  of the  $\varphi$  field, and to density-dependent matter couplings [67]. Various choices of the functions  $V(\varphi)$  and  $a(\varphi)$  can then reduce the  $\varphi$ -induced deviations from GR in dense environments while still allowing for significant deviations in different (*e.g.*, cosmological) regimes [68–72].

Other screening mechanisms have been invoked, based on an environment dependence mediated by (first or second) derivatives of a scalar degree of freedom. Roughly speaking, such mechanisms involve a (possibly effective) scalar degree of freedom  $\varphi$  that satisfies a field equation that is more general than Eq. (21.42) in that the left-hand side,  $\square_g\varphi$ , is replaced by a non-linear function of  $\varphi$ ,  $\partial\varphi$  and  $\partial^2\varphi$ . The presence of non-linear derivative self-interactions of  $\varphi$  can weaken the effective coupling of  $\varphi$  to matter. A simple toy-model showing this weakening would be to replace Eq. (21.42) by an equation of the form

$$Z(\varphi, \partial\varphi, \partial^2\varphi)\square_g\varphi = \frac{4\pi G}{c^4} \left( -\alpha(\varphi)T + \frac{\partial V(\varphi)}{\partial\varphi} \right). \quad (21.47)$$

Such an equation is equivalent, at a first level of approximation, to replacing the gravitational constant  $G$  entering Eq. (21.42) by  $G_{\text{eff}}(\varphi_0, \partial\varphi_0, \partial^2\varphi_0) \equiv G/Z_0$ , where  $Z_0 \equiv Z(\varphi_0, \partial\varphi_0, \partial^2\varphi_0)$ . This has a screening effect if  $Z_0 \gg 1$ . Indeed, the replacement  $G \rightarrow G_{\text{eff}}$  diminishes the strength of the interaction potential due to  $\varphi$  exchange by a factor of  $1/Z_0$ . In addition, the range of this interaction is also affected:  $m_0(\varphi_0) = \sqrt{4\pi G\partial^2 V(\varphi_0)/\partial\varphi_0^2} \rightarrow m_{0\text{eff}}(\varphi_0, \partial\varphi_0, \partial^2\varphi_0) = \sqrt{4\pi G_{\text{eff}}\partial^2 V(\varphi_0)/\partial\varphi_0^2} = Z_0^{-1/2}m_0$ .

Screening mechanisms based on such non-linear derivative self-interactions are often referred to as being “Vainshtein-like” because a similar mechanism was first invoked in Ref. [73] as a conjectural way to ensure that the extra degrees of freedom associated with a massive (rather than massless) graviton become effectively weakly coupled to matter within a large domain around gravitational sources. Here, one is considering massive deformations of the massless spin-2 metric field of GR by a very small mass,

possibly of cosmological scale:  $m_g \sim \hbar H_0 \sim 10^{-33}$  eV. The construction of ghost-free potential terms for a spin-2 field has turned out to be a delicate matter [74]. The phenomenology of a very-low-mass graviton is still partly uncontrolled, both because of the unknown extent to which the Vainshtein screening is really active, and because of subtle constraints linked to an eventual UV completion of the theory beyond the unusually low energy scale where it becomes strongly coupled:

$$\Lambda_{\text{strong coupling}} \sim (M_{\text{Planck}} m_0^2)^{1/3} \sim 10^{-13} \left( \frac{m_0}{\hbar H_0} \right)^{2/3} \text{ eV}. \quad (21.48)$$

The search for modified gravity theories incorporating an extra scalar degree of freedom potentially able to yield a Vainshtein-like screening led to writing down the following general class of tensor-scalar Lagrangian [75, 76]:

$$\begin{aligned} L_{\text{tot}}[g_{\mu\nu}, \varphi, \psi] = & G_2(\varphi, X) - G_3(\varphi, X) \square_g \varphi + G_4(\varphi, X) R \\ & + G_{4X}(\varphi, X) [(\square_g \varphi)^2 - \varphi^{\mu\nu} \varphi_{\mu\nu}] \\ & + G_5(\varphi, X) G^{\mu\nu} \varphi_{\mu\nu} - \frac{1}{6} G_{5X}(\varphi, X) (\square_g \varphi)^3 \\ & - 3 \square_g \varphi \varphi^{\mu\nu} + 2 \varphi_{\mu\nu} \varphi^{\mu\lambda} \varphi_{\lambda}^{\nu} + L_{\text{matter}}[g_{\mu\nu}, \psi]. \end{aligned} \quad (21.49)$$

Here  $g_{\mu\nu}$  denotes the matter-coupled metric,  $X \equiv -\frac{1}{2} g^{\mu\nu} \partial_\mu \varphi \partial_\nu \varphi$ ,  $\varphi_{\mu\nu} \equiv \nabla_\mu \nabla_\nu \varphi$ ,  $G^{\mu\nu} \equiv R^{\mu\nu} - \frac{1}{2} R g^{\mu\nu}$ , and the various coefficients  $G_n(\varphi, X)$  are arbitrary functions of two variables (with  $G_{nX} \equiv \partial G_n / \partial X$ ). The field equations derived from the Lagrangian of Eq. (21.49) are only of second order in derivatives in spite of the non-linear structure of  $L_{\text{tot}}$ . This implies that the tensor-scalar theories defined by Eq. (21.49) feature three degrees of freedom, corresponding to a massless spin-2 excitation (GW) and a spin-0 excitation. Contrary to the simpler tensor-scalar theories of Eq. (21.40), it is found that the speed of propagation of GWs implied by Eq. (21.49) is generically different from the speed of light:

$$\frac{c_{\text{GW}}^2}{c^2} = \frac{G_4 - X(\ddot{\varphi} G_{5X} + G_{5\varphi})}{G_4 - 2XG_{4X} - X(H\dot{\varphi} G_{5X} - G_{5\varphi})}. \quad (21.50)$$

More general modified gravity models have been proposed (see, e.g. Refs. [77, 78]). Apart from the simplest of them, most of these models have a rather artificial flavor, and do not lead to convincing alternative explanations either of dark matter or of dark energy. In addition, many of them do not lead (contrary to GR) to mathematically “well-posed” evolution problems [79–81]. This entails a serious challenge to deriving strong-field predictions for such models. It has been argued that many of these (dark-energy motivated) models should be viewed as effective field theory (EFT) approximations that need some sort of UV completion at an unusually low frequency scale [82]. In spite of these shortcomings, such models are conceptually interesting because they give examples of deviations for various predictions of GR, existing independently from each other, in various regimes. For instance, some special tensor-scalar models lead to black hole solutions modified by scalar-hair [83, 84]. For other types of black holes with scalar-hair, see Ref. [85]. This shows the interest of phenomenologically testing, in a democratic and agnostic way, all conceivable deviations from GR.

Let us now turn to briefly presenting current experimental results of various phenomenological tests of the main GR predictions recalled in Section 21.2 above.

## 21.4 Experimental tests of the Equivalence Principle (i.e., of the matter-gravity coupling)

### 21.4.1 Tests of the constancy of constants

Stringent limits on a possible time variation of the basic coupling constants have been obtained by analyzing a natural fission reactor phenomenon that took place at Oklo, Gabon, two billion years ago [86, 87]. These limits are at the  $1 \times 10^{-8}$  level for the fractional variation of the fine-structure constant  $\alpha_{\text{em}}$  [87], and at the

$4 \times 10^{-9}$  level for the fractional variation of the ratio  $m_q / \Lambda_{\text{QCD}}$  between the light quark masses and  $\Lambda_{\text{QCD}}$  [88]. The determination of the lifetime of Rhenium 187 from isotopic measurements of some meteorites dating back to the formation of the solar system (about 4.6 Gyr ago) yields comparably strong limits [89]. Measurements of absorption lines in astronomical spectra also give stringent limits on the variability of both  $\alpha_{\text{em}}$  and  $\mu = m_p / m_e$  at cosmological redshifts, e.g.,

$$\Delta \alpha_{\text{em}} / \alpha_{\text{em}} = (1.2 \pm 1.7_{\text{stat}} \pm 0.9_{\text{sys}}) \times 10^{-6}, \quad (21.51)$$

at redshifts  $z = 1.0\text{--}2.4$  [90], and

$$|\Delta \mu / \mu| < 4 \times 10^{-7} (95\% \text{ CL}), \quad (21.52)$$

at a redshift  $z = 0.88582$  [91]. There are also significant limits on the variation of  $\alpha_{\text{em}}$  and  $\mu = m_p / m_e$  at redshift  $z \sim 10^3$  from cosmic microwave background data, e.g.,  $\Delta \alpha_{\text{em}} / \alpha_{\text{em}} = (3.6 \pm 3.7) \times 10^{-3}$  [92]. Direct laboratory limits (based on monitoring the frequency ratio of several different atomic clocks) on the present time variation of  $\alpha_{\text{em}}$ ,  $\mu = m_p / m_e$ , and  $m_q / \Lambda_{\text{QCD}}$  have reached the levels [93]

$$\begin{aligned} d \ln(\alpha_{\text{em}}) / dt &= (-2.5 \pm 2.6) \times 10^{-17} \text{ yr}^{-1}, \\ d \ln(\mu) / dt &= (-1.5 \pm 3.0) \times 10^{-16} \text{ yr}^{-1}, \\ d \ln(m_q / \Lambda_{\text{QCD}}) / dt &= (7.1 \pm 4.4) \times 10^{-15} \text{ yr}^{-1}. \end{aligned} \quad (21.53)$$

There are also experimental limits on a possible dependence of coupling constants on the gravitational potential [93, 94].

Experimental limits on the present time variation of the gravitational constant, Eq. (21.33), have been derived from planetary ephemerides [95], lunar laser ranging [96], and binary-pulsar data [97, 98]. The most stringent limits come from lunar-laser-ranging data [96]:

$$\frac{\dot{G}_0}{G_0} = (7.1 \pm 7.6) \times 10^{-14} \text{ yr}^{-1}. \quad (21.54)$$

### 21.4.2 Tests of the isotropy of space and of Local Lorentz invariance

The highest precision tests of the isotropy of space have been performed by looking for possible quadrupolar shifts of nuclear energy levels [99]. The (null) results can be interpreted as testing the fact that the various pieces in the matter Lagrangian, Eq. (21.6), are indeed coupled to one and the same external metric  $g_{\mu\nu}$  to the  $10^{-29}$  level.

Stringent tests of possible violations of local Lorentz invariance in gravitational interactions have been obtained both from solar-system data [8] and pulsar data [100, 101]. For astrophysical constraints on possible Planck-scale violations of Lorentz invariance, see Ref. [102].

### 21.4.3 Tests of the universality of free fall (weak, and strong equivalence principles)

The universality of the acceleration of free fall has been verified, for laboratory bodies, both on the ground [103, 104] (at the  $10^{-13}$  level), and in space [105, 106] (at the  $10^{-14}$  level):

$$\begin{aligned} (\Delta a/a)_{\text{BeTi}} &= (0.3 \pm 1.8) \times 10^{-13}; \\ (\Delta a/a)_{\text{BeAl}} &= (-0.7 \pm 1.3) \times 10^{-13}; \\ (\Delta a/a)_{\text{TiPt}} &= (-1 \pm 9(\text{stat}) \pm 9(\text{syst})) \times 10^{-15}. \end{aligned} \quad (21.55)$$

The universality of free fall has also been verified when comparing the fall of classical and quantum objects ( $6 \times 10^{-9}$  level [107]), or of two quantum objects ( $(1 \pm 1.4) \times 10^{-9}$  level [108]; including a test that atoms prepared in a quantum superposition of two hyperfine states fall in the same way).

The universality of free fall of self-gravitating bodies (strong equivalence principle) has been verified in both the weak-gravity, and the strong-gravity regimes. The gravitational accelerations of the Earth and the Moon toward the Sun have been checked to agree at the  $10^{-13}$  level [96]

$$(\Delta a/a)_{\text{EarthMoon}} = (-3 \pm 5) \times 10^{-14}. \quad (21.56)$$

The latter result constrains the Nordtvedt PPN parameter [9]  $\eta \equiv 4\bar{\beta} - \bar{\gamma}$  to the  $10^{-4}$  level:

$$\eta = (-0.2 \pm 1.1) \times 10^{-4}. \quad (21.57)$$

See below for strong-field tests of the strong equivalence principle.

Finally, the universality of the gravitational redshift of clock rates has been verified at the  $10^{-4}$  level by comparing a hydrogen-maser clock flying on a rocket up to an altitude of about 10,000 km to a similar clock on the ground [109]. The redshift due to a height change of only 33 cm has been detected by comparing two optical clocks based on  $^{27}\text{Al}^+$  ions [110]. The gravitational redshift has also been detected in the orbit of a star near the supermassive black hole at the center of our Galaxy [111, 112], and its universality has been verified at the 5% level [113].

### 21.5 Tests of quasi-stationary, weak-field gravity

All currently performed gravitational experiments in the solar system, including perihelion advances of planetary orbits, the bending and delay of electromagnetic signals passing near the Sun, and very accurate ranging data to the Moon obtained by laser echoes, are compatible with the post-Newtonian results of Eq. (21.15), Eq. (21.13), and Eq. (21.14). The “gravito-magnetic” interactions  $\propto v_{AVB}$  contained in Eq. (21.13) are involved in many of these experimental tests. They have been particularly tested in lunar-laser-ranging data [114], in the combined LAGEOS-LARES satellite data [115, 116], and in the dedicated Gravity Probe B mission [117].

To assess in a quantitative manner the results of the various solar-system tests of gravity it is convenient to express them in terms of the PPN parameters defined above. The best current limit on the post-Einstein parameter  $\bar{\gamma} \equiv \gamma - 1$  is

$$\bar{\gamma} = (2.1 \pm 2.3) \times 10^{-5}, \quad (21.58)$$

as deduced from the additional Doppler shift experienced by radio-wave beams connecting the Earth to the Cassini spacecraft when they passed near the Sun [118].

The (cubic-vertex-related) post-Einstein parameter  $\bar{\beta} \equiv \beta - 1$  is constrained at the  $10^{-4}$  level both from a study of the global sensitivity of planetary ephemerides to post-Einstein parameters [95],

$$|\bar{\beta}| < 7 \times 10^{-5}, \quad (21.59)$$

and from lunar-laser-ranging data [96]

$$\bar{\beta} = (-4.5 \pm 5.6) \times 10^{-5}. \quad (21.60)$$

More stringent limits on  $\bar{\gamma}$  (*i.e.* the coupling of  $\varphi$  to matter) are obtained in dilaton-like models where scalar couplings violate the Equivalence Principle [119].

### 21.6 Tests of strong-field gravity (neutron stars and black holes)

Experimental tests of strong-field gravity have been obtained in various physical systems, notably binary pulsars and coalescing binary black holes.

It is convenient to quantitatively express binary-pulsar tests of strong-field gravity by using the PPK formalism defined above. We recall that the measurement of  $N$  phenomenological PPK parameters leads to  $N - 2$  tests of strong-field gravity. In all, *thirteen* tests of strong-field and/or radiative gravity have been obtained in the four different (double neutron-star) binary pulsar systems PSR1913+16 [10, 11, 120], PSR1534+12 [121–123], PSR J1141–6545 [124–127], and PSR J0737–3039 A,B [128–132]. These consist of  $N - 2 = 5 - 2 = 3$  tests from PSR1913+16;  $5 - 2 = 3$  tests from PSR1534+12;  $4 - 2 = 2$  tests from PSR J1141–6545; and  $7 - 2 = 5$  tests from PSR J0737–3039 (see, also, Ref. [133] for additional, less accurate tests of relativistic gravity). Among these tests, four of them (those involving the measurement of the PPK parameter  $\dot{P}_b$ ) probe radiative effects, and will be discussed in the following section. The four binary pulsar systems PSR1913+16, PSR1534+12, PSR J1141–6545, and PSR J0737–3039 A,B have given nine tests of quasi-static, strong-field gravity. GR passes all these tests within the measurement

accuracy. Let us only highlight here some of the most accurate strong-field tests.

In the binary pulsar PSR 1534+12 [121] one has measured *five* post-Keplerian parameters:  $k$ ,  $\gamma_{\text{timing}}$ ,  $r$ ,  $s$ , and (with less accuracy)  $\dot{P}_b$  [122, 123]. This yields *three* tests of relativistic gravity. Among these tests, the two involving the measurements of  $k$ ,  $\gamma_{\text{timing}}$ ,  $r$ , and  $s$  accurately probe strong field gravity, without mixing of radiative effects [122]. The most precise ( $10^{-3}$  level) of these pure strong-field tests is the one obtained by combining the measurements of  $k$ ,  $\gamma_{\text{timing}}$ , and  $s$ ; namely, [123],

$$\left[ \frac{s^{\text{obs}}}{s^{\text{GR}}[k^{\text{obs}}, \gamma_{\text{timing}}^{\text{obs}}]} \right]_{1534+12} = 1.002 \pm 0.002. \quad (21.61)$$

The discovery of the remarkable *double* binary pulsar PSR J0737–3039 A and B [128, 129] has led to the measurement of *seven* independent parameters [130–132]: five of them are the post-Keplerian parameters  $k$ ,  $\gamma_{\text{timing}}$ ,  $r$ ,  $s$ , and  $\dot{P}_b$  entering the relativistic timing formula of the fast-spinning pulsar PSR J0737–3039 A; a sixth is the ratio  $R = x_B/x_A$  between the projected semi-major axis of the more slowly spinning companion pulsar PSR J0737–3039 B, and that of PSR J0737–3039 A (the theoretical prediction for the ratio  $R = x_B/x_A$ , considered as a function of the (inertial) masses  $m_1 = m_A$  and  $m_2 = m_B$ , is  $R^{\text{theory}} = m_1/m_2 + O((v/c)^4)$  [13, 14], independently of the gravitational theory considered). Finally, the seventh parameter  $\Omega_{\text{SO,B}}$  is the angular rate of (spin-orbit) precession of PSR J0737–3039 B around the total angular momentum vector [131, 132]. These seven measurements give us *five* tests of relativistic gravity [130, 134, 135], four of which are quasi-static, strong-field tests. GR passes all those tests with flying colors [135]. The most accurate is at the  $5 \times 10^{-4}$  level:

$$\left[ \frac{s^{\text{obs}}}{s^{\text{GR}}[k^{\text{obs}}, R^{\text{obs}}]} \right]_{0737-3039} = 1.0000 \pm 0.0005. \quad (21.62)$$

Binary pulsar data on other types of pulsar systems can be used to test strong-field aspects of the “strong equivalence principle,” namely the GR prediction that strong-self-gravity objects (such as neutron stars) should fall with the same acceleration as weak-self-gravity objects (such as white-dwarfs) in the (external) gravitational field created by other objects (such as the Galaxy, or another white dwarf). The first binary-pulsar tests of this property have been obtained in nearly circular binary systems (made of a neutron star and a white dwarf) falling in the field of the Galaxy, and have led to strong-field confirmations (at the  $2 \times 10^{-3}$  level) of the strong equivalence principle [98, 136–138]. The remarkable discovery of the pulsar PSR J0337+1715 in a hierarchical triple system [139] has allowed one to derive a much more accurate test of the strong equivalence principle because the inner binary (comprising a pulsar and a close white-dwarf companion) falls toward the outer white-dwarf companion with an acceleration that is  $10^8$  times larger than the Galactic acceleration. This leads to a 95% confidence level limit on a possible fractional difference in free-fall acceleration of the pulsar and its close companion of [140]

$$|\Delta a/a| < 2.6 \times 10^{-6}. \quad (21.63)$$

This limit yields strong constraints on tensor-scalar gravity models.

Measurements over several years of the pulse profiles of various pulsars have detected secular changes compatible with the prediction [141] that the general relativistic spin-orbit coupling should cause a secular change in the orientation of the pulsar beam with respect to the line of sight (“geodetic precession”). Such confirmations of general-relativistic spin-orbit effects were obtained in PSR 1913+16 [142], PSR B1534+12 [123], PSR J1141–6545 [143], PSR J0737–3039 [131, 132], and PSR J1906+0746 [144, 145]. In some cases (notably PSR 1913+16 and PSR J1906+0746) the secular change in the orientation of the pulsar beam is expected to lead to the disappearance of the beam (as seen on the Earth) on a human time scale (the second pulsar in the double system PSR J0737–3039 already disappeared in March 2008 and is expected to reappear around 2035 [132]).

Recently, the ultimate strong-field regime of black holes has started to be quantitatively probed via GW observations. The LIGO-Virgo collaboration has detected (starting in September 2015) GW signals [146], which, besides testing the radiative structure of gravity (see next section), are in excellent qualitative and quantitative agreement with the structure and dynamics of black-hole horizons in GR. Because of the mixing of strong-field effects with radiative effects during the coalescence of two black holes, and because of the lack of detailed alternative-theory predictions for this process (see, however, Refs. [44–46]), it is not easy to set quantitative limits on possible strong-field deviations from GR, independently of radiative effects. Direct tests of the existence of black-hole horizons are scarce (see, however, the suggestion to look for GW echoes as a negative test [147]). The only sharp quantitative assessment on possible deviations from GR concerns the global agreement between the full observed GW signal of coalescing binary black holes, and the GR-predicted one. In particular, the noise-weighted correlation between the first observed strain signal GW150914 and the best-fit GR-predicted waveform was found to be  $\geq 96\%$  [49]. In other words, GR-violation effects that cannot be reabsorbed in a redefinition of physical parameters are limited (in a noise-weighted sense) to less than 4%.

Let us also mention that the Event Horizon Telescope collaboration has obtained event-horizon-scale images of the supermassive black hole candidate in the center of the giant elliptical galaxy M87 that are “consistent with expectations for the shadow of a Kerr black hole as predicted by general relativity” [148]. However, in view of modeling uncertainties, and of the limited accuracy of the imaging, no quantitative assessment of eventual deviations from GR can be made at this stage.

## 21.7 Tests of radiative gravity (both in binary-pulsar data and in GW data)

Experimental confirmations of the GR predictions for the radiative structure of gravity have been obtained both in binary-pulsar data and in the observation of GW signals from coalescing compact binaries (binary black holes and binary neutron stars).

Binary-pulsar observations involving the measurement of the orbital period derivative  $\dot{P}_b$  give *direct* experimental tests of the reality of gravitational radiation, and, in particular, an experimental confirmation that the speed of propagation of gravity  $c_g$  is equal to the speed of light  $c$  (indeed, as recalled above,  $\dot{P}_b$  is a consequence of the propagation of the gravitational interaction between the two neutron stars [12]). Even in the presence of screening mechanisms within the binary system, the value of  $\dot{P}_b$  yields a measurement of the speed of propagation of GWs at the  $10^{-2}$  level [149]. The currently most accurate binary-pulsar tests of the radiative properties of gravity come from the binary neutron-star systems PSR1913+16 and PSR J0737–3039 A,B, as well as from several neutron-star-white-dwarf systems, notably PSR J1738+0333.

After subtracting a small ( $\sim 10^{-14}$  level in  $\dot{P}_b^{\text{obs}} = (-2.423 \pm 0.001) \times 10^{-12}$ ), but significant, “Galactic” perturbing effect (linked to Galactic accelerations and to the pulsar proper motion) [150], one finds that the phenomenological test obtained by combining the measurements of the three PPK parameters ( $k - \gamma_{\text{timing}} - \dot{P}_b$ )<sub>1913+16</sub> is passed by GR with complete success [120]:

$$\left[ \frac{\dot{P}_b^{\text{obs}} - \dot{P}_b^{\text{gal}}}{\dot{P}_b^{\text{GR}}[k^{\text{obs}}, \gamma_{\text{timing}}^{\text{obs}}]} \right]_{1913+16} = 0.9983 \pm 0.0016. \quad (21.64)$$

Here  $\dot{P}_b^{\text{GR}}[k^{\text{obs}}, \gamma_{\text{timing}}^{\text{obs}}]$  is the result of inserting in  $\dot{P}_b^{\text{GR}}(m_1, m_2)$  the values of the masses predicted by the two equations  $k^{\text{obs}} = k^{\text{GR}}(m_1, m_2)$ , and  $\gamma_{\text{timing}}^{\text{obs}} = \gamma_{\text{timing}}^{\text{GR}}(m_1, m_2)$ . This yields experimental evidence for the reality of gravitational radiation damping forces at the  $(-1.7 \pm 1.6) \times 10^{-3}$  level.

Similarly, the combined measurement in PSR J0737–3039 A,B of the three parameters  $k$ ,  $R \equiv x_B/x_A$ , and  $\dot{P}_b$  yields another experimental test of the radiative structure of gravity at the  $10^{-3}$

level [130–132]:

$$\left[ \frac{\dot{P}_b^{\text{obs}}}{\dot{P}_b^{\text{GR}}[k^{\text{obs}}, R^{\text{obs}}]} \right]_{0737-3039} = 1.000 \pm 0.001. \quad (21.65)$$

In addition to the above tests, further very stringent tests of radiative gravity follow from the measurement of the orbital period decay  $\dot{P}_b$  of low-eccentricity pulsar-white dwarf systems. Notably, the system PSR J1738+0333 yields an intrinsic orbital decay of [151]

$$\left[ \dot{P}_b^{\text{obs}} - \dot{P}_b^{\text{gal}} \right]_{1738+0333} = (-25.9 \pm 3.2) \times 10^{-15}, \quad (21.66)$$

to be compared to

$$\left[ \dot{P}_b^{\text{GR}} \right]_{1738+0333} = (-27.7^{+1.5}_{-1.9}) \times 10^{-15}. \quad (21.67)$$

The fractional agreement between the (corrected) observed period decay and the GR-predicted one seems to be quantitatively less impressive than the double-neutron-star results cited above, but the crucial point is that asymmetric binary systems (such as neutron-star-white-dwarf ones) are strong emitters of dipolar gravitational radiation in tensor-scalar theories, with  $\dot{P}_b$  scaling (modulo matter-scalar couplings) like  $m_1 m_2 / (m_1 + m_2)^2 (v/c)^3$ , instead of the parametrically smaller GR-predicted quadrupolar radiation  $\dot{P}_b \sim (v/c)^5$  [7, 15]. In view of the very small absolute value of  $\dot{P}_b$ , this makes such systems (and notably PSR J1738+0333) very sensitive probes of tensor-scalar gravity [97, 151–154]. It is then useful to turn to a theory-dependent analysis of pulsar data. Such an analysis (see, *e.g.*, [17, 122, 151, 154]) leads to excluding a large portion of the parameter space of tensor-scalar gravity allowed by solar-system tests. As a result, the basic matter-scalar coupling  $\alpha_0^2$  is more strongly constrained, over most of the parameter space, than the best current solar-system limits of Eq. (21.58) (namely below the  $10^{-5}$  level) [151, 154].

We now turn to the tests of radiative gravity that can be deduced from the first two observing runs of the LIGO-Virgo collaboration (LVC) (the third observing run of the LVC has started on April 1, 2019, and has already issued many alerts). The first two observing runs of the LVC have reported the detection of GW signals emitted by the inspiral and coalescence of ten binary black hole systems, and one binary neutron star system [146] (see [155] for more claimed detections from the public LVC data). The network signal-to-noise ratio (SNR) of the reported events varies between 10 and 24 for binary black hole coalescences, and is equal to 33 for the binary neutron star event. All currently detected GW signals are consistent with GR predictions. Several phenomenological approaches were used and led to setting limits on possible deviations from GR.

Besides checking the agreement between the *full* observed GW signals and the corresponding best-fit full signals predicted by GR, attempts were made to test the consistency between two separate parts of the signals. A first attempt [156] separated: (i) the lower-frequency (LF) signal emitted during the inspiral phase (considered up to the innermost stable circular orbit); and (ii) the higher-frequency (HF) remaining signal emitted during the late-inspiral, the merger, and the ringdown. Separately fitting each of these partial signals to GR-based templates then leads to separate estimates of the binary’s parameters, leading to separate estimates of the mass  $M_f$  and dimensionless spin parameter  $a_f = J_f / (GM_f^2)$  of the final black hole that would be formed (in GR) by the coalescence of the two initial black holes. The consistency with GR then consists in testing whether the two estimates  $(M_f, a_f)_{\text{LF}}$  and  $(M_f, a_f)_{\text{HF}}$  are compatible with each other. They were found to be consistent within statistical errors of order 30% for seven selected binary black hole events (see Fig. 2 in [156]). A second attempt [157] separately considered the *post-merger signal* of coalescing black holes, and tried to quantify the presence and structure of the GR-predicted ringing modes in the latter post-merger signal. Measuring, for the first event GW150914 (by using a model of the post-merger signal including the first two ringing modes), the mass and spin of the final black hole,  $(M_f, a_f)_{\text{post-merger}}$ , has shown consistency, at the  $\sim 20\%$



level, with the corresponding values inferred (using GR predictions) from fitting the entire signal [157].

The parametrization of Eq. (21.38) for possible deviations in the frequency dependence of the Fourier-domain phase  $\psi(f)$  of the black hole coalescence GW signal was used to measure best-fit values for each fractional deviation parameter  $\delta\hat{p}_i$ , considered separately (the other ones being set to zero). In all cases, the posterior distribution for each  $\delta\hat{p}_i$  is consistent with the GR value, *i.e.*,  $\delta\hat{p}_i^{\text{GR}} = 0$  (see figures 3 and 4 in Ref. [156]). The current limits on  $\delta\hat{p}_i$  are (roughly) of order unity, except for the two parameters highlighted above:  $\delta\hat{p}_3$  (parameterizing the  $O((\frac{v}{c})^3)$  fractional correction to the LO, quadrupolar term); and  $\delta\hat{p}_{-2}$  (parameterizing a possible dipolar-radiation-related  $O((\frac{v}{c})^{-2})$  fractional correction to the LO, quadrupolar term). The current combined 90% upper bound on  $\delta\hat{p}_3$  is  $\sim 10\%$ , while the corresponding bound on  $\delta\hat{p}_{-2}$  is  $2 \times 10^{-3}$  (see figure 4 in Ref. [156]). See Ref. [158] for examples of the translation of these phenomenological constraints into bounds on specific theories.

As recalled above, GR predicts that the polarization content of GWs is pure helicity-2, *i.e.* described by the two independent components of a traceless tensor transverse to the propagation direction. A (massless) scalar excitation would add a pure-trace “breathing mode” in the plane transverse to the propagation direction. A phenomenological approach to generic metric theories of gravity would allow for up to six polarizations for a GW [159], namely two tensor, two vector and two scalar modes. The LVC tested possible polarization deviations from GR in the following way [33, 156]: they assumed that the phase evolution of the GW signal was the one predicted by GR, but they replaced the polarization structure of the signal either by a generic vector-like one, or by a generic scalar-like one. The best polarization constraints have been obtained from the GW170817 event. The latter very long ( $\sim 100$  s) and very loud (SNR  $\simeq 33$ ) event was convincingly interpreted as coming from a binary neutron star inspiral ( $\sim 40$  Mpc away), and was associated with a subsequent  $\gamma$ -ray burst, followed by transient counterparts across the electromagnetic spectrum [160]. The polarization analysis of the GW170817 data has given overwhelming evidence in favor of pure tensor polarization modes in comparison to pure vector or pure scalar modes with a base-ten logarithm of the Bayes factor of  $+20.81 \pm 0.08$  and  $+23.09 \pm 0.08$ , respectively [156].

GR also predicts that GWs are non dispersive, and propagate at the same speed as light. One can phenomenologically modify the GR-predicted GW phase evolution by adding the putative effect of an anomalous dispersion relation of the form  $E^2 = p^2 c^2 + A p^\alpha c^\alpha$ . GW data have been used to set bounds on the anomalous coefficient  $A$  for various values of the exponent  $\alpha$ . The best bounds come from the analysis of the GW170104 event (see figure 5 in [32]). The case  $\alpha = 0$  is equivalent to assuming that gravitons disperse as a massive particle [56]. Combined GW data lead to the following phenomenological limit on the graviton mass:  $m_g \leq 7.7 \times 10^{-23} \text{ eV}/c^2$  [32]. See Refs. [161, 162] for other graviton mass bounds.

Finally, a very constraining bound on the speed of propagation of gravity  $c_{\text{GW}}$  was derived from the observed time delay of 1.7 s between GW170817 and the associated  $\gamma$ -ray burst. Namely, the fractional difference between  $c_{\text{GW}}$  and  $c_{\text{light}} \equiv c$  is constrained to be [163]

$$-3 \times 10^{-15} < \frac{c_{\text{GW}} - c}{c} < +7 \times 10^{-16}. \quad (21.68)$$

When comparing the latter bound to the prediction Eq. (21.50) from general second-order tensor-scalar theories, Eq. (21.49), one is led to conclude that the coupling function  $G_5(\varphi, X)$  has to be ignored and that the coupling function  $G_4(\varphi, X)$  has to be restricted to depend only on  $\varphi$ . This drastically reduces the viable tensor-scalar modified-gravity models [164–167]. Observations from future GW detectors (both on the ground and in space) are expected to considerably strengthen the testing power of GW data [168, 169].

## 21.8 Conclusions

All present experimental tests are compatible with the predictions of the current “standard” theory of gravitation, Einstein’s General Relativity. Let us recap the main tests. The universality of the coupling between matter and gravity (Equivalence Principle) has been verified at around the  $10^{-14}$  level. Solar system experiments have tested the weak-field predictions of Einstein’s theory at the few times  $10^{-5}$  level. The propagation properties (in the near zone) of relativistic gravity, as well as several of its static strong-field aspects, have been verified at the  $10^{-3}$  level (or better) in several binary pulsar experiments. Interferometric detectors of gravitational radiation have given direct observational proofs of the existence, and properties, of gravitational waves (in the wave zone), and of the existence of coalescing black holes, and they have already set strong limits on possible deviations; in particular: an upper bound  $|\delta\hat{p}_{-2}| < 2 \times 10^{-3}$  on a possible dipolar contribution to the GW flux; the  $O(10^{-15})$  bound of Eq. (21.68) on the speed of gravity; and strong evidence for the pure-tensor polarization structure of gravitational waves. In addition, laboratory experiments have set strong constraints on sub-millimeter modifications of Newtonian gravity, while many different cosmological data sets have been used to set limits on possible GR deviations on cosmological scales [29]. In spite of the uneasiness of having to assume the existence of dark matter, and the presence of an unaturally small cosmological constant (as dark energy), General Relativity stands out as a uniquely successful description of gravity on all the scales that have been explored so far. There are no modified-gravity models which naturally pass all existing experimental tests, while either explaining away the need for dark matter or for dark energy.

## References

- [1] S. Weinberg, *Rev. Mod. Phys.* **61**, 1 (1989).
- [2] H. A. Buchdahl, *Phys. Rev.* **116**, 1027 (1959).
- [3] N. Chamel *et al.*, *Int. J. Mod. Phys. E* **22**, 1330018 (2013), [arXiv:1307.3995].
- [4] J. R. Oppenheimer and H. Snyder, *Phys. Rev.* **56**, 455 (1939).
- [5] R. P. Kerr, *Phys. Rev. Lett.* **11**, 237 (1963).
- [6] V. F. Mukhanov, H. A. Feldman and R. H. Brandenberger, *Phys. Rept.* **215**, 203 (1992).
- [7] C. M. Will, *Theory and Experiment in Gravitational Physics*, Cambridge University Press (2018).
- [8] C. M. Will, *Living Rev. Rel.* **17**, 4 (2014), [arXiv:1403.7377].
- [9] K. Nordvedt, *Phys. Rev.* **170**, 1186 (1968).
- [10] R. A. Hulse, *Rev. Mod. Phys.* **66**, 699 (1994).
- [11] J. H. Taylor, *Rev. Mod. Phys.* **66**, 711 (1994).
- [12] T. Damour and N. Deruelle, *Phys. Lett.* **A87**, 81 (1981); T. Damour, *C.R. Acad. Sci. Paris* **294**, 1335 (1982).
- [13] T. Damour and J. H. Taylor, *Phys. Rev.* **D45**, 1840 (1992).
- [14] T. Damour and N. Deruelle, *Ann. Inst. H. Poincaré A*, **44**, 263 (1986).
- [15] T. Damour and G. Esposito-Farese, *Class. Quant. Grav.* **9**, 2093 (1992).
- [16] C. M. Will and H. W. Zaglauer, *Astrophys. J.* **346**, 366 (1989).
- [17] T. Damour and G. Esposito-Farese, *Phys. Rev.* **D54**, 1474 (1996), [arXiv:gr-qc/9602056].
- [18] T. Damour and G. Esposito-Farese, *Phys. Rev.* **D58**, 042001 (1998), [arXiv:gr-qc/9803031].
- [19] J.-P. Uzan, *Gen. Rel. Grav.* **39**, 307 (2007), [arXiv:astro-ph/0605313].
- [20] R. Caldwell, A. Cooray and A. Melchiorri, *Phys. Rev.* **D76**, 023507 (2007), [arXiv:astro-ph/0703375].
- [21] P. Zhang *et al.*, *Phys. Rev. Lett.* **99**, 141302 (2007), [arXiv:0704.1932].
- [22] L. Amendola, M. Kunz and D. Sapone, *JCAP* **0804**, 013 (2008), [arXiv:0704.2421].

- [23] W. Hu and I. Sawicki, Phys. Rev. **D76**, 104043 (2007), [arXiv:0708.1190].
- [24] S. F. Daniel *et al.*, Phys. Rev. **D77**, 103513 (2008), [arXiv:0802.1068].
- [25] G.-B. Zhao *et al.*, Phys. Rev. **D79**, 083513 (2009), [arXiv:0809.3791].
- [26] J.-P. Uzan, Gen. Rel. Grav. **42**, 2219 (2010), [arXiv:0908.2243].
- [27] E. Bertschinger, Phil. Trans. Roy. Soc. Lond. **A369**, 4947 (2011), [arXiv:1111.4659].
- [28] T. Baker, P. G. Ferreira and C. Skordis, Phys. Rev. **D87**, 2, 024015 (2013), [arXiv:1209.2117].
- [29] M. Ishak, Living Rev. Rel. **22**, 1, 1 (2019), [arXiv:1806.10122].
- [30] B. P. Abbott *et al.* (LIGO Scientific, Virgo), Phys. Rev. Lett. **116**, 6, 061102 (2016), [arXiv:1602.03837].
- [31] B. P. Abbott *et al.* (LIGO Scientific, Virgo), Phys. Rev. Lett. **116**, 24, 241103 (2016), [arXiv:1606.04855].
- [32] B. P. Abbott *et al.* (LIGO Scientific, VIRGO), Phys. Rev. Lett. **118**, 22, 221101 (2017), [Erratum: Phys. Rev. Lett.121,no.12,129901(2018)], [arXiv:1706.01812].
- [33] B. P. Abbott *et al.* (LIGO Scientific, Virgo), Phys. Rev. Lett. **119**, 14, 141101 (2017), [arXiv:1709.09660].
- [34] B. P. Abbott *et al.* (LIGO Scientific, Virgo), Phys. Rev. Lett. **119**, 16, 161101 (2017), [arXiv:1710.05832].
- [35] B. P. Abbott *et al.* (LIGO Scientific, Virgo), Phys. Rev. **X6**, 4, 041015 (2016), [erratum: Phys. Rev.X8,no.3,039903(2018)], [arXiv:1606.04856].
- [36] A. Buonanno and T. Damour, Phys. Rev. **D62**, 064015 (2000), [arXiv:gr-qc/0001013].
- [37] L. Blanchet, Living Rev. Rel. **17**, 2 (2014), [arXiv:1310.1528].
- [38] F. Pretorius, Phys. Rev. Lett. **95**, 121101 (2005), [arXiv:gr-qc/0507014]; M. Campanelli *et al.*, Phys. Rev. Lett. **96**, 111101 (2006), [arXiv:gr-qc/0511048]; J. G. Baker *et al.*, Phys. Rev. Lett. **96**, 111102 (2006), [arXiv:gr-qc/0511103].
- [39] K. Yagi *et al.*, Phys. Rev. **D85**, 064022 (2012), [Erratum: Phys. Rev.D93,no.2,029902(2016)], [arXiv:1110.5950].
- [40] K. Yagi, L. C. Stein and N. Yunes, Phys. Rev. **D93**, 2, 024010 (2016), [arXiv:1510.02152].
- [41] K. Prabhu and L. C. Stein, Phys. Rev. **D98**, 2, 021503 (2018), [arXiv:1805.02668].
- [42] L. Bernard, Phys. Rev. **D98**, 4, 044004 (2018), [arXiv:1802.10201].
- [43] F.-L. Julié and E. Berti (2019), [arXiv:1909.05258].
- [44] M. Okounkova *et al.*, Phys. Rev. **D96**, 4, 044020 (2017), [arXiv:1705.07924].
- [45] H. Witek *et al.*, Phys. Rev. **D99**, 6, 064035 (2019), [arXiv:1810.05177].
- [46] M. Okounkova *et al.* (2019), [arXiv:1906.08789].
- [47] L. Blanchet and B. S. Sathyaprakash, Phys. Rev. Lett. **74**, 1067 (1995).
- [48] K. G. Arun *et al.*, Phys. Rev. **D74**, 024006 (2006), [arXiv:gr-qc/0604067].
- [49] B. P. Abbott *et al.* (LIGO Scientific, Virgo), Phys. Rev. Lett. **116**, 22, 221101 (2016), [Erratum: Phys. Rev. Lett.121,no.12,129902(2018)], [arXiv:1602.03841].
- [50] N. Yunes and F. Pretorius, Phys. Rev. **D80**, 122003 (2009), [arXiv:0909.3328].
- [51] S. Khan *et al.*, Phys. Rev. **D93**, 4, 044007 (2016), [arXiv:1508.07253].
- [52] C. V. Vishveshwara, Nature **227**, 936 (1970).
- [53] S. L. Detweiler, Astrophys. J. **239**, 292 (1980).
- [54] V. Cardoso *et al.*, Phys. Rev. **D99**, 10, 104077 (2019), [arXiv:1901.01265].
- [55] R. McManus *et al.*, Phys. Rev. **D100**, 4, 044061 (2019), [arXiv:1906.05155].
- [56] C. M. Will, Phys. Rev. **D57**, 2061 (1998), [arXiv:gr-qc/9709011].
- [57] M. Fierz, Helv. Phys. Acta **29**, 128 (1956).
- [58] E. G. Adelberger, B. R. Heckel and A. E. Nelson, Ann. Rev. Nucl. Part. Sci. **53**, 77 (2003), [hep-ph/0307284].
- [59] D. J. Kapner *et al.*, Phys. Rev. Lett. **98**, 021101 (2007), [hep-ph/0611184].
- [60] A. O. Sushkov *et al.*, Phys. Rev. Lett. **107**, 171101 (2011), [arXiv:1108.2547].
- [61] T. Damour and J. F. Donoghue, Phys. Rev. **D82**, 084033 (2010), [arXiv:1007.2792].
- [62] R. V. Wagoner, Phys. Rev. **D1**, 3209 (1970).
- [63] C. Brans and R. H. Dicke, Phys. Rev. **124**, 925 (1961), [142(1961)].
- [64] J. Alsing *et al.*, Phys. Rev. **D85**, 064041 (2012), [arXiv:1112.4903].
- [65] T. Damour and K. Nordtvedt, Phys. Rev. Lett. **70**, 2217 (1993).
- [66] T. Damour and A. M. Polyakov, Nucl. Phys. **B423**, 532 (1994), [hep-th/9401069].
- [67] K. A. Olive and M. Pospelov, Phys. Rev. **D77**, 043524 (2008), [arXiv:0709.3825].
- [68] J. Khoury and A. Weltman, Phys. Rev. Lett. **93**, 171104 (2004), [arXiv:astro-ph/0309300].
- [69] K. Hinterbichler and J. Khoury, Phys. Rev. Lett. **104**, 231301 (2010), [arXiv:1001.4525].
- [70] P. Brax *et al.*, Phys. Rev. **D82**, 063519 (2010), [arXiv:1005.3735].
- [71] A. Joyce *et al.*, Phys. Rept. **568**, 1 (2015), [arXiv:1407.0059].
- [72] C. Burrage and J. Sakstein, Living Rev. Rel. **21**, 1, 1 (2018), [arXiv:1709.09071].
- [73] A. I. Vainshtein, Phys. Lett. **39B**, 393 (1972).
- [74] C. de Rham, Living Rev. Rel. **17**, 7 (2014), [arXiv:1401.4173].
- [75] G. W. Horndeski, Int. J. Theor. Phys. **10**, 363 (1974).
- [76] C. Deffayet *et al.*, Phys. Rev. **D84**, 064039 (2011), [arXiv:1103.3260].
- [77] L. Heisenberg, Phys. Rept. **796**, 1 (2019), [arXiv:1807.01725].
- [78] T. Kobayashi, Rept. Prog. Phys. **82**, 8, 086901 (2019), [arXiv:1901.07183].
- [79] G. Papallo and H. S. Reall, Phys. Rev. **D96**, 4, 044019 (2017), [arXiv:1705.04370].
- [80] L. Bernard, L. Lehner and R. Luna, Phys. Rev. **D100**, 2, 024011 (2019), [arXiv:1904.12866].
- [81] A. D. Kovács, Phys. Rev. **D100**, 2, 024005 (2019), [arXiv:1904.00963].
- [82] C. de Rham and S. Melville, Phys. Rev. Lett. **121**, 22, 221101 (2018), [arXiv:1806.09417].
- [83] D. D. Doneva and S. S. Yazadjiev, Phys. Rev. Lett. **120**, 13, 131103 (2018), [arXiv:1711.01187].
- [84] H. O. Silva *et al.*, Phys. Rev. Lett. **120**, 13, 131104 (2018), [arXiv:1711.02080].
- [85] C. A. R. Herdeiro and E. Radu, Int. J. Mod. Phys. **D24**, 09, 1542014 (2015), [arXiv:1504.08209].
- [86] A.I. Shlyakhter, Nature **264**, 340 (1976).

- [87] T. Damour and F. Dyson, Nucl. Phys. **B480**, 37 (1996), [hep-ph/9606486]; C. R. Gould, E. I. Sharapov and S. K. Lamoreaux, Phys. Rev. **C74**, 024607 (2006), [arXiv:nucl-ex/0701019]; E. D. Davis and L. Hamdan, Phys. Rev. **C92**, 1, 014319 (2015), [arXiv:1503.06011]; Yu. V. Petrov *et al.*, Phys. Rev. **C74**, 064610 (2006), [hep-ph/0506186].
- [88] V. V. Flambaum and R. B. Wiringa, Phys. Rev. **C79**, 034302 (2009), [arXiv:0807.4943].
- [89] K. A. Olive *et al.*, Phys. Rev. **D69**, 027701 (2004), [arXiv:astro-ph/0309252].
- [90] M. T. Murphy, A. L. Malec and J. X. Prochaska, Mon. Not. Roy. Astron. Soc. **461**, 3, 2461 (2016), [arXiv:1606.06293].
- [91] N. Kanekar *et al.*, Mon. Not. Roy. Astron. Soc. **448**, 1, L104 (2015), [arXiv:1412.7757].
- [92] P. A. R. Ade *et al.* (Planck), Astron. Astrophys. **580**, A22 (2015), [arXiv:1406.7482].
- [93] T. Rosenband *et al.*, Science **319**, 1808 (2008); J. Guena *et al.*, Phys. Rev. Lett. **109**, 080801 (2012); R. M. Godun *et al.*, Phys. Rev. Lett. **113**, 21, 210801 (2014), [arXiv:1407.0164].
- [94] T. M. Fortier *et al.*, Phys. Rev. Lett. **98**, 070801 (2007); S. Blatt *et al.*, Phys. Rev. Lett. **100**, 140801 (2008), [arXiv:0801.1874]; T. Dent, Phys. Rev. Lett. **101**, 041102 (2008), [arXiv:0805.0318].
- [95] A. Fienga *et al.*, Cel. Mech. Dyn. Astr. **123**, Issue 2, 1 (2015).
- [96] F. Hofmann and J. Müller, Class. Quant. Grav. **35**, 3, 035015 (2018).
- [97] K. Lazaridis *et al.*, Mon. Not. R. Astron. Soc. **400**, 805 (2009), [arXiv:0908.0285].
- [98] W. W. Zhu *et al.*, Mon. Not. Roy. Astron. Soc. **482**, 3, 3249 (2019), [arXiv:1802.09206].
- [99] M. Smiciklas *et al.*, Phys. Rev. Lett. **107**, 171604 (2011), [arXiv:1106.0738].
- [100] J. F. Bell and T. Damour, Class. Quant. Grav. **13**, 3121 (1996), [arXiv:gr-qc/9606062].
- [101] L. Shao and N. Wex, Class. Quant. Grav. **29**, 215018 (2012), [arXiv:1209.4503].
- [102] S. Liberati, J. Phys. Conf. Ser. **631**, 1, 012011 (2015).
- [103] S. Schlamminger *et al.*, Phys. Rev. Lett. **100**, 041101 (2008), [arXiv:0712.0607].
- [104] T. A. Wagner *et al.*, Class. Quant. Grav. **29**, 184002 (2012), [arXiv:1207.2442].
- [105] P. Touboul *et al.*, Phys. Rev. Lett. **119**, 23, 231101 (2017), [arXiv:1712.01176].
- [106] P. Touboul *et al.* (MICROSCOPE), Class. Quant. Grav. **36**, 22, 225006 (2019), [arXiv:1909.10598].
- [107] S. Merlet *et al.*, Metrologia, **47**, L9-L11 (2010).
- [108] G. Rosi *et al.*, Nature Commun. **8**, 5529 (2017), [arXiv:1704.02296].
- [109] R.F.C. Vessot and M.W. Levine, Gen. Rel. Grav. **10**, 181 (1978); R. F. C. Vessot *et al.*, Phys. Rev. Lett. **45**, 2081 (1980).
- [110] C. W. Chou *et al.*, Science **329**, 1630 (2010).
- [111] R. Abuter *et al.* (GRAVITY), Astron. Astrophys. **615**, L15 (2018), [arXiv:1807.09409].
- [112] T. Do *et al.*, Science **365**, 6454, 664 (2019), [arXiv:1907.10731].
- [113] A. Amorim *et al.* (GRAVITY), Phys. Rev. Lett. **122**, 10, 101102 (2019), [arXiv:1902.04193].
- [114] J.G. Williams, S.G. Turyshev, and D.H. Boggs, Class. Quantum Grav. **29**, 184004 (2012).
- [115] I. Ciufolini and E. C. Pavlis, Nature **431**, 958 (2004).
- [116] I. Ciufolini *et al.*, Eur. Phys. J. **C76**, 3, 120 (2016), [arXiv:1603.09674].
- [117] C. W. F. Everitt *et al.*, Phys. Rev. Lett. **106**, 221101 (2011), [arXiv:1105.3456].
- [118] B. Bertotti, L. Iess and P. Tortora, Nature **425**, 374 (2003).
- [119] J. Bergé *et al.*, Phys. Rev. Lett. **120**, 14, 141101 (2018), [arXiv:1712.00483].
- [120] J. M. Weisberg and Y. Huang, Astrophys. J. **829**, 1, 55 (2016), [arXiv:1606.02744].
- [121] A. Wolszczan, Nature **350**, 688 (1991).
- [122] J. N. Taylor, A. Wolszczan and T. Damour, Nature **355**, 132 (1993).
- [123] E. Fonseca, I. H. Stairs and S. E. Thorsett, Astrophys. J. **787**, 82 (2014), [arXiv:1402.4836].
- [124] V. M. Kaspi *et al.*, Astrophys. J. **528**, 445 (2000), [arXiv:astro-ph/9906373].
- [125] S. M. Ord, M. Bailes and W. van Straten, Astrophys. J. **574**, L75 (2002), [arXiv:astro-ph/0204421].
- [126] M. Bailes *et al.*, Astrophys. J. **595**, L49 (2003), [arXiv:astro-ph/0307468].
- [127] N. D. R. Bhat, M. Bailes and J. P. W. Verbiest, Phys. Rev. **D77**, 124017 (2008), [arXiv:0804.0956].
- [128] M. Burgay *et al.*, Nature **426**, 531 (2003), [arXiv:astro-ph/0312071].
- [129] A. G. Lyne *et al.*, Science **303**, 1153 (2004), [arXiv:astro-ph/0401086].
- [130] M. Kramer *et al.*, Science **314**, 97 (2006), [arXiv:astro-ph/0609417].
- [131] R. P. Breton *et al.*, Science **321**, 104 (2008), [arXiv:0807.2644].
- [132] B. Perera *et al.*, Astrophys. J. **721**, 1193 (2010), [arXiv:1008.1097].
- [133] R. D. Ferdman *et al.*, Mon. Not. Roy. Astron. Soc. **443**, 3, 2183 (2014), [arXiv:1406.5507].
- [134] M. Kramer and N. Wex, Class. Quant. Grav. **26**, 073001 (2009).
- [135] M. Kramer, in *Neutron Stars and Pulsars: Challenges and Opportunities after 80 Years*; M. Kramer, IAU Symp. **291**, 19 (2013), [arXiv:1211.2457].
- [136] T. Damour and G. Schaefer, Phys. Rev. Lett. **66**, 2549 (1991).
- [137] M. E. Gonzalez *et al.*, Astrophys. J. **743**, 102 (2011), [arXiv:1109.5638].
- [138] P. C. C. Freire, M. Kramer and N. Wex, Class. Quant. Grav. **29**, 184007 (2012), [arXiv:1205.3751].
- [139] S. M. Ransom *et al.*, Nature **505**, 520 (2014), [arXiv:1401.0535].
- [140] A. M. Archibald *et al.*, Nature **559**, 7712, 73 (2018), [arXiv:1807.02059].
- [141] T. Damour and R. Ruffini, C. R. Acad. Sc. Paris **279**, série A, 971 (1974); B. M. Barker and R. F. O'Connell, Phys. Rev. **D12**, 329 (1975).
- [142] M. Kramer, Astrophys. J. **509**, 856 (1998), [arXiv:astro-ph/9808127]; J. M. Weisberg and J. H. Taylor, Astrophys. J. **576**, 942 (2002), [arXiv:astro-ph/0205280].
- [143] R. N. Manchester *et al.*, Astrophys. J. **710**, 1694 (2010), [arXiv:1001.1483].
- [144] J. van Leeuwen *et al.*, Astrophys. J. **798**, 2, 118 (2015), [arXiv:1411.1518].
- [145] G. Desvignes *et al.*, Science **365**, 6457, 1013 (2019).
- [146] B. P. Abbott *et al.* (LIGO Scientific, Virgo), Phys. Rev. **X9**, 3, 031040 (2019), [arXiv:1811.12907].
- [147] V. Cardoso and P. Pani, Nat. Astron. **1**, 9, 586 (2017), [arXiv:1709.01525].
- [148] K. Akiyama *et al.* (Event Horizon Telescope), Astrophys. J. **875**, 1, L1 (2019), [arXiv:1906.11238].

- [149] J. Beltran Jimenez, F. Piazza and H. Velten, *Phys. Rev. Lett.* **116**, 6, 061101 (2016), [arXiv:1507.05047].
- [150] T. Damour and J. H. Taylor, *Astrophys. J.* **366**, 501 (1991).
- [151] P. C. C. Freire *et al.*, *Mon. Not. Roy. Astron. Soc.* **423**, 3328 (2012), [arXiv:1205.1450].
- [152] J. Antoniadis *et al.*, *Science* **340**, 6131 (2013), [arXiv:1304.6875].
- [153] W. W. Zhu *et al.*, *Astrophys. J.* **809**, 1, 41 (2015), [arXiv:1504.00662].
- [154] L. Shao *et al.*, *Phys. Rev.* **X7**, 4, 041025 (2017), [arXiv:1704.07561].
- [155] T. Venumadhav *et al.* (2019), [arXiv:1904.07214].
- [156] B. P. Abbott *et al.* (LIGO Scientific, Virgo) (2019), [arXiv:1903.04467].
- [157] M. Isi *et al.*, *Phys. Rev. Lett.* **123**, 11, 111102 (2019), [arXiv:1905.00869].
- [158] N. Yunes, K. Yagi and F. Pretorius, *Phys. Rev.* **D94**, 8, 084002 (2016), [arXiv:1603.08955].
- [159] D. M. Eardley, D. L. Lee and A. P. Lightman, *Phys. Rev.* **D8**, 3308 (1973).
- [160] B. P. Abbott *et al.*, *Astrophys. J.* **848**, 2, L12 (2017), [arXiv:1710.05833].
- [161] C. de Rham *et al.*, *Rev. Mod. Phys.* **89**, 2, 025004 (2017), [arXiv:1606.08462].
- [162] C. M. Will, *Class. Quant. Grav.* **35**, 17, 17LT01 (2018), [arXiv:1805.10523].
- [163] B. P. Abbott *et al.* (LIGO Scientific, Virgo, Fermi-GBM, INTEGRAL), *Astrophys. J.* **848**, 2, L13 (2017), [arXiv:1710.05834].
- [164] T. Baker *et al.*, *Phys. Rev. Lett.* **119**, 25, 251301 (2017), [arXiv:1710.06394].
- [165] P. Creminelli and F. Vernizzi, *Phys. Rev. Lett.* **119**, 25, 251302 (2017), [arXiv:1710.05877].
- [166] J. Sakstein and B. Jain, *Phys. Rev. Lett.* **119**, 25, 251303 (2017), [arXiv:1710.05893].
- [167] J. M. Ezquiaga and M. Zumalacárregui, *Phys. Rev. Lett.* **119**, 25, 251304 (2017), [arXiv:1710.05901].
- [168] E. Barausse, N. Yunes and K. Chamberlain, *Phys. Rev. Lett.* **116**, 24, 241104 (2016), [arXiv:1603.04075].
- [169] K. Chamberlain and N. Yunes, *Phys. Rev.* **D96**, 8, 084039 (2017), [arXiv:1704.08268].

## 22. Big-Bang Cosmology

Revised August 2019 by K.A. Olive (Minnesota U.) and J.A. Peacock (Edinburgh U.).

### 22.1 Introduction to Standard Big-Bang Model

The observed expansion of the Universe [1–3] is a natural (almost inevitable) result of any homogeneous and isotropic cosmological model based on general relativity. However, by itself, the Hubble expansion does not provide sufficient evidence for what we generally refer to as the Big-Bang model of cosmology. While general relativity is in principle capable of describing the cosmology of any given distribution of matter, it is extremely fortunate that our Universe appears to be homogeneous and isotropic on large scales. Together, homogeneity and isotropy allow us to extend the Copernican Principle to the Cosmological Principle, stating that all spatial positions in the Universe are essentially equivalent.

The formulation of the Big-Bang model began in the 1940s with the work of George Gamow and his collaborators, Ralph Alpher and Robert Herman. In order to account for the possibility that the abundances of the elements had a cosmological origin, they proposed that the early Universe was once very hot and dense (enough so as to allow for the nucleosynthetic processing of hydrogen), and has subsequently expanded and cooled to its present state [4, 5]. In 1948, Alpher and Herman predicted that a direct consequence of this model is the presence of a relic background radiation with a temperature of order a few K [6, 7]. Of course this radiation was observed 16 years later as the Cosmic Microwave Background (CMB) [8]. Indeed, it was the observation of this radiation that singled out the Big-Bang model as the prime candidate to describe our Universe. Subsequent work on Big-Bang nucleosynthesis further confirmed the necessity of our hot and dense past. (See Sec. 22.3.7 for a brief discussion of BBN and the review on BBN – Sec. 24 of this *Review* for a detailed discussion of BBN.) These relativistic cosmological models face severe problems with their initial conditions, to which the best modern solution is inflationary cosmology, discussed in Sec. 22.3.5 and in – Sec. 23 of this *Review*. If correct, these ideas would strictly render the term ‘Big Bang’ redundant, since it was first coined by Hoyle to represent a criticism of the lack of understanding of the initial conditions.

#### 22.1.1 The Robertson-Walker Universe

The observed homogeneity and isotropy enable us to describe the overall geometry and evolution of the Universe in terms of two cosmological parameters accounting for the spatial curvature and the overall expansion (or contraction) of the Universe. These two quantities appear in the most general expression for a space-time metric that has a (3D) maximally symmetric subspace of a 4D space-time, known as the Robertson-Walker metric:

$$ds^2 = dt^2 - R^2(t) \left[ \frac{dr^2}{1 - kr^2} + r^2 (d\theta^2 + \sin^2 \theta d\phi^2) \right]. \quad (22.1)$$

Note that we adopt  $c = 1$  throughout. By rescaling the radial coordinate, we can choose the curvature constant  $k$  to take only the discrete values  $+1$ ,  $-1$ , or  $0$  corresponding to closed, open, or spatially flat geometries. In this case, it is often more convenient to re-express the metric as

$$ds^2 = dt^2 - R^2(t) [d\chi^2 + S_k^2(\chi) (d\theta^2 + \sin^2 \theta d\phi^2)], \quad (22.2)$$

where the function  $S_k(\chi)$  is  $(\sin \chi, \chi, \sinh \chi)$  for  $k = (+1, 0, -1)$ . The coordinate  $r$  [in Eq. (22.1)] and the ‘angle’  $\chi$  [in Eq. (22.2)] are both dimensionless; the dimensions are carried by the cosmological scale factor,  $R(t)$ , which determines proper distances in terms of the comoving coordinates. A common alternative is to define a dimensionless scale factor,  $a(t) = R(t)/R_0$ , where  $R_0 \equiv R(t_0)$  is  $R$  at the present epoch. It is also sometimes convenient to define a dimensionless or conformal time coordinate,  $\eta$ , by  $d\eta = dt/R(t)$ . Along constant spatial sections, the proper time is defined by the time coordinate,  $t$ . Similarly, for  $dt = d\theta = d\phi = 0$ , the proper distance is given by  $R(t)\chi$ . For standard texts on cosmological models see *e.g.*, Refs. [9–16].

#### 22.1.2 The redshift

The cosmological redshift is a direct consequence of the Hubble expansion, determined by  $R(t)$ . A local observer detecting light from a distant emitter sees a redshift in frequency. We can define the redshift as

$$z \equiv \frac{\nu_1 - \nu_2}{\nu_2} \simeq v_{12}, \quad (22.3)$$

where  $\nu_1$  is the frequency of the emitted light,  $\nu_2$  is the observed frequency, and  $v_{12}$  is the relative velocity between the emitter and the observer. While the definition,  $z = (\nu_1 - \nu_2)/\nu_2$  is valid in general, relating the redshift to a simple relative velocity is only correct on small scales (*i.e.*, less than cosmological scales) such that the expansion velocity is non-relativistic. For light signals, we can use the metric given by Eq. (22.1) and  $ds^2 = 0$  to write

$$v_{12} = \dot{R} \delta r = \frac{\dot{R}}{R} \delta t = \frac{\delta R}{R} = \frac{R_2 - R_1}{R_1}, \quad (22.4)$$

where  $\delta r(\delta t)$  is the radial coordinate (temporal) separation between the emitter and observer. Noting that physical distance,  $D$ , is  $R\delta r$  or  $\delta t$ , Eq. (22.4) gives us Hubble’s law,  $v = HD$ . In addition, we obtain the simple relation between the redshift and the scale factor

$$1 + z = \frac{\nu_1}{\nu_2} = \frac{R_2}{R_1}. \quad (22.5)$$

This result does not depend on the non-relativistic approximation.

#### 22.1.3 The Friedmann equations of motion

The cosmological equations of motion are derived from Einstein’s equations

$$\mathcal{R}_{\mu\nu} - \frac{1}{2} g_{\mu\nu} \mathcal{R} = 8\pi G_N T_{\mu\nu} + \Lambda g_{\mu\nu} \quad (22.6)$$

Gliner [17] and Zeldovich [18] have pioneered the modern view, in which the  $\Lambda$  term is set on the rhs and interpreted as an effective energy – momentum tensor  $T_{\mu\nu}$  for the vacuum of  $\Lambda g_{\mu\nu}/8\pi G_N$ . It is common to assume that the matter content of the Universe is a perfect fluid, for which

$$T_{\mu\nu} = -p g_{\mu\nu} + (p + \rho) u_\mu u_\nu, \quad (22.7)$$

where  $g_{\mu\nu}$  is the space-time metric described by Eq. (22.1),  $p$  is the isotropic pressure,  $\rho$  is the energy density and  $u = (1, 0, 0, 0)$  is the velocity vector for the isotropic fluid in co-moving coordinates. With the perfect fluid source, Einstein’s equations lead to the Friedmann equations

$$H^2 \equiv \left( \frac{\dot{R}}{R} \right)^2 = \frac{8\pi G_N \rho}{3} - \frac{k}{R^2} + \frac{\Lambda}{3}, \quad (22.8)$$

and

$$\frac{\ddot{R}}{R} = \frac{\Lambda}{3} - \frac{4\pi G_N}{3} (\rho + 3p), \quad (22.9)$$

where  $H(t)$  is the Hubble parameter and  $\Lambda$  is the cosmological constant. The first of these is sometimes called the Friedmann equation. Energy conservation via  $T^{\mu\nu}_{;\mu} = 0$ , leads to a third useful equation [which can also be derived from Eq. (22.8) and Eq. (22.9)]

$$\dot{\rho} = -3H(\rho + p). \quad (22.10)$$

Eq. (22.10) can also be simply derived as a consequence of the first law of thermodynamics.

Eq. (22.8) has a simple classical mechanical analog if we neglect (for the moment) the cosmological term  $\Lambda$ . By interpreting  $-k/R^2$  Newtonianly as a ‘total energy’, then we see that the evolution of the Universe is governed by a competition between the potential energy,  $8\pi G_N \rho/3$ , and the kinetic term  $(\dot{R}/R)^2$ . For  $\Lambda = 0$ , it is clear that the Universe must be expanding or contracting (except at the turning point prior to collapse in a closed Universe). The ultimate fate of the Universe is determined by the curvature constant  $k$ . For  $k = +1$ , the Universe will recollapse in a finite time, whereas for  $k = 0, -1$ , the Universe will expand indefinitely. These simple conclusions can be altered when  $\Lambda \neq 0$  or more generally with some component with  $(\rho + 3p) < 0$ .

### 22.1.4 Definition of cosmological parameters

In addition to the Hubble parameter, it is useful to define several other measurable cosmological parameters. The Friedmann equation can be used to define a critical density such that  $k = 0$  when  $\Lambda = 0$ ,

$$\begin{aligned}\rho_c &\equiv \frac{3H^2}{8\pi G_N} = 1.88 \times 10^{-26} h^2 \text{ kg m}^{-3} \\ &= 1.05 \times 10^{-5} h^2 \text{ GeV cm}^{-3},\end{aligned}\quad (22.11)$$

where the scaled Hubble parameter,  $h$ , is defined by

$$\begin{aligned}H &\equiv 100 h \text{ km s}^{-1} \text{ Mpc}^{-1} \\ \Rightarrow H^{-1} &= 9.778 h^{-1} \text{ Gyr} \\ &= 2998 h^{-1} \text{ Mpc}.\end{aligned}\quad (22.12)$$

The cosmological density parameter  $\Omega_{\text{tot}}$  is defined as the energy density relative to the critical density,

$$\Omega_{\text{tot}} = \rho/\rho_c. \quad (22.13)$$

Note that one can now rewrite the Friedmann equation as

$$k/R^2 = H^2(\Omega_{\text{tot}} - 1). \quad (22.14)$$

From Eq. (22.14), one can see that when  $\Omega_{\text{tot}} > 1$ ,  $k = +1$  and the Universe is closed, when  $\Omega_{\text{tot}} < 1$ ,  $k = -1$  and the Universe is open, and when  $\Omega_{\text{tot}} = 1$ ,  $k = 0$ , and the Universe is spatially flat.

It is often necessary to distinguish different contributions to the density. It is therefore convenient to define present-day density parameters for pressureless matter ( $\Omega_m$ ) and relativistic particles ( $\Omega_r$ ), plus the quantity  $\Omega_\Lambda = \Lambda/3H^2$ . In more general models, we may wish to drop the assumption that the vacuum energy density is constant, and we therefore denote the present-day density parameter of the vacuum by  $\Omega_v$ . The Friedmann equation then becomes

$$k/R_0^2 = H_0^2(\Omega_m + \Omega_r + \Omega_v - 1), \quad (22.15)$$

where the subscript 0 indicates present-day values. Thus, it is the sum of the densities in matter, relativistic particles, and vacuum that determines the overall sign of the curvature. Note that the quantity  $-k/R_0^2 H_0^2$  is sometimes referred to as  $\Omega_K$ . This usage is unfortunate: it encourages one to think of curvature as a contribution to the energy density of the Universe, which is not correct.

### 22.1.5 Standard Model solutions

Much of the history of the Universe in the standard Big-Bang model can be easily described by assuming that either matter or radiation dominates the total energy density. During inflation and again today the expansion rate for the Universe is accelerating, and domination by a cosmological constant or some other form of dark energy should be considered. In the following, we shall delineate the solutions to the Friedmann equation when a single component dominates the energy density. Each component is distinguished by an equation of state parameter  $w = p/\rho$ . We concentrate on solutions that expand at early times, although the Friedmann equation also permits a time-reversed contracting solution.

#### 22.1.5.1 Solutions for a general equation of state

Let us first assume a general equation of state parameter for a single component,  $w$ , which is constant. In this case, Eq. (22.10) can be written as  $\dot{\rho} = -3(1+w)\rho\dot{R}/R$  and is easily integrated to yield

$$\rho \propto R^{-3(1+w)}. \quad (22.16)$$

Note that at early times when  $R$  is small, the less singular curvature term  $k/R^2$  in the Friedmann equation can be neglected so long as  $w > -1/3$ . Curvature domination occurs at rather late times (if a cosmological constant term does not dominate sooner). For  $w \neq -1$ , one can insert this result into the Friedmann equation Eq. (22.8), and if one neglects the curvature and cosmological constant terms, it is easy to integrate the equation to obtain,

$$R(t) \propto t^{2/[3(1+w)]}. \quad (22.17)$$

#### 22.1.5.2 A Radiation-dominated Universe

In the early hot and dense Universe, it is appropriate to assume an equation of state corresponding to a gas of radiation (or relativistic particles) for which  $w = 1/3$ . In this case, Eq. (22.16) becomes  $\rho \propto R^{-4}$ . The ‘extra’ factor of  $1/R$  is due to the cosmological redshift; not only is the number density of particles in the radiation background decreasing as  $R^{-3}$  since volume scales as  $R^3$ , but in addition each particle’s energy is decreasing as  $E \propto \nu \propto R^{-1}$ . Similarly, one can substitute  $w = 1/3$  into Eq. (22.17) to obtain

$$R(t) \propto t^{1/2}; \quad H = 1/2t. \quad (22.18)$$

#### 22.1.5.3 A Matter-dominated Universe

At relatively late times, non-relativistic matter eventually dominates the energy density over radiation [see Eq. (22.3.8)]. A pressureless gas ( $w = 0$ ) leads to the expected dependence  $\rho \propto R^{-3}$  from Eq. (22.16) and, if  $k = 0$ , we obtain

$$R(t) \propto t^{2/3}; \quad H = 2/3t. \quad (22.19)$$

#### 22.1.5.4 A Universe dominated by vacuum energy

If there is a dominant source of vacuum energy,  $V_0$ , it would act as a cosmological constant with  $\Lambda = 8\pi G_N V_0$  and equation of state  $w = -1$ . In this case, the solution to the Friedmann equation when curvature is neglected is particularly simple and leads to an exponential expansion of the Universe:

$$R(t) \propto e^{\sqrt{\Lambda/3}t}. \quad (22.20)$$

More generally we could write

$$a(t) = \sinh^{2/3}(\sqrt{3\Lambda}t/2), \quad (22.21)$$

which describes a flat Universe containing both matter and vacuum energy, with  $a(t)$  being the scale factor normalized to unity when both components are equal.

A key parameter is the equation of state of the vacuum,  $w \equiv p/\rho$ : this need not be the  $w = -1$  of  $\Lambda$ , and may not even be constant [19–21]. There is much interest in the more general possibility of a dynamically evolving vacuum energy, for which the name ‘dark energy’ has become commonly used. A variety of techniques exist whereby the vacuum density as a function of time may be measured, usually expressed as the value of  $w$  as a function of epoch [22, 23]. The best current measurement of the equation of state (assumed constant, but without assuming zero curvature) is  $w = -1.028 \pm 0.031$  [24]. Unless stated otherwise, we will assume that the vacuum energy is a cosmological constant with  $w = -1$  exactly.

The presence of vacuum energy can dramatically alter the fate of the Universe. For example, if  $\Lambda < 0$ , the Universe will eventually recollapse independent of the sign of  $k$ . For large values of  $\Lambda > 0$  (larger than the Einstein static value needed to halt any cosmological expansion or contraction), even a closed Universe will expand forever. One way to quantify this is the deceleration parameter,  $q_0$ , defined as

$$q_0 = - \left. \frac{R\ddot{R}}{\dot{R}^2} \right|_0 = \frac{1}{2}\Omega_m + \Omega_r + \frac{(1+3w)}{2}\Omega_v. \quad (22.22)$$

This equation shows us that  $w < -1/3$  for the vacuum may lead to an accelerating expansion. To the continuing astonishment of cosmologists, such an effect has been observed; one piece of direct evidence is the supernova Hubble diagram [25–30] (see Fig. 22.1 below). Current data indicate that vacuum energy is indeed the largest contributor to the cosmological density budget, with  $\Omega_v = 0.685 \pm 0.007$  and  $\Omega_m = 0.315 \pm 0.007$  if  $k = 0$  is assumed [24].

The existence of this constituent is without doubt the greatest puzzle raised by the current cosmological model; the final section of this review discusses some of the ways in which the vacuum-energy problem is being addressed. For more details, see the review on Dark Energy – Sec. 28.

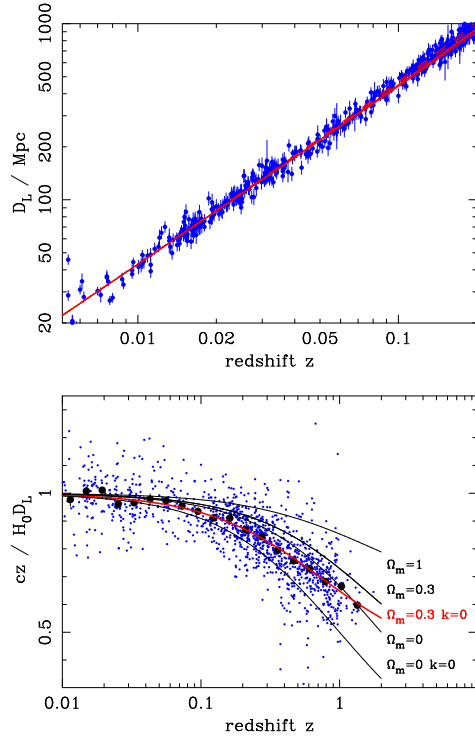


Figure 22.1: The type Ia supernova Hubble diagram, based on over 1200 publicly available supernova distance estimates [28–30]. The first panel shows that for  $z \ll 1$  the large-scale Hubble flow is indeed linear and uniform; the second panel shows an expanded scale, with the linear trend divided out, and with the redshift range extended to show how the Hubble law becomes nonlinear. ( $\Omega_r = 0$  is assumed.) Larger points with errors show median values in redshift bins. Comparison with the prediction of Friedmann models favors a vacuum-dominated Universe.

## 22.2 Introduction to Observational Cosmology

### 22.2.1 Fluxes, luminosities, and distances

The key quantities for observational cosmology can be deduced quite directly from the metric.

(1) The *proper* transverse size of an object seen by us to subtend an angle  $d\psi$  is its comoving size  $d\psi S_k(\chi)$  times the scale factor at the time of emission:

$$d\ell = d\psi R_0 S_k(\chi)/(1+z). \quad (22.23)$$

(2) The apparent flux density of an object is deduced by allowing its photons to flow through a sphere of current radius  $R_0 S_k(\chi)$ ; but photon energies and arrival rates are redshifted, and the bandwidth  $d\nu$  is reduced. The observed photons at frequency  $\nu_0$  were emitted at frequency  $\nu_0(1+z)$ , so the flux density is the luminosity at this frequency, divided by the total area, divided by  $1+z$ :

$$S_\nu(\nu_0) = \frac{L_\nu([1+z]\nu_0)}{4\pi R_0^2 S_k^2(\chi)(1+z)}. \quad (22.24)$$

These relations lead to the following common definitions:

$$\begin{aligned} \text{angular-diameter distance: } D_A &= (1+z)^{-1} R_0 S_k(\chi) \\ \text{luminosity distance: } D_L &= (1+z) R_0 S_k(\chi). \end{aligned} \quad (22.25)$$

These distance-redshift relations are expressed in terms of observables by using the equation of a null radial geodesic ( $R(t)d\chi =$

$dt$ ) plus the Friedmann equation:

$$\begin{aligned} R_0 d\chi &= \frac{1}{H(z)} dz = \frac{1}{H_0} [(1 - \Omega_m - \Omega_\nu - \Omega_r)(1+z)^2 \\ &\quad + \Omega_\nu(1+z)^{3+3w} + \Omega_m(1+z)^3 \\ &\quad + \Omega_r(1+z)^4]^{-1/2} dz. \end{aligned} \quad (22.26)$$

The main scale for the distance here is the Hubble length,  $1/H_0$ .

The flux density is the product of the specific intensity  $I_\nu$  and the solid angle  $d\Omega$  subtended by the source:  $S_\nu = I_\nu d\Omega$ . Combining the angular size and flux-density relations thus gives the relativistic version of surface-brightness conservation:

$$I_\nu(\nu_0) = \frac{B_\nu([1+z]\nu_0)}{(1+z)^3}, \quad (22.27)$$

where  $B_\nu$  is surface brightness (luminosity emitted into unit solid angle per unit area of source). We can integrate over  $\nu_0$  to obtain the corresponding total or bolometric formula:

$$I_{\text{tot}} = \frac{B_{\text{tot}}}{(1+z)^4}. \quad (22.28)$$

This cosmology-independent form expresses Liouville's Theorem: photon phase-space density is conserved along rays.

### 22.2.2 Distance data and geometrical tests of cosmology

In order to confront these theoretical predictions with data, we have to bridge the divide between two extremes. Nearby objects may have their distances measured quite easily, but their radial velocities are dominated by deviations from the ideal Hubble flow, which typically have a magnitude of several hundred  $\text{km s}^{-1}$ . On the other hand, objects at redshifts  $z \gtrsim 0.01$  will have observed recessional velocities that differ from their ideal values by  $\lesssim 10\%$ , but absolute distances are much harder to supply in this case. The traditional solution to this problem is the construction of the distance ladder: an interlocking set of methods for obtaining relative distances between various classes of object, which begins with absolute distances at the 10 to 100 pc level, and terminates with galaxies at significant redshifts. This is discussed in the article on Cosmological Parameters – Sec. 25.1 of this *Review*.

One of the key developments in this area has been the use of type Ia supernovae (SNe), which now allow measurement of relative distances with 5% precision. In combination with improved Cepheid data from the HST plus improved measurements of the distance to the LMC (or alternatively a direct geometrical distance to the maser galaxy NGC4258), SNe results extend the distance ladder to the point where deviations from uniform expansion are negligible, leading to the best existing Cepheid-based value for  $H_0$ :  $74.03 \pm 1.42 \text{ km s}^{-1} \text{ Mpc}^{-1}$  [31]. Better still, the analysis of high- $z$  SNe has allowed a simple and direct test of cosmological geometry to be carried out: as shown in Fig. 22.1 and Fig. 22.2, supernova data and measurements of CMB anisotropies strongly favor a  $k = 0$  model dominated by vacuum energy. It is worth noting that there is some tension ( $3.7\sigma$ ) between the Cepheid and CMB determinations of  $H_0$  (the latter is  $67.4 \pm 0.5$  [24]). While it is remarkable that the two very different methods give such similar results, the formal disagreement shows that either there are unidentified systematic errors or that some new post-CDM physics is required; there is no current consensus in the community on these alternatives. We do note that a recent analysis of SNe Ia with a calibration of the tip of the red-giant branch gives a result close to that of the CMB:  $69.8 \pm 0.8$  (stat.)  $\pm 1.7$  (sys.)  $\text{km s}^{-1} \text{ Mpc}^{-1}$  [32]. (See the review on Cosmological Parameters – Sec. 25.1 of this *Review* for a more comprehensive review of Hubble parameter determinations.)

### 22.2.3 Age of the Universe

The most striking conclusion of relativistic cosmology is that the Universe has not existed forever. The dynamical result for



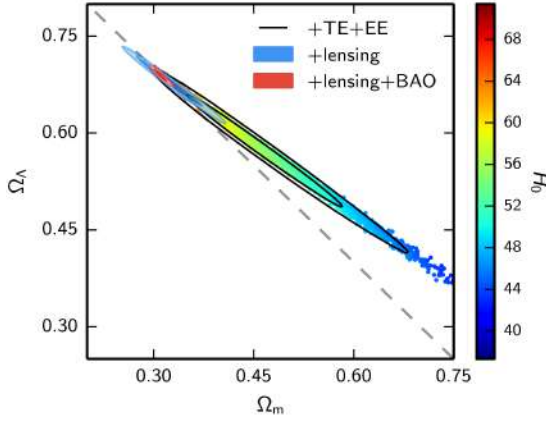


Figure 22.2: Likelihood-based probability densities over the plane  $\Omega_\Lambda$  (i.e.,  $\Omega_v$  assuming  $w = -1$ ) vs  $\Omega_m$ . The colored locus derives from *Planck* [33] and shows that the CMB alone requires a flat Universe  $\Omega_v + \Omega_m \simeq 1$  if the Hubble constant is not too high. The SNe Ia results [34] very nearly constrain the orthogonal combination  $\Omega_v - \Omega_m$ , and the intersection of these constraints directly favors a flat model with  $\Omega_m \simeq 0.3$ , as does the measurement of the Baryon Acoustic Oscillation lengthscale (for which a joint constraint is shown on this plot). The CMB alone is capable of breaking the degeneracy with  $H_0$  by using the measurements of gravitational lensing that can be made with modern high-resolution CMB data.

the age of the Universe may be written as

$$\begin{aligned} H_0 t_0 &= \int_0^\infty \frac{dz}{(1+z)H(z)} \\ &= \int_0^\infty \frac{dz}{(1+z) [(1+z)^2(1+\Omega_m z) - z(2+z)\Omega_v]^{1/2}}, \end{aligned} \quad (22.29)$$

where we have neglected  $\Omega_r$  and chosen  $w = -1$ . Over the range of interest ( $0.1 \lesssim \Omega_m \lesssim 1$ ,  $|\Omega_v| \lesssim 1$ ), this exact answer may be approximated to a few per cent accuracy by

$$H_0 t_0 \simeq \frac{2}{3} (0.7\Omega_m + 0.3 - 0.3\Omega_v)^{-0.3}. \quad (22.30)$$

For the special case that  $\Omega_m + \Omega_v = 1$ , the integral in Eq. (22.29) can be expressed analytically as

$$H_0 t_0 = \frac{2}{3\sqrt{\Omega_v}} \ln \frac{1 + \sqrt{\Omega_v}}{\sqrt{1 - \Omega_v}} \quad (\Omega_m < 1). \quad (22.31)$$

The most accurate means of obtaining ages for astronomical objects is based on the natural clocks provided by radioactive decay. The use of these clocks is complicated by a lack of knowledge of the initial conditions of the decay. In the Solar System, chemical fractionation of different elements helps pin down a precise age for the pre-Solar nebula of 4.6 Gyr, but for stars it is necessary to attempt an a priori calculation of the relative abundances of nuclei that result from supernova explosions. In this way, a lower limit for the age of stars in the local part of the Milky Way of about 11 Gyr is obtained [35, 36].

The other major means of obtaining cosmological age estimates is based on the theory of stellar evolution. In principle, the main-sequence turnoff point in the color-magnitude diagram of a globular cluster should yield a reliable age. But these have been controversial, owing to theoretical uncertainties in the evolution model – as well as observational uncertainties in the distance, dust extinction, and metallicity of clusters. The present consensus favors ages for the oldest clusters of about 13 Gyr [37].

These methods are all consistent with the age deduced from studies of structure formation, using the microwave background and large-scale structure:  $t_0 = 13.80 \pm 0.02$  Gyr [24], where the extra accuracy comes at the price of assuming the simple 6-parameter  $\Lambda$ CDM model to be true.

### 22.2.4 Horizon, isotropy, flatness problems

For photons, the radial equation of motion is just  $c dt = R d\chi$ . How far can a photon get in a given time? The answer is clearly

$$\Delta\chi = \int_{t_1}^{t_2} \frac{dt}{R(t)} \equiv \Delta\eta, \quad (22.32)$$

i.e., just the interval of conformal time. We can replace  $dt$  by  $dR/R$ , which the Friedmann equation says is  $\propto dR/\sqrt{\rho R^2}$  at early times. Thus, this integral converges if  $\rho R^2 \rightarrow \infty$  as  $t_1 \rightarrow 0$ , otherwise it diverges. Provided the equation of state is such that  $\rho$  changes faster than  $R^{-2}$ , light signals can only propagate a finite distance between the Big Bang and the present; there is then said to be a particle horizon. Such a horizon therefore exists in conventional Big-Bang models, which are dominated by radiation ( $\rho \propto R^{-4}$ ) at early times.

At late times, the integral for the horizon is largely determined by the matter-dominated phase, for which

$$D_H = R_0 \chi_H \equiv R_0 \int_0^{t(z)} \frac{dt}{R(t)} \simeq \frac{6000}{\sqrt{\Omega_m z}} h^{-1} \text{Mpc} \quad (z \gg 1). \quad (22.33)$$

The horizon at the time of formation of the microwave background ('last scattering':  $z \simeq 1100$ ) was thus of order 100 Mpc in size, subtending an angle of about  $1^\circ$ . Why then are the large number of causally disconnected regions we see on the microwave sky all at the same temperature? The Universe is very nearly isotropic and homogeneous, even though the initial conditions appear not to permit such a state to be constructed.

A related problem is that the  $\Omega = 1$  Universe is unstable:

$$\Omega(a) - 1 = \frac{\Omega - 1}{1 - \Omega + \Omega_v a^2 + \Omega_m a^{-1} + \Omega_r a^{-2}}, \quad (22.34)$$

where  $\Omega$  with no subscript is the total density parameter, and  $a(t) = R(t)/R_0$ . This requires  $\Omega(t)$  to be unity to arbitrary precision as the initial time tends to zero; a Universe of non-zero curvature today requires very finely tuned initial conditions.

## 22.3 The Hot Thermal Universe

### 22.3.1 Thermodynamics of the early Universe

As alluded to above, we expect that much of the early Universe can be described by a radiation-dominated equation of state. In addition, through much of the radiation-dominated period, thermal equilibrium is established by the rapid rate of particle interactions relative to the expansion rate of the Universe (see Sec. 22.3.3 below). In equilibrium, it is straightforward to compute the thermodynamic quantities,  $\rho$ ,  $p$ , and the entropy density,  $s$ . In general, the energy density for a given particle type  $i$  can be written as

$$\rho_i = \int E_i dn_{q_i}, \quad (22.35)$$

with the density of states given by

$$dn_{q_i} = \frac{g_i}{2\pi^2} (\exp[(E_{q_i} - \mu_i)/T_i] \pm 1)^{-1} q_i^2 dq_i, \quad (22.36)$$

where  $g_i$  counts the number of degrees of freedom for particle type  $i$ ,  $E_{q_i}^2 = m_i^2 + q_i^2$ ,  $\mu_i$  is the chemical potential, and the  $\pm$  corresponds to either Fermi or Bose statistics. Similarly, we can define the pressure of a perfect gas as

$$p_i = \frac{1}{3} \int \frac{q_i^2}{E_i} dn_{q_i}. \quad (22.37)$$

The number density of species  $i$  is simply

$$n_i = \int dn_{q_i}, \quad (22.38)$$

and the entropy density is

$$s_i = \frac{\rho_i + p_i - \mu_i n_i}{T_i}. \quad (22.39)$$



In the Standard Model, a chemical potential is often associated with baryon number, and since the net baryon density relative to the photon density is known to be very small (of order  $10^{-9}$ ), we can neglect any such chemical potential when computing total thermodynamic quantities.

For photons, we can compute all of the thermodynamic quantities rather easily. Taking  $g_i = 2$  for the 2 photon polarization states, we have (in units where  $\hbar = k_B = 1$ )

$$\rho_\gamma = \frac{\pi^2}{15} T^4, \quad p_\gamma = \frac{1}{3} \rho_\gamma, \quad s_\gamma = \frac{4\rho_\gamma}{3T}, \quad n_\gamma = \frac{2\zeta(3)}{\pi^2} T^3, \quad (22.40)$$

with  $2\zeta(3)/\pi^2 \simeq 0.2436$ . Note that Eq. (22.10) can be converted into an equation for entropy conservation. Recognizing that  $\dot{p} = s\dot{T}$ , Eq. (22.10) becomes

$$d(sR^3)/dt = 0. \quad (22.41)$$

For radiation, this corresponds to the relationship between expansion and cooling,  $T \propto R^{-1}$  in an adiabatically expanding Universe. Note also that both  $s$  and  $n_\gamma$  scale as  $T^3$ .

### 22.3.2 Radiation content of the Early Universe

At the very high temperatures associated with the early Universe, massive particles are pair produced, and are part of the thermal bath. If for a given particle species  $i$  we have  $T \gg m_i$ , then we can neglect the mass in Eq. (22.35) to Eq. (22.39), and the thermodynamic quantities are easily computed as in Eq. (22.40). In general, we can approximate the energy density (at high temperatures) by including only those particles with  $m_i \ll T$ . In this case, we have

$$\rho = \left( \sum_B g_B + \frac{7}{8} \sum_F g_F \right) \frac{\pi^2}{30} T^4 \equiv \frac{\pi^2}{30} N(T) T^4, \quad (22.42)$$

where  $g_{B(F)}$  is the number of degrees of freedom of each boson (fermion) and the sum runs over all boson and fermion states with  $m \ll T$ . The factor of  $7/8$  is due to the difference between the Fermi and Bose integrals. Eq. (22.42) defines the effective number of degrees of freedom,  $N(T)$ , by taking into account new particle degrees of freedom as the temperature is raised. This quantity, calculated from high temperature lattice QCD, is plotted in Fig. 22.3 [38]. Near the QCD transition, there is a slight difference between the coefficient of  $T^4$  for  $\rho$  and the coefficient of  $T^3$  for the entropy density  $s = (2\pi^2/45)N_s(T)T^3$  [39], as seen in the figure.

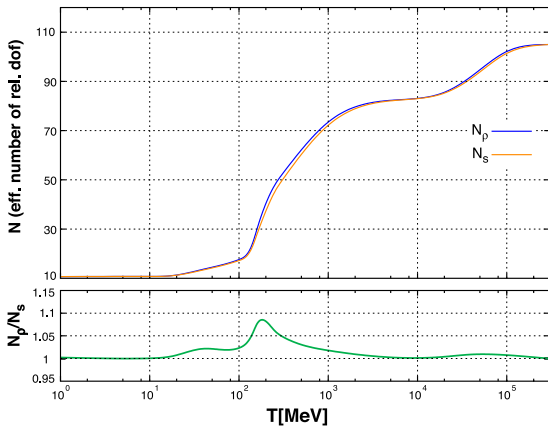


Figure 22.3: The effective numbers of relativistic degrees of freedom as a function of temperature. The sharp drop corresponds to the quark-hadron transition. The bottom panel shows the relative ratio between the number of degrees of freedom characterizing the energy density and the entropy.

The value of  $N(T)$  at any given temperature depends on the particle physics model. In the standard  $SU(3) \times SU(2) \times U(1)$  model, we can specify  $N(T)$  up to temperatures of  $O(100)$  GeV.

The change in  $N$  (ignoring mass effects) can be seen in the table below.

Temperature	New Particles	$4N(T)$
$T < m_e$	$\gamma$ 's + $\nu$ 's	29
$m_e < T < m_\mu$	$e^\pm$	43
$m_\mu < T < m_\pi$	$\mu^\pm$	57
$m_\pi < T < T_c^\dagger$	$\pi$ 's	69
$T_c < T < m_{\text{strange}}$	$\pi$ 's + $u, \bar{u}, d, \bar{d}$ + gluons	205
$m_s < T < m_{\text{charm}}$	$s, \bar{s}$	247
$m_c < T < m_\tau$	$c, \bar{c}$	289
$m_\tau < T < m_{\text{bottom}}$	$\tau^\pm$	303
$m_b < T < m_{W,Z}$	$b, \bar{b}$	345
$m_{W,Z} < T < m_{\text{Higgs}}$	$W^\pm, Z$	381
$m_H < T < m_{\text{top}}$	$H^0$	385
$m_t < T$	$t, \bar{t}$	427

$^\dagger T_c$  corresponds to the confinement-deconfinement transition between quarks and hadrons.

At higher temperatures,  $N(T)$  will be model-dependent. For example, in the minimal  $SU(5)$  model, one needs to add 24 states to  $N(T)$  for the charged and colored  $X$  and  $Y$  gauge bosons, another 24 from the adjoint Higgs, and another 6 scalar degrees of freedom (in addition to the 4 associated with the complex Higgs doublet already counted in the longitudinal components of  $W^\pm$  and  $Z$ , and in  $H$ ) from the  $\mathbf{5}$  of Higgs. Hence for  $T > m_X$  in minimal  $SU(5)$ ,  $N(T) = 160.75$ . In a supersymmetric model this would at least double.

In the radiation-dominated epoch, Eq. (22.10) can be integrated (neglecting the  $T$ -dependence of  $N$ ) giving us a relationship between the age of the Universe and its temperature

$$t = \left( \frac{90}{32\pi^3 G_N N(T)} \right)^{1/2} T^{-2}. \quad (22.43)$$

Put into a more convenient form

$$t T_{\text{MeV}}^2 = 2.4 [N(T)]^{-1/2}, \quad (22.44)$$

where  $t$  is measured in seconds and  $T_{\text{MeV}}$  in units of MeV.

### 22.3.3 Neutrinos and equilibrium

Due to the expansion of the Universe, certain rates may be too slow to either establish or maintain equilibrium. Quantitatively, for each particle  $i$ , as a minimal condition for equilibrium, we will require that some rate  $\Gamma_i$  involving that type be larger than the expansion rate of the Universe, or

$$\Gamma_i > H. \quad (22.45)$$

Recalling that the age of the Universe is determined by  $H^{-1}$ , this condition is equivalent to requiring that on average, at least one interaction has occurred over the lifetime of the Universe.

A good example for a process that goes in and out of equilibrium is the weak interaction of neutrinos. On dimensional grounds, one can estimate the thermally averaged scattering cross-section:

$$\langle \sigma v \rangle \sim O(10^{-2}) T^2 / m_W^4 \quad (22.46)$$

for  $T \lesssim m_W$ . Recalling that the number density of leptons is  $n \propto T^3$ , we can compare the weak interaction rate,  $\Gamma_{\text{wk}} \sim n \langle \sigma v \rangle$ , with the expansion rate,

$$H = \left( \frac{8\pi G_N \rho}{3} \right)^{1/2} = \left( \frac{8\pi^3}{90} N(T) \right)^{1/2} T^2 / M_P \quad (22.47) \\ \simeq 1.66 N(T)^{1/2} T^2 / M_P,$$

where the Planck mass  $M_P = G_N^{-1/2} = 1.22 \times 10^{19}$  GeV.

Neutrinos will be in equilibrium when  $\Gamma_{\text{wk}} > H$  or

$$T > (500 m_W^4 / M_P)^{1/3} \sim 1 \text{ MeV}. \quad (22.48)$$

However, this condition assumes  $T \ll m_W$ ; for higher temperatures, we should write  $\langle \sigma v \rangle \sim O(10^{-2})/T^2$ , so that  $\Gamma \sim 10^{-2} T$ . Thus, in the very early stages of expansion, at temperatures  $T \gtrsim 10^{-2} M_P / \sqrt{N}$ , equilibrium will not have been established.

Having attained a quasi-equilibrium stage, the Universe then cools further to the point where the interaction and expansion timescales match once again. The temperature at which these rates are equal is commonly referred to as the neutrino decoupling or freeze-out temperature and is defined by  $T_{\text{wk}}(T_d) = H(T_d)$ . For  $T < T_d$ , neutrinos drop out of equilibrium. The Universe becomes transparent to neutrinos and their momenta simply redshift with the cosmic expansion. The effective neutrino temperature will simply fall with  $T \sim 1/R$ .

Soon after decoupling,  $e^\pm$  pairs in the thermal background begin to annihilate (when  $T \lesssim m_e$ ). Because the neutrinos are decoupled, the energy released due to annihilation heats up the photon background relative to the neutrinos. The change in the photon temperature can be easily computed from entropy conservation. The neutrino entropy must be conserved separately from the entropy of interacting particles. A straightforward computation yields

$$T_\nu = (4/11)^{1/3} T_\gamma \simeq 1.9 \text{ K}. \quad (22.49)$$

The total entropy density is therefore given by the contribution from photons and 3 flavors of neutrinos

$$s = \frac{4}{3} \frac{\pi^2}{30} \left( 2 + \frac{21}{4} (T_\nu/T_\gamma)^3 \right) T_\gamma^3 = \frac{4}{3} \frac{\pi^2}{30} \left( 2 + \frac{21}{11} \right) T_\gamma^3 = 7.04 n_\gamma. \quad (22.50)$$

Similarly, the total relativistic energy density is given by

$$\rho_r = \frac{\pi^2}{30} \left[ 2 + \frac{21}{4} (T_\nu/T_\gamma)^4 \right] T_\gamma^4 \simeq 1.68 \rho_\gamma. \quad (22.51)$$

In practice, a small correction is needed to this, since neutrinos are not totally decoupled at  $e^\pm$  annihilation: the effective number of massless neutrino species is 3.045, rather than 3 [40, 41].

This expression ignores neutrino rest masses, but current oscillation data require at least one neutrino eigenstate to have a mass exceeding 0.05 eV. In this minimal case,  $\Omega_\nu h^2 = 6 \times 10^{-4}$ , so the neutrino contribution to the matter budget would be negligibly small (which is our normal assumption). However, a nearly degenerate pattern of mass eigenstates could allow larger densities, since oscillation experiments only measure differences in  $m^2$  values. Note that a 0.05-eV neutrino has  $T_\nu = m_\nu$  at  $z \simeq 296$ , so the above expression for the total present relativistic density is really only an extrapolation. However, neutrinos are almost certainly relativistic at all epochs where the radiation content of the Universe is dynamically significant.

### 22.3.4 Field Theory and Phase transitions

It is very likely that the Universe has undergone one or more phase transitions during the course of its evolution [42–45]. Our current vacuum state is described by  $SU(3)_c \times U(1)_{\text{em}}$ , which in the Standard Model is a remnant of an unbroken  $SU(3)_c \times SU(2)_L \times U(1)_Y$  gauge symmetry. Symmetry breaking occurs when a non-singlet gauge field (the Higgs field in the Standard Model) picks up a non-vanishing vacuum expectation value, determined by a scalar potential. For example, a simple (non-gauged) potential describing symmetry breaking is  $V(\phi) = \frac{1}{4} \lambda \phi^4 - \frac{1}{2} \mu^2 \phi^2 + V(0)$ . The resulting expectation value is simply  $\langle \phi \rangle = \mu/\sqrt{\lambda}$ .

In the early Universe, finite temperature radiative corrections typically add terms to the potential of the form  $\phi^2 T^2$ . Thus, at very high temperatures, the symmetry is restored and  $\langle \phi \rangle = 0$ . As the Universe cools, depending on the details of the potential, symmetry breaking will occur via a first-order phase transition in which the field tunnels through a potential barrier, or via a second-order transition in which the field evolves smoothly from one state to another (as would be the case for the above example potential).

The evolution of scalar fields can have a profound impact on the early Universe. The equation of motion for a scalar field  $\phi$  can be derived from the energy-momentum tensor

$$T_{\mu\nu} = \partial_\mu \phi \partial_\nu \phi - \frac{1}{2} g_{\mu\nu} \partial_\rho \phi \partial^\rho \phi - g_{\mu\nu} V(\phi). \quad (22.52)$$

By associating  $\rho = T_{00}$  and  $p = R^{-2}(t)T_{ii}$  we have

$$\begin{aligned} \rho &= \frac{1}{2} \dot{\phi}^2 + \frac{1}{2} R^{-2}(t) (\nabla \phi)^2 + V(\phi) \\ p &= \frac{1}{2} \dot{\phi}^2 - \frac{1}{6} R^{-2}(t) (\nabla \phi)^2 - V(\phi), \end{aligned} \quad (22.53)$$

and from Eq. (22.10) we can write the equation of motion (by considering a homogeneous region, we can ignore the gradient terms)

$$\ddot{\phi} + 3H\dot{\phi} = -\partial V/\partial \phi. \quad (22.54)$$

### 22.3.5 Inflation

**Inflation of early universe** In Sec. 22.2.4, we discussed some of the problems associated with the standard Big-Bang model. However, during a phase transition, our assumptions of an adiabatically expanding Universe are generally not valid. If, for example, a phase transition occurred in the early Universe such that the field evolved slowly from the symmetric state to the global minimum, the Universe may have been dominated by the vacuum energy density associated with the potential near  $\phi \simeq 0$ . During this period of slow evolution, the energy density due to radiation will fall below the vacuum energy density,  $\rho \ll V(0)$ . When this happens, the expansion rate will be dominated by the constant  $V(0)$ , and we obtain the exponentially expanding solution given in Eq. (22.20). When the field evolves towards the global minimum it will begin to oscillate about the minimum, energy will be released during its decay, and a hot thermal Universe will be restored. If released fast enough, it will produce radiation at a temperature  $NT_{\text{R}}^4 \lesssim V(0)$ . In this reheating process, entropy has been created and the final value of  $RT$  is greater than the initial value of  $RT$ . Thus, we see that, during a phase transition, the relation  $RT \sim \text{constant}$  need not hold true. This is the basis of the inflationary Universe scenario [46–48].

If, during the phase transition, the value of  $RT$  changed by a factor of  $O(10^{29})$ , the cosmological problems discussed above would be solved. The observed isotropy would be generated by the immense expansion; one small causal region could get blown up, and thus our entire visible Universe would have been in thermal contact some time in the past. In addition, the density parameter  $\Omega$  would have been driven to 1 (with exponential precision). Density perturbations will be stretched by the expansion,  $\lambda \sim R(t)$ . Thus it will appear that  $\lambda \gg H^{-1}$  or that the perturbations have left the horizon, where in fact the size of the causally connected region is now no longer simply  $H^{-1}$ . However, not only does inflation offer an explanation for large scale perturbations, it also offers a source for the perturbations themselves through quantum fluctuations.

Problems with early models of inflation based on either a first-order [49] or second-order [50, 51] phase transition of a Grand Unified Theory led to models invoking a completely new scalar field: the inflaton,  $\phi$ . The potential of this field,  $V(\phi)$ , needs to have a very low gradient and curvature in order to match observed metric fluctuations. For a more thorough discussion of the problems of early models and a host of current models being studied see the review on inflation – Sec. 23 of this *Review*. In most current inflation models, reheated bubbles typically do not percolate, so inflation is ‘eternal’ and continues with exponential expansion in the region outside bubbles. These causally disconnected bubble Universes constitute a ‘multiverse’, where low-energy physics can vary between different bubbles. This has led to a controversial ‘anthropic’ approach to cosmology [52–54], where observer selection within the multiverse can be introduced as a means of understanding e.g. why the observed level of vacuum energy is so low (because larger values suppress growth of structure).

### 22.3.6 Baryogenesis

The Universe appears to be populated exclusively with matter rather than antimatter. Indeed antimatter is only detected in accelerators or in cosmic rays. However, the presence of antimatter in the latter is understood to be the result of collisions of primary particles in the interstellar medium. There is in fact strong evidence against primary forms of antimatter in the Universe. Furthermore, the density of baryons compared to the density of photons is extremely small,  $\eta \sim 10^{-9}$ .

The production of a net baryon asymmetry requires baryon number violating interactions,  $C$  and  $CP$  violation, and a departure from thermal equilibrium [55]. The first two of these ingredients are expected to be contained in Grand Unified Theories (GUTs) as well as in the non-perturbative sector of the Standard Model; the third can be realized in an expanding Universe where, as we have seen, interactions come in and out of equilibrium.

There are several interesting and viable mechanisms for the production of the baryon asymmetry. While we can not review any of them here in any detail, we mention some of the important scenarios. In all cases, all three ingredients listed above are incorporated. One of the first mechanisms was based on the out of equilibrium decay of a massive particle such as a superheavy GUT gauge or Higgs boson [56, 57]. A novel mechanism involving the decay of flat directions in supersymmetric models is known as the Affleck-Dine scenario [58]. There is also the possibility of generating the baryon asymmetry at the electro-weak scale using the non-perturbative interactions of sphalerons [59]. Because these interactions conserve the sum of baryon and lepton number,  $B + L$ , it is possible to first generate a lepton asymmetry (*e.g.*, by the out-of-equilibrium decay of a superheavy right-handed neutrino), which is converted to a baryon asymmetry at the electro-weak scale [60]. This mechanism is known as leptobaryogenesis.

### 22.3.7 Nucleosynthesis

An essential element of the standard cosmological model is Big-Bang nucleosynthesis (BBN), the theory that predicts the abundances of the light element isotopes D,  $^3\text{He}$ ,  $^4\text{He}$ , and  $^7\text{Li}$ . Nucleosynthesis takes place at a temperature scale of order 1 MeV. The nuclear processes lead primarily to  $^4\text{He}$ , with a primordial mass fraction of about 25%. Lesser amounts of the other light elements are produced: about  $10^{-5}$  of D and  $^3\text{He}$  and about  $10^{-10}$  of  $^7\text{Li}$  by number relative to H. The abundances of the light elements depend almost solely on one key parameter, the baryon-to-photon ratio,  $\eta$ . The nucleosynthesis predictions can be compared with observational determinations of the abundances of the light elements. Consistency between theory and observations driven primarily by recent D/H measurements [61, 62] leads to a range of

$$5.8 \times 10^{-10} < \eta < 6.5 \times 10^{-10}. \quad (22.55)$$

$\eta$  is related to the fraction of  $\Omega$  contained in baryons:

$$\Omega_b = 3.66 \times 10^7 \eta h^{-2}, \quad (22.56)$$

or  $10^{10} \eta = 274 \Omega_b h^2$ . The *Planck* result [24] for  $\Omega_b h^2$  of  $0.0224 \pm 0.0002$  translates into a value of  $\eta = 6.12 \pm 0.04$ . This result can be used to ‘predict’ the light element abundances, which can in turn be compared with observation [63]. The resulting D/H abundance is in excellent agreement with that found in quasar absorption systems. It is in reasonable agreement with the helium abundance observed in extragalactic HII regions (once systematic uncertainties are accounted for), but is in poor agreement with the Li abundance observed in the atmospheres of halo dwarf stars [64]. See the review on BBN – Sec. 24 of this *Review* for a detailed discussion of BBN or references [65–68].

### 22.3.8 The transition to a matter-dominated Universe

In the Standard Model, the temperature (or redshift) at which the Universe undergoes a transition from a radiation-dominated to a matter-dominated Universe is determined by the amount of dark matter. Assuming three nearly massless neutrinos, the energy density in radiation at temperatures  $T \ll 1$  MeV, is given by

$$\rho_r = \frac{\pi^2}{30} \left[ 2 + \frac{21}{4} \left( \frac{4}{11} \right)^{4/3} \right] T^4. \quad (22.57)$$

In the absence of non-baryonic dark matter, the matter density can be written as

$$\rho_m = m_N \eta n_\gamma, \quad (22.58)$$

where  $m_N$  is the nucleon mass. Recalling that  $n_\gamma \propto T^3$  [cf. Eq. (22.40)], we can solve for the temperature or redshift at the matter-radiation equality when  $\rho_r = \rho_m$ ,

$$T_{\text{eq}} = 0.22 m_N \eta \quad \text{or} \quad (1 + z_{\text{eq}}) = 0.22 \eta \frac{m_N}{T_0}, \quad (22.59)$$

where  $T_0$  is the present temperature of the microwave background. For  $\eta = 6.1 \times 10^{-10}$ , this corresponds to a temperature  $T_{\text{eq}} \simeq 0.13$  eV or  $(1 + z_{\text{eq}}) \simeq 550$ . A transition this late would be problematic for structure formation (see Sec. 22.4.5).

The redshift of matter domination can be pushed back significantly if non-baryonic dark matter is present. If instead of Eq. (22.58), we write

$$\rho_m = \Omega_m \rho_c \left( \frac{T}{T_0} \right)^3, \quad (22.60)$$

we find that

$$T_{\text{eq}} = 0.9 \frac{\Omega_m \rho_c}{T_0^3} \quad \text{or} \quad (1 + z_{\text{eq}}) = 2.4 \times 10^4 \Omega_m h^2. \quad (22.61)$$

## 22.4 The Universe at late times

### 22.4.1 The CMB

One form of the infamous Olbers’ paradox says that, in Euclidean space, surface brightness is independent of distance. Every line of sight will terminate on matter that is hot enough to be ionized and so scatter photons:  $T \gtrsim 10^3$  K, and the sky should therefore shine as brightly as the surface of the Sun. The reason the night sky is dark is entirely due to the expansion, which cools the radiation temperature to 2.73 K. This gives a Planck function peaking at around 1 mm to produce the CMB.

The CMB spectrum is a very accurate match to a Planck function [69]. (See the review on CMB – Sec. 29 of this *Review*.) The COBE estimate of the temperature is [70]

$$T = 2.7255 \pm 0.0006 \text{ K}. \quad (22.62)$$

The lack of any distortion of the Planck spectrum is a strong physical constraint. It is very difficult to account for in any expanding Universe other than one that passes through a hot stage. Alternative schemes for generating the radiation, such as thermalization of starlight by dust grains, inevitably generate a superposition of temperatures. What is required in addition to thermal equilibrium is that  $T \propto 1/R$ , so that radiation from different parts of space arrive at an observer with the same apparent temperature.

Although it is common to speak of the CMB as originating at ‘recombination’, a more accurate terminology is the era of ‘last scattering’. In practice, this takes place at  $z \simeq 1100$ , almost independently of the main cosmological parameters, at which time the fractional ionization is very small. This occurred when the age of the Universe was about 370,000 years. But the CMB photons themselves were not generated at this point, and were the result of thermalization at  $z \sim 10^7$ . (See the review on CMB – Sec. 29 of this *Review* for a full discussion of the CMB.)

### 22.4.2 Matter in the Universe

One of the main tasks of cosmology is to measure the density of the Universe, and how this is divided between dark matter and baryons. The baryons consist partly of stars, with  $0.002 \lesssim \Omega_* \lesssim 0.003$  [71] but mainly inhabit the intergalactic medium (IGM). One powerful way in which this can be studied is via the absorption of light from distant luminous objects such as quasars. Even very small amounts of neutral hydrogen can absorb rest-frame UV photons (the Gunn-Peterson effect), and should suppress the continuum by a factor  $\exp(-\tau)$ , where

$$\tau \simeq 10^{4.62} h^{-1} \left[ \frac{n_{\text{HI}}(z)/m^{-3}}{(1+z)\sqrt{1+\Omega_m z}} \right], \quad (22.63)$$

and this expression applies while the Universe is matter dominated ( $z \gtrsim 1$  in the  $\Omega_m = 0.3$   $\Omega_v = 0.7$  model). At  $z < 6$ , the dominant effect on quasar spectra is a ‘forest’ of narrow absorption lines, which produce a mean  $\tau = 1$  in the Ly $\alpha$  forest at about  $z = 3$ , and so we have  $\Omega_{\text{HI}} \simeq 10^{-6.7} h^{-1}$ . This is such a small number that the IGM must be very highly ionized at these redshifts, apart from a few high-density clumps. But at  $z > 6$  there is good evidence for a ‘reionization’ era at which the general IGM is not so strongly ionized [72]. As discussed below, this ionized IGM at low  $z$  is also detectable via the secondary Compton scattering of CMB photons.

The Ly $\alpha$  forest is of great importance in pinning down the abundance of deuterium. Because electrons in deuterium differ in reduced mass by about 1 part in 4000 compared to hydrogen, each absorption system in the Ly $\alpha$  forest is accompanied by an offset deuterium line. By careful selection of systems with an optimal HI column density, a measurement of the D/H ratio can be made. This has now been done with high accuracy in 10 quasars, with consistent results [61]. Combining these determinations with the theory of primordial nucleosynthesis yields a baryon density of  $\Omega_b h^2 = 0.021 - 0.024$  (95% confidence) in excellent agreement with the Planck result. (See also the review on BBN – Sec. 24 of this *Review*.)

Ionized IGM can also be detected in emission when it is densely clumped, via bremsstrahlung radiation. This generates the spectacular X-ray emission from rich clusters of galaxies. Studies of this phenomenon allow us to achieve an accounting of the total baryonic material in clusters. Within the central  $\simeq 1$  Mpc, the masses in stars, X-ray emitting gas, and total dark matter can be determined with reasonable accuracy (perhaps 20% rms), and this allows a minimum baryon fraction to be determined [73, 74]:

$$\frac{M_{\text{baryons}}}{M_{\text{total}}} \gtrsim 0.009 + (0.066 \pm 0.003) h^{-3/2}. \quad (22.64)$$

Because clusters are the largest collapsed structures, it is reasonable to take this as applying to the Universe as a whole. This equation implies a minimum baryon fraction of perhaps 12% (for reasonable  $h$ ), which is too high for  $\Omega_m = 1$  if we take  $\Omega_b h^2 \simeq 0.02$  from nucleosynthesis. This is therefore one of the more robust arguments in favor of  $\Omega_m \simeq 0.3$ . (See the review on Cosmological Parameters – Sec. 25.1 of this *Review*.) This argument is also consistent with the inference on  $\Omega_m$  that can be made from Fig. 22.2.

This method is much more robust than the older classical technique for weighing the Universe: ‘ $L \times M/L$ ’. The overall light density of the Universe is reasonably well determined from redshift surveys of galaxies, so that a good determination of mass  $M$  and luminosity  $L$  for a single object suffices to determine  $\Omega_m$  – but only *if* the mass-to-light ratio were universal.

### 22.4.3 Gravitational lensing

A robust method for determining masses in cosmology is to use gravitational light deflection. Most systems can be treated as a geometrically thin gravitational lens, where the light bending is assumed to take place only at a single distance. Simple geometry then determines a mapping between the coordinates in the intrinsic source plane (S) and the observed image plane (I):

$$\alpha(D_L \theta_I) = \frac{D_S}{D_{LS}} (\theta_I - \theta_S), \quad (22.65)$$

where the angles  $\theta_I, \theta_S$ , and  $\alpha$  are in general two-dimensional vectors on the sky. The distances  $D_{LS}$  etc. are given by an extension of the usual distance-redshift formula:

$$D_{LS} = \frac{R_0 S_k (\chi_S - \chi_L)}{1 + z_S}. \quad (22.66)$$

This is the angular-diameter distance for objects on the source plane as perceived by an observer on the lens.

Solutions of this equation divide into weak lensing, where the mapping between source plane and image plane is one-to-one, and strong lensing, in which multiple imaging is possible. For circularly-symmetric lenses, an on-axis source is multiply imaged into a ‘caustic’ ring, whose radius is the Einstein radius:

$$\begin{aligned} \theta_E &= \left( 4GM \frac{D_{LS}}{D_L D_S} \right)^{1/2} \\ &= \left( \frac{M}{10^{11.09} M_\odot} \right)^{1/2} \left( \frac{D_L D_S / D_{LS}}{\text{Gpc}} \right)^{-1/2} \text{arcsec}. \end{aligned} \quad (22.67)$$

The observation of ‘arcs’ (segments of near-perfect Einstein rings) in rich clusters of galaxies has thus given very accurate masses for the central parts of clusters – generally in good agreement with other indicators, such as analysis of X-ray emission from the cluster IGM [75, 76].

Gravitational lensing has also developed into a particularly promising probe of cosmological structure on 10-Mpc to 100-Mpc scales. Weak image distortions manifest themselves as an additional ellipticity of galaxy images (‘shear’), which can be observed by averaging many images together (the corresponding flux amplification is less readily detected). The result is a ‘cosmic shear’ field of order 1% ellipticity, coherent over scales of around 30 arcmin, which is directly related to the cosmic mass field. For this reason, weak lensing is seen as potentially the cleanest probe of matter fluctuations, next to the CMB. Already, impressive results have been obtained in measuring cosmological parameters, based on survey data from only  $\sim 10^3 \text{ deg}^2$  [77, 78]. A particular strength of lensing is its ability to measure the amplitude of mass fluctuations; this can be deduced from the amplitude of CMB fluctuations, but only with low precision on account of the poorly-known optical depth due to Compton scattering after reionization. However, the effect of weak lensing on the CMB map itself can be detected via the induced non-Gaussian signal, and this gives the CMB greater internal power [79]. The main difficulty of principle with lensing is that part of the signal is generated by small-scale density fluctuations; thus a model is required for nonlinear evolution, including astrophysical effects that separate baryons and dark matter. In this respect, the CMB is a cleaner probe of the primordial fluctuations.

### 22.4.4 Density Fluctuations

The overall properties of the Universe are very close to being homogeneous; and yet telescopes reveal a wealth of detail on scales varying from single galaxies to large-scale structures of size exceeding 100 Mpc. The existence of these structures must be telling us something important about the initial conditions of the Big Bang, and about the physical processes that have operated subsequently. This motivates the study of the density perturbation field, defined as

$$\delta(\mathbf{x}) \equiv \frac{\rho(\mathbf{x}) - \langle \rho \rangle}{\langle \rho \rangle}. \quad (22.68)$$

A critical feature of the  $\delta$  field is that it inhabits a Universe that is isotropic and homogeneous in its large-scale properties. This suggests that the statistical properties of  $\delta$  should also be statistically homogeneous – *i.e.*, it is a stationary random process.

It is often convenient to describe  $\delta$  as a Fourier superposition:

$$\delta(\mathbf{x}) = \sum \delta_{\mathbf{k}} e^{-i\mathbf{k} \cdot \mathbf{x}}. \quad (22.69)$$

We avoid difficulties with an infinite Universe by applying periodic boundary conditions in a cube of some large volume  $V$ . The cross-terms vanish when we compute the variance in the field, which is just a sum over modes of the power spectrum:

$$\langle \delta^2 \rangle = \sum |\delta_{\mathbf{k}}|^2 \equiv \sum P(k). \quad (22.70)$$

Note that the statistical nature of the fluctuations must be isotropic, so we write  $P(k)$  rather than  $P(\mathbf{k})$ . The  $\langle \dots \rangle$  average here is a volume average. Cosmological density fields are an example of an ergodic process, in which the average over a large volume tends to the same answer as the average over a statistical ensemble.

The statistical properties of discrete objects sampled from the density field are often described in terms of  $N$ -point correlation functions, which represent the excess probability over random for finding one particle in each of  $N$  boxes in a given configuration. For the 2-point case, the correlation function is readily shown to be identical to the autocorrelation function of the  $\delta$  field:  $\xi(r) = \langle \delta(x)\delta(x+r) \rangle$ .

The power spectrum and correlation function are Fourier conjugates, and thus are equivalent descriptions of the density field (similarly,  $k$ -space equivalents exist for the higher-order correlations). It is convenient to take the limit  $V \rightarrow \infty$  and use  $k$ -space integrals, defining a dimensionless power spectrum, which measures the contribution to the fractional variance in density per unit logarithmic range of scale, as  $\Delta^2(k) = d\langle \delta^2 \rangle / d \ln k =$

$Vk^3P(k)/2\pi^2$ :

$$\xi(r) = \int \Delta^2(k) \frac{\sin kr}{kr} d \ln k; \quad \Delta^2(k) = \frac{2}{\pi} k^3 \int_0^\infty \xi(r) \frac{\sin kr}{kr} r^2 dr. \quad (22.71)$$

For many years, an adequate approximation to observational data on galaxies was  $\xi = (r/r_0)^{-\gamma}$ , with  $\gamma \simeq 1.8$  and  $r_0 \simeq 5 h^{-1}$  Mpc. Modern surveys are now able to probe into the large-scale linear regime where unaltered traces of the curved post-recombination spectrum can be detected [80–82].

#### 22.4.5 Formation of cosmological structure

The simplest model for the generation of cosmological structure is gravitational instability acting on some small initial fluctuations (for the origin of which a theory such as inflation is required). If the perturbations are adiabatic (*i.e.*, fractionally perturb number densities of photons and matter equally), the linear growth law for matter perturbations is simple:

$$\delta \propto \begin{cases} a^2(t) & (\text{radiation domination; } \Omega_r = 1); \\ a(t) & (\text{matter domination; } \Omega_m = 1). \end{cases} \quad (22.72)$$

For low-density Universes, the growth is slower:

$$d \ln \delta / d \ln a \simeq \Omega_m^\gamma(a), \quad (22.73)$$

where the parameter  $\gamma$  is close to 0.55 independent of the vacuum density [83, 84].

The alternative perturbation mode is isocurvature: only the equation of state changes, and the total density is initially unperturbed. These modes perturb the total entropy density, and thus induce additional large-scale CMB anisotropies [85]. Although the character of perturbations in the simplest inflationary theories are purely adiabatic, correlated adiabatic and isocurvature modes are predicted in many models; the simplest example is the curvaton, which is a scalar field that decays to yield a perturbed radiation density. If the matter content already exists at this time, the overall perturbation field will have a significant isocurvature component. Such a prediction is inconsistent with current CMB data [86], and most analyses of CMB and large-scale structure (LSS) data assume the adiabatic case to hold exactly.

Linear evolution preserves the shape of the power spectrum. However, a variety of processes mean that growth actually depends on the matter content.

1. Pressure opposes gravity effectively for wavelengths below the horizon length while the Universe is radiation dominated. The *comoving* horizon size at  $z_{\text{eq}}$  is therefore an important scale:

$$D_H(z_{\text{eq}}) = \frac{2(\sqrt{2}-1)}{(\Omega_m z_{\text{eq}})^{1/2} H_0} = \frac{16.0}{\Omega_m h^2} \text{Mpc}. \quad (22.74)$$

2. At early times, dark matter particles will undergo free streaming at the speed of light, and so erase all scales up to the horizon – a process that only ceases when the particles go nonrelativistic. For light massive neutrinos, this happens at  $z_{\text{eq}}$ ; all structure up to the horizon-scale power-spectrum break is in fact erased. Hot(cold) dark matter models are thus sometimes dubbed large(small)-scale damping models.
3. A further important scale arises where photon diffusion can erase perturbations in the matter – radiation fluid; this process is named Silk damping.

The overall effect is encapsulated in the transfer function, which gives the ratio of the late-time amplitude of a mode to its initial value (see Fig. 22.4). The overall power spectrum is thus the primordial scalar-mode power law, times the square of the transfer function:

$$P(k) \propto k^{n_s} T_k^2. \quad (22.75)$$

The most generic power-law index is  $n_s = 1$ : the ‘Zeldovich’ or ‘scale-invariant’ spectrum. Inflationary models tend to predict a small ‘tilt’:  $|n_s - 1| \lesssim 0.05$  [12, 13]. On the assumption that the dark matter is cold, the power spectrum then depends on 5 parameters:  $n_s$ ,  $h$ ,  $\Omega_b$ ,  $\Omega_c$  ( $\equiv \Omega_m - \Omega_b$ ), and an overall amplitude.

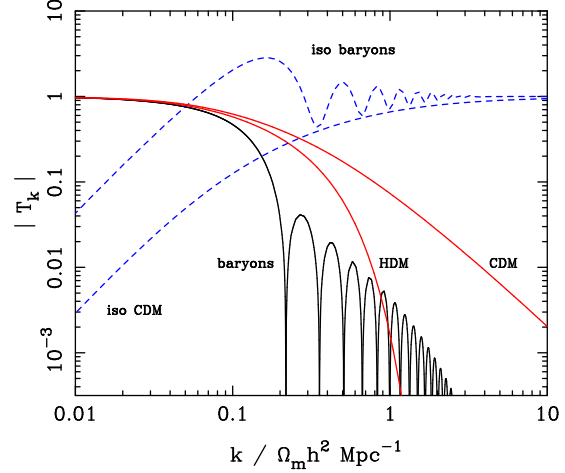


Figure 22.4: A plot of transfer functions for various models. For adiabatic models,  $T_k \rightarrow 1$  at small  $k$ , whereas the opposite is true for isocurvature models. For dark-matter models, the characteristic wavenumber scales proportional to  $\Omega_m h^2$ . The scaling for baryonic models does not obey this exactly; the plotted cases correspond to  $\Omega_m = 1$ ,  $h = 0.5$ .

The latter is often specified as  $\sigma_8$ , the linear-theory fractional rms in density when a spherical filter of radius  $8 h^{-1}$  Mpc is applied in linear theory. This scale can be probed directly via weak gravitational lensing, and also via its effect on the abundance of rich galaxy clusters. The favored value from the latter is approximately [87]

$$\sigma_8 \simeq [0.746 \pm 0.012 (\text{stat.}) \pm 0.022 (\text{sys.})] (\Omega_m/0.3)^{-0.47}, \quad (22.76)$$

which is rather similar to the normalization inferred from weak lensing:  $\sigma_8 \simeq [0.745 \pm 0.039] (\Omega_m/0.3)^{-0.5}$  [77]; or  $[0.782 \pm 0.027] (\Omega_m/0.3)^{-0.5}$  [78]. These figures are in  $> 2\sigma$  tension with the *Planck* values of  $(\sigma_8, \Omega_m) = (0.811 \pm 0.006, 0.315 \pm 0.007)$ . If real, such a discrepancy could indicate interesting new physics; but the current evidence is not strong enough to make such a claim.

A direct measure of mass inhomogeneity is valuable, since the galaxies inevitably are biased with respect to the mass. This means that the fractional fluctuations in galaxy number,  $\delta n/n$ , may differ from the mass fluctuations,  $\delta \rho/\rho$ . It is commonly assumed that the two fields obey some proportionality on large scales where the fluctuations are small,  $\delta n/n = b \delta \rho/\rho$ , but even this is not guaranteed [88].

The main shape of the transfer function is a break around the horizon scale at  $z_{\text{eq}}$ , which depends just on  $\Omega_m h$  when wavenumbers are measured in observable units ( $h \text{Mpc}^{-1}$ ). For reasonable baryon content, weak oscillations in the transfer function are also expected, and these BAOs (Baryon Acoustic Oscillations) have been clearly detected [89, 90]. As well as directly measuring the baryon fraction, the scale of the oscillations directly measures the acoustic horizon at decoupling; this can be used as an additional standard ruler for cosmological tests, and the BAO signature has become one of the most important applications of large galaxy surveys. Overall, current power-spectrum data [80–82] favor  $\Omega_m h \simeq 0.20$  and a baryon fraction of about 0.15 for  $n_s \simeq 1$  (see Fig. 22.5).

In principle, accurate data over a wide range of  $k$  could determine both  $\Omega_m h$  and  $n_s$ , but in practice there is a strong degeneracy between these. In order to constrain  $n_s$  itself, it is necessary to examine data on anisotropies in the CMB.

#### 22.4.6 CMB anisotropies

The CMB has a clear dipole anisotropy, of magnitude  $1.23 \times 10^{-3}$ . This is interpreted as being due to the Earth’s motion, which is equivalent to a peculiar velocity for the Milky Way of

$$v_{\text{MW}} \simeq 600 \text{ km s}^{-1} \quad \text{towards } (\ell, b) \simeq (270^\circ, 30^\circ). \quad (22.77)$$

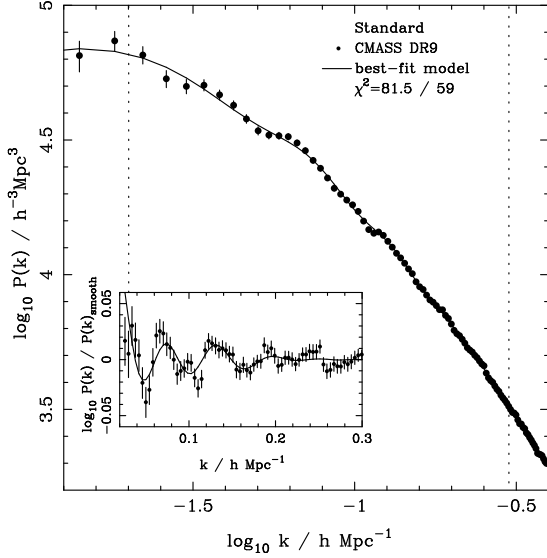


Figure 22.5: The galaxy power spectrum from the SDSS BOSS survey [82]. The solid points with error bars show the power estimate. The solid line shows a standard  $\Lambda$ CDM model with  $\Omega_b h^2 \simeq 0.02$  and  $\Omega_m h \simeq 0.2$ . The inset amplifies the region where BAO features are visible. The fact that these perturb the power by  $\sim 20\%$  rather than order unity is direct evidence that the matter content of the Universe is dominated by collisionless dark matter.

All higher-order multipole moments of the CMB are however much smaller (of order  $10^{-5}$ ), and interpreted as signatures of density fluctuations at last scattering ( $\simeq 1100$ ). To analyze these, the sky is expanded in spherical harmonics as explained in the review on the CMB – Sec. 29 of this *Review*. The dimensionless power per  $\ln k$  or ‘bandpower’ for the CMB is defined as

$$\mathcal{T}^2(\ell) = \frac{\ell(\ell+1)}{2\pi} C_\ell. \quad (22.78)$$

This function encodes information from the three distinct mechanisms that cause CMB anisotropies:

- (1) Gravitational (Sachs – Wolfe) perturbations. Photons from high-density regions at last scattering have to climb out of potential wells, and are thus redshifted.
- (2) Intrinsic (adiabatic) perturbations. In high-density regions, the coupling of matter and radiation can compress the radiation also, giving a higher temperature.
- (3) Velocity (Doppler) perturbations. The plasma has a non-zero velocity at recombination, which leads to Doppler shifts in frequency and hence shifts in brightness temperature.

Because the potential fluctuations obey Poisson’s equation,  $\nabla^2 \Phi = 4\pi G \rho \delta$ , and the velocity field satisfies the continuity equation  $\nabla \cdot \mathbf{u} = -\dot{\delta}$ , the resulting different powers of  $k$  ensure that the Sachs-Wolfe effect dominates on large scales and adiabatic effects on small scales.

The relation between angle and comoving distance on the last-scattering sphere requires the comoving angular-diameter distance to the last-scattering sphere; because of its high redshift, this is effectively identical to the horizon size at the present epoch,  $D_H$ :

$$\begin{aligned} D_H &= \frac{2}{\Omega_m H_0} \quad (\Omega_\nu = 0) \\ D_H &\simeq \frac{2}{\Omega_m^{0.4} H_0} \quad (\text{flat} : \Omega_m + \Omega_\nu = 1). \end{aligned} \quad (22.79)$$

These relations show how the CMB is strongly sensitive to curvature: the horizon length at last scattering is  $\propto 1/\sqrt{\Omega_m}$ , so that this subtends an angle that is virtually independent of  $\Omega_m$  for a flat model. Observations of a peak in the CMB power spectrum

at relatively large scales ( $\ell \simeq 221$ ) are thus strongly inconsistent with zero- $\Lambda$  models with low density: current CMB + BAO + lensing data require  $\Omega_m + \Omega_\nu = 0.999 \pm 0.004$  (95%) [24]. (See e.g., Fig. 22.2).

In addition to curvature, the CMB encodes information about several other key cosmological parameters. Within the compass of simple adiabatic CDM models, there are 9 of these:

$$\omega_c, \omega_b, \Omega_{\text{tot}}, h, \tau, n_s, n_t, r, Q. \quad (22.80)$$

The symbol  $\omega$  denotes the physical density,  $\Omega h^2$ : the transfer function depends only on the densities of CDM ( $\omega_c$ ) and baryons ( $\omega_b$ ). Transcribing the power spectrum at last scattering into an angular power spectrum brings in the total density parameter ( $\Omega_{\text{tot}} \equiv \Omega_m + \Omega_\nu = \Omega_c + \Omega_b + \Omega_\nu$ ) and  $h$ : there is a near-exact geometrical degeneracy [91] between these that keeps the angular-diameter distance to last scattering invariant, so that models with substantial spatial curvature and large vacuum energy cannot be ruled out without prior knowledge of the Hubble parameter. Alternatively, the CMB alone cannot measure the Hubble parameter without taking into account the line-of-sight information from CMB lensing.

A further possible degeneracy involves the tensor contribution to the CMB anisotropies. These are important at large scales (up to the horizon scales); for smaller scales, only scalar fluctuations (density perturbations) are important. Each of these components is characterized by a spectral index,  $n$ , and a ratio between the power spectra of tensors and scalars ( $r$ ). See the review on Cosmological Parameters – Sec. 25.1 of this *Review* for a technical definition of the  $r$  parameter. Finally, the overall amplitude of the spectrum must be specified ( $Q$ ), together with the optical depth to Compton scattering owing to recent reionization ( $\tau$ ). Adding a large tensor contribution reduces the contrast between low  $\ell$  and the peak at  $\ell \simeq 221$  (because the tensor spectrum has no acoustic component). The previous relative height of the peak can be recovered by increasing  $n_s$  to increase the small-scale power in the scalar component; this in turn over-predicts the power at  $\ell \sim 1000$ , but this effect can be counteracted by raising the baryon density [92]. This approximate 3-way degeneracy is broken as we increase the range of multipoles sampled.

The reason the tensor component is introduced, and why it is so important, is that it is the only non-generic prediction of inflation. Slow-roll models of inflation involve two dimensionless parameters:

$$\epsilon \equiv \frac{M_{\text{P}}^2}{16\pi} \left( \frac{V'}{V} \right)^2, \quad \eta \equiv \frac{M_{\text{P}}^2}{8\pi} \left( \frac{V''}{V} \right), \quad (22.81)$$

where  $V$  is the inflaton potential, and dashes denote derivatives with respect to the inflation field. In terms of these, the tensor-to-scalar ratio is  $r \simeq 16\epsilon$ , and the spectral indices are  $n_s = 1 - 6\epsilon + 2\eta$  and  $n_t = -2\epsilon$ . The natural expectation of inflation is that the quasi-exponential phase ends once the magnitudes of the slow-roll parameters become of order unity, so that both  $n_s \neq 1$  and a significant tensor component are expected. These predictions can be avoided in some models, but it is undeniable that observation of such features would be a great triumph for inflation. Cosmology therefore stands at a fascinating point given that the most recent CMB data reject the zero-tensor  $n_s = 1$  model at more than  $8\sigma$ :  $n_s = 0.965 \pm 0.004$  [24]. This rejection is strong enough that it is also able to break the tensor degeneracy, so that no model with  $n_s = 1$  is acceptable, whatever the value of  $r$ .

The current limit on  $r$  is  $< 0.06$  at 95% confidence [93]. In conjunction with the measured value of  $n_s$ , this upper limit sits close to the prediction of a linear potential (i.e.  $|\eta| \ll |\epsilon|$ ). Any further reduction in the limit on  $r$  will force  $\eta$  to be negative – i.e. a convex potential at the point where LSS scales were generated (sometimes called a ‘hilltop’), in contrast to simple early models such as  $V(\phi) = m^2 \phi^2$  or  $\lambda \phi^4$ , which are now excluded. Examples of models that are currently in excellent agreement with the Planck results are the Starobinsky model of  $\mathcal{R} + \mathcal{R}^2$  gravity [94], or the Higgs-inflation model where the Higgs field is non-minimally coupled [95]. Assuming 55 e-foldings of inflation, these models predict  $n_s = 0.965$  and  $r = 0.0035$ . Assuming that no systematic error in the CMB data can be identified, cosmology has thus



passed a critical hurdle in rejecting scale-invariant fluctuations. The years ahead will be devoted to the task of searching for the tensor fluctuations – for which the main tool will be the polarization of the CMB [14].

#### 22.4.6.1 CMB foregrounds

As the quality of CMB data improves, there is a growing interest in effects that arise along the line of sight. The CMB temperature is perturbed by dark-matter structures and by Compton scattering from ionized gas. In the former case, we have the integrated Sachs-Wolfe effect, which is sensitive to the time derivative of the gravitational potential. In the linear regime, this is damped when the Universe becomes  $\Lambda$ -dominated, and this is an independent way of detecting  $\Lambda$  [96]. The potential also causes gravitational lensing of the CMB: structures at  $z \simeq 1-2$  displace features on the CMB sky by about 2 arcmin over coherent degree-scale patches. Detection of these distortions allows a map to be made of overdensity projected from  $z = 0$  to 1100 [79]. This is a very powerful calibration for direct studies of gravitational lensing using galaxies. Finally, Comptonization affects the CMB in two ways: the thermal Sunyaev-Zeldovich effect measures the blurring of photon energies by hot gas, and the kinetic Sunyaev-Zeldovich effect is sensitive to the bulk velocity of the gas. Both these effects start to dominate over the intrinsic CMB fluctuations at multipoles  $\ell \gtrsim 2000$  [97].

#### 22.4.7 Probing dark energy and the nature of gravity

The most radical element of our current cosmological model is the dark energy that accelerates the expansion. The energy density of this component is approximately  $(2.2 \text{ meV})^4$  (for  $w = -1$ ,  $\Omega_v = 0.68$ ,  $h = 0.67$ ), or roughly  $10^{-123} M_{\text{p}}^4$ , and such an unnaturally small number is hard to understand. Various quantum effects (most simply, zero-point energy) should make contributions to the vacuum energy density. These may be truncated by new physics at high energy, but this presumably occurs at  $> 1 \text{ TeV}$  scales, not meV; thus the apparent energy scale of the vacuum is at least  $10^{15}$  times smaller than its natural value. A classic review of this situation is given by Weinberg [52], which lists extreme escape routes – especially the multiverse viewpoint, according to which low values of  $\Lambda$  are rare, but high values suppress the formation of structure and observers. It is certainly impressive that Weinberg used such reasoning to predict the value of  $\Lambda$  before any data strongly indicated a non-zero value.

But it may be that the phenomenon of dark energy is entirely illusory. The necessity for this constituent arises from using the Friedmann equation to describe the evolution of the cosmic expansion; if this equation is incorrect, it would require the replacement of Einstein's relativistic theory of gravity with some new alternative. A frontier of current cosmological research is to distinguish these possibilities [98, 99]. We also note that it has been suggested that dark energy might be an illusion even within general relativity, owing to an incorrect treatment of averaging in an inhomogeneous Universe [100, 101]. Most would argue that a standard Newtonian treatment of such issues should be adequate inside the cosmological horizon, but debate on this issue continues.

Dark Energy can differ from a classical cosmological constant in being a dynamical phenomenon [102, 103], *e.g.*, a rolling scalar field (sometimes dubbed 'quintessence'). Empirically, this means that it is endowed with two thermodynamic properties that astronomers can try to measure: the bulk equation of state, and the sound speed. If the sound speed is close to the speed of light, the effect of this property is confined to very large scales, and mainly manifests itself in the large-angle multipoles of the CMB anisotropies [104]. The equation of state parameter governs the rate of change of the vacuum density:  $d \ln \rho_v / d \ln a = -3(1+w)$ , so it can be accessed via the evolving expansion rate,  $H(a)$ . This can be measured most cleanly by using the inbuilt natural ruler of large-scale structure: the BAO horizon scale [105]:

$$D_{\text{BAO}} \simeq 147 (\Omega_{\text{m}} h^2 / 0.13)^{-0.25} (\Omega_{\text{b}} h^2 / 0.023)^{-0.08} \text{ Mpc}. \quad (22.82)$$

$H(a)$  is measured by radial clustering, since  $dr/dz = c/H$ ; clustering in the plane of the sky measures the integral of this. The expansion rate is also measured by the growth of density fluctuations, where the pressure-free growth equation for the density

perturbation is  $\ddot{\delta} + 2H(a)\dot{\delta} = 4\pi G\rho_0 \delta$ . Thus, both the scale and amplitude of density fluctuations are sensitive to  $w(a)$  – but only weakly. These observables change by only typically 0.2% for a 1% change in  $w$ . Current constraints [24] place a constant  $w$  to within 5–10% of  $-1$ , depending on the data combination chosen. A substantial improvement in this precision will require us to limit systematics in data to a few parts in 1000.

Testing whether theories of gravity require revision can also be done using data on cosmological inhomogeneities. Two separate issues arise, concerning the metric perturbation potentials  $\Psi$  and  $\Phi$ , which affect respectively the time and space parts of the metric. In Einstein gravity, these potentials are both equal to the Newtonian gravitational potential, which satisfies Poisson's equation:  $\nabla^2 \Phi / a^2 = 4\pi G \bar{\rho} \delta$ . Empirically, modifications of gravity require us to explore a change with scale and with time of the 'slip' ( $\Psi/\Phi$ ) and the effective  $G$  on the rhs of the Poisson equation. The former aspect can only be probed via gravitational lensing, whereas the latter can be addressed on 10–100 Mpc scales via the growth of clustering. Various schemes for parameterising modified gravity exist, but a practical approach is to assume that the growth rate can be tied to the density parameter:  $d \ln \delta / d \ln a = \Omega_{\text{m}}^{\gamma}(a)$  [83, 84]. The parameter  $\gamma$  is close to 0.55 for standard relativistic gravity, but can differ by around 0.1 from this value in many non-standard models. Clearly this parameterization is incomplete, since it explicitly rejects the possibility of early dark energy ( $\Omega_{\text{m}}(a) \rightarrow 1$  as  $a \rightarrow 0$ ), but it is a convenient way of capturing the power of various experiments. Current data are consistent with standard  $\Lambda$ CDM [106], and exclude variations in slip or effective  $G$  of larger than a few times 10%.

Current planning envisages a set of satellite probes that, a decade hence, will have pursued these fundamental tests via gravitational lensing measurements over thousands of square degrees,  $> 10^8$  redshifts, and photometry of  $> 1000$  supernovae (Euclid in Europe, WFIRST in the USA) [22, 23]. These experiments will measure both  $w$  and the perturbation growth rate to an accuracy of around 1%. The outcome will be either a validation of the standard relativistic vacuum-dominated Big Bang cosmology at a level of precision far beyond anything attempted to date, or the opening of entirely new directions in cosmological models. For a more complete discussion of dark energy and future probes see the review on Dark Energy – Sec. 28

#### References

- [1] V.M. Slipher, *Pop. Astr.* **23**, 21 (1915).
- [2] K. Lundmark, *Mon. Not. R. Astron. Soc* **84**, 747 (1924).
- [3] E. Hubble and M. L. Humason, *Astrophys. J.* **74**, 43 (1931).
- [4] G. Gamow, *Phys. Rev.* **70**, 572 (1946).
- [5] R. A. Alpher, H. Bethe and G. Gamow, *Phys. Rev.* **73**, 803 (1948).
- [6] R.A. Alpher and R.C. Herman, *Phys. Rev.* **74**, 1737 (1948).
- [7] R.A. Alpher and R.C. Herman, *Phys. Rev.* **75**, 1089 (1949).
- [8] A. A. Penzias and R. W. Wilson, *Astrophys. J.* **142**, 419 (1965).
- [9] P.J.E. Peebles, *Principles of Physical Cosmology*, Princeton University Press (1993).
- [10] G. Börner, *The Early Universe: Facts and Fiction*, Springer-Verlag (1988).
- [11] E.W. Kolb and M.S. Turner, *The Early Universe*, Addison-Wesley (1990).
- [12] J.A. Peacock, *Cosmological Physics*, Cambridge Univ. Press (1999).
- [13] A.R. Liddle and D. Lyth, *Cosmological Inflation and Large-Scale Structure*, Cambridge University Press (2000).
- [14] S. Dodelson, *Modern Cosmology*, Academic Press (2003).
- [15] V. Mukhanov, *Physical Foundations of Cosmology*, Cambridge University Press (2005).
- [16] S. Weinberg, *Cosmology*, Oxford Press (2008).
- [17] E.B. Gliner, *Sov. Phys. JETP* **22**, 378 (1966).

- [18] Ya. B. Zel'dovich, A. Krasinski and Ya. B. Zeldovich, *Sov. Phys. Usp.* **11**, 381 (1968), [*Usp. Fiz. Nauk*95,209(1968)].
- [19] P.M. Garnavich *et al.*, *Astrophys. J.* **507**, 74 (1998).
- [20] S. Perlmutter, M. S. Turner and M. J. White, *Phys. Rev. Lett.* **83**, 670 (1999), [*arXiv:astro-ph/9901052*].
- [21] I. Maor *et al.*, *Phys. Rev.* **D65**, 123003 (2002), [*arXiv:astro-ph/0112526*].
- [22] A. Albrecht *et al.* (2006), [*arXiv:astro-ph/0609591*].
- [23] J. A. Peacock *et al.* (2006), [*arXiv:astro-ph/0610906*].
- [24] N. Aghanim *et al.* (Planck) (2018), [*arXiv:1807.06209*].
- [25] A.G. Riess *et al.*, *Astrophys. J.* **116**, 1009 (1998).
- [26] S. Perlmutter *et al.* (Supernova Cosmology Project), *Astrophys. J.* **517**, 565 (1999), [*arXiv:astro-ph/9812133*].
- [27] A. G. Riess, *Publ. Astron. Soc. Pac.* **112**, 1284 (2000), [*arXiv:astro-ph/0005229*].
- [28] J. L. Tonry *et al.* (Supernova Search Team), *Astrophys. J.* **594**, 1 (2003), [*arXiv:astro-ph/0305008*].
- [29] R. Amanullah *et al.*, *Astrophys. J.* **716**, 712 (2010), [*arXiv:1004.1711*].
- [30] M. Betoul *et al.*, *Astron. & Astrophys.* **568**, A22 (2014).
- [31] A. G. Riess *et al.*, "*Astrophys. J.*" **876**, 85 (2019), [*arXiv:1903.07603*].
- [32] W. L. Freedman *et al.* (2019), [*arXiv:1907.05922*].
- [33] Planck Collab. 2015 Results XIII, *Astron. & Astrophys.* **594**, A13 (2016).
- [34] P. Astier *et al.*, *Astron. & Astrophys.* **447**, 31 (2006).
- [35] J. A. Johnson and M. Bolte, *Astrophys. J.* **554**, 888 (2001), [*arXiv:astro-ph/0103299*].
- [36] R. Cayrel *et al.*, *Nature* **409**, 691 (2001), [*arXiv:astro-ph/0104357*].
- [37] D. A. Vandenberg *et al.*, *Astrophys. J.* **775**, 134 (2013), [*arXiv:1308.2257*].
- [38] S. Borsanyi *et al.*, *Nature* **539**, 7627, 69 (2016), [*arXiv:1606.07494*].
- [39] M. Srednicki, R. Watkins and K. A. Olive, *Nucl. Phys.* **B310**, 693 (1988), [*247(1988)*].
- [40] G. Mangano *et al.*, *Phys. Lett.* **B534**, 8 (2002), [*arXiv:astro-ph/0111408*].
- [41] P. F. de Salas and S. Pastor, *JCAP* **7**, 051 (2016), [*arXiv:1606.06986*].
- [42] A. D. Linde, *Phys. Rev.* **D14**, 3345 (1976).
- [43] A. Linde, *Rept. on Prog. in Phys.* **42**, 389 (1979).
- [44] C.E. Vayonakis, *Surv. High Energy Physics* **5**, 87 (1986).
- [45] S.A. Bonometto and A. Masiero, *Nuovo Cimento* **9N5**, 1 (1986).
- [46] A. Linde, *Particle Physics And Inflationary Cosmology*, Harwood (1990).
- [47] K. A. Olive, *Phys. Rept.* **190**, 307 (1990).
- [48] D. H. Lyth and A. Riotto, *Phys. Rept.* **314**, 1 (1999), [*hep-ph/9807278*].
- [49] A. H. Guth, *Phys. Rev.* **D23**, 347 (1981), [*Adv. Ser. Astrophys. Cosmol.*3,139(1987)].
- [50] A. D. Linde, *Phys. Lett.* **108B**, 389 (1982), [*Adv. Ser. Astrophys. Cosmol.*3,149(1987)].
- [51] A. Albrecht and P. J. Steinhardt, *Phys. Rev. Lett.* **48**, 1220 (1982), [*Adv. Ser. Astrophys. Cosmol.*3,158(1987)].
- [52] S. Weinberg, *Rev. Mod. Phys.* **61**, 1 (1989).
- [53] L. Susskind 247–266 (2003), [*hep-th/0302219*].
- [54] B. Carr, *Universe or multiverse?* C.U.P. (2007).
- [55] A. D. Sakharov, *Pisma Zh. Eksp. Teor. Fiz.* **5**, 32 (1967), [*Usp. Fiz. Nauk*161,no.5,61(1991)].
- [56] S. Weinberg, *Phys. Rev. Lett.* **42**, 850 (1979).
- [57] D. Toussaint *et al.*, *Phys. Rev.* **D19**, 1036 (1979).
- [58] I. Affleck and M. Dine, *Nucl. Phys.* **B249**, 361 (1985).
- [59] V. A. Kuzmin, V. A. Rubakov and M. E. Shaposhnikov, *Phys. Lett.* **155B**, 36 (1985).
- [60] M. Fukugita and T. Yanagida, *Phys. Lett.* **B174**, 45 (1986).
- [61] S. Riemer-Sorensen and S. Jenssen, *Universe* **3**, 44 (2017).
- [62] R. J. Cooke, M. Pettini and C. C. Steidel, *Astrophys. J.* **855**, 2, 102 (2018), [*arXiv:1710.11129*].
- [63] R. H. Cyburt, B. D. Fields and K. A. Olive, *Phys. Lett.* **B567**, 227 (2003), [*arXiv:astro-ph/0302431*].
- [64] R. H. Cyburt, B. D. Fields and K. A. Olive, *JCAP* **0811**, 012 (2008), [*arXiv:0808.2818*].
- [65] K. A. Olive, G. Steigman and T. P. Walker, *Phys. Rept.* **333**, 389 (2000), [*arXiv:astro-ph/9905320*].
- [66] F. Iocco *et al.*, *Phys. Rept.* **472**, 1 (2009), [*arXiv:0809.0631*].
- [67] R. H. Cyburt *et al.*, *Rev. Mod. Phys.* **88**, 015004 (2016), [*arXiv:1505.01076*].
- [68] C. Pitrou *et al.*, *Phys. Rept.* **754**, 1 (2018), [*arXiv:1801.08023*].
- [69] D. J. Fixsen *et al.*, *Astrophys. J.* **473**, 576 (1996), [*arXiv:astro-ph/9605054*].
- [70] J. C. Mather *et al.*, *Astrophys. J.* **512**, 511 (1999), [*arXiv:astro-ph/9810373*].
- [71] S. Cole *et al.* (2dFGRS), *Mon. Not. Roy. Astron. Soc.* **326**, 255 (2001), [*arXiv:astro-ph/0012429*].
- [72] J. Schroeder, A. Mesinger and Z. Haiman, *Mon. Not. R. Astron. Soc.* **428**, 3058 (2012).
- [73] S. D. M. White *et al.*, *Nature* **366**, 429 (1993).
- [74] S. W. Allen, R. W. Schmidt and A. C. Fabian, *Mon. Not. Roy. Astron. Soc.* **334**, L11 (2002), [*arXiv:astro-ph/0205007*].
- [75] S. W. Allen, *Mon. Not. Roy. Astron. Soc.* **296**, 392 (1998), [*arXiv:astro-ph/9710217*].
- [76] G. P. Smith *et al.*, *Mon. Not. Roy. Astron. Soc.* **456**, 1, L74 (2016), [*arXiv:1511.01919*].
- [77] H. Hildebrandt *et al.*, *Mon. Not. Roy. Astron. Soc.* **465**, 1454 (2017), [*arXiv:1606.05338*].
- [78] M. A. Troxel *et al.*, "*Phys. Rev.*" **98**, 4, 043528 (2018), [*arXiv:1708.01538*].
- [79] Planck Collab. 2015 Results XV, *Astron. & Astrophys.* **594**, A15 (2016).
- [80] S. Cole *et al.* (2dFGRS), *Mon. Not. Roy. Astron. Soc.* **362**, 505 (2005), [*arXiv:astro-ph/0501174*].
- [81] W. J. Percival *et al.*, *Astrophys. J.* **657**, 645 (2007), [*arXiv:astro-ph/0608636*].
- [82] L. Anderson *et al.*, *Mon. Not. Roy. Astron. Soc.* **427**, 4, 3435 (2013), [*arXiv:1203.6594*].
- [83] E. Linder, *Phys. Rev.* **D72**, 43529 (2005).
- [84] D. Polarski and R. Gannouji, *Phys. Lett.* **B660**, 439 (2008), [*arXiv:0710.1510*].
- [85] G. Efstathiou and J. R. Bond, *Mon. Not. Roy. Astron. Soc.* **218**, 1, 103 (1986).
- [86] C. Gordon and A. Lewis, *Phys. Rev.* **D67**, 123513 (2003), [*arXiv:astro-ph/0212248*].
- [87] A. Vikhlinin *et al.*, *Astrophys. J.* **692**, 1060 (2009), [*arXiv:0812.2720*].
- [88] A. Dekel and O. Lahav, *Astrophys. J.* **520**, 24 (1999), [*arXiv:astro-ph/9806193*].
- [89] W. J. Percival *et al.*, *Mon. Not. Roy. Astron. Soc.* **381**, 1053 (2007), [*arXiv:0705.3323*].
- [90] W. J. Percival *et al.* (SDSS), *Mon. Not. Roy. Astron. Soc.* **401**, 2148 (2010), [*arXiv:0907.1660*].



- [91] G. Efstathiou and J. R. Bond, *Mon. Not. Roy. Astron. Soc.* **304**, 75 (1999), [arXiv:astro-ph/9807103].
- [92] G. Efstathiou *et al.* (2dFGRS), *Mon. Not. Roy. Astron. Soc.* **330**, L29 (2002), [arXiv:astro-ph/0109152].
- [93] P. A. R. Ade *et al.* (BICEP2, Keck Array), *Phys. Rev. Lett.* **121**, 221301 (2018), [arXiv:1810.05216].
- [94] A. A. Starobinsky, *Phys. Lett.* **B91**, 99 (1980), [771(1980)].
- [95] F. Bezrukov and M. Shaposhnikov, *JHEP* **07**, 089 (2009), [arXiv:0904.1537].
- [96] Planck Collab. 2015 Results XXI, *Astron. & Astrophys.* **594**, A21 (2016).
- [97] Planck Collab. 2015 Results XXII, *Astron. & Astrophys.* **594**, A22 (2016).
- [98] W. Hu and I. Sawicki, *Phys. Rev.* **D76**, 4043 (2007).
- [99] B. Jain and P. Zhang, *Phys. Rev.* **D78**, 3503 (2008).
- [100] D. L. Wiltshire, *Phys. Rev. Lett.* **99**, 251101 (2007), [arXiv:0709.0732].
- [101] T. Buchert, *Gen. Rel. Grav.* **40**, 467 (2008), [arXiv:0707.2153].
- [102] I. Zlatev, L.-M. Wang and P. J. Steinhardt, *Phys. Rev. Lett.* **82**, 896 (1999), [arXiv:astro-ph/9807002].
- [103] C. Armendariz-Picon, V. Mukhanov, and P.J. Steinhardt, *Phys. Rev.* **D63**, 3510 (2001).
- [104] S. DeDeo, R.R. Caldwell, and P.J. Steinhardt, *Phys. Rev.* **D67**, 3509 (2003).
- [105] W. Hu, *ASP Conf. Ser.* **339**, 215 (2005), [arXiv:astro-ph/0407158].
- [106] S. F. Daniel *et al.*, *Phys. Rev.* **D81**, 123508 (2010), [arXiv:1002.1962].

## 23. Inflation

Revised August 2019 by J. Ellis (King's Coll. London; CERN) and D. Wands (Portsmouth U.).

### 23.1 Motivation and Introduction

The standard Big-Bang model of cosmology provides a successful framework in which to understand the thermal history of our Universe and the growth of cosmic structure, but it is essentially incomplete. As described in Sec. 22.2.4, Big-Bang cosmology requires very specific initial conditions. It postulates a uniform cosmological background, described by a spatially-flat, homogeneous and isotropic Robertson-Walker (RW) metric (Eq. (22.1) in “Big Bang Cosmology” review), with scale factor  $R(t)$ . Within this setting, it also requires an initial almost scale-invariant distribution of primordial density perturbations as seen, for example, in the cosmic microwave background (CMB) radiation (described in Chap. 29, “Cosmic Microwave Background” review), on scales far larger than the causal horizon at the time the CMB photons last scattered.

The Hubble expansion rate,  $H \equiv \dot{R}/R$ , in a RW cosmology is given by the Friedmann constraint equation (Eq. (22.8) in “Big Bang Cosmology” review)

$$H^2 = \frac{8\pi\rho}{3M_P^2} + \frac{\Lambda}{3} - \frac{k}{R^2}, \quad (23.1)$$

where  $k/R^2$  is the intrinsic spatial curvature. We use natural units such that the speed of light  $c = 1$  and hence we have the Planck mass  $M_P = G_N^{-1/2} \simeq 10^{19}$  GeV (see “Astrophysical Constants and Parameters”). A cosmological constant,  $\Lambda$ , of the magnitude required to accelerate the Universe today (see Chap. 28, “Dark Energy” review) would have been completely negligible in the early Universe where the energy density  $\rho \gg M_P^2 \Lambda \sim 10^{-12} (\text{eV})^4$ . The standard early Universe cosmology, described in Sec. 22.1.5 in “Big Bang Cosmology” review, is thus dominated by non-relativistic matter ( $p_m \ll \rho_m$ ) or radiation ( $p_r = \rho_r/3$  for an isotropic distribution). This leads to a decelerating expansion with  $\ddot{R} < 0$ .

The hypothesis of inflation [1, 2] postulates a period of accelerated expansion,  $\ddot{R} > 0$ , in the very early Universe, preceding the standard radiation-dominated era, which offers a physical model for the origin of these initial conditions, as reviewed in [3–7]. Such a period of accelerated expansion (i) drives a curved Robertson-Walker spacetime (with spherical or hyperbolic spatial geometry) towards spatial flatness, and (ii) it also expands the causal horizon beyond the present Hubble length, so as to encompass all the scales relevant to describe the large-scale structure observed in our Universe today, via the following two mechanisms.

1. A spatially-flat universe with vanishing spatial curvature,  $k = 0$ , has the dimensionless density parameter  $\Omega_{tot} = 1$ , where we define (Eq. (22.13) in “Big Bang Cosmology” review; see Chap. 25.1, “Cosmological Parameters” review for more complete definitions)

$$\Omega_{tot} \equiv \frac{8\pi\rho_{tot}}{3M_P^2 H^2}, \quad (23.2)$$

with  $\rho_{tot} \equiv \rho + \Lambda M_P^2/8\pi$ . If we re-write the Friedmann constraint (Eq. (23.1)) in terms of  $\Omega_{tot}$  we have

$$1 - \Omega_{tot} = -\frac{k}{R^2}. \quad (23.3)$$

Observations require  $|1 - \Omega_{tot,0}| < 0.005$  today [8], where the subscript 0 denotes the present-day value. Taking the time derivative of Eq. (23.3) we obtain

$$\frac{d}{dt}(1 - \Omega_{tot}) = -2\frac{\ddot{R}}{\dot{R}}(1 - \Omega_{tot}). \quad (23.4)$$

Thus in a decelerating expansion,  $\dot{R} > 0$  and  $\ddot{R} < 0$ , any small initial deviation from spatial flatness grows,  $(d/dt)|1 - \Omega_{tot}| > 0$ . A small value such as  $|1 - \Omega_{tot,0}| < 0.005$  today requires an even smaller value at earlier times, e.g.,  $|1 - \Omega_{tot}| < 10^{-5}$  at

the last scattering of the CMB, which appears unlikely, unless for some reason space is exactly flat. However, an extended period of accelerated expansion in the very early Universe, with  $\dot{R} > 0$  and  $\ddot{R} > 0$  and hence  $(d/dt)|1 - \Omega_{tot}| < 0$ , can drive  $\Omega_{tot}$  sufficiently close to unity, so that  $|1 - \Omega_{tot,0}|$  remains unobservably small today, even after the radiation- and matter-dominated eras, for a wide range of initial values of  $\Omega_{tot}$ .

2. The comoving distance (the present-day proper distance) traversed by light between cosmic time  $t_1$  and  $t_2$  in an expanding universe can be written, (see Eq. (22.32) in “Big Bang Cosmology” review), as

$$D_0(t_1, t_2) = R_0 \int_{t_1}^{t_2} \frac{dt}{R(t)} = R_0 \int_{\ln R_1}^{\ln R_2} \frac{d(\ln R)}{\dot{R}}. \quad (23.5)$$

In standard decelerated (radiation- or matter-dominated) cosmology the integrand,  $1/\dot{R}$ , decreases towards the past, and there is a finite comoving distance traversed by light (a particle horizon) since the Big Bang ( $R_1 \rightarrow 0$ ). For example, the comoving size of the particle horizon at the CMB last-scattering surface ( $R_2 = R_{lss}$ ) corresponds to  $D_0 \sim 100$  Mpc, or approximately  $1^\circ$  on the CMB sky today (see Sec. 22.2.4 in “Big Bang Cosmology” review). However, during a period of inflation,  $1/\dot{R}$  increases towards the past, and hence the integral (Eq. (23.5)) diverges as  $R_1 \rightarrow 0$ , allowing an arbitrarily large causal horizon, dependent only upon the duration of the accelerated expansion. Assuming that the Universe inflates with a finite Hubble rate  $H_*$  at  $t_1 = t_*$ , ending with  $H_{end} < H_*$  at  $t_2 = t_{end}$ , we have

$$D_0(t_*, t_{end}) > \left(\frac{R_0}{R_{end}}\right) H_*^{-1} (e^{N_*} - 1), \quad (23.6)$$

where  $N_* \equiv \ln(R_{end}/R_*)$  describes the duration of inflation, measured in terms of the logarithmic expansion (or “e-folds”) from  $t_1 = t_*$  up to the end of inflation at  $t_2 = t_{end}$ , and  $R_0/R_{end}$  is the subsequent expansion from the end of inflation to the present day. If inflation occurs above the TeV scale, the comoving Hubble scale at the end of inflation,  $(R_0/R_{end})H_{end}^{-1}$ , is less than one astronomical unit ( $\sim 10^{11}$  m), and a causally-connected patch can encompass our entire observable Universe today, which has a size  $D_0 > 30$  Gpc, if there were more than 40 e-folds of inflation ( $N_* > 40$ ). If inflation occurs at the GUT scale ( $10^{15}$  GeV) then we require more than 60 e-folds.

Producing an accelerated expansion in general relativity requires an energy-momentum tensor with negative pressure,  $p < -\rho/3$  (see Eq. (22.9) in “Big Bang Cosmology” review and Chap. 28, “Dark Energy” review), quite different from the hot dense plasma of relativistic particles in the hot Big Bang. However a positive vacuum energy  $V > 0$  does exert a negative pressure,  $p_V = -\rho_V$ . The work done by the cosmological expansion must be negative in this case so that the local vacuum energy density remains constant in an expanding universe,  $\dot{\rho}_V = -3H(\rho_V + p_V) = 0$ . Therefore, a false vacuum state can drive an exponential expansion, corresponding to a de Sitter spacetime with a constant Hubble rate  $H^2 = 8\pi\rho_V/3M_P^2$  on spatially-flat hypersurfaces.

A constant vacuum energy  $V$ , equivalent to a cosmological constant  $\Lambda$  in the Friedmann equation Eq. (23.1), cannot provide a complete description of inflation in the early Universe, since inflation must necessarily have come to an end in order for the standard Big-Bang cosmology to follow. A phase transition to the present true vacuum is required to release the false vacuum energy into the energetic plasma of the hot Big Bang and produce the large total entropy of our observed Universe today. Thus we must necessarily study dynamical models of inflation, where the time-invariance of the false vacuum state is broken by a time-dependent field. A first-order phase transition would produce a very inhomogeneous Universe [9] unless a time-dependent scalar field leads to a rapidly changing percolation rate [10–12]. However,

a second-order phase transition [13, 14], controlled by a slowly-rolling scalar field, can lead to a smooth classical exit from the vacuum-dominated phase.

As a spectacular bonus, quantum fluctuations in that scalar field could provide a source of almost scale-invariant density fluctuations [15, 16], as detected in the CMB (see Chap. 29), which are thought to be the origin of the structures seen in the Universe today.

Accelerated expansion and primordial perturbations can also be produced in some modified gravity theories (e.g., [1, 17]), which introduce additional non-minimally coupled degrees of freedom. Such inflation models can often be conveniently studied by transforming variables to an ‘Einstein frame’ in which Einstein’s equations apply with minimally coupled scalar fields [18–20].

In the following we will review scalar field cosmology in general relativity and the spectra of primordial fluctuations produced during inflation, before studying selected inflation models.

### 23.2 Scalar Field Cosmology

The energy-momentum tensor for a canonical scalar field  $\phi$  with self-interaction potential  $V(\phi)$  is given in Eq. (22.52) in “Big Bang Cosmology” review. In a homogeneous background this corresponds to a perfect fluid with density

$$\rho = \frac{1}{2}\dot{\phi}^2 + V(\phi), \tag{23.7}$$

and isotropic pressure

$$p = \frac{1}{2}\dot{\phi}^2 - V(\phi), \tag{23.8}$$

while the 4-velocity is proportional to the gradient of the field,  $u^\mu \propto \nabla^\mu \phi$ .

A field with vanishing potential energy acts like a stiff fluid with  $p = \rho = \dot{\phi}^2/2$ , whereas if the time-dependence vanishes we have  $p = -\rho = -V$  and the scalar field is uniform in time and space. Thus a classical, potential-dominated scalar-field cosmology, with  $p \simeq -\rho$ , can naturally drive a quasi-de Sitter expansion; the slow time-evolution of the energy density weakly breaks the exact  $O(1, 3)$  symmetry of four-dimensional de Sitter spacetime down to a Robertson-Walker (RW) spacetime, where the scalar field plays the role of the cosmic time coordinate.

In a scalar-field RW cosmology the Friedmann constraint equation (Eq. (23.1)) reduces to

$$H^2 = \frac{8\pi}{3M_P^2} \left( \frac{1}{2}\dot{\phi}^2 + V \right) - \frac{k}{R^2}, \tag{23.9}$$

while energy conservation (Eq. (22.10) in “Big Bang Cosmology” review) for a homogeneous scalar field reduces to the Klein-Gordon equation of motion (Eq. (22.54) in “Big Bang Cosmology” review)

$$\ddot{\phi} = -3H\dot{\phi} - V'(\phi). \tag{23.10}$$

The evolution of the scalar field is thus driven by the potential gradient  $V' = dV/d\phi$ , subject to damping by the Hubble expansion  $3H\dot{\phi}$ .

If we define the Hubble slow-roll parameter

$$\epsilon_H \equiv -\frac{\dot{H}}{H^2}, \tag{23.11}$$

then we see that inflation ( $\dot{R} > 0$  and hence  $\dot{H} > -H^2$ ) requires  $\epsilon_H < 1$ . In this case the spatial curvature decreases relative to the scalar field energy density as the Universe expands. Hence in the following we drop the spatial curvature and consider a spatially-flat RW cosmology, assuming that inflation has lasted sufficiently long that our observable universe is very close to spatially flatness. However, we note that bubble nucleation, leading to a first-order phase transition during inflation, can lead to homogeneous hypersurfaces with a hyperbolic (‘open’) geometry, effectively resetting the spatial curvature inside the bubble [21]. This is the basis of so-called open inflation models [22–24], where inflation inside the bubble has a finite duration, leaving a finite negative spatial curvature.

In a scalar field-dominated cosmology (Eq. (23.11)) gives

$$\epsilon_H = \frac{3\dot{\phi}^2}{2V + \dot{\phi}^2}, \tag{23.12}$$

in which case we see that inflation requires a potential-dominated expansion,  $\dot{\phi}^2 < V$ .

#### 23.2.1 Slow-Roll Inflation

It is commonly assumed that the field acceleration term,  $\ddot{\phi}$ , in (Eq. (23.10)) can be neglected, in which case one can give an approximate solution for the inflationary attractor [25]. This slow-roll approximation reduces the second-order Klein-Gordon equation (Eq. (23.10)) to a first-order system, which is over-damped, with the potential gradient being approximately balanced against to the Hubble damping:

$$3H\dot{\phi} \simeq -V', \tag{23.13}$$

and at the same time that the Hubble expansion (Eq. (23.9)) is dominated by the potential energy

$$H^2 \simeq \frac{8\pi}{3M_P^2} V(\phi), \tag{23.14}$$

corresponding to  $\epsilon_H \ll 1$ .

A necessary condition for the validity of the slow-roll approximation is that the potential slow-roll parameters

$$\epsilon \equiv \frac{M_P^2}{16\pi} \left( \frac{V'}{V} \right)^2, \quad \eta \equiv \frac{M_P^2}{8\pi} \left( \frac{V''}{V} \right), \tag{23.15}$$

are small, i.e.,  $\epsilon \ll 1$  and  $|\eta| \ll 1$ , requiring the potential to be correspondingly flat. If we identify  $V''$  with the effective mass of the field, we see that the slow-roll approximation requires that the mass of the scalar field must be small compared with the Hubble scale. We note that the Hubble slow-roll parameter (Eq. (23.11)) coincides with the potential slow-roll parameter,  $\epsilon_H \simeq \epsilon$ , to leading order in the slow-roll approximation.

The slow-roll approximation allows one to determine the Hubble expansion rate as a function of the scalar field value, and vice versa. In particular, we can express, in terms of the scalar field value during inflation, the total logarithmic expansion, or number of “e-folds”:

$$\begin{aligned} N_* &\equiv \ln \left( \frac{R_{end}}{R_*} \right) \\ &= \int_{t_*}^{t_{end}} H dt \simeq - \int_{\phi_*}^{\phi_{end}} \sqrt{\frac{4\pi}{\epsilon}} \frac{d\phi}{M_P} \text{ for } V' > 0. \end{aligned} \tag{23.16}$$

Given that the slow-roll parameters are approximately constant during slow-roll inflation,  $d\epsilon/dN \simeq 2\epsilon(\eta - 2\epsilon) = \mathcal{O}(\epsilon^2)$ , we have

$$N_* \simeq \frac{4}{\sqrt{\epsilon}} \frac{\Delta\phi}{M_P}. \tag{23.17}$$

Since we require  $N > 40$  to solve the flatness, horizon and entropy problems of the standard Big Bang cosmology, we require either very slow roll,  $\epsilon < 0.01$ , or a large change in the value of the scalar field relative to the Planck scale,  $\Delta\phi > M_P$ .

#### 23.2.2 Reheating

Slow-roll inflation can lead to an exponentially large universe, close to spatial flatness and homogeneity, but the energy density is locked in the potential energy of the scalar field, and needs to be converted to particles and thermalised to recover a hot Big Bang cosmology at the end of inflation [26, 27]. This process is usually referred to as reheating, although there was not necessarily any preceding thermal era. Reheating can occur when the scalar field evolves towards the minimum of its potential, converting the potential energy first to kinetic energy. This can occur either through the breakdown of the slow-roll condition in single-field models, or due to an instability triggered by the inflaton reaching

a critical value, in multi-field models known as hybrid inflation models [28].

Close to a simple minimum, the scalar field potential can be described by a quadratic function,  $V = m^2\phi^2/2$ , where  $m$  is the mass of the field. We can obtain slow-roll inflation in such a potential at large field values,  $\phi \gg M_P$ . However, for  $\phi \ll M_P$  the field approaches an oscillatory solution:

$$\phi(t) \simeq \frac{M_P}{\sqrt{3\pi}} \frac{\sin(mt)}{mt}. \quad (23.18)$$

For  $|\phi| < M_P$  the Hubble rate drops below the inflaton mass,  $H < m$ , and the field oscillates many times over a Hubble time. Averaging over several oscillations,  $\Delta t \gg m^{-1}$ , we find  $\langle \dot{\phi}^2/2 \rangle_{\Delta t} \simeq \langle m^2\phi^2/2 \rangle_{\Delta t}$  and hence

$$\langle \rho \rangle_{\Delta t} \simeq \frac{M_P^2}{6\pi t^2}, \quad \langle p \rangle_{\Delta t} \simeq 0. \quad (23.19)$$

This coherent oscillating field corresponds to a condensate of non-relativistic massive inflaton particles, driving a matter-dominated era at the end of inflation, with scale factor  $R \propto t^{2/3}$ .

The inflaton condensate can lose energy through perturbative decays due to terms in the interaction Lagrangian, such as

$$\mathcal{L}_{int} \subset -\lambda_i \sigma \phi \chi_i^2 - \lambda_j \phi \bar{\psi}_j \psi_j \quad (23.20)$$

that couple the inflation to scalar fields  $\chi_i$  or fermions  $\psi_j$ , where  $\sigma$  has dimensions of mass and the  $\lambda_i$  are dimensionless couplings. When the mass of the inflaton is much larger than the decay products, the decay rate is given by [29]

$$\Gamma_i = \frac{\lambda_i^2 \sigma^2}{8\pi m}, \quad \Gamma_j = \frac{\lambda_j^2 m}{8\pi}. \quad (23.21)$$

These decay products must in turn thermalise with Standard Model particles before we recover conventional hot Big Bang cosmology. An upper limit on the reheating temperature after inflation is given by [27]

$$T_{rh} = 0.2 \left( \frac{100}{g_*} \right)^{1/4} \sqrt{M_P \Gamma_{tot}}, \quad (23.22)$$

where  $g_*$  is the effective number of degrees of freedom and  $\Gamma_{tot}$  is the total decay rate for the inflaton, which is required to be less than  $m$  for perturbative decay.

The baryon asymmetry of the Universe must be generated after the main release of entropy during inflation, which is an important constraint on possible models. Also, the fact that the inflaton mass is much larger than the mass scale of the Standard Model opens up the possibility that it may decay into massive stable or metastable particles that could be connected with dark matter, constraining possible models. For example, in the context of supergravity models the reheat temperature is constrained by the requirement that gravitinos are not overproduced, potentially destroying the successes of Big Bang nucleosynthesis. For a range of gravitino masses one must require  $T_{rh} < 10^9$  GeV [30, 31].

The process of inflaton decay and reheating can be significantly altered by interactions leading to space-time dependences in the effective masses of the fields. In particular, parametric resonance can lead to explosive, non-perturbative decay of the inflaton in some cases, a process often referred to as preheating [26, 32]. For example, an interaction term of the form

$$\mathcal{L}_{int} \subset -\lambda^2 \phi^2 \chi^2, \quad (23.23)$$

leads to a time-dependent effective mass for the  $\chi$  field as the inflaton  $\phi$  oscillates. This can lead to non-adiabatic particle production if the bare mass of the  $\chi$  field is small for large couplings or for rapid changes of the inflaton field. The process of preheating is highly model-dependent, but it highlights the possible role of non-thermal particle production after and even during inflation.

## 23.3 Primordial Perturbations from Inflation

Although inflation was originally discussed as a solution to the problem of initial conditions required for homogeneous and isotropic hot Big Bang cosmology, it was soon realised that inflation also offered a mechanism to generate the inhomogeneous initial conditions required for the formation of large-scale structure [15–17, 33].

### 23.3.1 Metric Perturbations

In a homogeneous classical inflationary cosmology driven by a scalar field, the inflaton field is uniform on constant-time hypersurfaces,  $\phi = \phi_0(t)$ . However, quantum fluctuations inevitably break the spatial symmetry leading to an inhomogeneous field:

$$\phi(t, x^i) = \phi_0(t) + \delta\phi(t, x^i). \quad (23.24)$$

At the same time, one should consider inhomogeneous perturbations of the RW spacetime metric (see, e.g., [34–36]):

$$ds^2 = (1 + 2A)dt^2 - 2RB_i dt dx^i - R^2 [(1 + 2C)\delta_{ij} + \partial_i \partial_j E + h_{ij}] dx^i dx^j, \quad (23.25)$$

where  $A$ ,  $B$ ,  $E$  and  $C$  are scalar perturbations while  $h_{ij}$  represents transverse and tracefree, tensor metric perturbations. Vector metric perturbations can be eliminated using Einstein constraint equations in a scalar field cosmology.

The tensor perturbations remain invariant under a temporal gauge transformation  $t \rightarrow t + \delta t(t, x^i)$ , but both the scalar field and the scalar metric perturbations transform. For example, we have

$$\delta\phi \rightarrow \delta\phi - \dot{\phi}_0 \delta t, \quad C \rightarrow C - H \delta t. \quad (23.26)$$

However, there are gauge invariant combinations, such as [37]

$$Q = \delta\phi - \frac{\dot{\phi}_0}{H} C, \quad (23.27)$$

which describes the scalar field perturbations on spatially-flat ( $C = 0$ ) hypersurfaces. This is simply related to the curvature perturbation on uniform-field ( $\delta\phi = 0$ ) hypersurfaces:

$$\mathcal{R} = C - \frac{H}{\dot{\phi}_0} \delta\phi = -\frac{H}{\dot{\phi}_0} Q, \quad (23.28)$$

which coincides in slow-roll inflation,  $\rho \simeq \rho(\phi)$ , with the curvature perturbation on uniform-density hypersurfaces [16]

$$\zeta = C - \frac{H}{\dot{\rho}_0} \delta\rho. \quad (23.29)$$

Thus scalar field and scalar metric perturbations are coupled by the evolution of the inflaton field.

### 23.3.2 Gravitational waves from inflation

The tensor metric perturbation,  $h_{ij}$  in Eq. (23.25), is gauge-invariant and decoupled from the scalar perturbations at first order. This represents the free excitations of the spacetime, i.e., gravitational waves, which are the simplest metric perturbations to study at linear order.

Each tensor mode, with wavevector  $\vec{k}$ , has two linearly-independent transverse and trace-free polarization states:

$$h_{ij}(\vec{k}) = h_{\vec{k}} q_{ij} + \bar{h}_{\vec{k}} \bar{q}_{ij}. \quad (23.30)$$

The linearised Einstein equations then yield the same evolution equation for the amplitude as that for a massless field in RW spacetime:

$$\ddot{h}_{\vec{k}} + 3H\dot{h}_{\vec{k}} + \frac{k^2}{R^2} h_{\vec{k}} = 0, \quad (23.31)$$

(and similarly for  $\bar{h}_{\vec{k}}$ ). This can be re-written in terms of the conformal time,  $\eta = \int dt/R$ , and the conformally rescaled field:

$$u_{\vec{k}} = \frac{M_P R h_{\vec{k}}}{\sqrt{32\pi}}. \quad (23.32)$$

This conformal field then obeys the wave equation for a canonical scalar field in Minkowski spacetime with a time-dependent mass:

$$u_{\vec{k}}'' + \left(k^2 - \frac{R''}{R}\right) u_{\vec{k}} = 0. \quad (23.33)$$

During slow-roll

$$\frac{R''}{R} \simeq (2 - \epsilon)R^2 H^2. \quad (23.34)$$

This makes it possible to quantise the linearised metric fluctuations,  $u_{\vec{k}} \rightarrow \hat{u}_{\vec{k}}$ , on sub-Hubble scales,  $k^2/R^2 \gg H^2$ , where the background expansion can be neglected.

Crucially, in an inflationary expansion, where  $\dot{R} > 0$ , the comoving Hubble length  $H^{-1}/R = 1/\dot{R}$  decreases with time. Thus all modes start inside the Hubble horizon and it is possible to take the initial field fluctuations to be in a vacuum state at early times or on small scales:

$$\langle u_{\vec{k}_1} u_{\vec{k}_2} \rangle = \frac{i}{2} (2\pi)^3 \delta^{(3)}(\vec{k}_1 + \vec{k}_2). \quad (23.35)$$

In terms of the amplitude of the tensor metric perturbations, this corresponds to

$$\langle h_{\vec{k}_1} h_{\vec{k}_2} \rangle = \frac{1}{2} \frac{\mathcal{P}_t(k_1)}{4\pi k_1^3} (2\pi)^3 \delta^{(3)}(\vec{k}_1 + \vec{k}_2), \quad (23.36)$$

where the factor 1/2 appears due to the two polarization states that contribute to the total tensor power spectrum:

$$\mathcal{P}_t(k) = \frac{64\pi}{M_P^2} \left(\frac{k}{2\pi R}\right)^2. \quad (23.37)$$

On super-Hubble scales,  $k^2/R^2 \ll H^2$ , we have the growing mode solution to Eq. (23.33),  $u_{\vec{k}} \propto R$ , corresponding to  $h_{\vec{k}} \rightarrow$  constant, i.e., tensor modes are frozen-in on super-Hubble scales, both during and after inflation. Thus, connecting the initial vacuum fluctuations on sub-Hubble scales to the late-time power spectrum for tensor modes at Hubble exit during inflation,  $k = R_* H_*$ , we obtain

$$\mathcal{P}_t(k) \simeq \frac{64\pi}{M_P^2} \left(\frac{H_*}{2\pi}\right)^2. \quad (23.38)$$

In the de Sitter limit,  $\epsilon \rightarrow 0$ , the Hubble rate becomes time-independent and the tensor spectrum on super-Hubble scales becomes scale-invariant [39]. However slow-roll evolution leads to weak time dependence of  $H_*$  and thus a scale-dependent spectrum on large scales, with a spectral tilt

$$n_t \equiv \frac{d \ln \mathcal{P}_T}{d \ln k} \simeq -2\epsilon_*. \quad (23.39)$$

### 23.3.3 Density Perturbations from single-field inflation

The inflaton field fluctuations on spatially-flat hypersurfaces are coupled to scalar metric perturbations at first order, but these can be eliminated using the Einstein constraint equations to yield an evolution equation

$$\ddot{Q}_{\vec{k}} + 3H\dot{Q}_{\vec{k}} + \left[\frac{k^2}{R^2} + V'' - \frac{8\pi}{M_P^2 R^3} \frac{d}{dt} \left(\frac{R^3 \dot{\phi}^2}{H}\right)\right] Q_{\vec{k}} = 0. \quad (23.40)$$

Terms proportional to  $M_P^{-2}$  represent the effect on the field fluctuations of gravity at first order. As can be seen, this vanishes in the limit of a constant background field, and hence is suppressed in the slow-roll limit, but it is of the same order as the effective mass,  $V'' = 3\eta H^2$ , so must be included if we wish to model deviations from exact de Sitter symmetry.

This wave equation can also be written in the canonical form for a free field in Minkowski spacetime if we define [37]

$$v_{\vec{k}} \equiv RQ_{\vec{k}}, \quad (23.41)$$

to yield

$$v_{\vec{k}}'' + \left(k^2 - \frac{z''}{z}\right) v_{\vec{k}} = 0, \quad (23.42)$$

where we define

$$z \equiv \frac{R\dot{\phi}}{H}, \quad \frac{z''}{z} \simeq (2 + 5\epsilon - 3\eta)R^2 H^2, \quad (23.43)$$

where the last approximate equality holds to leading order in the slow-roll approximation.

As previously done for gravitational waves, we quantise the linearised field fluctuations  $v_{\vec{k}} \rightarrow \hat{v}_{\vec{k}}$  on sub-Hubble scales,  $k^2/R^2 \gg H^2$ , where the background expansion can be neglected. Thus we impose

$$\langle v_{\vec{k}_1} v_{\vec{k}_2}' \rangle = \frac{i}{2} \delta^{(3)}(\vec{k}_1 + \vec{k}_2). \quad (23.44)$$

In terms of the field perturbations, this corresponds to

$$\langle Q_{\vec{k}_1} Q_{\vec{k}_2} \rangle = \frac{\mathcal{P}_Q(k_1)}{4\pi k_1^3} (2\pi)^3 \delta^{(3)}(\vec{k}_1 + \vec{k}_2), \quad (23.45)$$

where the power spectrum for vacuum field fluctuations on sub-Hubble scales,  $k^2/R^2 \gg H^2$ , is simply

$$\mathcal{P}_Q(k) = \left(\frac{k}{2\pi R}\right)^2, \quad (23.46)$$

yielding the classic result for the vacuum fluctuations for a massless field in de Sitter at Hubble exit,  $k = R_* H_*$ :

$$\mathcal{P}_Q(k) \simeq \left(\frac{H}{2\pi}\right)_*^2. \quad (23.47)$$

In practice there are slow-roll corrections due to the small but finite mass ( $\eta$ ) and field evolution ( $\epsilon$ ) [40].

Slow-roll corrections to the field fluctuations are small on sub-Hubble scales, but can become significant as the field and its perturbations evolve over time on super-Hubble scales. Thus it is helpful to work instead with the curvature perturbation,  $\zeta$  defined in equation (Eq. (23.29)), which remains constant on super-Hubble scales for adiabatic density perturbations both during and after inflation [16,41]. Thus we have an expression for the primordial curvature perturbation on super-Hubble scales produced by single-field inflation:

$$\mathcal{P}_\zeta(k) = \left[ \left(\frac{H}{\dot{\phi}}\right)^2 \mathcal{P}_Q(k) \right]_* \simeq \frac{4\pi}{M_P^2} \left[ \frac{1}{\epsilon} \left(\frac{H}{2\pi}\right)^2 \right]_*. \quad (23.48)$$

Comparing this with the primordial gravitational wave power spectrum (Eq. (23.38)) we obtain the tensor-to-scalar ratio for single-field slow-roll inflation

$$r \equiv \frac{\mathcal{P}_t}{\mathcal{P}_\zeta} \simeq 16\epsilon_*. \quad (23.49)$$

Note that the scalar amplitude is boosted by a factor  $1/\epsilon_*$  during slow-roll inflation, because small scalar field fluctuations can lead to relatively large curvature perturbations on hypersurfaces defined with respect to the density if the potential energy is only weakly dependent on the scalar field, as in slow-roll. Indeed, the de Sitter limit is singular, since the potential energy becomes independent of the scalar field at first order,  $\epsilon \rightarrow 0$ , and the curvature perturbation on uniform-density hypersurfaces becomes ill-defined.

We note that in single-field inflation the tensor-to-scalar ratio and the tensor tilt (Eq. (23.39)) at the same scale are both determined by the first slow-roll parameter at Hubble exit,  $\epsilon_*$ , giving rise to an important consistency test for single-field inflation:

$$n_t = -\frac{r}{8}. \quad (23.50)$$

This may be hard to verify if  $r$  is small, making any tensor tilt  $n_t$  difficult to measure. On the other hand, it does offer a way to rule out single-field slow-roll inflation if either  $r$  or  $n_t$  is large.

Given the relatively large scalar power spectrum, it has proved easier to measure the scalar tilt, conventionally defined as  $n_s - 1$ .

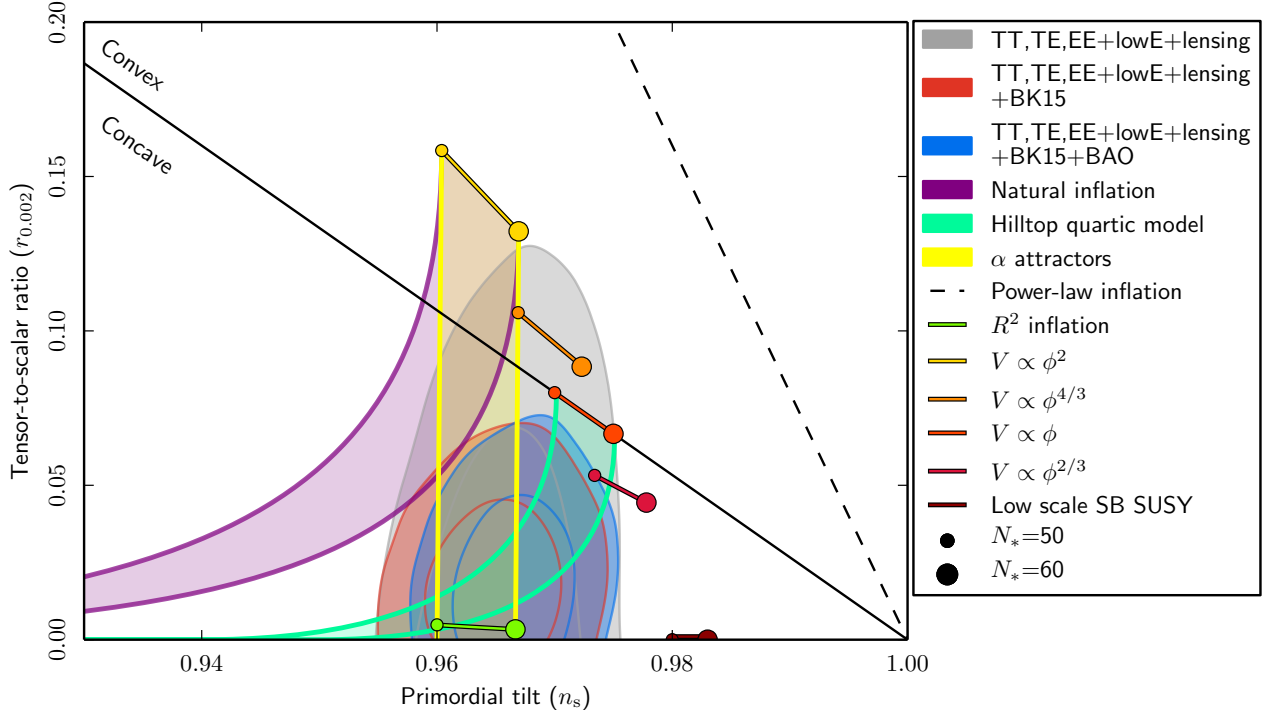


Figure 23.1: The marginalized joint 68 and 95% CL regions for the tilt in the scalar perturbation spectrum,  $n_s$ , and the relative magnitude of the tensor perturbations,  $r$ , obtained from the *Planck* 2018 and lensing data alone, and their combinations with BICEP2/Keck Array (BK15) and (optionally) BAO data, confronted with the predictions of some of the inflationary models discussed in this review. This figure is taken from [38].

Slow-roll corrections lead to slow time-dependence of both  $H_*$  and  $\epsilon_*$ , giving a weak scale-dependence of the scalar power spectrum:

$$n_s - 1 \equiv \frac{d \ln \mathcal{P}_\zeta}{d \ln k} \simeq -6\epsilon_* + 2\eta_*, \quad (23.51)$$

and a running of this tilt at second-order in slow-roll:

$$\frac{dn_s}{d \ln k} \simeq -8\epsilon_*(3\epsilon_* - 2\eta_*) - 2\xi_*^2, \quad (23.52)$$

where the running introduces a new slow-roll parameter at second-order:

$$\xi^2 = \frac{M_P^4}{64\pi^2} \frac{V'V'''}{V^2}. \quad (23.53)$$

### 23.3.4 Observational Bounds

The observed scale-dependence of the power spectrum makes it necessary to specify the comoving scale,  $k$ , at which quantities are constrained and hence the Hubble-exit time,  $k = a_* H_*$ , when the corresponding theoretical quantities are calculated during inflation. This is usually expressed in terms of the number of e-folds from the end of inflation [42]:

$$N_*(k) \simeq 67 - \ln \left( \frac{k}{a_0 H_0} \right) + \frac{1}{4} \ln \left( \frac{V_*^2}{M_P^4 \rho_{end}} \right) + \frac{1}{12} \ln \left( \frac{\rho_{rh}}{\rho_{end}} \right) - \frac{1}{12} \ln(g_*), \quad (23.54)$$

where  $H_0^{-1}/a_0$  is the present comoving Hubble length. Different models of reheating and and thus different reheat temperatures and densities,  $\rho_{rh}$  in Eq. (23.54), lead to a range of possible values for  $N_*$  corresponding to a fixed physical scale, and hence we have a range of observational predictions for a given inflation model, as seen in Fig. 23.1.

The *Planck* 2018 temperature and polarization data (see Chap. 29, ‘‘Cosmic Microwave Background’’ review) are consistent with a smooth featureless power spectrum over a range of comoving

wavenumbers,  $0.008 h^{-1} \text{ Mpc}^{-1} \leq k \leq 0.1 h \text{ Mpc}^{-1}$ . In the absence of running, the data measure the spectral index to be [38]

$$n_s = 0.9649 \pm 0.0042, \quad (23.55)$$

corresponding to a deviation from scale-invariance exceeding the  $7\sigma$  level. If running of the spectral tilt is included in the model, this is constrained to be [38]

$$\frac{dn_s}{d \ln k} = -0.0045 \pm 0.0067 \quad (23.56)$$

at the 95% CL, assuming no running of the running. A combined analysis of the *Planck* 2018 and BICEP2/Keck Array 2015 data [43] places an upper bound on the tensor-to-scalar ratio at  $k = 0.002 \text{ Mpc}^{-1}$  [38]

$$r < 0.06 \quad (23.57)$$

at the 95% CL.

These observational bounds can be converted into bounds on the slow-roll parameters and hence the potential during slow-roll inflation. Setting higher-order slow-roll parameters (beyond second-order in horizon-flow parameters [44]) to zero, the *Planck* collaboration obtain the following 95% CL bounds when lensing and BK15 data are included [38]

$$\epsilon < 0.0044, \quad (23.58)$$

$$\eta = -0.015 \pm 0.006, \quad (23.59)$$

$$\xi^2 = 0.0029_{-0.0069}^{+0.0073}, \quad (23.60)$$

which can be used to constrain models, as discussed in the next Section.

Fig. 23.1, which is taken from [38], compares observational CMB constraints on the tilt,  $n_s$ , in the spectrum of scalar perturbations and the ratio,  $r$ , between the magnitudes of tensor and scalar perturbations. Important rôles are played by data from the *Planck* satellite and on lensing, the BICEP2/Keck Array (BK15) and measurements of baryon acoustic oscillations (BAO). The reader is referred to [38] for technical details. These experimental constraints are compared with the predictions of some

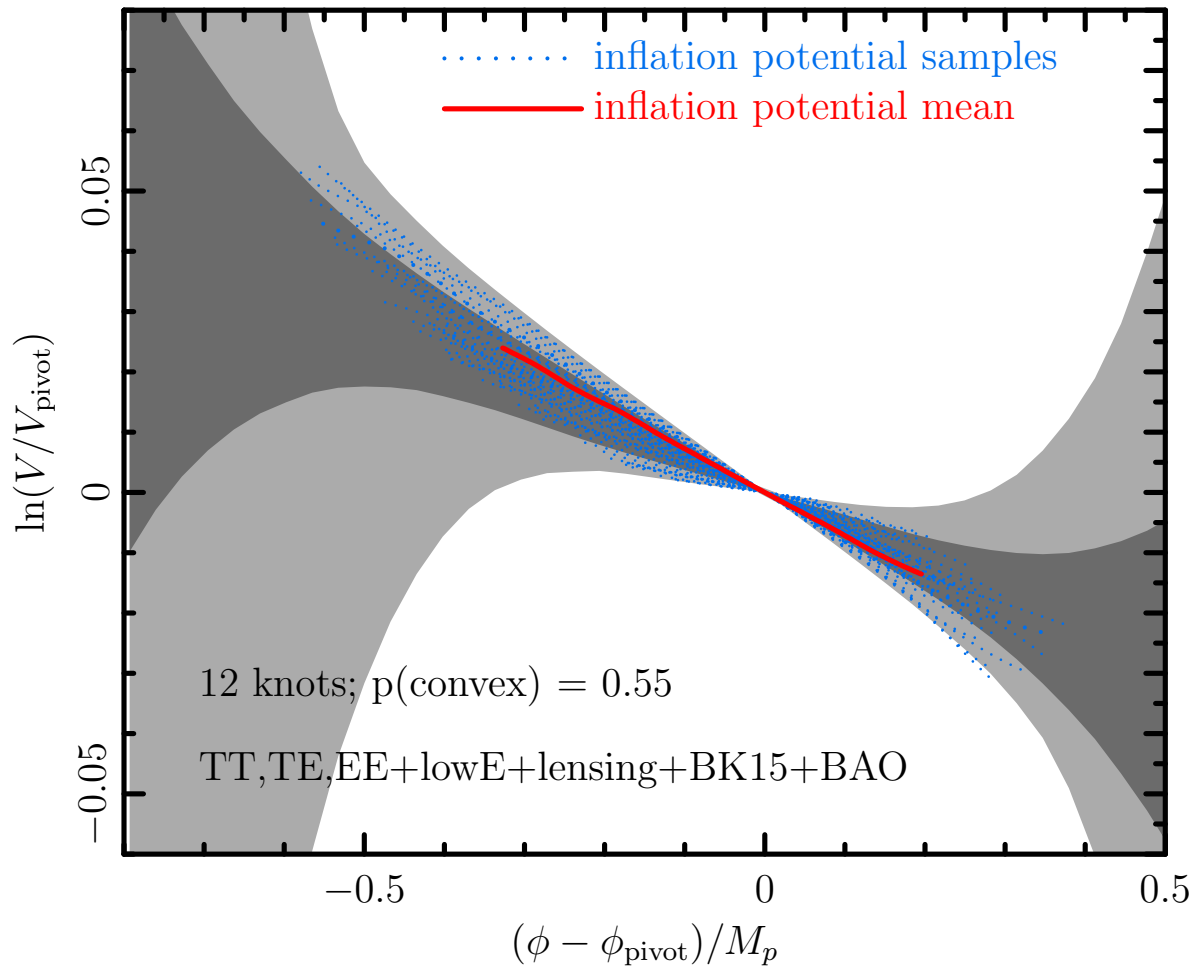


Figure 23.2: The result of reconstructing a single-field inflaton potential using a cubic-spline power-spectrum mode expansion and the the full *Planck*, lensing, BK15 and BAO data set. This figure is taken from [38].

of the inflationary models discussed in this review. Generally speaking, models with a concave potential are favored over those with a convex potential, and models with power-law inflation are now excluded, as opposed to models with de Sitter-like (quasi-)exponential expansion.

There is no significant evidence for local features within the range of inflaton field values probed by the data [38]. However, the data may be used to reconstruct partially the effective inflationary potential over a range of inflaton field values, assuming that it is suitably smooth. The result of one such exercise by the *Planck* collaboration [38] in the framework of a generic single-field inflaton potential is shown in Fig. 23.2. This reconstruction assumes a cubic-spline power-spectrum mode expansion and employs the full *Planck*, lensing, BK15 and BAO data set. The reader is again referred to [38] for technical details. We see that the effective inflaton potential is relatively well reconstructed over field values  $\phi$  within  $\pm 0.5$  of the chosen pivot value, but the potential is only very weakly constrained for larger values of  $|\phi - \phi_{pivot}|$ , providing wide scope for inflationary model-builders.

## 23.4 Models

### 23.4.1 Pioneering Models

The paradigm of the inflationary Universe was proposed in [2], where it was pointed out that an early period of (near-)exponential expansion, in addition to resolving the horizon and flatness problems of conventional Big-Bang cosmology as discussed above (the possibility of a de Sitter phase in the early history of the Universe was also proposed in the non-minimal gravity model of [1], with the motivation of avoiding an initial singularity), would also dilute the prior abundance of any unseen heavy, (meta-)stable particles, as exemplified by monopoles

in grand unified theories (GUTs; see Chap. 94, “Grand Unified Theories” review). The original proposal was that this inflationary expansion took place while the Universe was in a metastable state (a similar suggestion was made in [45, 46], where in [45] it was also pointed out that such a mechanism could address the horizon problem) and was terminated by a first-order transition due to tunnelling through a potential barrier. However, it was recognized already in [2] that this ‘old inflation’ scenario would need modification if the transition to the post-inflationary universe were to be completed smoothly without generating unacceptable inhomogeneities.

This ‘graceful exit’ problem was addressed in the ‘new inflation’ model of [13] (see also [14] and footnote [39] of [2]), which studied models based on an SU(5) GUT with an effective potential of the Coleman-Weinberg type (i.e., dominated by radiative corrections), in which inflation could occur during the roll-down from the local maximum of the potential towards a global minimum. However, it was realized that the Universe would evolve to a different minimum from the Standard Model [47], and it was also recognized that density fluctuations would necessarily be too large [15], since they were related to the GUT coupling strength.

These early models of inflation assumed initial conditions enforced by thermal equilibrium in the early Universe. However, this assumption was questionable: indeed, it was not made in the model of [1], in which a higher-order gravitational curvature term was assumed to arise from quantum corrections, and the assumption of initial thermal equilibrium was jettisoned in the ‘chaotic’ inflationary model of [48]. These are the inspirations for much recent inflationary model building, so we now discuss them in more detail, before reviewing contemporary models.

In this section we will work in natural units where we set the reduced Planck mass to unity, i.e.,  $8\pi/M_P^2 = 1$ . All masses are thus relative to the reduced Planck scale.

### 23.4.2 $R^2$ Inflation

The first-order Einstein-Hilbert action,  $(1/2) \int d^4x \sqrt{-g} R$ , where  $R$  is the Ricci scalar curvature, is the minimal possible theory consistent with general coordinate invariance. However, it is possible that there might be non-minimal corrections to this action, and the unique second-order possibility is

$$S = \frac{1}{2} \int d^4x \sqrt{-g} \left( R + \frac{R^2}{6M^2} \right). \quad (23.61)$$

It was pointed out in [1] that an  $R^2$  term could be generated by quantum effects, and that (Eq. (23.61)) could lead to de Sitter-like expansion of the Universe. Scalar density perturbations in this model were calculated in [17]. Because the initial phase was (almost) de Sitter, these perturbations were (approximately) scale-invariant, with magnitude  $\propto M$ . It was pointed out in [17] that requiring the scalar density perturbations to lie in the range  $10^{-3}$  to  $10^{-5}$ , consistent with upper limits at that time, would require  $M \sim 10^{-3}$  to  $10^{-5}$  in Planck units, and it was further suggested that these perturbations could lead to the observed large-scale structure of the Universe, including the formation of galaxies.

Although the action (Eq. (23.61)) does not contain an explicit scalar field, [17] reduced the calculation of density perturbations to that of fluctuations in the scalar curvature  $R$ , which could be identified (up to a factor) with a scalar field of mass  $M$ . The formal equivalence of  $R^2$  gravity (Eq. (23.61)) to a theory of gravity with a massive scalar  $\phi$  had been shown in [18], see also [19]. The effective scalar potential for what we would nowadays call the ‘inflaton’ [49] takes the form

$$S = \frac{1}{2} \int d^4x \sqrt{-g} \left[ R + (\partial_\mu \phi)^2 - \frac{3}{2} M^2 (1 - e^{-\sqrt{2/3} \phi})^2 \right] \quad (23.62)$$

when the action is written in the Einstein frame, and the potential is shown as the solid black line in Fig. 23.3. Using (Eq. (23.48)), one finds that the amplitude of the scalar density perturbations in this model is given by

$$\Delta_{\mathcal{R}} = \frac{3M^2}{8\pi^2} \sinh^4 \left( \frac{\phi}{\sqrt{6}} \right), \quad (23.63)$$

The measured magnitude of the density fluctuations in the CMB requires  $M \simeq 1.3 \times 10^{-5}$  in Planck units (assuming  $N_* \simeq 55$ ), so one of the open questions in this model is why  $M$  is so small. Obtaining  $N_* \simeq 55$  also requires an initial value of  $\phi \simeq 5.5$ , i.e., a super-Planckian initial condition, and another issue for this and many other models is how the form of the effective potential is protected and remains valid at such large field values. Using Eq. (23.51) one finds that  $n_s \simeq 0.965$  for  $N_* \simeq 55$  and using (Eq. (23.49)) one finds that  $r \simeq 0.0035$ . These predictions are consistent with the present data from *Planck* and other experiments, as seen in Fig. 23.1.

### 23.4.3 Chaotic Models with Power-Law Potentials

As has already been mentioned, a key innovation in inflationary model-building was the suggestion to abandon the questionable assumption of a thermal initial state, and consider ‘chaotic’ initial conditions with very general forms of potential [48]. (Indeed, the  $R^2$  model discussed above can be regarded as a prototype of this approach.) The chaotic approach was first proposed in the context of a simple power-law potential of the form  $\mu^{4-\alpha} \phi^\alpha$ , and the specific example of  $\lambda \phi^4$  was studied in [48]. Such models make the following predictions for the slow-roll parameters  $\epsilon$  and  $\eta$ :

$$\epsilon = \frac{1}{2} \left( \frac{\alpha}{\phi} \right)^2, \quad \eta = \frac{\alpha(\alpha-1)}{\phi^2}, \quad (23.64)$$

leading to the predictions

$$r \approx \frac{4\alpha}{N_*}, \quad n_s - 1 \approx -\frac{\alpha+2}{2N_*}, \quad (23.65)$$

which are shown in Fig. 23.1 for some illustrative values of  $\alpha$ . We note that the prediction of the original  $\phi^4$  model lies out of the frame, with values of  $r$  that are too large and values of  $n_s$  that are too small. The  $\phi^3$  model has similar problems, and would in any case require modification in order to have a well-defined minimum. The simplest possibility is  $\phi^2$ , but this is now also disfavored by the data, at the 95% CL if only the *Planck* data are considered, and more strongly if other data are included, as seen in Fig. 23.1. (For non-minimal models of quadratic inflation that avoid this problem, see, e.g., [51].)

Indeed, as can be seen in Fig. 23.1, all single-field models with a convex potential (i.e., one curving upwards) are disfavored compared to models with a concave potential.

### 23.4.4 Hilltop Models

This preference for a concave potential motivates interest in ‘hilltop’ models [52], whose starting-point is a potential of the form

$$V(\phi) = \Lambda^4 \left[ 1 - \left( \frac{\phi}{\mu} \right)^p + \dots \right], \quad (23.66)$$

where the  $\dots$  represent extra terms that yield a positive semi-definite potential. To first order in the slow-roll parameters, when  $x \equiv \phi/\mu$  is small, one has

$$n_s \simeq 1 - p(p-1)\mu^{-2} \frac{x^{p-2}}{(1-x^p)} - \frac{3}{8}r, \quad r \simeq 8p^2\mu^{-2} \frac{x^{2p-2}}{(1-x^p)^2}. \quad (23.67)$$

As seen in Fig. 23.1, a hilltop model with  $p = 4$  can be compatible with the *Planck* and other measurements, if  $\mu \gg M_P$ .

### 23.4.5 D-Brane Inflation

Many scenarios for inflation involving extra dimensions have been proposed, e.g., the possibility that observable physics resides on a three-dimensional brane, and that there is an inflationary potential that depends on the distance between our brane and an antibrane, with a potential of the form [53]

$$V(\phi) = \Lambda^4 \left[ 1 - \left( \frac{\mu}{\phi} \right)^p + \dots \right]. \quad (23.68)$$

In this scenario the effective potential vanishes in the limit  $\phi \rightarrow \infty$ , corresponding to complete separation between our brane and the antibrane. The predictions for  $n_s$  and  $r$  in this model can be obtained from (Eq. 23.67) by exchanging  $p \leftrightarrow -p$ , and are also consistent with the *Planck* and other data.

### 23.4.6 Natural Inflation

Also seen in Fig. 23.1 are the predictions of ‘natural inflation’ [54], in which one postulates a non-perturbative shift symmetry that suppresses quantum corrections, so that a hierarchically small scale of inflation,  $H \ll M_P$ , is technically natural. In the simplest models, there is a periodic potential of the form

$$V(\phi) = \Lambda^4 \left[ 1 + \cos \left( \frac{\phi}{f} \right) \right], \quad (23.69)$$

where  $f$  is a dimensional parameter reminiscent of an axion decay constant (see the next subsection) [55], which must have a value  $> M_P$ . Natural inflation can yield predictions similar to quadratic inflation (which are no longer favored, as already discussed), but can also yield an effective convex potential. Thus, it may lead to values of  $r$  that are acceptably small, but for values of  $n_s$  that are in tension with the data, as seen in Fig. 23.1.

### 23.4.7 Axion Monodromy Models

The effective potentials in stringy models [56,57] motivated by axion monodromy may be of the form

$$V(\phi) = \mu^{4-\alpha} \phi^\alpha + \Lambda^4 e^{-C \left( \frac{\phi}{\phi_0} \right)^{p_\Lambda}} \cos \left[ \gamma + \frac{\phi}{f} \left( \frac{\phi}{\phi_0} \right)^{p_f+1} \right], \quad (23.70)$$

where  $\mu, \Lambda, f$  and  $\phi_0$  are parameters with the dimension of mass, and  $C, p, p_\Lambda, p_f$  and  $\gamma$  are dimensionless constants, generalizing the potential ([54]) in the simplest models of natural inflation. The oscillations in (Eq. 23.70) are associated with the axion field, and powers  $p_\Lambda, p_f \neq 0$  may arise from  $\phi$ -dependent evolutions of



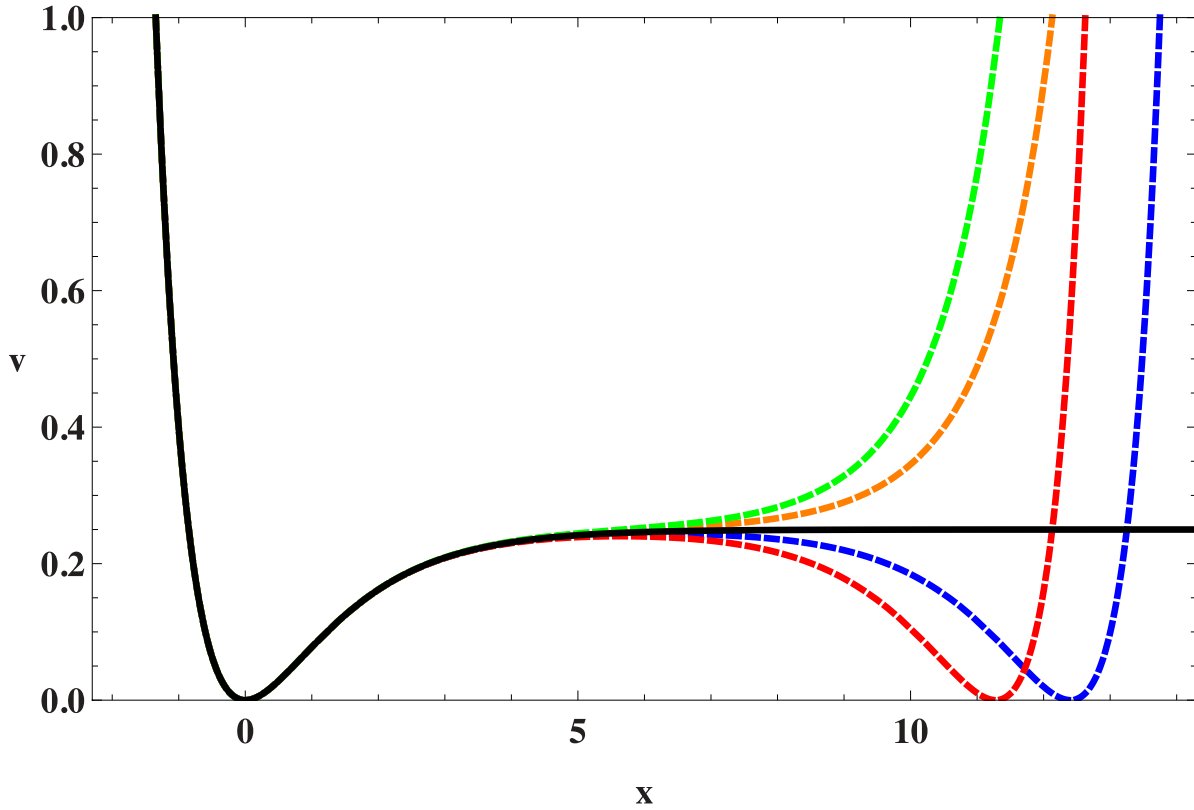


Figure 23.3: The inflationary potential  $V$  in the  $R^2$  model (solid black line) compared with its form in various no-scale models discussed in detail in [50] (dashed coloured lines).

string moduli. Since the exponential prefactor in (Eq. 23.70) is due to non-perturbative effects that may be strongly suppressed, the oscillations may be unobservably small. Specific string models having  $\phi^\alpha$  with  $\alpha = 4/3, 1$  or  $2/3$  have been constructed in [56,57], providing some motivation for the low-power models mentioned above.

As seen in Fig. 23.1, the simple axion monodromy models with the power  $\alpha = 4/3$  or  $1$  are no longer compatible with the current CMB data at the 95% CL, while  $\alpha = 2/3$  is only marginally compatible at 95% CL. The *Planck* Collaboration has also searched for characteristic effects associated with the second term in (Eq. (23.70)), such as a possible drift in the modulation amplitude (setting  $p_A = C = 0$ ), and a possible drifting frequency generated by  $p_f \neq 0$ , without finding any compelling evidence [38].

### 23.4.8 Higgs Inflation

Since the energy scale during inflation is commonly expected to lie between the Planck and TeV scales, it may serve as a useful bridge with contacts both to string theory or some other quantum theory of gravity, on the one side, and particle physics on the other side. However, as the above discussion shows, much of the activity in building models of inflation has been largely independent of specific connections with these subjects, though some examples of string-motivated models of inflation were mentioned above.

The most economical scenario for inflation might be to use as inflaton the only established scalar field, namely the Higgs field (see Chap.11, “Status of Higgs boson physics” review). A specific model assuming a non-minimal coupling of the Higgs field  $h$  to gravity was constructed in [58]. Its starting-point is the action

$$S = \int d^4x \sqrt{-g} \left[ \frac{M^2 + \xi h^2}{2} R + \frac{1}{2} \partial_\mu h \partial^\mu h - \frac{\lambda}{4} (h^2 - v^2)^2 \right], \tag{23.71}$$

where  $v$  is the Higgs vacuum expectation value. The model requires  $\xi \gg 1$ , in which case it can be rewritten in the Einstein

frame as

$$S = \int d^4x \sqrt{-g} \left[ \frac{1}{2} R + \frac{1}{2} \partial_\mu \chi \partial^\mu \chi - U(\chi) \right], \tag{23.72}$$

where the effective potential for the canonically-normalized inflaton field  $\chi$  has the form

$$U(\chi) = \frac{\lambda}{4\xi^2} \left[ 1 + \exp\left(-\frac{2\chi}{\sqrt{6}M_P}\right) \right]^{-2}, \tag{23.73}$$

which is similar to the effective potential of the  $R^2$  model at large field values. As such, the model inflates successfully if  $\xi \simeq 5 \times 10^4 m_h / (\sqrt{2}v)$ , with predictions for  $n_s$  and  $r$  that are indistinguishable from the predictions of the  $R^2$  model shown in Fig. 23.1.

This model is very appealing, but must confront several issues. One is to understand the value of  $\xi$ , and another is the possibility of unitarity violation. However, a more fundamental issue is whether the effective quartic Higgs coupling is positive at the scale of the Higgs field during inflation. Extrapolations of the effective potential in the Standard Model using the measured values of the masses of the Higgs boson and the top quark indicate that probably  $\lambda < 0$  at this scale [59], though there are still significant uncertainties associated with the appropriate input value of the top mass and the extrapolation to high renormalization scales.

### 23.4.9 Supersymmetric Models of Inflation

Supersymmetry [60] is widely considered to be a well-motivated possible extension of the Standard Model that might become apparent at the TeV scale. It is therefore natural to consider supersymmetric models of inflation. These were originally proposed because of the problems of the the new inflationary theory [13,14] based on the one-loop (Coleman-Weinberg) potential for breaking  $SU(5)$ . Several of these problems are related to the magnitude of the effective potential parameters: in any model of inflation based on an elementary scalar field, some parameter in the effective potential must be small in natural units, e.g., the quartic coupling

$\lambda$  in a chaotic model with a quartic potential, or the mass parameter  $\mu$  in a model of chaotic quadratic inflation. These parameters are renormalized multiplicatively in a supersymmetric theory, so that the quantum corrections to small values would be under control. Hence it was suggested that inflation cries out for supersymmetry [61], though non-supersymmetric resolutions of the problems of Coleman-Weinberg inflation are also possible: see, e.g., Ref. [62].

In the Standard Model there is only one scalar field that could be a candidate for the inflaton, namely the Higgs field discussed above, but even the minimal supersymmetric extension of the Standard Model (MSSM) contains many scalar fields. However, none of these is a promising candidate for the inflaton. The minimal extension of the MSSM that may contain a suitable candidate is the supersymmetric version of the minimal seesaw model of neutrino masses, which contains the three supersymmetric partners of the heavy singlet (right-handed) neutrinos. One of these singlet sneutrinos  $\tilde{\nu}$  could be the inflaton [63]: it would have a quadratic potential, the mass coefficient required would be  $\sim 10^{13}$  GeV, very much in the expected ball-park for singlet (right-handed) neutrino masses, and sneutrino inflaton decays also could give rise to the cosmological baryon asymmetry via leptogenesis. However, as seen in Fig. 23.1 and already discussed, a purely quadratic inflationary potential is no longer favored by the data. This difficulty could in principle be resolved in models with multiple sneutrinos [64], or by postulating a trilinear sneutrino coupling and hence a superpotential of Wess-Zumino type [65], which can yield successful inflation with predictions intermediate between those of natural inflation and hilltop inflation in Fig. 23.1.

Finally, we note that it is also possible to obtain inflation via supersymmetry breaking, as in the model [66] whose predictions are illustrated in Fig. 23.1.

### 23.4.10 Supergravity Models

Any model of early-Universe cosmology, and specifically inflation, must necessarily incorporate gravity. In the context of supersymmetry this requires an embedding in some supergravity theory [67, 68]. An  $\mathcal{N} = 1$  supergravity theory is specified by three functions: a Hermitian function of the matter scalar fields  $\phi^i$ , called the Kähler potential  $K$ , that describes its geometry, a holomorphic function of the superfields, called the superpotential  $W$ , which describes their interactions, and another holomorphic function  $f_{\alpha\beta}$ , which describes their couplings to gauge fields  $V_\alpha$  [69].

The simplest possibility is that the Kähler metric is flat:

$$K = \phi^i \phi_i^*, \quad (23.74)$$

where the sum is over all scalar fields in the theory, and the simplest inflationary model in minimal supergravity had the superpotential [70]

$$W = m^2(1 - \phi)^2, \quad (23.75)$$

Where  $\phi$  is the inflaton. However, this model predicts a tilted scalar perturbation spectrum,  $n_s = 0.933$ , which is now in serious disagreement with the data from *Planck* and other experiments shown in Fig. 23.1.

Moreover, there is a general problem that arises in any supergravity theory coupled to matter, namely that, since its effective scalar potential contains a factor of  $e^K$ , scalars typically receive squared masses  $\propto H^2 \sim V$ , where  $H$  is the Hubble parameter [71], an issue called the ‘ $\eta$  problem’. The theory given by (Eq. (23.75)) avoids this  $\eta$  problem, but a generic supergravity inflationary model encounters this problem of a large inflaton mass. Moreover, there are additional challenges for supergravity inflation associated with the spontaneous breaking of local supersymmetry [72–74].

Various approaches to the  $\eta$  problem in supergravity have been proposed, including the possibility of a shift symmetry [75], and one possibility that has attracted renewed attention recently is no-scale supergravity [76, 77]. This is a form of supergravity with a Kähler potential that can be written in the form [78]

$$K = -3 \ln \left( T + T^* - \frac{\sum_i |\phi^i|^2}{3} \right), \quad (23.76)$$

which has the special property that it naturally has a flat potential, at the classical level and before specifying a non-trivial superpotential. As such, no-scale supergravity is well-suited for constructing models of inflation. Adding to its attraction is the feature that compactifications of string theory to supersymmetric four-dimensional models yield effective supergravity theories of the no-scale type [79]. There are many examples of superpotentials that yield effective inflationary potentials for either the  $T$  field (which is akin to a modulus field in some string compactification) or a  $\phi$  field (generically representing matter) that are of the same form as the effective potential of the  $R^2$  model (Eq. (23.62)) when the magnitude of the inflaton field  $\gg 1$  in Planck units, as required to obtain sufficiently many e-folds of inflation,  $N_*$  [80, 81]. This framework also offers the possibility of using a suitable superpotential to construct models with effective potentials that are similar, but not identical, to the  $R^2$  model, as shown by the dashed coloured lines in Fig. 23.3.

### 23.4.11 Other Exponential Potential Models

This framework also offers the possibility [80] of constructing models in which the asymptotic constant value of the potential at large inflaton field values is approached via a different exponentially-suppressed term:

$$V(\phi) = A \left[ 1 - \delta e^{-B\phi} + \mathcal{O}(e^{-2B\phi}) \right], \quad (23.77)$$

where the magnitude of the scalar density perturbations fixes  $A$ , but  $\delta$  and  $B$  are regarded as free parameters. In the case of  $R^2$  inflation  $\delta = 2$  and  $B = \sqrt{2/3}$ . In a model such as (Eq. (23.77)), one finds at leading order in the small quantity  $e^{-B\phi}$  that

$$\begin{aligned} n_s &= 1 - 2B^2 \delta e^{-B\phi}, \\ r &= 8B^2 \delta^2 e^{-2B\phi}, \\ N_* &= \frac{1}{B^2 \delta} e^{+B\phi}. \end{aligned} \quad (23.78)$$

yielding the relations

$$n_s = 1 - \frac{2}{N_*}, \quad r = \frac{8}{B^2 N_*^2}. \quad (23.79)$$

This model leads to the class of predictions labelled by ‘ $\alpha$  attractors’ [82] in Fig. 23.1. There are generalizations of the simplest no-scale model (Eq. (23.76)) with prefactors before the  $\ln(\dots)$  that are 1 or 2, leading to larger values of  $B = \sqrt{2}$  or 1, respectively, and hence smaller values of  $r$  than in the  $R^2$  model.

## 23.5 Model Comparison

Given a particular inflationary model, one can obtain constraints on the model parameters, informed by the likelihood, corresponding to the probability of the data given a particular choice of parameters (see Sec. 40, ‘Statistics’ review). In the light of the detailed constraints on the statistical distribution of primordial perturbations now inferred from high-precision observations of the cosmic microwave background, it is also possible to make quantitative comparison of the statistical evidence for or against different inflationary models. This can be done either by comparing the logarithm of the maximum likelihood that can be obtained for the data using each model, i.e., the minimum  $\chi^2$  (with some correction for the number of free parameters in each model), or by a Bayesian model comparison [83] (see also Sec. 40.3.3 in ‘Statistics’ review).

In such a Bayesian model comparison one computes [7] the evidence,  $\mathcal{E}(\mathcal{D}|\mathcal{M}_A)$  for a model,  $\mathcal{M}_A$ , given the data  $\mathcal{D}$ . This corresponds to the likelihood,  $\mathcal{L}(\theta_{Aj}) = p(\mathcal{D}|\theta_{Aj}, \mathcal{M}_A)$ , integrated over the assumed prior distribution,  $\pi(\theta_{Aj}|\mathcal{M}_A)$ , for all the model parameters  $\theta_{Aj}$ :

$$\mathcal{E}(\mathcal{D}|\mathcal{M}_A) = \int \mathcal{L}(\theta_{Aj}) \pi(\theta_{Aj}|\mathcal{M}_A) d\theta_{Aj}. \quad (23.80)$$

The posterior probability of the model given the data follows from Bayes’ theorem

$$p(\mathcal{M}_A|\mathcal{D}) = \frac{\mathcal{E}(\mathcal{D}|\mathcal{M}_A) \pi(\mathcal{M}_A)}{p(\mathcal{D})}, \quad (23.81)$$

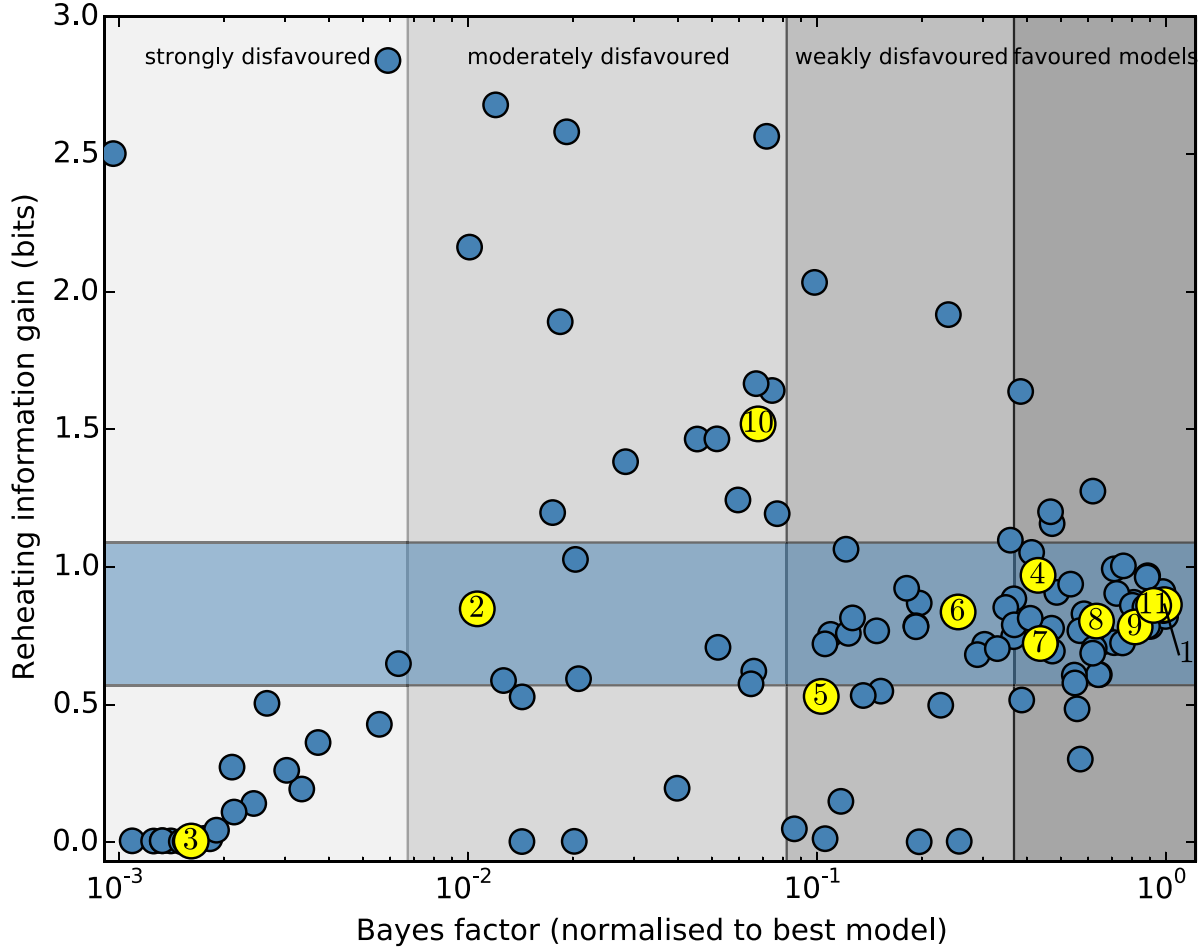


Figure 23.4: The Bayes factors calculated in [84] for a large sample of inflationary models using *Planck* 2015 data [85]. Those highlighted in yellow are featured in this review, according to the numbers listed in the text.

where the prior probability of the model is given by  $\pi(\mathcal{M}_A)$ . Assuming that all models are equally likely a priori,  $\pi(\mathcal{M}_A) = \pi(\mathcal{M}_B)$ , the relative probability of model  $A$  relative to a reference model, in the light of the data, is thus given by the Bayes factor

$$B_{A,ref} = \frac{\mathcal{E}(\mathcal{D}|\mathcal{M}_A)}{\mathcal{E}(\mathcal{D}|\mathcal{M}_{ref})}. \quad (23.82)$$

Computation of the multi-dimensional integral (Eq. (23.80)) is a challenging numerical task. Even using an efficient sampling algorithm requires hundreds of thousands of likelihood computations for each model, though slow-roll approximations can be used to calculate rapidly the primordial power spectrum using the APSIC numerical library [7] for a large number of single-field, slow-roll inflation models.

The change in  $\chi^2$  for selected slow-roll models relative to the Starobinsky  $R^2$  inflationary model, used as a reference, is given in Table 23.1 (taken from [38]). All the other inflation models require a substantial amplitude of tensor modes, and so have an increased  $\chi^2$  with respect to the Starobinsky and other models with a scalar tilt but small tensor modes. Table 23.1 also shows the Bayesian evidence for ( $\ln B_{A,ref} > 0$ ) or against ( $\ln B_{A,ref} < 0$ ) a selection of inflation models using the *Planck* analysis priors [38]. The Starobinsky  $R^2$  inflationary model may be chosen as a reference [38] that provides a good fit to current data. Higgs inflation [58] is indistinguishable using current data, making the model comparison “inconclusive” on the Jeffrey’s scale ( $|\ln B_{A,ref}| < 1$ ). (Recall, though, that this model is disfavoured by the measured values of the Higgs and top quark masses [59].) We note that although  $\alpha$ -attractor models can provide a good fit to the data, they are disfavoured relative to the Starobinsky model due to their larger prior volume. There is now strong evidence

( $|\ln B_{A,ref}| > 5$ ) against large-field models such as chaotic inflation with a quadratic or a quartic potential. Indeed, over 30% of the slow-roll inflation models considered in Ref. [7] are strongly disfavoured by the *Planck* data.

**Table 23.1:** Observational evidence for and against selected inflation models:  $\Delta\chi^2$  and the Bayes factors are calculated relative to the Starobinsky  $R^2$  inflationary model, which is treated as a reference. Results from *Planck* 2018 analysis [38].

Model	$\Delta\chi^2$	$\ln B_{A,ref}$
$R^2$ inflation	0	0
Power-law potential $\phi^{2/3}$	+4.0	-4.6
Power-law potential $\phi^2$	+21.6	< -10
Power-law potential $\phi^4$	+75.3	< -10
Natural inflation	+9.9	-6.6
Hilltop quartic model	-0.3	-1.4

The Bayes factors for a wide selection of slow-roll inflationary models are displayed in Fig. 23.4, which is adapted from Fig. 3 in [84], where more complete descriptions of the models and the calculations of the Bayes factors using *Planck* 2015 data [85] are given. Models discussed in this review are highlighted in yellow, and numbered as follows: (1)  $R^2$  inflation (Sec. 23.4.2) and models with similar predictions, such as Higgs inflation (Sec. 23.4.8) and no-scale supergravity inflation (Sec. 23.4.10); chaotic inflation models (2) with a  $\phi^2$  potential; (3) with a  $\phi^4$  potential; (4) with a  $\phi^{2/3}$  potential, and (5) with a  $\phi^p$  potential marginalising over  $p \in [0.2, 6]$  (Sec. 23.4.3); hilltop inflation models (6) with  $p = 2$ ;

(7) with  $p = 4$  and (8) marginalising over  $p$  (Sec. 23.4.4); (9) brane inflation (Sec. 23.4.5); (10) natural inflation (Sec. 23.4.6); (11) exponential potential models such as  $\alpha$ -attractors (Sec. 23.4.11). As seen in Fig. 23.4 and discussed in the next Section, constraints on reheating are starting to provide additional information about models of inflation.

### 23.6 Constraints on Reheating

One connection between inflation and particle physics is provided by inflaton decay, whose products are expected to have thermalized subsequently. As seen in (Eq. (23.54)), the number of e-folds required during inflation depends on details of this reheating process, including the matter density upon reheating, denoted by  $\rho_{th}$ , which depends in turn on the inflaton decay rate  $\Gamma_\phi$ . We see in Fig. 23.1 that, within any specific inflationary model, both  $n_s$  and particularly  $r$  are sensitive to the value of  $N_*$ . In particular, the one- $\sigma$  uncertainty in the experimental measurement of  $n_s$  is comparable to the variation in many model predictions for  $N_* \in [50, 60]$ . This implies that the data start to constrain scenarios for inflaton decay in many models. For example, it is clear from Fig. 23.1 that  $N_* = 60$  would be preferred over  $N_* = 50$  in a chaotic inflationary model with a quadratic potential.

As a specific example, let us consider  $R^2$  models and related models such as Higgs and no-scale inflation models that predict small values of  $r$  [86]. As seen in Fig. 23.1, within these models the combination of *Planck*, BICEP2/Keck Array and BAO data would require a limited range of  $n_s$ , corresponding to a limited range of  $N_*$ , as seen by comparing the left and right vertical axes in Fig. 23.5:

$$N_* \gtrsim 52 \quad (68\% \text{ CL}), \quad N_* \gtrsim 44 \quad (95\% \text{ CL}). \quad (23.83)$$

Within any specific model for inflaton decay, these bounds can be translated into constraints on the effective decay coupling. For example, if one postulates a two-body inflaton decay coupling  $y$ , the bounds (Eq. (23.83)) can be translated into bounds on  $y$ . This is illustrated in Fig. 23.5, where any value of  $N_*$  (on the left vertical axis), projected onto the diagonal line representing the correlation predicted in  $R^2$ -like models, corresponds to a specific value of the inflaton decay rate  $\Gamma_\phi/m$  (lower horizontal axis) and hence  $y$  (upper horizontal axis):

$$y \gtrsim 10^{-5} \quad (68\% \text{ CL}), \quad y \gtrsim 10^{-15} \quad (95\% \text{ CL}). \quad (23.84)$$

These bounds are not very constraining – although the 68% CL lower bound on  $y$  is already comparable with the electron Yukawa coupling – but can be expected to improve significantly in the coming years and thereby provide significant information on the connections between inflation and particle physics.

### 23.7 Beyond Single-Field Slow-Roll Inflation

There are numerous possible scenarios beyond the simplest single-field models of slow-roll inflation. These include theories in which non-canonical fields are considered, such as k-inflation [87] or DBI inflation [88], and multiple-field models, such as the curvaton scenario [89]. As well as altering the single-field predictions for the primordial curvature power spectrum (Eq. (23.48)) and the tensor-scalar ratio (Eq. (23.49)), they may introduce new quantities that vanish in single-field slow-roll models, such as isocurvature matter perturbations, corresponding to entropy fluctuations in the photon-to-matter ratio, at first order:

$$S_m = \frac{\delta n_m}{n_m} - \frac{\delta n_\gamma}{n_\gamma} = \frac{\delta \rho_m}{\rho_m} - \frac{3}{4} \frac{\delta \rho_\gamma}{\rho_\gamma}. \quad (23.85)$$

Another possibility is non-Gaussianity in the distribution of the primordial curvature perturbation (see Chap. 29, “Cosmic Microwave Background” review), encoded in higher-order correlators such as the primordial bispectrum [90]

$$\langle \zeta(\mathbf{k})\zeta(\mathbf{k}')\zeta(\mathbf{k}'') \rangle \equiv (2\pi)^3 \delta(\mathbf{k} + \mathbf{k}' + \mathbf{k}'') B_\zeta(k, k', k''), \quad (23.86)$$

which is often expressed in terms of a dimensionless non-linearity parameter

$$f_{NL} \propto B_\zeta(k, k', k'')/P_\zeta(k)P_\zeta(k').$$

The three-point function (Eq. (23.86)) can be thought of as defined on a triangle whose sides are  $\mathbf{k}, \mathbf{k}', \mathbf{k}''$ , of which only two are independent, since they sum to zero. Further assuming statistical isotropy ensures that the bispectrum depends only on the magnitudes of the three vectors,  $k, k'$  and  $k''$ . The search for  $f_{NL}$  and other non-Gaussian effects was a prime objective of the *Planck* data analysis [91, 92].

#### 23.7.1 Effective Field Theory of Inflation

Since slow-roll inflation is a phase of accelerated expansion with an almost constant Hubble parameter, one may think of inflation in terms of an effective theory where the de Sitter spacetime symmetry is spontaneously broken down to RW symmetry by the time-evolution of the Hubble rate,  $\dot{H} \neq 0$ . There is then a Goldstone boson,  $\pi$ , associated with the spontaneous breaking of time-translation invariance, which can be used to study model-independent properties of inflation. The Goldstone boson describes a spacetime-dependent shift of the time coordinate, corresponding to an adiabatic perturbation of the matter fields:

$$\delta\phi_i(t, \vec{x}) = \phi_i(t + \pi(t, \vec{x})) - \phi_i(t). \quad (23.87)$$

Thus adiabatic field fluctuations can be absorbed into the spatial metric perturbation,  $\mathcal{R}$  in Eq. (23.28) at first order, in the comoving gauge:

$$\mathcal{R} = -H\pi, \quad (23.88)$$

where we define  $\pi$  on spatially-flat hypersurfaces. In terms of inflaton field fluctuations, we can identify  $\pi \equiv \delta\phi/\dot{\phi}$ , but in principle this analysis is not restricted to inflation driven by scalar fields.

The low-energy effective action for  $\pi$  can be obtained by writing down the most general Lorentz-invariant action and expanding in terms of  $\pi$ . The second-order effective action for the free-field wave modes,  $\pi_k$ , to leading order in slow roll is then

$$S_\pi^{(2)} = - \int d^4x \sqrt{-g} \frac{M_P^2 \dot{H}}{c_s^2} \left[ \dot{\pi}_k^2 - \frac{c_s^2}{R^2} (\nabla\pi)^2 \right], \quad (23.89)$$

where  $\epsilon_H$  is the Hubble slow-roll parameter (Eq. (23.11)). We identify  $c_s^2$  with an effective sound speed, generalising canonical slow-roll inflation, which is recovered in the limit  $c_s^2 \rightarrow 1$ .

The scalar power spectrum on super-Hubble scales (Eq. (23.48)) is enhanced for a reduced sound speed, leading to a reduced tensor-scalar ratio (Eq. (23.49))

$$\mathcal{P}_\zeta(k) \simeq \frac{4\pi}{M_P^2} \frac{1}{c_s^2 \epsilon} \left( \frac{H}{2\pi} \right)^2, \quad r \simeq 16(c_s^2 \epsilon)_*. \quad (23.90)$$

At third perturbative order and to lowest order in derivatives, one obtains [94]

$$S_\pi^{(3)} = \int d^4x \sqrt{-g} \frac{M_P^2 (1 - c_s^2) \dot{H}}{c_s^2} \left[ \frac{\dot{\pi} (\nabla\pi)^2}{R^2} - \left( 1 + \frac{2}{3} \frac{\tilde{c}_3}{c_s^2} \right) \dot{\pi}^3 \right]. \quad (23.91)$$

Note that this expression vanishes for canonical fields with  $c_s^2 = 1$ . For  $c_s^2 \neq 1$  the cubic action is determined by the sound speed and an additional parameter  $\tilde{c}_3$ . Both terms in the cubic action give rise to primordial bispectra that are well approximated by equilateral bispectra. However, the shapes are not identical, so one can find a linear combination for which the equilateral bispectra of each term cancel, giving rise to a distinctive orthogonal-type bispectrum [94].

Analysis based on *Planck* 2018 temperature and polarization data has placed bounds on several bispectrum shapes including equilateral and orthogonal shapes [92]:

$$f_{NL}^{equil} = -26 \pm 47, \quad f_{NL}^{orthog} = -38 \pm 24 \quad (68\% \text{ CL}). \quad (23.92)$$

For the simplest case of a constant sound speed, and marginalising over  $\tilde{c}_3$ , this provides a bound on the inflaton sound speed [92]

$$c_s \geq 0.021 \quad (95\% \text{ CL}). \quad (23.93)$$

For a specific model such as DBI inflation [88], corresponding to  $\tilde{c}_3 = 3(1 - c_s^2)/2$ , one obtains a tighter bound [92]:

$$c_s^{DBI} \geq 0.086 \quad (95\% \text{ CL}). \quad (23.94)$$

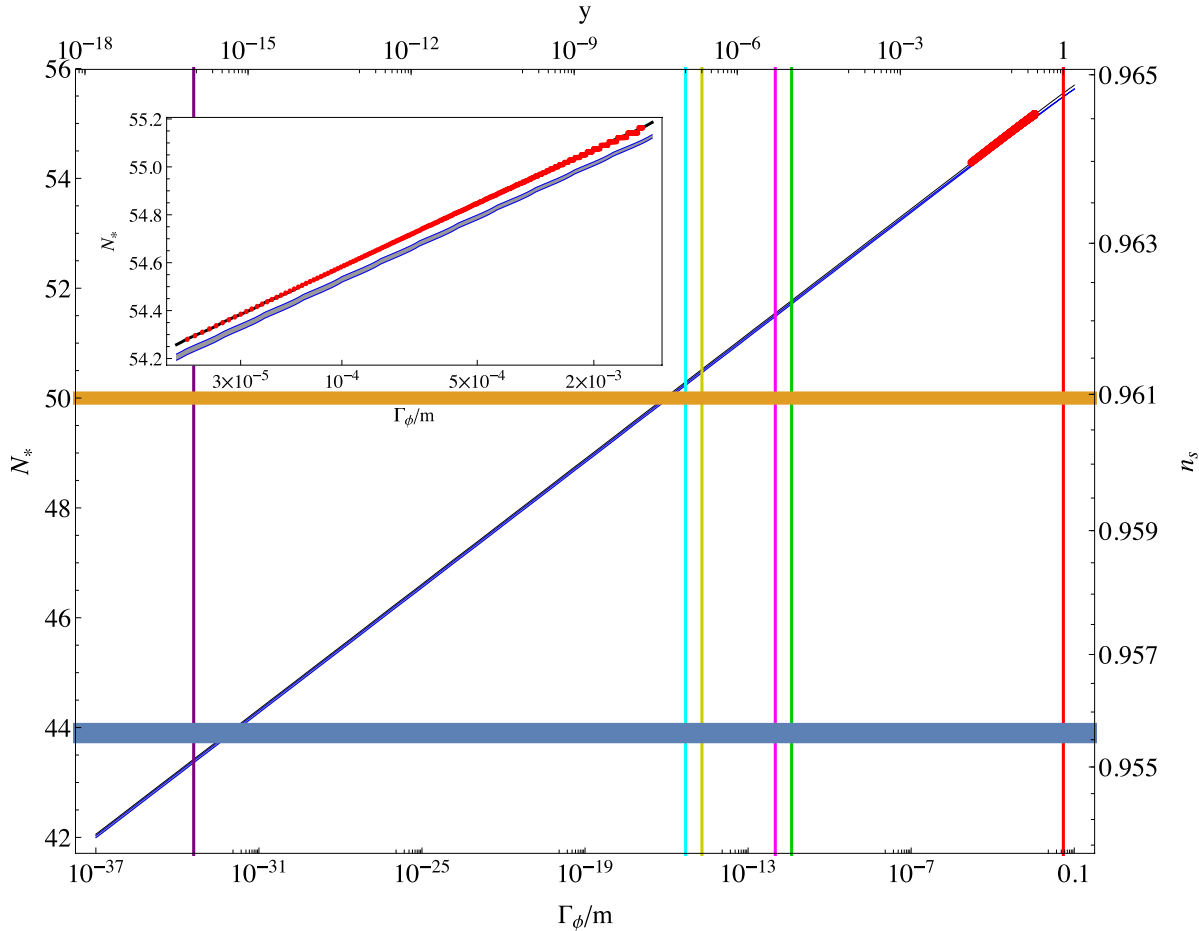


Figure 23.5: The values of  $N_*$  (left axis) and  $n_s$  (right axis) in  $R^2$  inflation and related models for a wide range of decay rates,  $\Gamma_\phi/m$ , (bottom axis) and corresponding two-body couplings,  $y$  (top axis). The diagonal red line segment shows full numerical results over a restricted range of  $\Gamma_\phi/m$  (which are shown in more detail in the insert), while the diagonal blue strip represents an analytical approximation described in [86]. The difference between these results is indistinguishable in the main plot, but is visible in the insert. The horizontal yellow and blue lines show the 68 and 95% CL lower limits from the *Planck* 2015 data [85], and the vertical coloured lines correspond to specific models of inflaton decay. Figure taken from [93].

The *Planck* team have analysed a wide range of non-Gaussian templates from different inflation models, including tests for deviations from an initial Bunch-Davies vacuum state, direction-dependent non-Gaussianity, and feature models with oscillatory bispectra [92]. No individual feature or resonance is above the three- $\sigma$  significance level after accounting for the look-elsewhere effect. These results are consistent with the simplest canonical, slow-roll inflation models, but do not rule out most alternative models; rather, bounds on primordial non-Gaussianity place important constraints on the parameter space for non-canonical models.

### 23.7.2 Multi-Field Fluctuations

There is a very large literature on two- and multi-field models of inflation, most of which lies beyond the scope of this review [95, 96]. However, two important general topics merit being mentioned here, namely residual isocurvature perturbations and the possibility of non-Gaussian effects in the primordial perturbations.

One might expect that other scalar fields besides the inflaton might have non-negligible values that evolve and fluctuate in parallel with the inflaton, without necessarily making the dominant contribution to the energy density during the inflationary epoch. However, the energy density in such a field might persist beyond the end of inflation before decaying, at which point it might come to dominate (or at least make a non-negligible contribution to) the total energy density. In such a case, its perturbations could end up generating the density perturbations detected in the CMB.

This could occur due to a late-decaying scalar field [89] or a field fluctuation that modulates the end of inflation [97] or the inflaton decay [98].

#### 23.7.2.1 Isocurvature Perturbations

Primordial perturbations arising in single-field slow-roll inflation are necessarily adiabatic, i.e., they affect the overall density without changing the ratios of different contributions, such as the photon-matter ratio,  $\delta(n_\gamma/n_m)/(n_\gamma/n_m)$ . This is because inflaton perturbations represent a local shift of the time, as described in section Sec. 23.7.1:

$$\pi = \frac{\delta n_\gamma}{\dot{n}_\gamma} = \frac{\delta n_m}{\dot{n}_m}. \quad (23.95)$$

However, any light scalar field (i.e., one with effective mass less than the Hubble scale) acquires a spectrum of nearly scale-invariant perturbations during inflation. Fluctuations orthogonal to the inflaton in field space are decoupled from the inflaton at Hubble-exit, but can affect the subsequent evolution of the density perturbation. In particular, they can give rise to local variations in the equation of state (non-adiabatic pressure perturbations) that can alter the primordial curvature perturbation  $\zeta$  on super-Hubble scales. Since these fluctuations are statistically independent of the inflaton perturbations at leading order in slow-roll [96], non-adiabatic field fluctuations can only increase the scalar power spectrum with respect to adiabatic perturbations at Hubble exit, while leaving the tensor modes unaffected at first perturbative order. Thus the single-field result for the

tensor-scalar ratio (Eq. (23.49)) becomes an inequality [99]

$$r \leq 16\epsilon_* . \quad (23.96)$$

Hence an observational upper bound on the tensor-scalar ratio does not bound the slow-roll parameter  $\epsilon$  in multi-field models.

If all the scalar fields present during inflation eventually decay completely into fully thermalized radiation, these field fluctuations are converted fully into adiabatic perturbations in the primordial plasma [100]. On the other hand, non-adiabatic field fluctuations can also leave behind primordial isocurvature perturbations (Eq. (23.85)) after inflation. In multi-field inflation models it is thus possible for non-adiabatic field fluctuations to generate both curvature and isocurvature perturbations leading to correlated primordial perturbations [101].

The amplitudes of any primordial isocurvature perturbations (Eq. (23.85)) are strongly constrained by the current CMB data, especially on large angular scales. Using temperature and low- $\ell$  polarization data yields the following bound on the amplitude of cold dark matter isocurvature perturbations at scale  $k = 0.002h^{-1}\text{Mpc}^{-1}$  (marginalising over the correlation angle and in the absence of primordial tensor perturbations) [38]:

$$\frac{\mathcal{P}_{S_m}}{\mathcal{P}_\zeta + \mathcal{P}_{S_m}} < 0.025 \text{ (95\% CL)} . \quad (23.97)$$

For fully (anti-)correlated isocurvature perturbations, corresponding to a single isocurvature field providing a source for both the curvature and residual isocurvature perturbations, the bounds become significantly tighter [38]:

$$\frac{\mathcal{P}_{S_m}}{\mathcal{P}_\zeta + \mathcal{P}_{S_m}} < 0.0002 \text{ (95\% CL), correlated} , \quad (23.98)$$

$$\frac{\mathcal{P}_{S_m}}{\mathcal{P}_\zeta + \mathcal{P}_{S_m}} < 0.003 \text{ (95\% CL), anti-correlated} \quad (23.99)$$

### 23.7.2.2 Local-Type Non-Gaussianity

Since non-adiabatic field fluctuations in multi-field inflation may lead to the evolution of the primordial curvature perturbation at all orders, it becomes possible to generate significant non-Gaussianity in the primordial curvature perturbation. Non-linear evolution on super-Hubble scales leads to local-type non-Gaussianity, where the local integrated expansion is a non-linear function of the local field values during inflation,  $N(\phi_i)$ . While the field fluctuations at Hubble exit,  $\delta\phi_{i*}$ , are Gaussian in the slow-roll limit, the curvature perturbation,  $\zeta = \delta N$ , becomes a non-Gaussian distribution [102]:

$$\zeta = \sum_i \frac{\partial N}{\partial \phi_i} \delta\phi_i + \frac{1}{2} \sum_{i,j} \frac{\partial^2 N}{\partial \phi_i \partial \phi_j} \delta\phi_i \delta\phi_j + \dots \quad (23.100)$$

with non-vanishing bispectrum in the squeezed limit ( $k_1 \approx k_2 \gg k_3$ ):

$$B_\zeta(k_1, k_2, k_3) \approx \frac{12}{5} f_{NL}^{local} \frac{\mathcal{P}_\zeta(k_1) \mathcal{P}_\zeta(k_3)}{4\pi k_1^3 4\pi k_3^3} , \quad (23.101)$$

where

$$\frac{6}{5} f_{NL}^{local} = \frac{\sum_{i,j} \frac{\partial^2 N}{\partial \phi_i \partial \phi_j}}{\left(\sum_i \frac{\partial N}{\partial \phi_i}\right)^2} . \quad (23.102)$$

Both equilateral and orthogonal bispectra, discussed above in the context of generalised single field inflation, vanish in the squeezed limit, enabling the three types of non-Gaussianity to be distinguished by observations, in principle.

Non-Gaussianity during multi-field inflation is highly model dependent, though  $f_{NL}^{local}$  can often be smaller than unity in multi-field slow-roll inflation [103]. Scenarios where a second light field plays a role during or after inflation can make distinctive predictions for  $f_{NL}^{local}$ , such as  $f_{NL}^{local} = -5/4$  in some curvaton scenarios [102, 104] or  $f_{NL}^{local} = 5$  in simple modulated reheating scenarios [98, 105]. By contrast the constancy of  $\zeta$  on super-Hubble

scales in single-field slow-roll inflation leads to a very small non-Gaussianity [106, 107], and in the squeezed limit we have the simple result  $f_{NL}^{local} = 5(1 - n_s)/12$  [108, 109].

A combined analysis of the *Planck* 2018 temperature and polarization data [92] yields the following range for  $f_{NL}^{local}$  defined in (Eq. (23.102)):

$$f_{NL}^{local} = -1 \pm 5 \text{ (68\% CL)} . \quad (23.103)$$

This sensitivity is sufficient to rule out parameter regimes giving rise to relatively large non-Gaussianity, but insufficient to probe  $f_{NL}^{local} = \mathcal{O}(\epsilon)$ , as expected in single-field models, or the range  $f_{NL}^{local} = \mathcal{O}(1)$  found in the simplest two-field models.

Local-type primordial non-Gaussianity can also give rise to a striking scale-dependent bias in the distribution of collapsed dark matter halos and thus the galaxy distribution [110, 111]. However, bounds from high-redshift galaxy surveys are not yet competitive with the best CMB constraints.

## 23.8 Initial Conditions and Fine-tuning

This review is based on the assumption that the inflationary paradigm is valid. However, it remains the object of many criticisms (see, e.g., [112]), many of them related to the perceived unnaturalness of the required initial conditions.

Most work on inflation is done in the context of RW cosmology, which assumes a high degree of symmetry, or small inhomogeneous perturbations (usually first order) about an RW cosmology. The isotropic RW space-time is an attractor for many homogeneous but anisotropic cosmologies in the presence of a false vacuum energy density [113], or a scalar field with suitable self-interaction potential energy [114, 115]. However it is much harder to establish the range of highly inhomogeneous initial conditions that yield a successful RW Universe, with only limited studies initially (see, e.g., [116, 117]). A related open question is the general nature of the pre-inflationary state of the inflaton and other fields that could have provided initial conditions suitable for inflation [112]. They would need to have satisfied non-trivial homogeneity and isotropy conditions, and one may ask how these could have arisen, whether these are plausible, and whether there may be some observable signature of the pre-inflationary state. These and other criticisms of inflation were addressed in [118], which presented studies of the sensitivity of inflation to the initial conditions. Complementing the studies reported in [118], there have been numerical relativity investigations of highly inhomogeneous initial conditions [119–121]. The general conclusion is that inflation is rather robust with respect to inhomogeneities in the initial conditions in both the scalar field profile and the extrinsic curvature, including large tensor perturbations.

To quantify the fine-tuning of initial conditions requires a measure in the space of possible cosmologies [122], however it has been argued that some of the measures historically used to frame this problem are formally invalid [123]. It is sometimes also objected that inflationary models predict the existence of a multiverse, and potentially a loss of predictive power [124], if it undergoes the process termed eternal inflation [125–127]. However, whether this is actually a bug or a feature remains a topic of debate [128, 129]. The existence of the multiverse is a purely philosophical problem, unless it has observable consequences, e.g., in the CMB.

One might expect signatures of any pre-inflationary state to appear at large angular scales, i.e., low multipoles  $\ell$ . Indeed, various anomalies have been noted in the large-scale CMB anisotropies, as also discussed in Chap. 29, the ‘‘Cosmic Microwave Background’’ review, including a possible suppression of the quadrupole and other very large-scale anisotropies, an apparent feature in the range  $\ell \approx 20$  to 30, and a possible hemispheric asymmetry. However, none of these are highly significant statistically, in view of the limitations due to cosmic variance [85]. They cannot yet be regarded as signatures of initial conditions, the multiverse or some pre-inflationary dynamics, such as might emerge from string theory.

A different kind of initial condition problem, called the trans-Planckian problem [130], is that the perturbations now seen in the CMB would have had wavelengths shorter than the Planck length at the onset of inflation. However, under quite general and

conservative assumptions the usual inflationary predictions would be quite robust [131], with the possibility of  $\mathcal{O}((H/m_P)^n)$  corrections that might have interesting signatures in the CMB [132].

When inflation was first proposed [1] [2] there was no evidence for the existence of scalar fields or the accelerated expansion of the universe. The situation has changed dramatically in recent years with the observational evidence that the cosmic expansion is currently accelerating and with the discovery of a scalar particle, namely the Higgs boson (see Chap. 11, “Status of Higgs boson physics” review). Combined with the lack of any widely accepted alternative model for the origin of cosmic structure, these discoveries have lent support to the idea of a primordial accelerated expansion driven by a scalar field, i.e., cosmological inflation. In parallel, successive CMB experiments have been consistent with generic predictions of inflationary models, although without yet providing irrefutable evidence. It was concluded in [118] that the inflationary paradigm is not currently in trouble. However, we note that inflation via a formally elementary scalar inflaton should probably only be regarded as an effective field theory valid at energy densities hierarchically smaller than the Planck scale. It should eventually be embedded in a suitable ultraviolet completion, on which inflationary dynamics may be our clearest window.

### 23.9 Future Probes of Inflation

Prospective future CMB experiments, both ground- and space-based are reviewed in the separate PDG “Cosmic Microwave Background” review, Chap. 29. The main emphasis in CMB experiments in the coming years will be on ground-based experiments providing improved measurements of  $B$ -mode polarization and greater sensitivity to the tensor-to-scalar ratio  $r$ , and more precise measurements at higher  $\ell$  that will constrain  $n_s$  better. As is apparent from Fig. 23.1 and the discussion of models such as  $R^2$  inflation, there is a strong incentive to reach a  $5\text{-}\sigma$  sensitivity to  $r \sim 3$  to  $4 \times 10^{-3}$ . This could be achieved with a moderately-sized space mission with large sky coverage [133], improvements in de-lensing and foreground measurements. The discussion in Sec. 23.3 (see also Fig. 23.5), also brought out the importance of reducing the uncertainty in  $n_s$ , as a way to constrain post-inflationary reheating and the connection to particle physics. CMB temperature anisotropies probe primordial density perturbations down to comoving scales of order 50 Mpc, beyond which scale secondary sources of anisotropy dominate. CMB spectral distortions could potentially constrain the amplitude and shape of primordial density perturbations on comoving scales from Mpc to kpc due to distortions caused by the Silk damping of pressure waves in the radiation dominated era, before the last scattering of the CMB photons but after the plasma can be fully thermalised [134].

Improved sensitivity to non-Gaussianities is also a priority. In addition to CMB measurements, future large-scale structure surveys will also have roles to play as probes into models of inflation, for which there are excellent prospects. High-redshift galaxy surveys are sensitive to local-type non-Gaussianity due to the scale-dependent bias induced on large scales. Current surveys such as eBOSS, probing out to redshift  $z \sim 2$ , can reach a precision  $\Delta f_{NL} \sim 15$ , from measurements of the galaxy power spectrum, or possibly  $\Delta f_{NL} \sim 10$ , if the galaxy bias can be determined independently [135]. Upcoming surveys such as DESI may reach  $\Delta f_{NL} \sim 4$  [136] comparable with the *Planck* sensitivity. In the future, radio surveys such as SKA will measure large-scale structure out to redshift  $z \sim 3$  [137], initially through mapping the intensity of the neutral hydrogen 21-cm line, and eventually through radio galaxy surveys which will probe local-type non-Gaussianity to  $f_{NL} \sim 1$ .

Galaxy clustering using DESI and *Euclid* satellite data could also constrain the running of the scalar tilt to a precision of  $\Delta\alpha_s \approx 0.0028$ , a factor of 2 improvement on *Planck* constraints, or a precision of 0.0016 using LSST data [136].

As an example of a proposed future satellite mission, *SPHEREx* [138] will use measurements of the galaxy power spectrum to target a measurement of the running of the scalar spectral index with a sensitivity  $\Delta\alpha_s \sim 10^{-3}$  and local-type primordial non-Gaussianity,  $\Delta f_{NL} \sim 1$ . Including information from the galaxy bispectrum one might reduce the measurement error on non-Gaussianity to  $\Delta f_{NL} \sim 0.2$ , making it possible to distin-

guish between single-field slow-roll models and alternatives such as the curvaton scenario for the origin of structure, which generate  $f_{NL} \sim 1$ .

#### Acknowledgements

The authors are grateful to Vincent Vennin for his careful reading of this manuscript and preparing Fig. 23.4 for this review. The work of J.E. was supported in part by the UK STFC via the research grant ST/L000258/1 and in part by the Estonian Research Council via a Mobilitas Plus grant. The work of D.W. was supported in part by the UK STFC research grants ST/N000668/1 and ST/S000550/1.

#### References

- [1] A. A. Starobinsky, Phys. Lett. **B91**, 99 (1980), [771(1980)].
- [2] A. H. Guth, Phys. Rev. **D23**, 347 (1981), [Adv. Ser. Astrophys. Cosmol.3,139(1987)].
- [3] K. A. Olive, Phys. Rept. **190**, 307 (1990).
- [4] D. H. Lyth and A. Riotto, Phys. Rept. **314**, 1 (1999), [hep-ph/9807278].
- [5] A.R. Liddle and D.H. Lyth, *Cosmological inflation and large-scale structure* (Cambridge University Press, 2000).
- [6] D. Baumann, in “Physics of the large and the small, TASI 09, proceedings of the Theoretical Advanced Study Institute in Elementary Particle Physics, Boulder, Colorado, USA, 1-26 June 2009,” 523–686 (2011), [arXiv:0907.5424].
- [7] J. Martin, C. Ringeval and V. Vennin, Phys. Dark Univ. **5-6**, 75 (2014), [arXiv:1303.3787]; J. Martin *et al.*, JCAP **1403**, 039 (2014), [arXiv:1312.3529]; J. Martin, Astrophys. Space Sci. Proc. **45**, 41 (2016), [arXiv:1502.05733].
- [8] P. A. R. Ade *et al.* (Planck), Astron. Astrophys. **594**, A13 (2016), [arXiv:1502.01589].
- [9] A. H. Guth and E. J. Weinberg, Nucl. Phys. **B212**, 321 (1983).
- [10] D. La and P. J. Steinhardt, Phys. Rev. Lett. **62**, 376 (1989), [Erratum: Phys. Rev. Lett.62,1066(1989)].
- [11] A. D. Linde, Phys. Lett. **B249**, 18 (1990).
- [12] F. C. Adams and K. Freese, Phys. Rev. **D43**, 353 (1991), [hep-ph/0504135].
- [13] A. D. Linde, Phys. Lett. **108B**, 389 (1982), [Adv. Ser. Astrophys. Cosmol.3,149(1987)].
- [14] A. Albrecht and P. J. Steinhardt, Phys. Rev. Lett. **48**, 1220 (1982), [Adv. Ser. Astrophys. Cosmol.3,158(1987)].
- [15] W. H. Press, Phys. Scripta **21**, 702 (1980); S. W. Hawking, Phys. Lett. **115B**, 295 (1982); A. A. Starobinsky, Phys. Lett. **117B**, 175 (1982); A. H. Guth and S. Y. Pi, Phys. Rev. Lett. **49**, 1110 (1982).
- [16] J. M. Bardeen, P. J. Steinhardt and M. S. Turner, Phys. Rev. **D28**, 679 (1983).
- [17] V. F. Mukhanov and G. V. Chibisov, JETP Lett. **33**, 532 (1981), [Pisma Zh. Eksp. Teor. Fiz.33,549(1981)].
- [18] K. S. Stelle, Gen. Rel. Grav. **9**, 353 (1978).
- [19] B. Whitt, Phys. Lett. **145B**, 176 (1984).
- [20] D. Wands, Class. Quant. Grav. **11**, 269 (1994), [arXiv:gr-qc/9307034].
- [21] S. R. Coleman and F. De Luccia, Phys. Rev. **D21**, 3305 (1980).
- [22] M. Sasaki *et al.*, Phys. Lett. **B317**, 510 (1993).
- [23] M. Bucher, A. S. Goldhaber and N. Turok, Phys. Rev. **D52**, 3314 (1995), [hep-ph/9411206].
- [24] A. D. Linde and A. Mezhlumian, Phys. Rev. **D52**, 6789 (1995), [arXiv:astro-ph/9506017].
- [25] A. R. Liddle, P. Parsons and J. D. Barrow, Phys. Rev. **D50**, 7222 (1994), [arXiv:astro-ph/9408015].
- [26] L. Kofman, A. D. Linde and A. A. Starobinsky, Phys. Rev. **D56**, 3258 (1997), [hep-ph/9704452].



- [27] B. A. Bassett, S. Tsujikawa and D. Wands, *Rev. Mod. Phys.* **78**, 537 (2006), [arXiv:astro-ph/0507632].
- [28] A. D. Linde, *Phys. Rev.* **D49**, 748 (1994), [arXiv:astro-ph/9307002].
- [29] A. D. Dolgov and A. D. Linde, *Phys. Lett.* **116B**, 329 (1982).
- [30] J. R. Ellis *et al.*, *Nucl. Phys.* **B238**, 453 (1984), [,223(1983)].
- [31] M. Kawasaki and T. Moroi, *Prog. Theor. Phys.* **93**, 879 (1995), [hep-ph/9403364].
- [32] J. H. Traschen and R. H. Brandenberger, *Phys. Rev.* **D42**, 2491 (1990).
- [33] G. V. Chibisov and V. F. Mukhanov, *Mon. Not. Roy. Astron. Soc.* **200**, 535 (1982).
- [34] H. Kodama and M. Sasaki, *Prog. Theor. Phys. Suppl.* **78**, 1 (1984).
- [35] V.F. Mukhanov, H.A. Feldman and R.H. Brandenberger, *Phys. Rept.* **215**, 203 (1992).
- [36] K. A. Malik and D. Wands, *Phys. Rept.* **475**, 1 (2009), [arXiv:0809.4944].
- [37] V. F. Mukhanov, *Sov. Phys. JETP* **67**, 1297 (1988), [*Zh. Eksp. Teor. Fiz.*94N7,1(1988)].
- [38] Y. Akrami *et al.* (Planck) (2018), [arXiv:1807.06211].
- [39] A. A. Starobinsky, *JETP Lett.* **30**, 682 (1979), [,767(1979)].
- [40] E. D. Stewart and D. H. Lyth, *Phys. Lett.* **B302**, 171 (1993), [arXiv:gr-qc/9302019].
- [41] D. Wands *et al.*, *Phys. Rev.* **D62**, 043527 (2000), [arXiv:astro-ph/0003278].
- [42] A. R. Liddle and S. M. Leach, *Phys. Rev.* **D68**, 103503 (2003), [arXiv:astro-ph/0305263].
- [43] P. A. R. Ade *et al.* (BICEP2, Keck Array), *Phys. Rev. Lett.* **121**, 221301 (2018), [arXiv:1810.05216].
- [44] S.M. Leach, A.R. Liddle, J. Martin, and D.J. Schwarz, *Phys. Rev.* **D66**, 23515 (2002).
- [45] D. Kazanas, *Astrophys. J.* **241**, L59 (1980).
- [46] K. Sato, *Mon. Not. Roy. Astron. Soc.* **195**, 467 (1981).
- [47] A. Billoire and K. Tamvakis, *Nucl. Phys.* **B200**, 329 (1982); J. D. Breit, S. Gupta and A. Zaks, *Phys. Rev. Lett.* **51**, 1007 (1983).
- [48] A. D. Linde, *Phys. Lett.* **129B**, 177 (1983).
- [49] D. V. Nanopoulos, K. A. Olive and M. Srednicki, *Phys. Lett.* **127B**, 30 (1983).
- [50] J. Ellis, D. V. Nanopoulos and K. A. Olive, *Phys. Rev. Lett.* **111**, 111301 (2013), [Erratum: *Phys. Rev. Lett.*111,no.12,129902(2013)], [arXiv:1305.1247].
- [51] T. S. Koivisto and F. R. Urban, *JCAP* **1503**, 03, 003 (2015), [arXiv:1407.3445].
- [52] L. Boubekeur and D. H. Lyth, *JCAP* **0507**, 010 (2005), [hep-ph/0502047].
- [53] G. R. Dvali, Q. Shafi and S. Solganik, in "4th European Meeting From the Planck Scale to the Electroweak Scale (Planck 2001) La Londe les Maures, Toulon, France, May 11-16, 2001," (2001), [hep-th/0105203]; J. Garcia-Bellido, R. Rabadan and F. Zamora, *JHEP* **01**, 036 (2002), [hep-th/0112147]; S. Kachru *et al.*, *JCAP* **0310**, 013 (2003), [hep-th/0308055].
- [54] F. C. Adams *et al.*, *Phys. Rev.* **D47**, 426 (1993), [hep-ph/9207245].
- [55] E. Pajer and M. Peloso, *Class. Quant. Grav.* **30**, 214002 (2013), [arXiv:1305.3557].
- [56] E. Silverstein and A. Westphal, *Phys. Rev.* **D78**, 106003 (2008), [arXiv:0803.3085].
- [57] L. McAllister, E. Silverstein and A. Westphal, *Phys. Rev.* **D82**, 046003 (2010), [arXiv:0808.0706].
- [58] F. L. Bezrukov and M. Shaposhnikov, *Phys. Lett.* **B659**, 703 (2008), [arXiv:0710.3755].
- [59] D. Buttazzo *et al.*, *JHEP* **12**, 089 (2013), [arXiv:1307.3536].
- [60] H. P. Nilles, *Phys. Rept.* **110**, 1 (1984); H. E. Haber and G. L. Kane, *Phys. Rept.* **117**, 75 (1985).
- [61] J.R. Ellis *et al.*, *Phys. Lett.* **118B**, 335 (1982).
- [62] N. Okada and Q. Shafi (2013), [arXiv:1311.0921].
- [63] H. Murayama *et al.*, *Phys. Rev. Lett.* **70**, 1912 (1993).
- [64] J. Ellis, M. Fairbairn and M. Sueiro, *JCAP* **1402**, 044 (2014), [arXiv:1312.1353].
- [65] D. Croon, J. Ellis and N. E. Mavromatos, *Phys. Lett.* **B724**, 165 (2013), [arXiv:1303.6253].
- [66] G. R. Dvali, Q. Shafi and R. K. Schaefer, *Phys. Rev. Lett.* **73**, 1886 (1994), [hep-ph/9406319].
- [67] D. V. Nanopoulos *et al.*, *Phys. Lett.* **123B**, 41 (1983).
- [68] A. B. Goncharov and A. D. Linde, *Phys. Lett.* **139B**, 27 (1984).
- [69] E. Cremmer *et al.*, *Nucl. Phys.* **B212**, 413 (1983), [,413(1982)].
- [70] R. Holman, P. Ramond and G. G. Ross, *Phys. Lett.* **137B**, 343 (1984).
- [71] E. J. Copeland *et al.*, *Phys. Rev.* **D49**, 6410 (1994), [arXiv:astro-ph/9401011]; E. D. Stewart, *Phys. Rev.* **D51**, 6847 (1995), [hep-ph/9405389].
- [72] G. D. Coughlan *et al.*, *Phys. Lett.* **131B**, 59 (1983); A. S. Goncharov, A. D. Linde and M. I. Vysotsky, *Phys. Lett.* **147B**, 279 (1984); T. Banks, D. B. Kaplan and A. E. Nelson, *Phys. Rev.* **D49**, 779 (1994), [hep-ph/9308292]; B. de Carlos *et al.*, *Phys. Lett.* **B318**, 447 (1993), [hep-ph/9308325]; M. Kawasaki, T. Moroi and T. Yanagida, *Phys. Lett.* **B370**, 52 (1996), [hep-ph/9509399].
- [73] J. R. Ellis, D. V. Nanopoulos and M. Quiros, *Phys. Lett.* **B174**, 176 (1986).
- [74] T. Moroi, M. Yamaguchi and T. Yanagida, *Phys. Lett.* **B342**, 105 (1995), [hep-ph/9409367].
- [75] M. Kawasaki, M. Yamaguchi and T. Yanagida, *Phys. Rev. Lett.* **85**, 3572 (2000), [hep-ph/0004243]; K. Nakayama, F. Takahashi and T. T. Yanagida, *JCAP* **1308**, 038 (2013), [arXiv:1305.5099].
- [76] E. Cremmer *et al.*, *Phys. Lett.* **133B**, 61 (1983).
- [77] A. S. Goncharov and A. D. Linde, *Class. Quant. Grav.* **1**, L75 (1984); C. Kounnas and M. Quiros, *Phys. Lett.* **151B**, 189 (1985).
- [78] J. R. Ellis, C. Kounnas and D. V. Nanopoulos, *Nucl. Phys.* **B247**, 373 (1984).
- [79] E. Witten, *Phys. Lett.* **155B**, 151 (1985).
- [80] J. Ellis, D. V. Nanopoulos and K. A. Olive, *JCAP* **1310**, 009 (2013), [arXiv:1307.3537].
- [81] J. Ellis *et al.*, *Class. Quant. Grav.* **33**, 9, 094001 (2016), [arXiv:1507.02308].
- [82] R. Kallosh, A. Linde and D. Roest, *JHEP* **11**, 198 (2013), [arXiv:1311.0472].
- [83] A. R. Liddle, *Mon. Not. Roy. Astron. Soc.* **377**, L74 (2007), [arXiv:astro-ph/0701113].
- [84] J. Martin, C. Ringeval and V. Vennin, *Phys. Rev.* **D93**, 10, 103532 (2016), [arXiv:1603.02606].
- [85] P. A. R. Ade *et al.* (Planck), *Astron. Astrophys.* **594**, A20 (2016), [arXiv:1502.02114].
- [86] C. T. Byrnes and E. R. M. Tarrant, *JCAP* **1507**, 007 (2015), [arXiv:1502.07339].
- [87] C. Armendariz-Picon, T. Damour and V. F. Mukhanov, *Phys. Lett.* **B458**, 209 (1999), [hep-th/9904075].
- [88] M. Alishahiha, E. Silverstein and D. Tong, *Phys. Rev.* **D70**, 123505 (2004), [hep-th/0404084].



- [89] K. Enqvist and M. S. Sloth, Nucl. Phys. **B626**, 395 (2002), [hep-ph/0109214]; D. H. Lyth and D. Wands, Phys. Lett. **B524**, 5 (2002), [hep-ph/0110002]; T. Moroi and T. Takahashi, Phys. Lett. **B522**, 215 (2001), [Erratum: Phys. Lett. **B539**, 303(2002)], [hep-ph/0110096].
- [90] N. Bartolo *et al.*, Phys. Rept. **402**, 103 (2004), [arXiv:astro-ph/0406398].
- [91] P. A. R. Ade *et al.* (Planck), Astron. Astrophys. **594**, A17 (2016), [arXiv:1502.01592].
- [92] Y. Akrami *et al.* (Planck) (2019), [arXiv:1905.05697].
- [93] J. Ellis *et al.*, JCAP **1507**, 07, 050 (2015), [arXiv:1505.06986].
- [94] L. Senatore, K. M. Smith and M. Zaldarriaga, JCAP **1001**, 028 (2010), [arXiv:0905.3746].
- [95] C. Gordon *et al.*, Phys. Rev. **D63**, 023506 (2001), [arXiv:astro-ph/0009131]; R. Easther *et al.*, Phys. Rev. Lett. **112**, 161302 (2014), [arXiv:1312.4035]; J. Ellis *et al.*, JCAP **1501**, 010 (2015), [arXiv:1409.8197]; S. Renaux-Petel and K. Turzynski, JCAP **1506**, 06, 010 (2015), [arXiv:1405.6195].
- [96] C. T. Byrnes and D. Wands, Phys. Rev. **D74**, 043529 (2006), [arXiv:astro-ph/0605679].
- [97] D. H. Lyth, JCAP **0511**, 006 (2005), [arXiv:astro-ph/0510443].
- [98] G. Dvali, A. Gruzinov and M. Zaldarriaga, Phys. Rev. **D69**, 023505 (2004), [arXiv:astro-ph/0303591].
- [99] D. Wands *et al.*, Phys. Rev. **D66**, 043520 (2002), [arXiv:astro-ph/0205253].
- [100] S. Weinberg, Phys. Rev. **D67**, 123504 (2003), [arXiv:astro-ph/0302326].
- [101] D. Langlois, Phys. Rev. **D59**, 123512 (1999), [arXiv:astro-ph/9906080].
- [102] D. H. Lyth and Y. Rodriguez, Phys. Rev. Lett. **95**, 121302 (2005), [arXiv:astro-ph/0504045].
- [103] F. Vernizzi and D. Wands, JCAP **0605**, 019 (2006), [arXiv:astro-ph/0603799].
- [104] M. Sasaki, J. Valiviita and D. Wands, Phys. Rev. **D74**, 103003 (2006), [arXiv:astro-ph/0607627].
- [105] G. Dvali, A. Gruzinov and M. Zaldarriaga, Phys. Rev. **D69**, 083505 (2004), [arXiv:astro-ph/0305548].
- [106] D. S. Salopek and J. R. Bond, Phys. Rev. **D43**, 1005 (1991).
- [107] A. Gangui *et al.*, Astrophys. J. **430**, 447 (1994), [arXiv:astro-ph/9312033].
- [108] J. M. Maldacena, JHEP **05**, 013 (2003), [arXiv:astro-ph/0210603].
- [109] V. Acquaviva *et al.*, Nucl. Phys. **B667**, 119 (2003), [arXiv:astro-ph/0209156].
- [110] N. Dalal *et al.*, Phys. Rev. **D77**, 123514 (2008), [arXiv:0710.4560].
- [111] S. Matarrese and L. Verde, Astrophys. J. **677**, L77 (2008), [arXiv:0801.4826].
- [112] A. Ijjas, P. J. Steinhardt and A. Loeb, Phys. Lett. **B723**, 261 (2013), [arXiv:1304.2785].
- [113] R. M. Wald, Phys. Rev. **D28**, 2118 (1983).
- [114] M. Heusler, Phys. Lett. **B253**, 33 (1991).
- [115] Y. Kitada and K.-i. Maeda, Phys. Rev. **D45**, 1416 (1992).
- [116] D. S. Goldwirth and T. Piran, Phys. Rept. **214**, 223 (1992).
- [117] T. Vachaspati and M. Trodden, Phys. Rev. **D61**, 023502 (1999), [arXiv:gr-qc/9811037].
- [118] D. Chowdhury *et al.* (2019), [arXiv:1902.03951].
- [119] W. E. East *et al.*, JCAP **1609**, 09, 010 (2016), [arXiv:1511.05143].
- [120] K. Clough *et al.*, JCAP **1709**, 09, 025 (2017), [arXiv:1608.04408].
- [121] K. Clough, R. Flauger and E. A. Lim, JCAP **1805**, 05, 065 (2018), [arXiv:1712.07352].
- [122] G. W. Gibbons, S. W. Hawking and J. M. Stewart, Nucl. Phys. **B281**, 736 (1987).
- [123] J. S. Schiffrin and R. M. Wald, Phys. Rev. **D86**, 023521 (2012), [arXiv:1202.1818].
- [124] A. Ijjas, P. J. Steinhardt and A. Loeb, Phys. Lett. **B736**, 142 (2014), [arXiv:1402.6980].
- [125] A. Vilenkin, Phys. Rev. **D27**, 2848 (1983).
- [126] A. D. Linde, Phys. Lett. **B175**, 395 (1986).
- [127] A. S. Goncharov, A. D. Linde and V. F. Mukhanov, Int. J. Mod. Phys. **A2**, 561 (1987).
- [128] A. H. Guth, D. I. Kaiser and Y. Nomura, Phys. Lett. **B733**, 112 (2014), [arXiv:1312.7619].
- [129] A. Linde, in “Proceedings, 100th Les Houches Summer School: Post-Planck Cosmology: Les Houches, France, July 8 - August 2, 2013,” 231–316 (2015), [arXiv:1402.0526].
- [130] J. Martin and R. H. Brandenberger, Phys. Rev. **D63**, 123501 (2001), [hep-th/0005209].
- [131] R. H. Brandenberger and J. Martin, Mod. Phys. Lett. **A16**, 999 (2001), [arXiv:astro-ph/0005432].
- [132] J. Martin and R. H. Brandenberger, in “Recent developments in theoretical and experimental general relativity, gravitation and relativistic field theories. Proceedings, 9th Marcel Grossmann Meeting, MG’9, Rome, Italy, July 2-8, 2000. Pts. A-C,” 2001–2002 (2000), [arXiv:astro-ph/0012031].
- [133] A. Kogut *et al.*, JCAP **1107**, 025 (2011), [arXiv:1105.2044].
- [134] J. Chluba, J. Hamann and S. P. Patil, Int. J. Mod. Phys. **D24**, 10, 1530023 (2015), [arXiv:1505.01834].
- [135] G.-B. Zhao *et al.*, Mon. Not. Roy. Astron. Soc. **457**, 3, 2377 (2016), [arXiv:1510.08216].
- [136] A. Font-Ribera *et al.*, JCAP **1405**, 023 (2014), [arXiv:1308.4164].
- [137] R. Maartens *et al.* (SKA Cosmology SWG), PoS **AASKA14**, 016 (2015), [arXiv:1501.04076].
- [138] O. Doré *et al.* (2014), [arXiv:1412.4872].

## 24. Big Bang Nucleosynthesis

Revised October 2019 by B.D. Fields (Astronomy, Illinois U.; Physics, Illinois U.), P. Molaro (INAF-OATS Trieste) and S. Sarkar (Rudolf Peierls, Oxford U.).

### 24.1 Abstract

Big-Bang nucleosynthesis (BBN) offers the deepest reliable probe of the early Universe, being based on well-understood Standard Model physics [1]. Predictions of the abundances of the light elements, D,  $^3\text{He}$ ,  $^4\text{He}$ , and  $^7\text{Li}$ , synthesized at the end of the *first three minutes*, are in good overall agreement with the primordial abundances inferred from observational data, thus validating the standard hot Big-Bang cosmology (see [2–5] for reviews). This is particularly impressive given that these abundances span nine orders of magnitude – from  $^4\text{He}/\text{H} \sim 0.08$  down to  $^7\text{Li}/\text{H} \sim 10^{-10}$  (ratios by number). Thus BBN provides powerful constraints on possible deviations from the standard cosmology, and on new physics beyond the Standard Model [6–9].

### 24.2 Theory

The synthesis of the light elements is sensitive to physical conditions in the early radiation-dominated era at a temperature  $T \sim 1$  MeV, corresponding to an age  $t \sim 1$  s. At higher temperatures, weak interactions were in thermal equilibrium, thus fixing the ratio of the neutron and proton number densities to be  $n/p = e^{-Q/T}$ , where  $Q = 1.293$  MeV is the neutron-proton mass difference. As the temperature dropped, the neutron-proton inter-conversion rate per nucleon,  $\Gamma_{n \leftrightarrow p} \sim G_{\text{F}}^2 T^5$ , fell faster than the Hubble expansion rate,  $H \sim \sqrt{g_* G_{\text{N}}} T^2$ , where  $g_*$  counts the number of relativistic particle species determining the energy density in radiation (see The Cosmological Parameters—Sec. 22 of this *Review*). This resulted in departure from chemical equilibrium (*freeze-out*) at  $T_{\text{fr}} \sim (g_* G_{\text{N}}/G_{\text{F}}^4)^{1/6} \simeq 1$  MeV. The neutron fraction at this time,  $n/p = e^{-Q/T_{\text{fr}}} \simeq 1/6$ , is thus sensitive to every known physical interaction, since  $Q$  is determined by both strong and electromagnetic interactions while  $T_{\text{fr}}$  depends on the weak as well as gravitational interactions. Moreover, the sensitivity to the Hubble expansion rate affords a probe of, *e.g.*, the number of relativistic neutrino species [10]. After freeze-out, the neutrons were free to  $\beta$ -decay, so the neutron fraction dropped to  $n/p \simeq 1/7$  by the time nuclear reactions began. A simplified analytic model of freeze-out yields the  $n/p$  ratio to an accuracy of  $\sim 1\%$  [11, 12].

The rates of these reactions depend on the density of baryons (strictly speaking, nucleons), which is usually expressed normalized to the relic blackbody photon density as  $\eta \equiv n_b/n_\gamma$ . As we shall see, all the light-element abundances can be explained with  $\eta_{10} \equiv \eta \times 10^{10}$  in the range 5.8–6.5 (95% CL). With  $n_\gamma$  fixed by the present CMB temperature 2.7255 K (see The Cosmological Parameters—Sec. 29 of this *Review*), this can be stated as the allowed range for the baryon mass density today,  $\rho_b = (3.9\text{--}4.6) \times 10^{-31}$  g cm $^{-3}$ , or as the baryonic fraction of the critical density,  $\Omega_b = \rho_b/\rho_{\text{crit}} \simeq \eta_{10} h^{-2}/274 = (0.021\text{--}0.024) h^{-2}$ , where  $h \equiv H_0/100$  km s $^{-1}$  Mpc $^{-1}$  is the present Hubble parameter (see The Cosmological Parameters—Sec. 25.1 of this *Review*).

The nucleosynthesis chain begins with the formation of deuterium in the process  $p(n, \gamma)\text{D}$ . However, photo-dissociation by the high number density of photons delays production of deuterium (and other complex nuclei) until well after  $T$  drops below the binding energy of deuterium,  $\Delta_{\text{D}} = 2.23$  MeV. The quantity  $\eta^{-1} e^{-\Delta_{\text{D}}/T}$ , *i.e.*, the number of photons per baryon above the deuterium photo-dissociation threshold, falls below unity at  $T \simeq 0.1$  MeV; nuclei can then begin to form without being immediately photo-dissociated again. Only 2-body reactions, such as  $\text{D}(p, \gamma)^3\text{He}$  and  $^3\text{He}(\text{D}, p)^4\text{He}$  are important because the density by this time has become rather low – comparable to that of air!

Nearly all neutrons end up bound in the most stable light element  $^4\text{He}$ . Heavier nuclei do not form in any significant quantity both because of the absence of stable nuclei with mass number 5 or 8 (which impedes nucleosynthesis via  $n^4\text{He}$ ,  $p^4\text{He}$  or  $^4\text{He}^4\text{He}$  reactions), and the large Coulomb barriers for reactions such as  $^3\text{He}(^4\text{He}, \gamma)^7\text{Li}$  and  $^3\text{He}(^4\text{He}, \gamma)^7\text{Be}$ . Hence the primordial mass fraction of  $^4\text{He}$ ,  $Y_{\text{p}} \equiv \rho(^4\text{He})/\rho_b$ , can be estimated by the simple

counting argument

$$Y_{\text{p}} = \frac{2(n/p)}{1 + n/p} \simeq 0.25 \quad (24.1)$$

where strictly speaking this gives the baryon fraction in  $^4\text{He}$ , which is what we will quote throughout. This differs slightly from the mass fraction due to small binding energy corrections.

There is little sensitivity here to the actual nuclear reaction rates, which are, however, important in determining the other ‘left-over’ abundances: D and  $^3\text{He}$  at the level of a few times  $10^{-5}$  by number relative to H, and  $^7\text{Li}/\text{H}$  at the level of about  $10^{-10}$  (when  $\eta_{10}$  is in the range 1–10). These values can be understood in terms of approximate analytic arguments [12, 13]. The experimental parameter most important in determining  $Y_{\text{p}}$  is the neutron lifetime,  $\tau_n$ , which normalizes (the inverse of)  $\Gamma_{n \leftrightarrow p}$ . Its value has recently been significantly revised downwards to  $\tau_n = 879.4 \pm 0.6$  s (see *N Baryons Listing*).

The elemental abundances shown in Fig. 24.1 as a function of  $\eta_{10}$  were calculated [14] using an updated version [15] of the Wagoner code [1]; other versions [16–19] too are publicly available. The  $^4\text{He}$  curve includes small corrections due to radiative processes at zero and finite temperatures [20], non-equilibrium neutrino heating during  $e^\pm$  annihilation [21], and finite nucleon mass effects [22]; the range primarily reflects the  $2\sigma$  uncertainty in the neutron lifetime. The spread in the curves for D,  $^3\text{He}$ , and  $^7\text{Li}$  corresponds to the  $2\sigma$  uncertainties in nuclear cross sections, as estimated by Monte Carlo methods [15, 23–25]. The input nuclear data have been carefully reassessed [2, 14, 15, 23–25, 25–29, 29], leading to improved precision for the abundance predictions. In particular, the uncertainty in  $^7\text{Li}/\text{H}$  at interesting values of  $\eta$  has been reduced recently by a factor  $\sim 2$ , a consequence of a similar reduction in the error budget [30] for the dominant mass-7 production channel  $^3\text{He}(^4\text{He}, \gamma)^7\text{Be}$ . Polynomial fits to the predicted abundances and the error correlation matrix have been given in refs. [24, 31]. The boxes in Fig 24.1 show the observationally inferred primordial abundances with their associated uncertainties, as discussed below.

### 24.3 Light Element Abundances

BBN theory predicts the universal abundances of D,  $^3\text{He}$ ,  $^4\text{He}$ , and  $^7\text{Li}$  which are essentially fixed by  $t \sim 180$  s. However, abundances are observed at much later epochs, after stellar nucleosynthesis commenced. Stars produce heavy elements such as C, N, O, and Fe (“metals”), while the ejected remains of stellar processing alters the light element abundances from their primordial values. Thus, one seeks astrophysical sites with low metal abundances to measure light element abundances that are closer to primordial.

BBN is the only significant source of deuterium which is entirely destroyed when it is cycled into stars [32]. Thus, any detection provides a lower limit to primordial D/H, and an upper limit on  $\eta_{10}$ . The best proxy to the primordial value of D is its measure in distant and chemically unprocessed matter, where stellar processing (astration) is minimal [32]. This has become possible with the advent of large telescopes, but after two decades of observational efforts we have only about a dozen determinations listed in Table 24.1 [33–46].

High-resolution spectra reveal the presence of D in high-redshift, low-metallicity quasar absorption systems via its isotope-shifted Lyman- $\alpha$  absorption features, though, unfortunately, these are often obscured or contaminated by the hydrogen features of the Lyman- $\alpha$  forest.

The nuclear reaction cross sections important for BBN have all been measured at the relevant energies. Recently however there have been substantial advances in the precision of light element observations (*e.g.*, D/H) and in the determination of cosmological parameters (*e.g.*, from *Planck*). This motivates corresponding improvement in BBN predictions and thus in the key reaction cross sections. For example, it has been suggested [48, 49] that  $\text{D}(p, \gamma)^3\text{He}$  measurements may suffer from systematic errors and be inferior to *ab initio* theory; if so, this could alter D/H abundances at a level that is now significant. Ongoing low-background cross section measurements should resolve this issue [50].

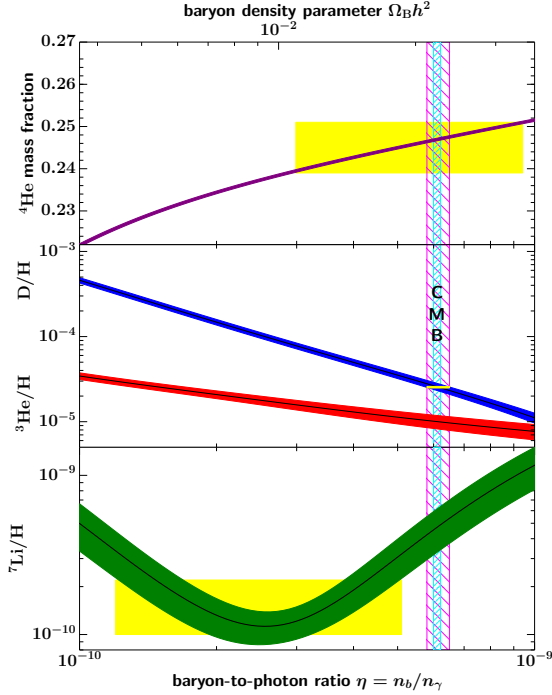


Figure 24.1: The primordial abundances of  ${}^4\text{He}$ , D,  ${}^3\text{He}$ , and  ${}^7\text{Li}$  as predicted by the standard model of Big-Bang nucleosynthesis — the bands show the 95% CL range [47]. Boxes indicate the observed light element abundances. The narrow vertical band indicates the CMB measure of the cosmic baryon density, while the wider band indicates the BBN D+ ${}^4\text{He}$  concordance range (both at 95% CL).

A few DLA systems show D lines resolved up to the higher members of the Lyman series. Recent determinations [37, 39] and re-analyses [38, 46, 51] provide strikingly improved precision over earlier work. A weighted mean of the 11 most precise measurements in Table 24.1 provides a value with a one percent precision:

$$D/H|_p \times 10^6 = (25.47 \pm 0.25). \quad (24.2)$$

Considering all the 16 extant determinations, the weighted mean is  $D/H|_p \times 10^6 = (25.36 \pm 0.26)$ , while different selections provide  $D/H|_p \times 10^6 = (25.27 \pm 0.30)$  [51] or  $D/H|_p \times 10^6 = (25.45 \pm 0.25)$  [52], all consistent with each other within  $1\sigma$ . Metallicities of the absorbers are  $(0.001 - 0.03) \times \text{Solar}$ , i.e. at a level where no significant astration is expected [34, 53]. D/H shows no correlation with metallicity, redshift, or the hydrogen column density  $N(\text{H}) (= \int_{\text{los}} n_{\text{H}} ds)$  integrated over the line-of-sight through the absorber. In the Galaxy D/H measurements are anti-correlated with metal abundances, which suggests that interstellar D partly resides in dust particles [54]. However, in the absorbers where deuterium is measured, the dust content is quite small as implied by Solar proportions of the abundances of refractory and non refractory elements. This is consistent with the measured D/H being truly representative of the primordial value.

The primordial  ${}^4\text{He}$  abundance is best determined through recombination emission lines of He and H in the most metal-poor extragalactic HII (ionized) regions, *viz.* blue compact galaxies, generally found at low redshift. There is now a large body of data on  ${}^4\text{He}$  and CNO in these galaxies, with over 1000 such systems in the Sloan Digital Sky Survey alone [59]. These data confirm that the stellar contribution to the helium abundance is positively correlated with metal production, so extrapolation to zero metallicity gives the primordial  ${}^4\text{He}$  abundance  $Y_p$ . However, HII regions are complex systems and several physical parameters enter in the He/H determination, notably the electron density and temperature, as well as reddening. Thus, systematic effects dominate the uncertainties in the abundance deter-

mination [60, 61]. A major step forward has been the inclusion of the He  $\lambda 10830$  infrared emission line which shows a strong dependence on the electron density and is thus useful to break the degeneracy with the temperature, allowing for a more robust helium abundance determination. In recent works the underlying  ${}^4\text{He}$  stellar absorption, and/or the newly derived values of the HeI-recombination and H-excitation-collisional coefficients are addressed and the  ${}^4\text{He}$  abundances have increased significantly. Some recent results are  $Y_p = 0.2451 \pm 0.0026$  [62],  $Y_p = 0.2449 \pm 0.0040$  [63] and  $Y_p = 0.2551 \pm 0.0022$  [59] — see Ref. [64] and references therein for previous determinations. Taking all this into account our recommended  ${}^4\text{He}$  abundance is

$$Y_p = 0.245 \pm 0.003, \quad (24.3)$$

but the matter is far from settled given that the measurements are only marginally consistent.

The best suited objects for the primordial  ${}^7\text{Li}$  determination are metal-poor stars in the Galactic halo, which have metallicities going down to  $10^{-6}$  of the Solar value [65]. Observations have long shown [66–69] that  ${}^7\text{Li}$  does not vary significantly in halo dwarfs with metallicities  $\lesssim 1/30$  of Solar — the *Spite plateau* [66, 70]. Recent observations show a puzzling drop in the Li/H abundance in metal-poor stars with  $[\text{Fe}/\text{H}] < -3.0$  [71–73]. This becomes particularly acute at the very low metallicity end where only one star out of the seven dwarfs with metallicities  $[\text{Fe}/\text{H}] \lesssim -4.5$  shows a  ${}^7\text{Li}$  abundance close to the Spite Plateau, while in the others where it ought to be present it is either lower or totally absent [65, 74]. The reason for the increase in scatter at low metallicity is unknown and prevents derivation of the primordial  ${}^7\text{Li}$  value by extrapolating to zero metallicity [72, 73].

The primordial  ${}^7\text{Li}$  in different samples of stars or globular clusters has been reported as  $\text{Li}/\text{H}|_p = (1.7 \pm 0.3) \times 10^{-10}$  [69],  $\text{Li}/\text{H}|_p = (2.19 \pm 0.28) \times 10^{-10}$  [75], and  $\text{Li}/\text{H}|_p = (1.86 \pm 0.23) \times 10^{-10}$  [76]. We note that different parameters (*e.g.*, the temperature) of the stellar atmosphere in which the  ${}^7\text{Li}$  absorption line is formed lead to slightly different values. To estimate the primordial  ${}^7\text{Li}$  value we consider only stars with metallicity in the range  $-2.8 < [\text{Fe}/\text{H}] < -1.5$  [73], where no scatter in excess of the observational errors is observed. This yields:

$$\text{Li}/\text{H}|_p = (1.6 \pm 0.3) \times 10^{-10}. \quad (24.4)$$

Strictly speaking the suggested primordial  ${}^7\text{Li}$  abundance should be considered a *lower bound* rather than a measure. In fact,  ${}^7\text{Li}$  in Pop II stars may have been partially destroyed due to mixing of the outer layers with the hotter interior [77]. Such processes can be constrained by the absence of significant scatter in  ${}^7\text{Li}$  versus  $T_{\text{eff}}$  [68], but  ${}^7\text{Li}$  depletion by a factor as large as  $\sim 1.8$  may have occurred [68, 78]. A recent model predicts that an initial  ${}^7\text{Li}$  abundance of  $\text{Li}/\text{H}|_p = 5.3 \times 10^{-10}$ , corresponding to the baryon density indicated by CMB and D/H abundance, is significantly destroyed in the pre-main-sequence phase and then partially restored by late accretion of fresh  ${}^7\text{Li}$  material ending onto the Spite Plateau [79, 80].

A  ${}^6\text{Li}$  plateau (analogous to the  ${}^7\text{Li}$  plateau) has also been claimed [81]. This has however been challenged by new observations and analyses which show that stellar convective motions can generate asymmetries in the line shape that mimic the presence of  ${}^6\text{Li}$  [82–84]. Recent high-precision measurements are sensitive to the tiny isotopic shift in absorption indicate  ${}^6\text{Li}/{}^7\text{Li} \leq 0.05$ , thus confirming that  ${}^7\text{Li}$  is dominant [81, 82].

The primordial abundance of  ${}^3\text{He}$  has the poorest observational determination of all of the light nuclides. The only data available come from the Solar system and from solar-metallicity HII regions in the Galaxy [85]. Therefore, inferring the primordial  ${}^3\text{He}$  abundance is problematic, compounded by the fact that stellar nucleosynthesis models for  ${}^3\text{He}$  are in conflict with observations. Consequently, we consider it inappropriate to use  ${}^3\text{He}$  (and also D+ ${}^3\text{He}$ ) as a cosmological probe.

**Table 24.1:** D/H measurements. For systems with multiple measurements we used the most recent one which is generally more precise.

QSO	$z_{em}$	$z_{em}$	$\log(NHI)$	[X/H]	(D/H) $\times 10^6$	Ref
QSO 2206–199	2.56	2.076	20.436 $\pm$ 0.008	-2.04	16.5 $\pm$ 3.5	[55]
QSO 0347–3819	3.22	3.025	20.63 $\pm$ 0.09	-1.25	22.4 $\pm$ 6.7	[56]
SDSS J1134+5742	3.52	3.411	17.95 $\pm$ 0.05	<-4.2	20.4 $\pm$ 6.1	[41]
QSO CTQ 247	3.02	2.621	20.45 $\pm$ 0.10	-1.99	28.0 $\pm$ 8.0	[43]
SDSS 1337+3152	3.17	3.168	20.41 $\pm$ 0.15	-2.68	12.0 $\pm$ 5.0	[57]
SDSS J1419+0829	3.03	3.049	20.392 $\pm$ 0.003	-1.92	25.1 $\pm$ 0.5	[36]
HS 0105+1619	2.65	2.536	19.40 $\pm$ 0.01	-1.77	25.8 $\pm$ 1.5	[36]
QSO B0913+0715	2.78	2.618	20.312 $\pm$ 0.008	-2.40	25.3 $\pm$ 1.0	[36]
SDSS J1358+0349	2.89	2.853	20.524 $\pm$ 0.006	-2.33	26.2 $\pm$ 0.7	[37]
SDSS J1358+6522	3.17	3.067	20.50 $\pm$ 0.01	-2.33	25.8 $\pm$ 1.0	[36]
SDSS J1558–0031	2.82	2.702	20.75 $\pm$ 0.03	-1.55	24.0 $\pm$ 1.4	[36]
PKS 1937–1009	3.78	3.256	18.09 $\pm$ 0.03	-1.87	24.5 $\pm$ 2.8	[58]
QSO J1444+2919	2.66	2.437	19.983 $\pm$ 0.010	-2.04	19.7 $\pm$ 3.3	[39]
PKS 1937–1009	3.78	3.572	17.925 $\pm$ 0.006	-2.26	26.2 $\pm$ 0.5	[46]
QSO 1009+2956	2.63	2.504	17.362 $\pm$ 0.005	-2.50	24.8 $\pm$ 4.1	[52]
QSO 1243+307	2.55	2.525	19.761 $\pm$ 0.026	-2.77	23.9 $\pm$ 1.0	[51]
Weighted mean of all 16					25.38 $\pm$ 0.25	
Weighted mean of the most recent 11					25.47 $\pm$ 0.25	

## 24.4 Concordance, Dark Matter, and the CMB

We now use the observed light element abundances to test the theory. We first consider standard BBN, which is based on Standard Model physics alone, so  $N_\nu = 3$  and the only free parameter is the baryon-to-photon ratio  $\eta$ . (The implications of BBN for physics beyond the Standard Model will be considered below). Thus, any abundance measurement determines  $\eta$ , and additional measurements overconstrain the theory and thereby provide a consistency check.

While the  $\eta$  ranges spanned by the boxes in Fig 24.1 do not all overlap, they are all within a factor  $\sim 2$  of each other. In particular, the lithium abundance corresponds to  $\eta$  values that are inconsistent with that of the (now very precise) D/H abundance as well as the less-constraining  $^4\text{He}$  abundance. This discrepancy marks the *lithium problem*. The problem could simply reflect difficulty in determining the primordial lithium abundance, or could hint at a more fundamental omission in the theory. The possibility that lithium reveals new physics is addressed in detail in the next section. If however we exclude the lithium constraint because its inferred abundance may suffer from systematic uncertainties, then D/H and  $^4\text{He}$  are in agreement. The concordant  $\eta$  range is essentially that implied by D/H, namely

$$5.8 \leq \eta_{10} \leq 6.5 \text{ (95\% CL)}. \quad (24.5)$$

Despite the lithium problem, the overall concordance remains remarkable: using only well-established microphysics we can extrapolate back to  $t \sim 1$  s to predict light element abundances spanning nine orders of magnitude, in approximate agreement with observation. This is a major success for the standard cosmology, and inspires confidence in extrapolation back to such early times.

This concordance provides a measure of the baryon content:

$$0.021 \leq \Omega_b h^2 \leq 0.024 \text{ (95\% CL)}, \quad (24.6)$$

a result that plays a key role in our understanding of the matter budget of the Universe. First of all  $\Omega_b \ll 1$ , *i.e.*, baryons cannot close the Universe [86]. Furthermore, the cosmic density of (optically) luminous matter is  $\Omega_{\text{lum}} \simeq 0.0024 h^{-1}$  [87], so that  $\Omega_b \gg \Omega_{\text{lum}}$ : most baryons are optically dark, probably in the form of a diffuse intergalactic medium [88]. Finally, given that  $\Omega_m \sim 0.3$  (see Dark Matter and Cosmological Parameters reviews), we infer that most matter in the Universe is not only dark, but also takes some non-baryonic (more precisely, non-nucleonic) form.

The BBN prediction for the cosmic baryon density can be tested through precision measurements of CMB temperature fluctuations (see Cosmic Microwave Background review). One can de-

termine  $\eta$  from the amplitudes of the acoustic peaks in the CMB angular power spectrum [89], making it possible to compare two measures of  $\eta$  using very different physics, at two widely separated epochs. In the standard cosmology, there is no change in  $\eta$  between BBN and CMB decoupling, thus, a comparison of  $\eta_{\text{BBN}}$  and  $\eta_{\text{CMB}}$  is a key test. Agreement would endorse the standard picture, while disagreement could point to new physics during/between the BBN and CMB epochs.

The analysis described in the Cosmic Microwave Background review, based on *Planck* TT, TE, EE + lowE data and lensing, yields  $\Omega_b h^2 = 0.02237 \pm 0.00015$  [90], which corresponds to  $\eta_{10} = 6.12 \pm 0.04$  [91]. This result depends weakly on the primordial helium abundance, and the fiducial *Planck* analysis uses BBN theory to fix  $Y_p(\eta)$ . Without BBN theory, the *Planck* TT, TE, EE + lowE data plus lensing give  $\Omega_b h^2 = 0.02230 \pm 0.00020$ , corresponding to  $\eta_{10} = 6.105 \pm 0.055$ . As shown in Fig. 24.1, this CMB estimate of the baryon density (narrow vertical band) is consistent with the BBN range, *i.e.*, in good agreement with the value inferred from high-redshift D/H measurements and local  $^4\text{He}$  determinations; together these observations span diverse environments from redshifts  $z \sim 1000$  to the present.

The  $^4\text{He}$  abundance is proportional to the  $n/p$  ratio when the weak-interaction rate falls behind the Hubble expansion rate at  $T_{\text{fr}} \sim 1$  MeV. The presence of additional neutrino flavors (or of any other relativistic species) at this time increases  $g_*$ , hence the expansion rate, leading to a larger value of  $T_{\text{fr}}$ ,  $n/p$ , and therefore  $Y_p$  [10, 92]. In the Standard Model at  $T = 1$  MeV,  $g_* = 5.5 + \frac{7}{4} N_\nu$ , where  $N_\nu$  is the *effective* number of (nearly) massless neutrino flavors. The helium curves in 24.1 were computed taking  $N_\nu = 3$ ; small corrections for non-equilibrium neutrino heating [21] are included in the thermal evolution and lead to an effective  $N_\nu = 3.045$  compared to assuming instantaneous neutrino freezeout (see The Cosmological Parameters—Sec. 22 of this Review). The computed  $^4\text{He}$  abundance scales as  $\Delta Y_p \simeq 0.013 \Delta N_\nu$  [11]. Clearly the central value for  $N_\nu$  from BBN will depend on  $\eta$ , which is independently determined (with weaker sensitivity to  $N_\nu$ ) by the adopted D or  $^7\text{Li}$  abundance. For example, if the best value for the observed primordial  $^4\text{He}$  abundance is 0.249, then, for  $\eta_{10} \sim 6$ , the central value for  $N_\nu$  is very close to 3. A maximum likelihood analysis on  $\eta$  and  $N_\nu$  based on  $^4\text{He}$  and D abundances nearly identical to those above finds the (correlated) 95% CL ranges to be  $5.6 < \eta_{10} < 6.6$  and  $2.3 < N_\nu < 3.4$  [5]. Identical results are obtained using a simpler method to extract such bounds based on  $\chi^2$  statistics, given a set of input abundances [93].

The CMB damping tail is sensitive to the primordial  $^4\text{He}$  abundance independently of both BBN and local  $^4\text{He}$  measurements

[94]. The *Planck* analysis using TT, TE, EE+lowE and lensing but not the BBN  $Y_p(\eta)$  relation gives a  ${}^4\text{He}$  mass fraction  $0.239^{+0.024}_{-0.025}$ , and nucleon fraction  $Y_p = 0.240^{+0.24}_{-0.25}$ , both at 95% CL [90]. This is consistent with the HII region helium abundance determination. Moreover, this value is consistent with the Standard ( $N_\nu = 3$ ) BBN prediction for  $Y_p$  with the *Planck*-determined baryon density.

This concordance represents a successful CMB-only test of BBN.

The precision determination of the baryon density using the CMB motivates using this as an input to BBN calculations. Within the context of the Standard Model, BBN then becomes a zero-parameter theory, and the light element abundances are completely determined to within the uncertainties in  $\eta_{\text{CMB}}$  and the BBN theoretical errors. Comparison with the observed abundances then can be used to test the astrophysics of post-BBN light element evolution [95]. Alternatively, one can consider possible physics beyond the Standard Model (*e.g.*, which might change the expansion rate during BBN) and then use all of the abundances to test such models; this is discussed in 23.6 below.

## 24.5 The Lithium Problem

As Fig. 24.1 shows, stellar Li/H measurements are inconsistent with the D/H (and CMB), given the error budgets we have quoted. Recent updates in nuclear cross sections and stellar abundance systematics *increase* the discrepancy to over  $5\sigma$ , depending on the stellar abundance analysis adopted [14]. For instance it is found  $\text{Li}/\text{H}|_p = (5.623 \pm 0.247) \times 10^{-10}$  in [96], *i.e.* a factor 3.5 higher than equation 24.4 and at a  $10\sigma$  CL.

The question then becomes pressing as to whether this mismatch comes from systematic errors in the observed abundances, and/or uncertainties in stellar astrophysics or nuclear inputs, or whether there might be new physics at work [9]. Nuclear inputs (cross sections) for BBN reactions are constrained by extensive laboratory measurements; to increase  ${}^7\text{Be}$  destruction requires enhancement of otherwise subdominant processes that can be attained by missed resonances in a few reactions such as  ${}^7\text{Be}(d, p)2\alpha$  if the compound nuclear state properties are particularly favorable [29, 97–99]. However, experimental searches have now closed off these possibilities [100–102], making a *nuclear fix* increasingly unlikely.

Another conventional means to solve the lithium problem is by *in situ* destruction over the long lifetimes of the host halo stars. Stellar depletion mechanisms include diffusion, rotationally induced mixing, or pre-main-sequence depletion. These effects certainly occur, but to reduce lithium to the required levels generally requires some *ad hoc* mechanism and fine tuning of the initial stellar parameters [79, 80, 103]. A putative signature of diffusion has been reported for the globular clusters NGC 6397 and NGC 6752, where the “turnoff” stars exhibit slightly lower (by a factor  $\sim 1.3$ ) abundances of Fe II TiII, ScII, CaI and MgI, than in more evolved stars [78, 104]. General features of diffusive models are a dispersion in the Li abundances and a pronounced downturn in the Li abundances at the hot end of the Li plateau. Some extra turbulence needs to be invoked to limit diffusion in the hotter stars and to restore uniform Li abundance along the Spite plateau [103]. Li destruction in the pre-Main sequence phase and partially restored by the accretion has been also proposed [80]

As nuclear and astrophysical solutions to the lithium problem become increasingly constrained (even if difficult to rule out definitively), the possibility of new physics arises. Nucleosynthesis models in which the baryon-to-photon ratio is inhomogeneous can alter abundances for a given  $\eta_{\text{BBN}}$ , but will overproduce  ${}^7\text{Li}$  [105]. Entropy generation by some non-standard process could have decreased  $\eta$  between the BBN era and CMB decoupling, however the lack of spectral distortions in the CMB rules out any significant energy injection up to a redshift  $z \sim 10^7$  [106]. The most intriguing resolution of the lithium problem thus involves new physics during BBN [7–9]

We summarize the general features of such solutions here, and later consider examples in the context of specific particle physics models. Many proposed solutions introduce perturbations to light-element formation during BBN; while all element abun-

dances may suffer perturbations, the interplay of  ${}^7\text{Li}$  and D is often the most important *i.e.* observations of D often provide the strongest constraints on the allowed perturbations to  ${}^7\text{Li}$ . In this connection it is important to note that the new, very precise determination of D/H will significantly constrain the ability of such models to ameliorate or solve the lithium problem.

A well studied class of models invokes the injection of suprathermal hadronic or electromagnetic particles due to decays of dark matter particles. The effects are complex and depend on the nature of the decaying particles and their branchings and spectra. However, the models that most successfully solve the lithium problem generally feature non-thermal nucleons, which dissociate all light elements. Dissociation of even a small fraction of  ${}^4\text{He}$  introduces a large abundance of free neutrons, which quickly thermalize. The thermal neutrons drive the  ${}^7\text{Be}(n, p){}^7\text{Li}$  conversion of  ${}^7\text{Be}$ . The resulting  ${}^7\text{Li}$  has a lower Coulomb barrier relative to  ${}^7\text{Be}$  and is readily destroyed via  ${}^7\text{Li}(p, \alpha){}^4\text{He}$  [107, 108]. But  ${}^4\text{He}$  dissociation also produces D directly as well as via nonthermal neutron  $n(p, \gamma)d$  reactions. This introduces a tension between Li/H reduction and D/H enhancement that becomes increasingly restrictive with the increasing precision of deuterium observations. Indeed, this now forces particle injection scenarios to make very small  ${}^7\text{Li}$  perturbations — far short of the level needed. An exception is a recent model wherein MeV-scale decays by construction avoid  ${}^4\text{He}$  dissociation and associated D/H overproduction, instead *borrowing* neutrons by dissociating only deuterons [109].

Another important class of models retains the standard cosmic particle content, but changes their interactions via time variations in the fundamental constants [110–115]. Here too, the details are model-dependent, but scenarios that solve or alleviate the lithium problem often feature perturbations to the deuteron binding energy. A weaker D binding leads to the D bottleneck being overcome later, so that element formation commences at a lower temperature and lower density. This leads in turn to slower nuclear rates that freeze out earlier. The net result is a *higher* final D/H, due to less efficient processing into  ${}^4\text{He}$ , but also *lower* Li, due to suppressed production via  ${}^3\text{He}(\alpha, \gamma){}^7\text{Be}$ .

The *cosmological lithium problem* remains an unresolved issue in BBN. Nevertheless, the remarkable concordance between the CMB and the D (as well as  ${}^4\text{He}$ ) abundance, is a non-trivial success, and provides important constraints on the early Universe.

## 24.6 Beyond the Standard Model

Given the simple physics underlying BBN, it is remarkable that it still provides the most effective test for the cosmological viability of ideas concerning physics beyond the Standard Model. Although baryogenesis and inflation must have occurred at higher temperatures in the early Universe, we do not as yet have ‘standard models’ for these, so BBN still marks the boundary between the established and the speculative in Big Bang cosmology. It might appear possible to push the boundary back to the quark-hadron transition at  $T \sim \Lambda_{\text{QCD}}$ , or electroweak symmetry breaking at  $T \sim 1/\sqrt{G_F}$ ; however, so far no observable relics of these epochs have been identified, either theoretically or observationally. Thus, although the Standard Model provides a precise description of physics up to the Fermi scale, cosmology cannot be traced in detail before the BBN era.

The CMB power spectrum in the damping tail is independently sensitive to  $N_\nu$  (*e.g.* [116]). The CMB value  $N_\nu^{\text{CMB}}$  probes the cosmic radiation content at (re)combination, so a discrepancy would imply new physics or astrophysics. Indeed, observations by the South Pole Telescope implied  $N_\nu^{\text{CMB}} = 3.85 \pm 0.62$  [117], prompting discussion of *dark radiation* such as sterile neutrinos [118]. However, *Planck* 2018 results give  $N_\nu^{\text{CMB}} = 2.92^{+0.36}_{+0.37}$ , 95% CL, when using *Planck* TT, TE, EE+lowE, a result quite consistent with the 3.045 of the Standard Model neutrinos [90].

Just as one can use the measured helium abundance to place limits on  $g_*$  [92, 111, 119–121], any changes in the strong, weak, electromagnetic, or gravitational coupling constants, arising *e.g.*, from the dynamics of new dimensions, can be similarly constrained [122], as can any speed-up of the expansion rate in, *e.g.*, scalar-tensor theories of gravity [123].

The limits on  $N_\nu$  can be translated into limits on other types of particles or particle masses that would affect the expansion rate

of the Universe during nucleosynthesis. For example, consider *sterile* neutrinos with only right-handed interactions of strength  $G_R < G_F$ . Such particles would decouple at higher temperature than (left-handed) neutrinos, so their number density ( $\propto T^3$ ) relative to neutrinos would be reduced by any subsequent entropy release, *e.g.*, due to annihilations of massive particles that become non-relativistic between the two decoupling temperatures. Thus (relativistic) particles with less than full strength weak interactions contribute less to the energy density than particles that remain in equilibrium up to the time of nucleosynthesis [124]. If we impose  $N_\nu < 4$  as an illustrative constraint, then the three right-handed neutrinos must have a temperature  $3(T_{\nu_R}/T_{\nu_L})^4 < 1$ . Since the temperature of the decoupled  $\nu_R$  is determined by entropy conservation (see The Cosmological Parameters—Sec. 22 of this Review),  $T_{\nu_R}/T_{\nu_L} = [(43/4)/g_*(T_d)]^{1/3} < 0.76$ , where  $T_d$  is the decoupling temperature of the  $\nu_R$ . This requires  $g_*(T_d) > 24$ , so decoupling must have occurred at  $T_d > 140$  MeV. The decoupling temperature is related to  $G_R$  through  $(G_R/G_F)^2 \sim (T_d/3 \text{ MeV})^{-3}$ , where 3 MeV is the decoupling temperature for  $\nu_L$ s. This yields a limit  $G_R \lesssim 10^{-2}G_F$ . The above argument sets lower limits on the masses of new  $Z'$  gauge bosons to which right-handed neutrinos would be coupled in models of superstrings [125], or extended technicolour [126]. Similarly a Dirac magnetic moment for neutrinos, which would allow the right-handed states to be produced through scattering and thus increase  $g_*$ , can be significantly constrained [127], as can any new interactions for neutrinos that have a similar effect [128–130]. Right-handed states can be populated directly by helicity-flip scattering if the neutrino mass is large enough, and this property has been used to infer a bound of  $m_{\nu_\tau} \lesssim 1$  MeV (taking  $N_\nu < 4$ ) [131]. If there is mixing between active and sterile neutrinos then the effect on BBN is more complicated [132, 133].

BBN limits on the cosmic expansion rate constrain supersymmetric scenarios in which the neutralino or gravitino are very light, so that they contribute to  $g_*$  [134]. A gravitino in the mass range  $\sim 10^{-4} - 10$  eV will affect the expansion rate of the Universe similarly to a light neutralino (which is however now probably ruled out by collider data, especially the decays of the Higgs-like boson). The net contribution to  $N_\nu$  then ranges between 0.74 and 1.69, depending on the gravitino and slepton masses [135].

The limit on the expansion rate during BBN can also be translated into bounds on the mass/lifetime of non-relativistic particles that decay during BBN. This results in an even faster speed-up rate, and typically also changes the entropy [136–138]. If the decays include Standard Model particles, the resulting electromagnetic [139] [95, 125, 140] and/or hadronic [141, 142] cascades can strongly perturb the light elements, which leads to even stronger constraints. Such arguments have been applied to rule out an MeV mass for  $\nu_\tau$ , which decays during nucleosynthesis [143].

Decaying-particle arguments have proved very effective in probing supersymmetry. Light-element abundances generally are complementary to accelerator data in constraining SUSY parameter space, with BBN reaching to values kinematically inaccessible to the LHC. Much recent interest has focused on the case in which the next-to-lightest supersymmetric particle is metastable and decays during or after BBN. The constraints on unstable particles discussed above imply stringent bounds on the allowed abundance of such particles [107]; if the metastable particle is charged (*e.g.*, the stau), then it is possible for it to form atom-like electromagnetic bound states with nuclei, and the resulting impact on light elements can be quite complex [8, 97, 144]. Moreover, SUSY decays can destroy  ${}^7\text{Li}$  and/or produce  ${}^6\text{Li}$ , leading to a possible supersymmetric solution to the lithium problems noted above [145] (see [7] for a review).

These arguments impose powerful constraints on supersymmetric inflationary cosmology [95, 125, 140–142], particularly thermal leptogenesis [146]. These limits can be evaded only if the gravitino is massive enough to decay before BBN, *i.e.*,  $m_{3/2} \gtrsim 50$  TeV [147] (which would be unnatural), or if it is in fact the lightest supersymmetric particle and thus stable [125, 140, 148, 149]. Similar constraints apply to moduli – very weakly coupled fields in string theory that obtain an electroweak-scale mass from supersymmetry breaking [150].

Finally, we mention that BBN places powerful constraints on the possibility that there are new large dimensions in nature, perhaps enabling the scale of quantum gravity to be as low as the electroweak scale [151]. Thus, Standard Model fields may be localized on a *brane*, while gravity alone propagates in the *bulk*. It has been further noted that the new dimensions may be non-compact, even infinite [152], and the cosmology of such models has attracted considerable attention. The expansion rate in the early Universe can be significantly modified, so BBN is able to set interesting constraints on such possibilities [153, 154].

## References

- [1] R. V. Wagoner, W. A. Fowler and F. Hoyle, *Astrophys. J.* **148**, 3 (1967).
- [2] D. N. Schramm and M. S. Turner, *Rev. Mod. Phys.* **70**, 303 (1998), [arXiv:astro-ph/9706069].
- [3] G. Steigman, *Ann. Rev. Nucl. Part. Sci.* **57**, 463 (2007), [arXiv:0712.1100].
- [4] F. Iocco *et al.*, *Phys. Rept.* **472**, 1 (2009), [arXiv:0809.0631].
- [5] R. H. Cyburt *et al.*, *Rev. Mod. Phys.* **88**, 015004 (2016), [arXiv:1505.01076].
- [6] S. Sarkar, *Rept. on Prog. in Phys.* **59**, 1493 (1996).
- [7] K. Jedamzik and M. Pospelov, *New J. Phys.* **11**, 105028 (2009), [arXiv:0906.2087].
- [8] M. Pospelov and J. Pradler, *Ann. Rev. Nucl. Part. Sci.* **60**, 539 (2010), [arXiv:1011.1054].
- [9] B. D. Fields, *Ann. Rev. Nucl. Part. Sci.* **61**, 47 (2011), [arXiv:1203.3551].
- [10] P. J. E. Peebles, *Phys. Rev. Lett.* **16**, 411 (1966).
- [11] J. Bernstein, L. S. Brown and G. Feinberg, *Rev. Mod. Phys.* **61**, 25 (1989).
- [12] S. Mukhanov, *Int. J. Theor. Phys.* **143**, 669 (2004).
- [13] R. Esmailzadeh, G. D. Starkman and S. Dimopoulos, *Astrophys. J.* **378**, 504 (1991).
- [14] R. H. Cyburt, B. D. Fields and K. A. Olive, *JCAP* **0811**, 012 (2008), [arXiv:0808.2818].
- [15] R. H. Cyburt, B. D. Fields and K. A. Olive, *New Astron.* **6**, 215 (2001), [arXiv:astro-ph/0102179].
- [16] L. Kawano, Technical Report FERMILAB-PUB-92-004-A (1992), URL <https://ui.adsabs.harvard.edu/abs/1992STIN...9225163K>.
- [17] O. Pisanti *et al.*, *Comput. Phys. Commun.* **178**, 956 (2008), [arXiv:0705.0290].
- [18] A. Arbey, *Comput. Phys. Commun.* **183**, 1822 (2012), [arXiv:1106.1363].
- [19] R. Consiglio *et al.*, *Computer Physics Communications* **233**, 237 (2018), [arXiv:1712.04378].
- [20] S. Esposito *et al.*, *Nucl. Phys.* **B568**, 421 (2000), [arXiv:astro-ph/9906232].
- [21] S. Dodelson and M. S. Turner, *Phys. Rev.* **D46**, 3372 (1992).
- [22] D. Seckel (1993), [hep-ph/9305311].
- [23] M. S. Smith, L. H. Kawano and R. A. Malaney, *Astrophys. J. Suppl.* **85**, 219 (1993).
- [24] G. Fiorentini *et al.*, *Phys. Rev.* **D58**, 063506 (1998), [arXiv:astro-ph/9803177].
- [25] A. Coc *et al.*, *Astrophys. J.* **744**, 158 (2012), [arXiv:1107.1117].
- [26] K. M. Nollett and S. Burles, *Phys. Rev.* **D61**, 123505 (2000), [arXiv:astro-ph/0001440].
- [27] R. H. Cyburt, *Phys. Rev.* **D70**, 023505 (2004), [arXiv:astro-ph/0401091].
- [28] P. D. Serpico *et al.*, *JCAP* **0412**, 010 (2004), [arXiv:astro-ph/0408076].
- [29] R. N. Boyd *et al.*, *Phys. Rev.* **D82**, 105005 (2010), [arXiv:1008.0848].

- [30] R.H. Cyburt and B. Davids, *Phys. Rev.* **C78**, 012 (2008).
- [31] S. Burles, K. M. Nollett and M. S. Turner, *Astrophys. J.* **552**, L1 (2001), [arXiv:astro-ph/0010171].
- [32] R. I. Epstein, J. M. Lattimer and D. N. Schramm, *Nature* **263**, 198 (1976).
- [33] S. D’Odorico *et al.*, *Astron. & Astrophys.* **368**, L21 (2001).
- [34] D. Romano *et al.*, *Mon. Not. Roy. Astron. Soc.* **369**, 295 (2006), [arXiv:astro-ph/0603190].
- [35] M. Pettini and D. V. Bowen, *Astrophys. J.* **560**, 41 (2001), [arXiv:astro-ph/0104474].
- [36] R. Cooke *et al.*, *Astrophys. J.* **781**, 1, 31 (2014), [arXiv:1308.3240].
- [37] R. J. Cooke *et al.*, *Astrophys. J.* **830**, 2, 148 (2016), [arXiv:1607.03900].
- [38] E.O. Zavarygin *et al.*, arXiv:1706.09512(2017).
- [39] S. A. Balashev *et al.*, *Mon. Not. Roy. Astron. Soc.* **458**, 2, 2188 (2016), [arXiv:1511.01797].
- [40] S. A. Levshakov *et al.*, *Astrophys. J.* **565**, 696 (2002), [arXiv:astro-ph/0105529].
- [41] M. Fumagalli, J. M. O’Meara and J. X. Prochaska, *Science* **334**, 1245 (2011), [arXiv:1111.2334].
- [42] R. Srianand *et al.*, *Mon. Not. Roy. Astron. Soc.* **405**, 1888 (2010), [arXiv:1002.4620].
- [43] P. Noterdaeme *et al.*, *Astron. & Astrophys.* **542**, L33 (2012), [arXiv:1205.3777].
- [44] M. Pettini and R. Cooke, *Mon. Not. Roy. Astron. Soc.* **425**, 2477 (2012), [arXiv:1205.3785].
- [45] S. Riemer-Sørensen *et al.*, *Mon. Not. Roy. Astron. Soc.* **447**, 2925 (2015), [arXiv:1412.4043].
- [46] S. Riemer-Sørensen *et al.*, *Mon. Not. Roy. Astron. Soc.* **468**, 3, 3239 (2017), [arXiv:1703.06656].
- [47] B. D. Fields *et al.*, *JCAP* (2019).
- [48] K. M. Nollett and G. P. Holder (2011), [arXiv:1112.2683].
- [49] L. E. Marcucci *et al.*, *Phys. Rev. Lett.* **116**, 10, 102501 (2016), [Erratum: *Phys. Rev. Lett.* 117, no.4, 049901(2016)], [arXiv:1510.07877].
- [50] C. Gustavino, *Euro. Phys. J. Web of Conferences*, 136, 01009 (2017).
- [51] R. J. Cooke, M. Pettini and C. C. Steidel, *Astrophys. J.* **855**, 2, 102 (2018), [arXiv:1710.11129].
- [52] E. O. Zavarygin *et al.*, *Mon. Not. R. Astron. Soc* **477**, 4, 5536 (2018), [arXiv:1706.09512].
- [53] F. van de Voort *et al.*, *Mon. Not. R. Astron. Soc* **477**, 1, 80 (2018), [arXiv:1704.08254].
- [54] J. L. Linsky *et al.*, *Astrophys. J.* **647**, 1106 (2006), [arXiv:astro-ph/0608308].
- [55] M. Pettini and D. V. Bowen, *Astrophys. J.* **560**, 1, 41 (2001), [arXiv:astro-ph/0104474].
- [56] S. D’Odorico, M. Dessauges-Zavadsky and P. Molaro, *Astron. & Astrophys.* **368**, L21 (2001), [arXiv:astro-ph/0102162].
- [57] R. Srianand *et al.*, *Mon. Not. R. Astron. Soc* **405**, 3, 1888 (2010), [arXiv:1002.4620].
- [58] S. Riemer-Sørensen *et al.*, *Mon. Not. R. Astron. Soc* **447**, 3, 2925 (2015), [arXiv:1412.4043].
- [59] Y. I. Izotov, T. X. Thuan and N. G. Guseva, *Mon. Not. Roy. Astron. Soc.* **445**, 1, 778 (2014), [arXiv:1408.6953].
- [60] Y. I. Izotov *et al.*, *Astrophys. J.* **527**, 757 (1999), [arXiv:astro-ph/9907228].
- [61] K. A. Olive and E. D. Skillman, *Astrophys. J.* **617**, 29 (2004), [arXiv:astro-ph/0405588].
- [62] M. Valerdi *et al.*, *Astrophys. J.* **876**, 2, 98 (2019), [arXiv:1904.01594].
- [63] E. Aver, K. A. Olive and E. D. Skillman, *JCAP* **1507**, 07, 011 (2015), [arXiv:1503.08146].
- [64] Y.I. Izotov *et al.*, *Astron. & Astrophys.* **558**, A57 (2013).
- [65] D. S. Aguado *et al.*, *Astrophys. J. Lett.* **874**, 2, L21 (2019), [arXiv:1904.04892].
- [66] M. Spite and F. Spite, *Nature* **297**, 483 (1982).
- [67] E. Vangioni-Flam *et al.*, *New Astron.* **4**, 245 (1999), [arXiv:astro-ph/9811327].
- [68] S. G. Ryan *et al.*, *Astrophys. J.* **530**, L57 (2000), [arXiv:astro-ph/9905211].
- [69] P. Bonifacio and P. Molaro, *Mon. Not. Roy. Astron. Soc.* **285**, 847 (1997), [arXiv:astro-ph/9611043].
- [70] R. Rebolo, P. Molaro and J. E. Beckman, *Astron. & Astrophys.* **192**, 192 (1988).
- [71] P. Bonifacio *et al.*, *Astron. & Astrophys.* **462**, 851 (2007).
- [72] W. Aoki *et al.*, *Astrophys. J.* **698**, 1803 (2009), [arXiv:0904.1448].
- [73] L. Sbordone *et al.*, *Astron. & Astrophys.* **522**, A26 (2010).
- [74] P. Bonifacio *et al.*, *Astron. & Astrophys.* **612**, A65 (2018), [arXiv:1801.03935].
- [75] P. Bonifacio *et al.*, *Astron. & Astrophys.* **390**, 91 (2002), [arXiv:astro-ph/0204332].
- [76] J. Melendez *et al.*, *Astron. & Astrophys.* **515**, L3 (2010).
- [77] M.H. Pinsonneault *et al.*, *Astrophys. J.* **574**, 389 (2002).
- [78] A. J. Korn *et al.*, *Nature* **442**, 657 (2006), [arXiv:astro-ph/0608201].
- [79] P. Molaro *et al.*, *Memorie della Soc. Astronomica Italiana Supp.* **22**, 233 (2012).
- [80] X. Fu *et al.*, *Mon. Not. R. Astron. Soc* **452**, 325 (2015).
- [81] M. Asplund *et al.*, *Astrophys. J.* **644**, 229 (2006), [arXiv:astro-ph/0510636].
- [82] K. Lind *et al.*, *Astron. & Astrophys.* **554**, 96 (2013).
- [83] R. Cayrel *et al.*, *Astron. & Astrophys.* **473**, L37 (2007).
- [84] M. Steffen *et al.*, *Memorie della Soc. Astronomica Italiana Supp.* **22**, 152 (2012).
- [85] D. S. Balsa and T. M. Bania, *Astrophys. J.* **156**, 6, 280 (2018), [arXiv:1810.09422].
- [86] H. Reeves *et al.*, *Astrophys. J.* **179**, 909 (1973).
- [87] M. Fukugita and P. J. E. Peebles, *Astrophys. J.* **616**, 643 (2004), [arXiv:astro-ph/0406095].
- [88] R. Cen and J. P. Ostriker, *Astrophys. J.* **514**, 1 (1999), [arXiv:astro-ph/9806281].
- [89] G. Jungman *et al.*, *Phys. Rev.* **D54**, 1332 (1996), [arXiv:astro-ph/9512139].
- [90] Planck Collaboration *et al.*, arXiv e-prints arXiv:1807.06209 (2018), [arXiv:1807.06209].
- [91] P.A.R. Ade *et al.*, *Astron. & Astrophys.* **594**, A13 (2016).
- [92] G. Steigman, D. N. Schramm and J. E. Gunn, *Phys. Lett.* **B66**, 202 (1977), [159(1977)].
- [93] E. Lisi, S. Sarkar and F. L. Villante, *Phys. Rev.* **D59**, 123520 (1999), [hep-ph/9901404].
- [94] R. Trotta and S. H. Hansen, *Phys. Rev.* **D69**, 023509 (2004), [arXiv:astro-ph/0306588].
- [95] R. H. Cyburt, B. D. Fields and K. A. Olive, *Phys. Lett.* **B567**, 227 (2003), [arXiv:astro-ph/0302431].
- [96] C. Pitrou *et al.*, *Phys. Rept.* **754**, 1 (2018), [arXiv:1801.08023].
- [97] R. H. Cyburt *et al.*, *JCAP* **1305**, 014 (2013), [arXiv:1303.0574].
- [98] N. Chakraborty, B. D. Fields and K. A. Olive, *Phys. Rev.* **D83**, 063006 (2011), [arXiv:1011.0722].
- [99] C. Broggin *et al.*, *JCAP* **1206**, 030 (2012), [arXiv:1202.5232].



- [100] P. D. O'Malley *et al.*, Phys. Rev. **C84**, 042801 (2011).
- [101] F. Hammache *et al.*, Phys. Rev. **C88**, 6, 062802 (2013), [arXiv:1312.0894].
- [102] M. W. Paris *et al.*, Nucl. Data Sheets **120**, 184 (2014), [arXiv:1304.3153].
- [103] O. Richard, G. Michaud and J. Richer, Astrophys. J. **619**, 538 (2005), [arXiv:astro-ph/0409672].
- [104] P. Gruyters *et al.*, Astron. Astrophys. **555**, 31 (2013).
- [105] K. Jedamzik and J. B. Rehm, Phys. Rev. **D64**, 023510 (2001), [arXiv:astro-ph/0101292].
- [106] D. J. Fixsen *et al.*, Astrophys. J. **473**, 576 (1996), [arXiv:astro-ph/9605054].
- [107] M. Kawasaki, K. Kohri and T. Moroi, Phys. Rev. **D71**, 083502 (2005), [arXiv:astro-ph/0408426].
- [108] K. Jedamzik, Phys. Rev. **D70**, 063524 (2004), [arXiv:astro-ph/0402344].
- [109] A. Goudelis, M. Pospelov and J. Pradler, Phys. Rev. Lett. **116**, 21, 211303 (2016), [arXiv:1510.08858].
- [110] J. D. Barrow, Phys. Rev. **D35**, 1805 (1987).
- [111] B. A. Campbell and K. A. Olive, Phys. Lett. **B345**, 429 (1995), [hep-ph/9411272].
- [112] L. Bergstrom, S. Iguri and H. Rubinstein, Phys. Rev. **D60**, 045005 (1999), [arXiv:astro-ph/9902157].
- [113] V. V. Flambaum and E. V. Shuryak, Phys. Rev. **D65**, 103503 (2002), [hep-ph/0201303].
- [114] A. Coc *et al.*, Phys. Rev. **D76**, 023511 (2007), [arXiv:astro-ph/0610733].
- [115] J. C. Berengut *et al.*, Phys. Rev. **D87**, 8, 085018 (2013), [arXiv:1301.1738].
- [116] Z. Hou *et al.*, Phys. Rev. **D87**, 083008 (2013), [arXiv:1104.2333].
- [117] R. Keisler *et al.*, Astrophys. J. **743**, 28 (2011), [arXiv:1105.3182].
- [118] J. Hamann *et al.*, Phys. Rev. Lett. **105**, 181301 (2010), [arXiv:1006.5276].
- [119] F. S. Accetta, L. M. Krauss and P. Romanelli, Phys. Lett. **B248**, 146 (1990).
- [120] K. M. Nollett and R. E. Lopez, Phys. Rev. **D66**, 063507 (2002), [arXiv:astro-ph/0204325].
- [121] C. Bambi, M. Giannotti and F. L. Villante, Phys. Rev. **D71**, 123524 (2005), [arXiv:astro-ph/0503502].
- [122] E. W. Kolb, M. J. Perry and T. P. Walker, Phys. Rev. **D33**, 869 (1986).
- [123] A. Coc *et al.*, Phys. Rev. **D73**, 083525 (2006), [arXiv:astro-ph/0601299].
- [124] K. A. Olive, D. N. Schramm and G. Steigman, Nucl. Phys. **B180**, 497 (1981).
- [125] J. R. Ellis *et al.*, Phys. Lett. **167B**, 457 (1986).
- [126] L. M. Krauss, J. Terning and T. Appelquist, Phys. Rev. Lett. **71**, 823 (1993), [hep-ph/9305265].
- [127] J. A. Morgan, Phys. Lett. **102B**, 247 (1981).
- [128] E. W. Kolb, M. S. Turner and T. P. Walker, Phys. Rev. **D34**, 2197 (1986).
- [129] J. A. Grifols and E. Masso, Mod. Phys. Lett. **A2**, 205 (1987).
- [130] K. S. Babu, R. N. Mohapatra and I. Z. Rothstein, Phys. Rev. Lett. **67**, 545 (1991).
- [131] A. D. Dolgov, S. H. Hansen and D. V. Semikoz, Nucl. Phys. **B524**, 621 (1998), [hep-ph/9712284].
- [132] K. Enqvist, K. Kainulainen and M. J. Thomson, Nucl. Phys. **B373**, 498 (1992).
- [133] A. D. Dolgov, Phys. Rept. **370**, 333 (2002), [hep-ph/0202122].
- [134] J. A. Grifols, R. N. Mohapatra and A. Riotto, Phys. Lett. **B400**, 124 (1997), [hep-ph/9612253].
- [135] H. K. Dreiner *et al.*, Phys. Rev. **D85**, 065027 (2012), [arXiv:1111.5715].
- [136] K. Sato and M. Kobayashi, Prog. Theor. Phys. **58**, 1775 (1977).
- [137] D. A. Dicus *et al.*, Phys. Rev. **D17**, 1529 (1978).
- [138] R. J. Scherrer and M. S. Turner, Astrophys. J. **331**, 19 (1988), [Astrophys. J.331,33(1988)].
- [139] D. Lindley, Mon. Not. R. Astron. Soc **188**, 15 (1979).
- [140] J. R. Ellis *et al.*, Nucl. Phys. **B373**, 399 (1992).
- [141] M. H. Reno and D. Seckel, Phys. Rev. **D37**, 3441 (1988).
- [142] S. Dimopoulos *et al.*, Nucl. Phys. **B311**, 699 (1989).
- [143] S. Sarkar and A. M. Cooper-Sarkar, Phys. Lett. **148B**, 347 (1984), [L.362(1984)].
- [144] M. Kawasaki, K. Kohri and T. Moroi, Phys. Lett. **B649**, 436 (2007), [hep-ph/0703122].
- [145] K. Jedamzik *et al.*, JCAP **0607**, 007 (2006), [hep-ph/0512044].
- [146] S. Davidson *et al.*, Phys. Rev. **466**, 105 (2008).
- [147] S. Weinberg, Phys. Rev. Lett. **48**, 1303 (1982).
- [148] R. H. Cyburt *et al.*, Phys. Rev. **D67**, 103521 (2003), [arXiv:astro-ph/0211258].
- [149] M. Bolz, A. Brandenburg and W. Buchmuller, Nucl. Phys. **B606**, 518 (2001), [Erratum: Nucl. Phys. B790,336(2008)], [hep-ph/0012052].
- [150] G. D. Coughlan *et al.*, Physics Letters B **131**, 1-3, 59 (1983).
- [151] N. Arkani-Hamed, S. Dimopoulos and G. R. Dvali, Phys. Rev. **D59**, 086004 (1999), [hep-ph/9807344].
- [152] L. Randall and R. Sundrum, Phys. Rev. Lett. **83**, 3370 (1999), [hep-ph/9905221].
- [153] J. M. Cline, C. Grojean and G. Servant, Phys. Rev. Lett. **83**, 4245 (1999), [hep-ph/9906523].
- [154] P. Binetruy *et al.*, Phys. Lett. **B477**, 285 (2000), [hep-th/9910219].



## 25. Cosmological Parameters

Updated September 2019, by O. Lahav (University College London) and A.R. Liddle (Perimeter Institute for Theoretical Physics and Universidade de Lisboa).

### 25.1 Parametrizing the Universe

Rapid advances in observational cosmology have led to the establishment of a precision cosmological model, with many of the key cosmological parameters determined to one or two significant figure accuracy. Particularly prominent are measurements of cosmic microwave background (CMB) anisotropies, with the highest precision observations being those of the *Planck* Satellite [1, 2] which supersede the landmark *WMAP* results [3, 4]. However the most accurate model of the Universe requires consideration of a range of observations, with complementary probes providing consistency checks, lifting parameter degeneracies, and enabling the strongest constraints to be placed.

The term ‘cosmological parameters’ is forever increasing in its scope, and nowadays often includes the parameterization of some functions, as well as simple numbers describing properties of the Universe. The original usage referred to the parameters describing the global dynamics of the Universe, such as its expansion rate and curvature. Now we wish to know how the matter budget of the Universe is built up from its constituents: baryons, photons, neutrinos, dark matter, and dark energy. We also need to describe the nature of perturbations in the Universe, through global statistical descriptors such as the matter and radiation power spectra. There may be additional parameters describing the physical state of the Universe, such as the ionization fraction as a function of time during the era since recombination. Typical comparisons of cosmological models with observational data now feature between five and ten parameters.

#### 25.1.1 The global description of the Universe

Ordinarily, the Universe is taken to be a perturbed Robertson–Walker space-time, with dynamics governed by Einstein’s equations. This is described in detail in the Big-Bang Cosmology chapter in this volume. Using the density parameters  $\Omega_i$  for the various matter species and  $\Omega_\Lambda$  for the cosmological constant, the Friedmann equation can be written

$$\sum_i \Omega_i + \Omega_\Lambda - 1 = \frac{k}{R^2 H^2}, \quad (25.1)$$

where the sum is over all the different species of material in the Universe. This equation applies at any epoch, but later in this article we will use the symbols  $\Omega_i$  and  $\Omega_\Lambda$  to refer specifically to the present-epoch values.

The complete present-epoch state of the homogeneous Universe can be described by giving the current-epoch values of all the density parameters and the Hubble constant  $h$  (the present-day Hubble parameter being written  $H_0 = 100h \text{ km s}^{-1} \text{ Mpc}^{-1}$ ). A typical collection would be baryons  $\Omega_b$ , photons  $\Omega_\gamma$ , neutrinos  $\Omega_\nu$ , and cold dark matter  $\Omega_c$  (given charge neutrality, the electron density is guaranteed to be too small to be worth considering separately and is effectively included with the baryons). The spatial curvature can then be determined from the other parameters using Eq. (25.1). The total present matter density  $\Omega_m = \Omega_c + \Omega_b$  may be used in place of the cold dark matter density  $\Omega_c$ .

These parameters also allow us to track the history of the Universe, at least back until an epoch where interactions allow interchanges between the densities of the different species; this is believed to have last happened at neutrino decoupling, shortly before Big-Bang Nucleosynthesis (BBN). To probe further back into the Universe’s history requires assumptions about particle interactions, and perhaps about the nature of physical laws themselves.

The standard neutrino sector has three flavors. For neutrinos of mass in the range  $5 \times 10^{-4} \text{ eV}$  to 1 MeV, the density parameter in neutrinos is predicted to be

$$\Omega_\nu h^2 = \frac{\sum m_\nu}{93.14 \text{ eV}}, \quad (25.2)$$

where the sum is over all families with mass in that range (higher masses need a more sophisticated calculation). We use units with

$c = 1$  throughout. Results on atmospheric and Solar neutrino oscillations [5] imply non-zero mass-squared differences between the three neutrino flavors. These oscillation experiments cannot tell us the absolute neutrino masses, but within the simple assumption of a mass hierarchy suggest a lower limit of approximately 0.06 eV for the sum of the neutrino masses (see the Neutrino chapter).

Even a mass this small has a potentially observable effect on the formation of structure, as neutrino free-streaming damps the growth of perturbations. Analyses commonly now either assume a neutrino mass sum fixed at this lower limit, or allow the neutrino mass sum to be a variable parameter. To date there is no decisive evidence of any effects from either neutrino masses or an otherwise non-standard neutrino sector, and observations impose quite stringent limits; see the Neutrinos in Cosmology chapter. However, we note that the inclusion of the neutrino mass sum as a free parameter can affect the derived values of other cosmological parameters.

#### 25.1.2 Inflation and perturbations

A complete model of the Universe should include a description of deviations from homogeneity, at least in a statistical way. Indeed, some of the most powerful probes of the parameters described above come from the evolution of perturbations, so their study is naturally intertwined with the determination of cosmological parameters.

There are many different notations used to describe the perturbations, both in terms of the quantity used to and the definition of the statistical measure. We use the dimensionless power spectrum  $\Delta^2$  as defined in the Big Bang Cosmology section (also denoted  $\mathcal{P}$  in some of the literature). If the perturbations obey Gaussian statistics, the power spectrum provides a complete description of their properties.

From a theoretical perspective, a useful quantity to describe the perturbations is the curvature perturbation  $\mathcal{R}$ , which measures the spatial curvature of a comoving slicing of the space-time. A simple case is the Harrison–Zeldovich spectrum, which corresponds to a constant  $\Delta_{\mathcal{R}}^2$ . More generally, one can approximate the spectrum by a power law, writing

$$\Delta_{\mathcal{R}}^2(k) = \Delta_{\mathcal{R}}^2(k_*) \left[ \frac{k}{k_*} \right]^{n_s - 1}, \quad (25.3)$$

where  $n_s$  is known as the spectral index, always defined so that  $n_s = 1$  for the Harrison–Zeldovich spectrum, and  $k_*$  is an arbitrarily chosen scale. The initial spectrum, defined at some early epoch of the Universe’s history, is usually taken to have a simple form such as this power law, and we will see that observations require  $n_s$  close to one. Subsequent evolution will modify the spectrum from its initial form.

The simplest mechanism for generating the observed perturbations is the inflationary cosmology, which posits a period of accelerated expansion in the Universe’s early stages [6, 7]. It is a useful working hypothesis that this is the sole mechanism for generating perturbations, and it may further be assumed to be the simplest class of inflationary model, where the dynamics are equivalent to that of a single scalar field  $\phi$  with canonical kinetic energy slowly rolling on a potential  $V(\phi)$ . One may seek to verify that this simple picture can match observations and to determine the properties of  $V(\phi)$  from the observational data. Alternatively, more complicated models, perhaps motivated by contemporary fundamental physics ideas, may be tested on a model-by-model basis (see more in the Inflation chapter in this volume).

Inflation generates perturbations through the amplification of quantum fluctuations, which are stretched to astrophysical scales by the rapid expansion. The simplest models generate two types, density perturbations that come from fluctuations in the scalar field and its corresponding scalar metric perturbation, and gravitational waves that are tensor metric fluctuations. The former experience gravitational instability and lead to structure formation, while the latter can influence the CMB anisotropies. Defining slow-roll parameters (with primes indicating derivatives with

respect to the scalar field) as

$$\epsilon = \frac{m_{\text{Pl}}^2}{16\pi} \left( \frac{V'}{V} \right)^2, \quad \eta = \frac{m_{\text{Pl}}^2}{8\pi} \frac{V''}{V}, \quad (25.4)$$

which should satisfy  $\epsilon, |\eta| \ll 1$ , the spectra can be computed using the slow-roll approximation as

$$\Delta_{\mathcal{R}}^2(k) \simeq \frac{8}{3m_{\text{Pl}}^4} \frac{V}{\epsilon} \Big|_{k=aH}, \quad \Delta_{\mathcal{t}}^2(k) \simeq \frac{128}{3m_{\text{Pl}}^4} V \Big|_{k=aH}. \quad (25.5)$$

In each case, the expressions on the right-hand side are to be evaluated when the scale  $k$  is equal to the Hubble radius during inflation. The symbol ‘ $\simeq$ ’ here indicates use of the slow-roll approximation, which is expected to be accurate to a few percent or better.

From these expressions, we can compute the spectral indices [8]:

$$n_s \simeq 1 - 6\epsilon + 2\eta \quad ; \quad n_t \simeq -2\epsilon. \quad (25.6)$$

Another useful quantity is the ratio of the two spectra, defined by

$$r \equiv \frac{\Delta_{\mathcal{t}}^2(k_*)}{\Delta_{\mathcal{R}}^2(k_*)}. \quad (25.7)$$

We have

$$r \simeq 16\epsilon \simeq -8n_t, \quad (25.8)$$

which is known as the consistency equation.

One could consider corrections to the power-law approximation, which we discuss later. However, for now we make the working assumption that the spectra can be approximated by such power laws. The consistency equation shows that  $r$  and  $n_t$  are not independent parameters, and so the simplest inflation models give initial conditions described by three parameters, usually taken as  $\Delta_{\mathcal{R}}^2$ ,  $n_s$ , and  $r$ , all to be evaluated at some scale  $k_*$ , usually the ‘statistical center’ of the range explored by the data. Alternatively, one could use the parametrization  $V$ ,  $\epsilon$ , and  $\eta$ , all evaluated at a point on the putative inflationary potential.

After the perturbations are created in the early Universe, they undergo a complex evolution up until the time they are observed in the present Universe. When the perturbations are small, this can be accurately followed using a linear theory numerical code such as CAMB or CLASS [9]. This works right up to the present for the CMB, but for density perturbations on small scales non-linear evolution is important and can be addressed by a variety of semi-analytical and numerical techniques. However the analysis is made, the outcome of the evolution is in principle determined by the cosmological model and by the parameters describing the initial perturbations, and hence can be used to determine them.

Of particular interest are CMB anisotropies. Both the total intensity and two independent polarization modes are predicted to have anisotropies. These can be described by the radiation angular power spectra  $C_\ell$  as defined in the CMB article in this volume, and again provide a complete description if the density perturbations are Gaussian.

### 25.1.3 The standard cosmological model

We now have most of the ingredients in place to describe the cosmological model. Beyond those of the previous subsections, we need a measure of the ionization state of the Universe. The Universe is known to be highly ionized at low redshifts (otherwise radiation from distant quasars would be heavily absorbed in the ultra-violet), and the ionized electrons can scatter microwave photons, altering the pattern of observed anisotropies. The most convenient parameter to describe this is the optical depth to scattering  $\tau$  (*i.e.*, the probability that a given photon scatters once); in the approximation of instantaneous and complete reionization, this could equivalently be described by the redshift of reionization  $z_{\text{ion}}$ .

As described in Sec. 25.4, models based on these parameters are able to give a good fit to the complete set of high-quality data available at present, and indeed some simplification is possible. Observations are consistent with spatial flatness, and the

inflation models so far described automatically generate negligible spatial curvature, so we can set  $k = 0$ ; the density parameters then must sum to unity, and so one of them can be eliminated. The neutrino energy density is often not taken as an independent parameter; provided that the neutrino sector has the standard interactions, the neutrino energy density, while relativistic, can be related to the photon density using thermal physics arguments, and a minimal assumption takes the neutrino mass sum to be that of the lowest mass solution to the neutrino oscillation constraints, namely 0.06 eV. In addition, there is no observational evidence for the existence of tensor perturbations (though the upper limits are fairly weak), and so  $r$  could be set to zero. This leaves seven parameters, which is the smallest set that can usefully be compared to the present cosmological data. This model is referred to by various names, including  $\Lambda$ CDM, the concordance cosmology, and the standard cosmological model.

Of these parameters, only  $\Omega_\gamma$  is accurately measured directly. The radiation density is dominated by the energy in the CMB, and the COBE satellite FIRAS experiment determined its temperature to be  $T = 2.7255 \pm 0.0006$  K [10],<sup>1</sup> corresponding to  $\Omega_\gamma = 2.47 \times 10^{-5} h^{-2}$ . It typically can be taken as fixed when fitting other data. Hence the minimum number of cosmological parameters varied in fits to data is six, though as described below there may additionally be many ‘nuisance’ parameters necessary to describe astrophysical processes influencing the data.

In addition to this minimal set, there is a range of other parameters that might prove important in future as the data-sets further improve, but for which there is so far no direct evidence, allowing them to be set to specific values for now. We discuss various speculative options in the next section. For completeness at this point, we mention one other interesting quantity, the helium fraction, which is a non-zero parameter that can affect the CMB anisotropies at a subtle level. It is usually fixed in microwave anisotropy studies, but the data are approaching a level where allowing its variation may become mandatory.

Most attention to date has been on parameter estimation, where a set of parameters is chosen by hand and the aim is to constrain them. Interest has been growing towards the higher-level inference problem of model selection, which compares different choices of parameter sets. Bayesian inference offers an attractive framework for cosmological model selection, setting a tension between model predictiveness and ability to fit the data [11].

#### 25.1.4 Derived parameters

The parameter list of the previous subsection is sufficient to give a complete description of cosmological models that agree with observational data. However, it is not a unique parameterization, and one could instead use parameters derived from that basic set. Parameters that can be obtained from the set given above include the age of the Universe, the present horizon distance, the present neutrino background temperature, the epoch of matter–radiation equality, the epochs of recombination and decoupling, the epoch of transition to an accelerating Universe, the baryon-to-photon ratio, and the baryon-to-dark-matter density ratio. In addition, the physical densities of the matter components,  $\Omega_i h^2$ , are often more useful than the density parameters. The density perturbation amplitude can be specified in many different ways other than the large-scale primordial amplitude, for instance, in terms of its effect on the CMB, or by specifying a short-scale quantity, a common choice being the present linear-theory mass dispersion on a scale of  $8 h^{-1}$  Mpc, known as  $\sigma_8$ .

Different types of observation are sensitive to different subsets of the full cosmological parameter set, and some are more naturally interpreted in terms of some of the derived parameters of this subsection than on the original base parameter set. In particular, most types of observation feature degeneracies whereby they are unable to separate the effects of simultaneously varying specific combinations of several of the base parameters.

<sup>1</sup>Unless stated otherwise, all quoted uncertainties in this article are  $1\sigma/68\%$  confidence and all upper limits are 95% confidence. Cosmological parameters sometimes have significantly non-Gaussian uncertainties. Throughout we have rounded central values, and especially uncertainties, from original sources, in cases where they appear to be given to excessive precision.

## 25.2 Extensions to the standard model

At present, there is no positive evidence in favor of extensions of the standard model. These are becoming increasingly constrained by the data, though there always remains the possibility of trace effects at a level below present observational capability.

### 25.2.1 More general perturbations

The standard cosmology assumes adiabatic, Gaussian perturbations. Adiabaticity means that all types of material in the Universe share a common perturbation, so that if the space-time is foliated by constant-density hypersurfaces, then all fluids and fields are homogeneous on those slices, with the perturbations completely described by the variation of the spatial curvature of the slices. Gaussianity means that the initial perturbations obey Gaussian statistics, with the amplitudes of waves of different wavenumbers being randomly drawn from a Gaussian distribution of width given by the power spectrum. Note that gravitational instability generates non-Gaussianity; in this context, Gaussianity refers to a property of the initial perturbations, before they evolve.

The simplest inflation models, based on one dynamical field, predict adiabatic perturbations and a level of non-Gaussianity that is too small to be detected by any experiment so far conceived. For present data, the primordial spectra are usually assumed to be power laws.

#### 25.2.1.1 Non-power-law spectra

For typical inflation models, it is an approximation to take the spectra as power laws, albeit usually a good one. As data quality improves, one might expect this approximation to come under pressure, requiring a more accurate description of the initial spectra, particularly for the density perturbations. In general, one can expand  $\ln \Delta_{\mathcal{R}}^2$  as

$$\ln \Delta_{\mathcal{R}}^2(k) = \ln \Delta_{\mathcal{R}}^2(k_*) + (n_{s,*} - 1) \ln \frac{k}{k_*} + \frac{1}{2} \frac{dn_s}{d \ln k} \Big|_* \ln^2 \frac{k}{k_*} + \dots, \quad (25.9)$$

where the coefficients are all evaluated at some scale  $k_*$ . The term  $dn_s/d \ln k|_*$  is often called the running of the spectral index [12]. Once non-power-law spectra are allowed, it is necessary to specify the scale  $k_*$  at which the spectral index is defined.

#### 25.2.1.2 Isocurvature perturbations

An isocurvature perturbation is one that leaves the total density unperturbed, while perturbing the relative amounts of different materials. If the Universe contains  $N$  fluids, there is one growing adiabatic mode and  $N-1$  growing isocurvature modes (for reviews see Ref. [7] and Ref. [13]). These can be excited, for example, in inflationary models where there are two or more fields that acquire dynamically-important perturbations. If one field decays to form normal matter, while the second survives to become the dark matter, this will generate a cold dark matter isocurvature perturbation.

In general, there are also correlations between the different modes, and so the full set of perturbations is described by a matrix giving the spectra and their correlations. Constraining such a general construct is challenging, though constraints on individual modes are beginning to become meaningful, with no evidence that any other than the adiabatic mode must be non-zero.

#### 25.2.1.3 Seeded perturbations

An alternative to laying down perturbations at very early epochs is that they are seeded throughout cosmic history, for instance by topological defects such as cosmic strings. It has long been excluded that these are the sole original of structure, but they could contribute part of the perturbation signal, current limits being just a few percent [14]. In particular, cosmic defects formed in a phase transition ending inflation is a plausible scenario for such a contribution.

#### 25.2.1.4 Non-Gaussianity

Multi-field inflation models can also generate primordial non-Gaussianity (reviewed, *e.g.*, in Ref. [7]). The extra fields can either be in the same sector of the underlying theory as the inflaton, or completely separate, an interesting example of the latter being the curvaton model [15]. Current upper limits on non-Gaussianity are

becoming stringent, but there remains strong motivation to push down those limits and perhaps reveal trace non-Gaussianity in the data. If non-Gaussianity is observed, its nature may favor an inflationary origin, or a different one such as topological defects.

### 25.2.2 Dark matter properties

Dark matter properties are discussed in the Dark Matter chapter in this volume. The simplest assumption concerning the dark matter is that it has no significant interactions with other matter, and that its particles have a negligible velocity as far as structure formation is concerned. Such dark matter is described as ‘cold,’ and candidates include the lightest supersymmetric particle, the axion, and primordial black holes. As far as astrophysicists are concerned, a complete specification of the relevant cold dark matter properties is given by the density parameter  $\Omega_c$ , though those seeking to detect it directly need also to know its interaction properties.

Cold dark matter is the standard assumption and gives an excellent fit to observations, except possibly on the shortest scales where there remains some controversy concerning the structure of dwarf galaxies and possible substructure in galaxy halos. It has long been excluded for all the dark matter to have a large velocity dispersion, so-called ‘hot’ dark matter, as it does not permit galaxies to form; for thermal relics the mass must be above about 1 keV to satisfy this constraint, though relics produced non-thermally, such as the axion, need not obey this limit. However, in future further parameters might need to be introduced to describe dark matter properties relevant to astrophysical observations. Suggestions that have been made include a modest velocity dispersion (warm dark matter) and dark matter self-interactions. There remains the possibility that the dark matter is comprised of two separate components, *e.g.*, a cold one and a hot one, an example being if massive neutrinos have a non-negligible effect.

### 25.2.3 Relativistic species

The number of relativistic species in the young Universe (omitting photons) is denoted  $N_{\text{eff}}$ . In the standard cosmological model only the three neutrino species contribute, and its baseline value is assumed fixed at 3.045 (the small shift from 3 is because of a slight predicted deviation from a thermal distribution [16]). However other species could contribute, for example an extra neutrino, possibly of sterile type, or massless Goldstone bosons or other scalars. It is hence interesting to study the effect of allowing this parameter to vary, and indeed although 3.045 is consistent with the data, most analyses currently suggest a somewhat higher value (*e.g.*, Ref. [17]).

### 25.2.4 Dark energy

While the standard cosmological model given above features a cosmological constant, in order to explain observations indicating that the Universe is presently accelerating, further possibilities exist under the general headings of ‘dark energy’ and ‘modified gravity’. These topics are described in detail in the Dark Energy chapter in this volume. This article focuses on the case of the cosmological constant, since this simple model is a good match to existing data. We note that more general treatments of dark energy/modified gravity will lead to weaker constraints on other parameters.

### 25.2.5 Complex ionization history

The full ionization history of the Universe is given by the ionization fraction as a function of redshift  $z$ . The simplest scenario takes the ionization to have the small residual value left after recombination up to some redshift  $z_{\text{ion}}$ , at which point the Universe instantaneously reionizes completely. Then there is a one-to-one correspondence between  $\tau$  and  $z_{\text{ion}}$  (that relation, however, also depending on other cosmological parameters). An accurate treatment of this process will track separate histories for hydrogen and helium. While currently rapid ionization appears to be a good approximation, as data improve a more complex ionization history may need to be considered.

### 25.2.6 Varying ‘constants’

Variation of the fundamental constants of Nature over cosmological times is another possible enhancement of the standard cosmology. There is a long history of study of variation of the

gravitational constant  $G_N$ , and more recently attention has been drawn to the possibility of small fractional variations in the fine-structure constant. There is presently no observational evidence for the former, which is tightly constrained by a variety of measurements. Evidence for the latter has been claimed from studies of spectral line shifts in quasar spectra at redshift  $z \approx 2$  [18], but this is presently controversial and in need of further observational study.

### 25.2.7 Cosmic topology

The usual hypothesis is that the Universe has the simplest topology consistent with its geometry, for example that a flat universe extends forever. Observations cannot tell us whether that is true, but they can test the possibility of a non-trivial topology on scales up to roughly the present Hubble scale. Extra parameters would be needed to specify both the type and scale of the topology; for example, a cuboidal topology would need specification of the three principal axis lengths and orientation. At present, there is no evidence for non-trivial cosmic topology [19].

## 25.3 Cosmological Probes

The goal of the observational cosmologist is to utilize astronomical information to derive cosmological parameters. The transformation from the observables to the parameters usually involves many assumptions about the nature of the data, as well as of the dark sector. Below we outline the physical processes involved in each of the major probes, and the main recent results. The first two subsections concern probes of the homogeneous Universe, while the remainder consider constraints from perturbations.

In addition to statistical uncertainties we note three sources of systematic uncertainties that will apply to the cosmological parameters of interest: (i) due to the assumptions on the cosmological model and its priors (*i.e.*, the number of assumed cosmological parameters and their allowed range); (ii) due to the uncertainty in the astrophysics of the objects (*e.g.*, light-curve fitting for supernovae or the mass–temperature relation of galaxy clusters); and (iii) due to instrumental and observational limitations (*e.g.*, the effect of ‘seeing’ on weak gravitational lensing measurements, or beam shape on CMB anisotropy measurements).

These systematics, the last two of which appear as ‘nuisance parameters’, pose a challenging problem to the statistical analysis. We attempt a statistical fit to the whole Universe with 6 to 12 parameters, but we might need to include hundreds of nuisance parameters, some of them highly correlated with the cosmological parameters of interest (for example time-dependent galaxy biasing could mimic the growth of mass fluctuations). Fortunately, there is some astrophysical prior knowledge on these effects, and a small number of physically-motivated free parameters would ideally be preferred in the cosmological parameter analysis.

### 25.3.1 Measures of the Hubble constant

In 1929, Edwin Hubble discovered the law of expansion of the Universe by measuring distances to nearby galaxies. The slope of the relation between the distance and recession velocity is defined to be the present-epoch Hubble constant,  $H_0$ . Astronomers argued for decades about the systematic uncertainties in various methods and derived values over the wide range  $40 \text{ km s}^{-1} \text{ Mpc}^{-1} \lesssim H_0 \lesssim 100 \text{ km s}^{-1} \text{ Mpc}^{-1}$ .

One of the most reliable results on the Hubble constant came from the Hubble Space Telescope (HST) Key Project [20]. This study used the empirical period–luminosity relation for Cepheid variable stars, and calibrated a number of secondary distance indicators—Type Ia Supernovae (SNe Ia), the Tully–Fisher relation, surface-brightness fluctuations, and Type II Supernovae. This approach was further extended, based on HST observations of 70 long-period Cepheids in the Large Magellanic Cloud, combined with Milky Way parallaxes and masers in NGC4258, to yield  $H_0 = 74.0 \pm 1.4 \text{ km s}^{-1} \text{ Mpc}^{-1}$  [21] (the SH0ES project). The major sources of uncertainty in this result are thought to be due to the heavy element abundance of the Cepheids and the distance to the fiducial nearby galaxy, the Large Magellanic Cloud, relative to which all Cepheid distances are measured.

Three other methods have been used recently. One is a calibration of the tip of the red-giant branch applied to Type Ia

supernovae, the Carnegie–Chicago Hubble Programme (CCHP) finding  $H_0 = 69.8 \pm 0.8 \text{ (stat.)} \pm 1.7 \text{ (sys.) km s}^{-1} \text{ Mpc}^{-1}$  [22]. The second uses the method of time delay in six gravitationally-lensed quasars, with the result  $H_0 = 73.3^{+1.7}_{-1.8} \text{ km s}^{-1} \text{ Mpc}^{-1}$  [23] (H0LiCOW). A third method that came to fruition recently is based on gravitational waves; the ‘bright standard siren’ applied to the binary neutron star GW170817 and the ‘dark standard siren’ implemented on the binary black hole GW170814 yield  $H_0 = 70^{+12}_{-8} \text{ km s}^{-1} \text{ Mpc}^{-1}$  [24] and  $H_0 = 75^{+40}_{-32} \text{ km s}^{-1} \text{ Mpc}^{-1}$  [25] respectively. With many more gravitational-wave events the future uncertainties on  $H_0$  from standard sirens will get smaller.

The determination of  $H_0$  by the *Planck* Collaboration [2] gives a lower value,  $H_0 = 67.4 \pm 0.5 \text{ km s}^{-1} \text{ Mpc}^{-1}$ . As discussed in their paper, there is strong degeneracy of  $H_0$  with other parameters, *e.g.*,  $\Omega_m$  and the neutrino mass. It is worth noting that using the ‘inverse distance ladder’ method gives a result  $H_0 = 67.8 \pm 1.3 \text{ km s}^{-1} \text{ Mpc}^{-1}$  [26], close to the *Planck* result. The inverse distance ladder relies on absolute-distance measurements from baryon acoustic oscillations (BAOs) to calibrate the intrinsic magnitude of the SNe Ia (rather than by nearby Cepheids and parallax). This measurement was derived from 207 spectroscopically-confirmed Type Ia supernovae from the Dark Energy Survey (DES), an additional 122 low-redshift SNe Ia, and measurements of BAOs. A combination of DES Y1 clustering and weak lensing with BAO and BBN (assuming  $\Lambda$ CDM) gives  $H_0 = 67.4^{+1.1}_{-1.2} \text{ km s}^{-1} \text{ Mpc}^{-1}$  [27].

The tension between the  $H_0$  values from *Planck* and the traditional cosmic distance ladder methods is of great interest and under investigation. For example, the SH0ES and H0LiCOW+SH0ES results deviate from *Planck* by  $4.4\sigma$  and  $5.3\sigma$  respectively, while the TRGB and standard-siren results lie between the *Planck* and cosmic ladder  $H_0$  values. There is possibly a trend for higher  $H_0$  derived from the nearby Universe and a lower  $H_0$  from the early Universe, which has led some researchers to propose a time-variation of the dark energy component or other exotic scenarios. Ongoing studies are addressing the question of whether the Hubble tension is due to systematics in at least one of the probes, or a signature of new physics.

Figure 25.1 shows a selection of recent  $H_0$  values, adapted from Ref. [28] which provides a very useful summary of the current status of the Hubble constant tension.

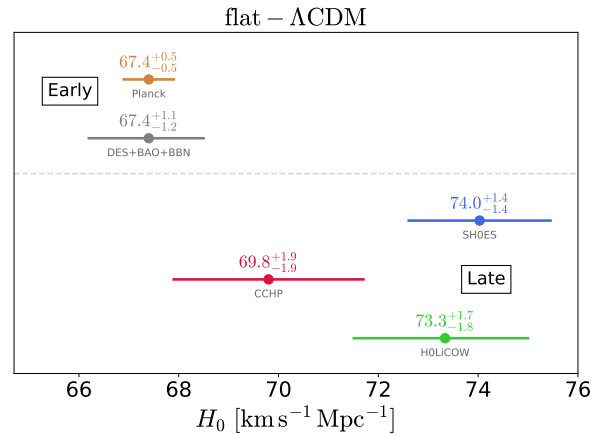


Figure 25.1: A selection of recent  $H_0$  measurements from the various projects as described in the text, divided into early and late Universe probes. The standard-siren determinations are omitted as they are too wide for the plot. Figure courtesy of Vivien Bonvin and Martin Millon, adapted from Ref. [28].

### 25.3.2 Supernovae as cosmological probes

Empirically, the peak luminosity of SNe Ia can be used as an efficient distance indicator (*e.g.*, Ref. [29]), thus allowing cosmology to be constrained via the distance–redshift relation. The favorite theoretical explanation for SNe Ia is the thermonuclear disruption

of carbon–oxygen white dwarfs. Although not perfect ‘standard candles’, it has been demonstrated that by correcting for a relation between the light-curve shape, color, and luminosity at maximum brightness, the dispersion of the measured luminosities can be greatly reduced. There are several possible systematic effects that may affect the accuracy of the use of SNe Ia as distance indicators, *e.g.*, evolution with redshift and interstellar extinction in the host galaxy and in the Milky Way.

Two major studies, the Supernova Cosmology Project and the High- $z$  Supernova Search Team, found evidence for an accelerating Universe [30], interpreted as due to a cosmological constant or a dark energy component. When combined with the CMB data (which indicate near flatness, *i.e.*,  $\Omega_m + \Omega_\Lambda \simeq 1$ ), the best-fit values were  $\Omega_m \approx 0.3$  and  $\Omega_\Lambda \approx 0.7$ . Most results in the literature are consistent with the  $w = -1$  cosmological constant case. One study [31] deduced, from a sample of 740 spectroscopically-confirmed SNe Ia, that  $\Omega_m = 0.295 \pm 0.034$  (stat+sym) for an assumed flat  $\Lambda$ CDM model. An analysis of a sample of spectroscopically-confirmed 207 DES SNe Ia combined with 122 low-redshift SNe [32] yielded  $\Omega_m = 0.331 \pm 0.038$  for an assumed flat  $\Lambda$ CDM model. In combination with the CMB, for a flat  $w$ CDM these data give  $w = -0.978 \pm 0.059$  and  $\Omega_m = 0.321 \pm 0.018$ , consistent with results from the JLA and Pantheon SNe Ia samples. Future experiments will refine constraints on the cosmic equation of state  $w(z)$ .

### 25.3.3 Cosmic microwave background

The physics of the CMB is described in detail in the CMB chapter in this volume. Before recombination, the baryons and photons are tightly coupled, and the perturbations oscillate in the potential wells generated primarily by the dark matter perturbations. After decoupling, the baryons are free to collapse into those potential wells. The CMB carries a record of conditions at the time of last scattering, often called primary anisotropies. In addition, it is affected by various processes as it propagates towards us, including the effect of a time-varying gravitational potential (the integrated Sachs–Wolfe effect), gravitational lensing, and scattering from ionized gas at low redshift.

The primary anisotropies, the integrated Sachs–Wolfe effect, and the scattering from a homogeneous distribution of ionized gas, can all be calculated using linear perturbation theory. Available codes include CAMB and CLASS [9], the former widely used embedded within the analysis package CosmoMC [33] and in higher-level analysis packages such as CosmoSIS [34] and CosmoLike [35]. Gravitational lensing is also calculated in these codes. Secondary effects, such as inhomogeneities in the reionization process, and scattering from gravitationally-collapsed gas (the Sunyaev–Zeldovich or SZ effect), require more complicated, and more uncertain, calculations.

The upshot is that the detailed pattern of anisotropies depends on all of the cosmological parameters. In a typical cosmology, the anisotropy power spectrum [usually plotted as  $\ell(\ell + 1)C_\ell$ ] features a flat plateau at large angular scales (small  $\ell$ ), followed by a series of oscillatory features at higher angular scales, the first and most prominent being at around one degree ( $\ell \simeq 200$ ). These features, known as acoustic peaks, represent the oscillations of the photon–baryon fluid around the time of decoupling. Some features can be closely related to specific parameters—for instance, the location in multipole space of the set of peaks probes the spatial geometry, while the relative heights of the peaks probe the baryon density—but many other parameters combine to determine the overall shape.

The 2018 data release from the *Planck* satellite [1] gives the most powerful results to date on the spectrum of CMB temperature anisotropies, with a precision determination of the temperature power spectrum to beyond  $\ell = 2000$ . The Atacama Cosmology Telescope (ACT) and South Pole Telescope (SPT) experiments extend these results to higher angular resolution, though without full-sky coverage. *Planck* and the polarisation-sensitive versions of ACT and SPT give the state of the art in measuring the spectrum of  $E$ -polarization anisotropies and the correlation spectrum between temperature and polarization. These are consistent with models based on the parameters we have described, and provide accurate determinations of many of those param-

eters [2]. Primordial  $B$ -mode polarization has not been detected (although the gravitational lensing effect on  $B$  modes has been measured).

The data provide an exquisite measurement of the location of the set of acoustic peaks, determining the angular-diameter distance of the last-scattering surface. In combination with other data this strongly constrains the spatial geometry, in a manner consistent with spatial flatness and excluding significantly-curved Universes. CMB data give a precision measurement of the age of the Universe. The CMB also gives a baryon density consistent with, and at higher precision than, that coming from BBN. It affirms the need for both dark matter and dark energy. It shows no evidence for dynamics of the dark energy, being consistent with a pure cosmological constant ( $w = -1$ ). The density perturbations are consistent with a power-law primordial spectrum, and there is no indication yet of tensor perturbations. The current best-fit for the reionization optical depth from CMB data,  $\tau = 0.054$ , is in line with models of how early structure formation induces reionization.

*Planck* has also made the first all-sky map of the CMB lensing field, which probes the entire matter distribution in the Universe and adds some additional constraining power to the CMB-only data-sets. These measurements are compatible with the expected effect in the standard cosmology.

### 25.3.4 Galaxy clustering

The power spectrum of density perturbations is affected by the nature of the dark matter. Within the  $\Lambda$ CDM model, the power spectrum shape depends primarily on the primordial power spectrum and on the combination  $\Omega_m h$ , which determines the horizon scale at matter–radiation equality, with a subdominant dependence on the baryon density. The matter distribution is most easily probed by observing the galaxy distribution, but this must be done with care since the galaxies do not perfectly trace the dark matter distribution. Rather, they are a ‘biased’ tracer of the dark matter [36]. The need to allow for such bias is emphasized by the observation that different types of galaxies show bias with respect to each other. In particular, scale-dependent and stochastic biasing may introduce a systematic effect on the determination of cosmological parameters from redshift surveys [37]. Prior knowledge from simulations of galaxy formation or from gravitational lensing data could help to quantify biasing. Furthermore, the observed 3D galaxy distribution is in redshift space, *i.e.*, the observed redshift is the sum of the Hubble expansion and the line-of-sight peculiar velocity, leading to linear and non-linear dynamical effects that also depend on the cosmological parameters. On the largest length scales, the galaxies are expected to trace the location of the dark matter, except for a constant multiplier  $b$  to the power spectrum, known as the linear bias parameter. On scales smaller than 20 Mpc or so, the clustering pattern is ‘squashed’ in the radial direction due to coherent infall, which depends approximately on the parameter  $\beta \equiv \Omega_m^{0.6}/b$  (on these shorter scales, more complicated forms of biasing are not excluded by the data). On scales of a few Mpc, there is an effect of elongation along the line of sight (colloquially known as the ‘finger of God’ effect) that depends on the galaxy velocity dispersion.

#### 25.3.4.1 Baryon acoustic oscillations

The power spectra of the 2-degree Field (2dF) Galaxy Redshift Survey and the Sloan Digital Sky Survey (SDSS) are well fit by a  $\Lambda$ CDM model and both surveys showed first evidence for baryon acoustic oscillations (BAOs) [38,39]. The Baryon Oscillation Spectroscopic Survey (BOSS) of luminous red galaxies (LRGs) in the SDSS (DR 12) found, using a sample of 1.2 million galaxies, consistency with  $w = -1.01 \pm 0.06$  [40] when combined with *Planck* 2015. Similar results for  $w$  were obtained by the WiggleZ survey [41].

#### 25.3.4.2 Redshift distortion

There is renewed interest in the ‘redshift distortion’ effect. This distortion depends on cosmological parameters [42] via the perturbation growth rate in linear theory  $f(z) = d \ln \delta / d \ln a \approx \Omega^\gamma(z)$ , where  $\gamma \simeq 0.55$  for the  $\Lambda$ CDM model and may be different for modified gravity models. By measuring  $f(z)$  it is feasible to constrain  $\gamma$  and rule out certain modified gravity models [43,44].

We note the degeneracy of the redshift-distortion pattern and the geometric distortion (the so-called Alcock–Paczynski effect [45]) *e.g.*, as illustrated by the WiggleZ survey [46] and the BOSS Survey [47].

#### 25.3.4.3 Limits on neutrino mass from galaxy surveys and other probes

Large-scale structure data place constraints on  $\Omega_\nu$  due to the neutrino free-streaming effect [48]. Presently there is no clear detection, and upper limits on neutrino mass are commonly estimated by comparing the observed galaxy power spectrum with a four-component model of baryons, cold dark matter, a cosmological constant, and massive neutrinos. Such analyses also assume that the primordial power spectrum is adiabatic, scale-invariant, and Gaussian. Potential systematic effects include biasing of the galaxy distribution and non-linearities of the power spectrum. An upper limit can also be derived from CMB anisotropies alone, while combination with additional cosmological data-sets can improve the results.

The most recent results on neutrino mass upper limits and other neutrino properties are summarised in the Neutrinos in Cosmology chapter in this volume. While the latest cosmological data do not yet constrain the sum of neutrino masses to below 0.2 eV, since the lower limit on this sum from oscillation experiments is 0.06 eV it is expected that future cosmological surveys will soon detect effects from the neutrino mass. Also, current cosmological datasets are in good agreement with the standard value for the effective number of neutrino species  $N_{\text{eff}} = 3.045$ .

#### 25.3.5 Clustering in the inter-galactic medium

It is commonly assumed, based on hydrodynamic simulations, that the neutral hydrogen in the inter-galactic medium (IGM) can be related to the underlying mass distribution. It is then possible to estimate the matter power spectrum on scales of a few megaparsecs from the absorption observed in quasar spectra, the so-called Lyman- $\alpha$  forest. The usual procedure is to measure the power spectrum of the transmitted flux, and then to infer the mass power spectrum. Photo-ionization heating by the ultraviolet background radiation and adiabatic cooling by the expansion of the Universe combine to give a simple power-law relation between the gas temperature and the baryon density. It also follows that there is a power-law relation between the optical depth  $\tau$  and  $\rho_b$ . Therefore, the observed flux  $F = \exp(-\tau)$  is strongly correlated with  $\rho_b$ , which itself traces the mass density. The matter and flux power spectra can be related by a biasing function that is calibrated from simulations.

A study of 266,590 quasars in the range  $1.77 < z < 3$  from SDSS was used to measure the BAO scale from the 3D correlation of Lyman- $\alpha$  and quasars [49]. Combined with the Lyman- $\alpha$  auto-correlation measurement presented in a companion paper [50] the BAO measurements at  $z = 2.34$  are within  $1.7\sigma$  of the *Planck* 2018  $\Lambda$ CDM model. The Lyman- $\alpha$  flux power spectrum has also been used to constrain the nature of dark matter, for example limiting the amount of warm dark matter [51].

#### 25.3.6 Weak gravitational lensing

Images of background galaxies are distorted by the gravitational effect of mass variations along the line of sight. Deep gravitational potential wells, such as galaxy clusters, generate ‘strong lensing’ leading to arcs, arcllets, and multiple images, while more moderate perturbations give rise to ‘weak lensing’. Weak lensing is now widely used to measure the mass power spectrum in selected regions of the sky (see Ref. [55] for reviews). Since the signal is weak, the image of deformed galaxy shapes (the ‘shear map’) must be analyzed statistically to measure the power spectrum, higher moments, and cosmological parameters. There are various systematic effects in the interpretation of weak lensing, *e.g.*, due to atmospheric distortions during observations, the redshift distribution of the background galaxies (usually depending on the accuracy of photometric redshifts), the intrinsic correlation of galaxy shapes, and non-linear modeling uncertainties.

As one example, the ‘Kilo-Degree Survey’ (KiDS), combined with the VISTA VIKING survey, used weak-lensing measure-

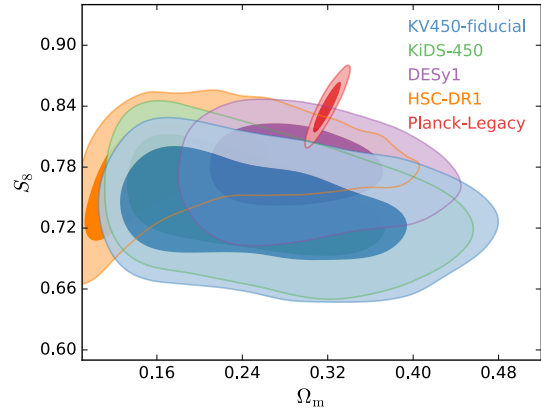


Figure 25.2: Marginalised posterior contours (inner 68% confidence level, outer 95% confidence level) in the  $\Omega_m$ – $S_8$  plane. Shown are the optical-only KiDS-450 analysis (green; Ref. [52]), the fiducial KiDS+VISTA-450 setup (blue; Ref. [52]), DES Year 1 using cosmic shear only (purple; Ref. [53]), HSC-DR1 cosmic shear (orange; Ref. [54]) and the *Planck* Legacy analysis (red; *Planck* Collaboration [2] using TT+TE+EE+lowE). Figure from Ref. [52].

ments over  $450 \text{ deg}^2$  to constrain the clumpiness parameter  $S_8 \equiv \sigma_8(\Omega_m/0.3)^{0.5} = 0.737^{+0.040}_{-0.036}$  [52]. This is lower by  $2.3\sigma$  than  $S_8$  derived from *Planck*. Figure 25.2 (which is Figure 4 from Ref. [52]) shows the  $\Omega_m$ – $S_8$  constraints derived from weak lensing of KiDS, DES, and HPC versus the CMB constraint from *Planck*. Variations in  $S_8$  among the weak-lensing surveys are mainly due to difference in the procedures for photometric redshift determinations. Results from weak lensing from DES, combined with other probes, are shown in the next section.

#### 25.3.7 Other probes

Other probes that have been used to constrain cosmological parameters, but that are not presently competitive in terms of accuracy, are the integrated Sachs–Wolfe effect [56] [57], the number density or composition of galaxy clusters [58], and galaxy peculiar velocities, which probe the mass fluctuations in the local Universe [59].

### 25.4 Bringing probes together

Although it contains two ingredients—dark matter and dark energy—which have not yet been verified by laboratory experiments, the  $\Lambda$ CDM model is almost universally accepted by cosmologists as the best description of the present data. The approximate values of some of the key parameters are  $\Omega_b \approx 0.05$ ,  $\Omega_c \approx 0.25$ ,  $\Omega_\Lambda \approx 0.70$ , and a Hubble constant  $h \approx 0.70$ . The spatial geometry is very close to flat (and usually assumed to be precisely flat), and the initial perturbations Gaussian, adiabatic, and nearly scale-invariant.

The most powerful data source is the CMB, which on its own supports all these main tenets. Values for some parameters, as given in Ref. [2], are reproduced in Table 25.1. These particular results presume a flat Universe. The constraints are somewhat strengthened by adding additional data-sets, BAO being shown in the Table as an example, though most of the constraining power resides in the CMB data. Similar constraints at lower precision were previously obtained by the *WMAP* collaboration.

If the assumption of spatial flatness is lifted, it turns out that the primary CMB on its own constrains the spatial curvature fairly weakly, due to a parameter degeneracy in the angular-diameter distance. However, inclusion of other data readily removes this degeneracy. Simply adding the *Planck* lensing measurement, and with the assumption that the dark energy is a cosmological constant, yields a 68% confidence constraint on  $\Omega_{\text{tot}} \equiv \sum \Omega_i + \Omega_\Lambda = 1.011 \pm 0.006$  and further adding BAO makes it  $0.9993 \pm 0.0019$  [2]. Results of this type are normally taken as justifying the restriction to flat cosmologies.

One derived parameter that is very robust is the age of the



**Table 25.1:** Parameter constraints reproduced from Ref. [2] (Table 2, column 5), with some additional rounding. Both columns assume the  $\Lambda$ CDM cosmology with a power-law initial spectrum, no tensors, spatial flatness, a cosmological constant as dark energy, and the sum of neutrino masses fixed to 0.06 eV. Above the line are the six parameter combinations actually fit to the data ( $\theta_{\text{MC}}$  is a measure of the sound horizon at last scattering); those below the line are derived from these. The first column uses *Planck* primary CMB data plus the *Planck* measurement of CMB lensing. This column gives our present recommended values. The second column adds in data from a compilation of BAO measurements described in Ref. [2]. The perturbation amplitude  $\Delta_{\mathcal{R}}^2$  (denoted  $A_s$  in the original paper) is specified at the scale  $0.05 \text{ Mpc}^{-1}$ . Uncertainties are shown at 68% confidence.

	<i>Planck</i> TT,TE,EE+lowE+lensing	+BAO
$\Omega_b h^2$	$0.02237 \pm 0.00015$	$0.02242 \pm 0.00014$
$\Omega_c h^2$	$0.1200 \pm 0.0012$	$0.1193 \pm 0.0009$
$100 \theta_{\text{MC}}$	$1.0409 \pm 0.0003$	$1.0410 \pm 0.0003$
$n_s$	$0.965 \pm 0.004$	$0.966 \pm 0.004$
$\tau$	$0.054 \pm 0.007$	$0.056 \pm 0.007$
$\ln(10^{10} \Delta_{\mathcal{R}}^2)$	$3.044 \pm 0.014$	$3.047 \pm 0.014$
$h$	$0.674 \pm 0.005$	$0.677 \pm 0.004$
$\sigma_8$	$0.811 \pm 0.006$	$0.810 \pm 0.006$
$\Omega_m$	$0.315 \pm 0.007$	$0.311 \pm 0.006$
$\Omega_\Lambda$	$0.685 \pm 0.007$	$0.689 \pm 0.006$

Universe, since there is a useful coincidence that for a flat Universe the position of the first peak is strongly correlated with the age. The CMB data give  $13.797 \pm 0.023$  Gyr (assuming flatness). This is in good agreement with the ages of the oldest globular clusters and with radioactive dating.

The baryon density  $\Omega_b$  is now measured with high accuracy from CMB data alone, and is consistent with and much more precise than the determination from BBN. The value quoted in the Big-Bang Nucleosynthesis chapter in this volume is  $0.021 \leq \Omega_b h^2 \leq 0.024$  (95% confidence).

While  $\Omega_\Lambda$  is measured to be non-zero with very high confidence, there is no evidence of evolution of the dark energy density. As described in the Dark Energy chapter in this volume, from a combination of CMB, weak gravitational lensing, SN, and BAO measurements, assuming a flat universe, Ref. [2] found  $w = -1.028 \pm 0.031$ , consistent with the cosmological constant case  $w = -1$ . Allowing more complicated forms of dark energy weakens the limits.

The data provide strong support for the main predictions of the simplest inflation models: spatial flatness and adiabatic, Gaussian, nearly scale-invariant density perturbations. But it is disappointing that there is no sign of primordial gravitational waves, with a 95% confidence upper limit from combining *Planck* with BICEP2/Keck Array BK15 data of  $r < 0.06$  at the scale  $0.002 \text{ Mpc}^{-1}$  [60] (weakening somewhat if running is allowed). The spectral index is clearly required to be less than one by current data, though the strength of that conclusion can weaken if additional parameters are included in the model fits.

Tests have been made for various types of non-Gaussianity, a particular example being a parameter  $f_{\text{NL}}$  that measures a quadratic contribution to the perturbations. Various non-Gaussian shapes are possible (see Ref. [61] for details), and current constraints on the popular ‘local’, ‘equilateral’, and ‘orthogonal’ types (combining temperature and polarization data) are  $f_{\text{NL}}^{\text{local}} = -1 \pm 5$ ,  $f_{\text{NL}}^{\text{equil}} = -26 \pm 47$ , and  $f_{\text{NL}}^{\text{ortho}} = -38 \pm 24$  respectively (these look weak, but prominent non-Gaussianity requires the product  $f_{\text{NL}} \Delta_{\mathcal{R}}$  to be large, and  $\Delta_{\mathcal{R}}$  is of order  $10^{-5}$ ). Clearly none of these give any indication of primordial non-gaussianity.

While the above results come from the CMB alone, other probes are becoming competitive (especially when considering more complex cosmological models), and so combination of data from different sources is of growing importance. We note that it has become fashionable to combine probes at the level of power-spectrum data vectors, taking into account nuisance parameters in each type of measurement. Recent examples include KiDS+GAMA [62] and Dark Energy Survey (DES) Year 1 [63]. For example, the DES analysis includes galaxy position–position clustering, galaxy–galaxy lensing, and weak lensing shear. Discussions on ‘tension’ in resulting cosmological parameters depend on the statistical approaches used. Commonly the cosmology community works within the Bayesian framework, and assesses agreement amongst data sets with respect to a model via Bayesian Evidence, essentially the denominator in Bayes’s theorem. As an example of results, combining DES Y1 with *Planck*, BAO measurements from SDSS, 6dF, and BOSS, and type Ia supernovae from the Joint Lightcurve Analysis (JLA) dataset has shown the datasets to be mutually compatible and yields very tight constraints on cosmological parameters:  $S_8 \equiv \sigma_8 (\Omega_m/0.3)^{0.5} = 0.799_{-0.009}^{+0.014}$ , and  $\Omega_m = 0.301_{-0.008}^{+0.006}$  in  $\Lambda$ CDM, and  $w = -1.00_{-0.05}^{+0.04}$  in  $w$ CDM [63]. The combined measurement of the Hubble constant within  $\Lambda$ CDM gives  $H_0 = 68.2 \pm 0.6 \text{ km s}^{-1} \text{ Mpc}^{-1}$ , still leaving some level of tension with the local measurements described earlier. Future analyses and the next generation of surveys will test for deviations from  $\Lambda$ CDM, for example epoch-dependent  $w(z)$  and modifications to General Relativity.

## 25.5 Outlook for the future

The concordance model is now well established, and there seems little room left for any dramatic revision of this paradigm. A measure of the strength of that statement is how difficult it has proven to formulate convincing alternatives.

Should there indeed be no major revision of the current paradigm, we can expect future developments to take one of two directions. Either the existing parameter set will continue to prove sufficient to explain the data, with the parameters subject to ever-tightening constraints, or it will become necessary to deploy new parameters. The latter outcome would be very much the more interesting, offering a route towards understanding new physical processes relevant to the cosmological evolution. There are many possibilities on offer for striking discoveries, for example:

- the cosmological effects of a neutrino mass may be unambiguously detected, shedding light on fundamental neutrino properties;
- detection of primordial non-Gaussianities would indicate that non-linear processes influence the perturbation generation mechanism;
- detection of variation in the dark-energy density (*i.e.*,  $w \neq -1$ ) would provide much-needed experimental input into its nature.

These provide more than enough motivation for continued efforts to test the cosmological model and improve its accuracy. Over the coming years, there are a wide range of new observations that will bring further precision to cosmological studies. Indeed, there are far too many for us to be able to mention them all here, and so we will just highlight a few areas.

The CMB observations will improve in several directions. A current frontier is the study of polarization, for which power spectrum measurements have now been made by several experiments. Detection of primordial  $B$ -mode anisotropies is the next major goal and a variety of projects are targeting this, though theory gives little guidance as to the likely signal level. Future CMB projects that are approved include *LiteBIRD* and the Simons Observatory.

An impressive array of cosmology surveys are already operational, under construction, or proposed, including the ground-based Hyper Suprime Camera (HSC) and Large Synoptic Survey Telescope (LSST) imaging surveys, spectroscopic surveys such as the Dark Energy Spectroscopic Instrument (DESI), and space missions *Euclid* and the Wide-Field Infrared Survey (WFIRST).

An exciting area for the future is radio surveys of the redshifted 21-cm line of hydrogen. Because of the intrinsic narrowness of this line, by tuning the bandpass the emission from narrow redshift slices of the Universe will be measured to extremely high redshift, probing the details of the reionization process at redshifts up to perhaps 20, as well as measuring large-scale features such as the BAOs. LOFAR and CHIME are the first instruments able to do this and have begun operations. In the longer term, the Square Kilometre Array (SKA) will take these studies to a precision level.

The development of the first precision cosmological model is a major achievement. However, it is important not to lose sight of the motivation for developing such a model, which is to understand the underlying physical processes at work governing the Universe's evolution. From that perspective, progress has been much less dramatic. For instance, there are many proposals for the nature of the dark matter, but no consensus as to which is correct. The nature of the dark energy remains a mystery. Even the baryon density, now measured to an accuracy of a percent, lacks an underlying theory able to predict it within orders of magnitude. Precision cosmology may have arrived, but at present many key questions remain to motivate and challenge the cosmology community.

### References

- [1] Y. Akrami *et al.* (Planck) (2018), [arXiv:1807.06205].
- [2] N. Aghanim *et al.* (Planck) (2018), [arXiv:1807.06209].
- [3] C. L. Bennett *et al.* (WMAP), *Astrophys. J. Suppl.* **208**, 20 (2013), [arXiv:1212.5225].
- [4] G. Hinshaw *et al.* (WMAP), *Astrophys. J. Suppl.* **208**, 19 (2013), [arXiv:1212.5226].
- [5] S. Fukuda *et al.* (Super-Kamiokande), *Phys. Rev. Lett.* **85**, 3999 (2000), [hep-ex/0009001]; Q. R. Ahmad *et al.* (SNO), *Phys. Rev. Lett.* **87**, 071301 (2001), [arXiv:nucl-ex/0106015].
- [6] E.W. Kolb and M.S. Turner, *The Early Universe*, Addison-Wesley (Redwood City, 1990).
- [7] D.H. Lyth and A.R. Liddle, *The Primordial Density Perturbation*, Cambridge University Press (2009).
- [8] A. R. Liddle and D. H. Lyth, *Phys. Lett.* **B291**, 391 (1992), [arXiv:astro-ph/9208007].
- [9] A. Lewis, A. Challinor and A. Lasenby, *Astrophys. J.* **538**, 473 (2000), [arXiv:astro-ph/9911177]; D. Blas, J. Lesgourgues and T. Tram, *JCAP* **1107**, 034 (2011), [arXiv:1104.2933].
- [10] D. J. Fixsen, *Astrophys. J.* **707**, 916 (2009), [arXiv:0911.1955].
- [11] M. Hobson *et al.* (eds), *Bayesian Methods in Cosmology*, Cambridge University Press (2009).
- [12] A. Kosowsky and M. S. Turner, *Phys. Rev.* **D52**, R1739 (1995), [arXiv:astro-ph/9504071].
- [13] K. A. Malik and D. Wands, *Phys. Rept.* **475**, 1 (2009), [arXiv:0809.4944].
- [14] P. A. R. Ade *et al.* (Planck), *Astron. Astrophys.* **571**, A25 (2014), [arXiv:1303.5085].
- [15] D. H. Lyth and D. Wands, *Phys. Lett.* **B524**, 5 (2002), [hep-ph/0110002]; K. Enqvist and M. S. Sloth, *Nucl. Phys.* **B626**, 395 (2002), [hep-ph/0109214]; T. Moroi and T. Takahashi, *Phys. Lett.* **B522**, 215 (2001), [Erratum: *Phys. Lett.* **B539**, 303 (2002)], [hep-ph/0110096].
- [16] P. F. de Salas and S. Pastor, *JCAP* **1607**, 07, 051 (2016), [arXiv:1606.06986].
- [17] S. Riemer-Sørensen, D. Parkinson, and T.M. Davis, *Publications of Astronomical Society of the Pacific* **30**, e029 (2013).
- [18] J. K. Webb *et al.*, *Phys. Rev. Lett.* **107**, 191101 (2011), [arXiv:1008.3907]; J. A. King *et al.*, *Mon. Not. Roy. Astron. Soc.* **422**, 3370 (2012), [arXiv:1202.4758]; P. Molaro *et al.*, *Astron. & Astrophys.* **555**, 68 (2013).
- [19] P. A. R. Ade *et al.* (Planck), *Astron. Astrophys.* **594**, A18 (2016), [arXiv:1502.01593].
- [20] W. L. Freedman *et al.* (HST), *Astrophys. J.* **553**, 47 (2001), [arXiv:astro-ph/0012376].
- [21] A. G. Riess *et al.*, *Astrophys. J.* **876**, 1, 85 (2019), [arXiv:1903.07603].
- [22] W.L. Freedman *et al.*, *Astrophys. J.* **882**, 34 (2019).
- [23] K. C. Wong *et al.* (2019), [arXiv:1907.04869].
- [24] B. P. Abbott *et al.* (LIGO Scientific, Virgo, 1M2H, Dark Energy Camera GW-E, DES, DLT40, Las Cumbres Observatory, VINROUGE, MASTER), *Nature* **551**, 7678, 85 (2017), [arXiv:1710.05835].
- [25] M. Soares-Santos *et al.* (DES, LIGO Scientific, Virgo), *Astrophys. J.* **876**, 1, L7 (2019), [arXiv:1901.01540].
- [26] E. Macaulay *et al.* (DES), *Mon. Not. Roy. Astron. Soc.* **486**, 2, 2184 (2019), [arXiv:1811.02376].
- [27] T. M. C. Abbott *et al.* (DES), *Mon. Not. Roy. Astron. Soc.* **480**, 3, 3879 (2018), [arXiv:1711.00403].
- [28] L. Verde, T. Treu and A. G. Riess, in "Nature Astronomy 2019," (2019), [arXiv:1907.10625].
- [29] B. Leibundgut, *Ann. Rev. Astron. Astrophys.* **39**, 67 (2001).
- [30] A. G. Riess *et al.* (Supernova Search Team), *Astron. J.* **116**, 1009 (1998), [arXiv:astro-ph/9805201]; P. M. Garnavich *et al.* (Supernova Search Team), *Astrophys. J.* **509**, 74 (1998), [arXiv:astro-ph/9806396]; S. Perlmutter *et al.* (Supernova Cosmology Project), *Astrophys. J.* **517**, 565 (1999), [arXiv:astro-ph/9812133].
- [31] M. Betoule *et al.* (SDSS), *Astron. Astrophys.* **568**, A22 (2014), [arXiv:1401.4064].
- [32] T. M. C. Abbott *et al.* (DES), *Astrophys. J.* **872**, 2, L30 (2019), [arXiv:1811.02374].
- [33] A. Lewis and S. Bridle, *Phys. Rev.* **D66**, 103511 (2002), [arXiv:astro-ph/0205436].
- [34] J. Zuntz *et al.*, *Astron. Comput.* **12**, 45 (2015), [arXiv:1409.3409].
- [35] E. Krause and T. Eifler, *Mon. Not. Roy. Astron. Soc.* **470**, 2, 2100 (2017), [arXiv:1601.05779].
- [36] N. Kaiser, *Astrophys. J.* **284**, L9 (1984).
- [37] A. Dekel and O. Lahav, *Astrophys. J.* **520**, 24 (1999), [arXiv:astro-ph/9806193].
- [38] D. J. Eisenstein *et al.* (SDSS), *Astrophys. J.* **633**, 560 (2005), [arXiv:astro-ph/0501171].
- [39] S. Cole *et al.* (2dFGRS), *Mon. Not. Roy. Astron. Soc.* **362**, 505 (2005), [arXiv:astro-ph/0501174].
- [40] S. Alam *et al.* (BOSS), *Mon. Not. Roy. Astron. Soc.* **470**, 3, 2617 (2017), [arXiv:1607.03155].
- [41] D. Parkinson *et al.*, *Phys. Rev.* **D86**, 103518 (2012), [arXiv:1210.2130].
- [42] N. Kaiser, *Mon. Not. Roy. Astron. Soc.* **227**, 1 (1987).
- [43] L. Guzzo *et al.*, *Nature* **451**, 541 (2008), [arXiv:0802.1944].
- [44] A. Nusser and M. Davis, *Astrophys. J.* **736**, 93 (2011), [arXiv:1101.1650].
- [45] C. Alcock and B. Paczynski, *Nature* **281**, 358 (1979).
- [46] C. Blake *et al.*, *Mon. Not. Roy. Astron. Soc.* **425**, 405 (2012), [arXiv:1204.3674].
- [47] H. Gil-Marín *et al.*, *Mon. Not. Roy. Astron. Soc.* **465**, 2, 1757 (2017), [arXiv:1606.00439].
- [48] J. Lesgourgues and S. Pastor, *Phys. Rept.* **429**, 307 (2006), [arXiv:astro-ph/0603494].
- [49] M. Blomqvist *et al.*, *Astron. Astrophys.* **629**, A86 (2019), [arXiv:1904.03430].
- [50] V. de Sainte Agathe *et al.*, *Astron. Astrophys.* **629**, A85 (2019), [arXiv:1904.03400].
- [51] M. Viel *et al.*, *Phys. Rev.* **D88**, 043502 (2013), [arXiv:1306.2314].



- [52] H. Hildebrandt *et al.*, *Astron. Astrophys.* **633**, A69 (2020), [arXiv:1812.06076].
- [53] M. A. Troxel *et al.* (DES), *Phys. Rev.* **D98**, 4, 043528 (2018), [arXiv:1708.01538].
- [54] Higake M. *et al.*, *Pub. Astron. Soc. Japan* **71**, 43 (2018).
- [55] A. Refregier, *Ann. Rev. Astron. Astrophys.* **41**, 645 (2003), [arXiv:astro-ph/0307212]; R. Massey *et al.*, *Nature* **445**, 286 (2007), [arXiv:astro-ph/0701594]; H. Hoekstra and B. Jain, *Ann. Rev. Nucl. Part. Sci.* **58**, 99 (2008), [arXiv:0805.0139].
- [56] R. G. Crittenden and N. Turok, *Phys. Rev. Lett.* **75**, 2642 (1995), [arXiv:astro-ph/9505120].
- [57] Planck Collab. 2015 Results XIX, *Astron. & Astrophys.* **594**, A21 (2016).
- [58] P. A. R. Ade *et al.* (Planck), *Astron. Astrophys.* **594**, A24 (2016), [arXiv:1502.01597].
- [59] A. Dekel, *Ann. Rev. Astron. Astrophys.* **32**, 371 (1994), [arXiv:astro-ph/9401022].
- [60] Y. Akrami *et al.* (Planck) (2018), [arXiv:1807.06211].
- [61] Y. Akrami *et al.* (Planck) (2019), [arXiv:1905.05697].
- [62] E. van Uitert *et al.*, *Mon. Not. Roy. Astron. Soc.* **476**, 4, 4662 (2018), [arXiv:1706.05004].
- [63] T. M. C. Abbott *et al.* (DES), *Phys. Rev.* **D98**, 4, 043526 (2018), [arXiv:1708.01530].

## 26. Neutrinos in Cosmology

Revised August 2019 by J. Lesgourgues (TTK, RWTH) and L. Verde (ICC, U. of Barcelona; ICREA, Barcelona).

### 26.1 Standard neutrino cosmology

Neutrino properties leave detectable imprints on cosmological observations that can then be used to constrain neutrino properties. This is a great example of the remarkable interconnection and interplay between nuclear physics, particle physics, astrophysics and cosmology (for general reviews see *e.g.*, [1–4]). Present cosmological data are already providing constraints on neutrino properties not only complementary but also competitive with terrestrial experiments; for instance, upper bounds on the total neutrino mass have shrunk by a factor of about 14 in the past 17 years. Forthcoming cosmological data may soon provide key information, not obtainable in other ways like *e.g.*, a measurement of the absolute neutrino mass scale. This new section is motivated by this exciting prospect.

A relic neutrino background pervading the Universe (the Cosmic Neutrino background,  $\nu\bar{\nu}$ ) is a generic prediction of the standard hot Big Bang model (see Big Bang Nucleosynthesis – Chap. 24 of this *Review*). While it has not yet been detected directly, it has been indirectly confirmed by the accurate agreement of predictions and observations of: *a*) the primordial abundance of light elements (see Big Bang Nucleosynthesis – Chap. 24 of this *Review*; *b*) the power spectrum of Cosmic Microwave Background (CMB) anisotropies (see Cosmic Microwave Background – Chap. 29 of this *Review*); and *c*) the large scale clustering of cosmological structures. Within the hot Big Bang model such good agreement would fail dramatically without a  $\nu\bar{\nu}$  with properties matching closely those predicted by the standard neutrino decoupling process (*i.e.*, involving only weak interactions).

We will illustrate below that cosmology is sensitive to the following neutrino properties: their density, related to the number of active (*i.e.*, left-handed, see Neutrino Mass, Mixing, and Oscillations – Chap. 14 of this *Review*) neutrino species, and their masses. At first order, cosmology is sensitive to the total neutrino mass, but is blind to the mixing angles and CP violation phase as discussed in Neutrino Mass, Mixing, and Oscillations (Chap. 14 of this *Review*). This makes cosmological constraints nicely complementary to measurements from terrestrial neutrino experiments.

The minimal cosmological model,  $\Lambda$ CDM, currently providing a good fit to most cosmological data sets (up to moderate tensions discussed in The Cosmological Parameters Chap. 25.1 of this *Review*), assumes that the only massless or light (sub-keV) relic particles since the Big Bang Nucleosynthesis (BBN) epoch are photons and active neutrinos. Extended models with light sterile neutrinos, light thermal axions or other light relics – sometimes referred to as “dark radiation” – would produce effects similar to, and potentially degenerate with, those of active neutrinos. Thus neutrino bounds are often discussed together with limits on such scenarios. In case of anomalies in cosmological data, it might not be obvious to discriminate between interpretation in terms of active neutrinos with non-standard decoupling, additional production mechanisms, non-standard interactions, etc., or in terms of some additional light particles. Such extensions are currently being explored as a possible way to resolve the  $H_0$  tension between late and early universe determinations, but are not widely favoured [5–8].

Hence neutrino density and mass bounds can be derived under the assumption of no additional massless or light relic particles, and the neutrino density measured in that way provides a test of standard (*i.e.*, involving only weak interactions) neutrino decoupling.

In that model, the three active neutrino types thermalize in the early Universe, with a negligible leptonic asymmetry. Then they can be viewed as three propagating mass eigenstates sharing the same temperature and identical Fermi-Dirac distributions, thus with no visible effects of flavour oscillations. Neutrinos decouple gradually from the thermal plasma at temperatures  $T \sim 2$  MeV. In the instantaneous neutrino decoupling limit, *i.e.*, assuming that neutrinos were fully decoupled at the time when electron-positrons annihilate and release entropy in the thermal bath, the neutrino-

to-photon density ratio between the time of electron-positron annihilation and the non-relativistic transition of neutrinos would be given by

$$\frac{\rho_\nu}{\rho_\gamma} = \frac{7}{8} N_{\text{eff}} \left( \frac{4}{11} \right)^{4/3}, \quad (26.1)$$

with  $N_{\text{eff}} = 3$ , and the last factor comes from the fourth power of the temperature ratio  $T_\nu/T_\gamma = (4/11)^{1/3}$  (see Big Bang Cosmology – Chap. 22 in this *Review*). In the above formula,  $N_{\text{eff}}$  is called the effective number of neutrino species because it can be viewed as a convenient parametrisation of the relativistic energy density of the Universe beyond that of photons, in units of one neutrino in the instantaneous decoupling limit. Precise simulations of neutrino decoupling and electron-positron annihilation, taking into account flavor oscillations, provide precise predictions for the actual phase-space distribution of relic neutrinos [9–12]. These distributions differ from the instantaneous decoupling approximation through a combination of a small shift in the photon temperature and small non-thermal distortions, all at the percent level. The final result for the density ratio  $\rho_\nu/\rho_\gamma$  in the relativistic regime can always be expressed as in Eq. (26.1), but with a different value of  $N_{\text{eff}}$ . The most recent analysis, that includes the effect of neutrino oscillations with the present values of the mixing parameters and an improved calculation of the collision terms, gives  $N_{\text{eff}} = 3.045$  [12]. The precise number density ratio  $n_\nu/n_\gamma$  can also be derived from such studies, and is important for computing the ratio  $\Omega_\nu h^2 / \sum_i m_i$  (ratio of the physical density of neutrinos in units of the critical density to the sum of neutrino masses) in the non-relativistic regime.

The neutrino temperature today,  $T_\nu^0 \simeq 1.7 \times 10^{-4}$  eV  $\simeq 1.9$  K, is smaller than at least two of the neutrino masses, since the two squared-mass differences are  $|\Delta m_{31}^2|^{1/2} > |\Delta m_{21}^2|^{1/2} > T_\nu^0$  (see Neutrino mass, Mixing, and oscillations – Chap. 14 of this *Review*). Thus at least two neutrino mass eigenstates are non-relativistic today and behave as a small “hot” fraction of the total dark matter (they cannot be all the dark matter, as explained in Chap. 27 in this *Review*). This fraction of hot dark matter can be probed by cosmological experiments, for two related reasons, as we now describe.

First, neutrinos are the only known particles behaving as radiation at early times (during the CMB acoustic oscillations) and dark matter at late times (during structure formation), which has consequences on the background evolution. Neutrinos become non-relativistic when their mass is equal to their average momentum, given for any Fermi-Dirac-distributed particle by  $\langle p \rangle = 3.15 T$ . Thus the redshift of the non-relativistic transition is given by  $z_i^{\text{nr}} = m_i / (3.15 T_\nu^0) - 1 = m_i / [0.53 \text{ meV}] - 1$  for each eigenstate of mass  $m_i$ , giving for instance  $z_i^{\text{nr}} = 110$  for  $m_i = 60$  meV, corresponding to a time deep inside the matter-dominated regime. Second, until the non-relativistic transition, neutrinos travel at the speed of light, and later on they move at a typical velocity  $\langle v_i/c \rangle = 3.15 T_\nu(z) / m_i = 0.53(1+z) \text{ meV} / m_i$ , which is several orders of magnitude larger than that of the dominant cold (or even of possibly warm) dark matter component(s). This brings their characteristic diffusion scale, called the “free-streaming length”, to cosmological relevant values, with consequences on gravitational clustering and the growth of structure.

Once neutrinos are non-relativistic, their energy density is given by  $\rho_\nu \simeq \sum m_i n_i$ . Since the number densities  $n_i$  are equal to each other (up to negligible corrections coming from flavour effects in the decoupling phase), the total mass ( $\sum m_\nu$ ) =  $m_1 + m_2 + m_3$  can be factorized out. It is possible that the lightest neutrino is still relativistic today, in which case this relation is slightly incorrect, but given that the total density is always strongly dominated by that of non-relativistic neutrinos, the error made is completely negligible. Using the expression for  $n_i/n_\gamma$  obtained from precise neutrino decoupling studies, and knowing  $n_\gamma$  from the measurement of the CMB temperature, one can compute  $\rho_\nu^0$ , the total neutrino density today, in units of the critical density  $\rho_{\text{crit}}^0$  [12]:

$$\Omega_\nu = \frac{\rho_\nu^0}{\rho_{\text{crit}}^0} = \frac{\sum m_\nu}{93.14 h^2 \text{ eV}}, \quad (26.2)$$

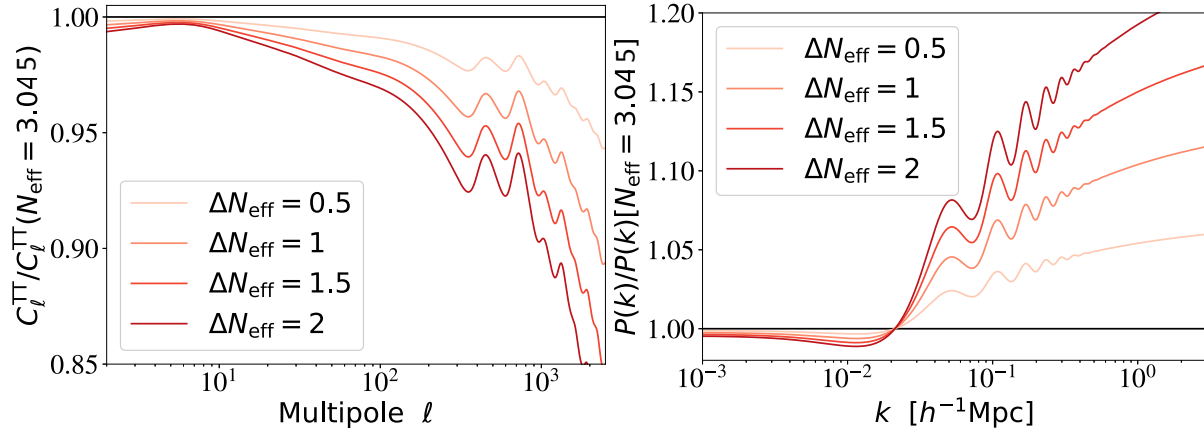


Figure 26.1: Ratio of the CMB  $C_\ell^{TT}$  (left, including lensing effects) and matter power spectrum  $P(k)$  (right, computed for each model in units of  $(h^{-1}\text{Mpc})^3$ ) for different values of  $\Delta N_{\text{eff}} \equiv N_{\text{eff}} - 3.045$  over those of a reference model with  $\Delta N_{\text{eff}} = 0$ . In order to minimize and better characterise the effect of  $N_{\text{eff}}$  on the CMB, the parameters that are kept fixed are  $\{z_{\text{eq}}, z_\Lambda, \omega_b, \tau\}$  and the primordial spectrum parameters. Fixing  $\{z_{\text{eq}}, z_\Lambda\}$  is equivalent to fixing the fractional density of total radiation, of total matter and of cosmological constant  $\{\Omega_r, \Omega_m, \Omega_\Lambda\}$  while increasing the Hubble parameter as a function of  $N_{\text{eff}}$ . The statistical errors on the  $C_\ell$  are  $\sim 1\%$  for a band power of  $\Delta\ell = 30$  at  $\ell \sim 1000$ . The error on  $P(k)$  is estimated to be of the order of 5%.

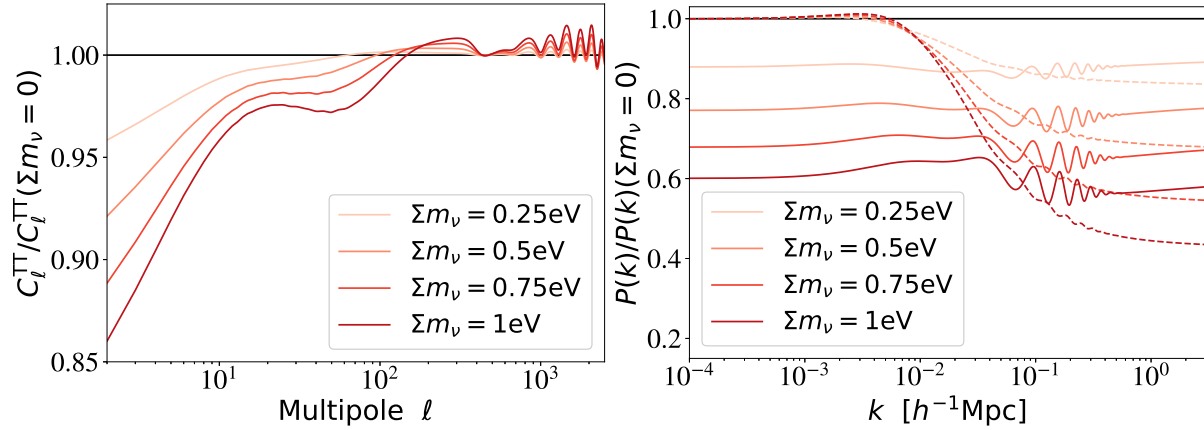


Figure 26.2: Ratio of the CMB  $C_\ell^{TT}$  and matter power spectrum  $P(k)$  (computed for each model in units of  $(h^{-1}\text{Mpc})^3$ ) for different values of  $\sum m_\nu$  over those of a reference model with massless neutrinos. In order to minimize and better characterise the effect of  $\sum m_\nu$  on the CMB, the parameters that are kept fixed are  $\omega_b, \omega_c, \tau$ , the angular scale of the sound horizon  $\theta_s$  and the primordial spectrum parameters (solid lines). This implies that we are increasing the Hubble parameter  $h$  as a function of  $\sum m_\nu$ . For the matter power spectrum, in order to single out the effect of neutrino free-streaming on  $P(k)$ , the dashed lines show the spectrum ratio when  $\{\omega_m, \omega_b, \Omega_\Lambda\}$  are kept fixed. For comparison, the error on  $P(k)$  is of the order of 5% with current observations, and the fractional  $C_\ell$  errors are of the order of  $1/\sqrt{\ell}$  at low  $\ell$ .

and the total neutrino average number density today:  $n_\nu^0 = 339.5 \text{ cm}^{-3}$ . Here  $h$  is the Hubble constant in units of  $100 \text{ km s}^{-1} \text{ Mpc}^{-1}$ .

## 26.2 Effects of neutrino properties on cosmological observables

As long as they are relativistic, *i.e.*, until some time deep inside the matter-dominated regime for neutrinos with a mass  $m_i \ll 3.15 T_\nu^{\text{eq}} \sim 1.5 \text{ eV}$  (see Big Bang Cosmology, Chap. 22 in this *Review*), neutrinos enhance the density of radiation: this effect is parameterised by  $N_{\text{eff}}$  and can be discussed separately from the effect of the mass that will be described later in this section. Increasing  $N_{\text{eff}}$  impacts the observable spectra of CMB anisotropies and matter fluctuations through background and perturbation effects.

### 26.2.1 Effect of $N_{\text{eff}}$ on the CMB

The background effects depend on what is kept fixed when increasing  $N_{\text{eff}}$ . If the densities of other species are kept fixed, a higher  $N_{\text{eff}}$  implies a smaller redshift of radiation-to-matter equality, with very strong effects on the CMB spectrum: when the amount of expansion between radiation-to-matter equality and

photon decoupling is larger, the CMB peaks are suppressed. This effect is not truly characteristic of the neutrino density, since it can be produced by varying several other parameters. Hence, to characterise the effect of  $N_{\text{eff}}$ , it is more useful and illuminating to enhance the density of total radiation, of total matter and of  $\Lambda$  by exactly the same amount, in order to keep the redshift of radiation-to-matter equality  $z_{\text{eq}}$  and matter-to- $\Lambda$  equality  $z_\Lambda$  fixed [4, 13, 14]. The primordial spectrum parameters, the baryon density  $\omega_b \equiv \Omega_b h^2$  and the optical depth to reionization  $\tau$  can be kept fixed at the same time, since we can simply vary  $N_{\text{eff}}$  together with the Hubble parameter  $h$  with fixed  $\{\omega_b, \Omega_c, \Omega_\Lambda\}$ . The impact of such a transformation is shown in Fig. 26.1 for the CMB temperature spectrum  $C_\ell^{TT}$  (defined in Chap. 29 in this *Review*) and for the matter power spectrum  $P(k)$  (defined in Chap. 22 in this *Review*) for several representative values of  $N_{\text{eff}}$ . These effects are within the reach of cosmological observations given current error bars, as discussed in Section 26.3.1 (for instance, with the *Planck* satellite data, the statistical error on the  $C_\ell$ 's is of the order of one per cent for a band power of  $\Delta\ell = 30$  at  $\ell \sim 1000$ ).

With this transformation, the main background effect of  $N_{\text{eff}}$

is an increase in the diffusion scale (or Silk damping scale, see Cosmic Microwave Background – Chap. 29 in this *Review*) at the time of decoupling, responsible for the decrease in  $C_\ell^{TT}$  at high  $\ell$ , plus smaller effects coming from a slight increase in the redshift of photon decoupling [4, 13, 14]. At the level of perturbations, a higher  $N_{\text{eff}}$  implies that photons feel gravitational forces from a denser neutrino component; this tends to decrease the acoustic peaks (because neutrinos are distributed in a smoother way than photons) and to shift them to larger scales / smaller multipoles (because photon perturbations traveling at the speed of sound in the photon-baryon fluid feel some dragging effect from neutrino perturbations travelling at the speed of light) [4, 13, 15]. The effect of increasing  $N_{\text{eff}}$  on the polarization spectrum features are the same as on the temperature spectrum: an increased Silk damping, and a shift in the acoustic peak amplitude and location - the latter effect is even more clear in the polarization spectrum, in which the location of acoustic peaks does not get further influenced by a Doppler effect like for temperature. The combination of these effects is truly characteristic of the radiation density parameter  $N_{\text{eff}}$  and cannot be mimicked by other parameters; thus  $N_{\text{eff}}$  can be accurately measured from the CMB alone. However, there are correlations between  $N_{\text{eff}}$  and other parameters. In particular, we have seen (Fig. 26.1) that in order to minimise the effect of  $N_{\text{eff}}$  on the CMB spectrum, one should vary  $h$  at the same time, hence there is a correlation between  $N_{\text{eff}}$  and  $h$ , which implies that independent measurements reducing the error bar on  $h$  also reduce that on  $N_{\text{eff}}$ . Note that this correlation is not equivalent to a perfect degeneracy, so both parameters can anyway be constrained with CMB data alone.

### 26.2.2 Effect of $N_{\text{eff}}$ on the matter spectrum

We have discussed the effect of increasing  $N_{\text{eff}}$  while keeping  $z_{\text{eq}}$  and  $\omega_b$  fixed, because the latter two quantities are very accurately constrained by CMB data. This implies that  $\omega_c$  increases with  $N_{\text{eff}}$ , and that the ratio  $\omega_b/\omega_c = \Omega_b/\Omega_c$  decreases. However, the ratio of baryonic-to-dark matter has a strong impact on the shape of the matter power spectrum, because until the time of decoupling of the baryons from the photons, CDM experiences gravitational collapse, while baryons are kept smoothly distributed by photon pressure and affected by acoustic oscillations. The decrease of  $\Omega_b/\Omega_c$  following from the increase of  $N_{\text{eff}}$  gives more weight to the most clustered of the two components, namely the dark matter one, and produces an enhancement of the small-scale matter power spectrum and a damping of the amplitude of baryon acoustic oscillations (BAOs), clearly visible in Fig. 26.1 (right plot). The scale of BAOs is also slightly shifted by the same neutrino dragging effect as for CMB peaks [19].

The increase in the small-scale matter power spectrum is also responsible for a last effect on the CMB spectra: the CMB last scattering surface is slightly more affected by weak lensing from large-scale structures. This tends to smooth the maxima, the minima, and the damping scale of the CMB spectra [20].

### 26.2.3 Effect of neutrino masses on the CMB

Neutrino eigenstates with a mass  $m_i \ll 0.57$  eV become non-relativistic after photon decoupling. They contribute to the non-relativistic matter budget today, but not at the time of equality or recombination. If we increase the neutrino mass while keeping fixed the density of baryons and dark matter ( $\omega_b$  and  $\omega_c$ ), the early cosmological evolution remains fixed and independent of the neutrino mass, until the time of the non-relativistic transition. Thus one might expect that the CMB temperature and polarisation power spectra are left invariant. This is not true for four reasons.

First, the neutrino density enhances the total non-relativistic density at late times,  $\omega_m = \omega_b + \omega_c + \omega_\nu$ , where  $\omega_\nu \equiv \Omega_\nu h^2$  is given as a function of the total mass  $\sum m_\nu$  by Eq. (26.2). The late background evolution impacts the CMB spectrum through the relation between scales on the last scattering surface and angles on the sky, and through the late ISW effect (see Cosmic Microwave Background – Chap. 29 of this *Review*). These two effects depend respectively on the angular diameter distance to recombination,  $d_A(z_{\text{rec}})$ , and on the redshift of matter-to- $\Lambda$  equality. Increasing  $\sum m_\nu$  tends to modify these two quantities. By playing with  $h$

and  $\Omega_\Lambda$ , it is possible to keep one of them fixed, but not both at the same time. Since the CMB measures the angular scale of acoustic oscillations with exquisite precision, and is only loosely sensitive to the late ISW effect due to cosmic variance, we choose in Fig. 26.2 to play with the Hubble parameter in order to maintain a fixed scale  $d_A(z_{\text{rec}})$ . With such a choice, an increase in neutrino mass comes together with a decrease in the late ISW effect explaining the depletion of the CMB spectrum for  $l \leq 20$ . The fact that both  $\sum m_\nu$  and  $h$  enter the expression of  $d_A(z_{\text{rec}})$  implies that measurements of the neutrino mass from CMB data are strongly correlated with  $h$ . Second, the non-relativistic transition of neutrinos affects the total pressure-to-density ratio of the universe, and causes a small variation of the metric fluctuations. If this transition takes place not too long after photon decoupling, this variation is observable through the early ISW effect [4, 21, 22]. It is responsible for the dip seen in Fig. 26.2 for  $20 \leq l \leq 200$ . Third, when the neutrino mass is higher, the CMB spectrum is less affected by the weak lensing effect induced by the large-scale structure at small redshift. This is due to a decrease in the matter power spectrum described in the next paragraphs. This reduced lensing effect is responsible for most of the oscillatory patterns visible in Fig. 26.2 (left plot) for  $l \geq 200$ . Fourth, the neutrinos with the smallest momenta start to be non-relativistic earlier than the average ones. The photon perturbations feel this through their gravitational coupling with neutrinos. This leads to a small enhancement of  $C_l^{TT}$  for  $l \geq 500$ , hardly visible on Fig. 26.2 because it is balanced by the lensing effect.

### 26.2.4 Effect of neutrino masses on the matter spectrum

The physical effect of neutrinos on the matter power spectrum is related to their velocity dispersion. Neutrinos free-stream over large distances without falling into small potential wells. The free-streaming scale is roughly defined as the distance travel by neutrinos over a Hubble time scale  $t_H = (a/\dot{a})$ , and approximates the scale below which neutrinos remain very smooth. On larger scales, they cluster in the same way as cold dark matter. The power spectrum of total matter fluctuations, related to the squared fluctuation  $\delta_m^2$  with  $\delta_m \equiv \delta_b + \delta_c + \delta_\nu$ , gets a negligible contribution from the neutrino component on small scales, and is reduced by a factor  $(1 - 2f_\nu)$ , where  $f_\nu = \omega_\nu/\omega_m$ . Additionally, on scales below the free-streaming scale, the growth of ordinary cold dark matter and baryon fluctuations is modified by the fact that neutrinos contribute to the background density, but not to the density fluctuations. This changes the balance between the gravitational forces responsible for clustering, and the Hubble friction term slowing it down. Thus the growth rate of CDM and baryon fluctuations is reduced [23]. This results today in an additional suppression of the small-scale linear matter power spectrum by approximately  $(1 - 6f_\nu)$ . These two effects sum up to a factor  $(1 - 8f_\nu)$  [24] (more precise approximations can be found in [2, 4]). The non-linear spectrum is even more suppressed on mildly non-linear scales [3, 25–29].

This effect is often illustrated by plots of the matter power spectrum ratio with fixed parameters  $\{\omega_m, \omega_b, \Omega_\Lambda\}$  and varying  $f_\nu$ , *i.e.*, with the CDM density adjusted to get a fixed total dark matter density [2, 4, 24] (see Fig. 26.2, right plot, dashed lines). This transformation does not leave the redshift of equality  $z_{\text{eq}}$  invariant, and has very large effects on the CMB spectra. If one follows the logic of minimizing CMB variations and fixing  $z_{\text{eq}}$  like in the previous paragraphs, the increase in  $\sum m_\nu$  must take place together with an increase of  $h$ , which tends to suppress the large-scale power spectrum, by approximately the same amount as the neutrino free-streaming effect [30]. In that case, the impact of neutrino masses on the matter power spectrum appears as an overall amplitude suppression, which can be seen in Fig. 26.2 (right plot, solid lines). The oscillations on intermediate wavenumbers come from a small shift in the BAO scale [30]. This global effect is not degenerate with a variation of the primordial spectrum amplitude  $A_s$ , because it only affects the matter power spectrum, and not the CMB spectra. However, the amplitude of the CMB temperature and polarization spectrum is given by the combination  $A_s e^{-2\tau}$ . Hence a measurement of  $\tau$  is necessary in order to fix  $A_s$  from CMB data, and avoid a parameter degeneracy between  $\sum m_\nu$  and  $A_s$  [30–32].

Table 26.1: Summary of  $N_{\text{eff}}$  constraints.

	Model	95%CL	Ref.
<b>CMB alone</b>			
P118[TT,TE,EE+lowE]	$\Lambda\text{CDM}+N_{\text{eff}}$	$2.92^{+0.36}_{-0.37}$	[16]
<b>CMB + background evolution + LSS</b>			
P118[TT,TE,EE+lowE+lensing] + BAO	$\Lambda\text{CDM}+N_{\text{eff}}$	$2.99^{+0.34}_{-0.33}$	[16]
” + BAO + R18	$\Lambda\text{CDM}+N_{\text{eff}}$	$3.27 \pm 0.15$ (68%CL)	[17]
”	” +5-params.	$2.85 \pm 0.23$ (68%CL)	[18]

A few of the neutrino mass effects described above –free-streaming scale, early ISW– depend on individual masses  $m_i$ , but most of them depend only on the total mass through  $f_\nu$  –suppression of the matter power spectrum, CMB lensing, shift in angular diameter distance–. Because the latter effects are easier to measure, cosmology is primarily sensitive to the total mass  $\sum m_\nu$  [33,34]. The possibility that future data sets might be able to measure individual masses or the mass hierarchy, despite systematic errors and parameter degeneracies, has recently become a subject of investigation [35,36].

### 26.3 Cosmological Constraints on neutrino properties

In this review we focus on cosmological constraints on the abundance and mass of ordinary active neutrinos. Several stringent but model-dependent constraints on non-standard neutrinos (*e.g.*, sterile neutrinos, active neutrinos with interactions beyond the weak force, unstable neutrinos with invisible decay, etc.) can also be found in the literature.

#### 26.3.1 Neutrino abundance

Table 26.1 shows a list of constraints on  $N_{\text{eff}}$  obtained with several combination of data sets. ‘P118’ denotes the *Planck* 2018 data, composed of a high- $\ell$  temperature+polarization likelihood (TT,TE,EE), low- $\ell$  polarization (low E) and CMB lensing spectrum likelihood (lensing) based on lensing extraction from quadratic estimators [16]. ‘BAO’ refers to measurements of the BAO scale (and hence of the angular diameter distance) from various recent data sets, described in detail in the references given in the table. ‘R18’ refers to the distance ladder local measurement of the Hubble scale from cepheids and supernovae [37].

Within the framework of a 7-parameter cosmological model ( $\Lambda\text{CDM}+N_{\text{eff}}$ ), the constraint on  $N_{\text{eff}}$  comes from the *Planck* 2018 data release [TT,TE,EE+lowE] is  $N_{\text{eff}} = 2.92^{+0.36}_{-0.37}$  (95%CL). This number is perfectly compatible with the prediction of the standard neutrino decoupling model,  $N_{\text{eff}} = 3.045$ , and can be viewed as a proof of self-consistency of the cosmological model.

The bounds can be tightened by adding information on the low-redshift background expansion from BAOs, or local  $H_0$  measurements. Finally, one can also add information on large scale structure (LSS), *i.e.*, on the growth rate and clustering amplitude of matter as a function of scale. However, LSS data are not very constraining for the  $N_{\text{eff}}$  parameter, and the only LSS data included in Table 26.1 is the measurement of the CMB lensing spectrum. All combinations of *Planck* 2018 data with BAO or CMB lensing constraints return measurements consistent with the standard expectation.

The situation is different with the inclusion of the low-redshift measurement of  $H_0$ , [37], known to be in tension with *Planck* in the  $\Lambda\text{CDM}$  framework. As explained in Section 26.2, the positive correlation between  $N_{\text{eff}}$  and  $h$  means that inclusion of the  $H_0$  measurement pushes  $N_{\text{eff}}$  to higher values,  $N_{\text{eff}} = 3.27 \pm 0.15$  (68%CL, P118[TT,TE,EE+lowE+lensing] + BAO+R18), but still compatible with the standard expectation at the  $\sim 1.5\sigma$  level.

It remains to be seen whether the  $> 3\sigma$  tension between CMB data and direct measurements of  $H_0$  results from systematics, or from a departure from the  $\Lambda\text{CDM}$  model [38,39].

The error bars on  $N_{\text{eff}}$  degrade mildly when the data are analysed in the context of more extended cosmological scenarios. Adding only the total neutrino mass as an 8th free parameter has a negligible impact on the bounds.

The authors of Ref. [18] take a more extreme point of view

and fit a 12-parameter model to P118[TT,TE,EE+lowE+lensing] data; they obtain  $N_{\text{eff}} = 2.95 \pm 0.24$  (68% CL), showing that it is very difficult with current cosmological data to accommodate shifts of more than 0.5 from the standard  $N_{\text{eff}}$  value, and to obtain good fits with, for instance, a fourth (sterile) thermalized neutrino. This is interesting since the anomalies in some oscillation data could be interpreted as evidence for at least one sterile neutrino with a large mixing angle, which would need to be thermalised unless non-standard interactions come into play [5]. In other words cosmology disfavors the explanation of the oscillations anomalies in terms of 1 or more extra neutrinos if they are thermalized.

#### 26.3.2 Are they really neutrinos, as expected?

While a value of  $N_{\text{eff}}$  significantly different from zero (at more than  $15\sigma$ ) and consistent with the expected number 3.045 yields a powerful indirect confirmation of the  $C\nu B$ , departures from standard  $N_{\text{eff}}$  could be caused by any ingredient affecting the early-time expansion rate of the Universe. Extra relativistic particles (either decoupled, self-interacting, or interacting with a dark sector), a background of gravitational waves, an oscillating scalar field with quartic potential, departures from Einstein gravity, or large extra dimensions are some of the possibilities for such ingredients. In principle one could even assume that the cosmic neutrino background never existed or has decayed (like in the “neutrinoless universe” model of [40]) while another dark radiation component is responsible for  $N_{\text{eff}}$ . At least, cosmological data allow to narrow the range of possible interpretations of  $N_{\text{eff}} \simeq 3$  to the presence of decoupled relativistic relics like standard neutrinos. Indeed, free-streaming particles leave specific signatures in the CMB and LSS spectra, because their density and pressure perturbations, bulk velocities and anisotropic stress also source the metric perturbations. These signatures can be tested in several ways.

A first approach consists of introducing a self-interaction term in the neutrino equations [6,7]. Ref. [8] finds that current CMB and BAO data are compatible with no self-interactions. The upper limit to the effective coupling constant  $G_{\text{eff}}$  for a Fermi-like four-fermions interaction at 95% confidence is  $\log_{10}(G_{\text{eff}}\text{MeV}^2) < -0.8$  for P115+BAO. Note however that neutrino self-interactions as strong as  $\log_{10}(G_{\text{eff}}\text{MeV}^2) \simeq -1.4$  could reconcile CMB+BAO data with the direct  $H_0$  measurement of Ref [37], but such interactions seem to be hardly compatible with BBN and laboratory constraints [41].

A second approach consists of introducing two phenomenological parameters,  $c_{\text{eff}}$  and  $c_{\text{vis}}$  (see *e.g.*, [42–44]):  $c_{\text{eff}}^2$  generalizes the linear relation between isotropic pressure perturbations and density perturbations, while  $c_{\text{vis}}^2$  modifies the neutrino anisotropic stress equation. While relativistic free-streaming species have  $(c_{\text{eff}}^2, c_{\text{vis}}^2) = (1/3, 1/3)$ , a perfect relativistic fluid would have  $(c_{\text{eff}}^2, c_{\text{vis}}^2) = (1/3, 0)$ . Other values do not necessarily refer to a concrete model, but make it possible to interpolate between these limits. *Planck* data strongly suggests  $(c_{\text{eff}}^2, c_{\text{vis}}^2) = (1/3, 1/3)$  [45,46].

Finally, Ref. [15] (resp. [19]) shows that current data are precise enough to detect the “neutrino drag” effect mentioned in Sec. 26.2 through the measurement of the CMB peak (resp. BAO) scale. These findings show that current cosmological data are able to detect not just the average density of some relativistic relics, but also their anisotropies.

**Table 26.2:** Summary of  $\sum m_\nu$  constraints.

	Model	95% CL (eV)	Ref.
<b>CMB alone</b>			
P118[TT+lowE]	$\Lambda$ CDM+ $\sum m_\nu$	< 0.54	[16]
P118[TT,TE,EE+lowE]	$\Lambda$ CDM+ $\sum m_\nu$	< 0.26	[16]
<b>CMB + probes of background evolution</b>			
P118[TT+lowE] + BAO	$\Lambda$ CDM+ $\sum m_\nu$	< 0.16	[16]
P118[TT,TE,EE+lowE] + BAO	$\Lambda$ CDM+ $\sum m_\nu$	< 0.13	[16]
P118[TT,TE,EE+lowE]+BAO	$\Lambda$ CDM+ $\sum m_\nu$ +5 params.	< 0.515	[18]
<b>CMB + LSS</b>			
P118[TT+lowE+lensing]	$\Lambda$ CDM+ $\sum m_\nu$	< 0.44	[16]
P118[TT,TE,EE+lowE+lensing]	$\Lambda$ CDM+ $\sum m_\nu$	< 0.24	[16]
<b>CMB + probes of background evolution + LSS</b>			
P118[TT+lowE+lensing] + BAO	$\Lambda$ CDM+ $\sum m_\nu$	< 0.13	[16]
P118[TT,TE,EE+lowE+lensing] + BAO	$\Lambda$ CDM+ $\sum m_\nu$	< 0.12	[16]
P118[TT,TE,EE+lowE+lensing] + BAO+Pantheon	$\Lambda$ CDM+ $\sum m_\nu$	< 0.11	[16]

### 26.3.3 Neutrino masses

Table 26.2 shows a list of constraints on  $\sum m_\nu$  obtained with several combinations of data sets. The acronyms “P118”, “BAO” and “R18” have been described in the previous subsection, while “Pantheon” refers to the supernovae Type Ia compilation of [47].

Given that most determinations of  $N_{\text{eff}}$  are compatible with the standard prediction,  $N_{\text{eff}} = 3.045$ , it is reasonable to adopt this value as a theoretical prior and to investigate neutrino mass constraints in the context of a minimal 7-parameter model,  $\Lambda$ CDM+ $\sum m_\nu$ . Under this assumption, the most robust constraints come from *Planck* 2018 temperature and polarization data alone:  $\sum m_\nu < 0.26$  eV (95%CL). Among the four effects of neutrino masses on the CMB spectra described before, current bounds are dominated by the first and the third effects (modified late background evolution, and distortions of the temperature and polarisation spectra through weak lensing).

Adding measurements of the BAO scale is crucial, since the measurement of the angular diameter distance at small redshift allows us to break parameter degeneracies, for instance between  $\sum m_\nu$  and  $h$ . Combined *Planck* 2018 data, BAO experiments give  $\sum m_\nu < 0.13$  eV (95%CL). Supernovae data are less constraining than BAO data for the neutrino mass determination.

Because the parameter correlation between  $\sum m_\nu$  and  $H_0$  is negative, the inclusion of R18 data provides stronger bounds on neutrinos masses, down to  $\sum m_\nu < 0.097$  eV (95% CL) when including P118[TT,TE,EE+lowE]+R18 [16], but such bounds are subject to caution, since they come from a combination of discrepant data sets (at the  $> 3\sigma$  level).

It is interesting to add LSS data sets, sensitive to the small-scale suppression of the matter power spectrum due to neutrino free-streaming. The bound from *Planck* 18 including lensing plus BAO is very strong,  $\sum m_\nu < 0.12$  eV (95%CL), which is comparable to previous bounds derived from *Planck* 15 in combination with Ly $\alpha$  forest data or other large-scale structure data [48–50]. It can even be tightened down to  $\sum m_\nu < 0.11$  eV by further adding supernovae data from the “Pantheon” compilation. The latter bound puts some pressure on the inverted mass hierarchy that requires  $\sum m_\nu > 0.11$  eV. It should however be noticed that the full DES 1-year data [51] prefer a lower  $\sigma_8$  value than the *Planck* best fit, relaxing the bound to  $\sum m_\nu < 0.14$  eV (95%CL, P118[TT,TE,EE+lowE+lensing] + BAO + DES) [16].

Upper bounds on neutrino masses become weaker when the data are analysed in the context of extended cosmological models, but only by a small amount. Floating  $N_{\text{eff}}$  instead of fixing it to 3.045 has no significant impact on the neutrino mass bounds reported in the previous paragraphs. Even in the extreme case considered by Ref. [18], with 12 free cosmological parameters, one can see in Table 26.2 that the bound from *Planck* 2018 (without lensing) + BAO increases from 0.13 eV to 0.52 eV (95% CL) only. This shows that current cosmological data are precise enough to disentangle the effect of several extended cosmological parameters, and that neutrino mass bounds are becoming increasingly robust.

### 26.4 Future prospects and outlook

The cosmic neutrino background has been detected indirectly at very high statistical significance. Direct detection experiments are now being planned, *e.g.*, at the Princeton Tritium Observatory for Light, Early-universe, Massive-neutrino Yield (PTOLEMY) [52]. The detection prospects crucially depend on the exact value of neutrino masses and on the enhancement of their density at the location of the Earth through gravitational clustering in the Milky Way and its sub-halos – an effect however expected to be small [53–55].

Over the past few years the upper limit on the sum of neutrino masses has become increasingly stringent, first indicating that the mass ordering is hierarchical and recently putting the inverted hierarchy under pressure and favouring the normal hierarchy (although quantitative estimates of how disfavoured the inverted hierarchy is vary depending on assumptions, see *e.g.* [56–58]) which has consequences for planning future double beta decay experiments.

Neutrino mass and density bounds are expected to keep improving significantly over the next years, thanks to new LSS experiments like DESI [59], Euclid [60], LSST [61], and SKA [62], or possible new CMB experiments like CMB-S4 [63], Pixie [64], CMBPol or CORE [65]. If the  $\Lambda$ CDM model is confirmed, and if neutrinos have standard properties, the total neutrino mass should be detected at the level of at least  $3-4\sigma$  even at the minimum level allowed by oscillations. This is the conclusion reached by several independent studies, using different dataset combinations (see *e.g.*, [32,66–71]). One should note that at the minimum level allowed by oscillations  $\sum m_\nu \sim 0.06$ , neutrinos constitute  $\sim 0.5\%$  of the Universe matter density, and their effects on the matter power spectrum is only at the 5% level, implying that exquisite control of systematic errors will be crucial to achieve the required accuracy. At this level, the information coming from the power spectrum shape is more powerful than that coming from geometrical measurements (*e.g.*, BAO). But exploiting the shape information requires improved understanding of the non-linear regime, and of galaxy bias for galaxy surveys. The fact that different surveys and different data set combinations have enough statistical power to reach this level, offers a much needed redundancy and the possibility to perform consistency checks which in turns helps immensely with the control of systematic errors and in making the measurement robust. Using the entire Universe as a particle detector, the on-going and future observational efforts hold the exciting prospect to provide a measurement of the sum of neutrino masses and possibly indication of their mass hierarchy.

#### References

- [1] A. D. Dolgov, Phys. Rept. **370**, 333 (2002), [hep-ph/0202122].
- [2] J. Lesgourgues and S. Pastor, Phys. Rept. **429**, 307 (2006), [arXiv:astro-ph/0603494].

- [3] S. Hannestad, *Prog. Part. Nucl. Phys.* **65**, 185 (2010), [arXiv:1007.0658].
- [4] J. Lesgourgues *et al.*, *Neutrino cosmology* (Cambridge University Press, 2013).
- [5] M. Archidiacono *et al.*, *JCAP* **1608**, 08, 067 (2016), [arXiv:1606.07673].
- [6] L. Lancaster *et al.*, *JCAP* **1707**, 07, 033 (2017), [arXiv:1704.06657].
- [7] I. M. Oldengott *et al.*, *JCAP* **1711**, 11, 027 (2017), [arXiv:1706.02123].
- [8] M. Park *et al.* (2019), [arXiv:1904.02625].
- [9] J. Birrell, C.-T. Yang and J. Rafelski, *Nucl. Phys.* **B890**, 481 (2014), [arXiv:1406.1759].
- [10] G. Mangano *et al.*, *Nucl. Phys.* **B729**, 221 (2005), [hep-ph/0506164].
- [11] E. Grohs *et al.*, *Phys. Rev.* **D93**, 8, 083522 (2016), [arXiv:1512.02205].
- [12] P. F. de Salas and S. Pastor, *JCAP* **1607**, 07, 051 (2016), [arXiv:1606.06986].
- [13] S. Bashinsky and U. Seljak, *Phys. Rev.* **D69**, 083002 (2004), [arXiv:astro-ph/0310198].
- [14] Z. Hou *et al.*, *Phys. Rev.* **D87**, 083008 (2013), [arXiv:1104.2333].
- [15] B. Follin *et al.*, *Phys. Rev. Lett.* **115**, 9, 091301 (2015), [arXiv:1503.07863].
- [16] N. Aghanim *et al.* (Planck) (2018), [arXiv:1807.06209].
- [17] Planck 2018 explanatory supplement, [wiki.cosmos.esa.int/planckpla2018/](http://wiki.cosmos.esa.int/planckpla2018/), “Mission Products: Cosmological parameters: Parameter Tables”.
- [18] E. Di Valentino, A. Melchiorri and J. Silk, arXiv:1908.01391 *Phys. Rev.* **D92**, 12,1302 (2015).
- [19] D. Baumann *et al.*, *Nature Phys.* **15**, 465 (2019), [arXiv:1803.10741].
- [20] A. Lewis and A. Challinor, *Phys. Rept.* **429**, 1 (2006), [arXiv:astro-ph/0601594].
- [21] J. Lesgourgues and S. Pastor, *Adv. High Energy Phys.* **2012**, 608515 (2012), [arXiv:1212.6154].
- [22] Z. Hou *et al.*, *Astrophys. J.* **782**, 74 (2014), [arXiv:1212.6267].
- [23] J. R. Bond, G. Efstathiou and J. Silk, *Phys. Rev. Lett.* **45**, 1980 (1980), [61(1980)].
- [24] W. Hu, D. J. Eisenstein and M. Tegmark, *Phys. Rev. Lett.* **80**, 5255 (1998), [arXiv:astro-ph/9712057].
- [25] S. Bird, M. Viel and M. G. Haehnelt, *Mon. Not. R. Astron. Soc.* **420**, 2551 (2012).
- [26] C. Wagner, L. Verde and R. Jimenez, *Astrophys. J.* **752**, L31 (2012), [arXiv:1203.5342].
- [27] C. J. Toderó Peixoto, V. de Souza and P. L. Biermann, *JCAP* **1507**, 07, 042 (2015), [arXiv:1502.00305].
- [28] J. Brandbyge and S. Hannestad, *JCAP* **1710**, 10, 015 (2017), [arXiv:1706.00025].
- [29] J. Adamek, R. Durrer and M. Kunz, *JCAP* **1711**, 11, 004 (2017), [arXiv:1707.06938].
- [30] M. Archidiacono *et al.*, *JCAP* **1702**, 02, 052 (2017), [arXiv:1610.09852].
- [31] A. Liu *et al.*, *Phys. Rev.* **D93**, 4, 043013 (2016), [arXiv:1509.08463].
- [32] R. Allison *et al.*, *Phys. Rev.* **D92**, 12, 123535 (2015), [arXiv:1509.07471].
- [33] J. Lesgourgues, S. Pastor and L. Perotto, *Phys. Rev.* **D70**, 045016 (2004), [hep-ph/0403296].
- [34] A. Slosar, *Phys. Rev.* **D73**, 123501 (2006), [arXiv:astro-ph/0602133].
- [35] R. Jimenez *et al.*, *JCAP* **1005**, 035 (2010), [arXiv:1003.5918].
- [36] R. Jimenez, C. P. Garay and L. Verde, *Phys. Dark Univ.* **15**, 31 (2017), [arXiv:1602.08430].
- [37] A. G. Riess *et al.*, *Astrophys. J.* **855**, 2, 136 (2018), [arXiv:1801.01120].
- [38] J. L. Bernal, L. Verde and A. G. Riess, *JCAP* **1610**, 10, 019 (2016), [arXiv:1607.05617].
- [39] L. Verde, T. Treu and A. G. Riess (2019), [arXiv:1907.10625].
- [40] J. F. Beacom, N. F. Bell and S. Dodelson, *Phys. Rev. Lett.* **93**, 121302 (2004), [arXiv:astro-ph/0404585].
- [41] N. Blinov *et al.* (2019), [arXiv:1905.02727].
- [42] W. Hu, *Astrophys. J.* **506**, 485 (1998), [arXiv:astro-ph/9801234].
- [43] W. Hu *et al.*, *Phys. Rev.* **D59**, 023512 (1999), [arXiv:astro-ph/9806362].
- [44] M. Gerbino, E. Di Valentino and N. Said, *Phys. Rev.* **D88**, 6, 063538 (2013), [arXiv:1304.7400].
- [45] B. Audren *et al.*, *JCAP* **1503**, 036 (2015), [arXiv:1412.5948].
- [46] P. A. R. Ade *et al.* (Planck), *Astron. Astrophys.* **594**, A13 (2016), [arXiv:1502.01589].
- [47] D. M. Scolnic *et al.*, *Astrophys. J.* **859**, 2, 101 (2018), [arXiv:1710.00845].
- [48] N. Palanque-Delabrouille *et al.*, *JCAP* **1511**, 11, 011 (2015), [arXiv:1506.05976].
- [49] A. J. Cuesta, V. Niro and L. Verde, *Phys. Dark Univ.* **13**, 77 (2016).
- [50] S. Vagnozzi *et al.*, *Phys. Rev.* **D96**, 12, 123503 (2017), [arXiv:1701.08172].
- [51] T. M. C. Abbott *et al.* (DES), *Phys. Rev.* **D98**, 4, 043526 (2018), [arXiv:1708.01530].
- [52] S. Betts *et al.*, in “Proceedings, 2013 Community Summer Study on the Future of U.S. Particle Physics: Snowmass on the Mississippi (CSS2013): Minneapolis, MN, USA, July 29-August 6, 2013,” (2013), [arXiv:1307.4738], URL <http://www.slac.stanford.edu/econf/C1307292/docs/submittedArxivFiles/1307.4738.pdf>.
- [53] A. Ringwald and Y. Y. Y. Wong, *JCAP* **0412**, 005 (2004), [hep-ph/0408241].
- [54] F. Villaescusa-Navarro *et al.*, *JCAP* **1303**, 019 (2013), [arXiv:1212.4855].
- [55] P. F. de Salas *et al.*, *JCAP* **1709**, 09, 034 (2017), [arXiv:1706.09850].
- [56] F. Simpson *et al.*, *JCAP* **1706**, 06, 029 (2017), [arXiv:1703.03425].
- [57] S. Hannestad and T. Schwetz, *JCAP* **1611**, 11, 035 (2016), [arXiv:1606.04691].
- [58] S. Roy Choudhury and S. Hannestad (2019), [arXiv:1907.12598].
- [59] A. Aghamousa *et al.* (DESI) (2016), [arXiv:1611.00036].
- [60] R. Laureijs *et al.* (EUCLID) (2011), [arXiv:1110.3193].
- [61] Paul A. Abell *et al.*, LSST Science and LSST Project Collaborations, <http://lss.fnal.gov/archive/test-tm/2000/fermilab-tm-2495-a.pdf> (2009) arXiv:0912.0201.
- [62] <http://www.skatelescope.org>.
- [63] K. N. Abazajian *et al.* (CMB-S4) (2016), [arXiv:1610.02743].
- [64] A. Kogut *et al.*, *JCAP* **1107**, 025 (2011), [arXiv:1105.2044].
- [65] J. Delabrouille *et al.* (CORE), *JCAP* **1804**, 04, 014 (2018), [arXiv:1706.04516].
- [66] C. Carbone *et al.*, *JCAP* **1103**, 030 (2011), [arXiv:1012.2868].
- [67] J. Hamann, S. Hannestad and Y. Y. Y. Wong, *JCAP* **1211**, 052 (2012), [arXiv:1209.1043].
- [68] B. Audren *et al.*, *JCAP* **1301**, 026 (2013), [arXiv:1210.2194].

- [69] R. Pearson and O. Zahn, Phys. Rev. **D89**, 4, 043516 (2014), [arXiv:1311.0905].
- [70] F. Villaescusa-Navarro, P. Bull and M. Viel, Astrophys. J. **814**, 2, 146 (2015), [arXiv:1507.05102].
- [71] T. Brinckmann *et al.*, JCAP **1901**, 059 (2019), [arXiv:1808.05955].



## 27. Dark Matter

Written August 2019 by L. Baudis (Zurich U.) and S. Profumo (UC Santa Cruz).

### 27.1 The case for dark matter

Modern cosmological models invariably include an electromagnetically close-to-neutral, non-baryonic matter species with negligible velocity from the standpoint of structure formation, generically referred to as “cold dark matter” (CDM; see The Big-Bang Cosmology—Sec. 22 of this *Review*). For the benchmark  $\Lambda$ CDM cosmology adopted in the Cosmological Parameters—Sec. 25.1 of this *Review*, the DM accounts for 26.4% of the critical density in the universe, or 84.4% of the total matter density. The nature of only a small fraction, between at least 0.5% (given neutrino oscillations) and at most 1.6% (from combined cosmological constraints), of the non-baryonic matter content of the universe is known: the three Standard Model neutrinos (see the Neutrino Masses, Mixing, and Oscillations—Sec. 14 of this *Review*). The fundamental makeup of the large majority of the DM is, as of yet, unknown.

Assuming the validity of General Relativity, DM is observed to be ubiquitous in gravitationally collapsed structures of size ranging from the smallest known galaxies [1] to galaxies of size comparable to the Milky Way [2], to groups and clusters of galaxies [3]. The mass-to-light ratio is observed to saturate at the largest collapsed scales to a value indicative, and close to, what inferred from other cosmological observations for the universe as a whole [4]. In such collapsed structures, the existence of DM is inferred directly using tracers of mass enclosed within a certain radius such as stellar velocity dispersion, rotation curves in axisymmetric systems, the virial theorem, gravitational lensing, and measures of the amount of non-dark, i.e. baryonic, mass such as stellar number counts and tracers of gas density such as X-ray emission [5]. The global DM abundance as determined from cosmological probes is discussed in Sec. 22.

The picture of structure formation in modern cosmology heavily relies on, and can be considered an independent and exceptionally strong motivation for, DM. Baryonic density fluctuations at CMB decoupling are observed to be at most on the order of  $\delta\rho_b/\rho_b|_{\text{rec}} \approx 10^{-3}$ ; since density perturbations grow linearly with the scale factor in the linear regime, absent any other matter fluid, one would predict that

$$\delta\rho_b/\rho_b|_{\text{today}} \approx \frac{\delta\rho_b/\rho_b|_{\text{rec}}}{a_{\text{rec}}} \approx 10^{-2}, \quad (27.1)$$

at odds with the observed highly non-linear structures in the universe,  $\delta\rho_b/\rho_b|_{\text{obs}} \gg 1$ . The presence of a dominant non-relativistic (“cold”) pressure-less matter component decoupled from the thermal bath well before recombination allows instead for the prediction of a matter power spectrum in remarkable agreement with observations [6].

Assuming deviations of gravitational interactions on large scales from general relativity or from its Newtonian limit, certain effects, attributed in the standard scenario to DM, can be explained by modified gravity [7]. Usually such theories mimic the effects otherwise attributed to DM on a limited range of scales, but fail globally, and especially at the largest scales. Key issues that at present appear highly problematic in the framework of theories of modified gravity without DM include (i) predicting the correct spectrum of density perturbations, (ii) predicting the observed anisotropy power spectrum of the CMB, and (iii) explaining weak lensing and X-ray observations of merging clusters such as 1E 0657-558 (the “Bullet” cluster) [8]. The inferred relative speed of gravitational and electromagnetic radiation in GW170817 additionally excludes a significant swath of modified theories of gravity where the two speeds (of gravitational and electromagnetic waves) differ [9].

### 27.2 Properties of dark matter candidates

**Electric charge:** The “darkness” of DM can be quantified based on constraints from the CMB and large-scale structure: if the DM is charged, or “milli-charged” (for instance via a kinetic mixing with a dark photon field, producing an effective

suppressed coupling to the visible photon field), it might impact the baryon-photon plasma during recombination; in turn, DM density fluctuations can be suppressed by radiation pressure and photon diffusion, additionally altering the baryon acoustic peak structure. [10] finds that the most stringent constraints stem from the requirement that the DM be completely decoupled from the baryon-photon plasma at recombination, yielding a maximal “milli-electric” charge, in units of the electron charge, of  $3.5 \times 10^{-7} (m_{\text{DM}}/1 \text{ GeV})^{0.58}$  for  $m_{\text{DM}} > 1 \text{ GeV}$ , and of  $4.0 \times 10^{-7} (m_{\text{DM}}/1 \text{ GeV})^{0.35}$  for  $m_{\text{DM}} < 1 \text{ GeV}$ . Limits also exist from structure formation on how optically dark and dissipationless the DM should be.

**Self-interactions:** Observations of merging clusters [8] and of the ellipticity of certain galaxies as inferred from X-rays [11] constrain the level of DM-DM self interactions. The figure of merit is the ratio of the DM-DM cross section and the DM mass [12] (see Ref. [13] for a review),  $\sigma_{\text{DM-DM}}/m_{\text{DM}} < 0.47 \text{ cm}^2/\text{g} \simeq 0.84 \text{ barn}/\text{GeV}$  at 95% C.L.. Assuming a velocity dependence in  $\sigma_{\text{DM-DM}}$ , “self-interacting DM” has been advocated as a possible solution to certain possible small-scale structure issues in the standard non-collisional ( $\sigma_{\text{DM-DM}} \simeq 0$ ) setup [13, 14] (see Sec. 27.4).

**Mass: Lower Limits:** Model-independent lower limits for very small DM masses are due to quantum effects: for fermionic DM particles, the phase-space density  $f(\vec{x}, \vec{p})$  is bounded from above due to Pauli’s exclusion principle,  $f < gh^{-3}$ , with  $g$  the number of internal degrees of freedom and  $h$  Planck’s constant; observations of the velocity dispersion (or, equivalently, measures of the enclosed mass) and physical density in dwarf galaxies, lead to a lower limit on fermionic DM masses, sometimes known as the Tremaine-Gunn limit [15]. Using the Fornax dwarf, Ref. [16] finds  $m_F > 70 \text{ eV}$ . More stringent limits can be drawn from Lyman- $\alpha$  observations, although such limits depend on the thermal history of the DM. In the case of bosonic DM, the Compton wavelength of an ultra-light species might erase small-scale structure, in conflict with CMB and large-scale structure [17], Lyman- $\alpha$  observations [18, 19], and measurements of high-redshift galaxy luminosity functions and the Milky Way satellite luminosity function [20–22]: these observations indicate that  $m_B \gtrsim 10^{-22} \text{ eV}$ .

**Mass: Upper Limits:** General upper limits exist on the mass of the DM constituent from the stability against tidal disruption of structures immersed in DM halos, such as galactic disks and globular clusters, and of individual small galaxies. The most stringent limits can be derived using wide halo binaries [23] and the stability of the star cluster within Eridanus II [24]. Such limits constrain an individual, point-like DM constituent, assuming it makes up 100% of the DM, to be lighter than around  $5 M_{\odot}$ . (Notice that the mass limits discussed here do not assume any specific production mechanism, and do not depend on the observed cosmological DM density).

**Stability:** The DM lifetime must be long compared to cosmological timescales [25].

### 27.3 Genesis of dark matter

The generation of DM in the early universe can proceed via thermal or non-thermal production, or both, or it may result from a particle-antiparticle asymmetry.

**Freeze-out:** The process of chemical decoupling from the high-temperature, high-density thermal bath (freeze-out) as a paradigm for particle production in the early universe is both a predictive and a successful one. The possibility that just like light elements, neutrinos, and CMB photons, particle DM also originated from a thermal decoupling process has thus garnered significant attention.

A particle species *chemically* decouples when the rate  $\Gamma$  for the species’ number-changing processes drops below the Hubble rate  $H$ . Rough estimates for the abundance of relics can be obtained by (i) calculating the freeze-out (i.e. “decoupling”) temperature  $T_{\text{f.o.}}$ , corresponding to  $H(T_{\text{f.o.}}) \sim \Gamma(T_{\text{f.o.}})$ , (ii) equating the comoving number density at freeze-out and today, eventually (iii) obtaining the physical density of relic particles today. This procedure assumes that entropy is conserved between  $T_{\text{f.o.}}$  and today, an assumption that could well be violated, especially for

heavy relics that decouple early, for instance by entropy injection episodes [26]. Notice also that the freeze-out calculation strongly depends on the assumed background cosmology, and changes e.g. if the early universe is not radiation-dominated around DM decoupling.

The calculation of the freeze-out relic abundance hinges on a Boltzmann equation relating the Liouville operator to the collision operator acting on the phase space density. Under a variety of simplifying assumptions including homogeneity and isotropy, it is possible to reduce the relevant equation for the number density  $n$  of a single species pair-annihilating with particles in the thermal bath via 2-to-2 processes to

$$\frac{dn}{dt} - 3Hn = -\langle\sigma v\rangle (n^2 - n_{\text{eq}}^2), \quad (27.2)$$

where  $\langle\sigma v\rangle$  is the thermally-averaged pair-annihilation cross section times relative velocity (see Ref. [27]), and  $n_{\text{eq}}$  is the equilibrium number density. Relics for which the freeze-out temperature is much larger than the particle mass (and thus that freeze-out as ultra-relativistic) are called *hot* relics; if the opposite is true, the relic is instead considered *cold*.

A straightforward calculation shows that to leading order the frozen-out density of *hot* relics is *linearly proportional to the relic particle mass*. The comoving number density  $Y = n/s$ , where  $s$  is the entropy density, for a hot relic is approximately given by its equilibrium value,

$$Y_{\text{f.o.}} \simeq Y_{\text{eq}} \simeq 0.278 \frac{g_{\text{eff}}}{g_{*s}}, \quad (27.3)$$

where  $g_{\text{eff}}$  is the relic's effective number of degrees of freedom, and  $g_{*s}$  is the number of entropic relativistic degrees of freedom, both calculated at  $T_{\text{f.o.}}$ . The resulting relic abundance, assuming an iso-entropic expansion, is

$$\Omega_{\text{hot}} h^2 = \frac{m Y_{\text{f.o.}} s_0 h^2}{\rho_c} \simeq \frac{m}{93 \text{ eV}}, \quad (27.4)$$

with  $s_0$  the entropy density today, and with the latter equality holding for the case of SM neutrinos, with a freeze-out temperature around 1 MeV (which enters in the final relic abundance through the degrees of freedom dependence on the right-hand-side of Eq. (27.3)).

For *cold* relics, the leading-order dependence of the relic abundance on the DM particle properties is an *inverse proportionality relation to the pair-annihilation cross section*,

$$\Omega_{\text{cold}} h^2 \simeq 0.1 \left( \frac{x_{\text{f.o.}}}{20} \right) \left( \frac{10^{-8} \text{ GeV}^{-2}}{\sigma_{DM+DM \leftrightarrow \text{anything}}} \right), \quad (27.5)$$

where  $x \equiv m_{\text{DM}}/T$ . In turn, the freeze-out temperature is approximately given by the solution to the equation

$$\sqrt{x} \cdot e^{-x} = (m_{\text{DM}} \cdot M_P \cdot \sigma_{DM+DM \leftrightarrow \text{anything}})^{-1}, \quad (27.6)$$

where  $M_P \simeq 2.435 \times 10^{18}$  GeV is the reduced Planck mass. As a result,  $T_{\text{f.o.}} \simeq m_{\text{DM}}/x_{\text{f.o.}}$ , with  $x_{\text{f.o.}}$  a number between 10 and 50, depending on the cross section, with only a logarithmic dependence on the DM mass. Since for electroweak-scale cross sections and masses  $\sigma_{DM+DM} \simeq 10^{-8} \text{ GeV}^{-2}$ , “weakly-interacting massive particles”, or WIMPs have gained exceptional popularity. Notice that Eq. (27.5) bears, however, no connection to the weak scale [28], despite the relation being known as “WIMP miracle”.

Numerous scenarios exist, including notably supersymmetry [29,30] and models with universal extra dimensions [31,32] where the relic abundance of the DM is controlled by processes involving a slightly heavier, unstable, co-annihilating species [33]. In this case the calculation of the abundance of the stable species proceeds similarly to what outlined above, with an effective pair-annihilation cross section that captures the effects of co-annihilation replacing the pair-annihilation cross section [30].

**Freeze-in:** Collisional processes can lead to the production of out-of-equilibrium particles that progressively accumulate over cosmic time, a process sometimes called *freeze-in*. The abundance

of the frozen-in particles produced at a given redshift depends on the product of the production rate times the Hubble time at that redshift. Freeze-in generally implies that the lightest observable-sector particles decay to the DM with relatively long lifetimes, giving peculiar signals at colliders (see e.g. [34]). Gravitinos are an example of DM candidates possibly produced via a freeze-in type scenario, albeit the portal coupling is in that case via a higher dimensional, Planck-suppressed operator [35].

**Cannibalization and other dark-sector number-changing processes:** Thermal processes can drive the abundance of the DM beyond simple 2-to-2 number-changing interactions. For instance, DM can “cannibalize” [36,37] itself if  $n \rightarrow 2$  processes exist. In this case, a critical aspect is whether or not the DM sector is in thermal contact with the Standard Model thermal bath. If it is,  $n \rightarrow 2$  processes can drive the relic abundance, e.g. in the Strongly Interacting Massive Particles (SIMP) scenario [38]. Models exist where the *kinetic decoupling* (i.e. the decoupling from the *thermal equilibrium velocity distribution*) of the two sectors drives the abundance of the DM (elastically decoupling relics, or ELDERS [39]). When the two sectors are not in thermal contact,  $n \rightarrow 2$  processes heat the DM sector dramatically, rapidly affecting the temperature ratio between the visible and dark sectors [36,38]. If the relevant cross sections are large enough, and the DM mass light enough, significant effects can arise in structure formation [36].

**Non-thermal production:** DM production can proceed via processes out of thermal equilibrium (“non-thermal” production). These include DM production via the decay of a “mother” particle [40,41] (or of topological defects [42], moduli [43] etc.) to the DM, or production via gravitational effects.

**Asymmetric DM:** An enticing alternative possibility for DM production is that of *asymmetric* DM [44,45]: the relic DM abundance arises from an asymmetry between anti-DM and DM. This asymmetry may or may not be related to the baryon-antibaryon asymmetry. If it is, then depending on the model and its thermal history, a relation exists between the mass of the DM and the proton mass. A variety of proposals have been put forward where alternately baryogenesis is explained from a DM sector asymmetry, or vice-versa (see e.g. Ref. [46] for a review).

**Primordial Black Holes production:** A qualitatively stand-alone class of DM candidates, primordial black holes (PBHs), arises from entirely different mechanisms from what reviewed above. PBHs are thought to originate from gravitational collapse of large density fluctuations in the early universe [47,48]. The over-densities could be produced in a variety of ways, such as topological defects like cosmic strings, necklaces or domain walls, curvature fluctuations from a period of ultra-slow-roll, a sound speed “resonance”, an early phase of matter domination, or sub-horizon phenomena including a phase transition and preheating. Albeit the calculation depends on the details of gravitational collapse, the formation time is connected to the PBH mass via  $M = \gamma M_{\text{PBH}} \simeq 2 \times 10^5 \gamma \left( \frac{t}{1 \text{ s}} \right) M_{\odot}$ , with  $\gamma \simeq (1/\sqrt{3})^3$  during radiation domination [49].

## 27.4 Density and velocity distribution of dark matter

### 27.4.1 Local density and velocity distribution

The density and distribution of DM in the Milky Way encipher relevant dynamical information about our Galaxy, and are particularly important for direct and indirect detection experiments. The *local density* ( $\rho_0$ ) is an average over a volume of a few hundred parsecs in the Solar neighbourhood.

To determine the local density from observations, two classes of methods are used [50]. So-called *local measures* rely on the vertical motion of tracer stars in the vicinity of the Sun, while *global measures* extrapolate  $\rho_0$  from the measured rotation curve, with additional assumptions about the Galactic halo shape. Conversely, by comparing the extrapolated local density with the one obtained from local measures, one can constrain the local shape of the Milky Way halo. A major source of uncertainty on  $\rho_0$  is the contribution of baryons (stars, gas, stellar remnants) to the local dynamical mass. For instance, the motion of tracer stars used in local measures is dictated by the total potential generated by

baryons and DM, and a robust baryonic census must be available to infer the additional contribution from DM. Recent determinations from global methods lie in the range  $(0.2 - 0.6) \text{ GeV/cm}^3$ , while new studies of the local DM density from *Gaia* satellite data yield  $(0.4 - 1.5) \text{ GeV/cm}^3$ , depending on the type of stars used in the study [51].

Other observational quantities that enter in the phase space distribution of DM, and provide constraints on mass models of the Milky Way are the local circular speed  $v_c$  and the escape velocity  $v_{esc}$ . The local circular speed is measured by various methods, roughly divided into measurements of the Sun's velocity with respect to an object assumed to be at rest with respect to the Galactic centre or direct measurements of the local radial force [52]. These methods yield values of  $v_c = (218 - 246) \text{ km/s}$ . A recent estimate of the escape velocity, defined as the speed above which objects are not gravitationally bound to our galaxy, is  $v_{esc} = 533^{+54}_{-41} \text{ km/s}$  [53].

The local velocity distribution of DM particles can not be measured directly at present, and is mostly derived from simulations. In general, experiments use the simplest, so-called *Standard Halo Model (SHM)* for their data analysis. It assumes an isotropic, isothermal sphere of DM particles with a density profile of  $\rho(r) \propto r^{-2}$ , for which the velocity distribution is Maxwellian, with a velocity dispersion  $\sigma_v = v_c/\sqrt{2}$ . This distribution, which formally extends to infinity, is truncated at  $v_{esc}$  [54]. Earlier high resolution, dark-matter-only simulations found velocity distributions that markedly deviated from a Maxwell-Boltzmann distribution [55] and in addition revealed components above the dominant smooth distribution, including narrow spikes due to tidal streams. Recent hydrodynamical simulations of Milky Way-like galaxies including baryons, which have a non-negligible effect on the DM distribution in the Solar neighbourhood, find velocity distributions that are indeed close to Maxwellian, arguing that the SHM is a good approximation [56–58].

Ultimately the goal is to determine the velocity distribution from observations (for example by studying the motion of stars that share the same kinematics as the DM), and the *Gaia* satellite data offers a unique opportunity to study the various stellar populations. Recently it was revealed that the local stellar halo has two components: a quasi-spherical, weakly rotating structure with metal-poor stars, and a flattened, radially anisotropic structure of metal-rich stars, which arose due to accretion of a large  $(10^{11-12} M_\odot)$  dwarf galaxy around  $(8-10) \times 10^9$  y ago [59]. The expectation is that the local DM halo shows a similar bimodal structure, and first velocity distributions of the two components - using the stellar populations as tracers - were inferred in [60]. In Ref. [61], an updated halo model is introduced: it includes the anisotropic structure seen in the *Gaia* data and provides an analytic expression for the velocity distribution. The value of the local DM density is updated to  $(0.55 \pm 0.17) \text{ GeV/cm}^3$ , where the 30% error accounts for the systematics. The circular rotation and the escape speeds are updated to  $v_c = (233 \pm 3) \text{ km/s}$  and  $v_{esc} = 528^{+24}_{-25} \text{ km/s}$ .

#### 27.4.2 Small-scale challenges

The  $\Lambda$ CDM framework is tremendously successful at explaining the observed large-scale structures of the Universe (corresponding to distances  $\geq 1 \text{ Mpc}$ , the typical inter-galactic distance), as well as the main properties of galaxies that form within DM haloes, see [62]. The observed large-scale structure is consistent with point-like, cold DM particles that interact purely via the gravitational force. But in the past decades, observations at scales below  $\sim 1 \text{ Mpc}$ , where structure formation becomes strongly nonlinear, turned out more problematic to be described within the  $\Lambda$ CDM model. The main *small-scale challenges* which received much attention in the recent literature [13, 62] are known as: the missing satellites problem, the cusp-core problem and the too-big-to-fail problem. Initially these issues, which are not all independent of one another, arose by comparing theoretical predictions from dark-matter-only simulations to observation. While their most likely solutions are in dissipative, baryonic physics (such as gas cooling, star formation, supernovae feedback), see the recent review in Ref. [63], the small-scale problems could in addition call for a

modification or an extension of the  $\Lambda$ CDM paradigm. Most importantly, the ever increasing amount of data on the satellites of the MW and M31 are used to constrain alternative DM models.

**The missing satellites problem:** High-resolution cosmological simulations of DM haloes the size of the MW predict hundreds or thousands of subhaloes with masses that are in principle large enough to allow for galaxy formation ( $> 10^7 M_\odot$ ). Yet less than  $\sim 100$  satellite galaxies with masses down to  $\sim 300 M_\odot$  are known to orbit our galaxy within 300 kpc. Galaxies in the field show a similar under-abundance. One solution could be that galaxy formation becomes increasingly inefficient as the halo mass drops, and thus the smallest DM haloes have naturally failed to form galaxies.

**The cusp-core problem:** The mass density profiles of DM haloes in  $\Lambda$ CDM simulations rise steeply at small radii,  $\rho(r) \propto r^{-\gamma}$ , with  $\gamma \simeq 0.8 - 1.4$  [64]. This is in contrast to the observed density profiles of many low-mass galaxies (albeit not all), the rotation curves of which are best fit with constant-density cores,  $\gamma \simeq 0 - 0.5$ . A related issue is that simulations predict more DM than measured in the central regions of galaxies (also known as the central density problem). A likely solution is that baryonic feedback modifies the structure of DM haloes. Hydrodynamic simulations which include the effects of baryons on galaxy formation have shown that baryonic feedback (e.g., supernova-driven blowouts) can erase the central cusps and produce core-like density profiles.

**The too-big-to-fail problem:** This problem is related to the fact that the local Universe contains fewer galaxies with large central densities ( $\simeq 10^{10} M_\odot$ ) compared to  $\Lambda$ CDM predictions. DM haloes of such masses are thought to be too massive to have failed to form stars (hence the name of the problem), especially if lower-mass subhaloes are capable of doing so. The bright MW satellites are generally associated with subhaloes (e.g., from the Aquarius and Via Lactea II  $\Lambda$ CDM simulations), however not with the most massive ones [65]. A similar issue is present in Andromeda and in field galaxies outside the Local Group. The solutions that were briefly mentioned above do not require modifications to the  $\Lambda$ CDM framework. Other solutions involve either modifications of linear theory predictions (via the nature of the DM particle, e.g., Warm DM - WDM) or modifications of nonlinear predictions (via DM models that involve a self-interaction of DM particles - SIDM) [62]. WDM models postulate particles with masses at the keV-scale, and the observed number of dark-matter-dominated satellites is used to set a lower limit on the number of subhaloes in the MW and thus a lower limit on the particle's mass [63]. Current constraints are in the range  $m_{WDM} > (1.6 - 2.3) \text{ keV}$ . Cosmological simulations with SIDM find that  $\sigma/m_{SIDM} \simeq (0.5-10) \text{ cm}^2/\text{g}$  can alleviate the cusp-core and too-big-to-fail problems, giving rise to DM cores in dwarf galaxies with sizes of  $(0.3-1.5) \text{ kpc}$  [13]. Galaxy clusters provide important constraints, and their large central DM densities prefer models with  $\sigma/m_{DM} \lesssim 0.1 \text{ cm}^2/\text{g}$  [66]. Thus, if SIDM is to solve the small-scale CDM problems (without considering the baryonic feedback however) and obey the constraints observed on the scales of clusters,  $\sigma$  must depend on the velocity of the particle: it must increase as the rms speed of the particle decreases from the scale of clusters ( $v \sim 10^3 \text{ km/s}$ ) to the scale of dwarf galaxies ( $v \sim 10 \text{ km/s}$ ).

## 27.5 Dark matter models

Particle DM model building is deeply intertwined with the question of the nature of physics beyond the Standard Model (BSM) of particle physics<sup>1</sup>. Directions in this area have followed a few strategies, including, but not limited to (1) pursuing DM candidates embedded in frameworks that include solutions to other open issues in particle physics, for example WIMPs in connection with electroweak-scale new physics that addresses the hierarchy problem, such as supersymmetry (see the Supersymmetry reviews Sec. 89 and 89); axions in connection with frameworks that address the strong CP problem (see Axions and Other Similar Particles—Sec. 91); sterile neutrinos in connection with the

<sup>1</sup>Notice that this includes the case of PBHs, as successful formation of the correct number density of PBHs involves new ingredients beyond standard cosmology and particle physics

problem of neutrino masses and mixing (see the Neutrino Masses, Mixing, and Oscillations—Sec. 14); or (2) *ad hoc*, or *bottom-up* models built with the intent of addressing or explaining a putative experimental (e.g. particle physical anomalies) or observational (e.g. astronomical) signal.

**WIMPs:** The WIMP paradigm has been a preferred framework chiefly because it often arises in beyond the Standard Model scenarios that address the hierarchy problem whilst also providing a simple mechanism to explain the observed relic abundance via the “WIMP miracle” described above. Perhaps the most notable example of a framework containing a paradigmatic WIMP is the minimal supersymmetric extension to the Standard Model, if the lightest supersymmetric particle is a neutralino (the mass eigenstate resulting from the mixing of the supersymmetric partners to the Higgses and to the SU(2) and hypercharge gauge bosons, and, possibly, of additional singlet scalars); purely SU(2) sneutrinos have long been ruled out by direct detection, but with suitable mixing with “inert” (gauge-singlet) sneutrinos they can also play the role of WIMP candidates. For more details see the the Supersymmetry—Sec. 89 and 90 in this *Review*. Other non-supersymmetric WIMP models include models with a Higgs or  $Z$  (or  $Z'$ ) portal, universal extra dimensions [32], and other models with extra (warped or flat) dimensions, little Higgs theories, technicolor and composite Higgs theories, among others (see e.g. the review in [67]).

**Axions and axion-like particles:** Axions are an especially compelling example of a broad category of DM candidates encompassing very light scalar or pseudoscalar fields. The QCD axion provides a solution to the strong  $CP$  problem, and is at present a viable DM candidate (see Sec. 91 for details on motivations, production mechanisms, and detection prospects for the QCD axion). Ultra-light, bosonic DM generally implies the imprint of quantum effects on macroscopic scales (hence the name of *wave* or *fuzzy* DM). Specifically, some of the small-scale issues mentioned in sec. 27.4 can be addressed if the de Broglie wavelength of the DM, of mass  $m_a$  and velocity  $v_a$ ,

$$\frac{\lambda}{2\pi} = \frac{\hbar}{m_a v_a} \simeq 1.9 \text{ kpc} \left( \frac{10^{-22} \text{ eV}}{m_a} \right) \left( \frac{10 \text{ km/s}}{v_a} \right) \quad (27.7)$$

is comparable to the size of the smallest observed gravitationally collapsed structures, roughly, for a self-gravitating system of mass  $M$ , a scale  $r \simeq GM/v^2$ . The typical expectation is the formation of a soliton-like core in the DM density profile of size  $\lambda$ , thus inversely proportional to the DM mass, with an upper limit on the central density of around

$$\rho_s \lesssim 7 M_\odot/\text{pc}^3 \left( \frac{m_a}{10^{-22} \text{ eV}} \right)^6 \left( \frac{M}{10^9 M_\odot} \right) \quad (27.8)$$

for a halo of virial mass  $M$ . Additionally, wave DM predicts that halos lighter than around  $10^7 (m_a/10^{-22} \text{ eV})^{-3/2} M_\odot$  should not exist [68], and that the number of halos in the local universe with a mass at or less  $10^9 (m_a/10^{-22} \text{ eV})^{-4/3} M_\odot$  [69] be significantly depleted, addressing in part the too big to fail and missing satellite problems (see Sec. 27.4 above). Light bosonic DM is necessarily produced non-thermally [70], and the connection with the visible sector need not, but might, exist.

**Dark photons:** Light *vector* bosons such as a “dark photon”  $V$  with a mass below  $m_V < 2m_e$ , can be cosmologically stable (depending upon its kinetic mixing coupling with the visible photon) and be a viable DM candidate. Light dark photons can be produced in the early universe through scattering or annihilation via processes such as  $\gamma e^\pm \rightarrow V e^\pm$  or  $e^+ e^- \rightarrow V \gamma$ , or via resonant photon-dark photon conversion, or from a condensate seeded by inflationary perturbations [71], or from a misalignment mechanism similar to the one commonly invoked for axion production; constraints on the parameter space stem from a combination of direct detection experiments, where the dark photon is absorbed and leads to a large ionization signal, from stellar cooling constraints from the Sun, horizontal branch stars, and red giants, and from CMB and the diffuse radiation from the  $V \rightarrow 3\gamma$  decay mode. More broadly, light dark (pseudo-)scalars and vectors can be best constrained with experiments that rely on their

wave-like behaviour and/or on their possible “portal” with the visible sector. A broad assortment of experiments is sensitive to the range of masses between  $10^{-22} \text{ eV}$  and  $10^{-2} \text{ eV}$ . Among these experimental efforts, the lowest masses are probed by torsion balance experiments [72, 73], atom interferometry [74], comagnetometers [75, 76], and even gravitational wave detectors [77]; at increasing masses, if the light bosons couple electromagnetically, they can generate effective currents which are detectable with different apparatus depending on the relevant, mass-dependent target frequency. The experimental portfolio includes the broadband axion search ABRACADABRA [78, 79], the LC resonator DM Radio [80], lumped-element LC resonators [81], and cavity resonators such as HAYSTAC [82] and ADMX [83].

**Sterile Neutrinos:** Sterile (gauge-singlet) neutrinos, assumed to share a Dirac mass term with ordinary, SU(2) $_L$ -active neutrinos, have long been considered viable DM candidates [84]. The mostly-sterile mass eigenstate participates in SU(2) $_L$  interactions via a mixing parameter  $\theta \ll 1$  that controls much of the particle’s phenomenology. In particular, the sterile neutrino possesses an inverse-lifetime on the order of  $\tau^{-1} \sim G_F^2 m_\nu^5 \theta^2$ , forcing the mixing to not exceed

$$\theta < 3.3 \times 10^{-4} \left( \frac{10 \text{ keV}}{m_\nu} \right)^5 \quad (27.9)$$

in order for the lifetime to exceed the age of the universe. While the main decay channel is to three active neutrinos, observationally the radiative decay mode to one neutrino plus a photon is much more relevant, giving rise to a quasi-monochromatic photon line at half the sterile neutrino mass. A recent tentative signal at 3.5 keV was reported from stacked observations of clusters of galaxies, individual clusters [85, 86], and the Galactic center [87] with both the XMM and Chandra X-ray observatories. The signal however was not detected in a large sample of galaxies and groups of galaxies [88] and dwarf galaxies [89], and especially Draco [90], shedding strong doubts on its sterile neutrino decay origin. Future observations with increased energy resolution might conclusively pinpoint the origin of the 3.5 keV emission [91].

**Models with rich dark sectors:** The absence of any conclusive signals from DM as a particle thus far motivates the hypothesis that the DM be charged under some new “hidden” dark-sector force, an idea that dates back many decades [92], including in the guise of “mirror DM” (more recently in the context of “neutral naturalness”). Top-down motivation for hidden-sector DM comes from string theory [93], although TeV-scale BSM framework such as supersymmetry and composite Higgs models can also naturally accommodate hidden sectors [94]. Although no coupling of the visible sector to the hidden sector need exist in principle, there are a few reasons to expect it [95]. The mass scale for hidden-sector DM is broader than, but overlapping with, that for WIMPs (this latter being limited to roughly between a few GeV and a few TeV). In particular, while some motivation exists for electroweak-scale hidden sectors, light, sub-GeV hidden sectors have a strong theoretical underpinning, and offer novel detection avenues and opportunities. The phenomenology of hidden-sector DM depends primarily on the nature of the force and its force carrier. The most-widely considered cases are (pseudo-)scalar and (axial-)vector mediators. Among the structures for the mediators’ coupling to the visible sector, renormalizable “portals” include the  $H^\dagger H$  operator, through Lagrangian terms of the type  $(\mu\phi + \lambda\phi^2)H^\dagger H$ , coupling to the hypercharge field strength  $B^{\mu\nu}$  via kinetic mixing,  $\epsilon' B_{\mu\nu} F'^{\mu\nu}$ , and the “neutrino” portal,  $y_n L H N$ , where  $L$  is the lepton doublet of any generation,  $N$  is a right-handed neutrino,  $H$  is the SM Higgs doublet, and  $y_n$  the Yukawa coupling. Other possibilities are for instance a vector mediator directly coupled to SM fermions charged under its corresponding symmetry [96], or a  $Z'$  associated to U(1) $_{B-L}$ . Additional possibilities, arising for instance from vector couplings to anomalous global symmetries of the SM like baryon or lepton number, also exist [95]. The accelerator program necessary to probe hidden-sector DM often involves small-scale colliders and fixed-target experiments, with experiments utilizing missing energy and momentum offering the best sensitivity. Beam-dump experiments can test large ranges of DM-mediator couplings as long as mediators decay or scatter

inside the detector (see e.g. the recent review [97]). Such experiments can also probe dark sectors with light vectors coupled to visible matter besides gauge kinetic mixing: an instance are neutrino trident scattering used to place bounds on e.g.  $L_\mu - L_\tau$   $Z'$  gauge bosons. Being virtually unconstrained, the phenomenology of dark sectors can be arbitrarily rich, with possibilities ranging from dark non-Abelian gauge interactions creating non-trivial self-interacting and/or particle number-changing dynamics, to models of “dynamical” DM, with multi-component, unstable DM candidates and a time-variable effective total DM abundance and equation of state [98].

## 27.6 Laboratory detection of dark matter

Laboratory searches for DM particles can be roughly classified in direct detection experiments, axion searches (see Axions and Other Similar Particles—Sec. 91), and searches at accelerators and colliders.

### 27.6.1 Searches at Accelerators and Colliders

Various searches for dark matter have been carried out by the CMS and ATLAS collaborations at the LHC in  $pp$  collisions [99–103]. In general, these assume that dark matter particles escape the detector without interacting leading to significant amounts of missing energy and momentum.

Searches for DM with the LHC and other colliders have targeted DM models that interact with the SM via Higgs or  $Z$  boson exchange, effective field theories with heavy mediators, UV-complete models such as supersymmetry, models with long-lived particles, and models with rich dark sectors. The experimental program correspondingly includes searches for invisible-particle production mediated by a SM boson, generic searches for invisible particles produced via new particle mediators, and specific searches for complete models.

There are a variety of types of signals for DM, as noted by Ref. [99]:

(a) the imbalance in the transverse momentum in an event due to the presence of DM particles, produced together with one Standard Model particle,

(b) a bump in the di-jet or di-lepton invariant mass distributions, or

(c) an excess of events in the di-jet angular distribution, produced by a dark matter mediator. No signal for DM has been observed in the LHC experiments so far. Instead limits are set on masses, couplings, and cross-sections. The latter can be compared with direct detection experiments.

Searches strategies are designed to optimize signal-to-noise by selecting specific search-specific cuts: a model-independent instance is initial-state electromagnetic or strong-interaction radiation plus missing transverse energy. Collider searches for DM inform, and are informed, by DM searches through direct or indirect detection (see below), and, if possible, by the inferred thermal relic DM abundance. The collider searches alone cannot prove that a discovery is of dark matter.

In the latter category, searches for DM with the LHC and other colliders have targeted DM models that interact with the SM via Higgs or  $Z$  boson exchange, effective field theories with heavy mediators, UV-complete models such as supersymmetry, models with long-lived particles, and models with rich dark sectors. The experimental program correspondingly includes searches for invisible-particle production mediated by a SM boson, generic searches for invisible particles produced via new particle mediators, and specific searches for complete models. Searches strategies are designed to optimize signal-to-noise by selecting specific search-specific cuts: a model-independent instance is initial-state electromagnetic or strong-interaction radiation plus missing transverse energy.

### 27.6.2 Direct detection formalism

Direct detection experiments mostly aim to observe elastic or inelastic scatters of Galactic DM particles with atomic nuclei, or with electrons in the detector material. Predicted event rates assume a certain mass and scattering cross section, as well as a set of astrophysical parameters: the local density  $\rho_0$ , the velocity distribution  $f(\vec{v})$ , and the escape velocity  $v_{esc}$  (see Sec. 27.4).

**Interactions with atomic nuclei:** For DM scattering off nuclei, the differential scattering rate  $R$  as a function of nuclear recoil energy  $E_R$  is

$$\frac{dR(E_R, t)}{dE_R} = N_T \frac{\rho_0}{m_{\text{DM}}} \int_{v > v_{\min}} v f(\vec{v} + \vec{v}_E(t)) \frac{d\sigma(E_R, v)}{dE_R} d^3v, \quad (27.10)$$

where  $N_T$  is the number of target nuclei,  $m_{\text{DM}}$  is the mass of the DM particles,  $v = |\vec{v}|$  is the speed of the particle in the experiment’s rest frame,  $f(\vec{v} + \vec{v}_E(t))$  is the velocity distribution in the Earth’s frame,  $v_{\min}$  is the minimum speed of the DM particles that can cause a recoil energy  $E_R$  and  $\sigma$  is the scattering cross section on the nucleus [29, 121]. For elastic scattering, the minimum velocity is  $v_{\min} = (m_N E_R / 2m_r^2)^{1/2}$ , with  $m_N$  being the mass of the nucleus, and  $m_r = (m_N m_{\text{DM}}) / (m_N + m_{\text{DM}})$  the reduced mass of the nucleus-DM system. In case of inelastic scattering, the minimum speed becomes  $v_{\min} = (m_N E_R / 2m_r^2)^{1/2} + E^* / (2m_N E_R)^{1/2}$ , with the nuclear excitation energy  $E^*$ , for part of the kinetic energy of the incoming particle will be spent on exciting the nucleus. The prompt de-excitation energy, if observed in addition to the nuclear recoil energy, will boost the region-of-interest to higher energies [122].

If one assumes the standard, leading order spin-independent (SI) and spin-dependent (SD) interactions, which couple to the charge/mass and spin of the nucleus, respectively, the differential cross section is proportional to the inverse squared speed of the DM particle,  $d\sigma/dE_R \propto v^{-2}$ , and the dependence on the velocity distribution can be expressed as:

$$g(v_{\min}, t) = \int_{v > v_{\min}} \frac{f(\vec{v} + \vec{v}_E(t))}{v} d^3v. \quad (27.11)$$

This functions allows for the comparison of various experimental results independently of the underlying velocity distribution [123], for a given DM mass. The time-integrated differential cross section is the sum of the SI and SD contributions:

$$\frac{d\sigma(E_R, v)}{dE_R} = \frac{m_N}{2m_r^2 v^2} (\sigma_0^{SI} F_{SI}^2(E_R) + \sigma_0^{SD} F_{SD}^2(E_R)), \quad (27.12)$$

where  $F^2(E_R)$  are the nuclear form factors and  $\sigma_0$  the cross sections in the limit of zero momentum transfer. Since the incoming particle velocity is  $v/c \sim 10^{-3}$ , the nuclear recoil energy is at most tens of keV (much smaller than typical nuclear binding energies per nucleon), and the momentum transfer  $q = (2m_N E_R)^{1/2} \sim \mathcal{O}(10\text{--}100\text{ MeV})$ . This implies that  $1/q$  can be of the same order as nuclear radii  $R \sim A^{1/3}$  fm, and that nuclei are not point-like from the perspective of a DM particle. The cross sections will thus involve nuclear form factors. These were calculated in [124] and [125] for the SI and SD case, respectively, for specific target nuclei, while the cross sections are often expressed in terms of single-nucleon cross sections and effective couplings of the DM particle to protons and neutrons. In the SI case, all the nucleons in the nucleus contribute coherently to the cross section (under the assumption of iso-spin independence in the DM couplings). Dominant sources of uncertainty are the nucleon sigma terms, especially for Higgs-dominated interactions, where the couplings are proportional to the quark masses. An overview is presented in Ref. [126]. For SD scattering, the nuclear spin contents due to the protons and neutrons must be considered.

The interactions of DM particles with nuclei can be treated in a non-relativistic effective field theory (NR-EFT) approach, which considers more general DM scenarios based on the lowest-order, four-field operators that describe the couplings to nucleons. These operators, which correspond to different types of interactions between the DM and quark fields, can be momentum- and velocity-dependent, and might be leading when momentum-independent interactions are suppressed, or even vanish in the limit of zero momentum [127, 128]. In Ref. [128, 129] all 15 operators (arising from 20 possible bilinear combinations between the DM and nucleon fields) which obey Galilean-invariance,  $T$ -symmetry and are Hermitian are written out up to quadratic order in  $q$ , and the

**Table 27.1:** Best constraints from direct detection experiments on the SI (at high  $>5$  GeV and low  $< 5$  GeV masses) and SD DM-nucleon couplings.

Experiment	Target	Fiducial mass [kg]	Cross section [cm <sup>2</sup> ]	DM mass [GeV]	Ref.
<b>Spin independent high mass (<math>&gt;5</math> GeV)</b>					
XENON1T	Xe	1042	$4.1 \times 10^{-47}$	30	[104]
PandaX-II	Xe	364	$8.6 \times 10^{-47}$	40	[105]
LUX	Xe	118	$1.1 \times 10^{-46}$	50	[106]
SuperCDMS	Ge	12	$1.0 \times 10^{-44}$	46	[107]
DarkSide-50	Ar	46	$1.14 \times 10^{-44}$	100	[108]
DEAP-3600	Ar	2000	$3.9 \times 10^{-45}$	100	[109]
<b>Spin independent low mass (<math>&lt;5</math> GeV)</b>					
LUX (Migdal)	Xe	118	$6.9 \times 10^{-38}$	2	[110]
XENON1T (Migdal)	Xe	1042	$3 \times 10^{-40}$	2	[111]
XENON1T (ionisation only)	Xe	1042	$3.6 \times 10^{-41}$	3	[112]
DarkSide-50 (ionisation only)	Ar	20	$1 \times 10^{-41}$	2	[113]
SuperCDMS (CDMSlite)	Ge	0.6	$2 \times 10^{-40}$	2	[114]
CRESST	CaWO <sub>4</sub> - O	0.024	$1 \times 10^{-39}$	2	[115]
NEWS-G	Ne	0.3	$1 \times 10^{-38}$	2	[116]
<b>Spin dependent proton</b>					
PICO60	C <sub>3</sub> F <sub>8</sub> - F	49	$3.2 \times 10^{-41}$	25	[117]
<b>Spin dependent neutron</b>					
XENON1T	Xe	1042	$6.3 \times 10^{-42}$	30	[118]
PandaX-II	Xe	364	$1.6 \times 10^{-41}$	40	[119]
LUX	Xe	118	$1.6 \times 10^{-41}$	35	[120]

nuclear response functions evaluated in shell-model calculations for DM targets made of F, Na, Ge, I and Xe isotopes. The connection to particle physics within the context of *simplified DM models* is made in Ref. [130, 131], where the simplified models assume a single DM particle with one mediator which couples it to quarks. More recently the DM-nucleus scattering was also analysed in the framework of chiral effective field theory (Ch-EFT), a low-energy effective theory of QCD, which allows for a consistent derivation of the nuclear responses beyond the leading-order expressions [132, 133]. Ch-EFT preserves the QCD symmetries, and predicts DM couplings to two nucleons (e.g., when the hypothetical particle couples to a virtual pion exchanged between the nucleons). It also provides a power counting that suggests a hierarchy of the various NR-EFT operators, which is however approximate given that the couplings between the DM and the Standard Model fields are not known. The generalised SI structure factors for spin-1/2 and spin-0 DM particles and various isotopes of F, Si, Ar, Ge and Xe employed in direct detection experiments are provided in Ref. [133].

**Scattering off bound electrons and absorption:** For DM particle masses below the GeV-scale, most searches for DM-nucleus scattering rapidly lose sensitivity, due to energy thresholds around a few 100 eV - few keV. As an example, a light DM particle with a mass of 100 MeV and  $v \propto 10^{-3}c$  will induce a nuclear recoil energy of about 0.5 eV in a target made of argon. Another strategy is to search for DM scattering off bound electrons, allowing for all of the kinetic energy (50 eV in the above case) to be transferred to the material [134]. The leading possibilities are ionisation, excitation, and molecular dissociation processes, which typically require energies of (1-10) eV, and thus allow to probe scattering of DM particles with masses down to the  $\mathcal{O}(\text{MeV})$  range.

For a bound electron with binding energy  $E_B$  DM particle masses of  $m_{\text{DM}} \geq 250 \text{ keV} \times E_B/1 \text{ eV}$  can in principle be probed. The signal depends on the material, and can consist of one or more electrons (in semiconductors, noble liquids, graphene), one or more photons (in scintillators) or phonons (in superconductors and superfluids) and quasiparticles (in superconductors). As an example, the differential event rate for ionisation in atoms is given by

$$\frac{dR_{\text{ion}}}{d \ln E_R} = N_T \frac{\rho_0}{m_{\text{DM}}} \frac{d\langle \sigma_{\text{ion}} v \rangle}{d \ln E_R}, \quad (27.13)$$

where  $E_R$  is the recoil energy transferred to the electron,  $\langle \sigma_{\text{ion}} v \rangle$  is the thermally averaged ionisation cross section and  $N_T$  is the number of target atoms per unit mass. The cross section is related

to the non relativistic DM-electron elastic scattering cross section ( $\sigma_e$ ):

$$\begin{aligned} \frac{dR_{\text{ion}}}{d \ln E_R} &= \frac{6.2}{A} \left( \frac{\rho_0}{0.4 \text{ GeV cm}^{-3}} \right) \left( \frac{\sigma_e}{10^{-40} \text{ cm}^2} \right) \left( \frac{10 \text{ MeV}}{m_{\text{DM}}} \right) \\ &\times \frac{d\langle \sigma_{\text{ion}} v \rangle / d \ln E_R}{10^{-3} \sigma_e} \frac{\text{events}}{\text{kg d}} \end{aligned} \quad (27.14)$$

Predicted differential rates in various materials (He, Ar, Ge, Xe) and for different particle masses are shown in [134], together with cross section sensitivities as a function of mass and expected background rates from neutrinos.

Two classes of DM candidates, axion-like-particles (ALPs) and dark (or hidden) photons (see Sec. 27.5), can be absorbed in a target material by interactions with bound electrons via the axioelectric effect, which is analogous to the photoelectric effect: a boson is absorbed by a bound electron, which is then ejected from the atom [71, 135, 136]. The dark photon arises in extensions of the SM by a new massive or massless  $U(1)'$  field, coupled to the SM  $U(1)_Y$  via a kinetic mixing term  $\kappa$ , see Sec. 27.5. The absorption cross section of a massive, NR particle  $m_V$  with coupling  $e' = e\kappa$  to electrons is (in natural units, and for energies  $E_V \ll m_e$ )

$$\sigma_{\text{abs}} = \frac{\alpha'}{\alpha} \left( \frac{E_V}{2m_e} \right)^2 \sigma_{\text{pe}}, \quad (27.15)$$

where  $\sigma_{\text{pe}}$  is the photoelectric cross section, and an analogue to the electromagnetic fine structure constant  $\alpha$  is introduced,  $\alpha' = (e\kappa)^2/4\pi$ . The rate per atom is

$$R \simeq \frac{\rho_0}{m_V} \times \kappa^2 \sigma_{\text{pe}}. \quad (27.16)$$

Since the kinetic energy of the dark photon is negligible compared to its rest energy, a mono-energetic peak at its mass is expected in the spectrum of a direct detection experiment. Dark photons with a thermally generated abundance are excluded by direct detection experiments [71], however non-thermal mechanisms (e.g., via perturbations during inflation) could create the relic abundance, see Section 27.3.

Similarly to axions, ALPs arise in the spontaneous breaking of a global symmetry, and are phenomenologically described by a mass  $m_a$  and a decay constant  $f_a$ . Unlike for QCD axions,

however, there is no strict relation between  $m_a$  and  $f_a$ . The coupling strength to electrons with mass  $m_e$  is parameterised by  $g_{ae} = 2m_e/f_a$ , and the absorption cross section of a particle with incoming velocity  $v_a$  is related to the cross section for the photoelectric effect as

$$\sigma_{abs} v_a \simeq \frac{3E_a^2}{4\pi\alpha f_a^2} \sigma_{pe} = \frac{3g_{ae}^2}{4\pi\alpha} \left(\frac{E_a}{2m_e}\right)^2 \sigma_{pe}. \quad (27.17)$$

As in the case of the dark photon, the signature is a monoenergetic peak at the mass of the particle, broadened by the energy resolution of the detector. Constraints on the couplings of ALPs and dark photons to electrons from direct detection experiments in  $m_a$  and  $m_V$  mass ranges from  $\sim (1 - 10^4)$  eV were derived in Ref. [137, 138], and compared to indirect limits from anomalous energy losses in the Sun, in red-giant and horizontal-branch stars. For a detailed discussion of axion and ALP searches, we refer to the *Axion* review.

### 27.6.3 Current and future direct detection technologies

Direct detection experiments aim to observe the small (keV-scale and below) and rare (fewer than  $\sim 1$  event/(kg y)) signals which are induced by DM particle scatters in a detector, mostly in the form of ionisation, scintillation or lattice vibrations. A majority of experiments detects more than one signal, which allows to distinguish between scattering off of electrons (electronic recoils, ER) and off of atomic nuclei (nuclear recoils, NR). A 3D position resolution is required to define central detector regions (or fiducial volumes) with low background rates from surrounding materials, and the distinction between single- versus multiple-scatters rejects a significant fraction of backgrounds, given that DM will scatter at most once. We refer to [139] for a recent review of the field.

**Specific signatures:** For NRs, the shape of the differential recoil spectrum is exponentially falling with recoil energy, and depends on the mass of the particle and on the nuclear mass. Unless  $m_{DM} \gg m_N$ ,  $m_{DM}$  can in principle be determined from the measured recoil spectrum, where multiple targets will provide tighter constraints [140]. The Earth's motion through the MW induces a seasonal variation of the total event rate and a forward-backward asymmetry in a directional signal [141, 142]. The annual modulation is due to the Earth's motion in the Galactic rest frame, which is a superposition of the Earth's rotation around the Sun and the Sun's rotation around the Galactic center. Since the Earth's orbital speed is much smaller than the Sun's speed, the expected amplitude of the modulation is  $\simeq 5\%$ . In the SHM, the period is one year, and the phase is 150 d (June 2), when both speeds add up maximally. This expectation is modified for different DM distributions, e.g. in the case of sub-structures such as clumps and streams [143, 144] and a DM disc [145]. In addition, the modulation changes phase at a specific recoil energy (known as crossing-energy) [146], which depends on the DM and nuclear mass, allowing to in principle determine  $m_{DM}$  if low energy thresholds can be achieved. A powerful signature is provided by the ability to detect the axis and direction of the recoiling nucleus. Since the DM flux in the laboratory frame is peaked in the direction of motion of the Sun towards the constellation Cygnus, the recoil spectrum is peaked in the opposite direction. The observation of such a dipole feature would provide a 'smoking-gun' evidence for DM, where the forward-backward rates can differ by a factor of  $\sim 10$ , depending on the energy threshold. Ref. [147] provides a recent review of the theoretical framework and of the discovery reach of directional detectors.

**Backgrounds, including neutrinos:** Early direct detection experiments employing low-background Ge spectrometers featured background levels around 2 events/(kg d keV), while the current generation of liquid Xe experiments reduced this noise by four orders of magnitude, to  $2 \times 10^{-4}$  events/(kg d keV). Nonetheless, the measured energy spectra are still dominated by interactions due to the radioactivity of detector components, followed by cosmic muons and their secondaries such as fast neutrons. The cosmic and environmental radiation are suppressed by going deep underground and surrounding the experiments with appropriate shielding structures (mainly large water Cherenkov detectors for the current and next-generation detectors). Activation of mate-

rials via cosmic-ray interactions produce long-lived radio-nuclides (e.g.,  $^{39}\text{Ar}$ ,  $^{60}\text{Co}$ ,  $^{68}\text{Ge}$ ,  $^{32}\text{Si}$ , etc), while long-lived, human-made isotopes ( $^{85}\text{Kr}$ ,  $^{137}\text{Cs}$ , etc) can mix with detector materials or generate surface backgrounds. For details, we refer to *Section 36.6* of this *Review*.

The final backgrounds will be due to the irreducible neutrino flux from the Sun, the atmosphere and the diffuse supernovae background [148]. Solar pp-neutrinos will dominate the electronic recoil background due to elastic neutrino-electron scatters, at a level of  $\sim (10 - 25)$  events/(t y) below energies of  $\sim 100$  keV, while coherent elastic neutrino-nucleus scatters (CE $\nu$ NS) from  $^8\text{B}$  solar neutrinos will induce up to  $\sim 10^3$  events/(t y) for high-A targets, at nuclear recoil energies below  $\sim$  few keV. Nuclear recoils from atmospheric neutrinos and the diffuse supernovae neutrino background will yield event rates in the range  $(1 - 5)$  events/(100 t y), depending on the detector material. In general,  $^8\text{B}$  and atmospheric neutrinos will impact light ( $\leq 6$  GeV) and heavy (100 GeV and above) DM searches for cross sections on nucleons below  $\sim 10^{-45}$  cm $^2$  and  $\sim 10^{-49}$  cm $^2$ , respectively. The precise cross sections where neutrinos constitute a dominant background depend however on the uncertainties on the flux of each neutrino source, and on the astrophysical parameters that enter in the DM signal models [149]. For very low energy thresholds to nuclear recoils, e.g. 10-30 eV in Ge and Si detectors, CE $\nu$ NS due to the  $^7\text{Be}$  neutrino flux become relevant for exposures of  $\sim 50$  kg y [150]. For DM searches with electron recoils via DM-electron scattering and dark photon or ALP absorption, solar neutrinos will also limit the sensitivity to DM masses in the range  $\sim (1-10^3)$  MeV and  $\sim (1-10^3)$  eV, respectively, for large exposures  $\sim 1$  t y, as shown in Ref. [151].

**Solid-state cryogenic detectors:** Current experiments using the bolometric technique (see *Section 36.5* of this *Review*), together with either charge or light readout, are SuperCDMS (Si, Ge) at Soudan [107], EDELWEISS (Ge) at the Laboratoire Souterrain de Modane (LSM) [152] and CRESST (CaWO $_3$ ) at the Laboratori Nazionali del Gran Sasso (LNGS) [115]. These experiments are optimised for low-mass DM searches, and can probe masses down to  $\sim 0.2$  GeV. CDMSlite also operates detectors at higher bias voltages to amplify the phonon signals produced by drifting charges and thus have access to light DM around 1.5 GeV [114]. The goal of their future phases is to probe the low-mass region down to cross sections of  $10^{-43}$ - $10^{-44}$  cm $^2$ . Much smaller, gram-scale versions of cryogenic detectors can have single-charge resolution and thus probe low-mass DM via inelastic electron recoils. A SuperCDMS single-charge sensitive Si detector placed upper limits on DM interacting with electrons for masses between  $(0.5 - 10^4)$  MeV, as well as on dark photon kinetic mixing for dark photon masses in the range  $(1.5 - 40)$  eV [153].

Germanium ionisation detectors operated at 77 K can reach sub-keV energy thresholds and low backgrounds, but lack the ability to distinguish electronic from nuclear recoils. The current CDEX-10 experiment [154], located at the China Jinping Underground Laboratory (CJPL), uses p-type, point-contact Ge detectors operated in liquid nitrogen, and probes DM masses down to 3 GeV. The neutrinoless double beta experiment Majorana Demonstrator at SURF has obtained constraints on the couplings of ALPs and dark photons to electrons, with masses between  $(6-100)$  keV [155].

**Noble liquids:** Liquid argon (LAr) and liquid xenon (LXe) are employed as DM targets, while R&D on liquid helium and neon is ongoing. We refer to Ref. [156] for a review of the liquid noble gas detector technology in low-energy physics, as well to *Section 36.4* of this *Review*. At present the best constraints on DM-nucleus interactions come from experiments using xenon: the LUX experiment which was operated at SURF [106], PandaX-II at CJPL [105] and XENON1T at LNGS [104]. These experiments probe particle masses down to  $\sim 6$  GeV (when using both light and charge signals) and the SI DM-nucleon cross section down to  $4.1 \times 10^{-47}$  cm $^2$  (at 30 GeV). LAr experiments use the powerful pulse shape discrimination (PSD) that allows for distinguishing between ER and NR events, at the expense of higher energy thresholds than in LXe. The DarkSide-50 TPC at LNGS [108] sets a minimum upper limit on the SI, DM-nucleon cross section



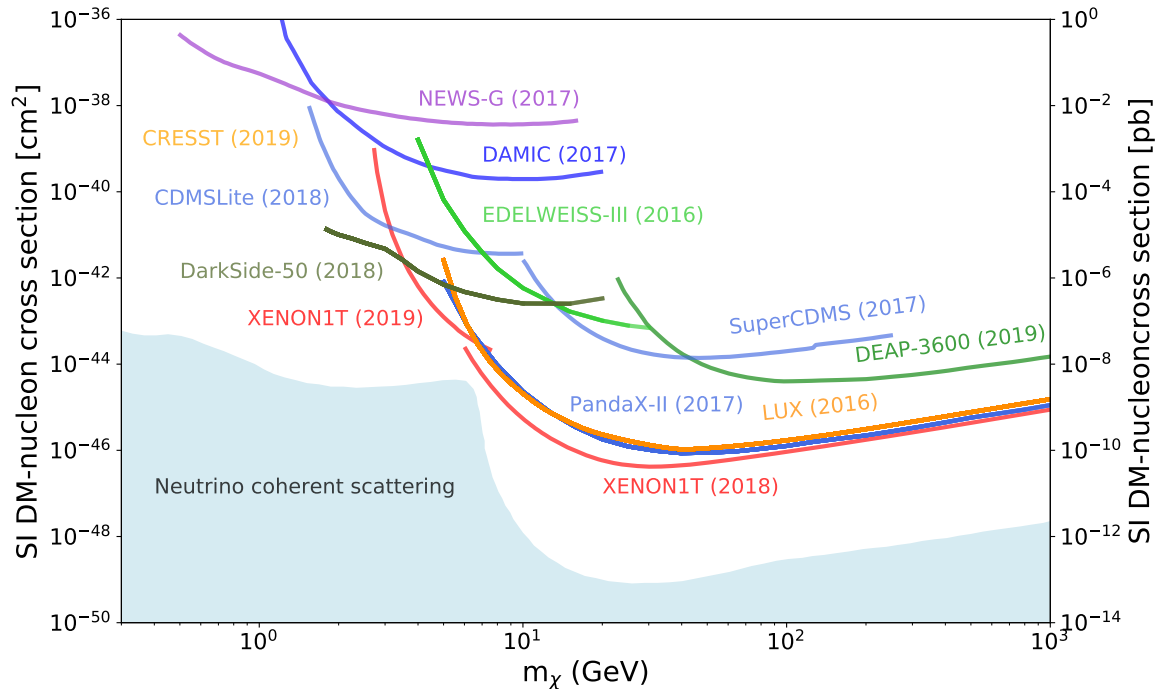


Figure 27.1: Upper limits on the SI DM-nucleon cross section as a function of DM mass.

of  $1.09 \times 10^{-44} \text{ cm}^2$  at 126 GeV, while the single-phase experiment DEAP-3600 at SNOLAB [109] constrains the SI cross section to values below  $3.9 \times 10^{-45} \text{ cm}^2$  at 100 GeV.

In noble liquids, sub-GeV DM particles can be searched for by observing inelastic, ER processes following a low-energy nuclear recoil: excitation and ionisation of the recoiling atom (the hypothetical Migdal effect) and a bremsstrahlung photon [157]. As an example, LUX and XENON1T constrained DM particle masses between (0.3 – 5) GeV via bremsstrahlung photons and Migdal electrons [110, 111]. Even lower masses are accessible when using the amplified, charge signal only, at the expense of giving up discrimination between ERs and NRs. XENON1T probed particle masses down to 60 MeV [112], while DarkSide-50 published constraints on WIMP masses as low as 1.8 GeV [113]. DM masses at the MeV-scale can also be probed by exploiting the scattering off electrons. The XENON1T experiment recently presented a light DM search with ionisation signals, with a background level of  $< 1 \text{ event}/(\text{t d keV})$  above 0.4 keV [112]. LXe TPCs also search for solar axions, Galactic ALPs and dark photons. PandaX-II and LUX set upper limits on the axion-electron coupling of  $3.5 \times 10^{-12}$  in the mass range ( $10^{-5} - 1$ ) eV for solar axions, and probe couplings around  $4 \times 10^{-13}$  in the mass range (1 – 10) keV for Galactic ALPs [158, 159].

The next generation of liquefied noble gas detectors, either in construction (DarkSide-20k [160], LZ [161], PandaX-4T [162], XENONnT [163]) or at the design and R&D stage (DARWIN [164]) will increase the sensitivity to various DM candidates by 1-2 orders of magnitude, with the ultimate goal of exploring the experimentally accessible parameter space, until the backgrounds from neutrinos will start dominating the event rates.

**Room temperature scintillators:** Several large DM experiments using high-purity NaI(Tl) crystals are acquiring data in various underground laboratories. Of these, DAMA/LIBRA at LNGS has the highest mass, 250 kg, and the largest exposure: 1.33 ty with an energy threshold of 1 keV and 2.46 ty with an energy threshold of 2 keV [165]. It is the only experiment in the field that reported an annually modulated event rate with a statistical significance of  $12.9 \sigma$  C.L. (20 annual cycles), with a modulation amplitude around 0.02 events/(kg d keV) in the energy region (1-4) keV. These findings were interpreted as due to DM interactions via nuclear or electronic recoils. The ANAIS experiment at Canfranc operates 112.5 kg of NaI(Tl) scintilla-

tors with an energy threshold of 1 keV and a background rate of 3.6 events/(kg d keV) in the (1-6) keV region. A first analysis of 1.5 y of data, for an exposure of 157.55 kg y is consistent with an absence of modulation [166], while 5 years of data are required to test the DAMA/LIBRA result at  $3 \sigma$ . The COSINE-100 experiment, located at the Yangyang Underground Laboratory, operates 106 kg of NaI(Tl) crystals in a liquid scintillator, with an energy threshold of 2 keV and a background rate of 2.7 events/(kg d keV). Results from a search based on 1.7 y of data (97.7 kg y exposure) in the (2-6) eV energy range are consistent, at 68.3% C.L., with both the null hypothesis and DAMA/LIBRA's best fit value in the same energy range. A larger exposure and a reduced energy threshold are required to test DAMA/LIBRA for  $3 \sigma$  coverage [167]. The SABRE experiment plans to operate a total of 50 kg of NaI(Tl) crystals, focussing on reaching a background level of 0.1 events/(kg d keV), an order of magnitude below DAMA/LIBRA [168]. Twin detectors will be installed at LNGS and at the Stawell Underground Physics Laboratory in the Southern hemisphere. While a DM-induced signal is expected to have the same phase in both hemispheres, seasonal or site-related effects would show different amplitudes and phases in the twin detectors. The COSINUS R&D project aims to develop a cryogenic scintillating bolometer with undoped NaI crystals with phonon and light readout, the ratio of which allows for particle discrimination. The hope is that it will shed light on the type of interactions responsible for the modulated signal [169].

**Room temperature ionisation detectors:** Silicon charged-coupled devices (CCDs) are employed for low-mass DM searches, as well as for hidden photon searches in the eV-mass range. Ionisation events induced in bulk silicon of high-resistivity, fully depleted CCDs are observed with charge resolutions around  $1-2 e^-$  and extremely low leakage currents, at the level of few  $e^- \text{ mm}^{-2} \text{ d}^{-1}$ . The position of an energy deposit is reconstructed in 3 dimensions and the particle type (electron, neutron, muon,  $\alpha$ -particles, etc) is reconstructed based on the recorded track pattern.

The DAMIC experiment at SNOLAB yielded new constraints on DM-electron scattering, and on the hidden-photon kinetic mixing parameter in the mass range (1-30) eV with an exposure of 7.6 kg d [170]. The SENSEI projects employs the skipper technology demonstrated in [171] to achieve single-electron sensitivity. A run with a prototype detector (0.0947 g) in a shallow



underground site at Fermilab yielded the most stringent direct-detection constraints on DM-electron scattering for masses in the range 500 keV–5 MeV, and on dark photon absorption below 12 eV [172]. The skipper technology will also be employed in the next stage of the DAMIC programme, DAMIC-M at LSM, which plans for a kg-size mass. The goal is to achieve thresholds of 2–3 electrons and to probe the DM-nucleon cross section down to  $\text{few} \times 10^{-43} \text{cm}^2$  around 2–3 GeV and the DM-electron cross section down to  $2 \times 10^{-41} \text{cm}^2$  at 10 MeV mass.

The NEWS-G collaboration operates spherical proportional counters [173] filled with a noble gas. Advantages of this technology are the low intrinsic electronic noise and a high amplification gain, allowing for low energy thresholds down to single-electron detection, and the possibility to use different light targets (He, Ne, etc.). A 60 cm diameter chamber operated at LSM with a gas mixture of Ne + CH<sub>4</sub> (0.7%) at 3.1 bar, excluded SI, WIMP-nucleon cross sections above  $4.4 \times 10^{-37} \text{cm}^2$  at 0.5 GeV after an exposure of 9.6 kg d [116] with an energy threshold  $\sim 100$  eV. The next iteration, a 140 cm sphere detector made of very low radioactivity copper (few  $\mu\text{Bq/kg}$  of <sup>238</sup>U and <sup>232</sup>Th) is under construction and is to start running at SNOLAB in 2019.

**Superheated liquid detectors:** Investigation of the spin-dependent interaction channel calls for target nuclei with uneven total angular momentum. A particularly favourable candidate is <sup>19</sup>F, the spin of which is carried mostly by the unpaired proton, yielding a cross section which is almost a factor of ten higher than of other employed nuclei with spin (e.g., <sup>23</sup>Na, <sup>73</sup>Ge, <sup>127</sup>I, <sup>129</sup>Xe, <sup>131</sup>Xe). Fluorine is part of the target of experiments using superheated liquids, such as the ones operated by the PICO [117] and MOSCAB [174] collaborations. A search in the PICO-60 C<sub>3</sub>F<sub>6</sub> bubble chamber at SNOLAB with an exposure of 1404 kg d and an energy threshold of 2.45 keV, yielded the most stringent constraint on the DM-proton SD cross section at  $3.2 \times 10^{-41} \text{cm}^2$  for a 25 GeV particle mass. In construction is a ton-scale detector (PICO-500) to be deployed in the cube area hall of SNOLAB. MOSCAB successfully built and tested a geyser-concept bubble chamber, the operation of which is based on a continuous process of evaporation and condensation, with the detector recovering its superheated state automatically after each event. After first results in a surface laboratory [174], the detector was moved underground to LNGS for science data taking.

**Directional detectors:** Detectors capable of measuring the direction of the recoiling nucleus would unequivocally confirm the Galactic origin of a signal and could probe the region below the neutrino floor [175, 176]. Because nuclear recoils have a range which is about 10 times smaller than the one of Compton recoils of the same energy, gaseous detectors have an excellent intrinsic background rejection if they can measure the range of events precisely. Several directional detectors are presently in operation: DRIFT in the Boulby Mine [177], DMTPC at the Waste Isolation Pivot Plant [178], MIMAC at LSM [179] and NEWAGE in the Kamioka laboratory [180]. A 1 m<sup>3</sup> detector has a typical mass of a few 100 g, depending on the target gas and its operating pressure, and can measure the sense of an incoming nuclear recoil above a few tens of keV.

A new technique is based on fine-grained nuclear emulsions (solid-state detectors with silver halide crystals uniformly dispersed in a gelatine film, where each crystal works as a sensor for charged particles), as proposed by the NEWSdm collaboration [181]. These act as target and nanometric tracking device, and the expected NR tracks are sub- $\mu\text{m}$  in size. Due to the small crystal size and larger number density, a superior spatial resolution compared to gaseous detectors is obtained. Simulations show that to reach the neutrino floor, exposures of 10 t y and 100 t y are required if a 30 nm and 50 nm threshold for detecting the track length is reached. This requires further R&D, since current emulsions allow for 100 nm tracking and target masses are around 1 kg, with 10 kg y exposures planned. A proposed approach for the directional detection of sub-GeV DM is to use two-dimensional materials such as monolayer graphene [182], from which the DM particle can eject electrons. Their energy and direction, correlated with the direction of the incoming DM, can be measured for instance with the proposed PTOLEMY experiment [183].

**New techniques:** To probe light (sub-GeV) DM particles, either via scatters off electrons or via couplings to phonons, new techniques beyond the ones discussed above are proposed. The DM particle mass that can be accessed in DM-electron scattering in noble liquids and semiconductors is limited by the minimum ionisation/excitation energy and the size of the band gap, respectively (at the  $\sim\text{eV}$ -scale). To reach lower energy thresholds, materials with smaller band gaps for electron excitations ( $\sim\text{meV}$ ), such as superconductors and superfluids, as well as Dirac materials were recently proposed [184–186]. These would in principle allow for the detection of keV-scale DM. Other ideas to detect keV–MeV scale DM are to observe NRs in superfluid He, via collective excitation modes in the fluid [187], or based on the breaking of chemical bonds between atoms [188].

Even lighter DM, with masses in the meV–eV range, could be detected via absorption on a conduction electron in a superconductor, followed by the emission of an athermal phonon [189]. Another proposed target for light DM are polar materials (for example GaAs, sapphire), which are especially sensitive for scattering through an ultralight dark photon, via excitation of single optical phonons [190]. If an anisotropic crystal such as sapphire is employed, a daily modulation interaction rate could be established [191]. A new class of detectors for bosonic DM, based on resonant absorption onto a gas of small polyatomic molecules, is proposed in [192]. The DM would effectively act as a laser that resonantly excites transitions in molecules when its mass closely matches the transition energy. While DM with SI couplings can efficiently excite phonons, it has been shown in [193] that if DM couples to the electron spin, magnon excitations (quanta of collective spin wave excitations) in materials with magnetic dipole order may also offer a promising detection avenue. Yet another approach for sub-GeV DM is to employ superconducting nanowires as both target and sensor, and first bounds on DM-electron interactions were already placed from a 4.3 ng tungsten-silicide prototype with a 0.8 eV energy threshold [194].

The detection of light DM via collective excitations in condensed matter systems and other methods is a rapidly evolving field, and a growing area of research at the interface of DM physics, condensed matter and materials science. We refer to Ref. [95, 195] for discussions of some of these new directions and models. Critical challenges are to detect these very small energy depositions, and to reliably assess the background noise.

Table 27.1 summarises the most stringent constraints on the DM-nucleon SI and SD cross sections, and Figure 27.1 shows the best constraints for SI couplings in the cross section versus DM mass parameter space, above masses of 0.3 GeV.

## 27.7 Astrophysical detection of dark matter

DM as a microscopic constituent can have measurable, macroscopic effects on astrophysical systems. Indirect DM detection refers to the search for the annihilation or decay debris from DM particles, resulting in detectable species, including especially gamma rays, neutrinos, and antimatter particles. The production rate of such particles depends on (i) the annihilation (or decay) rate (ii) the density of pairs (respectively, of individual particles) in the region of interest, and (iii) the number of final-state particles produced in one annihilation (decay) event. In formulae, the rate for production of a final state particle  $f$  per unit volume from DM annihilation can be cast as

$$\Gamma_f^A = c \frac{\rho_{\text{DM}}^2}{m_{\text{DM}}^2} \langle \sigma v \rangle N_f^A, \quad (27.18)$$

where  $\langle \sigma v \rangle$  indicates the thermally-averaged cross section for DM annihilation times relative velocity [27], calculated at the appropriate temperature,  $\rho_{\text{DM}}$  is the physical density of DM, and  $N_f^A$  is the number of final state particles  $f$  produced in one individual annihilation event. The constant  $c$  depends on whether the DM is its own antiparticle, in which case  $c = 1/2$ , or if there is a mixture of DM particles and antiparticles (in case there is no asymmetry,  $c = 1/4$ ). The analog for decay is

$$\Gamma_f^D = \frac{\rho_{\text{DM}}}{m_{\text{DM}}} \frac{1}{\tau_{\text{DM}}} N_f^D, \quad (27.19)$$

with the same conventions for the symbols, and where  $\tau_{\text{DM}}$  is the DM's lifetime.

**Gamma Rays:** DM annihilation to virtually any final state produces gamma rays: emission processes include the dominant two-photon decay mode of neutral pions resulting from the hadronization of strongly-interacting final states; final state radiation; and internal bremsstrahlung, the latter two including, possibly, the emission of massive gauge or Higgs bosons subsequently producing photons via their decay products. Similarly, neutrinos are produced from charged pion decay and from radiative processes. The flux of gamma rays and neutrinos is calculated integrating the rate  $\Gamma_f$  per steradian (simply meaning, for isotropic emission,  $\Gamma_f/(4\pi)$ ) along the line of sight within the appropriate angular region (the *differential* flux is obtained in the same way by simply replacing  $N_f$  with the differential flux at production, at the appropriate redshift in the case of cosmologically distant sources),

$$\phi_f = \int_{\Delta\Omega} d\Omega \int_{\text{l.o.s.}} dl \frac{\Gamma_f}{4\pi}. \quad (27.20)$$

It is customary to factor out, in the expression for the rate, a *particle physics* factor, depending upon the DM particle mass and its annihilation or decay rate, and an *astrophysical* factor, which only depends on the observational target. The latter is sometimes denoted with  $J_{\Delta\Omega}(\psi)$  with  $\psi$  indicating the direction of the line of sight. Although different conventions are in use, a common choice is to define

$$J_{\Delta\Omega}(\psi) = \int_{\Delta\Omega} \int_{\text{l.o.s.}(\psi)} \rho_{\text{DM}}^2(l, \Omega) dl d\Omega. \quad (27.21)$$

For a target with uniform density  $\rho$  and radius  $r$  at a distance  $d \gg r$ , such that the target is entirely within the solid angle  $\Delta\Omega$ ,

$$J \simeq \frac{4\pi r^3 \rho_{\text{DM}}^2}{3d^2}. \quad (27.22)$$

Searches for gamma-ray emission from DM annihilation have focused on targets chosen based on a variety of considerations, primarily intended to maximize signal to noise. Nearby dwarf spheroidal galaxies contain very small amounts of gas, and do not host any significant astrophysical background at gamma-ray or X-ray frequencies, and are thus an optimal target choice for DM searches. An accurate determination of the DM density profile in these objects results in somewhat large systematics when deriving constraints from the non-observation of emission from DM; future optical surveys will help pinpoint with greater accuracy stellar kinematics and thus reduce such uncertainty; a second target is the inner region of the Milky Way: while nearby and potentially hosting a large density of DM, the Galactic center region is however very bright at almost any wavelength, making the extraction of a signal highly problematic; nearby clusters of galaxies are also known to host significant astrophysical emission, but are potentially ideally suited to constrain DM decay. Finally, putative nearby DM clumps are also a possible source of a bright DM signal (albeit from an unknown direction), as is the annihilation of DM in all halos at all redshifts.

DM annihilation and decay can lead to striking spectral features. Since the process happens typically at very low particle velocities, if the DM pair-annihilates e.g. to two photons or two neutrinos, the final-state particles will be nearly monoenergetic, with an energy close to the DM particle mass and a width proportional to the DM velocity in units of  $c$  (if a  $\gamma\gamma$  line is present electroweak symmetry also implies a  $Z\gamma$  line, if kinematically allowed). No astrophysical processes are known to produce lines at gamma-ray or neutrino energies in the GeV and above (with, perhaps, the possible exception of cold pulsar winds [196]) making this channel virtually background-free. At lower energy, lines are expected from radiative decay modes of candidates such as sterile neutrinos (see Sec. 27.5). DM annihilation or decay can lead to additional spectral features besides lines. These include (one or more) “boxes” [197], produced by boosted final states decaying to monochromatic photons (such as e.g. neutral pions), or combinations thereof. Processes occurring at higher redshift can distort

these spectral features by smearing them to lower energies. Neglecting gamma-ray attenuation, the flux of gamma rays from all redshift can be cast as

$$\frac{dN_\gamma}{dE_\gamma}(E_\gamma) = \frac{c}{8\pi} \int \frac{\langle\sigma v\rangle \rho_{\text{DM}}(z) dz}{H(z)(1+z)^3 m_{\text{DM}}^2} \left( \frac{dN_\gamma}{dE'} \right)_{E'=E_\gamma(1+z)}. \quad (27.23)$$

While the calculation of the differential spectrum of gamma rays from a given final state  $f$ ,  $dN_f^i/dE_\gamma$ , is carried out using numerical tools, such as PYTHIA [198] that reproduce hadronization and particle decay for masses well above a few GeV, in the sub-GeV range gamma-ray production follows primarily from meson decay and radiative processes well outside the range of applicability of the Altarelli-Parisi splitting function. The MeV gamma-ray range will soon be probed with forthcoming satellites [199]. Recently a code that provides the expected gamma-ray spectrum for sub-GeV DM, **Hazma**, has become available [200].

Observations with the Fermi Large Area Telescope (LAT) and with ground-based facilities such as HESS, VERITAS, MAGIC, and HAWC have provided an unprecedented picture of the gamma-ray sky ideally suited to look for a signal from DM annihilation or decay for DM particles from a few GeV mass up to several TeV. The LAT has provided some of the most stringent constraints to-date on DM pair-annihilation for a variety of annihilation final states, chiefly from stacked observations of nearby satellite dwarf spheroidal galaxies [201]. Excesses of gamma rays over the expected diffuse and point-source background have been claimed, most importantly from the direction of the inner Galaxy, where a signal from DM annihilation might be especially bright [202, 203]. The nature of this excess is quite controversial: while the morphology and spectrum fall within what expected for a standard WIMP with a mass of a few tens of GeV [204], unresolved point sources, including especially an (expected) population of milli-second pulsars (MSPs) have been advocated as a possible plausible counterpart [205]. Statistical methods to discriminate between DM and MSPs have been utilized [206, 207], but recent studies indicate that such results might not be conclusive [208]. Large uncertainties in the Galactic diffuse background emission model are additionally known to exist, and possible plague the morphological and spectral information [209, 210]. Other notable potential gamma-ray excesses include a diffuse emission from the Andromeda galaxy (M31) [211–213], possibly in excess of what expected from cosmic-ray models [214]; and a diffuse emission at 511 keV energy in the inner Galaxy from Integral-SPI observations [215]; such emission has known astrophysical counterparts [216], as well as several proposed DM explanations (e.g. [217]).

While DM annihilation and decay typically occurs at low velocities, the possibility of “boosted” DM has also been considered [218]. In this case, the DM particle might dominantly pair-annihilate to a lighter dark species, which does interact with Standard Model particle, and could be detected with neutrino telescopes or direct detection experiments. Future facilities that promise to widen the reach of gamma-ray searches for DM include especially the Cherenkov Telescope Array (CTA), see fig. 27.2.

**Neutrinos:** DM can be captured in celestial bodies in significant amounts, depending on the DM scattering cross section off of nucleons, the DM mass, and the DM flux incident on the celestial body of interest. For DM masses at or around the GeV scale, evaporation from the celestial body plays an important role [219]. If enough DM accumulates, DM annihilation inside the celestial body can then lead to the production of Standard Model particles. Such particles can heat up the body, if they lose most of their energy before escaping. Utilizing models for heat production in planets, or stellar interior models in the case of stars, constraints can be put on DM particle properties. Of note are constraints from anomalous warming of cold planets such as Uranus [220], alterations to the stellar structure or the Sun's seismic activity [221], and anomalous Earth heat flow [222]. Alternately, DM annihilation in celestial bodies can result in the production of particles that can escape the body. Within the Standard Model, the only such instance is annihilation to neutrinos, but, similarly to the boosted DM case the DM can annihilate to a (stable or unstable) dark-sector particles, whose decay or interactions can be detected

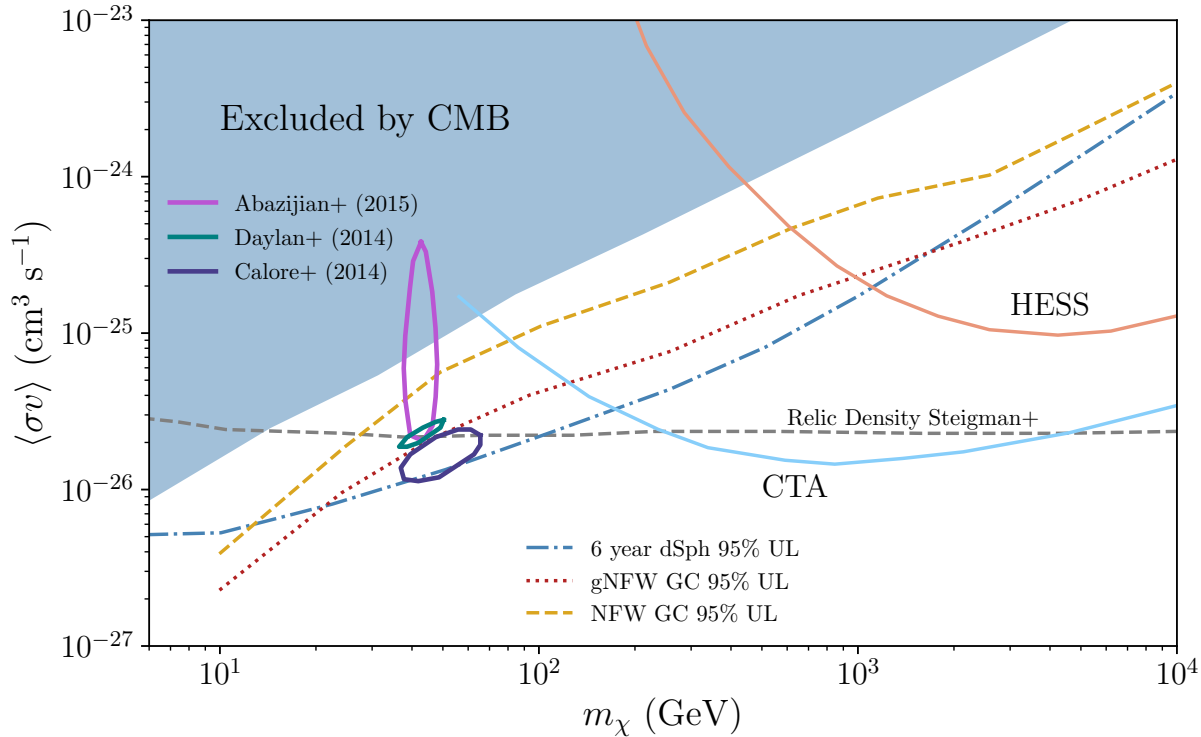


Figure 27.2: Upper limits and projected sensitivity from CTA on the pair-annihilation rate versus the DM mass from gamma-ray and CMB observations (figure courtesy of Logan Morrison).

on Earth [223,224]. For direct annihilation to neutrinos, given the lower limit on the DM mass from evaporation, the typical neutrino energies usually exceed the energy of neutrinos from the Sun, the best target for this type of searches, making this a virtually background-free DM search. Significant neutrino fluxes can only be achieved, however, if near-equilibration is reached between the capture and annihilation rates. In turn, this requires large-enough DM-nucleon scattering cross sections, to-date very close to the limits from direct detection (see sec. 27.6). Only spin-dependent cross section, and capture in the Sun usually provide large-enough neutrino fluxes. IceCube and ANTARES searches for an anomalous flux of high-energy neutrinos from the Sun yielded null results, which can be interpreted as constraints on spin-dependent nucleon-DM interactions under the assumption of equilibration and of specific annihilation final states [225,226]. Lower-threshold detectors, including DeepCore [227] and PINGU [228], can produce interesting limits on lower-mass DM candidates above the evaporation threshold.

**Cosmic-ray Antimatter:** Stable charged particles produced by decays of products of, or directly from DM annihilation or decay, populate the cosmic radiation and are a prime target for indirect DM searches. To maximize signal to noise, searches focus on relatively rare particle species, such as positrons, antiprotons, and antinuclei. While in certain models the production of particles and antiparticles is not symmetric [229], generally DM annihilation or decay produces as many particles as antiparticles in the final state. Charged particles produced by DM propagate and lose energy prior to reaching detectors. The transport of charged particles is customarily carried out in the context of diffusion models such as the Galactic “leaky box” setup, see e.g. [230]. While progress in constraining the uncertain propagation and energy-loss processes has been steady with improved data from new detectors such as PAMELA [231] and AMS-02 [232], the calculation of the particle flux at Earth from that at production suffers from significant uncertainties [230].

An excess of high-energy positrons over the standard secondary production from inelastic cosmic-ray interactions has been firmly established by several experiments, most recently and with the highest statistics by AMS-02 [233]. The excess has been ascribed

to DM annihilation, although strong constraints from the non-observation of corresponding anomalies in other channels, such as antiprotons and gamma rays, and the peculiar spectral shape, force DM models to be quite convoluted (see e.g. [234]). Alternatively, excess *primary* positrons can be produced in the magnetosphere of nearby pulsars [235,236]. This latter explanation was questioned in [237] in connection with the detection of a TeV halo around two candidate pulsars, leading to the determination of a highly suppressed diffusion coefficient within the pulsar nebula; with such low diffusion coefficient, positrons from the pulsars would not contribute significantly to the flux at Earth; Ref. [238], however, showed that likely the diffusion coefficient is not constant, and that if it increases outside the nebula, as expected from other cosmic-ray measurements, pulsars can still be considered as the counterpart to the positron excess. Other explanations for the excess, albeit somewhat controversial, and increasingly constrained by data, also exist [239,240].

The antiproton spectrum in the cosmic radiation as measured by AMS-02 [232] also exhibits features that might be considered as excess flux between 10 and 20 GeV, and energies above 100 GeV [241], which have been interpreted as possible signal of DM annihilation; more realistically, however, systematic uncertainties in the antiproton production cross section, in cosmic-ray transport, reacceleration at high energy and, at low energy, solar modulation make it extremely difficult to assess the robustness of the excesses [242,243].

Antinuclei such as anti-deuterium and anti-helium could also form as a result of DM annihilation or decay. While baryon number conservation forces the typical kinetic energy of antinuclei produced in inelastic cosmic-ray processes to large values, antinuclei arising from hadronization of DM-initiated jets have low energy, offering optimal signal-to-noise when a low-energy cut on the antinucleus kinetic energy is used [244–248]. Specific detector designs have been developed to single out low-energy cosmic-ray antinuclei (e.g.  $E < 0.25$  GeV/nucleon in the case of the General Antiparticle Spectrometer, or GAPS [249]). The detection of even a single antinucleus would have considerable importance as a possible sign of new physics [250].

**Multi-wavelength studies:** Electrons and positrons from

DM lose energy quite efficiently, radiating at a variety of wavelengths. This *secondary* radiative emission presents spectral and morphological features that might provide an important additional indirect detection channel. The most efficient energy loss mechanisms for high-energy electrons and positrons are inverse Compton (IC) up-scattering of background photons, and synchrotron radiation in the presence of magnetic fields. Depending on the DM mass, the emitted light from synchrotron peaks at MHz-GHz frequencies, while the IC emission at X-ray to gamma-ray frequencies, depending on the energy of the background radiation, typically ranging from CMB photons up to starlight photons [251–253]. The calculation of the secondary emission from DM entails both solving the transport of the electrons and positrons from DM, and for the radiative emission; codes exist that perform these calculations for certain astrophysical environments [254–256], with diffusion playing an increasingly critical role in smaller and smaller structures such as dwarf galaxies [252]. It has been demonstrated that for large magnetic fields and for certain final states, the synchrotron emission is more constraining than the gamma-ray emission [257].

**Stellar Physics:** Microscopic properties of the DM can meaningfully alter, and thus be constrained by, several astrophysical environments, from planets and stars, up to the universe as a whole. DM particles light enough to be produced in collisional processes inside stars, with typically temperatures in the keV, or supernovae, with energy scales in the MeV, lead to an additional energy-loss mechanism, if capable of escaping the system. If this is the case, the increased needed energy output would also result in an increased neutrino flux, leading to constraints on the masses and couplings of the DM, see e.g. [258] for a comprehensive review. DM annihilation can even have fueled early stages of stellar evolution, perhaps with measurable consequences [259]. DM capture in neutron stars could lead to the collapse of the star into black holes; the existence of neutron stars in DM-rich environments can thus be used to constrain the mass and interaction cross section of DM with nucleons [260] and even relatively light, but stable, primordial black holes [261].

**Cosmology:** Energy injection from DM processes in the early universe, as well as the contribution of DM to the effective relativistic degrees of freedom, are severely constrained from data on Big Bang Nucleosynthesis (see Sec. 24 in this *Review*) and on the energy and anisotropy power spectrum of the CMB (see Sec. 29). Codes exist that perform the calculation of the constraints on particle DM models [200,262].

**PBH Detection:** Macroscopic DM candidates can gravitationally perturb structure and compromise the stability of, for instance, globular clusters such as Eridanus II [24], and/or disrupt wide binaries [263]. This constrains the maximal mass of a macroscopic DM candidate to not much more than  $5 M_{\odot}$  [263] (see also [24]). In the specific case of primordial black holes, strong constraints also stem from the acceleration of charged particles around and after recombination, with significant effects on the CMB [264], albeit a lively debate exists over the accretion efficiency around such objects at high redshift [265,266]. Whether or not PBH in the solar-mass range can be 100% of the DM is therefore disputed at present. Other effects produced by macroscopic, massive DM candidates are the microlensing of stars [267, 268] and quasars [269], femtolensing of gamma-ray bursts [270], and neutron star capture [261]. It is important to note that recently constraints from both microlensing and femtolensing have been corrected after the realization of important finite-size source and wave effects [268, 271, 272], leaving a substantial window, at PBH masses  $10^{17} \lesssim M_{\text{BH}}/g \lesssim 10^{21}$  where PBH can be 100% of the DM. Light black holes,  $M_{\text{BH}} \lesssim 10^{17}$  g, are also constrained by the non-detection of products of evaporation [273].

## References

- [1] J. D. Simon, arXiv e-prints arXiv:1901.05465 (2019), [arXiv:1901.05465].
- [2] P. Salucci, *Astron. Astrophys. Rev.* **27**, 1, 2 (2019), [arXiv:1811.08843].
- [3] S. W. Allen, A. E. Evrard and A. B. Mantz, *Annual Review of Astronomy and Astrophysics* **49**, 1, 409 (2011),

- [arXiv:1103.4829].
- [4] N. A. Bahcall *et al.*, *ApJ* **541**, 1 (2000).
- [5] S. D. M. White, G. Efstathiou and C. S. Frenk, *Mon. Not. Roy. Astron. Soc.* **262**, 1023 (1993).
- [6] A. J. S. Hamilton and M. Tegmark, *Mon. Not. Roy. Astron. Soc.* **330**, 506 (2002), [arXiv:astro-ph/0008392].
- [7] B. Famaey and S. McGaugh, *Living Rev. Rel.* **15**, 10 (2012), [arXiv:1112.3960].
- [8] S. W. Randall *et al.*, *Astrophys. J.* **679**, 1173 (2008), [arXiv:0704.0261].
- [9] R. H. Sanders, *Int. J. Mod. Phys. D* **27**, 14, 14 (2018), [arXiv:1805.06804].
- [10] S. D. McDermott, H.-B. Yu and K. M. Zurek, *Phys. Rev. D* **83**, 063509 (2011), [arXiv:1011.2907].
- [11] D. A. Buote *et al.*, *Astrophys. J.* **577**, 183 (2002), [arXiv:astro-ph/0205469].
- [12] D. Harvey *et al.*, *Science* **347**, 1462 (2015), [arXiv:1503.07675].
- [13] S. Tulin and H.-B. Yu, *Phys. Rept.* **730**, 1 (2018), [arXiv:1705.02358].
- [14] D. N. Spergel and P. J. Steinhardt, *Phys. Rev. Lett.* **84**, 3760 (2000), [arXiv:astro-ph/9909386].
- [15] S. Tremaine and J. E. Gunn, *Phys. Rev. Lett.* **42**, 407 (1979), [66(1979)].
- [16] L. Randall, J. Scholtz and J. Unwin, *Mon. Not. Roy. Astron. Soc.* **467**, 2, 1515 (2017), [arXiv:1611.04590].
- [17] R. Hlozek *et al.*, *Phys. Rev. D* **91**, 10, 103512 (2015), [arXiv:1410.2896].
- [18] E. Armengaud *et al.*, *Mon. Not. Roy. Astron. Soc.* **471**, 4, 4606 (2017), [arXiv:1703.09126].
- [19] M. Nori *et al.*, *Mon. Not. Roy. Astron. Soc.* **482**, 3, 3227 (2019), [arXiv:1809.09619].
- [20] B. Bozek *et al.*, *Mon. Not. Roy. Astron. Soc.* **450**, 1, 209 (2015), [arXiv:1409.3544].
- [21] H.-Y. Schive *et al.*, *Astrophys. J.* **818**, 1, 89 (2016), [arXiv:1508.04621].
- [22] E. O. Nadler *et al.*, *Astrophys. J.* **878**, 2, L32 (2019), [*Astrophys. J. Lett.* 878,32(2019)], [arXiv:1904.10000].
- [23] M. A. Monroy-Rodríguez and C. Allen, *ApJ* **790**, 2, 159 (2014), [arXiv:1406.5169].
- [24] T. D. Brandt, *Astrophys. J.* **824**, 2, L31 (2016), [arXiv:1605.03665].
- [25] B. Audren *et al.*, *JCAP* **1412**, 12, 028 (2014), [arXiv:1407.2418].
- [26] M. Dutra *et al.*, *JCAP* **1803**, 037 (2018), [arXiv:1801.05447].
- [27] P. Gondolo and G. Gelmini, *Nucl. Phys.* **B360**, 145 (1991).
- [28] J. L. Feng and J. Kumar, *Phys. Rev. Lett.* **101**, 231301 (2008), [arXiv:0803.4196].
- [29] G. Jungman, M. Kamionkowski and K. Griest, *Phys. Rept.* **267**, 195 (1996), [hep-ph/9506380].
- [30] J. Edsjo *et al.*, *JCAP* **0304**, 001 (2003), [hep-ph/0301106].
- [31] G. Servant and T. M. P. Tait, *Nucl. Phys.* **B650**, 391 (2003), [hep-ph/0206071].
- [32] D. Hooper and S. Profumo, *Phys. Rept.* **453**, 29 (2007), [hep-ph/0701197].
- [33] K. Griest and D. Seckel, *Phys. Rev. D* **43**, 3191 (1991).
- [34] R. T. Co *et al.*, *JCAP* **1512**, 12, 024 (2015), [arXiv:1506.07532].
- [35] V. S. Rychkov and A. Strumia, *Phys. Rev. D* **75**, 075011 (2007), [hep-ph/0701104].
- [36] E. D. Carlson, M. E. Machacek and L. J. Hall, *Astrophys. J.* **398**, 43 (1992).

- [37] D. Pappadopulo, J. T. Ruderman and G. Trevisan, Phys. Rev. **D94**, 3, 035005 (2016), [arXiv:1602.04219].
- [38] Y. Hochberg *et al.*, Phys. Rev. Lett. **113**, 171301 (2014), [arXiv:1402.5143].
- [39] E. Kuflik *et al.*, Phys. Rev. Lett. **116**, 22, 221302 (2016), [arXiv:1512.04545].
- [40] W. B. Lin *et al.*, Phys. Rev. Lett. **86**, 954 (2001), [arXiv:astro-ph/0009003].
- [41] G. B. Gelmini and P. Gondolo, Phys. Rev. **D74**, 023510 (2006), [hep-ph/0602230].
- [42] M. Hindmarsh, R. Kirk and S. M. West, JCAP **1403**, 037 (2014), [arXiv:1311.1637].
- [43] T. Moroi and L. Randall, Nucl. Phys. **B570**, 455 (2000), [hep-ph/9906527].
- [44] P. Hut and K. A. Olive, Phys. Lett. **87B**, 144 (1979).
- [45] S. Nussinov, Phys. Lett. **165B**, 55 (1985).
- [46] K. M. Zurek, Phys. Rept. **537**, 91 (2014), [arXiv:1308.0338].
- [47] Y. B. Zel'dovich and I. D. Novikov, Soviet Ast. **10**, 602 (1967).
- [48] S. Hawking, Mon. Not. R. Astron. Soc **152**, 75 (1971).
- [49] B. J. Carr, ApJ **201**, 1 (1975).
- [50] J. I. Read, J. Phys. **G41**, 063101 (2014), [arXiv:1404.1938].
- [51] J. Buch, S. C. J. Leung and J. Fan, JCAP **1904**, 026 (2019), [arXiv:1808.05603].
- [52] J. Bovy *et al.*, Astrophys. J. **759**, 131 (2012), [arXiv:1209.0759].
- [53] T. Piffi *et al.*, Astron. Astrophys. **562**, A91 (2014), [arXiv:1309.4293].
- [54] A. M. Green, J. Phys. **G44**, 8, 084001 (2017), [arXiv:1703.10102].
- [55] M. Vogelsberger *et al.*, Mon. Not. Roy. Astron. Soc. **395**, 797 (2009), [arXiv:0812.0362].
- [56] C. Kelso *et al.*, JCAP **1608**, 071 (2016), [arXiv:1601.04725].
- [57] N. Bozorgnia *et al.*, JCAP **1605**, 05, 024 (2016), [arXiv:1601.04707].
- [58] J. D. Sloane *et al.*, Astrophys. J. **831**, 93 (2016), [arXiv:1601.05402].
- [59] A. Helmi *et al.*, Nature **7729**, 985 (2018).
- [60] L. Necib, M. Lisanti and V. Belokurov (2018), [arXiv:1807.02519].
- [61] N. W. Evans, C. A. J. O'Hare and C. McCabe, Phys. Rev. **D99**, 2, 023012 (2019), [arXiv:1810.11468].
- [62] J. S. Bullock and M. Boylan-Kolchin, Ann. Rev. Astron. Astrophys. **55**, 343 (2017), [arXiv:1707.04256].
- [63] J. Zavala and C. S. Frenk (2019), [arXiv:1907.11775].
- [64] J. F. Navarro *et al.*, Mon. Not. Roy. Astron. Soc. **402**, 21 (2010), [arXiv:0810.1522].
- [65] M. Boylan-Kolchin, J. S. Bullock and M. Kaplinghat, Mon. Not. Roy. Astron. Soc. **415**, L40 (2011), [arXiv:1103.0007].
- [66] K. E. Andrade *et al.* (2019), [arXiv:1901.00507].
- [67] G. Servant, in "Particle dark matter," 164–189 (2010).
- [68] L. Hui *et al.*, Phys. Rev. **D95**, 4, 043541 (2017), [arXiv:1610.08297].
- [69] A. Fattahi *et al.* (2016), [arXiv:1607.06479].
- [70] D. J. E. Marsh, Phys. Rept. **643**, 1 (2016), [arXiv:1510.07633].
- [71] H. An *et al.*, Phys. Lett. **B747**, 331 (2015), [arXiv:1412.8378].
- [72] P. W. Graham and S. Rajendran, Phys. Rev. **D88**, 035023 (2013), [arXiv:1306.6088].
- [73] P. W. Graham *et al.*, Phys. Rev. **D93**, 7, 075029 (2016), [arXiv:1512.06165].
- [74] A. Arvanitaki *et al.*, Phys. Rev. **D97**, 7, 075020 (2018), [arXiv:1606.04541].
- [75] P. W. Graham *et al.*, Phys. Rev. **D97**, 5, 055006 (2018), [arXiv:1709.07852].
- [76] I. M. Bloch *et al.* (2019), [arXiv:1907.03767].
- [77] A. Pierce, K. Riles and Y. Zhao, Phys. Rev. Lett. **121**, 6, 061102 (2018), [arXiv:1801.10161].
- [78] Y. Kahn, B. R. Safdi and J. Thaler, Phys. Rev. Lett. **117**, 14, 141801 (2016), [arXiv:1602.01086].
- [79] R. Henning *et al.* (ABRACADABRA), in "Proceedings, 13th Patras Workshop on Axions, WIMPs and WISPs, (PATRAS 2017): Thessaloniki, Greece, 15 May 2017 - 19, 2017," 28–31 (2018).
- [80] S. Chaudhuri *et al.*, Phys. Rev. **D92**, 7, 075012 (2015), [arXiv:1411.7382].
- [81] P. Sikivie, N. Sullivan and D. B. Tanner, Phys. Rev. Lett. **112**, 13, 131301 (2014), [arXiv:1310.8545].
- [82] B. M. Brubaker *et al.*, Phys. Rev. **D96**, 12, 123008 (2017), [arXiv:1706.08388].
- [83] G. Rybka (ADMX), Phys. Dark Univ. **4**, 14 (2014).
- [84] S. Dodelson and L. M. Widrow, Phys. Rev. Lett. **72**, 17 (1994), [hep-ph/9303287].
- [85] E. Bulbul *et al.*, Astrophys. J. **789**, 13 (2014), [arXiv:1402.2301].
- [86] A. Boyarsky *et al.*, Phys. Rev. Lett. **113**, 251301 (2014), [arXiv:1402.4119].
- [87] T. E. Jeltema and S. Profumo, Mon. Not. Roy. Astron. Soc. **450**, 2, 2143 (2015), [arXiv:1408.1699].
- [88] M. E. Anderson, E. Churazov and J. N. Bregman, Mon. Not. Roy. Astron. Soc. **452**, 4, 3905 (2015), [arXiv:1408.4115].
- [89] D. Malyshev, A. Neronov and D. Eckert, Phys. Rev. **D90**, 103506 (2014), [arXiv:1408.3531].
- [90] T. E. Jeltema and S. Profumo, Mon. Not. Roy. Astron. Soc. **458**, 4, 3592 (2016), [arXiv:1512.01239].
- [91] F. A. Aharonian *et al.* (Hitomi), Astrophys. J. **837**, 1, L15 (2017), [arXiv:1607.07420].
- [92] I. Yu. Kobzarev, L. B. Okun and I. Ya. Pomeranchuk, Sov. J. Nucl. Phys. **3**, 6, 837 (1966), [Yad. Fiz.3,1154(1966)].
- [93] M. J. Strassler and K. M. Zurek, Phys. Lett. **B651**, 374 (2007), [hep-ph/0604261].
- [94] M. J. Strassler (2006), [hep-ph/0607160].
- [95] M. Battaglieri *et al.*, in "U.S. Cosmic Visions: New Ideas in Dark Matter College Park, MD, USA, March 23–25, 2017," (2017), [arXiv:1707.04591], URL <http://lss.fnal.gov/archive/2017/conf/fermilab-conf-17-282-ae-ppd-t.pdf>.
- [96] Y. Kahn *et al.*, JHEP **05**, 002 (2017), [arXiv:1609.09072].
- [97] J. Alexander *et al.* (2016), [arXiv:1608.08632], URL <http://lss.fnal.gov/archive/2016/conf/fermilab-conf-16-421.pdf>.
- [98] K. R. Dienes and B. Thomas, Phys. Rev. **D85**, 083523 (2012), [arXiv:1106.4546].
- [99] N. Trevisani (ATLAS, CMS), Universe **4**, 11, 131 (2018).
- [100] E. Tolley (ATLAS), PoS **ICHEP2018**, 171 (2019).
- [101] W. C. Kalderon (ATLAS), PoS **DIS2018**, 085 (2018).
- [102] D. Vannerom (CMS), PoS **DIS2019**, 111 (2019).
- [103] G. Gómez-Ceballos (CMS), PoS **EDSU2018**, 014 (2018).
- [104] E. Aprile *et al.* (XENON), Phys. Rev. Lett. **121**, 11, 111302 (2018), [arXiv:1805.12562].
- [105] X. Cui *et al.* (PandaX-II), Phys. Rev. Lett. **119**, 18, 181302 (2017), [arXiv:1708.06917].
- [106] D. S. Akerib *et al.* (LUX), Phys. Rev. Lett. **118**, 2, 021303 (2017), [arXiv:1608.07648].

- [107] R. Agnese *et al.* (SuperCDMS), Phys. Rev. Lett. **120**, 6, 061802 (2018), [arXiv:1708.08869].
- [108] P. Agnes *et al.* (DarkSide), Phys. Rev. **D98**, 10, 102006 (2018), [arXiv:1802.07198].
- [109] R. Ajaj *et al.* (DEAP), Phys. Rev. **D100**, 022004 (2019), [arXiv:1902.04048].
- [110] D. S. Akerib *et al.* (LUX), Phys. Rev. Lett. **122**, 13, 131301 (2019), [arXiv:1811.11241].
- [111] E. Aprile *et al.* (XENON) (2019), [arXiv:1907.12771].
- [112] E. Aprile *et al.* (2019), [arXiv:1907.11485].
- [113] P. Agnes *et al.* (DarkSide), Phys. Rev. Lett. **121**, 8, 081307 (2018), [arXiv:1802.06994].
- [114] R. Agnese *et al.* (SuperCDMS), Phys. Rev. **D99**, 6, 062001 (2019), [arXiv:1808.09098].
- [115] A. H. Abdelhameed *et al.* (CRESST) (2019), [arXiv:1904.00498].
- [116] Q. Arnaud *et al.* (NEWS-G), Astropart. Phys. **97**, 54 (2018), [arXiv:1706.04934].
- [117] C. Amole *et al.* (PICO), Phys. Rev. **D100**, 2, 022001 (2019), [arXiv:1902.04031].
- [118] E. Aprile *et al.* (XENON), Phys. Rev. Lett. **122**, 14, 141301 (2019), [arXiv:1902.03234].
- [119] J. Xia *et al.* (PandaX-II), Phys. Lett. **B792**, 193 (2019), [arXiv:1807.01936].
- [120] D. S. Akerib *et al.* (LUX), Phys. Rev. Lett. **118**, 25, 251302 (2017), [arXiv:1705.03380].
- [121] J. D. Lewin and P. F. Smith, Astropart. Phys. **6**, 87 (1996).
- [122] J. R. Ellis, R. A. Flores and J. D. Lewin, Phys. Lett. **B212**, 375 (1988).
- [123] P. J. Fox, J. Liu and N. Weiner, Phys. Rev. **D83**, 103514 (2011), [arXiv:1011.1915].
- [124] L. Vietze *et al.*, Phys. Rev. **D91**, 4, 043520 (2015), [arXiv:1412.6091].
- [125] P. Klos *et al.*, Phys. Rev. **D88**, 8, 083516 (2013), [Erratum: Phys. Rev. **D89**, no.2, 029901 (2014)], [arXiv:1304.7684].
- [126] J. Ellis, N. Nagata and K. A. Olive, Eur. Phys. J. **C78**, 7, 569 (2018), [arXiv:1805.09795].
- [127] J. Fan, M. Reece and L.-T. Wang, JCAP **1011**, 042 (2010), [arXiv:1008.1591].
- [128] A. L. Fitzpatrick *et al.*, JCAP **1302**, 004 (2013), [arXiv:1203.3542].
- [129] N. Anand, A. L. Fitzpatrick and W. C. Haxton, Phys. Rev. **C89**, 6, 065501 (2014), [arXiv:1308.6288].
- [130] M. I. Gresham and K. M. Zurek, Phys. Rev. **D89**, 12, 123521 (2014), [arXiv:1401.3739].
- [131] J. B. Dent *et al.*, Phys. Rev. **D92**, 6, 063515 (2015), [arXiv:1505.03117].
- [132] D. Gazda, R. Catena and C. Forssén, Phys. Rev. **D95**, 10, 103011 (2017), [arXiv:1612.09165].
- [133] M. Hoferichter *et al.*, Phys. Rev. **D99**, 5, 055031 (2019), [arXiv:1812.05617].
- [134] R. Essig, J. Mardon and T. Volansky, Phys. Rev. **D85**, 076007 (2012), [arXiv:1108.5383].
- [135] F. T. Avignone, III *et al.*, Phys. Rev. **D35**, 2752 (1987).
- [136] M. Pospelov, A. Ritz and M. B. Voloshin, Phys. Rev. **D78**, 115012 (2008), [arXiv:0807.3279].
- [137] I. M. Bloch *et al.*, JHEP **06**, 087 (2017), [arXiv:1608.02123].
- [138] Y. Hochberg, T. Lin and K. M. Zurek, Phys. Rev. **D95**, 2, 023013 (2017), [arXiv:1608.01994].
- [139] M. Schumann (2019), [arXiv:1903.03026].
- [140] M. Pato *et al.*, Phys. Rev. **D83**, 083505 (2011), [arXiv:1012.3458].
- [141] A. K. Drukier, K. Freese and D. N. Spergel, Phys. Rev. **D33**, 3495 (1986).
- [142] D. N. Spergel, Phys. Rev. **D37**, 1353 (1988).
- [143] D. Stiff, L. M. Widrow and J. Frieman, Phys. Rev. **D64**, 083516 (2001), [arXiv:astro-ph/0106048].
- [144] K. Freese *et al.*, Phys. Rev. Lett. **92**, 111301 (2004), [arXiv:astro-ph/0310334].
- [145] T. Bruch *et al.*, Astrophys. J. **696**, 920 (2009), [arXiv:0804.2896].
- [146] M. J. Lewis and K. Freese, Phys. Rev. **D70**, 043501 (2004), [arXiv:astro-ph/0307190].
- [147] F. Mayet *et al.*, Phys. Rept. **627**, 1 (2016), [arXiv:1602.03781].
- [148] L. E. Strigari, New J. Phys. **11**, 105011 (2009), [arXiv:0903.3630].
- [149] C. A. J. O'Hare, Phys. Rev. **D94**, 6, 063527 (2016), [arXiv:1604.03858].
- [150] L. E. Strigari, Phys. Rev. **D93**, 10, 103534 (2016), [arXiv:1604.00729].
- [151] R. Essig, M. Sholapurkar and T.-T. Yu, Phys. Rev. **D97**, 9, 095029 (2018), [arXiv:1801.10159].
- [152] Q. Arnaud *et al.* (EDELWEISS), Phys. Rev. **D97**, 2, 022003 (2018), [arXiv:1707.04308].
- [153] R. Agnese *et al.* (SuperCDMS), Phys. Rev. Lett. **121**, 5, 051301 (2018), [Erratum: Phys. Rev. Lett. **122**, no.6, 069901 (2019)], [arXiv:1804.10697].
- [154] H. Jiang *et al.* (CDEX), Phys. Rev. Lett. **120**, 24, 241301 (2018), [arXiv:1802.09016].
- [155] N. Abgrall *et al.* (Majorana), Phys. Rev. Lett. **118**, 16, 161801 (2017), [arXiv:1612.00886].
- [156] V. Chepel and H. Araujo, JINST **8**, R04001 (2013), [arXiv:1207.2292].
- [157] M. J. Dolan, F. Kahlhoefer and C. McCabe, Phys. Rev. Lett. **121**, 10, 101801 (2018), [arXiv:1711.09906].
- [158] C. Fu *et al.* (PandaX), Phys. Rev. Lett. **119**, 18, 181806 (2017), [arXiv:1707.07921].
- [159] D. S. Akerib *et al.* (LUX), Phys. Rev. Lett. **118**, 26, 261301 (2017), [arXiv:1704.02297].
- [160] C. E. Aalseth *et al.*, Eur. Phys. J. Plus **133**, 131 (2018), [arXiv:1707.08145].
- [161] D. S. Akerib *et al.* (LUX-ZEPLIN) (2018), [arXiv:1802.06039].
- [162] H. Zhang *et al.* (PandaX), Sci. China Phys. Mech. Astron. **62**, 3, 31011 (2019), [arXiv:1806.02229].
- [163] E. Aprile *et al.* (XENON), JCAP **1604**, 04, 027 (2016), [arXiv:1512.07501].
- [164] J. Aalbers *et al.* (DARWIN), JCAP **1611**, 017 (2016), [arXiv:1606.07001].
- [165] R. Bernabei *et al.*, Universe **4**, 11, 116 (2018), [Nucl. Phys. Atom. Energy **19**, no.4, 307 (2018)], [arXiv:1805.10486].
- [166] J. Amaré *et al.*, Phys. Rev. Lett. **123**, 3, 031301 (2019), [arXiv:1903.03973].
- [167] G. Adhikari *et al.* (COSINE-100), Phys. Rev. Lett. **123**, 3, 031302 (2019), [arXiv:1903.10098].
- [168] G. D'Imperio *et al.* (Sabre), PoS **ICHEP2018**, 653 (2019).
- [169] K. Schäffner *et al.*, J. Low. Temp. Phys. **193**, 5-6, 1174 (2018).
- [170] A. Aguilar-Arevalo *et al.* (DAMIC) (2019), [arXiv:1907.12628].
- [171] J. Tiffenberg *et al.* (SENSEI), Phys. Rev. Lett. **119**, 13, 131802 (2017), [arXiv:1706.00028].
- [172] O. Abramoff *et al.* (SENSEI), Phys. Rev. Lett. **122**, 16, 161801 (2019), [arXiv:1901.10478].

- [173] I. Giomataris *et al.*, JINST **3**, P09007 (2008), [arXiv:0807.2802].
- [174] A. Antonicci *et al.* (MOSCAB), Eur. Phys. J. **C77**, 11, 752 (2017), [arXiv:1708.00101].
- [175] P. Grothaus, M. Fairbairn and J. Monroe, Phys. Rev. **D90**, 5, 055018 (2014), [arXiv:1406.5047].
- [176] C. A. J. O'Hare *et al.*, Phys. Rev. **D92**, 6, 063518 (2015), [arXiv:1505.08061].
- [177] J. B. R. Battat *et al.* (DRIFT), Astropart. Phys. **91**, 65 (2017), [arXiv:1701.00171].
- [178] C. Deaconu *et al.*, Phys. Rev. **D95**, 12, 122002 (2017), [arXiv:1705.05965].
- [179] Y. Tao *et al.* (2019), [arXiv:1903.02159].
- [180] T. Hashimoto *et al.*, AIP Conf. Proc. **1921**, 1, 070001 (2018), [arXiv:1707.09744].
- [181] G. De Lellis, EPJ Web Conf. **209**, 01019 (2019).
- [182] Y. Hochberg *et al.*, Phys. Lett. **B772**, 239 (2017), [arXiv:1606.08849].
- [183] E. Baracchini *et al.* (PTOLEMY) (2018), [arXiv:1808.01892].
- [184] Y. Hochberg, Y. Zhao and K. M. Zurek, Phys. Rev. Lett. **116**, 1, 011301 (2016), [arXiv:1504.07237].
- [185] Y. Hochberg *et al.*, JHEP **08**, 057 (2016), [arXiv:1512.04533].
- [186] Y. Hochberg *et al.*, Phys. Rev. **D97**, 1, 015004 (2018), [arXiv:1708.08929].
- [187] S. Knapen, T. Lin and K. M. Zurek, Phys. Rev. **D95**, 5, 056019 (2017), [arXiv:1611.06228].
- [188] R. Essig *et al.*, Phys. Rev. **D95**, 5, 056011 (2017), [arXiv:1608.02940].
- [189] Y. Hochberg, T. Lin and K. M. Zurek, Phys. Rev. **D94**, 1, 015019 (2016), [arXiv:1604.06800].
- [190] S. Knapen *et al.*, Phys. Lett. **B785**, 386 (2018), [arXiv:1712.06598].
- [191] S. Griffin *et al.*, Phys. Rev. **D98**, 11, 115034 (2018), [arXiv:1807.10291].
- [192] A. Arvanitaki, S. Dimopoulos and K. Van Tilburg, Phys. Rev. **X8**, 4, 041001 (2018), [arXiv:1709.05354].
- [193] T. Trickle, Z. Zhang and K. M. Zurek (2019), [arXiv:1905.13744].
- [194] Y. Hochberg *et al.*, Phys. Rev. Lett. **123**, 15, 151802 (2019), [arXiv:1903.05101].
- [195] T. Lin, PoS **333**, 009 (2019), [arXiv:1904.07915].
- [196] F. Aharonian, D. Khangulyan and D. Malyshev, Astron. Astrophys. **547**, A114 (2012), [arXiv:1207.0458].
- [197] K. K. Boddy *et al.*, Phys. Rev. **D94**, 9, 095027 (2016), [arXiv:1606.07440].
- [198] T. Sjöstrand (2019), [arXiv:1907.09874].
- [199] M. Tavani *et al.* (e-ASTROGAM), JHEAp **19**, 1 (2018), [arXiv:1711.01265].
- [200] A. Coogan, L. Morrison and S. Profumo (2019), [arXiv:1907.11846].
- [201] M. Ackermann *et al.* (Fermi-LAT), Phys. Rev. Lett. **115**, 23, 231301 (2015), [arXiv:1503.02641].
- [202] D. Hooper and L. Goodenough, Phys. Lett. **B697**, 412 (2011), [arXiv:1010.2752].
- [203] M. Ackermann *et al.* (Fermi-LAT), Astrophys. J. **840**, 1, 43 (2017), [arXiv:1704.03910].
- [204] F. Calore, I. Cholis and C. Weniger, JCAP **1503**, 038 (2015), [arXiv:1409.0042].
- [205] K. N. Abazajian and M. Kaplinghat, Phys. Rev. **D86**, 083511 (2012), [Erratum: Phys. Rev. **D87**, 129902 (2013)], [arXiv:1207.6047].
- [206] S. K. Lee, M. Lisanti and B. R. Safdi, JCAP **1505**, 05, 056 (2015), [arXiv:1412.6099].
- [207] T. Daylan *et al.*, Phys. Dark Univ. **12**, 1 (2016), [arXiv:1402.6703].
- [208] R. K. Leane and T. R. Slatyer (2019), [arXiv:1904.08430].
- [209] E. Carlson, T. Linden and S. Profumo, Phys. Rev. Lett. **117**, 11, 111101 (2016), [arXiv:1510.04698].
- [210] M. Ajello *et al.* (Fermi-LAT), Astrophys. J. **819**, 1, 44 (2016), [arXiv:1511.02938].
- [211] M. Ackermann *et al.* (Fermi-LAT), Astrophys. J. **836**, 2, 208 (2017), [arXiv:1702.08602].
- [212] A. McDaniel, T. Jeltema and S. Profumo, Phys. Rev. **D97**, 10, 103021 (2018), [arXiv:1802.05258].
- [213] C. Karwin *et al.* (2019), [arXiv:1903.10533].
- [214] A. McDaniel, T. Jeltema and S. Profumo, Phys. Rev. **D100**, 2, 023014 (2019), [arXiv:1903.06833].
- [215] R. L. Kinzer *et al.*, Astrophys. J. **559**, 282 (2001).
- [216] R. M. Bandyopadhyay *et al.*, Mon. Not. Roy. Astron. Soc. **392**, 1115 (2009), [arXiv:0810.3674].
- [217] D. P. Finkbeiner and N. Weiner, Phys. Rev. **D76**, 083519 (2007), [arXiv:astro-ph/0702587].
- [218] K. Agashe *et al.*, JCAP **1410**, 10, 062 (2014), [arXiv:1405.7370].
- [219] T. Damour and L. M. Krauss, Phys. Rev. Lett. **81**, 5726 (1998), [arXiv:astro-ph/9806165].
- [220] S. L. Adler, Phys. Lett. **B671**, 203 (2009), [arXiv:0808.2823].
- [221] J. Casanellas and I. Lopes, Astrophys. J. **765**, L21 (2013), [arXiv:1212.2985].
- [222] G. D. Mack, J. F. Beacom and G. Bertone, Phys. Rev. **D76**, 043523 (2007), [arXiv:0705.4298].
- [223] J. Smolinsky and P. Tanedo, Phys. Rev. **D95**, 7, 075015 (2017), [Erratum: Phys. Rev. **D96**, no.9, 099902 (2017)], [arXiv:1701.03168].
- [224] C. Niblaeus, A. Beniwal and J. Edsjo (2019), [arXiv:1903.11363].
- [225] M. G. Aartsen *et al.* (IceCube), JCAP **1604**, 04, 022 (2016), [arXiv:1601.00653].
- [226] S. Adrian-Martinez *et al.* (ANTARES), Phys. Lett. **B759**, 69 (2016), [arXiv:1603.02228].
- [227] C. R. Das *et al.*, Phys. Lett. **B725**, 297 (2013), [arXiv:1110.5095].
- [228] M. G. Aartsen *et al.* (IceCube), J. Phys. **G44**, 5, 054006 (2017), [arXiv:1607.02671].
- [229] Y. Zhao and K. M. Zurek, JHEP **07**, 017 (2014), [arXiv:1401.7664].
- [230] A. W. Strong, I. V. Moskalenko and V. S. Ptuskin, Ann. Rev. Nucl. Part. Sci. **57**, 285 (2007), [arXiv:astro-ph/0701517].
- [231] O. Adriani *et al.* (PAMELA), Phys. Rev. Lett. **111**, 081102 (2013), [arXiv:1308.0133].
- [232] M. Aguilar *et al.* (AMS), Phys. Rev. Lett. **117**, 9, 091103 (2016).
- [233] M. Aguilar *et al.* (AMS), Phys. Rev. Lett. **110**, 141102 (2013).
- [234] S. Profumo, F. Queiroz and C. Siqueira (2019), [arXiv:1903.07638].
- [235] D. Hooper, P. Blasi and P. D. Serpico, JCAP **0901**, 025 (2009), [arXiv:0810.1527].
- [236] S. Profumo, Central Eur. J. Phys. **10**, 1 (2011), [arXiv:0812.4457].
- [237] A. U. Abeysekara *et al.* (HAWC), Science **358**, 6365, 911 (2017), [arXiv:1711.06223].

- [238] S. Profumo *et al.*, Phys. Rev. **D97**, 12, 123008 (2018), [arXiv:1803.09731].
- [239] R. Cowsik, B. Burch and T. Madziwa-Nussinov, Astrophys. J. **786**, 124 (2014), [arXiv:1305.1242].
- [240] K. Blum, B. Katz and E. Waxman, Phys. Rev. Lett. **111**, 21, 211101 (2013), [arXiv:1305.1324].
- [241] M.-Y. Cui *et al.*, Phys. Rev. Lett. **118**, 19, 191101 (2017), [arXiv:1610.03840].
- [242] A. Reinert and M. W. Winkler, JCAP **1801**, 01, 055 (2018), [arXiv:1712.00002].
- [243] M. W. Winkler, JCAP **1702**, 02, 048 (2017), [arXiv:1701.04866].
- [244] F. Donato, N. Fornengo and P. Salati, Phys. Rev. **D62**, 043003 (2000), [hep-ph/9904481].
- [245] K. Mori *et al.*, Astrophys. J. **566**, 604 (2002), [arXiv:astro-ph/0109463].
- [246] H. Baer and S. Profumo, JCAP **0512**, 008 (2005), [arXiv:astro-ph/0510722].
- [247] E. Carlson *et al.*, Phys. Rev. **D89**, 7, 076005 (2014), [arXiv:1401.2461].
- [248] M. Cirelli *et al.*, JHEP **08**, 009 (2014), [arXiv:1401.4017].
- [249] R. Bird *et al.*, in “36th International Cosmic Ray Conference (ICRC 2019) Madison, Wisconsin, USA, July 24-August 1, 2019,” (2019), [arXiv:1908.03154].
- [250] A. Coogan and S. Profumo, Phys. Rev. **D96**, 8, 083020 (2017), [arXiv:1705.09664].
- [251] S. Colafrancesco, S. Profumo and P. Ullio, Astron. Astrophys. **455**, 21 (2006), [arXiv:astro-ph/0507575].
- [252] S. Colafrancesco, S. Profumo and P. Ullio, Phys. Rev. **D75**, 023513 (2007), [arXiv:astro-ph/0607073].
- [253] S. Profumo and P. Ullio (2010), [arXiv:1001.4086].
- [254] T. E. Jeltema and S. Profumo, JCAP **0811**, 003 (2008), [arXiv:0808.2641].
- [255] M. Cirelli *et al.*, JCAP **1103**, 051 (2011), [Erratum: JCAP1210,E01(2012)], [arXiv:1012.4515].
- [256] A. McDaniel *et al.*, JCAP **1709**, 09, 027 (2017), [arXiv:1705.09384].
- [257] E. Storm *et al.*, Astrophys. J. **768**, 106 (2013), [arXiv:1210.0872].
- [258] G. G. Raffelt, *Stars as laboratories for fundamental physics* (1996), ISBN 9780226702728, URL <http://wwwth.mpp.mpg.de/members/raffelt/mypapers/199613.pdf>.
- [259] D. Spolyar, K. Freese and P. Gondolo, Phys. Rev. Lett. **100**, 051101 (2008), [arXiv:0705.0521].
- [260] S. Dimopoulos, J. Preskill and F. Wilczek, Phys. Lett. **119B**, 320 (1982).
- [261] P. Pani and A. Loeb, JCAP **1406**, 026 (2014), [arXiv:1401.3025].
- [262] H. Liu, G. W. Ridgway and T. R. Slatyer (2019), [arXiv:1904.09296].
- [263] M. A. Monroy-Rodríguez and C. Allen, Astrophys. J. **790**, 2, 159 (2014), [arXiv:1406.5169].
- [264] M. Ricotti, J. P. Ostriker and K. J. Mack, Astrophys. J. **680**, 829 (2008), [arXiv:0709.0524].
- [265] S. Bird *et al.*, Phys. Rev. Lett. **116**, 20, 201301 (2016), [arXiv:1603.00464].
- [266] V. Poulin *et al.*, Phys. Rev. **D96**, 8, 083524 (2017), [arXiv:1707.04206].
- [267] P. Tisserand *et al.* (EROS-2), Astron. Astrophys. **469**, 387 (2007), [arXiv:astro-ph/0607207].
- [268] H. Niikura *et al.*, Nat. Astron. **3**, 6, 524 (2019), [arXiv:1701.02151].
- [269] E. Mediavilla *et al.*, Astrophys. J. **706**, 1451 (2009), [arXiv:0910.3645].
- [270] A. Barnacka, J. F. Glicenstein and R. Moderski, Phys. Rev. **D86**, 043001 (2012), [arXiv:1204.2056].
- [271] A. Katz *et al.*, JCAP **1812**, 005 (2018), [arXiv:1807.11495].
- [272] N. Smyth *et al.* (2019), [arXiv:1910.01285].
- [273] B. J. Carr *et al.*, Phys. Rev. **D81**, 104019 (2010), [arXiv:0912.5297].



## 28. Dark Energy

Revised August 2019 by D.H. Weinberg (Ohio State U.) and M. White (UC Berkeley; LBNL).

### 28.1 Repulsive Gravity and Cosmic Acceleration

In the first modern cosmological model, Einstein [1] modified his field equation of General Relativity (GR), introducing a “cosmological term” that enabled a solution with time-independent, spatially homogeneous matter density  $\rho_m$  and constant positive space curvature. Although Einstein did not frame it this way, one can view the “cosmological constant”  $\Lambda$  as representing a constant energy density of the vacuum [2], whose repulsive gravitational effect balances the attractive gravity of matter and thereby allows a static solution. After the development of dynamic cosmological models [3, 4] and the discovery of cosmic expansion [5], the cosmological term appeared unnecessary, and Einstein and de Sitter [6] advocated adopting an expanding, homogeneous and isotropic, spatially flat, matter-dominated Universe as the default cosmology until observations dictated otherwise. Such a model has matter density equal to the critical density,  $\Omega_m \equiv \rho_m/\rho_c = 1$ , and negligible contribution from other energy components [7].

By the mid-1990s, the Einstein-de Sitter model was showing numerous cracks, under the combined onslaught of data from the cosmic microwave background (CMB), large-scale galaxy clustering, and direct estimates of the matter density, the expansion rate ( $H_0$ ), and the age of the Universe. As noted in a number of papers from this time, introducing a cosmological constant offered a potential resolution of many of these tensions, yielding the most empirically successful version of the inflationary cold dark matter scenario. In the late 1990s, supernova surveys by two independent teams provided direct evidence for accelerating cosmic expansion [8, 9], establishing the cosmological constant model (with  $\Omega_m \simeq 0.3$ ,  $\Omega_\Lambda \simeq 0.7$ ) as the preferred alternative to the  $\Omega_m = 1$  scenario. Shortly thereafter, CMB evidence for a spatially flat Universe [10, 11], and thus for  $\Omega_{\text{tot}} \simeq 1$ , cemented the case for cosmic acceleration by firmly eliminating the free-expansion alternative with  $\Omega_m \ll 1$  and  $\Omega_\Lambda = 0$ . Today, the accelerating Universe is well established by multiple lines of independent evidence from a tight web of precise cosmological measurements.

As discussed in the Big Bang Cosmology article of this *Review* (Sec. 22), the scale factor  $R(t)$  of a homogeneous and isotropic Universe governed by GR grows at an accelerating rate if the pressure  $p < -\frac{1}{3}\rho$  (in  $c = 1$  units). A cosmological constant has  $\rho_\Lambda = \text{constant}$  and pressure  $p_\Lambda = -\rho_\Lambda$  (see Eq. 22.10), so it will drive acceleration if it dominates the total energy density. However, acceleration could arise from a more general form of “dark energy” that has negative pressure, typically specified in terms of the equation-of-state-parameter  $w = p/\rho$  ( $= -1$  for a cosmological constant). Furthermore, the conclusion that acceleration requires a new energy component beyond matter and radiation relies on the assumption that GR is the correct description of gravity on cosmological scales. The title of this article follows the common but inexact usage of “dark energy” as a catch-all term for the origin of cosmic acceleration, regardless of whether it arises from a new form of energy or a modification of GR. Our account here draws on the much longer review of cosmic acceleration by Ref. [12], which provides background explanation and extensive literature references for the discussion in Secs. 28.2 and 28.3.

Below we will use the abbreviation  $\Lambda$ CDM to refer to a model with cold dark matter, a cosmological constant, inflationary initial conditions, standard radiation and neutrino content, and a flat Universe with  $\Omega_{\text{tot}} = 1$  (though we will sometimes describe this model as “flat  $\Lambda$ CDM” to emphasize this last restriction). We will use  $w$ CDM to denote a model with the same assumptions but a free, constant value of  $w$ . Models with the prefix “o” (*e.g.*, o $w$ CDM) allow non-zero space curvature.

### 28.2 Theories of Cosmic Acceleration

#### 28.2.1 Dark Energy or Modified Gravity?

A cosmological constant is the mathematically simplest, and perhaps the physically simplest, theoretical explanation for the accelerating Universe. The problem is explaining its unnaturally small magnitude, as discussed in Sec. 22.4.7 of this *Review*. An alternative (which still requires finding a way to make the cos-

mological constant zero or at least negligibly small) is that the accelerating cosmic expansion is driven by a new form of energy such as a scalar field [13] with potential  $V(\phi)$ . The energy density and pressure of the field  $\phi(\mathbf{x})$  take the same forms as for inflationary scalar fields, given in Eq. (22.52) of the Big Bang Cosmology article. In the limit that  $\frac{1}{2}\dot{\phi}^2 \ll |V(\phi)|$ , the scalar field acts like a cosmological constant, with  $p_\phi \simeq -\rho_\phi$ . In this scenario, today’s cosmic acceleration is closely akin to the epoch of inflation, but with radically different energy and timescale.

More generally, the value of  $w = p_\phi/\rho_\phi$  in scalar field models evolves with time in a way that depends on  $V(\phi)$  and on the initial conditions  $(\phi_i, \dot{\phi}_i)$ ; some forms of  $V(\phi)$  have attractor solutions in which the late-time behavior is insensitive to initial values. Many forms of time evolution are possible, including ones where  $w$  is approximately constant and broad classes where  $w$  “freezes” towards or “thaws” away from  $w = -1$ , with the transition occurring when the field comes to dominate the total energy budget. If  $\rho_\phi$  is even approximately constant, then it becomes dynamically insignificant at high redshift, because the matter density scales as  $\rho_m \propto (1+z)^3$ . “Early dark energy” models are ones in which  $\rho_\phi$  is a small but not negligible fraction (*e.g.*, a few percent) of the total energy throughout the matter- and radiation-dominated eras, tracking the dominant component before itself coming to dominate at low redshift.

Instead of introducing a new energy component, one can attempt to modify gravity in a way that leads to accelerated expansion [14]. One option is to replace the Ricci scalar  $\mathcal{R}$  with a function  $\mathcal{R} + f(\mathcal{R})$  in the gravitational action [15]. Other changes can be more radical, such as introducing extra dimensions and allowing gravitons to “leak” off the brane that represents the observable Universe (the “DGP” model [16]). The DGP example has inspired a more general class of “galileon” and massive gravity models. Constructing viable modified gravity models is challenging, in part because it is easy to introduce theoretical inconsistencies (such as “ghost” fields with negative kinetic energy), but above all because GR is a theory with many high-precision empirical successes on solar system scales [17]. Modified gravity models typically invoke screening mechanisms that force model predictions to approach those of GR in regions of high density or strong gravitational potential. Screening offers potentially distinctive signatures, as the strength of gravity (*i.e.*, the effective value of  $G_N$ ) can vary by order unity in environments with different gravitational potentials.

More generally, one can search for signatures of modified gravity by comparing the history of cosmic structure growth to the history of cosmic expansion. Within GR, these two are linked by a consistency relation, as described below (Eq. (28.2)). Modifying gravity can change the predicted rate of structure growth, and it can make the growth rate dependent on scale or environment. In some circumstances, modifying gravity alters the combinations of potentials responsible for gravitational lensing and the dynamics of non-relativistic tracers (such as galaxies or stars) in different ways (see Sec. 22.4.7 in this *Review*), leading to order unity mismatches between the masses of objects inferred from lensing and those inferred from dynamics in unscreened environments.

At present there are no fully realized and empirically viable modified gravity theories that explain the observed level of cosmic acceleration. The constraints on  $f(\mathcal{R})$  models now force them so close to GR that they cannot produce acceleration without introducing a separate dark energy component [18]. The DGP model is empirically ruled out by several tests, including the expansion history, the integrated Sachs-Wolfe effect, and redshift-space distortion measurements of the structure growth rate [19]. The near-simultaneous arrival of gravitational waves and electromagnetic signals from the neutron star merger event GW170817, which shows that gravitational waves travel at almost exactly the speed of light, is a further strong constraint on modified gravity theories [20]. The elimination of models should be considered an important success of the program to empirically test theories of cosmic acceleration. However, it is worth recalling that there was no fully realized gravitational explanation for the precession of Mercury’s orbit prior to the completion of GR in 1915, and the fact that no complete and viable modified gravity theory exists

today does not mean that one will not arise in the future. In the meantime, we can continue empirical investigations that can tighten restrictions on such theories or perhaps point towards the gravitational sector as the origin of accelerating expansion.

### 28.2.2 Expansion History and Growth of Structure

The main line of empirical attack on dark energy is to measure the history of cosmic expansion and the history of matter clustering with the greatest achievable precision over a wide range of redshift. Within GR, the expansion rate  $H(z)$  is governed by the Friedmann equation (see the articles on Big Bang Cosmology and Cosmological Parameters—Secs. 22 and 25.1 in this *Review*). For dark energy with an equation of state  $w(z)$ , the cosmological constant contribution to the expansion,  $\Omega_\Lambda$ , is replaced by a redshift-dependent contribution. The evolution of the dark energy density follows from Eq. (22.10),

$$\begin{aligned} \Omega_{\text{de}} \frac{\rho_{\text{de}}(z)}{\rho_{\text{de}}(z=0)} &= \Omega_{\text{de}} \exp \left[ 3 \int_0^z [1 + w(z')] \frac{dz'}{1+z'} \right] \\ &= \Omega_{\text{de}} (1+z)^{3(1+w)}, \end{aligned} \quad (28.1)$$

where the second equality holds for constant  $w$ . If  $\Omega_m$ ,  $\Omega_r$ , and the present value of  $\Omega_{\text{tot}}$  are known, then measuring  $H(z)$  pins down  $w(z)$ . (Note that  $\Omega_{\text{de}}$  is the same quantity denoted  $\Omega_v$  in Sec. 22, but we have adopted the ‘de’ subscript to avoid implying that dark energy is necessarily a vacuum effect.)

While some observations can probe  $H(z)$  directly, others measure the distance-redshift relation. The basic relations between angular diameter distance or luminosity distance and  $H(z)$  are given in Ch. 22—and these are generally unaltered in time-dependent dark energy or modified gravity models. For convenience, in later sections, we will sometimes refer to the comoving angular distance,  $D_{A,c}(z) = (1+z)D_A(z)$ .

In GR-based linear perturbation theory, the density contrast  $\delta(\mathbf{x}, t) \equiv \rho(\mathbf{x}, t)/\bar{\rho}(t) - 1$  of pressureless matter grows in proportion to the linear growth function  $G(t)$  (not to be confused with the gravitational constant  $G_N$ ), which follows the differential equation

$$\ddot{G} + 2H(z)\dot{G} - \frac{3}{2}\Omega_m H_0^2 (1+z)^3 G = 0. \quad (28.2)$$

To a good approximation, the logarithmic derivative of  $G(z)$  is

$$f(z) \equiv -\frac{d \ln G}{d \ln(1+z)} \simeq \left[ \Omega_m (1+z)^3 \frac{H_0^2}{H^2(z)} \right]^\gamma, \quad (28.3)$$

where  $\gamma \simeq 0.55$  for relevant values of cosmological parameters [21]. In an  $\Omega_m = 1$  Universe,  $G(z) \propto (1+z)^{-1}$ , but growth slows when  $\Omega_m$  drops significantly below unity. One can integrate Eq. (28.3) to get an approximate integral relation between  $G(z)$  and  $H(z)$ , but the full (numerical) solution to Eq. (28.2) should be used for precision calculations. Even in the non-linear regime, the amplitude of clustering is determined mainly by  $G(z)$ , so observations of non-linear structure can be used to infer the linear  $G(z)$ , provided one has good theoretical modeling to relate the two.

In modified gravity models the growth rate of gravitational clustering may differ from the GR prediction. A general strategy to test modified gravity, therefore, is to measure both the expansion history and the growth history to see whether they yield consistent results for  $H(z)$  or  $w(z)$ .

### 28.2.3 Parameters

Constraining a general history of  $w(z)$  is nearly impossible, because the dark energy density, which affects  $H(z)$ , is given by an integral over  $w(z)$ , and distances and the growth factor involve a further integration over functions of  $H(z)$ . Oscillations in  $w(z)$  over a range  $\Delta z/(1+z) \ll 1$  are therefore extremely difficult to constrain. It has become conventional to phrase constraints or projected constraints on  $w(z)$  in terms of a linear evolution model,

$$w(a) = w_0 + w_a(1-a) = w_p + w_a(a_p - a), \quad (28.4)$$

where  $a \equiv (1+z)^{-1}$ ,  $w_0$  is the value of  $w$  at  $z = 0$ , and  $w_p$  is the value of  $w$  at a ‘pivot’ redshift  $z_p \equiv a_p^{-1} - 1$ , where it

is best constrained by a given set of experiments. For typical data combinations,  $z_p \simeq 0.5$ . This simple parameterization can provide a good approximation to the predictions of many physically motivated models for observables measured with percent-level precision. A widely used ‘Figure of Merit’ (FoM) for dark energy experiments [22] is the projected combination of errors  $[\sigma(w_p)\sigma(w_a)]^{-1}$ . Ambitious future experiments with 0.1–0.3% precision on observables can constrain richer descriptions of  $w(z)$ , which can be characterized by principal components.

There has been less convergence on a standard parameterization for describing modified gravity theories. Deviations from the GR-predicted growth rate can be described by a deviation  $\Delta\gamma$  in the index of Eq. (28.3), together with an overall multiplicative offset relative to the  $G(z)$  expected from extrapolating the CMB-measured fluctuation amplitude to low redshift. However, these two parameters may not accurately capture the growth predictions of all physically interesting models. Another important parameter to constrain is the ratio of the gravitational potentials governing space curvature and the acceleration of non-relativistic test particles. The possible phenomenology of modified gravity models is rich, which enables many consistency tests but complicates the task of constructing parameterized descriptions.

The more general set of cosmological parameters is discussed elsewhere in this *Review* (Sec. 25.1), but here we highlight a few that are particularly important to the dark energy discussion.

- The dimensionless Hubble parameter  $h \equiv H_0/100 \text{ km s}^{-1} \text{ Mpc}^{-1}$  determines the present day value of the critical density and the overall scaling of distances inferred from redshifts.
- $\Omega_m$  and  $\Omega_{\text{tot}}$  affect the expansion history and the distance-redshift relation.
- The sound horizon  $r_s = \int_0^{t_{\text{rec}}} c_s(t) dt/a(t)$ , the comoving distance that pressure waves can propagate between  $t = 0$  and recombination, determines the physical scale of the acoustic peaks in the CMB and the baryon acoustic oscillation (BAO) feature in low-redshift matter clustering [23].
- The amplitude of matter fluctuations, conventionally represented by the quantity  $\sigma_8(z)$ , scales the overall amplitude of growth measures such as weak lensing or redshift-space distortions (discussed in the next section).

Specifically,  $\sigma_8(z)$  refers to the rms fluctuation of the matter overdensity  $\rho/\bar{\rho}$  in spheres of radius  $8h^{-1}\text{Mpc}$ , computed from the linear theory matter power spectrum at redshift  $z$ , and  $\sigma_8$  on its own refers to the value at  $z = 0$  (just like our convention for  $\Omega_m$ ).

While discussions of dark energy are frequently phrased in terms of values and errors on quantities like  $w_p$ ,  $w_a$ ,  $\Delta\gamma$ , and  $\Omega_{\text{tot}}$ , parameter precision is the means to an end, not an end in itself. The underlying goal of empirical studies of cosmic acceleration is to address two physically profound questions:

1. Does acceleration arise from a breakdown of GR on cosmological scales or from a new energy component that exerts repulsive gravity within GR?
2. If acceleration is caused by a new energy component, is its energy density constant in space and time, as expected for a fundamental vacuum energy, or does it show variations that indicate a dynamical field?

Substantial progress towards answering these questions, in particular any definitive rejection of the cosmological constant ‘null hypothesis,’ would be a major breakthrough in cosmology and fundamental physics.

## 28.3 Observational Probes

We briefly summarize the observational probes that play the greatest role in current constraints on dark energy. Further discussion can be found in other articles of this *Review*, in particular Secs. 25.1 (Cosmological Parameters) and 29 (The Cosmic Microwave Background), and in Ref. [12], which provides extensive references to background literature. Recent observational results from these methods are discussed in Sec. 28.4.

### 28.3.1 Methods, Sensitivity, Systematics

**Cosmic Microwave Background Anisotropies:** Although CMB anisotropies provide limited information about dark energy on their own, CMB constraints on the geometry, matter content, and radiation content of the Universe play a critical role in dark energy studies when combined with low-redshift probes. In particular, CMB data supply measurements of  $\theta_s = r_s/D_{A,c}(z_{\text{rec}})$ , the angular size of the sound horizon at recombination, from the angular location of the acoustic peaks, measurements of  $\Omega_m h^2$  and  $\Omega_b h^2$  from the heights of the peaks, and normalization of the amplitude of matter fluctuations at  $z_{\text{rec}}$  from the amplitude of the CMB fluctuations themselves. *Planck* data yield a 0.18% determination of  $r_s$ , which scales as  $(\Omega_m h^2)^{-0.25}$  for cosmologies with standard matter and radiation content. The uncertainty in the matter fluctuation amplitude at the epoch of recombination is 0.5%. Secondary anisotropies, including the integrated Sachs-Wolfe effect, the Sunyaev-Zeldovich (SZ, [24]) effect, and weak lensing of primary anisotropies, provide additional information about dark energy by constraining low-redshift structure growth.

**Type Ia Supernovae (SN):** Type Ia supernovae, produced by the thermonuclear explosions of white dwarfs, exhibit 10–15% scatter in peak luminosity after correction for light curve duration (the time to rise and fall) and color (which is a diagnostic of dust extinction). Since the peak luminosity is not known *a priori*, supernova surveys constrain ratios of luminosity distances at different redshifts. If one is comparing a high-redshift sample to a local calibrator sample measured with much higher precision (and distances inferred from Hubble’s law), then one essentially measures the luminosity distance in  $h^{-1}\text{Mpc}$ , constraining the combination  $hD_L(z)$ . With distance uncertainties of 5–8% per well observed supernova, a sample of around 100 SNe is sufficient to achieve sub-percent statistical precision. The 1–2% systematic uncertainties in current samples are dominated by uncertainties associated with photometric calibration and dust extinction corrections plus the observed dependence of luminosity on host galaxy properties. Another potential systematic is redshift evolution of the supernova population itself, which can be tested by analyzing subsamples grouped by spectral properties or host galaxy properties to confirm that they yield consistent results.

**Baryon Acoustic Oscillations (BAO):** Pressure waves that propagate in the pre-recombination photon-baryon fluid imprint a characteristic scale in the clustering of matter and galaxies, which appears in the galaxy correlation function as a localized peak at the sound horizon scale  $r_s$ , or in the power spectrum as a series of oscillations. Since observed galaxy coordinates consist of angles and redshifts, measuring this “standard ruler” scale in a galaxy redshift survey determines the angular diameter distance  $D_A(z)$  and the expansion rate  $H(z)$ , which convert coordinate separations to comoving distances. Errors on the two quantities are correlated, and in existing galaxy surveys the best determined combination is approximately  $D_V(z) = [czD_{A,c}^2(z)/H(z)]^{1/3}$ . As an approximate rule of thumb, a survey that fully samples structures at redshift  $z$  over a comoving volume  $V$ , and is therefore limited by cosmic variance rather than shot noise, measures  $D_{A,c}(z)$  with a fractional error of  $0.005(V/10\text{Gpc}^3)^{-1/2}$  and  $H(z)$  with a fractional error 1.6–1.8 times higher. The most precise BAO measurements to date come from large galaxy redshift surveys probing  $z < 0.8$ , and these will be extended to higher redshifts by future projects. At redshifts  $z > 2$ , BAO can also be measured in the Lyman- $\alpha$  forest of intergalactic hydrogen absorption towards background quasars, where the fluctuating absorption pattern provides tens or hundreds of samples of the density field along each quasar sightline. For Lyman- $\alpha$  forest BAO, the best measured parameter combination is more heavily weighted towards  $H(z)$  because of strong redshift-space distortions that enhance clustering in the line-of-sight direction. Radio intensity mapping, which maps large-scale structure in redshifted 21-cm hydrogen emission without resolving individual galaxies, offers a potentially promising route to measuring BAO over large volumes at relatively low cost, but the technique is still under development. Photometric redshifts in optical imaging surveys can be used to measure BAO in the angular direction, though the typical distance precision is a factor of 3–4 lower compared to a well sampled spectroscopic survey

of the same area, and angular BAO measurements do not directly constrain  $H(z)$ . BAO distance measurements complement SN distance measurements by providing absolute rather than relative distances (with precise calibration of  $r_s$  from the CMB) and by having greater achievable precision at high redshift thanks to the increasing comoving volume available. Theoretical modeling suggests that BAO measurements from even the largest feasible redshift surveys will be limited by statistical rather than systematic uncertainties.

**Weak Gravitational Lensing:** Gravitational light bending by a clustered distribution of matter shears the shapes of higher redshift background galaxies in a spatially coherent manner, producing a correlated pattern of apparent ellipticities. By studying the weak lensing signal for source galaxies binned by photometric redshift (estimated from broad-band colors), one can probe the correlation of source ellipticities to deduce the clustering of intervening matter. “Galaxy-galaxy lensing” (GGL) uses the correlation between a shear map and a foreground galaxy sample to measure the average mass profile around the foreground galaxies, which can be combined with galaxy clustering to constrain total matter clustering. For a specified expansion history, the predicted signals scale approximately as  $\sigma_8 \Omega_m^\alpha$ , with  $\alpha \simeq 0.3\text{--}0.5$ . The predicted signals also depend on the distance-redshift relation, so weak lensing becomes more powerful in concert with SN or BAO measurements that can pin this relation down independently. The most challenging systematics are shape measurement biases, biases in the distribution of photometric redshifts, and intrinsic alignments of galaxy orientations that could contaminate the lensing-induced signal. Weak lensing of CMB anisotropies is an increasingly powerful tool, in part because it circumvents many of these observational and astrophysical systematics. Predicting the large-scale weak lensing signal is straightforward in principle, but the number of independent modes on large scales is small, and the inferences are therefore dominated by sample variance. Exploiting small-scale measurements, for tighter constraints, requires modeling the effects of complex physical processes such as star formation and feedback on the matter power spectrum. Strong gravitational lensing can also provide constraints on dark energy, either through time delay measurements that probe the absolute distance scale, or through measurements of multiple-redshift lenses that constrain distance ratios. The primary uncertainty for strong lensing constraints is modeling the mass distribution of the lens systems.

**Clusters of Galaxies:** Like weak lensing, the abundance of massive dark-matter halos probes structure growth by constraining  $\sigma_8 \Omega_m^\alpha$ , where  $\alpha \simeq 0.3\text{--}0.5$ . These halos can be identified as dense concentrations of galaxies or through the signatures of hot ( $10^7\text{--}10^8\text{K}$ ) gas in X-ray emission or SZ distortion of the CMB. The critical challenge in cluster cosmology is calibrating the relation  $P(M_{\text{halo}}|O)$  between the halo mass as predicted from theory and the observable  $O$  used for cluster identification. Measuring the stacked weak lensing signal from clusters has emerged as a promising approach to achieve percent-level accuracy in calibration of the mean relation, which is required for clusters to remain competitive with other growth probes. This method requires accurate modeling of completeness and contamination of cluster catalogs, projection effects on cluster selection and weak lensing measurements, and possible baryonic physics effects on the mass distribution within clusters.

**Redshift-Space Distortions (RSD) and the Alcock-Paczynski (AP) Effect:** Redshift-space distortions of galaxy clustering, induced by peculiar motions, probe structure growth by constraining the parameter combination  $f(z)\sigma_8(z)$ , where  $f(z)$  is the growth rate defined by Eq. (28.3). Uncertainties in theoretical modeling of non-linear gravitational evolution and the non-linear bias between the galaxy and matter distributions currently limit application of the method to large scales (comoving separations  $r \gtrsim 10h^{-1}\text{Mpc}$  or wavenumbers  $k \lesssim 0.2h\text{Mpc}^{-1}$ ). A second source of anisotropy arises if one adopts the wrong cosmological metric to convert angles and redshifts into comoving separations, a phenomenon known as the Alcock-Paczynski effect [26]. Demanding isotropy of clustering at redshift  $z$  constrains the parameter combination

**Table 28.1:** A selection of major dark-energy experiments, based on Ref. [25]. Abbreviations in the “Data” column refer to optical (Opt) or near-infrared (NIR) imaging (I) or spectroscopy (S). For spectroscopic experiments, the “Spec- $z$ ” column lists the primary redshift range for galaxies (gals), quasars (QSOs), or the Lyman- $\alpha$  forest (Ly $\alpha$ F). Abbreviations in the “Methods” column are weak lensing (WL), clusters (CL), supernovae (SN), baryon acoustic oscillations (BAO), and redshift-space distortions (RSD).

Project	Dates	Area/deg <sup>2</sup>	Data	Spec- $z$ Range	Methods
BOSS	2008–2014	10,000	Opt-S	0.3–0.7 (gals) 2–3.5 (Ly $\alpha$ F)	BAO/RSD
KiDS	2011–2019	1500	Opt-I	—	WL/CL
DES	2013–2019	5000	Opt-I	—	WL/CL SN/BAO
eBOSS	2014–2018	7500	Opt-S	0.6–2.0 (gal/QSO) 2–3.5 (Ly $\alpha$ F)	BAO/RSD
SuMIRE	2014–2024	1500	Opt-I	—	WL/CL
HETDEX	2017–2023	450	Opt/NIR-S	0.8–2.4 (gals)	BAO/RSD
DESI	2020–2025	14,000	Opt-S	1.9 < $z$ < 3.5 (gals)	BAO/RSD
LSST	2022–2032	20,000	Opt-S	0–1.7 (gals) 2–3.5 (Ly $\alpha$ F)	BAO/RSD
LSST	2022–2032	20,000	Opt-I	—	WL/CL SN/BAO
<i>Euclid</i>	2022–2028	15,000	Opt-I	—	WL/CL
<i>WFIRST</i>	2025–2030	2200	NIR-S	0.7–2.2 (gals)	BAO/RSD
<i>WFIRST</i>	2025–2030	2200	NIR-I	—	WL/CL/SN
<i>WFIRST</i>	2025–2030	2200	NIR-S	1.0–3.0 (gals)	BAO/RSD

$H(z)D_A(z)$ . The main challenge for the AP method is correcting for the anisotropy induced by peculiar velocity RSD.

*Low Redshift Measurement of  $H_0$ :* The value of  $H_0$  sets the current value of the critical density  $\rho_c = 3H_0^2/8\pi G_N$ , and combination with CMB measurements provides a long lever arm for constraining the evolution of dark energy. The challenge in conventional  $H_0$  measurements is establishing distances to galaxies that are “in the Hubble flow,” *i.e.*, far enough away that their peculiar velocities are small compared to the expansion velocity  $v = H_0 d$ . This can be done by building a ladder of distance indicators tied to stellar parallax on its lowest rung, or by using gravitational-lens time delays or geometrical measurements of maser data to circumvent this ladder.

### 28.3.2 Dark Energy Experiments

Most observational applications of these methods now take place in the context of large cosmological surveys, for which constraining dark energy and modified gravity theories is a central objective. Table 28.1 lists a selection of current and planned dark-energy experiments, taken originally from the Snowmass 2013 Dark Energy Facilities review [25], which focused on projects in which the U.S. has either a leading role or significant participation. References and links to further information about these projects can be found in Ref. [25]. We have adjusted some of the dates in this Table relative to those in Ref. [25] and added the European-led KiloDegree Survey (KiDS). Dates in the Table correspond to the duration of survey observations, and the final cosmological results frequently require 1–3 years of analysis and modeling beyond the end of data taking.

Beginning our discussion with imaging surveys, the Dark Energy Survey (DES) has observed 1/8 of the sky to a depth roughly 2 magnitudes deeper than the Sloan Digital Sky Survey (SDSS), enabling weak lensing measurements with much greater statistical precision, cluster measurements calibrated by weak lensing, and angular BAO measurements based on photometric redshifts. With repeat imaging over a smaller area, DES has identified thousands of Type Ia SNe, which together with spectroscopic follow-up data enable significant improvements on the current state-of-the-art for supernova (SN) cosmology. Cosmological results from weak lensing and galaxy clustering analyses of the first year DES data are presented in Ref. [27] and discussed further below, while the first cosmological results from the DES supernova survey are presented in Ref. [28]. The Hyper-Suprime Camera (HSC) on the Subaru 8.2-m telescope is carrying out a similar type of optical imaging survey, probing a smaller area than DES but to greater

depth. First cosmological results from HSC weak lensing are reported in Refs. [29, 30]. The HSC survey is one component of the Subaru Measurement of Images and Redshifts (SuMIRE) project. Beginning in the early 2020s, the dedicated Large Synoptic Survey Telescope (LSST) will scan the southern sky to SDSS-like depth every four nights. LSST imaging co-added over its decade-long primary survey will reach extraordinary depth, enabling weak lensing, cluster, and photometric BAO studies from billions of galaxies. Additionally, LSST time-domain monitoring will identify and measure light curves for thousands of Type Ia SNe per year.

Turning to spectroscopic surveys, the Baryon Oscillation Spectroscopic Survey (BOSS) and its successor eBOSS used fiber-fed optical spectrographs to map the redshift-space distributions of millions of galaxies and quasars. These 3-dimensional maps enable BAO and RSD measurements, and Lyman- $\alpha$  forest spectra of high-redshift quasars extend these measurements to redshifts  $z > 2$ . As discussed below, the BOSS Collaboration has now published BAO and RSD analyses of its final data sets, and eBOSS has released BAO measurements from quasar clustering at  $z = 1$ –2. The Hobby-Eberly Telescope Dark Energy Experiment (HETDEX) uses integral field spectrographs to detect Lyman- $\alpha$  emission-line galaxies at  $z \simeq 1.9$ –3.5, probing a small sky area but a substantial comoving volume. The Dark Energy Spectroscopic Instrument (DESI) will follow a strategy similar to BOSS/eBOSS but on a much grander scale, using a larger telescope (4-m vs. 2.5-m) and a much higher fiber multiplex (5000 vs. 1000) to survey an order-of-magnitude more galaxies. A new Prime Focus Spectrograph (PFS) for the Subaru telescope will enable the spectroscopic component of SuMIRE, with the large telescope aperture and wavelength sensitivity that extends to the near-infrared (NIR) allowing it to probe a higher redshift galaxy population than DESI, over a smaller area of sky.

Compared to ground-based observations, space observations afford higher angular resolution and a far lower NIR sky background. The *Euclid* and *WFIRST* (*Wide Field Infrared Survey Telescope*) missions will exploit these advantages, conducting large area imaging surveys for weak lensing and cluster studies and slitless spectroscopic surveys of emission-line galaxies for BAO and RSD studies. *WFIRST* will also incorporate an imaging and spectrophotometric supernova (SN) survey, extending to redshift  $z \simeq 1.7$ . Survey details are likely to evolve prior to launch, but in the current designs one can roughly characterize the difference between the *Euclid* and *WFIRST* dark-energy experiments as “wide vs. deep,” with planned survey areas of 15,000 deg<sup>2</sup> and

2200 deg<sup>2</sup>, respectively. For weak lensing shape measurements, *Euclid* will use a single wide optical filter, while *WFIRST* will use three NIR filters. The *Euclid* galaxy redshift survey will cover a large volume at relatively low space density, while the *WFIRST* survey will provide denser sampling of structure in a smaller volume. There are numerous synergies among the LSST, *Euclid*, and *WFIRST* dark energy programs, as discussed in Ref. [31].

### 28.4 Current Constraints on Expansion, Growth, and Dark Energy

The last decade has seen dramatic progress in measurements of the cosmic expansion history and structure growth, leading to much tighter constraints on the parameters of dark energy models. CMB data from the *WMAP* and *Planck* satellites and from higher resolution ground-based experiments have provided an exquisitely detailed picture of structure at the recombination epoch and the first CMB-based measures of low-redshift structure through lensing and SZ cluster counts. Cosmological supernova samples have increased in size from tens to many hundreds, with continuous coverage from  $z = 0$  to  $z \simeq 1.4$ , alongside major improvements in data quality, analysis methods, and detailed understanding of local populations. BAO measurements have advanced from the first detections to 1–2% precision at multiple redshifts, with increasingly sophisticated methods for testing systematics, fitting models, and evaluating statistical errors. Advances in X-ray, SZ, and weak-lensing observations of large samples of galaxy clusters allow a multi-faceted approach to mass calibration, improving statistical precision but also revealing sources of astrophysical uncertainty. Cluster constraints have been joined by the first precise matter-clustering constraints from cosmic-shear weak lensing and galaxy-galaxy lensing, and by redshift-space distortion measurements that probe different aspects of structure growth at somewhat lower precision. The precision of low-redshift  $H_0$  measurements has sharpened from the roughly 10% error of the *HST* Key Project [32] to 2–4% in recent analyses.

As an illustration of current measurements of the cosmic expansion history, Fig. 28.1 compares distance-redshift measurements from SN and BAO data to the predictions for a flat Universe with a cosmological constant. SN cosmology relies on compilation analyses that try to bring data from different surveys probing distinct redshift ranges to a common scale. Here we use the “joint light curve analysis” (JLA) sample of Ref. [34], who carried out a careful intercalibration of the 3-year Supernova Legacy Survey (SNLS3, [35]) and the full SDSS-II Supernova Survey [3] data in combination with several local supernova samples and high-redshift supernovae from *HST*. Results from the Union2.1 sample [36], which partly overlaps JLA but has different analysis procedures, would be similar. Other state-of-the-art supernova data sets include the Pan-STARRS1 sample incorporated in the PANTHEON compilation [37] and the first sample of spectroscopically confirmed supernovae from DES [28]. For illustration purposes, we have binned the JLA data in redshift and plotted the diagonal elements of the covariance matrix as error bars, and we have converted the SN luminosity distances to an equivalent comoving angular diameter distance. Because the peak luminosity of a fiducial SN Ia is an unknown free parameter, the SN distance measurements could all be shifted up and down by a constant multiplicative factor; cosmological information resides in the relative distances as a function of redshift. The normalization used here corresponds to a Hubble parameter  $h = 0.674$ .

The  $z < 2$  BAO data points come from the 6-degree-Field Galaxy Survey 6dFGS survey [39], the SDSS-II Main Galaxy Sample [40], the final galaxy clustering data set from BOSS [38], and the first BAO measurement from quasar clustering in eBOSS [41]. For the 6dFGS, SDSS-II, and eBOSS data points, values of  $D_V$  have been converted to  $D_{A,c}$ . The BOSS analysis measures  $D_{A,c}$  directly; we have taken values from the “BAO only” column of table 7 of Ref. [38]. At  $z = 2.34$  we plot  $D_{A,c}$  measured from the BAO analysis of the eBOSS Lyman- $\alpha$  forest auto-correlation and cross-correlation with quasars [42]. The BAO measurements are converted to absolute distances using the sound horizon scale  $r_s = 147.09$  Mpc from *Planck* 2018 CMB data, whose 0.18% uncertainty is small compared to the current BAO measurement er-

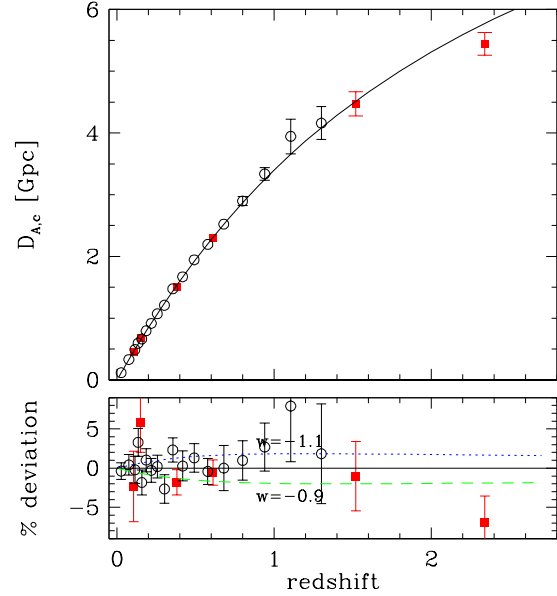


Figure 28.1: Distance-redshift relation measured from Type Ia SNe and BAO compared to the predictions (black curve) of a flat  $\Lambda$ CDM model with  $\Omega_m = 0.315$  and  $h = 0.674$ , the best-fit parameters inferred from *Planck* CMB data [33]. Circles show binned luminosity distances from the JLA SN sample [34], multiplied by  $(1+z)^{-1}$  to convert to comoving angular diameter distance. Red squares show BAO distance measurements from the 6dFGS, SDSS-II, BOSS, and eBOSS surveys (see text for details and references). The lower panel plots residuals from the  $\Lambda$ CDM prediction, with dashed and dotted curves that show the effect of changing  $w$  by  $\pm 0.1$  while all other parameters are held fixed. Note that the SN data points can be shifted up or down by a constant factor to account for freedom in the peak luminosity, while the BAO data points are calibrated to 0.2% precision by the sound horizon scale computed from *Planck* data. The errors on the BAO data points are approximately independent. In the upper panel, error bars are plotted only at  $z > 0.7$  to avoid visual confusion.

rors. The BOSS galaxy and eBOSS Lyman- $\alpha$  forest analyses also measure  $H(z)$  at the same redshifts, providing further leverage on expansion history that is not captured in Fig. 28.1.

The plotted cosmological model has  $\Omega_m = 0.315$  and  $h = 0.674$ , the best-fit values from *Planck* (TT+TE+EE+lowE+lensing) assuming  $w = -1$  and  $\Omega_{\text{tot}} = 1$  [33]. The SN, BAO, and CMB data sets, probing a wide range of redshifts with radically different techniques, are for the most part mutually consistent with the predictions of a flat  $\Lambda$ CDM cosmology. The eBOSS Lyman- $\alpha$  forest BAO measurements lie about  $1.7\sigma$  from the *Planck*  $\Lambda$ CDM prediction [42], notably closer than the  $2.3\sigma$  difference obtained with earlier BOSS data and discussed in the 2018 edition of this *Review*. Dotted and dashed curves in the lower panel of Fig. 28.1 show the effect of changing  $w$  by  $\pm 0.1$  with all other parameters held fixed, which leads to significantly worse agreement with the data. However, such a single-parameter comparison does not capture the impact of parameter degeneracies or the ability of complementary data sets to break them, and if one instead forced a match to CMB data by changing  $h$  and  $\Omega_m$  when changing  $w$  then the predicted BAO distances would diverge at  $z = 0$  rather than converging there.

Figure 28.2, taken from Ref. [38], presents constraints on models that allow a free but constant value of  $w$  with non-zero space curvature ( $ow$ CDM, left panel) or the evolving equation of state of Eq. (28.4) in a flat Universe ( $w_0w_a$ CDM, right panel). Green contours show constraints from the combination of *Planck* 2015 CMB data and the JLA supernova sample. Gray contours show the combination of *Planck* with BAO measurements from BOSS, 6dFGS, and SDSS-II. Red contours adopt a more aggressive anal-



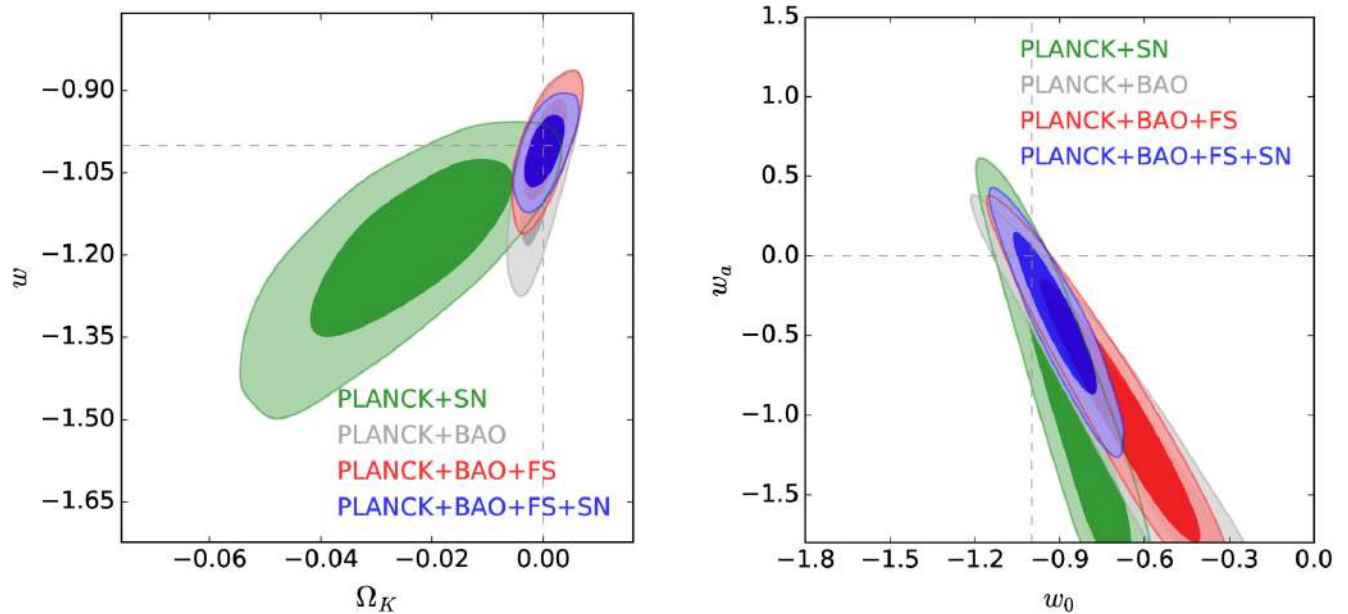


Figure 28.2: Constraints on dark energy model parameters from combinations of CMB, BAO, galaxy clustering, and supernova (SN) data, taken from Ref. [38]. The left panel shows 68% and 95% confidence contours in the  $ow$ CDM model, with constant equation-of-state parameter  $w$  and non-zero space curvature  $\Omega_K \equiv 1 - \Omega_{\text{tot}}$ . Green and gray contours show the combination of *Planck* CMB data with SN or BAO data, respectively. Red contours combine CMB, BAO, and the full shape (FS) of redshift-space galaxy clustering. Blue contours add SN data to this combination. The right panel shows confidence contours for the same data combinations in the  $w_0w_a$ CDM model, which assumes a flat Universe and an evolving equation of state with  $w(a) = w_0 + w_a(1 - a)$ .

ysis of the BOSS galaxy data that uses the full shape (FS) of the redshift-space power spectrum and correlation function, modeled via perturbation theory, in addition to the measurement of the BAO scale itself. The full shape analysis improves the constraining power of the data, primarily because measurement of the Alcock-Paczynski effect on sub-BAO scales helps to break the degeneracy between  $D_{A,c}(z)$  and  $H(z)$ . Blue contours show constraints from the full combination of CMB, BAO+FS, and SN data. Supernovae provide fine-grained relative distance measurements with good bin-by-bin precision at  $z < 0.7$  (see Fig. 28.1), which is complementary to BAO for constraining redshift evolution of  $w$ . In both classes of model, the flat  $\Lambda$ CDM parameters ( $w = w_0 = -1$ ,  $\Omega_K = w_a = 0$ ) lie within the 68% confidence contour.

The precision on dark energy parameters depends, of course, on both the data being considered and the flexibility of the model being assumed. For the  $ow$ CDM model and the Planck+BAO+FS+SN data combination, Ref. [38] finds  $w = -1.01 \pm 0.04$ . Assuming a flat Universe and incorporating *Planck* 2018 data and DES Year 1 weak lensing, in addition to BAO and SN, Ref. [33] finds

$$w = -1.028 \pm 0.031. \quad (28.5)$$

We consider either of these results to be a reasonable characterization of current knowledge about the dark energy equation of state. In the  $w_0w_a$ CDM model there is strong degeneracy between  $w_0$  and  $w_a$ , as one can see in Fig. 28.2. However, the value of  $w$  at the pivot redshift  $z_p = 0.29$  is well constrained by the Planck+BAO+FS+SN data combination, with  $w_p = -1.05 \pm 0.06$  [38]. The constraint on the evolution parameter, by contrast, remains poor even with this data combination,  $w_a = -0.39 \pm 0.34$ . For examinations of a wide range of dark energy, dark matter, neutrino content, and modified gravity models, see Refs. [33, 38, 43].

A flat  $\Lambda$ CDM model fit to *Planck* CMB data alone predicts  $H_0 = 67.4 \pm 0.5 \text{ km s}^{-1} \text{ Mpc}^{-1}$  (see Chapter 29 of this *Review*). This prediction and its error bar are sensitive to the assumptions of constant dark energy and a flat Universe. However, by adding BAO and supernova data one can construct an “inverse distance ladder” to measure  $H_0$  precisely, even with a general dark energy model and free curvature [44]. Ref. [45] applies this approach to obtain  $H_0 = 67.8 \pm 1.3 \text{ km s}^{-1} \text{ Mpc}^{-1}$ . As discussed in

Sec. 25.3.1 of this *Review*, recent measurements from low-redshift data yield higher values of  $H_0$ . Figure 28.3 compares the CMB-anchored  $H_0$  estimates cited above to distance-ladder estimates that use Cepheid [46] or tip-of-the-red-giant-branch (TRGB) [47] stars to calibrate SNe Ia luminosities, and to an entirely independent estimate that uses gravitational-lens time delays [48]. The Cepheid and lensing estimates are discrepant with the CMB-anchored estimates at a statistically significant level (Ref. [46] quotes  $4.4\sigma$  relative to *Planck*  $\Lambda$ CDM), while the TRGB calibration yields an intermediate result that is consistent with either the “high” or “low” values of  $H_0$ .

The tension in  $H_0$  could reflect some combination of statistical flukes and systematic errors in one or more of the data sets employed in these analyses. However, if the resolution lies in new physics rather than measurement errors, then this is probably physics that operates in the *pre-recombination* Universe, rescaling the BAO standard ruler in a way that shifts the  $\Lambda$ CDM and inverse-distance-ladder values upward. Models with extra relativistic degrees of freedom or dark energy that is dynamically significant in the early Universe can achieve this effect by increasing the early expansion rate, but they are tightly constrained by the damping tail of CMB anisotropies. A finely tuned model in which early dark energy decays rapidly after recombination can mitigate the tension between CMB data and local  $H_0$  measurements [49], though it still prefers  $H_0$  values below those of Ref. [46].

The amplitude of CMB anisotropies is proportional to the amplitude of density fluctuations present at recombination, and by assuming GR and a specified dark energy model one can extrapolate the growth of structure forward to the present day to predict  $\sigma_8$ . Probes of low-redshift structure yield constraints in the  $(\sigma_8, \Omega_m)$  plane, which can be summarized in terms of the parameter combination  $S_8 \equiv \sigma_8(\Omega_m/0.3)^{0.5}$ . As discussed in earlier editions of this *Review*, many but not all weak-lensing and cluster studies to date yield  $S_8$  values lower than those predicted for *Planck*-normalized  $\Lambda$ CDM. The right panel of Fig. 28.3 illustrates the current state-of-play, comparing a selection of recently published  $S_8$  estimates to the *Planck*+ $\Lambda$ CDM prediction of  $S_8 = 0.832 \pm 0.013$ .

The first four points show cosmic-shear weak-lensing estimates from the Deep Lens Survey [50], KiDS [51], DES [52], and HSC [29]. All of these estimates lie below the *Planck* central value,

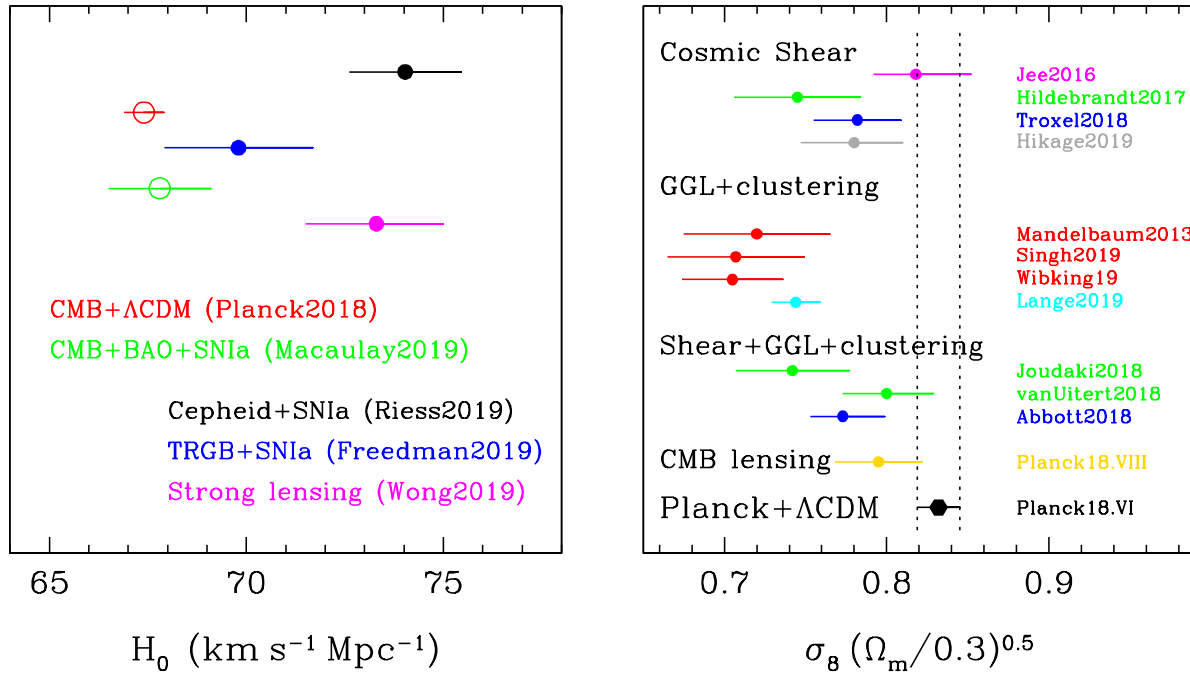


Figure 28.3: Tensions between low-redshift cosmological measurements and the predictions of a CMB-normalized  $\Lambda$ CDM model. All error bars are  $1\sigma$ ; see text for observational references. (Left) Open circles show values of  $H_0$  for flat  $\Lambda$ CDM with *Planck* parameters or a general dark energy model constrained by a combination of CMB, BAO, and supernova data. Filled circles show distance-ladder estimates based on Cepheid or TRGB calibration or an independent estimate using gravitational-lens time delays. (Right) Matter clustering characterized by the parameter combination  $\sigma_8(\Omega_m/0.3)^{0.5}$ , as predicted by a *Planck*-normalized  $\Lambda$ CDM model (vertical dotted lines, black hexagon) and estimated from weak gravitational lensing using cosmic shear, galaxy-galaxy lensing and galaxy clustering, or a combination of the two constraints. Points of the same color are based on the same weak-lensing data. The “CMB lensing” point shows the value of  $\sigma_8$  for  $\Omega_m = 0.3$  inferred from *Planck* CMB lensing, a measurement that is independent of the “Planck+ $\Lambda$ CDM” prediction and weighted to somewhat higher redshift than the other weak-lensing points.

though only the KiDS estimate is discrepant by  $\sim 2\sigma$ . The next four points use galaxy-galaxy lensing in combination with galaxy clustering. Ref. [53] used weak-lensing data from SDSS imaging and the SDSS main galaxy redshift catalog, restricting the analysis to scales well described by perturbation theory. Refs. [54] and [55] used the same weak-lensing data but the BOSS LOWZ galaxy sample, and they employed two quite different approaches to model the clustering and lensing signals into the strongly non-linear regime ( $r \approx 1 h^{-1} \text{Mpc}$ ) so that they could fully exploit the constraining power of the data. Ref. [56] found a strong discrepancy on these non-linear scales between the predictions of a *Planck*-normalized  $\Lambda$ CDM model and the galaxy-galaxy lensing of BOSS CMASS galaxies, measured from 250  $\text{deg}^2$  of deep imaging from the Canada-France-Hawaii Telescope. Ref. [57], plotted in Figure 28.3, revisited these data with a more general modeling approach and showed that the discrepancy persists over a range of redshift and galaxy stellar mass.

The third set of points in this panel shows  $S_8$  estimates that combine cosmic shear with galaxy-galaxy lensing and galaxy clustering (a.k.a. “ $3 \times 2$ ” analyses because they combine three 2-point correlations), restricted to fairly large scales in the perturbative regime. Refs. [58] and [59] use KiDS weak-lensing data but two different galaxy samples; although they are statistically consistent with each other, the difference of their central values illustrates the sensitivity to external data and analysis choices. Ref. [27] presents constraints from the  $3 \times 2$  analysis of the Year 1 DES data, which yields an  $S_8$  value lower than the *Planck* prediction but consistent at the  $\sim 2\sigma$  level.

The “CMB lensing” point shows the matter-clustering amplitude inferred from *Planck* CMB lensing; we have evaluated Eq. (38) of Ref. [60] at  $\Omega_m = 0.3$  and adopted the same fractional error. It is important to emphasize that this is a measurement of low-redshift clustering even though the background being lensed is the CMB. The CMB lensing kernels peak at  $z \lesssim 1$ , with tails to  $z \sim 5$ , so the effective redshift of the  $S_8$  measurement is somewhat

higher than that of the other weak-lensing data points. The result is consistent with the *Planck*+ $\Lambda$ CDM prediction at  $1\sigma$ , and it is also consistent with the lower value corresponding to the mean or median of the optical weak-lensing measurements.

No one of these analyses provides convincing evidence of a conflict with the  $\Lambda$ CDM cosmological model. However, the case for such a conflict has grown stronger as the low inferred clustering amplitude has persisted across multiple statistically independent weak-lensing surveys and multiple analysis methods. One possible explanation is that several of the weak lensing surveys are affected by a common, unrecognized, systematic bias. Another possibility is a true deviation between the clustering growth extrapolated forward from the early Universe and the clustering of matter at late times. The consistency of CMB lensing and Lyman- $\alpha$  forest measurements with  $\Lambda$ CDM clustering predictions suggests that any such deviation sets in mainly at  $z < 1$ , coinciding with the era of cosmic acceleration. Because the expansion history is well constrained by BAO and supernova data, it is difficult to change low-redshift matter clustering by simply changing the equation of state of dark energy. Instead, a deviation between predicted and observed clustering might point towards modified gravity, decaying dark matter, or coupling between dark matter and dark energy.

The next 2–3 years should see rapid progress on this conundrum. As the KiDS, DES, and HSC data sets grow in size, their statistical uncertainties will shrink, which will in turn enable more stringent internal cross-checks that test for consistent results from different redshift ranges, different scales, and different lens and source populations. Modeling methods that exploit non-linear scales will also be more stringently tested. Clusters of galaxies with weak-lensing mass calibration provide an alternative route to  $S_8$  measurement, with competitive statistical precision. Recent cluster-based  $S_8$  estimates span a wide range, some of them consistent with *Planck*+ $\Lambda$ CDM and others implying lower matter clustering, and we have not quoted results here because it is diffi-

cult to decide which are most reliable. However, the opportunity to combine multiple cluster samples with multiple weak-lensing surveys may lead to consistent and convincing measurements in the near future. CMB lensing constraints will improve with higher angular resolution data from the South Pole Telescope and the Atacama Cosmology Telescope and their successors. Finally, the DESI survey will soon allow the first RSD-based measurements of structure growth at the 1–2% level, providing an entirely distinct route to probe the clustering tension hinted at in Fig. 28.3.

## 28.5 Summary and Outlook

Figure 28.2 focuses on model parameter constraints, but to describe the observational situation it is more useful to characterize the precision, redshift range, and systematic uncertainties of the basic expansion and growth measurements. At present, supernova surveys constrain distance ratios at the 1–2% level in redshift bins of width  $\Delta z = 0.1$  over the range  $0 < z < 0.6$ , with larger but still interesting error bars out to  $z \simeq 1.3$ . These measurements are currently limited by systematics tied to photometric calibration, dust reddening, host-galaxy correlations, and possible evolution of the SN population. BAO surveys have measured the absolute distance scale (calibrated to the sound horizon  $r_s$ ) to 4% at  $z = 0.15$ , 1% at  $z = 0.38$  and  $z = 0.61$ , and 2% at  $z = 2.3$ . Multiple studies have used clusters of galaxies or weak-lensing cosmic shear or galaxy-galaxy lensing to measure a parameter combination  $\sigma_8 \Omega_m^\alpha$  with  $\alpha \simeq 0.3\text{--}0.5$ . The estimated errors of the most recent studies, including both statistical contributions and identified systematic uncertainties, are 3–5%. RSD measurements constrain the combination  $f(z)\sigma_8(z)$ , and recent determinations span the redshift range  $0 < z < 0.9$  with typical estimated errors of about 10%. These errors are dominated by statistics, but shrinking them further will require improvements in modeling non-linear effects on small scales. Distance-ladder estimates of  $H_0$  now span a small range, using overlapping data but distinct treatments of key steps; individual studies quote uncertainties of 2–5%, with similar statistical and systematic contributions. *Planck* data and higher resolution ground-based experiments now measure CMB anisotropies with exquisite precision; for example, CMB measurements now constrain the physical size of the BAO sound horizon to 0.2% and the angular scale of the sound horizon to 0.01%.

A flat  $\Lambda$ CDM model with standard radiation and neutrino content can fit the CMB data and the BAO and SN distance measurements to within their estimated uncertainties. The CMB+BAO parameters for this model are in significant tension with some but not all recent measurements of  $H_0$  determined from low-redshift data. The discrepancy could reflect underestimated systematic errors in one or more of the input data sets. If the conflict is real, then it may point to new physics in the pre-recombination Universe that rescales the sound horizon, such as early dark energy or extra relativistic degrees of freedom. Many measurements of low-redshift matter clustering from weak lensing lie below the predictions of a  $\Lambda$ CDM model extrapolated forward from the *Planck* CMB anisotropies. No one analysis presents a convincing conflict, but the difference persists across several independent data sets and analysis methods. If real, this discrepancy could point towards modified gravity, decaying dark matter, or coupling between dark matter and dark energy. However, none of the tensions present in the data yet provides compelling evidence for new physics.

Analyses of the final KiDS and DES weak-lensing data sets and the expanding HSC weak-lensing data set should yield measurements of matter clustering that have sharper statistical precision and more stringent tests of internal consistency. Fully exploiting these data will require further development of accurate models of matter clustering, galaxy clustering, and weak lensing by galaxy clusters into the fully non-linear regime, including robust methods of accounting for uncertainties in the baryonic mass distribution. It will also require further progress on the thorny challenge of photometric redshift calibration so that these uncertainties do not dominate the error budget. Higher signal-to-noise CMB lensing maps cross-correlated with galaxies will provide independent tests that avoid some of the systematic uncertainties of optical weak lensing.  $H_0$  measurements will improve with increasing numbers of Cepheid or TRGB distances to supernova host galaxies, improv-

ing *Gaia* parallaxes of Galactic Cepheids, increasing numbers of strong gravitational-lens time delays, and continued attention to the systematic uncertainties in each method. Improving measurements of the CMB damping tail from ground-based experiments will provide increasingly strong constraints on solutions involving pre-recombination physics.

After beginning operations in early 2020, the DESI galaxy redshift survey will quickly exceed the size of the existing SDSS and BOSS surveys, enabling high precision BAO measurements of expansion history at  $z \approx 0.7\text{--}1.4$  and, for the first time, percent-level measurements of structure growth through RSD. Precise BAO and RSD measurements at higher redshifts will come from DESI Lyman- $\alpha$  forest maps and the HETDEX and Subaru PFS galaxy surveys. The BAO measurements will complement increasingly precise measurements of the relative distance scale at  $z < 1$  from the DES photometric supernova sample and from improved local supernova samples ( $z < 0.1$ ) that provide a low-redshift anchor. Large galaxy samples will also enable more powerful applications of the Alcock-Paczynski effect, which can amplify the power of BAO and supernova distance measurements by converting them to constraints on the expansion rate  $H(z)$ .

The early-to-mid 2020s will see another major leap in observational capabilities with the advent of LSST, *Euclid*, and *WFIRST*. LSST will be the ultimate ground-based optical weak-lensing experiment, measuring several billion galaxy shapes over 20,000 deg<sup>2</sup> of the southern hemisphere sky, and it will detect and monitor many thousands of SNe per year. *Euclid* and *WFIRST* also have weak lensing as a primary science goal, taking advantage of the high angular resolution and extremely stable image quality achievable from space. Both missions plan large spectroscopic galaxy surveys, which will provide better sampling at high redshifts than DESI or PFS because of the lower infrared sky background above the atmosphere. *WFIRST* is also designed to carry out what should be the ultimate supernova cosmology experiment, with deep, high resolution, near-IR observations and the stable calibration achievable with a space platform. The 2020s will also see dramatic advances in CMB lensing from the Simons Observatory and, potentially, CMB-S4 and/or a space-based probe; cross-correlation with galaxy surveys allows precise tomographic measurements of clustering as a function of redshift.

If the anomalies suggested in Fig. 28.3 are real, then the experiments of the 2020s will map out their redshift, scale, and environment dependence in great detail, providing detailed empirical constraints on dynamical dark energy or modified gravity models. If these tensions dissipate with improved measurements, then the experiments of the 2020s will achieve much more stringent tests of the  $\Lambda$ CDM paradigm, with the potential to reveal deviations that are within the statistical uncertainties of current data. The critical clue to the origin of cosmic acceleration could also come from a surprising direction, such as laboratory or solar-system tests that challenge GR, time variation of fundamental “constants,” or anomalous behavior of gravity in some astronomical environments. Experimental advances along these multiple axes could confirm today’s relatively simple, but frustratingly incomplete, “standard model” of cosmology, or they could force yet another radical revision in our understanding of energy, or gravity, or the spacetime structure of the Universe.

## References

- [1] A. Einstein, Sitzungsber. Preuss. Akad. Wiss. Berlin (Math. Phys.), 142 (1917).
- [2] Ya. B. Zel’dovich, A. Krasinski and Ya. B. Zeldovich, Sov. Phys. Usp. **11**, 381 (1968), [Gen. Rel. Grav.40,1557(2008); Usp. Fiz. Nauk95,209(1968)].
- [3] A. Friedman, Z. Phys. **10**, 377 (1922), [Gen. Rel. Grav.31,1991(1999)].
- [4] G. Lemaître, Annales de la Societe Scientifique de Bruxelles **47**, 49 (1927).
- [5] E. Hubble, Proc. Nat. Acad. Sci. **15**, 168 (1929).
- [6] A. Einstein and W. de Sitter, Proc. Nat. Acad. Sci. **18**, 213 (1932).



- [7] For background and definitions, see Big-Bang Cosmology – Sec. 22 of this *Review*.
- [8] A. G. Riess *et al.* (Supernova Search Team), *Astron. J.* **116**, 1009 (1998), [arXiv:astro-ph/9805201].
- [9] S. Perlmutter *et al.* (Supernova Cosmology Project), *Astrophys. J.* **517**, 565 (1999), [arXiv:astro-ph/9812133].
- [10] P. de Bernardis *et al.* (Boomerang), *Nature* **404**, 955 (2000), [arXiv:astro-ph/0004404].
- [11] S. Hanany *et al.*, *Astrophys. J.* **545**, L5 (2000), [arXiv:astro-ph/0005123].
- [12] D. H. Weinberg *et al.*, *Phys. Rept.* **530**, 87 (2013), [arXiv:1201.2434].
- [13] C. Wetterich, *Nucl. Phys.* **B302**, 668 (1988), [arXiv:1711.03844].
- [14] A. Joyce *et al.*, *Phys. Rept.* **568**, 1 (2015), [arXiv:1407.0059].
- [15] S. M. Carroll *et al.*, *Phys. Rev.* **D70**, 043528 (2004), [arXiv:astro-ph/0306438].
- [16] G. R. Dvali, G. Gabadadze and M. Porrati, *Phys. Lett.* **B485**, 208 (2000), [hep-th/0005016].
- [17] C.M. Will, *Living Reviews in Relativity*, **9**, 3 (2006). See also the chapter on Experimental Tests of Gravitational Theory – in this *Review*.
- [18] J. Wang, L. Hui and J. Khoury, *Phys. Rev. Lett.* **109**, 241301 (2012), [arXiv:1208.4612].
- [19] M. Fairbairn and A. Goobar, *Phys. Lett.* **B642**, 432 (2006), [arXiv:astro-ph/0511029]; Y.-S. Song, I. Sawicki and W. Hu, *Phys. Rev.* **D75**, 064003 (2007), [arXiv:astro-ph/0606286]; C. Blake *et al.*, *Mon. Not. Roy. Astron. Soc.* **415**, 2876 (2011), [arXiv:1104.2948].
- [20] T. Baker *et al.*, *Phys. Rev. Lett.* **119**, 25, 251301 (2017), [arXiv:1710.06394].
- [21] E. V. Linder, *Phys. Rev.* **D72**, 043529 (2005), [arXiv:astro-ph/0507263].
- [22] This is essentially the FoM proposed in the Dark Energy Task Force (DETF) report, A. Albrecht *et al.*, [astro-ph/0609591](https://arxiv.org/abs/astro-ph/0609591), though they based their FoM on the area of the 95 in the  $w_0 - w_a$  plane.
- [23] For high accuracy, the impact of acoustic oscillations must be computed with a full Boltzmann code, but the simple integral for  $r_s$  captures the essential physics and the scaling with cosmological parameters.
- [24] R. A. Sunyaev and Ya. B. Zeldovich, *Astrophys. Space Sci.* **7**, 3 (1970).
- [25] D. Weinberg *et al.* (2013), [arXiv:1309.5380].
- [26] C. Alcock and B. Paczynski, *Nature* **281**, 358 (1979).
- [27] T. M. C. Abbott *et al.* (DES), *Phys. Rev.* **D98**, 4, 043526 (2018), [arXiv:1708.01530].
- [28] T. M. C. Abbott *et al.* (DES), *Astrophys. J.* **872**, 2, L30 (2019), [arXiv:1811.02374].
- [29] C. Hikage *et al.* (HSC), *Publ. Astron. Soc. Jap.* **71**, 2, Publications of the Astronomical Society of Japan, Volume 71, Issue 2, April 2019, 43, <https://doi.org/10.1093/pasj/psz010> (2019), [arXiv:1809.09148].
- [30] T. Hamana *et al.* (2019), [arXiv:1906.06041].
- [31] B. Jain *et al.* (2015), [arXiv:1501.07897].
- [32] W. L. Freedman *et al.* (HST), *Astrophys. J.* **553**, 47 (2001), [arXiv:astro-ph/0012376].
- [33] N. Aghanim *et al.* (Planck) (2018), [arXiv:1807.06209].
- [34] M. Betoule *et al.*, *Astron. & Astrophys.* **568**, 22 (2014).
- [35] M. Sullivan *et al.* (SNLS), *Astrophys. J.* **737**, 102 (2011), [arXiv:1104.1444].
- [36] N. Suzuki *et al.* (Supernova Cosmology Project), *Astrophys. J.* **746**, 85 (2012), [arXiv:1105.3470].
- [37] D. M. Scolnic *et al.*, *Astrophys. J.* **859**, 2, 101 (2018), [arXiv:1710.00845].
- [38] S. Alam *et al.* (BOSS), *Mon. Not. Roy. Astron. Soc.* **470**, 3, 2617 (2017), [arXiv:1607.03155].
- [39] F. Beutler *et al.*, *Mon. Not. Roy. Astron. Soc.* **416**, 3017 (2011), [arXiv:1106.3366].
- [40] A. J. Ross *et al.*, *Mon. Not. Roy. Astron. Soc.* **449**, 1, 835 (2015), [arXiv:1409.3242].
- [41] M. Ata *et al.*, *Mon. Not. Roy. Astron. Soc.* **473**, 4, 4773 (2018), [arXiv:1705.06373].
- [42] M. Blomqvist *et al.*, *Astron. Astrophys.* **629**, A86 (2019), [arXiv:1904.03430].
- [43] Planck Collab. 2015 Results XIV, *Astron. & Astrophys.* **594**, A14 (2016).
- [44] E. Aubourg *et al.*, *Phys. Rev.* **D92**, 12, 123516 (2015), [arXiv:1411.1074].
- [45] E. Macaulay *et al.* (DES), *Mon. Not. Roy. Astron. Soc.* **486**, 2, 2184 (2019), [arXiv:1811.02376].
- [46] A. G. Riess *et al.*, *Astrophys. J.* **876**, 1, 85 (2019), [arXiv:1903.07603].
- [47] W.L. Friedman, *Astron. J.* **882** (2019) 34.
- [48] K. C. Wong *et al.* (2019), [arXiv:1907.04869].
- [49] V. Poulin *et al.*, *Phys. Rev. Lett.* **122**, 22, 221301 (2019), [arXiv:1811.04083].
- [50] M. J. Jee *et al.*, *Astrophys. J.* **824**, 2, 77 (2016), [arXiv:1510.03962].
- [51] H. Hildebrandt *et al.*, *Mon. Not. Roy. Astron. Soc.* **465**, 1454 (2017), [arXiv:1606.05338].
- [52] M. A. Troxel *et al.* (DES), *Phys. Rev.* **D98**, 4, 043528 (2018), [arXiv:1708.01538].
- [53] R. Mandelbaum *et al.*, *Mon. Not. Roy. Astron. Soc.* **432**, 1544 (2013), [arXiv:1207.1120].
- [54] S. Singh *et al.*, *Mon. Not. Roy. Astron. Soc.* **491**, 1, 51 (2020), [arXiv:1811.06499].
- [55] B. D. Wibking *et al.*, *Mon. Not. Roy. Astron. Soc.* **492**, 2, 2872 (2020), [arXiv:1907.06293].
- [56] A. Leauthaud *et al.*, *Mon. Not. Roy. Astron. Soc.* **467**, 3, 3024 (2017), [arXiv:1611.08606].
- [57] J. U. Lange *et al.*, *Mon. Not. Roy. Astron. Soc.* **488**, 4, 5771 (2019), [arXiv:1906.08680].
- [58] S. Joudaki *et al.*, *Mon. Not. Roy. Astron. Soc.* **474**, 4, 4894 (2018), [arXiv:1707.06627].
- [59] E. van Uitert *et al.*, *Mon. Not. Roy. Astron. Soc.* **476**, 4, 4662 (2018), [arXiv:1706.05004].
- [60] N. Aghanim *et al.* (Planck) (2018), [arXiv:1807.06210].

## 29. Cosmic Microwave Background

Revised August 2019 by D. Scott (U. of British Columbia) and G.F. Smoot (HKUST; Paris U.; UC Berkeley; LBNL).

### 29.1 Introduction

The energy content in electromagnetic radiation from beyond our Galaxy is dominated by the cosmic microwave background (CMB), discovered in 1965 [1]. The spectrum of the CMB is well described by a blackbody function with  $T = 2.7255$  K. This spectral form is a main supporting pillar of the hot Big Bang model for the Universe. The lack of any observed deviations from a blackbody spectrum constrains physical processes over cosmic history at redshifts  $z \lesssim 10^7$  (see earlier versions of this review).

Currently the key CMB observable is the angular variation in temperature (or intensity) correlations, and to a growing extent polarization [2–4]. Since the first detection of these anisotropies by the Cosmic Background Explorer (*COBE*) satellite [5], there has been intense activity to map the sky at increasing levels of sensitivity and angular resolution by ground-based and balloon-borne measurements. These were joined in 2003 by the first results from NASA’s Wilkinson Microwave Anisotropy Probe (*WMAP*) [6], which were improved upon by analyses of data added every 2 years, culminating in the 9-year results [7]. In 2013 we had the first results [8] from the third generation CMB satellite, ESA’s *Planck* mission [9, 10], which were enhanced by results from the 2015 *Planck* data release [11, 12], and then the final 2018 *Planck* data release [13, 14]. Additionally, CMB anisotropies have been extended to smaller angular scales by ground-based experiments, particularly the Atacama Cosmology Telescope (ACT) [15] and the South Pole Telescope (SPT) [16]. Together these observations have led to a stunning confirmation of the ‘Standard Model of Cosmology.’ In combination with other astrophysical data, the CMB anisotropy measurements place quite precise constraints on a number of cosmological parameters, and have launched us into an era of precision cosmology. With the study of the CMB now past the half-century mark, the program to map temperature anisotropies is effectively wrapping up, and attention is increasingly focussing on polarization measurements as the future arena in which to test fundamental physics.

### 29.2 CMB Spectrum

It is well known that the spectrum of the microwave background is very precisely that of blackbody radiation, whose temperature evolves with redshift as  $T(z) = T_0(1+z)$  in an expanding universe. As a direct test of its cosmological origin, this relationship has been tested by measuring the strengths of emission and absorption lines in high-redshift systems [17].

Measurements of the spectrum are consistent with a blackbody distribution over more than three decades in frequency (there is a claim by ARCADE [18] of a possible unexpected extragalactic emission signal at low frequency, but the interpretation is debated [19]). All viable cosmological models predict a very nearly Planckian spectrum to within the current observational limits. Because of this, measurements of deviations from a blackbody spectrum have received little attention in recent years, with only a few exceptions. However, that situation will eventually change, since proposed experiments (such as PIXIE [20] and PRISM [21]) have the potential to dramatically improve the constraints on energy release in the early Universe. It now seems feasible to probe spectral distortion mechanisms that are *required* in the standard picture, such as those arising from the damping and dissipation of relatively small primordial perturbations, or the average effect of inverse Compton scattering. A more ambitious goal would be to reach the precision needed to detect the residual lines from the cosmological recombination of hydrogen and helium and hence test whether conditions at  $z \gtrsim 1000$  accurately follow those in the standard picture [22].

### 29.3 Description of CMB Anisotropies

Observations show that the CMB contains temperature anisotropies at the  $10^{-5}$  level and polarization anisotropies at the  $10^{-6}$  (and lower) level, over a wide range of angular scales. These anisotropies are usually expressed using a spherical harmonic expansion

of the CMB sky:

$$T(\theta, \phi) = \sum_{\ell m} a_{\ell m} Y_{\ell m}(\theta, \phi) \quad (29.1)$$

(with the linear polarization pattern written in a similar way using the so-called spin-2 spherical harmonics). Increasing angular resolution requires that the expansion goes to higher multipoles. Because there are only very weak phase correlations seen in the CMB sky and since we notice no preferred direction, the vast majority of the cosmological information is contained in the temperature 2-point function, *i.e.*, the variance as a function only of angular separation. Equivalently, the power per unit  $\ln \ell$  is  $\ell \sum_m |a_{\ell m}|^2 / 4\pi$ .

#### 29.3.1 The Monopole

The CMB has a mean temperature of  $T_\gamma = 2.7255 \pm 0.0006$  K ( $1\sigma$ ) [23], which can be considered as the monopole component of CMB maps,  $a_{00}$ . Since all mapping experiments involve difference measurements, they are insensitive to this average level; monopole measurements can only be made with absolute temperature devices, such as the FIRAS instrument on the *COBE* satellite [24]. The measured  $kT_\gamma$  is equivalent to  $0.234$  meV or  $4.60 \times 10^{-10} m_e c^2$ . A blackbody of the measured temperature has a number density  $n_\gamma = (2\zeta(3)/\pi^2) T_\gamma^3 \simeq 411 \text{ cm}^{-3}$ , energy density  $\rho_\gamma = (\pi^2/15) T_\gamma^4 \simeq 4.64 \times 10^{-34} \text{ g cm}^{-3} \simeq 0.260 \text{ eV cm}^{-3}$ , and a fraction of the critical density  $\Omega_\gamma \simeq 5.38 \times 10^{-5}$ .

#### 29.3.2 The Dipole

The largest anisotropy is in the  $\ell = 1$  (dipole) first spherical harmonic, with amplitude  $3.3621 \pm 0.0010$  mK [13]. The dipole is interpreted to be the result of the Doppler boosting of the monopole caused by the Solar System motion relative to the nearly isotropic blackbody field, as broadly confirmed by measurements of the radial velocities of local galaxies (*e.g.*, Ref. [25]); the intrinsic part of the signal is expected to be 2 orders of magnitude smaller (and fundamentally difficult to distinguish). The motion of an observer with velocity  $\beta \equiv v/c$  relative to an isotropic Planckian radiation field of temperature  $T_0$  produces a Lorentz-boosted temperature pattern

$$\begin{aligned} T(\theta) &= T_0(1 - \beta^2)^{1/2} / (1 - \beta \cos \theta) \\ &\simeq T_0 \left[ 1 + \beta \cos \theta + (\beta^2/2) \cos 2\theta + \text{O}(\beta^3) \right]. \end{aligned} \quad (29.2)$$

At every point in the sky, one observes a blackbody spectrum, with temperature  $T(\theta)$ . The spectrum of the dipole has been confirmed to be the differential of a blackbody spectrum [26]. At higher order there are additional effects arising from aberration and from modulation of the anisotropy pattern, which have also been observed [27].

The implied velocity for the Solar System barycenter is  $v = 369.82 \pm 0.11 \text{ km s}^{-1}$ , assuming a value  $T_0 = T_\gamma$ , towards  $(l, b) = (264.021^\circ \pm 0.011^\circ, 48.253^\circ \pm 0.005^\circ)$  [13]. Such a Solar System motion implies a velocity for the Galaxy and the Local Group of galaxies relative to the CMB. The derived value is  $v_{\text{LG}} = 620 \pm 15 \text{ km s}^{-1}$  towards  $(l, b) = (271.9^\circ \pm 2.0^\circ, 29.6^\circ \pm 1.4^\circ)$  [13], where most of the error comes from uncertainty in the velocity of the Solar System relative to the Local Group.

The dipole is a frame-dependent quantity, and one can thus determine the ‘CMB frame’ (in some sense this is a special frame) as that in which the CMB dipole would be zero. Any velocity of the receiver relative to the Earth and the Earth around the Sun is removed for the purposes of CMB anisotropy studies, while our velocity relative to the Local Group of galaxies and the Local Group’s motion relative to the CMB frame are normally removed for cosmological studies. The dipole is now routinely used as a primary calibrator for mapping experiments, either via the time-varying orbital motion of the Earth, or through the cosmological dipole measured by satellite experiments.

#### 29.3.3 Higher-Order Multipoles

The variations in the CMB temperature maps at higher multipoles ( $\ell \geq 2$ ) are interpreted as being mostly the result of per-

turbations in the density of the early Universe, manifesting themselves at the epoch of the last scattering of the CMB photons. In the hot Big Bang picture, the expansion of the Universe cools the plasma so that by a redshift  $z \simeq 1100$  (with little dependence on the details of the model), the hydrogen and helium nuclei can bind electrons into neutral atoms, a process usually referred to as recombination [28]. Before this epoch, the CMB photons were tightly coupled to the baryons, while afterwards they could freely stream towards us. By measuring the  $a_{\ell m}$ s we are thus learning directly about physical conditions in the early Universe.

A statistically-isotropic sky means that all  $m$ s are equivalent, *i.e.*, there is no preferred axis, so that the temperature correlation function between two positions on the sky depends only on angular separation and not orientation. Together with the assumption of Gaussian statistics (*i.e.*, no correlations between the modes), the 2-point function of the temperature field (or equivalently the power spectrum in  $\ell$ ) then fully characterizes the anisotropies. The power summed over all  $m$ s at each  $\ell$  is  $(2\ell+1)C_\ell/(4\pi)$ , where  $C_\ell \equiv \langle |a_{\ell m}|^2 \rangle$ . Thus averages of  $a_{\ell m}$ s over  $m$  can be used as estimators of the  $C_\ell$ s to constrain their expectation values, which are the quantities predicted by a theoretical model. For an idealized full-sky observation, the variance of each measured  $C_\ell$  (*i.e.*, the variance of the variance) is  $[2/(2\ell+1)]C_\ell^2$ . This sampling uncertainty (known as ‘cosmic variance’) comes about because each  $C_\ell$  is  $\chi^2$  distributed with  $(2\ell+1)$  degrees of freedom for our observable volume of the Universe. For fractional sky coverage,  $f_{\text{sky}}$ , this variance is increased by  $1/f_{\text{sky}}$  and the modes become partially correlated.

It is important to understand that theories predict the expectation value of the power spectrum, whereas our sky is a single realization. Hence the cosmic variance is an unavoidable source of uncertainty when constraining models; it dominates the scatter at lower  $\ell$ s, while the effects of instrumental noise and resolution dominate at higher  $\ell$ s [29].

Theoretical models generally predict that the  $a_{\ell m}$  modes are Gaussian random fields to high precision, matching the empirical tests, *e.g.*, standard slow-roll inflation’s non-Gaussian contribution is expected to be at least an order of magnitude below current observational limits [30]. Although non-Gaussianity of various forms is possible in early Universe models, tests show that Gaussianity is an extremely good simplifying approximation [31]. The only current indications of any non-Gaussianity or statistical anisotropy are some relatively weak signatures at large scales, seen in both *WMAP* [32] and *Planck* data [33], but not of high enough significance to reject the simplifying assumption. Nevertheless, models that deviate from the inflationary slow-roll conditions can have measurable non-Gaussian signatures. So while the current observational limits make the power spectrum the dominant probe of cosmology, it is worth noting that higher-order correlations are becoming a tool for constraining otherwise viable theories.

### 29.3.4 Angular Resolution and Binning

There is no one-to-one conversion between multipole  $\ell$  and the angle subtended by a particular spatial scale projected onto the sky. However, a single spherical harmonic  $Y_{\ell m}$  corresponds to angular variations of  $\theta \sim \pi/\ell$ . CMB maps contain anisotropy information from the size of the map (or in practice some fraction of that size) down to the beam-size of the instrument,  $\sigma$  (the standard deviation of the beam, in radians). One can think of the effect of a Gaussian beam as rolling off the power spectrum with the function  $e^{-\ell(\ell+1)\sigma^2}$ .

For less than full sky coverage, the  $\ell$  modes become correlated. Hence, experimental results are usually quoted as a series of ‘band powers,’ defined as estimators of  $\ell(\ell+1)C_\ell/2\pi$  over different ranges of  $\ell$ . Because of the strong foreground signals in the Galactic plane, even ‘all-sky’ surveys, such as *WMAP* and *Planck*, involve a cut sky. The amount of binning required to obtain uncorrelated estimates of power also depends on the map size.

## 29.4 Cosmological Parameters

The current ‘Standard Model’ of cosmology contains around 10 free parameters, only six of which are required to have non-null values (see The Cosmological Parameters—Sec. 25.1 of this *Re-*

*view*). The basic framework is the Friedmann-Robertson-Walker (FRW) metric (*i.e.*, a universe that is approximately homogeneous and isotropic on large scales), with density perturbations laid down at early times and evolving into today’s structures (see Big-Bang cosmology—Sec. 22 of this *Review*). The most general possible set of density variations is a linear combination of an adiabatic density perturbation and some isocurvature perturbations. Adiabatic means that there is no change to the entropy per particle for each species, *i.e.*,  $\delta\rho/\rho$  for matter is  $(3/4)\delta\rho/\rho$  for radiation. Isocurvature means that the set of individual density perturbations adds to zero, for example, matter perturbations compensate radiation perturbations so that the total energy density remains unperturbed, *i.e.*,  $\delta\rho$  for matter is  $-\delta\rho$  for radiation. These different modes give rise to distinct (temporal) phases during growth, with those of the adiabatic scenario being fully consistent with the data. Models that generate mainly isocurvature type perturbations (such as most topological defect scenarios) are not viable. However, an admixture of the adiabatic mode with up to 1.7% isocurvature contribution (depending on details of the mode) is still allowed [34].

### 29.4.1 Initial Condition Parameters

Within the adiabatic family of models, there is, in principle, a free function describing the variation of comoving curvature perturbations,  $\mathcal{R}(\mathbf{x}, t)$ . The great virtue of  $\mathcal{R}$  is that, on large scales, it is constant in time on super-horizon scales for a purely adiabatic perturbation. There are physical reasons to anticipate that the variance of these perturbations will be described well by a power law in scale, *i.e.*, in Fourier space  $\langle |\mathcal{R}|_k^2 \rangle \propto k^{n_s-4}$ , where  $k$  is wavenumber and  $n_s$  is spectral index as usually defined. So-called ‘scale-invariant’ initial conditions (meaning gravitational potential fluctuations that are independent of  $k$ ) correspond to  $n_s = 1$ . In inflationary models [35] (see Inflation—Sec. 23 of this *Review*), perturbations are generated by quantum fluctuations, which are set by the energy scale of inflation, together with the slope and higher derivatives of the inflationary potential. One generally expects that the Taylor series expansion of  $\ln \mathcal{R}_k(\ln k)$  has terms of steadily decreasing size. For the simplest models, there are thus two parameters describing the initial conditions for density perturbations, namely the amplitude and slope of the power spectrum. These can be explicitly defined, for example, through

$$\mathcal{P}_{\mathcal{R}}^2 \equiv k^3 \langle |\mathcal{R}|_k^2 \rangle / 2\pi^2 \simeq A_s (k/k_0)^{n_s-1}, \quad (29.3)$$

with  $A_s \equiv \mathcal{P}_{\mathcal{R}}^2(k_0)$  and  $k_0 = 0.05 \text{ Mpc}^{-1}$ , say. There are other equally valid definitions of the amplitude parameter (see also Secs. 22, 23, and 25.1 of this *Review*), and we caution that the relationships between some of them can be cosmology-dependent. In slow-roll inflationary models, this normalization is proportional to the combination  $V^3/(V')^2$ , for the inflationary potential  $V(\phi)$ . The slope  $n_s$  also involves  $V''$ , and so the combination of  $A_s$  and  $n_s$  can constrain potentials.

Inflation generates tensor (gravitational wave) modes, as well as scalar (density perturbation) modes. This fact introduces another parameter, measuring the amplitude of a possible tensor component, or equivalently the ratio of the tensor to scalar contributions. The tensor amplitude is  $A_t \propto V$ , and thus one expects a larger gravitational wave contribution in models where inflation happens at higher energies. The tensor power spectrum also has a slope, often denoted  $n_t$ , but since this seems unlikely to be measured in the near future (and there is also a consistency relation with tensor amplitude), it is sufficient for now to focus only on the amplitude of the gravitational wave component. It is most common to define the tensor contribution through  $r$ , the ratio of tensor to scalar perturbation spectra at some fixed value of  $k$  (*e.g.*,  $k = 0.002 \text{ Mpc}^{-1}$ , although it was historically defined in terms of the ratio of contributions at  $\ell = 2$ ). Different inflationary potentials will lead to different predictions, *e.g.*, for 50 e-folds  $\lambda\phi^4$  inflation gives  $r = 0.32$  and  $m^2\phi^2$  inflation gives  $r = 0.16$  (both now disfavored by the data), while other models can have arbitrarily small values of  $r$ . In any case, whatever the specific definition, and whether they come from inflation or something else, the ‘initial conditions’ give rise to a minimum of three parameters,  $A_s$ ,  $n_s$ , and  $r$ .

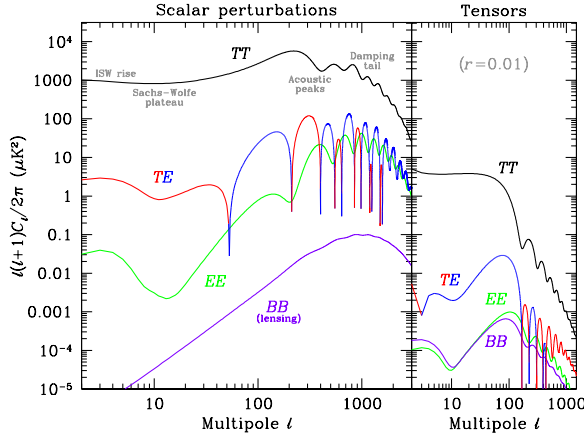


Figure 29.1: Theoretical CMB anisotropy power spectra, using the best-fitting  $\Lambda$ CDM model from *Planck*, calculated using CAMB. The panel on the left shows the theoretical expectation for scalar perturbations, while the panel on the right is for tensor perturbations, with an amplitude set to  $r = 0.01$  for illustration. Note that the horizontal axis is logarithmic here. For the well-measured scalar  $TT$  spectrum, the regions, each covering roughly a decade in  $\ell$ , are labeled as in the text: the ISW rise; Sachs-Wolfe plateau; acoustic peaks; and damping tail. The  $TE$  cross-correlation power spectrum changes sign, and that has been indicated by plotting the absolute value, but switching color for the negative parts.

### 29.4.2 Background Cosmology Parameters

The FRW cosmology requires an expansion parameter (the Hubble constant,  $H_0$ , often represented through  $H_0 = 100 h \text{ km s}^{-1} \text{ Mpc}^{-1}$ ) and several parameters to describe the matter and energy content of the Universe. These are usually given in terms of the critical density, *i.e.*, for species ‘x,’  $\Omega_x \equiv \rho_x / \rho_{\text{crit}}$ , where  $\rho_{\text{crit}} \equiv 3H_0^2 / 8\pi G$ . Since physical densities  $\rho_x \propto \Omega_x h^2 \equiv \omega_x$  are what govern the physics of the CMB anisotropies, it is these  $\omega$ s that are best constrained by CMB data. In particular, CMB observations constrain  $\Omega_b h^2$  for baryons and  $\Omega_c h^2$  for cold dark matter (with  $\rho_m = \rho_c + \rho_b$  for the sum).

The contribution of a cosmological constant  $\Lambda$  (or other form of dark energy, see Dark Energy—Sec. 28) is usually included together with a parameter that quantifies the curvature,  $\Omega_K \equiv 1 - \Omega_{\text{tot}}$ , where  $\Omega_{\text{tot}} = \Omega_m + \Omega_\Lambda$ . The radiation content, while in principle a free parameter, is precisely enough determined by the measurement of  $T_\gamma$  that it can be considered fixed, and makes a  $< 10^{-4}$  contribution to  $\Omega_{\text{tot}}$  today.

Astrophysical processes at relatively low redshift can also affect the  $C_\ell$ s, with a particularly significant effect coming through reionization. The Universe became reionized at some redshift  $z_i$ , long after recombination, affecting the CMB through the integrated Thomson scattering optical depth:

$$\tau = \int_0^{z_i} \sigma_T n_e(z) \frac{dt}{dz} dz, \quad (29.4)$$

where  $\sigma_T$  is the Thomson cross-section,  $n_e(z)$  is the number density of free electrons (which depends on astrophysics), and  $dt/dz$  is fixed by the background cosmology. In principle,  $\tau$  can be determined from the small-scale matter power spectrum, together with the physics of structure formation and radiative feedback processes; however, this is a sufficiently intricate calculation that in practice  $\tau$  needs to be considered as a free parameter.

Thus, we have eight basic cosmological parameters:  $A_s$ ,  $n_s$ ,  $r$ ,  $h$ ,  $\Omega_b h^2$ ,  $\Omega_c h^2$ ,  $\Omega_{\text{tot}}$ , and  $\tau$ . One can add additional parameters to this list, particularly when using the CMB in combination with other data sets. The next most relevant ones might be:  $\Omega_\nu h^2$ , the massive neutrino contribution;  $w$  ( $\equiv p/\rho$ ), the equation of state parameter for the dark energy; and  $dn_s/d \ln k$ , measuring deviations from a constant spectral index. To these 11 one could of course add further parameters describing additional physics, such as details of the reionization process, features in the ini-

tial power spectrum, a sub-dominant contribution of isocurvature modes, *etc.*

As well as these underlying parameters, there are other (dependent) quantities that can be obtained from them. Such derived parameters include the actual  $\Omega$ s of the various components (*e.g.*,  $\Omega_m$ ), the variance of density perturbations at particular scales (*e.g.*,  $\sigma_8$ ), the angular scale of the sound horizon ( $\theta_*$ ), the age of the Universe today ( $t_0$ ), the age of the Universe at recombination, reionization, *etc.* (see The Cosmological Parameters—Sec. 25.1).

## 29.5 Physics of Anisotropies

The cosmological parameters affect the anisotropies through the well understood physics of the evolution of linear perturbations within a background FRW cosmology. There are very effective, fast, and publicly-available software codes for computing the CMB temperature, polarization, and matter power spectra, *e.g.*, CMBFAST [36], CAMB [37], and CLASS [38]. These have been tested over a wide range of cosmological parameters and are considered to be accurate to much better than the 1% level [39], so that numerical errors are less than 10% of the parameter uncertainties for *Planck* [8].

For pedagogical purposes, it is easiest to focus on the temperature anisotropies, before moving to the polarization power spectra. A description of the physics underlying the  $C_\ell^{TT}$ s can be separated into four main regions (the first two combined below), as shown in the top left part of Fig. 29.1.

### 29.5.1 The ISW Rise, $\ell \lesssim 10$ , and Sachs-Wolfe Plateau, $10 \lesssim \ell \lesssim 100$

The horizon scale (or more precisely, the angle subtended by the Hubble radius) at last scattering corresponds to  $\ell \simeq 100$ . Anisotropies at larger scales have not evolved significantly, and hence directly reflect the ‘initial conditions.’ Temperature variations are  $\delta T/T = -(1/5)\mathcal{R}(\mathbf{x}_{\text{LSS}}) \simeq (1/3)\delta\phi/c^2$ , where  $\delta\phi$  is the perturbation to the gravitational potential, evaluated on the last scattering surface (LSS). This is a result of the combination of gravitational redshift and intrinsic temperature fluctuations, and is usually referred to as the Sachs-Wolfe effect [40].

Assuming that a nearly scale-invariant spectrum of curvature and corresponding density perturbations was laid down at early times (*i.e.*,  $n_s \simeq 1$ , meaning equal power per decade in  $k$ ), then  $\ell(\ell+1)C_\ell \simeq \text{constant}$  at low  $\ell$ s. This effect is hard to see unless the multipole axis is plotted logarithmically (as in Fig. 29.1, and part of Fig. 29.2).

Time variation of the potentials (*i.e.*, time-dependent metric perturbations) at late times leads to an upturn in the  $C_\ell$ s in the lowest several multipoles; any deviation from a total equation of state  $w = 0$  has such an effect. So the dominance of the dark energy at low redshift (see Dark Energy—Sec. 28) makes the lowest  $\ell$ s rise above the plateau. This is usually called the integrated Sachs-Wolfe effect (or ISW rise), since it comes from the line integral of  $\dot{\phi}$ ; it has been confirmed through correlations between the large-angle anisotropies and large-scale structure [41, 42]. Specific models can also give additional contributions at low  $\ell$  (*e.g.*, perturbations in the dark-energy component itself [43]), but typically these are buried in the cosmic variance.

In principle, the mechanism that produces primordial perturbations could generate scalar, vector, and tensor modes. However, the vector (vorticity) modes decay with the expansion of the Universe. The tensors (transverse trace-free perturbations to the metric) generate temperature anisotropies through the integrated effect of the locally-anisotropic expansion of space. Since the tensor modes also redshift away after they enter the horizon, they contribute only to angular scales above about  $1^\circ$  (see Fig. 29.1). Hence some fraction of the low- $\ell$  signal could be due to a gravitational wave contribution, although small amounts of tensors are essentially impossible to discriminate from other effects that might raise the level of the plateau. Nevertheless, the tensors *can* be distinguished using polarization information (see Sec. ??).

### 29.5.2 The Acoustic Peaks, $100 \lesssim \ell \lesssim 1000$

On sub-degree scales, the rich structure in the anisotropy spectrum is the consequence of gravity-driven acoustic oscillations oc-

curing before the atoms in the Universe became neutral [44]. Perturbations inside the horizon at last scattering have been able to evolve causally and produce anisotropy at the last-scattering epoch, which reflects this evolution. The frozen-in phases of these sound waves imprint a dependence on the cosmological parameters, which gives CMB anisotropies their great constraining power.

The underlying physics can be understood as follows. Before the Universe became neutral, the proton-electron plasma was tightly coupled to the photons, and these components behaved as a single ‘photon-baryon fluid.’ Perturbations in the gravitational potential, dominated by the dark-matter component, were steadily evolving. They drove oscillations in the photon-baryon fluid, with photon pressure providing most of the restoring force and baryons giving some additional inertia. The perturbations were quite small in amplitude,  $\mathcal{O}(10^{-5})$ , and so evolved linearly. That means each Fourier mode developed independently, and hence can be described as a driven harmonic oscillator, with frequency determined by the sound speed in the fluid. Thus the fluid density underwent oscillations, giving time variations in temperature. These combine with a velocity effect, which is  $\pi/2$  out of phase and has its amplitude reduced by the sound speed.

After the Universe recombined, the radiation decoupled from the baryons and could travel freely towards us. At that point, the (temporal) phases of the oscillations were frozen-in, and became projected on the sky as a harmonic series of peaks. The main peak is the mode that went through 1/4 of a period, reaching maximal compression. The even peaks are maximal *under*-densities, which are generally of smaller amplitude because the rebound has to fight against the baryon inertia. The troughs, which do not extend to zero power, are partially filled by the Doppler effect because they are at the velocity maxima.

The physical length scale associated with the peaks is the sound horizon at last scattering, which can be straightforwardly calculated. This length is projected onto the sky, leading to an angular scale that depends on the geometry of space, as well as the distance to last scattering. Hence the angular position of the peaks is a sensitive probe of a particular combination of cosmological parameters. In fact, the angular scale,  $\theta_*$ , is the most precisely measured observable, and hence is usually treated as an element of the cosmological parameter set.

One additional effect arises from reionization at redshift  $z_i$ . A fraction of photons ( $\tau$ ) will be isotropically scattered at  $z < z_i$ , partially erasing the anisotropies at angular scales smaller than those subtended by the Hubble radius at  $z_i$ . This corresponds typically to  $\ell$ s above about 10, depending on the specific reionization model. The acoustic peaks are therefore reduced by a factor  $e^{-2\tau}$  relative to the plateau.

These peaks were a clear theoretical prediction going back to about 1970 [45]. One can think of them as a snapshot of stochastic standing waves. Since the physics governing them is simple and their structure rich, one can see how they encode extractable information about the cosmological parameters. Their empirical existence started to become clear around 1994 [46], and the emergence, over the following decade, of a coherent series of acoustic peaks and troughs is a triumph of modern cosmology. This picture has received further confirmation with the detection in the power spectrum of galaxies (at redshifts  $z \lesssim 1$ ) of the imprint of these same acoustic oscillations in the baryon component [47], as well as through detection of the expected oscillations in CMB polarization power spectra (see Sec. 29.7).

### 29.5.3 The Damping Tail, $\ell \gtrsim 1000$

The recombination process is not instantaneous, which imparts a thickness to the last-scattering surface. This leads to a damping of the anisotropies at the highest  $\ell$ s, corresponding to scales smaller than that subtended by this thickness. One can also think of the photon-baryon fluid as having imperfect coupling, so that there is diffusion between the two components, and hence the amplitudes of the oscillations decrease with time. These effects lead to a damping of the  $C_{\ell s}$ , sometimes called Silk damping [48], which cuts off the anisotropies at multipoles above about 2000. So, although in principle it is possible to measure to ever smaller scales, this becomes increasingly difficult in practice.

### 29.5.4 Gravitational Lensing Effects

An extra effect at high  $\ell$ s comes from gravitational lensing, caused structures at low redshift along the line of sight to the last-scattering surface. The  $C_{\ell s}$  are convolved with a smoothing function in a calculable way, partially flattening the peaks and troughs, generating a power-law tail at the highest multipoles, and complicating the polarization signal [49]. The expected effects of lensing on the CMB have been definitively detected through the 4-point function, which correlates temperature gradients and small-scale anisotropies (enabling a map of the lensing potential to be constructed [50]), as well as through the smoothing effect on the shape of the  $C_{\ell s}$ . Lensing is important because it gives an independent estimate of  $A_s$ , breaking the parameter combination  $A_s e^{-2\tau}$  that is largely degenerate in the temperature anisotropy power spectra.

Lensing is an example of a ‘secondary effect,’ *i.e.*, the processing of anisotropies due to relatively nearby structures (see Sec. 29.8.2). Galaxies and clusters of galaxies give several such effects; all are expected to be of low amplitude, but are increasingly important at the highest  $\ell$ s. Such effects carry additional cosmological information (about evolving gravitational potentials in the low-redshift Universe) and are receiving more attention as experiments push to higher sensitivity and angular resolution. The lensing power spectrum can potentially constrain dark-energy evolution, while future measurements at high  $\ell$  are a particularly sensitive probe of the sum of the neutrino masses [51].

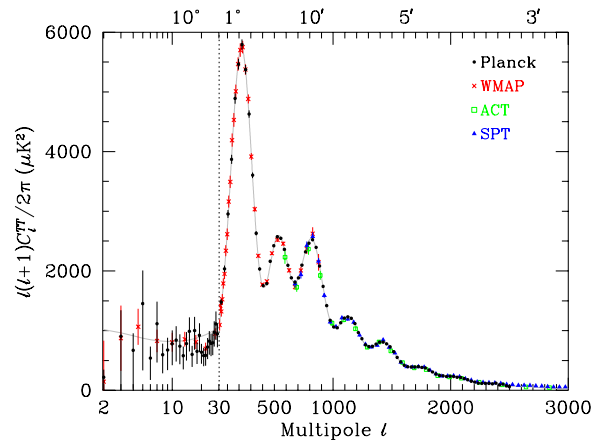


Figure 29.2: CMB temperature anisotropy band-power estimates from the *Planck*, *WMAP*, ACT, and SPT experiments. Note that the widths of the  $\ell$ -bands vary between experiments and have not been plotted. This figure represents only a selection of the most recent available experimental results, and some points with large error bars have been omitted. At the higher multipoles these band-powers involve subtraction of particular foreground models, and so proper analysis requires simultaneous fitting of CMB and foregrounds over multiple frequencies. The horizontal axis here is logarithmic for the lowest multipoles, to show the Sachs-Wolfe plateau, and linear for the other multipoles. The acoustic peaks and damping region are very clearly observed, with no need for a theoretical line to guide the eye; however, the curve plotted is the best-fit *Planck*  $\Lambda$ CDM model.

## 29.6 Current Temperature Anisotropy Data

There has been a steady improvement in the quality of CMB data that has led to the development of the present-day cosmological model. The most robust constraints currently available come from *Planck* satellite [52] [53] data (together with constraints from non-CMB cosmological data sets), although smaller-scale results from the ACT [54] and SPT [55] experiments are beginning to add useful constraining power. We plot power spectrum estimates from these experiments in Fig. 29.2, along with *WMAP* data [7] to show the consistency (see previous versions of this review for data from earlier experiments). Comparisons among data sets show consistency, both in maps and in derived power spectra (up



to systematic uncertainties in the overall calibration for some experiments). This makes it clear that systematic effects are largely under control.

The band-powers shown in Fig. 29.2 are in very good agreement with a ‘ $\Lambda$ CDM’ model. As described earlier, several (at least seven) of the peaks and troughs are quite apparent. For details of how these estimates were arrived at, the strength of correlations between band-powers, and other information required to properly interpret them, the original papers should be consulted.

## 29.7 CMB Polarization

Thomson scattering of an anisotropic radiation field also generates linear polarization and the CMB is predicted to be polarized, at the level of roughly 5% of the temperature anisotropies [56]. Polarization is a spin-2 field on the sky, and the algebra of the modes in  $\ell$ -space is strongly analogous to spin-orbit coupling in quantum mechanics [57]. The linear polarization pattern can be decomposed in a number of ways, with two quantities required for each pixel in a map, often given as the  $Q$  and  $U$  Stokes parameters. However, the most intuitive and physical decomposition is a geometrical one, splitting the polarization pattern into a part that comes from a divergence (often referred to as the ‘ $E$  mode’) and a part with a curl (called the ‘ $B$  mode’) [58]. More explicitly, the modes are defined in terms of second derivatives of the polarization amplitude, with the Hessian for the  $E$  modes having principal axes in the same sense as the polarization, while the  $B$ -mode pattern can be thought of as a  $45^\circ$  rotation of the  $E$ -mode pattern. Globally one sees that the  $E$  modes have  $(-1)^\ell$  parity (like the spherical harmonics), while the  $B$  modes have  $(-1)^{\ell+1}$  parity.

The existence of this linear polarization allows for six different cross-power spectra to be determined from data that measure the full temperature and polarization anisotropy information. Parity considerations make two of these zero, and we are left with four potential observables,  $C_\ell^{TT}$ ,  $C_\ell^{TE}$ ,  $C_\ell^{EE}$ , and  $C_\ell^{BB}$  (see Fig. 29.1). Because scalar perturbations have no handedness, the  $B$ -mode power spectrum can only be sourced by vectors or tensors. Moreover, since inflationary scalar perturbations give only  $E$  modes, while tensors generate roughly equal amounts of  $E$  and  $B$  modes, then the determination of a non-zero  $B$ -mode signal is a way to measure the gravitational-wave contribution (and thus potentially derive the energy scale of inflation). However, since the signal is expected to be rather weak, one must first eliminate the foreground contributions and other systematic effects down to very low levels. In addition, CMB lensing creates  $B$  modes from  $E$  modes, further complicating the extraction of a tensor signal.

Like with temperature, the polarization  $C_\ell$ s exhibit a series of acoustic peaks generated by the oscillating photon-baryon fluid. The main ‘ $EE$ ’ power spectrum has peaks that are out of phase with those in the ‘ $TT$ ’ spectrum because the polarization anisotropies are sourced by the fluid velocity. The ‘ $TE$ ’ part of the polarization and temperature patterns comes from correlations between density and velocity perturbations on the last-scattering surface, which can be both positive and negative, and is of larger amplitude than the  $EE$  signal. There is no polarization Sachs-Wolfe effect, and hence no large-angle plateau. However, scattering during a recent period of reionization can create a polarization ‘bump’ at large angular scales.

Because the polarization anisotropies have only a small fraction of the amplitude of the temperature anisotropies, they took longer to detect. The first measurement of a polarization signal came in 2002 from the DASI experiment [59], which provided a convincing detection, confirming the general paradigm, but of low enough significance that it lent no real constraint to models. Despite dramatic progress since then, it is still the case that polarization data mainly support the basic paradigm, while reducing error bars on parameters by only around 20%. However, there are exceptions to this, specifically in the reionization optical depth, and the potential to constrain primordial gravitational waves. Moreover the situation is expected to change dramatically as more of the available polarization modes are measured.

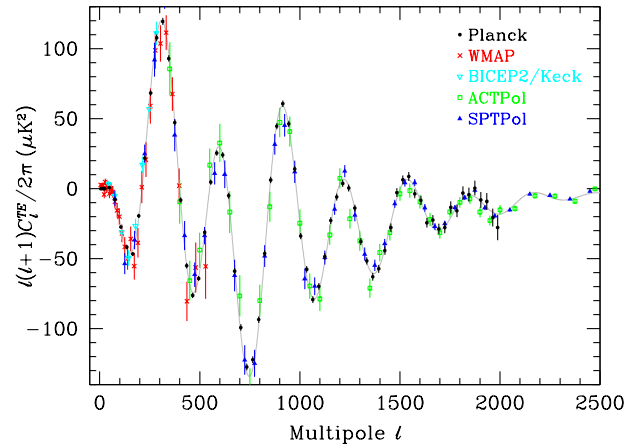


Figure 29.3: Cross-power spectrum band-powers of the temperature anisotropies and  $E$ -mode polarization signal from *Planck* (the low multipole data have been binned here), as well as *WMAP*, *BICEP2/Keck*, *ACTPol*, and *SPTPol*. The curve is the best fit to the *Planck* temperature, polarization, and lensing band-powers. Note that each band-power is an average over a range of multipoles, and hence to compare in detail with a model one has to integrate the theoretical curve through the band.

### 29.7.1 $T$ - $E$ Power Spectrum

Since the  $T$  and  $E$  skies are correlated, one has to measure the  $TE$  power spectrum, as well as  $TT$  and  $EE$ , in order to extract all the cosmological information. This  $TE$  signal has now been mapped out extremely accurately by *Planck* [53], and these band-powers are shown in Fig. 29.3, along with those from *WMAP* [60] and *BICEP2/Keck* [61], with *ACTPol* [62] [63] and *SPTPol* [64] extending to smaller angular scales. The anti-correlation at  $\ell \approx 150$  and the peak at  $\ell \approx 300$  were the first features to become distinct, but now a whole series of oscillations is clearly seen in this power spectrum (including at least six peaks and troughs [13]). The measured shape of the cross-correlation power spectrum provides supporting evidence for the general cosmological picture, as well as directly constraining the thickness of the last-scattering surface. Since the polarization anisotropies are generated in this scattering surface, the existence of correlations at angles above about a degree demonstrates that there were super-Hubble fluctuations at the recombination epoch. The sign of this correlation also confirms the adiabatic paradigm.

The overall picture of the source of CMB polarization and its oscillations has also been confirmed through tests that average the maps around both temperature hot spots and cold spots [65]. One sees precisely the expected patterns of radial and tangential polarization configurations, as well as the phase shift between polarization and temperature. This leaves no doubt that the oscillation picture is the correct one and that the polarization is coming from Thomson scattering at  $z \approx 1100$ .

### 29.7.2 $E$ - $E$ Power Spectrum

Experimental band-powers for  $C_\ell^{EE}$  from *Planck*, *WMAP*, *BICEP2/Keck Array* [61], *ACTPol* [63], and *SPTPol* [64] are shown in Fig. 29.4. Without the benefit of correlating with the temperature anisotropies (*i.e.*, measuring  $C_\ell^{TE}$ ), the polarization anisotropies are very weak and challenging to measure. Nevertheless, the oscillatory pattern is now well established and the data closely match the  $TT$ -derived theoretical prediction. In Fig. 29.4 one can clearly see the ‘shoulder’ expected at  $\ell \approx 140$ , the first main peak at  $\ell \approx 400$  (corresponding to the first trough in  $C_\ell^{TT}$ ), and the series of oscillations that is out of phase with those of the temperature anisotropy power spectrum (including four or five peaks and troughs [13]).

Perhaps the most unique result from the polarization measurements is at the largest angular scales ( $\ell < 10$ ) in  $C_\ell^{TE}$  and  $C_\ell^{EE}$ , where there is evidence for an excess signal (not visible in Fig. 29.4) compared to that expected from the temperature power

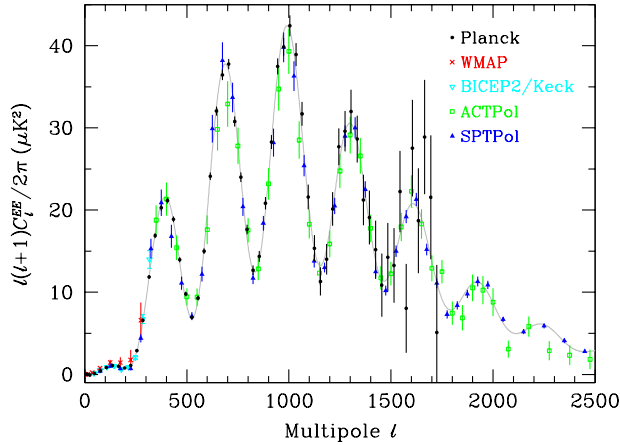


Figure 29.4: Power spectrum of  $E$ -mode polarization from *Planck*, together with *WMAP*, BICEP2/Keck, ACTPol, and SPTPol. Note that some band-powers with larger uncertainties have been omitted and that the unbinned *Planck* low- $\ell$  data have been binned here. Also plotted is the best-fit theoretical model from *Planck* temperature, polarization, and lensing data.

spectrum alone. This is precisely the signal anticipated from an early period of reionization, arising from Doppler shifts during the partial scattering at  $z < z_i$ . The amplitude of the signal indicates that the first stars, presumably the source of the ionizing radiation, formed around  $z \simeq 8$  (although the uncertainty is still quite large). Since this corresponds to scattering optical depth  $\tau \simeq 0.06$ , then roughly 6% of CMB photons were re-scattered at the reionization epoch, with the other 94% last scattering at  $z \simeq 1100$ . However, estimates of the amplitude of this reionization excess have come down since the first measurements by *WMAP* (indicating that this is an extremely difficult measurement to make) and the latest *Planck* results have reduced the value further [14].

### 29.7.3 $B$ - $B$ Power Spectrum

The expected amplitude of  $C_\ell^{BB}$  is very small, and so measurements of this polarization curl-mode are extremely challenging. The first indication of the existence of the  $BB$  signal came from the detection of the expected conversion of  $E$  modes to  $B$  modes by gravitational lensing, through a correlation technique using the lensing potential and polarization measurements from SPT [66]. However, the real promise of  $B$  modes lies in the detection of primordial gravitational waves at larger scales. This tensor signature could be seen either in the ‘recombination bump’ at around  $\ell = 100$  (caused by an ISW effect as gravitational waves redshift away at the last-scattering epoch) or the ‘reionization bump’ at  $\ell \lesssim 10$  (from additional scattering at low redshifts).

Results from the BICEP-2 experiment [67] in 2014 suggested a detection of the primordial  $B$ -mode signature around the recombination peak. BICEP-2 mapped a small part of the CMB sky with the best sensitivity level reached at that time (below 100 nK), but at a single frequency. Higher frequency data from *Planck* indicated that much of the BICEP2 signal was due to dust within our Galaxy, and a combined analysis by the BICEP-2, Keck Array, and *Planck* teams [68] indicated that the data are consistent with no primordial  $B$  modes. The current constraint from *Planck* data alone is  $r < 0.10$  (95% [14]) and this limit is reduced to  $r < 0.06$  with the inclusion of Keck Array data at 95 GHz [69].

Several experiments are continuing to push down the sensitivity of  $B$ -mode measurements, motivated by the enormous importance of a future detection of this telltale signature of inflation (or other physics at the highest energies). A compilation of experimental results for  $C_\ell^{BB}$  is shown in Fig. 29.5, coming from a combination of direct estimates of the  $B$  modes (BICEP2/Keck Array [61], POLARBEAR [70], SPTPol [71], and ACTPol [63]) and indirect determinations of the lensing  $B$  modes based on estimating the effect of measured lensing on measured  $E$  modes (*Planck* [72], SPT [66], and ACT [73]). Additional band-power estimates are expected from these and other experiments in the near future,

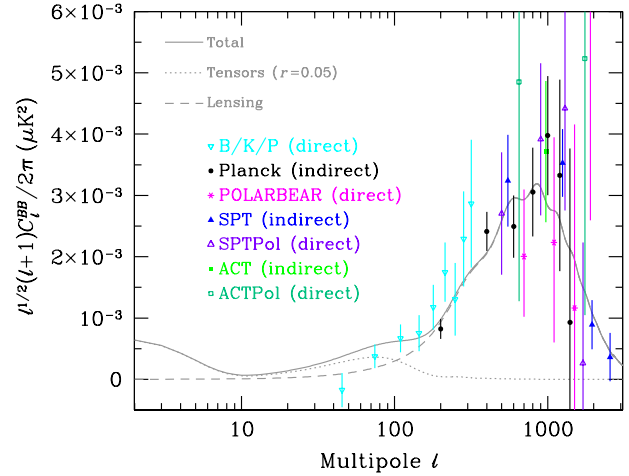


Figure 29.5: Power spectrum of  $B$ -mode polarization, including results from the BICEP2/Keck Array/*Planck* combined analysis (B/K/P), *Planck*, POLARBEAR, SPT, and ACT. Note that some of the measurements are direct estimates of  $B$  modes on the sky, while others are only sensitive to the lensing signal and come from combining  $E$ -mode and lensing potential measurements. Several earlier experiments reported upper limits, which are all off the top of this plot. A logarithmic horizontal axis is adopted here and the  $y$ -axis has been divided by a factor of  $\sqrt{\ell}$  in order to show all three theoretically expected contributions: the low- $\ell$  reionization bump; the  $\ell \simeq 100$  recombination peak; and the high- $\ell$  lensing signature. The dotted line is for a tensor (primordial gravitational wave) fraction  $r = 0.05$ , simply as an example, with all other cosmological parameters set at the best *Planck*-derived values, for which model the expected lensing  $B$  modes have also been shown with a dashed line.

with the Simons Observatory [74], the so-called ‘Stage 4’ CMB project [75] and the *LiteBIRD* satellite [76], holding great promise for pushing down to the  $r \sim 0.001$  level.

### 29.7.4 $\phi$ - $\phi$ Power Spectrum

One further CMB observable that can be measured is the gravitational lensing deflection, leading to the construction of a map of the lensing potential. The latest *Planck* results [77] give a map that is detected at the  $40\sigma$  level using a minimum-variance procedure from the 4-point function of temperature and polarization data. From this estimates can be constructed of  $C_\ell^{\phi\phi}$ , the lensing-potential power spectrum, and this is found to be consistent with predictions from the best-fit temperature and polarization model.

We can think of each sky pixel as possessing three independent quantities that can be measured, namely  $T$ ,  $E$ , and  $\phi$  (and potentially  $B$ , if that becomes detectable). Determining the constraining power comes down to counting  $Y_{\ell m}$  modes [78], as well as appreciating that some modes help to break particular parameter degeneracies. We have only scratched the surface of CMB lensing so far, and it is expected that future small-scale experiments will lead to dramatically more of the cosmological information being extracted. Further information can also be derived about the lower- $z$  Universe by cross-correlating CMB lensing with other cosmological tracers of large-scale structure. Additionally, small-scale lensing, combined with  $E$ -mode measurements, can be used to ‘delens’ CMB  $B$ -mode data, which will be important for pushing down into the  $r \lesssim 0.01$  regime [79].

## 29.8 Complications

There are a number of issues that complicate the interpretation of CMB anisotropy data (and are considered to be *signal* by many astrophysicists), some of which we sketch out below.

### 29.8.1 Foregrounds

The microwave sky contains significant emission from our Galaxy and from extragalactic sources [80]. Fortunately, the frequency dependence of these various sources is in general substan-

tially different from that of the CMB anisotropy signals. The combination of Galactic synchrotron, bremsstrahlung, and dust emission reaches a minimum at a frequency of roughly 100 GHz (or wavelength of about 3 mm). As one moves to greater angular resolution, the minimum moves to slightly higher frequencies, but becomes more sensitive to unresolved (point-like) sources.

At frequencies around 100 GHz, and for portions of the sky away from the Galactic plane, the foregrounds are typically 1 to 10% of the CMB anisotropies. By making observations at multiple frequencies, it is relatively straightforward to separate the various components and determine the CMB signal to the few per cent level. For greater sensitivity, it is necessary to use the spatial information and statistical properties of the foregrounds to separate them from the CMB. Furthermore, at higher  $\ell$ s it is essential to carefully model extragalactic foregrounds, particularly the clustering of infrared-emitting galaxies, which dominate the measured power spectrum as we move into the damping tail.

The foregrounds for CMB polarization follow a similar pattern to those for temperature, but are intrinsically brighter relative to CMB anisotropies. *WMAP* showed that the polarized foregrounds dominate at large angular scales, and that they must be well characterized in order to be discriminated [81]. *Planck* has shown that it is possible to characterize the foreground polarization signals, with synchrotron dominating at low frequencies and dust at high frequencies [82]. On smaller scales there are no strongly-polarized foregrounds, and hence it is in principle easier to measure foreground-free modes at high multipoles in polarization than in temperature. Although foreground contamination will no doubt become more complicated as we push down in sensitivity, and they will make analysis more difficult, for the time being, foreground contamination is not a fundamental limit for CMB experiments.

### 29.8.2 Secondary Anisotropies

With increasingly precise measurements of the primary anisotropies, there is growing theoretical and observational interest in ‘secondary anisotropies,’ pushing experiments to higher angular resolution and sensitivity. These secondary effects arise from the processing of the CMB due to ionization history and the evolution of structure, including gravitational lensing (which was already discussed) and patchy reionization effects [83]. Additional information can thus be extracted about the Universe at  $z \ll 1000$ . This tends to be most effectively done through correlating CMB maps with other cosmological probes of structure. Secondary signals are also typically non-Gaussian, unlike the primary CMB anisotropies.

A secondary signal of great current interest is the Sunyaev-Zeldovich (SZ) effect [84], which is Compton scattering ( $\gamma e \rightarrow \gamma' e'$ ) of the CMB photons by hot electron gas. This creates spectral distortions by transferring energy from the electrons to the photons. It is particularly important for clusters of galaxies, through which one observes a partially Comptonized spectrum, resulting in a decrement at radio wavelengths and an increment in the submillimeter.

The imprint on the CMB sky is of the form  $\Delta T/T = y f(x)$ , with the  $y$ -parameter being the integral of Thomson optical depth times  $kT_e/m_e c^2$  through the cluster, and  $f(x)$  describing the frequency dependence. This is simply  $x \coth(x/2) - 4$  for a non-relativistic gas (the electron temperature in a cluster is typically a few keV), where the dimensionless frequency  $x \equiv h\nu/kT_\gamma$ . As well as this ‘thermal’ SZ effect, there is also a smaller ‘kinetic’ effect due to the bulk motion of the cluster gas, giving  $\Delta T/T \sim \tau(v/c)$ , with either sign, but having the same spectrum as the primary CMB anisotropies.

A significant advantage in finding galaxy clusters via the SZ effect is that the signal is largely independent of redshift, so in principle clusters can be found to arbitrarily large distances. The SZ effect can be used to find and study individual clusters, and to obtain estimates of the Hubble constant. There is also the potential to constrain cosmological parameters, such as the clustering amplitude  $\sigma_8$  and the equation of state of the dark energy, through counts of detected clusters as a function of redshift. The promise of the method has been realized through detections of clusters purely through the SZ effect by SPT [85], ACT [86], and

*Planck* [87]. Results from *Planck* clusters [88] suggest a somewhat lower value of  $\sigma_8$  than inferred from CMB anisotropies, but there are still systematic uncertainties that might encompass the difference, and a more recent analysis of SPT-detected clusters shows better agreement [89]. Further analysis of scaling relations among cluster properties should enable more robust cosmological constraints to be placed in future, so that we can understand whether this ‘tension’ might be a sign of new physics.

### 29.8.3 Higher-order Statistics

Although most of the CMB anisotropy information is contained in the power spectra, there will also be weak signals present in higher-order statistics. These can measure any primordial non-Gaussianity in the perturbations, as well as non-linear growth of the fluctuations on small scales and other secondary effects (plus residual foreground contamination of course). There are an infinite variety of ways in which the CMB could be non-Gaussian [30]; however, there is a generic form to consider for the initial conditions, where a quadratic contribution to the curvature perturbations is parameterized through a dimensionless number  $f_{\text{NL}}$ . This weakly non-linear component can be constrained in several ways, the most popular being through measurements of the bispectrum (or 3-point function).

The constraints depend on the shape of the triangles in harmonic space, and it has become common to distinguish the ‘local’ or ‘squeezed’ configuration (in which one side is much smaller than the other two) from the ‘equilateral’ configuration. Other configurations are also relevant for specific theories, such as ‘orthogonal’ non-Gaussianity, which has positive correlations for  $k_1 \simeq 2k_2 \simeq 2k_3$ , and negative correlations for the equilateral configuration. The latest results from the *Planck* team [90] are  $f_{\text{NL}}^{\text{local}} = 1 \pm 5$ ,  $f_{\text{NL}}^{\text{equil}} = -26 \pm 47$ , and  $f_{\text{NL}}^{\text{ortho}} = -38 \pm 24$ .

These results are consistent with zero, but are at a level that is now interesting for model predictions. The amplitude of  $f_{\text{NL}}$  expected is small, so that a detection of  $f_{\text{NL}} \gg 1$  would rule out all single-field, slow-roll inflationary models. It is still possible to improve upon these *Planck* results, and it certainly seems feasible that a measurement of primordial non-Gaussianity may yet be within reach. *Non*-primordial detections of non-Gaussianity from expected signatures have already been made. For example, the bispectrum and trispectrum contain evidence of gravitational lensing, the ISW effect, and Doppler boosting. For now the primordial signal is elusive, but should it be detected, then detailed measurements of non-Gaussianity will become a unique probe of inflationary-era physics. Because of that, much effort continues to be devoted to honing predictions and measurement techniques, with the expectation that we will need to go beyond the CMB to dramatically improve the constraints.

### 29.8.4 Anomalies

Several features seen in the *Planck* data [33, 65, 91] confirm those found earlier with *WMAP* [32], showing mild deviations from a simple description of the data; these are often referred to as ‘anomalies.’ One such feature is the lack of power in the multipole range  $\ell \simeq 20\text{--}30$  [14] [53]. Other examples involve the breaking of statistical anisotropy, caused by alignment of the lowest multipoles, as well as a somewhat excessive cold spot and a power asymmetry between hemispheres. No such feature is significant at more than the roughly  $3\sigma$  level, and the importance of ‘a posteriori’ statistics here has been emphasized by many authors. Since these effects are at large angular scales, where cosmic variance dominates, the results will not increase in significance with more data, although there is the potential for more sensitive polarization measurements to provide independent tests.

## 29.9 Constraints on Cosmological Parameters

The most striking outcome of the last couple of decades of experimental results is that the standard cosmological paradigm continues to be in very good shape. A large amount of high-precision data on the power spectrum is adequately fit with fewer than 10 free parameters (and only six need non-trivial values). The framework is that of FRW models, which have nearly flat geometry, containing dark matter and dark energy, and with adiabatic perturbations having close to scale-invariant initial condi-



tions.

Within this basic picture, the values of the cosmological parameters can be constrained. Of course, more stringent bounds can be placed on models that cover a restricted parameter space, *e.g.*, assuming that  $\Omega_{\text{tot}} = 1$  or  $r = 0$ . More generally, the constraints depend upon the adopted prior probability distributions, even if they are implicit, for example by restricting the parameter freedom or their ranges (particularly where likelihoods peak near the boundaries), or by using different choices of other data in combination with the CMB. As the data become even more precise, these considerations will be less important, but for now we caution that restrictions on model space and choice of non-CMB data sets and priors need to be kept in mind when adopting specific parameter values and uncertainties.

There are some combinations of parameters that fit the CMB anisotropies almost equivalently. For example, there is a nearly exact geometric degeneracy, where any combination of  $\Omega_{\text{m}}$  and  $\Omega_{\Lambda}$  that provides the same angular-diameter distance to last scattering will give nearly identical  $C_{\ell}$ s. There are also other less exact degeneracies among the parameters. Such degeneracies can be broken when using the CMB results in combination with other cosmological data sets. Particularly useful are complementary constraints from baryon acoustic oscillations, galaxy clustering, the abundance of galaxy clusters, weak gravitational lensing measurements, and Type Ia supernova distances. For an overview of some of these other cosmological constraints, see The Cosmological Parameters—Sec. 25.1 of this *Review*.

Within the context of a 6-parameter family of models (which fixes  $\Omega_{\text{tot}} = 1$ ,  $dn_{\text{s}}/d\ln k = 0$ ,  $r = 0$ , and  $w = -1$ ) the *Planck* results for *TT*, together with *TE*, *EE*, and CMB lensing, yield [14]:  $\ln(10^{10} A_{\text{s}}) = 3.044 \pm 0.014$ ;  $n_{\text{s}} = 0.965 \pm 0.004$ ;  $\Omega_{\text{b}} h^2 = 0.02237 \pm 0.00015$ ;  $\Omega_{\text{c}} h^2 = 0.1200 \pm 0.0012$ ;  $100\theta_{*} = 1.04092 \pm 0.00031$ ; and  $\tau = 0.054 \pm 0.007$ . Other parameters can be derived from this basic set, including  $h = 0.674 \pm 0.005$ ,  $\Omega_{\Lambda} = 0.685 \pm 0.007 (= 1 - \Omega_{\text{m}})$  and  $\sigma_8 = 0.811 \pm 0.006$ . Somewhat different (although consistent) values are obtained using other data combinations, such as including BAO, supernova,  $H_0$ , or weak-lensing constraints (see Sec. 25.1 of this *Review*). However, the results quoted above are currently the best available from CMB data alone.

The standard cosmological model still fits the data well, with the error bars on the parameters continuing to shrink. Improved measurement of higher acoustic peaks has dramatically reduced the uncertainty in the  $\theta_{*}$  parameter, which is now detected at  $> 3000\sigma$ . The evidence for  $n_{\text{s}} < 1$  is now at the  $8\sigma$  level from *Planck* data alone. The value of the reionization optical depth has decreased compared with earlier estimates; it is convincingly detected, but still not at very high significance.

Constraints can also be placed on parameters beyond the basic six, particularly when including other astrophysical data sets. Relaxing the flatness assumption, the constraint on  $\Omega_{\text{tot}}$  is  $1.011 \pm 0.006$ . Note that for  $h$ , the CMB data alone provide only a very weak constraint if spatial flatness is not assumed. However, with the addition of other data (particularly powerful in this context being a compilation of BAO measurements; see Sec. 25.1 of this *Review*), the constraints on the Hubble constant and curvature improve considerably, leading to  $\Omega_{\text{tot}} = 0.9993 \pm 0.0019$  [14].

For  $\Omega_{\text{b}} h^2$  the CMB-derived value is generally consistent with completely independent constraints from Big Bang nucleosynthesis (see Sec. 24 of this *Review*). Related are constraints on additional neutrino-like relativistic degrees of freedom, which lead to  $N_{\text{eff}} = 2.99 \pm 0.17$  (including BAO), *i.e.*, no evidence for extra neutrino species.

The best limit on the tensor-to-scalar ratio is  $r < 0.06$  (measured at  $k = 0.002 \text{ Mpc}^{-1}$ ) from a combination of *Planck* and BICEP/Keck data. This limit depends on how the slope  $n_{\text{t}}$  is restricted and whether  $dn_{\text{s}}/d\ln k \neq 0$  is allowed. The joint constraints on  $n_{\text{s}}$  and  $r$  allow specific inflationary models to be tested [34, 92, 93]. Looking at the  $(n_{\text{s}}, r)$  plane, this means that  $m^2 \phi^2$  (mass-term quadratic) inflation is now disfavored by the data, as well as  $\lambda \phi^4$  (self-coupled) inflation.

The addition of the dark-energy equation of state  $w$  adds the partial degeneracy of being able to fit a ridge in  $(w, h)$  space,

extending to low values of both parameters. This degeneracy is broken when the CMB is used in combination with other data sets, *e.g.*, adding a compilation of BAO and supernova data gives  $w = -1.028 \pm 0.031$ . Constraints can also be placed on more general dark energy and modified-gravity models [94]. However, when extending the search space, one needs to be careful not to over-interpret some tensions between data sets as evidence for new physics.

For the reionization optical depth, a reanalysis of *Planck* data in 2016 resulted in a reduction in the value of  $\tau$ , with the tightest result giving  $\tau = 0.055 \pm 0.009$ , and the newest analysis gives similar numbers. This corresponds to  $z_{\text{i}} = 7.8\text{--}8.8$  (depending on the functional form of the reionization history), with an uncertainty of  $\pm 0.9$  [95]. This redshift is only slightly higher than that suggested from studies of absorption lines in high- $z$  quasar spectra [96] and Ly  $\alpha$ -emitting galaxies [97], perhaps hinting that the process of reionization was not as complex as previously suspected. The important constraint provided by CMB polarization, in combination with astrophysical measurements, thus allows us to investigate how the first stars formed and brought about the end of the cosmic dark ages.

## 29.10 Particle Physics Constraints

CMB data place limits on parameters that are directly relevant for particle physics models. For example, there is a limit on the sum of the masses of the neutrinos,  $\sum m_{\nu} < 0.12 \text{ eV}$  (95%) [14] coming from *Planck* together with BAO measurements (although limits are weaker when considering both  $N_{\text{eff}}$  and  $\sum m_{\nu}$  as free parameters). This assumes the usual number density of fermions, which decoupled when they were relativistic. The limit is tantalizingly only a factor of a few higher than the minimum value coming from neutrino mixing experiments (see Neutrino Mixings—Secs. 14 and 26). As well as being an indirect probe of the neutrino background, *Planck* data also require that the neutrino background has perturbations, *i.e.*, that it possesses a sound speed  $c_{\text{s}}^2 \simeq 1/3$ , as expected [12].

The current suite of data suggests that  $n_{\text{s}} < 1$ , with a best-fitting value about 0.035 below unity. This is already quite constraining for inflationary models, particularly along with  $r$  limits. There is no current evidence for running of the spectral index, with  $dn_{\text{s}}/d\ln k = -0.004 \pm 0.007$  from *Planck* alone [14] (with a similar value when BAO data are included), although this is less of a constraint on models. Similarly, primordial non-Gaussianity is being probed to interesting levels, although tests of simple inflationary models will only come with significant reductions in uncertainty.

The large-angle anomalies, such as the hemispheric modulation of power and the dip in power at  $\ell \simeq 20\text{--}30$ , have the potential to be hints of new physics. Such effects might be expected in a universe that has a large-scale power cut-off, or anisotropy in the initial power spectrum, or is topologically non-trivial. However, cosmic variance and *a posteriori* statistics limit the significance of these anomalies, absent the existence of a model that naturally yields some of these features (and ideally also predicting other phenomena that can be tested).

Constraints on ‘cosmic birefringence’ (*i.e.*, rotation of the plane of CMB polarization that generates non-zero *TB* and *EB* power) can be used to place limits on theories involving parity violation, Lorentz violation, or axion-photon mixing [98].

It is possible to place limits on additional areas of physics [99], for example annihilating dark matter [12, 12], primordial magnetic fields [100], and time variation of the fine-structure constant [101], as well as the neutrino chemical potential, a contribution of warm dark matter, topological defects, or physics beyond general relativity. Further particle physics constraints will follow as the smaller-scale and polarization measurements continue to improve.

The CMB anisotropy measurements precisely pin down physics at the time of last-scattering, and so any change of physics can be constrained if it affects the relevant energies or timescales. Future, higher sensitivity measurements of the CMB frequency spectrum will push the constraints back to cover energy injection at much earlier times ( $\sim 1$  year). Comparison of CMB and BBN observables extend these constraints to timescales of order seconds, and energies in the MeV range. And to the extent that inflation pro-

vides an effective description of the generation of perturbations, the inflationary observables may constrain physics at GUT-type energy scales.

More generally, careful measurement of the CMB power spectra and non-Gaussianity can in principle put constraints on physics at the highest energies, including ideas of string theory, extra dimensions, colliding branes, *etc.* At the moment any calculation of predictions appears to be far from definitive. However, there is a great deal of activity on implications of string theory for the early Universe, and hence a very real chance that there might be observational implications for specific scenarios.

### 29.11 Fundamental Lessons

More important than the precise values of parameters is what we have learned about the general features that describe our observable Universe. Beyond the basic hot Big Bang picture, the CMB has taught us that:

- the (observable) Universe is very close to isotropic;
- the Universe recombined at  $z \sim 1000$  and started to become ionized again at  $z \sim 10$ ;
- the geometry of the Universe is close to flat;
- both dark matter and dark energy are required;
- gravitational instability is sufficient to grow all of the observed large structures in the Universe;
- topological defects were not important for structure formation;
- there were ‘synchronized’ super-Hubble modes generated in the early Universe;
- the initial perturbations were predominantly adiabatic in nature;
- the primordial perturbation spectrum has a slightly red tilt;
- the perturbations had close to Gaussian (*i.e.*, maximally random) initial conditions.

These features form the basis of the cosmological standard model,  $\Lambda$ CDM, for which it is tempting to make an analogy with the Standard Model of particle physics (see earlier Sections of this *Review*). The cosmological model is much further from any underlying ‘fundamental theory,’ which might ultimately provide the values of the parameters from first principles. Nevertheless, any genuinely complete ‘theory of everything’ must include an explanation for the values of these cosmological parameters in addition to the parameters of the Standard Model of particle physics.

### 29.12 Future Directions

Given the significant progress in measuring the CMB sky, which has been instrumental in tying down the cosmological model, what can we anticipate for the future? There will be a steady improvement in the precision and confidence with which we can determine the appropriate cosmological parameters. Ground-based experiments operating at smaller angular scales will continue to place tighter constraints on the damping tail, lensing, and cross-correlations. New polarization experiments at small scales will probe further into the damping tail, without the limitation of extragalactic foregrounds. And polarization experiments at large angular scales will push down the limits on primordial  $B$  modes.

*Planck*, the third generation CMB satellite mission, was launched in May 2009, and has produced a large number of papers, including a set of cosmological studies based on the first two full surveys of the sky (accompanied by a public release of data products) in 2013, a further series coming from analysis of the full mission data release in 2015 (eight surveys for the Low Frequency Instrument and five surveys for the High Frequency Instrument), and a third series derived from a final analysis of the 2018 data release, including full constraints from polarization data.

A set of cosmological parameters is now known to percent-level accuracy, and that may seem sufficient for many people. However, we should certainly demand more of measurements that describe *the entire observable Universe!* Hence a lot of activity in the coming years will continue to focus on determining those parameters with increasing precision. This necessarily includes testing for consistency among different predictions of the cosmological

Standard Model, and searching for signals that might require additional physics.

A second area of focus will be the smaller-scale anisotropies and ‘secondary effects.’ There is a great deal of information about structure formation at  $z \ll 1000$  encoded in the CMB sky. This may involve higher-order statistics and cross-correlations with other large-scale structure tracers, as well as spectral signatures, with many experiments targeting the galaxy cluster SZ effect. The current status of CMB lensing is similar (in terms of total signal-to-noise) to the quality of the first CMB anisotropy measurements by *COBE*, and thus we can expect that experimental probes of lensing will improve dramatically in the coming years. All of these investigations can provide constraints on the dark-energy equation of state, for example, which is a major area of focus for several future cosmological surveys at optical wavelengths. CMB lensing also promises to yield a measurement of the sum of the neutrino masses.

A third direction is increasingly sensitive searches for specific signatures of physics at the highest energies. The most promising of these may be the primordial gravitational wave signals in  $C_{\ell}^{BB}$ , which could be a probe of the  $\sim 10^{16}$  GeV energy range. There are several ground- and balloon-based experiments underway that are designed to search for the polarization  $B$  modes. Additionally, non-Gaussianity holds the promise of constraining models beyond single-field slow-roll inflation.

Anisotropies in the CMB have proven to be the premier probe of cosmology and the early Universe. Theoretically the CMB involves well-understood physics in the linear regime, and is under very good calculational control. A substantial and improving set of observational data now exists. Systematics appear to be under control and are not currently a limiting factor. And so for the next several years we can expect an increasing amount of cosmological information to be gleaned from CMB anisotropies, with the prospect also of some genuine surprises.

### References

- [1] A. A. Penzias and R. W. Wilson, *Astrophys. J.* **142**, 419 (1965); R. H. Dicke *et al.*, *Astrophys. J.* **142**, 414 (1965).
- [2] M. White, D. Scott and J. Silk, *Ann. Rev. Astron. Astrophys.* **32**, 319 (1994).
- [3] W. Hu and S. Dodelson, *Ann. Rev. Astron. Astrophys.* **40**, 171 (2002).
- [4] A. Challinor and H. Peiris, in M. Novello and S. Perez, editors, “American Institute of Physics Conference Series,” volume 1132, 86–140 (2009), [arXiv:0903.5158].
- [5] G. F. Smoot *et al.*, *Astrophys. J. Lett.* **396**, L1 (1992).
- [6] C. L. Bennett *et al.*, *Astrophys. J. Supp.* **148**, 1 (2003).
- [7] G. Hinshaw *et al.*, *Astrophys. J. Supp.* **208**, 19 (2013), [arXiv:1212.5226].
- [8] Planck Collab. 2013 Results XVI, *Astron. Astrophys.* **571**, A16 (2014), [arXiv:1303.5076].
- [9] J. A. Tauber *et al.*, *Astron. Astrophys.* **520**, A1 (2010).
- [10] Planck Collab. 2013 Results I, *Astron. Astrophys.* **571**, A1 (2014), [arXiv:1303.5062].
- [11] Planck Collab. 2015 Results I, *Astron. Astrophys.* **594**, A1 (2016), [arXiv:1502.01582].
- [12] Planck Collab. 2015 Results XIII, *Astron. Astrophys.* **594**, A13 (2016), [arXiv:1502.01589].
- [13] Planck Collab. 2018 Results I, arXiv e-prints arXiv:1807.06205 (2018), [arXiv:1807.06205].
- [14] Planck Collab. 2018 Results VI, arXiv e-prints arXiv:1807.06209 (2018), [arXiv:1807.06209].
- [15] D. S. Swetz *et al.*, *Astrophys. J. Supp.* **194**, 41 (2011), [arXiv:1007.0290].
- [16] J. E. Carlstrom *et al.*, *Proc. Astron. Soc. Pacific* **123**, 568 (2011), [arXiv:0907.4445].
- [17] P. Noterdaeme *et al.*, *Astron. Astrophys.* **526**, L7 (2011), [arXiv:1012.3164]; S. Muller *et al.*, *Astron. & Astrophys.* **551**, A109 (2013), [arXiv:1212.5456].

- [18] D. J. Fixsen *et al.*, *Astrophys. J.* **734**, 5 (2011), [arXiv:0901.0555].
- [19] J. Singal *et al.*, *Pub. Astron. Soc. Pac.* **130**, 985, 036001 (2018).
- [20] A. Kogut *et al.*, in “Space Telescopes and Instrumentation 2014: Optical, Infrared, and Millimeter Wave,” volume 9143 of *Proc. SPIE*, 91431E (2014).
- [21] P. André *et al.*, *JCAP* **2014**, 2, 006 (2014), [arXiv:1310.1554].
- [22] V. Desjacques *et al.*, *Mon. Not. R. Astron. Soc.* **451**, 4460 (2015), [arXiv:1503.05589].
- [23] D. J. Fixsen, *Astrophys. J.* **707**, 916 (2009), [arXiv:0911.1955].
- [24] J. C. Mather *et al.*, *Astrophys. J.* **512**, 511 (1999).
- [25] Y. Hoffman, H. M. Courtois and R. B. Tully, *Mon. Not. R. Astron. Soc.* **449**, 4494 (2015), [arXiv:1503.05422].
- [26] D. J. Fixsen *et al.*, *Astrophys. J.* **420**, 445 (1994).
- [27] Planck Collab. 2013 Results XXVII, *Astron. Astrophys.* **571**, A27 (2014), [arXiv:1303.5087].
- [28] S. Seager, D. D. Sasselov and D. Scott, *Astrophys. J. Supp.* **128**, 407 (2000).
- [29] L. Knox, *Phys. Rev.* 4307–4318 (1995).
- [30] N. Bartolo *et al.*, *Phys. Rep.* **402**, 103 (2004).
- [31] Planck Collab. 2013 Results XXIV, *Astron. Astrophys.* **571**, A24 (2014), [arXiv:1303.5084].
- [32] C. L. Bennett *et al.*, *Astrophys. J. Supp.* **192**, 17 (2011), [arXiv:1001.4758].
- [33] Planck Collab. 2013 Results XXIII, *Astron. Astrophys.* **571**, A23 (2014), [arXiv:1303.5083].
- [34] Planck Collab. 2018 Results X, arXiv e-prints arXiv:1807.06211 (2018), [arXiv:1807.06211].
- [35] A. R. Liddle and D. H. Lyth, *Cosmological Inflation and Large-Scale Structure* (2000).
- [36] U. Seljak and M. Zaldarriaga, *Astrophys. J.* **469**, 437 (1996).
- [37] A. Lewis, A. Challinor and A. Lasenby, *Astrophys. J.* **538**, 473 (2000).
- [38] D. Blas, J. Lesgourgues and T. Tram, *J. Cosmology Astropart. Phys.* **7**, 034 (2011), [arXiv:1104.2933].
- [39] U. Seljak *et al.*, *Phys. Rev.* , 8, 083507 (2003).
- [40] R. K. Sachs and A. M. Wolfe, *Astrophys. J.* **147**, 73 (1967).
- [41] R. G. Crittenden and N. Turok, *Phys. Rev. Lett.* **76**, 575 (1996).
- [42] Planck Collab. 2015 Results XXI, *Astron. Astrophys.* **594**, A21 (2016), [arXiv:1502.01595].
- [43] W. Hu *et al.*, *Phys. Rev.* **59**, 2, 023512 (1999).
- [44] W. Hu, N. Sugiyama and J. Silk, *Nature* **386**, 37 (1997).
- [45] P. J. E. Peebles and J. T. Yu, *Astrophys. J.* **162**, 815 (1970); R. A. Sunyaev and Y. B. Zeldovich, *Astron. Astrophys. Supp.* **7**, 3 (1970).
- [46] D. Scott, J. Silk and M. White, *Science* **268**, 829 (1995).
- [47] D. J. Eisenstein, *New Astron. Rev.* **49**, 360 (2005).
- [48] J. Silk, *Astrophys. J.* **151**, 459 (1968).
- [49] M. Zaldarriaga and U. Seljak, *Phys. Rev.* , 2, 023003 (1998).
- [50] Planck Collab. 2013 Result XVII, *Astron. Astrophys.* **571**, A17 (2014), [arXiv:1303.5077].
- [51] M. Kaplinghat, L. Knox and Y.-S. Song, *Phys. Rev. Lett.* **91**, 24, 241301 (2003).
- [52] Planck Collab. 2013 Results XV, *Astron. Astrophys.* **571**, A15 (2014), [arXiv:1303.5075].
- [53] Planck Collab. 2018 Results V, arXiv e-prints arXiv:1907.12875 (2019), [arXiv:1907.12875].
- [54] S. Das *et al.*, *J. Cosmology Astropart. Phys.* **4**, 014 (2014), [arXiv:1301.1037].
- [55] K. T. Story *et al.*, *Astrophys. J.* **779**, 86 (2013), [arXiv:1210.7231].
- [56] W. Hu and M. White, *New Astron.* **2**, 323 (1997).
- [57] W. Hu and M. White, *Phys. Rev.* 596–615 (1997).
- [58] M. Zaldarriaga and U. Seljak, *Phys. Rev.* 1830–1840 (1997).
- [59] J. M. Kovac *et al.*, *Nature* **420**, 772 (2002).
- [60] D. Larson *et al.*, *Astrophys. J. Supp.* **192**, 16 (2011), [arXiv:1001.4635].
- [61] Keck Array and BICEP2 Collabs. V, *Astrophys. J.* **811**, 126 (2015), [arXiv:1502.00643].
- [62] S. Naess *et al.*, *J. Cosmology Astropart. Phys.* **10**, 007 (2014), [arXiv:1405.5524].
- [63] T. Louis *et al.*, *J. Cosmology Astropart. Phys.* **6**, 031 (2017), [arXiv:1610.02360].
- [64] A. T. Crites *et al.*, *Astrophys. J.* **805**, 36 (2015), [arXiv:1411.1042].
- [65] Planck Collab. 2018 Results VII, arXiv e-prints arXiv:1906.02552 (2019), [arXiv:1906.02552].
- [66] D. Hanson *et al.*, *Phys. Rev. Lett.* **111**, 14, 141301 (2013), [arXiv:1307.5830].
- [67] BICEP2 Collab., *Phys. Rev. Lett.* **112**, 24, 241101 (2014), [arXiv:1403.3985].
- [68] BICEP2/Keck and Planck Collabs., *Phys. Rev. Lett.* **114**, 10, 101301 (2015), [arXiv:1502.00612].
- [69] BICEP2 Collaboration and Keck Array Collaboration, *Phys. Rev. Lett.* **121**, 22, 221301 (2018).
- [70] POLARBEAR Collab., *Astrophys. J.* **848**, 121 (2017), [arXiv:1705.02907].
- [71] R. Keisler *et al.*, *Astrophys. J.* **807**, 151 (2015), [arXiv:1503.02315].
- [72] Planck Collab. 2015 Results XV, *Astron. Astrophys.* **594**, A15 (2016), [arXiv:1502.01591].
- [73] A. van Engelen *et al.*, *Astrophys. J.* **808**, 7 (2015), [arXiv:1412.0626].
- [74] P. Ade *et al.* (The Simons Observatory collaboration), *JCAP* **2019**, 2, 056 (2019).
- [75] K. N. Abazajian *et al.*, ArXiv e-prints (2016), [arXiv:1610.02743].
- [76] Y. Sekimoto *et al.*, in “Proc. SPIE,” volume 10698 of *Society of Photo-Optical Instrumentation Engineers (SPIE) Conference Series*, 106981Y (2018).
- [77] Planck Collab. 2018 Results VIII, arXiv e-prints arXiv:1807.06210 (2018), [arXiv:1807.06210].
- [78] D. Scott *et al.*, *JCAP* **2016**, 6, 046 (2016), [arXiv:1603.03550].
- [79] L. Knox and Y.-S. Song, *Phys. Rev. Lett.* **89**, 1, 011303 (2002), [arXiv:astro-ph/0202286]; M. Kesden, A. Cooray and M. Kamionkowski, *Phys. Rev. Lett.* **89**, 011304 (2002), [arXiv:astro-ph/0202434]; C. M. Hirata and U. Seljak, *Phys. Rev.* **D68**, 8, 083002 (2003), [arXiv:astro-ph/0306354].
- [80] Planck Collab. 2013 Results XII, *Astron. Astrophys.* **571**, A12 (2014), [arXiv:1303.5072].
- [81] B. Gold *et al.*, *Astrophys. J. Supp.* **192**, 15 (2011), [arXiv:1001.4555].
- [82] Planck Collab. Interm. Results XXX, *Astron. Astrophys.* **586**, A133 (2016), [arXiv:1409.5738].
- [83] M. Millea *et al.*, *Astrophys. J.* **746**, 4 (2012), [arXiv:1102.5195].
- [84] R. A. Sunyaev and I. B. Zeldovich, *Ann. Rev. Astron. Astrophys.* **18**, 537 (1980).
- [85] R. Williamson *et al.*, *Astrophys. J.* **738**, 139 (2011), [arXiv:1101.1290].
- [86] T. A. Marriage *et al.*, *Astrophys. J.* **737**, 61 (2011), [arXiv:1010.1065].

- [87] Planck Collab. Early Results VIII, *Astron. Astrophys.* **536**, A8 (2011), [arXiv:1101.2024].
- [88] Planck Collab. 2013 Results XX, *Astron. Astrophys.* **571**, A20 (2014), [arXiv:1303.5080].
- [89] T. de Haan *et al.*, *Astrophys. J.* **832**, 95 (2016), [arXiv:1603.06522].
- [90] Planck Collab. 2018 Results IX, arXiv e-prints arXiv:1905.05697 (2019), [arXiv:1905.05697].
- [91] Planck Collab. 2015 Results XVI, *Astron. Astrophys.* **594**, A16 (2016), [arXiv:1506.07135].
- [92] Planck Collab. 2013 Results XXII, *Astron. Astrophys.* **571**, A22 (2014), [arXiv:1303.5082].
- [93] Planck Collab. 2015 Results XX, *Astron. Astrophys.* **594**, A20 (2016), [arXiv:1502.02114].
- [94] Planck Collab. 2015 Results XIV, *Astron. Astrophys.* **594**, A14 (2016), [arXiv:1502.01590].
- [95] Planck Collab. Interm. Results XLVI, *Astron. Astrophys.* **596**, A107 (2016), [arXiv:1605.02985].
- [96] X. Fan, C. L. Carilli and B. Keating, *Ann. Rev. Astron. Astrophys.* **44**, 415 (2006).
- [97] T. R. Choudhury *et al.*, *Mon. Not. R. Astron. Soc.* **452**, 261 (2015), [arXiv:1412.4790].
- [98] B. Feng *et al.*, *Phys. Rev. Lett.* **96**, 22, 221302 (2006).
- [99] M. Kamionkowski and A. Kosowsky, *Ann. Rev. Nucl. Part. Sci.* **49**, 77 (1999).
- [100] Planck Collab. 2015 Results XIX, *Astron. Astrophys.* **594**, A19 (2016), [arXiv:1502.01594].
- [101] Planck Collab. Interm. Results XXIV, *Astron. Astrophys.* **580**, A22 (2015), [arXiv:1406.7482].

## 30. Cosmic Rays

Revised October 2019 by J.J. Beatty (Ohio State U.), J. Matthews (Louisiana State U.) and S.P. Wakely (Chicago U.; Chicago U., Kavli Inst.).

Cosmic rays are a population of energetic elementary particles and nuclei with a steeply falling near-power law spectrum extending from a few MeV to tens of Joules per particle. Primary cosmic rays can be measured directly by experiments in space or on balloons at energies where there is sufficient flux (§30.1). Atmospheric interactions of primary cosmic rays produce fluxes of secondary elementary particles which can be detected in the atmosphere (§30.2), at the Earth's surface (§30.3), and underground (§30.4). At high energies, air showers of particles generated by a single primary can be detected (§30.5). These showers can be reconstructed to determine the energy, direction, and composition of the incident particle. Energetic neutrinos are closely linked to high energy cosmic rays, both through their production at astrophysical sites of particle acceleration and by production during propagation of extremely high energy cosmic rays (§30.6).

## 30.1 Primary Spectra from Direct Measurements

The cosmic radiation incident at the top of the terrestrial atmosphere includes all stable charged particles and nuclei with lifetimes of order  $10^6$  years or longer. When discussing the astrophysical origin of cosmic rays, “primary” cosmic rays are those particles accelerated at astrophysical sources and “secondaries” are those particles produced in interaction of the primaries with interstellar gas<sup>1</sup>. Thus electrons, protons and helium, as well as carbon, oxygen, iron, and other nuclei synthesized in stars, are primaries. Nuclei such as lithium, beryllium, and boron (which are not abundant end-products of stellar nucleosynthesis) are secondaries. Antiprotons and positrons are also in large part secondary. Whether a small fraction of these particles may be primary is a question of current interest.

Apart from particles associated with solar flares<sup>2</sup>, the cosmic radiation comes from outside the solar system. The incoming charged particles are “modulated” by the solar wind, the expanding magnetized plasma generated by the Sun, which decelerates and partially excludes the lower energy galactic cosmic rays from the inner solar system. There is a significant anticorrelation between solar activity (which has an alternating eleven-year cycle) and the intensity of the cosmic rays with rigidities below about 10 GV. In addition, the lower-energy cosmic rays are affected by the geomagnetic field, which they must penetrate to reach the top of the atmosphere. Thus the intensity of any component of the cosmic radiation in the GeV range depends both on the location and time.

There are four different ways to describe the spectra of the components of the cosmic radiation: (1) By particles per unit rigidity. Propagation (and probably also acceleration) through cosmic magnetic fields depends on gyroradius or *magnetic rigidity*,  $R$ , which is gyroradius multiplied by the magnetic field strength:

$$R = \frac{pc}{Ze} = r_L B \quad (30.1)$$

(2) By particles per energy-per-nucleon. Fragmentation of nuclei propagating through the interstellar gas depends on energy per nucleon, since that quantity is approximately conserved when a nucleus breaks up on interaction with the gas. (3) By nucleons per energy-per-nucleon. Production of secondary cosmic rays in the atmosphere depends on the intensity of nucleons per energy-per-nucleon, approximately independently of whether the incident nucleons are free protons or bound in nuclei. (4) By particles per energy-per-nucleus. Air shower experiments that use the atmosphere as a calorimeter generally measure a quantity that is related to total energy per particle.

The units of differential intensity  $I$  are  $[\text{m}^{-2} \text{s}^{-1} \text{sr}^{-1} \mathcal{E}^{-1}]$ , where  $\mathcal{E}$  represents the units of one of the four variables listed above.

<sup>1</sup>‘Primary’ and ‘secondary’ are used in a different but analogous sense when discussing cosmic ray interactions in the atmosphere.

<sup>2</sup>Energetic particles accelerated by the Sun and at other sites within the heliosphere and at its boundary are outside the scope of this review

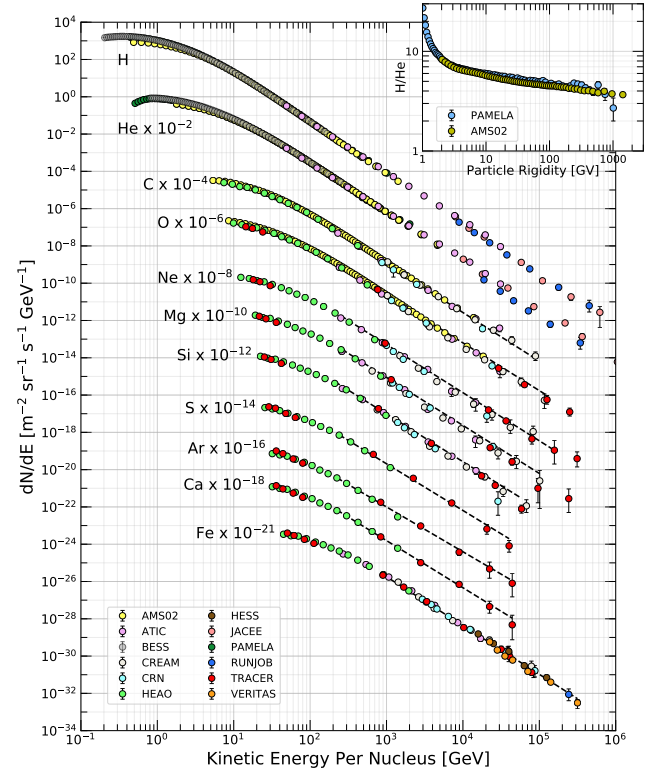


Figure 30.1: Fluxes of nuclei of the primary cosmic radiation in particles per energy-per-nucleus are plotted vs energy-per-nucleus using data from Refs. [1–13]. The inset shows the H/He ratio as a function of rigidity [1, 3].

The intensity of primary nucleons in the energy range from several GeV to somewhat beyond 100 TeV is given approximately by

$$I_N(E) \approx 1.8 \times 10^4 (E/1 \text{ GeV})^{-\alpha} \frac{\text{nucleons}}{\text{m}^2 \text{ s sr GeV}}, \quad (30.2)$$

where  $E$  is the energy-per-nucleon (including rest mass energy) and  $\alpha$  ( $\equiv \gamma + 1$ )  $\approx 2.7$  is the differential spectral index of the cosmic-ray flux and  $\gamma$  is the integral spectral index. About 74% of the primary nucleons are free protons and about 70% of the rest are nucleons bound in helium nuclei. The fractions of the primary nuclei are nearly constant over this energy range (with a few interesting variations, e.g. [1]). Fractions of both primary and secondary incident nuclei are listed in Table 30.1. Figure 30.1 shows the major nuclear components for kinetic energies greater than 0.22 GeV/nucleus. A useful compendium of experimental data for cosmic-ray nuclei and electrons is described in [14].

The composition and energy spectra of nuclei are typically interpreted in the context of propagation models, in which the sources of the primary cosmic radiation are located within the Galaxy [15]. The ratio of secondary to primary nuclei is observed to decrease with increasing energy, a fact often interpreted to mean that the lifetime of cosmic rays in the Galaxy decreases with energy. Measurements of radioactive “clock” isotopes in the low energy cosmic radiation are consistent with a lifetime in the Galaxy of about 15 Myr [16].

Cosmic rays are nearly isotropic at most energies due to diffusive propagation in the galactic magnetic field. Milagro [17], HAWC and IceCube [18], and the Tibet-III air shower array [19] have observed anisotropy at the level of about  $10^{-3}$  for cosmic rays with energy of a few TeV, possibly due to the direction of local Galactic magnetic fields, motion of the solar system in the Galaxy, and to the distribution of sources.

The spectrum of electrons and positrons incident at the top of

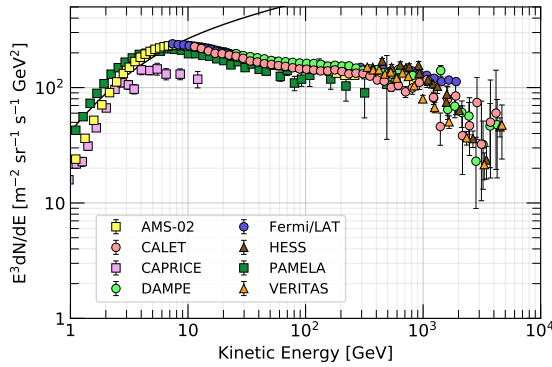


Figure 30.2: Differential spectrum of electrons plus positrons (except PAMELA data, which are electrons only) multiplied by  $E^3$  [20–28]. The line shows the proton spectrum [29] multiplied by 0.01.

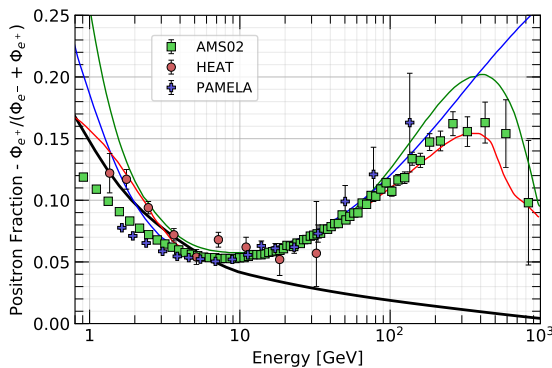


Figure 30.3: The positron fraction (ratio of the flux of  $e^+$  to the total flux of  $e^+$  and  $e^-$ ) [22, 30–32]. The heavy black line is a model of pure secondary production [33] and the three thin lines show three representative attempts to model the positron excess with different phenomena: green: dark matter decay [34]; blue: propagation physics [35]; red: production in pulsars [36]. The ratio below 10 GeV is dependent on the polarity of the solar magnetic field.

the atmosphere is generally expected to steepen by one power of  $E$  above an energy of 5 GeV because of radiative energy loss effects in the Galaxy. Most modern measurements of the combined electron+positron spectrum at high energy, which includes data from spectrometers, calorimeters, and ground-based air Cherenkov telescopes, reveal a relatively smooth spectrum to approximately 1 TeV, where evidence of a cutoff has been reported [24, 26, 28].

The PAMELA [30, 31] and AMS-02 [37, 38] satellite experi-

**Table 30.1:** Relative abundances  $F$  of cosmic-ray nuclei at 10.6 GeV/nucleon normalized to oxygen ( $\equiv 1$ ) [9]. The oxygen flux at kinetic energy of 10.6 GeV/nucleon is  $3.29 \times 10^{-2} (\text{m}^2 \text{ s sr GeV/nucleon})^{-1}$ . Abundances of hydrogen and helium are from Refs.(citerange) [2–4]. Note that one can not use these values to extend the cosmic-ray flux to high energy because the power law indices for each element may differ slightly.

$Z$	Element	$F$	$Z$	Element	$F$
1	H	550	13–14	Al-Si	0.19
2	He	34	15–16	P-S	0.03
3–5	Li-B	0.40	17–18	Cl-Ar	0.01
6–8	C-O	2.20	19–20	K-Ca	0.02
9–10	F-Ne	0.30	21–25	Sc-Mn	0.05
11–12	Na-Mg	0.22	26–28	Fe-Ni	0.12

ments measured the positron to electron ratio to increase above 10 GeV instead of the expected decrease [33] at higher energy, confirming earlier hints seen by the HEAT balloon-borne experiment [32]. The structure in the electron spectrum, as well as the increase in the positron fraction, may be related to contributions from individual nearby sources (supernova remnants or pulsars) emerging above a background suppressed at high energy by synchrotron losses [39]. Other explanations have invoked propagation effects [35] or dark matter decay/annihilation processes (see, e.g., [34]). The significant disagreement in the ratio below  $\sim 10$  GeV is attributable to differences in charge-sign dependent solar modulation effects present near Earth at the times of measurement.

The ratio of antiprotons to protons is  $\sim 2 \times 10^{-4}$  [40] at around 10–20 GeV, and there is clear evidence [41] for the kinematic suppression at lower energy that is the signature of secondary antiprotons. The  $\bar{p}/p$  ratio also shows a strong dependence on the phase and polarity of the solar cycle [42] in the opposite sense to that of the positron fraction. There is at this time no evidence for a significant primary component of antiprotons. No antihelium or antideuteron has been found in the cosmic radiation. The best measured upper limit on the ratio antihelium/helium is currently approximately  $1 \times 10^{-7}$  [43]. The upper limit on the flux of antideuterons around 1 GeV/nucleon is approximately  $2 \times 10^{-4} (\text{m}^2 \text{ s sr GeV/nucleon})^{-1}$  [44].

A useful method for calculating the effect of solar modulation including time, charge-sign, and rigidity-dependent effects is given in Ref. [45].

### 30.2 Cosmic Rays in the Atmosphere

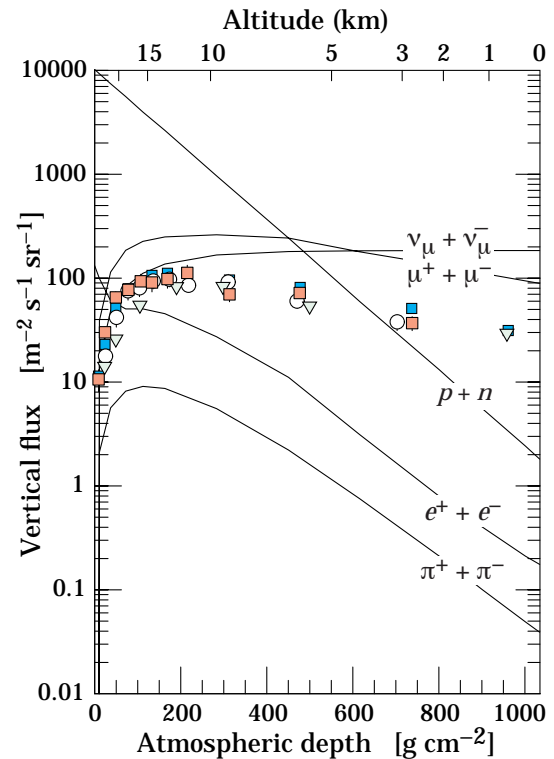


Figure 30.4: Vertical fluxes of cosmic rays in the atmosphere with  $E > 1$  GeV estimated from the nucleon flux of Eq. (30.2). The points show measurements of negative muons with  $E_\mu > 1$  GeV [46–51].

Figure 30.4 shows the vertical fluxes of the major cosmic-ray components in the atmosphere in the energy region where the particles are most numerous (except for electrons, which are most numerous near their critical energy, which is about 81 MeV in air). Except for protons and electrons near the top of the atmosphere,



all particles are produced in interactions of the primary<sup>3</sup> cosmic rays in the air. Muons and neutrinos are products of the decay chain of charged mesons, while electrons and photons originate in decays of neutral mesons.

Most measurements are made at ground level or near the top of the atmosphere, but there are also measurements of muons and electrons from airplanes and balloons. Fig. 30.4 shows measurements of negative muons [46–51]. Since  $\mu^+(\mu^-)$  are produced in association with  $\nu_\mu(\bar{\nu}_\mu)$ , the measurement of muons near the maximum of the intensity curve for the parent pions serves to calibrate the atmospheric  $\nu_\mu$  beam [52]. Because muons typically lose almost 2 GeV in passing through the atmosphere, the comparison near the production altitude is important for the sub-GeV range of  $\nu_\mu(\bar{\nu}_\mu)$  energies.

The flux of cosmic rays through the atmosphere is described by a set of coupled cascade equations with boundary conditions at the top of the atmosphere to match the primary spectrum. Numerical or Monte Carlo calculations are needed to account accurately for decay and energy-loss processes, and for the energy-dependences of the cross sections and of the primary spectral index  $\gamma$ . Approximate analytic solutions are, however, useful in limited regions of energy [53, 54]. For example, the vertical intensity of charged pions with energy  $E_\pi \ll \epsilon_\pi = 115$  GeV is

$$I_\pi(E_\pi, X) \approx \frac{Z_{N\pi}}{\lambda_N} I_N(E_\pi, 0) e^{-X/\Lambda} \frac{X E_\pi}{\epsilon_\pi} \quad (30.3)$$

where  $\Lambda$  is the characteristic length for exponential attenuation of the parent nucleon flux in the atmosphere. This expression has a maximum at  $X = \Lambda \approx 121 \pm 4$  g cm<sup>-2</sup> [55], which corresponds to an altitude of 15 kilometers. The quantity  $Z_{N\pi}$  is the spectrum-weighted moment of the inclusive distribution of charged pions in interactions of nucleons with nuclei of the atmosphere. The intensity of low-energy pions is much less than that of nucleons because  $Z_{N\pi} \approx 0.079$  is small and because most pions with energy much less than the critical energy  $\epsilon_\pi$  decay rather than interact.

### 30.3 Cosmic rays at the surface

#### 30.3.1 Muons

Muons are the most numerous charged particles at sea level (see Fig. 30.4). Most muons are produced high in the atmosphere (typically 15 km) and lose about 2 GeV to ionization before reaching the ground. Their energy and angular distribution reflect a convolution of the production spectrum, energy loss in the atmosphere, and decay. For example, 2.4 GeV muons have a decay length of 15 km, which is reduced to 8.7 km by energy loss. The mean energy of muons at the ground is  $\approx 4$  GeV. The energy spectrum is almost flat below 1 GeV, steepens gradually to reflect the primary spectrum in the 10–100 GeV range, and steepens further at higher energies because pions with  $E_\pi > \epsilon_\pi$  tend to interact in the atmosphere before they decay. Asymptotically ( $E_\mu \gg 1$  TeV), the energy spectrum of atmospheric muons is one power steeper than the primary spectrum. The integral intensity of vertical muons above 1 GeV/c at sea level is  $\approx 70$  m<sup>-2</sup>s<sup>-1</sup>sr<sup>-1</sup> [56] [57], with recent measurements [51, 58, 59] favoring a lower normalization by 10–15%. Experimentalists are familiar with this number in the form  $I \approx 1$  cm<sup>-2</sup> min<sup>-1</sup> for horizontal detectors. The overall angular distribution of muons at the ground as a function of zenith angle  $\theta$  is  $\propto \cos^2 \theta$ , which is characteristic of muons with  $E_\mu \sim 3$  GeV. At lower energy the angular distribution becomes increasingly steep, while at higher energy it flattens, approaching a sec  $\theta$  distribution for  $E_\mu \gg \epsilon_\pi$  and  $\theta < 70^\circ$ .

Figure 30.5 shows the muon energy spectrum at sea level for two angles. At large angles low energy muons decay before reaching the surface and high energy pions decay before they interact, thus the average muon energy increases. An approximate extrapolation formula valid when muon decay is negligible ( $E_\mu > 100/\cos \theta$  GeV) and the curvature of the Earth can be neglected ( $\theta < 70^\circ$ ) is

$$\frac{dN_\mu}{dE_\mu d\Omega} \approx \frac{0.14 E_\mu^{-2.7}}{\text{cm}^2 \text{ s sr GeV}} \times \left\{ \frac{1}{1 + \frac{1.1 E_\mu \cos \theta}{115 \text{ GeV}}} + \frac{0.054}{1 + \frac{1.1 E_\mu \cos \theta}{850 \text{ GeV}}} \right\} \quad (30.4)$$

where the two terms give the contribution of pions and charged kaons. Eq. (30.4) neglects a small contribution from charm and heavier flavors which is negligible except at very high energy [64].

The muon charge ratio reflects the excess of  $\pi^+$  over  $\pi^-$  and  $K^+$  over  $K^-$  in the forward fragmentation region of proton initiated interactions together with the fact that there are more free and bound protons than free and bound neutrons in the primary spectrum. The increase with energy of  $\mu^+/\mu^-$  shown in Fig. 30.6 reflects the increasing importance of kaons in the TeV range [65] and indicates a significant contribution of associated production by cosmic-ray protons ( $p \rightarrow \Lambda + K^+$ ). The same process is even more important for atmospheric neutrinos at high energy.

#### 30.3.2 Electromagnetic component

At the ground, this component consists of electrons, positrons, and photons primarily from cascades initiated by decay of neutral and charged mesons. Muon decay is the dominant source of low-energy electrons at sea level. Decay of neutral pions is more important at high altitude or when the energy threshold is high. Knock-on electrons also make a small contribution at low energy [66]. The integral vertical intensity of electrons plus positrons is very approximately 30, 6, and 0.2 m<sup>-2</sup>s<sup>-1</sup>sr<sup>-1</sup> above 10, 100, and 1000 MeV respectively [57, 67], but the exact numbers depend sensitively on altitude, and the angular dependence is complex because of the different altitude dependence of the different sources of electrons [66, 68]. The ratio of photons to electrons plus positrons is approximately 1.3 above 1 GeV and 1.7 below the critical energy [68].

#### 30.3.3 Nucleons

Nucleons above 1 GeV/c at ground level are degraded remnants of the primary cosmic radiation. The intensity is approximately  $I_N(E, 0) \times \exp(-X/\cos \theta \Lambda)$  for  $\theta < 70^\circ$ . At sea level, about 1/3 of the nucleons in the vertical direction are neutrons (up from  $\approx 10\%$  at the top of the atmosphere as the  $n/p$  ratio approaches equilib-

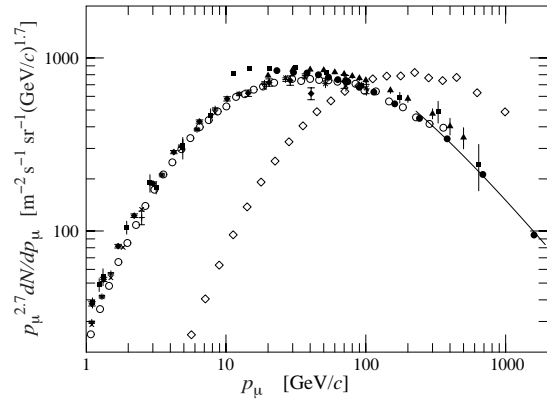


Figure 30.5: Spectrum of muons at  $\theta = 0^\circ$  ( $\diamond$  [56],  $\blacksquare$  [60],  $\blacktriangledown$  [61],  $\blacktriangle$  [62],  $\times$ ,  $+$  [58],  $\circ$  [51], and  $\bullet$  [59]) and  $\theta = 75^\circ$   $\diamond$  [63]). The line plots the result from Eq. (30.4) for vertical showers.

**Table 30.2:** Average muon range  $R$  and energy loss parameters calculated for standard rock. Range is given in km-water-equivalent, or  $10^5$  g cm<sup>-2</sup>.

$E_\mu$ GeV	$R$ km.w.e.	$a$ MeV g <sup>-1</sup> cm <sup>2</sup>	$b_{\text{brems}}$	$b_{\text{pair}}$	$b_{\text{nucl}}$ $10^{-6}$ g <sup>-1</sup> cm <sup>2</sup>	$\sum b_i$	$\sum b_{\text{ice}}$
10	0.05	2.17	0.70	0.70	0.50	1.90	1.66
100	0.41	2.44	1.10	1.53	0.41	3.04	2.51
1000	2.45	2.68	1.44	2.07	0.41	3.92	3.17
10000	6.09	2.93	1.62	2.27	0.46	4.35	3.78

<sup>3</sup>When discussing cosmic rays in the atmosphere, ‘primary’ is used to denote the original particle and ‘secondary’ to denote the particles produced in interactions.

rium). The integral intensity of vertical protons above 1 GeV/c at sea level is  $\approx 0.9 \text{ m}^{-2}\text{s}^{-1}\text{sr}^{-1}$  [57,69].

### 30.4 Cosmic Rays Underground

Only muons and neutrinos penetrate to significant depths underground. The muons produce tertiary fluxes of photons, electrons, and hadrons.

#### 30.4.1 Muons

As discussed in Section 34.6 of this *Review*, muons lose energy by ionization and by radiative processes: bremsstrahlung, direct production of  $e^+e^-$  pairs, and photonuclear interactions. The total muon energy loss may be expressed as a function of the amount of matter traversed as

$$-\frac{dE_\mu}{dX} = a + bE_\mu \quad (30.5)$$

where  $a$  is the ionization loss and  $b$  is the fractional energy loss by the three radiation processes. Both are slowly varying functions of energy. The quantity  $\epsilon \equiv a/b$  ( $\approx 500 \text{ GeV}$  in standard rock) defines a critical energy below which continuous ionization loss is more important than radiative losses. Table 30.2 shows  $a$  and  $b$  values for standard rock, and  $b$  for ice, as a function of muon energy. The second column of Table 30.2 shows the muon range in standard rock ( $A = 22$ ,  $Z = 11$ ,  $\rho = 2.65 \text{ g cm}^{-3}$ ). These parameters are quite sensitive to the chemical composition of the rock, which must be evaluated for each location.

The intensity of muons underground can be estimated from the muon intensity in the atmosphere and their rate of energy loss. To the extent that the mild energy dependence of  $a$  and  $b$  can be neglected, Eq. (30.5) can be integrated to provide the following relation between the energy  $E_{\mu,0}$  of a muon at production in the atmosphere and its average energy  $E_\mu$  after traversing a thickness  $X$  of rock (or ice or water):

$$E_{\mu,0} = (E_\mu + \epsilon)e^{bX} - \epsilon. \quad (30.6)$$

Especially at high energy, however, fluctuations are important and an accurate calculation requires a simulation that accounts for stochastic energy-loss processes [72].

There are two depth regimes for which Eq. (30.6) can be simplified. For  $X \ll b^{-1} \approx 2.5 \text{ km}$  water equivalent,  $E_{\mu,0} \approx E_\mu(X) + aX$ , while for  $X \gg b^{-1}$   $E_{\mu,0} \approx (\epsilon + E_\mu(X)) \exp(bX)$ . Thus at shallow depths the differential muon energy spectrum is approximately constant for  $E_\mu < aX$  and steepens to reflect the surface muon spectrum for  $E_\mu > aX$ , whereas for  $X > 2.5 \text{ km.w.e.}$  the differential spectrum underground is again constant for small muon energies but steepens to reflect the surface muon spectrum

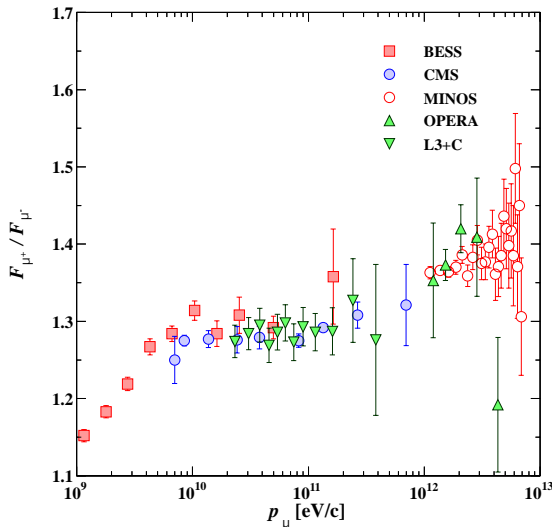


Figure 30.6: Muon charge ratio as a function of the muon momentum from Refs. [51, 59, 65, 70, 71].

for  $E_\mu > \epsilon \approx 0.5 \text{ TeV}$ . In the deep regime the shape is independent of depth although the intensity decreases exponentially with depth. In general the muon spectrum at slant depth  $X$  is

$$\frac{dN_\mu(X)}{dE_\mu} = \frac{dN_\mu}{dE_{\mu,0}} \frac{dE_{\mu,0}}{dE_\mu} = \frac{dN_\mu}{dE_{\mu,0}} e^{bX} \quad (30.7)$$

where  $E_{\mu,0}$  is the solution of Eq. (30.6) in the approximation neglecting fluctuations.

Fig. 30.7 shows the vertical muon intensity versus depth. In constructing this “depth-intensity curve,” each group has taken account of the angular distribution of the muons in the atmosphere, the map of the overburden at each detector, and the properties of the local medium in connecting measurements at various slant depths and zenith angles to the vertical intensity. Use of data from a range of angles allows a fixed detector to cover a wide range of depths. The flat portion of the curve is due to muons produced locally by charged-current interactions of  $\nu_\mu$ . The inset shows the vertical intensity curve for water and ice [79–82]. It is not as steep as the one for rock because of the lower muon energy loss in water.

#### 30.4.2 Neutrinos

Because neutrinos have small interaction cross sections, measurements of atmospheric neutrinos require a deep detector to avoid backgrounds. There are two types of measurements: contained (or semi-contained) events, in which the vertex is determined to originate inside the detector, and neutrino-induced muons. The latter are muons that enter the detector from zenith angles so large (*e.g.*, nearly horizontal or upward) that they cannot be muons produced in the atmosphere. In neither case is the neutrino flux measured directly. What is measured is a convolution of the neutrino flux and cross section with the properties

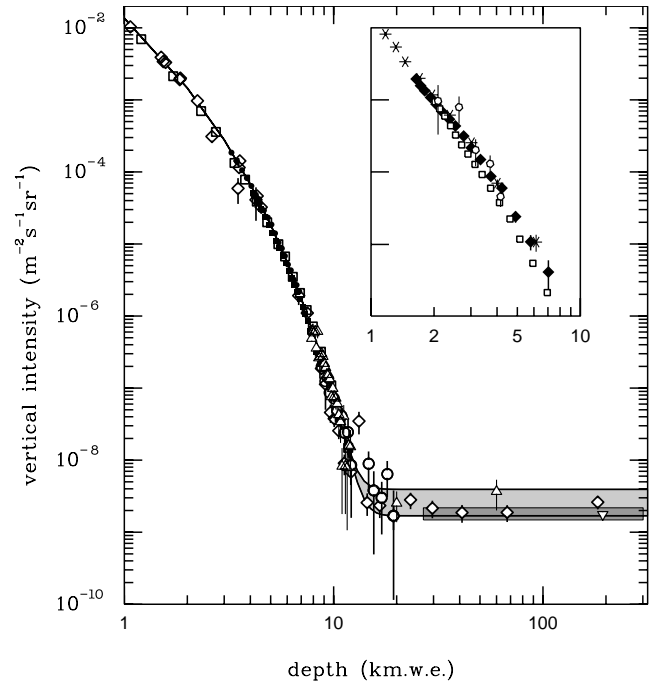


Figure 30.7: Vertical muon intensity vs depth (1 km.w.e. =  $10^5 \text{ g cm}^{-2}$  of standard rock). The experimental data are from:  $\diamond$ : the compilations of Crouch [73],  $\square$ : Baksanu [74],  $\circ$ : LVD [75],  $\bullet$ : MACRO [76],  $\blacksquare$ : Frejus [77], and  $\triangle$ : SNO [78]. The shaded area at large depths represents neutrino-induced muons of energy above 2 GeV. The upper line is for horizontal neutrino-induced muons, the lower one for vertically upward muons. Darker shading shows the muon flux measured by the SuperKamiokande experiment. The inset shows the vertical intensity curve for water and ice published in Refs. [79–82]. Additional data extending to slant depths of 13 km are available in [83].



**Table 30.3:** Measured fluxes ( $10^{-9} \text{ m}^{-2} \text{ s}^{-1} \text{ sr}^{-1}$ ) of neutrino-induced muons as a function of the effective minimum muon energy  $E_\mu$ .

$E_\mu >$	1 GeV	1 GeV	1 GeV	2 GeV	3 GeV	3 GeV
Ref.	CWI [84]	Baksan [85]	MACRO [86, 87]	IMB [88, 89]	Kam [90]	SuperK [91]
$F_\mu$	$2.17 \pm 0.21$	$2.77 \pm 0.17$	$2.29 \pm 0.15$	$2.26 \pm 0.11$	$1.94 \pm 0.12$	$1.74 \pm 0.07$

of the detector (which includes the surrounding medium in the case of entering muons). This section focuses on neutrinos below about 1 TeV. For discussion of atmospheric neutrinos in the TeV–PeV region including a prompt component produced by charmed meson decays, see Ref. [53].

Contained and semi-contained events reflect neutrinos in the sub-GeV to multi-GeV region where the product of increasing cross section and decreasing flux is maximum. In the GeV region the neutrino flux and its angular distribution depend on the geomagnetic location of the detector and, to a lesser extent, on the phase of the solar cycle. Naively, we expect  $\nu_\mu/\nu_e = 2$  from counting neutrinos of the two flavors coming from the chain of pion and muon decays. Contrary to expectation, however, the numbers of the two classes of events are similar rather than different by a factor of two. This is now understood to be a consequence of neutrino flavor oscillations [92]. (See the article on neutrino properties in this *Review*.)

Two well-understood properties of atmospheric cosmic rays provide a standard for comparison of the measurements of atmospheric neutrinos to expectation. These are the “sec  $\theta$  effect” and the “east-west effect” [93]. The former refers originally to the enhancement of the flux of  $> 10$  GeV muons (and neutrinos) at large zenith angles because the parent pions propagate more in the low density upper atmosphere where decay is enhanced relative to interaction. For neutrinos from muon decay, the enhancement near the horizontal becomes important for  $E_\nu > 1$  GeV and arises mainly from the increased pathlength through the atmosphere for muon decay in flight. Fig. 14.4 from Ref. [94] shows a comparison between measurement and expectation for the zenith angle dependence of multi-GeV electron-like (mostly  $\nu_e$ ) and muon-like (mostly  $\nu_\mu$ ) events separately. The  $\nu_e$  show an enhancement near the horizontal and approximate equality for nearly upward ( $\cos \theta \approx -1$ ) and nearly downward ( $\cos \theta \approx 1$ ) events. There is, however, a very significant deficit of upward ( $\cos \theta < 0$ )  $\nu_\mu$  events, which have long pathlengths comparable to the radius of the Earth. This feature is the principal signature for atmospheric neutrino oscillations [92].

Muons that enter the detector from outside after production in charged-current interactions of neutrinos naturally reflect a higher energy portion of the neutrino spectrum than contained events because the muon range increases with energy as well as the cross section. The relevant energy range is  $\sim 10 < E_\nu < 1000$  GeV, depending somewhat on angle. Neutrinos in this energy range show a sec  $\theta$  effect similar to muons (see Eq. (30.4)). This causes the flux of horizontal neutrino-induced muons to be approximately a factor two higher than the vertically upward flux. The upper and lower edges of the horizontal shaded region in Fig. 30.7 correspond to horizontal and vertical intensities of neutrino-induced muons. Table 30.3 gives the measured fluxes of upward-moving neutrino-induced muons averaged over the lower hemisphere. Generally the definition of minimum muon energy depends on where it passes through the detector. The tabulated effective minimum energy estimates the average over various accepted trajectories.

### 30.5 Air Showers

So far we have discussed inclusive or uncorrelated fluxes of various components of the cosmic radiation. An air shower is caused by a single cosmic ray with energy high enough for its cascade to be detectable at the ground. The shower has a hadronic core, which acts as a collimated source of electromagnetic subshowers, generated mostly from  $\pi^0 \rightarrow \gamma\gamma$  decays. The resulting electrons and positrons are the most numerous charged particles in the shower. The number of muons, produced by decays of charged mesons, is an order of magnitude lower. Air showers spread over a large area on the ground, and arrays of detectors operated for long times are useful for studying cosmic rays with primary en-

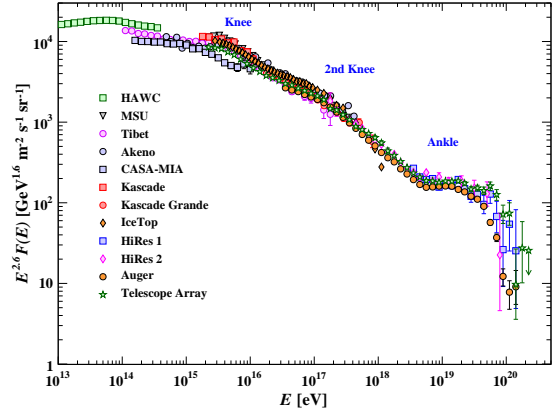


Figure 30.8: The all-particle spectrum as a function of  $E$  (energy-per-nucleus) from air shower measurements [95–105]

ergy  $E_0 > 100$  TeV, where the low flux makes measurements with small detectors in balloons and satellites difficult.

Greisen [106] gives the following approximate analytic expressions for the numbers and lateral distributions of particles in showers at ground level. The total number of muons  $N_\mu$  with energies above 1 GeV is

$$N_\mu(> 1\text{GeV}) \approx 0.95 \times 10^5 \left( N_e/10^6 \right)^{3/4}, \quad (30.8)$$

where  $N_e$  is the total number of charged particles in the shower (not just  $e^\pm$ ). The number of muons per square meter,  $\rho_\mu$ , as a function of the lateral distance  $r$  (in meters) from the center of the shower is

$$\rho_\mu = \frac{1.25 N_\mu}{2\pi \Gamma(1.25)} \left( \frac{1}{320} \right)^{1.25} r^{-0.75} \left( 1 + \frac{r}{320} \right)^{-2.5}, \quad (30.9)$$

where  $\Gamma$  is the gamma function. The number density of charged particles is

$$\rho_e = C_1(s, d, C_2) x^{(s-2)} (1+x)^{(s-4.5)} (1+C_2 x^d). \quad (30.10)$$

Here  $s$ ,  $d$ , and  $C_2$  are parameters in terms of which the overall normalization constant  $C_1(s, d, C_2)$  is given by

$$C_1(s, d, C_2) = \frac{N_e}{2\pi r_1^2} [B(s, 4.5 - 2s) C_2 B(s + d, 4.5 - d - 2s)]^{-1}, \quad (30.11)$$

where  $B(m, n)$  is the beta function. The values of the parameters depend on shower size ( $N_e$ ), depth in the atmosphere, identity of the primary nucleus, etc. For showers with  $N_e \approx 10^6$  at sea level, Greisen uses  $s = 1.25$ ,  $d = 1$ , and  $C_2 = 0.088$ . Finally,  $x$  is  $r/r_1$ , where  $r_1$  is the Molière radius, which depends on the density of the atmosphere and hence on the altitude at which showers are detected. At sea level  $r_1 \approx 78$  m. It increases with altitude as the air density decreases. (See the section on electromagnetic cascades in the article on the passage of particles through matter in this *Review*.)

The lateral spread of a shower is determined largely by Coulomb scattering of the many low-energy electrons and is characterized by the Molière radius. The lateral spread of the muons ( $\rho_\mu$ ) is larger and depends on the transverse momenta of the muons at production as well as multiple scattering.

There are large fluctuations in development from shower to shower, even for showers initiated by primaries of the same energy and mass—especially for small showers, which are usually

well past maximum development when observed at the ground. Thus the shower size  $N_e$  and primary energy  $E_0$  are only related in an average sense, and even this relation depends on depth in the atmosphere. One estimate of the relation is [98]

$$E_0 \sim 3.9 \times 10^6 \text{ GeV} (N_e/10^6)^{0.9} \quad (30.12)$$

for vertical showers with  $10^{14} < E < 10^{17}$  eV at  $920 \text{ g cm}^{-2}$  (965 m above sea level). As  $E_0$  increases, the shower maximum (on average) moves down into the atmosphere and the relation between  $N_e$  and  $E_0$  changes. Moreover, because of fluctuations,  $N_e$  as a function of  $E_0$  is not correctly obtained by inverting Eq. (30.12). At the maximum of shower development, there are approximately 2/3 particles per GeV of primary energy.

Cosmic ray shower development is sensitive to hadronic physics in the forward region above energies that can be probed at accelerators. Hadronic interaction models used to interpret air shower measurements now incorporate data from the LHC, reducing the extrapolation required. However, differences between the simulated and observed properties of showers remain. Most notably, the observed muon content of showers near  $10^{19}$  eV exceeds that given by models by 30–60% [107].

There are three common types of air shower detectors: shower arrays that measure a ground parameter related to shower size  $N_e$  and muon number  $N_\mu$  as well as the lateral distribution on the ground, optical Cherenkov and radio detectors that detect forward-beamed emission by the charged particles of the shower, and ‘fluorescence’ detectors that measure nitrogen scintillation excited by the charged particles in the shower. The fluorescence light is emitted isotropically so the showers can be observed from the side. Detection of radiofrequency emission from showers via geomagnetic and Askaryan mechanisms has been successfully employed in recent experiments [108]. Detailed simulations and cross-calibrations between different types of detectors are necessary to establish the primary energy spectrum from air-shower experiments.

Figure 30.8 shows the ‘all-particle’ spectrum. The differential energy spectrum has been multiplied by  $E^{2.6}$  in order to display the features of the steep spectrum that are otherwise difficult to discern. The steepening that occurs between  $10^{15}$  and  $10^{16}$  eV is known as the *knee* of the spectrum. Another steepening occurs around  $10^{17}$  eV, known as the *second knee*. The feature around  $10^{18.5}$  eV is called the *ankle* of the spectrum.

Air shower experiments typically have uncertain energy scales, dependent on an assumed composition and on the hadronic interaction model used when interpreting the data. Their systematic errors are therefore simplest when plotting  $\frac{dN}{d \ln E} = E \frac{dN}{dE}$ . When the spectrum is multiplied by a different power of energy, systematic errors in energy scale result in an apparent shift in the normalization of the spectrum; for example, when the spectrum is multiplied by  $E^{2.6}$  a systematic shift of 20% in the energy scale results in a 34% change in the normalization of the plotted flux. See Ref. [53], §2.5.2 for further discussion of this issue.

In the energy range above  $10^{17}$  eV, the fluorescence technique [109] is particularly useful because it can establish the primary energy in a nearly model-independent way by observing most of the longitudinal development of each shower, from which  $E_0$  is obtained by integrating the energy deposition in the atmosphere. The result, however, depends strongly on the light absorption in the atmosphere and the calculation of the detector’s aperture.

Assuming the cosmic-ray spectrum below  $10^{18}$  eV is of galactic origin, the knee could indicate that most cosmic accelerators in the Galaxy have reached their maximum energy for acceleration of protons. Some types of expanding supernova remnants, for example, are estimated not to be able to accelerate protons above energies in the range of  $10^{15}$  eV. Effects of propagation and confinement in the Galaxy [110] also need to be considered. A discussion of models of the knee may be found in Ref. [111].

The second knee may have a similar origin to the knee, but corresponding to steepening of the spectrum of heavy nuclei, particularly iron. The Cascade-Grande experiment has reported observation of a second steepening of the spectrum near  $8 \times 10^{16}$  eV, with evidence that this structure is accompanied by a transition to

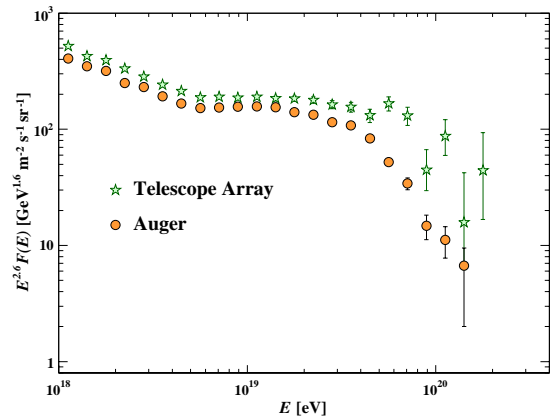


Figure 30.9: Expanded view of the highest energy portion of the cosmic-ray spectrum from data of the Pierre Auger Observatory [104] and the Telescope Array [105].

electron-poor showers resulting from heavy primaries [101]. Cascade Grande has also reported that the spectrum of light nuclei is steeper than the all-particle spectrum below the second knee and flattens in the vicinity of the second knee [112]. IceCube has performed a composition analysis using coincident surface (Ice-Top) and in-ice data, and finds that the mean logarithmic mass increases between  $5 \times 10^{15}$  eV and  $10^{17}$  eV [113]. Together, these data are suggestive that the knee and second knee may result from a *Peters cycle*, with a steepening of the spectrum of each primary element taking place at the same rigidity but different energy per particle [114].

The Auger and Telescope Array (TA) experiments have studied composition using the depth of shower maximum  $X_{max}$ , a quantity that correlates strongly with  $\ln(E/A)$  and with the interaction cross section of the primary particle. The Auger collaboration [115], using a post-LHC hadronic interaction model, reports a composition becoming light up to  $2 \times 10^{18}$  eV but then becoming heavier above that energy, with the mean mass intermediate between protons and iron at  $3 \times 10^{19}$  eV. The TA collaboration [116], using a different post-LHC model, has interpreted their data as implying a light primary composition (mainly p and He) of ultrahigh-energy cosmic-rays (UHECR) from  $1.3 \times 10^{18}$  to  $4 \times 10^{19}$  eV. Auger and TA have also conducted a thorough joint analysis [117] and state that, at the current level of statistics and understanding of systematics, both data sets are compatible with being drawn from the same parent distribution, and that the TA data is compatible both with a light composition below  $10^{19}$  eV and with the mixed composition above  $10^{19}$  eV as reported by Auger.

Possible contributions to the origin of the ankle include a higher energy population of particles overtaking a lower energy population, for example an extragalactic flux beginning to dominate over the Galactic flux (e.g. Ref. [109]). Another proposed mechanism is that the dip structure in the region of the ankle is due to  $p\gamma \rightarrow e^+ + e^-$  energy losses of extragalactic protons on the 2.7 K cosmic microwave radiation (CMB) [118].

If the cosmic-ray flux at the highest energies is extragalactic in origin, there should be a rapid steepening of the spectrum (called the GZK feature) around  $5 \times 10^{19}$  eV, resulting from the onset of inelastic interactions of UHE cosmic rays with the cosmic microwave background [119] [120]. Photo-dissociation of heavy nuclei in the mixed composition model [121] would have a similar effect. UHECR experiments have detected events of energy above  $10^{20}$  eV [109, 122]. The HiRes fluorescence experiment [103, 123] detected evidence of a suppression consistent with the GZK effect, and the Auger observatory [104] has also presented spectra showing this suppression based on surface detector measurements calibrated against fluorescence detectors using events detected in hybrid mode, i.e. with both the surface and the fluorescence detectors. The Telescope Array (TA) [105] has also presented a spectrum showing this suppression. The differential energy spec-

tra measured by the TA and by Auger agree within systematic errors below  $10^{19}$  eV (Fig. 30.9).

Cosmic rays above  $5 \times 10^{19}$  eV are predominantly from nearby sources ( $< 100$  Mpc). Auger has reported the observation of a dipole of amplitude  $6.6^{+1.2}_{-0.8}\%$  for cosmic rays with energies above  $8 \times 10^{18}$  eV. The direction of the dipole indicates an extragalactic origin for these particles [124]. There are also hints of structure at smaller angular scales. TA has reported a ‘hot spot’ in the Northern Hemisphere at energies above  $5.5 \times 10^{19}$  eV of radius  $\sim 25^\circ$  with a chance probability of this excess with respect to an isotropic distribution of  $2.1 \times 10^{-3}$  [125]. Auger has also reported an excess of events above  $3.7 \times 10^{19}$  eV in a region near the radio-loud active galaxy Centaurus A with a post-trial significance of  $3.9\sigma$ , and a correlation of the distribution of ultrahigh energy events with several catalogs of nearby astrophysical objects, with starburst galaxies giving the highest significance at  $4.5\sigma$  [126].

### 30.6 Neutrinos at High Energies

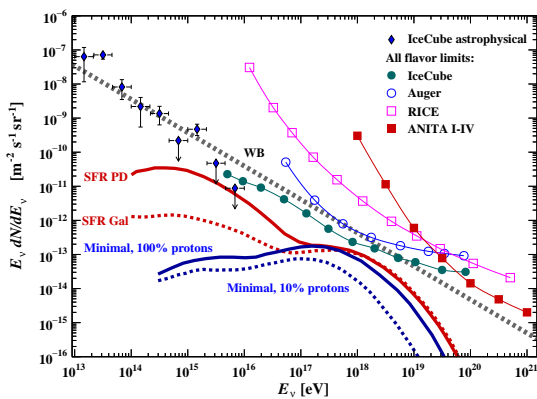


Figure 30.10: The best-fit IceCube *astrophysical* all-flavor neutrino flux [127]. Also shown are differential limits on the flux of *cosmogenic* neutrinos set by four experiments [128–131]. The IceCube limit on cosmogenic neutrinos accounts for a nuisance background of astrophysical neutrinos. The curves show the Waxman-Bahcall benchmark flux (solid grey) [132, 133], cosmogenic models with cosmic ray sources with maximum proton energy of  $10^{20.5}$  eV evolving with the star-formation rate in proton dip (solid red) and Galactic composition (dashed red) scenarios [134], and ‘minimal’ cosmogenic models with protons constituting 100% (solid blue) and 10% (dashed red) of the cosmic rays [135].

Neutrinos are expected to be produced in hadronic interactions in a variety of astrophysical objects. IceCube has reported a population of astrophysical neutrino events extending from tens of TeV to beyond ten PeV [127, 136, 137]. Multimessenger observations of the flaring blazar TXS 0506+056 have identified this object as a high-energy neutrino source [138, 139].

There is also expected to be a neutrino flux produced in cosmic ray GZK interactions. Measuring this *cosmogenic*<sup>4</sup> neutrino flux above  $10^{18}$  eV would help resolve the UHECR uncertainties mentioned above. One half of the energy that UHECR protons lose in photoproduction interactions that cause the GZK effects ends up in neutrinos [140]. Heavier nuclei produce lower energy neutrinos due to the lower energy of their constituent nucleons. The magnitude of the cosmogenic neutrino flux depends strongly on the cosmic-ray spectrum at acceleration, the cosmic-ray composition, the cosmological evolution of the cosmic-ray sources, and the energy of the Galactic-extragalactic transition.

The expected rate of cosmogenic neutrinos is lower than current limits obtained by IceCube [127], the Auger observatory [130], RICE [129, 141], and ANITA [131], which are shown in Fig. 30.10 together with a models for cosmogenic neutrino production [134, 135] and the Waxman-Bahcall benchmark flux of

neutrinos produced in cosmic ray sources [132, 133]. At production, the dominant component of neutrinos comes from  $\pi^\pm$  decays and has flavor content  $\nu_e:\nu_\mu:\nu_\tau = 1:2:0$ . After oscillations, the arriving cosmogenic neutrinos are expected to be a 1:1:1 mixture of flavors. The sensitivity of each experiment depends on neutrino flavor, and all limits are expressed as three-flavor limits assuming a 1:1:1 mixture.

### References

- [1] O. Adriani *et al.* (PAMELA), *Science* **332**, 69 (2011).
- [2] M. Aguilar *et al.* (AMS), *Phys. Rev. Lett.* **114**, 171103 (2015).
- [3] M. Aguilar *et al.* (AMS), *Phys. Rev. Lett.* **115**, 21, 211101 (2015).
- [4] K. Abe *et al.*, *Astrophys. J.* **822**, 2, 65 (2016).
- [5] M. J. Christ *et al.*, *Astrophys. J.* **502**, 278 (1998).
- [6] A.D. Panov *et al.* (ATIC Collab.), *Bull. Russian Acad. of Science, Physics*, **73**, 564 (2009).
- [7] V. A. Derbina *et al.* (RUNJOB), *Astrophys. J.* **628**, L41 (2005).
- [8] H. S. Ahn *et al.*, *Astrophys. J.* **707**, 593 (2009).
- [9] J.J. Engelmann *et al.* (HEAO3-C2 Collab.), *Astron. & Astrophys.* **233**, 96 (1990).
- [10] D. Müller *et al.* (CRN Collab.), *Astrophys. J.* **374**, 356 (1991).
- [11] M. Ave *et al.*, *Astrophys. J.* **678**, 262 (2008).
- [12] F. Aharonian *et al.* (H.E.S.S.), *Phys. Rev.* **D75**, 042004 (2007).
- [13] A. Archer *et al.* (VERITAS), *Phys. Rev.* **D98**, 2, 022009 (2018).
- [14] D. Maurin *et al.*, *Astron. & Astrophys.* **569**, A32 (2014).
- [15] A. W. Strong, I. V. Moskalenko and V. S. Ptuskin, *Ann. Rev. Nucl. Part. Sci.* **57**, 285 (2007).
- [16] R.A. Mewaldt *et al.*, *Space Science Reviews* 99,27(2001).
- [17] A. A. Abdo *et al.*, *Astrophys. J.* **698**, 2121 (2009).
- [18] A. U. Abeysekara *et al.* (HAWC, IceCube), *Astrophys. J.* **871**, 1, 96 (2019).
- [19] M. Amenomori *et al.*, *Astrophys. J.* **711**, 119 (2010).
- [20] O. Adriani *et al.* (PAMELA), *Phys. Rev. Lett.* **106**, 201101 (2011).
- [21] M. Boezio *et al.*, *Astrophys. J.* **532**, 653 (2000).
- [22] M. Aguilar *et al.* (AMS), *Phys. Rev. Lett.* **122**, 10, 101101 (2019).
- [23] S. Abdollahi *et al.* (Fermi-LAT), *Phys. Rev.* **D95**, 8, 082007 (2017).
- [24] G. Ambrosi *et al.* (DAMPE), *Nature* **552**, 63 (2017).
- [25] O. Adriani *et al.* (CALET), *Phys. Rev. Lett.* **122**, 18, 181102 (2019).
- [26] F. Aharonian *et al.* (H.E.S.S.), *Phys. Rev. Lett.* **101**, 261104 (2008).
- [27] F. Aharonian *et al.* (H.E.S.S.), *Astron. Astrophys.* **508**, 561 (2009).
- [28] A. Archer *et al.* (VERITAS), *Phys. Rev.* **D98**, 6, 062004 (2018).
- [29] Y. Shikaze *et al.*, *Astropart. Phys.* **28**, 154 (2007).
- [30] O. Adriani *et al.* (PAMELA), *Nature* **458**, 607 (2009).
- [31] O. Adriani *et al.*, *Phys. Rev. Lett.* **102**, 051101 (2009).
- [32] J.J. Beatty *et al.*, *Phys. Rev. Lett.* **93**, 24112 (2004).
- [33] I. V. Moskalenko and A. W. Strong, *Astrophys. J.* **493**, 694 (1998).
- [34] A. Ibarra, D. Tran and C. Weniger, *Int. J. Mod. Phys.* **A28**, 1330040 (2013).
- [35] D. Gaggero *et al.*, *Phys. Rev. Lett.* **111**, 021102 (2013).

<sup>4</sup>Here we use cosmogenic to denote neutrinos produced by photoproduction during propagation, and astrophysical to denote neutrinos produced by other mechanisms or close to sources.

- [36] P.-F. Yin *et al.*, Phys. Rev. **D88**, 2, 023001 (2013).
- [37] M. Aguilar *et al.* (AMS), Phys. Rev. Lett. **110**, 141102 (2013).
- [38] L. Accardo *et al.* (AMS), Phys. Rev. Lett. **113**, 121101 (2014).
- [39] J. Nishimura *et al.*, Adv. Space Research **19**, 767 (1997).
- [40] A. S. Beach *et al.*, Phys. Rev. Lett. **87**, 271101 (2001).
- [41] A. Yamamoto *et al.*, Adv. Space Research **42**, 443(2008).
- [42] Y. Asaoka *et al.*, Phys. Rev. Lett. **88**, 51101 (2002).
- [43] K. Abe *et al.*, Phys. Rev. Lett. **108**, 131301 (2012).
- [44] H. Fuke *et al.*, Phys. Rev. Lett. **95**, 081101 (2005).
- [45] I. Cholis, D. Hooper and T. Linden, Phys. Rev. **D93**, 4, 043016 (2016).
- [46] R. Bellotti *et al.*, Phys. Rev. **D53**, 35 (1996).
- [47] R. Bellotti *et al.* (WiZard/MASS2), Phys. Rev. **D60**, 052002 (1999).
- [48] M. Boezio *et al.* (WiZard/CAPRICE), Phys. Rev. **D62**, 032007 (2000).
- [49] M. Boezio *et al.*, Phys. Rev. **D67**, 072003 (2003).
- [50] S. Coutu *et al.*, Phys. Rev. **D62**, 032001 (2000).
- [51] S. Haino *et al.*, Phys. Lett. **B594**, 35 (2004).
- [52] T. Sanuki *et al.*, Phys. Rev. **D75**, 043005 (2007).
- [53] T.K. Gaisser, R. Engel, and E. Resconi, *Cosmic Rays and Particle Physics (second edition)*, Cambridge University Press (2016).
- [54] P. Lipari, Astropart. Phys. **1**, 195 (1993).
- [55] E. Mocchiutti *et al.*, in *Proc. 28th Int. Cosmic Ray Conf.*, Tsukuba, 1627 (2003). [<http://adsabs.harvard.edu/abs/2003ICRC...3.1627M>].
- [56] M. P. De Pascale *et al.*, J. Geophys. Res. **98**, A3, 3501 (1993).
- [57] P.K.F. Grieder, *Cosmic Rays at Earth*, Elsevier Science (2001).
- [58] J. Kremer *et al.*, Phys. Rev. Lett. **83**, 4241 (1999).
- [59] P. Achard *et al.* (L3), Phys. Lett. **B598**, 15 (2004).
- [60] O. C. Allkofer, K. Carstensen and D. W. Dau, Phys. Lett. **36B**, 425 (1971).
- [61] B. C. Rastin, J. Phys. **G10**, 1609 (1984).
- [62] C. A. Ayre *et al.*, J. Phys. **G1**, 584 (1975).
- [63] H. Jokisch *et al.*, Phys. Rev. **D19**, 1368 (1979).
- [64] C. G. S. Costa, Astropart. Phys. **16**, 193 (2001).
- [65] P. Adamson *et al.* (MINOS), Phys. Rev. **D76**, 052003 (2007).
- [66] S. Hayakawa, *Cosmic Ray Physics*, Wiley, Interscience, New York (1969).
- [67] R.R. Daniel and S.A. Stephens, Revs. Geophysics & Space Sci. **12**, 233 (1974).
- [68] K.P. Beuermann and G. Wibberenz, Can. J. Phys. **46**, S1034 (1968).
- [69] I. S. Diggory *et al.*, J. Phys. **A7**, 741 (1974).
- [70] V. Khachatryan *et al.* (CMS), Phys. Lett. **B692**, 83 (2010).
- [71] N. Agafonova *et al.* (OPERA), Eur. Phys. J. **C67**, 25 (2010).
- [72] P. Lipari and T. Stanev, Phys. Rev. **D44**, 3543 (1991).
- [73] M. Crouch, in *Proc. 20th Int. Cosmic Ray Conf.*, Moscow, **6**, 165 (1987) [<http://adsabs.harvard.edu/abs/1987ICRC...6..165C>].
- [74] Yu.M. Andreev, V.I. Gurentzov, and I.M. Kogai, in *Proc. 20th Int. Cosmic Ray Conf.*, Moscow, **6**, 200 (1987), [<http://adsabs.harvard.edu/abs/1987ICRC...6..200A>].
- [75] M. Aglietta *et al.* (LVD), Astropart. Phys. **3**, 311 (1995).
- [76] M. Ambrosio *et al.* (MACRO), Phys. Rev. **D52**, 3793 (1995).
- [77] C. Berger *et al.* (FREJUS), Phys. Rev. **D40**, 2163 (1989).
- [78] C. Waltham *et al.*, in *Proc. 27th Int. Cosmic Ray Conf.*, Hamburg, 991 (2001), [<http://adsabs.harvard.edu/abs/2001ICRC...3..991W>].
- [79] I. A. Belolaptikov *et al.* (BAIKAL), Astropart. Phys. **7**, 263 (1997).
- [80] J. Babson *et al.* (DUMAND), Phys. Rev. **D42**, 3613 (1990).
- [81] P. Desiati *et al.*, in *Proc. 28th Int. Cosmic Ray Conf.*, Tsukuba, 1373 (2003) [<http://adsabs.harvard.edu/abs/2003ICRC...3.1373D>].
- [82] T. Pradier (ANTARES), in "Proceedings, 43rd Rencontres de Moriond on Electroweak Interactions and Unified Theories: La Thuile, Italy, March 1-8, 2008," 423-430 (2008).
- [83] S. Aiello *et al.* (NEMO), Astropart. Phys. **66**, 1 (2015).
- [84] F. Reines *et al.*, Phys. Rev. Lett. **15**, 429 (1965).
- [85] M.M. Boliev *et al.*, in *Proc. 3rd Int. Workshop on Neutrino Telescopes* (ed. Milla Baldo Ceolin), 235 (1991).
- [86] M. Ambrosio *et al.* (MACRO), Phys. Lett. **B434**, 451 (1998).
- [87] F. Ronga (MACRO), in "Proceedings, 26th International Cosmic Ray Conference (ICRC), August 17-25, 1999, Salt Lake City: Invited, Rapporteur, and Highlight Papers," volume 2, 172 (1999), URL [http://krusty.physics.utah.edu/~icrc1999/root/vol2/h4\\_1\\_07.pdf](http://krusty.physics.utah.edu/~icrc1999/root/vol2/h4_1_07.pdf).
- [88] R. Becker-Szendy *et al.*, Phys. Rev. Lett. **69**, 1010 (1992).
- [89] *Proc. 25th Int. Conf. High-Energy Physics*, Singapore (eds. K.K. Phua and Y. Yamaguchi, World Scientific), 662 1991.
- [90] S. Hatakeyama *et al.* (Kamiokande), Phys. Rev. Lett. **81**, 2016 (1998).
- [91] Y. Fukuda *et al.* (Super-Kamiokande), Phys. Rev. Lett. **82**, 2644 (1999).
- [92] Y. Fukuda *et al.* (Super-Kamiokande), Phys. Rev. Lett. **81**, 1562 (1998).
- [93] T. Futagami *et al.* (Super-Kamiokande), Phys. Rev. Lett. **82**, 5194 (1999).
- [94] Y. Ashie *et al.* (Super-Kamiokande), Phys. Rev. **D71**, 112005 (2005).
- [95] R. Alfaro *et al.* (HAWC), Phys. Rev. **D96**, 12, 122001 (2017).
- [96] Yu. A. Fomin *et al.*, *Proc. 22nd Int. Cosmic Ray Conf.*, Dublin, **2**, 85 (1991) [<http://adsabs.harvard.edu/abs/1991ICRC...2..85F>].
- [97] M. Amenomori *et al.*, Astrophys. J. **268**, 1165 (2008).
- [98] M. Nagano *et al.*, J. Phys. **G10**, 1295 (1984).
- [99] M. A. K. Glasmacher *et al.*, Astropart. Phys. **10**, 291 (1999).
- [100] T. Antoni *et al.* (KASCADE), Astropart. Phys. **24**, 1 (2005).
- [101] W. D. Apel *et al.* (KASCADE Grande), Phys. Rev. Lett. **107**, 171104 (2011).
- [102] K. Andeen, M. Plum *et al.*, (IceCube Collab.), *Proceedings of Science (ICRC2019)*, 172 (2019).
- [103] R. U. Abbasi *et al.* (HiRes), Phys. Rev. Lett. **100**, 101101 (2008).
- [104] V. Verzi *et al.*, (Auger Collab.), *Proceedings of Science (ICRC2019)*, 450 (2019).
- [105] D. Ivanov *et al.*, (Telescope Array Collab.), *Proceedings of Science (ICRC2019)*, 298 (2019).
- [106] K. Greisen, Ann. Rev. Nucl. Sci. **10**, 63 (1960).
- [107] A. Aab *et al.* (Pierre Auger), Phys. Rev. Lett. **117**, 19, 192001 (2016).
- [108] T. Huege, Phys. Rept. **620**, 1 (2016).

- [109] D. J. Bird *et al.* (HiRes), *Astrophys. J.* **424**, 491 (1994).
- [110] V.S. Ptuskin *et al.*, *Astron. & Astrophys.* **268**, 726 (1993).
- [111] J. R. Hoerandel, *Astropart. Phys.* **21**, 241 (2004).
- [112] W. D. Apel *et al.*, *Phys. Rev.* **D87**, 081101 (2013), [arXiv:1304.7114].
- [113] M. G. Aartsen *et al.* (IceCube) (2019), [arXiv:1906.04317].
- [114] B. Peters, *Nuovo Cimento* **XXII**, 800 (1961).
- [115] J. Bellido *et al.* (Auger Collab.), *Proceedings of Science(ICRC2017)*, 506 (2017).
- [116] D. Ikeda *et al.* (TA Collab.), *Proceedings of Science(ICRC2017)*, 515 (2017).
- [117] V. de Souza *et al.* (TA and Auger Collabs.), *Proceedings of Science(ICRC2017)*, 522 (2017).
- [118] V. Berezhinsky, A. Z. Gazizov and S. I. Grigorieva, *Phys. Rev.* **D74**, 043005 (2006).
- [119] K. Greisen, *Phys. Rev. Lett.* **16**, 748 (1966).
- [120] G. T. Zatsepin and V. A. Kuzmin, *JETP Lett.* **4**, 78 (1966), [*Pisma Zh. Eksp. Teor. Fiz.*4,114(1966)].
- [121] D. Allard *et al.*, *Astron. & Astrophys.* **443**, L29 (2005).
- [122] M. Takeda *et al.*, *Astropart. Phys.* **19**, 447 (2003).
- [123] R. U. Abbasi *et al.* (HiRes), *Astropart. Phys.* **32**, 53 (2009).
- [124] E. Roulet *et al.*, (Auger Collab.), *Proceedings of Science (ICRC2019)*, 408 (2019).
- [125] K. Kawata *et al.*, (Telescope Array Collab.), *Proceedings of Science (ICRC2019)*, 310 (2019).
- [126] L. Caccianiga *et al.*, (Auger Collab.), *Proceedings of Science (ICRC2019)*, 206 (2019).
- [127] M. G. Aartsen *et al.* (IceCube), *Astrophys. J.* **809**, 1, 98 (2015).
- [128] M. G. Aartsen *et al.* (IceCube), *Phys. Rev.* **D98**, 6, 062003 (2018).
- [129] I. Kravchenko *et al.*, *Phys. Rev.* **D85**, 062004 (2012).
- [130] F. Pedrera *et al.*, (Auger Collab.), *Proceedings of Science (ICRC2019)*, 172 (2019).
- [131] C. Deaconu *et al.*, (ANITA Collab.), *Proceedings of Science (ICRC2019)*, 867 (2019).
- [132] E. Waxman and J. N. Bahcall, *Phys. Rev.* **D59**, 023002 (1999).
- [133] E. Waxman, 33–45 (2017).
- [134] K. Kotera, D. Allard and A. V. Olinto, *JCAP* **1010**, 013 (2010).
- [135] M. Ahlers and F. Halzen, *Phys. Rev.* **D86**, 083010 (2012).
- [136] M. G. Aartsen *et al.* (IceCube), *Science* **342**, 1242856 (2013).
- [137] M. G. Aartsen *et al.* (IceCube), *Phys. Rev. Lett.* **113**, 101101 (2014).
- [138] M. G. Aartsen *et al.* (IceCube, Fermi-LAT, MAGIC, AGILE, ASAS-SN, HAWC, H.E.S.S., INTEGRAL, Kanata, Kiso, Kapteyn, Liverpool Telescope, Subaru, Swift NuSTAR, VERITAS, VLA/17B-403), *Science* **361**, eaat1378 (2018).
- [139] M. G. Aartsen *et al.* (IceCube), *Science* **361**, 6398, 147 (2018).
- [140] V. S. Berezhinsky and G. T. Zatsepin, *Phys. Lett.* **28B**, 423 (1969).
- [141] I. Kravchenko *et al.*, *Phys. Rev.* **D73**, 082002 (2006).

## Experimental Methods and Colliders

31. Accelerator physics of colliders (rev.) . . . . .	521
32. High-energy collider parameters (rev.) . . . . .	529
33. Neutrino beam lines at high-energy proton synchrotrons (rev.)	534
34. Passage of particles through matter (rev.) . . . . .	535
35. Particle detectors at accelerators (rev.) . . . . .	551
36. Particle detectors for non-accelerator phys. (rev.) . . . . .	589
37. Radioactivity and radiation protection (rev.) . . . . .	612
38. Commonly used radioactive sources (rev.) . . . . .	618





## 31. Accelerator Physics of Colliders

Revised August 2019 by M.J. Syphers (Northern Illinois U.; FNAL) and F. Zimmermann (CERN).

This article provides background for the High-Energy Collider Parameter Tables that follow and some additional information.

### 31.1 Luminosity

The number of events,  $N_{exp}$ , is the product of the cross section of interest,  $\sigma_{exp}$ , and the time integral over the instantaneous luminosity,  $\mathcal{L}$ :

$$N_{exp} = \sigma_{exp} \times \int \mathcal{L}(t) dt. \quad (31.1)$$

Today's colliders all employ bunched beams. If two bunches containing  $n_1$  and  $n_2$  particles collide head-on with average collision frequency  $f_{coll}$ , a basic expression for the luminosity is

$$\mathcal{L} = f_{coll} \frac{n_1 n_2}{4\pi \sigma_x^* \sigma_y^*} \mathcal{F} \quad (31.2)$$

where  $\sigma_x^*$  and  $\sigma_y^*$  characterize the rms transverse beam sizes in the horizontal (bend) and vertical directions at the interaction point, and  $\mathcal{F}$  is a factor of order 1, that takes into account geometric effects such as a crossing angle and finite bunch length, and dynamic effects, such as the mutual focusing of the two beam during the collision. For a circular collider,  $f_{coll}$  equals the number of bunches per beam times the revolution frequency. In 31.2, it is assumed that the bunches are identical in transverse profile, that the profiles are Gaussian and independent of position along the bunch, and the particle distributions are not altered during bunch crossing. Nonzero beam crossing angles  $\theta_c$  in the horizontal plane and long bunches (rms bunch length  $\sigma_z$ ) will reduce the luminosity, e.g., by a factor  $\mathcal{F} \approx 1/(1 + \phi^2)^{1/2}$ , where the parameter  $\phi \equiv \theta_c \sigma_z / (2\sigma_x^*)$  is known as the Piwinski angle. Another luminosity reduction for long bunches is due to the "hourglass" effect (see below).

Whatever the distribution at the source, by the time the beam reaches high energy, the normal form is a useful approximation as suggested by the  $\sigma$ -notation. In the case of an electron storage ring, synchrotron radiation leads to a Gaussian distribution in equilibrium, but even in the absence of radiation the central limit theorem of probability and the diminished importance of space charge effects produce a similar result. Beam tails are often modelled by the superposition of a second Gaussian distribution with larger size and much lower intensity.

The luminosity may be obtained directly by measurement of the beam properties in Eq. 31.2. For continuous measurements, an expression similar to Eq. 31.1 with  $N_{ref}$  from a known reference cross section,  $\sigma_{ref}$ , may be used to determine  $\sigma_{exp}$  according to  $\sigma_{exp} = (N_{exp}/N_{ref})\sigma_{ref}$ .

In the Tables, luminosity is stated in units of  $\text{cm}^{-2}\text{s}^{-1}$ . Integrated luminosity, on the other hand, is usually quoted as the inverse of the standard measures of cross section such as femto-barns and, recently, attobarns. Subsequent sections in this report briefly expand on the dynamics behind collider design, comment on the realization of collider performance in a selection of today's facilities, and end with some remarks on future possibilities.

### 31.2 Beam Dynamics

The first concern of beam dynamics is stability. While a reference particle proceeds along the design, or reference, trajectory other particles in the bunch are to remain close by. Assume that the reference particle carries a right-handed Cartesian coordinate system, with the  $z$ -coordinate pointed in the direction of motion along the reference trajectory. The right-handed coordinate system would indicate the reference particle to travel clockwise around a storage ring. The independent variable is the distance  $s$  of the reference particle along this trajectory rather than time, and for simplicity this path is taken to be planar. The transverse coordinates are  $x$  and  $y$ , where  $\{x, z\}$  defines the plane of the reference trajectory.

Several time scales are involved, and the approximations used in writing the equations of motion reflect that circumstance. All of today's high energy colliders are alternating-gradient synchrotrons

or, respectively, storage rings [1,2], and the shortest time scale is that associated with transverse motion, that is described in terms of betatron oscillations, so called because of their analysis for the betatron accelerator species years ago. The linearized equations of motion of a particle displaced from the reference particle are

$$\begin{aligned} x'' + K_x x &= 0, & K_x &\equiv \frac{q}{p} \frac{\partial B}{\partial x} + \frac{1}{\rho^2} \\ y'' + K_y y &= 0, & K_y &\equiv -\frac{q}{p} \frac{\partial B}{\partial y} \\ z' &= -x/\rho \end{aligned} \quad (31.3)$$

where the magnetic field  $B(s)$  along the design trajectory is only in the  $y$  direction, contains only dipole and quadrupole terms, and is treated as static here. The radius of curvature due to the field on the reference orbit is  $\rho$ ;  $z$  represents the longitudinal distance from the reference particle;  $p$  and  $q$  are the particle's momentum and charge, respectively. The prime denotes  $d/ds$ . The pair  $(x, x')$  describes approximately-canonical variables. For more general cases (e.g. acceleration) one should use  $(x, p_x)$  instead, where  $p_x$  denotes the transverse momentum in the  $x$ -direction.

The equations for  $x$  and  $y$  are those of harmonic oscillators but with a restoring force periodic in  $s$ ; that is, they are instances of Hill's equation. The solution may be written in the form

$$x(s) = A_x \sqrt{\beta_x} \cos \psi_x \quad (31.4)$$

$$x'(s) = -\frac{A_x}{\sqrt{\beta_x}} [\alpha_x \cos \psi_x + \sin \psi_x] \quad (31.5)$$

where  $A_x$  is a constant of integration,  $\alpha_x \equiv -(1/2)d\beta_x(s)/ds$ , and the envelope of the motion is modulated by the *amplitude function*,  $\beta_x$ . A solution of the same form describes the motion in  $y$ . The subscripts will be suppressed in the following discussion.

The amplitude function satisfies

$$2\beta\beta'' - \beta'^2 + 4\beta^2 K = 4, \quad (31.6)$$

and in a region free of magnetic field it should be noted that the solution of Eq. 31.6 is a parabola. Expressing  $A$  in terms of  $x$ ,  $x'$  yields

$$\begin{aligned} A^2 &= \gamma x^2 + 2\alpha x x' + \beta x'^2 \\ &= \frac{1}{\beta} [x^2 + (\alpha x + \beta x')^2] \end{aligned} \quad (31.7)$$

with  $\gamma \equiv (1 + \alpha^2)/\beta$ . In a single pass system such as a linac, the *Courant-Snyder parameters*  $\alpha$ ,  $\beta$ ,  $\gamma$  may be selected to match the  $x$ ,  $x'$  distribution of the input beam; in a recursive system, the parameters are usually defined by the structure rather than by the beam.

The relationships between the parameters and the structure may be seen by treatment of a simple *lattice* consisting of equally-spaced thin-lens quadrupoles whose magnetic-field gradients are equal in magnitude but alternating in sign. For this discussion, the weak focusing effects of the bending magnets may be neglected. The propagation of  $X \equiv \{x, x'\}$  through a repetition period may be written  $X_2 = MX_1$ , with the matrix  $M = FODO$  composed of the matrices

$$F = \begin{pmatrix} 1 & 0 \\ -1/f & 1 \end{pmatrix}, \quad D = \begin{pmatrix} 1 & 0 \\ 1/f & 1 \end{pmatrix}, \quad O = \begin{pmatrix} 1 & L \\ 0 & 1 \end{pmatrix}, \quad (31.8)$$

where  $f$  is the magnitude of the focal length and  $L$  the lens spacing. Then

$$M = \begin{pmatrix} 1 + \frac{L}{f} & 2L + \frac{L^2}{f} \\ -\frac{L}{f^2} & 1 - \frac{L}{f} - \frac{L^2}{f^2} \end{pmatrix}. \quad (31.9)$$

The matrix for  $y$  is identical in form differing only by a change in sign of the terms linear in  $1/f$ . An eigenvector-eigenvalue analysis of the matrix  $M$  shows that the motion is stable provided  $f > L/2$ . While that criterion is easily met, in practice instability may be caused by many other factors, including the beam-beam interaction.

Standard focus-drift-defocus-drift, or *FODO*, cells such as characterized in simple form by Eq. 31.9 occupy most of the layout of



a large collider ring and may be used to set the scale of the amplitude function and related phase advance. Conversion of Eq. 31.4 to a matrix form equivalent to Eq. 31.9 (but more generally valid, i.e. for any stable periodic linear motion) gives

$$M = \begin{pmatrix} C + \alpha S & \beta S \\ -\gamma S & C - \alpha S \end{pmatrix} \quad (31.10)$$

where  $C \equiv \cos \Delta\psi$ ,  $S \equiv \sin \Delta\psi$ , and the relation between structure and amplitude function is specified by setting the values of the latter to be the same at both ends of the cell. By comparison of Eq. 31.9 and Eq. 31.10 one finds  $C = 1 - L^2/(2f^2)$ , so that the choice  $f = L/\sqrt{2}$  would give a phase advance  $\Delta\psi$  of 90 degrees for the standard cell. The amplitude function would have a maximum at the focusing quadrupole of magnitude  $\hat{\beta} = 2.7L$ , illustrating the relationship of alternating gradient focusing amplitudes to relatively local aspects of the design. Other functionalities such as injection, extraction, and HEP experiments are included by lattice sections matched to the standard cell parameters ( $\beta$ ,  $\alpha$ ) at the insertion points.

The phase advances according to  $d\psi/ds = 1/\beta$ ; that is,  $\beta$  also plays the role of a local  $\lambda/2\pi$ , and the *tune*,  $\nu$ , is the number of such oscillations per turn about the closed path. In the neighborhood of an interaction point (IP), the beam optics of the ring is configured so as to produce a narrow focus; the value of the amplitude function at this point is designated  $\beta^*$ .

The motion as it develops with  $s$  describes an ellipse in  $\{x, x' \equiv dx/ds\}$  phase space, the area of which is  $\pi A^2$ , where  $A$  is the constant in Eq. 31.4. If the interior of that ellipse is populated by an ensemble of non-interacting particles, that area, given the name *emittance* and denoted by  $\varepsilon$ , would change only with energy. More precisely, for a beam with a Gaussian distribution in  $x, x'$ , the area containing one standard deviation  $\sigma_x$ , divided by  $\pi$ , is used as the definition of emittance in the Tables:

$$\varepsilon_x \equiv \frac{\sigma_x^2}{\beta_x}, \quad (31.11)$$

with a corresponding expression in the other transverse direction,  $y$ . For most of the entries in the Tables the standard deviation is used as the beam radius.

At larger transverse amplitudes, due to the influence of nonlinear magnetic fields, the particle motion does not remain linear. Nonlinear fields arise, e.g., from the sextupole magnets deployed to correct the chromaticity (i.e., the change of focusing with particle momentum), or from persistent-current field errors in the superconducting magnets of hadron synchrotrons. At a certain amplitude the nonlinear particle motion ceases to be stable, and particles are lost after circulating for a possibly large number of turns. This limit of stability is called the “dynamic aperture”.

To complete the coordinates used to describe the particle motion, and to characterize the longitudinal behavior, we take as the variable conjugate to  $z$  the fractional momentum deviation  $\delta p/p$  from that of the reference particle. Radiofrequency electric fields in the  $s$  direction provide a means for longitudinal oscillations, and the frequency determines the bunch length. The frequency of this system appears in the Tables as does the rms value of  $\delta p/p$  characterized as “energy spread” of the beam.

For HEP bunch length is a significant quantity for a variety of reasons, but in the present context if the bunch length, or (with nonzero crossing angle) the effective interaction length, becomes larger than  $\beta^*$  the luminosity is adversely affected. This is because  $\beta$  grows parabolically as one proceeds away from the interaction point and so the beam size increases thus lowering the contribution to the luminosity from such locations. This is often called the “hourglass” effect.

In a storage ring, the bunch length tends to increase with higher bunch intensity due to the so-called longitudinal “impedance” or “wake fields”. Similar collective electromagnetic interactions with the beam environment can lead to longitudinal and transverse single- or multi-bunch instabilities [3,4], which may either increase energy spread or beam emittance, and even result in a beam loss.

Another major external electromagnetic field interaction, in the single particle context, is the production of synchrotron radiation

due to centripetal acceleration, given by the Larmor formula multiplied by a relativistic magnification factor of  $\gamma^4$  [5]. In the case of electron rings this process determines the equilibrium emittance through a balance between radiation damping and excitation of oscillations, and further serves as a barrier to future higher energy versions in this variety of collider. A more comprehensive discussion of betatron oscillations, longitudinal motion, and synchrotron radiation is available in the 2008 version of the PDG review [6].

Synchrotron radiation emitted during the collision in the field of the opposing beam is called beamstrahlung. Beamstrahlung is relevant for both linear colliders, where it may degrade the luminosity spectrum, and for future highest-energy circular colliders, where it may limit the beam lifetime, and also increases the energy spread and bunch length of the stored beam. For both types of colliders the beamstrahlung is mitigated by making the colliding beams as flat as possible at the interaction point ( $\sigma_x^* \gg \sigma_y^*$ ). The photon energy spectrum of the beamstrahlung is characterized by the parameter Upsilon  $\Upsilon = (2/3)\hbar\omega_c/E_b$  [7], with  $\hbar\omega_c$  denoting the critical photon energy and  $E_b$  the beam energy. The spectrum strongly deviates from the classical synchrotron radiation spectrum for  $\Upsilon$  approaching 1.

### 31.3 Road to High Luminosity

Eq. 31.2 can be recast in terms of emittances and amplitude functions as

$$\mathcal{L} = f \frac{n_1 n_2}{4\pi \sqrt{\varepsilon_x \beta_x^* \varepsilon_y \beta_y^*}} \mathcal{F}. \quad (31.12)$$

Under the assumption  $\mathcal{F} \approx 1$ , to achieve high luminosity, all one has to do is make high population bunches of low emittance collide at high frequency at locations where the beam optics provides as low values of the amplitude functions as possible.

Expressions for the reductions due to crossing angle and other effects can be found elsewhere [8]. While there are no fundamental limits to producing luminosity, there are certainly challenges. Here we have space to mention only a few of these. The beam-beam tune shift appears in the Tables. A bunch in beam 1 presents a (nonlinear) lens to a particle in beam 2 resulting in changes to the particle’s transverse tune with a range characterized by the (vertical) beam-beam parameter [8]

$$\xi_{y,2} = \frac{m_e r_e q_1 q_2 n_1 \beta_{y,2}^*}{2\pi m_{A,2} \gamma_2 \sigma_{y,1}^* (\sigma_{x,1}^* + \sigma_{y,1}^*)} \quad (31.13)$$

where  $r_e$  denotes the classical electron radius ( $r_e \approx 2.8 \times 10^{-15}$  m),  $m_e$  the electron mass,  $q_1$  ( $q_2$ ) the particle charge of beam 1 (2) in units of the elementary charge, and  $m_{A,2}$  the mass of beam-2 particles. The transverse oscillations are susceptible to resonant perturbations from a variety of sources such as imperfections in the magnetic guide field, so that certain values of the tune must be avoided. Accordingly, the tune spread arising from  $\xi$  is limited [9–11]. A glance at the Tables shows that electrons are more forgiving than protons thanks to the damping effects of synchrotron radiation; the  $\xi$ -values for the former are about an order of magnitude larger than those for protons. In linear colliders, the strength of the collision is measured by the ratio of the rms bunch length  $\sigma_z$  to the approximate (linear, thin-lens) beam-beam focal length. This ratio, called disruption parameter  $D_y$  [7], is related to  $\xi_y$  via  $D_y = 4\pi\sigma_z\xi_y/\beta_y^*$ . For hadron colliders, two fundamental luminosity limits are the beam lifetime, determined by burn-off in the collisions, and the radiation from the collision debris, which affects the equipment lifetime.

A subject of present intense interest is the *electron-cloud effect* [12,13]; actually a variety of related processes come under this heading. They typically involve a buildup of electron density in the vacuum chamber due to emission from the chamber walls stimulated by electrons or photons originating from the beam itself. For instance, there is a process closely resembling the multipacting effects familiar from radiofrequency system commissioning. Low energy electrons are ejected from the walls by photons from positron or proton beam-produced synchrotron radiation. These electrons are accelerated toward a beam bunch, but by the time they reach the center of the vacuum chamber the bunch has gone

and so the now-energetic electrons strike the opposite wall to produce more secondaries. These secondaries are now accelerated by a subsequent bunch, and so on. Among the disturbances that this electron accumulation can produce is an enhancement of the tune spread within the bunch; the near-cancellation of bunch-induced electric and magnetic fields is no longer in effect.

If the luminosity of Eq. 31.12 is rewritten in terms of the beam-beam parameter, Eq. 31.13, the emittance itself disappears. However, the emittance must be sufficiently small to realize a desired magnitude of beam-beam parameter, but once  $\xi_y$  reaches this limit, further lowering the emittance does not lead to higher luminosity.

For electron synchrotrons and storage rings, radiation damping provides an automatic route to achieve a small emittance. In fact, synchrotron radiation is of key importance in the design and optimization of  $e^+e^-$  colliders. While vacuum stability and electron clouds can be of concern in the positron rings, synchrotron radiation along with the restoration of longitudinal momentum by the RF system has the positive effect of generating very small transverse beam sizes and small momentum spread. Further reduction of beam size at the interaction points using standard beam optics techniques and successfully contending with high beam currents has led to record luminosities in these rings. To maximize integrated luminosity the beam can be “topped off” by injecting new particles without removing existing ones – a feature difficult to imitate in hadron colliders.

For hadrons, particularly antiprotons, two inventions have played a prominent role. Stochastic cooling [14] was employed first to prepare beams for the  $S\bar{p}pS$  and subsequently in the Tevatron, and to cool the beams at full energy in RHIC [15–17]. Electron cooling [18] was also used in the Tevatron, RHIC and LHC complexes to great advantage. Further innovations are underway driven by the needs of potential future projects; these are noted in the final section. For future energy-frontier hadron colliders, like the proposed FCC-hh and SPPC, also synchrotron radiation damping becomes an important cooling mechanism.

### 31.4 Recent High Energy Colliders

Collider accelerator physics of course goes far beyond the elements of the preceding sections. In this and the following section elaboration is made on various issues associated with some of the recently operating colliders, particularly factors which impact integrated luminosity. The various colliders utilizing hadrons each have unique characteristics and are, therefore, discussed separately. As space is limited, general references are provided where much further information can be obtained. A more complete list of recent colliders and their parameters can be found in the High-Energy Collider Parameters tables.

#### 31.4.1 Tevatron

The first synchrotron in history using superconducting magnets, the Tevatron [19], was the highest energy collider for 25 years. Its 4.5 T dipole magnets employed superconducting Nb-Ti cable operating at 4.5 K [20], requiring what was then the world’s largest cryogenic system [21]. Tevatron operation was terminated in September 2011, after delivering more than  $10 \text{ fb}^{-1}$  to the  $p\text{-}\bar{p}$  collider experiments CDF and D0. The route to high integrated luminosity in the Tevatron was governed by the antiproton production rate, the turn-around time to produce another store, and the resulting optimization of store time. The antiproton production complex [22] consisted of three 8 GeV  $\bar{p}$  accelerators — Accumulator, Debuncher, and Recycler — and employed 25 independent stochastic cooling systems and one high energy electron cooling set-up [23] to accumulate up to record high  $25 \times 10^{10} \bar{p}$  per hour. The proton and antiproton beams in the Tevatron circulated in a single vacuum pipe and thus were placed on separated orbits which wrapped around each other in a helical pattern outside of the interaction regions. As the available aperture was limited, the long-range encounters played an important role. Despite these limitations, a total beam-beam tuneshift parameter of  $N_{IP}\xi \approx 0.025\text{--}0.03$  was achieved, a record for hadron beams [24], where  $N_{IP}$  denotes the number of collision points (2 for the Tevatron). Other notable advances at the Tevatron included the first permanent-magnet-based high energy accelerator

(Recycler), novel longitudinal beam manipulation techniques such as *slip-stacking* and *momentum mining* [25,26], and the first use of electron lenses [27] for beam collimation and for compensation of long-range beam-beam effects. The Tevatron ultimately achieved luminosities a factor of 430 over its original design specification.

#### 31.4.2 HERA

HERA [28], operated between 1992 and 2007, delivered nearly  $1 \text{ fb}^{-1}$  of integrated luminosity to the electron-proton collider experiments H1 and ZEUS. HERA was the first high-energy lepton-hadron collider, and also the first facility to employ both applications of superconductivity: magnets and accelerating structures. The proton beams of HERA had a maximum energy of 920 GeV. The lepton beams (positrons or electrons) were provided by the existing DESY complex, and were accelerated to 27.5 GeV using conventional magnets. At collision a 4-times higher frequency RF system, compared with the injection RF, was used to generate shorter bunches, thus helping alleviate the hourglass effect at the collision points. The lepton beam naturally would become transversely polarized (within about 40 minutes) and “spin rotators” were implemented on either side of an IP to produce longitudinal polarization at the experiment.

#### 31.4.3 LEP

Installed in a tunnel of 27 km circumference, LEP [29] was the largest circular  $e^+e^-$  collider built so far. LEP was operated from 1989 to 2000 with beam energies ranging from 45.6 to 104.5 GeV and a maximum luminosity of  $10^{32} \text{ cm}^{-2}\text{s}^{-1}$ , at 98 GeV, surpassing all relevant design parameters. Up to about 60 GeV, LEP used resonant depolarization to precisely measure the beam energy [30,31].

#### 31.4.4 SLC

Based on an existing 3-km long S-band linac, the SLC [32] was the first and only linear collider. It was operated from 1987 to 1998 with a constant beam energy of 45.6 GeV, up to about 80% electron-beam polarization, quasi-flat beams, a final-focus optics with local chromatic correction based on four interleaved sextupoles and  $\beta_y^* \approx 1 \text{ mm}$ . In its last year, SLC achieved a peak luminosity of about  $3 \times 10^{30} \text{ cm}^{-2}\text{s}^{-1}$ , roughly half of the design value.

### 31.5 Present Collider Facilities

#### 31.5.1 LHC

The superconducting Large Hadron Collider [33] presently is the world’s highest energy collider. Early operations for HEP were first at 3.5 TeV (in 2011) and then 4 TeV per proton [34] (since 2012), with the beam energy increased to 6.5 TeV in 2015. The current status is best checked at the Web site [35]. In 2017 peak luminosities above  $2 \times 10^{34} \text{ cm}^{-2}\text{s}^{-1}$  (more than twice the design value) have been achieved. To meet its luminosity goals the LHC operates with a high beam current of approximately 0.5 A, leading to stored energies of several hundred MJ per beam. Component protection, beam collimation, and controlled energy deposition were given a high priority. Additionally, at energies of 5–7 TeV per particle, synchrotron radiation moves from being a curiosity to a challenge in a hadron accelerator for the first time. At design beam current the cryogenic system must remove roughly 7 kW due to synchrotron radiation, intercepted at a temperature of about 5–20 K. As the photons are emitted their interactions with the vacuum chamber wall can generate free electrons, with consequent “electron cloud” development. Much care was taken to design a special beam screen for the chamber to mitigate this issue. The two proton beams are contained in separate pipes throughout most of the circumference, and are brought together into a single pipe at the interaction points. The large number of bunches, and subsequent short bunch spacing, would lead to approximately 30 head-on collisions through 120 m of common beam pipe at each IP. Thus, a small crossing angle is employed, which reduces the luminosity by about 15%. Still, the bunches moving in one direction experience multiple long-range encounters with the counter-rotating bunches and the resulting perturbations of the particle motion continues to remain a concern. The luminosity scale is absolutely calibrated by the “van der Meer method” as was invented for the ISR [36], and followed by multiple, re-

dundant luminosity monitors (see for example [37] and references therein). The Tables also show the LHC luminosity performance in Pb-Pb collisions, which for the ATLAS and CMS experiments well exceeded the design value, while for the ALICE [38] experiment, the luminosity is “levelled” near the Pb-Pb design value of  $10^{27} \text{ cm}^{-2}\text{s}^{-1}$ . The LHC can also provide Pb-p collisions as it did in 2013 and 2016, and other ion-ion or ion-proton collisions, at different energies.

In the coming years, an ambitious upgrade program, HL-LHC [39, 40], has as its target an order-of-magnitude increase in integrated luminosity through the utilization of Nb<sub>3</sub>Sn superconducting magnets, superconducting compact “crab” cavities and luminosity leveling also for ATLAS and CMS as its key ingredients.

### 31.5.2 $e^+e^-$ Rings

Asymmetric energies of the two beams have allowed for the enhancement of  $B$ -physics research and for interesting interaction region designs. As the bunch spacing can be quite short, the lepton beams sometimes pass through each other at an angle, which may reduce the luminosity — unless the crossing angle can be taken advantage of. KEKB [41] installed high frequency “crab crossing” schemes to fully restore the geometric overlap of the colliding bunches. It attained over  $1 \text{ fb}^{-1}$  of integrated luminosity in a single day. A different collision approach, called “crab waist”, which relies on special sextupoles together with a large crossing angle, has been successfully implemented at DAΦNE [42]. The crab-waist collision scheme has also been partly realized at the KEKB upgrade, SuperKEKB, and it has indeed become a key ingredient for all proposed future  $e^+e^-$  circular colliders. SuperKEKB is aiming for luminosities of  $8 \times 10^{35} \text{ cm}^{-2}\text{s}^{-1}$  [43]. Other  $e^+e^-$  ring colliders currently in operation are BEPC-II, VEPP-2000 and VEPP-4M [43].

### 31.5.3 RHIC

The Relativistic Heavy Ion Collider [44] employs superconducting magnets, and collides combinations of fully-stripped ions such as H-H (p-p), p-Al, p-Au, d-Au, h-Au, Cu-Cu, Cu-Au, Zr-Zr, Ru-Ru, Au-Au, and U-U over a wide energy range [45]. The high charge per particle (+79 for gold, for instance) makes intra-beam scattering of particles within the bunch a special concern, even for seemingly moderate bunch intensities. In 2012, 3-D stochastic cooling was successfully implemented in RHIC [17] and is now routinely used. With stochastic cooling, steady increases in the bunch intensity, and numerous other upgrades, RHIC now operates at 44 times the Au-Au design average luminosity. Another special feature of accelerating heavy ions in RHIC is that the beams cross the “transition energy” during acceleration — a point where the derivative with respect to momentum of the revolution period is zero. This is more typical of low-energy accelerators, where the necessary phase jump required of the RF system is implemented rapidly and little time is spent near this condition. In the case of RHIC with heavy ions, the superconducting magnets do not ramp very quickly and the period of time spent crossing transition is long and must be dealt with carefully. For p-p operation the RHIC beams are always above their transition energy and so this condition is completely avoided. A RHIC physics program in search of a critical point in the nuclear matter phase diagram required operation below the nominal injection energy, and in order to reach the integrated luminosity goals the first bunched beam electron cooler was successfully commissioned for the lowest energies [46].

RHIC is also unique in its ability to accelerate and collide polarized proton beams. As proton beam polarization must be maintained from its low-energy source, successful acceleration through the myriad of depolarizing resonance conditions in high energy circular accelerators has taken years to accomplish. An energy of 255 GeV per proton with 55% final polarization per beam has been realized. As part of a scheme to compensate the head-on beam-beam effect, electron lenses operated routinely during the polarized proton operation at 100 GeV in 2015 [47].

Collisions between a RHIC proton beam and an electron beam stored in a new ring (eRHIC) is one of the two proposed configuration of a future US electron-ion collider (EIC) for nuclear physics

[48], the alternative being the addition of figure-8 hadron and electron storage rings to the CEBAF facility at JLAB (JLEIC).

## 31.6 Future High Energy Colliders and Prospects

Recent accomplishments of particle physics have been obtained through high-energy and high-intensity experiments using hadron-hadron, lepton-lepton, and lepton-proton colliders. Following the discovery of the Higgs particle at the LHC and in view of ongoing searches for “new physics” and rare phenomena, various options are under discussions and development to pursue future particle-physics research at higher energy and with appropriate luminosity. This is the basis for several new projects, ideas, and R&D activities, which can only briefly be summarized here. Specifically, the following projects are noted: an energy upgrade of the LHC based on 16 T dipole magnets (HE-LHC) [49], two approaches to an electron-positron linear collider [50, 51], larger 100-km circular tunnels supporting  $e^+e^-$  collisions up to either 240 [52] or 365 GeV [53] in the centre of mass along with a subsequent 70-140 TeV or 100-TeV proton-proton collider, possible future, or far future, muon-ring colliders [54, 55], and potential use of plasma acceleration and other advanced schemes. Complementary studies are ongoing of a high-energy lepton-hadron collider bringing into collision a 60-GeV electron beam from an energy-recovery linac with the 7 TeV protons circulating in the LHC (LHeC) [56, 57], or, much later, with the 50(35) TeV protons of the 100(70) TeV collider (FCC-eh, SPPC), and of  $\gamma\gamma$  collider Higgs factories based on recirculating electron linacs (e.g. SAPPHiRE [58]). Tentative parameters of some of the colliders discussed, or mentioned, in this section are summarized in Table 31.1 and Table 31.2.

### 31.6.1 Electron-Positron Linear Colliders

For more than four decades, efforts have been devoted to develop high-gradient technology  $e^+e^-$  colliders in order to overcome the synchrotron radiation limitations of circular  $e^+e^-$  machines in the TeV energy range.

The primary challenge confronting a high energy, high luminosity single pass collider design is the power requirement, so that measures must be taken to keep the demand within bounds as illustrated in a transformed Eq. 31.2 [60]:

$$\mathcal{L} \approx \frac{137}{8\pi r_e} \frac{P_{\text{wall}}}{E_{\text{cm}}} \frac{\eta}{\sigma_y^*} N_\gamma H_D. \quad (31.14)$$

Here,  $P_{\text{wall}}$  is the total wall-plug power of the collider,  $\eta \equiv P_b/P_{\text{wall}}$  the efficiency of converting wall-plug power into beam power  $P_b = f_{\text{coll}} n E_{\text{cm}}$ ,  $E_{\text{cm}}$  the cms energy,  $n (= n_1 = n_2)$  the bunch population, and  $\sigma_y^*$  the vertical rms beam size at the collision point. In formulating Eq. 31.14 the number of beamstrahlung photons emitted per  $e^\pm$ , was approximated as  $N_\gamma \approx 2\alpha r_e n / \sigma_y^*$ , where  $\alpha$  denotes the fine-structure constant. The management of  $P_{\text{wall}}$  leads to an upward push on the bunch population  $n$  with an attendant rise in the energy radiated due to the electromagnetic field of one bunch acting on the particles of the other. Keeping a significant fraction of the luminosity close to the nominal energy represents a design goal, which is met if  $N_\gamma$  does not exceed a value of about 1. A consequence is the use of flat beams, where  $N_\gamma$  is managed by the beam width, and luminosity adjusted by the beam height, thus the explicit appearance of the vertical beam size  $\sigma_y^*$ . The final factor in Eq. 31.14,  $H_D$ , represents the enhancement of luminosity due to the pinch effect during bunch crossing (the effect of which has been neglected in the expression for  $N_\gamma$ ).

The approach designated by the International Linear Collider (ILC) is presented in the Tables, and the contrast with the collision-point parameters of the circular colliders is striking, though reminiscent in direction of those of the SLAC Linear Collider. The ILC *Technical Design Report* [50, 61] has a baseline cms energy of 500 GeV with upgrade provision for 1 TeV, and luminosity comparable to the LHC; recent tendencies have been toward a baseline of 250 GeV. The ILC is based on superconducting accelerating structures of the 1.3 GHz TESLA variety. Progress toward higher field gradients and  $Q$  values continues to be made, with nitrogen-doping techniques being a recent example [62].

At CERN, a design effort is underway on the Compact Linear

**Table 31.1:** Tentative parameters of selected future  $e^+e^-$  high-energy colliders. Parameters associated with different beam energy scenarios are comma-separated.

	FCC-ee	CEPC	ILC	CLIC
Species	$e^+e^-$	$e^+e^-$	$e^+e^-$	$e^+e^-$
Beam energy (GeV)	46, 120, 183	46, 120	125, 250	190, 1500
Circumference / Length (km)	97.75	100	20.5, 31	11, 50
Interaction regions	2	2	1	1
Est. integrated luminosity per experiment ( $\text{ab}^{-1}/\text{year}$ )	26, 0.9, 0.17	4, 0.4	0.2, 0.2	0.2, 0.6
Peak luminosity ( $10^{34}/\text{cm}^2/\text{s}$ )	230, 8.5, 1.6	32, 3	1.4, 1.8	1.5, 6
Time between collisions ( $\mu\text{s}$ )	0.015, 0.75, 8.5	0.025, 0.68	0.55	0.0005
Energy spread (rms, $10^{-3}$ )	1.3, 1.65, 2.0	0.4, 1.0	$e^-$ : 1.9, 1.2 $e^+$ : 1.5, 0.7	3.5
Bunch length (rms, mm)	12.1, 5.3, 3.8	8.5, 3.3	0.3	0.09, 0.044
IP beam size ( $\mu\text{m}$ )	H: 6.3, 14, 38 V: 0.03, 0.04, 0.07	H: 5.9, 21 V: 0.04, 0.07	H: 0.52, 0.47 V: 0.008, 0.006	H: 0.15, 0.04 V: 0.003, 0.001
Injection energy (GeV)	on energy (topping off)	on energy (topping off)	5.0 (linac)	9.0 (linac)
Transv. rms emittance (pm)	H: 270, 630, 1340 V: 1, 1, 3	H: 170, 1210 V: 2, 3	H: 20, 10 V: 0.14, 0.07	H: 2.4, 0.22 V: 0.8, 0.01
$\beta^*$ at interaction point (cm)	H: 15, 30, 100 V: 0.08, 0.1, 0.16	H: 20, 36 V: 0.1, 0.15	H: 1.3, 2.2 V: 0.041, 0.048	H: 0.8, 0.69 V: 0.01, 0.0068
Full crossing angle (mrad)	30	33	14	20
Crossing scheme	crab waist	crab waist	crab crossing	crab crossing
Piwinski angle $\phi = \sigma_z \theta_c / (2\sigma_x^*)$	28.5, 5.8, 1.5	23.8, 2.6	0	0
Beam-beam param. $\xi_y (10^{-3})$	133, 118, 144	72, 109	n/a	n/a
Disruption parameter $D_y$	0.9, 1.1, 1.9	0.3, 1.0	34, 25	8, 12
Average Upsilon $\mathcal{U}$	0.0002, 0.0004, 0.0006	0.0001, 0.0005	0.03, 0.06	0.26, 3.4
RF frequency (MHz)	400, 400, 800	650	1300	11994
Particles per bunch ( $10^{10}$ )	17, 15, 27	8, 15	2	0.52, 0.37
Bunches per beam	16640, 328, 33	12000, 242	1312 (pulse)	352, 312 (trains at 50 Hz)
Average beam current (mA)	1390, 29, 5.4	19.2	6 (in train)	1660, 1200 (in train)
RF gradient (MV/m)	1.3, 9.8, 19.8	3.6, 19.7	31.5	72, 100
Polarization (%)	$\geq 10$ , 0, 0	5–10, 0	$e^-$ : 80% $e^+$ : 30%	$e^-$ : 70% at IP
SR power loss (MW)	100	64	n/a	n/a
Beam power/beam (MW)	n/a	n/a	5.3, 10.5	3, 14
Novel technology	—	—	high grad. SC RF	two-beam accel.

Collider (CLIC), each linac of which is itself a two-beam accelerator, in that a high energy, low current beam is fed by a low energy, high current driver [63]. The CLIC design employs normal conducting 12 GHz accelerating structures at a gradient of 100 MeV/m, some three times the current capability of the superconducting ILC cavities. The design cms energy is 3 TeV, though recent staging options – 0.38, 1.5, and 3 TeV – have been developed [51].

### 31.6.2 Future Circular Colliders

The discovery, in 2012, of the Higgs boson at the LHC has stimulated interest in constructing a large circular tunnel which could host a variety of energy-frontier machines, including high-energy electron-positron, proton-proton, and lepton-hadron colliders. Such projects are under study by a global collaboration hosted at CERN (FCC) [53, 64, 65] and another one centered in China (CEPC/SPPC) [52], following earlier proposals for a Very Large Hadron Collider (VLHC) [66] and a Very Large Lepton Collider (VLLC) in the US, which would have been housed in the same 230-km long tunnel.

The maximum beam energy of a hadron collider is directly proportional to the magnetic field and to the ring circumference. The LHC magnets, based on Nb-Ti superconductor, achieve a maximum operational field of 8.33 T. The HL-LHC project develops the technology of higher field Nb<sub>3</sub>Sn magnets as well as cables made from high-temperature superconductor (HTS). Nb<sub>3</sub>Sn dipoles could ultimately reach an operational field around 16 T, and HTS inserts, requiring new engineering materials and substantial dedicated R&D, could boost this further. More cost-effective hybrid magnet designs incorporating Nb-Ti, two types of Nb<sub>3</sub>Sn, and an inner layer of HTS providing fields of about

20 T have been examined [67]. However present project efforts are not utilizing this hybrid approach as of yet.

Aside from the magnets, the cryogenic beam vacuum system is another key component of any future hadron collider. A beam screen inside the cold bore of the magnets can intercept the synchrotron radiation at an elevated temperature, allowing a more efficient extraction of the synchrotron-radiation heat load. While the LHC beam screen has a temperature of 5–20 K, future, higher-energy machines are likely to raise this temperature to 50 K or 100 K.

Further substantial increases in collision energy are possible only with a larger tunnel. The FCC hadron collider (FCC-hh) [64, 68, 69], formerly called VHE-LHC, is based on a new tunnel of about 100 km circumference, which would allow exploring energies up to 100 TeV in the centre of mass with proton-proton collisions, using 16 T magnets. This new tunnel could also accommodate a high-luminosity circular  $e^+e^-$  Higgs factory (FCC-ee) as well as a lepton-hadron collider (FCC-eh). The SPPC is a 100 km hadron collider based on 12 T (later 24 T) iron-based high-temperature superconducting magnets, which could be installed in the same tunnel as the  $e^+e^-$  collider CEPC.

In order to serve as a Higgs factory a new circular  $e^+e^-$  collider needs to achieve a cms energy of at least 240 GeV. FCC-ee [53, 68] (formerly TLEP), installed in the  $\sim 100$  km tunnel of the FCC-hh, could reach even higher energies, e.g. 365 GeV cms for  $t\bar{t}$  production. At these energies, the luminosity, limited by the synchrotron radiation power, would still be above  $10^{34} \text{ cm}^{-2}\text{s}^{-1}$  at each of two or four collision points. At lower energies (Z pole and WW threshold) FCC-ee could deliver two to three orders of magnitude higher luminosities, and also profit from radiative self polarization for

**Table 31.2:** Tentative parameters of selected future high-energy hadronic colliders. Parameters associated with different beam energy scenarios for a  $\mu$  collider are comma-separated. Parameters of HL-LHC can be found in the High-Energy Collider Parameters review tables. The listed luminosity for the LHeC refers to parasitic operation in parallel to the HL-LHC  $pp$  collisions; it could be significantly increased for dedicated operation [59].

	LHeC	HE-LHC	FFC-hh	SPPC	$\mu$ collider
Species	$ep$	$pp$	$pp$	$pp$	$\mu^+\mu^-$
Beam Energy (TeV)	0.06( $e$ ), 7 ( $p$ )	13.5	50	37.5	0.063, 3
Circumference (km)	9( $e$ ), 26.7 ( $p$ )	26.7	97.75	100	0.3, 6
Interaction regions	1	2 (4)	4	2	1, 2
Estimated integrated luminosity per experiment ( $\text{ab}^{-1}/\text{year}$ )	0.1	0.5	0.2–1.0	0.4	0.001, 1.0
Peak luminosity ( $10^{34}/\text{cm}^2/\text{s}$ )	0.8	16	5–30	10	2.2, 71
Time between collisions ( $\mu\text{s}$ )	0.025	0.025	0.025	0.025	1, 20
Energy spread (rms, $10^{-3}$ )	0.03 ( $e$ ), 0.1( $p$ )	0.1	0.1	0.2	0.04, 1
Bunch length (rms, mm)	0.06 ( $e$ ), 75.5( $p$ )	80	80	75.5	63, 2
IP beam size ( $\mu\text{m}$ )	4.3 (round)	8.8	6.7–3.5 (init.)	6.8 (init.)	75, 1.5
Injection energy (GeV)	1( $e$ ), 450( $p$ )	1300	3300	2100	on energy
Transverse emittance (rms, nm)	0.45( $e$ ), 0.27( $p$ )	0.17	0.04 (init.)	0.06 (init.)	335, 0.9
$\beta^*$ , amplitude fcn. at IP (cm)	5.0( $e$ ), 7.0( $p$ )	45	110–30	75	1.7, 0.25
Beam-beam parameter/IP ( $10^{-3}$ )	–( $e$ ), 0.4( $p$ )	12	5–15	7.5	20, 90
RF frequency (MHz)	800( $e$ ), 400( $p$ )	400	400	400/200	805
Particles per bunch ( $10^{10}$ )	0.23( $e$ ), 22( $p$ )	22	10	15	400, 200
Bunches per beam	–( $e$ ), 2808( $p$ )	2808	10600	10080	1
Average beam current (mA)	15( $e$ ), 883( $p$ )	1120	500	730	640, 16 (peak)
Length of standard cell (m)	52.4( $e$ arc), 107( $p$ )	137	213	148	N/A
Phase advance per cell (deg)	310/90( $e$ H/V) 90( $p$ )	90	90	90	N/A
Peak magnetic field (T)	0.264( $e$ ), 8.33( $p$ )	16	16	12	10
Polarization (%)	90( $e$ ), 0( $p$ )	0	0	0	0
SR power loss/beam (MW)	30( $e$ ), 0.01( $p$ )	0.1	2.4	1.1	$3 \times 10^{-5}$ , 0.068
Novel technology	high-energy ERL	16T Nb <sub>3</sub> Sn magnets	16T Nb <sub>3</sub> Sn magnets	HTS magnets	muon prod.

precise energy calibration. The short beam lifetime at the high target luminosity, due to radiative Bhabha scattering, requires FCC-ee to be constructed as a double ring, where the collider rings operating at constant energy are complemented by a full-energy injector ring installed in the same tunnel to “top off” the collider current. Beamstrahlung, i.e. synchrotron radiation emitted during the collision in the field of the opposing beam, introduces an additional beam lifetime limitation depending on momentum acceptance (so that achieving sufficient off-momentum dynamic aperture becomes one of the design challenges), as well as some bunch lengthening.

### 31.6.3 Muon Collider

The muon to electron mass ratio of 210 implies less concern about synchrotron radiation by a factor of about  $2 \times 10^9$  and its  $2.2 \mu\text{s}$  lifetime means that it will last for some  $300B$  turns in a ring with an average bending magnets field of  $B$  (Tesla). Design effort became serious in the mid 1990s and a collider outline emerged quickly.

Removal of the synchrotron radiation barrier reduces the scale of a muon collider facility to a level compatible with on-site placement at existing accelerator laboratories. The Higgs production cross section in the s-channel is enhanced by a factor of  $(m_\mu/m_e)^2$  compared to that in  $e^+e^-$  collisions. The obvious advantage in colliding muons rather than protons is that the muon collider center of mass energy  $\sqrt{s}$ , is entirely available to produce short-distance reactions rather than being spread among proton constituents and, e.g., a 14 TeV muon collider with sufficient luminosity might be very effective as a direct exploration machine, with a physics potential similar to that of a 100 TeV proton-proton collider [70]. Muon colliders are expected to be more compact, power efficient and significantly less expensive than equivalent energy frontier hadron or  $e^+e^-$  machines, and a neutrino factory could

potentially be realized in the course of construction [71].

The challenges to luminosity achievement are clear and amenable to immediate study: targeting, collection, and emittance reduction are paramount, as well as the bunch manipulation required to produce  $> 10^{12}$  muons per bunch without emittance degradation. A multi-TeV c.m.e. high luminosity  $O(10^{34} \text{ cm}^{-2}\text{s}^{-1})$  muon collider would consist of [72, 73]: (i) a high power proton driver (SRF 8 GeV 2–4 MW  $H^-$  linac), (ii) pre-target accumulation and compressor rings, in which high intensity 1–3 ns long proton bunches are formed, (iii) a liquid-mercury target for converting the proton beam into a tertiary muon beam with energy of about 200 MeV, (iv) a multi-stage ionization cooling section that reduces transverse and longitudinal emittances and creates a low emittance beam, (v) a multistage acceleration system, possibly employing recirculating linear accelerators (RLA) to accelerate muons in a modest number of turns up to 2 TeV using superconducting RF technology, and, finally, (vi) a 2–6 km diameter collider ring located some 100 m underground, where counter-propagating muon beams are stored and collide over the roughly 1000–2000 turns corresponding to the muon lifetime.

Collection of muons from the decay of pions produced in proton-nucleus interactions results in a large initial 6D phase volume for the muons, which must be reduced (cooled) by a factor of  $10^6$ , otherwise, the luminosity reach will not exceed  $O(10^{31} \text{ cm}^{-2}\text{s}^{-1})$ . The technique of ionization cooling [74, 75] is uniquely applicable to muons because of their minimal interaction with matter [76]; a proof-of-principle was recently demonstrated in the pioneering MICE experiment at RAL [77]. Muon collider R&D has led to a number of remarkable advances in the past decade [78], including a novel concept to generate muon pairs at threshold using the annihilation of 45 GeV positrons with electrons at rest [79, 80], and alternative concepts based on laser-hadron collisions [55, 81, 82], all of which might allow low emittance beams to be obtained directly,

without any cooling.

### 31.6.4 Plasma Acceleration and Other Advanced Concepts

At the 1956 CERN Symposium, a paper by Veksler, in which he suggested acceleration of protons to the TeV scale using a bunch of electrons, anticipated current interest in plasma acceleration [83]. A half-century later this became more than a suggestion, with the demonstration, as a striking example, of electron energy doubling from 42 to 84 GeV over 85 cm at SLAC [84], the creation of a 1 GeV electron bunch with relatively small energy spread accelerated through a cm-scale plasma [85], and the achievement of proton-driven plasma acceleration of electrons at CERN [86].

Whether plasma acceleration will find application in an HEP facility is not yet clear, given the necessity of staging and phase-locking acceleration in multiple plasma chambers. However, strides continue to be made, as multi-stage coupling of independent laser plasma accelerators have been demonstrated recently [87]. Another critical issue is the power efficiency  $\eta$  for a collider based on plasma acceleration, whose luminosity would still be described by 31.14. Maintaining beam quality and beam position as well as the acceleration of high-repetition bunch trains are also primary feasibility issues, addressed by active R&D. For a recent status report on laser-plasma acceleration and the steps towards a future electron positron collider based on this technology, see [88].

Additional approaches aiming at accelerating gradients higher, or much higher, than those achievable with conventional metal cavities include the use of dielectric materials and, for the long-term future, crystals. Combining several innovative ideas, even a linear crystal muon collider driven by X-ray lasers has been proposed [89], as well as “accelerators on a chip” [90,91]. Not only the achievable accelerating gradient, but also the overall power efficiency, e.g. the attainable luminosity as a function of electrical input power, along with the beam stability [92] will determine the suitability of any novel technology for use in future high-energy accelerators.

### References

- [1] E. D. Courant and H. S. Snyder, *Annals Phys.* **3**, 1 (1958), *Annals Phys.*281,360(2000). This is the classic article on the alternating gradient synchrotron.
- [2] A. W. Chao *et al.*, editors, *Handbook of accelerator physics and engineering*, World Scientific, Hackensack, USA (2013), ISBN 9789814415842, URL <http://www.worldscientific.com/worldscibooks/10.1142/8543>.
- [3] A. W. Chao, *Physics of collective beam instabilities in high energy accelerators*, Wiley, New York, NY (1993), URL <https://cds.cern.ch/record/246480>.
- [4] K. Y. Ng, *Physics of intensity dependent beam instabilities*, World Scientific, Hoboken, NJ (2006), URL <https://cds.cern.ch/record/1012829>.
- [5] H. Wiedemann, in *Handbook of Accelerator Physics and Engineering* [2], *ibid*, Sec. 3.1.
- [6] C. Amsler *et al.* (Particle Data Group), *Phys. Lett.* **B667**, 1 (2008).
- [7] K. Yokoya and P. Chen, *Lect. Notes Phys.* **400**, 415 (1992).
- [8] M.A. Furman and M.S. Zisman, *Handbook of Accelerator Physics and Engineering* [2], *ibid*, Sec. 4.1.
- [9] R. Assmann and K. Cornelis, in “Particle accelerator. Proceedings, 7th European Conference, EPAC 2000, Vienna, Austria, June 26-30, 2000. Vol. 1-3,” 1187–1189 (2000), URL <http://weblib.cern.ch/abstract?CERN-SL-2000-046-0P>.
- [10] J. Gao, *Nucl. Instrum. Meth.* **A533**, 270 (2004).
- [11] K. Ohmi and F. Zimmermann, *Phys. Rev. ST Accel. Beams* **18**, 12, 121003 (2015).
- [12] M.A. Furman, *Handbook of Accelerator Physics and Engineering* [2], *ibid*, Sec. 2.4.14.
- [13] <http://ab-abp-rlc.web.cern.ch/ab-abp-rlc-ecloud/>. This site contains many references as well as videos of electron cloud simulations.
- [14] D. Mohl *et al.*, *Phys. Rept.* **58**, 73 (1980).
- [15] M. Blaskiewicz and J. M. Brennan, *Phys. Rev. ST Accel. Beams* **10**, 061001 (2007).
- [16] M. Blaskiewicz, J. M. Brennan and F. Severino, *Phys. Rev. Lett.* **100**, 174802 (2008).
- [17] M. Blaskiewicz, J. M. Brennan and K. Mernick, *Phys. Rev. Lett.* **105**, 094801 (2010).
- [18] G. I. Budker, *Sov. Atom. Energ.* **22**, 438 (1967), [*At. Energ.*22,346(1967)].
- [19] H. T. Edwards, *Ann. Rev. Nucl. Part. Sci.* **35**, 605 (1985).
- [20] A. Tollestrup and E. Todesco, in “Reviews Of Accelerator Science And Technology: Volume 1,” 185–210, World Scientific (2008).
- [21] W. Fowler, *Particle Accelerators* **26**, 179 (1990).
- [22] M. Church and J. Marriner, *Annual Review of Nuclear and Particle Science* **43**, 1, 253 (1993).
- [23] S. Nagaitsev *et al.*, *Physical Review Letters* **96**, 4, 044801 (2006).
- [24] V. Shiltsev *et al.*, *Physical Review Special Topics-Accelerators and Beams* **8**, 10, 101001 (2005).
- [25] K. Koba and J. Steimel, in “AIP Conference Proceedings,” volume 642, 223–225, AIP (2002).
- [26] C. Bhat, *Physics Letters A* **330**, 6, 481 (2004).
- [27] V. D. Shiltsev, *Electron lenses for super-colliders*, Springer (2016).
- [28] Brief history at [http://en.wikipedia.org/wiki/Hadron\\_Elektron\\_Ring\\_Anlage](http://en.wikipedia.org/wiki/Hadron_Elektron_Ring_Anlage).
- [29] R. Assmann, M. Lamont and S. Myers, *Nucl. Phys. Proc. Suppl.* **109B**, 17 (2002), [17(2002)].
- [30] R. Assmann *et al.*, *Eur. Phys. J.* **C6**, 187 (1999).
- [31] R. Assmann *et al.*, in “Proceedings, 1999 Particle Accelerator Conference (PAC’99): New York, New York, March 29-April 2, 1999,” 2999–3001 (1999), URL <http://accelconf.web.cern.ch/AccelConf/p99/PAPERS/THP23.PDF>.
- [32] N. Phinney, eConf **C00082**, MO102 (2000), [1(2000)], [arXiv:physics/0010008].
- [33] L. Evans, *Ann. Rev. Nucl. Part. Sci.* **61**, 435 (2011).
- [34] M. Draper, editor, *Proceedings, LHC Performance Workshop (Chamonix 2014)*, CERN, CERN, Geneva (2015), ISBN 9789290834137.
- [35] Detailed information from the multi-volume design report to present status may be found at <http://lhc.web.cern.ch/lhc/>.
- [36] S. van der Meer (1968).
- [37] G. Aad *et al.* (ATLAS), *Eur. Phys. J.* **C73**, 8, 2518 (2013), [arXiv:1302.4393].
- [38] <http://aliceinfo.cern.ch/Public/Welcome.html>.
- [39] <http://hilumilhc.web.cern.ch>.
- [40] G. Apollinari *et al.*, *CERN Yellow Rep. Monogr.* **4**, 1 (2017).
- [41] S. Kurokawa and E. Kikutani, *Nucl. Instrum. Meth.* **A499**, 1 (2003).
- [42] M. Zobov *et al.*, *Phys. Rev. Lett.* **104**, 174801 (2010).
- [43] An overview of electron-positron colliders past and present may be found in ICFA Beam Dynamics Newsletter No. 46, April 2009, <http://icfa-bd.kek.jp/>. A daily account of the luminosity progress at SuperKEKB may be found at <http://www-linac.kek.jp/skekb/snapshot/dailysnap.html>.
- [44] M. Harrison *et al.*, *Nucl. Instrum. Meth.* **A499**, 1 (2003).
- [45] <http://www.rhichome.bnl.gov/RHIC/Runs/>.
- [46] A. Fedotov, *et al.*, *Proceedings NAPAC 2019* (2019).
- [47] W. Fischer *et al.*, *Phys. Rev. Lett.* **115**, 26, 264801 (2015).
- [48] F. Pilat, in “Proceedings, 9th International Particle Accelerator Conference (IPAC 2018): Vancouver, BC Canada,” TUXGBD3 (2018).

- [49] F. Zimmermann *et al.*, The European Physical Journal Special Topics **228**, 5, 1109 (2019), ISSN 1951-6401, URL <https://doi.org/10.1140/epjst/e2019-900088-6>.
- [50] P. Bambade *et al.* (2019), [arXiv:1903.01629].
- [51] T. K. Charles *et al.* (CLICdp, CLIC), CERN Yellow Rep. Monogr. **1802**, 1 (2018), [arXiv:1812.06018].
- [52] CEPC Study Group (2018), [arXiv:1809.00285].
- [53] M. Benedikt *et al.*, The European Physical Journal Special Topics **228**, 2, 261 (2019).
- [54] D. Neuffer and V. Shiltsev, JINST **13**, 10, T10003 (2018), [arXiv:1811.10694].
- [55] F. Zimmermann MOPMF065 (2018), [J. Phys. Conf. Ser.1067,no.2,022017(2018)].
- [56] J. L. Abelleira Fernandez *et al.* (LHeC Study Group), J. Phys. **G39**, 075001 (2012), [arXiv:1206.2913].
- [57] J. L. Abelleira Fernandez *et al.* (LHeC Study Group) (2012), [arXiv:1211.5102].
- [58] S. A. Bogacz *et al.* (2012), [arXiv:1208.2827].
- [59] F. Bordry *et al.* (2018), [arXiv:1810.13022].
- [60] F. Zimmermann, AIP Conf. Proc. **592**, 1, 494 (2001).
- [61] <http://www.linearcollider.org/ILC/Publications/Technical-Design-Report>.
- [62] A. Grassellino *et al.*, Supercond. Sci. Technol. **26**, 102001 (2013), [arXiv:1306.0288].
- [63] <http://lcd.web.cern.ch/lcd/CDR/CDR.html>.
- [64] M. Benedikt *et al.*, The European Physical Journal Special Topics **228**, 4, 755 (2019), ISSN 1951-6401, URL <https://doi.org/10.1140/epjst/e2019-900087-0>.
- [65] M. Mangano *et al.*, The European Physical Journal C **79**, 6, 474 (2019), ISSN 1434-6052, URL <https://doi.org/10.1140/epjc/s10052-019-6904-3>.
- [66] <http://vlhc.org>.
- [67] E. Todesco and F. Zimmermann, editors, *Proceedings, EuCARD-AccNet-EuroLumi Workshop: The High-Energy Large Hadron Collider (HE-LHC10): Villa Bighi, Malta, Republic of Malta, October 14-16, 2010. EuCARD-AccNet-EuroLumi Workshop: The High-Energy Large Hadron Collider*, CERN, CERN, Geneva (2011), 29 lectures, 156 pages, published as CERN Yellow Report, URL <https://cds.cern.ch/record/1344820>.
- [68] <http://fcc.web.cern.ch>.
- [69] M. Benedikt, D. Schulte and F. Zimmermann, Phys. Rev. ST Accel. Beams **18**, 101002 (2015).
- [70] D. Neuffer and V. Shiltsev, Journal of Instrumentation **13**, 10, T10003 (2018).
- [71] [http://en.wikipedia.org/wiki/Neutrino\\_Factory](http://en.wikipedia.org/wiki/Neutrino_Factory).
- [72] C. M. Ankenbrandt *et al.*, Physical Review Special Topics Accelerators and Beams **2**, 8, 081001 (1999).
- [73] J.-P. Delahaye *et al.*, in “Proceedings, 2013 Community Summer Study on the Future of U.S. Particle Physics: Snowmass on the Mississippi (CSS2013): Minneapolis, MN, USA, July 29-August 6, 2013,” (2013), [arXiv:1308.0494], URL <http://www.slac.stanford.edu/econf/C1307292/docs/submittedArxivFiles/1308.0494.pdf>.
- [74] A. Skrinsky and V. Parkhomchuk, Sov. J. Part. Nucl **12**, 223, 210 (1981).
- [75] D. Neuffer, Particle Accelerators **14**, 75 (1983).
- [76] R. Palmer, Reviews of Accelerator Science and Technology **7**, 137 (2014).
- [77] M. Bogomilov *et al.*, arXiv preprint arXiv:1907.08562 (2019).
- [78] M. Boscolo, J. P. Delahaye and M. Palmer, Reviews of Accelerator Science and Technology **10**, 189 (2019), arXiv preprint arXiv:1808.01858.
- [79] M. Antonelli *et al.*, Nucl. Instrum. Meth. **A807**, 101 (2016), [arXiv:1509.04454].
- [80] M. Biagini *et al.*, in “Proceedings, 10th International Particle Accelerator Conference (IPAC2019): Melbourne, Australia, May 19-24, 2019,” MOZZPLS2 (2019).
- [81] C. Curatolo, F. Broggi and L. Serafini, Nucl. Instrum. Meth. **A865**, 128 (2017).
- [82] M. W. Krasny (2015), [arXiv:1511.07794].
- [83] V. I. Veksler (1956), URL <http://cds.cern.ch/record/1241563>.
- [84] I. Blumenfeld *et al.*, Nature **445**, 741 (2007).
- [85] W. P. Leemans *et al.*, Nature Phys. **2**, 696 (2006).
- [86] E. Gschwendtner and M. Turner (AWAKE) (2019), [arXiv:1901.04171].
- [87] S. Steinke *et al.*, Nature **530**, 7589, 190 (2016).
- [88] ALEGRO Collab., Towards an Advanced Linear International Collider, arXiv:1901.10370 .
- [89] V. D. Shiltsev, Phys. Usp. **55**, 965 (2012), [arXiv:1205.3087].
- [90] J. Breuer and P. Hommelhoff, Phys. Rev. Lett. **111**, 13, 134803 (2013), [arXiv:1308.0464].
- [91] E. A. Peralta *et al.*, Nature **503**, 91 (2013).
- [92] V. Lebedev, A. Burov and S. Nagaitsev, Phys. Rev. Accel. Beams **20**, 12, 121301 (2017), [Erratum: Phys. Rev. Accel. Beams **21**, 059901 (2018)], [arXiv:1701.01498].

## 32. High-Energy Collider Parameters

High-Energy Collider Parameters:  $e^+e^-$  Colliders (I)

**Table 32.1:** Updated in March 2020 with numbers received from representatives of the colliders (contact E. Pianori, LBNL). The table shows the parameter values achieved. Quantities are, where appropriate, r.m.s.; unless noted otherwise, energies refer to beam energy;  $H$  and  $V$  indicate horizontal and vertical directions; s.c. stands for superconducting. Parameters for the defunct SPEAR, DORIS, PETRA, PEP, TRISTAN, and VEPP-2M colliders may be found in our 1996 edition (Phys. Rev. **D54**, 1 July 1996, Part I).

	VEPP-2000 (Novosibirsk)	VEPP-4M (Novosibirsk)	BEPC (China)	BEPC-II (China)	DAΦNE (Frascati)
Physics start date	2010	1994	1989	2008	1999
Physics end date	—	—	2005	—	—
Maximum beam energy (GeV)	1.0	6	2.5	1.89 (2.35 max)	0.510
Delivered integrated luminosity per exp. ( $\text{fb}^{-1}$ )	0.25	0.05	0.11	24.6	$\approx 4.7$ in 2001-2007 $\approx 2.7$ w/crab-waist $\approx 1.8$ since Nov 2014
Luminosity ( $10^{30} \text{ cm}^{-2} \text{ s}^{-1}$ )	50	20	12.6 at 1.843 GeV 5 at 1.55 GeV	1000	453
Time between collisions ( $\mu\text{s}$ )	0.04	0.6	0.8	0.008	0.0027
Full crossing angle ( $\mu$ rad)	0	0	0	$2.2 \times 10^4$	$5 \times 10^4$
Energy spread (units $10^{-3}$ )	0.71	1	0.58 at 2.2 GeV	0.52	0.40
Bunch length (cm)	4	5	$\approx 5$	$\approx 1.2$	low current: 1 at 15mA: 2
Beam radius ( $10^{-6}$ m)	125 (round)	H:1000 V:30	H:890 V:37	H:347 V:4.5	H:260 V:4.8
Free space at interaction point (m)	$\pm 0.5$	$\pm 2$	$\pm 2.15$	$\pm 0.63$	$\pm 0.295$
Luminosity lifetime (hr)	continuous	2	7–12	1.5	0.2
Turn-around time (min)	continuous	18	32	4 (topping up)	2 (topping up)
Injection energy (GeV)	0.2–1.0	1.8	1.55	1.89	on energy
Transverse emittance ( $10^{-9}$ m)	H:150 V:150	H:200 V:20	H:660 V:28	H:121 V:1.56	H:260 V:2.6
$\beta^*$ , amplitude function at interaction point (m)	H:0.05 - 0.11 V:0.05 - 0.11	H:0.75 V:0.05	H:1.2 V:0.05	H:1.0 V:0.0129	H:0.26 V:0.009
Beam-beam tune shift per crossing (units $10^{-4}$ )	H:850 V:850	500	350	383	440 (crab-waist test)
RF frequency (MHz)	172	180	199.53	499.8	356
Particles per bunch (units $10^{10}$ )	8	15	20 at 2 GeV 11 at 1.55 GeV	3.8	$e^-$ : 3.2 $e^+$ : 2.1
Bunches per ring per species	1	2	1	119	100 to 105 (120 buckets)
Average beam current per species (mA)	160	80	40 at 2 GeV 22 at 1.55 GeV	851	$e^-$ : 1250 $e^+$ : 800
Circumference or length (km)	0.024	0.366	0.2404	0.23753	0.098
Interaction regions	2	1	2	1	1
Magnetic length of dipole (m)	1.1	2	1.6	outer ring: 1.6 inner ring: 1.41	outer ring: 1.2 inner ring: 1
Length of standard cell (m)	12	7.2	6.6	outer ring: 6.6 inner ring: 6.2	n/a
Phase advance per cell (deg)	H:745 V:385	65	$\approx 60$	60–90 non-standard cells	—
Dipoles in ring	8	78	40 + 4 weak	84 + 8 weak	8
Quadrupoles in ring	24 + 4 s.c.	150	68	134+2 s.c.	48
Peak magnetic field (T)	2.4	0.6	0.903 at 2.8 GeV	outer ring: 0.677 inner ring: 0.766	1.2



## High-Energy Collider Parameters: $e^+e^-$ Colliders (II)

**Table 32.2:** Updated in March 2020 with numbers received from representatives of the colliders (contact E. Pianori, LBNL). The table shows the parameter values achieved. Quantities are, where appropriate, r.m.s.; unless noted otherwise, energies refer to beam energy;  $H$  and  $V$  indicate horizontal and vertical directions; s.c. stands for superconducting. ILC and CLIC parameters are documented in the Accelerator physics of colliders review.

	CESR (Cornell)	CESR-C (Cornell)	LEP (CERN)	SLC (SLAC)
Physics start date	1979	2002	1989	1989
Physics end date	2002	2008	2000	1998
Maximum beam energy (GeV)	6	6	100 - 104.6	50
Delivered integrated luminosity per experiment ( $\text{fb}^{-1}$ )	41.5	2.0	0.221 at Z peak 0.501 at 65 – 100 GeV 0.275 at >100 GeV	0.022
Luminosity ( $10^{30} \text{ cm}^{-2}\text{s}^{-1}$ )	1280 at 5.3 GeV	76 at 2.08 GeV	24 at Z peak 100 at > 90 GeV	2.5
Time between collisions ( $\mu\text{s}$ )	0.014 to 0.22	0.014 to 0.22	22	8300
Full crossing angle ( $\mu$ rad)	$\pm 2000$	$\pm 3300$	0	0
Energy spread (units $10^{-3}$ )	0.6 at 5.3 GeV	0.82 at 2.08 GeV	0.7→1.5	1.2
Bunch length (cm)	1.8	1.2	1.0	0.1
Beam radius ( $\mu\text{m}$ )	H:460 V:4	H:340 V:6.5	H:200→300 V:2.5→8	H:1.5 V:0.5
Free space at interaction point (m)	$\pm 2.2$ ( $\pm 0.6$ to REC quads)	$\pm 2.2$ ( $\pm 0.3$ to PM quads)	$\pm 3.5$	$\pm 2.8$
Luminosity lifetime (hr)	2–3	2–3	20 at Z peak 10 at > 90 GeV	—
Turn-around time (min)	5 (topping up)	1.5 (topping up)	50	120 Hz (pulsed)
Injection energy (GeV)	1.8–6	1.5–6	22	45.64
Transverse emittance ( $10^{-9}$ m)	210 1	120 3.5	H:20–45 V:0.25→1	H:0.5 V:0.05
$\beta^*$ , amplitude function at interaction point (m)	1.0 0.018	0.94 0.012	1.5 0.05	0.0025 0.0015
Beam-beam tune shift per crossing ( $10^{-4}$ ) or disruption	250 620	$e^-$ : 420 ( $H$ ), 280 ( $V$ ) $e^+$ : 410 ( $H$ ), 270 ( $V$ )	830	0.75 ( $H$ ) 2.0 ( $V$ )
RF frequency (MHz)	500	500	352.2	2856
Particles per bunch (units $10^{10}$ )	1.15	4.7	45 in collision 60 in single beam	4.0
Bunches per ring per species	9 trains of 5 bunches	8 trains of 3 bunches	4 trains of 1 or 2	1
Average beam current per species (mA)	340	72	4 at Z peak 4→6 at > 90 GeV	0.0008
Beam polarization (%)	—	—	55 at 45 GeV 5 at 61 GeV	$e^-$ : 80
Circumference or length (km)	0.768	0.768	26.66	1.45 +1.47
Interaction regions	1	1	4	1
Magnetic length of dipole (m)	1.6–6.6	1.6–6.6	11.66/pair	2.5
Length of standard cell (m)	16	16	79	5.2
Phase advance per cell (deg)	45–90 (no standard cell)	45–90 (no standard cell)	102/90	108
Dipoles in ring	86	84	3280 + 24 inj. + 64 weak	460+440
Quadrupoles in ring	101 + 4 s.c.	101 + 4 s.c.	520 + 288 + 8 s.c.	—
Peak magnetic field (T)	0.3 / 0.8 at 8 GeV	0.3 / 0.8 at 8 GeV, 2.1 wigglers at 1.9 GeV	0.135	0.597

High-Energy Collider Parameters:  $e^+e^-$  Colliders (III)

**Table 32.3:** Updated in March 2020 with numbers received from representatives of the colliders (contact E. Pianori, LBNL). The table shows the parameter values achieved. Design parameters for SuperKEKEB may be found in our 2018 edition (Phys. Rev. **D98**, 030001 (2018)) Quantities are, where appropriate, r.m.s.; unless noted otherwise, energies refer to beam energy;  $H$  and  $V$  indicate horizontal and vertical directions; s.c. stands for superconducting.

	KEKB (KEK)	PEP-II (SLAC)	SuperKEKB (KEK)
Physics start date	1999	1999	2018
Physics end date	2010	2008	—
Maximum beam energy (GeV)	$e^-$ : 8.33 (8.0 nominal) $e^+$ : 3.64 (3.5 nominal)	$e^-$ : 7–12 (9.0 nominal) $e^+$ : 2.5–4 (3.1 nominal)	$e^-$ : 7 $e^+$ : 4
Delivered integrated luminosity per exp. ( $\text{fb}^{-1}$ )	1040	557	10.57
Luminosity ( $10^{30} \text{ cm}^{-2}\text{s}^{-1}$ )	21083	12069 (design: 3000)	$1.88 \times 10^4$
Time between collisions ( $\mu\text{s}$ )	0.00590 or 0.00786	0.0042	0.0065
Full crossing angle ( $\mu$ rad)	$\pm 11000^*$	0	$\pm 41500$
Energy spread (units $10^{-3}$ )	0.7	$e^-/e^+$ : 0.61/0.77	$e^-/e^+$ : 0.64/0.81
Bunch length (cm)	0.65	$e^-/e^+$ : 1.1/1.0	$e^-/e^+$ : 0.5/0.6
Beam radius ( $\mu\text{m}$ )	H: 124 ( $e^-$ ), 117 ( $e^+$ ) V: 1.9	157 4.7	$e^-$ : 16.6 ( $H$ ), 0.25 ( $V$ ) $e^+$ : 12.6 ( $H$ ), 0.25 ( $V$ )
Free space at interaction point (m)	+0.75/−0.58 (+300/−500) mrad cone	$\pm 0.2$ , $\pm 300$ mrad cone	$e^-$ : +1.20/−1.28, $e^+$ : +0.78/−0.73 (+300/−500) mrad cone
Luminosity lifetime (hr)	continuous	continuous	continuous
Turn-around time (min)	continuous	continuous	continuous
Injection energy (GeV)	$e^-/e^+$ : 8.0/3.5 (nominal)	$e^-/e^+$ : 9.0/3.1 (nominal)	$e^-/e^+$ : 7/4
Transverse emittance ( $10^{-9}$ m)	$e^-$ : 24 ( $57^\dagger$ ) ( $H$ ), 0.61 ( $V$ ) $e^+$ : 18 ( $55^\dagger$ ) ( $H$ ), 0.56 ( $V$ )	$e^-$ : 48 ( $H$ ), 1.8 ( $V$ ) $e^+$ : 24 ( $H$ ), 1.8 ( $V$ )	$e^-$ : 4.7 ( $H$ ), 0.061 ( $V$ ) $e^+$ : 2.0 ( $H$ ), 0.061 ( $V$ )
$\beta^*$ , amplitude function at interaction point (m)	$e^-$ : 1.2 ( $0.27^\dagger$ ) ( $H$ ), 0.0059 ( $V$ ) $e^+$ : 1.2 ( $0.23^\dagger$ ) ( $H$ ), 0.0059 ( $V$ )	$e^-$ : 0.50 ( $H$ ), 0.012 ( $V$ ) $e^+$ : 0.50 ( $H$ ), 0.012 ( $V$ )	$e^-$ : 0.060 ( $H$ ), $1 \times 10^{-3}$ ( $V$ ) $e^+$ : 0.080 ( $H$ ), $1 \times 10^{-3}$ ( $V$ )
Beam-beam tune shift per crossing (units $10^{-4}$ )	$e^-$ : 1020 ( $H$ ), 900 ( $V$ ) $e^+$ : 1270 ( $H$ ), 1290 ( $V$ )	$e^-$ : 703 ( $H$ ), 498 ( $V$ ) $e^+$ : 510 ( $H$ ), 727 ( $V$ )	$e^-$ : 12 ( $H$ ), 270 ( $V$ ) $e^+$ : 23 ( $H$ ), 270 ( $V$ )
RF frequency (MHz)	508.887	476	508.887
Particles per bunch (units $10^{10}$ )	$e^-/e^+$ : 4.7/6.4	$e^-/e^+$ : 5.2/8.0	$e^-/e^+$ : 2.76/3.52
Bunches per ring per species	1585	1732	1476
Average beam current per species (mA)	$e^-/e^+$ : 1188/1637	$e^-/e^+$ : 1960/3026	$e^-/e^+$ : 640/819
Beam polarization (%)	—	—	—
Circumference or length (km)	3.016	2.2	3.016
Interaction regions	1	1	1
Magnetic length of dipole (m)	$e^-/e^+$ : 5.86/0.915	$e^-/e^+$ : 5.4/0.45	$e^-/e^+$ : 5.9/4.0
Length of standard cell (m)	$e^-/e^+$ : 75.7/76.1	15.2	$e^-/e^+$ : 75.7/76.1
Phase advance per cell (deg)	450	$e^-/e^+$ : 60/90	450
Dipoles in ring	$e^-/e^+$ : 116/112	$e^-/e^+$ : 192/192	$e^-/e^+$ : 116/112
Quadrupoles in ring	$e^-/e^+$ : 452/452	$e^-/e^+$ : 290/326	$e^-/e^+$ : 466/460
Peak magnetic field (T)	$e^-/e^+$ : 0.25/0.72	$e^-/e^+$ : 0.18/0.75	$e^-/e^+$ : 0.22/0.19

\*KEKB was operated with crab crossing from 2007 to 2010.

$^\dagger$ With dynamic beam-beam effect.

High-Energy Collider Parameters:  $ep$ ,  $\bar{p}p$ ,  $pp$  Colliders

**Table 32.4:** Updated in March 2020 with numbers received from representatives of the colliders (contact E. Pianori, LBNL). The table shows the parameter values achieved. Parameters for the defunct  $Spp\bar{p}S$  collider may be found in our 2002 edition (Phys. Rev. D66, 010001 (2002)). Quantities are, where appropriate, r.m.s.; unless noted otherwise, energies refer to beam energy;  $H$  and  $V$  indicate horizontal and vertical directions; s.c. stands for superconducting.

	HERA (DESY)	TEVATRON* (Fermilab)	RHIC Brookhaven	LHC (CERN)		
Physics start date	1992	1987	2001	2009	2015	2026 (HL-LHC)
Physics end date	2007	2011	—	—		
Particles collided	$ep$	$p\bar{p}$	$pp$ (polarized)	$pp$		
Maximum beam energy (TeV)	$e$ : 0.030 $p$ : 0.92	0.980	0.255 55% polarization	4.0	6.5	7.0
Max. delivered integrated luminosity per exp. ( $\text{fb}^{-1}$ )	0.8	12	0.38 at 100 GeV 1.3 at 250/255 GeV	23.3 at 4.0 TeV 6.1 at 3.5 TeV	160	250/y
Luminosity ( $10^{30} \text{ cm}^{-2} \text{ s}^{-1}$ )	75	431	245 (pk) 160 (avg)	$7.7 \times 10^3$	$2.1 \times 10^4$	$5.0 \times 10^4$ (leveled)
Time between collisions (ns)	96	396	107	49.90	24.95	24.95
Full crossing angle ( $\mu$ rad)	0	0	0	290	$320 \rightarrow 260^\dagger$	500
Energy spread (units $10^{-3}$ )	$e$ : 0.91 $p$ : 0.2	0.14	0.15	0.1445	0.105	0.129
Bunch length (cm)	$e$ : 0.83 $p$ : 8.5	$p$ : 50 $\bar{p}$ : 45	60	9.4	8	9
Beam radius ( $10^{-6}$ m)	$e$ : 110 (H), 30 (V) $p$ : 111 (H), 30 (V)	$p$ : 28 $\bar{p}$ : 16	85	18.8	$8.5^\ddagger$	$7^\ddagger$
Free space at interaction point (m)	$\pm 2$	$\pm 6.5$	16	38	38	38
Initial luminosity decay time, $-L/(dL/dt)$ (hr)	10	6 (avg)	7.5	$\approx 6$	$\approx 8$	$\approx 7.5$ (leveled)
Turn-around time (min)	$e$ : 75, $p$ : 135	90	25	180	150	145
Injection energy (TeV)	$e$ : 0.012 $p$ : 0.040	0.15	0.023	0.450	0.450	0.450
Transverse emittance ( $10^{-9}$ m)	$e$ : 20 (H), 3.5 (V) $p$ : 5 (H), 5 (V)	$p$ : 3 $\bar{p}$ : 1	11	0.59	0.3	0.33
$\beta^*$ , ampl. function at interaction point (m)	$e$ : 0.6 (H), 0.26 (V) $p$ : 2.45 (H), 0.18 (V)	0.28	0.65	0.6	$0.3 \rightarrow 0.29^\S$	$0.6 \rightarrow 0.15^\S$
Beam-beam tune shift per crossing (units $10^{-4}$ )	$e$ : 190 (H), 450 (V) $p$ : 12 (H), 9 (V)	$p$ : 120 $\bar{p}$ : 120	73	72	45	86
RF frequency (MHz)	$e$ : 499.7 $p$ : 208.2/52.05	53	accel: 9 store: 28	400.8	400.8	400.8
Particles per bunch (units $10^{10}$ )	$e$ : 3 $p$ : 7	$p$ : 26 $\bar{p}$ : 9	18.5	16	11	22
Bunches per ring per species	$e$ : 189 $p$ : 180	36	111	1380	2556 2544 (i.r. 1/5 $^\P$ )	2760 2748 (i.r. 1/5 $^\P$ )
Average beam current per species (mA)	$e$ : 40 $p$ : 90	$p$ : 70 $\bar{p}$ : 24	257	400	510	1100
Circumference (km)	6.336	6.28	3.834	26.659		
Interaction regions	2 colliding beams 1 fixed target ( $e$ beam)	2 high $\mathcal{L}$	6 total, 2 high $\mathcal{L}$	4 total, 2 high $\mathcal{L}$		
Magnetic length of dipole (m)	$e$ : 9.185; $p$ : 8.82	6.12	9.45	14.3		
Length of standard cell (m)	$e$ : 23.5 $p$ : 47	59.5	29.7	106.90		
Phase advance per cell (deg)	$e$ : 60 $p$ : 90	67.8	84	90		
Dipoles in ring	$e$ : 396 $p$ : 416	774	192 per ring + 12 common	1232 main dipoles		
Quadrupoles in ring	$e$ : 580 $p$ : 280	216	246 per ring	482 2-in-1 24 1-in-1		
Magnet types	$e$ : C-shaped $p$ : s.c., col., warm iron	s.c., $\cos\theta$ warm iron	s.c., $\cos\theta$ cold iron	s.c., 2-in-1 cold iron		
Peak magnetic field (T)	$e$ : 0.274; $p$ : 5	4.4	3.5	8.3 $^\parallel$		

\*Other TEVATRON parameters:  $\bar{p}$  source accum. rate:  $25 \times 10^{10} \text{ hr}^{-1}$ ; max. no. of  $\bar{p}$  stored:  $3.4 \times 10^{12}$  (Accumulator),  $6.1 \times 10^{12}$  (Recycler).

$^\dagger$  Variable crossing angle decreasing during the fill with the reduction in bunch population

$^\ddagger$  Minimum beam radius during levelling

$^\S$   $\beta^*$  levelling

$^\P$  Number of bunches colliding at the interaction regions (i.r.) 1 (ATLAS) and 5 (CMS).

$^\parallel$  Value for design beam energy of 7 TeV.

## High-Energy Collider Parameters: Heavy Ion Colliders

**Table 32.5:** Updated in March 2020 with numbers received from representatives of the collider (contact E. Pianori, LBNL) The table shows the parameter values achieved. For the LHC, only maximum values for the ATLAS and CMS experiments are provided (ALICE and LHCb have different requirements for energy and luminosity). Design values for a high-luminosity upgrade are also given. Quantities are, where appropriate, r.m.s.; unless noted otherwise, energies refer to beam energy; s.c. stands for superconducting. pk and avg denote peak and average values.

	RHIC (Brookhaven)			LHC (CERN)			
Physics start date	2000	2012 / 2018 / 2018 / 2012 / 2004 2014 / 2002 / 2015 / 2015		2010	2012	2017	$\geq 2021$ (high lum.)*
Physics end date	—			—			
Particles collided	Au Au	U U / Zr Zr / Ru Ru / Cu Au Cu Cu / h Au d Au / p Au / p Al		Pb Pb	p Pb	Xe Xe	Pb Pb
Max. beam energy (TeV/n)	0.1	0.1		2.51	p:6.5 Pb:2.56	2.72	2.76
$\sqrt{s_{NN}}$ (TeV)	0.2	0.2		5.02	8.16	5.44	5.5
Max. delivered int. nucleon-pair lumin. per exp. ( $\text{pb}^{-1}$ )	2639 (at 100 GeV/n)	21 / 36 / 36.9 / 167 / 60 43 / 169 / 124 / 63 (all at 100 GeV/n)		77.8	194	0.05	$\approx 121/y$
Luminosity ( $10^{27} \text{ cm}^{-2} \text{ s}^{-1}$ )	pk: 15.5 avg: 8.7	pk: 0.4 / 4.8 / 3.8 / 12 / 21 170 / 850 / 880 / 7600 avg: 0.6 / 2.2 / 2.1 / 10 / 8 100 / 500 / 450 / 3800		6.1	900	0.4	6.4 (leveled)
Time between collisions (ns)	107	107 / 107 / 107 107/ 107 / 321 107 / 107 / 107 / 107		74.9 / 149.7	99.8 / 149.7	$\approx 5500$	49.9
Full crossing angle ( $\mu$ rad)	0	0		320	280	300	340
Energy spread (units $10^{-3}$ )	0.75	0.75		0.11	0.11	0.11	0.11
Bunch length (cm)	30	30		8.0	p / Pb: 9 / 11.5	11	7.9
Beam radius ( $10^{-6}$ m)	114 <sup>†</sup>	123 <sup>†</sup> / 87 <sup>†</sup> / 88 <sup>†</sup> / 163 <sup>†</sup> / 145 <sup>†</sup> 136 <sup>†</sup> / 124 <sup>†</sup> / 147 <sup>†</sup> / 128 <sup>†</sup>		21	19	12	17
Free space at inter. point (m)	16	16		38	38	38	38
Initial luminosity decay time, $-L/(dL/dt)$ (hr)	1	-0.35 <sup>‡</sup> / $\infty^{\S}$ / $\infty^{\S}$ / $\infty^{\ddagger}$ / 1.8 0.6 / $\infty^{\ddagger}$ / 0.5 / 0.25		3.3	$\approx 2$	$\approx 6$	$\infty$
Turn-around time (min)	30	60 <sup>¶</sup> / 40 <sup>¶</sup> / 40 <sup>¶</sup> / 160 <sup>¶</sup> / 90 <sup>¶</sup> 45 <sup>¶</sup> / 90 <sup>¶</sup> / 60 <sup>¶</sup> / 50 <sup>¶</sup>		$\approx 180$	150	180	$\approx 200$
Injection energy (TeV/n)	0.011	0.011		0.177	p / Pb: 0.45 / 0.177	0.188	0.177
Transverse emittance ( $10^{-9}$ m)	19 <sup>†</sup>	22 <sup>†</sup> / 10.7 <sup>†</sup> / 11.2 <sup>†</sup> / 38 <sup>†</sup> / 23 <sup>†</sup> 19 <sup>†</sup> / 22 <sup>†</sup> / 26 <sup>†</sup> / 21 <sup>†</sup>		0.85	0.29	0.3	0.5
$\beta^*$ , ampl. function at interaction point (m)	0.7	0.7 / 0.7 / 0.7 / 0.7 / 0.9 1.0 / 0.7 / 0.8 / 0.8		0.5	0.5	0.4	0.5
Beam-beam tune shift per crossing (units $10^{-4}$ )	39 <sup>†</sup>	6 <sup>†</sup> / 18 <sup>†</sup> / 21 <sup>†</sup> / 14 <sup>†</sup> , 14 <sup>†</sup> / 30 <sup>†</sup> / 42 <sup>†</sup> , 22 <sup>†</sup> 40 <sup>†</sup> , 27 <sup>†</sup> / 53 <sup>†</sup> , 41 <sup>†</sup> / 80 <sup>†</sup> , 59 <sup>†</sup>		15	15	$\approx 10$	11
RF frequency (MHz)	accel: 28, store: 197			400.8	400.8	400.8	400.8
Particles per bunch (units $10^{10}$ )	0.20	0.03 / 0.1 / 0.1 / 0.4, 0.13 / 0.45 4.5, 0.13 / 13, 0.20 / 22.5, 0.16 / 24, 1.1		0.022 (r.m.s.)	p:2.6 Pb:0.022	0.027	0.018
Bunches per ring per species	111	111 / 111 / 111 / 111 / 37 111 / 111 / 111 / 111		733	p:540 Pb:684	16	1232
Average beam current per species (mA)	224	38 / 56 / 61 / 160, 138 / 60 / 125, 143 181, 213 / 313, 176 / 334, 199		23.8	p:16 Pb:15	0.54	32
Circumference (km)	3.834			26.659			
Interaction regions	6 total, 2 high $\mathcal{L}$			4 total, 3 high $\mathcal{L}$			
Magnetic length of dipole (m)	9.45			14.3			
Length of standard cell (m)	29.7			106.90			
Phase advance per cell (deg)	93	84 / 84 / 84 / 84 / 84 93 / 84(d), 93 / 84(p), 93 / 84(p), 93		90			
Dipoles in ring	192 per ring, + 12 common			1232, main dipoles			
Quadrupoles in ring	246 per ring			482 2-in-1, 24 1-in-1			
Magnet Type	s.c. $\cos\theta$ , cold iron			s.c., 2 in 1, cold iron			
Peak magnetic field (T)	3.5			8.3			

\*High luminosity upgrade expected  $\geq 2021$ ; will extend throughout HL-LHC running. Very preliminary, conservative estimates.

<sup>†</sup>Initial value, possibly larger after cooling

<sup>‡</sup>Negative or infinite decay time is effect of cooling.

<sup>§</sup>luminosity leveled to flat after set to target value, with cooling

<sup>¶</sup>measured minimum, not theoretical

### 33. Neutrino Beam Lines at High-Energy Proton Synchrotrons

Revised August 2019 with numbers verified by representatives of the synchrotrons (contact C.-J. Lin, LBNL). For existing (future) neutrino beam lines the latest achieved (design) values are given.

The main source of neutrinos at proton synchrotrons is from the decay of pions and kaons produced by protons striking a nuclear target. There are different schemes to focus the secondary particles to enhance neutrino flux and/or tune the neutrino energy profile. In wide-band beams (WBB), the neutrino parent mesons are focused over a wide momentum range to obtain maximum neutrino intensity. In narrow-band beams (NBB), the secondary particles are first momentum-selected to produce a monochromatic parent beam. Another approach to generate a narrow-band neutrino spectrum is to select neutrinos that are emitted off-axis relative to the momentum of the parent mesons. For a comprehensive review of the topic, including other historical neutrino beam lines, see the article by S. E. Kopp, "Accelerator-based neutrino beams," Phys. Rept. **439**, 101 (2007).

	PS (CERN)				SPS (CERN)				PS (KEK)	Main Ring (JPARC)
	1963	1969	1972	1983	1977	1977	1995	2006	1999	2017
Date	1963	1969	1972	1983	1977	1977	1995	2006	1999	2017
Proton Kinetic Energy (GeV)	20.6	20.6	26	19	350	350	450	400	12	30 (50)
Protons per Cycle ( $10^{12}$ )	0.7	0.6	5	5	10	10	36	48	6	240 (330)
Cycle Time (s)	3	2.3	-	-	-	-	14.4	6	2.2	2.48 (3.5)
Beam Power (kW)	0.8	0.9	-	-	-	-	180	510	5	500 (750)
Target	-	-	-	-	-	-	Be	Graphite	Al	Graphite
Target Length (cm)	-	-	-	-	-	-	290	130	66	91
Secondary Focussing	1-horn WBB	3-horn WBB	2-horn WBB	bare target	dichromatic NBB	2-horn WBB	2-horn WBB	2-horn WBB	2-horn WBB	3-horn off-axis
Decay Pipe Length (m)	-	-	-	-	-	-	110	1090	200	96
$\langle E_\nu \rangle$ (GeV)	1.5	1.5	1.5	1	50,150 <sup>†</sup>	20	24.3	17	1.3	0.6
Experiments	HLBC, Spark Ch.	HLBC, Spark Ch.	GGM, Aachen-Padova	CDHS, CHARM	CDHS, CHARM, BEBC	GGM, CDHS, CHARM, BEBC	NOMAD, CHORUS	OPERA, ICARUS	K2K	T2K

	Main Ring (Fermilab)					Booster (Fermilab)	Main Injector (Fermilab)			
	1974	1979	1976	1991	1998	2002, (2020)	2005	2017	(2020)	(2026)
Date	1974	1979	1976	1991	1998	2002, (2020)	2005	2017	(2020)	(2026)
Proton Kinetic Energy (GeV)	300	400	350	800	800	8	120	120	120	(60 – 120)
Protons per Cycle ( $10^{12}$ )	10	10	13	10	12	4.5	37	54	(65)	(75)
Cycle Time (s)	-	-	-	60	60	0.2	2	1.333	(1.2)	(1.2)
Beam Power (kW)	-	-	-	20	25	29	350	720	(1000)	(1200)
Target	-	-	-	-	BeO	Be	Graphite	Graphite	Graphite	(Graphite)
Target Length (cm)	-	-	-	-	31	71	95	120	120	(150-220)
Secondary Focussing	dichromatic NBB	2-horn WBB	1-horn WBB	quad trip.	SSQT WBB	1-horn WBB	2-horn WBB	2-horn off-axis	2-horn off-axis	(3-horn WBB)
Decay Pipe Length (m)	400	400	400	400	400	50	675	675	675	(220)
$\langle E_\nu \rangle$ (GeV)	50,180 <sup>†</sup>	25	100	90,260	70,180	1	3-20 <sup>‡</sup>	2	2	(2.5)
Experiments	CITF, HPWF, 15' BC	15' BC	HPWF 15' BC	15' BC, CCFRR	NuTeV	MiniBooNE, SciBooNE, MicroBooNE, (SBND, ICARUS)	MINOS, MINERνA	NOνA, MINERνA, MINOS+	NOνA	LBNF/ DUNE

<sup>†</sup>Pion and kaon peaks in the momentum-selected channel.

<sup>‡</sup>Tunable WBB energy spectrum.

## 34. Passage of Particles Through Matter

Revised August 2019 by D.E. Groom (LBNL) and S.R. Klein (NSD LBLN).

34.1	Notation . . . . .	535
34.2	Electronic energy loss by heavy particles . . . . .	535
34.2.1	Moments and cross sections . . . . .	535
34.2.2	Maximum energy transfer in a single collision	535
34.2.3	Stopping power at intermediate energies . . . . .	536
34.2.4	Mean excitation energy . . . . .	538
34.2.5	Density effect . . . . .	538
34.2.6	Energy loss at low energies . . . . .	538
34.2.7	Energetic knock-on electrons ( $\delta$ rays) . . . . .	538
34.2.8	Restricted energy loss rates for relativistic ionizing particles . . . . .	539
34.2.9	Fluctuations in energy loss . . . . .	539
34.2.10	Energy loss in mixtures and compounds . . . . .	540
34.2.11	Ionization yields . . . . .	540
34.3	Multiple scattering through small angles . . . . .	540
34.4	Photon and electron interactions in matter . . . . .	541
34.4.1	Collision energy losses by $e^\pm$ . . . . .	541
34.4.2	Radiation length . . . . .	541
34.4.3	Bremsstrahlung energy loss by $e^\pm$ . . . . .	542
34.4.4	Critical energy . . . . .	542
34.4.5	Energy loss by photons . . . . .	543
34.4.6	Bremsstrahlung and pair production at very high energies . . . . .	543
34.4.7	Photonuclear and electronuclear interactions at still higher energies . . . . .	544
34.5	Electromagnetic cascades . . . . .	545
34.6	Muon energy loss at high energy . . . . .	546
34.7	Cherenkov and transition radiation . . . . .	547
34.7.1	Optical Cherenkov radiation . . . . .	547
34.7.2	Coherent radio Cherenkov radiation . . . . .	547
34.7.3	Transition radiation . . . . .	548

This review covers the interactions of photons and electrically charged particles in matter, concentrating on energies of interest for high-energy physics and astrophysics and processes of interest for particle detectors (ionization, Cherenkov radiation, transition radiation). Much of the focus is on particles heavier than electrons ( $\pi^\pm$ ,  $p$ , etc.). Although the charge number  $z$  of the projectile is included in the equations, only  $z = 1$  is discussed in detail. Muon radiative losses are discussed, as are photon/electron interactions at high to ultrahigh energies. Neutrons are not discussed.

## 34.1 Notation

The notation and important numerical values are shown in Table 34.1.

## 34.2 Electronic energy loss by heavy particles

## 34.2.1 Moments and cross sections

The electronic interactions of fast charged particles with speed  $v = \beta c$  occur in *single collisions with energy losses*  $W$  [1], leading to ionization, atomic, or collective excitation. Most frequently the energy losses are small (for 90% of all collisions the energy losses are less than 100 eV). In thin absorbers few collisions will take place and the total energy loss will show a large variance [1]; also see Sec. 34.2.9 below. For particles with charge  $ze$  more massive than electrons (“heavy” particles), scattering from free electrons is adequately described by the Rutherford differential cross section [2],

$$\frac{d\sigma_R(W; \beta)}{dW} = \frac{2\pi r_e^2 m_e c^2 z^2}{\beta^2} \frac{(1 - \beta^2 W/W_{\max})}{W^2}, \quad (34.1)$$

where  $W_{\max}$  is the maximum energy transfer possible in a single collision. But in matter electrons are not free.  $W$  must be finite and depends on atomic and bulk structure. For electrons bound in atoms Bethe [3] used “Born Theorie” to obtain the differential cross section

$$\frac{d\sigma_B(W; \beta)}{dW} = \frac{d\sigma_R(W; \beta)}{dW} B(W). \quad (34.2)$$

Electronic binding is accounted for by the correction factor  $B(W)$ . Examples of  $B(W)$  and  $d\sigma_B/dW$  can be seen in Figs. 5 and 6 of Ref. [1].

**Table 34.1:** Summary of variables used in this section. The kinematic variables  $\beta$  and  $\gamma$  have their usual relativistic meanings.

Symb.	Definition	Value or (usual) units
$m_e c^2$	electron mass $\times c^2$	0.510 998 950 00(15) MeV
$r_e$	classical electron radius $e^2/4\pi\epsilon_0 m_e c^2$	2.817 940 3262(13) fm
$\alpha$	fine structure constant $e^2/4\pi\epsilon_0 \hbar c$	1/137.035 999 084(21)
$N_A$	Avogadro’s number	6.022 140 76 $\times 10^{23}$ mol $^{-1}$
$\rho$	density	g cm $^{-3}$
$x$	mass per unit area	g cm $^{-2}$
$M$	incident particle mass	MeV/ $c^2$
$E$	incident part. energy $\gamma M c^2$	MeV
$T$	kinetic energy, $(\gamma - 1) M c^2$	MeV
$W$	energy transfer to an electron in a single collision	MeV
$W_{\max}$	Maximum possible energy transfer to an electron in a single collision	MeV
$k$	bremsstrahlung photon energy	MeV
$z$	charge number of incident particle	
$Z$	atomic number of absorber	
$A$	atomic mass of absorber	g mol $^{-1}$
$K$	$4\pi N_A r_e^2 m_e c^2$ (Coefficient for $dE/dx$ )	0.307 075 MeV mol $^{-1}$ cm $^2$
$I$	mean excitation energy	eV ( <i>Nota bene!</i> )
$\delta(\beta\gamma)$	density effect correction to ionization energy loss	
$\hbar\omega_p$	plasma energy $\sqrt{4\pi N_e r_e^3 m_e c^2}/\alpha$	$\sqrt{\rho(Z/A)} \times 28.816$ eV $\hookrightarrow \rho$ in g cm $^{-3}$
$N_e$	electron density	(units of $r_e$ ) $^{-3}$
$w_j$	weight fraction of the $j$ th element in a compound or mixt.	
$n_j$	$\alpha$ number of $j$ th kind of atoms in a compound or mixture	
$X_0$	radiation length	g cm $^{-2}$
$E_c$	critical energy for electrons	MeV
$E_{\mu c}$	critical energy for muons	GeV
$E_s$	scale energy $\sqrt{4\pi/\alpha} m_e c^2$	21.2052 MeV
$R_M$	Molière radius	g cm $^{-2}$

Bethe’s original theory applies only to energies above which atomic effects are not important. The free-electron cross section (Eq. (34.1)) can be used to extend the cross section to  $W_{\max}$ . At high energies  $\sigma_B$  is further modified by polarization of the medium, and this “density effect,” discussed in Sec. 34.2.5, must also be included. Smaller corrections are discussed below.

The mean number of collisions with energy loss between  $W$  and  $W + dW$  occurring in a distance  $\delta x$  is  $N_e \delta x (d\sigma/dW) dW$ , where  $d\sigma(W; \beta)/dW$  contains all contributions. It is convenient to define the moments

$$M_j(\beta) = N_e \delta x \int W^j \frac{d\sigma(W; \beta)}{dW} dW, \quad (34.3)$$

so that  $M_0$  is the mean number of collisions in  $\delta x$ ,  $M_1$  is the mean energy loss in  $\delta x$ ,  $(M_2 - M_1^2)$  is the variance, etc. The number of collisions is Poisson-distributed with mean  $M_0$ .  $N_e$  is either measured in electrons/g ( $N_e = N_A Z/A$ ) or electrons/cm $^3$  ( $N_e = N_A \rho Z/A$ ). The former is used throughout this chapter, since quantities of interest ( $dE/dx$ ,  $X_0$ , etc.) vary smoothly with composition when there is no density dependence.

## 34.2.2 Maximum energy transfer in a single collision

For a particle with mass  $M$ ,

$$W_{\max} = \frac{2m_e c^2 \beta^2 \gamma^2}{1 + 2\gamma m_e/M + (m_e/M)^2}. \quad (34.4)$$

In older references [2, 7] the “low-energy” approximation  $W_{\max} = 2m_e c^2 \beta^2 \gamma^2$ , valid for  $2\gamma m_e \ll M$ , is often implicit. For

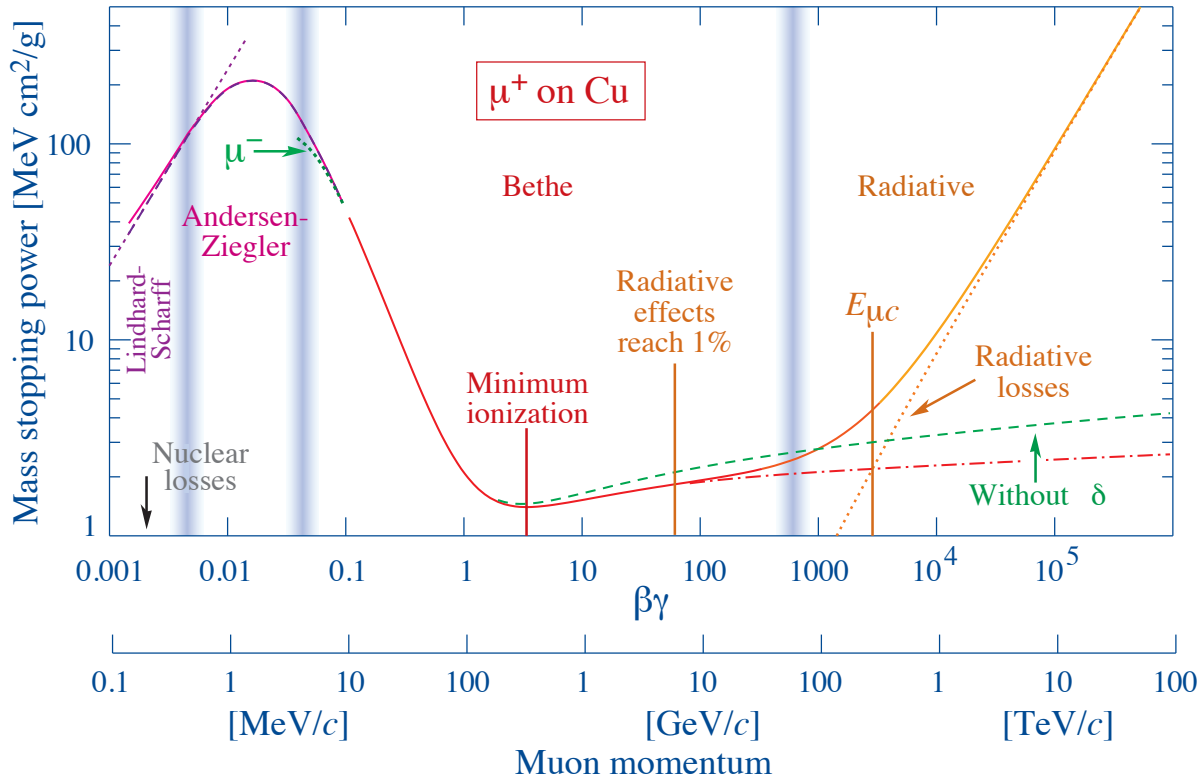


Figure 34.1: Mass stopping power ( $= \langle -dE/dx \rangle$ ) for positive muons in copper as a function of  $\beta\gamma = p/Mc$  over nine orders of magnitude in momentum (12 orders of magnitude in kinetic energy). Solid curves indicate the total stopping power. Data below the break at  $\beta\gamma \approx 0.1$  are taken from ICRU 49 [4] assuming only  $\beta$  dependence, and data at higher energies are from [5]. Vertical bands indicate boundaries between different approximations discussed in the text. The short dotted lines labeled “ $\mu^-$ ” illustrate the “Barkas effect”, the dependence of stopping power on projectile charge at very low energies [6].  $dE/dx$  in the radiative region is not simply a function of  $\beta$ .

a pion in copper, the error thus introduced into  $dE/dx$  is greater than 6% at 100 GeV. For  $2\gamma m_e \gg M$ ,  $W_{\max} = Mc^2 \beta^2 \gamma$ .

At energies of order 100 GeV, the maximum 4-momentum transfer to the electron can exceed 1 GeV/c, where hadronic structure effects modify the cross sections. This problem has been investigated by J.D. Jackson [8], who concluded that for incident hadrons (but not for large nuclei) corrections to  $dE/dx$  are negligible below energies where radiative effects dominate. While the cross section for rare hard collisions is modified, the average stopping power, dominated by many softer collisions, is almost unchanged.

### 34.2.3 Stopping power at intermediate energies

The mean rate of energy loss by moderately relativistic charged heavy particles is well described by the “Bethe equation,”

$$\left\langle -\frac{dE}{dx} \right\rangle = K z^2 \frac{Z}{A} \frac{1}{\beta^2} \left[ \frac{1}{2} \ln \frac{2m_e c^2 \beta^2 \gamma^2 W_{\max}}{I^2} - \beta^2 - \frac{\delta(\beta\gamma)}{2} \right]. \quad (34.5)$$

Eq. (34.5) is valid in the region  $0.1 \lesssim \beta\gamma \lesssim 1000$  with an accuracy of a few percent. Small corrections are discussed below.

This is the *mass stopping power*; with the symbol definitions and values given in Table 34.1, the units are  $\text{MeV g}^{-1} \text{cm}^2$ . As can be seen from Fig. 34.2,  $\langle dE/dx \rangle$  defined in this way is about the same for most materials, decreasing slowly with  $Z$ . The *linear stopping power*, in  $\text{MeV/cm}$ , is  $\rho \langle dE/dx \rangle$ , where  $\rho$  is the density in  $\text{g/cm}^3$ .

At  $\beta\gamma \sim 0.1$  the projectile velocity is comparable to atomic electron “velocities” (Sec. 34.2.6), and at  $\beta\gamma \sim 1000$  radiative effects begin to be important (Sec. 34.6). Both limits are  $Z$  dependent. A minor dependence on  $M$  at high energies is introduced through  $W_{\max}$ , but for all practical purposes  $\langle dE/dx \rangle$  in a given material is a function of  $\beta$  alone.

The stopping power at first falls as  $1/\beta^\alpha$  where  $\alpha \approx 1.4$ – $1.7$ ,

depending slightly on the incident particle’s mass and decreasing somewhat with  $Z$ , and reaches a broad minimum at  $\beta\gamma = 3.5$ – $3.0$  as  $Z$  goes from 7 to 100. It then inexorably rises as the argument of the logarithmic term increases. Two independent mechanisms contribute. Two thirds of the rise is produced by the explicit  $\beta^2 \gamma^2$  dependence through the relativistic flattening and extension of the particle’s electric field. Rather than producing ionization at greater and greater distances, the field polarizes the medium, cancelling the increase in the logarithmic term at high energies. This is taken into account by the density-effect correction  $\delta(\beta\gamma)$ . The other third is introduced by the  $\beta^2 \gamma$  dependence of  $W_{\max}$ , the maximum possible energy transfer to a recoil electron. “Hard collision” events increasingly extend the tail of the energy loss distribution, increasing the mean but with little effect on the position of the maximum, the most probable energy loss.

Few concepts in high-energy physics are as misused as  $dE/dx$ , since the mean is weighted by rare events with large single-collision energy losses. Even with samples of hundreds of events in a typical detector, the mean energy loss cannot be obtained dependably. Far better and more easily measured is the most probable energy loss, discussed in Sec. 34.2.9. The most probable energy loss in a typical detector is considerably smaller than the mean given by the Bethe equation. It does not continue to rise with the mean stopping power, but approaches a “Fermi plateau.”

In analysing TPC data (Sec. 35.6.5), the same end is often accomplished by using the mean of 50%–70% of the samples with the smallest signals as the estimator.

Although it must be used with cautions and caveats,  $\langle dE/dx \rangle$  as described in Eq. (34.5) still forms the basis of much of our understanding of energy loss by charged particles. Extensive tables are available [4, 5] and [pdg.lbl.gov/AtomicNuclearProperties/](http://pdg.lbl.gov/AtomicNuclearProperties/).

For heavy projectiles, like ions, additional terms are required to account for higher-order photon coupling to the target, and to account for the finite target radius. These can change  $dE/dx$  by a

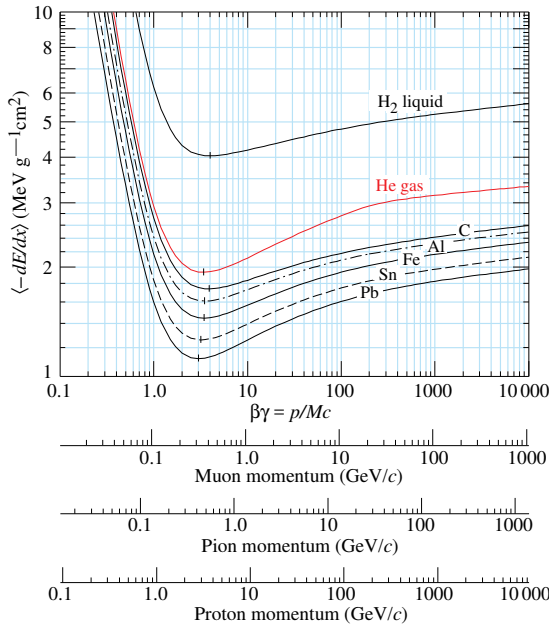


Figure 34.2: Mean energy loss rate in liquid (bubble chamber) hydrogen, gaseous helium, carbon, aluminum, iron, tin, and lead. Radiative effects, relevant for muons and pions, are not included. These become significant for muons in iron for  $\beta\gamma \gtrsim 1000$ , and at lower momenta for muons in higher- $Z$  absorbers. See Fig. 34.23.

factor of two or more for the heaviest nuclei in certain kinematic regimes [9].

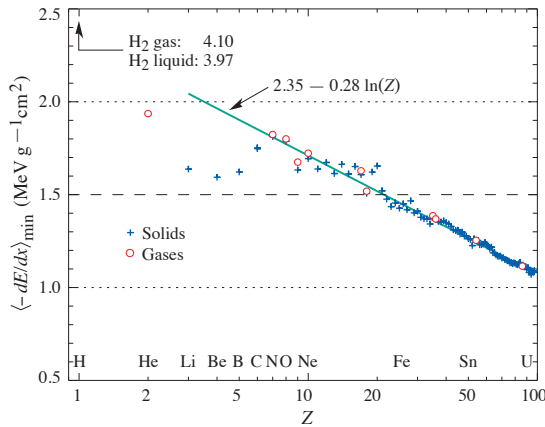


Figure 34.3: Mass stopping power at minimum ionization for the chemical elements. The straight line is fitted for  $Z > 6$ . A simple functional dependence on  $Z$  is not to be expected, since  $\langle -dE/dx \rangle$  also depends on other variables.

The function as computed for muons on copper is shown as the “Bethe” region of Fig. 34.1. Mean energy loss behavior below this region is discussed in Sec. 34.2.6, and the radiative effects at high energy are discussed in Sec. 34.6. Only in the Bethe region is it a function of  $\beta$  alone; the mass dependence is more complicated elsewhere. The stopping power in several other materials is shown in Fig. 34.2. Except in hydrogen, particles with the same velocity have similar rates of energy loss in different materials, although there is a slow decrease in the rate of energy loss with increasing  $Z$ . The qualitative behavior difference at high energies between a gas (He in the figure) and the other materials shown in the figure is due to the density-effect correction,  $\delta(\beta\gamma)$ , discussed in Sec. 34.2.5. The stopping power functions are characterized by broad minima whose position drops from  $\beta\gamma = 3.5$  to 3.0 as  $Z$  goes from 7 to 100. The values of minimum ionization as a function of atomic number are shown in Fig. 34.3.

In practical cases, most relativistic particles (e.g., cosmic-ray muons) have mean energy loss rates close to the minimum; they are “minimum-ionizing particles,” or mip’s.

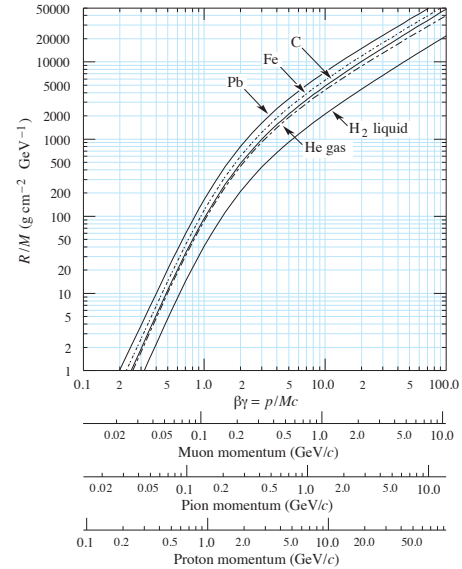


Figure 34.4: Range of heavy charged particles in liquid (bubble chamber) hydrogen, helium gas, carbon, iron, and lead. For example: For a  $K^+$  whose momentum is 700 MeV/ $c$ ,  $\beta\gamma = 1.42$ . For lead we read  $R/M \approx 396$ , and so the range is 195 g cm<sup>-2</sup> (17 cm).

Eq. (34.5) may be integrated to find the total (or partial) “continuous slowing-down approximation” (CSDA) range  $R$  for a particle which loses energy only through ionization and atomic excitation. Since  $dE/dx$  depends only on  $\beta$ ,  $R/M$  is a function of  $E/M$  or  $pc/M$ . In practice, range is a useful concept only for low-energy hadrons ( $R \lesssim \lambda_I$ , where  $\lambda_I$  is the nuclear interaction length), and for muons below a few hundred GeV (above which radiative effects dominate). Fig. 34.4 shows  $R/M$  as a function of  $\beta\gamma$  ( $= p/Mc$ ) for a variety of materials.

The mass scaling of  $dE/dx$  and range is valid for the electronic losses described by the Bethe equation, but not for radiative losses.

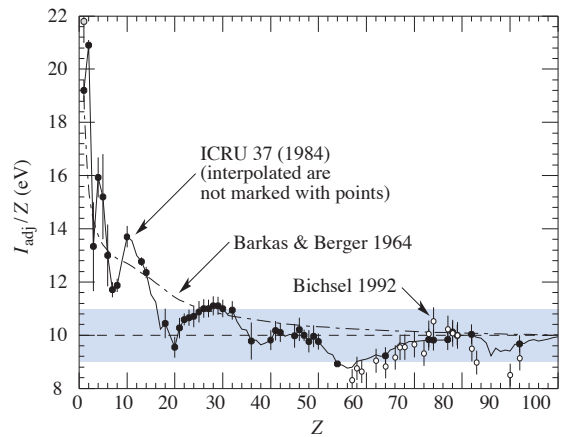


Figure 34.5: Mean excitation energies (divided by  $Z$ ) as adopted by the ICRU [10]. Those based on experimental measurements are shown by symbols with error flags; the interpolated values are simply joined. The grey point is for liquid H<sub>2</sub>; the black point at 19.2 eV is for H<sub>2</sub> gas. The open circles show more recent determinations by Bichsel [11]. The dash-dotted curve is from the approximate formula of Barkas [12] used in early editions of this Review.



### 34.2.4 Mean excitation energy

“The determination of the mean excitation energy is the principal non-trivial task in the evaluation of the Bethe stopping-power formula” [13]. Recommended values have varied substantially with time. Estimates based on experimental stopping-power measurements for protons, deuterons, and alpha particles and on oscillator-strength distributions and dielectric-response functions were given in ICRU 49 [4]. See also ICRU 37 [10]. These values, shown in Fig. 34.5, have since been widely used. Machine-readable versions can also be found [14].

### 34.2.5 Density effect

As the particle energy increases, its electric field flattens and extends, so that the distant-collision contribution to the logarithmic term in Eq. (34.5) increases as  $\beta^2\gamma^2$ . However, real media become polarized, limiting the field extension and effectively truncating this part of the logarithmic rise [2–5, 15, 16]. At very high energies,

$$\delta(\beta\gamma)/2 \rightarrow \ln(\hbar\omega_p/I) + \ln\beta\gamma - 1/2, \quad (34.6)$$

where  $\delta(\beta\gamma)/2$  is the density effect correction introduced in Eq. (34.5) and  $\hbar\omega_p$  is the plasma energy defined in Table 34.1. A comparison with Eq. (34.5) shows that  $|dE/dx|$  then grows as  $\ln T_{\max}$  rather than  $\ln\beta^2\gamma^2 T_{\max}$ , and that the mean excitation energy  $I$  is replaced by the plasma energy  $\hbar\omega_p$ . An example of the ionization stopping power as calculated with and without the density effect correction is shown in Fig. 34.1. Since the plasma frequency scales as the square root of the electron density, the correction is much larger for a liquid or solid than for a gas, as is illustrated in Fig. 34.2.

The density effect correction is usually computed using Sternheimer’s parameterization [15]:

$$\delta(\beta\gamma) = \begin{cases} 2(\ln 10)x - \bar{C} & \text{if } x \geq x_1; \\ 2(\ln 10)x - \bar{C} + a(x_1 - x)^k & \text{if } x_0 \leq x < x_1; \\ 0 & \text{if } x < x_0 \text{ (nonconductors);} \\ \delta_0 10^{2(x-x_0)} & \text{if } x < x_0 \text{ (conductors)} \end{cases} \quad (34.7)$$

Here  $x = \log_{10} \beta\gamma = \log_{10}(p/Mc)$ .  $\bar{C}$  (the negative of the  $C$  used in Ref. [15]) is obtained by equating the high-energy case of Eq. (34.7) with the limit given in Eq. (34.6). The other parameters are adjusted to give a best fit to the results of detailed calculations for momenta below  $Mc \exp(x_1)$ . For nonconductors the correction is 0 below  $\beta\gamma = 10^{x_0}$ , corresponding to 100–200 MeV for pions and 1–2 GeV for protons. For conductors it decreases rapidly below this point. Parameters for the elements and nearly 200 compounds and mixtures of interest are published in a variety of places, notably in Ref. [16]. A recipe for finding the coefficients for nontabulated materials is given by Sternheimer and Peierls [17] and is summarized in Ref. [5].

The remaining relativistic rise comes from the  $\beta^2\gamma$  growth of  $W_{\max}$ , which in turn is due to (rare) large energy transfers to a few electrons. When these events are excluded, the energy deposit in an absorbing layer approaches a constant value, the Fermi plateau (see Sec. 34.2.8 below). At even higher energies (e.g., > 332 GeV for muons in iron, and at a considerably higher energy for protons in iron), radiative effects are more important than ionization losses. These are especially relevant for high-energy muons, as discussed in Sec. 34.6.

### 34.2.6 Energy loss at low energies

The theory of energy loss by ionization and excitation as given by Bethe is based on a first-order Born approximation. It assumes free electrons, and should be valid when the projectile’s velocity is large compared to that of the atomic electrons. This presents a problem at low energies, where  $W_{\max}$  is less than the K shell binding energy. However, Mott showed that the Born approximation can be applied at energies much smaller than atomic binding energies [18]; the incident particle can be treated by classical mechanics since its wavelength is shorter than atomic dimensions. The Born method is actually better justified when its velocity is not large compared to the K electron velocity [19].

Higher-order corrections must still be made to extend the Bethe equation Eq. (34.5) to low energies, e.g. below 10 MeV for protons.

An improved approximation for the terms in the square brackets of Eq. (34.5) at low energies is obtained with

$$L(\beta) = L_a(\beta) - \frac{C(\beta)}{Z} + zL_1(\beta) + z^2L_2(\beta). \quad (34.8)$$

Here  $L_a$  is the square-bracketed terms of Eq. (34.5),  $C/Z$  is the sum of shell corrections and  $zL_1$  and  $z^2L_2$  are Barkas and Bloch correction terms [4, 20]. With these corrections, the Bethe treatment is accurate to about 1% down to  $\beta \approx 0.05$ , or about 1 MeV for protons.

*Shell correction  $-C/Z$ .* As the velocity of the projectile decreases, the contribution to the stopping power from K shell electrons decreases, and at even lower velocities contributions from L and higher shells further reduce it. The correction  $(C_K + C_L + \dots)/Z$  is included in the square brackets of Eq. (34.5). It is calculated and tabulated (for a few common materials) in a number of places; Refs. [4, 10, 20] are especially useful. As an example, the shell correction for a 30 MeV proton traversing aluminum is 0.6%, but increases to 9.9% as the proton’s energy decreases to 0.3 MeV.

*Barkas correction  $zL_1$ .* Qualitatively, one might imagine an atom’s electron cloud slightly recoiling at the approach of a negative projectile and being attracted toward an approaching positive projectile. Hence the stopping power for negative particles should be slightly smaller than the stopping power for positive particles. In a 1956 paper, Barkas *et al.* noted that negative pions possibly had a longer range than positive pions [6]. The effect has been measured for a number of negative/positive particle pairs, and more recently in detailed studies with antiprotons at the CERN LEAR facility [21]. Since no complete theory exists, an empirical approach is necessary. A 1972 harmonic-oscillator model by Ashley *et al.* [22] is often used; it has two parameters determined by experimental data.

*Bloch correction  $z^2L_2$ .* Bloch’s extension of Bethe’s theory introduced a low-energy correction that takes account of perturbations of the atomic wave functions. The form obtained by Lindhard and Sørensen [9] is used e.g. in Refs. [4, 20].

For the interval  $0.01 < \beta < 0.05$  there is no satisfactory theory. For protons, one usually relies on the phenomenological fitting formulae developed by Andersen and Ziegler [4, 23]. As tabulated in ICRU 49 [4], the nuclear plus electronic proton stopping power in copper is  $113 \text{ MeV cm}^2 \text{ g}^{-1}$  at  $T = 10 \text{ keV}$  ( $\beta\gamma = 0.005$ ), rises to a maximum of  $210 \text{ MeV cm}^2 \text{ g}^{-1}$  at  $T \approx 120 \text{ keV}$  ( $\beta\gamma = 0.016$ ), then falls to  $118 \text{ MeV cm}^2 \text{ g}^{-1}$  at  $T = 1 \text{ MeV}$  ( $\beta\gamma = 0.046$ ). Above 0.5–1.0 MeV the corrected Bethe theory is adequate.

For particles moving more slowly than  $\approx 0.01c$  (more or less the velocity of the outer atomic electrons), Lindhard has been quite successful in describing electronic stopping power, which is proportional to  $\beta$  [24]. Finally, we note that at even lower energies, e.g., for protons of less than several hundred eV, non-ionizing nuclear recoil energy loss dominates the total energy loss [4, 24, 25].

### 34.2.7 Energetic knock-on electrons ( $\delta$ rays)

The distribution of secondary electrons with kinetic energies  $T \gg I$  is [2]

$$\frac{d^2N}{dTdx} = \frac{1}{2} K z^2 \frac{Z}{A} \frac{1}{\beta^2} \frac{F(T)}{T^2} \quad (34.9)$$

for  $I \ll T \leq W_{\max}$ , where  $W_{\max}$  is given by Eq. (34.4). Here  $\beta$  is the velocity of the primary particle. The factor  $F$  is spin-dependent, but is about unity for  $T \ll W_{\max}$ . For spin-0 particles  $F(T) = (1 - \beta^2 T/W_{\max})$ ; forms for spins 1/2 and 1 are also given by Rossi [2] (Sec. 2.3, Eqs. 7 and 8). Additional formulae are given in [26]. Equation Eq. (34.9) is inaccurate for  $T$  close to  $I$  [27].

$\delta$  rays of even modest energy are rare. For a  $\beta \approx 1$  particle, for example, on average only one collision with  $T_e > 10 \text{ keV}$  will occur along a path length of 90 cm of argon gas [1].

A  $\delta$  ray with kinetic energy  $T_e$  and corresponding momentum  $p_e$  is produced at an angle  $\theta$  given by

$$\cos \theta = (T_e/p_e)(p_{\max}/W_{\max}), \quad (34.10)$$

where  $p_{\max}$  is the momentum of an electron with the maximum possible energy transfer  $W_{\max}$ .

### 34.2.8 Restricted energy loss rates for relativistic ionizing particles

Further insight can be obtained by examining the mean energy deposit by an ionizing particle when energy transfers are restricted to  $T \leq W_{\text{cut}} \leq W_{\text{max}}$ . The restricted energy loss rate is

$$-\frac{dE}{dx} \Big|_{T < W_{\text{cut}}} = K z^2 \frac{Z}{A} \frac{1}{\beta^2} \left[ \frac{1}{2} \ln \frac{2m_e c^2 \beta^2 \gamma^2 W_{\text{cut}}}{I^2} - \frac{\beta^2}{2} \left( 1 + \frac{W_{\text{cut}}}{W_{\text{max}}} \right) - \frac{\delta}{2} \right]. \quad (34.11)$$

This form approaches the normal Bethe function (Eq. (34.5)) as  $W_{\text{cut}} \rightarrow W_{\text{max}}$ . It can be verified that the difference between Eq. (34.5) and Eq. (34.11) is equal to  $\int_{W_{\text{cut}}}^{W_{\text{max}}} T(d^2N/dTdx)dT$ , where  $d^2N/dTdx$  is given by Eq. (34.9).

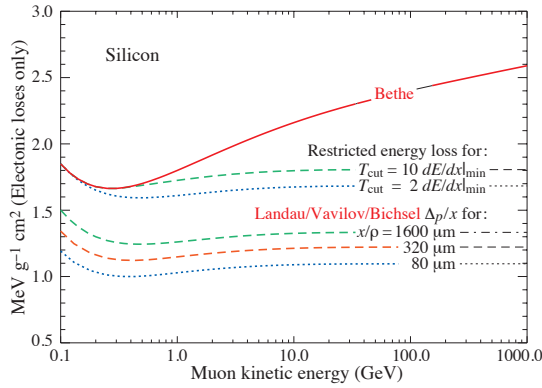


Figure 34.6: Bethe  $dE/dx$ , two examples of restricted energy loss, and the Landau most probable energy per unit thickness in silicon. The change of  $\Delta_p/x$  with thickness  $x$  illustrates its  $a \ln x + b$  dependence. Minimum ionization ( $dE/dx|_{\text{min}}$ ) is  $1.664 \text{ MeV g}^{-1} \text{ cm}^2$ . Radiative losses are excluded. The incident particles are muons.

Since  $W_{\text{cut}}$  replaces  $W_{\text{max}}$  in the argument of the logarithmic term of Eq. (34.5), the  $\beta\gamma$  term producing the relativistic rise in the close-collision part of  $dE/dx$  is replaced by a constant, and  $|dE/dx|_{T < W_{\text{cut}}}$  approaches the constant “Fermi plateau.” (The density effect correction  $\delta$  eliminates the explicit  $\beta\gamma$  dependence produced by the distant-collision contribution.) This behavior is illustrated in Fig. 34.6, where restricted loss rates for two examples of  $W_{\text{cut}}$  are shown in comparison with the full Bethe  $dE/dx$  and the Landau-Vavilov most probable energy loss (to be discussed in Sec. 34.2.9 below).

“Restricted energy loss” is cut at the total mean energy, not the single-collision energy above  $W_{\text{cut}}$ . It is of limited use. The most probable energy loss, discussed in the next Section, is far more useful in situations where single-particle energy loss is observed.

### 34.2.9 Fluctuations in energy loss

For detectors of moderate thickness  $x$  (e.g. scintillators or LAr cells),<sup>1</sup> the energy loss probability distribution  $f(\Delta; \beta\gamma, x)$  is adequately described by the highly-skewed Landau (or Landau-Vavilov) distribution [28, 29].

The most probable energy loss is [30]<sup>2</sup>

$$\Delta_p = \xi \left[ \ln \frac{2mc^2 \beta^2 \gamma^2}{I} + \ln \frac{\xi}{I} + j - \beta^2 - \delta(\beta\gamma) \right], \quad (34.12)$$

<sup>1</sup>“Moderate thickness” means  $G \lesssim 0.05\text{--}0.1$ , where  $G$  is given by Rossi Ref. [2], Eq. 2.7(10). It is Vavilov’s  $\kappa$  [28].  $G$  is proportional to the absorber’s thickness, and as such parameterizes the constants describing the Landau distribution. These are fairly insensitive to thickness for  $G \lesssim 0.1$ , the case for most detectors.

<sup>2</sup>Practical calculations can be expedited by using the tables of  $\delta$  and  $\beta$  from the text versions of the muon energy loss tables to be found at [pdg.lbl.gov/AtomicNuclearProperties](http://pdg.lbl.gov/AtomicNuclearProperties).

where  $\xi = (K/2) \langle Z/A \rangle z^2 (x/\beta^2) \text{ MeV}$  for a detector with a thickness  $x$  in  $\text{g cm}^{-2}$ , and  $j = 0.200$  [30].<sup>3</sup> While  $dE/dx$  is independent of thickness,  $\Delta_p/x$  scales as  $a \ln x + b$ . The density correction  $\delta(\beta\gamma)$  was not included in Landau’s or Vavilov’s work, but it was later included by Bichsel [30]. The high-energy behavior of  $\delta(\beta\gamma)$  (Eq. (34.6)) is such that

$$\Delta_p \xrightarrow{\beta\gamma \gtrsim 100} \xi \left[ \ln \frac{2mc^2 \xi}{(\hbar\omega_p)^2} + j \right]. \quad (34.13)$$

Thus the Landau-Vavilov most probable energy loss, like the restricted energy loss, reaches a Fermi plateau. The Bethe  $dE/dx$  and Landau-Vavilov-Bichsel  $\Delta_p/x$  in silicon are shown as a function of muon energy in Fig. 34.6. The energy deposit in the  $1600 \mu\text{m}$  case is roughly the same as in a 3 mm thick plastic scintillator.

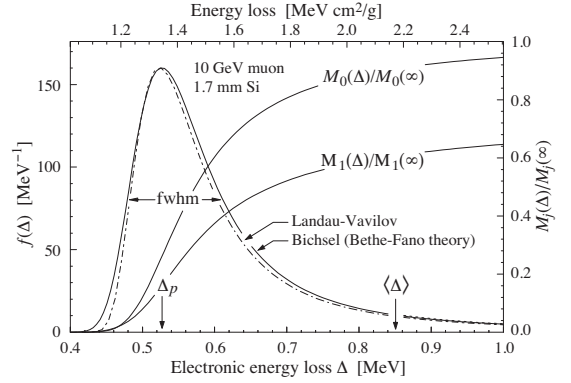


Figure 34.7: Electronic energy deposit distribution for a 10 GeV muon traversing 1.7 mm of silicon, the stopping power equivalent of about 0.3 cm of PVT-based scintillator [1, 11, 32]. The Landau-Vavilov function (dot-dashed) uses a Rutherford cross section without atomic binding corrections but with a kinetic energy transfer limit of  $W_{\text{max}}$ . The solid curve was calculated using Bethe-Fano theory.  $M_0(\Delta)$  and  $M_1(\Delta)$  are the cumulative 0th moment (mean number of collisions) and 1st moment (mean energy loss) in crossing the silicon. (See Sec. 34.2.1). The fwhm of the Landau-Vavilov function is about  $4\xi$  for detectors of moderate thickness.  $\Delta_p$  is the most probable energy loss, and  $\langle \Delta \rangle$  divided by the thickness is the Bethe ( $dE/dx$ ).

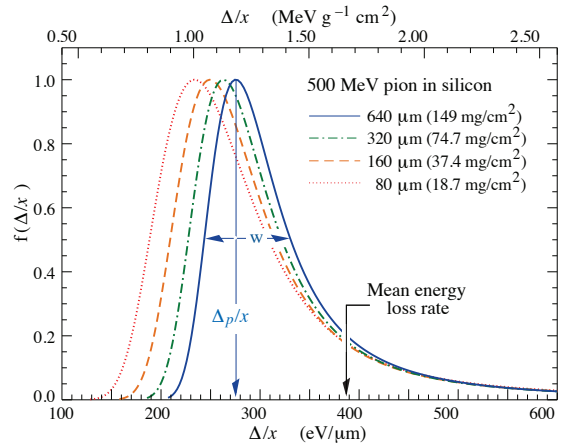


Figure 34.8: Straggling functions in silicon for 500 MeV pions, normalized to unity at the most probable value  $\Delta_p/x$ . The width  $w$  is the full width at half maximum.

The distribution function for the energy deposit by a 10 GeV muon going through a detector of about this thickness is shown

<sup>3</sup>Rossi [2], Talman [31], and others give somewhat different values for  $j$ . The most probable loss is not sensitive to its value.

in Fig. 34.7. In this case the most probable energy loss is 62% of the mean ( $M_1(\langle\Delta\rangle)/M_1(\infty)$ ). Folding in experimental resolution displaces the peak of the distribution, usually toward a higher value. 90% of the collisions ( $M_1(\langle\Delta\rangle)/M_1(\infty)$ ) contribute to energy deposits below the mean. It is the very rare high-energy-transfer collisions, extending to  $W_{\max}$  at several GeV, that drives the mean into the tail of the distribution. The large weight of these rare events makes the mean of an experimental distribution consisting of a few hundred events subject to large fluctuations and sensitive to cuts. *The mean of the energy loss given by the Bethe equation, Eq. (34.5), is thus ill-defined experimentally and is not useful for describing energy loss by single particles.*<sup>4</sup> It rises as  $\ln\gamma$  because  $W_{\max}$  increases as  $\gamma$  at high energies. *The most probable energy loss should be used.*

A practical example: For muons traversing 0.25 inches (0.64 cm) of PVT (polyvinyltoluene) based plastic scintillator, the ratio of the most probable  $E$  loss rate to the mean loss rate via the Bethe equation is [0.69, 0.57, 0.49, 0.42, 0.38] for  $T_\mu = [0.01, 0.1, 1, 10, 100]$  GeV. Radiative losses add less than 0.5% to the total mean energy deposit at 10 GeV, but add 7% at 100 GeV. The most probable  $E$  loss rate rises slightly beyond the minimum ionization energy, then is essentially constant.

The Landau distribution fails to describe energy loss in thin absorbers such as gas TPC cells [1] and Si detectors [30], as can be seen *e.g.* in Fig. 1 of Ref. [1] for an argon-filled TPC cell. Also see Talman [31]. While  $\Delta_p/x$  may be calculated adequately with Eq. (34.12), the distributions are significantly wider than the Landau width  $w = 4\xi$  Ref. [30], Fig. 15. Examples for 500 MeV pions incident on thin silicon detectors are shown in Fig. 34.8. For very thick absorbers the distribution is less skewed but never approaches a Gaussian.

The most probable energy loss, scaled to the mean loss at minimum ionization, is shown in Fig. 34.9 for several silicon detector thicknesses.

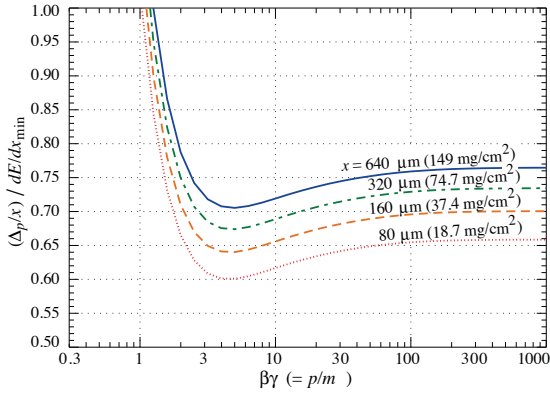


Figure 34.9: Most probable energy loss in silicon, scaled to the mean loss of a minimum ionizing particle,  $388 \text{ eV}/\mu\text{m}$  ( $1.66 \text{ MeV g}^{-1}\text{cm}^2$ ).

### 34.2.10 Energy loss in mixtures and compounds

A mixture or compound can be thought of as made up of thin layers of pure elements in the right proportion (Bragg additivity). In this case,

$$\left\langle \frac{dE}{dx} \right\rangle = \sum w_j \left\langle \frac{dE}{dx} \right\rangle_j, \quad (34.14)$$

where  $dE/dx|_j$  is the mean rate of energy loss (in  $\text{MeV g cm}^{-2}$ ) in the  $j$ th element. Eq. (34.5) can be inserted into Eq. (34.14) to find expressions for  $\langle Z/A \rangle$ ,  $\langle I \rangle$ , and  $\langle \delta \rangle$ ; for example,  $\langle Z/A \rangle = \sum w_j Z_j/A_j = \sum n_j Z_j / \sum n_j A_j$ . However,  $\langle I \rangle$  as defined this way is an underestimate, because in a compound electrons are more tightly bound than in the free elements, and  $\langle \delta \rangle$  as calculated this way has little relevance, because it is the electron density that matters. If possible, one uses the tables given in

<sup>4</sup>It does find application in dosimetry, where only bulk deposit is relevant.

Refs. [16, 33], or the recipes given in [17] (repeated in Ref. [5]), that include effective excitation energies and interpolation coefficients for calculating the density effect correction for the chemical elements and nearly 200 mixtures and compounds. Otherwise, use the recipe for  $\delta$  given in Refs. [5, 17], and calculate  $\langle I \rangle$  following the discussion in Ref. [13]. (Note the “13%” rule!)

### 34.2.11 Ionization yields

The Bethe equation describes energy loss via excitation and ionization. Many gaseous detectors (proportional counters or TPCs) or liquid ionization detectors count the number of electrons or positive ions from ionization, rather than the ionization energy. As a further complication, the electron liberated in the initial ionization often has enough energy to ionize other atoms or molecules; this process can happen several times. The number of electron-ion pairs per unit length is typically three or more times the original number. Ion or electron counting is a proxy for a direct  $dE/dx$  measurement. Calibrations link the number of observed ions to the traversing particle’s  $dE/dx$ .

The details depend on the gases (or liquids) and the particular detector involved. A useful discussion of the physics is provided in Sec.35.6 of this Review.

## 34.3 Multiple scattering through small angles

A charged particle traversing a medium is deflected by many small-angle scatters. Most of this deflection is due to Coulomb scattering from nuclei as described by the Rutherford cross section. (However, for hadronic projectiles, the strong interactions also contribute to multiple scattering.) For many small-angle scatters the net scattering and displacement distributions are Gaussian via the central limit theorem. Less frequent “hard” scatters produce non-Gaussian tails. These Coulomb scattering distributions are well-represented by the theory of Molière [34]. Accessible discussions are given by Rossi [2] and Jackson [35], and exhaustive reviews have been published by Scott [36] and Motz *et al.* [37]. Experimental measurements have been published by Bichsel [38] (low energy protons) and by Shen *et al.* [39] (relativistic pions, kaons, and protons).<sup>5</sup>

If we define

$$\theta_0 = \theta_{\text{plane}}^{\text{rms}} = \frac{1}{\sqrt{2}} \theta_{\text{space}}^{\text{rms}}, \quad (34.15)$$

then it is sufficient for many applications to use a Gaussian approximation for the central 98% of the projected angular distribution, with an rms width given by Lynch & Dahl [40]:

$$\begin{aligned} \theta_0 &= \frac{13.6 \text{ MeV}}{\beta c p} z \sqrt{\frac{x}{X_0}} \left[ 1 + 0.088 \log_{10} \left( \frac{x z^2}{X_0 \beta^2} \right) \right] \\ &= \frac{13.6 \text{ MeV}}{\beta c p} z \sqrt{\frac{x}{X_0}} \left[ 1 + 0.038 \ln \left( \frac{x z^2}{X_0 \beta^2} \right) \right] \end{aligned} \quad (34.16)$$

Here  $p$ ,  $\beta c$ , and  $z$  are the momentum, velocity, and charge number of the incident particle, and  $x/X_0$  is the thickness of the scattering medium in radiation lengths (defined below). This takes into account the  $p$  and  $z$  dependence quite well at small  $Z$ , but for large  $Z$  and small  $x$  the  $\beta$ -dependence is not well represented. Further improvements are discussed in Ref. [40].

Eq. (34.16) describes scattering from a single material, while the usual problem involves the multiple scattering of a particle traversing many different layers and mixtures. Since it is from a fit to a Molière distribution, it is incorrect to add the individual  $\theta_0$  contributions in quadrature; the result is systematically too small. It is much more accurate to apply Eq. (34.16) once, after finding  $x$  and  $X_0$  for the combined scatterer.

The nonprojected (space) and projected (plane) angular distributions are given approximately by [34]

$$\frac{1}{2\pi \theta_0^2} \exp \left( -\frac{\theta_{\text{space}}^2}{2\theta_0^2} \right) d\Omega, \quad (34.17)$$

<sup>5</sup>Shen *et al.*’s measurements show that Bethe’s simpler methods of including atomic electron effects agrees better with experiment than does Scott’s treatment.

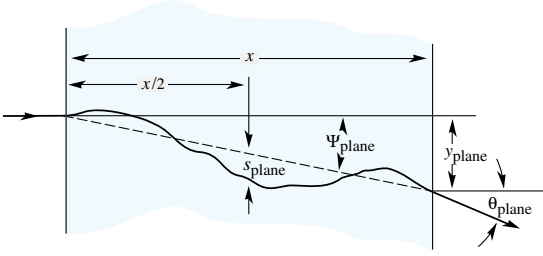


Figure 34.10: Quantities used to describe multiple Coulomb scattering. The particle is incident in the plane of the figure.

$$\frac{1}{\sqrt{2\pi}\theta_0} \exp\left(-\frac{\theta_{\text{plane}}^2}{2\theta_0^2}\right) d\theta_{\text{plane}}, \quad (34.18)$$

where  $\theta$  is the deflection angle. In this approximation,  $\theta_{\text{space}}^2 \approx (\theta_{\text{plane},x}^2 + \theta_{\text{plane},y}^2)$ , where the  $x$  and  $y$  axes are orthogonal to the direction of motion, and  $d\Omega \approx d\theta_{\text{plane},x} d\theta_{\text{plane},y}$ . Deflections into  $\theta_{\text{plane},x}$  and  $\theta_{\text{plane},y}$  are independent and identically distributed. Fig. 34.10 shows these and other quantities sometimes used to describe multiple Coulomb scattering. They are

$$\psi_{\text{plane}}^{\text{rms}} = \frac{1}{\sqrt{3}} \theta_{\text{plane}}^{\text{rms}} = \frac{1}{\sqrt{3}} \theta_0, \quad (34.19)$$

$$y_{\text{plane}}^{\text{rms}} = \frac{1}{\sqrt{3}} x \theta_{\text{plane}}^{\text{rms}} = \frac{1}{\sqrt{3}} x \theta_0, \quad (34.20)$$

$$s_{\text{plane}}^{\text{rms}} = \frac{1}{4\sqrt{3}} x \theta_{\text{plane}}^{\text{rms}} = \frac{1}{4\sqrt{3}} x \theta_0. \quad (34.21)$$

All the quantitative estimates in this section apply only in the limit of small  $\theta_{\text{plane}}^{\text{rms}}$  and in the absence of large-angle scatters. The random variables  $s$ ,  $\psi$ ,  $y$ , and  $\theta$  in a given plane are correlated. Obviously,  $y \approx x\psi$ . In addition,  $y$  and  $\theta$  have the correlation coefficient  $\rho_{y\theta} = \sqrt{3}/2 \approx 0.87$ . For Monte Carlo generation of a joint  $(y_{\text{plane}}, \theta_{\text{plane}})$  distribution, or for other calculations, it may be most convenient to work with independent Gaussian random variables  $(z_1, z_2)$  with mean zero and variance one, and then set

$$y_{\text{plane}} = z_1 x \theta_0 (1 - \rho_{y\theta}^2)^{1/2} / \sqrt{3} + z_2 \rho_{y\theta} x \theta_0 / \sqrt{3} \quad (34.22a)$$

$$= z_1 x \theta_0 / \sqrt{12} + z_2 x \theta_0 / 2; \quad (34.22b)$$

$$\theta_{\text{plane}} = z_2 \theta_0. \quad (34.22c)$$

Note that the second term for  $y_{\text{plane}}$  equals  $x\theta_{\text{plane}}/2$  and represents the displacement that would have occurred had the deflection  $\theta_{\text{plane}}$  all occurred at the single point  $x/2$ .

For heavy ions the multiple Coulomb scattering has been measured and compared with various theoretical distributions [41].

### 34.4 Photon and electron interactions in matter

At low energies electrons and positrons primarily lose energy by ionization, although other processes (Møller scattering, Bhabha scattering,  $e^+$  annihilation) contribute, as shown in Fig. 34.11. While ionization loss rates rise logarithmically with energy, bremsstrahlung losses rise nearly linearly (fractional loss is nearly independent of energy), and dominates above the critical energy (Sec. 34.4.4 below), a few tens of MeV in most materials

#### 34.4.1 Collision energy losses by $e^\pm$

Stopping power differs somewhat for electrons and positrons, and both differ from stopping power for heavy particles because of the kinematics, spin, charge, and the identity of the incident electron with the electrons that it ionizes. Complete discussions and tables can be found in Refs. [10, 13, 33].

For electrons, large energy transfers to atomic electrons (taken as free) are described by the Møller cross section. From Eq. (34.4), the maximum energy transfer in a single collision should be the entire kinetic energy,  $W_{\text{max}} = m_e c^2 (\gamma - 1)$ , but because the particles are identical, the maximum is half this,  $W_{\text{max}}/2$ . (The results are the same if the transferred energy is  $\epsilon$  or if the transferred energy is  $W_{\text{max}} - \epsilon$ . The stopping power is by convention calculated

for the faster of the two emerging electrons.) The first moment of the Møller cross section [26] (divided by  $dx$ ) is the stopping power:

$$\left\langle -\frac{dE}{dx} \right\rangle = \frac{1}{2} K \frac{Z}{A} \frac{1}{\beta^2} \left[ \ln \frac{m_e c^2 \beta^2 \gamma^2 \{m_e c^2 (\gamma - 1)/2\}}{I^2} + (1 - \beta^2) - \frac{2\gamma - 1}{\gamma^2} \ln 2 + \frac{1}{8} \left( \frac{\gamma - 1}{\gamma} \right)^2 - \delta \right] \quad (34.23)$$

The logarithmic term can be compared with the logarithmic term in the Bethe equation (Eq. (34.2)) by substituting  $W_{\text{max}} = m_e c^2 (\gamma - 1)/2$ .

Electron-positron scattering is described by the fairly complicated Bhabha cross section [26]. There is no identical particle problem, so  $W_{\text{max}} = m_e c^2 (\gamma - 1)$ . The first moment of the Bhabha equation yields

$$\left\langle -\frac{dE}{dx} \right\rangle = \frac{1}{2} K \frac{Z}{A} \frac{1}{\beta^2} \left[ \ln \frac{m_e c^2 \beta^2 \gamma^2 \{m_e c^2 (\gamma - 1)\}}{2I^2} + 2 \ln 2 - \frac{\beta^2}{12} \left( 23 + \frac{14}{\gamma + 1} + \frac{10}{(\gamma + 1)^2} + \frac{4}{(\gamma + 1)^3} \right) - \delta \right]. \quad (34.24)$$

Following ICRU 37 [10], the density effect correction  $\delta$  has been added to Uehling's equations [26] in both cases.

For heavy particles, shell corrections were developed assuming that the projectile is equivalent to a perturbing potential whose center moves with constant velocity. This assumption has no sound theoretical basis for electrons. The authors of ICRU 37 [10] estimated the possible error in omitting it by assuming the correction was twice as great as for a proton of the same velocity. At  $T = 10$  keV, the error was estimated to be  $\approx 2\%$  for water,  $\approx 9\%$  for Cu, and  $\approx 21\%$  for Au.

As shown in Fig. 34.11, stopping powers for  $e^-$ ,  $e^+$ , and heavy particles are not dramatically different. In silicon, the minimum value for electrons is  $1.50 \text{ MeV cm}^2/\text{g}$  (at  $\gamma = 3.3$ ); for positrons,  $1.46 \text{ MeV cm}^2/\text{g}$  (at  $\gamma = 3.7$ ), and for muons,  $1.66 \text{ MeV cm}^2/\text{g}$  (at  $\gamma = 3.58$ ).

#### 34.4.2 Radiation length

High-energy electrons predominantly lose energy in matter by bremsstrahlung, and high-energy photons by  $e^+e^-$  pair production. The characteristic amount of matter traversed for these related interactions is called the radiation length  $X_0$ , usually measured in  $\text{g cm}^{-2}$ . It is the mean distance over which a high-energy electron loses all but  $1/e$  of its energy by bremsstrahlung. It is also the appropriate scale length for describing high-energy electromagnetic cascades.  $X_0$  has been calculated and tabulated by Y.S. Tsai [42]:

$$\frac{1}{X_0} = 4\alpha r_e^2 \frac{N_A}{A} \left\{ Z^2 [L_{\text{rad}} - f(Z)] + Z L'_{\text{rad}} \right\}. \quad (34.25)$$

For  $A = 1 \text{ g mol}^{-1}$ ,  $4\alpha r_e^2 N_A/A = (716.408 \text{ g cm}^{-2})^{-1}$ .  $L_{\text{rad}}$  and  $L'_{\text{rad}}$  are given in Table 34.2. The function  $f(Z)$  is an infinite sum, but for elements up to uranium can be represented to 4-place accuracy by

$$f(Z) = a^2 \left[ (1 + a^2)^{-1} + 0.20206 - 0.0369 a^2 + 0.0083 a^4 - 0.002 a^6 \right], \quad (34.26)$$

where  $a = \alpha Z$  [43].

The radiation length in a mixture or compound may be approximated by

$$1/X_0 = \sum w_j / X_j, \quad (34.27)$$

where  $w_j$  and  $X_j$  are the fraction by weight and the radiation length for the  $j$ th element.

**Table 34.2:** Tsai's  $L_{\text{rad}}$  and  $L'_{\text{rad}}$ , for use in calculating the radiation length in an element using Eq. (34.25).

Element	$Z$	$L_{\text{rad}}$	$L'_{\text{rad}}$
H	1	5.31	6.144
He	2	4.79	5.621
Li	3	4.74	5.805
Be	4	4.71	5.924
Others	$> 4$	$\ln(184.15 Z^{-1/3})$	$\ln(1194 Z^{-2/3})$

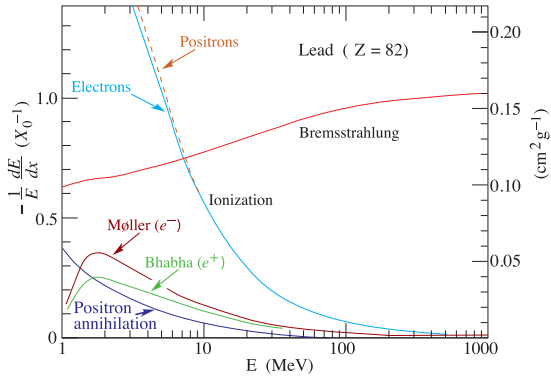


Figure 34.11: Fractional energy loss per radiation length in lead as a function of electron or positron energy. Electron (positron) scattering is considered as ionization when the energy loss per collision is below 0.255 MeV, and as Møller (Bhabha) scattering when it is above. Adapted from Fig. 3.2 from Messel and Crawford, *Electron-Photon Shower Distribution Function Tables for Lead, Copper, and Air Absorbers*, Pergamon Press, 1970. Messel and Crawford use  $X_0(\text{Pb}) = 5.82 \text{ g/cm}^2$ , but we have modified the figures to reflect the value given in the Table of Atomic and Nuclear Properties of Materials ( $X_0(\text{Pb}) = 6.37 \text{ g/cm}^2$ ).

**34.4.3 Bremsstrahlung energy loss by  $e^\pm$**

At very high energies and except at the high-energy tip of the bremsstrahlung spectrum, the cross section can be approximated in the “complete screening case” as [42]

$$d\sigma/dk = (1/k)4\alpha r_e^2 \left\{ \left( \frac{4}{3} - \frac{4}{3}y + y^2 \right) [Z^2(L_{\text{rad}} - f(Z)) + Z L'_{\text{rad}}] + \frac{1}{9}(1-y)(Z^2 + Z) \right\}, \tag{34.28}$$

where  $y = k/E$  is the fraction of the electron’s energy transferred to the radiated photon. At small  $y$  (the “infrared limit”) the term on the second line ranges from 1.7% (low  $Z$ ) to 2.5% (high  $Z$ ) of the total. If it is ignored and the first line simplified with the definition of  $X_0$  given in Eq. (34.25), we have

$$\frac{d\sigma}{dk} = \frac{A}{X_0 N_A k} \left( \frac{4}{3} - \frac{4}{3}y + y^2 \right). \tag{34.29}$$

This cross section (times  $k$ ) is shown by the top curve in Fig. 34.12.

This formula is accurate except near  $y = 1$ , where screening may become incomplete, and near  $y = 0$ , where the infrared divergence is removed by the interference of bremsstrahlung amplitudes from nearby scattering centers (the LPM effect) [44, 45] and dielectric suppression [46, 47]. These and other suppression effects in bulk media are discussed in Sec. 34.4.6.

With decreasing energy ( $E \lesssim 10 \text{ GeV}$ ) the high- $y$  cross section drops and the curves become rounded as  $y \rightarrow 1$ . Curves of this familiar shape can be seen in Rossi [2] (Figs. 2.11.2,3); see also the review by Koch & Motz [48].

Except at these extremes, and still in the complete-screening approximation, the number of photons with energies between  $k_{\text{min}}$

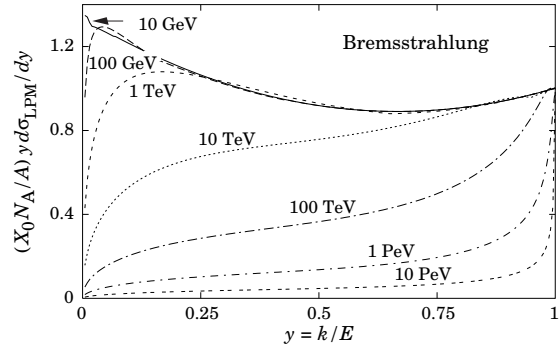


Figure 34.12: The normalized bremsstrahlung cross section  $k d\sigma_{LPM}/dk$  in lead versus the fractional photon energy  $y = k/E$ . The vertical axis has units of photons per radiation length.

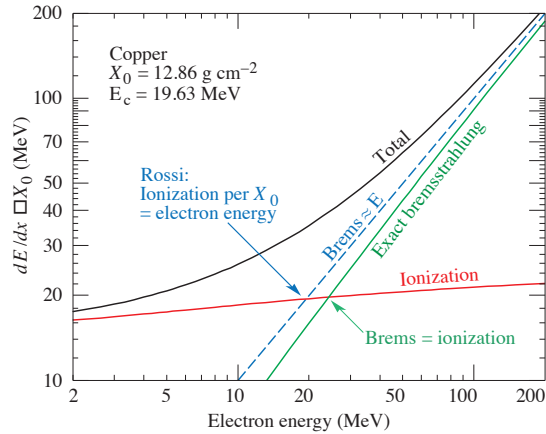


Figure 34.13: Two definitions of the critical energy  $E_c$ .

and  $k_{\text{max}}$  emitted by an electron travelling a distance  $d \ll X_0$  is

$$N_\gamma = \frac{d}{X_0} \left[ \frac{4}{3} \ln \left( \frac{k_{\text{max}}}{k_{\text{min}}} \right) - \frac{4(k_{\text{max}} - k_{\text{min}})}{3E} + \frac{k_{\text{max}}^2 - k_{\text{min}}^2}{2E^2} \right]. \tag{34.30}$$

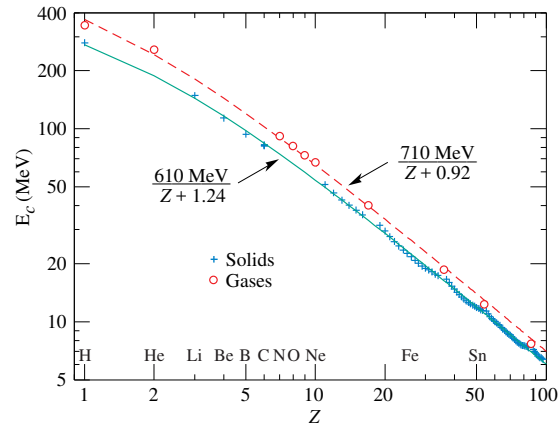


Figure 34.14: Electron critical energy for the chemical elements, using Rossi’s definition [2]. The fits shown are for solids and liquids (solid line) and gases (dashed line). The rms deviation is 2.2% for the solids and 4.0% for the gases.

**34.4.4 Critical energy**

An electron loses energy by bremsstrahlung at a rate nearly proportional to its energy, while the ionization loss rate varies only logarithmically with the electron energy. The *critical energy*  $E_c$  is sometimes defined as the energy at which the two loss rates



are equal [49]. Among alternate definitions is that of Rossi [2], who defines the critical energy as the energy at which the ionization loss per radiation length is equal to the electron energy. Equivalently, it is the same as the first definition with the approximation  $|dE/dx|_{\text{brems}} \approx E/X_0$ . This form has been found to describe transverse electromagnetic shower development more accurately (see below). These definitions are illustrated in the case of copper in Fig. 34.13.

The accuracy of approximate forms for  $E_c$  has been limited by the failure to distinguish between gases and solid or liquids, where there is a substantial difference in ionization at the relevant energy because of the density effect. We distinguish these two cases in Fig. 34.14. Fits were also made with functions of the form  $a/(Z+b)^\alpha$ , but  $\alpha$  was found to be essentially unity. Since  $E_c$  also depends on  $A$ ,  $I$ , and other factors, such forms are at best approximate.

Values of  $E_c$  for both electrons and positrons in more than 300 materials can be found at [pdg.lbl.gov/AtomicNuclearProperties](http://pdg.lbl.gov/AtomicNuclearProperties).

#### 34.4.5 Energy loss by photons

Contributions to the photon cross section in a light element (carbon) and a heavy element (lead) are shown in Fig. 34.15. At low energies it is seen that the photoelectric effect dominates, although Compton scattering, Rayleigh scattering, and photonuclear absorption also contribute. The photoelectric cross section is characterized by discontinuities (absorption edges) as thresholds for photoionization of various atomic levels are reached. Photon attenuation lengths for a variety of elements are shown in Fig. 34.16, and data for  $30 \text{ eV} < k < 100 \text{ GeV}$  for all elements are available from the web pages given in the caption. Here  $k$  is the photon energy.

The increasing domination of pair production as the energy increases is shown in Fig. 34.17. Using approximations similar to those used to obtain Eq. (34.29), Tsai's formula for the differential cross section [42] reduces to

$$\frac{d\sigma}{dx} = \frac{A}{X_0 N_A} \left[ 1 - \frac{4}{3}x(1-x) \right] \quad (34.31)$$

in the complete-screening limit valid at high energies. Here  $x = E/k$  is the fractional energy transfer to the pair-produced electron (or positron), and  $k$  is the incident photon energy. The cross section is very closely related to that for bremsstrahlung, since the Feynman diagrams are variants of one another. The cross section is of necessity symmetric between  $x$  and  $1-x$ , as can be seen by the solid curve in Fig. 34.18. See the review by Motz, Olsen, & Koch for a more detailed treatment [54]. Eq. (34.31) may be integrated to find the high-energy limit for the total  $e^+e^-$  pair-production cross section:

$$\sigma = \frac{7}{9}(A/X_0 N_A). \quad (34.32)$$

Equation Eq. (34.32) is accurate to within a few percent down to energies as low as 1 GeV, particularly for high- $Z$  materials.

#### 34.4.6 Bremsstrahlung and pair production at very high energies

At ultrahigh energies, Eqns. 34.28–34.32 will fail because of quantum mechanical interference between amplitudes from different scattering centers. Since the longitudinal momentum transfer to a given center is small ( $\propto k/E(E-k)$ , in the case of bremsstrahlung), the interaction is spread over a comparatively long distance called the formation length ( $\propto E(E-k)/k$ ) via the uncertainty principle. In alternate language, the formation length is the distance over which the highly relativistic electron and the photon “split apart.” The interference is usually destructive. Calculations of the “Landau-Pomeranchuk-Migdal” (LPM) effect may be made semi-classically based on the average multiple scattering, or more rigorously using a quantum transport approach [44, 45].

In amorphous media, bremsstrahlung is suppressed if the pho-

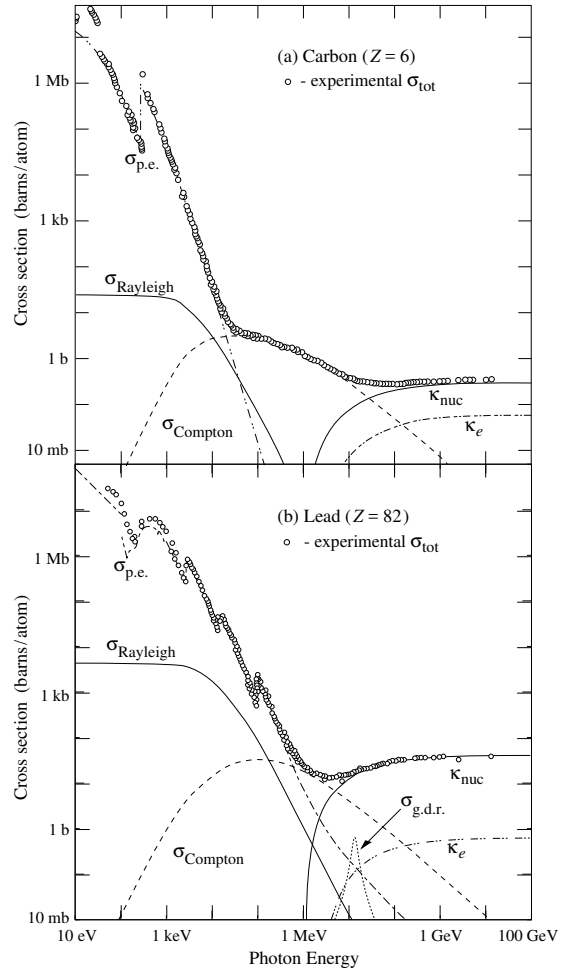


Figure 34.15: Photon total cross sections as a function of energy in carbon and lead, showing the contributions of different processes [50]:

- $\sigma_{\text{p.e.}}$  = Atomic photoelectric effect (electron ejection, photon absorption)
- $\sigma_{\text{Rayleigh}}$  = Rayleigh (coherent) scattering—atom neither ionized nor excited
- $\sigma_{\text{Compton}}$  = Incoherent scattering (Compton scattering off an electron)
- $\kappa_{\text{nuc}}$  = Pair production, nuclear field
- $\kappa_e$  = Pair production, electron field
- $\sigma_{\text{g.d.r.}}$  = Photonuclear interactions, most notably the Giant Dipole Resonance [51]. In these interactions, the target nucleus is usually broken up.

Original figures through the courtesy of John H. Hubbell (NIST).

ton energy  $k$  is less than  $E^2/(E + E_{LPM})$  [45], where<sup>6</sup>

$$E_{LPM} = (m_e c^2)^2 \alpha \frac{X_0}{4\pi\hbar c \rho} = (7.7 \text{ TeV/cm}) \times \frac{X_0}{\rho}. \quad (34.33)$$

Since physical distances are involved,  $X_0/\rho$ , in cm, appears. The energy-weighted bremsstrahlung spectrum for lead,  $k d\sigma_{LPM}/dk$ , is shown in Fig. 34.12. With appropriate scaling by  $X_0/\rho$ , other materials behave similarly.

For photons, pair production is reduced for  $E(k-E) > k E_{LPM}$ . The pair-production cross sections for different photon energies are shown in Fig. 34.18.

If  $k \ll E$ , several additional mechanisms can also produce suppression. When the formation length is long, even weak factors

<sup>6</sup>This definition differs from that of Ref. [55] by a factor of two.  $E_{LPM}$  scales as the 4th power of the mass of the incident particle, so that  $E_{LPM} = (1.4 \times 10^{10} \text{ TeV/cm}) \times X_0/\rho$  for a muon.

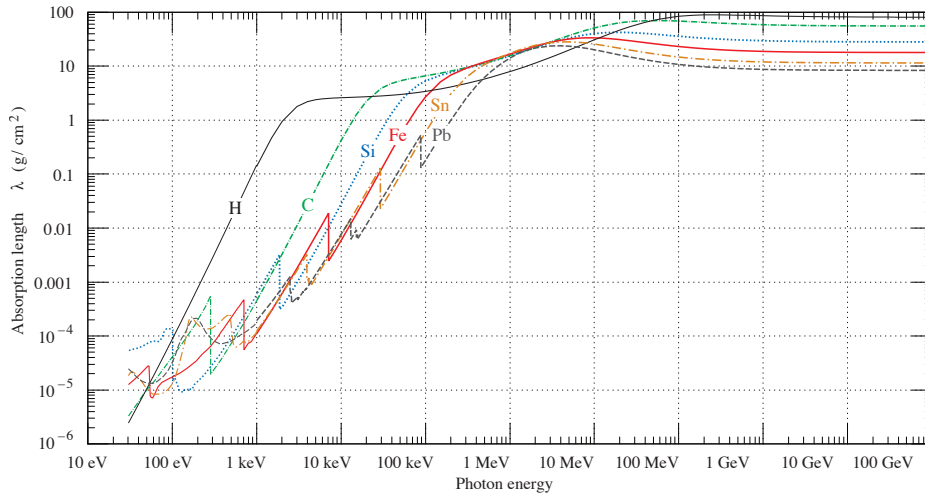


Figure 34.16: The photon mass attenuation length (or mean free path)  $\lambda = 1/(\mu/\rho)$  for various elemental absorbers as a function of photon energy. The mass attenuation coefficient is  $\mu/\rho$ , where  $\rho$  is the density. The intensity  $I$  remaining after traversal of thickness  $t$  (in mass/unit area) is given by  $I = I_0 \exp(-t/\lambda)$ . The accuracy is a few percent. For a chemical compound or mixture,  $1/\lambda_{\text{eff}} \approx \sum_{\text{elements}} w_Z/\lambda_Z$ , where  $w_Z$  is the proportion by weight of the element with atomic number  $Z$ . The processes responsible for attenuation are given in Fig. 34.11. Since coherent processes are included, not all these processes result in energy deposition. The data for  $30 \text{ eV} < E < 1 \text{ keV}$  are from Ref. [52], those for  $1 \text{ keV} < E < 100 \text{ GeV}$  from Ref. [53].

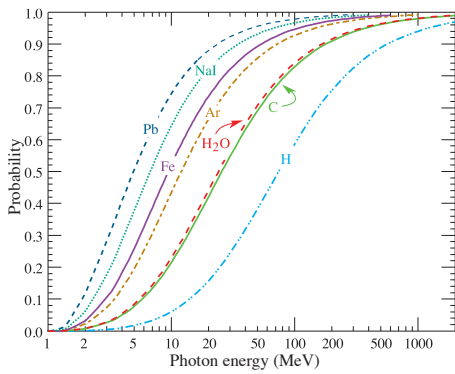


Figure 34.17: Probability  $P$  that a photon interaction will result in conversion to an  $e^+e^-$  pair. Except for a few-percent contribution from photonuclear absorption around 10 or 20 MeV, essentially all other interactions in this energy range result in Compton scattering off an atomic electron. For a photon attenuation length  $\lambda$  (Fig. 34.16), the probability that a given photon will produce an electron pair (without first Compton scattering) in thickness  $t$  of absorber is  $P[1 - \exp(-t/\lambda)]$ .

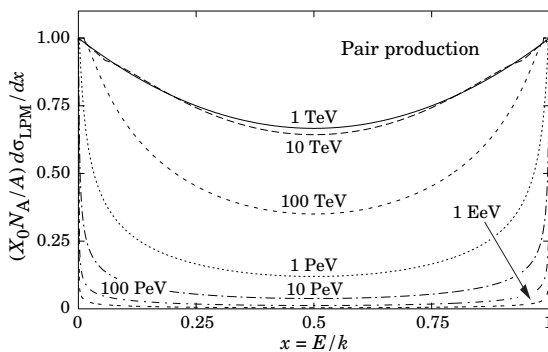


Figure 34.18: The normalized pair production cross section  $d\sigma_{LPM}/dx$ , versus fractional electron energy  $x = E/k$ .

can perturb the interaction. For example, the emitted photon can coherently forward scatter off of the electrons in the media. Because of this, for  $k < \omega_p E/m_e \sim 10^{-4}$ , bremsstrahlung is sup-

pressed by a factor  $(km_e/\omega_p E)^2$  [47]. Magnetic fields can also suppress bremsstrahlung.

In crystalline media, the situation is more complicated, with coherent enhancement or suppression possible. The cross section depends on the electron and photon energies and the angles between the particle direction and the crystalline axes [56].

#### 34.4.7 Photonuclear and electronuclear interactions at still higher energies

At still higher photon and electron energies, where the bremsstrahlung and pair production cross-sections are heavily suppressed by the LPM effect, photonuclear and electronuclear interactions predominate over electromagnetic interactions.

At photon energies above about  $10^{20}$  eV, for example, photons usually interact hadronically. The exact cross-over energy depends on the model used for the photonuclear interactions. These processes are illustrated in Fig. 34.19. At still higher energies ( $\gtrsim 10^{23}$  eV), photonuclear interactions can become coherent, with the photon interaction spread over multiple nuclei. Essentially, the photon coherently converts to a  $\rho^0$ , in a process that is somewhat similar to kaon regeneration [57].

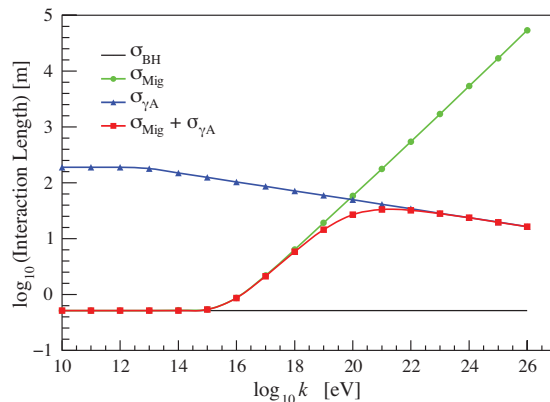


Figure 34.19: Interaction length for a photon in ice as a function of photon energy for the Bethe-Heitler (BH), LPM (Mig) and photonuclear ( $\gamma A$ ) cross sections [57]. The Bethe-Heitler interaction length is  $9X_0/7$ , and  $X_0$  is 0.393 m in ice.

Similar processes occur for electrons. As electron energies increase and the LPM effect suppresses bremsstrahlung, electronu-

clear interactions become more important. At energies above  $10^{21}$  eV, these electronuclear interactions dominate electron energy loss [57].

### 34.5 Electromagnetic cascades

When a high-energy electron or photon is incident on a thick absorber, it initiates an electromagnetic cascade as pair production and bremsstrahlung generate more electrons and photons with lower energy. The longitudinal development is governed by the high-energy part of the cascade, and therefore scales as the radiation length in the material. Electron energies eventually fall below the critical energy, and then dissipate their energy by ionization and excitation rather than by the generation of more shower particles. In describing shower behavior, it is therefore convenient to introduce the scale variables

$$t = x/X_0, \quad y = E/E_c, \quad (34.34)$$

so that distance is measured in units of radiation length and energy in units of critical energy.

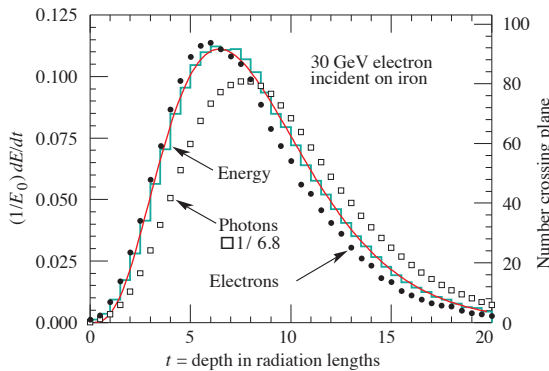


Figure 34.20: An EGS4 simulation of a 30 GeV electron-induced cascade in iron. The histogram shows fractional energy deposition per radiation length, and the curve is a gamma-function fit to the distribution. Circles indicate the number of electrons with total energy greater than 1.5 MeV crossing planes at  $X_0/2$  intervals (scale on right) and the squares the number of photons with  $E \geq 1.5$  MeV crossing the planes (scaled down to have same area as the electron distribution).

Longitudinal profiles from an EGS4 [58] simulation of a 30 GeV electron-induced cascade in iron are shown in Fig. 34.20. The number of particles crossing a plane (very close to Rossi's  $\Pi$  function [2]) is sensitive to the cutoff energy, here chosen as a total energy of 1.5 MeV for both electrons and photons. The electron number falls off more quickly than energy deposition. This is because, with increasing depth, a larger fraction of the cascade energy is carried by photons. Exactly what a calorimeter measures depends on the device, but it is not likely to be exactly any of the profiles shown. In gas counters it may be very close to the electron number, but in glass Cherenkov detectors and other devices with “thick” sensitive regions it is closer to the energy deposition (total track length). In such detectors the signal is proportional to the “detectable” track length  $T_d$ , which is in general less than the total track length  $T$ . Practical devices are sensitive to electrons with energy above some detection threshold  $E_d$ , and  $T_d = T F(E_d/E_c)$ . An analytic form for  $F(E_d/E_c)$  obtained by Rossi [2] is given by Fabjan in Ref. [59]; see also Amaldi [60].

The mean longitudinal profile of the energy deposition in an electromagnetic cascade is reasonably well described by a gamma distribution [61]:

$$\frac{dE}{dt} = E_0 b \frac{(bt)^{a-1} e^{-bt}}{\Gamma(a)} \quad (34.35)$$

The maximum  $t_{\max}$  occurs at  $(a-1)/b$ . We have made fits to shower profiles in elements ranging from carbon to uranium, at energies from 1 GeV to 100 GeV. The energy deposition profiles

are well described by Eq. (34.35) with

$$t_{\max} = (a-1)/b = 1.0 \times (\ln y + C_j), \quad j = e, \gamma, \quad (34.36)$$

where  $C_e = -0.5$  for electron-induced cascades and  $C_\gamma = +0.5$  for photon-induced cascades. To use Eq. (34.35), one finds  $(a-1)/b$  from Eq. (34.36) and Eq. (34.34), then finds  $a$  either by assuming  $b \approx 0.5$  or by finding a more accurate value from Fig. 34.21. The results are very similar for the electron number profiles, but there is some dependence on the atomic number of the medium. A similar form for the electron number maximum was obtained by Rossi in the context of his “Approximation B,” [2] (see Fabjan’s review in Ref. [59]), but with  $C_e = -1.0$  and  $C_\gamma = -0.5$ ; we regard this as superseded by the EGS4 result.

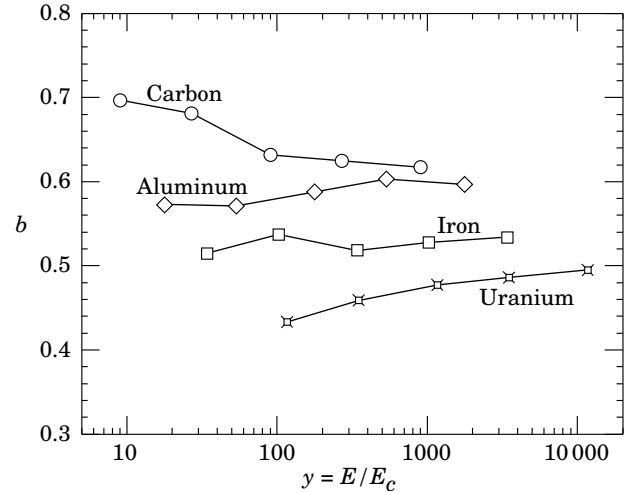


Figure 34.21: Fitted values of the scale factor  $b$  for energy deposition profiles obtained with EGS4 for a variety of elements for incident electrons with  $1 \leq E_0 \leq 100$  GeV. Values obtained for incident photons are essentially the same.

The “shower length”  $X_s = X_0/b$  is less conveniently parameterized, since  $b$  depends upon both  $Z$  and incident energy, as shown in Fig. 34.21. As a corollary of this  $Z$  dependence, the number of electrons crossing a plane near shower maximum is underestimated using Rossi’s approximation for carbon and seriously overestimated for uranium. Essentially the same  $b$  values are obtained for incident electrons and photons. For many purposes it is sufficient to take  $b \approx 0.5$ .

The length of showers initiated by ultra-high energy photons and electrons is somewhat greater than at lower energies since the first or first few interaction lengths are increased via the mechanisms discussed above.

The gamma function distribution is very flat near the origin, while the EGS4 cascade (or a real cascade) increases more rapidly. As a result Eq. (34.35) fails badly for about the first two radiation lengths; it was necessary to exclude this region in making fits.

Because fluctuations are important, Eq. (34.35) should be used only in applications where average behavior is adequate. Grindhammer *et al.* have developed fast simulation algorithms in which the variance and correlation of  $a$  and  $b$  are obtained by fitting Eq. (34.35) to individually simulated cascades, then generating profiles for cascades using  $a$  and  $b$  chosen from the correlated distributions [62].

The transverse development of electromagnetic showers in different materials scales fairly accurately with the *Molière radius*  $R_M$ , given by [63,64]

$$R_M = X_0 E_s/E_c, \quad (34.37)$$

where  $E_s \approx 21$  MeV (Table 34.1), and the Rossi definition of  $E_c$  is used.

In a material containing a weight fraction  $w_j$  of the element with critical energy  $E_{c_j}$  and radiation length  $X_j$ , the Molière radius is



given by

$$\frac{1}{R_M} = \frac{1}{E_s} \sum \frac{w_j E_{cj}}{X_j} \quad (34.38)$$

Measurements of the lateral distribution in electromagnetic cascades are shown in Refs. [63,64]. On the average, only 10% of the energy lies outside the cylinder with radius  $R_M$ . About 99% is contained inside of  $3.5R_M$ , but at this radius and beyond composition effects become important and the scaling with  $R_M$  fails. The distributions are characterized by a narrow core, and broaden as the shower develops. They are often represented as the sum of two Gaussians.

At high enough energies, the LPM effect (Sec. 34.4.6) reduces the cross sections for bremsstrahlung and pair production, and hence can cause significant elongation of electromagnetic cascades [45].

### 34.6 Muon energy loss at high energy

At sufficiently high energies, radiative processes become more important than ionization for all charged particles. For muons and pions in materials such as iron, this “critical energy” occurs at several hundred GeV. (There is no simple scaling with particle mass, but for protons the “critical energy” is much, much higher.) Radiative effects dominate the energy loss of energetic muons found in cosmic rays or produced at the newest accelerators. These processes are characterized by small cross sections, hard spectra, large energy fluctuations, and the associated generation of electromagnetic and (in the case of photonuclear interactions) hadronic showers [65–73]. As a consequence, at these energies the treatment of energy loss as a uniform and continuous process is for many purposes inadequate.

It is convenient to write the average rate of muon energy loss as [74]

$$-dE/dx = a(E) + b(E)E \quad (34.39)$$

Here  $a(E)$  is the ionization energy loss given by Eq. (34.5), and  $b(E)$  is the sum of  $e^+e^-$  pair production, bremsstrahlung, and photonuclear contributions. To the approximation that these slowly-varying functions are constant, the mean range  $x_0$  of a muon with initial energy  $E_0$  is given by

$$x_0 \approx (1/b) \ln(1 + E_0/E_{\mu c}), \quad (34.40)$$

where  $E_{\mu c} = a/b$ .

Fig. 34.22 shows contributions to  $b(E)$  for iron. Since  $a(E) \approx 0.002 \text{ GeV g}^{-1} \text{ cm}^2$ ,  $b(E)E$  dominates the energy loss above several hundred GeV, where  $b(E)$  is nearly constant. The rates of energy loss for muons in hydrogen, uranium, and iron are shown in Fig. 34.23 [5].

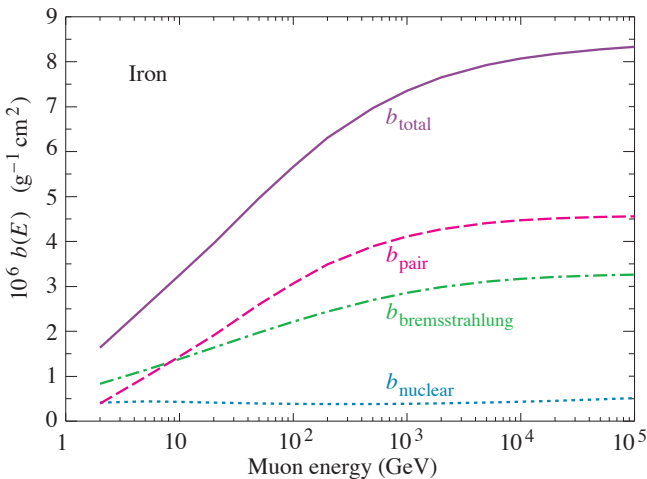


Figure 34.22: Contributions to the fractional energy loss by muons in iron due to  $e^+e^-$  pair production, bremsstrahlung, and photonuclear interactions, as obtained from Groom *et al.* [5] except for post-Born corrections to the cross section for direct pair production from atomic electrons.

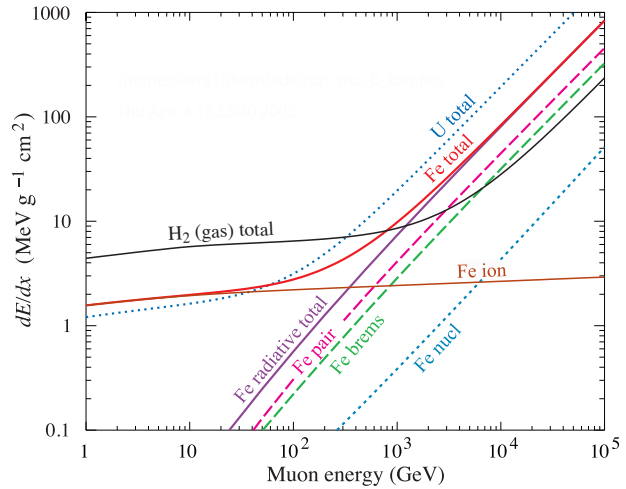


Figure 34.23: The average energy loss of a muon in hydrogen, iron, and uranium as a function of muon energy. Contributions to  $dE/dx$  in iron from ionization and pair production, bremsstrahlung and photonuclear interactions are also shown.

The “muon critical energy”  $E_{\mu c}$  can be defined more exactly as the energy at which radiative and ionization losses are equal, and can be found by solving  $E_{\mu c} = a(E_{\mu c})/b(E_{\mu c})$ . This definition corresponds to the solid-line intersection in Fig. 34.13, and is different from the Rossi definition we used for electrons. It serves the same function: below  $E_{\mu c}$  ionization losses dominate, and above  $E_{\mu c}$  radiative effects dominate. The dependence of  $E_{\mu c}$  on atomic number  $Z$  is shown in Fig. 34.24.

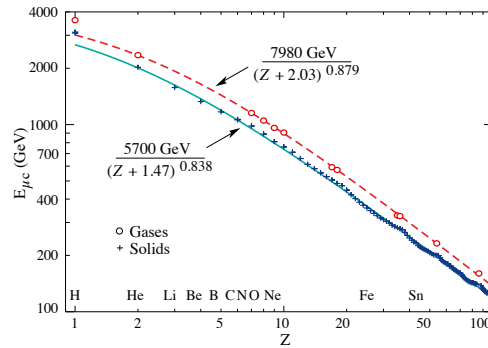


Figure 34.24: Muon critical energy for the chemical elements, defined as the energy at which radiative and ionization energy loss rates are equal [5]. The equality comes at a higher energy for gases than for solids or liquids with the same atomic number because of a smaller density effect reduction of the ionization losses. The fits shown in the figure exclude hydrogen. Alkali metals fall 3–4% above the fitted function, while most other solids are within 2% of the function. Among the gases the worst fit is for radon (2.7% high).

The radiative cross sections are expressed as functions of the fractional energy loss  $\nu$ . The bremsstrahlung cross section goes roughly as  $1/\nu$  over most of the range, while for the pair production case the distribution goes as  $\nu^{-3}$  to  $\nu^{-2}$  [75]. “Hard” losses are therefore more probable in bremsstrahlung, and in fact energy losses due to pair production may very nearly be treated as continuous. The simulated momentum distribution of an incident 1 TeV/c muon beam after it crosses 3 m of iron is shown in Fig. 34.25 [5]. The most probable loss is 8 GeV, or 3.4 MeV  $\text{g}^{-1} \text{ cm}^2$ . The full width at half maximum is 9 GeV/c, or 0.9%. The radiative tail is almost entirely due to bremsstrahlung, although most of the events in which more than 10% of the incident energy lost experienced relatively hard photonuclear interactions. The latter can exceed detector resolution [76], necessitating the

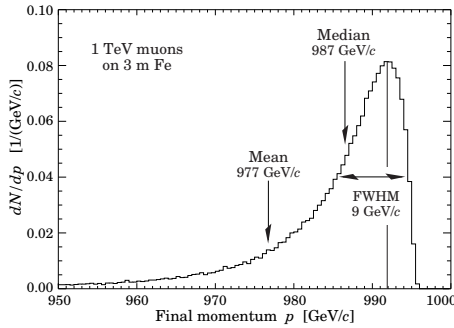


Figure 34.25: The momentum distribution of 1 TeV/c muons after traversing 3 m of iron as calculated by S.I. Striganov [5].

reconstruction of lost energy. Tables in Ref. [5] list the stopping power as  $9.82 \text{ MeV g}^{-1}\text{cm}^2$  for a 1 TeV muon, so that the mean loss should be 23 GeV ( $\approx 23 \text{ GeV}/c$ ), for a final momentum of 977 GeV/c, far below the peak. This agrees with the indicated mean calculated from the simulation. Electromagnetic and hadronic cascades in detector materials can obscure muon tracks in detector planes and reduce tracking efficiency [77].

### 34.7 Cherenkov and transition radiation [35, 78, 79]

A charged particle radiates if its velocity is greater than the local phase velocity of light (Cherenkov radiation) or if it crosses suddenly from one medium to another with different optical properties (transition radiation). Neither process is important for energy loss, but both are used in high-energy and cosmic-ray physics detectors.

#### 34.7.1 Optical Cherenkov radiation

The angle  $\theta_c$  of Cherenkov radiation, relative to the particle's direction, for a particle with velocity  $\beta c$  in a medium with index of refraction  $n$  is

$$\begin{aligned} \cos \theta_c &= (1/n\beta) \\ \text{or } \tan \theta_c &= \sqrt{\beta^2 n^2 - 1} \\ &\approx \sqrt{2(1 - 1/n\beta)} \quad \text{for small } \theta_c, \text{ e.g. in gases.} \end{aligned} \quad (34.41)$$

The threshold velocity  $\beta_t$  is  $1/n$ , and  $\gamma_t = 1/(1 - \beta_t^2)^{1/2}$ . Therefore,  $\beta_t \gamma_t = 1/(2\delta + \delta^2)^{1/2}$ , where  $\delta = n - 1$ . Values of  $\delta$  for various commonly used gases are given as a function of pressure and wavelength in Ref. [80]. See its Table 6.1 for values at atmospheric pressure. Data for other commonly used materials are given in Ref. [81].

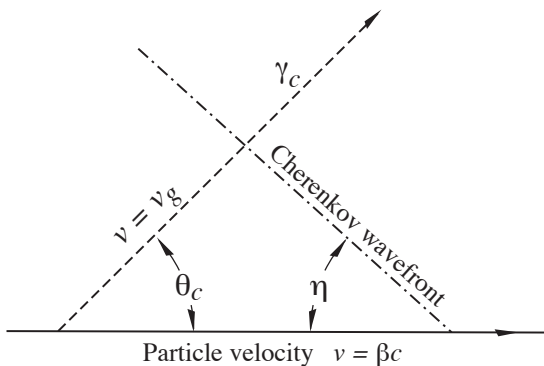


Figure 34.26: Cherenkov light emission and wavefront angles. In a dispersive medium,  $\theta_c + \eta \neq 90^\circ$ .

Practical Cherenkov radiator materials are dispersive. Let  $\omega$  be the photon's frequency, and let  $k = 2\pi/\lambda$  be its wavenumber. The photons propagate at the group velocity  $v_g = d\omega/dk = c/[n(\omega) + \omega(dn/d\omega)]$ . In a non-dispersive medium, this simplifies to  $v_g = c/n$ .

In his classical paper, Tamm [82] showed that for dispersive media the radiation is concentrated in a thin conical shell whose vertex is at the moving charge, and whose opening half-angle  $\eta$  is

$$\begin{aligned} \cot \eta &= \left[ \frac{d}{d\omega} (\omega \tan \theta_c) \right]_{\omega_0} \\ &= \left[ \tan \theta_c + \beta^2 \omega n(\omega) \frac{dn}{d\omega} \cot \theta_c \right]_{\omega_0}, \end{aligned} \quad (34.42)$$

where  $\omega_0$  is the central value of the small frequency range under consideration. (See Fig. 34.26.) This cone has a opening half-angle  $\eta$ , and, unless the medium is non-dispersive ( $dn/d\omega = 0$ ),  $\theta_c + \eta \neq 90^\circ$ . The Cherenkov wavefront 'sideslips' along with the particle [83]. This effect has timing implications for ring imaging Cherenkov counters [84], but it is probably unimportant for most applications.

The number of photons produced per unit path length of a particle with charge  $ze$  and per unit energy interval of the photons is

$$\begin{aligned} \frac{d^2 N}{dE dx} &= \frac{\alpha z^2}{hc} \sin^2 \theta_c = \frac{\alpha^2 z^2}{r_e m_e c^2} \left( 1 - \frac{1}{\beta^2 n^2(E)} \right) \\ &\approx 370 \sin^2 \theta_c(E) \text{ eV}^{-1} \text{ cm}^{-1} \quad (z = 1), \end{aligned} \quad (34.43)$$

or, equivalently,

$$\frac{d^2 N}{dx d\lambda} = \frac{2\pi \alpha z^2}{\lambda^2} \left( 1 - \frac{1}{\beta^2 n^2(\lambda)} \right). \quad (34.44)$$

The index of refraction  $n$  is a function of photon energy  $E = \hbar\omega$ , as is the sensitivity of the transducer used to detect the light. For practical use, Eq. (34.43) must be multiplied by the the transducer response function and integrated over the region for which  $\beta n(\omega) > 1$ . Further details are given in the discussion of Cherenkov detectors in the Particle Detectors section (Sec. 35.5 of this Review).

When two particles are close together (lateral separation  $\lesssim 1$  wavelength), the electromagnetic fields from the particles may add coherently, affecting the Cherenkov radiation. Because of their opposite charges, the radiation from an  $e^+e^-$  pair at close separation is suppressed compared to two independent leptons [85].

#### 34.7.2 Coherent radio Cherenkov radiation

Coherent Cherenkov radiation is produced by many charged particles with a non-zero net charge moving through matter on an approximately common "wavefront"—for example, the electrons and positrons in a high-energy electromagnetic cascade. The signals can be visible for energies above  $10^{16}$  eV; see Sec. 36.3.3.3 for more details. The phenomenon is called the Askaryan effect [86]. Near the end of a shower, when typical particle energies are below  $E_c$  (but still relativistic), a charge imbalance develops. Photons can Compton-scatter atomic electrons, and positrons can annihilate with atomic electrons to contribute even more photons which can in turn Compton scatter. These processes result in a roughly 20% excess of electrons over positrons in a shower. The net negative charge leads to coherent radio Cherenkov emission. The radiation includes a component from the decelerating charges (as in bremsstrahlung). Because the emission is coherent, the electric field strength is proportional to the shower energy, and the signal power increases as its square. The electric field strength also increases linearly with frequency, up to a maximum frequency determined by the lateral spread of the shower. This cutoff occurs at about 1 GHz in ice, and scales inversely with the Moliere radius. At low frequencies, the radiation is roughly isotropic, but, as the frequency rises toward the cutoff frequency, the radiation becomes increasingly peaked around the Cherenkov angle. The radiation is linearly polarized in the plane containing the shower axis and the photon direction. A measurement of the signal polarization can be used to help determine the shower direction. The characteristics of this radiation have been nicely demonstrated in a series of experiments at SLAC [87]. A detailed discussion of the radiation can be found in Ref. [88].

## 34.7.3 Transition radiation

The energy radiated when a particle with charge  $ze$  crosses the boundary between vacuum and a medium with plasma frequency  $\omega_p$  is

$$I = \alpha z^2 \gamma \hbar \omega_p / 3, \quad (34.45)$$

where

$$\hbar \omega_p = \sqrt{4\pi N_e r_e^3 m_e c^2 / \alpha} = \sqrt{\rho \text{ (in g/cm}^3\text{)} \langle Z/A \rangle} \times 28.81 \text{ eV}. \quad (34.46)$$

For styrene and similar materials,  $\hbar \omega_p \approx 20$  eV; for air it is 0.7 eV.

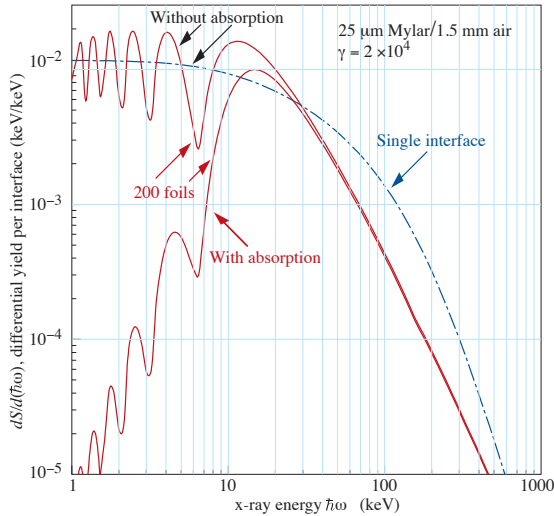


Figure 34.27: X-ray photon energy spectra for a radiator consisting of 200 25  $\mu\text{m}$  thick foils of Mylar with 1.5 mm spacing in air (solid lines) and for a single surface (dashed line). Curves are shown with and without absorption. Adapted from Ref. [89].

The number spectrum  $dN_\gamma/d(\hbar\omega)$  diverges logarithmically at low energies and decreases rapidly for  $\hbar\omega/\gamma\hbar\omega_p > 1$ . About half the energy is emitted in the range  $0.1 \leq \hbar\omega/\gamma\hbar\omega_p \leq 1$ . Inevitable absorption in a practical detector removes the divergence. For a particle with  $\gamma = 10^3$ , the radiated photons are in the soft x-ray range 2 to 40 keV. The  $\gamma$  dependence of the emitted energy thus comes from the hardening of the spectrum rather than from an increased quantum yield.

The number of photons with energy  $\hbar\omega > \hbar\omega_0$  is given by the answer to problem 13.15 in Ref. [35],

$$N_\gamma(\hbar\omega > \hbar\omega_0) = \frac{\alpha z^2}{\pi} \left[ \left( \ln \frac{\gamma \hbar \omega_p}{\hbar \omega_0} - 1 \right)^2 + \frac{\pi^2}{12} \right], \quad (34.47)$$

within corrections of order  $(\hbar\omega_0/\gamma\hbar\omega_p)^2$ . The number of photons above a fixed energy  $\hbar\omega_0 \ll \gamma\hbar\omega_p$  thus grows as  $(\ln \gamma)^2$ , but the number above a fixed fraction of  $\gamma\hbar\omega_p$  (as in the example above) is constant. For example, for  $\hbar\omega > \gamma\hbar\omega_p/10$ ,  $N_\gamma = 2.519 \alpha z^2 / \pi = 0.59\% \times z^2$ .

The particle stays “in phase” with the x ray over a distance called the formation length,  $d(\omega) = (2c/\omega)(1/\gamma^2 + \theta^2 + \omega_p^2/\omega^2)^{-1}$ . Most of the radiation is produced in this distance. Here  $\theta$  is the x-ray emission angle, characteristically  $1/\gamma$ . For  $\theta = 1/\gamma$  the formation length has a maximum at  $d(\gamma\omega_p/\sqrt{2}) = \gamma c/\sqrt{2}\omega_p$ . In practical situations it is tens of  $\mu\text{m}$ .

Since the useful x-ray yield from a single interface is low, in practical detectors it is enhanced by using a stack of  $N$  foil radiators—foils  $L$  thick, where  $L$  is typically several formation lengths—separated by gas-filled gaps. The amplitudes at successive interfaces interfere to cause oscillations about the single-interface spectrum. At increasing frequencies above the position of the last interference maximum ( $L/d(\omega) = \pi/2$ ), the formation zones, which have opposite phase, overlap more and more and the

spectrum saturates,  $dI/d\omega$  approaching zero as  $L/d(\omega) \rightarrow 0$ . This is illustrated in Fig. 34.27 for a realistic detector configuration.

For regular spacing of the layers fairly complicated analytic solutions for the intensity have been obtained [89,90]. Although one might expect the intensity of coherent radiation from the stack of foils to be proportional to  $N^2$ , the angular dependence of the formation length conspires to make the intensity  $\propto N$ .

## References

- [1] H. Bichsel, Nucl. Instrum. Meth. **A562**, 154 (2006).
- [2] B. Rossi, *High Energy Particles*, Prentice-Hall, Inc., Englewood Cliffs, NJ, 1952.
- [3] H.A. Bethe, *Zur Theorie des Durchgangs schneller Korpuskularstrahlen durch Materie*, H. Bethe, Ann. Phys. **5**, 325 (1930).
- [4] “Stopping Powers and Ranges for Protons and Alpha Particles,” ICRU Report No. 49 (1993); Tables and graphs are available at <http://physics.nist.gov/PhysRefData/Star/Text/PSTAR.html> and <http://physics.nist.gov/PhysRefData/Star/Text/ASTAR.html>.
- [5] D.E. Groom, N.V. Mokhov, and S.I. Striganov, “Muon stopping-power and range tables: 10 MeV–100 TeV,” Atomic Data and Nuclear Data Tables **78**, 183–356 (2001). Since submission of this paper it has become likely that post-Born corrections to the direct pair production cross section should be made. Code used to make Figs. 34.22–34.24 included these corrections [D.Yu. Ivanov *et al.*, Phys. Lett. **B442**, 453 (1998)]. The effect is negligible except at high  $Z$ . (It is less than 1% for iron.); Extensive printable and machine-readable tables are given at <http://pdg.lbl.gov/AtomicNuclearProperties/>.
- [6] W. H. Barkas, W. Birnbaum and F. M. Smith, Phys. Rev. **101**, 778 (1956).
- [7] U. Fano, Ann. Rev. Nucl. Sci. **13**, 1 (1963).
- [8] J. D. Jackson, Phys. Rev. **D59**, 017301 (1999).
- [9] J. Lindhard and A. H. Sørensen, Phys. Rev. **A53**, 2443 (1996).
- [10] “Stopping Powers for Electrons and Positrons,” ICRU Report No. 37 (1984); Tables and graphs are available at <http://physics.nist.gov/PhysRefData/Star/Text/ESTAR.html>.
- [11] H. Bichsel, Phys. Rev. **A46**, 5761 (1992).
- [12] W.H. Barkas and M.J. Berger, *Tables of Energy Losses and Ranges of Heavy Charged Particles*, NASA-SP-3013 (1964).
- [13] S.M. Seltzer and M.J. Berger, Int. J. of Applied Rad. **33**, 1189 (1982).
- [14] <http://physics.nist.gov/PhysRefData/XrayMassCoef/tab1.html>.
- [15] R. M. Sternheimer, Phys. Rev. **88**, 851 (1952).
- [16] R. M. Sternheimer, M. J. Berger and S. M. Seltzer, Atom. Data Nucl. Data Tabl. **30**, 261 (1984); Minor errors are corrected in Ref. 5. Chemical composition for the tabulated materials is given in Ref. 10.
- [17] R. M. Sternheimer and R. F. Peierls, Phys. Rev. **B3**, 3681 (1971).
- [18] N. F. Mott, Proceedings of the Cambridge Philosophical Society **27**, 553 (1931).
- [19] M. S. Livingston and H. A. Bethe, Rev. Mod. Phys. **9**, 245 (1937).
- [20] H. Bichsel, Phys. Rev. **A65**, 5, 052709 (2002).
- [21] S. P. Møller *et al.*, Phys. Rev. **A56**, 4, 2930 (1997).
- [22] J. C. Ashley, R. H. Ritchie and W. Brandt, Phys. Rev. **B5**, 2393 (1972).
- [23] H.H. Andersen and J.F. Ziegler, *Hydrogen: Stopping Powers and Ranges in All Elements*. Vol. 3 of *The Stopping and Ranges of Ions in Matter* (Pergamon Press 1977).

- [24] J. Lindhard, Kgl. Danske Videnskab. Selskab, Mat.-Fys. Medd. **28**, No. 8 (1954); J. Lindhard, M. Scharff, and H.E. Schiøtt, Kgl. Danske Videnskab. Selskab, Mat.-Fys. Medd. **33**, No. 14 (1963).
- [25] J.F. Ziegler, J.F. Biersac, and U. Littmark, *The Stopping and Range of Ions in Solids*, Pergamon Press 1985.
- [26] E.A. Uehling, Ann. Rev. Nucl. Sci. **4**, 315 (1954) (For heavy particles with unit charge, but  $e^\pm$  cross sections and stopping powers are also given).
- [27] N.F. Mott and H.S.W. Massey, *The Theory of Atomic Collisions*, Oxford Press, London, 1965.
- [28] P. V. Vavilov, Sov. Phys. JETP **5**, 749 (1957), [Zh. Eksp. Teor. Fiz.32,920(1957)].
- [29] L.D. Landau, J. Exp. Phys. (USSR) **8**, 201 (1944).
- [30] H. Bichsel, Rev. Mod. Phys. **60**, 663 (1988).
- [31] R. Talman, Nucl. Instrum. Meth. **159**, 189 (1979).
- [32] H. Bichsel, Ch. 87 in the Atomic, Molecular and Optical Physics Handbook, G.W.F. Drake, editor (Am. Inst. Phys. Press, Woodbury NY, 1996).
- [33] S.M. Seltzer and M.J. Berger, Int. J. of Applied Rad. **35**, 665 (1984). This paper corrects and extends the results of Ref. [13].
- [34] H. A. Bethe, Phys. Rev. **89**, 1256 (1953).
- [35] J.D. Jackson, *Classical Electrodynamics*, 3rd edition, (John Wiley and Sons, New York, 1998).
- [36] W. T. Scott, Rev. Mod. Phys. **35**, 231 (1963).
- [37] J. W. Motz, H. Olsen and H. W. Koch, Rev. Mod. Phys. **36**, 881 (1964).
- [38] H. Bichsel, Phys. Rev. **112**, 182 (1958).
- [39] G. Shen *et al.*, Phys. Rev. **D20**, 1584 (1979).
- [40] G. R. Lynch and O. I. Dahl, Nucl. Instrum. Meth. **B58**, 6 (1991).
- [41] M. Wong *et al.*, Med. Phys. **17**, 163 (1990).
- [42] Y.-S. Tsai, Rev. Mod. Phys. **46**, 815 (1974), [Erratum: Rev. Mod. Phys.49,521(1977)].
- [43] H. Davies, H. A. Bethe and L. C. Maximon, Phys. Rev. **93**, 788 (1954).
- [44] L. D. Landau and I. Pomeranchuk, Dokl. Akad. Nauk Ser. Fiz. **92**, 535 (1953); **92**, 735 (1953). These papers are available in English in L. Landau, *The Collected Papers of L.D. Landau*, Pergamon Press, 1965; A. B. Migdal, Phys. Rev. **103**, 1811 (1956).
- [45] S. Klein, Rev. Mod. Phys. **71**, 1501 (1999).
- [46] M.L. Ter-Mikaelian, SSSR **94**, 1033 (1954); M.L. Ter-Mikaelian, *High Energy Electromagnetic Processes in Condensed Media* (John Wiley and Sons, New York, 1972).
- [47] P. L. Anthony *et al.*, Phys. Rev. Lett. **76**, 3550 (1996).
- [48] H. W. Koch and J. W. Motz, Rev. Mod. Phys. **31**, 920 (1959).
- [49] M.J. Berger and S.M. Seltzer, "Tables of Energy Losses and Ranges of Electrons and Positrons," National Aeronautics and Space Administration Report NASA-SP-3012 (Washington DC 1964).
- [50] Curves for these and other elements, compounds, and mixtures may be obtained from <https://www.nist.gov/pml/xcom-photon-cross-sections-database>. The photon total cross section is approximately flat for at least two decades beyond the energy range shown.
- [51] B. L. Berman and S. C. Fultz, Rev. Mod. Phys. **47**, 713 (1975).
- [52] [http://www.cxro.lbl.gov/optical\\_constants/pert\\_form.html](http://www.cxro.lbl.gov/optical_constants/pert_form.html).
- [53] <https://physics.nist.gov/PhysRefData/XrayMassCoef/tab3.html>.
- [54] J. W. Motz, H. A. Olsen and H. W. Koch, Rev. Mod. Phys. **41**, 581 (1969).
- [55] P. L. Anthony *et al.*, Phys. Rev. Lett. **75**, 1949 (1995).
- [56] U. I. Uggerhøj, Rev. Mod. Phys. **77**, 1131 (2005).
- [57] L. Gerhardt and S. R. Klein, Phys. Rev. **D82**, 074017 (2010).
- [58] W.R. Nelson, H. Hirayama, and D.W.O. Rogers, "The EGS4 Code System," SLAC-265, Stanford Linear Accelerator Center (Dec. 1985).
- [59] *Experimental Techniques in High Energy Physics*, ed. T. Ferbel (Addison-Wesley, Menlo Park CA 1987).
- [60] U. Amaldi, Phys. Scripta **23**, 409 (1981).
- [61] E. Longo and I. Sestili, Nucl. Instrum. Meth. **128**, 283 (1975), [Erratum: Nucl. Instrum. Meth.135,587(1976)].
- [62] G. Grindhammer *et al.*, in *Proceedings of the 1988 Summer Study on High Energy Physics in the 1990's*, Snowmass, CO, June 27 – July 15, 1990, edited by F.J. Gilman and S. Jensen, (World Scientific, Teaneck, NJ, 1989) p. 151.
- [63] W. R. Nelson *et al.*, Phys. Rev. **149**, 201 (1966).
- [64] G. Bathow *et al.*, Nucl. Phys. **B20**, 592 (1970).
- [65] H. Bethe and W. Heitler, Proc. Roy. Soc. Lond. **A146**, 83 (1934); H.A. Bethe, *Proc. Cambridge Phil. Soc.* **30**, 542 (1934).
- [66] A.A. Petrukhin and V.V. Shestakov, Can. J. Phys. **46**, S377 (1968).
- [67] V.M. Galitskii and S.R. Kel'ner, Sov. Phys. JETP **25**, 948 (1967).
- [68] S.R. Kel'ner and Yu.D. Kotov, Sov. J. Nucl. Phys. **7**, 237 (1968).
- [69] R.P. Kokoulin and A.A. Petrukhin, in *Proceedings of the International Conference on Cosmic Rays*, Hobart, Australia, August 16–25, 1971, Vol. **4**, p. 2436.
- [70] A. I. Nikishov, Sov. J. Nucl. Phys. **27**, 677 (1978), [Yad. Fiz.27,1281(1978)].
- [71] Yu. M. Andreev, L. B. Bezrukov and E. V. Bugaev, Phys. Atom. Nucl. **57**, 2066 (1994), [Yad. Fiz.57,2146(1994)].
- [72] L. B. Bezrukov and E. V. Bugaev, Yad. Fiz. **33**, 1195 (1981), [Sov. J. Nucl. Phys.33,635(1981)].
- [73] N.V. Mokhov and C.C. James, The MARS Code System User's Guide, Fermilab-FN-1058-APC (2018), <https://mars.fnal.gov/>; N. Mokhov *et al.*, Prog. Nucl. Sci. Tech. **4**, 496 (2014).
- [74] P. H. Barrett *et al.*, Rev. Mod. Phys. **24**, 3, 133 (1952).
- [75] A. Van Ginneken, Nucl. Instrum. Meth. **A251**, 21 (1986).
- [76] U. Becker *et al.*, Nucl. Instrum. Meth. **A253**, 15 (1986).
- [77] J.J. Eastman and S.C. Loken, in *Proceedings of the Workshop on Experiments, Detectors, and Experimental Areas for the Supercollider*, Berkeley, CA, July 7–17, 1987, edited by R. Donaldson and M.G.D. Gilchriese (World Scientific, Singapore, 1988), p. 542.
- [78] *Methods of Experimental Physics*, L.C.L. Yuan and C.-S. Wu, editors, Academic Press, 1961, Vol. 5A, p. 163.
- [79] W.W.M. Allison and P.R.S. Wright, "The Physics of Charged Particle Identification:  $dE/dx$ , Cherenkov Radiation, and Transition Radiation," p. 371 in *Experimental Techniques in High Energy Physics*, T. Ferbel, editor, (Addison-Wesley 1987).
- [80] E.R. Hayes, R.A. Schluter, and A. Tamosaitis, "Index and Dispersion of Some Cherenkov Counter Gases," ANL-6916 (1964).
- [81] T. Ypsilantis, in "Proceedings of the Symposium on Particle Identification at High Luminosity Hadron Colliders, Apr 5-7, 1989 Batavia, Ill.," 0661–676 (1989).
- [82] I. Tamm, J. Phys. U.S.S.R., **1**, 439 (1939).
- [83] H. Motz and L.I. Schiff, Am. J. Phys. **21**, 258 (1953).
- [84] B. N. Ratcliff, Nucl. Instrum. Meth. **A502**, 211 (2003).
- [85] S. K. Mandal, S. R. Klein and J. D. Jackson, Phys. Rev. **D72**, 093003 (2005).

- [86] G. A. Askar'yan, Sov. Phys. JETP **14**, 2, 441 (1962), [Zh. Eksp. Teor. Fiz.41,616(1961)].
- [87] P. W. Gorham *et al.*, Phys. Rev. **D72**, 023002 (2005).
- [88] E. Zas, F. Halzen and T. Stanev, Phys. Rev. **D45**, 362 (1992).
- [89] M. L. Cherry *et al.*, Phys. Rev. **D10**, 3594 (1974); M. L. Cherry, Phys. Rev. **D17**, 2245 (1978).
- [90] B. Dolgoshein, Nucl. Instrum. Meth. **A326**, 434 (1993).

## 35. Particle Detectors at Accelerators

Revised 2019. See the various sections for authors.

35.1	Introduction . . . . .	551
35.2	Photon detectors . . . . .	551
35.2.1	Vacuum photodetectors . . . . .	552
35.2.2	Gaseous photon detectors . . . . .	553
35.2.3	Solid-state photon detectors . . . . .	553
35.3	Organic scintillators . . . . .	554
35.3.1	Scintillation mechanism . . . . .	554
35.3.2	Caveats and cautions . . . . .	555
35.3.3	Scintillating and wavelength-shifting fibers . . . . .	555
35.4	Inorganic scintillators . . . . .	555
35.5	Cherenkov detectors . . . . .	558
35.6	Gaseous detectors . . . . .	560
35.6.1	Energy loss and charge transport in gases . . . . .	560
35.6.2	Multi-Wire Proportional and Drift Chambers . . . . .	562
35.6.3	High Rate Effects . . . . .	563
35.6.4	Micro-Pattern Gas Detectors . . . . .	563
35.6.5	Time-projection chambers . . . . .	565
35.6.6	Transition radiation detectors (TRD's) . . . . .	567
35.6.7	Resistive-plate chambers . . . . .	568
35.7	Semiconductor detectors . . . . .	569
35.7.1	Materials Requirements . . . . .	569
35.7.2	Detector Configurations . . . . .	570
35.7.3	Signal Formation . . . . .	570
35.7.4	Radiation Damage . . . . .	571
35.8	Low-noise electronics . . . . .	571
35.9	Calorimeters . . . . .	573
35.9.1	Introduction . . . . .	573
35.9.2	Electromagnetic calorimeters . . . . .	574
35.9.3	Hadronic calorimeters . . . . .	575
35.9.4	Free electron drift velocities in liquid ionization chambers . . . . .	578
35.10	Accelerator-based neutrino detectors . . . . .	579
35.10.1	Introduction . . . . .	579
35.10.2	Signals and Backgrounds . . . . .	579
35.10.3	Instances of Neutrino Detector Technology . . . . .	579
35.10.4	Outlook . . . . .	582
35.11	Superconducting magnets for collider detectors . . . . .	582
35.11.1	Solenoid Magnets . . . . .	582
35.11.2	Properties of collider detector magnets . . . . .	583
35.11.3	Toroidal magnets . . . . .	584
35.12	Measurement of particle momenta in a uniform magnetic field . . . . .	584

### 35.1 Introduction

This review summarizes the detector technologies employed at accelerator particle physics experiments. Several of these detectors are also used in a non-accelerator context and examples of such applications will be provided. The detector techniques which are specific to non-accelerator particle physics experiments are the subject of Chap. 36. More detailed discussions of detectors and their underlying physics can be found in books by Ferbel [1], Kleinknecht [2], Knoll [3], Green [4], Leroy & Rancoita [5], and Grupen [6].

In Table 35.1 are given typical resolutions and deadtimes of common charged particle detectors. The quoted numbers are usually based on typical devices, and should be regarded only as rough approximations for new designs. The spatial resolution refers to the intrinsic detector resolution, i.e. without multiple scattering. We note that analog detector readout can provide better spatial resolution than digital readout by measuring the deposited charge in neighboring channels. Quoted ranges attempt to be representative of both possibilities. The time resolution is defined by how accurately the time at which a particle crossed the detector can be determined. The deadtime is the minimum separation in time between two resolved hits on the same channel. Typical performance of calorimetry and particle identification are provided in the relevant sections below.

**Table 35.1:** Typical resolutions and deadtimes of common charged particle detectors. Revised November 2011.

Detector Type	Intrinsic Spatial Resolution (rms)	Time Resolution	Dead Time
Resistive plate chamber	$\lesssim 10$ mm	1 ns (50 ps <sup>*</sup> )	—
Streamer chamber	$300 \mu\text{m}^\dagger$	$2 \mu\text{s}$	100 ms
Liquid argon drift [7]	$\sim 175\text{--}450 \mu\text{m}$	$\sim 200$ ns	$\sim 2 \mu\text{s}$
Scintillation tracker	$\sim 100 \mu\text{m}$	$100 \text{ps}/n^\ddagger$	10 ns
Bubble chamber	$10\text{--}150 \mu\text{m}$	1 ms	$50 \text{ms}^\S$
Proportional chamber	$50\text{--}100 \mu\text{m}^\P$	2 ns	20-200 ns
Drift chamber	$50\text{--}100 \mu\text{m}$	$2 \text{ns}^\parallel$	20-100 ns
Micro-pattern gas detect.	$30\text{--}40 \mu\text{m}$	$< 10$ ns	10-100 ns
Silicon strip	pitch/(3 to 7)**	few ns <sup>††</sup>	$\lesssim 50 \text{ns}^{\dagger\dagger}$
Silicon pixel	$\lesssim 10 \mu\text{m}$	few ns <sup>††</sup>	$\lesssim 50 \text{ns}^{\dagger\dagger}$
Emulsion	$1 \mu\text{m}$	—	—

\*For multiple-gap RPCs.

<sup>†</sup> $300 \mu\text{m}$  is for 1 mm pitch (wirespacing/ $\sqrt{12}$ ).

<sup>‡</sup> $n$  = index of refraction.

<sup>§</sup>Multiple pulsing time.

<sup>¶</sup>Delay line cathode readout can give  $\pm 150 \mu\text{m}$  parallel to anode wire.

<sup>||</sup>For two chambers

\*\*The highest resolution (“7”) is obtained for small-pitch detectors ( $\lesssim 25 \mu\text{m}$ ) with pulse-height-weighted center finding.

<sup>††</sup>Limited by the readout electronics [8]

### 35.2 Photon detectors

Revised August 2011 by D. Chakraborty (Northern Illinois U.) and T. Sumiyoshi (Tokyo Metropolitan U.).

Most detectors in high-energy, nuclear, and astrophysics rely on the detection of photons in or near the visible range,  $100 \text{nm} \lesssim \lambda \lesssim 1000 \text{nm}$ , or  $E \approx$  a few eV. This range covers scintillation and Cherenkov radiation as well as the light detected in many astronomical observations.

Generally, photodetection involves generating a detectable electrical signal proportional to the (usually very small) number of incident photons. The process involves three distinct steps:

1. generation of a primary photoelectron or electron-hole ( $e-h$ ) pair by an incident photon by the photoelectric or photoconductive effect,
2. amplification of the p.e. signal to detectable levels by one or more multiplicative bombardment steps and/or an avalanche process (usually), and,
3. collection of the secondary electrons to form the electrical signal.

The important characteristics of a photodetector include the following in statistical averages:

1. quantum efficiency (QE or  $\epsilon_Q$ ): the number of primary photoelectrons generated per incident photon ( $0 \leq \epsilon_Q \leq 1$ ; in silicon more than one  $e-h$  pair per incident photon can be generated for  $\lambda \lesssim 165 \text{nm}$ ),
2. collection efficiency (CE or  $\epsilon_C$ ): the overall acceptance factor other than the generation of photoelectrons ( $0 \leq \epsilon_C \leq 1$ ),
3. gain ( $G$ ): the number of electrons collected for each photoelectron generated,
4. dark current or dark noise: the electrical signal when there is no photon,
5. energy resolution: electronic noise (ENC or  $N_e$ ) and statistical fluctuations in the amplification process compound the Poisson distribution of  $n_\gamma$  photons from a given source:

$$\frac{\sigma(E)}{\langle E \rangle} = \sqrt{\frac{f_N}{n_\gamma \epsilon_Q \epsilon_C} + \left( \frac{N_e}{G n_\gamma \epsilon_Q \epsilon_C} \right)^2}, \quad (35.1)$$



where  $f_N$ , or the excess noise factor (ENF), is the contribution to the energy distribution variance due to amplification statistics [9],

6. dynamic range: the maximum signal available from the detector (this is usually expressed in units of the response to noise-equivalent power, or NEP, which is the optical input power that produces a signal-to-noise ratio of 1),
7. time dependence of the response: this includes the transit time, which is the time between the arrival of the photon and the electrical pulse, and the transit time spread, which contributes to the pulse rise time and width, and
8. rate capability: inversely proportional to the time needed, after the arrival of one photon, to get ready to receive the next.

The QE is a strong function of the photon wavelength ( $\lambda$ ), and is usually quoted at maximum, together with a range of  $\lambda$  where the QE is comparable to its maximum. Spatial uniformity and linearity with respect to the number of photons are highly desirable in a photodetector's response.

Optimization of these factors involves many trade-offs and vary widely between applications. For example, while a large gain is desirable, attempts to increase the gain for a given device also increases the ENF and after-pulsing ("echos" of the main pulse). In solid-state devices, a higher QE often requires a compromise in the timing properties. In other types, coverage of large areas by focusing increases the transit time spread.

Other important considerations also are highly application-specific. These include the photon flux and wavelength range, the total area to be covered and the efficiency required, the volume available to accommodate the detectors, characteristics of the environment such as chemical composition, temperature, magnetic field, ambient background, as well as ambient radiation of different types and, mode of operation (continuous or triggered), bias (high-voltage) requirements, power consumption, calibration needs, aging, cost, and so on. Several technologies employing different phenomena for the three steps described above, and many variants within each, offer a wide range of solutions to choose from. The salient features of the main technologies and the common variants are described below. Some key characteristics are summarized in Table 35.2.

### 35.2.1 Vacuum photodetectors

Vacuum photodetectors can be broadly subdivided into three types: photomultiplier tubes, microchannel plates, and hybrid photodetectors.

#### 35.2.1.1 Photomultiplier tubes

A versatile class of photon detectors, vacuum photomultiplier tubes (PMT) has been employed by a vast majority of all particle physics experiments to date [9]. Both "transmission-" and "reflection-type" PMT's are widely used. In the former, the photocathode material is deposited on the inside of a transparent window through which the photons enter, while in the latter, the photocathode material rests on a separate surface that the incident photons strike. The cathode material has a low work function, chosen for the wavelength band of interest. When a photon hits the cathode and liberates an electron (the photoelectric effect), the latter is accelerated and guided by electric fields to impinge on a secondary-emission electrode, or dynode, which then emits a few ( $\sim 5$ ) secondary electrons. The multiplication process is repeated typically 10 times in series to generate a sufficient number of electrons, which are collected at the anode for delivery to the external circuit. The total gain of a PMT depends on the applied high voltage  $V$  as  $G = AV^{kn}$ , where  $k \approx 0.7-0.8$  (depending on the dynode material),  $n$  is the number of dynodes in the chain, and  $A$  a constant (which also depends on  $n$ ). Typically,  $G$  is in the range of  $10^5-10^6$ . Pulse risetimes are usually in the few nanosecond range. With *e.g.* two-level discrimination the effective time resolution can be much better.

A large variety of PMT's, including many just recently developed, covers a wide span of wavelength ranges from infrared (IR) to extreme ultraviolet (XUV) [10]. They are categorized by the window materials, photocathode materials, dynode struc-

tures, anode configurations, *etc.* Common window materials are borosilicate glass for IR to near-UV, fused quartz and sapphire ( $\text{Al}_2\text{O}_3$ ) for UV, and  $\text{MgF}_2$  or LiF for XUV. The choice of photocathode materials include a variety of mostly Cs- and/or Sb-based compounds such as CsI, CsTe, bi-alkali (SbRbCs, SbKCs), multi-alkali (SbNa<sub>2</sub>KCs), GaAs(Cs), GaAsP, *etc.* Sensitive wavelengths and peak quantum efficiencies for these materials are summarized in Table-35.3. Typical dynode structures used in PMT's are circular cage, line focusing, box and grid, venetian blind, and fine mesh. In some cases, limited spatial resolution can be obtained by using a mosaic of multiple anodes. Fast PMT's with very large windows—measuring up to 508 mm across—have been developed in recent years for detection of Cherenkov radiation in neutrino experiments such as Super-Kamiokande and KamLAND among many others. Specially prepared low-radioactivity glass is used to make these PMT's, and they are also able to withstand the high pressure of the surrounding liquid.

PMT's are vulnerable to magnetic fields—sometimes even the geomagnetic field causes large orientation-dependent gain changes. A high-permeability metal shield is often necessary. However, proximity-focused PMT's, *e.g.* the fine-mesh types, can be used even in a high magnetic field ( $\geq 1$  T) if the electron drift direction is parallel to the field. CMS uses custom-made vacuum phototriodes (VPT) mounted on the back face of projective lead tungstate crystals to detect scintillation light in the endcap sections of its electromagnetic calorimeters, which are inside a 3.8 T superconducting solenoid. A VPT employs a single dynode (thus,  $G \approx 10$ ) placed close to the photocathode, and a mesh anode plane between the two, to help it cope with the strong magnetic field, which is not too unfavorably oriented with respect to the photodetector axis in the endcaps (within  $25^\circ$ ), but where the radiation level is too high for Avalanche Photodiodes (APD's) like those used in the barrel section.

#### 35.2.1.2 Microchannel plates

A typical Microchannel plate (MCP) photodetector consists of one or more  $\sim 2$  mm thick glass plates with densely packed  $O(10 \mu\text{m})$ -diameter cylindrical holes, or "channels", sitting between the transmission-type photocathode and anode planes, separated by  $O(1 \text{ mm})$  gaps. Instead of discrete dynodes, the inner surface of each cylindrical tube serves as a continuous dynode for the entire cascade of multiplicative bombardments initiated by a photoelectron. Gain fluctuations can be minimized by operating in a saturation mode, whence each channel is only capable of a binary output, but the sum of all channel outputs remains proportional to the number of photons received so long as the photon flux is low enough to ensure that the probability of a single channel receiving more than one photon during a single time gate is negligible. MCP's are thin, offer good spatial resolution, have excellent time resolution ( $\sim 20$  ps), and can tolerate random magnetic fields up to 0.1 T and axial fields up to  $\sim 1$  T. However, they suffer from relatively long recovery time per channel and short lifetime. MCP's are widely employed as image-intensifiers, although not so much in HEP or astrophysics.

#### 35.2.1.3 Hybrid photon detectors

Hybrid photon detectors (HPD) combine the sensitivity of a vacuum PMT with the excellent spatial and energy resolutions of a Si sensor [11]. A single photoelectron ejected from the photocathode is accelerated through a potential difference of  $\sim 20$  kV before it impinges on the silicon sensor/anode. The gain nearly equals the maximum number of  $e-h$  pairs that could be created from the entire kinetic energy of the accelerated electron:  $G \approx eV/w$ , where  $e$  is the electronic charge,  $V$  is the applied potential difference, and  $w \approx 3.7$  eV is the mean energy required to create an  $e-h$  pair in Si at room temperature. Since the gain is achieved in a single step, one might expect to have the excellent resolution of a simple Poisson statistic with large mean, but in fact it is even better, thanks to the Fano effect discussed in Sec. 35.7.

Low-noise electronics must be used to read out HPD's if one intends to take advantage of the low fluctuations in gain, *e.g.* when counting small numbers of photons. HPD's can have the same  $\epsilon_Q \epsilon_C$  and window geometries as PMT's and can be segmented down to  $\sim 50 \mu\text{m}$ . However, they require rather high biases and

**Table 35.2:** Representative characteristics of some photodetectors commonly used in particle physics. The time resolution of the devices listed here vary in the 10–2000 ps range.

Type	$\lambda$ (nm)	$\epsilon_Q \epsilon_C$	Gain	Risetime (ns)	Area (mm <sup>2</sup> )	1-p.e noise (Hz)	HV (V)	Price (USD)
PMT *	115–1700	0.15–0.25	$10^3$ – $10^7$	0.7–10	$10^2$ – $10^5$	$10$ – $10^4$	500–3000	100–5000
MCP*	100–650	0.01–0.10	$10^3$ – $10^7$	0.15–0.3	$10^2$ – $10^4$	0.1–200	500–3500	10–6000
HPD*	115–850	0.1–0.3	$10^3$ – $10^4$	7	$10^2$ – $10^5$	$10$ – $10^3$	$\sim 2 \times 10^4$	$\sim 600$
GPM*	115–500	0.15–0.3	$10^3$ – $10^6$	$O(0.1)$	$O(10)$	$10$ – $10^3$	300–2000	$O(10)$
APD	300–1700	$\sim 0.7$	$10$ – $10^8$	$O(1)$	$10$ – $10^3$	$1$ – $10^3$	400–1400	$O(100)$
PPD	320–900	0.15–0.3	$10^5$ – $10^6$	$\sim 1$	1–10	$O(10^6)$	30–60	$O(100)$
VLPC	500–600	$\sim 0.9$	$\sim 5 \times 10^4$	$\sim 10$	1	$O(10^4)$	$\sim 7$	$\sim 1$

\*These devices often come in multi-anode configurations. In such cases, area, noise, and price are to be considered on a “per readout-channel” basis.

will not function in a magnetic field. The exception is proximity-focused devices ( $\Rightarrow$  no (de)magnification) in an axial field. With time resolutions of  $\sim 10$  ps and superior rate capability, proximity-focused HPD’s can be an alternative to MCP’s. Current applications of HPD’s include the CMS hadronic calorimeter and the RICH detector in LHCb. Large-size HPD’s with sophisticated focusing may be suitable for future water Cherenkov experiments.

Hybrid APD’s (HAPD’s) add an avalanche multiplication step following the electron bombardment to boost the gain by a factor of  $\sim 50$ . This affords a higher gain and/or lower electrical bias, but also degrades the signal definition.

**Table 35.3:** Properties of photocathode and window materials commonly used in vacuum photodetectors.

Photocathode material	$\lambda$ (nm)	Window material	Peak $\epsilon_Q$ ( $\lambda/\text{nm}$ )
CsI	115–200	MgF <sub>2</sub>	0.11 (140)
CsTe	115–320	MgF <sub>2</sub>	0.14 (240)
Bi-alkali	300–650	Borosilicate	0.27 (390)
	160–650	Synthetic Silica	0.27 (390)
“Ultra Bi-alkali”	300–650	Borosilicate	0.43 (350)
	160–650	Synthetic Silica	0.43 (350)
Multi-alkali	300–850	Borosilicate	0.20 (360)
	160–850	Synthetic Silica	0.20 (360)
GaAs(Cs)*	160–930	Synthetic Silica	0.23 (280)
GaAsP(Cs)	300–750	Borosilicate	0.50 (500)
InP/InGaAsP <sup>†</sup>	350–1700	Borosilicate	0.01 (1100)

\*Reflection type photocathode is used.

<sup>†</sup>Requires cooling to  $\sim -80^\circ\text{C}$ .

### 35.2.2 Gaseous photon detectors

In gaseous photomultipliers (GPM) a photoelectron in a suitable gas mixture initiates an avalanche in a high-field region, producing a large number of secondary impact-ionization electrons. In principle the charge multiplication and collection processes are identical to those employed in gaseous tracking detectors such as multiwire proportional chambers, micromesh gaseous detectors (Micromegas), or gas electron multipliers (GEM). These are discussed in Sec. 35.6.4.

The devices can be divided into two types depending on the photocathode material. One type uses solid photocathode materials much in the same way as PMT’s. Since it is resistant to gas mixtures typically used in tracking chambers, CsI is a common choice. In the other type, photoionization occurs on suitable molecules vaporized and mixed in the drift volume. Most gases have photoionization work functions in excess of 10 eV, which would limit their sensitivity to wavelengths far too short. However, vapors of TMAE (tetrakis dimethyl-amine ethylene) or TEA (tri-ethyl-amine), which have smaller work functions (5.3 eV for TMAE and 7.5 eV for TEA), are suited for XUV photon detection [12]. Since devices like GEM’s offer sub-mm spatial resolution, GPM’s are often used as position-sensitive photon detectors.

They can be made into flat panels to cover large areas ( $O(1\text{ m}^2)$ ), can operate in high magnetic fields, and are relatively inexpensive. Many of the ring imaging Cherenkov (RICH) detectors to date have used GPM’s for the detection of Cherenkov light [13–16]. Special care must be taken to suppress the photon-feedback process in GPM’s. It is also important to maintain high purity of the gas as minute traces of O<sub>2</sub> can significantly degrade the detection efficiency.

### 35.2.3 Solid-state photon detectors

In a phase of rapid development, solid-state photodetectors are competing with vacuum- or gas-based devices for many existing applications and making way for a multitude of new ones. Compared to traditional vacuum- and gaseous photodetectors, solid-state devices are more compact, lightweight, rugged, tolerant to magnetic fields, and often cheaper. They also allow fine pixelization, are easy to integrate into large systems, and can operate at low electric potentials, while matching or exceeding most performance criteria. They are particularly well suited for detection of  $\gamma$ - and X-rays. Except for applications where coverage of very large areas or dynamic range is required, solid-state detectors are proving to be the better choice. Some hybrid devices attempt to combine the best features of different technologies while applications of nanotechnology are opening up exciting new possibilities.

Silicon photodiodes (PD) are widely used in high-energy physics as particle detectors and in a great number of applications (including solar cells!) as light detectors. The structure is discussed in some detail in Sec. 35.7. In its simplest form, the PD is a reverse-biased  $p$ - $n$  junction. Photons with energies above the indirect bandgap energy (wavelengths shorter than about 1050 nm, depending on the temperature) can create  $e$ - $h$  pairs (the photoconductive effect), which are collected on the  $p$  and  $n$  sides, respectively. Often, as in the PD’s used for crystal scintillator readout in CLEO, L3, Belle, BaBar, and GLAST, intrinsic silicon is doped to create a  $p$ - $i$ - $n$  structure. The reverse bias increases the thickness of the depleted region; in the case of these particular detectors, to full depletion at a depth of about 100  $\mu\text{m}$ . Increasing the depletion depth decreases the capacitance (and hence electronic noise) and extends the red response. Quantum efficiency can exceed 90%, but falls toward the red because of the increasing absorption length of light in silicon. The absorption length reaches 100  $\mu\text{m}$  at 985 nm. However, since  $G = 1$ , amplification is necessary. Optimal low-noise amplifiers are slow, but, even so, noise limits the minimum detectable signal in room-temperature devices to several hundred photons.

Very large arrays containing  $O(10^7)$  of  $O(10\ \mu\text{m}^2)$ -sized photodiodes pixelizing a plane are widely used to photograph all sorts of things from everyday subjects at visible wavelengths to crystal structures with X-rays and astronomical objects from infrared to UV. To limit the number of readout channels, these are made into charge-coupled devices (CCD), where pixel-to-pixel signal transfer takes place over thousands of synchronous cycles with sequential output through shift registers [17]. Thus, high spatial resolution is achieved at the expense of speed and timing precision. Custom-made CCD’s have virtually replaced photographic plates and other imagers for astronomy and in spacecraft. Typical QE’s



exceed 90% over much of the visible spectrum, and “thick” CCD’s have useful QE up to  $\lambda = 1 \mu\text{m}$ . Active Pixel Sensor (APS) arrays with a preamplifier on each pixel and CMOS processing afford higher speeds, but are challenged at longer wavelengths. Much R&D is underway to overcome the limitations of both CCD and CMOS imagers.

In APD’s, an exponential cascade of impact ionizations initiated by the original photogenerated  $e$ - $h$  pair under a large reverse-bias voltage leads to an avalanche breakdown [18–21]. As a result, detectable electrical response can be obtained from low-intensity optical signals down to single photons. Excellent junction uniformity is critical, and a guard ring is generally used as a protection against edge breakdown. Well-designed APD’s, such as those used in CMS’ crystal-based electromagnetic calorimeter, have achieved  $\epsilon_Q \epsilon_C \approx 0.7$  with sub-ns response time. The sensitive wavelength window and gain depend on the semiconductor used. The gain is typically 10–200 in linear and up to  $10^8$  in Geiger mode of operation. Stability and close monitoring of the operating temperature are important for linear-mode operation, and substantial cooling is often necessary. Position-sensitive APD’s use time information at multiple anodes to calculate the hit position.

One of the most promising recent developments in the field is that of devices consisting of large arrays ( $O(10^3)$ ) of tiny APD’s packed over a small area ( $O(1 \text{ mm}^2)$ ) and operated in a limited Geiger mode [22–24]. Among different names used for this class of photodetectors, “PPD” (for “Pixelized Photon Detector”) is most widely accepted (formerly “SiPM”). Although each cell only offers a binary output, linearity with respect to the number of photons is achieved by summing the cell outputs in the same way as with a MCP in saturation mode (see above). PPD’s are being adopted as the preferred solution for various purposes including medical imaging, *e.g.* positron emission tomography (PET). These compact, rugged, and economical devices allow auto-calibration through decent separation of photoelectron peaks and offer gains of  $O(10^6)$  at a moderate bias voltage ( $\sim 50 \text{ V}$ ). However, the single-photoelectron noise of a PPD, being the logical “or” of  $O(10^3)$  Geiger APD’s, is rather large:  $O(1 \text{ MHz/mm}^2)$  at room temperature. PPD’s are particularly well-suited for applications where triggered pulses of several photons are expected over a small area, *e.g.* fiber-guided scintillation light. Intense R&D is expected to lower the noise level and improve radiation hardness, resulting in coverage of larger areas and wider applications. Attempts are being made to combine the fabrication of the sensors and the front-end electronics (ASIC) in the same process with the goal of making PPD’s and other finely pixelized solid-state photodetectors extremely easy to use.

Of late, much R&D has been directed to  $p$ - $i$ - $n$  diode arrays based on thin polycrystalline diamond films formed by chemical vapor deposition (CVD) on a hot substrate ( $\sim 1000 \text{ K}$ ) from a hydrocarbon-containing gas mixture under low pressure ( $\sim 100 \text{ mbar}$ ). These devices have maximum sensitivity in the extreme- to moderate-UV region [25–27]. Many desirable characteristics, including high tolerance to radiation and temperature fluctuations, low dark noise, blindness to most of the solar radiation spectrum, and relatively low cost make them ideal for space-based UV/XUV astronomy, measurement of synchrotron radiation, and luminosity monitoring at (future) lepton collider(s).

Visible-light photon counters (VLPC) utilize the formation of an impurity band only 50 meV below the conduction band in As-doped Si to generate strong ( $G \approx 5 \times 10^4$ ) yet sharp response to single photons with  $\epsilon_Q \approx 0.9$  [28–30]. The smallness of the band gap considerably reduces the gain dispersion. Only a very small bias ( $\sim 7 \text{ V}$ ) is needed, but high sensitivity to infrared photons requires cooling below 10 K. The dark noise increases sharply and exponentially with both temperature and bias. The Run 2 DØ detector used 86000 VLPC’s to read the optical signal from its scintillating-fiber tracker and scintillator-strip preshower detectors.

### 35.3 Organic scintillators

Revised August 2017 by K.F. Johnson (Florida State U.).

Organic scintillators are broadly classed into three types, crystalline, liquid, and plastic, all of which utilize the ionization produced by charged particles (see Sec. 34.2 of this *Review*) to generate optical photons, usually in the blue to green wavelength regions [31]. Plastic scintillators are by far the most widely used, liquid organic scintillator is finding increased use, and crystal organic scintillators are practically unused in high-energy physics. Plastic scintillator densities range from 1.03 to 1.20  $\text{g cm}^{-3}$ . Typical photon yields are about 1 photon per 100 eV of energy deposit [32]. A one-cm-thick scintillator traversed by a minimum-ionizing particle will therefore yield  $\approx 2 \times 10^4$  photons. The resulting photoelectron signal will depend on the collection and transport efficiency of the optical package and the quantum efficiency of the photodetector.

Organic scintillator does not respond linearly to the ionization density. Very dense ionization columns emit less light than expected on the basis of  $dE/dx$  for minimum-ionizing particles. A widely used semi-empirical model by Birks posits that recombination and quenching effects between the excited molecules reduce the light yield [33]. These effects are more pronounced the greater the density of the excited molecules. Birks’ formula is

$$\frac{d\mathcal{L}}{dx} = \mathcal{L}_0 \frac{dE/dx}{1 + k_B dE/dx}, \quad (35.2)$$

where  $\mathcal{L}$  is the luminescence,  $\mathcal{L}_0$  is the luminescence at low specific ionization density, and  $k_B$  is Birks’ constant, which must be determined for each scintillator by measurement. Decay times are in the ns range; rise times are much faster.

The high light yield and fast response time allow the possibility of sub-ns timing resolution [34]. The fraction of light emitted during the decay “tail” can depend on the exciting particle. This allows pulse shape discrimination as a technique to carry out particle identification. Because of the hydrogen content (carbon to hydrogen ratio  $\approx 1$ ) plastic scintillator is sensitive to proton recoils from neutrons.

Ease of fabrication into desired shapes and low cost has made plastic scintillator a common detector element. In the form of scintillating fiber it has found widespread use in tracking and calorimetry [35].

Demand for large volume detectors has led to increased use of liquid organic scintillator, which has the same scintillation mechanism as plastic scintillator, due to its cost advantage. The containment vessel defines the detector shape; photodetectors or wavelighters may be immersed in the liquid.

#### 35.3.1 Scintillation mechanism

A charged particle traversing matter leaves behind it a wake of excited molecules. Certain types of molecules, however, will release a small fraction ( $\approx 3\%$ ) of this energy as optical photons. This process, scintillation, is especially marked in those organic substances which contain aromatic rings, such as polystyrene (PS) and polyvinyltoluene (PVT). Liquids which scintillate include toluene, xylene and pseudocumene.

In fluorescence, the initial excitation takes place via the absorption of a photon, and de-excitation by emission of a longer wavelength photon. Fluors are used as “wavelighters” to shift scintillation light to a more convenient wavelength. Occurring in complex molecules, the absorption and emission are spread out over a wide band of photon energies, and have some overlap, that is, there is some fraction of the emitted light which can be re-absorbed [36]. This “self-absorption” is undesirable for detector applications because it causes a shortened attenuation length. The wavelength difference between the major absorption and emission peaks is called the Stokes’ shift. It is usually the case that the greater the Stokes’ shift, the smaller the self absorption thus, a large Stokes’ shift is a desirable property for a fluor.

The plastic scintillators used in high-energy physics are binary or ternary solutions of selected fluors in a plastic base containing aromatic rings. (See appendix in Ref. [37] for a comprehensive list of components.) Virtually all plastic scintillators contain as a base either PVT or PS. PVT-based scintillator can be up to 50% brighter.

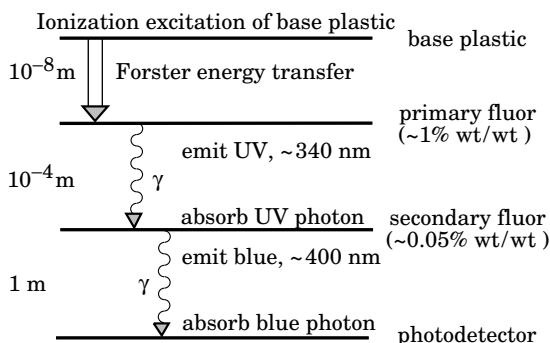


Figure 35.1: Cartoon of scintillation “ladder” depicting the operating mechanism of organic scintillator. Approximate fluor concentrations and energy transfer distances for the separate sub-processes are shown.

Ionization in the plastic base produces UV photons with short attenuation length (several mm). Longer attenuation lengths are obtained by dissolving a “primary” fluor in high concentration (1% by weight) into the base, which is selected to efficiently re-radiate absorbed energy at wavelengths where the base is more transparent (see Fig. 35.1).

The primary fluor has a second important function. The decay time of the scintillator base material can be quite long – in pure polystyrene it is 16 ns, for example. The addition of the primary fluor in high concentration can shorten the decay time by an order of magnitude and increase the total light yield. At the concentrations used (1% and greater), the average distance between a fluor molecule and an excited base unit is around 100 Å, much less than a wavelength of light. At these distances the predominant mode of energy transfer from base to fluor is not the radiation of a photon, but a resonant dipole-dipole interaction, first described by Foerster, which strongly couples the base and fluor [38]. The strong coupling sharply increases the speed and the light yield of the plastic scintillators.

Normally a fluor which fulfills other requirements is not adequate with respect to emission wavelength or attenuation length, so it is necessary to add yet another waveshifter (the “secondary” fluor), at fractional percent levels, and occasionally a third (not shown in Fig. 35.1).

External wavelength shifters are widely used to aid light collection in complex geometries. Scintillation light is captured by a lightpipe comprising a wave-shifting fluor dissolved in a non-scintillating base. The wavelength shifter must be insensitive to ionizing radiation and Cherenkov light. A typical wavelength shifter uses an acrylic base because of its good optical qualities, a single fluor to shift the light emerging from the plastic scintillator to the blue-green, and contains ultra-violet absorbing additives to deaden response to Cherenkov light.

By drastically increasing fluor concentrations beyond those discussed above, scintillators of increased radiation resistance or with special properties such as neutron/gamma discrimination may be made [39].

### 35.3.2 Caveats and cautions

Plastic scintillators are reliable, robust, and convenient. However, exposure to solvent vapors, high temperatures, mechanical flexing, irradiation, or rough handling will cause degradation. A The surface is particularly fragile region and can “craze” – develop microcracks which degrade transmission of light by total internal reflection. crazing is particularly likely where oils, solvents, or *fingerprints* have contacted the surface.

They have a long-lived luminescence which does not follow a simple exponential decay. Intensities at the  $10^{-4}$  level of the initial fluorescence can persist for hundreds of ns [31] [40].

They can decrease their light yield with increasing partial pressure of oxygen. This can be a 10% effect in an artificial atmosphere [41].

Their light yield may be changed by a magnetic field. Increases of  $\approx 3\%$  at 0.45 T have been reported [42].

Irradiation of plastic scintillator creates color centers which absorb light more strongly in the UV and blue than at longer wavelengths. This poorly understood effect appears as a reduction both of light yield and attenuation length. Radiation damage depends not only on the integrated dose, but on the dose rate, atmosphere, and temperature, before, during and after irradiation, as well as the materials properties of the base such as glass transition temperature, polymer chain length, *etc.* Annealing also occurs, accelerated by the diffusion of atmospheric oxygen and elevated temperatures. The phenomena are complex, unpredictable, and not well understood [43]. Since color centers are most disruptive at shorter wavelengths, the most reliable method of mitigating radiation damage is to shift emissions at every step to the longest practical wavelengths, *e.g.*, utilize fluors with large Stokes’ shifts (aka the “Better red than dead” strategy).

### 35.3.3 Scintillating and wavelength-shifting fibers

The clad optical fiber comprising scintillator and wavelength shifter (WLS) is particularly useful [44]. Since the initial demonstration of the scintillating fiber (SCIFI) calorimeter [45], SCIFI techniques have become mainstream [46]. SCIFI calorimeters are fast, dense, radiation hard, and can have leadglass-like resolution. SCIFI trackers can handle high rates and are radiation tolerant, but the low photon yield at the end of a long fiber (see below) requires use of sensitive photodetectors. WLS-only fiber readout of a calorimeter allows a very high level of hermeticity since the solid angle blocked by the fiber on its way to the photodetector is very small.

The sensitive region of scintillating fibers can be controlled by splicing them onto clear (non-scintillating/non-WLS) fibers.

A typical configuration would be fibers with a core of polystyrene-based scintillator or WLS (index of refraction  $n = 1.59$ ), surrounded by a cladding of PMMA ( $n = 1.49$ ) a few microns thick, or, for added light capture, with another cladding of fluorinated PMMA with  $n = 1.42$ , for an overall diameter of 0.5 to 1 mm. The fraction of generated light which is transported down the optical fiber is denoted the capture fraction and is about 6% for the single-clad fiber and 10% for the double-clad fiber. A minimum-ionizing particle traversing a high-quality 1 mm diameter fiber perpendicular to its axis will produce fewer than 2000 photons, of which about 200 are captured. Attenuation may eliminate 95% of these photons in a large collider tracker.

A scintillating or WLS fiber is often characterized by its attenuation length, over which the signal is attenuated to  $1/e$  of its original value. Factors determining attenuation length include re-absorption of emitted photons by the polymer base or dissolved fluors, the level of crystallinity of the base polymer, variation of photodetector sensitivity to emitted wavelengths, and the quality of the internal surface [47]. Attenuation lengths of several meters are obtained by high quality fibers.

## 35.4 Inorganic scintillators

Revised August 2019 by C.L. Woody (BNL) and R.-Y. Zhu (HEP California Inst. of Technology).

Inorganic crystals form a class of scintillating materials with much higher densities than organic plastic scintillators (typically  $\sim 4\text{--}8\text{ g/cm}^3$ ) with a variety of different properties for use as scintillation detectors. Due to their high density and high effective atomic number, they can be used in applications where high stopping power or a high conversion efficiency for electrons or photons is required. These include total absorption electromagnetic calorimeters (see Sec. 35.9.2), which consist of a totally active absorber (as opposed to a sampling calorimeter), as well as serving as gamma ray detectors over a wide range of energies. Many of these crystals also have very high light output, and can therefore provide excellent energy resolution down to very low energies ( $\sim$  few hundred keV).

Some crystals are intrinsic scintillators in which the luminescence is produced by a part of the crystal lattice itself. However, other crystals require the addition of a dopant, typically fluorescent ions such as thallium (Tl) or cerium (Ce) which is responsible for producing the scintillation light. However, in both cases, the

**Table 35.4:** Properties of several inorganic crystals. Most of the notation is defined in Sec. 6 of this Review.

Parameter:	$\rho$	MP	$X_0^*$	$R_M^*$	$dE/dx^*$	$\lambda_I^*$	$\tau_{\text{decay}}$	$\lambda_{\text{max}}$	$n^\dagger$	Relative output <sup>‡</sup>	Hygroscopic?	$d(\text{LY})/dT$ %/°C <sup>§</sup>
Units:	g/cm <sup>3</sup>	°C	cm	cm	MeV/cm	cm	ns	nm				
NaI(Tl)	3.67	651	2.59	4.13	4.8	42.9	245	410	1.85	100	yes	-0.2
BGO	7.13	1050	1.12	2.23	9.0	22.8	300	480	2.15	21	no	-0.9
BaF <sub>2</sub>	4.89	1280	2.03	3.10	6.5	30.7	650 <sup>s</sup> <0.6 <sup>f</sup>	300 <sup>s</sup> 220 <sup>f</sup>	1.50	36 <sup>s</sup> 4.1 <sup>f</sup>	no	-1.9 <sup>s</sup> 0.1 <sup>f</sup>
CsI(Tl)	4.51	621	1.86	3.57	5.6	39.3	1220	550	1.79	165	slight	0.4
CsI(Na)	4.51	621	1.86	3.57	5.6	39.3	690	420	1.84	88	yes	0.4
CsI(pure)	4.51	621	1.86	3.57	5.6	39.3	30 <sup>s</sup> 6 <sup>f</sup>	310	1.95	3.6 <sup>s</sup> 1.1 <sup>f</sup>	slight	-1.4
PbWO <sub>4</sub>	8.30	1123	0.89	2.00	10.1	20.7	30 <sup>s</sup> 10 <sup>f</sup>	425 <sup>s</sup> 420 <sup>f</sup>	2.20	0.3 <sup>s</sup> 0.077 <sup>f</sup>	no	-2.5
LSO(Ce)	7.40	2050	1.14	2.07	9.6	20.9	40	402	1.82	85	no	-0.2
PbF <sub>2</sub>	7.77	824	0.93	2.21	9.4	21.0	-	-	-	Cherenkov	no	-
CeF <sub>3</sub>	6.16	1460	1.70	2.41	8.42	23.2	30	340	1.62	7.3	no	0
LaBr <sub>3</sub> (Ce)	5.29	783	1.88	2.85	6.90	30.4	20	356	1.9	180	yes	0.2
CeBr <sub>3</sub>	5.23	722	1.96	2.97	6.65	31.5	17	371	1.9	165	yes	-0.1

\* Numerical values calculated using formulae in this review.

† Refractive index at the wavelength of the emission maximum.

‡ Relative light output measured for samples of 1.5 X<sub>0</sub> cube with a Tyvek paper wrapping and a full end face coupled to a photodetector. The quantum efficiencies of the photodetector are taken out.

§ Variation of light yield with temperature evaluated at the room temperature.

*f* = fast component, *s* = slow component

scintillation mechanism is the same. Energy is deposited in the crystal by ionization, either directly by charged particles, or by the conversion of photons into electrons or positrons which subsequently produce ionization. This energy is transferred to the luminescent centers which then radiate scintillation photons. The light yield  $L$  in terms of the number of scintillation photons produced per MeV of energy deposit in the crystal can be expressed as [48]

$$L = 10^6 S \cdot Q / (\beta \cdot E_g), \quad (35.3)$$

where  $\beta \cdot E_g$  is the energy required to create an e-h pair expressed as a multiple of the band gap energy  $E_g$  (eV),  $S$  is the efficiency of energy transfer to the luminescent center and  $Q$  is the quantum efficiency of the luminescent center. The values of  $\beta$ ,  $S$  and  $Q$  are crystal dependent and are the main factors in determining the intrinsic light yield of the scintillator. The decay time of the scintillator is mainly dominated by the decay time of the luminescent center.

Table-35.4 lists the basic properties of some commonly used inorganic crystals. NaI(Tl) is one of the most common and widely used scintillators, with an emission that is well matched to a bialkali photomultiplier tube, but it is highly hygroscopic and difficult to work with, and has a rather low density. CsI(Tl) and CsI(Na) have high light yield, low cost, and are mechanically robust (high plasticity and resistance to cracking). However, they need careful surface treatment and are slightly and highly hygroscopic respectively. Pure CsI has identical mechanical properties as CsI(Tl), but a faster emission at shorter wavelength and a much lower light output.

Undoped BaF<sub>2</sub> has a fast component with a less than 0.6 ns decay time, and is the fastest known scintillator. However, it also has a slow component with a much longer decay time ( $\sim 630$  ns). Bismuth germanate (Bi<sub>4</sub>Ge<sub>3</sub>O<sub>12</sub> or BGO) has a high density, and consequently a short radiation length  $X_0$  and Molière radius  $R_M$ . Similar to CsI(Tl), BGO's emission is well-matched to the spectral sensitivity of photodiodes, and it is easy to handle and not hygroscopic. Lead tungstate (PbWO<sub>4</sub> or PWO) has a very high density, with a very short  $X_0$  and  $R_M$ , but its intrinsic light yield is rather low.

Cerium doped lutetium oxyorthosilicate (Lu<sub>2</sub>SiO<sub>5</sub>:Ce, or LSO:Ce) [49] and cerium doped lutetium-yttrium oxyorthosilicate (Lu<sub>2(1-x)</sub>Y<sub>2x</sub>SiO<sub>5</sub>, LYSO:Ce) [50] are dense crystal scintillators which have a high light yield and a fast decay time. Only the properties of LSO:Ce are listed in Table-35.4 since the properties of LYSO:Ce are similar to that of LSO:Ce except a slightly lower density than LSO:Ce depending on the yttrium fraction (typically

5 to 10%) in LYSO:Ce. This material is also featured with excellent radiation hardness [51, 52], so is expected to be used where extraordinary radiation hardness is required.

Also listed in Table-35.4 are other fluoride crystals such as PbF<sub>2</sub> as a Cherenkov material and CeF<sub>3</sub>, which have been shown to provide excellent energy resolution in calorimeter applications. Table-35.4 also includes cerium doped lanthanum tri-halides, such as LaBr<sub>3</sub> [53] and CeBr<sub>3</sub> [54], which are brighter and faster than LSO:Ce, but they are highly hygroscopic and have a lower density. The FWHM energy resolution measured for these materials coupled to a PMT with bi-alkali photocathode for 0.662 MeV  $\gamma$ -rays from a <sup>137</sup>Cs source is about 3%, and has recently been improved to 2% by co-doping with cerium and strontium [55], which is the best among all inorganic crystal scintillators. For this reason, LaBr<sub>3</sub> and CeBr<sub>3</sub> are expected to be used in applications where a good energy resolution for low energy photons are required, such as homeland security.

Beside the crystals listed in Table-35.4, a number of new crystals are being developed that may have potential applications in high energy or nuclear physics. Of particular interest is the family of yttrium and lutetium perovskites and garnet, which include YAP (YAlO<sub>3</sub>:Ce), LuAP (LuAlO<sub>3</sub>:Ce), YAG (Y<sub>3</sub>Al<sub>5</sub>O<sub>12</sub>:Ce) and LuAG (Lu<sub>3</sub>Al<sub>5</sub>O<sub>12</sub>:Ce) and their mixed compositions. These have been shown to be linear over a large energy range [56], and have the potential for providing good intrinsic energy resolution.

Aiming at the best jet-mass resolution inorganic scintillators are being investigated for HEP calorimeters with dual readout for both Cherenkov and scintillation light to be used at future linear lepton colliders. These materials may be used for an electromagnetic calorimeter [57] or a homogeneous hadronic calorimetry (HHCAL) detector concept, including both electromagnetic and hadronic parts [58, 59]. Because of the unprecedented volume (70 to 100 m<sup>3</sup>) foreseen for the HHCAL detector concept the materials must be (1) dense (to minimize the leakage) and (2) cost-effective. It should also be UV transparent (for effective collection of the Cherenkov light) and allow for a clear discrimination between the Cherenkov and scintillation light. The preferred scintillation light is thus at a longer wavelength, and not necessarily bright or fast. Dense crystals, scintillating glasses and ceramics offer a very attractive implementation for this detector concept [60].

The fast scintillation light provides timing information about electromagnetic interactions and showers, which may be used to mitigate pile-up effects and/or for particle identification since the time development of electromagnetic and hadronic showers, as well as minimum ionizing particles, are different. The timing in-

formation is primarily determined by the scintillator rise time and decay time, and the number of photons produced. For fast timing, it is important to have a large number of photons emitted in the initial part of the scintillation pulse, e.g. in the first ns, since one is often measuring the arrival time of the particle in the crystal using the leading edge of the light pulse. A good example of this is BaF<sub>2</sub>, which has ~10% of its light in its fast component with a decay time of less than 0.6 ns. Recent investigation shows that doping with yttrium in BaF<sub>2</sub> reduces its slow component significantly, while keeping its ultrafast scintillation component unchanged [61, 62]. The light propagation can spread out the arrival time of the scintillation photons at the photodetector due to time dispersion [63]. The time response of the photodetector also plays a major role in achieving good time resolution with fast scintillating crystals.

Table-35.4 gives the light output of other crystals relative to NaI(Tl) and their dependence to the temperature variations measured for 1.5 X<sub>0</sub> cube crystal samples with a Tyvek paper wrapping and a full end face coupled to a photodetector [64]. The quantum efficiency of the photodetector is taken out to facilitate a direct comparison of crystal's light output. However, the useful signal produced by a scintillator is usually quoted in terms of the number of photoelectrons per MeV produced by a given photodetector. The relationship between the light yield (*LY*) in number of photons/MeV produced (*N*<sub>photons/MeV</sub>) and the light output in number of photoelectrons/MeV detected involves the factors for the light collection efficiency (*LC*) and the quantum efficiency (*QE*) of the photodetector:

$$N_{p.e.}/\text{MeV} = LY \cdot LC \cdot QE. \quad (35.4)$$

*LC* depends on the size and shape of the crystal, and includes effects such as the transmission of scintillation light within the crystal (i.e., the bulk attenuation length of the material), scattering from within the crystal, reflections and scattering from the crystal surfaces, and re-bouncing back into the crystal by wrapping materials. These factors can vary considerably depending on the sample, but can be in the range of ~10–60%. The internal light transmission depends on the intrinsic properties of the material, e.g. the density and type of the scattering centers and defects that can produce internal absorption within the crystal, and can be highly affected by factors such as radiation damage, as discussed below.

The quantum efficiency depends on the type of photodetector used to detect the scintillation light, which is typically ~15–30% for photomultiplier tubes and ~70% for silicon photodetectors for visible wavelengths. The quantum efficiency of the detector is usually highly wavelength dependent and should be matched to the particular crystal of interest to give the highest quantum yield at the wavelength corresponding to the peak of the scintillation emission. Fig. 35.2 shows the quantum efficiencies of two photodetectors, a Hamamatsu R2059 PMT with bi-alkali cathode and quartz window and a Hamamatsu S8664 avalanche photodiode (APD) as a function of wavelength. Also shown in the figure are emission spectra of three crystal scintillators, BGO, LSO:Ce/LYSO:Ce and CsI(Tl), and the numerical values of the emission weighted quantum efficiency. The area under each emission spectrum is proportional to crystal's light yield, as shown in Table-35.4, where the quantum efficiencies of the photodetector has been taken out. Results with different photodetectors can be significantly different. For example, the response of CsI(Tl) relative to NaI(Tl) with a standard photomultiplier tube with a bi-alkali photo-cathode, e.g. Hamamatsu R2059, would be 45 rather than 165 because of the photomultiplier's low quantum efficiency at longer wavelengths. For scintillators which emit in the UV, a detector with a quartz window should be used.

For very low energy applications (typically below 1 MeV), non-proportionality of the scintillation light yield may be important. It has been known for a long time that the conversion factor between the energy deposited in a crystal scintillator and the number of photons produced is not constant. It is also known that the energy resolution measured by all crystal scintillators for low energy  $\gamma$ -rays is significantly worse than the contribution from photo-electron statistics alone, indicating an intrinsic contribu-

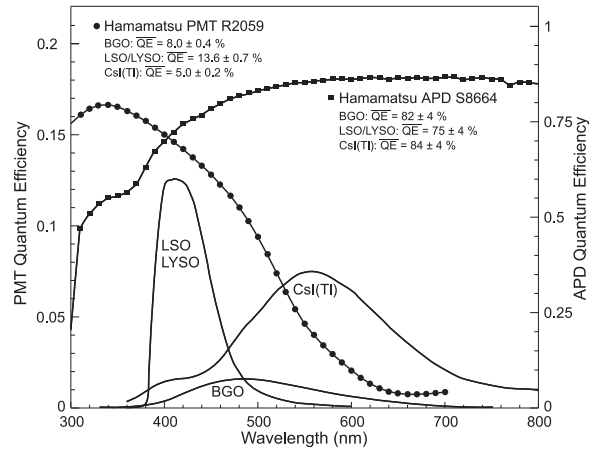


Figure 35.2: The quantum efficiencies of two photodetectors, a Hamamatsu R2059 PMT with bi-alkali cathode and a Hamamatsu S8664 avalanche photodiode (APD), are shown as a function of wavelength. Also shown in the figure are emission spectra of three crystal scintillators, BGO, LSO and CsI(Tl), and the numerical values of the emission weighted quantum efficiencies. The area under each emission spectrum is proportional to crystal's light yield.

tion from the scintillator itself. Precision measurement using low energy electron beam shows that this non-proportionality is crystal dependent [65]. Recent study on this issue also shows that this effect is also sample dependent even for the same crystal [66]. Further work is therefore needed to fully understand this subject.

One important issue related to the application of a crystal scintillator is its radiation hardness. Stability of its light output, or the ability to track and monitor the variation of its light output in a radiation environment, is required for high resolution and precision calibration [67]. All known crystal scintillators suffer from ionization dose induced radiation damage [68], where a common damage phenomenon is the appearance of radiation induced absorption caused by the formation of color centers originated from the impurities or point defects in the crystal. This radiation induced absorption reduces the light attenuation length in the crystal, and hence its light output. For crystals with high defect density, a severe reduction of light attenuation length may cause a distortion of the light response uniformity, leading to a degradation of the energy resolution. Additional radiation damage effects may include a reduced intrinsic scintillation light yield (damage to the luminescent centers) and an increased phosphorescence (afterglow). For crystals to be used in a high precision calorimeter in a radiation environment, its scintillation mechanism must not be damaged and its light attenuation length in the expected radiation environment must be long enough so that its light response uniformity, and thus its energy resolution, does not change.

While radiation damage induced by ionization dose is well understood [69], investigation is on-going to understand radiation damage caused by hadrons, including both charged hadrons [70] and neutrons [71]. Two additional fundamental processes may cause defects by hadrons: displacement damage and nuclear breakup. While charged hadrons can produce all three types of damage (and it's often difficult to separate them), neutrons can produce only the last two, and electrons and photons only produce ionization damage. Studies on hadron induced radiation damage to lead tungstate [72] show a proton-specific damage component caused by fragments from fission induced in lead and tungsten by particles in the hadronic shower. The fragments cause a severe, local damage to the crystalline lattice due to their extremely high energy loss over a short distance [72]. Recent investigation also sees evidence of neutron-specific damage in various crystals [71].

Most of the crystals listed in Table-35.4 have been used in high energy or nuclear physics experiments when the ultimate energy resolution for electrons and photons is desired. Examples are the Crystal Ball NaI(Tl) calorimeter at SPEAR, the L3 BGO

calorimeter at LEP, the CLEO CsI(Tl) calorimeter at CESR, the KTeV CsI calorimeter at the Tevatron, and the BaBar, BELLE and BES III CsI(Tl) calorimeters at PEP-II, KEK and BEPC II, respectively. Because of their high density and relative low cost, PWO calorimeters are used by CMS and ALICE at LHC, by CLAS and PrimEx at CEBAF and by PANDA at GSI. Similarly, PbF<sub>2</sub> calorimeters are used by the A4 experiment at MAINZ and by the g-2 experiment at Fermilab. A CsI calorimeter is being built for the Mu2e experiment at Fermilab. An LYSO:Ce calorimeter is being built for the COMET experiment at J-PARC, and an LYSO:Ce crystal-based precision timing layer is being built for the CMS experiment at the HL-LHC.

### 35.5 Cherenkov detectors

Revised July 2019 by B.N. Ratcliff (SLAC) and J. Schwiening (GSI Darmstadt).

Although devices using Cherenkov radiation are often thought of as only particle identification (PID) detectors, in practice they are used over a much broader range of applications including; (1) fast particle counters; (2) hadronic PID; (3) electromagnetic calorimeters (EMC); and (4) tracking detectors performing complete event reconstruction. Examples of applications from each category include; (1) the BaBar luminosity detector [73] and the Quartic fast timing counter for the ATLAS Forward Proton Detector, designed to measure small angle scatters at the LHC [74]; (2) the hadronic PID detectors at the B factory detectors—DIRC in BaBar [75], and the modern Imaging Aerogel and TOP counters at Belle II [76]; (3) the CMS Hadron Forward calorimeter based on Cherenkov light emitted in quartz fibers embedded in a steel absorber [77]; and (4) large water Cherenkov counters such as Super-Kamiokande [78].

Cherenkov counters contain two main elements; (1) a radiator through which the charged particle passes, and (2) a photodetector. As Cherenkov radiation is a weak source of photons, light collection and detection must be as efficient as possible. The refractive index  $n$  and the particle's path length through the radiator  $L$  appear in the Cherenkov relations allowing the tuning of these quantities for particular applications. One or more of the properties of Cherenkov radiation discussed in the Passages of Particles through Matter section (Sec. 34 of this *Review*) are utilized in Cherenkov detectors: the prompt emission of a light pulse; the existence of a velocity threshold for radiation; and the dependence of the Cherenkov cone half-angle  $\theta_c$  and the number of emitted photons on the velocity of the particle  $v_p$  and the refractive index  $n$  of the medium. The Cherenkov angle can be calculated as

$$\cos \theta_c = \frac{1}{n(E)\beta}, \quad (35.5)$$

where  $\beta = v_p/c$  with  $c$  being the speed of light, and  $E$  the photon energy. The number of photoelectrons ( $N_{p.e.}$ ) detected in a given device with radiator of length  $L$  is

$$N_{p.e.} = L \frac{\alpha^2 z^2}{r_e m_e c^2} \int \epsilon(E) \sin^2 \theta_c(E) dE, \quad (35.6)$$

where  $\epsilon(E)$  is the efficiency for collecting the Cherenkov light and transducing it into photoelectrons, and  $\alpha^2/(r_e m_e c^2) = 370 \text{ cm}^{-1} \text{ eV}^{-1}$ . The quantities  $\epsilon$  and  $\theta_c$  are functions of the photon energy. As the typical energy dependent variation of the index of refraction is modest, a quantity called the *Cherenkov detector quality factor*  $N_0$  can be defined as

$$N_0 = \frac{\alpha^2 z^2}{r_e m_e c^2} \int \epsilon dE, \quad (35.7)$$

so that, taking the charge number  $z = 1$  (the usual case in high-energy physics),

$$N_{p.e.} \approx LN_0(\sin^2 \theta_c). \quad (35.8)$$

This definition of the quality factor  $N_0$  is not universal, nor, indeed, very useful for those common situations where  $\epsilon$  factorizes as  $\epsilon = \epsilon_{\text{coll}}\epsilon_{\text{det}}$  with the geometrical photon collection efficiency ( $\epsilon_{\text{coll}}$ ) varying substantially for different tracks while the

photon detector efficiency ( $\epsilon_{\text{det}}$ ) remains nearly track independent. In this case, it can be useful to explicitly remove ( $\epsilon_{\text{coll}}$ ) from the definition of  $N_0$ . A typical value of  $N_0$  for a photomultiplier (PMT) detection system working in the visible and near UV, and collecting most of the Cherenkov light, is about  $100 \text{ cm}^{-1}$ . Practical counters, utilizing a variety of different photodetectors, have values ranging between about 30 and  $180 \text{ cm}^{-1}$ . Radiators can be chosen from a variety of transparent materials (Sec. 34 of this *Review* and Table 6.1). In addition to refractive index, the choice requires consideration of factors such as material density, radiation length and radiation hardness, transmission bandwidth, absorption length, chromatic dispersion, optical workability (for solids), availability, and cost. When the momenta of particles to be identified is high, the refractive index must be set close to one, so that the photon yield per unit length is low and a long particle path in the radiator is required. Recently, the gap in refractive index that has traditionally existed between gases and liquid or solid materials has been partially closed with transparent *silica aerogels* with indices that range between about 1.007 and 1.13.

Cherenkov counters may be classified as either *imaging* or *threshold* types, depending on whether they do or do not make use of Cherenkov angle ( $\theta_c$ ) information. Imaging counters may be used to track particles as well as identify them. The recent development of very fast photodetectors such as micro-channel plate PMTs (MCP PMT) (see 35.2 of this *Review*) also potentially allows very fast Cherenkov based time of flight (TOF) detectors of either class [79]. The track timing resolution of imaging detectors can be extremely good as it scales approximately as  $\frac{1}{\sqrt{N_{p.e.}}}$ .

*Threshold* Cherenkov detectors [80], in their simplest form, make a yes/no decision based on whether the particle is above or below the Cherenkov threshold velocity  $\beta_t = 1/n$ . A straightforward enhancement of such detectors uses the number of observed photoelectrons (or a calibrated pulse height) to discriminate between species or to set probabilities for each particle species [81]. This strategy can increase the momentum range of particle separation by a modest amount (to a momentum some 20% above the threshold momentum of the heavier particle in a typical case).

Careful designs give  $\langle \epsilon_{\text{coll}} \rangle \gtrsim 90\%$ . For a photomultiplier with a typical alkali cathode,  $\int \epsilon_{\text{det}} dE \approx 0.27 \text{ eV}$ , so that

$$N_{p.e.}/L \approx 90 \text{ cm}^{-1} (\sin^2 \theta_c) \quad (\text{i.e., } N_0 = 90 \text{ cm}^{-1}). \quad (35.9)$$

Suppose, for example, that  $n$  is chosen so that the threshold for species  $a$  is  $p_t$ ; that is, at this momentum species  $a$  has velocity  $\beta_a = 1/n$ . A second, lighter, species  $b$  with the same momentum has velocity  $\beta_b$ , so  $\cos \theta_c = \beta_a/\beta_b$ , and

$$N_{p.e.}/L \approx 90 \text{ cm}^{-1} \frac{m_a^2 - m_b^2}{p_t^2 + m_a^2}. \quad (35.10)$$

For  $K/\pi$  separation at  $p = p_t = 1(5) \text{ GeV}/c$ ,  $N_{p.e.}/L \approx 16(0.8) \text{ cm}^{-1}$  for  $\pi$ 's and (by design) 0 for  $K$ 's.

For limited path lengths  $N_{p.e.}$  will usually be small. The overall efficiency of the device is controlled by Poisson fluctuations, which can be especially critical for separation of species where one particle type is dominant. Moreover, the effective number of photoelectrons is often less than the average number calculated above due to additional equivalent noise from the photodetector (see the discussion of the excess noise factor in 35.2 of this *Review*). It is common to design for at least 10 photoelectrons for the high velocity particle in order to obtain a robust counter. As rejection of the particle that is below threshold depends on *not* seeing a signal, electronic and other background noise, especially overlapping tracks, can be important. Physics sources of light production for the below threshold particle, such as decay to an above threshold particle, scintillation light, or the production of delta rays in the radiator, often limit the separation attainable, and need to be carefully considered. Well designed, modern multi-channel counters, such as the ACC at Belle [82], can attain adequate particle separation performance over a substantial momentum range.

*Imaging* counters make the most powerful use of the information available by measuring the ring-correlated angles of emission



of the individual Cherenkov photons. They typically provide positive ID information both for the “wanted” and the “unwanted” particles, thus reducing mis-identification substantially. Since low-energy photon detectors can measure only the position (and, perhaps, a precise detection time) of the individual Cherenkov photons (not the angles directly), the photons must be “imaged” onto a detector so that their angles can be derived [83]. Typically the optics map the Cherenkov cone onto (a portion of) a distorted “circle” at the photodetector. Though the imaging process is directly analogous to familiar imaging techniques used in telescopes and other optical instruments, there is a somewhat bewildering variety of methods used in a wide variety of counter types with different names. Some of the imaging methods used include (1) focusing by a lens or mirror; (2) proximity focusing (i.e., focusing by limiting the emission region of the radiation); and (3) focusing through an aperture (a pinhole). In addition, the prompt Cherenkov emission coupled with the speed of some modern photon detectors allows the use of (4) time imaging, a method which is little used in conventional imaging technology, and may allow some separation with particle TOF. Finally, (5) correlated tracking (and event reconstruction) can be performed in large water counters by combining the individual space position and time of each photon together with the constraint that Cherenkov photons are emitted from each track at the same polar angle (Sec. 36.3.1 of this *Review*).

In a simple model of an imaging PID counter, the fractional error on the particle velocity ( $\delta_\beta$ ) is given by

$$\delta_\beta = \frac{\sigma_\beta}{\beta} = \tan \theta_c \sigma(\theta_c), \quad (35.11)$$

where

$$\sigma(\theta_c) = \frac{\langle \sigma(\theta_i) \rangle}{\sqrt{N_{p.e.}}} \oplus C, \quad (35.12)$$

and  $\langle \sigma(\theta_i) \rangle$  is the average single photoelectron resolution, as defined by the optics, detector resolution and the intrinsic chromaticity spread of the radiator index of refraction averaged over the photon detection bandwidth.  $C$  combines a number of other contributions to resolution including, (1) correlated terms such as tracking, alignment, and multiple scattering, (2) hit ambiguities, (3) background hits from random sources, and (4) hits coming from other tracks. The actual separation performance is also limited by physics effects such as decays in flight and particle interactions in the material of the detector. In many practical cases, the performance is limited by these effects.

For a  $\beta \approx 1$  particle of momentum ( $p$ ) well above threshold entering a radiator with index of refraction ( $n$ ), the number of  $\sigma$  separation ( $N_\sigma$ ) between particles of mass  $m_1$  and  $m_2$  is approximately

$$N_\sigma \approx \frac{|m_1^2 - m_2^2|}{2p^2 \sigma(\theta_c) \sqrt{n^2 - 1}}. \quad (35.13)$$

In practical counters, the angular resolution term  $\sigma(\theta_c)$  varies between about 0.1 and 5 mrad depending on the size, radiator, and photodetector type of the particular counter. The range of momenta over which a particular counter can separate particle species extends from the point at which the number of photons emitted becomes sufficient for the counter to operate efficiently as a threshold device ( $\sim 20\%$  above the threshold for the lighter species) to the value in the imaging region given by the equation above. For example, for  $\sigma(\theta_c) = 2$  mrad, a fused silica radiator ( $n = 1.474$ ), or a fluorocarbon gas radiator ( $C_5F_{12}$ ,  $n = 1.0017$ ), would separate  $\pi/K$ 's from the threshold region starting around 0.15(3) GeV/ $c$  through the imaging region up to about 4.2(18) GeV/ $c$  at better than  $3\sigma$ .

Many different imaging counters have been built during the last several decades [79]. Among the earliest examples of this class of counters are the very limited acceptance *Differential Cherenkov detectors*, designed for particle selection in high momentum beam lines. These devices use optical focusing and/or geometrical masking to select particles having velocities in a specified region. With careful design, a velocity resolution of  $\sigma_\beta/\beta \approx 10^{-4}$ – $10^{-5}$  can be obtained [80].

Practical multi-track *Ring-Imaging Cherenkov detectors* (generically called RICH counters) are a more recent development. RICH counters are sometimes further classified by ‘generations’ that differ based on historical timing, performance, design, and photodetection techniques.

Prototypical examples of first generation RICH counters are those used in the DELPHI and SLD detectors at the LEP and SLC Z factory  $e^+e^-$  colliders [79]. They have both liquid ( $C_6F_{14}$ ,  $n = 1.276$ ) and gas ( $C_5F_{12}$ ,  $n = 1.0017$ ) radiators, the former being proximity imaged with the latter using mirrors. The phototransducers are a TPC/wire-chamber combination. They are made sensitive to photons by doping the TPC gas (usually, ethane/methane) with  $\sim 0.05\%$  TMAE (tetrakis(dimethylamino)ethylene). Great attention to detail is required, (1) to avoid absorbing the UV photons to which TMAE is sensitive, (2) to avoid absorbing the single photoelectrons as they drift in the long TPC, and (3) to keep the chemically active TMAE vapor from interacting with materials in the system. In spite of their unforgiving operational characteristics, these counters attained good  $e/\pi/K/p$  separation over wide momentum ranges (from about 0.25 to 20 GeV/ $c$ ) during several years of operation at LEP and SLC. Related but smaller acceptance devices include the OMEGA RICH at the CERN SPS, and the RICH in the balloon-borne CAPRICE detector [79].

Later generation counters [79] generally operate at much higher rates, with more detection channels, than the first generation detectors just described. They also utilize faster, more forgiving photon detectors, covering different photon detection bandwidths. Radiator choices have broadened to include materials such as lithium fluoride, fused silica, and aerogel. Vacuum-based photodetection systems (e.g., single or multi anode PMTs, MCP-PMTs, or hybrid photodiodes (HPD)) have become increasingly common (see 35.2 of this *Review*). They handle high rates, and can be used with a wide choice of radiators. Examples include (1) the SELEX RICH at Fermilab, which mirror focuses the Cherenkov photons from a neon radiator onto a camera array made of  $\sim 2000$  PMTs to separate hadrons over a wide momentum range (to well above 200 GeV/ $c$  for heavy hadrons); (2) the NA62 RICH at CERN, which uses a 17 m long tank filled with neon gas as radiator and spherical mirrors to focus the photons on two arrays of 2000 PMTs to separate pions from muons for momenta between 15 and 35 GeV/ $c$ ; (3) the CBM RICH under construction at FAIR where the Cherenkov photons, produced in about 30 m<sup>3</sup> of CO<sub>2</sub> radiator gas, are mirror-focused on arrays of multi-anode PMTs (MaPMTs) with a total of about 55,000 pixels, to identify electrons with momenta up to 10 GeV/ $c$ ; and (4) the LHCb detector now running at the LHC. It uses two separate counters. One volume contains C<sub>4</sub>F<sub>10</sub> (originally in combination with aerogel, which was removed in 2015) while the second volume contains CF<sub>4</sub>. Photons are mirror-focused onto detector arrays of HPDs to cover a  $\pi/K$  separation momentum range between 1 and 150 GeV/ $c$ . Further upgrades, including the replacement of the HPDs by MaPMTs and improved readout electronics, are necessary to deal with increases in luminosity.

Other fast detection systems that use solid cesium iodide (CsI) photocathodes or triethylamine (TEA) doping in proportional chambers are useful with certain radiator types and geometries. Examples include (1) the CLEO-III RICH at CESR that uses a LiF radiator with TEA doped proportional chambers; (2) the ALICE detector at the LHC that uses proximity focused liquid ( $C_6F_{14}$  radiators and solid CsI photocathodes (similar photodetectors have been used for several years by the HADES and COMPASS detectors), and the hadron blind detector (HBD) in the PHENIX detector at RHIC that couples a low index CF<sub>4</sub> radiator to a photodetector based on electron multiplier (GEM) chambers with reflective CsI photocathodes [79].

Recent technological advances in the production of aerogel with improved transparency in the UV range and finely tuned refractive indices enable several new RICH designs. The innovative hybrid geometry of the CLAS12 RICH, with complex photon paths that feature multiple passes through the aerogel tiles, is only possible due to the improved scattering length of the aerogel. It minimizes the material inside of the detector acceptance as well as the

cost of the photon sensor array. Beam tests have demonstrated that the counter will be able to provide clean  $\pi/K$  separation up to 8 GeV/c. The forward endcap Aerogel RICH (ARICH) for the Belle II upgrade at KEKB, designed to provide clean  $\pi/K$  separation for momenta up to 3.5 GeV/c, is an example of the so-called focusing aerogel approach [84]. The radiator is a dual-layer aerogel, with a thickness of 20 mm for each layer and increasing refractive indices of  $n = 1.045$  and  $n = 1.055$  along the particle path. The Cherenkov ring images from the two layers overlap on the array of Hybrid Avalanche Photo Detectors (HAPDs), which provide efficient single photon detection in the 1.5 T magnetic field.

A DIRC (Detection [of] Internally Reflected Cherenkov [light]) is a distinctive, compact RICH subtype first used in the BaBar detector [75]. A DIRC “inverts” the usual RICH principle for use of light from the radiator by collecting and imaging the total internally reflected light rather than the transmitted light. It utilizes the optical material of the radiator in two ways, simultaneously: as a Cherenkov radiator and as a light pipe. The magnitudes of the photon angles are preserved during transport by the flat, rectangular cross section radiators, allowing the photons to be efficiently transported to a detector outside the path of the particle where they may be imaged in up to three independent dimensions (the usual two in space and, due to the long photon paths lengths, one in time). Because the index of refraction in the radiator is large ( $n \sim 1.47$  for fused silica), the momentum range with good  $\pi/K$  separation goes up to 4–5 GeV/c. It is plausible, but difficult, to extend it up to about 10 GeV/c with an improved design.

The BaBar experiment at the asymmetric PEP-II  $e^+e^-$  collider studied CP violation in  $\Upsilon(4S)$  decays. Excellent pion/kaon separation for particle momenta up to 4 GeV/c was required. The BaBar DIRC used 4.9 m long, rectangular bars made from synthetic fused silica as radiator and light guide. The photons were imaged via a “pin-hole” through an expansion region filled with 6 000 liters of purified water onto an array of 10 752 densely packed photomultiplier tubes placed at a distance of about 1.2 m from the bar end. During more than 8 years of operation, the BaBar DIRC achieved  $\pi/K$  separation of 2.5 standard deviations or more up to 4 GeV/c momentum. For a pion identification rate around 85% the DIRC provided a kaon misidentification rate well below 1% up to 3 GeV/c.

The next generation of DIRC detectors takes advantage of the new, very fast, pixelated photodetectors becoming available, such as MaPMTs and MCP-PMTs. They typically utilize either time imaging or lens/mirror-focused optics, or both, leading not only to a precision measurement of the Cherenkov angle, but in some cases, to a precise measurement of the particle time of flight, and/or to correction of the chromatic dispersion in the radiator. Examples [79] include (1) the Belle II Time of Propagation (TOP) counter that emphasizes precision timing for both Cherenkov imaging and TOF to perform  $\pi/K$  separation of at least 3 standard deviations up to 4 GeV/c; (2) the DIRC upgrade of the GlueX experiment at Jefferson Lab that places four decommissioned BaBar DIRC modules, coupled to upgraded optics and readout, perpendicular to the beamline and will be the first application of a DIRC in a detector endcap; (3) the PANDA Barrel DIRC at FAIR, to be installed in 2023, that will be the first DIRC counter to use lens focusing and is expected to provide more than 3 standard deviations  $\pi/K$  separation up to 3.5 GeV/c; and (4) the TORCH proposal being developed for an LHCb upgrade in 2024 which uses DIRC imaging for individual photons with fast photon detectors to provide particle separation via particle TOF with a precision of 10–15 ps per track over a flight path length of 9.5 m.

## 35.6 Gaseous detectors

### 35.6.1 Energy loss and charge transport in gases

Revised March 2010 by F. Sauli (CERN) and M. Titov (CEA Saclay, DSM/IRFU/SPP).

Gas-filled detectors localize the ionization produced by charged particles, generally after charge multiplication. The statistics of

ionization processes having asymmetries in the ionization trails, affect the coordinate determination deduced from the measurement of drift time, or of the center of gravity of the collected charge. For thin gas layers, the width of the energy loss distribution can be larger than its average, requiring multiple sample or truncated mean analysis to achieve good particle identification. In the truncated mean method for calculating  $\langle dE/dx \rangle$ , the ionization measurements along the track length are broken into many samples and then a fixed fraction of high-side (and sometimes also low-side) values are rejected [85].

The energy loss of charged particles and photons in matter is discussed in Sec. 34. Table 35.5 provides values of relevant parameters in some commonly used gases at NTP (normal temperature, 20° C, and pressure, 1 atm) for unit-charge minimum-ionizing particles (MIPs) [86, 87].

Values often differ, depending on the source, so those in the table should be taken only as approximate. For different conditions and for mixtures, and neglecting internal energy transfer processes (*e.g.*, Penning effect), one can scale the density,  $N_P$ , and  $N_T$  with temperature and pressure assuming a perfect gas law.

**Table 35.5:** Properties of noble and molecular gases at normal temperature and pressure (NTP: 20° C, one atm).  $E_X$ ,  $E_I$ : first excitation, ionization energy;  $W_I$ : average energy per ion pair;  $dE/dx|_{\min}$ ,  $N_P$ ,  $N_T$ : differential energy loss, primary and total number of electron-ion pairs per cm, for unit charge minimum ionizing particles.

Gas	Density, mg cm <sup>-3</sup>	$E_X$ eV	$E_I$ eV	$W_I$ eV	$dE/dx _{\min}$ keV cm <sup>-1</sup>	$N_P$ cm <sup>-1</sup>	$N_T$ cm <sup>-1</sup>
He	0.179	19.8	24.6	41.3	0.32	3.5	8
Ne	0.839	16.7	21.6	37	1.45	13	40
Ar	1.66	11.6	15.7	26	2.53	25	97
Xe	5.495	8.4	12.1	22	6.87	41	312
CH <sub>4</sub>	0.667	8.8	12.6	30	1.61	28	54
C <sub>2</sub> H <sub>6</sub>	1.26	8.2	11.5	26	2.91	48	112
iC <sub>4</sub> H <sub>10</sub>	2.49	6.5	10.6	26	5.67	90	220
CO <sub>2</sub>	1.84	7.0	13.8	34	3.35	35	100
CF <sub>4</sub>	3.78	10.0	16.0	54	6.38	63	120

When an ionizing particle passes through the gas it creates electron-ion pairs, but often the ejected electrons have sufficient energy to further ionize the medium. As shown in Table 35.5, the total number of electron-ion pairs ( $N_T$ ) is usually a few times larger than the number of primaries ( $N_P$ ).

The probability for a released electron to have an energy  $E$  or larger follows an approximate  $1/E^2$  dependence (Rutherford law), taking into account the electronic structure of the medium

The probability for a released electron to have an energy  $E$  or larger follows an approximate  $1/E^2$  dependence (Rutherford law), shown in Fig. 35.3 for Ar/CH<sub>4</sub> at NTP (dotted line, left scale). More detailed estimates taking into account the electronic structure of the medium are shown in the figure, for three values of the particle velocity factor  $\beta\gamma$  [88]. The dot-dashed line provides, on the right scale, the practical range of electrons (including scattering) of energy  $E$ . As an example, about 0.6% of released electrons have 1 keV or more energy, substantially increasing the ionization loss rate. The practical range of 1 keV electrons in argon (dot-dashed line, right scale) is 70  $\mu$ m and this can contribute to the error in the coordinate determination.

The number of electron-ion pairs per primary ionization, or cluster size, has an exponentially decreasing probability; for argon, there is about 1% probability for primary clusters to contain ten or more electron-ion pairs [89].

Once released in the gas, and under the influence of an applied electric field, electrons and ions drift in opposite directions and diffuse towards the electrodes. The drift velocity and diffusion of electrons depend very strongly on the nature of the gas. Large drift velocities are achieved by adding polyatomic gases (usually CH<sub>4</sub>, CO<sub>2</sub>, or CF<sub>4</sub>) having large inelastic cross sections at moderate energies, which results in “cooling” electrons into the energy range of the Ramsauer-Townsend minimum (at  $\sim 0.5$  eV) of the

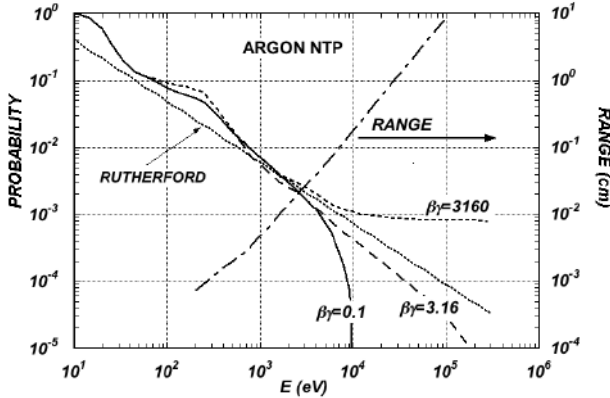


Figure 35.3: Probability of single collisions in which released electrons have an energy  $E$  or larger (left scale) and practical range of electrons in Ar/CH<sub>4</sub> (P10) at NTP (dot-dashed curve, right scale) [88].

elastic cross-section of argon. In a simple approximation, gas kinetic theory provides the drift velocity  $v$  as a function of the mean collision time  $\tau$  and the electric field  $E$ :  $v = eE\tau/m_e$  (Townsend's expression). In the presence of an external magnetic field, the Lorentz force acting on electrons between collisions deflects the drifting electrons and modifies the drift properties.

Once released in the gas, and under the influence of an applied electric field, electrons and ions drift in opposite directions and diffuse towards the electrodes. The scattering cross section is determined by the details of atomic and molecular structure. Therefore, the drift velocity and diffusion of electrons depend very strongly on the nature of the gas, specifically on the inelastic cross-section involving the rotational and vibrational levels of molecules. In noble gases, the inelastic cross section is zero below excitation and ionization thresholds. Large drift velocities are achieved by adding polyatomic gases (usually CH<sub>4</sub>, CO<sub>2</sub>, or CF<sub>4</sub>) having large inelastic cross sections at moderate energies, which results in "cooling" electrons into the energy range of the Ramsauer-Townsend minimum (at  $\sim 0.5$  eV) of the elastic cross-section of argon. The reduction in both the total electron scattering cross-section and the electron energy results in a large increase of electron drift velocity (for a compilation of electron-molecule cross sections see Ref. [90]). Another principal role of the polyatomic gas is to absorb the ultraviolet photons emitted by the excited noble gas atoms. Extensive collections of experimental data [91] and theoretical calculations based on transport theory [92] permit estimates of drift and diffusion properties in pure gases and their mixtures. In a simple approximation, gas kinetic theory provides the drift velocity  $v$  as a function of the mean collision time  $\tau$  and the electric field  $E$ :  $v = eE\tau/m_e$  (Townsend's expression). Values of drift velocity and diffusion for some commonly used gases at NTP are given in Fig. 35.4 and Fig. 35.5.

These have been computed with the MAGBOLTZ program [87]. For different conditions, the horizontal axis must be scaled inversely with the gas density. Standard deviations for longitudinal ( $\sigma_L$ ) and transverse diffusion ( $\sigma_T$ ) are given for one cm of drift, and scale with the square root of the drift distance. Since the collection time is inversely proportional to the drift velocity, diffusion is less in gases such as CF<sub>4</sub> that have high drift velocities. In the presence of an external magnetic field, the Lorentz force acting on electrons between collisions deflects the drifting electrons and modifies the drift properties. The electron trajectories, velocities and diffusion parameters can be computed with MAGBOLTZ. A simple theory, the friction force model, provides an expression for the vector drift velocity  $\mathbf{v}$  as a function of electric and magnetic field vectors  $\mathbf{E}$  and  $\mathbf{B}$ , of the Larmor frequency  $\omega = eB/m_e$ , and of the mean collision time  $\tau$ :

$$\mathbf{v} = \frac{e}{m_e} \frac{\tau}{1 + \omega^2 \tau^2} \left( \mathbf{E} + \frac{\omega \tau}{B} (\mathbf{E} \times \mathbf{B}) + \frac{\omega^2 \tau^2}{B^2} (\mathbf{E} \cdot \mathbf{B}) \mathbf{B} \right) \quad (35.14)$$

To a good approximation, and for moderate fields, one can as-

sume that the energy of the electrons is not affected by  $B$ , and use for  $\tau$  the values deduced from the drift velocity at  $B = 0$  (the Townsend expression). For  $\mathbf{E}$  perpendicular to  $\mathbf{B}$ , the drift angle to the relative to the electric field vector is  $\tan \theta_B = \omega \tau$  and  $v = (E/B)(\omega \tau / \sqrt{1 + \omega^2 \tau^2})$ . For parallel electric and magnetic fields, drift velocity and longitudinal diffusion are not affected, while the transverse diffusion can be strongly reduced:  $\sigma_T(B) = \sigma_T(B=0) / \sqrt{1 + \omega^2 \tau^2}$ . The dotted line in Fig. 35.5 represents  $\sigma_T$  for the classic Ar/CH<sub>4</sub> (90:10) mixture at 4 T. Large values of  $\omega \tau \sim 20$  at 5 T are consistent with the measurement of diffusion coefficient in Ar/CF<sub>4</sub>/iC<sub>4</sub>H<sub>10</sub> (95:3:2). This reduction is exploited in time projection chambers (Sec. 35.6.5) to improve spatial resolution.

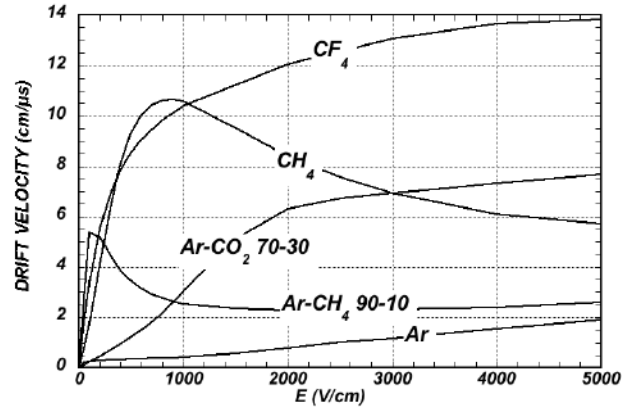


Figure 35.4: Computed electron drift velocity as a function of electric field in several gases at NTP and  $B = 0$  [87].

In mixtures containing electronegative molecules, such as O<sub>2</sub> or H<sub>2</sub>O, electrons can be captured to form negative ions. Capture cross-sections are strongly energy-dependent, and therefore the capture probability is a function of applied field. For example, the electron is attached to the oxygen molecule at energies below 1 eV. The three-body electron attachment coefficients may differ greatly for the same additive in different mixtures. As an example, at moderate fields (up to 1 kV/cm) the addition of 0.1% of oxygen to an Ar/CO<sub>2</sub> mixture results in an electron capture probability about twenty times larger than the same addition to Ar/CH<sub>4</sub>.

Carbon tetrafluoride is not electronegative at low and moderate fields, making its use attractive as drift gas due to its very low diffusion. However, CF<sub>4</sub> has a large electron capture cross section at fields above  $\sim 8$  kV/cm, before reaching avalanche field strengths. Depending on detector geometry, some signal reduction and resolution loss can be expected using this gas.

If the electric field is increased sufficiently, electrons gain enough energy between collisions to ionize molecules. Above a gas-dependent threshold, the mean free path for ionization,  $\lambda_i$ , decreases exponentially with the field; its inverse,  $\alpha = 1/\lambda_i$ , is the first Townsend coefficient. In wire chambers, most of the increase of avalanche particle density occurs very close to the anode wires, and a simple electrostatic consideration shows that the largest fraction of the detected signal is due to the motion of positive ions receding from the wires. The electron component, although very fast, contributes very little to the signal. This determines the characteristic shape of the detected signals in the proportional mode: a fast rise followed by a gradual increase.

The slow component, the so-called "ion tail" that limits the time resolution of the detector, is usually removed by differentiation of the signal. In uniform fields,  $N_0$  initial electrons multiply over a length  $x$  forming an electron avalanche of size  $N = N_0 e^{\alpha x}$ ;  $N/N_0$  is the gain of the detector. Fig. 35.6 shows examples of Townsend coefficients for several gas mixtures, computed with MAGBOLTZ [87].

Positive ions released by the primary ionization or produced in the avalanches drift and diffuse under the influence of the electric field. Negative ions may also be produced by electron attachment to gas molecules. The drift velocity of ions in the fields encoun-



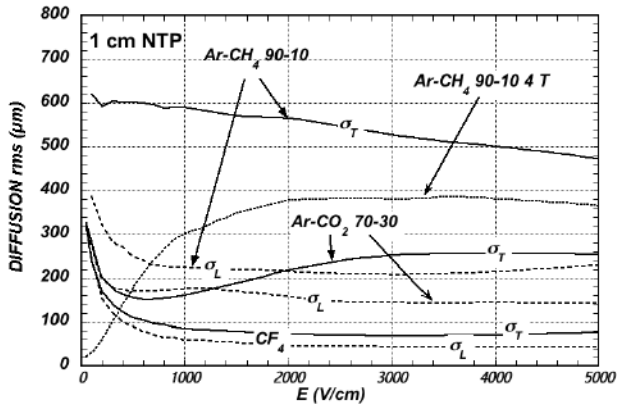


Figure 35.5: Electron longitudinal diffusion ( $\sigma_L$ ) (dashed lines) and transverse diffusion ( $\sigma_T$ ) (full lines) for 1 cm of drift at NTP and  $B = 0$ . The dotted line shows  $\sigma_T$  for the P10 mixture at 4 T [87].

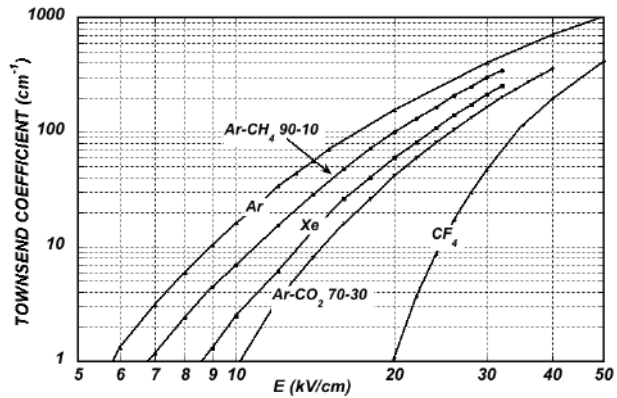


Figure 35.6: Computed first Townsend coefficient  $\alpha$  as a function of electric field in several gases at NTP [87].

tered in gaseous detectors (up to few kV/cm) is typically about three orders of magnitude less than for electrons. The ion mobility  $\mu$ , the ratio of drift velocity to electric field, is constant for a given ion type up to very high fields. Values of mobility at NTP for ions in their own and other gases are given in Table 35.6 [93]. For different temperatures and pressures, the mobility can be scaled inversely with the density assuming an ideal gas law. For mixtures, due to a very effective charge transfer mechanism, only ions with the lowest ionization potential survive after a short path in the gas. Both the lateral and transverse diffusion of ions are proportional to the square root of the drift time, with a coefficient that depends on temperature but not on the ion mass. Accumulation of ions in the gas drift volume may induce field distortions (see Sec. 35.6.5).

**Table 35.6:** Mobility of ions in gases at NTP [93].

Gas	Ion	Mobility $\mu$ ( $\text{cm}^2 \text{V}^{-1} \text{s}^{-1}$ )
He	$\text{He}^+$	10.4
Ne	$\text{Ne}^+$	4.7
Ar	$\text{Ar}^+$	1.54
Ar/ $\text{CH}_4$	$\text{CH}_4^+$	1.87
Ar/ $\text{CO}_2$	$\text{CO}_2^+$	1.72
$\text{CH}_4$	$\text{CH}_4^+$	2.26
$\text{CO}_2$	$\text{CO}_2^+$	1.09

**35.6.2 Multi-Wire Proportional and Drift Chambers**  
Revised March 2010 by F. Sauli (CERN) and M. Titov (CEA

Saclay, DSM/IRFU/SPP).

Single-wire counters that detect the ionization produced in a gas by a charged particle, followed by charge multiplication and collection around a thin wire have been used for decades. Good energy resolution is obtained in the proportional amplification mode, while very large saturated pulses can be detected in the streamer and Geiger modes [94].

Multiwire proportional chambers (MWPCs) [95,96], introduced in the late '60's, detect, localize and measure energy deposit by charged particles over large areas. A mesh of parallel anode wires at a suitable potential, inserted between two cathodes, acts almost as a set of independent proportional counters (see Fig. 35.7a). Electrons released in the gas volume drift towards the anodes and produce avalanches in the increasing field. Analytic expressions for the electric field can be found in many textbooks. The fields close to the wires  $E(r)$ , in the drift region  $E_D$ , and the capacitance  $C$  per unit length of anode wire are approximately given by

$$E(r) = \frac{CV_0}{2\pi\epsilon_0} \frac{1}{r} \quad E_D = \frac{CV_0}{2\epsilon_0 s} \quad C = \frac{2\pi\epsilon_0}{\pi(\ell/s) - \ln(2\pi a/s)}, \quad (35.15)$$

where  $r$  is the distance from the center of the anode,  $s$  the wire spacing,  $\ell$  and  $V_0$  the distance and potential difference between anode and cathode, and  $a$  the anode wire radius.

Because of electrostatic forces, anode wires are in equilibrium only for a perfect geometry. Small deviations result in forces displacing the wires alternatively below and above the symmetry plane, sometimes with catastrophic results. These displacement forces are countered by the mechanical tension of the wire, up to a maximum unsupported stable length,  $L_M$  [97], above which the wire deforms:

$$L_M = \frac{s}{CV_0} \sqrt{4\pi\epsilon_0 T_M} \quad (35.16)$$

The maximum tension  $T_M$  depends on the wire diameter and modulus of elasticity. Table 35.7 gives approximate values for tungsten and the corresponding maximum stable wire length under reasonable assumptions for the operating voltage ( $V_0 = 5 \text{ kV}$ ) [98]. Internal supports and spacers can be used in the construction of longer detectors to overcome limits on the wire length imposed by Eq. (35.16).

**Table 35.7:** Maximum tension  $T_M$  and stable unsupported length  $L_M$  for tungsten wires with spacing  $s$ , operated at  $V_0 = 5 \text{ kV}$ . No safety factor is included.

Wire diameter ( $\mu\text{m}$ )	$T_M$ (newton)	$s$ (mm)	$L_M$ (cm)
10	0.16	1	25
20	0.65	2	85

Detection of charge on the wires over a predefined threshold provides the transverse coordinate to the wire with an accuracy comparable to that of the wire spacing. The coordinate along each wire can be obtained by measuring the ratio of collected charge at the two ends of resistive wires. Making use of the charge profile induced on segmented cathodes, the so-called center-of-gravity (COG) method, permits localization of tracks to sub-mm accuracy. Due to the statistics of energy loss and asymmetric ionization clusters, the position accuracy is  $\sim 50 \mu\text{m}$  rms for tracks perpendicular to the wire plane, but degrades to  $\sim 250 \mu\text{m}$  at  $30^\circ$  to the normal [99]. The intrinsic bi-dimensional characteristic of the COG readout has found numerous applications in medical imaging.

Drift chambers, developed in the early '70's, can be used to estimate the longitudinal position of a track by exploiting the arrival time of electrons at the anodes if the time of interaction is known [100]. The distance between anode wires is usually several cm, allowing coverage of large areas at reduced cost. In the original design, a thicker wire (the field wire) at the proper voltage, placed between the anode wires, reduces the field at the mid-point between anodes and improves charge collection (Fig. 35.7b). In some drift chamber designs, and with the help of suitable voltages

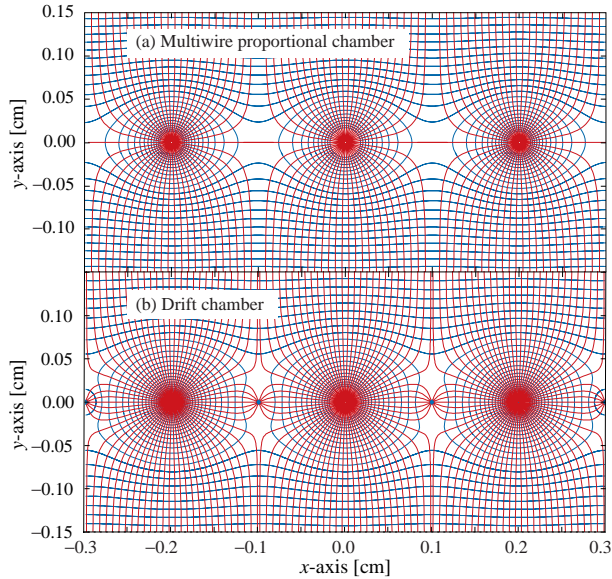


Figure 35.7: Electric field lines and equipotentials in (a) a multiwire proportional chamber and (b) a drift chamber.

applied to field-shaping electrodes, the electric field structure is adjusted to improve the linearity of space-to-drift-time relation, resulting in better spatial resolution [101].

Drift chambers can reach a longitudinal spatial resolution from timing measurement of order  $100 \mu\text{m}$  (rms) or better for minimum ionizing particles, depending on the geometry and operating conditions. However, a degradation of resolution is observed [102] due to primary ionization statistics for tracks close to the anode wires, caused by the spread in arrival time of the nearest ionization clusters. The effect can be reduced by operating the detector at higher pressures. Sampling the drift time on rows of anodes led to the concept of multiple arrays such as the multi-drift module [103] and the JET chamber [104]. A measurement of drift time, together with the recording of charge sharing from the two ends of the anode wires provides the coordinates of segments of tracks. The total charge gives information on the differential energy loss and is exploited for particle identification. The time projection chamber (TPC) [105] combines a measurement of drift time and charge induction on cathodes, to obtain excellent tracking for high multiplicity topologies occurring at moderate rates (see Sec. 35.6.5). In all cases, a good knowledge of electron drift velocity and diffusion properties is required. This has to be combined with the knowledge of the electric fields in the structures, computed with commercial or custom-developed software [106, 107]. For an overview of detectors exploiting the drift time for coordinate measurement see Refs. [108] and [97].

Multiwire and drift chambers have been operated with a variety of gas fillings and operating modes, depending on experimental requirements. The so-called “Magic Gas,” a mixture of argon, isobutane and Freon [96], permits very high and saturated gains ( $\sim 10^6$ ). This gas mixture was used in early wire chambers, but was found to be susceptible to severe aging processes. With present-day electronics, proportional gains around  $10^4$  are sufficient for detection of minimum ionizing particles, and noble gases with moderate amounts of polyatomic gases, such as methane or carbon dioxide, are used.

Although very powerful in terms of performance, multi-wire structures have reliability problems when used in harsh or hard-to-access environments, since a single broken wire can disable the entire detector. Introduced in the '80's, straw and drift tube systems make use of large arrays of wire counters encased in individual enclosures, each acting as an independent wire counter [109]. Techniques for low-cost mass production of these detectors have been developed for large experiments, such as the Transition Radiation Tracker and the Drift Tubes arrays for CERN's LHC ex-

periments [110].

### 35.6.3 High Rate Effects

Revised March 2010 by F. Sauli (CERN) and M. Titov (CEA Saclay, DSM/IRFU/SPP).

The production of positive ions in the avalanches and their slow drift before neutralization result in a rate-dependent accumulation of positive charge in the detector. This may result in significant field distortion, gain reduction and degradation of spatial resolution. As shown in Fig. 35.8 [111], the proportional gain drops above a charge production rate around  $10^9$  electrons per second and mm of wire, independently of the avalanche size. For a proportional gain of  $10^4$  and 100 electrons per track, this corresponds to a particle flux of  $10^3 \text{ s}^{-1} \text{ mm}^{-1}$  (1 kHz/mm<sup>2</sup> for 1 mm wire spacing).

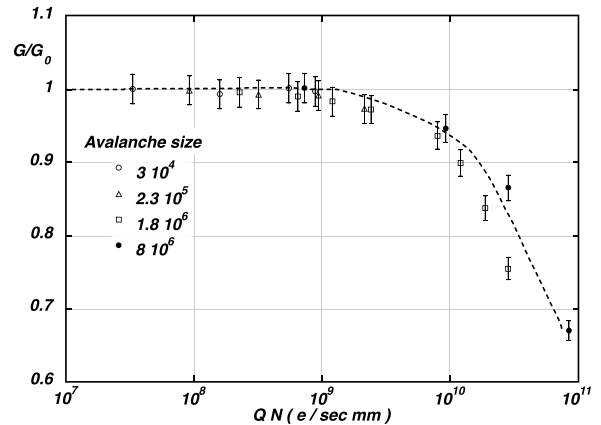


Figure 35.8: Charge rate dependence of normalized gas gain  $G/G_0$  (relative to zero counting rate) in proportional thin-wire detectors [111].  $Q$  is the total charge in single avalanche;  $N$  is the particle rate per wire length.

At high radiation fluxes, a fast degradation of detectors due to the formation of polymers deposits (aging) is often observed. The process has been extensively investigated, often with conflicting results. Several causes have been identified, including organic pollutants and silicone oils. Addition of small amounts of water in many (but not all) cases has been shown to extend the lifetime of the detectors. Addition of fluorinated gases (*e.g.*,  $\text{CF}_4$ ) or oxygen may result in an etching action that can overcome polymer formation, or even eliminate already existing deposits. However, the issue of long-term survival of gas detectors with these gases is controversial [112]. Under optimum operating conditions, a total collected charge of a few coulombs per cm of wire can usually be reached before noticeable degradation occurs. This corresponds, for one mm spacing and at a gain of  $10^4$ , to a total particle flux of  $\sim 10^{14}$  MIPs/cm<sup>2</sup>.

### 35.6.4 Micro-Pattern Gas Detectors

Revised March 2010 by F. Sauli (CERN) and M. Titov (CEA Saclay, DSM/IRFU/SPP).

Despite various improvements, position-sensitive detectors based on wire structures are limited by basic diffusion processes and space charge effects to localization accuracies of 50–100  $\mu\text{m}$  [113]. Modern photolithographic technology led to the development of novel Micro-Pattern Gas Detector (MPGD) concepts [114], revolutionizing cell size limitations for many gas detector applications. By using pitch size of a few hundred  $\mu\text{m}$ , an order of magnitude improvement in granularity over wire chambers, these detectors offer intrinsic high rate capability ( $> 10^6$  Hz/mm<sup>2</sup>), excellent spatial resolution ( $\sim 30 \mu\text{m}$ ), multi-particle resolution ( $\sim 500 \mu\text{m}$ ), and single photo-electron time resolution in the ns range.

The Micro-Strip Gas Chamber (MSGC), invented in 1988, was the first of the micro-structure gas chambers [115]. It consists of a set of tiny parallel metal strips laid on a thin resistive support, alternatively connected as anodes and cathodes. Owing to

the small anode-to-cathode distance ( $\sim 100 \mu\text{m}$ ), the fast collection of positive ions reduces space charge build-up, and provides a greatly increased rate capability. Unfortunately, the fragile electrode structure of the MSGC turned out to be easily destroyed by discharges induced by heavily ionizing particles [116]. Nevertheless, detailed studies of their properties, and in particular, on the radiation-induced processes leading to discharge breakdown, led to the development of the more powerful devices: GEM and Micromegas. These have improved reliability and radiation hardness. The absence of space-charge effects in GEM detectors at the highest rates reached so far and the fine granularity of MPGDs improve the maximum rate capability by more than two orders of magnitude (Fig. 35.9) [117] [118]. Even larger rate capability has been reported for Micromegas [119].

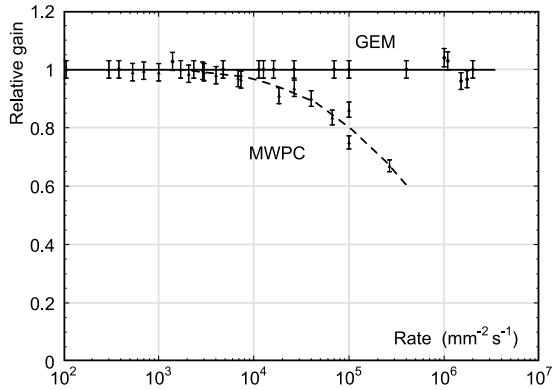


Figure 35.9: Normalized gas gain as a function of particle rate for MWPC [117] and GEM [118].

The Gas Electron Multiplier (GEM) detector consists of a thin-foil copper-insulator-copper sandwich chemically perforated to obtain a high density of holes in which avalanches occur [120]. The hole diameter is typically between  $25 \mu\text{m}$  and  $150 \mu\text{m}$ , while the corresponding distance between holes varies between  $50 \mu\text{m}$  and  $200 \mu\text{m}$ . The central insulator is usually (in the original design) the polymer Kapton, with a thickness of  $50 \mu\text{m}$ . Application of a potential difference between the two sides of the GEM generates the electric fields indicated in Fig. 35.10. Each hole acts as an independent proportional counter. Electrons released by the primary ionization particle in the upper conversion region (above the GEM foil) drift into the holes, where charge multiplication occurs in the high electric field ( $50\text{--}70 \text{ kV/cm}$ ). Most of avalanche electrons are transferred into the gap below the GEM. Several GEM foils can be cascaded, allowing the multi-layer GEM detectors to operate at overall gas gain above  $10^4$  in the presence of highly ionizing particles, while strongly reducing the risk of discharges. This is a major advantage of the GEM technology [121]. Localization can then be performed by collecting the charge on a patterned one- or two-dimensional readout board of arbitrary pattern, placed below the last GEM.

The micro-mesh gaseous structure (Micromegas) is a thin parallel-plate avalanche counter, as shown in Fig. 35.11 [122]. It consists of a drift region and a narrow multiplication gap ( $25\text{--}150 \mu\text{m}$ ) between a thin metal grid (micromesh) and the readout electrode (strips or pads of conductor printed on an insulator board). Electrons from the primary ionization drift through the holes of the mesh into the narrow multiplication gap, where they are amplified. The electric field is homogeneous both in the drift (electric field  $\sim 1 \text{ kV/cm}$ ) and amplification ( $50\text{--}70 \text{ kV/cm}$ ) gaps. In the narrow multiplication region, gain variations due to small variations of the amplification gap are approximately compensated by an inverse variation of the amplification coefficient, resulting in a more uniform gain. The small amplification gap produces a narrow avalanche, giving rise to excellent spatial resolution:  $12 \mu\text{m}$  accuracy, limited by the micro-mesh pitch, has been achieved for MIPs, as well as very good time resolution and energy resolution ( $\sim 12\%$  FWHM with  $6 \text{ keV x rays}$ ) [123].

The performance and robustness of GEM and Micromegas have

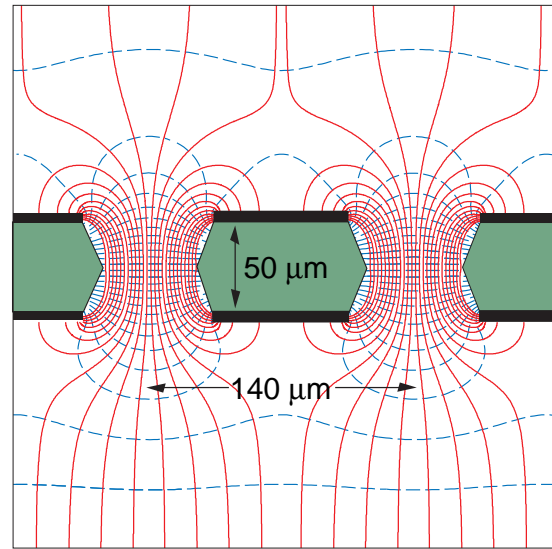


Figure 35.10: Schematic view and typical dimensions of the hole structure in the GEM amplification cell. Electric field lines (solid) and equipotentials (dashed) are shown.

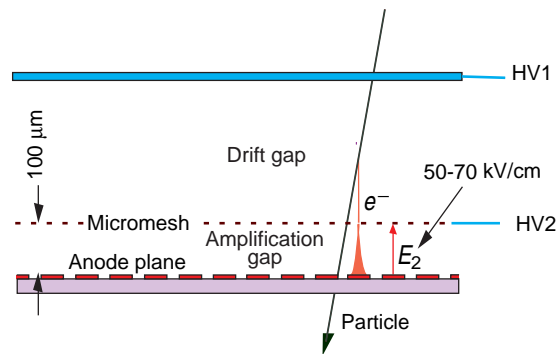


Figure 35.11: Schematic drawing of the Micromegas detector.

encouraged their use in high-energy and nuclear physics, UV and visible photon detection, astroparticle and neutrino physics, neutron detection and medical physics. Most structures were originally optimized for high-rate particle tracking in nuclear and high-energy physics experiments. COMPASS, a high-luminosity experiment at CERN, pioneered the use of large-area ( $\sim 40 \times 40 \text{ cm}^2$ ) GEM and Micromegas detectors close to the beam line with particle rates of  $25 \text{ kHz/mm}^2$ . Both technologies achieved a tracking efficiency of close to 100% at gas gains of about  $10^4$ , a spatial resolution of  $70\text{--}100 \mu\text{m}$  and a time resolution of  $\sim 10 \text{ ns}$ . GEM detectors are also used for triggering in the LHCb Muon System and for tracking in the TOTEM Telescopes. Both GEM and Micromegas devices are foreseen for the upgrade of the LHC experiments and for one of the readout options for the Time Projection Chamber (TPC) at the International Linear Collider (ILC). The development of new fabrication techniques—“bulk” Micromegas technology [124] and single-mask GEMs [125]—is a big step toward industrial production of large-size MPGDs. In some applications requiring very large-area coverage with moderate spatial resolution, coarse macro-patterned detectors, such as Thick GEMs (THGEM) [126] or patterned resistive-plate devices [127] might offer economically interesting solutions.

Sensitive and low-noise electronics enlarge the range of the MPGD applications. Recently, the GEM and Micromegas detectors were read out by high-granularity ( $\sim 50 \mu\text{m}$  pitch) CMOS chips assembled directly below the GEM or Micromegas amplification structures [128]. These detectors use the bump-bonding pads of a pixel chip as an integrated charge collecting anode. With this arrangement signals are induced at the input gate of a charge-



sensitive preamplifier (top metal layer of the CMOS chip). Every pixel is then directly connected to the amplification and digitization circuits, integrated in the underlying active layers of the CMOS technology, yielding timing and charge measurements as well as precise spatial information in 3D.

The operation of a MPGD with a Timepix CMOS chip has demonstrated the possibility of reconstructing 3D-space points of individual primary electron clusters with  $\sim 30 \mu\text{m}$  spatial resolution and event-time resolution with nanosecond precision. This has become indispensable for tracking and triggering and also for discriminating between ionizing tracks and photon conversions. The GEM, in conjunction with a CMOS ASIC,<sup>1</sup> can directly view the absorption process of a few keV x-ray quanta and simultaneously reconstruct the direction of emission, which is sensitive to the x-ray polarization. Thanks to these developments, a micro-pattern device with finely segmented CMOS readout can serve as a high-precision “electronic bubble chamber.” This may open new opportunities for x-ray polarimeters, detection of weakly interacting massive particles (WIMPs) and axions, Compton telescopes, and 3D imaging of nuclear recoils.

An elegant solution for the construction of the Micromegas with pixel readout is the integration of the amplification grid and CMOS chip by means of an advanced “wafer post-processing” technology [129]. This novel concept is called “Ingrid” (see Fig. 35.12). With this technique, the structure of a thin ( $1 \mu\text{m}$ ) aluminum grid is fabricated on top of an array of insulating pillars, which stands  $\sim 50 \mu\text{m}$  above the CMOS chip. The sub- $\mu\text{m}$  precision of the grid dimensions and avalanche gap size results in a uniform gas gain. The grid hole size, pitch and pattern can be easily adapted to match the geometry of any pixel readout chip.

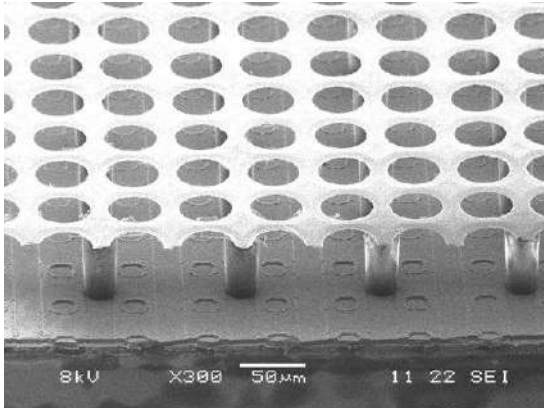


Figure 35.12: Photo of the Micromegas “Ingrid” detector. The grid holes can be accurately aligned with readout pixels of CMOS chip. The insulating pillars are centered between the grid holes, thus avoiding dead regions.

Recent developments in radiation hardness research with state-of-the-art MPGDs are reviewed in Ref. [130]. Earlier aging studies of GEM and Micromegas concepts revealed that they might be even less vulnerable to radiation-induced performance degradation than standard silicon microstrip detectors.

The RD51 collaboration was established in 2008 to further advance technological developments of micro-pattern detectors and associated electronic-readout systems for applications in basic and applied research [131].

### 35.6.5 Time-projection chambers

Revised August 2019 by C. Lippmann (GSI Darmstadt).

The Time Projection Chamber (TPC) concept was invented by David Nygren in the 1970’s [132]. It consists of a cylindrical or square field cage that is filled with a gaseous (or liquid) detection medium. Charged particles produce tracks of ionization electrons that drift in a uniform electric field towards a position-sensitive amplification stage which provides a 2D projection of the particle

trajectories. The third coordinate can be calculated from the arrival times of the drifted electrons. The start for this drift time measurement is usually derived from an external detector, e.g. a fast interaction trigger detector.

This section focuses on the gas-filled TPCs that are often used in particle or nuclear physics experiments at accelerators on account of their low material budget. For neutrino physics (Sec. 35.10) or for detecting rare events (Sec. 36.4), on the contrary, usually high density and large active mass are required, and a liquid detection medium is favored.

The TPC enables full 3D measurements of charged particle tracks, which gives it a distinct advantage over other tracking detector designs which record information only in two-dimensional detector planes and have less overall segmentation. The track points recorded in a TPC are basically adjacent, which facilitates the track finding enormously. This advantage is often exploited for pattern recognition in events with large numbers of particles, e.g. heavy-ion collisions. Two examples of modern large-volume gaseous TPCs are shown in (Figure 35.13) and (Figure 35.14).

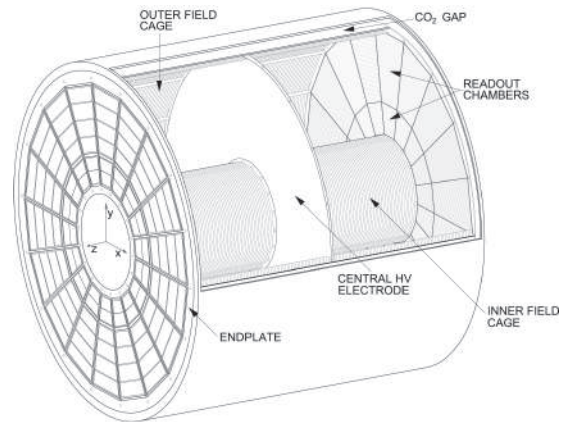


Figure 35.13: Schematic view of the ALICE TPC [133]. The drift volume with 5 m diameter is divided into two halves, each providing 2.5 m drift length.

Identification of the charged particles crossing the TPC is possible by simultaneously measuring their momentum and specific energy deposit through ionisation ( $dE/dx$ ). The momentum, as well as the charge sign, are calculated from a helix fit to the particle trajectory in the presence of a magnetic field (typically parallel to the drift field). For this application, precise spatial measurements in the plane transverse to the magnetic field are most important. The specific energy deposit is estimated from many charge measurements along the particle trajectory (e.g. one measurement per anode wire or per row of readout pads). As the charge collected per readout segment depends on the track angle and on the ambient conditions, the measured values are corrected for the effective length of the track segments and for variations of the gas temperature and pressure. The most probable value of the corrected signal amplitudes provides the best estimator for the specific energy deposit (see Sec. 34.2.3); it is usually approximated by the truncated mean, i.e. the average of the 50%–70% smallest values. The resulting particle identification performance is illustrated in (Figure 35.15), for the ALICE TPC.

The dependence of the achievable energy resolution on the number of measurements  $N$ , on the thickness of the sampling layers  $t$ , and on the gas pressure  $P$  can be estimated using an empirical formula [135]:

$$\sigma_{dE/dx} = 0.41 N^{-0.43} (tP)^{-0.32}. \quad (35.17)$$

Typical values at nominal pressure are  $\sigma_{dE/dx} = 4.5$  to 7.5%, with  $t = 0.4$  to 1.5 cm and  $N = 40$  up to more than 300. Due to the high gas pressure of 8.5 bar, the resolution achieved with the PEP-4/9 TPC was an unprecedented 3% [136].

The greatest challenges for a large TPC are due to the length of the drift of up to several meters. In particular, it can make

<sup>1</sup>Application Specific Integrated Circuit

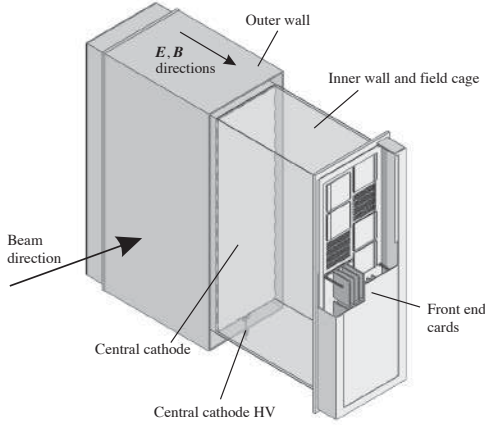


Figure 35.14: One of the 3 TPC modules for the near detector of the T2K experiment [134]. The size is  $2 \times 2 \times 0.8 \text{ m}^3$ . Micromegas devices are used for gas amplification and readout.

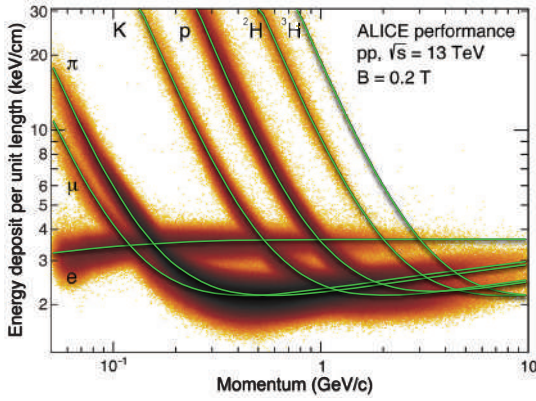


Figure 35.15: Energy deposit versus momentum measured in the ALICE TPC.

the device sensitive to small distortions in the electric field. Such distortions can arise from a number of sources, e.g. imperfections in the field cage construction or the presence of ions in the drift volume. The electron drift in a TPC in the presence of a magnetic field is defined by Eq. (35.14). The  $E \times B$  term of Eq. (35.14) vanishes for perfectly aligned electric and magnetic fields, which can however be difficult to achieve in practice. Furthermore, the electron drift depends on the  $\omega\tau$  factor, which is defined by the gas mixture and the magnetic field strength. The electrons will tend to follow the magnetic field lines for  $\omega\tau > 1$  or the electric field lines for  $\omega\tau < 1$ . The former mode of operation makes the TPC less sensitive to non-uniformities of the electric field, which is usually desirable.

The drift of the ionization electrons is superposed with a random diffusion motion which degrades their position information. The ultimate resolution of a single position measurement is limited to around

$$\sigma_x = \frac{\sigma_D \sqrt{L}}{\sqrt{n}}, \quad (35.18)$$

where  $\sigma_D$  is the transverse diffusion coefficient for 1 cm drift,  $L$  is the drift length in cm and  $n$  is the effective number of electrons collected. Without a magnetic field,  $\sigma_{D,B=0} \sqrt{L}$  is typically a few mm after a drift of  $L = 100 \text{ cm}$ . However, in a strong magnetic field parallel to the drift field, a large value of  $\omega\tau$  can significantly reduce diffusion:

$$\frac{\sigma_{D,B>0}}{\sigma_{D,B=0}} = \frac{1}{\sqrt{1 + \omega^2 \tau^2}}. \quad (35.19)$$

This factor can reach values of up to 10. In practice, the final resolution limit due to diffusion will typically be around  $\sigma_x = 100 \mu\text{m}$ .

The drift and diffusion of electrons depend strongly on the gas mixture. The optimal gas mixture varies according to the environment in which the TPC will operate. In all cases, the oxygen concentration must be kept very low (few ten parts per million in a large TPC) in order to avoid electron loss through attachment.

Ideally, the drift velocity should depend only weakly on the electric field at the nominal operating condition. The classic Ar/CH<sub>4</sub> (90:10) mixture, known as P10, has a drift velocity maximum of  $5 \text{ cm}/\mu\text{s}$  at an electric field of only  $125 \text{ V/cm}$  (Figure 35.4). In this regime, the electron arrival time is not affected by small variations in the ambient conditions. Moreover, low electric fields simplify the design and operation of the field cage. The mixture has a large transverse diffusion at  $B = 0$ , but this can be reduced significantly in a strong magnetic field due to the relatively large value of  $\omega\tau$ .

For some applications organic gases like CH<sub>4</sub> are not desirable since they may cause aging. An alternative is to replace CH<sub>4</sub> with CO<sub>2</sub>. An Ar/CO<sub>2</sub> (90:10) mixture features a low transverse diffusion at all magnetic field strengths, but does not provide a saturated drift velocity for the typical electric fields used in TPCs (up to a few  $100 \text{ V/cm}$ ), so it is quite sensitive to the ambient conditions. Freon admixtures like CF<sub>4</sub> can be an attractive option for a TPC as well, since the resulting gas mixtures provide high drift velocities at low electric fields. However, the use of CF<sub>4</sub> always needs to be thoroughly validated for compatibility with all materials of the detector and the gas system.

Historically, the amplification stages used in gaseous TPCs have been planes of anode wires operated in proportional mode. The performance is limited by effects related to the feature size of a few mm (wire spacing). Since near the wires the electric and magnetic fields are not parallel, the incoming ionisation electrons are displaced in the direction of the wires (“wire  $E \times B$  effect”), which degrades the resolution. The smaller feature sizes of Micro-Pattern Gas Detectors (MPGDs) like GEMs and Micromegas lead to many advantages as compared to wire planes (see Sec. 35.6.4). In particular,  $E \times B$  effects in the amplification stage are much smaller. Moreover, the signal induction process in MPGDs leads to a very narrow pad response, allowing for a much finer segmentation and improving the separation of two nearby tracks. Combinations of MPGDs with silicon sensors have resulted in the highest granularity readout systems so far (see Sec. 35.6.4). These devices make it possible to count the number of ionization clusters along the length of a track, which can, in principle, improve the particle identification capability. However, the big challenge for such a system is the huge number of readout channels for a TPC of a typical size.

The accumulation of the positive ions created by the ionization from the particle tracks can lead to time-dependent distortions of the drift field. Due to their low drift velocity, ions from many events may coexist in the drift volume. To reduce the effect of such a build-up of space charge, Argon can be replaced by Neon as the main component of the gas mixture. Neon features a lower number of ionisation electrons per unit of track length (see 35.5) and a higher ion mobility (see 35.6).

Of much greater concern are the ions produced in the gas amplification stage. In order to prevent them from entering the drift volume, large TPCs built until now usually have a gating grid. The gating grid can be switched to transparent mode (usually in the presence of an interaction trigger) to allow the ionization electrons to pass into the amplification region. After all electrons have reached the amplification region, it is usually closed such that it is rendered opaque to electrons and ions.

A gating grid implies a principal rate limitation to a few kHz. Different groups are therefore working towards the goal of continuous readout for applications where a triggered operation would lead to unacceptable data loss (e.g. ALICE [137], sPHENIX [138]).

New readout schemes using MPGDs enable continuous readout, as they can be optimised in order to limit the ion back-flow at the same effective gain as MWPCs. Extensive work has been carried out during the 2010's to design such readout structures. In ALICE and sPHENIX ion back-flow values below 1% are achieved with a thorough adjustment of the various fields in a quadruple GEM system. Similar levels of ion back-flow can be reached with Micromegas detectors [139].

On the other hand, combinations of MPGDs and a gating structure may be used for triggered operation.

### 35.6.6 Transition radiation detectors (TRD's)

Revised August 2019 by P. Nevski (BNL) and A. Romaniouk (MEPhI Moscow).

Transition radiation (TR) x-rays are produced when a highly relativistic particle ( $\gamma \gtrsim 10^3$ ) crosses a refractive index interface, as discussed in Sec. 34.7. Since the TR yield is about 1% per boundary crossing, radiation from multiple surface crossings (e.g., a stack of foils) is used in practical detectors. The x-rays, ranging from a few keV to a few dozen keV or more, are emitted in a forward direction at small angles (within few mrad) to the particle trajectory. The TR intensity for a single boundary crossing always increases with  $\gamma$ , but, for multiple boundary crossings, interference leads to saturation above a Lorentz factor  $\gamma_{\text{sat}} = 0.6 \omega_1 \sqrt{\ell_1 \ell_2} / c$  [140], where  $\omega_1$  is the radiator material plasma frequency,  $\ell_1$  is its thickness, and  $\ell_2$  the spacing between material elements. The probability density function of TR is a fairly complex function of  $\gamma$ , radiator parameters, angle ( $\theta$ ) and photon energy ( $\omega$ ). For well defined radiator parameters a measured two-dimensional energy vs angle distribution is in a very good agreement with the theory predictions [141]. Integration over the angle yields the TR spectrum, which typically features many maxima (see Sec. 34.7). Most of the TR energy is emitted near the last maximum of the spectra determined by radiator material parameters at  $\omega_{\text{max}} = \ell_1 \omega_1^2 / 2\pi c$ . The effective TR photon emission starts at about  $\gamma_{\text{thr}} = \ell_1 \omega_1 / c$ . By varying radiator parameters one may optimize the particle separation for a given range of the  $\gamma$ -factor. The angular distribution of TR photons has a few maxima and extends up to  $\theta_{\text{max}} = (1/\gamma^2 + \omega_1^2/\omega^2)^{1/2}$  [142]. For a single foil the largest part of the TR energy is emitted around the most probable angle  $\theta = (1/\gamma^2 + \omega_2^2/\omega^2)^{1/2}$ , where  $\omega_2$  is the plasma frequency of the gas surrounding the radiator material elements. However, in case of multiple interfaces, interference effects may significantly change this angle. For instance, for a stack of foils of 15.5  $\mu\text{m}$  thickness spaced by 210  $\mu\text{m}$  TR produced by 20 GeV electrons is emitted mostly around  $\theta \sim 0.9$  mrad [143].

In the simplest concept, a detector module might consist of a low- $Z$  TR radiator followed by a high- $Z$  active layer made of proportional counters filled with a Xe-rich gas mixture. The atomic number considerations follow from the dominant photoelectric absorption cross section per atom going roughly as  $Z^n/\omega^3$ , where  $n$  varies between 4 and 5 over the region of interest.<sup>2</sup> To minimize self-absorption, materials such as polypropylene, Mylar, carbon, and (rarely) lithium in the form of foils, fibers or foams are used as radiators. The TR signal in the active regions is in most cases superimposed upon the particle ionization losses, which are proportional to  $Z$ . In most of the detectors used in particle physics the radiator parameters are chosen to provide  $\gamma_{\text{sat}} \approx 2000$ . Those detectors normally work as threshold devices, ensuring the best electron/pion separation in the momentum range  $1 \text{ GeV}/c \lesssim p \lesssim 150 \text{ GeV}/c$ .

One can distinguish two design concepts—“thick” and “thin” detectors:

In “thick” detectors the radiator, optimized for a minimum total radiation length at maximum TR yield and total TR absorption in the detector, consists of few hundred foils (for instance 300 20  $\mu\text{m}$  thick polypropylene foils). Most of the TR photons are absorbed in the radiator itself. To maximise the number of TR photons reaching the detector, part of the radiator far from the active layers is often made of thicker foils, which shifts the x-ray

spectrum to higher energies. The detector thickness, about 2-4 cm for Xe-filled gas chambers, is optimized to absorb the incoming x-ray spectrum. A classical detector is composed of several similar modules which respond nearly independently. Such detectors were used in the UA2, NA34 and other experiments [144], and are being used in the ALICE experiment [145] [146].

In another TRD concept a fine granular radiator/detector structure exploits the soft part of the TR spectrum more efficiently and thereby may act also as an integral part of the tracking detector providing many points of measurements on the particle track. This can be achieved, for instance, by distributing small-diameter straw-tube detectors uniformly or in thin layers throughout the radiator material. Even with a relatively thin radiator stack, radiation below 4 keV is mostly lost in the radiators themselves. However, for photon energies above this value, the absorption is reduced and the radiation can be registered by several consecutive detector layers, thus creating a strong TR build-up effect. This approach allows to realise a TRD as an integral part of a tracking detector. Descriptions of detectors using this approach in both accelerator and space experiments can be found in [145, 147–150]. For example, in the ATLAS TR tracker (TRT), charged particles on average cross about 35 straw tube layers embedded in the radiator material [147]. The effective thickness of the Xe gas per straw is about 2.5 mm and the average number of foils per straw is about 40 with an effective foil thickness of about 18  $\mu\text{m}$ . In this approach straw walls also act as radiators and make some contribution to the TR spectrum.

Although the values mentioned above are typical for most of the plastic radiators used with Xe-based detectors, they vary significantly depending on the detector requirements. Careful simulations are usually needed to build a detector optimized for a particular application. For TRD simulations the codes are based on well understood TR emission formulas (see for instance [142]). They are realised as the stand-alone simulation programs [151] and GEANT4 based ones [152] and give both a good agreement of the TR energy spectra with data [141, 143, 153].

The discrimination between electrons and pions can be based on the charge deposition measured in each detection module, on the number of clusters – energy depositions observed above an optimal threshold (usually it is 5–7 keV), or on more sophisticated methods such as analyzing the pulse shape as a function of time. The total energy measurement technique is more suitable for thick gas volumes, which absorb most of the TR radiation and where the ionization loss fluctuations are relatively small. The cluster-counting method works better for detectors with thin gas layers, where the fluctuations of the ionization losses are bigger. Cluster-counting replaces the Landau-Vavilov distribution of background ionization energy losses with the Poisson statistics of  $\delta$ -electrons, responsible for the distribution tails. The latter distribution is narrower than the Landau-Vavilov distribution. In practice, most of the experiments use a likelihood method, which exploits detailed knowledge of the detector response for different particles and gives the best separation. The more parameters are considered, the better achievable separation power. For example, for the TRD in the AMS experiment the rejection power achieved in the real experiment is better by almost one order of magnitude than that obtained in the beam test if stringent criteria for track selection are applied, see in [150]. Another example is the neural network method used by the ALICE TRD (ALICE point in 35.16) which gives another factor of 2–3 in rejection power with respect to the likelihood method [145].

The major factor in the performance of any TRD is its overall length. This is illustrated in Fig. 35.16, which shows, for a variety of detectors, the pion efficiency at a fixed electron efficiency of 90% as a function of the overall detector length. As TRD performance depends on particle energy, the experimental data in this figure covering a range of particle energies from 1 GeV to 40 GeV, are rescaled to an energy of 10 GeV when possible. Phenomenologically, the rejection power against pions increases as  $5 \cdot 10^{L/38}$ , where the range of validity is  $L \approx 20\text{--}100$  cm. Apart from the beam energy variations, the observed scattering of the points in the plot reflects how effectively the detector space is used and how well the exact response to different particles is taken into account

<sup>2</sup>Photon absorption coefficients for the elements (via a NIST link), and  $dE/dx|_{\text{min}}$  and plasma energies for many materials are given in [pdg.lbl.gov/AtomicNuclearProperties](http://pdg.lbl.gov/AtomicNuclearProperties).



in the analysis. For instance, the ATLAS TRT was built as a compromise between TR and tracking requirements; that is why the test-beam prototype result (lower point) is better than the real End-Cap TRT performance at the LHC shown in Fig. 35.16 for different regions in the detector (in agreement with MC).

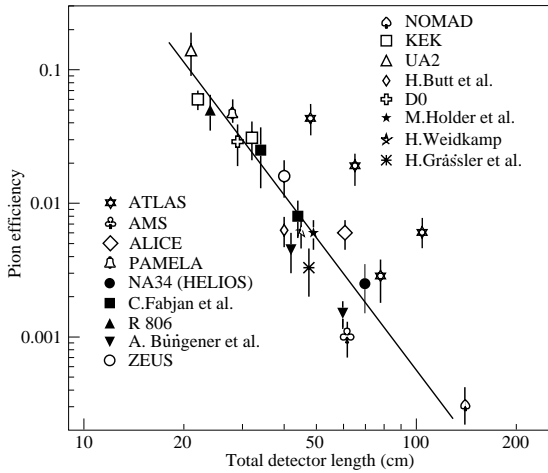


Figure 35.16: Pion efficiency measured (or predicted) for different TRDs as a function of the detector length for a fixed electron efficiency of 90%. The plot is based on the table given in [144]. Results from more recent detectors are added from [145, 148–150, 154].

In most cases, recent TRDs combine particle identification with charged-track measurement in the same detector [145, 149, 155]. This is particularly important for collider experiments, where the available space for the inner detector is very limited. For a modest increase of the radiation length due to the radiator ( $\sim 4\% X_0$ ), a significant enhancement of the electron identification was obtained in the case of the ATLAS TRT. Here, the combination of the two detector functions provides a powerful tool for electron identification even at very high particle densities.

In addition to the enhancement of the electron identification during offline data analysis, TRD signatures are often used in the trigger algorithms at collider experiments. The ALICE experiment [146] is a good example for the use of the TRD in a First Level Trigger. In the ATLAS experiment, the TRT information is used in the High Level Trigger (HLT) algorithms. At increasing luminosities, the electron trigger output rate becomes so high, that a significant increase of the calorimeter energy threshold is required to keep it at an acceptable level. This may affect the trigger efficiency of very important physics channels (e.g.  $W \rightarrow e\nu$  inclusive decay). Even a very soft TR cut at the HLT level, which preserves high electron efficiency (98%), allows to suppress a significant part of fake triggers and enhance the purity for physics events with electrons in a final state. The TRT also plays a crucial role in the studies where an electron suppression is required (e.g. hadronic mode of  $\tau$ -decays). TR information is a completely independent tool for electron identification and allows to study systematic uncertainties of other electron reconstruction methods.

Electron identification is not the only TRD application. Some TRDs for particle astrophysics are designed to directly measure the Lorentz factor of high-energy nuclei by using the quadratic dependence of the TR yield on nuclear charge; see, for instance, in [156]. The radiator configuration ( $\ell_1, \ell_2$ ) is tuned to extend the TR yield rise up to  $\gamma \approx 10^5$  using the more energetic part of the TR spectrum (up to 100 keV). High density radiator materials (such as Al) are the best for this purpose. Direct absorption of the TR-photons of these energies with thin detectors becomes problematic and TR detection methods based on Compton scattering have been proposed, see in [156].

The high granularity of the semiconductor pixel or microstrip detectors provides spatial separation of the TR photons and  $dE/dx$  losses at relatively modest distances between radiator and detector. These detectors may be the basis for novel devices which

combine precise tracking and PID properties [141, 143]. Use of the TR production angle in addition to its energy can help to improve PID properties of the TRD. The presence of a magnetic field could enhance the separation between TR photons and  $dE/dx$  losses [157]. New detector techniques for TRDs are also under consideration. GasPixel detectors allow to reconstruct a track segment with a space point accuracy of  $< 30 \mu\text{m}$  and exploit all details of the particle tracks to highlight individual TR clusters in the gas, see in [158]. Thin films of heavy scintillators might be a very attractive option for non-gas based TRD [159].

### 35.6.7 Resistive-plate chambers

Revised October 2019 by G. Aielli (Rome U. Tor Vergata).

The resistive-plate chamber (RPC) is a gaseous detector developed by R. Santonico and R. Cardarelli in the early 1980's [160]<sup>3</sup>. Although its original purpose was to provide a competitive alternative to large scintillator counters, the RPC's potential for timing tracker systems was quickly recognized given its high detection efficiency ( $>95\%$ ), excellent temporal and spatial resolutions and ease of constructing large-format single frame detectors. The RPC, as sketched in Fig. 35.17, is a large planar capacitor with two parallel high bulk resistivity electrode plates ( $10^9$ – $10^{13} \Omega\cdot\text{cm}$ ) separated by a set of insulating spacers. The spacers define a gap in the range from a few millimeters down to 0.1 mm with a precision of a few  $\sim \mu\text{m}$ . The gap is filled with a suitable atmospheric-pressure gas mixture which serves as a target for ionizing radiation. The gas gap thickness practically determines the time resolution of the RPC, on the other side the limit for reaching full detection efficiency (depending also on the gas density) is typically 1mm. Since the primary ionization for sub-millimeter gas gaps is insufficient, multiple gaps can be combined to ensure high detection efficiency [162]. The electrodes are most commonly made of high pressure phenolic-melaminic laminate (HPL), improperly referred to as "bakelite", or glass. A moderate electrode resistivity

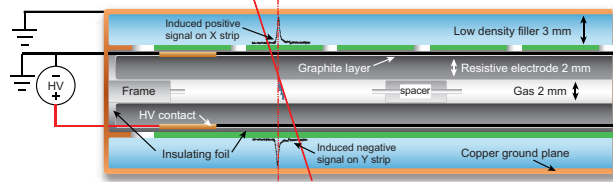


Figure 35.17: Schematic cross section of a generic single gap RPC.

( $\sim 10^5 \Omega/\square$ ) establishes a uniform electric field of several kV/mm across the gap, which initiates an electron avalanche following primary ionization. The above resistivity is low enough to ensure uniformity of the electric field, yet still transparent to fast signal transients from avalanches. Due to the high electrode resistivity in RPCs, the electrode time constant is much longer than discharge processes. Therefore only the locally-stored electrostatic energy contributes to the discharge, which prevents the formation of sparks and leaves the rest of the detector field unaffected. This field configuration and resistive feedback offers, besides the excellent time resolution, an excellent spacial localization of the discharge, without the need of micro-patterned electrodes. The gas-facing surface of HPL electrodes are commonly coated with a few  $\mu\text{m}$ -thick layer of polymerized linseed oil. This layer has a similar resistivity as the electrode, and is smooth to aid the uniformity of the electric field. It also protects the electrode from the free radicals generated in the discharge e.g. in presence of hydrocarbons or fluorocarbons. As with other gaseous detectors, the gas mixture is optimized for each specific application. In general it needs to contain a UV photons absorber, to quench the spurious counts and an electronegative component to limit the avalanche growth in presence of very high electric fields [163] [164]. According to a first order approximation, each primary ionization in an RPC is exponentially amplified according to its distance from the anode, due to the uniform field. Therefore RPC signals span a large dynamic range (unlike gaseous detectors where

<sup>3</sup>The RPC was based on earlier work on a spark counter with one metallic and one high-resistivity plate [161].

ionization and amplification occur in separate regions) following the exponential distribution, having the most probable signals toward the zero. For increasingly stronger fields, the avalanche exponential growth progressively saturates to linear and the signal amplitude distribution peak detaches from zero, making easier to distinguish the signal and the noise, [165], and finally reaches a strongly-saturated "streamer" transition which exhausts all the locally-available energy [166], generating an almost fixed amplitude signal. Any of this operating regimes can be used, in function of the front-end electronics sensitivity, and depending on the operating environment. A set of metallic readout electrodes (e.g. pads or strips) placed behind the resistive electrodes detect the charge pulse induced by the fast movement of the avalanche electrons. The signal is isotropically distributed with respect to the field direction and present with equal but opposite amplitude on the two electrodes. This feature allows for 2D localization of the signal with uniform spatial resolution. The induced charge density projected in 1D can be calculated for a simplified RPC model [167] as:  $\sigma(x) = A/\cosh[(x - \bar{x})/\delta]$  where  $\bar{x}$  is the center of the avalanche and  $\delta = (g+2d)/\pi$  depends on the gap and electrode width ( $g$  and  $d$ , respectively). The spatial extent of actual signals are generally larger than those given by this model [168] [169]. Conductivity of the graphite layer results in the most prominent broadening. Cross-talk from parasitic coupling of neighboring electrodes can also spread the signal spatially. Although the broadened charge distribution preserves most of the original spatial resolution, it can adversely impact signal clustering, so the detector layout must be calculated according to the expected application requirements. Sensitivity to high-frequency electron avalanche signals over large RPC areas requires a correspondingly adequate Faraday cage and readout structure design. To preserve the excellent timing features of the RPC signal, the front end electronics should have a short rise time (ideally  $\ll$  than the signal rise time) and low noise, although these requirements are usually in competition [170].

### 35.6.7.1 RPC types and applications

RPCs are generally classified in two categories depending on the gas gap structure: single gap RPCs (described above) and multiple gap RPCs (typically referred as mRPCs or timing RPCs). While they are both based on the same principle they have different construction techniques, performance and limitations, making them suitable for different applications. Due to its simplicity and robustness, the single gap RPC is ideal for covering very large surfaces. Typical detector systems can have sensitive surface areas up to  $\sim 10^4$  m<sup>2</sup>, with single module areas of a few m<sup>2</sup>, and a space-time resolution down to  $\sim 0.4$  ns  $\times$  100  $\mu$ m [171] [172]. Sensible examples are the ATLAS [173] and CMS [174] muon systems or ground and underground based cosmic rays and neutrino arrays [175]. Moreover, single gap RPCs have recently found an application in tracking calorimetry [176]. The mRPC allows for smaller gas gap thicknesses while still maintaining a sufficient gaseous target. The most common version [177] consists of a stack of floating glass electrodes separated by monofilament (i.e. fishing line), sandwiched between two external electrodes which provide the high-voltage bias. The floating glass electrodes assume a potential determined by the avalanche processes occurring between them. mRPCs have been largely used in TOF systems and in applications such as timing PET.

### 35.6.7.2 Time and space resolution

The RPC field configuration generates an avalanche which is strongly correlated in space and time to the original ionizing event. Space-time uncertainties generally arise from the statistical fluctuations of the ionization and multiplication processes, and from the characteristics of the readout and front-end electronics. The intrinsic signal latency is commonly in a few ns range, making the RPC suitable for applications where a low latency is essential. A higher time resolution and shorter signal duration is correlated with a thinner gas gap, although a higher electric field is required for sufficient avalanche development [177] [178]. Typical timing performances range from around 1 ns with a 2 mm gas gap, down to 20 ps for a stack of several 0.1 mm gaps [179]. The mechanical delicacy of sub-mm-gap structures makes this technique less suitable for very large detector areas. Digital strip

readouts are commonly used, with spatial resolution determined by the strip pitch and the cluster size ( $\sim 0.5$  cm). A more precise measurement of the charge in each strip involved in the cluster, and demonstrated recently, through charge centroid techniques that the RPC avalanche space-time localization is better than  $\sim 50$  ps  $\times$  40  $\mu$ m [180].

### 35.6.7.3 Rate capability and ageing

RPC rate capability is limited by the voltage drop on resistive electrodes,  $\Delta V = V_a - V_{\text{gas}} = I \cdot R$  [181]. Here  $V_a$  is the applied voltage,  $V_{\text{gas}}$  is the effective voltage on the gas,  $R = \rho \cdot d/S$  is the total electrode resistance and  $I$  is the working current. Expressing  $I$  as the particle flux  $\Phi$  times an average charge per avalanche  $\langle Q \rangle$  gives  $\Delta V/\Phi = \rho \cdot d \cdot \langle Q \rangle$ . A large  $I$  not only limits the rate capability but also affects the long term performance of the detector. Discharges deplete the conductive properties of HPL electrodes [182]. In the presence of fluorocarbons and water, discharges generate hydrofluoric acid (HF) which damages internal detector surfaces, particularly glass electrodes [183]. HF damage can be mitigated by preventing water vapor contamination (for glass electrodes) or by sufficient flushing of the gas gap (for HPL electrodes where water vapor is unavoidable). Operating in the streamer regime puts low requirements on the front end electronics sensitivity, but generally limits the counting rate capability to  $\sim 100$  Hz/cm<sup>2</sup> and requires stability over a large gain range. Higher-rate operation can be achieved by reducing gas gain in favor of electronic amplification, operating the detector in avalanche mode. Increasing concentrations of electronegative gases, such as C<sub>2</sub>H<sub>2</sub>F<sub>4</sub> and SF<sub>6</sub> [164], shifts the streamer transition to higher gains. The avalanche signal has a higher dynamic range, a drawback which can be compensated with appropriate electronics. With these techniques, stable performance at high rates (e.g. 10 kHz/cm<sup>2</sup>) has been achieved for large area single gap RPCs [170]. Complementary strategies rely on the natural redundancy and higher signal yield of multiple micro gap structures [184] and electrodes made with lower resistivity materials [185]. Lowering the electrode resistivity finds a limit in the increasing probability of discharge in presence of high uniform field, thus lowering the average charge per count, i.e. the applied electric field is also a gateway to further lower the electrode resistivity without spoiling the detector stability.

## 35.7 Semiconductor detectors

Revised November 2013 by H. Spieler (LBNL).

Semiconductor detectors provide a unique combination of energy and position resolution. In collider detectors they are most widely used as position sensing devices and photodetectors (Sec. 35.2).

Integrated circuit technology allows the formation of high-density micron-scale electrodes on large (15–20 cm diameter) wafers, providing excellent position resolution. Furthermore, the density of silicon and its small ionization energy yield adequate signals with active layers only 100–300  $\mu$ m thick, so the signals are also fast (typically tens of ns). The high energy resolution is a key parameter in x-ray, gamma, and charged particle spectroscopy, e.g., in neutrinoless double beta decay searches. Silicon and germanium are the most commonly used materials, but gallium-arsenide, CdTe, CdZnTe, and other materials are also useful. CdZnTe provides a higher stopping power and the ratio of Cd to Zn concentrations changes the bandgap. Ge detectors are commonly operated at liquid nitrogen temperature to reduce the bias current, which depends exponentially on temperature. Semiconductor detectors depend crucially on low-noise electronics (see Sec. 35.8), so the detection sensitivity is determined by signal charge and capacitance. For a comprehensive discussion of semiconductor detectors and electronics see [186] or the tutorial website <http://www-physics.lbl.gov/spieler>.

### 35.7.1 Materials Requirements

Semiconductor detectors are essentially solid state ionization chambers. Absorbed energy forms electron-hole pairs, i.e., negative and positive charge carriers, which under an applied electric field move towards their respective collection electrodes, where



they induce a signal current. The energy required to form an electron-hole pair is proportional to the bandgap. In tracking detectors the energy loss in the detector should be minimal, whereas for energy spectroscopy the stopping power should be maximized, so for gamma rays high- $Z$  materials are desirable.

Measurements on silicon photodiodes [187] show that for photon energies below 4 eV one electron-hole ( $e-h$ ) pair is formed per incident photon. The mean energy  $E_i$  required to produce an  $e-h$  pair peaks at 4.4 eV for a photon energy around 6 eV. Above  $\sim 1.5$  keV it assumes a constant value, 3.67 eV at room temperature. It is larger than the bandgap energy because momentum conservation requires excitation of lattice vibrations (phonons). For minimum-ionizing particles, the most probable charge deposition in a 300  $\mu\text{m}$  thick silicon detector is about 3.5 fC (22000 electrons). Other typical ionization energies are 2.96 eV in Ge, 4.2 eV in GaAs, and 4.43 eV in CdTe.

Since both electronic and lattice excitations are involved, the variance in the number of charge carriers  $N = E/E_i$  produced by an absorbed energy  $E$  is reduced by the Fano factor  $F$  (about 0.1 in Si and Ge). Thus,  $\sigma_N = \sqrt{FN}$  and the energy resolution  $\sigma_E/E = \sqrt{FE_i/E}$ . However, the measured signal fluctuations are usually dominated by electronic noise or energy loss fluctuations in the detector.

The electronic noise contributions depend on the pulse shaping in the signal processing electronics, so the choice of the shaping time is critical (see Sec. 35.8).

A smaller bandgap would produce a larger signal and improve energy resolution, but the intrinsic resistance of the material is critical. Thermal excitation, given by the Fermi-Dirac distribution, promotes electrons into the conduction band, so the thermally excited carrier concentration increases exponentially with decreasing bandgaps. In pure Si the carrier concentration is  $\sim 10^{10} \text{cm}^{-3}$  at 300 K, corresponding to a resistivity  $\rho \approx 400 \text{k}\Omega \text{cm}$ . In reality, crystal imperfections and minute impurity concentrations limit Si carrier concentrations to  $\sim 10^{11} \text{cm}^{-3}$  at 300 K, corresponding to a resistivity  $\rho \approx 40 \text{k}\Omega \text{cm}$ . In practice, resistivities up to 20  $\text{k}\Omega \text{cm}$  are available, with mass production ranging from 5 to 10  $\text{k}\Omega \text{cm}$ . Signal currents at keV scale energies are of order  $\mu\text{A}$ . However, for a resistivity of  $10^4 \Omega \text{cm}$  a 300  $\mu\text{m}$  thick sensor with  $1 \text{cm}^2$  area would have a resistance of 300  $\Omega$ , so 30 V would lead to a current flow of 100 mA and a power dissipation of 3 W. On the other hand, high-quality single crystals of Si and Ge can be grown economically with suitably large volumes, so to mitigate the effect of resistivity one resorts to reverse-biased diode structures. Although this reduces the bias current relative to a resistive material, the thermally excited leakage current can still be excessive at room temperature, so Ge diodes are typically operated at liquid nitrogen temperature (77 K).

A major effort is to find high- $Z$  materials with a bandgap that is sufficiently high to allow room-temperature operation while still providing good energy resolution. Compound semiconductors, *e.g.*, CdZnTe, can allow this, but typically suffer from charge collection problems, characterized by the product  $\mu\tau$  of mobility and carrier lifetime. In Si and Ge  $\mu\tau > 1 \text{cm}^2 \text{V}^{-1}$  for both electrons and holes, whereas in compound semiconductors it is in the range  $10^{-3}$ – $10^{-8}$ . Since for holes  $\mu\tau$  is typically an order of magnitude smaller than for electrons, detector configurations where the electron contribution to the charge signal dominates—*e.g.*, strip or pixel structures—can provide better performance.

### 35.7.2 Detector Configurations

A  $p-n$  junction operated at reverse bias forms a sensitive region depleted of mobile charge and sets up an electric field that sweeps charge liberated by radiation to the electrodes. Detectors typically use an asymmetric structure, *e.g.*, a highly doped  $p$  electrode and a lightly doped  $n$  region, so that the depletion region extends predominantly into the lightly doped volume.

In a planar device the thickness of the depleted region is

$$W = \sqrt{2\epsilon(V + V_{bi})/Ne} = \sqrt{2\rho\mu\epsilon(V + V_{bi})} \quad (35.20)$$

where  $V$  = external bias voltage

$V_{bi}$  = “built-in” voltage ( $\approx 0.5$  V for resistivities typically used in Si detectors)

$N$  = doping concentration

$e$  = electronic charge

$\epsilon$  = dielectric constant =  $11.9 \epsilon_0 \approx 1 \text{pF/cm}$  in Si

$\rho$  = resistivity (typically 1–10  $\text{k}\Omega \text{cm}$  in Si)

$\mu$  = charge carrier mobility

= 1350  $\text{cm}^2 \text{V}^{-1} \text{s}^{-1}$  for electrons in Si

= 450  $\text{cm}^2 \text{V}^{-1} \text{s}^{-1}$  for holes in Si

In Si

$$W = 0.5[\mu\text{m}\sqrt{\Omega\text{-cm} \cdot V}] \times \sqrt{\rho(V + V_{bi})} \text{ for } n\text{-type Si, and}$$

$$W = 0.3[\mu\text{m}\sqrt{\Omega\text{-cm} \cdot V}] \times \sqrt{\rho(V + V_{bi})} \text{ for } p\text{-type Si.}$$

The conductive  $p$  and  $n$  regions together with the depleted volume form a capacitor with the capacitance per unit area

$$C = \epsilon/W \approx 1 [\text{pF/cm}] / W \text{ in Si.} \quad (35.21)$$

In strip and pixel detectors the capacitance is dominated by the fringing capacitance to neighboring electrodes. For example, the strip-to-strip Si fringing capacitance is  $\sim 1$ – $1.5 \text{pF cm}^{-1}$  of strip length at a strip pitch of 25–50  $\mu\text{m}$ .

Large volume ( $\sim 10^2$ – $10^3 \text{cm}^3$ ) Ge detectors are commonly configured as coaxial detectors, *e.g.*, a cylindrical  $n$ -type crystal with 5–10 cm diameter and 10 cm length with an inner 5–10 mm diameter  $n^+$  electrode and an outer  $p^+$  layer forming the diode junction. Ge can be grown with very low impurity levels,  $10^9$ – $10^{10} \text{cm}^{-3}$  (HPGe), so these large volumes can be depleted with several kV.

### 35.7.3 Signal Formation

The signal pulse shape depends on the instantaneous carrier velocity  $v(x) = \mu E(x)$  and the electrode geometry, which determines the distribution of induced charge (*e.g.*, see [186], pp. 71–83). Charge collection time decreases with increasing bias voltage, and can be reduced further by operating the detector with “overbias,” *i.e.*, a bias voltage exceeding the value required to fully deplete the device. Note that in partial depletion the electric field goes to zero, whereas going beyond full depletion adds a constantly distributed field. The collection time is limited by velocity saturation at high fields (in Si approaching  $10^7 \text{cm/s}$  at  $E > 10^4 \text{V/cm}$ ); at an average field of  $10^4 \text{V/cm}$  the collection time is about 15 ps/ $\mu\text{m}$  for electrons and 30 ps/ $\mu\text{m}$  for holes. In typical fully-depleted detectors 300  $\mu\text{m}$  thick, electrons are collected within about 10 ns, and holes within about 25 ns.

Position resolution is limited by transverse diffusion during charge collection (typically 5  $\mu\text{m}$  for 300  $\mu\text{m}$  thickness) and by knock-on electrons. Resolutions of 2–4  $\mu\text{m}$  (rms) have been obtained in beam tests. In magnetic fields, the Lorentz drift deflects the electron and hole trajectories and the detector must be tilted to reduce spatial spreading (see “Hall effect” in semiconductor textbooks).

Electrodes can be in the form of cm-scale pads, strips, or  $\mu\text{m}$ -scale pixels. Various readout structures have been developed for pixels, *e.g.*, CCDs, DEPFETs, monolithic pixel devices that integrate sensor and electronics (MAPS), and hybrid pixel devices that utilize separate sensors and readout ICs connected by two-dimensional arrays of solder bumps. For an overview and further discussion see Ref. [186].

In gamma ray spectroscopy ( $E_\gamma > 10^2 \text{keV}$ ) Compton scattering dominates, so for a significant fraction of events the incident gamma energy is not completely absorbed, *i.e.*, the Compton scattered photon escapes from the detector and the energy deposited by the Compton electron is only a fraction of the total. Distinguishing multi-interaction events, *e.g.*, multiple Compton scatters with a final photoelectric absorption, from single Compton scatters allows background suppression. Since the individual interactions take place in different parts of the detector volume, these events can be distinguished by segmenting the outer electrode of a coaxial detector and analyzing the current pulse shapes. The

different collection times can be made more distinguishable by using “point” electrodes, where most of the signal is induced when charges are close to the electrode, similarly to strip or pixel detectors. Charge clusters arriving from different positions in the detector will arrive at different times and produce current pulses whose major components are separated in time. Point electrodes also reduce the electrode capacitance, which reduces electronic noise, but careful design is necessary to avoid low-field regions in the detector volume.

### 35.7.4 Radiation Damage

Radiation damage occurs through two basic mechanisms:

1. Bulk damage due to displacement of atoms from their lattice sites. This leads to increased leakage current, carrier trapping, and build-up of space charge that changes the required operating voltage. Displacement damage depends on the nonionizing energy loss and the energy imparted to the recoil atoms, which can initiate a chain of subsequent displacements, *i.e.*, damage clusters. Hence, it is critical to consider both particle type and energy.
2. Surface damage due to charge build-up in surface layers, which leads to increased surface leakage currents. In strip detectors the inter-strip isolation is affected. The effects of charge build-up are strongly dependent on the device structure and on fabrication details. Since the damage is proportional to the absorbed energy (when ionization dominates), the dose can be specified in rad (or Gray) independent of particle type.

The increase in reverse bias current due to bulk damage is  $\Delta I_r = \alpha \Phi$  per unit volume, where  $\Phi$  is the particle fluence and  $\alpha$  the damage coefficient ( $\alpha \approx 3 \times 10^{-17}$  A/cm for minimum ionizing protons and pions after long-term annealing;  $\alpha \approx 2 \times 10^{-17}$  A/cm for 1 MeV neutrons). The reverse bias current depends strongly on temperature

$$\frac{I_R(T_2)}{I_R(T_1)} = \left(\frac{T_2}{T_1}\right)^2 \exp\left[-\frac{E}{2k} \left(\frac{T_1 - T_2}{T_1 T_2}\right)\right] \quad (35.22)$$

where  $E = 1.2$  eV, so rather modest cooling can reduce the current substantially ( $\sim 6$ -fold current reduction in cooling from room temperature to  $0^\circ\text{C}$ ).

Displacement damage forms acceptor-like states. These trap electrons, building up a negative space charge, which in turn requires an increase in the applied voltage to sweep signal charge through the detector thickness. This has the same effect as a change in resistivity, *i.e.*, the required voltage drops initially with fluence, until the positive and negative space charge balance and very little voltage is required to collect all signal charge. At larger fluences the negative space charge dominates, and the required operating voltage increases ( $V \propto N$ ). The safe limit on operating voltage ultimately limits the detector lifetime. Strip detectors specifically designed for high voltages have been extensively operated at bias voltages  $>500$  V. Since the effect of radiation damage depends on the electronic activity of defects, various techniques have been applied to neutralize the damage sites. For example, additional doping with oxygen can increase the allowable charged hadron fluence roughly three-fold [188]. Detectors with columnar electrodes normal to the surface can also extend operational lifetime [189]. The increase in leakage current with fluence, on the other hand, appears to be unaffected by resistivity and whether the material is *n* or *p*-type. At fluences beyond  $10^{15}$   $\text{cm}^{-2}$  decreased carrier lifetime becomes critical [190] [191].

Strip and pixel detectors have remained functional at fluences beyond  $10^{15}$   $\text{cm}^{-2}$  for minimum ionizing protons. At this damage level, charge loss due to recombination and trapping becomes significant and the high signal-to-noise ratio obtainable with low-capacitance pixel structures extends detector lifetime. The higher mobility of electrons makes them less sensitive to carrier lifetime than holes, so detector configurations that emphasize the electron contribution to the charge signal are advantageous, *e.g.*,  $n^+$  strips or pixels on a *p*- or *n*-substrate. The occupancy of the defect charge states is strongly temperature dependent; competing processes can increase or decrease the re-

quired operating voltage. It is critical to choose the operating temperature judiciously ( $-10$  to  $0^\circ\text{C}$  in typical collider detectors) and limit warm-up periods during maintenance. For a more detailed summary see [192] and the web-sites of the ROSE and RD50 collaborations at <http://RD48.web.cern.ch/rd48> and <http://RD50.web.cern.ch/rd50>. Materials engineering, *e.g.*, introducing oxygen interstitials, can improve certain aspects and is under investigation. At high fluences diamond is an alternative, but operates as an insulator rather than a reverse-biased diode.

Currently, the lifetime of detector systems is still limited by the detectors; in the electronics use of standard “deep submicron” CMOS fabrication processes with appropriately designed circuitry has increased the radiation resistance to fluences  $> 10^{15}$   $\text{cm}^{-2}$  of minimum ionizing protons or pions. For a comprehensive discussion of radiation effects see [193].

## 35.8 Low-noise electronics

Revised November 2013 by H. Spieler (LBNL).

Many detectors rely critically on low-noise electronics, either to improve energy resolution or to allow a low detection threshold. A typical detector front-end is shown in Fig. 35.18.

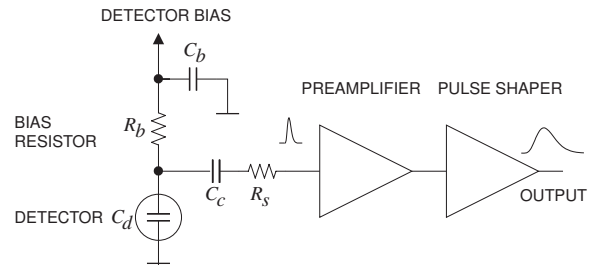


Figure 35.18: Typical detector front-end circuit.

The detector is represented by a capacitance  $C_d$ , a relevant model for most detectors. Bias voltage is applied through resistor  $R_b$  and the signal is coupled to the preamplifier through a blocking capacitor  $C_c$ . The series resistance  $R_s$  represents the sum of all resistances present in the input signal path, *e.g.* the electrode resistance, any input protection networks, and parasitic resistances in the input transistor. The preamplifier provides gain and feeds a pulse shaper, which tailors the overall frequency response to optimize signal-to-noise ratio while limiting the duration of the signal pulse to accommodate the signal pulse rate. Even if not explicitly stated, all amplifiers provide some form of pulse shaping due to their limited frequency response.

The equivalent circuit for the noise analysis (Fig. 35.19) includes both current and voltage noise sources. The leakage current of a semiconductor detector, for example, fluctuates due to continuous electron emission statistics. The statistical fluctuations in the charge measurement will scale with the square root of the total number of recorded charges, so this noise contribution increases with the width of the shaped output pulse. This “shot noise”  $i_{nd}$  is represented by a current noise generator in parallel with the detector. Resistors exhibit noise due to thermal velocity fluctuations of the charge carriers. This yields a constant noise power density vs. frequency, so increasing the bandwidth of the shaped output pulse, *i.e.* reducing the shaping time, will increase the noise. This noise source can be modeled either as a voltage or current generator. Generally, resistors shunting the input act as noise current sources and resistors in series with the input act as noise voltage sources (which is why some in the detector community refer to current and voltage noise as “parallel” and “series” noise). Since the bias resistor effectively shunts the input, as the capacitor  $C_b$  passes current fluctuations to ground, it acts as a current generator  $i_{nb}$  and its noise current has the same effect as the shot noise current from the detector. Any other shunt resistances can be incorporated in the same way. Conversely, the series resistor  $R_s$  acts as a voltage generator. The electronic noise of the amplifier is described fully by a combination of voltage and current sources at its input, shown as  $e_{na}$  and  $i_{na}$ .

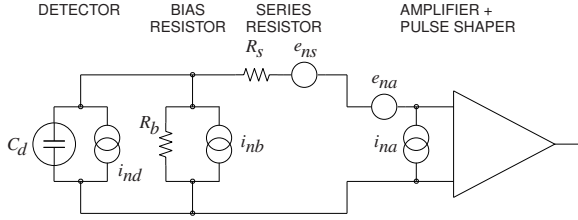


Figure 35.19: Equivalent circuit for noise analysis.

Shot noise and thermal noise have a “white” frequency distribution, *i.e.* the spectral power densities  $dP_n/df \propto di_n^2/df \propto de_n^2/df$  are constant with the magnitudes

$$\begin{aligned} i_{nd}^2 &= 2eI_d, \\ i_{nb}^2 &= \frac{4kT}{R_b}, \\ e_{ns}^2 &= 4kTR_s, \end{aligned} \quad (35.23)$$

where  $e$  is the electronic charge,  $I_d$  the detector bias current,  $k$  the Boltzmann constant and  $T$  the temperature. Typical amplifier noise parameters  $e_{na}$  and  $i_{na}$  are of order  $nV/\sqrt{\text{Hz}}$  and  $pA/\sqrt{\text{Hz}}$ . Trapping and detrapping processes in resistors, dielectrics and semiconductors can introduce additional fluctuations whose noise power frequently exhibits a  $1/f$  spectrum. The spectral density of the  $1/f$  noise voltage is

$$e_{nf}^2 = \frac{A_f}{f}, \quad (35.24)$$

where the noise coefficient  $A_f$  is device specific and of order  $10^{-10}$ – $10^{-12} \text{V}^2$ .

A fraction of the noise current flows through the detector capacitance, resulting in a frequency-dependent noise voltage  $i_n/(\omega C_d)$ , which is added to the noise voltage in the input circuit. Thus, the current noise contribution increases with lowering frequency, so its contribution increases with shaping pulse width. Since the individual noise contributions are random and uncorrelated, they add in quadrature. The total noise at the output of the pulse shaper is obtained by integrating over the full bandwidth of the system. Superimposed on repetitive detector signal pulses of constant magnitude, purely random noise produces a Gaussian signal distribution.

Since radiation detectors typically convert the deposited energy into charge, the system’s noise level is conveniently expressed as an equivalent noise charge  $Q_n$ , which is equal to the detector signal that yields a signal-to-noise ratio of one. The equivalent noise charge is commonly expressed in Coulombs, the corresponding number of electrons, or the equivalent deposited energy (eV). For a capacitive sensor

$$Q_n^2 = i_n^2 F_i T_S + e_n^2 F_v \frac{C^2}{T_S} + F_{vf} A_f C^2, \quad (35.25)$$

where  $C$  is the sum of all capacitances shunting the input,  $F_i$ ,  $F_v$ , and  $F_{vf}$  depend on the shape of the pulse determined by the shaper and  $T_S$  is a characteristic time, for example, the peaking time of a semi-gaussian pulse or the sampling interval in a correlated double sampler. The form factors  $F_i, F_v$  are easily calculated

$$F_i = \frac{1}{2T_S} \int_{-\infty}^{\infty} [W(t)]^2 dt, \quad F_v = \frac{T_S}{2} \int_{-\infty}^{\infty} \left[ \frac{dW(t)}{dt} \right]^2 dt, \quad (35.26)$$

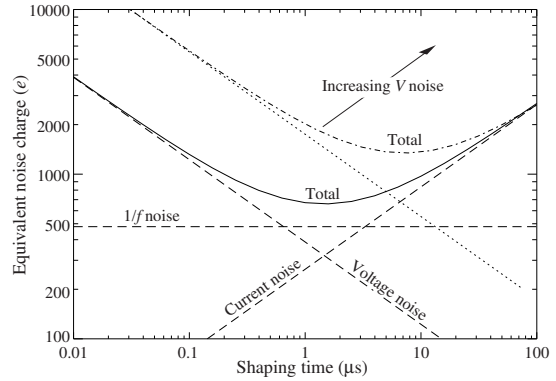
where for time-invariant pulse-shaping  $W(t)$  is simply the system’s impulse response (the output signal seen on an oscilloscope) for a short input pulse with the peak output signal normalized to unity. For more details see Refs. [194, 195] and [196, 197].

A pulse shaper formed by a single differentiator and integrator with equal time constants has  $F_i = F_v = 0.9$  and  $F_{vf} = 4$ , in-

dependent of the shaping time constant. The overall noise bandwidth, however, depends on the time constant, *i.e.* the characteristic time  $T_S$ . The contribution from noise currents increases with shaping time, *i.e.* pulse duration, whereas the voltage noise decreases with increasing shaping time, *i.e.* reduced bandwidth. Noise with a  $1/f$  spectrum depends only on the ratio of upper to lower cutoff frequencies (integrator to differentiator time constants), so for a given shaper topology the  $1/f$  contribution to  $Q_n$  is independent of  $T_S$ . Furthermore, the contribution of noise voltage sources to  $Q_n$  increases with detector capacitance. Pulse shapers can be designed to reduce the effect of current noise, *e.g.*, mitigate radiation damage. Increasing pulse symmetry tends to decrease  $F_i$  and increase  $F_v$  (*e.g.*, to 0.45 and 1.0 for a shaper with one  $CR$  differentiator and four cascaded integrators). For the circuit shown in Fig. 35.19,

$$\begin{aligned} Q_n^2 &= \left( 2eI_d + 4kT/R_b + i_{na}^2 \right) F_i T_S \\ &+ \left( 4kTR_s + e_{na}^2 \right) F_v C_d^2 / T_S + F_{vf} A_f C_d^2. \end{aligned} \quad (35.27)$$

As the characteristic time  $T_S$  is changed, the total noise goes through a minimum, where the current and voltage contributions are equal. Fig. 35.20 shows a typical example. At short shaping times the voltage noise dominates, whereas at long shaping times the current noise takes over. The noise minimum is flattened by the presence of  $1/f$  noise. Increasing the detector capacitance will increase the voltage noise and shift the noise minimum to longer shaping times.


 Figure 35.20: Equivalent noise charge *vs* shaping time. Changing the voltage or current noise contribution shifts the noise minimum. Increased voltage noise is shown as an example.

For quick estimates, one can use the following equation, which assumes an FET amplifier (negligible  $i_{na}$ ) and a simple  $CR$ – $RC$  shaper with time constants  $\tau$  (equal to the peaking time):

$$\begin{aligned} (Q_n/e)^2 &= 12 \left[ \frac{1}{\text{nA} \cdot \text{ns}} \right] I_d \tau + 6 \times 10^5 \left[ \frac{\text{k}\Omega}{\text{ns}} \right] \frac{\tau}{R_b} \\ &+ 3.6 \times 10^4 \left[ \frac{\text{ns}}{(\text{pF})^2 (\text{nV})^2 / \text{Hz}} \right] e_n^2 \frac{C^2}{\tau}. \end{aligned} \quad (35.28)$$

Noise is improved by reducing the detector capacitance and leakage current, judiciously selecting all resistances in the input circuit, and choosing the optimum shaping time constant. Another noise contribution to consider is that noise cross-couples from the neighboring front-ends in strip and pixel detectors through the inter-electrode capacitance.

The noise parameters of the amplifier depend primarily on the input device. In field effect transistors, the noise current contribution is very small, so reducing the detector leakage current and increasing the bias resistance will allow long shaping times with correspondingly lower noise. In bipolar transistors, the base current sets a lower bound on the noise current, so these devices are

best at short shaping times. In special cases where the noise of a transistor scales with geometry, *i.e.*, decreasing noise voltage with increasing input capacitance, the lowest noise is obtained when the input capacitance of the transistor is equal to the detector capacitance, albeit at the expense of power dissipation. Capacitive matching is useful with field-effect transistors, but not bipolar transistors. In bipolar transistors, the minimum obtainable noise is independent of shaping time, but only at the optimum collector current  $I_C$ , which does depend on shaping time.

$$Q_{n,\min}^2 = 4kT \frac{C}{\sqrt{\beta_{DC}}} \sqrt{F_i F_v} \quad \text{at} \quad I_c = \frac{kT}{e} C \sqrt{\beta_{DC}} \sqrt{\frac{F_v}{F_i}} \frac{1}{T_S}, \quad (35.29)$$

where  $\beta_{DC}$  is the DC current gain. For a  $CR$ - $RC$  shaper and  $\beta_{DC} = 100$ ,

$$Q_{n,\min}/e \approx 250 \sqrt{C/\text{pF}}. \quad (35.30)$$

Practical noise levels range from  $\sim 1e$  for CCD's at long shaping times to  $\sim 10^4 e$  in high-capacitance liquid argon calorimeters. Silicon strip detectors typically operate at  $\sim 10^3$  electrons, whereas pixel detectors with fast readout provide noise of several hundred electrons.

In timing measurements, the slope-to-noise ratio must be optimized, rather than the signal-to-noise ratio alone, so the rise time  $t_r$  of the pulse is important. The "jitter"  $\sigma_t$  of the timing distribution is

$$\sigma_t = \frac{\sigma_n}{(dS/dt)_{S_T}} \approx \frac{t_r}{S/N}, \quad (35.31)$$

where  $\sigma_n$  is the rms noise and the derivative of the signal  $dS/dt$  is evaluated at the trigger level  $S_T$ . To increase  $dS/dt$  without incurring excessive noise, the amplifier bandwidth should match the rise-time of the detector signal. The 10 to 90% rise time of an amplifier with bandwidth  $f_U$  is  $0.35/f_U$ . For example, an oscilloscope with 350 MHz bandwidth has a 1 ns rise time. When amplifiers are cascaded, which is invariably necessary, the individual rise times add in quadrature.

$$t_r \approx \sqrt{t_{r1}^2 + t_{r2}^2 + \dots + t_{rn}^2}. \quad (35.32)$$

Increasing signal-to-noise ratio also improves time resolution, so minimizing the total capacitance at the input is also important. At high signal-to-noise ratios, the time jitter can be much smaller than the rise time. The timing distribution may shift with signal level ("walk"), but this can be corrected by various means, either in hardware or software [198].

The basic principles discussed above apply to both analog and digital signal processing. In digital signal processing the pulse shaper shown in Fig. 35.18 is replaced by an analog to digital converter (ADC) followed by a digital processor that determines the pulse shape. Digital signal processing allows great flexibility in implementing filtering functions. The software can be changed readily to adapt to a wide variety of operating conditions and it is possible to implement filters that are impractical or even impossible using analog circuitry. However, this comes at the expense of increased circuit complexity and increased demands on the ADC compared to analog shaping.

If the sampling rate of the ADC is too low, high frequency components will be transferred to lower frequencies ("aliasing"). The sampling rate of the ADC must be high enough to capture the maximum frequency component of the input signal. Apart from missing information on the fast components of the pulse, under-sampling introduces spurious artifacts. If the frequency range of the input signal is much greater, the noise at the higher frequencies will be transferred to lower frequencies and increase the noise level in the frequency range of pulses formed in the subsequent digital shaper. The Nyquist criterion states that the sampling frequency must be at least twice the maximum relevant input frequency. This requires that the bandwidth of the circuitry preceding the ADC must be limited. The most reliable technique is to insert a low-pass filter.

The digitization process also introduces inherent noise, since the voltage range  $\Delta V$  corresponding to a minimum bit introduces

quasi-random fluctuations relative to the exact amplitude

$$\sigma_n = \frac{\Delta V}{\sqrt{12}}. \quad (35.33)$$

When the Nyquist condition is fulfilled the noise bandwidth  $\Delta f_n$  is spread nearly uniformly and extends to 1/2 the sampling frequency  $f_S$ , so the spectral noise density

$$e_n = \frac{\sigma_n}{\sqrt{\Delta f_n}} = \frac{\Delta V}{\sqrt{12}} \cdot \frac{1}{\sqrt{f_S/2}} = \frac{\Delta V}{\sqrt{6f_S}}. \quad (35.34)$$

Sampling at a higher frequency spreads the total noise over a larger frequency range, so oversampling can be used to increase the effective resolution. In practice, this quantization noise is increased by differential nonlinearity. Furthermore, the equivalent input noise of ADCs is often rather high, so the overall gain of the stages preceding the ADC must be sufficiently large for the preamplifier input noise to override.

When implemented properly, digital signal processing provides significant advantages in systems where the shape of detector signal pulses changes greatly, for example in large semiconductor detectors for gamma rays or in gaseous detectors (*e.g.* TPCs) where the duration of the current pulse varies with drift time, which can range over orders of magnitude. Where is analog signal processing best (most efficient)? In systems that require fast time response the high power requirements of high-speed ADCs are prohibitive. Systems that are not sensitive to pulse shape can use fixed shaper constants and rather simple filters, which can be either continuous or sampled. In high density systems that require small circuit area and low power (*e.g.* strip and pixel detectors), analog filtering often yields the required response and tends to be most efficient.

It is important to consider that additional noise is often introduced by external electronics, *e.g.* power supplies and digital systems. External noise can couple to the input. Often the "common grounding" allows additional noise current to couple to the current loop connecting the detector to the preamp. Recognizing additional noise sources and minimizing cross-coupling to the detector current loop is often important. Understanding basic physics and its practical effects is important in forming a broad view of the detector system and recognizing potential problems (*e.g.* modified data), rather than merely following standard recipes.

For a more detailed introduction to detector signal processing and electronics see Ref. [199] or the tutorial website <http://www-physics.lbl.gov/spieler>.

## 35.9 Calorimeters

### 35.9.1 Introduction

Revised August 2019 by D.E. Groom (LBNL).

A calorimeter is designed to measure a particle's (or jet's) energy and direction for an (ideally) contained electromagnetic (EM) or hadronic shower. The characteristic interaction distance for an electromagnetic interaction is the radiation length  $X_0$ , which ranges from  $13.8 \text{ g cm}^{-2}$  in iron to  $6.0 \text{ g cm}^{-2}$  in uranium.<sup>4</sup> Similarly, the characteristic nuclear interaction length  $\lambda_I$  varies from  $132.1 \text{ g cm}^{-2}$  (Fe) to  $209 \text{ g cm}^{-2}$  (U).<sup>5</sup> In either case, a calorimeter must be many interaction lengths deep, where "many" is determined by physical size, cost, and other factors. EM calorimeters tend to be  $15$ – $30 X_0$  deep, while hadronic calorimeters are usually compromised at  $5$ – $8 \lambda_I$ . In real experiments the shower begins in the EM calorimeter and then develops in a succession of different structures.

There is a premium on small  $\lambda_I/\rho$  and  $X_0/\rho$  (both with units of length). These quantities are shown for  $Z > 20$  for the chemical elements in Fig. 35.21. For the hadronic case, metallic absorbers in the W–Au region are best, followed by U. Elements in the Ru–Pd region are not used since they are too rare and expensive.

<sup>4</sup>  $X_0 = 120 \text{ g cm}^{-2} Z^{-2/3}$  to better than 5% for  $Z > 23$ .

<sup>5</sup>  $\lambda_I = 37.8 \text{ g cm}^{-2} A^{0.312}$  to within 0.8% for  $Z > 15$ .  
See [pdg.lbl.gov/AtomicNuclearProperties](http://pdg.lbl.gov/AtomicNuclearProperties) for actual values.

Given cost considerations, Fe, Cu, or Pb are generally appropriate. For EM calorimeters high  $Z$  is preferred; tungsten and lead are popular choices.

These considerations are for *sampling calorimeters* consisting of metallic absorber sandwiched or (threaded) with an active material which generates signal. The active medium may be a scintillator, an ionizing noble liquid, a gas, silicon, or a Cherenkov radiator. The average interaction length is thus greater than that of the absorber alone, sometimes substantially so.

There are also *homogeneous calorimeters*, in which the entire volume is sensitive, *i.e.*, contributes signal. Homogeneous calorimeters may be built with inorganic heavy (high density, high  $\langle Z \rangle$ ) scintillating crystals or non-scintillating Cherenkov radiators such as lead glass and lead fluoride. Scintillation light and/or ionization in noble liquids can be detected. Nuclear interaction lengths in inorganic crystals range from 17.8 cm (LuAlO<sub>3</sub>) to 42.2 cm (NaI). Popular choices have been BGO with  $\lambda_I = 22.3$  cm and  $X_0 = 1.12$  cm, and PbWO<sub>4</sub> (20.3 cm and 0.89 cm). Properties of these and other commonly used inorganic crystal scintillators can be found in Table-35.4.

Homogeneous calorimeters at accelerators are usually electromagnetic, but in non-accelerator physics experiments the sensitive medium can be water or ice, scintillator, or the atmosphere itself.

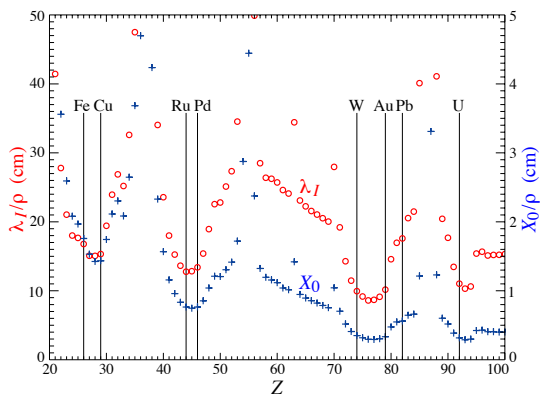


Figure 35.21: Nuclear interaction length  $\lambda_I/\rho$  (circles) and radiation length  $X_0/\rho$  (+'s) in cm for the chemical elements with  $Z > 20$  and  $\lambda_I < 50$  cm.

Comprehensive tables of particle-physics calorimeters are given as Appendix C in Ref. [200].

### 35.9.2 Electromagnetic calorimeters

Revised August 2019 by C.L. Woody (BNL) and R.-Y. Zhu (HEP California Inst. of Technology).

The development of electromagnetic showers is discussed in the section on “Passage of Particles Through Matter” (Sec. 34 of this *Review*). Formulae are given which approximately describe average showers, but since the physics of electromagnetic showers is well understood, a detailed and reliable Monte Carlo simulation is possible. EGS4 [201] and GEANT [202] have emerged as the standards.

Electromagnetic calorimeters are devices that are designed to measure the total energy of electrons and photons by total absorption. They come in two general categories: homogeneous and sampling. In a homogeneous calorimeter, all of the particle’s energy is deposited in the active detector volume and is used to produce a measurable signal (either scintillation light, Cherenkov light or charge). Homogeneous electromagnetic calorimeters are typically constructed using high density, high  $Z$  inorganic scintillating crystals such as BaF<sub>2</sub>, BGO, CsI, CsI(Tl), LYSO, NaI(Tl) and PWO, non-scintillating Cherenkov radiators such as lead glass and lead fluoride (PbF<sub>2</sub>), or ionizing noble liquids such as liquid argon, liquid krypton or liquid xenon. The properties of some commonly used inorganic crystal scintillators can be found in Table-35.4. Total absorption homogeneous calorimeters such as those built with heavy crystal scintillators provide the best energy resolution for

measuring electromagnetic showers and are generally used when the best possible performance is required, particularly at lower energies.

A sampling calorimeter consists of an active medium which generates a signal and a passive medium which functions as an absorber. In this case, most of the particle’s energy is deposited in the absorber and only a fraction of the energy is detected in the active medium. The ratio of energy in the sampling medium to the total energy in calorimeter is called the sampling fraction. The active medium may be a scintillator, an ionizing noble liquid, a semiconductor, or a gas ionization detector. The absorber is typically a heavy metal with a high  $Z$  such as lead, tungsten, iron, copper, or depleted uranium. The active material is interspersed with the passive absorber in a variety of ways, *e.g.* by using alternating plates of active material and absorber or embedding the active material, such as scintillating fibers, into the absorber. The main difficulty in this approach is extracting the signal from the active material. This can be done using a so-called “spaghetti” design, where scintillating fibers are brought to the front or back of the detector and read out. This can also be done with either wavelength shifting plates or fibers, such as in a so-called “shashlik” design where wavelength shifting fibers run through the stack of alternating scintillator and absorber plates and are read out at one end, or embedding wavelength shifting fibers in the scintillating plates which are then brought out to the edges or back of the detector and read out. For ionization detectors, there is also an “accordion” design where the absorber plates are folded into an accordion shape along with interspersed electrodes to collect the ionization charge [203]. While these readout schemes are generally more complicated than those for homogeneous calorimeters, the sampling calorimeter design allows the construction of large calorimeters at much lower cost than homogeneous calorimeters.

The energy resolution  $\sigma_E/E$  of a calorimeter can be parameterized as  $a/\sqrt{E} \oplus b \oplus c/E$ , where  $\oplus$  represents addition in quadrature and  $E$  is in GeV. The stochastic term  $a$  represents statistics-related fluctuations such as intrinsic shower fluctuations, photoelectron statistics, dead material at the front of the calorimeter, and sampling fluctuations for minimum ionizing particles. For a fixed number of radiation lengths, the stochastic term  $a$  for a sampling calorimeter is expected to be proportional to  $\sqrt{t/f}$ , where  $t$  is plate thickness and  $f$  is sampling fraction [204–206]. The stochastic term  $a$  is typically on the order of a few percent level for a homogeneous calorimeter, and is generally in the range of 10 to 20% for sampling calorimeters, depending on the sampling fraction.

The main contributions to the systematic, or constant, term  $b$  are detector non-uniformity and calibration uncertainties. In the case of hadronic cascades discussed below, non-compensation also contributes deviations from  $\sqrt{E}$  scaling. Another important contribution to the energy resolution of calorimeters that are used in high radiation environments such as high luminosity colliders is radiation damage of the active medium. Radiation damage can induce optical absorption in scintillating materials which reduces the measured light output and produces non-uniformities in light collection. This can be mitigated by developing radiation-hard active media [68], by reducing the signal path length [207] and by frequent *in situ* calibration and monitoring [67, 206]. With effort, the constant term  $b$  can be reduced to below one percent. The term  $c$  is due mainly to electronic noise summed over the readout channels required to measure the shower energy (typically a few Molière radii).

The position resolution depends on the effective Molière radius and the transverse granularity of the calorimeter. Like the energy resolution, it can be factored as  $a/\sqrt{E} \oplus b$ , where  $a$  is the stochastic term, typically on the order a few mm to 20 mm, and  $b$  can be as small as a fraction of mm for a dense calorimeter with fine granularity. Electromagnetic calorimeters may also provide directionality measurements for electrons and photons. This is particularly important for photon-related physics when there are uncertainties in the event origin, since photons are not detected by the tracking system of the overall experiment. The typical photon angular resolution is about  $45 \text{ mrad}/\sqrt{E}$ , which can be achieved by implementing longitudinal segmentation [203] for a



**Table 35.8:** Resolution of typical electromagnetic calorimeters.  $E$  is in GeV.

Technology (Experiment)	Depth	Energy resolution	Date
NaI(Tl) (Crystal Ball)	$20X_0$	$2.7\%/E^{1/4}$	1983
$\text{Bi}_4\text{Ge}_3\text{O}_{12}$ (BGO) (L3)	$22X_0$	$2\%/\sqrt{E} \oplus 0.7\%$	1993
CsI (KTeV)	$27X_0$	$2\%/\sqrt{E} \oplus 0.45\%$	1996
CsI(Tl) (BaBar)	$16\text{--}18X_0$	$2.3\%/E^{1/4} \oplus 1.4\%$	1999
CsI(Tl) (BELLE)	$16X_0$	1.7% for $E_\gamma > 3.5$ GeV	1998
CsI(Tl) (BES III)	$15X_0$	2.5% for $E_\gamma = 1$ GeV	2010
$\text{PbWO}_4$ (CMS)	$25X_0$	$3\%/\sqrt{E} \oplus 0.5\% \oplus 0.2/E$	1997
$\text{PbWO}_4$ (ALICE)	$19X_0$	$3.6\%/\sqrt{E} \oplus 1.2\%$	2008
Lead glass (OPAL)	$20.5X_0$	$5\%/\sqrt{E}$	1990
Liquid Kr (NA48)	$27X_0$	$3.2\%/\sqrt{E} \oplus 0.42\% \oplus 0.09/E$	1998
Scintillator/depleted U (ZEUS)	$20\text{--}30X_0$	$18\%/\sqrt{E}$	1988
Scintillator/Pb (CDF)	$18X_0$	$13.5\%/\sqrt{E}$	1988
Scintillator fiber/Pb spaghetti (KLOE)	$15X_0$	$5.7\%/\sqrt{E} \oplus 0.6\%$	1995
Liquid Ar/Pb (NA31)	$27X_0$	$7.5\%/\sqrt{E} \oplus 0.5\% \oplus 0.1/E$	1988
Liquid Ar/Pb (SLD)	$21X_0$	$8\%/\sqrt{E}$	1993
Liquid Ar/Pb (H1)	$20\text{--}30X_0$	$12\%/\sqrt{E} \oplus 1\%$	1998
Liquid Ar/depl. U (DØ)	$20.5X_0$	$16\%/\sqrt{E} \oplus 0.3\% \oplus 0.3/E$	1993
Liquid Ar/Pb accordion (ATLAS)	$25X_0$	$10\%/\sqrt{E} \oplus 0.4\% \oplus 0.3/E$	1996

sampling calorimeter or by adding a preshower detector [208] for a homogeneous calorimeter without longitudinal segmentation.

There have been many electromagnetic calorimeters built and used in particle physics experiments for a variety of applications. Table-35.8 provides a short list of the major ones used in some of the larger experiments. Also listed are calorimeter depths in radiation lengths ( $X_0$ ) and the achieved energy resolution. Whenever possible, the performance of the calorimeters *in situ* are quoted, which is usually in good agreement with prototype test beam results as well as EGS or GEANT simulations, provided that all systematic effects are properly included. Details about detector design and performance can be found in Appendix C of reference [206] and Proceedings of the International Conference series on Calorimetry in High Energy Physics.

### 35.9.3 Hadronic calorimeters

Revised August 2019 by D.E. Groom (LBNL).

Hadronic calorimetry [200, 209] is considerably more difficult than electromagnetic (EM) calorimetry due to the large differences in the character of energy deposition processes, the length of shower development, and the lumpy character of the depositions. Nuclear disassociation results in undetectable energy loss. For the same cascade containment fraction discussed in the previous section, the calorimeter would need to be  $\sim 10$  times deeper. Electromagnetic energy deposit from the decay of  $\pi^0$ 's produced in the cascade is usually detected with greater efficiency than are the hadronic parts of the cascade, themselves subject to large fluctuations in neutron production, undetectable energy loss to nuclear disassociation, and other effects [200].

Most large hadron calorimeters are parts of large  $4\pi$  detectors at colliding beam facilities. These have been sampling calorimeters: plates of absorber (Fe, Pb, U, or occasionally Cu or W) alternating with plastic scintillators (plates, tiles, bars, fibers), crystals, silicon, liquid argon (LAr), or gaseous detectors. The ionization is measured directly, or via scintillation or Cherenkov light observed by conventional photomultipliers (PMT's), photodiodes or silicon photomultipliers (SiPM's). Wavelength-shifting fibers are often used to solve difficult problems of geometry and light collection uniformity. There are as many variants of these schemes as there are calorimeters, including variations in geometry of the absorber and sensors, *e.g.*, scintillating fibers threading an absorber [210], and the "accordion" LAr detector [211]. The latter has zig-zag absorber plates to minimize channeling effects; the calorimeter is hermetic (no cracks), and plates are oriented so that cascades cross the same plate repeatedly. Another departure

from the traditional sandwich structure is the LAr-tube design shown in Fig. 35.22(a) [212].

Ideally the calorimeter is segmented in  $\phi$  and  $\theta$  (or  $\eta = -\ln \tan(\theta/2)$ ). An example, a wedge of the ATLAS central barrel calorimeter, is shown in Fig. 35.22(b) [213].

Calorimeters based on Cherenkov light detection are more usual in EM calorimeters, since comparatively little Cherenkov radiation is produced by the hadronic fraction of a shower. An important exception is the radiation-hard forward calorimeter in CMS, with iron absorber and quartz fibers read out by PMT's, and Cherenkov light detection is an essential half of dual-readout calorimetry.

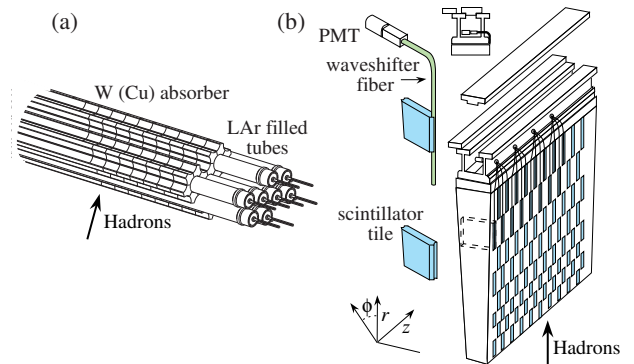


Figure 35.22: (a) ATLAS forward hadronic calorimeter structure (FCal2, 3) [212]. Tubes containing LAr are embedded in a mainly tungsten matrix. (b) ATLAS central calorimeter wedge; iron with plastic scintillator tile with wavelength-shifting fiber read-out [213].

The SICAPO collaboration has demonstrated the possibility of operating hadronic calorimeters using silicon sensors [214]. These satisfy the requirements required by the new generation of experiments, including compactness, high granularity, radiation hardness [215, 216], fast charge collection, and compensation via local hardening effects [217]. They are being studied for ILC detectors, and are part of the CMS HCAL upgrade.

High-granularity calorimeters play an increasingly important role. Greater segmentation has accordingly been an important part of LHC detector upgrades. For some time, the CALICE collaboration has built and tested an increasingly sophisticated

series of “tracking” calorimeters with a highly granular readout [218]. Most are EM (ECAL) and hadronic (HCAL) calorimeters with analog readout (scintillator plates), but digital (Sec. 35.6.7) and semidigital (Sec. 35.6.4) readouts are also explored. A recent example is a SiPM-on-tile readout HCAL with  $> 22,000$  channels [219].

Much of the following discussion assumes an idealized calorimeter, with the same structure throughout and without leakage.

In an inelastic hadronic collision a significant fraction  $f_{em}$  of the energy is removed from further hadronic interaction by the production of secondary  $\pi^0/\eta$ 's, whose decay photons generate high-energy electromagnetic showers. Charged secondaries ( $\pi^\pm, p, \dots$ ) deposit energy via ionization and excitation, but also interact with nuclei, producing evaporation neutrons, spallation protons and neutrons, and heavier spallation fragments. The charged collision products produce detectable ionization, as do the showering  $\gamma$ -rays from the prompt de-excitation of highly excited nuclei. The recoiling nuclei generate little or no detectable signal. The neutrons lose kinetic energy in elastic collisions, thermalize on a time scale of several  $\mu\text{s}$ , and are captured, with the production of more  $\gamma$ -rays—usually outside the acceptance gate of the electronics. Between endothermic spallation losses, nuclear recoils, and late neutron capture, a significant fraction of the hadronic energy (20%–40%, depending on the absorber and energy of the incident particle) is used to overcome nuclear binding energies and is therefore lost or “invisible.”

In contrast to EM showers, hadronic cascade processes are characterized by the production of relatively few high-energy particles. The lost energy and  $f_{em}$  are highly variable from event to event. Unless there is event-by-event knowledge of both the EM fraction and the invisible energy loss, the energy resolution of a hadron calorimeter is significantly worse than that of its EM counterpart.

The efficiency  $e$  with which EM deposit is detected varies from event to event, but because of the large multiplicity in EM showers the variation is small. In contrast, because a variable fraction of the hadronic energy deposit is detectable, the efficiency  $h$  with which hadronic energy is detected is subject to considerably larger fluctuations. It thus makes sense to consider the ratio  $h/e$  as a stochastic variable.

Most energy deposit is by very low-energy electrons and charged hadrons. Because so many generations are involved in a high-energy cascade, the hadron spectra in a given material are essentially independent of energy except for overall normalization [220,221]. For this reason  $\langle h/e \rangle$  is a robust concept, independently of hadron energy and species.

If the detection efficiency for the EM sector is  $e$  and that for the hadronic sector is  $h$ , then the ratio of the mean response to a pion relative to that for an electron is

$$\langle \pi/e \rangle = \langle f_{em} \rangle + \langle f_h \rangle \langle h/e \rangle = 1 - (1 - \langle h/e \rangle) \langle f_h \rangle \quad (35.35)$$

It has been shown by a simple induction argument and verified by simulation and experiment that the decrease in the average value of the hadronic energy fraction  $\langle f_h \rangle = 1 - \langle f_{em} \rangle$  as the projectile energy  $E$  increases is fairly well described by the power law [220,221]

$$\langle f_h \rangle \approx (E/E_0)^{m-1} \quad (\text{for } E > E_0), \quad (35.36)$$

at least up to a few hundred GeV. The exponent  $m$  depends logarithmically on the mean multiplicity and the mean fractional loss to  $\pi^0$  production in a single interaction. It is in the range 0.80–0.87, depending on the composition of the absorber. The scale factor  $E_0$ , roughly the energy for the onset of inelastic collisions, is 1 GeV or a little less for incident pions [221]. Both  $m$  and  $E_0$  must be obtained experimentally for a given calorimeter configuration.

Only the product  $(1 - \langle h/e \rangle)E_0^{1-m}$  can be obtained by measuring  $\langle \pi/e \rangle$  as a function of energy. Since  $1 - m$  is small and  $E_0 \approx 1$  GeV for pion-induced cascades, this fact is usually ignored and  $\langle h/e \rangle$  or the usual  $\langle e/h \rangle$  is reported.

In a hadron-nucleus collision a large fraction of the incident energy is carried by a “leading particle” with the same quark content as the incident hadron. If the projectile is a charged pion, the

leading particle is usually a pion, which can be neutral and hence contributes to the EM sector. This is not true for incident protons. The result is an increased mean hadronic fraction for incident protons: The power  $m$  is the same, but  $E_0 \approx 2.6$  GeV [221–224]. Data obtained by Akhurin *et al.* [223] with a quartz-fiber calorimeter indicate that proton-induced showers are shorter than pion-induced showers, and the resolution is substantially better. The “leading particle” effect evidently persists as the shower develops.

By definition,  $0 \leq f_{em} \leq 1$ . With increasing energy  $\langle f_{em} \rangle \rightarrow 1$ , while its variance,  $\sigma_{f_{em}}^2$ , decreases slowly [222]. For  $\langle h/e \rangle \neq 1$  (*noncompensation*), fluctuations in  $f_{em}$  significantly contribute to or even dominate the resolution. Since the  $f_{em}$  distribution has a high-energy tail, the calorimeter response is non-Gaussian with a high-energy tail if  $\langle h/e \rangle < 1$ . Noncompensation thus seriously degrades resolution and produces a nonlinear response. It is clearly desirable to *compensate* the response, *i.e.*, to design the calorimeter such that  $\langle h/e \rangle = 1$ . *This is possible only with a sampling calorimeter*, where several variables can be chosen or tuned:

1. Decrease the EM sensitivity. EM cross sections increase with  $Z$ ,<sup>||</sup> and most of the energy in an EM shower is deposited by low-energy electrons. A disproportionate fraction of the EM energy is thus deposited in the higher- $Z$  absorber. Lower- $Z$  cladding, such as the steel cladding on ZEUS U plates, preferentially absorbs low-energy  $\gamma$ 's in EM showers and thus also lowers the electronic response. The degree of EM signal suppression can be tuned by varying the sensor/absorber thickness ratio.

*Hardening:* The SICIPO collaboration has shown that the response of a W (or Pb) plate EM calorimeter is reduced by low- $Z$  absorbers (G10) in contact with the silicon sensors. This is understood to result of the G10 absorbing electrons below the critical energy ( $E_c$ ) in the W or Pb [225]. They also showed that interspersing low- $Z$  layers (Fe, with large  $E_c$ ) with high- $Z$  layers (Pb, low  $E_c$ ) dramatically modified the response of a hadron calorimeter. In either case, ionization energy losses begin to dominate below  $E_c$ . The energy spectrum of shower electrons becomes softer when moving from the Pb to the Fe, with the Fe producing the same filtering effect as G10.  $\langle e/h \rangle$  ranging from 0.89 to 1.11 was obtained with various combinations of Pb and Fe plates [217].

2. *Software compensation* provides another approach to decreasing the EM sensitivity. It takes advantage of the fact that in heavy absorbers the radiation length is much smaller than the nuclear interaction length. As a result, showers from  $\pi^0/\eta$  decay are fairly local. Given sufficient segmentation, the contribution of these “hot spots” can be given lower weight in summing the energy deposit, effectively decreasing  $f_{em}$ . Software compensation was first exploited in the CDMS detector [226]. Even with its few longitudinal segments, resolution was substantially improved for single particles of known high energy. It was further developed for the H1 [227] and ATLAS [228] detectors. Three-dimensional granularity considerably extends these techniques. For example, a 2007 CERN SPS study with the CALICE analog scintillator-steel hadronic calorimeter (AHCAL, with 7608 scintillator cells) obtained a 12–25% resolution improvement for 10–80 GeV incident  $\pi^\pm$ 's [229,230]. Jets are more problematical, in part because of the nonlinear response to the large fraction of their particles with  $E < 10$  GeV.
3. Increase the hadronic sensitivity. The abundant neutrons produced in the cascade have large  $n$ - $p$  elastic scattering cross sections, so that low-energy scattered protons are produced in hydrogenous sampling materials such as butane-filled proportional counters or plastic scintillator. The number of spallation neutrons is highly correlated with missing energy. (The maximal fractional energy loss when a neutron scatters from a nucleus with mass number  $A$  is  $4A/(1+A)^2$ .) The down side in the scintillator case is that the signal from a highly-ionizing stopping proton can be reduced by as much as 90%

<sup>||</sup>The asymptotic pair-production cross section scales roughly as  $Z^{0.75}$ , and  $|dE/dx|$  slowly decreases with increasing  $Z$ .

by recombination and quenching (Birks' Law, Eq. (35.2)).

4. Fabjan and Willis proposed that the additional signal generated in the aftermath of fission in  $^{238}\text{U}$  absorber plates should compensate nuclear fluctuations [231]. The production of fission fragments due to fast  $n$  capture was later observed [232]. However, while a very large amount of energy is released, it is mostly carried by low-velocity, very highly ionizing fission fragments produce very little observable signal because of recombination and quenching. In fact much of the compensation observed with the ZEUS and DØ  $^{238}\text{U}$ /scintillator calorimeters was mainly the result of mechanisms 1 and 3 above.

Motivated very much by the work of Brau, Gabriel, Brückmann, and Wigmans in 1985–87 [233–236], several groups explored a variety of compensation mechanisms and built calorimeters which were very nearly compensating. The degree of compensation was sensitive to the acceptance gate width, and so could be somewhat further tuned. Examples are given in Table 35.9.

Another approach to compensation is provided by a *dual-readout calorimeter*, in which the signal is sensed by two readout systems with highly contrasting  $\langle h/e \rangle$ . The concept, proposed by Mockett in 1983 [246], has been explored by a number of others since. Winn and Worstell, for example, proposed using an “orange” scintillator, observing the ionization contribution through an orange filter and the Cherenkov contribution through a blue filter [247]. The dual-readout technique was implemented by the DREAM collaboration in the late 1990's [248,249]. The test beam calorimeter consisted of copper tubes, each filled with scintillator and quartz fibers. If the two signals  $C$  and  $S$  (quartz and scintillator) are both normalized to electron response, then for each event Eq. (35.35)

$$\begin{aligned} C &= E[f_{em} + \langle h/e \rangle_C (1 - f_{em})] \\ S &= E[f_{em} + \langle h/e \rangle_S (1 - f_{em})]. \end{aligned} \quad (35.37)$$

On a scatter plot of  $C$  vs  $S$  (or  $C/E$  vs  $S/E$ ), events scatter about a line-segment locus, as shown in Fig. 35.23 [222]. With increasing energy the distribution moves upward along the locus and becomes tighter. Equations 35.37 are linear in  $1/E$  and  $f_{em}$ , and are easily solved to obtain estimators of the *corrected* energy and  $f_{em}$  for each event. Both are subject to resolution effects, but contributions due to fluctuations in  $f_{em}$  are eliminated. The solution for the corrected energy is given by [222]:

$$E = \frac{\xi S - C}{\xi - 1}, \quad \text{where } \xi = \frac{1 - \langle h/e \rangle_C}{1 - \langle h/e \rangle_S}. \quad (35.38)$$

Here  $\xi$  is the energy-independent slope of the event locus on a plot of  $C$  vs  $S$ . It can be found either from the fitted slope or by measuring  $\pi/e$  as a function of  $E$ . The slope  $\xi$  must be as far from unity as possible to optimize resolution, which in practical terms means that the scintillator readout of the calorimeter must be as compensating as possible [250].

The fractional energy resolution in an ideal calorimeter can be represented by

$$\frac{\sigma}{E} = \frac{a_1(E)}{\sqrt{E}} \oplus [1 - \langle h/e \rangle] \sigma_{f_{em}}, \quad (35.39)$$

where  $\sigma_{f_{em}}^2$  is the variance of  $f_{em}$  [222]. The coefficient  $a_1$  is expected to have mild energy dependence for a number of reasons. For example, the sampling variance contribution to  $a_1$  is  $(\pi/e)E$  rather than  $E$ .  $\sigma_{f_{em}}$  slowly decreases with increasing energy, as discussed above. Usually a plot of  $(\sigma/E)^2$  vs  $1/E$  is well described by a straight line (constant  $a_1$ ) with a finite intercept—the right term in Eq. (35.39), is called “the constant term.” Precise data show the slight downturn of  $a_1$  [210,222].

Although the usually-dominant contribution of the  $f_{em}$  distribution to the resolution can be minimized by compensation or the use of dual calorimetry, there remain significant contributions to the resolution:

1. Incomplete corrections for leakage, differences in light collection efficiency, and electronics calibration.

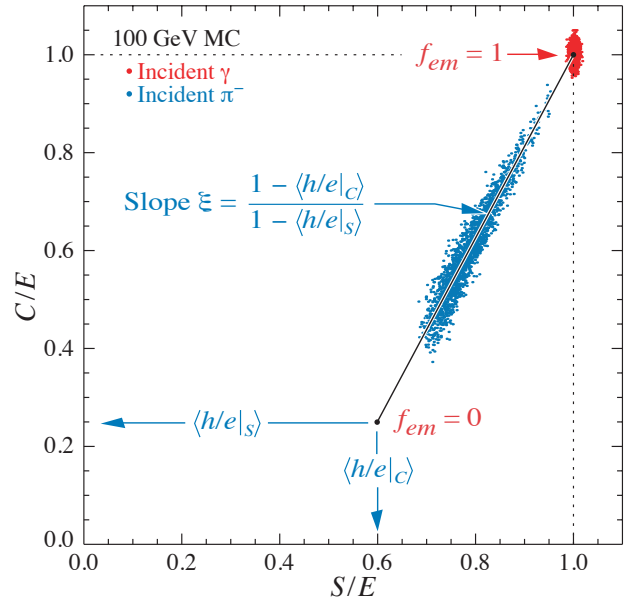


Figure 35.23: Scatter plot of Monte Carlo  $C/E$  (Cherenkov) vs  $S/E$  (scintillator) signals for individual events in a dual readout calorimeter. Hadronic events are shown in blue, and scatter about the indicated event locus. Electromagnetic events cluster about  $(C/E, S/E) = (1,1)$ . In this case worse resolution (fewer p.e.'s) was assumed for the Cherenkov events, leading to the “elliptical” distribution.

2. Readout transducer shot noise (usually photoelectron statistics), plus electronic noise.
3. Sampling fluctuations. Only a small part of the energy deposit takes place in the scintillator or other sensor, and that fraction is subject to large fluctuations. It depends on the sensor/absorber ratio, often chosen to achieve compensation. If this is the case, it is small in the scint/Fe and somewhat more forgiving in the scint/U case.
4. Intrinsic fluctuations. The many ways ionization can be produced in a hadronic shower have different detection efficiencies and are subject to stochastic fluctuations. In particular, a very large fraction of the hadronic energy is “invisible.” The lost fraction depends on the readout—it will be greater for a Cherenkov readout, less for an organic scintillator readout.

Except in a sampling calorimeter especially designed for the purpose, sampling and intrinsic resolution contributions cannot be separated. This may have been best studied by Drews *et al.* [240], who used a calorimeter in which even- and odd-numbered scintillators were separately read out. Sums and differences of the variances were used to separate sampling and intrinsic contributions.

The above discussion concerns stand-alone hadron calorimeters that exist only in test beams. In a collider experiment there is a central tracker in a magnetic field, then an EM calorimeter, a sequence of calorimeters, and finally a possible muon detector. Particle flow analysis uses all available information in analyzing the event [251,252]. The tracker supplies the charged particle positions and momenta, the EM calorimeter the  $\gamma$  energy (and some hadronic energy), and the hadron calorimeter the energy deposit from neutral hadrons as well as the most of the energy deposit from the particles observed in the tracker. Good calorimeter granularity is essential. Simulations via GEANT4 [253,254] support the analysis as well as the development of new analysis algorithms.

Despite the central importance of particle flow analysis, further discussion is beyond the scope of this specialized description of hadron calorimeters.

As a last topic, we discuss the mean spatial distribution of



**Table 35.9:** Examples of near-compensating sampling hadron calorimeters. For our present purposes some calorimeter structure variation and “constant terms” in the fitted resolution have been ignored.

Calorimeter	Passive	Active	Resolution	$\langle e/h \rangle$	Reference
(Akesson <i>et al.</i> )	U, U/Cu (3/5 m)	Scint (2.5mm)	$36\%/\sqrt{E}$	1.11	[237]
HELIOS	U (3 mm)	Scint (2.5 mm)	$34\%/\sqrt{E}$	$1.016 \pm 0.006$	[238]
(Drews <i>et al.</i> )	Pb (10 mm)	Scint (2.5 mm)	$44\%/\sqrt{E}$	$1.10 \pm 0.01$	[239, 240]
(Drews <i>et al.</i> )	U (3.2 mm)	Scint (3.0 mm)	$36\%/\sqrt{E}$	$1.02 \pm 0.01$	[240]
WA80	U (3 mm)	Scint (3 mm)	$67\%/\sqrt{E}$	1.12	[241]
ZEUS FCAL	U (3.0/3.2 mm)	Scint (2,5/3.0 mm)	$35\%/\sqrt{E}$	0.97	[242, 243]
SPACAL	Pb (4× scint vol)	1 mm scint fibers	$30\%/\sqrt{E}$	$1.15 \pm 0.02$	[244]
SICAPO	Fe/Pb	Si		$1.11-0.89^*$	[217]
DØ	U (6 mm) <sup>†</sup>	LAr (2 × 2.3)	$44\%/\sqrt{E}$	1.08	[245]

\* SICAPO: Various Fe/Pb configurations, G10 plates next to Si detectors.

† DØ: 1 mm G10 between LAr gaps may help compensation.

hadronic cascades. After the first interaction of the incident hadron, the average longitudinal distribution rises to a smooth peak whose position increases slowly with energy. The distribution becomes nearly exponential after several interaction lengths. Examples from the CDHS magnetized iron-scintillator sandwich calorimeter test beam calibration runs [255] and the ATLAS TileCal results [224] are shown in Fig. 35.24. Proton-induced cascades are somewhat shorter and broader than pion-induced cascades [224]. A gamma distribution fairly well describes the longitudinal development of an EM shower, as discussed in Sec. 34.5. Following this logic, Bock *et al.* suggested that the profile of a hadronic cascade could be fitted by the sum of two  $\Gamma$  distributions, one with a characteristic length  $X_0$  and the other with length  $\lambda_I$  [256, 257]. Fits to this 4-parameter function are commonly used, *e.g.*, by the ATLAS TileCal collaboration [224]. If the interaction point is not known (the usual case), the distribution must be convoluted with an exponential in the interaction length of the incident particle. Adragna *et al.* give an analytic form for the convoluted function [224].

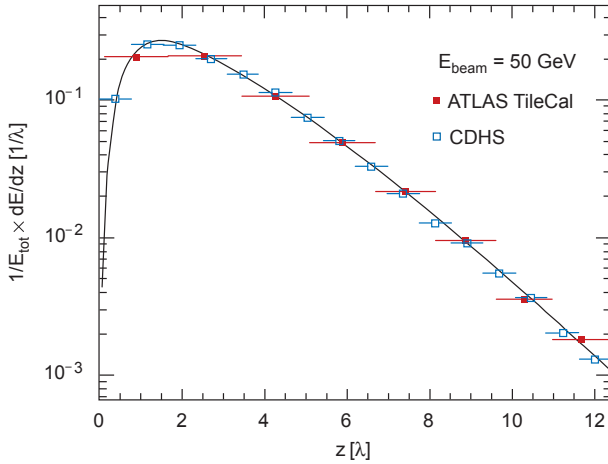


Figure 35.24: Mean profiles of  $\pi^+$  (mostly) induced cascades in the CDHS neutrino detector [255] and in the ATLAS tile calorimeter [224]. Measurements are front of the calorimeter, and so are convoluted with the first interaction distance.

The transverse energy deposit is characterized by a central core dominated by EM cascades, together with a wide “skirt” produced by wide-angle hadronic interactions [258].

While the average distributions might be useful in designing a calorimeter, they have little meaning for individual events, whose distributions are extremely variable because of the small number of particles involved early in the cascade.

Particle identification, primarily  $e-\pi$  discrimination, is accomplished in most calorimeters by observing the depth development. An EM shower is mostly contained in  $15X_0$  while a

hadronic shower takes about  $4\lambda_I$ . In high- $A$  absorbers such as Pb,  $X_0/\lambda_I \sim 0.03$ . In a fiber calorimeter, such as the RD52 dual-readout calorimeter,  $e-\pi$  discrimination is achieved by differences in the Cerenkov and scintillation signals, lateral spread, and timing differences, ultimately achieving about 500:1 discrimination [259].

### 35.9.4 Free electron drift velocities in liquid ionization chambers

Revised August 2009 by W. Walkowiak (Siegen U.).

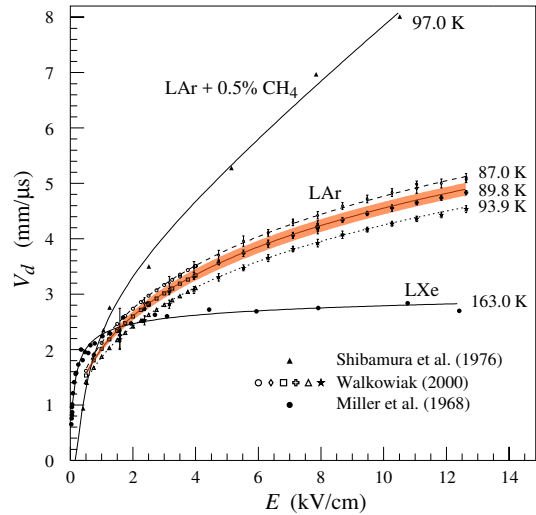


Figure 35.25: Drift velocity of free electrons as a function of electric field strength for LAr [260], LAr + 0.5% CH<sub>4</sub> [261] and LXe [262]. The average temperatures of the liquids are indicated. Results of a fit to an empirical function [263] are superimposed. In case of LAr at 91 K the error band for the global fit [260] including statistical and systematic errors as well as correlations of the data points is given. Only statistical errors are shown for the individual LAr data points.

Drift velocities of free electrons in LAr [260] are given as a function of electric field strength for different temperatures of the medium in Fig. 35.25. The drift velocities in LAr have been measured using a double-gridded drift chamber with electrons produced by a laser pulse on a gold-plated cathode. The average temperature gradient of the drift velocity of the free electrons in LAr is described [260] by

$$\frac{\Delta v_d}{\Delta T v_d} = (-1.72 \pm 0.08) \%/\text{K}. \quad (35.40)$$

Previous measurements [261, 262, 264, 265] range from 13% higher [262] to 18% lower [264] than these measurements. They

used different techniques and show drift velocities for free electrons which cannot be explained by the temperature dependence mentioned above.

Drift velocities of free electrons in LXe [261] as a function of electric field strength are also displayed in Fig. 35.25. The drift velocity saturates for  $|E| > 3$  kV/cm, and decreases with increasing temperature for LXe as well as measured e.g. by [266].

The addition of small concentrations of other molecules like  $N_2$ ,  $H_2$  and  $CH_4$  in solution to the liquid typically increases the drift velocities of free electrons above the saturation value [261, 264], see example for  $CH_4$  admixture to LAr in Fig. 35.25. Therefore, actual drift velocities are critically dependent on even small additions or contaminations.

## 35.10 Accelerator-based neutrino detectors

Revised August 2017 by M.O. Wascko (Imperial Coll. London).

### 35.10.1 Introduction

Accelerator-based neutrino experiments span many orders of magnitude in neutrino energy, from a few MeV to hundreds of GeV. This wide range of neutrino energy is driven by the many physics applications of accelerator-based neutrino beams. Foremost among them is neutrino oscillation, which varies as the ratio  $L/E_\nu$ , where  $L$  is the neutrino baseline (distance traveled), and  $E_\nu$  is the neutrino energy. But accelerator-based neutrino beams have also been used to study the nature of the weak interaction, to probe nucleon form factors and structure functions, and to study nuclear structure.

The first accelerator-based neutrino experiment used neutrinos from the decays of high energy pions in flight to show that the neutrinos emitted from pion decay are different from the neutrinos emitted by beta decay [267]. The field of accelerator-based neutrino experiments would likely not have expanded beyond this without Simon van der Meer's invention of the magnetic focusing horn [268], which significantly increased the flux of neutrinos aimed toward the detector. In this mini-review, we focus on experiments employing decay-in-flight beams—pions, kaons, charmed mesons, and taus—producing fluxes of neutrinos and antineutrinos from  $\sim 10$  MeV to  $\sim 100$  GeV.

Neutrino interactions with matter proceed only through the weak interaction, making the cross section extremely small and requiring high fluxes of neutrinos and large detector masses in order to achieve satisfactory event rates. Therefore, neutrino detector design is a balancing act taking into account sufficient numbers of nuclear targets (often achieved with inactive detector materials), adequate sampling/segmentation to ensure accurate reconstruction of the tracks and showers produced by neutrino-interaction secondary particles, and practical readout systems to allow timely analysis of data.

### 35.10.2 Signals and Backgrounds

The neutrino interaction processes available increase with increasing neutrino energy as interaction thresholds are crossed; in general neutrino-interaction cross sections grow with energy; for a detailed discussion of neutrino interactions see [269]. The multiplicity of secondary particles from each interaction process grows in complexity with neutrino energy, while the forward-boost due to increasing  $E_\nu$  compresses the occupied phase space in the lab frame, impacting detector designs. Because decay-in-flight beams produce neutrinos at well-defined times, leading to very small duty factors, the predominant backgrounds usually stem from unwanted beam-induced neutrino interactions, i.e. neutrinos interacting via other processes than the one being studied. A noteworthy exception is time projection chambers, wherein the long drift times can admit substantially more cosmic backgrounds than most other detection methods. Cosmic backgrounds are more rare at higher energies because the secondary particles produced by neutrino interactions yield detector signals that resemble cosmic backgrounds less and less.

Below, we describe a few of the dominant neutrino interaction processes, with a focus on the final state particle content and topologies.

### 35.10.2.1 Charged-Current Quasi-Elastic Scattering and Pion Production

Below  $\sim 2$  GeV neutrino energy, the dominant neutrino-nucleus interaction process is quasi-elastic (QE) scattering. In the charged current (CC) mode, the CCQE base neutrino reaction is  $\nu_\ell n \rightarrow \ell^- p$ , where  $\ell = e, \mu, \tau$ , and similarly for antineutrinos,  $\bar{\nu}_\ell p \rightarrow \ell^+ n$ . The final state particles are a charged lepton, and perhaps a recoiling nucleon if it is given enough energy to escape the nucleus. Detectors designed to observe this process should have good single-particle track resolution for muon neutrino interactions, but should have good  $\mu/e$  separation for electron neutrino interactions. Because the interaction cross section falls sharply with  $Q^2$ , the lepton typically carries away more of the neutrino's kinetic energy than the recoiling nucleon. The fraction of backward-scattered leptons is large, however, so detectors with  $4\pi$  coverage are desirable. The dominant backgrounds in this channel tend to come from single pion production events in which the pion is not detected.

Near 1 GeV, the quasi-elastic cross section is eclipsed by pion production processes. A typical single pion production ( $CC1\pi$ ) reaction is  $\nu_\ell n \rightarrow \ell^- \pi^+ n$ , but many more final state particle combinations are possible. Single pion production proceeds through the coherent channel and many incoherent processes, dominated by resonance production. With increasing neutrino energy, higher-order resonances can be excited, leading to multiple pions in the final state. Separating these processes from quasi-elastic scattering, and indeed from each other, requires tagging, and ideally reconstructing, the pions. Since these processes can produce neutral pions, electromagnetic (EM) shower reconstruction is more important here than it is for the quasi-elastic channel. The predominant backgrounds for pion production change with increasing neutrino energy. Detection of pion processes is also complicated because near threshold the quasi-elastic channel creates pion backgrounds through final state interactions of the recoiling nucleon, and at higher energies backgrounds come from migration of multiple pion events in which one or more pions is not detected.

### 35.10.2.2 Deep Inelastic Scattering

Beyond a few GeV, the neutrino has enough energy to probe the nucleon at the parton scale, leading to deep inelastic scattering (DIS). In the charged-current channel, the DIS neutrino reaction is  $\nu_\ell N \rightarrow \ell^- X$ , where  $N$  is a nucleon and  $X$  encompasses the entire recoiling hadronic system. The final state particle reconstruction revolves around accurate reconstruction of the lepton momentum and containment and reconstruction of the hadronic shower energy. Because of the high neutrino energies involved, DIS events are very forward boosted, and can have extremely long particle tracks. For this reason, detectors measuring DIS interactions must be large to contain the hadronic showers in the detector volume.

### 35.10.2.3 Neutral Currents

Neutrino interactions proceeding through the neutral current (NC) channel are identified by the lack of a charged lepton in the final state. For example, the NC elastic reaction is  $\nu_\ell N \rightarrow \nu_\ell N$ , and the NC DIS reaction is  $\nu_\ell N \rightarrow \nu_\ell X$ . NC interactions are suppressed relative to CC interactions by a factor involving the weak mixing angle; the primary backgrounds for NC interactions come from CC interactions in which the charged lepton is misidentified.

## 35.10.3 Instances of Neutrino Detector Technology

Below we describe many of the actual detectors that have been built and operated for use in accelerator-based neutrino beams.

### 35.10.3.1 Spark Chambers

In the first accelerator-based neutrino beam experiment, Lederman, Schwartz, and Steinberger [267] used an internally-triggered spark chamber detector, filled with 10 tons of Al planes and surrounded by external scintillator veto planes, to distinguish muon tracks from electron showers, and hence muon neutrinos from electron neutrinos. The inactive Al planes served as the neutrino interaction target and as radiators for EM shower development. The detector successfully showed the presence of muon tracks from neutrino interactions. It was also sensitive to the hadronic show-

**Table 35.10:** Properties of detectors for accelerator-based neutrino beams.

Name	Type	Target	Mass* (t)	Location	$\langle E_\nu \rangle$ (GeV)	Dates
Lederman et al.	Spark	Al	10	BNL	0.2–2	1962
CERN-spark	Spark	Al	20	CERN	1.5	1964
Serpukhov	Spark	Al	20	IHEP	4	1977
Aachen-Padova	Spark	Al	30	CERN	1.5	1976–77
Gargamelle	Bubble	Freon	6	CERN	1.5, 20	1972, 1977
BEBC	Bubble	H, D, Ne-H	2–42	CERN	50, 150 & 20	1977–84
SKAT	Bubble	Freon	8	IHEP	4	1977–1987
ANL-12ft	Bubble	H, D	1–2	ANL	0.5	1970
BNL-7ft	Bubble	H, D	0.4–0.9	BNL	1.3, 3	1976–82
Fermilab-15ft	Bubble	D, Ne	1–20	FNAL	50, 180 & 25, 100	1974–92
CITF	Iron	Fe	92	FNAL	50, 180	1977–83
CDHS	Iron	Fe	750	CERN	50, 150	1977–83
MINOS	Iron	Fe	980, 5.4k	FNAL	4–15	2005–2016
INGRID	Iron	Fe	99	J-PARC	0.7–3	2009–
Super-Kamiokande	Cherenkov	H <sub>2</sub> O	22,500	Kamioka	0.6	1996–
K2K-1kt	Cherenkov	H <sub>2</sub> O	25	KEK	0.8	1998–2004
MiniBooNE	Cherenkov	CH <sub>2</sub>	440	FNAL	0.6	2002–12
HWPF	Scintillation	CH <sub>2</sub>	2	FNAL	2	2014–
LSND	Scintillation	CH <sub>2</sub>	130	LANL	0.06	1993–98
NOvA	Scintillation	CH <sub>2</sub>	300, 14k	FNAL/Ash River	2	2013–
SciBar	Scintillation	CH	12	KEK/FNAL	0.8, 0.6	2004, 2007–8
ICARUS	LArTPC	Ar	760	LNGS	20	2006–12
Argoneut	LArTPC	Ar	0.025	FNAL	3	2009–10
MicroBooNE	LArTPC	Ar	170	FNAL	0.8	2014–
FNAL-E-531	Emulsion	Ag, Br	0.009	FNAL	25	1984
CHORUS	Emulsion	Ag, Br	1.6	CERN	20	1995
DONuT	Emulsion	Fe	0.26	FNAL	100	1997
OPERA	Emulsion	Pb	1.3k	LNGS	20	2006–12
NINJA	Emulsion	Fe	0.001	J-PARC	0.6	2016–
CHARM	Hybrid	CaCO <sub>3</sub>	150	CERN	20	1977
CHARM-II	Hybrid	glass	692	CERN	20	1983
BNL-E-734	Hybrid	CH <sub>2</sub>	172	BNL	1.3	1987
BNL-E-776	Hybrid	concrete	240	BNL	3	1990
NOMAD	Hybrid	CH	3	CERN	20	1995–98
CCFR	Hybrid	Fe	690	FNAL	90, 260	1991
NuTeV	Hybrid	Fe	690	FNAL	70, 180	1996–97
MINERvA	Hybrid	CH, H <sub>2</sub> O, Fe, Pb, C, He	8	FNAL	3, 8	2009–
T2K-ND280	Hybrid	CH, H <sub>2</sub> O, Pb, Cu	4	J-PARC	0.6	2009–

\*Fiducial.

ers induced by NC interactions, which were unknown at the time. In 1963, CERN also built and ran a large (20 ton) Al plane spark chamber in a wideband beam based on the PS accelerator [270]. More than a decade later, the Aachen-Padova [271] experiment at CERN employed a 30 ton Al spark chamber in the PS-WBB.

### 35.10.3.2 Bubble Chambers

Several large bubble chamber detectors were employed as accelerator neutrino detectors in the 1970s and 80s, performing many of the first studies of the properties of the weak interaction. Bubble chambers provide exquisite granularity in the reconstruction of secondary particles, allowing very accurate separation of interaction processes. However, the extremely slow and labor-intensive acquisition and analysis of the data from photographic film led to them being phased out in favor of electronically read out detectors.

The Gargamelle [272] detector at CERN used Freon and propane gas targets to make the first observation of neutrino-induced NC interactions and more. The BEBC [273] detector at CERN was a bubble chamber that was alternately filled with liquid hydrogen, deuterium, and a neon-hydrogen mixture; BEBC was also outfitted with a track-sensitive detector to improve event tagging, and sometimes used with a small emulsion chamber. The SKAT [274] Freon bubble chamber was exposed to wideband neutrino and antineutrino beams at the Serpukhov laboratory in the former Soviet Union. A series of American bubble chambers in the 1970's and 1980's made measurements on free nucleons that

are still crucial inputs for neutrino-nucleus scattering predictions. The 12-foot bubble chamber at ANL [275] in the USA used both deuterium and hydrogen targets, as did the 7-foot bubble chamber at BNL [276]. Fermilab's 15 foot bubble chamber [277] used deuterium and neon targets.

### 35.10.3.3 Iron Tracking Calorimeters

Because of the forward boost of high energy interactions, long detectors made of magnetized iron interspersed with active detector layers have been very successfully employed. The long magnetized detectors allow measurements of the momentum of penetrating muons. The iron planes also act as shower-inducing layers, allowing separation of EM and hadronic showers; the large number of iron planes provide enough mass for high statistics and/or shower containment. Magnetized iron spectrometers have been used for studies of the weak interaction, measurements of structure functions, and searches for neutrino oscillation. Non-magnetized iron detectors have also been successfully employed as neutrino monitors for oscillation experiments and also for neutrino-nucleus interaction studies.

The Caltech-Fermilab counter (CITF) [275] combined a 92 ton iron-scintillator target-calorimeter detector with a downstream toroidal magnet to perform early studies of weak interactions—including observations of neutral currents. The CDHS [278] detector used layers of magnetized iron modules interspersed with wire drift chambers, with a fiducial mass of 750 t, to detector neutrinos in the range 30–300 GeV. Within each iron module,

5 cm (or 15 cm) iron plates were interspersed with scintillation counters. The MINOS [279] detectors, a near detector of 980 t at FNAL and a far detector of 5400 t in the Soudan mine, were functionally identical magnetized iron calorimeters, comprised of iron plates interleaved with layers of 4 cm wide plastic scintillator strips in alternating orientations. The T2K [280] on-axis detector, INGRID, consists of 16 non-magnetized iron scintillator sandwich detectors, each with nine 6.5 cm iron plane (7.1 t total) interspersed between layers of 5 cm wide plastic scintillator strips readout out by multi-pixel photon counters (MPPCs) coupled to WLS fibers. Fourteen of the INGRID modules are arranged in a cross-hair configuration centered on the neutrino beam axis.

#### 35.10.3.4 Cherenkov Detectors

Open volume water Cherenkov detectors were originally built to search for proton decay. Large volumes of ultra-pure water were lined with photomultipliers to collect Cherenkov light emitted by the passage of relativistic charged particles. See Sec. 36.3.1 for a detailed discussion of deep liquid detectors for rare processes. The Cherenkov light, which has significant production in the visible range, appears on the walls of the detectors in distinctive ring patterns, and topological characteristics of the rings are employed to separate muon-induced rings from electron-induced with very high accuracy. As neutrino detectors, Cherenkov detectors optimize the design balance since the entire neutrino target is also active detector medium.

When used to detect  $\sim$  GeV neutrinos, the detector medium acts as a natural filter for final state particles below the Cherenkov threshold; this feature has been exploited successfully by the K2K, MiniBooNE (using mineral oil instead of water), and T2K neutrino oscillation experiments. This makes event reconstruction simple and robust since electrons and muons have very different signatures, but does require making assumptions when inferring neutrino energy since not all final state particles are observed. At higher energies Cherenkov detectors become less accurate because the overlapping rings from many final state particles become increasingly difficult to resolve.

The second-generation Cherenkov detector in Japan, Super-Kamiokande [78] (Super-K), comprises 22.5 kt of water viewed by 50 cm photomultiplier tubes with 40% photocathode coverage; it is surrounded by an outer detector region viewed by 20 cm photomultipliers. Super-K is the far detector for K2K and T2K, and is described in greater detail elsewhere in this review. The K2K experiment also employed a 1 kt water Cherenkov detector in the suite of near detectors [281], with 40% photocathode coverage. The MiniBooNE detector at FNAL was a 0.8 kt [282] mineral oil Cherenkov detector, with 20 cm photomultipliers giving 10% photocathode coverage, surrounded by a veto detector also with 20 cm photomultipliers.

#### 35.10.3.5 Scintillation Detectors

Liquid and solid scintillator detectors also employ fully (or nearly fully) active detector media. Typically organic scintillators, which emit into the ultraviolet range, are dissolved in mineral oil or plastic and read out by photomultipliers coupled to wavelength shifters (WLS). Open volume scintillation detectors lined with photomultipliers are conceptually similar to Cherenkov detectors, although energy reconstruction is calorimetric in nature as opposed to kinematic (see also Sec. 36.3.1). For higher energies and higher particle multiplicities, it becomes beneficial to use segmented detectors to help distinguish particle tracks and showers from each other.

The HWPf collaboration [283] employed a 2 t liquid scintillator total-absorption hadron calorimeter followed by a magnetic spectrometer to observe neutral current events in the early days of Fermilab. The LSND [284] detector at LANL was a 130 t open volume liquid scintillator detector employed to detect relatively low energy ( $<300$  MeV) neutrinos. The NOvA [285] detectors use segmented volumes of liquid scintillator in which the scintillation light is collected by WLS fibers in the segments that are coupled to avalanche photodiodes (APDs) at the ends of the volumes. The NOvA far detector, located in Ash River, MN, is comprised of 896 layers of 15.6 m long extruded PVC scintillator cells for a total mass of 14 kt; the NOvA near detector is comprised of 214 layers

of 4.1 m scintillator volumes for a total mass of 300 t. Both are placed in the NuMI beamline at  $0.8^\circ$  off-axis. The SciBar (Scintillation Bar) detector was originally built for K2K at KEK in Japan and then re-used for SciBooNE [286] at FNAL. SciBar used plastic scintillator strips with  $1.5\text{ cm} \times 2.5\text{ cm}$  rectangular cross section, read out by multianode photomultipliers (MAPMTs) coupled to WLS fibers, arranged in alternating horizontal and vertical layers. Both SciBooNE and K2K employed an EM calorimeter downstream of SciBar and a muon range detector (MRD) downstream of that.

#### 35.10.3.6 Liquid Argon Time Projection Chambers

Liquid argon time projection chambers (LAr-TPCs) were conceived in the 1970s as a way to achieve a fully active detector with sub-centimeter track reconstruction [287]. A massive volume of purified liquid argon is put under a strong electric field (hundreds of V/cm), so that the liberated electrons from the paths of ionizing particles can be drifted to the edge of the volume and read out, directly by collecting charge from wire planes or non-destructively through charge induction in the wire planes. A dual-phase readout method is also being developed, in which the charge is drifted vertically and then passed through an amplification region inside a gas volume above the liquid volume; the bottom of the liquid volume is equipped with a PMT array for detecting scintillation photons from the liquid argon. The first large scale LAr-TPC was the ICARUS T-600 module [288], comprising 760 t of liquid argon with a charge drift length of 1.5 m read out by wires with 3 mm pitch, which operated in LNGS, both standalone and also exposed to the CNGS high energy neutrino beam. The ICARUS detector has been transported to Fermilab and is being installed in an on-axis position in the Booster Neutrino Beamline, where it will also be exposed to off-axis neutrinos from the NuMI beamline. The ArgoNeuT [289] detector at FNAL, with fiducial mass 25 kg of argon read out with 4 mm pitch wires, was exposed to the NuMI neutrino and antineutrino beams. The MicroBooNE [290] detector at FNAL comprises 170 t of liquid Ar, read out with 3 mm wire pitch, which began collecting data in the Booster Neutrino Beam Oct 2015. A LAr-TPC has also been chosen as the detector design for the future DUNE neutrino oscillation experiment, from FNAL to Sanford Underground Research Facility; both single and dual phase modules are planned.

#### 35.10.3.7 Emulsion Detectors

Photographic film emulsions have been employed in particle physics experiments since the 1940s [291]. Thanks to advances in scanning technology and automation [292], they have been successfully employed as neutrino detectors. Emulsions are used for experiments observing CC tau neutrino interactions, where the short lifetime of the tau,  $\tau_\tau = 2.90 \times 10^{-13}$  s, leading to the short mean path length,  $c \times \tau = 87\ \mu\text{m}$ , requires extremely precise track resolution. They are employed in hybrid detectors in which the emulsion bricks are embedded inside fine-grained tracker detectors. In the data analysis, the tracker data are used to select events with characteristics typical of a tau decay in the final state, such as missing energy and unbalanced transverse momentum. The reconstructed tracks are projected back into an emulsion brick and used as the search seed for a neutrino interaction vertex.

E531 [293] at Fermilab tested many of the emulsion-tracker hybrid techniques employed by later neutrino experiments, in a detector with approximately 9 kg of emulsion target. The CHORUS [292] experiment at CERN used 1,600 kg of emulsion, in a hybrid detector with a fiber tracker, high resolution calorimeter, and muon spectrometer, to search for  $\nu_\mu \rightarrow \nu_\tau$  oscillation. The DONuT [294] experiment at FNAL used a hybrid detector, with 260 kg of emulsion bricks interspersed with fiber trackers, followed by a magnetic spectrometer, and calorimeter, to make the first direct observation of tau neutrino CC interactions. The OPERA [295] [296] [297] experiment used an automated hybrid emulsion detector, with 1,300 t of emulsion, to make the first direct observation of the appearance of  $\nu_\tau$  in a  $\nu_\mu$  beam. Recently, the NINJA collaboration has developed an emulsion cloud chamber detector to observe neutrinos in the J-PARC neutrino beam [298].

### 35.10.3.8 Hybrid Detectors

In the previous neutrino detector examples, one can point to a specific detection technology or configuration that defines a category of detectors. In this section we look at detectors that combine multiple elements or techniques, without one facet being specifically dominant or crucial; we call these detectors hybrids.

The CHARM detector [299] at CERN was built to study neutral-current interactions and search for muon neutrino oscillation. It was a fine-grained ionization calorimeter tracker with approximately 150 t of marble as neutrino target, surrounded by a magnetized iron muon system for tagging high angle muons, and followed downstream by a muon spectrometer. The CHARM II detector [300] at CERN comprised a target calorimeter followed by a downstream muon spectrometer. Each target calorimeter module consists of a 4.8 cm thick glass plate followed by a layer of plastic streamer tubes, with spacing 1 cm, instrumented with 2 cm wide pickup strips. Every fifth module is followed by a 3 cm thick scintillator layer. The total mass of the target calorimeter was 692 t.

The Brookhaven E-734 [301] detector was a tracking calorimeter made up of 172 t liquid scintillator modules interspersed with proportional drift tubes, followed by a dense EM calorimeter and a muon spectrometer downstream of that. The detector was exposed to a wideband horn-focused beam with peak neutrino energy near 1 GeV. The Brookhaven E-776 [302] experiment comprised a finely segmented EM calorimeter, with 2.54 cm concrete absorbers interspersed with planes of drift tubes and acrylic scintillation counters, with total mass 240 t, followed by a muon spectrometer.

The FNAL Lab-E neutrino detector was used by the CCFR [303] and NuTeV [304] collaborations to perform a series of experiments in the Fermilab high energy neutrino beam (50 GeV <  $E_\nu$  < 300 GeV). The detector was comprised of six iron target calorimeter modules, with 690 t total target mass, followed by three muon spectrometer modules, followed by two drift chambers. Each iron target calorimeter module comprised 5.2 cm thick steel plates interspersed with liquid scintillation counters and drift chambers.

The NOMAD [305] detector at CERN consisted of central tracker detector inside a 0.4 T dipole magnet (the magnet was originally used by the UA1 experiment at CERN) followed by a hadronic calorimeter and muon detectors downstream of the magnet. The main neutrino target is 3 t of drift chambers followed downstream by transition radiation detectors which are followed by an EM calorimeter. NOMAD was exposed to the same wideband neutrino beam as was CHORUS.

MINERvA [306] is a hybrid detector based around a central plastic scintillator tracker: 8.3 t of plastic scintillator strips with triangular cross section read out by MAPMTs coupled to WLS fibers. The scintillator tracker is surrounded by electromagnetic and hadronic calorimetry, which is achieved by interleaving thin lead (steel) layers between the scintillator layers for the ECAL (HCAL). MINERvA is situated upstream of the MINOS near detector which acts as a muon spectrometer. Upstream of the scintillator tracker is a nuclear target region containing inactive layers of C (graphite), Pb, Fe (steel), and O (water). MINERvA's physics goals span a wide range of neutrino-nucleus interaction studies, from form factors to nuclear effects.

T2K [280] in Japan employs two near detectors at 280 m from the neutrino beam target, one centered on the axis of the horn-focused J-PARC neutrino beam and one placed 2.5° off-axis. The on-axis detector, INGRID, is described above. The 2.5° off-axis detector, ND280, employs the UA1 magnet (at 0.2 T) previously used by NOMAD. Inside the magnet volume are three separate detector systems: the trackers, the Pi0 Detector (P0D), and several ECAL modules. The tracker detectors comprise two fine-grained scintillator detectors (FGDs), read out by MPPCs coupled to WLS fibers, interleaved between three gas TPCs read out by micromegas planes. The downstream FGD contains inactive water layers in addition to the scintillators. Upstream of the tracker is the P0D, a sampling tracker calorimeter with active detector materials comprising plastic scintillator read out by MPPCs and WLS fibers, and inactive sheets of brass radiators and refillable

water modules. Surrounding the tracker and P0D, but still inside the magnet, are lead-scintillator EM sampling calorimeters.

### 35.10.4 Outlook

Detectors for accelerator-based neutrino beams have been in use, and constantly evolving, for six decades now. The rich program of neutrino oscillation physics and attendant need for newer and better neutrino-nucleus scattering measurements means that more neutrino detectors with broader capabilities will be needed in the coming decades.

One of the most intriguing prospects is a large volume, high pressure gas time projection chamber (HPTPC). With the prospect of megawatt power accelerator-based neutrino beams, it is entirely feasible to collect high statistics data sets with a gas target. The low momentum thresholds for particle detection, and excellent momentum resolution and particle identification capabilities, of an HPTPC would open a new window into the physics of neutrino-nucleus scattering. Moreover, the ability to change the gas mixtures in the HPTPC would allow measurements in the same detector on multiple nuclear targets, which would, in turn, allow unprecedentedly accurate constraints and tuning of neutrino-nucleus interaction models.

## 35.11 Superconducting magnets for collider detectors

Revised August 2019 by Y. Makida (KEK).

### 35.11.1 Solenoid Magnets

In all cases SI unit are assumed, so that the magnetic field,  $B$ , is in Tesla, the stored energy,  $E$ , is in joules, the dimensions are in meters, and vacuum permeability of  $\mu_0 = 4\pi \times 10^{-7}$ .

The magnetic field ( $B$ ) in an simple solenoid with a flux return iron yoke, in which the magnetic field is lower than magnetic saturation of < 2 T, is given by

$$B = \frac{\mu_0 n I}{L} \quad (35.41)$$

where  $n$  is the number of turns,  $I$  is the current and  $L$  is the coil length.

In an air-core solenoid case, the central field is given by

$$B(0, 0) = \mu_0 n I \frac{1}{\sqrt{L^2 + 4R^2}}, \quad (35.42)$$

where  $R$  is the coil radius.

In most cases, momentum analysis is made by measuring the circular trajectory of the passing particles according to  $p = mv = qrB$ , where  $p$  is the momentum,  $m$  the mass,  $q$  the charge,  $r$  the bending radius. The sagitta,  $s$ , of the trajectory is given by

$$s = q B \ell^2 / 8p, \quad (35.43)$$

where  $\ell$  is the path length in the magnetic field. In a practical momentum measurement in colliding beam detectors, it is more effective to increase the magnetic volume than the field strength, since

$$dp/p \propto p/B \ell^2, \quad (35.44)$$

where  $\ell$  corresponds to the solenoid coil radius  $R$ . The energy stored in the magnetic field of any magnet is calculated by integrating  $B^2$  over all space:

$$E = \frac{1}{2\mu_0} \int B^2 dV \quad (35.45)$$

If the coil thin and inside an iron return yoke, (which is the case if it is to superconducting coil), then

$$E \approx (B^2/2\mu_0)\pi R^2 L. \quad (35.46)$$

For a detector in which the calorimetry is outside the aperture of the solenoid, the coil must be transparent in terms of radiation and absorption lengths. This usually means that the superconducting solenoid and its cryostat is of minimum real thickness and is made of a material with long radiation length. There are two major contributors to the thickness of a thin solenoid:

**Table 35.11:** Progress of superconducting magnets for particle physics detectors.

Experiment	Laboratory	$B$ [T]	Radius [m]	Length [m]	Energy [MJ]	$X/X_0$	$E/M$ [kJ/kg]
TOPAZ*	KEK	1.2	1.45	5.4	20	0.70	4.3
CDF*	Tsukuba/Fermi	1.5	1.5	5.07	30	0.84	5.4
VENUS*	KEK	0.75	1.75	5.64	12	0.52	2.8
AMY*	KEK	3	1.29	3	40	†	
CLEO-II*	Cornell	1.5	1.55	3.8	25	2.5	3.7
ALEPH*	Saclay/CERN	1.5	2.75	7.0	130	2.0	5.5
DELPHI*	RAL/CERN	1.2	2.8	7.4	109	1.7	4.2
ZEUS*	INFN/DESY	1.8	1.5	2.85	11	0.9	5.5
H1*	RAL/DESY	1.2	2.8	5.75	120	1.8	4.8
BaBar*	INFN/SLAC	1.5	1.5	3.46	27	†	3.6
D0*	Fermi	2.0	0.6	2.73	5.6	0.9	3.7
BELLE*	KEK	1.5	1.8	4	42	†	5.3
BES-III	IHEP	1.0	1.475	3.5	9.5	†	2.6
ATLAS-CS	ATLAS/CERN	2.0	1.25	5.3	38	0.66	7.0
ATLAS-BT	ATLAS/CERN	1	4.7–9.75	26	1080	(Toroid)†	
ATLAS-ET	ATLAS/CERN	1	0.825–5.35	5	2 × 250	(Toroid)†	
CMS	CMS/CERN	4	6	12.5	2600	†	12
SiD**	ILC	5	2.9	5.6	1560	†	12
ILD**	ILC	4	3.8	7.5	2300	†	13
SiD**	CLIC	5	2.8	6.2	2300	†	14
ILD**	CLIC	4	3.8	7.9	2300	†	
FCC**		6	6	23	54000	†	12

\* No longer in service  
\*\* Conceptual design in future  
† EM calorimeter is inside solenoid, so small  $X/X_0$  is not a goal

1. The conductor consisting of the current-carrying superconducting material (usually Nb-Ti/Cu) and the quench protecting stabilizer (usually aluminum) are wound on the inside of a structural support cylinder (usually aluminum also). The coil thickness scales as  $B^2R$ , so the thickness in radiation lengths ( $X_0$ ) is

$$t_{\text{coil}}/X_0 = (R/\sigma_h X_0)(B^2/2\mu_0), \quad (35.47)$$

where  $t_{\text{coil}}$  is the physical thickness of the coil,  $X_0$  the average radiation length of the coil/stabilizer material, and  $\sigma_h$  is the hoop stress in the coil [307].  $B^2/2\mu_0$  is the magnetic pressure. In large detector solenoids, the aluminum stabilizer and support cylinders dominate the thickness; the superconductor (Nb-Ti/Cu) contributes a smaller fraction. The main coil and support cylinder components typically contribute about 2/3 of the total thickness in radiation lengths.

2. Another contribution to the material comes from the outer cylindrical shell of the vacuum vessel. Since this shell is susceptible to buckling collapse, its thickness is determined by the diameter, length and the modulus of the material of which it is fabricated. The outer vacuum shell represents about 1/3 of the total thickness in radiation length.

### 35.11.2 Properties of collider detector magnets

The physical dimensions, central field stored energy and thickness in radiation lengths normal to the beam line of the superconducting solenoids associated with the major collider are given in Table 35.11 [308]. Fig. 35.26 shows thickness in radiation lengths as a function of  $B^2R$  in various collider detector solenoids.

The ratio of stored energy to cold mass ( $E/M$ ) is a useful performance measure. It can also be expressed as the ratio of the stress,  $\sigma_h$ , to twice the equivalent density,  $\rho$ , in the coil [307]:

$$\frac{E}{M} = \frac{E}{\rho 2\pi t_{\text{coil}} RL} \approx \frac{\sigma_h}{2\rho} \quad (35.48)$$

The  $E/M$  ratio in the coil is approximately equivalent to  $H$ ,\*\* the enthalpy of the coil, and it determines the average coil temperature rise after energy absorption in a quench:

$$E/M = H(T_2) - H(T_1) \approx H(T_2) \quad (35.49)$$

\*\* The enthalpy, or heat content, is called  $H$  in the thermodynamics literature. It is not to be confused with the magnetic field intensity  $B/\mu$ .

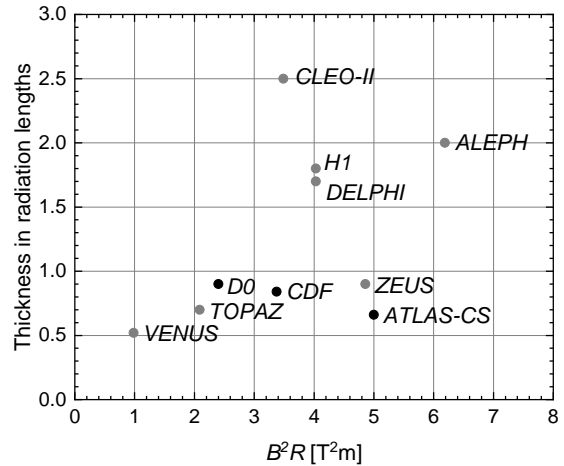


Figure 35.26: Magnet wall thickness in radiation length as a function of  $B^2R$  for various detector solenoids. Gray entries are for magnets no longer in use, and entries underlined are not listed in Table 35.11. Open circles are for magnets not designed to be “thin.” The SSC-SDC prototype provided important R&D for LHC magnets.

where  $T_2$  is the average coil temperature after the full energy absorption in a quench, and  $T_1$  is the initial temperature.  $E/M$  ratios of 5, 10, and 20 kJ/kg correspond to  $\sim 65$ ,  $\sim 80$ , and  $\sim 100$  K, respectively. The  $E/M$  ratios of various detector magnets are shown in Fig. 35.27 as a function of total stored energy. One would like the cold mass to be as small as possible to minimize the thickness, but temperature rise during a quench must also be minimized. An  $E/M$  ratio as large as 12 kJ/kg is designed into the CMS solenoid, with the possibility that about half of the stored energy can go to an external dump resistor. Thus the coil temperature can be kept below 80 K if the energy extraction system works well. The limit is set by the maximum temperature that the coil design can tolerate during a quench. This maximum local temperature should be  $<130$  K ( $50$  K +  $80$  K), so that thermal expansion effects, which are remarkable beyond 80 K, in

the coil are manageable less than 50 K.

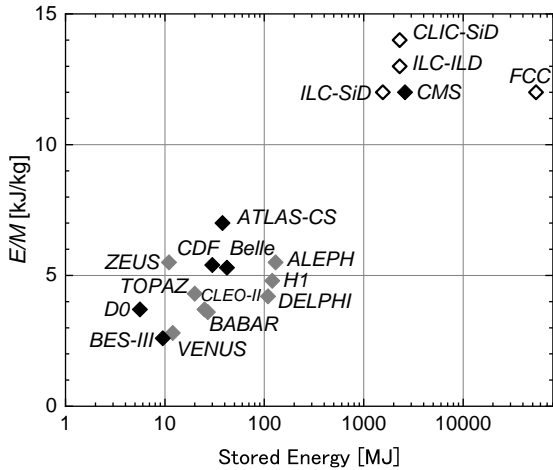


Figure 35.27: Ratio of stored energy to cold mass for major detector solenoids. Gray indicates magnets no longer in operation.

### 35.11.3 Toroidal magnets

Toroidal coils uniquely provide a closed magnetic field without the necessity of an iron flux-return yoke. Because no field exists at the collision point and along the beam line, there is, in principle, no effect on the beam. On the other hand, the field profile generally has  $1/r$  dependence. The particle momentum may be determined by measurements of the deflection angle combined with the sagitta. The deflection (bending) power  $BL$  is

$$BL \approx \int_{R_i}^{R_0} \frac{B_i R_i dR}{R \sin \theta} = \frac{B_i R_i}{\sin \theta} \ln(R_0/R_i), \quad (35.50)$$

where  $R_i$  is the inner coil radius,  $R_0$  is the outer coil radius, and  $\theta$  is the angle between the particle trajectory and the beam line axis. The momentum resolution given by the deflection may be expressed as

$$\frac{\Delta p}{p} \propto \frac{p}{BL} \approx \frac{p \sin \theta}{B_i R_i \ln(R_0/R_i)}. \quad (35.51)$$

The momentum resolution is better in the forward/backward (smaller  $\theta$ ) direction. The geometry has been found to be optimal when  $R_0/R_i \approx 3-4$ . In practical designs, the coil is divided into 6–12 lumped coils in order to have reasonable acceptance and accessibility. This causes the coil design to be much more complex. The mechanical structure needs to sustain the decentering force between adjacent coils, and the peak field in the coil is 3–5 times higher than the useful magnetic field for the momentum analysis [309].

## 35.12 Measurement of particle momenta in a uniform magnetic field

The trajectory of a particle with momentum  $p$  (in GeV/c) and charge  $ze$  in a constant magnetic field  $\vec{B}$  is a helix, with radius of curvature  $R$  and pitch angle  $\lambda$ . The radius of curvature and momentum component perpendicular to  $\vec{B}$  are related by

$$p \cos \lambda = 0.3 z B R, \quad (35.52)$$

where  $B$  is in tesla and  $R$  is in meters.

The distribution of measurements of the curvature  $k \equiv 1/R$  is approximately Gaussian. The curvature error for a large number of uniformly spaced measurements on the trajectory of a charged particle in a uniform magnetic field can be approximated by

$$(\delta k)^2 = (\delta k_{\text{res}})^2 + (\delta k_{\text{ms}})^2, \quad (35.53)$$

where  $\delta k$  = curvature error  
 $\delta k_{\text{res}}$  = curvature error due to finite measurement resolution  
 $\delta k_{\text{ms}}$  = curvature error due to multiple scattering.

If many ( $\geq 10$ ) uniformly spaced position measurements are made along a trajectory in a uniform medium,

$$\delta k_{\text{res}} = \frac{\epsilon}{L'} \sqrt{\frac{720}{N+4}}, \quad (35.54)$$

where  $N$  = number of points measured along track  
 $L'$  = the projected length of the track onto the bending plane  
 $\epsilon$  = measurement error for each point, perpendicular to the trajectory.

If a vertex constraint is applied at the origin of the track, the coefficient under the radical becomes 320.

For arbitrary spacing of coordinates  $s_i$  measured along the projected trajectory and with variable measurement errors  $\epsilon_i$  the curvature error  $\delta k_{\text{res}}$  is calculated from:

$$(\delta k_{\text{res}})^2 = \frac{4}{w} \frac{V_{ss}}{V_{ss} V_{s^2 s^2} - (V_{s^2})^2}, \quad (35.55)$$

where  $V$  are covariances defined as  $V_{s^m s^n} = \langle s^m s^n \rangle - s^m s^n$  with  $\rangle s^m = w^{-1} \sum (s_i^m / \epsilon_i^2)$  and  $w = \sum \epsilon_i^{-2}$ .

The contribution due to multiple Coulomb scattering is approximately

$$\delta k_{\text{ms}} \approx \frac{(0.016)(\text{GeV}/c)z}{Lp\beta \cos^2 \lambda} \sqrt{\frac{L}{X_0}}, \quad (35.56)$$

where  $p$  = momentum (GeV/c)  
 $z$  = charge of incident particle in units of  $e$   
 $L$  = the total track length  
 $X_0$  = radiation length of the scattering medium (in units of length; the  $X_0$  defined elsewhere must be multiplied by density)  
 $\beta$  = the kinematic variable  $v/c$ .

More accurate approximations for multiple scattering may be found in the section on Passage of Particles Through Matter (Sec. 34 of this Review). The contribution to the curvature error is given approximately by  $\delta k_{\text{ms}} \approx 8s_{\text{plane}}^{\text{rms}}/L^2$ , where  $s_{\text{plane}}^{\text{rms}}$  is defined there.

## References

- [1] T. Ferbel (ed.), *Experimental Techniques in High Energy Physics*, Addison-Wesley, Menlo Park, CA (1987).
- [2] K. Kleinknecht, *Detectors for Particle Radiation*, Cambridge University Press, Cambridge (1998).
- [3] G.F. Knoll, *Radiation Detection and Measurement*, 3rd edition, John Wiley & Sons, New York (1999).
- [4] D.R. Green, *The Physics of Particle Detectors*, Cambridge Monographs on Particle Physics, Nuclear Physics and Cosmology, Cambridge University Press, Cambridge (2000).
- [5] C. Leroy and P.-G. Rancoita, *Principles of Radiation Interaction in Matter and Detection*, World Scientific, Singapore (2004).
- [6] C. Grupen, *Particle Detectors*, Cambridge Monographs on Particle Physics, Nuclear Physics and Cosmology, Cambridge University Press (2008).
- [7] ICARUS Collab., ICARUS-TM/2001-09 [LGNS-EXP 13/89 add.2/01] (2001).
- [8] H. Spieler, *IEEE Trans.* **NS29**, 1142 (1982).
- [9] K. Arisaka, *Nucl. Instrum. Meth.* **A442**, 80 (2000).
- [10] T. Hakamata (ed.), *Photomultiplier Tubes: Basics and Applications*, 3rd edition, Hamamatsu Photonics K.K., Hamamatsu (2006).
- [11] A. Braem *et al.*, *Nucl. Instrum. Meth.* **A518**, 574 (2004).
- [12] R. Arnold *et al.*, *Nucl. Instrum. Meth.* **A314**, 465 (1992).
- [13] P. Mangeot *et al.*, *Nucl. Instrum. Methods* **A216**, 79 (1983).
- [14] R. Apsimon *et al.*, *IEEE Trans.* **NS33**, 112 (1986).
- [15] R. Arnold *et al.*, *Nucl. Instrum. Meth.* **A270**, 255 (1988).
- [16] D. Aston *et al.*, *Nucl. Instrum. Meth.* **A283**, 582 (1989).

- [17] J. Janesick, *Scientific charge-coupled devices*, SPIE Press, Bellingham, WA (2001).
- [18] R. Haitz *et al.*, *J. Appl. Phys.* **36**, 3123 (1965).
- [19] R. McIntyre, *IEEE Trans. Electron Devices* **13**, 164 (1966).
- [20] H. Dautet *et al.*, *Applied Optics*, **32**, 3894 (1993).
- [21] Perkin-Elmer Optoelectronics, *Avalanche Photodiodes: A User's Guide*, (2003).
- [22] P. Buzhan *et al.*, *Nucl. Instrum. Meth.* **A504**, 48 (2003).
- [23] Z. Sadygov *et al.*, *Nucl. Instrum. Methods* **A504**, 301 (2003).
- [24] V. Golovin and V. Savelev, *Nucl. Instrum. Meth.* **A518**, 560 (2004).
- [25] M. Landstrass *et al.*, *Diam. & Rel. Matter*, **2**, 1033 (1993).
- [26] R. McKeag and R. Jackman, *Diam. & Rel. Matter*, **7**, 513 (1998).
- [27] R. Brascia *et al.*, *Phys. Stat. Sol.* **199**, 113 (2003).
- [28] M. Petrov, M. Stapelbroek, and W. Kleinhans, *Appl. Phys. Lett.* **51**, 406 (1987).
- [29] M. Atac and M. Petrov, *IEEE Trans.* **NS36**, 163 (1989).
- [30] M. Atac *et al.*, *Nucl. Instrum. Meth.* **A314**, 56 (1992).
- [31] J.B. Birks, *The Theory and Practice of Scintillation Counting*, Pergamon, London (1964).
- [32] D. Clark, *Nucl. Instrum. Methods* **117**, 295 (1974).
- [33] J. B. Birks, *Proc. Phys. Soc.* **A64**, 874 (1951).
- [34] B. Bengston and M. Moszynski, *Nucl. Instrum. Methods* **117**, 227 (1974); J. Bialkowski *et al.*, *Nucl. Instrum. Methods* **117**, 221 (1974).
- [35] C. P. Achenbach (2004), [arXiv:nucl-ex/0404008].
- [36] I.B. Berlman, *Handbook of Fluorescence Spectra of Aromatic Molecules*, 2nd edition, Academic Press, New York (1971).
- [37] F. Sauli (ed.), *Instrumentation in High Energy Physics*, World Scientific, Singapore (1992), see pp. 218–279 by C. Zorn.
- [38] T. Foerster, *Ann. Phys.* **2**, 55 (1948).
- [39] N. Zaitseva *et al.*, *Nucl. Instrum. Methods* **A668**, 88 (2012).
- [40] J.M. Fluornoy, *Rad. Phys. and Chem.* **41**, 389 (1993).
- [41] D. Horstman and U. Holm, *Rad. Phys. and Chem.* **41**, 395 (1993).
- [42] D. Blomker *et al.*, *Nucl. Instrum. Meth.* **A311**, 505 (1992).
- [43] K.F. Johnson and R.L. Clough (eds.), *Proceedings of the International Conference on Radiation-Tolerant Plastic Scintillators and Detectors*, *Rad. Phys. and Chem.* **41** (1993).
- [44] S.R. Borenstein and R.C. Strand, *IEEE Trans.* **NS31**, 396 (1984).
- [45] P. Sonderegger, *Nucl. Instrum. Meth.* **A257**, 523 (1987).
- [46] P. Achenbach *et al.*, *Nucl. Instrum. Meth.* **A593**, 353 (2008), [arXiv:0802.2830].
- [47] C. M. Hawkes *et al.*, *Nucl. Instrum. Meth.* **A292**, 329 (1990).
- [48] S.E. Derenzo, W.-S. Choong and W.W. Moses, *Phys. Med. Biol.* **59**, 3261 (2014).
- [49] C. Melcher and J. Schweitzer, *Nucl. Instrum. Methods* **A314**, 212 (1992).
- [50] D.W. Cooke *et al.*, *J. Appl. Phys.* **88**, 7360 (2000).
- [51] J.M. Chen *et al.*, *IEEE Trans.* **NS54**, 718 (2007).
- [52] J.M. Chen *et al.*, *IEEE Trans.* **NS54**, 1319 (2007).
- [53] E.V.D. van Loef *et al.*, *Nucl. Instrum. Methods* **A486**, 254 (2002).
- [54] W. Drozdowski *et al.*, *IEEE Trans.* **NS55**, 1391 (2008).
- [55] M.S. Alekhin *et al.*, *Appl. Phys. Lett.* **102**, 161915 (2013).
- [56] C. Kuntner *et al.* (Crystal Clear), *Nucl. Instrum. Meth.* **A493**, 131 (2002).
- [57] N. Akchurin *et al.*, *Nucl. Instrum. Meth.* **A595**, 359 (2008).
- [58] A. Para, FERMILAB-CONF-11-519-CD (2011).
- [59] H. Wenzel *et al.*, FERMILAB-PUB-11-531-CD-E (2011).
- [60] R.H. Mao, L.Y. Zhang and R.Y. Zhu, *IEEE Trans.* **NS59**, 2229 (2012).
- [61] R. Y. Zhu, TIPP 2017, SPPHY 213, 70 (2018).
- [62] C. Hu *et al.*, *IEEE Trans.* **NS66**, DOI: 10.1109/TNS.2019.2918305 (2019).
- [63] W.W. Moses, W.-S. Choong and S.E. Derenzo, *Acta Physica Polonica* **B7**, 725 (2014).
- [64] R.H. Mao, L.Y. Zhang and R.Y. Zhu, *IEEE Trans.* **NS55**, 2425 (2008).
- [65] B.D. Rooney and J.D. Valentine, *IEEE Trans.* **NS44**, 509 (1997).
- [66] W.W. Moses *et al.*, *IEEE Trans.* **NS55**, 1049 (2008).
- [67] G. Gratta, H. Newman and R. Y. Zhu, *Ann. Rev. Nucl. Part. Sci.* **44**, 453 (1994).
- [68] R. Y. Zhu, *Nucl. Instrum. Meth.* **A413**, 297 (1998).
- [69] F. Yang *et al.*, *IEEE Trans.* **NS63**, 612 (2016).
- [70] F. Yang *et al.*, *IEEE Trans.* **NS64**, 665 (2017).
- [71] C. Hu *et al.*, *Journal of Physics: Conference Series (Calor2018)*, **1162** 012020 (2019).
- [72] G. Dissertori *et al.*, *Nucl. Instrum. Methods* **745**, 1 (2014), and references therein.
- [73] S. Ecklund, C. Field and G. Mazaheri, *Nucl. Instr. and Meth. Res. Sect.* **A463**, 68 (2001).
- [74] M. G. Albrow *et al.*, *JINST* **7**, P10027 (2012), [arXiv:1207.7248].
- [75] B. Aubert *et al.* (BaBar), *Nucl. Instr. and Meth. Res. Sect.* **A479**, 1 (2002), [hep-ex/0105044].
- [76] E. Torassa (Belle-II PID Group), *Nucl. Instr. and Meth. Res. Sect.* **A824**, 152 (2016).
- [77] G. Bayatian *et al.* (CMS), *Eur. Phys. J.* **C53**, 139 (2008).
- [78] Y. Fukuda *et al.* (Super-Kamiokande), *Nucl. Instrum. Meth.* **A501**, 418 (2003).
- [79] Proceedings of the International Workshops on Ring Imaging Cherenkov Detectors, *Nucl. Instr. and Meth. Res. Sect.* **A343**, 1 (1993); *Nucl. Instr. and Meth. Res. Sect.* **A371**, 1 (1996); *Nucl. Instr. and Meth. Res. Sect.* **A433**, 1 (1999); *Nucl. Instr. and Meth. Res. Sect.* **A502**, 1 (2003); *Nucl. Instr. and Meth. Res. Sect.* **A553**, 1 (2005); *Nucl. Instr. and Meth. Res. Sect.* **A595**, 1 (2008); *Nucl. Instr. and Meth. Res. Sect.* **A639**, 1 (2011); *Nucl. Instr. and Meth. Res. Sect.* **A766**, 1 (2014); *Nucl. Instr. and Meth. Res. Sect.* **A876**, 1 (2017); *Nucl. Instr. and Meth. Res. Sect.* **A 952**, 1 (2019).
- [80] J. Litt and R. Meunier, *Ann. Rev. Nucl. Part. Sci.* **23**, 1 (1973).
- [81] D. Bartlett *et al.*, *Nucl. Instr. and Meth. Res. Sect.* **A260**, 55 (1987).
- [82] A. Abashian *et al.*, *Nucl. Instr. and Meth. Res. Sect.* **A479**, 117 (2002).
- [83] B. N. Ratcliff, *Nucl. Instr. and Meth. Res. Sect.* **A502**, 211 (2003).
- [84] T. Iijima *et al.*, *Nucl. Instr. and Meth. Res. Sect.* **A548**, 383 (2005), [arXiv:physics/0504220].
- [85] W. Blum, W. Riegler, and L. Rolandi, *Particle Detection with Drift Chambers*, Springer-Verlag, Berlin (2008).
- [86] L.G. Christophorou, *Atomic and Molecular Radiation Physics*, John Wiley & Sons, Hoboken (1971).
- [87] <http://consult.cern.ch/writeup/magboltz/>.
- [88] H. Bichsel, *Nucl. Instrum. Meth.* **A562**, 154 (2006).



- [89] H. Fischle, J. Heintze and B. Schmidt, Nucl. Instrum. Meth. **A301**, 202 (1991).
- [90] <http://rjd.web.cern.ch/rjd/cgi-bin/cross>.
- [91] A. Peisert and F. Sauli (1984).
- [92] S. F. Biagi, Nucl. Instrum. Meth. **A421**, 1-2, 234 (1999).
- [93] E. McDaniel and E. Mason, *The Mobility and Diffusion of Ions in Gases*, John Wiley & Sons, Hoboken (1973); G. Schultz, G. Charpak and F. Sauli, Rev. Phys. Appl. **12**, 1, 67 (1977).
- [94] G.F. Knoll, *Radiation Detection and Measurement*, 3rd edition, John Wiley & Sons, New York (1999).
- [95] G. Charpak *et al.*, Nucl. Instrum. Methods **A62**, 262 (1968).
- [96] G. Charpak and F. Sauli, Ann. Rev. Nucl. Sci. **34**, 285 (1984).
- [97] W. Blum, W. Riegler, and L. Rolandi, *Particle Detection with Drift Chambers*, Springer-Verlag, Berlin (2008).
- [98] T. Ferbel (ed.), *Experimental Techniques in High Energy Physics*, Addison-Wesley, Menlo Park, CA (1987), see "Principles of Operation of Multiwire Proportional and Drift Chambers".
- [99] G. Charpak *et al.*, Nucl. Instrum. Methods **A167**, 455 (1979).
- [100] A.H. Walenta *et al.*, Nucl. Instrum. Methods **A92**, 373 (1971).
- [101] A. Breskin *et al.*, Nucl. Instrum. Methods **A124**, 189 (1975).
- [102] A. Breskin *et al.*, Nucl. Instrum. Methods **A156**, 147 (1978).
- [103] R. Bouclier *et al.*, Nucl. Instrum. Meth. **A265**, 78 (1988), [556(1987)].
- [104] H. Drumm *et al.*, Nucl. Instrum. Methods **A176**, 333 (1980).
- [105] D.R. Nygren and J.N. Marx, Phys. Today **31N10**, 46 (1978).
- [106] <http://consult.cern.ch/writeup/magboltz/>.
- [107] <http://www.ansoft.com>.
- [108] C. Grupen, *Particle Detectors*, Cambridge Monographs on Particle Physics, Nuclear Physics and Cosmology, Cambridge University Press (2008).
- [109] P. S. Baringer *et al.*, Nucl. Instrum. Meth. **A254**, 542 (1987).
- [110] J. Virdee, Phys. Reports **403**, 401 (2004).
- [111] A. H. Walenta, Phys. Scripta **23**, 354 (1981).
- [112] J. Va'vra, ICFA Instrum. Bull. **24**, 1 (2002), [1(2002)].
- [113] M. Aleksa *et al.*, Nucl. Instrum. Meth. **A446**, 435 (2000).
- [114] F. Sauli and A. Sharma, Ann. Rev. Nucl. Part. Sci. **49**, 341 (1999).
- [115] A. Oed, Nucl. Instrum. Meth. **A263**, 351 (1988), [124(1988)].
- [116] Y. Bagaturia *et al.* (HERA-B Inner Tracker), Nucl. Instrum. Meth. **A490**, 223 (2002), [ICFA Instrum. Bull.24,54(2002)], [hep-ex/0204011].
- [117] A. Breskin *et al.*, Nucl. Instrum. Methods **A124**, 189 (1975).
- [118] J. Benlloch *et al.*, IEEE Trans. **NS45**, 234 (1998).
- [119] Y. Giomataris, Nucl. Instrum. Meth. **A419**, 239 (1998).
- [120] F. Sauli, Nucl. Instrum. Meth. **A386**, 531 (1997); A. Bressan *et al.*, Nucl. Instrum. Meth. **A425**, 262 (1999).
- [121] S. Bachmann *et al.*, Nucl. Instrum. Meth. **A479**, 294 (2002); A. Bressan *et al.*, Nucl. Instrum. Meth. **A424**, 321 (1999).
- [122] Y. Giomataris *et al.*, Nucl. Instrum. Meth. **A376**, 29 (1996).
- [123] J. Derre *et al.*, Nucl. Instrum. Meth. **A459**, 523 (2001); G. Charpak *et al.*, Nucl. Instrum. Meth. **A478**, 26 (2002).
- [124] I. Giomataris *et al.*, Nucl. Instrum. Meth. **A560**, 405 (2006), [arXiv:physics/0501003].
- [125] S. Duarte Pinto *et al.*, IEEE NSS Conf. Record **N08-4**, 1426 (2008).
- [126] L. Periale *et al.*, Nucl. Instrum. Meth. **A478**, 377 (2002), [arXiv:physics/0106048]; R. Chechik *et al.*, Nucl. Instrum. Meth. **A535**, 303 (2004), [arXiv:physics/0404119]; A. Breskin *et al.*, Nucl. Instrum. Meth. **A598**, 107 (2009), [arXiv:0807.2026].
- [127] A. Di Mauro *et al.*, Nucl. Instrum. Meth. **A581**, 225 (2007), [arXiv:0706.0102].
- [128] R. Bellazzini *et al.*, Nucl. Instrum. Meth. **A535**, 477 (2004), [arXiv:physics/0403019]; M. Campbell *et al.*, Nucl. Instrum. Meth. **A540**, 295 (2005), [arXiv:physics/0409048]; A. Bamberger *et al.*, Nucl. Instrum. Meth. **A573**, 361 (2007), [arXiv:physics/0611229].
- [129] M. Chefderville *et al.*, Nucl. Instrum. Meth. **A556**, 490 (2006).
- [130] M. P. Titov, ICFA Instrum. Bull. **26**, 002 (2004), [199(2004)], [arXiv:physics/0403055].
- [131] <http://rd51-public.web.cern.ch/RD51-Public>.
- [132] D.R. Nygren and J.N. Marx, Phys. Today **31N10**, 46 (1978).
- [133] J. Alme *et al.*, Nucl. Instrum. Meth. **A622**, 316 (2010), [arXiv:1001.1950].
- [134] N. Abgrall *et al.* (T2K ND280 TPC), Nucl. Instrum. Meth. **A637**, 25 (2011), [arXiv:1012.0865].
- [135] A. H. Walenta *et al.*, Nucl. Instrum. Meth. **161**, 45 (1979).
- [136] H. Aihara *et al.*, IEEE Trans. **NS30**, 63 (1983).
- [137] T. A. collaboration (ALICE) (2014).
- [138] K. Dehmelt (sPHENIX), PoS **MPGD2017**, 044 (2019).
- [139] P. Colas, I. Giomataris and V. Lepeltier, Nucl. Instrum. Meth. **A535**, 226 (2004).
- [140] X. Artru, G. B. Yodh and G. Mennessier, Phys. Rev. **D12**, 1289 (1975).
- [141] E. J. Schioppa *et al.*, Nucl. Instrum. Meth. **A936**, 523 (2019).
- [142] M. L. Cherry *et al.*, Phys. Rev. **D10**, 3594 (1974).
- [143] J. Alozy *et al.*, Nucl. Instrum. Meth. **A927**, 1 (2019), [arXiv:1901.11265].
- [144] B. Dolgoshein, Nucl. Instrum. Meth. **A326**, 434 (1993).
- [145] A. Andronic and J. P. Wessels, Nucl. Instrum. Meth. **A666**, 130 (2012).
- [146] S. Acharya *et al.* (ALICE), Nucl. Instrum. Meth. **A881**, 88 (2018), [arXiv:1709.02743].
- [147] T. Akesson *et al.* (ATLAS TRT), Nucl. Instrum. Meth. **A522**, 131 (2004).
- [148] M. Ambriola *et al.*, Nucl. Instrum. Meth. **A522**, 77 (2004).
- [149] J. Adelman (ATLAS), Nucl. Instrum. Meth. **A706**, 33 (2013).
- [150] T. Kirn (AMS 02 TRD), Nucl. Instrum. Meth. **A706**, 43 (2013).
- [151] P. Nevski, Nucl. Instrum. Meth. **A522**, 116 (2004).
- [152] V. M. Grishin and S. S. Sadilov, Nucl. Instrum. Meth. **A522**, 122 (2004).
- [153] B. Beischer *et al.*, Nucl. Instrum. Meth. **A583**, 485 (2007).
- [154] T. Akesson *et al.* (ATLAS TRT), Nucl. Instrum. Meth. **A412**, 200 (1998).
- [155] M. Petris *et al.*, Nucl. Instrum. Meth. **A714**, 17 (2013).
- [156] M. L. Cherry, Nucl. Instrum. Meth. **A706**, 39 (2013).
- [157] M. Brigida *et al.*, Nucl. Instrum. Meth. **A706**, 69 (2013).

- [158] F. Hartjes *et al.*, Nucl. Instrum. Meth. **A706**, 59 (2013).
- [159] V. V. Berdnikov *et al.*, Nucl. Instrum. Meth. **A706**, 65 (2013).
- [160] R. Santonico and R. Cardarelli, Nucl. Instrum. Methods **A187**, 377 (1981).
- [161] V.V. Parkhomchuck, Yu.N. Pestov, and N.V. Petrovykh, Nucl. Instrum. Methods **93**, 269 (1971).
- [162] E. Cerron Zeballos *et al.*, Nucl. Instrum. Meth. **A374**, 132 (1996).
- [163] R. Cardarelli, A. Di Ciaccio and R. Santonico, Nucl. Instrum. Meth. **A333**, 399 (1993).
- [164] P. Camarri *et al.*, Nucl. Instrum. Meth. **A414**, 317 (1998).
- [165] G. Aielli *et al.*, Nucl. Instrum. Meth. **A508**, 6 (2003).
- [166] R. Cardarelli, R. Santonico and V. Makeev, Nucl. Instrum. Meth. **A382**, 470 (1996).
- [167] I. Crotty *et al.*, Nucl. Instrum. Methods **A505**, 203 (2006).
- [168] R. Santonico, Nucl. Instrum. Meth. **A456**, 1 (2000).
- [169] W. Riegler and D. Burgarth, Nucl. Instrum. Meth. **A481**, 130 (2002).
- [170] R. Cardarelli *et al.*, JINST **8**, P01003 (2013).
- [171] G. Aielli *et al.*, JINST **9**, 09, C09030 (2014).
- [172] R. Santonico, JINST **9**, 11, C11007 (2014).
- [173] G. Aad *et al.* (ATLAS), JINST **3**, S08003 (2008).
- [174] S. Chatrchyan *et al.* (CMS), JINST **3**, S08004 (2008).
- [175] R. Santonico, Nucl. Instrum. Meth. **A661**, S2 (2012).
- [176] M. Bedjidian *et al.*, JINST **6**, P02001 (2011), [arXiv:1011.5969].
- [177] P. Fonte, A. Smirnitsky and M. C. S. Williams (ALICE), Nucl. Instrum. Meth. **A443**, 201 (2000).
- [178] L. Paolozzi *et al.*, PoS **RPC2012**, 065 (2012).
- [179] S. An *et al.*, Nucl. Instrum. Meth. **A594**, 39 (2008).
- [180] C. Iacobaeus *et al.*, Nucl. Instrum. Meth. **A513**, 244 (2003), [arXiv:physics/0210006].
- [181] G. Aielli *et al.*, Nucl. Instrum. Meth. **A456**, 82 (2000).
- [182] G. Aielli *et al.*, IEEE Trans. **NS53**, 567 (2006).
- [183] H. Sakai *et al.*, Nucl. Instrum. Meth. **A484**, 153 (2002).
- [184] R. Santonico, JINST **8**, P04023 (2013).
- [185] L. Lopes *et al.*, Nucl. Instrum. Meth. **A533**, 69 (2004).
- [186] H. Spieler, *Semiconductor Detector Systems*, Oxford Univ. Press, Oxford (2005).
- [187] F. Scholze *et al.*, Nucl. Instrum. Methods **A439**, 208 (2000).
- [188] G. Lindstrom *et al.* (ROSE), Nucl. Instrum. Meth. **A465**, 60 (2000), [280(2000)].
- [189] C. Da Via *et al.*, Nucl. Instrum. Meth. **A509**, 86 (2003).
- [190] G. Kramberger *et al.*, Nucl. Instrum. Meth. **A481**, 297 (2002).
- [191] O. Krasel *et al.*, IEEE Trans. **NS51**, 3055 (2004).
- [192] G. Lindstrom, M. Moll and E. Fretwurst, Nucl. Instrum. Meth. **A426**, 1 (1999).
- [193] A. Holmes-Siedle and L. Adams, *Handbook of Radiation Effects*, 2nd edition, Oxford Univ. Press, Oxford (2002).
- [194] V. Radeka, IEEE Trans. **NS15**, 455 (1968).
- [195] V. Radeka, IEEE Trans. **NS21**, 51 (1974).
- [196] F. S. Goulding, Nucl. Instrum. Meth. **100**, 493 (1972).
- [197] F.S. Goulding and D.A. Landis, IEEE Trans. **NS29**, 1125 (1982).
- [198] H. Spieler, IEEE Trans. **NS29**, 1142 (1982).
- [199] H. Spieler, *Semiconductor Detector Systems*, Oxford Univ. Press, Oxford (2005).
- [200] R. Wigmans, *Calorimetry*, International Series of Monographs on Physics, Oxford University Press (2017).
- [201] W.R. Nelson, H. Hirayama, and D.W.O. Rogers, SLAC-265 (1985).
- [202] R. Brun *et al.*, CERN DD/EE/84-1 (1987).
- [203] ATLAS Collab., CERN/LHCC 96-41 (1996).
- [204] D. Hitlin *et al.*, Nucl. Instrum. Meth. **137**, 225 (1976).
- [205] W. J. Willis and V. Radeka, Nucl. Instrum. Meth. **120**, 221 (1974).
- [206] R. Wigmans, *Calorimetry: Energy Measurement in Particle Physics*, Inter. Series of Monographs on Phys. **107**, Second Edition, Oxford Scholarship Online (2017).
- [207] R.Y. Zhu, Journal of Physics: Conference Series **587**, 012055 (2015).
- [208] CMS Collab., CERN/LHCC 97-33 (1997).
- [209] C. Leroy and P. Rancoita, Rept. Prog. Phys. **63**, 505 (2000).
- [210] N. Akchurin *et al.*, Nucl. Instrum. Meth. **A399**, 202 (1997).
- [211] B. Aubert *et al.*, Nucl. Instrum. Meth. **A321**, 467 (1992).
- [212] A. Artamonov *et al.*, JINST **3**, P02010 (2008).
- [213] F. Ariztizabal *et al.* (RD-34), Nucl. Instrum. Meth. **A349**, 384 (1994).
- [214] E. Borchini *et al.* (SICAPO), Nucl. Instrum. Meth. **A279**, 57 (1989).
- [215] G. Abbiendi, R. G. Kellogg and D. M. Strom, in "Calorimetry in particle physics. Proceedings, 10th International Conference, CALOR 2002, Pasadena, USA, March 25-29, 2002," 287-295 (2002), [hep-ex/0206074].
- [216] S. C. Berridge *et al.*, IEEE Trans. Nucl. Sci. **39**, 1242 (1992).
- [217] E. Borchini *et al.*, IEEE Transactions on Nuclear Science **40**, 508 (1993).
- [218] <https://twiki.cern.ch/twiki/bin/view/CALICE/CaliceDetectors>.
- [219] F. Sefkow and F. Simon (CALICE), J. Phys. Conf. Ser. **1162**, 1, 012012 (2019), [arXiv:1808.09281].
- [220] D. E. Groom, in "ECFA Study Week on Instrumentation Technology for High Luminosity Hadron Colliders Barcelona, Spain, September 14-21, 1989," URL [http://lss.fnal.gov/cgi-bin/find\\_paper.pl?other/ssc/ssc-227.pdf](http://lss.fnal.gov/cgi-bin/find_paper.pl?other/ssc/ssc-227.pdf).
- [221] T. A. Gabriel *et al.*, Nucl. Instrum. Meth. **A338**, 336 (1994).
- [222] D. E. Groom, Nucl. Instrum. Meth. **A572**, 633 (2007), erratum: Nucl. Instrum. Meth. **A593**, 628 (2008).
- [223] N. Akchurin *et al.*, Nucl. Instr. Methods **A408**, 380 (1998); An energy-independent analysis of these data is given in [222].
- [224] P. Adragna *et al.*, Nucl. Instrum. Meth. **A615**, 158 (2010).
- [225] F. Lemeilleur *et al.*, Physics Letters B **222**, 3, 518 (1989), ISSN 0370-2693, URL <http://www.sciencedirect.com/science/article/pii/0370269389903560>.
- [226] H. Abramowicz *et al.*, Nucl. Instrum. Meth. **180**, 429 (1981).
- [227] B. Andrieu *et al.* (H1 Calorimeter Group), Nucl. Instrum. Meth. **A336**, 499 (1993).
- [228] C. Cojocaru *et al.* (ATLAS), Nucl. Instrum. Meth. **A531**, 3, 481 (2004).
- [229] C. Adloff *et al.* (CALICE), J. Instr. **7**, 09, P09017 (2012).
- [230] C. Adloff *et al.* (CALICE), JINST **8**, 07005 (2013).
- [231] C. W. Fabjan *et al.*, Phys. Lett. **60B**, 105 (1975).
- [232] C. Leroy, J. Sirois, and R. Wigmans, Nucl. Instrum. Methods **A252**, 4 (1986).
- [233] J. Brau *et al.*, Nucl. Instrum. Meth. **A238**, 489 (1985).
- [234] H. Brückmann and H. Kowalski, ZEUS Int. Note 86/026 DESY, Hamburg (1986).
- [235] R. Wigmans, Nucl. Instrum. Meth. **A259**, 389 (1987).
- [236] R. Wigmans, Nucl. Instrum. Meth. **A265**, 273 (1988).
- [237] T. Akesson *et al.*, Nucl. Instrum. Meth. **A241**, 17 (1985).

- [238] T. Akesson *et al.*, Nucl. Instrum. Meth. **A262**, 243 (1987).
- [239] E. Bernardi *et al.*, Nucl. Instrum. Meth. **A262**, 229 (1987).
- [240] G. Drews *et al.*, Nucl. Instrum. Meth. **A290**, 335 (1990).
- [241] G. R. Young *et al.*, Nucl. Instrum. Meth. **A279**, 503 (1989).
- [242] A. Andresen *et al.* (ZEUS Calorimeter Group, ZEUS), Nucl. Instrum. Meth. **A309**, 101 (1991).
- [243] [www-zeus.desy.de/bluebook/ch05/subsection2\\_4\\_15\\_3.html](http://www-zeus.desy.de/bluebook/ch05/subsection2_4_15_3.html).
- [244] D. Acosta *et al.*, Nucl. Instrum. Meth. **A308**, 481 (1991).
- [245] S. Abachi *et al.* (D0), Nucl. Instrum. Meth. **A338**, 185 (1994).
- [246] P. Mockett, SLAC-267, 335 (1983).
- [247] D.R. Winn and W.A. Worstell, "Compensating Hadron Calorimeters with Cerenkov Light", IEEE TNS, NS-36, 334 (1989).
- [248] R. Wigmans, *Proc. 7th Inter. Conf. on Calorimetry in High Energy Physics*, 182 World Scientific, River Edge, NJ, (1998);.
- [249] S. Lee, M. Livan and R. Wigmans, Rev. Mod. Phys. **90**, 2, 025002 (2018).
- [250] D. E. Groom, Nucl. Instrum. Meth. **A705**, 24 (2013).
- [251] J.-C. Brient, J. Phys. Conf. Ser. **160**, 012025 (2009).
- [252] F. Sefkow *et al.*, Rev. Mod. Phys. **88**, 015003 (2016).
- [253] J. Apostolakis *et al.*, J. Phys. Conf. Ser. **160**, 012073 (2009).
- [254] J. Allison *et al.*, Nucl. Instrum. Meth. **A835**, 186 (2016).
- [255] M. Holder *et al.*, Nucl. Instrum. Meth. **151**, 69 (1978).
- [256] R.K. Bock, T. Hansl-Kozanecka, and T.P. Shah, Nucl. Instrum. Methods **186**, 533 (1981) Y.A. Kulchitsky and V.B. Vinogradov, Nucl. Instrum. Methods **A455**, 499 (2000).
- [257] Y.A. Kulchitsky and V.B. Vinogradov, Nucl. Instrum. Methods **A455**, 499 (2000).
- [258] D. Acosta *et al.*, Nucl. Instrum. Meth. **A316**, 184 (1992).
- [259] N. Akchurin *et al.*, Nucl. Instrum. Meth. **A735**, 120 (2014).
- [260] W. Walkowiak, Nucl. Instrum. Meth. **A449**, 288 (2000).
- [261] E. Shibamura *et al.*, Nucl. Instrum. Methods **A316**, 184 (1975).
- [262] L. S. Miller, S. Howe and W. E. Spear, Phys. Rev. **166**, 871 (1968).
- [263] A.M. Kalinin *et al.*, ATLAS-LARG-NO-058 (1996).
- [264] K. Yoshino, U. Sowada and W. F. Schmidt, Phys. Rev. **A14**, 438 (1976).
- [265] A.O. Allen *et al.*, NSRDS-NBS-58 (1976).
- [266] P. Benetti *et al.*, Nucl. Instrum. Methods **A32**, 361 (1993).
- [267] G. Danby *et al.*, Phys. Rev. Lett. **9**, 36 (1962).
- [268] S. van der Meer (1961).
- [269] J. A. Formaggio and G. P. Zeller, Rev. Mod. Phys. **84**, 1307 (2012), [arXiv:1305.7513].
- [270] H. Faissner, "CERN Spark Chamber Neutrino Experiment", INSPIRE-1377455.
- [271] H. Faissner *et al.*, Phys. Lett. **68B**, 377 (1977).
- [272] F. J. Hasert *et al.* (Gargamelle Neutrino), Nucl. Phys. **B73**, 1 (1974).
- [273] N. Armenise *et al.* (BEBC TST Neutrino), Phys. Lett. **81B**, 385 (1979).
- [274] A.E. Asratien *et al.*, Phys. Lett. **79**, 497 (1978).
- [275] S. J. Barish *et al.*, Phys. Rev. **D16**, 3103 (1977).
- [276] N. J. Baker *et al.*, Phys. Rev. **D23**, 2499 (1981).
- [277] J. W. Chapman *et al.*, Phys. Rev. **D14**, 5 (1976).
- [278] M. Holder *et al.*, Nucl. Instrum. Meth. **148**, 235 (1978).
- [279] I. Ambats *et al.* (MINOS) (1998).
- [280] K. Abe *et al.* (T2K), Nucl. Instrum. Meth. **A659**, 106 (2011), [arXiv:1106.1238].
- [281] M. H. Ahn *et al.* (K2K), Phys. Rev. **D74**, 072003 (2006), [hep-ex/0606032].
- [282] A. A. Aguilar-Arevalo *et al.* (MiniBooNE), Nucl. Instrum. Meth. **A599**, 28 (2009), [arXiv:0806.4201].
- [283] A. C. Benvenuti *et al.*, Nucl. Instrum. Meth. **125**, 447 (1975).
- [284] C. Athanassopoulos *et al.* (LSND), Nucl. Instrum. Meth. **A388**, 149 (1997), [arXiv:nucl-ex/9605002].
- [285] D. S. Ayres *et al.* (NOvA) (2007).
- [286] K. Hiraide *et al.* (SciBooNE), Phys. Rev. **D78**, 112004 (2008), [arXiv:0811.0369].
- [287] C. Rubbia, CERN-EP-INT-77-08 (1977).
- [288] S. Amerio *et al.* (ICARUS), Nucl. Instrum. Meth. **A527**, 329 (2004).
- [289] C. Anderson *et al.*, JINST **7**, 10020 (2012).
- [290] H. Chen *et al.*, FERMILAB-PROPOSAL-0974 (2007).
- [291] D. H. Perkins, Nature **159**, 126 (1947).
- [292] S. Aoki *et al.*, Nucl. Instrum. Meth. **A447**, 361 (2000).
- [293] N. Uhida *et al.*, Nucl. Instrum. Methods **224**, 50 (1984).
- [294] K. Kodama *et al.*, Nucl. Instrum. Meth. **B93**, 340 (1994).
- [295] T. Adam *et al.*, Nucl. Instrum. Meth. **A577**, 523 (2007), [arXiv:physics/0701153].
- [296] D. Di Ferdinando (OPERA), Radiat. Meas. **44**, 840 (2009), [arXiv:0812.0451].
- [297] R. Acquafredda *et al.* (OPERA), New J. Phys. **8**, 303 (2006), [hep-ex/0611023].
- [298] T. Fukuda *et al.*, PTEP **2017**, no. 6, 063C02 (2017).
- [299] A. N. Diddens *et al.* (CERN-Hamburg-Amsterdam-Rome-Moscow), Nucl. Instrum. Meth. **178**, 27 (1980).
- [300] D. Geiregat *et al.* (CHARM-II), Nucl. Instrum. Meth. **A325**, 92 (1993).
- [301] L. A. Ahrens *et al.*, Nucl. Instrum. Meth. **A254**, 515 (1987).
- [302] G. Gidal, LBL-91 Suppl., Rev. (1985).
- [303] W. K. Sakumoto *et al.*, Nucl. Instrum. Meth. **A294**, 179 (1990).
- [304] D. A. Harris *et al.* (NuTeV), Nucl. Instrum. Meth. **A447**, 377 (2000), [hep-ex/9908056].
- [305] J. Altegoer *et al.* (NOMAD), Nucl. Instrum. Meth. **A404**, 96 (1998).
- [306] L. Aliaga *et al.* (MINERvA), Nucl. Instrum. Meth. **A743**, 130 (2014), [arXiv:1305.5199].
- [307] A. Yamamoto, Nucl. Instrum. Meth. **A453**, 445 (2000).
- [308] A. Yamamoto and Y. Makida, Nucl. Instrum. Meth. **A494**, 255 (2002).
- [309] T. M. Taylor, Phys. Scripta **23**, 459 (1981).
- [310] R. L. Gluckstern, Nucl. Instrum. Meth. **24**, 381 (1963).
- [311] V. Karimaki, Nucl. Instrum. Meth. **A410**, 284 (1998).

## 36. Particle Detectors for Non-Accelerator Physics

36.1	Introduction . . . . .	589
36.2	High-energy cosmic-ray hadron and gamma-ray detectors . . . . .	589
36.2.1	Atmospheric fluorescence detectors . . . . .	589
36.2.2	Atmospheric Cherenkov telescopes for high-energy gamma ray astronomy . . . . .	591
36.3	Large neutrino detectors . . . . .	592
36.3.1	Deep liquid detectors for rare processes . . . . .	592
36.3.2	Neutrino telescopes . . . . .	594
36.3.3	Radio emission from (ultra-)high energy particle showers . . . . .	598
36.4	Large time-projection chambers for rare event detection . . . . .	601
36.4.1	Dark matter and other low energy signals . . . . .	601
36.4.2	$0\nu\beta\beta$ Decay . . . . .	603
36.5	Sub-Kelvin detectors . . . . .	603
36.5.1	Equilibrium thermal detectors . . . . .	603
36.5.2	Nonequilibrium Detectors . . . . .	604
36.6	Low-radioactivity background techniques . . . . .	605
36.6.1	Defining the problem . . . . .	606
36.6.2	Environmental radioactivity . . . . .	606
36.6.3	Radioactive impurities in detector and shielding components . . . . .	606
36.6.4	Radon and its progeny . . . . .	607
36.6.5	Cosmic rays . . . . .	608
36.6.6	Neutrons . . . . .	608

### 36.1 Introduction

Non-accelerator experiments have become increasingly important in particle physics. These include cosmic ray experiments (with surface, space and underground detectors), neutrino oscillation measurements with solar and atmospheric neutrinos in underground laboratories, searches for neutrino-less double beta decays and dark matter candidates again in underground laboratories, and searches for more exotic phenomena. The detectors are in the majority of the cases different from those used at accelerators. Even when the detectors are based on the same physics (e. g. tracking detectors), they are employed in radically different ways. The methods range from atmospheric scintillation detectors to massive Cherenkov detectors, from large liquid scintillator detectors to dual phase TPCs, from ultrapure ionization calorimeters to cryogenic solid state detectors. With the exception of the cosmic ray detectors, techniques for producing and testing radiologically ultra-pure materials are constantly developed. Progress is linked to pushing forward the ultra-low background frontier. In this section, some important technologies relevant for detectors on the surface and underground are discussed. Space-based detectors also use some unique instrumentation, but these are beyond the present scope of this review.

### 36.2 High-energy cosmic-ray hadron and gamma-ray detectors

#### 36.2.1 Atmospheric fluorescence detectors

Revised August 2019 by L.R. Wiencke (Colorado School of Mines).

Cosmic-ray fluorescence detectors (FDs) use the atmosphere as a giant calorimeter to measure isotropic scintillation light that traces the development profiles of extensive air showers. An extensive air shower (EAS) is produced by the interactions of ultra high-energy ( $E > 10^{17}$  eV) subatomic particles in the stratosphere and upper troposphere. The amount of scintillation light generated by an EAS is proportional to the energy deposited in the atmosphere and nearly independent of the primary species. With energies extending beyond  $10^{20}$  eV these are the highest energy subatomic particles known to exist. In addition to particle arrival directions, energy spectra and primary composition, the astroparticle science investigated with FDs also includes multimessenger studies, searches for high energy photons, neutrinos, monopoles and deeply penetrating forms of dark matter.

Previous experiments with FDs included the pioneering Fly's Eye [1, 2], and the High Resolution Fly's Eye (HiRes and HiRes prototype) [3]. The current generation of experiments include the Telescope Array (TA) [4] in the northern hemisphere, and the much larger Pierre Auger Observatory (Auger) [5] in the southern hemisphere. Both are hybrid observatories. Their FD telescopes overlook sparse arrays of particle detectors on the ground. Select parameters are listed in Table 36.1. TA and Auger have each one FD site populated with additional telescopes that view up to  $60^\circ$  in elevation to measure lower EASs using a combination of scintillation and direct Cherenkov light. The Auger FD also measures UV scintillation that traces the development of atmospheric transient luminous events called "Elves" that are initiated by lightning [6]. At TA a prototype FD telescope, dubbed FAST [7], has observed EASs using wide field of view PMTs and fast timing.

The fluorescence light is emitted primarily between 290 and 430 nm (Figure 36.1) with major lines at 337, 357, and 391 nm, when relativistic charged particles, primarily electrons and positrons, excite nitrogen molecules in air, resulting in transitions of the 1P and 2P systems. Reviews and references for the pioneering and recent laboratory measurements of fluorescence yield,  $Y(\lambda, P, T, u)$ , including dependence on wavelength ( $\lambda$ ), temperature ( $T$ ), pressure ( $p$ ), and humidity ( $u$ ) may be found in Refs. [8–10]. The results of various laboratory experiments have been combined (Figure 36.2) to obtain an absolute average and uncertainty for  $Y(337 \text{ nm}, 800 \text{ hPa}, 293 \text{ K}, \text{ dry air})$  of  $7.04 \pm 0.24 \text{ ph/MeV}$  after corrections for different electron beam energies and other factors. The units of ph/MeV correspond to the number of fluorescence photons produced per MeV of energy deposited in the atmosphere by the electromagnetic component of an EAS.

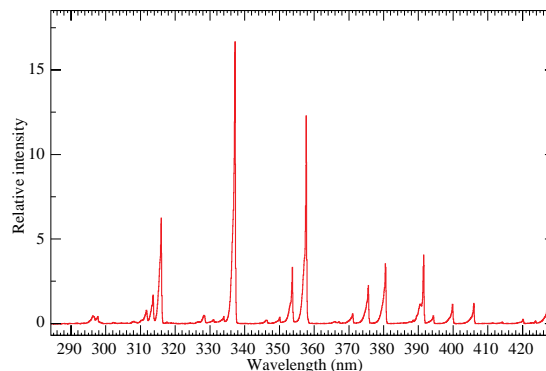


Figure 36.1: Measured fluorescence spectrum excited by 3 MeV electrons in dry air at 800 hPa and 293 K. Airfly experiment. Figure from Ref [11].

An FD element (telescope) consists of a non-tracking spherical mirror of less than astronomical quality, a close-packed “camera” of photomultiplier tubes (PMTs) near the focal plane, and a flash ADC readout system with a pulse and track-finding trigger scheme [5, 13]. The major experiments listed in Table 36.1 all use conventional PMTs (for example, Hamamatsu R9508 or Photonis XP3062) with grounded cathodes and AC coupled readout. Segmented mirrors have been fabricated from slumped or slumped/polished glass with an anodized aluminum coating or fabricated using shaped aluminum that was then chemically anodized with  $\text{AlMgSiO}_5$ . A broadband UV filter (custom fabricated or Schott MUG-6) reduces background light such as starlight, air-glow, man-made light pollution, and airplane strobe-lights.

At  $10^{20}$  eV, where the flux drops below 1 EAS/km<sup>2</sup>century, the aperture for an eye of adjacent FD telescopes that span the horizon can reach  $10^4 \text{ km}^2 \text{ sr}$ . FD operation requires (nearly) moonless nights and clear atmospheric conditions, which imposes a duty cycle of about 10%. Arrangements of LEDs, calibrated diffuse sources [14], pulsed UV lasers [15], LIDARs<sup>1</sup> and IR detectors

<sup>1</sup>LIDAR stands for “Light Detection and Ranging” and refers here to

**Table 36.1:** Parameters of major fluorescence detectors. Note 1: Year when all FD sites were operational. Note 2: At TA 1 of the 3 FD sites features 24 telescopes from the HiRes experiment. Note 3: A-C for one telescope where A is the full area and C the area obscured by the camera and support structures. Thus A-C is the effective light collecting area. For the modified Schmidt design at Auger, the area of the entrance pupil, A, is listed because the pupil is smaller than the mirror and thus defines the entrance aperture. For the other experiments, the area of the mirror, A, is listed

Observatory	Fly's Eye	HiRes	Telescope Array	Pierre Auger
Location	Dugway UT US	Dugway UT US	Delta UT US	Malargüe AR
Start-End	1981-1992	1996-2006	2008-present	2005-present
Sites (note 1)	2 (1986)	2 (1999)	3 (2008)	4 (2008)
Separation	3.3 km	12.6 km	31-40 km	39-62 km
Telescopes/site	67,18	21,42	12,12,14+10	6, 6, 6, 6+3
Pixel FOV	5.5°	1°	1°	1.5°
Telescope FOV	≈18° × ≈18°	16° × 13.5°	18° × 15° (note 2)	30° × 28.1°
Azi × Elv				
Light collection area (note 3)	1.95 m <sup>2</sup> - 0.25 m <sup>2</sup>	3.72 m <sup>2</sup> - 0.5 m <sup>2</sup>	6.8 m <sup>2</sup> - 0.85 m <sup>2</sup> (for 2 sites)	3.80 m <sup>2</sup> - 0.80 m <sup>2</sup> (modified schmidt)
Energy Scale	≤40%	≈20%	≈20%	14%
Uncertainty				

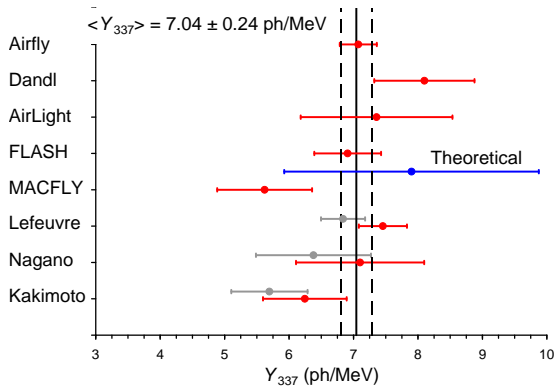


Figure 36.2: Fluorescence yield values and associated uncertainties at 337 nm ( $Y_{337}$ ) in dry air at 800 hPa and 293 K. The methodology and corrections that were applied to obtain the average and the uncertainty are discussed extensively in this reference. The vertical axis denotes different laboratory experiments that measured FY. The gray bars show three of the original measurements to illustrate the scale of the corrections applied. Figure from Ref [12].

that are sensitive to clouds are used for photometric calibration, atmospheric calibration [16], and determination of exposure [17]. For purposes of optical transmission, the atmosphere is treated as having a dominant molecular component and a secondary aerosol component. The latter is well described [18] by molecular scattering theory and models derived from radiosonde measurements. The aerosol component can include dust, haze and pollution and the aerosol optical depth profile must be measured on site in the UV during FD data taking.

The EAS generates a track consistent with a light source moving at  $v = c$  across the FOV. The number of photons ( $N_\gamma$ ) as a function of atmospheric depth ( $X$ ) can be expressed as [9]

$$\frac{dN_\gamma}{dX} = \frac{dE_{\text{dep}}^{\text{tot}}}{dX} \int Y(\lambda, P, T, u) \cdot \tau_{\text{atm}}(\lambda, X) \cdot \varepsilon_{\text{FD}}(\lambda) d\lambda, \quad (36.1)$$

where  $\tau_{\text{atm}}(\lambda, X)$  is the atmospheric transmission, including wavelength ( $\lambda$ ) dependence, and  $\varepsilon_{\text{FD}}(\lambda)$  is the FD efficiency.  $\varepsilon_{\text{FD}}(\lambda)$  includes geometric factors and collection efficiency of the optics, quantum efficiency of the PMTs, and other throughput factors. The typical systematic uncertainties,  $\tau_{\text{atm}}$  (10%) and  $\varepsilon_{\text{FD}}$  (photometric calibration 10%), currently dominate the systematic uncertainty the absolute EAS energy scale. FD energy resolu-

systems that measure atmospheric properties from the light scattered backwards from laser pulses directed into the sky.

tion, defined as event-to-event statistical uncertainty, is typically less than 10% for final data samples used for science analysis.

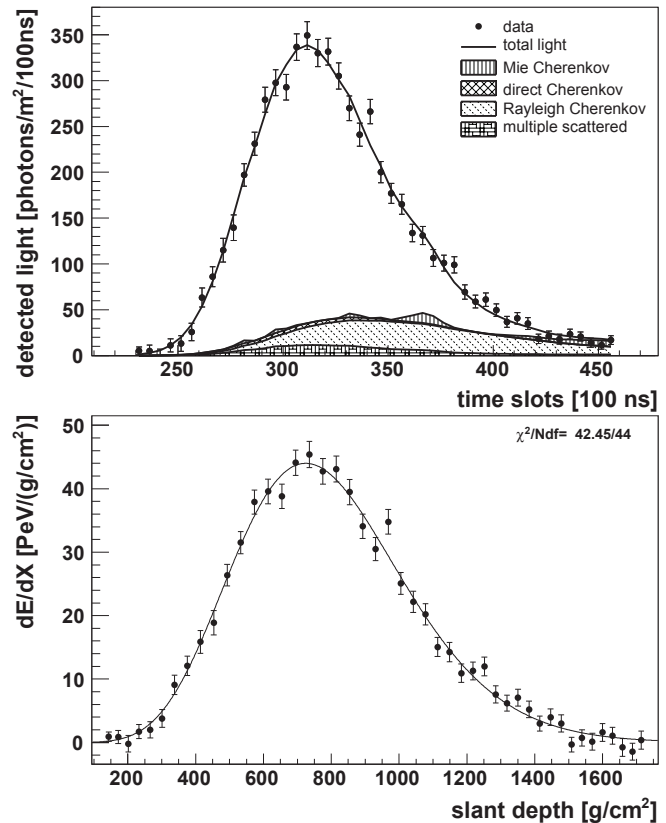


Figure 36.3: Example light profile (left) of one EAS recorded by the Pierre Auger FD and the corresponding profile (right) of energy deposited in the atmosphere vs atmospheric slant depth. The light profiles include the estimated components of Cherenkov light that have been scattered out of the forward beam by the molecular and aerosol (Mie) components of the atmosphere. The reconstructed energy of this EAS was  $3.0 \pm 0.2 \times 10^{19}$  eV. Figure from Ref [19].

Analysis methods to reconstruct the EAS profile and deconvolve the contributions of re-scattered scintillation light, and direct and scattered Cherenkov light are described in [1] and more recently in [20]. The EAS energy is typically obtained by integrating over the Gaisser-Hillas function [21]



$$E_{\text{cal}} = \int_0^{\infty} [w_{\text{max}} \left( \frac{X - X_0}{X_{\text{max}} - X_0} \right)^{(X_{\text{max}} - X_0)/\lambda} e^{(X_{\text{max}} - X)/\lambda}] dX, \quad (36.2)$$

where  $E_{\text{cal}}$  is the energy of electromagnetic energy component of the EAS and  $X_{\text{max}}$  is the atmospheric slant depth at which the shower reaches its maximum energy deposit rate. This maximum  $dE/dX$  is denoted as  $w_{\text{max}}$ .  $X_0$  and  $\lambda$  are two shape parameters. The energy of the primary cosmic ray is obtained by correcting  $E_{\text{cal}}$  upward by about 10% to account for the invisible energy carried by particles that do not interact in the atmosphere. Energy resolution,  $\Delta E/E$ , of 15-20% is achievable, provided the geometric fit of the EAS axis is constrained, typically by multi-eye stereo projection or hybrid observations, and the profile fit of EAS development along the track is constrained by the observed rise and fall about  $X_{\text{max}}$ . An example of a recorded EAS light profile and its corresponding  $dE/dX$  development profile are shown in Fig. 36.3.

The EAS generates a track consistent with a light source moving at  $v = c$  across the FOV. The number of photons ( $N_\gamma$ ) as a function of atmospheric depth ( $X$ ) can be expressed as [9]

R&D toward an FD in space is at the design and prototype phase. A proposed space based FD instrument [22] by the JEM-EUSO collaboration would look down on the earth's atmosphere from space to view a much larger area than ground based instruments. Prototypes that have been built and flown include the TUS instrument [23], operated 2016-2018 onboard the Lomonosov satellite, and two FD telescopes flown on stratospheric balloons in 2014 [24] and 2017 [25]. The prototype instrument Mini-EUSO [26] (25 cm diameter aperture), currently at the International Space Station (ISS), will survey terrestrial UV emission by looking down through a UV window from inside the ISS beginning late 2019. The proposed POEMMA twin-satellite space mission [27] would record scintillation and Cherenkov light from EASs the atmosphere to measure UHECRs and PeV scale cosmogenic tau neutrinos.

### 36.2.2 Atmospheric Cherenkov telescopes for high-energy gamma ray astronomy

Revised August 2019 by J. Holder (Delaware U.; Delaware U., Bartol Inst.).

A wide variety of astrophysical objects are now known to produce high-energy  $\gamma$ -ray photons. Leptonic or hadronic particles, accelerated to relativistic energies in the source, produce  $\gamma$ -rays typically through inverse Compton boosting of ambient photons or through the decay of neutral pions produced in hadronic interactions. At energies below  $\sim 30$  GeV,  $\gamma$ -ray emission can be efficiently detected using satellite or balloon-borne instrumentation, with an effective area approximately equal to the size of the detector (typically  $< 1$  m<sup>2</sup>). At higher energies, a technique with much larger effective collection area is desirable to measure astrophysical  $\gamma$ -ray fluxes, which decrease rapidly with increasing energy. Atmospheric Cherenkov detectors achieve effective collection areas of  $> 10^5$  m<sup>2</sup> by employing the Earth's atmosphere as an intrinsic part of the detection technique.

As described in Chapter 30, a hadronic cosmic ray or high energy  $\gamma$ -ray incident on the Earth's atmosphere triggers a particle cascade, or air shower. Relativistic charged particles in the cascade generate Cherenkov radiation, which is emitted along the shower direction, resulting in a light pool on the ground with a radius of  $\sim 130$  m. Cherenkov light is produced throughout the cascade development, with the maximum emission occurring when the number of particles in the cascade is largest, at an altitude of  $\sim 10$  km for primary energies of 100 GeV–1 TeV. Following absorption and scattering in the atmosphere, the Cherenkov light at ground level peaks at a wavelength,  $\lambda \approx 300$ –350 nm. The photon density is typically  $\sim 100$  photons/m<sup>2</sup> for a 1 TeV primary, arriving in a brief flash of a few nanoseconds duration. This Cherenkov pulse can be detected from any point within the light pool radius by using large reflecting surfaces to focus the Cherenkov light on to fast photon detectors (Fig. 36.4).

Modern atmospheric Cherenkov telescopes, such as those built and operated by the VERITAS [28], H.E.S.S. [29] and MAGIC [30]

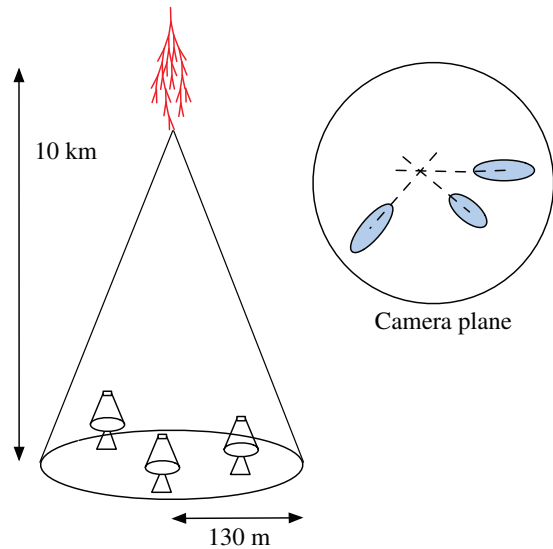


Figure 36.4: A schematic illustration of an imaging atmospheric Cherenkov telescope array. The primary particle initiates an air shower, resulting in a cone of Cherenkov radiation. Telescopes within the Cherenkov light pool record elliptical images; the intersection of the long axes of these images indicates the arrival direction of the primary, and hence the location of a  $\gamma$ -ray source in the sky

collaborations, consist of large ( $> 100$  m<sup>2</sup>) segmented mirrors on steerable altitude-azimuth mounts. A camera made from an array of photosensors is placed at the focus of each mirror and used to record a Cherenkov image of each air shower. In these imaging atmospheric Cherenkov telescopes, single-anode photomultiplier tubes (PMTs) have traditionally been used (2048, in the case of H.E.S.S. II), but silicon devices now feature in more modern designs. The telescope cameras typically cover a field-of-view of  $3 - 10^\circ$  in diameter. Images are recorded at kHz rates, the vast majority of which are due to showers with hadronic cosmic-ray primaries. The shape and orientation of the Cherenkov images are used to discriminate  $\gamma$ -ray photon events from this cosmic-ray background, and to reconstruct the photon energy and arrival direction.  $\gamma$ -ray images result from purely electromagnetic cascades and appear as narrow, elongated ellipses in the camera plane. The long axis of the ellipse corresponds to the vertical extension of the air shower, and points back towards the source position in the field-of-view. If multiple telescopes are used to view the same shower (“stereoscopy”), the source position is simply the intersection point of the various image axes. Cosmic-ray primaries produce secondaries with large transverse momenta, which initiate sub-showers. Their images are consequently wider and less regular than those with  $\gamma$ -ray primaries and, since the original charged particle has been deflected by Galactic magnetic fields before reaching the Earth, the images have no preferred orientation.

The measurable differences in Cherenkov image orientation and morphology provide the background discrimination which makes ground-based  $\gamma$ -ray astronomy possible. For point-like sources, such as distant active galactic nuclei, modern instruments can reject over 99.999% of the triggered cosmic-ray events, while retaining up to 50% of the  $\gamma$ -ray population. In the case of spatially extended sources, such as Galactic supernova remnants, the background rejection is less efficient, but the technique can be used to produce  $\gamma$ -ray maps of the emission from the source. The angular resolution depends upon the number of telescopes which view the image and the energy of the primary  $\gamma$ -ray, but is typically less than  $0.1^\circ$  per event (68% containment radius) at energies above a few hundred GeV.

The total Cherenkov yield from the air shower is proportional to the energy of the primary particle. The image intensity, combined with the reconstructed distance of the shower core from each

telescope, can therefore be used to estimate the primary energy. The energy resolution of this technique, also energy-dependent, is typically 15–20% at energies above a few hundred GeV. Energy spectra of  $\gamma$ -ray sources can be measured over a wide range, depending upon the instrument characteristics, source properties (flux, spectral slope, elevation angle, *etc.*), and exposure time. The effective energy range is typically from 30 GeV to 100 TeV and peak sensitivity lies in the range from 100 GeV to a few TeV.

The first astrophysical source to be convincingly detected using the imaging atmospheric Cherenkov technique was the Crab Nebula [31], with an integral flux of  $2.1 \times 10^{-11}$  photons  $\text{cm}^{-2} \text{s}^{-1}$  above 1 TeV [32]. Modern imaging atmospheric Cherenkov telescopes have sensitivity sufficient to detect sources with less than 1% of the Crab Nebula flux in a few tens of hours. The TeV source catalog now consists of over 200 sources (see e.g. Ref. [33]). A large fraction of these were detected by scanning the Galactic plane from the southern hemisphere with the H.E.S.S. telescope array [34]. Recent reviews of the field include [35] and [36], and a historical overview can be found in [37].

Major upgrades of the existing telescope arrays have recently been completed, including the addition of a 28 m diameter central telescope to H.E.S.S. (H.E.S.S. II). Development is also underway for the next generation instrument, the Cherenkov Telescope Array (CTA), which will consist of a northern and a southern hemisphere observatory, with a combined total of more than 100 telescopes [38]. Telescopes of three different sizes are planned, spread over an area of  $> 1 \text{ km}^2$ , providing wider energy coverage, improved angular and energy resolutions, and an order of magnitude improvement in sensitivity relative to existing imaging atmospheric Cherenkov telescopes. Baseline telescope designs are similar to existing devices, but exploit technological developments such as dual mirror optics and silicon photo-detectors.

### 36.3 Large neutrino detectors

#### 36.3.1 Deep liquid detectors for rare processes

Revised August 2018 by K. Scholberg (Duke U.) and C.W. Walter (Duke U.).

Deep, large detectors for rare processes tend to be multi-purpose with physics reach that includes not only solar, reactor, supernova and atmospheric neutrinos, but also searches for baryon number violation, searches for exotic particles such as magnetic monopoles, and neutrino and cosmic-ray astrophysics in different energy regimes. The detectors may also serve as targets for long-baseline neutrino beams for neutrino oscillation physics studies. In general, detector design considerations can be divided into high- and low-energy regimes, for which background and event reconstruction issues differ. The high-energy regime, from about 100 MeV to a few hundred GeV, is relevant for proton decay searches, atmospheric neutrinos and high-energy astrophysical neutrinos. The low-energy regime (a few tens of MeV or less) is relevant for supernova, solar, reactor and geological neutrinos.

Large water Cherenkov and scintillator detectors (see Table 36.2) usually consist of a volume of transparent liquid viewed by photomultiplier tubes (PMTs) (see Sec 35.2); the liquid serves as active target. PMT hit charges and times are recorded and digitized, and triggering is usually based on coincidence of PMT hits within a time window comparable to the detector's light-crossing time. Because photosensors lining an inner surface represent a driving cost that scales as surface area, very large volumes can be used for comparatively reasonable cost. Some detectors are segmented into subvolumes individually viewed by PMTs, and may include other detector elements (*e.g.*, tracking detectors). Devices to increase light collection, *e.g.*, reflectors or waveshifter plates, may be employed. A common configuration is to have at least one concentric outer layer of liquid material separated from the inner part of the detector to serve as shielding against ambient background. If optically separated and instrumented with PMTs, an outer layer may also serve as an active veto against entering cosmic rays and other background events. The PMTs for large detectors typically range in size from 20 cm to 51 cm diameter, and typical quantum efficiencies are in the 20–25% range for scintillation and water-Cherenkov photons. PMTs with higher quantum

efficiencies, 35% or higher, have recently become available. The active liquid volume requires purification and there may be continuous recirculation of liquid. For large homogeneous detectors, the event interaction vertex is determined using relative timing of PMT hits, and energy deposition is determined from the number of recorded photoelectrons. A “fiducial volume” is usually defined within the full detector volume, some distance away from the PMT array. Inside the fiducial volume, enough PMTs are illuminated per event that reconstruction is considered reliable, and furthermore, entering background from the enclosing walls is suppressed by a buffer of self-shielding. PMT and detector optical parameters are calibrated using laser, LED, or other light sources. Quality of event reconstruction typically depends on photoelectron yield, pixelization and timing.

Because in most cases one is searching for rare events, large detectors are usually sited underground to reduce cosmic-ray-related background (see Chapter 30). The minimum depth required varies according to the physics goals [39].

#### 36.3.1.1 Liquid scintillator detectors

Past and current large underground detectors based on hydrocarbon scintillators include LVD, MACRO, Baksan, Borexino, KamLAND and SNO+; JUNO is a future detector. Experiments at nuclear reactors include CHOOZ, Double CHOOZ, Daya Bay, and RENO. Organic liquid scintillators (see Section 35.3) for large detectors are chosen for high light yield and attenuation length, good stability, compatibility with other detector materials, high flash point, low toxicity, appropriate density for mechanical stability, and low cost. They may be doped with waveshifters and stabilizing agents. Popular choices are pseudocumene (1,2,4-trimethylbenzene) with a few g/L of the PPO (2,5-diphenyloxazole) fluor, and linear alkylbenzene (LAB). In a typical detector configuration there will be active or passive regions of undoped scintillator, non-scintillating mineral oil or water surrounding the inner neutrino target volume. A thin vessel or balloon made of nylon, acrylic or other material transparent to scintillation light may contain the inner target; if the scintillator is buoyant with respect to its buffer, ropes may hold the balloon in place. For phototube surface coverages in the 20–40% range, yields in the few hundreds of photoelectrons per MeV of energy deposition can be obtained. Typical energy resolution is about  $7\%/\sqrt{E(\text{MeV})}$ , and typical position reconstruction resolution is a few tens of cm at  $\sim 1 \text{ MeV}$ , scaling as  $\sim N^{-1/2}$ , where  $N$  is the number of photoelectrons detected.

Shallow detectors for reactor neutrino oscillation experiments require excellent muon veto capabilities. For  $\bar{\nu}_e$  detection via inverse beta decay on free protons,  $\bar{\nu}_e + p \rightarrow n + e^+$ , the neutron is captured by a proton on a  $\sim 180 \mu\text{s}$  timescale, resulting in a 2.2 MeV  $\gamma$  ray, observable by Compton scattering and which can be used as a tag in coincidence with the positron signal. The positron annihilation  $\gamma$  rays may also contribute. Inverse beta decay tagging may be improved by addition of Gd at  $\sim 0.1\%$  by mass, which for natural isotope abundance has a  $\sim 49,000$  barn cross-section for neutron capture (in contrast to the 0.3 barn cross-section for capture on free protons). Gd capture takes  $\sim 30 \mu\text{s}$ , and is followed by a cascade of  $\gamma$  rays adding up to about 8 MeV. Gadolinium doping of scintillator requires specialized formulation to ensure adequate attenuation length and stability.

Scintillation detectors have an advantage over water Cherenkov detectors in the lack of Cherenkov threshold and the high light yield. However, scintillation light emission is nearly isotropic, and therefore directional capabilities are relatively weak. Liquid scintillator is especially suitable for detection of low-energy events. Radioactive backgrounds are a serious issue, and include long-lived cosmogenics. To go below a few MeV, very careful selection of materials and purification of the scintillator is required (see Section 36.6). Fiducialization and tagging can reduce background. One can also dissolve neutrinoless double beta decay ( $0\nu\beta\beta$ ) isotopes in scintillator. This has been realized by KamLAND-Zen, which deployed a 1.5 m-radius balloon containing enriched Xe dissolved in scintillator inside KamLAND, and  $^{130}\text{Te}$  is planned for SNO+. Although for this approach, energy resolution is poor compared to other  $0\nu\beta\beta$  search experiments, the quantity of iso-

**Table 36.2:** Properties of large detectors for rare processes. If total target mass is divided into large submodules, the number of subdetectors is indicated in parentheses. Projects with first data expected in 2021 or later are indicated in italics.

Detector	Mass, kton (modules)	PMTs (diameter, cm)	$\xi$	p.e./MeV	Dates
Baksan	0.33, scint (3150)	1/module (15)	segmented	40	1980–
MACRO	0.56, scint (476)	2-4/module (20)	segmented	18	1989–2000
LVD	1, scint. (840)	3/module (15)	segmented	15	1992–
KamLAND	0.41*, scint	1325(43)+554(51) <sup>†</sup>	34%	460	2002–
Borexino	0.1*, scint	2212 (20)	30%	500	2007–
SNO+	0.78, scint <sup>‡</sup>	9394 (20)	47%	400–600	2019 (exp.)
CHOOZ	0.005, scint (Gd)	192 (20)	15%	130	1997–1998
Double Chooz	0.017, scint (Gd)(2)	534/module (20)	13%	180	2011–
Daya Bay	0.160, scint (Gd)(8)	192/module (20)	5.6% <sup>§</sup>	100	2011–
RENO	0.032, scint (Gd)(2)	342/module (25)	12.6%	100	2011–
<i>JUNO</i>	20.0*, scint	17613 (51)/25600 (8)	77.9%	1200	2021 (exp.)
IMB-1	3.3*, H <sub>2</sub> O	2048 (12.5)	1%	0.25	1982–1985
IMB-2	3.3*, H <sub>2</sub> O	2048 (20)	4.5%	1.1	1987–1990
Kam I	0.88/0.78*, H <sub>2</sub> O	1000/948 (51)	20%	3.4	1983–1985
Kam II	1.04*, H <sub>2</sub> O	948 (51)	20%	3.4	1986–1990
Kam III	1.04*, H <sub>2</sub> O	948 (51)	20% <sup>¶</sup>	4.3	1990–1995
SK I	22.5*, H <sub>2</sub> O	11146 (51)	40%	6	1996–2001
SK II	22.5*, H <sub>2</sub> O	5182 (51)	19%	3	2002–2005
SK III-V	22.5*, H <sub>2</sub> O	11129 (51)	40%	6	2006–
SK-Gd	22.5*, H <sub>2</sub> O (Gd)	11129 (51)	40%	6	2020 (exp.)
<i>Hyper-K</i>	187*, H <sub>2</sub> O <sup>  </sup>	40000 (51)	40%	12	2027 (exp.)
SNO	1, D <sub>2</sub> O/1.7, H <sub>2</sub> O	9438 (20)	31%**	9	1999–2006

\*Indicates typical fiducial mass used for data analysis; this may vary by physics topic.

<sup>†</sup>Measurements made before 2003 only considered data from the 43 cm PMTs.

<sup>‡</sup>SNO+ ran with water fill from May 2017 to July 2019.

<sup>§</sup>The effective Daya Bay coverage is 12% with top and bottom reflectors.

<sup>¶</sup>The effective Kamiokande III coverage was 25% with light collectors.

<sup>||</sup>A second staged module is planned.

\*\*The effective SNO coverage was 54% with light collectors.

tope can be so large that the kinematic signature of  $0\nu\beta\beta$  would be visible as a clear feature in the spectrum.

### 36.3.1.2 Water Cherenkov detectors

Very large imaging water detectors reconstruct ten-meter-scale Cherenkov rings produced by charged particles (see Section 35.5). The first such large detectors were IMB and Kamiokande. The only currently existing instance of this class of detector, with fiducial mass of 22.5 kton and total mass of 50 kton, is Super-Kamiokande (Super-K, SK). Hyper-Kamiokande (Hyper-K) plans at least one, and possibly two, detectors with 187-kton fiducial mass. For volumes of this scale, absorption and scattering of Cherenkov light are non-negligible, and a wavelength-dependent factor  $\exp(-d/L(\lambda))$  (where  $d$  is the distance from emission to the sensor and  $L(\lambda)$  is the attenuation length of the medium) must be included in the integral of Eq. (35.6) for the photoelectron yield. Attenuation lengths on the order of 100 meters have been achieved.

Cherenkov detectors are excellent electromagnetic calorimeters, and the number of Cherenkov photons produced by an  $e/\gamma$  is nearly proportional to its kinetic energy. For massive particles, the number of photons produced is also related to the energy, but not linearly. For any type of particle, the *visible energy*  $E_{\text{vis}}$  is defined as the energy of an electron which would produce the same number of Cherenkov photons. The number of collected photoelectrons depends on the scattering and attenuation in the water along with the photo-cathode coverage, quantum efficiency and the optical parameters of any external light collection systems or protective material surrounding them. Event-by-event corrections are made for geometry and attenuation. For a typical case, in water  $N_{\text{p.e.}} \sim 15 \xi E_{\text{vis}}(\text{MeV})$ , where  $\xi$  is the effective fractional photosensor coverage. Cherenkov photoelectron yield per MeV of energy is relatively small compared to that for scintillator, *e.g.*,  $\sim 6$  p.e./MeV for Super-K with a PMT surface coverage of  $\sim 40\%$ . In spite of light yield and Cherenkov threshold issues, the intrinsic directionality of Cherenkov light allows individual particle tracks to be reconstructed. Vertex and direction fits are performed us-

ing PMT hit charges and times, requiring that the hit pattern be consistent with a Cherenkov ring.

High-energy ( $\sim 100$  MeV or more) neutrinos from the atmosphere or beams interact with nucleons; for the nucleons bound inside the  $^{16}\text{O}$  nucleus, nuclear effects must be considered both at the interaction and as the particles leave the nucleus. Various event topologies can be distinguished by their timing and fit patterns, and by presence or absence of light in a veto. “Fully-contained” events are those for which the neutrino interaction final state particles do not leave the inner part of the detector; these have their energies relatively well measured. Neutrino interactions for which the lepton is not contained in the inner detector sample have higher-energy parent neutrino energy distributions. For example, in “partially-contained” events, the neutrino interacts inside the inner part of the detector but the lepton (almost always a muon, since only muons are penetrating) exits. “Upward-going muons” can arise from neutrinos which interact in the rock below the detector and create muons which enter the detector and either stop, or go all the way through (entering downward-going muons cannot be distinguished from cosmic rays). At high energies, multi-photoelectron hits are likely and the charge collected by each PMT (rather than the number of PMTs firing) must be used; this degrades the energy resolution to approximately  $2\%/\sqrt{\xi E_{\text{vis}}(\text{GeV})}$ . The absolute energy scale in this regime can be known to  $\sim 2\text{--}3\%$  using cosmic-ray muon energy deposition, Michel electrons and  $\pi^0$  from atmospheric neutrino interactions. Typical vertex resolutions for GeV energies are a few tens of cm [40]. Angular resolution for determination of the direction of a charged particle track is a few degrees. For a neutrino interaction, because some final-state particles are usually below Cherenkov threshold, knowledge of direction of the incoming neutrino direction itself is generally worse than that of the lepton direction, and dependent on neutrino energy.

Multiple particles in an interaction (so long as they are above Cherenkov threshold) may be reconstructed, allowing for the exclusive reconstruction of final states. In searches for proton decay,



multiple particles can be kinematically reconstructed to form a decaying nucleon. High-quality particle identification is also possible:  $\gamma$  rays and electrons shower, and electrons scatter, which results in fuzzy rings, whereas muons, pions and protons make sharp rings. These patterns can be quantitatively separated with high reliability using maximum likelihood methods [41]. A  $e/\mu$  misidentification probability of  $\sim 0.4\%/\xi$  in the sub-GeV range is consistent with the performance of several experiments for  $4\% < \xi < 40\%$ . Sources of background for high energy interactions include misidentified cosmic muons and anomalous light patterns when the PMTs sometimes “flash” and emit photons themselves. The latter class of events can be removed using its distinctive PMT signal patterns, which may be repeated. More information about high energy event selection and reconstruction may be found in reference [42].

In spite of the fairly low light yield, large water Cherenkov detectors may be employed for reconstructing low-energy events, down to *e.g.*  $\sim 4$ -5 MeV for Super-K [43]. Low-energy neutrino interactions of solar neutrinos in water are predominantly elastic scattering off atomic electrons; single electron events are then reconstructed. At solar neutrino energies, the visible energy resolution ( $\sim 30\%/\sqrt{\xi E_{\text{vis}}(\text{MeV})}$ ) is about 20% worse than photoelectron counting statistics would imply. Using an electron LINAC and/or nuclear sources, approximately 0.5% determination of the absolute energy scale has been achieved at solar neutrino energies. Angular resolution is limited by multiple scattering in this energy regime (25–30°). At these energies, radioactive backgrounds become a dominant issue. These backgrounds include radon in the water itself or emanated from detector materials, and  $\gamma$  rays from the rock and detector materials. In the few to few tens of MeV range, radioactive products of cosmic-ray-muon-induced spallation are troublesome, and are removed by proximity in time and space to preceding muons, at some cost in dead time. Gadolinium doping using 0.2%  $\text{Gd}_2(\text{SO}_4)_3$  is planned for Super-K to improve selection of low-energy  $\bar{\nu}_e$  and other events with accompanying neutrons [44].

The Sudbury Neutrino Observatory (SNO) detector [45] is the only instance of a large heavy water detector and deserves mention here. In addition to an outer 1.7 kton of light water, SNO contained 1 kton of  $\text{D}_2\text{O}$ , giving it unique sensitivity to neutrino neutral current ( $\nu_x + d \rightarrow \nu_x + p + n$ ), and charged current ( $\nu_e + d \rightarrow p + p + e^-$ ) deuteron breakup reactions. The neutrons were detected in three ways: In the first phase, via the reaction  $n + d \rightarrow t + \gamma + 6.25$  MeV; Cherenkov radiation from electrons Compton-scattered by the  $\gamma$  rays was observed. In the second phase, NaCl was dissolved in the water.  $^{35}\text{Cl}$  captures neutrons,  $n + ^{35}\text{Cl} \rightarrow ^{36}\text{Cl} + \gamma + 8.6$  MeV. The  $\gamma$  rays were observed via Compton scattering. In a final phase, specialized low-background  $^3\text{He}$  counters (“neutral current detectors” or NCDs) were deployed in the detector. These counters detected neutrons via  $n + ^3\text{He} \rightarrow p + t + 0.76$  MeV; ionization charge from energy loss of the products was recorded in proportional counters.

### 36.3.2 Neutrino telescopes

Revised August 2019 by U.F. Katz (Erlangen U.) and C. Spiering (DESY, Zeuten).

The primary goal of neutrino telescopes (NTs) is the detection of astrophysical neutrinos, in particularly those which are expected to accompany the production of high-energy cosmic rays in astrophysical accelerators. NTs in addition address a variety of other fundamental physics issues like indirect search for dark matter, study of neutrino oscillations, search for exotic particles like magnetic monopoles or study of cosmic rays and their interactions [46–48]. Electromagnetic radio frequency detectors for high energy neutrinos are discussed in “Radio emission from (ultra-) high energy particle showers” section 36.3.3.

NTs are large-volume arrays of “optical modules” (OMs) installed in open transparent media like water or ice, at depths that completely block the daylight. The OMs record the Cherenkov light induced by charged secondary particles produced in reactions of high-energy neutrinos in or around the instrumented volume. The neutrino energy,  $E_\nu$ , and direction can be reconstructed from the hit pattern recorded. NTs typically target an energy

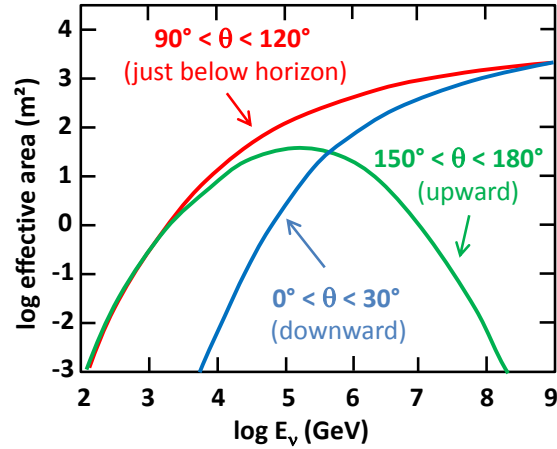


Figure 36.5: Effective  $\bar{\nu}_\mu$  area for IceCube as an example of a cubic-kilometre NT, as a function of neutrino energy for three intervals of the zenith angle  $\theta$ . The values shown here correspond to a specific event selection for point source searches.

range  $E_\nu \gtrsim 100$  GeV; sensitivity to lower energies is achieved in dedicated setups with denser instrumentation.

In detecting cosmic neutrinos, three sources of backgrounds have to be considered: (i) *atmospheric neutrinos* from cosmic-ray interactions in the atmosphere, which can be separated from cosmic neutrinos on a statistical basis, or, for down-going neutrinos, by vetoing accompanying muons; (ii) down-going punch-through *atmospheric muons* from cosmic-ray interactions, which are suppressed by several orders of magnitude with respect to the ground level due to the large detector depths. They can be further reduced by selecting upward-going or high-energy neutrinos or by self-veto methods; (iii) random backgrounds due to photomultiplier (PMT) dark counts,  $^{40}\text{K}$  decays (mainly in sea water) or bioluminescence (only water), which impact adversely on event recognition and reconstruction. Note that atmospheric neutrinos and muons allow for investigating neutrino oscillations and cosmic ray anisotropies, respectively.

Recently, it has become obvious that a precise measurement of the energy-zenith-distribution of atmospheric neutrinos may allow for determining the neutrino mass hierarchy by exploiting matter-induced oscillation effects in the Earth [49, 50].

Neutrinos can interact with target nucleons  $N$  through charged current ( $\bar{\nu}_\ell N \rightarrow \ell^\mp X$ , CC) or neutral current ( $\bar{\nu}_\ell N \rightarrow \bar{\nu}_\ell X$ , NC) processes. A CC reaction of a  $\bar{\nu}_\mu$  produces a muon track and a hadronic particle cascade, whereas all NC reactions and CC reactions of  $\bar{\nu}_\tau$  produce particle cascades only. CC interactions of  $\bar{\nu}_\tau$  can have either signature, depending on the  $\tau$  decay mode. In most astrophysical models, neutrinos are expected to be produced through the  $\pi/K \rightarrow \mu \rightarrow e$  decay chain, *i.e.*, with a flavour ratio  $\nu_e : \nu_\mu : \nu_\tau \approx 1 : 2 : 0$ . For sources outside the solar system, neutrino oscillations turn this ratio to  $\nu_e : \nu_\mu : \nu_\tau \approx 1 : 1 : 1$  upon arrival on Earth.

The total neutrino-nucleon cross section is about  $10^{-35}$   $\text{cm}^2$  at  $E_\nu = 1$  TeV and rises roughly linearly with  $E_\nu$  below this energy and as  $E_\nu^{0.3-0.5}$  above, flattening out towards high energies. The CC:NC cross-section ratio is about 2:1. At energies above some TeV, neutrino absorption in the Earth becomes noticeable; for vertically upward-moving neutrinos (zenith angle  $\theta = 180^\circ$ ), the survival probability is 74 (27, < 2)% for 10 (100, 1000) TeV. On average, between 50% (65%) and 75% of  $E_\nu$  is transferred to the final-state lepton in neutrino (antineutrino) reactions between 100 GeV and 10 PeV.

The final-state lepton follows the initial neutrino direction with a RMS mismatch angle  $\langle \phi_{\nu\ell} \rangle \approx 1.5^\circ/\sqrt{E_\nu [\text{TeV}]}$ , indicating the intrinsic kinematic limit to the angular resolution of NTs. For CC  $\bar{\nu}_\mu$  reactions at energies above about 10 TeV, the angular resolution is dominated by the muon reconstruction accuracy of a few times  $0.1^\circ$  at most. For muon energies  $E_\mu \gtrsim 1$  TeV, the increasing light emission due to radiative processes allows for re-

constructing  $E_\mu$  from the measured  $dE_\mu/dx$  with an accuracy of  $\sigma(\log E_\mu) \approx 0.3$ ; at lower energies,  $E_\mu$  can be estimated from the length of the muon track if it is contained in the detector. These properties make CC  $\bar{\nu}_\mu$  reactions the prime channel for the identification of individual astrophysical neutrino sources.

Hadronic and electromagnetic particle cascades at the relevant energies are 5–20 m long, *i.e.*, short compared to typical OM distances. The total amount of Cherenkov light provides a direct measurement of the cascade energy with an accuracy of about 20% at energies above 10 TeV and 10% beyond 100 TeV for events contained in the instrumented volume. Neutrino flavour and reaction mechanism can, however, hardly be determined and neutrinos from NC reactions or  $\tau$  decays may carry away significant “invisible” energy. Above 100 TeV, the average directional reconstruction accuracy of cascades is 10–15 degrees in polar ice and better than 2 degrees in water, the difference being due to the inhomogeneity of the ice and stronger light scattering in ice. These features, together with the small background of atmospheric  $\bar{\nu}_e$  and  $\bar{\nu}_\tau$  events, makes the cascade channel particularly interesting for searches for a diffuse, high-energy excess of extraterrestrial over atmospheric neutrinos. In water, cascade events can also be used for the search for point sources of cosmic neutrinos, albeit the inferior angular accuracy compared to muon tracks leads to a higher background from atmospheric neutrinos.

The detection efficiency of a NT is quantified by its effective area, *e.g.*, the fictitious area for which the full incoming neutrino flux would be recorded (see Figure 36.5). The increase with  $E_\nu$  is due to the rise of neutrino cross section and muon range, while neutrino absorption in the Earth causes the decrease at large  $\theta$ . Identification of downward-going neutrinos requires strong cuts

against atmospheric muons, hence the cut-off towards low  $E_\nu$ . Due to the small cross section, the effective area is many orders of magnitude smaller than the geometrical dimension of the detector; a  $\bar{\nu}_\mu$  with 1 TeV can, *e.g.*, be detected with a probability of the order  $10^{-6}$  if the NT is on its path.

Detection of upward-going muons allows for identifying neutrino interactions far outside the instrumented volume. This method, however, is only sensitive to CC  $\bar{\nu}_\mu$  interactions and cannot be extended to more than 5–10 degrees above the geometric horizon, where the background of atmospheric muons becomes prohibitive. Alternatively, one can select events that start inside the instrumented volume and thus remove incoming muons that generate early hits in the outer layers of the detector. Such a veto-based event selection is sensitive to neutrinos of all flavours from all directions, albeit with a reduced efficiency since a part of the instrumented volume is sacrificed for the veto. Such a muon veto, or vetoing events with a coincident signal in the surface array, also rejects down-going atmospheric neutrinos that are accompanied by muons from the same air shower and thus reduces the atmospheric-neutrino background. Actually, the breakthrough in detecting high-energy cosmic neutrinos has been achieved with this technique.

Note that the fields of view of NTs at the South Pole and in the Northern hemisphere are complementary for each reaction channel and neutrino energy.

### 36.3.2.1 The Projects

Table 36.3 lists past, present and future neutrino telescope projects and their main parameters.

**Table 36.3:** Past, present and future NT projects and their main parameters. The milestone years give the times of project start, of first data taking with partial configurations, of detector completion, and of project termination. Projects with first data expected past 2020 are indicated in italics. The size refers to the largest instrumented volume reached during the project development. See [48] for references to the different projects where unspecified.

Experiment	Milestones	Location	Size (km <sup>3</sup> )	Remarks
DUMAND	1978/–/–/1995	Pacific Ocean		Terminated due to technical/funding problems
NT-200	1980/1993/1998/2015	Lake Baikal	10 <sup>−4</sup>	First proof of principle
GVD [51]	2012/2015/–/–	Lake Baikal	0.5–1.5	High-energy $\nu$ astronomy first 5 clusters installed
NESTOR	1991/–/–/–	Med. Sea		2004 data taking with prototype
NEMO	1998/–/–/–	Med. Sea		R&D project, prototype tests
AMANDA	1990/1996/2000/2009	South Pole	0.015	First deep-ice NT
ANTARES	1997/2006/2008/–	Med. Sea	0.010	First deep-sea NT
IceCube	2001/2005/2010/–	South Pole	1.0	First km <sup>3</sup> -sized detector
<i>IceCube-Gen2</i> [52]	2014/–/–/–	South Pole	5–10	Planned extension of IceCube covering low and high energies, a surface array and radio detection
KM3NeT/ARCA [50]	2013/(2015)/–/–	Med. Sea	ca. 1	First construction phase started
KM3NeT/ORCA [50]	2014/(2017)/–/–	Med. Sea	0.003	Low-energy configuration for neutrino mass hierarchy
<i>KM3NeT Phase 3</i>	2013/–/–/–	Med. Sea	ca. 3	6 ARCA blocks + ORCA

### 36.3.2.2 Properties of media

The efficiency and quality of event reconstruction depend strongly on the optical properties (absorption and scattering length, intrinsic optical activity) of the medium in the spectral range of alkali photocathodes (300–550 nm). Large absorption lengths result in a better light collection, large scattering lengths in superior angular resolution. Deep-sea sites typically have effective scattering lengths of > 100 m and, at their peak transparency around 450 nm, absorption lengths of 50–65 m. The absorption length for Lake Baikal is 22–24 m. The properties of South Polar ice vary strongly with depth; at the peak transparency wave length (400 nm), the scattering length is between 5 and 75 m and the absorption length between 15 and 250 m, with the best values in the depth region 2200–2450 m and the worst ones in the layer

1950–2100 m.

Noise rates measured by 25 cm PMTs in deep polar ice are about 0.5 kHz per PMT and almost entirely due to radioactivity in the OM components. The corresponding rates in sea water are typically 60 kHz, mostly due to <sup>40</sup>K decays. Bioluminescence activity can locally cause rates on the MHz scale for seconds; the frequency and intensity of such “bursts” depends strongly on the sea current, the season, the geographic location, and the detector geometry. Experience from ANTARES shows that these backgrounds are manageable without a major loss of efficiency or experimental resolution.

### 36.3.2.3 Technical realisation

**Optical modules (OMs) and PMTs:** An OM is a pressure-tight glass sphere housing one or several PMTs with a time resolu-

tion in the nanosecond range, and in most cases also electronics for control, HV generation, operation of calibration LEDs, time synchronisation and signal digitisation.

Hybrid PMTs with 37 cm diameter have been used for NT-200, conventional hemispheric PMTs for AMANDA (20 cm) and for ANTARES, IceCube and Baikal-GVD (25 cm). A novel concept has been chosen for KM3NeT. The OMs (43 cm) are equipped with 31 PMTs (7.5 cm), plus control, calibration and digitisation electronics. The main advantages are that (i) the overall photocathode area exceeds that of a 25 cm PMT by more than a factor of 3; (ii) the individual readout of the PMTs results in a very good separation between one- and two-photoelectron signals which is essential for online data filtering and random background suppression; (iii) the hit pattern on an OM provides directional information; (iv) no mu-metal shielding against the Earth magnetic field is required. Figure 36.6 shows the OM designs of IceCube and KM3NeT.

**Readout and data filtering:** In current NTs the PMT data are digitised in situ, for ANTARES and Baikal-GVD in special electronics containers close to the OMs, for IceCube and KM3NeT inside the OMs. For IceCube, data are transmitted via electrical cables of up to 3.3 km length, depending on the location of the strings and the depth of the OMs; for ANTARES, KM3NeT and Baikal-GVD optical fibre connections have been chosen (several 10 km for the first two and 4 km for GVD).

The full digitised waveforms of the IceCube OMs are transmitted to the surface for pulses appearing in local coincidences on a string; for other pulses, only time and charge information is provided. For ANTARES (time and charge) and KM3NeT (time over threshold), all PMT signals above an adjustable noise threshold are sent to shore.

The raw data are subsequently processed on online computer farms, where multiplicity and topology-driven filter algorithms are applied to select event candidates. The filter output data rate is about 10 GByte/day for ANTARES and of the order 1 TByte/day for IceCube (100 GByte/day transferred via satellite) and KM3NeT.

**Calibration:** For efficient event recognition and reconstruction, the OM timing must be synchronised at the few-nanosecond level and the OM positions and orientations must be known to a few 10 cm and a few degrees, respectively. Time calibration is achieved by sending time synchronisation signals to the OM electronics and also by light calibration signals emitted in situ at known times by LED or laser flashers (ANTARES, KM3NeT). Precise position calibration is achieved by measuring the travel time of light calibration signals sent from OM to OM (IceCube) or acoustic signals sent from transducers at the sea floor to receivers on the detector strings (ANTARES, KM3NeT, Baikal-GVD). Absolute pointing and angular resolution can be determined by measuring the “shadow of the moon” (*i.e.*, the directional depletion of muons generated in cosmic-ray interactions). IceCube has shown that both are below  $1^\circ$ , confirming MC calculations which indicate a precision of  $\approx 0.5^\circ$  for energies above 10 TeV. For KM3NeT, simulations indicate that sub-degree precision in the absolute pointing can be reached within a few weeks of operation.

**Detector configurations:** IceCube (see Figure 36.7) consists of 5160 Digital OMs (DOMs) installed on 86 strings at depths of 1450 to 2450 m in the Antarctic ice; except for the DeepCore region, string distances are 125 m and vertical distances between OMs 17 m. 324 further DOMs are installed in IceTop, an array of detector stations on the ice surface above the strings. DeepCore is a high-density sub-array at large depths (*i.e.*, in the best ice layer) at the centre of IceCube.

The NT200 detector in Lake Baikal at a depth of 1100 m consisted of 8 strings attached to an umbrella-like frame, with 12 pairs of OMs per string. The diameter of the instrumented volume was 42 m, its height 70 m. Meanwhile (2019), the Baikal collaboration has installed the first five clusters of a future cubic-kilometre array. A first phase, covering a volume of about  $0.4 \text{ km}^3$ , will consist of 9 clusters, each with 288 OMs at 8 strings; its completion is scheduled for 2021. A next stage could comprise about 20 clusters and cover up to  $1.5 \text{ km}^3$ .

ANTARES comprises 12 strings with lateral distances of 60–

70 m, each carrying 25 triplets of OMs at vertical distances of 14.5 m. The OMs are located at depths of 2.1–2.4 km, starting 100 m above the sea floor. A further string carries devices for calibration and environmental monitoring. A system to investigate the feasibility of acoustic neutrino detection has also been implemented.

KM3NeT will consist of building blocks of 115 strings each, with 18 OMs per string. Operation of prototypes and the first strings deployed have successfully verified the KM3NeT technology [53]. In the upcoming phase 2.0 of its staged implementation, KM3NeT aims at two building blocks for neutrino astronomy, with vertical distances between OMs of 36 m and a lateral distance between adjacent strings of 90 m (ARCA, for *Astroparticle Research with Cosmics in the Abyss*) and at one block for the measurement of the neutrino mass hierarchy, with vertical distances between OMs of 9 m and a lateral distance between adjacent strings of about 20 m (ORCA, for *Oscillation Research with Cosmics in the Abyss*) [50]. A first installation phase of ARCA near Capo Passero, East of Sicily and of ORCA near Toulon has started in 2015 and comprises 24 (6 ARCA (ORCA) strings to be deployed by 2021 (2019). Completion of the full ARCA (ORCA) arrays is planned for 2026 (2024). The possibility of directing a neutrino beam from the Protvino accelerator to ORCA (P2O) is also under study [54].

### 36.3.2.4 Results

Atmospheric neutrino fluxes have been precisely measured with AMANDA and ANTARES ( $\bar{\nu}_\mu$ ) and with IceCube ( $\bar{\nu}_\mu$ ,  $\bar{\nu}_e$ ); the results are in agreement with predicted spectra.

In 2013, an excess of track and cascade events between 30 TeV and 1 PeV above background expectations was reported by IceCube; this analysis used the data taken in 2010 and 2011 and for the first time employed containment conditions and an atmospheric muon veto for suppression of down-going atmospheric neutrinos (High-Energy Starting Event analysis, HESE). The observed excess reached a significance of  $5.7\sigma$  in a subsequent analysis of 3 years of data [56] and increased in significance since then. It cannot be explained by atmospheric neutrinos and misidentified atmospheric muons alone. A consistent observation has also been made by ANTARES [57], albeit with much lower significance. The skymap of HESE and high-energy through-going muon events (see Figure 36.8) does not indicate statistically significant event clusters, nor deviations from an isotropic cosmic neutrino flux. Meanwhile the energy range of the IceCube HESE analysis has been extended down to 1 TeV and the high-energy excess confirmed; also, events with through-going muons showed a corresponding excess of cosmic origin. In [58], the various analyses have been combined. Assuming the cosmic neutrino flux to be isotropic, flavour-symmetric and  $\nu$ - $\bar{\nu}$ -symmetric at Earth, the all-flavour spectrum is well described by a power law with normalisation  $6.7^{+1.1}_{-1.2} \times 10^{-18} \text{ GeV}^{-1} \text{ s}^{-1} \text{ sr}^{-1} \text{ cm}^{-2}$  at 100 TeV and a spectral index  $-2.50 \pm 0.09$  for energies between 25 TeV and 2.8 PeV. A spectral index of  $-2$ , an often quoted benchmark value, is disfavoured with a significance of  $3.8\sigma$ .

Multi-messenger observations triggered by a high-energy IceCube neutrino event in 2017 (see Figure 36.9 for an event display), together with a neutrino excess from the same celestial direction in the 2014/15 archival IceCube data, yielded evidence for a first neutrino signal related to a known astronomical object, the blazar<sup>2</sup> TXS 0506+056 [59, 60]. Multi-messenger investigations in conjunction with gravitational waves, ultra-high-energy cosmic rays or gamma-ray observations have not revealed further matching neutrino signals to date. Also, no further astrophysical neutrino sources were found in a recent combined IceCube/ANTARES search for steady sources [61].

IceCube has reported an energy-dependent anisotropy of cosmic-ray induced muons and a measurement of the neutrino-nucleon cross section using neutrino absorption in Earth.

No indications for neutrino fluxes from dark matter annihilations or for other exotic phenomena have been found.

<sup>2</sup>An Active Galactic Nucleus with a relativistic jet outflow pointing to the observer.

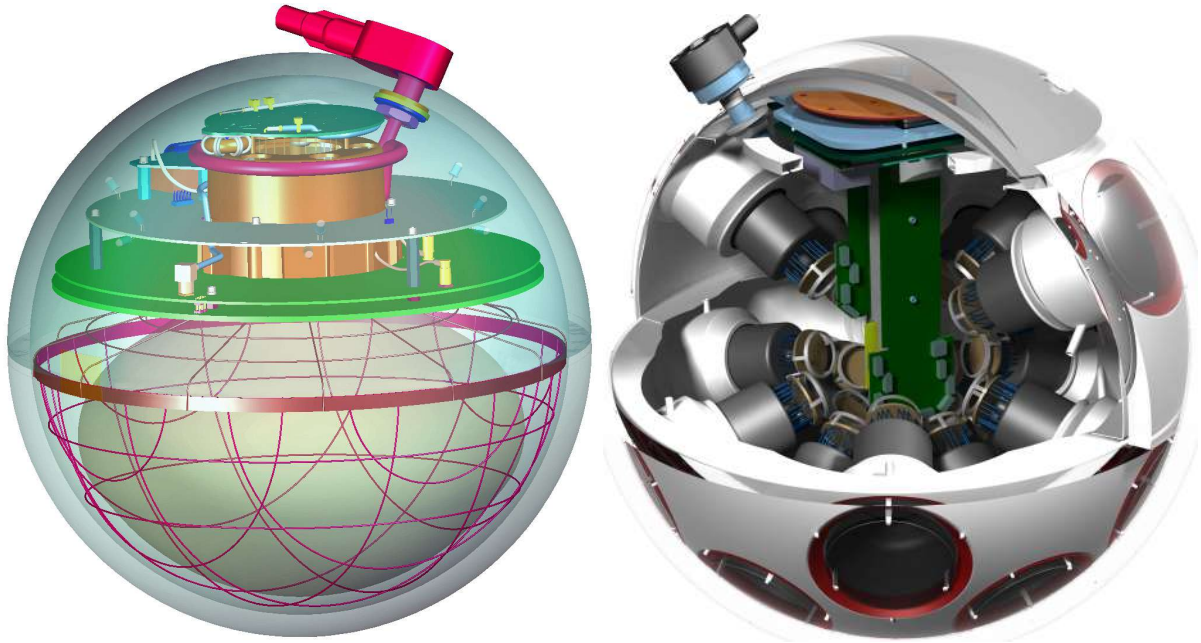


Figure 36.6: Schematic views of the digital OMs of IceCube (left) and KM3NeT (right).

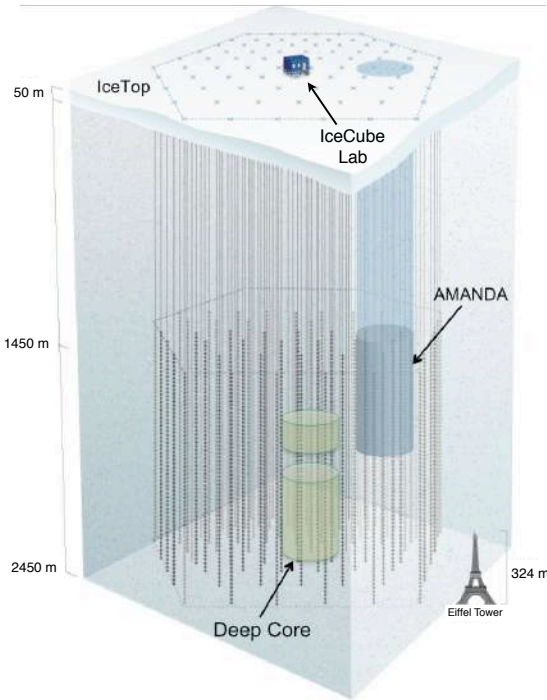


Figure 36.7: Schematic view of the IceCube neutrino observatory comprising the deep-ice detector including its nested dense part DeepCore, and the surface air shower array IceTop. The IceCube Lab houses data acquisition electronics and the computer farm for online processing. Operation of AMANDA was terminated in 2009.

At lower energies, down to 10 GeV, IceCube/DeepCore and ANTARES have identified clear signals of oscillations of atmospheric neutrinos. The closely spaced OMs of DeepCore allow for selecting a very pure sample of low-energy  $\bar{\nu}_\mu$  (6–56 GeV) that produce upward moving muons inside the detector. The neutrino energy is determined from the energy of the hadronic shower at the vertex and the muon range. Fits to the energy/zenith-dependent deficit of muon neutrinos provide constraints on the oscillation pa-

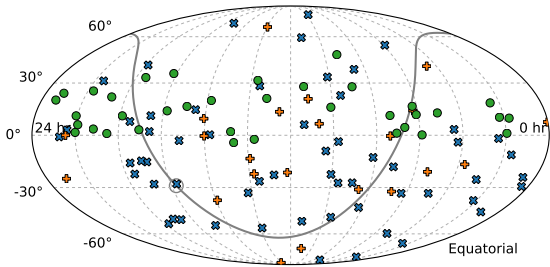


Figure 36.8: Arrival directions of IceCube candidate events for cosmic neutrinos in equatorial coordinates. The plot contains 82 HESE events, with shower-like events marked as blue  $\times$  and muon tracks as orange  $+$ , and in addition 36 through-going muons tracks with an energy deposit exceeding 200 TeV (green circles). Approximately 40% of the events are expected to originate from atmospheric backgrounds. The grey curve denotes the Galactic Plane and the grey circle the Galactic Centre (from [55]).

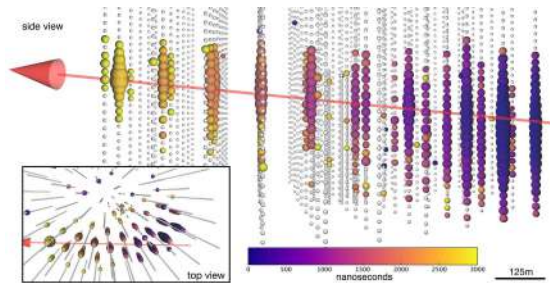


Figure 36.9: Display of the neutrino event IceCube-170922A pointing to the blazar TXS 0506+056. The deposited energy is 24 TeV, the neutrino energy is estimated to be 290 TeV. The colour code indicates the signal timing (blue: early; yellow: late), the size of the coloured circles is a logarithmic measure of the light intensity registered per DOM. The arrow indicates the reconstructed direction, corresponding to a zenith angle of  $5.7^{+0.5}_{-0.3}$  degrees below horizon. Figure from [59].

rameters  $\sin^2 \theta_{23}$  and  $\Delta m_{23}^2$ . The analysis of the same dependence for cascade-like events provides a  $3\sigma$  evidence for  $\nu_\tau$  appearance



– an important measurement to test the unitarity of the PNMS matrix [62].

See [63] and [64] for summaries of recent results of IceCube and ANTARES/KM3NeT, respectively.

### 36.3.2.5 Plans beyond 2020

Within the future IceCube-Gen2 project, it is planned to extend the sensitivity of IceCube towards both lower and higher energies. A substantially denser instrumentation of a sub-volume of DeepCore would lead to an energy threshold for neutrino detection of a few GeV, aiming primarily at measuring the neutrino mass hierarchy. For higher energies, a large-volume extension, combined with a powerful surface veto, is envisaged [52]. A very first phase with 7 closely spaced strings is in preparation for deployment in 2022/23, aiming to cover part of the low-energy program, to better calibrate the existing IceCube detector and the archival data, and to test new technologies. More information on the future extensions of GVD and KM3NeT are given above, in Table 36.3 and in [50].

### 36.3.3 Radio emission from (ultra-)high energy particle showers

Revised October 2019 by S.R. Klein (NSD LBNL; UC Berkeley).

Coherent radio-frequency (RF) electromagnetic radiation is an attractive signature to search for particle cascades produced by interactions of high-energy particles. RF signatures have been used to study both cosmic-ray air showers and to search for neutrino-induced showers. The difference in length scale ( $X_0$ ) between air and the solid materials used for other neutrino searches leads to surprisingly large differences in signal generation. This article will begin with neutrino-induced showers, with air showers covered in subsection 36.3.3.3. At lower energies, incoherent optical Cherenkov radiation is frequently used, as discussed in "Neutrino telescopes" section 36.3.2.

RF detectors can be used to search for energetic neutrinos from three types of sources: astrophysical objects (*i.e.* extending measurements the neutrino energy spectrum observed at TeV to PeV energies upward in energy), searching for cosmogenic neutrinos associated with cosmic-ray-cosmic microwave background radiation interactions, and searching for neutrinos from beyond-standard-model physics. These types are roughly associated with energies below  $10^{18}$  eV, the energy range  $10^{18}$  to  $10^{20}$  eV, and above  $10^{20}$  eV. Cosmogenic neutrinos are produced when ultra-high energy (UHE) protons with energy  $E > 4 \times 10^{19}$  eV interact with photons from the cosmic-microwave background radiation, infrared light from old stars, and other extragalactic background light. These protons are excited to a  $\Delta^+$  resonance which may decay via  $\Delta^+ \rightarrow n\pi^+$ , leading to the production of neutrinos with energies above  $10^{18}$  eV [65, 66]. Neutrinos are the only long-range probe of the ultra-high energy cosmos, because protons, heavier nuclei and photons with energies above  $5 \times 10^{19}$  eV are limited to ranges of less than 100 Mpc by interactions with the CMB and early starlight.

The cosmogenic neutrino signal depends heavily on the fraction of UHE cosmic-rays that are protons. For a 100% proton composition (disfavored by most data), observing a cosmogenic neutrino signal of at least a few events per year requires a detector with an active volume of about  $100 \text{ km}^3$ , made out of a non-conducting solid (or potentially liquid) medium, with a long absorption length for radio waves. The huge volumes require that this be a common material. A dense medium would reduce the detector volume, but, unfortunately, the available natural media have only moderate density. Optical Cherenkov and acoustical detectors are limited by short ( $< 300$  m) attenuation lengths [67] so would require a prohibitively expensive number of sensors. Radio-detection is the only current approach that can scale to this volume. The two most commonly used media are glacial ice, in Antarctica or Greenland, or the lunar regolith [68].

Electromagnetic and hadronic showers produce radio pulses via the Askaryan effect [69, 70], as discussed in "Passage of Particles Through Matter" review Sec. 34. The shower contains more electrons than positrons. At wavelengths longer than the transverse size of the shower, this leads to coherent Cherenkov emission, where the electric field scales as the square of the net charge ex-

cess. This may also be described more generally as being due to radiation from a time-varying net charge [71]; this latter description also applies to radio emission in cosmic-ray air showers.

High-frequency radiation is concentrated around the Cherenkov angle. Viewed directly on the Cherenkov cone, the electric field strength,  $\epsilon_{\text{Ch}}$  at a frequency  $f$  from an electromagnetic shower from a  $\nu_e$  may be roughly parameterized as [72, 73]

$$\epsilon_{\text{Ch}}(\text{V/mMHz}) = 2.53 \times 10^{-7} \frac{E_\nu}{1\text{TeV}} \frac{f}{f_c} \left[ \frac{1}{1 + (f/f_c)^{1.44}} \right]. \quad (36.3)$$

The electric field strength increases linearly with frequency, up to a cut-off frequency  $f_c$ , which is set by the transverse size of the shower [74, 75]. The maximum wavelength  $c/f_c$  is roughly the Moliere radius divided by  $\cos(\theta_C)$  where  $\theta_C$  is the Cherenkov angle. The cutoff frequencies depend on the density (which affects the Moliere radius). They are about 1 GHz in ice, and about 3 GHz in the lunar regolith. Near  $f_c$ , radiation is narrowly concentrated around the Cherenkov angle [74, 75]. At lower frequencies, the limited length of the emitting region leads to a broadening in emission angle around the Cherenkov cone. Away from  $\theta_C$ , the electric field from Eq. (36.3) is reduced by [72],

$$\frac{\epsilon}{\epsilon_{\text{Ch}}} = \exp \left( -\frac{1}{2} \frac{(\theta - \theta_C)^2}{(2.2^\circ \times [1\text{GHz}/f])^2} \right). \quad (36.4)$$

In both ice and the lunar regolith, the Cherenkov angle is about  $56^\circ$ . At very low frequencies, the distribution is very broad, with  $f = 50\text{MHz}$  corresponding to a shower with an angular spread of  $\sigma = 45^\circ$ .

More accurate calculations of the predicted radio signal from a neutrino require detailed Monte Carlo simulations. These simulations begin with a neutrino induced shower, and then calculate (directly or from a parameterization) the Askaryan signal. The Askaryan signal calculation is tough for two reasons. First, much of the excess charge comes from the lowest energy particles in the shower. Second, it is necessary to keep track of the phase of the signal from each particle, as well as the amplitude and the time (or frequency) dependence. This signal is then propagated through the medium and into an antenna model [73].

Along the Cherenkov cone, the 1 GHz maximum frequency leads to a generated pulse width of  $\approx 1$  nsec. This pulse broadens by dispersion as it propagates, particularly for signals from the Moon traversing the ionosphere. As long as the dispersion can be compensated for and backgrounds controlled, a large bandwidth detector is the most sensitive. Spectral information can be used to reject background, and to help reconstruct the neutrino direction, because the cutoff frequency depends on the observation angle with respect to the Cherenkov cone.

The electric field is linearly proportional to the neutrino energy, so the power (field strength squared) is proportional to the square of the neutrino energy. Since the signal is a radio wave, the field amplitude decreases as  $1/R$ , plus absorption in the intervening medium. The detection threshold is determined by the distance to the antenna and the noise characteristics of the detector. For an antenna located in the detection medium, the typical threshold is around  $10^{17}$  eV; for stand-off (remote sensing) detectors, the threshold rises roughly linearly with the distance. These thresholds can be reduced significantly by using directional antennas and/or combining the signals from multiple antennas using beam-forming techniques. Experiments have used both approaches to reduce trigger-level noise, or to reject background at the analysis level. For multi-element arrays, the threshold drops as the square root of number of antennas, since the signal adds in-phase while the backgrounds add with random phases [76].

Some common background sources are anthropogenic noise, antenna/preamp noise, cosmic-ray air showers, charge generated by blowing snow, lightning, and, at low frequencies, radiation from the Milky Way. The need to limit anthropogenic noise has led most experimental groups to select remote locations for their detectors.

Reconstruction of the neutrino arrival direction depends on several aspects of the signal. First, the direction from the antenna

to the interaction site must be determined. This can be done by using the relative timing from separated antennas, or using beam-forming techniques with multi-element arrays. If the radio signal encounters media where the index of refraction vary (like the firm of glacial ice), then it may be necessary to use ray-tracing techniques to follow the signal back to interaction point. The distance (and hence the neutrino energy) can be difficult to determine unless the signal can be triangulated, either using multiple, separated antennas, or observing two pulses with different flight paths (*i. e.* with one including a reflection) in a single antenna.

The neutrino arrival direction can be determined with respect to that direction via two angles, which are determined using very different methods. The first uses the measured frequency spectrum. Equation 36.4 can be used to determine the angular distance between the detector vector and the Cherenkov cone. The second angle can be determined by the polarization of the signal. The radio signal is produced with a linear polarization in the plane containing both the neutrino direction and the photon direction. These two angles can be combined to determine the direction, subject to a (usually) four-fold ambiguity, due to uncertainty as to whether the antenna is inside or outside the Cherenkov cone, and because the neutrino direction can be flipped  $180^\circ$  without affecting the observed signal. Often, some of these solutions can be rejected because they correspond to long path lengths through the Moon or the Earth, where the neutrino would be absorbed.

At energies above  $10^{16}$  eV in ice, the Landau-Pomeranchuk-Migdal effect lengthens electromagnetic showers, by reducing the cross-sections for bremsstrahlung and pair production [77]. The lengthening of the shower leads to a narrowing of the radio emission around the Cherenkov cone, and a reduction in high-frequency emission away from the cone [73]. At higher energies, this leads two separate components of the Askaryan radiation: an un-altered component from the hadronic portion of the shower (on average 20% of the total energy) and a an angularly narrowed component from the LPM-lengthened electromagnetic shower. The angular narrowing scales as  $E_\nu^{1/3}$ ; if these two components can be observed separately, they could, in principle, be combined to determine the inelasticity of the neutrino interaction [78], allowing for improved measurements of parton distributions, and searches for beyond-standard-model interactions.

At still higher energies, above  $10^{20}$  eV, the LPM effect becomes stronger, and the electromagnetic shower splits into multiple sub-showers with significant separation. When this separations become large enough, the subshowers will effectively become independent radiators, with the total emission showing substantial event-by-event variation, depending on the division into subshowers [77]. Because of this, many of the experiments that study higher energy (well above  $10^{20}$  eV) neutrinos focus on the hadronic shower from the struck nucleus. This contains an average of only about 20% of the energy, but with smaller large fluctuations.

Figure 36.10 shows some of the current limits from neutrino searches, including from prototype arrays. Except for LOFAR, which is fully operational, projected limits from future experiments are not shown in the figure.

One variation on the radio-detection approach is to look for radio signals from Earth-skimming  $\nu_\tau$ . Although  $\nu_\tau$  are much less commonly produced than  $\nu_\mu$  and  $\nu_e$ , as they travel astrophysical distances, oscillations lead to a  $\nu_e : \nu_\mu : \nu_\tau$  ratio near 1 : 1 : 1, for almost all non-exotic acceleration and propagation mechanisms [90].

If the  $\nu_\tau$  traverse the Earth and interact while traveling upward, near the surface, the resulting  $\tau^\pm$  may exit the Earth before decaying. 83% of the time, the decay produces a hadronic or electromagnetic shower in the atmosphere [91]. Experiments have searched for this upgoing shower, and for the resulting optical Cherenkov and coherent RF radiation. The threshold energy dependence for these searches depends on several factors, notably including the average  $\tau^\pm$  decay length, which increases linearly with energy; the Pierre Auger observatory set limits on the neutrino flux at energies above  $10^{17}$  eV [80]. Radio-detection efforts have similar or slightly higher thresholds. Detection in low-density (compared to rock or ice) air introduces a number of new complications, including the much larger length scale and the effects

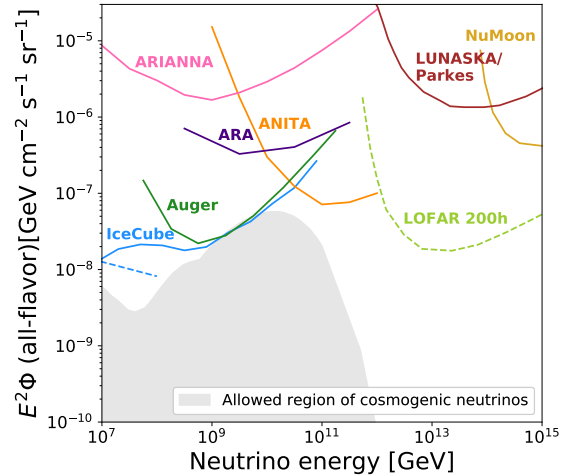


Figure 36.10: Representative 3-flavor (summed, assuming equal fluxes of each flavor) differential (over one decade in energy) limits from different experiments and prototype experiments. Shown are limits from the IceCube ultra-high energy  $\nu$  search [79], the Auger search for earth-skimming  $\nu_\tau$  [80], the LUNASKA/Parkes [81] and NuMoon lunar searches [82], the ANITA balloon experiment [83], ARA [84] and ARIANNA prototypes [85], along with projections for the LOFAR array [86]. The dashed blue line is the extrapolation of the IceCube through-going  $\nu_\mu$  flux measured at lower energies (few 10s of TeV to 10 PeV), with spectral index  $\alpha = -2.28$  [87]. Because of the long extrapolation, this should only be treated as a rough reference. The ARA and ARIANNA limits are from prototype arrays, and indicate the energy range that might be covered, with far higher sensitivity by larger arrays. The shaded area is the allowed region for neutrinos, from a recent global analysis that included the measured cosmic-ray spectrum and composition [88]. Thanks to Anna Nelles (DESY-Zeuthen) for preparing this figure, which is adapted from Ref. [89].

of the Earth's magnetic field. These issues are similar to those inherent in studies of radio signals from cosmic-ray air showers, discussed later.

The ANITA balloon-based radio-detection experiment has even reported two anomalous events [92] which the collaboration has indicated might be from Earth-skimming  $\nu_\tau$ . However, this interpretation is controversial.

A number of prototype  $\nu_\tau$  radio-detection experiments exist. The GRAND Collaboration recently proposed to deploy a 10,000 antenna array, eventually growing to 200,000 antennas spread over 200,000 km<sup>2</sup> [93]. The latter array would be sensitive to cosmogenic neutrinos, unless the UHE cosmic-ray flux is mostly heavier nuclei.

Magnetic monopoles would also emit radio waves, and neutrino experiments have also set monopole flux limits [94].

### 36.3.3.1 The Moon as a target

Because of its large size and non-conducting regolith, and the availability of large radio-telescopes, the Moon is an attractive target [95]. Conventional radio-telescopes are quite well suited to lunar neutrino searches, with natural beam widths not too dissimilar from the size of the Moon. Still, there are experimental challenges. The attenuation length is typically estimated to be  $9m/f(\text{GHz})$ , so only near-surface interactions can be studied. The composition of the lunar regolith is not well known, so there are significant uncertainties on this attenuation. And, there is a background from cosmic-ray interactions in the Moon. One big limitation of lunar experiments is that the 240,000 km target-antenna separation leads to neutrino energy thresholds above  $10^{20}$  eV.

The effective volume probed by experiments depends on the geometry, which itself depends on the frequency range used. At high frequencies  $f$ , the electric field strength is high, leading to a lower energy threshold, but the sensitive volume is limited because

the Cherenkov cone only points toward the Earth for a narrow range of geometries. Lower frequency radiation is more isotropic, so the effective volume is larger, but, because the electric field is weaker, the energy threshold is higher. The  $1/f$  dependence of the attenuation length in the lunar regolith further increases the effective volume at low frequencies. The frequency range affects the energy dependence of the sensitivity. As can be seen in Fig. 36.10, a low-frequency experiment like NuMoon (which covered 115-180 MHz) has good sensitivity, but only above about  $10^{14}$  GeV, while Lunaska/Parkes, which observed in the range 1200-1500 MHz, has a higher flux limit, but is sensitive above about  $10^{12.5}$  GeV.

With modern technology, it is increasingly viable to search over very broad frequency ranges [96]. One technical challenge is due to dispersion (frequency dependent time delays) in the ionosphere. Dispersion can be largely removed with a de-dispersion filter, using either analog circuitry or post-collection digital processing.

Lunar experiments use different techniques to reduce the anthropogenic background. Some experiments use multiple antennas, separated by at least hundreds of meters; by requiring a coincidence within a small time window, anthropogenic noise can be rejected. With good enough timing, beam-forming techniques can be used to further reduce the background. An alternative approach is to use beam forming with multiple feed antennas viewing a single reflector, to ensure that the signal points back to the moon.

In the near future, several large radio detector arrays should reach significantly lower limits. The LOFAR array is taking data with 36 detector clusters spread over Northwest Europe [86]. In the longer term, the Square Kilometer Array (SKA) with its  $1 \text{ km}^2$  effective area will push thresholds down to near  $10^{20}$  eV [96]. It should be noted that current limits and projected sensitivities are sensitive to many details, and different analyses make different assumptions. A recent review [97] compared different radio-detection experiments using a common framework, and found some significant shifts in sensitivities.

### 36.3.3.2 Ice-based detectors

Detecting neutrinos with a lower energy threshold requires a smaller antenna-target separation. Natural ice is an attractive medium for this, offering a stable construction platform, with radio attenuation lengths from over 300 m to 1 km. The attenuation length varies with the frequency and ice temperature, with higher attenuation in warmer ice.

Although glacial ice is mostly uniform, the top  $\approx 100$  m of ice, the 'firn,' exhibits a gradual transition from packed snow at the surface (typical density  $0.35 \text{ g/cm}^3$ ) to solid ice (density  $0.92 \text{ g/cm}^3$ ) below [98]. The thickness of the firn varies with location; it is thicker in central Antarctica than in the coastal ice sheets or in Greenland. The varying density has several implications.

The index of refraction depends linearly on the density, so radio waves curve downward in the firn. This bending reduces the effective volume of surface or aerial antennas. A surface antenna cannot see near-surface interactions at large horizontal distances. The bending also means that the arrival direction of radio waves do not point directly back to the neutrino source. One must use ray tracing to determine the direction of neutrino interactions.

The bending also creates an opportunity to measure the distance from the detector to the neutrino interaction. For some geometries with buried antennas, there may be two paths to the detector: one 'direct' path, with minor bending, and a second where the signal is bent beyond vertical, bouncing off the surface before reaching the antenna. By measuring the time difference between the two paths, the distance to the interaction vertex may be determined; this greatly improves the energy determination [99, 100].

There are also indications that the increase in firn density is non-monotonic [101, 102]. This can lead to a non-monotonic change in index of refraction which may create waveguides which trap a small fraction of the radio energy and propagate it horizontally.

In one type of experiment, antennas mounted on scientific balloons observe the ice from above. Radio signals from in-ice neutrino interactions propagate to the surface, traverse the ice-air

interface, and then travel to the balloon. The surface roughness of the ice can affect signals as they transition from the ice to the atmosphere. The best known example, ANITA, has made four flights around Antarctica, floating at an altitude around 35 km [103]. Its 32/40/48 (depending on the flight) dual-polarization horn antennas scanned the surrounding ice, out to the horizon (650 km away). Because of the small angle of incidence, ANITA could use polarization to separate signals from background;  $\nu$  signals should be vertically polarized, while most background from cosmic-ray air showers should be horizontally polarized.

Because of the significant source-detector separation, ANITA is most sensitive at energies above  $10^{19}$  eV, above the peak of the cosmogenic neutrino spectrum. As with all radio-detection experiments, ANITA had to contend with anthropogenic backgrounds. The ANITA collaboration uses their multiple antennas as a phased array to achieve good pointing accuracy. They rejected all events that pointed toward known or suspected areas of human habitation. By using the several-meter separation between antennas, they achieved a pointing accuracy of  $0.2\text{-}0.4^\circ$  in elevation, and  $0.5\text{-}1.1^\circ$  in azimuth. ANITA has set the most stringent flux limits yet on neutrinos with energies above  $10^{20}$  eV [83].

Other ice based experiments use antennas located within the active volume, allowing them to reach thresholds around  $10^{17}$  eV, or lower with phased array antennas. This approach was pioneered by the RICE experiment [104] which buried 18 half-wave dipole antennas in holes drilled for AMANDA at the South Pole, at depths from 100 to 300 m. The hardware was sensitive from 200 MHz to 1 GHz. Each antenna fed an in-situ preamplifier which transmitted the signals to surface digitizing electronics.

Two groups have deployed prototype arrays which have explored different detector concepts. The Askaryan Radio Array (ARA) deployed surface and buried antennas at the South Pole [105], while the Antarctic Ross Iceshelf Antenna Neutrino Array (ARIANNA) installed surface antennas on the Ross Ice Shelf [85], about 110 km north of McMurdo station. ARIANNA offered the possibility of detecting downward-going  $\nu$ , from the radio waves reflected off the ice-sea water interface on the bottom of the Ross Ice Shelf, while ARA took advantage of the colder ice at the South Pole, with its longer radio attenuation length. ARA buried antennas up to 200 m deep, be able to observe a larger portion of ice, due to the refraction of the signal in the firn. In contrast, ARIANNA deployed antennas just below the surface, allowing them to use high-gain, but large log periodic dipole antennas. Recently, phased-array trigger techniques have been demonstrated that can reduce the energy threshold by a factor of several [76, 106].

Both experiments use stations which operate independently, spaced far enough to maximize sensitivity, but where only a small fraction of neutrino events will be visible in multiple stations. Each station includes multiple antennas, which will include both horizontal and vertical polarization. The collaborations can determine the neutrino arrival direction (modulo a (usually) 4-fold directional ambiguity) by using relative timing to find the direction from the station to the interaction, and the neutrino arrival direction by using the frequency spectrum to find the angular distance from the Cherenkov cone and by measuring the linear polarization of the radio signal. The expected angular resolution is a few degrees.

Looking ahead, the RNO [89] and ARIANNA [107] Collaborations have proposed next-generation experiments combining the best features from ARA and ARIANNA. Both experiments have been proposed for the South Pole, although operation in Greenland may also be considered. Further out, the proposed IceCube Gen2 expansion includes a substantial radio array component [52]

### 36.3.3.3 Radio-detection of cosmic-ray air showers

The physics of radio-wave generation in air showers is more complex than for neutrino-induced showers [108], although there are enough similarities that some experiments are sensitive to both sources. Particularly in the upper atmosphere, air is much less dense than rock or ice, so the showers develop over much larger distance scales. These larger distance scales lead to significant effects from the Earth's magnetic field.

For cosmic-rays arrival directions that are perpendicular to the magnetic field, the field produces significant charge separation,

as electrons and positrons are bent in different directions as they propagate. This leads to a growing charge dipole (transverse current) [109]. This time-varying transverse current emits radiation, spread over the transverse size of the shower, with a Cherenkov ring around the primary trajectory. Electrons in the shower may also emit synchrotron radiation due to bending in the Earth's field. Since the radiating particles are moving relativistically downward, a ground-based observer sees a Lorentz contracted pulse which can have frequency components reaching the GHz range, limited by the thickness of the particle shower. However, for most geometries, the bulk of the energy is at frequencies below 100 MHz, and most experiments are focused at frequencies below that.

There is still a contribution from coherent radio Cherenkov signals, but it is subdominant. Its most notable effect is to create an azimuthal (around the shower axis) interference pattern, destroying the radial symmetry of the radiation [110].

Since they observe the atmosphere, one of the major issues for radio-detection experiments is anthropogenic noise. Most man-made noise has distinctive characteristics (such as being narrow-band, and coming from near the horizon) which makes it relatively easy to reject during data analysis, via narrow-band filters and other techniques [111]. However, these factors complicate triggering. This is even an issue in Antarctica, where communication radios and passing satellites can mimic showers, at least at the trigger level. For this reason, most experiments have used radio antennas in combination with at least one other detector technology, such as scintillation counters. One exception is ARIANNA, which is located in an uninhabited part of Antarctica, enabling them to self-trigger on air showers [112]. With careful choice of frequency band, it may be possible to reach PeV energies with Antarctic detectors [113]. In more populous areas, the triggering challenges are likely to be bigger.

Radio-detection can be used to determine the shower energy, as done by the Auger and Tunka-Rex experiments [114, 115]. Radio signals can also be used to infer the altitude for shower-maximum, where the shower contains the most particles, as done by the LOPES and Tunka-Rex collaborations [115, 116]. This altitude is sensitive to the cosmic-ray composition. Radio-detection is also useful for energy cross-calibrations between different experiments, and, with improved simulations, may be able to provide an independent energy scale calibration for air shower arrays.

### 36.4 Large time-projection chambers for rare event detection

Revised October 2019 by T. Shutt (SLAC).

Rare event searches require detectors that combine large target masses and low levels of radioactivity, and that are located deep underground to eliminate cosmic-ray related backgrounds. Past and present efforts include searches for the scattering of particle dark matter, neutrinoless double beta decay, and the measurement of solar neutrinos, while next generation experiments will also probe coherent scattering of solar, atmospheric and diffuse supernova background neutrinos. Large time project chambers (TPCs) [117], adapted from particle collider experiments, have emerged as a leading technology for these efforts. Events are measured in a central region confined by a field cage and usually filled with a liquid noble element target. Ionization electrons are drifted (in the  $z$  direction) to an anode region by use of electrode grids and field shaping rings, where their magnitude and  $x - y$  location is measured. In rare event searches (with no external trigger available) scintillation generated at the initial event site is also measured, and the time difference between this prompt signal and the later-arriving charge signal gives the event location in  $z$  for a known electron drift speed. Thus, 3D imaging is achieved in a monolithic central volume. The relatively slow readout due to the drift of charges ( $\sim 1/2$  ms/m at 1 kV/cm) [118] is not a major pile-up concern in low background experiments. Noble elements have relatively high light yields (comparable to or exceeding the best inorganic scintillators), and the charge signal can be amplified by multiplication or electroluminescence. Radioactive backgrounds are distinguished by event imaging, the separate measurements of charge and light, and scintillation pulse shape. For recent reviews

of noble element detectors, see [119] [120] [121] [122].

Methods for achieving very low radioactive backgrounds are discussed in general in section 35.6. The basic architecture of large TPCs is very favorable for this application because gas or liquid targets can be relatively easily purified, while the generally more radioactive readout and support materials are confined to the periphery. The 3D imaging of the TPC then allows self shielding in the target material, which is quite powerful when the target is large compared to mean scattering lengths of order  $\sim 10$  cm for  $\sim$  MeV neutrons and gammas from radioactivity. Most recent experiments have immersed the TPCs in hermetic water shields to eliminate external radioactive backgrounds, and several are also using an active scintillator inner layer to further veto backgrounds from detector materials. While other target fluids are possible, almost all recent efforts have used Xe and Ar. In LHe and LNe the mobility of electrons is  $\sim 10^3$  times lower than in the heavier noble elements due to the formation "bubbles" around electrons. [123] [124] It is worth noting that scintillation and electron drift are possible in a number of organic fluids, possibly providing a route to economical large detectors, but with much reduced performance compared to noble elements.

In noble element targets, all non-noble impurities are readily removed (e.g., by chemical reaction in a commercial getter) so that only radioactive noble isotopes are a significant background concern. Xe, Ne and He have no long lived radioactive isotopes (apart from the  $^{136}\text{Xe}$ , discussed below, and the very long-lived  $^{124}\text{Xe}$  [125]). Kr has  $\sim 0.3$  MBq/kg of the beta emitter  $^{85}\text{Kr}$  created by nuclear fuel reprocessing [126], making it unusable as a target, while the  $\sim 1$  Bq/kg level of the beta emitter  $^{39}\text{Ar}$  [127] is a nuisance for Ar-based experiments. Both of these can be backgrounds in other target materials, as can Rn emanating from detector components. Relatively low background materials are available for most of the structures surrounding the central target, with the exception of radioactive glasses and ceramics usually present in PMTs, feedthroughs and electrical components. Very low background PMTs with synthetic quartz windows, available over the last 15 years (see, e.g., [128]), have been a key enabling technology for dark matter searches. Radio-clean SiPMTs and related Si-based photon detectors are increasingly being used in cases where their dark rates (which are significantly higher than PMTs) can be tolerated.

An important technical challenge in liquid detectors is achieving the high voltages needed for electron drift and measurement. In general, quench gases which stabilize charge gain and speed electron transport in wire chambers cannot be used, since these absorb and/or quench scintillation light and can trap electrons. It is also important to suppress low-level emission of electrons and associated photons which can otherwise swamp low energy signals. Drift of electrons over meter scales with minimal loss from attachment on trace levels of dissolved impurities (e.g.,  $\text{O}_2$ ) has so far required continuous circulating purification.

#### 36.4.1 Dark matter and other low energy signals

A major goal of low background experiments is detection of WIMP (Weakly Interacting Massive Particle) dark matter through scattering on nuclei in a terrestrial detector (for a recent review, see [129]). Energy transfers are generally small, a few tens of keV at most. Liquid noble TPCs distinguish single nuclear recoils (NR) from dark matter from the dominant background of electron recoils (ER) from gamma rays and beta decays by rejecting multiple scatters, and, as described below, based on both the ratio of charge to light and the scintillation pulse shape. Neutrons are a NR background, but are present at much lower rates than gammas and betas, and also undergo significant multiple scattering. To detect small charge signals, a dual phase technique is used wherein electrons from interactions in the liquid target are drifted to the liquid surface and extracted with high field ( $\sim 5$  kV/cm) into the gas phase where they create an amplified electroluminescence signal which is usually measured by an array of PMTs located just above the liquid. (While both charge multiplication and electroluminescence are possible in liquid, they require very high fields created by very small electron structures and thus have not seen widespread adoption. For recent progress see [130]) This technique readily measures single electrons with  $\sim$



cm  $x - y$  resolution.

The measurement of the initial scintillation signal, by contrast, suffers from loss upon reflection from the TPC walls, and inefficiency in the readout, and usually limits the energy threshold. In LXe, the  $\sim 178$  nm wavelength is just long enough to be transmitted through high purity synthetic quartz PMTs windows, and, remarkably, PTFE immersed in LXe has  $\sim 97\%$  reflectivity. [131] The  $\sim 128$  nm scintillation light of LAr requires waveshifting (usually using TPB) both for reflectivity (usually on PTFE) and for efficient measurement. With both liquids, a second sensor array at the bottom of the TPC is used to maximize light collection, and total photon efficiencies have been in the 10-15% range. Typical raw yields for ER are several tens of electrons and photons per keV, and, in LXe, a NR threshold of  $\sim 5$  keV has been achieved [132].

The microscopic processes leading to signals in liquid nobles are complex. Energy deposited by an event generates pairs of free electron and ions, and also atoms in their lowest excited state. The latter rapidly form excimers which de-excite by emitting light. Excimers arise in both triplet and singlet states which have the same energy but different decay times. In an event track, some fraction of electrons recombine with ions, while the rest escape and are measured. Each recombined ion creates an additional excimer, and hence another photon. Finally, some part of the energy is lost as heat - a small fraction for ER but a dominant and energy dependent fraction for NR. The branching into these various modes depends on drift field, energy, and particle type, requiring extensive calibrations. These have largely been carried out for LXe (see, e.g., [133]), and have been incorporated into the NEST Monte Carlo framework. [134]

This complexity also gives rise to discrimination between ER and NR: for the same visible energy, the slower NR create short, denser tracks and generate a higher fraction of initial excitons, leading to a smaller ratio of measured charge to light. NR also generate a higher ratio of short-lived singlet state to long-lived triplet states than ER, so that the scintillation signal itself gives pulse shape discrimination (PSD). Charge/light discrimination has been well mapped in LXe, and, remarkably, is very high ( $>99.9\%$ ) below  $\sim 10$  keV for NR. [132] It has only recently been measured in LAr [135], and has not yet played an important role in LAr based experiments. Qualitatively, PSD is similar in LXe and LAr - strong at high energy and weak at low energy. However it is well mapped only in LAr where it is very high above  $\sim 50$  keV, achieving values above  $\sim 10^8$ . [136]

This extremely powerful PSD in LAr is sufficient to overcome the ER background from  $^{39}\text{Ar}$ , which is roughly  $10^7$  times higher than the fundamental low energy ER background from p-p solar neutrinos. In a multi-ton detector the event rate from  $^{39}\text{Ar}$  poses a significant pile-up challenge, and the DarkSide collaboration is pursuing  $^{39}\text{Ar}$  reduction through two methods. One, for which a factor 1400 reduction in  $\sim 50$  kg Ar has been demonstrated, is extracting "aged" Ar from underground (cosmic ray shielded) gas deposits in which the 269 yr half-life  $^{39}\text{Ar}$  has decayed. [137] The other method is removal by distillation. The need for  $^{39}\text{Ar}$  depleted Ar negates the much lower raw material cost of Ar compared to Xe. Kr must also be removed from both Xe and Ar experiments (and Ar must be from Xe experiments), comparatively easy tasks compared to isotopic separation. This is done through distillation or a chromatographic technique. In current LXe experiments the remaining dominant ER backgrounds is the beta decay of a daughter of  $^{222}\text{Rn}$  in the active LXe, where the Rn has emanated from detector materials or external plumbing. Rn will be even more important as experiments scale up in size, but can in principle be reduced by better materials screening and online Rn separation, again by either distillation or chromatography. Neutrons are in general some six orders of magnitude less abundant than gamma rays and betas in U and Th decay chains, but they naturally scatter in the WIMP energy range, and their single scatters cannot be discriminated against. Self shielding is less powerful for neutrons than gamma rays, so that they are an increasingly important background at the current ton scale and future larger experiments, both in Ar and Xe. Active outer shielding layers which tag and veto neutrons are being included in most

next generation experiments.

The WIMP sensitivity is a combination of backgrounds, discrimination, and WIMP scattering rates. The scattering rates are model dependent, but are in general dominated by spin-independent coherent scattering on the full nucleus. This has an  $A^2$  dependence, favoring high mass targets. The energy spectrum is close to a falling exponential, so that the lowest possible energy threshold maximizes sensitivity. Experiments using LXe TPCs have had the leading sensitivity for standard WIMP dark matter for well over a decade, for all but the lowest WIMP masses. The ton-scale XENON1T [138] achieved a WIMP-nucleon sensitivity of  $4.1 \times 10^{-47} \text{ cm}^2$  at 30 GeV mass, closely followed by PANDAX-II [139] and LUX [140]. The next generation  $\sim 7$  tonne experiments LZ [141] and XENONnT [142], and  $\sim 4$  tonne PandaX-4T [143] are currently in late stages of construction. The DarkSide program is carrying out WIMP searches with LAr TPCs. The 50 kg DarkSide-50 achieved a sensitivity  $\gtrsim 40$  times poorer than XENON1T. A 50 ton scale-up, DarkSide-20 is being pursued which features SiPMs instead of PMTs. [144]. (The best current limit using LAr is not from a TPC, but instead the scintillation-only DEAP-3600 experiment. [136])

LZ and XENONnT project sensitivity to WIMPs about a decade above the "floor" of coherent scattering of astrophysical neutrinos, which, absent a directional measurement (see below), are essentially indistinguishable from WIMPs. DARWIN, a proposed 50 ton LXe TPC would approach the practical limit set by this floor for WIMP masses above  $\sim 5$  GeV [145], while ARGO a  $\sim 200$  ton LAr detector would achieve similar sensitivity for WIMPs masses well above  $\sim 50$  GeV. [144]

There has been recent interest in models featuring low mass dark matter. These give rise to low energy recoils, and also strongly favor low mass target nuclei (despite the  $A^2$  rate penalty). This has led to renewed focus on events below the scintillation threshold, where the charge signal alone achieves very low threshold due to the gain of the electroluminescence readout. This preserves  $x - y$  spatial information, but only very weak depth information based on electron diffusion. Thus it is subject to the high backgrounds at the top and bottom of the active region, and decays of Rn daughters on grids. While the first such results came from XENON10, a recent result in LAr from DarkSide-50 extends to much lower dark matter mass because of the lower mass of Ar. To maximize the sensitivity of such searches in the future, studies have begun to understand and minimize the sources of electron backgrounds from both radioactivity and spurious sources such as field emission from grids. There is also an effort to develop a superfluid He TPC [146] read out with superconducting sensors (similar to the proposed HERON solar neutrino experiment). The rich set of signals in this case - scintillation, rotons, and ionization - potentially offer significant background rejection.

Measurement of NR recoil track direction would provide proof of the galactic origin of a dark matter signal since the prevailing WIMP direction varies on a daily basis as the earth spins. This cannot be achieved for the sub-micron tracks in any existing solid or liquid technology, but the mm-scale tracks in a low pressure gas (typically,  $P \sim 50$  Torr) could be imaged with sufficiently dense instrumentation. Directionality can be established with  $O(10^2)$  events by measuring just the track direction, while, with finer resolution that distinguishes the diffuse (dense) tail and dense (diffuse) head of NR (ER) tracks, only  $O(10)$  events are required. Such imaging requires a high energy threshold, decreasing WIMP sensitivity, but also powerfully rejecting less dense ER background tracks.

A variety of TPC configurations are being pursued to accomplish this, most with a  $\text{CF}_4$  target. The longest established effort, DRIFT, avoids diffusion washing out tracks for electron drift distances greater than  $\sim 20$  cm by attaching electrons to  $\text{CS}_2$ , which drifts with vastly reduced diffusion. Other efforts drift electrons directly and use a variety of techniques for their measurement: DMTPC (electroluminescence + CCDs), MIMAC (MicroMegas), NEWAGE (GEMs), and  $\text{D}^3$  (Si pixels). A related suggestion is that the amount of recombination in a high pressure Xe gas with an electron-cooling additive could be sensitive to the angle between the track and electric field [147], eliminating the need for

track imaging. Directional measurements appear to be the only possibility to push beyond the floor of coherent neutrino scatterers [148], though at the cost of enormous target mass and channel count.

### 36.4.2 $0\nu\beta\beta$ Decay

Another major class of rare event search is neutrinoless double beta decay ( $0\nu\beta\beta$ ). A limited set of nuclei are unstable against simultaneous beta decay of two neutrons. Fortunately, this includes the Xe isotope  $^{136}\text{Xe}$  (Q-value 2458 keV), which can be used as the active material in a detector, and which, as an inert gas, can also be more readily enriched from its natural 8.9% abundance than any other  $\beta\beta$  isotope. Observation of the lepton-number violating neutrinoless version of this decay would establish that neutrinos are Majorana particles and provide a direct measure of neutrino mass. For a recent review, see [149] [122]. The signal in  $0\nu\beta\beta$  decay is distinctive: the full Q-value energy of the nuclear decay appears as equal energy back-to-back recoil electrons. A large TPC is advantageous for observing this low rate decay for all the reasons described above. The first detector to observe the standard model process two neutrino double beta decay was a gaseous TPC which imaged the two electrons tracks from  $^{82}\text{Se}$  embedded in a foil. [150] Modern TPCs use Xe as the detector medium.

The dominant background is gamma rays originating outside the active volume. Most of these undergo multiple Compton-scatters which are efficiently recognized and rejected through sub-cm position resolution, though the few percent of gammas at this energy that photoabsorb are not. Self shielding of gamma rays in the double beta decay energy window is less powerful than in the low energy dark matter window, since in the former case there is some small probability of penetrating to some depth followed by the modestly small probability of photo-absorption. The latter case consists of three small probability processes: penetration to some depth, a very low-energy scatter, and the gamma exiting without a second interaction. Because of this and the fact that background and the signal are both electron recoils (i.e., NR/ER discrimination is of no value), the requirements on radioactivity in all the surrounding materials of a  $\beta\beta$  TPC are much more stringent than an otherwise similar dark matter detector, unless other background rejection tools are available. However  $\beta\beta$  searches are insensitive to low energy backgrounds (e.g.,  $^{85}\text{Kr}$  and  $^{39}\text{Ar}$ ) important for dark matter.

Very good energy resolution is crucial to avoid background from  $2\nu\beta\beta$  decays and gammas including the prominent 2615 keV line from  $^{208}\text{Tl}$  in the Th chain. Here a combined charge and light measurement largely eliminates the otherwise dominant fluctuations in charge and light. Because of the high energy of the  $\beta\beta$  signal, charge can be read out directly, and the scintillation measurement is easily tolerant of the dark rates of SiPMs. These goals have led  $\beta\beta$  detectors to have somewhat different optimization than dark matter detectors, although the next generation large Xe dark matter experiments (LZ, XENONnT, DARWIN) have significant  $\beta\beta$  reach.

The recently completed EXO-200 experiment used a single-phase LXe TPC with roughly 110 active kg of Xe enriched to 80.7%  $^{136}\text{Xe}$  to achieve one of the best  $\beta\beta$  search limits [151]. The energy resolution obtained is (FWHM) of 2.71% (at 2458 keV), and lower values in LXe appear possible. A multi-ton successor experiment, nEXO, has been proposed which would fully cover the inverted neutrino mass hierarchy. [152] EXO-200 featured LAAPDs for light readout, and direct charge readout, while nEXO will use SiPMs.

A related but different approach is to use high pressure gaseous Xe TPC. [153] The lower density requires a large apparatus for given target mass, but has two significant advantages. The larger track size allows the two-electron topology of  $0\nu\beta\beta$  events to be distinguished from single electrons from photoabsorption of background gammas. In addition, the low recombination fraction in the gas phase suppresses recombination fluctuations, allowing higher energy resolution. Recent progress with a 5 kg prototype by the NEXT collaboration has demonstrated the topology based discrimination, and, notably, 1% (FWHM) energy resolution. A

$\sim 100$  kg detector is now under construction, and ton-scale designs being studied. Finally, a long-standing idea that would provide definitive identification of a  $0\nu\beta\beta$  signal is to extract and tag the ionized Ba daughter via atomic physics techniques [154], either in gas or liquid and gas phases. Significant recent progress by both the EXO and NEXT collaborations has now achieved the key milestone of demonstrating single Ba ion sensitivity in test setups. [155] [156] [157]

## 36.5 Sub-Kelvin detectors

Revised August 2018 by K.D. Irwin (Stanford U.; SLAC).

Many particle physics experiments utilize detectors operated at temperatures below 1 K. These include WIMP searches, beta-decay experiments to measure the absolute mass of the electron neutrino, and searches for neutrinoless-double-beta decay ( $0\nu\beta\beta$ ) to probe the properties of Majorana neutrinos. Sub-Kelvin detectors also provide important cosmological constraints on particle physics through sensitive measurement of the cosmic microwave background (CMB). CMB measurements probe the physics of inflation at  $\sim 10^{16}$  GeV, and the absolute mass, hierarchy, and number of neutrino species.

Detectors that operate below 1 K benefit from reduced thermal noise and lower material specific heat and thermal conductivity. At these temperatures, superconducting materials, sensors with high responsivity, and cryogenic preamplifiers and multiplexers are available. We provide a simple overview of the techniques and the experiments using sub-K detectors. A useful review of the broad application of low-temperature detectors is provided in [158], and the proceedings of the International Workshop on Low Temperature Detectors [159] provide an overview of the field.

Sub-Kelvin detectors can be categorized as equilibrium thermal detectors or non-equilibrium detectors. Equilibrium detectors measure a temperature rise in a material when energy is deposited. Non-equilibrium detectors are based on the measurement of prompt, non-equilibrated signals and on the excitation of materials with an energy gap.

### 36.5.1 Equilibrium thermal detectors

An equilibrium thermal detector consists of a thermometer and absorber with combined heat capacity  $C$  coupled to a heat bath through a weak thermal conductance  $G$ . The rise time of a thermal detector is limited by the internal equilibration time of the thermometer-absorber system and the electrical time constant of the thermometer. The thermal relaxation time over which heat escapes to the heat bath is  $\tau = C/G$ . Thermal detectors are often designed so that an energy input to the absorber is thermalized and equilibrated through the absorber and thermometer on timescales shorter than  $\tau$ , making the operation particularly simple. An equilibrium thermal detector can be operated as either a calorimeter, which measures an incident energy deposition  $E$ , or as a bolometer, which measures an incident power  $P$ .

In a calorimeter, an energy  $E$  deposited by a particle interaction causes a transient change in the temperature  $\Delta T = E/C$ , where the heat capacity  $C$  can be dominated by the phonons in a lattice, the quasiparticle excitations in a superconductor, or the electronic heat capacity of a metal. The thermodynamic energy fluctuations in the absorber and thermometer have variance

$$\Delta E_{\text{rms}}^2 = k_{\text{B}} T^2 C \quad (36.5)$$

when operated near equilibrium, where  $\Delta E_{\text{rms}}$  is the root-mean-square energy fluctuation,  $k_{\text{B}}$  is the Boltzmann constant and  $T$  is the equilibrium temperature. When a sufficiently sensitive thermometer is used, and the energy is thermalized at frequencies large compared to the thermal response frequency ( $f_{\text{th}} = 1/2\pi\tau$ ), the signal-to-noise ratio is nonzero at frequencies higher than  $f_{\text{th}}$ . In this case, detector energy resolution can be somewhat better than  $\Delta E_{\text{rms}}$  [160]. Deviations from the ideal calorimeter model can cause excess noise and position and energy dependence in the signal shape, leading to degradation in achieved energy resolution.

In a bolometer, a power  $P$  deposited by a stream of particles causes a change in the equilibrium temperature  $\Delta T = P/G$ . The weak thermal conductance  $G$  to the heat bath is usually limited by

**Table 36.4:** Some selected experiments using sub-Kelvin equilibrium bolometers to measure the CMB. These experiments constrain the physics of inflation and the absolute mass, hierarchy, and number of neutrino species. The experiment location determines the part of the sky that is observed. The size of the aperture determines the angular resolution. The table also indicates the type of sensor used, the number of sensors, the frequency range, and the number of frequency bands. The number of sensors and frequency range and bands for ongoing upgrades are provided for some experiments in parentheses.

Sub-K CMB Experiment	Location	Aperture	Sensor type	# Sensors (planned)	Frequency (planned)	Bands (planned)
<b>Ground-based</b>						
Atacama Cosmology Telescope (2007–)	Chile	6 m	TES	1,800 (5,334)	90–150 GHz (28–220 GHz)	2 (5)
BICEP/Keck (2006–)	South Pole	26/68 cm	TES	3,200	95–220 GHz	3
CLASS (2015–)	Chile	60 cm	TES	36 (5,108)	40 GHz (40–220 GHz)	1 (4)
POLARBEAR / Simons (2012–)	Chile	3.5 m	TES	1,274 (22,764)	150 GHz (90–220 GHz)	1 (3)
South Pole Telescope (2007–)	South Pole	10 m	TES	1,536 (16,260)	95–150 GHz (95–220 GHz)	2 (3)
<b>Balloon</b>						
EBEX (2013–)	McMurdo	1.5 m	TES	~1,000	150–410 GHz	3
PIPER (2016–)	New Mexico	2 m	TES	5,120	200–600 GHz	4
SPIDER (2014–)	McMurdo	30 cm	TES	1,959	90–280 GHz	3
<b>Satellite</b>						
Planck HFI (2003–)	L2	1.5 m	NTD	52	100–857 GHz	9

the flow of heat through a phonon or electron system. The thermodynamic power fluctuations in the absorber and thermometer have power spectral density

$$S_P = NEP^2 = 4k_B T^2 G \quad (36.6)$$

when operated near equilibrium, where the units of NEP (noise equivalent power) are  $W/\sqrt{\text{Hz}}$ .

The minimization of thermodynamic energy and power fluctuations is a primary motivation for the use of sub-Kelvin thermal detectors. These low temperatures also enable the use of materials and structures with extremely low  $C$  and  $G$ , and the use of superconducting materials and amplifiers.

When very large absorbers are required (e.g. WIMP dark matter searches), dielectric crystals with extremely low specific heat are often used. These materials are operated well below the Debye temperature  $T_D$  of a crystal, where the specific heat scales as  $T^3$ . In this low-temperature limit, the dimensionless phononic heat capacity at fixed volume reduces to

$$\frac{C_V}{N k_B} = \frac{12 \pi^4}{5} \left( \frac{T}{T_D} \right)^3, \quad (36.7)$$

where  $N$  is the number of atoms in the crystal. Normal metals have higher low-temperature specific heat than dielectric crystals, but they also have superior thermalization properties, making them attractive for some applications in which extreme precision and high energy resolution are required (e.g. beta endpoint experiments to measure neutrino mass using  $^{163}\text{Ho}$ ). At low temperature, the heat capacity of normal metals is dominated by electrons, and is linear in temperature, with convenient form

$$C = \frac{\rho}{A} \gamma V T, \quad (36.8)$$

where  $V$  is the sample volume,  $\gamma$  is the molar specific heat of the material,  $\rho$  is the mass density, and  $A$  is the atomic weight. Superconducting absorbers are also used. Superconductors combine some of the thermalization advantages of normal metals with the lower specific heats associated with insulators when operated well below  $T_c$ , where the electronic heat capacity freezes out, and the material is dominated by phononic heat capacity. At higher temperatures, superconducting materials have more complicated heat capacities, but at their transition temperature  $T_c$ , BCS theory predicts that the electronic heat capacity of a superconductor is  $\sim 2.43$  times the normal metal value.

When very low thermal conductances are required for power measurement (e.g. the measurement of the cosmic microwave

background), the weak thermal link is sometimes provided by thin membranes of non-stoichiometric silicon nitride. The thermal conductance of these membranes is:

$$G = 4\sigma A T^3 \xi, \quad (36.9)$$

where  $\sigma$  has a value of  $15.7 \text{ mW/cm}^2\text{K}^4$ ,  $A$  is the cross-sectional area perpendicular to the heat flow, and  $\xi$  is a numerical factor with a value of one in the case of specular surface scattering but less than one for diffuse surface scattering. The thermal impedance between the electron and phonon systems can also limit the thermal conductance.

The most commonly used sub-Kelvin thermometer is the superconducting transition-edge sensor (TES) [161]. The TES consists of a superconductor biased at the transition temperature  $T_c$ , in the region between the superconducting and normal state, where its resistance is a strong function of temperature. The TES is voltage biased. The Joule power provides strong negative electrothermal feedback, which improves linearity, speeds up response to faster than  $\tau = C/G$ , and provides tolerance for  $T_c$  variation between multiple TESs in a large array. The current flowing through a TES is read out by a superconducting quantum interference device (SQUID) amplifier. These amplifiers can be cryogenically multiplexed, allowing a large number of TES devices to be read out with a small number of wires to room temperature.

Neutron-transmutation-doped (NTD) germanium and implanted silicon semiconductors read out by cryogenic FET amplifiers are also used as thermometers [160]. Their electrical resistance is exponentially dependent on  $1/T$ , and is determined by phonon-assisted hopping conduction between impurity sites. Finally, the temperature dependence of the permeability of a paramagnetic material is used as a thermometer. Detectors using these thermometers are referred to as metallic magnetic calorimeters (MMC) [162]. These detectors operate without dissipation and are inductively readout by SQUIDS.

Equilibrium thermal detectors are simple, and they have important advantages in precision measurements because of their insensitivity to statistical variations in energy down-conversion pathways, as long as the incident energy equilibrates into an equilibrium thermal distribution that can be measured by a thermometer.

### 36.5.2 Nonequilibrium Detectors

Nonequilibrium detectors use many of the same principles and techniques as equilibrium detectors, but are also sensitive to details of the energy down-conversion before thermalization. Sub-Kelvin nonequilibrium detectors measure athermal phonon sig-

**Table 36.5:** Selected experiments using sub-Kelvin calorimeters. The table shows only currently operated experiments, and is not exhaustive. WIMP experiments search for dark matter, and beta-decay and neutrinoless double beta decay ( $0\nu\beta\beta$ ) experiments constrain neutrino mass, hierarchy, and Majorana nature. The experiment location determines the characteristics of the radioactive background. The dates of current program phase, detection mode (equilibrium or nonequilibrium phonon measurements, and measurement of ionization or scintillation signals), the absorber and total mass, the sensor type, and the number of sensors and crystals (if different) are given. Many sub-K calorimeter experiments are also in planning and construction phases, including EURECA (dark matter), HOLMES and NuMECs (beta decay), and CUPID-0 ( $0\nu\beta\beta$  decay). Many of the existing experiments are being upgraded to larger mass absorbers, different absorber materials, or lower energy threshold.

Sub-K Calorimeter	Location	Detection mode	Absorber Total mass	Sensor type	# Sensor # Crystal
<b>WIMP</b>					
CRESST II (2003–)	Gran Sasso Italy	Noneq. phon. and scint.	CaWO <sub>4</sub> 5.4 kg	TES	18
EDELWEISS III (2015–)	LSM Modane France	Eq. thermal and ion.	Ge 22 kg	NTD Ge +HEMT	36
SuperCDMS (2012–)	Soudan, USA SNOLAB, Canada	Noneq. phon. and ion.	Ge 9 kg	TES +JFET	120 15
<b>Beta decay</b>					
ECHO (2012–)	Heidelberg Germany	Eq. thermal	Au: <sup>163</sup> Ho 0.2μg	MMC	16
<b><math>0\nu\beta\beta</math> decay</b>					
CUORE (2015–)	Gran Sasso Italy	Eq. thermal	TeO <sub>2</sub> 741 kg	NTD Ge	988
AMoRe Pilot (2015–)	Yang Yang S. Korea	Noneq. phon. and scint.	CaMoO <sub>4</sub> 1.5 kg	MMC	5
LUCIFER (2010–)	Gran Sasso Italy	Eq. thermal and scint.	ZnSe 431 g	NTD Ge	1

nals in a dielectric crystal, electron-hole pairs in a semiconductor crystal, athermal quasiparticle excitations in a superconductor, photon emission from a scintillator, or a combination of two of the above to better discriminate recoils from nuclei or electrons. Because the phonons are athermal, sub-Kelvin nonequilibrium detectors can use absorbers with larger heat capacity, and they use information about the details of energy down-conversion pathways in order to better discriminate signal from background.

In WIMP and neutrino experiments using sub-Kelvin dielectric semiconductors, the recoil energy is typically  $\gtrsim 0.1$  keV. The majority of the energy is deposited in phonons and a minority in ionization and, in some cases, scintillation. The semiconductor bandgap is typically  $\sim$  eV, and  $k_B T < 10 \mu\text{eV}$  at  $T < 1$  K. Thus, high-energy charge pairs and athermal phonons are initially produced. The charge pairs cascade quickly to the gap edge. The high-energy phonons experience isotopic scattering and anharmonic decay, which downshifts the phonon spectrum until the phonon mean free path approaches the characteristic dimension of the absorber. If the crystal is sufficiently pure, these phonons propagate ballistically, preserving information about the interaction location. They are not thermalized, and thus not affected by an increase in the crystal heat capacity, allowing the use of larger absorbers. Sensors similar to those used in sub-K equilibrium thermal detectors measure the athermal phonons at the crystal surface.

Superconductors can also be used as absorbers in sub-Kelvin detectors when  $T \ll T_c$ . The superconducting gap is typically  $\sim$  meV. Energy absorption breaks Cooper pairs and produces quasiparticles. These particles cascade to the superconducting gap edge, and then recombine after a material-dependent lifetime. During the quasiparticle lifetime, they diffuse through the material. In superconductors with large mean free path, the diffusion length can be more than 1 mm, allowing diffusion to a detector.

In some experiments (e.g. SuperCDMS and CRESST), athermal phonons and quasiparticle diffusion are combined to increase achievable absorber mass. Athermal phonons in a three-dimensional dielectric crystal break Cooper pairs in a two-dimensional superconducting film on the detector surface. The resulting quasiparticles diffuse to thermal sensors (typically a TES) where they are absorbed and detected. While thin superconducting films have diffusion lengths shorter than the diffusion lengths in single crystal superconductors, segmenting the films into small

sections and coupling them to multiple TES sensors allows the instrumentation of large absorber volume. The TES sensors can be wired in parallel to combine their output signal.

The combined measurement of the phonon signal and a secondary signal (ionization or scintillation) can provide a powerful discrimination of signal from background events. Nuclear-recoil events in WIMP searches produce proportionally smaller ionization or scintillation signal than electron-scattering events. Since many of the background events are electron recoils, this discrimination provides a powerful veto. Similarly, beta-decay events produce proportionally smaller scintillation signal than alpha-particle events, allowing rejection of alpha backgrounds in neutrino experiments.

Combined phonon and ionization measurement has been implemented in experiments including CDMS I/II, SuperCDMS, and EDELWEISS I/II/III. These experiments use semiconductor crystal absorbers, in which dark-matter scattering events would produce recoiling particles and generate electron-hole pairs and phonons. The electron-hole pairs are separated and drifted to the surface of the crystal by applying an electric field, where they are measured by a JFET or HEMT using similar techniques to those used in 77 K Ge x-ray spectrometers. However, the field strength must be much lower in sub-K detectors to limit the generation of phonon signals by the Neganov-Luke effect, which can confuse the background discrimination. For detectors with very low threshold, the Neganov-Luke effect can also be used to detect generated charge through the induced phonon signal.

Combined phonon and scintillation measurement has been implemented in CRESST II, ROSEBUD, AMoRE and LUCIFER. For example, the CRESST-II experiment uses CaWO<sub>4</sub> crystal absorbers, and measures both the phonon signal and the scintillation signal with TES calorimeters. A wide variety of scintillating crystals are under consideration, including different tungstates and molybdates, BaF<sub>2</sub>, ZnSe, and bismuth germanate (BGO).

### 36.6 Low-radioactivity background techniques

Revised November 2019 by A. Piepke (Alabama U.).

The physics reach of low-energy rare-event experiments is often limited by background caused by radioactivity. The problems to be addressed span a wide range of energies, particle types, and interactions. Experiments searching for double beta decay, low energy solar neutrinos or neutrino interactions at nuclear reactors

are often concerned about electron recoils and therefore  $\beta$ -decays and  $\gamma$ -ray scattering. The energy scales of interest reach from few keV to few MeV. Dark Matter searches, looking for nuclear recoils, often focus their attention on neutron-induced energy deposits, with electron recoils being of secondary importance. While the energy scales of interest are typically in the keV range, the hadronic physics responsible for the neutron production and interaction spans MeV to GeV. The utilized detector technologies are just as varied, including, among others, large liquid scintillation detectors, solid state calorimeters, gaseous and liquid tracking detectors and crystal scintillators. Except for reactor bound experiments, these searches are typically performed underground to limit the impact of the cosmic radiation. The depth requirements vary depending on the problem and the chosen detector concept. Depending on the chosen detector design, the separation of the physics signal from this unwanted interference can be achieved on an event-by-event basis by active event tagging, utilizing some unique event features, or by reducing the flux of the background-creating radiation by appropriate shielding, material selection and surface cleaning. In all cases, the background rate is proportional to the flux of the interfering radiation. Its reduction is, thus, essential for realizing the full physics potential of the experiment. In this context, “low energy” may be defined as the regime of natural, anthropogenic, or cosmogenic radioactivity; all at energies of up to about 10 MeV. See [163] [164] for in-depth reviews of this subject. Following the classification of [163], sources of background may be categorized into the following classes:

1. environmental radioactivity,
2. radio-impurities in detector or shielding components,
3. radon and its progeny,
4. cosmic rays,
5. neutrons from natural fission, ( $\alpha, n$ ) reactions and from cosmic-ray muon spallation and capture.

### 36.6.1 Defining the problem

The application defines the requirements. Background goals can be as demanding as a few low-energy events per year in a ton-size detector. The maximal strength of the physics signal of interest can often be estimated theoretically or from limits derived by earlier experiments. The experiments are then designed for the desired signal-to-background ratio. This requires finding the right balance between “clarity of measurement”, ease of construction, schedule and budget.

It is good practice to use detector simulations to translate the background requirements into limits for the radioactivity content of various detector components, requirements for radiation shielding, and allowable cosmic-ray fluxes. This strategy allows the identification of the most critical components early and facilitates the allocation of analysis and development resources in a rational way. The CERN code GEANT4 [165] is a widely used tool for this purpose. It has incorporated sufficient nuclear physics to allow accurate background estimations. Custom-written event generators, modeling *e.g.*, particle correlations in complex decay schemes, deviations from allowed beta spectra or  $\gamma - \gamma$ -angular correlations, are used as well.

### 36.6.2 Environmental radioactivity

The long-lived, naturally occurring radio-nuclides  $^{40}\text{K}$ ,  $^{232}\text{Th}$ , and  $^{238}\text{U}$  have average abundances of 1.6, 11 and 2.7 ppm (corresponding to 412, 45 and 33 Bq/kg, respectively) in the earth’s crust, with large local variations [166]. In most applications,  $\gamma$  radiation emitted in the decay of natural radioactivity and its unstable daughters constitutes the dominant contribution to the local radiation field. Typical low-background applications require levels of natural radioactivity on the order of ppb or ppt in the detector components. Passive or active shielding is used to suppress external  $\gamma$  radiation down to an equivalent level. Fig 36.11 shows the attenuation length  $\lambda(E_\gamma)$  as a function of  $\gamma$ -ray energy  $E_\gamma$  for three common shielding materials: water, copper, lead. Assuming exponential damping, the thickness  $\ell$  required to reduce the external flux by a factor  $f > 1$ , is:

$$\ell = \lambda(E_\gamma) \cdot \ln f. \quad (36.10)$$

At 100 keV, a typical energy scale for dark matter searches (or 2.615 MeV for a typical double-beta decay experiment), attenuation by a factor  $f = 10^5$  requires 67(269) cm of  $\text{H}_2\text{O}$ , 2.8(34) cm of Cu, or 0.18(23) cm of Pb. Such estimates allow for an order-of-magnitude determination of the experiment dimensions.

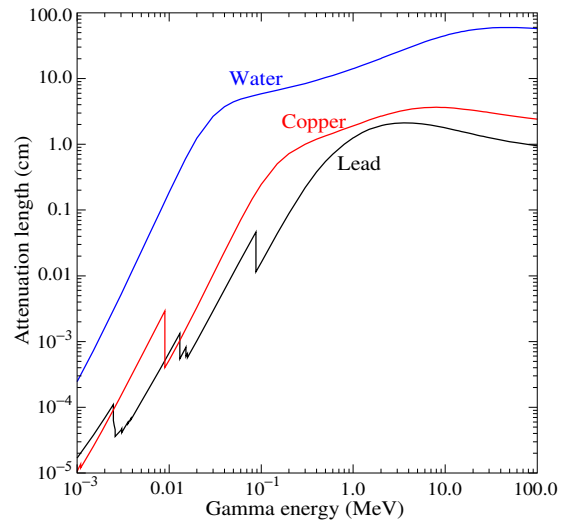


Figure 36.11:  $\gamma$ -ray attenuation lengths in some common shielding materials. The mass attenuation data has been taken from the NIST data base XCOM; see “Atomic Nuclear Properties” at [pdg.lbl.gov](http://pdg.lbl.gov).

As discussed in the following section, shielding materials contain radioactivity too. Consequently, they are chosen such as to contribute as little as possible to the overall background budget. The shielding materials discussed above, when properly selected, fit that requirement. Th/U concentrations in selected  $\text{H}_2\text{O}$ , Cu and Pb are  $\leq 0.1$  ppt [167],  $\leq 0.5$  ppt [168] and  $\leq 1$  ppt [169], respectively. Although cost effectively available in bulk quantity, steel is often not utilized as it can contain Th/U at concentrations of  $\leq 1$  ppb.

A precise estimation of the the magnitude of the external gamma-ray background, including scattering and the effect of analysis-energy cuts, requires Monte Carlo simulations based on the knowledge of the radioactivity present in the laboratory. Detailed modeling of the  $\gamma$ -ray flux in a large laboratory, or inside the hermetic shielding, needs to cope with a very small probability of generating any signal in the detector. It is often advantageous to calculate the solid angle of the detector to the background sources and mass attenuation of the radiation shield separately, or to employ importance sampling. The former method can lead to loss of energy-direction correlations while in the latter has to balance CPU-time consumption against the loss of statistical independence. These approaches reduce the computation time required for a statistically meaningful number of detector hits to manageable levels.

Water is commonly used as shielding medium for large detectors. It can be obtained cheaply and purified effectively in large quantity. Water purification technology is commercially available. Ultra-pure water, instrumented with photomultiplier tubes, can serve as active cosmic-ray veto system. Water is also an effective neutron moderator and shield. In more recent underground experiments that involve detectors operating at cryogenic temperature, liquefied gases (*e.g.* argon) are being used for shielding as well.

### 36.6.3 Radioactive impurities in detector and shielding components

After suppressing the effect of external radioactivity, radioactive impurities, contained in the detector components or attached to their surfaces, become important. Every material contains radioactivity at some level. The activity can be natural, cosmogenic, man-made, or a combination of them. The determination of the

activity content of a specific material or component requires case-by-case analyses, and is rarely obtainable from the manufacturer. However, there are some general rules that can be used to guide the pre-selection. For detectors designed to look for electrons (for example in double-beta decay searches or neutrino detection via inverse beta decay or elastic scattering), intrinsic radioactivity is often the principal source of background. For devices detecting nuclear recoils (for example in dark matter searches), this is often of secondary importance as ionization signals can be actively discriminated on an event-by-event basis. In the latter case radioactive decay-induced nuclear reactions, resulting in the emission of energetic neutrons, become a concern. Scattering of these neutrons on the detector material can lead to nuclear-recoil and, thus, background.

For natural radioactivity, a rule of thumb is that refined materials are more radiopure than their source in nature. Substances with high standard reduction potential tend to be cleaner as the refining process preferentially segregates K, Th, and U from electrodeposited materials. For example, Al is often found to contain considerable amounts of Th and U, while electrolytic Cu is very low in primordial activities. K, Th, and U tend to exist as or form compounds with low vapor pressure. Plastics or liquid hydrocarbons, having been refined by distillation, are often quite radiopure. Zone refining utilizes differences in solubility in the liquid and solid phase of the host material to segregate unwanted impurities. This technique is often used in the production of semiconductor detectors. Depending on the material processing, differences in standard reduction potential, boiling point and vapor pressure (for example for U and Ra) may lead to a breakage of decay chain equilibrium. Tabulated radioassay results for a wide range of materials can be found in Refs. [170], [169], [171] and [168]. Radioassay results from previous experiments are being archived at an online database [167].

The long-lived  $^{238}\text{U}$  daughter  $^{210}\text{Pb}$  ( $T_{1/2}=22.3\text{ y}$ ) is found in all shielding lead. It is a background concern at low energies. This is due to the relatively high endpoint energy ( $Q_{\beta}=1.162\text{ MeV}$ ) of its beta-unstable daughter  $^{210}\text{Bi}$ . Lead refined from selected low-U ore typically has specific activities of about 5–30 Bq/kg. For applications that require lower specific activity, ancient lead (for example from Roman ships) is sometimes used. Because the ore processing and lead refining removed most of the  $^{238}\text{U}$ , the  $^{210}\text{Pb}$  decayed during the long waiting time to the level supported by the U-content of the refined lead. Lining the lead with copper to range out the low-energy radiation is another remedy. However, intermediate- $Z$  materials carry additional cosmogenic-activation risks when handled above ground, as will be discussed below.  $^{210}\text{Pb}$  is also found in solders, even lead free types.

Man-made radioactivity, released during above-ground nuclear testing and nuclear power production, is a source of background. The fission product  $^{137}\text{Cs}$  can often be found attached to the surface of materials. The radioactive noble gas  $^{85}\text{Kr}$ , released into the atmosphere by nuclear reactors and nuclear fuel re-processing, is sometimes a background concern, especially due to its high solubility in organic materials. Post-World War II steel typically contains a few tens of mBq/kg of  $^{60}\text{Co}$ .

Surface activity is not a material property per se but is added during manufacturing and handling. Surface contamination can be effectively removed by clean machining, solvent washing, etching, leaching with dilute acid or their combination. However, different chemical elements for example the decay chain members Ra, Po and Pb have different attachment characteristics and, therefore may react differently to solvents, leading to incomplete cleaning and chain equilibrium breakage. The assembly of low-background detectors is often performed in controlled enclosures (e.g. clean rooms or glove boxes) to avoid contaminating surfaces with environmental substances, such as dust, containing radioactivity at much higher concentrations than the detector components. Due to the small size of dust particles, a fairly large fraction of  $^{226}\text{Ra}$   $\alpha$ -decays results in  $^{222}\text{Rn}$  being ejected into the surrounding gas. This fraction can approach 20% for ultra fine dust. Because of its low reactivity, radon can then spread throughout the detector. When not being processed, components are best stored in sealed bags to limit dust deposition on the surface, even inside

clean rooms, and to separate them from radon contained in the air. Nylon bags are also good radon barriers. Storage of parts under vacuum is an alternative solution to limit dust deposition and radon daughter attachment. Surface contamination with environmental dust can be quantified by means of wipe-testing with acid or alcohol wetted Whatman 41 filters. Analysis of acid cleaned paper wipes by means of mass spectroscopy or neutron activation analysis is capable of detecting less than 1 pg/cm<sup>2</sup> of Th and U.

The most demanding low-rate experiments require screening of *all* components for low levels of radioactivity, which can be a time consuming task. The requirements for activity characterization depend on the experiment, the location and amount of a particular component. Monte Carlo simulations are used to quantify these requirements. Sensitivities of the order  $\mu\text{Bq/kg}$  or less are sometimes required for the most critical detector components. At such a level of sensitivity, the characterization becomes a challenging problem in itself. Low-background  $\alpha$ ,  $\beta$ , and  $\gamma$ -ray counting, mass spectroscopy, and neutron activation analysis are commonly used diagnostic techniques.

#### 36.6.4 Radon and its progeny

The noble gas  $^{222}\text{Rn}$ , a pure  $\alpha$ -emitter, is a  $^{238}\text{U}$  decay product. Due to its relatively long half-life of 3.8 d it is released by surface soil and is found in the atmosphere everywhere.  $^{220}\text{Rn}$  (a  $^{232}\text{Th}$  decay product) is unimportant for most low-background experiments because of its short half-life of 55.6 s. It has only very little time to escape from its host material before decaying, with its daughters being immobile. The  $^{222}\text{Rn}$  activity of air ranges from 10 to 100 mBq/L outdoors and 100 to thousands of mBq/L indoors. The natural radon concentration depends on the weather and shows daily and seasonal variations. Radon levels are lowest above the oceans. For electron detectors, it is not the Rn itself that creates background, but its progeny  $^{214}\text{Pb}$ ,  $^{214}\text{Bi}$ ,  $^{210}\text{Bi}$ , which emit energetic beta and  $\gamma$  radiation. Thus, not only the detector itself has to be separated from contact with air, but also air-containing internal voids can be a background concern. Radon is soluble in water and even more so in organic solvents. For large liquid scintillation detectors, radon mobility due to convection and diffusion is a concern. To define a scale: typical double-beta-decay searches are restricted to  $< \mu\text{Bq/kg}_{\text{detector}}$  (or 1 decay per  $\text{kg}_{\text{detector}}$  and per 11.6 days) activities of  $^{222}\text{Rn}$  in the active medium. This corresponds to a steady-state population of 0.5 atoms/ $\text{kg}_{\text{detector}}$ . The decay of Rn itself is a concern for some recoil type detectors, as nuclear recoil energies in  $\alpha$  decays are substantial (100 keV in the case of  $^{222}\text{Rn}$  decays).

Low-background detectors are often kept sealed from the air and continuously flushed with boil-off nitrogen, which contains only small amounts of Rn. For the most demanding applications, the nitrogen is purified by multiple distillations, or by using pressure swing adsorption chromatography. Then only the Rn out-gassing of the piping (due to its intrinsic U content) determines the radon concentration. Radon diffuses readily through thin plastic barriers. If the detector is to be isolated from its environment by means of a membrane, the choice of material is important [172].

Prolonged exposure of detector components or raw materials to air leads to the accumulation of the long-lived radon daughter  $^{210}\text{Pb}$  on surfaces. Due to its low  $Q$ -value of 63.5 keV,  $^{210}\text{Pb}$  itself is only a problem when extreme low energy response is important. However, because of its higher  $Q$ -value, the lead daughter  $^{210}\text{Bi}$ , is a concern up to the MeV scale. The alpha unstable Bi-daughter  $^{210}\text{Po}$  ( $E_{\alpha} = 5304\text{ keV}$ ) contributes not only to the alpha background but can also induce the emission of energetic neutrons via ( $\alpha, n$ ) reactions on low- $Z$  materials (such as F, C, Si...etc.). The neutrons, in turn, may capture on other detector components, creating energetic background. The ( $\alpha, n$ ) reaction yield induced by the  $\alpha$  decay of  $^{210}\text{Po}$  is typically small (about  $6 \cdot 10^{-6} n/\alpha$  in Teflon, for example). This creates a memory effect, the air exposure history impacts the ( $\alpha, n$ ) background component.

Some data is available on the deposition of radon daughters from air onto materials, see e.g. [173], [174] and [175]. This data indicates a large spread of effective radon daughter collection distances ranging from a few  $cm$  to a few  $m$  in air. This large spread may indicate dependence on hidden, uncontrolled variables. These considerations limit the allowable air exposure

time but only within a wide range. Many experiments therefore adopt to perform the assembly of detector components in a radon-reduced atmosphere to counter this uncertainty.

In case raw materials (e.g. in the form of granules) were exposed to air at the production site, the bulk (instead of the surface as discussed before) of the finished detector components may be loaded with  $^{210}\text{Pb}$  and its daughters. These are difficult to detect as no energetic gamma radiation is emitted in their decays. Careful air-exposure management is the only way to reduce this source of background. This can be achieved by storing the parts under a protective low-radon cover gas or keeping them sealed from radon.

State-of-the-art detectors can detect radon outgassing even at the level of few atoms. Solid state, scintillation, or gas detectors utilize alpha spectroscopy or are exploiting the fast  $\beta - \alpha$  decay sequences of  $^{214}\text{Bi}$  and  $^{214}\text{Po}$ . The efficiency of these devices is sometimes boosted by electrostatic collection of radon ions from a large gas volume onto a small detector. Cryogenic radon collection can also boost the radon sensitivity. Radon outgassing measurement campaigns, similar to the radioactivity measurements discussed above, are conducted by collaborations to assure that the internal radon production stays within its allowance.

### 36.6.5 Cosmic rays

Cosmic radiation, discussed in detail in Chapter 30, is a source of background for just about any non-accelerator experiment. Primary cosmic rays are about 90% protons, 9% alpha particles, and the rest heavier nuclei (Fig 30.1). They are totally attenuated within the first few  $\text{hg}/\text{cm}^2$  of atmospheric thickness. At sea level secondary particles ( $\pi^\pm : p : e^\pm : n : \mu^\pm$ ) are observed with relative intensities 1 : 13 : 340 : 480 : 1420 ([176]; also see Fig 30.3).

All but the muon and the neutron components are readily absorbed by overburden such as building ceilings and passive shielding. Only if there is very little overburden ( $\lesssim 10 \text{ g}/\text{cm}^2$  [163]) do pions and protons need to be considered when estimating the production rate of cosmogenic radioactivity.

Sensitive experiments are, thus, operated deep underground where essentially only muons can penetrate. As shown in Fig-30.7, the muon intensity falls off rapidly with depth. Active detection systems, capable of tagging events correlated in time with cosmic-ray activity, are needed, depending on the overburden.

The muonic background is related to low-radioactivity techniques insofar as photo-nuclear interactions with atomic nuclei can produce long-lived radioactivity directly or indirectly via the creation of neutrons. This happens at any overburden, however, at strongly depth dependent rates. Muon bremsstrahlung, created in high- $Z$  shielding materials, contributes to the low energy background too. Active muon detection systems are effective in reducing cosmogenic background, but only for activities with sufficiently short half-lives, allowing vetoing with reasonable detector dead time.

Cosmogenic activation of detector components at the surface can be an issue for low-background experiments. Proper management of parts and materials above ground during manufacturing and detector assembly minimizes the accumulation of long-lived activity. Cosmogenic activation is most important for intermediate- $Z$  materials such as Cu and Fe. For the most demanding applications, metals are stored and transported under sufficient shielding to stop the hadronic component of the cosmic rays. Parts can be stored underground for long periods before being used. Underground machine shops are sometimes used to limit the duration of exposure at the surface. Some experiments are even electro-forming copper underground.

### 36.6.6 Neutrons

Neutrons contribute to the background of low-energy experiments in different ways: directly through nuclear recoil in the detector medium, and indirectly, through the production of radio-nuclides, capture  $\gamma$ s and inelastic scattering inside the detector and its components. The indirect mechanisms allow even remote materials to contribute to the background by means of penetrating  $\gamma$  radiation. Neutrons are thus an important source of low-energy background. They are produced in different ways:

1. At the earth's surface the flux of cosmic-ray secondary neutrons is exceeded only by that of muons;
2. Energetic tertiary neutrons are produced by cosmic-ray muons by nuclear spallation in the detector and laboratory walls;
3. In high- $Z$  materials, often used in radiation shields, nuclear capture of negative muons results in the emission of neutrons;
4. Natural radioactivity has a neutron component through spontaneous fission and  $(\alpha, n)$ -reactions.

A calculation with the hadronic simulation code FLUKA [177], using the known energy distribution of secondary neutrons at the earth's surface [178], yields a mass attenuation of  $1.5 \text{ hg}/\text{cm}^2$  in concrete for secondary neutrons. In case energy-dependent neutron-capture cross sections are known, such calculations can be used to obtain the production rate of particular radio-nuclides.

At an overburden of only few meters water equivalent, neutron production by muons becomes the dominant mechanism. Neutron production rates are high in high- $Z$  shielding materials. A high- $Z$  radiation shield, discussed earlier as being effective in reducing background due to external radioactivity, thus acts as a source for cosmogenic tertiary high-energy neutrons. Depending on the overburden and the radioactivity content of the laboratory, there is an optimal shielding thickness. Water shields, although bulky, are an attractive alternative due to their low neutron production yield and self-shielding.

Shields made from plastic or water are commonly used to reduce the neutron flux. The shield is sometimes doped with a substance having a high thermal neutron capture cross section (such as boron) to absorb thermal neutrons more quickly. The hydrogen, contained in these shields, serves as a target for elastic scattering, and is effective in reducing the neutron energy. Neutrons from natural radioactivity have relatively low energies and can be effectively suppressed by a neutron shield. Ideally, such a neutron shield should be inside the lead to be effective for tertiary neutrons. However, this is rarely done as it increases the neutron production target (in form of the passive shield), and the costs increase as the cube of the linear dimensions. An active cosmic-ray veto is an effective solution, correlating a neutron with its parent muon. This solution works best if the veto system is as far away from the detector as feasible (outside the radiation shield) in order to correlate as many background-producing muons with neutrons as possible. The vetoed time after a muon hit needs to be sufficiently long to assure muon bremsstrahlung and neutron-induced backgrounds are sufficiently suppressed. An upper limit to the allowable veto period is given by the veto-induced deadtime, which is related to the muon hit rate on the veto detector. This consideration also constitutes the limiting factor for the physical size of the veto system (besides the cost). The background caused by neutron-induced radioactivity with live-times far exceeding the veto time cannot be addressed in this way. Moving the detector deep underground, and thus reducing the muon flux, is the only technique that addresses all sources of cosmogenic the neutron background.

### References

- [1] R. M. Baltrusaitis *et al.*, Nucl. Instrum. Meth. **A240**, 410 (1985).
- [2] D. J. Bird *et al.* (HiRes), Astrophys. J. **424**, 491 (1994).
- [3] T. Abu-Zayyad *et al.*, Nucl. Instrum. Meth. **A450**, 253 (2000).
- [4] H. Tokuno *et al.*, Nucl. Instrum. Meth. **A676**, 54 (2012), [arXiv:1201.0002].
- [5] J. Abraham *et al.* (Pierre Auger), Nucl. Instrum. Meth. **A620**, 227 (2010), [arXiv:0907.4282].
- [6] R. Mussa and G. Ciaccio (Pierre Auger), Eur. Phys. J. Plus **127**, 94 (2012).
- [7] T. Fujii *et al.*, Astropart. Phys. **74**, 64 (2016), [arXiv:1504.00692].
- [8] F. Arqueros, J. R. Hoerandel and B. Keilhauer, Nucl. Instrum. Meth. **A597**, 23 (2008), [arXiv:0807.3844].



- [9] F. Arqueros, J. R. Hoerandel and B. Keilhauer, Nucl. Instrum. Meth. **A597**, 1 (2008), [arXiv:0807.3760].
- [10] J. Rosado, F. Blanco and F. Arqueros, Astropart. Phys. **34**, 164 (2010), [arXiv:1004.3971].
- [11] M. Ave *et al.* (AIRFLY), Astropart. Phys. **28**, 41 (2007), [arXiv:astro-ph/0703132].
- [12] J. Rosado, F. Blanco and F. Arqueros, Astropart. Phys. **55**, 51 (2014), [arXiv:1401.4310].
- [13] J. H. Boyer *et al.*, Nucl. Instrum. Meth. **A482**, 457 (2002).
- [14] J. T. Brack *et al.*, Astropart. Phys. **20**, 653 (2004).
- [15] B. Fick *et al.*, JINST **1**, 11, P11003 (2006).
- [16] J. Abraham *et al.* (Pierre Auger), Astropart. Phys. **33**, 108 (2010), [arXiv:1002.0366].
- [17] P. Abreu *et al.* (Pierre Auger), Astropart. Phys. **34**, 368 (2011), [arXiv:1010.6162].
- [18] R. Thalman *et al.* Journal of Quantitative Spectroscopy and Radiative Transfer, **147**, 171 (2014), Erratum-ibid. **189**, 281 (2017).
- [19] J. Abraham *et al.* [Pierre Auger Collab.], Nucl. Instrum. Methods **A789**, 172 (2015).
- [20] M. Unger *et al.*, Nucl. Instrum. Meth. **A588**, 433 (2008), [arXiv:0801.4309].
- [21] T.K. Gaisser and A.M. Hillas, *Proc. 15th Int. Cosmic Ray Conf. Bulgarska Akademiia na Naukite, Conf. Papers* **8**, 353 (1978), (archived at <http://adsabs.harvard.edu/abs/1977ICRC....8..353G>).
- [22] A. Huang, G. Medina-Tanco and A. Santangelo, Experimental Astronomy **40**, 1 (2015).
- [23] P. A. Klimov *et al.*, Space Sci. Rev. **212**, 3-4, 1687 (2017), [arXiv:1706.04976].
- [24] G. Abdellaoui *et al.* (JEM-EUSO), Journal of Instrumentation **13**, 5 (2018), ISSN 17480221.
- [25] L. Wiencke and A. Olinto (JEM-EUSO), PoS **ICRC2017**, 1097 (2018).
- [26] F. Capel *et al.*, Advances in Space Research **62**, 2954 (2018).
- [27] A. V. Olinto *et al.*, PoS **ICRC2017**, 542 (2018), [35,542(2017)], [arXiv:1708.07599].
- [28] J. Holder *et al.*, AIP Conf. Proc. **1085**, 657 (2009), [arXiv:0810.0474].
- [29] F. Aharonian *et al.* (H.E.S.S.), Astron. Astrophys. **457**, 899 (2006), [arXiv:astro-ph/0607333].
- [30] J. Albert *et al.* (MAGIC), Astrophys. J. **674**, 1037 (2008), [arXiv:0705.3244].
- [31] T. C. Weekes *et al.*, Astrophys. J. **342**, 379 (1989).
- [32] A. M. Hillas *et al.*, Astrophys. J. **503**, 744 (1998).
- [33] <http://tevcat.uchicago.edu/>.
- [34] F. Aharonian *et al.* (H.E.S.S.), Astrophys. J. **636**, 777 (2006), [arXiv:astro-ph/0510397].
- [35] M. de Naurois and D. Mazin, Comptes Rendus Physique **16**, 610 (2015), [arXiv:1511.00463].
- [36] N. Park, PoS **ICRC2017**, arXiv:1808.10495 (2018), [arXiv:1808.10495].
- [37] A. M. Hillas, Astropart. Phys. **43**, 19 (2013).
- [38] B. S. Acharya *et al.* (CTA Consortium), Astropart. Phys. **43**, 3 (2013).
- [39] A. Bernstein *et al.*, *Report on the Depth Requirements for a Massive Detector at Homestake* (2009), [arXiv:0907.4183].
- [40] Y. Ashie *et al.* (Super-Kamiokande), Phys. Rev. **D71**, 112005 (2005), [hep-ex/0501064].
- [41] S. Kasuga *et al.*, Phys. Lett. **B374**, 238 (1996).
- [42] M. Shiozawa (Super-Kamiokande), Nucl. Instrum. Meth. **A433**, 240 (1999).
- [43] K. Abe *et al.* (Super-Kamiokande), Phys. Rev. **D83**, 052010 (2011), [arXiv:1010.0118].
- [44] J. F. Beacom and M. R. Vagins, Phys. Rev. Lett. **93**, 171101 (2004), [hep-ph/0309300].
- [45] J. Boger *et al.* (SNO), Nucl. Instrum. Meth. **A449**, 172 (2000), [arXiv:nucl-ex/9910016].
- [46] T. K. Gaisser, F. Halzen and T. Stanev, Phys. Rept. **258**, 173 (1995), [Erratum: Phys. Rept.271,355(1996)], [hep-ph/9410384].
- [47] J.G. Learned and K. Mannheim, Ann. Rev. Nucl. and Part. Sci. **50**, 679 (2000).
- [48] U. F. Katz and C. Spiering, Prog. Part. Nucl. Phys. **67**, 651 (2012), [arXiv:1111.0507].
- [49] M. G. Aartsen *et al.* (IceCube), J. Phys. **G44**, 5, 054006 (2017), [arXiv:1607.02671].
- [50] S. Adrián-Martínez *et al.* (KM3NeT), J. Phys. **G43**, 8, 084001 (2016), [arXiv:1601.07459].
- [51] A. D. Avrorin *et al.*, Phys. Part. Nucl. **46**, 2, 211 (2015).
- [52] M. G. Aartsen *et al.* (IceCube) (2014), [arXiv:1412.5106].
- [53] S. Adrián-Martínez *et al.* (KM3NeT), Eur. Phys. J. **C74**, 9, 3056 (2014), [arXiv:1405.0839].
- [54] A. V. Akimov *et al.*, Eur. Phys. J. **C79**, 9, 758 (2019), [arXiv:1902.06083].
- [55] C. Kopper (for the IceCube Collab.), contribution to ICRC2017.
- [56] M. G. Aartsen *et al.* (IceCube), Phys. Rev. Lett. **113**, 101101 (2014), [arXiv:1405.5303].
- [57] A. Albert *et al.* (ANTARES), Astrophys. J. **853**, 1, L7 (2018), [arXiv:1711.07212].
- [58] M. G. Aartsen *et al.* (IceCube), Phys. Rev. **D91**, 7, 072004 (2015), [arXiv:1410.7227].
- [59] M. G. Aartsen *et al.* (IceCube, Fermi-LAT, MAGIC, AGILE, ASAS-SN, HAWC, H.E.S.S., INTEGRAL, Kanata, Kiso, Kapteyn, Liverpool Telescope, Subaru, Swift NuSTAR, VERITAS, VLA/17B-403), Science **361**, 6398, eaat1378 (2018), [arXiv:1807.08816].
- [60] M. G. Aartsen *et al.* (IceCube), Science **361**, 6398, 147 (2018), [arXiv:1807.08794].
- [61] G. Illuminati (for the ANTARES and IceCube Collabs.), contribution to ICRC2019.
- [62] M. G. Aartsen *et al.* (IceCube), Phys. Rev. **D99**, 3, 032007 (2019), [arXiv:1901.05366].
- [63] D. Williams (for the IceCube Collab.), contribution to ICRC2019.
- [64] R. Coniglione (for the ANTARES and KM3NeT Collabs.), contribution to ICRC2019.
- [65] K. Greisen, Phys. Rev. Lett. **16**, 748 (1966).
- [66] G. T. Zatsepin and V. A. Kuzmin, JETP Lett. **4**, 78 (1966), [Pisma Zh. Eksp. Teor. Fiz.4,114(1966)].
- [67] R. Abbasi *et al.* (IceCube), Astropart. Phys. **34**, 382 (2011), [arXiv:1004.1694].
- [68] S. R. Klein, Nucl. Phys. Proc. Supl. **229-232**, 284 (2012), [arXiv:1012.1407].
- [69] G. A. Askar'yan, Sov. Phys. JETP **14**, 2, 441 (1962), [Zh. Eksp. Teor. Fiz.41,616(1961)].
- [70] G.A. Askaryan, Sov. Phys. JETP **21**, 658 (1965).
- [71] C. W. James *et al.*, Phys. Rev. **E84**, 056602 (2011), [arXiv:1007.4146].
- [72] J. Alvarez-Muniz, R. A. Vazquez and E. Zas, Phys. Rev. **D62**, 063001 (2000), [arXiv:astro-ph/0003315].
- [73] C. Glaser *et al.* (2019), [arXiv:1906.01670].
- [74] D. Saltzberg *et al.*, Phys. Rev. Lett. **86**, 2802 (2001), [hep-ex/0011001].
- [75] O. Scholten *et al.*, J. Phys. Conf. Ser. **81**, 012004 (2007).



- [76] A. G. Viereg, K. Bechtol and A. Romero-Wolf, *JCAP* **1602**, 02, 005 (2016), [arXiv:1504.08006].
- [77] L. Gerhardt and S. R. Klein, *Phys. Rev.* **D82**, 074017 (2010), [arXiv:1007.0039].
- [78] J. Alvarez-Muniz, R. A. Vazquez and E. Zas, *Phys. Rev.* **D61**, 023001 (2000), [arXiv:astro-ph/9901278].
- [79] M. G. Aartsen *et al.* (IceCube), *Phys. Rev.* **D98**, 6, 062003 (2018), [arXiv:1807.01820].
- [80] A. Aab *et al.* (Pierre Auger), *JCAP* **1910**, 10, 022 (2019), [arXiv:1906.07422].
- [81] J. D. Bray *et al.*, *Phys. Rev.* **D91**, 6, 063002 (2015), [arXiv:1502.03313].
- [82] O. Scholten *et al.*, *Phys. Rev. Lett.* **103**, 191301 (2009), [arXiv:0910.4745].
- [83] P. W. Gorham *et al.* (ANITA), *Phys. Rev.* **D99**, 12, 122001 (2019), [arXiv:1902.04005].
- [84] P. Allison *et al.* (ARA), in “36th International Cosmic Ray Conference (ICRC 2019) Madison, Wisconsin, USA, July 24-August 1, 2019,” (2019), [arXiv:1907.11125].
- [85] A. Anker *et al.* (2019), [arXiv:1909.00840].
- [86] T. Winchen *et al.*, *J. Phys. Conf. Ser.* **1181**, 1, 012077 (2019), [arXiv:1903.08472].
- [87] J. Stettner (IceCube), in “HAWC Contributions to the 36th International Cosmic Ray Conference (ICRC2019),” (2019), [arXiv:1908.09551].
- [88] A. van Vliet, J. R. Horandel and R. Alves Batista, *PoS ICRC2017*, 562 (2018), [35,562(2017)], [arXiv:1707.04511].
- [89] J. A. Aguilar *et al.* (2019), [arXiv:1907.12526].
- [90] J. G. Learned and S. Pakvasa, *Astropart. Phys.* **3**, 267 (1995), [hep-ph/9405296].
- [91] J. L. Feng *et al.*, *Phys. Rev. Lett.* **88**, 161102 (2002), [hep-ph/0105067].
- [92] P. W. Gorham *et al.* (ANITA), *Phys. Rev. Lett.* **121**, 16, 161102 (2018), [arXiv:1803.05088].
- [93] J. Álvarez Muñiz *et al.* (GRAND), *Sci. China Phys. Mech. Astron.* **63**, 1, 219501 (2020), [arXiv:1810.09994].
- [94] M. Detrixhe *et al.* (ANITA-II), *Phys. Rev.* **D83**, 023513 (2011), [arXiv:1008.1282].
- [95] R.D. Dagkesamanskii and I.M. Zheleznykh, *Sov. Phys. JETP Lett.* **50**, 233 (1989).
- [96] C. W. James *et al.*, *EPJ Web Conf.* **135**, 04001 (2017), [arXiv:1704.05336].
- [97] J. D. Bray, *Astropart. Phys.* **77**, 1 (2016), [arXiv:1601.02980].
- [98] J.A. Dowdeswell and S. Evans, *Rept. on Prog. in Phys.* **67**, 1821 (2004).
- [99] P. Allison *et al.*, *Astropart. Phys.* **108**, 63 (2019), [arXiv:1712.03301].
- [100] A. Anker *et al.*, *JCAP* **1911**, 030 (2019), [arXiv:1909.02677].
- [101] S. W. Barwick *et al.*, *JCAP* **1807**, 07, 055 (2018), [arXiv:1804.10430].
- [102] C. Deaconu *et al.*, *Phys. Rev.* **D98**, 4, 043010 (2018), [arXiv:1805.12576].
- [103] P. W. Gorham *et al.* (ANITA), *Phys. Rev. Lett.* **103**, 051103 (2009), [arXiv:0812.2715].
- [104] I. Kravchenko *et al.*, *Phys. Rev.* **D73**, 082002 (2006), [arXiv:astro-ph/0601148].
- [105] P. Allison *et al.* (ARA), *Phys. Rev.* **D93**, 8, 082003 (2016), [arXiv:1507.08991].
- [106] J. Avva *et al.*, *Nucl. Instrum. Meth.* **A869**, 46 (2017), [arXiv:1605.03525].
- [107] A. Anker *et al.* (ARIANNA), *Adv. Space Res.* **64**, 2595 (2019), [arXiv:1903.01609].
- [108] F. G. Schroder, *Prog. Part. Nucl. Phys.* **93**, 1 (2017), [arXiv:1607.08781].
- [109] T. Huege, *Braz. J. Phys.* **44**, 520 (2014), [1294(2013)], [arXiv:1310.6927].
- [110] S. Buitink *et al.*, *Phys. Rev.* **D90**, 8, 082003 (2014), [arXiv:1408.7001].
- [111] T. Huege, *Phys. Rept.* **620**, 1 (2016), [arXiv:1601.07426].
- [112] S. W. Barwick *et al.*, *Astropart. Phys.* **90**, 50 (2017), [arXiv:1612.04473].
- [113] A. Balagopal V. *et al.*, *Eur. Phys. J.* **C78**, 2, 111 (2018), [erratum: *Eur. Phys. J.* **C78**, 1017 (2018)], [arXiv:1712.09042].
- [114] A. Aab *et al.* (Pierre Auger), *Phys. Rev. Lett.* **116**, 24, 241101 (2016), [arXiv:1605.02564].
- [115] P. A. Bezyazeev *et al.*, *Phys. Rev.* **D97**, 12, 122004 (2018), [arXiv:1803.06862].
- [116] W. D. Apel *et al.* (LOPES), *Phys. Rev.* **D90**, 6, 062001 (2014), [arXiv:1408.2346].
- [117] D. R. Nygren, in “Proceedings, 1975 PEP Summer Study, Berkeley, July 28-August 20, 1975,” 126–133 (1975).
- [118] L. S. Miller, S. Howe and W. E. Spear, *Phys. Rev.* **166**, 871 (1968), URL <https://link.aps.org/doi/10.1103/PhysRev.166.871>.
- [119] E. Aprile and T. Doke, *Rev. Mod. Phys.* **82**, 2053 (2010), [arXiv:0910.4956].
- [120] V. Chepel and H. Araujo, *JINST* **8**, R04001 (2013), [arXiv:1207.2292].
- [121] D. Gonzalez-Diaz, F. Monrabal and S. Murphy, *Nucl. Instrum. Meth.* **A878**, 200 (2018), [arXiv:1710.01018].
- [122] J. J. Gomez-Cadenas, F. Monrabal Capilla and P. Ferrario, *Front.in Phys.* **7**, 51 (2019), [arXiv:1903.02435].
- [123] H. J. Maris, *Journal of the Physical Society of Japan* **77**, 11, 111008 (2008), URL <https://doi.org/10.1143/JPSJ.77.111008>.
- [124] L. Bruschi, G. Mazzi and M. Santini, *Phys. Rev. Lett.* **28**, 1504 (1972), URL <https://link.aps.org/doi/10.1103/PhysRevLett.28.1504>.
- [125] E. Aprile *et al.*, *Nature* **568**, 7753, 532 (2019), URL <https://doi.org/10.1038/s41586-019-1124-4>.
- [126] K. Winger *et al.*, *Journal of Environmental Radioactivity* **80**, 2, 183 (2005), ISSN 0265-931X, URL <http://www.sciencedirect.com/science/article/pii/S0265931X04002887>.
- [127] H. Loosli, *Earth and Planetary Science Letters* **63**, 1, 51 (1983), ISSN 0012-821X, URL <http://www.sciencedirect.com/science/article/pii/0012821X83900213>.
- [128] E. Aprile *et al.* (XENON), *Eur. Phys. J.* **C75**, 11, 546 (2015), [arXiv:1503.07698].
- [129] M. Schumann, *J. Phys.* **G46**, 10, 103003 (2019), [arXiv:1903.03026].
- [130] E. Aprile *et al.*, *JINST* **9**, 11, P11012 (2014), [arXiv:1408.6206].
- [131] F. Neves *et al.*, *JINST* **12**, 01, P01017 (2017), [arXiv:1612.07965].
- [132] D. S. Akerib *et al.* (LUX Collaboration), *Phys. Rev. D* **97**, 102008 (2018), URL <https://link.aps.org/doi/10.1103/PhysRevD.97.102008>.
- [133] D. S. Akerib *et al.* (LUX), *Phys. Rev.* **D95**, 1, 012008 (2017), [arXiv:1610.02076].
- [134] M. Szydagis *et al.*, *Journal of Instrumentation* **6**, 10, P10002 (2011), URL <https://doi.org/10.1088%2F1748-0221%2F6%2F10%2Fp10002>.
- [135] M. Kimura *et al.*, *Phys. Rev.* **D100**, 3, 032002 (2019), [arXiv:1902.01501].
- [136] R. Ajaj *et al.* (DEAP), *Phys. Rev.* **D100**, 2, 022004 (2019), [arXiv:1902.04048].

- [137] P. Agnes *et al.* (DarkSide), Phys. Rev. **D93**, 8, 081101 (2016), [Addendum: Phys. Rev.D95,no.6,069901(2017)], [arXiv:1510.00702].
- [138] E. Aprile *et al.* (XENON), Phys. Rev. Lett. **119**, 18, 181301 (2017), [arXiv:1705.06655].
- [139] X. Cui *et al.* (PandaX-II), Phys. Rev. Lett. **119**, 18, 181302 (2017), [arXiv:1708.06917].
- [140] D. S. Akerib *et al.*, Phys. Rev. Lett. **118**, 25, 251302 (2017).
- [141] D. S. Akerib *et al.* (LUX-ZEPLIN) (2018), [arXiv:1802.06039].
- [142] E. Aprile *et al.* (XENON), JCAP **1604**, 04, 027 (2016), [arXiv:1512.07501].
- [143] H. Zhang *et al.* (PandaX), Sci. China Phys. Mech. Astron. **62**, 3, 31011 (2019), [arXiv:1806.02229].
- [144] C. E. Aalseth *et al.*, Eur. Phys. J. Plus **133**, 131 (2018), [arXiv:1707.08145].
- [145] J. Aalbers *et al.*, Journal of Cosmology and Astroparticle Physics **2016**, 11, 017 (2016), URL <https://doi.org/10.1088%2F1475-7516%2F2016%2F11%2F017>.
- [146] W. Guo and D. N. McKinsey, Phys. Rev. **D87**, 11, 115001 (2013), [arXiv:1302.0534].
- [147] D. R. Nygren, J. Phys. Conf. Ser. **460**, 012006 (2013).
- [148] C. A. J. O'Hare *et al.*, Phys. Rev. **D92**, 6, 063518 (2015), [arXiv:1505.08061].
- [149] S. M. Bilenky and C. Giunti, Mod. Phys. Lett. **A27**, 1230015 (2012), [arXiv:1203.5250].
- [150] S. R. Elliott, A. A. Hahn and M. K. Moe, Phys. Rev. Lett. **59**, 2020 (1987), URL <http://link.aps.org/doi/10.1103/PhysRevLett.59.2020>.
- [151] G. Anton *et al.* (EXO-200), Phys. Rev. Lett. **123**, 16, 161802 (2019), [arXiv:1906.02723].
- [152] S. A. Kharusi *et al.* (nEXO) (2018), [arXiv:1805.11142].
- [153] D. Nygren, Nucl. Instrum. Meth. **A603**, 337 (2009).
- [154] M. K. Moe, Phys. Rev. **C44**, 931 (1991), [1019(1991)].
- [155] A. D. McDonald *et al.*, Phys. Rev. Lett. **120**, 13, 132504 (2018), [arXiv:1711.04782].
- [156] C. Chambers *et al.* (nEXO), Nature **569**, 7755, 203 (2019), [arXiv:1806.10694].
- [157] P. Thapa *et al.* (2019), [arXiv:1904.05901].
- [158] C. Enss, editor, *Cryogenic particle detection*, volume 99 of *Topics in applied physics*, Springer, Berlin, Germany (2005).
- [159] E. Shirokoff (ed.), *Proc. 15th Int. Workshop on Low Temperature Detectors (LTD-15)*, J. Low Temp. Phys. **176**, 131–1108 (2014).
- [160] S.H. Moseley, J.C. Mather, and D. McCammon, J. Appl. Phys. **56**, 1257 (1984).
- [161] K.D. Irwin, Appl. Phys. Lett. **66**, 1998 (1995).
- [162] S.R. Bandler *et al.*, J. Low. Temp. Phys. **93**, 709 (1993).
- [163] G. Heusser, Ann. Rev. Nucl. Part. Sci. **45**, 543 (1995).
- [164] J. A. Formaggio and C. J. Martoff, Ann. Rev. Nucl. Part. Sci. **54**, 361 (2004).
- [165] S. Agostinelli *et al.* (GEANT4), Nucl. Instrum. Meth. **A506**, 250 (2003).
- [166] U. N. S. C. on the Effects of Atomic Radiation, *Sources and Effects of Ionizing Radiation*, p233, United Nations (2010).
- [167] <http://www.radiopurity.org>.
- [168] N. Abgrall *et al.*, Nucl. Instrum. Meth. **A828**, 22 (2016), [arXiv:1601.03779].
- [169] D. S. Leonard *et al.*, Nucl. Instrum. Meth. **A591**, 490 (2008), [arXiv:0709.4524].
- [170] J. Jagam and J. Simpson, Nucl. Instrum. Meth. **A324**, 389 (1993).
- [171] D. S. Leonard *et al.*, Nucl. Instrum. Meth. **A871**, 169 (2017), [arXiv:1703.10799].
- [172] M. Wojcik *et al.*, Nucl. Instrum. Meth. **A449**, 158 (2000).
- [173] V. E. Guiseppe *et al.*, AIP Conf. Proc. **1338**, 95 (2011), [arXiv:1101.0126].
- [174] M. Stein *et al.*, Nucl. Instrum. Meth. **A880**, 92 (2018), [arXiv:1708.09476].
- [175] E. S. Morrison *et al.*, AIP Conf. Proc. **1921**, 1, 090002 (2018), [arXiv:1708.08534].
- [176] National Council on Radiation Protection and Measurement, Report 94, Bethesda, MD (1987).
- [177] T. Boehlen *et al.*, Nuclear Data Sheets **120**, 211 (2014), <http://www.fluka.org/fluka.php>.
- [178] M.S. Gordon *et al.*, IEEE Trans. **NS51**, 3427 (2004).

## 37. Radioactivity and Radiation Protection

Revised August 2019 by S. Roesler and M. Silari (CERN).

## 37.1. Definitions [1,2,3]

It would be desirable if legal protection limits could be expressed in directly measurable *physical quantities*. However, this does not allow quantifying biological effects of the exposure of the human body and its detriment to ionizing radiation.

For this reason, protection limits are expressed in terms of so-called *protection quantities* which, although calculable, are not measurable. Protection quantities quantify the extent of exposure of the human body to ionizing radiation from both whole and partial body external irradiation and from intakes of radionuclides.

In order to demonstrate compliance with dose limits, so-called *operational quantities* are typically used, which aim at providing conservative estimates of protection quantities. Often radiation protection detectors used for individual and area monitoring are calibrated in terms of operational quantities and, thus, these quantities become “measurable”.

## 37.1.1. Physical quantities :

• **Fluence**,  $\Phi$  (unit:  $1/\text{m}^2$ ): The fluence is the quotient of the sum of the particle track lengths  $dl$  in the volume  $dV$

$$\Phi = dl/dV . \quad (37.1)$$

It can also be expressed in terms of number of particles  $dN$  incident upon a small sphere of cross-sectional area  $da$

$$\Phi = dN/da .$$

• **Absorbed dose**,  $D$  (unit: gray,  $1 \text{ Gy}=1 \text{ J/kg}=100 \text{ rad}$ ): The absorbed dose is the energy imparted by ionizing radiation in a volume element of a specified material divided by the mass of this volume element.

• **Kerma**,  $K$  (unit: gray): Kerma is the sum of the initial kinetic energies of all charged particles set in motion by indirectly ionizing radiation in a volume element of the specified material divided by the mass of this volume element.

• **Linear energy transfer,  $L$  or LET** (unit:  $\text{J/m}$ , often given in  $\text{keV}/\mu\text{m}$ ,  $1 \text{ keV}/\mu\text{m} \approx 1.602 \times 10^{-10} \text{ J/m}$ ): The linear energy transfer is the mean energy,  $dE$ , lost by a charged particle owing to collisions with electrons in traversing a distance  $dl$  in matter. *Low-LET radiation*: X rays and gamma rays (accompanied by charged particles due to interactions with the surrounding medium) or light charged particles such as electrons that produce sparse ionizing events far apart at a molecular scale ( $L < 10 \text{ keV}/\mu\text{m}$ ). *High-LET radiation*: neutrons and heavy charged particles that produce ionizing events densely spaced at a molecular scale ( $L > 10 \text{ keV}/\mu\text{m}$ ). While the above LET definition refers to electronic stopping power only, at low energy nuclear stopping power could be a significant fraction of the total stopping power.

• **Activity**,  $A$  (unit: becquerel,  $1 \text{ Bq}=1/\text{s}=27 \text{ pCi}$ ): Activity is the expectation value of the number of nuclear decays occurring in a given quantity of material per unit time.

## 37.1.2. Protection quantities :

• **Organ absorbed dose**,  $D_T$  (unit: gray): The mean absorbed dose in an organ or tissue  $T$  of mass  $m_T$  is defined as

$$D_T = \frac{1}{m_T} \int_{m_T} D dm .$$

• **Equivalent dose**,  $H_T$  (unit: sievert,  $1 \text{ Sv}=100 \text{ rem}$ ): The equivalent dose  $H_T$  in an organ or tissue  $T$  is equal to the sum of the absorbed doses  $D_{T,R}$  in the organ or tissue caused by different radiation types  $R$  weighted with so-called radiation weighting factors  $w_R$ :

$$H_T = \sum_R w_R \times D_{T,R} . \quad (37.2)$$

Table 37.1: Radiation weighting factors,  $w_R$ .

Radiation type	$w_R$
Photons, electrons and muons	1
Neutrons, $E_n < 1 \text{ MeV}$	$2.5 + 18.2 \times \exp[-(\ln E_n)^2/6]$
$1 \text{ MeV} \leq E_n \leq 50 \text{ MeV}$	$5.0 + 17.0 \times \exp[-(\ln(2E_n))^2/6]$
$E_n > 50 \text{ MeV}$	$2.5 + 3.25 \times \exp[-(\ln(0.04E_n))^2/6]$
Protons and charged pions	2
Alpha particles, fission fragments, heavy ions	20

It expresses long-term risks (primarily cancer and leukemia) from low-level chronic exposure. The values for  $w_R$  recommended by ICRP [2] are given in Table 37.1.

• **Effective dose**,  $E$  (unit: sievert): The sum of the equivalent doses, weighted by the tissue weighting factors  $w_T$  ( $\sum_T w_T = 1$ ) of several organs and tissues  $T$  of the body that are considered to be most sensitive [2], is called “effective dose”:

$$E = \sum_T w_T \times H_T . \quad (37.3)$$

## 37.1.3. Operational quantities :

• **Dose equivalent**,  $H$  (unit: sievert): The dose equivalent at a point in tissue is given by

$$H = D \times Q \quad (37.4)$$

where  $D$  is the absorbed dose and  $Q$  is the quality factor at that point. The quality factor at a point in tissue, is given by:

$$Q = \frac{1}{D} \int_{L=0}^{\infty} Q(L) D_L dL$$

where  $D_L$  is the distribution of  $D$  in unrestricted linear energy transfer  $L$  at the point of interest, and  $Q(L)$  is the quality factor as a function of  $L$ . The integration is to be performed over  $D_L$ , due to all charged particles, excluding their secondary electrons.

• **Ambient dose equivalent**,  $H^*(10)$  (unit: sievert): The dose equivalent at a point in a radiation field that would be produced by the corresponding expanded and aligned field in a 30 cm diameter sphere of unit density tissue (ICRU sphere) at a depth of 10 mm on the radius vector opposing the direction of the aligned field. Ambient dose equivalent is the operational quantity for *area monitoring*.

• **Personal dose equivalent**,  $H_p(d)$  (unit: sievert): The dose equivalent in ICRU tissue at an appropriate depth,  $d$ , below a specified point on the human body. The specified point is normally taken to be where the individual dosimeter is worn. For the assessment of effective dose,  $H_p(10)$  with a depth  $d = 10 \text{ mm}$  is chosen, and for the assessment of the dose to the skin and to the hands and feet the personal dose equivalent,  $H_p(0.07)$ , with a depth  $d = 0.07 \text{ mm}$ , is used. Personal dose equivalent is the operational quantity for *individual monitoring*.

## 37.1.4. Dose conversion coefficients :

Dose conversion coefficients allow direct calculation of protection or operational quantities from particle fluence and are functions of particle type, energy and irradiation configuration. The most common coefficients are those for effective dose and ambient dose equivalent. The former are based on simulations in which the dose to organs of anthropomorphic phantoms is calculated for approximate actual conditions of exposure, such as irradiation of the front of the body (anterior-posterior irradiation) or isotropic irradiation.

Conversion coefficients from fluence to effective dose are given for anterior-posterior irradiation and various particles in Fig. 37.1 [4]. For example, the effective dose from an anterior-posterior irradiation in a field of 1-MeV neutrons with a fluence of 1 neutron per  $\text{cm}^2$  is about 290 pSv. In Monte Carlo simulations such coefficients allow multiplication with fluence at scoring time such that effective dose to a human body at the considered location is directly obtained.

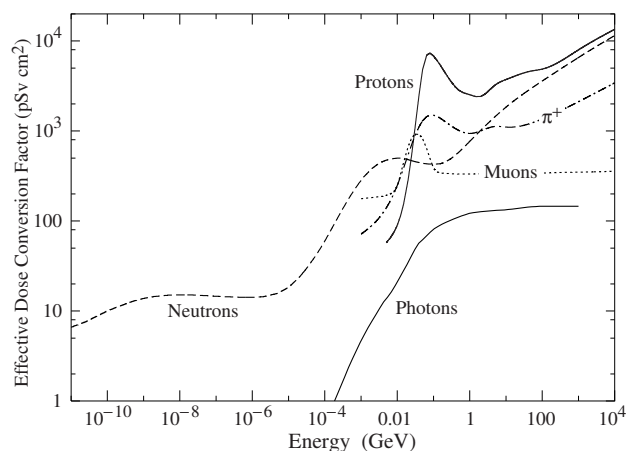


**Figure 37.1:** Fluence to effective dose conversion coefficients for anterior-posterior irradiation and various particles [4].

### 37.2. Radiation levels [5]

- **Natural background radiation:** On a worldwide average, the annual whole-body dose equivalent due to all sources of natural background radiation ranges from 1.0 to 13 mSv (0.1–1.3 rem) with an annual average of 2.4 mSv [6]. In certain areas values up to 50 mSv (5 rem) have been measured. A large fraction (typically more than 50%) originates from inhaled natural radioactivity, mostly radon and radon daughters. The latter can vary by more than one order of magnitude: it is 0.1–0.2 mSv in open areas, 2 mSv on average in a house and more than 20 mSv in poorly ventilated mines.
- **Cosmic ray background radiation:** At sea level, the whole-body dose equivalent due to cosmic ray background radiation is dominated by muons; at higher altitudes also nucleons contribute. Dose equivalent rates range from less than 0.1  $\mu$ Sv/h at sea level to a few  $\mu$ Sv/h at aircraft altitudes. Details on cosmic ray fluence levels are given in the Cosmic Rays section (Sec. 30 of this *Review*).

### 37.3. Health effects of ionizing radiation

Radiation can cause two types of health effects, deterministic and stochastic:

- **Deterministic effects** are tissue reactions which cause injury to a population of cells if a given threshold of absorbed dose is exceeded. The severity of the reaction increases with dose. The quantity in use for tissue reactions is the absorbed dose,  $D$ . When particles other than photons and electrons (low-*LET* radiation) are involved, a Relative Biological Effectiveness (*RBE*)-weighted dose may be used. The *RBE* of a given radiation is the reciprocal of the ratio of the absorbed dose of that radiation to the absorbed dose of a reference radiation (usually X rays) required to produce the same degree of biological effect. It is a complex quantity that depends on many factors such as cell type, dose rate, fractionation, etc.
- **Stochastic effects** are malignant diseases and heritable effects for which the probability of an effect occurring, but not its severity, is a function of dose without threshold.
- **Lethal dose:** The whole-body dose from penetrating ionizing radiation resulting in 50% mortality in 30 days (assuming no medical treatment) is 2.5–4.5 Gy (250–450 rad)<sup>†</sup>, as measured internally on the body longitudinal center line. The surface dose varies due to variable body attenuation and may be a strong function of energy.
- **Cancer induction:** The cancer induction probability is about 5% per Sv on average for the entire population [3].
- **Recommended effective dose limits:** The International Commission on Radiological Protection (ICRP) recommends a limit for radiation workers of 20 mSv effective dose per year averaged over 5 years, with the provision that the dose should not exceed 50 mSv in any single year [3]. The limit in the EU-countries and Switzerland is

<sup>†</sup> *RBE*-weighted when necessary

20 mSv per year, in the U.S. it is 50 mSv per year (5 rem per year). Many physics laboratories in the U.S. and elsewhere set lower limits. The effective dose limit for general public is typically 1 mSv per year.

### 37.4. Prompt neutrons at accelerators

Neutrons dominate the radiation environment outside thick shielding (*e.g.*, > 1 m of concrete) for high energy (> a few hundred MeV) electron and hadron accelerators. In addition, for accelerators with energies above about 10 GeV, muons contribute significantly at small angles with regard to the beam, even behind several meters of shielding. Another special case are synchrotron light sources where particular care has to be taken to shield the very intense low-energy photons extracted from the electron synchrotron into the experimental areas. Due to its importance at high energy accelerators this section focuses on prompt neutrons.

#### 37.4.1. Electron accelerators :

At electron accelerators, neutrons are generated via photonuclear reactions from bremsstrahlung photons. Neutron production takes place above a threshold value which varies from 10 to 19 MeV for light nuclei (with important exceptions, such as 2.23 MeV for deuterium and 1.67 MeV for beryllium) and from 4 to 6 MeV for heavy nuclei. It is commonly described by different mechanisms depending on the photon energy: the giant dipole resonance interactions (from threshold up to about 30 MeV, often the dominant process), the quasi-deuteron effect (between 30 MeV and a few hundred MeV), the delta resonance mechanism (between 200 MeV and a few GeV) and the vector meson dominance model at higher energies.

The giant dipole resonance reaction consists in a collective excitation of the nucleus, in which neutrons and protons oscillate in the direction of the photon electric field. The oscillation is damped by friction in a few cycles, with the photon energy being transferred to the nucleus in a process similar to evaporation. Nucleons emitted in the dipolar interaction have an anisotropic angular distribution, with a maximum at  $90^\circ$ , while those leaving the nucleus as a result of evaporation are emitted isotropically with a Maxwellian energy distribution described as [7]:

$$\frac{dN}{dE_n} = \frac{E_n}{T^2} e^{-E_n/T}, \quad (37.5)$$

where  $T$  is a nuclear ‘temperature’ (in units of MeV) characteristic of the particular target nucleus and its excitation energy. For heavy nuclei the ‘temperature’ generally lies in the range of  $T = 0.5$ – $1.0$  MeV. Neutron yields from semi-infinite targets per kW of electron beam power are plotted in Fig. 37.2 as a function of the electron beam energy [7].

While for thick targets neutron production is mainly due to photonuclear interactions, for thin targets (thickness of fractions of the radiation length) electronuclear interactions are the dominating process.

Typical neutron energy spectra outside of concrete (80 cm thick, 2.35 g/cm<sup>3</sup>) and iron (40 cm thick) shields are shown in Fig. 37.3. In order to compare these spectra to those caused by proton beams (see below) the spectra are scaled by a factor of 100, which roughly corresponds to the difference in the high energy hadronic cross sections for photons and hadrons (*e.g.*, the fine structure constant). The shape of these spectra are generally characterized by a low-energy peak at around 1 MeV (evaporation neutrons) and a high-energy shoulder at around 70–80 MeV. In case of concrete shielding, the spectrum also shows a pronounced peak at thermal neutron energies.

#### 37.4.2. Proton accelerators :

At proton accelerators, neutron yields emitted per incident proton by different target materials are roughly independent of proton energy between 20 MeV and 1 GeV, and are given by the ratio C : Al : Cu-Fe : Sn : Ta-Pb = 0.3 : 0.6 : 1.0 : 1.5 : 1.7 [10]. Above about 1 GeV, the neutron yield is proportional to  $E^m$ , where  $0.80 \leq m \leq 0.85$  [11].

Typical neutron energy spectra outside of concrete and iron shielding are shown in Fig. 37.3. Here, the radiation fields are caused

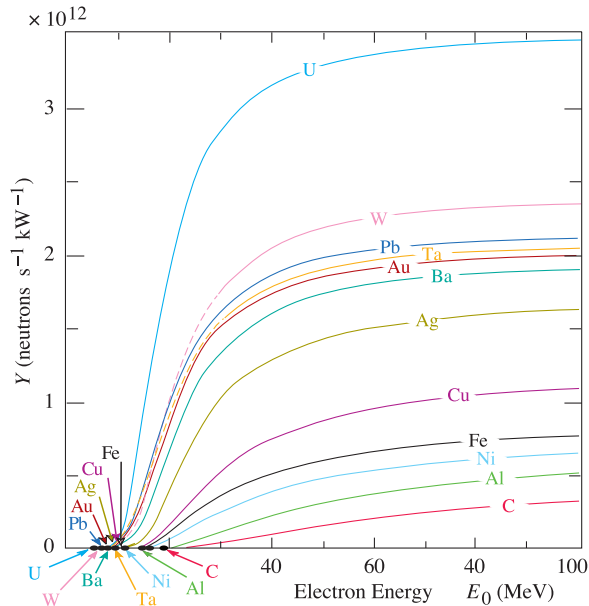


**Figure 37.2:** Neutron yields from semi-infinite targets per kW of electron beam power, as a function of the electron beam energy, disregarding target self-shielding [7].

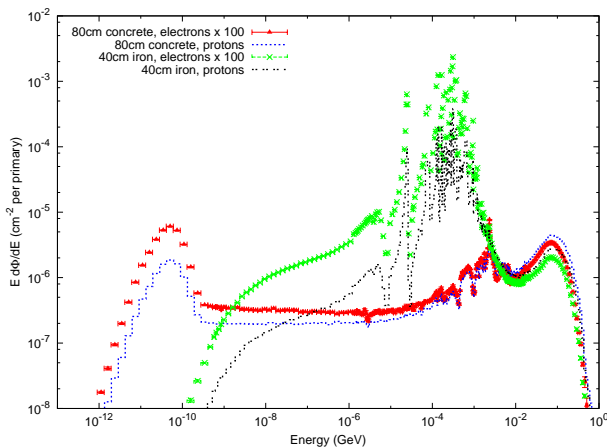


**Figure 37.3:** Neutron energy spectra calculated with the FLUKA code [8,9] from 25 GeV proton and electron beams on a thick copper target. Spectra are evaluated at  $90^\circ$  to the beam direction behind 80 cm of concrete or 40 cm of iron. All spectra are normalized per beam particle. For better visualization, spectra for electron beam are multiplied by a factor of 100.

by a 25 GeV proton beam interacting with a thick copper target. The comparison of these spectra with those for an electron beam of the same energy reflects the difference in the hadronic cross sections between photons and hadrons above a few 100 MeV. Differences are increasing towards lower energies because of different interaction mechanisms. Furthermore, the slight shift in energy above about 100 MeV follows from the fact that the energies of the interacting photons are lower than 25 GeV. Apart from this the shapes of the two spectra are similar.

The neutron-attenuation length is shown in Fig. 37.4 for concrete and mono-energetic broad-beam conditions. It reaches an asymptotic value of about  $117 \text{ g/cm}^2$  above 200 MeV. As the cascade through thick shielding is carried by particles with energies between about 100 MeV and 300 MeV (in this energy range non-elastic cross sections are at minimum and are dominated by quasi-elastic processes leading to low attenuation) this value is equal to the equilibrium attenuation length for particles emitted at 90 degrees in concrete.

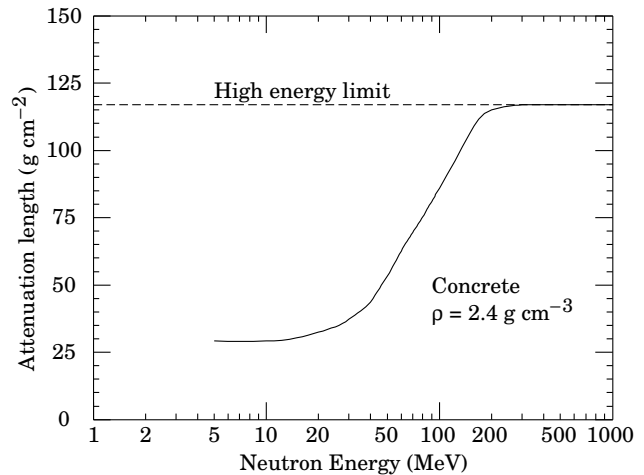


**Figure 37.4:** The variation of the attenuation length for mono-energetic neutrons in concrete as a function of neutron energy [10].

### 37.5. Photon sources

The dose equivalent rate in tissue (in mSv/h) from a gamma point source emitting one photon of energy  $E$  (in MeV) per second at a distance of 1 m is  $4.6 \times 10^{-9} \mu_{en}/\rho E$ , where  $\mu_{en}/\rho$  is the mass energy absorption coefficient. The latter has a value of  $0.029 \pm 0.004 \text{ cm}^2/\text{g}$  for photons in tissue over an energy range between 60 keV and 2 MeV (see Ref. 12 for tabulated values).

Similarly, the dose equivalent rate in tissue (in mSv/h) at the surface of a semi-infinite slab of uniformly activated material containing 1 Bq/g of a gamma emitter of energy  $E$  (in MeV) is  $2.9 \times 10^{-4} R_\mu E$ , where  $R_\mu$  is the ratio of the mass energy absorption coefficients of the photons in tissue and in the material.

### 37.6. Accelerator-induced radioactivity

Typical medium- and long-lived activation products in metallic components of accelerators are  $^{22}\text{Na}$ ,  $^{46}\text{Sc}$ ,  $^{48}\text{V}$ ,  $^{51}\text{Cr}$ ,  $^{54}\text{Mn}$ ,  $^{55}\text{Fe}$ ,  $^{59}\text{Fe}$ ,  $^{56}\text{Co}$ ,  $^{57}\text{Co}$ ,  $^{58}\text{Co}$ ,  $^{60}\text{Co}$ ,  $^{63}\text{Ni}$  and  $^{65}\text{Zn}$ . Gamma-emitting nuclides dominate doses by external irradiation at longer decay times (more than one day) while at short decay times  $\beta^+$  emitters are also important (through photons produced by  $\beta^+$  annihilation). Due to their short range,  $\beta^-$  emitters are relevant, for example, only for dose to the skin and eyes or for doses due to inhalation or ingestion. Fig. 37.5 and Fig. 37.6 show the contributions of gamma and  $\beta^+$  emitters to the total dose rate at 12.4 cm distance to a copper sample [13]. The sample was activated by the stray radiation field created by a 120 GeV mixed hadron beam dumped in a copper target during about 8 hours at intensities between  $10^7 - 10^8$  hadrons per second. Typically, dose rates at a certain decay time are mainly determined by radionuclides having a half-life of the order of the decay time. Extended irradiation periods might be an exception to this general rule as in this case the activity of long-lived nuclides can build up sufficiently so that it dominates that one of short-lived even at short cooling times.

Activation in concrete is dominated by  $^{24}\text{Na}$  (short decay time) and  $^{22}\text{Na}$  (long decay time). Both nuclides can be produced either by low-energy neutron reactions on the sodium-component in the concrete or by spallation reactions on silicon, calcium and other constituents such as aluminum. At long decay times nuclides of radiological interest in activated concrete can also be  $^{60}\text{Co}$ ,  $^{152}\text{Eu}$ ,  $^{154}\text{Eu}$  and  $^{134}\text{Cs}$ , all of which produced by  $(n,\gamma)$ -reactions with traces of natural cobalt, europium and cesium. Thus, such trace elements might be important even if their content in concrete is only a few parts per million or less by weight.

The explicit simulation of radionuclide production with general-purpose Monte Carlo codes has become the most commonly applied method to calculate induced radioactivity and its radiological consequences [13] (see also Sec. 37.8). They are complemented by

analytical codes based on folding particle fluence spectra with nuclide production cross sections. ActiWiz [14,15] is an example of such a code targeting the domain of radiological characterization and material optimization. It allows for calculating nuclide inventories by convolution of fluence spectra with nuclide production data for 85 chemical elements and arbitrary compounds from threshold to an energy of 100 TeV.

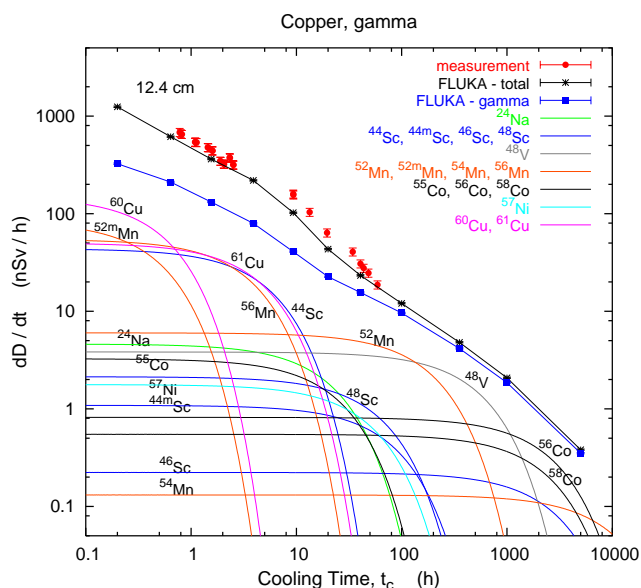


**Figure 37.5:** Contribution of individual gamma-emitting nuclides to the total dose rate at 12.4 cm distance to an activated copper sample [13].

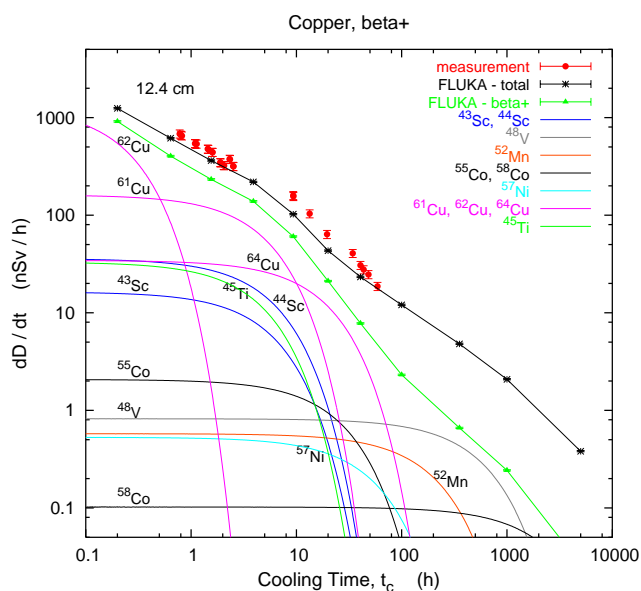


**Figure 37.6:** Contribution of individual positron-emitting nuclides to the total dose rate at 12.4 cm distance to an activated copper sample [13].

### 37.7. Radiation protection instrumentation

The capacity to distinguish and measure the high-LET (mostly neutrons) and the low-LET components (photons, electrons, muons) of the radiation field at workplaces is of primary importance to evaluate the exposure of personnel. At proton machines the prompt dose equivalent outside a shield is mainly due to neutrons, with some contribution from photons and, to a minor extent, charged particles. At high-energy electron accelerators the dominant stray radiation during operation consists of high-energy neutrons, because the shielding is normally thick enough to absorb most of the bremsstrahlung photons. Most of the personnel exposure at accelerator facilities is often received during maintenance interventions, and is due to gamma/beta radiation coming from residual radioactivity in accelerator components.

Radiation detectors used both for radiation surveys and area monitoring are normally calibrated in ambient dose equivalent  $H^*(10)$ .

#### 37.7.1. Neutron detectors :

• **Rem counters:** A rem counter [16] is a portable detector consisting of a thermal neutron counter embedded in a polyethylene moderator, with a response function that approximately follows the curve of the conversion coefficients from neutron fluence to  $H^*(10)$  over a wide energy range. Conventional rem counters provide a response to neutrons up to approximately 10-15 MeV, extended-range units are heavier as they include a high-A converter but correctly measure  $H^*(10)$  up to several hundred MeV [17].

• **Bonner Sphere Spectrometer (BSS):** A BSS [18] is made up of a thermal neutron detector at the centre of moderating spheres of different diameters made of polyethylene (PE) or a combination of PE and a high-A material to enhance its response to high energy neutrons (similar to rem counters). Each sphere has a different response function versus neutron energy, and the neutron energy, at which the sensitivity peaks, increases with sphere diameter. The energy resolution of the system is rather low but satisfactory for radiation protection purposes. The neutron spectrum is obtained by unfolding the experimental counts of the BSS with its response matrix by a computer code that is often based on an iterative algorithm such as GRAVEL [19] and MAXED [20]. BSS exist in active (using  $^3\text{He}$  or  $\text{BF}_3$  proportional counters or  $^6\text{LiI}$  scintillators) and passive versions (using CR-39 track detectors or LiF), for use *e.g.* in strongly pulsed fields. With  $^3\text{He}$  counters the discrimination with respect to gamma rays and noise is excellent.

• **Bubble detectors:** A bubble detector [21] is a dosimeter based on a super-heated emulsion (super-heated droplets suspended in a gel) contained in a vial and acting as a continuously sensitive, miniature bubble chamber. The total number of bubbles evolved from the radiation-induced nucleation of drops gives an integrated measure of the total neutron exposure. Various techniques exist to record and count the bubbles, *e.g.*, visual inspection, automated reading with video cameras or acoustic counting. Bubble detectors are insensitive to low-LET radiation. Super-heated emulsions are used as personal, area and environmental dosimeters, as well as neutron spectrometers.

• **Track etched detectors:** Track etched detectors (TEDs) [22] are based on the preferential dissolution of suitable, mostly insulator, materials along the damage trails of charged particles of sufficiently high-energy deposition density. The detectors are effectively not sensitive to radiation which deposits the energy through the interactions of particles with low LET. These dosimeters are generally able to determine neutron ambient dose equivalent down to around 100  $\mu\text{Sv}$ . They are used both as personal dosimeters and for area monitoring, *e.g.*, in BSS.

#### 37.7.2. Photon detectors [23] :

• **GM counters:** Geiger Müller (GM) counters are low cost devices simple to operate. They work in pulse mode and since they only count radiation-induced events, any spectrometric information is lost. In general they are calibrated in terms of air kerma, for instance in a  $^{60}\text{Co}$  field. The response of GM counters to photons is constant within 15% for energies up to 2 MeV and shows considerable energy dependence above.



• **Ionization chambers:** Ionization chambers are gas-filled detectors used both as hand-held instruments (*e.g.*, for radiation surveys) and environmental monitors. They are normally operated in current mode although pulse-mode operation is also possible. They possess a relatively flat response to a wide range of X- and gamma ray energies (typically from 10 keV to several MeV), can measure radiation over a wide intensity range and are capable of discriminating between the beta and gamma components of a radiation field (by use of, *e.g.*, a beta window). Pressurized ion chambers (filled, *e.g.*, with Ar or H gas to several tens of bars) are used for environmental monitoring applications. They have good sensitivity to neutrons and charged hadrons in addition to low LET radiation (gammas and muons), with the response function to the former being strongly non-linear with energy.

• **Scintillators:** Scintillation-based detectors are used in radiation protection as hand-held probes and in fixed installations, *e.g.*, portal monitors. A scintillation detector or counter is obtained coupling a scintillator to an electronic light sensor such as a photomultiplier tube (PMT), a photodiode or a silicon photomultiplier (SiPM). There is a wide range of scintillating materials, inorganic (such as CsI and BGO), organic or plastic; they find application in both photon dosimetry and spectrometry.

### 37.7.3. Operation in pulsed radiation fields :

There are many practical situations with particle accelerators used for scientific, industrial and medical applications where the time structure of the stray radiation limits the use of active monitors or requires specifically designed electronics. Pulsed neutron and gamma fields may be present because of beam losses at, *e.g.*, targets, collimators and beam dumps. The time duration of a single burst can range from a few ns to about 1 ms with a typical repetition rate in the range 0.1–100 Hz. Conventional detectors generally suffer from dead time effects and have strong limitations in the measurements of pulsed fields. Severe under response has been observed, *e.g.*, in commercial rem counters, with tremendous underestimation of the ambient dose equivalent,  $H^*(10)$ , up to three orders of magnitude. The common techniques used to correct the response of radiation detectors which include dead-time corrections operate properly in a steady-state radiation field, whereas it is much more difficult to cope with dead time losses in a pulsed radiation field of unknown time structure and burst dose. Generally speaking the monitoring instrumentation must be chosen on the basis of the knowledge of the radiation field. Detectors with specifically designed electronics must be employed in pulsed field conditions, such as the recently developed LUPIN [24] in place of conventional rem counters for neutrons. If real-time monitoring is not required, passive detectors or dosimeters such as TEDs mentioned in Sec. 37.7.1 or LiF mentioned in Sec. 37.7.4 can be employed, as they are insensitive to the time structure of the radiation.

### 37.7.4. Personal dosimeters :

Personal dosimeters, calibrated in  $H_p(10)$ , are worn by persons exposed to ionizing radiation for professional reasons to record the dose received. They are typically passive detectors, either film, track etched detectors,  $^6\text{Li}/^7\text{Li}$ -based dosimeters (*e.g.* LiF), optically stimulated luminescence (OSL) or radiophotoluminescence detectors (RPL) but semi-active dosimeters using miniaturized ion-chambers also exist, like the Direct Ion Storage (DIS) dosimeters in use at CERN.

Electronic personal dosimeters are small active units for on-line monitoring of individual exposure, designed to be worn on the body. They can give an alarm on both the integral dose received or dose rate once a pre-set threshold is exceeded.

## 37.8. Monte Carlo codes for radiation protection studies

The use of general-purpose particle interaction and transport Monte Carlo codes is often the most accurate and efficient choice for assessing radiation protection quantities at accelerators. Due to the vast spread of such codes to all areas of particle physics and the associated extensive benchmarking with experimental data, the modeling has

reached an unprecedented accuracy. Furthermore, most codes allow the user to simulate all aspects of a high energy particle cascade in one and the same run: from the first interaction of a TeV nucleus over the transport and re-interactions (hadronic and electromagnetic) of the produced secondaries, to detailed nuclear fragmentation, the calculation of radioactive decays and even of the electromagnetic shower caused by the radiation from such decays. A brief account of the codes most widely used for radiation protection studies at high energy accelerators is given in the following.

• **FLUKA [8,9]:** FLUKA is a general-purpose particle interaction and transport code. It comprises all features needed for radiation protection, such as detailed hadronic and nuclear interaction models up to 10 PeV, full coupling between hadronic and electromagnetic processes and numerous variance reduction options. The latter include weight windows, region importance biasing, and leading particle, interaction, and decay length biasing (among others). The capabilities of FLUKA are unique for studies of induced radioactivity, especially with regard to nuclide production, decay, and transport of residual radiation. In particular, particle cascades by prompt and residual radiation are simulated in parallel based on the microscopic models for nuclide production and a solution of the Bateman equations for activity build-up and decay.

• **GEANT4 [25,26,27]:** GEANT4 is an object-oriented toolkit consisting of a kernel that provides the framework for particle transport, including tracking, geometry description, material specifications, management of events and interfaces to external graphics systems. The kernel also provides interfaces to physics processes. It allows the user to freely select the physics models that best serve the particular application needs. Implementations of interaction models exist over an extended range of energies, from optical photons and thermal neutrons to high-energy interactions required for the simulation of accelerator and cosmic ray experiments. To facilitate the use of variance reduction techniques, general-purpose biasing methods such as importance biasing, weight windows, and a weight cut-off method have been introduced directly into the toolkit. Other variance reduction methods, such as leading particle biasing for hadronic processes, come with the respective physics packages.

• **MARS15 [28,29]:** The MARS15 code system is a set of Monte Carlo programs for the simulation of hadronic and electromagnetic cascades. It covers a wide energy range: 1 keV to 100 TeV for muons, charged hadrons, heavy ions and electromagnetic showers; and 0.00215 eV to 100 TeV for neutrons. Hadron-nucleus interactions as well as practically all other strong, weak and electromagnetic interactions in the entire energy range can be simulated either inclusively or exclusively. MARS15 uses ENDFB-VII nuclear data to handle interactions of neutrons with energies below 14 MeV. Several variance reduction techniques, such as weight windows, particle splitting, and Russian roulette, are available. A tagging module allows tagging the origin of a given signal for source term or sensitivity analyses. The geometry module allows either a basic solid body representation option or a ROOT-based powerful engine. Further features of MARS15 include a MAD-MARS merge for a convenient creation of accelerator models and multi-turn tracking and cascade simulation in accelerator and beamline lattices.

• **MCNP6 [30,31]:** MCNP6 is the latest version of the Monte Carlo N-Particle transport (MCNP) family of neutron interaction and transport codes and, therefore, features one of the most comprehensive and detailed descriptions of the related physical processes. It transports 37 different particle types, including ions and electromagnetic particles. The neutron interaction and transport modules use standard evaluated data libraries mixed with physics models where such libraries are not available. The transport is continuous in energy. MCNP6 contains one of the most powerful implementations of variance reduction techniques. Spherical mesh weight windows can be created by a generator in order to focus the simulation time on certain spatial regions of interest. In addition, a more generalized phase space biasing is also possible through energy- and time-dependent weight windows. Other biasing options include pulse-height tallies with variance reduction and criticality source convergence acceleration.

• **PHITS [32,33]**: The Particle and Heavy-Ion Transport code System PHITS was among the first general-purpose codes to simulate the transport and interactions of heavy ions in a wide energy range, from 10 MeV/nucleon to 100 GeV/nucleon. It is based on the high-energy hadron transport code NMTC/JAM that was extended to heavy ions. The transport of low-energy neutrons employs cross sections from evaluated nuclear data libraries such as ENDF and JENDL below 20 MeV. Electromagnetic interactions are simulated based on the ITS code in the energy range between 1 keV and 100 MeV for electrons and positrons and between 1 keV and 100 GeV for photons. Several variance reduction techniques, including weight windows and region importance biasing, are available.

#### References:

1. International Commission on Radiation Units and Measurements, *Fundamental Quantities and Units for Ionizing Radiation*, ICRU Report 60 (1998).
2. ICRP, 2010. *Conversion Coefficients for Radiological Protection Quantities for External Radiation Exposures*, ICRP Publication 116, Annals of the ICRP 40(2-5).
3. ICRP Publication 103, *The 2007 Recommendations of the International Commission on Radiological Protection*, Annals of the ICRP, Elsevier (2007).
4. M. Pelliccioni, *Radiation Protection Dosimetry* **88**, 279 (2000).
5. E. Pochin, *Nuclear Radiation: Risks and Benefits*, Clarendon Press, Oxford, 1983.
6. United Nations, *Report of the United Nations Scientific Committee on the Effect of Atomic Radiation*, General Assembly, Official Records A/63/46 (2008).
7. W.P. Swanson, *Radiological Safety Aspects of the Operation of Electron Linear Accelerators*, IAEA Technical Reports Series No. 188 (1979).
8. A. Ferrari, *et al.*, FLUKA: A Multi-particle Transport Code, CERN-2005-010 (2005), <http://www.fluka.org>.
9. T.T. Böhlen, *et al.*, The FLUKA code: Developments and Challenges for High Energy and Medical Applications, *Nuclear Data Sheets* **120**, 211 (2014).
10. R.H. Thomas and G.R. Stevenson, *Radiological Safety Aspects of the Operation of Proton Accelerators*, IAEA Technical Report Series No. 283 (1988).
11. T.A. Gabriel, *et al.*, *Nucl. Instrum. Methods* **A338**, 336 (1994).
12. <http://physics.nist.gov/PhysRefData/XrayMassCoef/cover.html>.
13. S. Roesler, *et al.*, "Simulation of Remanent Dose Rates and Benchmark Measurements at the CERN-EU High Energy Reference Field Facility," in *Proceedings of the Sixth International Meeting on Nuclear Applications of Accelerator Technology*, San Diego, CA, 1-5 June 2003, 655–662 (2003).
14. C. Theis and H. Vincke, "The use of ActiWiz in operational radiation protection," in *Proceedings of the Twelfth Meeting of Task-Force on Shielding Aspects of Accelerators, Targets and Irradiation Facilities of Accelerator Technology, SATIF12 FNAL*, 28-30 April 2014, Nuclear Science Report NEA/NSC/R 3, (2015).
15. C. Theis and H. Vincke, "ActiWiz3 an overview of the concepts, architecture and new features," CERN Technical Note CERN-RP-2016-117-REPORTS-TN (2016), <http://actiwiz.web.cern.ch>.
16. I.O. Andersson and J. Braun, A neutron rem counter with uniform sensitivity from 0.025 eV to 10 MeV in *Proceedings of the IAEA Symposium on Neutron dosimetry*, IAEA, Vienna, Vol. II, 87–95, (1963).
17. C. Birattari, *et al.*, *Radiation Protection Dosimetry* **76**, 135 (1998).
18. R.L. Bramblett, R.I. Ewing and T.W. Bonner, *Nucl. Instrum. Methods* **9**, 1 (1960).
19. M. Matzke, PTB, Braunschweig PTBN-19, (1994).
20. M. Reginatto and P. Goldhagen, *Health Physics* **77**, 579 (1999).
21. F. d'Errico, *Nucl. Instrum. Methods* **B184**, 229 (2001).
22. K. Becker, Dosimetric applications of track etching, in *Topics in Radiation Dosimetry* Ed. F.H. Attix, Academic Press, London, 79–143, (1972).
23. G.F. Knoll, *Radiation detection and measurements*, Wiley (2010).
24. M. Caresana, *et al.*, A new version of the LUPIN detector: Improvements and latest experimental verification, *Review of Scientific Instruments* **85**, 065102 (2014).
25. S. Agostinelli, *et al.*, *Nucl. Instrum. Methods* **A506**, 250 (2003).
26. J. Allison, *et al.*, *IEEE Transactions on Nuclear Science* **53**, 270 (2006).
27. J. Allison, *et al.*, *Nucl. Instrum. Methods* **A835**, 186 (2016), <http://geant4.cern.ch>.
28. N.V. Mokhov and C.C. James The MARS Code System Users Guide, Fermilab-FN-1058-APC (2018), <https://mars.fnal.gov>.
29. N.V. Mokhov, *et al.*, *Prog. Nucl. Sci. Technol.* **4**, 496 (2014).
30. D. Pelowitz, *et al.*, Los Alamos National Laboratory report, LA-CP-14-00745 (2014), <https://mcnp.lanl.gov>.
31. J.T. Goorley, *et al.*, *Nuclear Technology* **180**, 298 (2012).
32. T. Sato, *et al.*, *Journal of Nuclear Science and Technology* **55**, 684 (2018).
33. T. Sato, *et al.*, PHITS Particle and Heavy Ion Transport code System, Version 3.10 (2019), <https://phits.jaea.go.jp>.



## 38. Commonly Used Radioactive Sources

Table 38.1. Revised September 2019 by D.E. Groom (LBNL).

Nuclide	Half-life	Type of decay	Particle		Photon		
			Energy (MeV)	Emission prob.	Energy (MeV)	Emission prob.	
$^{22}_{11}\text{Na}$	2.603 y	$\beta^+$ , EC	0.546	90%	0.511 1.275	Annih. 100%	
$^{51}_{24}\text{Cr}$	27.70 d	EC			0.320 V K x rays	10% 100%	
Neutrino calibration source							
$^{54}_{25}\text{Mn}$	0.855 y	EC			0.835 Cr K x rays	100% 26%	
$^{55}_{26}\text{Fe}$	2.747 y	EC			Mn K x rays: 0.00590 0.00649	24.4% 2.86%	
$^{57}_{27}\text{Co}$	271.8 d	EC			0.014 0.122 0.136	9% 86% 11%	
					Fe K x rays	58%	
$^{60}_{27}\text{Co}$	5.271 y	$\beta^-$	0.317	99.9%	1.173 1.333	99.9% 99.9%	
$^{68}_{32}\text{Ge}$	271.0 d	EC			Ga K x rays	42%	
$\rightarrow ^{68}_{31}\text{Ga}$	67.8 m	$\beta^+$ , EC	1.899	90%	0.511 1.077	Annih. 3%	
$^{90}_{38}\text{Sr}$	28.8 y	$\beta^-$	0.546	100%			
$\rightarrow ^{90}_{39}\text{Y}$	2.67 d	$\beta^-$	2.279	100%			
$^{106}_{44}\text{Ru}$	371.5 d	$\beta^-$	0.039	100%			
$\rightarrow ^{106}_{45}\text{Rh}$	30.1 s	$\beta^-$	3.546	79%	0.512 0.622	21% 10%	
$^{109}_{48}\text{Cd}$	1.265 y	EC	0.063 0.084	$e^-$ 42% $e^-$ 44%	0.088 Ag K x rays	3.7% 100%	
$^{113}_{50}\text{Sn}$	115.1 d	EC	0.364 0.388	$e^-$ 28% $e^-$ 6%	0.392 In K x rays	65% 97%	
$^{137}_{55}\text{Cs}$	30.0 y	$\beta^-$	0.514 1.176	94% 6%	0.662	85%	
$^{133}_{56}\text{Ba}$	10.55 y	EC	0.045 0.075	$e^-$ 50% $e^-$ 6%	0.081 0.356	33% 62%	
					Cs K x rays	121%	
$^{152}_{63}\text{Eu}$	13.537 y	EC $\beta^-$		72.1% 27.9%	Many $\gamma$ 's 0.1218–1.408 MeV		
$^{207}_{83}\text{Bi}$	32.9 y	EC	0.481 0.975 1.047	$e^-$ 2% $e^-$ 7% $e^-$ 2%	0.569 1.063 1.770	98% 75% 7%	
					Pb K x rays	78%	
$^{228}_{90}\text{Th}$	1.912 y	6 $\alpha$ : 3 $\beta^-$ :	5.341 to 8.785 0.334 to 2.246		0.239 0.583 2.614	44% 31% 36%	
		( $\rightarrow ^{224}_{88}\text{Ra}$ ( 361 d	$\rightarrow ^{220}_{86}\text{Rn}$ 55.8 s	$\rightarrow ^{216}_{84}\text{Po}$ 0.148 s	$\rightarrow ^{212}_{82}\text{Pb}$ 10.64 h	$\rightarrow ^{212}_{83}\text{Bi}$ 60.54 m	$\rightarrow ^{212}_{84}\text{Po}$ 300 ns)
$^{241}_{95}\text{Am}$	432.6 y	$\alpha$	5.443 5.486	13% 84%	0.060 Np L x rays	36% 38%	
$^{241}_{95}\text{Am/Be}$	432.6 y	$6 \times 10^{-5}$ neutrons ( $\langle E \rangle = 4$ MeV) and $4 \times 10^{-5}$ $\gamma$ 's (4.43 MeV from $^9_4\text{Be}(\alpha, n)$ )					
$^{244}_{96}\text{Cm}$	18.11 y	$\alpha$	5.763 5.805	24% 76%	Pu L x rays	$\sim 9\%$	
$^{252}_{98}\text{Cf}$	2.645 y	$\alpha$ (97%)	6.076 6.118	15% 82%			
		Fission (3.1%): Average 7.8 $\gamma$ 's/fission; $\langle E_\gamma \rangle = 0.88$ MeV $\approx 4$ neutrons/fission; $\langle E_n \rangle = 2.14$ MeV					

“Emission probability” is the probability per decay of a given emission; because of cascades these may total more than 100%. Only principal emissions are listed. EC means electron capture, and  $e^-$  means monoenergetic internal conversion (Auger) electron. The intensity of 0.511 MeV  $e^+e^-$  annihilation photons depends upon the number of stopped positrons. Endpoint  $\beta^\pm$  energies are listed. In some cases when energies are closely spaced, the  $\gamma$ -ray values are approximate weighted averages. Radiation from short-lived daughter isotopes is included where relevant.

Half-lives, energies, and intensities may be found in [www-pub.iaea.org/books/IAEABooks/7551/Update-of-X-Ray-and-Gamma-Ray-Decay-Data-Standards-for-Detector-Calibration-and-Other-Applications](http://www-pub.iaea.org/books/IAEABooks/7551/Update-of-X-Ray-and-Gamma-Ray-Decay-Data-Standards-for-Detector-Calibration-and-Other-Applications), IAEA (2007) or Nuclear Data Sheets ([www.journals.elsevier.com/nuclear-data-sheets](http://www.journals.elsevier.com/nuclear-data-sheets)) (2007).

Neutron sources: See *e.g.* “Neutron Calibration Sources in the Daya Bay Experiment,” J. Liu *et al.*, Nuclear Instrum. Methods **A797**, 260 (2005) (arXiv.1504.07911).

$^{51}\text{Cr}$  calibration of neutrino detectors is discussed in *e.g.* J.N. Abdurashitov *et al.* [SAGE Collaboration], Phys. Rev. **C59**, 2246 (1999). The use of  $^{75}_{34}\text{Se}$  and other isotopes has also been proposed.

**Mathematical Tools or Statistics, Monte Carlo, Group Theory**

39. Probability (rev.) . . . . .	621
40. Statistics (rev.) . . . . .	626
41. Monte Carlo techniques (rev.) . . . . .	642
42. Monte Carlo event generators . . . . .	646
43. Monte Carlo neutrino event generators (rev.) . . . . .	657
44. Monte Carlo particle numbering scheme (rev.) . . . . .	661
45. Clebsch-Gordan coefficients, spherical harmonics, and $d$ functions	665
46. SU(3) isoscalar factors and representation matrices . . . . .	666
47. SU( $n$ ) multiplets and Young diagrams . . . . .	667



## 39. Probability

Revised August 2019 by G. Cowan (RHUL).

### 39.1 General

[1–8] An abstract definition of probability can be given by considering a set  $S$ , called the sample space, and possible subsets  $A, B, \dots$ , the interpretation of which is left open. The probability  $P$  is a real-valued function defined by the following axioms due to Kolmogorov [9]:

1. For every subset  $A$  in  $S$ ,  $P(A) \geq 0$ ;
2. For disjoint subsets (*i.e.*,  $A \cap B = \emptyset$ ),  $P(A \cup B) = P(A) + P(B)$ ;
3.  $P(S) = 1$ .

In addition, one defines the conditional probability  $P(A|B)$  (read as  $P$  of  $A$  given  $B$ ) as

$$P(A|B) = \frac{P(A \cap B)}{P(B)}. \quad (39.1)$$

From this definition and using the fact that  $A \cap B$  and  $B \cap A$  are the same, one obtains *Bayes' theorem*,

$$P(A|B) = \frac{P(B|A)P(A)}{P(B)}. \quad (39.2)$$

From the three axioms of probability and the definition of conditional probability, one obtains the *law of total probability*,

$$P(B) = \sum_i P(B|A_i)P(A_i), \quad (39.3)$$

for any subset  $B$  and for disjoint  $A_i$  with  $\cup_i A_i = S$ . This can be combined with Bayes' theorem (Eq. (39.2)) to give

$$P(A|B) = \frac{P(B|A)P(A)}{\sum_i P(B|A_i)P(A_i)}, \quad (39.4)$$

where the subset  $A$  could, for example, be one of the  $A_i$ .

The most commonly used interpretation of the elements of the sample space are outcomes of a repeatable experiment. The probability  $P(A)$  is assigned a value equal to the limiting frequency of occurrence of  $A$ . This interpretation forms the basis of *frequentist statistics*.

The elements of the sample space might also be interpreted as *hypotheses*, *i.e.*, statements that are either true or false, such as ‘The mass of the  $W$  boson lies between 80.3 and 80.5 GeV.’ Upon repetition of a measurement, however, such statements are either always true or always false, *i.e.*, the corresponding probabilities in the frequentist interpretation are either 0 or 1. Using *subjective probability*, however,  $P(A)$  is interpreted as the degree of belief that the hypothesis  $A$  is true. Subjective probability is used in *Bayesian* (as opposed to frequentist) statistics. Bayes' theorem can be written

$$P(\text{theory}|\text{data}) \propto P(\text{data}|\text{theory})P(\text{theory}), \quad (39.5)$$

where ‘theory’ represents some hypothesis and ‘data’ is the outcome of the experiment. Here  $P(\text{theory})$  is the *prior* probability for the theory, which reflects the experimenter's degree of belief before carrying out the measurement, and  $P(\text{data}|\text{theory})$  is the probability to have gotten the data actually obtained, given the theory, which is also called the *likelihood*.

Bayesian statistics provides no fundamental rule for obtaining the prior probability, which may depend on previous measurements, theoretical prejudices, *etc.* Once this has been specified, however, Eq. (39.5) tells how the probability for the theory must be modified in the light of the new data to give the *posterior* probability,  $P(\text{theory}|\text{data})$ . As Eq. (39.5) is stated as a proportionality, the probability must be normalized by summing (or integrating) over all possible hypotheses.

### 39.2 Random variables

A *random variable* is a numerical characteristic assigned to an element of the sample space. In the frequency interpretation of probability, it corresponds to an outcome of a repeatable experiment. Let  $x$  be a possible outcome of an observation. If  $x$  can take on any value from a continuous range, we write  $f(x; \theta)dx$  as the probability that the measurement's outcome lies between  $x$  and  $x + dx$ . The function  $f(x; \theta)$  is called the *probability density function* (p.d.f.), which may depend on one or more parameters  $\theta$ . If  $x$  can take on only discrete values (*e.g.*, the non-negative integers), then we use  $f(x; \theta)$  to denote the probability to find the value  $x$ . In the following the term p.d.f. is often taken to cover both the continuous and discrete cases, although technically the term density should only be used in the continuous case.

The p.d.f. is always normalized to unity. Both  $x$  and  $\theta$  may have multiple components and are then often written as vectors. If  $\theta$  is unknown, we may wish to estimate its value from a given set of measurements of  $x$ ; this is a central topic of *statistics* (see Sec. 40).

The *cumulative distribution function*  $F(a)$  is the probability that  $x \leq a$ :

$$F(a) = \int_{-\infty}^a f(x) dx. \quad (39.6)$$

Here and below, if  $x$  is discrete-valued, the integral is replaced by a sum. The endpoint  $a$  is expressly included in the integral or sum. Then  $0 \leq F(x) \leq 1$ ,  $F(x)$  is nondecreasing, and  $P(a < x \leq b) = F(b) - F(a)$ . If  $x$  is discrete,  $F(x)$  is flat except at allowed values of  $x$ , where it has discontinuous jumps equal to  $f(x)$ .

Any function of random variables is itself a random variable, with (in general) a different p.d.f. The *expectation value* of any function  $u(x)$  is

$$E[u(x)] = \int_{-\infty}^{\infty} u(x) f(x) dx, \quad (39.7)$$

assuming the integral is finite. The expectation value is linear, *i.e.*, for any two functions  $u$  and  $v$  of  $x$  and constants  $c_1$  and  $c_2$ ,  $E[c_1 u + c_2 v] = c_1 E[u] + c_2 E[v]$ .

The  $n^{\text{th}}$  moment of a random variable  $x$  is

$$\alpha_n \equiv E[x^n] = \int_{-\infty}^{\infty} x^n f(x) dx, \quad (39.8a)$$

and the  $n^{\text{th}}$  central moment of  $x$  (or moment about the mean,  $\alpha_1$ ) is

$$m_n \equiv E[(x - \alpha_1)^n] = \int_{-\infty}^{\infty} (x - \alpha_1)^n f(x) dx. \quad (39.8b)$$

The most commonly used moments are the mean  $\mu$  and variance  $\sigma^2$ :

$$\mu \equiv \alpha_1, \quad (39.9a)$$

$$\sigma^2 \equiv V[x] \equiv m_2 = \alpha_2 - \mu^2. \quad (39.9b)$$

The mean is the location of the ‘center of mass’ of the p.d.f., and the variance is a measure of the square of its width. Note that  $V[cx + k] = c^2 V[x]$ . It is often convenient to use the *standard deviation* of  $x$ ,  $\sigma$ , defined as the square root of the variance.

Any odd moment about the mean is a measure of the skewness of the p.d.f. The simplest of these is the dimensionless coefficient of skewness  $\gamma_1 = m_3/\sigma^3$ .

The fourth central moment  $m_4$  provides a convenient measure of the tails of a distribution. For the Gaussian distribution (see Sec. 39.4), one has  $m_4 = 3\sigma^4$ . The *kurtosis* is defined as  $\gamma_2 = m_4/\sigma^4 - 3$ , *i.e.*, it is zero for a Gaussian, positive for a *leptokurtic* distribution with longer tails, and negative for a *platykurtic* distribution with tails that die off more quickly than those of a Gaussian.

The *quantile*  $x_\alpha$  is the value of the random variable  $x$  at which the cumulative distribution is equal to  $\alpha$ . That is, the quantile

is the inverse of the cumulative distribution function, *i.e.*,  $x_\alpha = F^{-1}(\alpha)$ . An important special case is the *median*,  $x_{\text{med}}$ , defined by  $F(x_{\text{med}}) = 1/2$ , *i.e.*, half the probability lies above and half lies below  $x_{\text{med}}$ . (More rigorously,  $x_{\text{med}}$  is a median if  $P(x \geq x_{\text{med}}) \geq 1/2$  and  $P(x \leq x_{\text{med}}) \geq 1/2$ . If only one value exists, it is called ‘*the median*.’)

Under a monotonic change of variable  $x \rightarrow y(x)$ , the quantiles of a distribution (and hence also the median) obey  $y_\alpha = y(x_\alpha)$ . In general the expectation value and *mode* (most probable value) of a distribution do not, however, transform in this way.

Let  $x$  and  $y$  be two random variables with a *joint* p.d.f.  $f(x, y)$ . The *marginal* p.d.f. of  $x$  (the distribution of  $x$  with  $y$  unobserved) is

$$f_1(x) = \int_{-\infty}^{\infty} f(x, y) dy, \tag{39.10}$$

and similarly for the marginal p.d.f.  $f_2(y)$ . The *conditional* p.d.f. of  $y$  given fixed  $x$  (with  $f_1(x) \neq 0$ ) is defined by  $f_3(y|x) = f(x, y)/f_1(x)$ , and similarly  $f_4(x|y) = f(x, y)/f_2(y)$ . From these, we immediately obtain Bayes’ theorem (see Eqs. (39.2) and (39.4)),

$$f_4(x|y) = \frac{f_3(y|x)f_1(x)}{f_2(y)} = \frac{f_3(y|x)f_1(x)}{\int f_3(y|x')f_1(x') dx'}. \tag{39.11}$$

The mean of  $x$  is

$$\mu_x = \int_{-\infty}^{\infty} \int_{-\infty}^{\infty} x f(x, y) dx dy = \int_{-\infty}^{\infty} x f_1(x) dx, \tag{39.12}$$

and similarly for  $y$ . The *covariance* of  $x$  and  $y$  is

$$\text{cov}[x, y] = E[(x - \mu_x)(y - \mu_y)] = E[xy] - \mu_x \mu_y. \tag{39.13}$$

A dimensionless measure of the covariance of  $x$  and  $y$  is given by the *correlation coefficient*,

$$\rho_{xy} = \text{cov}[x, y]/\sigma_x \sigma_y, \tag{39.14}$$

where  $\sigma_x$  and  $\sigma_y$  are the standard deviations of  $x$  and  $y$ . It can be shown that  $-1 \leq \rho_{xy} \leq 1$ .

Two random variables  $x$  and  $y$  are *independent* if and only if

$$f(x, y) = f_1(x)f_2(y). \tag{39.15}$$

If  $x$  and  $y$  are independent, then  $\rho_{xy} = 0$ ; the converse is not necessarily true. If  $x$  and  $y$  are independent,  $E[u(x)v(y)] = E[u(x)]E[v(y)]$ , and  $V[x+y] = V[x] + V[y]$ ; otherwise,  $V[x+y] = V[x] + V[y] + 2\text{cov}[x, y]$ , and  $E[uv]$  does not necessarily factorize.

Consider a set of  $n$  continuous random variables  $\mathbf{x} = (x_1, \dots, x_n)$  with joint p.d.f.  $f(\mathbf{x})$ , and a set of  $n$  new variables  $\mathbf{y} = (y_1, \dots, y_n)$ , related to  $\mathbf{x}$  by means of a function  $\mathbf{y}(\mathbf{x})$  that is one-to-one, *i.e.*, the inverse  $\mathbf{x}(\mathbf{y})$  exists. The joint p.d.f. for  $\mathbf{y}$  is given by

$$g(\mathbf{y}) = f(\mathbf{x}(\mathbf{y}))|J|, \tag{39.16}$$

where  $|J|$  is the absolute value of the determinant of the square matrix  $J_{ij} = \partial x_i / \partial y_j$  (the Jacobian determinant). If the transformation from  $\mathbf{x}$  to  $\mathbf{y}$  is not one-to-one, the  $\mathbf{x}$ -space must be broken into regions where the function  $\mathbf{y}(\mathbf{x})$  can be inverted, and the contributions to  $g(\mathbf{y})$  from each region summed.

Given a set of functions  $\mathbf{y} = (y_1, \dots, y_m)$  with  $m < n$ , one can construct  $n - m$  additional independent functions, apply the procedure above, then integrate the resulting  $g(\mathbf{y})$  over the unwanted  $y_i$  to find the marginal distribution of those of interest.

For a one-to-one transformation of discrete random variables, the probability is obtained by simple substitution; no Jacobian is necessary because in this case  $f$  is a probability rather than a probability density. If the transformation is not one-to-one, then one must sum the probabilities for all values of the original variable that contribute to a given value of the transformed variable. If  $f$  depends on a set of parameters  $\theta$ , a change to a different parameter set  $\eta(\theta)$  is made by simple substitution; no Jacobian is used.

### 39.3 Characteristic functions

The characteristic function  $\phi(u)$  associated with the p.d.f.  $f(x)$  is essentially its Fourier transform, or the expectation value of  $e^{iux}$ :

$$\phi(u) = E[e^{iux}] = \int_{-\infty}^{\infty} e^{iux} f(x) dx. \tag{39.17}$$

Once  $\phi(u)$  is specified, the p.d.f.  $f(x)$  is uniquely determined and vice versa; knowing one is equivalent to the other. Characteristic functions are useful in deriving a number of important results about moments and sums of random variables.

It follows from Eqs. (39.8) and (39.17) that the  $n^{\text{th}}$  moment of a random variable  $x$  that follows  $f(x)$  is given by

$$i^{-n} \left. \frac{d^n \phi}{du^n} \right|_{u=0} = \int_{-\infty}^{\infty} x^n f(x) dx = \alpha_n. \tag{39.18}$$

Thus it is often easy to calculate all the moments of a distribution defined by  $\phi(u)$ , even when  $f(x)$  cannot be written down explicitly.

If the p.d.f.s  $f_1(x)$  and  $f_2(y)$  for independent random variables  $x$  and  $y$  have characteristic functions  $\phi_1(u)$  and  $\phi_2(u)$ , then the characteristic function of the weighted sum  $ax + by$  is  $\phi_1(au)\phi_2(bu)$ . The rules of addition for several important distributions (*e.g.*, that the sum of two Gaussian distributed variables also follows a Gaussian distribution) easily follow from this observation.

Let the (partial) characteristic function corresponding to the conditional p.d.f.  $f_2(x|z)$  be  $\phi_2(u|z)$ , and the p.d.f. of  $z$  be  $f_1(z)$ . The characteristic function after integration over the conditional value is

$$\phi(u) = \int \phi_2(u|z)f_1(z) dz. \tag{39.19}$$

Suppose we can write  $\phi_2$  in the form

$$\phi_2(u|z) = A(u)e^{ig(u)z}. \tag{39.20}$$

Then

$$\phi(u) = A(u)\phi_1(g(u)). \tag{39.21}$$

The cumulants (semi-invariants)  $\kappa_n$  of a distribution with characteristic function  $\phi(u)$  are defined by the relation

$$\phi(u) = \exp \left[ \sum_{n=1}^{\infty} \frac{\kappa_n}{n!} (iu)^n \right] = \exp \left( i\kappa_1 u - \frac{1}{2} \kappa_2 u^2 + \dots \right). \tag{39.22}$$

The values  $\kappa_n$  are related to the moments  $\alpha_n$  and  $m_n$ . The first few relations are

$$\begin{aligned} \kappa_1 &= \alpha_1 (= \mu, \text{ the mean}) \\ \kappa_2 &= m_2 = \alpha_2 - \alpha_1^2 (= \sigma^2, \text{ the variance}) \\ \kappa_3 &= m_3 = \alpha_3 - 3\alpha_1 \alpha_2 + 2\alpha_1^3. \end{aligned} \tag{39.23}$$

### 39.4 Commonly used probability distributions

Table 39.1 gives a number of common probability density functions and corresponding characteristic functions, means, and variances. Further information may be found in Refs. [1–8] [10], and [11], which has particularly detailed tables. Monte Carlo techniques for generating each of them may be found in our Sec. 41.4 and in Ref. [10]. We comment below on all except the trivial uniform distribution.

#### 39.4.1 Binomial and multinomial distributions

A random process with exactly two possible outcomes which occur with fixed probabilities is called a *Bernoulli* process. If the probability of obtaining a certain outcome (a ‘‘success’’) in an individual trial is  $p$ , then the probability of obtaining exactly  $r$  successes ( $r = 0, 1, 2, \dots, N$ ) in  $N$  independent trials, without regard to the order of the successes and failures, is given by the binomial distribution  $f(r; N, p)$  in Table 39.1. If  $r$  and  $s$  are binomially distributed with parameters  $(N_r, p)$  and  $(N_s, p)$ , then  $t = r + s$  follows a binomial distribution with parameters  $(N_r + N_s, p)$ . If

there are  $m$  possible outcomes for each trial having probabilities  $p_1, p_2, \dots, p_m$ , then the joint probability to find  $r_1, r_2, \dots, r_m$  of each outcome after a total of  $N$  independent trials is given by the multinomial distribution as shown in Table 39.1. We can regard outcome  $i$  as “success” and all the rest as “failure”, so individually, any of the  $r_i$  follow a binomial distribution for  $N$  trials and a success probability  $p_i$ .

**39.4.2 Poisson distribution**

The Poisson distribution  $f(n; \nu)$  gives the probability of finding exactly  $n$  events in a given interval of  $x$  (e.g., space or time) when the events occur independently of one another and of  $x$  at an average rate of  $\nu$  per the given interval. The variance  $\sigma^2$  equals  $\nu$ . It is the limiting case  $p \rightarrow 0, N \rightarrow \infty, Np = \nu$  of the binomial distribution. The Poisson distribution approaches the Gaussian distribution for large  $\nu$ .

For example, a large number of radioactive nuclei of a given type will result in a certain number of decays in a fixed time interval. If this interval is small compared to the mean lifetime, then the probability for a given nucleus to decay is small, and thus the number of decays in the time interval is well modeled as a Poisson variable.

**39.4.3 Normal or Gaussian distribution**

The normal (or Gaussian) probability density function  $f(x; \mu, \sigma^2)$  given in Table 39.1 has mean  $E[x] = \mu$  and variance  $V[x] = \sigma^2$ . Comparison of the characteristic function  $\phi(u)$  given in Table 39.1 with Eq. (39.22) shows that all cumulants  $\kappa_n$  beyond  $\kappa_2$  vanish; this is a unique property of the Gaussian distribution. Some other properties are:

$$\begin{aligned} P(x \text{ in range } \mu \pm \sigma) &= 0.6827, \\ P(x \text{ in range } \mu \pm 0.6745\sigma) &= 0.5, \\ E[|x - \mu|] &= \sqrt{2/\pi}\sigma = 0.7979\sigma, \\ \text{half-width at half maximum} &= \sqrt{2 \ln 2}\sigma = 1.177\sigma. \end{aligned}$$

For a Gaussian with  $\mu = 0$  and  $\sigma^2 = 1$  (the *standard normal*)

$$f(x_1, x_2; \mu_1, \mu_2, \sigma_1, \sigma_2, \rho) = \frac{1}{2\pi\sigma_1\sigma_2\sqrt{1-\rho^2}} \times \exp \left\{ \frac{-1}{2(1-\rho^2)} \left[ \frac{(x_1 - \mu_1)^2}{\sigma_1^2} - \frac{2\rho(x_1 - \mu_1)(x_2 - \mu_2)}{\sigma_1\sigma_2} + \frac{(x_2 - \mu_2)^2}{\sigma_2^2} \right] \right\}. \quad (39.26)$$

The characteristic function for the multivariate Gaussian is

$$\phi(\mathbf{u}; \boldsymbol{\mu}, V) = \exp \left[ i\boldsymbol{\mu} \cdot \mathbf{u} - \frac{1}{2}\mathbf{u}^T V \mathbf{u} \right]. \quad (39.27)$$

If the components of  $\mathbf{x}$  are independent, then Eq. (39.27) is the product of the characteristic functions of  $n$  Gaussians.

For an  $n$ -dimensional Gaussian distribution for  $\mathbf{x}$  with mean  $\boldsymbol{\mu}$  and covariance matrix  $V$ , the marginal distribution for any single  $x_i$  is a one-dimensional Gaussian with mean  $\mu_i$  and variance  $V_{ii}$ . The equation  $(\mathbf{x} - \mathbf{a})^T V^{-1}(\mathbf{x} - \mathbf{a}) = C$ , where  $C$  is any positive number, defines an  $n$ -dimensional ellipse centered about  $\mathbf{a}$ . If  $\mathbf{a}$  is equal to the mean  $\boldsymbol{\mu}$ , then  $C$  is a random variable obeying the  $\chi^2$  distribution for  $n$  degrees of freedom, which is discussed in the following section. The probability that  $\mathbf{x}$  lies outside the ellipsoid for a given value of  $C$  is given by  $1 - F_{\chi^2}(C; n)$ , where  $F_{\chi^2}$  is the cumulative  $\chi^2$  distribution. This may be read from Fig. 40.1. For example, the “ $s$ -standard-deviation ellipsoid” occurs at  $C = s^2$ . For the two-variable case ( $n = 2$ ), the point  $\mathbf{x}$  lies outside the one-standard-deviation ellipsoid with 61% probability. The use of these ellipsoids as indicators of probable error is described in Sec. 40.4.2.2; the validity of those indicators assumes that  $\boldsymbol{\mu}$  and  $V$  are correct.

**39.4.4 Log-normal distribution**

If a random variable  $y$  follows a Gaussian distribution with mean  $\mu$  and variance  $\sigma^2$ , then  $x = e^y$  follows a log-normal distribution, as given in Table 39.1. As a consequence of the central limit theorem described in Sec. 39.4.3, the distribution of the product of a large number of positive random variables approaches

the cumulative distribution, often written  $\Phi(x)$ , is related to the error function erf by

$$F(x; 0, 1) \equiv \Phi(x) = \frac{1}{2} \left[ 1 + \text{erf}(x/\sqrt{2}) \right]. \quad (39.24)$$

The error function and standard Gaussian are tabulated in many references (e.g., Ref. [11, 12]) and are available in software packages such as ROOT [13]. For a mean  $\mu$  and variance  $\sigma^2$ , replace  $x$  by  $(x - \mu)/\sigma$ . The probability of  $x$  in a given range can be calculated with Eq. (40.70).

For  $x$  and  $y$  independent and normally distributed,  $z = ax + by$  follows a normal p.d.f.  $f(z; a\mu_x + b\mu_y, a^2\sigma_x^2 + b^2\sigma_y^2)$ ; that is, the weighted means and variances add.

The Gaussian derives its importance in large part from the *central limit theorem*:

If independent random variables  $x_1, \dots, x_n$  are distributed according to any p.d.f. with finite mean and variance, then the sum  $y = \sum_{i=1}^n x_i$  will have a p.d.f. that approaches a Gaussian for large  $n$ . If the p.d.f.s of the  $x_i$  are not identical, the theorem still holds under somewhat more restrictive conditions. The mean and variance are given by the sums of corresponding terms from the individual  $x_i$ . Therefore, the sum of a large number of fluctuations  $x_i$  will be distributed as a Gaussian, even if the  $x_i$  themselves are not.

For a set of  $n$  Gaussian random variables  $\mathbf{x}$  with means  $\boldsymbol{\mu}$  and covariances  $V_{ij} = \text{cov}[x_i, x_j]$ , the p.d.f. for the one-dimensional Gaussian is generalized to

$$f(\mathbf{x}; \boldsymbol{\mu}, V) = \frac{1}{(2\pi)^{n/2} \sqrt{|V|}} \exp \left[ -\frac{1}{2}(\mathbf{x} - \boldsymbol{\mu})^T V^{-1}(\mathbf{x} - \boldsymbol{\mu}) \right], \quad (39.25)$$

where the determinant  $|V|$  must be greater than 0. For diagonal  $V$  (independent variables),  $f(\mathbf{x}; \boldsymbol{\mu}, V)$  is the product of the p.d.f.s of  $n$  Gaussian distributions.

For  $n = 2$ ,  $f(\mathbf{x}; \boldsymbol{\mu}, V)$  is

a log-normal. It is bounded below by zero and is thus well suited for modeling quantities that are intrinsically non-negative such as an efficiency. One can implement a log-normal model for a random variable  $x$  by defining  $y = \ln x$  so that  $y$  follows a Gaussian distribution.

**39.4.5  $\chi^2$  distribution**

If  $x_1, \dots, x_n$  are independent Gaussian random variables, the sum  $z = \sum_{i=1}^n (x_i - \mu_i)^2 / \sigma_i^2$  follows the  $\chi^2$  p.d.f. with  $n$  degrees of freedom, which we denote by  $\chi^2(n)$ . More generally, for  $n$  correlated Gaussian variables as components of a vector  $\mathbf{X}$  with covariance matrix  $V$ ,  $z = \mathbf{X}^T V^{-1} \mathbf{X}$  follows  $\chi^2(n)$  as in the previous section. For a set of  $z_i$ , each of which follows  $\chi^2(n_i)$ ,  $\sum z_i$  follows  $\chi^2(\sum n_i)$ . For large  $n$ , the  $\chi^2$  p.d.f. approaches a Gaussian with a mean and variance given by  $\mu = n$  and  $\sigma^2 = 2n$ , respectively (here the formulae for  $\mu$  and  $\sigma^2$  are valid for all  $n$ ).

The  $\chi^2$  p.d.f. is often used in evaluating the level of compatibility between observed data and a hypothesis for the p.d.f. that the data might follow. This is discussed further in Sec. 40.3.2 on significance tests.

**39.4.6 Student’s  $t$  distribution**

Suppose that  $y$  and  $x_1, \dots, x_n$  are independent and Gaussian distributed with mean 0 and variance 1. We then define

$$z = \sum_{i=1}^n x_i^2 \quad \text{and} \quad t = \frac{y}{\sqrt{z/n}}. \quad (39.28)$$

The variable  $z$  thus follows a  $\chi^2(n)$  distribution. Then  $t$  is distributed according to Student’s  $t$  distribution with  $n$  degrees of

**Table 39.1:** Some common probability density functions, with corresponding characteristic functions and means and variances. In the Table,  $\Gamma(k)$  is the gamma function, equal to  $(k - 1)!$  when  $k$  is an integer;  ${}_1F_1$  is the confluent hypergeometric function of the 1st kind [11].

Distribution	Probability density function $f$ (variable; parameters)	Characteristic function $\phi(u)$	Mean	Variance
Uniform	$f(x; a, b) = \begin{cases} 1/(b - a) & a \leq x \leq b \\ 0 & \text{otherwise} \end{cases}$	$\frac{e^{ibu} - e^{iau}}{(b-a)iu}$	$\frac{a+b}{2}$	$\frac{(b-a)^2}{12}$
Binomial	$f(r; N, p) = \frac{N!}{r!(N-r)!} p^r q^{N-r}$ $r = 0, 1, 2, \dots, N; \quad 0 \leq p \leq 1; \quad q = 1 - p$	$(q + pe^{iu})^N$	$Np$	$Npq$
Multinomial	$f(r_1, \dots, r_m; N, p_1, \dots, p_m) = \frac{N!}{r_1! \dots r_m!} p_1^{r_1} \dots p_m^{r_m}$	$(\sum_{k=1}^m p_k e^{iu_k})^N$	$E[r_i] = Np_i$	$\text{cov}[r_i, r_j] = Np_i(\delta_{ij} - p_j)$
Poisson	$f(n; \nu) = \frac{\nu^n e^{-\nu}}{n!}; \quad n = 0, 1, 2, \dots; \quad \nu > 0$	$\exp[\nu(e^{iu} - 1)]$	$\nu$	$\nu$
Normal (Gaussian)	$f(x; \mu, \sigma^2) = \frac{1}{\sigma\sqrt{2\pi}} \exp(-(x - \mu)^2/2\sigma^2)$	$\exp(i\mu u - \frac{1}{2}\sigma^2 u^2)$	$\mu$	$\sigma^2$
Multivariate Gaussian	$f(\mathbf{x}; \boldsymbol{\mu}, \mathbf{V}) = \frac{1}{(2\pi)^{n/2} \sqrt{ \mathbf{V} }} \times \exp[-\frac{1}{2}(\mathbf{x} - \boldsymbol{\mu})^T \mathbf{V}^{-1}(\mathbf{x} - \boldsymbol{\mu})]$ $-\infty < x_j < \infty; \quad -\infty < \mu_j < \infty; \quad  \mathbf{V}  > 0$	$\exp[i\boldsymbol{\mu} \cdot \mathbf{u} - \frac{1}{2}\mathbf{u}^T \mathbf{V} \mathbf{u}]$	$\mathbf{u}$	$V_{jk}$
Log-normal	$f(x; \mu, \sigma^2) = \frac{1}{\sigma\sqrt{2\pi}} \frac{1}{x} \exp(-(\ln x - \mu)^2/2\sigma^2)$ $0 < x < \infty; \quad -\infty < \mu < \infty; \quad \sigma > 0$	—	$\exp(\mu + \sigma^2/2)$	$\exp(2\mu + \sigma^2) \times [\exp(\sigma^2) - 1]$
$\chi^2$	$f(z; n) = \frac{z^{n/2-1} e^{-z/2}}{2^{n/2} \Gamma(n/2)}; \quad z \geq 0$	$(1 - 2iu)^{-n/2}$	$n$	$2n$
Student's $t$	$f(t; n) = \frac{1}{\sqrt{n\pi}} \frac{\Gamma[(n+1)/2]}{\Gamma(n/2)} \left(1 + \frac{t^2}{n}\right)^{-(n+1)/2}$ $-\infty < t < \infty; \quad n \text{ not required to be integer}$	—	$0$ for $n > 1$	$n/(n - 2)$ for $n > 2$
Gamma	$f(x; \lambda, k) = \frac{x^{k-1} \lambda^k e^{-\lambda x}}{\Gamma(k)}; \quad 0 \leq x < \infty; \quad k \text{ not required to be integer}$	$(1 - iu/\lambda)^{-k}$	$k/\lambda$	$k/\lambda^2$
Beta	$f(x; \alpha, \beta) = \frac{\Gamma(\alpha+\beta)}{\Gamma(\alpha)\Gamma(\beta)} x^{\alpha-1} (1-x)^{\beta-1}$ $0 \leq x \leq 1$	${}_1F_1(\alpha; \alpha + \beta; iu)$	$\frac{\alpha}{\alpha+\beta}$	$\frac{\alpha\beta}{(\alpha+\beta)^2(\alpha+\beta+1)}$

freedom,  $f(t; n)$ , given in Table 39.1.

If defined through gamma functions as in Table 39.1, the parameter  $n$  is not required to be an integer. As  $n \rightarrow \infty$ , the distribution approaches a Gaussian, and for  $n = 1$  it is a *Cauchy* or *Breit-Wigner* distribution.

As an example, consider the *sample mean*  $\bar{x} = \sum x_i/n$  and the *sample variance*  $s^2 = \sum (x_i - \bar{x})^2/(n-1)$  for normally distributed  $x_i$  with unknown mean  $\mu$  and variance  $\sigma^2$ . The sample mean has a Gaussian distribution with a variance  $\sigma^2/n$ , so the variable  $(\bar{x} - \mu)/\sqrt{\sigma^2/n}$  is normal with mean 0 and variance 1. The quantity  $(n-1)s^2/\sigma^2$  is independent of this and follows  $\chi^2(n-1)$ . The ratio

$$t = \frac{(\bar{x} - \mu)/\sqrt{\sigma^2/n}}{\sqrt{(n-1)s^2/\sigma^2(n-1)}} = \frac{\bar{x} - \mu}{\sqrt{s^2/n}} \tag{39.29}$$

is distributed as  $f(t; n - 1)$ . The unknown variance  $\sigma^2$  cancels, and  $t$  can be used to test the hypothesis that the true mean is some particular value  $\mu$ .

### 39.4.7 Gamma distribution

For a process that generates events as a function of  $x$  (e.g., space or time) according to a Poisson distribution, the distance in  $x$  from an arbitrary starting point (which may be some particular event) to the  $k^{\text{th}}$  event follows a *gamma* distribution,  $f(x; \lambda, k)$ . The Poisson parameter  $\mu$  is  $\lambda$  per unit  $x$ . The special case  $k = 1$  (i.e.,  $f(x; \lambda, 1) = \lambda e^{-\lambda x}$ ) is called the *exponential* distribution. A sum of  $k'$  exponential random variables  $x_i$  is distributed as  $f(\sum x_i; \lambda, k')$ .

The parameter  $k$  is not required to be an integer. For  $\lambda = 1/2$  and  $k = n/2$ , the gamma distribution reduces to the  $\chi^2(n)$  distribution.

### 39.4.8 Beta distribution

The beta distribution describes a continuous random variable  $x$  in the interval  $[0, 1]$ . By scaling and translation one can easily

generalize it to have arbitrary endpoints. In Bayesian inference about the parameter  $p$  of a binomial process, if the prior p.d.f. is a beta distribution  $f(p; \alpha, \beta)$  then the observation of  $r$  successes out of  $N$  trials gives a posterior beta distribution  $f(p; r + \alpha, N - r + \beta)$  (Bayesian methods are discussed further in Sec. 40). The uniform distribution is a beta distribution with  $\alpha = \beta = 1$ .

### References

- [1] H. Cramér, *Mathematical Methods of Statistics*, (Princeton Univ. Press, New Jersey, 1958).
- [2] A. Stuart and J.K. Ord, *Kendall's Advanced Theory of Statistics*, Vol. 1 *Distribution Theory* 6th Ed., (Halsted Press, New York, 1994), and earlier editions by Kendall and Stuart.
- [3] F.E. James, *Statistical Methods in Experimental Physics*, 2nd Ed., (World Scientific, Singapore, 2006).
- [4] L. Lyons, *Statistics for Nuclear and Particle Physicists*, (Cambridge University Press, New York, 1986).
- [5] B.R. Roe, *Probability and Statistics in Experimental Physics*, 2nd Ed., (Springer, New York, 2001).
- [6] R.J. Barlow, *Statistics: A Guide to the Use of Statistical Methods in the Physical Sciences*, (John Wiley, New York, 1989).
- [7] S. Brandt, *Data Analysis*, 3rd Ed., (Springer, New York, 1999).
- [8] G. Cowan, *Statistical Data Analysis*, (Oxford University Press, Oxford, 1998).
- [9] A.N. Kolmogorov, *Grundbegriffe der Wahrscheinlichkeitstheorie*, (Springer, Berlin, 1933); *Foundations of the Theory of Probability*, 2nd Ed., (Chelsea, New York 1956).
- [10] Ch. Walck, *Hand-book on Statistical Distributions for Experimentalists*, University of Stockholm Internal Report SUP-PFY/96-01, available from [www.physto.se/~walck](http://www.physto.se/~walck).
- [11] M. Abramowitz and I. Stegun, eds., *Handbook of Mathematical Functions*, (Dover, New York, 1972).

- [12] F.W.J. Olver *et al.*, eds., NIST Handbook of Mathematical Functions, (Cambridge University Press, 2010); A companion Digital Library of Mathematical Functions is available at [dlmf.nist.gov](http://dlmf.nist.gov).
- [13] R. Brun and F. Rademakers, Nucl. Instrum. Meth. **A389**, 81 (1997); See also [root.cern.ch](http://root.cern.ch).



## 40. Statistics

Revised October 2019 by G. Cowan (RHUL).

This chapter gives an overview of statistical methods used in high-energy physics. In statistics, we are interested in using a given sample of data to make inferences about a probabilistic model, *e.g.*, to assess the model's validity or to determine the values of its parameters. There are two main approaches to statistical inference, which we may call frequentist and Bayesian.

In frequentist statistics, probability is interpreted as the frequency of the outcome of a repeatable experiment. The most important tools in this framework are parameter estimation, covered in Section 40.2, statistical tests, discussed in Section 40.3, and confidence intervals, which are constructed so as to cover the true value of a parameter with a specified probability, as described in Section 40.4.2. Note that in frequentist statistics one does not define a probability for a hypothesis or for the value of a parameter.

In Bayesian statistics, the interpretation of probability is more general and includes *degree of belief* (called subjective probability). One can then speak of a probability density function (p.d.f.) for a parameter, which expresses one's state of knowledge about where its true value lies. Bayesian methods provide a natural means to include additional information, which in general may be subjective; in fact they *require* prior probabilities for the hypotheses (or parameters) in question, *i.e.*, the degree of belief about the parameters' values, before carrying out the measurement. Using Bayes' theorem (Eq. (39.4)), the prior degree of belief is updated by the data from the experiment. Bayesian methods for interval estimation are discussed in Sections 40.4.1 and 40.4.2.4.

For many inference problems, the frequentist and Bayesian approaches give similar numerical values, even though they answer different questions and are based on fundamentally different interpretations of probability. In some important cases, however, the two approaches may yield very different results. For a discussion of Bayesian vs. non-Bayesian methods, see references written by a statistician [1], by a physicist [2], or the detailed comparison in Ref. [3].

### 40.1 Fundamental concepts

Consider an experiment whose outcome is characterized by one or more data values, which we can write as a vector  $\mathbf{x}$ . A *hypothesis*  $H$  is a statement about the probability for the data, often written  $P(\mathbf{x}|H)$ . (We will usually use a capital letter for a probability and lower case for a probability density. Often the term p.d.f. is used loosely to refer to either a probability or a probability density.) This could, for example, define completely the p.d.f. for the data (a *simple* hypothesis), or it could specify only the functional form of the p.d.f., with the values of one or more parameters not determined (a *composite* hypothesis).

If the probability  $P(\mathbf{x}|H)$  for data  $\mathbf{x}$  is regarded as a function of the hypothesis  $H$ , then it is called the *likelihood* of  $H$ , usually written  $L(H)$ . Often the hypothesis is characterized by one or more parameters  $\theta$ , in which case  $L(\theta) = P(\mathbf{x}|\theta)$  is called the likelihood function.

In some cases one can obtain at least approximate frequentist results using the likelihood evaluated only with the data obtained. In general, however, the frequentist approach requires a full specification of the probability model  $P(\mathbf{x}|H)$  both as a function of the data  $\mathbf{x}$  and hypothesis  $H$ .

In the Bayesian approach, inference is based on the posterior probability for  $H$  given the data  $\mathbf{x}$ , which represents one's degree of belief that  $H$  is true given the data. This is obtained from Bayes' theorem (39.4), which can be written

$$P(H|\mathbf{x}) = \frac{P(\mathbf{x}|H)\pi(H)}{\int P(\mathbf{x}|H')\pi(H')dH'} \quad (40.1)$$

Here  $P(\mathbf{x}|H)$  is the likelihood for  $H$ , which depends only on the data actually obtained. The quantity  $\pi(H)$  is the prior probability for  $H$ , which represents one's degree of belief for  $H$  before carrying out the measurement. The integral in the denominator (or sum, for discrete hypotheses) serves as a normalization factor. If  $H$  is characterized by a continuous parameter  $\theta$  then the posterior

probability is a p.d.f.  $p(\theta|\mathbf{x})$ . Note that the likelihood function itself is not a p.d.f. for  $\theta$ .

### 40.2 Parameter estimation

Here we review *point estimation* of parameters, first with an overview of the frequentist approach and its two most important methods, maximum likelihood and least squares, treated in Sections 40.2.2 and 40.2.3. The Bayesian approach is outlined in Sec. 40.2.5.

An *estimator*  $\hat{\theta}$  (written with a hat) is a function of the data used to estimate the value of the parameter  $\theta$ . Sometimes the word 'estimate' is used to denote the value of the estimator when evaluated with given data. There is no fundamental rule dictating how an estimator must be constructed. One tries, therefore, to choose that estimator which has the best properties. The most important of these are (a) *consistency*, (b) *bias*, (c) *efficiency*, and (d) *robustness*.

(a) An estimator is said to be *consistent* if the estimate  $\hat{\theta}$  converges in probability (see Ref. [3]) to the true value  $\theta$  as the amount of data increases. This property is so important that it is possessed by all commonly used estimators.

(b) The *bias*,  $b = E[\hat{\theta}] - \theta$ , is the difference between the expectation value of the estimator and the true value of the parameter. The expectation value is taken over a hypothetical set of similar experiments in which  $\hat{\theta}$  is constructed in the same way. When  $b = 0$ , the estimator is said to be unbiased. The bias depends on the chosen metric, *i.e.*, if  $\hat{\theta}$  is an unbiased estimator of  $\theta$ , then  $\hat{\theta}^2$  is not in general an unbiased estimator for  $\theta^2$ .

(c) *Efficiency* is the ratio of the minimum possible variance for any estimator of  $\theta$  to the variance  $V[\hat{\theta}]$  of the estimator  $\hat{\theta}$ . For the case of a single parameter, under rather general conditions the minimum variance is given by the Rao-Cramér-Fréchet bound,

$$\sigma_{\min}^2 = \left(1 + \frac{\partial b}{\partial \theta}\right)^2 / I(\theta), \quad (40.2)$$

where

$$I(\theta) = E \left[ \left( \frac{\partial \ln L}{\partial \theta} \right)^2 \right] = -E \left[ \frac{\partial^2 \ln L}{\partial \theta^2} \right] \quad (40.3)$$

is the *Fisher information*,  $L$  is the likelihood, and the operator  $E[\ ]$  in (40.3) is the expectation value with respect to the data. For the final equality to hold, the range of allowed data values must not depend on  $\theta$ .

The *mean-squared error*,

$$\text{MSE} = E[(\hat{\theta} - \theta)^2] = V[\hat{\theta}] + b^2, \quad (40.4)$$

is a measure of an estimator's quality which combines bias and variance.

(d) *Robustness* is the property of being insensitive to departures from assumptions in the p.d.f., *e.g.*, owing to uncertainties in the distribution's tails.

It is not in general possible to optimize simultaneously for all the measures of estimator quality described above. For some common estimators, the properties above are known exactly. More generally, it is possible to evaluate them by Monte Carlo simulation. Note that they will in general depend on the unknown  $\theta$ .

#### 40.2.1 Estimators for mean, variance, and median

Suppose we have a set of  $n$  independent measurements,  $x_1, \dots, x_n$ , each assumed to follow a p.d.f. with unknown mean  $\mu$  and unknown variance  $\sigma^2$  (the measurements do not necessarily have to follow a Gaussian distribution). Then

$$\hat{\mu} = \frac{1}{n} \sum_{i=1}^n x_i \quad (40.5)$$

$$\hat{\sigma}^2 = \frac{1}{n-1} \sum_{i=1}^n (x_i - \hat{\mu})^2 \quad (40.6)$$

are unbiased estimators of  $\mu$  and  $\sigma^2$ . The variance of  $\hat{\mu}$  is  $\sigma^2/n$  and the variance of  $\hat{\sigma}^2$  is

$$V[\hat{\sigma}^2] = \frac{1}{n} \left( m_4 - \frac{n-3}{n-1} \sigma^4 \right), \quad (40.7)$$

where  $m_4$  is the 4<sup>th</sup> central moment of  $x$  (see Eq. (39.8)). For Gaussian distributed  $x_i$ , this becomes  $2\sigma^4/(n-1)$  for any  $n \geq 2$ , and for large  $n$  the standard deviation of  $\hat{\sigma}$  is  $\sigma/\sqrt{2n}$ . For any  $n$  and Gaussian  $x_i$ ,  $\hat{\mu}$  is an efficient estimator for  $\mu$ , and the estimators  $\hat{\mu}$  and  $\hat{\sigma}^2$  are uncorrelated. Otherwise the arithmetic mean (40.5) is not necessarily the most efficient estimator; this is discussed further in Sec. 8.7 of Ref. [4].

If  $\sigma^2$  is known, it does not improve the estimate  $\hat{\mu}$ , as can be seen from Eq. (40.5); however, if  $\mu$  is known, one can substitute it for  $\hat{\mu}$  in Eq. (40.6) and replace  $n-1$  by  $n$  to obtain an estimator of  $\sigma^2$  still with zero bias but smaller variance. If the  $x_i$  have different, known variances  $\sigma_i^2$ , then the weighted average

$$\hat{\mu} = \frac{1}{w} \sum_{i=1}^n w_i x_i, \quad (40.8)$$

where  $w_i = 1/\sigma_i^2$  and  $w = \sum_i w_i$ , is an unbiased estimator for  $\mu$  with a smaller variance than an unweighted average. The standard deviation of  $\hat{\mu}$  is  $1/\sqrt{w}$ .

As an estimator for the median  $x_{\text{med}}$ , one can use the value  $\hat{x}_{\text{med}}$  such that half the  $x_i$  are below and half above (the sample median). If there are an even number of observations and the sample median lies between two observed values, the estimator is set by convention to their arithmetic average. If the p.d.f. of  $x$  has the form  $f(x-\mu)$  and  $\mu$  is both mean and median, then for large  $n$  the variance of the sample median approaches  $1/[4nf^2(0)]$ , provided  $f(0) > 0$ . Although estimating the median can often be more difficult computationally than the mean, the resulting estimator is generally more robust, as it is insensitive to the exact shape of the tails of a distribution.

**40.2.2 The method of maximum likelihood**

Suppose we have a set of measured quantities  $\mathbf{x}$  and the likelihood  $L(\boldsymbol{\theta}) = P(\mathbf{x}|\boldsymbol{\theta})$  for a set of parameters  $\boldsymbol{\theta} = (\theta_1, \dots, \theta_N)$ . The *maximum likelihood* (ML) estimators for  $\boldsymbol{\theta}$  are defined as the values that give the maximum of  $L$ . Because of the properties of the logarithm, it is usually easier to work with  $\ln L$ , and since both are maximized for the same parameter values  $\boldsymbol{\theta}$ , the ML estimators can be found by solving the *likelihood equations*,

$$\frac{\partial \ln L}{\partial \theta_i} = 0, \quad i = 1, \dots, N. \quad (40.9)$$

Often the solution must be found numerically. Maximum likelihood estimators are important because they are asymptotically (*i.e.*, for large data samples) unbiased, efficient and have a Gaussian sampling distribution under quite general conditions, and the method has a wide range of applicability.

In general the likelihood function is obtained from the probability of the data under assumption of the parameters. An important special case is when the data consist of *i.i.d.* (independent and identically distributed) values. Here one has a set of  $n$  statistically independent quantities  $\mathbf{x} = (x_1, \dots, x_n)$ , where each component follows the same p.d.f.  $f(x; \boldsymbol{\theta})$ . In this case the joint p.d.f. of the data sample factorizes and the likelihood function is

$$L(\boldsymbol{\theta}) = \prod_{i=1}^n f(x_i; \boldsymbol{\theta}). \quad (40.10)$$

In this case the number of events  $n$  is regarded as fixed. If however the probability to observe  $n$  events itself depends on the parameters  $\boldsymbol{\theta}$ , then this dependence should be included in the likelihood. For example, if  $n$  follows a Poisson distribution with mean  $\mu$  and the independent  $x$  values all follow  $f(x; \boldsymbol{\theta})$ , then the likelihood becomes

$$L(\boldsymbol{\theta}) = \frac{\mu^n}{n!} e^{-\mu} \prod_{i=1}^n f(x_i; \boldsymbol{\theta}). \quad (40.11)$$

Equation (40.11) is often called the *extended likelihood* (see, *e.g.*, Refs. [5–7]). If  $\mu$  is given as a function of  $\boldsymbol{\theta}$ , then including the probability for  $n$  given  $\boldsymbol{\theta}$  in the likelihood provides additional information about the parameters. This therefore leads to a reduction in their statistical uncertainties and in general changes their estimated values.

In evaluating the likelihood function, it is important that any normalization factors in the p.d.f. that involve  $\boldsymbol{\theta}$  be included. However, we will only be interested in the maximum of  $L$  and in ratios of  $L$  at different values of the parameters; hence any multiplicative factors that do not involve the parameters that we want to estimate may be dropped, including factors that depend on the data but not on  $\boldsymbol{\theta}$ .

Under a one-to-one change of parameters from  $\boldsymbol{\theta}$  to  $\boldsymbol{\eta}$ , the ML estimators  $\hat{\boldsymbol{\theta}}$  transform to  $\boldsymbol{\eta}(\hat{\boldsymbol{\theta}})$ . That is, the ML solution is invariant under change of parameter. However, other properties of ML estimators, in particular the bias, are not invariant under change of parameter.

The inverse  $V^{-1}$  of the covariance matrix  $V_{ij} = \text{cov}[\hat{\theta}_i, \hat{\theta}_j]$  for a set of ML estimators can be estimated by using

$$(\hat{V}^{-1})_{ij} = - \left. \frac{\partial^2 \ln L}{\partial \theta_i \partial \theta_j} \right|_{\hat{\boldsymbol{\theta}}}. \quad (40.12)$$

For finite samples, however, Eq. (40.12) can result in a misestimation of the variances. In the large sample limit (or in a linear model with Gaussian data),  $L$  has a Gaussian form and  $\ln L$  is (hyper)parabolic. In this case,  $s$  times the standard deviations  $\sigma_i$  of the estimators for the parameters can be obtained from the hypersurface defined by the  $\boldsymbol{\theta}$  such that

$$\ln L(\boldsymbol{\theta}) = \ln L_{\text{max}} - s^2/2, \quad (40.13)$$

where  $\ln L_{\text{max}}$  is the value of  $\ln L$  at the solution point (compare with Eq. (40.73)). The minimum and maximum values of  $\theta_i$  on the hypersurface then give an approximate  $s$ -standard deviation confidence interval for  $\theta_i$  (see Section 40.4.2.2).

**40.2.2.1 ML with binned data**

If the total number of data values  $x_i$ , ( $i = 1, \dots, n_{\text{tot}}$ ), is small, the unbinned maximum likelihood method, *i.e.*, use of Equation (40.10) (or (40.11) for extended ML), is preferred since binning can only result in a loss of information, and hence larger statistical errors for the parameter estimates. If the sample is large, it can be convenient to bin the values in a histogram with  $N$  bins, so that one obtains a vector of data  $\mathbf{n} = (n_1, \dots, n_N)$  with expectation values  $\boldsymbol{\mu} = E[\mathbf{n}]$  and probabilities  $f(\mathbf{n}; \boldsymbol{\mu})$ . Suppose the mean values  $\boldsymbol{\mu}$  can be determined as a function of a set of parameters  $\boldsymbol{\theta}$ . Then one may maximize the likelihood function based on the contents of the bins.

As mentioned in Sec. 40.2.2, the total number of events  $n_{\text{tot}} = \sum_i n_i$  can be regarded either as fixed or as a random variable. If it is fixed, the histogram follows a multinomial distribution,

$$f_M(\mathbf{n}; \boldsymbol{\theta}) = \frac{n_{\text{tot}}!}{n_1! \dots n_N!} p_1^{n_1} \dots p_N^{n_N}, \quad (40.14)$$

where we assume the probabilities  $p_i$  are given functions of the parameters  $\boldsymbol{\theta}$ . The distribution can be written equivalently in terms of the expected number of events in each bin,  $\mu_i = n_{\text{tot}} p_i$ . If the  $n_i$  are regarded as independent and Poisson distributed, then the data are instead described by a product of Poisson probabilities,

$$f_P(\mathbf{n}; \boldsymbol{\theta}) = \prod_{i=1}^N \frac{\mu_i^{n_i}}{n_i!} e^{-\mu_i}, \quad (40.15)$$

where the mean values  $\mu_i$  are given functions of  $\boldsymbol{\theta}$ . The total number of events  $n_{\text{tot}}$  thus follows a Poisson distribution with mean  $\mu_{\text{tot}} = \sum_i \mu_i$ .

When using maximum likelihood with binned data, one can find the ML estimators and at the same time obtain a statistic usable for a test of goodness-of-fit (see Sec. 40.3.2). Maximizing the likelihood  $L(\boldsymbol{\theta}) = f_{M/P}(\mathbf{n}; \boldsymbol{\theta})$  is equivalent to maximizing

the likelihood ratio  $\lambda(\theta) = f_{M/P}(n; \theta) / f(n; \hat{\mu})$ , where in the denominator  $f(n; \mu)$  is a model with an adjustable parameter for each bin,  $\mu = (\mu_1, \dots, \mu_N)$ , and the corresponding estimators are  $\hat{\mu} = (n_1, \dots, n_N)$  (called the “saturated model”). Equivalently one often minimizes the quantity  $-2 \ln \lambda(\theta)$ . For independent Poisson distributed  $n_i$  this is [8]

$$-2 \ln \lambda(\theta) = 2 \sum_{i=1}^N \left[ \mu_i(\theta) - n_i + n_i \ln \frac{n_i}{\mu_i(\theta)} \right], \quad (40.16)$$

where for bins with  $n_i = 0$ , the last term in (40.16) is zero. The expression (40.16) without the terms  $\mu_i - n_i$  also gives  $-2 \ln \lambda(\theta)$  for multinomially distributed  $n_i$ , *i.e.*, when the total number of entries is regarded as fixed. In the limit of zero bin width, minimizing (40.16) is equivalent to maximizing the unbinned extended likelihood function (40.11); in the corresponding multinomial case without the  $\mu_i - n_i$  terms one obtains Eq. (40.10).

A smaller value of  $-2 \ln \lambda(\hat{\theta})$  corresponds to better agreement between the data and the hypothesized form of  $\mu(\theta)$ . The value of  $-2 \ln \lambda(\hat{\theta})$  can thus be translated into a *p*-value as a measure of goodness-of-fit, as described in Sec. 40.3.2. Assuming the model is correct, then according to Wilks’ theorem [9], for sufficiently large  $\mu_i$  and provided certain regularity conditions are met, the minimum of  $-2 \ln \lambda$  as defined by Eq. (40.16) follows a  $\chi^2$  distribution (see, *e.g.*, Ref. [8]). If there are  $N$  bins and  $m$  fitted parameters, then the number of degrees of freedom for the  $\chi^2$  distribution is  $N - m$  if the data are treated as Poisson-distributed, and  $N - m - 1$  if the  $n_i$  are multinomially distributed.

Suppose the  $n_i$  are Poisson-distributed and the overall normalization  $\mu_{\text{tot}} = \sum_i \mu_i$  is taken as an adjustable parameter, so that  $\mu_i = \mu_{\text{tot}} p_i(\theta)$ , where the probability to be in the *i*th bin,  $p_i(\theta)$ , does not depend on  $\mu_{\text{tot}}$ . Then by minimizing Eq. (40.16), one obtains that the area under the fitted function is equal to the sum of the histogram contents, *i.e.*,  $\sum_i \hat{\mu}_i = \sum_i n_i$ . This is a property not possessed by the estimators from the method of least squares (see, *e.g.*, Sec. 40.2.3 and Ref. [7]).

40.2.2.2 *Frequentist treatment of nuisance parameters*

Suppose we want to determine the values of parameters  $\theta$  using a set of measurements  $x$  described by a probability model  $P_x(x|\theta)$ . In general the model is not perfect, which is to say it cannot provide an accurate description of the data even at the most optimal point of its parameter space. As a result, the estimated parameters can have a systematic bias.

One can improve the model by including in it additional parameters. That is,  $P_x(x|\theta)$  is replaced by a more general model  $P_x(x|\theta, \nu)$ , which depends on parameters of interest  $\theta$  and *nuisance parameters*  $\nu$ . The additional parameters are not of intrinsic interest but must be included for the model to be accurate for some point in the enlarged parameter space.

Although including additional parameters may eliminate or at least reduce the effect of systematic uncertainties, their presence will result in increased statistical uncertainties for the parameters of interest. This occurs because the estimators for the nuisance parameters and those of interest will in general be correlated, which results in an enlargement of the contour defined by Eq. (40.13).

To reduce the impact of the nuisance parameters one often tries to constrain their values by means of control or calibration measurements, say, having data  $y$ . For example, some components of  $y$  could represent estimates of the nuisance parameters, often from separate experiments. Suppose the measurements  $y$  are statistically independent from  $x$  and are described by a model  $P_y(y|\nu)$ . The joint model for both  $x$  and  $y$  is in this case therefore the product of the probabilities for  $x$  and  $y$ , and thus the likelihood function for the full set of parameters is

$$L(\theta, \nu) = P_x(x|\theta, \nu) P_y(y|\nu). \quad (40.17)$$

Note that in this case if one wants to simulate the experiment by means of Monte Carlo, both the primary and control measurements,  $x$  and  $y$ , must be generated for each repetition under assumption of fixed values for the parameters  $\theta$  and  $\nu$ .

Using all of the parameters  $(\theta, \nu)$  in Eq. (40.13) to find the statistical errors in the parameters of interest  $\theta$  is equivalent to using the *profile likelihood*, which depends only on  $\theta$ . It is defined as

$$L_p(\theta) = L(\theta, \hat{\hat{\nu}}(\theta)), \quad (40.18)$$

where the double-hat notation indicates the profiled values of the parameters  $\nu$ , defined as the values that maximize  $L$  for the specified  $\theta$ . The profile likelihood is discussed further in Section 40.3.2.1 in connection with hypothesis tests.

40.2.3 *The method of least squares*

The *method of least squares* (LS) coincides with the method of maximum likelihood in the following special case. Consider a set of  $N$  independent measurements  $y_i$  at known points  $x_i$ . The measurement  $y_i$  is assumed to be Gaussian distributed with mean  $\mu(x_i; \theta)$  and known variance  $\sigma_i^2$ . The goal is to construct estimators for the unknown parameters  $\theta$ . The log-likelihood function contains the sum of squares

$$\chi^2(\theta) = -2 \ln L(\theta) + \text{constant} = \sum_{i=1}^N \frac{(y_i - \mu(x_i; \theta))^2}{\sigma_i^2}. \quad (40.19)$$

The parameter values that maximize  $L$  are the same as those which minimize  $\chi^2$ .

The minimum of the chi-square function in Equation (40.19) defines the least-squares estimators  $\hat{\theta}$  for the more general case where the  $y_i$  are not Gaussian distributed as long as they are independent. If they are not independent but rather have a covariance matrix  $V_{ij} = \text{cov}[y_i, y_j]$ , then the LS estimators are determined by the minimum of

$$\chi^2(\theta) = (\mathbf{y} - \boldsymbol{\mu}(\theta))^T V^{-1} (\mathbf{y} - \boldsymbol{\mu}(\theta)), \quad (40.20)$$

where  $\mathbf{y} = (y_1, \dots, y_N)$  is the (column) vector of measurements,  $\boldsymbol{\mu}(\theta)$  is the corresponding vector of predicted values, and the superscript  $T$  denotes the transpose. If the  $y_i$  are not Gaussian distributed, then the LS and ML estimators will not in general coincide.

Often one further restricts the problem to the case where  $\mu(x_i; \theta)$  is a linear function of the parameters, *i.e.*,

$$\mu(x_i; \theta) = \sum_{j=1}^m \theta_j h_j(x_i). \quad (40.21)$$

Here the  $h_j(x)$  are  $m$  linearly independent functions, *e.g.*,  $1, x, x^2, \dots, x^{m-1}$  or Legendre polynomials. We require  $m < N$  and at least  $m$  of the  $x_i$  must be distinct.

Minimizing  $\chi^2$  in this case with  $m$  parameters reduces to solving a system of  $m$  linear equations. Defining  $H_{ij} = h_j(x_i)$  and minimizing  $\chi^2$  by setting its derivatives with respect to the  $\theta_i$  equal to zero gives the LS estimators,

$$\hat{\theta} = (H^T V^{-1} H)^{-1} H^T V^{-1} \mathbf{y} \equiv D \mathbf{y}. \quad (40.22)$$

The covariance matrix for the estimators  $U_{ij} = \text{cov}[\hat{\theta}_i, \hat{\theta}_j]$  is given by

$$U = D V D^T = (H^T V^{-1} H)^{-1}, \quad (40.23)$$

or equivalently, its inverse  $U^{-1}$  can be found from

$$(U^{-1})_{ij} = \frac{1}{2} \frac{\partial^2 \chi^2}{\partial \theta_i \partial \theta_j} \Big|_{\theta=\hat{\theta}} = \sum_{k,l=1}^m h_i(x_k) (V^{-1})_{kl} h_j(x_l). \quad (40.24)$$

The LS estimators can also be found from the expression

$$\hat{\theta} = U \mathbf{g}, \quad (40.25)$$

where the vector  $\mathbf{g}$  is defined by

$$\mathbf{g}_i = \sum_{j,k=1}^m y_j h_i(x_k) (V^{-1})_{jk}. \quad (40.26)$$

For the case of uncorrelated  $y_i$ , for example, one can use (40.25) with

$$(U^{-1})_{ij} = \sum_{k=1}^N \frac{h_i(x_k)h_j(x_k)}{\sigma_k^2}, \quad (40.27)$$

$$g_i = \sum_{k=1}^N \frac{y_k h_i(x_k)}{\sigma_k^2}. \quad (40.28)$$

Expanding  $\chi^2(\boldsymbol{\theta})$  about  $\hat{\boldsymbol{\theta}}$ , one finds that the contour in parameter space defined by

$$\chi^2(\boldsymbol{\theta}) = \chi^2(\hat{\boldsymbol{\theta}}) + 1 = \chi_{\min}^2 + 1 \quad (40.29)$$

has tangent planes located at plus-or-minus-one standard deviation  $\sigma_{\hat{\boldsymbol{\theta}}}$  from the LS estimates  $\hat{\boldsymbol{\theta}}$  (the relation is approximate if the fit function  $\mu(x; \boldsymbol{\theta})$  is nonlinear in the parameters).

In constructing the quantity  $\chi^2(\boldsymbol{\theta})$  one requires the variances or, in the case of correlated measurements, the covariance matrix. Often these quantities are not known *a priori* and must be estimated from the data. In this case the least-squares and maximum-likelihood methods are no longer exactly equivalent even for Gaussian distributed measurements. An important example is where the measured value  $y_i$  represents the event count in a histogram bin. If, for example,  $y_i$  represents a Poisson variable, for which the variance is equal to the mean, then one can either estimate the variance from the predicted value,  $\mu(x_i; \boldsymbol{\theta})$ , or from the observed number itself,  $y_i$ . In the first option, the variances become functions of the parameters, and as a result the estimators may need to be found numerically. The second option can be undefined if  $y_i$  is zero, and for small  $y_i$ , the variance will be poorly estimated. In either case, one should constrain the normalization of the fitted curve to the correct value, *i.e.*, one should determine the area under the fitted curve directly from the number of entries in the histogram (see Ref. [7], Section 7.4). As noted in Sec. 40.2.2.1, this issue is avoided when using the method of extended maximum likelihood with binned data by minimizing Eq. (40.16). In that case if the expected number of events  $\mu_{\text{tot}}$  does not depend on the other fitted parameters  $\boldsymbol{\theta}$ , then its extended ML estimator is equal to the observed total number of events.

As the minimum value of the  $\chi^2$  represents the level of agreement between the measurements and the fitted function, it can be used for assessing the goodness-of-fit; this is discussed further in Section 40.3.2.

#### 40.2.4 Parameter estimation with constraints

In some applications one is interested in using a set of measured quantities  $\mathbf{y} = (y_1, \dots, y_N)$  to estimate a set of parameters  $\boldsymbol{\theta} = (\theta_1, \dots, \theta_M)$  subject to a number of constraints. For example, one may have measured coordinates from two tracks, and one wishes to estimate their momentum vectors subject to the constraint that the tracks have a common vertex. The parameters can also include momenta of undetected particles such as neutrinos, as long as the constraints from conservation of energy and momentum and from known masses of particles involved in the reaction chain provide enough information for these quantities to be inferred.

A set of  $K$  constraints can be given in the form of equations

$$c_k(\boldsymbol{\theta}) = 0, \quad k = 1, \dots, K. \quad (40.30)$$

In some problems it may be possible to define a new set of parameters  $\boldsymbol{\eta} = (\eta_1, \dots, \eta_L)$  with  $L = M - K$  such that every point in  $\boldsymbol{\eta}$ -space automatically satisfies the constraints. If this is possible then the problem reduces to one of estimating  $\boldsymbol{\eta}$  with, *e.g.*, maximum likelihood or least squares and then transforming the estimators back into  $\boldsymbol{\theta}$ -space.

In many cases it may be difficult or impossible to find an appropriate transformation  $\boldsymbol{\eta}(\boldsymbol{\theta})$ . Suppose that the parameters are determined through minimizing an objective function such as  $\chi^2(\boldsymbol{\theta})$  in the method of least squares. Here one may enforce the con-

straints by finding the stationary points of the *Lagrange function*

$$\mathcal{L}(\boldsymbol{\theta}, \boldsymbol{\lambda}, \mathbf{y}) = \chi^2(\boldsymbol{\theta}, \mathbf{y}) + \sum_{k=1}^K \lambda_k c_k(\boldsymbol{\theta}) \quad (40.31)$$

with respect to both the parameters  $\boldsymbol{\theta}$  and a set of *Lagrange multipliers*  $\boldsymbol{\lambda} = (\lambda_1, \dots, \lambda_K)$ . Combining the parameters and Lagrange multipliers into an  $(M + K)$ -component vector  $\boldsymbol{\gamma} = (\theta_1, \dots, \theta_M, \lambda_1, \dots, \lambda_K)$ , the solutions for  $\boldsymbol{\gamma}$ , *i.e.*, the estimators  $\hat{\boldsymbol{\gamma}}$ , are found (*e.g.*, numerically) from the system of equations

$$F_i(\boldsymbol{\gamma}, \mathbf{y}) \equiv \frac{\partial \mathcal{L}}{\partial \gamma_i} = 0, \quad i = 1, \dots, M + K. \quad (40.32)$$

To obtain the covariance matrix of the estimated parameters one can find solutions  $\hat{\boldsymbol{\gamma}}$  corresponding to the expectation values of the data  $\langle \mathbf{y} \rangle$  and expand  $F_i(\hat{\boldsymbol{\gamma}}, \mathbf{y})$  to first order about these values. This gives (see, *e.g.*, Sec. 11.6 of Ref. [7]) linearized approximations for the estimators,  $\hat{\boldsymbol{\gamma}}(\mathbf{y}) \approx \hat{\boldsymbol{\gamma}} + C(\mathbf{y} - \langle \mathbf{y} \rangle)$ , where the matrix  $C = -A^{-1}B$ , and  $A$  and  $B$  are given by

$$A_{ij} = \left[ \frac{\partial F_i}{\partial \gamma_j} \right]_{\hat{\boldsymbol{\gamma}}, \langle \mathbf{y} \rangle} \quad \text{and} \quad B_{ij} = \left[ \frac{\partial F_i}{\partial y_j} \right]_{\hat{\boldsymbol{\gamma}}, \langle \mathbf{y} \rangle}. \quad (40.33)$$

In practice the values  $\langle \mathbf{y} \rangle$  and corresponding solutions  $\hat{\boldsymbol{\gamma}}$  are estimated using the data from the actual measurement. Using this approximation for  $\hat{\boldsymbol{\gamma}}(\mathbf{y})$ , one can find the covariance matrix  $U_{ij} = \text{cov}[\hat{\gamma}_i, \hat{\gamma}_j]$  of the the estimators for the  $\gamma_i$  in terms of that of the data  $V_{ij} = \text{cov}[y_i, y_j]$  using error propagation (*cf.* Eqs. (40.42) and (40.43)),

$$U = CVC^T. \quad (40.34)$$

The upper-left  $M \times M$  block of the matrix  $U$  gives the covariance matrix for the estimated parameters  $\text{cov}[\hat{\theta}_i, \hat{\theta}_j]$ . One can show for linear constraints that  $\text{cov}[\hat{\theta}_i, \hat{\theta}_j]$  is also given by the upper-left  $M \times M$  block of  $2A^{-1}$ . If the parameters are estimated using the method of least squares, then the number of degrees of freedom for the distribution of the minimized  $\chi^2$  is increased by the number of constraints, *i.e.*, it becomes  $N - M + K$ . Further details can be found in, *e.g.*, Ch. 8 of Ref. [4] and Ch. 7 of Ref. [10].

#### 40.2.5 The Bayesian approach

In the frequentist methods discussed above, probability is associated only with data, not with the value of a parameter. This is no longer the case in Bayesian statistics, however, which we introduce in this section. For general introductions to Bayesian statistics see, *e.g.*, Refs. [11–14].

Suppose the outcome of an experiment is characterized by a vector of data  $\mathbf{x}$ , whose probability distribution depends on an unknown parameter (or parameters)  $\boldsymbol{\theta}$  that we wish to determine. In Bayesian statistics, all knowledge about  $\boldsymbol{\theta}$  is summarized by the posterior p.d.f.  $p(\boldsymbol{\theta}|\mathbf{x})$ , whose integral over any given region gives the degree of belief for  $\boldsymbol{\theta}$  to take on values in that region, given the data  $\mathbf{x}$ . It is obtained by using Bayes' theorem,

$$p(\boldsymbol{\theta}|\mathbf{x}) = \frac{P(\mathbf{x}|\boldsymbol{\theta})\pi(\boldsymbol{\theta})}{\int P(\mathbf{x}|\boldsymbol{\theta}')\pi(\boldsymbol{\theta}') d\boldsymbol{\theta}'}, \quad (40.35)$$

where  $P(\mathbf{x}|\boldsymbol{\theta})$  is the likelihood function, *i.e.*, the joint p.d.f. for the data viewed as a function of  $\boldsymbol{\theta}$ , evaluated with the data actually obtained in the experiment, and  $\pi(\boldsymbol{\theta})$  is the prior p.d.f. for  $\boldsymbol{\theta}$ . Note that the denominator in Eq. (40.35) serves to normalize the posterior p.d.f. to unity.

As it can be difficult to report the full posterior p.d.f.  $p(\boldsymbol{\theta}|\mathbf{x})$ , one would usually summarize it with statistics such as the mean (or median) value, and covariance matrix. In addition one may construct intervals with a given probability content, as is discussed in Sec. 40.4.1 on Bayesian interval estimation.

##### 40.2.5.1 Priors

Bayesian statistics supplies no unique rule for determining the prior  $\pi(\boldsymbol{\theta})$ ; this reflects the analyst's subjective degree of belief (or state of knowledge) about  $\boldsymbol{\theta}$  before the measurement was carried out. For the result to be of value to the broader community,

whose members may not share these beliefs, it is important to carry out a *sensitivity analysis*, that is, to show how the result changes under a reasonable variation of the prior probabilities.

One might like to construct  $\pi(\theta)$  to represent complete ignorance about the parameters by setting it equal to a constant. A problem here is that if the prior p.d.f. is flat in  $\theta$ , then it is not flat for a nonlinear function of  $\theta$ , and so a different parametrization of the problem would lead in general to a non-equivalent posterior p.d.f.

For the special case of a constant prior, one can see from Bayes' theorem (40.35) that the posterior is proportional to the likelihood, and therefore the mode (peak position) of the posterior is equal to the ML estimator. The posterior mode, however, will change in general upon a transformation of parameter. One may use as the Bayesian estimator a summary statistic other than the mode, such as the median, which is invariant under parameter transformation. But this will not in general coincide with the ML estimator.

The difficult and subjective nature of encoding personal knowledge into priors has led to what is called *objective Bayesian statistics*, where prior probabilities are based not on an actual degree of belief but rather derived from formal rules. These give, for example, priors which are invariant under a transformation of parameters, or ones which result in a maximum gain in information for a given set of measurements. For an extensive review see, e.g., [15].

Objective priors do not in general reflect degree of belief, but they could in some cases be taken as possible, although perhaps extreme, subjective priors. The posterior probabilities as well therefore do not necessarily reflect a degree of belief. However one may regard investigating a variety of objective priors to be an important part of the sensitivity analysis. Furthermore, use of objective priors with Bayes' theorem can be viewed as a recipe for producing estimators or intervals which have desirable frequentist properties.

An important procedure for deriving objective priors is due to Jeffreys. According to *Jeffreys' rule* one takes the prior as

$$\pi(\theta) \propto \sqrt{\det(I(\theta))}, \tag{40.36}$$

where

$$I_{ij}(\theta) = -E \left[ \frac{\partial^2 \ln P(x|\theta)}{\partial \theta_i \partial \theta_j} \right] \tag{40.37}$$

is the *Fisher information matrix*. One can show that the Jeffreys prior leads to inference that is invariant under a transformation of parameters. One should note that the Jeffreys prior does not in general correspond to one's degree of belief about the value of a parameter. As examples, the Jeffreys prior for the mean  $\mu$  of a Gaussian distribution is a constant, and for the mean of a Poisson distribution one finds  $\pi(\mu) \propto 1/\sqrt{\mu}$ .

Neither the constant nor  $1/\sqrt{\mu}$  priors can be normalized to unit area and are therefore said to be *improper*. This can be allowed because the prior always appears multiplied by the likelihood function, and if the likelihood falls to zero sufficiently quickly then one may have a normalizable posterior density.

An important type of objective prior is the reference prior due to Bernardo and Berger [16]. To find the reference prior for a given problem one considers the Kullback-Leibler divergence  $D_n[\pi, p]$  of the posterior  $p(\theta|x)$  relative to a prior  $\pi(\theta)$ , obtained from a set of i.i.d. data  $\mathbf{x} = (x_1, \dots, x_n)$ :

$$D_n[\pi, p] = \int p(\theta|x) \ln \frac{p(\theta|x)}{\pi(\theta)} d\theta. \tag{40.38}$$

This is effectively a measure of the gain in information provided by the data. The reference prior is chosen so that the expectation value of this information gain is maximized for the limiting case of  $n \rightarrow \infty$ , where the expectation is computed with respect to the marginal distribution of the data,

$$p(\mathbf{x}) = \int p(\mathbf{x}|\theta)\pi(\theta) d\theta. \tag{40.39}$$

For a single, continuous parameter the reference prior is usually identical to the Jeffreys prior. In the multiparameter case an iterative algorithm exists, which requires sorting the parameters by order of inferential importance. Often the result does not depend on this order, but when it does, this can be part of a sensitivity analysis. Further discussion and applications to particle physics problems can be found in Ref. [17].

#### 40.2.5.2 Bayesian treatment of nuisance parameters

As discussed in Sec. 40.2.2, a model may depend on parameters of interest  $\theta$  as well as on nuisance parameters  $\nu$ , which must be included for an accurate description of the data. Knowledge about the values of  $\nu$  may be supplied by control measurements, theoretical insights, physical constraints, etc. Suppose, for example, one has data  $\mathbf{y}$  from a control measurement which is characterized by a probability  $P_{\mathbf{y}}(\mathbf{y}|\nu)$ . Suppose further that before carrying out the control measurement one's state of knowledge about  $\nu$  is described by an initial prior  $\pi_0(\nu)$ , which in practice is often taken to be a constant or in any case very broad. By using Bayes' theorem (40.1) one obtains the updated prior  $\pi(\nu)$  (i.e., now  $\pi(\nu) = \pi(\nu|\mathbf{y})$ , the probability for  $\nu$  given  $\mathbf{y}$ ),

$$\pi(\nu|\mathbf{y}) \propto P(\mathbf{y}|\nu)\pi_0(\nu). \tag{40.40}$$

In the absence of a model for  $P(\mathbf{y}|\nu)$  one may make some reasonable but *ad hoc* choices. For a single nuisance parameter  $\nu$ , for example, one might characterize the uncertainty by a p.d.f.  $\pi(\nu)$  centered about its nominal value with a certain standard deviation  $\sigma_\nu$ . Often a Gaussian p.d.f. provides a reasonable model for one's degree of belief about a nuisance parameter; in other cases, more complicated shapes may be appropriate. If, for example, the parameter represents a non-negative quantity then a log-normal or gamma p.d.f. can be a more natural choice than a Gaussian truncated at zero. Note also that truncation of the prior of a nuisance parameter  $\nu$  at zero will in general make  $\pi(\nu)$  nonzero at  $\nu = 0$ , which can lead to an unnormalizable posterior for a parameter of interest that appears multiplied by  $\nu$ .

The likelihood function, prior, and posterior p.d.f.s all depend on both  $\theta$  and  $\nu$ , and are related by Bayes' theorem, as usual. Note that the likelihood here only refers to the primary measurement  $\mathbf{x}$ . Once any control measurements  $\mathbf{y}$  are used to find the updated prior  $\pi(\nu)$  for the nuisance parameters, this information is fully encapsulated in  $\pi(\nu)$  and the control measurements do not appear further.

One can obtain the posterior p.d.f. for  $\theta$  alone by integrating over the nuisance parameters, i.e.,

$$p(\theta|x) = \int p(\theta, \nu|x) d\nu. \tag{40.41}$$

Such integrals can often not be carried out in closed form, and if the number of nuisance parameters is large, then they can be difficult to compute with standard Monte Carlo methods. *Markov Chain Monte Carlo* (MCMC) techniques are often used for computing integrals of this type (see Sec. 41.5).

#### 40.2.6 Propagation of errors

Consider a set of  $n$  quantities  $\theta = (\theta_1, \dots, \theta_n)$  and a set of  $m$  functions  $\eta(\theta) = (\eta_1(\theta), \dots, \eta_m(\theta))$ . Suppose we have estimated  $\hat{\theta} = (\hat{\theta}_1, \dots, \hat{\theta}_n)$ , using, say, maximum-likelihood or least-squares, and we also know or have estimated the covariance matrix  $V_{ij} = \text{cov}[\hat{\theta}_i, \hat{\theta}_j]$ . The goal of *error propagation* is to determine the covariance matrix for the functions,  $U_{ij} = \text{cov}[\hat{\eta}_i, \hat{\eta}_j]$ , where  $\hat{\eta} = \eta(\hat{\theta})$ . In particular, the diagonal elements  $U_{ii} = V[\hat{\eta}_i]$  give the variances. The new covariance matrix can be found by expanding the functions  $\eta(\theta)$  about the estimates  $\hat{\theta}$  to first order in a Taylor series. Using this one finds

$$U_{ij} \approx \sum_{k,l} \frac{\partial \eta_i}{\partial \theta_k} \frac{\partial \eta_j}{\partial \theta_l} \Big|_{\hat{\theta}} V_{kl}. \tag{40.42}$$

This can be written in matrix notation as  $U \approx AVA^T$  where the matrix of derivatives  $A$  is

$$A_{ij} = \frac{\partial \eta_i}{\partial \theta_j} \Big|_{\hat{\theta}}, \quad (40.43)$$

and  $A^T$  is its transpose. The approximation is exact if  $\boldsymbol{\eta}(\boldsymbol{\theta})$  is linear (it holds, for example, in Equation (40.23)). If this is not the case, the approximation can break down if, for example,  $\boldsymbol{\eta}(\boldsymbol{\theta})$  is significantly nonlinear close to  $\hat{\boldsymbol{\theta}}$  in a region of a size comparable to the standard deviations of  $\hat{\boldsymbol{\theta}}$ .

### 40.3 Statistical tests

In addition to estimating parameters, one often wants to assess the validity of certain statements concerning the data's underlying distribution. Frequentist *hypothesis tests*, described in Sec. 40.3.1, provide a rule for accepting or rejecting hypotheses depending on the outcome of a measurement. In *significance tests*, covered in Sec. 40.3.2, one gives the probability to obtain a level of incompatibility with a certain hypothesis that is greater than or equal to the level observed with the actual data. In the Bayesian approach, the corresponding procedure is based fundamentally on the posterior probabilities of the competing hypotheses. In Sec. 40.3.3 we describe a related construct called the Bayes factor, which can be used to quantify the degree to which the data prefer one or another hypothesis.

#### 40.3.1 Hypothesis tests

A frequentist *test* of a hypothesis (often called the null hypothesis,  $H_0$ ) is a rule that states for which data values  $\boldsymbol{x}$  the hypothesis is rejected. A region of  $\boldsymbol{x}$ -space called the critical region,  $w$ , is specified such that there is no more than a given probability under  $H_0$ ,  $\alpha$ , called the *size* or *significance level* of the test, to find  $\boldsymbol{x} \in w$ . If the data are discrete, it may not be possible to find a critical region with exact probability content  $\alpha$ , and thus we require  $P(\boldsymbol{x} \in w|H_0) \leq \alpha$ . If the data are observed in the critical region,  $H_0$  is rejected.

The data  $\boldsymbol{x}$  used to construct a test could be, for example, a set of values that characterizes an individual event. In this case the test corresponds to classification as, *e.g.*, signal or background. Alternatively the data could represent a set of values from a collection of events. Often one is interested in knowing whether all of the events are of a certain type (background), or whether the sample contains at least some events of a new type (signal). Here the background-only hypothesis plays the role of  $H_0$ , and in the alternative  $H_1$  both signal and background are present. Rejecting  $H_0$  is, from the standpoint of frequentist statistics, the required step to establish discovery of the signal process.

The critical region is not unique. Its choice should take into account the probabilities for the data predicted by some alternative hypothesis (or set of alternatives)  $H_1$ . Rejecting  $H_0$  if it is true is called a *type-I error*, and occurs by construction with probability no greater than  $\alpha$ . Not rejecting  $H_0$  if an alternative  $H_1$  is true is called a *type-II error*, and for a given test this will have a certain probability  $\beta = P(\boldsymbol{x} \notin w|H_1)$ . The quantity  $1 - \beta$  is called the *power* of the test of  $H_0$  with respect to the alternative  $H_1$ . A strategy for defining the critical region can therefore be to maximize the power with respect to some alternative (or alternatives) given a fixed size  $\alpha$ .

To maximize the power of a test of  $H_0$  with respect to the alternative  $H_1$ , the *Neyman–Pearson lemma* states that the critical region  $w$  should be chosen such that for all data values  $\boldsymbol{x}$  inside  $w$ , the likelihood ratio

$$\lambda(\boldsymbol{x}) = \frac{f(\boldsymbol{x}|H_1)}{f(\boldsymbol{x}|H_0)} \quad (40.44)$$

is greater than or equal to a given constant  $c_\alpha$ , and everywhere outside the critical region one has  $\lambda(\boldsymbol{x}) < c_\alpha$ , where the value of  $c_\alpha$  is determined by the size of the test  $\alpha$ . Here  $H_0$  and  $H_1$  must be simple hypotheses, *i.e.*, they should not contain undetermined parameters.

It is convenient to define the test using a scalar function of the data  $\boldsymbol{x}$  called a *test statistic*,  $t(\boldsymbol{x})$ , such that the boundary

of the critical region is given by a surface of constant  $t(\boldsymbol{x})$ . The Neyman–Pearson lemma is equivalent to the statement that the likelihood ratio (40.44) represents the optimal test statistic. It can be difficult in practice, however, to determine  $\lambda(\boldsymbol{x})$ , since this requires knowledge of the joint p.d.f.s  $f(\boldsymbol{x}|H_0)$  and  $f(\boldsymbol{x}|H_1)$ . Often one does not have explicit formulae for these, but rather Monte Carlo models that allow one to generate instances of  $\boldsymbol{x}$  that follow the p.d.f.s.

In the case where the likelihood ratio (40.44) cannot be used explicitly, there exist a variety of other multivariate methods for constructing a test statistic that may approach its performance. These are based on machine-learning algorithms that use samples of *training data* corresponding to the hypotheses in question, often generated from Monte Carlo models. Methods often used in HEP include *Fisher Discriminants*, *Neural Networks*, *Boosted Decision Trees* and *Support Vector Machines*. Descriptions of these and other methods can be found in Refs. [18–21], in *Proceedings of the PHYSTAT* conference series [22], and in the HEP Community White Paper [23]. Software for HEP includes the TMVA [24] and `scikit-learn` [25] packages.

An important issue in constructing a test is the choice of variables that enter into the data vector  $\boldsymbol{x}$ . For purposes of classification one may choose, for example, to form certain functions of particle momenta such as, *e.g.*, invariant masses that are felt to be physically meaningful in the context of a particular event type. It may be difficult to know, however, whether there may exist further features that would help distinguish between signal and background. Recently, so-called *Deep Neural Networks* containing several or more hidden layers have been applied in HEP [26, 27]; these allow one to use directly as inputs the elements of the data vector  $\boldsymbol{x}$  (features) that represent lower-level quantities such as individual particle momenta, rather than needing to first construct “by hand” higher level features. Each hidden layer then allows the network to construct significant high-level features in an automatic way.

The multivariate algorithms designed to classify events into signal and background types also form the basis of tests of the hypothesis that a sample of events consists of background only. Such a test can be constructed using the distributions of the test statistic  $t(\boldsymbol{x})$  for event classification obtained from a multivariate algorithm such as a Neural Network output. The distributions  $p(t|s)$  and  $p(t|b)$  for signal and background events, respectively, are used to construct the likelihood ratio of the signal-plus-background hypothesis relative to that of background only. To the extent that the test statistic  $t(\boldsymbol{x})$  approximates the likelihood ratio (or a monotonic function thereof) for individual events given by (40.44), the resulting test of the background-only hypothesis for the event sample will have maximum power with respect to the signal-plus-background alternative (see Ref. [28]).

#### 40.3.2 Tests of significance (goodness-of-fit)

Often one wants to quantify the level of agreement between the data and a hypothesis without explicit reference to alternative hypotheses. This can be done by defining a statistic  $t$  whose value reflects in some way the level of agreement between the data and the hypothesis. The analyst must decide what values of the statistic correspond to better or worse levels of agreement with the hypothesis in question; the choice will in general depend on the relevant alternative hypotheses.

The hypothesis in question,  $H_0$ , will determine the p.d.f.  $f(t|H_0)$  for the statistic. The significance of a discrepancy between the data and what one expects under the assumption of  $H_0$  is quantified by giving the *p-value*, defined as the probability to find  $t$  in the region of equal or lesser compatibility with  $H_0$  than the level of compatibility observed with the actual data. For example, if  $t$  is defined such that large values correspond to poor agreement with the hypothesis, then the *p-value* would be

$$p = \int_{t_{\text{obs}}}^{\infty} f(t|H_0) dt, \quad (40.45)$$

where  $t_{\text{obs}}$  is the value of the statistic obtained in the actual experiment.

The  $p$ -value is a function of the data, and is therefore itself a random variable. If the hypothesis used to compute the  $p$ -value is true, then for continuous data  $p$  will be uniformly distributed between zero and one. Note that the  $p$ -value is not the probability for the hypothesis; in frequentist statistics, this is not defined.

The  $p$ -value should not be confused with the size (significance level) of a test, or the confidence level of a confidence interval (Section 40.4), both of which are pre-specified constants. We may formulate a hypothesis test, however, by defining the critical region to correspond to the data outcomes that give the lowest  $p$ -values, so that finding  $p \leq \alpha$  implies that the data outcome was in the critical region. When constructing a  $p$ -value, one generally chooses the region of data space deemed to have lower compatibility with the model being tested as one having higher compatibility with a given alternative, such that the corresponding test will have a high power with respect to this alternative.

When searching for a new phenomenon, one tries to reject the hypothesis  $H_0$  that the data are consistent with known (*e.g.*, Standard Model) processes. If the  $p$ -value of  $H_0$  is sufficiently low, then one is willing to accept that some alternative hypothesis is true. Often one converts the  $p$ -value into an equivalent significance  $Z$ , defined so that a  $Z$  standard deviation upward fluctuation of a Gaussian random variable would have an upper tail area equal to  $p$ , *i.e.*,

$$Z = \Phi^{-1}(1 - p). \quad (40.46)$$

Here  $\Phi$  is the cumulative distribution of the standard Gaussian, and  $\Phi^{-1}$  is its inverse (quantile) function. Often in HEP the level of significance where an effect is said to qualify as a discovery is  $Z = 5$ , *i.e.*, a  $5\sigma$  effect, corresponding to a  $p$ -value of  $2.87 \times 10^{-7}$ . One's actual degree of belief that a new process is present, however, will depend in general on other factors as well, such as the plausibility of the new signal hypothesis and the degree to which it can describe the data, one's confidence in the model that led to the observed  $p$ -value, and possible corrections for multiple observations out of which one focuses on the smallest  $p$ -value obtained (the "look-elsewhere effect", discussed in Section 40.3.2.2).

#### 40.3.2.1 Treatment of nuisance parameters for frequentist tests

Suppose one wants to test hypothetical values of parameters  $\theta$ , but the model also contains nuisance parameters  $\nu$ . To find a  $p$ -value for  $\theta$  we can construct a test statistic  $q_\theta$  such that larger values constitute increasing incompatibility between the data and the hypothesis. Then for an observed value of the statistic  $q_{\theta, \text{obs}}$ , the  $p$ -value of  $\theta$  is

$$p_\theta(\nu) = \int_{q_{\theta, \text{obs}}}^{\infty} f(q_\theta | \theta, \nu) dq_\theta, \quad (40.47)$$

which depends in general on the nuisance parameters  $\nu$ . In the strict frequentist approach,  $\theta$  is rejected only if the  $p$ -value is less than  $\alpha$  for all possible values of the nuisance parameters.

The difficulty described above is effectively solved if we can define the test statistic  $q_\theta$  in such a way that its distribution  $f(q_\theta | \theta)$  is independent of the nuisance parameters. Although exact independence is only found in special cases, it can be achieved approximately by use of the *profile likelihood ratio*. This is given by the profile likelihood from Eq.(40.18) divided by the value of the likelihood at its maximum, *i.e.*, when evaluated with the ML estimators  $\hat{\theta}$  and  $\hat{\nu}$ :

$$\lambda_p(\theta) = \frac{L(\theta, \hat{\nu}(\theta))}{L(\hat{\theta}, \hat{\nu})}. \quad (40.48)$$

Wilks' theorem [9] states that, providing certain general conditions are satisfied, the distribution of  $-2 \ln \lambda_p(\theta)$ , under assumption of  $\theta$ , approaches a  $\chi^2$  distribution in the limit where the data sample is very large, independent of the values of the nuisance parameters  $\nu$ . Here the number of degrees of freedom is equal to the number of components of  $\theta$ . More details on use of the profile likelihood are given in Refs. [29, 30] and in contributions to the PHYSTAT conferences [22]; explicit formulae for special cases can be found in Ref. [31]. Further discussion on how to incorporate systematic uncertainties into  $p$ -values can be found in Ref. [32].

Even with use of the profile likelihood ratio, for a finite data sample the  $p$ -value of hypothesized parameters  $\theta$  will retain in general some dependence on the nuisance parameters  $\nu$ . Ideally one would find the maximum of  $p_\theta(\nu)$  from Eq. (40.47) explicitly, but that is often impractical. An approximate and computationally feasible technique is to use  $p_\theta(\hat{\nu}(\theta))$ , where  $\hat{\nu}(\theta)$  are the profiled values of the nuisance parameters as defined in Section 40.2.2.2. The resulting  $p$ -value is correct if the true values of the nuisance parameters are equal to the profiled values used; otherwise it could be either too high or too low. This is discussed further in Section 40.4.2 on confidence intervals.

One may also treat model uncertainties in a Bayesian manner but then use the resulting model in a frequentist test. Suppose the uncertainty in a set of nuisance parameters  $\nu$  is characterized by a Bayesian prior p.d.f.  $\pi(\nu)$ . This can be used to construct the marginal (also called the prior predictive) model for the data  $x$  and parameters of interest  $\theta$ ,

$$P_m(x|\theta) = \int P(x|\theta, \nu)\pi(\nu) d\nu. \quad (40.49)$$

The marginal model does not represent the probability of data that would be generated if one were really to repeat the experiment, as in that case one would assume that the nuisance parameters do not vary. Rather, the marginal model represents a situation in which every repetition of the experiment is carried out with new values of  $\nu$ , randomly sampled from  $\pi(\nu)$ . It is in effect an average of models each with a given  $\nu$ , where the average is carried out with respect to the prior p.d.f.  $\pi(\nu)$ .

The marginal model for the data  $x$  can be used to determine the distribution of a test statistic  $Q$ , which can be written

$$P_m(Q|\theta) = \int P(Q|\theta, \nu)\pi(\nu) d\nu. \quad (40.50)$$

In a search for a new signal process, the test statistic can be based on the ratio of likelihoods corresponding to the experiments where signal and background events are both present,  $L_{s+b}$ , to that of background only,  $L_b$ . Often the likelihoods are evaluated with the profiled values of the nuisance parameters, which may give improved performance. It is important to note, however, that it is through use of the marginal model for the distribution of  $Q$  that the uncertainties related to the nuisance parameters are incorporated into the result of the test. Different choices for the test statistic itself only result in variations of the power of the test with respect to different alternatives.

#### 40.3.2.2 The look-elsewhere effect

The "look-elsewhere effect" relates to multiple measurements used to test a single hypothesis. The classic example is when one searches in a distribution for a peak whose position is not predicted in advance. Here the no-peak hypothesis is tested using data in a given range of the distribution. In the frequentist approach the correct  $p$ -value of the no-peak hypothesis is the probability, assuming background only, to find a signal as significant as the one found or more so anywhere in the search region. This can be substantially higher than the probability to find a peak of equal or greater significance in the particular place where it appeared. There is in general some ambiguity as to what constitutes the relevant search region or even the broader set of relevant measurements. Although the desired  $p$ -value is well defined once the search region has been fixed, an exact treatment can require extensive computation.

The "brute-force" solution to this problem by Monte Carlo involves generating data under the background-only hypothesis and for each data set, fitting a peak of unknown position and recording a measure of its significance. To establish a discovery one often requires a  $p$ -value smaller than  $2.87 \times 10^{-7}$ , corresponding to a  $5\sigma$  or larger effect. Determining this with Monte Carlo thus requires generating and fitting a very large number of experiments, perhaps several times  $10^7$ . In contrast, if the position of the peak is fixed, then the fit to the distribution is much easier, and furthermore one can in many cases use formulae valid for sufficiently large samples that bypass completely the need for Monte Carlo

(see, e.g., [31]). However, this fixed-position or “local”  $p$ -value would not be correct in general, as it assumes the position of the peak was known in advance.

A method that allows one to modify the local  $p$ -value computed under assumption of a fixed position to obtain an approximation to the correct “global” value using a relatively simple calculation is described in Ref. [33]. Suppose a test statistic  $q_0$ , defined so that larger values indicate increasing disagreement with the data, is observed to have a value  $u$ . Furthermore suppose the model contains a nuisance parameter  $\theta$  (such as the peak position) which is only defined under the signal model (there is no peak in the background-only model). An approximation for the global  $p$ -value is found to be

$$p_{\text{global}} \approx p_{\text{local}} + \langle N_u \rangle, \quad (40.51)$$

where  $\langle N_u \rangle$ , which is much smaller than one in cases of interest, is the mean number of “upcrossings” of the statistic  $q_0$  above the level  $u$  in the range of the nuisance parameter considered (e.g., the mass range).

The value of  $\langle N_u \rangle$  can be estimated from the number of upcrossings  $\langle N_{u_0} \rangle$  above some much lower value,  $u_0$ , by using a relation due to Davis [34],

$$\langle N_u \rangle \approx \langle N_{u_0} \rangle e^{-(u-u_0)/2}. \quad (40.52)$$

By choosing  $u_0$  sufficiently low, the value of  $\langle N_u \rangle$  can be estimated by simulating only a very small number of experiments, or even from the observed data, rather than the  $10^7$  needed if one is dealing with a  $5\sigma$  effect.

#### 40.3.2.3 Goodness-of-fit with the method of least squares

When estimating parameters using the method of least squares, one obtains the minimum value of the quantity  $\chi^2$  (40.19). This statistic can be used to test the *goodness-of-fit*, i.e., the test provides a measure of the significance of a discrepancy between the data and the hypothesized functional form used in the fit. It may also happen that no parameters are estimated from the data, but that one simply wants to compare a histogram, e.g., a vector of Poisson distributed numbers  $\mathbf{n} = (n_1, \dots, n_N)$ , with a hypothesis for their expectation values  $\mu_i = E[n_i]$ . As the distribution is Poisson with variances  $\sigma_i^2 = \mu_i$ , the  $\chi^2$  (40.19) becomes *Pearson’s  $\chi^2$  statistic*,

$$\chi^2 = \sum_{i=1}^N \frac{(n_i - \mu_i)^2}{\mu_i}. \quad (40.53)$$

If the hypothesis  $\boldsymbol{\mu} = (\mu_1, \dots, \mu_N)$  is correct, and if the expected values  $\mu_i$  in (40.53) are sufficiently large (or equivalently, if the measurements  $n_i$  can be treated as following a Gaussian distribution), then the  $\chi^2$  statistic will follow the  $\chi^2$  p.d.f. with the number of degrees of freedom equal to the number of measurements  $N$  minus the number of fitted parameters.

Alternatively, one may fit parameters and evaluate goodness-of-fit by minimizing  $-2 \ln \lambda$  from Eq. (40.16). One finds that the distribution of this statistic approaches the asymptotic limit faster than does Pearson’s  $\chi^2$ . Therefore if one uses the asymptotic  $\chi^2$  p.d.f. as the statistic’s approximate sampling distribution to compute a  $p$ -value, one obtains in general a more accurate result from  $-2 \ln \lambda$  than from Pearson’s  $\chi^2$  (see Ref. [8] and references therein).

Assuming the goodness-of-fit statistic follows a  $\chi^2$  p.d.f., the  $p$ -value for the hypothesis is then

$$p = \int_{\chi^2}^{\infty} f(z; n_d) dz, \quad (40.54)$$

where  $f(z; n_d)$  is the  $\chi^2$  p.d.f. and  $n_d$  is the appropriate number of degrees of freedom. Values are shown in Fig. 40.1 or obtained from the ROOT function `TMath::Prob`. If the conditions for using the  $\chi^2$  p.d.f. do not hold, the statistic can still be defined as before, but its p.d.f. must be determined by other means in order to obtain the  $p$ -value, e.g., using a Monte Carlo calculation.

Since the mean of the  $\chi^2$  distribution is equal to  $n_d$ , one expects in a “reasonable” experiment to obtain  $\chi^2 \approx n_d$ . Hence the quantity  $\chi^2/n_d$  is sometimes reported. Since the p.d.f. of  $\chi^2/n_d$

depends on  $n_d$ , however, one must report  $n_d$  as well if one wishes to determine the  $p$ -value. The  $p$ -values obtained for different values of  $\chi^2/n_d$  are shown in Fig. 40.2.

If the minimized  $\chi^2$  value indicates a low level of agreement between data and hypothesis, one may be tempted to expect a high degree of uncertainty for any fitted parameters. Poor goodness-of-fit, however, does not mean that one will have large statistical errors for parameter estimates. If, for example, the error bars (or covariance matrix) used in constructing the  $\chi^2$  are underestimated, then this will lead to underestimated statistical errors for the fitted parameters. The standard deviations of estimators that one finds from, say, Eq. (40.13) reflect how widely the estimates would be distributed if one were to repeat the measurement many times, assuming that the hypothesis and measurement errors used in the  $\chi^2$  are also correct. They do not include the systematic error which may result from an incorrect hypothesis or incorrectly estimated measurement errors in the  $\chi^2$ .

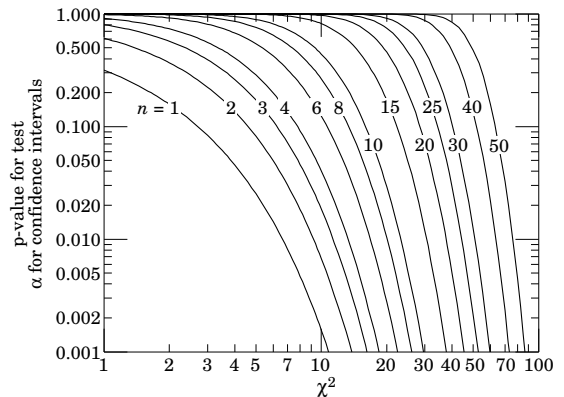


Figure 40.1: One minus the  $\chi^2$  cumulative distribution,  $1 - F(\chi^2; n)$ , for  $n$  degrees of freedom. This gives the  $p$ -value for the  $\chi^2$  goodness-of-fit test as well as one minus the coverage probability for confidence intervals (see Sec. 40.4.2.2).

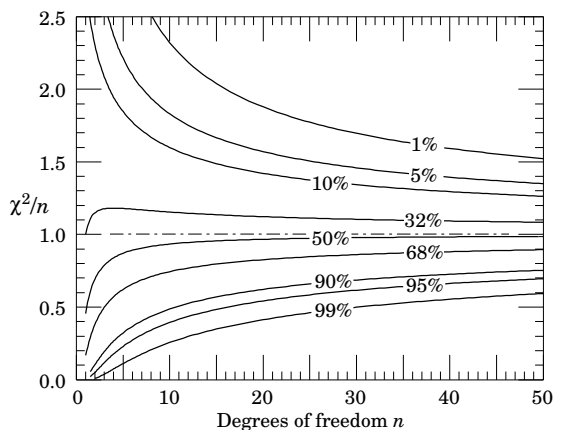


Figure 40.2: The ‘reduced’  $\chi^2$ , equal to  $\chi^2/n$ , for  $n$  degrees of freedom. The curves show as a function of  $n$  the  $\chi^2/n$  that corresponds to a given  $p$ -value.

#### 40.3.3 Bayes factors

In Bayesian statistics, all of one’s knowledge about a model is contained in its posterior probability, which one obtains using Bayes’ theorem (Eq. (40.35)). Thus one could reject a hypothesis  $H$  if its posterior probability  $P(H|\mathbf{x})$  is sufficiently small. The difficulty here is that  $P(H|\mathbf{x})$  is proportional to the prior probability  $P(H)$ , and there will not be a consensus about the prior probabilities for the existence of new phenomena. Nevertheless one can construct a quantity called the Bayes factor (described below), which can be used to quantify the degree to which the



data prefer one hypothesis over another, and is independent of their prior probabilities.

Consider two models (hypotheses),  $H_i$  and  $H_j$ , described by vectors of parameters  $\theta_i$  and  $\theta_j$ , respectively. Some of the components will be common to both models and others may be distinct. The full prior probability for each model can be written in the form

$$\pi(H_i, \theta_i) = P(H_i)\pi(\theta_i|H_i). \quad (40.55)$$

Here  $P(H_i)$  is the overall prior probability for  $H_i$ , and  $\pi(\theta_i|H_i)$  is the normalized p.d.f. of its parameters. For each model, the posterior probability is found using Bayes' theorem,

$$P(H_i|\mathbf{x}) = \frac{\int P(\mathbf{x}|\theta_i, H_i)P(H_i)\pi(\theta_i|H_i) d\theta_i}{P(\mathbf{x})}, \quad (40.56)$$

where the integration is carried out over the internal parameters  $\theta_i$  of the model. The ratio of posterior probabilities for the models is therefore

$$\frac{P(H_i|\mathbf{x})}{P(H_j|\mathbf{x})} = \frac{\int P(\mathbf{x}|\theta_i, H_i)\pi(\theta_i|H_i) d\theta_i}{\int P(\mathbf{x}|\theta_j, H_j)\pi(\theta_j|H_j) d\theta_j} \frac{P(H_i)}{P(H_j)}. \quad (40.57)$$

The *Bayes factor* is defined as

$$B_{ij} = \frac{\int P(\mathbf{x}|\theta_i, H_i)\pi(\theta_i|H_i) d\theta_i}{\int P(\mathbf{x}|\theta_j, H_j)\pi(\theta_j|H_j) d\theta_j}. \quad (40.58)$$

This gives what the ratio of posterior probabilities for models  $i$  and  $j$  would be if the overall prior probabilities for the two models were equal. If the models have no nuisance parameters, *i.e.*, no internal parameters described by priors, then the Bayes factor is simply the likelihood ratio. The Bayes factor therefore shows by how much the probability ratio of model  $i$  to model  $j$  changes in the light of the data, and thus can be viewed as a numerical measure of evidence supplied by the data in favour of one hypothesis over the other.

Although the Bayes factor is by construction independent of the overall prior probabilities  $P(H_i)$  and  $P(H_j)$ , it does require priors for all internal parameters of a model, *i.e.*, one needs the functions  $\pi(\theta_i|H_i)$  and  $\pi(\theta_j|H_j)$ . In a Bayesian analysis where one is only interested in the posterior p.d.f. of a parameter, it may be acceptable to take an unnormalizable function for the prior (an improper prior) as long as the product of likelihood and prior can be normalized. But improper priors are only defined up to an arbitrary multiplicative constant, and so the Bayes factor would depend on this constant. Furthermore, although the range of a constant normalized prior is unimportant for parameter determination (provided it is wider than the likelihood), this is not so for the Bayes factor when such a prior is used for only one of the hypotheses. So to compute a Bayes factor, all internal parameters must be described by normalized priors that represent meaningful probabilities over the entire range where they are defined.

An exception to this rule may be considered when the identical parameter appears in the models for both numerator and denominator of the Bayes factor. In this case one can argue that the arbitrary constants would cancel. One must exercise some caution, however, as parameters with the same name and physical meaning may still play different roles in the two models.

Both integrals in Equation (40.58) are of the form

$$m = \int P(\mathbf{x}|\theta)\pi(\theta) d\theta, \quad (40.59)$$

which is the marginal likelihood seen previously in Eq. (40.49) (in some fields this quantity is called the *evidence*). Computing marginal likelihoods can be difficult; in many cases it can be done with the nested sampling algorithm [35] as implemented, *e.g.*, in the program `MultiNest` [36]. A review of Bayes factors can be found in Ref. [37].

## 40.4 Intervals and limits

When the goal of an experiment is to determine a parameter  $\theta$ , the result is usually expressed by quoting, in addition to the point estimate, some sort of interval which reflects the statistical precision of the measurement. In the simplest case, this can be given by the parameter's estimated value  $\hat{\theta}$  plus or minus an estimate of the standard deviation of  $\hat{\theta}$ ,  $\hat{\sigma}_{\hat{\theta}}$ . If, however, the p.d.f. of the estimator is not Gaussian or if there are physical boundaries on the possible values of the parameter, then one usually quotes instead an interval according to one of the procedures described below.

In reporting an interval or limit, the experimenter may wish to

- communicate as objectively as possible the result of the experiment;
- provide an interval that is constructed to cover on average the true value of the parameter with a specified probability;
- provide the information needed by the consumer of the result to draw conclusions about the parameter or to make a particular decision;
- draw conclusions about the parameter that incorporate stated prior beliefs.

With a sufficiently large data sample, the point estimate and standard deviation (or for the multiparameter case, the parameter estimates and covariance matrix) satisfy essentially all of these goals. For finite data samples, no single method for quoting an interval will achieve all of them.

In addition to the goals listed above, the choice of method may be influenced by practical considerations such as ease of producing an interval from the results of several measurements. Of course the experimenter is not restricted to quoting a single interval or limit; one may choose, for example, first to communicate the result with a confidence interval having certain frequentist properties, and then in addition to draw conclusions about a parameter using a judiciously chosen subjective Bayesian prior. It is recommended, however, that there be a clear separation between these two aspects of reporting a result. In the remainder of this section, we assess the extent to which various types of intervals achieve the goals stated here.

### 40.4.1 Bayesian intervals

As described in Sec. 40.2.5, a Bayesian posterior probability may be used to determine regions that will have a given probability of containing the true value of a parameter. In the single parameter case, for example, an interval (called a Bayesian or credible interval)  $[\theta_{\text{lo}}, \theta_{\text{up}}]$  can be determined which contains a given fraction  $1 - \alpha$  of the posterior probability, *i.e.*,

$$1 - \alpha = \int_{\theta_{\text{lo}}}^{\theta_{\text{up}}} p(\theta|\mathbf{x}) d\theta. \quad (40.60)$$

Sometimes an upper or lower limit is desired, *i.e.*,  $\theta_{\text{lo}}$  or  $\theta_{\text{up}}$  can be set to a physical boundary or to plus or minus infinity. In other cases, one might be interested in the set of  $\theta$  values for which  $p(\theta|\mathbf{x})$  is higher than for any  $\theta$  not belonging to the set, which may constitute a single interval or a set of disjoint regions; these are called highest posterior density (HPD) intervals. Note that HPD intervals are not invariant under a nonlinear transformation of the parameter.

If a parameter is constrained to be non-negative, then the prior p.d.f. can simply be set to zero for negative values. An important example is the case of a Poisson variable  $n$ , which counts signal events with unknown mean  $s$ , as well as background with mean  $b$ , assumed known. For the signal mean  $s$ , one often uses the prior

$$\pi(s) = \begin{cases} 0 & s < 0 \\ 1 & s \geq 0 \end{cases}. \quad (40.61)$$

This prior may be regarded as providing an interval whose frequentist properties can be studied, rather than as representing a degree of belief. For example, to obtain an upper limit on  $s$ , one may proceed as follows. The likelihood for  $s$  is given by the Poisson distribution for  $n$  with mean  $s + b$ ,

$$P(n|s) = \frac{(s+b)^n}{n!} e^{-(s+b)}, \quad (40.62)$$

along with the prior (40.61) in (40.35) gives the posterior density for  $s$ . An upper limit  $s_{\text{up}}$  at confidence level (or here, rather, *credibility* level)  $1 - \alpha$  can be obtained by requiring

$$1 - \alpha = \int_{-\infty}^{s_{\text{up}}} p(s|n) ds = \frac{\int_{-\infty}^{s_{\text{up}}} P(n|s) \pi(s) ds}{\int_{-\infty}^{\infty} P(n|s) \pi(s) ds}, \quad (40.63)$$

where the lower limit of integration is effectively zero because of the cut-off in  $\pi(s)$ . By relating the integrals in Eq. (40.63) to incomplete gamma functions, the solution for the upper limit is found to be

$$s_{\text{up}} = \frac{1}{2} F_{\chi^2}^{-1} [p, 2(n+1)] - b, \quad (40.64)$$

where  $F_{\chi^2}^{-1}$  is the quantile of the  $\chi^2$  distribution (inverse of the cumulative distribution). Here the quantity  $p$  is

$$p = 1 - \alpha \left( 1 - F_{\chi^2} [2b, 2(n+1)] \right), \quad (40.65)$$

where  $F_{\chi^2}$  is the cumulative  $\chi^2$  distribution. For both  $F_{\chi^2}$  and  $F_{\chi^2}^{-1}$  above, the argument  $2(n+1)$  gives the number of degrees of freedom. For the special case of  $b = 0$ , the limit reduces to

$$s_{\text{up}} = \frac{1}{2} F_{\chi^2}^{-1} (1 - \alpha; 2(n+1)). \quad (40.66)$$

It happens that for the case of  $b = 0$ , the upper limit from Eq. (40.66) coincides numerically with the frequentist upper limit discussed in Section 40.4.2.3. Values for  $1 - \alpha = 0.9$  and  $0.95$  are given by the values  $\mu_{\text{up}}$  in Table 40.3. The frequentist properties of confidence intervals for the Poisson mean found in this way are discussed in Refs. [2] and [38].

As in any Bayesian analysis, it is important to show how the result changes under assumption of different prior probabilities. For example, one could consider the Jeffreys prior as described in Sec. 40.2.5. For this problem one finds the Jeffreys prior  $\pi(s) \propto 1/\sqrt{s+b}$  for  $s \geq 0$  and zero otherwise. As with the constant prior, one would not regard this as representing one's prior beliefs about  $s$ , both because it is improper and also as it depends on  $b$ . Rather it is used with Bayes' theorem to produce an interval whose frequentist properties can be studied.

If the model contains nuisance parameters then these are eliminated by marginalizing, as in Eq. (40.41), to obtain the p.d.f. for the parameters of interest. For example, if the parameter  $b$  in the Poisson counting problem above were to be characterized by a prior p.d.f.  $\pi(b)$ , then one would first use Bayes' theorem to find  $p(s, b|n)$ . This is then marginalized to find  $p(s|n) = \int p(s, b|n) \pi(b) db$ , from which one may determine an interval for  $s$ . One may not be certain whether to extend a model by including more nuisance parameters. In this case, a Bayes factor may be used to determine to what extent the data prefer a model with additional parameters, as described in Section 40.3.3.

#### 40.4.2 Frequentist confidence intervals

The unqualified phrase "confidence intervals" refers to frequentist intervals obtained with a procedure due to Neyman [39], described below. The boundary of the interval (or in the multiparameter case, region) is given by a specific function of the data, which would fluctuate if one were to repeat the experiment many times. The *coverage probability* refers to the fraction of intervals in such an ensemble that contain the true parameter value. Confidence intervals are constructed so as to have a coverage probability greater than or equal to a given *confidence level*, regardless of the true parameter's value. It is important to note that in the frequentist approach, such a probability is not meaningful for a fixed interval. In this section we discuss several techniques for producing intervals that have, at least approximately, this property of coverage.

##### 40.4.2.1 The Neyman construction for confidence intervals

Consider a p.d.f.  $f(x; \theta)$  where  $x$  represents the outcome of the experiment and  $\theta$  is the unknown parameter for which we want to construct a confidence interval. The variable  $x$  could (and often does) represent an estimator for  $\theta$ . Using  $f(x; \theta)$ , we can find using a pre-defined rule and probability  $1 - \alpha$  for every value of  $\theta$ , a set of values  $x_1(\theta, \alpha)$  and  $x_2(\theta, \alpha)$  such that

$$P(x_1 < x < x_2; \theta) = \int_{x_1}^{x_2} f(x; \theta) dx \geq 1 - \alpha. \quad (40.67)$$

If  $x$  is discrete, the integral is replaced by the corresponding sum. In that case there may not exist a range of  $x$  values whose summed probability is exactly equal to a given value of  $1 - \alpha$ , and one requires by convention  $P(x_1 < x < x_2; \theta) \geq 1 - \alpha$ .

This is illustrated for continuous  $x$  in Fig. 40.3: a horizontal line segment  $[x_1(\theta, \alpha), x_2(\theta, \alpha)]$  is drawn for representative values of  $\theta$ . The union of such intervals for all values of  $\theta$ , designated in the figure as  $D(\alpha)$ , is known as a *confidence belt*. Typically the curves  $x_1(\theta, \alpha)$  and  $x_2(\theta, \alpha)$  are monotonic functions of  $\theta$ , which we assume for this discussion.

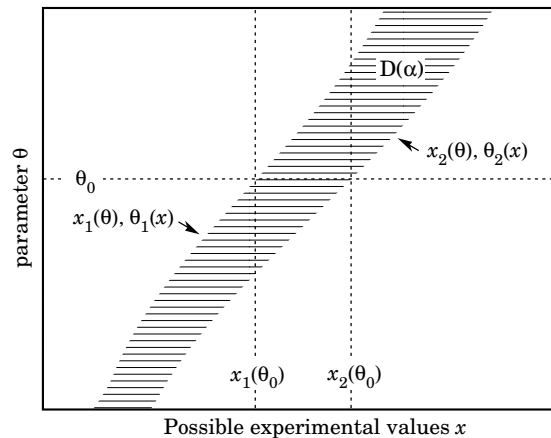


Figure 40.3: Construction of the confidence belt (see text).

Upon performing an experiment to measure  $x$  and obtaining a value  $x_0$ , one draws a vertical line through  $x_0$ . The confidence interval for  $\theta$  is the set of all values of  $\theta$  for which the corresponding line segment  $[x_1(\theta, \alpha), x_2(\theta, \alpha)]$  is intercepted by this vertical line. Such confidence intervals are said to have a *confidence level* (CL) equal to  $1 - \alpha$ .

Now suppose that the true value of  $\theta$  is  $\theta_0$ , indicated in the figure. We see from the figure that  $\theta_0$  lies between  $\theta_1(x)$  and  $\theta_2(x)$  if and only if  $x$  lies between  $x_1(\theta_0)$  and  $x_2(\theta_0)$ . The two events thus have the same probability, and since this is true for any value  $\theta_0$ , we can drop the subscript 0 and obtain

$$1 - \alpha = P(x_1(\theta) < x < x_2(\theta)) = P(\theta_2(x) < \theta < \theta_1(x)). \quad (40.68)$$

In this probability statement,  $\theta_1(x)$  and  $\theta_2(x)$ , *i.e.*, the endpoints of the interval, are the random variables and  $\theta$  is an unknown constant. If the experiment were to be repeated a large number of times, the interval  $[\theta_1, \theta_2]$  would vary, covering the fixed value  $\theta$  in a fraction  $1 - \alpha$  of the experiments.

The condition of coverage in Eq. (40.67) does not determine  $x_1$  and  $x_2$  uniquely, and additional criteria are needed. One possibility is to choose *central intervals* such that the probabilities to find  $x$  below  $x_1$  and above  $x_2$  are each  $\alpha/2$ . In other cases, one may want to report only an upper or lower limit, in which case one of  $P(x \leq x_1)$  or  $P(x \geq x_2)$  can be set to  $\alpha$  and the other to zero. Another principle based on *likelihood ratio ordering* for determining which values of  $x$  should be included in the confidence belt is discussed below.

When the observed random variable  $x$  is continuous, the coverage probability obtained with the Neyman construction is  $1 - \alpha$ , regardless of the true value of the parameter. Because of the requirement  $P(x_1 < x < x_2) \geq 1 - \alpha$  when  $x$  is discrete, one obtains

in that case confidence intervals that include the true parameter with a probability greater than or equal to  $1 - \alpha$ .

An equivalent method of constructing confidence intervals is to consider a test (see Sec. 40.3) of the hypothesis that the parameter's true value is  $\theta$  (assume one constructs a test for all physical values of  $\theta$ ). One then excludes all values of  $\theta$  where the hypothesis would be rejected in a test of size  $\alpha$  or less. The remaining values constitute the confidence interval at confidence level  $1 - \alpha$ . If the critical region of the test is characterized by having a  $p$ -value  $p_\theta \leq \alpha$ , then the endpoints of the confidence interval are found in practice by solving  $p_\theta = \alpha$  for  $\theta$ .

In the procedure outlined above, one is still free to choose the test to be used; this corresponds to the freedom in the Neyman construction as to which values of the data are included in the confidence belt. One possibility is to use a test statistic based on the *likelihood ratio*,

$$\lambda(\theta) = \frac{f(x; \theta)}{f(x; \hat{\theta})}, \quad (40.69)$$

where  $\hat{\theta}$  is the value of the parameter which, out of all allowed values, maximizes  $f(x; \theta)$ . This results in the intervals described in Ref. [40] by Feldman and Cousins. The same intervals can be obtained from the Neyman construction described above by including in the confidence belt those values of  $x$  which give the greatest values of  $\lambda(\theta)$ .

If the model contains nuisance parameters  $\nu$ , then these can be incorporated into the test (or the  $p$ -values) used to determine the limit by profiling as discussed in Section 40.3.2.1. As mentioned there, the strict frequentist approach is to regard the parameter of interest  $\theta$  as excluded only if it is rejected for all possible values of  $\nu$ . The resulting interval for  $\theta$  will then cover the true value with a probability greater than or equal to the nominal confidence level for all points in  $\nu$ -space.

If the  $p$ -value is based on the profiled values of the nuisance parameters, *i.e.*, with  $\nu = \hat{\nu}(\theta)$  used in Eq. (40.47), then the resulting interval for the parameter of interest will have the correct coverage if the true values of  $\nu$  are equal to the profiled values. Otherwise the coverage probability may be too high or too low. This procedure has been called *profile construction* in HEP [41] (see also [32]).

#### 40.4.2.2 Gaussian distributed measurements

An important example of constructing a confidence interval is when the data consists of a single random variable  $x$  that follows a Gaussian distribution; this is often the case when  $x$  represents an estimator for a parameter and one has a sufficiently large data sample. If there is more than one parameter being estimated, the multivariate Gaussian is used. For the univariate case with known  $\sigma$ , the probability that the measured value  $x$  will fall within  $\pm\delta$  of the true value  $\mu$  is

$$1 - \alpha = \frac{1}{\sqrt{2\pi}\sigma} \int_{\mu-\delta}^{\mu+\delta} e^{-(x-\mu)^2/2\sigma^2} dx = \text{erf}\left(\frac{\delta}{\sqrt{2}\sigma}\right) = 2\Phi\left(\frac{\delta}{\sigma}\right) - 1, \quad (40.70)$$

where erf is the Gaussian error function, which is rewritten in the final equality using  $\Phi$ , the Gaussian cumulative distribution. Fig. 40.4 shows a  $\delta = 1.64\sigma$  confidence interval unshaded. The choice  $\delta = \sigma$  gives an interval called the *standard error* which has  $1 - \alpha = 68.27\%$  if  $\sigma$  is known. Values of  $\alpha$  for other frequently used choices of  $\delta$  are given in Table 40.1.

We can set a one-sided (upper or lower) limit by excluding above  $x + \delta$  (or below  $x - \delta$ ). The values of  $\alpha$  for such limits are half the values in Table 40.1.

The relation (40.70) can be re-expressed using the cumulative distribution function for the  $\chi^2$  distribution as

$$\alpha = 1 - F(\chi^2; n), \quad (40.71)$$

for  $\chi^2 = (\delta/\sigma)^2$  and  $n = 1$  degree of freedom. This can be seen as the  $n = 1$  curve in Fig. 40.1 or obtained by using the ROOT function `TMath::Prob`. For multivariate measurements of, say,  $n$  parameter estimates  $\hat{\theta} = (\hat{\theta}_1, \dots, \hat{\theta}_n)$ , construction of the confidence

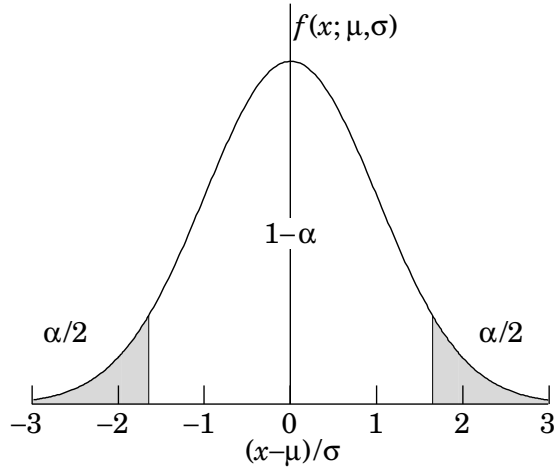


Figure 40.4: Illustration of a symmetric 90% confidence interval (unshaded) for a Gaussian-distributed measurement of a single quantity. Integrated probabilities, defined by  $\alpha = 0.1$ , are as shown.

Table 40.1: Area of the tails  $\alpha$  outside  $\pm\delta$  from the mean of a Gaussian distribution.

$\alpha$	$\delta$	$\alpha$	$\delta$
0.3173	$1\sigma$	0.2	$1.28\sigma$
$4.55 \times 10^{-2}$	$2\sigma$	0.1	$1.64\sigma$
$2.7 \times 10^{-3}$	$3\sigma$	0.05	$1.96\sigma$
$6.3 \times 10^{-5}$	$4\sigma$	0.01	$2.58\sigma$
$5.7 \times 10^{-7}$	$5\sigma$	0.001	$3.29\sigma$
$2.0 \times 10^{-9}$	$6\sigma$	$10^{-4}$	$3.89\sigma$

region requires the full covariance matrix  $V_{ij} = \text{cov}[\hat{\theta}_i, \hat{\theta}_j]$ , which can be estimated as described in Sections 40.2.2 and 40.2.3. Under fairly general conditions with the methods of maximum-likelihood or least-squares in the large sample limit, the estimators will be distributed according to a multivariate Gaussian centered about the true (unknown) values  $\theta$ , and furthermore, the likelihood function itself will take on a Gaussian shape.

The standard error ellipse for the pair  $(\hat{\theta}_i, \hat{\theta}_j)$  is shown in Fig. 40.5, corresponding to a contour  $\chi^2 = \chi^2_{\text{min}} + 1$  or  $\ln L = \ln L_{\text{max}} - 1/2$ . The ellipse is centered about the estimated values  $\hat{\theta}_i$ , and the tangents to the ellipse give the standard deviations of the estimators,  $\sigma_i$  and  $\sigma_j$ . The angle of the major axis of the ellipse is given by

$$\tan 2\phi = \frac{2\rho_{ij}\sigma_i\sigma_j}{\sigma_j^2 - \sigma_i^2}, \quad (40.72)$$

where  $\rho_{ij} = \text{cov}[\hat{\theta}_i, \hat{\theta}_j]/\sigma_i\sigma_j$  is the correlation coefficient.

The correlation coefficient can be visualized as the fraction of the distance  $\sigma_i$  from the ellipse's horizontal center-line at which the ellipse becomes tangent to vertical, *i.e.*, at the distance  $\rho_{ij}\sigma_i$  below the center-line as shown. As  $\rho_{ij}$  goes to  $+1$  or  $-1$ , the ellipse thins to a diagonal line.

It could happen that one of the parameters, say,  $\theta_j$ , is known from previous measurements to a precision much better than  $\sigma_j$ , so that the current measurement contributes almost nothing to the knowledge of  $\theta_j$ . However, the current measurement of  $\theta_i$  and its dependence on  $\theta_j$  may still be important. In this case, instead of quoting both parameter estimates and their correlation, one sometimes reports the value of  $\theta_i$ , which minimizes  $\chi^2$  at a fixed value of  $\theta_j$ , such as the PDG best value. This  $\theta_i$  value lies along the dotted line between the points where the ellipse becomes tangent to vertical, and has statistical error  $\sigma_{\text{inner}}$  as shown on the figure, where  $\sigma_{\text{inner}} = (1 - \rho_{ij}^2)^{1/2}\sigma_i$ . Instead of the correlation  $\rho_{ij}$ , one reports the dependency  $d\hat{\theta}_i/d\theta_j$ , which is the slope of the dotted line. This slope is related to the correlation coefficient by

$$d\hat{\theta}_i/d\theta_j = \rho_{ij} \times \frac{\sigma_i}{\sigma_j}.$$

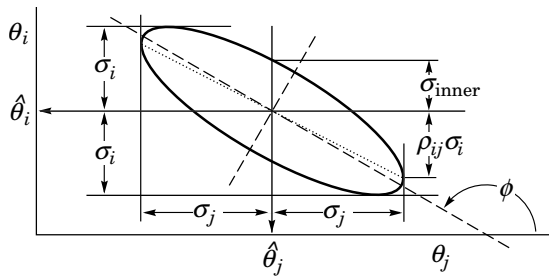


Figure 40.5: Standard error ellipse for the estimators  $\hat{\theta}_i$  and  $\hat{\theta}_j$ . In the case shown the correlation is negative.

As in the single-variable case, because of the symmetry of the Gaussian function between  $\theta$  and  $\hat{\theta}$ , one finds that contours of constant  $\ln L$  or  $\chi^2$  cover the true values with a certain, fixed probability. That is, the confidence region is determined by

$$\ln L(\theta) \geq \ln L_{\max} - \Delta \ln L, \quad (40.73)$$

or where a  $\chi^2$  has been defined for use with the method of least-squares,

$$\chi^2(\theta) \leq \chi^2_{\min} + \Delta \chi^2. \quad (40.74)$$

Values of  $\Delta \chi^2$  or  $2\Delta \ln L$  are given in Table 40.2 for several values of the coverage probability  $1 - \alpha$  and number of fitted parameters  $m$ . For Gaussian distributed data, these are related by  $\Delta \chi^2 = 2\Delta \ln L = F_{\chi_m^2}^{-1}(1 - \alpha)$ , where  $F_{\chi_m^2}^{-1}$  is the chi-square quantile (inverse of the cumulative distribution) for  $m$  degrees of freedom.

**Table 40.2:** Values of  $\Delta \chi^2$  or  $2\Delta \ln L$  corresponding to a coverage probability  $1 - \alpha$  in the large data sample limit, for joint estimation of  $m$  parameters.

$(1 - \alpha)$ (%)	$m = 1$	$m = 2$	$m = 3$
68.27	1.00	2.30	3.53
90.	2.71	4.61	6.25
95.	3.84	5.99	7.82
95.45	4.00	6.18	8.03
99.	6.63	9.21	11.34
99.73	9.00	11.83	14.16

For non-Gaussian data samples, the probability for the regions determined by Equations (40.73) or (40.74) to cover the true value of  $\theta$  becomes independent of  $\theta$  only in the large-sample limit. So for a finite data sample these are not exact confidence regions according to our previous definition. Nevertheless, they can still have a coverage probability only weakly dependent on the true parameter, and approximately as given in Table 40.2. In any case, the coverage probability of the intervals or regions obtained according to this procedure can in principle be determined as a function of the true parameter(s), for example, using a Monte Carlo calculation.

One of the practical advantages of intervals that can be constructed from the log-likelihood function or  $\chi^2$  is that it is relatively simple to produce the interval for the combination of several experiments. If  $N$  independent measurements result in log-likelihood functions  $\ln L_i(\theta)$ , then the combined log-likelihood function is simply the sum,

$$\ln L(\theta) = \sum_{i=1}^N \ln L_i(\theta). \quad (40.75)$$

This can then be used to determine an approximate confidence interval or region with Eq. (40.73), just as with a single experiment.

#### 40.4.2.3 Poisson or binomial data

Another important class of measurements consists of counting a certain number of events,  $n$ . In this section, we will assume these are all events of the desired type, *i.e.*, there is no background. If  $n$  represents the number of events produced in a reaction with cross section  $\sigma$ , say, in a fixed integrated luminosity  $\mathcal{L}$ , then it follows a Poisson distribution with mean  $\mu = \sigma \mathcal{L}$ . If, on the other hand, one has selected a larger sample of  $N$  events and found  $n$  of them to have a particular property, then  $n$  follows a binomial distribution where the parameter  $p$  gives the probability for the event to possess the property in question. This is appropriate, *e.g.*, for estimates of branching ratios or selection efficiencies based on a given total number of events.

For the case of Poisson distributed  $n$ , limits on the mean value  $\mu$  can be found from the Neyman procedure as discussed in Section 40.4.2.1 with  $n$  used directly as the statistic  $x$ . The upper and lower limits are found to be

$$\mu_{lo} = \frac{1}{2} F_{\chi^2}^{-1}(\alpha_{lo}; 2n), \quad (40.76a)$$

$$\mu_{up} = \frac{1}{2} F_{\chi^2}^{-1}(1 - \alpha_{up}; 2(n + 1)), \quad (40.76b)$$

where confidence levels of  $1 - \alpha_{lo}$  and  $1 - \alpha_{up}$  refer separately to the corresponding intervals  $\mu \geq \mu_{lo}$  and  $\mu \leq \mu_{up}$ , and  $F_{\chi^2}^{-1}$  is the quantile of the  $\chi^2$  distribution (inverse of the cumulative distribution). For central confidence intervals at confidence level  $1 - \alpha$ , set  $\alpha_{lo} = \alpha_{up} = \alpha/2$ .

**Table 40.3:** Lower and upper (one-sided) limits for the mean  $\mu$  of a Poisson variable given  $n$  observed events in the absence of background, for confidence levels of 90% and 95%.

$n$	$1 - \alpha = 90\%$		$1 - \alpha = 95\%$	
	$\mu_{lo}$	$\mu_{up}$	$\mu_{lo}$	$\mu_{up}$
0	–	2.30	–	3.00
1	0.105	3.89	0.051	4.74
2	0.532	5.32	0.355	6.30
3	1.10	6.68	0.818	7.75
4	1.74	7.99	1.37	9.15
5	2.43	9.27	1.97	10.51
6	3.15	10.53	2.61	11.84
7	3.89	11.77	3.29	13.15
8	4.66	12.99	3.98	14.43
9	5.43	14.21	4.70	15.71
10	6.22	15.41	5.43	16.96

It happens that the upper limit from Eq. (40.76b) coincides numerically with the Bayesian upper limit for a Poisson parameter, using a uniform prior p.d.f. for  $\mu$ . Values for confidence levels of 90% and 95% are shown in Table 40.3. For the case of binomially distributed  $n$  successes out of  $N$  trials with probability of success  $p$ , the upper and lower limits on  $p$  are found to be

$$p_{lo} = \frac{n F_F^{-1}[\alpha_{lo}; 2n, 2(N - n + 1)]}{N - n + 1 + n F_F^{-1}[\alpha_{lo}; 2n, 2(N - n + 1)]}, \quad (40.77a)$$

$$p_{up} = \frac{(n + 1) F_F^{-1}[1 - \alpha_{up}; 2(n + 1), 2(N - n)]}{(N - n) + (n + 1) F_F^{-1}[1 - \alpha_{up}; 2(n + 1), 2(N - n)]}. \quad (40.77b)$$

Here  $F_F^{-1}$  is the quantile of the  $F$  distribution (also called the Fisher-Snedecor distribution; see Ref. [4]).

#### 40.4.2.4 Parameter exclusion in cases of low sensitivity

An important example of a statistical test arises in the search for a new signal process. Suppose the parameter  $\mu$  is defined such that it is proportional to the signal cross section. A statistical test may be carried out for hypothesized values of  $\mu$ , which may be done by computing a  $p$ -value,  $p_\mu$ , for all  $\mu$ . Those values not rejected in a test of size  $\alpha$ , *i.e.*, for which one does not find  $p_\mu \leq \alpha$ , constitute a confidence interval with confidence level  $1 - \alpha$ .

In general one will find that for some regions in the parameter space of the signal model, the predictions for data are almost indistinguishable from those of the background-only model. This corresponds to the case where  $\mu$  is very small, as would occur, *e.g.*, in a search for a new particle with a mass so high that its production rate in a given experiment is negligible. That is, one has essentially no experimental sensitivity to such a model.

One would prefer that if the sensitivity to a model (or a point in a model's parameter space) is very low, then it should not be excluded. Even if the outcomes predicted with or without signal are identical, however, the probability to reject the signal model will equal  $\alpha$ , the type-I error rate. As one often takes  $\alpha$  to be 5%, this would mean that in a large number of searches covering a broad range of a signal model's parameter space, there would inevitably be excluded regions in which the experimental sensitivity is very small, and thus one may question whether it is justified to regard such parameter values as disfavored.

Exclusion of models to which one has little or no sensitivity occurs, for example, if the data fluctuate very low relative to the expectation of the background-only hypothesis. In this case the resulting upper limit on  $\mu$  may be anomalously low. As a means of controlling this effect one often determines the mean or median limit under assumption of the background-only hypothesis, as discussed in Sec. 40.5.

One way to mitigate the problem of excluding models to which one is not sensitive is the  $CL_s$  method, where the measure used to test a parameter is increased for decreasing sensitivity [42, 43]. The procedure is based on a statistic called  $CL_s$ , which is defined as

$$CL_s = \frac{p_\mu}{1 - p_b}, \quad (40.78)$$

where  $p_b$  is the  $p$ -value of the background-only hypothesis. In the usual formulation of the method, both  $p_\mu$  and  $p_b$  are defined using a single test statistic, and the definition of  $CL_s$  above assumes this statistic is continuous; more details can be found in Refs. [42, 43].

A point in a model's parameter space is regarded as excluded if one finds  $CL_s \leq \alpha$ . As the denominator in Eq. (40.78) is always less than or equal to unity, the exclusion criterion based on  $CL_s$  is more stringent than the usual requirement  $p_\mu \leq \alpha$ . In this sense the  $CL_s$  procedure is conservative, and the coverage probability of the corresponding intervals will exceed the nominal confidence level  $1 - \alpha$ . If the experimental sensitivity to a given value of  $\mu$  is very low, then one finds that as  $p_\mu$  decreases, so does the denominator  $1 - p_b$ , and thus the condition  $CL_s \leq \alpha$  is effectively prevented from being satisfied. In this way the exclusion of parameters in the case of low sensitivity is suppressed.

The  $CL_s$  procedure has the attractive feature that the resulting intervals coincide with those obtained from the Bayesian method in two important cases: the mean value of a Poisson or Gaussian distributed measurement with a constant prior. The  $CL_s$  intervals overcover for all values of the parameter  $\mu$ , however, by an amount that depends on  $\mu$ .

The problem of excluding parameter values to which one has little sensitivity is particularly acute when one wants to set a one-sided limit, *e.g.*, an upper limit on a cross section. Here one tests a value of a rate parameter  $\mu$  against the alternative of a lower rate, and therefore the critical region of the test is taken to correspond to data outcomes with a low event yield. If the number of events found in the search region fluctuates low enough, however, it can happen that all physically meaningful signal parameter values, including those to which one has very little sensitivity, are rejected by the test.

Another solution to this problem, therefore, is to replace the one-sided test by one based on the likelihood ratio, where the critical region is not restricted to low rates. This is the approach followed in the Feldman-Cousins procedure described in Section 40.4.2.1. The critical region for the test of a given value of  $\mu$  contains data values characteristic of both higher and lower rates. As a result, for a given observed rate one can in general obtain a two-sided interval. If, however, the parameter estimate  $\hat{\mu}$  is sufficiently close to the lower limit of zero, then only high values of  $\mu$  are rejected, and the lower edge of the confidence interval is at zero. Note, however, that the coverage property of

$1 - \alpha$  pertains to the entire interval, not to the probability for the upper edge  $\mu_{\text{up}}$  to be greater than the true value  $\mu$ . For parameter estimates increasingly far away from the boundary, *i.e.*, for increasing signal significance, the point  $\mu = 0$  is excluded and the interval has nonzero upper and lower edges.

An additional difficulty arises when a parameter estimate is not significantly far away from the boundary, in which case it is natural to report a one-sided confidence interval (often an upper limit). It is straightforward to force the Neyman prescription to produce only an upper limit by setting  $x_2 = \infty$  in Eq. (40.67). Then  $x_1$  is uniquely determined and the upper limit can be obtained. If, however, the data come out such that the parameter estimate is not so close to the boundary, one might wish to report a central confidence interval (*i.e.*, an interval based on a two-sided test with equal upper and lower tail areas). As pointed out by Feldman and Cousins [40], if the decision to report an upper limit or two-sided interval is made by looking at the data ("flip-flopping"), then in general there will be parameter values for which the resulting intervals have a coverage probability less than  $1 - \alpha$ . With the confidence intervals suggested in [40], the prescription determines whether the interval is one- or two-sided in a way which preserves the coverage probability (and are thus said to be *unified*).

The intervals according to this method for the mean of Poisson variable in the absence of background are given in Table 40.4. (Note that  $\alpha$  in Ref. [40] is defined following Neyman [39] as the coverage probability; this is opposite the modern convention used here in which the coverage probability is  $1 - \alpha$ .) The values of  $1 - \alpha$  given here refer to the coverage of the true parameter by the whole interval  $[\mu_1, \mu_2]$ . In Table 40.3 for the one-sided upper limit, however,  $1 - \alpha$  refers to the probability to have  $\mu_{\text{up}} \geq \mu$  (or  $\mu_{\text{lo}} \leq \mu$  for lower limits).

**Table 40.4:** Unified confidence intervals  $[\mu_1, \mu_2]$  for a the mean of a Poisson variable given  $n$  observed events in the absence of background, for confidence levels of 90% and 95%.

$n$	$1 - \alpha = 90\%$		$1 - \alpha = 95\%$	
	$\mu_1$	$\mu_2$	$\mu_1$	$\mu_2$
0	0.00	2.44	0.00	3.09
1	0.11	4.36	0.05	5.14
2	0.53	5.91	0.36	6.72
3	1.10	7.42	0.82	8.25
4	1.47	8.60	1.37	9.76
5	1.84	9.99	1.84	11.26
6	2.21	11.47	2.21	12.75
7	3.56	12.53	2.58	13.81
8	3.96	13.99	2.94	15.29
9	4.36	15.30	4.36	16.77
10	5.50	16.50	4.75	17.82

A potential difficulty with unified intervals arises if, for example, one constructs such an interval for a Poisson parameter  $s$  of some yet to be discovered signal process with, say,  $1 - \alpha = 0.9$ . If the true signal parameter is zero, or in any case much less than the expected background, one will usually obtain a one-sided upper limit on  $s$ . In a certain fraction of the experiments, however, a two-sided interval for  $s$  will result. Since, however, one typically chooses  $1 - \alpha$  to be only 0.9 or 0.95 when setting limits, the value  $s = 0$  may be found below the lower edge of the interval before the existence of the effect is well established. It must then be communicated carefully that in excluding  $s = 0$  at, say, 90% or 95% confidence level from the interval, one is not necessarily claiming to have discovered the effect, for which one would usually require a higher level of significance (*e.g.*,  $5\sigma$ ).

Another possibility is to construct a Bayesian interval as described in Section 40.4.1. The presence of the boundary can be incorporated simply by setting the prior density to zero in the unphysical region. More specifically, the prior may be chosen using formal rules such as the reference prior or Jeffreys prior mentioned in Sec. 40.2.5.

In HEP a widely used prior for the mean  $\mu$  of a Poisson distributed measurement has been the uniform distribution for

$\mu \geq 0$ . This prior does not follow from any fundamental rule nor can it be regarded as reflecting a reasonable degree of belief, since the prior probability for  $\mu$  to lie between any two finite values is zero. The procedure above can be more appropriately regarded as a way for obtaining intervals with frequentist properties that can be investigated. The resulting upper limits have a coverage probability that depends on the true value of the Poisson parameter, and is nowhere smaller than the stated probability content. Lower limits and two-sided intervals for the Poisson mean based on flat priors undercover, however, for some values of the parameter, although to an extent that in practical cases may not be too severe [2, 38].

In any case, it is important to always report sufficient information so that the result can be combined with other measurements. Often this means giving an unbiased estimator and its standard deviation, even if the estimated value is in the unphysical region.

It can also be useful with a frequentist interval to calculate its subjective probability content using the posterior p.d.f. based on one or several reasonable guesses for the prior p.d.f. If it turns out to be significantly less than the stated confidence level, this warns that it would be particularly misleading to draw conclusions about the parameter's value from the interval alone.

### 40.5 Experimental sensitivity

In this section we describe methods for characterizing the sensitivity of a search for a new physics signal. As discussed in Sec. 40.3, an experimental analysis can often be formulated as a test of hypothetical model parameters. Therefore we may quantify the sensitivity by giving the results that we expect from such a test under specific assumptions about the signal process.

Here to be concrete we will consider a parameter  $\mu$  proportional to the rate of a signal process, although the concepts described in this section may be easily generalized to other parameters. One may wish to establish discovery of the signal process by testing and rejecting the hypothesis that  $\mu = 0$ , and in addition one often wants to test nonzero values of  $\mu$  to construct a confidence interval (e.g., limits) as described in Sec. 40.4. In the frequentist framework, the result of each tested value of  $\mu$  is the  $p$ -value  $p_\mu$  or equivalently the significance  $Z_\mu = \Phi^{-1}(1 - p_\mu)$ , where as usual  $\Phi$  is the standard Gaussian cumulative distribution and its inverse  $\Phi^{-1}$  is the standard Gaussian quantile.

Prior to carrying out the experiment, one generally wants to quantify what significance  $Z_\mu$  is expected under given assumptions for the presence or absence of the signal process. Specifically, for the significance of a test of  $\mu = 0$  (the discovery significance) one usually quotes the  $Z_0$  one would expect if the signal is present at a given nominal rate, which we can define in general to correspond to  $\mu = 1$ . For limits, one often gives the expected limit under assumption of the background-only ( $\mu = 0$ ) model. These quantities are used to optimize the analysis and to quantify the experimental sensitivity, that is, to characterize how likely it is to make a discovery if the signal is present, and to say what values of  $\mu$  one may be able to exclude if the signal is in fact absent.

First we clarify the notion of *expected significance*. Because the significance  $Z_\mu$  is a function of the data, it is itself a random quantity characterized by a certain sampling distribution. This distribution depends on the assumed value of  $\mu$ , which is not necessarily the same as the hypothesized value of  $\mu$  being tested. We may therefore consider the distribution  $f(Z_\mu|\mu')$ , i.e., the distribution of  $Z_\mu$  that would be obtained by considering data samples generated under assumption of  $\mu'$ . In a similar way one can talk about the sampling distribution of an upper limit for  $\mu$ ,  $f(\mu_{\text{up}}|\mu')$ .

One can identify the expected significance or limit with either the mean or median of these distributions, but the median may be preferred since it is invariant under monotonic transformations. For example, the monotonic relation between  $p$ -value and significance,  $p = 1 - \Phi(Z)$ , then gives  $\text{med}[p_\mu|\mu'] = 1 - \Phi(\text{med}[Z_\mu|\mu'])$ , whereas the corresponding relation does not hold in general for the mean.

In some cases one may be able to write down approximate formulae for the distributions of  $Z_\mu$  and for limits, but more generally they must be determined from Monte Carlo calculations. In many

cases of interest, the significance  $Z_\mu$  and the limits on  $\mu$  will have approximate Gaussian distributions.

As an example, consider a Poisson counting experiment, where the result consists of an observed number  $n$  of events, modeled as a Poisson distributed variable with a mean of  $\mu s + b$ . Here  $s$  and  $b$ , the expected numbers of events from signal and background processes, are taken to be known. If we are interested in discovering the signal process we test and try to reject the hypothesis  $\mu = 0$ . To characterize the experimental sensitivity, we want to give the discovery significance expected under the assumption of  $\mu = 1$ .

In the limit where its mean value is large, the Poisson variable  $n$  can be approximated as an almost continuous Gaussian variable with mean  $\mu s + b$  and standard deviation  $\sigma = \sqrt{\mu s + b}$ . In the usual case where a physical signal model corresponds to  $\mu > 0$ , the  $p$ -value of  $\mu = 0$  is the probability to find  $n$  greater than or equal to the value observed,

$$p_0 = \Phi\left(\frac{n-b}{\sqrt{b}}\right), \quad (40.79)$$

and the corresponding significance is  $Z_0 = \Phi^{-1}(1 - p_0) = (n - b)/\sqrt{b}$ . The median (here equal to the mean) of  $n$  assuming  $\mu = 1$  is  $s + b$ , and therefore the median discovery significance is

$$\text{med}[Z_0|\mu = 1] = \frac{s}{\sqrt{b}}. \quad (40.80)$$

The figure of merit “ $s/\sqrt{b}$ ” has been widely used in HEP as a measure of expected discovery significance. A better approximation for the Poisson counting experiment, however, may be obtained by testing  $\mu = 0$  using the likelihood ratio (40.48)  $\lambda(0) = L(0)/L(\hat{\mu})$ , where

$$L(\mu) = \frac{(\mu s + b)^n}{n!} e^{-(\mu s + b)} \quad (40.81)$$

is the likelihood function,  $\hat{\mu} = (n - b)/s$  is the ML estimator. In this example there are no nuisance parameters, as  $s$  and  $b$  are taken to be known. For the case where the relevant signal models correspond to positive  $\mu$ , one may test the  $\mu = 0$  hypothesis with the statistic  $q_0 = -2 \ln \lambda(0)$  when  $\hat{\mu} > 0$ , i.e., an excess is observed, and  $q_0 = 0$  otherwise. One can show (see, e.g., [31]) that in the large-sample limit, the discovery significance is then  $Z_0 = \sqrt{q_0}$ , for which one finds

$$Z_0 = \sqrt{2 \left( n \ln \frac{n}{b} + b - n \right)} \quad (40.82)$$

for  $n > b$  and  $Z_0 = 0$  otherwise. To approximate the expected discovery significance assuming  $\mu = 1$ , one may simply replace  $n$  with the expected value  $E[n|\mu = 1] = s + b$  (the so-called “Asimov data set”), giving

$$\text{med}[Z_0|\mu = 1] = \sqrt{2 \left( (s + b) \ln \left( 1 + \frac{s}{b} \right) - s \right)}. \quad (40.83)$$

This has been shown in Ref. [31] to provide a good approximation to the median discovery significance for values of  $s$  of several and for  $b$  well below unity. The right-hand side of Eq. (40.83) reduces to  $s/\sqrt{b}$  in the limit  $s \ll b$ .

Beyond the simple Poisson counting experiment, in general one may test values of a parameter  $\mu$  with more complicated functions of the measured data to obtain a  $p$ -value  $p_\mu$ , and from this one can quote the equivalent significance  $Z_\mu$  or find, e.g., an upper limit  $\mu_{\text{up}}$ . In this case as well one may quantify the experimental sensitivity by giving the significance  $Z_\mu$  expected if the data are generated with a different value of the parameter  $\mu'$ . In some problems, finding the sampling distribution of the significance or limits may be possible using large-sample formulae as described, e.g., in Ref. [31]. In other cases a Monte Carlo study may be needed. Using whatever method of calculation is most appropriate, one usually quotes the expected (mean or, preferably, median) significance or limit as the primary measures of experimental sensitivity.

Even if the true signal is present at its nominal rate, the actual discovery significance  $Z_0$  obtained from the real data is subject to statistical fluctuations and will not in general be equal to its expected value. In an analogous way, the observed limit will differ from the expected limit even if the signal is absent. Upon observing such a difference one would like to know how large this is compared to expected statistical fluctuations. Therefore, in addition to the observed significance and limits it is useful to communicate not only their expected values but also a measure of the width of their distributions.

As the distributions of significance and limits are often well approximated by a Gaussian, one may indicate the intervals corresponding to plus-or-minus one and/or two standard deviations. If the distributions are significantly non-Gaussian, one may use instead the quantiles that give the same probability content, *i.e.*, [0.1587, 0.8413] for  $\pm 1\sigma$ , [0.02275, 0.97725] for  $\pm 2\sigma$ . An upper limit found significantly below the background-only expectation may indicate a strong downward fluctuation of the data, or perhaps as well an incorrect estimate of the background rate.

The procedures described above pertain to frequentist hypothesis tests and limits. Bayesian limits, just like those found from a frequentist procedure, are functions of the data and one may therefore find, usually with approximations or Monte Carlo studies, their sampling distribution and corresponding mean (or, preferably, median) and standard deviation.

When trying to establish discovery of a signal process, the Bayesian approach may employ a Bayes factor as described in Sec. 40.3.3. In the case of the Poisson counting experiment with the likelihood from Eq. (40.81), the log of the Bayes factor that compares  $\mu = 1$  to  $\mu = 0$  is  $\ln B_{10} = \ln(L(1)/L(0)) = n \ln(1 + s/b) - s$ . That is, the expectation value, assuming  $\mu = 1$ , of  $\ln B_{10}$  for this problem is

$$E[\ln B_{10} | \mu = 1] = (s + b) \ln \left( 1 + \frac{s}{b} \right) - s. \quad (40.84)$$

Comparing this to Eq. (40.83), one finds  $\text{med}[Z_0 | 1] = \sqrt{2E[\ln B_{10} | 1]}$ . Thus for this particular problem the frequentist median discovery significance can be related to the corresponding Bayes factor in a simple way.

In some analyses, the goal may not be to establish discovery of a signal process but rather to measure, as accurately as possible, the signal rate. If we consider again the Poisson counting experiment described by the likelihood function of Eq. (40.81), the ML estimator  $\hat{\mu} = (n - b)/s$  has a variance, assuming  $\mu = 1$ , of

$$V[\hat{\mu}] = V \left[ \frac{n - b}{s} \right] = \frac{1}{s^2} V[n] = \frac{s + b}{s^2}, \quad (40.85)$$

so that the standard deviation of  $\hat{\mu}$  is  $\sigma_{\hat{\mu}} = \sqrt{s + b}/s$ . One may therefore use  $s/\sqrt{s + b}$  as a figure of merit to be maximized in order to obtain the best measurement accuracy of a rate parameter. The quantity  $s/\sqrt{s + b}$  is also the expected significance with which one rejects  $s$  assuming the signal is absent, and thus can be used to optimize the expected upper limit on  $s$ .

## References

- [1] B. Efron, *Am. Stat.* **40**, 11 (1986).
- [2] R. D. Cousins, *Am. J. Phys.* **63**, 398 (1995).
- [3] A. Stuart, J.K. Ord, and S. Arnold, *Kendall's Advanced Theory of Statistics*, Vol. 2A: *Classical Inference and the Linear Model*, 6th ed., Oxford Univ. Press (1999), and earlier editions by Kendall and Stuart. The likelihood-ratio ordering principle is described at the beginning of Ch. 23. Chapter 26 compares different schools of statistical inference.
- [4] F. James, *Statistical methods in experimental physics* (2006), ISBN 9789812567956.
- [5] L. Lyons, *Statistics for Nuclear and Particle Physicists* (1986), ISBN 9780521379342, URL <http://www.cambridge.org/uk/catalogue/catalogue.asp?isbn=0521255406>.
- [6] R. J. Barlow, *Nucl. Instrum. Meth.* **A297**, 496 (1990).
- [7] G. Cowan, *Statistical data analysis* (1998), ISBN 9780198501565.
- [8] S. Baker and R. D. Cousins, *Nucl. Instrum. Meth.* **221**, 437 (1984).
- [9] S. S. Wilks, *Annals Math. Statist.* **9**, 1, 60 (1938).
- [10] O. Behnke *et al.*, editors, *Data analysis in high energy physics*, Wiley-VCH, Weinheim, Germany (2013), ISBN 9783527410583, 9783527653447, 9783527653430, URL <http://www.wiley-vch.de/publish/dt/books/ISBN3-527-41058-9>.
- [11] A. O'Hagan and J.J. Forster, *Bayesian Inference*, (2nd edition, volume 2B of *Kendall's Advanced Theory of Statistics*, Arnold, London, 2004).
- [12] D. Sivia and J. Skilling, *Data Analysis: A Bayesian Tutorial*, (Oxford University Press, 2006).
- [13] P.C. Gregory, *Bayesian Logical Data Analysis for the Physical Sciences*, (Cambridge University Press, 2005).
- [14] J.M. Bernardo and A.F.M. Smith, *Bayesian Theory*, (Wiley, 2000).
- [15] Robert E. Kass and Larry Wasserman, *J. Am. Stat. Assoc.* **91**, 1343 (1996).
- [16] J.M. Bernardo, *J. R. Statist. Soc.* **B41**, 113 (1979); J.M. Bernardo and J.O. Berger, *J. Am. Stat. Assoc.* **84**, 200 (1989). See also J.M. Bernardo, *Reference Analysis*, in *Handbook of Statistics*, 25 (D.K. Dey and C.R. Rao, eds.), 17-90, Elsevier (2005) and references therein.
- [17] L. Demortier, S. Jain and H. B. Prosper, *Phys. Rev.* **D82**, 034002 (2010), [arXiv:1002.1111].
- [18] Christopher M. Bishop, *Pattern Recognition and Machine Learning*, (Springer, New York, 2006).
- [19] T. Hastie, R. Tibshirani, and J. Friedman, *The Elements of Statistical Learning*, (2nd edition, Springer, New York, 2009).
- [20] A. Webb, *Statistical Pattern Recognition*, 2nd ed., (Wiley, New York, 2002).
- [21] L.I. Kuncheva, *Combining Pattern Classifiers*, (Wiley, New York, 2004).
- [22] Links to the *Proceedings of the PHYSTAT* conference series (Durham 2002, Stanford 2003, Oxford 2005, and Geneva 2007, 2011) can be found at [phystat.org](http://phystat.org).
- [23] K. Albertsson *et al.* (2018), [arXiv:1807.02876].
- [24] A. Hocker *et al.* (2007), [arXiv:physics/0703039]; Software available from [tmva.sourceforge.net](http://tmva.sourceforge.net).
- [25] F. Pedregosa *et al.*, *J. Machine Learning Res.* **12**, 2825 (2011), [arXiv:1201.0490].
- [26] P. Baldi, P. Sadowski and D. Whiteson, *Nature Commun.* **5**, 4308 (2014), [arXiv:1402.4735].
- [27] D. Guest, K. Cranmer and D. Whiteson, *Ann. Rev. Nucl. Part. Sci.* **68**, 161 (2018), [arXiv:1806.11484].
- [28] K. Cranmer, J. Pavez and G. Louppe (2015), [arXiv:1506.02169].
- [29] N. Reid, *Likelihood Inference in the Presence of Nuisance Parameters*, *Proceedings of PHYSTAT2003*, L. Lyons, R. Mount, and R. Reitmeyer, eds., eConf C030908, Stanford, 2003.
- [30] W. A. Rolke, A. M. Lopez and J. Conrad, *Nucl. Instrum. Meth.* **A551**, 493 (2005), [arXiv:physics/0403059].
- [31] G. Cowan *et al.*, *Eur. Phys. J.* **C71**, 1554 (2011), [Erratum: *Eur. Phys. J.* **C73**, 2501 (2013)], [arXiv:1007.1727].
- [32] L. Demortier, *P-Values and Nuisance Parameters*, *Proceedings of PHYSTAT 2007*, CERN-2008-001, p. 23.
- [33] E. Gross and O. Vitells, *Eur. Phys. J.* **C70**, 525 (2010), [arXiv:1005.1891].
- [34] R. B. Davies, *Biometrika* **74**, 33 (1987).
- [35] J. Skilling, *Nested Sampling*, *AIP Conference Proceedings*, **735**, 395-405 (2004).
- [36] F. Feroz, M. P. Hobson and M. Bridges, *Mon. Not. Roy. Astron. Soc.* **398**, 1601 (2009), [arXiv:0809.3437].

- [37] R. E. Kass and A. E. Raftery, *J. Am. Statist. Assoc.* **90**, 430, 773 (1995).
- [38] B. P. Roe and M. B. Woodroffe, *Phys. Rev.* **D63**, 013009 (2001), [hep-ex/0007048].
- [39] J. Neyman, *Phil. Trans. Roy. Soc. Lond.* **A236**, 767, 333 (1937); Reprinted in *A Selection of Early Statistical Papers on J. Neyman*, (University of California Press, Berkeley, 1967).
- [40] G. J. Feldman and R. D. Cousins, *Phys. Rev.* **D57**, 3873 (1998), [arXiv:physics/9711021]; This paper does not specify what to do if the ordering principle gives equal rank to some values of  $x$ . Eq. 21.6 of Ref. [3] gives the rule: all such points are included in the acceptance region (the domain  $D(\alpha)$ )/ Some authors have assumed the contrary, and shown that one can then jbtain null intervals.
- [41] K. Cranmer, in “Statistical Problems in Particle Physics, Astrophysics and Cosmology (PHYSTAT 05): Proceedings, Oxford, UK, September 12-15, 2005,” 112–123 (2005), [arXiv:physics/0511028], URL [http://www.physics.ox.ac.uk/phystat05/proceedings/files//Cranmer\\_LHCStatisticalChallenges.ps](http://www.physics.ox.ac.uk/phystat05/proceedings/files//Cranmer_LHCStatisticalChallenges.ps).
- [42] A. L. Read, in “Workshop on confidence limits, CERN, Geneva, Switzerland, 17-18 Jan 2000: Proceedings,” 81–101 (2000), URL <http://weblib.cern.ch/abstract?CERN-OPEN-2000-205>.
- [43] T. Junk, *Nucl. Instrum. Meth.* **A434**, 435 (1999), [hep-ex/9902006].



## 41. Monte Carlo Techniques

Revised August 2019 by G. Cowan (RHUL).

Monte Carlo techniques are often the only practical way to evaluate difficult integrals or to sample random variables governed by complicated probability density functions. Here we describe an assortment of methods for sampling some commonly occurring probability density functions.

### 41.1 Sampling the uniform distribution

Most Monte Carlo sampling or integration techniques assume a “random number generator,” which generates uniform statistically independent values on the half open interval  $[0, 1)$ ; for reviews see, *e.g.*, Refs. [1, 2].

Uniform random number generators are available in software libraries such as CLHEP [3], and ROOT [4]. For example, in addition to a basic congruential generator TRandom (see below), ROOT provides three more sophisticated routines: TRandom1 implements the RANLUX generator [5] based on the method by Lüscher, and allows the user to select different quality levels, trading off quality with speed; TRandom2 is based on the maximally equidistributed combined Tausworthe generator by L’Ecuyer [6]; the TRandom3 generator implements the Mersenne twister algorithm of Matsumoto and Nishimura [7]. All of the algorithms produce a periodic sequence of numbers, and to obtain effectively random values, one must not use more than a small subset of a single period. The Mersenne twister algorithm has an extremely long period of  $2^{19937} - 1$ .

The performance of the generators can be investigated with tests such as DIEHARD [8] or TestU01 [9]. Many commonly available congruential generators fail these tests and often have sequences (typically with periods less than  $2^{32}$ ), which can be easily exhausted on modern computers. A short period is a problem for the TRandom generator in ROOT, which, however, has the advantage that its state is stored in a single 32-bit word. The generators TRandom1, TRandom2, or TRandom3 have much longer periods, with TRandom3 being recommended by the ROOT authors as providing the best combination of speed and good random properties. For further information see, *e.g.*, Ref. [10].

### 41.2 Inverse transform method

If the desired probability density function is  $f(x)$  on the range  $-\infty < x < \infty$ , its cumulative distribution function (expressing the probability that  $x \leq a$ ) is given by Eq. (39.6). If  $a$  is chosen with probability density  $f(a)$ , then the integrated probability up to point  $a$ ,  $F(a)$ , is itself a random variable which will occur with uniform probability density on  $[0, 1]$ . Suppose  $u$  is generated according to a uniformly distributed in  $(0, 1)$ . If  $x$  can take on any value, and ignoring the endpoints, we can then find a unique  $x$  chosen from the p.d.f.  $f(x)$  for a given  $u$  if we set

$$u = F(x) , \tag{41.1}$$

provided we can find an inverse of  $F$ , defined by

$$x = F^{-1}(u) . \tag{41.2}$$

This method is shown in Fig. 41.1a. It is most convenient when one can calculate by hand the inverse function of the indefinite integral of  $f$ . This is the case for some common functions  $f(x)$  such as  $\exp(x)$ ,  $(1 - x)^n$ , and  $1/(1 + x^2)$  (Cauchy or Breit-Wigner), although it does not necessarily produce the fastest generator. Standard libraries contain software to implement this method numerically, working from functions or histograms in one or more dimensions, *e.g.*, the UNU.RAN package [11], available in ROOT. For a discrete distribution,  $F(x)$  will have a discontinuous jump of size  $f(x_k)$  at each allowed  $x_k, k = 1, 2, \dots$ . Choose  $u$  from a uniform distribution on  $(0,1)$  as before. Find  $x_k$  such that

$$F(x_{k-1}) < u \leq F(x_k) \equiv \text{Prob} (x \leq x_k) = \sum_{i=1}^k f(x_i) ; \tag{41.3}$$

then  $x_k$  is the value we seek (note:  $F(x_0) \equiv 0$ ). This algorithm is illustrated in Fig. 41.1b.

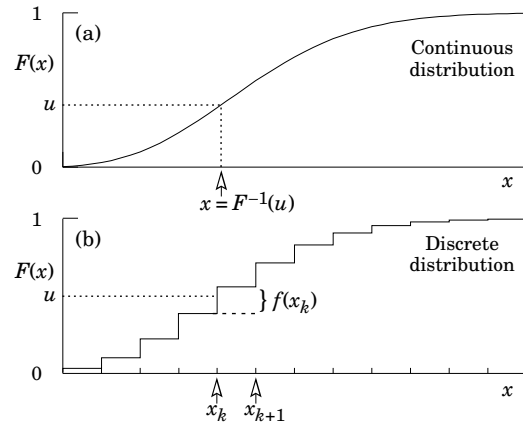


Figure 41.1: Use of a random number  $u$  chosen from a uniform distribution  $(0,1)$  to find a random number  $x$  from a distribution with cumulative distribution function  $F(x)$ .

### 41.3 Acceptance-rejection method (Von Neumann)

Very commonly an analytic form for  $F(x)$  is unknown or too complex to work with, so that obtaining an inverse as in Eq. (41.2) is impractical. We suppose that for any given value of  $x$ , the probability density function  $f(x)$  can be computed, and further that enough is known about  $f(x)$  that we can enclose it entirely inside a shape which is  $C$  times an easily generated distribution  $h(x)$ , as illustrated in Fig. 41.2. That is,  $Ch(x) \geq f(x)$  must hold for all  $x$ . Frequently  $h(x)$  is uniform or is a normalized

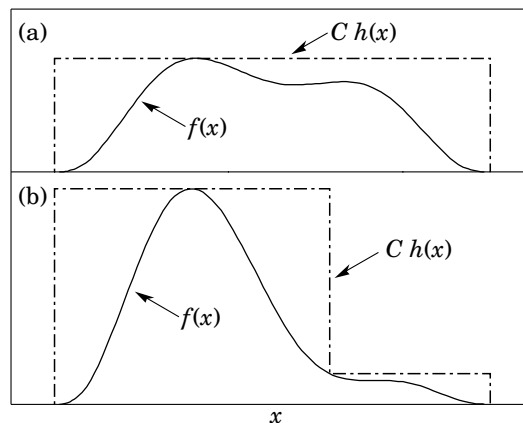


Figure 41.2: Illustration of the acceptance-rejection method. Random points are chosen inside the upper bounding figure, and rejected if the ordinate exceeds  $f(x)$ . The lower figure illustrates a method to increase the efficiency (see text).

sum of uniform distributions. Note that both  $f(x)$  and  $h(x)$  must be normalized to unit area, and therefore, the proportionality constant  $C > 1$ . To generate  $f(x)$ , first generate a candidate  $x$  according to  $h(x)$ . Calculate  $f(x)$  and the height of the envelope  $Ch(x)$ ; generate  $u$  and test if  $uCh(x) \leq f(x)$ . If so, accept  $x$ ; if not reject  $x$  and try again. If we regard  $x$  and  $uCh(x)$  as the abscissa and ordinate of a point in a two-dimensional plot, these points will populate the entire area  $Ch(x)$  in a smooth manner; then we accept those which fall under  $f(x)$ . The efficiency is the ratio of areas, which must equal  $1/C$ ; therefore we must keep  $C$  as close as possible to 1.0. Therefore, we try to choose  $Ch(x)$  to be as close to  $f(x)$  as convenience dictates, as in the lower part of Fig. 41.2.

### 41.4 Algorithms

Algorithms for generating random numbers belonging to many different distributions are given for example by Press [12], Ahrens and Dieter [13], Rubinstein [14], Devroye [15], Walck [16] and Gentle [17]. For many distributions, alternative algorithms exist, varying in complexity, speed, and accuracy. For time-critical applications, these algorithms may be coded in-line to remove the significant overhead often encountered in making function calls.

In the examples given below, we use the notation for the variables and parameters given in Table 39.1. Variables named “ $u$ ” are assumed to be independent and uniform on  $[0,1]$ . Denominators must be verified to be non-zero where relevant.

#### 41.4.1 Exponential decay

This is a common application of the inverse transform method, and uses the fact that if  $u$  is uniformly distributed in  $[0, 1]$ , then  $(1 - u)$  is as well. Consider an exponential p.d.f.  $f(t) = (1/\tau) \exp(-t/\tau)$  that is truncated so as to lie between two values,  $a$  and  $b$ , and renormalized to unit area. To generate decay times  $t$  according to this p.d.f., first let  $\alpha = \exp(-a/\tau)$  and  $\beta = \exp(-b/\tau)$ ; then generate  $u$  and let

$$t = -\tau \ln(\beta + u(\alpha - \beta)). \tag{41.4}$$

For  $(a, b) = (0, \infty)$ , we have simply  $t = -\tau \ln u$ . (See also Sec. 41.4.6.)

#### 41.4.2 Isotropic direction in 3D

Isotropy means the density is proportional to solid angle, the differential element of which is  $d\Omega = d(\cos \theta)d\phi$ . Hence  $\cos \theta$  is uniform  $(2u_1 - 1)$  and  $\phi$  is uniform  $(2\pi u_2)$ . For alternative generation of  $\sin \phi$  and  $\cos \phi$ , see the next subsection.

#### 41.4.3 Sine and cosine of random angle in 2D

Generate  $u_1$  and  $u_2$ . Then  $v_1 = 2u_1 - 1$  is uniform on  $(-1,1)$ , and  $v_2 = u_2$  is uniform on  $(0,1)$ . Calculate  $r^2 = v_1^2 + v_2^2$ . If  $r^2 > 1$ , start over. Otherwise, the sine ( $S$ ) and cosine ( $C$ ) of a random angle (*i.e.*, uniformly distributed between zero and  $2\pi$ ) are given by

$$S = 2v_1v_2/r^2 \quad \text{and} \quad C = (v_1^2 - v_2^2)/r^2. \tag{41.5}$$

#### 41.4.4 Gaussian distribution

If  $u_1$  and  $u_2$  are uniform on  $(0,1)$ , then

$$z_1 = \sin(2\pi u_1)\sqrt{-2 \ln u_2} \quad \text{and} \quad z_2 = \cos(2\pi u_1)\sqrt{-2 \ln u_2} \tag{41.6}$$

are independent and Gaussian distributed with mean 0 and  $\sigma = 1$ .

There are many variants of this basic algorithm, which may be faster. For example, construct  $v_1 = 2u_1 - 1$  and  $v_2 = 2u_2 - 1$ , which are uniform on  $(-1,1)$ . Calculate  $r^2 = v_1^2 + v_2^2$ , and if  $r^2 > 1$  start over. If  $r^2 < 1$ , it is uniform on  $(0,1)$ . Then

$$z_1 = v_1 \sqrt{\frac{-2 \ln r^2}{r^2}} \quad \text{and} \quad z_2 = v_2 \sqrt{\frac{-2 \ln r^2}{r^2}} \tag{41.7}$$

are independent numbers chosen from a normal distribution with mean 0 and variance 1.  $z'_i = \mu + \sigma z_i$  distributes with mean  $\mu$  and variance  $\sigma^2$ .

For a multivariate Gaussian with an  $n \times n$  covariance matrix  $V$ , one can start by generating  $n$  independent Gaussian variables,  $\{\eta_j\}$ , with mean 0 and variance 1 as above. Then the new set  $\{x_i\}$  is obtained as  $x_i = \mu_i + \sum_j L_{ij}\eta_j$ , where  $\mu_i$  is the mean of  $x_i$ , and  $L_{ij}$  are the components of  $L$ , the unique lower triangular matrix that fulfils  $V = LL^T$ . The matrix  $L$  can be easily computed by the following recursive relation (Cholesky’s method):

$$L_{jj} = \left( V_{jj} - \sum_{k=1}^{j-1} L_{jk}^2 \right)^{1/2}, \tag{41.8a}$$

$$L_{ij} = \frac{V_{ij} - \sum_{k=1}^{j-1} L_{ik}L_{jk}}{L_{jj}}, \quad j = 1, \dots, n; \quad i = j + 1, \dots, n, \tag{41.8b}$$

where  $V_{ij} = \rho_{ij}\sigma_i\sigma_j$  are the components of  $V$ . For  $n = 2$  one has

$$L = \begin{pmatrix} \sigma_1 & 0 \\ \rho\sigma_2 & \sqrt{1 - \rho^2}\sigma_2 \end{pmatrix}, \tag{41.9}$$

and therefore the correlated Gaussian variables are generated as  $x_1 = \mu_1 + \sigma_1\eta_1$ ,  $x_2 = \mu_2 + \rho\sigma_2\eta_1 + \sqrt{1 - \rho^2}\sigma_2\eta_2$ .

#### 41.4.5 $\chi^2(n)$ distribution

To generate a variable following the  $\chi^2$  distribution for  $n$  degrees of freedom, use the Gamma distribution with  $k = n/2$  and  $\lambda = 1/2$  using the method of Sec. 41.4.6.

#### 41.4.6 Gamma distribution

All of the following algorithms are given for  $\lambda = 1$ . For  $\lambda \neq 1$ , divide the resulting random number  $x$  by  $\lambda$ .

- If  $k = 1$  (the exponential distribution), accept  $x = -\ln u$ . (See also Sec. 41.4.1.)
- If  $0 < k < 1$ , initialize with  $v_1 = (e+k)/e$  (with  $e = 2.71828\dots$  being the natural log base). Generate  $u_1, u_2$ . Define  $v_2 = v_1 u_1$ .

**Case 1:**  $v_2 \leq 1$ . Define  $x = v_2^{1/k}$ . If  $u_2 \leq e^{-x}$ , accept  $x$  and stop, else restart by generating new  $u_1, u_2$ .

**Case 2:**  $v_2 > 1$ . Define  $x = -\ln([v_1 - v_2]/k)$ . If  $u_2 \leq x^{k-1}$ , accept  $x$  and stop, else restart by generating new  $u_1, u_2$ . Note that, for  $k < 1$ , the probability density has a pole at  $x = 0$ , so that return values of zero due to underflow must be accepted or otherwise dealt with.

- Otherwise, if  $k > 1$ , initialize with  $c = 3k - 0.75$ . Generate  $u_1$  and compute  $v_1 = u_1(1 - u_1)$  and  $v_2 = (u_1 - 0.5)\sqrt{c/v_1}$ . If  $x = k + v_2 - 1 \leq 0$ , go back and generate new  $u_1$ ; otherwise generate  $u_2$  and compute  $v_3 = 64v_1^3u_2^2$ . If  $v_3 \leq 1 - 2v_2^2/x$  or if  $\ln v_3 \leq 2\{[k - 1] \ln[x/(k - 1)] - v_2\}$ , accept  $x$  and stop; otherwise go back and generate new  $u_1$ .

#### 41.4.7 Binomial distribution

Begin with  $k = 0$  and generate  $u$  uniform in  $[0, 1)$ . Compute  $P_k = (1 - p)^n$  and store  $P_k$  into  $B$ . If  $u \leq B$  accept  $r_k = k$  and stop. Otherwise, increment  $k$  by one; compute the next  $P_k$  as  $P_k \cdot (p/(1 - p)) \cdot (n - k)/(k + 1)$ ; add this to  $B$ . Again, if  $u \leq B$ , accept  $r_k = k$  and stop, otherwise iterate until a value is accepted. If  $p > 1/2$ , it will be more efficient to generate  $r$  from  $f(r; n, q)$ , *i.e.*, with  $p$  and  $q$  interchanged, and then set  $r_k = n - r$ .

#### 41.4.8 Poisson distribution

Iterate until a successful choice is made: Begin with  $k = 1$  and set  $A = 1$  to start. Generate  $u$ . Replace  $A$  with  $uA$ ; if now  $A < \exp(-\mu)$ , where  $\mu$  is the Poisson parameter, accept  $n_k = k - 1$  and stop. Otherwise increment  $k$  by 1, generate a new  $u$  and repeat, always starting with the value of  $A$  left from the previous try.

Note that the Poisson generator used in ROOT’s `TRandom` classes before version 5.12 (including the derived classes `TRandom1`, `TRandom2`, `TRandom3`) uses a Gaussian approximation when  $\mu$  exceeds a given threshold. This may be satisfactory (and much faster) for some applications. To do this, generate  $z$  from a Gaussian with zero mean and unit standard deviation; then use  $x = \max(0, [\mu + z\sqrt{\mu} + 0.5])$  where  $[\ ]$  signifies the greatest integer  $\leq$  the expression. The routines from Numerical Recipes [12] and CLHEP’s routine `RandPoisson` do not make this approximation (see, *e.g.*, Ref. [10]).

#### 41.4.9 Student’s $t$ distribution

Generate  $u_1$  and  $u_2$  uniform in  $(0,1)$ ; then  $t = \sin(2\pi u_1)[n(u_2^{-2/n} - 1)]^{1/2}$  follows the Student’s  $t$  distribution for  $n > 0$  degrees of freedom ( $n$  not necessarily an integer).

Alternatively, generate  $x$  from a Gaussian with mean 0 and  $\sigma^2 = 1$  according to the method of 41.4.4. Next generate  $y$ ,

an independent gamma random variate, according to 41.4.6 with  $\lambda = 1/2$  and  $k = n/2$ . Then  $z = x/\sqrt{y/n}$  is distributed as a  $t$  with  $n$  degrees of freedom.

For the special case  $n = 1$ , the Breit-Wigner distribution, generate  $u_1$  and  $u_2$ ; set  $v_1 = 2u_1 - 1$  and  $v_2 = 2u_2 - 1$ . If  $v_1^2 + v_2^2 \leq 1$  accept  $z = v_1/v_2$  as a Breit-Wigner distribution with unit area, center at 0.0, and FWHM 2.0. Otherwise start over. For center  $M_0$  and FWHM  $\Gamma$ , use  $W = z\Gamma/2 + M_0$ .

#### 41.4.10 Beta distribution

The choice of an appropriate algorithm for generation of beta distributed random numbers depends on the values of the parameters  $\alpha$  and  $\beta$ . For, e.g.,  $\alpha = 1$ , one can use the transformation method to find  $x = 1 - u^{1/\beta}$ , and similarly if  $\beta = 1$  one has  $x = u^{1/\alpha}$ . For more general cases see, e.g., Refs. [16, 17] and references therein.

### 41.5 Markov Chain Monte Carlo

In applications involving generation of random numbers following a multivariate distribution with a high number of dimensions, the transformation method may not be possible and the acceptance-rejection technique may have too low of an efficiency to be practical. If it is not required to have independent random values, but only that they follow a certain distribution, then Markov Chain Monte Carlo (MCMC) methods can be used. In depth treatments of MCMC can be found, e.g., in the texts by Robert and Casella [18], Liu [19], and the review by Neal [20]. HEP-oriented software for MCMC is available from the Bayesian Analysis Toolkit (BAT) [21].

MCMC is particularly useful in connection with Bayesian statistics, where a p.d.f.  $p(\theta)$  for an  $n$ -dimensional vector of parameters  $\theta = (\theta_1, \dots, \theta_n)$  is obtained, and one needs the marginal distribution of a subset of the components. Here one samples  $\theta$  from  $p(\theta)$  and simply records the marginal distribution for the components of interest.

A simple and broadly applicable MCMC method is the Metropolis-Hastings algorithm, which allows one to generate multidimensional points  $\theta$  distributed according to a target p.d.f. that is proportional to a given function  $p(\theta)$ . It is not necessary to have  $p(\theta)$  normalized to unit area, which is useful in Bayesian statistics, as posterior probability densities are often determined only up to an unknown normalization constant.

To generate points that follow  $p(\theta)$ , one first needs a proposal p.d.f.  $q(\theta; \theta_0)$ , which can be (almost) any p.d.f. from which independent random values  $\theta$  can be generated, and which contains as a parameter another point in the same space  $\theta_0$ . For example, a multivariate Gaussian centered about  $\theta_0$  can be used. Beginning at an arbitrary starting point  $\theta_0$ , the Hastings algorithm iterates the following steps:

1. Generate a value  $\theta$  using the proposal density  $q(\theta; \theta_0)$ ;
2. Form the Hastings test ratio,  $\alpha = \min\left[1, \frac{p(\theta)q(\theta_0; \theta)}{p(\theta_0)q(\theta; \theta_0)}\right]$ ;
3. Generate a value  $u$  uniformly distributed in  $[0, 1]$ ;
4. If  $u \leq \alpha$ , take  $\theta_1 = \theta$ . Otherwise, repeat the old point, i.e.,  $\theta_1 = \theta_0$ .
5. Set  $\theta_0 = \theta_1$  and return to step 1.

If one takes the proposal density to be symmetric in  $\theta$  and  $\theta_0$ , then this is the *Metropolis-Hastings* algorithm, and the test ratio becomes  $\alpha = \min[1, p(\theta)/p(\theta_0)]$ . That is, if the proposed  $\theta$  is at a value of probability higher than  $\theta_0$ , the step is taken. If the proposed step is rejected, the old point is repeated.

Methods for assessing and optimizing the performance of the algorithm are discussed in, e.g., Refs. [18–20]. One can, for example, examine the autocorrelation as a function of the lag  $k$ , i.e., the correlation of a sampled point with that  $k$  steps removed. This should decrease as quickly as possible for increasing  $k$ .

Generally one chooses the proposal density so as to optimize some quality measure such as the autocorrelation. For certain problems it has been shown that one achieves optimal performance

when the acceptance fraction, that is, the fraction of points with  $u \leq \alpha$ , is around 40%. This can be adjusted by varying the width of the proposal density. For example, one can use for the proposal p.d.f. a multivariate Gaussian with the same covariance matrix as that of the target p.d.f., but scaled by a constant.

### 41.6 Generative Adversarial Networks

Recent developments in Machine Learning have led to new types of Monte Carlo methods based on generative models. The goal is to generate events each consisting of a vector of quantities  $\mathbf{x}$ , which could represent the set of pixels in an image or energy deposits in the cells of a calorimeter. Suppose, however, that we do not have direct access to the underlying probability density  $f(\mathbf{x})$ , but rather we only have an implicit model (e.g., a computer program able to simulate the complexities of the physical system), which can provide a set of events usable as training data. In the case of a calorimeter, for example, this could represent real events from a control measurement or simply the output from a detailed simulation.

Generative models such as such as Variational Autoencoders (VAEs) [22, 23] and Generative Adversarial Networks (GANs) [24] are algorithms for generating events that mimic the training data. Recently GANs have been investigated in HEP for simulation of energy deposits in calorimeters, so far in a simplified setting. They are able to generate events that capture detailed properties of those from a detailed Monte Carlo simulation but require far less computing time (for a recent example see, e.g., Ref. [25]).

Here we sketch the main ideas behind GANs used to simulate a random vector  $\mathbf{x}$ . This follows some distribution  $f(\mathbf{x})$  which itself is not known, but we have a set of instances (events)  $\mathbf{x}_1, \dots, \mathbf{x}_N$  as training data, here regarded as representative of the true distribution. We seek a function (the generator)  $G(\mathbf{z})$  which takes as input a vector of random numbers  $\mathbf{z}$  and produces directly as output an event vector, i.e.,  $\mathbf{x} = G(\mathbf{z})$ . The method is in this sense similar to the transformation method described in 41.2, but here both the function  $G$  and the input of random values  $\mathbf{z}$  are multidimensional. As a prototypical example we can take the components of  $\mathbf{z}$  as independent and Gaussian distributed about zero with unit variance.

The GAN makes use of two functions, the generator  $G(\mathbf{z})$  and a discriminator  $D(\mathbf{x})$ . The generator tries to produce events  $\mathbf{x}$  that mimic the (real) training data and thus look as if they were sampled from the unknown distribution  $f(\mathbf{x})$ . Simultaneously, the discriminator is trained to do its best to distinguish the generated events from the real ones.

To find the function  $G(\mathbf{z})$  that generates events that are as similar as possible to the training data, one may use a Deep Neural Network (DNN), i.e., a neural network with a sufficiently large number of hidden layers, and thus having a large set of parameters  $\theta_g$ . This is needed so that network is capable of modelling accurately the potentially complex density  $f(\mathbf{x})$ . The input layer corresponds to the components of the random vector  $\mathbf{z}$  and the multidimensional output layer to  $\mathbf{x}$ . The goal is thus reduced to finding optimal values of the parameters  $\theta_g$  using the training data.

The discriminator function  $D(\mathbf{x}; \theta_d)$  can also be a DNN containing parameters  $\theta_d$ . It takes as input an event (an instance in  $\mathbf{x}$ -space) and provides a single scalar output in  $[0, 1]$ , which should be as close as possible to zero for generated and one for real events.

The parameters of the generator and discriminator are chosen such that the function

$$V(\theta_g, \theta_d) = E_{\mathbf{x}}[\log(D(\mathbf{x}; \theta_d))] + E_{\mathbf{z}}[\log(1 - D(G(\mathbf{z}; \theta_g); \theta_d))] \quad (41.10)$$

is minimized with respect to  $\theta_g$  and simultaneously maximized with respect to  $\theta_d$ . For the expectation value in the first term,  $\mathbf{x}$  is sampled from the (real) training data; for the second term  $\mathbf{z}$  follows its given distribution, e.g., a multivariate standard Gaussian. That is, the discriminator is adjusted to maximize the probability that it will correctly identify an event as real or generated, and simultaneously the generator is tuned such that it produces

events which appear as real as possible when evaluated by the discriminator.

Challenges with GANs such as difficulty training the networks are an active area of research in Machine Learning. Once an optimal set of parameters is found, the transformation  $\mathbf{x} = G(\mathbf{z}; \theta_g)$  can be used to generate events in  $\mathbf{x}$ -space that capture detailed properties of the training data. Further information on applications, network architecture and training procedures can be found in, e.g., Ref. [25] and references therein.

### References

- [1] F. James, *Comput. Phys. Commun.* **60**, 329 (1990).
- [2] P. L'Ecuyer, *Proc. 1997 Winter Simulation Conference*, IEEE Press, Dec. 1997, 127–134.
- [3] L. Lonnblad, *Comput. Phys. Commun.* **84**, 307 (1994).
- [4] R. Brun and F. Rademakers, *Nucl. Instrum. Meth.* **A389**, 81 (1997); See also `root.cern.ch`.
- [5] F. James, *Comput. Phys. Commun.* **79**, 111 (1994), [Erratum: *Comput. Phys. Commun.* 97,357(1996)]; M. Luscher, *Comput. Phys. Commun.* **79**, 100 (1994), [hep-lat/9309020].
- [6] P. L'Ecuyer, *Mathematics of Computation*, **65**, 213 (1996) and **65**, 225 (1999).
- [7] M. Matsumoto and T. Nishimura, *ACM Transactions on Modeling and Computer Simulation*, Vol. 8, No. 1, January 1998, 3–30.
- [8] Much of DIEHARD is described in: G. Marsaglia, *A Current View of Random Number Generators*, keynote address, *Computer Science and Statistics: 16th Symposium on the Interface*, Elsevier (1985).
- [9] P. L'Ecuyer and R. Simard, *ACM Transactions on Mathematical Software* 33, 4, Article 1, December 2007.
- [10] J. Heinrich, CDF Note CDF/MEMO/STATISTICS/PUBLIC/8032, 2006.
- [11] UNU.RAN is described at `statmath.wu.ac.at/software/unuran`; See also W. Hörmann, J. Leydold, and G. Derflinger, *Automatic Nonuniform Random Variate Generation*, (Springer, New York, 2004).
- [12] W.H. Press *et al.*, *Numerical Recipes*, 3rd edition, (Cambridge University Press, New York, 2007).
- [13] J.H. Ahrens and U. Dieter, *Computing* **12**, 223 (1974).
- [14] R.Y. Rubinstein, *Simulation and the Monte Carlo Method*, (John Wiley and Sons, Inc., New York, 1981).
- [15] L. Devroye, *Non-Uniform Random Variate Generation*, (Springer-Verlag, New York, 1986); Available online at `luc.devroye.org/rnbookindex.html`.
- [16] C. Walck, *Handbook on Statistical Distributions for Experimentalists*, University of Stockholm Report SUF-PFY/96-01, available from `www.fysik.su.se/~walck`.
- [17] J.E. Gentle, *Random Number Generation and Monte Carlo Methods*, 2nd ed., (Springer, New York, 2003).
- [18] C.P. Robert and G. Casella, *Monte Carlo Statistical Methods*, 2nd ed., (Springer, New York, 2004).
- [19] J.S. Liu, *Monte Carlo Strategies in Scientific Computing*, (Springer, New York, 2001).
- [20] R.M. Neal, *Probabilistic Inference Using Markov Chain Monte Carlo Methods*, Technical Report CRG-TR-93-1, Dept. of Computer Science, University of Toronto, available from `www.cs.toronto.edu/~radford/res-mcmc.html`.
- [21] A. Caldwell, D. Kollar, K. Kröninger, *Comput. Phys. Commun.* **180** (2009) pages 2197-2209.
- [22] D.P. Kingma and M. Welling, *Auto-Encoding Variational Bayes*, Int. Conf. on Learning Representations, ICLR, 2014; E-print: arXiv:1312.6114 [stat.ML].
- [23] D.J. Rezende, S. Mohamed and D. Wierstra, *Stochastic Backpropagation and Approximate Inference in Deep Generative Models*, Proc. 31st Int. Conf. on Machine Learning, Beijing, 2014. JMLR: W&CP vol. 32; E-print: arXiv:1401.4082 [stat.ML].
- [24] I.J. Goodfellow *et al.*, *Generative Adversarial Nets*, Proceedings of Advances in Neural Information Processing Systems 27 (Z. Ghahramani *et al.*, eds., NIPS 2014) pages 2672–2680; E-print: arXiv:1406.2661 [stat.ML].
- [25] M. Paganini, L. de Oliveira and B. Nachman, *Phys. Rev. Lett.* **120**, 4, 042003 (2018), [arXiv:1705.02355].

## 42. Monte Carlo Event Generators

Revised September 2017 by P. Nason (INFN, Milan) and P.Z. Skands (Monash University).

General-purpose Monte Carlo (GPMC) generators like HERWIG [1,2,3], PYTHIA [4,5], and SHERPA [6], provide detailed simulations of high-energy collisions. They play an essential role in QCD modeling (in particular for aspects beyond fixed-order perturbative QCD) and in data analysis and the planning of new experiments, where they are used together with detector simulation to estimate signals and backgrounds in high-energy processes. They are built from several components, that describe the physics starting from very short distance scales, up to the typical scale of hadron formation and decay. Since QCD is weakly interacting at short distances (below a femtometer), the components of the GPMC dealing with short-distance physics are based upon perturbation theory. At larger distances, all soft hadronic phenomena, like hadronization and the formation of the underlying event in hadron collisions, cannot be computed from first principles at present, and one must rely upon QCD-inspired models.

The purpose of this review is to illustrate the main components of these generators. It is divided into four sections. The first one deals with short-distance, perturbative phenomena. The basic concepts leading to the simulations of the dominant QCD processes are illustrated here. In the second section, the nonperturbative transition from partons to hadrons (“hadronization”) is treated. The two most popular hadronization models, the string and cluster models, are illustrated. The basics of the implementation of decay chains of unstable “primary” hadrons into stable “secondaries” is also illustrated here. In the third section, models for soft hadron physics are discussed. These include models for the underlying event and for minimum-bias interactions. Issues of Bose-Einstein and color-reconnection effects are also discussed here. The fourth section briefly introduces the challenges of MC uncertainty estimates and tuning.

We use natural units throughout, such that  $c = 1$  and  $\hbar = 1$ , with energy, momenta and masses measured in GeV, and time and distances measured in  $\text{GeV}^{-1}$ .

### 42.1. Short-distance physics in GPMC generators

The short-distance components of a GPMC generator deal with the computation of the primary process at hand, with decays of short-lived particles, and with the generation of QCD and QED radiation. QCD radiation is computable in perturbation theory as long as the time scales involved are well below  $1/\Lambda$ , where  $\Lambda$  is a typical hadronic scale of few hundred MeV. Because of the presence of logarithmic enhancements due to both collinear and soft emissions, this description involves an indefinite number of final-state particles that are emitted at time scales below  $1/\Lambda$ . In  $e^+e^-$  annihilation into hadrons, for example, the time scale of the primary process is of the order of the inverse of the annihilation energy  $Q$ . Collinear and soft emissions take place at all time scales between  $1/Q$  and  $1/\Lambda$ . Technically, the computation of the dominant collinear and soft radiation is carried out by the so called shower algorithms. Historically, such algorithms were first developed for resummation of collinear singularities, leading to the so called “Parton Shower” algorithms. We will briefly describe this approach in this section. We stress, however, that many modern generators adopt approaches that focus initially upon soft singularities, leading to the so called “Dipole Showers” discussed in Sec. 42.1.3.

Collinear singularities arise when the angle between two emitted light partons becomes small. For example, in a process in which a quark and a gluon are emitted, if the angle  $\theta$  among them is very small (and is smaller than the angles among all other pairs of light partons in the process) the squared amplitude factorizes as follows

$$|M_{qg}|^2 d\Phi_{qg} \approx |M_q|^2 d\Phi_q \frac{\alpha_s}{2\pi} P_{q,gg}(z) dz \frac{d\phi}{2\pi} \frac{d\theta^2}{\theta^2} \quad (42.1)$$

where  $M_{qg}$ ,  $d\Phi_{qg}$  are the amplitude and phase space when both the gluon and the quark are emitted;  $M_q$ ,  $d\Phi_q$  are the amplitude and phase space when only the quark is emitted;  $z = E_q/(E_q + E_g)$  is the fraction of energy carried by the quark;  $\phi$  is the azimuth of the splitting plane, and  $P_{q,gg}(z) = C_F(1+z^2)/(1-z)$  is the Altarelli-Parisi

splitting kernel for gluon emission from a quark line, with color factor  $C_F = 4/3$ . The factorized form of Eq. (42.1) is due to the fact that for small angle the process is dominated by a single amplitude in which the splitting quark is almost on shell and hence propagates for long distances. We define the energy scale corresponding to the inverse of this distance as the *hardness* of the splitting process, so that larger hardness corresponds to shorter distance. We can define the hardness  $t$  as the product  $E^2\theta^2$ , or as the virtuality of the splitting parton  $p^2$ , or as a measure of the relative transverse momentum in the splitting such as the  $k_t$  of an emitted parton relative to its parent, defined by  $p^2 = 2E^2z(1-z)(1-\cos\theta) \approx z(1-z)E^2\theta^2$ ,  $k_T^2 = z^2(1-z)^2E^2\theta^2$ . (42.2)

If the region of small values of  $z$  and  $1-z$  was not important, these definitions would be equivalent. In QCD we also have soft divergences, arising when soft gluons are emitted. In Eq. (42.1) they appear as  $z \rightarrow 1$ , because of the  $1/(1-z)$  singularity of  $P_{q,gg}(z)$ . Thus, we expect that the choice of the appropriate ordering variable will be relevant when dealing with soft divergences (see Sec. 42.3). The  $d\theta^2/\theta^2$  factor in Eq. (42.1) can be equivalently written in terms of the hardness  $dt/t$ . After integration it gives rise to a logarithmic factor  $\log(Q^2/\Lambda^2)$ . We can have many subsequent splittings, that we can describe by applying Eq. (42.1) recursively, as long as the splittings are strongly ordered in decreasing hardness. This means that, from a typical final-state configuration, by clustering together final-state parton pairs with the smallest hardness recursively, we can reconstruct a branching tree, that may be viewed as the splitting history of the event. We stress that all hardness values between the hardness of the primary process and the cutoff scale  $\Lambda$  are equally involved here. The collinear approximation is applied recursively to splitting processes that have much smaller hardness with respect to all previous ones.

By integrating over the phase space, a process with  $n$  collinear splittings will be of order  $(\alpha_s(Q^2) \log(Q^2/\Lambda^2))^n$  with respect to the primary process. Since  $\alpha_s(Q^2) \propto 1/\log(Q^2/\Lambda^2)$  [7], these corrections are not small. The so-called KLN theorem [8,9] guarantees that large logarithmic enhancements arising from final-state collinear splitting cancel against the virtual corrections in inclusive cross sections, order by order in perturbation theory. Furthermore, the factorization theorem guarantees that initial-state collinear singularities can be factorized into the parton density functions (PDFs) [7]. Therefore, the cross section for the basic process remains accurate up to corrections of higher orders in  $\alpha_s(Q)$ , provided it is interpreted as an inclusive cross section, rather than as a bare partonic cross section. For example, the leading order (LO) cross section for  $e^+e^- \rightarrow q\bar{q}$  is a good LO estimate of the  $e^+e^-$  cross section for the production of a pair of quarks accompanied by an arbitrary number of collinear and soft gluons, but is not a good estimate of the cross section for the production of a  $q\bar{q}$  pair with no extra radiation. In summary, perturbation theory at fixed order can yield increasingly accurate predictions for inclusive observables, but cannot be used to describe the indefinite sequence of collinear and soft radiations that accompany the hard partons.

Parton-Shower algorithms are used to compute the cross section for generic hard processes including all dominant collinear radiation. These algorithms begin with the generation of the kinematics of the basic process, performed with a probability proportional to its LO partonic cross section. This is interpreted physically as the inclusive cross section for the basic process, followed by an arbitrary sequence of shower splittings. The algorithm then assigns a probability to each splitting sequence, so that the initial LO cross section is partitioned into the cross sections for a multitude of final states of arbitrary multiplicity, with their sum equal to the cross section of the primary process. This property of the GPMCs reflects the KLN cancellation mentioned earlier, and it is often called “unitarity of the shower process”, a name that reminds us that the KLN cancellation itself is a consequence of unitarity. The fact that a quantum mechanical process can be described in terms of composition of probabilities, rather than amplitudes, follows from the collinear approximation. In fact, because of strong ordering, a radiated parton cannot be collinear to more than one parton in the amplitude, and this suppresses interference effects.

We now illustrate the basic parton-shower algorithm, as first introduced in Ref. 11. (For more pedagogical introductions see Ref. 18

and references therein.) For simplicity, we consider the example of  $e^+e^-$  annihilation into  $q\bar{q}$  pairs, where we only have to deal with final state radiation (FSR). We consider all final states that can be built by dressing the  $q$  and  $\bar{q}$  partons with an indefinite number of splitting processes. By recursively clustering together final state parton pairs with the smallest relative hardness, from each final state configuration we can construct two trees rooted at the  $q$  and  $\bar{q}$  partons. The momenta of all intermediate lines of the tree diagrams are then uniquely determined from the final-state momenta. Hardnesses in the trees are ordered. One assigns to each splitting vertex the hardness  $t$ , the energy fractions  $z$  and  $1-z$  of the two generated partons, and the azimuth  $\phi$  of the splitting process with respect to the momentum of the incoming parton. For definiteness, we assume that  $z$  and  $\phi$  are defined in the center-of-mass (CM) frame of the  $e^+e^-$  collision. The differential cross section for a given final state is given by the product of the differential cross section for the initial  $e^+e^- \rightarrow q\bar{q}$  process, multiplied by a factor

$$\Delta_i(t_m, t_n) \frac{\alpha_S(t)}{2\pi} P_{i,jk}(z) \frac{dt_m}{t_m} dz \frac{d\phi}{2\pi} \quad (42.3)$$

for each intermediate line arising from the  $n^{\text{th}}$  and ending in the  $m^{\text{th}}$  splitting vertex.  $\Delta(t_m, t_n)$  is the so-called Sudakov form factor

$$\Delta_i(t_m, t_n) = \exp \left[ - \int_{t_m}^{t_n} \frac{dq^2}{q^2} \frac{\alpha_S(q^2)}{2\pi} \sum_{jk} P_{i,jk}(z) dz \frac{d\phi}{2\pi} \right]. \quad (42.4)$$

The suffixes  $i$  and  $jk$  represent the parton species of the incoming and final partons, respectively, and  $P_{i,jk}(z)$  are the Altarelli-Parisi [12] splitting kernels. Notice that the endpoints on the  $z$  integration depend upon the definition of hardness. For example, in case of virtuality or transverse momentum ordering, the  $z$  integration is automatically cut-off near the extremes, see eq. (1.2). When this is not the case (as, for example, for angular ordering) an explicit cut-off on  $z$  must be introduced, corresponding to the requirement that an emission must have some minimum energy to be distinguishable from no emission. For lines originating at the primary vertex, the scale  $t_n$  is replaced by the typical scale of the primary process and for lines ending without any further splitting the scale  $t_m$  is replaced by  $t_0$ , an infrared cutoff defined by the shower hadronization scale (at which the charges are screened by hadronization) or, for an unstable particle, its width (a source cannot emit radiation with a period exceeding its lifetime).

Eq. (42.3) can be obtained by iterating formula Eq. (42.1) recursively, with two important corrections: a) the strong coupling is evaluated at a scale corresponding to the hardness of the splitting process; b) the presence of the Sudakov form factor. Both these modifications arise from the inclusion of all collinear-dominant virtual corrections.

Notice that the Sudakov form factor for a small hardness interval  $\Delta_i(t, t + \delta t)$  is equal to one minus the integrated emission probability of Eq. (42.3), i.e. it can be interpreted as the probability of no emission in the interval  $t, t + \delta t$ . From this, it immediately follows that  $\Delta_i(t_m, t_n)$  can be interpreted as the no-emission probability in the full  $t_m, t_n$  interval. This interpretation allows to formulate the shower process as a probabilistic algorithm. We first notice that  $0 < \Delta_i(t_m, t_n) \leq 1$ , where the upper extreme is reached for  $t_m = t_n$ , and the lower extreme is approached for  $t_m = t_0$ . Starting from each of the partons in the primary process (e.g.,  $e^+e^- \rightarrow q\bar{q}$ ), event generation then proceeds recursively as follows. Given a parton exiting a vertex with hardness  $t_n$ , (taken to be of order the annihilation scale  $Q^2$  for the first branching) one seeks a solution of the equation  $r = \Delta_i(t_m, t_n)$ , with  $r \in [0, 1]$  a uniform random number, and solves it for the hardness of the next branching  $t_m$ . If  $t_m \leq t_0$ , no splitting is generated and the line is interpreted as a final parton. If  $t_m > t_0$ , a branching is generated at the scale  $t_m$ . Its  $z$  value and the final parton species  $jk$  are generated with a probability proportional to  $P_{i,jk}(z)$ . The azimuth is generated uniformly, neglecting angular correlations (see Sec. 42.1.1). This procedure is started with each of the primary process partons, and is applied recursively to all generated partons. It

may generate an arbitrary number of partons, and it stops when no final-state partons undergo further splitting.

The four-momenta of the final-state partons are reconstructed from the momenta of the initial ones, and from the whole sequence of splitting variables, subject to overall momentum conservation. Different algorithms employ different strategies to treat recoil effects due to momentum conservation, which may be applied either locally for each splitting, or globally for the entire set of partons (a procedure called *momentum reshuffling*.) This has a subleading effect with respect to the collinear approximation.

We emphasize that the shower cross sections described above can be derived from perturbative QCD by keeping only the collinear-dominant real and virtual contributions to the cross section. As such it is unproductive for large-angle radiation. It is thus unsafe to rely upon Parton Shower Monte Carlo alone to compute backgrounds to new physics signals that are characterized by several widely separated jets.

A Shower Monte Carlo builds its final state as if it developed from an iterative process, often with each intermediate stage made available to the user. It should be remarked that the meaning of these intermediate stages is only relevant within the approximation adopted by the generator, and could also differ in different implementations.

#### 42.1.1. Angular correlations :

In gluon-splitting processes ( $g \rightarrow q\bar{q}$ ,  $g \rightarrow gg$ ) in the collinear approximation, the distribution of the split pair is not uniform in azimuth, and the Altarelli-Parisi splitting functions are recovered only after azimuthal averaging. This dependence is due to the interference of positive and negative helicity states for the gluon that undergoes splitting. Spin correlations propagate through the splitting process, and determine acasual correlations of the EPR kind [13]. A method to partially account for these effects was introduced in Ref. 14, in which the azimuthal correlation between two successive splittings is computed by averaging over polarizations. This can then be applied at each branching step. Acasual correlations are argued to be small, and are discarded with this method, that is still used in PYTHIA [4]. A method that fully includes spin correlation effects was later proposed [15], and has been implemented in HERWIG [16,3].

#### 42.1.2. Initial-state radiation :

Initial-state radiation (ISR) arises because incoming particles may undergo collinear radiation before entering the hard-scattering process. In doing so, they acquire a non-vanishing transverse momentum, and their virtuality becomes negative (spacelike). It turns out to be convenient to develop the ISR shower starting with the highest hardness (i.e. with the hard process) and ending with the smallest (i.e. with the incoming parton in the hadron). Unlike the case of FSR, however, hardness ordering is opposite to time ordering in the ISR case. A corresponding backwards-evolution algorithm was formulated by Sjöstrand [17], and was basically adopted in all shower models. It can be illustrated by considering a primary interaction initiated by a quark where no collinear emission of hardness  $\geq t$  have taken place, and the same process where the quark also emits a collinear gluon of hardness  $t$ . The respective cross sections are proportional to

$$|M_q(x)|^2 dx f_q(x, t), \text{ and } |M_q(x)|^2 dx \frac{\alpha_S(t)}{2\pi} f_q(x/z, t) P_{q,gg}(z) dz \frac{d\phi}{2\pi} \frac{dt}{t}. \quad (42.5)$$

Here  $f_q$  is the quark PDF in the incoming hadron,  $x$  is the fraction of momentum of the incoming quark that enters the basic process, while  $x/z$  is the fraction of momentum of the incoming quark *before* it emits the collinear gluon. The elementary *emission probability* is the ratio of the second over the first expression in Eq. (42.5). In analogy with the final state radiation case, this ratio will appear in the exponent of the Sudakov form factor, that (after the inclusion of all splitting subprocesses) is given by

$$\Delta_i^{\text{ISR}}(t, t') = \exp \left[ - \int_{t'}^t \frac{dt''}{t''} \frac{\alpha_S(t'')}{2\pi} \int_x^1 \frac{dz}{z} \sum_{jk} P_{j,ik}(z) \frac{f_j(t'', x/z)}{f_i(t'', x)} \right]. \quad (42.6)$$

Notice that there are two uses of the PDFs: they are used to compute the cross section for the basic hard process, and they control

ISR via backward evolution. Since the evolution is generated with leading-logarithmic accuracy, it is acceptable to use two different PDF sets for these two tasks, provided they agree at the LO level.

In the context of GPMC evolution, each ISR emission generates a finite amount of transverse momentum. Details on how the recoils generated by these transverse “kicks” are distributed among other partons in the event, in particular the ones involved in the hard process, constitute one of the main areas of difference between existing algorithms, see Ref. 18. An additional  $\mathcal{O}(1 \text{ GeV})$  of “primordial  $k_T$ ” is typically added, to represent the sum of unresolved and/or non-perturbative motion below the shower cutoff scale.

#### 42.1.3. Soft emissions and QCD coherence :

Soft singularities arise in QCD due to the real or virtual emission of soft gluons. For example, the cross section for the emission of a soft gluon in  $e^+e^-$  annihilation into hadrons is given by

$$\begin{aligned} d\sigma_{q\bar{q}g} &\approx d\sigma_{q\bar{q}} \frac{4}{3} (4\pi\alpha_s) \left[ \frac{2 p_q \cdot p_{\bar{q}}}{p_q \cdot l p_{\bar{q}} \cdot l} \right] \frac{d^3l}{2l^0(2\pi)^3} \\ &= d\sigma_{q\bar{q}} \frac{\alpha_s}{2\pi} \frac{4}{3} \frac{d\phi}{l^0} \frac{d\cos\theta}{2\pi} \frac{1}{1-\cos^2\theta}, \end{aligned} \quad (42.7)$$

where  $p_q$ ,  $p_{\bar{q}}$  and  $l$  are the quark, antiquark and gluon momentum, and  $\theta$  and  $\phi$  are the polar and azimuthal angle of the gluon momentum with respect to the quark direction. Since the gluon is soft, we may assume that  $p_q$  and  $p_{\bar{q}}$  are unaffected by the gluon emission. The soft singularity is manifest in the  $d\phi^0/l^0$  factor. Notice that also collinear singularities are present at the same time when  $\theta \rightarrow 0$  and  $\theta \rightarrow \pi$ , corresponding to the gluon becoming collinear to either the quark or the antiquark. It is easy to check that in the collinear limits Eq. (42.7) becomes equivalent to Eq. (42.1) with  $P_{q,gg}(z) = (4/3)2/(1-z)$ , i.e. the limiting form of  $P_{q,gg}(z)$  when  $z$  approaches 1. Thus, soft singularities coexist with collinear ones, so that two potentially large logarithms can arise simultaneously due to gluon emission.

Unlike the case of collinear emission, soft emission is not tied to a single emitting particle. The amplitude for the emission of a soft gluon from an external (incoming or outgoing) line with momentum  $p$  is proportional to  $p \cdot \epsilon/p \cdot l$ . When squaring the amplitude, products like the one appearing in the square bracket of Eq. (42.1) arise for all pairs of external particles, with the product of a single emission amplitude with itself appearing only if  $p^2 > 0$ , i.e. for massive coloured particles. Thus interference plays here a crucial role. This is unlike the case of collinear singularities, where because of strong ordering a radiated parton cannot be collinear to more than one other parton.

It was shown in a set of publications (see Ref. 19) that, within the conventional parton-shower formalism based on collinear factorization, the region of collinear and soft emissions can be correctly described by using the angle of the emissions as the ordering variable, rather than the virtuality, and by setting the argument of  $\alpha_s$  at the splitting vertex equal to the relative parton transverse momentum after the splitting. Physically, the ordering in angle approximates the coherent interference arising from large-angle soft emission from a bunch of collinear partons. Without this effect, the particle multiplicity would grow too rapidly with energy, in conflict with  $e^+e^-$  data. For this reason, angular ordering is used as the default evolution variable in all versions of HERWIG (see Ref. 20). To partially account for soft interference effects, an angular veto is imposed on the virtuality-ordered evolution in PYTHIA 6 [21].

A radical alternative formulation of QCD cascades first proposed in Ref. 22 focuses upon soft emission, rather than collinear emission, as the basic splitting mechanism. It then becomes natural to consider a branching process where it is a parton pair (i.e. a dipole) rather than a single parton, that emits a soft parton. Adding a suitable correction for non-soft, collinear partons, one can simultaneously achieve the correct logarithmic structure for both the collinear and soft emissions in the so called leading color approximation, i.e. when terms suppressed by a power of the number of colors are neglected. The ARIADNE [23] and VINCIA [25] programs are based on this approach. Dipole-type showers [26] are also used by default in SHERPA [27] and exist as an option in HERWIG [28]. An alternative dipole-based model is available in PYTHIA and SHERPA via the DIRE [29]

plugin. The  $p_{\perp}$ -ordered showers in PYTHIA 6 and 8 represent a hybrid, combining collinear splitting kernels with dipole kinematics [30].

#### 42.1.4. Resummation :

It is notoriously difficult to assess the accuracy of shower Monte Carlos in comparison with QCD resummation calculations [7]. The latter start from the definition of a specific infrared-safe observable, which develops towers of large logarithms in certain regions of phase space. A dedicated resummation calculation must in general be performed for each new observable. The predictions of shower MCs, on the other hand, are cast in terms of complete sets of final-state momenta, on which one can evaluate any observable; i.e., the shower algorithm itself is normally independent of the specific observable(s) under study.

Generally, shower MCs perform much better than strict LL resummations; this is related to their inclusion of several universal but formally subleading aspects. But there are no guarantees. A shower MC may do well for some specific observables, and not for others. At present, it is difficult to make more precise and general statements than that. Instead, it is common to specify what kind of corrections are included. Typically, collinear emissions are accounted for, although not always including angular correlations. Soft emissions are dealt with to some extent via angular ordering or dipole approaches. The most important and ubiquitous aspects beyond the strict LL approximation are momentum conservation and optimised scale choices. The former is obviously physical, hence including it should yield better results than not doing so (indeed, momentum conservation does become an aspect of QCD resummation calculations beyond LL), although the precise way of how the resulting recoil effects are handled in the shower is ambiguous. The latter can be tied, e.g., to reaching NLL accuracy for soft emissions for observables such as the transverse momentum of Drell-Yan pairs [101].

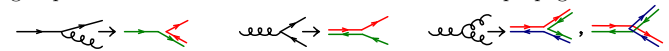
#### 42.1.5. Massive quarks :

Quark masses act as a cut-off on collinear singularities. If the mass of a quark is below, or of the order of  $\Lambda$ , its effect in the shower is small. For larger quark masses, like in  $c$ ,  $b$ , or  $t$  production, it is the mass, rather than the typical hadronic scale, that cuts off collinear radiation. For a quark with energy  $E$  and mass  $m_Q$ , the divergent behavior  $d\theta/\theta$  of the collinear splitting process is regulated for  $\theta \leq \theta_0 = m_Q/E$ . We thus expect less collinear activity for heavy quarks than for light ones, which in turn is the reason why heavy quarks carry a larger fraction of the momentum acquired in the hard production process.

This feature can be implemented with different levels of sophistication. Using the fact that soft emission exhibits a zero at zero emission angle, older parton shower algorithms simply limited the shower emission to be not smaller than the angle  $\theta_0$ . More modern approaches are used in both PYTHIA, where mass effects are included using a kind of matrix-element correction method [31], and in HERWIG++ and SHERPA, where a generalization of the Altarelli-Parisi splitting kernel is used for massive quarks [32].

#### 42.1.6. Color information :

In event generators, quarks and antiquarks are represented by color lines, with arrows indicating the direction of color flow. In the limit of infinitely many colors (called the leading color approximation), each such line can be associated with a unique label; the probability for two quarks (or antiquarks) to have the same color (anticolor) vanishes. Moreover, in the same limit gluons can be represented by a pair of color lines with opposite arrows, as can be realised e.g. from the SU(3) group relation  $8 = 3 \otimes \bar{3} \ominus 1$ . The rules for color propagation are:



During the shower development, partons are connected by color lines. We can have a quark directly connected by a color line to an antiquark, or via an arbitrary number of intermediate gluons, as shown in Fig. 42.1. It is also possible for a set of gluons to be connected cyclically in color, as e.g. in the decay  $\Upsilon \rightarrow ggg$ .

The color information is used in angular-ordered showers, where the angle of color-connected partons (i.e. partons connected by the same color line) determines the initial angle for the shower development, and in dipole showers, where dipoles are always color-connected partons. It is also used in hadronization models, where the initial strings or



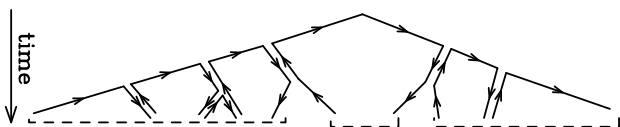


**Figure 42.1:** Color development of a shower in  $e^+e^-$  annihilation. Color-neutral clusters of partons are indicated by the dashed under-brackets.

clusters used for hadronization are formed by color-neutral clusters of partons.

#### 42.1.7. Electromagnetic corrections :

The physics of photon emission from light charged particles can also be treated with a shower MC algorithm. High-energy electrons and quarks, for example, are accompanied by bremsstrahlung photons. Also here, similarly to the QCD case, electromagnetic corrections are of order  $\alpha_{\text{em}} \ln(Q/m)$ , where  $m$  is the mass of the radiating particle, or even of order  $\alpha_{\text{em}} \ln(Q/m) \ln(E_\gamma/E)$  in the region where soft photon emission is important, so that, especially for the case of electrons, their inclusion in the simulation process is mandatory. This is done in most of the GPMC's (for a recent comparative study see [33]). The specialized generator PHOTOS [34] is sometimes used as an afterburner for an improved treatment of QED radiation in non-hadronic resonance decays.

For photon emissions off leptons, the shower can be continued down to virtualities arbitrarily close to the lepton mass shell (unlike the case in QCD). In practice, an infrared cutoff is still required for the shower algorithm to terminate. Therefore, there is always an energy cut-off for emitted photons that depends upon the implementations [33]. In the case of electrons, this energy is typically of the order of its mass. Electromagnetic radiation below this scale is not enhanced by collinear singularities, and is thus bound to be soft, so that the electron momentum is not affected by it.

For photons emitted from quarks, we have instead the obvious limitation that the photon wavelength cannot exceed the typical hadronic size. Longer-wavelength photons are in fact emitted by hadrons, rather than quarks. This last effect is in practice never modeled by existing shower MC implementations. Thus, electromagnetic radiation from quarks is cut off at a typical hadronic scale. Finally, hadron (and  $\tau$ ) decays involving charged particles can produce additional soft bremsstrahlung. This is implemented in a general way in HERWIG++/HERWIG 7 [35] and SHERPA [36].

#### 42.1.8. Beyond-the-Standard-Model Physics :

The inclusion of processes for physics beyond the Standard Model (BSM) in event generators is to some extent only a matter of implementing the relevant hard processes and (chains of) decays, with the level of difficulty depending on the complexity of the model and the degree of automation [37,38]. Notable exceptions are long-lived colored particles [39], particles in exotic color representations, and particles showering under new gauge symmetries, with a growing set of implementations documented in the individual GPMC manuals. Further complications that may be relevant are finite-width effects (discussed in Sec. 42.1.9) and the assumed threshold behavior.

In addition to code-specific implementations [18], there are a few commonly adopted standards that are useful for transferring information and events between codes. Currently, the most important of these is the Les Houches Event File (LHEF) standard [40], normally used to transfer parton-level events from a hard-process generator to a shower generator. Another important standard is the Supersymmetry Les Houches Accord (SLHA) format [41], originally used to transfer information on supersymmetric particle spectra and couplings, but by now extended to apply also to more general BSM frameworks and incorporated within the LHEF standard [42].

#### 42.1.9. Decay Chains and Particle Widths :

In most BSM processes and some SM ones, an important aspect of the event simulation is how decays of short-lived particles, such as top quarks, EW and Higgs bosons, and new BSM resonances, are

handled. We here briefly summarize the spectrum of possibilities, but emphasize that there is no universal standard. Users are advised to check whether the treatment of a given code is adequate for the physics study at hand.

The appearance of an unstable resonance as a physical particle at an intermediate stage of the event generation implies that its production and decay processes are treated as being factorized. This is valid up to corrections of order  $\Gamma/m_0$ , with  $\Gamma$  the width and  $m_0$  the pole mass. States whose widths are a substantial fraction of their mass should instead be treated as intrinsically off-shell internal propagator lines.

For states treated as physical particles, two aspects are relevant: the mass distribution of the decaying particle itself and the distributions of its decay products. For the former, matrix-element generators often use a simple  $\delta$  function at  $m_0$ . The next level up, typically used in GPMCs, is to use a Breit-Wigner distribution (relativistic or non-relativistic), which formally resums higher-order virtual corrections to the mass distribution. Note, however, that this still only generates an improved picture for moderate fluctuations away from  $m_0$ . Similarly to above, particles that are significantly off-shell (in units of  $\Gamma$ ) should not be treated as resonant, but rather as internal off-shell propagator lines. In most GPMCs, further refinements are included, for instance by letting  $\Gamma$  be a function of  $m$  (“running widths”) and by limiting the magnitude of the allowed fluctuations away from  $m_0$ . We finally point out that recently NLO+PS generators have appeared that can deal with resonances including off-shell effects, non-resonance contributions and interference of radiation generated in resonance decay and production, see [24] and references therein.

For the distributions of the decay products, the simplest treatment is again to assign them their respective  $m_0$  values, with a uniform phase-space distribution. A more sophisticated treatment distributes the decay products according to the differential decay matrix elements, capturing at least the internal dynamics and helicity structure of the decay process, including EPR-like correlations. Further refinements include polarizations of the external states [43] and assigning the decay products their own Breit-Wigner distributions, the latter of which opens the possibility to include also intrinsically off-shell decay channels, like  $H \rightarrow WW^*$ .

GPMC manuals often give instructions on how to include new decay modes, at varying levels of sophistications ranging from simple uniform phase-space sampling (which the user can reweight a posteriori) and step-function thresholds, to fully matrix-element weighted decay implementations including potential off-shell / threshold effects.

During subsequent showering of the decay products, most parton-shower models will preserve the total invariant mass of the decayed resonance, so as not to skew the original resonance shape. In the context of passing externally generated LHEF files [40] to a GPMC for showering, note that this is only possible if the intermediate resonances are present (with status code 2) in the LHEF event record [44].

#### 42.1.10. Matching with Matrix Elements :

Shower algorithms are based upon a combination of the collinear (small-angle) and soft (small-energy) approximations and are thus normally inaccurate for hard, wide-angle emissions (i.e., additional well-resolved jets). They also contain only the leading singular pieces of next-to-leading order (NLO) and higher corrections to the basic process.

Traditional GPMCs, like HERWIG and PYTHIA, have included for a long time the so called Matrix Element Corrections (MEC), first formulated in Ref. 45 with later developments summarized in Ref. 18. They are typically available for  $2 \rightarrow 1$  or  $1 \rightarrow 2$  processes, like DIS, vector boson and Higgs production and decays, and top decays. The MEC corrects the emission of the hardest jet at large angles, so that it becomes exact at LO. A generalization of the method to multiple emissions was formulated recently [46].

Aside from MECs implemented directly in the GPMCs, the improvements on the parton-shower description of hard collisions have been made in two main directions: the so called Matrix Elements and Parton Shower matching (ME+PS from now on), and the matching of NLO calculations and Parton Showers (NLO+PS). We now discuss



each of these, and then briefly summarise techniques becoming available for combining them.

The ME+PS method allows one to use tree-level matrix elements for hard, large-angle emissions. It was first formulated in the so-called CKKW paper [47], and several variants have appeared, including the CKKW-L, MLM, and pseudoshower methods, see Refs. 48, 18 for summaries. So called “Truncated Showers” are required [49] to maintain color coherence when interfacing to angular-ordered parton showers, and care must be taken to use consistent  $\alpha_S$  choices for the real (ME-driven) and virtual (PS-driven) corrections [50].

In the ME+PS method one typically starts by generating LO matrix elements for the production of the basic process plus a certain number  $\leq n$  of other partons. A minimum separation is imposed on the produced partons, requiring, for example, that the relative transverse momentum in any pair of partons is above a given cut  $Q_{\text{cut}}$ . One then reweights these amplitudes in such a way that, in the strongly ordered region, the virtual effects that are included in the shower algorithm (i.e. running couplings and Sudakov form factors) are also accounted for. At this stage, before parton showers are added, the generated configurations are tree-level accurate at large angle, and at small angle they match the results of the shower algorithm, except that there are no emissions below the scale  $Q_{\text{cut}}$ , and no final states with more than  $n$  partons. These kinematic configurations are thus fed into a GPMC, that must generate all splittings with relative transverse momentum below the scale  $Q_{\text{cut}}$ , for initial events with less than  $n$  partons, or below the scale of the smallest pair transverse momentum, for events with  $n$  partons. The matching parameter  $Q_{\text{cut}}$  must be chosen to be large enough for fixed-order perturbation theory to hold, but small enough so that the shower is accurate for emissions below it. Notice that the accuracy achieved with MEC is equivalent to that of ME+PS with  $n = 1$ , where MEC has the advantage of not having a matching parameter  $Q_{\text{cut}}$ .

The popularity of the ME+PS method is due to the fact that processes with many jets appear often as backgrounds to new-physics searches. These jets are typically required to be well separated, and to have large transverse momenta. These kinematical configurations are exactly those for which pure shower algorithms are unreliable, hence it is mandatory to describe them using at least LO matrix elements.

Several ME+PS implementations use existing LO generators, like ALPGEN [51], MADGRAPH [52], and others summarized in Ref. 48, for the calculation of the matrix elements, and feed the partonic events to a GPMC like PYTHIA or HERWIG using the Les Houches Interface for User Processes (LHI/LHEF) [44,40]. SHERPA and HERWIG 7 also include their own matrix-element generators.

The NLO+PS methods promote the accuracy of the generation of the basic process from LO to NLO in QCD. They must thus include the radiation of one extra parton with tree-level accuracy, since this radiation constitutes a NLO correction to the basic process. They must also include NLO virtual corrections. They can be viewed as an extension of the MEC methods with the inclusion of NLO virtual corrections. They are however more general, since they are applicable to processes of arbitrary complexity. Two of these methods are now widely used: MC@NLO [53] and POWHEG [49,54], with several alternative methods now also being pursued, see Ref. 18 and references therein.

NLO+PS generators produce NLO accurate distributions for inclusive quantities, and generate the hardest jet with tree-level accuracy. It should be recalled, though, that in  $2 \rightarrow 1$  processes like  $Z/W$  production, GPMCs including MEC and weighted by a constant  $K$  factor may perform nearly as well, and, if suitably tuned, may even yield a better description of data. In this context, note also that the optimal tuning of an NLO+PS generator may well be different from that of the pure PS.

Several NLO+PS processes are implemented in the MC@NLO program [53], together with the new AMC@NLO development [55], and in the POWHEG BOX framework [54]. HERWIG 7 supports now its own variants of POWHEG and MC@NLO for several processes. SHERPA instead implements a variant of the MC@NLO method.

For applications that require an accurate description of more than one hard, large-angle jet associated with the primary process, ME+PS schemes are still superior to NLO+PS ones. Ideally, one

would like to improve NLO generators in such a way that also the production of associated jets achieves NLO accuracy. The FFX [57], UNLOPS [58], MiNLO [59] and MEPS@NLO [60] methods address this problem. In turn, its solution is a prerequisite for the construction of NNLO+PS generators, that in fact have already appeared for the  $gg \rightarrow H$  and Drell-Yan processes (see ref. [61] and references therein).

## 42.2. Hadronization Models

In the context of GPMCs, *hadronization* denotes the process by which a set of colored partons (*after* showering) is transformed into a set of “primary hadrons”, which may then subsequently decay further (to “secondary hadrons”). This non-perturbative transition takes place at the *hadronization scale*  $Q_{\text{had}}$ , which by construction is equal to the infrared cutoff of the parton shower. In the absence of a first-principles solution to the relevant dynamics, GPMCs use QCD-inspired phenomenological models to describe this transition.

An important result in “quenched” lattice QCD (see Chap. 17 of PDG book) is that the potential energy between two partons with opposite color charges grows linearly with their separation, at distances greater than about a femtometer. This is known as “linear confinement”, and it forms the starting point for the *string model of hadronization*, discussed below in Sec. 42.2.1. Alternatively, a property of perturbative QCD called “preconfinement” is the basis of the *cluster model of hadronization*, discussed in Sec. 42.2.2.

A key difference between MC hadronization models and the fragmentation-function (FF) formalism used to describe inclusive hadron spectra in perturbative QCD (see Chap. 9 and Chap. 19 of PDG book) is that FFs can be defined at an arbitrary perturbative scale  $Q$  while MC hadronization models are intrinsically defined at the scale  $Q_{\text{had}}$ . Direct comparisons are therefore only meaningful if the perturbative evolution between  $Q$  and  $Q_{\text{had}}$  is taken into account. FFs are calculable in pQCD, given a non-perturbative initial condition obtained by fits to hadron spectra. In the MC context, one can prove that the correct QCD evolution of the FFs arises from the shower formalism, with the hadronization model providing an explicit parameterization of the non-perturbative component. However, the MC modeling of shower and hadronization includes much more information on the final state since it is fully exclusive (i.e., it addresses all particles in the final state explicitly), while FFs only describe inclusive spectra. This exclusivity also enables MC models to make use of the color-flow information coming from the perturbative shower evolution (see Sec. 42.1.6) to determine between which partons confining potentials should arise. E.g., in the string picture, the nonperturbative limit of a QCD dipole is a string piece [62].

Given an exact hadronization model, its dependence on the scale  $Q_{\text{had}}$  should in principle be compensated by the corresponding scale dependence of the shower algorithm, which stops generating branchings at the scale  $Q_{\text{had}}$ . However, due to their complicated and fully exclusive nature, it is generally not possible to enforce this compensation automatically in MC models. One must therefore be aware that the nonperturbative model parameters must be “retuned” by hand if the infrared cutoff is modified. Any other changes to the perturbative part of the calculation, such as matching to further (fixed-order or resummed) coefficients, may also necessitate a retuning. Tuning is discussed briefly in Sec. 42.4.

Finally, it should be emphasized that the so-called “parton level” that can be obtained by switching off hadronization in a GPMC, is not a universal concept, since each model defines  $Q_{\text{had}}$  differently (e.g. via a cutoff in  $p_{\perp}$ , invariant mass, etc., with different tunes using different values for the cutoff). Comparisons to distributions at this level may therefore be used to provide an idea of the overall impact of hadronization corrections within a given model, but should be avoided in the context of physical observables.

### 42.2.1. The String Model :

Starting from early concepts [63], several hadronization models based on strings have been proposed [18]. Of these, the most widely used today is the so-called Lund model [64,65], implemented in PYTHIA [4,5]. We concentrate on that particular model here, though many of the overall concepts would be shared by any string-inspired method.

Consider a color-connected quark-antiquark pair emerging from the parton shower (like the  $\bar{q}q$  pair in the center of Fig. 42.1). As the charges move apart, linear confinement implies that a potential  $V(r) = \kappa r$  is reached for large distances  $r$ . (At short distances, there is a Coulomb term  $\propto 1/r$  as well, but this is neglected in the Lund string.) This potential describes a string with tension  $\kappa \sim 1 \text{ GeV/fm} \sim 0.2 \text{ GeV}^2$ . The physical picture is that of a color flux tube being stretched between the  $q$  and the  $\bar{q}$ .

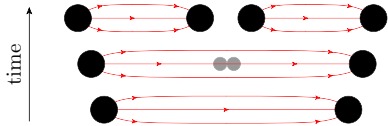


**Figure 42.2:** Illustration of string breaking by quark pair-creation in the string field.

As the string grows, the nonperturbative creation of quark-antiquark pairs can break the string, via the process illustrated in Fig. 42.2. The model is Lorentz invariant, so considerations involving boosted string systems are straightforward, involving the usual Lorentz effects. More complicated configurations involving intermediate gluons are treated by representing gluons as transverse “kinks”, illustrated in Fig. 42.3, and considerations involving boosted string systems are subject to the usual Lorentz effects. In the leading-color approximation, the order of these kinks follows directly from the color ordering produced by the parton shower, cf. the  $\bar{q}gggq$  and  $\bar{q}gq$  systems on the left and right part of Fig. 42.1. (Modifications to this order, by possible color reconnection/rearrangement effects, are discussed in Sec. 42.3.3.)

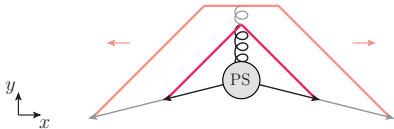


**Figure 42.3:** Schematic illustration of an  $e^+e^- \rightarrow q\bar{q}$  configuration emerging from the parton shower (PS). Snapshots of string positions are shown at two different times (full and shaded lines respectively). The gluon forms a transverse kink which grows in the  $y$  direction until all the gluon’s kinetic energy has been used up.

Thus gluons effectively build up a transverse structure in the originally one-dimensional object, with infinitely soft ones smoothly absorbed into the string. Note: cyclic topologies made entirely of gluons (closed strings) are also possible, e.g. in decays such as  $H \rightarrow gg$  or  $\Upsilon \rightarrow ggg$ . The space-time evolution is more involved when kinks are taken into account [65], but no additional free parameters need to be introduced. The main difference between quark and gluon hadronization stems from the fact that gluons are connected to two string pieces (one on either side), while quarks are only connected to a single string piece. Hence, the relative rate of energy loss per unit invariant time — and consequently also the rate of hadron production — is larger by a factor of 2 for gluons (similar to the ratio of color Casimirs  $C_A/C_F = 2.25$ ).

To convert a set of partons to hadrons, the first step is thus to map color-connected pairs of partons to string pieces, with quarks as endpoints and gluons as kinks. Next, the strings evolve, with a constant probability density for string breaks to occur per unit string space-time area. In this context, it is important to note that the individual string breaks are causally disconnected [65], hence they do not have to be generated in any particular time-ordered sequence. This is exploited in the Lund model to allow to consider the formation of a single on-shell hadron at a time, in an order that corresponds to decreasing average absolute rapidity (along the string). Selecting randomly between the left and right sides of the string, the first hadron to be generated is thus the “outermost” one, formed by combining

the original hadronizing endpoint quark (or antiquark)  $q_0$  with an antiquark (or quark)  $\bar{q}_1$  produced by a breakup. The new leftover quark (or antiquark)  $q_1$  becomes the string endpoint for the next iteration, in a Markov chain which continues, alternating randomly between the left and right ends of the string, until finally a small last bit of string is decayed directly to two hadrons, with no energy left over.

For each breakup vertex, quantum mechanical tunneling is assumed to control the masses and  $p_\perp$  kicks (transverse to the string axis, in a frame in which the string itself has no transverse motion) that can be produced, leading to a Gaussian suppression

$$\text{Prob}(m_q^2, p_{\perp q}^2) \propto \exp\left(\frac{-\pi m_q^2}{\kappa}\right) \exp\left(\frac{-\pi p_{\perp q}^2}{\kappa}\right), \quad (42.8)$$

where  $m_q$  is the mass of the produced quark flavor and  $p_\perp$  is the nonperturbative transverse momentum imparted to it by the breakup process, with a universal average value of  $\langle p_{\perp q}^2 \rangle = \kappa/\pi \sim (250 \text{ MeV})^2$ . The antiquark has the same mass and opposite  $p_\perp$ .

In an MC model with a fixed shower cutoff  $t_0$ , the effective amount of  $p_\perp$  in string breaks may be larger than the purely nonperturbative  $\kappa/\pi$  above, to account for effects of additional (unresolved) radiation below  $t_0$ .

From the mass term in Eq. (42.8), one concludes that charm and bottom quarks are too heavy to be produced in string breaks, while strange quarks will be suppressed relative to up and down ones. Lacking unambiguous and precise mass definitions for light quarks, however, the effective amount of strangeness suppression is normally extracted from experimental data, using observables such as  $K/\pi$  and  $K^*/\rho$  ratios.

Baryon production can also be incorporated, by allowing string breaks to produce pairs of *diquarks*, loosely bound states of two quarks in an overall  $\bar{3}$  representation. Again, since diquark masses are difficult to define, the relative rate of diquark to quark production is extracted, e.g. from the  $p/\pi$  ratio. Since the perturbative shower splittings do not produce diquarks, the optimal value for this parameter is mildly correlated with the amount of  $g \rightarrow q\bar{q}$  splittings produced by the shower. More advanced scenarios for baryon production have also been proposed, see Ref. 65. Within the PYTHIA framework, a hadronization model including baryon string junctions [66] is also available.

The next step of the algorithm is the assignment of the produced quarks within hadron multiplets. Using a nonrelativistic classification of spin states, the hadronizing  $q$  may combine with the  $\bar{q}'$  from a newly created breakup to produce a meson — or baryon, if diquarks are involved — of a given spin  $S$  and angular momentum  $L$ . The lowest-lying pseudoscalar and vector meson multiplets, and spin-1/2 and -3/2 baryons, are assumed to dominate in a string framework<sup>1</sup>, but individual rates are not predicted by the model. This is therefore the sector that contains the largest amount of free parameters. The ratio  $V/P$  of vectors to pseudoscalars is expected to be 3, but in practice it is only in the  $B$  meson sector that this is approximately true. For lighter flavors, the difference in phase space caused by the  $V-P$  mass splittings implies a suppression of vector production. When extracting the corresponding parameters from data, it is advisable to begin with the heaviest states, since so-called feed-down from the decays of higher-lying hadron states complicates the extraction for lighter particles, see Sec. 42.2.3. For baryons, additional parameters control the relative rates of spin-1 diquarks vs. spin-0 ones.

With  $p_\perp^2$  and  $m^2$  now fixed, the final step is to select the longitudinal momentum component of the created hadron along the string axis. This is parameterized by a nonperturbative *fragmentation function*,  $f(z)$ , which governs the probability for a hadron to take a fraction  $z \in [0, 1]$  of the total available momentum. In a string framework, the requirement that the hadronization be independent of

<sup>1</sup> PYTHIA includes the lightest pseudoscalar and vector mesons, with the four  $L = 1$  multiplets (scalar, tensor, and 2 pseudovectors) available but disabled by default, largely because several states are poorly known and thus may result in a worse overall description when included. For baryons, the lightest spin-1/2 and -3/2 multiplets are included.

the sequence in which breakups are considered (causality) imposes a “left-right symmetry” which strongly constrains the functional form of  $f(z)$ , with the solution

$$f(z) \propto \frac{1}{z} (1-z)^a \exp\left(-\frac{b(m_h^2 + p_{\perp h}^2)}{z}\right). \quad (42.9)$$

This is known as the Lund symmetric fragmentation function (normalized to unit integral). The dimensionless parameter  $a$  dampens the hard tail of the fragmentation function, towards  $z \rightarrow 1$ , and may in principle be flavor-dependent, while  $b$ , with dimension  $\text{GeV}^{-2}$ , is a universal constant related to the string tension [65] which determines the behavior in the soft limit,  $z \rightarrow 0$ . Note that the dependence on the hadron mass,  $m_h$ , in  $f(z)$  implies that heavier hadrons have higher  $\langle z \rangle$ .

As a by-product, the probability distribution in invariant time  $\tau$  of  $q'\bar{q}$  breakup vertices, or equivalently  $\Gamma = (\kappa\tau)^2$ , is also obtained, with  $dP/d\Gamma \propto \Gamma^a \exp(-b\Gamma)$  implying an area law for the color flux, and the average breakup time lying along a hyperbola of constant invariant time  $\tau_0 \sim 10^{-23}\text{s}$  [65].

For massive endpoints (e.g.  $c$  and  $b$  quarks), which do not move along straight lightcone sections, the exponential suppression with string area leads to modifications of the form  $f(z) \rightarrow f(z)/z^{bm_Q^2}$ , with  $m_Q$  the mass of the heavy quark [67]. Although different forms, such as the Peterson formula [68], can also be used to describe inclusive heavy-meson spectra (see Sec 19.8 of PDG book), such choices are not strictly consistent with causality in the string framework.

#### 42.2.2. The Cluster Model :

The cluster hadronization model is based on *preconfinement*, i.e., on the observation [69,70] that the color structure of a perturbative QCD shower evolution at any scale  $Q_0$  is such that color-singlet subsystems of partons (labeled “clusters”) occur with a universal invariant mass distribution which is power suppressed at large masses. For any starting scale  $Q \gg Q_0 \gg \Lambda_{\text{QCD}}$ , only the number of such clusters depends on  $Q$ , while the shape of their mass distribution only depends on  $Q_0$  and on  $\Lambda_{\text{QCD}}$ .

Following early models based on this universality [11,71], the cluster model developed by Webber [72] has for many years been a hallmark of the HERWIG generators, with an alternative implementation [73] now available in the SHERPA generator. The key idea, in addition to preconfinement, is to force “by hand” all gluons to split into quark-antiquark pairs at the end of the parton shower. Compared with the string description, this effectively amounts to viewing gluons as “seeds” for string breaks, rather than as kinks in a continuous object. After the splittings, a new set of low-mass color-singlet clusters is obtained, formed only by quark-antiquark pairs. These can be decayed to on-shell hadrons in a simple manner, with the relative yields of different hadron species mainly governed by their masses and the size of the phase space.

The algorithm starts by generating the forced  $g \rightarrow q\bar{q}$  breakups, and by assigning flavors and momenta to the produced quark pairs. For a typical shower cutoff corresponding to a gluon virtuality of  $Q_{\text{had}} \sim 1\text{GeV}$ , the  $p_{\perp}$  generated by the splittings can be neglected. The constituent light-quark masses,  $m_{u,d} \sim 300\text{MeV}$  and  $m_s \sim 450\text{MeV}$ , imply a suppression (typically even an absence) of strangeness production. In principle, the model also allows for diquarks to be produced at this stage, but due to the larger constituent masses this would only become relevant for shower cutoffs larger than  $1\text{GeV}$ .

If a cluster formed in this way has an invariant mass above some cutoff value, typically 3–4 GeV, it is forced to undergo sequential  $1 \rightarrow 2$  cluster breakups, along an axis defined by the constituent partons of the original cluster, until all sub-cluster masses fall below the cutoff value. Due to the preservation of the original axis in these breakups, this treatment has some resemblance to the string-like picture, though the nonperturbative  $p_{\perp}$  kicks generated in this way are generally larger, up to half the allowed cluster mass.

Next, on the low-mass side of the spectrum, some clusters are allowed to decay directly to a single hadron, with nearby clusters

absorbing any excess momentum. This improves the description of the high- $z$  part of the spectrum — where the hadron carries almost all the momentum of its parent jet — at the cost of introducing one additional parameter, controlling the probability for single-hadron cluster decay.

Having obtained a final distribution of small-mass clusters, now with a strict cutoff at 3–4 GeV and with the component destined to decay to single hadrons already removed, the remaining clusters are interpreted as a smoothed-out spectrum of excited mesons, each of which decays isotropically to two hadrons, with relative probabilities proportional to the available phase space for each possible two-hadron combination that is consistent with the cluster’s internal flavors, including spin degeneracy. It is important that all the light members (containing only  $uds$ ) of each hadron multiplet be included, as the absence of members can lead to unphysical isospin or SU(3) flavor violation. Typically, the lightest pseudoscalar, vector, scalar, even and odd charge conjugation pseudovector, and tensor multiplets of light mesons are included. In addition, some excited vector multiplets of light mesons may be available. For baryons, usually only the lightest flavor-octet, -decuplet and -singlet baryons are present, although both the HERWIG++ and SHERPA implementations now include some heavier baryon multiplets as well.

Differently from the string model, the mechanism of phase-space suppression employed here leads to a natural enhancement of the lighter pseudoscalars, and no parameters beyond the spectrum of hadron masses need to be introduced at this point. The phase space also limits the transverse momenta of the produced hadrons relative to the jet axis.

Note that, since the masses and decays of excited heavy-flavor hadrons in particular are not well known, there is some freedom in the model to adjust these, which in turn will affect their relative phase-space populations.

#### 42.2.3. Hadron and $\tau$ Decays :

Of the so-called primary hadrons, originating directly from string breaks and/or cluster decays (see above), many are unstable and so decay further, until a set of particles is obtained that can be considered stable on time scales relevant to the given measurement. (A typical hadron-collider definition of a “stable particle”  $c\tau \geq 10\text{mm}$  includes weakly-decaying strange hadrons  $K$ ,  $\Lambda$ ,  $\Sigma^{\pm}$ ,  $\bar{\Sigma}^{\pm}$ ,  $\Xi$ ,  $\Omega$ .) The decay modeling can therefore have a significant impact on final particle yields and spectra, especially for the lowest-lying hadronic states, which receive the largest relative contributions from decays (feed-down). This interplay also implies that hadronization parameters may need to be retuned if significant changes to the decay treatment are made.

Particle summary tables, such as those given elsewhere in this *Review*, represent a condensed summary of the available experimental measurements and hence may be incomplete and/or exhibit inconsistencies within the experimental precision. In an MC decay package, on the other hand, all information must be quantified and consistent, with all branching ratios summing to unity. When adapting particle summary information for use in a decay package, a number of choices must therefore be made. The amount of ambiguity increases as more excited hadron multiplets are added to the simulation, about which less and less is known from experiment, with each GPMC making its own choices.

A related choice is how to distribute the decay products differentially in phase space, in particular which matrix elements to use. Historically, MC generators contained matrix elements only for selected (generator-specific) classes of hadron and  $\tau$  decays, coupled with a Breit-Wigner smearing of the masses, truncated at the edges of the physical decay phase space (the treatment of decay thresholds can be important for certain modes [18]). A more sophisticated treatment can then be obtained by reweighting the generated events using the obtained particle four-momenta and/or by using specialized external packages such as EVTGEN [74] for hadron decays and TAUOLA [75] for  $\tau$  decays.

More recently, HERWIG++ and SHERPA include helicity-dependence in  $\tau$  decays [76,6], with a more limited treatment available in PYTHIA 8 [5]. The HERWIG++ and SHERPA generators have also included significantly improved internal simulations of hadronic

decays, which include spin correlations between those decays for which matrix elements are used. Photon-bremstrahlung effects are discussed in Sec. 42.1.7.

HERWIG++ and PYTHIA include the probability for  $B$  mesons to oscillate into  $\bar{B}$  ones before decay. SHERPA and EVTGEN also include CP-violating effects and, for common decay modes of the neutral meson and its antiparticle, the interference between the direct decay and oscillation followed by decay.

We end on a note of warning on double counting. This may occur if a particle can decay via an intermediate on-shell resonance. An example is  $a_1 \rightarrow \pi\pi\pi$  which may proceed via  $a_1 \rightarrow \rho\pi$ ,  $\rho \rightarrow \pi\pi$ . If these decay channels of the  $a_1$  are both included, each with their full partial width, a double counting of the on-shell  $a_1 \rightarrow \rho\pi$  contribution would result. Such cases are normally dealt with consistently in the default MC generator packages, so this warning is mostly for users that wish to edit decay tables on their own.

### 42.3. Models for Soft Hadron-Hadron Physics

#### 42.3.1. Minimum-Bias and Diffraction :

The term “minimum bias” (MB) originates from the experimental requirement of a minimal number of tracks (or hits) in a given instrumented region. In order to make MC predictions for such observables, all possible contributions to the relevant phase-space region must be accounted for. There are essentially four types of physics processes, which together make up the total hadron-hadron ( $hh$ ) cross section: 1) elastic scattering<sup>2</sup>:  $hh \rightarrow hh$ , 2) single diffractive dissociation:  $hh \rightarrow h + \text{gap} + X$ , with  $X$  denoting anything that is not the original beam particle, and “gap” denoting a rapidity region devoid of observed activity; 3) double diffractive dissociation:  $hh \rightarrow X + \text{gap} + X$ , and 4) inelastic non-diffractive scattering: everything else. A fifth class may also be defined, called central diffraction ( $hh \rightarrow h + \text{gap} + X + \text{gap} + h$ ). Note that different terminologies exist [77]: in experimental settings, diffraction is typically defined by an observable gap, of some minimal size in rapidity, while in the MC context, each diffractive physics process produces a whole spectrum of gaps, with small ones suppressed but not excluded.

The inelastic non-diffractive part of the cross section is typically modeled either by smoothly regulating and extending the perturbative QCD scattering cross sections all the way to zero  $p_\perp$  [78] (PYTHIA and SHERPA), or by regulating the QCD cross sections with a sharp cutoff [79] and adding a separate class of nonperturbative scatterings below that scale [80] (HERWIG). See also Sec. 42.3.2. In all cases, the most important ingredients are: 1) the IR regularization of the perturbative scattering cross sections, including their PDF dependence, 2) the assumed matter distribution of the colliding hadrons, possibly including multi-parton correlations [66] and/or  $x$  dependence [81], and 3) additional soft-QCD effects such as color reconnections, discussed in Sec. 42.3.3.

Currently, there are essentially three methods for simulating diffraction in the main MC models: 1) in PYTHIA 6, one picks a diffractive mass according to parameterized cross sections  $\propto dM^2/M^2$  [82]. This mass is represented as a string, which is hadronized as described in Sec. 42.2.1, though differences in the effective scale of the hadronization may necessitate a (re)tuning of the hadronization parameters for diffraction; 2) in PYTHIA 8, the high-mass tail beyond  $M \sim 10$  GeV is augmented by a partonic description in terms of pomeron PDFs [83], allowing diffractive jet production including showers and underlying event [84]; 3) the PHOJET and DPMJET programs also include central diffraction and rely directly on a formulation in terms of pomerons (color-singlet multi-gluon states) [85–87]. . Cut pomerons correspond to exchanges of soft gluons while uncut ones give elastic and diffractive topologies as well as virtual corrections that help preserve unitarity. So-called “hard pomerons” provide a transition to the perturbative regime. Hadronization is still handled using the Lund string model, so there is some overlap with the above models at the hadronization stage.

<sup>2</sup> The QED elastic cross section diverges and is normally a non-default option.

In addition, a pomeron-based package exists for HERWIG [88], and an effort is underway to construct an MC implementation of the “KMR” model [89] within the SHERPA generator. Color reconnections (Sec. 42.3.3) may also play a role in creating rapidity gaps and the underlying event (Sec. 42.3.2) in filling them.

#### 42.3.2. Underlying Event and Jet Pedestals :

In the GPMC context, “underlying event” (UE) denotes any additional activity *beyond* the basic process and its associated ISR and FSR activity. The UE is thus only defined in the context of events selected with a “hard” (i.e., high- $p_\perp$ ) trigger which defines the basic process at hand. (This is distinct from the MB selection which does not require any hard perturbative activity.) The dominant contribution to the UE is believed to come from additional color exchanges between the colliding hadronic states. These multiple exchanges can be modeled either as additional perturbative (mainly  $t$ -channel gluon) exchanges, called multiple parton-parton interactions (MPI), or nonperturbatively using so-called cut pomerons (roughly equivalent to exchange of gluons with  $p_\perp \rightarrow 0$ ). The experimental observation that events with a hard trigger are accompanied by a higher-than-average level of associated activity (UE particle densities and related quantities are greater than those of MB events at the same CM energy) is called the “jet pedestal” effect.

The most clearly identifiable consequence of MPI is arguably the possibility of observing several hard parton-parton interactions in one and the same hadron-hadron event. Typically, these are QCD  $2 \rightarrow 2$  interactions, which produce additional back-to-back jet pairs, with each pair having a small value of  $\text{sum}(\vec{p}_\perp)$ . The fraction of MPI that give rise to additional reconstructible jets is, however, small. Soft interactions, that exchange color and a small amount of momentum without giving rise to observable jets, are much more plentiful, and can give significant corrections to the color flow and total scattered energy of the event. This affects the final-state activity in a more global way, increasing hadron-multiplicity and summed  $E_T$  distributions, and contributing to the break-up of the beam remnants in the forward direction.

The first detailed Monte Carlo model for perturbative MPI was proposed in Ref. 78, and with some variation this still forms the basis for most modern implementations. Some useful additional references can be found in Ref. 18. The first crucial observation is that the  $t$ -channel propagators appearing in perturbative QCD  $2 \rightarrow 2$  scattering almost go on shell at low  $p_\perp$ , causing the differential cross sections to behave roughly as

$$d\sigma_{2 \rightarrow 2} \propto \frac{dt}{t^2} \sim \frac{dp_\perp^2}{p_\perp^4} . \quad (42.10)$$

This cross section represents the inclusive scattering of partons against partons in perturbative QCD, summed over all partons. Thus, if a single hadron-hadron scattering contains *two* parton-parton interactions, that event will contribute twice to the parton-parton cross section  $\sigma_{2 \rightarrow 2}$  but only once to the hadron-hadron one  $\sigma_{\text{tot}}$ , and so on. In the limit that all the parton-parton interactions are independent and equivalent, one has

$$\sigma_{2 \rightarrow 2} = \langle n \rangle \sigma_{\text{tot}} , \quad (42.11)$$

with  $\langle n \rangle$  the average number of parton-parton interactions, typically defined with some minimal  $p_\perp > p_{\perp \text{min}}$  to render the parton-parton cross section finite. The probability for  $n$  parton-parton scatterings then follows a Poisson distribution,

$$\mathcal{P}_n = \langle n \rangle^n \frac{\exp(-\langle n \rangle)}{n!} . \quad (42.12)$$

This simple argument expresses unitarity; instead of the total hadron-hadron interaction cross section diverging as the parton-parton  $p_\perp \rightarrow 0$  (which would violate unitarity), we have restated the problem so that it is now the *number of parton-parton interactions per hadron-hadron collision* that diverges, with the total hadron-hadron cross section remaining finite. At LHC energies, the parton-parton scattering cross sections computed using the LO QCD cross section folded with modern PDFs become larger than the total  $pp$  one for  $p_{\perp \text{min}}$  values of

order 4–5 GeV (see e.g. [90,91]). One therefore expects the average number of perturbative MPI to exceed unity at around that scale.

Two ingredients remain to fully regulate the remaining divergence. Firstly, the interactions cannot use up more momentum than is available in the parent hadron. This suppresses the large- $n$  tail of the estimate above. In PYTHIA-based models, the MPI are ordered in  $p_{\perp}$ , and the parton densities for each successive interaction are explicitly constructed so that the sum of  $x$  fractions can never be greater than unity. In the HERWIG models, the Poisson estimate of  $\langle n \rangle$  above is used as an initial guess, but the generation of actual MPI is stopped once the energy-momentum conservation limit is reached. Both of these approaches generate momentum (conservation) correlations among the MPI.

The second ingredient invoked to suppress the number of interactions, at low  $p_{\perp}$  and  $x$ , is color screening; if the wavelength  $\sim 1/p_{\perp}$  of an exchanged colored parton becomes larger than a typical color-anticolor separation distance, it will only see an *average* color charge that vanishes in the limit  $p_{\perp} \rightarrow 0$ . This provides an infrared cutoff for MPI similar to that provided by the hadronization scale for parton showers. A first estimate of the color-screening cutoff would be the proton size,  $p_{\perp\text{min}} \approx \hbar/r_p \approx 0.3 \text{ GeV} \approx \Lambda_{\text{QCD}}$ , but empirically this appears to be far too low. In current models, one replaces the proton radius  $r_p$  in the above formula by a “typical color screening distance,” i.e., an average size of a region within which the net compensation of a given color charge occurs. This number is not known from first principles [89] and is perceived of simply as an effective cutoff parameter. The simplest choice is to introduce a step function  $\Theta(p_{\perp} - p_{\perp\text{min}})$ . Alternatively, one may note that the jet cross section is divergent like  $\alpha_S^2(p_{\perp}^2)/p_{\perp}^4$ , cf. Eq. (42.10), and that therefore a factor

$$\frac{\alpha_S^2(p_{\perp 0}^2 + p_{\perp}^2)}{\alpha_S^2(p_{\perp}^2)} \frac{p_{\perp 0}^4}{(p_{\perp 0}^2 + p_{\perp}^2)^2} \quad (42.13)$$

would smoothly regulate the divergences, now with  $p_{\perp 0}$  as the free parameter. Regardless of whether it is imposed as a smooth (PYTHIA and SHERPA) or steep (HERWIG++) function, this is effectively the main “tuning” parameter in such models.

Note that the numerical value obtained for the cross section depends upon the PDF set used, and therefore the optimal value to use for the cutoff will also depend on this choice. Note also that the cutoff does not have to be energy-independent. Higher energies imply that parton densities can be probed at smaller  $x$  values, where the number of partons rapidly increases. Partons then become closer packed and the color screening distance  $d$  decreases. The uncertainty on the energy and/or  $x$  scaling of the cutoff is a major concern when extrapolating between different collider energies [92].

We now turn to the origin of the observational fact that hard jets appear to sit on top of a higher “pedestal” of underlying activity than events with no hard jets. This is interpreted as a consequence of impact-parameter-dependence: in peripheral collisions, only a small fraction of events contain any high- $p_{\perp}$  activity, whereas central collisions are more likely to contain at least one hard scattering; a high- $p_{\perp}$  triggered sample will therefore be biased towards small impact parameters,  $b$ . The ability of a model to describe the shape of the pedestal (e.g. to describe both MB and UE distributions simultaneously) therefore depends upon its modeling of the  $b$ -dependence, and correspondingly the impact-parameter shape constitutes another main tuning parameter.

For each impact parameter  $b$ , the number of interactions  $\tilde{n}(b)$  can still be assumed to be distributed according to Eq. (42.12), again modulo momentum conservation, but now with the mean value of the Poisson distribution depending on impact parameter,  $\langle \tilde{n}(b) \rangle$ . This causes the final  $n$ -distribution (integrated over  $b$ ) to be wider than a Poissonian.

Finally, there are two perturbative modeling aspects which go beyond the introduction of MPI themselves: 1) parton showers off the MPI, and 2) perturbative parton-rescattering effects. Without showers, MPI models would generate very sharp peaks for back-to-back MPI jets, caused by unshowered partons passed directly to

the hadronization model. However, with the exception of the oldest PYTHIA6 model, all GPMC models do include such showers [18], and hence should exhibit more realistic (i.e., broader and more decorrelated) MPI jets. On the initial-state side, the main questions are whether and how correlated multi-parton densities are taken into account and, as discussed previously, how the showers are regulated at low  $p_{\perp}$  and/or low  $x$ . Although none of the MC models currently impose a rigorous correlated multi-parton evolution, all of them include some elementary aspects. The most significant for parton-level results is arguably momentum conservation, which is enforced explicitly in all the models. The so-called “interleaved” models [30] attempt to go a step further, generating an explicitly correlated multi-parton evolution in which flavor sum rules are imposed to conserve, e.g. the total numbers of valence and sea quarks [66].

Perturbative rescattering in the final state can occur if partons are allowed to undergo several distinct interactions, with showering activity possibly taking place in-between. This has so far not been studied extensively, but a first exploratory model is available [93]. In the initial state, parton rescattering/recombination effects have so far not been included in any of the GPMC models.

#### 42.3.3. Bose-Einstein and Color-Reconnection Effects :

In the context of  $e^+e^-$  collisions, Bose-Einstein (BE) correlations have mostly been discussed as a source of uncertainty on high-precision  $W$  mass determinations at LEP [94]. In hadron-hadron (and nucleus-nucleus) collisions, however, BE correlations are used extensively to study the space-time structure of hadronizing matter (“femtoscopy”).

In MC models of hadronization, each string break or particle/cluster decay is normally factorized from all other ones. This reduces the number of variables that must be considered in each step, but also makes it intrinsically difficult to introduce correlations among particles from different breaks/decays. In GPMCs, a few semi-classical models are available within the PYTHIA 6 and 8 generators [95], in which the BE effect is mimicked by an attractive interaction between pairs of identical particles in the final state, with no higher correlations included. Variants of this model differ mainly by the assumed shape of the correlation function and how overall momentum conservation is handled.

As discussed in Sec. 42.2, leading-color (“planar”) color flows are used to set up the hadronizing systems (clusters or strings) at the hadronization stage. If the systems do not overlap significantly in space and time, subleading-color ambiguities and/or nonperturbative reconections are expected to be small. However, if the density of displaced color charges is sufficiently high that several systems can overlap significantly, full-color and/or reconnection effects should become progressively larger.

In the specific context of MPI, a crucial question is how color is neutralized *between* different MPI systems, including the remnants. The large rapidity differences involved imply large invariant masses (though normally low  $p_{\perp}$ ), and hence large amounts of (soft) particle production. Indeed, in the context of soft-inclusive physics, it is these “inter-system” strings/clusters that furnish the dominant particle-production mechanism, and hence their modeling is an essential part of the soft-physics description, affecting topics such as MB/UE multiplicity and  $p_{\perp}$  distributions, rapidity gaps, and precision mass measurements. Reviews of color-reconnection effects can be found in Refs. 18,96.

#### 42.4. Uncertainties and Tuning

The accuracy that can be achieved by a GPMC model depends on the sophistication of the theory models it incorporates, on the available constraints on its free parameters, and on the nature of the observable(s) under study. Using existing data (or more accurate theory calculations) to constrain the model parameters is referred to as generator tuning. Although tuned models do tend to yield improved results also for observables that they have not been tuned to, the question of evaluating the remaining uncertainties reliably is still far from solved. It is worth noting, however, that all of the GPMCs now provide options for automatic evaluation of perturbative shower uncertainties (e.g., via renormalization-scale variations), in the form

of vectors of alternative event weights [97,98,99] although significant weight fluctuations can be a problem for processes with many or large shower phase spaces. One must be aware that these variations are not necessarily exhaustive and care must be taken in their interpretation. Nonperturbative uncertainties must normally still be evaluated by varying salient model parameters by hand. A general method called eigentunes [100] is also available, based on global fits to data.

Typically, the overall event properties are determined by only a few, very important parameters, such as the value of  $\alpha_S$ , for perturbative corrections, and the shape of the fragmentation functions, for nonperturbative ones. More parameters may then be introduced to describe successively more detailed aspects (e.g., the rates and decays of individual hadron species), but these should have progressively less impact on the overall modeling. One may therefore take a factorized approach, first constraining the perturbative parameters and thereafter the nonperturbative ones, in order of decreasing significance to the overall modeling. Furthermore, by identifying which measurements are most sensitive to each parameter, this ordering can be reflected in the way that data is selected and applied to constrain the models. Thus, measurements sensitive to global event properties would typically be applied first, to constrain the most inclusive parameters, and so on for progressively more exclusive aspects.

At LO $\times$ LL, perturbation theory is doing well if it agrees with an IR safe measurement within  $\sim 10\%$ . It would therefore not make much sense to tune a GPMC beyond roughly 5% (it might even be dangerous, due to overfitting). The advent of NLO Monte Carlos may reduce this number slightly, but only for quantities for which one expects NLO precision. For quantities governed by nonperturbative physics, uncertainties are larger. For some quantities, e.g. ones for which the underlying modeling is known to be poor, an order-of-magnitude agreement or worse may have to be accepted. Note further that the unitarity of shower and hadronization models implies that the Born-level cross-section normalization is not tunable, hence in tuning contexts one tends to focus on the shapes of distributions rather than their normalizations.

In the context of LO $\times$ LL GPMC tuning, subleading aspects of coupling-constant and PDF choices are relevant. In particular, one should be aware that the choice of QCD  $\Lambda$  parameter  $\Lambda_{\overline{\text{MS}}} = 1.569\Lambda_{\overline{\text{MS}}}$  (for 5 active flavors) improves the predictions of coherent shower algorithms at the NLL level for a class of relevant observables [101], and hence this scheme is often considered the baseline for shower tuning. The question of LO vs. NLO PDFs is more involved [18], but it should be emphasized that the gluon PDF at (very) low  $x$  is important for determining the level of the underlying event in MPI models (Sec. 42.3.2), and hence the MB/UE tuning (and energy scaling [92]) is linked to the choice of PDF in such models. Further issues and an example of a specific recipe that could be followed in a realistic set-up can be found in Ref. 90. A useful online resource can be found at the mcplots.cern.ch web site [102], based on the RIVET tool [103].

Recent years have seen the emergence of automated tools to reduce the amount of both computer and manpower required for tuning [100]. Automating the human expert input is more difficult. In the tools currently on the market, this is addressed by a combination of input solicited from the GPMC authors (e.g., which parameters and ranges to consider, which observables constitute a complete set, etc) and a set of weights determining the relative priority given to each bin in each distribution. The final result is therefore still subjective but at least reproducible. When backed by careful demonstrations of sensitivities, correlations, and uncertainties, the quality of the resulting tunes is by now competitive. The field is still burgeoning, with future sophistications to be expected.

#### References:

1. G. Corcella *et al.*, JHEP **0101**, 010 (2001), hep-ph/0011363.
2. M.Bähr *et al.*, Eur. Phys. J. **C58**, 639 (2008), arXiv:0803.0883.
3. J. Bellm *et al.*, Eur. Phys. J. **C76**, 196 (2016), arXiv:1512.01178.
4. T. Sjöstrand, S. Mrenna, and P. Z. Skands, JHEP **05**, 026 (2006), hep-ph/0603175.
5. T. Sjöstrand *et al.*, Comp. Phys. Comm. **191**, 159 (2015), arXiv:1410.3012.
6. T. Gleisberg *et al.*, JHEP **0902**, 007 (2009), arXiv:0811.4622.
7. QCD summary, PDG..
8. T. Kinoshita, J. Math. Phys. **3**, 650 (1962).
9. T. Lee and M. Nauenberg, Phys. Rev. **133**, 1549 (1964).
10. A. Buckley *et al.*, arXiv:1101.2599, and references therein..
11. G.C. Fox and S. Wolfram, Nucl. Phys. **B168**, 285 (1980).
12. G. Altarelli and G. Parisi, Nucl. Phys. **B126**, 298 (1977).
13. A. Einstein, B. Podolsky, and N. Rosen, Phys. Rev. **47**, 777 (1935).
14. B.R. Webber, Phys. Lett. **B193**, 91 (1987).
15. J.C. Collins, Nucl. Phys. **B304**, 794 (1988).
16. I.G. Knowles, Comp. Phys. Comm. **58**, 271 (1990).
17. T. Sjöstrand, Phys. Lett. **B157**, 321 (1985).
18. A. Buckley *et al.*, Phys. Reports **504**, 145 (2011), arXiv:1101.2599.
19. G. Marchesini and B.R. Webber, Nucl. Phys. **B310**, 461 (1988).
20. S. Gieseke, P. Stephens, and B. Webber, JHEP **0312**, 045 (2003), hep-ph/0310083.
21. M. Bengtsson and T. Sjöstrand, Nucl. Phys. **B289**, 810 (1987).
22. G. Gustafson and U. Pettersson, Nucl. Phys. **B306**, 746 (1988).
23. L. Lönnblad, Comp. Phys. Comm. **71**, 15 (1992).
24. T. Ježo *et al.*, Eur. Phys. J. **C76**, 691 (2016), arXiv:1607.04538.
25. W.T. Giele, D.A. Kosower, and P.Z. Skands, Phys. Rev. **D78**, 014026 (2008), arXiv:0707.3652.
26. Z. Nagy and D.E. Soper, JHEP **0510**, 024 (2005), hep-ph/0503053.
27. S. Schumann and F. Krauss, JHEP **0803**, 038 (2008), arXiv:0709.1027.
28. S. Plätzer and S. Gieseke, Eur. Phys. J. **C72**, 2187 (2012), arXiv:1109.6256.
29. S. Höche and S. Prestel, Eur. Phys. J. **C75**, 461 (2015), arXiv:1506.05057.
30. T. Sjöstrand and P.Z. Skands, Eur. Phys. J. **C39**, 129 (2005), hep-ph/0408302.
31. E. Norrbin and T. Sjöstrand, Nucl. Phys. **B603**, 297 (2001), hep-ph/0010012.
32. S. Catani *et al.*, Nucl. Phys. **B627**, 189 (2002), hep-ph/0201036.
33. J. Cambranos *et al.*, (2013), arXiv:1305.2124.
34. N. Davidson, T. Przedzinski, and Z. Was, (2010), arXiv:1011.0937.
35. K. Hamilton and P. Richardson, JHEP **0607**, 010 (2006), hep-ph/0603034.
36. M. Schönherr and F. Krauss, JHEP **0812**, 018 (2008), arXiv:0810.5071.
37. A. Semenov, Comp. Phys. Comm. **180**, 431 (2009), arXiv:0805.0555.
38. N.D. Christensen and C. Duhr, Comp. Phys. Comm. **180**, 1614 (2009), arXiv:0806.4194.
39. M. Fairbairn *et al.*, Phys. Reports **438**, 1 (2007), hep-ph/0611040.
40. J. Alwall *et al.*, Comp. Phys. Comm. **176**, 300 (2007), hep-ph/0609017.
41. P.Z. Skands *et al.*, JHEP **0407**, 036 (2004), hep-ph/0311123.
42. J. Alwall *et al.*, (2007), arXiv:0712.3311.
43. P. Richardson, JHEP **0111**, 029 (2001), hep-ph/0110108.
44. E. Boos *et al.*, (2007), hep-ph/0109068.
45. M. Bengtsson and T. Sjöstrand, Phys. Lett. **B185**, 435 (1987).
46. W. T. Giele, D. A. Kosower and P. Z. Skands, Phys. Rev. **D84**, 054003 (2011), arXiv:1102.2126.
47. S. Catani *et al.*, JHEP **11**, 063 (2001), hep-ph/0109231.
48. J. Alwall *et al.*, Eur. Phys. J. **C53**, 473 (2008), arXiv:0706.2569.
49. P. Nason, JHEP **11**, 040 (2004), hep-ph/0409146.
50. B. Cooper *et al.*, Eur. Phys. J. **C72**, 2078 (2012), arXiv:1109.5295.
51. M.L. Mangano *et al.*, JHEP **0307**, 001 (2003), hep-ph/0206293.
52. J. Alwall *et al.*, JHEP **1106**, 128 (2011), arXiv:1106.0522.

53. S. Frixione and B.R. Webber, JHEP **06**, 029 (2002), [hep-ph/0204244](#).
54. S. Alioli *et al.*, JHEP **1006**, 043 (2010), [arXiv:1002.2581](#).
55. J. Alwall *et al.*, JHEP **07**, 079 (2014), [arXiv:1405.0301](#).
56. S. Alioli, K. Hamilton, and E. Re, JHEP **09**, 104 (2011), [arXiv:1108.0909](#).
57. R. Frederix and S. Frixione, JHEP **12**, 061 (2012), [arXiv:1209.6215](#).
58. L. Lönnblad and S. Prestel, JHEP **03**, 166 (2013), [arXiv:1211.7278](#).
59. K. Hamilton, P. Nason and G. Zanderighi, JHEP **10**, 155 (2012), [arXiv:1206.3572](#).
60. S. Höche *et al.*, JHEP **04**, 027 (2013), [arXiv:1207.5030](#).
61. K. Hamilton, P. Nason and G. Zanderighi, JHEP **05**, 140 (2015), [arXiv:1501.04637](#).
62. G. Gustafson, Phys. Lett. **B175**, 453 (1986).
63. X. Artru and G. Mennessier, Nucl. Phys. **B70**, 93 (1974).
64. B. Andersson *et al.*, Phys. Reports **97**, 31 (1983).
65. B. Andersson, Camb. Monogr. Part. Phys. Nucl. Phys. Cosmol. **7** (1997).
66. T. Sjöstrand and P.Z. Skands, JHEP **0403**, 053 (2004), [hep-ph/0402078](#).
67. M. Bowler, Z. Phys. **C11**, 169 (1981).
68. C. Peterson *et al.*, Phys. Rev. **D27**, 105 (1983).
69. D. Amati and G. Veneziano, Phys. Lett. **B83**, 87 (1979).
70. A. Bassetto, M. Ciafaloni, and G. Marchesini, Phys. Lett. **B83**, 207 (1979).
71. R.D. Field and S. Wolfram, Nucl. Phys. **B213**, 65 (1983).
72. B.R. Webber, Nucl. Phys. **B238**, 492 (1984).
73. J.-C. Winter, F. Krauss, and G. Soff, Eur. Phys. J. **C36**, 381 (2004), [hep-ph/0311085](#).
74. D. Lange, Nucl. Instrum. Methods **A462**, 152 (2001).
75. S. Jadach *et al.*, Comp. Phys. Comm. **76**, 361 (1993).
76. D. Grellscheid and P. Richardson, (2007), [arXiv:0710.1951](#).
77. V. Khoze *et al.*, Eur. Phys. J. **C69**, 85 (2010), [arXiv:1005.4839](#).
78. T. Sjöstrand and M. van Zijl, Phys. Rev. **D36**, 2019 (1987).
79. J.M. Butterworth, J.R. Forshaw, and M.H. Seymour, Z. Phys. **C72**, 637 (1996), [hep-ph/9601371](#).
80. M. Bähr *et al.*, (2009), [arXiv:0905.4671](#).
81. R. Corke and T. Sjöstrand, JHEP **1105**, 009 (2011), [1101.5953](#).
82. G.A. Schuler and T. Sjöstrand, Phys. Rev. **D49**, 2257 (1994).
83. G. Ingelman and P. Schlein, Phys. Lett. **B152**, 256 (1985).
84. S. Navin, (2010), [arXiv:1005.3894](#).
85. P. Aurenche *et al.*, Comp. Phys. Comm. **83**, 107 (1994), [hep-ph/9402351](#).
86. F.W. Bopp, R. Engel, and J. Ranft, (1998), [hep-ph/9803437](#).
87. S. Roesler, R. Engel, and J. Ranft, p. 1033 (2000), [hep-ph/0012252](#).
88. B.E. Cox and J.R. Forshaw, Comp. Phys. Comm. **144**, 104 (2002), [hep-ph/0010303](#).
89. M. Ryskin, A. Martin, and V. Khoze, Eur. Phys. J. **C71**, 1617 (2011), [arXiv:1102.2844](#).
90. P. Skands, S. Carrazza and J. Rojo, Eur. Phys. J. **C74**, 3024 (2014), [arXiv:1404.5630](#).
91. M. Bähr, J.M. Butterworth, and M.H. Seymour, JHEP **01**, 065 (2009), [arXiv:0806.2949](#).
92. H. Schulz and P.Z. Skands, Eur. Phys. J. **C71**, 1644 (2011), [arXiv:1103.3649](#).
93. R. Corke and T. Sjöstrand, JHEP **01**, 035 (2009), [arXiv:0911.1901](#).
94. LEP Electroweak Working Group, (2005), [hep-ex/0511027](#).
95. L. Lönnblad and T. Sjöstrand, Eur. Phys. J. **C2**, 165 (1998), [hep-ph/9711460](#).
96. J. R. Christiansen and P. Z. Skands, JHEP **08**, 003 (2015), [arXiv:1505.01681](#).
97. J. Bellm *et al.*, Phys. Rev. **D94**, 034028 (2016), [arXiv:1605.08256](#).
98. S. Mrenna and P. Skands, Phys. Rev. **D94**, 074005 (2016), [arXiv:1605.08352](#).
99. E. Bothmann, M. Schnherr and S. Schumann, Eur. Phys. J. **C76**, 590 (2016), [arXiv:1606.08753](#).
100. A. Buckley *et al.*, Eur. Phys. J. **C65**, 331 (2010), [arXiv:0907.2973](#).
101. S. Catani, B. R. Webber, and G. Marchesini, Nucl. Phys. **B349**, 635 (1991).
102. A. Karneyeu *et al.*, Eur. Phys. J. **C74**, 2714 (2013), [arXiv:1306.3436](#).
103. A. Buckley *et al.*, Comp. Phys. Comm. **184**, 2803 (2010), [arXiv:1003.0694](#).



## 43. Monte Carlo Neutrino Generators

Revised August 2019 by H. Gallagher (Tufts U.) and Y. Hayato (Kamioka Observatory, ICRR, UTokyo).

Monte Carlo neutrino generators are programs or libraries which simulate neutrino interactions with electrons, nucleons and nuclei. In this capacity their usual task is to take an input neutrino and nucleus and produce a set of 4-vectors for particles emerging from the interaction, which are then input to full detector simulations. Since these generators have to simulate not only the initial interaction of neutrinos with target particles, but re-interactions of the generated particles in the nucleus, they contain a wide range of elementary particle and nuclear physics. Viewed more broadly, they are the access point for neutrino experimentalists to the theory inputs needed for analysis. Examples include cross section libraries for event rate calculations and parameter uncertainties and reweighting tools for systematic error evaluation.

Neutrino experiments typically operate in neutrino beams that are neither completely pure nor mono-energetic. Generators are a crucial component in the convolution of beam flux, neutrino interaction physics, and detector response that is necessary to make predictions about observable quantities. Similarly they are used to relate reconstructed quantities back to true quantities. In these various capacities they are used from the detector design stage through the extraction of physics measurements from reconstructed observables. Monte Carlo neutrino generators play unique and important roles in the experimental study of neutrino interactions and oscillations.

There are several neutrino event generators available, such as ANIS [1], GENIE [2], GiBUU [3, 4], MARLEY [5], NEGN [6], NEUT [7], NUANCE [8], the FLUKA routines NUNDIS/NUNRES [9] [10], and NuWro [11], as well as tools to facilitate cross-generator comparisons [12]. Historically, experiments would develop their own generators. This was often because they were focused on a particular measurement, energy range, or target, and wanted to ensure that the best physics was included for it. These ‘home-grown’ generators were often tuned primarily or exclusively to the neutrino data most similar to the data that the experiment would be collecting. A major advance in the field was the introduction of conference series devoted to the topic of neutrino interaction physics, NuINT (<https://nuint2017.physics.utoronto.ca>) and NuFACT (<https://indico.uu.se/event/324/>) in particular. Event generator comparisons have been a regular staple of the NuINT conference series from its inception, and a great deal of information on this topic can be found in the Proceedings of these meetings. These meetings have facilitated experiment-theory discussions leading to the first generator developed by a theory group (NuWro) [11], the extension of established nuclear interaction codes (FLUKA and GiBUU) to include neutrino-nuclear processes [3] [4] [9] [10], and inclusion of theorists in existing generator development teams.

These activities have led to more careful scrutiny of the crucial nuclear theory inputs to these generators, which is evaluated in particular through comparisons to electron-scattering data. At this point in time all simulation codes face challenges in describing the full extent of the lepton scattering data, and the tension between incorporating the best available theory versus obtaining the best agreement with the data plays out in a variety of ways within the field. For the field to make progress, inclusion of state of the art theory needs to be coupled to global analyses that correctly incorporate correlations between measurements. Given the rapid pace of new data and the complexity of analyses, this is a significant challenge for the field in the coming years.

There are many neutrino experiments which use various sources of neutrinos, from reactors, accelerators, the atmosphere, and astrophysical sources, thereby covering a range of energies from MeV to TeV. Much of the emphasis has been on the few-GeV region in the generators, as this is the relevant energy range for short- and long-baseline neutrino oscillation experiments. These generators use the impulse approximation, which treats the nucleus as a collection of independent nucleons and the primary interaction occurs between the probe and a single nucleon, for most

of the initial interaction, and subsequently simulates the interactions of secondary particles in the nucleus in semi-classical ways. Semi-classical hadron transport approaches are commonly used as they are able to simulate a variety of nuclei in a single model, and for practical considerations as these approaches are fast. However, there are several challenges facing these simulations coming mainly from the complexity of the nuclear physics, and avoiding double counting in combining perturbative and non-perturbative models for the neutrino-nucleon scattering processes. The overall validity of this impulse approximation-based scheme, and in particular the importance of scattering channels that involve more than one nucleon, is a crucial question that is the topic of much current work. While generators share many common ingredients, differences in implementation, parameter values, and approaches to avoid double counting can yield dramatically different predictions [13]. In the following sections, interaction models and their implementations including the interactions of generated particles in the nuclei are described.

In order to assure its validity, neutrino event generators are tuned and validated against a wide variety of data, including data from photon, charged lepton, neutrino, and hadron probes. The results from these external data tuning exercises are important for experiments as they quantify the uncertainty on model parameters, needed by experiments in the evaluation of generator-related systematic errors. Electron scattering data plays an important role in determining the vector contribution to the form-factors and structure functions, as well as in evaluating specific aspects of the nuclear model [14]. Hadron scattering data is used in validating the nuclear model, in particular of interactions between hadrons produced in the primary interaction and the residual target nucleus (final state interactions). Tuning of neutrino-nucleon scattering and hadronization models relies heavily on the previous generation of high energy neutrino scattering and hydrogen and deuterium bubble chamber experiments, and more recent data from the K2K, MiniBooNE, NOMAD, SciBooNE, MINOS, T2K, ArgoNEUT, MINERvA, NOvA, MicroBooNE, and SBND experiments either has been, or will be, used for this purpose.

### 43.1 Neutrino-Nucleon Scattering

Event generators typically begin with free-nucleon cross sections which are then embedded into a nuclear physics model. The most important processes are quasi-elastic (elastic for neutral current (NC)) scattering, resonance production, and non-resonant inelastic scattering, which make comparable contributions for few-GeV interactions. The neutrino cross sections in this energy range can be seen in Figures 51.1 through 51.3 of this *Review*.

#### 43.1.1 Quasi-Elastic Scattering

The cross section for the neutrino nucleon charged current quasi-elastic scattering is described in terms of the leptonic and hadronic weak currents, where dominant contributions to the hadronic current come from the vector (V) and axial-vector (A) form factors. Contributions from the pseudo-scalar form factor (P) are typically small for muon and electron neutrinos and are related to the axial form factor (A) assuming partially conserved axial currents (PCAC). The vector form factors are related via the conserved vector current (CVC) hypothesis to those measured by precise electron scattering experiments, which are known to have some deviation from the simple dipole form [15]. Therefore, most of the generators use parametrizations of this form factor taken directly from the data. For the axial form factor there is no such precise experiment, and most of the generators use a dipole form [16]. Generally, the value of axial form factor at  $q^2 = 0$  ( $q$  is the four-momentum transfer) is extracted from the polarized nucleon beta decay experiment. However, the selection of the axial vector mass parameter depends on each generator, with values typically around  $1.00 \text{ GeV}/c^2$ . Recently, there are several attempts to use the other functions for the axial form factors [17, 18] and some generators have already implemented these form factors [19].

#### 43.1.2 Resonance Production

Most generators use the prescriptions of Rein-Sehgal [20] to simulate neutrino-induced single pion production. To obtain the



cross section for a particular channel, they calculate the amplitude for the production of each resonance multiplied by the probability for the decay of that resonance into that particular channel. Implementation differences include the number of resonances included, whether the amplitudes are added coherently or incoherently, the invariant mass range over which the model is used, how non-resonant backgrounds are included, inclusion of lepton mass terms, and the model parameter values (in particular the axial mass). In this model it is also possible to calculate the cross-sections of single photon, kaon and  $\eta$  productions by changing the decay probability of the resonances, which are included in some of the programs. However, it is known that discrepancies exist between the recent pion electro/photoproduction data and the results from the simulation data with the same framework, i.e. vector part of this model. There are several attempts to overcome this issue [21] and some of the generators started using more appropriate form factors. Recently, there is another attempt to further improve the model itself and make it possible to reproduce both electron and neutrino scatterings [22]. This work is expected to be implemented in the generators soon. GiBUU and NuWro generators do not use the Rein-Sehgal model, and instead rely directly on electro-production data for the vector contribution and fit bubble chamber data to determine the remaining parameters for the axial contribution [23–25]. The dynamical coupled-channel model, which has been developed to simulate various electro- and photo-meson productions, was extended to simulate the neutrino single pion production [26]. This model is also being implemented and expected to be available in some of the generators in future.

#### 43.1.3 Deep and Shallow Inelastic Scattering

For this process the fundamental target shifts from the nucleon to its quark constituents. Therefore, the generators use the standard expression for the constructions for the nucleon structure functions  $F_2$  and  $xF_3$  from parton distributions for high  $Q^2$  (the DIS regime:  $W > 2 \text{ GeV}/c^2$  and  $Q^2 > 1 \text{ GeV}^2$ ) to calculate direction and momentum of lepton. The first challenge is in extending this picture to the lower values of  $Q^2$  and  $W$  that dominate the available phase space for few-GeV interactions (the so-called ‘shallow inelastic scattering’, or SIS regime). GRV98LO parton distribution functions [27] with the corrections proposed in [28] are widely used, while others [9] implement their own modifications to the parton distributions at low  $Q^2$ . Both DIS and SIS generates hadrons but their production depends on each generator’s implementation of a hadronization model as described in the next section. There are various difficulties not only in the actual hadronization but the relation with the single meson production. It is necessary to avoid double counting between the resonance and SIS/DIS models, and all generators are different in this regard. The scheme chosen can have a significant impact on the results of simulations at a few-GeV neutrino energies.

### 43.2 Hadronization Models

For hadrons produced via baryonic resonances, the underlying model amplitudes and resonance branching fractions can be used to fully characterize the hadronic system. For non-resonant production, a hadronization model is required. Most generators use PYTHIA [29] for this purpose, although some with modified parameters. In addition some implement their own models to handle invariant masses that are too low for PYTHIA, typically somewhere around  $2.0 \text{ GeV}/c^2$ . Such models rely heavily on measurements of neutrino hadro-production in high-resolution devices, such as bubble chambers and the CHORUS [30] and NOMAD experiments [31], to construct empirical parametrizations that reproduce the key features of the data [32, 33]. The basic ingredients are the empirical observations that average charged particle multiplicities increase logarithmically with the invariant mass of the hadronic system, and that the distribution of charged particle multiplicities about this average are described by a single function (an observation known as KNO scaling [34]). Neutral particles are assumed to be produced with an average multiplicity that is 50% of the charged particle multiplicity. Simple parametrizations to more accurately reproduce differences observed in the forward/backward hemispheres of hadronic systems are included in GENIE, NEUT, and NuWro.

### 43.3 Nuclear Physics

The nuclear physics relevant to neutrino-nucleus scattering at few-GeV energies is complicated, involving Fermi motion, nuclear binding, Pauli blocking, in-medium modifications of form factors and hadronization, intranuclear rescattering of hadrons, and many-body scattering mechanisms including long- and short-range nucleon-nucleon correlations.

#### 43.3.1 Treatments of scattering kinematics in nucleus

In order to obtain the cross-section off nucleons in the nucleus, it is necessary to take into account various in-medium effects. Most of the models used for neutrino-nuclear scattering kinematics were developed in the context of few-GeV inclusive electron scattering, by experiments going back nearly 50 years. The basic models employed in event generators rely on impulse approximation schemes, the most simple of which is the Relativistic Fermi Gas Model. The most common implementations have been the Smith-Moniz [35] and Bodek-Ritchie [36] models. However, the results from neutrino-nucleus scattering experiments in 2000 and afterwards, such as K2K, MiniBooNE have shown large discrepancies from the naive expectation from the models. Most striking differences are a suppression of forward going muons (low  $Q^2$ ), a high  $Q^2$  enhancement in the event rate, and an overall larger than expected number of observed events. In order to reproduce the data, the quasi-elastic axial mass was used as the effective parameter and increased by roughly 20% from the nominal values obtained by an earlier generation of bubble chamber experiments using hydrogen or deuterium [16]. These inconsistency between nucleon and nucleus targets suggests that the simple nuclear model is not appropriate in describing the data. Moreover, these simple Fermi-Gas models are not expected to describe the kinematical distributions of final state nucleons. Actually, recent hadronic energy measurements by MINERvA have shown that the simple global Fermi-gas model is not appropriate to reproduce the small energy deposit. Therefore, several generators have to implement better models, such as local Fermi-Gas model or more sophisticated models. Within the electron scattering community, the analogous calculations have for decades relied on spectral functions, which incorporate information about nucleon momenta and binding energies in the impulse approximation scheme. Therefore, most of the generators have implemented the spectral functions in their latest releases.

Actually, the discrepancies in small  $q^2$  could not be solved alone by just introducing the local Fermi-gas model nor spectral function models. This implies that the additional medium correction effects are needed to be taken into account. One of the implemented solutions is the local Fermi-Gas model with medium correction calculated using the random phase approximation, which is known to give large suppression in small  $q^2$ . Although, the fundamental parts of the models are same, actual implementations are quite different between the generators. Especially, the constructions of the final state hadron kinematics are quite different. Especially for the quasi-elastic scattering case, treatment of the nucleon masses in the nucleus, the binding and the separation energies are sometimes quite different. Recently, Super-Scaling model with relativistic mean field theory effects (SuSAv2) [37] was also implemented.

The cause of the discrepancy of small  $q^2$  seems to be identified but the issue of the observed interaction rates are not solved. This implies that there must be some interaction channels which are missing and not considered in the generators.

These led to a revisit of the role played by scattering from multi-particle/hole states in the nucleus, and the experimental search for evidence of these scattering channels is an area of intense experimental interest [38]. The contribution of these scattering processes is an extremely active area of theoretical research as well, with significant implications for generators and analyses [39]. Several approaches, ranging from strictly phenomenological descriptions to full theoretical calculations, have recently been incorporated into generators [40–42]. One example of a phenomenological approach utilizes an Effective Spectral Function [43] and a Transverse Enhancement Model [44], which together encapsulate information derived from electron scattering experiments at relevant kinematics. The microscopic model of Nieves and collab-

orators is now available in GENIE and NEUT [45, 46]. SuSAv2 model also has capability to simulate this multi-nucleon quasi-elastic like interaction and is also implemented in GENIE.

One of the challenges in incorporating full theoretical models of these processes is that they are typically slow, so generators have developed new approaches whereby much of the computation is done offline, and the generators simply read in the hadronic tensor components. This allows for a full prediction of the lepton kinematics, however the ability to simulate the hadronic component of these multinucleon states then relies on separate models. The other challenges is that the theoretical models are not designed to describe exclusive final states. Precisely speaking, some of the neutrino interactions could not be separated each other because of the interference between those channels. Also, there are limitation of the model itself to describe some of the kinematic regions. However, the generators need to simulate final all the state particles and thus, several assumptions are made by authors of the generators from time to time.

Also, it is known from photo and electro-nuclear scattering that the Delta width is affected by Pauli blocking and collisional broadening. These effects are included in some, but not all generators.

When scattering from a nucleus, coherent scattering of various kinds is possible. Most simulations incorporate, at least, neutral and charged coherent single pion production. While the interaction rate for these interactions is typically around a percent of the total yield, the unique kinematic features of these events can make them potential backgrounds for oscillation searches. Implemented in Monte Carlo are several PCAC-based methods [47, 48], and microscopic models [49, 50], valid at lower neutrino energies, have also been implemented in several generators. One of the commonly used model by Rein and Sehgal [47] predicts much larger charged current cross-section compared to the recent measurements of MINER $\nu$ A and T2K gives a few times smaller cross-section for the charged current coherent pion production. However, the cross-section is sensitive to the pion cross-section used in the model as parameters and improved models with lepton mass correction [48] give better agreement with the recent data. This improved model is implemented in most of the generators.

### 43.3.2 Hadron Production in Nuclei

Neutrino pion production is one of the dominant interactions in a few-GeV region and the interaction cross sections of pions in nucleus from those interactions are quite large. Therefore, the interactions of pions in nucleus changes the kinematics of the pions and can have large effects on the results of simulations at these energies. Most generators implement this physics through an intranuclear cascade simulation. In generators which utilize cascade models, a hadron, which has been formed in the nucleus, is moved step by step until it interacts with the other nucleon or escapes from the nucleus. The probabilities of each interaction in nucleus are usually given as the mean free paths and used to determine whether the hadron is interacted or not. If the hadron is found to be interacted, appropriate interactions are selected and simulated. Usually, absorption, elastic, charge exchange, and inelastic scatterings including particle productions are simulated as intranuclear interactions. The determination method of the kinematics for the final state particles heavily depends on the generators but most of them use experimentally validated models to simulate hadron interactions in nucleus. No two interanuclear cascade simulations implemented in neutrino event generators are the same. In all cases hadrons propagate from an interaction vertex chosen based on the density distribution of the target nucleus. In determining the generated position of the hadrons in nucleus, the concept of the formation length is sometimes employed. Based on this idea, the hadronization process is not instantaneous and it takes some time before generating the hadrons [11]. The basis for formation times are measurements at relatively high energy and  $Q^2$ , and most generators that employ the concept do not apply them to resonance interactions.

GiBUU does not employ an intranuclear cascade simulation, instead, it utilizes a semi-classical transport model in coupled channels that describes the space-time evolution of a many body system in the presence of potentials and a collision term [3]. This approach assures consistency between nuclear effects in the initial

state, such as Fermi motion, Pauli blocking, hadron self-energies, and modified cross sections, and the final state, such as particle re-interactions, since the two are derived from the same model. This model has been previously used to describe a wide variety of nuclear interaction data. Similarly, the hadronic simulation of the NUNDIS/NUNRES programs are handled by the well-established FLUKA hadronic simulation package [9].

### References

- [1] A. Gazizov and M. P. Kowalski, *Comput. Phys. Commun.* **172**, 203 (2005), [arXiv:astro-ph/0406439].
- [2] C. Andreopoulos *et al.*, *Nucl. Instrum. Meth.* **A614**, 87 (2010), [arXiv:0905.2517].
- [3] O. Buss *et al.*, *Phys. Rept.* **512**, 1 (2012), [arXiv:1106.1344].
- [4] K. Gallmeister, U. Mosel and J. Weil, *Phys. Rev.* **C94**, 3, 035502 (2016), [arXiv:1605.09391].
- [5] S. Gardiner, C. Grant, E. Panic, and R. Svoboda, <http://www.marleygen.org>.
- [6] D. Autiero, *Nucl. Phys. Proc. Suppl.* **139**, 253 (2005).
- [7] Y. Hayato, *Nucl. Phys. Proc. Suppl.* **112**, 171 (2002).
- [8] D. Casper, *Nucl. Phys. Proc. Suppl.* **112**, 161 (2002), [hep-ph/0208030].
- [9] G. Battistoni *et al.*, *Acta Phys. Polon.* **B40**, 2491 (2009).
- [10] T. T. Böhlen *et al.*, *Nucl. Data Sheets* **120**, 211 (2014).
- [11] T. Golan, C. Juszczak and J. T. Sobczyk, *Phys. Rev.* **C86**, 015505 (2012), [arXiv:1202.4197].
- [12] P. Stowell *et al.*, *JINST* **12**, 01, P01016 (2017), [arXiv:1612.07393].
- [13] S. Boyd *et al.*, *AIP Conf. Proc.* **1189**, 1, 60 (2009).
- [14] O. Benhar, D. day and I. Sick, *Rev. Mod. Phys.* **80**, 189 (2008), [arXiv:nucl-ex/0603029].
- [15] A. Bodek *et al.*, *Eur. Phys. J.* **C53**, 349 (2008), [arXiv:0708.1946].
- [16] H. Gallagher, G. Garvey and G. P. Zeller, *Ann. Rev. Nucl. Part. Sci.* **61**, 355 (2011).
- [17] E. Tomasi-Gustafsson, G. I. Gakh and C. Adamuscin, *Phys. Rev.* **C73**, 045204 (2006), [arXiv:nucl-th/0512039].
- [18] B. Bhattacharya, R. J. Hill and G. Paz, *Phys. Rev.* **D84**, 073006 (2011), [arXiv:1108.0423].
- [19] A. S. Meyer *et al.*, *Phys. Rev.* **D93**, 11, 113015 (2016), [arXiv:1603.03048].
- [20] D. Rein and L. M. Sehgal, *Annals Phys.* **133**, 79 (1981).
- [21] K. M. Graczyk and J. T. Sobczyk, *Phys. Rev.* **D77**, 053001 (2008), [Erratum: *Phys. Rev.* **D79**, 079903 (2009)], [arXiv:0707.3561].
- [22] M. Kabirnezhad, *Phys. Rev.* **D97**, 1, 013002 (2018), [arXiv:1711.02403].
- [23] O. Lalakulich and E. A. Paschos, *Phys. Rev.* **D71**, 074003 (2005), [hep-ph/0501109].
- [24] J. A. Nowak, *Phys. Scripta* **T127**, 70 (2006), [hep-ph/0607081].
- [25] L. Alvarez-Ruso, S. K. Singh and M. J. Vicente Vacas, *Phys. Rev.* **C57**, 2693 (1998), [arXiv:nucl-th/9712058].
- [26] S. X. Nakamura, H. Kamano and T. Sato, *Phys. Rev.* **D92**, 7, 074024 (2015), [arXiv:1506.03403].
- [27] M. Glück, E. Reya and A. Vogt, *Eur. Phys. J.* **C5**, 461 (1998), [hep-ph/9806404].
- [28] A. Bodek and U. K. Yang, *J. Phys.* **G29**, 1899 (2003), [hep-ex/0210024].
- [29] T. Sjostrand, S. Mrenna and P. Z. Skands, *JHEP* **05**, 026 (2006), [hep-ph/0603175].
- [30] A. Kayis-Topaksu *et al.* (CHORUS), *Eur. Phys. J.* **C51**, 775 (2007), [arXiv:0707.1586].
- [31] J. Altegoer *et al.* (NOMAD), *Phys. Lett.* **B445**, 439 (1999).

- [32] T. Yang *et al.*, Eur. Phys. J. **C63**, 1 (2009), [arXiv:0904.4043].
- [33] J. A. Nowak and J. T. Sobczyk, Acta Phys. Polon. **B37**, 2371 (2006), [hep-ph/0608108].
- [34] Z. Koba, H. B. Nielsen and P. Olesen, Nucl. Phys. **B40**, 317 (1972).
- [35] R. A. Smith and E. J. Moniz, Nucl. Phys. **B43**, 605 (1972), [Erratum: Nucl. Phys. B101,547(1975)].
- [36] A. Bodek and J. L. Ritchie, Phys. Rev. **D24**, 1400 (1981).
- [37] J. A. Caballero *et al.*, Phys. Lett. **B653**, 366 (2007), [arXiv:0705.1429].
- [38] P. A. Rodrigues *et al.* (MINERvA), Phys. Rev. Lett. **116**, 071802 (2016), [Addendum: Phys. Rev. Lett. 121, no. 20, 209902 (2018)], [arXiv:1511.05944].
- [39] L. Alvarez-Ruso *et al.*, Prog. Part. Nucl. Phys. **100**, 1 (2018), [arXiv:1706.03621].
- [40] T. Katori, AIP Conf. Proc. **1663**, 1, 030001 (2015), [arXiv:1304.6014].
- [41] M. Alam *et al.* (2015), [arXiv:1512.06882].
- [42] C. Wilkinson *et al.*, Phys. Rev. **D93**, 7, 072010 (2016), [arXiv:1601.05592].
- [43] A. Bodek, M. E. Christy and B. Coopersmith, Eur. Phys. J. **C74**, 10, 3091 (2014), [arXiv:1405.0583].
- [44] A. Bodek, H. S. Budd and M. E. Christy, Eur. Phys. J. **C71**, 1726 (2011), [arXiv:1106.0340].
- [45] J. Nieves, I. Ruiz Simo and M. J. Vicente Vacas, Phys. Rev. **C83**, 045501 (2011), [arXiv:1102.2777].
- [46] R. Gran *et al.*, Phys. Rev. **D88**, 11, 113007 (2013), [arXiv:1307.8105].
- [47] D. Rein and L. M. Sehgal, Nucl. Phys. **B223**, 29 (1983).
- [48] C. Berger and L. M. Sehgal, Phys. Rev. **D79**, 053003 (2009), [arXiv:0812.2653].
- [49] L. Alvarez-Ruso *et al.*, Phys. Rev. **C75**, 055501 (2007), [Erratum: Phys. Rev. C80, 019906 (2009)], [arXiv:nucl-th/0701098].
- [50] L. Alvarez-Ruso, L. S. Geng and M. J. Vicente Vacas, Phys. Rev. **C76**, 068501 (2007), [Erratum: Phys. Rev. C80, 029904 (2009)], [arXiv:0707.2172].

## 44. Monte Carlo Particle Numbering Scheme

Revised August 2019 by F. Krauss (Durham U.), S. Navas (Dp.de Fisica. U. de Granada), P. Richardson (Durham U.) and T. Sjöstrand (Lund U.).

The Monte Carlo particle numbering scheme presented here is intended to facilitate interfacing between event generators, detector simulators, and analysis packages used in particle physics. The numbering scheme was introduced in 1988 [1] and a revised version [2, 3] was adopted in 1998 in order to allow systematic inclusion of quark model states which are as yet undiscovered and hypothetical particles such as SUSY particles. The numbering scheme is used in several event generators, *e.g.* HERWIG, PYTHIA, and SHERPA, and interfaces, *e.g.* /HEPEVT/ and HepMC.

The general form is a 7-digit number:

$$\pm n \ n_r \ n_L \ n_{q_1} \ n_{q_2} \ n_{q_3} \ n_J .$$

This encodes information about the particle's spin, flavor content, and internal quantum numbers. The details are as follows:

1. Particles are given positive numbers, antiparticles negative numbers. The PDG convention for mesons is used, so that  $K^+$  and  $B^+$  are particles.
2. Quarks and leptons are numbered consecutively starting from 1 and 11 respectively; to do this they are first ordered by family and within families by weak isospin.
3. In composite quark systems (diquarks, mesons, and baryons)  $n_{q_{1-3}}$  are quark numbers used to specify the quark content, while the rightmost digit  $n_J = 2J + 1$  gives the system's spin (except for the  $K_S^0$  and  $K_L^0$ ). The scheme does not cover particles of spin  $J > 4$ .
4. Diquarks have 4-digit numbers with  $n_{q_1} \geq n_{q_2}$  and  $n_{q_3} = 0$ .
5. The numbering of mesons is guided by the nonrelativistic ( $L$ - $S$  decoupled) quark model, as listed in Tables 15.2, 15.3, and 15.4.
  - (a) The numbers specifying the meson's quark content conform to the convention  $n_{q_1} = 0$  and  $n_{q_2} \geq n_{q_3}$ . The special case  $K_L^0$  is the sole exception to this rule.
  - (b) The quark numbers of flavorless, light ( $u, d, s$ ) mesons are: 11 for the member of the isotriplet ( $\pi^0, \rho^0, \dots$ ), 22 for the lighter isosinglet ( $\eta, \omega, \dots$ ), and 33 for the heavier isosinglet ( $\eta', \phi, \dots$ ). Since isosinglet mesons are often large mixtures of  $u\bar{u} + d\bar{d}$  and  $s\bar{s}$  states, 22 and 33 are assigned by mass and do not necessarily specify the dominant quark composition.
  - (c) The special numbers 310 and 130 are given to the  $K_S^0$  and  $K_L^0$  respectively.
  - (d) The fifth digit  $n_L$  is reserved to distinguish mesons of the same total ( $J$ ) but different spin ( $S$ ) and orbital ( $L$ ) angular momentum quantum numbers. For  $J > 0$  the numbers are: ( $L, S$ ) = ( $J - 1, 1$ )  $n_L = 0$ , ( $J, 0$ )  $n_L = 1$ , ( $J, 1$ )  $n_L = 2$  and ( $J + 1, 1$ )  $n_L = 3$ . For the exceptional case  $J = 0$  the numbers are ( $0, 0$ )  $n_L = 0$  and ( $1, 1$ )  $n_L = 1$  (*i.e.*  $n_L = L$ ). See Table 44.1.
  - (e) If a set of physical mesons correspond to a (non-negligible) mixture of basis states, differing in their internal quantum numbers, then the lightest physical state gets the smallest basis state number. For example the  $K_1(1270)$  is numbered 10313 ( $1^1P_1 K_{1B}$ ) and the  $K_1(1400)$  is numbered 20313 ( $1^3P_1 K_{1A}$ ).
  - (f) The sixth digit  $n_r$  is used to label mesons radially excited above the ground state.
  - (g) Numbers have been assigned for complete  $n_r = 0$   $S$ - and  $P$ -wave multiplets, even where states remain to be identified.
  - (h) In some instances assignments within the  $q\bar{q}$  meson model are only tentative; here best guess assignments are made.
  - (i) Many states appearing in the Meson Listings are not yet assigned within the  $q\bar{q}$  model. Here  $n_{q_{2-3}}$  and  $n_J$

**Table 44.1:** Meson numbering logic. Here  $qq$  stands for  $n_{q_2} n_{q_3}$ .

$J$	$L = J - 1, S = 1$			$L = J, S = 0$			$L = J, S = 1$			$L = J + 1, S = 1$		
	code	$J^{PC}$	$L$	code	$J^{PC}$	$L$	code	$J^{PC}$	$L$	code	$J^{PC}$	$L$
0	—	—	—	00qq1	0 <sup>-+</sup>	0	—	—	—	10qq1	0 <sup>++</sup>	1
1	00qq3	1 <sup>--</sup>	0	10qq3	1 <sup>+-</sup>	1	20qq3	1 <sup>++</sup>	1	30qq3	1 <sup>--</sup>	2
2	00qq5	2 <sup>++</sup>	1	10qq5	2 <sup>-+</sup>	2	20qq5	2 <sup>--</sup>	2	30qq5	2 <sup>++</sup>	3
3	00qq7	3 <sup>-</sup>	2	10qq7	3 <sup>+-</sup>	3	20qq7	3 <sup>++</sup>	3	30qq7	3 <sup>-</sup>	4
4	00qq9	4 <sup>++</sup>	3	10qq9	4 <sup>-+</sup>	4	20qq9	4 <sup>--</sup>	4	30qq9	4 <sup>++</sup>	5

are assigned according to the state's likely flavors and spin; all such unassigned light isoscalar states are given the flavor code 22. Within these groups  $n_L = 0, 1, 2, \dots$  is used to distinguish states of increasing mass. These states are flagged using  $n = 9$ . It is to be expected that these numbers will evolve as the nature of the states are elucidated. Codes are assigned to all mesons which are listed in the one-page table at the end of the Meson Summary Table as long as they have a preferred or established spin. Additional heavy meson states expected from heavy quark spectroscopy are also assigned codes.

6. The numbering of baryons is again guided by the nonrelativistic quark model, see Table 15.7. This numbering scheme is illustrated through a few examples in Table 44.2.
  - (a) The numbers specifying a baryon's quark content are such that in general  $n_{q_1} \geq n_{q_2} \geq n_{q_3}$ .
  - (b) Two states exist for  $J = 1/2$  baryons containing 3 different types of quarks. In the lighter baryon ( $\Lambda, \Xi, \Omega, \dots$ ) the light quarks are in an antisymmetric ( $J = 0$ ) state while for the heavier baryon ( $\Sigma^0, \Xi', \Omega', \dots$ ) they are in a symmetric ( $J = 1$ ) state. In this situation  $n_{q_2}$  and  $n_{q_3}$  are reversed for the lighter state, so that the smaller number corresponds to the lighter baryon.
  - (c) For excited baryons a scheme is adopted, where the  $n_r$  label is used to denote the excitation bands in the harmonic oscillator model, see Sec. 15.4. Using the notation employed there,  $n_r$  is given by the  $N$ -index of the  $D_N$  band identifier.
  - (d) Further degeneracies of excited hadron multiplets with the same excitation number  $n_r$  and spin  $J$  are lifted by labelling such multiplets with the  $n_L$  index according to their mass, as given by its  $N$  or  $\Delta$ -equivalent.
  - (e) In such excited multiplets extra singlets may occur, the  $\Lambda(1520)$  being a prominent example. In such cases the ordering is reversed such that the heaviest quark label is pushed to the last position:  $n_{q_3} > n_{q_1} > n_{q_2}$ .
  - (f) For pentaquark states  $n = 9$ ,  $n_r n_L n_{q_1} n_{q_2}$  gives the four quark numbers in order  $n_r \geq n_L \geq n_{q_1} \geq n_{q_2}$ ,  $n_{q_3}$  gives the antiquark number, and  $n_J = 2J + 1$ , with the assumption that  $J = 1/2$  for the states currently reported.
7. The gluon, when considered as a gauge boson, has official number 21. In codes for glueballs, however, 9 is used to allow a notation in close analogy with that of hadrons.
8. The pomeron and odderon trajectories and a generic reggeon trajectory of states in QCD are assigned codes 990, 9990, and 110 respectively, where the final 0 indicates the indeterminate nature of the spin, and the other digits reflect the expected "valence" flavor content. We do not attempt a complete classification of all reggeon trajectories, since there is currently no need to distinguish a specific such trajectory from its lowest-lying member.
9. Two-digit numbers in the range 21–30 are provided for the Standard Model gauge bosons and Higgs.
10. Codes 81–100 are reserved for generator-specific pseudoparticles and concepts. Codes 901–930, 1901–1930, 2901–2930, and 3901–3930 are for additional components of Standard Model parton distribution functions, where the latter three

**Table 44.2:** Some examples of octet (top) and decuplet (bottom) members for the numbering scheme for excited baryons. Here  $qqq$  stands for  $n_{q_1}n_{q_2}n_{q_3}$ . See the text for the definition of the notation. The numbers in parenthesis correspond to the mass of the baryons. The states marked as (?) are not experimentally confirmed.

$J^P$	$(D, L_N^P)$	$n_r n_L n_{q_1} n_{q_2} n_{q_3} n_J$	$N$	$\Lambda_8$	$\Sigma$	$\Xi$	$\Lambda_1$
Octet							
1/2 <sup>+</sup>	(56, 0 <sub>0</sub> <sup>+</sup> )	00qqq2	(939)	(1116)	(1193)	(1318)	—
1/2 <sup>+</sup>	(56, 0 <sub>2</sub> <sup>+</sup> )	20qqq2	(1440)	(1600)	(1660)	(1690)	—
1/2 <sup>+</sup>	(70, 0 <sub>2</sub> <sup>+</sup> )	21qqq2	(1710)	(1810)	(1880)	(?)	(?)
1/2 <sup>-</sup>	(70, 1 <sub>1</sub> <sup>-</sup> )	10qqq2	(1535)	(1670)	(1620)	(1750)	(1405)
$J^P$	$(D, L_N^P)$	$n_r n_L n_{q_1} n_{q_2} n_{q_3} n_J$	$\Delta$	$\Sigma$	$\Xi$	$\Omega$	
Decuplet							
3/2 <sup>+</sup>	(56, 0 <sub>0</sub> <sup>+</sup> )	00qqq4	(1232)	(1385)	(1530)	(333)	372
3/2 <sup>+</sup>	(56, 0 <sub>2</sub> <sup>+</sup> )	20qqq4	(1600)	(1690)	(?)	(?)	
1/2 <sup>-</sup>	(70, 1 <sub>1</sub> <sup>-</sup> )	11qqq2	(1620)	(1750)	(?)	(?)	
3/2 <sup>-</sup>	(70, 1 <sub>1</sub> <sup>-</sup> )	12qqq4	(1700)	(?)	(?)	(?)	

ranges are intended to distinguish left/ right/ longitudinal components. Codes 998 and 999 are reserved for GEANT tracking purposes.

11. The search for physics beyond the Standard Model is an active area, so these codes are also standardized as far as possible.
  - (a) A standard fourth generation of fermions is included by analogy with the first three.
  - (b) The graviton and the boson content of a two-Higgs-doublet scenario and of additional SU(2)×U(1) groups are found in the range 31–40.
  - (c) “One-of-a-kind” exotic particles are assigned numbers in the range 41–80. The subrange 61–80 can be used for new heavier fermions in generic models, where partners to the SM fermions would have codes offset by 60. If required, however, other assignments could be made.
  - (d) Fundamental supersymmetric particles are identified by adding a nonzero  $n$  to the particle number. The superpartner of a boson or a left-handed fermion has  $n = 1$  while the superpartner of a right-handed fermion has  $n = 2$ . When mixing occurs, such as between the winos and charged Higgsinos to give charginos, or between left and right sfermions, the lighter physical state is given the smaller basis state number.
  - (e) Technicolor states have  $n = 3$ , with technifermions treated like ordinary fermions. States which are ordinary color singlets have  $n_r = 0$ . Color octets have  $n_r = 1$ . If a state has non-trivial quantum numbers under the topcolor groups SU(3)<sub>1</sub> × SU(3)<sub>2</sub>, the quantum numbers are specified by tech, $ij$ , where  $i$  and  $j$  are 1 or 2.  $n_L$  is then  $2i + j$ . The colon,  $V_8$ , is a heavy gluon color octet and thus is 3100021.
  - (f) Excited (composite) quarks and leptons are identified by setting  $n = 4$  and  $n_r = 0$ .
  - (g) Within several scenarios of new physics, it is possible to have colored particles sufficiently long-lived for color-singlet hadronic states to form around them. In the context of supersymmetric scenarios, these states are called  $R$ -hadrons, since they carry odd  $R$ -parity.  $R$ -hadron codes, defined here, should be viewed as templates for corresponding codes also in other scenarios, for any long-lived particle that is either an unflavored color octet or a flavored color triplet. The  $R$ -hadron code is obtained by combining the SUSY particle code with a code for the light degrees of freedom, with as many intermediate zeros removed from the former as required to make place for the latter at the end. (To exemplify, a sparticle  $n00000n_{\bar{q}}$  combined with quarks  $q_1$  and  $q_2$  obtains code  $n00n_{\bar{q}}n_{q_1}n_{q_2}n_J$ .) Specifically, the new-particle spin decouples in the limit of large masses, so that the final  $n_J$  digit is defined by the spin state of the light-quark system alone. An appropriate number of  $n_q$  digits is used to define the ordinary-quark content. As usual, 9

rather than 21 is used to denote a gluon/gluino in composite states. The sign of the hadron agrees with that of the constituent new particle (a color triplet) where there is a distinct new antiparticle, and else is defined as for normal hadrons. Particle names are  $R$  with the flavor content as lower index.

- (h) A black hole in models with extra dimensions has code 5000040. Kaluza-Klein excitations in models with extra dimensions have  $n = 5$  or  $n = 6$ , to distinguish excitations of left- or right-handed fermions or, in case of mixing, the lighter or heavier state (cf. 11d). The nonzero  $n_r$  digit gives the radial excitation number, in scenarios where the level spacing allow these to be distinguished. Should the model also contain supersymmetry, excited SUSY states would be denoted by an  $n_r > 0$ , with  $n = 1$  or 2 as usual. Should some colored states be long-lived enough that hadrons would form around them, the coding strategy of 11g applies, with the initial two  $nn_r$  digits preserved in the combined code.
  - (i) Magnetic monopoles and dyons are assumed to have one unit of Dirac monopole charge and a variable integer number  $n_{q_1}n_{q_2}n_{q_3}$  units of electric charge. Codes  $411n_{q_1}n_{q_2}n_{q_3}0$  are then used when the magnetic and electrical charge sign agree and  $412n_{q_1}n_{q_2}n_{q_3}0$  when they disagree, with the overall sign of the particle set by the magnetic charge. For now no spin information is provided.
  - (j) The nature of Dark Matter (DM) is not known, and therefore a definitive classification is too early. Candidates within specific scenarios are classified therein, such as 1000022 for the lightest neutralino. Generic fundamental states can be given temporary codes in the range 51 - 60, with 51, 52 and 53 reserved for spin 0, 1/2 and 1 ones (this could also be an axion state). Generic mediators of s-channel DM pair creation or annihilation can be given codes 54 and 55 for spin 0 or 1 ones. Separate antiparticles, with negative codes, may or may not exist. More elaborate new scenarios should be constructed with  $n = 5$  and  $n_r = 9$ .
  - (k) Hidden Valley particles have  $n = 4$  and  $n_r = 9$ , and trailing numbers in agreement with their nearest-analog standard particles, as far as possible. Thus 4900021 is the gauge boson  $g_v$  of a confining gauge field, 490000 $n_{q_v}$  and 490001 $n_{\ell_v}$  fundamental constituents charged or not under this, 4900022 is the  $\gamma_v$  of a non-confining field, and 4900 $n_{q_v1}n_{q_v2}n_J$  a Hidden Valley meson.
12. Occasionally program authors add their own states. To avoid confusion, these should be flagged by setting  $nn_r = 99$ .
  13. Concerning the non-99 numbers, it may be noted that only quarks, excited quarks, squarks, and diquarks have  $n_{q_3} = 0$ ; only diquarks, baryons (including pentaquarks), and the odderon have  $n_{q_1} \neq 0$ ; and only mesons, the reggeon, and the pomeron have  $n_{q_1} = 0$  and  $n_{q_2} \neq 0$ . Concerning mesons



CHARMED MESONS		$B_c^{*+}$	10541	$\Upsilon(11020)$	9010553	CHARMED BARYONS		BOTTOM BARYONS	
$D^+$	411	$B_c^{*+}$	543	$\chi_{b2}(1P)$	555	$\Lambda_c^+$	4122	$\Lambda_b^0$	5122
$D^0$	421	$B_{c1}(L)^+$	10543	$\eta_{b2}(1D)$	10555	$\Sigma_c^{++}$	4222	$\Sigma_b^-$	5112
$D_0^*(2400)^+$	10411	$B_{c1}(H)^+$	20543	$\Upsilon_2(1D)$	20555	$\Sigma_c^+$	4212	$\Sigma_b^0$	5212
$D_0^*(2400)^0$	10421	$B_{c2}^{*+}$	545	$\chi_{b2}(2P)$	100555	$\Sigma_c^0$	4112	$\Sigma_b^+$	5222
$D^*(2010)^+$	413	<hr/> <b><math>c\bar{c}</math> MESONS</b> <hr/>		$\eta_{b2}(2D)$	110555	$\Sigma_c^{*+}$	4224	$\Sigma_b^{*-}$	5114
$D^*(2007)^0$	423	$\eta_c(1S)$	441	$\Upsilon_2(2D)$	120555	$\Sigma_c^{*0}$	4214	$\Sigma_b^{*0}$	5214
$D_1(2420)^+$	10413	$\chi_{c0}(1P)$	10441	$\chi_{b2}(3P)$	200555	$\Sigma_c^{*+}$	4114	$\Sigma_b^{*+}$	5224
$D_1(2420)^0$	10423	$\eta_c(2S)$	100441	$\Upsilon_3(1D)$	557	$\Xi_c^+$	4232	$\Xi_b^-$	5132
$D_1(H)^+$	20413	$J/\psi(1S)$	443	$\Upsilon_3(2D)$	100557	$\Xi_c^0$	4132	$\Xi_b^0$	5232
$D_2^*(2430)^0$	20423	$h_c(1P)$	10443	<hr/> <b>LIGHT BARYONS</b> <hr/>		$\Xi_c^{'+}$	4322	$\Xi_b^-$	5312
$D_2^*(2460)^+$	415	$\chi_{c1}(1P)$	20443	$p$	2212	$\Xi_c^{'0}$	4312	$\Xi_b^0$	5322
$D_2^*(2460)^0$	425	$\psi(2S)$	100443	$n$	2112	$\Xi_c^{*+}$	4324	$\Xi_b^+$	5314
$D_s^+$	431	$\psi(3770)$	30443	$\Delta^{++}$	2224	$\Xi_c^{*0}$	4314	$\Xi_b^0$	5324
$D_{s0}^*(2317)^+$	10431	$\psi(4040)$	9000443	$\Delta^+$	2214	$\Omega_c^0$	4332	$\Omega_b^-$	5332
$D_s^{*+}$	433	$\psi(4160)$	9010443	$\Delta^0$	2114	$\Omega_c^{*0}$	4334	$\Omega_b^{*-}$	5334
$D_{s1}(2536)^+$	10433	$\psi(4415)$	9020443	$\Delta^-$	1114	$\Xi_{cc}^+$	4412	$\Xi_{bc}^0$	5142
$D_{s1}(2460)^+$	20433	$\chi_{c2}(1P)$	445	<hr/> <b>STRANGE BARYONS</b> <hr/>		$\Xi_{cc}^{*+}$	4414	$\Xi_{bc}^+$	5242
$D_{s2}^*(2573)^+$	435	$\chi_{c2}(3930)$	100445	$\Lambda$	3122	$\Xi_{cc}^{*0}$	4424	$\Xi_{bc}^+$	5412
<hr/> <b>BOTTOM MESONS</b> <hr/>		<hr/> <b><math>b\bar{b}</math> MESONS</b> <hr/>		$\Sigma^+$	3222	$\Xi_{cc}^+$	4432	$\Xi_{bc}^0$	5422
$B^0$	511	$\eta_b(1S)$	551	$\Sigma^0$	3212	$\Xi_{cc}^{*+}$	4434	$\Xi_{bc}^0$	5424
$B^+$	521	$\chi_{b0}(1P)$	10551	$\Sigma^-$	3112	$\Xi_{cc}^{*0}$	4444	$\Omega_{bc}^0$	5342
$B_s^{*0}$	10511	$\eta_b(2S)$	100551	$\Sigma^{*+}$	3224 <sup>c</sup>	$\Omega_{bc}^{*0}$	5434	$\Omega_{bc}^{*0}$	5434
$B_0^{*+}$	10521	$\chi_{b0}(2P)$	110551	$\Sigma^{*0}$	3214 <sup>c</sup>	$\Omega_{bc}^{*+}$	5444	$\Omega_{bc}^{*+}$	5444
$B_s^{*0}$	513	$\eta_b(3S)$	200551	$\Sigma^{*-}$	3114 <sup>c</sup>	$\Xi_{bc}^{*+}$	5512	$\Xi_{bc}^{*+}$	5512
$B^{*+}$	523	$\chi_{b0}(3P)$	210551	$\Xi^0$	3322	$\Xi_{bc}^{*0}$	5522	$\Xi_{bc}^{*0}$	5522
$B_1(L)^0$	10513	$\Upsilon(1S)$	553	$\Xi^-$	3312	$\Xi_{bc}^{*+}$	5514	$\Xi_{bc}^{*+}$	5514
$B_1(L)^+$	10523	$h_b(1P)$	10553	$\Xi^{*0}$	3324 <sup>c</sup>	$\Xi_{bc}^{*0}$	5524	$\Xi_{bc}^{*0}$	5524
$B_1(H)^0$	20513	$\chi_{b1}(1P)$	20553	$\Xi^{*-}$	3314 <sup>c</sup>	$\Omega_{bc}^{*+}$	5532	$\Omega_{bc}^{*+}$	5532
$B_1(H)^+$	20523	$\Upsilon_1(1D)$	30553	$\Omega^-$	3334	$\Omega_{bc}^{*0}$	5542	$\Omega_{bc}^{*0}$	5542
$B_2^{*0}$	515	$\Upsilon(2S)$	100553	<hr/> <b>PENTAQUARKS</b> <hr/>		$\Theta^+$	9221132		
$B_2^{*+}$	525	$\Upsilon(3S)$	200553			$\Phi^{--}$	9331122		
$B_s^0$	531	$h_b(2P)$	110553						
$B_{s0}^{*0}$	10531	$\chi_{b1}(2P)$	120553						
$B_s^{*0}$	533	$\Upsilon_1(2D)$	130553						
$B_{s1}(L)^0$	10533	$\Upsilon(3S)$	200553						
$B_{s1}(H)^0$	20533	$h_b(3P)$	210553						
$B_s^{*0}$	535	$\chi_{b1}(3P)$	220553						
$B_c^+$	541	$\Upsilon(4S)$	300553						
		$\Upsilon(10860)$	9000553						

**Footnotes to the Tables:**

\*) Numbers or names in bold face are new or have changed since the 2018 *Review*.

a) Particular in the third generation, the left and right fermion states may mix, as shown. The lighter mixed state is given the smaller number.

b) The physical  $\tilde{\chi}$  states are admixtures of the pure  $\tilde{\gamma}$ ,  $\tilde{Z}^0$ ,  $\tilde{W}^+$ ,  $\tilde{H}_1^0$ ,  $\tilde{H}_2^0$ , and  $\tilde{H}^+$  states.

c)  $\Sigma^*$  and  $\Xi^*$  are alternate names for  $\Sigma(1385)$  and  $\Xi(1530)$ .

This text and full lists of particle numbers can be found on-

line [5].

**References**

[1] G. P. Yost *et al.* (Particle Data Group), Phys. Lett. **B204**, 1 (1988).  
 [2] I.G.Knowles *et al.*, CERN 96-01, p. 103.  
 [3] C. Caso *et al.* (Particle Data Group), Eur. Phys. J. **C3**, 1 (1998).  
 [4] G. Audi *et al.*, Nucl. Phys. **A729**, 3 (2003).  
 [5] <http://pdg.lbl.gov/current/mc-particle-id>.

45. Clebsch-Gordan Coefficients, Spherical Harmonics, and *d* Functions

Note: A square-root sign is to be understood over *every* coefficient, e.g., for  $-8/15$  read  $-\sqrt{8/15}$ .

Notation:  $\begin{matrix} J & J & \dots \\ M & M & \dots \end{matrix}$

$$1/2 \times 1/2$$

1		
+1/2	1/2	0
+1/2	1/2	0
-1/2	1/2	-1/2
-1/2	-1/2	1

$$Y_1^0 = \sqrt{\frac{3}{4\pi}} \cos \theta$$

$$Y_1^1 = -\sqrt{\frac{3}{8\pi}} \sin \theta e^{i\phi}$$

$$Y_2^0 = \sqrt{\frac{5}{4\pi}} \left( \frac{3}{2} \cos^2 \theta - \frac{1}{2} \right)$$

$$Y_2^1 = -\sqrt{\frac{15}{8\pi}} \sin \theta \cos \theta e^{i\phi}$$

$$Y_2^2 = \frac{1}{4} \sqrt{\frac{15}{2\pi}} \sin^2 \theta e^{2i\phi}$$

$$2 \times 1/2$$

5/2	3/2
+5/2	1
+2+1/2	1
1/5	4/5
4/5	-1/5
5/2	3/2
1/2	1/2

$m_1$	$m_2$	Coefficients
$m_1$	$m_2$	
$\vdots$	$\vdots$	

$$1 \times 1/2$$

3/2	1/2
+3/2	1
+1+1/2	1
1/3	2/3
2/3	-1/3
3/2	1/2
1/2	-1/2

$$2 \times 1$$

3	2
+3	2
+2+1	1
1/3	2/3
2/3	-1/3
3	2
2	1

$$1 \times 1$$

2	1
+2	1
+1+1	1
1/2	1/2
1/2	-1/2
2	1
1	0

$$Y_\ell^{-m} = (-1)^m Y_\ell^{m*}$$

0	-1	1/2	1/2	2
-1	0	1/2	-1/2	-2
-1	-1	1	1	1

$$3/2 \times 1$$

5/2	3/2
+5/2	1
+3/2+1	1
2/5	3/5
3/5	-2/5
5/2	3/2
1/2	1/2

$$d_{\ell, m, 0}^\ell = \sqrt{\frac{4\pi}{2\ell+1}} Y_\ell^m e^{-im\phi}$$

$$\langle j_1 j_2 m_1 m_2 | j_1 j_2 J M \rangle = (-1)^{J-j_1-j_2} \langle j_2 j_1 m_2 m_1 | j_2 j_1 J M \rangle$$

$$2 \times 3/2$$

7/2	5/2
+7/2	1
+2+3/2	1
3/7	4/7
4/7	-3/7
7/2	5/2
3/2	3/2

$$2 \times 2$$

4	3
+4	3
+2+2	1
1/2	1/2
1/2	-1/2
4	3
3	2

3/14	1/2	2/7
+1	1	0
3/14	-1/2	2/7
1/4	3/10	3/7
3/7	1/5	-1/14
3/10	-1/5	-1/14
3/10	3/10	1

4	3	2	1
+4	3	2	1
+2	1	0	0
1/70	1/10	2/7	2/5
8/35	2/5	1/14	-1/10
18/35	0	-2/7	0
8/35	-2/5	1/14	1/10
1/70	-1/10	2/7	-2/5

4	3	2	1
+4	3	2	1
+2	1	0	0
1/14	3/10	3/7	1/5
3/7	1/5	-1/14	-3/10
3/7	-1/5	-1/14	3/10
3/7	3/7	-1/5	1

4	3	2	1
+4	3	2	1
+2	1	0	0
1/14	3/10	3/7	1/5
3/7	1/5	-1/14	-3/10
3/7	-1/5	-1/14	3/10
3/7	3/7	-1/5	1

$$d_{3/2, 3/2}^{3/2} = \frac{1 + \cos \theta}{2} \cos \frac{\theta}{2}$$

$$d_{3/2, 1/2}^{3/2} = -\sqrt{3} \frac{1 + \cos \theta}{2} \sin \frac{\theta}{2}$$

$$d_{3/2, -1/2}^{3/2} = \sqrt{3} \frac{1 - \cos \theta}{2} \cos \frac{\theta}{2}$$

$$d_{3/2, -3/2}^{3/2} = -\frac{1 - \cos \theta}{2} \sin \frac{\theta}{2}$$

$$d_{1/2, 1/2}^{3/2} = \frac{3 \cos \theta - 1}{2} \cos \frac{\theta}{2}$$

$$d_{1/2, -1/2}^{3/2} = -\frac{3 \cos \theta + 1}{2} \sin \frac{\theta}{2}$$

$$d_{2, 2}^2 = \left( \frac{1 + \cos \theta}{2} \right)^2$$

$$d_{2, 1}^2 = -\frac{1 + \cos \theta}{2} \sin \theta$$

$$d_{2, 0}^2 = \frac{\sqrt{6}}{4} \sin^2 \theta$$

$$d_{2, -1}^2 = -\frac{1 - \cos \theta}{2} \sin \theta$$

$$d_{2, -2}^2 = \left( \frac{1 - \cos \theta}{2} \right)^2$$

$$3/2 \times 3/2$$

3	2
+3	2
+3/2+3/2	1
1/2	1/2
1/2	-1/2
3	2
2	1

1/5	1/2	3/10
3/5	0	-2/5
1/5	-1/2	3/10
3/2	1/2	1/2
1/20	1/4	9/20
1/20	1/4	-1/20
9/20	-1/4	-1/20
1/20	-1/4	9/20

1/35	6/35	2/5	2/5
12/35	5/14	0	-3/10
18/35	-3/35	-1/5	1/5
4/35	-27/70	2/5	-1/10
7/2	5/2	3/2	1/2
0	-1/2	-1/2	-1/2
7/2	5/2	3/2	1/2
12/35	5/14	0	3/10
1/35	-6/35	2/5	-2/5

4	3	2	1	0
+4	3	2	1	0
+2	1	0	0	0
1/70	1/10	2/7	2/5	1/5
8/35	2/5	1/14	-1/10	-1/5
18/35	0	-2/7	0	1/5
8/35	-2/5	1/14	1/10	-1/5
1/70	-1/10	2/7	-2/5	1/5

4	3	2	1	0
+4	3	2	1	0
+2	1	0	0	0
1/14	3/10	3/7	1/5	1/5
3/7	1/5	-1/14	-3/10	-1/5
3/7	-1/5	-1/14	3/10	1/5
3/7	3/7	-1/5	1/5	1

0	-2	3/14	1/2	2/7
-1	-1	4/7	0	-3/7
-2	0	3/14	-1/2	2/7
-1	-2	1/2	1/2	4
-2	-1	1/2	-1/2	-4

4	3	2	1	0
+4	3	2	1	0
+2	1	0	0	0
1/14	3/10	3/7	1/5	1/5
3/7	1/5	-1/14	-3/10	-1/5
3/7	-1/5	-1/14	3/10	1/5
3/7	3/7	-1/5	1/5	1

$$d_{0,0}^1 = \cos \theta$$

$$d_{1/2, 1/2}^{1/2} = \cos \frac{\theta}{2}$$

$$d_{1/2, -1/2}^{1/2} = -\sin \frac{\theta}{2}$$

$$d_{1,1}^1 = \frac{1 + \cos \theta}{2}$$

$$d_{1,0}^1 = -\frac{\sin \theta}{\sqrt{2}}$$

$$d_{1,-1}^1 = \frac{1 - \cos \theta}{2}$$

3	2	1	0	0
+3	2	1	0	0
+2	1	0	0	0
1/20	1/4	9/20	1/4	1/4
1/20	1/4	-1/20	-1/4	1/4
9/20	-1/4	-1/20	1/4	1/4
1/20	-1/4	9/20	-1/4	1/4

1/5	1/2	3/10	1/2	1/2
3/5	0	-2/5	0	0
1/5	-1/2	3/10	0	0
3/2	1/2	1/2	1	0
1/20	1/4	9/20	1/4	1/4
1/20	1/4	-1/20	-1/4	1/4
9/20	-1/4	-1/20	1/4	1/4
1/20	-1/4	9/20	-1/4	1/4

1/5	1/2	3/10	1/2	1/2
3/5	0	-2/5	0	0
1/5	-1/2	3/10	0	0
3/2	1/2	1/2	1	0
1/20	1/4	9/20	1/4	1/4
1/20	1/4	-1/20	-1/4	1/4
9/20	-1/4	-1/20	1/4	1/4
1/20	-1/4	9/20	-1/4	1/4

1/5	1/2	3/10	1/2	1/2
3/5	0	-2/5	0	0
1/5	-1/2	3/10	0	0
3/2	1/2	1/2	1	0
1/20	1/4	9/20	1/4	1/4
1/20	1/4	-1/20	-1/4	1/4
9/20	-1/4	-1/20	1/4	1/4
1/20	-1/4	9/20	-1/4	1/4

4	3	2	1	0
+4	3	2	1	0
+2	1	0	0	0
1/14	3/10	3/7	1/5	1/5
3/7	1/5	-1/14	-3/10	-1/5
3/7	-1/5	-1/14	3/10	1/5
3/7	3/7	-1/5	1/5	1

4	3	2	1	0
+4	3	2	1	0
+2	1	0	0	0
1/14	3/10	3/7	1/5	1/5
3/7	1/5	-1/14	-3/10	-1/5
3/7	-1/5	-1/14	3/10	1/5
3/7	3/7	-1/5	1/5	1

**Figure 45.1:** The sign convention is that of Wigner (*Group Theory*, Academic Press, New York, 1959), also used by Condon and Shortley (*The Theory of Atomic Spectra*, Cambridge Univ. Press, New York, 1953), Rose (*Elementary Theory of Angular Momentum*, Wiley, New York, 1957), and Cohen (*Tables of the Clebsch-Gordan Coefficients*, North American Rockwell Science Center, Thousand Oaks, Calif., 1974).

Downloaded from https://academic.oup.com/ptep/article/2020/8/083C01/5891211 by guest on 12 November 2020



### 46. SU(3) isoscalar factors and representation matrices

Written by R.L. Kelly (LBNL).

The most commonly used SU(3) isoscalar factors, corresponding to the singlet, octet, and decuplet content of  $8 \otimes 8$  and  $10 \otimes 8$ , are shown at the right. The notation uses particle names to identify the coefficients, so that the pattern of relative couplings may be seen at a glance. We illustrate the use of the coefficients below. See J.J de Swart, Rev. Mod. Phys. **35**, 916 (1963) for detailed explanations and phase conventions.

A  $\sqrt{\quad}$  is to be understood over every integer in the matrices; the exponent 1/2 on each matrix is a reminder of this. For example, the  $\Xi \rightarrow \Omega K$  element of the  $10 \rightarrow 10 \otimes 8$  matrix is  $-\sqrt{6}/\sqrt{24} = -1/2$ .

Intramultiplet relative decay strengths may be read directly from the matrices. For example, in decuplet  $\rightarrow$  octet + octet decays, the ratio of  $\Omega^* \rightarrow \Xi \bar{K}$  and  $\Delta \rightarrow N \pi$  partial widths is, from the  $10 \rightarrow 8 \times 8$  matrix,

$$\frac{\Gamma(\Omega^* \rightarrow \Xi \bar{K})}{\Gamma(\Delta \rightarrow N \pi)} = \frac{12}{6} \times (\text{phase space factors}). \quad (46.1)$$

Including isospin Clebsch-Gordan coefficients, we obtain, e.g.,

$$\frac{\Gamma(\Omega^{*-} \rightarrow \Xi^0 K^-)}{\Gamma(\Delta^+ \rightarrow p \pi^0)} = \frac{1/2}{2/3} \times \frac{12}{6} \times p.s.f. = \frac{3}{2} \times p.s.f. \quad (46.2)$$

Partial widths for  $8 \rightarrow 8 \otimes 8$  involve a linear superposition of  $8_1$  (symmetric) and  $8_2$  (antisymmetric) couplings. For example,

$$\Gamma(\Xi^* \rightarrow \Xi \pi) \sim \left( -\sqrt{\frac{9}{20}} g_1 + \sqrt{\frac{3}{12}} g_2 \right)^2. \quad (46.3)$$

The relations between  $g_1$  and  $g_2$  (with de Swart's normalization) and the standard  $D$  and  $F$  couplings that appear in the interaction Lagrangian,

$$\mathcal{L} = -\sqrt{2} D Tr(\{\bar{B}, B\}M) + \sqrt{2} F Tr([\bar{B}, B]M), \quad (46.4)$$

where  $[\bar{B}, B] \equiv \bar{B}B - B\bar{B}$  and  $\{\bar{B}, B\} \equiv \bar{B}B + B\bar{B}$ , are

$$D = \frac{\sqrt{30}}{40} g_1, \quad F = \frac{\sqrt{6}}{24} g_2. \quad (46.5)$$

Thus, for example,

$$\Gamma(\Xi^* \rightarrow \Xi \pi) \sim (F - D)^2 \sim (1 - 2\alpha)^2, \quad (46.6)$$

where  $\alpha \equiv F/(D + F)$ . (This definition of  $\alpha$  is de Swart's. The alternative  $D/(D + F)$ , due to Gell-Mann, is also used.)

The generators of SU(3) transformations,  $\lambda_a$  ( $a = 1, 8$ ), are  $3 \times 3$  matrices that obey the following commutation and anticommutation relationships:

$$[\lambda_a, \lambda_b] \equiv \lambda_a \lambda_b - \lambda_b \lambda_a = 2i f_{abc} \lambda_c \quad (46.7)$$

$$\{\lambda_a, \lambda_b\} \equiv \lambda_a \lambda_b + \lambda_b \lambda_a = \frac{4}{3} \delta_{ab} I + 2d_{abc} \lambda_c, \quad (46.8)$$

where  $I$  is the  $3 \times 3$  identity matrix, and  $\delta_{ab}$  is the Kronecker delta symbol. The  $f_{abc}$  are odd under the permutation of any pair of indices, while the  $d_{abc}$  are even. The nonzero values are

$1 \rightarrow 8 \otimes 8$

$$(\Lambda) \rightarrow (N \bar{K} \Sigma \pi \Lambda \eta \Xi K) = \frac{1}{\sqrt{8}} (2 \ 3 \ -1 \ -2)^{1/2}$$

$8_1 \rightarrow 8 \otimes 8$

$$\begin{pmatrix} N \\ \Sigma \\ \Lambda \\ \Xi \end{pmatrix} \rightarrow \begin{pmatrix} N\pi & N\eta & \Sigma K & \Lambda K \\ N\bar{K} & \Sigma\pi & \Lambda\pi & \Sigma\eta & \Xi K \\ N\bar{K} & \Sigma\pi & \Lambda\eta & \Xi K \\ \Sigma\bar{K} & \Lambda\bar{K} & \Xi\pi & \Xi\eta \end{pmatrix} = \frac{1}{\sqrt{20}} \begin{pmatrix} 9 & -1 & -9 & -1 \\ -6 & 0 & 4 & 4 & -6 \\ 2 & -12 & -4 & -2 \\ 9 & -1 & -9 & -1 \end{pmatrix}^{1/2}$$

$8_2 \rightarrow 8 \otimes 8$

$$\begin{pmatrix} N \\ \Sigma \\ \Lambda \\ \Xi \end{pmatrix} \rightarrow \begin{pmatrix} N\pi & N\eta & \Sigma K & \Lambda K \\ N\bar{K} & \Sigma\pi & \Lambda\pi & \Sigma\eta & \Xi K \\ N\bar{K} & \Sigma\pi & \Lambda\eta & \Xi K \\ \Sigma\bar{K} & \Lambda\bar{K} & \Xi\pi & \Xi\eta \end{pmatrix} = \frac{1}{\sqrt{12}} \begin{pmatrix} 3 & 3 & 3 & -3 \\ 2 & 8 & 0 & 0 & -2 \\ 6 & 0 & 0 & 6 \\ 3 & 3 & 3 & -3 \end{pmatrix}^{1/2}$$

$10 \rightarrow 8 \otimes 8$

$$\begin{pmatrix} \Delta \\ \Sigma \\ \Xi \\ \Omega \end{pmatrix} \rightarrow \begin{pmatrix} N\pi & \Sigma K \\ N\bar{K} & \Sigma\pi & \Lambda\pi & \Sigma\eta & \Xi K \\ \Sigma\bar{K} & \Lambda\bar{K} & \Xi\pi & \Xi\eta \\ \Xi\bar{K} \end{pmatrix} = \frac{1}{\sqrt{12}} \begin{pmatrix} -6 & 6 \\ -2 & 2 & -3 & 3 & 2 \\ 3 & -3 & 3 & 3 \\ 12 \end{pmatrix}^{1/2}$$

$8 \rightarrow 10 \otimes 8$

$$\begin{pmatrix} N \\ \Sigma \\ \Lambda \\ \Xi \end{pmatrix} \rightarrow \begin{pmatrix} \Delta\pi & \Sigma K \\ \Delta\bar{K} & \Sigma\pi & \Sigma\eta & \Xi K \\ \Sigma\pi & \Xi K \\ \Sigma\bar{K} & \Xi\pi & \Xi\eta & \Omega K \end{pmatrix} = \frac{1}{\sqrt{15}} \begin{pmatrix} -12 & 3 \\ 8 & -2 & -3 & 2 \\ -9 & 6 \\ 3 & -3 & -3 & 6 \end{pmatrix}^{1/2}$$

$10 \rightarrow 10 \otimes 8$

$$\begin{pmatrix} \Delta \\ \Sigma \\ \Xi \\ \Omega \end{pmatrix} \rightarrow \begin{pmatrix} \Delta\pi & \Delta\eta & \Sigma K \\ \Delta\bar{K} & \Sigma\pi & \Sigma\eta & \Xi K \\ \Sigma\bar{K} & \Xi\pi & \Xi\eta & \Omega K \\ \Xi\bar{K} & \Omega\eta \end{pmatrix} = \frac{1}{\sqrt{24}} \begin{pmatrix} 15 & 3 & -6 \\ 8 & 8 & 0 & -8 \\ 12 & 3 & -3 & -6 \\ 12 & -12 \end{pmatrix}^{1/2}$$

$abc$	$f_{abc}$	$abc$	$d_{abc}$	$abc$	$d_{abc}$
123	1	118	$1/\sqrt{3}$	355	1/2
147	1/2	146	1/2	366	-1/2
156	-1/2	157	1/2	377	-1/2
246	1/2	228	$1/\sqrt{3}$	448	$-1/(2\sqrt{3})$
257	1/2	247	-1/2	558	$-1/(2\sqrt{3})$
345	1/2	256	1/2	668	$-1/(2\sqrt{3})$
367	-1/2	338	$1/\sqrt{3}$	778	$-1/(2\sqrt{3})$
458	$\sqrt{3}/2$	344	1/2	888	$-1/\sqrt{3}$
678	$\sqrt{3}/2$				

The  $\lambda_a$ 's are

$$\lambda_1 = \begin{pmatrix} 0 & 1 & 0 \\ 1 & 0 & 0 \\ 0 & 0 & 0 \end{pmatrix} \quad \lambda_2 = \begin{pmatrix} 0 & -i & 0 \\ i & 0 & 0 \\ 0 & 0 & 0 \end{pmatrix} \quad \lambda_3 = \begin{pmatrix} 1 & 0 & 0 \\ 0 & -1 & 0 \\ 0 & 0 & 0 \end{pmatrix}$$

$$\lambda_4 = \begin{pmatrix} 0 & 0 & 1 \\ 0 & 0 & 0 \\ 1 & 0 & 0 \end{pmatrix} \quad \lambda_5 = \begin{pmatrix} 0 & 0 & -i \\ 0 & 0 & 0 \\ i & 0 & 0 \end{pmatrix} \quad \lambda_6 = \begin{pmatrix} 0 & 0 & 0 \\ 0 & 0 & 1 \\ 0 & 1 & 0 \end{pmatrix}$$

$$\lambda_7 = \begin{pmatrix} 0 & 0 & 0 \\ 0 & 0 & -i \\ 0 & i & 0 \end{pmatrix} \quad \lambda_8 = \frac{1}{\sqrt{3}} \begin{pmatrix} 1 & 0 & 0 \\ 0 & 1 & 0 \\ 0 & 0 & -2 \end{pmatrix}$$

Equation (46.7) defines the Lie algebra of SU(3). A general  $d$ -dimensional representation is given by a set of  $d \times d$  matrices satisfying Eq. (46.7) with the  $f_{abc}$  given above. Equation (46.8) is specific to the defining 3-dimensional representation.

## 47. SU(n) Multiplets and Young Diagrams

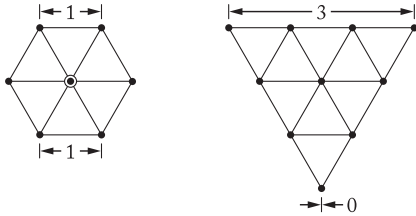
Written by C.G. Wohl (LBNL).

This note tells (1) how SU(n) particle multiplets are identified or labeled, (2) how to find the number of particles in a multiplet from its label, (3) how to draw the Young diagram for a multiplet, and (4) how to use Young diagrams to determine the overall multiplet structure of a composite system, such as a 3-quark or a meson-baryon system.

In much of the literature, the word “representation” is used where we use “multiplet,” and “tableau” is used where we use “diagram.”

### 47.1. Multiplet labels

An SU(n) multiplet is uniquely identified by a string of (n-1) nonnegative integers: (α, β, γ, ...). Any such set of integers specifies a multiplet. For an SU(2) multiplet such as an isospin multiplet, the single integer α is the number of steps from one end of the multiplet to the other (i.e., it is one fewer than the number of particles in the multiplet). In SU(3), the two integers α and β are the numbers of steps across the top and bottom levels of the multiplet diagram. Thus the labels for the SU(3) octet and decuplet



are (1,1) and (3,0). For larger n, the interpretation of the integers in terms of the geometry of the multiplets, which exist in an (n-1)-dimensional space, is not so readily apparent.

The label for the SU(n) singlet is (0,0, ..., 0). In a flavor SU(n), the n quarks together form a (1,0, ..., 0) multiplet, and the n antiquarks belong to a (0, ..., 0, 1) multiplet. These two multiplets are conjugate to one another, which means their labels are related by (α, β, ...) ↔ (... , β, α).

### 47.2. Number of particles

The number of particles in a multiplet, N = N(α, β, ...), is given as follows (note the pattern of the equations).

In SU(2), N = N(α) is

$$N = \frac{(\alpha + 1)}{1} \tag{47.1}$$

In SU(3), N = N(α, β) is

$$N = \frac{(\alpha + 1)}{1} \cdot \frac{(\beta + 1)}{1} \cdot \frac{(\alpha + \beta + 2)}{2} \tag{47.2}$$

In SU(4), N = N(α, β, γ) is

$$N = \frac{(\alpha+1)}{1} \cdot \frac{(\beta+1)}{1} \cdot \frac{(\gamma+1)}{1} \cdot \frac{(\alpha+\beta+2)}{2} \cdot \frac{(\beta+\gamma+2)}{2} \cdot \frac{(\alpha+\beta+\gamma+3)}{3} \tag{47.3}$$

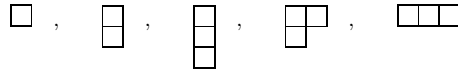
Note that in Eq. (47.3) there is no factor with (α + γ + 2): only a consecutive sequence of the label integers appears in any factor. One more example should make the pattern clear for any SU(n). In SU(5), N = N(α, β, γ, δ) is

$$N = \frac{(\alpha+1)}{1} \cdot \frac{(\beta+1)}{1} \cdot \frac{(\gamma+1)}{1} \cdot \frac{(\delta+1)}{1} \cdot \frac{(\alpha+\beta+2)}{2} \cdot \frac{(\beta+\gamma+2)}{2} \cdot \frac{(\gamma+\delta+2)}{2} \cdot \frac{(\alpha+\beta+\gamma+3)}{3} \cdot \frac{(\beta+\gamma+\delta+3)}{3} \cdot \frac{(\alpha+\beta+\gamma+\delta+4)}{4} \tag{47.4}$$

From the symmetry of these equations, it is clear that multiplets that are conjugate to one another have the same number of particles, but so can other multiplets. For example, the SU(4) multiplets (3,0,0) and (1,1,0) each have 20 particles. Try the equations and see.

### 47.3. Young diagrams

A Young diagram consists of an array of boxes (or some other symbol) arranged in one or more left-justified rows, with each row being at least as long as the row beneath. The correspondence between a diagram and a multiplet label is: The top row juts out α boxes to the right past the end of the second row, the second row juts out β boxes to the right past the end of the third row, etc. A diagram in SU(n) has at most n rows. There can be any number of “completed” columns of n boxes buttressing the left of a diagram; these don’t affect the label. Thus in SU(3) the diagrams



represent the multiplets (1,0), (0,1), (0,0), (1,1), and (3,0). In any SU(n), the quark multiplet is represented by a single box, the antiquark multiplet by a column of (n-1) boxes, and a singlet by a completed column of n boxes.

### 47.4. Coupling multiplets together

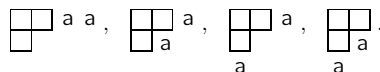
The following recipe tells how to find the multiplets that occur in coupling two multiplets together. To couple together more than two multiplets, first couple two, then couple a third with each of the multiplets obtained from the first two, etc.

First a definition: A sequence of the letters a, b, c, ... is admissible if at any point in the sequence at least as many a’s have occurred as b’s, at least as many b’s have occurred as c’s, etc. Thus abcd and aabc are admissible sequences and abb and acb are not. Now the recipe:

(a) Draw the Young diagrams for the two multiplets, but in one of the diagrams replace the boxes in the first row with a’s, the boxes in the second row with b’s, etc. Thus, to couple two SU(3) octets (such as the π-meson octet and the baryon octet), we start with and

. The unlettered diagram forms the upper left-hand corner of all the enlarged diagrams constructed below.

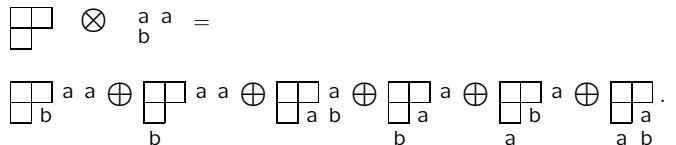
(b) Add the a’s from the lettered diagram to the right-hand ends of the rows of the unlettered diagram to form all possible legitimate Young diagrams that have no more than one a per column. In general, there will be several distinct diagrams, and all the a’s appear in each diagram. At this stage, for the coupling of the two SU(3) octets, we have:



(c) Use the b’s to further enlarge the diagrams already obtained, subject to the same rules. Then throw away any diagram in which the full sequence of letters formed by reading right to left in the first row, then the second row, etc., is not admissible.

(d) Proceed as in (c) with the c’s (if any), etc.

The final result of the coupling of the two SU(3) octets is:



Here only the diagrams with admissible sequences of a’s and b’s and with fewer than four rows (since n = 3) have been kept. In terms of multiplet labels, the above may be written

$$(1, 1) \otimes (1, 1) = (2, 2) \oplus (3, 0) \oplus (0, 3) \oplus (1, 1) \oplus (1, 1) \oplus (0, 0) .$$

In terms of numbers of particles, it may be written

$$8 \otimes 8 = 27 \oplus 10 \oplus \overline{10} \oplus 8 \oplus 8 \oplus 1 .$$

The product of the numbers on the left here is equal to the sum on the right, a useful check. (See also Sec. 15 on the Quark Model.)



## Kinematics, Cross-Section Formulae, and Plots

48. Kinematics (rev.) . . . . .	671
49. Resonances (rev.) . . . . .	675
50. Cross-section formulae for specific processes (rev.) . . . . .	682
51. Neutrino cross section measurements (rev.) . . . . .	691
52. Plots of cross sections and related quantities (rev.) . . . . .	696



## 48. Kinematics

Reviewed August 2019 by D. Miller (Glasgow), D.R. Tovey (Sheffield) and January 2000 by J.D. Jackson (LBNL).

Throughout this section units are used in which  $\hbar = c = 1$ . The following conversions are useful:  $\hbar c = 197.3$  MeV fm,  $(\hbar c)^2 = 0.3894$  (GeV)<sup>2</sup> mb.

### 48.1 Lorentz transformations

The energy  $E$  and 3-momentum  $\mathbf{p}$  of a particle of mass  $m$  form a 4-vector  $p = (E, \mathbf{p})$  whose square  $p^2 \equiv E^2 - |\mathbf{p}|^2 = m^2$ . The velocity of the particle is  $\beta = \mathbf{p}/E$ . The energy and momentum  $(E^*, \mathbf{p}^*)$  viewed from a frame moving with velocity  $\beta_f$  are given by

$$\begin{pmatrix} E^* \\ p_{\parallel}^* \end{pmatrix} = \begin{pmatrix} \gamma_f & -\gamma_f \beta_f \\ -\gamma_f \beta_f & \gamma_f \end{pmatrix} \begin{pmatrix} E \\ p_{\parallel} \end{pmatrix}, \quad p_T^* = p_T, \quad (48.1)$$

where  $\gamma_f = (1 - \beta_f^2)^{-1/2}$  and  $p_T$  ( $p_{\parallel}$ ) are the components of  $\mathbf{p}$  perpendicular (parallel) to  $\beta_f$ . Other 4-vectors, such as the space-time coordinates of events, of course transform in the same way. The scalar product of two 4-momenta  $p_1 \cdot p_2 = E_1 E_2 - \mathbf{p}_1 \cdot \mathbf{p}_2$  is invariant (frame independent).

### 48.2 Center-of-mass energy and momentum

In the collision of two particles of masses  $m_1$  and  $m_2$  the total center-of-mass energy can be expressed in the Lorentz-invariant form

$$\begin{aligned} E_{\text{cm}} &= [(E_1 + E_2)^2 - (\mathbf{p}_1 + \mathbf{p}_2)^2]^{1/2}, \\ &= [m_1^2 + m_2^2 + 2E_1 E_2 (1 - \beta_1 \beta_2 \cos \theta)]^{1/2}, \end{aligned} \quad (48.2)$$

where  $\theta$  is the angle between the particles. In the frame where one particle (of mass  $m_2$ ) is at rest (lab frame),

$$E_{\text{cm}} = (m_1^2 + m_2^2 + 2E_{1\text{lab}} m_2)^{1/2}. \quad (48.3)$$

The velocity of the center-of-mass in the lab frame is

$$\beta_{\text{cm}} = \mathbf{p}_{\text{lab}} / (E_{1\text{lab}} + m_2), \quad (48.4)$$

where  $\mathbf{p}_{\text{lab}} \equiv \mathbf{p}_{1\text{lab}}$  and

$$\gamma_{\text{cm}} = (E_{1\text{lab}} + m_2) / E_{\text{cm}}. \quad (48.5)$$

The c.m. momenta of particles 1 and 2 are of magnitude

$$p_{\text{cm}} = p_{\text{lab}} \frac{m_2}{E_{\text{cm}}}. \quad (48.6)$$

For example, if a 0.80 GeV/c kaon beam is incident on a proton target, the center of mass energy is 1.699 GeV and the center of mass momentum of either particle is 0.442 GeV/c. It is also useful to note that

$$E_{\text{cm}} dE_{\text{cm}} = m_2 dE_{1\text{lab}} = m_2 \beta_{1\text{lab}} dp_{1\text{lab}}. \quad (48.7)$$

### 48.3 Lorentz-invariant amplitudes

The matrix elements for a scattering or decay process are written in terms of an invariant amplitude  $-i\mathcal{M}$ . As an example, the  $S$ -matrix for  $2 \rightarrow 2$  scattering is related to  $\mathcal{M}$  by

$$\begin{aligned} \langle p'_1 p'_2 | S | p_1 p_2 \rangle &= I - i(2\pi)^4 \delta^4(p_1 + p_2 - p'_1 - p'_2) \\ &\times \frac{\mathcal{M}(p_1, p_2; p'_1, p'_2)}{(2E_1)^{1/2} (2E_2)^{1/2} (2E'_1)^{1/2} (2E'_2)^{1/2}}. \end{aligned} \quad (48.8)$$

The state normalization is such that

$$\langle p' | p \rangle = (2\pi)^3 \delta^3(\mathbf{p} - \mathbf{p}'). \quad (48.9)$$

For a  $2 \rightarrow 2$  scattering process producing unstable particles  $1'$  and  $2'$  decaying via  $1' \rightarrow 3'4'$  and  $2' \rightarrow 5'6'$  the matrix element

for the complete process can be written in the narrow width approximation as:

$$\begin{aligned} \mathcal{M}(12 \rightarrow 3'4'5'6') &= \\ \sum_{h_{1'}, h_{2'}} &\frac{\mathcal{M}(12 \rightarrow 1'2') \mathcal{M}(1' \rightarrow 3'4') \mathcal{M}(2' \rightarrow 5'6')}{(m_{3'4'}^2 - m_{1'}^2 + im_{1'}\Gamma_{1'}) (m_{5'6'}^2 - m_{2'}^2 + im_{2'}\Gamma_{2'})}. \end{aligned} \quad (48.10)$$

Here,  $m_{ij}$  is the invariant mass of particles  $i$  and  $j$ ,  $m_k$  and  $\Gamma_k$  are the mass and total width of particle  $k$ , and the sum runs over the helicities of the intermediate particles. This enables the cross section for such a process to be written as the product of the cross section for the initial  $2 \rightarrow 2$  scattering process with the branching ratios (relative partial decay rates) of the subsequent decays.

### 48.4 Particle decays

The partial decay rate of a particle of mass  $M$  into  $n$  bodies in its rest frame is given in terms of the Lorentz-invariant matrix element  $\mathcal{M}$  by

$$d\Gamma = \frac{(2\pi)^4}{2M} |\mathcal{M}|^2 d\Phi_n(P; p_1, \dots, p_n), \quad (48.11)$$

where  $d\Phi_n$  is an element of  $n$ -body phase space given by

$$d\Phi_n(P; p_1, \dots, p_n) = \delta^4(P - \sum_{i=1}^n p_i) \prod_{i=1}^n \frac{d^3 p_i}{(2\pi)^3 2E_i}. \quad (48.12)$$

This phase space can be generated recursively, viz.

$$\begin{aligned} d\Phi_n(P; p_1, \dots, p_n) &= d\Phi_j(q; p_1, \dots, p_j) \\ &\times d\Phi_{n-j+1}(P; q, p_{j+1}, \dots, p_n) (2\pi)^3 dq^2, \end{aligned} \quad (48.13)$$

where  $q^2 = (\sum_{i=1}^j E_i)^2 - |\sum_{i=1}^j \mathbf{p}_i|^2$ . This form is particularly useful in the case where a particle decays into another particle that subsequently decays.

#### 48.4.1 Survival probability

If a particle of mass  $M$  has mean proper lifetime  $\tau (= 1/\Gamma)$  and has momentum  $(E, \mathbf{p})$ , then the probability that it lives for a time  $t_0$  or greater before decaying is given by

$$P(t_0) = e^{-t_0 \Gamma/\gamma} = e^{-Mt_0 \Gamma/E}, \quad (48.14)$$

and the probability that it travels a distance  $x_0$  or greater is

$$P(x_0) = e^{-Mx_0 \Gamma/|\mathbf{p}|}. \quad (48.15)$$

#### 48.4.2 Two-body decays

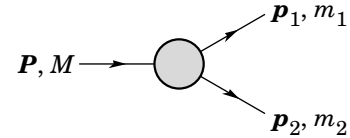


Figure 48.1: Definitions of variables for two-body decays.

In the rest frame of a particle of mass  $M$ , decaying into 2 particles labeled 1 and 2,

$$E_1 = \frac{M^2 - m_2^2 + m_1^2}{2M}, \quad (48.16)$$

$$\begin{aligned} |\mathbf{p}_1| &= |\mathbf{p}_2| \\ &= \frac{[(M^2 - (m_1 + m_2)^2)(M^2 - (m_1 - m_2)^2)]^{1/2}}{2M}, \end{aligned} \quad (48.17)$$

and

$$d\Gamma = \frac{1}{32\pi^2} |\mathcal{M}|^2 \frac{|\mathbf{p}_1|}{M^2} d\Omega, \quad (48.18)$$

where  $d\Omega = d\phi_1 d(\cos\theta_1)$  is the solid angle of particle 1. The invariant mass  $M$  can be determined from the energies and momenta using Eq. (48.2) with  $M = E_{\text{cm}}$ .

## 48.4.3 Three-body decays

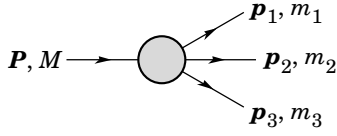


Figure 48.2: Definitions of variables for three-body decays.

Defining  $p_{ij} = p_i + p_j$  and  $m_{ij}^2 = p_{ij}^2$ , then  $m_{12}^2 + m_{23}^2 + m_{13}^2 = M^2 + m_1^2 + m_2^2 + m_3^2$  and  $m_{12}^2 = (P - p_3)^2 = M^2 + m_3^2 - 2ME_3$ , where  $E_3$  is the energy of particle 3 in the rest frame of  $M$ . In that frame, the momenta of the three decay particles lie in a plane. The relative orientation of these three momenta is fixed if their energies are known. The momenta can therefore be specified in space by giving three Euler angles  $(\alpha, \beta, \gamma)$  that specify the orientation of the final system relative to the initial particle. The direction of any one of the particles relative to the frame in which the initial particle is described can be specified in space by two angles  $(\alpha, \beta)$  while a third angle,  $\gamma$ , can be set as the azimuthal angle of a second particle around the first [1]. Then

$$d\Gamma = \frac{1}{(2\pi)^5} \frac{1}{16M} |\mathcal{M}|^2 dE_1 dE_3 d\alpha d(\cos\beta) d\gamma. \quad (48.19)$$

Alternatively

$$d\Gamma = \frac{1}{(2\pi)^5} \frac{1}{16M^2} |\mathcal{M}|^2 |\mathbf{p}_1^*| |\mathbf{p}_3| dm_{12} d\Omega_1^* d\Omega_3, \quad (48.20)$$

where  $(|\mathbf{p}_1^*|, \Omega_1^*)$  is the momentum of particle 1 in the rest frame of 1 and 2, and  $\Omega_3$  is the angle of particle 3 in the rest frame of the decaying particle.  $|\mathbf{p}_1^*|$  and  $|\mathbf{p}_3|$  are given by

$$|\mathbf{p}_1^*| = \frac{[(m_{12}^2 - (m_1 + m_2)^2)(m_{12}^2 - (m_1 - m_2)^2)]^{1/2}}{2m_{12}}, \quad (48.21a)$$

and

$$|\mathbf{p}_3| = \frac{[(M^2 - (m_{12} + m_3)^2)(M^2 - (m_{12} - m_3)^2)]^{1/2}}{2M}. \quad (48.21b)$$

[Compare with Eq. (48.17).]

If the decaying particle is a scalar or we average over its spin states, then integration over the angles in Eq. (48.19) gives

$$\begin{aligned} d\Gamma &= \frac{1}{(2\pi)^3} \frac{1}{8M} |\overline{\mathcal{M}}|^2 dE_1 dE_3 \\ &= \frac{1}{(2\pi)^3} \frac{1}{32M^3} |\overline{\mathcal{M}}|^2 dm_{12}^2 dm_{23}^2. \end{aligned} \quad (48.22)$$

This is the standard form for the Dalitz plot.

## 48.4.3.1 Dalitz plot

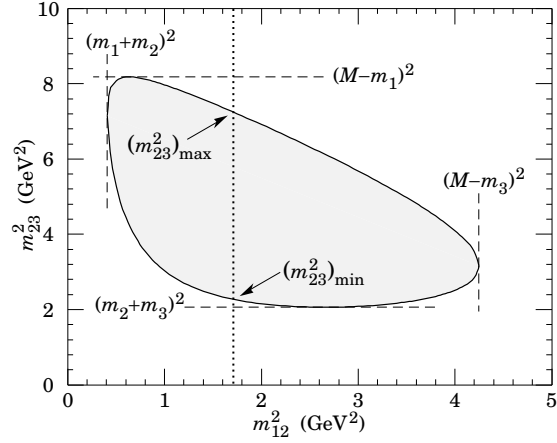
For a given value of  $m_{12}^2$ , the range of  $m_{23}^2$  is determined by its values when  $\mathbf{p}_2$  is parallel or antiparallel to  $\mathbf{p}_3$ :

$$(E_2^* + E_3^*)^2 - \left( \sqrt{E_2^{*2} - m_2^2} - \sqrt{E_3^{*2} - m_3^2} \right)^2, \quad (48.23a)$$

$$(E_2^* + E_3^*)^2 - \left( \sqrt{E_2^{*2} - m_2^2} + \sqrt{E_3^{*2} - m_3^2} \right)^2. \quad (48.23b)$$

Here  $E_2^* = (m_{12}^2 - m_1^2 + m_2^2)/2m_{12}$  and  $E_3^* = (M^2 - m_{12}^2 - m_3^2)/2m_{12}$  are the energies of particles 2 and 3 in the  $m_{12}$  rest frame. The scatter plot in  $m_{12}^2$  and  $m_{23}^2$  is called a Dalitz plot. If  $|\overline{\mathcal{M}}|^2$  is constant, the allowed region of the plot will be uniformly populated with events [see Eq. (48.22)]. A nonuniformity

in the plot gives immediate information on  $|\mathcal{M}|^2$ . For example, in the case of  $D \rightarrow K\pi\pi$ , bands appear when  $m_{(K\pi)} = m_{K^*(892)}$ , reflecting the appearance of the decay chain  $D \rightarrow K^*(892)\pi \rightarrow K\pi\pi$ .

Figure 48.3: Dalitz plot for a three-body final state. In this example, the state is  $\pi^+ \bar{K}^0 p$  at 3 GeV. Four-momentum conservation restricts events to the shaded region.

## 48.4.4 Kinematic limits

## 48.4.4.1 Three-body decays

In a three-body decay (Fig. 48.2) the maximum of  $|\mathbf{p}_3|$ , [given by Eq. (48.21)], is achieved when  $m_{12} = m_1 + m_2$ , *i.e.*, particles 1 and 2 have the same vector velocity in the rest frame of the decaying particle. If, in addition,  $m_3 > m_1, m_2$ , then  $|\mathbf{p}_3|_{\max} > |\mathbf{p}_1|_{\max}, |\mathbf{p}_2|_{\max}$ . The distribution of  $m_{12}$  values possesses an end-point or maximum value at  $m_{12} = M - m_3$ . This can be used to constrain the mass difference of a parent particle and one invisible decay product.

## 48.4.4.2 Sequential two-body decays

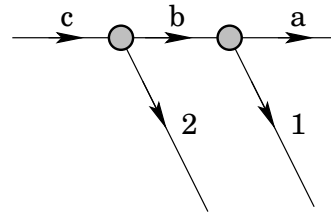


Figure 48.4: Particles participating in sequential two-body decay chain. Particles labeled 1 and 2 are visible while the particle terminating the chain (a) is invisible.

When a heavy particle initiates a sequential chain of two-body decays terminating in an invisible particle, constraints on the masses of the states participating in the chain can be obtained from end-points and thresholds in invariant mass distributions of the aggregated decay products. For the two-step decay chain depicted in Fig. 48.4 the invariant mass distribution of the two visible particles possesses an end-point given by:

$$(m_{12}^{\max})^2 = \frac{(m_c^2 - m_b^2)(m_b^2 - m_a^2)}{m_b^2}, \quad (48.24)$$

provided particles 1 and 2 are massless. If visible particle 1 has non-zero mass  $m_1$  then Eq. (48.24) is replaced by

$$(m_{12}^{\max})^2 = m_1^2 + \frac{(m_c^2 - m_b^2)}{2m_b^2} \times \left( m_1^2 + m_b^2 - m_a^2 + \sqrt{(-m_1^2 + m_b^2 - m_a^2)^2 - 4m_1^2 m_a^2} \right) \quad (48.25)$$

See Refs. [2] and [3] for other cases.

#### 48.4.5 Multibody decays

The above results may be generalized to final states containing any number of particles by combining some of the particles into “effective particles” and treating the final states as 2 or 3 “effective particle” states. Thus, if  $p_{ijk\dots} = p_i + p_j + p_k + \dots$ , then

$$m_{ijk\dots} = \sqrt{p_{ijk\dots}^2}, \quad (48.26)$$

and  $m_{ijk\dots}$  may be used in place of *e.g.*,  $m_{12}$  in the relations in Sec. 48.4.3 or Sec. 48.4.4 above.

### 48.5 Cross sections

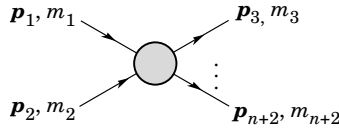


Figure 48.5: Definitions of variables for production of an  $n$ -body final state.

The differential cross section is given by

$$d\sigma = \frac{(2\pi)^4 |\mathcal{M}|^2}{4\sqrt{(p_1 \cdot p_2)^2 - m_1^2 m_2^2}} \times d\Phi_n(p_1 + p_2; p_3, \dots, p_{n+2}). \quad (48.27)$$

[See Eq. (48.12).] In the rest frame of  $m_2$ (lab),

$$\sqrt{(p_1 \cdot p_2)^2 - m_1^2 m_2^2} = m_2 p_{1\text{lab}}; \quad (48.28a)$$

while in the center-of-mass frame

$$\sqrt{(p_1 \cdot p_2)^2 - m_1^2 m_2^2} = p_{1\text{cm}} \sqrt{s}. \quad (48.28b)$$

#### 48.5.1 Two-body reactions

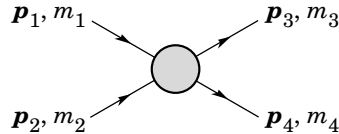


Figure 48.6: Definitions of variables for a two-body final state.

Two particles of momenta  $p_1$  and  $p_2$  and masses  $m_1$  and  $m_2$  scatter to particles of momenta  $p_3$  and  $p_4$  and masses  $m_3$  and  $m_4$ ; the Lorentz-invariant Mandelstam variables are defined by

$$s = (p_1 + p_2)^2 = (p_3 + p_4)^2 = m_1^2 + 2E_1 E_2 - 2\mathbf{p}_1 \cdot \mathbf{p}_2 + m_2^2, \quad (48.29)$$

$$t = (p_1 - p_3)^2 = (p_2 - p_4)^2 = m_1^2 - 2E_1 E_3 + 2\mathbf{p}_1 \cdot \mathbf{p}_3 + m_3^2, \quad (48.30)$$

$$u = (p_1 - p_4)^2 = (p_2 - p_3)^2 = m_1^2 - 2E_1 E_4 + 2\mathbf{p}_1 \cdot \mathbf{p}_4 + m_4^2, \quad (48.31)$$

and they satisfy

$$s + t + u = m_1^2 + m_2^2 + m_3^2 + m_4^2. \quad (48.32)$$

The two-body cross section may be written as

$$\frac{d\sigma}{dt} = \frac{1}{64\pi s} \frac{1}{|\mathbf{p}_{1\text{cm}}|^2} |\mathcal{M}|^2. \quad (48.33)$$

In the center-of-mass frame

$$\begin{aligned} t &= (E_{1\text{cm}} - E_{3\text{cm}})^2 - (p_{1\text{cm}} - p_{3\text{cm}})^2 \\ &\quad - 4p_{1\text{cm}} p_{3\text{cm}} \sin^2(\theta_{\text{cm}}/2) \\ &= t_0 - 4p_{1\text{cm}} p_{3\text{cm}} \sin^2(\theta_{\text{cm}}/2), \end{aligned} \quad (48.34)$$

where  $\theta_{\text{cm}}$  is the angle between particle 1 and 3. The limiting values  $t_0$  ( $\theta_{\text{cm}} = 0$ ) and  $t_1$  ( $\theta_{\text{cm}} = \pi$ ) for  $2 \rightarrow 2$  scattering are

$$t_0(t_1) = \left[ \frac{m_1^2 - m_3^2 - m_2^2 + m_4^2}{2\sqrt{s}} \right]^2 - (p_{1\text{cm}} \mp p_{3\text{cm}})^2. \quad (48.35)$$

In the literature the notation  $t_{\text{min}}$  ( $t_{\text{max}}$ ) for  $t_0$  ( $t_1$ ) is sometimes used, which should be discouraged since  $t_0 > t_1$ . The center-of-mass energies and momenta of the incoming particles are

$$E_{1\text{cm}} = \frac{s + m_1^2 - m_2^2}{2\sqrt{s}}, \quad E_{2\text{cm}} = \frac{s + m_2^2 - m_1^2}{2\sqrt{s}}, \quad (48.36)$$

For  $E_{3\text{cm}}$  and  $E_{4\text{cm}}$ , change  $m_1$  to  $m_3$  and  $m_2$  to  $m_4$ . Then

$$p_{i\text{cm}} = \sqrt{E_{i\text{cm}}^2 - m_i^2} \text{ and } p_{1\text{cm}} = \frac{p_{1\text{lab}} m_2}{\sqrt{s}}. \quad (48.37)$$

Here the subscript lab refers to the frame where particle 2 is at rest. [For other relations see Eqs. (48.2)–(48.4).]

#### 48.5.2 Inclusive reactions

Choose some direction (usually the beam direction) for the  $z$ -axis; then the energy and momentum of a particle can be written as

$$E = m_T \cosh y, \quad p_x, p_y, p_z = m_T \sinh y, \quad (48.38)$$

where  $m_T$ , conventionally called the ‘transverse mass’, is given by

$$m_T^2 = m^2 + p_x^2 + p_y^2. \quad (48.39)$$

and the rapidity  $y$  is defined by

$$\begin{aligned} y &= \frac{1}{2} \ln \left( \frac{E + p_z}{E - p_z} \right) \\ &= \ln \left( \frac{E + p_z}{m_T} \right) = \tanh^{-1} \left( \frac{p_z}{E} \right). \end{aligned} \quad (48.40)$$

Note that the definition of the transverse mass in Eq. (48.39) differs from that used by experimentalists at hadron colliders (see Sec. 48.6.1 below). Under a boost in the  $z$ -direction to a frame with velocity  $\beta$ ,  $y \rightarrow y - \tanh^{-1} \beta$ . Hence the shape of the rapidity distribution  $dN/dy$  is invariant, as are differences in rapidity. The invariant cross section may also be rewritten

$$E \frac{d^3\sigma}{d^3p} = \frac{d^3\sigma}{d\phi dy p_T dp_T} \Rightarrow \frac{d^2\sigma}{\pi dy d(p_T^2)}. \quad (48.41)$$

The second form is obtained using the identity  $dy/dp_z = 1/E$ , and the third form represents the average over  $\phi$ .

Feynman’s  $x$  variable is given by

$$x = \frac{p_z}{p_{z\text{max}}} \approx \frac{E + p_z}{(E + p_z)_{\text{max}}} \quad (p_T \ll |p_z|). \quad (48.42)$$

In the c.m. frame,

$$x \approx \frac{2p_{z\text{cm}}}{\sqrt{s}} = \frac{2m_T \sinh y_{\text{cm}}}{\sqrt{s}} \quad (48.43)$$

and

$$= (y_{\text{cm}})_{\text{max}} = \ln(\sqrt{s}/m). \quad (48.44)$$

The invariant mass  $M$  of the two-particle system described in Sec. 48.4.2 can be written in terms of these variables as

$$M^2 = m_1^2 + m_2^2 + 2[E_T(1)E_T(2) \cosh \Delta y - \mathbf{p}_T(1) \cdot \mathbf{p}_T(2)], \quad (48.45)$$

where

$$E_T(i) = \sqrt{|\mathbf{p}_T(i)|^2 + m_i^2}, \quad (48.46)$$

and  $\mathbf{p}_T(i)$  denotes the transverse momentum vector of particle  $i$ .



For  $p \gg m$ , the rapidity [Eq. (48.40)] may be expanded to obtain

$$y = \frac{1}{2} \ln \frac{\cos^2(\theta/2) + m^2/4p^2 + \dots}{\sin^2(\theta/2) + m^2/4p^2 + \dots} \approx -\ln \tan(\theta/2) \equiv \eta \quad (48.47)$$

where  $\cos \theta = p_z/p$ . The pseudorapidity  $\eta$  defined by the second line is approximately equal to the rapidity  $y$  for  $p \gg m$  and  $\theta \gg 1/\gamma$ , and in any case can be measured when the mass and momentum of the particle are unknown. From the definition one can obtain the identities

$$\sinh \eta = \cot \theta, \quad \cosh \eta = 1/\sin \theta, \quad \tanh \eta = \cos \theta. \quad (48.48)$$

## 48.6 Transverse variables

At hadron colliders, a significant and unknown proportion of the energy of the incoming hadrons in each event escapes down the beam-pipe. Consequently if invisible particles are created in the final state, their net momentum can only be constrained in the plane transverse to the beam direction. Defining the  $z$ -axis as the beam direction, this net momentum is equal to the missing transverse energy vector

$$\mathbf{E}_T^{\text{miss}} = -\sum_i \mathbf{p}_T(i), \quad (48.49)$$

where the sum runs over the transverse momenta of all visible final state particles.

### 48.6.1 Single production with semi-invisible final state

Consider a single heavy particle of mass  $M$  produced in association with visible particles which decays as in Fig. 48.1 to two particles, of which one (labeled particle 1) is invisible. The mass of the parent particle can be constrained with the quantity  $M_T$  defined by

$$M_T^2 \equiv [E_T(1) + E_T(2)]^2 - [\mathbf{p}_T(1) + \mathbf{p}_T(2)]^2 = m_1^2 + m_2^2 + 2[E_T(1)E_T(2) - \mathbf{p}_T(1) \cdot \mathbf{p}_T(2)], \quad (48.50)$$

where

$$\mathbf{p}_T(1) = \mathbf{E}_T^{\text{miss}}. \quad (48.51)$$

This quantity is called the ‘transverse mass’ by hadron collider experimentalists but it should be noted that it is quite different from that used in the description of inclusive reactions [Eq. (48.39)]. The distribution of event  $M_T$  values possesses an end-point at  $M_T^{\text{max}} = M$ . If  $m_1 = m_2 = 0$  then

$$M_T^2 = 2|\mathbf{p}_T(1)||\mathbf{p}_T(2)|(1 - \cos \phi_{12}), \quad (48.52)$$

where  $\phi_{ij}$  is defined as the angle between particles  $i$  and  $j$  in the transverse plane.

### 48.6.2 Pair production with semi-invisible final states

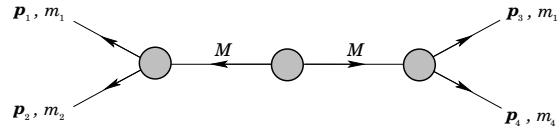


Figure 48.7: Definitions of variables for pair production of semi-invisible final states. Particles 1 and 3 are invisible while particles 2 and 4 are visible.

Consider two identical heavy particles of mass  $M$  produced such that their combined center-of-mass is at rest in the transverse plane (Fig. 48.7). Each particle decays to a final state consisting of an invisible particle of fixed mass  $m_1$  together with an additional visible particle.  $M$  and  $m_1$  can be constrained with the variables  $M_{T2}$  and  $M_{CT}$  which are defined in Refs. [4] and [5].

### References

- [1] J.D. Jackson in *High Energy Physics, Les Houches 1965 Summer School*, GORDON AND BREACH Science Publishers (1965), p. 348.
- [2] I. Hinchliffe *et al.*, Phys. Rev. **D55**, 5520 (1997), [hep-ph/9610544].
- [3] B. C. Allanach *et al.*, JHEP **09**, 004 (2000), [hep-ph/0007009].
- [4] C. G. Lester and D. J. Summers, Phys. Lett. **B463**, 99 (1999), [hep-ph/9906349].
- [5] D. R. Tovey, JHEP **04**, 034 (2008), [arXiv:0802.2879].

## 49. Resonances

Revised August 2019 by D.M. Asner (BNL), C. Hanhart (Jülich) and E. Klempt (Bonn U.).

### 49.1 General Considerations

Perturbative methods can be applied to systems of quarks and gluons only for large momentum transfers (see review on ‘Quantum Chromodynamics’) and, under certain conditions, to some properties of systems that contain heavy quarks or very large momentum scales (see review on ‘Heavy-Quark and Soft-Collinear Effective Theory’). Dealing with Quantum Chromodynamics (QCD) in the low momentum transfer region is a very complicated, non-perturbative problem. The physical states appear as poles of the  $S$ -matrix either on physical sheet (bound states) or on the unphysical sheets (resonances) and manifest themselves as structures in experimental observables.

Resonances can show up either in so-called formation experiments, typically of the kind

$$A + B \rightarrow \mathbf{R} \rightarrow C_1 + \dots + C_n,$$

where they become visible in an energy scan (a perfect example of this being the  $R$ -function measured in  $e^+e^-$  annihilations — *cf.* the corresponding plots in the review on ‘Plots of Cross Sections and Related Quantities’), or together with a spectator particle  $S$  in production experiments of the kind

$$\begin{aligned} A + B &\rightarrow \mathbf{R} + S \rightarrow [C_1 + \dots + C_n] + S, \\ Z &\rightarrow \mathbf{R} + S \rightarrow [C_1 + \dots + C_n] + S. \end{aligned}$$

where the first reaction corresponds to an associated production, the second is a decay (see ‘Review of Multibody Charm Analyses’). In the latter case the resonance properties are commonly extracted from a Dalitz plot analysis (see review on ‘Kinematics’) or projections thereof.

Resonance phenomena are very rich: while typical hadronic widths are of the order of 100 MeV (*e.g.*, for the meson resonances  $\rho(770)$  or  $\psi(4040)$  or the baryon resonance  $\Delta(1232)$ ) corresponding to a lifetime of  $10^{-23}$  s, the widths can also be as small as a few MeV (*e.g.* of  $\phi(1020)$  or  $J/\psi$ ) or as large as several hundred

MeV (*e.g.* of the meson resonances  $f_0(500)$  or  $D_1(2430)$  or the baryon resonance  $N(2190)$ ).

Typically, a resonance appears as a peak in the total cross section. If the structure is narrow and if there are no relevant thresholds or other resonances nearby, the resonance properties may be extracted employing a standard Breit-Wigner parameterization, if necessary improved by using an energy-dependent width (*cf.* Sec. 49.3.1 of this review). However, in general, unitarity and analyticity call for the use of more refined tools. When there are overlapping resonances with the same quantum numbers, the resonance terms should not simply be added but combined in a non-trivial way either in a  $K$ -matrix approximation (*cf.* Sec. 49.3.2 of this review) or using other advanced methods (*cf.* Sec. 49.3.6 of this review). Additional constraints from the  $S$ -matrix allow one to build more reliable amplitudes and in turn to reduce the systematic uncertainties of the resonance parameters: pole locations and residues. In addition, for broad resonances there is no direct relation anymore between pole location and the total width/lifetime — then the pole residues need to be used in order to quantify the decay properties.

For simplicity, throughout this review the formulas are given for distinguishable, scalar particles. The additional complications that appear in the presence of spins can be controlled in the helicity framework developed by Jacob and Wick [1], or in a non-covariant [2] or covariant [3] tensor operator formalism. Within these approaches, sequential (cascade) decays are commonly treated as a coherent sum of two-body interactions. Most of the expressions below are given for two-body kinematics.

#### 49.1.1 Properties of the $S$ -matrix

The unitary operator that connects asymptotic *in* and *out* states is called the  $S$ -matrix. The scattering amplitude is defined as the interacting part of the  $S$  matrix. For the case of two interacting particles, it reads: (*cf.* Eq. (8) of the review on ‘Kinematics’ but note: we here use a different sign convention as well as a different normalisation of the fields to be consistent with most books on field theory)

$$i(2\pi)^4 \delta^4(p_1 + p_2 - p'_1 - p'_2) \mathcal{M}(p_1, p_2; p_1, p'_2)_{ba} = {}_{\text{out}} \langle p'_1 p'_2, b | S - 1 | p_1 p_2, a \rangle_{\text{in}} \quad (49.1)$$

where  $|p_1 p_2, a\rangle$  and  $|p'_1 p'_2, b\rangle$  are asymptotic states of two non-interacting particles with momentum  $p_1, p_2$  and  $p'_1, p'_2$ . The channel labels  $a$  and  $b$  are multi-indices specifying all additional properties of the channel. In general,  $\mathcal{M}$  is a matrix in channel space. For single particle states we employ the common relativistic normalization,

$$\langle p' | p \rangle = (2\pi)^3 2E_p \delta^3(\vec{p}' - \vec{p}), \quad (49.2)$$

with  $E_p = \sqrt{\vec{p}^2 + m^2}$ . The scattering amplitude an analytic function of the Mandelstam variables  $s, t$  and  $u$  up to poles and kinematic singularities. Branch points appear whenever there is a channel opening — at each two-particle threshold the number of Riemann sheets doubles. Triangle topologies can induce logarithmic singularities on the unphysical sheets often called triangle singularities (TS) [4–6]. Analyticity and unitarity principles of the  $S$ -matrix put strong constraints to the function  $\mathcal{M}(s, t)$ . Poles refer either to bound states or to resonances. The former poles are located on the physical sheet, the latter are located on unphysical sheets. Naturally those located on the unphysical sheet closest to the physical one, often called the second sheet, have usually the largest impact on observables. Moreover, as follows from analyticity, if there is a pole at some complex value of  $s$ , there must be another pole at its complex conjugate value,  $s^*$ . The pole with a negative imaginary part is closer to the physical axis and thus influences the observables in the vicinity of the resonance region more strongly (see Fig. 49.1). However, at the threshold both poles are always equally important. If there are

resonances in subsystems of multi-particle states, branch points appear in the complex plane of the unphysical sheet(s) [6]. Any of these singularities can lead to some structure in the observables (see also Ref. [7]). If certain kinematical constraints are met, especially the TS can mimic resonance signals, as claimed in Refs. [8–13] or could in certain channels lead to significant shifts of resonance signals [14]. For a partial-wave-projected amplitude (see Sec. 49.1.3) additional singularities not related to resonance physics may emerge as a result of the partial-wave projection [15].

Further constraints come, *e.g.*, from crossing symmetry and duality [16]. Approaches based on analyticity and crossing symmetry, implemented via dispersion theory, like the Roy equations [17] or variants thereof, were developed and applied to  $\pi\pi \rightarrow \pi\pi$  scattering [18–20],  $\pi K$  scattering [21],  $\gamma\gamma \rightarrow \pi\pi$  [22] as well as pion-nucleon scattering [23].

#### 49.1.2 Consequences from unitarity

In what follows, scattering amplitudes  $\mathcal{M}$  and production amplitudes  $\mathcal{A}$  will be distinguished, since unitarity puts different constraints on these. For the production amplitudes we require that the initial state is weakly coupled and, hence, the probability of the time-reversed reaction is negligibly small compared to the other coupled channels.

The discontinuity of the scattering amplitude over the unitarity

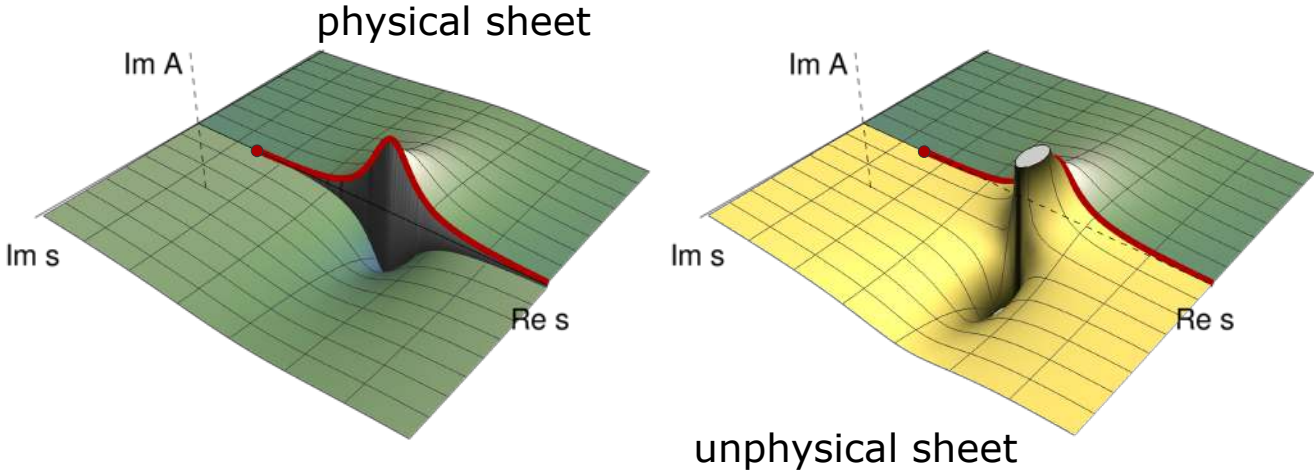


Figure 49.1: Imaginary part of a typical single-channel scattering amplitude with an isolated resonance. The solid red line shows the physical range of the Mandelstam variable  $s$ : It is real valued and starts from threshold shown by the red dot. The left plot shows the imaginary part of the amplitude in the complex  $S$ -plane that corresponds to the first physical sheet (green surface). The right plot shows analytic continuation of the same amplitude to the lower plane of the unphysical sheet (yellow surface). The latter contains the resonance pole. The two sheets are connected smoothly along the real axis above the threshold.

cut is constrained by unitarity [24] to

$$\text{Disc } \mathcal{M}_{ba} = [\mathcal{M}_{ba} - \mathcal{M}_{ab}^*] = i(2\pi)^4 \sum_c \int d\Phi_c \mathcal{M}_{cb}^* \mathcal{M}_{ca}, \quad (49.3)$$

with  $\Phi_c$  being the invariant phase space for channel  $c$ . The sum includes only open channels, *i.e.* those for which the production threshold is below the energy of the scattered system. Using time-reversal symmetry, and  $\text{Disc } \mathcal{M}(s, t) = 2i \text{Im}(\mathcal{M}(s + i\epsilon, t))$  for the  $s$ -channel, the optical theorem follows

$$\text{Im } \mathcal{M}_{aa}(s, 0) = 2q_a \sqrt{s} \sigma_{\text{tot}}(a \rightarrow \text{anything}), \quad (49.4)$$

where  $q_a$  denotes the relative momentum of the particles of channel  $a$  (see Eq. (17) of the review on “Kinematics”). The value  $t = 0$  in Eq. (49.4) corresponds to forward scattering.

The unitarity relation for a production amplitude for a channel  $a$  is given by

$$[\mathcal{A}_a - \mathcal{A}_a^*] = i(2\pi)^4 \sum_c \int d\Phi_c \mathcal{M}_{ca}^* \mathcal{A}_c. \quad (49.5)$$

One application of the two-body-unitarity constraint from Eq. (49.5) is studies of the three-body decays in the Khuri-Treiman framework [25]. The standard procedure here is to derive the equations for the production amplitude for small values of the mass of the decaying particle in the scattering domain and relate it to the decay kinematics by an analytic continuation in the decay mass. Note that in this kinematics the connection between imaginary part and discontinuity employed to derive Eq. (49.4) no longer holds. The method was successfully applied to various decays of light mesons,  $\eta \rightarrow 3\pi$  in Refs. [26–28],  $\phi/\omega \rightarrow 3\pi$  in Ref. [29,30],  $\eta' \rightarrow \eta\pi\pi$  in Ref. [31], as well as to the charm-mesons decays  $D^+ \rightarrow K^0/\pi^0/\pi^+$  [32,33].

### 49.1.3 Partial-wave decomposition

It is often convenient to expand the scattering amplitude in partial waves. Since resonances have a well-defined spin, in the  $s$ -channel they appear only in the corresponding partial waves. For scalar particles only one may write

$$\mathcal{M}_{ba}(s, t) = \sum_{j=0}^{\infty} (2j+1) \mathcal{M}_{ba}^j(s) P_j(\cos(\theta)), \quad (49.6)$$

where  $j$  denotes the total angular momentum. For scalar particles it coincides with the orbital angular momentum of the particle

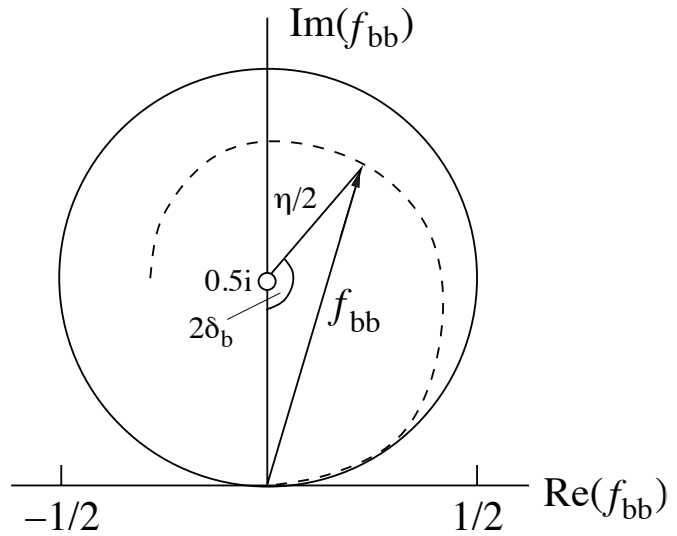


Figure 49.2: Argand plot showing a diagonal element of a partial-wave amplitude,  $a_{bb}$ , as a function of energy. The amplitude leaves the unitary circle (solid line) as soon as inelasticity sets in,  $\eta < 1$  (dashed line).

pairs in the initial and the final state. To simplify notations we will drop the label  $j$  for the single-argument function  $\mathcal{M}_{ba}(s)$ . The unitarity constraint for  $\mathcal{M}_{ba}(s)$  reads,

$$\text{Im } \mathcal{M}_{ba} = \sum_c \mathcal{M}_{cb}^* \rho_c \mathcal{M}_{ca} \quad (49.7)$$

with  $\rho_c$  being a factor that is related to the two-body phase space in Eq. (12) of the review on “Kinematics”,

$$\rho_c(s) = \frac{(2\pi)^4}{2} \int d\Phi_2 = \frac{1}{16\pi} \frac{2|\vec{q}_c|}{\sqrt{s}}. \quad (49.8)$$

The partial-wave amplitudes  $f_{ba}(s)$  are connected to  $\mathcal{M}_{ba}(s)$  via

$$f_{ba}(s) = \sqrt{\rho_b} \mathcal{M}_{ba}(s) \sqrt{\rho_a}. \quad (49.9)$$

From this definition it follows for the unitarity condition that  $\text{Im } f_{ba}^{-1} = -\delta_{ba}$ . Moreover,  $\mathbb{I} + 2if$  is a unitary matrix. Hence, it

can be parameterized as,

$$f_{bb} = (\eta_b \exp(2i\delta_b) - 1)/2i, \quad (49.10)$$

where  $\delta_b$  denotes the phase shift for the scattering from channel  $b$  to channel  $b$ ,  $\eta_b$  is elasticity parameter — also called inelasticity. One has  $0 \leq \eta_b \leq 1$ , where  $\eta_b = 1$  refers to purely elastic scattering. The evolution with energy of a partial-wave amplitude  $f_{bb}$  can be displayed as a trajectory in an Argand plot, as shown in Fig. 49.2. In case of a two-channel problem,  $\eta_b = \eta_a = \eta$ , and the off-diagonal element is  $f_{ba} = \sqrt{1 - \eta^2}/2 \exp(i(\delta_b + \delta_a))$ .

The partial-wave-projected production amplitude  $\mathcal{A}(s)$  (the label  $j$  is dropped for consistency) is also constrained by unitarity. From Eq. (49.5) follows,

$$\text{Im } \mathcal{A}_a = \sum_b \mathcal{M}_{ab}^* \rho_b \mathcal{A}_b, \quad (49.11)$$

where the sum runs over all open channels. For purely elastic scattering, where the sum collapses to just the channel  $a$ , the Watson theorem, stating that the phase of  $\mathcal{A}_a$  agrees with that of  $\mathcal{M}_{aa}$ , follows straightforwardly, since the left-hand side of Eq. (49.11) is a real number.

## 49.2 Properties of resonances

The main characteristics of a resonance is its pole position,  $s_R$ , in the complex  $s$ -plane that is independent of the reaction studied. The more traditional parameters mass  $M_R$  and total width  $\Gamma_R$  may be introduced via the pole parameters

$$\sqrt{s_R} = M_R - i\Gamma_R/2. \quad (49.12)$$

Note that the standard Breit-Wigner parameters  $M_{BW}$  and  $\Gamma_{BW}$ , also introduced below, in general deviate from the pole parameters, *e.g.*, due to finite width effects and the influence of thresholds.

In addition to the pole location a resonance is characterized also by its residues that quantify its couplings to the various channels and allow one to define branching ratios. In the Meson Particle Listings the two-photon width of  $f_0(500)$  is defined in terms of the corresponding residue. The Baryon Particle Listings give the elastic pole residues and normalized transition residues. However, different conventions are used in the two sectors, which are shortly outlined here.

In the close vicinity of the resonance pole the scattering matrix  $\mathcal{M}$  can be written as

$$\lim_{s \rightarrow s_R} (s - s_R) \mathcal{M}_{ba} = -\mathcal{R}_{ba}. \quad (49.13)$$

The residues may be calculated via an integration along a closed contour around the pole using

$$\mathcal{R}_{ba} = -\frac{1}{2\pi i} \oint ds \mathcal{M}_{ba}. \quad (49.14)$$

The factorization of the residue  $(\mathcal{R}_{ba})^2 = \mathcal{R}_{aa} \times \mathcal{R}_{bb}$  allows one to introduce pole couplings according to

$$\tilde{g}_a = \mathcal{R}_{ba} / \sqrt{\mathcal{R}_{bb}}. \quad (49.15)$$

The pole couplings are the only quantities that characterize the transition strength of a given resonance to some channel  $a$  independently of how the particular resonance was produced. One may define a partial width and a branching fraction even for a broad resonance via

$$\Gamma_{R \rightarrow a} = \frac{|\tilde{g}_a|^2}{M_R} \rho_a(M_R^2) \quad \text{and} \quad \text{Br}_a = \Gamma_{R \rightarrow a} / \Gamma_R, \quad (49.16)$$

where  $M_R$  and  $\Gamma_R$  were introduced in Eq. (49.12). This expression was used to define a two-photon width for the broad  $f_0(500)$  (also called  $\sigma$ ) [34, 35]. Eq. (49.16) defines a partial-decay width independent of the reaction used to extract the parameters. For a narrow resonance it maps smoothly onto the other common definition of the branching fraction, discussed in Eq. (49.22).

In the baryon sector it is common to define the residue with respect to the partial-wave amplitudes  $f_{ba}(s)$  defined in Eq. (49.9) and with respect to  $\sqrt{s}$  instead of  $s$ . Accordingly in the baryon listings the elastic pole residue, which refers to  $\pi N \rightarrow \pi N$  scattering, is related to the residues introduced above via

$$r_{\pi N, \pi N} = \frac{\rho_{\pi N}(s_R)}{\sqrt{4s_R}} \mathcal{R}_{\pi N, \pi N}, \quad (49.17)$$

where the phase-space factor is to be evaluated at the pole.

## 49.3 Common parameterizations

Up to a few exceptions where sophisticated dispersive methods can be used or one restricts oneself to a very small energy range, there is in general no universal model-independent recipe to build the scattering amplitude. The resonance parameters extracted should not depend on the approach used, however, assuming that the amplitude fits relevant data of sufficient quality well. Deviations of resonance parameters obtained in different models which equally-well describe the data must be attributed to the systematic theory uncertainties.

### 49.3.1 The Breit-Wigner parameterization

First we focus on the most common case of resonances that appear in production reactions and consider the simplest approximation that is only appropriate for a narrow resonance located far from all relevant thresholds. In this case, one may use the constant-width Breit-Wigner parameterization,

$$\mathcal{A}(s) = \frac{\tilde{\alpha}}{M_{BW}^2 - s - i\sqrt{s}\Gamma_{BW}} \approx \frac{\tilde{\alpha}}{M_{BW}^2 - s - iM_{BW}\Gamma_{BW}}, \quad (49.18)$$

where  $\tilde{\alpha}$  contains the resonance coupling to the source as well as to the final state. It is common to replace  $\sqrt{s}$  by  $M_{BW}$  as done in the right expression.

To use a constant partial width for a resonance coupling to some channel  $a$  in an analysis is justified only, if  $2(M_R - \sqrt{s_{\text{thr}_a})}/\Gamma_R \gg 1$ , where  $\sqrt{s_{\text{thr}_a}}$  denotes the location of the threshold for channel  $a$ . Otherwise, it is important to build in the appropriate threshold behavior and use the energy-dependent expression for the denominator.

$$\mathcal{A}_a(s) = \frac{\alpha g_a n_a(s)}{M_{BW}^2 - s - i \sum_b g_b^2 \rho_b(s) n_b^2(s)}, \quad (49.19)$$

where the sum in the denominator is taken over all open channels,  $n_a$  combines the threshold and barrier factors,  $n_a = (q_a/q_0)^{l_a} F_{l_a}(q_a, q_0)$ , with  $l_a$  being the orbital angular momentum in channel  $a$ ,  $q_a$  is given by Eq. (17) of the review on “Kinematics”, and  $q_0$  denotes a momentum scale. The factor  $(q_a)^{l_a}$  guarantees the correct threshold behavior. The rapid growth of this factor for angular momenta  $l > 0$  is commonly compensated at higher energies by a phenomenological form factor, here denoted by  $F_{l_a}(q_a, q_0)$ . Often the Blatt-Weisskopf form factors are used [36–38], where  $F_j(q, q_0) = F_j(q/q_0)$  and, *e.g.*  $F_0^2(z) = 1$ ,  $F_1^2(z) = 1/(1+z)$  and  $F_2^2(z) = 1/(9+3z+z^2)$ . The denominator can be written as  $M_{BW}^2 - s - iM_{BW}\Gamma_{\text{tot}}(s)$ , with

$$\Gamma_{\text{tot}}(s) = \sum_b \Gamma_b(s) \quad (49.20)$$

for the energy-dependent total width. An often used parameterization for the partial width  $\Gamma_a(s)$  trades the coupling for the resonance width:

$$\Gamma_a(s) = \Gamma_{BW a} \frac{\rho_a(s)}{\rho_a(M_{BW}^2)} \left( \frac{q_a}{q_{aR}} \right)^{2l_a} \frac{F_{l_a}^2(q_a, q_0)}{F_{l_a}^2(q_{aR}, q_0)}. \quad (49.21)$$

Here  $q_{aR}$  are the values of the break-up momentum evaluated at  $s = M_{BW}^2$ . The Breit-Wigner parameters  $M_{BW}$  and  $\Gamma_{BW}$  in Eq. (49.18) as well as the coupling  $g_a$  in Eq. (49.19) allow for an effective description of resonance phenomena but in general do not have strict physical meaning. The mass and width agree with the pole parameters only if the resonance is narrow in the sense

defined above. Otherwise, the Breit-Wigner parameters deviate from the pole parameters and are in general reaction dependent.

Branching fractions for individual, isolated resonances may be

$$\text{Br}'_a = \frac{\int_{s_{\text{thr},a}}^{\infty} ds \frac{|g_a|^2 n_a^2 \rho_a(s)}{|M_{\text{BW}}^2 - s - iM_{\text{BW}}\Gamma_{\text{tot}}(s)|^2}}{\sum_c \int_{s_{\text{thr},c}}^{\infty} ds \frac{|g_c|^2 n_c^2 \rho_c(s)}{|M_{\text{BW}}^2 - s - iM_{\text{BW}}\Gamma_{\text{tot}}(s)|^2}}, \quad (49.23)$$

is also often used.

If there is more than one resonance in one partial wave that significantly couples to the same channel, it is in general incorrect to use a sum of Breit-Wigner functions, for this usually leads to violation of unitarity constraints. Then, more refined methods should be used, like the  $K$ -matrix approximation described in the next section.

### 49.3.2 $K$ -matrix approximation and Flatté parameterizations

The  $K$ -matrix method is a general construction for coupled-channel scattering amplitudes  $\mathcal{M}_{ba}$  that guarantees two-particle unitarity, but does not allow for the inclusion of left-hand cuts [39]. The amplitude reads,

$$n_b \mathcal{M}_{ba}^{-1} n_a = \mathcal{K}_{ba}^{-1} - i\delta_{ba} \rho_a n_a^2, \quad (49.24)$$

where  $\mathcal{K}_{ba}$  is an arbitrary real function. The factor  $n_a$  becomes important for the waves with non-zero angular momentum. As mentioned before  $n_a = q_a^{l_a}$  or  $n_a = (q_a/q_0)^{l_a} F_{l_a}(q_a, q_0)$ .

As there is no unique rigorous recipe to build  $\mathcal{K}$ , various parameterizations thereof have to be studied, in order to get access to the theoretical systematic uncertainty. One possible choice for the  $K$ -matrix is

$$\mathcal{K}_{ba}(s) = \sum_R \frac{g_b^R g_a^R}{M_R^2 - s} + \sum_{i=0}^{N_{\text{b.g.}}} b_{ba}^{(i)} s^i, \quad (49.25)$$

where  $M_R$  is referred to as the bare mass of the resonance  $R$ ,  $g_a^R$  is the bare coupling of the resonance  $R$  to the channel  $a$  and the  $b_{ba}^{(i)}$  are matrices parameterizing the non-pole parts of the  $K$ -matrix. As long as all parameters appearing in Eq. (49.25) are real the amplitude is unitary. From the ansatz given above the scattering amplitude  $\mathcal{M}$  can be calculated directly using the matrix form,

$$\mathcal{M} = n[1 - \mathcal{K} i \rho n^2]^{-1} \mathcal{K} n. \quad (49.26)$$

This solution also applies in those cases in which the inverse of  $\mathcal{K}$  does not exist.

As an alternative to Eq. (49.25), the same functional form as on the right side of Eq. (49.25) can be used to parameterize the inverse  $K$ -matrix, called by authors of Ref. [40] the  $M$ -matrix. The  $K$ -matrix framework is extensively used to parameterize the scattering amplitudes needed to analyse the data from lattice QCD calculations [41–43]

One notices that the evaluation of the  $K$ -matrix amplitude for the multichannel problem requires an analytic continuation already on the real axis. For a given closed channel  $c$  (the channel  $c$  is called closed, if  $s < s_{\text{thr},c}$ ), the factor  $q_c(s)$  that enters  $\rho_c$  and  $n_c$  has to be calculated below the corresponding threshold, *i.e.* in the unphysical region of the particular channel  $c$ . This is done using analytic continuation as described *e.g.* in Refs. [44, 45]:

$$q_c = i\sqrt{-q_c^2} \quad \text{for} \quad q_c^2 < 0. \quad (49.27)$$

The resulting line shape above and below the threshold of channel  $c$  is called the Flatté parameterization [44]. The continuation given

introduced based on the parameters introduced above:

$$\text{Br}'_a = \frac{\Gamma_{\text{BW}a}}{\Gamma_{\text{BW,tot}}} \quad (49.22)$$

where  $\Gamma_{\text{BW,tot}} = \sum_a \Gamma_{\text{BW}a}$  denotes the total width evaluated at the Breit-Wigner mass.

The branching fraction definition based on a probability of the decay to a certain channel,

above stays on the physical sheet. To reach the unphysical sheet the negative square root needs to be chosen. If the coupling of a resonance to the channel opening nearby is very strong, the Flatté parameterization shows a scaling invariance and does not allow for an extraction of individual partial decay widths, but only of ratios [46]. The position of the resonance poles can be determined by a study of the zeros of the analytic function  $\det[1 - \mathcal{K} i \rho n^2]$ . Due to the  $\rho$  factor, this determinant has a complicated multisheet structure, however, the closest unphysical sheet is always the one which is determined by the heaviest threshold below the studied point  $s$ .

### 49.3.3 Scattering-length approximation

A scattering length,  $a$ , is introduced as the first term in an expansion of the scattering phase shift introduced in Eq. (49.10). For  $S$ -waves one finds

$$q \cot \delta = 1/a + O(q^2), \quad (49.28)$$

where  $q$  is a break-up momentum of the scattering system. In this approximation, the scattering amplitude reads

$$\mathcal{M}(s) = \frac{8\pi\sqrt{s}}{1/a - iq(s)}. \quad (49.29)$$

The scattering length is proportional to the value of the amplitude at threshold. The sign of the scattering length is a matter of convention — notably in nuclear physics a sign convention different from Eq. (49.28) is common. A scattering length approximation is applicable only in a very limited energy range, however, might well be appropriate to analyse the recently discovered narrow near-threshold states [47, 48] from this point of view, *e.g.*, in Refs. [49–51]. Moreover, it is possible to introduce the effect of a weakly coupled lower channel. To see this one might start from

$$\mathcal{K} = \begin{pmatrix} \gamma & \beta \\ \beta & 0 \end{pmatrix}, \quad (49.30)$$

with  $\beta, \gamma$  being real numbers. It leads to

$$\mathcal{M}_{\text{el.}}(s) = \frac{1}{1/(\gamma + i\beta^2 \rho_{\text{inel.}}(s)) - i\rho(s)}, \quad (49.31)$$

with  $\rho_{\text{inel.}}(s)$  being the phase-space factor of the inelastic channel. The scattering length for the amplitude in Eq. (49.31) obtains an imaginary part due to the coupling to the lower channel,

$$a = \frac{1}{8\pi\sqrt{s_{\text{thr}}}} (\gamma + i\beta^2 \rho_{\text{inel.}}(s_{\text{thr}})). \quad (49.32)$$

If the function  $\beta^2 \rho_{\text{inel.}}(s)$  does not vary significantly in the energy range studied, the scattering length approximation with a complex value is justified. For large values of  $a$  the amplitude of Eq. (49.31) develops a near threshold pole located on the physical or unphysical sheet for negative or positive values of  $\gamma$ , respectively. While easy to use, it is important to stress, however, that the approximation in Eq. (49.30) is a specific choice of the dynamic function that produces a single pole near the physical

region pointing at a hadronic molecule nature of the state studied [51–53]. For practical analyses, various modifications of the parameterization have to be tested.

#### 49.3.4 Two methods to build the production amplitude

When the unitary scattering amplitude is fixed, it can be used to build the production amplitude in a way that it is consistent with unitarity [38, 54].

1. The  $Q$ -vector approach is discussed in Ref. [38, 40, 55]. It reads,

$$A_a(s) = \sum_c \mathcal{M}_{ac}(s) Q_c(s) / n_c, \quad Q_c(s) = \sum_i Q_c^{(i)} s^i. \quad (49.33)$$

The unitarity condition of Eq. (49.11) is satisfied when  $Q_c(s)$  is a real function and in particular does not have singularities above the lowest threshold for all channels  $c$ . Besides these conditions  $Q_c(s)$  is arbitrary. Note that in the  $Q$ -vector approach the left hand cuts of the scattering matrix  $\mathcal{M}_{ac}(s)$  get imported to the production amplitude which might generate a wrong analytic structure. If this problem is relevant needs to be investigated on a case-by-case basis. In a study of  $\gamma\gamma \rightarrow \pi\pi$ , cf. Ref. [34, 35] a low-order polynomial is claimed to be sufficient to parametrize the energy dependence of the function  $Q_c(s)$ . The  $Q$ -vector method is convenient, if the full matrix  $\mathcal{M}$  is known, cf. Ref. [40].

2. The  $P$ -vector is a parameterization that exploits the  $K$ -matrix of the scattering amplitude [39, 54]. It contains two components: the background term  $B_c$  that is coupled to the  $K$ -matrix via an intermediate loop represented by the  $i\rho$  factor, and the “direct” resonance production term with couplings  $\alpha_c^R$ :

$$A_a(s) = n_a \sum_c \left[ 1 - \mathcal{K} i\rho n^2 \right]_{ac}^{-1} P_c, \quad P_c = \sum_R \frac{\alpha_c^R g_c^R}{M_R^2 - s} + B_c. \quad (49.34)$$

Again, unitarity requires the parameters  $B_c$  and  $\alpha_c^R$  to be real. Importantly, the masses  $M_R$  need to agree with those in  $\mathcal{K}$  in Eq. (49.25).

An important difference between the methods is to be noticed [54]: When the two-particle scattering amplitude goes to zero, the production amplitude in the  $Q$ -vector method vanishes for finite values of  $Q_c$ , while it stays finite in the  $P$ -vector approach. An advanced version of the  $P$ -vector approach that exploits analytic properties of production amplitude [54, 56, 57] is widely used, e.g. in the dispersive Khuri-Treiman framework [25, 58] for construction of three-body-decay amplitude.

#### 49.3.5 Further improvements: Chew-Mandelstam function

The  $K$ -matrix described above usually allows one to get a proper fit of physical amplitudes and it is easy to deal with, however, it also has an important deficit: it violates constraints from analyticity — e.g.,  $\rho_a$ , given by Eq. (49.8), is ill-defined at  $s = 0$ , and for unequal masses it develops an unphysical cut (see Fig. 49.3). A method to improve the analytic properties was suggested in Refs. [59–63]. It replaces the phase-space factor  $i\rho_a(s)$  in Eq. (49.24) by the analytic function  $\Sigma_a(s)$  that produces the identical imaginary part on the right-hand cut. This function is called the Chew-Mandelstam function and for  $S$ -waves it reads [56, 61]:

$$\Sigma_a(s) = \frac{1}{16\pi^2} \left[ \frac{2q_a}{\sqrt{s}} \log \frac{m_1^2 + m_2^2 - s + 2\sqrt{s}q_a}{2m_1 m_2} \right. \quad (49.35)$$

$$\left. - (m_1^2 - m_2^2) \left( \frac{1}{s} - \frac{1}{(m_1 + m_2)^2} \right) \log \frac{m_1}{m_2} \right], \quad (49.36)$$

where  $m_1$  and  $m_2$  are masses of the final-state particles in channel  $a$ ,  $s_{\text{thr}_a} = (m_1 + m_2)^2$ . The function along the real axis is plotted on the right pane of Fig. 49.1. For channels with  $j > 0$ , the threshold behavior has to be incorporated properly. This can be

done, e.g., by computing the dispersion integral

$$\Sigma_a(s + i0) = \frac{s - s_{\text{thr}_a}}{\pi} \int_{s_{\text{thr}_a}}^{\infty} \frac{\rho_a(s') n_a^2(s')}{(s' - s_{\text{thr}_a})(s' - s - i0)} ds'. \quad (49.37)$$

A further discussion of the calculation of the Chew-Mandelstam function can be found in Ref. [64].

If there is only a single resonance in a given channel, it is possible to feed the imaginary part of the Breit-Wigner function, Eq. (49.19) with an energy-dependent width, directly into a dispersion integral to get a resonance propagator with the correct analytic structure [65, 66].

#### 49.3.6 Two-potential decomposition

The other advanced technique to construct the scattering amplitude which is widely used in the literature [67–71] is based on the two-potential formalism [72]. The method is usually formulated for the full unprojected amplitude  $\mathcal{M}_{ba}(s, t)$ , however, in order to simplify the discussion we present the equations in the partial-wave-projected form.

The scattering amplitude  $\mathcal{M}$  is decomposed into a pole part and a non-pole part, often called background (b.g.)

$$\mathcal{M}(s) = \mathcal{M}^{\text{b.g.}}(s) + \mathcal{M}^{\text{pole}}(s). \quad (49.38)$$

The splitting given in Eq. (49.38) is not unique and model-dependent (see, e.g., the discussions in Refs. [73, 74]). The background scattering matrix is assumed to be unitary by itself. One option is to parameterize it, e.g. at low energies directly in terms of phase shifts and inelasticities — see, e.g., Refs. [71, 75]. In this case the vertex functions  $\Omega(s)_{ab}$  introduced below can be written in terms of an Omnes matrix [75], which reduces to the well known Omnes function in the single channel case [57]. Alternatively, it can be computed based on some potential,  $V^{\text{b.g.}}$ , fed into a proper scattering equation.

The complete amplitude  $\mathcal{M}$  of Eq. (49.38) is unitary if the pole part is chosen as

$$\mathcal{M}^{\text{pole}}(s) = \Omega(s) [1 - V^{\text{R}}(s) \Sigma^u(s)]^{-1} V^{\text{R}}(s) \Omega^T(s). \quad (49.39)$$

where the resonance potential reads in channel space

$$V_{ab}^{\text{R}}(s) = \sum_R \frac{g_a^R g_b^R}{M_R^2 - s}, \quad (49.40)$$

$\Sigma_{ab}^u$  denotes the self-energy matrix, and  $g_a^R$  and  $M_R$  denote the bare coupling of the resonance  $R$  to channel  $a$  and its bare mass, respectively. A relation analogous to Eq. (49.5) holds for the normalized vertex functions, however, with the final state interaction provided by  $\mathcal{M}^{\text{b.g.}}$ .

$$\text{Disc } \Omega_{ab}(s) = 2i \sum_c \mathcal{M}_{ca}^{\text{b.g.}*}(s) \rho_c(s) \Omega_{cb}(s). \quad (49.41)$$

The discontinuity of the self-energy matrix  $\Sigma^u(s)$  is

$$\text{Disc } \Sigma_{ab}^u(s) = 2i \sum_c \Omega_{ca}^*(s) \rho_c(s) \Omega_{cb}(s). \quad (49.42)$$

The real part of  $\Sigma^u$  can be calculated from Eq. (49.42) via a properly subtracted dispersion integral. If  $\mathcal{M}^{\text{b.g.}}$  is unitary, the use of Eq. (49.39) leads to a unitary full amplitude, cf. Eq. (49.38). However, the pole term alone is unitary only for a vanishing background amplitude. In this situation the amplitude just described reduces to the analytically improved  $K$ -matrix of Sec. 49.3.5. While the omission of non-pole terms is a bad approximation for, e.g., scalar-isoscalar  $\pi\pi$  interactions at low energies [76], it typically works well for higher partial waves.

The algebra of the two potential splitting presented in Eq. (49.38) is found to be very practical in various other cases, beyond the pole-background separation. It was employed in Refs. [71, 75] to treat the pion vector and scalar form factor, respectively, over a sizable energy range including inelasticities. A

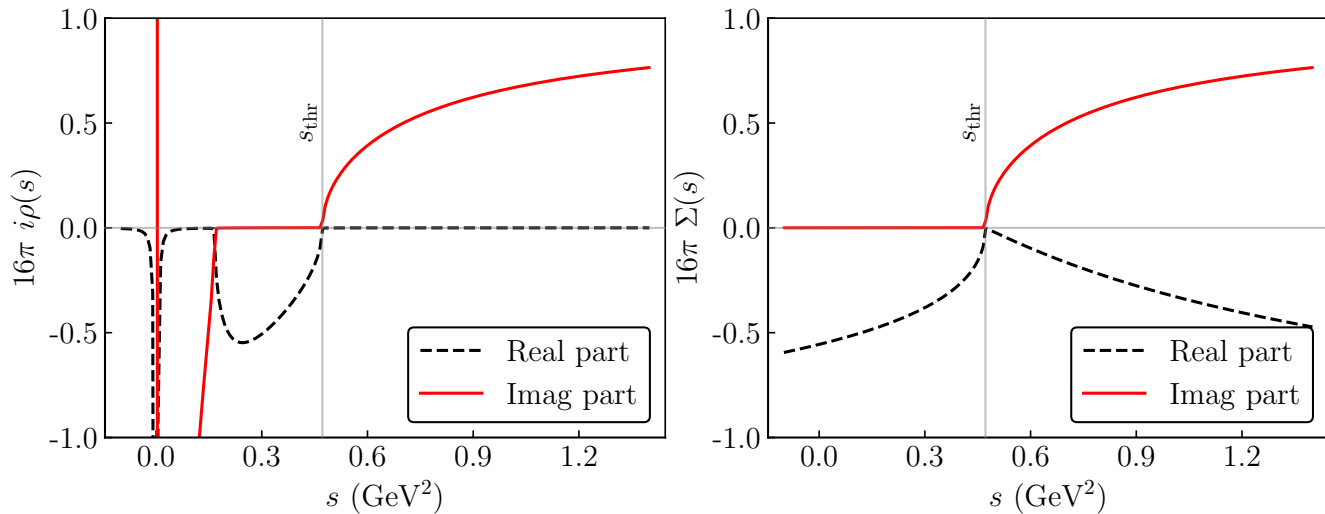


Figure 49.3: Comparison of the  $i\rho$  function (left plot) to the Chew-Mandelstam function from Eq. (49.36) (right plot), evaluated for the case of  $S$ -wave  $\eta\pi$  scattering. The values of  $s$  are taken slightly above the real axis,  $s + i0$ . The solid red line shows the imaginary part that is the same for both functions above threshold. The dashed black line presents the real part. One finds indications of the unphysical left-hand singularities of the function  $i\rho$  on the left plot, while the Chew-Mandelstam function is analytic below the two-particle threshold.

similar decomposition applied to the  $3 \rightarrow 3$  scattering problem provided a way to isolate the non-separable one-particle exchange singularity from the short-range resonance interaction [77].

#### Acknowledgement

We are very grateful to Mikhail Mikhasenko, who gave vital input to improve this review.

#### References

- [1] M. Jacob and G. C. Wick, *Annals Phys.* **7**, 404 (1959), [*Annals Phys.*281,774(2000)].
- [2] C. Zemach, *Phys. Rev.* **140B**, 97, 109 (1965).
- [3] A. V. Anisovich *et al.*, *J. Phys.* **G28**, 15 (2002), [hep-ph/0105330].
- [4] L. Landau, *Nucl. Phys.* **13**, 181 (1959).
- [5] R. Cutkosky, *J. Math. Phys.* **1**, 429 (1960).
- [6] V. N. Gribov, Y. L. Dokshitzer and J. Nyiri, *Strong Interactions of Hadrons at High Energies – Gribov Lectures on Theoretical Physics*, Cambridge University Press, Cambridge (2009).
- [7] A rapid change in an amplitude is not an unambiguous signal of a singularity of the  $S$ -matrix [78], however, for realistic interactions this connection holds.
- [8] S. Coleman and R. E. Norton, *Nuovo Cim.* **38**, 438 (1965).
- [9] C. Schmid, *Phys. Rev.* **154**, 5, 1363 (1967).
- [10] I. J. R. Aitchison and C. Kacser, *Il Nuovo Cimento A* (1965-1970) **40**, 2, 576 (1965), ISSN 1826-9869, URL <https://doi.org/10.1007/BF02721045>.
- [11] M. Mikhasenko, B. Ketzner and A. Sarantsev, *Phys. Rev.* **D91**, 9, 094015 (2015), [arXiv:1501.07023].
- [12] M. Bayar *et al.*, *Phys. Rev.* **D94**, 7, 074039 (2016), [arXiv:1609.04133].
- [13] F. Aceti, L. R. Dai and E. Oset, *Phys. Rev.* **D94**, 9, 096015 (2016), [arXiv:1606.06893].
- [14] J.-J. Wu *et al.*, *Phys. Rev. Lett.* **108**, 081803 (2012), [arXiv:1108.3772].
- [15] G. Höhler, *Pion-Nucleon Scattering – Methods and Results of Phenomenological Analyses*, Springer-Verlag Berlin, Heidelberg, New York, 1983.
- [16] M. Fukugita and K. Igi, *Phys. Rept.* **31**, 237 (1977).
- [17] S. M. Roy, *Phys. Lett.* **36B**, 353 (1971).
- [18] B. Ananthanarayan *et al.*, *Phys. Rept.* **353**, 207 (2001), [hep-ph/0005297].
- [19] G. Colangelo, J. Gasser and H. Leutwyler, *Nucl. Phys.* **B603**, 125 (2001), [hep-ph/0103088].
- [20] R. Garcia-Martin *et al.*, *Phys. Rev.* **D83**, 074004 (2011), [arXiv:1102.2183].
- [21] P. Buettiker, S. Descotes-Genon and B. Moussallam, *Eur. Phys. J.* **C33**, 409 (2004), [hep-ph/0310283].
- [22] M. Hoferichter, D. R. Phillips and C. Schat, *Eur. Phys. J.* **C71**, 1743 (2011), [arXiv:1106.4147].
- [23] M. Hoferichter *et al.*, *Phys. Rept.* **625**, 1 (2016), [arXiv:1510.06039].
- [24] M. P. Peskin and D. V. Schroeder, *An Introduction to Quantum Field Theory*, Westview Press, 1995.
- [25] N. N. Khuri and S. B. Treiman, *Phys. Rev.* **119**, 1115 (1960).
- [26] P. Guo *et al.*, *Phys. Lett.* **B771**, 497 (2017), [arXiv:1608.01447].
- [27] M. Albaladejo and B. Moussallam, *Eur. Phys. J.* **C77**, 8, 508 (2017), [arXiv:1702.04931].
- [28] G. Colangelo *et al.*, *Eur. Phys. J.* **C78**, 11, 947 (2018), [arXiv:1807.11937].
- [29] F. Niecknig, B. Kubis and S. P. Schneider, *Eur. Phys. J.* **C72**, 2014 (2012), [arXiv:1203.2501].
- [30] I. V. Danilkin *et al.*, *Phys. Rev.* **D91**, 9, 094029 (2015), [arXiv:1409.7708].
- [31] T. Isken *et al.*, *Eur. Phys. J.* **C77**, 7, 489 (2017), [arXiv:1705.04339].
- [32] F. Niecknig and B. Kubis, *JHEP* **10**, 142 (2015), [arXiv:1509.03188].
- [33] F. Niecknig and B. Kubis, *Phys. Lett.* **B780**, 471 (2018), [arXiv:1708.00446].
- [34] D. Morgan and M. R. Pennington, *Z. Phys.* **C37**, 431 (1988), [Erratum: *Z. Phys.*C39,590(1988)].
- [35] D. Morgan and M. R. Pennington, *Z. Phys.* **C48**, 623 (1990).
- [36] J. M. Blatt and V. F. Weisskopf, *Theoretical nuclear physics*, Springer, New York (1952), ISBN 9780471080190.
- [37] F. Von Hippel and C. Quigg, *Phys. Rev.* **D5**, 624 (1972).
- [38] S. U. Chung *et al.*, *Annalen Phys.* **4**, 404 (1995).
- [39] I. J. R. Aitchison, *Nucl. Phys.* **A189**, 417 (1972).

- [40] K. L. Au, D. Morgan and M. R. Pennington, *Phys. Rev.* **D35**, 1633 (1987).
- [41] J. J. Dudek, R. G. Edwards and D. J. Wilson (Hadron Spectrum), *Phys. Rev.* **D93**, 9, 094506 (2016), [arXiv:1602.05122].
- [42] R. A. Briceno *et al.*, *Phys. Rev.* **D97**, 5, 054513 (2018), [arXiv:1708.06667].
- [43] A. J. Woss *et al.* (2019), [arXiv:1904.04136].
- [44] S. M. Flatte, *Phys. Lett.* **63B**, 224 (1976).
- [45] V. V. Anisovich and A. V. Sarantsev, *Eur. Phys. J.* **A16**, 229 (2003), [hep-ph/0204328].
- [46] V. Baru *et al.*, *Eur. Phys. J.* **A23**, 523 (2005), [arXiv:nucl-th/0410099].
- [47] S. K. Choi *et al.* (Belle), *Phys. Rev. Lett.* **91**, 262001 (2003), [hep-ex/0309032].
- [48] R. Aaij *et al.* (LHCb), *Phys. Rev. Lett.* **122**, 22, 222001 (2019), [arXiv:1904.03947].
- [49] E. Braaten and J. Stapleton, *Phys. Rev.* **D81**, 014019 (2010), [arXiv:0907.3167].
- [50] V. Baru *et al.*, *Eur. Phys. J.* **A44**, 93 (2010), [arXiv:1001.0369].
- [51] C. Fernández-Ramírez *et al.* (JPAC), *Phys. Rev. Lett.* **123**, 9, 092001 (2019), [arXiv:1904.10021].
- [52] D. Morgan, *Nucl. Phys.* **A543**, 632 (1992).
- [53] V. Baru *et al.*, *Phys. Lett.* **B586**, 53 (2004), [hep-ph/0308129].
- [54] I. J. R. Aitchison (2015), [arXiv:1507.02697].
- [55] R. N. Cahn and P. V. Landshoff, *Nucl. Phys.* **B266**, 451 (1986).
- [56] J. L. Basdevant and E. L. Berger, *Phys. Rev.* **D16**, 657 (1977).
- [57] R. Omnes, *Nuovo Cim.* **8**, 316 (1958).
- [58] I. J. R. Aitchison and R. Pasquier, *Phys. Rev.* **152**, 4, 1274 (1966).
- [59] G. J. Gounaris and J. J. Sakurai, *Phys. Rev. Lett.* **21**, 244 (1968).
- [60] M. R. Pennington *et al.*, *Eur. Phys. J.* **C56**, 1 (2008), [arXiv:0803.3389].
- [61] J. A. Oller and E. Oset, *Phys. Rev.* **D60**, 074023 (1999), [hep-ph/9809337].
- [62] N. N. Achasov and A. V. Kiselev, *Phys. Rev.* **D83**, 054008 (2011), [arXiv:1011.4446].
- [63] A. V. Anisovich *et al.*, *Phys. Rev.* **D84**, 076001 (2011).
- [64] J. H. Reid and N. N. Trofimennoff, *J. Math. Phys.* **25**, 3540 (1984).
- [65] E. L. Lomon and S. Pacetti, *Phys. Rev.* **D85**, 113004 (2012), [Erratum: *Phys. Rev.* **D86**, 039901(2012)], [arXiv:1201.6126].
- [66] B. Moussallam, *Eur. Phys. J.* **C73**, 2539 (2013), [arXiv:1305.3143].
- [67] I. R. Afnan and B. Blankleider, *Phys. Rev.* **C22**, 1638 (1980).
- [68] A. D. Lahiff and I. R. Afnan, *Phys. Rev.* **C60**, 024608 (1999), [arXiv:nucl-th/9903058].
- [69] A. Matsuyama, T. Sato and T. S. H. Lee, *Phys. Rept.* **439**, 193 (2007), [arXiv:nucl-th/0608051].
- [70] D. Ronchen *et al.*, *Eur. Phys. J.* **A49**, 44 (2013), [arXiv:1211.6998].
- [71] C. Hanhart, *Phys. Lett.* **B715**, 170 (2012), [arXiv:1203.6839].
- [72] K. Nakano, *Phys. Rev.* **C26**, 1123 (1982).
- [73] D. Djukanovic, J. Gegelia and S. Scherer, *Phys. Rev.* **D76**, 037501 (2007), [arXiv:0707.2030].
- [74] M. Doring *et al.*, *Phys. Lett.* **B681**, 26 (2009), [arXiv:0903.1781].
- [75] S. Ropertz, C. Hanhart and B. Kubis, *Eur. Phys. J.* **C78**, 12, 1000 (2018), [arXiv:1809.06867].
- [76] J. Gasser and U. G. Meissner, *Nucl. Phys.* **B357**, 90 (1991).
- [77] M. Mikhasenko *et al.*, *JHEP* **08**, 080 (2019), [arXiv:1904.11894].
- [78] G. Calucci, L. Fonda and G. C. Ghirardi, *Phys. Rev.* **166**, 1719 (1968).



## 50. Cross-Section Formulae for Specific Processes

Revised August 2019 by H. Baer (Oklahoma U.) and R.N. Cahn (LBNL).

### PART I: STANDARD MODEL PROCESSES

Setting aside leptonproduction (for which, see Sec. 16 of this *Review*), the cross sections of primary interest are those with light incident particles,  $e^+e^-$ ,  $\gamma\gamma$ ,  $q\bar{q}$ ,  $gq$ ,  $gg$ , etc., where  $g$  and  $q$  represent gluons and light quarks. The produced particles include both light particles and heavy ones -  $t$ ,  $W$ ,  $Z$ , and the Higgs boson  $H$ . We provide the production cross sections calculated within the Standard Model for several such processes.

#### 50.1 Resonance Formation

Resonant cross sections are generally described by the Breit-Wigner formula (Sec. 18 of this *Review*).

$$\sigma(E) = \frac{2J+1}{(2S_1+1)(2S_2+1)} \frac{4\pi}{k^2} \left[ \frac{\Gamma^2/4}{(E-E_0)^2 + \Gamma^2/4} \right] B_{in} B_{out}, \quad (50.1)$$

where  $E$  is the c.m. energy,  $J$  is the spin of the resonance, and the number of polarization states of the two incident particles are  $2S_1+1$  and  $2S_2+1$ . The c.m. momentum in the initial state is  $k$ ,  $E_0$  is the c.m. energy at the resonance, and  $\Gamma$  is the full width at half maximum height of the resonance. The branching fraction for the resonance into the initial-state channel is  $B_{in}$  and into the final-state channel is  $B_{out}$ . For a narrow resonance, the factor in square brackets may be replaced by  $\pi\Gamma\delta(E-E_0)/2$ .

#### 50.2 Production of light particles

The production of point-like, spin-1/2 fermions in  $e^+e^-$  annihilation through a virtual photon,  $e^+e^- \rightarrow \gamma^* \rightarrow f\bar{f}$ , at c.m. energy squared  $s$  is given by

$$\frac{d\sigma}{d\Omega} = N_c \frac{\alpha^2}{4s} \beta [1 + \cos^2\theta + (1-\beta^2)\sin^2\theta] Q_f^2, \quad (50.2)$$

where  $\beta$  is  $v/c$  for the produced fermions in the c.m.,  $\theta$  is the c.m. scattering angle, and  $Q_f$  is the charge of the fermion. The factor  $N_c$  is 1 for charged leptons and 3 for quarks. In the ultrarelativistic limit,  $\beta \rightarrow 1$ ,

$$\sigma = N_c Q_f^2 \frac{4\pi\alpha^2}{3s} = N_c Q_f^2 \frac{86.8 \text{ nb}}{s(\text{GeV}^2)}. \quad (50.3)$$

The cross section for the annihilation of a  $q\bar{q}$  pair into a distinct pair  $q'\bar{q}'$  through a gluon is completely analogous up to color factors, with the replacement  $\alpha \rightarrow \alpha_s$ . Treating all quarks as massless, averaging over the colors of the initial quarks and defining  $t = -s \sin^2(\theta/2)$ ,  $u = -s \cos^2(\theta/2)$ , one finds [1]

$$\frac{d\sigma}{d\Omega}(q\bar{q} \rightarrow q'\bar{q}') = \frac{\alpha_s^2}{9s} \frac{t^2 + u^2}{s^2}. \quad (50.4)$$

Crossing symmetry gives

$$\frac{d\sigma}{d\Omega}(qq' \rightarrow qq') = \frac{\alpha_s^2}{9s} \frac{s^2 + u^2}{t^2}. \quad (50.5)$$

If the quarks  $q$  and  $q'$  are identical, we have

$$\frac{d\sigma}{d\Omega}(q\bar{q} \rightarrow q\bar{q}) = \frac{\alpha_s^2}{9s} \left[ \frac{t^2 + u^2}{s^2} + \frac{s^2 + u^2}{t^2} - \frac{2u^2}{3st} \right], \quad (50.6)$$

and by crossing

$$\frac{d\sigma}{d\Omega}(qq \rightarrow qq) = \frac{\alpha_s^2}{9s} \left[ \frac{t^2 + s^2}{u^2} + \frac{s^2 + u^2}{t^2} - \frac{2s^2}{3ut} \right]. \quad (50.7)$$

Annihilation of  $e^+e^-$  into  $\gamma\gamma$  has the cross section

$$\frac{d\sigma}{d\Omega}(e^+e^- \rightarrow \gamma\gamma) = \frac{\alpha^2}{2s} \frac{u^2 + t^2}{tu}. \quad (50.8)$$

The related QCD process also has a triple-gluon coupling. The cross section is

$$\frac{d\sigma}{d\Omega}(q\bar{q} \rightarrow gg) = \frac{8\alpha_s^2}{27s} (t^2 + u^2) \left( \frac{1}{tu} - \frac{9}{4s^2} \right). \quad (50.9)$$

The crossed reactions are

$$\frac{d\sigma}{d\Omega}(qg \rightarrow qg) = \frac{\alpha_s^2}{9s} (s^2 + u^2) \left( -\frac{1}{su} + \frac{9}{4t^2} \right) \quad (50.10)$$

and

$$\frac{d\sigma}{d\Omega}(gg \rightarrow q\bar{q}) = \frac{\alpha_s^2}{24s} (t^2 + u^2) \left( \frac{1}{tu} - \frac{9}{4s^2} \right). \quad (50.11)$$

Finally,

$$\frac{d\sigma}{d\Omega}(gg \rightarrow gg) = \frac{9\alpha_s^2}{8s} \left( 3 - \frac{ut}{s^2} - \frac{su}{t^2} - \frac{st}{u^2} \right). \quad (50.12)$$

Lepton-quark scattering is analogous (neglecting  $Z$  exchange)

$$\frac{d\sigma}{d\Omega}(eq \rightarrow eq) = \frac{\alpha^2}{2s} e_q^2 \frac{s^2 + u^2}{t^2}. \quad (50.13)$$

where  $e_q$  is the charge of the quark. For neutrino scattering with the four-Fermi interaction

$$\frac{d\sigma}{d\Omega}(\nu d \rightarrow \ell^- u) = \frac{G_F^2 s}{4\pi^2}, \quad (50.14)$$

where the Cabibbo angle suppression is ignored. Similarly

$$\frac{d\sigma}{d\Omega}(\nu \bar{u} \rightarrow \ell^- \bar{d}) = \frac{G_F^2 s}{4\pi^2} \frac{(1 + \cos\theta)^2}{4}. \quad (50.15)$$

To obtain the formulae for deep inelastic scattering (presented in more detail in Section 18) we consider quarks of type  $i$  carrying a fraction  $x = Q^2/(2M\nu)$  of the nucleon's energy, where  $\nu = E - E'$  is the energy lost by the lepton in the nucleon rest frame. With  $y = \nu/E$  we have the correspondences

$$1 + \cos\theta \rightarrow 2(1-y),$$

$$d\Omega_{cm} \rightarrow 4\pi f_i(x) dx dy, \quad (50.16)$$

where the latter incorporates the quark distribution,  $f_i(x)$ . In this way we find

$$\begin{aligned} \frac{d\sigma}{dx dy}(eN \rightarrow eX) &= \frac{4\pi\alpha^2 x s}{Q^4} \frac{1}{2} [1 + (1-y)^2] \\ &\times \left[ \frac{4}{9}(u(x) + \bar{u}(x) + \dots) + \frac{1}{9}(d(x) + \bar{d}(x) + \dots) \right] \end{aligned} \quad (50.17)$$

where now  $s = 2ME$  is the cm energy squared for the electron-nucleon collision and we have suppressed contributions from higher mass quarks.

Similarly,

$$\frac{d\sigma}{dx dy}(\nu N \rightarrow \ell^- X) = \frac{G_F^2 x s}{\pi} [(d(x) + \dots) + (1-y)^2(\bar{u}(x) + \dots)] \quad (50.18)$$

and

$$\frac{d\sigma}{dx dy}(\bar{\nu} N \rightarrow \ell^+ X) = \frac{G_F^2 x s}{\pi} [(\bar{d}(x) + \dots) + (1-y)^2(u(x) + \dots)]. \quad (50.19)$$

Quasi-elastic neutrino scattering ( $\nu_\mu n \rightarrow \mu^- p$ ,  $\bar{\nu}_\mu p \rightarrow \mu^+ n$ ) is directly related to the crossed reaction, neutron decay. The formula for the differential cross section is presented, for example, in N.J. Baker *et al.*, Phys. Rev. **D23**, 2499 (1981).

### 50.3 Hadroproduction of heavy quarks

For hadroproduction of heavy quarks  $Q = c, b, t$ , it is important to include mass effects in the formulae. For  $q\bar{q} \rightarrow Q\bar{Q}$ , one has

$$\frac{d\sigma}{d\Omega}(q\bar{q} \rightarrow Q\bar{Q}) = \frac{\alpha_s^2}{9s^3} \sqrt{1 - \frac{4m_Q^2}{s}} \left[ (m_Q^2 - t)^2 + (m_Q^2 - u)^2 + 2m_Q^2 s \right], \quad (50.20)$$

while for  $gg \rightarrow Q\bar{Q}$  one has

$$\begin{aligned} \frac{d\sigma}{d\Omega}(gg \rightarrow Q\bar{Q}) &= \frac{\alpha_s^2}{32s} \sqrt{1 - \frac{4m_Q^2}{s}} \left[ \frac{6}{s^2} (m_Q^2 - t)(m_Q^2 - u) - \right. \\ &\quad \left. - \frac{m_Q^2 (s - 4m_Q^2)}{3(m_Q^2 - t)(m_Q^2 - u)} + \frac{4}{3} \frac{(m_Q^2 - t)(m_Q^2 - u) - 2m_Q^2 (m_Q^2 + t)}{(m_Q^2 - t)^2} \right. \\ &\quad \left. + \frac{4}{3} \frac{(m_Q^2 - t)(m_Q^2 - u) - 2m_Q^2 (m_Q^2 + u)}{(m_Q^2 - u)^2} - 3 \frac{(m_Q^2 - t)(m_Q^2 - u) + m_Q^2 (u - t)}{s(m_Q^2 - t)} \right. \\ &\quad \left. - 3 \frac{(m_Q^2 - t)(m_Q^2 - u) + m_Q^2 (t - u)}{s(m_Q^2 - u)} \right]. \quad (50.21) \end{aligned}$$

### 50.4 Production of Weak Gauge Bosons

#### 50.4.1 $W$ and $Z$ resonant production

Resonant production of a single  $W$  or  $Z$  is governed by the partial widths

$$\Gamma(W \rightarrow \ell_i \bar{\nu}_i) = \frac{\sqrt{2} G_F m_W^3}{12\pi} \quad (50.22)$$

$$\Gamma(W \rightarrow q_i \bar{q}_j) = 3 \frac{\sqrt{2} G_F |V_{ij}|^2 m_W^3}{12\pi} \quad (50.23)$$

$$\begin{aligned} \Gamma(Z \rightarrow f\bar{f}) &= N_c \frac{\sqrt{2} G_F m_Z^3}{6\pi} \\ &\quad \times \left[ (T_3 - Q_f \sin^2 \theta_W)^2 + (Q_f \sin^2 \theta_W)^2 \right]. \quad (50.24) \end{aligned}$$

The weak mixing angle is  $\theta_W$ . The CKM matrix elements are indicated by  $V_{ij}$  and  $N_c$  is 3 for  $q\bar{q}$  final states and 1 for leptonic final states.

The full differential cross section for  $f_i \bar{f}_j \rightarrow (W, Z) \rightarrow f_i' \bar{f}_j'$  is given by

$$\begin{aligned} \frac{d\sigma}{d\Omega} &= \frac{N_c^f}{N_c^i} \cdot \frac{1}{256\pi^2 s} \cdot \frac{s^2}{(s - M^2)^2 + s\Gamma^2} \\ &\quad \times \left[ (L^2 + R^2)(L'^2 + R'^2)(1 + \cos^2 \theta) \right. \\ &\quad \left. + (L^2 - R^2)(L'^2 - R'^2) 2 \cos \theta \right] \quad (50.25) \end{aligned}$$

where  $M$  is the mass of the  $W$  or  $Z$ . The couplings for the  $W$  are  $L = (8G_F m_W^2 / \sqrt{2})^{1/2} V_{ij} / \sqrt{2}$ ;  $R = 0$  where  $V_{ij}$  is the corresponding CKM matrix element, with an analogous expression for  $L'$  and  $R'$ . For  $Z$ , the couplings are  $L = (8G_F m_Z^2 / \sqrt{2})^{1/2} (T_3 -$

$\sin^2 \theta_W Q)$ ;  $R = -(8G_F m_Z^2 / \sqrt{2})^{1/2} \sin^2 \theta_W Q$ , where  $T_3$  is the weak isospin of the initial left-handed fermion and  $Q$  is the initial fermion's electric charge. The expressions for  $L'$  and  $R'$  are analogous. The color factors  $N_c^{i,f}$  are 3 for initial or final quarks and 1 for initial or final leptons.

#### 50.4.2 Production of pairs of weak gauge bosons

The cross section for  $f\bar{f} \rightarrow W^+ W^-$  is given in term of the couplings of the left-handed and right-handed fermion  $f$ ,  $\ell = 2(T_3 - Qx_W)$ ,  $r = -2Qx_W$ , where  $T_3$  is the third component of weak isospin for the left-handed  $f$ ,  $Q$  is its electric charge (in units of the proton charge), and  $x_W = \sin^2 \theta_W$ :

$$\begin{aligned} \frac{d\sigma}{dt} &= \frac{2\pi\alpha^2}{N_c s^2} \left\{ \left[ \left( Q + \frac{\ell + r}{4x_W} \frac{s}{s - m_Z^2} \right)^2 \right. \right. \\ &\quad \left. \left. + \left( \frac{\ell - r}{4x_W} \frac{s}{s - m_Z^2} \right)^2 \right] A(s, t, u) \right. \\ &\quad \left. + \frac{1}{2x_W} \left( Q + \frac{\ell}{2x_W} \frac{s}{s - m_Z^2} \right) \right. \\ &\quad \left. (\Theta(-Q)I(s, t, u) - \Theta(Q)I(s, u, t)) \right. \\ &\quad \left. + \frac{1}{8x_W^2} (\Theta(-Q)E(s, t, u) + \Theta(Q)E(s, u, t)) \right\}, \quad (50.26) \end{aligned}$$

where  $\Theta(x)$  is 1 for  $x > 0$  and 0 for  $x < 0$ , and where

$$\begin{aligned} A(s, t, u) &= \left( \frac{tu}{m_W^4} - 1 \right) \left( \frac{1}{4} - \frac{m_W^2}{s} + 3 \frac{m_W^4}{s^2} \right) + \frac{s}{m_W^2} - 4, \\ I(s, t, u) &= \left( \frac{tu}{m_W^4} - 1 \right) \left( \frac{1}{4} - \frac{m_W^2}{2s} - \frac{m_W^4}{st} \right) + \frac{s}{m_W^2} - 2 + 2 \frac{m_W^2}{t}, \\ E(s, t, u) &= \left( \frac{tu}{m_W^4} - 1 \right) \left( \frac{1}{4} + \frac{m_W^4}{t^2} \right) + \frac{s}{m_W^2}, \quad (50.27) \end{aligned}$$

and  $s, t, u$  are the usual Mandelstam variables with  $s = (p_f + p_{\bar{f}})^2$ ,  $t = (p_f - p_{W^-})^2$ ,  $u = (p_f - p_{W^+})^2$ . The factor  $N_c$  is 3 for quarks and 1 for leptons.

The analogous cross-section for  $q_i \bar{q}_j \rightarrow W^\pm Z^0$  is

$$\begin{aligned} \frac{d\sigma}{dt} &= \frac{\pi\alpha^2 |V_{ij}|^2}{6s^2 x_W^2} \left\{ \left( \frac{1}{s - m_W^2} \right)^2 \left[ \left( \frac{9 - 8x_W}{4} \right) (ut - m_W^2 m_Z^2) \right. \right. \\ &\quad \left. \left. + (8x_W - 6) s (m_W^2 + m_Z^2) \right] \right. \\ &\quad \left. + \left[ \frac{ut - m_W^2 m_Z^2 - s(m_W^2 + m_Z^2)}{s - m_W^2} \right] \left[ \frac{\ell_j}{t} - \frac{\ell_i}{u} \right] \right. \\ &\quad \left. + \frac{ut - m_W^2 m_Z^2}{4(1 - x_W)} \left[ \frac{\ell_j^2}{t^2} + \frac{\ell_i^2}{u^2} \right] + \frac{s(m_W^2 + m_Z^2)}{2(1 - x_W)} \frac{\ell_i \ell_j}{tu} \right\}, \quad (50.28) \end{aligned}$$

where  $\ell_i$  and  $\ell_j$  are the couplings of the left-handed  $q_i$  and  $q_j$  as defined above. The CKM matrix element between  $q_i$  and  $q_j$  is  $V_{ij}$ .

The cross section for  $q_i \bar{q}_i \rightarrow Z^0 Z^0$  is

$$\frac{d\sigma}{dt} = \frac{\pi\alpha^2}{96} \frac{\ell_i^4 + r_i^4}{x_W^2 (1 - x_W^2)^2 s^2} \left[ \frac{t}{u} + \frac{u}{t} + \frac{4m_Z^2 s}{tu} - m_Z^4 \left( \frac{1}{t^2} + \frac{1}{u^2} \right) \right]. \quad (50.29)$$

## 50.5 Production of Higgs Bosons

### 50.5.1 Resonant Production

The Higgs boson of the Standard Model can be produced resonantly in the collisions of quarks, leptons,  $W$  or  $Z$  bosons, gluons, or photons. The production cross section is thus controlled by the partial width of the Higgs boson into the entrance channel and its total width. The branching fractions for the Standard Model Higgs boson are shown in Fig. 1 of the ‘‘Searches for Higgs bosons’’ review in the Particle Listings section, as a function of the Higgs boson mass. The partial widths are given by the relations

$$\Gamma(H \rightarrow f\bar{f}) = \frac{G_F m_f^2 m_H N_c}{4\pi\sqrt{2}} (1 - 4m_f^2/m_H^2)^{3/2}, \quad (50.30)$$

$$\Gamma(H \rightarrow W^+W^-) = \frac{G_F m_H^3 \beta_W}{32\pi\sqrt{2}} (4 - 4a_W + 3a_W^2), \quad (50.31)$$

$$\Gamma(H \rightarrow ZZ) = \frac{G_F m_H^3 \beta_Z}{64\pi\sqrt{2}} (4 - 4a_Z + 3a_Z^2), \quad (50.32)$$

where  $N_c$  is 3 for quarks and 1 for leptons and where  $a_W = 1 - \beta_W^2 = 4m_W^2/m_H^2$  and  $a_Z = 1 - \beta_Z^2 = 4m_Z^2/m_H^2$ . The decay to two gluons proceeds through quark loops, with the  $t$  quark dominating [2]. Explicitly,

$$\Gamma(H \rightarrow gg) = \frac{\alpha_s^2 G_F m_H^3}{36\pi^3 \sqrt{2}} \left| \sum_q I(m_q^2/m_H^2) \right|^2, \quad (50.33)$$

where  $I(z)$  is complex for  $z < 1/4$ . For  $z < 2 \times 10^{-3}$ ,  $|I(z)|$  is small so the light quarks contribute negligibly. For  $m_H < 2m_t$ ,  $z > 1/4$  and

$$I(z) = 3 \left[ 2z + 2z(1 - 4z) \left( \sin^{-1} \frac{1}{2\sqrt{z}} \right)^2 \right], \quad (50.34)$$

which has the limit  $I(z) \rightarrow 1$  as  $z \rightarrow \infty$ .

### 50.5.2 Higgs Boson Production in $W^*$ and $Z^*$ decay

The Standard Model Higgs boson can be produced in the decay of a virtual  $W$  or  $Z$  (‘‘Higgstrahlung’’) [3,4]: In particular, if  $k$  is the c.m. momentum of the Higgs boson,

$$\sigma(q_i \bar{q}_j \rightarrow WH) = \frac{\pi\alpha^2 |V_{ij}|^2}{36 \sin^4 \theta_W} \frac{2k}{\sqrt{s}} \frac{k^2 + 3m_W^2}{(s - m_W^2)^2} \quad (50.35)$$

$$\sigma(f\bar{f} \rightarrow ZH) = \frac{2\pi\alpha^2 (\ell_f^2 + r_f^2)}{48N_c \sin^4 \theta_W \cos^4 \theta_W} \frac{2k}{\sqrt{s}} \frac{k^2 + 3m_Z^2}{(s - m_Z^2)^2}, \quad (50.36)$$

where  $\ell$  and  $r$  are defined as above.

### 50.5.3 $W$ and $Z$ Fusion

Just as high-energy electrons can be regarded as sources of virtual photon beams, at very high energies they are sources of virtual  $W$  and  $Z$  beams. For Higgs boson production, it is the longitudinal components of the  $W$ s and  $Z$ s that are important [5]. The distribution of longitudinal  $W$ s carrying a fraction  $y$  of the electron’s energy is [6]

$$f(y) = \frac{g^2}{16\pi^2} \frac{1-y}{y}, \quad (50.37)$$

where  $g = e/\sin\theta_W$ . In the limit  $s \gg m_H \gg m_W$ , the partial decay rate is  $\Gamma(H \rightarrow W_L W_L) = (g^2/64\pi)(m_H^3/m_W^2)$  and in the equivalent  $W$  approximation [7]

$$\sigma(e^+e^- \rightarrow \bar{\nu}_e \nu_e H) = \frac{1}{16m_W^2} \left( \frac{\alpha}{\sin^2 \theta_W} \right)^3 \times \left[ \left( 1 + \frac{m_H^2}{s} \right) \log \frac{s}{m_H^2} - 2 + 2 \frac{m_H^2}{s} \right]. \quad (50.38)$$

There are significant corrections to this relation when  $m_H$  is not large compared to  $m_W$  [8]. For  $m_H = 150$  GeV, the estimate is too high by 51% for  $\sqrt{s} = 1000$  GeV, 32% too high at  $\sqrt{s} = 2000$  GeV, and 22% too high at  $\sqrt{s} = 4000$  GeV. Fusion of  $ZZ$  to make a Higgs boson can be treated similarly. Identical formulae apply for Higgs production in the collisions of quarks whose charges permit the emission of a  $W^+$  and a  $W^-$ , except that QCD corrections and CKM matrix elements are required. Even in the absence of QCD corrections, the fine-structure constant ought to be evaluated at the scale of the collision, say  $m_W$ . All quarks contribute to the  $ZZ$  fusion process.

### 50.6 Inclusive hadronic reactions

One-particle inclusive cross sections  $E d^3\sigma/d^3p$  for the production of a particle of momentum  $p$  are conveniently expressed in terms of rapidity  $y$  (see above) and the momentum  $p_T$  transverse to the beam direction (in the c.m.):

$$E \frac{d^3\sigma}{d^3p} = \frac{d^3\sigma}{d\phi dy p_T dp_T}. \quad (50.39)$$

In appropriate circumstances, the cross section may be decomposed as a partonic cross section multiplied by the probabilities of finding partons of the prescribed momenta:

$$\sigma_{\text{hadronic}} = \sum_{ij} \int dx_1 dx_2 f_i(x_1) f_j(x_2) d\hat{\sigma}_{\text{partonic}}, \quad (50.40)$$

The probability that a parton of type  $i$  carries a fraction of the incident particle’s that lies between  $x_1$  and  $x_1 + dx_1$  is  $f_i(x_1)dx_1$  and similarly for partons in the other incident particle. The partonic collision is specified by its c.m. energy squared  $\hat{s} = x_1 x_2 s$  and the momentum transfer squared  $\hat{t}$ . The final hadronic state is more conveniently specified by the rapidities  $y_1, y_2$  of the two jets resulting from the collision and the transverse momentum  $p_T$ . The connection between the differentials is

$$dx_1 dx_2 d\hat{t} = dy_1 dy_2 \frac{\hat{s}}{s} dp_T^2, \quad (50.41)$$

so that

$$\frac{d^3\sigma}{dy_1 dy_2 dp_T^2} = \frac{\hat{s}}{s} \left[ f_i(x_1) f_j(x_2) \frac{d\hat{\sigma}}{d\hat{t}}(\hat{s}, \hat{t}, \hat{u}) + f_i(x_2) f_j(x_1) \frac{d\hat{\sigma}}{d\hat{t}}(\hat{s}, \hat{u}, \hat{t}) \right], \quad (50.42)$$

where we have taken into account the possibility that the incident parton types might arise from either incident particle. The second term should be dropped if the types are identical:  $i = j$ .

### 50.7 Two-photon processes

In the Weizsäcker-Williams picture, a high-energy electron beam is accompanied by a spectrum of virtual photons of energies  $\omega$  and invariant-mass squared  $q^2 = -Q^2$ , for which the photon number density is

$$dn = \frac{\alpha}{\pi} \left[ 1 - \frac{\omega}{E} + \frac{\omega^2}{E^2} - \frac{m_e^2 \omega^2}{Q^2 E^2} \right] \frac{d\omega}{\omega} \frac{dQ^2}{Q^2}, \quad (50.43)$$

where  $E$  is the energy of the electron beam. The cross section for  $e^+e^- \rightarrow e^+e^- X$  is then [9]

$$d\sigma_{e^+e^- \rightarrow e^+e^- X}(s) = dn_1 dn_2 d\sigma_{\gamma\gamma \rightarrow X}(W^2), \quad (50.44)$$

where  $W^2 = m_X^2$ . Integrating from the lower limit  $Q^2 = m_e^2 \frac{\omega_i^2}{E_i(E_i - \omega_i)}$  to a maximum  $Q^2$  gives

$$\sigma_{e^+e^- \rightarrow e^+e^- X}(s) = \frac{\alpha^2}{\pi^2} \int_{z_{th}}^1 \frac{dz}{z} \times \left[ \left( \ln \frac{Q_{max}^2}{zm_e^2} - 1 \right)^2 f(z) + \frac{1}{3} (\ln z)^3 \right] \sigma_{\gamma\gamma \rightarrow X}(zs), \quad (50.45)$$

where

$$f(z) = \left(1 + \frac{1}{2}z\right)^2 \ln(1/z) - \frac{1}{2}(1-z)(3+z). \quad (50.46)$$

The appropriate value of  $Q_{max}^2$  depends on the properties of the produced system  $X$ . For production of hadronic systems,  $Q_{max}^2 \approx m_\rho^2$ , while for lepton-pair production,  $Q^2 \approx W^2$ . For production of a resonance with spin  $J \neq 1$ , we have

$$\sigma_{e^+e^- \rightarrow e^+e^- R}(s) = (2J+1) \frac{8\alpha^2 \Gamma_{R \rightarrow \gamma\gamma}}{m_R^3} \times \left[ f(m_R^2/s) \left( \ln \frac{m_V^2 s}{m_e^2 m_R^2} - 1 \right)^2 - \frac{1}{3} \left( \ln \frac{s}{M_R^2} \right)^3 \right], \quad (50.47)$$

where  $m_V$  is the mass that enters into the form factor for the  $\gamma\gamma \rightarrow R$  transition, typically  $m_\rho$ .

## PART II: PROCESSES BEYOND THE STANDARD MODEL

### 50.8 Production of supersymmetric particles

In supersymmetric (SUSY) theories (see Supersymmetric Particle Searches in this *Review*), every boson has a fermionic superpartner, and every fermion has a bosonic superpartner. The minimal supersymmetric Standard Model (MSSM) is a direct supersymmetrization of the Standard Model (SM), although a second Higgs doublet is needed to avoid triangle anomalies [10]. Under *soft* SUSY breaking, superpartner masses are lifted above the SM particle masses. In weak scale SUSY, the superpartners are invoked to stabilize the weak scale under radiative corrections, so the superpartners are expected to have masses of order the TeV scale.

#### 50.8.1 Gluino and squark production

The superpartners of gluons are the color octet, spin- $\frac{1}{2}$  gluinos ( $\tilde{g}$ ), while each helicity component of quark flavor has a spin-0 squark partner, *e.g.*  $\tilde{q}_L$  and  $\tilde{q}_R$ . Third generation left- and right- squarks are expected to have large mixing, resulting in mass eigenstates  $\tilde{q}_1$  and  $\tilde{q}_2$ , with  $m_{\tilde{q}_1} < m_{\tilde{q}_2}$  (here,  $q$  denotes any of the SM flavors of quarks and  $\tilde{q}_i$  the corresponding flavor and type ( $i = L, R$  or  $1, 2$ ) of squark). Gluino pair production ( $\tilde{g}\tilde{g}$ ) takes place via either glue-gluon or quark-antiquark annihilation [11].

The subprocess cross sections are usually presented as differential distributions in the Mandelstam variables  $s$ ,  $t$  and  $u$ . Note that for a  $2 \rightarrow 2$  scattering subprocess  $ab \rightarrow cd$ , the Mandelstam variable  $s = (p_a + p_b)^2 = (p_c + p_d)^2$ , where  $p_a$  is the 4-momentum of particle  $a$ , and so forth. The variable  $t = (p_c - p_a)^2$ , where  $c$  and  $a$  are taken conventionally to be the most similar particles in the subprocess. The variable  $u$  would then be equal to  $(p_d - p_a)^2$ . Note that since  $s$ ,  $t$  and  $u$  are squares of 4-vectors, they are invariants in any inertial reference frame.

Gluino pair production at hadron colliders is described by:

$$\frac{d\sigma}{dt}(gg \rightarrow \tilde{g}\tilde{g}) = \frac{9\pi\alpha_s^2}{4s^2} \left\{ \frac{2(m_g^2 - t)(m_g^2 - u)}{s^2} + \frac{(m_g^2 - t)(m_g^2 - u) - 2m_g^2(m_g^2 + t)}{(m_g^2 - t)^2} + \frac{(m_g^2 - t)(m_g^2 - u) - 2m_g^2(m_g^2 + u)}{(m_g^2 - u)^2} + \frac{m_g^2(s - 4m_g^2)}{(m_g^2 - t)(m_g^2 - u)} \right\},$$

$$\left. \frac{(m_g^2 - t)(m_g^2 - u) + m_g^2(u - t)}{s(m_g^2 - t)} - \frac{(m_g^2 - t)(m_g^2 - u) + m_g^2(t - u)}{s(m_g^2 - u)} \right\}, \quad (50.48)$$

where  $\alpha_s$  is the strong fine structure constant. Also,

$$\frac{d\sigma}{dt}(q\bar{q} \rightarrow \tilde{g}\tilde{g}) = \frac{8\pi\alpha_s^2}{9s^2} \left\{ \frac{4}{3} \left( \frac{m_g^2 - t}{m_q^2 - t} \right)^2 + \frac{4}{3} \left( \frac{m_g^2 - u}{m_q^2 - u} \right)^2 + \frac{3}{s^2} [(m_g^2 - t)^2 + (m_g^2 - u)^2 + 2m_g^2 s] - 3 \frac{[(m_g^2 - t)^2 + m_g^2 s]}{s(m_q^2 - t)} - 3 \frac{[(m_g^2 - u)^2 + m_g^2 s]}{s(m_q^2 - u)} + \frac{1}{3} \frac{m_g^2 s}{(m_q^2 - t)(m_q^2 - u)} \right\}. \quad (50.49)$$

Gluinos can also be produced in association with squarks:  $\tilde{g}\tilde{q}_i$  production, where  $\tilde{q}_i$  represents any of the various types (left, right- or mixed) and flavors of squarks. The subprocess cross section is independent of whether the squark is the right-, left- or mixed type:

$$\frac{d\sigma}{dt}(gq \rightarrow \tilde{g}\tilde{q}_i) = \frac{\pi\alpha_s^2}{24s^2} \frac{[\frac{16}{3}(s^2 + (m_{\tilde{q}_i}^2 - u)^2) + \frac{4}{3}s(m_{\tilde{q}_i}^2 - u)]}{s(m_g^2 - t)(m_{\tilde{q}_i}^2 - u)^2} \times \left( (m_g^2 - u)^2 + (m_{\tilde{q}_i}^2 - m_g^2)^2 + \frac{2sm_g^2(m_{\tilde{q}_i}^2 - m_g^2)}{(m_g^2 - t)} \right). \quad (50.50)$$

There are many different subprocesses for production of squark pairs. Since left- and right- squarks generally have different masses and different decay patterns, we present the differential cross section for each subprocess of  $\tilde{q}_i$  ( $i = L, R$  or  $1, 2$ ) separately. (In early literature, the following formulae were often combined into a single equation which didn't differentiate the various squark types.) The result for  $gg \rightarrow \tilde{q}_i\tilde{q}_i$  is:

$$\frac{d\sigma}{dt}(gg \rightarrow \tilde{q}_i\tilde{q}_i) = \frac{\pi\alpha_s^2}{4s^2} \left\{ \frac{1}{3} \left( \frac{m_q^2 + t}{m_q^2 - t} \right)^2 + \frac{1}{3} \left( \frac{m_q^2 + u}{m_q^2 - u} \right)^2 + \frac{3}{32s^2} (8s(4m_q^2 - s) + 4(u - t)^2) + \frac{7}{12} - \frac{1}{48} \frac{(4m_q^2 - s)^2}{(m_q^2 - t)(m_q^2 - u)} + \frac{3}{32} \frac{[(t - u)(4m_q^2 + 4t - s) - 2(m_q^2 - u)(6m_q^2 + 2t - s)]}{s(m_q^2 - t)} + \frac{3}{32} \frac{[(u - t)(4m_q^2 + 4u - s) - 2(m_q^2 - t)(6m_q^2 + 2u - s)]}{s(m_q^2 - u)} + \frac{7}{96} \frac{[4m_q^2 + 4t - s]}{m_q^2 - t} + \frac{7}{96} \frac{[4m_q^2 + 4u - s]}{m_q^2 - u} \right\}, \quad (50.51)$$

which has an obvious  $u \leftrightarrow t$  symmetry.

For  $q\bar{q} \rightarrow \tilde{q}_i\tilde{q}_i$  with the same initial and final state flavors, we have

$$\frac{d\sigma}{dt}(q\bar{q} \rightarrow \tilde{q}_i\tilde{q}_i) = \frac{2\pi\alpha_s^2}{9s^2} \left\{ \frac{1}{(t - m_{\tilde{q}_i}^2)^2} + \frac{2}{s^2} - \frac{2/3}{s(t - m_{\tilde{q}_i}^2)} \right\} \times [-st - (t - m_{\tilde{q}_i}^2)^2], \quad (50.52)$$

while if initial and final state flavors are different ( $q\bar{q} \rightarrow \tilde{q}'_i\tilde{q}'_i$ ) we instead have

$$\frac{d\sigma}{dt}(q\bar{q} \rightarrow \tilde{q}'_i\tilde{q}'_i) = \frac{4\pi\alpha_s^2}{9s^4} \left[ -st - (t - m_{\tilde{q}'_i}^2)^2 \right]. \quad (50.53)$$

If the two initial state quarks are of different flavors, then we have

$$\frac{d\sigma}{dt}(q\bar{q}' \rightarrow \tilde{q}_i\tilde{q}'_i) = \frac{2\pi\alpha_s^2}{9s^2} \frac{-st - (t - m_{\tilde{q}_i}^2)^2}{(t - m_{\tilde{q}'_i}^2)^2}. \quad (50.54)$$

If the initial quarks are of different flavor and final state squarks are of different type ( $i \neq j$ ) then

$$\frac{d\sigma}{dt}(q\bar{q}' \rightarrow \tilde{q}_i\tilde{q}'_j) = \frac{2\pi\alpha_s^2}{9s^2} \frac{m_{\tilde{q}'_j}^2 s}{(t - m_{\tilde{q}_i}^2)^2}. \quad (50.55)$$

For same-flavor initial state quarks, but final state unlike-type squarks, we also have

$$\frac{d\sigma}{dt}(q\bar{q} \rightarrow \tilde{q}_i\tilde{q}'_j) = \frac{2\pi\alpha_s^2}{9s^2} \frac{m_{\tilde{q}'_j}^2 s}{(t - m_{\tilde{q}_i}^2)^2}. \quad (50.56)$$

There also exist cross sections for quark-quark annihilation to squark pairs. For same flavor quark-quark annihilation to same flavor/same type final state squarks,

$$\begin{aligned} \frac{d\sigma}{dt}(qq \rightarrow \tilde{q}_i\tilde{q}_i) &= \\ &= \frac{\pi\alpha_s^2}{9s^2} m_{\tilde{q}_i}^2 s \left\{ \frac{1}{(t - m_{\tilde{q}_i}^2)^2} + \frac{1}{(u - m_{\tilde{q}_i}^2)^2} - \frac{2/3}{(t - m_{\tilde{q}_i}^2)(u - m_{\tilde{q}_i}^2)} \right\}, \end{aligned} \quad (50.57)$$

while if the final type squarks are different ( $i \neq j$ ), we have

$$\begin{aligned} \frac{d\sigma}{dt}(qq \rightarrow \tilde{q}_i\tilde{q}_j) &= \\ &= \frac{2\pi\alpha_s^2}{9s^2} \times \\ &\left\{ \frac{[-st - (t - m_{\tilde{q}_i}^2)(t - m_{\tilde{q}_j}^2)]}{(t - m_{\tilde{q}_i}^2)} + \frac{[-su - (u - m_{\tilde{q}_i}^2)(u - m_{\tilde{q}_j}^2)]}{(u - m_{\tilde{q}_j}^2)} \right\}. \end{aligned} \quad (50.58)$$

If initial/final state flavors are different, but final state squark types are the same, then

$$\frac{d\sigma}{dt}(q\bar{q}' \rightarrow \tilde{q}_i\tilde{q}'_i) = \frac{2\pi\alpha_s^2}{9s^2} \frac{m_{\tilde{q}'_i}^2 s}{(t - m_{\tilde{q}_i}^2)^2}. \quad (50.59)$$

If initial quark flavors are different and final squark types are different, then

$$\frac{d\sigma}{dt}(q\bar{q}' \rightarrow \tilde{q}_i\tilde{q}'_j) = \frac{2\pi\alpha_s^2}{9s^2} \frac{-st - (t - m_{\tilde{q}_i}^2)(t - m_{\tilde{q}'_j}^2)}{(t - m_{\tilde{q}_i}^2)^2}. \quad (50.60)$$

### 50.8.2 Gluino and squark associated production

In the MSSM, the charged spin- $\frac{1}{2}$  winos and higgsinos mix to make chargino states  $\chi_{1,2}^{\pm}$ , with  $m_{\chi_{1,2}^{\pm}} < m_{\chi_{3,4}^{\pm}}$ . The spin- $\frac{1}{2}$  neutral bino, wino and higgsino fields mix to give four neutralino mass eigenstates  $\chi_{1,2,3,4}^0$  ordered according to mass. We sometimes denote the charginos and neutralinos collectively as -inos for notational simplicity

For gluino and squark production in association with charginos and neutralinos [12], the quark-squark-neutralino couplings<sup>1</sup> are

<sup>1</sup>The couplings  $A_{\tilde{\chi}_i^0}^f$  and  $B_{\tilde{\chi}_i^0}^f$  are given explicitly in Ref. [13] in Eq. (8.87). Also, the couplings  $A_{\tilde{\chi}_i^-}^d$  and  $A_{\tilde{\chi}_i^-}^u$  are given in Eq. (8.93). The couplings  $X_i^j$  and  $Y_i^j$  are given by Eq. (8.103), while the  $x_i$  and  $y_i$  couplings are given in Eq. (8.100). Finally, the couplings  $W_{ij}$  are given in Eq. (8.101).

defined by the interaction Lagrangian terms

$$\mathcal{L}_{\tilde{f}f\tilde{\chi}_i^0} = \left[ iA_{\tilde{\chi}_i^0}^f \tilde{f}_L^{\dagger} \tilde{\chi}_i^0 P_L f + iB_{\tilde{\chi}_i^0}^f \tilde{f}_R^{\dagger} \tilde{\chi}_i^0 P_R f + \text{h.c.} \right]$$

, where  $A_{\tilde{\chi}_i^0}^f$  and  $B_{\tilde{\chi}_i^0}^f$  are coupling constants involving gauge couplings, neutralino mixing elements and in the case of third generation fermions, Yukawa couplings. Their form depends on the conventions used for setting up the MSSM Lagrangian, and can be found in various reviews [14] and textbooks [13,15].  $P_L$  and  $P_R$  are the usual left- and right- spinor projection operators and  $f$  denotes any of the SM fermions  $u, d, e, \nu_e, \dots$ . The fermion-sfermion- chargino couplings have the form  $\mathcal{L} = \left[ iA_{\tilde{\chi}_i^-}^d \tilde{u}_L^{\dagger} \tilde{\chi}_i^- P_L d + iA_{\tilde{\chi}_i^-}^u \tilde{d}_L^{\dagger} \tilde{\chi}_i^- P_L u + \text{h.c.} \right]$  for  $u$  and  $d$  quarks, where the  $A_{\tilde{\chi}_i^-}^d$  and  $A_{\tilde{\chi}_i^-}^u$  couplings are again convention-dependent, and can be found in textbooks. The superscript  $c$  denotes ‘‘charge conjugate spinor’’, defined by  $\psi^c \equiv C\bar{\psi}^T$ .

The subprocess cross sections for chargino-squark associated production occur via squark exchange and are given by

$$\frac{d\sigma}{dt}(\tilde{u}g \rightarrow \tilde{\chi}_i^- \tilde{d}_L) = \frac{\alpha_s}{24s^2} |A_{\tilde{\chi}_i^-}^u|^2 \psi(m_{\tilde{d}_L}, m_{\tilde{\chi}_i^-}, t), \quad (50.61)$$

$$\frac{d\sigma}{dt}(d\tilde{g} \rightarrow \tilde{\chi}_i^- \tilde{u}_L) = \frac{\alpha_s}{24s^2} |A_{\tilde{\chi}_i^-}^d|^2 \psi(m_{\tilde{u}_L}, m_{\tilde{\chi}_i^-}, t), \quad (50.62)$$

while neutralino-squark production is given by

$$\frac{d\sigma}{dt}(q\bar{q} \rightarrow \tilde{\chi}_i^0 \tilde{q}) = \frac{\alpha_s}{24s^2} \left( |A_{\tilde{\chi}_i^0}^q|^2 + |B_{\tilde{\chi}_i^0}^q|^2 \right) \psi(m_{\tilde{q}}, m_{\tilde{\chi}_i^0}, t), \quad (50.63)$$

where

$$\begin{aligned} \psi(m_1, m_2, t) &= \frac{s + t - m_1^2}{2s} - \frac{m_1^2(m_2^2 - t)}{(m_1^2 - t)^2} \\ &+ \frac{t(m_2^2 - m_1^2) + m_2^2(s - m_2^2 + m_1^2)}{s(m_1^2 - t)}. \end{aligned} \quad (50.64)$$

Here, the variable  $t$  is given by the square of ‘‘squark-minus-quark’’ four-momentum. The neutralino-gluino associated production cross section also occurs via squark exchange and is given by

$$\begin{aligned} \frac{d\sigma}{dt}(q\bar{q} \rightarrow \tilde{\chi}_i^0 \tilde{g}) &= \frac{\alpha_s}{18s^2} \left( |A_{\tilde{\chi}_i^0}^q|^2 + |B_{\tilde{\chi}_i^0}^q|^2 \right) \left[ \frac{(m_{\tilde{\chi}_i^0}^2 - t)(m_{\tilde{g}}^2 - t)}{(m_{\tilde{q}}^2 - t)^2} \right. \\ &+ \left. \frac{(m_{\tilde{\chi}_i^0}^2 - u)(m_{\tilde{g}}^2 - u)}{(m_{\tilde{q}}^2 - u)^2} - \frac{2\eta_i \eta_{\tilde{g}} m_{\tilde{g}} m_{\tilde{\chi}_i^0} s}{(m_{\tilde{q}}^2 - t)(m_{\tilde{q}}^2 - u)} \right], \end{aligned} \quad (50.65)$$

where  $\eta_i$  is the sign of the neutralino mass eigenvalue and  $\eta_{\tilde{g}}$  is the sign of the gluino mass eigenvalue. We also have chargino-gluino associated production:

$$\begin{aligned} \frac{d\sigma}{dt}(\tilde{u}d \rightarrow \tilde{\chi}_i^- \tilde{g}) &= \frac{\alpha_s}{18s^2} \left[ |A_{\tilde{\chi}_i^-}^u|^2 \frac{(m_{\tilde{\chi}_i^-}^2 - t)(m_{\tilde{g}}^2 - t)}{(m_{\tilde{d}_L}^2 - t)^2} \right. \\ &+ \left. |A_{\tilde{\chi}_i^-}^d|^2 \frac{(m_{\tilde{\chi}_i^-}^2 - u)(m_{\tilde{g}}^2 - u)}{(m_{\tilde{u}_L}^2 - u)^2} + \frac{2\eta_{\tilde{g}} \text{Re}(A_{\tilde{\chi}_i^-}^u A_{\tilde{\chi}_i^-}^d)}{(m_{\tilde{d}_L}^2 - t)(m_{\tilde{u}_L}^2 - u)} m_{\tilde{g}} m_{\tilde{\chi}_i^-} s \right], \end{aligned} \quad (50.66)$$

where  $\hat{t} = (\tilde{g} - d)^2$  and in the third term one must take the real part of the in general complex coupling constant product.

### 50.8.3 Slepton and sneutrino production

The subprocess cross section for  $\tilde{\ell}_L \bar{\nu}_{\ell L}$  production ( $\ell = e$  or  $\mu$ ) occurs via  $s$ -channel  $W$  exchange and is given by

$$\frac{d\sigma}{dt}(d\bar{u} \rightarrow \tilde{\ell}_L \bar{\nu}_{\ell L}) = \frac{g^4 |D_W(s)|^2}{192\pi s^2} \left( tu - m_{\tilde{\ell}_L}^2 m_{\tilde{\nu}_{\ell L}}^2 \right), \quad (50.67)$$

where  $D_W(s) = 1/(s - M_W^2 + iM_W\Gamma_W)$  is the  $W$ -boson propagator denominator. The production of  $\tilde{\tau}_1 \bar{\nu}_\tau$  is given as above, but replacing  $m_{\tilde{\ell}_L} \rightarrow m_{\tilde{\tau}_1}$ ,  $m_{\tilde{\nu}_{\ell L}} \rightarrow m_{\tilde{\nu}_\tau}$  and multiplying by an overall factor of  $\cos^2 \theta_\tau$  (where  $\theta_\tau$  is the tau-slepton mixing angle). Similar substitutions hold for  $\tilde{\tau}_2 \bar{\nu}_\tau$  production, except the overall factor is  $\sin^2 \theta_\tau$ .

**Table 50.1:** The constants  $\alpha_f$  and  $\beta_f$  that appear in in the SM neutral current Lagrangian. Here  $t \equiv \tan \theta_W$  and  $c \equiv \cot \theta_W$ .

$f$	$q_f$	$\alpha_f$	$\beta_f$
$\ell$	-1	$\frac{1}{4}(3t - c)$	$\frac{1}{4}(t + c)$
$\nu_\ell$	0	$\frac{1}{4}(t + c)$	$-\frac{1}{4}(t + c)$
$u$	$\frac{2}{3}$	$-\frac{5}{12}t + \frac{1}{4}c$	$-\frac{1}{4}(t + c)$
$d$	$-\frac{1}{3}$	$\frac{1}{12}t - \frac{1}{4}c$	$\frac{1}{4}(t + c)$

The subprocess cross section for  $\tilde{\ell}_L \bar{\ell}_L$  production occurs via  $s$ -channel  $\gamma$  and  $Z$  exchange, and depends on the neutral current interaction, with fermion couplings to  $\gamma$  and  $Z^0$  given by  $\mathcal{L}_{\text{neutral}} = -eq_f \bar{f} \gamma^\mu f A_\mu + e \bar{f} \gamma^\mu (\alpha_f + \beta_f \gamma_5) f Z_\mu$  (with values of  $q_f$ ,  $\alpha_f$ , and  $\beta_f$  given in Table-50.1).

The subprocess cross section is given by

$$\begin{aligned} \frac{d\sigma}{dt}(q\bar{q} \rightarrow \tilde{\ell}_L \bar{\ell}_L) &= \frac{e^4}{24\pi s^2} \left( tu - m_{\tilde{\ell}_L}^4 \right) \times \\ &\left\{ \frac{q_\ell^2 q_q^2}{s^2} + (\alpha_\ell - \beta_\ell)^2 (\alpha_q^2 + \beta_q^2) |D_Z(s)|^2 \right. \\ &\left. + \frac{2q_\ell q_q \alpha_q (\alpha_\ell - \beta_\ell) (s - M_Z^2)}{s} |D_Z(s)|^2 \right\}, \quad (50.68) \end{aligned}$$

where  $D_Z(s) = 1/(s - M_Z^2 + iM_Z\Gamma_Z)$ . The cross section for sneutrino production is given by the same formula, but with  $\alpha_\ell$ ,  $\beta_\ell$ ,  $q_\ell$  and  $m_{\tilde{\ell}_L}$  replaced by  $\alpha_\nu$ ,  $\beta_\nu$ , 0 and  $m_{\tilde{\nu}_L}$ , respectively. The cross section for  $\tilde{\tau}_1 \bar{\tau}_1$  production is obtained by replacing  $m_{\tilde{\ell}_L} \rightarrow m_{\tilde{\tau}_1}$  and  $\beta_\ell \rightarrow \beta_\ell \cos 2\theta_\tau$ . The cross section for  $\tilde{\ell}_R \bar{\ell}_R$  production is given by substituting  $\alpha_\ell - \beta_\ell \rightarrow \alpha_\ell + \beta_\ell$  and  $m_{\tilde{\ell}_L} \rightarrow m_{\tilde{\ell}_R}$  in the equation above. The cross section for  $\tilde{\tau}_2 \bar{\tau}_2$  production is obtained from the formula for  $\tilde{\ell}_R \bar{\ell}_R$  production by replacing  $m_{\tilde{\ell}_R} \rightarrow m_{\tilde{\tau}_2}$  and  $\beta_\ell \rightarrow \beta_\ell \cos 2\theta_\tau$ .

Finally, the cross section for  $\tilde{\tau}_1 \bar{\tau}_2$  production occurs only via  $Z$  exchange, and is given by

$$\begin{aligned} \frac{d\sigma}{dt}(q\bar{q} \rightarrow \tilde{\tau}_1 \bar{\tau}_2) &= \frac{d\sigma}{dt}(q\bar{q} \rightarrow \tilde{\tau}_1 \bar{\tau}_2) = \\ &\frac{e^4}{24\pi s^2} (\alpha_q^2 + \beta_q^2) \beta_\ell^2 \sin^2 2\theta_\tau |D_Z(s)|^2 (ut - m_{\tilde{\tau}_1}^2 m_{\tilde{\tau}_2}^2). \quad (50.69) \end{aligned}$$

### 50.8.4 Chargino and neutralino pair production

#### 50.8.4.1 $\tilde{\chi}_i^- \tilde{\chi}_j^0$ production

The subprocess cross section for  $d\bar{u} \rightarrow \tilde{\chi}_i^- \tilde{\chi}_j^0$  depends on Lagrangian couplings

$$\mathcal{L}_{W\bar{u}d} = -\frac{g}{\sqrt{2}} \bar{u} \gamma_\mu P_L d W^{+\mu} + \text{h.c.}$$

$$\mathcal{L}_{W\tilde{\chi}_i^- \tilde{\chi}_j^0} = -g(-i)^{\theta_j} \bar{\tilde{\chi}}_i^- [X_i^j + Y_i^j \gamma_5] \gamma_\mu \tilde{\chi}_j^0 W^{-\mu} + \text{h.c.}$$

$$\mathcal{L}_{q\bar{q}\tilde{\chi}_i^-} = iA_{\tilde{\chi}_i^-}^d \bar{u}_L^\dagger \tilde{\chi}_i^- P_L d + iA_{\tilde{\chi}_i^-}^u \bar{d}_L^\dagger \tilde{\chi}_i^- P_L u + \text{h.c.}$$

and

$$\mathcal{L}_{q\bar{q}\tilde{\chi}_j^0} = iA_{\tilde{\chi}_j^0}^q \bar{q}_L^\dagger \tilde{\chi}_j^0 P_L q + \text{h.c.}$$

Contributing diagrams include  $W$  exchange and also  $\tilde{d}_L$  and  $\tilde{u}_L$  squark exchange. The  $X_i^j$  and  $Y_i^j$  couplings are new, and again convention-dependent: the cross section formulae works if the interaction Lagrangian is written in the above form, so that the couplings can be suitably extracted. The term  $\theta_j = 0$  (1) if  $m_{\tilde{\chi}_j^0} > 0$  ( $< 0$ ); it comes about because the neutralino field must be re-defined by a  $-i\gamma_5$  transformation if its mass eigenvalue is negative [13]. The subprocess cross section is given in terms of dot products of four momenta, where particle labels are used to denote their four-momenta; note that all mass terms in the cross section formulae are positive definite, so that the signs of mass eigenstates have been absorbed into the Lagrangian couplings, as for instance in Ref. [13]. We then have

$$\frac{d\sigma}{dt}(d\bar{u} \rightarrow \tilde{\chi}_i^- \tilde{\chi}_j^0) = \frac{1}{192\pi s^2}$$

$$\left[ T_W + T_{\tilde{d}_L} + T_{\tilde{u}_L} + T_{W\tilde{d}_L} + T_{W\tilde{u}_L} + T_{\tilde{d}_L\tilde{u}_L} \right] \quad (50.70)$$

where

$$\begin{aligned} T_W &= 8g^4 |D_W(s)|^2 \left\{ [X_i^{j2} + Y_i^{j2}] (\tilde{\chi}_j^0 \cdot d\tilde{\chi}_i^- \cdot \bar{u} + \tilde{\chi}_j^0 \cdot \bar{u}\tilde{\chi}_i^- \cdot d) \right. \\ &+ 2(X_i^j Y_i^j) (\tilde{\chi}_j^0 \cdot d\tilde{\chi}_i^- \cdot \bar{u} - \tilde{\chi}_j^0 \cdot \bar{u}\tilde{\chi}_i^- \cdot d) \\ &\left. + [X_i^{j2} - Y_i^{j2}] m_{\tilde{\chi}_i^-} m_{\tilde{\chi}_j^0} d \cdot \bar{u} \right\}, \quad (50.71) \end{aligned}$$

$$T_{\tilde{d}_L} = \frac{4|A_{\tilde{\chi}_i^-}^u|^2 |A_{\tilde{\chi}_j^0}^d|^2}{[(\tilde{\chi}_i^- - \bar{u})^2 - m_{\tilde{d}_L}^2]^2} d \cdot \tilde{\chi}_j^0 \tilde{\chi}_i^- \cdot \bar{u}, \quad (50.72)$$

$$T_{\tilde{u}_L} = \frac{4|A_{\tilde{\chi}_i^-}^d|^2 |A_{\tilde{\chi}_j^0}^u|^2}{[(\tilde{\chi}_j^0 - \bar{u})^2 - m_{\tilde{u}_L}^2]^2} \bar{u} \cdot \tilde{\chi}_j^0 \tilde{\chi}_i^- \cdot d \quad (50.73)$$

$$\begin{aligned} T_{W\tilde{d}_L} &= \frac{-\sqrt{2}g^2 \text{Re}[A_{\tilde{\chi}_j^0}^{d*} A_{\tilde{\chi}_i^-}^u (-i)^{\theta_j}] (s - M_W^2) |D_W(s)|^2}{(\tilde{\chi}_i^- - \bar{u})^2 - m_{\tilde{d}_L}^2} \\ &\times \left\{ 8(X_i^j + Y_i^j) \tilde{\chi}_j^0 \cdot d\bar{u} \cdot \tilde{\chi}_i^- + 4(X_i^j - Y_i^j) m_{\tilde{\chi}_i^-} m_{\tilde{\chi}_j^0} d \cdot \bar{u} \right\} \quad (50.74) \end{aligned}$$

$$\begin{aligned} T_{W\tilde{u}_L} &= \frac{\sqrt{2}g^2 \text{Re}[A_{\tilde{\chi}_i^-}^{d*} A_{\tilde{\chi}_j^0}^u (-i)^{\theta_j}] (s - M_W^2) |D_W(s)|^2}{(\tilde{\chi}_j^0 - \bar{u})^2 - m_{\tilde{u}_L}^2} \\ &\times \left\{ 8(X_i^j - Y_i^j) \tilde{\chi}_j^0 \cdot \bar{u}d \cdot \tilde{\chi}_i^- + 4(X_i^j + Y_i^j) m_{\tilde{\chi}_i^-} m_{\tilde{\chi}_j^0} d \cdot \bar{u} \right\} \quad (50.75) \end{aligned}$$

and

$$T_{\tilde{d}_L\tilde{u}_L} = -\frac{4\text{Re}[A_{\tilde{\chi}_j^0}^d A_{\tilde{\chi}_i^-}^{u*} A_{\tilde{\chi}_i^-}^{d*} A_{\tilde{\chi}_j^0}^u] m_{\tilde{\chi}_i^-} m_{\tilde{\chi}_j^0} d \cdot \bar{u}}{[(\tilde{\chi}_i^- - \bar{u})^2 - m_{\tilde{d}_L}^2][(\tilde{\chi}_j^0 - \bar{u})^2 - m_{\tilde{u}_L}^2]}. \quad (50.76)$$

## 50.8.4.2 Chargino pair production

The subprocess cross section for  $d\bar{d} \rightarrow \tilde{\chi}_i^- \tilde{\chi}_i^+$  ( $i = 1, 2$ ) depends on Lagrangian couplings  $\mathcal{L} = e\tilde{\chi}_i^- \gamma_\mu \tilde{\chi}_i^- A^\mu - e \cot \theta_W \tilde{\chi}_i^- \gamma_\mu (x_i - y_i \gamma_5) \tilde{\chi}_i^- Z^\mu$  and also  $\mathcal{L} \ni iA_{\tilde{\chi}_i^-}^d \tilde{u}_L^\dagger \tilde{\chi}_i^- P_L d + iA_{\tilde{\chi}_i^-}^u \tilde{d}_L^\dagger \tilde{\chi}_i^- P_L u + \text{h.c.}$

Contributing diagrams include  $s$ -channel  $\gamma$ ,  $Z^0$  exchange and  $t$ -channel  $\tilde{u}_L$  exchange [16, 17]. The couplings  $x_i$  and  $y_i$  are again new and as usual convention-dependent.

The subprocess cross section is given by

$$\frac{d\sigma}{dt}(d\bar{d} \rightarrow \tilde{\chi}_i^- \tilde{\chi}_i^+) = \frac{1}{192\pi s^2} [T_\gamma + T_Z + T_{\tilde{u}_L} + T_{\gamma Z} + T_{\gamma \tilde{u}_L} + T_{Z\tilde{u}_L}] \quad (50.77)$$

where

$$T_\gamma = \frac{32e^4 q_d^2}{s^2} \left[ d \cdot \tilde{\chi}_i^+ \bar{d} \cdot \tilde{\chi}_i^- + d \cdot \tilde{\chi}_i^- \bar{d} \cdot \tilde{\chi}_i^+ + m_{\tilde{\chi}_i^-}^2 d \cdot \bar{d} \right] \quad (50.78)$$

$$T_Z = 32e^4 \cot^2 \theta_W |D_Z(s)|^2$$

$$\left\{ (\alpha_d^2 + \beta_d^2)(x_i^2 + y_i^2) \left[ d \cdot \tilde{\chi}_i^+ \bar{d} \cdot \tilde{\chi}_i^- + d \cdot \tilde{\chi}_i^- \bar{d} \cdot \tilde{\chi}_i^+ + m_{\tilde{\chi}_i^-}^2 d \cdot \bar{d} \right] \right. \\ \left. \mp 4\alpha_d \beta_d x_i y_i \left[ d \cdot \tilde{\chi}_i^+ \bar{d} \cdot \tilde{\chi}_i^- - d \cdot \tilde{\chi}_i^- \bar{d} \cdot \tilde{\chi}_i^+ \right] - 2y_i^2 (\alpha_d^2 + \beta_d^2) m_{\tilde{\chi}_i^-}^2 d \cdot \bar{d} \right\} \quad (50.79)$$

$$T_{\tilde{u}_L} = \frac{4|A_{\tilde{\chi}_i^-}^d|^4}{[(d - \tilde{\chi}_i^-)^2 - m_{\tilde{u}_L}^2]^2} d \cdot \tilde{\chi}_i^- \bar{d} \cdot \tilde{\chi}_i^+ \quad (50.80)$$

$$T_{\gamma Z} = \frac{64e^4 \cot \theta_W q_d (s - M_Z^2) |D_Z(s)|^2}{s} \times \\ \left\{ \alpha_d x_i \left( d \cdot \tilde{\chi}_i^+ \bar{d} \cdot \tilde{\chi}_i^- + d \cdot \tilde{\chi}_i^- \bar{d} \cdot \tilde{\chi}_i^+ + m_{\tilde{\chi}_i^-}^2 d \cdot \bar{d} \right) \right. \\ \left. \pm \beta_d y_i \left( d \cdot \tilde{\chi}_i^- \bar{d} \cdot \tilde{\chi}_i^+ - d \cdot \tilde{\chi}_i^+ \bar{d} \cdot \tilde{\chi}_i^- \right) \right\} \quad (50.81)$$

$$T_{\gamma \tilde{u}_L} = \mp \frac{8e^2 q_d}{s} \frac{|A_{\tilde{\chi}_i^-}^d|^2}{[(d - \tilde{\chi}_i^-)^2 - m_{\tilde{u}_L}^2]} \left\{ 2\bar{d} \cdot \tilde{\chi}_i^+ d \cdot \tilde{\chi}_i^- + m_{\tilde{\chi}_i^-}^2 d \cdot \bar{d} \right\} \quad (50.82)$$

and

$$T_{Z\tilde{u}_L} = \mp 8e^2 \cot \theta_W |D_Z(s)|^2 \frac{|A_{\tilde{\chi}_i^-}^d|^2 (s - M_Z^2)}{[(d - \tilde{\chi}_i^-)^2 - m_{\tilde{u}_L}^2]} (\alpha_d - \beta_d) \\ \times \left\{ 2(x_i \mp y_i) d \cdot \tilde{\chi}_i^- \bar{d} \cdot \tilde{\chi}_i^+ + m_{\tilde{\chi}_i^-}^2 (x_i \pm y_i) d \cdot \bar{d} \right\} \quad (50.83)$$

using the upper of the sign choices.

The cross section for  $u\bar{u} \rightarrow \tilde{\chi}_i^+ \tilde{\chi}_i^-$  can be obtained from the above by replacing  $\alpha_d \rightarrow \alpha_u$ ,  $\beta_d \rightarrow \beta_u$ ,  $q_d \rightarrow q_u$ ,  $\tilde{u}_L \rightarrow \tilde{d}_L$ ,  $A_{\tilde{\chi}_i^-}^d \rightarrow A_{\tilde{\chi}_i^-}^u$ ,  $d \rightarrow \bar{u}$ ,  $\bar{d} \rightarrow u$  and adopting the lower of the sign choices everywhere.

The cross section for  $q\bar{q} \rightarrow \tilde{\chi}_1^- \tilde{\chi}_2^+$ ,  $\tilde{\chi}_1^+ \tilde{\chi}_2^-$  can occur via  $Z$  and  $\tilde{q}_L$  exchange. It is usually much smaller than  $\tilde{\chi}_{1,2}^- \tilde{\chi}_{1,2}^+$  production, so the cross section will not be presented here. It can be found in Appendix A of Ref. [13].

## 50.8.4.3 Neutralino pair production

Neutralino pair production via  $q\bar{q}$  fusion takes place via  $s$ -channel  $Z$  exchange plus  $t$ - and  $u$ -channel left- and right- squark exchange (5 diagrams) [17, 18]. The Lagrangian couplings (see previous footnote\*) needed include terms given above plus terms of the form  $\mathcal{L} = W_{ij} \tilde{\chi}_i^- \gamma_\mu (\gamma_5)^{\theta_i + \theta_j + 1} \tilde{\chi}_j^0 Z^\mu$ . The couplings  $W_{ij}$

depend only on the *higgsino* components of the neutralinos  $i$  and  $j$ . The subprocess cross section is given by:

$$\frac{d\sigma}{dt}(q\bar{q} \rightarrow \tilde{\chi}_i^0 \tilde{\chi}_j^0) = \frac{1}{192\pi s^2} [T_Z + T_{\tilde{q}_L} + T_{\tilde{q}_R} + T_{Z\tilde{q}_L} + T_{Z\tilde{q}_R}] \quad (50.84)$$

where

$$T_Z = 128e^2 |W_{ij}|^2 (\alpha_q^2 + \beta_q^2) |D_Z(s)|^2 \\ \left[ q \cdot \tilde{\chi}_i^0 \bar{q} \cdot \tilde{\chi}_j^0 + q \cdot \tilde{\chi}_j^0 \bar{q} \cdot \tilde{\chi}_i^0 - \eta_i \eta_j m_{\tilde{\chi}_i^0} m_{\tilde{\chi}_j^0} q \cdot \bar{q} \right], \quad (50.85)$$

$$T_{\tilde{q}_L} = 4|A_{\tilde{\chi}_i^0}^q|^2 |A_{\tilde{\chi}_j^0}^q|^2 \left\{ \frac{q \cdot \tilde{\chi}_i^0 \bar{q} \cdot \tilde{\chi}_j^0}{[(\tilde{\chi}_i^0 - q)^2 - m_{\tilde{q}_L}^2]^2} + \frac{q \cdot \tilde{\chi}_j^0 \bar{q} \cdot \tilde{\chi}_i^0}{[(\tilde{\chi}_j^0 - q)^2 - m_{\tilde{q}_L}^2]^2} \right. \\ \left. - \eta_i \eta_j \frac{m_{\tilde{\chi}_i^0} m_{\tilde{\chi}_j^0} q \cdot \bar{q}}{[(\tilde{\chi}_i^0 - q)^2 - m_{\tilde{q}_L}^2][(\tilde{\chi}_j^0 - q)^2 - m_{\tilde{q}_L}^2]} \right\} \quad (50.86)$$

$$T_{\tilde{q}_R} = 4|B_{\tilde{\chi}_i^0}^q|^2 |B_{\tilde{\chi}_j^0}^q|^2 \left\{ \frac{q \cdot \tilde{\chi}_i^0 \bar{q} \cdot \tilde{\chi}_j^0}{[(\tilde{\chi}_i^0 - q)^2 - m_{\tilde{q}_R}^2]^2} + \frac{q \cdot \tilde{\chi}_j^0 \bar{q} \cdot \tilde{\chi}_i^0}{[(\tilde{\chi}_j^0 - q)^2 - m_{\tilde{q}_R}^2]^2} \right. \\ \left. - \eta_i \eta_j \frac{m_{\tilde{\chi}_i^0} m_{\tilde{\chi}_j^0} q \cdot \bar{q}}{[(\tilde{\chi}_i^0 - q)^2 - m_{\tilde{q}_R}^2][(\tilde{\chi}_j^0 - q)^2 - m_{\tilde{q}_R}^2]} \right\} \quad (50.87)$$

$$T_{Z\tilde{q}_L} = 16e(\alpha_q - \beta_q)(s - M_Z^2) |D_Z(s)|^2$$

$$\left\{ \frac{Re(W_{ij} A_{\tilde{\chi}_i^0}^{q*} A_{\tilde{\chi}_j^0}^q)}{[(\tilde{\chi}_i^0 - q)^2 - m_{\tilde{q}_L}^2]} \left[ 2q \cdot \tilde{\chi}_i^0 \bar{q} \cdot \tilde{\chi}_j^0 - \eta_i \eta_j m_{\tilde{\chi}_i^0} m_{\tilde{\chi}_j^0} q \cdot \bar{q} \right] \right. \\ \left. + \eta_i \eta_j \frac{Re(W_{ij} A_{\tilde{\chi}_i^0}^q A_{\tilde{\chi}_j^0}^{q*})}{[(\tilde{\chi}_j^0 - q)^2 - m_{\tilde{q}_L}^2]} \left[ 2q \cdot \tilde{\chi}_j^0 \bar{q} \cdot \tilde{\chi}_i^0 - \eta_i \eta_j m_{\tilde{\chi}_i^0} m_{\tilde{\chi}_j^0} q \cdot \bar{q} \right] \right\} \quad (50.88)$$

$$T_{Z\tilde{q}_R} = 16e(\alpha_q + \beta_q)(s - M_Z^2) |D_Z(s)|^2$$

$$\left\{ \frac{Re(W_{ij} B_{\tilde{\chi}_i^0}^{q*} B_{\tilde{\chi}_j^0}^q)}{[(\tilde{\chi}_i^0 - q)^2 - m_{\tilde{q}_R}^2]} \left[ 2q \cdot \tilde{\chi}_i^0 \bar{q} \cdot \tilde{\chi}_j^0 - \eta_i \eta_j m_{\tilde{\chi}_i^0} m_{\tilde{\chi}_j^0} q \cdot \bar{q} \right] \right. \\ \left. - \frac{Re(W_{ij} B_{\tilde{\chi}_i^0}^q B_{\tilde{\chi}_j^0}^{q*})}{[(\tilde{\chi}_j^0 - q)^2 - m_{\tilde{q}_R}^2]} \left[ 2q \cdot \tilde{\chi}_j^0 \bar{q} \cdot \tilde{\chi}_i^0 - \eta_i \eta_j m_{\tilde{\chi}_i^0} m_{\tilde{\chi}_j^0} q \cdot \bar{q} \right] \right\}. \quad (50.89)$$

As before,  $\eta_i = \pm 1$  corresponding to whether the neutralino mass eigenvalue is positive or negative. When  $i = j$  in the above formula, one must remember to integrate over just  $2\pi$  steradians of solid angle to avoid double counting in the total cross section.

## 50.9 Universal extra dimensions

In the Universal Extra Dimension (UED) model of Ref. [19] (see Ref. [20] for a review of models with extra spacetime dimensions), the Standard Model is embedded in a five dimensional theory, where the fifth dimension is compactified on an  $S_1/Z_2$  orbifold. Each SM chirality state is then the zero mode of an infinite tower of Kaluza-Klein excitations labelled by  $n = 0 - \infty$ . A KK parity is usually assumed to hold, where each state is assigned KK-parity  $P = (-1)^n$ . If the compactification scale is around a TeV, then the  $n = 1$  (or even higher) KK modes may be accessible to collider searches.

Of interest for hadron colliders are the production of massive  $n \geq 1$  quark or gluon pairs. These production cross sections have been calculated in Ref. [21, 22]. We list here results for the  $n = 1$  case only with  $M_1 = 1/R$  ( $R$  is the compactification radius) and  $s$ ,  $t$  and  $u$  are the usual Mandelstam variables; more general formulae can be found in Ref. [22]. The superscript \* stands for any KK excited state, while  $\bullet$  stands for left chirality states and  $\circ$  stands for right chirality states.

$$\frac{d\sigma}{dt} = \frac{1}{16\pi s^2} T \quad (50.90)$$

where

$$T(q\bar{q} \rightarrow g^* g^*) = \frac{2g_s^4}{27} \left[ M_1^2 \left( -\frac{4s^3}{t'^2 u'^2} + \frac{57s}{t'u'} - \frac{108}{s} \right) + \frac{20s^2}{t'u'} - 93 + \frac{108t'u'}{s^2} \right] \quad (50.91)$$

and

$$T(gg \rightarrow g^* g^*) = \frac{9g_s^4}{27} \left[ 3M_1^4 \frac{s^2 + t'^2 + u'^2}{t'^2 u'^2} - 3M_1^2 \frac{s^2 + t'^2 + u'^2}{st'u'} + 1 + \frac{(s^2 + t'^2 + u'^2)^3}{4s^2 t'^2 u'^2} - \frac{t'u'}{s^2} \right] \quad (50.92)$$

where  $t' = t - M_1^2$  and  $u' = u - M_1^2$ .

Also,

$$T(q\bar{q} \rightarrow q_1^* \bar{q}_1^*) = \frac{4g_s^4}{9} \left[ \frac{2M_1^2}{s} + \frac{t'^2 + u'^2}{s^2} \right],$$

$$T(q\bar{q} \rightarrow q_1^* \bar{q}_1^*) = \frac{g_s^4}{9} \left[ 2M_1^2 \left( \frac{4}{s} + \frac{s}{t'^2} - \frac{1}{t'} \right) + \frac{23}{6} + \frac{2s^2}{t'^2} + \frac{8s}{3t'} + \frac{6t'}{s} + \frac{8t'^2}{s^2} \right],$$

$$T(qq \rightarrow q_1^* \bar{q}_1^*) = \frac{g_s^4}{27} \left[ M_1^2 \left( 6 \frac{t'}{u'^2} + 6 \frac{u'}{t'^2} - \frac{s}{t'u'} \right) + 2 \left( 3 \frac{t'^2}{u'^2} + 3 \frac{u'^2}{t'^2} + 4 \frac{s^2}{t'u'} - 5 \right) \right],$$

$$T(gg \rightarrow q_1^* \bar{q}_1^*) = g_s^4 \left[ M_1^4 \frac{-4}{t'u'} \left( \frac{s^2}{6t'u'} - \frac{3}{8} \right) + M_1^2 \frac{4}{s} \left( \frac{s^2}{6t'u'} - \frac{3}{8} \right) + \frac{s^2}{6t'u'} - \frac{17}{24} + \frac{3t'u'}{4s^2} \right],$$

$$T(gq \rightarrow g^* q_1^*) = \frac{-g_s^4}{3} \left[ \frac{5s^2}{12t'^2} + \frac{s^3}{t'^2 u'} + \frac{11su'}{6t'^2} + \frac{5u'^2}{12t'^2} + \frac{u'^3}{st'^2} \right],$$

$$T(q\bar{q}' \rightarrow q_1^* \bar{q}_1^*) = \frac{g_s^4}{18} \left[ 4M_1^4 \frac{s}{t'^2} + 5 + 4 \frac{s^2}{t'^2} + 8 \frac{s}{t'} \right],$$

$$T(qq' \rightarrow q_1^* q_1^*) = \frac{2g_s^4}{9} \left[ -M_1^2 \frac{s}{t'^2} + \frac{1}{4} + \frac{s^2}{t'^2} \right],$$

$$T(qq \rightarrow q_1^* q_1^{\circ}) =$$

$$\frac{g_s^4}{9} \left[ M_1^2 \left( \frac{2s^3}{t'^2 u'^2} - \frac{4s}{t'u'} \right) + 2 \frac{s^4}{t'^2 u'^2} - 8 \frac{s^2}{t'u'} + 5 \right],$$

$$T(q\bar{q}' \rightarrow q_1^* \bar{q}_1^{\circ}) = \frac{g_s^4}{9} \left[ 2M_1^2 \left( \frac{1}{t'} + \frac{u'}{t'^2} \right) + \frac{5}{2} + \frac{4u'}{t'} + \frac{2u'^2}{t'^2} \right],$$

and

$$T(qq' \rightarrow q_1^* q_1^{\circ}) = \frac{g_s^4}{9} \left[ -2M_1^2 \left( \frac{1}{t'} + \frac{u'}{t'^2} \right) + \frac{1}{2} + \frac{2u'^2}{t'^2} \right].$$

## 50.10 Large extra dimensions

In the ADD theory [23] with large extra dimensions (LED), the SM particles are confined to a 3-brane, while gravity propagates in the bulk. It is assumed that the  $n$  extra dimensions are compactified on an  $n$ -dimensional torus of volume  $(2\pi r)^n$ , so that the fundamental  $4+n$  dimensional Planck scale  $M_*$  is related to the usual 4-dimensional Planck scale  $M_{Pl}$  by  $M_{Pl}^2 = M_*^{n+2} (2\pi r)^n$ . If  $M_* \sim 1$  TeV, then the  $M_W - M_{Pl}$  hierarchy problem is just due to gravity propagating in the large extra dimensions.

In these theories, the KK-excited graviton states  $G_{\mu\nu}^n$ , for  $n = 1 - \infty$  can be produced at collider experiments. The graviton couplings to matter are suppressed by  $1/M_{Pl}$ , so that graviton emission cross sections  $d\sigma/dt \sim 1/M_{Pl}^2$ . However, the mass splittings between the excited graviton states can be tiny, so the graviton eigenstates are usually approximated by a continuum distribution. A summation (integration) over all allowed graviton emissions ends up cancelling the  $1/M_{Pl}^2$  factor, so that observable cross section rates can be attained. Some of the fundamental production formulae for a KK graviton (denoted  $G$ ) of mass  $m$  at hadron colliders include the subprocesses

$$\frac{d\sigma_m}{dt}(f\bar{f} \rightarrow \gamma G) = \frac{\alpha Q_f^2}{16N_f} \frac{1}{sM_{Pl}^2} F_1\left(\frac{t}{s}, \frac{m^2}{s}\right), \quad (50.93)$$

where  $Q_f$  is the charge of fermion  $f$  and  $N_f$  is the number of QCD colors of  $f$ . Also,

$$\frac{d\sigma_m}{dt}(q\bar{q} \rightarrow gG) = \frac{\alpha_s}{36} \frac{1}{sM_{Pl}^2} F_1\left(\frac{t}{s}, \frac{m^2}{s}\right), \quad (50.94)$$

$$\frac{d\sigma_m}{dt}(qg \rightarrow qG) = \frac{\alpha_s}{96} \frac{1}{sM_{Pl}^2} F_2\left(\frac{t}{s}, \frac{m^2}{s}\right), \quad (50.95)$$

$$\frac{d\sigma_m}{dt}(gg \rightarrow gG) = \frac{3\alpha_s}{16} \frac{1}{sM_{Pl}^2} F_3\left(\frac{t}{s}, \frac{m^2}{s}\right), \quad (50.96)$$

where

$$F_1(x, y) = \frac{1}{x(y-1-x)} \left[ -4x(1+x)(1+2x+2x^2) + y(1+6x+18x^2+16x^3) - 6y^2x(1+2x) + y^3(1+4x) \right] \quad (50.97)$$

$$F_2(x, y) = -(y-1-x)F_1\left(\frac{x}{y-1-x}, \frac{y}{y-1-x}\right) \quad (50.98)$$

and

$$F_3(x, y) = \frac{1}{x(y-1-x)} \left[ 1 + 2x + 3x^2 + 2x^3 + x^4 - 2y(1+x^3) + 3y^2(1+x^2) - 2y^3(1+x) + y^4 \right] \quad (50.99)$$

These formulae must then be multiplied by the graviton density of states formula  $dN = S_{n-1} \frac{M_{Pl}^2}{M_*^{n+2}} m^{n-1} dm$  to gain the cross section

$$\frac{d^2\sigma}{dtdm} = S_{n-1} \frac{M_{Pl}^2}{M_*^{n+2}} m^{n-1} \frac{d\sigma_m}{dt} \quad (50.100)$$

where  $S_n = \frac{(2\pi)^{n/2}}{\Gamma(n/2)}$  is the surface area of an  $n$ -dimensional sphere of unit radius.

Virtual graviton processes can also be searched for at colliders. For instance, in Ref. [24] the cross section for Drell-Yan production of lepton pairs via gluon fusion was calculated, where it is found that, in the center-of-mass system

$$\frac{d\sigma}{dz}(gg \rightarrow \ell^+ \ell^-) = \frac{\lambda^2 s^3}{64\pi M_*^8} (1-z^2)(1+z^2) \quad (50.101)$$

where  $z = \cos\theta$  and  $\lambda$  is a model-dependent coupling constant  $\sim 1$ . Formulae for Drell-Yan production via  $q\bar{q}$  fusion can also be found in Refs. [24, 25].



### 50.11 Warped extra dimensions

In the Randall-Sundrum model [26] of warped extra dimensions, the arena for physics is a 5-d anti-deSitter ( $AdS_5$ ) spacetime, for which a non-factorizable metric exists with a metric warp factor  $e^{-2\sigma(\phi)}$ . It is assumed that two opposite tension 3-branes exist within  $AdS_5$  at the two ends of an  $S_1/Z_2$  orbifold parametrized by co-ordinate  $\phi$  which runs from  $0-\pi$ . The 4-D solution of the Einstein equations yields  $\sigma(\phi) = kr_c|\phi|$ , where  $r_c$  is the compactification radius of the extra dimension and  $k \sim M_{Pl}$ . The 4-D effective action allows one to identify  $\overline{M}_{Pl}^2 = \frac{M^3}{k}(1 - e^{-2kr_c\pi})$ , where  $M$  is the 5-D Planck scale. Physical particles on the TeV scale (SM) brane have mass  $m = e^{-kr_c\pi}m_0$ , where  $m_0$  is a fundamental mass of order the Planck scale. Thus, the weak scale-Planck scale hierarchy occurs due to the existence of the exponential warp factor if  $kr_c \sim 12$ .

In the simplest versions of the RS model, the TeV-scale brane contains only SM particles plus a tower of KK gravitons. The RS gravitons have mass  $m_n = kx_n e^{-kr_c\pi}$ , where the  $x_i$  are roots of Bessel functions  $J_1(x_n) = 0$ , with  $x_1 \simeq 3.83$ ,  $x_2 \simeq 7.02$  etc. While the RS zero-mode graviton couplings suppressed by  $1/\overline{M}_{Pl}$  and are thus inconsequential for collider searches, the  $n = 1$  and higher modes have couplings suppressed instead by  $A_\pi = e^{-kr_c\pi}\overline{M}_{Pl} \sim TeV$ . The  $n = 1$  RS graviton should have width  $\Gamma_1 = \rho m_1 x_1^2 (k/\overline{M}_{Pl})^2$ , where  $\rho$  is a constant depending on how many decay modes are open. The formulae for dilepton production via virtual RS graviton exchange can be gained from the above formulae for the ADD scenario via the replacement [27]

$$\frac{\lambda}{M_*^4} \rightarrow \frac{i^2}{8\Lambda_\pi^2} \sum_{n=1}^{\infty} \frac{1}{s - m_n^2 + im_n\Gamma_n}. \quad (50.102)$$

#### References

- [1] J. F. Owens, E. Reya and M. Gluck, Phys. Rev. **D18**, 1501 (1978).
- [2] F. Wilczek, Phys. Rev. Lett. **39**, 1304 (1977).
- [3] B. L. Ioffe and V. A. Khoze, Sov. J. Part. Nucl. **9**, 50 (1978), [Fiz. Elem. Chast. Atom. Yadra9,118(1978)].
- [4] J. R. Ellis, M. K. Gaillard and D. V. Nanopoulos, Nucl. Phys. **B106**, 292 (1976).
- [5] R. N. Cahn and S. Dawson, Phys. Lett. **136B**, 196 (1984), [Erratum: Phys. Lett.138B,464(1984)].
- [6] S. Dawson, Nucl. Phys. **B249**, 42 (1985).
- [7] M. S. Chanowitz and M. K. Gaillard, Phys. Lett. **142B**, 85 (1984).
- [8] R. N. Cahn, Nucl. Phys. **B255**, 341 (1985), [Erratum: Nucl. Phys.B262,744(1985)].
- [9] V. M. Budnev *et al.*, Phys. Rept. **15**, 181 (1975), see for an exhaustive treatment.
- [10] See *e.g.* H.Haber, *Supersymmetry, Part I (Theory), this Review*.
- [11] P. R. Harrison and C. H. Llewellyn Smith, Nucl. Phys. **B213**, 223 (1983), [Erratum: Nucl. Phys.B223,542(1983)]; S. Dawson, E. Eichten and C. Quigg, Phys. Rev. **D31**, 1581 (1985); V. D. Barger *et al.*, Phys. Rev. **D31**, 528 (1985); H. Baer and X. Tata, Phys. Lett. **160B**, 159 (1985).
- [12] H. Baer, D. D. Karatas and X. Tata, Phys. Rev. **D42**, 2259 (1990).
- [13] Weak Scale Supersymmetry: From Superfields to Scattering Events, H. Baer and X. Tata (Cambridge University Press) 2006.
- [14] H. E. Haber and G. L. Kane, Phys. Rept. **117**, 75 (1985).
- [15] Theory and Phenomenology of Sparticles, M. Drees, R. Godbole, and P. Roy (World Scientific) 2005.
- [16] A. Bartl, H. Fraas and W. Majerotto, Z. Phys. **C30**, 441 (1986).
- [17] H. Baer *et al.*, Int. J. Mod. Phys. **A4**, 4111 (1989).
- [18] A. Bartl, H. Fraas and W. Majerotto, Nucl. Phys. **B278**, 1 (1986).
- [19] T. Appelquist, H.-C. Cheng and B. A. Dobrescu, Phys. Rev. **D64**, 035002 (2001), [hep-ph/0012100].
- [20] For a review of models with extra spacetime dimensions, see G. Giudice and J. Wells, *Extra Dimensions, this Review*.
- [21] J. M. Smillie and B. R. Webber, JHEP **10**, 069 (2005), [hep-ph/0507170].
- [22] C. Macesanu, C. D. McMullen and S. Nandi, Phys. Rev. **D66**, 015009 (2002), [hep-ph/0201300].
- [23] N. Arkani-Hamed, S. Dimopoulos and G. R. Dvali, Phys. Lett. **B429**, 263 (1998), [hep-ph/9803315]; N. Arkani-Hamed, S. Dimopoulos and G. R. Dvali, Phys. Rev. **D59**, 086004 (1999), [hep-ph/9807344].
- [24] J. L. Hewett, Phys. Rev. Lett. **82**, 4765 (1999), [hep-ph/9811356].
- [25] G. F. Giudice, R. Rattazzi and J. D. Wells, Nucl. Phys. **B544**, 3 (1999), [hep-ph/9811291]; E. A. Mirabelli, M. Perelstein and M. E. Peskin, Phys. Rev. Lett. **82**, 2236 (1999), [hep-ph/9811337]; T. Han, J. D. Lykken and R.-J. Zhang, Phys. Rev. **D59**, 105006 (1999), [hep-ph/9811350].
- [26] L. Randall and R. Sundrum, Phys. Rev. Lett. **83**, 3370 (1999), [hep-ph/9905221].
- [27] H. Davoudiasl, J. L. Hewett and T. G. Rizzo, Phys. Rev. Lett. **84**, 2080 (2000), [hep-ph/9909255].

## 51. Neutrino Cross Section Measurements

Revised August 2019 by G.P. Zeller (FNAL).

Neutrino cross sections are an essential ingredient in all neutrino experiments. Interest in neutrino scattering has recently increased due to the need for such information in the interpretation of neutrino oscillation data [1]. Historically, neutrino scattering results on both charged current (CC) and neutral current (NC) channels have been collected over many decades using a variety of targets, analysis techniques, and detector technologies. With the advent of intense neutrino sources constructed for neutrino oscillation investigations, experiments are now remeasuring these cross sections with a renewed appreciation for nuclear effects<sup>1</sup> and the importance of improved neutrino flux estimations. This work summarizes accelerator-based neutrino cross section measurements performed in the  $\sim 0.1 - 300$  GeV range with an emphasis on inclusive, quasi-elastic (pionless), and pion production processes, areas where we have the most experimental input at present (Table 51.1). For a more comprehensive discussion of neutrino cross sections, including neutrino-electron elastic scattering and lower energy neutrino measurements, the reader is directed to a review of this subject [2]. Here, we survey existing experimental data on neutrino interactions and do not attempt to provide a census of the associated theoretical calculations [3], which are both critical and plentiful, or the important constraints being gleaned from electron-nucleus scattering as input to neutrino event generators.

**Table 51.1:** List of beam properties, nuclear targets, and run durations for modern accelerator-based neutrino experiments studying neutrino scattering.

Experiment	beam	$\langle E_\nu \rangle, \langle E\bar{\nu} \rangle$ GeV	neutrino target(s)	run period
ArgoNeuT	$\nu, \bar{\nu}$	4.3, 3.6	Ar	2009 – 2010
ICARUS (at CNGS)	$\nu$	20.0	Ar	2010 – 2012
K2K	$\nu$	1.3	CH, H <sub>2</sub> O	2003 – 2004
MicroBooNE	$\nu$	0.8	Ar	2015 –
MINERvA	$\nu, \bar{\nu}$	3.5 (LE), 5.5 (ME)	He, C, CH, H <sub>2</sub> O, Fe, Pb	2009 – 2019
MiniBooNE	$\nu, \bar{\nu}$	0.8, 0.7	CH <sub>2</sub>	2002 – 2019
MINOS	$\nu, \bar{\nu}$	3.5, 6.1	Fe	2004 – 2016
NOMAD	$\nu, \bar{\nu}$	23.4, 19.7	C-based	1995 – 1998
NOvA	$\nu, \bar{\nu}$	2.0, 2.0	CH <sub>2</sub>	2010 –
SciBooNE	$\nu, \bar{\nu}$	0.8, 0.7	CH	2007 – 2008
T2K	$\nu, \bar{\nu}$	0.6, 0.6	CH, H <sub>2</sub> O, Fe	2010 –

### 51.1 Inclusive Scattering

Over the years, many experiments have measured the total inclusive charged current cross section for neutrino ( $\nu_\mu N \rightarrow \mu^- X$ ) and antineutrino ( $\bar{\nu}_\mu N \rightarrow \mu^+ X$ ) scattering off nucleons covering a broad range of neutrino energies. As can be seen in Fig. 51.1, the inclusive cross section approaches a linear dependence on neutrino energy. This behavior is expected for point-like scattering of neutrinos from quarks, an assumption which breaks down at lower energies. Modern measurements of such inclusive scattering cross sections and their target nuclei are summarized in Table 51.2.

To provide a more complete picture, single and double differential cross sections for such inclusive scattering processes have been reported – these include measurements on iron from NuTeV [4] and, more recently, on a variety of nuclear targets from ArgoNeuT [5, 6], MicroBooNE [7], MINERvA [8], and T2K [9, 10]. More recently, MicroBooNE has measured the multiplicity of charged tracks emanating from neutrino scattering on argon [11] and T2K has reported detailed ratios of CC cross sections on hydrocarbon, water, and iron [12]. T2K has also provided the first measurement of the antineutrino CC inclusive cross section at low energy [13]

<sup>1</sup>Nuclear effects refer to kinematic and final state effects which impact neutrino scattering off nuclei. Such effects can be significant and are particularly relevant given that modern neutrino experiments make use of nuclear targets to increase their event yields.

<sup>2</sup>In the case of deuterium, many experiments additionally observed the spectator proton.

(Fig. 51.1). At high energy, the inclusive cross section is dominated by deep inelastic scattering (DIS). Several neutrino experiments have measured DIS cross sections for specific targets and final states, for example, MINERvA has measured ratios of muon neutrino inclusive and DIS cross sections on a variety of nuclear targets including lead, iron, and carbon [14, 15]. Other experiments have measured opposite-sign dimuon production, the most recent being from CHORUS [16], NOMAD [17], and NuTeV [18]. At lower neutrino energies, the inclusive cross section is an additionally complex combination of quasi-elastic scattering and pion production processes, two areas we discuss next.

**Table 51.2:** Published measurements of neutrino and antineutrino CC inclusive cross sections from modern accelerator-based neutrino experiments.

experiment	measurement	target
ArgoNeuT	$\nu_\mu$ [5, 6], $\bar{\nu}_\mu$ [6]	Ar
MicroBooNE	$\nu_\mu$ [7]	Ar
MINERvA	$\nu_\mu$ [8, 14, 15, 19], $\bar{\nu}_\mu$ [19], $\bar{\nu}_\mu/\nu_\mu$ [20]	CH, C/CH, Fe/CH, Pb/CH
MINOS	$\nu_\mu$ [21], $\bar{\nu}_\mu$ [21]	Fe
NOMAD	$\nu_\mu$ [22]	C
SciBooNE	$\nu_\mu$ [23]	CH
T2K	$\nu_\mu$ [9, 10, 12, 24, 25], $\nu_e$ [26, 27], $\bar{\nu}_\mu/\nu_\mu$ [13]	CH, H <sub>2</sub> O, Fe

### 51.2 Quasi-elastic scattering

Quasi-elastic (QE) scattering is the dominant neutrino interaction for neutrino energies less than  $\sim 1$  GeV and represents a large fraction of the signal samples in many neutrino oscillation experiments, which is why this process has received considerable attention in recent years. Historically, neutrino (antineutrino) quasi-elastic scattering refers to the process,  $\nu_\mu n \rightarrow \mu^- p$  ( $\bar{\nu}_\mu p \rightarrow \mu^+ n$ ), where a charged lepton and single nucleon are ejected in the elastic interaction of a neutrino (or antineutrino) with a nucleon in the target material. This is the final state one would strictly observe, for example, in scattering off of a *free* nucleon target. There were many early measurements of neutrino QE scattering that span back to the 1970's [2]. In many of these initial measurements, bubble chamber experiments employed light targets (hydrogen or deuterium) and required both the detection of the final state muon and single nucleon<sup>2</sup>; thus the final state was clear and elastic kinematic conditions could be verified. The situation is more complicated, of course, for heavier nuclear targets used in modern neutrino experiments. In this case, nuclear effects can impact the size and shape of the cross section as well as the final state composition, kinematics, and topology. Due to intranuclear hadron rescattering and the effects of correlations between target nucleons, additional particles may be ejected in the final state; hence, a QE interaction on a nuclear target does not necessarily imply the ejection of a lepton and a *single* nucleon. One therefore needs to take care in defining what one means by neutrino QE scattering when scattering off targets heavier than hydrogen or deuterium. Because of this, modern experiments tend to instead report cross sections for processes involving pionless (e.g., nucleon-only) final states, often referred to as CC  $0\pi$  or QE-like reactions in recent literature. Such measurements are summarized in Table 51.3. Many modern experiments have also recently opted to report nucleon-only cross sections as a function of final state particle kinematics [28–36]. Such distributions can be more difficult to directly compare between experiments but are much less model-dependent and provide more stringent tests of the theory than historical cross sections as a function of neutrino energy ( $E_\nu$ ) or 4-momentum transfer ( $Q^2$ ). Recent work has been done to develop a means to directly compare experimental measurements produced in these less model-dependent forms [37].

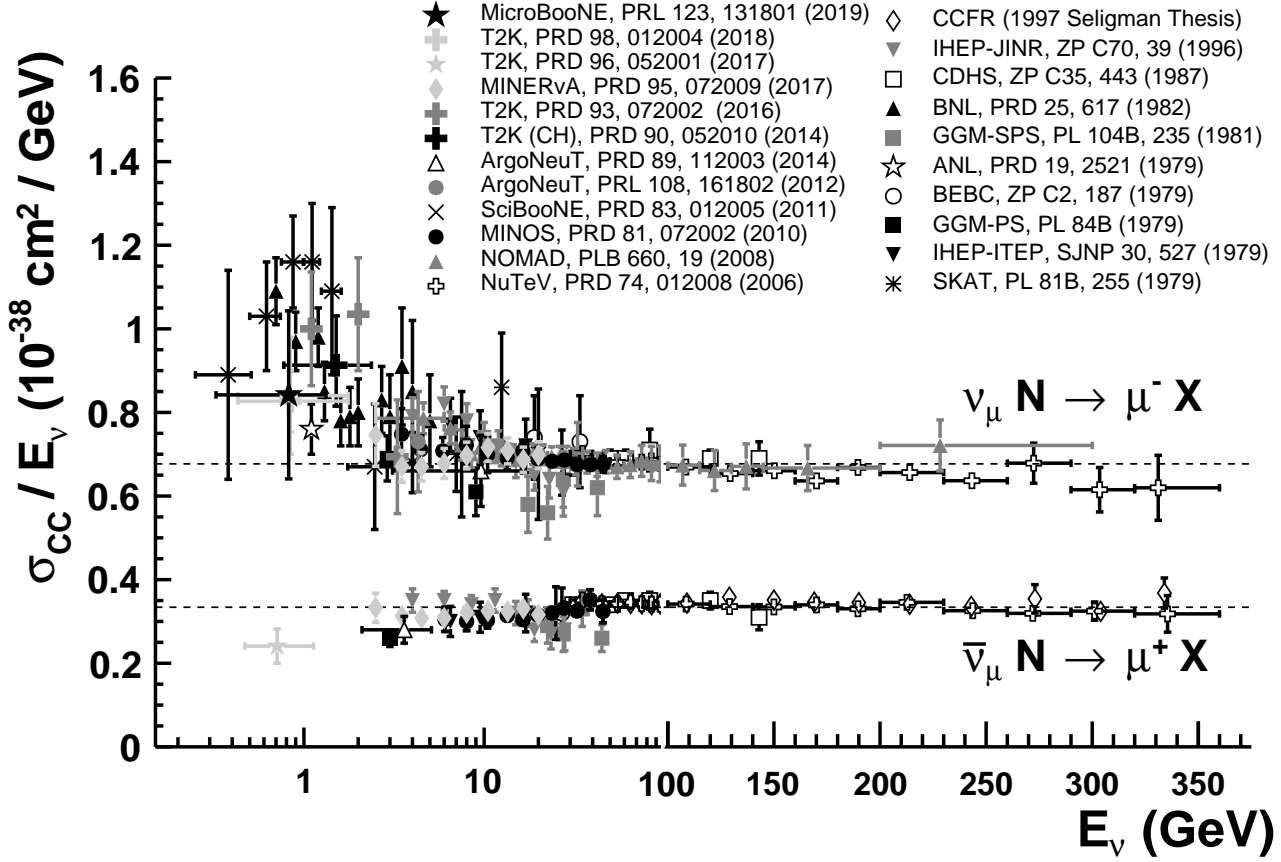


Figure 51.1: Measurements of per nucleon  $\nu_\mu$  and  $\bar{\nu}_\mu$  CC inclusive scattering cross sections divided by neutrino energy as a function of neutrino energy. Note the transition between logarithmic and linear scales occurring at 100 GeV. Neutrino cross sections are typically twice as large as their corresponding antineutrino counterparts, although this difference can be larger at lower energies. NC cross sections (not shown) are generally smaller compared to the CC case.

**Table 51.3:** Published measurements of CC and NC scattering cross sections with nucleon-only final states from modern neutrino experiments.

experiment	measurement	target
ArgoNeuT	2p [38]	Ar
K2K	$M_A$ [39]	H <sub>2</sub> O
MINERvA	$\frac{d\sigma}{dQ^2}$ [40–42], 1p [43], $\nu_e$ [44], $\frac{d^2\sigma}{dp_T dp_{  }}$ [28, 29], $\frac{d\sigma}{dp_n} \frac{d\sigma}{d\delta\alpha_T}$ [30], $\frac{d^2\sigma}{dE_{avail} dq_3}$ [45]	CH, Fe, Pb
MiniBooNE	$\frac{d^2\sigma}{dT_\mu d\theta_\mu}$ [31, 32], $M_A$ [46], NC [47, 48]	CH <sub>2</sub>
MINOS	$M_A$ [49]	Fe
NOMAD	$M_A$ , $\sigma(E_\nu)$ [50]	C
Super-K	NC [51]	H <sub>2</sub> O
T2K	$\frac{d^2\sigma}{dT_\mu d\theta_\mu}$ [33–35], $\sigma(E_\nu)$ [52], $M_A$ [53], NC [54], $\frac{d\sigma}{d\delta p_T} \frac{d\sigma}{d\delta\alpha_T}$ [36]	CH, H <sub>2</sub> O

The topic of neutrino QE scattering began drawing increased attention following the first double differential cross section measurements of this process that revealed a significantly larger cross section than originally anticipated, predominantly in the backwards muon scattering region [31, 32]. Such an enhancement was observed many years prior in transverse electron-nucleus scattering [55] and was attributed to the presence of correlations between target nucleons in the nucleus. As a result, the impact of such nuclear effects on neutrino QE scattering has recently become the subject of intense experimental and theoretical scrutiny with implications on event rates, nucleon emission, neutrino energy reconstruction, and neutrino versus antineutrino cross sections. The reader is referred to reviews of the situation in [3, 56, 57]. To help drive further progress in understanding the underlying nuclear contributions, pionless (e.g., nucleon-only)

cross sections have been reported for the first time in the form of double-differential distributions by MiniBooNE [31, 32], MINERvA [28, 29, 45], and T2K [33–35]. Such double-differential cross sections in terms of final state particle kinematics reduce some of the model-dependence of the reported data, provide the most robust measurements available, and allow a more rigorous two-dimensional test of the underlying nuclear theory. MINERvA and T2K have been especially prolific in recent years in probing this interaction process (Table 51.3). Neutrino experiments have also launched dedicated studies of the hadronic side of these interactions, including ArgoNeuT [38, 58], MINERvA [43], and T2K [36]. MINERvA has been the first modern experiment to measure neutron emission in antineutrino interactions [59]. In addition, the exploration of transverse kinematic variables in neutrino scattering is allowing better constraints on the various contributions to the

cross section, including recent evaluations from MINERvA [28–30] and T2K [36]. With the MiniBooNE results having first revealed these additional complexities in neutrino-nucleus QE scattering, measurements from multiple neutrino experiments, on other targets, and using additional kinematics are crucial for getting a better handle on the underlying nuclear physics impacting neutrino-nucleus interactions. What we once thought was “simple” QE scattering is in fact not so simple.

In addition to such charged current investigations, measurements of the neutral current counterpart of this channel have also been performed. The most recent NC elastic scattering cross section measurements include those from BNL E734 [60], MiniBooNE [47, 48], Super-K [51], and T2K [54]. A number of measurements of the Cabibbo-suppressed antineutrino QE hyperon production cross section have additionally been reported [61, 62], although not in recent years.

### 51.3 Pion Production

In addition to such elastic scattering processes, neutrinos can also inelastically scatter producing a nucleon excited state ( $\Delta$ ,  $N^*$ ). Such baryonic resonances quickly decay, most often to a nucleon and single-pion final state. Historically, experiments have measured various exclusive final states associated with these reactions, the majority of which have been on hydrogen and deuterium targets [2]. There have been several recent re-analyses of this data to better understand the consistency between data sets [63], nucleon form factors [64], and non-resonant contributions [65]. Also, modern measurements of neutrino-induced pion production have since been performed on a variety of nuclear targets (Table 51.4).

**Table 51.4:** Summary of modern measurements of NC and CC scattering cross sections involving a pion (or pions) in the final state.

experiment	$\pi^\pm$	$\pi^0$	target
	measurement	measurement	
ArgoNeuT	CC [66]	NC [67]	Ar
K2K	CC [68, 69]	CC [70], NC [71]	CH, H <sub>2</sub> O
MicroBooNE	–	CC [72]	Ar
MINERvA	CC [73–77]	CC [74, 78, 79], NC [80]	CH
MiniBooNE	CC [81, 82]	CC [83], NC [84, 85]	CH <sub>2</sub>
MINOS	–	NC [86]	Fe
NOMAD	–	NC [87]	C
NOvA	–	NC [88]	C
SciBooNE	CC [89]	NC [90, 91]	CH
T2K	CC [92, 93]	–	CH, H <sub>2</sub> O

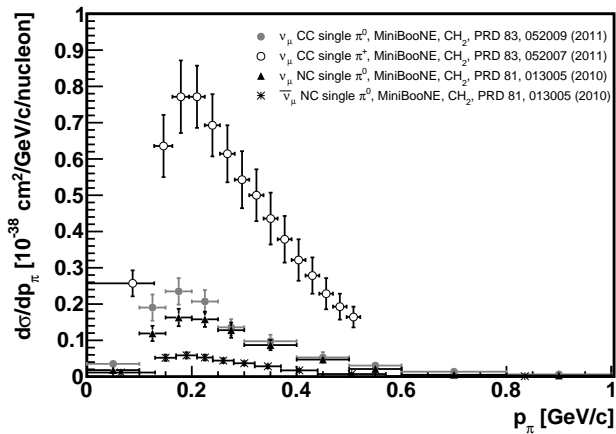


Figure 51.2: Differential cross sections for CC and NC pion production from MiniBooNE at a mean neutrino energy of 0.8 GeV. Shown here are the measurements as a function of the momentum of the outgoing pion in the interaction, a kinematic that is particularly sensitive to final state interactions. Other distributions are also available in the publications listed in the legend.

In addition to resonance production processes, neutrinos can also coherently scatter off of the entire nucleus and produce a distinctly forward-scattered single pion final state. Both CC ( $\nu_\mu A \rightarrow \mu^- A\pi^+$ ,  $\bar{\nu}_\mu A \rightarrow \mu^+ A\pi^-$ ) and NC ( $\nu_\mu A \rightarrow \nu_\mu A\pi^0$ ,  $\bar{\nu}_\mu A \rightarrow \bar{\nu}_\mu A\pi^0$ ) processes are possible in this case. Even though the level of coherent pion production is small compared to their resonant counterpart, observations exist across a broad energy range and on multiple nuclear targets [94]. More recently, several modern neutrino experiments have either measured or set limits on coherent pion production cross sections including ArgoNeuT [66], K2K [69], MINERvA [75, 77], MiniBooNE [85], MINOS [86], NOMAD [87], NOvA [88], SciBooNE [89, 91], and T2K [69].

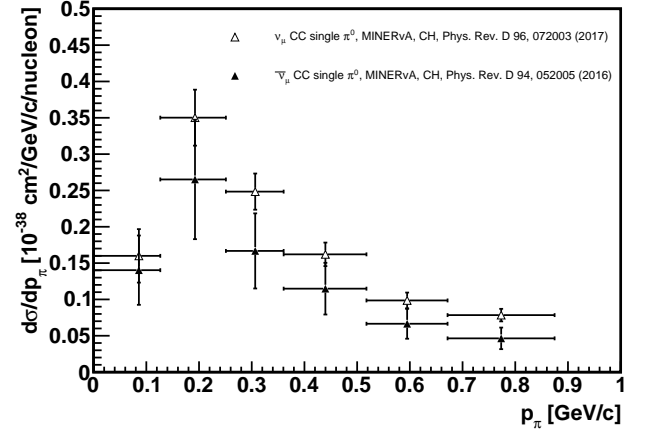


Figure 51.3: Differential cross sections for neutrino ( $W < 1.4$  GeV) and antineutrino ( $W < 1.8$  GeV) CC  $\pi^0$  production from MINERvA at a mean neutrino energy of 3.3 GeV. Shown here are the measurements as a function of the momentum of the outgoing pion in the interaction, a kinematic that is particularly sensitive to final state interactions. Other distributions are available in the publications listed in the legend as well as for charged pion production [74].

As with QE scattering, a new appreciation for the significance of nuclear effects has surfaced in pion production channels, again due to the use of heavy nuclear targets in modern neutrino experiments. Many experiments have been careful to report cross sections for various detected final states, thereby not correcting for large and uncertain nuclear effects (e.g., pion rescattering, charge exchange, and absorption) which can introduce significant sources of uncertainty and model dependence. Providing the most comprehensive survey of neutrino single-pion production to date, MiniBooNE has published a total of 16 single- and double-differential cross sections for both the final state muon (in the case of CC scattering) and pions in these interactions; thus, providing the first measurements of these distributions (Fig. 51.2) [81–84]. MINERvA has recently produced similar kinematic measurements at higher neutrino energies (Fig. 51.3) [74, 76, 79] and T2K at lower energies [92]. Importantly, MINERvA has been working towards an improved nuclear model that can describe all of the pion reaction channels simultaneously, an issue that many experiments have struggled with up until now [74]. ArgoNeuT [67] and MicroBooNE [72] have been adding new information on single pion production in argon. Regardless of the interaction channel or target material, differential cross section measurements in terms of observed final state particle kinematics are preferred for their reduced model dependence and for the additional kinematic information they provide. Such a new direction has been the focus of modern measurements as opposed to the reporting of more model-dependent, historical cross sections as a function of  $E_\nu$  or  $Q^2$ . Together with similar results for other interaction channels, a better understanding and modeling of nuclear effects will be possible moving forward. MINERvA [95] has already taken a large step in this direction by explicitly tuning the physics in existing neutrino event generators to best fit the experimental data on pion production.

It should be noted that baryonic resonances can also decay to multi-pion, other mesonic ( $K$ ,  $\eta$ ,  $\rho$ , etc.), and even photon final states. Experimental results for these channels are typically sparse or non-existent [2]; however, photon production processes can be an important background for  $\nu_\mu \rightarrow \nu_e$  appearance searches and thus have become the focus of recent experimental investigations, most notably in NOMAD [96] and T2K [97]. There have also been several recent measurements of kaon final states produced in neutrino NC and CC scattering in MINERvA [98–100] that are providing needed background constraints for certain nucleon decay searches.

#### 51.4 Outlook

Currently operating experiments will continue to produce additional neutrino cross section measurements as they accumulate additional statistics, while a few new experiments will soon be coming online. Analysis of a broad energy range of data from MINERvA is providing some of the most detailed analysis of nuclear effects in neutrino interactions by examining multiple nuclei in a single experiment. Data from ArgoNeuT, ICARUS, Micro-BooNE, and SBND will probe deeper into complex neutrino final states using the superior capabilities of liquid argon time projection chambers, while the T2K and NOvA near detectors will continue to collect high statistics samples in intense neutrino beams. Together with dedicated discussions between the experiments on how best to report neutrino cross section measurements [101] and accompanying improvements in nuclear model calculations [3], these investigations are crucial for significantly advancing our understanding of neutrino-nucleus scattering.

#### 51.5 Acknowledgments

The author thanks Anne Schukraft (Fermilab) for her help in preparing the plots and content of this review.

#### References

- [1] O. Benhar *et al.*, Phys. Rept. **700**, 1 (2017), [arXiv:1501.06448].
- [2] J. A. Formaggio and G. P. Zeller, Rev. Mod. Phys. **84**, 1307 (2012), [arXiv:1305.7513].
- [3] L. Alvarez-Ruso *et al.*, Prog. Part. Nucl. Phys. **100**, 1 (2018), [arXiv:1706.03621].
- [4] M. Tzanov *et al.* (NuTeV), Phys. Rev. **D74**, 012008 (2006), [hep-ex/0509010].
- [5] C. Anderson *et al.* (ArgoNeuT), Phys. Rev. Lett. **108**, 161802 (2012), [arXiv:1111.0103].
- [6] R. Acciarri *et al.* (ArgoNeuT), Phys. Rev. **D89**, 11, 112003 (2014), [arXiv:1404.4809].
- [7] P. Abratenko *et al.* (MicroBooNE), Phys. Rev. Lett. **123**, 13, 131801 (2019), [arXiv:1905.09694].
- [8] P. A. Rodrigues *et al.* (MINERvA), Phys. Rev. Lett. **116**, 071802 (2016), [Addendum: Phys. Rev. Lett.121,no.20,209902(2018)], [arXiv:1511.05944].
- [9] K. Abe *et al.* (T2K), Phys. Rev. **D87**, 9, 092003 (2013), [arXiv:1302.4908].
- [10] K. Abe *et al.* (T2K), Phys. Rev. **D98**, 012004 (2018), [arXiv:1801.05148].
- [11] C. Adams *et al.* (MicroBooNE), Eur. Phys. J. **C79**, 3, 248 (2019), [arXiv:1805.06887].
- [12] K. Abe *et al.* (T2K) (2019), [arXiv:1904.09611].
- [13] K. Abe *et al.* (T2K), Phys. Rev. **D96**, 5, 052001 (2017), [arXiv:1706.04257].
- [14] B. G. Tice *et al.* (MINERvA), Phys. Rev. Lett. **112**, 23, 231801 (2014), [arXiv:1403.2103].
- [15] J. Mousseau *et al.* (MINERvA), Phys. Rev. **D93**, 7, 071101 (2016), [arXiv:1601.06313].
- [16] A. Kayis-Topaksu *et al.* (CHORUS), Nucl. Phys. **B798**, 1 (2008), [arXiv:0804.1869].
- [17] O. Samoylov *et al.* (NOMAD), Nucl. Phys. **B876**, 339 (2013), [arXiv:1308.4750].
- [18] D. Mason *et al.* (NuTeV), Phys. Rev. Lett. **99**, 192001 (2007).
- [19] J. Devan *et al.* (MINERvA), Phys. Rev. **D94**, 11, 112007 (2016), [arXiv:1610.04746].
- [20] L. Ren *et al.* (MINERvA), Phys. Rev. **D95**, 7, 072009 (2017), [Addendum: Phys. Rev.D97,no.1,019902(2018)], [arXiv:1701.04857].
- [21] P. Adamson *et al.* (MINOS), Phys. Rev. **D81**, 072002 (2010), [arXiv:0910.2201].
- [22] Q. Wu *et al.* (NOMAD), Phys. Lett. **B660**, 19 (2008), [arXiv:0711.1183].
- [23] Y. Nakajima *et al.* (SciBooNE), Phys. Rev. **D83**, 012005 (2011), [arXiv:1011.2131].
- [24] K. Abe *et al.* (T2K), Phys. Rev. **D90**, 5, 052010 (2014), [arXiv:1407.4256].
- [25] K. Abe *et al.* (T2K), Phys. Rev. **D93**, 7, 072002 (2016), [arXiv:1509.06940].
- [26] K. Abe *et al.* (T2K), Phys. Rev. Lett. **113**, 24, 241803 (2014), [arXiv:1407.7389].
- [27] K. Abe *et al.* (T2K), Phys. Rev. **D91**, 112010 (2015), [arXiv:1503.08815].
- [28] D. Ruterbories *et al.* (MINERvA), Phys. Rev. **D99**, 1, 012004 (2019), [arXiv:1811.02774].
- [29] C. E. Patrick *et al.* (MINERvA), Phys. Rev. **D97**, 5, 052002 (2018), [arXiv:1801.01197].
- [30] X. G. Lu *et al.* (MINERvA), Phys. Rev. Lett. **121**, 2, 022504 (2018), [arXiv:1805.05486].
- [31] A. A. Aguilar-Arevalo *et al.* (MiniBooNE), Phys. Rev. **D81**, 092005 (2010), [arXiv:1002.2680].
- [32] A. A. Aguilar-Arevalo *et al.* (MiniBooNE), Phys. Rev. **D88**, 3, 032001 (2013), [arXiv:1301.7067].
- [33] K. Abe *et al.* (T2K), Phys. Rev. **D93**, 11, 112012 (2016), [arXiv:1602.03652].
- [34] K. Abe *et al.* (T2K), Phys. Rev. **D97**, 1, 012001 (2018), [arXiv:1708.06771].
- [35] K. Abe *et al.* (2019), [arXiv:1908.10249].
- [36] K. Abe *et al.* (T2K), Phys. Rev. **D98**, 3, 032003 (2018), [arXiv:1802.05078].
- [37] K. Mahn, C. Marshall and C. Wilkinson, Ann. Rev. Nucl. Part. Sci. **68**, 105 (2018), [arXiv:1803.08848].
- [38] R. Acciarri *et al.* (ArgoNeuT), Phys. Rev. **D90**, 1, 012008 (2014), [arXiv:1405.4261].
- [39] R. Gran *et al.* (K2K), Phys. Rev. **D74**, 052002 (2006), [hep-ex/0603034].
- [40] G. A. Fiorentini *et al.* (MINERvA), Phys. Rev. Lett. **111**, 022502 (2013), [arXiv:1305.2243].
- [41] L. Fields *et al.* (MINERvA), Phys. Rev. Lett. **111**, 2, 022501 (2013), [arXiv:1305.2234].
- [42] M. Betancourt *et al.* (MINERvA), Phys. Rev. Lett. **119**, 8, 082001 (2017), [arXiv:1705.03791].
- [43] T. Walton *et al.* (MINERvA), Phys. Rev. **D91**, 7, 071301 (2015), [arXiv:1409.4497].
- [44] J. Wolcott *et al.* (MINERvA), Phys. Rev. Lett. **116**, 8, 081802 (2016), [arXiv:1509.05729].
- [45] R. Gran *et al.* (MINERvA), Phys. Rev. Lett. **120**, 22, 221805 (2018), [arXiv:1803.09377].
- [46] A. A. Aguilar-Arevalo *et al.* (MiniBooNE), Phys. Rev. Lett. **100**, 032301 (2008), [arXiv:0706.0926].
- [47] A. A. Aguilar-Arevalo *et al.* (MiniBooNE), Phys. Rev. **D82**, 092005 (2010), [arXiv:1007.4730].
- [48] A. A. Aguilar-Arevalo *et al.* (MiniBooNE), Phys. Rev. **D91**, 1, 012004 (2015), [arXiv:1309.7257].
- [49] P. Adamson *et al.* (MINOS), Phys. Rev. **D91**, 1, 012005 (2015), [arXiv:1410.8613].

- [50] V. Lyubushkin *et al.* (NOMAD), *Eur. Phys. J.* **C63**, 355 (2009), [arXiv:0812.4543].
- [51] L. Wan *et al.* (Super-Kamiokande), *Phys. Rev.* **D99**, 3, 032005 (2019), [arXiv:1901.05281].
- [52] K. Abe *et al.* (T2K), *Phys. Rev.* **D91**, 11, 112002 (2015), [arXiv:1503.07452].
- [53] K. Abe *et al.* (T2K), *Phys. Rev.* **D92**, 11, 112003 (2015), [arXiv:1411.6264].
- [54] K. Abe *et al.* (T2K), *Phys. Rev.* **D90**, 7, 072012 (2014), [arXiv:1403.3140].
- [55] J. Carlson *et al.*, *Phys. Rev.* **C65**, 024002 (2002), [arXiv:nucl-th/0106047].
- [56] H. Gallagher, G. Garvey and G. P. Zeller, *Ann. Rev. Nucl. Part. Sci.* **61**, 355 (2011).
- [57] G. T. Garvey *et al.*, *Phys. Rept.* **580**, 1 (2015), [arXiv:1412.4294].
- [58] O. Palamara (ArgoNeuT), *JPS Conf. Proc.* **12**, 010017 (2016).
- [59] M. Elkins *et al.* (MINERvA), *Phys. Rev.* **D100**, 5, 052002 (2019), [arXiv:1901.04892].
- [60] L. A. Ahrens *et al.*, *Phys. Rev.* **D35**, 785 (1987).
- [61] J. Brunner *et al.* (SKAT), *Z. Phys.* **C45**, 551 (1990).
- [62] V. V. Ammosov *et al.*, *Z. Phys.* **C36**, 377 (1987); O. Erriquez *et al.*, *Phys. Lett.* **70B**, 383 (1977); T. Eichten *et al.*, *Phys. Lett.* **40B**, 593 (1972).
- [63] C. Wilkinson *et al.*, *Phys. Rev.* **D90**, 11, 112017 (2014), [arXiv:1411.4482].
- [64] A. S. Meyer *et al.*, *Phys. Rev.* **D93**, 11, 113015 (2016), [arXiv:1603.03048].
- [65] P. Rodrigues, C. Wilkinson and K. McFarland, *Eur. Phys. J.* **C76**, 8, 474 (2016), [arXiv:1601.01888].
- [66] R. Acciarri *et al.* (ArgoNeuT), *Phys. Rev. Lett.* **113**, 26, 261801 (2014), [erratum: *Phys. Rev. Lett.* 114, no. 3, 039901 (2015)], [arXiv:1408.0598].
- [67] R. Acciarri *et al.* (ArgoNeuT), *Phys. Rev.* **D96**, 1, 012006 (2017), [arXiv:1511.00941].
- [68] A. Rodriguez *et al.* (K2K), *Phys. Rev.* **D78**, 032003 (2008), [arXiv:0805.0186].
- [69] M. Hasegawa *et al.* (K2K), *Phys. Rev. Lett.* **95**, 252301 (2005), [hep-ex/0506008].
- [70] C. Mariani *et al.* (K2K), *Phys. Rev.* **D83**, 054023 (2011), [arXiv:1012.1794].
- [71] S. Nakayama *et al.* (K2K), *Phys. Lett.* **B619**, 255 (2005), [hep-ex/0408134].
- [72] C. Adams *et al.* (MicroBooNE), *Phys. Rev.* **D99**, 9, 091102 (2019), [arXiv:1811.02700].
- [73] B. Eberly *et al.* (MINERvA), *Phys. Rev.* **D92**, 9, 092008 (2015), [arXiv:1406.6415].
- [74] C. L. McGivern *et al.* (MINERvA), *Phys. Rev.* **D94**, 5, 052005 (2016), [arXiv:1606.07127].
- [75] A. Higuera *et al.* (MINERvA), *Phys. Rev. Lett.* **113**, 26, 261802 (2014), [arXiv:1409.3835].
- [76] T. Le *et al.* (MINERvA), *Phys. Rev.* **D100**, 5, 052008 (2019), [arXiv:1906.08300].
- [77] A. Mislivec *et al.* (MINERvA), *Phys. Rev.* **D97**, 3, 032014 (2018), [arXiv:1711.01178].
- [78] T. Le *et al.* (MINERvA), *Phys. Lett.* **B749**, 130 (2015), [arXiv:1503.02107].
- [79] O. Altinok *et al.* (MINERvA), *Phys. Rev.* **D96**, 7, 072003 (2017), [arXiv:1708.03723].
- [80] J. Wolcott *et al.* (MINERvA), *Phys. Rev. Lett.* **117**, 11, 111801 (2016), [arXiv:1604.01728].
- [81] A. A. Aguilar-Arevalo *et al.* (MiniBooNE), *Phys. Rev.* **D83**, 052007 (2011), [arXiv:1011.3572].
- [82] A. A. Aguilar-Arevalo *et al.* (MiniBooNE), *Phys. Rev. Lett.* **103**, 081801 (2009), [arXiv:0904.3159].
- [83] A. A. Aguilar-Arevalo *et al.* (MiniBooNE), *Phys. Rev.* **D83**, 052009 (2011), [arXiv:1010.3264].
- [84] A. A. Aguilar-Arevalo *et al.* (MiniBooNE), *Phys. Rev.* **D81**, 013005 (2010), [arXiv:0911.2063].
- [85] A. A. Aguilar-Arevalo *et al.* (MiniBooNE), *Phys. Lett.* **B664**, 41 (2008), [arXiv:0803.3423].
- [86] P. Adamson *et al.* (MINOS), *Phys. Rev.* **D94**, 7, 072006 (2016), [arXiv:1608.05702].
- [87] C. T. Kullenberg *et al.* (NOMAD), *Phys. Lett.* **B682**, 177 (2009), [arXiv:0910.0062].
- [88] M. A. Acero *et al.* (NOvA) (2019), [arXiv:1902.00558].
- [89] K. Hiraida *et al.* (SciBooNE), *Phys. Rev.* **D78**, 112004 (2008), [arXiv:0811.0369].
- [90] Y. Kurimoto *et al.* (SciBooNE), *Phys. Rev.* **D81**, 033004 (2010), [arXiv:0910.5768].
- [91] Y. Kurimoto *et al.* (SciBooNE), *Phys. Rev.* **D81**, 111102 (2010), [arXiv:1005.0059].
- [92] K. Abe *et al.* (T2K), *Phys. Rev.* **D95**, 1, 012010 (2017), [arXiv:1605.07964].
- [93] K. Abe *et al.* (T2K), *Phys. Rev. Lett.* **117**, 19, 192501 (2016), [arXiv:1604.04406].
- [94] P. Vilain *et al.* (CHARM-II), *Phys. Lett.* **B313**, 267 (1993); A compilation of historical coherent pion production data.
- [95] P. Stowell *et al.* (MINERvA), *Phys. Rev.* **D100**, 7, 072005 (2019), [arXiv:1903.01558].
- [96] C. T. Kullenberg *et al.* (NOMAD), *Phys. Lett.* **B706**, 268 (2012), [arXiv:1111.3713].
- [97] K. Abe *et al.* (T2K), *J. Phys.* **G46**, 8, 08LT01 (2019), [arXiv:1902.03848].
- [98] C. M. Marshall *et al.* (MINERvA), *Phys. Rev.* **D94**, 1, 012002 (2016), [arXiv:1604.03920].
- [99] C. M. Marshall *et al.* (MINERvA), *Phys. Rev. Lett.* **119**, 1, 011802 (2017), [arXiv:1611.02224].
- [100] Z. Wang *et al.* (MINERvA), *Phys. Rev. Lett.* **117**, 6, 061802 (2016), [arXiv:1606.08890].
- [101] M. Betancourt *et al.*, *Phys. Rept.* **773-774**, 1 (2018), [arXiv:1805.07378].

## 52. Plots of Cross Sections and Related Quantities

Updated in 2019. See various sections for details.

52.1	Pseudorapidity Distributions in $pp$ and $\bar{p}p$ Interactions . . . . .	696
52.2	Average Hadron Multiplicities in Hadronic $e^+e^-$ Annihilation Events . . . . .	697
52.3	$\sigma$ and $R$ in $e^+e^-$ Collisions . . . . .	699
52.4	Annihilation Cross Section Near $M_Z$ . . . . .	701
52.5	Total Hadronic Cross Sections . . . . .	702

52.1 Pseudorapidity Distributions in  $pp$  and  $\bar{p}p$  Interactions

Revised August 2013 by D.R. Ward (Cavendish Lab.).

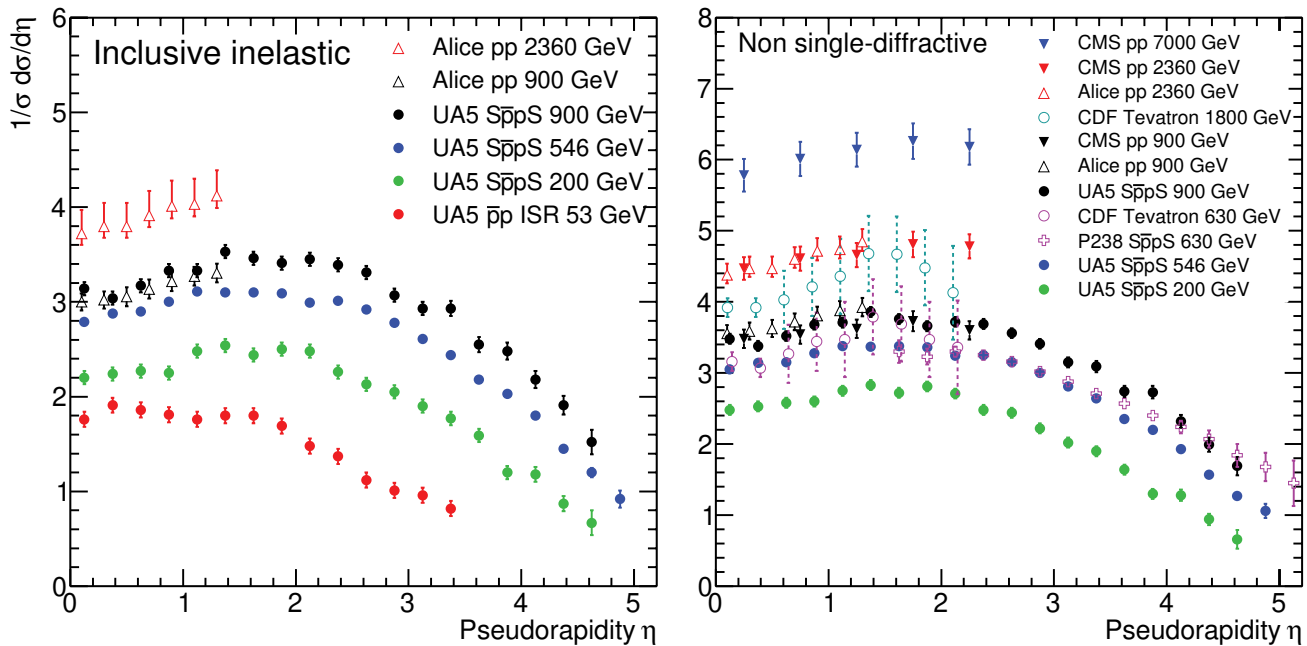
Pseudorapidity Distributions in  $pp$  and  $\bar{p}p$  Interactions

Figure 52.1: Charged particle pseudorapidity distributions in  $\bar{p}p$  collisions for  $53 \text{ GeV} \leq \sqrt{s} \leq 1800 \text{ GeV}$ . UA5 data from the  $S\bar{p}pS$  are taken from [1], and from the ISR from [2]. The UA5 data are shown for both the full inelastic cross-section and with singly diffractive events excluded. Additional non single-diffractive measurements are available from CDF at the Tevatron [3] and from P238 at the  $S\bar{p}pS$  [4]. These may be compared with both inclusive and non single-diffractive measurements in  $pp$  collisions at the LHC from ALICE [5] and for non single-diffractive interactions from CMS [6, 7]. (Courtesy of D.R. Ward, Cambridge Univ., 2013)

52.2 Average Hadron Multiplicities in Hadronic  $e^+e^-$  Annihilation Events

Revised August 2019 by O. Biebel (Ludwig-Maximilians U.).

**Table 52.1:** Average hadron multiplicities per hadronic  $e^+e^-$  annihilation event at  $\sqrt{s} \approx 10, 29\text{--}35, 91,$  and  $130\text{--}200$  GeV. The rates given include decay products from resonances with  $c\tau < 10$  cm, and include the corresponding anti-particle state. Correlations of the systematic uncertainties were considered for the calculation of the averages. Quoted errors are not increased by scale factor  $S$ .

Particle	$\sqrt{s} \approx 10$ GeV	$\sqrt{s} = 29\text{--}35$ GeV	$\sqrt{s} = 91$ GeV	$\sqrt{s} = 130\text{--}200$ GeV	References
<b>Pseudoscalar mesons:</b>					
$\pi^+$	$6.52 \pm 0.11$	$3 \pm 0.4$	$17.02 \pm 0.19$	$21.24 \pm 0.39$	[8–17]
$\pi^0$	$3.2 \pm 0.35$	$83 \pm 0.28$	$9.42 \pm 0.32$		[12, 18–23]
$K^+$	$0.953 \pm 0.018$	$1.48 \pm 0.09$	$2.228 \pm 0.059$	$2.82 \pm 0.19$	[9–17, 24, 25]
$K^0$	$0.91 \pm 0.05$	$1.48 \pm 0.07$	$2.049 \pm 0.026$	$2.10 \pm 0.12$	[12, 17, 20, 26–36]
$\eta$	$0.20 \pm 0.04$	$0.61 \pm 0.07$	$1.049 \pm 0.080$		[12, 18, 19, 22, 23, 37–40]
$\eta'(958)$	$0.03 \pm 0.01$	$0.26 \pm 0.10$	$0.152 \pm 0.020$		[20, 39, 41–43]
$D^+$	$0.194 \pm 0.019^{(a)}$	$0.17 \pm 0.03$	$0.175 \pm 0.016$		[12, 44–47]
$D^0$	$0.446 \pm 0.032^{(a)}$	$0.45 \pm 0.07$	$0.454 \pm 0.030$		[12, 44–47]
$D_s^+$	$0.063 \pm 0.014^{(a)}$	$0.45 \pm 0.20^{(b)}$	$0.131 \pm 0.021$		[8, 39, 44, 47–49]
$B^{(c)}$	—	—	$0.134 \pm 0.016^{(d)}$		[46, 50]
$B^+$	—	—	$0.141 \pm 0.004^{(d)}$		[51]
$B_s^0$	—	—	$0.054 \pm 0.011^{(d)}$		[52, 53]
<b>Scalar mesons:</b>					
$f_0(980)$	$0.024 \pm 0.006$	$0.05 \pm 0.02^{(e)}$	$0.146 \pm 0.012$		[41, 54–56]
$a_0(980)^\pm$	—	—	$0.27 \pm 0.11^{(f)}$		[43]
<b>Vector mesons:</b>					
$\rho(770)^0$	$0.35 \pm 0.04$	$0.81 \pm 0.08$	$1.231 \pm 0.098$		[9, 12, 55, 57, 58]
$\rho(770)^\pm$	—	—	$2.40 \pm 0.43^{(f)}$		[43]
$\omega(782)$	$0.30 \pm 0.08$	—	$1.016 \pm 0.065$		[40, 42, 43, 57]
$K^*(892)^+$	$0.27 \pm 0.03$	$0.64 \pm 0.05$	$0.714 \pm 0.055$		[9, 12, 33, 57, 59, 60]
$K^*(892)^0$	$0.29 \pm 0.03$	$0.56 \pm 0.06$	$0.738 \pm 0.024$		[9, 12, 36, 57, 58, 61, 62]
$\phi(1020)$	$0.044 \pm 0.003$	$0.085 \pm 0.011$	$0.0963 \pm 0.0032$		[12, 36, 56–58, 61]
$D^*(2010)^+$	$0.177 \pm 0.022^{(a)}$	$0.43 \pm 0.07$	$0.1937 \pm 0.0057^{(g)}$		[12, 44–46, 63, 64]
$D^*(2007)^0$	$0.168 \pm 0.019^{(a)}$	$0.27 \pm 0.11$	—		[12, 44, 45]
$D_s^*(2112)^+$	$0.048 \pm 0.014^{(a)}$	—	$0.101 \pm 0.048^{(h)}$		[48, 65]
$B^{*(i)}$	—	—	$0.288 \pm 0.026$		[66, 67]
$J/\psi(1S)$	$0.00050 \pm 0.00005^{(a)}$	—	$0.0052 \pm 0.0004^{(j)}$		[68–73]
$\psi(2S)$	—	—	$0.0023 \pm 0.0004^{(j)}$		[71, 73, 74]
$\Upsilon(1S)$	—	—	$0.00014 \pm 0.00007^{(j)}$		[75]
<b>Pseudovector mesons:</b>					
$f_1(1285)$	—	—	$0.165 \pm 0.051$		[76]
$f_1(1420)$	—	—	$0.056 \pm 0.012$		[76]
$\chi_{c1}(3510)$	—	—	$0.0041 \pm 0.0011^{(j)}$		[71, 74]
<b>Tensor mesons:</b>					
$f_2(1270)$	$0.09 \pm 0.02$	$0.14 \pm 0.04$	$0.166 \pm 0.020$		[54–56, 77]
$f_2'(1525)$	—	—	$0.012 \pm 0.006$		[55]
$K_2^*(1430)^+$	—	$0.09 \pm 0.03$	—		[55, 78]
$K_2^*(1430)^0$	—	$0.12 \pm 0.06$	$0.084 \pm 0.022$		[54, 55, 79]
$B^{** (k)}$	—	—	$0.118 \pm 0.024$		[80]
$D_{s1}^\pm$	—	—	$0.0052 \pm 0.0011^{(l)}$		[81]
$D_{s2}^\pm$	—	—	$0.0083 \pm 0.0031^{(l)}$		[81]
<b>Baryons:</b>					
$p$	$0.266 \pm 0.008$	$0.640 \pm 0.050$	$1.050 \pm 0.032$	$1.41 \pm 0.18$	[10, 13–17, 24, 25, 77]
$\Lambda$	$0.093 \pm 0.006^{(a)}$	$0.205 \pm 0.010$	$0.3915 \pm 0.0065$	$0.39 \pm 0.03$	[17, 20, 34, 36, 77, 82–85]
$\Sigma^0$	$0.0221 \pm 0.0018^{(a)}$	—	$0.078 \pm 0.010$		[10, 59, 82, 86–88]
$\Sigma^-$	—	—	$0.081 \pm 0.010$		[88, 89]
$\Sigma^+$	—	—	$0.107 \pm 0.011$		[87, 88]
$\Sigma^\pm$	—	—	$0.174 \pm 0.009$		[84, 88]
$\Xi^-$	$0.0055 \pm 0.0004^{(a)}$	$0.0176 \pm 0.0027$	$0.0262 \pm 0.0009$		[9, 59, 77, 82–85]
$\Delta(1232)^{++}$	$0.040 \pm 0.010$	—	$0.085 \pm 0.014$		[90–92]
$\Sigma(1385)^-$	$0.006 \pm 0.002$	$0.017 \pm 0.004$	$0.0240 \pm 0.0017$		[59, 82, 84, 85, 93]
$\Sigma(1385)^+$	$0.0062 \pm 0.0011^{(a)}$	$0.017 \pm 0.004$	$0.0239 \pm 0.0015$		[59, 82–85, 93]

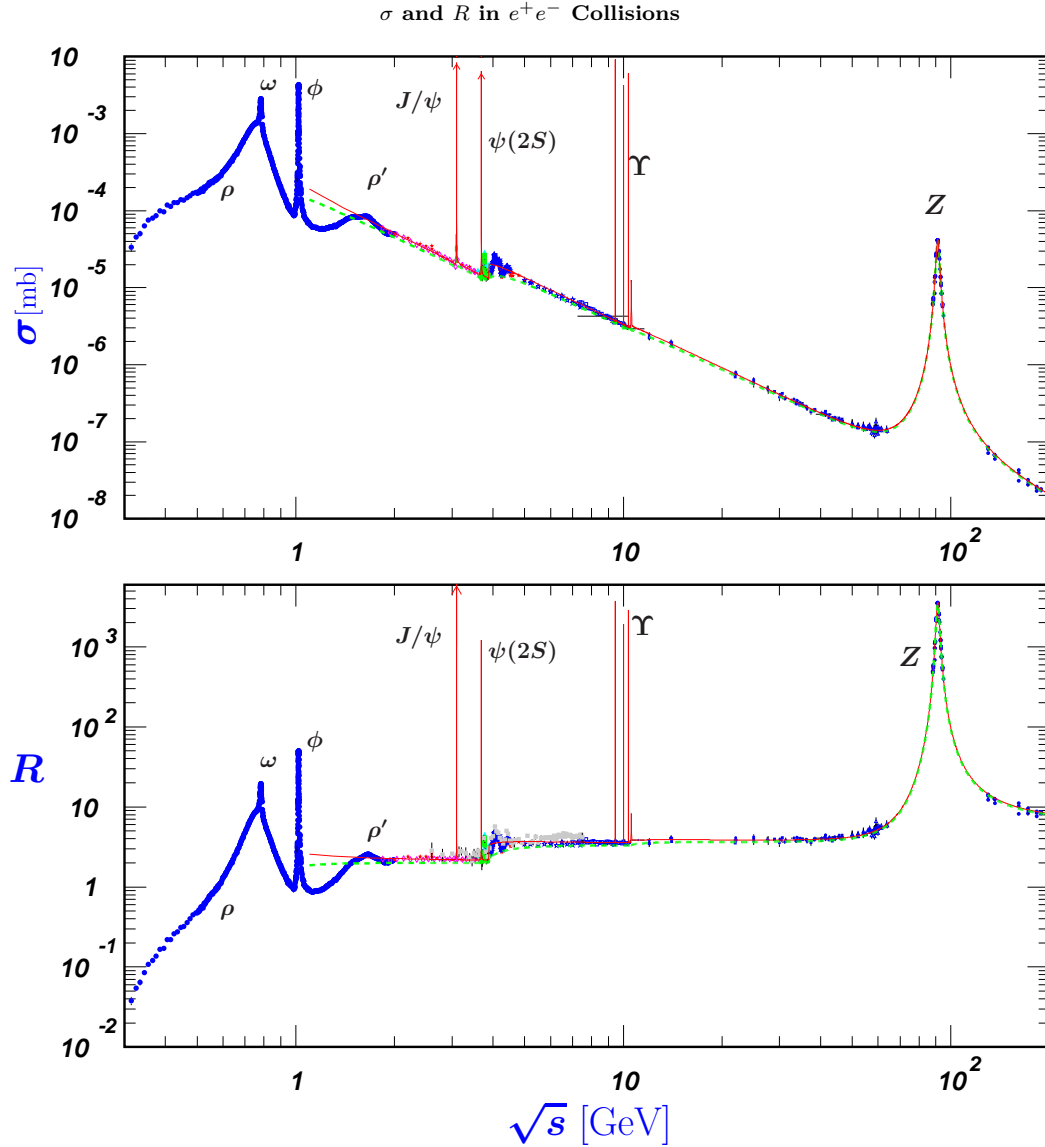


Particle	$\sqrt{s} \approx 10$ GeV	$\sqrt{s} = 29\text{--}35$ GeV	$\sqrt{s} = 91$ GeV	$\sqrt{s} = 130\text{--}200$ GeV
$\Sigma(1385)^\pm$	$0.0106 \pm 0.0020$	$0.033 \pm 0.008$	$0.0472 \pm 0.0027$	[59, 82, 84, 85, 93]
$\Xi(1530)^0$	$0.00130 \pm 0.00010^{(a)}$	—	$0.00694 \pm 0.00049$	[59, 82, 83, 85, 94]
$\Omega^-$	$0.00060 \pm 0.00033^{(a)}$	$0.014 \pm 0.007$	$0.00124 \pm 0.00018$	[59, 77, 82, 83, 85, 86]
$\Lambda_c^+$	$0.0479 \pm 0.0038^{(a,m)}$	$0.110 \pm 0.050$	$0.078 \pm 0.017$	[47, 49, 77, 83, 95]
$\Lambda_b^0$	—	—	$0.031 \pm 0.016$	[96]
$\Sigma_c^0$	$0.0025 \pm 0.0004^{(a)}$	—	—	[83]
$\Lambda(1520)$	$0.0046 \pm 0.0004^{(a)}$	—	$0.0222 \pm 0.0027$	[83, 85, 89, 97]

- (a)  $\sigma_{\text{had}} = 3.33 \pm 0.05 \pm 0.21$  nb (CLEO: [98]) has been used in converting the measured cross sections to average hadron multiplicities.
- (b)  $B(D_s \rightarrow \eta\pi, \eta'\pi)$  was used (RPP 1994).
- (c) Comprises both charged and neutral  $B$  meson states.
- (d) The Standard Model  $B(Z \rightarrow b\bar{b}) = 0.217$  was used.
- (e)  $x_p = p/p_{\text{beam}} > 0.1$  only.
- (f) Both charge states.
- (g)  $B(D^*(2010)^+ \rightarrow D^0\pi^+) \times B(D^0 \rightarrow K^-\pi^+)$  has been used (RPP 2000).
- (h)  $B(D_s^* \rightarrow D_s^+\gamma)$ ,  $B(D_s^+ \rightarrow \phi\pi^+)$ ,  $B(\phi \rightarrow K^+K^-)$  have been used (RPP 1998).
- (i) Any charge state (*i.e.*,  $B_d^*$ ,  $B_u^*$ , or  $B_s^*$ ).
- (j)  $B(Z \rightarrow \text{hadrons}) = 0.699$  was used (RPP 1994).
- (k) Any charge state (*i.e.*,  $B_d^{**}$ ,  $B_u^{**}$ , or  $B_s^{**}$ ).
- (l) Assumes  $B(D_{s1}^+ \rightarrow D^{*+}K^0 + D^{*0}K^+) = 100\%$  and  $B(D_{s2}^+ \rightarrow D^0K^+) = 45\%$ .
- (m) The value was derived from the cross section of  $\Lambda_c^+ \rightarrow p\pi K$  using (a) and assuming the branching fraction to be  $(5.0 \pm 1.3)\%$  (RPP 2004).

#### References grouped by collaboration for Table-52.1:

- RPP: [12]
- ALEPH: [13, 20, 40, 58, 59, 63, 70, 81],
- ARGUS: [8, 24, 37, 41, 57, 82, 90, 97],
- BaBar: [10, 48, 68, 95],
- Belle: [44, 69, 83],
- CELLO: [19, 26],
- CLEO: [9, 45, 49, 98],
- Crystal Ball: [38],
- DELPHI: [14, 17, 21, 25, 33, 46, 50–52, 55, 61, 66, 71, 76, 80, 84, 86, 89, 91, 94],
- HRS: [27, 54, 78, 93],
- L3: [22, 34, 42, 67, 72, 74, 87]
- MARK II: [29, 39],
- JADE: [18, 28],
- OPAL: [15, 23, 35, 43, 47, 53, 56, 60, 62, 64, 65, 73, 75, 79, 85, 88, 92, 96],
- PLUTO: [30]
- SLD: [16, 36],
- TASSO: [31]
- TPC: [32].

52.3  $\sigma$  and  $R$  in  $e^+e^-$  Collisions

**Figure 52.2:** World data on the total cross section of  $e^+e^- \rightarrow \text{hadrons}$  and the ratio  $R(s) = \sigma(e^+e^- \rightarrow \text{hadrons}, s) / \sigma(e^+e^- \rightarrow \mu^+\mu^-, s)$ .  $\sigma(e^+e^- \rightarrow \text{hadrons}, s)$  is the experimental cross section corrected for initial state radiation and electron-positron vertex loops,  $\sigma(e^+e^- \rightarrow \mu^+\mu^-, s) = 4\pi\alpha^2(s)/3s$ . Data errors are total below 2 GeV and statistical above 2 GeV. The curves are an educative guide: the broken one (green) is a naive quark-parton model prediction, and the solid one (red) is 3-loop pQCD prediction (see “Quantum Chromodynamics” section of this *Review*, Eq. (9.7) or, for more details [99], Breit-Wigner parameterizations of  $J/\psi$ ,  $\psi(2S)$ , and  $\Upsilon(nS)$ ,  $n = 1, 2, 3, 4$  are also shown. The full list of references to the original data and the details of the  $R$  ratio extraction from them can be found in [100]. Corresponding computer-readable data files are available at <http://pdg.lbl.gov/current/xsect/>. (Courtesy of the COMPAS (Protvino) and HEPDATA (Durham) Groups, August 2019. Corrections by P. Janot (CERN) and M. Schmitt (Northwestern U.))

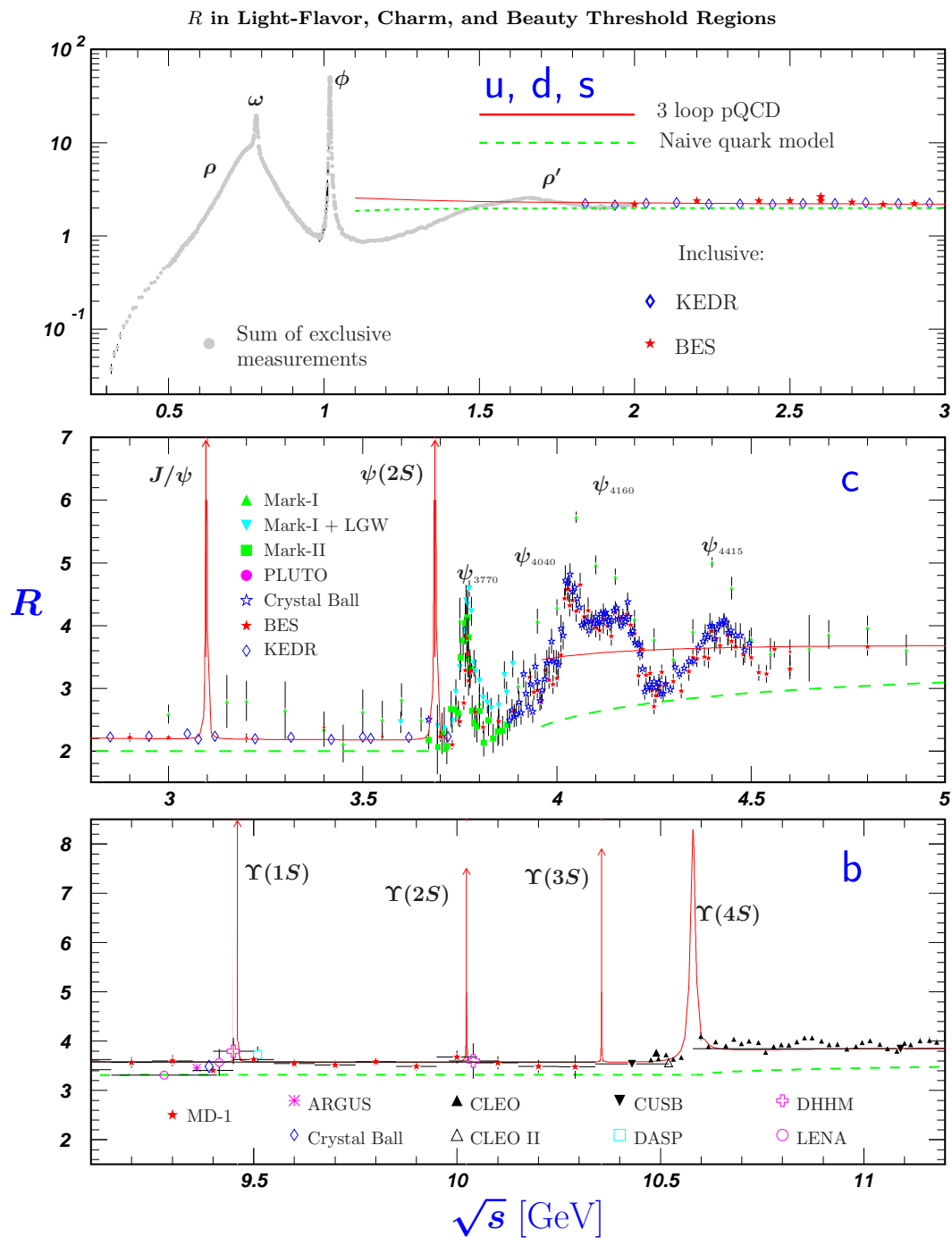


**Figure 52.3:**  $R$  in the light-flavor, charm, and beauty threshold regions. Data errors are total below 2 GeV and statistical above 2 GeV. The curves are the same as in Fig. 52.2. **Note:** CLEO data above  $\Upsilon(4S)$  were not fully corrected for radiative effects, and we retain them on the plot only for illustrative purposes with a normalization factor of 0.8. The full list of references to the original data and the details of the  $R$  ratio extraction from them can be found in [100]. The computer-readable data are available at <http://pdg.lbl.gov/current/xsect/>. (Courtesy of the COMPAS (Protvino) and HEPDATA (Durham) Groups, August 2019.)

52.4 Annihilation Cross Section Near  $M_Z$ 

Courtesy of M. Grünewald and the LEP Electroweak Working Group, 2007.

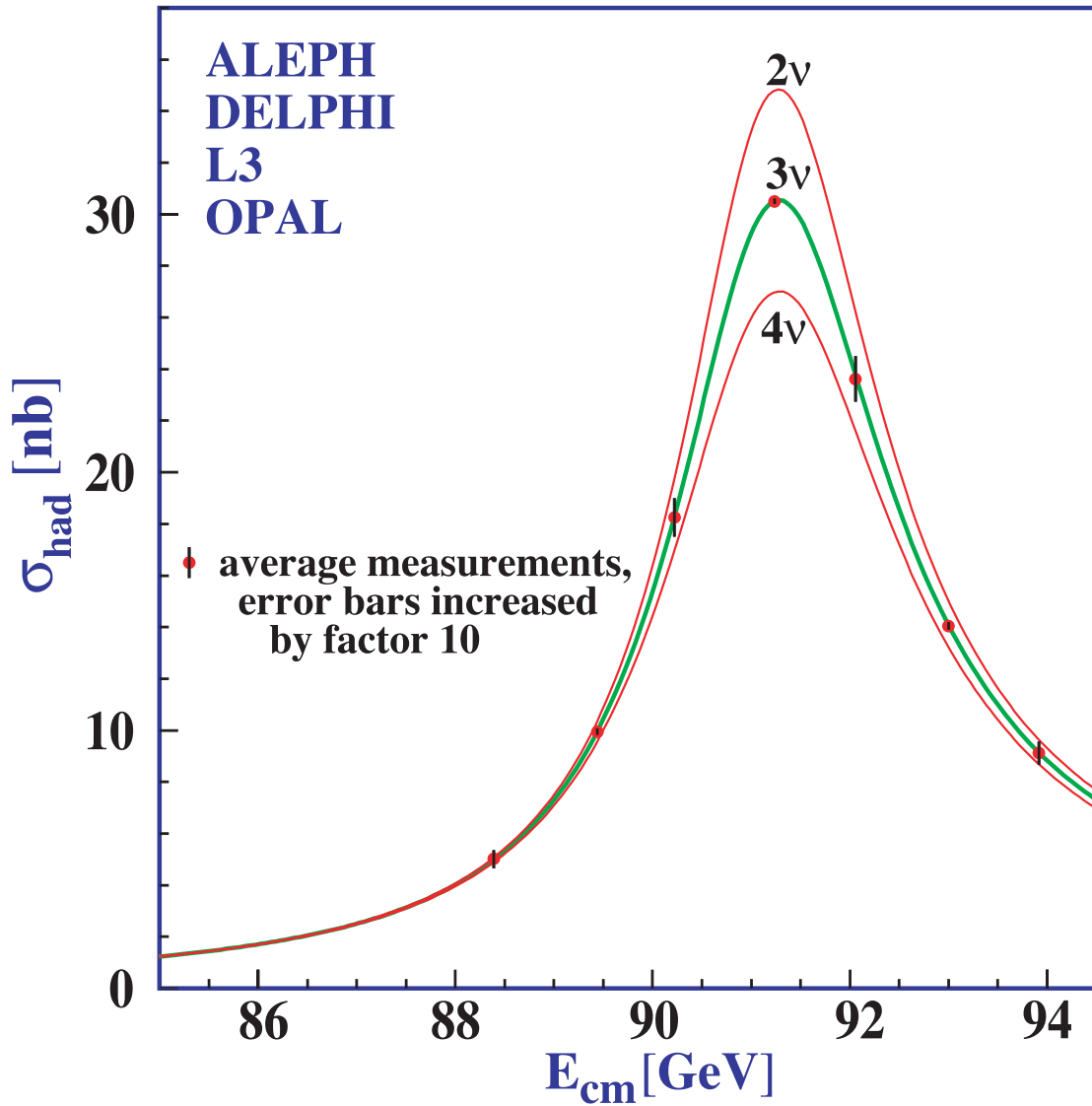


**Figure 52.4:** Combined data from the ALEPH, DELPHI, L3, and OPAL Collaborations for the cross section in  $e^+e^-$  annihilation into hadronic final states as a function of the center-of-mass energy near the Z pole. The curves show the predictions of the Standard Model with two, three, and four species of light neutrinos. The asymmetry of the curve is produced by initial-state radiation. Note that the error bars have been increased by a factor ten for display purposes. References: ALEPH [101], DELPHI [102], L3 [103], OPAL [104], Combination [105],

## 52.5 Total Hadronic Cross Sections

Revised August 2019 by COMPAS Group (NRC KI – IHEP, Protvino).

In this section, plots of total cross section for various processes are presented. The plots include data from hadronic collisions such as  $pp$  and  $\bar{p}p$ , as well as  $\gamma p$ ,  $\gamma d$ , and  $\gamma\gamma$  processes. The cross section data provide crucial inputs to the study of QCD physics. In particular, to probe the non-perturbative part of QCD processes which are described by a number of diffractive models. We begin by introducing some models of diffractive scatterings and listing references for further reading.

Diffractive scattering here means scattering of hadrons at small angles and exhibiting typical diffraction pattern in angular distribution of scattered particles. Beyond purely elastic scattering diffraction phenomena include inelastic processes with large rapidity gaps: those of single and double diffractive dissociation and “central diffractive” events. In distinction from the most of other processes considered in the SM diffraction processes (DP) are related to large spatio-temporal scales growing with energy of collision. Being caused by strong interactions DP are a subject of the fundamental strong interaction theory, QCD, and hereby a part of the longstanding problem of QCD at large distances.

One of the most important basic notions and tools in general theoretical framework related to the diffractive processes is the notion of the Regge poles, or Reggeons, generalizing the simple one-particle exchange (of Yukawa type) by virtual particles of fixed spin to exchanges by states with “running spin” dependent on the transferred momenta [106,107]. The simplest case of the one-Reggeon exchange amplitude is given by the amplitude (at high c.m. energy  $\sqrt{s}$  and fixed (small) transferred momentum squared,  $t$ ):  $T(s, t) = \beta(t)s^{\alpha(t)}$  which qualitatively exhibits many typical features of generic diffractive processes (e.g. the growth of the interaction radius with energy). In practice the single-pole Reggeon model is insufficient for many diffractive processes but still serves a building block for more sophisticated schemes. Up to now no firm results concerning Regge trajectories  $\alpha(t)$  and Regge residues  $\beta(t)$  were obtained from the first principles of QCD. General principles imply that both  $\alpha(t)$  and  $\beta(t)$  are analytic functions with right cuts from some  $t_0 > 0$  to positive infinity.

The theoretical requisite for analyzing diffractive phenomena is therefore represented by various model approaches. The more commonly discussed models in the literatures are:

- **Regge -Eikonal approach** [108–115]: this approach automatically satisfy the  $s$ -channel unitarity condition and generalizes the impact parameter approximation to the relativistic case.
- **Regge pole models with minimal corrections due to two-Reggeon exchanges** [116–118]: in this model, contribution of the leading trajectory is supplemented by a two-Reggeon exchange with arbitrary coefficient chosen from the fitting details.
- **$U$ -matrix (or resonance) approach** [119,120]: the unitarity respecting approach with the scattering amplitude defined by a reaction matrix.
- **Direct functional modelling of the amplitudes without Regge trajectories** [121,122]: this approach appeals to only very general properties of the amplitudes leaving aside all dynamical assumptions and mostly aiming at the best phenomenological description of the data.
- **Quasi-classical approach** [123–126]: based on the observation that diffractive processes deal with high quantum numbers, in particular with large number of virtual quanta.

For readers who are interested in examples of both total and elastic cross section parametrizations and fits, see previous edition of the *Plots of Cross Sections and Related Quantities* review [127]. For the cross section plots shown in the following pages, the example fits are using parametrizations as described in [127] with the fit range starting at about  $\sqrt{s} = 5$  GeV.

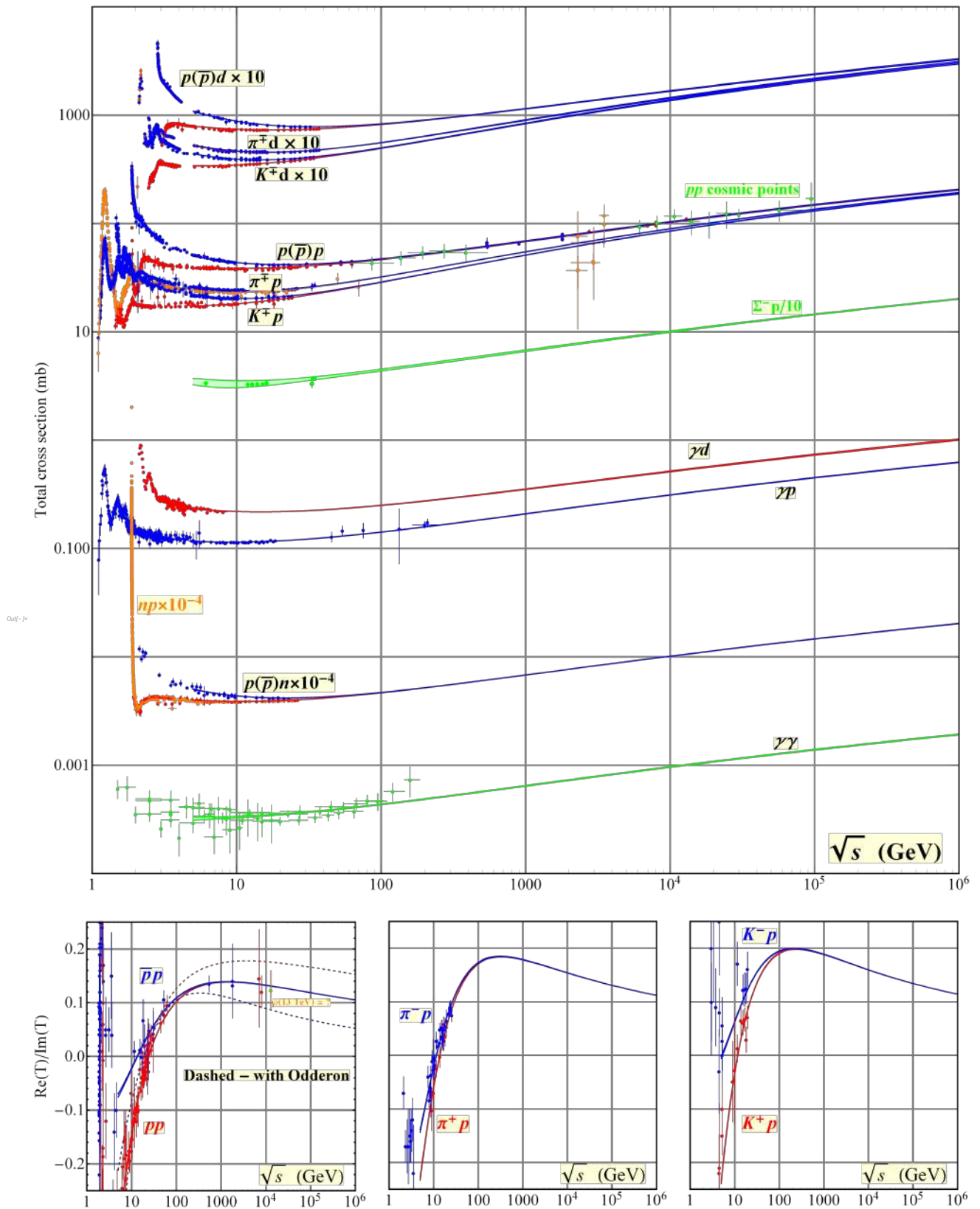


**Figure 52.5:** Summary of hadronic,  $\gamma p$ ,  $\gamma d$ , and  $\gamma\gamma$  total cross sections, and ratio of the real to imaginary parts of the forward hadronic amplitudes. Corresponding computer-readable data files may be found at <http://pdg.lbl.gov/current/xsect/>. (Courtesy of the COMPAS group, NRC KI – IHEP, Protvino, August 2019.)

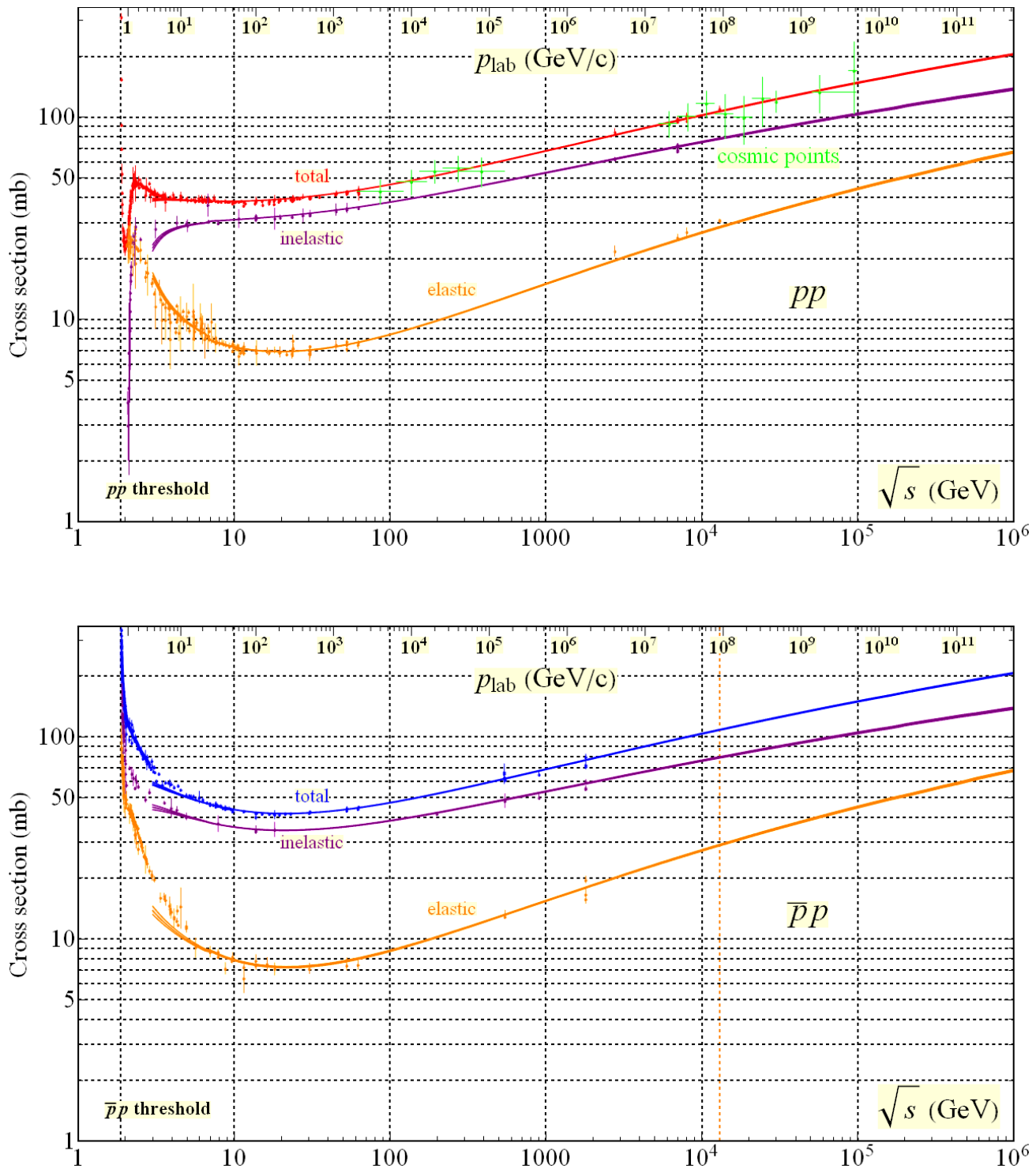


**Figure 52.6:** Total and elastic cross sections for  $pp$  and  $\bar{p}p$  collisions as a function of laboratory beam momentum and total center-of-mass energy.  $\sigma_{\text{el}}$  is computed using the nuclear part of the elastic scattering amplitude [126]. Corresponding computer-readable data files may be found at <http://pdg.lbl.gov/current/xsect/>. (Courtesy of the COMPAS group, NRC KI – IHEP, Protvino, August 2019.)

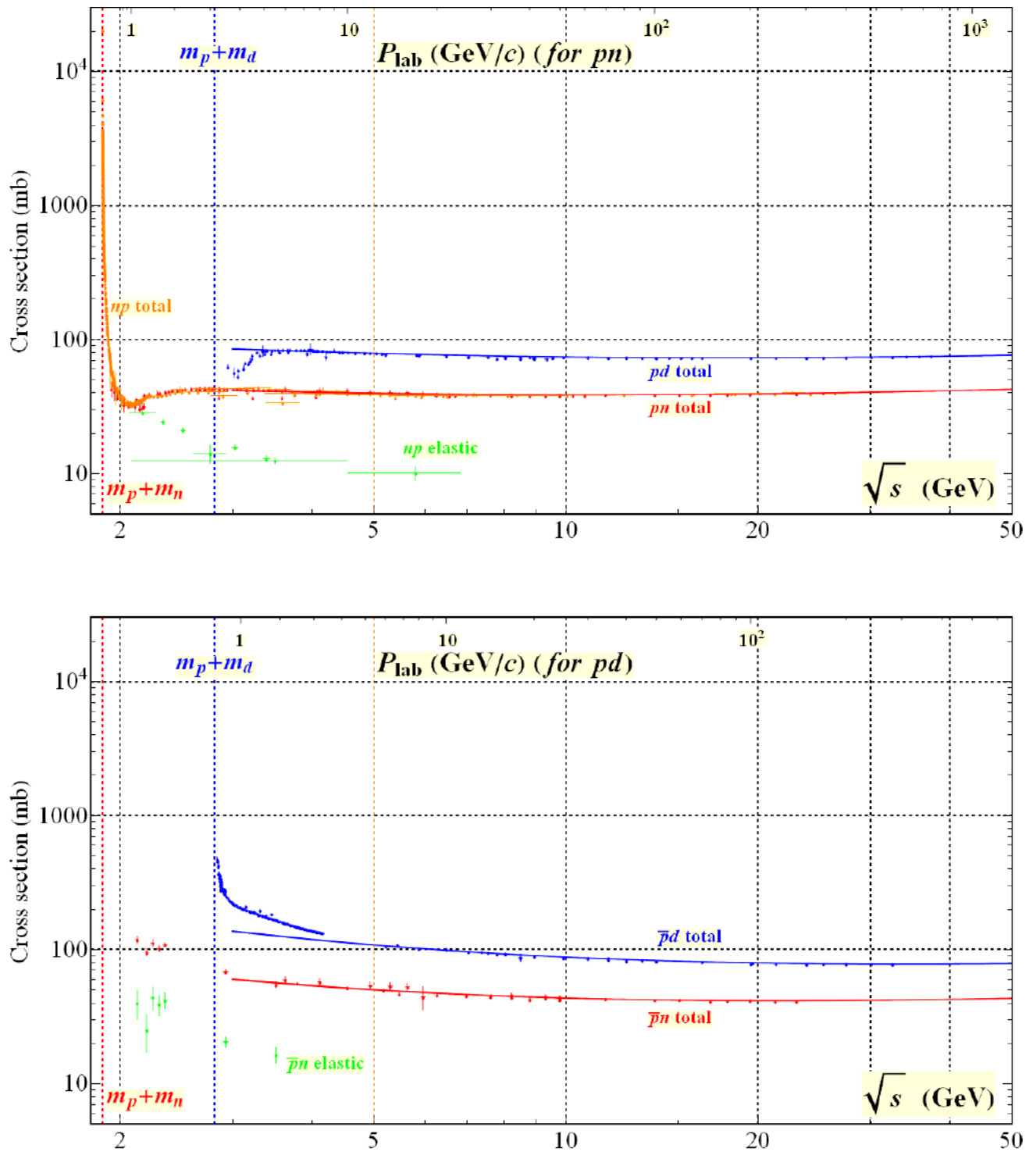


**Figure 52.7:** Total and elastic cross sections for  $pd$  (total only),  $np$ ,  $\bar{p}d$  (total only), and  $\bar{p}n$  collisions as a function of laboratory beam momentum and total center-of-mass energy. Corresponding computer-readable data files may be found at <http://pdg.lbl.gov/current/xsect/>. (Courtesy of the COMPAS Group, NRC KI – IHEP, Protvino, August 2019.)



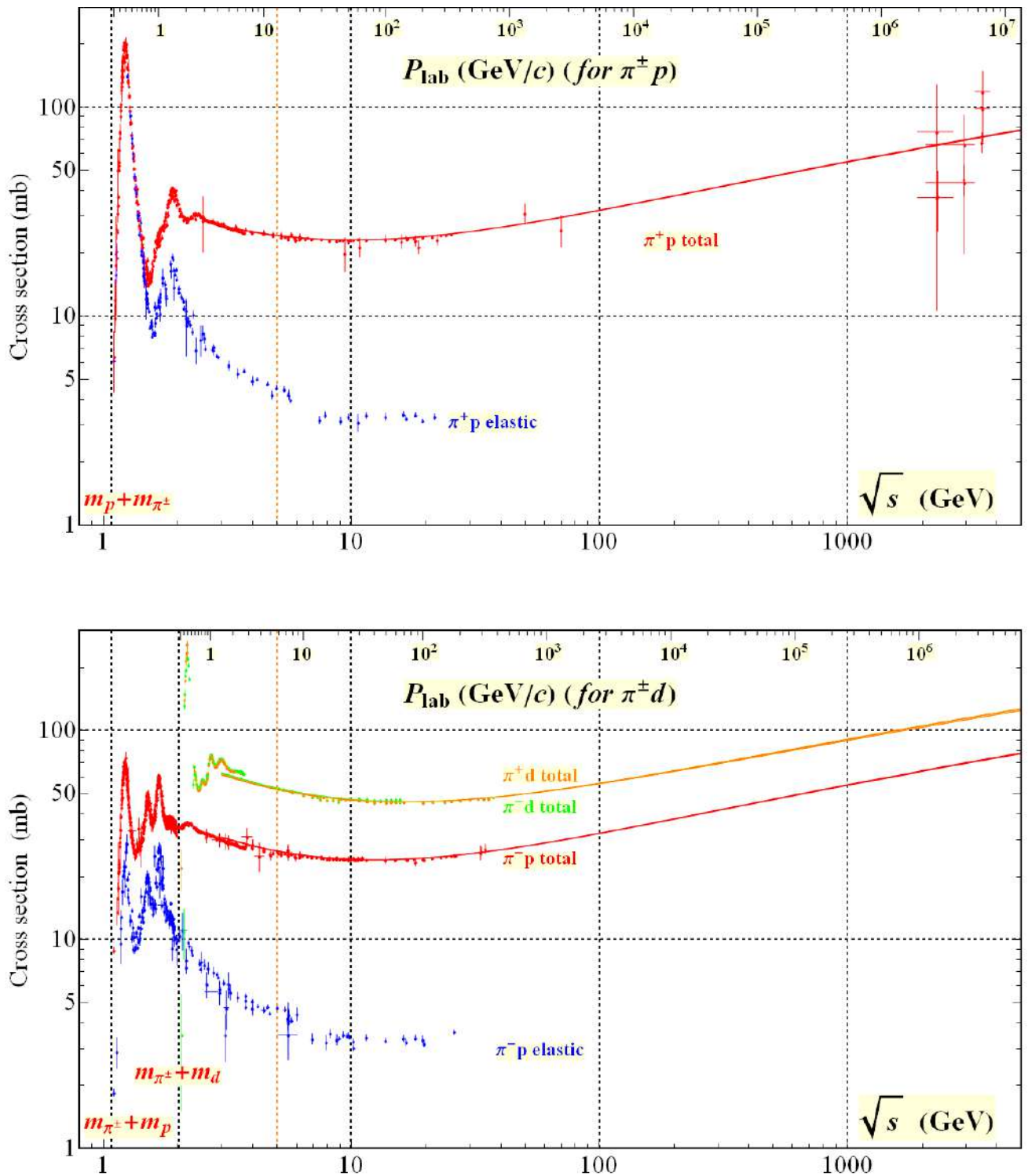


**Figure 52.8:** Total and elastic cross sections for  $\pi^\pm p$  and  $\pi^\pm d$  (total only) collisions as a function of laboratory beam momentum and total center-of-mass energy. Corresponding computer-readable data files may be found at <http://pdg.lbl.gov/current/xsect/>. (Courtesy of the COMPAS Group, NRC KI – IHEP, Protvino, August 2019.)

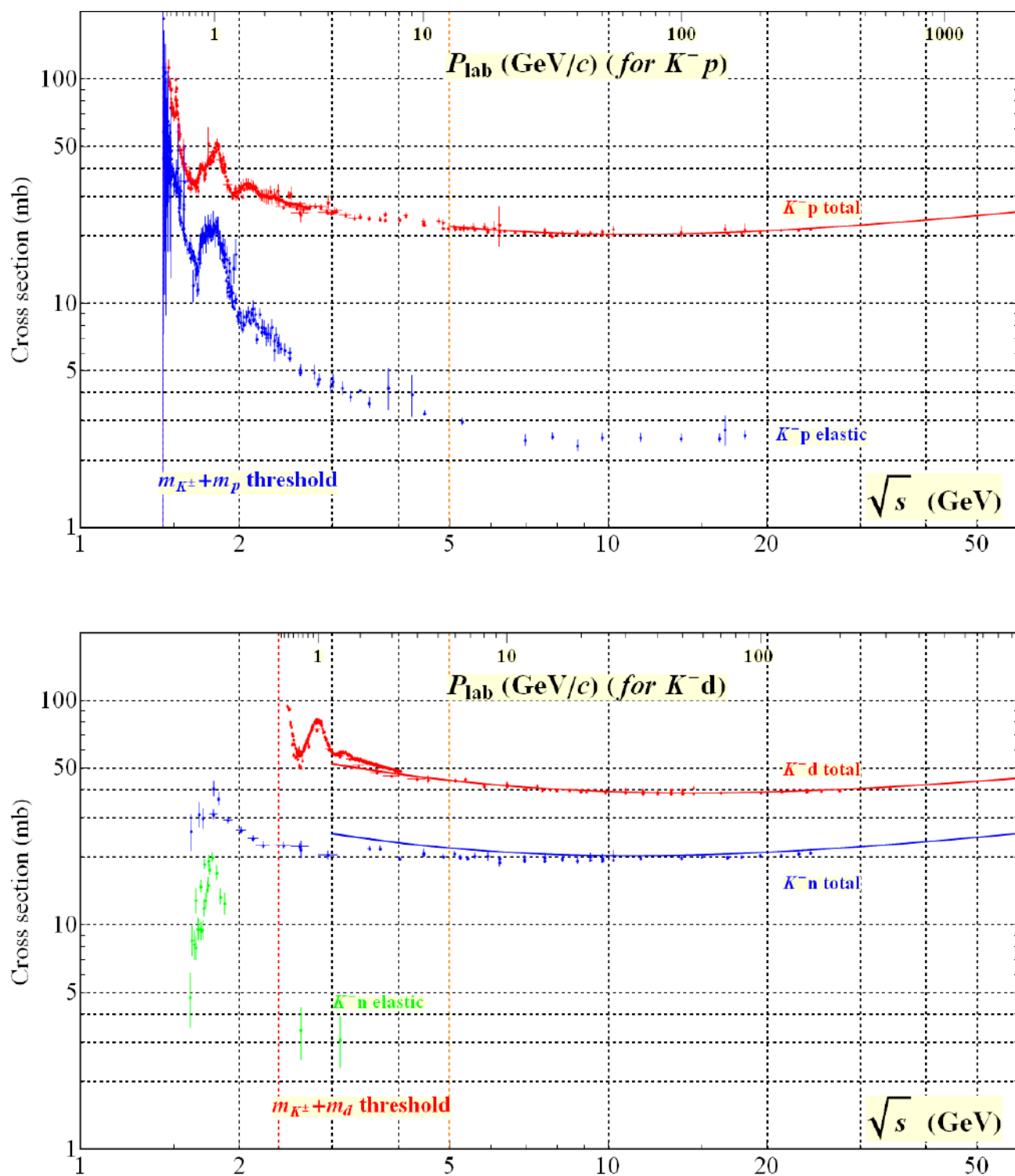


**Figure 52.9:** Total and elastic cross sections for  $K^-p$  and  $K^-d$  (total only), and  $K^-n$  collisions as a function of laboratory beam momentum and total center-of-mass energy. Corresponding computer-readable data files may be found at <http://pdg.lbl.gov/current/xsect/>. (Courtesy of the COMPAS Group, NRC KI – IHEP, Protvino, August 2019.)

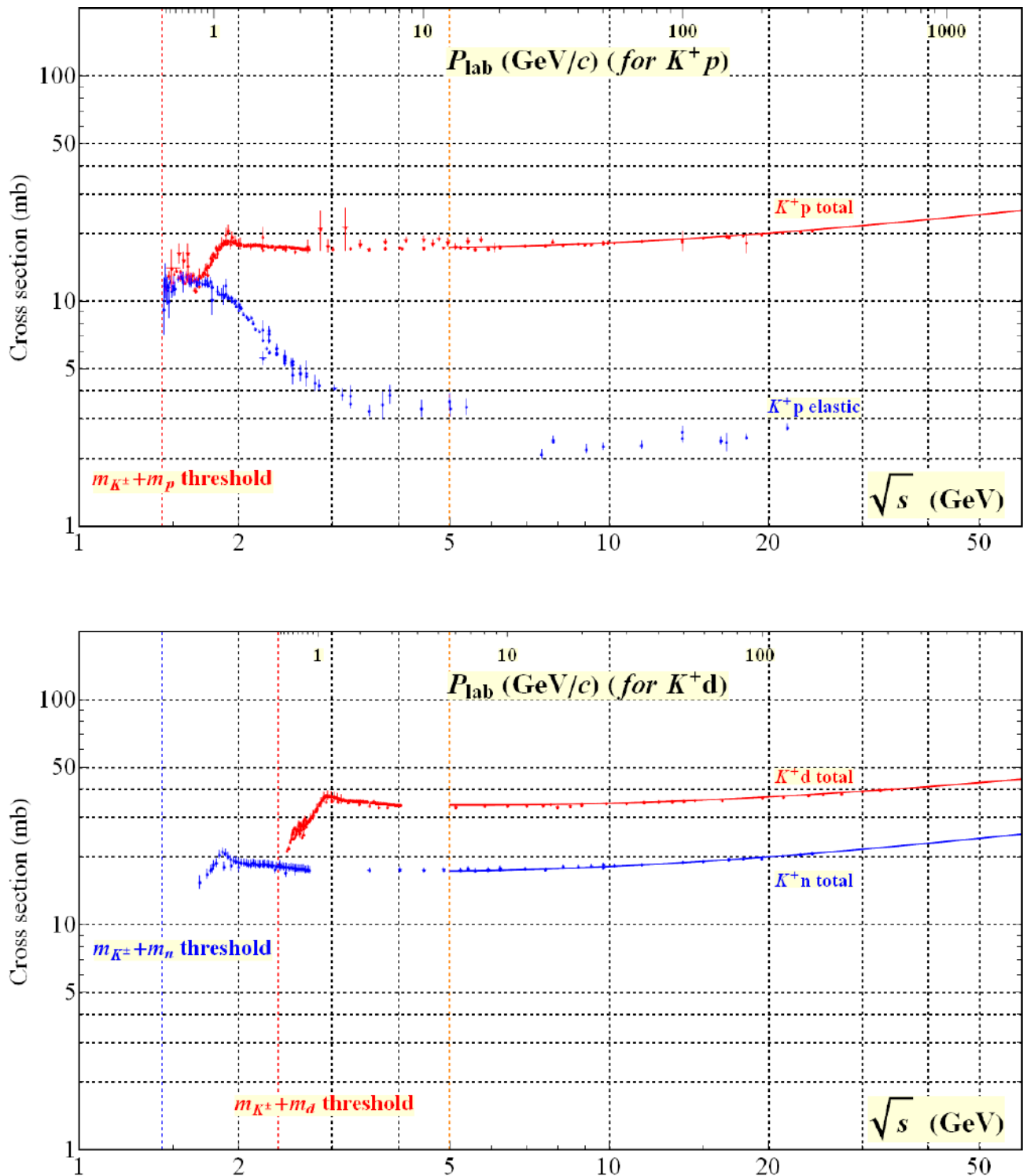


**Figure 52.10:** Total and elastic cross sections for  $K^+p$  and total cross sections for  $K^+d$  and  $K^+n$  collisions as a function of laboratory beam momentum and total center-of-mass energy. Corresponding computer-readable data files may be found at <http://pdg.lbl.gov/current/xsect/>. (Courtesy of the COMPAS Group, NRC KI – IHEP, Protvino, August 2019.)

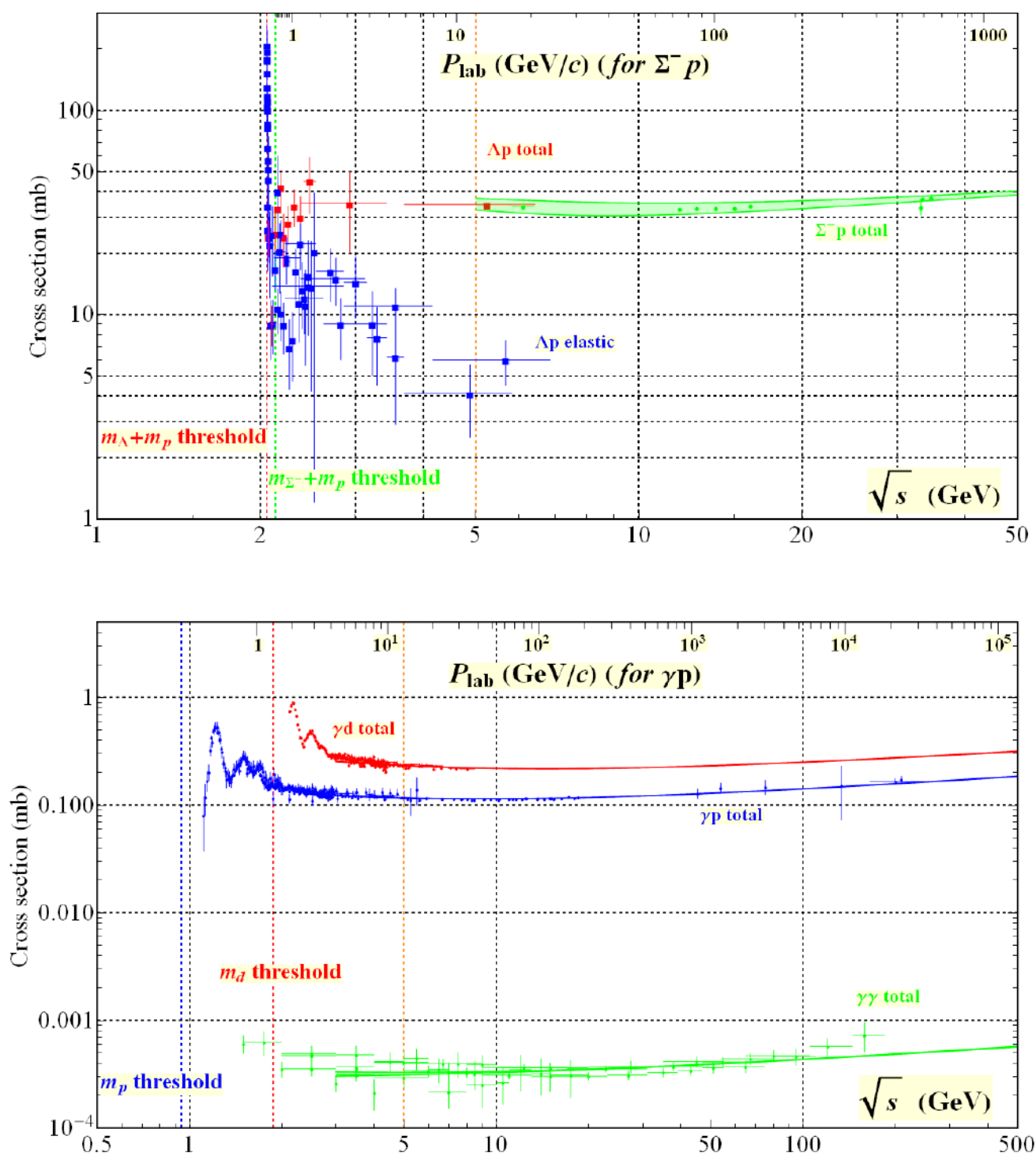


**Figure 52.11:** Total and elastic cross sections for  $\Delta p$ , total cross section for  $\Sigma^- p$ , and total hadronic cross sections for  $\gamma d$ ,  $\gamma p$ , and  $\gamma\gamma$  collisions as a function of laboratory beam momentum and the total center-of-mass energy. Corresponding computer-readable data files may be found at <http://pdg.lbl.gov/current/xsect/>. (Courtesy of the COMPAS group, NRC KI – IHEP, Protvino, August 2019.)

## References

- [1] G. J. Alner *et al.* (UA5), *Z. Phys.* **C33**, 1 (1986).
- [2] K. Alpgard *et al.* (UA5), *Phys. Lett.* **112B**, 183 (1982).
- [3] F. Abe *et al.* (CDF), *Phys. Rev.* **D41**, 2330 (1990), [119(1989)].
- [4] R. Harr *et al.*, *Phys. Lett.* **B401**, 176 (1997), [hep-ex/9703002].
- [5] K. Aamodt *et al.* (ALICE), *Eur. Phys. J.* **C68**, 89 (2010), [arXiv:1004.3034].
- [6] V. Khachatryan *et al.* (CMS), *JHEP* **02**, 041 (2010), [arXiv:1002.0621].
- [7] V. Khachatryan *et al.* (CMS), *Phys. Rev. Lett.* **105**, 022002 (2010), [arXiv:1005.3299].
- [8] H. Albrecht *et al.* (ARGUS), *Z. Phys.* **C54**, 1 (1992).
- [9] S. Behrends *et al.* (CLEO), *Phys. Rev.* **D31**, 2161 (1985).
- [10] J. P. Lees *et al.* (BaBar), *Phys. Rev.* **D88**, 032011 (2013), [arXiv:1306.2895].
- [11] H. Albrecht *et al.*, *Phys. Lett.* **102B**, 291 (1981).
- [12] K. Hikasa *et al.* (Particle Data Group), *Phys. Rev.* **D45**, S1 (1992), [Erratum: *Phys. Rev.*D46,5210(1992)].
- [13] R. Barate *et al.* (ALEPH), *Eur. Phys. J.* **C5**, 205 (1998).
- [14] P. Abreu *et al.* (DELPHI), *Eur. Phys. J.* **C5**, 585 (1998).
- [15] R. Akers *et al.* (OPAL), *Z. Phys.* **C63**, 181 (1994).
- [16] K. Abe *et al.* (SLD), *Phys. Rev.* **D69**, 072003 (2004), [hep-ex/0310017].
- [17] P. Abreu *et al.* (DELPHI), *Eur. Phys. J.* **C18**, 203 (2000), [Erratum: *Eur. Phys. J.*C25,493(2002)], [hep-ex/0103031].
- [18] D. D. Pitzl *et al.* (JADE), *Z. Phys.* **C46**, 1 (1990), [Erratum: *Z. Phys.*C47,676(1990)].
- [19] H. J. Behrend *et al.* (CELLO), *Z. Phys.* **C47**, 1 (1990).
- [20] R. Barate *et al.* (ALEPH), *Eur. Phys. J.* **C16**, 613 (2000).
- [21] W. Adam *et al.* (DELPHI), *Z. Phys.* **C69**, 561 (1996).
- [22] M. Acciarri *et al.* (L3), *Phys. Lett.* **B371**, 126 (1996).
- [23] G. Abbiendi *et al.* (OPAL), *Eur. Phys. J.* **C17**, 373 (2000), [hep-ex/0007017].
- [24] H. Albrecht *et al.* (ARGUS), *Z. Phys.* **C44**, 547 (1989).
- [25] P. Abreu *et al.* (DELPHI), *Nucl. Phys.* **B444**, 3 (1995).
- [26] H. J. Behrend *et al.* (CELLO), *Z. Phys.* **C46**, 397 (1990).
- [27] M. Derrick *et al.*, *Phys. Rev.* **D35**, 2639 (1987).
- [28] W. Bartel *et al.* (JADE), *Z. Phys.* **C20**, 187 (1983).
- [29] H. Schellman *et al.*, *Phys. Rev.* **D31**, 3013 (1985).
- [30] C. Berger *et al.* (PLUTO), *Phys. Lett.* **104B**, 79 (1981).
- [31] M. Althoff *et al.* (TASSO), *Z. Phys.* **C27**, 27 (1985).
- [32] H. Aihara *et al.* (TPC/Two Gamma), *Phys. Rev. Lett.* **53**, 2378 (1984).
- [33] P. Abreu *et al.* (DELPHI), *Z. Phys.* **C65**, 587 (1995).
- [34] M. Acciarri *et al.* (L3), *Phys. Lett.* **B407**, 389 (1997), [Erratum: *Phys. Lett.*B427,409(1998)].
- [35] R. Akers *et al.* (OPAL), *Z. Phys.* **C67**, 389 (1995).
- [36] K. Abe *et al.* (SLD), *Phys. Rev.* **D59**, 052001 (1999), [hep-ex/9805029].
- [37] H. Albrecht *et al.* (ARGUS), *Z. Phys.* **C46**, 15 (1990).
- [38] C. Bieler *et al.* (Crystal Ball), *Z. Phys.* **C49**, 225 (1991).
- [39] G. Wormser *et al.*, *Phys. Rev. Lett.* **61**, 1057 (1988).
- [40] A. Heister *et al.* (ALEPH), *Phys. Lett.* **B528**, 19 (2002), [hep-ex/0201012].
- [41] H. Albrecht *et al.* (ARGUS), *Z. Phys.* **C58**, 199 (1993).
- [42] M. Acciarri *et al.* (L3), *Phys. Lett.* **B393**, 465 (1997).
- [43] K. Ackerstaff *et al.* (OPAL), *Eur. Phys. J.* **C5**, 411 (1998), [hep-ex/9805011].
- [44] R. Seuster *et al.* (Belle), *Phys. Rev.* **D73**, 032002 (2006), [hep-ex/0506068].
- [45] M. Artuso *et al.* (CLEO), *Phys. Rev.* **D70**, 112001 (2004), [hep-ex/0402040].
- [46] P. Abreu *et al.* (DELPHI), *Z. Phys.* **C59**, 533 (1993), [Erratum: *Z. Phys.*C65,709(1995)].
- [47] G. Alexander *et al.* (OPAL), *Z. Phys.* **C72**, 1 (1996).
- [48] B. Aubert *et al.* (BaBar), *Phys. Rev.* **D65**, 091104 (2002), [hep-ex/0201041].
- [49] D. Bortoletto *et al.* (CLEO), *Phys. Rev.* **D37**, 1719 (1988), [Erratum: *Phys. Rev.*D39,1471(1989)].
- [50] P. Abreu *et al.* (DELPHI), *Z. Phys.* **C57**, 181 (1993).
- [51] J. Abdallah *et al.* (DELPHI), *Phys. Lett.* **B576**, 29 (2003), [hep-ex/0311005].
- [52] P. Abreu *et al.* (DELPHI), *Z. Phys.* **C61**, 407 (1994).
- [53] R. Akers *et al.* (OPAL), *Z. Phys.* **C66**, 555 (1995).
- [54] S. Abachi *et al.*, *Phys. Rev. Lett.* **57**, 1990 (1986).
- [55] P. Abreu *et al.* (DELPHI), *Phys. Lett.* **B449**, 364 (1999).
- [56] K. Ackerstaff *et al.* (OPAL), *Eur. Phys. J.* **C4**, 19 (1998), [hep-ex/9802013].
- [57] H. Albrecht *et al.* (ARGUS), *Z. Phys.* **C61**, 1 (1994).
- [58] D. Buskulic *et al.* (ALEPH), *Z. Phys.* **C69**, 379 (1996).
- [59] R. Barate *et al.* (ALEPH), *Phys. Rept.* **294**, 1 (1998).
- [60] P. D. Acton *et al.* (OPAL), *Phys. Lett.* **B305**, 407 (1993).
- [61] P. Abreu *et al.* (DELPHI), *Z. Phys.* **C73**, 61 (1996).
- [62] K. Ackerstaff *et al.* (OPAL), *Phys. Lett.* **B412**, 210 (1997), [hep-ex/9708022].
- [63] R. Barate *et al.* (ALEPH), *Eur. Phys. J.* **C16**, 597 (2000), [hep-ex/9909032].
- [64] K. Ackerstaff *et al.* (OPAL), *Eur. Phys. J.* **C1**, 439 (1998), [hep-ex/9708021].
- [65] K. Ackerstaff *et al.* (OPAL), *Eur. Phys. J.* **C5**, 1 (1998), [hep-ex/9802008].
- [66] P. Abreu *et al.* (DELPHI), *Z. Phys.* **C68**, 353 (1995).
- [67] M. Acciarri *et al.* (L3), *Phys. Lett.* **B345**, 589 (1995).
- [68] B. Aubert *et al.* (BaBar), *Phys. Rev. Lett.* **87**, 162002 (2001), [hep-ex/0106044].
- [69] K. Abe *et al.* (Belle), *Phys. Rev. Lett.* **88**, 052001 (2002), [hep-ex/0110012].
- [70] D. Buskulic *et al.* (ALEPH), *Phys. Lett.* **B295**, 396 (1992).
- [71] P. Abreu *et al.* (DELPHI), *Phys. Lett.* **B341**, 109 (1994).
- [72] M. Acciarri *et al.* (L3), *Phys. Lett.* **B453**, 94 (1999).
- [73] G. Alexander *et al.* (OPAL), *Z. Phys.* **C70**, 197 (1996).
- [74] M. Acciarri *et al.* (L3), *Phys. Lett.* **B407**, 351 (1997).
- [75] G. Alexander *et al.* (OPAL), *Phys. Lett.* **B370**, 185 (1996).
- [76] J. Abdallah *et al.* (DELPHI), *Phys. Lett.* **B569**, 129 (2003), [hep-ex/0309057].
- [77] A. De Angelis, *J. Phys.* **G19**, 1233 (1993).
- [78] S. Abachi *et al.*, *Phys. Lett.* **B199**, 151 (1987).
- [79] R. Akers *et al.* (OPAL), *Z. Phys.* **C68**, 1 (1995).
- [80] P. Abreu *et al.* (DELPHI), *Phys. Lett.* **B345**, 598 (1995).
- [81] A. Heister *et al.* (ALEPH), *Phys. Lett.* **B526**, 34 (2002), [hep-ex/0112010].
- [82] H. Albrecht *et al.* (ARGUS), *Z. Phys.* **C39**, 177 (1988).
- [83] M. Niiyama *et al.* (Belle), *Phys. Rev.* **D97**, 7, 072005 (2018), [arXiv:1706.06791].
- [84] P. Abreu *et al.* (DELPHI), *Z. Phys.* **C67**, 543 (1995).
- [85] G. Alexander *et al.* (OPAL), *Z. Phys.* **C73**, 569 (1997).
- [86] W. Adam *et al.* (DELPHI), *Z. Phys.* **C70**, 371 (1996).
- [87] M. Acciarri *et al.* (L3), *Phys. Lett.* **B479**, 79 (2000), [hep-ex/0002066].

- [88] G. Alexander *et al.* (OPAL), *Z. Phys.* **C73**, 587 (1997).
- [89] P. Abreu *et al.* (DELPHI), *Phys. Lett.* **B475**, 429 (2000), [hep-ex/0103020].
- [90] H. Albrecht *et al.* (ARGUS), *Phys. Lett.* **B230**, 169 (1989).
- [91] P. Abreu *et al.* (DELPHI), *Phys. Lett.* **B361**, 207 (1995).
- [92] G. Alexander *et al.* (OPAL), *Phys. Lett.* **B358**, 162 (1995).
- [93] S. Abachi *et al.*, *Phys. Rev. Lett.* **58**, 2627 (1987), [Erratum: *Phys. Rev. Lett.*59,2388(1987)].
- [94] J. Abdallah *et al.* (DELPHI), *Eur. Phys. J.* **C44**, 299 (2005), [hep-ex/0510023].
- [95] B. Aubert *et al.* (BaBar), *Phys. Rev.* **D75**, 012003 (2007), [hep-ex/0609004].
- [96] P. D. Acton *et al.* (OPAL), *Phys. Lett.* **B281**, 394 (1992).
- [97] H. Albrecht *et al.* (ARGUS), *Phys. Rept.* **276**, 223 (1996).
- [98] R. Giles *et al.* (CLEO), *Phys. Rev.* **D29**, 1285 (1984).
- [99] K. G. Chetyrkin, R. V. Harlander and J. H. Kuhn, *Nucl. Phys.* **B586**, 56 (2000), [Erratum: *Nucl. Phys.*B634,413(2002)], [hep-ph/0005139].
- [100] V. V. Ezhela, S. B. Lugovsky and O. V. Zenin (2003), [hep-ph/0312114].
- [101] R. Barate *et al.* (ALEPH), *Eur. Phys. J.* **C14**, 1 (2000).
- [102] P. Abreu *et al.* (DELPHI), *Eur. Phys. J.* **C16**, 371 (2000).
- [103] M. Acciarri *et al.* (L3), *Eur. Phys. J.* **C16**, 1 (2000), [hep-ex/0002046].
- [104] G. Abbiendi *et al.* (OPAL), *Eur. Phys. J.* **C19**, 587 (2001), [hep-ex/0012018].
- [105] S. Schael *et al.* (ALEPH, DELPHI, L3, OPAL, SLD, LEP Electroweak Working Group, SLD Electroweak Group, SLD Heavy Flavour Group), *Phys. Rept.* **427**, 257 (2006), [hep-ex/0509008].
- [106] P. Collins, *An Introduction to Regge Theory and High-Energy Physics*, Cambridge Monographs on Mathematical Physics, Cambridge Univ. Press, Cambridge, UK (2009), ISBN 9780521110358.
- [107] G. Pancheri and Y. N. Srivastava, *Eur. Phys. J.* **C77**, 3, 150 (2017), [arXiv:1610.10038].
- [108] L. A. Harland-Lang, V. A. Khoze and M. G. Ryskin, *Int. J. Mod. Phys.* **A30**, 1542013 (2015).
- [109] V. A. Petrov and A. Prokudin, *Phys. Rev.* **D87**, 3, 036003 (2013), [arXiv:1212.1924].
- [110] C. Bourrely, J. Soffer and T. T. Wu, *Eur. Phys. J.* **C28**, 97 (2003), [hep-ph/0210264].
- [111] M. M. Block *et al.*, *Phys. Rev.* **D92**, 1, 014030 (2015), [arXiv:1505.04842].
- [112] O. V. Selyugin, *Phys. Rev.* **D91**, 11, 113003 (2015), [Erratum: *Phys. Rev.*D92,no.9,099901(2015)], [arXiv:1505.02426].
- [113] L. G. Dakhno and V. A. Nikonov, *Eur. Phys. J.* **A5**, 209 (1999), [hep-ph/9902320].
- [114] A. A. Godizov, *Phys. Lett.* **B735**, 57 (2014), [arXiv:1404.2851].
- [115] E. Gotsman, E. M. Levin and U. Maor, *Phys. Rev.* **D49**, R4321 (1994), [hep-ph/9310257].
- [116] A. Donnachie and P. V. Landshoff, *Phys. Lett.* **B727**, 500 (2013), [Erratum: *Phys. Lett.*B750,669(2015)], [arXiv:1309.1292].
- [117] E. Martynov, *Phys. Rev.* **D87**, 11, 114018 (2013), [arXiv:1305.3093].
- [118] L. Jenkovszky, *Nuovo Cim.* **C037**, 02, 99 (2014).
- [119] S. M. Troshin and N. E. Tyurin, *Int. J. Mod. Phys.* **A32**, 17, 1750103 (2017), [arXiv:1704.00443].
- [120] V. V. Anisovich, *Phys. Usp.* **58**, 10, 963 (2015).
- [121] D. A. Fagundes, M. J. Menon and P. V. R. G. Silva, *Nucl. Phys.* **A946**, 194 (2016), [arXiv:1509.04108].
- [122] E. Martynov and B. Nicolescu, *Eur. Phys. J.* **C56**, 57 (2008), [arXiv:0712.1685].
- [123] W. Heisenberg, *Z. Phys.* **133**, 65 (1952).
- [124] J. R. Cudell *et al.*, *Phys. Rev.* **D65**, 074024 (2002), [hep-ph/0107219].
- [125] H. Nastase and J. Sonnenschein, *Phys. Rev.* **D92**, 105028 (2015), [arXiv:1504.01328].
- [126] V. I. Belousov *et al.*, *Phys. Atom. Nucl.* **79**, 1, 113 (2016), [*Yad. Fiz.*79,no.1,55(2016)].
- [127] C. Patrignani *et al.* (Particle Data Group), *Chin. Phys.* **C40**, 10, 100001 (2016).



## Particle Properties

### Gauge Bosons

53. Mass and width of the $W$ boson (rev.)	715
54. $Z$ boson	717

### Charged Leptons

55. Muon anomalous magnetic moment (rev.)	722
56. Muon decay parameters (rev.)	725
57. $\tau$ branching fractions (rev.)	728
58. $\tau$ -lepton decay parameters	731

### Quarks

59. Quark masses (rev.)	733
60. Top quark (rev.)	741

### Mesons

61. Form factors for rad. pion & kaon decays (rev.)	762
62. Scalar mesons below 2 GeV (rev.)	764
63. Pseudoscalar and pseudovector mesons in the 1400 MeV region (rev.)	771
64. Rare kaon decays (rev.)	774
65. $CPT$ invariance tests in neutral kaon decay (rev.)	779
66. $V_{ud}$ , $V_{us}$ , Cabibbo angle, and CKM unitarity (rev.)	781
67. $CP$ -violation in $K_L$ decays	784
68. Review of multibody charm analyses (rev.)	788
69. $D^0-\bar{D}^0$ mixing (rev.)	792
70. $D_s^+$ branching fractions (rev.)	801
71. Leptonic decays of charged pseudoscalar mesons (rev.)	803
72. Production and decay of $b$ -flavored hadrons (rev.)	814
73. Polarization in $B$ decays (rev.)	824
74. $B^0-\bar{B}^0$ mixing (rev.)	828
75. Semileptonic $B$ decays, $V_{cb}$ and $V_{ub}$ (rev.)	835
76. CKM angles from $B$ hadrons, Determination of (new)	849
77. Spectroscopy of mesons containing two heavy quarks (rev.)	854
78. Non- $q\bar{q}$ mesons (rev.)	861

### Baryons

79. Baryon decay parameters	868
80. $N$ and $\Delta$ resonances (rev.)	869
81. Baryon magnetic moments	874
82. $\Lambda$ and $\Sigma$ resonances (rev.)	875
83. Pole structure of the $\Lambda(1405)$ region (rev.)	878
84. Charmed baryons (rev.)	879
85. Pentaquarks (rev.)	881

## Notes in Volume 2

Extraction of triple gauge couplings (TGC's)	1017
Anomalous $ZZ\gamma$ , $Z\gamma\gamma$ , and $ZZV$ couplings	1042
Anomalous $W/Z$ quartic couplings	1043
Neutrino properties (rev.)	1135
Sum of neutrino masses (rev.)	1138
Number of light neutrino types from collider experiments	1143
Neutrinoless double- $\beta$ decay (rev.)	1145
Three-neutrino mixing parameters (rev.)	1155
$\rho(770)$ (rev.)	1221
$\rho(1450)$ and the $\rho(1700)$ (rev.)	1302
Charged kaon mass	1337
Dalitz plot parameters for $K \rightarrow 3\pi$ decays	1345
$K_{\ell 3}^{\pm}$ and $K_{\ell 3}^0$ form factors	1347
$CP$ -violation in $K_S \rightarrow 3\pi$	1357
Heavy Flavor Averaging Group (rev.)	1465
Charmonium system (rev.)	1668
Branching ratios of $\psi(2S)$ and $\chi_{c0,1,2}$ (rev.)	1698
Bottomonium system (rev.)	1782
Width determination of the $\Upsilon$ states	1782
$\Sigma(1670)$ region	1938
Radiative hyperon decays	1960
$\Xi$ resonances	1964





## 53. Mass and Width of the W Boson

Revised June 2019 by M.W. Grünewald (U. College Dublin) and A. Gurtu (Kyung Hee U.).

Precision determination of the W-mass is of great importance in testing the internal consistency of the Standard Model. From the time of its discovery in 1983, the W-boson has been studied and its mass determined in  $p\bar{p}$  and  $e^+e^-$  interactions; it is currently studied in pp interactions at the LHC. The W mass and width definition used here corresponds to a Breit-Wigner with mass-dependent width.

Production of on-shell W bosons at hadron colliders is tagged by the high  $p_T$  charged lepton from its decay. Owing to the unknown parton-parton effective energy and missing energy in the longitudinal direction, the collider experiments reconstruct the transverse mass of the W, and derive the W mass from comparing the transverse mass distribution with Monte Carlo predictions as a function of  $M_W$ . These analyses use the electron and muon decay modes of the W boson.

In the  $e^+e^-$  collider (LEP) a precise knowledge of the beam energy enables one to determine the  $e^+e^- \rightarrow W^+W^-$  cross section as a function of center of mass energy, as well as to reconstruct the W mass precisely from its decay products, even if one of them decays leptonically. Close to the  $W^+W^-$  threshold (161 GeV), the dependence of the W-pair production cross section on  $M_W$  is large, and this was used to determine  $M_W$ . At higher energies (172 to 209 GeV) this dependence is much weaker and W-bosons were directly reconstructed and the mass determined as the invariant mass of its decay products, improving the resolution with a kinematic fit.

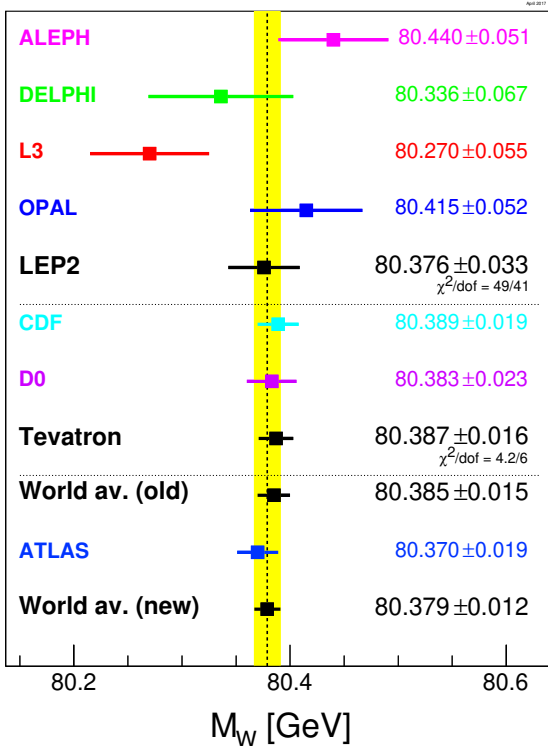


**Figure 53.1:** Measurements of the W-boson mass by the LEP, Tevatron and LHC experiments.

In order to compute the LEP average W mass, each experiment provided its measured W mass for the  $q\bar{q}q\bar{q}$  and  $q\bar{q}l\bar{\nu}_\ell$ ,  $\ell = e, \mu, \tau$  channels at each center-of-mass energy, along with a detailed break-up of errors: statistical, uncorrelated, partially correlated and fully correlated systematics [1]. These have been combined to obtain a LEP W mass of  $M_W = 80.376 \pm 0.033$  GeV. Errors due to uncertainties in LEP energy (9 MeV), and possible effect of color reconnection (CR) and Bose-Einstein correlations (BEC) between quarks from different W's (8 MeV) are included. The mass difference between  $q\bar{q}q\bar{q}$  and

$q\bar{q}l\bar{\nu}_\ell$  final states (due to possible CR and BEC effects) is  $-12 \pm 45$  MeV. In a similar manner, the width results obtained at LEP have been combined, resulting in  $\Gamma_W = 2.195 \pm 0.083$  GeV [1].

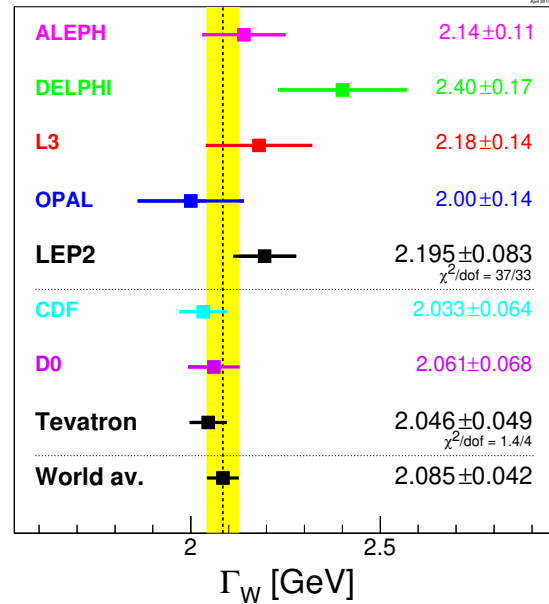


**Figure 53.2:** Measurements of the W-boson width by the LEP and Tevatron experiments.

The two Tevatron experiments have also identified common systematic errors. Between the two experiments, uncertainties due to the parton distribution functions, radiative corrections, and choice of mass (width) in the width (mass) measurements are treated as correlated. An average W width of  $\Gamma_W = 2.046 \pm 0.049$  GeV [2] is obtained. Errors of 20 MeV and 7 MeV accounting for PDF and radiative correction uncertainties in this width combination dominate the correlated uncertainties. At the 2011/12 winter conferences, the CDF and D0 experiments have presented new results for the mass of the W boson based on  $2 - 4 \text{ fb}^{-1}$  of Run-II data,  $80.387 \pm 0.019$  GeV [3] and  $80.375 \pm 0.023$  GeV [4], respectively. The W-mass determination from the Tevatron experiments has thus become very precise. Combining all Tevatron results from Run-I and Run-II using an improved treatment of correlations, a new average of  $80.387 \pm 0.016$  GeV is obtained [5], with common uncertainties of 10 MeV (PDF) and 4 MeV (radiative corrections).

Good agreement between the LEP and Tevatron results is observed. Combining these results, assuming no common systematic uncertainties between the LEP and the Tevatron measurements, yields an average W mass of  $M_W = 80.385 \pm 0.015$  GeV and a W width of  $\Gamma_W = 2.085 \pm 0.042$  GeV.

At the 2016/17 winter conferences, the ATLAS collaboration presented a measurement of the mass of the W boson in pp collisions at  $\sqrt{s} = 7$  TeV,  $M_W = 80.370 \pm 0.019$  GeV, since then published [6], which is compatible with the above world average and of similar precision to the best measurements of CDF and D0. Assuming a Tevatron/LHC common PDF uncertainty of 7 MeV [7], this results in a new world average of  $M_W = 80.379 \pm 0.012$  GeV.

The LEP, Tevatron and LHC results on mass and width, which are based on all results available, are compared in Fig. 53.1 and Fig. 53.2. The Standard Model prediction from the electroweak fit, including Z-pole data and  $m_{\text{top}}$  and  $M_H$  measurements, gives a W-boson mass of  $M_W = 80.354 \pm 0.007$  GeV and a W-boson width of  $\Gamma_W = 2.091 \pm 0.001$  GeV [8].

## References:

1. The LEP Collaborations: ALEPH, DELPHI, L3, OPAL, the LEP Electroweak Working Group, CERN-PH-EP/2013-022, [arXiv:1302.3415 \[hep-ex\]](#), Phys.Rept. 532 (2013) 119-244.
2. The Tevatron Electroweak Working Group, for the CDF and D0 Collaborations: *Combination of CDF and D0 Results on the Width of the  $W$  Boson*, March 2010, [arXiv:1003.2826 \[hep-ex\]](#).
3. The CDF Collaboration, *Precise measurement of the  $W$ -boson mass with the CDF II detector*, [arXiv:1203.0275 \[hep-ex\]](#), Phys. Rev. Lett. **108**, 151803 (2012).
4. The D0 Collaboration, *Measurement of the  $W$  Boson Mass with the D0 Detector*, [arXiv:1203.0293 \[hep-ex\]](#), Phys. Rev. Lett. **108**, 151804 (2012).
5. The CDF and D0 Collabs: *Combination of CDF and D0  $W$ -Boson Mass Measurements*, July 2013, [arXiv:1307.7627 \[hep-ex\]](#), Phys. Rev. **D88**, 052018 (2013).
6. The ATLAS Collaboration, *Measurement of the  $W$ -boson mass in  $pp$  collisions at  $\sqrt{s} = 7$  TeV with the ATLAS detector*, January 2017, [arXiv:1701.07240 \[hep-ex\]](#), Eur.Phys.J. C78 (2018) no.2, 110.
7. Jens Erler, *Precision in  $EW$  measurements at Run 2 and beyond*, Talk presented at the *52nd Rencontres de Moriond EW*, March 2017.
8. J. Haller et al., *Update of the global electroweak fit and constraints on two-Higgs-doublet models*, Eur. Phys. J. C78, 675 (2018).

## 54. Z Boson

Revised September 2013 by M.W. Gr unewald (U. College Dublin and U. Ghent) and A. Gurtu (Formerly Tata Inst.).

Precision measurements at the  $Z$ -boson resonance using electron–positron colliding beams began in 1989 at the SLC and at LEP. During 1989–95, the four LEP experiments (ALEPH, DELPHI, L3, OPAL) made high-statistics studies of the production and decay properties of the  $Z$ . Although the SLD experiment at the SLC collected much lower statistics, it was able to match the precision of LEP experiments in determining the effective electroweak mixing angle  $\sin^2\bar{\theta}_W$  and the rates of  $Z$  decay to  $b$ - and  $c$ -quarks, owing to availability of polarized electron beams, small beam size, and stable beam spot.

The  $Z$ -boson properties reported in this section may broadly be categorized as:

- The standard ‘lineshape’ parameters of the  $Z$  consisting of its mass,  $M_Z$ , its total width,  $\Gamma_Z$ , and its partial decay widths,  $\Gamma(\text{hadrons})$ , and  $\Gamma(\ell\bar{\ell})$  where  $\ell = e, \mu, \tau, \nu$ ;
- $Z$  asymmetries in leptonic decays and extraction of  $Z$  couplings to charged and neutral leptons;
- The  $b$ - and  $c$ -quark-related partial widths and charge asymmetries which require special techniques;
- Determination of  $Z$  decay modes and the search for modes that violate known conservation laws;
- Average particle multiplicities in hadronic  $Z$  decay;
- $Z$  anomalous couplings.

The effective vector and axial-vector coupling constants describing the  $Z$ -to-fermion coupling are also measured in  $p\bar{p}$  and  $ep$  collisions at the Tevatron and at HERA. The corresponding cross-section formulae are given in Section 39 (Cross-section formulae for specific processes) and Section 16 (Structure Functions) in this *Review*. In this minireview, we concentrate on the measurements in  $e^+e^-$  collisions at LEP and SLC.

The standard ‘lineshape’ parameters of the  $Z$  are determined from an analysis of the production cross sections of these final states in  $e^+e^-$  collisions. The  $Z \rightarrow \nu\bar{\nu}(\gamma)$  state is identified directly by detecting single photon production and indirectly by subtracting the visible partial widths from the total width. Inclusion in this analysis of the forward-backward asymmetry of charged leptons,  $A_{FB}^{(0,\ell)}$ , of the  $\tau$  polarization,  $P(\tau)$ , and its forward-backward asymmetry,  $P(\tau)^{fb}$ , enables the separate determination of the effective vector ( $\bar{g}_V$ ) and axial vector ( $\bar{g}_A$ ) couplings of the  $Z$  to these leptons and the ratio ( $\bar{g}_V/\bar{g}_A$ ), which is related to the effective electroweak mixing angle  $\sin^2\bar{\theta}_W$  (see the ‘‘Electroweak Model and Constraints on New Physics’’ review).

Determination of the  $b$ - and  $c$ -quark-related partial widths and charge asymmetries involves tagging the  $b$  and  $c$  quarks for which various methods are employed: requiring the presence of a high momentum prompt lepton in the event with high transverse momentum with respect to the accompanying jet; impact parameter and lifetime tagging using precision vertex measurement with high-resolution detectors; application of neural-network techniques to classify events as  $b$  or non- $b$  on a statistical basis using event–shape variables; and using the presence of a charmed meson ( $D/D^*$ ) or a kaon as a tag.

### 54.1. $Z$ -parameter determination

LEP was run at energy points on and around the  $Z$  mass (88–94 GeV) constituting an energy ‘scan.’ The shape of the cross-section variation around the  $Z$  peak can be described by a Breit-Wigner ansatz with an energy-dependent total width [1–3]. The **three** main properties of this distribution, viz., the **position** of the peak, the **width** of the distribution, and the **height** of the peak, determine respectively the values of  $M_Z$ ,  $\Gamma_Z$ , and  $\Gamma(e^+e^-) \times \Gamma(f\bar{f})$ , where  $\Gamma(e^+e^-)$  and  $\Gamma(f\bar{f})$  are the electron and fermion partial widths of the  $Z$ . The quantitative determination of these parameters is done by writing analytic expressions for these cross sections in terms of the parameters, and fitting the calculated cross sections to the measured ones by varying these parameters, taking properly into account all the

errors. Single-photon exchange ( $\sigma_\gamma^0$ ) and  $\gamma$ - $Z$  interference ( $\sigma_{\gamma Z}^0$ ) are included, and the large ( $\sim 25\%$ ) initial-state radiation (ISR) effects are taken into account by convoluting the analytic expressions over a ‘Radiator Function’ [1–5]  $H(s, s')$ . Thus for the process  $e^+e^- \rightarrow f\bar{f}$ :

$$\sigma_f(s) = \int H(s, s') \sigma_f^0(s') ds' \quad (54.1)$$

$$\sigma_f^0(s) = \sigma_Z^0 + \sigma_\gamma^0 + \sigma_{\gamma Z}^0 \quad (54.2)$$

$$\sigma_Z^0 = \frac{12\pi}{M_Z^2} \frac{\Gamma(e^+e^-)\Gamma(f\bar{f})}{\Gamma_Z^2} \frac{s \Gamma_Z^2}{(s - M_Z^2)^2 + s^2\Gamma_Z^2/M_Z^2} \quad (54.3)$$

$$\sigma_\gamma^0 = \frac{4\pi\alpha^2(s)}{3s} Q_f^2 N_c^f \quad (54.4)$$

$$\begin{aligned} \sigma_{\gamma Z}^0 = & -\frac{2\sqrt{2}\alpha(s)}{3} (Q_f G_F N_c^f \mathcal{G}_V^f \mathcal{G}_V^f) \\ & \times \frac{(s - M_Z^2)M_Z^2}{(s - M_Z^2)^2 + s^2\Gamma_Z^2/M_Z^2} \end{aligned} \quad (54.5)$$

where  $Q_f$  is the charge of the fermion,  $N_c^f = 3$  for quarks and 1 for leptons, and  $\mathcal{G}_V^f$  is the vector coupling of the  $Z$  to the fermion-antifermion pair  $f\bar{f}$ .

Since  $\sigma_{\gamma Z}^0$  is expected to be much less than  $\sigma_Z^0$ , the LEP Collaborations have generally calculated the interference term in the framework of the Standard Model. This fixing of  $\sigma_{\gamma Z}^0$  leads to a tighter constraint on  $M_Z$ , and consequently a smaller error on its fitted value. It is possible to relax this constraint and carry out the fit within the S-matrix framework, which is briefly described in the next section.

In the above framework, the QED radiative corrections have been explicitly taken into account by convoluting over the ISR and allowing the electromagnetic coupling constant to run [6]:  $\alpha(s) = \alpha/(1 - \Delta\alpha)$ . On the other hand, weak radiative corrections that depend upon the assumptions of the electroweak theory and on the values of  $M_{\text{top}}$  and  $M_{\text{Higgs}}$  are accounted for by **absorbing them into the couplings**, which are then called the *effective* couplings  $\mathcal{G}_V$  and  $\mathcal{G}_A$  (or alternatively the effective parameters of the  $*$  scheme of Kennedy and Lynn [7].)

$\mathcal{G}_V^f$  and  $\mathcal{G}_A^f$  are complex numbers with small imaginary parts. As experimental data does not allow simultaneous extraction of both real and imaginary parts of the effective couplings, the convention  $g_A^f = \text{Re}(\mathcal{G}_A^f)$  and  $g_V^f = \text{Re}(\mathcal{G}_V^f)$  is used and the imaginary parts are added in the fitting code [4].

Defining

$$A_f = 2 \frac{g_V^f \cdot g_A^f}{(g_V^f)^2 + (g_A^f)^2} \quad (54.6)$$

the lowest-order expressions for the various lepton-related asymmetries on the  $Z$  pole are [8–10]  $A_{FB}^{(0,\ell)} = (3/4)A_e A_f$ ,  $P(\tau) = -A_\tau$ ,  $P(\tau)^{fb} = -(3/4)A_e$ ,  $A_{LR} = A_e$ . The full analysis takes into account the energy-dependence of the asymmetries. Experimentally  $A_{LR}$  is defined as  $(\sigma_L - \sigma_R)/(\sigma_L + \sigma_R)$ , where  $\sigma_{L(R)}$  are the  $e^+e^- \rightarrow Z$  production cross sections with left- (right)-handed electrons.

The definition of the partial decay width of the  $Z$  to  $f\bar{f}$  includes the effects of QED and QCD final-state corrections, as well as the contribution due to the imaginary parts of the couplings:

$$\Gamma(f\bar{f}) = \frac{G_F M_Z^3}{6\sqrt{2}\pi} N_c^f (|\mathcal{G}_A^f|^2 R_A^f + |\mathcal{G}_V^f|^2 R_V^f) + \Delta_{ew/\text{QCD}} \quad (54.7)$$

where  $R_V^f$  and  $R_A^f$  are radiator factors to account for final state QED and QCD corrections, as well as effects due to nonzero fermion masses, and  $\Delta_{ew/\text{QCD}}$  represents the non-factorizable electroweak/QCD corrections.

### 54.2. S-matrix approach to the Z

While most experimental analyses of LEP/SLC data have followed the ‘Breit-Wigner’ approach, an alternative S-matrix-based analysis is also possible. The Z, like all unstable particles, is associated with a complex pole in the S matrix. The pole position is process-independent and gauge-invariant. The mass,  $\overline{M}_Z$ , and width,  $\overline{\Gamma}_Z$ , can be defined in terms of the pole in the energy plane via [11–14]

$$\overline{s} = \overline{M}_Z^2 - i\overline{M}_Z\overline{\Gamma}_Z \quad (54.8)$$

leading to the relations

$$\begin{aligned} \overline{M}_Z &= M_Z / \sqrt{1 + \Gamma_Z^2 / M_Z^2} \\ &\approx M_Z - 34.1 \text{ MeV} \end{aligned} \quad (54.9)$$

$$\begin{aligned} \overline{\Gamma}_Z &= \Gamma_Z / \sqrt{1 + \Gamma_Z^2 / M_Z^2} \\ &\approx \Gamma_Z - 0.9 \text{ MeV} . \end{aligned} \quad (54.10)$$

The LEP collaborations [15] have analyzed their data using the S-matrix approach as defined in Eq. (54.8), in addition to the conventional one. They observe a downward shift in the Z mass as expected.

### 54.3. Handling the large-angle $e^+e^-$ final state

Unlike other  $f\overline{f}$  decay final states of the Z, the  $e^+e^-$  final state has a contribution not only from the s-channel but also from the t-channel and s-t interference. The full amplitude is not amenable to fast calculation, which is essential if one has to carry out minimization fits within reasonable computer time. The usual procedure is to calculate the non-s channel part of the cross section separately using the Standard Model programs ALIBABA [16] or TOPAZO [17], with the measured value of  $M_{\text{top}}$ , and  $M_{\text{Higgs}} = 150 \text{ GeV}$ , and add it to the s-channel cross section calculated as for other channels. This leads to two additional sources of error in the analysis: firstly, the theoretical calculation in ALIBABA itself is known to be accurate to  $\sim 0.5\%$ , and secondly, there is uncertainty due to the error on  $M_{\text{top}}$  and the unknown value of  $M_{\text{Higgs}}$  (100–1000 GeV). These errors are propagated into the analysis by including them in the systematic error on the  $e^+e^-$  final state. As these errors are common to the four LEP experiments, this is taken into account when performing the LEP average.

### 54.4. Errors due to uncertainty in LEP energy determination

The systematic errors related to the LEP energy measurement, see Refs. 18–23, can be classified as:

- The absolute energy scale error;
- Energy-point-to-energy-point errors due to the nonlinear response of the magnets to the exciting currents;
- Energy-point-to-energy-point errors due to possible higher-order effects in the relationship between the dipole field and beam energy;
- Energy reproducibility errors due to various unknown uncertainties in temperatures, tidal effects, corrector settings, RF status, etc.

Precise energy calibration was done outside normal data-taking using the resonant depolarization technique. Run-time energies were determined every 10 minutes by measuring the relevant machine parameters and using a model which takes into account all the known effects, including leakage currents produced by trains in the Geneva area and the tidal effects due to gravitational forces of the Sun and the Moon. The LEP Energy Working Group has provided a covariance matrix from the determination of LEP energies for the different running periods during 1993–1995 [18].

### 54.5. Choice of fit parameters

The LEP Collaborations have chosen the following primary set of parameters for fitting:  $M_Z$ ,  $\Gamma_Z$ ,  $\sigma_{\text{hadron}}^0$ ,  $R(\text{lepton})$ ,  $A_{FB}^{(0,\ell)}$ , where  $R(\text{lepton}) = \Gamma(\text{hadrons})/\Gamma(\text{lepton})$ ,  $\sigma_{\text{hadron}}^0 = 12\pi\Gamma(e^+e^-)\Gamma(\text{hadrons})/M_Z^2\Gamma_Z^2$ . With a knowledge of these fitted parameters and their covariance matrix, any other parameter can be derived. The main advantage of these parameters is that they form a physics motivated set of parameters with much reduced correlations.

Thus, the most general fit carried out to cross section and asymmetry data determines the **nine parameters**:  $M_Z$ ,  $\Gamma_Z$ ,  $\sigma_{\text{hadron}}^0$ ,  $R(e)$ ,  $R(\mu)$ ,  $R(\tau)$ ,  $A_{FB}^{(0,e)}$ ,  $A_{FB}^{(0,\mu)}$ ,  $A_{FB}^{(0,\tau)}$ . Assumption of lepton universality leads to a **five-parameter fit** determining  $M_Z$ ,  $\Gamma_Z$ ,  $\sigma_{\text{hadron}}^0$ ,  $R(\text{lepton})$ ,  $A_{FB}^{(0,\ell)}$ .

### 54.6. Combining results from LEP and SLC experiments

With a steady increase in statistics over the years and improved understanding of the common systematic errors between LEP experiments, the procedures for combining results have evolved continuously [24]. The Line Shape Sub-group of the LEP Electroweak Working Group investigated the effects of these common errors, and devised a combination procedure for the precise determination of the Z parameters from LEP experiments. Using these procedures, this note also gives the results after combining the final parameter sets from the four experiments, and these are the results quoted as the fit results in the Z listings below. Transformation of variables leads to values of derived parameters like partial decay widths and branching ratios to hadrons and leptons. Finally, transforming the LEP combined nine parameter set to  $(M_Z, \Gamma_Z, \sigma_{\text{hadron}}^0, g_A^f, g_V^f, f = e, \mu, \tau)$  using the average values of lepton asymmetry parameters ( $A_e, A_\mu, A_\tau$ ) as constraints, leads to the best fitted values of the vector and axial-vector couplings ( $g_V, g_A$ ) of the charged leptons to the Z.

Brief remarks on the handling of common errors and their magnitudes are given below. The identified common errors are those coming from

- LEP energy-calibration uncertainties, and
- the theoretical uncertainties in (i) the luminosity determination using small angle Bhabha scattering, (ii) estimating the non-s channel contribution to large angle Bhabha scattering, (iii) the calculation of QED radiative effects, and (iv) the parametrization of the cross section in terms of the parameter set used.

### 54.7. Common LEP energy errors

All the collaborations incorporate in their fit the full LEP energy error matrix as provided by the LEP energy group for their intersection region [18]. The effect of these errors is separated out from that of other errors by carrying out fits with energy errors scaled up and down by  $\sim 10\%$  and redoing the fits. From the observed changes in the overall error matrix, the covariance matrix of the common energy errors is determined. Common LEP energy errors lead to uncertainties on  $M_Z$ ,  $\Gamma_Z$ , and  $\sigma_{\text{hadron}}^0$  of 1.7, 1.2 MeV, and 0.011 nb, respectively.

### 54.8. Common luminosity errors

BHLUMI 4.04 [25] is used by all LEP collaborations for small-angle Bhabha scattering leading to a common uncertainty in their measured cross sections of 0.061% [26]. BHLUMI does not include a correction for production of light fermion pairs. OPAL explicitly corrects for this effect and reduces their luminosity uncertainty to 0.054%, which is taken fully correlated with the other experiments. The other three experiments among themselves have a common uncertainty of 0.061%.

### 54.9. Common non-*s* channel uncertainties

The same standard model programs ALIBABA [16] and TOPAZ0 [17] are used to calculate the non-*s* channel contribution to the large angle Bhabha scattering [27]. As this contribution is a function of the *Z* mass, which itself is a variable in the fit, it is parametrized as a function of  $M_Z$  by each collaboration to properly track this contribution as  $M_Z$  varies in the fit. The common errors on  $R_e$  and  $A_{FB}^{(0,e)}$  are 0.024 and 0.0014 respectively, and are correlated between them.

### 54.10. Common theoretical uncertainties: QED

There are large initial-state photon and fermion pair radiation effects near the *Z* resonance, for which the best currently available evaluations include contributions up to  $\mathcal{O}(\alpha^3)$ . To estimate the remaining uncertainties, different schemes are incorporated in the standard model programs ZFITTER [5], TOPAZ0 [17], and MIZA [28]. Comparing the different options leads to error estimates of 0.3 and 0.2 MeV on  $M_Z$  and  $\Gamma_Z$  respectively, and of 0.02% on  $\sigma_{\text{hadron}}^\circ$ .

### 54.11. Common theoretical uncertainties: parametrization of lineshape and asymmetries

To estimate uncertainties arising from ambiguities in the model-independent parametrization of the differential cross-section near the *Z* resonance, results from TOPAZ0 and ZFITTER were compared by using ZFITTER to fit the cross sections and asymmetries calculated using TOPAZ0. The resulting uncertainties on  $M_Z$ ,  $\Gamma_Z$ ,  $\sigma_{\text{hadron}}^\circ$ ,  $R(\text{lepton})$ , and  $A_{FB}^{(0,\ell)}$  are 0.1 MeV, 0.1 MeV, 0.001 nb, 0.004, and 0.0001 respectively.

Thus, the overall theoretical errors on  $M_Z$ ,  $\Gamma_Z$ ,  $\sigma_{\text{hadron}}^\circ$  are 0.3 MeV, 0.2 MeV, and 0.008 nb respectively; on each  $R(\text{lepton})$  is 0.004 and on each  $A_{FB}^{(0,\ell)}$  is 0.0001. Within the set of three  $R(\text{lepton})$ 's and the set of three  $A_{FB}^{(0,\ell)}$ 's, the respective errors are fully correlated.

All the theory-related errors mentioned above utilize Standard Model programs which need the Higgs mass and running electromagnetic coupling constant as inputs; uncertainties on these inputs will also lead to common errors. All LEP collaborations used the same set of inputs for Standard Model calculations:  $M_Z = 91.187$  GeV, the Fermi constant  $G_F = (1.16637 \pm 0.00001) \times 10^{-5}$  GeV<sup>-2</sup> [29],  $\alpha^{(5)}(M_Z) = 1/128.877 \pm 0.090$  [30],  $\alpha_s(M_Z) = 0.119$  [31],  $M_{\text{top}} = 174.3 \pm 5.1$  GeV [31] and  $M_{\text{Higgs}} = 150$  GeV. The only observable effect, on  $M_Z$ , is due to the variation of  $M_{\text{Higgs}}$  between 100–1000 GeV (due to the variation of the  $\gamma/Z$  interference term which is taken from the Standard Model):  $M_Z$  changes by +0.23 MeV per unit change in  $\log_{10} M_{\text{Higgs}}/\text{GeV}$ , which is not an error but a correction to be applied once  $M_{\text{Higgs}}$  is determined. The effect is much smaller than the error on  $M_Z$  ( $\pm 2.1$  MeV).

### 54.12. Methodology of combining the LEP experimental results

The LEP experimental results actually used for combination are slightly modified from those published by the experiments (which are given in the Listings below). This has been done in order to facilitate the procedure by making the inputs more consistent. These modified results are given explicitly in [24]. The main differences compared to the published results are (a) consistent use of ZFITTER 6.23 and TOPAZ0 (the published ALEPH results used ZFITTER 6.10); (b) use of the combined energy-error matrix, which makes a difference of 0.1 MeV on the  $M_Z$  and  $\Gamma_Z$  for L3 only as at that intersection the RF modeling uncertainties are the largest.

Thus, nine-parameter sets from all four experiments with their covariance matrices are used together with all the common errors correlations. A grand covariance matrix,  $V$ , is constructed and a combined nine-parameter set is obtained by minimizing  $\chi^2 = \Delta^T V^{-1} \Delta$ , where  $\Delta$  is the vector of residuals of the combined parameter set to the results of individual experiments. Imposing

lepton universality in the combination results in the combined five parameter set.

### 54.13. Study of $Z \rightarrow b\bar{b}$ and $Z \rightarrow c\bar{c}$

In the sector of *c*- and *b*-physics, the LEP experiments have measured the ratios of partial widths  $R_b = \Gamma(Z \rightarrow b\bar{b})/\Gamma(Z \rightarrow \text{hadrons})$ , and  $R_c = \Gamma(Z \rightarrow c\bar{c})/\Gamma(Z \rightarrow \text{hadrons})$ , and the forward-backward (charge) asymmetries  $A_{FB}^{b\bar{b}}$  and  $A_{FB}^{c\bar{c}}$ . The SLD experiment at SLC has measured the ratios  $R_c$  and  $R_b$  and, utilizing the polarization of the electron beam, was able to obtain the final state coupling parameters  $A_b$  and  $A_c$  from a measurement of the left-right forward-backward asymmetry of *b*- and *c*-quarks. The high precision measurement of  $R_c$  at SLD was made possible owing to the small beam size and very stable beam spot at SLC, coupled with a highly precise CCD pixel detector. Several of the analyses have also determined other quantities, in particular the semileptonic branching ratios,  $B(b \rightarrow \ell^-)$ ,  $B(b \rightarrow c \rightarrow \ell^+)$ , and  $B(c \rightarrow \ell^+)$ , the average time-integrated  $B^0\bar{B}^0$  mixing parameter  $\bar{\chi}$  and the probabilities for a *c*-quark to fragment into a  $D^+$ , a  $D_s$ , a  $D^{*+}$ , or a charmed baryon. The latter measurements do not concern properties of the *Z* boson, and hence they do not appear in the Listing below. However, for completeness, we will report at the end of this minireview their values as obtained fitting the data contained in the *Z* section. All these quantities are correlated with the electroweak parameters, and since the mixture of *b* hadrons is different from the one at the  $\Upsilon(4S)$ , their values might differ from those measured at the  $\Upsilon(4S)$ .

All the above quantities are correlated to each other since:

- Several analyses (for example the lepton fits) determine more than one parameter simultaneously;
- Some of the electroweak parameters depend explicitly on the values of other parameters (for example  $R_b$  depends on  $R_c$ );
- Common tagging and analysis techniques produce common systematic uncertainties.

The LEP Electroweak Heavy Flavour Working Group has developed [32] a procedure for combining the measurements taking into account known sources of correlation. The combining procedure determines fourteen parameters: the six parameters of interest in the electroweak sector,  $R_b$ ,  $R_c$ ,  $A_{FB}^{b\bar{b}}$ ,  $A_{FB}^{c\bar{c}}$ ,  $A_b$  and  $A_c$  and, in addition,  $B(b \rightarrow \ell^-)$ ,  $B(b \rightarrow c \rightarrow \ell^+)$ ,  $B(c \rightarrow \ell^+)$ ,  $\bar{\chi}$ ,  $f(D^+)$ ,  $f(D_s)$ ,  $f(c_{\text{baryon}})$  and  $P(c \rightarrow D^{*+}) \times B(D^{*+} \rightarrow \pi^+ D^0)$ , to take into account their correlations with the electroweak parameters. Before the fit both the peak and off-peak asymmetries are translated to the common energy  $\sqrt{s} = 91.26$  GeV using the predicted energy-dependence from ZFITTER [5].

### 54.14. Summary of the measurements and of the various kinds of analysis

The measurements of  $R_b$  and  $R_c$  fall into two classes. In the first, named single-tag measurement, a method for selecting *b* and *c* events is applied and the number of tagged events is counted. A second technique, named double-tag measurement, has the advantage that the tagging efficiency is directly derived from the data thereby reducing the systematic error on the measurement.

The measurements in the *b*- and *c*-sector can be essentially grouped in the following categories:

- Lifetime (and lepton) double-tagging measurements of  $R_b$ . These are the most precise measurements of  $R_b$  and obviously dominate the combined result. The main sources of systematics come from the charm contamination and from estimating the hemisphere *b*-tagging efficiency correlation;
- Analyses with  $D/D^{*\pm}$  to measure  $R_c$ . These measurements make use of several different tagging techniques (inclusive/exclusive double tag, exclusive double tag, reconstruction of all weakly decaying charmed states) and no assumptions are made on the energy-dependence of charm fragmentation;
- A measurement of  $R_c$  using single leptons and assuming  $B(b \rightarrow c \rightarrow \ell^+)$ ;

- Lepton fits which use hadronic events with one or more leptons in the final state to measure the asymmetries  $A_{FB}^{b\bar{b}}$  and  $A_{FB}^{c\bar{c}}$ . Each analysis usually gives several other electroweak parameters. The dominant sources of systematics are due to lepton identification, to other semileptonic branching ratios and to the modeling of the semileptonic decay;
- Measurements of  $A_{FB}^{b\bar{b}}$  using lifetime tagged events with a hemisphere charge measurement. These measurements dominate the combined result;
- Analyses with  $D/D^{*\pm}$  to measure  $A_{FB}^{c\bar{c}}$  or simultaneously  $A_{FB}^{b\bar{b}}$  and  $A_{FB}^{c\bar{c}}$ ;
- Measurements of  $A_b$  and  $A_c$  from SLD, using several tagging methods (lepton, kaon,  $D/D^*$ , and vertex mass). These quantities are directly extracted from a measurement of the left–right forward–backward asymmetry in  $c\bar{c}$  and  $b\bar{b}$  production using a polarized electron beam.

### 54.15. Averaging procedure

All the measurements are provided by the LEP and SLD Collaborations in the form of tables with a detailed breakdown of the systematic errors of each measurement and its dependence on other electroweak parameters.

The averaging proceeds via the following steps:

- Define and propagate a consistent set of external inputs such as branching ratios, hadron lifetimes, fragmentation models *etc.* All the measurements are checked to ensure that all use a common set of assumptions (for instance, since the QCD corrections for the forward–backward asymmetries are strongly dependent on the experimental conditions, the data are corrected before combining);
- Form the full (statistical and systematic) covariance matrix of the measurements. The systematic correlations between different analyses are calculated from the detailed error breakdown in the measurement tables. The correlations relating several measurements made by the same analysis are also used;
- Take into account any explicit dependence of a measurement on the other electroweak parameters. As an example of this dependence, we illustrate the case of the double-tag measurement of  $R_b$ , where  $c$ -quarks constitute the main background. The normalization of the charm contribution is not usually fixed by the data and the measurement of  $R_b$  depends on the assumed value of  $R_c$ , which can be written as:

$$R_b = R_b^{\text{meas}} + a(R_c) \frac{(R_c - R_c^{\text{used}})}{R_c}, \quad (54.11)$$

where  $R_b^{\text{meas}}$  is the result of the analysis which assumed a value of  $R_c = R_c^{\text{used}}$  and  $a(R_c)$  is the constant which gives the dependence on  $R_c$ ;

- Perform a  $\chi^2$  minimization with respect to the combined electroweak parameters.

After the fit the average peak asymmetries  $A_{FB}^{c\bar{c}}$  and  $A_{FB}^{b\bar{b}}$  are corrected for the energy shift from 91.26 GeV to  $M_Z$  and for QED (initial state radiation),  $\gamma$  exchange, and  $\gamma Z$  interference effects, to obtain the corresponding pole asymmetries  $A_{FB}^{0,c}$  and  $A_{FB}^{0,b}$ .

This averaging procedure, using the fourteen parameters described above, and applied to the data contained in the Z particle listing below, gives the following results (where the last 8 parameters do not depend directly on the Z):

$$\begin{aligned} R_b^0 &= 0.21629 \pm 0.00066 \\ R_c^0 &= 0.1721 \pm 0.0030 \\ A_{FB}^{0,b} &= 0.0992 \pm 0.0016 \\ A_{FB}^{0,c} &= 0.0707 \pm 0.0035 \end{aligned}$$

$$A_b = 0.923 \pm 0.020$$

$$A_c = 0.670 \pm 0.027$$

$$B(b \rightarrow \ell^-) = 0.1071 \pm 0.0022$$

$$B(b \rightarrow c \rightarrow \ell^+) = 0.0801 \pm 0.0018$$

$$B(c \rightarrow \ell^+) = 0.0969 \pm 0.0031$$

$$\bar{\chi} = 0.1250 \pm 0.0039$$

$$f(D^+) = 0.235 \pm 0.016$$

$$f(D_s) = 0.126 \pm 0.026$$

$$f(c_{\text{baryon}}) = 0.093 \pm 0.022$$

$$P(c \rightarrow D^{*+}) \times B(D^{*+} \rightarrow \pi^+ D^0) = 0.1622 \pm 0.0048$$

Among the non–electroweak observables, the B semileptonic branching fraction  $B(b \rightarrow \ell^-)$  is of special interest, since the dominant error source on this quantity is the dependence on the semileptonic decay model for  $b \rightarrow \ell^-$ , with  $\Delta B(b \rightarrow \ell^-)_{b \rightarrow \ell^- \text{-model}} = 0.0012$ . Extensive studies have been made to understand the size of this error. Among the electroweak quantities, the quark asymmetries with leptons depend also on the semileptonic decay model, while the asymmetries using other methods usually do not. The fit implicitly requires that the different methods give consistent results and this effectively constrains the decay model, and thus reduces in principle the error from this source in the fit result.

To obtain a conservative estimate of the modelling error, the above fit has been repeated removing all asymmetry measurements. The results of the fit on B–decay related observables are [24]:  $B(b \rightarrow \ell^-) = 0.1069 \pm 0.0022$ , with  $\Delta B(b \rightarrow \ell^-)_{b \rightarrow \ell^- \text{-model}} = 0.0013$ ,  $B(b \rightarrow c \rightarrow \ell^+) = 0.0802 \pm 0.0019$  and  $\bar{\chi} = 0.1259 \pm 0.0042$ .

#### References:

1. R.N. Cahn, Phys. Rev. **D36**, 2666 (1987).
2. F.A. Berends *et al.*, “Z Physics at LEP 1,” CERN Report 89-08 (1989), Vol. 1, eds. G. Altarelli, R. Kleiss, and C. Verzegnassi, p. 89.
3. A. Borrelli *et al.*, Nucl. Phys. **B333**, 357 (1990).
4. D. Bardin and G. Passarino, “Upgrading of Precision Calculations for Electroweak Observables,” hep-ph/9803425; D. Bardin, G. Passarino, and M. Grunewald, “Precision Calculation Project Report,” hep-ph/9902452.
5. D. Bardin *et al.*, Z. Phys. **C44**, 493 (1989); Comp. Phys. Comm. **59**, 303 (1990); D. Bardin *et al.*, Nucl. Phys. **B351**, 1 (1991); Phys. Lett. **B255**, 290 (1991), and CERN-TH/6443/92 (1992); Comp. Phys. Comm. **133**, 229 (2001).
6. G. Burgers *et al.*, “Z Physics at LEP 1,” CERN Report 89-08 (1989), Vol. 1, eds. G. Altarelli, R. Kleiss, and C. Verzegnassi, p. 55.
7. D.C. Kennedy and B.W. Lynn, Nucl. Phys. **B322**, 1 (1989).
8. M. Consoli *et al.*, “Z Physics at LEP 1,” CERN Report 89-08 (1989), Vol. 1, eds. G. Altarelli, R. Kleiss, and C. Verzegnassi, p. 7.
9. M. Bohm *et al.*, *ibid*, p. 203.
10. S. Jadach *et al.*, *ibid*, p. 235.
11. R. Stuart, Phys. Lett. **B262**, 113 (1991).
12. A. Sirlin, Phys. Rev. Lett. **67**, 2127 (1991).
13. A. Leike, T. Riemann, and J. Rose, Phys. Lett. **B273**, 513 (1991).
14. See also D. Bardin *et al.*, Phys. Lett. **B206**, 539 (1988).
15. The LEP Collaborations: ALEPH, DELPHI, L3, OPAL, the LEP Electroweak Working Group, CERN-PH-EP/2013-022, arXiv:1302.3415 [hep-ex], Phys.Rept. 532 (2013) 119-244.
16. W. Beenakker, F.A. Berends, and S.C. van der Marck, Nucl. Phys. **B349**, 323 (1991).

17. G. Montagna *et al.*, Nucl. Phys. **B401**, 3 (1993); Comp. Phys. Comm. **76**, 328 (1993); Comp. Phys. Comm. **93**, 120 (1996); G. Montagna *et al.*, Comp. Phys. Comm. **117**, 278 (1999).
18. R. Assmann *et al.*, (Working Group on LEP Energy), Eur. Phys. J. **C6**, 187 (1999).
19. R. Assmann *et al.*, (Working Group on LEP Energy), Z. Phys. **C66**, 567 (1995).
20. L. Arnaudon *et al.*, (Working Group on LEP Energy and LEP Collabs.), Phys. Lett. **B307**, 187 (1993).
21. L. Arnaudon *et al.*, (Working Group on LEP Energy), CERN-PPE/92-125 (1992).
22. L. Arnaudon *et al.*, Phys. Lett. **B284**, 431 (1992).
23. R. Bailey *et al.*, 'LEP Energy Calibration' CERN-SL-90-95-AP, *Proceedings of the "2<sup>nd</sup> European Particle Accelerator Conference*, Nice, France, 12–16 June 1990, pp. 1765-1767.
24. The LEP Collabs.: ALEPH, DELPHI, L3, OPAL, the LEP Electroweak Working Group, and the SLD Heavy Flavour Group: Phys. Reports **427**, 257 (2006).
25. S. Jadach *et al.*, BHLUMI 4.04, Comp. Phys. Comm. **102**, 229 (1997);  
S. Jadach and O. Nicosini, Event generators for Bhabha scattering, in Physics at LEP2, CERN-96-01 Vol. 2, February 1996.
26. B.F.L. Ward *et al.*, Phys. Lett. **B450**, 262 (1999).
27. W. Beenakker and G. Passarino, Phys. Lett. **B425**, 199 (1998).
28. M. Martinez *et al.*, Z. Phys. **C49**, 645 (1991);  
M. Martinez and F. Teubert, Z. Phys. **C65**, 267 (1995), updated with results summarized in S. Jadach, B. Pietrzyk, and M. Skrzypek, Phys. Lett. **B456**, 77 (1999) and Reports of the working group on precision calculations for the *Z* resonance, CERN 95-03, ed. D. Bardin, W. Hollik, and G. Passarino, and references therein.
29. T. van Ritbergen and R. Stuart, Phys. Lett. **B437**, 201 (1998); Phys. Rev. Lett. **82**, 488 (1999).
30. S. Eidelman and F. Jegerlehner, Z. Phys. **C67**, 585 (1995);  
M. Steinhauser, Phys. Lett. **B429**, 158 (1998).
31. Particle Data Group (D.E. Groom *et al.*), Eur. Phys. J. **C15**, 1 (2000).
32. The LEP Experiments: ALEPH, DELPHI, L3, and OPAL Nucl. Instrum. Methods **A378**, 101 (1996).



## 55. Muon Anomalous Magnetic Moment

Updated August 2019 by A. Hoecker (CERN) and W.J. Marciano (BNL).

The Dirac equation predicts a muon magnetic moment,  $\vec{M} = g\mu \frac{e}{2m_\mu} \vec{S}$ , with gyromagnetic ratio  $g_\mu = 2$ . Quantum loop effects lead to a small calculable deviation from  $g_\mu = 2$ , parameterized by the anomalous magnetic moment

$$a_\mu \equiv \frac{g_\mu - 2}{2}. \quad (55.1)$$

That quantity can be accurately measured and, within the Standard Model (SM) framework, precisely predicted. Hence, comparison of experiment and theory tests the SM at its quantum loop level. A deviation in  $a_\mu^{\text{exp}}$  from the SM expectation would signal effects of new physics, with current sensitivity reaching up to mass scales of  $\mathcal{O}(\text{TeV})$  [1,2]. For recent thorough muon  $g - 2$  reviews, see e.g. Refs. [3–5].

The E821 experiment at Brookhaven National Lab (BNL) studied the precession of  $\mu^+$  and  $\mu^-$  in a constant external magnetic field as they circulated in a confining storage ring. It found<sup>1</sup> [6]

$$\begin{aligned} a_{\mu^+}^{\text{exp}} &= 11\,659\,204(6)(5) \times 10^{-10}, \\ a_{\mu^-}^{\text{exp}} &= 11\,659\,215(8)(3) \times 10^{-10}, \end{aligned} \quad (55.2)$$

where the first errors are statistical and the second systematic. Assuming CPT invariance and taking into account correlations between systematic uncertainties, one finds for their average [6,7]

$$a_\mu^{\text{exp}} = 11\,659\,209.1(5.4)(3.3) \times 10^{-10}. \quad (55.3)$$

These results represent about a factor of 14 improvement over the classic CERN experiments of the 1970's [8]. Improvement of the measurement by a factor of four by setting up the E821 storage ring at Fermilab, and utilizing a cleaner and more intense muon beam and improved detectors [9] is in progress with the commissioning of the experiment having started in 2017. First results are expected in 2019. Another muon  $g - 2$  experiment with similar sensitivity but using an alternative zero-electric-field technique with a low-emittance and low-momentum muon beam is currently under construction at J-PARC in Japan [10].

The SM prediction for  $a_\mu^{\text{SM}}$  is generally divided into three parts (see Fig. 55.1 for representative Feynman diagrams)

$$a_\mu^{\text{SM}} = a_\mu^{\text{QED}} + a_\mu^{\text{EW}} + a_\mu^{\text{Had}}. \quad (55.4)$$

The QED part includes all photonic and leptonic ( $e, \mu, \tau$ ) loops starting with the classic  $\alpha/2\pi$  Schwinger contribution. It has been computed through 5 loops [11]

$$\begin{aligned} a_\mu^{\text{QED}} &= \frac{\alpha}{2\pi} + 0.765\,857\,425(17) \left(\frac{\alpha}{\pi}\right)^2 + 24.050\,509\,96(32) \left(\frac{\alpha}{\pi}\right)^3 \\ &\quad + 130.879\,6(6\,3) \left(\frac{\alpha}{\pi}\right)^4 + 752.2(1.0) \left(\frac{\alpha}{\pi}\right)^5 + \dots \end{aligned} \quad (55.5)$$

with little change in the coefficients since our last update of this review. Employing  $\alpha^{-1} = 137.035\,999\,046(27)$ , obtained from the precise measurements of  $h/m_{\text{Cs}}$  [12], the Rydberg constant, and  $m_{\text{Cs}}/m_e$  leads to [11]

$$a_\mu^{\text{QED}} = 116\,584\,718.92(0.03) \times 10^{-11}, \quad (55.6)$$

where the small error results mainly from the uncertainty in  $\alpha$ .

<sup>1</sup> The results reported by the experiment have been updated in Eqs. (55.2) and (55.3) to the newest value for the absolute muon-to-proton magnetic ratio  $\lambda = 3.183\,345\,107(84)$  [7]. The change induced in  $a_\mu^{\text{exp}}$  with respect to the value of  $\lambda = 3.183\,345\,39(10)$  used in Ref. 6 amounts to  $+1.12 \times 10^{-10}$ .

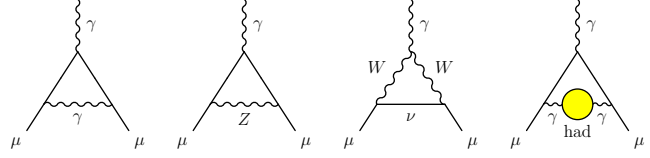


**Figure 55.1:** Representative diagrams contributing to  $a_\mu^{\text{SM}}$ . From left to right: first order QED (Schwinger term), lowest-order weak, lowest-order hadronic.

Loop contributions involving heavy  $W^\pm, Z$  or Higgs particles are collectively labeled as  $a_\mu^{\text{EW}}$ . They are suppressed by at least a factor of  $(\alpha/\pi) \cdot (m_\mu^2/m_W^2) \simeq 4 \times 10^{-9}$ . At 1-loop order [13]

$$\begin{aligned} a_\mu^{\text{EW}}[\text{1-loop}] &= \frac{G_\mu m_\mu^2}{8\sqrt{2}\pi^2} \left[ \frac{5}{3} + \frac{1}{3} (1 - 4\sin^2\theta_W)^2 \right] + \mathcal{O}\left(\frac{m_\mu^2}{M_W^2}\right) + \mathcal{O}\left(\frac{m_\mu^2}{m_H^2}\right) \\ &= 194.8 \times 10^{-11}, \end{aligned} \quad (55.7)$$

for  $\sin^2\theta_W \equiv 1 - M_W^2/M_Z^2 \simeq 0.223$ , and where  $G_\mu \simeq 1.166 \times 10^{-5} \text{ GeV}^{-2}$  is the Fermi coupling constant. Two-loop corrections are relatively large and negative [14]. For a Higgs boson mass of 125 GeV it amounts to  $a_\mu^{\text{EW}}[\text{2-loop}] = -41.2(1.0) \times 10^{-11}$  [14], where the uncertainty stems from quark triangle loops. The 3-loop leading logarithms are negligible,  $\mathcal{O}(10^{-12})$  [14,15]. A recent full 2-loop numerical evaluation of the electroweak correction [16] reproduces the total 1+2-loop contribution when adjusted for appropriate light quark masses

$$a_\mu^{\text{EW}} = 153.6(1.0) \times 10^{-11}. \quad (55.8)$$

Hadronic (quark and gluon) loop contributions to  $a_\mu^{\text{SM}}$  give rise to its main theoretical uncertainties. At present, those effects are not precisely calculable from first principles, but such an approach, at least partially, may become possible as lattice QCD matures [17]. Instead, one currently relies on a dispersion relation approach to evaluate the lowest-order  $\mathcal{O}(\alpha^2)$  hadronic vacuum polarization contribution  $a_\mu^{\text{Had}}[\text{LO}]$  from corresponding cross section measurements [18]

$$a_\mu^{\text{Had}}[\text{LO}] = \frac{1}{3} \left(\frac{\alpha}{\pi}\right)^2 \int_{m_\pi^2}^{\infty} ds \frac{K(s)}{s} R^{(0)}(s), \quad (55.9)$$

where  $K(s)$  is a QED kernel function [19], and where  $R^{(0)}(s)$  denotes the ratio of the bare<sup>2</sup> cross section for  $e^+e^-$  annihilation into hadrons to the pointlike muon-pair cross section at center-of-mass energy  $\sqrt{s}$ . The function  $K(s) \sim 1/s$  in Eq. (55.9) emphasizes the low-energy part of the integral so that  $a_\mu^{\text{Had}}[\text{LO}]$  is dominated by the  $\rho(770) \rightarrow \pi^+\pi^-$  resonance.

The analysis of Eq. (55.9) results in the representative value [20]

$$a_\mu^{\text{Had}}[\text{LO}] = 6\,939(39)(7) \times 10^{-11}, \quad (55.10)$$

where the first error is experimental, dominated by systematic uncertainties in the  $e^+e^- \rightarrow$  hadrons cross-section data, and the second due to perturbative QCD, which is used at intermediate and large energies in the dispersion integral to predict the contribution from the quark-antiquark continuum. The experimental precision is currently limited by a discrepancy between the most precise  $\pi^+\pi^-$  data from the BABAR and KLOE experiments [20]. Other recent evaluations [31,32] of  $a_\mu^{\text{Had}}[\text{LO}]$  find consistent results with Eq. (55.10).

Alternatively, one can use precise vector spectral functions from  $\tau \rightarrow \nu_\tau +$  hadrons decays [21] that can be related to isovector  $e^+e^- \rightarrow$  hadrons cross sections by isospin symmetry. Analyses replaced  $e^+e^-$  data in the two-pion and four-pion channels by

<sup>2</sup> The bare cross section is defined as the measured cross section corrected for initial-state radiation, electron-vertex loop contributions and vacuum-polarization effects in the photon propagator. However, QED effects in the hadron vertex and final state, as photon radiation, are included.

the corresponding isospin-transformed  $\tau$  data, and applied isospin-violating corrections [22]. Owing to the progress in the precision of the  $e^+e^-$  data, the  $\tau$  data are now less precise and less reliable due to additional theoretical uncertainties, so that recent  $a_\mu^{\text{Had}}[\text{LO}]$  evaluations ignored them.

Higher order hadronic contributions are obtained from dispersion relations using the same  $e^+e^- \rightarrow$  hadrons data [23], giving  $a_\mu^{\text{Had,Disp}}[\text{NLO}] = (-98.7 \pm 0.9) \times 10^{-11}$  and  $a_\mu^{\text{Had,Disp}}[\text{NNLO}] = (12.4 \pm 0.1) \times 10^{-11}$  [24], along with model-dependent estimates of the hadronic light-by-light scattering contribution,  $a_\mu^{\text{Had,LBL}}[\text{NLO}]$ , motivated by large- $N_C$  QCD [25–30].<sup>3</sup> Following [29], one finds for the sum of the three terms

$$a_\mu^{\text{Had}}[\text{N(N)LO}] = 19(26) \times 10^{-11}, \quad (55.11)$$

where the error is dominated by hadronic light-by-light uncertainty.

Adding Eqs. (55.6), (55.8), (55.10) and (55.11) gives the representative SM prediction

$$a_\mu^{\text{SM}} = 116\,591\,830(1)(40)(26) \times 10^{-11}, \quad (55.12)$$

where the errors are due to the electroweak, lowest-order hadronic, and higher-order hadronic contributions, respectively. The difference between experiment and theory

$$\Delta a_\mu = a_\mu^{\text{exp}} - a_\mu^{\text{SM}} = 261(63)(48) \times 10^{-11}, \quad (55.13)$$

where the errors are from experiment and theory prediction (with all errors combined in quadrature), respectively, represents an interesting but not conclusive discrepancy of 3.3 times the combined  $1\sigma$  error. All the recent estimates for the hadronic contribution compiled in Fig. 55.2 exhibit similar discrepancies.

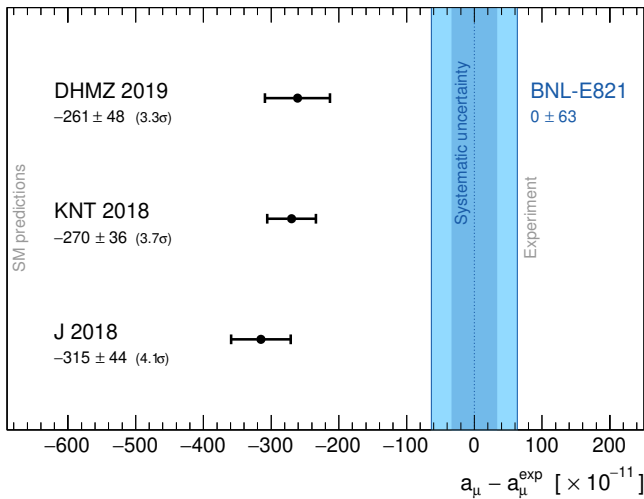


**Figure 55.2:** Compilation of recent results for  $a_\mu$  (in units of  $10^{-11}$ ), subtracted by the central value of the experimental average (55.3). The shaded (dark shaded) vertical band indicates the total (systematic) experimental uncertainty. The SM predictions are taken from: DHMZ 2019 [20], KNT 2018 [31], and J 2017 [32]. Note that the quoted errors in the figure do not include the uncertainty on the subtracted experimental value. To obtain for each theory calculation a result equivalent to Eq. (55.13), the errors from theory and experiment must be added in quadrature.

<sup>3</sup> Some representative recent estimates of the hadronic light-by-light scattering contribution,  $a_\mu^{\text{Had,LBL}}[\text{NLO}]$  are:  $105(26) \times 10^{-11}$  [29],  $110(40) \times 10^{-11}$  [25],  $136(25) \times 10^{-11}$  [26]. An approach based on dispersion relations is proposed in [28].

An exciting interpretation is that  $\Delta a_\mu$  may be a new physics signal with supersymmetric particle loops as the leading candidate explanation. Such a scenario is quite natural, since generically, supersymmetric models predict [1] an additional contribution to  $a_\mu^{\text{SM}}$

$$a_\mu^{\text{SUSY}} \simeq \pm 130 \times 10^{-11} \cdot \left( \frac{100 \text{ GeV}}{m_{\text{SUSY}}} \right)^2 \tan\beta, \quad (55.14)$$

where  $m_{\text{SUSY}}$  is a representative supersymmetric mass scale,  $\tan\beta \simeq 3\text{--}40$  a potential enhancement factor, and  $\pm 1$  corresponds to the sign of the  $\mu$  term in the supersymmetric Lagrangian. Supersymmetric particles in the mass range 100–500 GeV could be the source of the deviation  $\Delta a_\mu$ . If so, those particles should be directly observable at the Large Hadron Collider at CERN. So far, there is however no direct evidence in support of the supersymmetry interpretation.

New physics effects [1] other than supersymmetry could also explain a non-vanishing  $\Delta a_\mu$ . A popular scenario involves the “dark photon”, a relatively light hypothetical vector boson from the dark matter sector that couples to our world of particle physics through mixing with the ordinary photon [33–35]. As a result, it couples to ordinary charged particles with strength  $\varepsilon \cdot e$  and gives rise to an additional muon anomalous magnetic moment contribution

$$a_\mu^{\text{dark photon}} = \frac{\alpha}{2\pi} \varepsilon^2 F(m_V/m_\mu), \quad (55.15)$$

where  $F(x) = \int_0^1 2z(1-z)^2 / [(1-z)^2 + x^2z] dz$ . For values of  $\varepsilon \sim 1\text{--}2 \times 10^{-3}$  and  $m_V \sim 10\text{--}100$  MeV, the dark photon, which was originally motivated by cosmology, can provide a viable solution to the muon  $g-2$  discrepancy. However, recent experimental constraints disfavor such a scenario [36] under the assumption that the dark photon decays primarily into charged lepton pairs. Direct searches for the dark photon continue to be well motivated [37], but with primary guidance coming from phenomena outside the muon anomalous magnetic moment discrepancy. More recent popular solutions to the muon anomaly discrepancy have focused on loop contributions coming from relatively light new scalar or pseudoscalar particle appendages from physics beyond the SM.

## References:

1. A. Czarnecki and W.J. Marciano, Phys. Rev. **D64**, 013014 (2001).
2. M. Davier and W.J. Marciano, Ann. Rev. Nucl. and Part. Sci. **54**, 115 (2004).
3. J. Miller, E. de Rafael, and B. Lee Roberts, Rept. Prog. Phys. **70**, 795 (2007).
4. F. Jegerlehner and A. Nyffeler, Phys. Reports **477**, 1 (2009).
5. J.P. Miller *et al.*, Ann. Rev. Nucl. and Part. Sci. **62**, 237 (2012).
6. G.W. Bennett *et al.*, Phys. Rev. Lett. **89**, 101804 (2002); Erratum *ibid.* Phys. Rev. Lett. **89**, 129903 (2002); G.W. Bennett *et al.*, Phys. Rev. Lett. **92**, 161802 (2004); G.W. Bennett *et al.*, Phys. Rev. **D73**, 072003 (2006).
7. P.J. Mohr, B.N. Taylor, and D.B. Newell, CODATA Group, Rev. Mod. Phys. **84**, 1527 (2012).
8. J. Bailey *et al.*, Nucl. Phys. **B150**, 1 (1979).
9. J. Grange *et al.*, FERMILAB-DESIGN-2014-02, arXiv:1501.06858 (2015).
10. M. Abe *et al.*, Prog. Theor. Exp. Phys. 053C02 (2019), arXiv:1901.03047.
11. T. Aoyama *et al.*, Phys. Rev. Lett. **109**, 111808 (2012); T. Aoyama *et al.*, Phys. Rev. Lett. **109**, 111807 (2012); T. Kinoshita and M. Nio, Phys. Rev. **D73**, 013003 (2006); T. Aoyama *et al.*, Phys. Rev. Lett. **99**, 110406 (2007); T. Kinoshita and M. Nio, Phys. Rev. **D70**, 113001 (2004); T. Kinoshita, Nucl. Phys. **B144**, 206 (2005)(Proc. Supp.); T. Kinoshita and M. Nio, Phys. Rev. **D73**, 053007 (2006); S. Laporta, Phys. Lett. **B772**, 232 (2017); A. Kurz *et al.*, Phys. Rev. **D93**, 053017 (2016); A.L. Kataev, arXiv:hep-ph/0602098 (2006); M. Passera, J. Phys. **G31**, 75 (2005).
12. R.H. Parker *et al.*, Science **Vol. 360**, Issue 6385, 191 (2018).

13. R. Jackiw and S. Weinberg, Phys. Rev. **D5**, 2396 (1972);  
G. Altarelli *et al.*, Phys. Lett. **B40**, 415 (1972);  
I. Bars and M. Yoshimura, Phys. Rev. **D6**, 374 (1972);  
K. Fujikawa, B.W. Lee, and A.I. Sanda, Phys. Rev. **D6**, 2923 (1972).
14. C. Gnendiger, D. Stöckinger, H. Stöckinger-Kim, Phys. Rev. **D88**, 053005 (2013);  
A. Czarnecki *et al.*, Phys. Rev. **D67**, 073006 (2003);  
Erratum *ibid.* Phys. Rev. **D73**, 119901 (2006);  
S. Heinemeyer, D. Stockinger, and G. Weiglein, Nucl. Phys. **B699**, 103 (2004);  
T. Gribouk and A. Czarnecki, Phys. Rev. **D72**, 053016 (2005);  
A. Czarnecki, B. Krause, and W.J. Marciano, Phys. Rev. Lett. **76**, 3267 (1996);  
A. Czarnecki, B. Krause, and W.J. Marciano, Phys. Rev. **D52**, 2619, (1995);  
S. Peris, M. Perrottet, and E. de Rafael, Phys. Lett. **B355**, 523 (1995);  
T. Kukhto *et al.*, Nucl. Phys. **B371**, 567 (1992).
15. G. Degrossi and G.F. Giudice, Phys. Rev. **D58**, 053007 (1998).
16. T. Ishikawa, N. Nakazawa, and Y. Yasui, Phys. Rev. **D99**, 073004 (2019).
17. BMW Collaboration, Phys. Rev. Lett. **121**, 022002 (2018);  
HPQCD Collaboration, [arXiv:1902.04223](https://arxiv.org/abs/1902.04223) (2019);  
RBC and UKQCD Collaborations, Phys. Rev. Lett. **121**, 022003 (2018);  
A. Gérardin *et al.*, Phys. Rev. **D100**, 014510 (2019);  
D. Giusti, F. Sanfilippo, and S. Simula, Phys. Rev. **D98**, 114504 (2018);  
B. Chakraborty *et al.*, Phys. Rev. **D96**, 034516 (2017);  
T. Blum *et al.*, Phys. Rev. **D96**, 034515 (2017);  
T. Blum, Phys. Rev. Lett. **118**, 022005 (2017);  
B. Chakraborty *et al.*, Phys. Rev. **D93**, 074509 (2016);  
C. Lehner, [arXiv:1710.06874](https://arxiv.org/abs/1710.06874) (2017).
18. C. Bouchiat and L. Michel, J. Phys. Radium **22**, 121 (1961);  
M. Gourdin and E. de Rafael, Nucl. Phys. **B10**, 667 (1969).
19. S.J. Brodsky and E. de Rafael, Phys. Rev. **168**, 1620 (1968).
20. M. Davier *et al.*, [arXiv:1908.00921](https://arxiv.org/abs/1908.00921) (2019).
21. R. Alemany *et al.*, Eur. Phys. J. **C2**, 123 (1998).
22. M. Davier *et al.*, Eur. Phys. J. **C71**, 1515 (2011).
23. B. Krause, Phys. Lett. **B390**, 392 (1997).
24. A. Kurz *et al.*, Phys. Lett. **B734**, 144 (2014).
25. J. Bijnens and J. Prades, Mod. Phys. Lett. **A22**, 767 (2007).
26. K. Melnikov and A. Vainshtein, Phys. Rev. **D70**, 113006 (2004).
27. M. Knecht and A. Nyffeler, Phys. Rev. **D65**, 073034 (2002);  
M. Knecht *et al.*, Phys. Rev. Lett. **88**, 071802 (2002).
28. G. Colangelo *et al.*, JHEP **1409**, 091 (2014).
29. J. Prades, E. de Rafael, and A. Vainshtein, Advanced series on directions in high energy physics 20, Editors B.L. Roberts and W. Marciano, [arXiv:0901.0306](https://arxiv.org/abs/0901.0306) (2009).
30. E. de Rafael, Phys. Lett. **B322**, 239 (1994).
31. A. Keshavarzi, D. Nomura, and T. Teubner, Phys. Rev. **D97**, 114025 (2018).
32. F. Jegerlehner, EPJ Web of Conferences **166**, 00022 (2018).
33. P. Fayet, Phys. Rev. **D75**, 115017 (2007).
34. M. Pospelov, Phys. Rev. **D80**, 095002 (2009).
35. D. Tucker-Smith and I. Yavin, Phys. Rev. **D83**, 101702 (R)(2011).
36. NA48/2 Collaboration (J.R. Batley *et al.*), Phys. Lett. **B746**, 178 (2015).
37. J. Alexander *et al.*, Dark Sectors 2016 Workshop: Community Report, [arXiv:1608.08632](https://arxiv.org/abs/1608.08632) (2017).

## 56. Muon Decay Parameters

Revised March 2019 by W. Fetscher (ETH Zurich) and H.-J. Gerber (ETH Zurich).

### 56.1 Introduction:

All measurements in direct muon decay,  $\mu^- \rightarrow e^- + 2$  neutrals, and its inverse,  $\nu_\mu + e^- \rightarrow \mu^- +$  neutral, are successfully described by the “ $V$ - $A$  interaction,” which is a particular case of a local, derivative-free, lepton-number-conserving, four-fermion interaction [1]. As shown below, within this framework, the Standard Model assumptions, such as the  $V$ - $A$  form and the nature of the neutrals ( $\nu_\mu$  and  $\bar{\nu}_e$ ), and hence the doublet assignments  $(\nu_e e^-)_L$  and  $(\nu_\mu \mu^-)_L$ , have been determined from experiments [2, 3]. All considerations on muon decay are valid for the leptonic tau decays  $\tau^- \rightarrow \ell^- + \nu_\tau + \bar{\nu}_\ell$  with the replacements  $m_\mu \rightarrow m_\tau$ ,  $m_e \rightarrow m_{\ell}$ ,  $\ell^- = e^-, \mu^-$ .

### 56.2 Parameters:

The differential decay probability to obtain an  $e^\pm$  with (reduced) energy between  $x$  and  $x + dx$ , emitted in the direction  $\hat{\mathbf{x}}_3$  at an angle between  $\vartheta$  and  $\vartheta + d\vartheta$  with respect to the muon polarization vector  $\mathbf{P}_\mu$ , and with its spin parallel to the arbitrary direction  $\hat{\boldsymbol{\zeta}}$ , neglecting radiative corrections, is given by

$$\begin{aligned} \frac{d^2\Gamma}{dx d\cos\vartheta} &= \frac{m_\mu}{4\pi^3} W_{e\mu}^4 G_F^2 \sqrt{x^2 - x_0^2} \\ &\times (F_{\text{IS}}(x) \pm P_\mu \cos\vartheta F_{\text{AS}}(x)) \\ &\times [1 + \hat{\boldsymbol{\zeta}} \cdot \mathbf{P}_e(x, \vartheta)]. \end{aligned} \quad (56.1)$$

Here,  $W_{e\mu} = \max(E_e) = (m_\mu^2 + m_e^2)/2m_\mu$  is the maximum  $e^\pm$  energy,  $x = E_e/W_{e\mu}$  is the reduced energy,  $x_0 = m_e/W_{e\mu} = 9.67 \times 10^{-3}$ , and  $P_\mu = |\mathbf{P}_\mu|$  is the degree of muon polarization.  $\hat{\boldsymbol{\zeta}}$  is the direction in which a perfect polarization-sensitive electron detector is most sensitive. The isotropic part of the spectrum,  $F_{\text{IS}}(x)$ , the anisotropic part  $F_{\text{AS}}(x)$ , and the electron polarization,  $\mathbf{P}_e(x, \vartheta)$ , may be parametrized by the Michel parameter  $\rho$  [1], by  $\eta$  [4], by  $\xi$  and  $\delta$  [5, 6], *etc.* These are bilinear combinations of the coupling constants  $g_{e\mu}^\gamma$ , which occur in the matrix element (given below).

If the masses of the neutrinos as well as  $x_0^2$  are neglected, the energy and angular distribution of the electron in the rest frame of a muon ( $\mu^\pm$ ) measured by a polarization insensitive detector, is given by

$$\begin{aligned} \frac{d^2\Gamma}{dx d\cos\vartheta} &\sim x^2 \cdot \left\{ 3(1-x) + \frac{2\rho}{3}(4x-3) + 3\eta x_0(1-x)/x \right. \\ &\left. \pm P_\mu \cdot \boldsymbol{\xi} \cdot \cos\vartheta \left[ 1-x + \frac{2\delta}{3}(4x-3) \right] \right\}. \end{aligned} \quad (56.2)$$

Here,  $\vartheta$  is the angle between the electron momentum and the muon spin, and  $x \equiv 2E_e/m_\mu$ . For the Standard Model coupling, we obtain  $\rho = \xi\delta = 3/4$ ,  $\xi = 1$ ,  $\eta = 0$  and the differential decay rate is

$$\frac{d^2\Gamma}{dx d\cos\vartheta} = \frac{G_F^2 m_\mu^5}{192\pi^3} [3 - 2x \pm P_\mu \cos\vartheta(2x-1)] \cdot x^2. \quad (56.3)$$

The coefficient in front of the square bracket is the total decay rate.

If only the neutrino masses are neglected, and if the  $e^\pm$  polarization is detected, then the functions in Eq. (56.1) become

$$F_{\text{IS}}(x) = x(1-x) + \frac{2}{3}\rho(4x^2 - 3x - x_0^2) + \eta \cdot x_0(1-x) \quad (56.4a)$$

$$\begin{aligned} F_{\text{AS}}(x) &= \frac{1}{3}\xi \sqrt{x^2 - x_0^2} \\ &\times \left[ (1-x) + \frac{2}{3}\delta \left\{ (4x-3) + \left( \sqrt{1-x_0^2} - 1 \right) \right\} \right] \end{aligned} \quad (56.4b)$$

$$\mathbf{P}_e(x, \vartheta) = P_{T_1} \cdot \hat{\mathbf{x}}_1 + P_{T_2} \cdot \hat{\mathbf{x}}_2 + P_L \cdot \hat{\mathbf{x}}_3 \quad (56.4c)$$

Here  $\hat{\mathbf{x}}_1$ ,  $\hat{\mathbf{x}}_2$ , and  $\hat{\mathbf{x}}_3$  are orthogonal unit vectors defined as follows:

$$\begin{aligned} \hat{\mathbf{x}}_3 &\text{ is along the } e \text{ momentum } \mathbf{p}_e \\ \frac{\hat{\mathbf{x}}_3 \times \mathbf{P}_\mu}{|\hat{\mathbf{x}}_3 \times \mathbf{P}_\mu|} &= \hat{\mathbf{x}}_2 \text{ is transverse to } \mathbf{p}_e \text{ and perpendicular to} \\ &\text{“the decay plane”} \\ \hat{\mathbf{x}}_2 \times \hat{\mathbf{x}}_3 &= \hat{\mathbf{x}}_1 \text{ is transverse to } \mathbf{p}_e \text{ and in the decay plane} \end{aligned}$$

The components of  $\mathbf{P}_e$  then are given by

$$P_{T_1}(x, \vartheta) = P_\mu \sin\vartheta \cdot F_{T_1}(x) / \{F_{\text{IS}}(x) \pm P_\mu \cos\vartheta \cdot F_{\text{AS}}(x)\} \quad (56.5a)$$

$$P_{T_2}(x, \vartheta) = P_\mu \sin\vartheta \cdot F_{T_2}(x) / \{F_{\text{IS}}(x) \pm P_\mu \cos\vartheta \cdot F_{\text{AS}}(x)\} \quad (56.5b)$$

$$P_L(x, \vartheta) = \frac{\pm F_{\text{IP}}(x) + P_\mu \cos\vartheta \cdot F_{\text{AP}}(x)}{F_{\text{IS}}(x) \pm P_\mu \cos\vartheta \cdot F_{\text{AS}}(x)}, \quad (56.5c)$$

where

$$F_{T_1}(x) = \frac{1}{12} \left\{ -2 \left[ \xi'' + 12 \left( \rho - \frac{3}{4} \right) \right] (1-x)x_0 - 3\eta(x^2 - x_0^2) + \eta''(-3x^2 + 4x - x_0^2) \right\} \quad (56.6a)$$

$$F_{T_2}(x) = \frac{1}{3} \sqrt{x^2 - x_0^2} \cdot \left\{ 3 \frac{\alpha'}{A} (1-x) + 2 \frac{\beta'}{A} \sqrt{1-x_0^2} \right\} \quad (56.6b)$$

$$F_{\text{IP}}(x) = \frac{1}{54} \sqrt{x^2 - x_0^2} \cdot \left\{ 9\xi' \left( -2x + 2 + \sqrt{1-x_0^2} \right) + 4\xi \left( \delta - \frac{3}{4} \right) 4x - 4 + \sqrt{1-x_0^2} \right\} \quad (56.6c)$$

$$F_{\text{AP}}(x) = \frac{1}{6} \left\{ \xi'' (2x^2 - x - x_0^2) + 4 \left( \rho - \frac{3}{4} \right) (4x^2 - 3x - x_0^2) + 2\eta''(1-x)x_0 \right\}. \quad (56.6d)$$

For the experimental values of the parameters  $\rho$ ,  $\xi$ ,  $\xi'$ ,  $\xi''$ ,  $\delta$ ,  $\eta$ ,  $\eta''$ ,  $\alpha/A$ ,  $\beta/A$ ,  $\alpha'/A$ ,  $\beta'/A$ , which are not all independent, see the Data Listings below. Experiments in the past have also been analyzed using the parameters  $a$ ,  $b$ ,  $c$ ,  $a'$ ,  $b'$ ,  $c'$ ,  $\alpha/A$ ,  $\beta/A$ ,  $\alpha'/A$ ,  $\beta'/A$  (and  $\eta = (\alpha - 2\beta)/2A$ ), as defined by Kinoshita and Sirlin [5] [6]. They serve as a model-independent summary of all possible measurements on the decay electron (see Listings below). The relations between the two sets of parameters are

$$\rho - \frac{3}{4} = \frac{3}{4}(-a + 2c)/A \quad (56.7a)$$

$$\eta = (\alpha - 2\beta)/A \quad (56.7b)$$

$$\eta'' = (3\alpha + 2\beta)/A \quad (56.7c)$$

$$\delta - \frac{3}{4} = \frac{9}{4} \cdot \frac{(a' - 2c')/A}{1 - [a + 3a' + 4(b + b') + 6c - 14c']/A} \quad (56.7d)$$

$$1 - \xi \frac{\delta}{\rho} = 4 \frac{[(b + b') + 2(c - c')]/A}{1 - (a - 2c)/A} \quad (56.7e)$$

$$1 - \xi = \left[ (a + a') + 4(b + b') + 6(c + c') \right] / A \quad (56.7f)$$

$$1 - \xi'' = (-2a + 20c)/A \quad (56.7g)$$

$$\text{with } A = a + 4b + 6c \quad (56.7h)$$

The differential decay probability to obtain a *left-handed*  $\nu_e$  with (reduced) energy between  $y$  and  $y + dy$ , neglecting radiative corrections as well as the masses of the electron and of the neutrinos, is given by [7]

$$\frac{d\Gamma}{dy} = \frac{m_\mu^5 G_F^2}{16\pi^3} \cdot Q_L^{\nu_e} \cdot y^2 \left\{ (1-y) - \omega_L \cdot \left( y - \frac{3}{4} \right) \right\}. \quad (56.8)$$

Here,  $y = 2 E_{\nu_e}/m_\mu$ .  $Q_L^{\nu_e}$  and  $\omega_L$  are parameters.  $\omega_L$  is the neutrino analog of the spectral shape parameter  $\rho$  of Michel. Since in the Standard Model,  $Q_L^{\nu_e} = 1$ ,  $\omega_L = 0$ , the measurement of  $d\Gamma/dy$  has allowed a null-test of the Standard Model (see Listings below).

**Table 56.1:** Coupling constants  $g_{\varepsilon\mu}^\gamma$  and some combinations of them. Ninety-percent confidence level experimental limits. The limits on  $|g_{LL}^S|$  and  $|g_{LR}^V|$  are from [8–10], and the others from a general analysis of muon decay measurements. Top three rows: [11], fourth row: [12], next three rows: [13], last row: [14]. The experimental uncertainty on the muon polarization in pion decay is included. Note that, by definition,  $|g_{\varepsilon\mu}^S| \leq 2$ ,  $|g_{\varepsilon\mu}^V| \leq 1$  and  $|g_{\varepsilon\mu}^T| \leq 1/\sqrt{3}$ .

$ g_{RR}^S  < 0.035$	$ g_{RR}^V  < 0.017$	$ g_{RR}^T  \equiv 0$
$ g_{LR}^S  < 0.050$	$ g_{LR}^V  < 0.023$	$ g_{LR}^T  < 0.015$
$ g_{RL}^S  < 0.420$	$ g_{RL}^V  < 0.105$	$ g_{RL}^T  < 0.105$
$ g_{LL}^S  < 0.550$	$ g_{LL}^V  > 0.960$	$ g_{LL}^T  \equiv 0$
$ g_{LR}^S + 6g_{LR}^T  < 0.143$	$ g_{RL}^S + 6g_{RL}^T  < 0.418$	
$ g_{LR}^S + 2g_{LR}^T  < 0.108$	$ g_{RL}^S + 2g_{RL}^T  < 0.417$	
$ g_{LR}^S - 2g_{LR}^T  < 0.070$	$ g_{RL}^S - 2g_{RL}^T  < 0.418$	
$Q_{RR} + Q_{LR} < 8.2 \times 10^{-4}$		

### 56.3 Matrix element:

All results in direct muon decay (energy spectra of the electron and of the neutrinos, polarizations, and angular distributions), and in inverse muon decay (the reaction cross section) at energies well below  $m_W c^2$ , may be parametrized in terms of amplitudes  $g_{\varepsilon\mu}^\gamma$  and the Fermi coupling constant  $G_F$ , using the matrix element

$$\frac{4G_F}{\sqrt{2}} \sum_{\substack{\gamma=S,V,T \\ \varepsilon,\mu=R,L}} g_{\varepsilon\mu}^\gamma \langle \bar{e}_\varepsilon | \Gamma^\gamma | (\nu_e)_n \rangle \langle \bar{\nu}_\mu \rangle_m | \Gamma_\gamma | \mu_\mu \rangle \quad (56.9)$$

We use the notation of Fetscher *et al.* [2], who in turn use the sign conventions and definitions of Scheck [15]. Here,  $\gamma = S, V, T$  indicates a scalar, vector, or tensor interaction; and  $\varepsilon, \mu = R, L$  indicate a right- or left-handed chirality of the electron or muon. The chiralities  $n$  and  $m$  of the  $\nu_e$  and  $\bar{\nu}_\mu$  are then determined by the values of  $\gamma, \varepsilon$ , and  $\mu$ . The particles are represented by fields of definite chirality [16].

As shown by Langacker and London [17], explicit lepton-number nonconservation still leads to a matrix element equivalent to Eq. (56.9). They conclude that it is not possible, even in principle, to test lepton-number conservation in (leptonic) muon decay if the final neutrinos are massless and are not observed.

The ten complex amplitudes  $g_{\varepsilon\mu}^\gamma$  ( $g_{RR}^T$  and  $g_{LL}^T$  are identically zero) and  $G_F$  constitute 19 independent (real) parameters to be determined by experiment. The Standard Model interaction corresponds to one single amplitude  $g_{LL}^V$  being unity and all the others being zero.

The (direct) muon decay experiments are compatible with an arbitrary mix of the scalar and vector amplitudes  $g_{LL}^S$  and  $g_{LL}^V$  – in the extreme even with purely scalar  $g_{LL}^S = 2$ ,  $g_{LL}^V = 0$ . The decision in favour of the Standard Model comes from the quantitative observation of inverse muon decay, which would be forbidden for pure  $g_{LL}^S$  [2].

### 56.4 Experimental determination of $V-A$ :

In order to determine the amplitudes  $g_{\varepsilon\mu}^\gamma$  uniquely from experiment, the following set of equations, where the left-hand sides

represent experimental results, has to be solved.

$$a = 16 \left( |g_{RL}^V|^2 + |g_{LR}^V|^2 \right) + |g_{RL}^S + 6g_{RL}^T|^2 + |g_{LR}^S + 6g_{LR}^T|^2 \quad (56.10a)$$

$$a' = 16 \left( |g_{RL}^V|^2 - |g_{LR}^V|^2 \right) + |g_{RL}^S + 6g_{RL}^T|^2 - |g_{LR}^S + 6g_{LR}^T|^2 \quad (56.10b)$$

$$\alpha = 8 \operatorname{Re} \left\{ g_{RL}^V \left( g_{LR}^{S*} + 6g_{LR}^{T*} \right) + g_{LR}^V \left( g_{RL}^{S*} + 6g_{RL}^{T*} \right) \right\} \quad (56.10c)$$

$$a' = 8 \operatorname{Im} \left\{ g_{RL}^V \left( g_{LR}^{S*} + 6g_{LR}^{T*} \right) - g_{LR}^V \left( g_{RL}^{S*} + 6g_{RL}^{T*} \right) \right\} \quad (56.10d)$$

$$b = 4 \left( |g_{RR}^V|^2 + |g_{LL}^V|^2 \right) + |g_{RR}^S|^2 + |g_{LL}^S|^2 \quad (56.10e)$$

$$b' = 4 \left( |g_{RR}^V|^2 - |g_{LL}^V|^2 \right) + |g_{RR}^S|^2 - |g_{LL}^S|^2 \quad (56.10f)$$

$$c = \frac{1}{2} \left\{ |g_{RL}^S|^2 - 2|g_{RL}^T|^2 + |g_{LR}^S|^2 - 2|g_{LR}^T|^2 \right\} \quad (56.10g)$$

$$c' = \frac{1}{2} \left\{ |g_{RL}^S|^2 - 2|g_{RL}^T|^2 - |g_{LR}^S|^2 + 2|g_{LR}^T|^2 \right\} \quad (56.10h)$$

and

$$Q_L^{\nu_e} = 1 - \left\{ \frac{1}{4}|g_{LR}^S|^2 + \frac{1}{4}|g_{LL}^S|^2 + |g_{RR}^V|^2 + |g_{RL}^V|^2 + 3|g_{LR}^T|^2 \right\} \quad (56.10i)$$

$$\omega_L = \frac{3}{4} \frac{|g_{RR}^S|^2 + 4|g_{LR}^V|^2 + |g_{RL}^S|^2 + 2|g_{LR}^T|^2}{|g_{RL}^S|^2 + |g_{RR}^S|^2 + 4|g_{LL}^V|^2 + 4|g_{LR}^V|^2 + 12|g_{RL}^T|^2} \quad (56.10j)$$

It has been noted earlier by C. Jarlskog [18], that certain experiments observing the decay electron are especially informative if they yield the  $V-A$  values. The complete solution is now found as follows. Fetscher *et al.* [2] introduced four probabilities  $Q_{\varepsilon\mu}(\varepsilon, \mu = R, L)$  for the decay of a  $\mu$ -handed muon into an  $\varepsilon$ -handed electron, and showed that there exist upper bounds on  $Q_{RR}$ ,  $Q_{LR}$ , and  $Q_{RL}$ , and a lower bound on  $Q_{LL}$ . These probabilities are given in terms of the  $g_{\varepsilon\mu}^\gamma$ 's by

$$Q_{\varepsilon\mu} = \frac{1}{4}|g_{\varepsilon\mu}^S|^2 + |g_{\varepsilon\mu}^V|^2 + 3(1 - \delta_{\varepsilon\mu})|g_{\varepsilon\mu}^T|^2 \quad (56.11)$$

where  $\delta_{\varepsilon\mu} = 1$  for  $\varepsilon = \mu$ , and  $\delta_{\varepsilon\mu} = 0$  for  $\varepsilon \neq \mu$ . They are related to the parameters  $a$ ,  $b$ ,  $c$ ,  $a'$ ,  $b'$ , and  $c'$  by

$$Q_{RR} = 2(b + b')/A \quad (56.12a)$$

$$Q_{LR} = [(a - a') + 6(c - c')]/2A \quad (56.12b)$$

$$Q_{RL} = [(a + a') + 6(c + c')]/2A \quad (56.12c)$$

$$Q_{LL} = 2(b - b')/A \quad (56.12d)$$

with  $A = 16$ . In the Standard Model,  $Q_{LL} = 1$  and the others are zero.

Since the upper bounds on  $Q_{RR}$ ,  $Q_{LR}$ , and  $Q_{RL}$  are found to be small, and since the helicity of the  $\nu_\mu$  in pion decay is known from experiment [19, 20] to very high precision to be  $-1$  [21], the cross section  $S$  of *inverse* muon decay, normalized to the  $V-A$  value, yields [2]

$$|g_{LL}^S|^2 \leq 4(1 - S) \quad (56.13a)$$

and

$$|g_{LL}^V|^2 = S. \quad (56.13b)$$

Thus the Standard Model assumption of a pure  $V-A$  leptonic charged weak interaction of  $e$  and  $\mu$  is derived (within errors)

from experiments at energies far below the mass of the  $W^\pm$ : Eq. (56.13 b) gives a lower limit for  $V-A$ , and Eqs. (56.12 a, b, c) and (56.13 a) give upper limits for the other four-fermion interactions. The existence of such upper limits may also be seen from  $Q_{RR} + Q_{RL} = (1 - \xi')/2$  ( $e^+$  longitudinal polarization) and  $Q_{RR} + Q_{LR} = \frac{1}{2}(1 + \xi/3 - 16\xi\delta/9)$  (decay asymmetry). Table 56.1 gives the current experimental limits on the magnitudes of the  $g_{\bar{e}\mu}^\gamma$ 's. More stringent limits on the six coupling constants  $g_{LR}^S, g_{LR}^V, g_{LR}^T, g_{RL}^S, g_{RL}^V,$  and  $g_{RL}^T$  have been derived from upper limits on the neutrino mass [22]. Limits on the "charge retention" coordinates, as used in the older literature (*e.g.*, Ref. [23]), are given by Burkard *et al.* [24].

### References

- [1] L. Michel, Proc. Phys. Soc. **A63**, 514 (1950).
- [2] W. Fetscher, H. J. Gerber and K. F. Johnson, Phys. Lett. **B173**, 102 (1986).
- [3] P. Langacker, Comments Nucl. Part. Phys. **19**, 1, 1 (1989).
- [4] C. Bouchiat and L. Michel, Phys. Rev. **106**, 170 (1957).
- [5] T. Kinoshita and A. Sirlin, Phys. Rev. **107**, 593 (1957).
- [6] T. Kinoshita and A. Sirlin, Phys. Rev. **108**, 844 (1957).
- [7] W. Fetscher, Phys. Rev. **D49**, 5945 (1994).
- [8] S. R. Mishra *et al.*, Phys. Lett. **B252**, 170 (1990).
- [9] S. R. Mishra, private communication.
- [10] P. Vilain *et al.* (CHARM-II), Phys. Lett. **B364**, 121 (1995).
- [11] A. Hillairet *et al.* (TWIST), Phys. Rev. **D85**, 092013 (2012), [arXiv:1112.3606].
- [12] R. P. MacDonald *et al.* (TWIST), Phys. Rev. **D78**, 032010 (2008), [arXiv:0807.1125].
- [13] C. A. Gagliardi, R. E. Tribble and N. J. Williams, Phys. Rev. **D72**, 073002 (2005), [hep-ph/0509069].
- [14] R. Bayes *et al.* (TWIST), Phys. Rev. Lett. **106**, 041804 (2011).
- [15] F. Scheck, in *Electroweak and Strong Interactions* (Springer Verlag, 1996).
- [16] K. Mursula and F. Scheck, Nucl. Phys. **B253**, 189 (1985).
- [17] P. Langacker and D. London, Phys. Rev. **D39**, 266 (1989).
- [18] C. Jarlskog, Nucl. Phys. **75**, 659 (1966).
- [19] A. Jodidio *et al.*, Phys. Rev. **D34**, 1967 (1986), [Erratum: Phys. Rev. **D37**, 237 (1988)].
- [20] L. P. Roesch *et al.*, Helv. Phys. Acta **55**, 74 (1982).
- [21] W. Fetscher, Phys. Lett. **140B**, 117 (1984).
- [22] G. Prezeau and A. Kurylov, Phys. Rev. Lett. **95**, 101802 (2005), [hep-ph/0409193].
- [23] S. E. Derenzo, Phys. Rev. **181**, 1854 (1969).
- [24] H. Burkard *et al.*, Phys. Lett. **160B**, 343 (1985).

57.  $\tau$  Branching Fractions

Revised May 2019 by Sw. Banerjee (Louisville U.) and A. Lusiani (SNS, Pisa; INFN, Pisa).

57.1  $\tau$  Branching Fractions

The  $\tau$  Listings contains 244 entries that correspond to either a  $\tau$  partial decay fraction into a specific decay mode (branching fraction) or a ratio of two  $\tau$  partial decay fractions (branching ratio). Experimental information provides values for 147 of these quantities, upper limits for 61 branching fractions to Lepton Family number, Lepton number, or Baryon number violating modes, and 36 additional upper limits for other modes. A total of 170 measurements of  $\tau$  branching fraction and branching ratio measurements is used for a global fit that determines 129 quantities.

57.2 The constrained fit to  $\tau$  branching fractions

The  $\tau$  branching fractions fit uses the reported values, uncertainties and statistical correlations of the  $\tau$  branching fractions and branching ratios measurements. Asymmetric uncertainties are symmetrized as  $\sigma_{\text{symm}}^2 = (\sigma_+^2 + \sigma_-^2)/2$ . Additionally, the most precise experimental inputs are treated according to how they depend on external parameters on the basis of their documentation [1]. The  $\tau$  measurements may depend on parameters such as the  $\tau$  pair production cross-section in  $e^+e^-$  annihilations at the  $\Upsilon(4S)$  peak. In some cases, measurements reported in different papers by the same collaboration may depend on common parameters like the estimate of the integrated luminosity or of particle identification efficiencies. For all the significant detected dependencies, the  $\tau$  measurements and their uncertainties are updated to account for the updated values of the external parameters. The dependencies on common systematic effects are also determined in size and sign, and all the common systematic dependencies of different measurements are used together with the published statistical and systematic uncertainties and correlations in order to compute a single all-inclusive variance and covariance matrix of the experimental inputs of the fit.

The fit procedure parameters correspond to  $\tau$  quantities that are fit to the experimental measurements while respecting relations described by a series of constraint equations. All the experimental inputs and all the constraint equations are reported in the  $\tau$  Listings section that follows this review. With respect to the 2016, 2017 and 2018 editions, the fit uses one more experimental measurement, published by the BaBar collaboration in 2018, on  $\mathcal{B}(\tau \rightarrow K^- K^0 \nu_\tau)$  [2]. If only a few measurements are correlated, the correlation coefficients are listed in the footnote for each measurement (see for example  $\Gamma(\text{particle}^- \geq 0 \text{ neutrals} \geq 0 K^0 \nu_\tau \text{ ("1-prong")})/\Gamma_{\text{total}}$ ). If a large number of measurements are correlated, then the full correlation matrix is listed in the footnote to the measurement that first appears in the  $\tau$  Listings. Footnotes to the other measurements refer to the first one. For example, the large correlation matrices for the branching fraction or ratio measurements contained in Refs. [3] [4] are listed in Footnotes to the  $\Gamma(e^- \bar{\nu}_e \nu_\tau)/\Gamma_{\text{total}}$  and  $\Gamma(h^- \nu_\tau)/\Gamma_{\text{total}}$  measurements respectively. The constraints between the  $\tau$  branching fractions and ratios include coefficients that correspond to physical quantities, like for instance the branching fractions of the  $\eta$  and  $\omega$  mesons. All quantities are taken from the 2018 edition of the Review of Particle Physics. Their uncertainties are neglected in the fit.

We obtain the branching fraction of  $\tau \rightarrow a_1^- (\rightarrow \pi^- \gamma) \nu_\tau$  using the ALEPH estimate for  $\mathcal{B}(a_1^- \rightarrow \pi^- \gamma)$  [3], which uses the measurement of  $\Gamma(a_1^- \rightarrow \pi^- \gamma)$  [5]. In the fit, we assume that  $\mathcal{B}(\tau^- \rightarrow a_1^- \nu_\tau)$  is equal to  $\mathcal{B}(\tau \rightarrow \pi^- \pi^- \pi^+ \nu_\tau \text{ (ex. } K^0, \omega)) + \mathcal{B}(\tau \rightarrow \pi^- 2\pi^0 \nu_\tau \text{ (ex. } K^0))$ , neglecting the observed but negligible branching fractions to other modes, including  $\mathcal{B}(a_1^- \rightarrow \pi^- \gamma)$ .

In some cases, constraints describe approximate relations that nevertheless hold within the present experimental precision. For instance, the constraint  $\mathcal{B}(\tau \rightarrow K^- K^- K^+ \nu_\tau) = \mathcal{B}(\tau \rightarrow K^- \phi \nu_\tau) \times \mathcal{B}(\phi \rightarrow K^+ K^-)$  is justified within the current experimental evidence.

In the fit, scale factors are applied to the published uncertainties of measurements only if significant inconsistency between different measurements remain after accounting for all relevant uncertainties and correlations. After examining the data and the fit pulls,

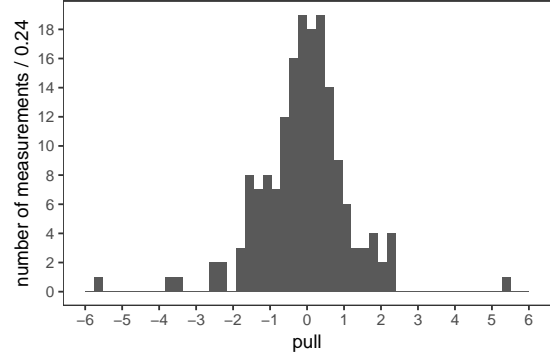


Figure 57.1: Pulls of individual measurements against the respective fitted quantity. No scale factor is used.

it has been decided to apply just one scale factor of 5.4 on the measurements of  $\mathcal{B}(\tau \rightarrow K^- K^- K^+ \nu_\tau)$ . The scale factor has been computed and applied according to the standard PDG procedure. Without the scale factor applied, the  $\chi^2$  probability of the fit is about 2%. On a per-measurement basis, the pull distribution in figure 57.1 indicates that just a few measurements have more than  $3\sigma$  pulls. (The uncertainties to obtain the pulls are computed using the measurements variance matrix and the variance matrix of the result, accounting for the fact that the variance matrix of the result is obtained from the measurement variance with the fit.) The pull probability distribution in figure 57.2 is reasonably flat. With many measurements some entries on the tails of the normal distribution must be expected. There are 170 pulls, one per measurement. They are partially correlated, and the effective number of independent pulls is equal to the number of degrees of freedom of the fit, 125. Only the  $\tau \rightarrow K^- K^- K^+ \nu_\tau$  decay mode has a pull that is inconsistent at the level of more than  $3\sigma$  even if considered as the largest pull in a set of 125. This confirms the choice of adopting just that one scale factor.

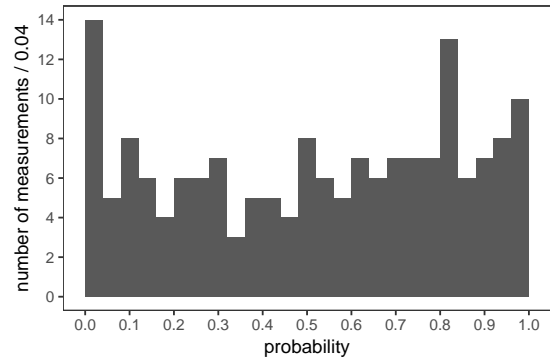


Figure 57.2: Probability of individual measurement pulls against the respective fitted quantity. No scale factor is used.

After scaling the error, the constrained fit has a  $\chi^2$  of 135 for 125 degrees of freedom, corresponding to a  $\chi^2$  probability of 26%. We use 170 measurements and 84 constraints on the branching fractions and ratios to determine 129 quantities, consisting of 112 branching fractions and 17 branching ratios. A total of 85 quantities have at least one measurement in the fit. The constraints include the unitarity constraint on the sum of all the exclusive  $\tau$  decay modes,  $\mathcal{B}_{\text{all}} = 1$ . If the unitarity constraint is released, the fit result for  $\mathcal{B}_{\text{all}}$  is consistent with unitarity with  $1 - \mathcal{B}_{\text{all}} = (0.00 \pm 0.10)\%$ .

For the convenience of summarizing the fit results, we list in the following the values and uncertainties for a set of 46 “basis” decay modes, from which all remaining branching fractions and ratios can be obtained using the constraints. The basis decay modes are not intended to sum up to 1. Since some basis quantities represent multiple branching fractions that are related by constraint

equations, they are properly weighted and the unitarity constraint corresponds to a linear combination whose coefficients are listed in the following. The correlation matrix between the basis modes is reported in the  $\tau$  Listings.

decay mode	fit result (%)	coefficient
$\mu^- \bar{\nu}_\mu \nu_\tau$	$17.3937 \pm 0.0384$	1.0000
$e^- \bar{\nu}_e \nu_\tau$	$17.8175 \pm 0.0399$	1.0000
$\pi^- \nu_\tau$	$10.8164 \pm 0.0512$	1.0000
$K^- \nu_\tau$	$0.6964 \pm 0.0096$	1.0000
$\pi^- \pi^0 \nu_\tau$	$25.4941 \pm 0.0893$	1.0000
$K^- \pi^0 \nu_\tau$	$0.4328 \pm 0.0148$	1.0000
$\pi^- 2\pi^0 \nu_\tau$ (ex. $K^0$ )	$9.2595 \pm 0.0964$	1.0021
$K^- 2\pi^0 \nu_\tau$ (ex. $K^0$ )	$0.0647 \pm 0.0218$	1.0000
$\pi^- 3\pi^0 \nu_\tau$ (ex. $K^0$ )	$1.0429 \pm 0.0707$	1.0000
$K^- 3\pi^0 \nu_\tau$ (ex. $K^0, \eta$ )	$0.0478 \pm 0.0212$	1.0000
$h^- 4\pi^0 \nu_\tau$ (ex. $K^0, \eta$ )	$0.1118 \pm 0.0391$	1.0000
$\pi^- \bar{K}^0 \nu_\tau$	$0.8384 \pm 0.0138$	1.0000
$K^- K^0 \nu_\tau$	$0.1486 \pm 0.0034$	1.0000
$\pi^- \bar{K}^0 \pi^0 \nu_\tau$	$0.3817 \pm 0.0129$	1.0000
$K^- \pi^0 K^0 \nu_\tau$	$0.1500 \pm 0.0070$	1.0000
$\pi^- \bar{K}^0 2\pi^0 \nu_\tau$ (ex. $K^0$ )	$0.0263 \pm 0.0226$	1.0000
$\pi^- K_S^0 K_S^0 \nu_\tau$	$0.0235 \pm 0.0006$	2.0000
$\pi^- K_S^0 K_L^0 \nu_\tau$	$0.1081 \pm 0.0241$	1.0000
$\pi^- \pi^0 K_S^0 K_S^0 \nu_\tau$	$0.0018 \pm 0.0002$	2.0000
$\pi^- \pi^0 K_S^0 K_L^0 \nu_\tau$	$0.0325 \pm 0.0119$	1.0000
$\bar{K}^0 h^- h^- h^+ \nu_\tau$	$0.0247 \pm 0.0199$	1.0000
$\pi^- \pi^- \pi^+ \nu_\tau$ (ex. $K^0, \omega$ )	$8.9868 \pm 0.0513$	1.0021
$\pi^- \pi^- \pi^+ \pi^0 \nu_\tau$ (ex. $K^0, \omega$ )	$2.7404 \pm 0.0710$	1.0000
$h^- h^- h^+ 2\pi^0 \nu_\tau$ (ex. $K^0, \omega, \eta$ )	$0.0981 \pm 0.0356$	1.0000
$\pi^- K^- K^+ \nu_\tau$	$0.1435 \pm 0.0027$	1.0000
$\pi^- K^- K^+ \pi^0 \nu_\tau$	$0.0061 \pm 0.0018$	1.0000
$K^- \pi^0 \eta \nu_\tau$	$0.1389 \pm 0.0072$	1.0000
$K^- \eta \nu_\tau$	$0.0155 \pm 0.0008$	1.0000
$K^- \pi^0 \eta \nu_\tau$	$0.0048 \pm 0.0012$	1.0000
$\pi^- \bar{K}^0 \eta \nu_\tau$	$0.0094 \pm 0.0015$	1.0000
$\pi^- \pi^+ \pi^- \eta \nu_\tau$ (ex. $K^0$ )	$0.0220 \pm 0.0013$	1.0000
$K^- \omega \nu_\tau$	$0.0410 \pm 0.0092$	1.0000
$h^- \pi^0 \omega \nu_\tau$	$0.4085 \pm 0.0419$	1.0000
$K^- \phi \nu_\tau$	$0.0044 \pm 0.0016$	0.8320
$\pi^- \omega \nu_\tau$	$1.9494 \pm 0.0645$	1.0000
$K^- \pi^- \pi^+ \nu_\tau$ (ex. $K^0, \omega$ )	$0.2927 \pm 0.0068$	1.0000
$K^- \pi^- \pi^+ \pi^0 \nu_\tau$ (ex. $K^0, \omega, \eta$ )	$0.0394 \pm 0.0142$	1.0000
$\pi^- 2\pi^0 \omega \nu_\tau$ (ex. $K^0$ )	$0.0072 \pm 0.0016$	1.0000
$2\pi^- \pi^+ 3\pi^0 \nu_\tau$ (ex. $K^0, \eta, \omega, f_1$ )	$0.0014 \pm 0.0027$	1.0000
$3\pi^- 2\pi^+ \nu_\tau$ (ex. $K^0, \omega, f_1$ )	$0.0775 \pm 0.0030$	1.0000
$K^- 2\pi^- 2\pi^+ \nu_\tau$ (ex. $K^0$ )	$0.0001 \pm 0.0001$	1.0000
$2\pi^- \pi^+ \omega \nu_\tau$ (ex. $K^0$ )	$0.0084 \pm 0.0006$	1.0000
$3\pi^- 2\pi^+ \pi^0 \nu_\tau$ (ex. $K^0, \eta, \omega, f_1$ )	$0.0038 \pm 0.0009$	1.0000
$K^- 2\pi^- 2\pi^+ \pi^0 \nu_\tau$ (ex. $K^0$ )	$0.0001 \pm 0.0001$	1.0000
$\pi^- f_1 \nu_\tau$ ( $f_1 \rightarrow 2\pi^- 2\pi^+$ )	$0.0052 \pm 0.0004$	1.0000
$\pi^- 2\pi^0 \eta \nu_\tau$	$0.0195 \pm 0.0038$	1.0000

In defining the fit constraints and in selecting the modes that sum up to one we made some assumptions and choices. We assume that some channels, like  $\tau^- \rightarrow \pi^- K^+ \pi^- \geq 0\pi^0 \nu_\tau$  and  $\tau^- \rightarrow \pi^+ K^- K^- \geq 0\pi^0 \nu_\tau$ , have negligible branching fractions as expected from the Standard Model, even if the experimental limits for these branching fractions are not very stringent. The 95% confidence level upper limits are  $\mathcal{B}(\tau^- \rightarrow \pi^- K^+ \pi^- \geq 0\pi^0 \nu_\tau) < 0.25\%$  and  $\mathcal{B}(\tau^- \rightarrow \pi^+ K^- K^- \geq 0\pi^0 \nu_\tau) < 0.09\%$ , values not so different from measured branching fractions for allowed 3-prong modes containing charged kaons. For decays to final states containing one neutral kaon we assume that the branching fraction with the  $K_L^0$  are the same as the corresponding one with a  $K_S^0$ . On decays with two neutral kaons we assume that the branching fractions with  $K_L^0 K_L^0$  are the same as the ones with  $K_S^0 K_S^0$ .

### 57.3 BaBar and Belle measure on average lower branching fractions and ratios.

We compare the BaBar and Belle measurements with the results of a fit where all their measurements have been excluded. We find that that BaBar and Belle measure on average lower  $\tau$  branching

fractions and ratios than the other experiments. Figures 57.3 and 57.4 show histograms of the 28 normalized differences between the  $B$ -factory measurements and the respective non- $B$ -factory fit results. The normalization is the uncertainty on the difference. The average normalized difference between the two sets of measurements is  $-0.8\sigma$  ( $-0.7\sigma$  for the 16 Belle measurements and  $-0.8\sigma$  for the 12 BaBar measurements).

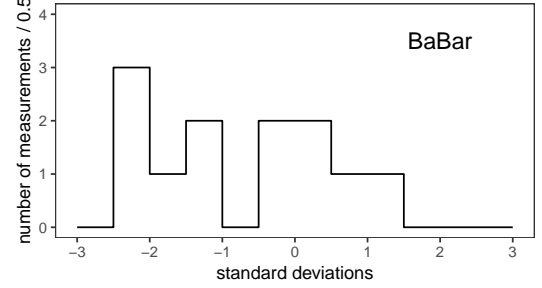


Figure 57.3: Distribution of the normalized difference between 12 measurements of branching fractions and ratios published by the BaBar collaboration and the respective averages computed using only non- $B$ -factory measurements.

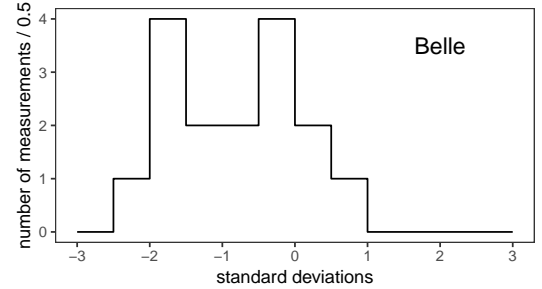


Figure 57.4: Distribution of the normalized difference between 16 measurements of branching fractions and ratios published by the Belle collaboration and the respective averages computed using only non- $B$ -factory measurements.

### 57.4 Overconsistency of Leptonic Branching Fraction Measurements.

As observed in the previous editions of this review, measurements of the leptonic branching fractions are more consistent with each other than expected from the quoted errors on the individual measurements. The  $\chi^2$  is 0.34 for  $\mathcal{B}_e$  and 0.08 for  $\mathcal{B}_\mu$ . Assuming normal errors, the probability of a smaller  $\chi^2$  is 1.3% for  $\mathcal{B}_e$  and 0.08% for  $\mathcal{B}_\mu$ .

### 57.5 Technical implementation of the fit

The fit computes a set of quantities denoted with  $q_i$  by minimizing a  $\chi^2$  while respecting a series of equality constraints on the  $q_i$ . The  $\chi^2$  is computed using the measurements  $m_i$  and their covariance matrix  $E_{ij}$  as  $\chi^2 = (m_i - A_{ik} q_k)^t E_{ij}^{-1} (m_j - A_{jl} q_l)$ , where the model matrix  $A_{ij}$  is used to get the vector of the predicted measurements  $m'_i$  from the vector of the fit parameters  $q_j$  as  $m'_i = A_{ij} q_j$ . In this particular implementation the measurements are grouped by the quantity that they measure, and all quantities with at least one measurement correspond to a fit parameter. Therefore, the matrix  $A_{ij}$  has one row per measurement  $m_i$  and one column per fitted quantity  $q_j$ , with unity coefficients for the rows and column that identify a measurement  $m_i$  of the quantity  $q_j$ , respectively. The constraints are equations involving the fit parameters. The fit does not impose limitations on the functional form of the constraints. In summary, the fit requires:

$$\min [\chi^2(q_k)] = \min [(m_i - A_{ik} q_k)^t E_{ij}^{-1} (m_j - A_{jl} q_l)] \quad (57.1)$$

$$\text{subjected to } f_r(q_s) - c_r = 0, \quad (57.2)$$

where the left term of Eq. 57.2 defines the constraint expressions. Using the method of Lagrange multipliers, a set of equations is



obtained by taking the derivatives with respect to the fitted quantities  $q_k$  and the Lagrange multipliers  $\lambda_r$  of the sum of the  $\chi^2$  and the constraint expressions multiplied by the Lagrange multipliers  $\lambda_r$ , one for each constraint:

$$\begin{aligned} \min \left[ (A_{ik}q_k - m_i)^t E_{ij}^{-1} (A_{jl}q_l - m_j) + 2\lambda_r (f_r(q_s) - c_r) \right] = \\ = \min \left[ \tilde{\chi}^2(q_k, \lambda_r) \right] , \\ (\partial/\partial q_k, \partial/\partial \lambda_r) \left[ \tilde{\chi}^2(q_k, \lambda_r) \right] = 0 . \end{aligned} \quad (57.3)$$

Eq. 57.3 defines a set of equations for the vector of the unknowns  $(q_k, \lambda_r)$ , some of which may be non-linear, in case of non-linear constraints. An iterative minimization procedure approximates at each step the non-linear constraint expressions by their first order Taylor expansion around the current values of the fitted quantities,  $\bar{q}_s$ :

$$f_r(q_s) - c_r = f_r(\bar{q}_s) + \left. \frac{\partial f_r(q_s)}{\partial q_s} \right|_{\bar{q}_s} (q_s - \bar{q}_s) - c_r ,$$

which can be written as

$$B_{rs}q_s - c'_r ,$$

where  $c'_r$  are the resulting constant known terms, independent of  $q_s$  at first order. After linearization, the differentiation by  $q_k$  and  $\lambda_r$  is trivial and leads to a set of linear equations

$$A_{ki}^t E_{ij}^{-1} A_{jl}q_l + B_{kr}^t \lambda_r = A_{ki}^t E_{ij}^{-1} m_j , \quad (57.4)$$

$$B_{rs}q_s = c'_r , \quad (57.5)$$

which can be expressed as

$$F_{ij}u_j = v_i , \quad (57.6)$$

where  $u_j = (q_k, \lambda_r)$  and  $v_i$  is the vector of the known constant terms running over the index  $k$  and then  $r$  in the right terms of Eq. 57.4 and Eq. 57.5, respectively. Solving the equation set in Eq. 57.6 by matrix inversion gives the the fitted quantities and their variance and covariance matrix, using the measurements and their variance and covariance matrix. The fit procedure starts by computing the linear approximation of the non-linear constraint expressions around the quantities seed values. With an iterative procedure, the unknowns are updated at each step by solving the equations and the equations are then linearized around the updated values, until the variation of the fitted unknowns is reduced below a numerically small threshold.

#### References

- [1] D. Asner *et al.* (Heavy Flavor Averaging Group) (2010), [arXiv:1010.1589].
- [2] J. P. Lees *et al.* (BaBar), Phys. Rev. **D98**, 3, 032010 (2018), [arXiv:1806.10280].
- [3] S. Schael *et al.* (ALEPH), Phys. Rept. **421**, 191 (2005), [hep-ex/0506072].
- [4] J. Abdallah *et al.* (DELPHI), Eur. Phys. J. **C46**, 1 (2006), [hep-ex/0603044].
- [5] M. Zielinski *et al.*, Phys. Rev. Lett. **52**, 1195 (1984).

## 58. $\tau$ -Lepton Decay Parameters

Updated August 2011 by A. Stahl (RWTH Aachen).

The purpose of the measurements of the decay parameters (also known as Michel parameters) of the  $\tau$  is to determine the structure (spin and chirality) of the current mediating its decays.

### 58.1. Leptonic Decays:

The Michel parameters are extracted from the energy spectrum of the charged daughter lepton  $\ell = e, \mu$  in the decays  $\tau \rightarrow \ell \nu_\ell \nu_\tau$ . Ignoring radiative corrections, neglecting terms of order  $(m_\ell/m_\tau)^2$  and  $(m_\tau/\sqrt{s})^2$ , and setting the neutrino masses to zero, the spectrum in the laboratory frame reads

$$\frac{d\Gamma}{dx} = \frac{G_{\tau\ell}^2 m_\tau^5}{192 \pi^3} \times \left\{ f_0(x) + \rho f_1(x) + \eta \frac{m_\ell}{m_\tau} f_2(x) - P_\tau [\xi g_1(x) + \xi \delta g_2(x)] \right\}, \quad (58.1)$$

with

$$\begin{aligned} f_0(x) &= 2 - 6x^2 + 4x^3 \\ f_1(x) &= -\frac{4}{9} + 4x^2 - \frac{32}{9}x^3 & g_1(x) &= -\frac{2}{3} + 4x - 6x^2 + \frac{8}{3}x^3 \\ f_2(x) &= 12(1-x)^2 & g_2(x) &= \frac{4}{9} - \frac{16}{3}x + 12x^2 - \frac{64}{9}x^3. \end{aligned}$$

The quantity  $x$  is the fractional energy of the daughter lepton  $\ell$ , *i.e.*,  $x = E_\ell/E_{\ell,max} \approx E_\ell/(\sqrt{s}/2)$  and  $P_\tau$  is the polarization of the tau leptons. The integrated decay width is given by

$$\Gamma = \frac{G_{\tau\ell}^2 m_\tau^5}{192 \pi^3} \left( 1 + 4\eta \frac{m_\ell}{m_\tau} \right). \quad (58.2)$$

The situation is similar to muon decays  $\mu \rightarrow e \nu_e \nu_\mu$ . The generalized matrix element with the couplings  $g_{\ell\mu}^\gamma$  and their relations to the Michel parameters  $\rho, \eta, \xi$ , and  $\delta$  have been described in the ‘‘Note on Muon Decay Parameters.’’ The Standard Model expectations are 3/4, 0, 1, and 3/4, respectively. For more details, see Ref. 1.

### 58.2. Hadronic Decays:

In the case of hadronic decays  $\tau \rightarrow h \nu_\tau$ , with  $h = \pi, \rho$ , or  $a_1$ , the ansatz is restricted to purely vectorial currents. The matrix element is

$$\frac{G_{\tau h}}{\sqrt{2}} \sum_{\lambda=R,L} g_\lambda \langle \bar{\Psi}_\omega(\nu_\tau) | \gamma^\mu | \Psi_\lambda(\tau) \rangle J_\mu^h \quad (58.3)$$

with the hadronic current  $J_\mu^h$ . The neutrino chirality  $\omega$  is uniquely determined from  $\lambda$ . The spectrum depends only on a single parameter  $\xi_h$

$$\frac{d^n \Gamma}{dx_1 dx_2 \dots dx_n} = f(\vec{x}) + \xi_h P_\tau g(\vec{x}), \quad (58.4)$$

with  $f$  and  $g$  being channel-dependent functions of the  $n$  observables  $\vec{x} = (x_1, x_2, \dots, x_n)$  (see Ref. 2). The parameter  $\xi_h$  is related to the couplings through

$$\xi_h = |g_L|^2 - |g_R|^2. \quad (58.5)$$

$\xi_h$  is the negative of the chirality of the  $\tau$  neutrino in these decays. In the Standard Model,  $\xi_h = 1$ . Also included in the Data Listings for  $\xi_h$  are measurements of the neutrino helicity which coincide with  $\xi_h$ , if the neutrino is massless (ASNER 00 [3], ACKERSTAFF 97R [4], AKERS 95P [5], ALBRECHT 93C [6], and ALBRECHT 90I [7]).

### 58.3. Combination of Measurements:

The individual measurements are combined, taking into account the correlations between the parameters. In a first fit, universality between the two leptonic decays, and between all hadronic decays, is assumed. A second fit is made without these assumptions. The results of the two fits are provided as OUR FIT in the Data Listings below in the tables whose title includes ‘‘(e or mu)’’ or ‘‘(all hadronic modes)’’, and ‘‘(e),’’ ‘‘(mu)’’ *etc.*, respectively. The measurements show good agreement with the Standard Model. The  $\chi^2$  values with respect to the Standard model predictions are 24.1 for 41 degrees of freedom and 26.8 for 56 degrees of freedom, respectively. The correlations are reduced through this combination to less than 20%, with the exception of  $\rho$  and  $\eta$  which are correlated by +23%, for the fit with universality and by +70% for  $\tau \rightarrow \mu \nu_\mu \nu_\tau$ .

### 58.4. Model-independent Analysis:

From the Michel parameters, limits can be derived on the couplings  $g_{\ell\lambda}^\kappa$  without further model assumptions. In the Standard model  $g_{LL}^V = 1$  (leptonic decays), and  $g_L = 1$  (hadronic decays) and all other couplings vanish. First, the partial decay widths have to be compared to the Standard Model predictions to derive limits on the normalization of the couplings  $A_x = G_{\tau x}^2/G_F^2$  with Fermi’s constant  $G_F$ :

$$\begin{aligned} A_e &= 1.0029 \pm 0.0046, \\ A_\mu &= 0.981 \pm 0.018, \\ A_\pi &= 1.0020 \pm 0.0073. \end{aligned} \quad (58.6)$$

Then limits on the couplings (95% CL) can be extracted (see Ref. 8 and Ref. 9). Without the assumption of universality, the limits given in Table 58.1 are derived.

**Table 58.1:** Coupling constants  $g_{\ell\mu}^\gamma$ . 95% confidence level experimental limits. The limits include the quoted values of  $A_e, A_\mu$ , and  $A_\pi$  and assume  $A_\rho = A_{a_1} = 1$ .

$\tau \rightarrow e \nu_e \nu_\tau$		
$ g_{RR}^S  < 0.70$	$ g_{RR}^V  < 0.17$	$ g_{RR}^T  \equiv 0$
$ g_{LR}^S  < 0.99$	$ g_{LR}^V  < 0.13$	$ g_{LR}^T  < 0.082$
$ g_{RL}^S  < 2.01$	$ g_{RL}^V  < 0.52$	$ g_{RL}^T  < 0.51$
$ g_{LL}^S  < 2.01$	$ g_{LL}^V  < 1.005$	$ g_{LL}^T  \equiv 0$
$\tau \rightarrow \mu \nu_\mu \nu_\tau$		
$ g_{RR}^S  < 0.72$	$ g_{RR}^V  < 0.18$	$ g_{RR}^T  \equiv 0$
$ g_{LR}^S  < 0.95$	$ g_{LR}^V  < 0.12$	$ g_{LR}^T  < 0.079$
$ g_{RL}^S  < 2.01$	$ g_{RL}^V  < 0.52$	$ g_{RL}^T  < 0.51$
$ g_{LL}^S  < 2.01$	$ g_{LL}^V  < 1.005$	$ g_{LL}^T  \equiv 0$
$\tau \rightarrow \pi \nu_\tau$		
$ g_V^V  < 0.15$	$ g_L^V  > 0.992$	
$\tau \rightarrow \rho \nu_\tau$		
$ g_R^V  < 0.10$	$ g_L^V  > 0.995$	
$\tau \rightarrow a_1 \nu_\tau$		
$ g_R^V  < 0.16$	$ g_L^V  > 0.987$	

### 58.5. Model-dependent Interpretation:

More stringent limits can be derived assuming specific models. For example, in the framework of a two Higgs doublet model, the measurements correspond to a limit of  $m_{H^\pm} > 1.9 \text{ GeV} \times \tan \beta$  on the mass of the charged Higgs boson, or a limit of 253 GeV on the mass of the second  $W$  boson in left-right symmetric models for arbitrary mixing (both 95% CL). See Ref. 9 and Ref. 10.

#### References:

1. F. Scheck, Phys. Reports **44**, 187 (1978);  
W. Fetscher and H.J. Gerber in *Precision Tests of the Standard Model*, edited by P. Langacker, World Scientific, 1993;  
A. Stahl, *Physics with  $\tau$  Leptons*, Springer Tracts in Modern Physics.
2. M. Davier *et al.*, Phys. Lett. **B306**, 411 (1993).

3. CLEO Collab., D.M. Asner *et al.*, Phys. Rev. **D61**, 012002 (2000).
4. OPAL Collab., K. Ackerstaff *et al.*, Z. Phys. **C75**, 593 (1997).
5. OPAL Collab., R. Akers *et al.*, Z. Phys. **C67**, 45 (1995).
6. ARGUS Collab., H. Albrecht *et al.*, Z. Phys. **C58**, 61 (1993).
7. ARGUS Collab., H. Albrecht *et al.*, Phys. Lett. **B250**, 164 (1990).
8. OPAL Collab., K. Ackerstaff *et al.*, Eur. Phys. J. **C8**, 3 (1999).
9. A. Stahl, Nucl. Phys. (Proc. Supp.) **B76**, 173 (1999).
10. M.-T. Dova *et al.*, Phys. Rev. **D58**, 015005 (1998);  
T. Hebbeker and W. Lohmann, Z. Phys. **C74**, 399 (1997);  
A. Pich and J.P. Silva, Phys. Rev. **D52**, 4006 (1995).

## 59. Quark Masses

Updated August 2019 by A.V. Manohar (UC, San Diego), L.P. Lellouch (CNRS & Aix-Marseille U.), and R.M. Barnett (LBNL).

### 59.1. Introduction

This note discusses some of the theoretical issues relevant for the determination of quark masses, which are fundamental parameters of the Standard Model of particle physics. Unlike the leptons, quarks are confined inside hadrons and are not observed as physical particles. Quark masses therefore cannot be measured directly, but must be determined indirectly through their influence on hadronic properties. Although one often speaks loosely of quark masses as one would of the mass of the electron or muon, any quantitative statement about the value of a quark mass must make careful reference to the particular theoretical framework that is used to define it. It is important to keep this *scheme dependence* in mind when using the quark mass values tabulated in the data listings.

Historically, the first determinations of quark masses were performed using quark models. These are usually called constituent quark masses and are of order 350 MeV for the  $u$  and  $d$  quarks. Constituent quark masses model the effects of dynamical chiral symmetry breaking discussed below, and are not directly related to the quark mass parameters  $m_q$  of the QCD Lagrangian of Eq. (59.1). The resulting masses only make sense in the limited context of a particular quark model, and cannot be related to the quark mass parameters,  $m_q$ , of the Standard Model. In order to discuss quark masses at a fundamental level, definitions based on quantum field theory must be used, and the purpose of this note is to discuss these definitions and the corresponding determinations of the values of the masses.

### 59.2. Mass parameters and the QCD Lagrangian

The QCD [1] Lagrangian is

$$\mathcal{L} = \sum_{q=u,d,s,\dots,t} \bar{q} (i\not{D} - m_q) q - \frac{1}{2} \text{tr} G_{\mu\nu} G^{\mu\nu}, \quad (59.1)$$

where the sum runs over the quark flavors  $u, d, s, c, b$  and  $t$ .  $\not{D} = (\partial_\mu - igA_\mu) \gamma^\mu$  is the gauge covariant derivative,  $A_\mu$  is the  $su(3)$ -valued gluon field,  $G_{\mu\nu} = \frac{i}{g} [D_\mu, D_\nu]$  is the gluon field strength,  $m_q$  is the mass parameter of quark flavor  $q$ , and  $q$  is the quark Dirac field. After renormalization, the QCD Lagrangian Eq. (59.1) gives finite values for physical quantities, such as scattering amplitudes. Renormalization is a procedure that invokes a subtraction scheme to render the amplitudes finite, and requires the introduction of a dimensionful scale parameter  $\mu$ . The mass parameters in the QCD Lagrangian Eq. (59.1) depend on the renormalization scheme used to define the theory, and also on the scale parameter  $\mu$ . The most commonly used renormalization scheme for QCD perturbation theory is the  $\overline{\text{MS}}$  scheme.

The QCD Lagrangian has a chiral symmetry in the limit that the quark masses vanish. This symmetry is spontaneously broken by dynamical chiral symmetry breaking, and explicitly broken by the quark masses. The non-perturbative scale of dynamical chiral symmetry breaking,  $\Lambda_\chi$ , is around 1 GeV [2]. It is conventional to call quarks heavy if  $m_q > \Lambda_\chi$ , so that explicit chiral symmetry breaking dominates ( $c, b$ , and  $t$  quarks are heavy), and light if  $m_q < \Lambda_\chi$ , so that spontaneous chiral symmetry breaking dominates (the  $u$  and  $d$  are light and the  $s$  is considered to be light when using  $SU(3)_L \times SU(3)_R$  chiral perturbation theory). The determination of light- and heavy-quark masses is considered separately in Sec. 59.4 and Sec. 59.5 below.

At high energies or short distances, non-perturbative effects, such as chiral symmetry breaking, become small and one can, in principle, determine quark masses by analyzing mass-dependent effects using QCD perturbation theory. Such computations are conventionally performed using the  $\overline{\text{MS}}$  scheme at a scale  $\mu \gg \Lambda_\chi$ , and give the  $\overline{\text{MS}}$  “running” mass  $\overline{m}(\mu)$ . We use the  $\overline{\text{MS}}$  scheme when reporting quark masses; one can readily convert these values into other schemes using perturbation theory.

The  $\mu$  dependence of  $\overline{m}(\mu)$  at short distances can be calculated using the renormalization group (RG) equation,

$$\mu^2 \frac{d\overline{m}(\mu)}{d\mu^2} = -\gamma(\overline{\alpha}_s(\mu)) \overline{m}(\mu), \quad (59.2)$$

where  $\gamma$  is the anomalous dimension which is now known to four-loop order in perturbation theory [3,4].  $\overline{\alpha}_s$  is the coupling constant [1] in the  $\overline{\text{MS}}$  scheme. Defining the expansion coefficients  $\gamma_r$  by

$$\gamma(\overline{\alpha}_s) \equiv \sum_{r=1}^{\infty} \gamma_r \left( \frac{\overline{\alpha}_s}{4\pi} \right)^r,$$

the first four coefficients are given by

$$\begin{aligned} \gamma_1 &= 4, \\ \gamma_2 &= \frac{202}{3} - \frac{20N_L}{9}, \\ \gamma_3 &= 1249 + \left( -\frac{2216}{27} - \frac{160}{3} \zeta(3) \right) N_L - \frac{140}{81} N_L^2, \\ \gamma_4 &= \frac{4603055}{162} + \frac{135680}{27} \zeta(3) - 8800 \zeta(5) \\ &\quad + \left( -\frac{91723}{27} - \frac{34192}{9} \zeta(3) + 880 \zeta(4) + \frac{18400}{9} \zeta(5) \right) N_L \\ &\quad + \left( \frac{5242}{243} + \frac{800}{9} \zeta(3) - \frac{160}{3} \zeta(4) \right) N_L^2 \\ &\quad + \left( -\frac{332}{243} + \frac{64}{27} \zeta(3) \right) N_L^3, \end{aligned}$$

where  $N_L$  is the number of active light quark flavors at the scale  $\mu$ , i.e. flavors with masses  $< \mu$ , and  $\zeta$  is the Riemann zeta function ( $\zeta(3) \simeq 1.2020569$ ,  $\zeta(4) \simeq 1.0823232$ , and  $\zeta(5) \simeq 1.0369278$ ). Eq. (59.2) must be solved in conjunction with the RG equation for  $\overline{\alpha}_s(\mu)$  given in [1]. In addition, as the renormalization scale crosses quark mass thresholds one needs to match the scale dependence of  $\overline{m}$  below and above the threshold. There are finite threshold corrections; the necessary formulae can be found in Ref. [5].

### 59.3. Lattice QCD

The use of lattice QCD calculations for *ab initio* determinations of the fundamental parameters of QCD, including the coupling constant and quark masses (except for the top-quark mass) is a very active area of research (see the review on Lattice Quantum Chromodynamics in this *Review*). Here we only briefly recall those features which are required for the determination of quark masses. In order to determine the lattice spacing ( $a$ , i.e. the distance between neighboring points of the lattice) and quark masses, one computes a convenient and appropriate set of physical quantities (frequently chosen to be a set of hadronic masses) for a variety of input values of the quark masses in units of the lattice spacing. These input quark masses are then tuned to their true (physical) values by requiring that the calculation correctly reproduces the set of physical quantities being used for the calibration.

The resulting values of the quark masses are bare quark masses, corresponding to a particular discretization of QCD and with the lattice spacing as the ultraviolet cut-off. In order for these results to be useful in phenomenological applications, it is necessary to relate them to renormalized masses defined in some standard renormalization scheme such as  $\overline{\text{MS}}$ . Provided that both the ultraviolet cut-off  $a^{-1}$  and the renormalization scale  $\mu$  are much greater than  $\Lambda_{\text{QCD}}$ , the bare and renormalized masses can be related in perturbation theory. However, in order to avoid uncertainties due to the unknown higher-order coefficients in lattice perturbation theory, most results obtained recently use *non-perturbative renormalization* to relate the bare masses to those defined in renormalization schemes which can be realized directly in lattice QCD (e.g. those obtained from quark and gluon Green functions at specified momenta in the Landau gauge [6]

or those defined using finite-volume techniques and the Schrödinger functional [7], but not  $\overline{\text{MS}}$  that is only defined for dimensional regularization). These methods require  $\mu \gg \Lambda_{\text{QCD}}$  so that unwanted (non-perturbative) corrections proportional to inverse powers of  $\mu$ , which appear in some approaches, remain small corrections that can be identified and removed. This condition is also necessary so that matching to other schemes can be performed reliably in perturbation theory. Moreover, these methods require  $a^{-1} \gg \mu$  so that cutoff effects are small enough to be extrapolated away. Thus, the calculations are repeated for finer and finer lattices spacings and the continuum limit,  $a \rightarrow 0$ , of these non-perturbatively renormalized masses is taken to eliminate all cutoff effects. The conversion to the  $\overline{\text{MS}}$  scheme is then performed using continuum perturbation theory, which is more readily obtained to higher orders and is usually better behaved than its lattice counterpart.

It is important to note that the issues surrounding the renormalization of quark masses disappear when considering pairwise ratios of these masses (up to electromagnetic effects for quarks of different charge, which are negligible compared to other uncertainties at present). Indeed, if the same scheme and scale are implemented, QCD renormalization factors are identical for all quark flavors, and these factors therefore cancel exactly in quark-mass ratios. In particular, this means that these ratios are scheme and scale independent. Moreover, these ratios suffer little from the uncertainties in the determination of the lattice scale because they are dimensionless. Thus, quark-mass ratios are typically determined with significantly higher precision using lattice QCD than are the individual masses.

The determination of quark masses using lattice simulations is well established and the current emphasis is on the reduction and control of the systematic uncertainties. With improved algorithms and access to more powerful computing resources, the precision of the results has improved immensely in recent years. Vacuum polarization effects are included with  $N_f = 2$ ,  $2 + 1$  or  $N_f = 2 + 1 + 1$  flavors of sea quarks. The number 2 here indicates that the up and down quarks are degenerate. Simulations with  $2 + 1$  and  $2 + 1 + 1$  flavors represent controlled approximations to physical QCD at the low energies considered for quark mass determinations, up to corrections of  $O((\Lambda_{\text{QCD}}/m_c)^2/N_c)$  and  $O((\Lambda_{\text{QCD}}/m_b)^2/N_c)$ , respectively. This is not the case for simulations with  $N_f = 2$  or in which vacuum polarization effects are completely neglected (this is the so-called *quenched* approximation) and results obtained in such frameworks will not enter the discussion here.

Particularly pleasing is the observation that different formulations of lattice QCD, with different systematic uncertainties, yield results which are largely consistent with each other. This gives us broad confidence in the estimates of the systematic errors. As the precision of the results approaches (or even exceeds in some cases) 1%, isospin breaking effects, including electromagnetic corrections need to be included and this is beginning to be done as will be discussed below. In particular, a reliable estimate of these effects is required for determining the individual  $u$  and  $d$  quark masses.

Members of the lattice QCD community have organized a Flavour Lattice Averaging Group (FLAG) which critically reviews quantities computed in lattice QCD relevant to flavor physics, including the determination of quark masses, against stated quality criteria and presents its view of the current status of the results. The latest edition reviews lattice results published before September 30th 2018 [8]. Since that deadline, only a single lattice determination of quark masses has appeared [9]. It is a computation of  $m_c$  and  $m_b$  in  $N_f = 2 + 1$  QCD, based on the method of Euclidean-time moments of pseudoscalar, two-point functions of  $c\bar{c}$  quark-bilinear operators described below. Its results are fully consistent with the lattice averages quoted later.

## 59.4. Light quarks

In this section we review the determination of the masses of the light quarks  $u$ ,  $d$  and  $s$  from lattice simulations and then discuss the consequences of the approximate chiral symmetry.

### 59.4.1. Lattice QCD results :

The most reliable determinations of the strange quark mass  $m_s$  and of the average of the up and down quark masses  $m_{ud} = (m_u + m_d)/2$  are obtained from lattice simulations. As explained in Sec. 59.3 above, the simulations are generally performed with degenerate up and down quarks ( $m_u = m_d$ ) and so it is the average which is obtained directly from the computations. Below we discuss the derivation of  $m_u$  and  $m_d$  separately, but we start by briefly presenting our estimate of the current status of the latest lattice results in the isospin symmetric limit. The FLAG Review [8] bases its summary numbers for these quark masses largely on references [10–15] for  $N_f = 2 + 1$  and references [16–19] for  $N_f = 2 + 1 + 1$  flavors of sea quarks, which its authors consider to have the most reliable estimates of the systematic uncertainties. For  $N_f = 2 + 1$  flavors, they quote  $\overline{m}_{ud} = (3.364 \pm 0.041)$  MeV,  $\overline{m}_s = (92.03 \pm 0.88)$  MeV and  $(\overline{m}_s/\overline{m}_{ud}) = 27.42 \pm 0.12$ . These numbers are  $\overline{m}_{ud} = (3.410 \pm 0.043)$  MeV,  $\overline{m}_s = (93.44 \pm 0.68)$  MeV and  $(\overline{m}_s/\overline{m}_{ud}) = 27.23 \pm 0.10$  for  $N_f = 2 + 1 + 1$  simulations. The masses are given in the  $\overline{\text{MS}}$  scheme at a renormalization scale of 2 GeV. Because of the systematic errors, these results are not simply the combinations of all the results in quadrature, but include a judgement of the remaining uncertainties. Since the different collaborations use different formulations of lattice QCD, the (relatively small) variations of the results between the groups provides important information about the reliability of the estimates.

Despite being reported in the  $\overline{\text{MS}}$  scheme at a renormalization scale of 2 GeV, the results for  $\overline{m}_{ud}$  and  $\overline{m}_s$  in the two frameworks differ in their renormalization schemes, since  $N_f = 2 + 1$  results are renormalized with  $N_L = 3$  and  $N_f = 2 + 1 + 1$  ones with  $N_L = 4$ . Thus, for a comparison, in principle one should convert the results to the same scheme. This is not the case for  $(\overline{m}_s/\overline{m}_{ud})$ , where renormalization factors cancel. The conversion of the  $N_f = 2 + 1$  results to the  $N_L = 4$  scheme can be performed, for instance, by running them down to the charm threshold in the  $N_L = 3$  theory, matching the results to the  $N_L = 4$  theory and running them back up to 2 GeV in that theory. Such a conversion, however, leads to shifts in the values of the quark masses that are well within the quoted errors. Thus, we choose simply to average the results from the two frameworks, yielding as a final lattice QCD estimate in the  $\overline{\text{MS}}$  scheme at  $\mu = 2$  GeV in the  $N_L = 4$  theory:

$$\overline{m}_{ud} = (3.39 \pm 0.04) \text{ MeV} \quad (59.3)$$

$$\overline{m}_s = (92.9 \pm 0.7) \text{ MeV}, \quad (59.4)$$

and

$$\frac{\overline{m}_s}{\overline{m}_{ud}} = 27.37 \pm 0.10. \quad (59.5)$$

where the error bars encompass statistical and systematic errors combined in quadrature. In performing these averages, the only slight tension found is in  $\overline{m}_s$  where the weighted average carries a  $\chi^2/dof = 1.6$ , used to increase the error by the usual  $\sqrt{\chi^2/dof}$  scale factor. Note also that we do not allow the errors to become smaller than those on the individual averages because of possible common systematics.

To obtain the individual values of  $\overline{m}_u$  and  $\overline{m}_d$  requires the introduction of isospin breaking effects, including electromagnetism. This is now being done completely using lattice field theory, albeit neglecting electromagnetic effects in the sea in most cases (see the computation of the neutron-proton mass splitting [20] for an exception). The effect of this neglect on the  $u$  and  $d$  quark masses has been estimated in [21], to induce a contribution to the uncertainty that ranges from about 3% in  $\overline{m}_u/\overline{m}_d$  to less than 1% in  $\overline{m}_d$ . FLAG has reviewed these quantities in [8]. Again, they separate results obtained from  $N_f = 2 + 1$  and  $N_f = 2 + 1 + 1$  simulations. For the former, their final averages are the results of [21], and for the latter, those of [22]. Thus, for  $N_f = 2 + 1$  they quote  $\overline{m}_u = 2.27(9)$  MeV,  $\overline{m}_d = 4.67(9)$  MeV,  $(\overline{m}_u/\overline{m}_d) = 0.485(19)$  and, for  $N_f = 2 + 1 + 1$ ,  $\overline{m}_u = 2.50(17)$  MeV,  $\overline{m}_d = 4.88(20)$  MeV,  $(\overline{m}_u/\overline{m}_d) = 0.513(31)$ . As for the light quark masses in the isospin limit, we average the results obtained with different numbers of sea-quark flavors. Here, only the  $\overline{m}_u$  average has a  $\chi^2/dof = 1.4 > 1$ , and its error is thus appropriately

scaled. Again, we do not allow the errors to become smaller than those on the individual averages because of possible common systematics. Thus, we give as a final lattice QCD estimate in the  $\overline{\text{MS}}$  scheme at  $\mu = 2 \text{ GeV}$  in the  $N_L = 4$  theory:

$$\overline{m}_u = 2.32(10) \text{ MeV}, \quad \overline{m}_d = 4.71(9) \text{ MeV}, \quad \frac{\overline{m}_u}{\overline{m}_d} = 0.493(19). \quad (59.6)$$

Of particular importance is the fact that  $m_u \neq 0$  to more than 20 standard deviations, since there would have been no strong  $CP$  problem had  $m_u$  been equal to zero.

The results for the light quark masses given in the listings are dominated by the lattice values, since most continuum extractions have larger uncertainties.

#### 59.4.2. Chiral Perturbation Theory :

For light quarks, one can use the techniques of chiral perturbation theory [23–25] to extract quark mass ratios. The mass term for light quarks in the QCD Lagrangian is

$$\overline{\Psi} M \Psi = \overline{\Psi}_L M \Psi_R + \overline{\Psi}_R M^\dagger \Psi_L, \quad (59.7)$$

where  $M$  is the light quark mass matrix,

$$M = \begin{pmatrix} m_u & 0 & 0 \\ 0 & m_d & 0 \\ 0 & 0 & m_s \end{pmatrix}, \quad (59.8)$$

$\Psi = (u, d, s)$ , and  $L$  and  $R$  are the left- and right-chiral components of  $\Psi$  given by  $\Psi_{L,R} = P_{L,R} \Psi$ ,  $P_L = (1 - \gamma_5)/2$ ,  $P_R = (1 + \gamma_5)/2$ . The mass term is the only term in the QCD Lagrangian that mixes left- and right-handed quarks. In the limit  $M \rightarrow 0$ , there is an independent  $\text{SU}(3) \times \text{U}(1)$  flavor symmetry for the left- and right-handed quarks. The vector  $\text{U}(1)$  symmetry is baryon number; the axial  $\text{U}(1)$  symmetry of the classical theory is broken in the quantum theory due to the anomaly. The remaining  $G_\chi = \text{SU}(3)_L \times \text{SU}(3)_R$  chiral symmetry of the QCD Lagrangian is spontaneously broken to  $\text{SU}(3)_V$ , which, in the limit  $M \rightarrow 0$ , leads to eight massless Goldstone bosons, the  $\pi$ 's,  $K$ 's, and  $\eta$ .

The symmetry  $G_\chi$  is only an approximate symmetry, since it is explicitly broken by the quark mass matrix  $M$ . The Goldstone bosons acquire masses which can be computed in a systematic expansion in  $M$ , in terms of low-energy constants, which are unknown non-perturbative parameters of the effective theory, and are not fixed by the symmetries. One treats the quark mass matrix  $M$  as an external field that transforms under  $G_\chi$  as  $M \rightarrow L M R^\dagger$ , where  $\Psi_L \rightarrow L \Psi_L$  and  $\Psi_R \rightarrow R \Psi_R$  are the  $\text{SU}(3)_L$  and  $\text{SU}(3)_R$  transformations, and writes down the most general Lagrangian invariant under  $G_\chi$ . Then one sets  $M$  to its given constant value Eq. (59.8), which implements the symmetry breaking. To first order in  $M$  one finds that [26]

$$\begin{aligned} m_{\pi^0}^2 &= B(m_u + m_d), \\ m_{\pi^\pm}^2 &= B(m_u + m_d) + \Delta_{\text{em}}, \\ m_{K^0}^2 &= m_{\overline{K}^0}^2 = B(m_d + m_s), \\ m_{K^\pm}^2 &= B(m_u + m_s) + \Delta_{\text{em}}, \\ m_\eta^2 &= \frac{1}{3} B(m_u + m_d + 4m_s), \end{aligned} \quad (59.9)$$

with two unknown constants  $B$  and  $\Delta_{\text{em}}$ , the electromagnetic mass difference. From Eq. (59.9), one can determine the quark mass ratios [26]

$$\begin{aligned} \frac{m_u}{m_d} &= \frac{2m_{\pi^0}^2 - m_{\pi^+}^2 + m_{K^+}^2 - m_{\overline{K}^0}^2}{m_{K^0}^2 - m_{K^+}^2 + m_{\pi^+}^2} = 0.56, \\ \frac{m_s}{m_d} &= \frac{m_{K^0}^2 + m_{K^+}^2 - m_{\pi^+}^2}{m_{K^0}^2 + m_{\pi^+}^2 - m_{K^+}^2} = 20.2, \end{aligned} \quad (59.10)$$

to lowest order in chiral perturbation theory, with an error which will be estimated below. Since the mass ratios extracted using chiral perturbation theory use the symmetry transformation property of  $M$  under the chiral symmetry  $G_\chi$ , it is important to use a renormalization scheme for QCD that does not change this transformation law. Any mass independent subtraction scheme such as  $\overline{\text{MS}}$  is suitable. The ratios of quark masses are scale independent in such a scheme (up to electromagnetic corrections), and Eq. (59.10) can be taken to be the ratio of  $\overline{\text{MS}}$  masses. Chiral perturbation theory cannot determine the overall scale of the quark masses, since it uses only the symmetry properties of  $M$ , and any multiple of  $M$  has the same  $G_\chi$  transformation law as  $M$ .

Chiral perturbation theory is a systematic expansion in powers of the light quark masses. The typical expansion parameter is  $m_K^2/\Lambda_\chi^2 \sim 0.25$  if one uses  $\text{SU}(3)$  chiral symmetry, and  $m_\pi^2/\Lambda_\chi^2 \sim 0.02$  if instead one uses  $\text{SU}(2)$  chiral symmetry. Electromagnetic effects at the few percent level also break  $\text{SU}(2)$  and  $\text{SU}(3)$  symmetry. The mass formulæ Eq. (59.9) were derived using  $\text{SU}(3)$  chiral symmetry, and are expected to have approximately a 25% uncertainty due to second order corrections. This estimate of the uncertainty is consistent with the lattice results summarized in Eq. (59.4)–Eq. (59.5).

There is a subtlety which arises when one tries to determine quark mass ratios at second order in chiral perturbation theory. The second order quark mass term [27]

$$\left(M^\dagger\right)^{-1} \det M^\dagger \quad (59.11)$$

(which can be generated by instantons) transforms in the same way under  $G_\chi$  as  $M$ . Chiral perturbation theory cannot distinguish between  $M$  and  $(M^\dagger)^{-1} \det M^\dagger$ ; one can make the replacement  $M \rightarrow M(\lambda) = M + \lambda M (M^\dagger M)^{-1} \det M^\dagger$  in the chiral Lagrangian,

$$\begin{aligned} M(\lambda) &= \text{diag}(m_u(\lambda), m_d(\lambda), m_s(\lambda)) \\ &= \text{diag}(m_u + \lambda m_d m_s, m_d + \lambda m_u m_s, m_s + \lambda m_u m_d), \end{aligned} \quad (59.12)$$

and leave all observables unchanged.

The combination

$$\left(\frac{m_u}{m_d}\right)^2 + \frac{1}{Q^2} \left(\frac{m_s}{m_d}\right)^2 = 1 \quad (59.13)$$

where

$$Q^2 = \frac{m_s^2 - m_{ud}^2}{m_d^2 - m_u^2}, \quad m_{ud} = \frac{1}{2}(m_u + m_d),$$

is insensitive to the transformation in Eq. (59.12). Eq. (59.13) gives an ellipse in the  $m_u/m_d - m_s/m_d$  plane. The ellipse is well-determined by chiral perturbation theory, but the exact location on the ellipse, and the absolute normalization of the quark masses, has larger uncertainties.  $Q$  is determined to be 22.1(7) from  $\eta \rightarrow 3\pi$  decay and the electromagnetic contribution to the  $K^+ - K^0$  and  $\pi^+ - \pi^0$  mass differences [28]. Lattice QCD collaborations have also reported determinations of  $Q$ . Using  $N_f = 2 + 1$  simulations, [21] obtains  $Q = 23.4(6)$  and [22] determines  $Q = 23.8(1.1)$  with  $N_f = 2 + 1 + 1$  simulations, which are fully compatible. The  $N_f = 2 + 1$  result is about 2 standard deviations larger than the one from phenomenology given above [28]. These values can also be compared to the leading-order result for  $Q$  in  $\text{SU}(3)$  chiral perturbation theory, that can be derived using Eq. (59.9) and the values for the relevant meson masses given in this review. This result also holds to next-to-leading order, thus:  $Q^{\text{NLO}} = 24.3$ .

The absolute normalization of the quark masses cannot be determined using chiral perturbation theory. Other methods, such as lattice simulations discussed above, or spectral function sum rules [29,30] for hadronic correlation functions reviewed next, are necessary.

### 59.4.3. Sum rules :

Sum rule methods have been used extensively to determine quark masses and for illustration we briefly discuss here their application to hadronic  $\tau$  decays [31]. Other applications involve very similar techniques.

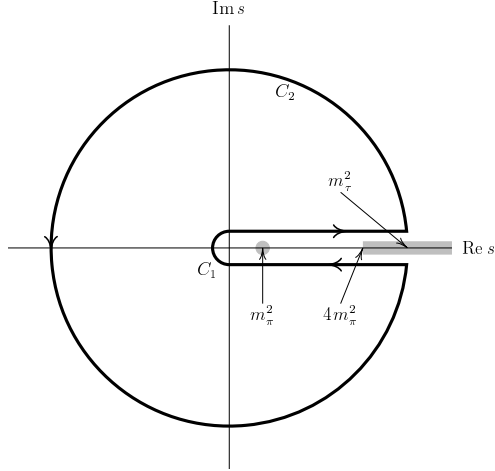


**Figure 59.1:** The analytic structure of  $\Pi(s)$  in the complex  $s$ -plane. The contours  $C_1$  and  $C_2$  are the integration contours discussed in the text, and the integral over the closed contour  $C_1 + C_2$  vanishes.  $m_\tau^2$  has not been drawn to scale;  $m_\tau^2 \sim 40(4m_\pi^2)$ .

The experimentally measured quantity is  $R_\tau$ ,

$$\frac{dR_\tau}{ds} = \frac{d\Gamma/ds(\tau^- \rightarrow \text{hadrons} + \nu_\tau(\gamma))}{\Gamma(\tau^- \rightarrow e^-\bar{\nu}_e\nu_\tau(\gamma))} \quad (59.14)$$

the hadronic invariant mass spectrum in semihadronic  $\tau$  decay, normalized to the leptonic  $\tau$  decay rate. It is useful to define  $q$  as the total momentum of the hadronic final state, so  $s = q^2$  is the hadronic invariant mass. The total hadronic  $\tau$  decay rate  $R_\tau$  is then given by integrating  $dR_\tau/ds$  over the kinematically allowed range  $0 \leq s \leq M_\tau^2$ .

$R_\tau$  can be written as

$$R_\tau = 12\pi \int_0^{M_\tau^2} \frac{ds}{M_\tau^2} \left(1 - \frac{s}{M_\tau^2}\right)^2 \times \left[ \left(1 + 2\frac{s}{M_\tau^2}\right) \text{Im} \Pi^T(s) + \text{Im} \Pi^L(s) \right] \quad (59.15)$$

where the hadronic spectral functions  $\Pi^{L,T}$  are defined from the time-ordered correlation function of two weak currents ( $j^\mu(x)$  and  $j^\nu(0)$ ) by

$$\Pi^{\mu\nu}(q) = i \int d^4x e^{iq \cdot x} \langle 0 | T(j^\mu(x) j^\nu(0)^\dagger) | 0 \rangle, \quad (59.16)$$

$$\Pi^{\mu\nu}(q) = (-g^{\mu\nu} + q^\mu q^\nu) \Pi^T(s) + q^\mu q^\nu \Pi^L(s), \quad (59.17)$$

and the decomposition Eq. (59.17) is the most general possible structure consistent with Lorentz invariance.

By the optical theorem, the imaginary part of  $\Pi^{\mu\nu}$  is proportional to the total cross-section for the current to produce all possible states. A detailed analysis including the phase space factors leads to Eq. (59.15). The spectral functions  $\Pi^{L,T}(s)$  are analytic in the complex  $s$  plane, with singularities along the real axis. There is an isolated pole at  $s = m_\pi^2$ , and single- and multi-particle singularities for  $s \geq 4m_\pi^2$ , the two-particle threshold. The discontinuity along the real axis is  $\Pi^{L,T}(s+i0^+) - \Pi^{L,T}(s-i0^+) = 2i \text{Im} \Pi^{L,T}(s)$ . As a result, Eq. (59.15) can be rewritten with the replacement  $\text{Im} \Pi^{L,T}(s) \rightarrow -i \Pi^{L,T}(s)/2$ , and the integration being over the contour  $C_1$ . Finally, the contour

$C_1$  can be deformed to  $-C_2$  without crossing any singularities, and so leaving the integral unchanged, i.e. the integral over the closed contour  $C_1 + C_2$  vanishes. One can derive a series of sum rules analogous to Eq. (59.15) by weighting the differential  $\tau$  hadronic decay rate by different powers of the hadronic invariant mass [32],

$$R_\tau^{kl} = \int_0^{M_\tau^2} ds \left(1 - \frac{s}{M_\tau^2}\right)^k \left(\frac{s}{M_\tau^2}\right)^l \frac{dR_\tau}{ds} \quad (59.18)$$

where  $dR_\tau/ds$  is the hadronic invariant mass distribution in  $\tau$  decay normalized to the leptonic decay rate. This leads to the final form of the sum rule(s),

$$R_\tau^{kl} = -6\pi i \int_{C_2} \frac{ds}{M_\tau^2} \left(1 - \frac{s}{M_\tau^2}\right)^{2+k} \left(\frac{s}{M_\tau^2}\right)^l \times \left[ \left(1 + 2\frac{s}{M_\tau^2}\right) \Pi^T(s) + \Pi^L(s) \right]. \quad (59.19)$$

The manipulations so far are completely rigorous and exact, relying only on the general analytic structure of quantum field theory. The left-hand side of the sum rule Eq. (59.19) is obtained from experiment. The right hand-side can be computed for  $s$  far away from any physical cuts using the operator product expansion (OPE) for the time-ordered product of currents in Eq. (59.16), and QCD perturbation theory. The OPE is an expansion for the time-ordered product Eq. (59.16) in a series of local operators, and is an expansion about the  $q \rightarrow \infty$  limit. It gives  $\Pi^{L,T}(s)$  as an expansion in powers of  $\alpha_s(s)$  and  $\Lambda_{\text{QCD}}^2/s$ , and is valid when  $s$  is far (in units of  $\Lambda_{\text{QCD}}^2$ ) from any singularities in the complex  $s$ -plane.

The OPE gives  $\Pi^{L,T}(s)$  as a series in  $\alpha_s$ , quark masses, and various non-perturbative vacuum matrix elements. By computing  $\Pi^{L,T}(s)$  theoretically, and comparing with the experimental values of  $R_\tau^{kl}$ , one determines various parameters such as  $\alpha_s$  and the quark masses. The theoretical uncertainties in using Eq. (59.19) arise from neglected higher order corrections (both perturbative and non-perturbative), and because the OPE is no longer valid near the real axis, where  $\Pi^{L,T}$  have singularities. The contribution of neglected higher order corrections can be estimated as for any other perturbative computation. The error due to the failure of the OPE is more difficult to estimate. In Eq. (59.19), the OPE fails on the endpoints of  $C_2$  that touch the real axis at  $s = M_\tau^2$ . The weight factor  $(1 - s/M_\tau^2)$  in Eq. (59.19) vanishes at this point, so the importance of the endpoint can be reduced by choosing larger values of  $k$ .

Light quark masses are often determined using QCD sum rules [30], which are similar to the  $\tau$  sum rules. One takes the correlator of two light-quark-bilinear operators (e.g. an axial vector current), as in Eq. (59.16), and computes their Laplace transforms or moments

$$\mathcal{L}_n(\tau) = \int_0^\infty ds s^n e^{-\tau s} \text{Im} \Pi(s), \quad \mathcal{M}_n(Q^2) = \int_0^\infty \frac{ds}{(s+Q^2)^n} \text{Im} \Pi(s)$$

to get Laplace or moment sum rules, respectively. The quark masses are extracted by comparing the theoretical and experimental values of  $\mathcal{L}_n(\tau)$  and  $\mathcal{M}_n(Q^2)$ . Considerable theoretical effort has gone into optimizing  $n$  and  $Q^2$  to improve the precision of the resulting light quark masses.

## 59.5. Heavy quarks

### 59.5.1. Continuum approaches and results :

For heavy quark physics one can exploit the fact that  $m_Q \gg \Lambda_{\text{QCD}}$  to construct effective theories ( $m_Q$  is the mass of the heavy quark  $Q$ ). The masses and decay rates of hadrons containing a single heavy quark, such as the  $B$  and  $D$  mesons can be determined using the heavy quark effective theory (HQET) [33]. The theoretical calculations involve radiative corrections computed in perturbation theory with an expansion in  $\alpha_s(m_Q)$  and non-perturbative corrections with an expansion in powers of  $\Lambda_{\text{QCD}}/m_Q$ . Due to the asymptotic nature of the QCD perturbation series, the two kinds of corrections are intimately related; an example of this are renormalon effects in the

perturbative expansion which are associated with non-perturbative corrections.

Systems containing two heavy quarks such as the  $\Upsilon$  or  $J/\Psi$  are treated using non-relativistic QCD (NRQCD) [34]. The typical momentum and energy transfers in these systems are  $\alpha_s m_Q$ , and  $\alpha_s^2 m_Q$ , respectively, so these bound states are sensitive to scales much smaller than  $m_Q$ . However, smeared observables, such as the cross-section for  $e^+e^- \rightarrow \bar{b}b$  averaged over some range of  $s$  that includes several bound state energy levels, are better behaved and only sensitive to scales near  $m_Q$ . For this reason, most determinations of the  $c, b$  quark masses using perturbative calculations compare smeared observables with experiment [35–37]. The method is similar to that outlined for  $\tau$  decays. The current correlator in Eq. (59.16) is the electromagnetic current, and the experimental data is the value of  $R(s)$  in the threshold region for  $e^+e^- \rightarrow Q\bar{Q}$ . The theoretical values for the moments are computed using renormalization group improved calculations in non-relativistic QCD.

There are many continuum extractions of the  $c$  and  $b$  quark masses, some with quoted errors of 10 MeV or smaller. There are systematic effects of comparable size, which are typically not included in these error estimates. Reference [38], for example, shows that even though the error estimate of  $m_c$  using the rapid convergence of the  $\alpha_s$  perturbation series is only a few MeV, the central value of  $m_c$  can differ by a much larger amount depending on which algorithm (all of which are formally equally good) is used to determine  $m_c$  from the data. This leads to a systematic error from perturbation theory of around 20 MeV for the  $c$  quark and 25 MeV for the  $b$  quark. Electromagnetic effects, which also are important at this precision, are often not included. For this reason, we inflate the errors on the continuum extractions of  $m_c$  and  $m_b$ . The average values of  $m_c$  and  $m_b$  from continuum determinations are (see Sec. G for the 1S scheme)

$$\begin{aligned} \overline{m}_c(\overline{m}_c) &= (1.280 \pm 0.025) \text{ GeV}, \\ \overline{m}_b(\overline{m}_b) &= (4.18 \pm 0.03) \text{ GeV}, \quad m_b^{1S} = (4.65 \pm 0.03) \text{ GeV}. \end{aligned}$$

### 59.5.2. Lattice approaches and results :

Lattice simulations of QCD lead to discretization errors which are powers of  $am_Q$  (modulated by logarithms); the power depends on the formulation of lattice QCD being used and in most cases is quadratic. Clearly these errors can be reduced by performing simulations at smaller lattice spacings, but also by using *improved* discretizations of the theory. Recently, with more powerful computing resources, better algorithms and techniques, it has become possible to perform simulations in the charm quark region and beyond, also decreasing the extrapolation which has to be performed to reach the  $b$ -quark.

Traditionally the charm quark mass is obtained by tuning its bare, simulation value to reproduce the physical mass of charmonium mesons or of the  $D, D_s$  mesons (requiring a more precise tuning of the light quark masses). This mass can then be renormalized to the  $\overline{\text{MS}}$  scheme using the methods discussed for the light quarks.

An alternative approach for obtaining the  $\overline{\text{MS}}$  mass from the tuned bare quark mass was proposed in [39]. Euclidean-time moments of pseudoscalar, two-point functions of  $c\bar{c}$  quark-bilinear operators can readily be computed on the lattice and extrapolated to the continuum limit where they can be compared to perturbative calculations of the same quantities at 4-loop order. In this way, both the strong coupling constant and the charm quark mass can be determined with remarkably small errors. As this approach uses the same perturbative expressions for two-point correlators as the continuum determinations discussed above, it suffers from similar perturbation-theory, systematic errors. FLAG [8] has reviewed lattice determinations of the charm quark mass obtained using both approaches. The most advanced calculations are performed with  $N_f = 2 + 1 + 1$  simulations. For these, the quoted average is

$$\overline{m}_c(\overline{m}_c) = 1.280(13) \text{ GeV},$$

based on the calculations performed in [17,16,40,18,19], in good agreement with the continuum result quoted above, but with a smaller

error. It is worth noting that while three [17,18,19] of the four calculations entering this average agree, the fourth [16,40] is about two standard deviations larger, and this is taken into account in the error bar. It should also be remembered that these results were obtained in QCD with exact isospin symmetry, though isospin breaking corrections to the physical inputs, including electromagnetism, are accounted for using phenomenology.

Historically, the main approach to controlling the discretization errors in lattice studies of  $b$  quark physics was to perform simulations of effective theories such as HQET and NRQCD. This remains an important technique, both in its own right and in providing additional information for extrapolations from lower masses to the bottom region. Using effective theories,  $m_b$  is obtained from what is essentially a computation of the difference of  $M_{H_b} - m_b$ , where  $M_{H_b}$  is the mass of a hadron  $H_b$  containing a  $b$ -quark. The relative error on  $m_b$  is therefore much smaller than that for  $M_{H_b} - m_b$ . The principal systematic errors are the matching of the effective theories to QCD and the presence of power divergences in  $a^{-1}$  in the  $1/m_b$  corrections which have to be subtracted numerically. A procedure for performing these subtractions fully non-perturbatively was proposed and implemented for the first time in [41].

The most recent lattice QCD determinations of the  $b$  quark mass rely on a variety of approaches, including Euclidean-time moments of correlation functions with [42] or without NRQCD [17] and HQET based interpolations [43,44] or extrapolations [18] from above the charm to the  $b$  region. The overall agreement of the results obtained using these very different approaches, which have different systematic errors, is a confirmation that the various groups control these uncertainties. As the range of heavy-quark masses which can be used in numerical simulations increases, results obtained by extrapolating the results to  $b$ -physics are becoming ever more reliable (see e.g. [18]) . FLAG's compilation [8] of the above  $N_f = 2 + 1 + 1$  results yields

$$\overline{m}_b(\overline{m}_b) = 4.198(12) \text{ GeV}.$$

Again, this result is compatible with the average value of continuum results, but with a significantly smaller uncertainty.

As explained in Sec. 59.3, ratios of quark masses can have significantly smaller errors than the individual masses if they are computed in the same lattice QCD framework and in the same renormalization scheme at identical scales. This led HPQCD to leverage their precise determination of  $m_c$  [39] to determine  $m_s$  and  $m_{ud}$  [57], through a precise computation of  $m_c/m_s$  [57] and of  $m_s/m_{ud}$  [58]. This  $N_f = 2 + 1$  calculation was updated using  $N_f = 2 + 1 + 1$  simulations in [17]. The ratio  $m_s/m_c$  was also computed in [15,59] with  $N_f = 2 + 1$  simulations and in [16,18] with  $N_f = 2 + 1 + 1$  ones. Based on [57,59], FLAG quotes [8]  $m_c/m_s = 11.82(16)$  for  $N_f = 2 + 1$ , and  $m_c/m_s = 11.768(33)$  for  $N_f = 2 + 1 + 1$ , based on [16,17,18], where a 50% stretch of the combined error was applied due to a tension between the results of [16] and [17]. As a final lattice number we give the  $N_f = 2 + 1 + 1$  average

$$m_c/m_s = 11.768(33),$$

which is renormalization scheme and scale independent.

The ratio  $m_b/m_c$  has also been computed on the lattice. The most advanced calculations have been performed with  $N_f = 2 + 1 + 1$  simulations [17,43,18]. Averaging these results using the FLAG [8] procedure yields

$$m_b/m_c = 4.576(11),$$

where a scale factor of  $\sqrt{\chi^2/dof} = 1.45$  has been applied to the error bar. Indeed, [43] contributes 3.3 to the total  $\chi^2$ .

### 59.5.3. Warnings concerning the use of the pole mass :

For an observable particle such as the electron, the position of the pole in the propagator is the definition of its mass. In QCD this definition of the quark mass is known as the pole mass. It is known that the on-shell quark propagator has no infrared divergences in perturbation theory [45,46], so this provides a perturbative definition of the quark mass. However, the pole mass cannot be used to arbitrarily high accuracy because of non-perturbative infrared effects



in QCD. In fact the full quark propagator has no pole because the quarks are confined, so that the pole mass cannot be defined outside of perturbation theory. The relation between the pole mass  $m_Q$  and the  $\overline{\text{MS}}$  mass  $\overline{m}_Q$ , used throughout this review, is known to three loops [47–50]

$$m_Q = \overline{m}_Q(\overline{m}_Q) \left\{ 1 + \frac{4\overline{\alpha}_s(\overline{m}_Q)}{3\pi} + \left[ -1.0414 \sum_q \left( 1 - \frac{4}{3} \frac{\overline{m}_q}{\overline{m}_Q} \right) + 13.4434 \right] \left[ \frac{\overline{\alpha}_s(\overline{m}_Q)}{\pi} \right]^2 + \left[ 0.6527 N_L^2 - 26.655 N_L + 190.595 \right] \left[ \frac{\overline{\alpha}_s(\overline{m}_Q)}{\pi} \right]^3 \right\}, \quad (59.20)$$

where  $\overline{\alpha}_s(\mu)$  is the strong interaction coupling constants in the  $\overline{\text{MS}}$  scheme, and the sum over  $q$  extends over the  $N_L$  flavors lighter than  $Q$ . The complete mass dependence of the  $\alpha_s^2$  term can be found in [47]; the mass dependence of the  $\alpha_s^3$  term is not known. For the  $b$ -quark, Eq. (59.20) reads

$$m_b = \overline{m}_b(\overline{m}_b) [1 + 0.10 + 0.05 + 0.03], \quad (59.21)$$

where the contributions from the different orders in  $\alpha_s$  are shown explicitly. The two and three loop corrections are comparable in size and have the same sign as the one loop term. This is a signal of the asymptotic nature of the perturbation series (there is a renormalon in the pole mass [51]). Such a badly behaved perturbation expansion can be avoided by directly extracting, from data, the mass defined in the  $\overline{\text{MS}}$  (used in this review) or other short-distance schemes (see below), without invoking the pole mass as an intermediate step.

### 59.6. Numerical values and caveats

The quark masses in the particle data listings have been obtained by using a wide variety of methods. Each method involves its own set of approximations and uncertainties. In most cases, the errors are an estimate of the size of neglected higher-order corrections or other uncertainties. The expansion parameters for some of the approximations are not very small (for example, they are  $m_K^2/\Lambda_\chi^2 \sim 0.25$  for the SU(3) chiral expansion and  $\Lambda_{\text{QCD}}/m_b \sim 0.1$  for the heavy-quark expansion), so an unexpectedly large coefficient in a neglected higher-order term could significantly alter the results. Thus, before using a particular result, it is important to understand the possible limitations of the approach used to obtain it. It is also important to note that the quark mass values can be significantly different in the different schemes.

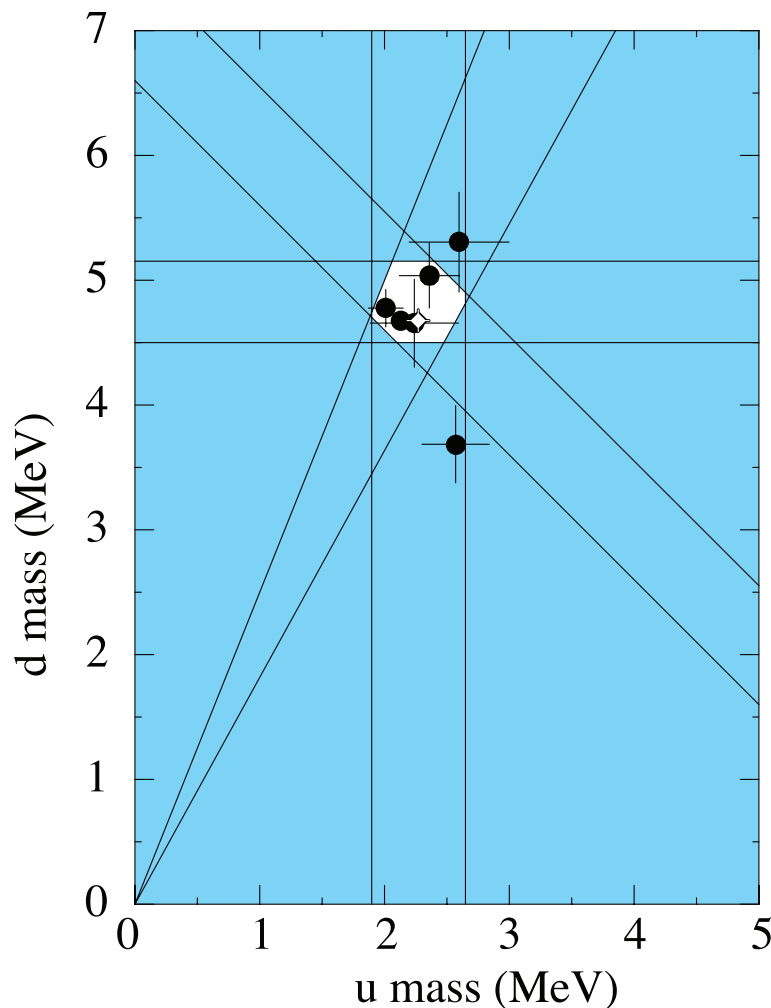


**Figure 59.2:** The allowed region (shown in white) for up quark and down quark masses renormalized in the  $\overline{\text{MS}}$  scheme at 2 GeV. This region was determined in part from papers reporting values for  $m_u$  and  $m_d$  (data points shown) and in part from an analysis of the allowed ranges of other mass parameters (see Fig. 59.3). The parameter  $(m_u + m_d)/2$  yields the two downward-sloping lines, while  $m_u/m_d$  yields the two rising lines originating at (0,0). There are two overlapping data points, so one of them is shown as a white diamond (it has very small error bars).

We have specified all masses in the  $\overline{\text{MS}}$  scheme. For light quarks, the renormalization scale has been chosen to be  $\mu = 2 \text{ GeV}$ . Quoting these masses at smaller values of  $\mu$ , where perturbative corrections become significantly larger, would introduce unnecessary uncertainties in the results. In fact, as lattice calculations, performed on finer and finer lattices, allow to determine quark masses, fully non-perturbatively, at larger and larger values of  $\mu$ , it may become advantageous to quote quark mass results at renormalization scales above  $2 \text{ GeV}$ , where perturbative uncertainties are smaller.

Given the small size of the charm quark mass, in the future it may become advantageous to quote its value at larger values of  $\mu$  so as not to introduce unnecessary perturbative uncertainties (see discussion above). Analyses of inclusive  $B$  meson decays have shown that other mass definitions lead to a better behaved perturbation series than for the  $\overline{\text{MS}}$  mass, and hence to more accurate mass values [52,53,54,56]. Thus, we have chosen to also give values for one of these, the  $b$  quark mass in the 1S-scheme [52,53]. Other schemes that have been proposed are the PS-scheme [54], the kinetic scheme [55] and, most

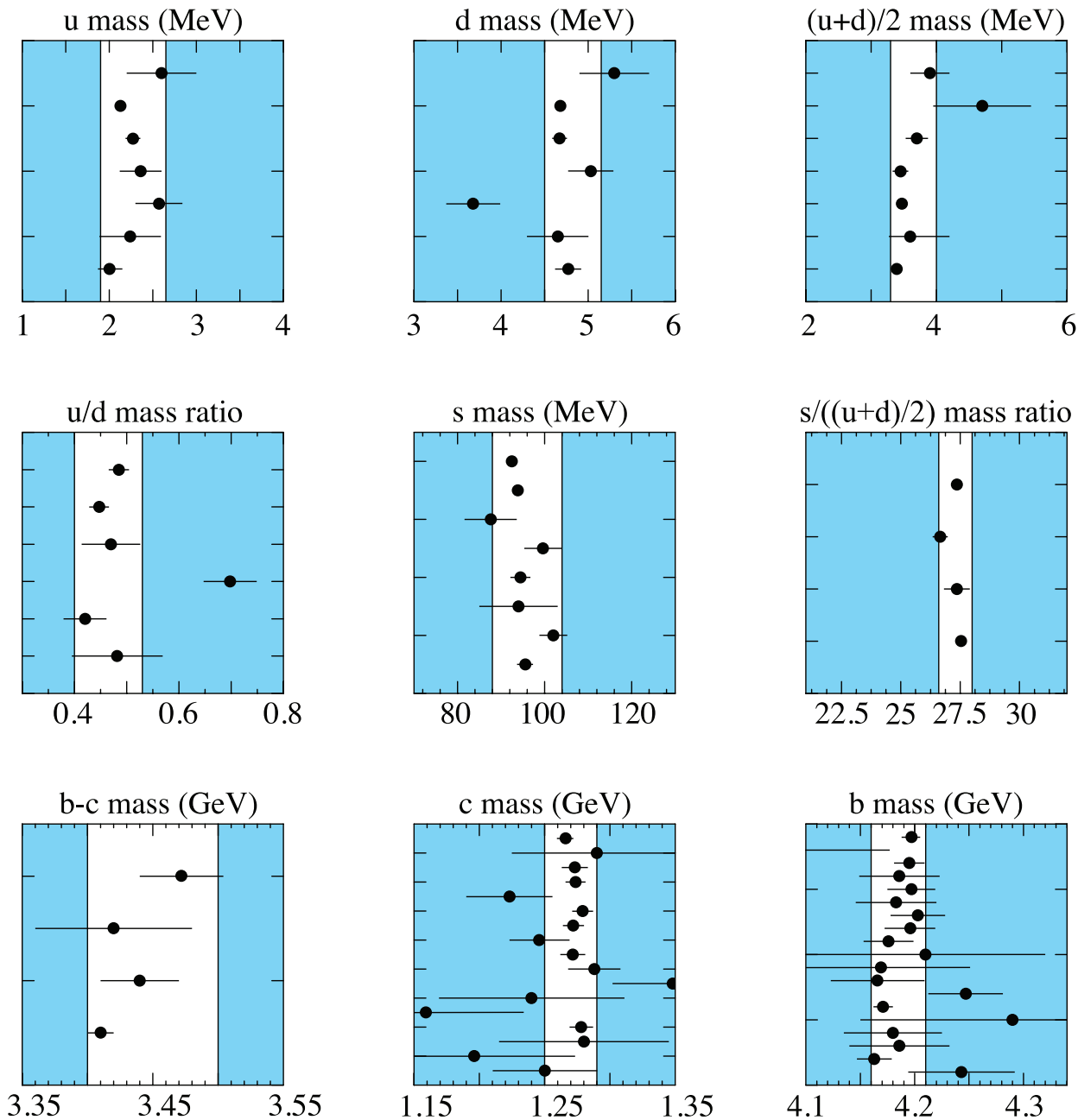


**Figure 59.3:** The values of each quark mass parameter taken from the Data Listings. The points are in chronological order with the more recent measurements at the top. The shaded regions indicate values excluded by our evaluations; some regions were determined in part through examination of Fig. 59.2.

The heavy quark masses obtained using HQET, QCD sum rules, or lattice gauge theory are consistent with each other if they are all converted into the same scheme and scale. For these quarks it is conventional to choose the renormalization scale equal to the quark mass, so we have quoted  $\overline{m}_Q(\mu)$  at  $\mu = \overline{m}_Q$  for the  $c$  and  $b$  quarks.

recently, the minimal renormalon-subtracted mass (MRS) [56] used in the lattice calculation [18].

If necessary, we have converted values in the original papers to our chosen scheme using two-loop formulae. It is important to realize that our conversions introduce significant additional errors. In converting to the  $\overline{\text{MS}}$   $b$ -quark mass, for example, the three-loop

conversions from the 1S and pole masses give values about 35 MeV and 135 MeV lower than the two-loop conversions. The uncertainty in  $\alpha_s(M_Z) = 0.1179 \pm 0.0010$  [1] gives an uncertainty of  $\pm 9$  MeV and  $\pm 21$  MeV respectively in the same conversions. We have not added these additional errors when we do our conversions. The  $\alpha_s$  value in the conversion is correlated with the  $\alpha_s$  value used in determining the quark mass, so the conversion error is not a simple additional error on the quark mass.

#### References:

1. See the review of QCD in this volume..
2. A.V. Manohar and H. Georgi, Nucl. Phys. **B234**, 189 (1984).
3. K.G. Chetyrkin, Phys. Lett. **B404**, 161 (1997).
4. J.A.M. Vermaseren, S.A. Larin, and T. van Ritbergen, Phys. Lett. **B405**, 327 (1997).
5. K.G. Chetyrkin, B.A. Kniehl, and M. Steinhauser, Nucl. Phys. **B510**, 61 (1998).
6. G. Martinelli *et al.*, Nucl. Phys. **B445**, 81 (1995).
7. K. Jansen *et al.*, Phys. Lett. **B372**, 275 (1996).
8. S. Aoki *et al.* [Flavour Lattice Averaging Group], [arXiv:1902.08191 [hep-lat]].
9. P. Petreczky and J. H. Weber, arXiv:1901.06424 [hep-lat].
10. A. Bazavov *et al.* [MILC collaboration], PoS **CD09** (2009) 007.
11. A. Bazavov *et al.*, PoS **LATTICE2010** (2010) 083.
12. S. Durr *et al.*, Phys. Lett. **B701**, 265 (2011).
13. S. Durr *et al.*, JHEP **1108**, 148 (2011).
14. T. Blum *et al.* [RBC and UKQCD collaborations], Phys. Rev. **D93**, 074505 (2016).
15. Y. Maetzawa and P. Petreczky, Phys. Rev. **D94**, 034507 (2016).
16. N. Carrasco *et al.* [ETM collaboration], Nucl. Phys. **B887**, 19 (2014).
17. B. Chakraborty *et al.* [HPQCD collaboration], Phys. Rev. **D91**, 054508 (2015).
18. A. Bazavov *et al.* [Fermilab Lattice and MILC and TUMQCD collaborations], Phys. Rev. **D98**, 054517 (2018).
19. A. T. Lytle *et al.* [HPQCD collaboration], Phys. Rev. **D98**, 014513 (2018).
20. S. Borsanyi *et al.* [BMW collaboration], Science **347**, 1452 (2015).
21. Z. Fodor *et al.* [BMW collaboration], Phys. Rev. Lett. **117**, 082001 (2016).
22. D. Giusti, V. Lubicz, C. Tarantino, G. Martinelli, S. Sanfilippo, S. Simula and N. Tantalo [RM123 collaboration], Phys. Rev. **D95**, 114504 (2017).
23. S. Weinberg, Physica **96A**, 327 (1979).
24. J. Gasser and H. Leutwyler, Ann. Phys. **158**, 142 (1984).
25. For a review, see A. Pich, Rept. on Prog. in Phys. **58**, 563 (1995).
26. S. Weinberg, Trans. N.Y. Acad. Sci. **38**, 185 (1977).
27. D.B. Kaplan and A.V. Manohar, Phys. Rev. Lett. **56**, 2004 (1986).
28. G. Colangelo, S. Lanz, H. Leutwyler and E. Passemar, Eur. Phys. J. C **78**, no. 11, 947 (2018).
29. S. Weinberg, Phys. Rev. Lett. **18**, 507 (1967).
30. M.A. Shifman, A.I. Vainshtein, and V.I. Zakharov, Nucl. Phys. **B147**, 385 (1979).
31. E. Braaten, S. Narison, and A. Pich, Nucl. Phys. **B373**, 581 (1992).
32. F. Le Diberder and A. Pich, Phys. Lett. **B286**, 147 (1992) doi:10.1016/0370-2693(92)90172-Z.
33. N. Isgur and M.B. Wise, Phys. Lett. **B232**, 113 (1989), *ibid*, **B237**, 527 (1990).
34. G.T. Bodwin, E. Braaten, and G.P. Lepage, Phys. Rev. **D51**, 1125 (1995).
35. A.H. Hoang, Phys. Rev. **D61**, 034005 (2000).
36. K. Melnikov and A. Yelkhovsky, Phys. Rev. **D59**, 114009 (1999).
37. M. Beneke and A. Signer, Phys. Lett. **B471**, 233 (1999).
38. B. Dehnadi, A. H. Hoang, V. Mateu and S. M. Zebarjad, JHEP **1309**, 103 (2013).
39. I. Allison *et al.* [HPQCD collaboration], Phys. Rev. **D78**, 054513 (2008).
40. C. Alexandrou, V. Drach, K. Jansen, C. Kallidonis and G. Koutsou, Phys. Rev. D **90**, no. 7, 074501 (2014).
41. J. Heitger *et al.* [ALPHA collaboration], JHEP **0402**, 022 (2004).
42. B. Colquhoun, R. J. Dowdall, C. T. H. Davies, K. Hornbostel and G. P. Lepage [HPQCD collaboration], Phys. Rev. D **91**, no. 7, 074514 (2015).
43. A. Bussone *et al.* [ETM collaboration], Phys. Rev. D **93**, no. 11, 114505 (2016).
44. P. Gambino, A. Melis and S. Simula, Phys. Rev. D **96**, no. 1, 014511 (2017).
45. R. Tarrach, Nucl. Phys. **B183**, 384 (1981).
46. A. Kronfeld, Phys. Rev. **D58**, 051501 (1998).
47. N. Gray *et al.*, Z. Phys. **C48**, 673 (1990).
48. D.J. Broadhurst, N. Gray, and K. Schilcher, Z. Phys. **C52**, 111 (1991).
49. K.G. Chetyrkin and M. Steinhauser, Phys. Rev. Lett. **83**, 4001 (1999).
50. K. Melnikov and T. van Ritbergen, Phys. Lett. **B482**, 99 (2000).
51. M. Beneke and V. M. Braun, Nucl. Phys. B **426**, 301 (1994).
52. A.H. Hoang, Z. Ligeti, A.V. Manohar, Phys. Rev. Lett. **82**, 277 (1999).
53. A.H. Hoang, Z. Ligeti, A.V. Manohar, Phys. Rev. **D59**, 074017 (1999).
54. M. Beneke, Phys. Lett. **B434**, 115 (1998).
55. P. Gambino and N. Uraltsev, Eur. Phys. J. **C34**, 181 (2004).
56. N. Brambilla *et al.* [TUMQCD collaboration], Phys. Rev. D **97**, no. 3, 034503 (2018).
57. C.T.H. Davies *et al.* [HPQCD collaboration], Phys. Rev. Lett. **104**, 132003 (2010).
58. A. Bazavov *et al.* [MILC Collaboration], Rev. Mod. Phys. **82**, 1349 (2010).
59. Y. B. Yang *et al.* [ $\chi$ QCD collaboration], Phys. Rev. D **92**, no. 3, 034517 (2015).

## 60. Top Quark

Revised August 2019 by T.M. Liss (City Coll. of New York), F. Maltoni (CP3 U. catholique de Louvain; Bologna U.) and A. Quadt (Göttingen U.).

### 60.1 Introduction

In the Standard Model (SM), the left-handed top quark is the  $Q = 2/3, T_3 = +1/2$  member of the weak-isospin doublet containing the bottom quark, while the right-handed top is an  $SU(2)_L$  singlet (see, e.g., the review “Electroweak Model and Constraints on New Physics”). Its phenomenology is driven by its large mass. Being heavier than a  $W$  boson, it is the only quark that decays semi-weakly, i.e., into a real  $W$  boson and a  $b$  quark. Therefore, it has a very short lifetime and decays before hadronization can occur. In addition, it is the only quark whose Yukawa coupling to the Higgs boson is of order unity. For these reasons, the top quark plays a special role in the Standard Model and in many extensions thereof. Top quark physics provides a unique laboratory where our understanding of the strong interactions, both in the perturbative and non-perturbative regimes, can be tested. An accurate knowledge of its properties (mass, couplings, production cross sections, decay branching ratios, *etc.*) can bring key information on fundamental interactions at the electroweak symmetry-breaking scale and beyond. This review provides a concise discussion of the experimental and theoretical issues involved in the determination of the top-quark properties.

### 60.2 Top-quark production at the Tevatron and LHC

In hadron collisions, top quarks are produced dominantly in pairs through the processes  $q\bar{q} \rightarrow t\bar{t}$  and  $gg \rightarrow t\bar{t}$ , at leading order in QCD. Approximately 85% of the production cross section at the Tevatron ( $p\bar{p}$  at 1.96 TeV) is from  $q\bar{q}$  annihilation, with the remainder from gluon-gluon fusion, while at LHC ( $pp$ ) energies about 90% of the production is from the latter process at  $\sqrt{s} = 14$  TeV ( $\approx 80\%$  at  $\sqrt{s} = 7$  TeV).

Predictions for the top-quark production total cross sections are available at next-to-next-to leading order (NNLO) [1, 2], also including next-to-next-to-leading-log (NNLL) soft gluon resummation. Assuming a top-quark mass of 173.3 GeV/ $c^2$ , close to the Tevatron + LHC average [3], the resulting theoretical prediction of the top-quark pair cross-section at NNLO+NNLL accuracy at the Tevatron at  $\sqrt{s} = 1.96$  TeV is  $\sigma_{t\bar{t}} = 7.16^{+0.11+0.17}_{-0.20-0.12}$  pb where the first uncertainty is from scale dependence and the second from parton distribution functions. At the LHC, assuming a top-quark mass of 172.5 GeV/ $c^2$  the cross sections are:  $\sigma_{t\bar{t}} = 177.3^{+4.6+9.0}_{-6.0-9.0}$  pb at  $\sqrt{s} = 7$  TeV,  $\sigma_{t\bar{t}} = 252.9^{+6.4+11.5}_{-8.6-11.5}$  pb at  $\sqrt{s} = 8$  TeV,  $\sigma_{t\bar{t}} = 831.8^{+19.8+35.1}_{-29.2-35.1}$  pb at  $\sqrt{s} = 13$  TeV, and  $\sigma_{t\bar{t}} = 984.5^{+23.2+41.3}_{-34.7-41.3}$  pb at  $\sqrt{s} = 14$  TeV [1].

Electroweak single top-quark production mechanisms, namely from  $q\bar{q}' \rightarrow t\bar{b}$  [4],  $qb \rightarrow q't$  [5], mediated by virtual  $s$ -channel and  $t$ -channel  $W$ -bosons, and  $Wt$ -associated production, through  $bg \rightarrow W^-t$ , lead to somewhat smaller cross sections. For example,  $t$ -channel production, while suppressed by the weak coupling with respect to the strong pair production, is kinematically enhanced, resulting in a sizeable cross section both at Tevatron and LHC energies. At the Tevatron, the  $t$ - and  $s$ -channel cross sections for top quarks are identical to those for antitop quarks, while at the LHC they are not, due to the charge-asymmetric initial state. Approximate NNLO cross sections for  $t$ -channel single top-quark production ( $t + \bar{t}$ ) are calculated for  $m_t = 173.3$  GeV/ $c^2$  to be  $2.06^{+0.13}_{-0.13}$  pb in  $p\bar{p}$  collisions at  $\sqrt{s} = 1.96$  TeV (scale and parton distribution functions uncertainties are combined in quadrature) [6]. Recently, calculations at NNLO accuracy for the  $t$ -channel cross section at the LHC have appeared [7, 8], predicting ( $m_t = 172.5$  GeV/ $c^2$ ):  $\sigma_{t+\bar{t}} = 64.0^{+0.77}_{-0.38}$  pb at  $\sqrt{s} = 7$  TeV,  $\sigma_{t+\bar{t}} = 84.6^{+1.0}_{-0.51}$  pb at  $\sqrt{s} = 8$  TeV,  $\sigma_{t+\bar{t}} = 215^{+2.1}_{-1.3}$  pb at  $\sqrt{s} = 13$  TeV, and  $\sigma_{t+\bar{t}} = 245^{+2.7}_{-1.3}$  pb at  $\sqrt{s} = 14$  TeV, where the quoted uncertainties are from scale variation only. For the  $s$ -channel, NNLO approximated calculations yield  $1.03^{+0.05}_{-0.05}$  pb for the Tevatron, and  $4.5^{+0.2}_{-0.2}(5.5^{+0.2}_{-0.2})$  pb for  $\sqrt{s} = 7$  (8) TeV at the LHC, with 69% (31%) of top (anti-top) quarks [9]. While negligible at the Tevatron, at LHC energies the  $Wt$ -associated

production becomes relevant. At  $\sqrt{s} = 7$  (8) TeV, an approximate NNLO calculation gives  $15.5^{+1.2}_{-1.2}(22.1^{+1.5}_{-1.5})$  pb ( $t + \bar{t}$ ), with an equal proportion of top and anti-top quarks [10].

Assuming  $|V_{tb}| \gg |V_{td}|, |V_{ts}|$  (see the review “The CKM Quark-Mixing Matrix” for more information), the cross sections for single top production are proportional to  $|V_{tb}|^2$ , and no extra hypothesis is needed on the number of quark families or on the unitarity of the CKM matrix in extracting  $|V_{tb}|$ . Separate measurements of the  $s$ - and  $t$ -channel processes provide sensitivity to physics beyond the Standard Model [11].

With a mass above the  $Wb$  threshold, and  $|V_{tb}| \gg |V_{td}|, |V_{ts}|$ , the decay width of the top quark is expected to be dominated by the two-body channel  $t \rightarrow Wb$ . Neglecting terms of order  $m_b^2/m_t^2$ ,  $\alpha_s^2$ , and  $(\alpha_s/\pi)M_W^2/m_t^2$ , the width predicted in the SM at NLO is [12]:

$$\Gamma_t = \frac{G_F m_t^3}{8\pi\sqrt{2}} \left(1 - \frac{M_W^2}{m_t^2}\right)^2 \left(1 + 2\frac{M_W^2}{m_t^2}\right) \left[1 - \frac{2\alpha_s}{3\pi} \left(\frac{2\pi^2}{3} - \frac{5}{2}\right)\right], \quad (60.1)$$

where  $m_t$  refers to the top-quark pole mass. The width for a value of  $m_t = 173.3$  GeV/ $c^2$  is 1.35 GeV/ $c^2$  (we use  $\alpha_s(M_Z) = 0.118$ ) and increases with mass. With its correspondingly short lifetime of  $\approx 0.5 \times 10^{-24}$  s, the top quark is expected to decay before top-flavored hadrons or  $t\bar{t}$ -quarkonium-bound states can form [13]. In fact, since the decay time is close to the would-be-resonance binding time, a peak will be visible in  $e^+e^-$  scattering at the  $t\bar{t}$  threshold [14] and it is in principle present (yet very difficult to measure) in hadron collisions, too [15]. The order  $\alpha_s^2$  QCD corrections to  $\Gamma_t$  are also available [16], thereby improving the overall theoretical accuracy to better than 1%.

The final states for the leading pair-production process can be divided into three classes:

- A.  $t\bar{t} \rightarrow W^+ b W^- \bar{b} \rightarrow q\bar{q}' b q'' \bar{q}''' \bar{b}$ , (45.7%)
- B.  $t\bar{t} \rightarrow W^+ b W^- \bar{b} \rightarrow q\bar{q}' b \ell^- \bar{\nu}_\ell \bar{b} + \ell^+ \nu_\ell b q'' \bar{q}''' \bar{b}$ , (43.8%)
- C.  $t\bar{t} \rightarrow W^+ b W^- \bar{b} \rightarrow \ell^+ \nu_\ell b \ell'^- \bar{\nu}_{\ell'}$ . (10.5%)

The quarks in the final state evolve into jets of hadrons. A, B, and C are referred to as the all-hadronic, lepton+jets ( $\ell$ +jets), and dilepton ( $\ell\ell$ ) channels, respectively. Their relative contributions, including hadronic corrections, are given in parentheses assuming lepton universality. While  $\ell$  in the above processes refers to  $e$ ,  $\mu$ , or  $\tau$ , most of the analyses distinguish the  $e$  and  $\mu$  from the  $\tau$  channel, which is more difficult to reconstruct. Therefore, in what follows, we will use  $\ell$  to refer to  $e$  or  $\mu$ , unless otherwise noted. Here, typically leptonic decays of  $\tau$  are included. In addition to the quarks resulting from the top-quark decays, extra QCD radiation (quarks and gluons) from the colored particles in the event can lead to extra jets.

The number of jets reconstructed in the detectors depends on the decay kinematics, as well as on the algorithm for reconstructing jets used by the analysis. Information on the transverse momenta of neutrinos is obtained from the imbalance in transverse momentum measured in each event (missing  $p_T$ , which is here also called missing  $E_T$ ).

The identification of top quarks in the electroweak single top channel is much more difficult than in the QCD  $t\bar{t}$  channel, due to a less distinctive signature and significantly larger backgrounds, mostly due to  $t\bar{t}$  and  $W$ +jets production.

Fully exclusive predictions via Monte Carlo generators for the  $t\bar{t}$  and single top production processes at NLO accuracy in QCD, including top-quark decays and possibly off-shell effects are available [17, 18] through the MC@NLO [19] and POWHEG [20] methods.

Besides fully inclusive QCD or EW top-quark production, more exclusive final states can be accessed at hadron colliders, whose cross sections are typically much smaller, yet can provide key information on the properties of the top quark. For all relevant final states (e.g.,  $t\bar{t}V$ ,  $t\bar{t}VV$  with  $V = \gamma, W, Z$ ,  $t\bar{t}H$ ,  $t\bar{t}$ +jets,  $t\bar{t}b\bar{b}$ ,  $t\bar{t}t\bar{t}$ ) automatic or semi-automatic predictions at NLO accuracy in QCD also in the form of event generators, i.e., interfaced

to parton-shower programs, are available (see the review “Monte Carlo event generators” for more information).

### 60.3 Top-quark measurements

Since the discovery of the top quark, direct measurements of  $t\bar{t}$  production have been made at six center-of-mass energies in  $pp$  or  $p\bar{p}$  and one in  $pPb$  collisions, providing stringent tests of QCD. The first measurements were made in Run I at the Tevatron at  $\sqrt{s} = 1.8$  TeV. In Run II at the Tevatron relatively precise measurements were made at  $\sqrt{s} = 1.96$  TeV. Finally, beginning in 2010, measurements have been made at the LHC at  $\sqrt{s} = 7$  TeV,  $\sqrt{s} = 8$  TeV, and  $\sqrt{s} = 13$  TeV, and recently also in a dedicated low energy run at  $\sqrt{s} = 5.02$  TeV and at 8.16 TeV in  $pPb$  collisions.

Production of single top quarks through electroweak interactions has now been measured with good precision at the Tevatron at  $\sqrt{s} = 1.96$  TeV, and at the LHC at  $\sqrt{s} = 7$  TeV,  $\sqrt{s} = 8$  TeV, and also at  $\sqrt{s} = 13$  TeV. Measurements at the Tevatron have managed to separate the  $s$ - and  $t$ -channel production cross sections, and at the LHC, the  $tW$  mechanism as well, though the  $t$ -channel is measured with best precision to date. The measurements allow an extraction of the CKM matrix element  $V_{tb}$ . Also more exclusive production modes and top-quark properties have been measured in single-top production.

With approximately 10 fb<sup>-1</sup> of Tevatron data, and almost 5 fb<sup>-1</sup> at 7 TeV, 20 fb<sup>-1</sup> at 8 TeV and 139 fb<sup>-1</sup> at 13 TeV at the LHC, many properties of the top quark have been measured with high precision. These include properties related to the production mechanism, such as  $t\bar{t}$  spin correlations, forward-backward or charge asymmetries, and differential production cross sections, as well as properties related to the  $tWb$  decay vertex, such as the helicity of the  $W$ -bosons from the top-quark decay. Also studies of the  $t\bar{t}\gamma$ ,  $t\bar{t}Z$  vertices as well as contact  $t\bar{t}b\bar{b}$ , and  $t\bar{t}t\bar{t}$  interactions have been made. In addition, many searches for physics beyond the Standard Model or  $t\bar{t}h$  or  $th$  production are being performed with increasing reach in both production and decay channels.

In the following sections we review the current status of measurements of the characteristics of the top quark.

#### 60.3.1 Top-quark production

##### 60.3.1.1 $t\bar{t}$ production

Fig. 60.1 summarizes the  $t\bar{t}$  production cross-section measurements from both the Tevatron and LHC. Please note that some cross section measurements at the LHC have luminosity-related uncertainties which have improved in the meantime [21]. The most recent measurement from DØ [22] ( $p\bar{p}$  at  $\sqrt{s} = 1.96$  TeV), combining the measurements from the dilepton and lepton plus jets final states in 9.7 fb<sup>-1</sup>, is  $7.26 \pm 0.13^{+0.57}_{-0.50}$  pb.

From CDF the most precise measurement made recently [23] is in 8.8 fb<sup>-1</sup> in the dilepton channel requiring at least one  $b$ -tag, yielding  $7.09 \pm 0.84$  pb. Both of these measurements assume a top-quark mass of 172.5 GeV/c<sup>2</sup>. The dependence of the cross-section measurements on the value chosen for the mass is less than that of the theory calculations because it only affects the determination of the acceptance. In some analyses also the shape of topological variables might be modified.

Combining the recent cross section measurements with older ones in other channels yields  $\sigma_{t\bar{t}} = 7.63 \pm 0.50$  pb (6.6%) for CDF,  $\sigma_{t\bar{t}} = 7.56 \pm 0.59$  pb (7.8%) for DØ and  $\sigma_{t\bar{t}} = 7.60 \pm 0.41$  pb (5.4%) for the Tevatron combination [24] in good agreement with the SM expectation of  $7.35^{+0.28}_{-0.33}$  pb at NNLO+NNLL in perturbative QCD [1] for a top mass of 172.5 GeV. The contributions to the uncertainty are 0.20 pb from statistical sources, 0.29 pb from systematic sources, and 0.21 pb from the uncertainty on the integrated luminosity.

CDF has measured the  $t\bar{t}$  production cross section in the dilepton channel with one hadronically decaying tau in 9.0 fb<sup>-1</sup>, yielding  $\sigma_{t\bar{t}} = 8.1 \pm 2.1$  pb. By separately identifying the single-tau and the ditau components, they measure the branching fraction of the top quark into the tau lepton, tau neutrino, and bottom quark to be  $(9.6 \pm 2.8)\%$  [25]. CDF also performs measurements of the  $t\bar{t}$  production cross section normalized to the  $Z$  production cross section in order to reduce the impact of the luminosity uncertainty [26].

DØ has performed a measurement of differential  $t\bar{t}$  cross sections in 9.7 fb<sup>-1</sup> of lepton+jets data as a function of the transverse momentum and absolute value of the rapidity of the top quarks as well as of the invariant mass of the  $t\bar{t}$  pair [27]. Observed differential cross sections are consistent with SM predictions.

The LHC experiments ATLAS and CMS use similar techniques to measure the  $t\bar{t}$  cross section in  $pp$  collisions. The most precise measurements come from the dilepton channel, and in particular the  $e\mu$  channel. At  $\sqrt{s} = 7$  TeV, ATLAS uses 4.6 fb<sup>-1</sup> of  $e\mu$  events in which they select an extremely clean sample and determine the  $t\bar{t}$  cross section simultaneously with the efficiency to reconstruct and tag  $b$ -jets, yielding  $\sigma_{t\bar{t}} = 182.9 \pm 7.1$  pb, corresponding to 3.9% precision [28]. Other measurements by ATLAS at  $\sqrt{s} = 7$  TeV, include a measurement in 0.7 fb<sup>-1</sup> in the lepton+jets channel [29], in the dilepton channel [30], and in 1.02 fb<sup>-1</sup> in the all-hadronic channel [31], which together yield a combined value of  $\sigma_{t\bar{t}} = 177 \pm 3(stat.)^{+8}_{-7}(syst.) \pm 7(lumi.)$  pb (6.2%) assuming  $m_t = 172.5$  GeV/c<sup>2</sup> [32]. In 4.7 fb<sup>-1</sup> of all-hadronic events, they obtain  $\sigma_{t\bar{t}} = 168 \pm 62$  pb [33]. Further analyses in the hadronic  $\tau$  plus jets channel in 1.67 fb<sup>-1</sup> [34] and the hadronic  $\tau$  + lepton channel in 2.05 fb<sup>-1</sup> [35], and the all-hadronic channel in 4.7 fb<sup>-1</sup> [33] yield consistent albeit less precise results. Another simultaneous measurement of the  $t\bar{t}, W^+W^-$ , and  $Z/\gamma^* \rightarrow \tau\tau$  cross section using the full 7 TeV dataset with 4.6 fb<sup>-1</sup> yields  $\sigma_{t\bar{t}} = 181 \pm 11$  pb, corresponding to a 6% precision [36]. The most precise measurement from CMS at  $\sqrt{s} = 7$  TeV is also obtained in the dilepton channel, where they measure  $\sigma_{t\bar{t}} = 162 \pm 2(stat.) \pm 5(syst.) \pm 4(lumi.)$  pb, corresponding to a 4.2% precision [37]. Other measurements at  $\sqrt{s} = 7$  TeV from CMS include measurements with 2.3 fb<sup>-1</sup> in the  $e/\mu$ +jets channel [38], with 3.5 fb<sup>-1</sup> in the all-hadronic channel [39], with 2.2 fb<sup>-1</sup> in the lepton+ $\tau$  channel [40], and with 3.9 fb<sup>-1</sup> in the  $\tau$ +jets channel [41]. ATLAS and CMS also provide a combined cross section at  $\sqrt{s} = 7$  TeV of  $173.3 \pm 2.3(stat.) \pm 7.6(syst.) \pm 6.3(lumi.)$  pb using slightly older results based on 0.7 – 1.1 fb<sup>-1</sup> [42].

At  $\sqrt{s} = 8$  TeV, ATLAS measures the  $t\bar{t}$  cross section with 20.3 fb<sup>-1</sup> using  $e\mu$  dilepton events, with a simultaneous measurement of the  $b$ -tagging efficiency, yielding  $\sigma_{t\bar{t}} = 242.4 \pm 1.7(stat.) \pm 5.5(syst.) \pm 7.5(lumi.) \pm 4.2(\text{beam energy})$  pb [43] assuming  $m_t = 172.5$  GeV/c<sup>2</sup>, which corresponds to a 4.7% precision. In the lepton+jets channel, they measure  $\sigma_{t\bar{t}} = 260 \pm 1(stat.)^{+20}_{-23}(syst.) \pm 8(lumi.) \pm 4(\text{beam energy})$  pb [29] in 20.3 fb<sup>-1</sup> using a likelihood discriminant fit and  $b$ -jet identification. Subsequently, ATLAS performed a new analysis in 20.2 fb<sup>-1</sup> lepton+jets events. They model the  $W$ +jets background using  $Z$ +jets data and employ neural networks in three jet-multiplicity and  $b$ -jet multiplicity regions for the signal and background separation, yielding  $\sigma_{t\bar{t}} = 248.3 \pm 0.7(stat.) \pm 13.4(syst.) \pm 4.7(lumi.)$  pb [44]. ATLAS also performed a cross section measurement in the hadronic  $\tau$ +jets channel yielding consistent, albeit less precise results [45]. CMS performs a template fit to the  $M_{b\bar{b}}$  mass distribution using 19.6 fb<sup>-1</sup> in the lepton+jets channel yielding  $\sigma_{t\bar{t}} = 228.5 \pm 3.8(stat.) \pm 13.7(syst.) \pm 6(lumi.)$  pb [46, 47]. These 8 TeV measurements are in agreement with QCD predictions up to NLO accuracy. In the  $e\mu$  channel, initially using 5.3 fb<sup>-1</sup> [47] and then using 19.7 fb<sup>-1</sup>, the cross sections are extracted using a binned likelihood fit to multi-differential final state distributions related to identified  $b$  quark and other jets in the event, yielding  $\sigma_{t\bar{t}} = 244.9 \pm 1.4(stat.)^{+6.3}_{-5.5}(syst.) \pm 6.4(lumi.)$  pb [48]. The cross section and its ratio between 7 TeV and 8 TeV measurements are found to be consistent with pQCD calculations. The cross section is also measured in the hadronic  $\tau$ +jets channel, yielding  $\sigma_{t\bar{t}} = 257 \pm 3(stat.) \pm 24(syst.) \pm 7(lumi.)$  pb [49] and in the all-hadronic final state giving  $\sigma_{t\bar{t}} = 275.6 \pm 6.1(stat.) \pm 37.8(syst.) \pm 7.2(lumi.)$  pb [50]. In combination of the most precise  $e\mu$  measurements in 5.3 – 20.3 fb<sup>-1</sup>, ATLAS and CMS together yield at 8 TeV  $\sigma_{t\bar{t}} = 241.5 \pm 1.4(stat.) \pm 5.7(syst.) \pm 6.2(lumi.)$  pb [51], which corresponds to a 3.5% precision, challenging the precision of the corresponding theoretical predictions. The LHCb collaboration presented the first observation of top-quark production in the forward region in  $pp$ -collisions. The  $W+b$  final state with  $W \rightarrow \mu\nu$  is reconstructed using muons with a transverse momentum,  $p_{T\mu}$ , larger than 25 GeV in the pseudorapidity range  $2.0 < \eta < 4.5$ .

The  $b$ -jets are required to have  $50 \text{ GeV} < p_T < 100 \text{ GeV}$  and  $2.2 < \eta < 4.2$ , while the transverse component of the sum of the muon and  $b$ -jet momenta must satisfy  $p_T > 20 \text{ GeV}$ . The results are based on data corresponding to integrated luminosities of 1.0 and  $2.0 \text{ fb}^{-1}$  collected at center-of-mass energies of 7 and 8 TeV by LHCb. The inclusive top quark production cross sections in the fiducial region are  $\sigma_{t\bar{t}} = 239 \pm 53(\text{stat.}) \pm 38(\text{syst.}) \text{ pb}$  at 7 TeV, and  $\sigma_{t\bar{t}} = 289 \pm 43(\text{stat.}) \pm 46(\text{syst.}) \text{ pb}$  at 8 TeV [52].

ATLAS and CMS have also measured the  $t\bar{t}$  production cross section with Run-II data at  $\sqrt{s} = 13 \text{ TeV}$ . In the  $e\mu$  events with at least one  $b$ -tag, ATLAS uses  $78 \text{ pb}^{-1}$  and obtains  $\sigma_{t\bar{t}} = 825 \pm 114 \text{ pb}$  [53]. This measurement is updated with lepton identification and trigger efficiencies to give  $\sigma_{t\bar{t}} = 829 \pm 50(\text{stat.}) \pm 56(\text{syst.}) \pm 83(\text{lumi.}) \text{ pb}$  [54]. In this note, ATLAS also presents a  $t\bar{t}$  cross section measurement in the  $ee$  and  $\mu\mu$  dilepton channel with one and two  $b$ -tags using a counting approach, yielding  $\sigma_{t\bar{t}} = 749 \pm 57(\text{stat.}) \pm 79(\text{syst.}) \pm 74(\text{lumi.}) \text{ pb}$ . In the lepton-plus-jets channel, using  $85 \text{ pb}^{-1}$ , the cross-section is extracted by counting the number of events with exactly one electron or muon and at least four jets, at least one of which is identified as originating from a  $b$ -quark, yielding  $\sigma_{t\bar{t}} = 817 \pm 13(\text{stat.}) \pm 103(\text{syst.}) \pm 88(\text{lumi.}) \text{ pb}$ , both assuming  $m_t = 172.5 \text{ GeV}$  [54]. The cross section measurement in the  $e\mu$  channel counting events with one or with two  $b$ -tags is also repeated using  $3.2 \text{ pb}^{-1}$  and yields  $\sigma_{t\bar{t}} = 818 \pm 8(\text{stat.}) \pm 27(\text{syst.}) \pm 19(\text{lumi.}) \pm 12(\text{beam.}) \text{ pb}$  [55], consistent with theoretical QCD calculations at NNLO. Very recently, ATLAS measures the inclusive  $t\bar{t}$  cross section in  $139 \text{ fb}^{-1}$  in the lepton-plus-jets channel through a profile-likelihood fit to be  $\sigma_{t\bar{t}} = 830.4 \pm 0.4(\text{stat.})^{+38.2}_{-37.0}(\text{syst.}) \text{ pb}$ , with a relative uncertainty of 4.6% [56]. The result is consistent with the theoretical calculations at NLO order in QCD perturbation theory. In  $36.1 \text{ fb}^{-1}$  of  $e\mu$  data with one or two  $b$ -tags, ATLAS measures the  $t\bar{t}$  cross section to  $\sigma_{t\bar{t}} = 826.4 \pm 3.6(\text{stat.}) \pm 11.5(\text{syst.}) \pm 15.7(\text{lumi.}) \pm 1.9(\text{beam.}) \text{ pb}$ , giving a total of 2.4%. This measurement is also used to determine the top quark pole mass and to derive ratios and double ratios of  $t\bar{t}$  and  $Z$  cross-sections at different energies as well as absolute and normalised differential cross-sections as functions of single lepton and dilepton kinematic variables [57]. CMS uses  $43 \text{ pb}^{-1}$  in the  $e\mu$  channel to measure  $\sigma_{t\bar{t}} = 746 \pm 58(\text{stat.}) \pm 53(\text{syst.}) \pm 36(\text{lumi.}) \text{ pb}$ , in agreement with the expectation from the standard model [58]. Using  $2.2 \text{ fb}^{-1}$  in the  $e\mu$  channel with at least one  $b$ -jet, CMS measures  $\sigma_{t\bar{t}} = 815 \pm 9(\text{stat.}) \pm 38(\text{syst.}) \pm 19(\text{lumi.}) \text{ pb}$ , in agreement with the expectation from the Standard Model [59]. A first measurement of the total inclusive and the normalized differential cross section in the lepton-plus-jets channel is made in  $42 \text{ pb}^{-1}$  yielding  $\sigma_{t\bar{t}} = 836 \pm 27(\text{stat.}) \pm 88(\text{syst.}) \pm 100(\text{lumi.}) \text{ pb}$  [60]. In  $2.2 \text{ fb}^{-1}$ , lepton-plus-jets events are categorized according to the accompanying jet multiplicity. From a likelihood fit to the invariant mass distribution of the isolated lepton and a  $b$ -jet, the cross section is measured to be  $\sigma_{t\bar{t}} = 888 \pm 2(\text{stat.})^{+26}_{-28}(\text{syst.}) \pm 20(\text{lumi.}) \text{ pb}$ , in agreement with the SM prediction [61]. This result is also used to extract the top-quark mass. Using  $35.9 \text{ fb}^{-1}$  of dilepton data, CMS measures the  $t\bar{t}$  cross section using a likelihood fit  $\sigma_{t\bar{t}} = 803 \pm 2(\text{stat.}) \pm 25(\text{syst.}) \pm 20(\text{lumi.}) \text{ pb}$ , in agreement with the expectation from the SM calculation at NLO order. This result is also used to extract the top quark mass and the strong coupling constant [62]. Very recently, using the same dataset in the dilepton channel with a hadronically decaying  $\tau$ , they measure  $\sigma_{t\bar{t}} = 781 \pm 7(\text{stat.}) \pm 62(\text{syst.}) \pm 20(\text{lumi.}) \text{ pb}$  [63]. In the all-hadronic channel, CMS uses  $2.53 \text{ fb}^{-1}$  of data, yielding a cross section of  $\sigma_{t\bar{t}} = 834 \pm 25(\text{stat.}) \pm 23(\text{lumi.}) \text{ pb}$  [64]. Also differential cross sections as a function of the leading top quark transverse momentum are measured. As general feature found across channels, it is found that measured top quark  $p_T$  spectrum is significantly softer than the theory predictions.

In addition, CMS has also measured the top-quark pair production cross section in a special LHC run with  $\sqrt{s} = 5.02 \text{ TeV}$ , accumulating  $27.4 \text{ pb}^{-1}$ . The measurement is performed by analyzing events with at least one charged lepton. The measured cross section is  $\sigma_{t\bar{t}} = 69.5 \pm 8.4 \text{ pb}$  [65], in agreement with the expectation from the Standard Model. In order to test consistency of the cross-section measurements with some systematic uncertain-

ties cancelling out while testing pQCD and PDFs, cross-section ratios between measurements at 7 TeV and at 8 TeV are performed and cited in several cases. In other cases, the cross-section ratio between  $t\bar{t}$ - and  $Z$ -production is determined as that is independent of luminosity uncertainties, but keeps its sensitivity to the ratio of gluon versus quark PDFs. These experimental results should be compared to the theoretical calculations at NNLO+NNLL that yield  $7.16^{+0.20}_{-0.23} \text{ pb}$  for top-quark mass of  $173.3 \text{ GeV}/c^2$  [1] at  $\sqrt{s} = 1.96 \text{ TeV}$ , and for top-quark mass of  $173.2 \text{ GeV}/c^2$   $\sigma_{t\bar{t}} = 173.6^{+4.5+8.9}_{-5.9-8.9} \text{ pb}$  at  $\sqrt{s} = 7 \text{ TeV}$ ,  $\sigma_{t\bar{t}} = 247.7^{+6.3+11.5}_{-8.5-11.5} \text{ pb}$  at  $\sqrt{s} = 8 \text{ TeV}$ , and  $\sigma_{t\bar{t}} = 816.0^{+19.4+34.4}_{-28.6-34.4} \text{ pb}$  at  $\sqrt{s} = 13 \text{ TeV}$ , at the LHC [1]. CMS also performed a measurement of top-quark pair production in  $pPb$  heavy ion collisions at  $\sqrt{s} = 8.16 \text{ TeV}$  in  $174 \text{ nb}^{-1}$  of lepton+jets events. They measure a cross section of  $\sigma_{t\bar{t}} = 45 \pm 8 \text{ pb}$ , which is consistent with pQCD calculations and with the scaled  $pp$  data [66].

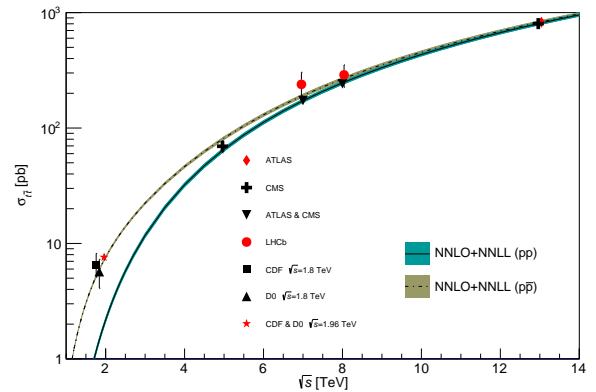


Figure 60.1: Measured and predicted  $t\bar{t}$  production cross sections from Tevatron energies in  $p\bar{p}$  collisions to LHC energies in  $pp$  collisions. Tevatron data points at  $\sqrt{s} = 1.8 \text{ TeV}$  are from Refs. [67, 68]. Those at  $\sqrt{s} = 1.96 \text{ TeV}$  are from Refs. [22–24]. The ATLAS, CMS, and LHCb data points are from Refs. [28, 37, 42, 47, 51, 52, 55, 62], and [65], respectively. Theory curves and uncertainties are generated using [1] for  $m_t = 172.5 \text{ GeV}/c^2$ , the  $m_t$  value assumed in the cross-section measurements. Figure adapted from Ref. [69].

In Fig. 60.1, one sees the importance of  $p\bar{p}$  at Tevatron energies where the valence antiquarks in the antiprotons contribute to the dominant  $q\bar{q}$  production mechanism. At LHC energies, the dominant production mode is gluon-gluon fusion and the  $pp$ - $p\bar{p}$  difference nearly disappears. The excellent agreement of these measurements with the theory calculations is a strong validation of QCD and the soft-gluon resummation techniques employed in the calculations. The measurements reach high precision and provide stringent tests of pQCD calculations at NNLO+NNLL level including their respective PDF uncertainties.

Most of these measurements assume a  $t \rightarrow Wb$  branching ratio of 100%. CDF and D0 have made direct measurements of the  $t \rightarrow Wb$  branching ratio [70]. Comparing the number of events with 0, 1 and 2 tagged  $b$  jets in the lepton+jets channel, and also in the dilepton channel, using the known  $b$ -tagging efficiency, the ratio  $R = B(t \rightarrow Wb) / \sum_{q=d,s,b} B(t \rightarrow Wq)$  can be extracted. In  $5.4 \text{ fb}^{-1}$  of data, D0 measures  $R = 0.90 \pm 0.04$ ,  $2.5\sigma$  from unity. The currently most precise measurement was made by CMS in  $19.7 \text{ fb}^{-1}$  at  $\sqrt{s} = 8 \text{ TeV}$ . They find  $R = 1.014 \pm 0.003(\text{stat.}) \pm 0.032(\text{syst.})$  and  $R > 0.955$  at 95% C.L. [71]. A significant deviation of  $R$  from unity would imply either non-SM top-quark decay (for example a flavor-changing neutral-current decay), or a fourth generation of quarks.

Thanks to the large available event samples, the Tevatron and the LHC experiments also performed differential cross-section measurements in  $t\bar{t}$  production. Such measurements are crucial, as they allow even more stringent tests of perturbative QCD as description of the production mechanism, allow the extraction or the use of PDF fits, and enhance the sensitivity to possible

new physics contributions, especially now that NNLO predictions for the main differential observables in  $t\bar{t}$  prediction have become available [72] and recently confirmed [2]. Furthermore, such measurements reduce the uncertainty in the description of  $t\bar{t}$  production as background in Higgs physics and searches for rare processes or beyond Standard Model physics. Differential cross sections are typically measured by a selection of candidate events, their kinematic reconstruction and subsequent unfolding of the obtained event counts in bins of kinematic distributions in order to correct for detector resolution effects, acceptance and migration effects. In some cases a bin-by-bin unfolding is used, while other analyses use more sophisticated techniques.

Experiments at Tevatron and LHC measure the differential cross section with respect to the  $t\bar{t}$  invariant mass,  $d\sigma/dM_{t\bar{t}}$ . The spectra are fully corrected for detector efficiency and resolution effects and are compared to several Monte Carlo simulations as well as selected theoretical calculations.

Using  $9.45 \text{ fb}^{-1}$ , CDF measured  $d\sigma/dM_{t\bar{t}}$  in the lepton+jets channel providing sensitivity to a variety of exotic particles decaying into  $t\bar{t}$  pairs [73]. In  $9.7 \text{ fb}^{-1}$  of lepton+jets data, DØ measured the differential  $t\bar{t}$  production cross section with respect to the transverse momentum and absolute rapidity of the top quarks as well as of the invariant mass of the  $t\bar{t}$  pair [27], which are all found to be in good agreement with the SM predictions.

ATLAS measured the differential  $t\bar{t}$  production cross section with respect to the top-quark transverse momentum, and of the mass, transverse momentum and rapidity of the top quark, the antitop quark as well as the  $t\bar{t}$  system in  $4.6 \text{ fb}^{-1}$  at  $\sqrt{s} = 7 \text{ TeV}$  in the lepton+jets channel [74–76]. It is found that data is softer than all predictions for higher values of the mass of the  $t\bar{t}$  system as well as in the tail of the top-quark  $p_T$  spectrum beginning at 200 GeV, particularly in the case of the **Alpgen+Herwig** generator. The  $M_{t\bar{t}}$  spectrum is not well described by NLO+NNLL calculations and there are also disagreements between the measured rapidity of the  $t\bar{t}$  system spectrum and the **MC@NLO+Herwig** and **POWHEG+Herwig** generators, both evaluated with the CT10 PDF set. All distributions show a preference for HERAPDF1.5 when used for the NLO QCD predictions. In  $5.0 \text{ fb}^{-1}$  of  $\sqrt{s} = 7 \text{ TeV}$  data in the lepton+jets and the dilepton channels, CMS measured normalised differential  $t\bar{t}$  cross sections with respect to kinematic properties of the final-state charged leptons and jets associated to  $b$ -quarks, as well as those of the top quarks and the  $t\bar{t}$  system. The data are compared with several predictions from perturbative QCD calculations and found to be consistent [77]. ATLAS uses  $4.6 \text{ fb}^{-1}$  of data at 7 TeV and  $20.2 \text{ fb}^{-1}$  at 8 TeV to measure the differential  $t\bar{t}$  cross section in the dilepton final state as a function of the mass, the transverse momentum and the rapidity of the  $t\bar{t}$  system [78]. The results are compared with different Monte Carlo generators and theoretical calculations of  $t\bar{t}$  production and found to be consistent with the majority of predictions in a wide kinematic range. Using  $20.3 \text{ fb}^{-1}$  of  $t\bar{t}$  events in the lepton+jets channel, ATLAS measures the normalized differential cross sections of  $t\bar{t}$  production as a function of the top-quark,  $t\bar{t}$  system and event-level kinematic observables [79]. The observables have been chosen to emphasize the  $t\bar{t}$  production process and to be sensitive to effects of initial- and final-state radiation, to the different parton distribution functions, and to non-resonant processes and higher-order corrections. The results are in fair agreement with the predictions over a wide kinematic range. Nevertheless, most generators predict a harder top-quark transverse momentum distribution at high values than what is observed in the data. Predictions beyond NLO accuracy improve the agreement with data at high top-quark transverse momenta. Using the current settings in the Monte Carlo programs and parton distribution functions, the rapidity distributions are not well modelled by any generator under consideration. However, the level of agreement is improved when more recent sets of parton distribution functions are used. Using  $20.3 \text{ fb}^{-1}$  of 8 TeV data, ATLAS performed a dedicated differential  $t\bar{t}$  cross-section measurement of highly boosted top quarks in the lepton+jets channel, where the hadronically decaying top quark has a transverse momentum above 300 GeV [80]. Jet substructure techniques are employed to identify top quarks, which are reconstructed with an anti- $k_t$  jet with a radius param-

eters  $R = 1.0$ . The predictions of NLO and LO matrix element plus parton shower Monte Carlo generators are found to generally overestimate the measured cross sections.

Using  $5.0 \text{ fb}^{-1}$  of data at 7 TeV and  $19.7 \text{ fb}^{-1}$  at 8 TeV in the lepton+jets channel, CMS reports measurements of normalized differential cross sections for  $t\bar{t}$  production with respect to four kinematic event variables: the missing transverse energy; the scalar sum of the jet transverse momentum ( $p_T$ ); the scalar sum of the  $p_T$  of all objects in the event; and the  $p_T$  of leptonically decaying  $W$  bosons from top quark decays [81]. No significant deviations from the predictions of several SM event generators are observed. Using the full  $19.7 \text{ fb}^{-1}$  data in the  $e\mu$  channel, CMS measures normalized double-differential cross sections for  $t\bar{t}$  production as a function of various pairs of observables characterizing the kinematics of the top quark and  $t\bar{t}$  system [82]. The data are compared to calculations using perturbative QCD at NLO and approximate NNLO orders. They are also compared to predictions of Monte Carlo event generators that complement fixed-order computations with parton showers, hadronization, and multiple-parton interactions. Overall agreement is observed with the predictions, which is improved when the latest global sets (as determined here by CMS) of proton parton distribution functions are used. The inclusion of the measured  $t\bar{t}$  cross sections in a fit of parametrized parton distribution functions is shown to have significant impact on the gluon distribution [82]. Another analysis at high transverse momentum regime for the top quarks, is performed by the CMS collaboration in  $19.7 \text{ fb}^{-1}$  at  $\sqrt{s} = 8 \text{ TeV}$  [83]. The measurement is performed for events in electron/muon plus jets final states where the hadronically decaying top quark is reconstructed as a single large-radius jet and identified as a top candidate using jet substructure techniques. The integrated cross section is measured at particle-level within a fiducial region resembling the detector-level selection as well as at parton-level. At particle-level, the fiducial cross section is measured to be  $\sigma_{t\bar{t}} = 1.28 \pm 0.09(\text{stat.} + \text{syst.}) \pm 0.10(\text{pdf}) \pm 0.09(\text{scales}) \pm 0.03(\text{lumi.})$  pb for  $p_T > 400 \text{ GeV}$ . At parton-level, it translates to  $\sigma_{t\bar{t}} = 1.44 \pm 0.10(\text{stat.} + \text{syst.}) \pm 0.13(\text{pdf}) \pm 0.15(\text{scales}) \pm 0.04(\text{lumi.})$  pb.

At parton-level, interactions between incoming partons (quarks or gluons) are considered via a gauge interaction yielding final state partons. While such interactions can be well described theoretically, partons are not visible in the detector. At the particle-level, visible and measurable hadrons, i.e. bound states of quarks and anti-quarks, are considered to form jets. The hadronisation process takes us from one level to the other.

In  $19.7 \text{ fb}^{-1}$  at  $\sqrt{s} = 8 \text{ TeV}$ , CMS repeated those measurements in the lepton+jets and in the dilepton channels [84]. While the overall precision is improved, no significant deviations from the Standard Model are found, yet a softer spectrum for the top quark at high  $p_T$  with respect to theoretical available predictions has been observed. This behaviour has been also observed in the all-hadronic final state [85], where also a total cross measurement is performed, yielding  $\sigma_{t\bar{t}} = 275.6 \pm 6.1(\text{stat}) \pm 37.8(\text{syst}) \pm 7.2(\text{lumi})$  pb is obtained. In  $3.2 \text{ fb}^{-1}$  at  $\sqrt{s} = 13 \text{ TeV}$ , ATLAS measured the differential  $t\bar{t}$  cross section as a function of the transverse momentum and absolute rapidity of the top quark, and of the transverse momentum, absolute rapidity and invariant mass of the  $t\bar{t}$  system [86,87]. The measured differential cross sections are compared to predictions of NLO generators matched to parton showers and the measurements are found to be consistent with all models within the experimental uncertainties with the exception of the Powheg-Box+ Herwig++ predictions, which differ significantly from the data in both the transverse momentum of the top quark and the mass of the  $t\bar{t}$  system. Using  $3.2 \text{ fb}^{-1}$  of data in the lepton+jets channel, ATLAS measured the differential cross sections of  $t\bar{t}$  production in fiducial phase-spaces as a function of top-quark and  $t\bar{t}$  system kinematic observables [88]. Two separate selections are applied that each focus on different top-quark momentum regions, referred to as resolved and boosted topologies of the  $t\bar{t}$  final state. The measured spectra are corrected for detector effects and are compared to several Monte Carlo simulations by means of calculated  $\chi^2$  and  $p$ -values. At a center-of-mass energy of 13 TeV, ATLAS presents a measurement of the boosted top quark



differential cross section in the all-hadronic decay mode [89]. They require two top-quark candidates, one with  $p_T > 500$  GeV and a second with  $p_T > 350$  GeV, with each candidate reconstructed as an anti- $k_T$  jet with radius parameter  $R = 1.0$ . The top-quark candidates are separated from the multijet background using the jet substructure and the presence of a  $b$ -quark tag in each jet. The observed kinematic distributions are unfolded to recover the differential cross sections in a limited phase-space region and compared with SM predictions, showing agreement. In addition, ATLAS measures the differential  $t\bar{t}$  cross section of highly boosted top-quarks decaying to all-hadronic final states in  $36.1 \text{ fb}^{-1}$  using jet substructure information [90]. In  $36 \text{ fb}^{-1}$ , ATLAS measures the single- and double-differential  $t\bar{t}$  cross-section in the lepton + jets channel at particle and parton level. Two topologies, resolved and boosted, are considered and the results are presented as a function of several kinematic variables characterising the top and  $t\bar{t}$  system and jet multiplicities. Overall, there is good agreement between the theoretical predictions and the data [91]. In  $2.1 \text{ fb}^{-1}$  at  $\sqrt{s} = 13$  TeV, CMS measures the normalized differential cross sections for  $t\bar{t}$  production in the dilepton channels as a function of the kinematic properties of the leptons, jets from bottom quark hadronization, top quarks, and top quark pairs at the particle and parton levels [92]. The results are compared to several Monte Carlo generators that implement calculations up to NLO in perturbative QCD interfaced with parton showering, and also to fixed-order theoretical calculations of top quark pair production up to NNLO, showing agreement. In  $2.3 \text{ fb}^{-1}$  of events in the lepton+jets channel, CMS measures the differential and double-differential cross sections for the  $t\bar{t}$  production as a function of jet multiplicity and of kinematic variables of the top quarks and the  $t\bar{t}$  system [93]. The differential cross sections are presented at particle level, within a phase space close to the experimental acceptance, and at parton level in the full phase space. The results are compared to several SM predictions. Using  $35.9 \text{ fb}^{-1}$ , CMS measures the differential  $t\bar{t}$  cross section in the single-lepton decay channel, as a function of a number of kinematic event variables. The data are compared to a variety of state-of-the-art LO and NLO simulations [94]. In  $35.8 \text{ fb}^{-1}$ , CMS measures the differential and double-differential  $t\bar{t}$  cross sections in the lepton-plus-jets channel as a function of kinematic variables of the top quarks and the top quark-antiquark ( $t\bar{t}$ ) system. In addition, kinematic variables and multiplicities of jets associated with the  $t\bar{t}$  production are measured. The kinematic variables of the top quarks and the  $t\bar{t}$  system are reasonably described in general, though none predict all the measured distributions. In particular, the transverse momentum distribution of the top quarks is more steeply falling than predicted. The kinematic distributions and multiplicities of jets are adequately modeled by certain combinations of NLO calculations and parton shower models [95]. In the dilepton channel, CMS measures differential  $t\bar{t}$  cross sections in  $35.9 \text{ fb}^{-1}$  as functions of kinematic observables of the top quarks and their decay products, the  $t\bar{t}$  system, and the total number of jets in the event. All results are compared with SM predictions from Monte Carlo simulations with NLO accuracy in QCD at matrix-element level interfaced to parton-shower simulations. Where possible, parton-level results are compared to calculations with beyond-NLO precision in QCD. Significant disagreement is observed between data and all predictions for several observables. The measurements are used to constrain the top quark chromomagnetic dipole moment in an effective field theory framework at NLO in QCD and to extract  $t\bar{t}$  and leptonic charge asymmetries [96]. In  $35.9 \text{ fb}^{-1}$  of dilepton events, CMS measures normalised multi-differential  $t\bar{t}$  cross sections as a function of the kinematic properties of the top quark and of the  $t\bar{t}$  system at parton level in the full phase space. A triple-differential measurement is performed as a function of the invariant mass and rapidity of the  $t\bar{t}$  system and the multiplicity of additional jets at particle level. The data are compared to predictions of Monte Carlo event generators that complement NLO QCD calculations with parton showers. The measurement is used to extract the strong coupling constant and the top-quark pole mass and parton distribution functions [97]. Further cross-section measurements are performed by ATLAS for  $t\bar{t}$ +heavy flavour [98] and  $t\bar{t}$ +jets production as well as the differential measurement of

the jet multiplicity in  $t\bar{t}$  events [99, 100]. Here, MC@NLO+Herwig MC is found to predict too few events at higher jet multiplicities. In addition, CMS measured the cross-section ratio  $\sigma_{t\bar{t}bb}/\sigma_{t\bar{t}jj}$  using  $19.6 \text{ fb}^{-1}$  of 8 TeV data [101]. This is of high relevance for top quark production as background to searches, for example for measurements of  $t\bar{t}h$  production and ongoing searches for 4-top quark production. Later, ATLAS also measured the  $t\bar{t}$  production cross section along with as the branching ratios into channels with leptons and quarks using  $4.6 \text{ fb}^{-1}$  of 7 TeV data [102]. They find agreement with the standard model at the level of a few percent. In  $36.1 \text{ fb}^{-1}$ , ATLAS measures the  $t\bar{t}bb$  cross section in the dilepton and the lepton-plus-jet channels. Results are presented at particle level in the form of inclusive cross-sections of  $t\bar{t}$  final states with three and four  $b$ -jets as well as differential cross-sections as a function of global event properties and properties of  $b$ -jet pairs. The measured inclusive fiducial cross-sections generally exceed the  $t\bar{t}bb$  predictions from various NLO matrix element calculations matched to a parton shower, but are compatible within the total uncertainties [103]. In  $2.3 \text{ fb}^{-1}$ , CMS measures the  $t\bar{t}bb$  cross section in the dilepton channel [104]. They also determine the cross section ratio  $\sigma_{t\bar{t}bb}/\sigma_{t\bar{t}jj}$ . In  $35.9 \text{ fb}^{-1}$ , CMS recently measured the cross section  $t\bar{t}bb$  as well as the cross section ratio  $\sigma_{t\bar{t}bb}/\sigma_{t\bar{t}jj}$  in the dilepton and the lepton+jets channel [105]. They fit the distribution of the  $b$  tagging discriminant variable of the two jets that do not belong to the  $t\bar{t}$  decay. In the same dataset, CMS measures the  $t\bar{t}bb$  cross section in the all-jet channel by selecting events containing at least eight jets, of which at least two are identified as  $b$ -jets. A combination of multivariate analysis techniques is used to reduce the large background from multijet events not containing a top quark pair, and to help discriminate between jets originating from top quark decays and other additional jets. The measured cross sections are found to be larger than theoretical predictions by a factor of 1.5-2.4, corresponding to 1-2 standard deviations [106].

### 60.3.1.2 Single-top production

Single-top quark production was first observed in 2009 by DØ [107] and CDF [108, 109] at the Tevatron. The production cross section at the Tevatron is roughly half that of the  $t\bar{t}$  cross section, but the final state with a single  $W$ -boson and typically two jets is less distinct than that for  $t\bar{t}$  and much more difficult to distinguish from the background of  $W$ +jets and other sources. A comprehensive review of the first observation and the techniques used to extract the signal from the backgrounds can be found in [110].

The dominant production at the Tevatron is through  $s$ -channel and  $t$ -channel  $W$ -boson exchange. Associated production with a  $W$ -boson ( $tW$  production) has a cross section that is too small to observe at the Tevatron. The  $t$ -channel process is  $qb \rightarrow q't$ , while the  $s$ -channel process is  $q\bar{q}' \rightarrow t\bar{b}$ . The  $s$ - and  $t$ -channel productions can be separated kinematically. This is of particular interest because potential physics beyond the Standard Model, such as fourth-generation quarks, heavy  $W$  and  $Z$  bosons, flavor-changing-neutral-currents [11], or a charged Higgs boson, would affect the  $s$ - and  $t$ -channels differently. However, the separation is difficult and initial observations and measurements at the Tevatron by both experiments were of combined  $s + t$ -channel production. The two experiments combined their measurements for maximum precision with a resulting  $s+t$ -channel production cross section of  $2.76_{-0.47}^{+0.58}$  pb [111]. The measured value assumes a top-quark mass of  $170 \text{ GeV}/c^2$ . The mass dependence of the result comes both from the acceptance dependence and from the  $t\bar{t}$  background evaluation. Also the shape of discriminating topological variables is sensitive to  $m_t$ . The dependence on  $m_T$  is therefore not necessarily a simple linear dependence but amounts to only a few tenths of picobarns over the range  $170 - 175 \text{ GeV}/c^2$ . The measured value agrees well with the theoretical calculation at  $m_t = 173 \text{ GeV}/c^2$  of  $\sigma_{s+t} = 3.12$  pb (including both top and anti-top production) [6, 9].

Using the full Run-II data set of up to  $9.7 \text{ fb}^{-1}$ , CDF and DØ have measured the  $t$ -channel single-top quark production to be  $\sigma_{t+\bar{t}} = 2.25_{-0.31}^{+0.29}$  pb [112, 113]. In the same publication, they also present the simultaneously measured  $s-$  and  $t-$ channel cross



sections and the  $s+t$  combined cross section measurement resulting in  $\sigma_{s+t} = 3.30_{-0.40}^{+0.52}$  pb, without assuming the SM ratio of  $\sigma_s/\sigma_t$ . The modulus of the CKM matrix element obtained from the  $s+t$ -channel measurement is  $|V_{tb}| = 1.02_{-0.05}^{+0.06}$  and its value is used to set a lower limit of  $|V_{tb}| > 0.92$  at 95% C.L. Those results are in good agreement with the theoretical value at the mass  $172.5 \text{ GeV}/c^2$  of  $\sigma_t = 2.08 \pm 0.13$  pb [6]. It should be noted that the theory citations here list cross sections for  $t$  or  $\bar{t}$  alone, whereas the experiments measure the sum. At the Tevatron, these cross sections are equal. The theory values quoted here already include this factor of two.

Using datasets of  $9.7 \text{ fb}^{-1}$  each, CDF and DØ combine their analyses and report the first observation of single-top-quark production in the  $s$ -channel, yielding  $\sigma_s = 1.29_{-0.24}^{+0.26}$  pb [114]. The probability of observing a statistical fluctuation of the background of the given size is  $1.8 \times 10^{-10}$ , corresponding to a significance of 6.3 standard deviations.

At the LHC, the  $t$ -channel cross section is expected to be more than three times as large as  $s$ -channel and  $tW$  production, combined. Both ATLAS and CMS have measured single top production cross sections at  $\sqrt{s} = 7 \text{ TeV}$  in  $pp$  collisions (assuming  $m_t = 172.5 \text{ GeV}/c^2$  unless noted otherwise).

Using  $4.59 \text{ fb}^{-1}$  of data at  $\sqrt{s} = 7 \text{ TeV}$ , ATLAS measures the  $t$ -channel single-top quark cross section in the lepton plus 2 or 3 jets channel with one  $b$ -tag by fitting the distribution of a multivariate discriminant constructed with a neural network, yielding  $\sigma_t = 46 \pm 6$  pb,  $\sigma_{\bar{t}} = 23 \pm 4$  pb with a ratio  $R_t = \sigma_t/\sigma_{\bar{t}} = 2.04 \pm 0.18$  and  $\sigma_{t+\bar{t}} = 68 \pm 8$  pb, consistent with SM expectations [115,116]. CMS follows two approaches in  $1.6 \text{ fb}^{-1}$  of lepton plus jets events. The first approach exploits the distributions of the pseudorapidity of the recoil jet and reconstructed top-quark mass using background estimates determined from control samples in data. The second approach is based on multivariate analysis techniques that probe the compatibility of the candidate events with the signal. They find  $\sigma_{t+\bar{t}}^{t\text{-channel}} = 67.2 \pm 6.1$  pb, and  $|V_{tb}| = 1.020 \pm 0.046(\text{exp.}) \pm 0.017(\text{th.})$  [117].

At  $\sqrt{s} = 8 \text{ TeV}$ , both experiments repeat and refine their measurements. ATLAS uses  $20.2 \text{ fb}^{-1}$  of data. Total, fiducial and differential cross-sections are measured for both top-quark and top-antiquark production [118]. An artificial neural network is employed to separate signal from background. The fiducial cross-section is measured with a precision of 5.8% (top quark) and 7.8% (top antiquark), respectively. The total cross-sections are measured to be  $\sigma_t^{t\text{-channel}}(tq) = 56.7_{-3.8}^{+4.3}$  pb for top-quark production and  $\sigma_{\bar{t}}^{t\text{-channel}}(\bar{t}q) = 32.9_{-2.7}^{+3.0}$  pb for top-antiquark production, in agreement with the SM prediction. In addition, the ratio of top-quark to top-antiquark production cross-sections is determined to be  $R_t = 1.72 \pm 0.09$ . The total cross-section is used to extract the  $Wtb$  coupling:  $f_{LV} \cdot |V_{tb}| = 1.029 \pm 0.048$ , which corresponds to  $|V_{tb}| > 0.92$  at the 95% confidence level, when assuming  $f_{LV} = 1$  and restricting the range of  $|V_{tb}|$  to the interval  $[0, 1]$ . The differential cross-sections as a function of the transverse momentum and rapidity of both the top quark and the top antiquark are measured at both the parton and particle levels. The transverse momentum and rapidity differential cross-sections of the accompanying jet from the  $t$ -channel scattering are measured at particle level. All measurements are compared to various Monte Carlo predictions as well as to fixed-order QCD calculations where available. The SM predictions provide good descriptions of the data. Using the same dataset, ATLAS probes the  $Wtb$  vertex structure from polarisation observables in  $t$ -channel single-top quark events. The polarisation observables are extracted from asymmetries in angular distributions measured with respect to spin quantisation axes appropriately chosen for the top quark and the  $W$ -boson. The asymmetry measurements are performed at parton level by correcting the observed angular distributions for detector effects and hadronisation after subtracting the background contributions. The measured top-quark and  $W$ -boson polarisation values are in agreement with the Standard Model predictions [119]. CMS uses  $19.7 \text{ fb}^{-1}$  in the electron or muon plus jets channel, exploiting the pseudorapidity distribution of the recoil jet. They find

$\sigma_t = 53.8 \pm 1.5(\text{stat.}) \pm 4.4(\text{syst.})$  pb and  $\sigma_{\bar{t}} = 27.6 \pm 1.3(\text{stat.}) \pm 3.7(\text{syst.})$  pb, resulting in an inclusive  $t$ -channel cross section of  $\sigma_{t+\bar{t}} = 83.6 \pm 2.3(\text{stat.}) \pm 7.4(\text{syst.})$  [120]. They measure a cross section ratio of  $R_t = \sigma_t/\sigma_{\bar{t}} = 1.95 \pm 0.10(\text{stat.}) \pm 0.19(\text{syst.})$ , in agreement with the SM. The CKM matrix element  $V_{tb}$  is extracted to be  $|V_{tb}| = 0.998 \pm 0.038(\text{exp.}) \pm 0.016(\text{th.})$ . Later, CMS has also provided a fiducial cross section measurement for  $t$ -channel single top at  $\sqrt{s} = 8 \text{ TeV}$  with  $19.7 \text{ fb}^{-1}$  of data in signal events with exactly one muon or electron and two jets, one of which is associated with a  $b$ -hadron [121]. The definition of the fiducial phase space follows closely the constraints imposed by event-selection criteria and detector acceptance. The total fiducial cross section is measured using different generators at next-to-leading order plus parton-shower accuracy. Using as reference the aMC@NLO MC predictions in the four-flavour scheme a  $\sigma_t^{\text{fid}} = 3.38 \pm 0.25(\text{exp.}) \pm 0.20(\text{th.})$  pb is obtained, in good agreement with the theory predictions. At 13 TeV, ATLAS uses  $3.2 \text{ fb}^{-1}$  to measurement the  $t$ -channel cross section. Using a binned maximum-likelihood fit to the discriminant distribution of a neural network, the cross-sections are determined to be  $\sigma_t(tq) = 156 \pm 5(\text{stat.}) \pm 27(\text{syst.}) \pm 3(\text{lumi.})$  pb and  $\sigma(\bar{t}q) = 91 \pm 4(\text{stat.}) \pm 18(\text{syst.}) \pm 2(\text{lumi.})$  pb [122]. The cross-section ratio is measured to be  $R_t = \sigma_t/\sigma_{\bar{t}} = 1.72 \pm 0.09(\text{stat.}) \pm 0.18(\text{syst.})$ . All results are in agreement with SM predictions. A measurement of the  $t$ -channel single top-quark cross section is also available at 13 TeV with the CMS detector, corresponding to an integrated luminosity of  $2.2 \text{ fb}^{-1}$ . Fits to the transverse  $W$ -mass and the output of an artificial neural network allow the determination of the background and the signal contribution. The measured cross-section is  $\sigma_t = 238 \pm 13 \pm 29$  pb [123]. The CKM matrix is determined to  $|V_{tb}| = 1.05 \pm 0.07(\text{exp.}) \pm 0.02(\text{th.})$ . Using  $35.9 \text{ fb}^{-1}$  of data, CMS performs measurements of the  $t$ -channel cross sections of single top quarks and antiquarks in the  $t$  channel, and their ratio. Events with one muon or electron are selected, and different categories of jet and  $b$ -jet multiplicity and multivariate discriminators are applied to separate the signal from the background, resulting in  $\sigma_t(tq) = 136 \pm 1(\text{stat}) \pm 22(\text{syst})$  pb and  $\sigma_{\bar{t}}(\bar{t}q) = 82 \pm 1(\text{stat}) \pm 14(\text{syst})$  pb, respectively, and their ratio is  $1.66 \pm 0.02(\text{stat}) \pm 0.05(\text{syst})$ . The results are in agreement with the predictions from the Standard Model [124].

The predicted cross section for  $tW$  process at the LHC  $\sqrt{s} = 7 \text{ TeV}$  is  $15.6 \pm 1.2$  pb [10]. This is of interest because it probes the  $Wtb$  vertex in a different kinematic region than  $s$ - and  $t$ -channel production, and because of its similarity to the associated production of a charged-Higgs boson and a top quark. The signal is difficult to extract because of its similarity to the  $t\bar{t}$  signature. Furthermore, it is difficult to uniquely define because at NLO a subset of diagrams have the same final state as  $t\bar{t}$  and the two interfere [125]. The cross section is calculated using the *diagram removal* technique [126] to define the signal process. In the *diagram removal* technique the interfering diagrams are removed, at the amplitude level, from the signal definition (an alternative technique, *diagram subtraction* removes these diagrams at the cross-section level and yields similar results [126]). These techniques work provided the selection cuts are defined such that the interference effects are small, which is usually the case.

Both, ATLAS and CMS, also provide evidence for the associate  $tW$  production at  $\sqrt{s} = 7 \text{ TeV}$  [127, 128]. ATLAS uses  $2.05 \text{ fb}^{-1}$  in the dilepton plus missing  $E_T$  plus jets channel, where a template fit to the final classifier distributions resulting from boosted decision trees as signal to background separation is performed. The result is incompatible with the background-only hypothesis at the  $3.3\sigma$  ( $3.4\sigma$  expected) level, yielding  $\sigma_{tW} = 16.8 \pm 2.9(\text{stat.}) \pm 4.9(\text{syst.})$  pb and  $|V_{tb}| = 1.03_{-0.19}^{+0.16}$  [127]. CMS uses  $4.9 \text{ fb}^{-1}$  in the dilepton plus jets channel with at least one  $b$ -tag. A multivariate analysis based on kinematic properties is utilized to separate the  $t\bar{t}$  background from the signal. The observed signal has a significance of  $4.0\sigma$  and corresponds to a cross section of  $\sigma_{tW} = 16_{-4}^{+5}$  pb [128].

Both experiments repeated their  $tW$ -analyses at  $\sqrt{s} = 8 \text{ TeV}$ . ATLAS uses  $20.3 \text{ fb}^{-1}$  to select events with two leptons and one central  $b$ -jet. The  $tW$  signal is separated from the backgrounds using boosted decision trees, each of which combines a number

of discriminating variables into one classifier. Production of  $tW$  events is observed with a significance of  $7.7\sigma$ . The cross section is extracted in a profile likelihood fit to the classifier output distributions. The  $tW$  cross section, inclusive of decay modes, is measured to be  $\sigma_{tW} = 23.0 \pm 1.3(\text{stat.})_{-3.5}^{+3.2}(\text{syst.}) \pm 1.1(\text{lumi.})$  pb, yielding a value for the CKM matrix element  $|V_{tb}| = 1.01 \pm 0.10$  and a lower limit of 0.80 at the 95% C.L. [129]. A fiducial cross section is also measured. CMS uses  $12.2 \text{ fb}^{-1}$  in events with two leptons and a jet originated from a  $b$  quark. A multivariate analysis based on kinematic properties is utilized to separate the signal and background. The  $tW$  associate production signal is observed at the level of  $6.1\sigma$ , yielding  $\sigma_{tW} = 23.4 \pm 5.4$  pb and  $|V_{tb}| = 1.03 \pm 0.12(\text{exp.}) \pm 0.04(\text{th.})$  [130]. ATLAS and CMS also combine their measurements and obtain  $\sigma_{tW} = 25.0 \pm 1.4(\text{stat.}) \pm 4.4(\text{syst.}) \pm 0.7(\text{lumi.})$  pb =  $25.0 \pm 4.7$  pb [131], in agreement with the NLO+NNLL expectation. They extract a 95% C.L. lower limit on the CKM matrix element of  $|V_{tb}| > 0.79$ .

At 13 TeV in the  $tW$ -channel, ATLAS uses  $3.2 \text{ fb}^{-1}$  of events with two opposite sign isolated leptons and at least one jet; they are separated into signal and control regions based on their jet multiplicity and the number of jets with  $b$ -tags. Signal is separated from background in two regions using boosted decision trees. The cross section is extracted by fitting templates to the data distributions, and is measured to be  $\sigma_{tW} = 94 \pm 10(\text{stat.})_{-22}^{+28}(\text{syst.}) \pm 2(\text{lumi.})$  pb [132]. The measurement is in agreement with the SM prediction. CMS uses  $36 \text{ fb}^{-1}$  of events with two opposite sign isolated leptons, one tight and one loose jet and one  $b$ -tag. Signal and background is separated in categories depending on the number of jets and the subset of  $b$ -tagged jets using a boosted decision tree. A maximum likelihood fits yields  $\sigma_{tW} = 63.1 \pm 6.6$  pb [133].

The  $s$ -channel production cross section is expected to be  $4.6 \pm 0.3$  pb for  $m_t = 173 \text{ GeV}/c^2$  at  $\sqrt{s} = 7 \text{ TeV}$  [9]. At ATLAS, a search for  $s$ -channel single top quark production is performed in  $0.7 \text{ fb}^{-1}$  at 7 TeV using events containing one lepton, missing transverse energy and two  $b$ -jets. Using a cut-based analysis, an observed (expected) upper limit at 95% C.L. on the  $s$ -channel cross-section of  $\sigma_s < 26.5$  (20.5) pb is obtained [134]. At 8 TeV, ATLAS uses  $20.3 \text{ fb}^{-1}$  of data with one lepton, large missing transverse momentum and exactly two  $b$ -tagged jets. They perform a maximum-likelihood fit of a discriminant based on a Matrix Element Method and optimized in order to separate single top-quark  $s$ -channel events from the main background contributions which are top-quark pair production and  $W$  boson production in association with heavy flavour jets. They find  $\sigma_s = 4.8 \pm 0.8(\text{stat.})_{-1.3}^{+1.6}(\text{syst.})$  pb with a signal significance of 3.2 standard deviations [135], which provides first evidence for  $s$ -channel single-top production at 8 TeV. The signal is extracted through a maximum-likelihood fit to the distribution of a multivariate discriminant defined using boosted decision trees to separate the expected signal contribution from background processes. At 7 TeV and 8 TeV, CMS uses  $5.1 \text{ fb}^{-1}$  and  $19.3 \text{ fb}^{-1}$ , respectively, and analyses leptonic decay modes by performing a maximum likelihood fit to a multivariate discriminant defined using a Boosted Decision Tree, yielding cross sections of  $\sigma_s = 7.1 \pm 8.1$  pb and  $\sigma_s = 13.4 \pm 7.3$  pb, respectively, and a best fit value of  $2.0 \pm 0.9$  for the combined ratio of the measured  $\sigma_s$  values and the ones expected in the Standard Model [136]. The signal significance is 2.5 standard deviations. ATLAS and CMS present the combinations of their single-top-quark production cross-section measurements, using Run-I data corresponding to integrated luminosities of  $1.17$  to  $5.1 \text{ fb}^{-1}$  at  $\sqrt{s} = 7 \text{ TeV}$  and  $12.2$  to  $20.3 \text{ fb}^{-1}$  at  $\sqrt{s} = 8 \text{ TeV}$ . These combinations are performed per centre-of-mass energy and for each production mode:  $t$ -channel,  $tW$ , and  $s$ -channel. The combined  $t$ -channel cross-sections are  $67.5 \pm 5.7$  pb and  $87.7 \pm 5.8$  pb at  $\sqrt{s} = 7$  and 8 TeV, respectively. The combined  $tW$  cross-sections are  $16.3 \pm 4.1$  pb and  $23.1 \pm 3.6$  pb at  $\sqrt{s} = 7$  and 8 TeV, respectively. For the  $s$ -channel cross-section, the combination yields  $4.9 \pm 1.4$  pb at  $\sqrt{s} = 8 \text{ TeV}$ . The square of the magnitude of the CKM matrix element  $V_{tb}$  multiplied by a form factor  $f_{LV}$  is determined for each production mode and centre-of-mass energy, using the ratio of the measured cross-section to its theoretical prediction. All combined measurements are consistent with their corresponding SM pre-

dictions [137]. Both, ATLAS and CMS, also measured the electroweak production of single top-quarks in association with a  $Z$ -boson, see section C.2.4 of this review.

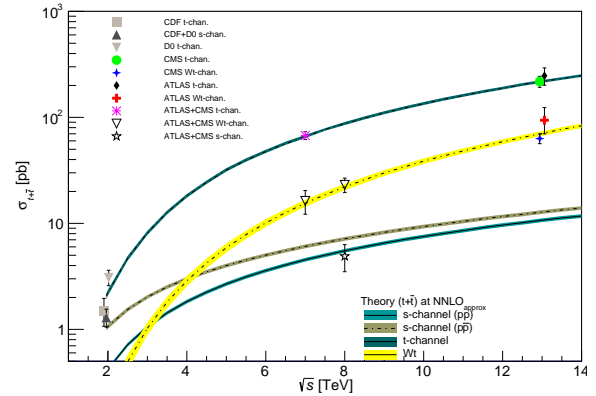


Figure 60.2: Measured and predicted single top production cross sections from Tevatron energies in  $p\bar{p}$  collisions to LHC energies in  $pp$  collisions. Tevatron data points at  $\sqrt{s} = 1.96 \text{ TeV}$  are from Refs. [113, 114]. The ATLAS and CMS data points at  $\sqrt{s} = 7 \text{ TeV}$  are from Refs. [115, 117, 127, 128, 134, 136]. The ones at  $\sqrt{s} = 8 \text{ TeV}$  are from Refs. [118, 120, 129, 130, 135, 136]. The ones at  $\sqrt{s} = 13 \text{ TeV}$  are from Refs. [122, 123]. Theory curves are generated using [6, 9, 10].

Fig. 60.2 provides a summary of all single top cross-section measurements at the Tevatron and the LHC as a function of the center-of-mass energy. All cross-section measurements are very well described by the theory calculation within their uncertainty.

Thanks to the large statistics now available at the LHC, both CMS and ATLAS experiments also performed differential cross-section measurements in single-top  $t$ -channel production [115], [138]. Such measurements are extremely useful as they test our understanding of both QCD and EW top-quark interactions. The CMS collaboration has measured differential single top quark  $t$ -channel production cross sections as functions of the transverse momentum and the absolute value of the rapidity of the top quark. The analysis is performed in the leptonic decay channels of the top quark, with either a muon or an electron in the final state, using data collected with the CMS experiment at the LHC at  $\sqrt{s} = 8 \text{ TeV}$  and corresponding to an integrated luminosity of  $19.7 \text{ fb}^{-1}$ . Neural networks are used to discriminate the signal process from the various background contributions. The results are found to agree with predictions from Monte Carlo generators [138]. Using the same data set and under the assumption that the spin analyzing power of a charged lepton is 100% as predicted in the SM, they are also able to measure the polarization of the top quark  $P_t = 0.82 \pm 0.12(\text{stat.}) \pm 0.32(\text{syst.})$  [139]. At 13 TeV, using  $35.9 \text{ fb}^{-1}$ , CMS measures the differential  $t$ -channel cross sections, for the first time in single-top production, and charge ratios for  $t$ -channel single top quark production [140]. The results are found to be in agreement with SM predictions using various NLO event generators and sets of parton distribution functions. Additionally, the spin asymmetry, sensitive to the top quark polarisation, is determined from the differential distribution of the polarisation angle at parton level to be  $0.439 \pm 0.062$ , in agreement with the SM prediction. This disfavors the results obtained at 8 TeV.

ATLAS has measured the differential  $tW$  cross section in  $36.1 \text{ fb}^{-1}$  at 13 TeV with respect to the energy of the  $b$ -jet, the energy of the system of the two leptons and  $b$ -jet, and the transverse mass or mass of combinations of leptons, the  $b$ -jet and neutrinos [141].

In  $35.9 \text{ fb}^{-1}$ , CMS managed to establish the first evidence for the production of a single top quark in association with a photon [142]. A multivariate discriminant based on topological and kinematic event properties is employed to separate signal from background processes. An excess above the background-only hypothesis is observed, with a significance of 4.4 standard deviations.

## 60.3.1.3 Top-Quark Forward-Backward &amp; Charge Asymmetry

A forward-backward asymmetry in  $t\bar{t}$  production at a  $p\bar{p}$  collider arises starting at order  $\alpha_S^3$  in QCD from the interference between the Born amplitude  $q\bar{q} \rightarrow t\bar{t}$  with 1-loop box production diagrams and between diagrams with initial- and final-state gluon radiation. The asymmetry,  $A_{FB}$ , is defined by

$$A_{FB} = \frac{N(\Delta y > 0) - N(\Delta y < 0)}{N(\Delta y > 0) + N(\Delta y < 0)}, \quad (60.2)$$

where  $\Delta y = y_t - y_{\bar{t}}$  is the rapidity difference between the top- and the anti-top quark. Calculations at  $\alpha_S^3$  predict a measurable  $A_{FB}$  at the Tevatron. The most recent calculations up to order  $\alpha_S^4$ , including electromagnetic and electroweak corrections, yield a predicted asymmetry of  $\approx(9.5 \pm 0.7)\%$  [143]. This is about 10% higher than the previous calculation at NLO [144, 145], and improves the agreement with experiment.

Both CDF and DØ measured asymmetry values in excess of the SM prediction, fueling speculation about exotic production mechanisms (see, for example, [146] and references therein). The first measurement of this asymmetry by DØ in  $0.9 \text{ fb}^{-1}$  [147] found an asymmetry at the detector level of  $(12 \pm 8)\%$ . The first CDF measurement in  $1.9 \text{ fb}^{-1}$  [148] yielded  $(24 \pm 14)\%$  at parton level. Both values were higher, though statistically consistent with the SM expectation. With the addition of more data, the uncertainties have been reduced, and the central values, if somewhat smaller, have remained consistent with the first measurements. At the same time, the improved calculations from theory have increased the predicted asymmetry values to the point where the discrepancy is no longer statistically significant.

CDF and DØ have now combined results using the full Tevatron dataset at  $\sqrt{s} = 1.96 \text{ TeV}$  [149]. Three combined asymmetries are reported:  $A_{FB}^{t\bar{t}}$  as defined in Eq. 2 for fully-reconstructed  $t\bar{t}$  events, a single-lepton asymmetry,  $A_{FB}^{\ell}$  defined as in Eq. 2 but with  $\Delta y$  replaced by the product of the lepton charge and pseudo-rapidity, and a dilepton asymmetry,  $A_{FB}^{\ell\ell}$ , defined as in Eq. 2 but with  $\Delta y$  replaced by  $\Delta\eta$  between the two leptons. The combined results are  $A_{FB}^{t\bar{t}} = 0.128 \pm 0.021 \pm 0.014$ ,  $A_{FB}^{\ell} = 0.073 \pm 0.016 \pm 0.012$ , and  $A_{FB}^{\ell\ell} = 0.108 \pm 0.043 \pm 0.016$ , where the first uncertainty is statistical and the second systematic. These are to be compared to SM predictions at NNLO QCD and NLO electroweak of  $A_{FB}^{t\bar{t}} = 0.095 \pm 0.007$  [143],  $A_{FB}^{\ell} = 0.038 \pm 0.003$ , and  $A_{FB}^{\ell\ell} = 0.048 \pm 0.004$  [145], respectively. Both experiments have also measured differential asymmetries, in bins of  $M_{t\bar{t}}$ ,  $\Delta y$ ,  $q_\ell \times \eta_\ell$ , and  $\Delta\eta_{\ell\ell}$ , with consistent results, though the growth of  $A_{FB}^{t\bar{t}}$  with increasing  $M_{t\bar{t}}$  and  $\Delta y$  appears somewhat more rapid than the SM prediction [149].

At the LHC, where the dominant  $t\bar{t}$  production mechanism is the charge-symmetric gluon-gluon fusion, the measurement is more difficult. For the sub-dominant  $q\bar{q}$  production mechanism, the symmetric  $pp$  collision does not define a forward and backward direction. Instead, the charge asymmetry,  $A_C$ , is defined in terms of a positive versus a negative  $t - \bar{t}$  rapidity difference,  $\Delta y$

$$A_C^{t\bar{t}} = \frac{N(\Delta|y| > 0) - N(\Delta|y| < 0)}{N(\Delta|y| > 0) + N(\Delta|y| < 0)}. \quad (60.3)$$

Both CMS and ATLAS have measured  $A_C$  in the LHC dataset. Using lepton+jets events in  $4.7 \text{ fb}^{-1}$  of data at  $\sqrt{s} = 7 \text{ TeV}$ , ATLAS measures  $A_C^{t\bar{t}} = (0.6 \pm 1.0)\%$  [150]. ATLAS has reported on the same measurement performed at  $\sqrt{s} = 8 \text{ TeV}$  with  $20.3 \text{ fb}^{-1}$  of data, with a result of  $A_C^{t\bar{t}} = (0.009 \pm 0.005)$  [151]. In the dilepton channel at  $\sqrt{s} = 8 \text{ TeV}$ , ATLAS measures [152]  $A_C^{t\bar{t}} = 0.021 \pm 0.016$ , and  $A_C^{\ell\ell} = 0.008 \pm 0.006$  (defined in terms of the  $\Delta\eta$  of the two leptons) in agreement with the SM predictions of  $(1.11 \pm 0.04)\%$  and  $(0.64 \pm 0.03)\%$ , respectively [145]. Using lepton+jets events CMS has measured  $A_C$  at both  $\sqrt{s} = 7$  and  $8 \text{ TeV}$ . They measure  $A_C^{t\bar{t}} = (0.4 \pm 1.5)\%$  and  $A_C^{\ell\ell} = (0.33 \pm 0.26(\text{stat.}) \pm 0.33(\text{sys.}))\%$  in  $5.0 \text{ fb}^{-1}$  at  $\sqrt{s} = 7 \text{ TeV}$  and in  $19.7 \text{ fb}^{-1}$  at  $\sqrt{s} = 8 \text{ TeV}$ , respectively [153, 154]. Both measurements are consistent with the SM expectations of

$A_C^{t\bar{t}} = 1.23 \pm 0.05\%$  at  $\sqrt{s} = 7 \text{ TeV}$  and  $1.11 \pm 0.04\%$  at  $\sqrt{s} = 8 \text{ TeV}$  [145], although the uncertainties are still too large for a precision test. In  $19.5 \text{ fb}^{-1}$  of dilepton events at  $\sqrt{s} = 8 \text{ TeV}$ , CMS measures  $A_C^{t\bar{t}} = 0.011 \pm .013$  and  $A_C^{\ell\ell} = 0.003 \pm 0.007$  [155], consistent with SM expectations [156].

In their 7 and 8 TeV analyses ATLAS and CMS also provide differential measurements as a function of  $M_{t\bar{t}}$  and the transverse momentum  $p_T$  and rapidity  $y$  of the  $t\bar{t}$  system. To reduce model-dependence, the CMS Collaboration has performed a measurement in a reduced fiducial phase space [157], with a result of  $A_C = -0.0035 \pm 0.0072(\text{stat.}) \pm 0.0031(\text{sys.})$ , in agreement with SM expectations.

To specifically address the dependence of the asymmetry on  $M_{t\bar{t}}$ , ATLAS has performed a measurement in boosted  $t\bar{t}$  events [158]. In  $20.3 \text{ fb}^{-1}$  of data at  $\sqrt{s} = 8 \text{ TeV}$ , in events with  $M_{t\bar{t}} > 0.75 \text{ TeV}$ , and  $|\Delta|y| < 2$ , ATLAS measures  $A_C^{t\bar{t}} = (4.2 \pm 3.2)\%$  compared to a NLO SM prediction of  $(1.60 \pm 0.04)\%$ . The measurement is also presented in three bins of  $M_{t\bar{t}}$ , each in agreement, though with large uncertainties, with the SM expectations.

Both ATLAS and CMS have measured asymmetries in the distribution of leptons from  $t\bar{t}$  decays. ATLAS, in  $4.6 \text{ fb}^{-1}$  of  $\sqrt{s} = 7 \text{ TeV}$  data, has measured  $A^{\ell\ell} = (2.4 \pm 1.5(\text{stat.}) \pm 0.9(\text{sys.}))\%$  in dilepton events [159]. Using a neutrino weighting technique in the same dataset to reconstruct the top quarks, ATLAS measures  $A_C = (2.1 \pm 2.5(\text{stat.}) \pm 1.7(\text{sys.}))\%$ . CMS, in  $5.0 \text{ fb}^{-1}$  of  $\sqrt{s} = 7 \text{ TeV}$  data, uses dilepton events to measure  $A_C = (1.0 \pm 1.5(\text{stat.}) \pm 0.6(\text{sys.}))\%$ , where a matrix weighting technique is used to reconstruct the top quarks, and  $A^{\ell\ell} = (0.9 \pm 1.0(\text{stat.}) \pm 0.6(\text{sys.}))\%$  [160]. An earlier result using lepton+jets events from the same CMS dataset found  $A_C = (0.4 \pm 1.0 \pm 1.1)\%$  [153]. Combined results from ATLAS and CMS have recently been released [161]. At  $\sqrt{s} = 7 \text{ TeV}$  the combined result is  $A_C = (0.5 \pm 0.7(\text{stat.}) \pm 0.6(\text{sys.}))\%$ , and at  $\sqrt{s} = 8 \text{ TeV}$  it is  $A_C = (0.55 \pm 0.23 \pm 0.25)\%$ . These results are all consistent, within their large uncertainties, with the SM expectations of  $A^{\ell\ell} = (0.70 \pm 0.03)\%$  and  $A_C = (1.23 \pm 0.05)\%$  [145].

A model-independent comparison of the Tevatron and LHC results is made difficult by the differing  $t\bar{t}$  production mechanisms at work at the two accelerators and by the symmetric nature of the  $pp$  collisions at the LHC. A recent result from the CMS Collaboration [162] in  $35.9 \text{ fb}^{-1}$  of lepton plus jets events at  $\sqrt{s} = 13 \text{ TeV}$ , uses a likelihood analysis in to separate the  $q\bar{q}$  process from production via gluon-gluon and gluon-quark interactions and extract  $A_{FB} = 0.048_{-0.084}^{+0.088}(\text{stat.}) \pm 0.028(\text{sys.})$ . In addition, given a particular model of BSM physics, a comparison can be obtained through the resulting asymmetry predicted by the model at the two machines, see for example [158].

## 60.3.2 Top-Quark Properties

## 60.3.2.1 Top-Quark Mass Measurements

The most precisely studied property of the top quark is its mass. The top-quark mass has been measured in the lepton+jets, the dilepton, and the all-jets channel by all four Tevatron and LHC experiments. The latest and/or most precise results are summarized in Table 60.1. The lepton+jets channel yields the most precise single measurements because of good signal to background ratio (in particular after  $b$ -tagging) and the presence of only a single neutrino in the final state. The momentum of a single neutrino can be reconstructed (up to a quadratic ambiguity) via the missing  $E_T$  measurement and the constraint that the lepton and neutrino momenta reconstruct to the known  $W$  boson mass. In the large data samples available at the LHC, measurements in the dilepton channel can be competitive and certainly complementary to those in the lepton+jets final state.

A large number of techniques have now been applied to measuring the top-quark mass. The original ‘template method’ [163], in which Monte Carlo templates of reconstructed mass distributions are fit to data, has evolved into a precision tool in the lepton+jets channel, where the systematic uncertainty due to the jet energy scale (JES) uncertainty is controlled by a simultaneous, *in situ* fit to the  $W \rightarrow jj$  hypothesis [164]. All the latest measurements in the lepton+jets and the all-jets channels use this technique in one way or another. In  $20.2 \text{ fb}^{-1}$  of data at  $\sqrt{s} = 8 \text{ TeV}$  in the lep-

ton+jets channel, ATLAS achieves a total uncertainty of 0.53% with a statistical component of 0.23% [165]. The measurement is based on a 3-dimensional template fit, determining the top-quark mass, the global jet energy scale and a  $b$ -to-light jet energy scale factor. The most precise CMS result in the lepton+jets channel uses an ideogram method and comes from a so-called ‘hybrid’ approach in which the prior knowledge about the jet energy scale is incorporated as a Gaussian constraint, with a width determined by the uncertainty on the jet energy corrections. In  $19.7 \text{ fb}^{-1}$  of  $\sqrt{s} = 8 \text{ TeV}$  data, CMS achieves a total uncertainty of 0.30% with a statistical component of 0.09% with the hybrid approach [166]. Using this same method, CMS has recently released the first top-mass measurement from  $\sqrt{s} = 13 \text{ TeV}$  data. Using  $35.9 \text{ fb}^{-1}$  of lepton+jets events they measure the top mass with a precision of 0.36%, with a statistical component of 0.05% [167]. The measurements at  $\sqrt{s} = 13 \text{ TeV}$  include, for the first time, an uncertainty due to ‘color reconnection’ [168,169]. In this same dataset, CMS has extracted a top mass from highly boosted top-quark decays by selecting events in which the hadronic-side top decay is reconstructed as a single jet with  $P_T > 400 \text{ GeV}$ . The cross section as a function of jet mass is unfolded at the particle level to extract a top mass with a precision of 1.4% [170].

The template method is complemented by the ‘matrix element’ method. This method was first applied by the DØ Collaboration [171], and is similar to a technique originally suggested by Kondo *et al.* [172] and Dalitz and Goldstein [173]. In the matrix element method a probability for each event is calculated as a function of the top-quark mass, using a LO matrix element for the production and decay of  $t\bar{t}$  pairs. The *in situ* calibration of dijet pairs to the  $W \rightarrow jj$  hypothesis is now also used with the matrix element technique to constrain the jet energy scale uncertainty. In the lepton+jets channel, DØ uses the full Tevatron dataset of  $9.7 \text{ fb}^{-1}$  and yields an uncertainty of about 0.43% [174].

In the dilepton channel, the signal to background is typically very good, but reconstruction of the mass is non-trivial because there are two neutrinos in the final state, yielding a kinematically unconstrained system. A variety of techniques have been developed to handle this. An analytic solution to the problem has been proposed [175], but this has not yet been used in the mass measurement. One of the most precise measurements in the dilepton channel comes from using the invariant mass of the charged lepton and  $b$ -quark system ( $M_{\ell b}$ ), which is sensitive to the top-quark mass and avoids the kinematic difficulties of the two-neutrino final state. In  $4.6 \text{ fb}^{-1}$  of  $\sqrt{s} = 7 \text{ TeV}$  data, ATLAS has measured the top-quark mass in the dilepton channel to a precision of 0.53% using a template fit to the  $M_{\ell b}$  distribution [176]. Using  $19.7 \text{ fb}^{-1}$  of data at  $\sqrt{s} = 8 \text{ TeV}$ , CMS has released [177] a mass measurement in the dilepton channel based on a simultaneous fit to  $M_{\ell b}$  and a transverse-mass-like variable  $M_{T2}$  [178]. The most precise result in this analysis, which comes from a linear combination of fits with the jet energy scale fixed at its nominal value and one that simultaneously determines the top mass and jet energy scale, has a total uncertainty of 0.54%. At the LHC, because of their precision, these techniques have largely displaced a number of earlier techniques in the dilepton channel, though these techniques are still included, and described, in the combined results from CMS, reported in Ref. [166].

In the neutrino weighting technique, used by CDF to analyze the full Run 2 dilepton dataset of  $9.1 \text{ fb}^{-1}$ , a weight is assigned by assuming a top-quark mass value and applying energy-momentum conservation to the top-quark decay, resulting in up to four possible pairs of solutions for the neutrino and anti-neutrino momenta. The missing  $E_T$  calculated in this way is then compared to the observed missing  $E_T$  to assign a weight [182]. The CDF result achieves a precision of 1.8% using a combination of neutrino weighting and an ‘alternative mass’, which is insensitive to the jet energy scale [183]. The alternative mass depends on the angles between the leptons and the leading jets and the lepton four-momenta.

In the all-jets channel there is no ambiguity due to neutrino momenta, but the signal to background is significantly poorer due to the severe QCD multijets background. The emphasis therefore has been on background modeling, and reduction through event

selection. The most recent measurement in the all-jets channel, by CMS in  $35.9 \text{ fb}^{-1}$  of  $\sqrt{s} = 13 \text{ TeV}$  data [179], uses an ideogram method and a 2-dimensional simultaneous fit for  $m_t$  and the jet energy scale to extract the top-quark mass and achieves a precision of 0.36%. A recent measurement from ATLAS [180] uses a template fit to the ratio of three-jet ( $m_t$ ) to two-jet ( $M_W$ ) mass in the all-hadronic channel, the two-jet denominator provides an *in situ* fit to the  $W \rightarrow jj$  hypothesis. In  $20.2 \text{ fb}^{-1}$  of data at  $\sqrt{s} = 8 \text{ TeV}$ , the result has a precision of 0.65%. A measurement from CDF in  $9.3 \text{ fb}^{-1}$  uses a two-dimensional template fit and achieves a precision of 1.1% [184].

The CMS Collaboration has, for the first time, extracted a top-quark mass measurement from single-top events [185], something not previously done because of the poor signal to background ratio. The mass is extracted from the invariant mass of the muon, bottom quark, and missing transverse energy. In  $19.7 \text{ fb}^{-1}$  of data at  $\sqrt{s} = 8 \text{ TeV}$ , a precision of 0.71% is achieved.

A dominant systematic uncertainty in these methods is the understanding of the jet energy scale, and so several techniques have been developed that have little sensitivity to the jet energy scale uncertainty. In addition to Reference [183] mentioned above, these include the measurement of the top-quark mass using the following techniques: Fitting of the lepton  $p_T$  spectrum of candidate events [186]; fitting of the transverse decay length of the  $b$ -jet ( $L_{xy}$ ) [187]; fitting the invariant mass of a lepton from the  $W$ -decay and a muon from the semileptonic  $b$  decay [188], kinematic properties of secondary vertices from  $b$ -quark fragmentation [189], the invariant mass of the  $J/\psi + \ell$  system in events in which a  $b$ -quark fragments to a  $J/\psi$  particle [190], fitting the  $b$ -jet energy peak [191], and dilepton kinematics in  $e\mu$  events [192].

Several measurements have now been made in which the top-quark mass is extracted from the measured  $t\bar{t}$  cross section using the theoretical relationship between the mass and the production cross section. These determinations make use of predictions calculated at higher orders, where the top mass enters as an input parameter defined in a given scheme. At variance with the usual methods, which involve the kinematic properties of the final states and therefore the pole mass, this approach can also directly determine a short-distance mass, such as the  $\overline{\text{MS}}$  mass [193]. With an alternative method ATLAS recently extracted the top-quark pole mass using  $t\bar{t}$  events with at least one additional jet, basing the measurement on the relationship between the differential rate of gluon radiation and the mass of the quark [194]. A similar analysis by CMS used the differential cross section as a function of the invariant mass of the  $t\bar{t}$  system and the leading jet not associated with the top decays [195].

Each of the experiments has produced a measurement combining its various results. The combined measurement from CMS with up to  $19.7 \text{ fb}^{-1}$  of data achieves statistical and systematic uncertainties of 0.08% and 0.27%, respectively [166]. The combined measurement from ATLAS, with up to  $20.3 \text{ fb}^{-1}$  yields statistical and systematic uncertainties of 0.14% and 0.24%, respectively [165]. CDF has combined measurements with up to  $9.3 \text{ fb}^{-1}$  [196] and achieves a statistical precision of 0.33% and a systematic uncertainty of 0.43%. DØ achieves a 0.33% statistical+JES and a 0.28% systematic uncertainty by combining results in  $9.7 \text{ fb}^{-1}$  [197].

Combined measurements from the Tevatron experiments and from the LHC experiments take into account the correlations between different measurements from a single experiment and between measurements from different experiments. The Tevatron average [181], using up to  $9.7 \text{ fb}^{-1}$  of data, now has a precision of 0.37%. The LHC combination, using up to  $4.9 \text{ fb}^{-1}$  of data, has a precision of 0.56% [198], where more work on systematic uncertainties is required. A Tevatron-LHC combination has been released, combining the results of all four experiments, using the full Tevatron dataset and the  $\sqrt{s} = 7 \text{ TeV}$  LHC data, with a resulting precision of 0.44% [3].

The direct measurements of the top-quark mass, such as those shown in Table 60.1, correspond to the parameter used in the Monte Carlo generators, which is generally agreed to be the pole mass. The relation between the pole mass and short-distance

**Table 60.1:** Measurements of top-quark mass from Tevatron and LHC.  $\int \mathcal{L} dt$  is given in  $\text{fb}^{-1}$ . The results are a selection of both published and preliminary (not yet submitted for publication as of September 2019) measurements. For a complete set of published results see the Listings. Statistical uncertainties are listed first, followed by systematic uncertainties.

$m_t$ (GeV/ $c^2$ )	Source	$\int \mathcal{L} dt$	Ref.	Channel
$172.08 \pm 0.25 \pm 0.41$	ATLAS	20.2	[165]	$\ell$ +jets+ $\ell\ell$ +All jets
$172.44 \pm 0.13 \pm 0.47$	CMS	19.7	[166]	$\ell$ +jets+ $\ell\ell$ +All jets
$172.35 \pm 0.16 \pm 0.48$	CMS	19.7	[166]	$\ell$ +jets
$172.34 \pm 0.20 \pm 0.70$	CMS	35.9	[179]	$\ell\ell$
$173.72 \pm 0.55 \pm 1.01$	ATLAS	20.2	[180]	All jets
$172.25 \pm 0.08 \pm 0.62$	CMS	35.9	[167]	$\ell$ +jets
$174.30 \pm 0.35 \pm 0.54$	CDF,DØ (I+II)	$\leq 9.7$	[181]	publ. or prelim.
$173.34 \pm 0.27 \pm 0.71$	Tevatron+LHC	$\leq 8.7 + \leq 4.9$	[3]	publ. or prelim.

masses, such as  $\overline{M\overline{S}}$ , is affected by non-perturbative effects. Recent calculations evaluate the size of this ambiguity to be below 250 MeV and therefore still smaller than the current measurement uncertainty [199, 200].

As a result of renormalization at higher-orders in perturbation theory, the top quark mass depends on the scale at which it is evaluated. The CMS collaboration has made the first measurement of the so-called running of the top-quark mass in the  $\overline{M\overline{S}}$  scheme [201]. The running mass is extracted from a measurement of the differential cross section as a function of the  $t\bar{t}$  invariant mass, unfolded back to the parton level, in  $e\mu$  final states. The running mass varies by about 15% from  $M_{t\bar{t}} = 400$  GeV to  $M_{t\bar{t}} \approx 1$  TeV, in good agreement with the renormalization group calculation at one-loop level. Compared to the hypothesis of no running, the significance of the measured running is  $2.6\sigma$ .

With the discovery of a Higgs boson at the LHC with a mass of about 125 GeV/ $c^2$  [202, 203], the precision measurement of the top-quark mass takes a central role in the question of the stability of the electroweak vacuum because top-quark radiative corrections tend to drive the Higgs quartic coupling,  $\lambda$ , negative, potentially leading to an unstable vacuum. A recent calculation at NNLO [204] leads to the conclusion of vacuum stability for a Higgs mass satisfying  $M_H \geq 129.4 \pm 5.6$  GeV/ $c^2$  [205]. Given the uncertainty, a Higgs mass of 125 GeV/ $c^2$  satisfies the limit, but the central values of the Higgs and top-quark masses put the electroweak vacuum squarely in the metastable region. The uncertainty is dominated by the precision of the top-quark mass measurement and its interpretation as the pole mass. For more details, see the Higgs boson review in this volume.

As a test of the CPT-symmetry, the mass difference of top- and antitop-quarks  $\Delta m_t = m_t - m_{\bar{t}}$ , which is expected to be zero, can be measured. CDF measures the mass difference in  $8.7 \text{ fb}^{-1}$  of 1.96 TeV data in the lepton+jets channel using a template method to find  $\Delta m_t = -1.95 \pm 1.11(\text{stat.}) \pm 0.59(\text{syst.})$  GeV/ $c^2$  [206] while DØ uses  $3.6 \text{ fb}^{-1}$  of lepton+jets events and the matrix element method with at least one  $b$ -tag. They find  $\Delta m_t = 0.8 \pm 1.8(\text{stat.}) \pm 0.5(\text{syst.})$  GeV/ $c^2$  [207]. In  $4.7 \text{ fb}^{-1}$  of 7 TeV data, ATLAS measures the mass difference in lepton+jets events with a double  $b$ -tag requirement and hence very low background to find  $\Delta m_t = 0.67 \pm 0.61(\text{stat.}) \pm 0.41(\text{syst.})$  GeV/ $c^2$  [208]. CMS measures the top-quark mass difference in  $5 \text{ fb}^{-1}$  of 7 TeV data in the lepton+jets channel and finds  $\Delta m_t = -0.44 \pm 0.46(\text{stat.}) \pm 0.27(\text{syst.})$  GeV/ $c^2$  [209]. They repeat this measurement with  $19.6 \text{ fb}^{-1}$  of 8 TeV data to find  $\Delta m_t = -0.15 \pm 0.19(\text{stat.}) \pm 0.09(\text{syst.})$  GeV/ $c^2$  [210]. All measurements are consistent with the SM expectation.

### 60.3.2.2 Top-Quark Spin Correlations, Polarization, and Width

One of the unique features of the top quark is that it decays before its spin can be flipped by the strong interaction. Thus the top-quark polarization is directly observable via the angular distribution of its decay products and it is possible to define and measure observables sensitive to the top-quark spin and its production mechanism. Although the top- and antitop-quarks produced by strong interactions in hadron collisions are essentially unpolarized, the spins of  $t$  and  $\bar{t}$  are correlated. For QCD production at threshold, the  $t\bar{t}$  system is produced in a  $^3S_1$  state with parallel spins for  $q\bar{q}$  annihilation or in a  $^1S_0$  state with antiparal-

lel spins for gluon-gluon fusion. The situations at the Tevatron, where the production is primarily from  $q\bar{q}$  annihilation, and at the LHC, where the production is primarily from gluon-gluon fusion, are therefore somewhat complementary. However, at the LHC production of  $t\bar{t}$  pairs at large invariant mass occurs primarily via fusion of gluons with opposite helicities, and the  $t\bar{t}$  pairs so produced have parallel spins as in production at the Tevatron via  $q\bar{q}$  annihilation. The direction of the top-quark spin is 100% correlated to the angular distributions of the down-type fermion (charged leptons or  $d$ -type quarks) in the decay. The joint angular distribution [211–213]

$$\frac{1}{\sigma} \frac{d^2\sigma}{d(\cos\theta_+)d(\cos\theta_-)} = \frac{1}{4}(1 + B_+ \cos\theta_+ + B_- \cos\theta_- + \kappa \cdot \cos\theta_+ \cdot \cos\theta_-), \quad (60.4)$$

where  $\theta_+$  and  $\theta_-$  are the angles of the daughters in the top-quark rest frame with respect to a particular spin quantization axis (assumed here to be the same for  $\theta_+$  and  $\theta_-$ ), is a very sensitive observable. The maximum value for  $\kappa$ , 0.782 at NLO at the Tevatron [214], is found in the off-diagonal basis [211], while at the LHC the value at NLO is 0.326 in the helicity basis [214]. The coefficients  $B_+$  and  $B_-$  are near zero in the SM because the top quarks are unpolarized in  $t\bar{t}$  production. In place of  $\kappa$ ,  $A\alpha_+\alpha_-$  is often used, where  $\alpha_i$  is the spin analyzing power, and  $A$  is the spin correlation coefficient, defined as

$$A = \frac{N(\uparrow\uparrow) + N(\downarrow\downarrow) - N(\uparrow\downarrow) - N(\downarrow\uparrow)}{N(\uparrow\uparrow) + N(\downarrow\downarrow) + N(\uparrow\downarrow) + N(\downarrow\uparrow)}, \quad (60.5)$$

where the first arrow represents the direction of the top-quark spin along a chosen quantization axis, and the second arrow represents the same for the antitop-quark. The spin analyzing power  $\alpha_i$  is +0.998 for positively charged leptons, -0.966 for down-type quarks from  $W$  decays, and -0.393 for bottom quarks [215]. The sign of  $\alpha$  flips for the respective antiparticles. The spin correlation could be modified by a new  $t\bar{t}$  production mechanism such as through a  $Z'$  boson, Kaluza-Klein gluons, a dark-matter mediator, or a Higgs boson.

The experiments typically use a Monte Carlo to provide templates for the measured distributions, or alternatively a matrix-element technique, and fit a parameter  $f$ , representing the fraction of events with the expected Standard Model correlation, with  $(1-f)$  the fraction with no correlation. The correlation coefficient is extracted via  $A_{\text{meas}} = f \cdot A_{\text{SM}}$ . A ‘fraction’  $f > 1$  means that the measured correlation coefficient is larger than the Standard Model expectation.

CDF used  $5.1 \text{ fb}^{-1}$  in the dilepton channel to measure the correlation coefficient in the beam axis [216]. The measurement was made using the expected distributions of  $(\cos\theta_+, \cos\theta_-)$  and  $(\cos\theta_b, \cos\theta_{\bar{b}})$  of the charged leptons or the  $b$ -quarks in the  $t\bar{t}$  signal and background templates to calculate a likelihood of observed reconstructed distributions as a function of assumed  $\kappa$ . They determined the 68% confidence interval for the correlation coefficient  $\kappa$  as  $-0.52 < \kappa < 0.61$  or  $\kappa = 0.04 \pm 0.56$  assuming  $m_t = 172.5$  GeV/ $c^2$ .

CDF also analyzed lepton+jets events in  $5.3 \text{ fb}^{-1}$  [217] assuming  $m_t = 172.5$  GeV/ $c^2$ . They form three separate tem-

plates - the same-spin template, the opposite-spin template, and the background template for the 2-dimensional distributions in  $\cos(\theta_l)\cos(\theta_d)$  vs.  $\cos(\theta_l)\cos(\theta_b)$ . The fit to the data in the helicity basis returns an opposite helicity fraction of  $F_{OH} = 0.74 \pm 0.24(stat.) \pm 0.11(syst.)$ . Converting this to the spin correlation coefficient yields  $\kappa_{helicity} = 0.48 \pm 0.48(stat.) \pm 0.22(syst.)$ . In the beamline basis, they find an opposite spin fraction of  $F_{OS} = 0.86 \pm 0.32(stat.) \pm 0.13(syst.)$  which can be converted into a correlation coefficient of  $\kappa_{beam} = 0.72 \pm 0.64(stat.) \pm 0.26(syst.)$ .

$D\bar{O}$  performed a measurement of the ratio  $f$  of events with correlated  $t$  and  $\bar{t}$  spins to the total number of  $t\bar{t}$  events. Combining dilepton and lepton plus jets events, and using a matrix-element technique in  $9.7 \text{ fb}^{-1}$  of Tevatron data,  $D\bar{O}$  measures  $f = 1.16 \pm 0.21$ , corresponding to  $A_{exp.} = 0.89 \pm 0.22(stat. + syst.)$  in the off-diagonal basis [218].

In Ref. [219]  $D\bar{O}$  presents a measurement of top-quark polarization in  $t\bar{t}$  production at the Tevatron. In  $9.7 \text{ fb}^{-1}$  of  $p\bar{p}$  collisions,  $D\bar{O}$  uses lepton angular distributions in lepton+jets events to measure polarization in the beam, helicity, and transverse bases. The measurements are, respectively,  $0.081 \pm 0.048$ ,  $-0.102 \pm 0.061$  and,  $0.040 \pm 0.035$ , where the beam-basis result is a combination with an earlier  $D\bar{O}$  result in dilepton events [220]. These results are all consistent near-zero polarization, as predicted in the SM.

Spin correlations have been conclusively measured at the LHC by both the ATLAS and CMS collaborations. In the dominant gluon fusion production mode for  $t\bar{t}$  pairs at the LHC, the angular distribution between the two leptons in  $t\bar{t}$  decays to dileptons is sensitive to the degree of spin correlation [221].

Measurements have been made at 7, 8, and now 13 TeV. While there is some interest in the  $\sqrt{s}$  dependence of the correlations as a test of the production mechanism ( $q\bar{q}$  vs gluon-gluon and possible sensitivity to new physics) the earlier measurements at 7 and 8 TeV [222–227] had relatively large uncertainties and have now been overtaken by the high-statistics 13 TeV measurements, which we review here.

The most recent result from ATLAS, in  $36.1 \text{ fb}^{-1}$  at  $\sqrt{s} = 13 \text{ TeV}$ , uses  $\Delta\phi$ , the azimuthal angle between the two charged leptons in  $e\mu$  events in an analysis that also measures the differential cross sections in  $\Delta\phi$  and  $\Delta\eta$  between the two leptons [228]. The result, measured by comparison with NLO Monte Carlo generators, is  $f = 1.249 \pm 0.024 \pm 0.061 \pm 0.040$ , where the uncertainties are statistical, systematic, and theoretical, is again greater than 1.0. Whereas the previous results were statistically consistent with the Standard Model expectation of 1.0, this result is inconsistent at the level of  $3.2\sigma$ . The NLO generators are NLO in QCD only (and only at the production level). Including electroweak couplings produces an expected Standard Model distribution consistent with the data, but results in a large scale uncertainty, giving  $f = 1.03 \pm 0.13$ .

In  $35.9 \text{ fb}^{-1}$  of data at  $\sqrt{s} = 13 \text{ TeV}$ , CMS has measured spin correlations in dilepton events using  $\Delta\phi$  and found  $f = 1.05 \pm 0.03 \pm 0.08^{+0.09}_{-0.12}$  [229], where the uncertainties are statistical, systematic, and theoretical. The correlation is also measured using the coefficient  $\kappa$  in Eq. 60.4 (called  $-C_{ij}$  in Reference [229]) using three orthogonal spin quantization axes defined in Ref. [230]. All results are consistent with  $f = 1$ . Measurements of the coefficients  $B_i$  in Eq. 60.4 in this analysis, which are expected to be nearly zero in the SM, yield  $B_+ = 0.005 \pm 0.023$  and  $B_- = 0.007 \pm 0.023$ , consistent with the SM predictions at NLO of  $0.0040^{+0.0017}_{-0.0012}$  [230]. These results are part of a complete study of the top-quark spin density matrix at  $\sqrt{s} = 13 \text{ TeV}$ , through the measurement of the coefficients of Eq. 60.4.

In a similar ATLAS measurement at  $\sqrt{s} = 8 \text{ TeV}$  [231], the spin-correlation coefficient  $\kappa$  is measured in the helicity basis to be  $\kappa = 0.296 \pm 0.093$  in good agreement with the SM expectation of 0.318 (corresponding to a central value of  $f$  of 0.931). The polarization coefficients,  $B$ , in Eq. 60.4 are measured, also in the helicity basis, to be  $B_+ = -0.044 \pm 0.038$  and  $B_- = -0.064 \pm 0.040$ , consistent with the SM predictions of  $0.0030 \pm 0.0010$  and  $0.0034 \pm 0.00104$ , respectively.

Observation of top-quark spin correlations requires a top-quark lifetime less than the spin decorrelation timescale [232]. The top-quark width, inversely proportional to its lifetime, is expected

to be of order  $1 \text{ GeV}/c^2$  (Eq. 1). Early measurements made at CDF [233] and CMS [234] established confidence-level intervals for the width, but did not have the sensitivity to make a direct measurement.

The first direct measurement comes from an ATLAS analysis that directly fits reconstructed lepton+jets events in  $20.2 \text{ fb}^{-1}$  of data at  $\sqrt{s} = 8 \text{ TeV}$ . They find  $\Gamma_t = 1.76 \pm 0.33^{+0.79}_{-0.68} \text{ GeV}/c^2$  [235]. A more recent measurement from ATLAS with  $139 \text{ fb}^{-1}$  of data at  $\sqrt{s} = 13 \text{ TeV}$  [236], uses a template fit to the lepton- $b$ -quark invariant mass in dilepton final states. The result,  $\Gamma_t = (1.9 \pm 0.5) \text{ GeV}/c^2$ , is the most precise measurement to date.

The total width of the top-quark can also be determined from the partial decay width  $\Gamma(t \rightarrow Wb)$  and the branching fraction  $B(t \rightarrow Wb)$ .  $D\bar{O}$  obtains  $\Gamma(t \rightarrow Wb)$  from the measured  $t$ -channel cross section for single top-quark production in  $5.4 \text{ fb}^{-1}$ , and  $B(t \rightarrow Wb)$  is extracted from a measurement of the ratio  $R = B(t \rightarrow Wb)/B(t \rightarrow Wq)$  in  $t\bar{t}$  events in lepton+jets channels with 0, 1 and 2  $b$ -tags. Assuming  $B(t \rightarrow Wq) = 1$ , where  $q$  includes any kinematically accessible quark, the result is:  $\Gamma_t = 2.00^{+0.47}_{-0.43} \text{ GeV}/c^2$  which translates to a top-quark lifetime of  $\tau_t = (3.29^{+0.90}_{-0.63}) \times 10^{-25} \text{ s}$ . Assuming a high mass fourth generation  $b'$  quark and unitarity of the four-generation quark-mixing matrix, they set the first upper limit on  $|V_{tb'}| < 0.59$  at 95% C.L. [237]. A similar analysis has been performed by CMS in  $19.7 \text{ fb}^{-1}$  of  $\sqrt{s} = 8 \text{ TeV}$  data. It provides a better determination of the total width with respect to the measurement by  $D\bar{O}$  giving  $\Gamma_t = 1.36 \pm 0.02(stat.)^{+0.14}_{-0.11}(syst.) \text{ GeV}/c^2$  [71].

### 60.3.2.3 $W$ -Boson Helicity in Top-Quark Decay

The Standard Model dictates that the top quark has the same vector-minus-axial-vector ( $V - A$ ) charged-current weak interactions  $\left(-i\frac{g}{\sqrt{2}}V_{tb}\gamma^\mu\frac{1}{2}(1 - \gamma_5)\right)$  as all the other fermions. In the SM, the fraction of top-quark decays to longitudinally polarized  $W$  bosons is proportional to its Yukawa coupling and hence enhanced with respect to the weak coupling. It is expected to be [238]  $\mathcal{F}_0^{\text{SM}} \approx x/(1+x)$ ,  $x = m_t^2/2M_W^2$  ( $\mathcal{F}_0^{\text{SM}} \sim 70\%$  for  $m_t = 175 \text{ GeV}/c^2$ ). Fractions of left-handed, right-handed, or longitudinal  $W$  bosons are denoted as  $\mathcal{F}_-$ ,  $\mathcal{F}_+$ , and  $\mathcal{F}_0$  respectively. In the SM,  $\mathcal{F}_-$  is expected to be  $\approx 30\%$  and  $\mathcal{F}_+ \approx 0\%$ . Predictions for the  $W$  polarization fractions at NNLO in QCD are available [239].

The Tevatron and the LHC experiments use various techniques to measure the helicity of the  $W$  boson in top-quark decays, in both the lepton+jets and in dilepton channels in  $t\bar{t}$  production.

The first method uses a kinematic fit, similar to that used in the lepton+jets mass analyses, but with the top-quark mass constrained to a fixed value, to improve the reconstruction of final-state observables, and render the under-constrained dilepton channel solvable. Alternatively, in the dilepton channel the final-state momenta can also be obtained through an algebraic solution of the kinematics. The distribution of the helicity angle ( $\cos\theta^*$ ) between the lepton and the  $b$  quark in the  $W$  rest frame provides the most direct measure of the  $W$  helicity. In a simplified version of this approach, the  $\cos\theta^*$  distribution is reduced to a forward-backward asymmetry.

The second method ( $p_T^\ell$ ) uses the different lepton  $p_T$  spectra from longitudinally or transversely polarized  $W$ -decays to determine the relative contributions.

A third method uses the invariant mass of the lepton and the  $b$ -quark in top-quark decays ( $M_{\ell b}^2$ ) as an observable, which is directly related to  $\cos\theta^*$ .

At the LHC, top-quark pairs in the dilepton channels are reconstructed by solving a set of six independent kinematic equations in the missing transverse energy in  $x$ - and in  $y$ -direction, two  $W$ -masses, and the two top/antitop-quark masses. In addition, the two jets with the largest  $p_T$  in the event are interpreted as  $b$ -jets. The pairing of the jets to the charged leptons is based on the minimization of the sum of invariant masses  $M_{min}$ . Simulations show that this criterion gives the correct pairing in 68% of the events.

Finally, the Matrix Element Method (MEM) has also been used [172], in which a likelihood is formed from a product of event probabilities calculated from the MEM for a given set of measured



kinematic variables and assumed  $W$ -helicity fractions.

The results of recent CDF,  $D\bar{O}$ , ATLAS, and CMS analyses are summarized in Table 60.2. The datasets are now large enough to allow for a simultaneous fit of  $\mathcal{F}_0$ ,  $\mathcal{F}_-$  and  $\mathcal{F}_+$ , which we denote by ‘3-param’ or  $\mathcal{F}_0$  and  $\mathcal{F}_+$ , which we denote by ‘2-param’ in the table. Results with either  $\mathcal{F}_0$  or  $\mathcal{F}_+$  fixed at its SM value are denoted ‘1-param’. For the simultaneous fits, the correlation coefficient between the two values is about  $-0.8$ . A complete set of published results can be found in the Listings. All results are in agreement with the SM expectation.

CDF and  $D\bar{O}$  combined their results based on  $2.7 - 5.4 \text{ fb}^{-1}$  [240] for a top-quark mass of  $172.5 \text{ GeV}/c^2$ . ATLAS presents results from  $1.04 \text{ fb}^{-1}$  of  $\sqrt{s} = 7 \text{ TeV}$  data using a template method for the  $\cos\theta^*$  distribution and angular asymmetries from the unfolded  $\cos\theta^*$  distribution in the lepton+jets and the dilepton channel [241]. CMS performs a similar measurement based on template fits to the  $\cos\theta^*$  distribution with  $5.0 \text{ fb}^{-1}$  of  $7 \text{ TeV}$  data in the lepton+jets final state [242]. As the polarization of the  $W$  bosons in top-quark decays is sensitive to the  $Wtb$  vertex Lorentz structure and anomalous couplings, both experiments also derive limits on anomalous contributions to the  $Wtb$  couplings. Recently, both experiments also combined their results from  $7 \text{ TeV}$  data to obtain values on the helicity fractions as well as limits on anomalous couplings [243].

At  $8 \text{ TeV}$ , ATLAS came out with a measurement of the  $W$ -helicity fractions in  $20.2 \text{ fb}^{-1}$  in lepton+jets events with at least one  $b$ -tag [244]. Using  $19.8 \text{ fb}^{-1}$  of  $8 \text{ TeV}$  data, CMS measured the  $W$ -helicity in lepton + 4 jet events with two  $b$ -tags [245]. In  $t\bar{t}$  events with two opposite-sign leptons (electron or muon) in the final state in this dataset, CMS applied six kinematic constraints on the kinematics of the produced particles [246]. Also, using the same dataset a first measurement of the  $W$ -boson helicity in top-quark decays was made in electroweak single top production [247], yielding similarly precise and consistent results.

#### 60.3.2.4 Top-Quark Electroweak Charges and Couplings

The top quark is the only quark whose electric charge has not been measured through production at threshold in  $e^+e^-$  collisions. Furthermore, it is the only quark whose electromagnetic coupling has not been observed and studied until recently. Since the CDF and  $D\bar{O}$  analyses on top-quark production did not associate the  $b$ ,  $\bar{b}$ , and  $W^\pm$  uniquely to the top or antitop, decays such as  $t \rightarrow W^+\bar{b}, \bar{t} \rightarrow W^-b$  were not excluded. A charge  $4/3$  quark of this kind is consistent with current electroweak precision data. The  $Z \rightarrow \ell^+\ell^-$  and  $Z \rightarrow b\bar{b}$  data, in particular the discrepancy between  $A_{LR}$  from SLC at SLAC and  $A_{FB}^{0,b}$  of  $b$ -quarks and  $A_{FB}^{0,\ell}$  of leptons from LEP at CERN, can be fitted with a top quark of mass  $m_t = 270 \text{ GeV}/c^2$ , provided that the right-handed  $b$  quark mixes with the isospin  $+1/2$  component of an exotic doublet of charge  $-1/3$  and  $-4/3$  quarks,  $(Q_1, Q_4)_R$  [249, 250]. Also the third component of the top quark’s weak isospin has not been measured so far.

$D\bar{O}$  studied the top-quark charge in double-tagged lepton+jets events, CDF did it in single tagged lepton+jets and dilepton events. Assuming the top- and antitop-quarks have equal but opposite electric charge, then reconstructing the charge of the  $b$ -quark through jet charge discrimination techniques, the  $|Q_{top}| = 4/3$  and  $|Q_{top}| = 2/3$  scenarios can be differentiated. For the exotic model of Chang *et al.* [250] with a top-quark charge  $|Q_{top}| = 4/3$ , CDF excluded the model at 99% C.L. [251] in  $5.6 \text{ fb}^{-1}$ , while  $D\bar{O}$  excluded the model at a significance greater than 5 standard deviations using  $5.3 \text{ fb}^{-1}$  and set an upper limit of 0.46 on the fraction of such quarks in the selected sample [252]. These results indicate that the observed particle is indeed consistent with being a SM  $|Q| = 2/3$  quark.

In  $2.05 \text{ fb}^{-1}$  at  $\sqrt{s} = 7 \text{ TeV}$ , ATLAS performed a similar analysis, reconstructing the  $b$ -quark charge either via a jet-charge technique or via the lepton charge in soft muon decays in combination with a kinematic likelihood fit. They measure the top-quark charge to be  $0.64 \pm 0.02(stat.) \pm 0.08(sys.)$  from the charges of the top-quark decay products in single lepton  $t\bar{t}$  events, and hence exclude the exotic scenario with charge  $-4/3$  at more than  $8\sigma$  [253].

In  $4.6 \text{ fb}^{-1}$  at  $\sqrt{s} = 7 \text{ TeV}$ , CMS discriminates between the SM

and the exotic top-quark charge scenario in the muon+jets final states in  $t\bar{t}$  events. They exploit the charge correlation between high- $p_t$  muons from  $W$ -boson decays and soft muons from  $B$ -hadron decays in  $b$ -jets. Using an asymmetry technique, where  $A = -1$  represent the exotic  $Q = -4/3$  scenario and  $A = +1$  the SM  $Q = +2/3$  scenario, they find  $A_{meas} = 0.97 \pm 0.12(stat.) \pm 0.31(sys.)$ , which agrees with the Standard Model expectation and excludes the exotic scenario at 99.9% C.L. [254].

The electromagnetic or the weak coupling of the top quark can be probed directly by investigating  $t\bar{t}$  events with an additional gauge boson, such as  $t\bar{t}\gamma$ ,  $t\bar{t}W$ , and  $t\bar{t}Z$  events. The corresponding coupling can be extracted from the corresponding cross section or extracted from effective field theory (EFT) fits to various measured distributions and differential cross sections.

CDF performed a search for events containing a lepton, a photon, significant missing transverse momentum, and a jet identified as containing a  $b$ -quark and at least three jets and large total transverse energy in  $6.0 \text{ fb}^{-1}$ . They reported evidence for the observation of  $t\bar{t}\gamma$  production with a cross section  $\sigma_{t\bar{t}\gamma} = 0.18 \pm 0.08 \text{ pb}$  and a ratio of  $\sigma_{t\bar{t}\gamma}/\sigma_{t\bar{t}} = 0.024 \pm 0.009$  [255].

ATLAS performed a first measurement of the  $t\bar{t}\gamma$  cross section in pp collisions at  $\sqrt{s} = 7 \text{ TeV}$  using  $4.6 \text{ fb}^{-1}$  of data. Events are selected that contain a large transverse momentum electron or muon and a large transverse momentum photon, yielding 140 and 222 events in the electron and muon samples, respectively. The production of  $t\bar{t}\gamma$  events was observed with a significance of 5.3 standard deviations. The resulting cross section times branching ratio into the single lepton channel for  $t\bar{t}\gamma$  production with a photon with transverse momentum above 20 GeV is  $\sigma^{fid.}(t\bar{t}\gamma) \times BR = 63 \pm 8(stat.)_{-13}^{+17}(sys.) \pm 1(lumi.) \text{ pb}$  per lepton flavour [256], which is consistent with leading-order theoretical calculations.

At  $8 \text{ TeV}$ , ATLAS has used  $20.2 \text{ fb}^{-1}$  of data to measure the  $t\bar{t}\gamma$  cross section with a photon above 15 GeV and  $|\eta| < 2.37$ . The fiducial cross section is measured to be  $139 \pm 18 \text{ fb}$  [257], in good agreement with the NLO prediction [258]. Using  $19.7 \text{ fb}^{-1}$  of data at  $8 \text{ TeV}$ , CMS performed a similar measurement of the  $t\bar{t}\gamma$  production cross section in the lepton+jets decay mode with a photon transverse momentum above 25 GeV and  $|\eta| < 1.44$ . They obtain a normalized cross section  $\mathcal{R} = \sigma_{t\bar{t}\gamma}/\sigma_{t\bar{t}} = (5.7 \pm 1.8) \times 10^{-4}$  in  $e$ -jets and  $(4.7 \pm 1.3) \times 10^{-4}$  in  $\mu$ -jets. The fiducial  $t\bar{t}\gamma$  cross section is obtained by multiplying by the measured  $t\bar{t}$  fiducial cross section of  $244.9 \pm 1.4(stat.)_{-5.5}^{+6.3}(sys.) \pm 6.4(lumi.) \text{ pb}$ . Extrapolating to the full phase space, the result is  $\sigma_{t\bar{t}\gamma} \times BR = (515 \pm 108) \text{ fb}$ , per lepton+jets final state [259], in good agreement with the theoretical prediction.

At  $\sqrt{s} = 13 \text{ TeV}$ , using  $36.1 \text{ fb}^{-1}$  of single-lepton and dilepton events with exactly one photon, ATLAS measures the  $t\bar{t}\gamma$  cross section. They employ neural network algorithms to separate the signal from the backgrounds. The fiducial cross-sections are measured to be  $521 \pm 9(stat.) \pm 41(sys.) \text{ fb}$  and  $69 \pm 3(stat.) \pm 4(sys.) \text{ fb}$  for the single-lepton and dilepton channels, respectively. The differential cross-sections are measured as a function of photon transverse momentum, photon absolute pseudorapidity, and angular distance between the photon and its closest lepton in both channels, as well as azimuthal opening angle and absolute pseudorapidity difference between the two leptons in the dilepton channel. All measurements are in agreement with the theoretical predictions [260]. Very recently, ATLAS uses  $139 \text{ fb}^{-1}$  of  $\sqrt{s} = 13 \text{ TeV}$   $e\mu + \gamma$  events with at least two jets, out of which at least one is  $b$ -tagged, to measure the inclusive and differential cross-sections for the production of a top-quark pair in association with a photon. The fiducial cross-section is measured to be  $44.2 \pm 2.6 \text{ fb}$ . Differential cross-sections as functions of several observables are compared to state-of-the-art Monte Carlo simulations and next-to-leading order theoretical calculations. These include cross-sections as functions of the photon transverse momentum and absolute pseudorapidity and angular variables related to the photon and the leptons and between the two leptons in the event. All measurements are in agreement with the predictions [261]. In  $35.9 \text{ fb}^{-1}$  of lepton-plus-photon-plus-jets events, CMS manages to establish the first evidence for the associated production of a single-top quark and a photon at  $\sqrt{s} = 13 \text{ TeV}$ . They employ

**Table 60.2:** Measurement and 95% C.L. upper limits of the  $W$  helicity in top-quark decays. The table includes both preliminary, as of October 2019, and published results. A full set of published results is given in the Listings.

$W$ Helicity	Source	$\int \mathcal{L} dt$ ( $\text{fb}^{-1}$ )	Ref.	Method
$\mathcal{F}_0 = 0.722 \pm 0.081$	CDF+DØ Run II	2.7-5.4	[240]	$\cos \theta^*$ 2-param
$\mathcal{F}_0 = 0.682 \pm 0.057$	CDF+DØ Run II	2.7-5.4	[240]	$\cos \theta^*$ 1-param
$\mathcal{F}_0 = 0.726 \pm 0.094$	CDF Run II	8.7	[248]	ME 2-param
$\mathcal{F}_0 = 0.67 \pm 0.07$	ATLAS (7 TeV)	1.0	[241]	$\cos \theta^*$ 3-param
$\mathcal{F}_0 = 0.682 \pm 0.045$	CMS (7 TeV)	5.0	[242]	$\cos \theta^*$ 3-param
$\mathcal{F}_0 = 0.626 \pm 0.059$	ATLAS+CMS (7 TeV)	2.2	[243]	$\cos \theta^*$ 3-param
$\mathcal{F}_0 = 0.709 \pm 0.019$	ATLAS (8 TeV)	20.2	[244]	$\cos \theta^*$ 3-param
$\mathcal{F}_0 = 0.681 \pm 0.026$	CMS (8 TeV)	19.8	[245]	$\cos \theta^*$ 3-param
$\mathcal{F}_0 = 0.653 \pm 0.029$	CMS (8 TeV)	19.7	[246]	$\cos \theta^*$ 3-param
$\mathcal{F}_0 = 0.720 \pm 0.054$	CMS (8 TeV)	19.7	[247]	$\cos \theta^*$ 3-param
$\mathcal{F}_+ = -0.033 \pm 0.046$	CDF+DØ Run II	2.7-5.4	[240]	$\cos \theta^*$ 2-param
$\mathcal{F}_+ = -0.015 \pm 0.035$	CDF+DØ Run II	2.7-5.4	[240]	$\cos \theta^*$ 1-param
$\mathcal{F}_+ = -0.045 \pm 0.073$	CDF Run II	8.7	[248]	ME 2-param
$\mathcal{F}_+ = 0.01 \pm 0.05$	ATLAS (7 TeV)	1.0	[241]	$\cos \theta^*$ 3-param
$\mathcal{F}_+ = 0.008 \pm 0.018$	CMS (7 TeV)	5.0	[242]	$\cos \theta^*$ 3-param
$\mathcal{F}_+ = 0.015 \pm 0.034$	ATLAS+CMS (7 TeV)	2.2	[243]	$\cos \theta^*$ 3-param
$\mathcal{F}_+ = -0.008 \pm 0.014$	ATLAS (8 TeV)	20.2	[244]	$\cos \theta^*$ 3-param
$\mathcal{F}_+ = -0.004 \pm 0.015$	CMS (8 TeV)	19.8	[245]	$\cos \theta^*$ 3-param
$\mathcal{F}_+ = 0.018 \pm 0.027$	CMS (8 TeV)	19.7	[246]	$\cos \theta^*$ 3-param
$\mathcal{F}_+ = -0.018 \pm 0.022$	CMS (8 TeV)	19.7	[247]	$\cos \theta^*$ 3-param

a multivariate discriminant based on topological and kinematic event properties to separate signal from background processes. An excess above the background-only hypothesis is observed, with a significance of 4.4 standard deviations. A fiducial cross section is measured for isolated photons with transverse momentum greater than 25 GeV in the central region of the detector. The measured product of the cross section and branching fraction is  $\sigma(pp \rightarrow t\gamma j)B(t \rightarrow \mu\gamma b) = 115 \pm 17(stat) \pm 30(syst)$  fb, which is consistent with the SM prediction [262]. A precision test of the vector and axial vector couplings in  $t\bar{t}\gamma$  events or searches for possible tensor couplings of top-quarks to photons will only be feasible with an integrated luminosity of several hundred  $\text{fb}^{-1}$  in the future [263].

ATLAS and CMS have also studied the associate production of top-antitop quark pairs along with an electroweak gauge boson, where in the Standard Model the  $W$ -boson is expected to be produced via initial state radiation, while the  $Z$ -boson can also be radiated from a final-state top-quark and hence provides sensitivity to the top-quark neutral current weak gauge coupling, which implies a sensitivity to the third component of the top-quark's weak isospin, which has not been measured so far.

CMS performed measurements of the  $t\bar{t}W$  and  $t\bar{t}Z$  production cross section at  $\sqrt{s} = 7$  TeV with  $5 \text{ fb}^{-1}$ , yielding  $\sigma_{t\bar{t}V} = 0.43_{-0.15}^{+0.17}(stat.)_{-0.07}^{+0.09}(syst.)$  pb ( $V = Z, W$ ) and  $\sigma_{t\bar{t}Z} = 0.28_{-0.11}^{+0.14}(stat.)_{-0.03}^{+0.06}(syst.)$  fb, at about 3 standard deviations significance [264] and compatible with the SM expectations of  $0.306_{-0.053}^{+0.031}$  pb and  $0.137_{-0.016}^{+0.012}$  pb, respectively [265, 266]. ATLAS performed a similar analysis with  $4.7 \text{ fb}^{-1}$  in the three-lepton channel and set an upper limit of 0.71 pb at 95% C.L. [267].

Using  $20.3 \text{ fb}^{-1}$  of 8 TeV data, ATLAS performs a simultaneous measurement of the  $t\bar{t}W$  and  $t\bar{t}Z$  cross section. They observe the  $t\bar{t}W$  and  $t\bar{t}Z$  production at the  $5.0\sigma$  and  $4.2\sigma$  level, respectively, yielding  $\sigma_{t\bar{t}W} = 369_{-91}^{+100}$  fb and  $\sigma_{t\bar{t}Z} = 176_{-52}^{+58}$  fb [268]. CMS performs an analysis where signal events are identified by matching reconstructed objects in the detector to specific final state particles from  $t\bar{t}W$  and  $t\bar{t}Z$  decays using  $19.5 \text{ fb}^{-1}$  of 8 TeV data. They obtain  $\sigma_{t\bar{t}W} = 382_{-102}^{+117}$  fb and  $\sigma_{t\bar{t}Z} = 242_{-55}^{+65}$  fb, yielding a significance of 4.8 and 6.4 standard, respectively [269]. These measurements are used to set bounds on five anomalous dimension-six operators that would affect the  $t\bar{t}W$  and  $t\bar{t}Z$  cross sections.

The most recent measurements in these channels are made at 13 TeV from ATLAS and CMS in multilepton final states. ATLAS made a measurement using  $36.1 \text{ fb}^{-1}$  of events with two, three or four leptons. In multiple regions, the  $t\bar{t}Z$  and  $t\bar{t}W$  cross

sections are simultaneously measured using a combined fit to all regions, yielding  $\sigma_{t\bar{t}Z} = 0.95 \pm 0.08(stat) \pm 0.10(syst)$  pb and  $\sigma_{t\bar{t}W} = 0.87 \pm 0.13(stat) \pm 0.14(syst)$  pb [270] to be compared with the NLO+NLL (QCD) and NLO (EW) SM predictions,  $\sigma_{t\bar{t}W} = 579_{-9\%}^{+14\%}$  fb and  $\sigma_{t\bar{t}Z} = 811_{-10\%}^{+11\%}$  fb [271].

CMS uses  $35.9 \text{ fb}^{-1}$  of data to measure  $t\bar{t}W$  and  $t\bar{t}Z$  production cross sections of  $0.77_{-0.11}^{+0.12}$  pb and  $0.99_{-0.08}^{+0.09}$  pb, and significances over the background-only hypotheses of  $5.5\sigma$  and  $9.5\sigma$ , respectively [272], firmly establishing the observation of these processes. Very recently, CMS measured the inclusive  $t\bar{t}Z$  cross section in  $77.5 \text{ fb}^{-1}$  of events with three or four charged leptons, and the  $Z$  boson is detected through its decay to an oppositely charged lepton pair. The production cross section is measured to be  $\sigma(t\bar{t}Z) = 0.95 \pm 0.05(stat) \pm 0.06(syst)$  pb. This measurement includes differential cross sections as functions of the transverse momentum of the  $Z$  boson and the angular distribution of the negatively charged lepton from the  $Z$  boson decay as well as stringent direct limits on the anomalous  $tZ$  couplings [273].

The electroweak couplings can also be probed in single-top production in association with a  $Z$  boson. The  $pp \rightarrow tZq$  process at the LHC probes both the  $WWZ$  coupling in the case where the  $Z$  emerges from the  $t$ -channel  $W$  in single-top production and, in the case where the  $Z$  is radiated from the top quark, the  $tZ$  coupling. A CMS search at 8 TeV produced a hint of a  $tZq$  signal in tri-lepton events, with a significance compared to the background-only hypothesis of  $2.4\sigma$  [274]. At 13 TeV the signal has begun to emerge. In  $35.9 \text{ fb}^{-1}$  of events with three leptons, the  $tZq$  production cross section is measured to be  $\sigma_{tZq} = 123_{-31}^{+33}(stat)_{-23}^{+29}(syst)$  fb, where  $l$  also includes tau leptons, with observed and expected significances of 3.7 and 3.1 standard deviations, respectively [262].

Searches for and now also measurements of the associate production of a top-antitop quark pair along with a Higgs boson,  $t\bar{t}h$ , with various subsequent decays provide sensitivity to the top-Higgs Yukawa coupling. For further details, see the review on "Higgs".

### 60.3.3 Searches for Physics Beyond the Standard Model

The top quark plays a special role in the SM. Being the only quark with a coupling to the Higgs boson of order one, it provides the most important contributions to the quadratic radiative corrections to the Higgs mass exposing the issue of the naturalness of the SM. It is therefore very common for models where the naturalness problem is addressed to have new physics associated with the top quark. In SUSY, for instance, naturalness predicts the scalar top partners to be the lightest among the squarks and to



be accessible at the LHC energies (see the review ‘‘Supersymmetry: Theory’’). In models where the Higgs is a pseudo-Goldstone boson, such as Little Higgs models, naturalness predicts the existence of partners of the top quarks with the same spin and color, but with different electroweak couplings, the so-called vectorial  $t'$ . Stops and  $t'$ 's are expected to have sizeable branching ratios to top quarks. Another intriguing prediction of SUSY models with universal couplings at the unification scale is that for a top-quark mass close to the measured value, the running of the Yukawa coupling down to 1 TeV naturally leads to the radiative breaking of the electroweak symmetry [275]. In fact, the top quark plays a role in the dynamics of electroweak symmetry breaking in many models [276]. One example is topcolor [277], where a large top-quark mass can be generated through the formation of a dynamic  $t\bar{t}$  condensate,  $X$ , which is formed by a new strong gauge force coupling preferentially to the third generation. Another example is topcolor-assisted technicolor [278], predicting the existence of a heavy  $Z'$  boson that couples preferentially to the third generation of quarks. If light enough such a state might be directly accessible at the present hadron collider energies, or if too heavy, lead to four-top interactions possibly visible in the  $t\bar{t}t\bar{t}$  final state. This final state has been recently observed by CMS [279] and limits are provided by ATLAS [280].

Current strategies to search for new physics in top-quark events at hadron colliders are either tailored to the discovery of specific models or model independent. They can be broadly divided in two classes. In the first class new resonant states are looked for through decay processes involving the top quarks. Current searches for bosonic resonances in  $t\bar{t}$  final states, or for direct stop and  $t'$  production, or for a charged Higgs in  $H^+ \rightarrow t\bar{b}$  fall in the category. On the other hand, if new states are too heavy to be directly produced, they might still give rise to deviations from the SM predictions for the strength and Lorentz form of the top-quark couplings to other SM particles. Accurate SM predictions and measurements are therefore needed and the results be efficiently interpreted in the framework of an effective field theory [281,282] as done for example in recent analyses sensitive to the strength and structure of the top quark couplings [270,279]. Global effective field theory interpretations based on publicly available measurements in the top quark sector have also appeared [283–285].

### 60.3.3.1 New Physics in Top Quark Production

Theoretical [286,287] and experimental efforts have been devoted to the searches of  $t\bar{t}$  resonances.

At the Tevatron, both the CDF and DØ collaborations have searched for resonant production of  $t\bar{t}$  pairs in the lepton+jets channel [288,289]. In both analyses, the data indicate no evidence of resonant production of  $t\bar{t}$  pairs. They place upper limits on the production cross section times branching fraction to  $t\bar{t}$  in comparison to the prediction for a narrow ( $\Gamma_{Z'} = 0.012M_{Z'}$ ) leptophobic topcolor  $Z'$  boson. Within this model, they exclude  $Z'$  bosons with masses below 915 (CDF-full data set) and 835 (DØ, 5 fb $^{-1}$ ) GeV/ $c^2$  at the 95% C.L. These limits turn out to be independent of couplings of the  $t\bar{t}$  resonance (pure vector, pure axial-vector, or SM-like  $Z'$ ). A similar analysis has been performed by CDF in the all-hadronic channel using 2.8 fb $^{-1}$  of data [290].

At the LHC, both the CMS and ATLAS collaborations have searched for resonant production of  $t\bar{t}$  pairs, employing different techniques and final-state signatures (all-hadronic, lepton+jets, dilepton) at  $\sqrt{s} = 7, 8$  and 13 TeV. In the low mass range, from the  $t\bar{t}$  threshold to about one TeV/ $c^2$ , standard techniques based on the reconstruction of each of the decay objects (lepton, jets and  $b$ -jets, missing  $E_T$ ) are used to identify the top quarks, while at higher invariant mass, the top quarks are boosted and the decay products more collimated and can appear as large-radius jets with substructure. Dedicated reconstruction techniques have been developed in recent years for boosted top quarks [291] that are currently employed at the LHC. Most of the analyses are model-independent (i.e., no assumption on the quantum numbers of the resonance is made) yet they assume a small width and no signal-background interference.

Using lepton+jets and fully hadronic channels in a data set corresponding to an integrated luminosity of 35.9 fb $^{-1}$  at 13 TeV, the CMS collaboration finds no significant deviations from the SM

background [292]. In particular, the existence of a leptophobic topcolor particle  $Z'$  is excluded at the 95% confidence level for resonances in the mass range  $0.6 < M_{Z'} < 3.8$  TeV/ $c^2$ ,  $0.5 < M_{Z'} < 5.25$  TeV/ $c^2$ , and  $0.5 < M_{Z'} < 6.65$  TeV/ $c^2$  for  $\Gamma_{Z'} = 1\%, 10\%, 30\%M_{Z'}$ , respectively [293]. Kaluza-Klein excitations of a gluon with  $M_{G_{KK}} < 4.55$  TeV/ $c^2$  (at 95% confidence level) in the Randall-Sundrum model are also excluded.

The ATLAS collaboration has performed a search for resonant  $t\bar{t}$  production in the lepton+jets channel using 36.1 fb $^{-1}$  of proton-proton (pp) collision data collected at a center-of-mass energy  $\sqrt{s} = 13$  TeV [294]. A search for local excesses in the number of data events compared to the Standard Model expectation in the  $t\bar{t}$  invariant mass spectrum is performed. No evidence for a  $t\bar{t}$  resonance is found and 95% confidence-level limits on the production rate are determined for massive states predicted in several benchmark models. For instance, a narrow leptophobic topcolor  $Z'$  boson with a mass below 3.0 TeV/ $c^2$  is excluded. A Kaluza-Klein excitation of the graviton is excluded for masses in the range  $0.45$  TeV/ $c^2 < m_G < 0.65$  TeV/ $c^2$ . A Kaluza-Klein excitation of the gluon in a Randall-Sundrum model is excluded for masses below 3.8 TeV/ $c^2$ .

ATLAS has also conducted a search for resonances in the all-jet final state at 13 TeV corresponding to an integrated luminosity of 36.1 fb $^{-1}$  [295]. The  $t\bar{t}$  events are reconstructed by selecting two top quarks in their fully hadronic decay modes. The invariant mass distribution of the two reconstructed top-quark candidates is examined for resonant production of new particles with various spins and decay widths. No significant deviation from the Standard Model prediction is observed and limits are set on the production cross-section times branching fraction for new hypothetical  $Z'$  bosons, dark-matter mediators, Kaluza-Klein gravitons and Kaluza-Klein gluons. For example, the  $Z'$  in the topcolor-assisted-technicolor model is excluded for masses up to 3.1–3.6 TeV, the dark-matter mediators in a simplified framework are excluded in the mass ranges from 0.8 to 0.9 TeV/ $c^2$  and from 2.0 to 2.2 TeV/ $c^2$ , and the Kaluza-Klein gluon is excluded for masses up to 3.4 TeV/ $c^2$ , depending on the decay widths of the particles.

Heavy charged bosons, such as  $W'$  or  $H^+$ , can also be searched for in  $t\bar{b}, tj$  final states (for more information see the review ‘‘ $W'$ -boson searches’’ and ‘‘Higgs Bosons: theory and searches’’), while heavy fermion resonances, such as vectorial or excited quarks, in final states such as  $tZ, tH, tW, bW$ .

CMS has performed several searches in this context, the most stringent limits coming from those at  $\sqrt{s} = 13$  TeV [296–302]. For instance, a  $W' \rightarrow t\bar{b}$  has been searched for in lepton+jets in 35.9 fb $^{-1}$ . No evidence has been found for a right-handed  $W'$  boson and masses below 3.6 TeV/ $c^2$  are excluded at 95% confidence level providing the most stringent limits for right-handed  $W'$  bosons in the top and bottom quark decay channel to date [296].

Single production of a vector-like quark decaying to a  $W$  boson and a top quark, with one lepton in the final state, also been searched in the same data set. No significant deviation from the standard model background expectation is observed. Exclusion limits at 95% confidence level are set on the product of the production cross section and branching fraction as a function of the vector-like quark mass, which range from 0.3 to 0.03 pb for vector-like quark masses of 700 to 2000 GeV/ $c^2$ . Mass exclusion limits up to 1660 GeV/ $c^2$  are obtained, depending on the vector-like quark type, coupling, and decay width. These represent the most stringent exclusion limits for the single production of vector-like quarks in this channel. [303]

In the same data set, searches for pair production of vector-like  $T$  or  $B$  quarks in fully hadronic final states have been performed based on two different techniques. A first cut-based analysis targets the  $bW$  decay mode of the  $T$  quark, while a second analysis, a multi-classification algorithm is deployed to label candidate jets as originating from top quarks, and  $W, Z$ , and  $H$ . Both analyses probe all possible branching fraction combinations of the  $T$  and  $B$  quarks and set limits at 95% confidence level on their masses, ranging from 740 to 1370 GeV/ $c^2$  [304].

ATLAS has performed searches for heavy bosons and fermions decaying to one top quark at  $\sqrt{s} = 7, 8$  and 13 TeV. A  $W' \rightarrow t\bar{b}$

has been searched for at 13 TeV in lepton+jets in  $36.1 \text{ fb}^{-1}$ . No evidence has been found for a right-handed  $W'$  boson with a mass below  $3.25 \text{ TeV}/c^2$  are excluded at 95% [305]. ATLAS has conducted a search for the single and pair production of a new charge  $+2/3$  quark ( $T$ ) decaying via  $T \rightarrow Zt$  (and also  $-1/3$  quark ( $B$ ) decaying via  $B \rightarrow Zb$ ) in a dataset corresponding to  $36.1 \text{ fb}^{-1}$  luminosity at  $\sqrt{s} = 13 \text{ TeV}$  [306]. The final state used is characterized by the presence of b-tagged jets, as well as a  $Z$  boson with high transverse momentum, which is reconstructed from a pair of opposite-sign same-flavor leptons. No significant excess of events above the SM expectation is observed, and upper limits are derived for vector-like quarks of various masses in a two-dimensional plane of branching ratios. Under branching ratio assumptions corresponding to a weak-isospin singlet scenario, a  $T$  quark with mass lower than  $1030 \text{ GeV}/c^2$  ( $1010 \text{ GeV}/c^2$  for a  $B$  quark) is excluded at the 95% confidence level. Under branching ratio assumptions corresponding to a particular weak-isospin doublet scenario, a  $T$  quark with mass lower than  $1210 \text{ GeV}/c^2$  ( $1140 \text{ GeV}/c^2$  for a  $B$  quark) is excluded at the 95% confidence level.

In the same dataset, ATLAS combines the searches for pair-produced vector-like partners of the top and bottom quarks in various decay channels ( $T \rightarrow Zt/Wb/Ht, B \rightarrow Zb/Wt/Hb$ ). The observed data are found to be in good agreement with the Standard Model background prediction in all individual searches. Therefore, combined 95% confidence-level upper limits are set on the production cross-section for a range of vector-like quark scenarios, significantly improving upon the reach of the individual searches. Model-independent limits are set assuming the vector-like quarks decay to Standard Model particles. A singlet  $T$  is excluded for masses below  $1.31 \text{ TeV}/c^2$  and a singlet  $B$  is excluded for masses below  $1.22 \text{ TeV}/c^2$ . Assuming a weak isospin ( $T, B$ ) doublet and  $|V_{Tb}| \ll |V_{tB}|$ ,  $T$  and  $B$  masses below  $1.37 \text{ TeV GeV}/c^2$  are excluded [307].

In many models top-quark partners preferably decay to top quarks and weakly interacting neutral stable particles, i.e., possibly dark matter candidates, that are not detected. An observable especially sensitive to new physics effects in  $t\bar{t}$  production is therefore the missing transverse momentum.

CMS has presented a differential cross section measurement of top-quark pair and single production with missing transverse energy and corresponding interpretations in the context of dark matter (effective and simplified) models at 8 and 13 TeV [308–311]. The results obtained so far are consistent with the SM expectations. In particular the search performed at 13 TeV [311] is based on  $35.9 \text{ fb}^{-1}$  of integrated luminosity. Upper limits are derived on the production cross section and interpreted in terms of a simplified model with a scalar/pseudoscalar mediator. Scalar and pseudoscalar mediator particles with masses below 290 and  $300 \text{ GeV}/c^2$ , respectively, are excluded at 95% confidence level, assuming a dark matter particle mass of  $1 \text{ GeV}/c^2$  and mediator couplings to fermions and dark matter particles equal to unity.

A search for top squarks at a center-of-mass energy of 13 TeV in  $36 \text{ fb}^{-1}$  of data has been performed by ATLAS [312] in final states with one isolated electron or muon, several energetic jets, and missing transverse momentum. The analysis also targets spin-0 mediator models, where the mediator decays into a pair of dark-matter particles and is produced in association with a pair of top quarks. No significant excess over the Standard Model prediction is observed. For pair-produced top-squarks decaying into top quarks, top-squark masses up to  $940 \text{ GeV}/c^2$  are excluded. Stringent exclusion limits are also derived for all other considered top-squark decay scenarios. For the spin-0 mediator models, upper limits are set on the visible cross-section.

Flavor-changing-neutral-currents (FCNC) are hugely suppressed in the SM as non zero contributions only arise at one-loop and are proportional to the splitting between the quark masses. In the case of the top quark  $B(t \rightarrow Bq)$  with  $B = g, \gamma, Z, H$  and  $q = u, c$  are predicted to be order of  $10^{-12}$  ( $t \rightarrow cg$ ) or much smaller [313]. Several observables are accessible at colliders to test and constrain such couplings.

CMS has performed several studies on the search for FCNC in top-quark production. They have considered single-top quark production in the  $t$ -channel in  $5 \text{ fb}^{-1}$  integrated luminosity at 7 TeV

and  $19.7 \text{ fb}^{-1}$  integrated luminosity at 8 TeV [314]. Events with the top quark decaying into a muon, neutrino and two or three jets are selected. The upper limits on effective coupling strength can be translated to the 95% upper limits on the corresponding branching ratios  $B(t \rightarrow gu) \leq 2.0 \cdot 10^{-5}$ ,  $B(t \rightarrow gc) \leq 4.1 \cdot 10^{-4}$ . They have performed a search for a single top quark produced in association with a photon in  $19.1 \text{ fb}^{-1}$  integrated luminosity at 8 TeV [315]. The event selection requires the presence of one isolated muon and jets in the final state. The upper limits on effective coupling strength can be translated to the 95% upper limits on the corresponding branching ratios  $B(t \rightarrow \gamma u) \leq 0.0161\%$ ,  $B(t \rightarrow \gamma c) \leq 0.182\%$ .

Recently, a search for flavor-changing neutral currents in associated production of a top quark with a Higgs boson decaying into  $b\bar{b}$  has also been presented by CMS, corresponding to an integrated luminosity of  $35.9 \text{ fb}^{-1}$  at 13 TeV. Two complementary channels are considered: top quark pair production, with FCNC decay of the top quark or antiquark, and single top associated production. A final state with one isolated lepton and at least three reconstructed jets, among which at least two are identified as  $b$  quark jets, is considered. No significant deviation is observed from predicted background and upper limits at 95% confidence level are set on the branching ratios of top quark decays,  $B(t \rightarrow uH) < 0.47\%$  and  $B(t \rightarrow cH) < 0.47\%$  [316], which are similar to the combined limits on all decay channels obtained with the full data set at 8 TeV [317].

ATLAS has presented results on the search for single top-quark production via FCNC's in strong interactions using data collected at  $\sqrt{s}=8 \text{ TeV}$  and corresponding to an integrated luminosity of  $20.3 \text{ fb}^{-1}$ . Flavor-changing-neutral-current events are searched for in which a light quark ( $u$  or  $c$ ) interacts with a gluon to produce a single top quark, either with or without the associated production of another light quark or gluon. Candidate events of top quarks decaying into leptons and jets are selected and classified into signal- and background-like events using a neural network. The observed 95% C.L. limit is  $\sigma_{qq \rightarrow t} \times B(t \rightarrow Wb) < 3.4 \text{ pb}$  that can be interpreted as limits on the branching ratios,  $B(t \rightarrow ug) < 4 \cdot 10^{-5}$  and  $B(t \rightarrow cg) < 1.7 \cdot 10^{-4}$  [318].

ATLAS has set limits on the coupling of a top quark, a photon, and an up or charm quark using  $81 \text{ fb}^{-1}$  of data 13 TeV. Events with a photon, an electron or muon, a b-tagged jet, and missing transverse momentum are selected. The data are consistent with the background-only hypothesis, and limits are set on the strength of the  $tq\gamma$  coupling in an effective field theory. These are also interpreted as 95% CL upper limits on  $t \rightarrow u\gamma$  branching ratio via a left-handed (right-handed) interaction of  $2.8 \times 10^{-5}$  ( $6.1 \times 10^{-5}$ ) and on the  $t \rightarrow c\gamma$  branching ratio for of  $22 \times 10^{-5}$  ( $18 \times 10^{-5}$ ) [319].

Constraints on FCNC couplings of the top quark can also be obtained from searches for anomalous single top-quark production in  $e^+e^-$  collisions, via the process  $e^+e^- \rightarrow \gamma, Z^* \rightarrow t\bar{q}$  and its charge-conjugate ( $q = u, c$ ), or in  $e^\pm p$  collisions, via the process  $e^\pm u \rightarrow e^\pm t$ . For a leptonic  $W$  decay, the topology is at least a high- $p_T$  lepton, a high- $p_T$  jet and missing  $E_T$ , while for a hadronic  $W$ -decay, the topology is three high- $p_T$  jets. Limits on the cross section for this reaction have been obtained by the LEP collaborations [320] in  $e^+e^-$  collisions, and by H1 [321] and ZEUS [322] in  $e^\pm p$  collisions. When interpreted in terms of branching ratios in top decay [323,324], the LEP limits lead to typical 95% C.L. upper bounds of  $B(t \rightarrow qZ) < 0.137$ . Assuming no coupling to the  $Z$  boson, the 95% C.L. limits on the anomalous FCNC coupling  $\kappa_\gamma < 0.13$  and  $< 0.27$  by ZEUS and H1, respectively, are stronger than the CDF limit of  $\kappa_\gamma < 0.42$ , and improve over LEP sensitivity in that domain. The H1 limit is slightly weaker than the ZEUS limit due to an observed excess of five-candidate events over an expected background of  $3.2 \pm 0.4$ . If this excess is attributed to FCNC top-quark production, this leads to a total cross section of  $\sigma(ep \rightarrow e + t + X, \sqrt{s} = 319 \text{ GeV}) < 0.25 \text{ pb}$  [321,325].

### 60.3.3.2 New Physics in Top-Quark decays

The large sample of top quarks produced at the Tevatron and the LHC allows to measure or set stringent limits on the branching ratios of rare top-quark decays. For example, the existence of a light  $H^+$  can be constrained by looking for  $t \rightarrow H^+b$  decay, in

particular with tau-leptons in the final state (for more information see the review “Higgs Bosons: theory and searches”).

A first class of searches for new physics focuses on the structure of the  $Wtb$  vertex. Using up to  $2.7 \text{ fb}^{-1}$  of data,  $D\bar{O}$  has measured the  $Wtb$  coupling form factors by combining information from the  $W$ -boson helicity in top-quark decays in  $t\bar{t}$  events and single top-quark production, allowing to place limits on the left-handed and right-handed vector and tensor couplings [326–328].

ATLAS has published the results of a search for  $CP$ -violation in the decay of single top quarks produced in the  $t$ -channel where the top quarks are predicted to be highly polarized, using the lepton+jets final state [329]. The data analyzed are from  $pp$  collisions at  $\sqrt{s} = 7 \text{ TeV}$  and correspond to an integrated luminosity of  $4.7 \text{ fb}^{-1}$ . In the Standard Model, the couplings at the  $Wtb$  vertex are left-handed, right-handed couplings being absent. A forward-backward asymmetry with respect to the normal to the plane defined by the  $W$ -momentum and the top-quark polarization has been used to probe the complex phase of a possibly non-zero value of the right-handed coupling, signaling a source of  $CP$ -violation beyond the SM. The measured value of the asymmetry is  $0.031 \pm 0.065(\text{stat.})_{-0.031}^{+0.029}(\text{syst.})$  in good agreement with the Standard Model.

A second class of searches focuses on FCNC's in the top-quark decays. Both, CDF and  $D\bar{O}$ , have provided the first limits for FCNC's in Run I and II. The most recent results from CDF give  $B(t \rightarrow qZ) < 3.7\%$  and  $B(t \rightarrow q\gamma) < 3.2\%$  at the 95% C.L. [330] while  $D\bar{O}$  [331, 332] sets  $B(t \rightarrow qZ) (q = u, c \text{ quarks}) < 3.2\%$  at 95% C.L.,  $B(t \rightarrow gu) < 2.0 \cdot 10^{-4}$ , and  $B(t \rightarrow gc) < 3.9 \cdot 10^{-3}$  at the 95% C.L. At the LHC, CMS has used a sample at a center-of-mass energy of 8 TeV corresponding to  $19.7 \text{ fb}^{-1}$  of integrated luminosity to perform a search for flavor changing neutral current top-quark decay  $t \rightarrow Zq$ . Events with a topology compatible with the decay chain  $t\bar{t} \rightarrow Wb + Zq \rightarrow \ell\nu b + \ell\ell q$  are searched for. There is no excess seen in the observed number of events relative to the SM prediction; thus no evidence for flavor changing neutral current in top-quark decays is found. A combination with a previous search at 7 TeV excludes a  $t \rightarrow Zq$  branching fraction greater than 0.05% at the 95% confidence level [333]. CMS has also performed a search for the production of a single top quark in association with a  $Z$  boson in the same data set at 8 TeV. Final states with three leptons (electrons or muons) and at least one jet are investigated. Exclusion limits at 95% confidence level on the branching fractions are found to be  $B(t \rightarrow uZ) < 0.022\%$  and  $B(t \rightarrow cZ) < 0.049\%$  [334].

The ATLAS collaboration has also searched for FCNC processes in  $31.1 \text{ fb}^{-1}$  of  $t\bar{t}$  events at a center-of-mass energy of 13 TeV, with one top quark decaying through FCNC ( $t \rightarrow qZ$ ) and the other through the SM dominant mode ( $t \rightarrow bW$ ). Only the decays of the  $Z$  boson to charged leptons and leptonic  $W$  boson decays were considered as signal, leading to a final state topology characterized by the presence of three isolated leptons, at least two jets and missing transverse energy from the undetected neutrino. No evidence for an FCNC signal was found. An upper limit on the  $t \rightarrow qZ$  branching ratio of  $B(t \rightarrow Zu(c)) < 1.7(2.4) \times 10^{-4}$  is set at the 95% confidence level [335].

Another search for FCNCs is the interactions of a top-quark to a Higgs boson and a light parton,  $tqH$ ,  $q = u, c$ . The CMS collaboration has performed a search using a sample at a center-of-mass energy of 13 TeV corresponding to  $35.9 \text{ fb}^{-1}$  of integrated luminosity, [336], combining single top quark FCNC production in association with the Higgs boson ( $pp \rightarrow tH$ ), and top quark pair production with FCNC decay of the top quark ( $t \rightarrow qH$ ). The combined analysis sets an upper limit on the  $t \rightarrow u/cH$  branching ratios of  $B(t \rightarrow u/cH) < 0.47\%$  at 95% confidence level. The ATLAS collaboration considers  $t \rightarrow qH$ ,  $q = u, c$  with  $36.1 \text{ fb}^{-1}$  of  $t\bar{t}$  events at  $\sqrt{s} = 13 \text{ TeV}$ . A combined measurement including  $H \rightarrow bb$  and  $H \rightarrow \tau\tau$  modes yields a 95% C.L. upper limit of 0.11% and 0.12% on the branching ratios of  $B(t \rightarrow cH)$  and  $B(t \rightarrow uH)$ , respectively [337].

## 60.4 Outlook

Top-quark physics at hadron colliders has developed into precision physics. Various properties of the top quark have been measured with high precision, where the LHC has by now surpassed

the Tevatron precision and reach in the majority of relevant observables. Several  $\sqrt{s}$ -dependent physics quantities, such as the production cross-section, have been measured at several energies at the Tevatron and the LHC. Up to now, all measurements are consistent with the SM predictions and allow stringent tests of the underlying production mechanisms by strong and weak interactions. Given the very large event samples available at the LHC, top-quark properties will be further determined in  $t\bar{t}$  as well as in electroweak single top-quark production. At the Tevatron, the  $t$ - and  $s$ -channels for electroweak single top-quark production have been measured separately. At the LHC, quick progress has been achieved in the last years making all three relevant channels measured with more than 5 sigma significance. Furthermore,  $t\bar{t}\gamma$ ,  $t\bar{t}Z$ , and  $t\bar{t}W$  together with  $t\bar{t}H$  associated production have started to provide key information on the top-quark electroweak couplings. At the same time various models of physics beyond the SM involving top-quark production are being constrained. With the first results from LHC Run-II at a higher center-of-mass energy and much higher luminosity starting to be released, top-quark physics has the potential to shed light on open questions and new aspects of physics at the TeV scale.

CDF note references can be retrieved from

<https://www-cdf.fnal.gov/physics/new/top/top.html>,  
and  $D\bar{O}$  note references from

<https://www-d0.fnal.gov/Run2Physics/WWW/documents/Run2Results.htm>,

and ATLAS note references from

<https://twiki.cern.ch/twiki/bin/view/AtlasPublic/TopPublicResults>,

and CMS note references from

<https://twiki.cern.ch/twiki/bin/view/CMSPublic/PhysicsResultsTOP>.

## References

- [1] M. Czakon, P. Fiedler and A. Mitov, Phys. Rev. Lett. **110**, 252004 (2013), [arXiv:1303.6254].
- [2] S. Catani *et al.*, JHEP **07**, 100 (2019), [arXiv:1906.06535].
- [3] ATLAS, CMS, CDF, & D0 Collab, Phys. Rev. Lett. , 110, 25204 (2013); [arXiv:403,4427].
- [4] S. Cortese and R. Petronzio, Phys. Lett. **B253**, 494 (1991).
- [5] S. S. D. Willenbrock and D. A. Dicus, Phys. Rev. **D34**, 155 (1986).
- [6] N. Kidonakis, Phys. Rev. **D83**, 091503 (2011), [arXiv:1103.2792].
- [7] M. Brucherseifer, F. Caola and K. Melnikov, Phys. Lett. **B736**, 58 (2014), [arXiv:1404.7116].
- [8] E. L. Berger, J. Gao and H. X. Zhu, JHEP **11**, 158 (2017), [arXiv:1708.09405].
- [9] N. Kidonakis, Phys. Rev. **D81**, 054028 (2010), [arXiv:1001.5034].
- [10] N. Kidonakis, Phys. Rev. **D82**, 054018 (2010), [arXiv:1005.4451].
- [11] T. M. P. Tait and C. P. Yuan, Phys. Rev. **D63**, 014018 (2000), [hep-ph/0007298].
- [12] M. Jezabek and J. H. Kuhn, Nucl. Phys. **B314**, 1 (1989).
- [13] I. I. Y. Bigi *et al.*, Phys. Lett. **B181**, 157 (1986).
- [14] A. H. Hoang *et al.*, Phys. Rev. **D65**, 014014 (2002), [hep-ph/0107144].
- [15] K. Hagiwara, Y. Sumino and H. Yokoya, Phys. Lett. **B666**, 71 (2008), [arXiv:0804.1014].
- [16] A. Czarnecki and K. Melnikov, Nucl. Phys. **B544**, 520 (1999), [hep-ph/9806244]; K. G. Chetyrkin *et al.*, Phys. Rev. **D60**, 114015 (1999), [hep-ph/9906273].
- [17] S. Frixione, P. Nason and B. R. Webber, JHEP **08**, 007 (2003), [hep-ph/0305252]; W. Kim and H. Shin, JHEP **07**, 070 (2007), [arXiv:0706.3563]; S. Frixione, P. Nason and G. Ridolfi, JHEP **09**, 126 (2007), [arXiv:0707.3088]; J. M. Campbell *et al.*, JHEP **04**, 114 (2015), [arXiv:1412.1828]; T. Ježo *et al.*, Eur. Phys. J. **C76**, 12, 691 (2016), [arXiv:1607.04538].

- [18] S. Frixione *et al.*, JHEP **03**, 092 (2006), [hep-ph/0512250]; V. Marotta and A. Naddeo, JHEP **08**, 029 (2008), [arXiv:0810.4759]; S. Alioli *et al.*, JHEP **09**, 111 (2009), [Erratum: JHEP02,011(2010)], [arXiv:0907.4076]; E. Re, Eur. Phys. J. **C71**, 1547 (2011), [arXiv:1009.2450]; R. Frederix, E. Re and P. Torrielli, JHEP **09**, 130 (2012), [arXiv:1207.5391]; R. Frederix *et al.*, JHEP **06**, 027 (2016), [arXiv:1603.01178].
- [19] S. Frixione and B. R. Webber, JHEP **06**, 029 (2002), [hep-ph/0204244].
- [20] P. Nason, JHEP **11**, 040 (2004), [hep-ph/0409146].
- [21] E. Todesco and J. Wenninger, Phys. Rev. Accel. Beams **20**, 8, 081003 (2017).
- [22] V. M. Abazov *et al.* (D0), Phys. Rev. **D94**, 092004 (2016), [arXiv:1605.06168].
- [23] T. Aaltonen *et al.* (CDF), Phys. Rev. **D88**, 091103 (2013), [arXiv:1304.7961].
- [24] T. A. Aaltonen *et al.* (CDF, D0), Phys. Rev. **D89**, 7, 072001 (2014), [arXiv:1309.7570].
- [25] T. A. Aaltonen *et al.* (CDF), Phys. Rev. **D89**, 9, 091101 (2014), [arXiv:1402.6728].
- [26] T. Aaltonen *et al.* (CDF), Phys. Rev. Lett. **105**, 012001 (2010), [arXiv:1004.3224].
- [27] V. M. Abazov *et al.* (D0), Phys. Rev. **D90**, 9, 092006 (2014), [arXiv:1401.5785].
- [28] G. Aad *et al.* (ATLAS), Eur. Phys. J. **C74**, 10, 3109 (2014), [Addendum: Eur. Phys. J.C76,no.11,642(2016)], [arXiv:1406.5375].
- [29] G. Aad *et al.* (ATLAS), Phys. Rev. **D91**, 11, 112013 (2015), [arXiv:1504.04251].
- [30] G. Aad *et al.* (ATLAS), JHEP **05**, 059 (2012), [arXiv:1202.4892].
- [31] ATLAS Collab., ATLAS-CONF-2011-140.
- [32] ATLAS Collab., ATLAS-CONF-2012-024.
- [33] ATLAS Collab., ATLAS-CONF-2012-031.
- [34] G. Aad *et al.* (ATLAS), Eur. Phys. J. **C73**, 3, 2328 (2013), [arXiv:1211.7205].
- [35] G. Aad *et al.* (ATLAS), Phys. Lett. **B717**, 89 (2012), [arXiv:1205.2067].
- [36] G. Aad *et al.* (ATLAS), Phys. Rev. **D91**, 5, 052005 (2015), [arXiv:1407.0573].
- [37] S. Chatrchyan *et al.* (CMS), JHEP **11**, 067 (2012), [arXiv:1208.2671].
- [38] S. Chatrchyan *et al.* (CMS), Phys. Lett. **B720**, 83 (2013), [arXiv:1212.6682].
- [39] S. Chatrchyan *et al.* (CMS), JHEP **05**, 065 (2013), [arXiv:1302.0508].
- [40] S. Chatrchyan *et al.* (CMS), Phys. Rev. **D85**, 112007 (2012), [arXiv:1203.6810].
- [41] S. Chatrchyan *et al.* (CMS), Eur. Phys. J. **C73**, 4, 2386 (2013), [arXiv:1301.5755].
- [42] ATLAS & CMS Collab., ATLAS-CONF-2012-134, CMS-PAS-TOP-12-003.
- [43] G. Aad *et al.* (ATLAS), Eur. Phys. J. **C74**, 10, 3109 (2014), [Addendum: Eur. Phys. J.C76,no.11,642(2016)], [arXiv:1406.5375].
- [44] M. Aaboud *et al.* (ATLAS), Eur. Phys. J. **C78**, 487 (2018), [arXiv:1712.06857].
- [45] M. Aaboud *et al.* (ATLAS), Phys. Rev. **D95**, 7, 072003 (2017), [arXiv:1702.08839].
- [46] V. Khachatryan *et al.* (CMS), Eur. Phys. J. **C77**, 1, 15 (2017), [arXiv:1602.09024].
- [47] S. Chatrchyan *et al.* (CMS), JHEP **02**, 024 (2014), [Erratum: JHEP02,102(2014)], [arXiv:1312.7582].
- [48] V. Khachatryan *et al.* (CMS), JHEP **08**, 029 (2016), [arXiv:1603.02303].
- [49] V. Khachatryan *et al.* (CMS), Phys. Lett. **B739**, 23 (2014), [arXiv:1407.6643].
- [50] V. Khachatryan *et al.* (CMS), Eur. Phys. J. **C76**, 3, 128 (2016), [arXiv:1509.06076].
- [51] ATLAS Collab., ATLAS-CONF-2014-053, CMS Collab., CMS-PAS-TOP-14-016.
- [52] R. Aaij *et al.* (LHCb), Phys. Rev. Lett. **115**, 11, 112001 (2015), [arXiv:1506.00903].
- [53] ATLAS Collab., ATLAS-CONF-2015-033.
- [54] ATLAS collab., ATLAS-CONF-2015-049.
- [55] M. Aaboud *et al.* (ATLAS), Phys. Lett. **B761**, 136 (2016), [Erratum: Phys. Lett.B772,879(2017)], [arXiv:1606.02699].
- [56] ATLAS Collab., ATLAS-CONF-2019-044.
- [57] ATLAS Collab., ATLAS-CONF-2019-041 (2019).
- [58] V. Khachatryan *et al.* (CMS), Phys. Rev. Lett. **116**, 5, 052002 (2016), [arXiv:1510.05302].
- [59] V. Khachatryan *et al.* (CMS), Eur. Phys. J. **C77**, 172 (2017), [arXiv:1611.04040].
- [60] CMS Collab., CMS-PAS-TOP-15-005.
- [61] A. M. Sirunyan *et al.* (CMS), JHEP **09**, 051 (2017), [arXiv:1701.06228].
- [62] A. M. Sirunyan *et al.* (CMS), Eur. Phys. J. **C79**, 5, 368 (2019), [arXiv:1812.10505].
- [63] CMS Collab., CMS-PAS-TOP-18-005.
- [64] CMS Collab., CMS-PAS-TOP-16-013.
- [65] A. M. Sirunyan *et al.* (CMS), JHEP **03**, 115 (2018), [arXiv:1711.03143].
- [66] A. M. Sirunyan *et al.* (CMS), Phys. Rev. Lett. **119**, 24, 242001 (2017), [arXiv:1709.07411].
- [67] V. M. Abazov *et al.* (D0), Phys. Rev. **D67**, 012004 (2003), [hep-ex/0205019].
- [68] T. Affolder *et al.* (CDF), Phys. Rev. **D64**, 032002 (2001), [Erratum: Phys. Rev.D67,119901(2003)], [hep-ex/0101036].
- [69] ATLAS Collab., ATLAS-CONF-2011-108.
- [70] V. M. Abazov *et al.* (D0), Phys. Rev. Lett. **107**, 121802 (2011), [arXiv:1106.5436]; D. Acosta *et al.* (CDF), Phys. Rev. Lett. **95**, 102002 (2005), [hep-ex/0505091].
- [71] V. Khachatryan *et al.* (CMS), Phys. Lett. **B736**, 33 (2014), [arXiv:1404.2292].
- [72] M. Czakon, D. Heymes and A. Mitov, Phys. Rev. Lett. **116**, 8, 082003 (2016), [arXiv:1511.00549].
- [73] T. Aaltonen *et al.* (CDF), Phys. Rev. Lett. **110**, 12, 121802 (2013), [arXiv:1211.5363].
- [74] G. Aad *et al.* (ATLAS), Eur. Phys. J. **C73**, 1, 2261 (2013), [arXiv:1207.5644].
- [75] G. Aad *et al.* (ATLAS), Phys. Rev. **D90**, 7, 072004 (2014), [arXiv:1407.0371].
- [76] G. Aad *et al.* (ATLAS), JHEP **06**, 100 (2015), [arXiv:1502.05923].
- [77] S. Chatrchyan *et al.* (CMS), Eur. Phys. J. **C73**, 3, 2339 (2013), [arXiv:1211.2220].
- [78] M. Aaboud *et al.* (ATLAS), Phys. Rev. **D94**, 9, 092003 (2016), [arXiv:1607.07281].
- [79] G. Aad *et al.* (ATLAS), Eur. Phys. J. **C76**, 10, 538 (2016), [arXiv:1511.04716].
- [80] G. Aad *et al.* (ATLAS), Phys. Rev. **D93**, 3, 032009 (2016), [arXiv:1510.03818].
- [81] V. Khachatryan *et al.* (CMS), Phys. Rev. **D94**, 5, 052006 (2016), [arXiv:1607.00837].
- [82] A. M. Sirunyan *et al.* (CMS), Eur. Phys. J. **C77**, 7, 459 (2017), [arXiv:1703.01630].

- [83] V. Khachatryan *et al.* (CMS), Phys. Rev. **D94**, 7, 072002 (2016), [arXiv:1605.00116].
- [84] V. Khachatryan *et al.* (CMS), Eur. Phys. J. **C75**, 11, 542 (2015), [arXiv:1505.04480].
- [85] V. Khachatryan *et al.* (CMS), Eur. Phys. J. **C76**, 3, 128 (2016), [arXiv:1509.06076].
- [86] M. Aaboud *et al.* (ATLAS), Eur. Phys. J. **C77**, 5, 292 (2017), [arXiv:1612.05220].
- [87] CMS Collab., CMS-PAS-TOP-15-010.
- [88] M. Aaboud *et al.* (ATLAS), JHEP **11**, 191 (2017), [arXiv:1708.00727].
- [89] ATLAS collab., ATLAS-CONF-2016-100.
- [90] M. Aaboud *et al.* (ATLAS), Phys. Rev. **D98**, 1, 012003 (2018), [arXiv:1801.02052].
- [91] G. Aad *et al.* (ATLAS) (2019), [arXiv:1908.07305].
- [92] A. M. Sirunyan *et al.* (CMS), JHEP **04**, 060 (2018), [arXiv:1708.07638].
- [93] V. Khachatryan *et al.* (CMS), Phys. Rev. **D95**, 9, 092001 (2017), [arXiv:1610.04191].
- [94] A. M. Sirunyan *et al.* (CMS), JHEP **06**, 002 (2018), [arXiv:1803.03991].
- [95] A. M. Sirunyan *et al.* (CMS), Phys. Rev. **D97**, 11, 112003 (2018), [arXiv:1803.08856].
- [96] A. M. Sirunyan *et al.* (CMS), JHEP **02**, 149 (2019), [arXiv:1811.06625].
- [97] A. M. Sirunyan *et al.* (CMS), Submitted to: Eur. Phys. J. (2019), [arXiv:1904.05237].
- [98] G. Aad *et al.* (ATLAS), Eur. Phys. J. **C76**, 1, 11 (2016), [arXiv:1508.06868].
- [99] G. Aad *et al.* (ATLAS), JHEP **01**, 020 (2015), [arXiv:1407.0891].
- [100] S. Chatrchyan *et al.* (CMS), Eur. Phys. J. **C74**, 3014 (2015), [Erratum: Eur. Phys. J. **C75**, no.5, 216(2015)], [arXiv:1404.3171].
- [101] V. Khachatryan *et al.* (CMS), Phys. Lett. **B746**, 132 (2015), [arXiv:1411.5621].
- [102] G. Aad *et al.* (ATLAS), Phys. Rev. **D92**, 7, 072005 (2015), [arXiv:1506.05074].
- [103] M. Aaboud *et al.* (ATLAS), JHEP **04**, 046 (2019), [arXiv:1811.12113].
- [104] A. M. Sirunyan *et al.* (CMS), Phys. Lett. **B776**, 355 (2018), [arXiv:1705.10141].
- [105] CMS Collab., CMS-PAS-TOP-18-002.
- [106] A. M. Sirunyan *et al.* (CMS) (2019), [arXiv:1909.05306].
- [107] V. M. Abazov *et al.* (D0), Phys. Rev. Lett. **103**, 092001 (2009), [arXiv:0903.0850]; V. M. Abazov *et al.* (D0), Phys. Rev. **D78**, 012005 (2008), [arXiv:0803.0739]; V. M. Abazov *et al.* (D0), Phys. Rev. Lett. **98**, 181802 (2007), [hep-ex/0612052].
- [108] T. Aaltonen *et al.* (CDF), Phys. Rev. Lett. **103**, 092002 (2009), [arXiv:0903.0885]; T. Aaltonen *et al.* (CDF), Phys. Rev. **D81**, 072003 (2010), [arXiv:1001.4577].
- [109] T. Aaltonen *et al.* (CDF), Phys. Rev. **D82**, 112005 (2010), [arXiv:1004.1181].
- [110] A. Heinson and T. R. Junk, Ann. Rev. Nucl. Part. Sci. **61**, 171 (2011), [arXiv:1101.1275].
- [111] Tevatron Electroweak Working Group, (2009), [arXiv:0908.2171].
- [112] CDF Collab., CDF conference note 11113 (2014), DØ Collab., DØ conference note 6448 (2014).
- [113] T. A. Aaltonen *et al.* (CDF, D0), Phys. Rev. Lett. **115**, 15, 152003 (2015), [arXiv:1503.05027].
- [114] T. A. Aaltonen *et al.* (CDF, D0), Phys. Rev. Lett. **112**, 231803 (2014), [arXiv:1402.5126].
- [115] G. Aad *et al.* (ATLAS), Phys. Rev. **D90**, 11, 112006 (2014), [arXiv:1406.7844].
- [116] G. Aad *et al.* (ATLAS), Phys. Lett. **B717**, 330 (2012), [arXiv:1205.3130].
- [117] S. Chatrchyan *et al.* (CMS), JHEP **12**, 035 (2012), [arXiv:1209.4533].
- [118] M. Aaboud *et al.* (ATLAS), Eur. Phys. J. **C77**, 8, 531 (2017), [arXiv:1702.02859].
- [119] M. Aaboud *et al.* (ATLAS), JHEP **04**, 124 (2017), [arXiv:1702.08309].
- [120] V. Khachatryan *et al.* (CMS), JHEP **06**, 090 (2014), [arXiv:1403.7366].
- [121] CMS Collab., CMS-PAS-TOP-15-007.
- [122] M. Aaboud *et al.* (ATLAS), JHEP **04**, 086 (2017), [arXiv:1609.03920].
- [123] A. M. Sirunyan *et al.* (CMS), Phys. Lett. **B772**, 752 (2017), [arXiv:1610.00678].
- [124] A. M. Sirunyan *et al.* (CMS) (2018), [arXiv:1812.10514].
- [125] C. D. White *et al.*, JHEP **11**, 074 (2009), [arXiv:0908.0631].
- [126] S. Frixione *et al.*, JHEP **07**, 029 (2008), [arXiv:0805.3067].
- [127] G. Aad *et al.* (ATLAS), Phys. Lett. **B716**, 142 (2012), [arXiv:1205.5764].
- [128] S. Chatrchyan *et al.* (CMS), Phys. Rev. Lett. **110**, 022003 (2013), [arXiv:1209.3489].
- [129] G. Aad *et al.* (ATLAS), JHEP **01**, 064 (2016), [arXiv:1510.03752].
- [130] S. Chatrchyan *et al.* (CMS), Phys. Rev. Lett. **112**, 23, 231802 (2014), [arXiv:1401.2942].
- [131] ATLAS Collab., ATLAS-CONF-2014-052, CMS Collab., CMS-PAS-TOP-14-009.
- [132] M. Aaboud *et al.* (ATLAS), JHEP **01**, 063 (2018), [arXiv:1612.07231].
- [133] A. M. Sirunyan *et al.* (CMS), JHEP **10**, 117 (2018), [arXiv:1805.07399].
- [134] ATLAS Collab., ATLAS-CONF-2011-118.
- [135] G. Aad *et al.* (ATLAS), Phys. Lett. **B756**, 228 (2016), [arXiv:1511.05980].
- [136] V. Khachatryan *et al.* (CMS), JHEP **09**, 027 (2016), [arXiv:1603.02555].
- [137] M. Aaboud *et al.* (ATLAS, CMS), JHEP **05**, 088 (2019), [arXiv:1902.07158].
- [138] CMS Collab., CMS-PAS-TOP-14-004.
- [139] CMS Collab., CMS-PAS-TOP-13-001.
- [140] A. M. Sirunyan *et al.* (CMS) (2019), [arXiv:1907.08330].
- [141] ATLAS collab., ATLAS-CONF-2016-012.
- [142] A. M. Sirunyan *et al.* (CMS), Phys. Rev. Lett. **121**, 22, 221802 (2018), [arXiv:1808.02913].
- [143] M. Czakon, P. Fiedler and A. Mitov, Phys. Rev. Lett. **115**, 5, 052001 (2015), [arXiv:1411.3007].
- [144] W. Hollik and D. Pagani, Phys. Rev. **D84**, 093003 (2011), [arXiv:1107.2606].
- [145] W. Bernreuther and Z.-G. Si, Phys. Rev. **D86**, 034026 (2012), [arXiv:1205.6580].
- [146] S. Jung *et al.*, Phys. Rev. **D81**, 015004 (2010), [arXiv:0907.4112].
- [147] V. M. Abazov *et al.* (D0), Phys. Rev. Lett. **100**, 142002 (2008), [arXiv:0712.0851].
- [148] T. Aaltonen *et al.* (CDF), Phys. Rev. Lett. **101**, 202001 (2008), [arXiv:0806.2472].
- [149] T. A. Aaltonen *et al.* (CDF, D0), Phys. Rev. Lett. **120**, 4, 042001 (2018), [arXiv:1709.04894].
- [150] G. Aad *et al.* (ATLAS), JHEP **02**, 107 (2014), [arXiv:1311.6724].

- [151] G. Aad *et al.* (ATLAS), Eur. Phys. J. **C76**, 2, 87 (2016), [Erratum: Eur. Phys. J. **C77**, 564(2017)], [arXiv:1509.02358].
- [152] G. Aad *et al.* (ATLAS), Phys. Rev. **D94**, 3, 032006 (2016), [arXiv:1604.05538].
- [153] S. Chatrchyan *et al.* (CMS), Phys. Lett. **B717**, 129 (2012), [arXiv:1207.0065].
- [154] V. Khachatryan *et al.* (CMS), Phys. Rev. **D93**, 3, 034014 (2016), [arXiv:1508.03862].
- [155] V. Khachatryan *et al.* (CMS), Phys. Lett. **B760**, 365 (2016), [arXiv:1603.06221].
- [156] M. Czakon *et al.*, Phys. Rev. **D98**, 1, 014003 (2018), [arXiv:1711.03945].
- [157] V. Khachatryan *et al.* (CMS), Phys. Lett. **B757**, 154 (2016), [arXiv:1507.03119].
- [158] G. Aad *et al.* (ATLAS), Phys. Lett. **B756**, 52 (2016), [arXiv:1512.06092].
- [159] G. Aad *et al.* (ATLAS), JHEP **05**, 061 (2015), [arXiv:1501.07383].
- [160] S. Chatrchyan *et al.* (CMS), JHEP **04**, 191 (2014), [arXiv:1402.3803].
- [161] M. Aaboud *et al.* (ATLAS, CMS), JHEP **04**, 033 (2018), [arXiv:1709.05327].
- [162] C. Collaboration (CMS) (2019).
- [163] F. Abe *et al.* (CDF), Phys. Rev. **D50**, 2966 (1994).
- [164] A. Abulencia *et al.* (CDF), Phys. Rev. **D73**, 032003 (2006), [hep-ex/0510048].
- [165] M. Aaboud *et al.* (ATLAS), Eur. Phys. J. **C79**, 4, 290 (2019), [arXiv:1810.01772].
- [166] V. Khachatryan *et al.* (CMS), Phys. Rev. **D93**, 7, 072004 (2016), [arXiv:1509.04044].
- [167] A. M. Sirunyan *et al.* (CMS), Eur. Phys. J. **C78**, 11, 891 (2018), [arXiv:1805.01428].
- [168] S. Argyropoulos and T. Sjöstrand, JHEP **11**, 043 (2014), [arXiv:1407.6653].
- [169] J. R. Christiansen and P. Z. Skands, JHEP **08**, 003 (2015), [arXiv:1505.01681].
- [170] C. Collaboration (CMS) (2019).
- [171] V. M. Abazov *et al.* (D0), Nature **429**, 638 (2004), [hep-ex/0406031].
- [172] K. Kondo, T. Chikamatsu and S. H. Kim, J. Phys. Soc. Jap. **62**, 1177 (1993).
- [173] R. H. Dalitz and G. R. Goldstein, Phys. Rev. **D45**, 1531 (1992); R. H. Dalitz and G. R. Goldstein, Phys. Lett. **B287**, 225 (1992).
- [174] V. M. Abazov *et al.* (D0), Phys. Rev. Lett. **113**, 032002 (2014), [arXiv:1405.1756].
- [175] L. Sonnenschein, Phys. Rev. **D73**, 054015 (2006), [Erratum: Phys. Rev. **D78**, 079902(2008)], [hep-ph/0603011].
- [176] G. Aad *et al.* (ATLAS), Eur. Phys. J. **C75**, 7, 330 (2015), [arXiv:1503.05427].
- [177] A. M. Sirunyan *et al.* (CMS), Phys. Rev. **D96**, 3, 032002 (2017), [arXiv:1704.06142].
- [178] C. G. Lester and D. J. Summers, Phys. Lett. **B463**, 99 (1999), [hep-ph/9906349].
- [179] A. M. Sirunyan *et al.* (CMS), Eur. Phys. J. **C79**, 4, 313 (2019), [arXiv:1812.10534].
- [180] M. Aaboud *et al.* (ATLAS), JHEP **09**, 118 (2017), [arXiv:1702.07546].
- [181] The Tevatron Electroweak Working Group and Aaltonen, T., For the CDF and D0 Collab., arXiv:1608.01881, FERMI-LAB-CONF-16-298-E.
- [182] B. Abbott *et al.* (D0), Phys. Rev. **D60**, 052001 (1999), [hep-ex/9808029]; F. Abe *et al.* (CDF), Phys. Rev. Lett. **82**, 271 (1999), [Erratum: Phys. Rev. Lett. **82**, 2808(1999)], [hep-ex/9810029].
- [183] T. Aaltonen *et al.* (CDF), Phys. Rev. **D92**, 3, 032003 (2015), [arXiv:1505.00500].
- [184] T. A. Aaltonen *et al.* (CDF), Phys. Rev. **D90**, 9, 091101 (2014), [arXiv:1409.4906].
- [185] A. M. Sirunyan *et al.* (CMS), Eur. Phys. J. **C77**, 5, 354 (2017), [arXiv:1703.02530].
- [186] T. Aaltonen *et al.* (CDF), Phys. Lett. **B698**, 371 (2011), [arXiv:1101.4926].
- [187] CMS Collab., CMS-PAS-TOP-12-030.
- [188] T. Aaltonen *et al.* (CDF), Phys. Rev. **D80**, 051104 (2009), [arXiv:0906.5371].
- [189] V. Khachatryan *et al.* (CMS), Phys. Rev. **D93**, 9, 092006 (2016), [arXiv:1603.06536].
- [190] V. Khachatryan *et al.* (CMS), JHEP **12**, 123 (2016), [arXiv:1608.03560].
- [191] CMS Collab., CMS-PAS-TOP-15-002.
- [192] CMS Collab., CMS-PAS-TOP-16-002.
- [193] V. M. Abazov *et al.* (D0), Phys. Rev. Lett. **100**, 192004 (2008), [arXiv:0803.2779]; S. Chatrchyan *et al.* (CMS), Phys. Lett. **B728**, 496 (2014), [Erratum: Phys. Lett. **B738**, 526(2014)], [arXiv:1307.1907]; V. M. Abazov *et al.* (D0), Phys. Lett. **B703**, 422 (2011), [arXiv:1104.2887]; ATLAS Collab., ATLAS-CONF-2019-041; U. Langenfeld, S. Moch and P. Uwer, Phys. Rev. **D80**, 054009 (2009), [arXiv:0906.5273].
- [194] G. Aad *et al.* (ATLAS) (2019), [arXiv:1905.02302].
- [195] CMS Collab., CMS-PAS-TOP-13-006 (2016).
- [196] CDF Collab., CDF conference note 11080 (2014).
- [197] V. M. Abazov *et al.* (D0), Phys. Rev. **D91**, 11, 112003 (2015), [arXiv:1501.07912].
- [198] CMS Collab., CMS-PAS-TOP-13-005.
- [199] M. Beneke *et al.*, Phys. Lett. **B775**, 63 (2017), [arXiv:1605.03609].
- [200] A. H. Hoang, C. Lepenik and M. Preisser, JHEP **09**, 099 (2017), [arXiv:1706.08526].
- [201] C. Collaboration (CMS) (2019), [arXiv:1909.09193].
- [202] G. Aad *et al.* (ATLAS), Phys. Lett. **B716**, 1 (2012), [arXiv:1207.7214].
- [203] S. Chatrchyan *et al.* (CMS), Phys. Lett. **B716**, 30 (2012), [arXiv:1207.7235].
- [204] G. Degrossi *et al.*, JHEP **08**, 098 (2012), [arXiv:1205.6497].
- [205] S. Alekhin, A. Djouadi and S. Moch, Phys. Lett. **B716**, 214 (2012), [arXiv:1207.0980].
- [206] T. Aaltonen *et al.* (CDF), Phys. Rev. **D87**, 5, 052013 (2013), [arXiv:1210.6131].
- [207] V. M. Abazov *et al.* (D0), Phys. Rev. **D84**, 052005 (2011), [arXiv:1106.2063].
- [208] G. Aad *et al.* (ATLAS), Phys. Lett. **B728**, 363 (2014), [arXiv:1310.6527].
- [209] S. Chatrchyan *et al.* (CMS), JHEP **06**, 109 (2012), [arXiv:1204.2807].
- [210] S. Chatrchyan *et al.* (CMS), Phys. Lett. **B770**, 50 (2017), [arXiv:1610.09551].
- [211] G. Mahlon and S. J. Parke, Phys. Rev. **D53**, 4886 (1996), [hep-ph/9512264]; G. Mahlon and S. J. Parke, Phys. Lett. **B411**, 173 (1997), [hep-ph/9706304].
- [212] G.R. Goldstein, in *Spin 96: Proceedings of the 12th International Symposium on High Energy Spin Physics*, Amsterdam, 1996, ed. C.W. Jager (World Scientific, Singapore, 1997), p. 328.
- [213] T. Stelzer and S. Willenbrock, Phys. Lett. **B374**, 169 (1996), [hep-ph/9512292].
- [214] W. Bernreuther *et al.*, Nucl. Phys. **B690**, 81 (2004), [hep-ph/0403035].

- [215] A. Brandenburg, Z. G. Si and P. Uwer, Phys. Lett. **B539**, 235 (2002), [hep-ph/0205023].
- [216] CDF Collab., CDF conference note 10719 (2011).
- [217] CDF Collab., CDF conference note 10211 (2010).
- [218] V. M. Abazov *et al.* (D0), Phys. Lett. **B757**, 199 (2016), [arXiv:1512.08818].
- [219] V. M. Abazov *et al.* (D0), Phys. Rev. **D95**, 1, 011101 (2017), [arXiv:1607.07627].
- [220] V. M. Abazov *et al.* (D0), Phys. Rev. **D92**, 052007 (2015), [arXiv:1507.05666].
- [221] G. Mahlon and S. J. Parke, Phys. Rev. **D81**, 074024 (2010), [arXiv:1001.3422].
- [222] G. Aad *et al.* (ATLAS), Phys. Rev. **D90**, 11, 112016 (2014), [arXiv:1407.4314].
- [223] G. Aad *et al.* (ATLAS), Phys. Rev. Lett. **114**, 14, 142001 (2015), [arXiv:1412.4742].
- [224] G. Aad *et al.* (ATLAS), Phys. Rev. **D93**, 1, 012002 (2016), [arXiv:1510.07478].
- [225] S. Chatrchyan *et al.* (CMS), Phys. Rev. Lett. **112**, 18, 182001 (2014), [arXiv:1311.3924].
- [226] V. Khachatryan *et al.* (CMS), Phys. Lett. **B758**, 321 (2016), [arXiv:1511.06170].
- [227] V. Khachatryan *et al.* (CMS), Phys. Rev. **D93**, 5, 052007 (2016), [arXiv:1601.01107].
- [228] M. Aaboud *et al.* (ATLAS), Submitted to: Eur. Phys. J. (2019), [arXiv:1903.07570].
- [229] A. M. Sirunyan *et al.* (CMS), Phys. Rev. **D100**, 7, 072002 (2019), [arXiv:1907.03729].
- [230] W. Bernreuther, D. Heisler and Z.-G. Si, JHEP **12**, 026 (2015), [arXiv:1508.05271].
- [231] M. Aaboud *et al.* (ATLAS), JHEP **03**, 113 (2017), [arXiv:1612.07004].
- [232] A. F. Falk and M. E. Peskin, Phys. Rev. **D49**, 3320 (1994), [hep-ph/9308241].
- [233] T. A. Aaltonen *et al.* (CDF), Phys. Rev. Lett. **111**, 20, 202001 (2013), [arXiv:1308.4050].
- [234] CMS Collab., CMS-PAS-TOP-16-019.
- [235] M. Aaboud *et al.* (ATLAS), Eur. Phys. J. **C78**, 2, 129 (2018), [arXiv:1709.04207].
- [236] ATLAS-CONF-2019-038.
- [237] V. M. Abazov *et al.* (D0), Phys. Rev. **D85**, 091104 (2012), [arXiv:1201.4156].
- [238] G. L. Kane, G. A. Ladinsky and C. P. Yuan, Phys. Rev. **D45**, 124 (1992).
- [239] A. Czarnecki, J. G. Korner and J. H. Piclum, Phys. Rev. **D81**, 111503 (2010), [arXiv:1005.2625].
- [240] T. Aaltonen *et al.* (CDF, D0), Phys. Rev. **D85**, 071106 (2012), [arXiv:1202.5272].
- [241] G. Aad *et al.* (ATLAS), JHEP **06**, 088 (2012), [arXiv:1205.2484].
- [242] S. Chatrchyan *et al.* (CMS), JHEP **10**, 167 (2013), [arXiv:1308.3879].
- [243] ATLAS and CMS Collab., ATLAS-CONF-2013-033, CMS-PAS-TOP-11-025.
- [244] M. Aaboud *et al.* (ATLAS), Eur. Phys. J. **C77**, 4, 264 (2017), [Erratum: Eur. Phys. J. C79, no.1, 19(2019)], [arXiv:1612.02577].
- [245] V. Khachatryan *et al.* (CMS), Phys. Lett. **B762**, 512 (2016), [arXiv:1605.09047].
- [246] CMS Collab., CMS-PAS-TOP-14-017.
- [247] V. Khachatryan *et al.* (CMS), JHEP **01**, 053 (2015), [arXiv:1410.1154].
- [248] T. Aaltonen *et al.* (CDF), Phys. Rev. **D87**, 3, 031104 (2013), [arXiv:1211.4523].
- [249] D. Choudhury, T. M. P. Tait and C. E. M. Wagner, Phys. Rev. **D65**, 053002 (2002), [hep-ph/0109097].
- [250] D. Chang, W.-F. Chang and E. Ma, Phys. Rev. **D59**, 091503 (1999), [hep-ph/9810531]; D. Chang, W.-F. Chang and E. Ma, Phys. Rev. **D61**, 037301 (2000), [hep-ph/9909537].
- [251] T. Aaltonen *et al.* (CDF), Phys. Rev. **D88**, 3, 032003 (2013), [arXiv:1304.4141].
- [252] V. M. Abazov *et al.* (D0), Phys. Rev. **D90**, 5, 051101 (2014), [Erratum: Phys. Rev. D90, no.7, 079904(2014)], [arXiv:1407.4837].
- [253] G. Aad *et al.* (ATLAS), JHEP **11**, 031 (2011).
- [254] CMS Collab., CMS-PAS-TOP-11-031.
- [255] T. Aaltonen *et al.* (CDF), Phys. Rev. **D84**, 031104 (2011), [arXiv:1106.3970].
- [256] G. Aad *et al.* (ATLAS), Phys. Rev. **D91**, 7, 072007 (2015), [arXiv:1502.00586].
- [257] M. Aaboud *et al.* (ATLAS), JHEP **11**, 086 (2017), [arXiv:1706.03046].
- [258] K. Melnikov, M. Schulze and A. Scharf, Phys. Rev. **D83**, 074013 (2011), [arXiv:1102.1967].
- [259] A. M. Sirunyan *et al.* (CMS), JHEP **10**, 006 (2017), [arXiv:1706.08128].
- [260] M. Aaboud *et al.* (ATLAS), Eur. Phys. J. **C79**, 5, 382 (2019), [arXiv:1812.01697].
- [261] ATLAS Collab., ATLAS-CONF-2019-042.
- [262] A. M. Sirunyan *et al.* (CMS), Phys. Lett. **B779**, 358 (2018), [arXiv:1712.02825].
- [263] M. Cepeda *et al.* (HL/HE WG2 group) (2019), [arXiv:1902.00134].
- [264] S. Chatrchyan *et al.* (CMS), Phys. Rev. Lett. **110**, 172002 (2013), [arXiv:1303.3239].
- [265] J. M. Campbell and R. K. Ellis, JHEP **07**, 052 (2012), [arXiv:1204.5678].
- [266] M. V. Garzelli *et al.*, JHEP **11**, 056 (2012), [arXiv:1208.2665].
- [267] ATLAS Collab., ATLAS-CONF-2012-126.
- [268] G. Aad *et al.* (ATLAS), JHEP **11**, 172 (2015), [arXiv:1509.05276].
- [269] V. Khachatryan *et al.* (CMS), JHEP **01**, 096 (2016), [arXiv:1510.01131].
- [270] M. Aaboud *et al.* (ATLAS), Phys. Rev. **D99**, 7, 072009 (2019), [arXiv:1901.03584].
- [271] A. Broggio *et al.*, JHEP **08**, 039 (2019), [arXiv:1907.04343].
- [272] A. M. Sirunyan *et al.* (CMS), JHEP **08**, 011 (2018), [arXiv:1711.02547].
- [273] (2019), [arXiv:1907.11270].
- [274] A. M. Sirunyan *et al.* (CMS), JHEP **07**, 003 (2017), [arXiv:1702.01404].
- [275] S. P. Martin 1–98 (1997), [Adv. Ser. Direct. High Energy Phys. 18, 1(1998)], [hep-ph/9709356].
- [276] C. T. Hill and E. H. Simmons, Phys. Rept. **381**, 235 (2003), [Erratum: Phys. Rept. 390, 553(2004)], [hep-ph/0203079].
- [277] C. T. Hill, Phys. Lett. **B266**, 419 (1991).
- [278] C. T. Hill, Phys. Lett. **B345**, 483 (1995), [hep-ph/9411426].
- [279] A. M. Sirunyan *et al.* (CMS) (2019), [arXiv:1908.06463].
- [280] M. Aaboud *et al.* (ATLAS), Phys. Rev. **D99**, 5, 052009 (2019), [arXiv:1811.02305].
- [281] C. Zhang and S. Willenbrock, Phys. Rev. **D83**, 034006 (2011), [arXiv:1008.3869].
- [282] J. A. Aguilar-Saavedra, Nucl. Phys. **B843**, 638 (2011), [Erratum: Nucl. Phys. B851, 443(2011)], [arXiv:1008.3562].
- [283] A. Buckley *et al.*, JHEP **04**, 015 (2016), [arXiv:1512.03360].

- [284] N. P. Hartland *et al.*, JHEP **04**, 100 (2019), [arXiv:1901.05965].
- [285] I. Brivio *et al.* (2019), [arXiv:1910.03606].
- [286] V. Barger, T. Han and D. G. E. Walker, Phys. Rev. Lett. **100**, 031801 (2008), [hep-ph/0612016].
- [287] R. Frederix and F. Maltoni, JHEP **01**, 047 (2009), [arXiv:0712.2355].
- [288] T. Aaltonen *et al.* (CDF), Phys. Rev. Lett. **110**, 12, 121802 (2013), [arXiv:1211.5363].
- [289] D. Acosta *et al.* (CDF), Phys. Rev. Lett. **94**, 211801 (2005), [hep-ex/0501050].
- [290] T. Aaltonen *et al.* (CDF), Phys. Rev. **D84**, 072003 (2011), [arXiv:1108.4755].
- [291] A. Altheimer *et al.*, J. Phys. **G39**, 063001 (2012), [arXiv:1201.0008].
- [292] A. M. Sirunyan *et al.* (CMS), JHEP **04**, 031 (2019), [arXiv:1810.05905].
- [293] A. M. Sirunyan *et al.* (CMS), JHEP **07**, 001 (2017), [arXiv:1704.03366].
- [294] M. Aaboud *et al.* (ATLAS), Eur. Phys. J. **C78**, 7, 565 (2018), [arXiv:1804.10823].
- [295] M. Aaboud *et al.* (ATLAS), Phys. Rev. **D99**, 9, 092004 (2019), [arXiv:1902.10077].
- [296] A. M. Sirunyan *et al.* (CMS), Phys. Lett. **B777**, 39 (2018), [arXiv:1708.08539].
- [297] A. M. Sirunyan *et al.* (CMS), Phys. Lett. **B781**, 574 (2018), [arXiv:1708.01062].
- [298] A. M. Sirunyan *et al.* (CMS), JHEP **08**, 073 (2017), [arXiv:1705.10967].
- [299] A. M. Sirunyan *et al.* (CMS), Phys. Lett. **B772**, 634 (2017), [arXiv:1701.08328].
- [300] V. Khachatryan *et al.* (CMS), Phys. Lett. **B771**, 80 (2017), [arXiv:1612.00999].
- [301] A. M. Sirunyan *et al.* (CMS), JHEP **04**, 136 (2017), [arXiv:1612.05336].
- [302] A. M. Sirunyan *et al.* (CMS), JHEP **05**, 029 (2017), [arXiv:1701.07409].
- [303] A. M. Sirunyan *et al.* (CMS), Eur. Phys. J. **C79**, 90 (2019), [arXiv:1809.08597].
- [304] A. M. Sirunyan *et al.* (CMS), Phys. Rev. **D100**, 7, 072001 (2019), [arXiv:1906.11903].
- [305] M. Aaboud *et al.* (ATLAS), Phys. Lett. **B788**, 347 (2019), [arXiv:1807.10473].
- [306] M. Aaboud *et al.* (ATLAS), Phys. Rev. **D98**, 11, 112010 (2018), [arXiv:1806.10555].
- [307] M. Aaboud *et al.* (ATLAS), Phys. Rev. Lett. **121**, 21, 211801 (2018), [arXiv:1808.02343].
- [308] CMS Collab. CMS-PAS-TOP-12-042 (2013).
- [309] V. Khachatryan *et al.* (CMS), JHEP **06**, 121 (2015), [arXiv:1504.03198].
- [310] A. M. Sirunyan *et al.* (CMS), Eur. Phys. J. **C77**, 12, 845 (2017), [arXiv:1706.02581].
- [311] A. M. Sirunyan *et al.* (CMS), JHEP **03**, 141 (2019), [arXiv:1901.01553].
- [312] M. Aaboud *et al.* (ATLAS), JHEP **06**, 108 (2018), [arXiv:1711.11520].
- [313] J. A. Aguilar-Saavedra, Acta Phys. Polon. **B35**, 2695 (2004), [hep-ph/0409342].
- [314] V. Khachatryan *et al.* (CMS), JHEP **02**, 028 (2017), [arXiv:1610.03545].
- [315] CMS Collab., CMS-PAS-TOP-14-003.
- [316] CMS Collab., CMS-PAS-TOP-17-003.
- [317] V. Khachatryan *et al.* (CMS), JHEP **02**, 079 (2017), [arXiv:1610.04857].
- [318] G. Aad *et al.* (ATLAS), Eur. Phys. J. **C76**, 2, 55 (2016), [arXiv:1509.00294].
- [319] G. Aad *et al.* (ATLAS), Phys. Lett. **B800**, 135082 (2020), [arXiv:1908.08461].
- [320] A. Heister *et al.* (ALEPH), Phys. Lett. **B543**, 173 (2002), [hep-ex/0206070]; J. Abdallah *et al.* (DELPHI), Phys. Lett. **B590**, 21 (2004), [hep-ex/0404014]; P. Achard *et al.* (L3), Phys. Lett. **B549**, 290 (2002), [hep-ex/0210041]; G. Abbiendi *et al.* (OPAL), Phys. Lett. **B521**, 181 (2001), [hep-ex/0110009].
- [321] F. D. Aaron *et al.* (H1), Phys. Lett. **B678**, 450 (2009), [arXiv:0904.3876].
- [322] H. Abramowicz *et al.* (ZEUS), Phys. Lett. **B708**, 27 (2012), [arXiv:1111.3901].
- [323] M. Beneke *et al.*, in “1999 CERN Workshop on standard model physics (and more) at the LHC, CERN, Geneva, Switzerland, 25-26 May: Proceedings,” 419–529 (2000), [hep-ph/0003033], URL <http://weblib.cern.ch/abstract?CERN-TH-2000-100>.
- [324] V. F. Obraztsov, S. R. Slabospitsky and O. P. Yushchenko, Phys. Lett. **B426**, 393 (1998), [hep-ph/9712394].
- [325] T. Carli, D. Dannheim and L. Bellagamba, Mod. Phys. Lett. **A19**, 1881 (2004), [hep-ph/0402012].
- [326] V. M. Abazov *et al.* (D0), Phys. Rev. Lett. **102**, 092002 (2009), [arXiv:0901.0151].
- [327] V. M. Abazov *et al.* (DØ Collab.), DØ conference note 5838 (2009).
- [328] V. M. Abazov *et al.* (D0), Phys. Lett. **B708**, 21 (2012), [arXiv:1110.4592].
- [329] ATLAS Collab., ATLAS-CONF-2013-032.
- [330] T. Aaltonen *et al.* (CDF), Phys. Rev. Lett. **101**, 192002 (2008), [arXiv:0805.2109].
- [331] V. M. Abazov *et al.* (D0), Phys. Lett. **B701**, 313 (2011), [arXiv:1103.4574].
- [332] V. M. Abazov *et al.* (D0), Phys. Lett. **B693**, 81 (2010), [arXiv:1006.3575].
- [333] S. Chatrchyan *et al.* (CMS), Phys. Rev. Lett. **112**, 17, 171802 (2014), [arXiv:1312.4194].
- [334] A. M. Sirunyan *et al.* (CMS), JHEP **07**, 003 (2017), [arXiv:1702.01404].
- [335] M. Aaboud *et al.* (ATLAS), JHEP **07**, 176 (2018), [arXiv:1803.09923].
- [336] A. M. Sirunyan *et al.* (CMS), JHEP **06**, 102 (2018), [arXiv:1712.02399].
- [337] M. Aaboud *et al.* (ATLAS), JHEP **05**, 123 (2019), [arXiv:1812.11568].



## 61. Form Factors for Radiative Pion and Kaon Decays

Revised August 2019 by M.A. Bychkov (Virginia U.) and G. D'Ambrosio (INFN, Napoli).

The radiative decays,  $\pi^\pm \rightarrow l^\pm \nu \gamma$  and  $K^\pm \rightarrow l^\pm \nu \gamma$ , with  $l$  standing for an  $e$  or a  $\mu$ , and  $\gamma$  for a real or virtual photon ( $e^+e^-$  pair), provide a powerful tool to investigate the hadronic structure of pions and kaons. The structure-dependent part  $SD_i$  of the amplitude describes the emission of photons from virtual hadronic states, and is parametrized in terms of form factors  $V, A$ , (vector, axial vector), in the standard description [1–4]. Note that in the Listings and some literature, equivalent nomenclature  $F_V$  and  $F_A$  for the vector and axial form factors is often used. Exotic, non-standard contributions like  $i = T, S$  (tensor, scalar) have also been considered. Apart from the SD terms, there is also the Inner Bremsstrahlung amplitude, IB, corresponding to photon radiation from external charged particles and described by Low theorem in terms of the physical decay  $\pi^\pm(K^\pm) \rightarrow l^\pm \nu$ . Experiments try to optimize their kinematics so as to minimize the IB part of the amplitude.

The SD amplitude in its standard form is given as

$$M(SD_V) = \frac{-eG_F U_{qq'}}{\sqrt{2}m_P} \epsilon^\mu l^\nu V^P \epsilon_{\mu\nu\sigma\tau} k^\sigma q^\tau \quad (61.1)$$

$$M(SD_A) = \frac{-ieG_F U_{qq'}}{\sqrt{2}m_P} \epsilon^\mu l^\nu \{A^P [(qk - k^2)g_{\mu\nu} - q_\mu k_\nu] + R^P k^2 g_{\mu\nu}\}, \quad (61.2)$$

which contains an additional axial form factor  $R^P$  which only can be accessed if the photon remains virtual.  $U_{qq'}$  is the Cabibbo-Kobayashi-Maskawa mixing-matrix element;  $\epsilon^\mu$  is the polarization vector of the photon (or the effective vertex,  $\epsilon^\mu = (e/k^2)\bar{u}(p_-)\gamma^\mu v(p_+)$ , of the  $e^+e^-$  pair);  $\ell^\nu = \bar{u}(p_\nu)\gamma^\nu(1 - \gamma_5)v(p_\ell)$  is the lepton-neutrino current;  $q$  and  $k$  are the meson and photon four-momenta ( $k = p_+ + p_-$  for virtual photons); and  $P$  stands for  $\pi$  or  $K$ .

For decay processes where the photon is real, the partial decay width can be written in analytical form as a sum of IB, SD, and IB/SD interference terms INT [1,4]:

$$\frac{d^2\Gamma_{P \rightarrow \ell\nu\gamma}}{dx dy} = \frac{d^2(\Gamma_{IB} + \Gamma_{SD} + \Gamma_{INT})}{dx dy}$$

$$= \frac{\alpha}{2\pi} \Gamma_{P \rightarrow \ell\nu} \frac{1}{(1-r)^2} \left\{ \text{IB}(x, y) + \frac{1}{r} \left( \frac{m_P}{2f_P} \right)^2 \left[ (V+A)^2 \text{SD}^+(x, y) + (V-A)^2 \text{SD}^-(x, y) \right] + \epsilon_P \frac{m_P}{f_P} \left[ (V+A) S_{INT}^+(x, y) + (V-A) S_{INT}^-(x, y) \right] \right\}. \quad (61.3)$$

Here

$$\text{IB}(x, y) = \left[ \frac{1-y+r}{x^2(x+y-1-r)} \right] \left[ x^2 + 2(1-x)(1-r) - \frac{2xr(1-r)}{x+y-1-r} \right]$$

$$\text{SD}^+(x, y) = (x+y-1-r) \left[ (x+y-1)(1-x) - r \right]$$

$$\text{SD}^-(x, y) = (1-y+r) \left[ (1-x)(1-y) + r \right]$$

$$S_{INT}^+(x, y) = \left[ \frac{1-y+r}{x(x+y-1-r)} \right] \left[ (1-x)(1-x-y) + r \right]$$

$$S_{INT}^-(x, y) = \left[ \frac{1-y+r}{x(x+y-1-r)} \right] \left[ x^2 - (1-x)(1-x-y) - r \right] \quad (61.4)$$

where  $x = 2E_\gamma/m_P$ ,  $y = 2E_\ell/m_P$ ,  $r = (m_\ell/m_P)^2$ ,  $f_P$  is the meson decay constant, and  $\epsilon_P$  is +1 for pions and -1 for kaons. The

structure dependent terms  $SD^+$  and  $SD^-$  are shown in Fig. 1. The  $SD^-$  term is maximized in the same kinematic region where overwhelming IB term dominates (along  $x+y=1$  diagonal). Thus experimental yields with less background are dominated by  $SD^+$  contribution and proportional to  $A^P + V^P$  making simultaneous precise determination of the form factors difficult.

Recently, formulas 61.3 and 61.4 have been extended to describe polarized distributions in radiative meson and muon decays [5].

The ‘‘helicity’’ factor  $r$  is responsible for the enhancement of the SD over the IB amplitude in the decays  $\pi^\pm \rightarrow e^\pm \nu \gamma$ , while  $\pi^\pm \rightarrow \mu^\pm \nu \gamma$  is dominated by IB. Interference terms are important for the decay  $K^\pm \rightarrow \mu^\pm \nu \gamma$  [6], but contribute only a few percent correction to pion decays. However, they provide the basis for determining the signs of  $V$  and  $A$ . Radiative corrections to the decay  $\pi^+ \rightarrow e^+ \nu \gamma$  have to be taken into account in the analysis of the precision experiments. They make up to 4% corrections in the total decay rate [7]. In  $\pi^\pm \rightarrow e^\pm \nu e^+ e^-$  and  $K^\pm \rightarrow \ell^\pm \nu e^+ e^-$  decays, all three form factors,  $V^P$ ,  $A^P$ , and  $R^P$ , can be determined [8, 9].

Theoretically, the first non-trivial  $\chi PT$  contributions to  $A^P$  and  $V^P$  appear at  $\mathcal{O}(p^4)$  [4], respectively from Gasser-Leutwyler coefficients,  $L_i$ 's, and the anomalous lagrangian:

$$A^P = \frac{4\sqrt{2}M_P}{F_\pi} (L_9^r + L_{10}^r), \quad V^P = \frac{\sqrt{2}M_P}{8\pi^2 F_\pi}. \quad (61.5)$$

In case of the kaon  $A^K = 0.042$  and  $V^K = 0.096$ .  $\mathcal{O}(p^6)$  contributions to  $A^K$  can be predicted accurately: they are flat in the momentum dependence and shift the  $\mathcal{O}(p^4)$  value to 0.034.  $\mathcal{O}(p^6)$  contributions to  $V^K$  are model dependent and can be approximated by a form factor linearly dependent on momentum. For example, when looking at the spread of results obtained within two different models, the constant piece of this linear form factor is shifted to  $0.078 \pm 0.005$  [1, 2, 4].

We give the experimental  $\pi^\pm$  form factors  $V^\pi$ ,  $A^\pi$ , and  $R^\pi$  in the Listings. In the  $K^\pm$  Listings, we give the extracted sum  $A^K + V^K$  and difference  $A^K - V^K$ , as well as  $V^K$ ,  $A^K$  and  $R^K$ . In particular KLOE has measured for the constant piece of the form factor  $A^K + V^K = 0.125 \pm 0.007 \pm 0.001$  [10] while ISTRA+,  $V^K - A^K = 0.21 \pm 0.04 \pm 0.04$  [11].

The pion vector form factor,  $V^\pi$ , is related via CVC (Conserved Vector Current) to the  $\pi^0 \rightarrow \gamma\gamma$  decay width. The constant term is given by  $|V^\pi(0)| = (1/\alpha)\sqrt{2}\Gamma_{\pi^0 \rightarrow \gamma\gamma}/\pi m_{\pi^0}$  [3]. The resulting value,  $V^\pi(0) = 0.0259(9)$ , has been confirmed by calculations based on chiral perturbation theory ( $\chi PT$ ) [4], and by two experiments given in the Listings. A recent experiment by the PIBETA collaboration [12] obtained a  $V^\pi(0)$  that is in excellent agreement with the CVC hypothesis. It also measured the slope parameter  $a$  in  $V^\pi(s) = V^\pi(0)(1 + a \cdot s)$ , where  $s = (1 - 2E_\gamma/m_\pi)^2$ , and  $E_\gamma$  is the gamma energy in the pion rest frame:  $a = 0.095 \pm 0.058$ . A functional dependence on  $s$  is expected for all form factors. It becomes non-negligible in the case of  $V^\pi(s)$  when a wide range of photon momenta is recorded; proper treatment in the analysis of  $K$  decays is mandatory.

The form factor,  $R^P$ , can be related to the electromagnetic radius,  $r_P$ , of the meson [2]:  $R^P = \frac{1}{3}m_P f_P (r_P^2)$  using PCAC (Partial Conserved Axial vector Current).

In lowest order  $\chi PT$ , the ratio  $A^\pi/V^\pi$  is related to the pion electric polarizability  $\alpha_E = [\alpha/(8\pi^2 m_\pi f_\pi^2)] \times A^\pi/V^\pi$  [13]. Direct experimental and theoretical status of pion polarizability studies currently is not settled. Most recent theoretical predictions from  $\chi PT$  [14] and experimental results from COMPASS collaboration [15] favor a small value of pion polarizability  $\alpha_\pi \sim (2 \div 3) \times 10^{-4} \text{ fm}^3$ . Dispersive analysis of  $\gamma\gamma \rightarrow \pi^+\pi^-$  crosssection [16] and experimental results from MAMI collaboration [17] report a much larger value of  $\alpha_\pi \sim 6 \times 10^{-4} \text{ fm}^3$ . Precise measurement of the pion form factors by PIBETA collaboration favors smaller values of polarizability  $\alpha_\pi = 2.7_{-0.5}^{+0.6} \times 10^{-4} \text{ fm}^3$ .

Several searches for the exotic form factors  $F_T^\pi$ ,  $F_T^K$  (tensor), and  $F_S^K$  (scalar) have been pursued in the past. In particular,  $F_T^\pi$  has been brought into focus by experimental as well as theoretical work [18]. New high-statistics data from the PIBETA collabora-

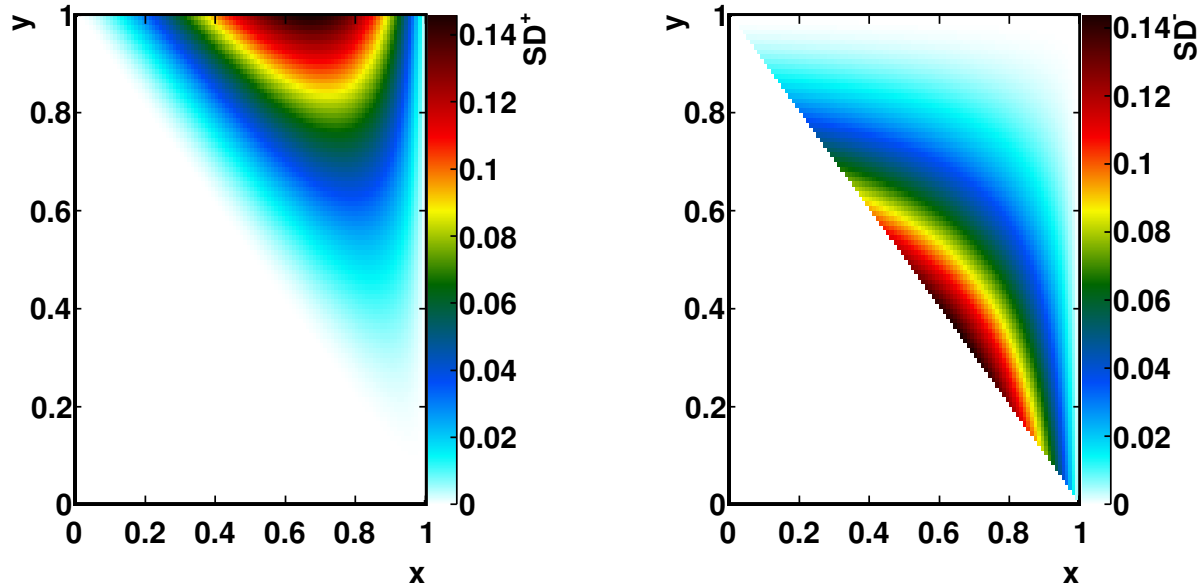


Figure 61.1: Components of the structure dependent terms of the decay width. Left:  $SD^+$ , right:  $SD^-$

tion have been re-analyzed together with an additional data set optimized for low backgrounds in the radiative pion decay. In particular, lower beam rates have been used in order to reduce the accidental background, thereby making the treatment of systematic uncertainties easier and more reliable. The PIBETA analysis now restricts  $F_T^\pi$  to the range  $-5.2 \times 10^{-4} < F_T^\pi < 4.0 \times 10^{-4}$  at a 90% confidence limit [12]. This result is in excellent agreement with the most recent theoretical work [4].

Precision measurements of radiative pion and kaon decays are effective tools to study QCD in the non-perturbative region and are of interest beyond the scope of radiative decays. Meanwhile other processes such as  $\pi^+ \rightarrow e^+\nu$  that seem to be better suited to search for new physics at the precision frontier are currently studied. The advantages of such process are the very accurate and reliable theoretical predictions and the more straightforward experimental analysis.

#### References

- [1] D. A. Bryman, P. Depommier and C. Leroy, Phys. Rept. **88**, 151 (1982), see our note on “Decay Constants of Charged Pseudoscalar Mesons” elsewhere in this *Review*; S. G. Brown and S. A. Bludman, Phys. Rev. **136**, B1160 (1964); P. DeBaenst and J. Pestieau, Nuovo Cimento **A53**, 137 (1968).
- [2] W. T. Chu, T. Ebata and D. M. Scott, Phys. Rev. **166**, 1577 (1968); D. Yu. Bardin and E. A. Ivanov, Sov. J. Part. Nucl. **7**, 286 (1976), [Fiz. Elem. Chast. Atom. Yadra7,726(1976)]; A. Kersch and F. Scheck, Nucl. Phys. **B263**, 475 (1986).
- [3] V.G. Vaks and B.L. Ioffe, Nuovo Cimento **10**, 342 (1958); V.F. Muller, Z. Phys. **173**, 438 (1963).
- [4] C. Q. Geng, I.-L. Ho and T. H. Wu, Nucl. Phys. **B684**, 281 (2004), [hep-ph/0306165]; J. Bijnens and P. Talavera, Nucl. Phys. **B489**, 387 (1997), [hep-ph/9610269]; V. Mateu and J. Portoles, Eur. Phys. J. **C52**, 325 (2007), [arXiv:0706.1039]; R. Unterdorfer and H. Pichl, Eur. Phys. J. **C55**, 273 (2008), [arXiv:0801.2482]; V. Cirigliano *et al.*, Rev. Mod. Phys. **84**, 399 (2012), [arXiv:1107.6001].
- [5] E. Gabrielli and L. Trentadue, Nucl. Phys. **B792**, 48 (2008), [hep-ph/0507191].
- [6] S. Adler *et al.* (E787), Phys. Rev. Lett. **85**, 2256 (2000), [hep-ex/0003019].
- [7] E. A. Kuraev, Yu. M. Bystritsky and E. P. Velicheva, Phys. Rev. **D69**, 114004 (2004), [hep-ph/0310275]; R. Unterdorfer and H. Pichl have treated radiative corrections of the structure terms to lowest order within  $\chi PT$  for the first time. See the reference under [4].
- [8] S. Egli *et al.* (SINDRUM), Phys. Lett. **B175**, 97 (1986).
- [9] A. A. Poblaguev *et al.*, Phys. Rev. Lett. **89**, 061803 (2002), [hep-ex/0204006].
- [10] F. Ambrosino *et al.* (KLOE), Eur. Phys. J. **C64**, 627 (2009), [Erratum: Eur. Phys. J.65,703(2010)], [arXiv:0907.3594].
- [11] V. A. Duk *et al.* (ISTRA+), Phys. Lett. **B695**, 59 (2011), [arXiv:1005.3517].
- [12] D. Pocanic *et al.*, Phys. Rev. Lett. **93**, 181803 (2004), [hep-ex/0312030]; E. Frlez *et al.*, Phys. Rev. Lett. **93**, 181804 (2004), [hep-ex/0312029]; M. Bychkov *et al.*, Phys. Rev. Lett. **103**, 051802 (2009), [arXiv:0804.1815].
- [13] J. F. Donoghue and B. R. Holstein, Phys. Rev. **D40**, 2378 (1989).
- [14] J. Gasser, M. A. Ivanov and M. E. Sainio, Nucl. Phys. **B745**, 84 (2006), [hep-ph/0602234].
- [15] C. Adolph *et al.* (COMPASS), Phys. Rev. Lett. **114**, 062002 (2015), [arXiv:1405.6377].
- [16] L. V. Fil’kov and V. L. Kashevarov, Phys. Rev. **C73**, 035210 (2006), [arXiv:nucl-th/0512047].
- [17] J. Ahrens *et al.*, Eur. Phys. J. **A23**, 113 (2005), [arXiv:nucl-ex/0407011].
- [18] A. A. Poblaguev, Phys. Lett. **B238**, 108 (1990); V. N. Bolotov *et al.*, Phys. Lett. **B243**, 308 (1990); V. M. Belyaev and I. I. Kogan, Phys. Lett. **B280**, 238 (1992); A. V. Chernyshev *et al.*, Mod. Phys. Lett. **A12**, 1669 (1997); A. A. Poblaguev, Phys. Rev. **D68**, 054020 (2003), [hep-ph/0307166]; M. V. Chizhov, Phys. Part. Nucl. Lett. **2**, 193 (2005), [Pisma Fiz. Elem. Chast. Atom. Yadra2005,no.4,7(2005)], [hep-ph/0402105].

## 62. Scalar Mesons below 2 GeV

Revised August 2019 by C. Amsler (Stefan Meyer Inst.), S. Eidelman (Budker Inst., Novosibirsk; Novosibirsk U.), T. Gutsche (Tübingen U.), C. Hanhart (Jülich) and S. Spanier (Tennessee U.).

### 62.1 Introduction

In contrast to the vector and tensor mesons, the identification of the scalar mesons is a long-standing puzzle. Scalar resonances are difficult to resolve because some of them have large decay widths which cause a strong overlap between resonances and background. In addition, several decay channels sometimes open up within a short mass interval (*e.g.* at the  $K\bar{K}$  and  $\eta\eta$  thresholds), producing cusps in the line shapes of the near-by resonances. Furthermore, one expects non- $q\bar{q}$  scalar objects, such as glueballs and multi-quark states in the mass range below 2 GeV (for reviews see, *e.g.*, Refs. [1–5] and the mini-review on *non- $q\bar{q}$  states* in this Review of Particle Physics (RPP)).

Light scalars are produced, for example, in  $\pi N$  scattering on polarized/unpolarized targets,  $p\bar{p}$  annihilation, central hadronic production,  $J/\psi$ ,  $B$ -,  $D$ - and  $K$ -meson decays,  $\gamma\gamma$  formation, and  $\phi$  radiative decays. Especially for the lightest scalar mesons simple parameterizations fail and more advanced theory tools are necessary to extract the resonance parameters from data. In the analyses available in the literature fundamental properties of the amplitudes such as unitarity, analyticity, Lorentz invariance, chiral and flavor symmetry are implemented at different levels of rigor. Especially, chiral symmetry implies the appearance of zeros close to the threshold in elastic  $S$ -wave scattering amplitudes involving soft pions [6, 7], which may be shifted or removed in associated production processes [8]. The methods employed are the  $K$ -matrix formalism, the  $N/D$ -method, the Dalitz–Tuan ansatz, unitarized quark models with coupled channels, effective chiral field theories and the linear sigma model, *etc.* Dynamics near the lowest two-body thresholds in some analyses are described by crossed channel ( $t$ ,  $u$ ) meson exchange or with an effective range parameterization instead of, or in addition to, resonant features in the  $s$ -channel. Dispersion theoretical approaches are applied to pin down the location of resonance poles for the low-lying states [9–12].

The mass and width of a resonance are found from the position of the nearest pole in the process amplitude ( $T$ -matrix or  $S$ -matrix) at an unphysical sheet of the complex energy plane, traditionally labeled as

$$\sqrt{s_{\text{Pole}}} = M - i\Gamma/2. \quad (62.1)$$

It is important to note that the pole of a Breit-Wigner parameterization agrees with this pole position only for narrow and well-separated resonances, far away from the opening of decay channels. For a detailed discussion of this issue we refer to the review on *Resonances* in this RPP.

In this note, we discuss the light scalars below 2 GeV organized in the listings under the entries ( $I = 1/2$ )  $K_0^*(700)$  (or  $\kappa$ ),  $K_0^*(1430)$ , ( $I = 1$ )  $a_0(980)$ ,  $a_0(1450)$ , and ( $I = 0$ )  $f_0(500)$  (or  $\sigma$ ),  $f_0(980)$ ,  $f_0(1370)$ ,  $f_0(1500)$ , and  $f_0(1710)$ . This list is minimal and does not necessarily exhaust the list of actual resonances. The ( $I = 2$ )  $\pi\pi$  and ( $I = 3/2$ )  $K\pi$  phase shifts do not exhibit any resonant behavior.

### 62.2 The $I = 1/2$ States

The  $K_0^*(1430)$  [13] is perhaps the least controversial of the light scalar mesons. The  $K\pi$   $S$ -wave scattering has two possible isospin channels,  $I=1/2$  and  $I=3/2$ . The  $I=3/2$  wave is elastic and repulsive up to 1.7 GeV [14] and contains no known resonances. The  $I=1/2$   $K\pi$  phase shift, measured from about 100 MeV above threshold in  $Kp$  production, rises smoothly, passes  $90^\circ$  at 1350 MeV, and continues to rise to about  $170^\circ$  at 1600 MeV. The first important inelastic threshold is  $K\eta'(958)$ . In the inelastic region the continuation of the amplitude is uncertain since the partial-wave decomposition has several solutions. The data are extrapolated towards the  $K\pi$  threshold using effective range type formulas [13, 15] or chiral perturbation predictions [16, 17]. From analyses using unitarized amplitudes there is agreement on the presence of a resonance pole around 1410 MeV having a width of

about 300 MeV. With reduced model dependence, Ref. [18] finds a larger width of 500 MeV.

Similar to the situation for the  $f_0(500)$ , discussed in the next section, the presence and properties of the light  $K_0^*(700)$  (or  $\kappa$ ) meson in the 700–900 MeV region are difficult to establish since it appears to have a very large width ( $\Gamma \approx 500$  MeV) and resides close to the  $K\pi$  threshold. Hadronic  $D$ - and  $B$ -meson decays provide additional data points in the vicinity of the  $K\pi$  threshold and are discussed in detail in the *Review on Multibody Charm Analyses* in this RPP. Precision information from semileptonic  $D$  decays avoiding the theoretically more demanding final states with three strongly interacting particles is not available. BES II [19] (re-analyzed in [20]) finds a  $K_0^*(700)$ -like structure in  $J/\psi$  decays to  $\bar{K}^{*0}(892)K^+\pi^-$  where  $K_0^*(700)$  recoils against the  $K^*(892)$ . Also clean with respect to final-state interaction is the decay  $\tau^- \rightarrow K_S^0\pi^-\nu_\tau$  studied by Belle [21], with  $K_0^*(700)$  parameters fixed to those of Ref. [19].

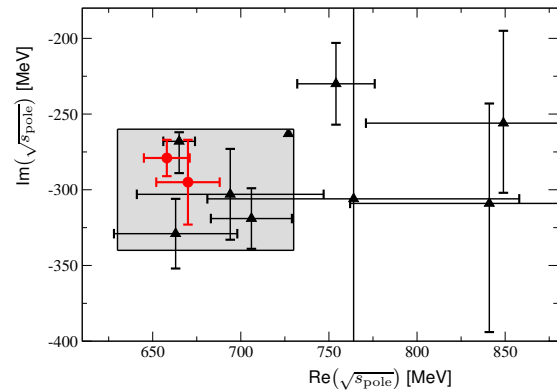


Figure 62.1: Location of the  $K_0^*(700)$  (or  $\kappa$ ) poles in the complex energy plane. Circles denote the results of the most refined analyses based on dispersion relations, while all other analyses quoted in the listings are denoted by triangles. The corresponding references are given in the listing.

Some authors find a  $K_0^*(700)$  pole in their phenomenological analysis (see, *e.g.*, [22–33]), while others do not need to include it in their fits (see, *e.g.*, [17, 34–37]). Similarly to the case of the  $f_0(500)$  discussed below, all works including constraints from chiral symmetry at low energies naturally seem to find a light  $K_0^*(700)$  below 800 MeV, see, *e.g.*, [38–42]. In these works the  $K_0^*(700)$ ,  $f_0(500)$ ,  $f_0(980)$  and  $a_0(980)$  appear to form a nonet [39, 40]. Additional evidence for this assignment is presented in Ref. [12], where the couplings of the nine states to  $q\bar{q}$  sources were compared. The same low-lying scalar nonet was also found earlier in the unitarized quark model of Ref. [41]. The analysis of Ref. [43] is based on the Roy-Steiner equations, which include analyticity and crossing symmetry. Ref. [44] uses the Padé method to extract pole parameters after refitting scattering data constrained to satisfy forward dispersion relations. Both arrive at compatible pole positions for the  $K_0^*(700)$  that are consistent with the pole parameters deduced either from other theoretical methods or Breit-Wigner fits. This is illustrated in Fig. 62.1. The compilation in this figure is used as justification for the range of pole parameters of the  $K_0^*(700)$  we quote as "our estimate", namely

$$\sqrt{s_{\text{Pole}}^{\kappa}} = (630 - 730) - i(260 - 340) \text{ MeV}. \quad (62.2)$$

### 62.3 The $I = 1$ States

Two isovector scalar states are known below 2 GeV, the  $a_0(980)$  and the  $a_0(1450)$ . Independent of any model, the  $K\bar{K}$  component in the  $a_0(980)$  wave function must be large: it lies just below the opening of the  $K\bar{K}$  channel to which it strongly couples [15, 45]. This generates an important cusp-like behavior in the resonant amplitude. Hence, its mass and width parameters are strongly distorted. To reveal its true coupling constants, a coupled-channel model with energy-dependent widths and mass

shift contributions is necessary. All listed  $a_0(980)$  measurements agree on a mass position value near 980 MeV, but the width takes values between 50 and 100 MeV, mostly due to the different models. For example, the analysis of the  $p\bar{p}$ -annihilation data [15] using a unitary  $K$ -matrix description finds a width as determined from the  $T$ -matrix pole of  $92 \pm 8$  MeV, while the observed width of the peak in the  $\pi\eta$  mass spectrum is about 45 MeV.

The relative coupling  $K\bar{K}/\pi\eta$  is determined indirectly from  $f_1(1285)$  [46–48] or  $\eta(1410)$  decays [49–51], from the line shape observed in the  $\pi\eta$  decay mode [52–55], or from the coupled-channel analysis of the  $\pi\pi\eta$  and  $K\bar{K}\pi$  final states of  $p\bar{p}$  annihilation at rest [15].

The  $a_0(1450)$  is seen in  $p\bar{p}$  annihilation experiments with stopped and higher momenta antiprotons, with a mass of about 1450 MeV or close to the  $a_2(1320)$  meson which is typically a dominant feature. A contribution from  $a_0(1450)$  is also found in the analysis of the  $D^\pm \rightarrow K^+K^-\pi^\pm$  [56] and  $D^0 \rightarrow K_S^0K^\pm\pi^\mp$  [57] decay.

## 62.4 The $I = 0$ States

The  $I = 0$ ,  $J^{PC} = 0^{++}$  sector is the most complex one, both experimentally and theoretically. The data have been obtained from the  $\pi\pi$ ,  $K\bar{K}$ ,  $\eta\eta$ ,  $4\pi$ , and  $\eta\eta'(958)$  systems produced in  $S$ -wave. Analyses based on several different production processes conclude that probably four poles are needed in the mass range from  $\pi\pi$  threshold to about 1600 MeV. The claimed isoscalar resonances are found under separate entries  $f_0(500)$  (or  $\sigma$ ),  $f_0(980)$ ,  $f_0(1370)$ , and  $f_0(1500)$ .

For discussions of the  $\pi\pi$   $S$  wave below the  $K\bar{K}$  threshold and on the long history of the  $f_0(500)$ , which was suggested in linear sigma models more than 50 years ago, see our reviews in previous editions and the review [5].

Information on the  $\pi\pi$   $S$ -wave phase shift  $\delta_J^I = \delta_0^0$  was already extracted many years ago from  $\pi N$  scattering [58–60], and near threshold from the  $K_{e4}$ -decay [61]. The kaon decays were later revisited leading to consistent data, however, with very much improved statistics [62, 63]. The reported  $\pi\pi \rightarrow K\bar{K}$  cross sections [64–67] have large uncertainties. The  $\pi N$  data have been analyzed in combination with high-statistics data (see entries labeled as RVUE for re-analyses of the data). The  $2\pi^0$  invariant mass spectra of the  $p\bar{p}$  annihilation at rest [68–70] and the central collision [71] do not show a distinct resonance structure below 900 MeV, but these data are consistently described with the standard solution for  $\pi N$  data [59, 72], which allows for the existence of the broad  $f_0(500)$ . An enhancement is observed in the  $\pi^+\pi^-$  invariant mass near threshold in the decays  $D^+ \rightarrow \pi^+\pi^-\pi^+$  [73–75] and  $J/\psi \rightarrow \omega\pi^+\pi^-$  [76, 77], and in  $\psi(2S) \rightarrow J/\psi\pi^+\pi^-$  with very limited phase space [78, 79].

The precise  $f_0(500)$  (or  $\sigma$ ) pole is difficult to establish because of its large width, and because it can certainly not be modeled by a naive Breit-Wigner resonance. The  $\pi\pi$  scattering amplitude shows an unusual energy dependence due to the presence of a zero in the unphysical regime close to the threshold [6, 7], required by chiral symmetry, and possibly due to crossed channel exchanges, the  $f_0(1370)$ , and other dynamical features. However, most of the analyses listed under  $f_0(500)$  agree on a pole position near  $(500 - i250)$  MeV. In particular, analyses of  $\pi\pi$  data that include unitarity,  $\pi\pi$  threshold behavior, strongly constrained by the  $K_{e4}$  data, and the chiral symmetry constraints from Adler zeroes and/or scattering lengths find a light  $f_0(500)$ , see, e.g., [80, 81].

Precise pole positions with an uncertainty of less than 20 MeV (see our table for the  $T$ -matrix pole) were extracted by use of Roy equations, which are twice subtracted dispersion relations derived from crossing symmetry and analyticity. In Ref. [10] the subtraction constants were fixed to the  $S$ -wave scattering lengths  $a_0^0$  and  $a_2^0$  derived from matching Roy equations and two-loop chiral perturbation theory [9]. The only additional relevant input to fix the  $f_0(500)$  pole turned out to be the  $\pi\pi$ -wave phase shifts at 800 MeV. The analysis was improved further in Ref. [12]. Alternatively, in Ref. [11] only data were used as input inside Roy equations. In that reference also once-subtracted Roy-like equations, called GKPY equations, were used, since the extrapolation

into the complex plane based on the twice subtracted equations leads to larger uncertainties mainly due to the limited experimental information on the isospin-2  $\pi\pi$  scattering length. Ref. [82] uses Padé approximants for the analytic continuation. All these extractions find consistent results. Using analyticity and unitarity only to describe data from  $K_{2\pi}$  and  $K_{e4}$  decays, Ref. [83] finds consistent values for the pole position and the scattering length  $a_0^0$ . The importance of the  $\pi\pi$  scattering data for fixing the  $f_0(500)$  pole is nicely illustrated by comparing analyses of  $p\bar{p} \rightarrow 3\pi^0$  omitting [68, 84] or including [69, 85] information on  $\pi\pi$  scattering: while the former analyses find an extremely broad structure above 1 GeV, the latter find  $f_0(500)$  masses of the order of 400 MeV.

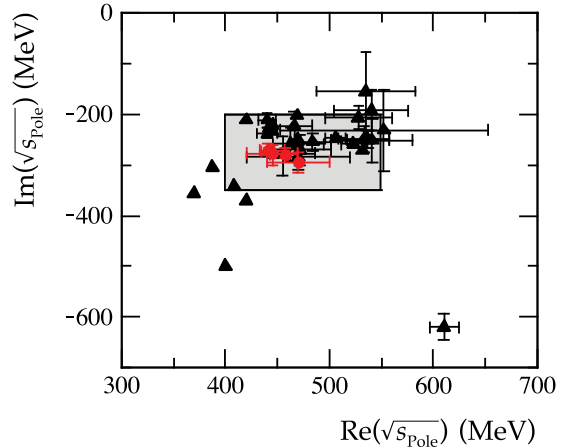


Figure 62.2: Location of the  $f_0(500)$  (or  $\sigma$ ) poles in the complex energy plane. Circles denote the recent analyses based on Roy(-like) dispersion relations, while all other analyses are denoted by triangles. The corresponding references are given in the listing.

As a result of the sensitivity of the extracted  $f_0(500)$  pole position on the high accuracy low energy  $\pi\pi$  scattering data [62, 63], the currently quoted range of pole positions for the  $f_0(500)$ , namely

$$\sqrt{s_{\text{Pole}}} = (400 - 550) - i(200 - 350) \text{ MeV}, \quad (62.3)$$

in the listing was fixed including only those analyses consistent with these data, Refs. [26] [29] [39] [41] [42] [54] [69] [78–81, 83] [75, 86–99] as well as the advanced dispersion analyses [9–12, 82]. The pole positions from those references are compared to the range of pole positions quoted above in Fig. 62.2. Note that this range is labeled as 'our estimate' — it is not an average over the quoted analyses but is chosen to include the bulk of the analyses consistent with the mentioned criteria. An averaging procedure is not justified, since the analyses use overlapping or identical data sets.

If one uses just the most advanced dispersive analyses of Refs. [9–12] shown as solid dots in Fig. 62.2 to determine the pole location of the  $f_0(500)$  the range narrows down to [5]

$$\sqrt{s_{\text{Pole}}} = (449_{-16}^{+22}) - i(275 \pm 12) \text{ MeV}, \quad (62.4)$$

which is labeled as 'conservative dispersive estimate' in this reference.

Due to the large strong width of the  $f_0(500)$  an extraction of its two-photon width directly from data is not possible. Thus, the values for  $\Gamma(\gamma\gamma)$  quoted in the literature as well as the listing are based on the expression in the narrow width approximation [100]  $\Gamma(\gamma\gamma) \simeq \alpha^2 |g_\gamma|^2 / (4\text{Re}(\sqrt{s_{\text{Pole}}}))$  where  $g_\gamma$  is derived from the residue at the  $f_0(500)$  pole to two photons and  $\alpha$  denotes the electromagnetic fine structure constant. The explicit form of the expression may vary between different authors due to different definitions of the coupling constant, however, the expression given for  $\Gamma(\gamma\gamma)$  is free of ambiguities. According to Refs. [101, 102], the data for  $f_0(500) \rightarrow \gamma\gamma$  are consistent with what is expected for a

two-step process of  $\gamma\gamma \rightarrow \pi^+\pi^-$  via pion exchange in the  $t$ - and  $u$ -channel, followed by a final state interaction  $\pi^+\pi^- \rightarrow \pi^0\pi^0$ . The same conclusion is drawn in Ref. [103] where the bulk part of the  $f_0(500) \rightarrow \gamma\gamma$  decay width is dominated by re-scattering. Therefore, it might be difficult to learn anything new about the nature of the  $f_0(500)$  from its  $\gamma\gamma$  coupling. For the most recent work on  $\gamma\gamma \rightarrow \pi\pi$ , see [83–106]. There are theoretical indications (e.g., [107–137]) that the  $f_0(500)$  pole behaves differently from a  $q\bar{q}$ -state – see next section and the mini-review on *non  $q\bar{q}$ -states* in this RPP for details.

The  $f_0(980)$  overlaps strongly with the background represented mainly by the  $f_0(500)$  and the  $f_0(1370)$ . This can lead to a dip in the  $\pi\pi$  spectrum at the  $K\bar{K}$  threshold. It changes from a dip into a peak structure in the  $\pi^0\pi^0$  invariant mass spectrum of the reaction  $\pi^-p \rightarrow \pi^0\pi^0n$  [111], with increasing four-momentum transfer to the  $\pi^0\pi^0$  system, which means increasing the  $a_1$ -exchange contribution in the amplitude, while the  $\pi$ -exchange decreases. The  $f_0(500)$  and the  $f_0(980)$  are also observed in data for radiative decays ( $\phi \rightarrow f_0\gamma$ ) from SND [112,113], CMD2 [114], and KLOE [115,116]. A dispersive analysis was used to simultaneously pin down the pole parameters of both the  $f_0(500)$  and the  $f_0(980)$  [11]; the uncertainty in the pole position quoted for the latter state is of the order of 10 MeV, only. We now quote for the mass

$$M_{f_0(980)} = 990 \pm 20 \text{ MeV} . \quad (62.5)$$

which is a range not an average, but is labeled as 'our estimate'.

Analyses of  $\gamma\gamma \rightarrow \pi\pi$  data [117–119] underline the importance of the  $K\bar{K}$  coupling of  $f_0(980)$ , while the resulting two-photon width of the  $f_0(980)$  cannot be determined precisely [120]. The prominent appearance of the  $f_0(980)$  in the semileptonic  $D_s$  decays and decays of  $B$  and  $B_s$ -mesons implies a dominant ( $\bar{s}s$ ) component: those decays occur via weak transitions that alternatively result in  $\phi(1020)$  production. Ratios of decay rates of  $B$  and/or  $B_s$  mesons into  $J/\psi$  plus  $f_0(980)$  or  $f_0(500)$  were proposed to allow for an extraction of the flavor mixing angle and to probe the tetraquark nature of those mesons within a certain model [121] [122]. The phenomenological fits of the LHCb collaboration using the isobar model do neither allow for a contribution of the  $f_0(980)$  in the  $B \rightarrow J/\psi\pi\pi$  [123] nor for an  $f_0(500)$  in  $B_s \rightarrow J/\psi\pi\pi$  decays [124]. From the former analysis the authors conclude that their data is incompatible with a model where  $f_0(500)$  and  $f_0(980)$  are formed from two quarks and two antiquarks (tetraquarks) at the eight standard deviation level. In addition, they extract an upper limit for the mixing angle of 17° at 90% C.L. between the  $f_0(980)$  and the  $f_0(500)$  that would correspond to a substantial ( $\bar{s}s$ ) content in  $f_0(980)$  [123]. However, in a dispersive analysis of the same data that allows for a model-independent inclusion of the hadronic final state interactions in Ref. [125] a substantial  $f_0(980)$  contribution is also found in the  $B$ -decays putting into question the conclusions of Ref. [123].

Let us now deal with the  $f_0$ 's above 1 GeV. A meson resonance that is very well studied experimentally, is the  $f_0(1500)$  seen by the Crystal Barrel experiment in five decay modes:  $\pi\pi$ ,  $K\bar{K}$ ,  $\eta\eta$ ,  $\eta\eta'(958)$ , and  $4\pi$  [15,69,70]. Due to its interference with the  $f_0(1370)$  (and  $f_0(1710)$ ), the peak attributed to the  $f_0(1500)$  can appear shifted in invariant mass spectra. Therefore, the application of simple Breit-Wigner forms arrives at slightly different resonance masses for  $f_0(1500)$ . Analyses of central-production data of the likewise five decay modes Refs. [126,127] agree on the description of the  $S$ -wave with the one above. The  $p\bar{p}$ ,  $p\bar{n}/n\bar{p}$  measurements [70,128–130] show a single enhancement at 1400 MeV in the invariant  $4\pi$  mass spectra, which is resolved into  $f_0(1370)$  and  $f_0(1500)$  [131] [132]. The data on  $4\pi$  from central production [133] require both resonances, too, but disagree on the relative content of  $\rho\rho$  and  $f_0(500)f_0(500)$  in  $4\pi$ . All investigations agree that the  $4\pi$  decay mode represents about half of the  $f_0(1500)$  decay width and is dominant for  $f_0(1370)$ .

The determination of the  $\pi\pi$  coupling of  $f_0(1370)$  is aggravated by the strong overlap with the broad  $f_0(500)$  and  $f_0(1500)$ . Since it does not show up prominently in the  $2\pi$  spectra, its mass and width are difficult to determine. Multichannel analyses of hadronically produced two- and three-body final states agree on

a mass between 1300 MeV and 1400 MeV and a narrow  $f_0(1500)$ , but arrive at a somewhat smaller width for  $f_0(1370)$ .

The existence of the  $f_0(1370)$  is questioned in the analysis of the  $\pi^-p \rightarrow \pi^-\pi^-\pi^+p$  data from COMPASS [138]. However,  $D^0 \rightarrow \pi^+\pi^-\pi^+\pi^-$  data from CLEO-c require a contribution from  $f_0(500)f_0(1370) \rightarrow 4\pi$  [139].

## 62.5 Interpretation of the scalars below 1 GeV

In the literature, many suggestions are discussed, such as conventional  $q\bar{q}$  mesons, compact ( $qq$ )( $\bar{q}\bar{q}$ ) structures (tetraquarks) or meson-meson bound states. In addition, one expects a scalar glueball in this mass range. In reality, there can be superpositions of these components, and one often depends on models to determine the dominant one. Although we have seen progress in recent years, this question remains open. Here, we mention some of the present conclusions.

The  $f_0(980)$  and  $a_0(980)$  are often interpreted as compact tetraquark states [134–137,140] or  $K\bar{K}$  bound states [141]. The insight into their internal structure using two-photon widths [113] [142–148] is not conclusive. The  $f_0(980)$  appears as a peak structure in  $J/\psi \rightarrow \phi\pi^+\pi^-$  and in  $D_s$  decays without  $f_0(500)$  background, while being nearly invisible in  $J/\psi \rightarrow \omega\pi^+\pi^-$ . Based on that observation it is suggested that  $f_0(980)$  has a large  $s\bar{s}$  component, which according to Ref. [149] is surrounded by a virtual  $K\bar{K}$  cloud (see also Ref. [150]). Data on radiative decays ( $\phi \rightarrow f_0\gamma$  and  $\phi \rightarrow a_0\gamma$ ) from SND, CMD2, and KLOE (see above) are consistent with a prominent role of kaon loops. This observation is interpreted as evidence for a compact four-quark [151] or a molecular [152,153] nature of these states. Details of this controversy are given in the comments [154,155]; see also Ref. [156]. It remains quite possible that the states  $f_0(980)$  and  $a_0(980)$ , together with the  $f_0(500)$  and the  $K_0^*(700)$ , form a new low-mass state nonet of predominantly four-quark states, where at larger distances the quarks recombine into a pair of pseudoscalar mesons creating a meson cloud (see, e.g., Ref. [157]). Different QCD sum rule studies [158–162] do not agree on a tetraquark configuration for the same particle group.

Models that start directly from chiral Lagrangians, either in non-linear [25,42,80,152] or in linear [163–169] realization, predict the existence of the  $f_0(500)$  meson near 500 MeV. Here the  $f_0(500)$ ,  $a_0(980)$ ,  $f_0(980)$ , and  $K_0^*(700)$  (in some models the  $K_0^*(1430)$ ) would form a nonet (not necessarily  $q\bar{q}$ ). In the linear sigma models the lightest pseudoscalars appear as their chiral partners. In these models the light  $f_0(500)$  is often referred to as the "Higgs boson of strong interactions", since here the  $f_0(500)$  plays a role similar to the Higgs particle in electro-weak symmetry breaking: within the linear sigma models it is important for the mechanism of chiral symmetry breaking, which generates most of the proton mass, and what is referred to as the constituent quark mass.

In the non-linear approaches of Refs. [25] and [80] the above resonances together with the low lying vector states are generated starting from chiral perturbation theory predictions near the first open channel, and then by extending the predictions to the resonance regions using unitarity and analyticity.

Ref. [163] uses a framework with explicit resonances that are unitarized and coupled to the light pseudoscalars in a chirally invariant way. Evidence for a non- $\bar{q}q$  nature of the lightest scalar resonances is derived from their mixing scheme. In Ref. [164] the scheme is extended and applied to the decay  $\eta' \rightarrow \eta\pi\pi$ , which lead to the same conclusions. To identify the nature of the resonances generated from scattering equations, in Ref. [170] the large  $N_c$  behavior of the poles was studied, with the conclusion that, while the light vector states behave consistent with what is predicted for  $\bar{q}q$  states, the light scalars behave very differently. This finding provides strong support for a non- $\bar{q}q$  nature of the light scalar resonances. Note, the more refined study of Ref. [107] found, in case of the  $f_0(500)$ , in addition to a dominant non- $\bar{q}q$  nature, indications for a subdominant  $\bar{q}q$  component located around 1 GeV. Additional support for the non- $\bar{q}q$  nature of the  $f_0(500)$  is given in Ref. [171], where the connection between the pole of resonances and their Regge trajectories is analyzed.

A model-independent method to identify hadronic molecules goes back to a proposal by Weinberg [172], shown to be equiva-



lent to the pole counting arguments of [173–182] in Ref. [176]. The formalism allows one to extract the amount of molecular component in the wave function from the effective coupling constant of a physical state to a nearby continuum channel. It can be applied to near threshold states only and provided strong evidence that the  $f_0(980)$  is a  $\bar{K}K$  molecule, while the situation turned out to be less clear for the  $a_0(980)$  (see also Refs. [146, 148]) Further insights into  $a_0(980)$  and  $f_0(980)$  are expected from their mixing [177]. The corresponding signal predicted in Refs. [178, 179] was recently observed at BES III [180]. It turned out that in order to get a quantitative understanding of those data in addition to the mixing mechanism itself, some detailed understanding of the production mechanism seems necessary [181].

In the unitarized quark model with coupled  $q\bar{q}$  and meson-meson channels, the light scalars can be understood as additional manifestations of bare  $q\bar{q}$  confinement states, strongly mass shifted from the 1.3 - 1.5 GeV region and very distorted due to the strong  $^3P_0$  coupling to  $S$ -wave two-meson decay channels [182, 183]. Thus, in these models the light scalar nonet comprising the  $f_0(500)$ ,  $f_0(980)$ ,  $K_0^*(700)$ , and  $a_0(980)$ , as well as the nonet consisting of the  $f_0(1370)$ ,  $f_0(1500)$  (or  $f_0(1710)$ ),  $K_0^*(1430)$ , and  $a_0(1450)$ , respectively, are two manifestations of the same bare input states (see also Ref. [184]).

Other models with different groupings of the observed resonances exist and may, *e.g.*, be found in earlier versions of this review.

## 62.6 Interpretation of the $f_0$ 's above 1 GeV

The  $f_0(1370)$  and  $f_0(1500)$  decay mostly into pions ( $2\pi$  and  $4\pi$ ) while the  $f_0(1710)$  decays mainly into the  $K\bar{K}$  final states. The  $K\bar{K}$  decay branching ratio of the  $f_0(1500)$  is small [126] [185].

If one uses the naive quark model, it is natural to assume that the  $f_0(1370)$ ,  $a_0(1450)$ , and the  $K_0^*(1430)$  are in the same SU(3) flavor nonet, being the  $(u\bar{u} + d\bar{d})$ ,  $u\bar{d}$  and  $u\bar{s}$  states, probably mixing with the light scalars [186], while the  $f_0(1710)$  is the  $s\bar{s}$  state. Indeed, the production of  $f_0(1710)$  (and  $f_2'(1525)$ ) is observed in  $p\bar{p}$  annihilation [187] but the rate is suppressed compared to  $f_0(1500)$  (respectively,  $f_2(1270)$ ), as would be expected from the OZI rule for  $s\bar{s}$  states. The  $f_0(1500)$  would also qualify as a  $(u\bar{u} + d\bar{d})$  state, although it is very narrow compared to the other states and too light to be the first radial excitation.

However, in  $\gamma\gamma$  collisions leading to  $K_S^0 K_S^0$  [188] a spin-0 signal is observed at the  $f_0(1710)$  mass (together with a dominant spin-2 component), while the  $f_0(1500)$  is not observed in  $\gamma\gamma \rightarrow K\bar{K}$  nor  $\pi^+\pi^-$  [189]. In  $\gamma\gamma$  collisions leading to  $\pi^0\pi^0$  Ref. [190] reports the observation of a scalar around 1470 MeV albeit with large uncertainties on the mass and  $\gamma\gamma$  couplings. This state could be the  $f_0(1370)$  or the  $f_0(1500)$ . The upper limit from  $\pi^+\pi^-$  [189] excludes a large  $n\bar{n}$  (here  $n$  stands for the two lightest quarks) content for the  $f_0(1500)$  and hence points to a mainly  $s\bar{s}$  state [191]. This appears to contradict the small  $K\bar{K}$  decay branching ratio of the  $f_0(1500)$  and makes a  $q\bar{q}$  assignment difficult for this state. Hence the  $f_0(1500)$  could be mainly glue due the absence of a  $2\gamma$ -coupling, while the  $f_0(1710)$  coupling to  $2\gamma$  would be compatible with an  $s\bar{s}$  state. This is in accord with the recent high-statistics Belle data in  $\gamma\gamma \rightarrow K_S^0 K_S^0$  [192] in which the  $f_0(1500)$  is absent, while a prominent peak at 1710 MeV is observed with quantum numbers  $0^{++}$ , compatible with the formation of an  $s\bar{s}$  state. However, the  $2\gamma$ -couplings are sensitive to glue mixing with  $q\bar{q}$  [193].

Note that an isovector scalar, possibly the  $a_0(1450)$  (albeit at a lower mass of 1317 MeV) is observed in  $\gamma\gamma$  collisions leading to  $\eta\pi^0$  [194]. The state interferes destructively with the non-resonant background, but its  $\gamma\gamma$  coupling is comparable to that of the  $a_2(1320)$ , in accord with simple predictions (see, *e.g.*, Ref. [191]).

The small width of  $f_0(1500)$ , and its enhanced production at low transverse momentum transfer in central collisions [195–197] also favor  $f_0(1500)$  to be non- $q\bar{q}$ . In the mixing scheme of Ref. [193], which uses central production data from WA102 and the recent hadronic  $J/\psi$  decay data from BES [198, 199], glue is shared between  $f_0(1370)$ ,  $f_0(1500)$  and  $f_0(1710)$ . The  $f_0(1370)$  is mainly  $n\bar{n}$ , the  $f_0(1500)$  mainly glue and the  $f_0(1710)$  dominantly  $s\bar{s}$ . This agrees with previous analyses [200, 201].

However, alternative schemes have been proposed (*e.g.*, in [202–208], for detailed reviews see, *e.g.*, Ref. [1] and the mini-review on *non- $q\bar{q}$  states* in this Review of Particle Physics (RPP)). In Ref. [208], a large  $K^+K^-$  scalar signal reported by Belle in  $B$  decays into  $KK\bar{K}$  [209], compatible with the  $f_0(1500)$ , is explained as due to constructive interference with a broad glueball background. However, the Belle data are inconsistent with the BaBar measurements which show instead a broad scalar at this mass for  $B$  decays into both  $K^\pm K^\pm K^\mp$  [210] and  $K^+K^-\pi^0$  [211].

The  $f_0(1500)$  has also been proposed as a tetraquarks state [212]. Whether the  $f_0(1500)$  is observed in 'gluon rich' radiative  $J/\psi$  decays is debatable [213] because of the limited amount of data - more data for this and the  $\gamma\gamma$  mode are needed. In Ref. [214], further refined in Ref. [215],  $f_0(1370)$  and  $f_0(1710)$  (together with  $f_2(1270)$  and  $f_2'(1525)$ ) were interpreted as bound systems of two vector mesons. This picture could be tested in radiative  $J/\psi$  decays [216] as well as radiative decays of the states themselves [217]. The vector-vector component of the  $f_0(1710)$  might also be the origin of the enhancement seen in  $J/\psi \rightarrow \gamma\phi\omega$  near threshold [218] observed at BES [219]. Note that the results of Refs. [214] [215] were challenged in Ref. [220] where in a covariant formalism, *e.g.*, the  $f_2(1270)$  did not emerge as a  $\rho\rho$ -bound state.

## References

- [1] C. Amsler and N. A. Tornqvist, Phys. Rept. **389**, 61 (2004).
- [2] D. V. Bugg, Phys. Rept. **397**, 257 (2004), [hep-ex/0412045].
- [3] F. E. Close and N. A. Tornqvist, J. Phys. **G28**, R249 (2002), [hep-ph/0204205].
- [4] E. Klempt and A. Zaitsev, Phys. Rept. **454**, 1 (2007), [arXiv:0708.4016].
- [5] J. R. Pelaez, Phys. Rept. **658**, 1 (2016), [arXiv:1510.00653].
- [6] S. L. Adler, Phys. Rev. **137**, B1022 (1965), [140(1964)].
- [7] S. L. Adler, Phys. Rev. **139**, B1638 (1965), [152(1965)].
- [8] J. A. Oller, Phys. Rev. **D71**, 054030 (2005), [hep-ph/0411105].
- [9] G. Colangelo, J. Gasser and H. Leutwyler, Nucl. Phys. **B603**, 125 (2001), [hep-ph/0103088].
- [10] I. Caprini, G. Colangelo, and H. Leutwyler, Phys. Rev. Lett. **96**, 132001 (2006).
- [11] R. Garcia-Martin *et al.*, Phys. Rev. Lett. **107**, 072001 (2011), [arXiv:1107.1635].
- [12] B. Moussallam, Eur. Phys. J. **C71**, 1814 (2011), [arXiv:1110.6074].
- [13] D. Aston *et al.*, Nucl. Phys. **B296**, 493 (1988).
- [14] P. Estabrooks *et al.*, Nucl. Phys. **B133**, 490 (1978).
- [15] A. Abele *et al.*, Phys. Rev. **D57**, 3860 (1998).
- [16] V. Bernard, N. Kaiser and U. G. Meissner, Phys. Rev. **D43**, 2757 (1991).
- [17] S. N. Cherry and M. R. Pennington, Nucl. Phys. **A688**, 823 (2001), [hep-ph/0005208].
- [18] J. M. Link *et al.* (FOCUS), Phys. Lett. **B648**, 156 (2007), [hep-ex/0612032].
- [19] M. Ablikim *et al.* (BES), Phys. Lett. **B633**, 681 (2006), [hep-ex/0506055].
- [20] F.-K. Guo *et al.*, Nucl. Phys. **A773**, 78 (2006), [hep-ph/0509050].
- [21] D. Epifanov *et al.* (Belle), Phys. Lett. **B654**, 65 (2007), [arXiv:0706.2231].
- [22] C. Cawlfeld *et al.* (CLEO), Phys. Rev. **D74**, 031108 (2006), [hep-ex/0606045].
- [23] A. V. Anisovich and A. V. Sarantsev, Phys. Lett. **B413**, 137 (1997), [hep-ph/9705401].
- [24] R. Delbourgo and M. D. Scadron, Int. J. Mod. Phys. **A13**, 657 (1998), [hep-ph/9807504].

- [25] J. A. Oller, E. Oset and J. R. Pelaez, Phys. Rev. **D59**, 074001 (1999), [Erratum: Phys. Rev.D75,099903(2007)], [hep-ph/9804209].
- [26] J. A. Oller and E. Oset, Phys. Rev. **D60**, 074023 (1999), [hep-ph/9809337].
- [27] C. M. Shakin and H. Wang, Phys. Rev. **D63**, 014019 (2001).
- [28] M. D. Scadron *et al.*, Nucl. Phys. **A724**, 391 (2003), [hep-ph/0211275].
- [29] D. V. Bugg, Phys. Lett. **B572**, 1 (2003), [Erratum: Phys. Lett.B595,556(2004)].
- [30] M. Ishida, Prog. Theor. Phys. Suppl. **149**, 190 (2003), [hep-ph/0212383].
- [31] H. Q. Zheng *et al.*, Nucl. Phys. **A733**, 235 (2004), [hep-ph/0310293].
- [32] Z. Y. Zhou and H. Q. Zheng, Nucl. Phys. **A775**, 212 (2006), [hep-ph/0603062].
- [33] J. M. Link *et al.* (FOCUS), Phys. Lett. **B653**, 1 (2007), [arXiv:0705.2248].
- [34] B. Aubert *et al.* (BaBar), Phys. Rev. **D76**, 011102 (2007), [arXiv:0704.3593].
- [35] S. Kopp *et al.* (CLEO), Phys. Rev. **D63**, 092001 (2001), [hep-ex/0011065].
- [36] J. M. Link *et al.* (FOCUS), Phys. Lett. **B535**, 43 (2002), [hep-ex/0203031].
- [37] J. M. Link *et al.* (FOCUS), Phys. Lett. **B621**, 72 (2005), [hep-ex/0503043].
- [38] M. Jamin, J. A. Oller and A. Pich, Nucl. Phys. **B587**, 331 (2000), [hep-ph/0006045].
- [39] D. Black *et al.*, Phys. Rev. **D64**, 014031 (2001), [hep-ph/0012278].
- [40] J. A. Oller, Nucl. Phys. **A727**, 353 (2003), [hep-ph/0306031].
- [41] E. van Beveren *et al.*, Z. Phys. **C30**, 615 (1986), [arXiv:0710.4067].
- [42] J. R. Pelaez, Mod. Phys. Lett. **A19**, 2879 (2004), [hep-ph/0411107].
- [43] S. Descotes-Genon and B. Moussallam, Eur. Phys. J. **C48**, 553 (2006), [hep-ph/0607133].
- [44] J. R. Peláez, A. Rodas and J. Ruiz de Elvira, Eur. Phys. J. **C77**, 2, 91 (2017), [arXiv:1612.07966].
- [45] M. Bargiotti *et al.* (OBELIX), Eur. Phys. J. **C26**, 371 (2003).
- [46] D. Barberis *et al.* (WA102), Phys. Lett. **B440**, 225 (1998), [hep-ex/9810003].
- [47] M. J. Corden *et al.*, Nucl. Phys. **B144**, 253 (1978).
- [48] C. Defoix *et al.*, Nucl. Phys. **B44**, 125 (1972).
- [49] Z. Bai *et al.* (MARK-III), Phys. Rev. Lett. **65**, 2507 (1990).
- [50] T. Bolton *et al.*, Phys. Rev. Lett. **69**, 1328 (1992).
- [51] C. Amsler *et al.* (Crystal Barrel), Phys. Lett. **B353**, 571 (1995).
- [52] S. M. Flatte, Phys. Lett. **63B**, 224 (1976).
- [53] C. Amsler *et al.* (Crystal Barrel), Phys. Lett. **B333**, 277 (1994).
- [54] G. Janssen *et al.*, Phys. Rev. **D52**, 2690 (1995), [arXiv:nucl-th/9411021].
- [55] D. V. Bugg, Phys. Rev. **D78**, 074023 (2008), [arXiv:0808.2706].
- [56] P. Rubin *et al.* (CLEO), Phys. Rev. **D78**, 072003 (2008), [arXiv:0807.4545].
- [57] R. Aaij *et al.* (LHCb), Phys. Rev. **D93**, 5, 052018 (2016), [arXiv:1509.06628].
- [58] S. D. Protopopescu *et al.*, Phys. Rev. **D7**, 1279 (1973).
- [59] G. Grayer *et al.*, Nucl. Phys. **B75**, 189 (1974).
- [60] H. Becker *et al.* (CERN-Cracow-Munich), Nucl. Phys. **B151**, 46 (1979).
- [61] L. Rosselet *et al.*, Phys. Rev. **D15**, 574 (1977).
- [62] S. Pislak *et al.* (BNL-E865), Phys. Rev. Lett. **87**, 221801 (2001), [Erratum: Phys. Rev. Lett.105,019901(2010)], [hep-ex/0106071].
- [63] J. R. Batley *et al.* (NA48-2), Eur. Phys. J. **C70**, 635 (2010).
- [64] W. Wetzel *et al.*, Nucl. Phys. **B115**, 208 (1976).
- [65] V. A. Polychronakos *et al.*, Phys. Rev. **D19**, 1317 (1979).
- [66] D. H. Cohen *et al.*, Phys. Rev. **D22**, 2595 (1980).
- [67] A. Etkin *et al.*, Phys. Rev. **D25**, 1786 (1982).
- [68] C. Amsler *et al.*, Phys. Lett. **B342**, 433 (1995).
- [69] C. Amsler *et al.* (Crystal Barrel), Phys. Lett. **B355**, 425 (1995).
- [70] A. Abele *et al.* (Crystal Barrel), Phys. Lett. **B380**, 453 (1996).
- [71] D.M. Alde *et al.*, Phys. Lett. **B397**, 250 (1997).
- [72] R. Kaminski, L. Lesniak and K. Rybicki, Z. Phys. **C74**, 79 (1997), [hep-ph/9606362].
- [73] E. M. Aitala *et al.* (E791), Phys. Rev. Lett. **86**, 770 (2001), [hep-ex/0007028].
- [74] J. M. Link *et al.* (FOCUS), Phys. Lett. **B585**, 200 (2004), [hep-ex/0312040].
- [75] G. Bonvicini *et al.* (CLEO), Phys. Rev. **D76**, 012001 (2007), [arXiv:0704.3954].
- [76] J. E. Augustin *et al.* (DM2), Nucl. Phys. **B320**, 1 (1989).
- [77] M. Ablikim *et al.* (BES), Phys. Lett. **B598**, 149 (2004), [hep-ex/0406038].
- [78] A. Gallegos, J. L. Lucio M. and J. Pestieau, Phys. Rev. **D69**, 074033 (2004), [hep-ph/0311133].
- [79] M. Ablikim *et al.* (BES), Phys. Lett. **B645**, 19 (2007), [hep-ex/0610023].
- [80] A. Dobado and J. R. Pelaez, Phys. Rev. **D56**, 3057 (1997), [hep-ph/9604416].
- [81] I. Caprini, Phys. Rev. **D77**, 114019 (2008), [arXiv:0804.3504].
- [82] P. Masjuan, J. Ruiz de Elvira, J.J. Sanz-Cillero, Phys. Rev. **D90**, 097901 (2014).
- [83] F. J. Yndurain, R. Garcia-Martin and J. R. Pelaez, Phys. Rev. **D76**, 074034 (2007), [hep-ph/0701025].
- [84] V.V. Anisovich *et al.*, Sov. Phys. Usp. **41**, 419 (1998).
- [85] V. V. Anisovich, Int. J. Mod. Phys. **A21**, 3615 (2006), [hep-ph/0510409].
- [86] B. S. Zou and D. V. Bugg, Phys. Rev. **D48**, R3948 (1993).
- [87] N. A. Tornqvist and M. Roos, Phys. Rev. Lett. **76**, 1575 (1996), [hep-ph/9511210].
- [88] R. Kaminski, L. Lesniak and J. P. Maillet, Phys. Rev. **D50**, 3145 (1994), [hep-ph/9403264].
- [89] N. N. Achasov and G. N. Shestakov, Phys. Rev. **D49**, 5779 (1994).
- [90] M. P. Locher, V. E. Markushin and H. Q. Zheng, Eur. Phys. J. **C4**, 317 (1998), [hep-ph/9705230].
- [91] J. A. Oller and E. Oset, Nucl. Phys. **A620**, 438 (1997), [Erratum: Nucl. Phys.A652,407(1999)], [hep-ph/9702314].
- [92] T. Hannah, Phys. Rev. **D60**, 017502 (1999), [hep-ph/9905236].
- [93] R. Kaminski, L. Lesniak and B. Loiseau, Phys. Lett. **B413**, 130 (1997), [hep-ph/9707377].
- [94] R. Kaminski, L. Lesniak and B. Loiseau, Eur. Phys. J. **C9**, 141 (1999), [hep-ph/9810386].
- [95] M. Ishida *et al.*, Prog. Theor. Phys. **104**, 203 (2000), [hep-ph/0005251].
- [96] Y.S. Surovtsev *et al.*, Phys. Rev. **D61**, 054024 (2001).

- [97] M. Ishida *et al.*, Phys. Lett. **B518**, 47 (2001).
- [98] Z. Y. Zhou *et al.*, JHEP **02**, 043 (2005), [hep-ph/0406271].
- [99] D. V. Bugg, J. Phys. **G34**, 151 (2007), [hep-ph/0608081].
- [100] D. Morgan and M. R. Pennington, Z. Phys. **C48**, 623 (1990).
- [101] M. R. Pennington, Phys. Rev. Lett. **97**, 011601 (2006).
- [102] M. R. Pennington, Mod. Phys. Lett. **A22**, 1439 (2007), [arXiv:0705.3314].
- [103] G. Mennessier, S. Narison and W. Ochs, Phys. Lett. **B665**, 205 (2008), [arXiv:0804.4452].
- [104] R. Garcia-Martin and B. Moussallam, Eur. Phys. J. **C70**, 155 (2010), [arXiv:1006.5373].
- [105] M. Hoferichter, D. R. Phillips and C. Schat, Eur. Phys. J. **C71**, 1743 (2011), [arXiv:1106.4147].
- [106] L.-Y. Dai and M. R. Pennington, Phys. Rev. **D90**, 3, 036004 (2014), [arXiv:1404.7524].
- [107] J. R. Pelaez and G. Rios, Phys. Rev. Lett. **97**, 242002 (2006), [hep-ph/0610397].
- [108] H.-X. Chen, A. Hosaka and S.-L. Zhu, Phys. Lett. **B650**, 369 (2007), [hep-ph/0609163].
- [109] F. Giacosa, Phys. Rev. **D75**, 054007 (2007), [hep-ph/0611388].
- [110] L. Maiani *et al.*, Eur. Phys. J. **C50**, 609 (2007), [hep-ph/0604018].
- [111] N. N. Achasov and G. N. Shestakov, Phys. Rev. **D58**, 054011 (1998), [hep-ph/9802286].
- [112] M. N. Achasov *et al.*, Phys. Lett. **B479**, 53 (2000), [hep-ex/0003031].
- [113] M. N. Achasov *et al.*, Phys. Lett. **B485**, 349 (2000), [hep-ex/0005017].
- [114] R. R. Akhmetshin *et al.* (CMD-2), Phys. Lett. **B462**, 371 (1999), [hep-ex/9907005].
- [115] A. Aloisio *et al.* (KLOE), Phys. Lett. **B536**, 209 (2002), [hep-ex/0204012].
- [116] F. Ambrosino *et al.* (KLOE), Eur. Phys. J. **C49**, 473 (2007), [hep-ex/0609009].
- [117] M. Boglione and M. R. Pennington, Eur. Phys. J. **C9**, 11 (1999), [hep-ph/9812258].
- [118] T. Mori *et al.* (Belle), Phys. Rev. **D75**, 051101 (2007), [hep-ex/0610038].
- [119] N. N. Achasov and G. N. Shestakov, Phys. Rev. **D77**, 074020 (2008), [arXiv:0712.0885].
- [120] M. R. Pennington *et al.*, Eur. Phys. J. **C56**, 1 (2008), [arXiv:0803.3389].
- [121] R. Fleischer, R. Knegjens and G. Ricciardi, Eur. Phys. J. **C71**, 1832 (2011), [arXiv:1109.1112].
- [122] S. Stone and L. Zhang, Phys. Rev. Lett. **111**, 6, 062001 (2013), [arXiv:1305.6554].
- [123] R. Aaij *et al.* (LHCb), Phys. Rev. **D90**, 1, 012003 (2014), [arXiv:1404.5673].
- [124] R. Aaij *et al.* (LHCb), Phys. Rev. **D89**, 9, 092006 (2014), [arXiv:1402.6248].
- [125] J. T. Daub, C. Hanhart and B. Kubis, JHEP **02**, 009 (2016), [arXiv:1508.06841].
- [126] D. Barberis *et al.* (WA102), Phys. Lett. **B462**, 462 (1999), [hep-ex/9907055].
- [127] D. Barberis *et al.* (WA102), Phys. Lett. **B479**, 59 (2000), [hep-ex/0003033].
- [128] M. Gaspero, Nucl. Phys. **A562**, 407 (1993).
- [129] A. Adamo *et al.*, Nucl. Phys. **A558**, 13C (1993).
- [130] C. Amsler *et al.* (Crystal Barrel), Phys. Lett. **B322**, 431 (1994).
- [131] A. Abele *et al.* (Crystal Barrel), Eur. Phys. J. **C19**, 667 (2001).
- [132] A. Abele *et al.* (CRYSTAL BARREL), Eur. Phys. J. **C21**, 261 (2001).
- [133] D. Barberis *et al.* (WA102), Phys. Lett. **B471**, 440 (2000), [hep-ex/9912005].
- [134] R. L. Jaffe, Phys. Rev. **D15**, 267 (1977).
- [135] M. G. Alford and R. L. Jaffe, Nucl. Phys. **B578**, 367 (2000), [hep-lat/0001023].
- [136] L. Maiani *et al.*, Phys. Rev. Lett. **93**, 212002 (2004), [hep-ph/0407017].
- [137] L. Maiani, A. D. Polosa and V. Riquer, Phys. Lett. **B651**, 129 (2007), [hep-ph/0703272].
- [138] C. Adolph *et al.* (COMPASS), Phys. Rev. **D95**, 3, 032004 (2017), [arXiv:1509.00992].
- [139] P. d'Argent *et al.*, JHEP **05**, 143 (2017), [arXiv:1703.08505].
- [140] G. 't Hooft *et al.*, Phys. Lett. **B662**, 424 (2008), [arXiv:0801.2288].
- [141] J. D. Weinstein and N. Isgur, Phys. Rev. **D41**, 2236 (1990).
- [142] T. Barnes, Phys. Lett. **165B**, 434 (1985).
- [143] Z. P. Li, F. E. Close and T. Barnes, Phys. Rev. **D43**, 2161 (1991).
- [144] R. Delbourgo, D.-s. Liu and M. D. Scadron, Phys. Lett. **B446**, 332 (1999), [hep-ph/9811474].
- [145] J. L. Lucio Martinez and M. Napsuciale, Phys. Lett. **B454**, 365 (1999), [hep-ph/9903234].
- [146] C. Hanhart *et al.*, Phys. Rev. **D75**, 074015 (2007), [hep-ph/0701214].
- [147] R. H. Lemmer, Phys. Lett. **B650**, 152 (2007), [hep-ph/0701027].
- [148] T. Branz, T. Gutsche and V. E. Lyubovitskij, Eur. Phys. J. **A37**, 303 (2008), [arXiv:0712.0354].
- [149] A. Deandrea *et al.*, Phys. Lett. **B502**, 79 (2001), [hep-ph/0012120].
- [150] K. M. Ecklund *et al.* (CLEO), Phys. Rev. **D80**, 052009 (2009), [arXiv:0907.3201].
- [151] N. N. Achasov and V. N. Ivanchenko, Nucl. Phys. **B315**, 465 (1989).
- [152] J. A. Oller, Nucl. Phys. **A714**, 161 (2003), [hep-ph/0205121].
- [153] Yu. S. Kalashnikova *et al.*, Eur. Phys. J. **A24**, 437 (2005), [hep-ph/0412340].
- [154] Yu. S. Kalashnikova *et al.*, Phys. Rev. **D78**, 058501 (2008), [arXiv:0711.2902].
- [155] N. N. Achasov and A. V. Kiselev, Phys. Rev. **D78**, 058502 (2008), [arXiv:0806.2993].
- [156] M. Boglione and M. R. Pennington, Eur. Phys. J. **C30**, 503 (2003), [hep-ph/0303200].
- [157] F. Giacosa and G. Pagliara, Phys. Rev. **C76**, 065204 (2007), [arXiv:0707.3594].
- [158] S. Narison, Nucl. Phys. **B96**, 244 (2001).
- [159] H.-J. Lee, Eur. Phys. J. **A30**, 423 (2006), [hep-ph/0512212].
- [160] H.-X. Chen, A. Hosaka and S.-L. Zhu, Phys. Rev. **D76**, 094025 (2007), [arXiv:0707.4586].
- [161] J. Sugiyama *et al.*, Phys. Rev. **D76**, 114010 (2007), [arXiv:0707.2533].
- [162] T. Kojo and D. Jido, Phys. Rev. **D78**, 114005 (2008), [arXiv:0802.2372].
- [163] D. Black *et al.*, Phys. Rev. **D59**, 074026 (1999), [hep-ph/9808415].
- [164] A. H. Fariborz *et al.*, Phys. Rev. **D90**, 3, 033009 (2014), [arXiv:1407.3870].



- [165] M. D. Scadron, Eur. Phys. J. **C6**, 141 (1999), [hep-ph/9710317].
- [166] M. Ishida, Prog. Theor. Phys. **101**, 661 (1999), [hep-ph/9902260].
- [167] N. A. Tornqvist, Eur. Phys. J. **C11**, 359 (1999), [hep-ph/9905282].
- [168] M. Napsuciale and S. Rodriguez, Phys. Lett. **B603**, 195 (2004), [hep-ph/0403072].
- [169] M. Napsuciale and S. Rodriguez, Phys. Rev. **D70**, 094043 (2004), [hep-ph/0407037].
- [170] J. R. Pelaez, Phys. Rev. Lett. **92**, 102001 (2004), [hep-ph/0309292].
- [171] J. T. Londergan *et al.*, Phys. Lett. **B729**, 9 (2014), [arXiv:1311.7552].
- [172] S. Weinberg, Phys. Rev. **130**, 776 (1963).
- [173] D. Morgan and M. R. Pennington, Phys. Lett. **B258**, 444 (1991), [Erratum: Phys. Lett. **B269**, 477 (1991)].
- [174] D. Morgan, Nucl. Phys. **A543**, 632 (1992).
- [175] N. A. Tornqvist, Phys. Rev. **D51**, 5312 (1995), [hep-ph/9403234].
- [176] V. Baru *et al.*, Phys. Lett. **B586**, 53 (2004), [hep-ph/0308129].
- [177] N. N. Achasov, S. A. Devyanin and G. N. Shestakov, Phys. Lett. **88B**, 367 (1979).
- [178] J.-J. Wu, Q. Zhao and B. S. Zou, Phys. Rev. **D75**, 114012 (2007), [arXiv:0704.3652].
- [179] C. Hanhart, B. Kubis and J. R. Pelaez, Phys. Rev. **D76**, 074028 (2007), [arXiv:0707.0262].
- [180] M. Ablikim *et al.* (BESIII), Phys. Rev. **D83**, 032003 (2011), [arXiv:1012.5131].
- [181] L. Roca, Phys. Rev. **D88**, 014045 (2013), [arXiv:1210.4742].
- [182] N. A. Tornqvist, Z. Phys. **C68**, 647 (1995), [hep-ph/9504372].
- [183] E. van Beveren and G. Rupp, Eur. Phys. J. **C22**, 493 (2001), [hep-ex/0106077].
- [184] M. Boglione and M. R. Pennington, Phys. Rev. **D65**, 114010 (2002), [hep-ph/0203149].
- [185] A. Abele *et al.* (Crystal Barrel), Phys. Lett. **B385**, 425 (1996).
- [186] D. Black, A. H. Fariborz and J. Schechter, Phys. Rev. **D61**, 074001 (2000), [hep-ph/9907516].
- [187] C. Amsler *et al.* (Crystal Barrel), Phys. Lett. **B639**, 165 (2006).
- [188] M. Acciarri *et al.* (L3), Phys. Lett. **B501**, 173 (2001), [hep-ex/0011037].
- [189] R. Barate *et al.* (ALEPH), Phys. Lett. **B472**, 189 (2000), [hep-ex/9911022].
- [190] S. Uehara *et al.* (Belle), Phys. Rev. **D78**, 052004 (2008), [arXiv:0805.3387].
- [191] C. Amsler, Phys. Lett. **B541**, 22 (2002), [hep-ph/0206104].
- [192] S. Uehara, *et al.*, Prog. Theor. Exp. Phys. **2013**, 123C01 (2013).
- [193] F. E. Close and Q. Zhao, Phys. Rev. **D71**, 094022 (2005), [hep-ph/0504043].
- [194] S. Uehara *et al.* (Belle), Phys. Rev. **D80**, 032001 (2009), [arXiv:0906.1464].
- [195] F. E. Close and A. Kirk, Phys. Lett. **B397**, 333 (1997), [hep-ph/9701222].
- [196] F. E. Close, Phys. Lett. **B419**, 387 (1998), [hep-ph/9710450].
- [197] A. Kirk, Phys. Lett. **B489**, 29 (2000), [hep-ph/0008053].
- [198] M. Ablikim *et al.* (BES), Phys. Lett. **B603**, 138 (2004), [hep-ex/0409007].
- [199] M. Ablikim *et al.* (BES), Phys. Lett. **B607**, 243 (2005), [hep-ex/0411001].
- [200] C. Amsler and F. E. Close, Phys. Rev. **D53**, 295 (1996), [hep-ph/9507326].
- [201] F. E. Close and A. Kirk, Eur. Phys. J. **C21**, 531 (2001), [hep-ph/0103173].
- [202] P. Minkowski and W. Ochs, Eur. Phys. J. **C9**, 283 (1999), [hep-ph/9811518].
- [203] W.-J. Lee and D. Weingarten, Phys. Rev. **D61**, 014015 (2000), [hep-lat/9910008].
- [204] M. Chanowitz, Phys. Rev. Lett. **95**, 172001 (2005), [hep-ph/0506125].
- [205] F. Brünner and A. Rebhan, Phys. Rev. Lett. **115**, 131601 (2015), [arXiv:1504.05815].
- [206] S. Janowski, F. Giacosa and D. H. Rischke, Phys. Rev. **D90**, 11, 114005 (2014), [arXiv:1408.4921].
- [207] M. Albaladejo and J. A. Oller, Phys. Rev. Lett. **101**, 252002 (2008), [arXiv:0801.4929].
- [208] P. Minkowski and W. Ochs, Eur. Phys. J. **C39**, 71 (2005), [hep-ph/0404194].
- [209] A. Garmash *et al.* (Belle), Phys. Rev. **D71**, 092003 (2005), [hep-ex/0412066].
- [210] B. Aubert *et al.* (BaBar), Phys. Rev. **D74**, 032003 (2006), [hep-ex/0605003].
- [211] B. Aubert *et al.* (BaBar), Phys. Rev. Lett. **99**, 161802 (2007), [arXiv:0706.3885].
- [212] L. Zou *et al.*, Phys. Rev. **D99**, 114024 (2019).
- [213] M. Ablikim *et al.*, Phys. Lett. **B642**, 441 (2006), [hep-ex/0603048].
- [214] R. Molina, D. Nicmorus and E. Oset, Phys. Rev. **D78**, 114018 (2008), [arXiv:0809.2233].
- [215] C. García-Recio *et al.*, Phys. Rev. **D87**, 9, 096006 (2013), [arXiv:1304.1021].
- [216] L. S. Geng *et al.*, Eur. Phys. J. **A44**, 305 (2010), [arXiv:0910.5192].
- [217] T. Branz, L. S. Geng and E. Oset, Phys. Rev. **D81**, 054037 (2010), [arXiv:0911.0206].
- [218] A. Martínez Torres *et al.*, Phys. Lett. **B719**, 388 (2013), [arXiv:1210.6392].
- [219] M. Ablikim *et al.* (BES), Phys. Rev. Lett. **96**, 162002 (2006), [hep-ex/0602031].
- [220] D. Gülmez, U. G. Meißner and J. A. Oller, Eur. Phys. J. **C77**, 7, 460 (2017), [arXiv:1611.00168].

### 63. Pseudoscalar and Pseudovector Mesons in the 1400 MeV Region

Revised August 2019 by C. Amsler (Stefan Meyer Inst.) and A. Masoni (INFN, Cagliari).

This minireview deals with some of the  $0^{-+}$  and  $1^{++}$  mesons reported in the 1200–1500 MeV region, namely the  $\eta(1295)$ ,  $\eta(1405)$ ,  $\eta(1475)$ ,  $f_1(1285)$ ,  $f_1(1420)$ ,  $a_1(1420)$  and  $f_1(1510)$ . The first observation of a pseudoscalar resonance around 1400 MeV – the  $\eta(1440)$  – was made in  $p\bar{p}$  annihilation at rest into  $\eta(1440)\pi^+\pi^-$ ,  $\eta(1440) \rightarrow K\bar{K}\pi$  [1]. This state was reported to decay into  $a_0(980)\pi$  and  $K^*(892)\bar{K}$  with roughly equal contributions. The  $\eta(1440)$  was also observed in radiative  $J/\psi(1S)$  decay into  $K\bar{K}\pi$  [2–4] and  $\gamma\rho$  [5] and was in the eighties considered as a glueball candidate

However, two pseudoscalars are now observed in this mass region, the  $\eta(1405)$  and  $\eta(1475)$ . The former decays mainly through  $a_0(980)\pi$  (or direct  $K\bar{K}\pi$ ) and the latter mainly to  $K^*(892)\bar{K}$ . The simultaneous observation of two pseudoscalars is reported in three production mechanisms:  $\pi^-p$  [6, 7]; radiative  $J/\psi(1S)$  decay [8, 9]; and  $p\bar{p}$  annihilation at rest [10–13]. All of them give values for the masses, widths, and decay modes that are in reasonable agreement. (However, Ref. [9] favors a state decaying into  $K^*(892)\bar{K}$  at a lower mass than the state decaying into  $a_0(980)\pi$ .) In  $J/\psi(1S)$  radiative decay, the  $\eta(1405)$  decays into  $K\bar{K}\pi$  through  $a_0(980)\pi$ , and hence a signal is also expected in the  $\eta\pi\pi$  mass spectrum. This was indeed observed by MARK III in  $\eta\pi^+\pi^-$  [14], which reported a mass of 1400 MeV, in line with the existence of the  $\eta(1405)$  decaying into  $a_0(980)\pi$ .

BESII [15] observes an enhancement in  $K^+K^-\pi^0$  around 1.44 GeV in  $J/\psi(1S)$  decay, recoiling against an  $\omega$  (but not a  $\phi$ ) without resolving the presence of two states nor performing a spin-parity analysis, due to low statistics. This state could also be the  $f_1(1420)$  (see below). On the other hand, BESII observes  $\eta(1405) \rightarrow \eta\pi\pi$  in  $J/\psi(1S)$  decay, recoiling against an  $\omega$  [16]. A single unresolved broad peak is also observed by BESIII in the decay  $\psi(2S) \rightarrow \omega K^*K$  which could be due to  $\eta(1405)$ ,  $\eta(1475)$  and  $f_1(1420)$  [17]. The  $\eta(1405)$  is also observed in  $p\bar{p}$  annihilation at rest into  $\eta\pi^+\pi^-\pi^0\pi^0$ , where it decays into  $\eta\pi\pi$  [18]. The intermediate  $a_0(980)\pi$  accounts for roughly half of the  $\eta\pi\pi$  signal, in agreement with MARK III [14] and DM2 [4].

Whether one or two pseudoscalar mesons exist in this mass region is still an open issue. According to Ref. [19] the splitting of a single state is due to nodes in the decay amplitudes which differ in  $\eta\pi\pi$  and  $K^*(892)\bar{K}$ . Based on the isospin violating decay  $J/\psi(1S) \rightarrow \gamma 3\pi$  observed by BESIII [20] the splitting could also be due to a triangular singularity mixing  $\eta\pi\pi$  and  $K^*(892)\bar{K}$  [21, 22]. In a further paper [23], using the approach of [21], the authors conclude that the BESIII results can be reproduced either with the  $\eta(1405)$  or the  $\eta(1475)$ , or by a mixture of these two states.

The  $\eta(1295)$  has been observed by four  $\pi^-p$  experiments [7, 24–26], and evidence is reported in  $p\bar{p}$  annihilation [27–29]. In  $J/\psi(1S)$  radiative decay, the  $\eta(1295)$  signal is evident in the  $0^{-+}$   $\eta\pi\pi$  wave of the DM2 data [9]. Also BaBar [30] reports evidence for a signal around 1295 MeV in  $B$  decays into  $\eta\pi\pi K$ . Nonetheless, the existence of the  $\eta(1295)$  is questioned in Refs. [19] and [31] in which the authors also claim the existence of a single pseudoscalar meson at 1440 MeV, the first radial excitation of the  $\eta$ . This conclusion is mainly based on a PhD thesis of the annihilation channel  $p\bar{p} \rightarrow 4\pi\eta$  with Crystal Barrel data [32].

Since the  $\eta(1295)$  has been reported by several experiments, using different production mechanisms, let us assume this state to be established. The  $\eta(1475)$  could then be the first radial excitation of the  $\eta'$ , with the  $\eta(1295)$  being the first radial excitation of the  $\eta$ . Ideal mixing, suggested by the  $\eta(1295)$  and  $\pi(1300)$  mass degeneracy, would then imply that the second isoscalar in the nonet is mainly  $s\bar{s}$ , and hence couples to  $K^*\bar{K}$ , in agreement with properties of the  $\eta(1475)$ . Also, its width matches the expected width for the radially excited  $s\bar{s}$  state [33, 34]. A study of radial excitations of pseudoscalar mesons [35] favors the  $s\bar{s}$  interpretation of the  $\eta(1475)$ . However, due to the strong kinematical suppression the data are not sufficient to exclude a sizeable  $s\bar{s}$  admixture also in the  $\eta(1405)$ .

The  $K\bar{K}\pi$  and  $\eta\pi\pi$  channels were studied in  $\gamma\gamma$  collisions by

L3 [36]. The analysis led to a clear  $\eta(1475)$  signal in  $K\bar{K}\pi$ , decaying into  $K^*\bar{K}$ , very well identified in the untagged data sample, where contamination from spin 1 resonances is not allowed. At the same time, L3 [36] did not observe the  $\eta(1405)$ , neither in  $K\bar{K}\pi$  nor in  $\eta\pi\pi$ . The observation of the  $\eta(1475)$ , combined with the absence of an  $\eta(1405)$  signal, strengthens the two-resonances hypothesis. Since gluonium production is presumably suppressed in  $\gamma\gamma$  collisions, the L3 results [36] suggest that  $\eta(1405)$  has a large gluonic content (see also Refs. [37] and [38]). The L3 result is somewhat in disagreement with that of CLEO-II, which did not observe any pseudoscalar signal in  $\gamma\gamma \rightarrow \eta(1475) \rightarrow K_S^0 K^\pm \pi^\mp$  [39]. However, more data are required. Moreover, after the CLEO-II result, L3 performed a further analysis with full statistics [40], confirming their previous evidence for the  $\eta(1475)$ . The CLEO upper limit [39] for  $\Gamma_{\gamma\gamma}(\eta(1475))$ , and the L3 results [40], are consistent with the world average for the  $\eta(1475)$  width.

BaBar [30] also reports the  $\eta(1475)$  in  $B$  decays into  $K\bar{K}^*$  recoiling against a  $K$ , but upper limits only are given for the  $\eta(1405)$ . As mentioned above, in  $B$  decays into  $\eta\pi\pi K$  the  $\eta(1295) \rightarrow \eta\pi\pi$  is observed while only upper limits are given for the  $\eta(1405)$ . The  $f_1(1420)$  (and  $f_1(1285)$ ) are not seen.

Under the assumption that two pseudoscalars exist in the 1400 MeV region, the  $\eta(1405)$  could be a glueball, but this interpretation for the  $\eta(1405)$  is not favored by lattice gauge theories which predict the  $0^{-+}$  state above 2 GeV [41, 42] (see also the article on the “Quark model” in this issue of the Review). However, the  $\eta(1405)$  is an excellent candidate for the  $0^{-+}$  glueball in the flux-tube model [43]. In this model, the  $0^{++}$   $f_0(1500)$  glueball is also naturally related to a  $0^{-+}$  glueball with mass degeneracy broken in QCD. Also, Ref. [44] shows that the pseudoscalar glueball could lie at a lower mass than predicted from lattice calculation. In this model the  $\eta(1405)$  appears as the natural glueball candidate, see also Refs. [45–47]. A detailed review of the experimental situation is available in Ref. [48].

Let us now deal with the  $1^{++}$  mesons. The pseudovector nonet is believed to consist of the isovector  $a_1(1260)$ , the isoscalars  $f_1(1285)$  and  $f_1(1420)$ , and the  $K_{1A}$ , which is a superposition with mixing angle  $\sim 34^\circ$  of  $K_1(1270)$  and  $K_1(1400)$  [49]. The  $f_1(1285)$  could also be a  $K^*\bar{K}$  molecule [50] or as a tetraquark state [51] and the  $f_1(1420)$  a  $K^*\bar{K}$  molecule, due to the proximity of the  $K^*\bar{K}$  threshold [52]. LHCb has analyzed the decays  $\bar{B}^0$  and  $\bar{B}_s^0 \rightarrow J/\psi(1S)f_1(1285)$  and determined the nonet mixing angle to be consistent with a mostly  $u\bar{u} + d\bar{d}$  structure [53] without specifying the identity of its isoscalar partner. This is consistent with earlier determinations assuming the  $f_1(1420)$  as the isoscalar partner [54] and the ratio of  $\bar{B}^0/\bar{B}_s^0$  decay rates excludes the tetraquark interpretation of this state [53].

The  $f_1(1420)$ , decaying into  $K^*\bar{K}$ , was first reported in  $\pi^-p$  reactions at 4 GeV/c [55]. However, later analyses found that the 1400–1500 MeV region was far more complex [56–58]. A reanalysis of the MARK III data in radiative  $J/\psi(1S)$  decay into  $K\bar{K}\pi$  [8] shows the  $f_1(1420)$  decaying into  $K^*\bar{K}$ . A  $C=+1$  state is also seen in tagged  $\gamma\gamma$  collisions (*e.g.*, Ref. [59]).

In  $\pi^-p \rightarrow \eta\pi\pi n$  charge-exchange reactions at 8–9 GeV/c the  $\eta\pi\pi$  mass spectrum is dominated by the  $\eta(1440)$  and  $\eta(1295)$  [24, 60], and at 100 GeV/c Ref. [25] reports the  $\eta(1295)$  and  $\eta(1440)$  decaying into  $\eta\pi^0\pi^0$  with a weak  $f_1(1285)$  signal, and no evidence for the  $f_1(1420)$ .

Axial ( $1^{++}$ ) mesons are not observed in  $p\bar{p}$  annihilation at rest in liquid hydrogen, which proceeds dominantly through  $S$ -wave annihilation. However, in gaseous hydrogen,  $P$ -wave annihilation is enhanced and, indeed, Ref. [11] reports  $f_1(1420)$  decaying into  $K^*\bar{K}$ . The  $f_1(1420)$ , decaying into  $K\bar{K}\pi$ , is also seen in  $pp$  central production, together with the  $f_1(1285)$ . The latter decays via  $a_0(980)\pi$ , and the former only via  $K^*\bar{K}$ , while the  $\eta(1440)$  is absent [61, 62]. The  $K_S^0 K_S^0 \pi^0$  decay mode of the  $f_1(1420)$  establishes unambiguously  $C=+1$ . On the other hand, there is no evidence for any state decaying into  $\eta\pi\pi$  around 1400 MeV, and hence the  $\eta\pi\pi$  mode of the  $f_1(1420)$  must be suppressed [63].

The COMPASS Collaboration has recently reported an isovector state at 1411 MeV, the  $a_1(1420)$  [64] [65]. This relatively

narrow state (161 MeV) is produced by diffractive dissociation with 190 GeV pions in  $\pi N \rightarrow 3\pi N$ , decays into  $f_0(980)\pi \rightarrow 3\pi$  (P-wave) and has therefore the quantum numbers  $(I^G)J^{PC} = (1^-)1^{++}$ . The pseudovector nonet already contains the established  $a_1(1260)$  as the  $I = 1$  state. As mentioned above, the  $f_1(1420)$  has been interpreted as a  $K^*\bar{K}$  molecule [52]. The new  $a_1(1420)$  could be its isovector partner. Arguments favoring the  $f_1(1420)$  being a hybrid  $q\bar{q}g$  meson [66] or a four-quark state [67] were also put forward. The  $q\bar{q}$  state would then remain to be identified, with the  $f_1(1510)$  (see below) as a candidate. However, alternative explanations are suggested: A single  $1^{++}$  isovector around 1400 MeV, can lead to two peaks in the  $3\pi$  mass spectrum, depending on the production mechanism,  $\rho\pi$  [68] or  $K^*\bar{K} \rightarrow K\bar{K}\pi \rightarrow f_0(980)\pi$  [69] for the  $a_1(1260)$  and  $f_0(980)\pi$  for the  $a_1(1420)$ .

A similar mechanism is invoked for the  $f_1(1420)$ , which is claimed to result from the  $K^*\bar{K}$  and  $a_0(980)\pi$  decay modes of the  $f_1(1285)$  [70]. The absence of  $f_1(1420)$  in  $K^-p$  [71] indeed argues against the  $f_1(1420)$  being the  $s\bar{s}$  member of the  $1^{++}$  nonet. However, the  $f_1(1420)$  was reported in  $K^-p$  but not in  $\pi^-p$  [72], while two experiments do not observe the  $f_1(1510)$  in  $K^-p$  [72,73]. The latter is also not seen in central collisions [62], nor  $\gamma\gamma$  collisions [74], although, surprisingly for an  $s\bar{s}$  state, a signal is reported in  $4\pi$  decays [75].

We now turn to the experimental evidence for the  $f_1(1510)$  which competes with the  $f_1(1420)$  to be the  $s\bar{s}$   $1^{++}$  meson. The  $f_1(1510)$  was seen in  $K^-p \rightarrow \Lambda K\bar{K}\pi$  at 4 GeV/c [76], and at 11 GeV/c [71]. Evidence is also reported in  $\pi^-p$  at 8 GeV/c, based on the phase motion of the  $1^{++}$   $K^*\bar{K}$  wave [58]. A somewhat broader  $1^{++}$  signal is also observed in  $J/\psi(1S) \rightarrow \gamma\eta\pi^+\pi^-$  [77] as well as a small signal in  $J/\psi(1S) \rightarrow \gamma\eta'\pi^+\pi^-$ , attributed to the  $f_1(1510)$  [78]. The  $f_1(1510)$  is not well established [79].

Summarizing, there is evidence for two isovector  $1^{++}$  states in the 1400 MeV region, the  $a_1(1260)$  and  $a_1(1420)$ , which cannot be both  $q\bar{q}$  states. These two states could stem from the same pole, or the latter be exotic (tetraquark or hybrid) or a molecular state. The  $f_1(1285)$  and the  $f_1(1420)$  are well known but their nature ( $q\bar{q}$ , tetraquark or molecular) remains to be established. In the  $0^{-+}$  sector there is evidence for two pseudoscalars in the 1400 MeV region, the  $\eta(1405)$  and  $\eta(1475)$ , decaying into  $a_0(980)\pi$  and  $K^*\bar{K}$ , respectively. These two structures could originate from a single pole. Doubts have been expressed on the existence of the  $\eta(1295)$ . The  $f_1(1510)$  remains to be firmly established.

### References

- [1] P. H. Baillon *et al.*, Nuovo Cim. **A50**, 393 (1967).
- [2] D. L. Scharre *et al.*, Phys. Lett. **97B**, 329 (1980).
- [3] C. Edwards *et al.*, Phys. Rev. Lett. **49**, 259 (1982), [Erratum: Phys. Rev. Lett.50,219(1983)].
- [4] J. E. Augustin *et al.* (DM2), Phys. Rev. **D42**, 10 (1990).
- [5] J. Z. Bai *et al.* (BES), Phys. Lett. **B594**, 47 (2004), [hep-ex/0403008].
- [6] M. G. Rath *et al.*, Phys. Rev. **D40**, 693 (1989).
- [7] G. S. Adams *et al.* (E852), Phys. Lett. **B516**, 264 (2001), [hep-ex/0107042].
- [8] Z. Bai *et al.* (MARK-III), Phys. Rev. Lett. **65**, 2507 (1990).
- [9] J. E. Augustin *et al.* (DM2), Phys. Rev. **D46**, 1951 (1992).
- [10] A. Bertin *et al.* (OBELIX), Phys. Lett. **B361**, 187 (1995).
- [11] A. Bertin *et al.* (OBELIX), Phys. Lett. **B400**, 226 (1997).
- [12] C. Cicalo *et al.* (OBELIX), Phys. Lett. **B462**, 453 (1999).
- [13] F. Nichitiu *et al.* (OBELIX), Phys. Lett. **B545**, 261 (2002).
- [14] T. Bolton *et al.*, Phys. Rev. Lett. **69**, 1328 (1992).
- [15] M. Ablikim *et al.* (BES), Phys. Rev. **D77**, 032005 (2008), [arXiv:0712.1411].
- [16] M. Ablikim *et al.* (BESIII), Phys. Rev. Lett. **107**, 182001 (2011), [arXiv:1107.1806].
- [17] M. Ablikim *et al.* (BESIII), Phys. Rev. **D87**, 092006 (2013), [arXiv:1303.6360].
- [18] C. Amsler *et al.* (Crystal Barrel), Phys. Lett. **B358**, 389 (1995).
- [19] E. Klempt and A. Zaitsev, Phys. Rept. **454**, 1 (2007), [arXiv:0708.4016].
- [20] M. Ablikim *et al.* (BESIII), Phys. Rev. Lett. **108**, 182001 (2012), [arXiv:1201.2737].
- [21] J.-J. Wu *et al.*, Phys. Rev. Lett. **108**, 081803 (2012), [arXiv:1108.3772].
- [22] X.-G. Wu *et al.*, Phys. Rev. **D87**, 1, 014023 (2013), [arXiv:1211.2148].
- [23] F. Aceti *et al.*, Phys. Rev. **D86**, 114007 (2012), [arXiv:1209.6507].
- [24] S. Fukui *et al.*, Phys. Lett. **B267**, 293 (1991), [,293(1991)].
- [25] D. Alde *et al.* (GAMS), Phys. Atom. Nucl. **60**, 386 (1997), [Yad. Fiz.60,458(1997)].
- [26] J. J. Manak *et al.* (E852), Phys. Rev. **D62**, 012003 (2000), [hep-ex/0001051].
- [27] A. V. Anisovich *et al.*, Nucl. Phys. **A690**, 567 (2001).
- [28] A. Abele *et al.*, Phys. Rev. **D57**, 3860 (1998).
- [29] C. Amsler *et al.*, Eur. Phys. J. **C33**, 23 (2004).
- [30] B. Aubert *et al.* (BaBar), Phys. Rev. Lett. **101**, 091801 (2008), [arXiv:0804.0411].
- [31] E. Klempt, Int. J. Mod. Phys. **A21**, 739 (2006).
- [32] J. Reinhardt, PhD Thesis, University of Bonn (2003), unpublished.
- [33] F. E. Close and A. Kirk, Phys. Lett. **B397**, 333 (1997), [hep-ph/9701222].
- [34] T. Barnes *et al.*, Phys. Rev. **D55**, 4157 (1997), [hep-ph/9609339].
- [35] T. Gutsche, V. E. Lyubovitskij and M. C. Tichy, Phys. Rev. **D79**, 014036 (2009), [arXiv:0811.0668].
- [36] M. Acciarri *et al.* (L3), Phys. Lett. **B501**, 1 (2001), [hep-ex/0011035].
- [37] F. E. Close, G. R. Farrar and Z.-p. Li, Phys. Rev. **D55**, 5749 (1997), [hep-ph/9610280].
- [38] D. M. Li, H. Yu and S. S. Fang, Eur. Phys. J. **C28**, 335 (2003).
- [39] R. Ahohe *et al.* (CLEO), Phys. Rev. **D71**, 072001 (2005), [hep-ex/0501026].
- [40] P. Achard *et al.* (L3), JHEP **03**, 018 (2007).
- [41] G. S. Bali *et al.* (UKQCD), Phys. Lett. **B309**, 378 (1993), [hep-lat/9304012].
- [42] C. J. Morningstar and M. J. Peardon, Phys. Rev. **D60**, 034509 (1999), [hep-lat/9901004].
- [43] L. Faddeev, A. J. Niemi and U. Wiedner, Phys. Rev. **D70**, 114033 (2004), [hep-ph/0308240].
- [44] H.-Y. Cheng, H.-n. Li and K.-F. Liu, Phys. Rev. **D79**, 014024 (2009), [arXiv:0811.2577].
- [45] G. Li, Q. Zhao and C.-H. Chang, J. Phys. **G35**, 055002 (2008), [hep-ph/0701020].
- [46] T. Gutsche, V. E. Lyubovitskij and M. C. Tichy, Phys. Rev. **D80**, 014014 (2009), [arXiv:0904.3414].
- [47] B. A. Li, Phys. Rev. **D81**, 114002 (2010), [arXiv:0912.2323].
- [48] A. Masoni, C. Cicalo and G. L. Usai, J. Phys. **G32**, R293 (2006).
- [49] H.-Y. Cheng, Phys. Lett. **B707**, 116 (2012), [arXiv:1110.2249].
- [50] F. Aceti, J.-J. Xie and E. Oset, Phys. Lett. **B750**, 609 (2015), [arXiv:1505.06134].
- [51] S. Stone and L. Zhang, Phys. Rev. Lett. **111**, 6, 062001 (2013), [arXiv:1305.6554].
- [52] R. S. Longacre, Phys. Rev. **D42**, 874 (1990).

- [53] R. Aaij *et al.* (LHCb), Phys. Rev. Lett. **112**, 9, 091802 (2014), [arXiv:1310.2145].
- [54] G. Gidal *et al.*, Phys. Rev. Lett. **59**, 2012 (1987).
- [55] C. Dionisi *et al.* (CERN-College de France-Madrid-Stockholm), Nucl. Phys. **B169**, 1 (1980).
- [56] S. U. Chung *et al.*, Phys. Rev. Lett. **55**, 779 (1985), [Erratum: Phys. Rev. Lett.55,2093(1985)].
- [57] D. F. Reeves *et al.*, Phys. Rev. **D34**, 1960 (1986).
- [58] A. Birman *et al.*, Phys. Rev. Lett. **61**, 1557 (1988), [Erratum: Phys. Rev. Lett.62,1577(1989)].
- [59] H. J. Behrend *et al.* (CELLO), Z. Phys. **C42**, 367 (1989).
- [60] A. Ando *et al.*, Phys. Rev. Lett. **57**, 1296 (1986).
- [61] T. A. Armstrong *et al.* (WA76), Phys. Lett. **B221**, 216 (1989).
- [62] D. Barberis *et al.* (WA102), Phys. Lett. **B413**, 225 (1997), [hep-ex/9707022].
- [63] T. A. Armstrong *et al.* (WA76, Athens-Bari-Birmingham-CERN-College de France), Z. Phys. **C52**, 389 (1991).
- [64] C. Adolph *et al.* (COMPASS), Phys. Rev. Lett. **115**, 8, 082001 (2015), [arXiv:1501.05732].
- [65] M. Aghasyan *et al.* (COMPASS), Phys. Rev. **D98**, 9, 092003 (2018), [arXiv:1802.05913].
- [66] S. Ishida *et al.*, Prog. Theor. Phys. **82**, 119 (1989).
- [67] D.O. Caldwell, *Hadron 89 Conf., Ajaccio, Corsica*, p. 127.
- [68] J.-L. Basdevant and E. L. Berger, Phys. Rev. Lett. **114**, 19, 192001 (2015), [arXiv:1504.05955].
- [69] M. Mikhasenko, B. Ketzer and A. Sarantsev, Phys. Rev. **D91**, 9, 094015 (2015), [arXiv:1501.07023].
- [70] V. R. Debastiani *et al.*, Phys. Rev. **D95**, 3, 034015 (2017), [arXiv:1611.05383].
- [71] D. Aston *et al.*, Phys. Lett. **B201**, 573 (1988).
- [72] P. F. Ermolov *et al.*, Sov. J. Nucl. Phys. **39**, 738 (1984), [Yad. Fiz.39,1170(1984)].
- [73] J. Dowd *et al.*, Nucl. Phys. Proc. Suppl. **21**, 11 (1991).
- [74] H. Aihara *et al.* (TPC/Two Gamma), Phys. Rev. **D38**, 1 (1988).
- [75] D. A. Bauer *et al.* (TPC/Two Gamma), Phys. Rev. **D48**, 3976 (1993).
- [76] P. Gavillet *et al.*, Z. Phys. **C16**, 119 (1982).
- [77] J. Z. Bai *et al.* (BES), Phys. Lett. **B446**, 356 (1999).
- [78] M. Ablikim *et al.* (BESIII), Phys. Rev. Lett. **106**, 072002 (2011), [arXiv:1012.3510].
- [79] F. E. Close and A. Kirk, Z. Phys. **C76**, 469 (1997), [hep-ph/9706543].

## 64. Rare Kaon Decays

Revised August 2019 by L. Littenberg (BNL) and G. Valencia (Monash U.).

## 64.1 Introduction

There are several useful reviews on rare kaon decays and related topics [1–12]. Activity in rare kaon decays can be divided roughly into four categories:

1. Searches for explicit violations of the Standard Model (SM)
2. The golden modes:  $K \rightarrow \pi\nu\bar{\nu}$
3. Other constraints on SM parameters
4. Studies of strong interactions at low energy.

The paradigm of Category 1 is the lepton flavor violating decay  $K_L \rightarrow \mu e$ . Category 2 includes the two modes that can be calculated with negligible theoretical uncertainty,  $K^+ \rightarrow \pi^+\nu\bar{\nu}$  and  $K_L \rightarrow \pi^0\nu\bar{\nu}$ . These modes can lead to precision determinations of CKM parameters or, in combination with other measurements of these parameters, they can constrain new interactions. They constitute the main focus of the current experimental kaon program. Category 3 is focused on decays with charged leptons, such as  $K_L \rightarrow \pi^0\ell^+\ell^-$  or  $K_L \rightarrow \ell^+\ell^-$  where  $\ell \equiv e, \mu$ . These modes are sensitive to CKM parameters but they suffer from multiple hadronic uncertainties that can be addressed, at least in part, through a systematic study of the peripheral modes indicated in Fig. 64.1. The interplay between Categories 3-4 and their complementarity to Category 2 is illustrated in the figure. Category 4 includes reactions like  $K^+ \rightarrow \pi^+\ell^+\ell^-$  where long distance contributions are dominant and which constitute a testing ground for the ideas of chiral perturbation theory. Other decays in this category are  $K_L \rightarrow \pi^0\gamma\gamma$  and  $K_L \rightarrow \ell^+\ell^-\gamma$ . The former is important in understanding a  $CP$ -conserving contribution to  $K_L \rightarrow \pi^0\ell^+\ell^-$ , whereas the latter could shed light on long distance contributions to  $K_L \rightarrow \mu^+\mu^-$ .

## 64.2 Explicit violations of the Standard Model

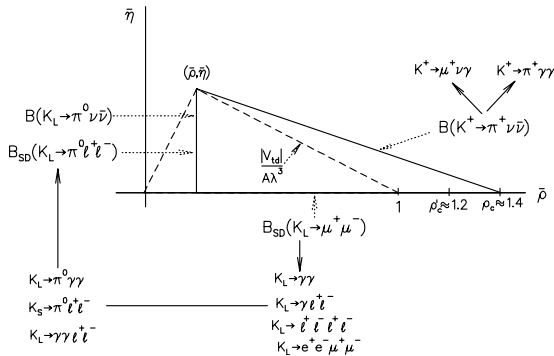


Figure 64.1: Role of rare kaon decays in determining the unitarity triangle. The solid arrows point to auxiliary modes needed to interpret the main results, or potential backgrounds to them.

Much activity has focussed on searches for lepton flavor violation (LFV). This is motivated by the fact that many extensions of the minimal Standard Model violate lepton flavor and by the potential to access very high energy scales. For example, the tree-level exchange of a LFV vector boson of mass  $M_X$  that couples to left-handed fermions with electroweak strength and without mixing angles yields  $B(K_L \rightarrow \mu e) = 4.7 \times 10^{-12} (148 \text{ TeV}/M_X)^4$  [2]. This simple dimensional analysis may be used to read from Table 64.1 that the reaction  $K_L \rightarrow \mu e$  is already probing scales of over 100 TeV. Table 64.1 summarizes the present experimental situation vis-à-vis LFV. The decays  $K_L \rightarrow \mu^\pm e^\mp$  and  $K^+ \rightarrow \pi^+ e^\mp \mu^\pm$  (or  $K_L \rightarrow \pi^0 e^\mp \mu^\pm$ ) provide complementary information on potential family number violating interactions, since the former is sensitive to parity-odd couplings and the latter is sensitive to parity-even couplings.

Limits on certain lepton-number violating (LNV) kaon decays also have been obtained, with recent interest arising from their role in constraining possible extensions of the neutrino sector [13,

14], and we list those in the table as well. Related searches in  $\mu$  and  $\tau$  processes are discussed in our section “Tests of Conservation Laws.”

**Table 64.1:** Searches for lepton flavor and lepton number violation in  $K$  decay

LFV mode	90% CL upper limit	Experiment	Yr./Ref.	Type
$K^+ \rightarrow \pi^+ e^- \mu^+$	$1.3 \times 10^{-11}$	BNL-865	2005/ [15]	LFV
$K^+ \rightarrow \pi^+ e^+ \mu^-$	$5.2 \times 10^{-10}$	BNL-865	2000/ [16]	LFV
$K_L \rightarrow \mu e$	$4.7 \times 10^{-12}$	BNL-871	1998/ [17]	LFV
$K_L \rightarrow \pi^0 e \mu$	$7.6 \times 10^{-11}$	KTeV	2008/ [18]	LFV
$K_L \rightarrow \pi^0 \pi^0 e \mu$	$1.7 \times 10^{-10}$	KTeV	2008/ [18]	LFV
$K^+ \rightarrow \pi^- e^+ e^+$	$2.2 \times 10^{-10}$	NA-62	2019/ [19]	LNV
$K^+ \rightarrow \pi^- \mu^+ \mu^+$	$4.2 \times 10^{-11}$	NA-62	2019/ [19]	LNV
$K^\pm \rightarrow \pi^\mp \mu^\pm \mu^\pm$	$8.6 \times 10^{-11}$	NA48/2	2017/ [20]	LNV
$K_L \rightarrow e^\pm e^\pm \mu^\mp \mu^\mp$	$4.12 \times 10^{-11}$	KTeV	2003/ [21]	LNV
$K^+ \rightarrow \pi^- \mu^+ e^+$	$5.0 \times 10^{-10}$	BNL-865	2000/ [16]	LNVF

Physics beyond the SM is also pursued through the search for  $K^+ \rightarrow \pi^+ X^0$ , where  $X^0$  is a new light particle. The searches cover both long-lived particles (*e.g.*, hyperphoton, axion, familon, *etc.*), and short-lived ones that decay to muon, electron or photon pairs. The 90% CL upper limit on  $K^+ \rightarrow \pi^+ X^0$  is  $7.3 \times 10^{-11}$  [22] for the case of massless  $X^0$ ; additional results as a function of the  $X^0$  mass can be found in [23]. Recently these limits have been reinterpreted in connection with a dark photon [24] or dark Z [25]. Such vectors have also been sought in their  $e^+e^-$  decay mode by NA48/2 [26]. Additional bounds for a short lived pseudoscalar  $X^0$  decaying to muons or photons are  $B(K_L \rightarrow \pi^0 \pi^0 \mu^+ \mu^-) < 1 \times 10^{-10}$  [27] and  $B(K_L \rightarrow \pi^0 \pi^0 \gamma \gamma) < 2.4 \times 10^{-7}$  [28].

64.3 The golden modes:  $K \rightarrow \pi\nu\bar{\nu}$ 

In the SM, the decay  $K^+ \rightarrow \pi^+\nu\bar{\nu}$  is dominated by one-loop diagrams with top-quark intermediate states while long-distance contributions are known to be quite small [29–31]. This permits a precise calculation of this rate in terms of SM parameters. Studies of this process are thus motivated by the possibility of detecting non-SM physics when comparing with the results of global fits [32, 33].

The branching ratio can be written in a compact form that exhibits the different ingredients that go into the calculation [34],

$$B(K^+ \rightarrow \pi^+\nu\bar{\nu}(\gamma)) = \kappa_+(1 + \Delta_{\text{EM}}) \left[ \left( \frac{\text{Im}(V_{ts}^* V_{td})}{\lambda^5} X_t \right)^2 + \left( \frac{\text{Re}(V_{cs}^* V_{cd})}{\lambda} (P_c + \delta P_{c,u}) + \frac{\text{Re}(V_{ts}^* V_{td})}{\lambda^5} X_t \right)^2 \right]. \quad (64.1)$$

The parameters in Eq. 64.1 incorporate the *a priori* unknown hadronic matrix element in terms of the very well-measured  $K_{e3}$  rate [29] in  $\kappa_+$ ; long distance QED corrections in  $\Delta_{\text{EM}}$  [35]; the Inami-Lim function for the short distance top-quark contribution [36] including NLO QCD corrections [37, 38] and the two-loop electroweak correction [34], all in  $X_t$ ; and the charm-quark contributions due to short distance effects including NNLO QCD corrections [39, 40] and NLO electroweak corrections via  $P_c$  [41], as well as certain long distance effects via  $\delta P_{c,u}$  [31, 42]. An interesting approximate way to cast this result in terms of the CKM parameters  $\lambda$ ,  $V_{cb}$ ,  $\bar{\rho}$  and  $\bar{\eta}$  (see our Section on “The Cabibbo-Kobayashi-Maskawa mixing matrix”) [43] is:

$$B(K^+ \rightarrow \pi^+\nu\bar{\nu}) \approx 1.6 \times 10^{-5} |V_{cb}|^4 [\sigma \bar{\eta}^2 + (\rho_c - \bar{\rho})^2], \quad (64.2)$$

where  $\rho_c \approx 1.45$  and  $\sigma \equiv \frac{1}{(1 - \frac{1}{2}\lambda^2)^2}$ . Thus,  $B(K^+ \rightarrow \pi^+\nu\bar{\nu})$  determines an ellipse in the  $\bar{\rho}$ ,  $\bar{\eta}$  plane with center  $(\rho_c, 0)$  and semiaxes  $\approx \frac{1}{|V_{cb}|^2} \sqrt{\frac{B(K^+ \rightarrow \pi^+\nu\bar{\nu})}{1.6 \times 10^{-5}}}$  and  $\frac{1}{\sigma |V_{cb}|^2} \sqrt{\frac{B(K^+ \rightarrow \pi^+\nu\bar{\nu})}{1.6 \times 10^{-5}}}$ .

BNL-787 observed two candidate events [44, 45] in the clean high  $\pi^+$  momentum and one event [46] in the low-momentum region. The successor experiment BNL-949 observed one more

in the high-momentum region [22] and three more in the low-momentum region [47], yielding a branching ratio of  $(1.73_{-1.05}^{+1.15}) \times 10^{-10}$  [23].

The NA62 experiment, performed with in-flight decays at CERN, aims to reach a sensitivity of  $\sim 10^{-12}$ /event. NA62 was commissioned in 2015 and has taken data in 2016, 2017 and 2018. The short 2016 run resulted in the observation of one event over an expected background of 0.152 events, which allowed a 95% C.L. limit of  $14 \times 10^{-10}$  to be set [48]. Very recently, preliminary results from the 2017 run have been announced. Two additional events were observed, over an expected background of 1.5 events. Combining this data with that of 2016, they obtain a 90% C.L. limit of  $1.85 \times 10^{-10}$  [49].

Using the latest CKMfitter input [32], we estimate  $B(K^+ \rightarrow \pi^+ \nu \bar{\nu}) = (8.5 \pm 0.5) \times 10^{-11}$ , near the lower end of the measurement of BNL-787 and 949. However, current parametric uncertainty in the CKM angles can result in numbers with central values differing from this one by up to 10% [50].

The second golden mode is the neutral counterpart to our preceding discussion:  $K_L \rightarrow \pi^0 \nu \bar{\nu}$ . It is dominantly  $CP$ -violating and free of hadronic uncertainties [29, 51, 52]. In the Standard Model, this mode is dominated by an intermediate top-quark state and does not suffer from the small uncertainty associated with the charm-quark intermediate state that affects  $K^+ \rightarrow \pi^+ \nu \bar{\nu}$ . The branching ratio is given by Ref. [43]:

$$B(K_L \rightarrow \pi^0 \nu \bar{\nu}) = \kappa_L \left( \frac{\text{Im}(V_{ts}^* V_{td})}{\lambda^5} X_t \right)^2 \approx 7.6 \times 10^{-5} |V_{cb}|^4 \bar{\eta}^2. \quad (64.3)$$

As with the charged mode, the hadronic matrix element can be related to that measured in  $K_{\ell 3}$  decay and is parameterized in  $\kappa_L$ .

Our estimate for the branching ratio, using the latest CKMfitter input [32], is  $(3.0 \pm 0.2) \times 10^{-11}$ . But similarly to the charged kaon case, parametric uncertainty in the CKM angles can result in a central value that differs from this one by up to almost 20% [50].

Grossman and Nir (GN) [53] pointed out that, in a nearly model-independent manner, the two golden modes satisfy the relation  $B(K_L \rightarrow \pi^0 \nu \bar{\nu}) \lesssim 4.4 B(K^+ \rightarrow \pi^+ \nu \bar{\nu})$ . Using the BNL 787/949 90% CL bound on  $K^+ \rightarrow \pi^+ \nu \bar{\nu}$ , GN then predict  $B(K_L \rightarrow \pi^0 \nu \bar{\nu}) < 1.46 \times 10^{-9}$ . Using instead the latest NA62 result, the GN upper bound becomes  $B(K_L \rightarrow \pi^0 \nu \bar{\nu}) < 8.14 \times 10^{-10}$  as can be seen in Figure 64.2.

The KOTO experiment at J-PARC, whose initial goal is to observe this decay, has been running since 2013 and in 2018 published a 90% CL upper limit of  $3.0 \times 10^{-9}$  [54], based on their 2015 data. They have run every year since, making incremental upgrades to the experimental configuration between runs.

It was pointed out in a recent paper that the GN bound obtained from the BNL result applies to the three body decay  $K_L \rightarrow \pi^0 \nu \bar{\nu}$  and not necessarily to two body modes such as  $K_L \rightarrow \pi^0 X^0$ . In this case KOTO can provide interesting constraints on new physics even at the current sensitivity level [55]. Using the 2015 data, they have established a 90% CL upper limit of  $2.4 \times 10^{-9}$  on  $K_L \rightarrow \pi^0 X^0$  for  $m_{X^0} \approx m_{\pi^0}$  [54].

Much theoretical work has explored beyond the SM scenarios that can populate this window as well as their correlations with other rare processes outside kaon physics. Although it would be relatively straight forward to establish the existence of new physics by observing deviations from their SM values in the  $K \rightarrow \pi \nu \bar{\nu}$  modes, it would take much more extensive global fits to pinpoint the origin of any such deviation. Partial summaries with references can be found in Refs. [9, 56–58]. There has also been a recent classification of the different possibilities in terms of the neutrino couplings [59], and several studies on the effect of neutrinos with different lepton flavor. [60–62].

The current theoretical and experimental situation for the golden modes is summarized in Fig. 64.2. The red area corresponds to the  $1\sigma$  SM prediction we obtain with the latest input available from CKMfitter (summer 2018) [32]. The yellow region shows the result established by the combined BNL-787 and BNL-949 results, whereas the green region marks the new 90% CL upper bound from NA62 for  $K^+ \rightarrow \pi^+ \nu \bar{\nu}$ . The black shaded region

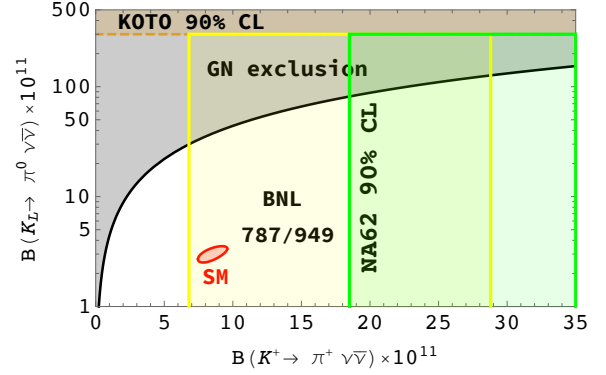


Figure 64.2: Summary of current situation for the golden modes  $K \rightarrow \pi \nu \bar{\nu}$ . The red ellipse shows the  $1\sigma$  SM prediction with input from CKMfitter; the yellow region corresponds to the BNL  $1\sigma$  measurement; the vertical green line marks the 90% CL upper bound from NA62, with the corresponding exclusion region shaded green; and the dashed orange line marks the 90% CL KOTO upper bound. The black shaded region shows the GN exclusion.

marks the GN exclusion, which lies significantly above the SM expectation leaving a large window for discovery of new physics contributions by experiments seeking to measure  $B(K_L \rightarrow \pi^0 \nu \bar{\nu})$ . The 90% CL upper bound on this mode from KOTO is shown as a dashed orange line, and is seen to still lie in the GN excluded zone.

Related modes with one extra pion,  $K \rightarrow \pi \pi \nu \bar{\nu}$ , are similarly dominated by short distance contributions [63–65]. However, they occur at much lower rates with branching ratios of order  $10^{-13}$ . The current best bound comes from KEK-391a, it is  $B(K_L \rightarrow \pi^0 \pi^0 \nu \bar{\nu}) < 8.1 \times 10^{-7}$  at 90% CL [66]. There is also a bound  $B(K^+ \rightarrow \pi^+ \pi^0 \nu \bar{\nu}) < 4.3 \times 10^{-5}$  at 90% CL [67] from BNL-787.

#### 64.4 Other constraints on Standard Model parameters

The decay  $K_L \rightarrow \mu^+ \mu^-$  has a short distance contribution sensitive to the CKM parameter  $\bar{\rho}$ , given by [43]:

$$B_{SD}(K_L \rightarrow \mu^+ \mu^-) \approx 2.7 \times 10^{-4} |V_{cb}|^4 (\rho'_c - \bar{\rho})^2 \quad (64.4)$$

where  $\rho'_c$  depends on the charm quark mass and is approximately 1.2. This decay, however, is dominated by a long-distance contribution from a two-photon intermediate state. The absorptive (imaginary) part of the long-distance component is determined by the measured rate for  $K_L \rightarrow \gamma \gamma$  to be  $B_{\text{abs}}(K_L \rightarrow \mu^+ \mu^-) = (6.64 \pm 0.07) \times 10^{-9}$ ; and it almost completely saturates the observed rate  $B(K_L \rightarrow \mu^+ \mu^-) = (6.84 \pm 0.11) \times 10^{-9}$  [68]. The difference between the observed rate and the absorptive component can be attributed to the (coherent) sum of the short-distance amplitude and the real part of the long-distance amplitude. The latter cannot be derived directly from experiment [69], but can be estimated with certain assumptions [70, 71].

By contrast, the decay  $K_L \rightarrow e^+ e^-$  is completely dominated by long distance physics and is easier to estimate. The result,  $B(K_L \rightarrow e^+ e^-) \sim 9 \times 10^{-12}$  [69, 72], is in good agreement with the BNL-871 measurement,  $(8.7_{-4.1}^{+5.7}) \times 10^{-12}$  [73].

The mode  $K_S \rightarrow \mu^+ \mu^-$  similarly has a short distance contribution proportional to the square of the CKM parameter  $\bar{\eta}$  entering at the  $10^{-13}$  level [10]. It also has long distance contributions arising from the two photon intermediate state which result in a rate  $B(K_S \rightarrow \mu^+ \mu^-)_{LD} = 5.1 \times 10^{-12}$  [10]. A 90% CL limit  $B(K_S \rightarrow \mu^+ \mu^-) < 2.1 \times 10^{-10}$  was recently obtained by LHCb [74, 75]. The interplay between  $K_L \rightarrow \mu^+ \mu^-$  and  $K_S \rightarrow \mu^+ \mu^-$  has been the subject of [76, 77].

The decay  $K_L \rightarrow \pi^0 e^+ e^-$  is sensitive to the CKM parameter  $\eta$  through its  $CP$ -violating component. There are both direct and indirect  $CP$ -violating amplitudes that can interfere. The direct  $CP$ -violating amplitude is short distance dominated and has been calculated in detail within the SM [5]. The indirect  $CP$ -violating

amplitude can be inferred from a measurement of  $K_S \rightarrow \pi^0 e^+ e^-$ . The complete  $CP$ -violating contribution to the rate can be written as [78–80]:

$$B_{CPV} \approx 10^{-12} \left[ 15.7 |a_S|^2 \pm 1.4 \left( \frac{|V_{cb}|^2 \bar{\eta}}{10^{-4}} \right) |a_S| + 0.12 \left( \frac{|V_{cb}|^2 \bar{\eta}}{10^{-4}} \right)^2 \right] \quad (64.5)$$

where the three terms correspond to the indirect  $CP$  violation, the interference, and the direct  $CP$  violation, respectively. The parameter  $a_S$  has been extracted by NA48/1 from a measurement of  $K_S \rightarrow \pi^0 e^+ e^-$  with the result  $|a_S| = 1.06_{-0.21}^{+0.26} \pm 0.07$  [81], as well as from a measurement of  $K_S \rightarrow \pi^0 \mu^+ \mu^-$  with the result  $|a_S| = 1.54_{-0.32}^{+0.40} \pm 0.06$  [82]. With current constraints on the CKM parameters, and assuming a positive sign for the interference term [80, 83], this implies that  $B_{CPV}(K_L \rightarrow \pi^0 e^+ e^-) \approx (3.1 \pm 0.9) \times 10^{-11}$ , where the three contributions to the central value from indirect, interference and direct  $CP$  violation are  $(1.76, 0.9, 0.45) \times 10^{-11}$  respectively. It should be noted that more recent studies suggest a much larger uncertainty in the value of  $a_S$  [84]. The complete  $CP$  violating amplitude for the related mode  $K_L \rightarrow \pi^0 \mu^+ \mu^-$  is predicted to be  $B_{CPV}(K_L \rightarrow \pi^0 \mu^+ \mu^-) \approx (1.4 \pm 0.5) \times 10^{-11}$  [10, 85].

$K_L \rightarrow \pi^0 e^+ e^-$  also has a  $CP$ -conserving component dominated by a two-photon intermediate state. This component can be decomposed into an absorptive and a dispersive part. The absorptive part can be extracted from the measurement of the low  $m_{\gamma\gamma}$  region of the  $K_L \rightarrow \pi^0 \gamma\gamma$  spectrum. The rate and the shape of the distribution  $d\Gamma/dm_{\gamma\gamma}$  in  $K_L \rightarrow \pi^0 \gamma\gamma$  are well described in chiral perturbation theory in terms of three (*a priori*) unknown parameters [86–89].

Both KTeV and NA48 have studied the mode  $K_L \rightarrow \pi^0 \gamma\gamma$ , reporting similar results. KTeV finds  $B(K_L \rightarrow \pi^0 \gamma\gamma) = (1.29 \pm 0.03_{\text{stat}} \pm 0.05_{\text{sys}}) \times 10^{-6}$  [90], while NA48 finds  $B(K_L \rightarrow \pi^0 \gamma\gamma) = (1.36 \pm 0.03_{\text{stat}} \pm 0.03_{\text{sys}} \pm 0.03_{\text{norm}}) \times 10^{-6}$  [91]. Both experiments are consistent with a negligible rate in the low  $m_{\gamma\gamma}$  region, suggesting a very small  $CP$ -conserving component  $B_{CP}(K_L \rightarrow \pi^0 e^+ e^-) \sim \mathcal{O}(10^{-13})$  [80, 89, 91]. There remains some model dependence in the estimate of the dispersive part of the  $CP$ -conserving  $K_L \rightarrow \pi^0 e^+ e^-$  [80].

The related process,  $K_L \rightarrow \pi^0 \gamma e^+ e^-$ , is potentially an additional background to  $K_L \rightarrow \pi^0 e^+ e^-$  in some region of phase space [92]. This process has been observed with a branching ratio of  $(1.62 \pm 0.14_{\text{stat}} \pm 0.09_{\text{sys}}) \times 10^{-8}$  [93].

The decay  $K_L \rightarrow \gamma \gamma e^+ e^-$  constitutes the dominant background to  $K_L \rightarrow \pi^0 e^+ e^-$ . It was first observed by BNL-845 [94], and subsequently confirmed with a much larger sample by KTeV [95]. It has been estimated that this background will enter at about the  $10^{-10}$  level [96, 97], comparable to or larger than the signal level. Because of this, the observation of  $K_L \rightarrow \pi^0 e^+ e^-$  at the SM level will depend on background subtraction with good statistics. Possible alternative strategies are discussed in Ref. [80] and references cited therein.

The 90% CL upper bound for the process  $K_L \rightarrow \pi^0 e^+ e^-$  is  $2.8 \times 10^{-10}$  [97]. For the closely related muonic process, the published upper bound is  $B(K_L \rightarrow \pi^0 \mu^+ \mu^-) \leq 3.8 \times 10^{-10}$  [98], compared with the SM prediction of  $(1.5 \pm 0.3) \times 10^{-11}$  [85] (assuming positive interference between the direct- and indirect- $CP$  violating components).

A study of  $K_L \rightarrow \pi^0 \mu^+ \mu^-$  has indicated that it might be possible to extract the direct  $CP$ -violating contribution by a joint study of the Dalitz plot variables and the components of the  $\mu^+$  polarization [99]. The latter tends to be quite substantial so that large statistics may not be necessary.

Combined information from  $K_L \rightarrow \pi^0 \ell^+ \ell^-$  as well as  $K_L \rightarrow \mu^+ \mu^-$  complements the  $K \rightarrow \pi \nu \bar{\nu}$  measurements in constraining physics beyond the SM [100].

## 64.5 Other long distance dominated modes

The decays  $K^+ \rightarrow \pi^+ \ell^+ \ell^-$  ( $\ell = e$  or  $\mu$ ) have received considerable attention. The rate and spectrum have been measured for both the electron and muon modes [101–106]. The theoretical status of these modes has been summarized recently [84, 107].

The measurements have been used to exclude new physics such as a dark photon [24]. Ref. [78, 79] has proposed a parameterization inspired by chiral perturbation theory, which provides a successful description of data but indicates the presence of large corrections beyond leading order. More work is needed to fully understand the origin of these large corrections. The mode  $K^+ \rightarrow \pi^+ \pi^0 e^+ e^-$ , recently analyzed by NA48/2 [108], is also dominated by long distance physics but it has been argued that measuring asymmetries can provide information on the short distance components [109]. The related mode  $K_S \rightarrow \pi^+ \pi^- e^+ e^-$ , which was measured by NA48/1 [110], has received new interest by LHCb [111] as an important background to other rare decays. An update of the theory for these modes can be found in [112].

The decay  $K^+ \rightarrow \pi^+ \gamma\gamma$  can be predicted in terms of one unknown parameter to leading order in  $\chi$ PT resulting in a correlation between the rate and the diphoton mass spectrum [113]. Certain important corrections at the next order are also known [114]. The rate was first measured by E787 [115], and more recently NA48/2 [116] has obtained a more precise result with a 6% error, as well as the corresponding spectrum fits. The most recent, and precise, result is from NA62 based on a sample of 232 events [117] but is still insufficient to distinguish between the leading order and next order  $\chi$ PT parameterizations.

Much information has been recorded by KTeV and NA48 on the rates and spectrum for the Dalitz pair conversion modes  $K_L \rightarrow \ell^+ \ell^- \gamma$  [118, 119], and  $K_L \rightarrow \ell^+ \ell^- \ell'^+ \ell'^-$  for  $\ell, \ell' = e$  or  $\mu$  [21, 120]. More recently, LHCb has performed preliminary studies of  $K_S \rightarrow \ell^+ \ell^- \ell'^+ \ell'^-$  [111]. All these results are used to test hadronic models and should eventually help unravel the underlying physics in  $K_L \rightarrow \mu^+ \mu^-$  [71, 76, 121].

## References

- [1] L. Littenberg and G. Valencia, *Ann. Rev. Nucl. Part. Sci.* **43**, 729 (1993), [hep-ph/9303225].
- [2] J. L. Ritchie and S. G. Wojcicki, *Rev. Mod. Phys.* **65**, 1149 (1993).
- [3] B. Winstein and L. Wolfenstein, *Rev. Mod. Phys.* **65**, 1113 (1993).
- [4] A. Pich, *Rept. Prog. Phys.* **58**, 563 (1995), [hep-ph/9502366].
- [5] G. Buchalla, A. J. Buras and M. E. Lautenbacher, *Rev. Mod. Phys.* **68**, 1125 (1996), [hep-ph/9512380].
- [6] G. D'Ambrosio and G. Isidori, *Int. J. Mod. Phys. A* **13**, 1 (1998), [hep-ph/9611284].
- [7] P. Buchholz and B. Renk, *Prog. Part. Nucl. Phys.* **39**, 253 (1997).
- [8] A. R. Barker and S. H. Kettell, *Ann. Rev. Nucl. Part. Sci.* **50**, 249 (2000), [hep-ex/0009024].
- [9] A. J. Buras, F. Schwab and S. Uhlig, *Rev. Mod. Phys.* **80**, 965 (2008), [hep-ph/0405132].
- [10] V. Cirigliano *et al.*, *Rev. Mod. Phys.* **84**, 399 (2012), [arXiv:1107.6001].
- [11] D. Bryman *et al.*, *Ann. Rev. Nucl. Part. Sci.* **61**, 331 (2011).
- [12] T. K. Komatsubara, *Prog. Part. Nucl. Phys.* **67**, 995 (2012), [arXiv:1203.6437].
- [13] A. Atre *et al.*, *JHEP* **05**, 030 (2009), [arXiv:0901.3589].
- [14] L. S. Littenberg and R. Shrock, *Phys. Lett.* **B491**, 285 (2000), [hep-ph/0005285].
- [15] A. Sher *et al.*, *Phys. Rev.* **D72**, 012005 (2005), [hep-ex/0502020].
- [16] R. Appel *et al.*, *Phys. Rev. Lett.* **85**, 2877 (2000), [hep-ex/0006003].
- [17] D. Ambrose *et al.* (BNL), *Phys. Rev. Lett.* **81**, 5734 (1998), [hep-ex/9811038].



- [18] E. Abouzaid *et al.* (KTeV), Phys. Rev. Lett. **100**, 131803 (2008), [arXiv:0711.3472].
- [19] E. Cortina Gil *et al.* (NA62), Phys. Lett. **B797**, 134794 (2019), [arXiv:1905.07770].
- [20] J. R. Batley *et al.* (NA48/2), Phys. Lett. **B769**, 67 (2017), [arXiv:1612.04723].
- [21] A. Alavi-Harati *et al.* (KTeV), Phys. Rev. Lett. **90**, 141801 (2003), [hep-ex/0212002].
- [22] V. V. Anisimovsky *et al.* (E949), Phys. Rev. Lett. **93**, 031801 (2004), [hep-ex/0403036].
- [23] A. V. Artamonov *et al.* (BNL-E949), Phys. Rev. **D79**, 092004 (2009), [arXiv:0903.0030].
- [24] M. Pospelov, Phys. Rev. **D80**, 095002 (2009), [arXiv:0811.1030].
- [25] H. Davoudiasl, H.-S. Lee and W. J. Marciano, Phys. Rev. **D89**, 9, 095006 (2014), [arXiv:1402.3620].
- [26] J. R. Batley *et al.* (NA48/2), Phys. Lett. **B746**, 178 (2015), [arXiv:1504.00607].
- [27] E. Abouzaid *et al.* (KTeV), Phys. Rev. Lett. **107**, 201803 (2011), [arXiv:1105.4800].
- [28] Y. C. Tung *et al.* (E391a), Phys. Rev. Lett. **102**, 051802 (2009), [arXiv:0810.4222].
- [29] J. S. Hagelin and L. S. Littenberg, Prog. Part. Nucl. Phys. **23**, 1 (1989).
- [30] M. Lu and M. B. Wise, Phys. Lett. **B324**, 461 (1994), [hep-ph/9401204].
- [31] A. F. Falk, A. Lewandowski and A. A. Petrov, Phys. Lett. **B505**, 107 (2001), [hep-ph/0012099].
- [32] J. Charles *et al.*, Phys. Rev. **D84**, 033005 (2011), [arXiv:1106.4041].
- [33] M. Bona *et al.* (UTfit), JHEP **03**, 049 (2008), [arXiv:0707.0636].
- [34] J. Brod, M. Gorbahn and E. Stamou, Phys. Rev. **D83**, 034030 (2011), [arXiv:1009.0947].
- [35] F. Mescia and C. Smith, Phys. Rev. **D76**, 034017 (2007), [arXiv:0705.2025].
- [36] T. Inami and C. S. Lim, Prog. Theor. Phys. **65**, 297 (1981), [Erratum: Prog. Theor. Phys.65,1772(1981)].
- [37] G. Buchalla and A. J. Buras, Nucl. Phys. **B548**, 309 (1999), [hep-ph/9901288].
- [38] M. Misiak and J. Urban, Phys. Lett. **B451**, 161 (1999), [hep-ph/9901278].
- [39] A. J. Buras *et al.*, Phys. Rev. Lett. **95**, 261805 (2005), [hep-ph/0508165].
- [40] A. J. Buras *et al.*, JHEP **11**, 002 (2006), [Erratum: JHEP11,167(2012)], [hep-ph/0603079].
- [41] J. Brod and M. Gorbahn, Phys. Rev. **D78**, 034006 (2008), [arXiv:0805.4119].
- [42] G. Isidori, F. Mescia and C. Smith, Nucl. Phys. **B718**, 319 (2005), [hep-ph/0503107].
- [43] A. J. Buras and R. Fleischer, Adv. Ser. Direct. High Energy Phys. **15**, 65 (1998), [65(1997)], [hep-ph/9704376].
- [44] S. Adler *et al.* (E787), Phys. Rev. Lett. **88**, 041803 (2002), [hep-ex/0111091].
- [45] S. Adler *et al.* (E787), Phys. Rev. Lett. **84**, 3768 (2000), [hep-ex/0002015].
- [46] S. S. Adler *et al.* (E787), Phys. Lett. **B537**, 211 (2002), [hep-ex/0201037].
- [47] A. V. Artamonov *et al.* (E949), Phys. Rev. Lett. **101**, 191802 (2008), [arXiv:0808.2459].
- [48] E. Cortina Gil *et al.* (NA62), Phys. Lett. **B791**, 156 (2019), [arXiv:1811.08508].
- [49] G. Ruggiero, NA62 collaboration “Latest measurement of  $K^+ \rightarrow \pi^+ \nu \bar{\nu}$  with the NA62 experiment at CERN”, talk at KAON 2019, [https://indico.cern.ch/event/769729/].
- [50] A. J. Buras *et al.*, JHEP **11**, 033 (2015), [arXiv:1503.02693].
- [51] L. S. Littenberg, Phys. Rev. **D39**, 3322 (1989).
- [52] G. Buchalla and G. Isidori, Phys. Lett. **B440**, 170 (1998), [hep-ph/9806501].
- [53] Y. Grossman and Y. Nir, Phys. Lett. **B398**, 163 (1997), [hep-ph/9701313].
- [54] J. K. Ahn *et al.* (KOTO), Phys. Rev. Lett. **122**, 2, 021802 (2019), [arXiv:1810.09655].
- [55] K. Fuyuto, W.-S. Hou and M. Kohda, Phys. Rev. Lett. **114**, 171802 (2015), [arXiv:1412.4397].
- [56] G. D’Ambrosio and G. Isidori, Phys. Lett. **B530**, 108 (2002), [hep-ph/0112135].
- [57] D. Bryman *et al.*, Int. J. Mod. Phys. **A21**, 487 (2006), [hep-ph/0505171].
- [58] A. J. Buras, D. Buttazzo and R. Knegjens, JHEP **11**, 166 (2015), [arXiv:1507.08672].
- [59] X.-G. He, G. Valencia and K. Wong, Eur. Phys. J. **C78**, 6, 472 (2018), [arXiv:1804.07449].
- [60] M. Bordone *et al.*, Eur. Phys. J. **C77**, 9, 618 (2017), [arXiv:1705.10729].
- [61] X.-G. He, J. Tandean and G. Valencia, JHEP **07**, 022 (2019), [arXiv:1903.01242].
- [62] X.-G. He, J. Tandean and G. Valencia, Phys. Lett. **B797**, 134842 (2019), [arXiv:1904.04043].
- [63] L. S. Littenberg and G. Valencia, Phys. Lett. **B385**, 379 (1996), [hep-ph/9512413].
- [64] C.-W. Chiang and F. J. Gilman, Phys. Rev. **D62**, 094026 (2000), [hep-ph/0007063].
- [65] C. Q. Geng, I. J. Hsu and Y. C. Lin, Phys. Rev. **D50**, 5744 (1994), [hep-ph/9406313].
- [66] R. Ogata *et al.* (E391a), Phys. Rev. **D84**, 052009 (2011), [arXiv:1106.3404].
- [67] S. Adler *et al.* (E787), Phys. Rev. **D63**, 032004 (2001), [hep-ex/0009055].
- [68] D. Ambrose *et al.* (E871), Phys. Rev. Lett. **84**, 1389 (2000).
- [69] G. Valencia, Nucl. Phys. **B517**, 339 (1998), [hep-ph/9711377].
- [70] G. D’Ambrosio, G. Isidori and J. Portoles, Phys. Lett. **B423**, 385 (1998), [hep-ph/9708326].
- [71] G. Isidori and R. Unterdorfer, JHEP **01**, 009 (2004), [hep-ph/0311084].
- [72] D. Gomez Dumm and A. Pich, Phys. Rev. Lett. **80**, 4633 (1998), [hep-ph/9801298].
- [73] D. Ambrose *et al.* (BNL E871), Phys. Rev. Lett. **81**, 4309 (1998), [hep-ex/9810007].
- [74] R. Aaij *et al.* (LHCb), Eur. Phys. J. **C77**, 10, 678 (2017), [arXiv:1706.00758].
- [75] Miguel Ramos Pernas, LHCb collaboration “Search for  $K_S \rightarrow \mu^+ \mu^-$  at LHCb”, talk at KAON 2019, [https://indico.cern.ch/event/769729/].
- [76] G. D’Ambrosio and T. Kitahara, Phys. Rev. Lett. **119**, 20, 201802 (2017), [arXiv:1707.06999].
- [77] V. Chobanova *et al.*, JHEP **05**, 024 (2018), [arXiv:1711.11030].
- [78] G. D’Ambrosio *et al.*, JHEP **08**, 004 (1998), [hep-ph/9808289].
- [79] C. Dib, I. Dunietz and F. J. Gilman, Phys. Rev. **D39**, 2639 (1989).
- [80] G. Buchalla, G. D’Ambrosio and G. Isidori, Nucl. Phys. **B672**, 387 (2003), [hep-ph/0308008].
- [81] J. R. Batley *et al.* (NA48/1), Phys. Lett. **B576**, 43 (2003), [hep-ex/0309075].
- [82] J. R. Batley *et al.* (NA48/1), Phys. Lett. **B599**, 197 (2004), [hep-ex/0409011].



- [83] S. Friot, D. Greynat and E. De Rafael, Phys. Lett. **B595**, 301 (2004), [hep-ph/0404136].
- [84] G. D'Ambrosio, D. Greynat and M. Knecht, JHEP **02**, 049 (2019), [arXiv:1812.00735].
- [85] G. Isidori, C. Smith and R. Unterdorfer, Eur. Phys. J. **C36**, 57 (2004), [hep-ph/0404127].
- [86] G. Ecker, A. Pich and E. de Rafael, Phys. Lett. **B237**, 481 (1990).
- [87] L. Cappiello, G. D'Ambrosio and M. Miragliuolo, Phys. Lett. **B298**, 423 (1993).
- [88] A. G. Cohen, G. Ecker and A. Pich, Phys. Lett. **B304**, 347 (1993).
- [89] F. Gabbiani and G. Valencia, Phys. Rev. **D66**, 074006 (2002), [hep-ph/0207189].
- [90] E. Abouzaid *et al.* (KTeV), Phys. Rev. **D77**, 112004 (2008), [arXiv:0805.0031].
- [91] A. Lai *et al.* (NA48), Phys. Lett. **B536**, 229 (2002), [hep-ex/0205010].
- [92] J. F. Donoghue and F. Gabbiani, Phys. Rev. **D56**, 1605 (1997), [hep-ph/9702278].
- [93] E. Abouzaid *et al.* (KTeV), Phys. Rev. **D76**, 052001 (2007), [arXiv:0706.4074].
- [94] W. M. Morse *et al.*, Phys. Rev. **D45**, 36 (1992).
- [95] A. Alavi-Harati *et al.* (KTeV), Phys. Rev. **D64**, 012003 (2001), [hep-ex/0010059].
- [96] H. B. Greenlee, Phys. Rev. **D42**, 3724 (1990).
- [97] A. Alavi-Harati *et al.* (KTeV), Phys. Rev. Lett. **93**, 021805 (2004), [hep-ex/0309072].
- [98] A. Alavi-Harati *et al.* (KTeV), Phys. Rev. Lett. **84**, 5279 (2000), [hep-ex/0001006].
- [99] M. V. Diwan, H. Ma and T. L. Trueman, Phys. Rev. **D65**, 054020 (2002), [hep-ph/0112350].
- [100] F. Mescia, C. Smith and S. Trine, JHEP **08**, 088 (2006), [hep-ph/0606081].
- [101] R. Appel *et al.* (E865), Phys. Rev. Lett. **83**, 4482 (1999), [hep-ex/9907045].
- [102] J. R. Batley *et al.* (NA48/2), Phys. Lett. **B677**, 246 (2009), [arXiv:0903.3130].
- [103] S. Adler *et al.* (E787), Phys. Rev. Lett. **79**, 4756 (1997), [hep-ex/9708012].
- [104] H. Ma *et al.* (e865), Phys. Rev. Lett. **84**, 2580 (2000), [hep-ex/9910047].
- [105] H. K. Park *et al.* (HyperCP), Phys. Rev. Lett. **88**, 111801 (2002), [hep-ex/0110033].
- [106] J. R. Batley *et al.* (NA48/2), Phys. Lett. **B697**, 107 (2011), [arXiv:1011.4817].
- [107] G. D'Ambrosio, D. Greynat and M. Knecht, Phys. Lett. (2019), [arXiv:1906.03046].
- [108] J. R. Batley *et al.* (NA48/2), Phys. Lett. **B788**, 552 (2019), [arXiv:1809.02873].
- [109] L. Cappiello *et al.*, Eur. Phys. J. **C72**, 1872 (2012), [Erratum: Eur. Phys. J. C72,2208(2012)], [arXiv:1112.5184].
- [110] J. R. Batley *et al.* (NA48/1), Phys. Lett. **B694**, 301 (2011).
- [111] C. Marin Benito (LHCb), J. Phys. Conf. Ser. **800**, 1, 012031 (2017).
- [112] L. Cappiello, O. Catà and G. D'Ambrosio, Eur. Phys. J. **C78**, 3, 265 (2018), [arXiv:1712.10270].
- [113] G. Ecker, A. Pich and E. de Rafael, Nucl. Phys. **B303**, 665 (1988).
- [114] G. D'Ambrosio and J. Portoles, Phys. Lett. **B386**, 403 (1996), [Erratum: Phys. Lett. B395,389(1997)], [hep-ph/9606213].
- [115] P. Kitching *et al.* (E787), Phys. Rev. Lett. **79**, 4079 (1997), [hep-ex/9708011].
- [116] J. R. Batley *et al.* (NA48/2), Phys. Lett. **B730**, 141 (2014), [arXiv:1310.5499].
- [117] C. Lazzeroni *et al.* (NA62), Phys. Lett. **B732**, 65 (2014), [arXiv:1402.4334].
- [118] A. Alavi-Harati *et al.* (KTeV), Phys. Rev. Lett. **87**, 071801 (2001).
- [119] E. Abouzaid *et al.* (KTeV), Phys. Rev. Lett. **99**, 051804 (2007), [hep-ex/0702039].
- [120] V. Fanti *et al.* (NA48), Phys. Lett. **B458**, 553 (1999).
- [121] G. D'Ambrosio, D. Greynat and G. Vulvert, Eur. Phys. J. **C73**, 12, 2678 (2013), [arXiv:1309.5736].

## 65. CPT Invariance Tests in Neutral Kaon Decay

Revised August 2019 by M. Antonelli (INFN, Frascati), G. D'Ambrosio (INFN, Napoli) and M.S. Sozzi (Pisa U.).

*CPT* theorem is based on three assumptions: quantum field theory, locality, and Lorentz invariance, and thus it is a fundamental probe of our basic understanding of particle physics. Strangeness oscillation in  $K^0 - \bar{K}^0$  system, described by the equation

$$i \frac{d}{dt} \begin{bmatrix} K^0 \\ \bar{K}^0 \end{bmatrix} = [M - i\Gamma/2] \begin{bmatrix} K^0 \\ \bar{K}^0 \end{bmatrix},$$

where  $M$  and  $\Gamma$  are hermitian matrices (see PDG review [1], references [2,3], and KLOE paper [4] for notations and previous literature), allows a very accurate test of *CPT* symmetry; indeed since *CPT* requires  $M_{11} = M_{22}$  and  $\Gamma_{11} = \Gamma_{22}$ , the mass and width eigenstates,  $K_{S,L}$ , have a *CPT*-violating piece,  $\delta$ , in addition to the usual *CPT*-conserving parameter  $\epsilon$ :

$$K_{S,L} = \frac{1}{\sqrt{2(1+|\epsilon_{S,L}|^2)}} \left[ (1+\epsilon_{S,L}) K^0 \pm (1-\epsilon_{S,L}) \bar{K}^0 \right]$$

$$\epsilon_{S,L} = \frac{-i\Im(M_{12}) - \frac{1}{2}\Im(\Gamma_{12}) \mp \frac{1}{2} [M_{11} - M_{22} - \frac{i}{2}(\Gamma_{11} - \Gamma_{22})]}{m_L - m_S + i(\Gamma_S - \Gamma_L)/2}$$

$$\equiv \epsilon \pm \delta. \quad (65.1)$$

Using the phase convention  $\Im(\Gamma_{12}) = 0$ , we determine the phase of  $\epsilon$  to be  $\varphi_{SW} \equiv \arctan \frac{2(m_L - m_S)}{\Gamma_S - \Gamma_L}$ . Imposing unitarity to an arbitrary combination of  $K^0$  and  $\bar{K}^0$  wave functions, we obtain the Bell-Steinberger relation [5] connecting *CP* and *CPT* violation in the mass matrix to *CP* and *CPT* violation in the decay; in fact, neglecting  $\mathcal{O}(\epsilon)$  corrections to the coefficient of the *CPT*-violating parameter,  $\delta$ , we can write [4]

$$\left[ \frac{\Gamma_S + \Gamma_L}{\Gamma_S - \Gamma_L} + i \tan \phi_{SW} \right] \left[ \frac{\Re(\epsilon)}{1+|\epsilon|^2} - i\Im(\delta) \right] = \frac{1}{\Gamma_S - \Gamma_L} \sum_f A_L(f) A_S^*(f), \quad (65.2)$$

where  $A_{L,S}(f) \equiv A(K_{L,S} \rightarrow f)$ . We stress that this relation is phase-convention-independent. The advantage of the neutral kaon system is that only a few decay modes give significant contributions to the r.h.s. in Eq. (65.2); in fact, defining for the hadronic modes

$$\alpha_i \equiv \frac{1}{\Gamma_S} \langle A_L(i) A_S^*(i) \rangle = \eta_i \mathcal{B}(K_S \rightarrow i),$$

$$i = \pi^0 \pi^0, \pi^+ \pi^- (\gamma), 3\pi^0, \pi^0 \pi^+ \pi^- (\gamma), \quad (65.3)$$

the recent data from CPLEAR, KLOE, KTeV, and NA48 have led to the following determinations (the analysis described in Ref. [4] has been updated by using the recent measurements of  $K_L$  branching ratios from KTeV [6, 7], NA48 [8, 9], the results described in the *CP* violation in  $K_L$  decays minireview, and the KLOE result [10])

$$\alpha_{\pi^+ \pi^-} = ((1.121 \pm 0.010) + i(1.061 \pm 0.010)) \times 10^{-3},$$

$$\alpha_{\pi^0 \pi^0} = ((0.493 \pm 0.005) + i(0.471 \pm 0.005)) \times 10^{-3},$$

$$\alpha_{\pi^+ \pi^- \pi^0} = ((0 \pm 2) + i(0 \pm 2)) \times 10^{-6},$$

$$|\alpha_{\pi^0 \pi^0 \pi^0}| < 1.5 \times 10^{-6} \text{ at 95\% CL.} \quad (65.4)$$

The semileptonic contribution to the right-handed side of Eq. (65.2) requires the determination of several observables: we

define [2, 3]

$$\begin{aligned} \mathcal{A}(K^0 \rightarrow \pi^- l^+ \nu) &= \mathcal{A}_0(1 - y), \\ \mathcal{A}(K^0 \rightarrow \pi^+ l^- \nu) &= \mathcal{A}_0^*(1 + y^*)(x_+ - x_-)^*, \\ \mathcal{A}(\bar{K}^0 \rightarrow \pi^+ l^- \nu) &= \mathcal{A}_0^*(1 + y^*), \\ \mathcal{A}(\bar{K}^0 \rightarrow \pi^- l^+ \nu) &= \mathcal{A}_0(1 - y)(x_+ + x_-), \end{aligned} \quad (65.5)$$

where  $x_+$  ( $x_-$ ) describes the violation of the  $\Delta S = \Delta Q$  rule in *CPT*-conserving (violating) decay amplitudes, and  $y$  parametrizes *CPT* violation for  $\Delta S = \Delta Q$  transitions. Taking advantage of their tagged  $K^0(\bar{K}^0)$  beams, CPLEAR has measured  $\Im(x_+)$ ,  $\Re(x_-)$ ,  $\Im(\delta)$ , and  $\Re(\delta)$  [11]. These determinations have been improved in Ref. [4] by including the information  $A_S - A_L = 4[\Re(\delta) + \Re(x_-)]$  (valid at first order in the small parameters), where  $A_{L,S}$  are the  $K_L$  and  $K_S$  semileptonic charge asymmetries, respectively, from the PDG [12] and the new KLOE semileptonic measurement [13]. Here we are also including the *T*-violating asymmetry measurement from CPLEAR [14] with a finer binning than appearing in the published article.

**Table 65.1:** Values, errors, and correlation coefficients for  $\Re(\delta)$ ,  $\Im(\delta)$ ,  $\Re(x_-)$ ,  $\Im(x_+)$ , and  $A_S + A_L$  obtained from a combined fit, including KLOE [4, 13] and CPLEAR [14].

	value	Correlations coefficients			
$\Re(\delta)$	$(4.3 \pm 2.7) \times 10^{-4}$	1			
$\Im(\delta)$	$(-0.9 \pm 0.6) \times 10^{-2}$	-0.40	1		
$\Re(x_-)$	$(-0.22 \pm 0.10) \times 10^{-2}$	-0.14	-0.30	1	
$\Im(x_+)$	$(0.06 \pm 0.19) \times 10^{-2}$	-0.12	-0.02	0.34	1
$A_S + A_L$	$(-0.23 \pm 0.38) \times 10^{-2}$	-0.12	-0.29	0.94	0.18

The value  $A_S + A_L$  in Table 65.1 can be directly included in the semileptonic contributions to the Bell Steinberger relations in Eq. (65.2)

$$\begin{aligned} \sum_{\pi l \nu} \langle A_L(\pi l \nu) A_S^*(\pi l \nu) \rangle \\ = 2\Gamma(K_L \rightarrow \pi l \nu) (\Re(\epsilon) - \Re(y) - i(\Im(x_+) + \Im(\delta))) \\ = 2\Gamma(K_L \rightarrow \pi l \nu) ((A_S + A_L)/4 - i(\Im(x_+) + \Im(\delta))). \end{aligned} \quad (65.6)$$

Defining

$$\alpha_{\pi l \nu} \equiv \frac{1}{\Gamma_S} \sum_{\pi l \nu} \langle A_L(\pi l \nu) A_S^*(\pi l \nu) \rangle + 2i \frac{\tau_{K_S}}{\tau_{K_L}} \mathcal{B}(K_L \rightarrow \pi l \nu) \Im(\delta), \quad (65.7)$$

we find:

$$\alpha_{\pi l \nu} = ((-0.1 \pm 0.2) + i(-0.1 \pm 0.5)) \times 10^{-5}. \quad (65.8)$$

**Table 65.2:** Summary of results: values, errors, and correlation coefficients for  $\Re(\epsilon)$ ,  $\Im(\delta)$ ,  $\Re(\delta)$ , and  $\Re(x_-)$ .

	value	Correlations coefficients			
$\Re(\epsilon)$	$(161.2 \pm 0.5) \times 10^{-5}$	+1			
$\Im(\delta)$	$(-0.3 \pm 1.4) \times 10^{-5}$	+0.08	1		
$\Re(\delta)$	$(2.6 \pm 2.5) \times 10^{-4}$	+0.00	-0.05	1	
$\Re(x_-)$	$(-2.7 \pm 1.0) \times 10^{-3}$	+0.05	0.13	-0.30	1

Inserting the values of the  $\alpha$  parameters into Eq. (65.2), we find

$$\begin{aligned} \Re(\epsilon) &= (161.2 \pm 0.5) \times 10^{-5}, \\ \Im(\delta) &= (-0.3 \pm 1.4) \times 10^{-5}. \end{aligned} \quad (65.9)$$

The complete information on Eq. (65.9) is given in Table 65.2. Now the agreement with *CPT* conservation,  $\Im(\delta) = \Re(\delta) = \Re(x_-) = 0$ , is at 18% C.L.

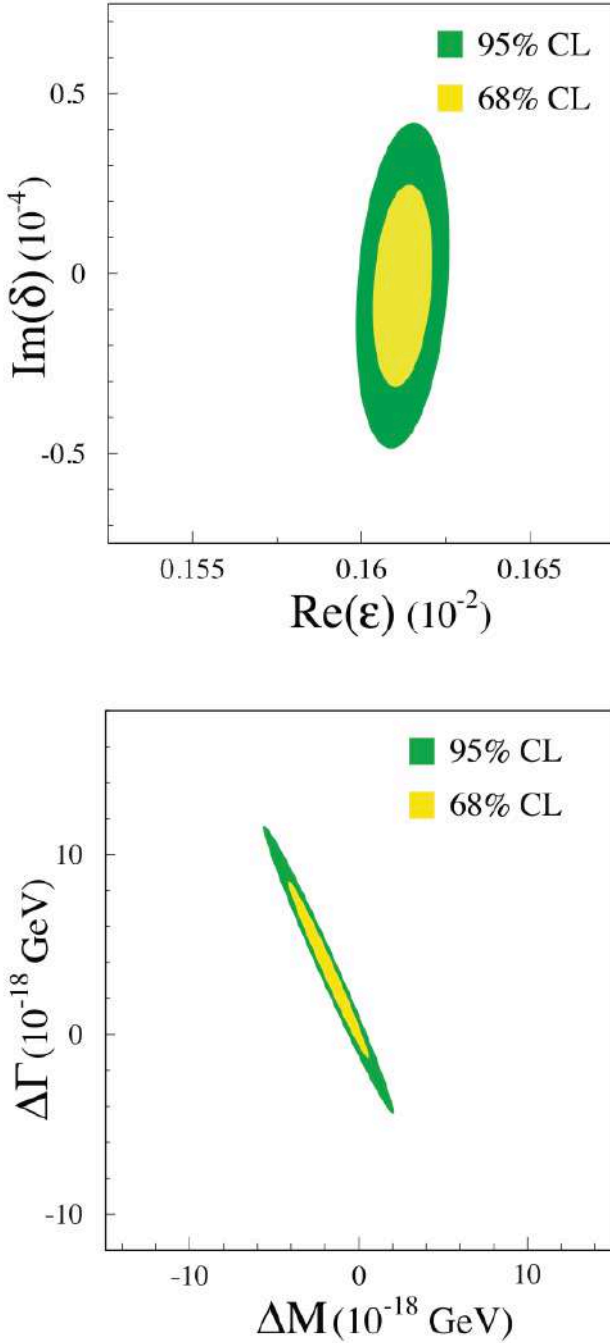


Figure 65.1: Top: allowed region at 68% and 95% C.L. in the  $\Re(\epsilon)$ ,  $\Im(\delta)$  plane. Bottom: allowed region at 68% and 95% C.L. in the  $\Delta M$ ,  $\Delta\Gamma$  plane.

The allowed region in the  $\Re(\epsilon) - \Im(\delta)$  plane at 68% CL and 95% C.L. is shown in the top panel of Fig. 65.1.

The process giving the largest contribution to the size of the allowed region is  $K_L \rightarrow \pi^+\pi^-$ , through the uncertainty on  $\phi_{+-}$ .

The limits on  $\Im(\delta)$  and  $\Re(\delta)$  can be used to constrain the  $K^0 - \bar{K}^0$  mass and width difference

$$\delta = \frac{i(m_{K^0} - m_{\bar{K}^0}) + \frac{1}{2}(\Gamma_{K^0} - \Gamma_{\bar{K}^0})}{\Gamma_S - \Gamma_L} \cos\phi_{SW} e^{i\phi_{SW}} [1 + \mathcal{O}(\epsilon)].$$

The allowed region in the  $\Delta M = (m_{K^0} - m_{\bar{K}^0})$ ,  $\Delta\Gamma = (\Gamma_{K^0} - \Gamma_{\bar{K}^0})$  plane is shown in the bottom panel of Fig. 65.1. As a result, we improve on the previous limits (see for instance, P. Bloch in Ref. [12]) and in the limit  $\Gamma_{K^0} - \Gamma_{\bar{K}^0} = 0$  we obtain

$$-4.0 \times 10^{-19} \text{ GeV} < m_{K^0} - m_{\bar{K}^0} < 4.0 \times 10^{-19} \text{ GeV} \quad \text{at 95 \% C.L.}$$

#### References

- [1] See the “CP Violation in Meson Decays,” in this *Review*.
- [2] L. Maiani, “CP And CPT Violation in Neutral Kaon Decays,” L. Maiani, G. Pancheri, and N. Paver, *The Second DAΦNE Physics Handbook*, Vol. 1,2.
- [3] G. D’Ambrosio, G. Isidori and A. Pugliese, in “2nd DAΦNE Physics Handbook:63-96,” 63–96 (1994), [hep-ph/9411389], URL <http://preprints.cern.ch/cgi-bin/setlink?base=preprint&categ=cern&id=th-7504-94>.
- [4] G. D’Ambrosio and G. Isidori (KLOE), *JHEP* **12**, 011 (2006), [hep-ex/0610034].
- [5] J. S. Bell and J. Steinberger, in “Wolfenstein, L. (ed.): CP violation, 42-57. (In Oxford International Symposium Conference on Elementary Particles),” 195–208, 221–222 (1966), (See Book Index).
- [6] T. Alexopoulos *et al.* (KTeV), *Phys. Rev.* **D70**, 092006 (2004), [hep-ex/0406002].
- [7] E. Abouzaid *et al.* (KTeV), *Phys. Rev.* **D83**, 092001 (2011), [arXiv:1011.0127].
- [8] A. Lai *et al.* (NA48), *Phys. Lett.* **B645**, 26 (2007), [hep-ex/0611052]; A. Lai *et al.* (NA48), *Phys. Lett.* **B602**, 41 (2004), [hep-ex/0410059].
- [9] We thanks G. Isidori and M. Palutan for their contribution to the original analysis [4] performed with KLOE data.
- [10] D. Babusci *et al.* (KLOE), *Phys. Lett.* **B723**, 54 (2013), [arXiv:1301.7623].
- [11] A. Angelopoulos *et al.* (CPLEAR), *Phys. Lett.* **B444**, 52 (1998).
- [12] W. M. Yao *et al.* (Particle Data Group), *J. Phys.* **G33**, 1 (2006).
- [13] A. Anastasi *et al.* (KLOE-2), *JHEP* **09**, 021 (2018), [arXiv:1806.08654].
- [14] P. Bloch, M. Fidecaro, private communication of the data in a finer binning format; A. Angelopoulos *et al.* (CPLEAR), *Phys. Lett.* **B444**, 43 (1998).

## 66. $V_{ud}$ , $V_{us}$ , the Cabibbo Angle, and CKM Unitarity

Updated November 2019 by E. Blucher (Univ. of Chicago) and W.J. Marciano (BNL)

The Cabibbo-Kobayashi-Maskawa (CKM) [1,2] three-generation quark mixing matrix written in terms of the Wolfenstein parameters  $(\lambda, A, \rho, \eta)$  [3] nicely illustrates the orthonormality constraint of unitarity as well as central role played by  $\lambda$ .

$$V_{\text{CKM}} = \begin{pmatrix} V_{ud} & V_{us} & V_{ub} \\ V_{cd} & V_{cs} & V_{cb} \\ V_{td} & V_{ts} & V_{tb} \end{pmatrix} = \begin{pmatrix} 1 - \lambda^2/2 & \lambda & A\lambda^3(\rho - i\eta) \\ -\lambda & 1 - \lambda^2/2 & A\lambda^2 \\ A\lambda^3(1 - \rho - i\eta) & -A\lambda^2 & 1 \end{pmatrix} + \mathcal{O}(\lambda^4). \quad (66.1)$$

That cornerstone is a carryover from the two-generation Cabibbo angle,  $\lambda = \sin(\theta_{\text{Cabibbo}}) = V_{us}$ . Its value is an important component in tests of CKM unitarity.

For some time, the precise value of  $\lambda$  was controversial, with kaon decays suggesting [4]  $\lambda \simeq 0.220$ , while indirect determinations via  $V_{ud}$  obtained from nuclear  $\beta$ -decays implied a somewhat larger  $\lambda \simeq 0.225 - 0.230$ . This difference resulted in a 2 – 2.5 sigma deviation from the first row unitarity requirement

$$|V_{ud}|^2 + |V_{us}|^2 + |V_{ub}|^2 = 1, \quad (66.2)$$

a potential signal [5] for new physics effects. Below, we describe the current status of  $V_{ud}$ ,  $V_{us}$ , and their associated unitarity test in Eq. (66.2). (Since  $|V_{ub}|^2 \simeq 1.7 \times 10^{-5}$  is negligibly small, it is ignored in this discussion.) Eq. (66.2) is currently the most stringent test of unitarity in the CKM matrix. However, as we shall see, it is again showing signs of 2 to 3 sigma inconsistency.

### 66.1. $V_{ud}$

Precise values of  $V_{ud}$  have been obtained from superallowed nuclear, neutron and pion beta decays. Currently, the best determination of  $V_{ud}$  comes from analysis of a set of 14 measured superallowed nuclear beta-decays [5] ( $0^+ \rightarrow 0^+$  transitions). Measuring their half-lives,  $t$ , and  $Q$  values gives the decay rate factors,  $f$ , which lead to a precise determination of  $V_{ud}$  via [6–10]. . . Based on those studies, one finds the average [11]

$$|V_{ud}|^2 = 0.97148(20)/(1 + \Delta_R^V), \quad (66.3)$$

where  $\Delta_R^V$  denotes the so-called inner or universal electroweak radiative corrections (RC) to superallowed nuclear beta decays. A dispersion relation (DR) calculational approach [12] to quantum loop corrections, specifically the gamma-W box diagram, gives  $\Delta_R^V = 0.02467(22)$ . Because of its small uncertainty and more rigorous theoretical footing, we use that value below. A somewhat different approach [13] found  $\Delta_R^V = 0.02426(32)$ . These recent values are roughly consistent. Both are larger than the 2018 PDG value of  $0.02361(38)$ . Implications and possible nuclear physics modifications of those studies are still under scrutiny [14]. Nevertheless, currently the 14 most precisely measured superallowed transitions [11] lead to the DR based weighted average of

$$V_{ud} = 0.97370(10)_{\text{exp.,nucl.}}(10)_{\text{RC}} \text{ (superallowed)}, \quad (66.4)$$

which, assuming unitarity, corresponds to the relatively large  $\lambda = 0.2278(6)$ . This recent determination of  $V_{ud}$  has shifted significantly down compared to the 2018 value [11] of  $0.97420(21)$ . Taken at face value, that reduced  $V_{ud}$  would seem to violate the first row unitarity requirement and thus suggest the presence of “new physics”.

Measurements of the neutron lifetime,  $\tau_n$ , the ratio of axial-vector/vector couplings,  $g_A \equiv G_A/G_V$ , via neutron decay asymmetries combined with the inner radiative corrections can also be used to determine  $V_{ud}$ :

$$|V_{ud}|^2 = \frac{5024.7 \text{ s}}{\tau_n(1 + 3g_A^2)(1 + \Delta_R^V)}, \quad (66.5)$$

where  $\Delta_R^V$  represents the same inner electroweak radiative corrections [7,8] as discussed above.

Using the current world averages

$$\begin{aligned} \tau_n^{\text{ave}} &= 879.4(6) \text{ s} \quad (1.5 \text{ PDG scale factor}) \\ g_A^{\text{ave}} &= 1.2762(5) \end{aligned} \quad (66.6)$$

leads to

$$|V_{ud}| = 0.9733(3)_{\tau_n(3)} g_A(1)_{\text{RC}}, \quad (66.7)$$

for an inner radiative correction of  $0.02467(22)$  while for  $0.02426(32)$  it increases to  $0.9735(5)$ . Those values are both low, compared with CKM unitarity expectations and the superallowed nuclear beta decay result reported above. Reconciliation suggests a shorter neutron lifetime near 878 s or a somewhat smaller  $g_A$ . Future neutron studies [15] are expected to resolve any current inconsistencies and significantly reduce the uncertainties in  $g_A$  and  $\tau_n$ .

The PIBETA experiment at PSI measured the very small ( $\mathcal{O}(10^{-8})$ ) branching ratio for  $\pi^+ \rightarrow \pi^0 e^+ \nu_e$  with about  $\pm 0.6\%$  precision. Its result gives [16]

$$|V_{ud}| = 0.9739(27) \left[ \frac{BR(\pi^+ \rightarrow e^+ \nu_e(\gamma))}{1.2325 \times 10^{-4}} \right]^{\frac{1}{2}} \quad (66.8)$$

which is normalized using the very precisely measured  $BR(\pi^+ \rightarrow e^+ \nu_e(\gamma)) = 1.2325(23) \times 10^{-4}$  [6], rather than the theoretical branching ratio of  $1.2350(2) \times 10^{-4}$  which if used, would increase  $|V_{ud}|$  to  $0.9749(27)$ . Theoretical uncertainties in pion beta decay are very small and would allow for a factor of 2 to 3 improvement of its small branching ratio. However, it would be difficult to have it compete with superallowed beta decays or future neutron decay efforts at direct  $|V_{ud}|$  determination.

### 66.2. $V_{us}$

$|V_{us}|$  may be directly obtained from kaon decays, hyperon decays, and tau decays. Early determinations most often used  $K\ell 3$  decays:

$$\Gamma_{K\ell 3} = \frac{G_F^2 M_K^5}{192\pi^3} S_{EW} (1 + \delta_K^\ell + \delta_{SU2}) C^2 |V_{us}|^2 f_+^2(0) I_K^\ell. \quad (66.9)$$

Here,  $\ell$  refers to either  $e$  or  $\mu$ ,  $G_F$  is the Fermi constant,  $M_K$  is the kaon mass,  $S_{EW}$  is the short-distance radiative correction,  $\delta_K^\ell$  is the mode-dependent long-distance radiative correction,  $f_+(0)$  is the calculated form factor at zero momentum transfer for the  $\ell\nu$  system, and  $I_K^\ell$  is the phase-space integral, which depends on measured semileptonic form factors. For charged kaon decays,  $\delta_{SU2}$  is the deviation from one of the ratio of  $f_+(0)$  for the charged to neutral kaon decay; it is zero for the neutral kaon.  $C^2$  is 1 (1/2) for neutral (charged) kaon decays. Most early determinations of  $|V_{us}|$  were based solely on  $K \rightarrow \pi e \nu$  decays;  $K \rightarrow \pi \mu \nu$  decays were not used because of large uncertainties in  $I_K^\mu$ . The experimental measurements are the semileptonic decay widths (based on the semileptonic branching fractions and lifetime) and form factors (allowing calculation of the phase space integrals). Theory is needed for  $S_{EW}$ ,  $\delta_K^\ell$ ,  $\delta_{SU2}$ , and  $f_+(0)$ .

Many measurements during the last 15 years have resulted in a shift in  $|V_{us}|$ . Most importantly, the  $K \rightarrow \pi e \nu$  branching fractions are significantly different than earlier PDG averages, probably as a result of inadequate treatment of radiation in older experiments. This effect was first observed by BNL E865 [17] in the charged kaon system and then by KTeV [18,19] in the neutral kaon system; subsequent measurements were made by KLOE [20–23], NA48 [24–26], and ISTRA+ [27]. Current averages (*e.g.*, by the PDG [28] or Flavianet [29]) of the semileptonic branching fractions are based only on recent, high-statistics experiments where the treatment of radiation is clear. In addition to measurements of branching fractions, new measurements of lifetimes [30] and form factors [31–35], have resulted in improved precision for all of the experimental inputs to  $|V_{us}|$ . Precise measurements of form factors for  $K_{\mu 3}$  decay make it possible to use both semileptonic decay modes to extract  $V_{us}$ .

Following the analysis of Moulson [36], the Flavianet group [29], and more recent updates [37], one finds, after including the isospin violating effect,  $\delta_{SU2}$ , the values of  $|V_{us}|f_+(0)$  in Table 66.1. The average of these measurements, including correlation effects [36], gives

$$f_+(0)|V_{us}| = 0.2165(4). \quad (66.10)$$

Lattice QCD calculations of  $f_+(0)$  have been carried out for 2, 2+1, and 2+1+1 quark flavors and range from about 0.96 to 0.97. Here, we use recent FLAG averages [38] for 2+1 and 2+1+1 flavors:

$$\begin{aligned} f_+(0) &= 0.9677(27) \quad N_f = 2 + 1 \\ f_+(0) &= 0.9706(27) \quad N_f = 2 + 1 + 1 \end{aligned} \quad (66.11)$$

One finds from Eq. (66.10) and Eq. (66.11),

$$\begin{aligned} |V_{us}| &= 0.2237(4)_{\text{exp+RC}}(6)_{\text{lattice}} \quad (N_f = 2 + 1, K\ell3 \text{ decays}) \\ &= 0.2231(4)_{\text{exp+RC}}(6)_{\text{lattice}} \quad (N_f = 2 + 1 + 1, K\ell3 \text{ decays}) \end{aligned} \quad (66.12)$$

**Table 66.1:**  $|V_{us}|f_+(0)$  from  $K\ell3$ .

Decay Mode	$ V_{us} f_+(0)$
$K^\pm e3$	$0.2169 \pm 0.0008$
$K^\pm \mu3$	$0.2167 \pm 0.0011$
$K_L e3$	$0.2164 \pm 0.0006$
$K_L \mu3$	$0.2167 \pm 0.0006$
$K_S e3$	$0.2156 \pm 0.0013$
Average (including correlation effects [36])	$0.2165 \pm 0.0004$

A value of  $V_{us}$  can also be obtained from a comparison of the radiative inclusive decay rates for  $K \rightarrow \mu\nu(\gamma)$  and  $\pi \rightarrow \mu\nu(\gamma)$  combined with a lattice gauge theory calculation of  $f_{K^+}/f_{\pi^+}$  via

$$\frac{|V_{us}|f_{K^+}}{|V_{ud}|f_{\pi^+}} = 0.23871(20) \left[ \frac{\Gamma(K \rightarrow \mu\nu(\gamma))}{\Gamma(\pi \rightarrow \mu\nu(\gamma))} \right]^{\frac{1}{2}} \quad (66.13)$$

with the small error coming from electroweak radiative corrections [39]. Employing

$$\frac{\Gamma(K \rightarrow \mu\nu(\gamma))}{\Gamma(\pi \rightarrow \mu\nu(\gamma))} = 1.3367(28), \quad (66.14)$$

which includes  $\Gamma(K \rightarrow \mu\nu(\gamma)) = 5.134(11) \times 10^7 \text{s}^{-1}$  [36,40], leads to

$$\frac{|V_{us}|f_{K^+}}{|V_{ud}|f_{\pi^+}} = 0.27600(37). \quad (66.15)$$

Employing the FLAG [38] lattice QCD averages for the isospin broken decay constants

$$\begin{aligned} \frac{f_{K^+}}{f_{\pi^+}} &= 1.1917(37) \quad N_f = 2 + 1 \\ &= 1.1932(19) \quad N_f = 2 + 1 + 1. \end{aligned} \quad (66.16)$$

along with the value of  $|V_{ud}|$  in Eq. (66.4) leads to

$$\begin{aligned} |V_{us}| &= 0.2255(8) \quad (N_f = 2 + 1, K\mu2 \text{ decays}) \\ &= 0.2252(5) \quad (N_f = 2 + 1 + 1, K\mu2 \text{ decays}) \end{aligned} \quad (66.17)$$

Together, weighted averages of the  $K\ell3$  (Eq. (66.12)) and  $K\mu2$  (Eq. (66.17)) values give similar results for  $N_f = 2 + 1$  and  $2 + 1 + 1$  flavors:

$$\begin{aligned} |V_{us}| &= 0.2245(5) \quad N_f = 2 + 1 \\ |V_{us}| &= 0.2245(4) \quad N_f = 2 + 1 + 1. \end{aligned} \quad (66.18)$$

Note that the differences between  $K\ell3$  and  $K\mu2$  values for  $V_{us}$  differ by 2 and 3 sigma, respectively, for  $N_f = 2 + 1$  and  $2 + 1 + 1$  flavors. One should, therefore, scale the uncertainties in Eq. (66.18) accordingly. For that reason, we employ an error scale factor of 2 in the uncertainty,  $|V_{us}| = 0.2245(8)$ , when we consider the first row test of CKM unitarity.

It should be mentioned that hyperon decay fits suggest [41]

$$|V_{us}| = 0.2250(27) \quad (\text{Hyperon Decays}) \quad (66.19)$$

modulo SU(3) breaking effects that could shift that value up or down. We note that a representative effort [42] that incorporates SU(3) breaking found  $V_{us} = 0.226(5)$ . Strangeness changing tau decays, averaging both inclusive and exclusive measurements, give [43]

$$|V_{us}| = 0.2221(13) \quad (\text{Tau Decays}), \quad (66.20)$$

which differs by about 2 sigma from the kaon determination discussed above, and would, if combined with  $V_{ud}$  from super-allowed beta decays, lead to a 4 sigma deviation from unitarity. This discrepancy results mainly from the inclusive tau decay results that rely on Finite Energy Sum Rule techniques and assumptions, as well as experimental uncertainties. Recent investigation of that approach suggests a larger value for  $V_{us}$ , which is more in accord with other determinations [44].

Employing the values of  $V_{ud}$  and  $V_{us}$  with an error scale factor of 2 from Eq. (66.4) and Eq. (66.18), respectively, leads to the unitarity consistency check

$$|V_{ud}|^2 + |V_{us}|^2 + |V_{ub}|^2 = 0.9985(3)(4). \quad (66.21)$$

where the first error is the uncertainty from  $|V_{ud}|^2$  and the second error is the uncertainty from  $|V_{us}|^2$  for both  $N_f = 2 + 1 + 1$  and  $N_f = 2 + 1$ . One finds an overall 3 sigma deviation from unitarity. That deviation could be due a problem with  $|V_{ud}|$  theory (RC or NP), the lattice determination of  $f_+(0)$  or new physics.

### 66.3. CKM Unitarity Constraints

The current 3 sigma experimental disagreement with unitarity,  $|V_{ud}|^2 + |V_{us}|^2 + |V_{ub}|^2 = 0.9985(5)$ , still provides strong confirmation of Standard Model radiative corrections (which range between 3-4% depending on the nucleus used) at a high significance level [45]. In addition, it implies constraints on ‘‘New Physics’’ effects at both the tree and quantum loop levels. Those effects could be in the form of contributions to nuclear beta decays,  $K$  decays and/or muon decays, with the last of these providing normalization via the muon lifetime [46], which is used to obtain the Fermi constant,  $G_\mu = 1.1663787(6) \times 10^{-5} \text{GeV}^{-2}$ .

In the following examples, we illustrate the implications of CKM unitarity for (1) exotic muon decays [47] (beyond ordinary muon decay  $\mu^+ \rightarrow e^+ \nu_e \bar{\nu}_\mu$ ) and (2) new heavy quark mixing  $V_{uD}$  [48]. Other examples in the literature [49,50] include  $Z_\chi$  boson quantum loop effects, supersymmetry, leptoquarks, compositeness etc.

#### Exotic Muon Decays

If additional lepton flavor violating decays such as  $\mu^+ \rightarrow e^+ \bar{\nu}_e \nu_\mu$  (wrong neutrinos) occur, they would cause confusion in searches for neutrino oscillations at, for example, muon storage rings/neutrino factories or other neutrino sources from muon decays. Calling the rate for all such decays  $\Gamma(\text{exotic } \mu \text{ decays})$ , they should be subtracted before the extraction of  $G_\mu$  and normalization of the CKM matrix. Since that is not done and unitarity works, one has (at one-sided 95% CL)

$$|V_{ud}|^2 + |V_{us}|^2 + |V_{ub}|^2 = 1 - BR(\text{exotic } \mu \text{ decays}) \geq 0.9977 \quad (66.22)$$

or

$$BR(\text{exotic } \mu \text{ decays}) \leq 0.0023. \quad (66.23)$$

This bound is a factor of 10 better than the direct experimental bound on  $\mu^+ \rightarrow e^+ \bar{\nu}_e \nu_\mu$ .

## New Heavy Quark Mixing

Heavy  $D$  quarks naturally occur in fourth quark generation models and some heavy quark “new physics” scenarios such as  $E_6$  grand unification. Their mixing with ordinary quarks gives rise to  $V_{uD}$ , which is constrained by unitarity (one sided 95% CL)

$$\begin{aligned} |V_{ud}|^2 + |V_{us}|^2 + |V_{ub}|^2 &= 1 - |V_{uD}|^2 \geq 0.9977 \\ |V_{uD}| &\leq 0.05. \end{aligned} \quad (66.24)$$

A similar constraint applies to heavy neutrino mixing and the couplings  $V_{\mu N}$  and  $V_{eN}$ .

## References:

1. N. Cabibbo, Phys. Rev. Lett. **10**, 531 (1963).
2. M. Kobayashi and T. Maskawa, Prog. Theor. Phys. **49**, 652 (1973).
3. L. Wolfenstein, Phys. Rev. Lett. **51**, 1945 (1983).
4. S. Eidelman *et al.* [Particle Data Group], Phys. Lett. **B592**, 1 (2004).
5. I.S. Towner and J.C. Hardy Rep. Prog. Phys. **73**, 046301 (2010).
6. W.J. Marciano and A. Sirlin, Phys. Rev. Lett. **71**, 3629 (1993).
7. A. Czarnecki, W.J. Marciano, and A. Sirlin, Phys. Rev. **D70**, 093006 (2004) [hep-ph/0406324].
8. W.J. Marciano and A. Sirlin, Phys. Rev. Lett. **96**, 032002 (2006) [hep-ph/0510099].
9. I.S. Towner and J.C. Hardy, Phys. Rev. **C77**, 025501 (2008).
10. J.C. Hardy and I.S. Towner, Phys. Rev. **C79**, 055502 (2009).
11. J.C. Hardy and I.S. Towner, Phys. Rev. **C91**, 0255012 (2015); PoS **CKM 2016**, 028 (2016).
12. C. Y. Seng, M. Gorchtein, H. H. Patel, and M. J. Ramsey-Musolf, Phys. Rev. Lett. **121**, 241804 (2018).
13. A. Czarnecki, W. J. Marciano, and A. Sirlin, Phys. Rev. **D100**, 073008 (2019).
14. C. Y. Seng, M. Gorchtein, and M. J. Ramsey-Musolf, Phys. Rev. **D100**, 013001 (2019); M. Gorchtein, Phys. Rev. **D123**, 042503 (2019).
15. H. Abele, Prog. in Part. Nucl. Phys. **60**, 1 (2008).
16. D. Poganic *et al.*, Phys. Rev. Lett. **93**, 181803 (2004) [hep-ex/0312030]; A. Czarnecki, W. J. Marciano and A. Sirlin, arXiv:1911.04685 [hep-ph].
17. A. Sher *et al.*, Phys. Rev. Lett. **91**, 261802 (2003).
18. T. Alexopoulos *et al.* [KTeV Collab.], Phys. Rev. Lett. **93**, 181802 (2004) [hep-ex/0406001].
19. T. Alexopoulos *et al.* [KTeV Collab.], Phys. Rev. **D70**, 092006 (2004) [hep-ex/0406002].
20. F. Ambrosino *et al.* [KLOE Collab.], Phys. Lett. **B632**, 43 (2006) [hep-ex/0508027].
21. F. Ambrosino *et al.* [KLOE Collab.], Phys. Lett. **B638**, 140 (2006) [hep-ex/0603041].
22. F. Ambrosino *et al.* [KLOE Collab.], Phys. Lett. **B636**, 173 (2006) [hep-ex/0601026].
23. F. Ambrosino *et al.* [KLOE Collab.], PoS **HEP2005**, 287 (2006) [hep-ex/0510028].
24. A. Lai *et al.* [NA48 Collab.], Phys. Lett. **B602**, 41 (2004) [hep-ex/0410059].
25. A. Lai *et al.* [NA48 Collab.], Phys. Lett. **B645**, 26 (2007) [hep-ex/0611052].
26. J.R. Batley *et al.* [NA48/2 Collab.], Eur. Phys. J. **C50**, 329 (2007) [hep-ex/0702015].
27. V.I. Romanovsky *et al.*, [hep-ex/0704.2052].
28. K.A. Olive *et al.* [Particle Data Group], Chin. Phys. C **38**, 090001 (2014).
29. Flavianet Working Group on Precise SM Tests in K Decays, M. Antonelli *et al.*, Eur. Phys. J. **C69**, 399 (2010). For a detailed review, see M. Antonelli *et al.*, [hep-ph/0907.5386].
30. F. Ambrosino *et al.* [KLOE Collab.], Phys. Lett. **B626**, 15 (2005) [hep-ex/0507088].
31. T. Alexopoulos *et al.* [KTeV Collab.], Phys. Rev. **D70**, 092007 (2004) [hep-ex/0406003].
32. E. Abouzaid *et al.* [KTeV Collab.], Phys. Rev. **D74**, 097101 (2006) [hep-ex/0608058].
33. F. Ambrosino *et al.* [KLOE Collab.], Phys. Lett. **B636**, 166 (2006) [hep-ex/0601038].
34. A. Lai *et al.* [NA48 Collab.], Phys. Lett. **B604**, 1 (2004) [hep-ex/0410065].
35. O.P. Yushchenko *et al.*, Phys. Lett. **B589**, 111 (2004) [hep-ex/0404030].
36. M. Moulson, [hep-ex/1704.04104]; PoS **CKM 2016**, 033 (2017).
37. E. Passemar, talk at CKM2018, <https://zenodo.org/record/2565480>.
38. S. Aoki *et al.* [Flavour Lattice Averaging Group], arXiv:1902.08191 [hep-lat] based on A. Bazavov *et al.*, Phys. Rev. Lett. **112**, 112001 (2014) [arXiv:1312.1228 [hep-ph]]; N. Carrasco, P. Lami, V. Lubich, L. Riggio, S. Simula and C. Tarantino, Phys. Rev. **D93**, 114512 (2016) [arXiv:1602.04113 [hep-lat]]; A. Bazavov *et al.*, Phys. Rev. **D87**, 073012 (2013) [arXiv:1212.4993 [hep-lat]]; P. A. Boyle *et al.* [RBC/UKQCD Collaboration], JHEP **1506**, 164 (2015) [arXiv:1504.01692 [hep-lat]] A. Bazavov *et al.*, Phys. Rev. **D98**, 074512 (2018) [arXiv:1712.09262 [hep-lat]]; T. Blum *et al.* [RBC and UKQCD Collaborations], Phys. Rev. **D93**, 074505 (2016) [arXiv:1411.7017 [hep-lat]]; R. J. Dowdall, C. T. H. Davies, G. P. Lepage and C. McNeile, Phys. Rev. **D88**, 074504 (2013) [arXiv:1303.1670 [hep-lat]]; N. Carrasco *et al.*, Phys. Rev. **D91**, 054507 (2015) [arXiv:1411.7908 [hep-lat]]; E. Follana *et al.* [HPQCD and UKQCD Collaborations], Phys. Rev. Lett. **100**, 062002 (2008) [arXiv:0706.1726 [hep-lat]]; A. Bazavov *et al.* [MILC Collaboration], PoS **LATTICE 2010**, 074 (2010) [arXiv:1012.0868 [hep-lat]]; S. Durr *et al.*, Phys. Rev. **D81**, 054507 (2010) [arXiv:1001.4692 [hep-lat]]; S. Durr *et al.*, Phys. Rev. **D95**, 054513 (2017) [arXiv:1601.05998 [hep-lat]] V. G. Bornyakov *et al.* [QCDSF-UKQCD Collaboration], Phys. Lett. **B767**, 366 (2017) [arXiv:1612.04798 [hep-lat]].
39. V. Cirigliano and H. Neufeld, Phys. Lett. **B700**, 7 (2011); W.J. Marciano, Phys. Rev. Lett. **93**, 231803 (2004) [hep-ph/0402299].
40. D. Babusci *et al.* [KLOE Collab.], Phys. Lett. **B738**, 128 (2014) [arXiv:1407.2028].
41. N. Cabibbo, E.C. Swallow, and R. Winston, Phys. Rev. Lett. **92**, 251803 (2004) [hep-ph/0307214].
42. V. Mateu and A. Pich, JHEP **0510**, 041 (2005).
43. Y. S. Amhis *et al.* [HFLAV Collaboration], arXiv:1909.12524 [hep-ex].
44. R. J. Hudspith, R. Lewis, K. Maltman and J. Zanotti, Phys. Lett. **B781**, 206 (2018) [arXiv:1702.01767 [hep-ph]]; P. Boyle *et al.* [RBC and UKQCD Collaborations], Phys. Rev. Lett. **121**, 202003 (2018) [arXiv:1803.07228 [hep-lat]].
45. A. Sirlin, Rev. Mod. Phys. **50**, 573 (1978).
46. D. Webber *et al.* [MuLan Collab.], Phys. Rev. Lett. **106**, 041803 (2011); V. Tishchenko *et al.* [MuLan Collab.], Phys. Rev. **D87**, 052003 (2013).
47. K.S. Babu and S. Pakvasa, hep-ph/0204236.
48. W. Marciano and A. Sirlin, Phys. Rev. Lett. **56**, 22 (1986); P. Langacker and D. London, Phys. Rev. **D38**, 886 (1988).
49. W. Marciano and A. Sirlin, Phys. Rev. **D35**, 1672 (1987).
50. R. Barbieri *et al.*, Phys. Lett. **156B**, 348 (1985); K. Hagiwara *et al.*, Phys. Rev. Lett. **75**, 3605 (1995); A. Kurylov and M. Ramsey-Musolf, Phys. Rev. Lett. **88**, 071804 (2000); S. Bauman, J. Erler, and M. Ramsey-Musolf, Phys. Rev. **D87**, 035012 (2013).

67. CP Violation in  $K_L$  Decays

Updated April 2016 by L. Wolfenstein (Carnegie-Mellon University), C.-J. Lin (LBNL), and T.G. Trippe (LBNL).

The symmetries  $C$  (particle-antiparticle interchange) and  $P$  (space inversion) hold for strong and electromagnetic interactions. After the discovery of large  $C$  and  $P$  violation in the weak interactions, it appeared that the product  $CP$  was a good symmetry. In 1964  $CP$  violation was observed in  $K^0$  decays at a level given by the parameter  $\epsilon \approx 2.3 \times 10^{-3}$ .

A unified treatment of  $CP$  violation in  $K$ ,  $D$ ,  $B$ , and  $B_s$  mesons is given in “ $CP$  Violation in Meson Decays” by D. Kirkby and Y. Nir in this *Review*. A more detailed review including a thorough discussion of the experimental techniques used to determine  $CP$  violation parameters is given in a book by K. Kleinknecht [1]. Here we give a concise summary of the formalism needed to define the parameters of  $CP$  violation in  $K_L$  decays, and a description of our fits for the best values of these parameters.

67.1. Formalism for  $CP$  violation in Kaon decay

$CP$  violation has been observed in the semi-leptonic decays  $K_L^0 \rightarrow \pi^\pm \ell^\pm \nu$ , and in the nonleptonic decay  $K_L^0 \rightarrow 2\pi$ . The experimental numbers that have been measured are

$$A_L = \frac{\Gamma(K_L^0 \rightarrow \pi^- \ell^+ \nu) - \Gamma(K_L^0 \rightarrow \pi^+ \ell^- \nu)}{\Gamma(K_L^0 \rightarrow \pi^- \ell^+ \nu) + \Gamma(K_L^0 \rightarrow \pi^+ \ell^- \nu)} \quad (67.1a)$$

$$\begin{aligned} \eta_{+-} &= A(K_L^0 \rightarrow \pi^+ \pi^-) / A(K_S^0 \rightarrow \pi^+ \pi^-) \\ &= |\eta_{+-}| e^{i\phi_{+-}} \end{aligned} \quad (67.1b)$$

$$\begin{aligned} \eta_{00} &= A(K_L^0 \rightarrow \pi^0 \pi^0) / A(K_S^0 \rightarrow \pi^0 \pi^0) \\ &= |\eta_{00}| e^{i\phi_{00}}. \end{aligned} \quad (67.1c)$$

$CP$  violation can occur either in the  $K^0 - \bar{K}^0$  mixing or in the decay amplitudes. Assuming  $CPT$  invariance, the mass eigenstates of the  $K^0 - \bar{K}^0$  system can be written

$$|K_S\rangle = p|K^0\rangle + q|\bar{K}^0\rangle, \quad |K_L\rangle = p|K^0\rangle - q|\bar{K}^0\rangle. \quad (67.2)$$

If  $CP$  invariance held, we would have  $q = p$  so that  $K_S$  would be  $CP$ -even and  $K_L$   $CP$ -odd. (We define  $|\bar{K}^0\rangle$  as  $CP|K^0\rangle$ .)  $CP$  violation in  $K^0 - \bar{K}^0$  mixing is then given by the parameter  $\tilde{\epsilon}$  where

$$\frac{p}{q} = \frac{(1 + \tilde{\epsilon})}{(1 - \tilde{\epsilon})}. \quad (67.3)$$

$CP$  violation can also occur in the decay amplitudes

$$A(K^0 \rightarrow \pi\pi(I)) = A_I e^{i\delta_I}, \quad A(\bar{K}^0 \rightarrow \pi\pi(I)) = A_I^* e^{i\delta_I}, \quad (67.4)$$

where  $I$  is the isospin of  $\pi\pi$ ,  $\delta_I$  is the final-state phase shift, and  $A_I$  would be real if  $CP$  invariance held. The  $CP$ -violating observables are usually expressed in terms of  $\epsilon$  and  $\epsilon'$  defined by

$$\eta_{+-} = \epsilon + \epsilon', \quad \eta_{00} = \epsilon - 2\epsilon'. \quad (67.5a)$$

One can then show [2]

$$\epsilon = \tilde{\epsilon} + i (\text{Im } A_0 / \text{Re } A_0), \quad (67.5b)$$

$$\sqrt{2}\epsilon' = i e^{i(\delta_2 - \delta_0)} (\text{Re } A_2 / \text{Re } A_0) (\text{Im } A_2 / \text{Re } A_2 - \text{Im } A_0 / \text{Re } A_0), \quad (67.5c)$$

$$A_L = 2\text{Re } \epsilon / (1 + |\epsilon|^2) \approx 2\text{Re } \epsilon. \quad (67.5d)$$

In Eqs. (67.5a), small corrections [3] of order  $\epsilon' \times \text{Re}(A_2/A_0)$  are neglected, and Eq. (67.5d) assumes the  $\Delta S = \Delta Q$  rule.

The quantities  $\text{Im } A_0$ ,  $\text{Im } A_2$ , and  $\text{Im } \tilde{\epsilon}$  depend on the choice of phase convention, since one can change the phases of  $K^0$  and  $\bar{K}^0$  by a transformation of the strange quark state  $|s\rangle \rightarrow |s\rangle e^{i\alpha}$ ; of course, observables are unchanged. It is possible by a choice of phase convention to set  $\text{Im } A_0$  or  $\text{Im } A_2$  or  $\text{Im } \tilde{\epsilon}$  to zero, but none of these is zero with the usual phase conventions in the Standard Model. The choice  $\text{Im } A_0 = 0$  is called the Wu-Yang phase convention [4], in which

case  $\epsilon = \tilde{\epsilon}$ . The value of  $\epsilon'$  is independent of phase convention, and a nonzero value demonstrates  $CP$  violation in the decay amplitudes, referred to as direct  $CP$  violation. The possibility that direct  $CP$  violation is essentially zero, and that  $CP$  violation occurs only in the mixing matrix, was referred to as the superweak theory [5].

By applying  $CPT$  invariance and unitarity the phase of  $\epsilon$  is given approximately by

$$\phi_\epsilon \approx \tan^{-1} \frac{2(m_{K_L} - m_{K_S})}{\Gamma_{K_S} - \Gamma_{K_L}} \approx 43.52 \pm 0.05^\circ, \quad (67.6a)$$

while Eq. (67.5c) gives the phase of  $\epsilon'$  to be

$$\phi_{\epsilon'} = \delta_2 - \delta_0 + \frac{\pi}{2} \approx 42.3 \pm 1.5^\circ, \quad (67.6b)$$

where the numerical value is based on an analysis of  $\pi - \pi$  scattering using chiral perturbation theory [6]. The approximation in Eq. (67.6a) depends on the assumption that direct  $CP$  violation is very small in all  $K^0$  decays. This is expected to be good to a few tenths of a degree, as indicated by the small value of  $\epsilon'$  and of  $\eta_{+-}$  and  $\eta_{00}$ , the  $CP$ -violation parameters in the decays  $K_S \rightarrow \pi^+ \pi^- \pi^0$  [7], and  $K_S \rightarrow \pi^0 \pi^0 \pi^0$  [8]. The relation in Eq. (67.6a) is exact in the superweak theory, so this is sometimes called the superweak-phase  $\phi_{\text{SW}}$ . An important point for the analysis is that  $\cos(\phi_{\epsilon'} - \phi_\epsilon) \simeq 1$ . The consequence is that only two real quantities need be measured, the magnitude of  $\epsilon$  and the value of  $(\epsilon'/\epsilon)$ , including its sign. The measured quantity  $|\eta_{00}/\eta_{+-}|^2$  is very close to unity so that we can write

$$|\eta_{00}/\eta_{+-}|^2 \approx 1 - 6\text{Re}(\epsilon'/\epsilon) \approx 1 - 6\epsilon'/\epsilon, \quad (67.7a)$$

$$\text{Re}(\epsilon'/\epsilon) \approx \frac{1}{3}(1 - |\eta_{00}/\eta_{+-}|). \quad (67.7b)$$

From the experimental measurements in this edition of the *Review*, and the fits discussed in the next section, one finds

$$|\epsilon| = (2.228 \pm 0.011) \times 10^{-3}, \quad (67.8a)$$

$$\phi_\epsilon = (43.5 \pm 0.5)^\circ, \quad (67.8b)$$

$$\text{Re}(\epsilon'/\epsilon) \approx \epsilon'/\epsilon = (1.66 \pm 0.23) \times 10^{-3}, \quad (67.8c)$$

$$\phi_{+-} = (43.4 \pm 0.5)^\circ, \quad (67.8d)$$

$$\phi_{00} - \phi_{+-} = (0.34 \pm 0.32)^\circ, \quad (67.8e)$$

$$A_L = (3.32 \pm 0.06) \times 10^{-3}. \quad (67.8f)$$

Direct  $CP$  violation, as indicated by  $\epsilon'/\epsilon$ , is expected in the Standard Model. However, the numerical value cannot be reliably predicted because of theoretical uncertainties [9]. The value of  $A_L$  agrees with Eq. (67.5d). The values of  $\phi_{+-}$  and  $\phi_{00} - \phi_{+-}$  are used to set limits on  $CPT$  violation [see “Tests of Conservation Laws”].

67.2. Fits for  $K_L^0$   $CP$ -violation parameters

In recent years,  $K_L^0$   $CP$ -violation experiments have improved our knowledge of  $CP$ -violation parameters, and their consistency with the expectations of  $CPT$  invariance and unitarity. To determine the best values of the  $CP$ -violation parameters in  $K_L^0 \rightarrow \pi^+ \pi^-$  and  $\pi^0 \pi^0$  decay, we make two types of fits, one for the phases  $\phi_{+-}$  and  $\phi_{00}$  jointly with  $\Delta m$  and  $\tau_S$ , and the other for the amplitudes  $|\eta_{+-}|$  and  $|\eta_{00}|$  jointly with the  $K_L^0 \rightarrow \pi\pi$  branching fractions.

67.2.1. Fits to  $\phi_{+-}$ ,  $\phi_{00}$ ,  $\Delta\phi$ ,  $\Delta m$ , and  $\tau_S$  data :

These are joint fits to the data on  $\phi_{+-}$ ,  $\phi_{00}$ , the phase difference  $\Delta\phi = \phi_{00} - \phi_{+-}$ , the  $K_L^0 - K_S^0$  mass difference  $\Delta m$ , and the  $K_S^0$  mean life  $\tau_S$ , including the effects of correlations.

Measurements of  $\phi_{+-}$  and  $\phi_{00}$  are highly correlated with  $\Delta m$  and  $\tau_S$ . Some measurements of  $\tau_S$  are correlated with  $\Delta m$ . The correlations are given in the footnotes of the  $\phi_{+-}$  and  $\phi_{00}$  sections of the  $K_L^0$  Listings, and the  $\tau_S$  section of the  $K_S^0$  Listings.

In most cases, the correlations are quoted as 100%, *i.e.*, with the value and error of  $\phi_{+-}$  or  $\phi_{00}$  given at a fixed value of  $\Delta m$  and  $\tau_S$ , with additional terms specifying the dependence of the value on  $\Delta m$  and  $\tau_S$ . These cases lead to diagonal bands in Figs. 67.1 and 67.2. The KTeV experiment [10] quotes its results as values of  $\Delta m$ ,  $\tau_S$ ,  $\phi_\epsilon$ ,  $\text{Re}(\epsilon'/\epsilon)$ , and  $\text{Im}(\epsilon'/\epsilon)$  with correlations, leading to the ellipses labeled “b.” The correlations for the KTeV measurements are given in the  $\text{Im}(\epsilon'/\epsilon)$  section of the  $K_L^0$  Listings. For small  $|\epsilon'/\epsilon|$ ,  $\phi_{+-} \approx \phi_\epsilon + \text{Im}(\epsilon'/\epsilon)$ .

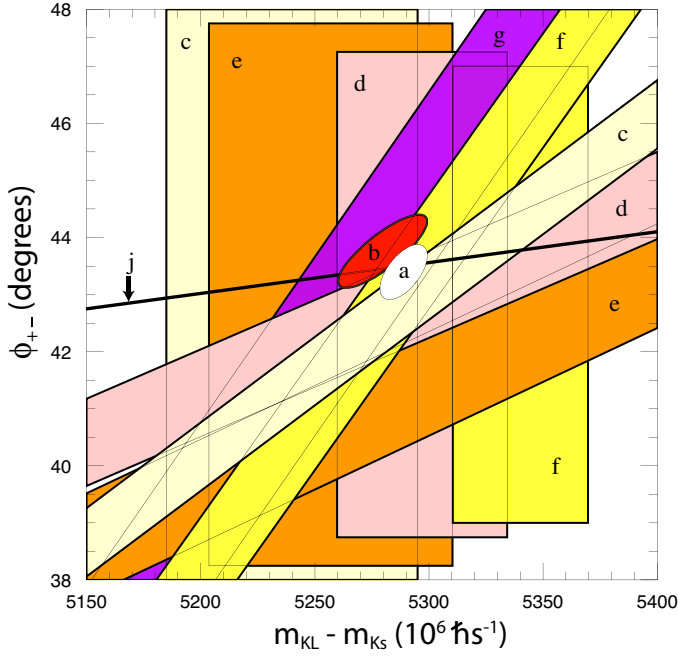


**Figure 67.1:**  $\phi_{+-}$  vs  $\Delta m$  for experiments which do not assume  $CPT$  invariance.  $\Delta m$  measurements appear as vertical bands spanning  $\Delta m \pm 1\sigma$ , cut near the top and bottom to aid the eye. Most  $\phi_{+-}$  measurements appear as diagonal bands spanning  $\phi_{+-} \pm \sigma_\phi$ . Data are labeled by letters: “b”–FNAL KTeV, “c”–CERN CPLEAR, “d”–FNAL E773, “e”–FNAL E731, “f”–CERN, “g”–CERN NA31, and are cited in Table 67.1. The narrow band “j” shows  $\phi_{SW}$ . The ellipse “a” shows the  $\chi^2 = 1$  contour of the fit result.

**Table 67.1:** References, Document ID’s, and sources corresponding to the letter labels in the figures. The data are given in the  $\phi_{+-}$  and  $\Delta m$  sections of the  $K_L$  Listings, and the  $\tau_S$  section of the  $K_S$  Listings.

Label	Source	PDG Document ID	Ref.
a	this Review	OUR FIT	
b	FNAL KTeV	ABOUZAID 11	[10]
c	CERN CPLEAR	APOSTOLAKIS 99C	[11]
d	FNAL E773	SCHWINGENHEUER 95	[12]
e	FNAL E731	GIBBONS 93,93C	[13,14]
f	CERN	GEWENIGER 74B,74C	[15,16]
g	CERN NA31	CAROSI 90	[17]
h	CERN NA48	LAI 02C	[18]
i	CERN NA31	BERTANZA 97	[19]
j	this Review	SUPERWEAK 16	

The data on  $\tau_S$ ,  $\Delta m$ , and  $\phi_{+-}$  shown in Figs. 67.1 and 67.2 are combined with data on  $\phi_{00}$  and  $\phi_{00} - \phi_{+-}$  in two fits, one without assuming  $CPT$ , and the other with this assumption. The results without assuming  $CPT$  are shown as ellipses labeled “a.” These ellipses are seen to be in good agreement with the superweak phase

$$\phi_{SW} = \tan^{-1} \left( \frac{2\Delta m}{\Delta\Gamma} \right) = \tan^{-1} \left( \frac{2\Delta m \tau_S \tau_L}{\hbar(\tau_L - \tau_S)} \right). \quad (67.9)$$

In Figs. 67.1 and 67.2,  $\phi_{SW}$  is shown as narrow bands labeled “j.”

Table 67.2 column 2, “Fit w/o  $CPT$ ,” gives the resulting fitted parameters, while Table 67.3 gives the correlation matrix for this fit. The white ellipses labeled “a” in Fig. 67.1 and Fig. 67.2 are the  $\chi^2 = 1$  contours for this fit.

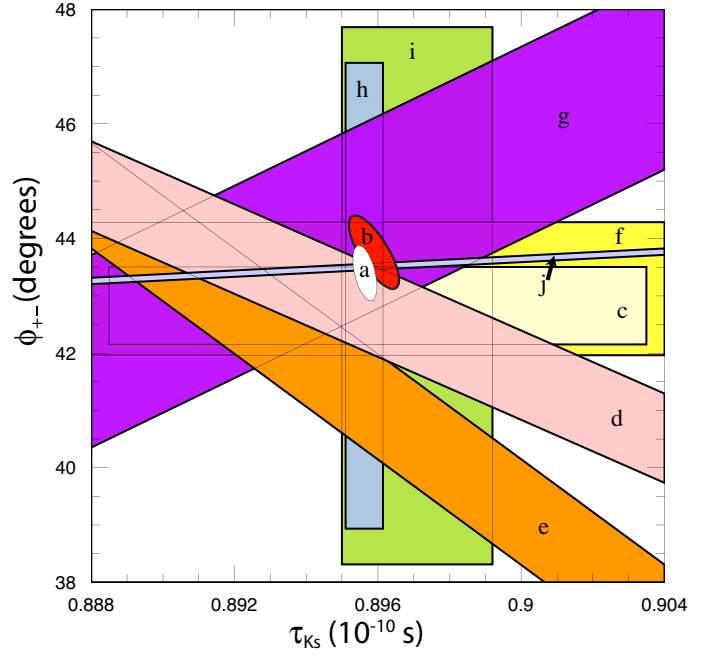


**Figure 67.2:**  $\phi_{+-}$  vs  $\tau_S$ .  $\tau_S$  measurements appear as vertical bands spanning  $\tau_S \pm 1\sigma$ , some of which are cut near the top and bottom to aid the eye. Most  $\phi_{+-}$  measurements appear as diagonal or horizontal bands spanning  $\phi_{+-} \pm \sigma_\phi$ . Data are labeled by letters: “b”–FNAL KTeV, “c”–CERN CPLEAR, “d”–FNAL E773, “e”–FNAL E731, “f”–CERN, “g”–CERN NA31, “h”–CERN NA48, “i”–CERN NA31, and are cited in Table 67.1. The narrow band “j” shows  $\phi_{SW}$ . The ellipse “a” shows the fit result’s  $\chi^2 = 1$  contour.

For experiments which have dependencies on unseen fit parameters, that is, parameters other than those shown on the x or y axis of the figure, their band positions are evaluated using the fit results and their band widths include the fitted uncertainty in the unseen parameters. This is also true for the  $\phi_{SW}$  bands.

If  $CPT$  invariance and unitarity are assumed, then by Eq. (67.6a), the phase of  $\epsilon$  is constrained to be approximately equal to

$$\phi_{SW} = (43.50258 \pm 0.00021)^\circ + 54.1(\Delta m - 0.5289)^\circ + 32.0(\tau_S - 0.89564)^\circ \quad (67.10)$$

where we have linearized the  $\Delta m$  and  $\tau_S$  dependence of Eq. (67.9). The error  $\pm 0.00021$  is due to the uncertainty in  $\tau_L$ . Here  $\Delta m$  has units  $10^{10} \text{ h s}^{-1}$  and  $\tau_S$  has units  $10^{-10} \text{ s}$ .

If in addition we use the observation that  $\text{Re}(\epsilon'/\epsilon) \ll 1$  and  $\cos(\phi_{\epsilon'} - \phi_\epsilon) \simeq 1$ , as well as the numerical value of  $\phi_{\epsilon'}$  given in Eq. (67.6b), then Eqs. (67.5a), which are sketched in Fig. 67.3, lead to the constraint

$$\begin{aligned} \phi_{00} - \phi_{+-} &\approx -3 \text{Im} \left( \frac{\epsilon'}{\epsilon} \right) \\ &\approx -3 \text{Re} \left( \frac{\epsilon'}{\epsilon} \right) \tan(\phi_{\epsilon'} - \phi_\epsilon) \\ &\approx 0.006^\circ \pm 0.008^\circ, \end{aligned} \quad (67.11)$$

so that  $\phi_{+-} \approx \phi_{00} \approx \phi_\epsilon \approx \phi_{SW}$ .

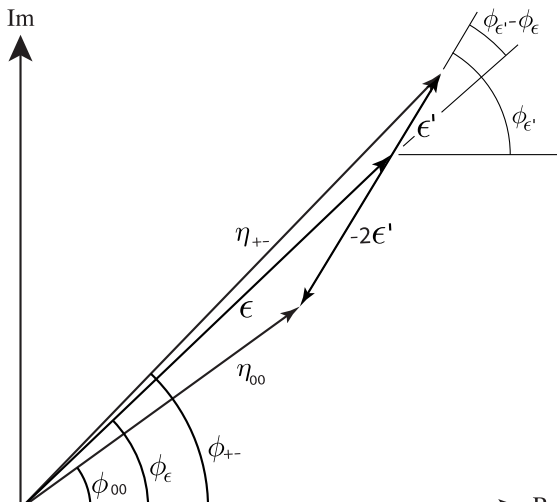
In the fit assuming  $CPT$ , we constrain  $\phi_\epsilon = \phi_{SW}$  using the linear expression in Eq. (67.10), and constrain  $\phi_{00} - \phi_{+-}$  using Eq. (67.11). These constraints are inserted into the Listings with the Document ID of SUPERWEAK 16. Some additional data for which the authors assumed  $CPT$  are added to this fit or substitute for other less precise data for which the authors did not make this assumption. See the Listings for details.

The results of this fit are shown in Table 67.2, column 3, “Fit w/ $CPT$ ,” and the correlation matrix is shown in Table 67.4. The  $\Delta m$  precision is improved by the  $CPT$  assumption.



**Table 67.2:** Fit results for  $\phi_{+-}$ ,  $\Delta m$ ,  $\tau_S$ ,  $\phi_{00}$ ,  $\Delta\phi = \phi_{00} - \phi_{+-}$ , and  $\phi_\epsilon$  without and with the  $CPT$  assumption.

Quantity(units)	Fit w/o $CPT$	Fit w/ $CPT$
$\phi_{+-}(\circ)$	$43.4 \pm 0.5$ (S=1.2)	$43.51 \pm 0.05$ (S=1.2)
$\Delta m(10^{10} \hbar s^{-1})$	$0.5289 \pm 0.0010$	$0.5293 \pm 0.0009$ (S=1.3)
$\tau_S(10^{-10} s)$	$0.89564 \pm 0.00033$	$0.8954 \pm 0.0004$ (S=1.1)
$\phi_{00}(\circ)$	$43.7 \pm 0.6$ (S=1.2)	$43.52 \pm 0.05$ (S=1.3)
$\Delta\phi(\circ)$	$0.34 \pm 0.32$	$0.006 \pm 0.014$ (S=1.7)
$\phi_\epsilon(\circ)$	$43.5 \pm 0.5$ (S=1.3)	$43.52 \pm 0.05$ (S=1.2)
$\chi^2$	16.4	20.0
# Deg. Free.	14	16

**Figure 67.3:** Sketch of Eqs. (67.5a). Not to scale.**Table 67.3:** Correlation matrix for the results of the fit without the  $CPT$  assumption

	$\phi_{+-}$	$\Delta m$	$\tau_S$	$\phi_{00}$	$\Delta\phi$	$\phi_\epsilon$
$\phi_{+-}$	1.000	0.596	-0.488	0.827	-0.040	0.976
$\Delta m$	0.596	1.000	-0.572	0.487	-0.035	0.580
$\tau_S$	-0.488	-0.572	1.000	-0.423	-0.014	-0.484
$\phi_{00}$	0.827	0.487	-0.423	1.000	0.529	0.929
$\Delta\phi$	-0.040	-0.035	-0.014	0.529	1.000	0.178
$\phi_\epsilon$	0.976	0.580	-0.484	0.929	0.178	1.000

**Table 67.4:** Correlation matrix for the results of the fit with the  $CPT$  assumption

	$\phi_{+-}$	$\Delta m$	$\tau_S$	$\phi_{00}$	$\Delta\phi$	$\phi_\epsilon$
$\phi_{+-}$	1.000	0.972	-0.311	0.957	-0.105	0.995
$\Delta m$	0.972	1.000	-0.509	0.958	-0.007	0.977
$\tau_S$	-0.311	-0.509	1.000	-0.306	0.004	-0.312
$\phi_{00}$	0.957	0.958	-0.306	1.000	0.189	0.981
$\Delta\phi$	-0.105	-0.007	0.004	0.189	1.000	-0.006
$\phi_\epsilon$	0.995	0.977	-0.312	0.981	-0.006	1.000

**67.2.2. Fits for  $\epsilon'/\epsilon$ ,  $|\eta_{+-}|$ ,  $|\eta_{00}|$ , and  $B(K_L \rightarrow \pi\pi)$  :**

We list measurements of  $|\eta_{+-}|$ ,  $|\eta_{00}|$ ,  $|\eta_{00}/\eta_{+-}|$ , and  $\epsilon'/\epsilon$ . Independent information on  $|\eta_{+-}|$  and  $|\eta_{00}|$  can be obtained from measurements of the  $K_L^0$  and  $K_S^0$  lifetimes ( $\tau_L$ ,  $\tau_S$ ), and branching ratios ( $B$ ) to  $\pi\pi$ , using the relations

$$|\eta_{+-}| = \left[ \frac{B(K_L^0 \rightarrow \pi^+\pi^-)}{\tau_L} \frac{\tau_S}{B(K_S^0 \rightarrow \pi^+\pi^-)} \right]^{1/2}, \quad (67.12a)$$

$$|\eta_{00}| = \left[ \frac{B(K_L^0 \rightarrow \pi^0\pi^0)}{\tau_L} \frac{\tau_S}{B(K_S^0 \rightarrow \pi^0\pi^0)} \right]^{1/2}. \quad (67.12b)$$

For historical reasons, the branching ratio fits and the  $CP$ -violation fits are done separately, but we want to include the influence of  $|\eta_{+-}|$ ,  $|\eta_{00}|$ ,  $|\eta_{00}/\eta_{+-}|$ , and  $\epsilon'/\epsilon$  measurements on  $B(K_L^0 \rightarrow \pi^+\pi^-)$  and  $B(K_L^0 \rightarrow \pi^0\pi^0)$  and vice versa. We approximate a global fit to all of these measurements by first performing two independent fits: 1) BRFIT, a fit to the  $K_L^0$  branching ratios, rates, and mean life, and 2) ETAFIT, a fit to the  $|\eta_{+-}|$ ,  $|\eta_{00}|$ ,  $|\eta_{+-}/\eta_{00}|$ , and  $\epsilon'/\epsilon$  measurements. The results from fit 1, along with the  $K_S^0$  values from this edition, are used to compute values of  $|\eta_{+-}|$  and  $|\eta_{00}|$ , which are included as measurements in the  $|\eta_{00}|$  and  $|\eta_{+-}|$  sections with a document ID of BRFIT 16. Thus, the fit values of  $|\eta_{+-}|$  and  $|\eta_{00}|$  given in this edition include both the direct measurements and the results from the branching ratio fit.

The process is reversed in order to include the direct  $|\eta|$  measurements in the branching ratio fit. The results from fit 2 above (before including BRFIT 16 values) are used along with the  $K_L^0$  and  $K_S^0$  mean lives and the  $K_S^0 \rightarrow \pi\pi$  branching fractions to compute the  $K_L^0$  branching ratio  $\Gamma(K_L^0 \rightarrow \pi^0\pi^0)/\Gamma(K_L^0 \rightarrow \pi^+\pi^-)$ . This branching ratio value is included as a measurement in the branching ratio section with a document ID of ETAFIT 16. Thus, the  $K_L^0$  branching ratio fit values in this edition include the results of the direct measurement of  $|\eta_{00}/\eta_{+-}|$  and  $\epsilon'/\epsilon$ . Most individual measurements of  $|\eta_{+-}|$  and  $|\eta_{00}|$  enter our fits directly via the corresponding measurements of  $\Gamma(K_L^0 \rightarrow \pi^+\pi^-)/\Gamma(\text{total})$  and  $\Gamma(K_L^0 \rightarrow \pi^0\pi^0)/\Gamma(\text{total})$ , and those that do not have too large errors to have any influence on the fitted values of these branching ratios. A more detailed discussion of these fits is given in the 1990 edition of this *Review* [20].

**References:**

1. K. Kleinknecht, "Uncovering  $CP$  violation: experimental clarification in the neutral  $K$  meson and  $B$  meson systems," *Springer Tracts in Modern Physics*, vol. 195 (Springer Verlag 2003).
2. B. Winstein and L. Wolfenstein, *Rev. Mod. Phys.* **65**, 1113 (1993).
3. M.S. Sozzi, *Eur. Phys. J.* **C36**, 37 (2004).
4. T.T. Wu and C.N. Yang, *Phys. Rev. Lett.* **13**, 380 (1964).
5. L. Wolfenstein, *Phys. Rev. Lett.* **13**, 562 (1964); L. Wolfenstein, *Comm. Nucl. Part. Phys.* **21**, 275 (1994).
6. G. Colangelo, J. Gasser, and H. Leutwyler, *Nucl. Phys.* **B603**, 125 (2001).
7. R. Adler *et al.*, (CPLEAR Collab.), *Phys. Lett.* **B407**, 193 (1997); P. Bloch, *Proceedings of Workshop on K Physics* (Orsay 1996), ed. L. Iconomidou-Fayard, Edition Frontieres, Gif-sur-Yvette, France (1997) p. 307.
8. A. Lai *et al.*, *Phys. Lett.* **B610**, 165 (2005).
9. G. Buchalla, A.J. Buras, and M.E. Lautenbacher, *Rev. Mod. Phys.* **68**, 1125 (1996); S. Bosch *et al.*, *Nucl. Phys.* **B565**, 3 (2000); S. Bertolini, M. Fabrichesi, and J.O. Egg, *Rev. Mod. Phys.* **72**, 65 (2000).
10. E. Abouzaid *et al.*, *Phys. Rev.* **D83**, 092001 (2011).
11. A. Apostolakis *et al.*, *Phys. Lett.* **B458**, 545 (1999).
12. B. Schwingerheuer *et al.*, *Phys. Rev. Lett.* **74**, 4376 (1995).
13. L.K. Gibbons *et al.*, *Phys. Rev. Lett.* **70**, 1199 (1993) and footnote in Ref. 12.
14. L.K. Gibbons, Thesis, RX-1487, Univ. of Chicago, 1993.
15. C. Geweniger *et al.*, *Phys. Lett.* **48B**, 487 (1974).

16. C. Geweniger *et al.*, Phys. Lett. **52B**, 108 (1974).
17. R. Carosi *et al.*, Phys. Lett. **B237**, 303 (1990).
18. A. Lai *et al.*, Phys. Lett. **B537**, 28 (2002).
19. L. Bertanza *et al.*, Z. Phys. **C73**, 629 (1997).
20. J.J. Hernandez *et al.*, Particle Data Group, Phys. Lett. **B239**, 1 (1990).

## 68. Review of Multibody Charm Analyses

Revised 2019 by D. M. Asner (Brookhaven National Laboratory) and J. Rademacker (University of Bristol)

### 68.1. Kinematics & Models

The differential decay rate to a point  $\mathbf{s} = (s_1, \dots, s_n)$  in  $n$  dimensional phase space can be expressed as

$$d\Gamma = |\mathcal{M}(\mathbf{s})|^2 \left| \frac{\partial^n \phi}{\partial (s_1 \dots s_n)} \right| d^n s \quad (68.1)$$

where  $|\partial^n \phi / \partial (s_1 \dots s_n)|$  represents the density of states at  $\mathbf{s}$ , and  $\mathcal{M}$  the matrix element for the decay at that point in phase space, which is 2, 5, 8, ... dimensional for  $D$  decays to 3, 4, 5, ... spinless particles. Additional parameters are required to fully describe decays involving particles with non-zero spin in the initial or final state.

For the important case of  $D$  decays to 3 pseudoscalars, the decay kinematics can be represented in a two dimensional Dalitz plot [1]. This is usually parametrized in terms of  $s_{12} \equiv (p_1 + p_2)^2$  and  $s_{23} \equiv (p_2 + p_3)^2$ , where  $p_1, p_2, p_3$  are the four-momenta of the final state particles. In terms of these variables, phase-space density is constant across the kinematically allowed region, so that any structure seen in the Dalitz plot is a direct consequence of the dynamics encoded in  $|\mathcal{M}|^2$ . Note that here, because the 3-momenta of the decay products are confined to a plane, no parity violating kinematic observables can be constructed (unless they also violate rotational invariance). This is not the case for decays to four or more particles. These can therefore not be unambiguously described in terms of analogously-defined variables  $s_{ij}, s_{ijk}$ , which are parity-even. The use of parity-odd observables in four body decays is discussed below.

In the widely-used isobar approach, the matrix element  $\mathcal{M}$  is modeled as a sum of interfering decay amplitudes, each proceeding through resonant two-body decays [2]. See Refs. 2–4 for a review of resonance phenomenology. In most analyses, each resonance is described by a Breit-Wigner [5] or Flatté [6] lineshape, and the model includes a non-resonant term with a constant phase and magnitude. This approach has well-known theoretical limitations, such as the violation of unitarity and analyticity, which can break the relationship between magnitude and phase across phase space. This motivates the use of more sophisticated descriptions, especially for broad, overlapping resonances (frequently found in S-wave components) where these limitations are particularly problematic. In charm analyses, these approaches have included the K-matrix approach [5–8] which respects two-body unitarity; the use of LASS scattering data [9]; dispersive methods [10–13]; methods based on chiral symmetry [14–16], QCD factorisation (although this seems better suited to  $B$  decays) [17–19]; and quasi model-independent parametrizations which use generic lineshapes, with minimal theory input and many free parameters, for a subset of resonances [20–23]. An important example, with a rich resonance structure, is  $D^0 \rightarrow K_S \pi^+ \pi^-$ , which is a key channel in Charge-Parity ( $CP$ ) violation and charm mixing analyses. The first analysis by CLEO [24] described the Dalitz plot with 5k signal events with 10 resonant components. This and later analyses by Belle [25] and CDF [26] model the Dalitz plot as a sum of Breit Wigner and Flatté line shapes, and a non-resonant component. BaBar [27] on the other hand use a K-matrix description for the  $\pi\pi$  S-wave based on [28] and input from LASS scattering data for the  $K - \pi$  S-wave, with no need to add a non-resonant component to describe the data. This approach is also followed in the latest analysis of this channel, published jointly by BaBar and Belle [29]. In total 18 resonant components, including four doubly Cabibbo suppressed ones, are required to describe the Dalitz plot with 1.1M  $D^0 \rightarrow K_S \pi^+ \pi^-$  events. Belle's and BaBar's data have been re-analyzed by [17] in a QCD factorization framework, using line-shape parametrizations for the S [30,31] and P wave [11] contributions that preserve 2-body unitarity and analyticity. The measurements give compatible results for the components they share.

The field of amplitude analyses remains very active. Publications since the last update of this review two years ago include Dalitz plot analyses of  $D_s^+ \rightarrow \pi^+ \pi^0 \eta$  by BES III [32];  $D^+ \rightarrow K^+ K^- K^+$  by LHCb [33];  $D^0 \rightarrow \pi^+ \pi^- \pi^0$  by BaBar [34]; BaBar and Belle's joint

analysis of  $D^0 \rightarrow K_S \pi^+ \pi^-$  [29]; and a re-analysis of  $D^+ \rightarrow K_S \pi^0 \pi^+$  and  $D^+ \rightarrow K^- \pi^+ \pi^+$  data from FOCUS, CLEO and BES III by Niecknig and Kubis [13]. Ahn, Yang and Nam developed amplitude models for  $\Lambda_c^+ \rightarrow K^- p \pi^+$  and  $\Lambda_c^+ \rightarrow K_S p \pi^0$  [35] based on BELLE data [36]. There has also been significant progress in four body amplitude analyses:  $D^0 \rightarrow K^+ K^- \pi^+ \pi^-$  and  $D^0 \rightarrow \pi^+ \pi^- \pi^+ \pi^-$  using CLEO data [22];  $D^+ \rightarrow K_S \pi^+ \pi^+ \pi^-$ ,  $D^0 \rightarrow K^- \pi^+ \pi^- \pi^+$  and  $D^0 \rightarrow K^- \pi^+ \pi^0 \pi^0$  by BES III [37–39]; and  $D^0 \rightarrow K^+ K^- \pi^+ \pi^-$ ,  $D^0 \rightarrow K^\mp \pi^\pm \pi^\mp \pi^\pm$  [23,40] by LHCb. Noteworthy is the increasing sophistication of recent amplitude analyses, most of which go substantially beyond the isobar model with Breit Wigner and Flatté lineshapes. However, with the notable exception of [13] and [33], they remain within the isobar framework which describes the decay as a series of 2-body processes; even if these are modeled with increasing sophistication, the approach ignores long-range hadronic effects such as re-scattering and does not respect 3 (or 4)-body unitarity and analyticity.

Several groups work on improved models. Dispersive techniques, which respect 3-body unitarity and analyticity, have been successfully applied to regions of the  $D^+ \rightarrow K^- \pi^+ \pi^+$  and  $D^+ \rightarrow K_S \pi^0 \pi^+$  Dalitz plots below the  $\eta/K$  threshold [12,13], where they provide a good description of the data with fewer fit parameters than the isobar approach. Ref. [41] uses a unitary coupled channel approach to describe  $D^+ \rightarrow K^- \pi^+ \pi^+$ , which has no restrictions on the kinematic range, but requires additional parameters to describe the Dalitz plot above the  $\eta/K$  threshold. Using an effective chiral Lagrangian, the authors of Ref. [16] provide a description of the annihilation contribution to the decay amplitude which respects 3-body unitarity. This approach provides a good description of LHCb  $D^+ \rightarrow K^+ K^- K^+$  data, with fewer parameters than an equivalent isobar model [33].

Limitations in the theoretical description of interfering resonances are the leading source of systematic uncertainty in many analyses. This is set to become increasingly problematic given the statistical precision achievable with the vast, clean charm samples available at the B factories, LHCb, and their upgrades. In some cases, the model uncertainty can be removed through model-independent methods, often relying on input from the charm threshold, as discussed below. Ref. 42 expand the scope and applicability of the quasi model-independent approach in amplitude fits. At the same time, increasingly sophisticated models are being developed, and applied to data.

### 68.2. Applications of multibody charm analyses

Amplitude analyses provide sensitivity to both relative magnitudes and phases of the interfering decay amplitudes. It is especially this sensitivity to phases that makes amplitude analyses such a uniquely powerful tool for studying a wide range of phenomena. Here we concentrate on their use for  $CP$  violation and mixing measurements in charm, and charm inputs to  $CP$  violation analyses in  $B$  meson decays (see also [43,44]). The properties of light-meson resonances determined in  $D$  amplitude analyses are reported in the light-unflavored-meson section of this Review.

#### 68.2.1. Time-integrated searches for $CP$ violation in charm :

Comparing the results of amplitude fits for  $CP$ -conjugate decay modes provides a measure of  $CP$  violation. Recent  $CP$  violation searches using this method include amplitude analyses of  $D^0 \rightarrow K_S^0 K^\pm \pi^\mp$  and  $D^0 \rightarrow K^+ K^- \pi^+ \pi^-$  by LHCb [45,40], and  $D^0 \rightarrow K^+ K^- \pi^+ \pi^-$ ,  $D^0 \rightarrow \pi^+ \pi^- \pi^+ \pi^-$  [46,22] using CLEO data.

A widely-used amplitude model-independent technique to search for local  $CP$  violation is based on performing a  $\chi^2$  comparison of  $CP$ -conjugate phase-space distributions. This method was pioneered by BaBar [47] and developed further in [48–50], with recent results reported by BaBar [51] and LHCb in  $D^\pm \rightarrow K^+ K^- \pi^\pm$  [52,53], CDF in  $D^0 \rightarrow K_S \pi^+ \pi^-$  [26], and LHCb in  $D^+ \rightarrow \pi^- \pi^+ \pi^+$  [55],  $D^0 \rightarrow K^+ K^- \pi^+ \pi^-$  and  $D^0 \rightarrow \pi^+ \pi^- \pi^+ \pi^-$  [50]. Un-binned methods can increase the sensitivity [54] and have been applied by LHCb to  $D^+ \rightarrow \pi^- \pi^+ \pi^+$ ,  $D^0 \rightarrow \pi^+ \pi^- \pi^0$  and  $D^0 \rightarrow \pi^+ \pi^- \pi^+ \pi^-$  [55,56,73].

An alternative model-independent approach is based on constructing observables in four body decays that are odd under motion reversal

(“naive T”) [58–66], which is equivalent to  $P$  for scalar particles [66]. One such observable is  $C_T = \vec{p}_2 \cdot (\vec{p}_3 \times \vec{p}_4) = (1/m_D)\epsilon_{\alpha\beta\gamma\delta} p_1^\alpha p_2^\beta p_3^\gamma p_4^\delta$ , where  $\vec{p}_i$  are the decay products’ three momenta in the decay’s restframe, and  $p_i$  are their four-momenta. Identical particles (as in  $D^0 \rightarrow K^+ \pi^- \pi^+ \pi^-$ ) are ordered by momentum magnitude. Comparing the  $P$  violating asymmetry  $A_T \equiv \frac{\Gamma(C_T > 0) - \Gamma(C_T < 0)}{\Gamma(C_T > 0) + \Gamma(C_T < 0)}$  with its  $C$ -conjugate in  $\bar{D}^0$  decays, provides sensitivity to  $CP$  violation. Searches for  $CP$  violation in this manner have been carried out for  $D^0 \rightarrow K^+ K^- \pi^+ \pi^-$  by FOCUS, BaBar, LHCb and Belle [67,68,69,70], where LHCb increase the sensitivity of the method by analysing the data in bins of phase space, and Belle’s analysis considers several new, hitherto unused  $P$ -odd variables;  $D^+ \rightarrow K^+ K_S \pi^+ \pi^-$  and  $D_s^+ \rightarrow K^+ K_S \pi^+ \pi^-$  by BaBar [71]; and  $D^0 \rightarrow K_S \pi^+ \pi^- \pi^0$  by Belle [72]. LHCb’s unbinned comparison of kinematic distributions in  $D^0, \bar{D}^0 \rightarrow \pi^+ \pi^- \pi^+ \pi^-$  is sensitive to  $CP$  violation in both  $P$  even and  $P$ -odd kinematic variables [73].

The results of all measurements described in this section are compatible with  $CP$  conservation in charm. Given the recent discovery of  $CP$  violation in  $D^0 \rightarrow K^+ K^-$ ,  $D^0 \rightarrow \pi^+ \pi^-$  decays, and in view of the vast data samples about to be collected, one might expect this to change in the foreseeable future.

**68.2.2. Charm Mixing and  $CP$  violation** : Time-dependent amplitude analyses in decays to final states that are accessible to both  $D^0$  and  $\bar{D}^0$  have unique sensitivity to mixing parameters. A Dalitz plot analysis of a self-conjugate final state, such as  $K_S \pi^+ \pi^-$  and  $K_S K^+ K^-$ , allows the measurement of the phase difference between the relevant  $D^0$  and  $\bar{D}^0$  decay amplitudes, and thus a direct measurement of  $x$  and  $y$ , the normalised mass and width difference of the  $D^0 - \bar{D}^0$  system’s mass eigenstates. This is in contrast to decays like  $D^0 \rightarrow K \pi$  [74] which only provide access to the decay-specific parameters  $x'^2, y'$ . Multibody charm analyses are also sensitive to  $CP$  violation in mixing and in the interference between mixing and decay; these results are summarised in [43,44].

**68.2.3.  $CP$  violation in decays of Beauty to Charm** : Neutral  $D$  mesons originating from  $B^- \rightarrow DK^-$  (here denoted as  $D_{B^-}$ ) are a superposition of  $D^0$  and  $\bar{D}^0$  with a relative phase that depends on the CKM unitarity triangle parameter  $\gamma/\phi_3$ ,

$$D_{B^-} \propto D^0 + r_B e^{i(\delta_B - \gamma)} \bar{D}^0,$$

where  $\delta_B$  is a  $CP$  conserving strong phase, and  $r_B \sim 0.1$ . In the corresponding  $CP$ -conjugate expression,  $\gamma/\phi_3$  changes sign. An amplitude analysis of the subsequent decay of the  $D_{B^\pm}$  to a state accessible to both  $D^0$  and  $\bar{D}^0$  allows the measurement of  $\gamma/\phi_3$  [75–79]. The method generalizes to similar  $B$  hadron decays, such as  $B^0 \rightarrow DK^{*0}$ . Measurements based on this technique have been reported by BaBar [80,81], Belle [25,82] and LHCb [83–92]. The most precise individual results come from the study of  $D_{B^-} \rightarrow K_S \pi^+ \pi^-$  and  $D_{B^-} \rightarrow K_S K^+ K^-$  with an uncertainty of  $\sim 10^\circ$  [25,80,82,86,92]; combining measurements in multiple decay modes leads to a current uncertainty on  $\gamma/\phi_3$  of less than  $6^\circ$ .

The interference between mixing and decay in  $B^0 \rightarrow D^0 h^0$  with  $h^0 = \pi^0, \eta, \omega$  provides sensitivity to  $\beta$ , which can be extracted from the Dalitz plot of the subsequent  $D^0 \rightarrow K_S \pi^+ \pi^-$  decay [29,93–96]. The combined BaBar/Belle analysis based on this technique resolved the ambiguity in  $\beta$  present in other measurements, such as  $B^0 \rightarrow J/\psi K_S$ , in favour of the solution compatible with other unitarity triangle constraints [29].

### 68.3. Model Independent Methods and the Charm Threshold

The precision measurement of mixing or  $CP$  violation parameters such  $\gamma/\phi_3$  from multibody charm decays requires as input the phase-differences between the  $D^0$  and  $\bar{D}^0$  amplitudes across phase space, as well as their magnitudes, for each final state of interest. While the magnitudes are fairly easily measured, the phase information requires either amplitude models with reliable phase motion, or model-independent approaches.

Model-independent measurements of the relevant phase differences rely on interference effects in the decays of well-defined coherent superpositions of  $D^0$  and  $\bar{D}^0$ . These are accessible at the charm threshold, where CLEO-c and BES III operate [43,97–104]. Charm mixing also results in a (time-dependent)  $D^0 - \bar{D}^0$  superposition, that can be used to measure the relevant phase information as input to  $\gamma/\phi_3$  measurements. This method is particularly powerful in doubly Cabibbo-suppressed decays such as  $D^0 \rightarrow K^+ \pi^- \pi^+ \pi^-$ , and when used in combination with threshold data [105,106]. Under some circumstances, with large data sets, the relevant strong phases and  $\gamma/\phi_3$  can be extracted simultaneously without external input, for example in simultaneous analysis of the  $B^0 \rightarrow DK^+ \pi^-$  Dalitz plot and that of the subsequent  $D \rightarrow K_S \pi^+ \pi^-$  decay [115]. However, the global effort to achieve a measurement of  $\gamma/\phi_3$  to sub-degree precision will continue to rely critically on input from the charm threshold.

The model-independent phase information is provided either integrated over the entire phase space of the decay, or in sub-regions/bins. The results can be expressed in terms of one complex parameter  $Z = R e^{-i\delta} = c + is$  per pair of  $CP$ -conjugate bins, with magnitude  $R \leq 1$ . Larger  $R$  values lead to higher sensitivity to  $\gamma/\phi_3$ . Amplitude models can be used to optimise the binning for sensitivity to  $\gamma/\phi_3$ , without introducing a model-dependent bias in the result.

CLEO-c data have been analyzed to provide binned  $Z$  for the self-conjugate decays  $D^0 \rightarrow K_S \pi^+ \pi^-$ ,  $D^0 \rightarrow K_S K^+ K^-$ ,  $D^0 \rightarrow \pi^+ \pi^- \pi^+ \pi^-$ , and  $D^0 \rightarrow K_S \pi^- \pi^+ \pi^0$  [107–110]; and phase space-integrated values for  $D^0, \bar{D}^0 \rightarrow K_S K^+ \pi^-$ ,  $K^+ \pi^- \pi^0$  and  $K^+ \pi^- \pi^+ \pi^-$  [111,112]. Adding input from LHCb’s charm mixing analysis significantly improves the constraints on  $Z$  for  $D^0, \bar{D}^0 \rightarrow K^+ \pi^- \pi^+ \pi^-$  [112,113]. A recent study based on LHCb’s  $D^0, \bar{D}^0 \rightarrow K^+ \pi^- \pi^+ \pi^-$  amplitude models [23] and CLEO-c data indicates that a binned analysis of  $D^0, \bar{D}^0 \rightarrow K^+ \pi^- \pi^+ \pi^-$  could lead to the most precise individual measurement of  $\gamma/\phi_3$  [114]. For self-conjugate decays such as  $D^0 \rightarrow \pi^+ \pi^- \pi^0$ , analysed with a single pair of bins,  $Z$  is real-valued, and usually expressed in terms of the  $CP$ -even fraction  $F_+ \equiv \frac{1}{2}(\text{Re}(Z) + 1)$ , defined such that a  $CP$ -even eigenstate has  $F_+ = 1$ , while a  $CP$ -odd eigenstate has  $F_+ = 0$  [102]. Recent analyses of CLEO-c data reveal that  $D^0 \rightarrow \pi^+ \pi^- \pi^0$  is compatible with being completely  $CP$ -even with  $F_+ = 0.973 \pm 0.017$ , while  $D^0 \rightarrow K^+ K^- \pi^0$  has  $F_+ = 0.732 \pm 0.055$ ,  $D^0 \rightarrow \pi^+ \pi^- \pi^+ \pi^-$  has  $F_+ = 0.769 \pm 0.023$  and  $D^0 \rightarrow K_S \pi^+ \pi^- \pi^0$  has  $0.238 \pm 0.020$  [103,109,110].

It is interesting to compare these values with those obtained from amplitude models as a cross check of the models’ phase-motion.  $F_+^{4\pi \text{ model}} = 0.729 \pm 0.020$  calculated from Ref. 22’s  $D^0 \rightarrow \pi^+ \pi^- \pi^+ \pi^-$  model, compares well to the measured value given above, as does  $Z^{K3\pi \text{ model}} = 0.459 \pm 0.025$  [23] to  $Z^{K3\pi \text{ meas}} = (0.32_{-0.13}^{+0.17}) \exp(-i(128_{-17}^{+28}^\circ))$  [112,113]. Binwise comparisons for  $D^0 \rightarrow K_S \pi^+ \pi^-$ ,  $D^0 \rightarrow K_S K^+ K^-$ ,  $D^0 \rightarrow \pi^+ \pi^- \pi^+ \pi^-$ , and  $D^0, \bar{D}^0 \rightarrow K^+ \pi^- \pi^+ \pi^-$  can be found in [107–109,114].

### 68.4. Summary

Multibody charm decays offer a rich phenomenology, including unique sensitivity to  $CP$  violation and charm mixing. This is a highly dynamic field with many new results (some of which we presented here) and rapidly increasing, high quality datasets. These datasets constitute a huge opportunity, but also a challenge to improve the theoretical descriptions of soft hadronic effects in multibody decays. For some measurements, model-independent methods, many relying on input from the charm threshold, provide a way of removing model-induced uncertainties. At the same time, substantial progress in the theoretical description of multibody decays is being made.

#### References:

1. R.H. Dalitz, *Phil. Mag.* **44**, 1068 (1953).
2. M. Bauer, B. Stech, and M. Wirbel, *Z. Phys.* **C4**, 103 (1987); P. Bedaque, A. Das, and V.S. Mathur, *Phys. Rev.* **D49**, 269 (1994); L.-L. Chau and H.-Y. Cheng, *Phys. Rev.* **D36**, 137 (1987); K. Terasaki, *Int. J. Mod. Phys.* **A10**, 3207 (1995); F. Buccella, M. Lusignoli, and A. Pugliese, *Phys. Lett.* **B379**, 249 (1996).

3. J.D. Jackson, *Nuovo Cimento* **34**, 1644 (1964).
4. See the note on Resonances in this *Review*.
5. E.P. Wigner, *Phys. Rev.* **70**, 15 (1946).
6. S. M. Flatté, *Phys. Lett.* **63B**, 224 (1976) *Phys. Lett.* **63B**, 224 (1976).
7. S.U. Chung *et al.*, *Ann. Phys.* **4**, 404 (1995).
8. I.J.R. Aitchison, *Nucl. Phys.* **A189**, 417 (1972).
9. D. Aston *et al.* (LASS Collab.), *Nucl. Phys.* **B296**, 493 (1988).
10. R. Omnes, *Nuovo Cimento* **8**, 316 (1958).
11. C. Hanhart, *Phys. Lett.* **B715**, 170 (2012).
12. F. Niecknig and B. Kubis, *JHEP* **1510**, 142 (2015).
13. F. Niecknig and B. Kubis, *Phys. Lett.* **B780**, 471 (2018).
14. P. C. Magalhães and M. R. Robilotta, *Phys. Rev. D* **92**, 094005(2015).
15. P. C. Magalhães *et al.*, *Phys. Rev. D* **84**, 094001(2011).
16. R. T. Aoude, P. C. Magalhães, A. C. Dos Reis and M. R. Robilotta, *Phys. Rev.* **D97**, 5,056021 (2018).
17. J.P. Dedonder *et al.* *Phys. Rev.* **D89**, 094018 (2014).
18. D. Boito, J.-P. Dedonder, B. El-Bennich, R. Escribano, R. Kaminski, L. Lesniak and B. Loiseau, *Phys. Rev.* **D96**, 11,113003 (2017).
19. R. Klein, T. Mannel, J. Virto and K. K. Vos, *JHEP* **1710**, 117 (2017).
20. E.M. Aitala *et al.* (E791 Collab.), *Phys. Rev.* **D73**, 032004 (2006) [*Phys. Rev.* **D74**, 059901 (E)(2006)].
21. G. Bonvicini *et al.* (CLEO Collab.), *Phys. Rev.* **D78**, 052001 (2008).
22. P. d'Argent *et al.*, *JHEP* **1705**, 142 (2017).
23. R. Aaij *et al.* [LHCb Collaboration], *Eur. Phys. J.* **C78**, 6,443 (2018).
24. H. Muramatsu *et al.* (CLEO Collab.), *Phys. Rev. Lett.* **89**, 251802 (2002).
25. A. Poluektov *et al.* (Belle Collab.), *Phys. Rev.* **D81**, 112002 (2010).
26. T. Aaltonen *et al.* (CDF Collab.), *Phys. Rev.* **D86**, 032007 (2012).
27. P. del Amo Sanchez *et al.* (BaBar Collab.), *Phys. Rev. Lett.* **105**, 081803 (2010).
28. V. V. Anisovich and A. V. Sarantsev, *Eur. Phys. J.* **A16**, 229 (2018).
29. I. Adachi *et al.* [BaBar and Belle Collaborations], *Phys. Rev. Lett.* **121**, 26,261801 (2018) *Phys. Rev.* **D98**, 11,112012 (2018).
30. B. El-Bennich *et al.* *Phys. Rev.* **D79**, 094005 (2009) [*Phys. Rev.* **D83**, 039903(E) (2011)].
31. J.P. Dedonder *et al.* *Acta Phys. Polon. B* **42** (2011) 2013.
32. M. Ablikim *et al.* [BESIII Collaboration], arXiv:1903.04118 [hep-ex]. (remove if still unpublished by end of review, otherwise update).
33. R. Aaij *et al.* [LHCb Collaboration], *JHEP* **1904**, 063 (2019).
34. J. P. Lees *et al.* [BaBar Collaboration], *Phys. Rev. D* **93**, 11,112014(2016).
35. J. K. Ahn, S. Yang and S. I. Nam, *Phys. Rev. D* **100**, 3,034027(2019).
36. analysing data published in S. B. Yang *et al.* [Belle Collaboration], *Phys. Rev. Lett.* **117**, 1,011801 (2016).
37. M. Ablikim *et al.* [BESIII Collaboration], arXiv:1901.05936 [hep-ex]. (remove if still unpublished by end of the review, otherwise update).
38. M. Ablikim *et al.* [BESIII Collaboration], *Phys. Rev. D* **95**, 7,072010(2017).
39. M. Ablikim *et al.* [BESIII Collaboration], *Phys. Rev.* **D99**, 9,092008 (2019).
40. R. Aaij *et al.* [LHCb Collaboration], *JHEP* **1902**, 126 (2019).
41. S. X. Nakamura, *Phys. Rev. D* **93**, 1,014005(2016).
42. F. Krinner, D. Greenwald, D. Ryabchikov, B. Grube and S. Paul, *Phys. Rev. D* **97**, 11,114008(2018).
43. See the note on  $D^0-\bar{D}^0$  Mixing in this *Review*.
44. See the note CP violation in the quark sector in this *Review*.
45. R. Aaij *et al.* [LHCb Collaboration], *Phys. Rev.* **D93**, 052018 (2016).
46. M. Artuso *et al.* (CLEO Collab.), *Phys. Rev.* **D85**, 122002 (2012).
47. B. Aubert *et al.* (BABAR Collab.), *Phys. Rev.* **D78**, 051102 (2008).
48. I. Bediaga *et al.*, *Phys. Rev.* **D80**, 096006 (2009).
49. I. Bediaga *et al.*, *Phys. Rev.* **D86**, 036005 (2012).
50. R. Aaij *et al.* (LHCb Collab.), *Phys. Lett.* **B726**, 623 (2013).
51. J.P. Lees *et al.* (BaBar Collab.), *Phys. Rev.* **D87**, 052010 (2013).
52. R. Aaij *et al.* (LHCb Collab.), *Phys. Rev.* **D84**, 112008 (2011).
53. R. Aaij *et al.* (LHCb Collab.), *JHEP* **1306**, 112 (2013).
54. M. Williams, *Phys. Rev.* **D84**, 054015 (2011).
55. R. Aaij *et al.* (LHCb Collab.), *Phys. Lett.* **B728**, 585 (2014).
56. R. Aaij *et al.* (LHCb Collab.), *Phys. Lett.* **B740**, 158 (2015).
57. R. Aaij *et al.* [LHCb Collaboration], *Phys. Lett.* **B769**, 345 (2017).
58. E. Golowich and G. Valencia, *Phys. Rev.* **D40**, 112, (1989).
59. G. Valencia, *Phys. Rev.* **D39**, 3339 (1989).
60. W. Bensalem and D. London, *Phys. Rev.* **D64**, 116003 (2001).
61. I.I.Y. Bigi, hep-ph/0107102.
62. W. Bensalem, A. Datta, and D. London, *Phys. Rev.* **D66**, 094004 (2002).
63. W. Bensalem, A. Datta, and D. London, *Phys. Lett.* **B538**, 309 (2002).
64. A. Datta and D. London, *Int. J. Mod. Phys.* **A19**, 2505 (2004).
65. M. Gronau and J.L. Rosner, *Phys. Rev.* **D84**, 096013 (2011).
66. G. Durieux and Y. Grossman, *Phys. Rev.* **D92**, 076013 (2015).
67. J.M. Link *et al.* (FOCUS Collab.), *Phys. Lett.* **B622**, 239 (2005).
68. P. del Amo Sanchez *et al.* (BaBar Collab.), *Phys. Rev.* **D81**, 111103 (2010).
69. R. Aaij *et al.* (LHCb Collab.), *JHEP* **1410**, 005 (2014).
70. J. B. Kim *et al.* [Belle Collaboration], *Phys. Rev.* **D99**, 1,011104 (2019).
71. J.P. Lees *et al.* (BaBar Collab.), *Phys. Rev.* **D84**, 031103 (2011).
72. K. Prasanth *et al.* [Belle Collaboration], *Phys. Rev.* **D95**, 9,091101 (2017).
73. R. Aaij *et al.* [LHCb Collaboration], *Phys. Lett.* **B769**, 345 (2017).
74. D.M. Asner *et al.* (CLEO Collab.), *Phys. Rev.* **D72**, 012001 (2005).
75. M. Gronau and D. Wyler, *Phys. Lett.* **B265**, 172 (1991).
76. M. Gronau and D. London, *Phys. Lett.* **B253**, 483 (1991).
77. D. Atwood *et al.*, *Phys. Rev. Lett.* **78**, 17, 3257 (1997).
78. A. Poluektov *et al.* (Belle Collab.), *Phys. Rev.* **D70**, 7, 072003 (2004).
79. J. Rademacker and G. Wilkinson, *Phys. Lett.* **B647**, 400 (2007).
80. P. del Amo Sanchez *et al.* (BaBar Collab.), *Phys. Rev. Lett.* **105**, 121801 (2010).
81. J.P. Lees *et al.* (BaBar Collab.), *Phys. Rev.* **D84**, 012002 (2011).
82. H. Aihara *et al.* (Belle Collab.), *Phys. Rev.* **D85**, 112014 (2012).
83. R. Aaij *et al.* (LHCb Collab.), *Phys. Lett.* **B726**, 151 (2013).
84. R. Aaij *et al.* (LHCb Collab.), *Phys. Lett.* **B723**, 44 (2013).
85. R. Aaij *et al.* (LHCb Collab.), *Phys. Lett.* **B718**, 43 (2012).
86. R. Aaij *et al.* (LHCb Collab.), *JHEP* **1410**, 97 (2014).
87. R. Aaij *et al.* (LHCb Collab.), *Phys. Lett.* **B733**, 36 (2014).
88. R. Aaij *et al.* (LHCb Collab.), *Nucl. Phys.* **B888**, 169 (2014).
89. R. Aaij *et al.* (LHCb Collab.), *Phys. Rev.* **D91**, 112014 (2015).
90. R. Aaij *et al.* [LHCb Collaboration], *JHEP* **1606**, 131 (2016).
91. R. Aaij *et al.* [LHCb Collaboration], *JHEP* **1612**, 087 (2016).
92. R. Aaij *et al.* [LHCb Collaboration], *JHEP* **1808**, 176 (2018), Erratum: *JHEP* **1810**, 107 (2018).
93. A. Bondar, T. Gershon and P. Krokovny, *Phys. Lett.* **B624**, 1 (2005).
94. P. Krokovny *et al.* [Belle Collaboration], *Phys. Rev. Lett.* **97**, 1,081801 (2006).
95. B. Aubert *et al.* [BaBar Collaboration], *Phys. Rev. Lett.* **99**, 231802 (2007).

96. V. Vorobyev *et al.* [Belle Collaboration], Phys. Rev. **D94**, 5,052004 (2016).
97. A. Giri *et al.*, Phys. Rev. **D68**, 5, 054018 (2003).
98. D. Atwood and A. Soni, Phys. Rev. **D68**, 033003 (2003).
99. S. Malde and G. Wilkinson, Phys. Lett. **B701**, 353 (2011).
100. A. Bondar *et al.*, Phys. Rev. **D82**, 034033 (2010).
101. C. Thomas and G. Wilkinson, JHEP **1210**, 184 (2012).
102. M. Nayak *et al.* Phys. Lett. **B740**, 1 (2015).
103. S. Malde *et al.* Phys. Lett. **B747**, 9 (2015).
104. S. Malde, C. Thomas, and G. Wilkinson, Phys. Rev. **D91**, 094032 (2015).
105. S. Harnew and J. Rademacker, Phys. Lett. **B728**, 296 (2014).
106. S. Harnew and J. Rademacker, JHEP **1503**, 169 (2015).
107. J. Libby *et al.* (CLEO Collab.), Phys. Rev. **D82**, 112006 (2010).
108. R.A. Briere *et al.* (CLEO Collab.), Phys. Rev. **D80**, 032002 (2009).
109. S. Harnew *et al.*, JHEP **1801**, 144 (2018).
110. P.K. Resmi *et al.*, JHEP **1801**, 082 (2018).
111. J. Insler *et al.* (CLEO Collab.), Phys. Rev. **D85**, 092016 (2012) erratum Phys. Rev. D 94,9,09905(2016).
112. T. Evans *et al.*, Phys. Lett. **B757**, 520 (2017), erratum Phys. Lett. **B765**, 402, (2017).
113. R. Aaij *et al.* [LHCb Collaboration], Phys. Rev. Lett. **117**, 24,241801 (2016).
114. T. Evans *et al.*, arXiv:1909.10196 [hep-ex].
115. D. Craik, T. Gershon and A. Poluektov, Phys. Rev. **D97**, 5,056002 (2018).

69.  $D^0$ - $\bar{D}^0$  Mixing

Revised August 2019 by D.M. Asner (BNL) and A.J. Schwartz (Cincinnati U.).

The formalism for  $D^0$ - $\bar{D}^0$  mixing is closely related to that for  $CP$  violation, which is also presented in the note “ $CP$  Violation in the Quark Sector” in this *Review*. The time evolution of the  $D^0$ - $\bar{D}^0$  system is described by the Schrödinger equation

$$i \frac{\partial}{\partial t} \begin{pmatrix} D^0(t) \\ \bar{D}^0(t) \end{pmatrix} = \left( \mathbf{M} - \frac{i}{2} \mathbf{\Gamma} \right) \begin{pmatrix} D^0(t) \\ \bar{D}^0(t) \end{pmatrix}, \quad (69.1)$$

where the  $\mathbf{M}$  and  $\mathbf{\Gamma}$  matrices are Hermitian, and  $CPT$  invariance requires that  $M_{11} = M_{22} \equiv M$  and  $\Gamma_{11} = \Gamma_{22} \equiv \Gamma$ . The off-diagonal elements of  $\mathbf{M}$  and  $\mathbf{\Gamma}$  are referred to as the dispersive and absorptive parts, respectively, of the mixing. The mass eigenstates  $D_1$  and  $D_2$  of the Hamiltonian  $\mathbf{M} - i\mathbf{\Gamma}/2$  are defined as

$$|D_{1,2}\rangle \equiv p|D^0\rangle \pm q|\bar{D}^0\rangle, \quad (69.2)$$

where normalization imposes  $|p|^2 + |q|^2 = 1$ . If  $p = q$ , then the mass eigenstates are  $CP$  eigenstates and  $CP$  is conserved. Our phase convention is  $CP|D^0\rangle = -|\bar{D}^0\rangle$ , which implies that, in the absence of  $CP$  violation,  $D_2$  is  $CP$ -even and  $D_1$  is  $CP$ -odd.

The eigenvalues of  $\mathbf{M} - i\mathbf{\Gamma}/2$  are

$$\omega_{1,2} = \left( M - \frac{i}{2} \Gamma \right) \pm \frac{q}{p} \left( M_{12} - \frac{i}{2} \Gamma_{12} \right) \equiv m_{1,2} - \frac{i}{2} \Gamma_{1,2}, \quad (69.3)$$

where  $m_{1,2}$  and  $\Gamma_{1,2}$  are real and correspond to the masses and decay widths, respectively, of the  $D_{1,2}$  mass eigenstates. As the trace  $\Gamma_{11} + \Gamma_{22} = 2\Gamma$  is unchanged by diagonalizing  $\mathbf{\Gamma}$ ,  $\Gamma = (\Gamma_1 + \Gamma_2)/2$ , i.e., the mean decay width. Solving for the eigenstates of the eigenvalues yields

$$\left( \frac{q}{p} \right)^2 = \frac{M_{12}^* - \frac{i}{2} \Gamma_{12}^*}{M_{12} - \frac{i}{2} \Gamma_{12}}. \quad (69.4)$$

If  $CP$  is conserved,  $(q/p) = 1$  and thus  $M_{12}$  and  $\Gamma_{12}$  must be real. In this case the difference in eigenvalues is  $\Delta m \equiv m_2 - m_1 = 2M_{12}$  and  $\Delta\Gamma \equiv \Gamma_2 - \Gamma_1 = 2\Gamma_{12}$ . The signs of  $\Delta m$  and  $\Delta\Gamma$  are difficult to predict from theory and thus must be determined experimentally.

We define dimensionless mixing parameters  $x$  and  $y$  as

$$x \equiv \frac{\Delta m}{\Gamma} \quad (69.5)$$

$$y \equiv \frac{\Delta\Gamma}{2\Gamma}. \quad (69.6)$$

These parameters are measured in several ways. The most precise values are obtained using the time dependence of  $D^0$  decays. For all methods, the initial flavor of the  $D^0$  or  $\bar{D}^0$  (at the production point) must be determined. The most common method used for this is to reconstruct  $D^{*+} \rightarrow D^0\pi^+$  or  $D^{*-} \rightarrow \bar{D}^0\pi^-$  decays; the charge of the accompanying pion (which has low momentum in the lab frame and is often referred to as the “soft” pion) determines the flavor of the neutral  $D$ . BaBar and LHCb have also identified the flavor of the neutral  $D$  by reconstructing semileptonic  $B^+ \rightarrow \bar{D}^0\ell^+\nu$ ,  $B^0 \rightarrow D^{*-}\ell^+\nu$ ,  $B^- \rightarrow D^0\ell^-\nu$ , and  $\bar{B}^0 \rightarrow D^{*+}\ell^-\nu$  decays; in this case the charge of the accompanying lepton determines the  $D$  flavor. At  $e^+e^-$  collider experiments such as Belle, BaBar, and BESIII, the  $D$  flavor can also be determined by fully reconstructing a  $D$  decay on the “opposite side” of an event, i.e., recoiling against the signal-side  $D$  decay.

At BESIII, where  $DD$  pairs are produced near their threshold via  $e^+e^- \rightarrow \psi(3770) \rightarrow D^0\bar{D}^0$ , there is relatively little background and the purity of opposite-side tagging is equivalent to that achieved using  $D^{*\pm}$  decays. However, BESIII operates at a symmetric  $e^+e^-$  collider, and the  $DD$  pairs are produced almost at rest in the lab frame. As a consequence, the  $D$ 's do not travel any appreciable distance before decaying, and time-dependent analyses are not possible. To overcome this, measurements of mixing at BESIII utilize the quantum coherence of the initial  $\psi(3770) \rightarrow D^0\bar{D}^0$  state and time-integrated measurements [1–5].

## 69.1 Time-Dependent Analyses

We extend the formalism of this *Review*'s note on “ $CP$  Violation in Meson Decays.” Our notation is as follows: Cabibbo-favored (“right-sign”) decay amplitudes are denoted  $\bar{A}_f \equiv \langle f|H|\bar{D}^0\rangle$  and  $A_{\bar{f}} \equiv \langle \bar{f}|H|D^0\rangle$ ; i.e., the final state is  $f = K^+\ell^-\nu$ ,  $K^+\pi^-$ ,  $K^+\pi^-\pi^0$ , etc. Doubly-Cabibbo-suppressed (“wrong-sign”) decay amplitudes are denoted  $A_f \equiv \langle f|H|D^0\rangle$  and  $\bar{A}_{\bar{f}} \equiv \langle \bar{f}|H|\bar{D}^0\rangle$ .

Starting from a pure  $|D^0\rangle$  or  $|\bar{D}^0\rangle$  state at  $t = 0$ , the time-dependent decay rates to wrong-sign final states are

$$r(t) \equiv |\langle f|H|D^0(t)\rangle|^2 = |\bar{A}_f|^2 \left| \frac{q}{p} \right|^2 |g_+(t)\lambda_f^{-1} + g_-(t)|^2 \quad (69.7)$$

$$\bar{r}(t) \equiv |\langle \bar{f}|H|\bar{D}^0(t)\rangle|^2 = |A_{\bar{f}}|^2 \left| \frac{p}{q} \right|^2 |g_+(t)\lambda_{\bar{f}} + g_-(t)|^2, \quad (69.8)$$

where

$$\lambda_f \equiv \frac{q\bar{A}_f}{pA_f}, \quad \lambda_{\bar{f}} \equiv \frac{q\bar{A}_{\bar{f}}}{pA_{\bar{f}}}, \quad (69.9)$$

and

$$g_{\pm}(t) = \frac{1}{2} (e^{-i\omega_1 t} \pm e^{-i\omega_2 t}). \quad (69.10)$$

A change in convention for the relative phase of  $D^0$  and  $\bar{D}^0$  would cancel between  $q/p$  and  $\bar{A}_f/A_f$  (or  $\bar{A}_{\bar{f}}/A_{\bar{f}}$ ), leaving  $\lambda_f$  (or  $\lambda_{\bar{f}}$ ) unchanged. For multibody final states, these equations apply separately to each point in phase-space. Integrating over regions of phase-space can lead to enhanced sensitivity to  $CP$  violation; see the discussion below on multibody decays and the “Review of Multibody Charm Analyses” in this *Review* [6]. As the mixing parameters  $x$  and  $y$  are very small,  $r(t)$  and  $\bar{r}(t)$  are usually expanded to second order in  $x$  and  $y$ .

## 69.2 Semileptonic decays

Consider the final state  $f = K^+\ell^-\bar{\nu}_\ell$ , where  $A_f = \bar{A}_{\bar{f}} = 0$  is an excellent approximation in the Standard Model. The final state  $f$  is accessible from a  $D^0$  only via mixing,<sup>1</sup> and the decay rate is

$$r(t) = |\bar{A}_f|^2 \left| \frac{q}{p} \right|^2 |g_-(t)|^2 \approx |\bar{A}_f|^2 \left| \frac{q}{p} \right|^2 \left( \frac{x^2 + y^2}{4} \right) (\Gamma t)^2 e^{-\Gamma t}. \quad (69.11)$$

For  $\bar{r}(t)$ ,  $q/p$  is replaced by  $p/q$ . In the Standard Model,  $CP$  violation in charm mixing is small and  $|q/p| \approx 1$ . In the limit of  $CP$  conservation,  $r(t) = \bar{r}(t)$ , and the time-integrated mixing rate relative to the time-integrated right-sign decay rate for semileptonic decays is

$$\frac{\int_0^\infty r(t) dt}{\int_0^\infty |\bar{A}_f|^2 e^{-\Gamma t} dt} = \frac{x^2 + y^2}{2} \equiv R_M. \quad (69.12)$$

Table 69.1 summarizes results for  $R_M$  from semileptonic decays; the world average from the Heavy Flavor Averaging Group (HFLAV) [7] is  $R_M = (1.30 \pm 2.69) \times 10^{-4}$ .

69.3 Wrong-sign decays to hadronic non- $CP$  eigenstates

Consider the final state  $f = K^+\pi^-$ , i.e.,  $A_f$  and  $\bar{A}_{\bar{f}}$  are doubly Cabibbo-suppressed. Allowing for  $CP$  violation, the ratio of decay amplitudes can be parameterized as

$$\frac{A_f}{\bar{A}_f} = -\sqrt{R_D^+} e^{-i\delta_f}, \quad \frac{\bar{A}_{\bar{f}}}{A_{\bar{f}}} = -\sqrt{R_D^-} e^{-i\delta_f}, \quad (69.13)$$

where  $\delta_f$  is the strong phase difference. The minus sign orig-

<sup>1</sup>There exists a doubly Cabibbo-suppressed amplitude in which the  $c$  and  $\bar{u}$  quarks exchange a  $W$ , and then the resulting  $d$  quark (from  $c$ ) decays semileptonically. We neglect this second-order process.

**Table 69.1:** Results for  $R_M$  in  $D^0$  semileptonic decays. The HFLAV average assumes reported statistical and systematic uncertainties are uncorrelated. When a single uncertainty is listed, that corresponds to statistical and systematic uncertainties combined. The measurements with an asterisk (\*) have been superseded and thus are not included in the HFLAV average.

Year	Experiment	Final state(s)	$R_M (\times 10^{-3})$	90% C.L. ( $\times 10^{-3}$ )
2008	Belle ( $492 \text{ fb}^{-1}$ ) [8]	$K^{(*)+}e^{-}\bar{\nu}_e$	$0.13 \pm 0.22 \pm 0.20$	$< 0.61$
2007	BaBar ( $344 \text{ fb}^{-1}$ ) [9]	$K^{(*)+}e^{-}\bar{\nu}_e$	$0.04^{+0.70}_{-0.60}$	$(-1.3, 1.2)$
2005	CLEO ( $9.0 \text{ fb}^{-1}$ ) [10]	$K^{(*)+}e^{-}\bar{\nu}_e$	$1.6 \pm 2.9 \pm 2.9$	$< 7.8$
1996	E791 ( $2 \times 10^{10}$ evts) [11]	$K^+\ell^{-}\bar{\nu}_\ell$	$1.1^{+3.0}_{-2.7}{}^{+0.0}_{-0.1}$	$< 5.0$
<b>HFLAV Average [7]</b>			<b><math>0.130 \pm 0.269</math></b>	
2005*	Belle ( $253 \text{ fb}^{-1}$ ) [12]	$K^{(*)+}e^{-}\bar{\nu}_e$	$0.02 \pm 0.47 \pm 0.14$	$< 1.0$
2004*	BaBar ( $87 \text{ fb}^{-1}$ ) [13]	$K^{(*)+}e^{-}\bar{\nu}_e$	$2.3 \pm 1.2 \pm 0.4$	$< 4.2$

**Table 69.2:** Results for  $R$ ,  $R_D$ , and  $A_D$  as measured using  $D^0 \rightarrow K^\pm \pi^\mp$  decays. When a single uncertainty is listed, that corresponds to statistical and systematic uncertainties combined. The measurements with an asterisk (\*) have been superseded and thus are not included in the HFLAV average. The measurements with a dagger (†) are not included in the HFLAV average due to poorer precision.

Year	Experiment	$R (\times 10^{-3})$	$R_D (\times 10^{-3})$	$A_D (\%)$
2018	LHCb ( $5.0 \text{ fb}^{-1} D^*$ tag) [14]	—	$3.454 \pm 0.031$	$-0.01 \pm 0.91$
2017	LHCb ( $3.0 \text{ fb}^{-1} B$ tag) [15]	—	$3.48 \pm 0.10$	—
2014	Belle ( $976 \text{ fb}^{-1}$ ) [16]	$3.86 \pm 0.06$	$3.53 \pm 0.13$	—
2013	CDF ( $9.6 \text{ fb}^{-1}$ ) [17]	$4.30 \pm 0.05$	$3.51 \pm 0.35$	—
2007	BaBar ( $384 \text{ fb}^{-1}$ ) [18]	$3.53 \pm 0.08 \pm 0.04$	$3.03 \pm 0.16 \pm 0.10$	$-2.1 \pm 5.2 \pm 1.5$
<b>HFLAV Average [7]</b>			<b><math>3.435 \pm 0.022</math></b>	<b><math>-0.55^{+0.49}_{-0.51}</math></b>
2013b*	LHCb ( $3.0 \text{ fb}^{-1} D^*$ tag) [19]	—	$3.568 \pm 0.066$	$-0.7 \pm 1.9$
2013a*	LHCb ( $1.0 \text{ fb}^{-1}$ ) [20]	$4.25 \pm 0.04$	$3.52 \pm 0.15$	—
2008*	CDF ( $1.5 \text{ fb}^{-1}$ ) [21]	$4.15 \pm 0.10$	$3.04 \pm 0.55$	—
2006*	Belle ( $400 \text{ fb}^{-1}$ ) [22]	$3.77 \pm 0.08 \pm 0.05$	$3.64 \pm 0.18$	$2.3 \pm 4.7$
2005†	FOCUS ( $234$ evts) [23]	$4.29^{+0.63}_{-0.61} \pm 0.27$	$5.17^{+1.47}_{-1.58} \pm 0.76$	$13^{+33}_{-25} \pm 10$
2000†	CLEO ( $9.0 \text{ fb}^{-1}$ ) [24]	$3.32^{+0.63}_{-0.65} \pm 0.40$	$4.8 \pm 1.2 \pm 0.4$	$-1^{+16}_{-17} \pm 1$
1998†	E791 ( $5643$ evts) [25]	$6.8^{+3.4}_{-3.3} \pm 0.7$	—	—

inates from the weak phase difference between the amplitudes, specifically, the relative signs of  $V_{us}$  and  $V_{cd}$ . The parameters  $R_D^+$  and  $R_D^-$  are the ratios of the doubly Cabibbo-suppressed (DCS) decay rate to the Cabibbo-favored (CF) decay rate. From the relevant CKM matrix elements, one estimates  $R_D^+, R_D^- \sim \tan^4 \theta_c$ , where  $\theta_c$  is the Cabibbo angle. With this parameterization, Eq. (69.9) becomes

$$\lambda_f^{-1} = \frac{p}{q} \frac{A_f}{\bar{A}_f} = -\sqrt{R_D^+} \left| \frac{p}{q} \right| e^{-i(\delta_f + \phi)} \quad (69.14)$$

$$\lambda_{\bar{f}} = \frac{q}{p} \frac{\bar{A}_{\bar{f}}}{A_{\bar{f}}} = -\sqrt{R_D^-} \left| \frac{q}{p} \right| e^{-i(\delta_f - \phi)}, \quad (69.15)$$

where  $\phi$  is a weak phase difference. In the Standard Model, the weak phase of  $A_f/\bar{A}_f$  or  $\bar{A}_{\bar{f}}/A_{\bar{f}}$  is, to excellent approximation,  $-1$ , which is already factored out, and thus  $\phi = \text{Arg}(q/p)$ . As  $\phi$  is essentially independent of the final state, it is referred to as “universal.”  $CP$  violation in mixing is characterized by  $|q/p| \neq |p/q| \neq 1$ .  $CP$  violation in the decay amplitudes  $A_f, \bar{A}_f, A_{\bar{f}}, \bar{A}_{\bar{f}}$  is referred to as *direct CP* violation and is parameterized by  $A_D \equiv (R_D^+ - R_D^-)/(R_D^+ + R_D^-)$ . The mean value is denoted  $R_D \equiv (R_D^+ + R_D^-)/2$ .

With these definitions, we expand the decay rates Eqs. (69.7) and (69.8) to second order in the small mixing parameters  $x$  and  $y$  to obtain [26, 27]:

$$r(t) = \left| \bar{A}_f \right|^2 e^{-\Gamma t} \times [R_D(1 + A_D) + \sqrt{R_D(1 + A_D)} \left| \frac{q}{p} \right| y'_+( \Gamma t ) + \left| \frac{q}{p} \right|^2 \frac{(x'_+{}^2 + y'_+{}^2)}{4} (\Gamma t)^2]$$

and

$$\bar{r}(t) = \left| A_{\bar{f}} \right|^2 e^{-\Gamma t} \times [R_D(1 - A_D) + \sqrt{R_D(1 - A_D)} \left| \frac{p}{q} \right| y'_-( \Gamma t ) + \left| \frac{p}{q} \right|^2 \frac{(x'_-{}^2 + y'_-{}^2)}{4} (\Gamma t)^2],$$

where

$$\begin{aligned} x'_\pm &= x \cos(\delta_f \pm \phi) + y \sin(\delta_f \pm \phi) \\ &\equiv x' \cos \phi \pm y' \sin \phi, \end{aligned} \quad (69.16)$$

$$\begin{aligned} y'_\pm &= y \cos(\delta_f \pm \phi) - x \sin(\delta_f \pm \phi) \\ &\equiv y' \cos \phi \mp x' \sin \phi, \end{aligned} \quad (69.17)$$

and

$$x' = x \cos \delta_f + y \sin \delta_f \quad (69.18)$$

$$y' = y \cos \delta_f - x \sin \delta_f. \quad (69.19)$$

In Eqs. (69.16) and (69.16), a fourth term  $R_D(1 \pm A_D)(x'_\pm{}^2 - y'_\pm{}^2)/4 \times (\Gamma t)^2$  has been dropped, as, for the range of decay times measured by experiments, it is negligible relative to the other terms.

The parameters  $(x', y')$  are the mixing parameters  $(x, y)$  rotated by the strong phase  $\delta_f$ . The parameters  $(x'_\pm, y'_\pm)$  are the parameters  $(x', y')$  rotated by the weak phase  $\pm \phi$ . Note that  $x'_+{}^2 + y'_+{}^2 = x'_-{}^2 + y'_-{}^2 = x'^2 + y'^2 = x^2 + y^2$ . Comparing Eqs. (69.16) and (69.16), one sees that  $r(t) \neq \bar{r}(t)$  ( $CP$  is violated) if either  $A_D \neq 0$ ,  $|q/p| \neq 1$ , or  $\phi \neq 0$ . These three inequalities correspond, respectively, to the three types of  $CP$  violation: in the (doubly Cabibbo-suppressed) decay amplitudes; in the mixing; and due to interference between a mixed amplitude and an unmixed decay amplitude. Whereas  $CP$  violation in the decay amplitudes is parameterized by  $A_D$ ,  $CP$  violation in the mixing is parameterized by  $A_M \equiv (|q/p| - |p/q|)/(|q/p| + |p/q|)$ .



**Table 69.3:** Results for  $x'^2$  and  $y'$ , as measured using  $D^0 \rightarrow K^\pm \pi^\mp$  decays. When a single uncertainty is listed, that corresponds to statistical and systematic uncertainties combined. The measurements with an asterisk (\*) have been superseded and thus are not included in the HFLAV global fit. The measurements with a dagger ( $\dagger$ ) are not included in the HFLAV global fit due to poorer precision. All confidence limits and intervals correspond to 95% C.L. The Belle 2006 results restrict  $x'^2$  to the physical region. The BaBar confidence intervals are obtained from the fit, whereas Belle uses a Feldman-Cousins method, and CDF uses a Bayesian method.

Year	Experiment	No $CP$ violation		Allowing for $CP$ violation	
		$x'^2 (\times 10^{-3})$	$y' (\%)$	$x'^2 (\times 10^{-3})$	$y' (\%)$
2018	LHCb ( $5.0 \text{ fb}^{-1}$ $D^*$ tag) [14]	$0.039 \pm 0.027$	$0.528 \pm 0.052$	$\begin{cases} D^0: 0.061 \pm 0.037 \\ \bar{D}^0: 0.016 \pm 0.039 \end{cases}$	$\begin{cases} 0.501 \pm 0.074 \\ 0.554 \pm 0.074 \end{cases}$
2017	LHCb ( $3.0 \text{ fb}^{-1}$ $B$ tag) [15]	$0.028 \pm 0.310$	$0.46 \pm 0.37$	$\begin{cases} D^0: -0.019 \pm 0.447 \\ \bar{D}^0: 0.079 \pm 0.433 \end{cases}$	$\begin{cases} 0.581 \pm 0.526 \\ 0.332 \pm 0.523 \end{cases}$
2014	Belle ( $976 \text{ fb}^{-1}$ ) [16]	$0.09 \pm 0.22$	$0.46 \pm 0.34$	—	—
2013	CDF ( $9.6 \text{ fb}^{-1}$ ) [17]	$0.08 \pm 0.18$	$0.43 \pm 0.43$	—	—
2007	BaBar ( $384 \text{ fb}^{-1}$ ) [18]	$-0.22 \pm 0.37$	$0.97 \pm 0.54$	$\begin{cases} D^0: -0.24 \pm 0.52 \\ \bar{D}^0: -0.20 \pm 0.50 \end{cases}$	$\begin{cases} 0.98 \pm 0.78 \\ 0.96 \pm 0.75 \end{cases}$
2006	Belle ( $400 \text{ fb}^{-1}$ ) [22]	$(0.18^{+0.21}_{-0.23})^*$	$(0.06^{+0.40}_{-0.39})^*$	$< 0.72$	$-2.8 < y' < 2.1$
2013b*	LHCb ( $3.0 \text{ fb}^{-1}$ $D^*$ tag) [19]	$0.055 \pm 0.049$	$0.48 \pm 0.10$	$\begin{cases} D^0: 0.049 \pm 0.070 \\ \bar{D}^0: 0.060 \pm 0.068 \end{cases}$	$\begin{cases} 0.51 \pm 0.14 \\ 0.45 \pm 0.14 \end{cases}$
2013a*	LHCb ( $1.0 \text{ fb}^{-1}$ ) [20]	$-0.09 \pm 0.13$	$0.72 \pm 0.24$	—	—
2008*	CDF ( $1.5 \text{ fb}^{-1}$ ) [21]	$-0.12 \pm 0.35$	$0.85 \pm 0.76$	—	—
2005 $\dagger$	FOCUS (234 evts) [23]	$< 8.3$	$-7.2 < y' < 4.1$	$< 8.0$	$-11.2 < y' < 6.7$
2000 $\dagger$	CLEO ( $9.0 \text{ fb}^{-1}$ ) [24]	$0.00 \pm 0.23$	$-2.3^{+1.3}_{-1.4}$	$0.00 \pm 0.23$	$-2.5^{+1.4}_{-1.6}$
1998 $\dagger$	E791 (5643 evts) [25]	$< 17$	$< 13$	—	—

**Table 69.4:** Results from time-dependent multibody analyses. The errors are statistical, systematic, and, when a third error is listed, due to the decay-model, respectively. The measurement with an asterisk (\*) has been superseded and thus is not included in the HFLAV global fit. The measurement with a dagger ( $\dagger$ ) is not included in the HFLAV global fit due to poorer precision. The 2019 LHCb result utilizes strong-phase measurements from CLEO-c [28] and thus is decay-model independent. This fit determines  $CP$ -violating parameters  $\Delta x$  and  $\Delta y$ ; the translation of these parameters to  $|q/p|$  and  $\phi$  is given in Ref. [29].

No $CP$ Violation				
Year	Experiment	Final State(s)	$x (\times 10^{-3})$	$y (\times 10^{-3})$
2019	LHCb ( $3.0 \text{ fb}^{-1}$ $B$ tag) [30]	$K_S^0 \pi^+ \pi^-$	$2.7 \pm 1.6 \pm 0.4$	$7.4 \pm 3.6 \pm 1.1$
2016	LHCb ( $1.0 \text{ fb}^{-1}$ $D^*$ tag) [31]	$K_S^0 \pi^+ \pi^-$	$-8.6 \pm 5.3 \pm 1.7$	$0.3 \pm 4.6 \pm 1.3$
2016	BaBar ( $468 \text{ fb}^{-1}$ ) [32]	$\pi^+ \pi^- \pi^0$	$15 \pm 12 \pm 6$	$2 \pm 9 \pm 5$
2014	Belle ( $921 \text{ fb}^{-1}$ ) [33]	$K_S^0 \pi^+ \pi^-$	$5.6 \pm 1.9^{+0.3+0.6}_{-0.9-0.9}$	$3.0 \pm 1.5^{+0.4+0.3}_{-0.5-0.6}$
2010	BaBar ( $469 \text{ fb}^{-1}$ ) [34]	$\begin{cases} K_S^0 \pi^+ \pi^- \\ K_S^0 K^+ K^- \end{cases}$	$1.6 \pm 2.3 \pm 1.2 \pm 0.8$	$5.7 \pm 2.0 \pm 1.3 \pm 0.7$
2007*	Belle ( $540 \text{ fb}^{-1}$ ) [35]	$K_S^0 \pi^+ \pi^-$	$8.0 \pm 2.9^{+0.9+1.0}_{-0.7-1.4}$	$3.3 \pm 2.4^{+0.8+0.6}_{-1.2-0.8}$
2005 $\dagger$	CLEO ( $9.0 \text{ fb}^{-1}$ ) [36]	$K_S^0 \pi^+ \pi^-$	$19^{+32}_{-33} \pm 4 \pm 4$	$-14 \pm 24 \pm 8 \pm 4$

With $CP$ Violation				
Year	Experiment	Final State(s)	$ q/p $	$\phi$
2019	LHCb ( $3.0 \text{ fb}^{-1}$ ) [30]	$K_S^0 \pi^+ \pi^-$	$\begin{cases} 1.05^{+0.22}_{-0.17} \\ \Delta x \times 10^{-3} = \\ -0.53 \pm 0.70 \pm 0.22 \end{cases}$	$\begin{cases} (-5.2^{+6.3}_{-9.2})^\circ \\ \Delta y \times 10^{-3} = \\ 0.6 \pm 1.6 \pm 0.3 \end{cases}$
2014	Belle ( $921 \text{ fb}^{-1}$ ) [33]	$K_S^0 \pi^+ \pi^-$	$0.90^{+0.16+0.05+0.06}_{-0.15-0.04-0.05}$	$(-6 \pm 11 \pm 3^{+3}_{-4})^\circ$
2007* $\ddagger$	Belle ( $540 \text{ fb}^{-1}$ ) [35]	$K_S^0 \pi^+ \pi^-$	$0.86^{+0.30+0.06}_{-0.29-0.03} \pm 0.08$	$(-14^{+16+5+2}_{-18-3-4})^\circ$

$\ddagger$ This result allows for all  $CP$  violations and is superseded by Ref. [33], which assumes no direct  $CP$  violation in doubly Cabibbo-suppressed decays.

In the limit of  $CP$  conservation,  $A_D = 0$ ,  $|q/p| = 1$ , and  $\phi = 0$ . In this case

$$r(t) = \bar{r}(t) = \left| A_{\bar{f}} \right|^2 e^{-\Gamma t} \left[ R_D + \sqrt{R_D} y' (\Gamma t) + \frac{x'^2 + y'^2}{4} (\Gamma t)^2 \right], \quad (69.20)$$

and the number of wrong-sign decays divided by the number of right-sign decays is

$$R = \frac{\int_0^\infty r(t) dt}{\int_0^\infty \left| A_{\bar{f}} \right|^2 e^{-\Gamma t} dt} = R_D + \sqrt{R_D} y' + \frac{x'^2 + y'^2}{2}. \quad (69.21)$$

The ratio  $R$  is straightforward to measure, as there is no time-dependence. In Table 69.2 we report measurements of  $R$ ,  $R_D$ , and  $A_D$  in  $D^0 \rightarrow K^+ \pi^-$  decays, and HFLAV world averages [7] obtained from a global fit that allows for both mixing and  $CP$  violation. Typically, the experimental fitted parameters are  $R_D$ ,  $x'^2$ , and  $y'$ ; the results for  $x'^2$  and  $y'$  are summarized in Table 69.3. Allowing for  $CP$  violation, the parameters  $(R_D^+, x'^2, y'_+)$  and  $(R_D^-, x'^2, y'_-)$  [or equivalently  $(R_D, A_D)$  instead of  $(R_D^+, R_D^-)$ ] are obtained by separately fitting  $D^0 \rightarrow K^+ \pi^-$  and  $\bar{D}^0 \rightarrow K^- \pi^+$  event samples.

Extraction of the mixing parameters  $x$  and  $y$  from measurements of  $x'$  and  $y'$  requires knowledge of the strong phase difference  $\delta_{K\pi}$ . This can be determined from the decay rates of  $D_\pm \rightarrow K^+ \pi^-$ , where  $D_+$  ( $D_-$ ) denotes the  $CP$ -even ( $CP$ -odd)

**Table 69.5:** Results for  $y_{CP}$  and  $A_\Gamma$  from  $D^0 \rightarrow K^+K^-$  and  $D^0 \rightarrow \pi^+\pi^-$  decays. When a single uncertainty is listed, that corresponds to statistical and systematic uncertainties combined. The measurements with an asterisk (\*) have been superseded and thus are not included in the HFLAV average. Results from LHCb labeled “ $B$  tag” have the  $D^0$  or  $\bar{D}^0$  flavor identified via  $B^\pm \rightarrow D\mu^\pm\nu_\mu X$  decays.

Year	Experiment	final state(s)	$y_{CP}$ (%)	$A_\Gamma (\times 10^{-3})$
2020	LHCb (8.4 fb $^{-1}$ $B+D^*$ tags) [37]	$K^+K^- + \pi^+\pi^-$	—	$-0.29 \pm 0.20 \pm 0.06$
2020	LHCb (5.4 fb $^{-1}$ $B$ tag) [37]	$K^+K^-$	—	$-0.43 \pm 0.36 \pm 0.05$
2020	LHCb (5.4 fb $^{-1}$ $B$ tag) [37]	$\pi^+\pi^-$	—	$0.22 \pm 0.70 \pm 0.08$
2019	LHCb (3 fb $^{-1}$ $B$ tag) [38]	$K^+K^- + \pi^+\pi^-$	$0.57 \pm 0.13 \pm 0.09$	—
2017	LHCb (3 fb $^{-1}$ $D^*$ tag) [39]	$K^+K^- + \pi^+\pi^-$	—	$-0.13 \pm 0.28 \pm 0.10$
2017	LHCb (3 fb $^{-1}$ $D^*$ tag) [39]	$K^+K^-$	—	$-0.30 \pm 0.32 \pm 0.10$
2017	LHCb (3 fb $^{-1}$ $D^*$ tag) [39]	$\pi^+\pi^-$	—	$0.46 \pm 0.58 \pm 0.12$
2016	Belle (976 fb $^{-1}$ ) [40]	$K^+K^- + \pi^+\pi^-$	$1.11 \pm 0.22 \pm 0.09$	$-0.3 \pm 2.0 \pm 0.7$
2015	LHCb (3 fb $^{-1}$ $B$ tag) [41]	$K^+K^- + \pi^+\pi^-$	—	$-1.25 \pm 0.73$
2015	LHCb (3 fb $^{-1}$ $B$ tag) [41]	$K^+K^-$	—	$-1.34 \pm 0.77^{+0.26}_{-0.34}$
2015	LHCb (3 fb $^{-1}$ $B$ tag) [41]	$\pi^+\pi^-$	—	$-0.92 \pm 1.45^{+0.25}_{-0.33}$
2015	BES III (2.9 fb $^{-1}$ ) [42]	$\left\{ \begin{array}{l} K^+K^-, \pi^+\pi^- \\ K_S^0\pi^0, K_S^0\pi^0\pi^0 \\ K_S^0\eta, K_S^0\omega \end{array} \right.$	$-2.0 \pm 1.3 \pm 0.7$	—
2014	CDF (9.7 fb $^{-1}$ ) [43]	$K^+K^- + \pi^+\pi^-$	—	$-1.2 \pm 1.2$
2014	CDF (9.7 fb $^{-1}$ ) [43]	$K^+K^-$	—	$-1.9 \pm 1.5 \pm 0.4$
2014	CDF (9.7 fb $^{-1}$ ) [43]	$\pi^+\pi^-$	—	$-0.1 \pm 1.8 \pm 0.3$
2012	BaBar (468 fb $^{-1}$ ) [44]	$K^+K^- + \pi^+\pi^-$	$0.72 \pm 0.18 \pm 0.12$	$0.9 \pm 2.6 \pm 0.6$
2009	Belle (673 fb $^{-1}$ ) [45]	$K_S^0 K^+K^-$	$0.11 \pm 0.61 \pm 0.52$	—
2002	CLEO (9.0 fb $^{-1}$ ) [46]	$K^+K^- + \pi^+\pi^-$	$-1.2 \pm 2.5 \pm 1.4$	—
2000	FOCUS ( $1 \times 10^6$ evts) [47]	$K^+K^-$	$3.42 \pm 1.39 \pm 0.74$	—
1999	E791 ( $2 \times 10^{10}$ evts) [48]	$K^+K^-$	$0.73 \pm 2.89 \pm 1.03$	—
<b>HFLAV Average [7]</b>			<b><math>0.715 \pm 0.111</math></b>	<b><math>-0.32 \pm 0.26</math></b>
2013*	LHCb (1.0 fb $^{-1}$ $D^*$ tag) [49]	$K^+K^-$	—	$-0.35 \pm 0.62 \pm 0.12$
2013*	LHCb (1.0 fb $^{-1}$ $D^*$ tag) [49]	$\pi^+\pi^-$	—	$0.33 \pm 1.06 \pm 0.14$
2011* $\ddagger$	LHCb (29 pb $^{-1}$ $D^*$ tag) [50]	$K^+K^-$	$0.55 \pm 0.63 \pm 0.41$	$-5.9 \pm 5.9 \pm 2.1$
2009*	BaBar (384 fb $^{-1}$ ) [51]	$K^+K^-$	$1.16 \pm 0.22 \pm 0.18$	—
2008*	BaBar (384 fb $^{-1}$ ) [52]	$K^+K^- + \pi^+\pi^-$	$1.03 \pm 0.33 \pm 0.19$	$2.6 \pm 3.6 \pm 0.8$
2007*	Belle (540 fb $^{-1}$ ) [53]	$K^+K^- + \pi^+\pi^-$	$1.31 \pm 0.32 \pm 0.25$	$0.1 \pm 3.0 \pm 1.5$
2003*	BaBar (91 fb $^{-1}$ ) [54]	$K^+K^- + \pi^+\pi^-$	$0.8 \pm 0.4^{+0.5}_{-0.4}$	—
2001*	Belle (23.4 fb $^{-1}$ ) [55]	$K^+K^-$	$-0.5 \pm 1.0^{+0.7}_{-0.8}$	—

$\ddagger$ This result for  $y_{CP}$  is not superseded but is not included in the HFLAV average due to having some correlations with, and much poorer precision than, the result of Ref. [38].

eigenstate. Since  $|D_\pm\rangle = (|D^0\rangle \mp |\bar{D}^0\rangle)/\sqrt{2}$ ,

$$\sqrt{2}A(D_\pm \rightarrow K^+\pi^-) = A(D^0 \rightarrow K^+\pi^-) \mp A(\bar{D}^0 \rightarrow K^+\pi^-). \quad (69.22)$$

Squaring this amplitude and using Eq. (69.13) yields the relation

$$\cos\delta_{K\pi} = \frac{|A(D_+ \rightarrow K^+\pi^-)|^2 - |A(D_- \rightarrow K^+\pi^-)|^2}{2|A(D^0 \rightarrow K^+\pi^-)||A(\bar{D}^0 \rightarrow K^+\pi^-)|}. \quad (69.23)$$

Measuring the right-hand side is possible only if one can identify pure  $D_+$ ,  $D_-$ ,  $D^0$ , and  $\bar{D}^0$  initial states. This is accomplished at CLEOc and BESIII utilizing the processes  $e^+e^- \rightarrow \psi(3770) \rightarrow \bar{D}^0 D^0 \rightarrow (f_{CP})(K^+\pi^-)$ , or  $\psi(3770) \rightarrow \bar{D}^0 D^0 \rightarrow (f_{\bar{D}^0})(K^+\pi^-)$ . In the first case, quantum coherence and  $CP$  symmetry insures that the  $K^+\pi^-$  state originates from a neutral  $D$  with  $CP$  opposite that of  $f_{CP}$ . In the second case, at the time when the  $\bar{D}^0$  decays, the opposite side is  $D^0$ . However, it can potentially mix to  $\bar{D}^0$  before decaying to  $K^+\pi^-$ , and this introduces some dependence on the mixing parameters  $x$  and  $y$ . This dependence is seen explicitly in the observable

$$A_{K\pi}^{CP} \equiv \frac{|A(D_- \rightarrow K^-\pi^+)|^2 - |A(D_+ \rightarrow K^-\pi^+)|^2}{|A(D_- \rightarrow K^-\pi^+)|^2 + |A(D_+ \rightarrow K^-\pi^+)|^2}. \quad (69.24)$$

To lowest order in the mixing parameters [56],

$$A_{K\pi}^{CP} = \frac{2\sqrt{R_D} \cos\delta_{K\pi} + y}{1 + R}, \quad (69.25)$$

where  $R$  is defined in Eq. (69.21).

### 69.3.1 Wrong-sign decays to multibody final states

For multibody final states, Eqs. (69.13)-(69.21) apply essentially to each point in phase-space. Although  $x$  and  $y$  do not vary across phase-space, knowledge of the resonant substructure is needed to extrapolate the strong phase difference  $\delta$  from point to point to determine  $x$  and  $y$ . Alternatively, model-independent methods to determine  $x$  and  $y$  require knowledge of the relative phases of  $D^0$  and  $\bar{D}^0$  decay amplitudes across the phase-space distribution [6]. This required phase information can be measured at the charm threshold, where CLEO-c and BESIII took data.

A time-dependent analysis of  $D^0 \rightarrow K^+\pi^-\pi^0$  decays at BaBar [66,67] determined the *relative* strong phase variation across the Dalitz plot and reported  $x'' = (2.61^{+0.57}_{-0.68} \pm 0.39)\%$  and  $y'' = (-0.06^{+0.55}_{-0.64} \pm 0.34)\%$ . These mixing parameters are defined as

$$\begin{aligned} x'' &= x \cos\delta_{K\pi\pi^0} + y \sin\delta_{K\pi\pi^0} \\ y'' &= y \cos\delta_{K\pi\pi^0} - x \sin\delta_{K\pi\pi^0}, \end{aligned} \quad (69.26)$$

in analogy with  $x'$ ,  $y'$ , and  $\delta_{K\pi}$  of Eqs. (69.18) and (69.19). Here,  $\delta_{K\pi\pi^0}$  is the strong phase difference between the amplitudes  $A(D^0 \rightarrow K^+\pi^-\pi^0)$  and  $A(\bar{D}^0 \rightarrow K^+\pi^-\pi^0)$  at a “reference point” of the Dalitz plot. In this case the reference point chosen is  $m_{\pi^-\pi^0} = m_{\rho^-}$ . The strong phase difference  $\delta_{K\pi\pi^0}$  can be determined in a manner similar to that for  $\delta_{K\pi}$ : by using Eq. (69.23) and quantum-correlated measurements of the branching fractions  $B(D_+ \rightarrow K^+\rho^-)$ ,  $B(D_- \rightarrow K^+\rho^-)$ ,  $B(D^0 \rightarrow K^+\rho^-)$ , and  $B(\bar{D}^0 \rightarrow K^+\rho^-)$  in  $e^+e^- \rightarrow \psi(3770)$  events.

For the decay modes  $D^0$  and  $\bar{D}^0 \rightarrow K^+\pi^-\pi^+\pi^-$ , Belle measured  $R = (0.324 \pm 0.008 \pm 0.007)\%$  [68]. Subsequently, a phase-space-integrated analysis from LHCb [69] measured the product of a coherence factor  $R_D^{K^3\pi}$  and the strong-phase-rotated mixing

**Table 69.6:** Results for the difference in time-integrated  $CP$  asymmetries  $\Delta A_{CP}$  between  $D^0 \rightarrow K^+K^-$  and  $D^0 \rightarrow \pi^+\pi^-$  decays. When a single uncertainty is listed, that corresponds to statistical and systematic uncertainties combined. The measurements with an asterisk (\*) have been either superseded or combined with subsequent results and thus are not included in the HFLAV global fit.

Year	Experiment	$\Delta A_{CP} (\times 10^{-3})$
2019	LHCb (8.9 fb $^{-1}$ $B+D^*$ tags) [57]	$-1.54 \pm 0.29$
2013	CDF (9.7 fb $^{-1}$ $D^*$ tag) [58]	$-6.2 \pm 2.1 \pm 1.0$
2008	BaBar (386 fb $^{-1}$ ) [59]	$2.4 \pm 6.2 \pm 2.6$
2008	Belle (540 fb $^{-1}$ ) [60]	$-8.6 \pm 6.0 \pm 0.7$
2016*	LHCb (3.0 fb $^{-1}$ $D^*$ tag) [61]	$-1.0 \pm 0.8 \pm 0.3$
2014*	LHCb (3.0 fb $^{-1}$ $B$ tag) [62]	$1.4 \pm 1.6 \pm 0.8$
2013*	LHCb (1.0 fb $^{-1}$ $B$ tag) [63]	$4.9 \pm 3.0 \pm 1.4$
2012*	LHCb (0.62 fb $^{-1}$ $D^*$ tag) [64]	$-8.2 \pm 2.1 \pm 1.1$
2012 $^\ddagger$	Belle (976 fb $^{-1}$ ) [65]	$-8.7 \pm 4.1 \pm 0.6$

$^\ddagger$ This preliminary result was not published and thus is not included in the HFLAV global fit.

**Table 69.7:** HFLAV global fit results (see text) [7].

Parameter	No $CP$ Violation	No $CP$ Violation in DCS Decays	All $CP$ Violation Allowed	95% C.L. Interval $CPV$ Allowed
$x$ (%)	$0.50^{+0.13}_{-0.14}$	$0.43^{+0.10}_{-0.11}$	$0.39^{+0.11}_{-0.12}$	[0.16, 0.61]
$y$ (%)	$0.62 \pm 0.07$	$0.63 \pm 0.06$	$0.651^{+0.063}_{-0.069}$	[0.51, 0.77]
$\delta_{K\pi}$ ( $^\circ$ )	$8.9^{+8.2}_{-8.9}$	$9.3^{+8.3}_{-9.2}$	$12.1^{+8.6}_{-10.2}$	[-10.4, 28.2]
$R_D$ (%)	$0.344 \pm 0.002$	$0.344 \pm 0.002$	$0.344 \pm 0.002$	[0.339, 0.348]
$A_D$ (%)	—	—	$-0.55^{+0.49}_{-0.51}$	[-1.5, 0.4]
$ q/p $	—	$0.998 \pm 0.008$	$0.969^{+0.050}_{-0.045}$	[0.89, 1.07]
$\phi$ ( $^\circ$ )	—	$0.08 \pm 0.31$	$-3.9^{+4.5}_{-4.6}$	[-13.2, 5.1]
$\delta_{K\pi\pi}$ ( $^\circ$ )	$18.5^{+22.7}_{-23.4}$	$22.1^{+22.6}_{-23.4}$	$25.8^{+23.0}_{-23.8}$	[-21.3, 70.3]
$A_{CP}^{\pi\pi}$ (%)	—	$0.05 \pm 0.16$	$0.06 \pm 0.16$	[-0.25, 0.38]
$A_{CP}^{KK}$ (%)	—	$-0.11 \pm 0.16$	$-0.09 \pm 0.16$	[-0.40, 0.22]
$x_{12}$ (%)	—	$0.43^{+0.10}_{-0.11}$	—	[0.22, 0.63]
$y_{12}$ (%)	—	$0.63 \pm 0.06$	—	[0.50, 0.75]
$\phi_{12}$ ( $^\circ$ )	—	$-0.25^{+0.96}_{-0.99}$	—	[-2.5, 1.8]

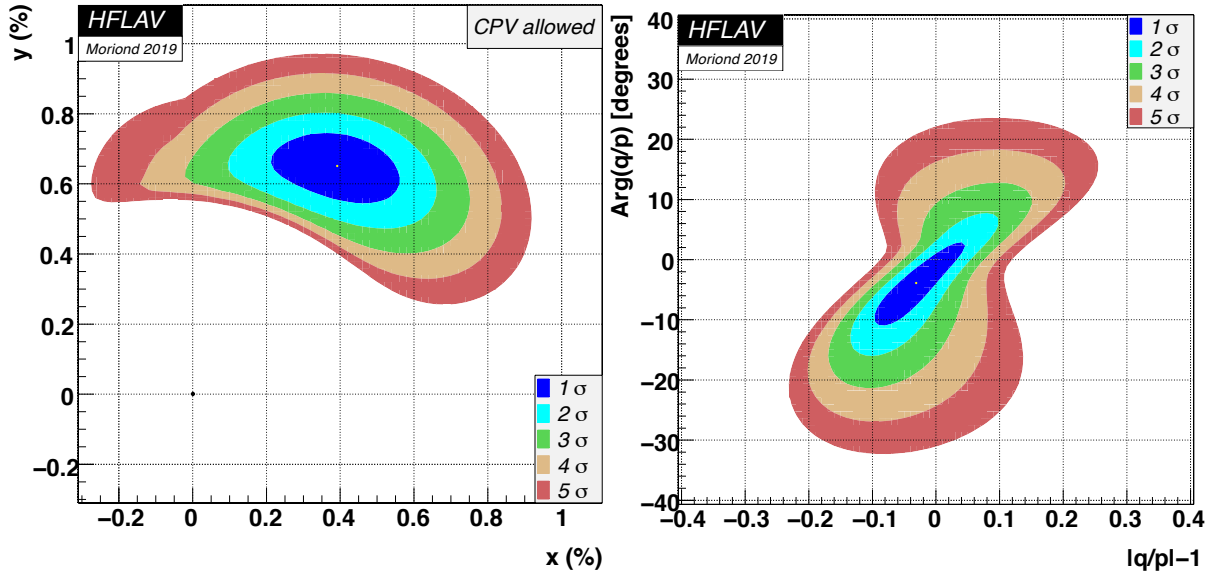


**Figure 69.1:** Two-dimensional  $1\sigma$ - $5\sigma$  contours for  $(x, y)$  (left) and for  $(|q/p|, \text{Arg}(q/p))$  (right) as obtained by HFLAV [7], from measurements of  $D^0 \rightarrow K^{(*)}\ell\nu$ ,  $h^+h^-$ ,  $K^+\pi^-$ ,  $K^+\pi^-\pi^0$ ,  $K^+\pi^-\pi^+\pi^-$ ,  $K_S^0\pi^+\pi^-$ ,  $K_S^0K^+K^-$ , and  $\pi^+\pi^-\pi^0$  decays, and double-tagged branching fractions measured at the  $\psi(3770)$  resonance.

parameter  $y''_{K3\pi}$ . This measurement resulted in an observation of charm mixing with  $8.2\sigma$  significance.

Both the sign and magnitude of  $x$  and  $y$  without strong phases entering or sign ambiguity can be measured using the time-dependent resonant substructure of multibody  $D^0$  decays [35, 36]. In  $D^0 \rightarrow K_S^0\pi^+\pi^-$ , the DCS and CF decay amplitudes populate the same Dalitz plot, which allows for di-

rect measurement of the relative strong phases. Belle [33, 35], BaBar [34], and CLEO [70] have measured the relative strong phase between  $D^0 \rightarrow K^*(892)^-\pi^+$  and  $D^0 \rightarrow K^*(892)^+\pi^-$  to be  $(173.9 \pm 0.7 \text{ (stat. only)})^\circ$ ,  $(177.6 \pm 1.1 \text{ (stat. only)})^\circ$ , and  $(189 \pm 10 \pm 3^{+15}_{-5})^\circ$ , respectively. These results are close to the  $180^\circ$  expected from Cabibbo factors and a small strong phase. Two LHCb measurements [30, 31] of  $x, y$  are decay-model inde-

pendent, i.e., the model of resonances in the intermediate state is replaced by strong-phase measurements from CLEO-c [28]. Table 69.4 summarizes mixing results from time-dependent multi-body analyses. World average values for the measurements listed are given later, as a result of the HFLAV global fit.

In addition, Belle [33,35] has measured the relative strong phase (statistical errors only) and the ratio  $R$  (central values only) of the DCS fit fraction relative to the CF fit fraction for five excited  $K$  states:  $K^*(892)^+\pi^-$ ,  $K_0^*(1430)^+\pi^-$ ,  $K_2^*(1430)^+\pi^-$ ,  $K^*(1410)^+\pi^-$ , and  $K^*(1680)^+\pi^-$ . Similarly, BaBar [34, 71, 72] has reported central values of  $R$  for  $K^*(892)^+\pi^-$ ,  $K_0^*(1430)^+\pi^-$ , and  $K_2^*(1430)^+\pi^-$ . The systematic uncertainties on  $R$  are not evaluated. Large differences in  $R$  are observed among these final states, which indicates interesting hadronic effects.

### 69.4 Decays to $CP$ Eigenstates

When the final state  $f$  is a  $CP$  eigenstate, there is no distinction between  $f$  and  $\bar{f}$ . Thus  $A_f = A_{\bar{f}}$  and  $\bar{A}_{\bar{f}} = \bar{A}_f$ . We denote final states with  $CP$  eigenvalues  $\pm 1$  by  $f_{\pm}$  and write  $\lambda_{\pm}$  for  $\lambda_{f_{\pm}}$ .

The quantity  $y$  may be measured by comparing the rate for  $D^0$  decays to  $CP$  eigenstates such as  $K^+K^-$  with the rate to non- $CP$  states such as  $K^-\pi^+$  [27]. If decays to  $K^+K^-$  have a shorter effective lifetime than those to  $K^-\pi^+$ , then  $\Gamma_+ > \Gamma_-$ , or, since  $CP$  violation is very small,  $\Gamma_2 > \Gamma_1$  and  $y$  is positive.

In the limit of small mixing ( $x, y \ll 1$ ) and the absence of direct  $CP$  violation in DCS decays ( $A_D = 0$ ), one can write

$$\lambda_{\pm} = \left| \frac{q}{p} \right| e^{\pm i\phi}. \quad (69.27)$$

In this scenario, to a good approximation, the decay rates for states that are initially  $D^0$  and  $\bar{D}^0$  to a  $CP$  eigenstate have exponential time dependence:

$$r_{\pm}(t) \propto \exp(-\Gamma_{\pm} t) \quad (69.28)$$

$$\bar{r}_{\pm}(t) \propto \exp(-\bar{\Gamma}_{\pm} t). \quad (69.29)$$

The effective decay widths are given by

$$\Gamma_{\pm} = 1 \pm \left| \frac{q}{p} \right| (y \cos \phi - x \sin \phi), \quad (69.30)$$

$$\bar{\Gamma}_{\pm} = 1 \pm \left| \frac{p}{q} \right| (y \cos \phi + x \sin \phi). \quad (69.31)$$

Thus the effective decay rate to a  $CP$  eigenstate combining both  $D^0$  and  $\bar{D}^0$  decays is

$$r_{\pm}(t) + \bar{r}_{\pm}(t) \propto e^{-(1 \pm y_{CP})t}, \quad (69.32)$$

where

$$y_{CP} = \frac{1}{2} \left( \left| \frac{q}{p} \right| + \left| \frac{p}{q} \right| \right) y \cos \phi - \frac{1}{2} \left( \left| \frac{q}{p} \right| - \left| \frac{p}{q} \right| \right) x \sin \phi \quad (69.33)$$

$$\approx y \cos \phi - A_M x \sin \phi. \quad (69.34)$$

If  $CP$  is conserved,  $y_{CP} = y$ . Almost all measurements of  $y_{CP}$  are relative to the  $D^0 \rightarrow K^-\pi^+$  decay rate. Belle [45] has reported  $y_{CP}$  also for the final state  $K_S^0 K^+K^-$ , which is dominated by the  $CP$ -odd final state  $K_S^0 \phi$ . Table 69.5 summarizes the current status of measurements.

In addition to  $y_{CP}$ , Belle [40], BaBar [44], LHCb [50], and CDF [43] have reported measurements of the decay-rate asymmetry for  $CP$ -even final states

$$A_{\Gamma} \equiv \frac{\Gamma_+ - \bar{\Gamma}_+}{\Gamma_+ + \bar{\Gamma}_+} = \frac{(1/\tau_+) - (1/\bar{\tau}_+)}{(1/\tau_+) + (1/\bar{\tau}_+)} = \frac{\bar{\tau}_+ - \tau_+}{\bar{\tau}_+ + \tau_+} \quad (69.35)$$

$$\approx \frac{1}{2} \left( \left| \frac{q}{p} \right| - \left| \frac{p}{q} \right| \right) y \cos \phi - \frac{1}{2} \left( \left| \frac{q}{p} \right| + \left| \frac{p}{q} \right| \right) x \sin \phi \quad (69.36)$$

$$\approx A_M y \cos \phi - x \sin \phi. \quad (69.37)$$

If  $CP$  is conserved,  $A_{\Gamma} = 0$ .

The asymmetry  $A_{\Gamma}$  relates to the full decay width. An asymmetry in partial widths is referred to as  $A_{CP}$  and is final-state dependent:

$$A_{CP} \equiv \frac{\Gamma(D^0 \rightarrow f) - \Gamma(\bar{D}^0 \rightarrow \bar{f})}{\Gamma(D^0 \rightarrow f) + \Gamma(\bar{D}^0 \rightarrow \bar{f})}. \quad (69.38)$$

Unlike  $A_{\Gamma}$ ,  $A_{CP}$  is a time-integrated quantity, i.e., it does not require measuring decay times. For neutral  $D$  decays,  $A_{CP}$  receives contributions from both direct (in the decay amplitudes) and indirect (due to mixing) processes:  $A_{CP}(D^0 \rightarrow f) = A_{CP}^f + A_{CP}^{\text{indirect}}$ . The latter indirect contribution depends on the mixing parameters  $x$  and  $y$ :

$$\begin{aligned} A_{CP}^{\text{indirect}} &= \frac{1}{2} \left( \left| \frac{q}{p} \right| + \left| \frac{p}{q} \right| \right) x \sin \phi - \frac{1}{2} \left( \left| \frac{q}{p} \right| - \left| \frac{p}{q} \right| \right) y \cos \phi \\ &= -A_{\Gamma}. \end{aligned} \quad (69.39)$$

Numerous measurements of  $A_{CP}$  for decays to  $CP$  eigenstates are listed in this *Review* [73]. Table 69.6 summarizes the current status of measurements of the difference in  $A_{CP}$  for  $D^0 \rightarrow K^+K^-$  and  $D^0 \rightarrow \pi^+\pi^-$  decays:  $\Delta A_{CP} \equiv A_{CP}(K^+K^-) - A_{CP}(\pi^+\pi^-)$ . Measuring the difference is advantageous, as numerous systematic uncertainties cancel. As  $A_{CP}^{\text{indirect}}$  is universal (independent of final state), it subtracts out of the difference  $\Delta A_{CP}$ . However, at hadron experiments such as LHCb, there are differences in efficiencies between  $K^+K^-$  and  $\pi^+\pi^-$  final states, and a small contribution to  $\Delta A_{CP}$  remains. The most recent result from LHCb [57], based on  $8.9 \text{ fb}^{-1}$  of data, differs from zero with a statistical significance of  $5.3\sigma$ . Thus, this measurement constitutes the first observation of  $CP$  violation in charm meson or charm baryon decays. These  $CP$  asymmetries are included in HFLAV's global fit for charm mixing parameters discussed below; the fit shows that the  $CP$  violation observed is due to the direct contributions  $A_{CP}^{KK}$  and  $A_{CP}^{\pi\pi}$ .

### 69.5 Quantum-correlated $D^0\bar{D}^0$ Analyses

Measurements of  $R_D$ ,  $\cos \delta_{K\pi}$ ,  $\sin \delta_{K\pi}$ ,  $x$ , and  $y$  can be obtained from a combined fit to time-integrated yields of single-tagged (ST) and double-tagged (DT)  $D^0\bar{D}^0$  events produced at the  $\psi(3770)$  resonance [74,75]. Single-tagged events are those in which either the  $D^0$  or  $\bar{D}^0$  decay is reconstructed (identified), and the other neutral  $D$  decays generically. Double-tagged events are those in which both  $D^0$  and  $\bar{D}^0$  decays are identified. Due to quantum correlations, the decay of a  $D^0, \bar{D}^0, D_+$ , or  $D_-$  projects the other neutral  $D$  into a state  $\bar{D}^0, D^0, D_-$ , and  $D_+$ , respectively. The  $CP$ -specific  $D_-$  and  $D_+$  decays (or, neglecting  $CP$  violation,  $D_1$  and  $D_2$  decays) include interference between  $D^0$  and  $\bar{D}^0$  amplitudes, and this provides sensitivity to  $R_D$  and  $\cos \delta_{K\pi}$ . The flavor-specific  $D^0$  and  $\bar{D}^0$  decays include interference between  $D_1$  and  $D_2$  amplitudes, and this provides sensitivity to  $x$  and  $y$ . For details of this method, see Refs. [1–5].

BESIII has reported results using  $2.92 \text{ fb}^{-1}$  of  $e^+e^- \rightarrow \psi(3770)$  data, where the quantum-correlated  $D^0\bar{D}^0$  pairs are produced in a  $C = -1$  state. They measure  $y_{CP} = (-2.0 \pm 1.3 \pm 0.7)\%$  [42] from DT yields using a  $CP$  eigenstate tag for one  $D$  and a semileptonic tag for the other; and they measure  $A_{K\pi}^{CP} = (12.7 \pm 1.3 \pm 0.7)\%$  [56] from DT yields using a  $CP$  tag for one  $D$  and a  $K^{\pm}\pi^{\mp}$  tag for the other. For  $y_{CP}$ , the  $CP$  eigenstates used are  $K^-K^+$  ( $f_+$ ),  $\pi^+\pi^-$  ( $f_+$ ),  $K_S^0\pi^0\pi^0$  ( $f_+$ ),  $K_S^0\pi^0$  ( $f_-$ ),  $K_S^0\eta$  ( $f_-$ ), and  $K_S^0\omega$  ( $f_-$ ). For  $A_{K\pi}^{CP}$ , additional  $CP$  eigenstates included are  $\pi^0\pi^0$  ( $f_+$ ) and  $\rho^0\pi^0$  ( $f_+$ ). Using external inputs for  $R_D$  and  $y$  from HFLAV [76], and  $R$  from the PDG [77] (see Eq. (69.25)), BESIII obtains  $\cos \delta_{K\pi} = 1.02 \pm 0.11 \pm 0.06 \pm 0.01$  [56], where the third uncertainty is due to the external inputs.

CLEO-c has reported results using  $0.82 \text{ fb}^{-1}$  of  $e^+e^- \rightarrow \psi(3770)$  data [78–80]. The values of  $y$ ,  $R_M$ ,  $\cos \delta_{K\pi}$ , and  $\sin \delta_{K\pi}$  are determined from a combined fit to the ST (hadronic only) and DT yields. The DT yields include events in which one  $D$  is reconstructed in a hadronic mode and the other  $D$  is partially reconstructed in either  $D \rightarrow K^{\mp}e^{\pm}\nu$  or  $D \rightarrow K^{\mp}\mu^{\pm}\nu$ .

The CLEO-c analysis obtains  $\cos \delta_{K\pi} = 0.81^{+0.22+0.07}_{-0.18-0.05}$  and  $\sin \delta_{K\pi} = -0.01 \pm 0.41 \pm 0.04$ . These fits allow  $\cos \delta_{K\pi}$ ,  $\sin \delta_{K\pi}$ , and  $x^2$  to be unphysical. Constraining  $\cos \delta_{K\pi}$  and  $\sin \delta_{K\pi}$  to the physical range  $[-1, +1]$  (i.e., interpreting  $\delta_{K\pi}$  as an angle) and also using external inputs for  $x$ ,  $y$  and  $y_{CP}$  from HFLAV [81], CLEO-c obtains  $\delta_{K\pi} = (18^{+11}_{-17})^\circ$  [80].

## 69.6 Summary of Experimental Results

Several recent results indicate that charm mixing is at the upper end of the range of Standard Model predictions. For  $D^0 \rightarrow K^+\pi^-$ , LHCb [19, 20], CDF [17], and Belle [16] each exclude the no-mixing hypothesis by more than 5 standard deviations. For  $y_{CP}$  in  $D^0 \rightarrow K^+K^-$  and  $\pi^+\pi^-$ , BaBar [44], Belle [40], and LHCb [38] measure  $3.3\sigma$ ,  $4.7\sigma$ , and  $3.6\sigma$  effects, respectively. The most sensitive measurements of  $x$  and  $y$  are from  $D^0 \rightarrow K_S^0\pi^+\pi^-$  decays at Belle [33] and LHCb [30]. In a similar analysis using  $D^0 \rightarrow K_S^0\pi^+\pi^-$  and  $D^0 \rightarrow K_S^0K^+K^-$  decays, BaBar [34] finds the no-mixing solution excluded at  $1.9\sigma$ . LHCb [69] has reported the observation of charm mixing in  $D^0 \rightarrow K^+\pi^-\pi^+\pi^-$  with  $8.2\sigma$  significance. However, the strong phase difference for this decay is not known, and thus  $x$  and  $y$  cannot be extracted. The current situation would benefit from better knowledge of the strong phase difference  $\delta_{K\pi}$  than provided by the current CLEO-c [80] and BESIII [56] results, and knowledge of the strong phase difference  $\delta_{K\pi\pi\pi}$ . Such knowledge would allow one to extract  $x$  and  $y$  from  $D^0 \rightarrow K^+\pi^-$  measurements of  $(x', y')$ , and from  $D^0 \rightarrow K^+\pi^-\pi^+\pi^-$  measurements of  $(x'', y'')$ . In fact, the most precise knowledge of  $\delta_{K\pi}$  comes from combining measurements of  $y'$  (Table 69.3) with measurements of  $y$  (Table 69.4) and  $y_{CP}$  (Table 69.5), as done in the HFLAV global fit described below.

The experimental data consistently indicate that the  $D^0$  and  $\bar{D}^0$  mesons mix. The mixing is presumably dominated by long-range processes. Under the assumption that the observed mixing is due entirely to non-Standard Model processes, significant constraints on New Physics models can be obtained [82]. A serious limitation to the interpretation of charm mixing in terms of New Physics is the theoretical uncertainty on the Standard Model predictions [83, 84].

## 69.7 HFLAV Global Fit for Charm Mixing Parameters

The Heavy Flavor Averaging Group (HFLAV) performs a global fit to all relevant mixing measurements to obtain world average values for 10 fitted parameters:  $x$ ,  $y$ ,  $\delta_{K\pi}$ ,  $\delta_{K\pi\pi^0}$ ,  $R_D(K^+\pi^-)$ ,  $A_D(K^+\pi^-)$ ,  $|q/p|$ ,  $\text{Arg}(q/p) \equiv \phi$ , and the direct  $CP$ -violating asymmetries  $A_{CP}^{K^+K^-}$  and  $A_{CP}^{\pi^+\pi^-}$ . Correlations among observables are taken into account by using the error matrices provided by the experiments. Measurements of  $D^0 \rightarrow K^{(*)+\ell^-\bar{\nu}}$ ,  $K^+K^-$ ,  $\pi^+\pi^-$ ,  $K^+\pi^-$ ,  $K^+\pi^-\pi^0$ ,  $K^+\pi^-\pi^+\pi^-$ ,  $K_S^0\pi^+\pi^-$ ,  $K_S^0K^+K^-$ , and  $\pi^+\pi^-\pi^0$  decays are used, as well as CLEO-c and BESIII results for double-tagged branching fractions measured at the  $\psi(3770)$ . There are three observables input to the fit that are themselves world average values calculated by HFLAV:  $R_M$  from  $D^0 \rightarrow K^{(*)+\ell^-\bar{\nu}}$  decays (Table 69.1), and  $y_{CP}$  and  $A_\Gamma$  from  $D^0 \rightarrow f_{CP}$  decays (Table 69.5). A measurement by LHCb of  $R_M$  using  $D^0 \rightarrow K^+\pi^-\pi^+\pi^-$  decays is input separately. Details of the fitting procedure are given in Ref. [7].

The results of the fit as of March 2019 are listed in Table 69.7. Three separate fits are performed: (a) assuming no  $CP$  violation; (b) assuming no  $CP$  violation in doubly Cabibbo-suppressed decays; and (c) allowing all  $CP$  violation. The second fit (b) corresponds to the theory expectation [85, 86]; in this case four fitted parameters are reduced to three using the relationship  $\tan \phi = (x/y) \cdot (1 - |q/p|^2)/(1 + |q/p|^2)$  [85–87]. Alternatively, one can fit for the three parameters  $x_{12} \equiv 2|M_{12}|/\Gamma$ ,  $y_{12} \equiv |F_{12}|/\Gamma$ , and  $\phi_{12} \equiv \text{Arg}(M_{12}/F_{12})$ , from which  $x$ ,  $y$ ,  $|q/p|$ , and  $\phi$  can be derived.

Confidence contours in the two dimensions  $(x, y)$  and  $(|q/p|, \phi)$  from the fit are plotted in Fig. 69.1. These contours are obtained by letting, for any point in the two-dimensional plane, all other fit parameters take their preferred values. The  $1\sigma$ – $5\sigma$  boundaries drawn are the loci of points in which the  $\chi^2$  has risen above the minimum by 2.30, 6.18, 11.83, 19.33, and 28.67 units. The fit

excludes the no-mixing point  $x=y=0$  at more than  $11.5\sigma$ , when  $CP$  violation is allowed. The fit is consistent with no  $CP$  violation ( $|q/p|=1$ ,  $\phi=0$ ) at the 63% confidence level.

One-dimensional likelihood functions for parameters are obtained by allowing, for any value of the parameter, all other fit parameters to take their preferred values. The resulting likelihood functions give central values, 68.3% C.L. intervals, and 95% C.L. intervals as listed in Table 69.7. The parameter ranges  $x \leq 0$  and  $y \leq 0$  are excluded at  $3.1\sigma$  and  $>11.4\sigma$  significance, respectively. The  $\chi^2$  of the fit is 60.7 for  $49 - 10 = 39$  degrees of freedom, indicating some disagreement among the measurements.

From the results of the HFLAV averaging, the following can be concluded: (1) Since  $CP$  violation is small and  $y_{CP}$  is positive, the  $CP$ -even state is shorter-lived, as in the  $K^0\bar{K}^0$  system. (2) However, since  $x$  appears to be positive, the  $CP$ -even state is heavier, unlike in the  $K^0\bar{K}^0$  system. (3) The strong phase difference  $\delta_{K\pi}$  is consistent with the  $SU(3)$  expectation of zero, and large values are unlikely (its magnitude is  $< 30^\circ$  at 95% C.L.) (4) While direct  $CP$  violation has now been observed in  $D$  decays, there is no evidence for indirect  $CP$  violation, i.e.,  $|q/p| \neq 1$  or  $\phi \neq 0$ . Observing such  $CP$  violation at the current level of sensitivity would indicate new physics.

## 69.8 Future Data

Current results are based primarily upon CLEO-c ( $0.82 \text{ fb}^{-1}$  of  $e^+e^- \rightarrow \psi(3770)$  data), Belle and BaBar ( $\sim 1.4 \text{ ab}^{-1}$  of  $e^+e^- \rightarrow Y(4S)$  data), and LHCb Runs 1 and 2 ( $3.0 \text{ fb}^{-1} + 5.9 \text{ fb}^{-1}$  of  $pp$  collision data at  $\sqrt{s} = 7, 8, 13 \text{ TeV}$ ).

BESIII has accumulated  $2.9 \text{ fb}^{-1}$  of  $e^+e^- \rightarrow \psi(3770)$  data and plans to collect up to  $20 \text{ fb}^{-1}$  in the next few years. These data should provide strong phase measurements that enable improved model-independent determinations of mixing parameters from Belle II and LHCb. In 2019, Belle II began accumulating  $50 \text{ ab}^{-1}$  of  $e^+e^- \rightarrow Y(4S)$  data [88], which is expected to take approximately ten years to collect. At LHCb, Run 2 was completed in 2018, Run 3 is planned for 2021–23, and Run 4 is planned for 2026–29 [89]. The goal for Runs 3+4 is to accumulate an additional  $50 \text{ fb}^{-1}$  of  $pp$  data at  $\sqrt{s} = 14 \text{ TeV}$ . These data, along with the large  $e^+e^-$  dataset from Belle II, should provide significantly greater sensitivity to  $D^0$ - $\bar{D}^0$  mixing and direct and indirect  $CP$  violation in  $D^0$  decays.

## References

- [1] D. M. Asner and W. M. Sun, Phys. Rev. **D73**, 034024 (2006), [Erratum: Phys. Rev. **D77**, 019901 (2008)], [hep-ph/0507238].
- [2] D. Atwood and A. A. Petrov, Phys. Rev. **D71**, 054032 (2005), [hep-ph/0207165].
- [3] M. Gronau, Y. Grossman and J. L. Rosner, Phys. Lett. **B508**, 37 (2001), [hep-ph/0103110].
- [4] Z.-z. Xing, Phys. Rev. **D55**, 196 (1997), [hep-ph/9606422].
- [5] M. Goldhaber and J. L. Rosner, Phys. Rev. **D15**, 1254 (1977).
- [6] See “Review of Multibody Charm Analyses” in this *Review*.
- [7] Y. Amhis *et al.* (Heavy Flavor Averaging Group) (2019), [arXiv:1909.12524].
- [8] U. Bitenc *et al.* (Belle), Phys. Rev. **D77**, 112003 (2008), [arXiv:0802.2952].
- [9] B. Aubert *et al.* (BaBar), Phys. Rev. **D76**, 014018 (2007), [arXiv:0705.0704].
- [10] C. Cawlfeld *et al.* (CLEO), Phys. Rev. **D71**, 077101 (2005), [hep-ex/0502012].
- [11] E. M. Aitala *et al.* (E791), Phys. Rev. Lett. **77**, 2384 (1996), [hep-ex/9606016].
- [12] U. Bitenc *et al.* (Belle), Phys. Rev. **D72**, 071101 (2005), [hep-ex/0507020].
- [13] B. Aubert *et al.* (BaBar), Phys. Rev. **D70**, 091102 (2004), [hep-ex/0408066].
- [14] R. Aaij *et al.* (LHCb), Phys. Rev. **D97**, 3, 031101 (2018), [arXiv:1712.03220].

- [15] R. Aaij *et al.* (LHCb), Phys. Rev. **D95**, 5, 052004 (2017), [Erratum: Phys. Rev. **D96**, 099907 (2017)], [arXiv:1611.06143].
- [16] B. R. Ko *et al.* (Belle), Phys. Rev. Lett. **112**, 11, 111801 (2014), [Addendum: Phys. Rev. Lett. **112**, 139903 (2014)], [arXiv:1401.3402].
- [17] T. A. Aaltonen *et al.* (CDF), Phys. Rev. Lett. **111**, 23, 231802 (2013), [arXiv:1309.4078].
- [18] B. Aubert *et al.* (BaBar), Phys. Rev. Lett. **98**, 211802 (2007), [hep-ex/0703020].
- [19] R. Aaij *et al.* (LHCb), Phys. Rev. Lett. **111**, 25, 251801 (2013), [arXiv:1309.6534].
- [20] R. Aaij *et al.* (LHCb), Phys. Rev. Lett. **110**, 10, 101802 (2013), [arXiv:1211.1230].
- [21] T. Aaltonen *et al.* (CDF), Phys. Rev. Lett. **100**, 121802 (2008), [arXiv:0712.1567].
- [22] L. M. Zhang *et al.* (Belle), Phys. Rev. Lett. **96**, 151801 (2006), [hep-ex/0601029].
- [23] J. M. Link *et al.* (FOCUS), Phys. Lett. **B618**, 23 (2005), [hep-ex/0412034].
- [24] R. Godang *et al.* (CLEO), Phys. Rev. Lett. **84**, 5038 (2000), [hep-ex/0001060].
- [25] E. M. Aitala *et al.* (E791), Phys. Rev. **D57**, 13 (1998), [hep-ex/9608018].
- [26] Y. Nir, Lectures given at 27th SLAC Summer Institute on Particle Physics: “ $CP$  Violation in and Beyond the Standard Model (SSI 99),” Stanford, California, 7-16 July 1999. Published in Trieste 1999, *Particle Physics*, pp. 165-243.
- [27] S. Bergmann *et al.*, Phys. Lett. **B486**, 418 (2000), [hep-ph/0005181].
- [28] J. Libby *et al.* (CLEO), Phys. Rev. **D82**, 112006 (2010), [arXiv:1010.2817].
- [29] A. Di Canto *et al.*, Phys. Rev. **D99**, 1, 012007 (2019), [arXiv:1811.01032].
- [30] R. Aaij *et al.* (LHCb), Phys. Rev. Lett. **122**, 23, 231802 (2019), [arXiv:1903.03074].
- [31] R. Aaij *et al.* (LHCb), JHEP **04**, 033 (2016), [arXiv:1510.01664].
- [32] J. P. Lees *et al.* (BaBar), Phys. Rev. **D93**, 11, 112014 (2016), [arXiv:1604.00857].
- [33] T. Peng *et al.* (Belle), Phys. Rev. **D89**, 9, 091103 (2014), [arXiv:1404.2412].
- [34] P. del Amo Sanchez *et al.* (BaBar), Phys. Rev. Lett. **105**, 081803 (2010), [arXiv:1004.5053].
- [35] K. Abe *et al.* (Belle), Phys. Rev. Lett. **99**, 131803 (2007), [arXiv:0704.1000].
- [36] D. M. Asner *et al.* (CLEO), Phys. Rev. **D72**, 012001 (2005), [hep-ex/0503045].
- [37] R. Aaij *et al.* (LHCb), Phys. Rev. **D101**, 1, 012005 (2020), [arXiv:1911.01114].
- [38] R. Aaij *et al.* (LHCb), Phys. Rev. Lett. **122**, 1, 011802 (2019), [arXiv:1810.06874].
- [39] R. Aaij *et al.* (LHCb), Phys. Rev. Lett. **118**, 26, 261803 (2017), [arXiv:1702.06490].
- [40] M. Starič *et al.* (Belle), Phys. Lett. **B753**, 412 (2016), [arXiv:1509.08266].
- [41] R. Aaij *et al.* (LHCb), JHEP **04**, 043 (2015), [arXiv:1501.06777].
- [42] M. Ablikim *et al.* (BESIII), Phys. Lett. **B744**, 339 (2015), [arXiv:1501.01378].
- [43] T. A. Aaltonen *et al.* (CDF), Phys. Rev. **D90**, 11, 111103 (2014), [arXiv:1410.5435].
- [44] J. P. Lees *et al.* (BaBar), Phys. Rev. **D87**, 1, 012004 (2013), [arXiv:1209.3896].
- [45] A. Zupanc *et al.* (Belle), Phys. Rev. **D80**, 052006 (2009), [arXiv:0905.4185].
- [46] S. E. Csorna *et al.* (CLEO), Phys. Rev. **D65**, 092001 (2002), [hep-ex/0111024].
- [47] J. M. Link *et al.* (FOCUS), Phys. Lett. **B485**, 62 (2000), [hep-ex/0004034].
- [48] E. M. Aitala *et al.* (E791), Phys. Rev. Lett. **83**, 32 (1999), [hep-ex/9903012].
- [49] R. Aaij *et al.* (LHCb), Phys. Rev. Lett. **112**, 4, 041801 (2014), [arXiv:1310.7201].
- [50] R. Aaij *et al.* (LHCb), JHEP **04**, 129 (2012), [arXiv:1112.4698].
- [51] B. Aubert *et al.* (BaBar), Phys. Rev. **D80**, 071103 (2009), [arXiv:0908.0761].
- [52] B. Aubert *et al.* (BaBar), Phys. Rev. **D78**, 011105 (2008), [arXiv:0712.2249].
- [53] M. Staric *et al.* (BELLE), Phys. Rev. Lett. **98**, 211803 (2007), [65(2007)], [hep-ex/0703036].
- [54] B. Aubert *et al.* (BaBar), Phys. Rev. Lett. **91**, 121801 (2003), [hep-ex/0306003].
- [55] K. Abe *et al.* (Belle), Phys. Rev. Lett. **88**, 162001 (2002), [hep-ex/0111026].
- [56] M. Ablikim *et al.* (BESIII), Phys. Lett. **B734**, 227 (2014), [arXiv:1404.4691].
- [57] R. Aaij *et al.* (LHCb), Phys. Rev. Lett. **122**, 21, 211803 (2019), [arXiv:1903.08726].
- [58] T. Aaltonen *et al.* (CDF), Phys. Rev. Lett. **109**, 111801 (2012), [arXiv:1207.2158].
- [59] B. Aubert *et al.* (BaBar), Phys. Rev. Lett. **100**, 061803 (2008), [arXiv:0709.2715].
- [60] M. Staric *et al.* (Belle), Phys. Lett. **B670**, 190 (2008), [arXiv:0807.0148].
- [61] R. Aaij *et al.* (LHCb), Phys. Rev. Lett. **116**, 19, 191601 (2016), [arXiv:1602.03160].
- [62] R. Aaij *et al.* (LHCb), JHEP **07**, 041 (2014), [arXiv:1405.2797].
- [63] R. Aaij *et al.* (LHCb), Phys. Lett. **B723**, 33 (2013), [arXiv:1303.2614].
- [64] R. Aaij *et al.* (LHCb), Phys. Rev. Lett. **108**, 111602 (2012), [arXiv:1112.0938].
- [65] B. R. Ko (Belle), in “7th International Workshop on the CKM Unitarity Triangle (CKM 2012) Cincinnati, Ohio, USA, September 28-October 2, 2012,” (2012), [arXiv:1212.5320].
- [66] B. Aubert *et al.* (BaBar), Phys. Rev. Lett. **97**, 221803 (2006), [hep-ex/0608006].
- [67] B. Aubert *et al.* (BaBar), Phys. Rev. Lett. **103**, 211801 (2009), [arXiv:0807.4544].
- [68] E. White *et al.* (Belle), Phys. Rev. **D88**, 5, 051101 (2013), [arXiv:1307.5935].
- [69] R. Aaij *et al.* (LHCb), Phys. Rev. Lett. **116**, 24, 241801 (2016), [arXiv:1602.07224].
- [70] H. Muramatsu *et al.* (CLEO), Phys. Rev. Lett. **89**, 251802 (2002), [Erratum: Phys. Rev. Lett. **90**, 059901 (2003)], [hep-ex/0207067].
- [71] B. Aubert *et al.* (BaBar), Phys. Rev. Lett. **95**, 121802 (2005), [hep-ex/0504039].
- [72] B. Aubert *et al.* (BaBar), Phys. Rev. **D78**, 034023 (2008), [arXiv:0804.2089].
- [73] See the tabulation of  $A_{CP}$  results in the  $D^0$  and  $D^+$  Listings in this *Review*.
- [74] R.A. Briere *et al.*, (CLEO Collab.), CLNS 01-1742, (2001).
- [75] D. M. Asner *et al.*, (BES-III Collab.), Int. J. Mod. Phys. **A**, 24 (2009).
- [76] Heavy Flavor Averaging Group, [https://hflav-eos.web.cern.ch/hflav-eos/charm/CHARM13/results\\_mix\\_cpv.html](https://hflav-eos.web.cern.ch/hflav-eos/charm/CHARM13/results_mix_cpv.html).

- [77] J. Beringer *et al.* (Particle Data Group), Phys. Rev. **D86**, 010001 (2012).
- [78] J. L. Rosner *et al.* (CLEO), Phys. Rev. Lett. **100**, 221801 (2008), [arXiv:0802.2264].
- [79] D. M. Asner *et al.* (CLEO), Phys. Rev. **D78**, 012001 (2008), [arXiv:0802.2268].
- [80] D. M. Asner *et al.* (CLEO), Phys. Rev. **D86**, 112001 (2012), [arXiv:1210.0939].
- [81] Heavy Flavor Averaging Group, [https://hflav-eos.web.cern.ch/hflav-eos/charm/March12/results\\_mix\\_cpv.html](https://hflav-eos.web.cern.ch/hflav-eos/charm/March12/results_mix_cpv.html).
- [82] E. Golowich *et al.*, Phys. Rev. **D76**, 095009 (2007), [arXiv:0705.3650].
- [83] G. Isidori *et al.*, Phys. Lett. **B711**, 46 (2012), [arXiv:1111.4987].
- [84] E. Franco, S. Mishima and L. Silvestrini, JHEP **05**, 140 (2012), [arXiv:1203.3131].
- [85] Y. Grossman, Y. Nir and G. Perez, Phys. Rev. Lett. **103**, 071602 (2009), [arXiv:0904.0305].
- [86] A. L. Kagan and M. D. Sokoloff, Phys. Rev. **D80**, 076008 (2009), [arXiv:0907.3917].
- [87] M. Ciuchini *et al.*, Phys. Lett. **B655**, 162 (2007), [hep-ph/0703204].
- [88] E. Kou *et al.* (Belle-II) (2018), [arXiv:1808.10567].
- [89] R. Aaij *et al.* (LHCb) (2018), [arXiv:1808.08865].

## 70. $D_s^+$ Branching Fractions

Updated September 2019 by J.L. Rosner (University of Chicago) and C.G. Wohl (LBNL).

Figure 70.1 shows a partial breakdown of the  $D_s^+$  branching fractions. The rest of this note is about how the figure was constructed. The values shown make heavy use of CLEO measurements of inclusive branching fractions [1]. For references to other data cited in the following, see the Listings.

### 70.1. Modes with leptons

The bottom (18.0 ± 1.0)% of Fig. 70.1 shows the fractions for the modes that include leptons. The measured  $K^0 e^+ \nu_e$  and  $K^{*0} e^+ \nu_e$  fractions have been doubled to take account of the corresponding  $\mu^+ \nu_\mu$  fractions. The sum of the exclusive  $X e^+ \nu_e$  fractions is (6.0 ± 0.3)%, consistent with an inclusive semileptonic measurement of (6.5 ± 0.4)%. There seems to be little missing here.

### 70.2. Inclusive hadronic $K\bar{K}$ fractions

The Cabibbo-favored  $c \rightarrow s$  decay in  $D_s^+$  decay produces a final state with both an  $s$  and an  $\bar{s}$ ; and thus modes with a  $K\bar{K}$  pair or with an  $\eta$ ,  $\omega$ ,  $\eta'$ , or  $\phi$  predominate (as may already be seen in Fig. 70.1 in the semileptonic fractions). We consider the  $K\bar{K}$  modes first. A complete picture of the exclusive  $K\bar{K}$  charge modes is not yet possible, because branching fractions for many of those modes have not yet been measured. However, CLEO has measured the inclusive  $K^+$ ,  $K^-$ ,  $K_S^0$ ,  $K^+ K^-$ ,  $K^+ K_S^0$ ,  $K^- K_S^0$ , and  $2K_S^0$  fractions (these include modes with leptons) [1]. And each of these inclusive fractions with a  $K_S^0$  is equal to the corresponding fraction with a  $K_L^0$ :  $f(K^+ K_L^0) = f(K^+ K_S^0)$ ,  $f(2K_L^0) = f(2K_S^0)$ , etc. Therefore, of all inclusive fractions pairing a  $K^+$ ,  $K_S^0$ , or  $K_L^0$  with a  $K^-$ ,  $K_S^0$ , or  $K_L^0$ , we know all but  $f(K_S^0 K_L^0)$ .

We can get that fraction. The total  $K_S^0$  fraction is

$$f(K_S^0) = f(K^+ K_S^0) + f(K^- K_S^0) + 2f(2K_S^0) + f(K_S^0 K_L^0) + f(\text{single } K_S^0),$$

where  $f(\text{single } K_S^0)$  is the sum of the branching fractions for modes such as  $K_S^0 \pi^+ 2\pi^0$  with a  $K_S^0$  and no second  $K$ . The  $K_S^0 \pi^+ 2\pi^0$  mode is in fact the only unmeasured single- $K_S^0$  mode (throughout, we shall assume that fractions for modes with a  $K$  or  $K\bar{K}$  and more than three pions are negligible), and we shall take its fraction to be the same as for the  $K_S^0 2\pi^+ \pi^-$  mode, (0.30 ± 0.11)%. Any reasonable deviation from this value would be too small to matter much in the following. Adding the several small single- $K_S^0$  branching fractions, including those from semileptonic modes, we get  $f(\text{single } K_S^0) = (1.7 \pm 0.2)\%$ .

Using this, we have:

$$\begin{aligned} f(K_S^0 K_L^0) &= f(K_S^0) - f(K^+ K_S^0) - f(K^- K_S^0) \\ &\quad - 2f(2K_S^0) - f(\text{single } K_S^0) \\ &= (19.0 \pm 1.1) - (5.8 \pm 0.5) - (1.9 \pm 0.4) \\ &\quad - 2 \times (1.7 \pm 0.3) - (1.7 \pm 0.2) \\ &= (6.2 \pm 1.4)\% . \end{aligned}$$

Here and below we treat the errors as uncorrelated, although often they are not. However, our main aim is to get numbers for Fig. 70.1; errors are secondary.

There is a check on our result: The  $\phi$  inclusive branching fraction is (15.7 ± 1.0)%, of which 34%, or (5.34 ± 0.34)% of  $D_s^+$  decays, produces a  $K_S^0 K_L^0$ . Our  $f(K_S^0 K_L^0) = (6.2 \pm 1.4)\%$  has to be at least this large—and it is, within the sizable error.

We now have all the inclusive  $K\bar{K}$  fractions. We use  $f(K^+ K^-) = 2 f(K^+ K_S^0)$ , and likewise for  $f(K^- K^0)$ . For  $K^+ K^-$  and  $K_S^0 K_L^0$ , we subtract off the contributions from  $\phi l^+ \nu$  decay to get the purely

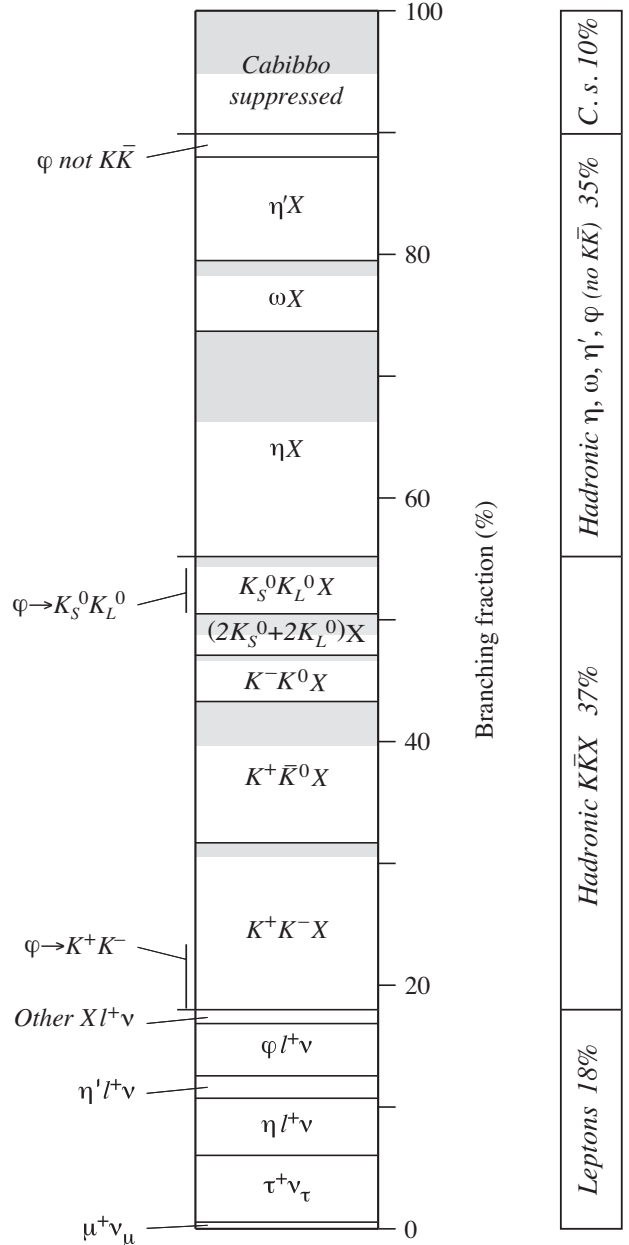


**Figure 70.1:** A partial breakdown of  $D_s^+$  branching fractions. The hadronic bins in the left column show inclusive fractions. Shading within a bin shows how much of the inclusive fraction is not yet accounted for by adding up all the relevant exclusive fractions. The inclusive hadronic  $\phi$  fraction is spread over three bins, in proportion to its decay fractions into  $K^+ K^-$ ,  $K_S^0 K_L^0$ , and no- $K\bar{K}$  modes.

hadronic  $K\bar{K}$  inclusive fractions:

$$\begin{aligned} f(K^+ K^-, \text{hadronic}) &= (15.8 \pm 0.7) - (2.1 \pm 0.3) \\ &= (13.7 \pm 0.8)\% \\ f(K^+ \bar{K}^0, \text{hadronic}) &= (11.6 \pm 1.0)\% \\ f(K^- K^0, \text{hadronic}) &= (3.8 \pm 0.8)\% \\ f(2K_S^0 + 2K_L^0, \text{hadronic}) &= (3.4 \pm 0.6)\% \\ f(K_S^0 K_L^0, \text{hadronic}) &= (6.2 \pm 1.4) - (1.5 \pm 0.2) \\ &= (4.7 \pm 1.4)\% . \end{aligned}$$

The fractions are shown in Fig. 70.1. They total (37.2 ± 2.2)% of  $D_s^+$  decays.



We can add more information to the figure by summing up measured branching fractions for exclusive modes within each bin:

$K^+K^-$  modes—The sum of measured  $K^+K^-\pi^+$ ,  $K^+K^-\pi^+\pi^0$ , and  $K^+K^-\pi^+\pi^-\pi^0$  branching fractions is  $(12.6 \pm 0.6)\%$ . That leaves  $(1.1 \pm 1.0)\%$  for the  $K^+K^-\pi^+\pi^0$  mode, which is the only other  $K^+K^-$  mode with three or fewer pions. In Fig. 70.1, this unmeasured part of the  $K^+K^-$  bin is shaded.

$K^+\bar{K}^0$  modes—Two times the sum of the measured  $K^+K_S^0$ ,  $K^+K_L^0\pi^0$ , and  $K^+K_S^0\pi^+\pi^-$  branching fractions is  $(8.0 \pm 0.5)\%$ . This leaves  $(3.6 \pm 1.1)\%$  for the unmeasured  $K^+\bar{K}^0$  modes (there are three such modes with three or fewer pions). This is shaded in the figure.

$K^-K^0$  modes—Twice the  $K^-K_S^0\pi^+$  fraction is  $(3.4 \pm 0.2)\%$ , which leaves about  $(0.4 \pm 0.8)\%$  for  $K^-K^0\pi^+\pi^0$ , the only other  $K^-K^0$  mode with three or fewer pions.

$2K_S^0 + 2K_L^0$  modes—The  $2K_S^0\pi^+$  and  $2K_S^0\pi^+\pi^-$  fractions sum to  $(0.86 \pm 0.07)\%$ ; this times two (for the corresponding  $2K_L^0$  modes) is  $(1.72 \pm 0.14)\%$ . This leaves about  $(1.7 \pm 0.7)\%$  for other  $2K_S^0 + 2K_L^0$  modes.

$K_S^0K_L^0$  modes—Most of the  $K_S^0K_L^0$  fraction is accounted for by  $\phi$  decays (see below).

### 70.3. Inclusive hadronic $\eta$ , $\omega$ , $\eta'$ , and $\phi$ fractions

These are easier. We start with the inclusive branching fractions, and then, to avoid double counting, subtract: (1) fractions for modes with leptons; (2)  $\eta$  mesons that are included in the inclusive  $\eta'$  fraction; and (3)  $K^+K^-$  and  $K_S^0K_L^0$  from  $\phi$  decays:

$$f(\eta \text{ hadronic}) = f(\eta \text{ inclusive}) - 0.65 f(\eta' \text{ inclusive})$$

$$-f(\eta\ell^+\nu) = (18.5 \pm 3.0)\%$$

$$f(\omega \text{ hadronic}) = f(\omega \text{ inclusive}) - 0.026 f(\eta' \text{ inclusive}) \\ = (5.8 \pm 1.4)\%$$

$$f(\eta' \text{ hadronic}) = f(\eta' \text{ inclusive}) - f(\eta'\ell^+\nu) \\ = (8.5 \pm 1.5)\%$$

$$f(\phi \text{ hadronic, } \not\rightarrow K\bar{K}) = 0.17 [f(\phi \text{ inclusive}) - f(\phi\ell^+\nu)] \\ = (1.9 \pm 0.2)\% .$$

The factors 0.65, 0.026, and 0.17 are the  $\eta' \rightarrow \eta$ ,  $\eta' \rightarrow \omega$ , and  $\phi \rightarrow K\bar{K}$  branching fractions. Figure 70.1 shows the results; the sum is  $(34.7 \pm 3.6)\%$ , which is about equal to the hadronic  $K\bar{K}$  total.

Note that the bin marked  $\phi$  near the top of Fig. 70.1 includes neither the  $\phi\ell^+\nu$  decays nor the 83% of other  $\phi$  decays that produce a  $K\bar{K}$  pair. There is twice as much  $\phi$  in the  $K_S^0K_L^0$  bin, and nearly three times as much in the  $K^+K^-$  bin. These contributions are indicated in those bins.

Again, we can show how much of each bin is accounted for by measured exclusive branching fractions:

$\eta$  modes—The sum of  $\eta\pi^+$ ,  $\eta\pi^+\pi^0$  (nearly all  $\eta\rho^+$ ), and  $\eta K^+$  branching fractions is  $(11.1 \pm 1.2)\%$ , which leaves a good part of the inclusive hadronic  $\eta$  fraction,  $(18.5 \pm 3.0)\%$ , to be accounted for. This is shaded in the figure.

$\omega$  modes—The sum of  $\omega\pi^+$ ,  $\omega\pi^+\pi^0$ , and  $\omega 2\pi^+\pi^-$  fractions is  $(4.6 \pm 0.9)\%$ , which is nearly as large as the inclusive hadronic  $\omega$  fraction,  $(5.8 \pm 1.4)\%$ .

$\eta'$  modes—The sum of  $\eta'\pi^+$ ,  $\eta'\rho^+$ , and  $\eta'K^+$  fractions is  $(9.9 \pm 1.5)\%$ , which is larger than but not in serious disagreement with the inclusive hadronic  $\eta'$  fraction,  $(8.5 \pm 1.5)\%$ .

### 70.4. Cabibbo-suppressed modes

The sum of the fractions for modes with a  $K\bar{K}$ ,  $\eta$ ,  $\omega$ ,  $\eta'$ , or leptons is  $(89.9 \pm 4.4)\%$ . The remaining  $(10.1 \pm 4.4)\%$  is to Cabibbo-suppressed modes, mainly single- $K$  pions and multiple-pion modes (see below). However, it should be noted that some small parts of the modes already discussed are Cabibbo-suppressed. For example, the  $(1.1 \pm 0.2)\%$  of  $D_s^+$  decays to  $K^0\ell\nu$  or  $K^{*0}\ell\nu$  is already in the  $X\ell\nu$  bin in Fig. 70.1. And the inclusive measurements of  $\eta$ ,  $\omega$ , and  $\eta'$  fractions do not distinguish between (and therefore include both) Cabibbo-allowed and -suppressed modes. We shall not try to make a separation here.

$K^0 + \text{pions}$ —Above, we found that  $f(\text{single } K_S^0) = (1.7 \pm 0.2)\%$ . Subtracting semileptonic fractions with a  $K_S^0$  leaves  $(1.3 \pm 0.2)\%$ . The hadronic single- $K^0$  fraction is twice this, about  $(2.6 \pm 0.4)\%$ . The sum of measured  $K^0\pi^+$ ,  $K^0\pi^+\pi^0$ , and  $K^0\pi^+\pi^-$  fractions is  $(1.8 \pm 0.3)\%$ , about two-thirds as much.

$K^+ + \text{pions}$ —The  $K^+\pi^0$  and  $K^+\pi^+\pi^-$  fractions sum to  $(0.72 \pm 0.05)\%$ . The total  $K^+$  fraction wanted here is probably in the 1-to-2% range.

$\text{Multi-pions}$ —The  $2\pi^+\pi^-$ ,  $\pi^+2\pi^0$ , and  $3\pi^+2\pi^-$  fractions total  $(2.5 \pm 0.2)\%$ . Modes not measured might double this.

The sum of the actually measured fractions is, including the semileptonics,  $(4.9 \pm 0.3)\%$ . The error on our Cabibbo-suppressed total,  $(10.1 \pm 4.4)\%$  is too large to know how much we might be missing.

### References:

1. S. Dobbs *et al.*, Phys. Rev. **D79**, 112008 (2009).

## 71. Leptonic Decays of Charged Pseudoscalar Mesons

Revised September 2019 by J.L. Rosner (Chicago U.), S.L. Stone (Syracuse U.) and R. Van de Water (FNAL).

### 71.1 Introduction

Charged mesons formed from a quark and antiquark can decay to a lepton-neutrino pair when these objects annihilate via a virtual  $W$  boson. Fig. 71.1 illustrates this process for the purely leptonic decay of a  $D^+$  meson.

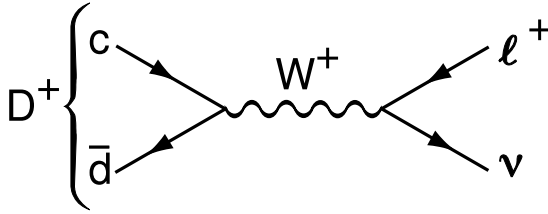


Figure 71.1: The annihilation process for pure  $D^+$  leptonic decays in the standard model.

Similar quark-antiquark annihilations via a virtual  $W^+$  to the  $\ell^+\nu$  final states occur for the  $\pi^+$ ,  $K^+$ ,  $D_s^+$ , and  $B^+$  mesons. (Whenever pseudoscalar-meson charges are specified in this article, use of the charge-conjugate particles and corresponding decays are also implied.) Let  $P$  be any of these pseudoscalar mesons. To lowest order, the decay width is

$$\Gamma^{(0)}(P \rightarrow \ell\nu) = \frac{G_F^2}{8\pi} f_P^2 m_\ell^2 M_P \left(1 - \frac{m_\ell^2}{M_P^2}\right)^2 |V_{q_1 q_2}|^2. \quad (71.1)$$

Here  $M_P$  is the  $P$  mass,  $m_\ell$  is the  $\ell$  mass,  $V_{q_1 q_2}$  is the Cabibbo-Kobayashi-Maskawa (CKM) matrix element between the quarks  $q_1 q_2$  in  $P$ , and  $G_F$  is the Fermi coupling constant. The decay constant  $f_P$  is proportional to the matrix element of the axial current between the one- $P$ -meson state and the vacuum:

$$\langle 0 | \bar{q}_1 \gamma_\mu \gamma_5 q_2 | P(p) \rangle = i p_\mu f_P, \quad (71.2)$$

and can be thought of as the “wavefunction overlap” of the quark and antiquark. In this article we use the convention in which  $f_\pi \approx 130$  MeV. For brevity, we will often denote the purely leptonic decay width in Eq. (71.1) by  $\Gamma^{(0)}$ .

The decay of  $P^\pm$  starts with a spin-0 meson, and ends up with a left-handed neutrino or right-handed antineutrino. By angular momentum conservation, the  $\ell^\pm$  must then also be left-handed or right-handed, respectively. In the  $m_\ell = 0$  limit, the decay is forbidden, and can only occur as a result of the finite  $\ell$  mass. This helicity suppression is the origin of the  $m_\ell^2$  dependence of the decay width.

Experimentally, it is difficult to isolate events in which there are *only* a lepton and neutrino in the final state from those with a lepton, neutrino, and soft photon. Thus, radiative contributions must be removed from the experimental measurements *a posteriori* to obtain  $\Gamma^{(0)}$ . The radiative contributions can be broken into three pieces: the short-distance contribution to leptonic and semileptonic decays mediated by a  $W^\pm$  boson that accounts for electroweak corrections not included in the definition of  $G_F$ , the long-distance internal bremsstrahlung (IB) contribution, and the contribution from photon emission that depends upon the hadron’s structure. The universal electroweak correction was calculated at  $\mathcal{O}(\alpha)$  by Sirlin [1], and increases the purely leptonic decay rate by  $\sim 1.8$ – $2.2\%$  depending on the decaying meson. The  $\mathcal{O}(\alpha)$  IB contribution was calculated by Kinoshita [2], and again is universal for all leptonic decays at this order. Numerically, the universal long-distance contribution lowers the purely leptonic decay rate by  $\sim 0.4$ – $2.4\%$ , where the correction is smallest for pions and largest for  $D_{(s)}$  mesons. The structure-dependent contributions have been estimated within various effective theories to increase the purely leptonic rate by one to a few percent [3–8].

In this review we treat the radiative corrections differently for the light, charm, and bottom meson systems for several reasons. First, the experimental uncertainties on the decay widths vary

substantially. Thus, while the inclusion of radiative corrections is essential for the pion, kaon, and  $D$ -meson decay widths, which have been measured to (sub)-percent precision, radiative corrections can be neglected (for now) for  $B \rightarrow \tau\nu$  decay. Second, the photons are treated differently on the experimental side for the different decay processes. For pions and kaons, the experimental measurements of  $\Gamma_{P\ell 2[\gamma]}$  are fully inclusive, while for  $D$  mesons, the experiments impose cuts on the energy of any neutral cluster deposited in the calorimeter, which reduce the soft-photon background substantially. Some experiments also remove the QED bremsstrahlung in the leading-logarithmic approximation using the PHOTOS Monte-Carlo generator [9]. Third, the theoretical knowledge of the structure-dependent corrections varies for each meson system.

Once radiative corrections have been accounted for, measurements of purely leptonic decay branching fractions and lifetimes allow an experimental determination of the product  $|V_{q_1 q_2}| f_P$ . If the decay constant  $f_P$  is known to sufficient precision from theory, one can obtain the corresponding CKM element within the standard model. If, on the other hand, one takes the value of  $|V_{q_1 q_2}|$  assuming CKM unitarity, one can infer an “experimental measurement” of the decay constant that can then be compared with theory.

The importance of measuring  $\Gamma(P \rightarrow \ell\nu)$  depends on the particle being considered. Leptonic decays of charged pseudoscalar mesons occur at tree level within the standard model. Thus one does not expect large new-physics contributions to measurements of  $\Gamma(P \rightarrow \ell\nu)$  for the lighter mesons  $P = \pi^+, K^+$ , and these processes in principle provide clean standard-model determinations of  $|V_{ud}|$  and  $|V_{us}|$ . The situation is different for leptonic decays of charm and bottom mesons. The presence of new heavy particles such as charged Higgs bosons or leptoquarks could lead to observable effects in  $\Gamma(P \rightarrow \ell\nu)$  for  $P = D_{(s)}^+, B^+$  [10–14]. Thus the determination of  $|V_{ub}|$  from  $B^+ \rightarrow \tau\nu$  decay, in particular, should be considered a probe of new physics. More generally, the ratio of leptonic decays to  $\tau\nu$  over  $\mu\nu$  final states probes lepton universality [10, 15].

The determinations of CKM elements from leptonic decays of charged pseudoscalar mesons provide complementary information to those from other decay processes. The decay  $P \rightarrow \ell\nu$  proceeds in the standard model via the axial-vector current  $\bar{q}_1 \gamma_\mu \gamma_5 q_2$ , whereas semileptonic pseudoscalar meson decays  $P_1 \rightarrow P_2 \ell\nu$  proceed via the vector current  $\bar{q}_1 \gamma_\mu q_2$ . Thus the comparison of determinations of  $|V_{q_1 q_2}|$  from leptonic and semileptonic decays tests the  $V - A$  structure of the standard-model electroweak charged-current interaction. More generally, a small right-handed admixture to the standard-model weak current would lead to discrepancies between  $|V_{q_1 q_2}|$  obtained from leptonic pseudoscalar-meson decays, exclusive semileptonic pseudoscalar-meson decays, exclusive semileptonic baryon decays, and inclusive semileptonic decays [16, 17].

Both measurements of the decay rates  $\Gamma(P \rightarrow \ell\nu)$  and theoretical calculations of the decay constants  $f_P$  for  $P = \pi^+, K^+, D_{(s)}^+$  from numerical lattice-QCD simulations are now quite precise. As a result, the elements of the first row of the CKM matrix  $|V_{ud}|$  and  $|V_{us}|$  can be obtained to sub-percent precision from  $\pi^+ \rightarrow \ell\nu$  and  $K^+ \rightarrow \ell\nu$ , where the limiting error is from theory. The elements of the second row of the CKM matrix  $|V_{cd(s)}|$  can be obtained from leptonic decays of charged pseudoscalar mesons to few-percent precision, where here the limiting error is from experiment. These enable stringent tests of the unitarity of the first and second rows of the CKM matrix.

This review is organized as follows. Because the experimental and theoretical issues associated with measurements of pions and kaons, charmed mesons, and bottom mesons differ, we discuss each one separately. We begin with the pion and kaon system in Sec. 71.2. First, in Sec. 71.2.1 we review current measurements of the experimental decay rates. We provide tables of branching-ratio measurements and determinations of the product  $|V_{ud(s)}| f_{\pi^+(K^+)}$ , as well as average values for these quantities including correlations and other effects needed to combine results.

Then, in Sec. 71.2.2 we summarize the status of theoretical calculations of the decay constants. We provide tables of recent lattice-QCD results for  $f_{\pi^+}$ ,  $f_{K^+}$ , and their ratio from simulations including dynamical  $u$ ,  $d$ ,  $s$ , and (in some cases  $c$ ) quarks, along with averages including correlations and strong SU(2)-isospin breaking corrections as needed. We next discuss the charmed meson system in Sec. 71.3, again reviewing current experimental rate measurements in Sec. 71.3.1 and theoretical decay-constant calculations in Sec. 71.3.2. Last, we discuss the bottom meson system in Sec. 71.4, following the same organization as the two previous sections. For almost all of the decay constants presented in Secs. 71.2.2, 71.3.2, and 71.4.2, we take as our preferred values the four-flavor averages from 2019 Flavor Lattice Averaging Group (FLAG) review [18], which incorporate all lattice-QCD results that appeared before 30 September 2018. There have not been any new decay-constant results that would qualify for the FLAG average since then.

After having established the status of both experimental measurements and theoretical calculations of leptonic charged pseudoscalar-meson decays, we discuss some implications for phenomenology in Sec. 71.5. For each process discussed in Secs. 71.2–71.4, we combine the average  $\mathcal{B}(P \rightarrow \ell\nu)$  with the decay constant  $f_P$  to infer the associated CKM matrix element. We then compare these results with determinations of the same CKM elements from other processes. We also use the CKM elements obtained from leptonic decays to test the unitarity of the first and second rows of the CKM matrix. Further, as in previous reviews, we combine the experimental  $\mathcal{B}(P \rightarrow \ell\nu)$ s with the associated CKM elements obtained from CKM unitarity to infer “experimental” values for the decay constants. The comparison of these values with theory provides a test of lattice and other QCD approaches, assuming that new-physics contributions to these processes are not significant.

## 71.2 Pions and kaons

### 71.2.1 Experimental rate measurements

Experimental rate measurements of pion and kaon leptonic decays are fully radiation inclusive. Following Refs. [19, 20], and references therein, we combine the  $\mathcal{O}(\alpha)$  radiative corrections to the purely leptonic rate as follows:

$$\Gamma(P \rightarrow \ell\nu[\gamma]) = \Gamma(P \rightarrow \ell\nu) \left[ 1 + \frac{\alpha}{\pi} C_P \right], \quad (71.3)$$

where  $P = \pi, K$ . The full expressions for  $C_\pi$  and  $C_K$  are given in Eq. (114) of Ref. [5]. In addition to the universal short- [1] and long-distance [2] corrections,  $C_\pi$  and  $C_K$  include hadronic-structure dependent contributions [3] through  $\mathcal{O}(\alpha p^4)$  in chiral perturbation theory ( $\chi$ Pt), where  $p$  is the pion or kaon momentum. The inclusion of radiative corrections to the purely leptonic rates is numerically important given the level of precision achieved on the experimental measurements of the  $\pi^\pm \rightarrow \mu^\pm \nu$  and  $K^\pm \rightarrow \mu^\pm \nu$  decay widths.

We evaluate  $\delta_P \equiv (\alpha/\pi)C_P$  using the latest experimentally-measured meson and lepton masses and coupling constants from the Particle Data group [21], and taking the low-energy constants (LECs) that parameterize the hadronic contributions from Refs. [5, 22, 23]. Because the finite non-logarithmic parts of the LECs were estimated within the large- $N_C$  approximation assuming that contributions from the lowest-lying resonances dominate, we conservatively assign a 100% uncertainty to the LECs, which leads to a  $\pm 0.9$  error in  $C_{\pi, K}$ .<sup>1</sup> We obtain the following correction factors to the individual charged pion and kaon decay widths:

$$\delta_\pi = 0.0176(21) \quad \text{and} \quad \delta_K = 0.0107(21). \quad (71.4)$$

The error on the ratio of kaon-to-pion leptonic decay widths is under better theoretical control because the hadronic contributions

<sup>1</sup>This uncertainty on  $C_{\pi, K}$  is smaller than the error estimated by Marciano and Sirlin in Ref. [24], which predates the calculations of the hadronic-structure contributions in Refs. [3, 5, 22, 23]. The hadronic LECs incorporate the large short-distance electroweak logarithm discussed in Ref. [24], and their dependence on the chiral renormalization scale cancels the scale-dependence induced by chiral loops, thereby removing the dominant scale uncertainty of the Marciano–Sirlin analysis [24].

from low-energy constants estimated within the large- $N_C$  framework cancel at lowest order in the chiral expansion. For the ratio, we use the correction factor

$$\delta_{K/\pi} = -0.0069(17), \quad (71.5)$$

where we take the estimated error due to higher-order corrections in the chiral expansion from Ref. [25].

There have been no new measurements of the pion leptonic decay rate since our previous review [26]. The sum of branching fractions for  $\pi^- \rightarrow \mu^- \bar{\nu}$  and  $\pi^- \rightarrow \mu^- \bar{\nu} \gamma$  is 99.98770(4)% [21]. Together with the lifetime 26.033(5) ns [21] this implies  $\Gamma(\pi^- \rightarrow \mu^- \bar{\nu}[\gamma]) = 3.8408(7) \times 10^7 \text{ s}^{-1}$ . We then subtract the estimated radiative correction factor  $\delta_\pi$  in Eq. (71.4) to obtain the purely leptonic rate  $\Gamma^{(0)}(\pi^- \rightarrow \mu^- \bar{\nu})$ . Using this rate and the masses from the 2014 PDG review [21] in Eq. (71.1) gives

$$f_{\pi^-} |V_{ud}| = (127.13 \pm 0.02 \pm 0.13) \text{ MeV}, \quad (71.6)$$

where the errors are from the experimental rate measurement and the radiative correction factor, respectively.

The uncertainty on  $f_{\pi^-} |V_{ud}|$  is dominated by that from the theoretical estimate of the hadronic structure-dependent radiative corrections. Recently the first direct lattice-QCD calculation of the radiative corrections to the pion and kaon leptonic decay rates was performed by the RM123-Soton Collaboration [8]. The results for both  $\delta_\pi = 0.0153(19)$  and  $\delta_K = 0.0088(9)$ , which are given in the Gasser-Rusetsky-Scimemi scheme [27], are compatible with our chiral-perturbation-theory estimates above and have smaller quoted uncertainties, especially for  $\delta_K$ . While independent confirmation of these results is needed, they demonstrate a promising approach for reducing the theoretical uncertainties on the pion and kaon leptonic decay rates in the future.

The world average for the  $K \rightarrow \mu\nu$  decay rate is obtained from a global fit of several kaon-decay branching ratios and lifetime measurements, and was last updated by the FlaviaNet Working Group on Kaon Decays in 2014 [37]. Thus, the radiation-inclusive branching ratio  $\mathcal{B}(K^- \rightarrow \mu^- \bar{\nu}[\gamma]) = 63.58(11)\%$  and lifetime  $\tau_{K^\pm} = 12.384(15)$  ns are unchanged from our previous review. These measurements imply  $\Gamma(K^- \rightarrow \mu^- \bar{\nu}[\gamma]) = 5.134(11) \times 10^7 \text{ s}^{-1}$ . As before, we subtract  $\delta_K$  in Eq. (71.4) from the radiation-inclusive decay width to obtain  $\Gamma^{(0)}(K^- \rightarrow \mu^- \bar{\nu})$ . We then use Eq. (71.1) to obtain

$$f_{K^+} |V_{us}| = (35.09 \pm 0.04 \pm 0.04) \text{ MeV}, \quad (71.7)$$

where the errors are from the experimental rate measurement and the radiative correction factor, respectively.

Short-distance radiative corrections cancel in the ratio of pion-to-kaon decay rates [38]:

$$\frac{\Gamma_{K\ell 2[\gamma]}}{\Gamma_{\pi\ell 2[\gamma]}} = \frac{|V_{us}|^2 f_{K^-}^2}{|V_{ud}|^2 f_{\pi^-}^2} \frac{m_K(1 - m_\ell^2/m_K^2)^2}{m_\pi(1 - m_\ell^2/m_\pi^2)^2} (1 + \delta_{K/\pi}), \quad (71.8)$$

where  $\delta_{K/\pi}$  is given in Eq. (71.5). The left-hand side of Eq. (71.8) is 1.3367(28), which implies

$$\frac{|V_{us}| f_{K^-}}{|V_{ud}| f_{\pi^-}} = 0.27599 \pm 0.00029 \pm 0.00024, \quad (71.9)$$

where the first uncertainty is from the branching fractions and the second is from  $\delta_{K/\pi}$ . Here, the estimated error on the hadronic structure-dependent radiative corrections is commensurate with the experimental error.

In summary, the main experimental results pertaining to charged pion and kaon leptonic decays are

$$|V_{ud}| f_{\pi^-} = (127.13 \pm 0.02 \pm 0.13) \text{ MeV}, \quad (71.10)$$

$$|V_{us}| f_{K^+} = (35.09 \pm 0.04 \pm 0.04) \text{ MeV}, \quad (71.11)$$

$$\frac{|V_{us}| f_{K^+}}{|V_{ud}| f_{\pi^-}} = 0.27599 \pm 0.00029 \pm 0.00024, \quad (71.12)$$

where the errors are from the experimental uncertainties in the branching fractions and the theoretical uncertainties in the radiative correction factors  $\delta_P$ , respectively. All of these values are the same as in our previous review [26].

**Table 71.1:** Recent published lattice-QCD results for  $f_{\pi^+}$ ,  $f_{K^+}$ , and their ratio. The upper and lower panels show  $(2+1+1)$ -flavor and  $(2+1)$ -flavor determinations, respectively. When two errors are shown, they are statistical and systematic, respectively. Results for  $f_{\pi}$  and  $f_K$  in the isospin-symmetric limit  $m_u = m_d$  are noted with an “ $\ddagger$ ”; they are corrected for isospin breaking via Eq. (71.13) before computing the averages.

Reference	$N_f$	$f_{\pi^+}$ (MeV)	$f_{K^+}$ (MeV)	$f_{K^+}/f_{\pi^+}$
Fermilab/MILC 17 [28] *	2+1+1	–	–	1.1950(15) $^{(+6)}_{(-18)}$
ETM 14 [29] *	2+1+1	–	154.4(1.5)(1.3)	1.184(12)(11)
Fermilab/MILC 14 [7] *	2+1+1	–	155.92(13) $^{(+42)}_{(-34)}$	1.1956(10) $^{(+26)}_{(-18)}$ †
HPQCD 13 [30] *	2+1+1	–	155.37(20)(28)	1.1916(15)(16)
FLAG 19 average [18]	2+1+1	–	155.7(3)	1.1932(19)
QCDSF/UKQCD 16 [31]	2+1	–	–	1.190(10)(13)
BMW 16 [32]	2+1	–	–	1.178(10)(26)
RBC/UKQCD 14 [33] ‡	2+1	130.19(89)	155.51(83)	1.1945(45)
MILC 10 [34]	2+1	129.2(0.4)(1.4)	156.1(4) $^{(+6)}_{(-9)}$	1.197(2) $^{(+3)}_{(-7)}$
BMW 10 [35] ‡	2+1	–	–	1.192(7)(6)
HPQCD/UKQCD 07 [36] ‡	2+1	132(2)	157(2)	1.189(2)(7)
FLAG 19 average [18]	2+1	130.2(8)	155.7(7)	1.1917(37)

\*PDG 2014 value of  $f_{\pi^+} = 130.41(21)$  MeV used to set absolute lattice scale.

†Superseded by  $f_{K^+}/f_{\pi^+}$  from Fermilab/MILC 17.

### 71.2.2 Theoretical decay-constant calculations

Table 71.1 presents recent published results for the charged pion and kaon decay constants and their ratio from numerical lattice-QCD simulations with three ( $N_f = 2 + 1$ ) or four flavors ( $N_f = 2 + 1 + 1$ ) of dynamical quarks. The uncertainties on both the individual decay constants and their ratio are at the sub-percent level. The  $SU(3)$ -breaking ratio  $f_{K^+}/f_{\pi^+}$  can be obtained with especially small errors because statistical errors associated with the Monte Carlo simulations are correlated between the numerator and denominator, as are some systematics. The results in Table 71.1 were obtained using several independent sets of gauge-field configurations, and a variety of lattice fermion actions that are sensitive to different systematic uncertainties.<sup>2</sup> Thus, the good agreement between them indicates that the lattice-QCD uncertainties are controlled and the associated error estimates are reliable.<sup>3</sup>

Table 71.1 also shows the three- and four-flavor averages for the pion and kaon decay constants and their ratio from the 2019 Flavour Lattice Averaging Group (FLAG) review [18] in the lines labeled “FLAG 19 average.” There is no four-flavor average for the pion decay constant in Table 71.1 because all of the four-flavor calculations use the quantity  $f_{\pi^+}$  as an input to fix the absolute lattice scale needed to convert from lattice-spacing units to GeV [7, 29, 30].

All of the results in Table 71.1 were obtained using isospin-symmetric gauge-field configurations, *i.e.*, the dynamical up and down quarks have the same mass. Fortunately, however, the dominant effect of strong-isospin breaking is easily included in lattice-QCD calculations as follows. Because the up-down mass difference  $\Delta m_{ud} \equiv (m_u - m_d) \sim -2.5$  MeV [18, 49] is much less than typical hadronic scales, the strong-isospin breaking corrections to physical observables can systematically be expanded in the small parameter  $\delta m_{ud} \equiv \Delta m_{ud}/\Lambda_{\text{QCD}}$ . The leading strong-isospin-breaking corrections to pseudoscalar-meson decay constants arise from the light *valence* quarks in the initial- and final-state hadrons. (See, *e.g.*, the discussion in Ref. [50], for a detailed discussion of isospin-breaking effects in pion and kaon observables.) Thus, to include the effect of nondegenerate up- and down-quark masses, most recent lattice-QCD calculations of  $f_{\pi^+}$  and  $f_{K^+}$  evaluate the masses of the valence quarks in the pion at the physical  $m_u$  and  $m_d$ , and the mass of the valence light quark in the kaon at the physical  $m_u$ .

This procedure yields a correction to the kaon decay constant below 0.5%. Consequently, strong-isospin breaking corrections from the light sea-quark masses – which are suppressed by an additional power of  $\delta m_{ud}$  – can be neglected given present uncertainties.

Some earlier lattice-QCD calculations, however, only provide the decay constants and their ratio in the  $SU(2)$  isospin-symmetric limit [33, 35, 36]. The Flavour Lattice Averaging Group corrects these results for strong-isospin breaking using chiral perturbation theory before including them in the averages. The leading strong-isospin-breaking corrections to the pion and kaon decay constants in  $\chi$ PT can be parameterized as [25, 51]

$$f_{\pi^+} = f_{\pi}, \quad f_{K^+} = f_K \sqrt{1 + \delta_{\text{SU}(2)}}, \quad (71.13)$$

where  $f_{\pi}$  and  $f_K$  denote the values of the decay constants in the isospin-symmetric limit. The pion decay constant does not receive corrections linear in  $m_u - m_d$  because of the  $G$ -parity symmetry of the pion triplet, so at first order the  $\delta m_{ud}$  expansion, strong-isospin breaking corrections are characterized by a single parameter,  $\delta_{\text{SU}(2)}$ . Next-to-leading order  $\chi$ PT yields numerical values for  $\delta_{\text{SU}(2)}$  of approximately  $-0.004$ . Recent direct lattice-QCD calculations of  $\delta_{\text{SU}(2)}$  give larger values of around  $-0.005$  to  $-0.008$  [8, 28–30, 50, 52], but further studies are needed. Thus, to be conservative, FLAG includes an uncertainty of 100% on the  $\chi$ PT estimate for  $\delta_{\text{SU}(2)}$  when correcting those decay-constant values that are quoted in the isospin-symmetric limit.

The errors on the decay-constant results in Table 71.1 obtained from  $(2+1)$ -flavor lattice-QCD simulations do not include an estimate of the systematic uncertainty from the omission of charm sea quarks in the simulation. Consequently, when the uncertainty on the  $(2+1+1)$ -flavor FLAG average is comparable to or better than that on the  $(2+1)$ -flavor FLAG average, we simply use the four-flavor average as our preferred value. This is not possible, however, for the pion decay constant. To account for this, we first estimate the systematic uncertainty on pseudoscalar-meson decay constants associated with the omission of charm sea quarks. We then add this estimate in quadrature to the quoted error on the  $(2+1)$ -flavor FLAG average for  $f_{\pi^+}$  to obtain our preferred value.

The error introduced by omitting charm sea quarks can be roughly estimated by expanding the charm-quark determinant in powers of  $1/m_c$  [53]; the resulting leading contribution is of order  $\alpha_s (\Lambda_{\text{QCD}}/2m_c)^2$  [54]. Taking the  $\overline{\text{MS}}$  values  $\overline{m}_c(\overline{m}_c) = 1.275$  GeV,  $\overline{\Lambda}_{\text{QCD}} \sim 340$  MeV from FLAG [40], and  $\overline{\alpha}(\overline{m}_c) \sim 0.4$ , leads to an estimate of about 0.7% for the contribution to the decay constants from charm sea quarks. We can compare this power-counting estimate of charm sea-quark contributions with

<sup>2</sup>See the PDG mini-review on “Lattice Quantum Chromodynamics” [39] for a general review of numerical lattice-QCD simulations. Details on the different methods used in modern lattice-QCD calculations are provided in Appendix A of the FLAG “Review[s] of lattice results concerning low energy particle physics” [18, 40, 41].

<sup>3</sup>See the review by Kronfeld [42] for a summary of the large body of evidence validating the methods employed in modern lattice-QCD simulations.

**Table 71.2:** Experimental results for  $\mathcal{B}(D^+ \rightarrow \mu^+\nu[\gamma])$ ,  $\mathcal{B}(D^+ \rightarrow \tau^+\nu[\gamma])$ , and  $|V_{cd}|f_{D^+}$ . The systematic errors on the inferred values of  $|V_{cd}|f_{D^+}$  include those from the  $D^+$  lifetime and mass. The error from radiative corrections is only included in the entries labeled “our average.”

Experiment	Mode	$\mathcal{B}$	$ V_{cd} f_{D^+}$ (MeV)
CLEO-c [43, 44]	$\mu^+\nu$	$(3.93 \pm 0.35 \pm 0.09) \times 10^{-4}$	$46.70 \pm 2.10 \pm 0.55$
CLEO-c [43, 44]	$\mu^+\nu + \tau^+\nu$	$(3.82 \pm 0.32 \pm 0.09) \times 10^{-4}$	$46.00 \pm 1.91 \pm 0.56$
BES III [45]	$\mu^+\nu$	$(3.71 \pm 0.19 \pm 0.06) \times 10^{-4}$	$45.33 \pm 1.17 \pm 0.38$
Our average	Lines 2+3	$(3.74 \pm 0.17) \times 10^{-4}$	$45.50 \pm 1.22$
CLEO-c [46, 47]	$\tau^+\nu$ ( $\pi^+\bar{\nu}$ )	$< 1.2 \times 10^{-3}$	
BES III [48]	$\tau^+\nu$ ( $\pi^+\bar{\nu}$ )	$(1.20 \pm 0.24 \pm 0.12) \times 10^{-3}$	$49.95 \pm 2.48$
Our average	$\mu^+\nu + \tau^+\nu$		$46.17 \pm 1.16$

the observed differences between the (2+1)- and (2+1+1)-flavor lattice-QCD averages for kaon,  $D_{(s)}$ -meson, and  $B_{(s)}$ -decay constants in Tables 71.1, 71.4, and 71.6. Looking at Table 71.1, the three- and four-flavor averages for  $f_{K^+}$  agree to much better than our simple power-counting estimate. Inspection of Tables 71.4 and 71.6 shows, however, that charm sea-quark effects of this size are still allowed for both  $D_{(s)}$ -meson and  $B_{(s)}$ -meson decay constants.

Our final preferred theoretical values for the charged pion and kaon decay constants are

$$f_{\pi^+} = 130.2(1.2) \text{ MeV}, \quad f_{K^+} = 155.7(3) \text{ MeV}, \quad \frac{f_{K^+}}{f_{\pi^+}} = 1.193(2), \quad (71.14)$$

where  $f_{K^+}$  and  $f_{K^+}/f_{\pi^+}$  are simply the four-flavor FLAG 2019 averages [18], and  $f_{\pi^+}$  is the three-flavor FLAG 2019 average with the error increased by the estimated 0.7% charm sea-quark contribution. The errors on all three quantities in Eq. (71.14) have decreased since our previous review [26, 55].

## 71.3 Charmed mesons

### 71.3.1 Experimental rate measurements

Measurements have been made of the branching fractions for  $D^+$  and  $D_s^+$  mesons decaying to both  $\mu^+\nu$  and  $\tau^+\nu$  final states. The CLEO-c, BES, and BES III experiments have made measurements of  $D^+$  decays using  $e^+e^-$  collisions at the  $\psi(3770)$  resonant energy where  $D^-D^+$  pairs are copiously produced. They fully reconstruct one of the  $D^+$ s; for concreteness, we will take this to be the  $D^-$ . Counting the number of these events provides the normalization for the branching fraction measurement. The experimental analyses then proceed by identifying a candidate  $\mu^+$  and forming the missing-mass squared,  $MM^2 = (E_{\text{CM}} - E_{D^-})^2 - (\vec{p}_{\text{CM}} - \vec{p}_{D^-} - \vec{p}_{\mu^+})^2$ , where  $E_{\text{CM}}$  and  $p_{\text{CM}}$  are the center-of-mass energy (which is known) and momentum (which equals zero in  $e^+e^-$  collisions). A peak at zero  $MM^2$  implies the existence of a missing neutrino, and hence the  $\mu^+\nu$  decay of the  $D^+$ . CLEO-c does not explicitly identify the muon, so their data consists of a combination of  $\mu^+\nu$  and  $\tau^+\nu$ ,  $\tau^+ \rightarrow \pi^+\nu$  events. This permits them to do two fits: in one they fit for the individual components, and in the other they fix the ratio of  $\tau^+\nu/\mu^+\nu$  events to be that given by the standard-model expectation. Thus, the former measurement should be used for new-physics searches, and the latter for standard-model predictions. Our average uses the fixed-ratio value.

Table 71.2 shows the available measurements of  $D^+ \rightarrow \mu^+\nu$ , as an upper limit on  $D^+ \rightarrow \tau^+\nu$  from CLEO-c and the first measurement of this decay from BES III. To extract the values of  $|V_{cd}|f_{D^+}$  via Eq. (71.1), we use values of  $m_{D^+} = 1.86961$  GeV and the well-measured  $D^+$  lifetime of 1.040(7) ps [64], and apply radiative corrections as described below. For calculating the average  $\mu^+\nu$  number, we use the CLEO-c result from  $\mu^+\nu + \tau^+\nu$ .

To obtain the purely leptonic rates  $\Gamma^{(0)}(D^+ \rightarrow \mu^+(\tau^+)\nu)$ , we subtract the radiative contributions as in Sec. 71.2.1, but use numerical values for the corrections appropriate for  $D$  mesons. First, we reduce both the  $\mu^+\nu$  and  $\tau^+\nu$  branching fractions in Table 71.2 by 1.8%, which is the universal short-distance electroweak contribution of Sirlin [1] evaluated using the  $D$ -meson mass for the factorization scale. We do not adjust the experimental rates

by the universal long-distance correction [2]. This is because QED bremsstrahlung contributions have already been subtracted at leading-log order from the measurements in Table 71.2 using Monte-Carlo estimates computed with PHOTOS [9]. The  $\mu^+\nu$  rates should also be reduced by the 1% estimate of the structure-dependent contributions from Dobrescu and Kronfeld [14]. This correction accounts for tree-level radiative processes in which the  $D$  meson decays into a real photon and an off-shell vector meson, which subsequently decays weakly to a charged lepton and neutrino. It is estimated using Eq. (12) of Burdman *et al.* [4] with the CLEO-c cut on the photon energy from Ref. [65], which is typical of all the measurements. We do not need to apply the structure-dependent correction to the  $\mu^+\nu$  branching fractions in Table 71.2, however, because the experiments have already included it in their quoted results. Therefore, in summary, we reduce both the  $D^+ \rightarrow \mu^+\nu$  and the  $D^+ \rightarrow \tau^+\nu$  rates by 1.8% to account for radiative corrections. It is worth noting, however, that the universal long-distance electromagnetic contribution estimated for point-like charged mesons by Kinoshita [2], which we are not including because IB contributions are already subtracted from the measurements via PHOTOS, would *increase* both rates by about 2.5%.

We now discuss the  $D_s^+$  decay process. Measurements of the leptonic decay rate have been made by several groups and are listed in Table 71.3. We exclude older values obtained by normalizing to  $D_s^+$  decay modes that are not well defined. Many measurements, for example, used the  $\phi\pi^+$  mode. This decay is a subset of the  $D_s^+ \rightarrow K^+K^-\pi^+$  channel which has interferences from other modes populating the  $K^+K^-$  mass region near the  $\phi$ , the most prominent of which is the  $f_0(980)$ . Thus, the extraction of the effective  $\phi\pi^+$  rate is sensitive to the mass resolution of the experiment and the cuts used to define the  $\phi$  mass region [66].<sup>4</sup>

To find  $D_s$  decays in the  $\mu^+\nu$  signal channels, the experiments rely on fully reconstructing all of the final state particles except for the neutrino and using a missing-mass technique to infer the existence of the neutrino. CLEO and BES III use  $e^+e^- \rightarrow D_s D_s^*$  collisions at 4170 MeV, while Babar and Belle use  $e^+e^- \rightarrow DK n \pi D_s^*$  collisions at energies near the  $\Upsilon(4S)$ . CLEO and BES III do a similar analysis as was done for the  $D^+$  above. Babar and Belle do a similar  $MM^2$  calculation by using the reconstructed hadrons, the photon from the  $D_s^{*+}$  decay and a detected  $\mu^+$ . To get the normalization they do a  $MM^2$  fit without the  $\mu^+$  and use the signal at the  $D_s^+$  mass squared to determine the total  $D_s^+$  yield.

When selecting the  $\tau^+ \rightarrow \pi^+\bar{\nu}$  and  $\tau^+ \rightarrow \rho^+\bar{\nu}$  decay modes, CLEO uses both the calculation of the missing-mass and the fact that there should be no extra energy in the event beyond that deposited by the measured tagged  $D_s^-$  and the  $\tau^+$  decay products. The  $\tau^+ \rightarrow e^+\nu\bar{\nu}$  mode, however, uses only extra energy. Babar and Belle also use the extra energy to discriminate signal from background in their  $\tau^+\nu$  measurements. BES III uses  $\tau^+ \rightarrow \pi^+\bar{\nu}$  decays, where they calculate the  $MM^2$  and discriminate against  $\mu^+$  from  $D_s^+ \rightarrow \mu^+\nu$  decays.

When extracting  $|V_{cs}|f_{D_s^+}$  via Eq. (71.1), we first apply the -1.8% universal electroweak correction [1] to all of the  $\mu^+\nu$  and

<sup>4</sup>We have not included the BaBar result for  $\mathcal{B}(D_s^+ \rightarrow \mu^+\nu)$  reported in Ref. [67] because this measurement determined the ratio of the leptonic decay rate to the hadronic decay rate  $\Gamma(D_s^+ \rightarrow \ell^+\nu)/\Gamma(D_s^+ \rightarrow \phi\pi^+)$ .

**Table 71.3:** Experimental results for  $\mathcal{B}(D_s^+ \rightarrow \mu^+\nu[\gamma])$ ,  $\mathcal{B}(D_s^+ \rightarrow \tau^+\nu[\gamma])$ , and  $|V_{cs}|f_{D_s^+}$ . The systematic errors on the inferred values of  $|V_{cs}|f_{D_s^+}$  include those from the  $D^+$  lifetime and mass. The entries labeled “our average” take into account correlations between systematic errors common to the experiments, and also include errors from radiative corrections.

Experiment	Mode	$\mathcal{B}(\%)$	$ V_{cs} f_{D_s^+}$ (MeV)
CLEO-c [46, 47]	$\mu^+\nu$	$(0.565 \pm 0.045 \pm 0.017)$	$247.6 \pm 9.9 \pm 4.1$
BaBar* [57]	$\mu^+\nu$	$(0.602 \pm 0.038 \pm 0.034)$	$254.3 \pm 8.0 \pm 7.4$
Belle [58]	$\mu^+\nu$	$(0.531 \pm 0.028 \pm 0.020)$	$238.8 \pm 6.3 \pm 4.8$
BES III [59]	$\mu^+\nu$	$(0.549 \pm 0.016 \pm 0.015)$	$244.9 \pm 3.6 \pm 3.7$
Our average	$\mu^+\nu$	$(0.552 \pm 0.016)$	$244.0 \pm 5.2$
CLEO-c [46, 47]	$\tau^+\nu$ ( $\pi^+\bar{\nu}$ )	$(6.42 \pm 0.81 \pm 0.18)$	$267.3 \pm 16.9 \pm 4.2$
CLEO-c [60]	$\tau^+\nu$ ( $\rho^+\bar{\nu}$ )	$(5.52 \pm 0.57 \pm 0.21)$	$247.9 \pm 12.8 \pm 5.0$
CLEO-c [61, 62]	$\tau^+\nu$ ( $e^+\nu\bar{\nu}$ )	$(5.30 \pm 0.47 \pm 0.22)$	$242.9 \pm 10.8 \pm 5.3$
BaBar [57]	$\tau^+\nu$ ( $e^+(\mu^+)\nu\bar{\nu}$ )	$(5.00 \pm 0.35 \pm 0.49)$	$236.9 \pm 8.3 \pm 11.7$
Belle [58]	$\tau^+\nu$ ( $\pi^+\bar{\nu}$ )	$(6.04 \pm 0.43^{+0.46}_{-0.40})$	$260.3 \pm 9.3^{+10.1}_{-8.8}$
Belle [58]	$\tau^+\nu$ ( $e^+\nu\bar{\nu}$ )	$(5.37 \pm 0.33^{+0.35}_{-0.31})$	$244.5 \pm 7.5^{+8.2}_{-7.4}$
Belle [58]	$\tau^+\nu$ ( $\mu^+\nu\bar{\nu}$ )	$(5.86 \pm 0.37^{+0.34}_{-0.59})$	$255.4 \pm 8.0^{+7.6}_{-13.1}$
BES III [63]	$\tau^+\nu$ ( $\pi^+\bar{\nu}$ )	$(0.483 \pm 0.65 \pm 0.26)$	$231.9 \pm 15.7 \pm 6.5$
Our average	$\tau^+\nu$	$(5.51 \pm 0.20)$	$248.3 \pm 6.1$
Our average	$\mu^+\nu + \tau^+\nu$		$245.7 \pm 4.6$

\*We do not use a previous unpublished BaBar result from a subsample of data that uses a different technique for obtaining the branching fraction normalization [56].

$\tau^+\nu$  branching fractions in Table 71.3; this is the same as for  $D^+$  mesons. We also decrease the Babar and Belle  $\mu^+\nu$  branching fractions by the 1% structure-dependent correction [14]. This correction was already included in CLEO and BES results for the  $\mu^+\nu$  branching fractions in Table 71.3. We use the masses and lifetimes  $m_{D_s^+} = 1.96834(7)$  GeV,  $m_{\tau^+} = 1.7686(12)$  GeV, and  $\tau_{D_s^+} = 0.504(4)$  ps [64]. The inferred values for  $f_{D_s^+}|V_{cs}|$  are in good agreement for the  $\mu^+\nu$  and  $\tau^+\nu$  decay modes.

It is clear from the discussion of radiative corrections in this section that they are less well understood theoretically for  $D^+$  and  $D_s^+$  meson decays than for pions and kaons. We therefore assign a 2.8% systematic uncertainty to the purely leptonic decay rates, which is the full size of the applied radiative corrections. This translates to a 1.4% error on the products of the decay constant times CKM matrix element. Putting everything together, the main experimental pertaining charmed meson leptonic decays are (see the bottom lines of Tables 71.2 and 71.3):

$$|V_{cd}|f_{D^+} = 46.2 \pm 1.0 \pm 0.6 \text{ MeV}, \quad (71.15)$$

$$|V_{cs}|f_{D_s^+} = 245.7 \pm 3.1 \pm 3.4 \text{ MeV}, \quad (71.16)$$

where the errors are from the measured branching fractions and the applied radiative corrections, respectively.

### 71.3.2 Theoretical decay-constant calculations

Table 71.4 presents recent theoretical calculations of charmed heavy-light meson decay constants and their ratio in the isospin-symmetric limit  $m_u = m_d$ . (As in Sec. 71.2.2, we denote the physical  $D^+$ -meson decay constant by  $f_{D^+}$ , and use  $f_D$  for the isospin-symmetric value.) The upper two panels show results from lattice-QCD simulations with three ( $N_f = 2 + 1$ ) or four flavors ( $N_f = 2 + 1 + 1$ ) of dynamical quarks. Although there are fewer available results than for the pion and kaon sector, both  $f_D$  and  $f_{D_s}$  have been obtained using multiple sets of gauge-field configurations with different lattice fermion actions, providing independent confirmation. For comparison, the bottom panel of Table 71.4 shows QCD-model calculations of the  $D$ - and  $D_s$ -meson decay constants for which uncertainty estimates are provided. The lattice and non-lattice results agree, but numerical lattice-QCD simulations have now reached significantly greater precision than other approaches.

The lattice-QCD decay-constant results in Table 71.4 were all obtained using isospin-symmetric gauge-field configurations. As discussed in Sec. 71.2.2, however, the leading strong-isospin breaking corrections to heavy-light pseudoscalar-meson decay constants can be accounted for by using the physical down (or up) quark in

the  $D$  (or  $B$ ) meson. Strong-isospin breaking corrections to heavy-strange meson decay constants are roughly an order-of-magnitude smaller because there are no light valence quarks involved. Recently, the Fermilab Lattice and MILC Collaborations used this approach to calculate directly the dominant strong-isospin breaking corrections to both  $f_D$  and  $f_B$ , finding [28]

$$f_{D^+} - f_D = 0.58(1)(7) \text{ MeV}, \quad f_{B^+} - f_B = -0.53(5)(7) \text{ MeV}. \quad (71.17)$$

These results agree with independent estimates of the strong-isospin-breaking corrections to heavy-light meson decay constants from Borelized sum rules [80]. Combined with the determinations of  $f_D$  and  $f_B$  from the same work, Eq. (71.17) implies that the corrections to the SU(3)-flavor breaking ratios are

$$\frac{f_{D_s}}{f_{D^+}} = \frac{f_{D_s}}{f_D} (1 - 0.0027(3)), \quad \frac{f_{B_s}}{f_{B^+}} = \frac{f_{B_s}}{f_B} (1 + 0.0028(5)). \quad (71.18)$$

These estimated strong-isospin-breaking corrections to  $f_D$  and  $f_{D_s}/f_D$  above are commensurate with the uncertainties on the (2+1+1)-flavor FLAG averages in Table 71.4. Consequently, it is important to account isospin-breaking effects before combining the theoretical decay constants with the corresponding experimental decay rates.

To obtain the charged  $D^+$ -meson decay constant, we apply the correction in Eq. (71.17) to the (2+1+1)-flavor 2019 FLAG average for the  $D$ -meson decay constant in the isospin-symmetric limit. Similarly we use Eq. (71.18) to correct the (2+1+1)-flavor 2019 FLAG average for  $f_{D_s}/f_D$ . We take the four-flavor FLAG 2019 average for  $f_{D_s}$  directly. Our final preferred theoretical values for the charmed pseudoscalar-meson decay constants are

$$\begin{aligned} f_{D^+} &= 212.6(7) \text{ MeV}, \\ f_{D_s} &= 249.9(5) \text{ MeV}, \\ \frac{f_{D_s}}{f_{D^+}} &= 1.175(2). \end{aligned} \quad (71.19)$$

For all three quantities in Eq. (71.19), the uncertainties are roughly half the size of those in our previous review [26, 55].

**Table 71.4:** Recent theoretical determinations of  $f_D$ ,  $f_{D_s}$ , and their ratio in the isospin-symmetric limit. The upper panels show results from lattice-QCD simulations with  $(2 + 1 + 1)$  and  $(2 + 1)$  dynamical quark flavors, respectively. Statistical and systematic errors are quoted separately. The bottom panel shows estimates from QCD sum rules (QCD SR) and the light-front quark model (LFQM). These are not used to obtain our preferred decay-constant values.

Reference	Method	$N_f$	$f_D$ (MeV)	$f_{D_s}$ (MeV)	$f_{D_s}/f_D$
Fermilab/MILC 17 [28]	LQCD	2+1+1	212.1(0.3)(0.5)	249.9(0.3)(0.3)	1.1782(06)(15) <sup>*</sup>
ETM 14 [29]	LQCD	2+1+1	207.4(3.7)(0.9)	247.2(3.9)(1.4)	1.192(19)(11)
FLAG 19 average [18]	LQCD	2+1+1	212.0(0.7)	249.9(0.5)	1.1783(16)
RBC/UKQCD 18 [68] <sup>†</sup>	LQCD	2+1	–	–	1.1652(35) <sub>(<sup>+120</sup><sub>-57</sub>)</sub>
RBC/UKQCD 17 [69]	LQCD	2+1	208.7(2.8) <sub>(<sup>+2.1</sup><sub>-1.8</sub>)</sub>	246.4(1.3) <sub>(<sup>+1.3</sup><sub>-1.9</sub>)</sub>	1.1667(77) <sub>(<sup>+52</sup><sub>-43</sub>)</sub>
$\chi$ QCD 14 [70]	LQCD	2+1	–	254(2)(4)	–
HPQCD 12 [71]	LQCD	2+1	208.3(1.0)(3.3)	–	1.187(4)(12)
Fermilab/MILC 11 [72]	LQCD	2+1	218.9(9.2)(6.6)	260.1(8.9)(6.1)	1.188(14)(21)
HPQCD 10 [73]	LQCD	2+1	–	248.0(1.4)(2.1)	–
FLAG 19 average [18]	LQCD	2+1	209.0(2.4)	248.0(1.6)	1.174(7)
Wang 15 [74] <sup>‡</sup>	QCD SR	–	208(10)	240(10)	1.15(6)
Gelhausen 13 [75]	QCD SR	–	201 <sub>(<sup>+12</sup><sub>-13</sub>)</sub>	238 <sub>(<sup>+13</sup><sub>-23</sub>)</sub>	1.15 <sub>(<sup>+0.04</sup><sub>-0.05</sub>)</sub>
Narison 12 [76]	QCD SR	–	204(6)	246(6)	1.21(4)
Lucha 11 [77]	QCD SR	–	206.2(8.9)	245.3(16.3)	1.193(26)
Hwang 09 [78]	LFQM	–	–	264.5(17.5) <sup>§</sup>	1.29(7)

<sup>\*</sup>Ref. [28] provides values for  $f_D$  and  $f_{D_s}$  in the isospin-symmetric limit, but not for their ratio. Here we infer the central value from those of the individual decay constants, and take the statistical and systematic errors to be the same as for the physical ratio  $f_{D_s}/f_D$ .

<sup>†</sup>Preprint submitted to the arXiv and JHEP after the deadline for inclusion in the 2019 FLAG review.

<sup>‡</sup>Obtained using  $m_c^{\text{MS}}$ ; results using  $m_c^{\text{pole}}$  are also given in the paper.

<sup>§</sup>Obtained by combining PDG value  $f_D = 205.8(8.9)$  MeV [79] with  $f_{D_s}/f_D$  from this work.

## 71.4 Bottom mesons

### 71.4.1 Experimental rate measurements

The Belle and BaBar collaborations have found evidence for  $B^- \rightarrow \tau^- \bar{\nu}$  decay in  $e^+e^- \rightarrow B^-B^+$  collisions at the  $\Upsilon(4S)$  energy. The analysis relies on reconstructing a hadronic or semileptonic  $B$  decay tag, finding a  $\tau$  candidate in the remaining track and photon candidates, and examining the extra energy in the event which should be close to zero for a real  $\tau^-$  decay to  $e^- \nu \bar{\nu}$  or  $\mu^- \nu \bar{\nu}$  opposite a  $B^+$  tag. While the BaBar results have remained unchanged, Belle reanalyzed both samples of their data. The branching fraction using hadronic tags changed from  $1.79^{+0.56+0.46}_{-0.49-0.51} \times 10^{-4}$  [81] to  $0.72^{+0.27}_{-0.25} \pm 0.11 \times 10^{-4}$  [82], while the corresponding change using semileptonic tags was from  $1.54^{+0.38+0.29}_{-0.37-0.31}$  to  $1.25 \pm 0.28 \pm 0.27$ . These changes demonstrate the difficulty of the analysis. The results are listed in Table 71.5.

**Table 71.5:** Experimental results for  $\mathcal{B}(B^- \rightarrow \tau^- \bar{\nu})$  and  $|V_{ub}|f_{B^+}$ . To extract the values of  $|V_{ub}|f_{B^+}$  via Eq. (71.1), we use the PDG 2018 value of the  $B^+$  lifetime of  $1.638 \pm 0.004$  ps, and the  $\tau^+$  and  $B^+$  masses of 1.77686 and 5.27933 GeV, respectively.

Experiment	Tag	$\mathcal{B}$ (units of $10^{-4}$ )	$ V_{ub} f_{B^+}$ (MeV)
Belle [82]	Hadronic	$0.72^{+0.27}_{-0.25} \pm 0.11$	
Belle [83]	Semileptonic	$1.25 \pm 0.28 \pm 0.27$	
Belle [83]	Average	$0.91 \pm 0.22$	$0.72 \pm 0.09$
BaBar [84]	Hadronic	$1.83^{+0.53}_{-0.49} \pm 0.24$	
BaBar [85]	Semileptonic	$1.7 \pm 0.8 \pm 0.2$	
BaBar [84]	Average	$1.79 \pm 0.48$	$1.01 \pm 0.14$
Our average		$1.06 \pm 0.20$	$0.77 \pm 0.07$

Because there are large backgrounds under the signals for these measurements, as well as substantial systematic errors, the significances of the individual results are still below the  $5\sigma$  discovery threshold. Belle quotes  $4.6\sigma$  for their combined hadronic and semileptonic tags, while BaBar quotes  $3.3\sigma$  and  $2.3\sigma$ , for hadronic and semileptonic tags. Greater precision is necessary to determine if any effects beyond the Standard Model are present.

We do not correct the measured branching ratios in Table 71.5 for radiative corrections because the experimental uncertainties are so large. The radiative corrections are expected to be bigger, however, for  $B \rightarrow \mu\nu$  leptonic decays because the corrections are

no longer helicity suppressed [6], and may be a significant fraction of the purely leptonic rate. More theoretical work is needed to understand radiative corrections to leptonic  $B$  decays in anticipation of future measurements with greater precision, and of new decay channels.

### 71.4.2 Theoretical decay-constant calculations

Table 71.6 presents recent theoretical calculations of bottom heavy-light meson decay constants and their ratio in the isospin-symmetric limit  $m_u = m_d$ . The upper two panels show results from lattice-QCD simulations with three ( $N_f = 2 + 1$ ) or four flavors ( $N_f = 2 + 1 + 1$ ) of dynamical quarks. For all decay constants, calculations using different gauge-field configurations, light-quark actions, and  $b$ -quark actions provide independent confirmation. For comparison, the bottom panel of Table 71.6 shows QCD-model calculations of the  $B^-$  and  $B_s^-$ -meson decay constants for which uncertainty estimates are provided. These are consistent with the lattice values, but with much larger uncertainties.

The lattice-QCD decay-constant results in Table 71.6 were all obtained using isospin-symmetric gauge-field configurations. Some calculations, however, account for the dominant effect of strong-isospin-breaking by using the correct value for the valence light-quark mass in the  $B$  meson ( $m_u$  for  $f_{B^+}$  and  $m_d$  for  $f_{B^0}$ ). Early estimates of the strong-isospin-breaking correction obtained  $f_{B^+} - f_B \sim 2$  MeV [88, 90], which would significant given the present lattice-QCD uncertainties. It turns out, however, that these calculations inadvertently introduced a spurious sea-quark contribution, and therefore overestimated the size of the effect. A more recent calculation by the Fermilab/MILC Collaboration finds very little evidence for isospin violation ( $f_{B^+} - f_B \sim 0.5$  MeV) [28], which is more than two times smaller than the total uncertainties on present lattice-QCD calculations. For this reason, we quote isospin averages in the current review.

Our preferred theoretical values for the bottom pseudoscalar-meson decay constants are

$$\begin{aligned}
 f_B &= 190.0(1.3) \text{ MeV}, \\
 f_{B_s} &= 230.0(1.3) \text{ MeV}, \\
 \frac{f_{B_s}}{f_B} &= 1.209(5),
 \end{aligned} \tag{71.20}$$

which are simply the  $N_f = 2 + 1 + 1$  FLAG 2019 averages [18]. Because the uncertainties on the three-flavor results in Table 71.6

**Table 71.6:** Recent theoretical determinations of  $f_B$ ,  $f_{B_s}$ , and their ratio in the isospin-symmetric limit. The upper panels show results from lattice-QCD simulations with  $(2+1+1)$  and  $(2+1)$  dynamical quark flavors, respectively. When available, statistical and systematic errors are quoted separately. The bottom panel shows estimates from the relativistic potential model (RPM), QCD sum rules, and the light-front quark model, which are not used to obtain our preferred decay-constant values.

Reference	Method	$N_f$	$f_B$ (MeV)	$f_{B_s}$ (MeV)	$f_{B_s}/f_B$
FNAL/MILC 17 [28]	LQCD	2+1+1	189.9(1.4)	230.7(1.2)	1.2180(49)
HPQCD 17 [86]*	LQCD	2+1+1	196(6)	236(7)	1.207(7)
ETM 16 [87]	LQCD	2+1+1	193(6)	229(5)	1.184(25)
HPQCD 13 [88]	LQCD	2+1+1	186(4)	224(5)	1.217(8)
FLAG 19 average [18]	LQCD	2+1+1	190.0(1.3)	230.3(1.3)	1.209(5)
Aoki 14 [89] <sup>†</sup>	LQCD	2+1	218.8(6.5)(30.8)	263.5(4.8)(36.7)	1.193(20)(44)
RBC/UKQCD 14 [90] <sup>‡</sup>	LQCD	2+1	195.6(6.4)(13.3)	235.4(5.2)(11.1)	1.223(14)(70)
HPQCD 12 [91]	LQCD	2+1	191(1)(8)	228(3)(10)	1.188(12)(13)
HPQCD 12 [91]	LQCD	2+1	189(3)(3)*	–	–
HPQCD 11 [92]	LQCD	2+1	–	225(3)(3)	–
Fermilab/MILC 11 [72]	LQCD	2+1	196.9(5.5)(7.0)	242.0(5.1)(8.0)	1.229(13)(23)
FLAG 19 average [18]	LQCD	2+1	192.0(4.3)	228.4(3.7)	1.201(16)
Sun 16 [93] <sup>§</sup>	RPM		219(15)	266(19)	1.21(9)
Wang 15 [74] <sup>§</sup>	QCD SR		194(15)	231(16)	1.19(10)
Baker 13 [94]	QCD SR		186(14)	222(12)	1.19(4)
Lucha 13 [95]	QCD SR		192.0(14.6)	228.0(19.8)	1.184(24)
Gelhausen 13 [75]	QCD SR		207 <sup>(+17)</sup> <sub>(-9)</sub>	242 <sup>(+17)</sup> <sub>(-12)</sub>	1.17 <sup>(+3)</sup> <sub>(-4)</sub>
Narison 12 [76]	QCD SR		206(7)	234(5)	1.14(3)
Hwang 09 [78]	LFQM		–	270.0(42.8) <sup>¶</sup>	1.32(8)

\*Re-analysis of data from HPQCD 13.

<sup>†</sup>Obtained with static  $b$  quarks (*i.e.*  $m_b \rightarrow \infty$ ).

<sup>‡</sup>Ref. [90] does not provide results in the isospin-symmetric limit, so we show  $f_{B^+}$  and  $f_{B_s}/f_{B^+}$  for this work. dsdecaycons:foot:ddag3

<sup>§</sup>Obtained using  $m_b^{\overline{\text{MS}}}$ ; results using  $m_b^{\text{pole}}$  are also given in the paper.

<sup>¶</sup>Obtained by combining PDG value  $f_B = 204(31)$  MeV [79] with  $f_{B_s}/f_B$  from this work. dsdecaycons:foot:mpar3

are substantially larger than those on the four-flavor results, including them in the average leaves the central values unchanged, and decreases the errors only slightly.

## 71.5 Phenomenological implications

### 71.5.1 $|V_{ud}|$ , $|V_{us}|$ , and status of first-row unitarity

Using the average values for  $f_{\pi^+}|V_{ud}|$ ,  $f_{K^+}|V_{us}|$ , and their ratio from Eqs. (71.10)–(71.12) and for  $f_{\pi^+}$ ,  $f_{K^+}$ , and their ratio from Eq. (71.14), we obtain the following determinations of the CKM matrix elements  $|V_{ud}|$ ,  $|V_{us}|$ , and their ratio from leptonic decays within the standard model:

$$|V_{ud}| = 0.9764(2)(90)(10), \quad |V_{us}| = 0.2254(3)(4)(3),$$

$$\frac{|V_{us}|}{|V_{ud}|} = 0.2313(2)4(2), \quad (71.21)$$

where the errors are from the experimental branching fraction(s), the pseudoscalar decay constant(s), and radiative corrections, respectively. These results enable a precise test of the unitarity of the first row of the CKM matrix from leptonic decays alone (the contribution from  $|V_{ub}|$  is negligible). Using the values of  $|V_{ud}|$  and  $|V_{us}|$  from Eq. (71.21), we find

$$|V_{ud}|^2 + |V_{us}|^2 + |V_{ub}|^2 - 1 = 0.004(18), \quad (71.22)$$

which is consistent with three-generation unitarity at the few-percent level.

The determinations of  $|V_{ud}|$  and  $|V_{us}|$  from leptonic decays in Eq. (71.21) can be compared to those obtained from other processes. The result above for  $|V_{ud}|$  agrees with the determination from superallowed  $\beta$ -decay,  $|V_{ud}| = 0.97420(21)$  [96], but has an error about forty times larger that is primarily due to the uncertainty in the theoretical determination of  $f_{\pi^+}$ . The CKM element  $|V_{us}|$  can be determined from semileptonic  $K^+ \rightarrow \pi^0 \ell^+ \nu$  decay. Here experimental measurements provide a value for the product  $f_+^{K\pi}(0)|V_{us}|$ , where  $f_+^{K\pi}(0)$  is the form-factor at zero four-momentum transfer between the initial state kaon and the final state pion. Taking the most recent experimental determination

of  $|V_{us}|f_+^{K\pi}(0) = 0.2165(4)$  from Moulson [37]<sup>5</sup> and the 2019  $(2+1+1)$ -flavor FLAG average for  $f_+(0)^{K\pi} = 0.9706(27)$  [18] based on the calculations of ETM [100] and Fermilab/MILC [101] gives  $|V_{us}| = 0.2231(6)_{\text{LQCD}}(4)_{\text{exp}}$  from  $K_{\ell 3}$  decay. The determinations of  $|V_{us}|$  from leptonic and semileptonic kaon decays are both quite precise (with the error from leptonic decay being about 25% smaller), but the central values differ by  $2.5\sigma$ . (This difference would be reduced to  $1.8\sigma$ , but not eliminated, using the  $(2+1)$ -flavor FLAG average for  $f_+(0)^{K\pi} = 0.9677(27)$  instead.) Finally, the combination of the ratio  $|V_{us}|/|V_{ud}|$  from leptonic decays [Eq. (71.21)] with  $|V_{ud}|$  from  $\beta$  decay implies an alternative determination of  $|V_{us}| = 0.2254(5)$  which agrees with the value from leptonic kaon decay, but disagrees with the  $K_{\ell 3}$ -decay result at the  $1.8\sigma$  level.

Given the roughly  $2\sigma$  tension between  $|V_{us}|$  from leptonic and semileptonic kaon decays, it is important to scrutinize the uncertainties on the theoretical and experimental inputs to  $|V_{us}|$  and other elements of the first row of the CKM matrix. Recently, Seng *et al.* introduced a new approach for calculating radiative corrections to neutron and nuclear beta decays using dispersion relations [102–105]. These calculations imply a lower value of  $|V_{ud}| = 0.97395(23)$  than the Hardy and Towner analysis [106] by almost  $1\sigma$ . An independent calculation of the radiative corrections by Czarnecki and Marciano using QCD sum rules yields similar results [107]. Using this value of  $|V_{ud}|$  with the determination of  $|V_{us}|$  from leptonic kaon decays in Eq. (71.21), we obtain  $|V_{ud}|^2 + |V_{us}|^2 + |V_{ub}|^2 - 1 = -0.0006(5)$ , again (roughly) consistent with first-row unitarity.

Last, we combine the experimental measurement of  $f_{\pi^+}|V_{ud}|$  in Eq. (71.10) with  $|V_{ud}|$  from superallowed  $\beta$ -decay [96] to infer an “experimental” value for the pion decay constant:

$$f_{\pi^-}^{\text{“exp”}} = 130.50(2)(3)(13) \text{ MeV}, \quad (71.23)$$

<sup>5</sup>This is an update of the 2010 Flavianet review [38] that includes new measurements of the  $K_S$  lifetime [97, 98],  $\text{Re}(\epsilon'/\epsilon)$  [98], and  $\mathcal{B}(K^\pm \rightarrow \pi^\pm \pi^+ \pi^-)$  [99]. The latter measurement is the primary source of the reduced error on  $\mathcal{B}(K_{\ell 3})$ , via the constraint that the sum of all branching ratios must equal unity.



where the uncertainties are from the errors on  $\Gamma$ ,  $|V_{ud}|$ , and higher-order corrections, respectively. Many recent (2+1+1)-flavor lattice-QCD calculations use this quantity to set the overall physical scale in their simulations, *e.g.*, Refs. [7, 28–30]. Conversely, comparing  $f_{\pi^-}^{\text{exp}}$  with the 2019 FLAG (2+1)-flavor average  $f_{\pi^+} = 130.2(8)$  MeV, which only includes lattice-QCD results that employ observables to set the scale [31–36], provides a test of lattice-QCD methods. The values are in good agreement within present uncertainties. We do not quote an “experimental” value for the kaon decay constant because the value of  $|V_{us}|$  is less clear given the  $\sim 2\sigma$  tension between the values of  $|V_{us}|$  obtained from leptonic and semileptonic kaon decays.

### 71.5.2 $|V_{cd}|$ , $|V_{cs}|$ , and status of second-row unitarity

Using the average values for  $|V_{cd}|f_{D^+}$  and  $|V_{cs}|f_{D_s^+}$  from Eqs. (71.15) and (71.16), and for  $f_{D^+}$  and  $f_{D_s^+}$  from Eq. (71.19), we obtain the following determinations of the CKM matrix elements  $|V_{cd}|$  and  $|V_{cs}|$  from leptonic decays within the standard model:

$$|V_{cd}| = 0.217(5)(3)(1) \quad \text{and} \quad |V_{cs}| = 0.983(13)(14)(2), \quad (71.24)$$

where the errors are from the measured branching fractions, radiative corrections, and decay constants, respectively. These results enable a test of the unitarity of the second row of the CKM matrix. We obtain

$$|V_{cd}|^2 + |V_{cs}|^2 + |V_{cb}|^2 - 1 = 0.016(37), \quad (71.25)$$

in agreement with three-generation unitarity.

The uncertainty on  $|V_{cd}|$  in Eq. (71.24) is limited by the measurement error on the  $D^+ \rightarrow \mu^+\nu$  decay rate. For  $|V_{cs}|$ , however, the experimental and radiative-correction errors are commensurate. It is worth noting that the value of  $|V_{cs}|$  from leptonic  $D_s$  decays has decreased substantially from the value of 1.007(17) in the previous version of this review [26, 55], and is now below unity as expected in the three-generation CKM framework. This change is due to our new, more consistent treatment of the radiative corrections, which lower the purely leptonic decay rates for the  $\mu^+\nu$  and  $\tau^+\nu$  channels by 2.8% and 1%, respectively. We emphasize, however, that we have taken a generous 100% uncertainty on these estimates, and that more theoretical work is needed to really pin down the sizes of the radiative corrections to  $D_{(s)}$ -meson leptonic decays.

The CKM matrix elements  $|V_{cd}|$  and  $|V_{cs}|$  can also be obtained from semileptonic  $D^+ \rightarrow \pi^0\ell^+\nu$  and  $D_s^+ \rightarrow K^0\ell^+\nu$  decays, respectively. Here experimental measurements determine the product of the form factor times the CKM element, and theory provides the value for the form factor at zero four-momentum transfer between the initial  $D_{(s)}$  meson and the final pion or kaon. The latest experimental averages from the Heavy Flavor Averaging Group (HFLAV) are  $f_+^{D\pi}(0)|V_{cd}| = 0.1426(19)$  and  $f_+^{D_s K}(0)|V_{cs}| = 0.7226(34)$  [108]. There are not enough published lattice-QCD calculations of the zero-momentum  $D_{(s)}$ -meson semileptonic form factors with  $N_f \geq 3$  to permit an average by the FLAG Collaboration. Taking the most precise three-flavor form-factor results  $f_+^{D\pi}(0) = 0.666(29)$  and  $f_+^{D_s K}(0) = 0.747(19)$  from the HPQCD Collaboration [109, 110] gives for the CKM matrix elements  $|V_{cd}| = 0.2141(97)$  and  $|V_{cs}| = 0.967(25)$ , in agreement with those from leptonic decays in Eq. (71.24). A newer, four-flavor calculation of the form factors by the ETM Collaboration, however, yields a smaller value of  $f_+^{D\pi}(0) = 0.612(35)$  by  $1.2\sigma$  and a larger  $f_+^{D_s K}(0) = 0.765(31)$  by  $0.5\sigma$ . These imply  $|V_{cd}| = 0.233(14)$  and  $|V_{cs}| = 0.945(39)$ , which are about  $1\sigma$  above and below the values from leptonic decays in Eq. (71.24), respectively. Independent lattice-QCD calculations of the  $D^+ \rightarrow \pi^0\ell^+\nu$  and  $D_s^+ \rightarrow K^0\ell^+\nu$  form factors now in progress [111, 112] may help clarify the picture.

We can combine the experimental measurements of  $f_{D^+}|V_{cd}|$  and  $f_{D_s^+}|V_{cs}|$  from Tables 71.2 and 71.3 with  $|V_{cd}| = 0.22438(44)$  and  $|V_{cs}| = 0.97359(10)$  from the PDG 2018 global unitarity-triangle analysis [64] to infer “experimental” values for the decay

constants within the standard model. We take the CKM elements from the global fit because they are based on many input quantities, thereby reducing the sensitivity to any one outlying measurement or calculation. We obtain for the decay constants

$$\begin{aligned} f_{D^+}^{\text{exp}} &= 205.8(4.5)(0.4)(2.7) \text{ MeV}, \\ f_{D_s^+}^{\text{exp}} &= 252.4(3.2)(0.03)(3.5) \text{ MeV}, \\ \left(\frac{f_{D_s^+}}{f_{D^+}}\right)^{\text{exp}} &= 1.226(31)(2)(3). \end{aligned} \quad (71.26)$$

where the uncertainties are from the errors on  $\Gamma^{(0)}$ , CKM matrix elements, and radiative corrections, respectively. For the decay-constant ratio, we expect most of the radiative corrections to cancel, and therefore multiply the 1.4% error from Sec. 71.3.1 by the SU(3)-breaking factor  $(m_s - m_d)/\Lambda_{\text{QCD}} \sim 1/5$ . The “experimental” values  $f_{D^+}$  ( $f_{D_s^+}/f_{D^+}$ ) are about  $1.3\sigma$  lower ( $1.6\sigma$  higher) than the (2+1+1)-flavor lattice-QCD averages in Eq. (71.19). The CKM matrix element  $|V_{cd}|$  is, however, proportional to  $|V_{us}|$  within the Wolfenstein parameterization [113, 114]. Thus, resolving the inconsistencies between determinations of  $|V_{us}|$  from leptonic and semileptonic decays discussed in Sec. 71.5.1 may also reduce the mild tensions observed here.

Last, we can test lepton-flavor universality in charm meson decays by checking the following relationship derived from Eq. (71.1):

$$\frac{\Gamma(D_s^+ \rightarrow \tau^+\nu)}{\Gamma(D_s^+ \rightarrow \mu^+\nu)} = \frac{m_\tau^2(1 - m_\tau^2/M_{D_s}^2)^2}{m_\mu^2(1 - m_\mu^2/M_{D_s}^2)^2} = 9.75, \quad (71.27)$$

where the uncertainties from the masses are negligible to the number of digits quoted. The measured ratio of  $\tau^+\nu$  to  $\mu^+\nu$  rates is  $9.98 \pm 0.46$ , consistent with the standard-model expectation.

### 71.5.3 $|V_{ub}|$ and other applications

Using the average value for  $|V_{ub}|f_{B^+}$  from Table 71.5, and for  $f_{B^+}$  from Eq. (71.20), we obtain the following determination of the CKM matrix element  $|V_{ub}|$  from leptonic decays within the standard model:

$$|V_{ub}| = 4.05(37)(3) \times 10^{-3}, \quad (71.28)$$

where the errors are from experiment and theory, respectively. One should bear in mind when interpreting Eq. (71.28) that none of the experimental measurements that enter the average for  $|V_{ub}|f_{B^+}$  have individually reached the  $5\sigma$  discovery level (see Sec. 71.4.1). Further, decays involving the third generation of quarks and leptons may be particularly sensitive to new physics associated with electroweak symmetry breaking due to their larger masses [10, 12], so Eq. (71.28) is more likely to be influenced by new physics than the determinations of the elements of the first and second rows of the CKM matrix in the previous sections.

The CKM element  $|V_{ub}|$  can also be obtained from semileptonic  $B$ -meson decays. For more than a decade, there has remained a persistent 2-3 $\sigma$  tension between the determinations of  $|V_{ub}|$  from exclusive  $B \rightarrow \pi\ell\nu$  decay and from inclusive  $B \rightarrow X_u\ell\nu$  decay, where  $X_u$  denotes all hadrons which contain a constituent up quark [21, 108, 115–118]. The currently most precise determination of  $|V_{ub}|^{\text{excl}} = 3.73(14) \times 10^{-3}$  is obtained from a joint  $z$ -fit by FLAG [18] of the vector and scalar form factors  $f_+^{B\pi}(q^2)$  and  $f_0^{B\pi}(q^2)$  calculated in (2+1)-flavor lattice QCD [119–121] and experimental measurements of the differential decay rate from BaBar [122, 123] and Belle [124, 125]. On the other hand, the PDG 2018 inclusive determination obtained using the theoretical frameworks in Refs. [126–128] is  $|V_{ub}|^{\text{incl}} = 4.49(28) \times 10^{-3}$  [64, 129]. The value of  $|V_{ub}|$  from leptonic  $B \rightarrow \tau\nu$  decay in Eq. (71.28) splits the difference between the inclusive and exclusive determinations, and is compatible (within large uncertainties) with both.

Given the large uncertainties on the experimental measurements of  $\mathcal{B}(B^- \rightarrow \tau^-\bar{\nu})$ , and the more than  $2\sigma$  disagreement between  $|V_{ub}|$  obtained from inclusive and exclusive semileptonic  $B$  decays, we do not present an “experimental” value of the decay constant  $f_{B^+}$ .

## Acknowledgements

We thank V. Cirigliano, C. Davies, A. El Khadra, A. Khodjamirian, A. Kronfeld, J. Laiho, W. Marciano, M. Moulson, S. Narison, S. Sharpe, and Z.-G. Wang for useful discussions on this and previous versions of the review. We thank M. Della Morte and S. Simula for valuable feedback on the manuscript, and for providing information on the 2019 FLAG lattice averages. We gratefully acknowledge support of the U. S. National Science Foundation and the U. S. Department of Energy through Grant No. DE-FG02-13ER41598. The work of J. L. R. was performed in part at the Aspen Center for Physics, which is supported by National Science Foundation grant PHY-1066293. Fermilab is operated by the Fermi Research Alliance, LLC, under Contract No. DE-AC02-07CH11359 with the U.S. Department of Energy, Office of Science, Office of High Energy Physics.

## References

- [1] A. Sirlin, Nucl. Phys. **B196**, 83 (1982).
- [2] T. Kinoshita, Phys. Rev. Lett. **2**, 477 (1959).
- [3] M. Knecht *et al.*, Eur. Phys. J. **C12**, 469 (2000), [hep-ph/9909284].
- [4] G. Burdman, J. T. Goldman and D. Wyler, Phys. Rev. **D51**, 111 (1995), [hep-ph/9405425].
- [5] V. Cirigliano and I. Rosell, JHEP **10**, 005 (2007), [arXiv:0707.4464].
- [6] D. Becirevic, B. Haas and E. Kou, Phys. Lett. **B681**, 257 (2009), [arXiv:0907.1845].
- [7] A. Bazavov *et al.* (Fermilab Lattice and MILC), Phys. Rev. **D90**, 074509 (2014), [arXiv:1407.3772].
- [8] M. Di Carlo *et al.*, Phys. Rev. **D100**, 034514 (2019), [arXiv:1904.08731].
- [9] E. Barberio and Z. Was, Comput. Phys. Commun. **79**, 291 (1994).
- [10] W.-S. Hou, Phys. Rev. **D48**, 2342 (1993).
- [11] A. G. Akeroyd and S. Recksiegel, Phys. Lett. **B554**, 38 (2003), [hep-ph/0210376].
- [12] A. G. Akeroyd and S. Recksiegel, J. Phys. **G29**, 2311 (2003), [hep-ph/0306037].
- [13] A. G. Akeroyd, Prog. Theor. Phys. **111**, 295 (2004), [hep-ph/0308260].
- [14] B. A. Dobrescu and A. S. Kronfeld, Phys. Rev. Lett. **100**, 241802 (2008), [arXiv:0803.0512].
- [15] J. L. Hewett, in “Heavy flavor physics. Proceedings, LISHEP 95, LAFEX International School on High-Energy Physics, session C, cbt Workshop, Rio de Janeiro, Brazil, February 21-23, 1995,” 171–187 (1995), [hep-ph/9505246], URL <http://www-public.slac.stanford.edu/sciDoc/docMeta.aspx?slacPubNumber=SLAC-PUB-6821>.
- [16] A. Crivellin, Phys. Rev. **D81**, 031301 (2010), [arXiv:0907.2461].
- [17] F. U. Bernlochner, Z. Ligeti and S. Turczyk, Phys. Rev. **D90**, 094003 (2014), [arXiv:1408.2516].
- [18] S. Aoki *et al.* (Flavour Lattice Averaging Group) (2019), [arXiv:1902.08191].
- [19] W. J. Marciano, Phys. Rev. Lett. **93**, 231803 (2004), [hep-ph/0402299].
- [20] V. Cirigliano *et al.*, Rev. Mod. Phys. **84**, 399 (2012), [arXiv:1107.6001].
- [21] K. A. Olive *et al.* (Particle Data Group), Chin. Phys. **C38**, 090001 (2014).
- [22] B. Ananthanarayan and B. Moussallam, JHEP **06**, 047 (2004), [hep-ph/0405206].
- [23] S. Descotes-Genon and B. Moussallam, Eur. Phys. J. **C42**, 403 (2005), [hep-ph/0505077].
- [24] W. J. Marciano and A. Sirlin, Phys. Rev. Lett. **71**, 3629 (1993).
- [25] V. Cirigliano and H. Neufeld, Phys. Lett. **B700**, 7 (2011), [arXiv:1102.0563].
- [26] J. L. Rosner, S. Stone and R. S. Van de Water (2015), review prepared for PDG 2015 edition, [arXiv:1509.02220].
- [27] J. Gasser, A. Rusetsky and I. Scimemi, Eur. Phys. J. **C32**, 97 (2003), [hep-ph/0305260].
- [28] A. Bazavov *et al.*, Phys. Rev. **D98**, 7, 074512 (2018), [arXiv:1712.09262].
- [29] N. Carrasco *et al.* (ETM), Phys. Rev. **D91**, 054507 (2015), [arXiv:1411.7908].
- [30] R. Dowdall *et al.* (HPQCD), Phys. Rev. **D88**, 074504 (2013), [arXiv:1303.1670].
- [31] V. G. Bornyakov *et al.* (QCDSF-UKQCD), Phys. Lett. **B767**, 366 (2017), [arXiv:1612.04798].
- [32] S. Durr *et al.*, Phys. Rev. **D95**, 5, 054513 (2017), [arXiv:1601.05998].
- [33] T. Blum *et al.* (RBC, UKQCD), Phys. Rev. **D93**, 074505 (2016), [arXiv:1411.7017].
- [34] A. Bazavov *et al.* (MILC), PoS **LATTICE2010**, 074 (2010), [arXiv:1012.0868].
- [35] S. Durr *et al.* (BMW), Phys. Rev. **D81**, 054507 (2010), [arXiv:1001.4692].
- [36] E. Follana *et al.* (HPQCD, UKQCD), Phys. Rev. Lett. **100**, 062002 (2008), [arXiv:0706.1726].
- [37] M. Moulson, in “8th International Workshop on the CKM Unitarity Triangle (CKM2014) Vienna, Austria, September 8-12, 2014,” (2014), [arXiv:1411.5252].
- [38] M. Antonelli *et al.* (FlaviaNet Working Group on Kaon Decays), Eur. Phys. J. **C69**, 399 (2010), [arXiv:1005.2323].
- [39] S. Hashimoto, J. Laiho and S. R. Sharpe, “Lattice Quantum Chromodynamics,” <http://pdg.lbl.gov/2019/reviews/rpp2018-rev-lattice-qcd.pdf> (2017), review prepared for PDG 2018 edition.
- [40] S. Aoki *et al.* (Flavour Lattice Averaging Group), Eur. Phys. J. **C74**, 2890 (2014), [arXiv:1310.8555].
- [41] S. Aoki *et al.*, Eur. Phys. J. **C77**, 2, 112 (2017), [arXiv:1607.00299].
- [42] A. S. Kronfeld, Ann. Rev. Nucl. Part. Sci. **62**, 265 (2012), [arXiv:1203.1204].
- [43] M. Artuso *et al.* (CLEO), Phys. Rev. Lett. **95**, 251801 (2005), [hep-ex/0508057].
- [44] B. I. Eisenstein *et al.* (CLEO), Phys. Rev. **D78**, 052003 (2008), [arXiv:0806.2112].
- [45] M. Ablikim *et al.* (BESIII), Phys. Rev. **D89**, 051104 (2014), [arXiv:1312.0374].
- [46] M. Artuso *et al.* (CLEO), Phys. Rev. Lett. **99**, 071802 (2007), [arXiv:0704.0629].
- [47] J. P. Alexander *et al.* (CLEO), Phys. Rev. **D79**, 052001 (2009), [arXiv:0901.1216].
- [48] M. Ablikim *et al.* (BESIII) (2019), [arXiv:1908.08877].
- [49] A. V. Manohar, C. T. Sachrajda and R. M. Barnett, “Quark Masses,” <http://pdg.lbl.gov/2019/reviews/rpp2018-rev-quark-masses.pdf> (2018), review prepared for PDG 2018 update.
- [50] G. M. de Divitiis *et al.*, JHEP **04**, 124 (2012), [arXiv:1110.6294].
- [51] J. Gasser and H. Leutwyler, Nucl. Phys. **B250**, 465 (1985).
- [52] G. M. de Divitiis *et al.* (RM123), Phys. Rev. **D87**, 11, 114505 (2013), [arXiv:1303.4896].
- [53] M. Nobes (2005), [hep-lat/0501009].
- [54] A. Bazavov *et al.* (Fermilab Lattice, MILC), Phys. Rev. **D93**, 11, 113016 (2016), [arXiv:1602.03560].
- [55] C. Patrignani *et al.* (Particle Data Group), Chin. Phys. **C40**, 10, 100001 (2016).

- [56] J. P. Lees *et al.* (BaBar) (2010), [arXiv:1003.3063].
- [57] P. del Amo Sanchez *et al.* (BaBar), Phys. Rev. **D82**, 091103 (2010), [Erratum: Phys. Rev.D91,no.1,019901(2015)], [arXiv:1008.4080].
- [58] A. Zupanc *et al.* (Belle), JHEP **1309**, 139 (2013), [arXiv:1307.6240].
- [59] M. Ablikim *et al.* (BESIII), Phys. Rev. Lett. **122**, 071802 (2019), [arXiv:1811.10890].
- [60] P. Naik *et al.* (CLEO), Phys. Rev. **D80**, 112004 (2009), [arXiv:0910.3602].
- [61] K. M. Ecklund *et al.* (CLEO), Phys. Rev. Lett. **100**, 161801 (2008), [arXiv:0712.1175].
- [62] P. U. E. Onyisi *et al.* (CLEO), Phys. Rev. **D79**, 052002 (2009), [arXiv:0901.1147].
- [63] M. Ablikim *et al.* (BESIII), Phys. Rev. **D94**, 072004 (2016), [arXiv:1608.06732].
- [64] M. Tanabashi *et al.* (Particle Data Group), Phys. Rev. **D98**, 3, 030001 (2018).
- [65] T. K. Pedlar *et al.* (CLEO), Phys. Rev. **D76**, 072002 (2007), [arXiv:0704.0437].
- [66] J. P. Alexander *et al.* (CLEO), Phys. Rev. Lett. **100**, 161804 (2008), [arXiv:0801.0680].
- [67] B. Aubert *et al.* (BaBar), Phys. Rev. Lett. **98**, 141801 (2007), [hep-ex/0607094].
- [68] P. A. Boyle *et al.* (RBC/UKQCD) (2018), [arXiv:1812.08791].
- [69] P. A. Boyle *et al.*, JHEP **12**, 008 (2017), [arXiv:1701.02644].
- [70] Y.-B. Yang *et al.* ( $\chi$ QCD), Phys. Rev. **D92**, 034517 (2015), [arXiv:1410.3343].
- [71] H. Na *et al.* (HPQCD), Phys. Rev. **D86**, 054510 (2012), [arXiv:1206.4936].
- [72] A. Bazavov *et al.* (Fermilab Lattice and MILC), Phys. Rev. **D85**, 114506 (2012), [arXiv:1112.3051].
- [73] C. T. H. Davies *et al.* (HPQCD), Phys. Rev. **D82**, 114504 (2010), [arXiv:1008.4018].
- [74] Z.-G. Wang, Eur. Phys. J. **C75**, 427 (2015), [arXiv:1506.01993].
- [75] P. Gelhausen *et al.*, Phys.Rev. **D88**, 014015 (2013), [arXiv:1305.5432].
- [76] S. Narison, Phys. Lett. **B718**, 1321 (2013), [arXiv:1209.2023].
- [77] W. Lucha, D. Melikhov and S. Simula, Phys. Lett. **B701**, 82 (2011), [arXiv:1101.5986].
- [78] C.-W. Hwang, Phys. Rev. **D81**, 054022 (2010), [arXiv:0910.0145].
- [79] C. Amsler *et al.* (Particle Data Group), Phys. Lett. **B667**, 1 (2008), and 2009 partial update for the 2010 edition.
- [80] W. Lucha, D. Melikhov and S. Simula, Eur. Phys. J. **C78**, 2, 168 (2018), [Erratum: Eur. Phys. J.C78,no.11,936(2018)], [arXiv:1702.07537].
- [81] K. Ikado *et al.* (Belle), Phys. Rev. Lett. **97**, 251802 (2006), [hep-ex/0604018].
- [82] I. Adachi *et al.* (Belle), Phys. Rev. Lett. **110**, 131801 (2013), [arXiv:1208.4678].
- [83] B. Kronenbitter *et al.* (Belle), Phys. Rev. **D92**, 051102 (2015), [arXiv:1503.05613].
- [84] J. P. Lees *et al.* (BaBar), Phys. Rev. **D88**, 031102 (2013), [arXiv:1207.0698].
- [85] B. Aubert *et al.* (BaBar), Phys. Rev. **D81**, 051101 (2010), [arXiv:0912.2453].
- [86] C. Hughes, C. T. H. Davies and C. J. Monahan, Phys. Rev. **D97**, 5, 054509 (2018), [arXiv:1711.09981].
- [87] A. Bussone *et al.* (ETM), Phys. Rev. **D93**, 11, 114505 (2016), [arXiv:1603.04306].
- [88] R. Dowdall *et al.* (HPQCD), Phys. Rev. Lett. **110**, 222003 (2013), [arXiv:1302.2644].
- [89] Y. Aoki *et al.*, Phys. Rev. **D91**, 114505 (2015), [arXiv:1406.6192].
- [90] N. H. Christ *et al.* (RBC/UKQCD), Phys. Rev. **D91**, 054502 (2015), [arXiv:1404.4670].
- [91] H. Na *et al.* (HPQCD), Phys. Rev. **D86**, 034506 (2012), [arXiv:1202.4914].
- [92] C. McNeile *et al.* (HPQCD), Phys. Rev. **D85**, 031503 (2012), [arXiv:1110.4510].
- [93] H.-K. Sun and M.-Z. Yang, Phys. Rev. **D95**, 11, 113001 (2017), [arXiv:1609.08958].
- [94] M. J. Baker *et al.*, JHEP **07**, 032 (2014), [arXiv:1310.0941].
- [95] W. Lucha, D. Melikhov and S. Simula, Phys.Rev. **D88**, 056011 (2013), [arXiv:1305.7099].
- [96] J. Hardy and I. S. Towner, PoS **CKM2016**, 028 (2016).
- [97] F. Ambrosino *et al.* (KLOE), Eur. Phys. J. **C71**, 1604 (2011), [arXiv:1011.2668].
- [98] E. Abouzaid *et al.* (KTeV), Phys. Rev. **D83**, 092001 (2011), [arXiv:1011.0127].
- [99] D. Babusci *et al.* (KLOE KLOE-2), Phys. Lett. **B738**, 128 (2014), [arXiv:1407.2028].
- [100] N. Carrasco *et al.*, Phys. Rev. **D93**, 11, 114512 (2016), [arXiv:1602.04113].
- [101] A. Bazavov *et al.* (Fermilab Lattice and MILC), Phys. Rev. Lett. **112**, 112001 (2014), [arXiv:1312.1228].
- [102] C.-Y. Seng *et al.*, Phys. Rev. Lett. **121**, 241804 (2018), [arXiv:1807.10197].
- [103] C. Y. Seng, M. Gorchtein and M. J. Ramsey-Musolf, Phys. Rev. **D100**, 013001 (2019), [arXiv:1812.03352].
- [104] M. Gorchtein, Phys. Rev. Lett. **123**, 042503 (2019), [arXiv:1812.04229].
- [105] C.-Y. Seng and U.-G. Meißner, Phys. Rev. Lett. **122**, 211802 (2019), [arXiv:1903.07969].
- [106] J. C. Hardy and I. S. Towner, Phys. Rev. **C91**, 025501 (2015), [arXiv:1411.5987].
- [107] A. Czarnecki, W. J. Marciano and A. Sirlin (2019), [arXiv:1907.06737].
- [108] Y. Amhis *et al.* (HFLAV), Eur. Phys. J. **C77**, 12, 895 (2017), [arXiv:1612.07233].
- [109] H. Na *et al.* (HPQCD), Phys. Rev. **D82**, 114506 (2010), [arXiv:1008.4562].
- [110] H. Na *et al.* (HPQCD), Phys. Rev. **D84**, 114505 (2011), [arXiv:1109.1501].
- [111] B. Chakraborty *et al.*, EPJ Web Conf. **175**, 13027 (2018), [arXiv:1710.07334].
- [112] R. Li *et al.* (Fermilab Lattice, MILC), PoS **LAT-TICE2018**, 269 (2019), [arXiv:1901.08989].
- [113] L. Wolfenstein, Phys. Rev. Lett. **51**, 1945 (1983).
- [114] J. Charles *et al.* (CKMfitter Group), Eur. Phys. J. **C41**, 1 (2005), updated results and plots available at: <http://ckmfitter.in2p3.fr>, [hep-ph/0406184].
- [115] M. Antonelli *et al.*, Phys. Rept. **494**, 197 (2010), [arXiv:0907.5386].
- [116] J. N. Butler *et al.* (Quark Flavor Physics Working Group), in “Community Summer Study 2013: Snowmass on the Mississippi (CSS2013) Minneapolis, MN, USA, July 29-August 6, 2013,” (2013), [arXiv:1311.1076], URL <http://www.slac.stanford.edu/econf/C1307292/docs/IntensityFrontier/QuarkF1-15.pdf>.
- [117] Y. Amhis *et al.* (Heavy Flavor Averaging Group) (2014), [arXiv:1412.7515].
- [118] A. J. Bevan *et al.* (Belle, BaBar), Eur. Phys. J. **C74**, 3026 (2014), [arXiv:1406.6311].

- [119] E. Dalgic *et al.*, Phys. Rev. **D73**, 074502 (2006), [Erratum: Phys. Rev.D75,119906(2007)], [hep-lat/0601021].
- [120] J. M. Flynn *et al.* (RBC/UKQCD), Phys. Rev. **D91**, 074510 (2015), [arXiv:1501.05373].
- [121] J. A. Bailey *et al.* (Fermilab Lattice, MILC), Phys. Rev. **D92**, 014024 (2015), [arXiv:1503.07839].
- [122] P. del Amo Sanchez *et al.* (BaBar), Phys. Rev. **D83**, 032007 (2011), [arXiv:1005.3288].
- [123] J. P. Lees *et al.* (BaBar), Phys. Rev. **D86**, 092004 (2012), [arXiv:1208.1253].
- [124] H. Ha *et al.* (Belle), Phys. Rev. **D83**, 071101 (2011), [arXiv:1012.0090].
- [125] A. Sibidanov *et al.* (Belle), Phys.Rev. **D88**, 032005 (2013), [arXiv:1306.2781].
- [126] S. W. Bosch *et al.*, Phys. Rev. Lett. **93**, 221801 (2004), [hep-ph/0403223].
- [127] J. R. Andersen and E. Gardi, JHEP **01**, 097 (2006), [hep-ph/0509360].
- [128] P. Gambino *et al.*, JHEP **10**, 058 (2007), [arXiv:0707.2493].
- [129] R. Kowalewski and T. Mannel, “Semileptonic  $b$ -Hadron Decays, Determination of  $V_{cb}$ ,  $V_{ub}$ ,” <http://pdg.lbl.gov/2019/reviews/rpp2018-rev-vcb-vub.pdf> (2017), review prepared for PDG 2018 update.

## 72. Production and Decay of *b*-flavored Hadrons

Revised April 2020 by P. Eerola (Helsinki U.), M. Kreps (Warwick U.) and Y. Kwon (Yonsei U., Seoul).

The *b* quark belongs to the third generation of quarks and is the weak-doublet partner of the *t* quark. The existence of the third-generation quark doublet was proposed in 1973 by Kobayashi and Maskawa [1] in their model of the quark mixing matrix (“CKM” matrix), and confirmed four years later by the first observation of a *b* $\bar{b}$  meson [2]. In the KM model, *CP* violation is explained within the Standard Model (SM) by an irreducible phase of the  $3 \times 3$  unitary matrix. The regular pattern of the three lepton and quark families is one of the most intriguing puzzles in particle physics. The existence of families gives rise to many of the free parameters in the SM, including the fermion masses, and the elements of the CKM matrix.

Since the *b* quark is the lighter element of the third-generation quark doublet, the decays of *b*-flavored hadrons occur via generation-changing processes through CKM matrix. Because of this, and the fact that the CKM matrix is close to a  $3 \times 3$  unit matrix, many interesting features such as loop and box diagrams, flavor oscillations, as well as large *CP* asymmetries, can be observed in the weak decays of *b*-flavored hadrons.

The CKM matrix is parameterized by three real parameters and one complex phase. This complex phase can become a source of *CP* violation in *B* meson decays. A crucial milestone was the first observation of *CP* violation in the *B* meson system in 2001, by the BaBar [3] and Belle [4] collaborations. They measured a large value for the parameter  $\sin 2\beta$  ( $= \sin 2\phi_1$ ) [5], almost four decades after the discovery of a small *CP* asymmetry in neutral kaons. A more detailed discussion of the CKM matrix and *CP* violation can be found elsewhere in this Review [6, 7].

The structure of this mini-review is organized as follows. After a discussion of *b*-quark production and current results on spectroscopy, we discuss lifetimes of *b*-flavored hadrons. We then discuss some basic properties of *B*-meson decays, followed by summaries of hadronic, rare, and electroweak penguin decays of *B*-mesons. There are separate mini-reviews for  $B^0$ - $\bar{B}^0$  mixing [8] and the extraction of the CKM matrix elements  $V_{cb}$  and  $V_{ub}$  from *B*-meson decays [9] in this Review.

### 72.1 Production and spectroscopy

The bound states of a  $\bar{b}$  antiquark and a *u*, *d*, *s*, or *c* quark are referred to as the  $B_u$  ( $B^+$ ),  $B_d$  ( $B^0$ ),  $B_s$  ( $B_s^0$ ), and  $B_c$  ( $B_c^+$ ) mesons, respectively. The  $B_c^+$  is the heaviest of the ground-state *b*-flavored mesons, and the most difficult to produce: it was observed for the first time in the semileptonic mode by CDF in 1998 [10], but its mass was accurately determined only in 2006, from the fully reconstructed mode  $B_c^+ \rightarrow J/\psi\pi^+$  [11]. Many exclusive decay channels can now be used for the accurate mass measurements, given the large statistics available at the LHC. Currently the most precise measurement is made by LHCb using the  $B_c^+ \rightarrow J/\psi D^0 K^+$  decay, yielding  $m(B_c^+) = 6274.28 \pm 1.40 \pm 0.32$  MeV/ $c^2$  [12].

The first excited meson is called the *B\** meson, while  $B^{**}$  is the generic name for the four orbitally excited ( $L = 1$ ) *B*-meson states that correspond to the *P*-wave mesons in the charm system,  $D^{**}$ . Excited states of the  $B_s^0$  meson are similarly named  $B_s^*$  and  $B_s^{**}$ . Of the possible bound  $\bar{b}b$  states, the  $\Upsilon(nS)$  and  $\chi_{b,J}(nP)$  states are well studied.

The pseudoscalar ground state  $\eta_b$  has been observed for the first time by BaBar [13] indirectly through the decay  $\Upsilon(3S) \rightarrow \gamma\eta_b$ , and then confirmed by Babar in  $\Upsilon(2S)$  decays [14] and CLEO in  $\Upsilon(3S)$  decays [15]. The most accurate mass and width measurements come now from Belle, using decays  $\Upsilon(5S) \rightarrow h_b(1P)\pi^+\pi^-$ ,  $h_b(1P) \rightarrow \gamma\eta_b(1S)$  [16] and  $\Upsilon(4S) \rightarrow \eta h_b(1P)$ ,  $h_b(1P) \rightarrow \gamma\eta_b(1S)$  [17]. Belle has also reported first evidence for the  $\eta_b(2S)$  in the  $h_b(2P) \rightarrow \eta_b(2S)\gamma$  transition [16]. See Ref. [18] for classification and naming of these and other states.

Experimental studies of *b* decays have been performed in  $e^+e^-$  collisions at the  $\Upsilon(4S)$  (ARGUS, CLEO, Belle, BaBar) and  $\Upsilon(5S)$  (CLEO, Belle) resonances. The full data samples of BaBar and Belle are  $560 \text{ fb}^{-1}$  and  $1020 \text{ fb}^{-1}$ , respectively, of which  $433 \text{ fb}^{-1}$  and  $710 \text{ fb}^{-1}$  are at the  $\Upsilon(4S)$  resonance. The Belle II experiment at SuperKEKB has started recording data in 2019, and the

experiment has so far collected about  $12.4 \text{ fb}^{-1}$  of data (March 2020). The  $e^+e^- \rightarrow b\bar{b}$  production cross-section at the  $\Upsilon(4S)$  ( $\Upsilon(5S)$ ) resonance is about 1.1 nb (0.3 nb). At the *Z* resonance (SLC, LEP) all species of *b*-flavored hadrons could be studied for the first time. The  $e^+e^- \rightarrow b\bar{b}$  production cross-section at the *Z* resonance is about 6.6 nb.

High-energy  $p\bar{p}$  (Tevatron) and  $pp$  collisions (LHC) produce *b*-flavored hadrons of all species with large cross-sections. At the Tevatron ( $\sqrt{s} = 1.96$  TeV) the visible cross section  $\sigma(p\bar{p} \rightarrow bX, |\eta| < 1)$  is about  $30 \mu\text{b}$ . CDF and D0 experiments at the Tevatron have accumulated by the end of their running about  $10 \text{ fb}^{-1}$  each.

At the LHC  $pp$  collider at  $\sqrt{s} = 7 - 13$  TeV, the visible *b*-hadron cross section at the LHCb experiment with pseudorapidity acceptance  $2 < \eta < 5$  has been measured to be  $\sim 72 \mu\text{b}$  at 7 TeV and  $\sim 144 \mu\text{b}$  at 13 TeV [19] (cross section at 13 TeV corrected in Erratum). LHCb has collected about  $1 \text{ fb}^{-1}$  at 7 TeV,  $2 \text{ fb}^{-1}$  at 8 TeV, and close to  $5.9 \text{ fb}^{-1}$  at 13 TeV during LHC Runs 1 and 2. CMS and ATLAS have collected each about  $5 \text{ fb}^{-1}$  of data at  $\sqrt{s} = 7$ ,  $20 \text{ fb}^{-1}$  at 8 TeV and about  $150 \text{ fb}^{-1}$  at 13 TeV during LHC Runs 1 and 2. The LHCb experiment is undergoing currently major upgrade. The LHC operation is planned to resume in 2021.

In hadron collisions, production happens as  $b\bar{b}$  pairs via leading order flavor creation or higher order processes such as gluon-splitting. Single *b*-quarks can be produced by flavor excitation. The total *b*-production cross section is an interesting test of our understanding of leading and higher order QCD processes. With a wealth of measurements at LHC and at Tevatron (see Ref. [19] and references therein), and improved calculations [20], there is a reasonable agreement between measurements and predictions.

Each quark of a  $b\bar{b}$  pair produced in hadron collisions hadronizes separately and incoherently from the other, but it is still possible to obtain a statistical indication of the charge of a produced *b*/ $\bar{b}$  quark (“flavor tag” or “charge tag”) from the accompanying particles produced in the hadronization process, or from the decay products of the other quark. The momentum spectrum of produced *b*-quarks typically peaks near the *b*-quark mass, and extends to much higher momenta, dropping by about a decade for every ten GeV. Typical decay lengths are of the order of a centimeter at 13 TeV  $pp$  collisions; the resolution for the decay vertex must be more precise than this to resolve the fast oscillations of  $B_s^0$  mesons.

In  $e^+e^-$  colliders, since the *B* mesons are very slow in the  $\Upsilon(4S)$  rest frame, asymmetric beam energies are used to boost the decay products to allow time-dependent measurements that are crucial for the study of *CP* violation. At KEKB, the boost was  $\beta\gamma = 0.43$ , while PEP-II used a slightly larger boost,  $\beta\gamma = 0.55$ . The typical *B*-meson decay length is dilated from  $\approx 20 \mu\text{m}$  to  $\approx 200 \mu\text{m}$ . At SuperKEKB the boost is lower,  $\beta\gamma = 0.28$ , which puts more demanding requirements on the track reconstruction precision at Belle II to reach a resolution in decay time measurements similar to Belle. The two *B* mesons produced in  $\Upsilon(4S)$  decay are in a coherent quantum state, which makes it easier than in hadron collisions to infer the charge state of one *B* meson from observation of the other; however, the coherence also requires determination of the decay time of both mesons, rather than just one, in order to perform time-dependent *CP*-violation measurements. For  $B_s^0$ , which can be produced at  $\Upsilon(5S)$  the situation is less favourable, as boost is not high enough to provide sufficient time resolution to resolve the fast  $B_s^0$  oscillations.

For the measurement of branching fractions, the initial composition of the data sample must be known. The  $\Upsilon(4S)$  resonance decays predominantly to  $B^0\bar{B}^0$  and  $B^+B^-$ ; the current experimental upper limit for non- $B\bar{B}$  decays of the  $\Upsilon(4S)$  is less than 4% at the 95% confidence level (CL) [21]. The observed modes of this category are decays to lower  $\Upsilon$  states and a pion pair,  $\eta$ , or  $\eta'$ , measured branching fractions being of order  $10^{-4} - 10^{-5}$  [22], and decays to  $h_b(1P)\eta$  with branching fraction of order  $10^{-3}$  [17].

The ratio  $f_+/f_0$  of the fractions of charged to neutral *B* productions from  $\Upsilon(4S)$  decays has been measured by CLEO, BaBar, and Belle in various ways. They typically use pairs of isospin-related decays of  $B^+$  and  $B^0$ , such that it can be assumed that

$\Gamma(B^+ \rightarrow x^+) = \Gamma(B^0 \rightarrow x^0)$ . In this way, the ratio of the number of events observed in these modes is proportional to  $(f_+ \tau_+)/ (f_0 \tau_0)$  [23, 24]. BaBar has also performed an independent measurement of  $f_0$  with a different method that does not require isospin symmetry or the value of the lifetime ratio, based on the number of events with one or two reconstructed  $B^0 \rightarrow D^{*-} \ell^+ \nu$  decays [25]. The combined result, from the current average of  $\tau_+/\tau_0$ , is  $f_+/f_0 = 1.058 \pm 0.024$  [26]. The result is consistent within  $2.4\sigma$  with equal production of  $B^+B^-$  and  $B^0\bar{B}^0$  pairs, and we assume  $f_+/f_0 = 1$  in this mini-review except where explicitly stated otherwise. This assumption is also supported by the near equality of the  $B^+$  and  $B^0$  masses: our fit yields  $m(B^0) = 5279.65 \pm 0.12$  MeV/ $c^2$ ,  $m(B^+) = 5279.34 \pm 0.12$  MeV/ $c^2$ , and  $m(B^0) - m(B^+) = 0.31 \pm 0.05$  MeV/ $c^2$ .

Data collected at the  $\Upsilon(5S)$  resonance gave CLEO, Belle and BaBar access to  $B_s^0$  decays. In  $\Upsilon(5S)$  decays there are seven possible final states including a pair of non-strange  $B$  mesons and 0, 1 or 2 pions, and three with a pair of strange  $B$  mesons ( $B_s^* \bar{B}_s^{*0}$ ,  $B_s^* \bar{B}_s^0$ , and  $B_s^0 \bar{B}_s^0$ ). The fraction of events with a pair of  $B_s^0$  mesons over the total number of events with a pair of  $b$ -flavored hadrons has been measured to be  $f_s[\Upsilon(5S)] = 0.199^{+0.030}_{-0.029}$  [27], of which 88% is  $B_s^* \bar{B}_s^0$  events. However, the small boost of  $B_s^0$  mesons produced in this way prevents resolution of their fast oscillations for time-dependent measurements; these are only accessible in hadron collisions (or at the  $Z$  peak).

In high-energy collisions, the produced  $b$  or  $\bar{b}$  quarks can hadronize with different probabilities into the full spectrum of  $b$ -hadrons, either in their ground or excited states. The hadronization does not have to be identical in  $p\bar{p}$  or  $pp$  collisions and in  $Z$  decay, because of the different momentum distributions of the  $b$ -quark in these processes; the sample used in the  $p\bar{p}$  measurements has momenta close to the  $b$  mass, rather than  $m_Z/2$ . The available data from Tevatron and LHC show that the production fractions  $f_d$ ,  $f_u$ ,  $f_s$ , and  $f_{\text{baryon}}$  of  $B^0$ ,  $B^+$ ,  $B_s^0$ , and  $b$  baryons, respectively, of weakly decaying  $b$  hadrons depend on the kinematics of the produced  $b$  hadron. The production fractions of  $b$  hadrons are discussed in more detail in the  $B^0 - \bar{B}^0$  mixing section in this Review [8].

Excited  $B$ -meson states have been thoroughly studied by CLEO, LEP, CUSB, D0 and CDF (an admixture of  $B$  mesons) and LHCb ( $B^{*+}$ -meson). The current world average of the  $B^* - B$  mass difference is  $45.21 \pm 0.21$  MeV/ $c^2$ . Excited  $B_s^*$ -meson states have been observed in  $\Upsilon(5S)$  decays by CUSB, CLEO and Belle.

For orbitally excited  $B$  meson states, with relative angular momentum  $L=1$  of the two quarks, there exist four states  $(J, j_q) = (0, 1/2), (1, 1/2), (1, 3/2), (2, 3/2)$ , where  $j_q$  is the total angular momentum of the light  $u$ ,  $d$  or  $s$  quark and  $J$  is the total angular momentum of the  $B$  meson. These states are collectively called as  $B_{(s)}^{**}$  mesons. The  $j_q = 1/2$  states are named  $B_{(s)0}^*$  ( $J = 0$ ) and  $B_{(s)1}$  ( $J = 1$ ) mesons, while the states with  $j_q = 3/2$  are named  $B_{(s)1}$  ( $J = 1$ ) and  $B_{(s)2}^*$  ( $J = 2$ ) mesons. The states with  $j_q = 1/2$  can decay through an  $S$ -wave transition and are expected to have a large width, but the  $j_q = 3/2$  states are narrow  $D$ -wave decays. Evidence for  $B^{**}$  production has been initially obtained at LEP as a broad  $B\pi$  resonance [28] or a  $B^+K^-$  enhancement [29]. Detailed results have been obtained for the narrow states  $B_1(5721)^{0,+}$  and  $B_2(5747)^{0,+}$  at the Tevatron and by LHCb, and clear enhancements compatible with the higher mass states  $B_J(5840)^{0,+}$  and  $B_J(5970)^{0,+}$  have been observed [30, 31]. Also the narrow  $B_s^{**}$  states  $B_{s1}(5830)^0$  and  $B_{s2}(5840)^0$  have been measured at the CDF [30], LHCb [32], and CMS [33].

Excited states of  $B_c^+$  mesons will provide important information about the strong potential. A  $B_c^+ \pi^+ \pi^-$  resonance has been observed for the first time by ATLAS [34]. The mass of the resonance has been measured precisely by CMS and LHCb as  $6871.6 \pm 1.1$  MeV/ $c^2$  [35, 36]. The resonance may be interpreted as the second  $S$ -wave state of the  $B_c^+$  meson,  $B_c^+(2S)$ , but the quantum numbers are to be confirmed.

Baryon states containing a  $b$  quark are labeled according to the same scheme used for non- $b$  baryons, with the addition of a  $b$  subscript [18]. The first observed  $b$  baryon was the  $\Lambda_b^0$  (quark composition  $udb$ ). Thanks to the large samples accumulated at

the Tevatron and specially at the LHC many new  $b$  baryons have been found. The masses of all these new baryons have been measured to a precision of a few MeV/ $c^2$ , and found to be in agreement with predictions from Heavy Quark Effective Theory (HQET).

Clear signals of four strongly-decaying baryon states,  $\Sigma_b^+$ ,  $\Sigma_b^{*+}$  ( $uub$ ),  $\Sigma_b^-$ ,  $\Sigma_b^{*-}$  ( $ddb$ ) have been obtained by CDF [37] and LHCb [38]. LHCb has also observed two new mass peaks in the  $\Lambda_b^0 \pi^\pm$  systems, consistent with single resonances and named as  $\Sigma_b^\pm(6097)$  [38]. The nature of these resonances is, however, not yet clear. The isodoublet of strange  $b$  baryons  $\Xi_b^0$  ( $usb$ ) and  $\Xi_b^\pm$  ( $dsb$ ) has been observed by CDF and D0 [39]. Masses, lifetimes, and branching ratios have been accurately measured by LHCb [40] and CDF [41]. LHCb has also measured several parameters sensitive to  $P$  and  $CP$  violation [42]. Other observed  $\Xi_b$  baryons are spin-3/2 states  $\Xi_b(5945)^0$  ( $\Xi_b^{*0}$ ) [43, 44] and  $\Xi_b(5955)^{-}$  [45], a spin-1/2 state  $\Xi_b'(5935)^-$  [45], and a resonance state  $\Xi_b^-(6227)$  [46]. The doubly-strange bottom baryon  $\Omega_b^-$  has been observed first by D0 and CDF [47]. Mass and mean life have been measured precisely by LHCb [48] and CDF [41].

The so-called exotic states have raised a lot of interest recently. While many exotic states were seen in the charm sector, in bottom sector there are fewer seen. The D0 Collaboration claimed a narrow state  $X(5568)$  decaying into a  $B_s^0 \pi^\pm$  final state [49]. While this would be an interesting addition to the observed states as the first exotic state with constituent quarks with four different flavours ( $b, s, u, d$ ), analysis by LHCb yields negative result [50]. Also CMS finds no such a state [51].

## 72.2 Lifetimes

Precise lifetimes are key in extracting the weak parameters that are important for understanding the role of the CKM matrix in  $CP$  violation, such as the determination of  $V_{cb}$  and  $B_s^0 \bar{B}_s^0$  mixing parameters. In the naive spectator model, the heavy quark can decay only via the external spectator mechanism, and thus, the lifetimes of all mesons and baryons containing  $b$  quarks would be equal. Non-spectator effects, such as the interference between contributing amplitudes, modify this simple picture and give rise to a lifetime hierarchy for  $b$ -flavored hadrons similar to the one in the charm sector. However, since the lifetime differences are expected to scale as  $1/m_Q^2$ , where  $m_Q$  is the mass of the heavy quark, the variations in the  $b$  system are expected to be only 10% or less [52, 53]. We expect:

$$\tau(B^+) \geq \tau(B^0) \approx \tau(B_s^0) > \tau(\Lambda_b^0) \gg \tau(B_c^+) . \quad (72.1)$$

For the  $B_c^+$ , both quarks decay weakly, so the lifetime is much shorter.

Measurements of the lifetimes of the different  $b$ -flavored hadrons thus provide a means to determine the importance of non-spectator mechanisms in the  $b$  sector. Availability of large samples of fully-reconstructed decays of different  $b$ -hadron species has resulted in precise measurements with small statistical and systematic uncertainties ( $\sim 1\%$ ). The world averages given in Table 72.1 have been determined by the Heavy Flavor Averaging Group (HFLAV) [27].

**Table 72.1:** Summary of i world-average  $b$ -hadron lifetime measurements. For the  $B_s^0$  lifetimes, see text below.

Particle	Lifetime [ps]
$B^+$	$1.638 \pm 0.004$
$B^0$	$1.519 \pm 0.004$
$B_s^0$	$1.515 \pm 0.004$
$B_s^0$	$1.423 \pm 0.005$
$B_s^{0L}$	$1.620 \pm 0.007$
$B_c^+$	$0.510 \pm 0.009$
$\Lambda_b^0$	$1.471 \pm 0.009$
$\Xi_b^-$	$1.572 \pm 0.040$
$\Xi_b^0$	$1.480 \pm 0.030$
$\Omega_b^-$	$1.64^{+0.18}_{-0.17}$

The  $B_s^0$  lifetime in Table 72.1 is defined as  $1/\Gamma_s$ , where  $\Gamma_s$  is the average width of the light (L) and heavy (H) mass eigenstates,  $(\Gamma_L + \Gamma_H)/2$ . In the absence of  $CP$  violation, the light (heavy)  $B_s^0$  mass eigenstate is the  $CP$ -even ( $CP$ -odd) eigenstate. Thus, the lifetime of the light (heavy) mass eigenstate can be measured from  $CP$ -even (odd) final states. The lifetimes can also be obtained from time-dependent angular analysis of  $B_s^0 \rightarrow J/\psi\phi$  decays.

The short  $B_c^+$  lifetime is in good agreement with predictions [54]. With large samples of  $B_c^+$  mesons at the LHC precision on the lifetimes can still improve. The measurement using semileptonic decays gives  $\tau_{B_c^+} = 0.509 \pm 0.008 \pm 0.012$  ps [55] while using decays  $B_c^+ \rightarrow J/\psi\pi^+$  yields  $\tau_{B_c^+} = 0.5134 \pm 0.0110 \pm 0.0057$  ps [56]. Each of these is more precise than the combination of all previous experiments.

The recent  $A_b^0$  lifetime measurements from LHC experiments and CDF are precise and favour lifetime close to the lifetime of  $B^0$  meson, in agreement with theory.

For precision comparisons with theory, lifetime ratios are more sensitive. Experimentally it is found [27]:

$$\frac{\tau_{B^+}}{\tau_{B^0}} = 1.076 \pm 0.004, \quad \frac{\tau_{B_s^0}}{\tau_{B^0}} = 0.998 \pm 0.004,$$

$$\frac{\tau_{A_b^0}}{\tau_{B^0}} = 0.969 \pm 0.006,$$

while recent Heavy Quark Expansion (HQE) predictions give [53]:

$$\frac{\tau_{B^+}}{\tau_{B^0}} = 1.04_{-0.01}^{+0.05} \pm 0.02 \pm 0.01, \quad \frac{\tau_{B_s^0}}{\tau_{B^0}} = 1.001 \pm 0.002,$$

$$\frac{\tau_{A_b^0}}{\tau_{B^0}} = 0.935 \pm 0.054.$$

The ratio of  $B^+$  to  $B^0$  lifetimes has a precision of better than 1%, and is significantly different from 1.0, in agreement with predictions [52]. The ratio of  $B_s^0$  to  $B^0$  lifetimes is expected to be very close to 1.0.

For a detailed discussion on neutral  $B^0$  and  $B_s^0$  oscillation and relevant  $CP$  violation measurements see Ref. [8].

### 72.3 Features of decays

The ground states of *b*-flavored hadrons decay via weak interactions. In most decays of the *b*-flavored hadrons, where the *b*-quark is accompanied by lighter partner quarks (*d*, *u*, *s*, or *c*), the decay modes are well described by the decay of the *b* quark (spectator model) [57]. The dominant decay mode of a *b* quark is  $b \rightarrow cW^{*-}$  (referred to as a “tree” or “spectator” decay), where the virtual *W* materializes either into a pair of leptons  $l\bar{\nu}$  (“semileptonic decay”), or into a pair of quarks which then hadronizes. The transition  $b \rightarrow u$  is suppressed by  $|V_{ub}/V_{cb}|^2 \sim (0.1)^2$  relative to  $b \rightarrow c$  transitions. The decays in which the spectator quark combines with one of the quarks from  $W^*$  to form one of the final state hadrons are suppressed by a factor  $\sim (1/3)^2$ , because the colors of the two quarks from different sources must match (“color-suppression”).

Semileptonic *B* decays  $B \rightarrow X_c l \nu$  and  $B \rightarrow X_u l \nu$  provide an excellent way to measure the magnitude of the CKM elements  $|V_{cb}|$  and  $|V_{ub}|$  respectively, because the strong interaction effects are much simplified due to the two leptons in the final state. Both exclusive and inclusive decays can be used with dominant uncertainties being complementary. For exclusive decay analysis, knowledge of the form factors for the exclusive hadronic system  $X_{c(u)}$  is required. For inclusive analysis, it is usually necessary to restrict the available phase-space of the decay products to suppress backgrounds; subsequently uncertainties are introduced in the extrapolation to the full phase-space. Moreover, restriction to a small corner of the phase-space may result in breakdown of the operator-product expansion scheme, thus making theoretical calculations unreliable. One of the recent unexpected results was determination of  $|V_{ub}|$  using  $A_b^0 \rightarrow p\mu^-\bar{\nu}_\mu$  decays by LHCb [58]. Besides, there have been measurements of inclusive semileptonic decays rates of  $B_s^0$  [59] and  $B_c^+$  [60] mesons. A more detailed discussion of *B* semileptonic decays and the extraction of  $|V_{cb}|$  and  $|V_{ub}|$  is given elsewhere in this *Review* [9].

On the other hand, hadronic *B* decays are complicated because of strong interaction effects caused by the surrounding cloud of light quarks and gluons. While this complicates the extraction of CKM matrix elements, it also provides a great opportunity to study perturbative and non-perturbative QCD, hadronization, and Final State Interaction (FSI) effects.

Many aspects of *B* decays can be understood through the Heavy Quark Effective Theory (HQET) [61]. This has been particularly successful for semileptonic decays. For further discussion of HQET, see for instance Ref. [62]. For hadronic decays, one typically uses effective Hamiltonian calculations that rely on a perturbative expansion with Wilson coefficients. In addition, some form of the factorization hypothesis is commonly used, where, in analogy with semileptonic decays, two-body hadronic decays of *B* mesons are expressed as the product of two independent hadronic currents, one describing the formation of a charm meson (in case of the dominant  $b \rightarrow cW^{*-}$  decays), and the other the hadronization of the remaining  $\bar{u}d$  (or  $\bar{c}s$ ) system from the virtual  $W^-$ . Qualitatively, for *B* decays with a large energy release, e.g.  $b \rightarrow uW^{*-}$  transitions, the  $\bar{u}d$  pair (produced as a color singlet) travels fast enough to leave the interaction region without influencing the charm meson. This is known to work well for the dominant spectator decays [63]. There are several common implementations of these ideas for hadronic *B* decays, the most common of which are QCD factorization (QCDF) [64–67], perturbative QCD (pQCD) [68–72], and soft collinear effective theory (SCET) [73–75].

The transitions  $b \rightarrow s$  and  $b \rightarrow d$  are flavor-changing neutral-current (FCNC) processes. Although they are not allowed in the SM as a tree-process, they can occur via more complicated loop diagrams (denoted “penguin” decays). The rates for  $b \rightarrow s$  penguin decays are comparable to the CKM-suppressed  $b \rightarrow u$  tree processes. Pure-penguin decays were first established by the observation of  $B \rightarrow K^*(892)\gamma$  [76]. Penguin processes involving  $b \rightarrow d$  transitions are further suppressed by CKM, and have been observed for  $B \rightarrow (\rho/\omega)\gamma$  decays [77, 78]. LHCb has observed a  $b \rightarrow d$  penguin transition in the  $B^+ \rightarrow \pi^+\mu^+\mu^-$  mode and measured its branching fraction to be  $(1.83 \pm 0.24 \pm 0.05) \times 10^{-8}$  [79].

Other decay processes discussed in this *Review* include *W*-exchange (a *W* is exchanged between initial-state quarks), penguin annihilation (the gluon from a penguin loop attaches to the spectator quark, similar to an exchange diagram), and pure-annihilation (the initial quarks annihilate to a virtual *W*, which then decays). Some observed decay modes such as  $B^0 \rightarrow D_s^- K^+$ , may be interpreted as evidence of a *W*-exchange process [80]. The evidence for the purely leptonic decay  $B^+ \rightarrow \tau^+\nu$  from Belle [81] and BaBar [82] is the first sign of a pure annihilation decay. The average branching fraction is  $(1.09 \pm 0.24) \times 10^{-4}$ , which is somewhat larger than, though consistent with, the value expected in the SM. A substantial region of parameter space of charged Higgs mass vs.  $\tan\beta$  is excluded by the measurements of this mode. A dedicated discussion of purely leptonic decays of charged pseudoscalar mesons is given elsewhere in this *Review* [83].

### 72.4 Dominant hadronic decays

Most of the hadronic *B* decays involve  $b \rightarrow c$  transition at the quark level, resulting in a charmed hadron or charmonium in the final state. Other types of hadronic decays are very rare and will be discussed separately in the next section. The experimental results on hadronic *B* decays have steadily improved over the years, and the measurements have reached sufficient precision to challenge our understanding of the dynamics of these decays. With good particle detection and hadron identification capabilities of *B*-factory detectors, a substantial fraction (roughly on the order of a few per mill) of hadronic *B* decay events can be fully reconstructed. In particular, good performances for detecting  $\pi^0$  and other neutral particles helped Belle and BaBar to make comprehensive measurements of the decays  $\bar{B}^0 \rightarrow D^{(*)0}h^0$  [84], where  $h^0$  stands for light neutral mesons such as  $\pi^0, \eta^{(\prime)}, \rho^0, \omega$ . The measurements are being complemented by LHCb, in decays like  $B^0 \rightarrow D^0\pi^+\pi^-$  [85], where no neutral particles reconstruction is needed. These decays proceed through color-suppressed diagrams, hence they provide useful tests on the factorization models.

Because of the kinematic constraint of  $\Upsilon(4S) \rightarrow B\bar{B}$ , the energy sum of the final-state particles of a  $B$  meson decay is always equal to one half of the total energy in the center of mass frame. As a result, the two variables,  $\Delta E$  (energy difference) and  $M_B$  ( $B$  candidate mass with a beam-energy constraint) are very effective for reducing combinatorial background both from  $\Upsilon(4S)$  and  $e^+e^- \rightarrow q\bar{q}$  continuum events. In particular, the energy-constraint in  $M_B$  improves the signal resolution by almost an order of magnitude.

The kinematically clean environment of  $B$  meson decays provides an excellent opportunity to search for new states. For instance, quark-level  $b \rightarrow c\bar{c}s$  decays have been used to search for new charmonium and charm-strange mesons and study their properties in detail. While narrow charm-strange states  $D_{s0}^*(2317)$  [86] and  $D_{s1}(2460)$  [87] were discovered by BaBar and CLEO, respectively, the properties of these new states were revealed by studying the  $B$  meson decays,  $B \rightarrow DD_{s0}^*(2317)$  and  $B \rightarrow DD_{s1}(2460)$  by Belle [88] and BaBar [89]. Another example is Dalitz plot analysis of decay  $B_s^0 \rightarrow \bar{D}^0 K^- \pi^+$  in which the decay to spin-3 resonance was observed for the first time [90].

Information on  $B_s^0$ ,  $B_c^+$  and  $\Lambda_b^0$  decays have been remarkably improved with recent studies of large samples from LHCb. Noticeable additions in  $B_s$  include decay modes to  $D_s^{(*)+} D_s^{(*)-}$ ,  $\bar{D}^0 \bar{K}^0$ , and  $J/\psi \bar{K}^*(892)^0$ . The  $B_s^0 \rightarrow D_s^{(*)+} D_s^{(*)-}$  decays were first observed by CDF [91], followed by Belle [92]. LHCb has improved the precision with  $\mathcal{B}(B_s^0 \rightarrow D_s^{(*)+} D_s^{(*)-}) = (3.07 \pm 0.22 \pm 0.33)\%$  [93], which suggests that  $B_s^0 \rightarrow D_s^{(*)+} D_s^{(*)-}$  decays do not saturate the  $CP$ -even modes of the  $B_s$  decays. The  $B_s^0 \rightarrow \bar{D}^0 \bar{K}^0$  decay occurs mostly via a color-suppressed tree diagram, and has a small theoretical uncertainty in the SM, thus this mode can significantly improve the determination of the  $CP$ -violation angle  $\phi_s$ . LHCb has observed this decay and the branching fraction is  $(4.3 \pm 0.5 \pm 0.7) \times 10^{-4}$  [94]. The  $B_s^0 \rightarrow J/\psi \bar{K}^*(892)^0$  decay can be used to constrain the penguin pollution in determining  $\phi_s$ . LHCb has updated the branching fraction and measured the  $CP$  asymmetries of this decay, thereby constraining the penguin pollution in  $\phi_s$  [95], although a much more stringent constraint on penguin pollution can come from  $B^0 \rightarrow J/\psi \rho^0$  which has been observed by BaBar [96] and LHCb [97]. The  $B_c^+ \rightarrow B_s^0 \pi^+$  decay is unique as the only observed mode of  $b$ -flavored hadron decays where the partner quark decays ( $c$  in this case) while the  $b$  quark remains a spectator. LHCb has observed this mode and measured  $[\sigma(B_c^+)/\sigma(B_s^0)] \times \mathcal{B}(B_c^+ \rightarrow B_s^0 \pi^+) = (2.37 \pm 0.31 \pm 0.11_{-0.13}^{+0.17}) \times 10^{-3}$  [98]. In addition, LHCb [99] and ATLAS [100] have measured  $B_c^+ \rightarrow J/\psi D_s^{(*)+}$ , which, by comparing with  $B_c^+ \rightarrow B_s^0 \pi^+$ , provides a ratio of exclusive  $b \rightarrow c$  and  $c \rightarrow s$  decays of  $B_c^+$ . For  $\Lambda_b^0 \rightarrow \Lambda_c^+ \pi^+ \pi^- \pi^-$  [101], not only the total rate is measured, but also structure involving decays through excited  $\Lambda_c$  and  $\Sigma_c$  baryons.

In addition, a variety of exotic particles that do not fit the conventional meson spectroscopy have been discovered in  $B$  decays. Belle found the  $X(3872)$  state by studying  $B^+ \rightarrow J/\psi \pi^+ \pi^- K^+$  [102], which was confirmed by CDF [103], D0 [104] and BaBar [105]. Production of  $X(3872)$  has been studied by the LHC experiments, LHCb [106], CMS [107] and ATLAS [108].

A charged charmonium-like state  $X(4430)^\pm$  that decays to  $\psi(2S)\pi^\pm$  was observed by Belle in  $B \rightarrow \psi(2S)K\pi^\pm$  [109]. Since it is charged, it could not be an ordinary charmonium state. A high-statistics study by LHCb confirmed the existence of the  $X(4430)^\pm$  in decays  $B \rightarrow \psi(2S)K\pi^\pm$  [110], demonstrated its resonance character by studying the phase motion, unambiguously determined its spin-parity, and saw evidence for another state. In a Dalitz plot analysis of  $\bar{B}^0 \rightarrow J/\psi K^- \pi^+$  [111], Belle has found another state, labelled as  $X(4200)^+$  in this Review, adding to the list of exotic charged charmonium-like states. In an amplitude analysis of the decay  $\Lambda_b^0 \rightarrow J/\psi p K^-$ , LHCb observed exotic structures, labelled as  $P_c(4380)^+$  and  $P_c(4450)^+$  in this Review, in the  $J/\psi p$  channel [112]. The subsequent analysis with significantly increased statistics observed additional state and resolved the peak at 4450 MeV/ $c^2$  as being due to the two states close in the mass [113]. They are referred to as charmonium-pentaquark states. More detailed discussions of exotic meson-like states and pentaquarks are

given elsewhere in this Review [114].

## 72.5 Rare hadronic decays

All  $B$ -meson decays that do not occur through the  $b \rightarrow c$  transition are usually called rare  $B$  decays. These include both semileptonic and hadronic  $b \rightarrow u$  decays that are suppressed at leading order by the small CKM matrix element  $V_{ub}$ , as well as higher-order  $b \rightarrow s(d)$  processes such as electroweak and gluonic penguin decays. In this section, we review hadronic rare  $B$  decays, while electroweak penguin decays and others are discussed in the next.

Charmless  $B$  meson decays into two-body hadronic final states such as  $B \rightarrow \pi\pi$  and  $K\pi$  are experimentally clean, and provide good opportunities to probe new physics and search for indirect and direct  $CP$  violations. Since the final state particles in these decays tend to have larger momenta than average  $B$  decay products, the event environment is cleaner than for  $b \rightarrow c$  decays. Branching fractions are typically around  $10^{-5}$ . Over the past decade, many such modes have been observed not only by  $e^+e^-$  collider experiments such as BaBar and Belle, but also by hadron collider experiments such as CDF ( $p\bar{p}$ ) and LHCb ( $pp$ ). In the latter cases, huge data samples of the modes with all charged final-state particles have been reconstructed by triggering on the impact parameter of the charged tracks. This has also allowed observation of charmless decays of the  $B_s$ , in final states such as  $\phi\phi$  [115, 116],  $K^+K^-$  [117, 118], and  $K^- \pi^+$  [118, 119], and of charmless decays of the  $\Lambda_b^0$  baryon [119]. The large samples available at LHCb experiment allow to perform also time-dependent  $CP$  violation measurements [120, 121]. Charmless  $B_s$  modes are related to corresponding  $B^0$  modes by  $U$ -spin symmetry, and are determined by similar amplitudes. Combining the observables from  $B_s^0$  and  $B^0$  modes is a further way of eliminating hadronic uncertainties and extracting relevant CKM information [122].

Because of relatively high-momenta for final state particles, the dominant source of background in  $e^+e^-$  collisions is  $q\bar{q}$  continuum events; sophisticated background suppression techniques exploiting event shape variables are essential for these analyses. In hadron collisions, the dominant background comes from QCD or partially reconstructed heavy flavors, and is similarly suppressed by a combination of kinematic and isolation requirements. The results are in general consistent among the experiments.

Most rare decay modes including  $B^0 \rightarrow K^+ \pi^-$  have contributions from both  $b \rightarrow u$  tree and  $b \rightarrow sg$  penguin processes. If the size of the two contributions are comparable, the interference between them may result in direct  $CP$  violation, seen experimentally as a charge asymmetry in the decay rate measurement. BaBar [123], Belle [124], CDF [117], and LHCb [120] have measured the direct  $CP$  violating asymmetry in  $B^0 \rightarrow K^+ \pi^-$  decays. Direct  $CP$  violation has been observed in this decay with a significance of more than  $5\sigma$ . The world average value of the asymmetry is now rather precise,  $A_{CP}(K^+ \pi^-) = -0.083 \pm 0.004$ . The  $CP$  asymmetry in  $B^+ \rightarrow K^+ \pi^0$  mode has been measured by BaBar [125] and Belle [124] with the average value  $A_{CP}(K^+ \pi^0) = 0.037 \pm 0.021$ . These two asymmetries differ by more than  $5\sigma$  significance, in contrast to a naive expectation based on simplified picture in the SM. For more detailed tests, there are sum rules [126] that relate the decay rates and decay-rate asymmetries between the four  $K\pi$  charge states. With the future improvements via Belle II and upgraded LHCb, the measurements are expected to become precise enough to test these sum rules. The  $CP$  asymmetry in the  $\pi^+ K^-$  mode has also been measured in  $B_s^0$  decays, by CDF [117] and LHCb [120]. The combined value is  $A_{CP}(B_s^0 \rightarrow \pi^+ K^-) = 0.221 \pm 0.015$ .

In addition to  $B_{(s)} \rightarrow K\pi$  modes, significant ( $> 3\sigma$ ) non-zero  $CP$  asymmetries have been measured in several other rare decay modes:  $A_{CP}(B^+ \rightarrow \rho^0 K^+) = 0.37 \pm 0.10$  [127],  $A_{CP}(B^+ \rightarrow \eta K^+) = -0.37 \pm 0.08$  [128],  $A_{CP}(B^0 \rightarrow \eta K^{*0}) = 0.19 \pm 0.05$  [129], and  $A_{CP}(B^+ \rightarrow f_2(1270)K^+) = -0.68_{-0.17}^{+0.19}$  [127]. In at least the first two cases, a large direct  $CP$  violation might be expected since the penguin amplitude is suppressed so the tree and penguin amplitudes may have comparable magnitudes. There are also measurements by LHCb of  $CP$  asymmetries in several 3-body modes:  $A_{CP}(B^+ \rightarrow \pi^+ \pi^- \pi^+) = 0.057 \pm 0.013$ ,  $A_{CP}(B^+ \rightarrow K^+ \pi^- \pi^+) = 0.027 \pm 0.008$ ,  $A_{CP}(B^+ \rightarrow K^+ K^- \pi^+) = -0.122 \pm 0.0021$ , and  $A_{CP}(B^+ \rightarrow K^+ K^- K^+) = -0.033 \pm 0.008$  [130, 131].



Many of these analyses now include Dalitz plot treatments with many intermediate resonances.

BaBar [132] and Belle [124, 133] have observed the decays  $B^+ \rightarrow \bar{K}^0 K^+$  and  $B^0 \rightarrow K^0 \bar{K}^0$ . The world-average branching fractions are  $\mathcal{B}(B^0 \rightarrow K^0 \bar{K}^0) = (1.21 \pm 0.16) \times 10^{-6}$  and  $\mathcal{B}(B^+ \rightarrow \bar{K}^0 K^+) = (1.31 \pm 0.17) \times 10^{-6}$ . These are the first observations of hadronic  $b \rightarrow d$  transitions, with significance bigger than  $5\sigma$  for all four measurements.  $CP$  asymmetries have been measured for these modes, but with large errors. LHCb has observed  $B^0 \rightarrow K^+ K^-$  mode which occurs via a weak-annihilation process and is the rarest hadronic  $B$ -meson decay thus far observed, with  $\mathcal{B}(B^0 \rightarrow K^+ K^-) = (7.80 \pm 1.52) \times 10^{-8}$  [134].  $B_s^0 \rightarrow K^+ K^-$  decay mode, which occurs mostly via  $b \rightarrow s$  penguin process, has been observed by Belle [135], CDF [136] and LHCb [118]. The average branching fraction is  $\mathcal{B}(B_s^0 \rightarrow K^+ K^-) = (25.4 \pm 1.6) \times 10^{-6}$ . Belle has also observed  $B_s^0 \rightarrow K^0 \bar{K}^0$  which also occurs via  $b \rightarrow s$  penguin transition in the SM. The branching fraction is  $(1.96_{-0.56}^{+0.62}) \times 10^{-5}$  [137].

The decay  $B^0 \rightarrow \pi^+ \pi^-$  can be used to extract the CKM angle  $\alpha$  (for details see elsewhere in this *Review* [138]). This is complicated by the presence of significant contributions from penguin diagrams. An isospin analysis [139] can be used to untangle the penguin complications. The decay  $B^0 \rightarrow \pi^0 \pi^0$  is crucial in this analysis. Both BaBar and Belle have observed  $B^0 \rightarrow \pi^0 \pi^0$ , with a mild tension in the measured branching fractions:  $(1.83 \pm 0.25) \times 10^{-6}$  for BaBar [123] and  $(1.31 \pm 0.26) \times 10^{-6}$  for Belle [140]. It turns out that the amount of penguin pollution in the  $B \rightarrow \pi\pi$  system is rather large. In the past few years, measurements in the  $B^0 \rightarrow \rho\rho$  system have produced more precise values of  $\alpha$ , since penguin amplitudes are generally smaller for decays with vector mesons. An important ingredient in the analysis is the  $B^0 \rightarrow \rho^0 \rho^0$  branching fraction. The average of measurements from BaBar [141] and Belle [142] yields a branching fraction of  $(0.96 \pm 0.15) \times 10^{-6}$ . This is only 3% of the  $\rho^+ \rho^-$  branching fraction, much smaller than the corresponding ratio ( $\gtrsim 20\%$ ) in the  $\pi\pi$  system.

Since  $B \rightarrow \rho\rho$  has two vector mesons in the final state, the  $CP$  eigenvalue of the final state depends on the longitudinal polarization fraction  $f_L$  for the decay. Therefore, a measurement of  $f_L$  is needed to extract the CKM angle  $\alpha$ . Both BaBar and Belle have measured  $f_L$  for the decays  $\rho^+ \rho^-$  [143] and  $\rho^+ \rho^0$  [144] and in both cases the measurements show  $f_L > 0.9$ , making a complete angular analysis unnecessary. In  $B^0 \rightarrow \rho^0 \rho^0$ ,  $f_L$  is measured by BaBar [141], Belle [142] and LHCb [145], with the average value being  $0.71_{-0.09}^{+0.08}$ .

By analyzing the angular distributions of the  $B$  decays to two vector mesons, we can learn a lot about both weak- and strong-interaction dynamics in  $B$  decays. Decays that are penguin-dominated surprisingly have values of  $f_L$  near 0.5. The list of such decays has now grown to include  $B \rightarrow \phi K^*(892)$ ,  $B \rightarrow \rho K^*(892)$ , and  $B \rightarrow \omega K^*(892)$ . The reasons for this "polarization puzzle" are not fully understood. A detailed description of the angular analysis of  $B$  decays to two vector mesons can be found in a separate mini-review [146] in this *Review*.

## 72.6 Electroweak penguin decays

Electroweak decays are one-loop FCNC decays proceeding through penguin or box Feynman diagrams with final state including real photon or pair of leptons. Such decays were first observed by CLEO experiment when it observed decay  $B \rightarrow K^*(892)\gamma$  [76]. Since then significant amount of experimental information was obtained. Branching fractions for these decays are  $10^{-5}$  or less, which makes them excellent candidates for searches for new physics beyond SM. Often several observables are available, which allows for stringent tests of the SM.

Starting with radiative decays, experimentally easiest to study are exclusive decays with a fully reconstructed final state. The best studied decay in this class is  $B \rightarrow K^*(892)\gamma$  seen by CLEO, Belle, BaBar experiments [147–149] with world average branching fraction  $\mathcal{B}(B^0 \rightarrow K^*(892)^0 \gamma) = (41.8 \pm 2.5) \times 10^{-6}$ . Decays through several other kaon resonances such as  $B \rightarrow K_1(1270)\gamma$ ,  $K_2^*(1430)\gamma$ , etc. were studied at B-factories [150–153]. It is worth to mention decay  $B^+ \rightarrow K^+ \pi^+ \pi^- \gamma$  for which besides measure-

ments of the branching fraction [151, 154, 155] one can also use the angular distribution to access photon polarisation. Such a measurement was done by the LHCb experiment, which was able to clearly demonstrate that the photon in  $B^+ \rightarrow K^+ \pi^+ \pi^- \gamma$  decay is polarised [156]. Unfortunately given non-trivial hadronic structure, more work is needed before turning this into test of the SM. The latest addition to the observed exclusive radiative decays is  $B_s^0 \rightarrow \phi\gamma$ , seen by the Belle and LHCb experiments [157, 158] with an average branching fraction of  $(3.4 \pm 0.4) \times 10^{-5}$ .

Compared to  $b \rightarrow s\gamma$ , the  $b \rightarrow d\gamma$  transitions such as  $B \rightarrow \rho\gamma$ , are suppressed by the CKM elements ratio  $|V_{td}/V_{ts}|^2$ . Both Belle and BaBar have observed these decays [77, 78]. The world average  $\mathcal{B}(B \rightarrow (\rho, \omega)\gamma) = (1.30 \pm 0.23) \times 10^{-6}$ . This can be used to calculate  $|V_{td}/V_{ts}|$  [159]; the measured values are  $0.195_{-0.024}^{+0.025}$  from Belle [77] and  $0.233_{-0.032}^{+0.033}$  from BaBar [78].

The observed radiative penguin branching fractions can constrain a large class of SM extensions [160]. However, due to the uncertainties in the hadronization, only the inclusive  $b \rightarrow s\gamma$  rate can be reliably compared with theoretical calculations. This rate can be measured from the endpoint of the inclusive photon spectrum in  $B$  decay. By combining the measurements of  $B \rightarrow X_s \gamma$  from the CLEO, BaBar, and Belle experiments [161–163], HFLAV obtains the new average:  $\mathcal{B}(B \rightarrow X_s \gamma) = (3.32 \pm 0.15) \times 10^{-4}$  [27] for  $E_\gamma \geq 1.6$  GeV, averaging over  $B^+$  and  $B^0$ . Consistent but less precise results have been reported by ALEPH for inclusive  $b$ -hadrons produced at the  $Z$ , which includes also contribution from  $B_s^0$  and  $A_b^0$  hadrons. Using the sum of seven exclusive final states, the BaBar experiment measured the branching fraction of inclusive  $b \rightarrow d\gamma$  decays to be  $(9.2 \pm 2.0 \pm 2.3) \times 10^{-6}$  [164]. The measured branching fraction can be compared to theoretical calculations. Recent calculations of  $\mathcal{B}(b \rightarrow s\gamma)$  at NNLO level predict for the  $E_\gamma \geq 1.6$  GeV values of  $(3.36 \pm 0.23) \times 10^{-4}$  for  $b \rightarrow s\gamma$  and  $(1.73_{-0.22}^{+0.12}) \times 10^{-5}$  for  $b \rightarrow d\gamma$  decays [165].

The  $CP$  asymmetry in  $b \rightarrow s\gamma$  is extensively studied theoretically both in the SM and beyond [166]. According to the SM, the  $CP$  asymmetry in  $b \rightarrow s\gamma$  is smaller than 1%, but some non-SM models allow significantly larger  $CP$  asymmetry ( $\sim 10\%$ ) without altering the branching fraction. The current world average is  $A_{CP} = 0.015 \pm 0.011$ , again dominated by BaBar and Belle [167]. In addition to the  $CP$  asymmetry, BaBar and Belle also measured the isospin asymmetry  $\Delta_{0-} = -0.006 \pm 0.020$  in  $b \rightarrow s\gamma$  measured using sum of exclusive decays [167, 168]. An alternative measurement using full reconstruction of the companion  $B$  in the hadronic decay modes yields a consistent, but less precise result [169]. Both Belle and BaBar experiments measured the isospin asymmetry in exclusive  $B \rightarrow K^*(892)\gamma$  decay with average of  $6.3 \pm 1.7\%$  [148, 149] and therefore providing evidence for the non-zero isospin asymmetry.

In addition, experiments have measured the inclusive photon energy spectrum for  $b \rightarrow s\gamma$ , and by analyzing the shape of the spectrum they obtain the first and second moments for photon energies. Belle has measured these moments covering the widest range in the photon energy ( $1.7 < E_\gamma < 2.8$  GeV) [163]. The measurement by BaBar has slightly smaller range with lower limit at 1.8 GeV [170]. These results can be used to extract non-perturbative HQET parameters that are needed for precise determination of the CKM matrix element  $V_{ub}$ .

Additional information on FCNC processes can be obtained from  $b \rightarrow s\ell^+ \ell^-$  decays. These processes are studied as a function of dilepton invariant mass squared,  $q^2$ . Different  $q^2$  regions are sensitive to different physics. Starting at the very low  $q^2$  decays exhibit sensitivity to the same physics as the radiative decays. Then for the  $q^2$  in region 1.1 to 6.0 GeV<sup>2</sup>/c<sup>4</sup> the SM and new physics have best chance to compete. At the high  $q^2$  above the  $\psi(2S)$  mass, the interference of SM and new physics is to some extent complementary to that in lower  $q^2$ . Regions around  $J/\psi$  and  $\psi(2S)$  is normally excluded from measurements as these are dominated by the  $b \rightarrow c$  transitions to charmonia. For exclusive decays, theory predictions require calculations of hadronic form factors. With current theory predictions, the most useful are measurements within the  $q^2$  regions 1.1 to 6.0 GeV<sup>2</sup>/c<sup>4</sup> and from 16.0 GeV<sup>2</sup>/c<sup>4</sup> up to the kinematic limit. From this reason in the listing we provide results mainly in those two regions.

Similar as for radiative decays, also for the  $b \rightarrow s\ell^+\ell^-$  decays the inclusive measurements provide some benefits. Both Belle and BaBar performed such measurement without reconstructing hadronic part exclusively and measure a branching fraction of  $(5.8 \pm 1.3) \times 10^{-6}$  [171]. Unfortunately this measurement is not trivially possible at hadron colliders and also does not easily allow the angular distributions of the decay products to be exploited. One alternative is to extract information on the inclusive decay as sum of exclusive decays. Such a measurement was performed by Belle [172], but in this case the difficulty lies in extrapolation for the missing hadronic states.

Turning to the exclusive decays, the initial measurements performed by B-factories typically averaged between charged and neutral  $B$  mesons as well as between  $e^+e^-$  and  $\mu^+\mu^-$  final states. The experiments CDF, LHCb, ATLAS and CMS are much better suited for the  $\mu^+\mu^-$  final states compared to the  $e^+e^-$  final states. As such most measurements at hadron colliders are done only with  $\mu^+\mu^-$  decays and by separating charged and neutral  $B$  mesons. The best studied decays are  $B^+ \rightarrow K^+\ell^+\ell^-$  and  $B^0 \rightarrow K^*(892)^0\ell^+\ell^-$ . At hadron colliders other  $b$  hadrons are produced and as such CDF and LHCb experiments did observe also  $B_s^0 \rightarrow \phi\mu^+\mu^-$  [173, 174],  $A_b^0 \rightarrow \Lambda\mu^+\mu^-$  [173, 175] and  $A_b^0 \rightarrow pK^-\mu^+\mu^-$  decays [176]. The total branching fractions integrated over whole  $q^2$  regions are  $(5.5 \pm 0.7) \times 10^{-7}$  for  $B^+ \rightarrow K^+e^+e^-$ ,  $(4.41 \pm 0.23) \times 10^{-7}$  for  $B^+ \rightarrow K^+\mu^+\mu^-$ ,  $(1.03_{-0.17}^{+0.19}) \times 10^{-6}$  for  $B^0 \rightarrow K^*(892)^0e^+e^-$  and  $(0.94 \pm 0.05) \times 10^{-6}$  for  $B^0 \rightarrow K^*(892)^0\mu^+\mu^-$  decays [177–180]. The total branching fractions for  $B_s^0 \rightarrow \phi\mu^+\mu^-$  and  $A_b^0 \rightarrow \Lambda\mu^+\mu^-$  decays are  $(8.2 \pm 1.2) \times 10^{-7}$  [173, 174] and  $(1.08 \pm 0.28) \times 10^{-6}$  [173, 175] respectively. With increased precision of  $B^0 \rightarrow K^*(892)^0\ell^+\ell^-$  decay, there is a question on what fraction of the seen branching fraction is due to the  $K^*(892)^0$  resonance and what fraction is due to the  $K\pi$  in  $s$ -wave. This has been studied by LHCb which found that the  $K\pi$  in  $s$ -wave fraction varies between 1% and about 10% depending on the  $q^2$  region [180]. It should be noted, that for all relevant  $B$  meson decays the branching fractions so far studied are consistently below the SM expectation.

In the  $b \rightarrow s\ell^+\ell^-$  decays angular distributions offer rich source of information. For the decays  $B^+ \rightarrow K^+\ell^+\ell^-$  and  $B^0 \rightarrow K^*(892)^0\ell^+\ell^-$  full angular analysis was already performed [181–186], while for other decays only partial angular analyses are available [174, 187]. Recently a lot of progress was done by constructing observables, which have reduced theory uncertainties and measurements of these are done. Most notably the observable called  $P'_5$  [188] shows a discrepancy with the SM in the  $q^2$  region which is highly sensitive to new physics [185, 186]. Measurements of the  $CP$  asymmetries [176, 178, 189], the isospin asymmetry [177–179] were also performed. All these measurements are well consistent with the small  $ACP$  and small isospin asymmetry expected in the SM [190]. With statistics available at the LHC, the measurement of phase difference between long- and short-distance contribution in  $B^+ \rightarrow K^+\mu^+\mu^-$  decays became possible [191].

With the data samples available at LHC, the lepton universality in  $b \rightarrow s\ell^+\ell^-$  can be tested. While in the SM decays to electron-positron and muon pairs are expected to be same up to small corrections due to the different masses of leptons, in extensions of the SM this does not have to hold. The angular analysis of  $B^0 \rightarrow K^*(892)^0e^+e^-$  decays was performed by LHCb at low dilepton invariant masses [192] and Belle in several regions over whole  $q^2$  range [186]. The most notable result on lepton universality test is the ratio of branching fractions between  $B^+ \rightarrow K^+\mu^+\mu^-$  and  $B^+ \rightarrow K^+e^+e^-$  and between  $B^0 \rightarrow K^*(892)^0\mu^+\mu^-$  and  $B^0 \rightarrow K^*(892)^0e^+e^-$  decays. In both cases, the measurements by LHCb show similar discrepancy from the SM, each being in the region of  $2.1$ – $2.6\sigma$  [193, 194]. Recently, LHCb experiment performed similar test with  $A_b^0 \rightarrow pK^-\ell^+\ell^-$  decays [195].

While  $b \rightarrow d\ell^+\ell^-$  decays are further suppressed, they recently became accessible. Signals were observed for  $B^+ \rightarrow \pi^+\mu^+\mu^-$  [79],  $B^0 \rightarrow \pi^+\pi^-\mu^+\mu^-$  [196] and  $A_b^0 \rightarrow p\pi^-\mu^+\mu^-$  [197] decays. The total branching fractions are only quantities measured and these are about  $2 \times 10^{-8}$  for the meson decays and about  $7 \times 10^{-8}$  for the  $A_b^0$  decay.

Finally the decays  $B_{(s)}^0 \rightarrow e^+e^-$  and  $\mu^+\mu^-$  are interesting since they only proceed at second order in weak interactions in the SM, but may have large contributions from supersymmetric loops, proportional to  $(\tan\beta)^6$ . First limits were published 30 years ago and since then experiments at Tevatron,  $B$ -factories and LHC gradually improved those and effectively excluded whole models of new physics and significantly constrained allowed parameter space of others. For the decays to  $\mu^+\mu^-$ , Tevatron experiments pushed the limits down to roughly factor of 5–10 above the SM expectation [198, 199]. The long journey in the search for these decays culminated in 2012, when first evidence for  $B_s^0 \rightarrow \mu^+\mu^-$  decay was seen [200]. Subsequently, LHC experiments ATLAS [201], CMS [202] and LHCb [203] observed statistically significant signal for  $B_s^0 \rightarrow \mu^+\mu^-$  decay. The average branching fraction is found to be  $(3.0 \pm 0.4) \times 10^{-9}$ . In experiments at hadron colliders searches for  $B^0 \rightarrow \mu^+\mu^-$  decays are performed at the same time. The best limit on  $B(B^0 \rightarrow \mu^+\mu^-) < 3.4 \times 10^{-10}$  at 95% C.L. [203]. The limits for the  $e^+e^-$  modes are:  $< 2.8 \times 10^{-7}$  and  $< 8.3 \times 10^{-8}$ , respectively, for  $B_s^0$  and  $B^0$  [204]. The searches for decays to  $\tau^+\tau^-$  are more challenging with current best limits of  $B(B^0 \rightarrow \tau^+\tau^-) < 2.1 \times 10^{-3}$  and  $B(B_s^0 \rightarrow \tau^+\tau^-) < 6.8 \times 10^{-3}$  at 95% C.L. [205]. All existing measurements of  $B^0$  and  $B_s^0$  decays to same flavour dilepton pair is consistent with SM expectation [206]. With  $B_s^0 \rightarrow \mu^+\mu^-$  decay observed, it was suggested that the effective lifetime is useful further test of the decay [207]. Attempt was made by LHCb experiment, but its precision is not yet sufficient to provide test of the SM [203]. It will take couple of years until interesting precision is reached. The searches were also performed for lepton flavour violating decays to two leptons with best limits in  $e^\pm\mu^\mp$  channel, where limits are  $< 3.7 \times 10^{-9}$  for  $B^0$  and  $< 1.4 \times 10^{-8}$  for  $B_s^0$ , at 95% confidence level [208].

Several theory groups performed global analysis of electroweak decays concluding that significant tension between data and SM is present [209]. The tension can be relieved by new physics beyond SM. For more detailed reviews see e.g. Ref. [210].

## 72.7 Summary and Outlook

The study of  $B$  mesons continues to be one of the most productive fields in particle physics. With the two asymmetric  $B$ -factory experiments Belle and BaBar, we now have a combined data sample of well over  $1 \text{ ab}^{-1}$ .  $CP$  violation has been firmly established in many decays of  $B$  mesons. Evidence for direct  $CP$  violation has been observed. Many rare decays resulting from hadronic  $b \rightarrow u$  transitions and  $b \rightarrow s(d)$  penguin decays have been observed, and the emerging pattern is still full of surprises. Despite the remarkable successes of the  $B$ -factory experiments, many fundamental questions in the flavor sector remain unanswered.

At Fermilab, CDF and D0 each has accumulated about  $10 \text{ fb}^{-1}$ , which is the equivalent of about  $10^{12}$   $b$ -hadrons produced. In spite of the low trigger efficiency of hadronic experiments, a selection of modes have been reconstructed in large quantities, giving a start to a program of studies on  $B_s$  and  $b$ -flavored baryons, in which a first major step has been the determination of the  $B_s$  oscillation frequency.

As Tevatron and  $B$ -factories finished their taking data, the new experiments at the LHC have become very active. LHCb has collected about  $1 \text{ fb}^{-1}$  at 7 TeV,  $2 \text{ fb}^{-1}$  at 8 TeV, and close to  $5.9 \text{ fb}^{-1}$  at 13 TeV during LHC Runs 1 and 2. CMS and ATLAS have collected each about  $5 \text{ fb}^{-1}$  of data at  $\sqrt{s} = 7 \text{ TeV}$ ,  $20 \text{ fb}^{-1}$  at 8 TeV and about  $150 \text{ fb}^{-1}$  at 13 TeV during LHC Runs 1 and 2. LHCb, which is dedicated to the studies of  $b$ - and  $c$ -hadrons, has a data sample that is for many decays larger than the sum of all previous experiments. With it, we are entering to regime of precision physics even for many rare decays, which allows much more detailed measurements.

The Belle II experiment at the SuperKEKB has started recording data in 2019 and has so far collected about  $12.4 \text{ fb}^{-1}$  of data (March 2020). The aim to increase sample to  $\sim 50 \text{ ab}^{-1}$  will make it possible to explore the indirect evidence of new physics beyond the SM in the heavy-flavor particles ( $b$ ,  $c$ , and  $\tau$ ), in a way that is complementary to the LHC. In the same time period, LHCb Collaboration is working on the upgrade of its detector,

installation of which is ongoing. The aim of the upgrade is to increase flexibility of the trigger, which will allow about a factor of five increase in instantaneous luminosity and of about a factor of two in efficiencies on triggering on purely hadronic decays. The plan is to integrate about  $50 \text{ fb}^{-1}$  of data starting from 2021.

These experiments promise a rich spectrum of rare and precise measurements that have the potential to fundamentally affecting our understanding of the SM and *CP*-violating phenomena.

### References

- [1] M. Kobayashi and T. Maskawa, *Prog. Theor. Phys.* **49**, 652 (1973).
- [2] S. W. Herb *et al.*, *Phys. Rev. Lett.* **39**, 252 (1977).
- [3] B. Aubert *et al.* (BaBar), *Phys. Rev. Lett.* **87**, 091801 (2001), [hep-ex/0107013].
- [4] K. Abe *et al.* (Belle), *Phys. Rev. Lett.* **87**, 091802 (2001), [hep-ex/0107061].
- [5] Currently two different notations ( $\phi_1, \phi_2, \phi_3$ ) and ( $\alpha, \beta, \gamma$ ) are used in the literature for CKM unitarity angles. In this mini-review, we use the latter notation following the other mini-reviews in this *Review*. The two notations are related by  $\phi_1 = \beta$ ,  $\phi_2 = \alpha$  and  $\phi_3 = \gamma$ .
- [6] See the “*CP* Violation in Meson Decays” by D. Kirkby and Y. Nir in this *Review*.
- [7] See the “CKM Quark Mixing Matrix,” by A. Cecucci, Z. Ligeti, and Y. Sakai, in this *Review*.
- [8] See the note on “ $B^0 - \bar{B}^0$  mixing,” by O. Schneider in this *Review*.
- [9] See the “Determination of  $|V_{cb}|$  and  $|V_{ub}|$ ,” by R. Kowalewski and T. Mannel in this *Review*.
- [10] F. Abe *et al.* (CDF), *Phys. Rev. Lett.* **81**, 2432 (1998), [hep-ex/9805034]; F. Abe *et al.* (CDF), *Phys. Rev.* **D58**, 112004 (1998), [hep-ex/9804014].
- [11] A. Abulencia *et al.* (CDF), *Phys. Rev. Lett.* **96**, 082002 (2006), [hep-ex/0505076].
- [12] R. Aaij *et al.* (LHCb), *Phys. Rev.* **D95**, 3, 032005 (2017), [arXiv:1612.07421].
- [13] B. Aubert *et al.* (BaBar), *Phys. Rev. Lett.* **101**, 071801 (2008), [Erratum: *Phys. Rev. Lett.* 102,029901(2009)], [arXiv:0807.1086].
- [14] B. Aubert *et al.* (BaBar), *Phys. Rev. Lett.* **103**, 161801 (2009), [arXiv:0903.1124].
- [15] G. Bonvicini *et al.* (CLEO), *Phys. Rev.* **D81**, 031104 (2010), [arXiv:0909.5474].
- [16] R. Mizuk *et al.* (Belle), *Phys. Rev. Lett.* **109**, 232002 (2012), [arXiv:1205.6351].
- [17] U. Tamponi *et al.* (Belle), *Phys. Rev. Lett.* **115**, 14, 142001 (2015), [arXiv:1506.08914].
- [18] See the note on “Naming scheme for hadrons,” by M. Roos and C.G. Wohl in this *Review*.
- [19] R. Aaij *et al.* (LHCb), *Phys. Rev. Lett.* **118**, 5, 052002 (2017), [Erratum: *Phys. Rev. Lett.* 119,no.16,169901(2017)], [arXiv:1612.05140].
- [20] M. Cacciari *et al.*, *JHEP* **10**, 137 (2012), [arXiv:1205.6344]; B. A. Kniehl *et al.*, *Phys. Rev.* **D84**, 094026 (2011), [arXiv:1109.2472]; M. Cacciari, M. L. Mangano and P. Nason, *Eur. Phys. J.* **C75**, 12, 610 (2015), [arXiv:1507.06197].
- [21] B. Barish *et al.* (CLEO), *Phys. Rev. Lett.* **76**, 1570 (1996).
- [22] E. Guido *et al.* (Belle), *Phys. Rev. Lett.* **121**, 062001 (2018), [arXiv:1803.10303]; E. Guido *et al.* (Belle), *Phys. Rev.* **D96**, 052005 (2017), [arXiv:1707.04973]; A. Sokolov *et al.* (Belle), *Phys. Rev.* **D79**, 051103 (2009), [arXiv:0901.1431]; B. Aubert *et al.* (BaBar), *Phys. Rev.* **D78**, 112002 (2008), [arXiv:0807.2014].
- [23] J. P. Alexander *et al.* (CLEO), *Phys. Rev. Lett.* **86**, 2737 (2001), [hep-ex/0006002]; S. B. Athar *et al.* (CLEO), *Phys. Rev.* **D66**, 052003 (2002), [hep-ex/0202033].
- [24] N. C. Hastings *et al.* (Belle), *Phys. Rev.* **D67**, 052004 (2003), [hep-ex/0212033].
- [25] B. Aubert *et al.* (BaBar), *Phys. Rev. Lett.* **95**, 042001 (2005), [hep-ex/0504001].
- [26] Y. Amhis *et al.* (HFLAV), *Eur. Phys. J.* **C77**, 12, 895 (2017), [arXiv:1612.07233].
- [27] Y. S. Amhis *et al.* (HFLAV) (2019), and online update at <https://hflav.web.cern.ch/content/lifetimes-and-oscillation-parameters>, [arXiv:1909.12524].
- [28] P. Abreu *et al.* (DELPHI), *Phys. Lett.* **B345**, 598 (1995).
- [29] R. Akers *et al.* (OPAL), *Z. Phys.* **C66**, 19 (1995).
- [30] T. A. Aaltonen *et al.* (CDF), *Phys. Rev.* **D90**, 1, 012013 (2014), [arXiv:1309.5961].
- [31] R. Aaij *et al.* (LHCb), *JHEP* **04**, 024 (2015), [arXiv:1502.02638].
- [32] R. Aaij *et al.* (LHCb), *Phys. Rev. Lett.* **110**, 15, 151803 (2013), [arXiv:1211.5994].
- [33] A. M. Sirunyan *et al.* (CMS), *Eur. Phys. J.* **C78**, 939 (2018), [arXiv:1809.03578].
- [34] G. Aad *et al.* (ATLAS), *Phys. Rev. Lett.* **113**, 21, 212004 (2014), [arXiv:1407.1032].
- [35] A. Sirunyan *et al.* (CMS), *Phys. Rev. Lett.* **122**, 132001 (2019), [arXiv:1902.00571].
- [36] R. Aaij *et al.* (LHCb), *Phys. Rev. Lett.* **122**, 232001 (2019), [arXiv:1904.00081].
- [37] T. Aaltonen *et al.* (CDF), *Phys. Rev. Lett.* **99**, 202001 (2007), [arXiv:0706.3868]; T. Aaltonen *et al.* (CDF), *Phys. Rev.* **D85**, 092011 (2012), [arXiv:1112.2808].
- [38] R. Aaij *et al.* (LHCb), *Phys. Rev. Lett.* **122**, 012001 (2019), [arXiv:1809.07752].
- [39] V. M. Abazov *et al.* (D0), *Phys. Rev. Lett.* **99**, 052001 (2007), [arXiv:0706.1690]; T. Aaltonen *et al.* (CDF), *Phys. Rev. Lett.* **99**, 052002 (2007), [arXiv:0707.0589].
- [40] R. Aaij *et al.* (LHCb), *Phys. Rev. Lett.* **113**, 032001 (2014), [arXiv:1405.7223]; R. Aaij *et al.* (LHCb), *Phys. Lett.* **B736**, 154 (2014), [arXiv:1405.1543]; R. Aaij *et al.* (LHCb), *Phys. Rev.* **D89**, 3, 032001 (2014), [arXiv:1311.4823]; R. Aaij *et al.* (LHCb), *Phys. Rev. Lett.* **113**, 24, 242002 (2014), [arXiv:1409.8568]; R. Aaij *et al.* (LHCb), *Phys. Rev. Lett.* **115**, 24, 241801 (2015), [arXiv:1510.03829]; R. Aaij *et al.* (LHCb), *Phys. Rev. Lett.* **118**, 7, 071801 (2017), [arXiv:1612.02244]; R. Aaij *et al.* (LHCb), *Phys. Lett.* **B722**, 265 (2017), [arXiv:1701.05274]; R. Aaij *et al.* (LHCb), *Phys. Rev. Lett.* **118**, 071801 (2017), [arXiv:1612.02244]; R. Aaij *et al.* (LHCb), *JHEP* **02**, 98 (2018), [arXiv:1711.05490]; R. Aaij *et al.* (LHCb), *Phys. Rev.* **D99**, 052006 (2019), [arXiv:1901.07075].
- [41] T. A. Aaltonen *et al.* (CDF), *Phys. Rev.* **D89**, 7, 072014 (2014), [arXiv:1403.8126].
- [42] R. Aaij *et al.* (LHCb), *JHEP* **08**, 039 (2018), [arXiv:1805.03941].
- [43] S. Chatrchyan *et al.* (CMS), *Phys. Rev. Lett.* **108**, 252002 (2012), [arXiv:1204.5955].
- [44] R. Aaij *et al.* (LHCb), *JHEP* **1605**, 161 (2016), [arXiv:1604.03896].
- [45] R. Aaij *et al.* (LHCb), *Phys. Rev. Lett.* **114**, 062004 (2015), [arXiv:1411.4849].
- [46] R. Aaij *et al.* (LHCb), *Phys. Rev. Lett.* **121**, 072002 (2018), [arXiv:1805.09418].
- [47] V. M. Abazov *et al.* (D0), *Phys. Rev. Lett.* **101**, 232002 (2008), [arXiv:0808.4142]; T. Aaltonen *et al.* (CDF), *Phys. Rev.* **D80**, 072003 (2009), [arXiv:0905.3123].
- [48] R. Aaij *et al.* (LHCb), *Phys. Rev. Lett.* **110**, 18, 182001 (2013), [arXiv:1302.1072]; R. Aaij *et al.* (LHCb), *Phys. Lett.* **B736**, 154 (2014), [arXiv:1405.1543]; R. Aaij *et al.* (LHCb), *Phys. Rev.* **D93**, 9, 092007 (2016), [arXiv:1604.01412].

- [49] V. M. Abazov *et al.* (D0), Phys. Rev. Lett. **117**, 2, 022003 (2016), [arXiv:1602.07588]; V. M. Abazov *et al.* (D0), Phys. Rev. **D97**, 092004 (2018), [arXiv:1712.10176].
- [50] R. Aaij *et al.* (LHCb), Phys. Rev. Lett. **117**, 15, 152003 (2016), [Addendum: Phys. Rev. Lett.118,no.10,109904(2017)], [arXiv:1608.00435].
- [51] A. Sirunyan *et al.* (CMS), Phys. Rev. Lett. **120**, 202005 (2018), [arXiv:1712.06144].
- [52] C. Tarantino, Eur. Phys. J. **C33**, S895 (2004), [hep-ph/0310241]; F. Gabbiani, A. I. Onishchenko and A. A. Petrov, Phys. Rev. **D70**, 094031 (2004), [hep-ph/0407004]; F. Gabbiani, A. I. Onishchenko and A. A. Petrov, Phys. Rev. **D68**, 114006 (2003), [hep-ph/0303235].
- [53] A. Lenz, Int. J. Mod. Phys. **A30**, 10, 1543005 (2015), [arXiv:1405.3601].
- [54] C.-H. Chang *et al.*, Phys. Rev. **D64**, 014003 (2001), [hep-ph/0007162]; V. V. Kiselev, A. E. Kovalsky and A. K. Likhoded, Nucl. Phys. **B585**, 353 (2000), [hep-ph/0002127]; A. Yu. Anisimov *et al.*, Phys. Lett. **B452**, 129 (1999), [hep-ph/9812514]; M. Beneke and G. Buchalla, Phys. Rev. **D53**, 4991 (1996), [hep-ph/9601249].
- [55] R. Aaij *et al.* (LHCb), Eur. Phys. J. **C74**, 5, 2839 (2014), [arXiv:1401.6932].
- [56] R. Aaij *et al.* (LHCb), Phys. Lett. **B742**, 29 (2015), [arXiv:1411.6899].
- [57] The  $B_c$  is a special case, where a weak decay of the  $c$  quark is also possible, but the spectator model still applies.
- [58] R. Aaij *et al.* (LHCb), Nature Phys. **11**, 743 (2015), [arXiv:1504.01568].
- [59] J. P. Lees *et al.* (BaBar), Phys. Rev. **D85**, 011101 (2012), [arXiv:1110.5600]; C. Oswald *et al.* (Belle), Phys. Rev. **D87**, 7, 072008 (2013), [Erratum: Phys. Rev.D90,no.11,119901(2014)], [arXiv:1212.6400]; C. Oswald *et al.* (Belle), Phys. Rev. **D92**, 7, 072013 (2015), [arXiv:1504.02004].
- [60] T. A. Aaltonen *et al.* (CDF), Phys. Rev. **D93**, 5, 052001 (2016), [arXiv:1601.03819].
- [61] B. Grinstein, Nucl. Phys. **B339**, 253 (1990); H. Georgi, Phys. Lett. **B240**, 447 (1990); A. F. Falk *et al.*, Nucl. Phys. **B343**, 1 (1990); E. Eichten and B. R. Hill, Phys. Lett. **B234**, 511 (1990).
- [62] "Heavy-Quark and Soft-Collinear Effective Theory" by C.W. Bauer and M. Neubert in this *Review*.
- [63] M. Neubert, "Aspects of QCD Factorization," hep-ph/0110093, *Proceedings of HF9*, Pasadena (2001) and references therein; Z. Ligeti, M. E. Luke and M. B. Wise, Phys. Lett. **B507**, 142 (2001), [hep-ph/0103020].
- [64] M. Beneke *et al.*, Phys. Rev. Lett. **83**, 1914 (1999), [hep-ph/9905312].
- [65] M. Beneke *et al.*, Nucl. Phys. **B591**, 313 (2000), [hep-ph/0006124].
- [66] M. Beneke *et al.*, Nucl. Phys. **B606**, 245 (2001), [hep-ph/0104110].
- [67] M. Beneke and M. Neubert, Nucl. Phys. **B675**, 333 (2003), [hep-ph/0308039].
- [68] Y.-Y. Keum, H.-n. Li and A. I. Sanda, Phys. Lett. **B504**, 6 (2001), [hep-ph/0004004].
- [69] Y. Y. Keum, H.-N. Li and A. I. Sanda, Phys. Rev. **D63**, 054008 (2001), [hep-ph/0004173].
- [70] Y.-Y. Keum and H.-n. Li, Phys. Rev. **D63**, 074006 (2001), [hep-ph/0006001].
- [71] C.-D. Lu, K. Ukai and M.-Z. Yang, Phys. Rev. **D63**, 074009 (2001), [hep-ph/0004213].
- [72] C.-D. Lu and M.-Z. Yang, Eur. Phys. J. **C23**, 275 (2002), [hep-ph/0011238].
- [73] C. W. Bauer, S. Fleming and M. E. Luke, Phys. Rev. **D63**, 014006 (2000), [hep-ph/0005275].
- [74] C. W. Bauer *et al.*, Phys. Rev. **D63**, 114020 (2001), [hep-ph/0011336].
- [75] C. W. Bauer and I. W. Stewart, Phys. Lett. **B516**, 134 (2001), [hep-ph/0107001].
- [76] R. Ammar *et al.* (CLEO), Phys. Rev. Lett. **71**, 674 (1993).
- [77] N. Taniguchi *et al.* (Belle), Phys. Rev. Lett. **101**, 111801 (2008), [Erratum: Phys. Rev. Lett.101,129904(2008)], [arXiv:0804.4770].
- [78] B. Aubert *et al.* (BaBar), Phys. Rev. **D78**, 112001 (2008), [arXiv:0808.1379].
- [79] R. Aaij *et al.* (LHCb), JHEP **10**, 034 (2015), [arXiv:1509.00414].
- [80] P. Krokovny *et al.* (Belle), Phys. Rev. Lett. **89**, 231804 (2002), [hep-ex/0207077]; B. Aubert *et al.* (BaBar), Phys. Rev. Lett. **98**, 081801 (2007), [hep-ex/0604012].
- [81] B. Kronenbitter *et al.* (Belle), Phys. Rev. **D92**, 5, 051102 (2015), [arXiv:1503.05613]; I. Adachi *et al.* (Belle), Phys. Rev. Lett. **110**, 13, 131801 (2013), [arXiv:1208.4678].
- [82] J. P. Lees *et al.* (BaBar), Phys. Rev. **D88**, 3, 031102 (2013), [arXiv:1207.0698]; B. Aubert *et al.* (BaBar), Phys. Rev. **D81**, 051101 (2010), [arXiv:0912.2453].
- [83] See the "Leptonic decays of charged pseudoscalar mesons," by J. Rosner, S. Stone, and R. Van de Water, in this *Review*.
- [84] J. P. Lees *et al.* (BaBar), Phys. Rev. **D84**, 112007 (2011), [Erratum: Phys. Rev.D87,no.3,039901(2013)], [arXiv:1107.5751]; S. Blyth *et al.* (Belle), Phys. Rev. **D74**, 092002 (2006), [hep-ex/0607029].
- [85] R. Aaij *et al.* (LHCb), Phys. Rev. D **92**, 3, 032002 (2015), [arXiv:1505.01710].
- [86] B. Aubert *et al.* (BaBar), Phys. Rev. Lett. **90**, 242001 (2003), [hep-ex/0304021].
- [87] D. Besson *et al.* (CLEO), Phys. Rev. **D68**, 032002 (2003), [Erratum: Phys. Rev.D75,119908(2007)], [hep-ex/0305100].
- [88] P. Krokovny *et al.* (Belle), Phys. Rev. Lett. **91**, 262002 (2003), [hep-ex/0308019]; Y. Mikami *et al.* (Belle), Phys. Rev. Lett. **92**, 012002 (2004), [hep-ex/0307052].
- [89] B. Aubert *et al.* (BaBar), Phys. Rev. Lett. **93**, 181801 (2004), [hep-ex/0408041].
- [90] R. Aaij *et al.* (LHCb), Phys. Rev. Lett. **113**, 162001 (2014), [arXiv:1407.7574].
- [91] T. Aaltonen *et al.* (CDF), Phys. Rev. Lett. **108**, 201801 (2012), [arXiv:1204.0536].
- [92] S. Esen *et al.* (Belle), Phys. Rev. **D87**, 3, 031101 (2013), [arXiv:1208.0323].
- [93] R. Aaij *et al.* (LHCb), Phys. Rev. **D93**, 9, 092008 (2016), [arXiv:1602.07543].
- [94] R. Aaij *et al.* (LHCb), Phys. Rev. Lett. **116**, 16, 161802 (2016), [arXiv:1603.02408].
- [95] R. Aaij *et al.* (LHCb), JHEP **11**, 082 (2015), [arXiv:1509.00400].
- [96] B. Aubert *et al.* (BaBar), Phys. Rev. **D76**, 031101 (2007), [arXiv:0704.1266].
- [97] R. Aaij *et al.* (LHCb), Phys. Rev. **D90**, 1, 012003 (2014), [arXiv:1404.5673].
- [98] R. Aaij *et al.* (LHCb), Phys. Rev. Lett. **111**, 18, 181801 (2013), [arXiv:1308.4544].
- [99] R. Aaij *et al.* (LHCb), Phys. Rev. **D87**, 11, 112012 (2013), [Addendum: Phys. Rev.D89,no.1,019901(2014)], [arXiv:1304.4530].
- [100] G. Aad *et al.* (ATLAS), Eur. Phys. J. **C76**, 1, 4 (2016), [arXiv:1507.07099].
- [101] R. Aaij *et al.* (LHCb), Phys. Rev. **D84**, 092001 (2011), [Erratum: Phys. Rev.D85,039904(2012)], [arXiv:1109.6831]; T. Aaltonen *et al.* (CDF), Phys. Rev. **D85**, 032003 (2012), [arXiv:1112.3334].

- [102] S. K. Choi *et al.* (Belle), Phys. Rev. Lett. **91**, 262001 (2003), [hep-ex/0309032].
- [103] D. Acosta *et al.* (CDF), Phys. Rev. Lett. **93**, 072001 (2004), [hep-ex/0312021].
- [104] V. M. Abazov *et al.* (D0), Phys. Rev. Lett. **93**, 162002 (2004), [hep-ex/0405004].
- [105] B. Aubert *et al.* (BaBar), Phys. Rev. **D71**, 071103 (2005), [hep-ex/0406022].
- [106] R. Aaij *et al.* (LHCb), Eur. Phys. J. **C72**, 1972 (2012), [arXiv:1112.5310].
- [107] S. Chatrchyan *et al.* (CMS), JHEP **04**, 154 (2013), [arXiv:1302.3968].
- [108] M. Aaboud *et al.* (ATLAS), JHEP **01**, 117 (2017), [arXiv:1610.09303].
- [109] S. K. Choi *et al.* (Belle), Phys. Rev. Lett. **100**, 142001 (2008), [arXiv:0708.1790]; R. Mizuk *et al.* (Belle), Phys. Rev. **D80**, 031104 (2009), [arXiv:0905.2869].
- [110] R. Aaij *et al.* (LHCb), Phys. Rev. Lett. **112**, 22, 222002 (2014), [arXiv:1404.1903]; R. Aaij *et al.* (LHCb), Phys. Rev. **D92**, 11, 112009 (2015), [arXiv:1510.01951].
- [111] K. Chilikin *et al.* (Belle), Phys. Rev. **D90**, 11, 112009 (2014), [arXiv:1408.6457].
- [112] R. Aaij *et al.* (LHCb), Phys. Rev. Lett. **115**, 072001 (2015), [arXiv:1507.03414].
- [113] R. Aaij *et al.* (LHCb), Phys. Rev. Lett. **122**, 22, 222001 (2019), [arXiv:1904.03947].
- [114] See the “Non- $q\bar{q}$  mesons,” by C. Amsler and C. Hanhart, and “Pentaquarks,” by M. Karliner and T. Skwarnicki, in this *Review*.
- [115] T. Aaltonen *et al.* (CDF), Phys. Rev. Lett. **107**, 261802 (2011), [arXiv:1107.4999].
- [116] R. Aaij *et al.* (LHCb), JHEP **10**, 053 (2015), [arXiv:1508.00788].
- [117] T. A. Aaltonen *et al.* (CDF), Phys. Rev. Lett. **113**, 24, 242001 (2014), [arXiv:1403.5586].
- [118] R. Aaij *et al.* (LHCb), JHEP **10**, 037 (2012), [arXiv:1206.2794].
- [119] T. Aaltonen *et al.* (CDF), Phys. Rev. Lett. **103**, 031801 (2009), [arXiv:0812.4271].
- [120] R. Aaij *et al.* (LHCb), Phys. Rev. D **98**, 3, 032004 (2018), [arXiv:1805.06759].
- [121] R. Aaij *et al.* (LHCb), JHEP **12**, 155 (2019), [arXiv:1907.10003].
- [122] R. Fleischer, Phys. Lett. **B459**, 306 (1999), [hep-ph/9903456]; D. London and J. Matias, Phys. Rev. **D70**, 031502 (2004), [hep-ph/0404009].
- [123] J. P. Lees *et al.* (BaBar), Phys. Rev. **D87**, 5, 052009 (2013), [arXiv:1206.3525].
- [124] Y. T. Duh *et al.* (Belle), Phys. Rev. **D87**, 3, 031103 (2013), [arXiv:1210.1348].
- [125] B. Aubert *et al.* (BaBar), Phys. Rev. **D76**, 091102 (2007), [arXiv:0707.2798].
- [126] M. Gronau and J. L. Rosner, Phys. Rev. **D71**, 074019 (2005), [hep-ph/0503131]; M. Gronau, Phys. Lett. **B627**, 82 (2005), [hep-ph/0508047].
- [127] B. Aubert *et al.* (BaBar), Phys. Rev. **D78**, 012004 (2008), [arXiv:0803.4451]; A. Garmash *et al.* (Belle), Phys. Rev. Lett. **96**, 251803 (2006), [hep-ex/0512066].
- [128] C. T. Hoi *et al.* (Belle), Phys. Rev. Lett. **108**, 031801 (2012), [arXiv:1110.2000]; B. Aubert *et al.* (BaBar), Phys. Rev. **D80**, 112002 (2009), [arXiv:0907.1743].
- [129] B. Aubert *et al.* (BaBar), Phys. Rev. Lett. **97**, 201802 (2006), [hep-ex/0608005]; C. H. Wang *et al.* (Belle), Phys. Rev. **D75**, 092005 (2007), [hep-ex/0701057].
- [130] R. Aaij *et al.* (LHCb), Phys. Rev. **D90**, 11, 112004 (2014), [arXiv:1408.5373].
- [131] C.-L. Hsu *et al.* (Belle), Phys. Rev. D **96**, 3, 031101 (2017), [arXiv:1705.02640].
- [132] B. Aubert *et al.* (BaBar), Phys. Rev. Lett. **97**, 171805 (2006), [hep-ex/0608036].
- [133] K. Abe *et al.* (Belle), Phys. Rev. Lett. **98**, 181804 (2007), [hep-ex/0608049].
- [134] R. Aaij *et al.* (LHCb), Phys. Rev. Lett. **118**, 8, 081801 (2017), [arXiv:1610.08288].
- [135] C. C. Peng *et al.* (Belle), Phys. Rev. **D82**, 072007 (2010), [arXiv:1006.5115].
- [136] T. Aaltonen *et al.* (CDF), Phys. Rev. Lett. **106**, 181802 (2011), [arXiv:1103.5762].
- [137] B. Pal *et al.* (Belle), Phys. Rev. Lett. **116**, 16, 161801 (2016), [arXiv:1512.02145].
- [138] See the “Determination of CKM angles from B hadrons,” by T. Gershon, M. Kenzie, and K. Trabelsi, in this *Review*.
- [139] M. Gronau and D. London, Phys. Rev. Lett. **65**, 3381 (1990).
- [140] T. Julius *et al.* (Belle), Phys. Rev. **D96**, 3, 032007 (2017), [arXiv:1705.02083].
- [141] B. Aubert *et al.* (BaBar), Phys. Rev. **D78**, 071104 (2008), [arXiv:0807.4977].
- [142] P. Vanhoefer *et al.* (Belle), Phys. Rev. **D89**, 072008 (2014), [Addendum: Phys. Rev. D89,119903(2014)], [arXiv:1212.4015].
- [143] B. Aubert *et al.* (BaBar), Phys. Rev. **D76**, 052007 (2007), [arXiv:0705.2157]; A. Somov *et al.* (Belle), Phys. Rev. Lett. **96**, 171801 (2006), [hep-ex/0601024].
- [144] B. Aubert *et al.* (BaBar), Phys. Rev. Lett. **102**, 141802 (2009), [arXiv:0901.3522]; J. Zhang *et al.* (Belle), Phys. Rev. Lett. **91**, 221801 (2003), [hep-ex/0306007].
- [145] R. Aaij *et al.* (LHCb), Phys. Lett. **B747**, 468 (2015), [arXiv:1503.07770].
- [146] See the “Polarization in *B* Decays,” by A. Gritsan in this *Review*.
- [147] T. E. Coan *et al.* (CLEO), Phys. Rev. Lett. **84**, 5283 (2000), [hep-ex/9912057].
- [148] T. Horiguchi *et al.* (Belle), Phys. Rev. Lett. **119**, 19, 191802 (2017), [arXiv:1707.00394].
- [149] B. Aubert *et al.* (BaBar), Phys. Rev. Lett. **103**, 211802 (2009), [arXiv:0906.2177].
- [150] B. Aubert *et al.* (BaBar), Phys. Rev. **D70**, 091105 (2004), [hep-ex/0409035].
- [151] H. Yang *et al.* (Belle), Phys. Rev. Lett. **94**, 111802 (2005), [hep-ex/0412039].
- [152] S. Nishida *et al.* (Belle), Phys. Lett. **B610**, 23 (2005), [hep-ex/0411065].
- [153] B. Aubert *et al.* (BaBar), Phys. Rev. **D74**, 031102 (2006), [hep-ex/0603054].
- [154] B. Aubert *et al.* (BaBar), Phys. Rev. Lett. **98**, 211804 (2007), [Erratum: Phys. Rev. Lett.100,199905(2008)], [hep-ex/0507031].
- [155] P. del Amo Sanchez *et al.* (BaBar), Phys. Rev. **D93**, 5, 052013 (2016), [arXiv:1512.03579].
- [156] R. Aaij *et al.* (LHCb), Phys. Rev. Lett. **112**, 16, 161801 (2014), [arXiv:1402.6852].
- [157] J. Wicht *et al.* (Belle), Phys. Rev. Lett. **100**, 121801 (2008), [arXiv:0712.2659]; D. Dutta *et al.* (Belle), Phys. Rev. **D91**, 1, 011101 (2015), [arXiv:1411.7771].
- [158] R. Aaij *et al.* (LHCb), Nucl. Phys. **B867**, 1 (2013), [arXiv:1209.0313].

- [159] A. Ali, E. Lunghi and A. Ya. Parkhomenko, Phys. Lett. **B595**, 323 (2004), [hep-ph/0405075]; P. Ball, G. W. Jones and R. Zwicky, Phys. Rev. **D75**, 054004 (2007), [hep-ph/0612081].
- [160] J. L. Hewett, Phys. Rev. Lett. **70**, 1045 (1993), [hep-ph/9211256].
- [161] S. Chen *et al.* (CLEO), Phys. Rev. Lett. **87**, 251807 (2001), [hep-ex/0108032].
- [162] J. P. Lees *et al.* (BaBar), Phys. Rev. **D86**, 112008 (2012), [arXiv:1207.5772].
- [163] A. Limosani *et al.* (Belle), Phys. Rev. Lett. **103**, 241801 (2009), [arXiv:0907.1384]; T. Saito *et al.* (Belle), Phys. Rev. **D91**, 5, 052004 (2015), [arXiv:1411.7198].
- [164] P. del Amo Sanchez *et al.* (BaBar), Phys. Rev. **D82**, 051101 (2010), [arXiv:1005.4087].
- [165] M. Misiak *et al.*, Phys. Rev. Lett. **114**, 22, 221801 (2015), [arXiv:1503.01789]; M. Czakon *et al.*, JHEP **04**, 168 (2015), [arXiv:1503.01791].
- [166] L. Wolfenstein and Y. L. Wu, Phys. Rev. Lett. **73**, 2809 (1994), [hep-ph/9410253]; G. M. Asatrian and A. Ioannianian, Phys. Rev. **D54**, 5642 (1996), [hep-ph/9603318]; M. Ciuchini, E. Gabrielli and G. F. Giudice, Phys. Lett. **B388**, 353 (1996), [Erratum: Phys. Lett. **B393**, 489 (1997)], [hep-ph/9604438]; S. Baek and P. Ko, Phys. Rev. Lett. **83**, 488 (1999), [hep-ph/9812229]; A. L. Kagan and M. Neubert, Phys. Rev. **D58**, 094012 (1998), [hep-ph/9803368]; K. Kiers, A. Soni and G.-H. Wu, Phys. Rev. **D62**, 116004 (2000), [hep-ph/0006280].
- [167] S. Watanuki *et al.* (Belle), Phys. Rev. D **99**, 3, 032012 (2019), [arXiv:1807.04236]; J. P. Lees *et al.* (BaBar), Phys. Rev. **D90**, 9, 092001 (2014), [arXiv:1406.0534].
- [168] B. Aubert *et al.* (BaBar), Phys. Rev. **D72**, 052004 (2005), [hep-ex/0508004].
- [169] B. Aubert *et al.* (BaBar), Phys. Rev. **D77**, 051103 (2008), [arXiv:0711.4889].
- [170] J. P. Lees *et al.* (BaBar), Phys. Rev. Lett. **109**, 191801 (2012), [arXiv:1207.2690].
- [171] M. Iwasaki *et al.* (Belle), Phys. Rev. **D72**, 092005 (2005), [hep-ex/0503044]; J. P. Lees *et al.* (BaBar), Phys. Rev. Lett. **112**, 211802 (2014), [arXiv:1312.5364].
- [172] Y. Sato *et al.* (Belle), Phys. Rev. **D93**, 3, 032008 (2016), [Addendum: Phys. Rev. **D93**, no.5, 059901 (2016)], [arXiv:1402.7134].
- [173] T. Aaltonen *et al.* (CDF), Phys. Rev. Lett. **107**, 201802 (2011), [arXiv:1107.3753].
- [174] R. Aaij *et al.* (LHCb), JHEP **07**, 084 (2013), [arXiv:1305.2168]; R. Aaij *et al.* (LHCb), JHEP **09**, 179 (2015), [arXiv:1506.08777].
- [175] R. Aaij *et al.* (LHCb), Phys. Lett. **B725**, 25 (2013), [arXiv:1306.2577].
- [176] R. Aaij *et al.* (LHCb), JHEP **06**, 108 (2017), [arXiv:1703.00256].
- [177] J. T. Wei *et al.* (Belle), Phys. Rev. Lett. **103**, 171801 (2009), [arXiv:0904.0770].
- [178] J. P. Lees *et al.* (BaBar), Phys. Rev. **D86**, 032012 (2012), [arXiv:1204.3933].
- [179] R. Aaij *et al.* (LHCb), JHEP **06**, 133 (2014), [arXiv:1403.8044].
- [180] R. Aaij *et al.* (LHCb), JHEP **11**, 047 (2016), [Erratum: JHEP **04**, 142 (2017)], [arXiv:1606.04731].
- [181] T. Aaltonen *et al.* (CDF), Phys. Rev. Lett. **108**, 081807 (2012), [arXiv:1108.0695].
- [182] R. Aaij *et al.* (LHCb), JHEP **05**, 082 (2014), [arXiv:1403.8045].
- [183] S. Chatrchyan *et al.* (CMS), Phys. Lett. **B727**, 77 (2013), [arXiv:1308.3409].
- [184] V. Khachatryan *et al.* (CMS), Phys. Lett. **B753**, 424 (2016), [arXiv:1507.08126].
- [185] R. Aaij *et al.* (LHCb), JHEP **02**, 104 (2016), [arXiv:1512.04442].
- [186] S. Wehle *et al.* (Belle), Phys. Rev. Lett. **118**, 11, 111801 (2017), [arXiv:1612.05014].
- [187] R. Aaij *et al.* (LHCb), JHEP **06**, 115 (2015), [Erratum: JHEP **09**, 145 (2018)], [arXiv:1503.07138].
- [188] S. Descotes-Genon *et al.*, JHEP **01**, 048 (2013), [arXiv:1207.2753].
- [189] R. Aaij *et al.* (LHCb), JHEP **09**, 177 (2014), [arXiv:1408.0978].
- [190] J. Lyon and R. Zwicky, Phys. Rev. **D88**, 9, 094004 (2013), [arXiv:1305.4797].
- [191] R. Aaij *et al.* (LHCb), Eur. Phys. J. **C77**, 3, 161 (2017), [arXiv:1612.06764].
- [192] R. Aaij *et al.* (LHCb), JHEP **04**, 064 (2015), [arXiv:1501.03038].
- [193] R. Aaij *et al.* (LHCb), Phys. Rev. Lett. **122**, 19, 191801 (2019), [arXiv:1903.09252].
- [194] R. Aaij *et al.* (LHCb), JHEP **08**, 055 (2017), [arXiv:1705.05802].
- [195] R. Aaij *et al.* (LHCb) (2019), [arXiv:1912.08139].
- [196] R. Aaij *et al.* (LHCb), Phys. Lett. **B743**, 46 (2015), [arXiv:1412.6433].
- [197] R. Aaij *et al.* (LHCb), JHEP **04**, 029 (2017), [arXiv:1701.08705].
- [198] T. Aaltonen *et al.* (CDF), Phys. Rev. Lett. **107**, 191801 (2011), [Addendum: Phys. Rev. Lett. **107**, no.23, 239903 (2011)], [arXiv:1107.2304].
- [199] V. M. Abazov *et al.* (D0), Phys. Rev. **D87**, 7, 072006 (2013), [arXiv:1301.4507].
- [200] R. Aaij *et al.* (LHCb), Phys. Rev. Lett. **110**, 2, 021801 (2013), [arXiv:1211.2674].
- [201] M. Aaboud *et al.* (ATLAS), JHEP **04**, 098 (2019), [arXiv:1812.03017].
- [202] S. Chatrchyan *et al.* (CMS), Phys. Rev. Lett. **111**, 101804 (2013), [arXiv:1307.5025].
- [203] R. Aaij *et al.* (LHCb), Phys. Rev. Lett. **118**, 19, 191801 (2017), [arXiv:1703.05747].
- [204] T. Aaltonen *et al.* (CDF), Phys. Rev. Lett. **102**, 201801 (2009), [arXiv:0901.3803].
- [205] R. Aaij *et al.* (LHCb), Phys. Rev. Lett. **118**, 25, 251802 (2017), [arXiv:1703.02508].
- [206] C. Bobeth *et al.*, Phys. Rev. Lett. **112**, 101801 (2014), [arXiv:1311.0903].
- [207] K. De Bruyn *et al.*, Phys. Rev. Lett. **109**, 041801 (2012), [arXiv:1204.1737]; A. J. Buras *et al.*, JHEP **07**, 77 (2013), [arXiv:1303.3820].
- [208] R. Aaij *et al.* (LHCb), Phys. Rev. Lett. **111**, 141801 (2013), [arXiv:1307.4889].
- [209] J. Aebischer *et al.*, Eur. Phys. J. C **80**, 3, 252 (2020), [arXiv:1903.10434]; F. Beaujean, C. Bobeth and D. van Dyk, Eur. Phys. J. **C74**, 2897 (2014), [Erratum: Eur. Phys. J. **C74**, 3179 (2014)], [arXiv:1310.2478]; M. Algueró *et al.*, JHEP **07**, 096 (2019), [arXiv:1902.04900]; A. Arbey *et al.*, Phys. Rev. D **100**, 1, 015045 (2019), [arXiv:1904.08399].
- [210] T. Blake, G. Lanfranchi and D. M. Straub, Prog. Part. Nucl. Phys. **92**, 50 (2017), [arXiv:1606.00916]; J. Albrecht, S. Reichert and D. van Dyk, Int. J. Mod. Phys. A **33**, 18n19, 1830016 (2018), [arXiv:1806.05010].

73. Polarization in  $B$  Decays

Revised August 2019 by A. V. Gritsan (Johns Hopkins University).

We review the notation used in polarization measurements in particle production and decay, with a particular emphasis on the  $B$  decays and the  $CP$ -violating observables in polarization measurements. We look at several examples of vector-vector and vector-tensor  $B$  meson decays, while more details about the theory and experimental results in  $B$  decays can be found in a separate mini-review [1] in this Review.

Figure 73.1 illustrates angular observables in an example of the sequential process  $ab \rightarrow X \rightarrow P_1 P_2 \rightarrow (p_{11} p_{12})(p_{21} p_{22})$  [2]. The angular distributions are of particular interest because they are sensitive to spin correlations and reveal properties of particles and their interactions, such as quantum numbers and couplings. In the case of a spin-zero particle  $X$ , such as  $B$  meson or a Higgs boson, there are no spin correlations in the production mechanism and the decay chain is to be analyzed. The angular distribution of decay products can be expressed as a function of three helicity angles which describe the alignment of the particles in the decay chain. The analyzer of the  $B$ -daughter polarization is normally chosen for two-body decays, as the direction of the daughters in the center-of-mass of the parent (*e.g.*,  $\rho \rightarrow 2\pi$ ) [3], and for three-body decays as the normal to the decay plane (*e.g.*,  $\omega \rightarrow 3\pi$ ) [4]. An equivalent set of transversity angles is sometimes used in polarization analyses [5]. The differential decay width depends on complex amplitudes  $A_{\lambda_1 \lambda_2}$ , corresponding to the  $X$ -daughter helicity states  $\lambda_i$ .

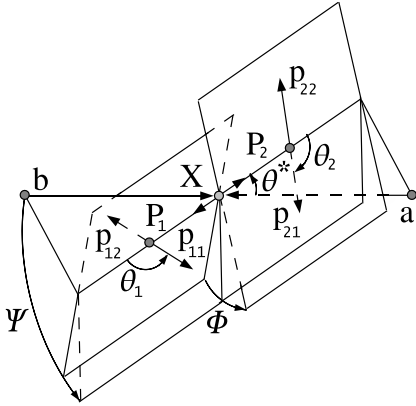


**Figure 73.1:** Definition of the production and helicity angles in the sequential process  $ab \rightarrow X \rightarrow P_1 P_2 \rightarrow (p_{11} p_{12})(p_{21} p_{22})$ . The three helicity angles include  $\theta_1$  and  $\theta_2$ , defined in the rest frame of the two daughters  $P_1$  and  $P_2$ , and  $\Phi$ , defined in the  $X$  frame as the angle between the two decay planes. The two production angles  $\theta^*$  and  $\Psi$  are defined in the  $X$  frame, where  $\Psi$  is the angle between the production plane and the average of the two decay planes.

In the case of a spin-zero  $B$ -meson decay, its daughter helicities are constrained to  $\lambda_1 = \lambda_2 = \lambda$ . Therefore we simplify amplitude notation as  $A_\lambda$ . Moreover, most  $B$ -decay polarization analyses are limited to the case when the spin of one of the  $B$ -meson daughters is 1. In that case, there are only three independent amplitudes corresponding to  $\lambda = 0$  or  $\pm 1$  [6], where the last two can be expressed in terms of parity-even and parity-odd amplitudes  $A_{\parallel, \perp} = (A_{+1} \pm A_{-1})/\sqrt{2}$ . The overall decay amplitude involves three complex terms proportional to the above amplitudes and the Wigner  $d$  functions of helicity angles. The exact angular dependence would depend on the quantum numbers of the  $B$ -meson daughters and of their decay products, and can be found in the literature [6,7]. When both  $B$ -meson daughters are tensor mesons and the smaller of the two daughter spins is  $J_1 > 1$ , this formalism can be easily extended by introducing the parity-even and parity-odd amplitudes of higher order  $A_{\parallel n, \perp n} = (A_{+n} \pm A_{-n})/\sqrt{2}$ , with  $1 < n \leq J_1$ , while the general angular parameterization may be found in Ref. 7. However, we limit the following discussion to

$J_1 = 1$ . The differential decay rate would involve six real quantities  $\alpha_i$ , including interference terms,

$$\frac{d\Gamma}{\Gamma d \cos \theta_1 d \cos \theta_2 d\Phi} = \sum_i \alpha_i f_i(\cos \theta_1, \cos \theta_2, \Phi), \quad (73.1)$$

where each  $f_i(\cos \theta_1, \cos \theta_2, \Phi)$  has unique angular dependence specific to particle quantum numbers, and the  $\alpha_i$  parameters are defined as:

$$\alpha_1 = \frac{|A_0|^2}{\sum |A_\lambda|^2} = f_L, \quad (73.2)$$

$$\alpha_2 = \frac{|A_{\parallel}|^2 + |A_{\perp}|^2}{\sum |A_\lambda|^2} = (1 - f_L), \quad (73.3)$$

$$\alpha_3 = \frac{|A_{\parallel}|^2 - |A_{\perp}|^2}{\sum |A_\lambda|^2} = (1 - f_L - 2f_{\perp}), \quad (73.4)$$

$$\alpha_4 = \frac{\Im m(A_{\perp} A_{\parallel}^*)}{\sum |A_\lambda|^2} = \sqrt{f_{\perp}(1 - f_L - f_{\perp})} \sin(\phi_{\perp} - \phi_{\parallel}), \quad (73.5)$$

$$\alpha_5 = \frac{\Re e(A_{\parallel} A_0^*)}{\sum |A_\lambda|^2} = \sqrt{f_L(1 - f_L - f_{\perp})} \cos(\phi_{\parallel}), \quad (73.6)$$

$$\alpha_6 = \frac{\Im m(A_{\perp} A_0^*)}{\sum |A_\lambda|^2} = \sqrt{f_{\perp} f_L} \sin(\phi_{\perp}), \quad (73.7)$$

where the amplitudes have been expressed with the help of polarization parameters  $f_L$ ,  $f_{\perp}$ ,  $\phi_{\parallel}$ , and  $\phi_{\perp}$  defined in Table 73.1. Note that the terms proportional to  $\Re e(A_{\perp} A_{\parallel}^*)$ ,  $\Im m(A_{\parallel} A_0^*)$ , and  $\Re e(A_{\perp} A_0^*)$  are absent in Eqs. (2-7). However, these terms may appear for some three-body decays of a  $B$ -meson daughter, see Ref. 7.

**Table 73.1:** Rate, polarization, and  $CP$ -asymmetry parameters defined for the  $B$ -meson decays to mesons with non-zero spin. Numerical examples are shown for the average of the  $B^0 \rightarrow \varphi K^*(892)^0$  decay measurements obtained from BABAR [8], Belle [9], and LHCb [10]. The first six parameters are defined under the assumption of no  $CP$  violation in decay, while they are averaged between the  $\bar{B}$  and  $B$  parameters in general. The last six parameters involve differences between the  $\bar{B}$  and  $B$  meson decay parameters. The phase convention  $\delta_0$  is chosen with respect to a single  $A_{00}$  amplitude from a reference  $B$  decay mode, which is  $B^0 \rightarrow \varphi K_0^*(1430)^0$  for numerical results.

parameter	definition	average
$\mathcal{B}$	$\Gamma/\Gamma_{\text{total}}$	$(10.1^{+0.6}_{-0.5}) \times 10^{-6}$
$f_L$	$ A_0 ^2/\sum  A_\lambda ^2$	$0.497 \pm 0.017$
$f_{\perp}$	$ A_{\perp} ^2/\sum  A_\lambda ^2$	$0.225 \pm 0.015$
$\phi_{\parallel} - \pi$	$\arg(A_{\parallel}/A_0) - \pi$	$-0.712 \pm 0.058$
$\phi_{\perp} - \pi$	$\arg(A_{\perp}/A_0) - \pi$	$-0.615 \pm 0.056$
$\delta_0 - \pi$	$\arg(A_{00}/A_0) - \pi$	$-0.26 \pm 0.10$
$A_{CP}$	$(\bar{\Gamma} - \Gamma)/(\bar{\Gamma} + \Gamma)$	$-0.003 \pm 0.038$
$A_{CP}^0$	$(\bar{f}_L - f_L)/(\bar{f}_L + f_L)$	$-0.007 \pm 0.030$
$A_{CP}^{\perp}$	$(\bar{f}_{\perp} - f_{\perp})/(\bar{f}_{\perp} + f_{\perp})$	$-0.014 \pm 0.057$
$\Delta\phi_{\parallel}$	$(\bar{\phi}_{\parallel} - \phi_{\parallel})/2$	$+0.051 \pm 0.053$
$\Delta\phi_{\perp}$	$(\bar{\phi}_{\perp} - \phi_{\perp} - \pi)/2$	$+0.075 \pm 0.050$
$\Delta\delta_0$	$(\bar{\delta}_0 - \delta_0)/2$	$+0.13 \pm 0.08$

Overall, six real parameters describe three complex amplitudes  $A_0$ ,  $A_{\parallel}$ , and  $A_{\perp}$ . These could be chosen to be the four polarization parameters  $f_L$ ,  $f_{\perp}$ ,  $\phi_{\parallel}$ , and  $\phi_{\perp}$ , one overall size normalization, such as decay rate  $\Gamma$ , or branching fraction  $\mathcal{B}$ , and one overall phase  $\delta_0$ . The phase convention is arbitrary for an isolated  $B$  decay mode. However, for several  $B$  decays, the relative phase could produce meaningful and observable effects through interference with other  $B$  decays with the same final states, such as for  $B \rightarrow VK_J^*$  with  $J = 0, 1, 2, 3, 4, \dots$ . The phase could be referenced to the single  $B \rightarrow VK_0^*$  amplitude  $A_{00}$  in

such a case, as shown in Table 73.1. Here  $V$  stands for any spin-one vector meson.

Moreover,  $CP$  violation can be tested in the angular distribution of the decay as the difference between the  $B$  and  $\bar{B}$ . Each of the six real parameters describing the three complex amplitudes would have a counterpart  $CP$ -asymmetry term, corresponding to three direct- $CP$  asymmetries in three amplitudes, and three  $CP$ -violating phase differences, equivalent to the phase measurements from the mixing-induced  $CP$  asymmetries in the time evolution of  $B$ -decays [1]. In Table 73.1 and Ref. 11, these are chosen to be the direct- $CP$  asymmetries in the overall decay rate  $\mathcal{A}_{CP}$ , in the  $f_L$  fraction  $\mathcal{A}_{CP}^0$ , and in the  $f_\perp$  fraction  $\mathcal{A}_{CP}^\perp$ , and three weak phase differences:

$$\Delta\phi_{\parallel} = \frac{1}{2}\arg(\bar{A}_{\parallel}A_0/A_{\parallel}\bar{A}_0), \quad (73.8)$$

$$\Delta\phi_{\perp} = \frac{1}{2}\arg(\bar{A}_{\perp}A_0/A_{\perp}\bar{A}_0) - \frac{\pi}{2}, \quad (73.9)$$

$$\Delta\delta_0 = \frac{1}{2}\arg(\bar{A}_{00}A_0/A_{00}\bar{A}_0). \quad (73.10)$$

The  $\frac{\pi}{2}$  term in Eq. (73.9) reflects the fact that  $A_{\perp}$  and  $\bar{A}_{\perp}$  differ in phase by  $\pi$  if  $CP$  is conserved. The two parameters  $\Delta\phi_{\parallel}$  and  $\Delta\phi_{\perp}$  are equivalent to triple-product asymmetries constructed from the vectors describing the decay angular distribution [12]. The  $CP$ -violating phase difference in the reference decay mode [11] is, in the Wolfenstein CKM quark-mixing phase convention,

$$\Delta\phi_{00} = \frac{1}{2}\arg(A_{00}/\bar{A}_{00}). \quad (73.11)$$

This can be measured only together with the mixing-induced phase difference for some of the neutral  $B$ -meson decays similar to other mixing-induced  $CP$  asymmetry measurements [1].

It may not always be possible to have a phase-reference decay mode which would define  $\delta_0$  and  $\Delta\delta_0$  parameters. In that case, it may be possible to define the phase difference directly similarly to Eq. (73.11):

$$\Delta\phi_0 = \frac{1}{2}\arg(A_0/\bar{A}_0). \quad (73.12)$$

One can measure the angles of the CKM unitarity triangle, assuming Standard Model contributions to the  $\Delta\phi_0$  and  $B$ -mixing phases. Examples include measurements of  $\beta = \phi_1$  with  $B \rightarrow J/\psi K^*$  and  $\alpha = \phi_2$  with  $B \rightarrow \rho\rho$ .

Most of the  $B$  decays that arise from tree-level  $b \rightarrow c$  transitions have the amplitude hierarchy  $|A_0| > |A_+| > |A_-|$  which is expected from analyses based on quark-helicity conservation [13]. The larger the mass of the vector-meson daughters, the weaker the inequality. The  $B$  meson decays to heavy vector particles with charm, such as  $B \rightarrow J/\psi K^*$ ,  $\psi(2S)K^*$ ,  $\chi_{c1}K^*$ ,  $D^*\rho$ ,  $D^*K^*$ ,  $D^*D^*$ , and  $D^*D_s^*$ , show a substantial fraction of the amplitudes corresponding to transverse polarization of the vector mesons ( $A_{\pm 1}$ ), in agreement with the factorization prediction. The detailed amplitude analysis of the  $B \rightarrow J/\psi K^*$  decays has been performed by the BABAR [14], Belle [15], CDF [16], CLEO [17], D0 [18], and LHCb [19] collaborations. Most analyses are performed under the assumption of the absence of direct  $CP$  violation. The parameter values are given in the particle listing of this *Review*. The difference between the strong phases  $\phi_{\parallel}$  and  $\phi_{\perp}$  deviates significantly from zero. The measurements [14,15] of  $CP$ -violating terms similar to those in  $B \rightarrow \varphi K^*$  [11] shown in Table 73.1 are consistent with zero.

In addition, the mixing-induced  $CP$ -violating asymmetry is measured in the  $B^0 \rightarrow J/\psi K^{*0}$  decay [1,14,15] where angular analysis allows one to separate  $CP$ -eigenstate amplitudes. This allows one to resolve the sign ambiguity of the  $\cos 2\beta$  ( $\cos 2\phi_1$ ) term that appears in the time-dependent angular distribution due to interference of parity-even and parity-odd terms. This analysis relies on the knowledge of discrete ambiguities in the strong phases  $\phi_{\parallel}$  and  $\phi_{\perp}$ , as discussed below. The BABAR experiment used a method based on the dependence on the  $K\pi$  invariant mass of the interference between the  $S$ - and  $P$ -waves to resolve the discrete ambiguity in the determination of the strong phases ( $\phi_{\parallel}, \phi_{\perp}$ ) in  $B \rightarrow J/\psi K^*$  decays [14]. The result

is in agreement with the amplitude hierarchy expectation [13]. The CDF [20], D0 [21], and LHCb [22] experiments have studied the  $B_s^0 \rightarrow J/\psi(K^+K^-)$ ,  $J/\psi(\pi^+\pi^-)$ ,  $\psi(K^+\pi^-)$  decays and provided the lifetime, polarization, and phase measurements.

The amplitude hierarchy  $|A_0| \gg |A_+| \gg |A_-|$  was expected in  $B$  decays to light vector particles in both penguin transitions [23,24] and tree-level transitions [13]. There is confirmation by the BABAR and Belle experiments of predominantly longitudinal polarization in the tree-level  $b \rightarrow u$  transition, such as  $B^0 \rightarrow \rho^+\rho^-$  [25],  $B^+ \rightarrow \rho^0\rho^+$  [26], and  $B^+ \rightarrow \omega\rho^+$  [27]; this is consistent with the analysis of the quark helicity conservation [13]. Because the longitudinal amplitude dominates the decay, a detailed amplitude analysis is not possible with current  $B$  samples, and limits on the transverse amplitude fraction are obtained. The small branching fractions of  $B^0 \rightarrow \rho^0\rho^0, \omega\rho^0, \omega\omega$  [29–31,27] indicate that  $b \rightarrow d$  penguin pollution is small in the charmless, strangeless vector-vector  $B$  decays. There is a measurement of large longitudinal polarization in  $B^0 \rightarrow \rho^0\rho^0$  [29–31] decays. The fraction of transverse polarization is large in decays to heavier mesons such as  $B^0 \rightarrow a_1(1260)^+a_1(1260)^-$  [28].

The interest in the polarization and  $CP$ -asymmetry measurements in penguin transition, such as  $b \rightarrow s$  decays  $B \rightarrow \varphi K^*$ ,  $\rho K^*$ ,  $\omega K^*$ , or  $B_s^0 \rightarrow \varphi\varphi$ ,  $K^*K^*$ , and  $b \rightarrow d$  decay  $B \rightarrow K^*\bar{K}^*$ , is motivated by their potential sensitivity to physics beyond the Standard Model. The decay amplitudes for  $B \rightarrow \varphi K^*$  have been measured by the BABAR, Belle, and LHCb experiments [11,9,32,33,10]. The fractions of longitudinal polarization are  $f_L = 0.50 \pm 0.05$  for the  $B^+ \rightarrow \varphi K^{*+}$  decay and  $f_L = 0.497 \pm 0.017$  for the  $B^0 \rightarrow \varphi K^{*0}$  decay. These indicate significant departure from the naive expectation of predominant longitudinal polarization, suggesting other contributions to the decay amplitude, previously neglected, either within the Standard Model, such as penguin annihilation [34] or QCD rescattering [35], or from physics beyond the Standard Model [36]. The complete set of twelve amplitude parameters measured in the  $B^0 \rightarrow \varphi K^{*0}$  decay is given in Table 73.1. Several other parameters could be constructed from the above twelve parameters, as suggested in Ref. 37.

The discrete ambiguity in the phase ( $\phi_{\parallel}, \phi_{\perp}, \Delta\phi_{\parallel}, \Delta\phi_{\perp}$ ) measurements has been resolved by BABAR in favor of  $|A_+| \gg |A_-|$  through interference between the  $S$ - and  $P$ -waves of  $K\pi$ . The search for vector-tensor and vector-axialvector  $B \rightarrow \varphi K_J^{(*)}$  decays with  $J = 1, 2, 3, 4$  revealed a large fraction of longitudinal polarization in the decay  $B \rightarrow \varphi K_2^*(1430)$  with  $f_L = 0.90_{-0.07}^{+0.06}$  [11,38], but large contribution of transverse amplitude in  $B \rightarrow \varphi K_1(1270)$  with  $f_L = 0.46_{-0.15}^{+0.13}$  [39].

Like  $B \rightarrow \varphi K^*$ , the decays  $B \rightarrow \rho K^*$  and  $B \rightarrow \omega K^*$  may be sensitive to New Physics. Measurements of the longitudinal polarization fraction in  $B \rightarrow \rho K^*$  [40] and in both vector-vector and vector-tensor final states of  $B \rightarrow \omega K_J^*$  [27] by BABAR and Belle reveal a large fraction of transverse polarization, indicating an anomaly similar to  $B \rightarrow \varphi K^*$  except for a different pattern in vector-tensor final states. An angular analysis of the  $B^0 \rightarrow \rho^0 K^{*0}$  decay mode by LHCb [41] provides much higher precision and indicates remarkably small longitudinal polarization fraction and a significant direct  $CP$  asymmetry observed in angular distributions of  $B \rightarrow VV$  decays for the first time. A large transverse polarization is also observed in the  $B_s^0 \rightarrow \varphi\varphi$  decay by CDF [42] and LHCb [43],  $B_s^0 \rightarrow K^{*0}\bar{K}^{*0}$  decays by LHCb [44], and  $B_s^0 \rightarrow \varphi K^{*0}$  decays by LHCb [45]. At the same time, measurement of the polarization in the  $b \rightarrow d$  penguin decays  $B \rightarrow K^*\bar{K}^*$  indicates a large fraction of longitudinal polarization [44,46]. The LHCb experiment has also provided the very first polarization results on the tensor-tensor, as well as vector-tensor, decays of the  $B_s^0$  meson in the  $(K\pi)(K\pi)$  final state [44]. The polarization pattern in penguin-dominated  $B$ -meson decays is not fully understood [34–36].

The three-body semileptonic  $B$ -meson decays, such as  $B \rightarrow V\ell_1\ell_2$ , share many features with the two-body  $B \rightarrow VV$  decays. Their differential decay width can be parameterized with the two helicity angles defined in the  $V$  and  $(\ell_1\ell_2)$  frames and with the azimuthal angle, as defined in Fig. 73.1. However, since the  $(\ell_1\ell_2)$  pair does not come from an on-shell particle, the angular distribution is unique to each point in the dilepton mass  $m_{\ell\ell}$  spectrum. The polarization



measurements as a function of  $m_{\ell\ell}$  provide complementary information on physics beyond the Standard Model, as discussed for  $B \rightarrow K^*\ell^+\ell^-$  and  $B_s \rightarrow \phi\ell^+\ell^-$  decays in Ref. 47. The data in these modes have been analyzed by the BABAR, Belle, CDF, CMS, and LHCb experiments [48–53].

The examples of the angular distributions and observables in  $B \rightarrow K^*\ell^+\ell^-$  are discussed in Ref. 47. Two angular observables have been measured in this decay in certain ranges of the dilepton mass  $m_{\ell\ell}$ . One parameter is the fraction of longitudinal polarization  $F_L$ , which is determined by the  $K^*$  angular distribution and is similar to  $f_L$  defined for exclusive two-body decays. The other parameter is the forward-backward asymmetry of the lepton pair  $A_{FB}$ , which is the asymmetry of the decay rate with positive and negative values of  $\cos\theta_1$ . A complete set of observables and angular terms has been adopted by the LHCb collaboration [52] following Ref. 47 with the  $F_L$ ,  $A_{FB}$ , and  $S_3 - S_9$  coefficients in the angular distributions. Additional set of optimized observables  $P_i^{(\prime)}$  is derived from those, for example  $P_2 = 2A_{FB}/(3 - 3F_L)$  and  $P_5' = S_5/\sqrt{F_L(1 - F_L)}$ . These observables have the advantage that the leading form-factor uncertainties cancel. There have been hints of deviations from SM in the measurement of  $P_5'$  and lepton flavor universality [48–53].

In summary, there has been considerable interest in the polarization measurements of  $B$ -meson decays because they reveal both weak- and strong-interaction dynamics [34–36] [54]. New measurements will further elucidate the pattern of spin alignment measurements in rare  $B$  decays, and further test the Standard Model and strong interaction dynamics, including the non-factorizable contributions to the  $B$ -decay amplitudes.

#### References:

1. M. Kreps, Y. Kwon, and P. Eerola, “Production and Decay of  $b$ -Flavored Hadrons,” mini-review in this *Review*.
2. For an example and further references see Y.Y. Gao *et al.*, Phys. Rev. **D81**, 075022 (2010).
3. M. Jacob and G. C. Wick, Ann. Phys. **7**, 404 (1959).
4. S. M. Berman and M. Jacob, Phys. Rev. **139**, 1023 (1965).
5. I. Dunietz *et al.*, Phys. Rev. **D43**, 2193 (1991).
6. G. Kramer and W.F. Palmer, Phys. Rev. **D45**, 193 (1992).
7. A. Datta *et al.*, Phys. Rev. **D77**, 114025 (2008).
8. BABAR Collab., B. Aubert *et al.*, Phys. Rev. **D78**, 092008 (2008).
9. Belle Collab., M. Prim *et al.*, Phys. Rev. **D88**, 072004 (2013).
10. LHCb Collab., R. Aaij *et al.*, JHEP **05**, 069 (2014).
11. BABAR Collab., B. Aubert *et al.*, Phys. Rev. Lett. **93**, 231804 (2004); Phys. Rev. Lett. **98**, 051801 (2007); Phys. Rev. **D78**, 092008 (2008).
12. G. Valencia, Phys. Rev. **D39**, 3339 (1998); A. Datta and D. London, Int. J. Mod. Phys. **A19**, 2505 (2004).
13. A. Ali *et al.*, Z. Phys. **C1**, 269 (1979); M. Suzuki, Phys. Rev. **D64**, 117503 (2001).
14. BABAR Collab., B. Aubert *et al.*, Phys. Rev. **D71**, 032005 (2005); Phys. Rev. **D76**, 031102 (2007).
15. Belle Collab., R. Itoh *et al.*, Phys. Rev. Lett. **95**, 091601 (2005) Phys. Rev. **D88**, 072004 (2013).
16. CDF Collab., T. Affolder *et al.*, Phys. Rev. Lett. **85**, 4668 (2000); CDF Collab., D. Acosta *et al.*, Phys. Rev. Lett. **94**, 101803 (2005).
17. CLEO Collab., C. P. Jessop, Phys. Rev. Lett. **79**, 4533 (1997).
18. D0 Collab., V. M. Abazov *et al.*, Phys. Rev. Lett. **102**, 032001 (2009).
19. LHCb Collab., R. Aaij *et al.*, Phys. Rev. **D88**, 052002 (2013).
20. CDF Collab., T. Aaltonen *et al.*, Phys. Rev. Lett. **100**, 121803 (2008); Phys. Rev. **D85**, 072002 (2012).
21. D0 Collab., V. M. Abazov *et al.*, Phys. Rev. Lett. **98**, 121801 (2007); Phys. Rev. **D85**, 032006 (2012).
22. LHCb Collab., R. Aaij *et al.*, Phys. Rev. Lett. **108**, 101803 (2012); Phys. Rev. Lett. **114**, 041801 (2015); Phys. Lett. **B747**, 484 (2015); JHEP **1511**, 082 (2015); JHEP **1708**, 037 (2017).
23. H.Y. Cheng and K.C. Yang, Phys. Lett. **B511**, 40 (2001); C.H. Chen, Y.Y. Keum, and H.n. Li, Phys. Rev. **D66**, 054013 (2002).
24. A.L.Kagan, Phys. Lett. **B601**, 151 (2004); Y. Grossman, Int. J. Mod. Phys. **A19**, 907 (2004).
25. BABAR Collab., B. Aubert *et al.*, Phys. Rev. **D76**, 052007 (2007); Belle Collab., A. Somov *et al.*, Phys. Rev. **D93**, 032010 (2016).
26. Belle Collab., J. Zhang *et al.*, Phys. Rev. Lett. **91**, 221801 (2003); BABAR Collab., B. Aubert *et al.*, Phys. Rev. Lett. **102**, 141802 (2009).
27. BABAR Collab., B. Aubert *et al.*, Phys. Rev. **D74**, 051102 (2006); Phys. Rev. **D79**, 052005 (2009).
28. BABAR Collab., B. Aubert *et al.*, Phys. Rev. **D80**, 092007 (2009).
29. BABAR Collab., B. Aubert *et al.*, Phys. Rev. **D78**, 071104 (2008).
30. Belle Collab., I. Adachi *et al.*, Phys. Rev. **D89**, 072008 (2014).
31. LHCb Collab., R. Aaij *et al.*, Phys. Lett. **B747**, 468 (2015).
32. Belle Collab., K.F. Chen *et al.*, Phys. Rev. Lett. **94**, 221804 (2005).
33. BABAR Collab., B. Aubert *et al.*, Phys. Rev. Lett. **99**, 201802 (2007).
34. A.L. Kagan, Phys. Lett. **B601**, 151 (2004); H.n. Li and S. Mishima, Phys. Rev. **D71**, 054025 (2005); C.-H. Chen *et al.*, Phys. Rev. **D72**, 054011 (2005); M. Beneke *et al.*, Phys. Rev. Lett. **96**, 141801 (2006); C.-H. Chen and C.-Q. Geng, Phys. Rev. **D75**, 054010 (2007); A. Datta *et al.*, Phys. Rev. **D76**, 034015 (2007); M. Beneke, J. Rohrer, and D. Yang, Nucl. Phys. **B774**, 64 (2007); H.-Y. Cheng and K.-C. Yang, Phys. Rev. **D78**, 094001 (2008).
35. C. W. Bauer *et al.*, Phys. Rev. **D70**, 054015 (2004); P. Colangelo *et al.*, Phys. Lett. **B597**, 291 (2004); M. Ladisa *et al.*, Phys. Rev. **D70**, 114025 (2004); H. Y. Cheng *et al.*, Phys. Rev. **D71**, 014030 (2005); H. Y. Cheng and K. C. Yang, Phys. Rev. **D83**, 034001 (2011).
36. Y. Grossman, Int. J. Mod. Phys. **A19**, 907 (2004); E. Alvarez *et al.*, Phys. Rev. **D70**, 115014 (2004); P.K. Das and K.C. Yang, Phys. Rev. **D71**, 094002 (2005); C.H. Chen and C.Q. Geng, Phys. Rev. **D71**, 115004 (2005); Y.D. Yang *et al.*, Phys. Rev. **D72**, 015009 (2005); K.C. Yang, Phys. Rev. **72**, 034009 (2005); S. Baek, Phys. Rev. **D72**, 094008 (2005); C.S. Huang *et al.*, Phys. Rev. **D73**, 034026 (2006); C.H. Chen and H. Hatanaka, Phys. Rev. **D73**, 075003 (2006); A. Faessler *et al.*, Phys. Rev. **D75**, 074029 (2007).
37. D. London, N. Sinha, and R. Sinha, Phys. Rev. **D69**, 11401 (2004).
38. BABAR Collab., B. Aubert *et al.*, Phys. Rev. **D76**, 051103 (2007).
39. BABAR Collab., B. Aubert *et al.*, Phys. Rev. Lett. **101**, 161801 (2008).
40. Belle Collab., J. Zhang *et al.*, Phys. Rev. Lett. **95**, 141801 (2005); BABAR Collab., B. Aubert *et al.*, Phys. Rev. Lett. **97**, 201801 (2006); Phys. Rev. **D83**, 051101 (2011); Phys. Rev. **D85**, 072005 (2012).
41. LHCb Collab., R. Aaij *et al.*, JHEP **05**, 026 (2019).
42. CDF Collab., T. Aaltonen *et al.*, Phys. Rev. Lett. **107**, 261802 (2011).
43. LHCb Collab., R. Aaij *et al.*, Phys. Lett. **B713**, 369 (2012); Phys. Rev. **D90**, 052011 (2014); arXiv:1907.10003 [hep-ex].
44. LHCb Collab., R. Aaij *et al.*, Phys. Lett. **B709**, 50 (2012); JHEP **1507**, 166 (2015); JHEP **03**, 140 (2018); JHEP **07**, 032 (2019).
45. LHCb Collab., R. Aaij *et al.*, JHEP **1311**, 092 (2013).
46. BABAR Collab., B. Aubert *et al.*, Phys. Rev. Lett. **100**, 081801 (2008); Phys. Rev. **D79**, 051102 (2009).
47. G. Burdman, Phys. Rev. **D52**, 6400 (1995); F. Kruger and J. Matias, Phys. Rev. **D71**, 094009 (2005); E. Lunghi and J. Matias, JHEP **0704**, 058 (2007); W. Altmannshofer *et al.*, JHEP **0901**, 019 (2009); J. Matias *et al.*, JHEP **1204**, 104 (2012); S. Descotes-Genon *et al.*, JHEP **1301**, 048 (2013).
48. BABAR Collab., B. Aubert *et al.*, Phys. Rev. **D79**, 031102 (2009); J. P. Lees *et al.*, Phys. Rev. **D93**, 052015 (2016).
49. Belle Collab., J.-T. Wei *et al.*, Phys. Rev. Lett. **103**, 171801 (2009); S. Wehle *et al.*, Phys. Rev. Lett. **118**, 111801 (2017).

- 
50. CDF Collab., T. Aaltonen *et al.*, Phys. Rev. Lett. **108**, 081807 (2012).
51. CMS Collab., S. Chatrchyan *et al.*, Phys. Lett. **B727**, 77 (2013); V. Khachatryan *et al.*, Phys. Lett. **B753**, 424 (2016); A. M. Sirunyan *et al.*, Phys. Lett. **B781**, 517 (2018).
52. LHCb Collab., R. Aaij *et al.*, JHEP **1308**, 131 (2013); JHEP **1504**, 064 (2015); JHEP **1602**, 104 (2016); JHEP **1611**, 047 (2016); JHEP **1612**, 065 (2016); JHEP **1708**, 055 (2017).
53. LHCb Collab., R. Aaij *et al.*, JHEP **1509**, 179 (2015).
54. C.H. Chen and H.n. Li, Phys. Rev. **D71**, 114008 (2005).

74.  $B^0-\bar{B}^0$  Mixing

Revised March 2020 by O. Schneider (EPFL).

There are two neutral  $B^0-\bar{B}^0$  meson systems,  $B_d^0-\bar{B}_d^0$  and  $B_s^0-\bar{B}_s^0$  (generically denoted  $B_q^0-\bar{B}_q^0$ ,  $q = s, d$ ), which exhibit particle-antiparticle mixing [1]. This mixing phenomenon is described in Ref. [2]. In the following, we adopt the notation introduced in Ref. [2], and assume  $CPT$  conservation throughout. In each system, the light (L) and heavy (H) mass eigenstates,

$$|B_{L,H}\rangle = p|B_q^0\rangle \pm q|\bar{B}_q^0\rangle, \quad (74.1)$$

have a mass difference  $\Delta m_q = m_H - m_L > 0$ , a total decay width difference  $\Delta\Gamma_q = \Gamma_L - \Gamma_H$  and an average decay width  $\Gamma_q = (\Gamma_L + \Gamma_H)/2$ . In the absence of  $CP$  violation in the mixing,  $|q/p| = 1$ , the differences are given by  $\Delta m_q = 2|M_{12}|$  and  $|\Delta\Gamma_q| = 2|I_{12}|$ , where  $M_{12}$  and  $I_{12}$  are the off-diagonal elements of the mass and decay matrices [2]. The evolution of a pure  $|B_q^0\rangle$  or  $|\bar{B}_q^0\rangle$  state at  $t = 0$  is given by

$$|B_q^0(t)\rangle = g_+(t)|B_q^0\rangle + \frac{q}{p}g_-(t)|\bar{B}_q^0\rangle, \quad (74.2)$$

$$|\bar{B}_q^0(t)\rangle = g_+(t)|\bar{B}_q^0\rangle + \frac{p}{q}g_-(t)|B_q^0\rangle, \quad (74.3)$$

which means that the flavor states remain unchanged (+) or oscillate into each other (-) with time-dependent probabilities proportional to

$$|g_{\pm}(t)|^2 = \frac{e^{-\Gamma_q t}}{2} \left[ \cosh\left(\frac{\Delta\Gamma_q}{2}t\right) \pm \cos(\Delta m_q t) \right]. \quad (74.4)$$

In the absence of  $CP$  violation, the time-integrated mixing probability  $\int |g_-(t)|^2 dt / (\int |g_-(t)|^2 dt + \int |g_+(t)|^2 dt)$  is given by

$$\chi_q = \frac{x_q^2 + y_q^2}{2(x_q^2 + 1)}, \quad \text{where } x_q = \frac{\Delta m_q}{\Gamma_q}, \quad y_q = \frac{\Delta\Gamma_q}{2\Gamma_q}. \quad (74.5)$$

### 74.1 Standard Model predictions and phenomenology

In the Standard Model, the transitions  $B_q^0 \rightarrow \bar{B}_q^0$  and  $\bar{B}_q^0 \rightarrow B_q^0$  are due to the weak interaction. They are described, at the lowest order, by box diagrams involving two  $W$  bosons and two up-type quarks (see Fig. 74.1), as is the case for  $K^0 - \bar{K}^0$  mixing. However, the long range interactions arising from intermediate virtual states are negligible for the neutral  $B$  meson systems, because the large  $B$  mass is off the region of hadronic resonances. The calculation of the dispersive and absorptive parts of the box diagrams yields the following predictions for the off-diagonal element of the mass and decay matrices [3],

$$M_{12} = -\frac{G_F^2 m_W^2 \eta_B m_{B_q} B_{B_q} f_{B_q}^2}{12\pi^2} S_0(m_t^2/m_W^2) (V_{tq}^* V_{tb})^2, \quad (74.6)$$

$$\begin{aligned} \Gamma_{12} = & \frac{G_F^2 m_b^2 \eta'_B m_{B_q} B_{B_q} f_{B_q}^2}{8\pi} \\ & \times \left[ (V_{tq}^* V_{tb})^2 + V_{tq}^* V_{tb} V_{cq}^* V_{cb} \mathcal{O}\left(\frac{m_c^2}{m_b^2}\right) \right. \\ & \left. + (V_{cq}^* V_{cb})^2 \mathcal{O}\left(\frac{m_c^4}{m_b^4}\right) \right], \quad (74.7) \end{aligned}$$

where  $G_F$  is the Fermi constant,  $m_W$  the  $W$  boson mass, and  $m_i$  the mass of quark  $i$ ;  $m_{B_q}$ ,  $f_{B_q}$  and  $B_{B_q}$  are the  $B_q^0$  mass, weak decay constant and bag parameter, respectively. The known function  $S_0(x_t)$  can be approximated very well by  $0.784 x_t^{0.76}$  [4], and  $V_{ij}$  are the elements of the CKM matrix [5]. The QCD corrections  $\eta_B$  and  $\eta'_B$  are of order unity. The only non-negligible contributions to  $M_{12}$  are from box diagrams involving two top quarks. The phases of  $M_{12}$  and  $\Gamma_{12}$  satisfy

$$\phi_M - \phi_\Gamma = \pi + \mathcal{O}\left(\frac{m_c^2}{m_b^2}\right), \quad (74.8)$$

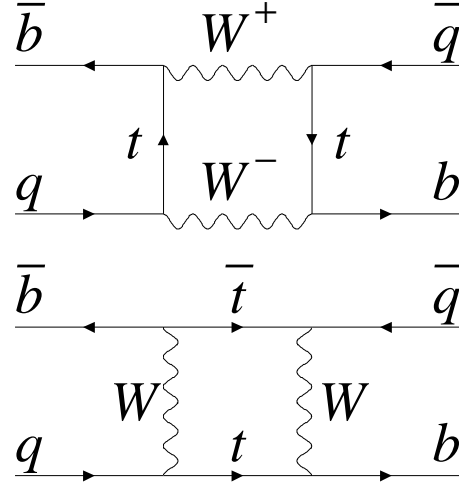


Figure 74.1: Dominant box diagrams for the  $B_q^0 \rightarrow \bar{B}_q^0$  transitions ( $q = d$  or  $s$ ). Similar diagrams exist where one or both  $t$  quarks are replaced with  $c$  or  $u$  quarks.

implying that the mass eigenstates have mass and width differences of opposite signs. This means that, like in the  $K^0-\bar{K}^0$  system, the heavy state is expected to have a smaller decay width than that of the light state:  $\Gamma_H < \Gamma_L$ . Hence,  $\Delta\Gamma_q = \Gamma_L - \Gamma_H$  is expected to be positive in the Standard Model.

Furthermore, the quantity

$$\left| \frac{\Gamma_{12}}{M_{12}} \right| \simeq \frac{3\pi}{2} \frac{m_b^2}{m_W^2} \frac{1}{S_0(m_t^2/m_W^2)} \sim \mathcal{O}\left(\frac{m_b^2}{m_t^2}\right) \quad (74.9)$$

is small, and a power expansion of  $|q/p|^2$  yields

$$\left| \frac{q}{p} \right|^2 = 1 + \left| \frac{\Gamma_{12}}{M_{12}} \right| \sin(\phi_M - \phi_\Gamma) + \mathcal{O}\left(\left| \frac{\Gamma_{12}}{M_{12}} \right|^2\right). \quad (74.10)$$

Therefore, considering both Eqs. (74.8) and (74.9), the  $CP$ -violating parameter

$$1 - \left| \frac{q}{p} \right|^2 \simeq \text{Im}\left(\frac{\Gamma_{12}}{M_{12}}\right) \quad (74.11)$$

is expected to be very small:  $\sim \mathcal{O}(10^{-3})$  for the  $B_d^0-\bar{B}_d^0$  system and  $\lesssim \mathcal{O}(10^{-4})$  for the  $B_s^0-\bar{B}_s^0$  system [6].

In the approximation of negligible  $CP$  violation in mixing, the ratio  $\Delta\Gamma_q/\Delta m_q$  is equal to the small quantity  $|\Gamma_{12}/M_{12}|$  of Eq. (74.9); it is hence independent of CKM matrix elements, *i.e.*, the same for the  $B_d^0-\bar{B}_d^0$  and  $B_s^0-\bar{B}_s^0$  systems. Calculations [7] yield  $\sim 5 \times 10^{-3}$  with a  $\sim 20\%$  uncertainty. Given the published experimental knowledge [8] on the mixing parameter  $x_q$

$$\begin{cases} x_d = 0.769 \pm 0.004 & (B_d^0-\bar{B}_d^0 \text{ system}) \\ x_s = 26.89 \pm 0.07 & (B_s^0-\bar{B}_s^0 \text{ system}) \end{cases}, \quad (74.12)$$

the Standard Model thus predicts that  $\Delta\Gamma_d/\Gamma_d$  is very small (below 1%), but  $\Delta\Gamma_s/\Gamma_s$  considerably larger ( $\sim 10\%$ ). These width differences are caused by the existence of final states to which both the  $B_q^0$  and  $\bar{B}_q^0$  mesons can decay. Such decays involve  $b \rightarrow c\bar{c}q$  quark-level transitions, which are Cabibbo-suppressed if  $q = d$  and Cabibbo-allowed if  $q = s$ .

A complete set of Standard Model predictions for all mixing parameters in both the  $B_d^0-\bar{B}_d^0$  and  $B_s^0-\bar{B}_s^0$  systems can be found in Ref. [9].

## 74.2 Experimental issues and methods for oscillation analyses

Time-integrated measurements of  $B^0$ - $\bar{B}^0$  mixing were published for the first time in 1987 by UA1 [10] and ARGUS [11], and since then by many other experiments. These measurements are typically based on counting same-sign and opposite-sign lepton pairs from the semileptonic decay of the produced  $b\bar{b}$  pairs. Such analyses cannot easily separate the contributions from the different  $b$ -hadron species, therefore, the clean environment of  $\Upsilon(4S)$  machines (where only  $B_d^0$  and charged  $B_u$  mesons are produced) is in principle best suited to measure  $\chi_d$ .

However, better sensitivity is obtained from time-dependent analyses aiming at the direct measurement of the oscillation frequencies  $\Delta m_d$  and  $\Delta m_s$ , from the proper time distributions of  $B_d^0$  or  $B_s^0$  candidates identified through their decay in (mostly) flavor-specific modes, and suitably tagged as mixed or unmixed. This is particularly true for the  $B_s^0$ - $\bar{B}_s^0$  system, where the large value of  $x_s$  implies maximal mixing, *i.e.*,  $\chi_s \simeq 1/2$ . In such analyses, the  $B_d^0$  or  $B_s^0$  mesons are either fully reconstructed, partially reconstructed from a charm meson, selected from a lepton with the characteristics of a  $b \rightarrow \ell^-$  decay, or selected from a reconstructed displaced vertex. At high-energy colliders (LEP, SLC, Tevatron, LHC), the proper time  $t = \frac{m_B}{p} L$  is measured from the distance  $L$  between the production vertex and the  $B$  decay vertex, and from an estimate of the  $B$  momentum  $p$ . At asymmetric  $B$  factories (KEKB, PEP-II), producing  $e^+e^- \rightarrow \Upsilon(4S) \rightarrow B_d^0 \bar{B}_d^0$  events with a boost  $\beta\gamma$  ( $= 0.425, 0.55$ ), the proper time difference between the two  $B$  candidates is estimated as  $\Delta t \simeq \frac{\Delta z}{\beta\gamma c}$ , where  $\Delta z$  is the spatial separation between the two  $B$  decay vertices along the boost direction. In all cases, the good resolution needed on the vertex positions is obtained with silicon detectors.

The average statistical significance  $\mathcal{S}$  of a  $B_q^0$  oscillation signal can be approximated as [12]

$$\mathcal{S} \approx \sqrt{N/2} f_{\text{sig}} (1 - 2\eta) e^{-(\Delta m_q \sigma_t)^2/2}, \quad (74.13)$$

where  $N$  is the number of selected and tagged candidates,  $f_{\text{sig}}$  is the fraction of signal in that sample,  $\eta$  is the total mistag probability, and  $\sigma_t$  is the resolution on proper time (or proper time difference). The quantity  $\mathcal{S}$  decreases very quickly as  $\Delta m_q$  increases; this dependence is controlled by  $\sigma_t$ , which is therefore a critical parameter for  $\Delta m_s$  analyses. At high-energy colliders, the proper time resolution  $\sigma_t \sim \frac{m_B}{(p)} \sigma_L \oplus t \frac{\sigma_p}{p}$  includes a constant contribution due to the decay length resolution  $\sigma_L$  (typically 0.04–0.3 ps), and a term due to the relative momentum resolution  $\sigma_p/p$  (typically 10–20% for partially reconstructed decays), which increases with proper time. At  $B$  factories, the boost of the  $B$  mesons is estimated from the known beam energies, and the term due to the spatial resolution dominates (typically 1–1.5 ps because of the much smaller  $B$  boost).

In order to tag a  $B_q^0$  candidate as mixed or unmixed, it is necessary to determine its flavor both in the initial state and in the final state. The initial and final state mistag probabilities,  $\eta_i$  and  $\eta_f$ , degrade  $\mathcal{S}$  by a total factor  $(1 - 2\eta) = (1 - 2\eta_i)(1 - 2\eta_f)$ . In lepton-based analyses, the final state is tagged by the charge of the lepton from  $b \rightarrow \ell^-$  decays; the largest contribution to  $\eta_f$  is then due to  $\bar{b} \rightarrow \bar{c} \rightarrow \ell^-$  decays. Alternatively, the charge of a reconstructed charm meson ( $D^{*-}$  from  $B_d^0$  or  $D_s^-$  from  $B_s^0$ ), or that of a kaon hypothesized to come from a  $b \rightarrow c \rightarrow s$  decay [13], can be used. For fully-inclusive analyses based on topological vertexing, final-state tagging techniques include jet-charge [14] and charge-dipole [15, 16] methods. At high-energy colliders, the methods to tag the initial state (*i.e.*, the state at production), can be divided into two groups: the ones that tag the initial charge of the  $\bar{b}$  quark contained in the  $B_q^0$  candidate itself (same-side tag), and the ones that tag the initial charge of the other  $b$  quark produced in the event (opposite-side tag). On the same side, the sign of a charged pion, kaon or proton from the primary vertex is correlated with the production state of the  $B_q^0$  meson if that particle is a decay product of a  $B^{**}$  state or the first in the fragmentation chain [17, 18]. Jet- and vertex-charge techniques work on both sides and on the opposite side, respec-

tively. Finally, the charge of a lepton from  $b \rightarrow \ell^-$ , of a kaon from  $b \rightarrow c \rightarrow s$  or of a charm hadron from  $b \rightarrow c$  [19] can be used as an opposite-side tag, keeping in mind that its performance is degraded due to integrated mixing. At SLC, the beam polarization produced a sizeable forward-backward asymmetry in the  $Z \rightarrow b\bar{b}$  decays, and provided another very interesting and effective initial state tag based on the polar angle of the  $B_q^0$  candidate [15]. Initial state tags have also been combined to reach  $\eta_i \sim 26\%$  at LEP [18, 20] or 22% at SLD [15] with full efficiency. In the case  $\eta_f = 0$ , this corresponds to an effective tagging efficiency  $Q = \epsilon D^2 = \epsilon(1 - 2\eta)^2$ , where  $\epsilon$  is the tagging efficiency, in the range 23–31%. The equivalent figure achieved by CDF during Tevatron Run I was  $\sim 3.5\%$  (see tagging summary on page 160 of Ref. [21]), reflecting the fact that tagging is more difficult at hadron colliders. The CDF and DØ analyses of Tevatron Run II data reached  $\epsilon D^2 = (1.8 \pm 0.1)\%$  [22] and  $(2.5 \pm 0.2)\%$  [23] for opposite-side tagging, while same-side kaon tagging (for  $B_s^0$  analyses) contributed an additional 3.7–4.8% at CDF [22], and pushed the combined performance to  $(4.7 \pm 0.5)\%$  at DØ [24]. LHCb, operating in the forward region at the LHC where the environment is different in terms of track multiplicity and  $b$ -hadron production kinematics, has reported  $\epsilon D^2 = (2.10 \pm 0.25)\%$  [25] for opposite-side tagging,  $(1.80 \pm 0.26)\%$  [26] for same-side kaon tagging, and  $(2.11 \pm 0.11)\%$  [27] for same-side pion and proton tagging; the combined figure ranges typically between  $(3.73 \pm 0.15)\%$  [28] and  $(5.33 \pm 0.25)\%$  [29] depending on the mode in which the tagged  $B_s^0$  meson is reconstructed, and reaches up to  $(8.1 \pm 0.6)\%$  [30] for hadronic  $B_d^0$  modes.

At  $B$  factories, the flavor of a  $B_d^0$  meson at production cannot be determined, since the two neutral  $B$  mesons produced in a  $\Upsilon(4S)$  decay evolve in a coherent  $P$ -wave state where they keep opposite flavors at any time. However, as soon as one of them decays, the other follows a time-evolution given by Eqs. (74.2) or (74.3), where  $t$  is replaced with  $\Delta t$  (which will take negative values half of the time). Hence, the “initial state” tag of a  $B$  can be taken as the final-state tag of the other  $B$ . Effective tagging efficiencies of 30% are achieved by BaBar and Belle [31], using different techniques including  $b \rightarrow \ell^-$  and  $b \rightarrow c \rightarrow s$  tags. It is worth noting that, in this case, mixing of the other  $B$  (*i.e.*, the coherent mixing occurring before the first  $B$  decay) does not contribute to the mistag probability.

Before the experimental observation of a decay-width difference, oscillation analyses typically neglected  $\Delta\Gamma_q$  in Eq. (74.4), and described the time dependence with the functions  $\Gamma_q e^{-\Gamma_q t} (1 \pm \cos(\Delta m_q t))/2$  (high-energy colliders) or  $\Gamma_d e^{-\Gamma_d |\Delta t|} (1 \pm \cos(\Delta m_d \Delta t))/4$  (asymmetric  $\Upsilon(4S)$  machines). As can be seen from Eq. (74.4), a non-zero value of  $\Delta\Gamma_q$  would effectively reduce the oscillation amplitude with a small time-dependent factor that would be very difficult to distinguish from time resolution effects. Measurements of  $\Delta m_q$  are usually extracted from the data using a maximum likelihood fit.

## 74.3 $\Delta m_d$ and $\Delta\Gamma_d$ measurements

Many  $B_d^0$ - $\bar{B}_d^0$  oscillations analyses have been published [32] by the ALEPH [33], DELPHI [16, 34], L3 [35], OPAL [36, 37], BaBar [38], Belle [39], CDF [17], DØ [23], and LHCb [40–43] collaborations. Although a variety of different techniques have been used, the individual  $\Delta m_d$  results obtained at LEP and Tevatron have remarkably similar precision. Their average is compatible with the recent and more precise measurements at the asymmetric  $B$  factories and the LHC. The systematic uncertainties are not negligible; they are often dominated by sample composition, mistag probability, or  $b$ -hadron lifetime contributions. Before being combined, the measurements are adjusted on the basis of a common set of input values, including the  $b$ -hadron lifetimes and fractions published in this *Review*. Some measurements are statistically correlated. Systematic correlations arise both from common physics sources (fragmentation fractions, lifetimes, branching ratios of  $b$  hadrons), and from purely experimental or algorithmic effects (efficiency, resolution, tagging, background description). Combining all measurements [16, 17, 23, 33–43] and accounting for all identified correlations yields  $\Delta m_d = 0.5065 \pm 0.0016(\text{stat}) \pm 0.0011(\text{syst}) \text{ ps}^{-1}$  [8], a result dominated by the latest LHCb measurement with

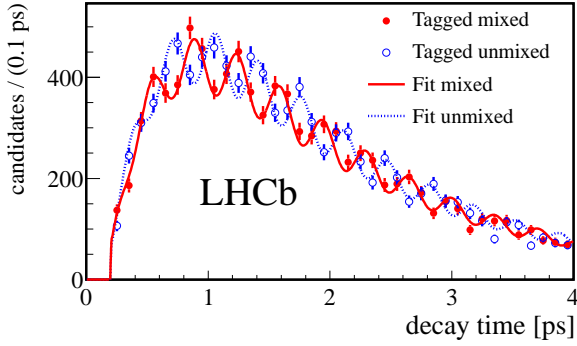


Figure 74.2: Proper time distribution of  $B_s^0 \rightarrow D_s^- \pi^+$  candidates tagged as mixed (red) or unmixed (blue) in the LHCb experiment, displaying  $B_s^0-\bar{B}_s^0$  oscillations (from Ref. [54]).

$B^0 \rightarrow D^{(*)-} \mu^+ \nu_\mu X$  decays [43].

On the other hand, ARGUS and CLEO have published time-integrated measurements [44–46], which average to  $\chi_d = 0.182 \pm 0.015$ . Following Ref. [46], the width difference  $\Delta\Gamma_d$  could in principle be extracted from the measured value of  $\Gamma_d$  and the above averages for  $\Delta m_d$  and  $\chi_d$  (see Eq. (74.5)), provided that  $\Delta\Gamma_d$  has a negligible impact on the  $\Delta m_d$  measurements. However, direct time-dependent studies published by DELPHI [16], BaBar [47], Belle [48], LHCb [49], ATLAS [50] and CMS [51] provide stronger constraints, which can be combined to yield [8]

$$\Delta\Gamma_d/\Gamma_d = +0.001 \pm 0.010. \quad (74.14)$$

Assuming  $\Delta\Gamma_d = 0$  and no  $CP$  violation in mixing, and using the  $B_d^0$  lifetime average of  $1.519 \pm 0.004$  ps [8], the  $\Delta m_d$  and  $\chi_d$  results are combined to yield the world average

$$\Delta m_d = 0.5065 \pm 0.0019 \text{ ps}^{-1} \quad (74.15)$$

or, equivalently,

$$\chi_d = 0.1858 \pm 0.0011. \quad (74.16)$$

This  $\Delta m_d$  value provides an estimate of  $2|M_{12}|$ , and can be used with Eq. (74.6) to extract  $|V_{td}|$  within the Standard Model [52]. The main experimental uncertainties on the result come from  $m_t$  and  $\Delta m_d$ , but are still completely negligible with respect to the uncertainty due to the hadronic matrix element  $f_{B_d} \sqrt{B_{B_d}} = 225 \pm 9$  MeV [53] obtained from three-flavor lattice QCD calculations.

#### 74.4 $\Delta m_s$ and $\Delta\Gamma_s$ measurements

After many years of intense search at LEP and SLC,  $B_s^0-\bar{B}_s^0$  oscillations were first observed in 2006 by CDF using  $1 \text{ fb}^{-1}$  of Tevatron Run II data [22]. More recently LHCb observed  $B_s^0-\bar{B}_s^0$  oscillations independently with  $B_s^0 \rightarrow D_s^- \pi^+$  [40, 54],  $B_s^0 \rightarrow D_s^- \mu^+ \nu X$  [42] and even  $B_s^0 \rightarrow J/\psi K^+ K^-$  [28] decays, using between 1 and  $4.9 \text{ fb}^{-1}$  of data collected at the LHC until 2016. Taking systematic correlations into account, the average of all published measurements of  $\Delta m_s$  [22, 28, 40, 42, 54] is

$$\Delta m_s = 17.749 \pm 0.019(\text{stat}) \pm 0.007(\text{syst}) \text{ ps}^{-1}, \quad (74.17)$$

dominated by LHCb (see Fig. 74.2) and still statistically limited.

The information on  $|V_{ts}|$  obtained in the framework of the Standard Model is hampered by the hadronic uncertainty, as in the  $B_d^0$  case. However, several uncertainties cancel in the frequency ratio

$$\frac{\Delta m_s}{\Delta m_d} = \frac{m_{B_s}}{m_{B_d}} \xi^2 \left| \frac{V_{ts}}{V_{td}} \right|^2, \quad (74.18)$$

where the SU(3) flavor-symmetry breaking factor  $\xi = (f_{B_s} \sqrt{B_{B_s}})/(f_{B_d} \sqrt{B_{B_d}}) = 1.206 \pm 0.017$  is obtained from a

combination of three-flavor lattice QCD calculations [53] dominated by the results of Ref. [55]. Using the measurements of Eqs. (74.15) and (74.17), one can extract

$$\left| \frac{V_{td}}{V_{ts}} \right| = 0.2054 \pm 0.0004(\text{exp}) \pm 0.0029(\text{lattice}), \quad (74.19)$$

in good agreement with (but much more precise than) the value obtained from the ratio of the  $b \rightarrow d\gamma$  and  $b \rightarrow s\gamma$  transition rates observed at the  $B$  factories [52].

The CKM matrix can be constrained using experimental results on observables such as  $\Delta m_d$ ,  $\Delta m_s$ ,  $|V_{ub}/V_{cb}|$ ,  $\epsilon_K$ , and  $\sin(2\beta)$  together with theoretical inputs and unitarity conditions [52, 56, 57]. The constraint from our knowledge on the ratio  $\Delta m_s/\Delta m_d$  is more effective in limiting the position of the apex of the CKM unitarity triangle than the one obtained from the  $\Delta m_d$  measurements alone, due to the reduced hadronic uncertainty in Eq. (74.18). We also note that the measured value of  $\Delta m_s$  is consistent with the Standard Model prediction obtained from CKM fits where no experimental information on  $\Delta m_s$  is used, *e.g.*,  $17.25 \pm 0.85 \text{ ps}^{-1}$  [56] or  $16.70_{-0.45}^{+0.73} \text{ ps}^{-1}$  [57].

Information on  $\Delta\Gamma_s$  can be obtained from the study of the proper time distribution of untagged  $B_s^0$  samples [58]. In the case of an inclusive  $B_s^0$  selection [59], or a flavor-specific (semileptonic or hadronic)  $B_s^0$  decay selection [20, 60–62], both the short- and long-lived components are present, and the proper time distribution is a superposition of two exponentials with decay constants  $\Gamma_{L,H} = \Gamma_s \pm \Delta\Gamma_s/2$ . In principle, this provides sensitivity to both  $\Gamma_s$  and  $(\Delta\Gamma_s/\Gamma_s)^2$ . Ignoring  $\Delta\Gamma_s$  and fitting for a single exponential leads to an estimate of  $1/\Gamma_s$  (called effective lifetime) with a relative bias proportional to  $(\Delta\Gamma_s/\Gamma_s)^2$ . An alternative approach, sensitive to first order in  $\Delta\Gamma_s/\Gamma_s$ , is to determine the effective lifetime of untagged  $B_s^0$  decays to pure  $CP$  eigenstates; measurements exist for  $B_s^0 \rightarrow D_s^+ D_s^-$  [61],  $B_s^0 \rightarrow K^+ K^-$  [62, 63],  $B_s^0 \rightarrow J/\psi\eta$  [64],  $B_s^0 \rightarrow J/\psi f_0(980)$  [65],  $B_s^0 \rightarrow J/\psi\pi^+\pi^-$  [51, 66],  $B_s^0 \rightarrow J/\psi K_S^0$  [67], and  $B_s^0 \rightarrow \mu^+\mu^-$  [68]. The extraction of  $1/\Gamma_s$  and  $\Delta\Gamma_s$  from such measurements, discussed in detail in Ref. [69], requires additional information in the form of theoretical assumptions or external inputs on weak phases and hadronic parameters. In what follows, we only use the effective lifetimes of decays to  $CP$ -even ( $D_s^+ D_s^-$ ,  $J/\psi\eta$ ) and  $CP$ -odd ( $J/\psi f_0(980)$ ,  $J/\psi\pi^+\pi^-$ ) final states where  $CP$  conservation can be assumed.

The best sensitivity to  $1/\Gamma_s$  and  $\Delta\Gamma_s$  is achieved by the time-dependent measurements of the  $B_s^0 \rightarrow J/\psi K^+ K^-$  (including  $B_s^0 \rightarrow J/\psi\phi$ ) and  $B_s^0 \rightarrow \psi(2S)\phi$  decay rates performed at CDF [70], DØ [71], ATLAS [72, 73], CMS [74] and LHCb [28, 75, 76], where the  $CP$ -even and  $CP$ -odd amplitudes are separated statistically through a full angular analysis. The LHCb collaboration analyzes the  $B_s^0 \rightarrow J/\psi K^+ K^-$  decay considering that the  $K^+ K^-$  system can be in a P-wave or S-wave state, and measures the dependence of the strong phase difference between the P-wave and S-wave amplitudes as a function of the  $K^+ K^-$  invariant mass [28, 77]; this allows the unambiguous determination of the sign of  $\Delta\Gamma_s$ , which is found to be positive. All these studies use both untagged and tagged  $B_s^0$  candidates and are optimized for the measurement of the  $CP$ -violating phase  $\phi_s^{c\bar{c}s}$ , defined as the weak phase difference between the  $B_s^0-\bar{B}_s^0$  mixing amplitude and the  $b \rightarrow c\bar{c}s$  decay amplitude. As reported below in Eq. (74.28), the current experimental average of  $\phi_s^{c\bar{c}s}$  is consistent with zero. Assuming no  $CP$  violation (*i.e.*,  $\phi_s^{c\bar{c}s} = 0$ ) a combination [8] of the published  $B_s^0 \rightarrow J/\psi K^+ K^-$ ,  $J/\psi\phi$  and  $\psi(2S)\phi$  analyses [28, 70–72, 74–76] and of effective lifetime measurements with flavor-specific [20, 60–62] and pure  $CP$  [51, 61, 64–66] final states yields

$$\Delta\Gamma_s = +0.085 \pm 0.004 \text{ ps}^{-1} \text{ and } 1/\Gamma_s = 1.515 \pm 0.004 \text{ ps}, \quad (74.20)$$

or, equivalently,

$$1/\Gamma_L = 1.423 \pm 0.005 \text{ ps} \text{ and } 1/\Gamma_H = 1.620 \pm 0.007 \text{ ps}, \quad (74.21)$$

in good agreement with the Standard Model prediction  $\Delta\Gamma_s = 0.088 \pm 0.020 \text{ ps}^{-1}$  [9].

Estimates of  $\Delta\Gamma_s/\Gamma_s$  obtained from measurements of the  $B_s^0 \rightarrow D_s^{(*)+} D_s^{(*)-}$  branching fractions are not included in the average,

**Table 74.1:**  $\bar{\chi}$  and  $b$ -hadron fractions (see text).

	in $Z$ decays [8]	at Tevatron [8]	at LHC [89–91]
$\bar{\chi}$	$0.1259 \pm 0.0042$	$0.147 \pm 0.011$	
$f_u = f_d$	$0.408 \pm 0.007$	$0.344 \pm 0.021$	
$f_s$	$0.100 \pm 0.008$	$0.115 \pm 0.013$	
$f_{\text{baryon}}$	$0.084 \pm 0.011$	$0.198 \pm 0.046$	
$f_s/f_d$	$0.246 \pm 0.023$	$0.333 \pm 0.040$	$0.247 \pm 0.009$

since they are based on the questionable [7] assumption that these decays account for all  $CP$ -even final states.

### 74.5 Average $b$ -hadron mixing probability and $b$ -hadron production fractions at high energy

Mixing measurements can significantly improve our knowledge on the fractions  $f_u$ ,  $f_d$ ,  $f_s$ , and  $f_{\text{baryon}}$ , defined as the fractions of  $B_u$ ,  $B_d^0$ ,  $B_s^0$ , and  $b$ -baryons in an unbiased sample of weakly-decaying  $b$  hadrons produced in high-energy collisions. Indeed, time-integrated mixing analyses using lepton pairs from  $b\bar{b}$  events at high energy measure the quantity

$$\bar{\chi} = f'_d \chi_d + f'_s \chi_s, \quad (74.22)$$

where  $f'_q$  ( $q = s, d$ ) is the  $B_q^0$  fraction in a sample of semileptonic  $b$ -hadron decays. Assuming that all  $b$  hadrons have the same semileptonic decay width implies  $f'_q = f_q/(\Gamma_q \tau_b)$ , where  $\tau_b$  is the average  $b$ -hadron lifetime. Hence  $\bar{\chi}$  measurements performed at LEP [78] and Tevatron [79, 80], together with  $\chi_d$  given in Eq. (74.16) and the very good approximation  $\chi_s = 1/2$  (in fact  $\chi_s = 0.499312 \pm 0.000004$  from Eqs. (74.5), (74.17) and (74.20)), provide constraints on  $f_d$  and  $f_s$ .

The LEP experiments have measured  $\mathcal{B}(\bar{b} \rightarrow B_s^0) \times \mathcal{B}(B_s^0 \rightarrow D_s^- \ell^+ \nu_\ell X)$  [81],  $\mathcal{B}(b \rightarrow A_b^0) \times \mathcal{B}(A_b^0 \rightarrow A_c^+ \ell^- \bar{\nu}_\ell X)$  [82], and  $\mathcal{B}(b \rightarrow \Xi_b^-) \times \mathcal{B}(\Xi_b^- \rightarrow \Xi^- \ell^- \bar{\nu}_\ell X)$  [83] from partially reconstructed final states including a lepton,  $f_{\text{baryon}}$  from protons identified in  $b$  events [84], and the production rate of charged  $b$  hadrons [85]. The  $b$ -hadron fraction ratios measured at CDF are based on double semileptonic  $K^* \mu \mu$  and  $\phi \mu \mu$  final states [86] and lepton-charm final states [87]; in addition CDF and DØ have both measured strange  $b$ -baryon production [88]. On the other hand, fraction ratios have been studied by LHCb using fully reconstructed hadronic  $B_s^0$  and  $B_d^0$  decays [89], as well as semileptonic decays of  $A_b^0$ ,  $B_s^0$ ,  $B_d^0$  and  $B_u$  [90]. ATLAS has measured  $f_s/f_d$  using  $B_s^0 \rightarrow J/\psi \phi$  and  $B^0 \rightarrow J/\psi K^{*0}$  decays [91]. Both CDF and LHCb observe that the ratio  $f_{A_b^0}/(f_u + f_d)$  decreases with the transverse momentum of the lepton+charm system, indicating that the  $b$ -hadron fractions are not the same in different environments. A combination of the available information from LEP and Tevatron yields, under the constraints  $f_u = f_d$ ,  $f_u + f_d + f_s + f_{\text{baryon}} = 1$  and Eq. (74.22), the averages of the first two columns of Table 74.1, while the third column shows the average of LHC measurements of  $f_s/f_u = f_s/f_d$ , which are all compatible. The  $B_c^+$  fraction, neglected in the above constraints, has been measured for the first time by LHCb to be  $(0.26 \pm 0.06)\%$  [92].

### 74.6 $CP$ -violation studies

Evidence for  $CP$  violation in  $B_q^0$ - $\bar{B}_q^0$  mixing has been searched for, both with flavor-specific and inclusive  $B_q^0$  decays, in samples where the initial flavor state is tagged, usually with a lepton from the other  $b$ -hadron in the event. In the case of semileptonic (or other flavor-specific) decays, where the final-state tag is also available, the following asymmetry [2]

$$\mathcal{A}_{\text{SL}}^q = \frac{N(\bar{B}_q^0(t) \rightarrow \ell^+ \nu_\ell X) - N(B_q^0(t) \rightarrow \ell^- \bar{\nu}_\ell X)}{N(\bar{B}_q^0(t) \rightarrow \ell^+ \nu_\ell X) + N(B_q^0(t) \rightarrow \ell^- \bar{\nu}_\ell X)} \simeq 1 - |q/p|^2 \quad (74.23)$$

has been measured either in time-integrated analyses at CLEO [46, 93], BaBar [94], CDF [95], DØ [96–98] and LHCb [99], or in time-dependent analyses at LEP [37, 100], BaBar [47, 101] and

Belle [102]. In the inclusive case, also investigated at LEP [100, 103], no final-state tag is used, and the asymmetry [104]

$$\begin{aligned} & \frac{N(\bar{B}_q^0(t) \rightarrow \text{all}) - N(B_q^0(t) \rightarrow \text{all})}{N(\bar{B}_q^0(t) \rightarrow \text{all}) + N(B_q^0(t) \rightarrow \text{all})} \\ & \simeq \mathcal{A}_{\text{SL}}^q \left[ \sin^2 \left( \frac{\Delta m_q t}{2} \right) - \frac{x_q}{2} \sin(\Delta m_q t) \right] \end{aligned} \quad (74.24)$$

must be measured as a function of the proper time to extract information on  $CP$  violation. In addition LHCb has studied the time dependence of the charge asymmetry of  $B^0 \rightarrow D^{(*)-} \mu^+ \nu_\mu X$  decays without tagging the initial state [105], which would be equal to

$$\frac{N(D^{(*)-} \mu^+ \nu_\mu X) - N(D^{(*)+} \mu^- \bar{\nu}_\mu X)}{N(D^{(*)-} \mu^+ \nu_\mu X) + N(D^{(*)+} \mu^- \bar{\nu}_\mu X)} = \mathcal{A}_{\text{SL}}^d \frac{1 - \cos(\Delta m_d t)}{2} \quad (74.25)$$

in absence of detection and production asymmetries.

The DØ collaboration measured a like-sign dimuon charge asymmetry in semileptonic  $b$  decays that deviates by  $2.8\sigma$  from the tiny Standard Model prediction and concluded, from a more refined analysis in bins of muon impact parameters, that the overall discrepancy is at the level of  $3.6\sigma$  [96]. In all other cases, asymmetries compatible with zero (and the Standard Model [9]) have been found, with a precision limited by the available statistics. Several of the analyses at high energy don't disentangle the  $B_d^0$  and  $B_s^0$  contributions, and either quote a mean asymmetry or a measurement of  $\mathcal{A}_{\text{SL}}^d$  assuming  $\mathcal{A}_{\text{SL}}^s = 0$ : we no longer include these in the average. An exception is the dimuon DØ analysis [96], which separates the two contributions by exploiting their dependence on the muon impact parameter cut. The resulting measurements of  $\mathcal{A}_{\text{SL}}^d$  and  $\mathcal{A}_{\text{SL}}^s$  are then both compatible with the Standard Model. They are also correlated. We therefore perform a two-dimensional average of the measurements of Refs. [46, 47, 93, 94, 96–99, 101, 102, 105] and obtain [8]

$$\mathcal{A}_{\text{SL}}^d = -0.0021 \pm 0.0017_{\text{stat}}/p|_d = 1.0010 \pm 0.0008, \quad (74.26)$$

$$\mathcal{A}_{\text{SL}}^s = -0.0006 \pm 0.0023_{\text{stat}}/p|_s = 1.0003 \pm 0.0014, \quad (74.27)$$

with a correlation coefficient of  $-0.054$  between  $\mathcal{A}_{\text{SL}}^d$  and  $\mathcal{A}_{\text{SL}}^s$ . These results show no evidence of  $CP$  violation and don't constrain yet the Standard Model.

$CP$  violation induced by  $B_s^0$ - $\bar{B}_s^0$  mixing in  $b \rightarrow c\bar{c}s$  decays has been a field of very active study in the past decade. In addition to the previously mentioned  $B_s^0 \rightarrow J/\psi K^+ K^-$  (including  $B_s^0 \rightarrow J/\psi \phi$ ) and  $B_s^0 \rightarrow \psi(2S)\phi$  studies, the decay modes  $B_s^0 \rightarrow J/\psi \pi^+ \pi^-$  (including  $B_s^0 \rightarrow J/\psi f_0(980)$ ) [106] and  $B_s^0 \rightarrow D_s^+ D_s^-$  [29] have also been analyzed by LHCb to measure  $\phi_s^{c\bar{c}s}$ , without the need for an angular analysis. The  $J/\psi \pi^+ \pi^-$  final state has been shown indeed to be (very close to) a pure  $CP$ -odd state [107]. A two-dimensional fit [8] of all published results [28, 29, 70–72, 74–76, 106] in the  $(\phi_s^{c\bar{c}s}, \Delta\Gamma_s)$  plane yields

$$\phi_s^{c\bar{c}s} = -0.051 \pm 0.023. \quad (74.28)$$

Adding to this fit the new ATLAS results recently submitted for publication [73] leads to the preliminary average  $\phi_s^{c\bar{c}s} = -0.057 \pm 0.021$ , with the overall situation shown on Fig. 74.3. This experimental value is consistent with the Standard Model prediction for  $\phi_s^{c\bar{c}s}$ , which is equal to  $-2\beta_s = -2 \arg(-V_{ts} V_{tb}^*)/(V_{cs} V_{cb}^*) = -0.0370^{+0.0007}_{-0.0008}$  [57] assuming negligible Penguin pollution.

### 74.7 Summary

$B^0$ - $\bar{B}^0$  mixing has been and still is a field of intense study. The mass differences in the  $B_d^0$ - $\bar{B}_d^0$  and  $B_s^0$ - $\bar{B}_s^0$  systems are known to relative precisions of 0.38% and 0.11%, respectively. The non-zero decay width difference in the  $B_s^0$ - $\bar{B}_s^0$  system is well established, with a relative difference of  $\Delta\Gamma_s/\Gamma_s = (12.9 \pm 0.6)\%$ , meaning that the heavy state of the  $B_s^0$ - $\bar{B}_s^0$  system lives  $\sim 14\%$  longer than the light state. In contrast, the relative decay width difference in the  $B_d^0$ - $\bar{B}_d^0$  system,  $\Delta\Gamma_d/\Gamma_d = (0.1 \pm 1.0)\%$ , is still consistent with



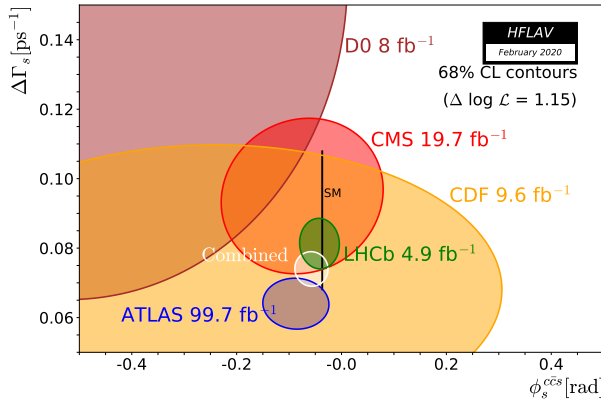


Figure 74.3: 68% CL contours in the  $(\phi_s^{c\bar{c}s}, \Delta\Gamma_s)$  plane, showing all measurements from CDF [70], DØ [71], ATLAS [72, 73], CMS [74] and LHCb [28, 29, 75, 76, 106], with their preliminary average [8]. The very thin black rectangle represents the Standard Model predictions of  $\phi_s^{c\bar{c}s}$  [57] and  $\Delta\Gamma_s$  [9].

zero.  $CP$  violation in  $B_d^0-\bar{B}_d^0$  or  $B_s^0-\bar{B}_s^0$  mixing has not been observed yet, with precisions on the semileptonic asymmetries below 0.3%.  $CP$  violation induced by  $B_s^0-\bar{B}_s^0$  mixing in  $b \rightarrow c\bar{c}s$  transitions has not yet been observed either, with an uncertainty on the  $\phi_s^{c\bar{c}s}$  phase of 23 mrad. Despite the recent improvements, all observations remain consistent with the Standard Model expectations.

However, the measurements where New Physics might show up are still statistically limited. More results are awaited from the LHC experiments and Belle II, with promising prospects for the investigation of the  $CP$ -violating phase  $\arg(-M_{12}/\Gamma_{12})$  and an improved determination of  $\phi_s^{c\bar{c}s}$ .

Mixing studies have clearly reached the stage of precision measurements, where much effort is needed, both on the experimental and theoretical sides, in particular to further reduce the hadronic uncertainties of lattice QCD calculations. In the long term, a stringent check of the consistency of the  $B_d^0$  and  $B_s^0$  mixing amplitudes (magnitudes and phases) with all other measured flavor-physics observables will be possible within the Standard Model, leading to very tight limits on (or otherwise a long-awaited surprise about) New Physics.

## References

- [1] T. D. Lee and C. S. Wu, *Ann. Rev. Nucl. Part. Sci.* **16**, 511 (1966); I. I. Bigi and A. I. Sanda, *Camb. Monogr. Part. Phys. Nucl. Phys. Cosmol.* **9**, 1 (2009), second edition, first published in 2000; G. C. Branco, L. Lavoura and J. P. Silva, *Int. Ser. Monogr. Phys.* **103**, 1 (1999).
- [2] See the review on  $CP$  violation in the quark sector by T. Gershon and Y. Nir in this publication.
- [3] A. J. Buras, W. Slominski and H. Steger, *Nucl. Phys.* **B245**, 369 (1984).
- [4] T. Inami and C. S. Lim, *Prog. Theor. Phys.* **65**, 297 (1981), erratum *ibid.* **65**, 1772 (1981); for the power-like approximation, see A. J. Buras and R. Fleischer, page 91 in “Heavy Flavours II,” eds. A. J. Buras and M. Lindner, Singapore World Scientific (1998).
- [5] M. Kobayashi and T. Maskawa, *Prog. Theor. Phys.* **49**, 652 (1973).
- [6] I. I. Bigi *et al.*, in “ $CP$  violation,” ed. C. Jarlskog, Singapore World Scientific (1989).
- [7] A. Lenz and U. Nierste (2011), [arXiv:1102.4274]; A. Lenz and U. Nierste, *JHEP* **06**, 072 (2007), [hep-ph/0612167].
- [8] Y. Amhis *et al.* (HFLAV) (2019), [arXiv:1909.12524]; the combined results on  $b$ -hadron fractions, lifetimes and mixing parameters published in this *Review* have been obtained by the  $B$  oscillations working group of the Heavy Flavor

Averaging (HFLAV) group, using the methods and procedures described in Chapter 4 of the above paper, after updating the list of inputs; for more information, see <https://hflav.web.cern.ch/>.

- [9] T. Jubb *et al.*, *Nucl. Phys.* **B915**, 431 (2017), [arXiv:1603.07770]; M. Artuso, G. Borissov and A. Lenz, *Rev. Mod. Phys.* **88**, 045002 (2016), [arXiv:1511.09466].
- [10] C. Albajar *et al.* (UA1), *Phys. Lett.* **B186**, 247 (1987), erratum *ibid.* **B197**, 565 (1987).
- [11] H. Albrecht *et al.* (ARGUS), *Phys. Lett.* **B192**, 245 (1987).
- [12] H. G. Moser and A. Roussarie, *Nucl. Instrum. Meth.* **A384**, 491 (1997).
- [13] SLD collab., SLAC-PUB-7228, SLAC-PUB-7229, and SLAC-PUB-7230, *28th Int. Conf. on High Energy Physics*, Warsaw (1996); J. L. Wittlin, *A measurement of the time dependence of  $B_d^0-\bar{B}_d^0$  mixing with kaon tagging*, Ph.D. thesis, Massachusetts U., Amherst (2001), URL <http://www.lib.umi.com/dissertations/fullcit?p3027272>.
- [14] ALEPH collab., contrib. 596 to *Int. Europhysics Conf. on High Energy Physics*, Jerusalem (1997).
- [15] K. Abe *et al.* (SLD), *Phys. Rev.* **D67**, 012006 (2003), [hep-ex/0209002].
- [16] J. Abdallah *et al.* (DELPHI), *Eur. Phys. J.* **C28**, 155 (2003), [hep-ex/0303032].
- [17] F. Abe *et al.* (CDF), *Phys. Rev. Lett.* **80**, 2057 (1998), [hep-ex/9712004]; F. Abe *et al.* (CDF), *Phys. Rev.* **D59**, 032001 (1999), [hep-ex/9806026]; F. Abe *et al.* (CDF), *Phys. Rev.* **D60**, 051101 (1999); F. Abe *et al.* (CDF), *Phys. Rev.* **D60**, 072003 (1999), [hep-ex/9903011]; T. Affolder *et al.* (CDF), *Phys. Rev.* **D60**, 112004 (1999), [hep-ex/9907053].
- [18] R. Barate *et al.* (ALEPH), *Eur. Phys. J.* **C4**, 367 (1998); R. Barate *et al.* (ALEPH), *Eur. Phys. J.* **C7**, 553 (1999), [hep-ex/9811018].
- [19] R. Aaij *et al.* (LHCb), *JINST* **10**, P10005 (2015), [arXiv:1507.07892].
- [20] P. Abreu *et al.* (DELPHI), *Eur. Phys. J.* **C16**, 555 (2000), [hep-ex/0107077].
- [21] K. Anikeev *et al.* (2002), [hep-ph/0201071].
- [22] A. Abulencia *et al.* (CDF), *Phys. Rev. Lett.* **97**, 242003 (2006), [hep-ex/0609040].
- [23] V. M. Abazov *et al.* (DØ), *Phys. Rev.* **D74**, 112002 (2006), [hep-ex/0609034].
- [24] V. M. Abazov *et al.* (DØ), *Phys. Rev. Lett.* **101**, 241801 (2008), [arXiv:0802.2255].
- [25] R. Aaij *et al.* (LHCb), *Eur. Phys. J.* **C72**, 2022 (2012), [arXiv:1202.4979].
- [26] R. Aaij *et al.* (LHCb), *JINST* **11**, P05010 (2016), [arXiv:1602.07252].
- [27] R. Aaij *et al.* (LHCb), *Eur. Phys. J.* **C77**, 238 (2017), [arXiv:1610.06019].
- [28] R. Aaij *et al.* (LHCb), *Phys. Rev. Lett.* **114**, 041801 (2015), [arXiv:1411.3104]; R. Aaij *et al.* (LHCb), *Eur. Phys. J.* **C79**, 706 (2019), erratum to appear, [arXiv:1906.08356].
- [29] R. Aaij *et al.* (LHCb), *Phys. Rev. Lett.* **113**, 211801 (2014), [arXiv:1409.4619].
- [30] R. Aaij *et al.* (LHCb), *Phys. Rev. Lett.* **117**, 261801 (2016), [arXiv:1608.06620].
- [31] B. Aubert *et al.* (BaBar), *Phys. Rev. Lett.* **94**, 161803 (2005), [hep-ex/0408127]; K. F. Chen *et al.* (Belle), *Phys. Rev.* **D72**, 012004 (2005), [hep-ex/0504023].
- [32] Throughout this document we omit references of results that have been replaced by new published measurements.
- [33] D. Buskulic *et al.* (ALEPH), *Z. Phys.* **C75**, 397 (1997).
- [34] P. Abreu *et al.* (DELPHI), *Z. Phys.* **C76**, 579 (1997).
- [35] M. Acciarri *et al.* (L3), *Eur. Phys. J.* **C5**, 195 (1998).

- [36] G. Alexander *et al.* (OPAL), *Z. Phys.* **C72**, 377 (1996); K. Ackerstaff *et al.* (OPAL), *Z. Phys.* **C76**, 417 (1997), [hep-ex/9707010]; G. Abbiendi *et al.* (OPAL), *Phys. Lett.* **B493**, 266 (2000), [hep-ex/0010013].
- [37] K. Ackerstaff *et al.* (OPAL), *Z. Phys.* **C76**, 401 (1997), [hep-ex/9707009].
- [38] B. Aubert *et al.* (BaBar), *Phys. Rev. Lett.* **88**, 221802 (2002), [hep-ex/0112044]; B. Aubert *et al.* (BaBar), *Phys. Rev.* **D66**, 032003 (2002), [hep-ex/0201020]; B. Aubert *et al.* (BaBar), *Phys. Rev. Lett.* **88**, 221803 (2002), [hep-ex/0112045]; B. Aubert *et al.* (BaBar), *Phys. Rev.* **D67**, 072002 (2003), [hep-ex/0212017]; B. Aubert *et al.* (BaBar), *Phys. Rev.* **D73**, 012004 (2006), [hep-ex/0507054].
- [39] N. C. Hastings *et al.* (Belle), *Phys. Rev.* **D67**, 052004 (2003), [hep-ex/0212033]; Y. Zheng *et al.* (Belle), *Phys. Rev.* **D67**, 092004 (2003), [hep-ex/0211065]; K. Abe *et al.* (Belle), *Phys. Rev.* **D71**, 072003 (2005), erratum *ibid.* **D71**, 079903 (2005), [hep-ex/0408111].
- [40] R. Aaij *et al.* (LHCb), *Phys. Lett.* **B709**, 177 (2012), [arXiv:1112.4311].
- [41] R. Aaij *et al.* (LHCb), *Phys. Lett.* **B719**, 318 (2013), [arXiv:1210.6750].
- [42] R. Aaij *et al.* (LHCb), *Eur. Phys. J.* **C73**, 2655 (2013), [arXiv:1308.1302].
- [43] P. Huang *et al.*, *Eur. Phys. J.* **C76**, 422 (2016), [arXiv:1505.03672].
- [44] H. Albrecht *et al.* (ARGUS), *Z. Phys.* **C55**, 357 (1992); H. Albrecht *et al.* (ARGUS), *Phys. Lett.* **B324**, 249 (1994).
- [45] J. E. Bartelt *et al.* (CLEO), *Phys. Rev. Lett.* **71**, 1680 (1993).
- [46] B. H. Behrens *et al.* (CLEO), *Phys. Lett.* **B490**, 36 (2000), [hep-ex/0005013].
- [47] B. Aubert *et al.* (BaBar), *Phys. Rev. Lett.* **92**, 181801 (2004), [hep-ex/0311037]; B. Aubert *et al.* (BaBar), *Phys. Rev.* **D70**, 012007 (2004), [hep-ex/0403002].
- [48] T. Higuchi *et al.*, *Phys. Rev.* **D85**, 071105 (2012), [arXiv:1203.0930].
- [49] R. Aaij *et al.* (LHCb), *JHEP* **04**, 114 (2014), [arXiv:1402.2554].
- [50] M. Aaboud *et al.* (ATLAS), *JHEP* **06**, 081 (2016), [arXiv:1605.07485].
- [51] A. M. Sirunyan *et al.* (CMS), *Eur. Phys. J.* **C78**, 457 (2018), erratum *ibid.* **C78**, 561 (2018), [arXiv:1710.08949].
- [52] See the review on the CKM quark-mixing matrix by A. Cecucci, Z. Ligeti, and Y. Sakai in this publication.
- [53] S. Aoki *et al.* (Flavour Lattice Averaging Group) (2019), [arXiv:1902.08191].
- [54] R. Aaij *et al.* (LHCb), *New J. Phys.* **15**, 053021 (2013), [arXiv:1304.4741].
- [55] A. Bazavov *et al.* (Fermilab Lattice and MILC), *Phys. Rev.* **D93**, 113016 (2016), [arXiv:1602.03560].
- [56] M. Bona *et al.* (UTfit), *JHEP* **10**, 081 (2006), [hep-ph/0606167]; updated results at <http://www.utfit.org/>.
- [57] J. Charles *et al.*, *Phys. Rev.* **D91**, 073007 (2015), [arXiv:1501.05013]; updated results at <http://ckmfitter.in2p3.fr/>.
- [58] K. Hartkorn and H. G. Moser, *Eur. Phys. J.* **C8**, 381 (1999).
- [59] M. Acciarri *et al.* (L3), *Phys. Lett.* **B438**, 417 (1998).
- [60] D. Buskulic *et al.* (ALEPH), *Phys. Lett.* **B377**, 205 (1996); K. Ackerstaff *et al.* (OPAL), *Phys. Lett.* **B426**, 161 (1998), [hep-ex/9802002]; F. Abe *et al.* (CDF), *Phys. Rev.* **D59**, 032004 (1999), [hep-ex/9808003]; V. M. Abazov *et al.* (DØ), *Phys. Rev. Lett.* **114**, 062001 (2015), [arXiv:1410.1568]; T. Aaltonen *et al.* (CDF), *Phys. Rev. Lett.* **107**, 272001 (2011), [arXiv:1103.1864]; R. Aaij *et al.* (LHCb), *Phys. Rev. Lett.* **113**, 172001 (2014), [arXiv:1407.5873]; R. Aaij *et al.* (LHCb), *Phys. Rev. Lett.* **119**, 101801 (2017), [arXiv:1705.03475].
- [61] R. Aaij *et al.* (LHCb), *Phys. Rev. Lett.* **112**, 111802 (2014), [arXiv:1312.1217].
- [62] R. Aaij *et al.* (LHCb), *Phys. Lett.* **B736**, 446 (2014), [arXiv:1406.7204].
- [63] R. Aaij *et al.* (LHCb), *Phys. Lett.* **B707**, 349 (2012), [arXiv:1111.0521].
- [64] R. Aaij *et al.* (LHCb), *Phys. Lett.* **B762**, 484 (2016), [arXiv:1607.06314].
- [65] T. Aaltonen *et al.* (CDF), *Phys. Rev.* **D84**, 052012 (2011), [arXiv:1106.3682]; V. M. Abazov *et al.* (DØ), *Phys. Rev.* **D94**, 012001 (2016), [arXiv:1603.01302].
- [66] R. Aaij *et al.* (LHCb), *Phys. Rev.* **D87**, 112010 (2013), [arXiv:1304.2600].
- [67] R. Aaij *et al.* (LHCb), *Nucl. Phys.* **B873**, 275 (2013), [arXiv:1304.4500].
- [68] R. Aaij *et al.* (LHCb), *Phys. Rev. Lett.* **118**, 191801 (2017), [arXiv:1703.05747].
- [69] R. Fleischer and R. Knegjens, *Eur. Phys. J.* **C71**, 1789 (2011), [arXiv:1109.5115].
- [70] T. Aaltonen *et al.* (CDF), *Phys. Rev. Lett.* **109**, 171802 (2012), [arXiv:1208.2967].
- [71] V. M. Abazov *et al.* (DØ), *Phys. Rev.* **D85**, 032006 (2012), [arXiv:1109.3166].
- [72] G. Aad *et al.* (ATLAS), *Phys. Rev.* **D90**, 052007 (2014), [arXiv:1407.1796]; G. Aad *et al.* (ATLAS), *JHEP* **08**, 147 (2016), [arXiv:1601.03297].
- [73] G. Aad *et al.* (ATLAS) (2020), [arXiv:2001.07115].
- [74] V. Khachatryan *et al.* (CMS), *Phys. Lett.* **B757**, 97 (2016), [arXiv:1507.07527].
- [75] R. Aaij *et al.* (LHCb), *JHEP* **08**, 037 (2017), [arXiv:1704.08217].
- [76] R. Aaij *et al.* (LHCb), *Phys. Lett.* **B762**, 253 (2016), [arXiv:1608.04855].
- [77] R. Aaij *et al.* (LHCb), *Phys. Rev. Lett.* **108**, 241801 (2012), [arXiv:1202.4717].
- [78] S. Schael *et al.* (ALEPH, DELPHI, L3, OPAL, SLD, LEP Electroweak Working Group, SLD Electroweak Group, SLD Heavy Flavour Group), *Phys. Rept.* **427**, 257 (2006), [hep-ex/0509008]; we use the  $\bar{\chi}$  average given in Eq. (5.39).
- [79] D. Acosta *et al.* (CDF), *Phys. Rev.* **D69**, 012002 (2004), [hep-ex/0309030].
- [80] V. M. Abazov *et al.* (DØ), *Phys. Rev.* **D74**, 092001 (2006), [hep-ex/0609014].
- [81] P. Abreu *et al.* (DELPHI), *Phys. Lett.* **B289**, 199 (1992); P. D. Acton *et al.* (OPAL), *Phys. Lett.* **B295**, 357 (1992); D. Buskulic *et al.* (ALEPH), *Phys. Lett.* **B361**, 221 (1995).
- [82] P. Abreu *et al.* (DELPHI), *Z. Phys.* **C68**, 375 (1995); R. Barate *et al.* (ALEPH), *Eur. Phys. J.* **C2**, 197 (1998).
- [83] D. Buskulic *et al.* (ALEPH), *Phys. Lett.* **B384**, 449 (1996); J. Abdallah *et al.* (DELPHI), *Eur. Phys. J.* **C44**, 299 (2005), [hep-ex/0510023].
- [84] R. Barate *et al.* (ALEPH), *Eur. Phys. J.* **C5**, 205 (1998).
- [85] J. Abdallah *et al.* (DELPHI), *Phys. Lett.* **B576**, 29 (2003), [hep-ex/0311005].
- [86] F. Abe *et al.* (CDF), *Phys. Rev.* **D60**, 092005 (1999).
- [87] T. Aaltonen *et al.* (CDF), *Phys. Rev.* **D77**, 072003 (2008), [arXiv:0801.4375]; T. Affolder *et al.* (CDF), *Phys. Rev. Lett.* **84**, 1663 (2000), [hep-ex/9909011]; the measurement of  $f_{\text{baryon}}/f_d$  in the latter paper has been updated based on; T. Aaltonen *et al.* (CDF), *Phys. Rev.* **D79**, 032001 (2009), [arXiv:0810.3213].
- [88] V. M. Abazov *et al.* (DØ), *Phys. Rev. Lett.* **99**, 052001 (2007), [arXiv:0706.1690]; V. M. Abazov *et al.* (DØ), *Phys. Rev. Lett.* **101**, 232002 (2008), [arXiv:0808.4142]; T. Aaltonen *et al.* (CDF), *Phys. Rev.* **D80**, 072003 (2009), [arXiv:0905.3123].



- [89] R. Aaij *et al.* (LHCb), JHEP **04**, 001 (2013), [arXiv:1301.5286]; the LHCb average of  $f_s/f_d$  has been updated in LHCb collab., LHCb-CONF-2013-011 (2013).
- [90] R. Aaij *et al.* (LHCb), Phys. Rev. **D85**, 032008 (2012), [arXiv:1111.2357]; R. Aaij *et al.* (LHCb), Phys. Rev. **D100**, 031102 (2019), [arXiv:1902.06794].
- [91] G. Aad *et al.* (ATLAS), Phys. Rev. Lett. **115**, 262001 (2015), [arXiv:1507.08925].
- [92] R. Aaij *et al.* (LHCb), Phys. Rev. **D100**, 112006 (2019), [arXiv:1910.13404].
- [93] D. E. Jaffe *et al.* (CLEO), Phys. Rev. Lett. **86**, 5000 (2001), [hep-ex/0101006].
- [94] J. P. Lees *et al.* (BaBar), Phys. Rev. Lett. **114**, 081801 (2015), [arXiv:1411.1842].
- [95] F. Abe *et al.* (CDF), Phys. Rev. **D55**, 2546 (1997).
- [96] V. M. Abazov *et al.* (DØ), Phys. Rev. **D89**, 012002 (2014), [arXiv:1310.0447].
- [97] V. M. Abazov *et al.* (DØ), Phys. Rev. **D86**, 072009 (2012), [arXiv:1208.5813].
- [98] V. M. Abazov *et al.* (DØ), Phys. Rev. Lett. **110**, 011801 (2013), [arXiv:1207.1769].
- [99] R. Aaij *et al.* (LHCb), Phys. Rev. Lett. **117**, 061803 (2016), erratum *ibid.* **118**, 129903 (2017), [arXiv:1605.09768].
- [100] R. Barate *et al.* (ALEPH), Eur. Phys. J. **C20**, 431 (2001).
- [101] J. P. Lees *et al.* (BaBar), Phys. Rev. Lett. **111**, 101802 (2013), erratum *ibid.* **111**, 159901 (2013), [arXiv:1305.1575].
- [102] E. Nakano *et al.* (Belle), Phys. Rev. **D73**, 112002 (2006), [hep-ex/0505017].
- [103] G. Abbiendi *et al.* (OPAL), Eur. Phys. J. **C12**, 609 (2000), [hep-ex/9901017].
- [104] M. Beneke, G. Buchalla and I. Dunietz, Phys. Lett. **B393**, 132 (1997), [hep-ph/9609357]; I. Dunietz, Eur. Phys. J. **C7**, 197 (1999), [hep-ph/9806521].
- [105] R. Aaij *et al.* (LHCb), Phys. Rev. Lett. **114**, 041601 (2015), [arXiv:1409.8586].
- [106] R. Aaij *et al.* (LHCb), Phys. Lett. **B736**, 186 (2014), [arXiv:1405.4140]; R. Aaij *et al.* (LHCb), Phys. Lett. **B797**, 134789 (2019), [arXiv:1903.05530].
- [107] R. Aaij *et al.* (LHCb), Phys. Rev. **D86**, 052006 (2012), [arXiv:1204.5643].

## 75. Semileptonic $b$ -Hadron Decays, Determination of $V_{cb}$ , $V_{ub}$

Revised August 2019 by T. Mannel (Siegen U.) and P. Urquijo (School of Phys. U. of Melbourne).

### 75.1 Introduction

Precision determinations of  $|V_{ub}|$  and  $|V_{cb}|$  are central to testing the CKM sector of the Standard Model, and complement the measurements of CP asymmetries in  $B$  decays. The length of the side of the unitarity triangle opposite the well-measured angle  $\beta$  is proportional to the ratio  $|V_{ub}|/|V_{cb}|$ ; its precise determination is a high priority of the heavy-flavor physics program.

The transitions  $b \rightarrow c\ell\bar{\nu}_\ell$  and  $b \rightarrow u\ell\bar{\nu}_\ell$  (where  $\ell$  refers to an electron or muon) each provide two avenues for determining these CKM matrix elements, namely through inclusive (i.e. the sum over all possible hadronic states) and exclusive final states (decays involving a specific meson,  $X = D, D^*, \pi, \rho$  etc.). While the purely leptonic final states in the decays  $B_c^- \rightarrow \tau\bar{\nu}$ ,  $B^- \rightarrow \tau\bar{\nu}$ , and  $B^- \rightarrow \mu\bar{\nu}$  are theoretically very simple, we do not use this information at present since none of the measurements has reached a competitive level of precision and thus the focus is on exclusive and inclusive semileptonic decays. This article and the values quoted here update the previous review [1].

The theory underlying the different determinations of  $|V_{qb}|$  is mature, in particular for  $|V_{cb}|$ . Most of the theoretical approaches use the fact that the masses  $m_b$  and  $m_c$  of the  $b$  and the  $c$  quark are large compared to the scale  $\Lambda_{\text{QCD}}$  that determines low-energy hadronic physics. Thus the basis for precise calculations is a systematic expansion in powers of  $\Lambda/m_b$ , where  $\Lambda \sim 500 - 700$  MeV is a hadronic scale of the order of  $\Lambda_{\text{QCD}}$ . Such an expansion can be formulated in the framework of an effective field theory which is described in a separate RPP mini-review [2].

Aside from this there has been significant progress over the last decade in lattice simulations of QCD which is a first-principles method for non-perturbative QCD calculations. Increased computer power as well as improved theoretical methods allow us to include also heavy quarks in this calculations, and thus the results from lattice QCD play an essential role in many of the determinations discussed here. We do not need to describe lattice methods here, they are discussed in a separate RPP mini-review [3].

The measurements discussed in this review are of branching fractions, ratios of branching fractions, and decay kinematic distributions. The determinations of  $|V_{cb}|$  and  $|V_{ub}|$  also require a measurement of the total decay widths of the corresponding  $b$  hadrons, determined from lifetimes, which is the subject of a separate RPP mini-review [4]. The measurements of inclusive semileptonic decays relevant to this review come primarily from  $e^+e^- B$  factories operating at the  $\Upsilon(4S)$  resonance, while the measurements of exclusive semileptonic decays come from both the  $e^+e^- B$  factories and from the LHCb experiment at CERN.

Semileptonic  $B$  meson decay amplitudes to electrons and muons are well measured and consistent with the SM, and thus are dominated by the Standard-Model  $W$  boson exchange, which is expected to be largely free from any impact of non-Standard Model physics. The decays  $\bar{B} \rightarrow D^{(*)}\tau\bar{\nu}_\tau$ , however, may become sensitive to effects beyond the Standard Model due to the large mass of the  $\tau$  lepton. For example, modifications in the Higgs sector such as a charged Higgs boson, may couple to the mass of the leptons, breaking lepton universality beyond the Standard Model. The currently observed anomalies in these decay could be an indication of new physics.

Many of the numerical results quoted in this review have been provided by the Heavy Flavor Averaging Group (HFLAV) [5].

### 75.2 Determination of $|V_{cb}|$

*Summary:* The determination of  $|V_{cb}|$  from inclusive decays has a relative uncertainty of about 2%; the limitations arise mainly from our ignorance of higher-order perturbative and non-perturbative corrections. Exclusive  $\bar{B} \rightarrow D^*\ell\bar{\nu}_\ell$  decays provide a determination of  $|V_{cb}|$  with a relative precision of about 2%, with comparable contributions from theory and experiment; the value determined from  $\bar{B} \rightarrow D\ell\bar{\nu}_\ell$  decays is consistent and has an uncertainty of 3%. However, as discussed below, recent work has

raised questions about these determinations. We choose to quote a less constraining value from exclusive decays.

The values obtained from the inclusive and exclusive determinations discussed below are:

$$|V_{cb}| = (42.2 \pm 0.8) \times 10^{-3} \quad (\text{inclusive}) \quad (75.1)$$

$$|V_{cb}| = (39.5 \pm 0.9) \times 10^{-3} \quad (\text{exclusive}). \quad (75.2)$$

An average of these determinations has  $p(\chi^2) = 2\%$ , so we scale the error by  $\sqrt{\chi^2/1} = 2.4$  to find

$$|V_{cb}| = (41.0 \pm 1.4) \times 10^{-3} \quad (\text{average}). \quad (75.3)$$

Given the only marginal consistency this average should be treated with caution.

#### 75.2.1 $|V_{cb}|$ from exclusive decays

Exclusive determinations of  $|V_{cb}|$  make use of semileptonic  $B$  decays into the ground state charmed mesons  $D$  and  $D^*$ . Based on Lorentz-invariance these decays are collectively described in terms of six independent form factors, which depend on the variable  $w \equiv v \cdot v'$ , where  $v$  and  $v'$  are the four velocities of the initial and final-state hadrons. In the rest frame of the decay this variable corresponds to the Lorentz factor of the final state  $D^{(*)}$  meson. Heavy Quark Symmetry (HQS) [6] [7] predicts that in the infinite mass limit the six form factors collapse into a single one, which is normalized at the ‘‘zero recoil point’’  $w = 1$ , the point of maximum momentum transfer to the leptons.

The determination of  $|V_{cb}|$  requires a calculation of the form factors. One possibility is to use the normalization of the form factor at  $w = 1$ , however, a precise determination requires to include corrections to the HQS prediction for the normalization as well as some information on the shape of the form factors near the point  $w = 1$ . These calculations utilize Heavy Quark Effective Theory, which is discussed in a separate RPP mini-review [2]. Some of the form factors are normalized at  $w = 1$  due to HQS, and this normalization is protected against linear corrections [8], and thus the leading corrections to the normalization are of order  $\Lambda_{\text{QCD}}^2/m_c^2$ . For the form factors that vanish in the infinite mass limit the corrections are in general linear in  $\Lambda_{\text{QCD}}/m_c$ .

In addition to these corrections, there are perturbatively calculable corrections from hard gluons as well as QED radiative corrections, which will be discussed in the relevant sections.

#### 75.2.2 $\bar{B} \rightarrow D^*\ell\bar{\nu}_\ell$

The decay rate for  $\bar{B} \rightarrow D^*\ell\bar{\nu}_\ell$  is given by

$$\frac{d\Gamma}{dw}(\bar{B} \rightarrow D^*\ell\bar{\nu}_\ell) = \frac{G_F^2 m_B^5}{48\pi^3} |V_{cb}|^2 (w^2 - 1)^{1/2} P(w) (\eta_{\text{ew}} \mathcal{F}(w))^2, \quad (75.4)$$

where  $P(w)$  is a phase space factor,

$$P(w) = r^3 (1 - r)^2 (w + 1)^2 \left( 1 + \frac{4w}{w + 1} \frac{1 - 2rw + r^2}{(1 - r)^2} \right). \quad (75.5)$$

with  $r = m_{D^*}/m_B$ . The form factor  $\mathcal{F}(w)$  can be expressed in terms of the vector and axial vector form factors

$$\begin{aligned} \frac{\langle D^*(v', \epsilon) | \bar{e}\gamma^\mu b | B(v) \rangle}{\sqrt{m_B m_{D^*}}} &= h_V(w) \epsilon^{\mu\nu\rho\sigma} v_{B,\nu} v_{D^*,\rho} \epsilon_\sigma^*, \\ \frac{\langle D^*(v', \epsilon) | \bar{e}\gamma^\mu \gamma^5 b | B(v) \rangle}{\sqrt{m_B m_{D^*}}} &= i h_{A_1}(w) (1 + w) \epsilon^{*\mu} \\ &\quad - i [h_{A_2}(w) v_B^\mu + h_{A_3}(w) v_{D^*}^\mu] \epsilon^* \cdot v_B \end{aligned}$$

as

$$P(w) |\mathcal{F}(w)|^2 = |h_{A_1}(w)|^2 \left\{ 2 \frac{r^2 - 2rw + 1}{(1 - r)^2} \left[ 1 + \frac{w - 1}{w + 1} R_1^2(w) \right] + \left[ 1 + \frac{w - 1}{1 - r} (1 - R_2(w)) \right]^2 \right\},$$

where the ratios  $R_1$  and  $R_2$  are given by

$$R_1(w) = \frac{h_V(w)}{h_{A_1}(w)}, \quad R_2(w) = \frac{h_{A_3}(w) + r h_{A_2}(w)}{h_{A_1}(w)}. \quad (75.6)$$

Note that  $\mathcal{F}$  at  $w = 1$  is unity by HQS in the infinite-mass limit [9–12]. Usually the decay rate formulae for semileptonic  $B$  decays assume massless leptons. The effect is typically very small, but for the muon case can be non-negligible in fits to data at high hadronic recoil.

The factor  $\eta_{ew} = 1.0066 \pm 0.0050$  accounts for the leading electroweak corrections to the four-fermion operator mediating the semileptonic decay [13], and includes an estimated uncertainty for missing long-distance QED radiative corrections [14].

The determination of  $V_{cb}$  using the normalization at  $w = 1$  involves an extrapolation to the zero-recoil point, for which a parametrization of the shape of  $\mathcal{F}(w)$  is needed. Convenient parametrizations make use of analyticity and unitarity constraints on the form factors and are expressed in terms of the variable

$$z = \frac{\sqrt{w+1} - \sqrt{2}}{\sqrt{w+1} + \sqrt{2}}, \quad (75.7)$$

originating from a conformal transformation. In terms of this variable the form factors (generically denoted as  $F$ ) may be written as [15–17]

$$F(z) = \frac{1}{P_F(z)\phi_F(z)} \sum_{n=0}^{\infty} a_n z^n \quad (75.8)$$

where the sum is bounded,  $\sum |a_n|^2 < 1$ . Furthermore, the function  $P_F(z)$  takes into account the resonances in the  $(\bar{c}b)$  system below the  $\bar{D}B$  threshold, and the weighting functions  $\phi_F(z)$  are derived from the unitarity constraint on the corresponding form factor. The values of  $z$  relevant to the decay are  $0 \leq z \leq 0.06$ , hence only very few terms are needed in the series in  $z$ . Eq. (75.8) will be referred to as the “BGL” expansion.

A frequently used parametrization proposed in Ref. [18] is a simple one-parameter form

$$h_{A_1}(w) = h_{A_1}(1) [1 - 8\rho^2 z + (53\rho^2 - 15)z^2 + (231\rho^2 - 91)z^3] \quad (75.9)$$

which has the slope  $\rho$  and of the form factor and the value  $h_{A_1}(1)$  as the only parameters. Furthermore, the ratios  $R_1(w)$  and  $R_1(w)$  are expanded in  $w - 1$ . However, this simple CLN parametrization is inconsistent in subleading orders of the  $1/m_{c/b}$  expansion [17, 19–22], and thus the recent fits are based on the BGL expansion. Typical fits include up to three parameters  $a_n$  in (75.8) for the different form factors.

The theoretical analysis of  $F(w)$  requires, aside from the perturbative calculation of QCD short-distance radiative correction [23], the treatment of non-perturbative aspects. The state-of-the-art input comes from lattice QCD calculations which include a realistic description of the sea quarks using  $2 + 1$  or  $2 + 1 + 1$  flavors and finite  $b$  and  $c$  masses.

Currently available are lattice results only for the value  $\mathcal{F}(1)$  at the non-recoil point [14, 24] with a total uncertainty at the (1–2)% level. The main contributions to this uncertainty in case of the Fermilab/MILC calculation are from the chiral extrapolation from the light quark masses used in the numerical lattice computation to realistic up and down quark masses, and from discretization errors. In the HPQCD calculation, the dominant source of uncertainty is the perturbative matching calculation for the heavy-light currents. These sources of uncertainty will be reduced with larger lattice sizes and smaller lattice spacings. The average of the two lattice predictions [25] is

$$\mathcal{F}(1) = 0.904 \pm 0.012, \quad (75.10)$$

Lattice calculations for values of  $F(w)$  for  $w \neq 1$  are underway, but not yet available.

Non-lattice estimates based on zero-recoil sum rules for the form factor tend to yield lower central values for  $\mathcal{F}(1)$  [26–28]. Omitting the contributions from excited states, the sum rules indicate that  $\mathcal{F}(1) < 0.93$ . Including an estimate for the contribution of the excited states yields  $\mathcal{F}(1) = 0.86 \pm 0.01 \pm 0.02$  [28, 29] where the second uncertainty accounts for the excited states.

Many experiments [30–40] have measured the differential decay rate as a function of  $w$ , employing a variety of methods: using

either  $B^+$  or  $B^0$  decays, with or without  $B$ -tagging, and with or without explicit reconstruction of the transition pion from  $D^* \rightarrow D$  decays. These measurements are input to a four-dimensional fit [5] for  $\eta_{ew}\mathcal{F}(1)|V_{cb}|$ ,  $\rho_{A_1}^2$  and the form-factor ratios  $R_1 \propto A_2/A_1$  and  $R_2 \propto V/A_1$ . The fit has a  $p$ -value of 0.8%, so we scale the uncertainty by a factor  $\sqrt{\chi^2/23}$  to give  $\eta_{ew}\mathcal{F}(1)|V_{cb}| = (35.27 \pm 0.52) \times 10^{-3}$  (CLN).

The leading sources of uncertainty on  $\eta_{ew}\mathcal{F}(1)|V_{cb}|$  are due to detection efficiencies and  $D^{(*)}$  decay branching fractions. Note that the  $\bar{B} \rightarrow D^*\ell\bar{\nu}_\ell$  form factor in the fit is parameterized using the CLN form, which has the drawbacks discussed previously.

Using the value from Eq. 75.10 for  $\mathcal{F}(1)$  and accounting for the electroweak correction gives

$$|V_{cb}| = (38.8 \pm 0.6 \pm 0.6) \times 10^{-3} (\bar{B} \rightarrow D^*\ell\bar{\nu}_\ell, \text{ LQCD, CLN}). \quad (75.11)$$

Not yet included in the average is the most recent measurement from Babar [41], which finds consistent results using the CLN form.

A safer approach is to use the more general BGL form-factor parameterization [17, 19]. Two experiments have recently published analyses with BGL based parametrizations at a given order in the expansion [40, 41]. The Belle analysis [40] is based on an untagged approach in the mode  $\bar{B}^0 \rightarrow D^{*+}\ell\bar{\nu}_\ell$  and measures 1- $d$  projections in bins of the hadronic recoil  $w$ , and angular variables  $\cos\theta_\ell$ ,  $\cos\theta_V$ , and  $\chi$ . The Babar analysis [41] is based on a hadronic tagged sample, and performs a full 4- $d$  unbinned analysis of neutral and charged  $B$  decay modes. Only the BGL form factors are fit in this analysis, not the normalisation, which based on the world average  $\bar{B} \rightarrow D^*\ell\bar{\nu}_\ell$  branching fraction.

At present only Ref. [40] publishes the fully-differential decay rate data and associated covariance matrix. An earlier preliminary measurement by Belle [39] also provided fully-differential decay rate data, used in a number of phenomenology analyses [17, 19], but was not published.

The BGL fit results from Ref. [40],  $|V_{cb}| = (38.4 \pm 1.0) \times 10^{-3}$ , and Ref. [41],  $|V_{cb}| = (38.4 \pm 0.9) \times 10^{-3}$ , are consistent with result from the fit with the CLN parametrization, Eq. 75.11. Both studies report fit results at low order in the three BGL expansion terms, ranging from zero-order to second-order in the Belle analysis, and first order for all terms in the Babar analysis. Studies of the impact of higher order expansions based on the Belle published decay rate data have been reported in Refs. [20, 21], where it is shown that the fit uncertainty on  $|V_{cb}|$  increases by approximately 50% with respect to the results reported at lower order. This is due to larger number of degrees of freedom allowed in the higher order expansions, however beyond second order there is very little information gain with the current measurements. Form-factor ratios are found to be consistent with HQET predictions based on fits to the published measurements. Without a combination of the two results at this stage, we choose to quote the arithmetic average of the results from Ref. [40, 41], where the central values are the same. The nominal result for  $|V_{cb}|$  is therefore

$$|V_{cb}| = (38.4 \pm 0.7 \pm 0.5 \pm 1.0) \times 10^{-3} (\bar{B} \rightarrow D^*\ell\bar{\nu}_\ell, \text{ LQCD, BGL}), \quad (75.12)$$

where the first uncertainty is experimental, the second is from LQCD, and the third is an additional uncertainty added by the authors to compensate for higher order expansion terms in the fit. Lattice QCD results for form factors away from zero recoil will be essential to control higher order terms in the BGL fit.

### 75.2.3 $\bar{B} \rightarrow D\ell\bar{\nu}_\ell$

The differential rate for  $\bar{B} \rightarrow D\ell\bar{\nu}_\ell$  is given by

$$\begin{aligned} \frac{d\Gamma}{dw}(\bar{B} \rightarrow D\ell\bar{\nu}_\ell) = \\ \frac{G_F^2}{48\pi^3} |V_{cb}|^2 (m_B + m_D)^2 m_D^3 (w^2 - 1)^{3/2} (\eta_{ew}\mathcal{G}(w))^2. \end{aligned} \quad (75.13)$$

The form factor is defined in terms of

$$\frac{\langle D(v') | \bar{c} \gamma^\mu b | B(v) \rangle}{\sqrt{m_B m_D}} = h_+(w) (v_B + v_D)^\mu + h_-(w) (v_B - v_D)^\mu \quad (75.14)$$

and reads

$$\mathcal{G}(w) = h_+(w) - \frac{m_B - m_D}{m_B + m_D} h_-(w), \quad (75.15)$$

where  $h_+$  is normalized to unity due to HQS and  $h_-$  vanishes in the infinite-mass limit. Thus

$$\mathcal{G}(1) = 1 + \mathcal{O} \left( \left( \frac{m_B - m_D}{m_B + m_D} \right)^2 \frac{\Lambda_{\text{QCD}}}{m_c} \right) \quad (75.16)$$

and the corrections to the HQET predictions are of order  $1/m$  in contrast to the case of  $F(1)$ .

The normalization,  $\mathcal{G}(1)$ , is obtained from QCD lattice calculations with realistic sea quarks and finite  $b$  and  $c$  masses. The most recent value for  $\mathcal{G}(1)$  is derived in Ref. [42] and is

$$\mathcal{G}(1) = 1.054 \pm 0.004 \pm 0.008 \quad (75.17)$$

Based on a parametrization of the shape of  $\mathcal{G}(w)$  a value of  $|V_{cb}|$  can be extracted. However,  $w \sim 1$  is a region with poor experimental precision given the low decay rate in this kinematic corner.

In fact, lattice calculations for the form factor  $\mathcal{G}(w)$  (including sea quarks and finite  $b$  and  $c$  masses) are now available for values  $w \neq 1$ , thus providing information over a range of  $z$  values (see Eq. (75.7)) [42, 43]. This lattice input can be used in a simultaneous fit, along with the differential branching fraction, in a form-factor expansion in  $z$  [15–17, 44].

The most precise measurements of  $\bar{B} \rightarrow D \ell \bar{\nu}_\ell$  [37, 45, 46] dominate the CLN average [5] value,  $\eta_{\text{ew}} \mathcal{G}(1) |V_{cb}| = (42.00 \pm 1.00) \times 10^{-3}$ . Note that this average corresponds to measurements that are fit to the CLN form factor parameterization; the same concerns expressed above for  $\bar{B} \rightarrow D^* \ell \bar{\nu}_\ell$  apply here. Using the value from Eq. (75.17) for  $\mathcal{G}(1)$  and accounting for the electroweak correction as above gives

$$|V_{cb}| = (39.6 \pm 0.9 \pm 0.3) \times 10^{-3} \quad (\bar{B} \rightarrow D \ell \bar{\nu}_\ell, \text{ LQCD, CLN}), \quad (75.18)$$

where the first uncertainty is from experiment, and the second is from lattice QCD, as well as the electroweak corrections.

Studies have also been conducted using the general BCL form-factor parametrization ( $z$ -expansion from Ref. Ref. [44]), combining binned measurements from Belle [46] and Babar [45] with lattice QCD determinations of the form factors as a function of the recoil parameter in the lowest third of the kinematically allowed region [25]. Only Ref. [46] published the full measurement covariance matrix, while Ref. [45] provides the statistical uncertainty covariance. Nevertheless, Ref. [46] is more precise and dominates the average [25], giving

$$|V_{cb}| = (40.1 \pm 1.0) \times 10^{-3} \quad (\bar{B} \rightarrow D \ell \bar{\nu}_\ell, \text{ LQCD, BCL}). \quad (75.19)$$

This result is consistent with the value reported in Ref. [47].

The  $|V_{cb}|$  averages from  $\bar{B} \rightarrow D^* \ell \bar{\nu}_\ell$  and  $\bar{B} \rightarrow D \ell \bar{\nu}_\ell$  decays using the BGL and BCL forms, respectively, are reasonably consistent. The correlations between the lattice uncertainties for  $\bar{B} \rightarrow D^* \ell \bar{\nu}_\ell$  and  $\bar{B} \rightarrow D \ell \bar{\nu}_\ell$  are discussed in Ref. [25], and considered to be 100% for the statistical uncertainty component. We assume an experimental uncertainty correlation of order 20% and combine the results, giving

$$|V_{cb}| = (39.5 \pm 0.9) \times 10^{-3} \quad (\text{exclusive}). \quad (75.20)$$

#### 75.2.4 $|V_{cb}|$ from inclusive decays

Measurements of the total semileptonic branching decay rate, along with moments of the lepton energy and hadronic invariant mass spectra in inclusive semileptonic  $b \rightarrow c$  transitions, can be used for a precision determination of  $|V_{cb}|$ . The total semileptonic decay rate can be calculated quite reliably in terms of non-perturbative parameters that can be extracted from the information contained in the moments.

#### 75.2.5 Inclusive semileptonic rate

The theoretical foundation for the calculation of the total semileptonic rate is the Operator Product Expansion (OPE) which yields the Heavy Quark Expansion (HQE) [48, 49]. Details can be found in the RPP mini-review on Effective Theories [2].

The OPE result for the total rate can be written schematically (details can be found, *e.g.*, in Ref. [50]) as

$$\begin{aligned} \Gamma = & |V_{cb}|^2 \frac{G_F^2 m_b^5(\mu)}{192\pi^3} \eta_{\text{ew}} \times \\ & \left[ z_0^{(0)}(r) + \frac{\alpha_s(\mu)}{\pi} z_0^{(1)}(r) + \left( \frac{\alpha_s(\mu)}{\pi} \right)^2 z_0^{(2)}(r) + \dots \right. \\ & + \frac{\mu_\pi^2}{m_b^2} \left( z_2^{(0)}(r) + \frac{\alpha_s(\mu)}{\pi} z_2^{(1)}(r) + \dots \right) \\ & + \frac{\mu_G^2}{m_b^2} \left( y_2^{(0)}(r) + \frac{\alpha_s(\mu)}{\pi} y_2^{(1)}(r) + \dots \right) \\ & + \frac{\rho_D^3}{m_b^3} \left( z_3^{(0)}(r) + \frac{\alpha_s(\mu)}{\pi} z_3^{(1)}(r) + \dots \right) \\ & \left. + \frac{\rho_{LS}^3}{m_b^3} \left( y_3^{(0)}(r) + \frac{\alpha_s(\mu)}{\pi} y_3^{(1)}(r) + \dots \right) + \dots \right] \quad (75.21) \end{aligned}$$

where  $r$  is the ratio  $m_c/m_b$  and the  $y_i$  and  $z_i$  are perturbatively calculable Wilson coefficients functions that appear at different orders of the heavy mass expansion.

The parameters  $\mu_\pi$ ,  $\mu_G$ ,  $\rho_D$  and  $\rho_{LS}$  constitute the non-perturbative input into the heavy quark expansion; they correspond to certain matrix elements to be discussed below. In the same way the HQE can be set up for the moments of distributions of charged-lepton energy, hadronic invariant mass and hadronic energy, *e.g.*

$$\langle E_e^n \rangle_{E_e > E_{\text{cut}}} = \int_{E_{\text{cut}}}^{E_{\text{max}}} \frac{d\Gamma}{dE_e} E_e^n dE_e \bigg/ \int_{E_{\text{cut}}}^{E_{\text{max}}} \frac{d\Gamma}{dE_e} dE_e. \quad (75.22)$$

The coefficients of the HQE are known up to order  $1/m_b^5$  at tree level [51–54]. The leading term  $z_0^{(i)}$  is the parton model, and is known completely to order  $\alpha_s$  and  $\alpha_s^2$  [55–57]. The terms of order  $\alpha_s^{n+1} \beta_0^n$  (where  $\beta_0$  is the first coefficient of the QCD  $\beta$  function,  $\beta_0 = (33 - 2n_f)/3$ ) have been included by the usual BLM procedure [50, 58, 59]. Corrections of order  $\alpha_s \mu_\pi^2/m_b^2$  have been computed in Ref. [60] and Ref. [61], while the  $\alpha_s \mu_G^2/m_b^2$  terms have been calculated in Ref. [62] and Ref. [63].

Starting at order  $1/m_b^3$  contributions with an infrared sensitivity to the charm mass,  $m_c$ , appear [51, 53, 64, 65]. At order  $1/m_b^3$  this “intrinsic charm” contribution manifests as a  $\log(m_c)$  in the coefficient of the Darwin term  $\rho_D^3$ . At higher orders, terms such as  $1/m_b^3 \times 1/m_c^2$  and  $\alpha_s(m_c) 1/m_b^3 \times 1/m_c$  appear, which are comparable in size to the contributions of order  $1/m_b^4$ .

The HQE parameters are given in terms of forward matrix elements of local operators; the parameters entering the expansion for orders up to  $1/m_b^3$  are  $(D_\perp^\mu = (g_{\mu\nu} - v_\mu v_\nu) D^\nu, \text{ where } v = p_B/M_B \text{ is the four-velocity of the } B \text{ meson})$

$$\begin{aligned} \bar{\Lambda} &= M_B - m_b, \\ \mu_\pi^2 &= -\langle B | \bar{b} (iD_\perp)^2 b | B \rangle, \\ \mu_G^2 &= \langle B | \bar{b} (iD_\perp^\mu) (iD_\perp^\nu) \sigma_{\mu\nu} b | B \rangle, \\ \rho_D^3 &= \langle B | \bar{b} (iD_{\perp\mu}) (ivD) (iD_\perp^\nu) b | B \rangle, \\ \rho_{LS}^3 &= \langle B | \bar{b} (iD_\perp^\mu) (ivD) (iD_\perp^\nu) \sigma_{\mu\nu} b | B \rangle. \end{aligned} \quad (75.23)$$

These parameters still depend on the heavy quark mass. Sometimes the infinite mass limits of these parameters  $\bar{\Lambda} \rightarrow \bar{\Lambda}_{\text{HQET}}$ ,  $\mu_\pi^2 \rightarrow -\lambda_1$ ,  $\mu_G^2 \rightarrow 3\lambda_2$ ,  $\rho_D^3 \rightarrow \rho_1$  and  $\rho_{LS}^3 \rightarrow 3\rho_2$ , are used instead. Beyond  $1/m^3$  the number of independent HQE parameters starts to proliferate [66]. In general, there are 13 parameters (at tree level) up to order  $1/m^4$  and 31 (at tree level) up to order  $1/m^5$ , not including  $\bar{\Lambda}$ . The HQE parameters of the orders  $1/m^4$

and  $1/m_b^5$  have been estimated in Ref. [54, 67], their impact on the  $|V_{cb}|$  determination has been studied in Ref. [68]. However, it has been pointed out recently that one may reduce the number of independent parameters in the HQE by exploiting reparametrization invariance, which is a symmetry of the HQE stemming from Lorentz invariance of QCD [69]. For a subset of observables this allows us to reduce the number of parameters to three up to order  $1/m^3$  ( $\rho_{LS}$  can be absorbed into  $\mu_G^2$  by a re-definition) and to 8 up to order  $1/m^4$  [70].

The rates and the spectra depend strongly on the definition  $m_b$  (or equivalently of  $\bar{\Lambda}$ ). This makes the discussion of renormalization issues mandatory, since the size of QCD corrections is strongly correlated with the definitions used for the quark masses. For example, it is well known (see eg. [71]) that using the pole mass definition for heavy quark masses leads to a perturbative series for the decay rates that does not converge very well.

This motivates the use of “short-distance” mass definitions, such as the kinetic scheme [26] or the 1S scheme [72–74]. Both schemes are well suited for the HQE, since they allow the choice of the renormalization scale  $\mu \leq m_b$ . Furthermore, they both can be extracted from other observables to a sufficient precision, such that a precise determination of  $|V_{cb}|$  becomes possible, despite of the strong quark-mass dependence of the total rate.

The 1S scheme eliminates the  $b$  quark pole mass by relating it to the perturbative expression for the mass of the 1S state of the  $\Upsilon$  system. The  $b$  quark mass in the 1S scheme is is half of the perturbatively calculated mass of the 1S state of the  $\Upsilon$  system. The best determination of the  $b$  quark mass in the 1S scheme is obtained from sum rules for  $e^+e^- \rightarrow b\bar{b}$  [75].

A second alternative is the so-called “kinetic mass”  $m_b^{\text{kin}}(\mu)$ , which is the mass entering the non-relativistic expression for the kinetic energy of a heavy quark, and which is defined using heavy-quark sum rules [26].

### 75.2.6 Determination of HQE Parameters and $|V_{cb}|$

Several experiments have measured moments in  $\bar{B} \rightarrow X_c \ell \bar{\nu}_\ell$  decays [76–84] as a function of the minimum lepton momentum. The measurements of the moments of the electron energy spectrum (0<sup>th</sup>-3<sup>rd</sup>) and of the squared hadronic mass spectrum (0<sup>th</sup>-2<sup>nd</sup>) have statistical uncertainties that are roughly equal to their systematic uncertainties. The 3<sup>rd</sup> order hadronic mass spectrum moments have also been measured by some experiments, with relatively large statistical uncertainty. The sets of moments measured within each experiment have strong correlations; their use in a global fit requires fully specified statistical and systematic covariance matrices. Measurements of photon energy moments (0<sup>th</sup>-2<sup>nd</sup>) in  $B \rightarrow X_s \gamma$  decays [85–89] as a function of the minimum accepted photon energy are also used in some fits; the dominant uncertainties on these measurements are statistical.

Global fits [84, 86, 90–95] to the full set of moments have been performed in the 1S and kinetic schemes. The semileptonic moments alone determine a linear combination of  $m_b$  and  $m_c$  very accurately but leave the orthogonal combination poorly determined (See e.g. [96]); additional input is required to allow a precise determination of  $m_b$ . This additional information can come from the radiative  $B \rightarrow X_s \gamma$  moments (with the caveat that the OPE for  $b \rightarrow s \gamma$  breaks down beyond leading order in  $\Lambda_{\text{QCD}}/m_b$ ), which provide complementary information on  $m_b$  and  $\mu_\pi^2$ , or from precise determinations of the charm quark mass [97, 98]. The values obtained in the kinetic scheme fits [5, 94, 95] with these two constraints are consistent. Based on the charm quark mass constraint  $m_c^{\overline{\text{MS}}}(3 \text{ GeV}) = 0.986 \pm 0.013 \text{ GeV}$  [99], a fit in the kinetic scheme [5] obtains

$$|V_{cb}| = (42.19 \pm 0.78) \times 10^{-3} \quad (75.24)$$

$$m_b^{\text{kin}} = 4.554 \pm 0.018 \text{ GeV} \quad (75.25)$$

$$\mu_\pi^2(\text{kin}) = 0.464 \pm 0.076 \text{ GeV}^2, \quad (75.26)$$

where the errors include experimental and theoretical uncertainties. Theoretical uncertainties from higher orders in  $1/m$  as well as in  $\alpha_s$  are estimated and included in performing the fits. Similar values for the parameters are obtained with a variety of assumptions about the theoretical uncertainties and their correlations.

The  $\chi^2/\text{dof}$  is well below unity in all fits, which could suggest that the theoretical uncertainties may be overestimated. However, while one could obtain a satisfactory fit with smaller uncertainties, this would result in unrealistically small uncertainties on the extracted HQE parameters, which are used as input to other calculations (e.g. the determination of  $|V_{ub}|$ ). The mass in the  $\overline{\text{MS}}$  scheme corresponding to Eq. (75.25) is  $m_b^{\overline{\text{MS}}} = 4.19 \pm 0.04 \text{ GeV}$ , where the uncertainty includes a contribution from the translation between mass schemes; this can be compared with a value obtained using relativistic sum rules [99],  $m_b^{\overline{\text{MS}}} = 4.163 \pm 0.016 \text{ GeV}$ , which provides a non-trivial cross-check.

A fit to the measured moments in the 1S scheme [5, 86, 93] gives

$$|V_{cb}| = (41.98 \pm 0.45) \times 10^{-3} \quad (75.27)$$

$$m_b^{1\text{S}} = 4.691 \pm 0.037 \text{ GeV} \quad (75.28)$$

$$\lambda_1(1\text{S}) = -0.362 \pm 0.067 \text{ GeV}^2, \quad (75.29)$$

This fit uses moments measurements from semileptonic and radiative decays and constrains the chromomagnetic operator using the  $B^*-B$  and  $D^*-D$  mass differences, but does not include the constraint on  $m_c$  nor the full NNLO corrections.

The fits in the two renormalization schemes give consistent results for  $|V_{cb}|$  and, after translation to a common renormalization scheme, for  $m_b$  and  $\mu_\pi^2$ . We take the fit in the kinetic scheme [95], which includes higher-order corrections and results in a more conservative uncertainty, as the inclusive determination of  $|V_{cb}|$ :

$$|V_{cb}| = (42.2 \pm 0.8) \times 10^{-3} \text{ (inclusive)}. \quad (75.30)$$

The precision of the global fit results can be further improved by calculating higher-order perturbative corrections to the coefficients of the HQE parameters. The inclusion of still-higher-order moments, if they can be measured with the required precision, may improve the sensitivity of the fits to higher-order terms in the HQE.

### 75.3 Determination of $|V_{ub}|$

*Summary:* Currently the best determinations of  $|V_{ub}|$  are from  $\bar{B} \rightarrow \pi \ell \bar{\nu}_\ell$  decays, where combined fits to theory and experimental data as a function of  $q^2$  provide a precision of about 4%; the uncertainties from experiment and theory are comparable in size. Determinations based on inclusive semileptonic decays are based on different observables and use different strategies to suppress the  $b \rightarrow c$  background. Most of the determinations are consistent and provide a precision of about 7%, with comparable contributions to the uncertainty from experiment and theory. The exception is the most recent Babar analysis, which observes significant model dependence.

The values obtained from inclusive and exclusive determinations are

$$|V_{ub}| = (4.25 \pm 0.12 \pm_{0.14}^{0.15} \pm 0.23) \times 10^{-3} \text{ (inclusive)}, \quad (75.31)$$

$$|V_{ub}| = (3.70 \pm 0.10 \pm 0.12) \times 10^{-3} \text{ (exclusive)}, \quad (75.32)$$

where the last uncertainty on the inclusive result was added by the authors of this review and is discussed below.

The exclusive and inclusive determinations are independent, and the dominant uncertainties are on multiplicative factors.

To combine these values, the inclusive and exclusive values are weighted by their relative errors and the uncertainties are treated as normally distributed. The resulting average has  $p(\chi^2) = 10\%$ , so we scale the error by  $\sqrt{\chi^2/1} = 1.6$  to find

$$|V_{ub}| = (3.82 \pm 0.24) \times 10^{-3} \text{ (average)}. \quad (75.33)$$

Given the somewhat poor consistency between the two determinations, this average should be treated with caution.

#### 75.3.1 $|V_{ub}|$ from inclusive decays

The theoretical description of inclusive  $\bar{B} \rightarrow X_u \ell \bar{\nu}_\ell$  decays is based on the Heavy Quark Expansion and leads to a predicted total decay rate with uncertainties below 5% [73, 100]. However,

the total decay rate is hard to measure due to the large background from CKM-favored  $\bar{B} \rightarrow X_c \ell \bar{\nu}_\ell$  transitions, and hence the theoretical methods differ from the  $\bar{B} \rightarrow X_c \ell \bar{\nu}_\ell$  case. For a calculation of the partial decay rate in regions of phase space where  $\bar{B} \rightarrow X_c \ell \bar{\nu}_\ell$  decays are suppressed one cannot use the HQE as for  $b \rightarrow c$ , rather the one needs to introduce non-perturbative distribution functions, the “shape functions” (SF) [101,102]. Their exact form is not known, but its moments can be related to the HQE parameters known e.g from the  $b \rightarrow c$  case.

The shape functions become important when the light-cone momentum component  $P_+ \equiv E_X - |P_X|$  is not large compared to  $\Lambda_{QCD}$ , as is the case near the endpoint of the  $\bar{B} \rightarrow X_u \ell \bar{\nu}_\ell$  lepton spectrum. Partial rates for  $\bar{B} \rightarrow X_u \ell \bar{\nu}_\ell$  are predicted and measured in a variety of kinematic regions that differ in their sensitivity to shape-function effects.

At leading order in  $1/m_b$  only a single shape function (SF) appears, which is universal for all heavy-to-light transitions [101, 102] and can be extracted in  $\bar{B} \rightarrow X_s \gamma$  decays. At subleading order in  $1/m_b$ , several shape functions appear [103], along with “resolved photon contributions” specific for  $\bar{B} \rightarrow X_s \gamma$  [104,105], and thus the prescriptions that relate directly the partial rates for  $\bar{B} \rightarrow X_s \gamma$  and  $\bar{B} \rightarrow X_u \ell \bar{\nu}_\ell$  decays [106–114] are limited to leading order in  $1/m_b$ .

Existing approaches use parametrizations of the leading SF that respect constraints on the normalization and on the first and second moments, which are given in terms of the HQE parameters  $\bar{\Lambda} = M_B - m_b$  and  $\mu_\pi^2$ , respectively. The relations between SF moments and the HQE parameters are known to second order in  $\alpha_s$  [115]; as a result, measurements of HQE parameters from global fits to  $\bar{B} \rightarrow X_c \ell \bar{\nu}_\ell$  and  $\bar{B} \rightarrow X_s \gamma$  moments can be used to constrain the SF moments, as well as to provide accurate values of  $m_b$  and other parameters for use in determining  $|V_{ub}|$ . Flexible parametrizations of the SF using orthogonal basis functions [116] or artificial neural networks [117] would allow global fits to inclusive  $B$  meson decay data that incorporate the known short-distance contributions and renormalization properties of the SF.

HFLAV performs fits on the basis of several approaches, with varying degrees of model dependence. We will consider here the approaches documented in Ref. [118] (BLNP), Ref. [119] (GGOU) and Ref. [120] (DGE).

The triple differential rate in the variables

$$P_\ell = M_B - 2E_\ell, \quad P_- = E_X + |\vec{P}_X|, \quad P_+ = E_X - |\vec{P}_X| \quad (75.34)$$

is

$$\frac{d^3\Gamma}{dP_+ dP_- dP_\ell} = \frac{G_F^2 |V_{ub}|^2}{16\pi^2} (M_B - P_+) \quad (75.35)$$

$$\left\{ (P_- - P_\ell)(M_B - P_- + P_\ell - P_+) \mathcal{F}_1 \right.$$

$$\left. + (M_B - P_-)(P_- - P_+) \mathcal{F}_2 + (P_- - P_\ell)(P_\ell - P_+) \mathcal{F}_3 \right\}.$$

The “structure functions”,  $\mathcal{F}_i$ , can be calculated using factorization theorems that have been proven to subleading order in the  $1/m_b$  expansion [121].

The BLNP [118] calculation uses these factorization theorems to write the  $\mathcal{F}_i$  terms as functions of perturbatively calculable hard coefficients  $H$  and jet functions  $J$ , which are convolved with the (soft) light-cone distribution functions  $S$ , which is the shape functions of the  $B$  meson. The calculation of  $\mathcal{O}(\alpha_s^2)$  contributions [122,123] is not yet complete and is not included in the  $|V_{ub}|$  determination given below.

The leading order term in the  $1/m_b$  expansion of the  $\mathcal{F}_i$  terms contains a single non-perturbative function and is calculated to subleading order in  $\alpha_s$ , while at subleading order in the  $1/m_b$  expansion there are several independent non-perturbative functions that have been calculated only at tree level in the  $\alpha_s$  expansion.

A distinct approach (GGOU) [119] uses a hard, Wilsonian cut-off that matches the definition of the kinetic mass. The non-perturbative input is similar to what is used in BLNP, but the shape functions are defined differently. In particular, they are defined at finite  $m_b$  and depend on the light-cone component  $k_+$  of the  $b$  quark momentum and on the momentum transfer  $q^2$  to the

leptons. These functions include subleading effects to all orders; as a result they are non-universal, with one shape function corresponding to each structure function in Eq. (75.35). Their  $k_+$  moments can be computed in the OPE and related to observables and to the shape functions defined in Ref. [118].

Going to subleading order in  $\alpha_s$  requires the definition of a renormalization scheme for the HQE parameters and for the SF. The relation between the moments of the SF and the forward matrix elements of local operators appearing the HQE is plagued by ultraviolet problems and requires additional renormalization. A scheme for improving this behavior was suggested in Ref. [118] and Ref. [124], which introduce a definition of the quark mass (the so-called shape-function scheme) based on the first moment of the measured  $\bar{B} \rightarrow X_s \gamma$  photon energy spectrum. Likewise, the HQE parameters can be defined from measured moments of spectra, corresponding to moments of the SF.

There are various ideas to model the SF, but this requires additional assumptions. One approach (DGE) is the so-called “dressed gluon exponentiation” [120], where the perturbative result is continued into the infrared regime using the renormalon structure obtained in the large  $\beta_0$  limit, where  $\beta_0$  has been defined following Eq. (75.21). Other approaches make even stronger assumptions, such as in Ref. [125], which assumes an analytic behavior for the strong coupling in the infrared to perform an extrapolation of perturbation theory.

In order to reduce sensitivity to SF uncertainties, measurements that use a combination of cuts on the leptonic momentum transfer  $q^2$  and the hadronic invariant mass  $m_X$ , as suggested in Ref. [126,127], have been made. In general, efforts to extend the experimental measurements of  $\bar{B} \rightarrow X_u \ell \bar{\nu}_\ell$  into charm-dominated regions (in order to reduce SF uncertainties) lead to an increased experimental sensitivity to the modeling of  $\bar{B} \rightarrow X_u \ell \bar{\nu}_\ell$  decays, resulting in measured partial rates with an undesirable level of model dependence. The measurements quoted below have used a variety of functional forms to parametrize the leading SF; a specific error budget for one determination is quoted in the next section. In no case is the parametrization uncertainty estimated to be more than a 2% on  $|V_{ub}|$ .

Weak Annihilation [119, 128, 129] (WA) can in principle contribute significantly in the high- $q^2$  region of  $\bar{B} \rightarrow X_u \ell \bar{\nu}_\ell$  decays. Estimates based on semileptonic  $D_s$  decays [65,126,127,129] lead to a  $\sim 2\%$  uncertainty on the total  $\bar{B} \rightarrow X_u \ell \bar{\nu}_\ell$  rate from the  $\mathcal{Y}(4S)$ . The  $q^2$  spectrum of the WA contribution is not well known, but from the OPE it is expected to contribute predominantly at high  $q^2$ . More recent theoretical investigations [65,130,131] and a direct search [132] indicate that WA is a small effect, but may become a significant source of uncertainty for  $|V_{ub}|$  measurements that accept only a small fraction of the full  $\bar{B} \rightarrow X_u \ell \bar{\nu}_\ell$  phase space.

### 75.3.2 Measurements

We summarize the measurements used in the determination of  $|V_{ub}|$  below. Given the improved precision and more rigorous theoretical interpretation of more recent measurements, determinations [133–136] done with LEP data are not considered in this review.

Inclusive electron momentum measurements [137–139] reconstruct a single charged electron to determine a partial decay rate for  $\bar{B} \rightarrow X_u \ell \bar{\nu}_\ell$  near the kinematic endpoint. This results in a selection efficiency of order 50% and only modest sensitivity to the modeling of detector response. The inclusive electron momentum spectrum from  $B\bar{B}$  events, after subtraction of the  $e^+e^- \rightarrow q\bar{q}$  continuum background, is fitted to a model  $\bar{B} \rightarrow X_u \ell \bar{\nu}_\ell$  spectrum and several components ( $D\ell\bar{\nu}_\ell$ ,  $D^*\ell\bar{\nu}_\ell$ , ...) of the  $\bar{B} \rightarrow X_c \ell \bar{\nu}_\ell$  background; the dominant uncertainties are related to this subtraction and modelling. The decay rate can be cleanly extracted for  $E_e > 2.3$  GeV, but this is deep in the SF region, where theoretical uncertainties are large. More recent measurements have increased the accessed phase phase. The resulting  $|V_{ub}|$  values for various  $E_e$  cuts are given in Table 75.1.

The most recent measurement [140] from BABAR is based on the inclusive electron spectrum and determines the partial branching fraction and  $|V_{ub}|$  for  $E_e > 0.8$  GeV. The analysis shows that the partial branching fraction measurements can have sig-

nal model dependence when the kinematic acceptance includes regions dominated by  $\bar{B} \rightarrow X_c \ell \bar{\nu}_\ell$  background. The model dependence enters primarily through the partial branching fractions, and arises because the signal yield fit has sensitivity to  $\bar{B} \rightarrow X_u \ell \bar{\nu}_\ell$  decays only in regions with good signal to noise.

An untagged “neutrino reconstruction” measurement [141] from BABAR uses a combination [142] of a high-energy electron with a measurement of the missing momentum vector. This allows  $S/B \sim 0.7$  for  $E_e > 2.0$  GeV and a  $\approx 5\%$  selection efficiency, but at the cost of a smaller accepted phase space for  $\bar{B} \rightarrow X_u \ell \bar{\nu}_\ell$  decays and uncertainties associated with the determination of the missing momentum. The corresponding values for  $|V_{ub}|$  are given in Table 75.1.

The large samples accumulated at the  $B$  factories allow studies in which one  $B$  meson is fully reconstructed and the recoiling  $B$  decays semileptonically [143–146]. The experiments can fully reconstruct a “tag”  $B$  candidate in about 0.5% (0.3%) of  $B^+ B^-$  ( $B^0 \bar{B}^0$ ) events. An electron or muon with center-of-mass momentum above 1.0 GeV is required amongst the charged tracks not assigned to the tag  $B$  and the remaining particles are assigned to the  $X_u$  system. The full set of kinematic properties ( $E_\ell$ ,  $m_X$ ,  $q^2$ , etc.) are available for studying the semileptonically decaying  $B$ , making possible selections that accept up to 90% of the full  $\bar{B} \rightarrow X_u \ell \bar{\nu}_\ell$  rate; however, the sensitivity to  $\bar{B} \rightarrow X_u \ell \bar{\nu}_\ell$  decays is still driven by the regions where  $\bar{B} \rightarrow X_c \ell \bar{\nu}_\ell$  decays are suppressed. Despite requirements (e.g. on the square of the missing mass) aimed at rejecting events with additional missing particles, undetected or mis-measured particles from  $\bar{B} \rightarrow X_c \ell \bar{\nu}_\ell$  decay (e.g.,  $K_L^0$  and additional neutrinos) remain an important source of uncertainty.

BABAR [143] and Belle [144, 145] have measured partial rates with cuts on  $m_X$ ,  $m_X$  and  $q^2$ ,  $P_+$  and  $E_\ell$  using the recoil method. In each case the experimental systematics have significant contributions from the modeling of  $\bar{B} \rightarrow X_u \ell \bar{\nu}_\ell$  and  $\bar{B} \rightarrow X_c \ell \bar{\nu}_\ell$  decays and from the detector response to charged particles, photons and neutral hadrons. The corresponding  $|V_{ub}|$  values are given in Table 75.1.

### 75.3.3 $|V_{ub}|$ from inclusive partial rates

The measured partial rates and theoretical calculations from BLNP, GGOU and DGE described previously are used to determine  $|V_{ub}|$  from all measured partial  $\bar{B} \rightarrow X_u \ell \bar{\nu}_\ell$  rates [5]; selected values are given in Table 75.1. The correlations amongst the multiple BABAR recoil-based measurements [143] are fully accounted for in the average. The statistical correlations amongst the other measurements used in the average are small (due to small overlaps among signal events and large differences in  $S/B$  ratios) and have been ignored. Correlated systematic and theoretical errors are taken into account, both within an experiment and between experiments. As an illustration of the relative sizes of the uncertainties entering  $|V_{ub}|$  we give the error breakdown for the GGOU average: statistical—1.6%; experimental—1.6%;  $\bar{B} \rightarrow X_c \ell \bar{\nu}_\ell$  modeling—0.9%;  $\bar{B} \rightarrow X_u \ell \bar{\nu}_\ell$  modeling—1.5%; HQE parameters ( $m_b$ )—1.9%; higher-order corrections—1.5%;  $q^2$  modeling—1.3%; Weak Annihilation— $^{+0.0}_{-1.1}\%$ ; SF parametrization—0.1%.

The averages quoted here are based on the following  $m_b$  values:  $m_b^{SF} = 4.582 \pm 0.023 \pm 0.018$  GeV for BLNP,  $m_b^{\text{kin}} = 4.554 \pm 0.018$  GeV for GGOU, and  $m_b^{\overline{MS}} = 4.188 \pm 0.043$  GeV for DGE. The  $m_b^{\text{kin}}$  value is determined in a global fit to moments in the kinetic scheme; this value is translated into  $m_b^{SF}$  and  $m_b^{\overline{MS}}$  at fixed order in  $\alpha_s$ . The second uncertainty quoted on  $m_b$  arises from the scheme translation.

Hadronization uncertainties also impact the  $|V_{ub}|$  determination. The theoretical expressions are valid at the parton level and do not incorporate any resonant structure (e.g.  $\bar{B} \rightarrow \pi \ell \bar{\nu}_\ell$ ); this must be added to the simulated  $\bar{B} \rightarrow X_u \ell \bar{\nu}_\ell$  event samples, since the detailed final state multiplicity and structure impacts the estimates of experimental acceptance and efficiency. The experiments have adopted procedures to input resonant structure while preserving the appropriate behavior in the kinematic variables ( $q^2$ ,  $E_\ell$ ,  $m_X$ ) averaged over the sample, but these prescriptions are *ad hoc* and ultimately require *in situ* calibration. The resulting uncertainties have been estimated to be  $\sim 1$ -2% on  $|V_{ub}|$ .

All calculations yield compatible  $|V_{ub}|$  values and similar error estimates. The arithmetic mean of the values and errors is  $|V_{ub}| = (4.25 \pm 0.12_{\text{exp}} \pm 0.15_{\text{theo}}) \times 10^{-3}$ , although there is a spread of approximately 10% in the evaluations with the three theoretical models. For reasons discussed below, we assign an additional uncertainty due to model dependence that is not reflected in the HFLAV averages. As highlighted in the BABAR analysis [140], model dependence entering measurement procedures can be sizeable, and is not consistently treated across analyses. Many of the analyses shown in Table 75.1 were based on partial branching fraction measurements determined in a single model (i.e. the one used by that analysis when simulating  $\bar{B} \rightarrow X_u \ell \bar{\nu}_\ell$  decays), although in some cases simulated events were weighted to match the expected spectra in other models and the differences introduced as systematic uncertainties, e.g. Ref. [145]. The  $|V_{ub}|$  value quoted by HFLAV for each model are, typically, derived from this unique partial branching fraction combined with another model-specific partial rate calculation. This translation from a single partial branching fraction into  $|V_{ub}|$  values in different models suffers, in principle, from the difficulties made explicit in the recent BABAR measurement. The model dependence in the partial branching fraction is sensitive to how the model predictions compare in the restricted region with good signal-to-noise, not by how they compare when integrated over the full kinematic range used in the fit. This effect needs to be accounted for by the experiments; the published results are insufficient to determine it. To account for the range in results using the different theoretical models, we take half of the spread of the averages as an additional systematic uncertainty, denoted  $\Delta\text{BF}$ . With this addition, the inclusive  $|V_{ub}|$  average is

$$|V_{ub}| = (4.25 \pm 0.12_{\text{exp}} \pm 0.15_{\text{theo}} \pm 0.23_{\Delta\text{BF}}) \times 10^{-3} \quad (\text{inclusive}), \quad (75.36)$$

### 75.3.4 $|V_{ub}|$ from exclusive decays

Exclusive charmless semileptonic decays offer a complementary means of determining  $|V_{ub}|$ . For the experiments, the specification of the final state provides better background rejection, but the branching fraction to a specific final state is typically only a few percent of that for inclusive decays. For theory, the calculation of the form factors for  $\bar{B} \rightarrow X_u \ell \bar{\nu}_\ell$  decays is challenging, but brings in a different set of uncertainties from those encountered in inclusive decays. In this review we focus on  $\bar{B} \rightarrow \pi \ell \bar{\nu}_\ell$ , as it is the most promising decay mode for both experiment and theory. Measurements of other exclusive  $\bar{B} \rightarrow X_u \ell \bar{\nu}_\ell$  decays can be found in Refs. [147–160].

### 75.3.5 $\bar{B} \rightarrow \pi \ell \bar{\nu}_\ell$ form factor calculations

The relevant form factors for the decay  $\bar{B} \rightarrow \pi \ell \bar{\nu}_\ell$  are usually defined as

$$\langle \pi(p_\pi) | V^\mu | B(p_B) \rangle = f_+(q^2) \left[ p_B^\mu + p_\pi^\mu - \frac{m_B^2 - m_\pi^2}{q^2} q^\mu \right] + f_0(q^2) \frac{m_B^2 - m_\pi^2}{q^2} q^\mu \quad (75.37)$$

in terms of which the rate becomes (in the limit  $m_\ell \rightarrow 0$ )

$$\frac{d\Gamma}{dq^2} = \frac{G_F^2 |V_{ub}|^2}{24\pi^3} |p_\pi|^3 |f_+(q^2)|^2, \quad (75.38)$$

where  $p_\pi$  is the pion momentum in the  $B$  meson rest frame.

Currently available non-perturbative methods for the calculation of the form factors include lattice QCD (LQCD) and light-cone sum rules (LCSR). The two methods are complementary in phase space, since the lattice calculation is restricted to the kinematical range of high momentum transfer,  $q^2$ , to the leptons, while light-cone sum rules provide information near  $q^2 = 0$ . Interpolations between these two regions can be constrained by unitarity and analyticity.

Lattice simulations for  $B \rightarrow \pi \ell \bar{\nu}$  and  $B_s \rightarrow K \ell \bar{\nu}$  transitions, where quark loop effects are fully incorporated, have been performed by the Fermilab/MILC [161, 162], HPQCD [163, 164] and RBC/UKQCD [165] collaborations. The calculations differ in the

**Table 75.1:**  $|V_{ub}|$  (in units of  $10^{-5}$ ) from inclusive  $\bar{B} \rightarrow X_u \ell \bar{\nu}_\ell$  measurements. The first uncertainty on  $|V_{ub}|$  is experimental, while the second includes both theoretical and HQE parameter uncertainties. The values are generally listed in order of increasing kinematic acceptance,  $f_u$  (0.19 to 0.90), except for the BABAR  $E_e > 0.8$  GeV measurement; those below the horizontal bar are based on recoil methods.

Ref.	cut (GeV)	BLNP	GGOU	DGE
CLEO [137]	$E_e > 2.1$	$422 \pm 49$	$423 \pm 49$	$386 \pm 45$
BABAR [141]	$E_e - q^2$	$471 \pm 32$	not available	$435 \pm 29$
BABAR [139]	$E_e > 2.0$	$452 \pm 26$	$452 \pm 26$	$430 \pm 24$
Belle [138]	$E_e > 1.9$	$493 \pm 46$	$495 \pm 46$	$482 \pm 45$
BABAR [140]	$E_e > 0.8$	$441 \pm 12$	$396 \pm 10$	$385 \pm 11$
<hr/>				
BABAR [143]	$q^2 > 8$ $m_X < 1.7$	$432 \pm 23$	$433 \pm 23$	$424 \pm 22$
BABAR [143]	$P_+ < 0.66$	$409 \pm 25$	$425 \pm 26$	$417 \pm 25$
BABAR [143]	$m_X < 1.7$	$403 \pm 22$	$410 \pm 23$	$422 \pm 23$
BABAR [143]	$E_\ell > 1$	$433 \pm 24$	$444 \pm 24$	$445 \pm 24$
Belle [145]	$E_\ell > 1$	$450 \pm 27$	$462 \pm 28$	$462 \pm 28$
<hr/>				
HFLAV [5]	Combination	$444^{+13+21}_{-14-22}$	$432 \pm 12$	$399 \pm 10$

way the  $b$  quark is simulated. While HPQCD is using nonrelativistic QCD, Fermilab/MILC and RBC/UKQCD are using relativistic  $b$  quarks with the Fermilab and Columbia heavy-quark formulations. The results agree within the quoted errors. The form factor  $f_+$  evaluated at  $q^2 = 20 \text{ GeV}^2$  has an estimated uncertainty of 3.4%, where the leading contribution is due to the chiral-continuum extrapolation fit, which includes statistical and heavy-quark discretization errors. However, the lattice simulations are restricted to the region of large  $q^2$ , i.e. the region  $q_{\text{max}}^2 > q^2 \gtrsim 15 \text{ GeV}^2$ .

The extrapolation to small values of  $q^2$  is performed using guidance from analyticity and unitarity. Making use of the heavy-quark limit, stringent constraints on the shape of the form factor can be derived [166], and the conformal mapping of the kinematical variables onto the complex unit disc yields a rapidly converging series in the variable

$$z = \frac{\sqrt{t_+ - t_-} - \sqrt{t_+ - q^2}}{\sqrt{t_+ - t_-} + \sqrt{t_+ - q^2}}, \quad (75.39)$$

where  $t_\pm = (M_B \pm m_\pi)^2$ . The use of lattice data in combination with experimental measurements of the differential decay rate provides a stringent constraint on the shape of the form factor in addition to precise determination of  $|V_{ub}|$  [167].

Another established non-perturbative approach to obtain the form factors is through Light-Cone QCD Sum Rules (LCSR), which, however, are not at the same footing as LQCD. LCSR provide an estimate for the product  $f_B f_+(q^2)$ , valid in the region  $0 < q^2 \lesssim 12 \text{ GeV}^2$ . The determination of  $f_+(q^2)$  itself requires knowledge of the decay constant  $f_B$ , which is usually obtained by replacing  $f_B$  by its two-point QCD (SVZ) sum rule [168] in terms of perturbative and condensate contributions. The advantage of this procedure is the approximate cancellation of various theoretical uncertainties in the ratio  $(f_B f_+)/f_B$ .

The LCSR for  $f_B f_+$  is based on the light-cone OPE of the relevant vacuum-to-pion correlation function, calculated in full QCD at finite  $b$ -quark mass. The resulting expressions comprise a triple expansion: in the twist  $t$  of the operators near the light-cone, in  $\alpha_s$ , and in the deviation of the pion distribution amplitudes from their asymptotic form, which is fixed from conformal symmetry. The state-of-the-art calculations include the leading twists two, three and four with full one-loop  $\alpha_s$  corrections [169, 170] and partial two-loop corrections [171]. Higher-twist contributions have been investigated in Ref. [172], which turn out to be small. Nevertheless, estimates based on LCSR are always affected by an systematic uncertainty, which is hard to quantify.

A detailed statistical analysis including the various correlations has been performed in Ref. [173], also including unitarity bounds on the form factor. The results obtained are fully compatible with the lattice QCD calculations of the form factor. For a de-

termination of  $V_{ub}$  one may use the partial rate expressed by the integral

$$\begin{aligned} \Delta\zeta(0, q_{\text{max}}^2) &= \frac{G_F^2}{24\pi^3} \int_0^{q_{\text{max}}^2} dq^2 p_\pi^3 |f_+(q^2)|^2 \\ &= \frac{1}{|V_{ub}|^2 \tau_{B_0}} \int_0^{q_{\text{max}}^2} dq^2 \frac{d\mathcal{B}(B \rightarrow \pi \ell \nu)}{dq^2}, \quad (75.40) \end{aligned}$$

for which the light-cone sum rule gives [173]

$$\Delta\zeta(0, 12 \text{ GeV}^2) = 5.25^{+0.68}_{-0.54} \text{ ps}^{-1}. \quad (75.41)$$

The uncertainty in this integral is about ten percent, which translates to a theoretical uncertainty of about five percent for the determination of  $V_{ub}$  with this method.

### 75.3.6 $\bar{B} \rightarrow \pi \ell \bar{\nu}_\ell$ measurements

The  $\bar{B} \rightarrow \pi \ell \bar{\nu}_\ell$  measurements fall into two broad classes: untagged, in which case the reconstruction of the missing momentum of the event serves as an estimator for the unseen neutrino, and tagged, in which the second  $B$  meson in the event is fully reconstructed in either a hadronic or semileptonic decay mode. The tagged measurements have better  $q^2$  resolution, high and uniform acceptance and  $S/B$  as high as 10, but lower statistical power. The untagged measurements have somewhat higher background ( $S/B < 1$ ) and make slightly more restrictive kinematic cuts, but still provide statistical power precision on the  $q^2$  dependence of the form factor.

CLEO has analyzed  $\bar{B} \rightarrow \pi \ell \bar{\nu}_\ell$  and  $\bar{B} \rightarrow \rho \ell \bar{\nu}_\ell$  using an untagged analysis [154–156]. Similar analyses have been done at BABAR [157–160] and Belle [174]. The leading systematic uncertainties in the untagged  $\bar{B} \rightarrow \pi \ell \bar{\nu}_\ell$  analyses are associated with modeling the missing momentum reconstruction, with background from  $\bar{B} \rightarrow X_u \ell \bar{\nu}_\ell$  decays and  $e^+e^- \rightarrow q\bar{q}$  continuum events, and with varying the form factor used to model  $\bar{B} \rightarrow \rho \ell \bar{\nu}_\ell$  decays.

Analyses [149, 175] based on reconstructing a  $B$  in the  $\bar{D}^{(*)} \ell^+ \nu_\ell$  decay mode and looking for a  $\bar{B} \rightarrow \pi \ell \bar{\nu}_\ell$  or  $\bar{B} \rightarrow \rho \ell \bar{\nu}_\ell$  decay amongst the remaining particles in the event make use of the fact that the  $B$  and  $\bar{B}$  are back-to-back in the  $\Upsilon(4S)$  frame to construct a discriminant variable that provides a signal-to-noise ratio above unity for all  $q^2$  bins. A related technique was discussed in Ref. [176]. BABAR [175] and Belle [147] have also used their samples of  $B$  mesons reconstructed in hadronic decay modes to measure exclusive charmless semileptonic decays, resulting in very clean but smaller samples. The dominant systematic uncertainties in the tagged analyses arise from tag calibration.



$|V_{ub}|$  can be obtained from the average  $\bar{B} \rightarrow \pi \ell \bar{\nu}_\ell$  branching fraction and the measured  $q^2$  spectrum. Fits to the  $q^2$  spectrum using a theoretically motivated parametrization (e.g. "BCL" from Ref. [44]) remove most of the model dependence from theoretical uncertainties in the shape of the spectrum. The most sensitive method for determining  $|V_{ub}|$  from  $\bar{B} \rightarrow \pi \ell \bar{\nu}_\ell$  decays employs a simultaneous fit [5, 161, 166, 167, 177, 178] to measured experimental partial rates and lattice points versus  $q^2$  (or  $z$ ) to determine  $|V_{ub}|$  and the first few coefficients of the expansion of the form factor in  $z$ . We quote the result from Ref. [5], which uses as experimental input an average of the measurements in Refs. [147, 157, 160, 174] and an average [179] of the LQCD input from Ref. [161] and Ref. [165]. The probability of the  $q^2$  measurement average is 6%. The average for the total  $B^0 \rightarrow \pi^- \ell^+ \nu_\ell$  branching fraction is obtained by summing up the partial branching fractions:

$$\mathcal{B}(B^0 \rightarrow \pi^- \ell^+ \nu_\ell) = (1.50 \pm 0.02_{\text{stat}} \pm 0.06_{\text{syst}}) \times 10^{-4} \quad (75.42)$$

The corresponding value of  $|V_{ub}|$  with this approach is found to be

$$|V_{ub}| = (3.70 \pm 0.10 \pm 0.12) \times 10^{-3} \quad (\text{exclusive}), \quad (75.43)$$

where the first uncertainty is experimental and the second is from theory. Adding an additional constraint using input [171] from LCSR gives [5]  $|V_{ub}| = (3.67 \pm 0.09 \pm 0.12) \times 10^{-3}$  (exclusive, LQCD+LCSR). Consistent results for  $|V_{ub}|$  were found in a fit reported in Ref. [25].

#### 75.4 Semileptonic $b$ -baryon decays and determination of $|V_{ub}|/|V_{cb}|$

*Summary:* A significant sample of  $\Lambda_b^0$  baryons is available at the LHCb experiment, and methods have been developed to study their semileptonic decays. Both  $\Lambda_b^0 \rightarrow p \mu \bar{\nu}$  and  $\Lambda_b^0 \rightarrow \Lambda_c^+ \mu \bar{\nu}$  decays have been measured at LHCb, and the ratio of branching fractions to these two decay modes is used to determine the ratio  $|V_{ub}|/|V_{cb}|$ . Averaging the LHCb determination with those obtained from inclusive and exclusive  $B$  meson decays, we find

$$|V_{ub}|/|V_{cb}| = 0.092 \pm 0.008 \quad (\text{average}) \quad (75.44)$$

where the average has  $p(\chi^2) = 0.9\%$  and the uncertainty has been scaled by a factor  $\sqrt{\chi^2/2} = 2.2$ . In light of the poor consistency of the three determinations considered, the average should be treated with caution.

##### 75.4.1 $\Lambda_b^0 \rightarrow \Lambda_c^+ \mu \bar{\nu}$ and $\Lambda_b^0 \rightarrow p \mu \bar{\nu}$

The  $\Lambda_b^0 \rightarrow \Lambda_c^+$  and  $\Lambda_b^0 \rightarrow p$  semileptonic transitions are described in terms of six form factors each. The three form factors corresponding to the vector current can be defined as [180]

$$\begin{aligned} \langle F(p', s') | \bar{q} \gamma_\mu b | \Lambda_b^0(p, s) \rangle &= \bar{u}_F(p', s') \left\{ f_0(q^2) (M_{\Lambda_b^0} - m_F) \frac{q_\mu}{q^2} \right. \\ &+ f_+(q^2) \frac{M_{\Lambda_b^0} + m_F}{s_+} \left( p_\mu + p'_\mu - \frac{q_\mu}{q^2} (M_{\Lambda_b^0}^2 - m_F^2) \right) \\ &\left. + f_\perp(q^2) \left( \gamma_\mu - \frac{2m_F}{s_+} p_\mu - \frac{2M_{\Lambda_b^0}}{s_+} p'_\mu \right) \right\} u_{\Lambda_b^0}(p, s), \end{aligned} \quad (75.45)$$

where  $F = p$  or  $\Lambda_c^+$  and where we define  $s_\pm = (M_{\Lambda_b^0} \pm m_F)^2 - q^2$ . At vanishing momentum transfer,  $q^2 \rightarrow 0$ , the kinematic constraint  $f_0(0) = f_+(0)$  holds. The form factors are defined in such a way that they correspond to time-like (scalar), longitudinal and transverse polarization with respect to the momentum-transfer  $q^\mu$  for  $f_0$ ,  $f_+$  and  $f_\perp$ , respectively. Furthermore we have chosen the normalization in such a way that for  $f_0, f_+, f_\perp \rightarrow 1$  one recovers the expression for point-like baryons.

Likewise, the expression for the axial-vector current is

$$\begin{aligned} \langle F(p', s') | \bar{q} \gamma_\mu \gamma_5 b | \Lambda_b^0(p, s) \rangle &= \\ &- \bar{u}_F(p', s') \gamma_5 \left\{ g_0(q^2) (M_{\Lambda_b^0} + m_F) \frac{q_\mu}{q^2} \right. \\ &+ g_+(q^2) \frac{M_{\Lambda_b^0} - m_F}{s_-} \left( p_\mu + p'_\mu - \frac{q_\mu}{q^2} (M_{\Lambda_b^0}^2 - m_F^2) \right) \\ &\left. + g_\perp(q^2) \left( \gamma_\mu + \frac{2m_F}{s_-} p_\mu - \frac{2M_{\Lambda_b^0}}{s_-} p'_\mu \right) \right\} u_{\Lambda_b^0}(p, s), \end{aligned} \quad (75.46)$$

with the kinematic constraint  $g_0(0) = g_+(0)$  at  $q^2 \rightarrow 0$ .

The form factors have been discussed in the heavy quark limit; assuming both  $b$  and  $c$  as heavy, all the form factors  $f_i$  and  $g_i$  for the case  $\Lambda_b^0 \rightarrow \Lambda_c^+ \mu \nu$  turn out to be identical [180]

$$f_0 = f_+ = f_\perp = g_0 = g_+ = g_\perp = \xi_B \quad (75.47)$$

and equal to the Isgur Wise function  $\xi_B$  for baryons. In the limit of a light baryon in the final state, the number of independent form factors is still reduced to two through the heavy quark symmetries of the  $\Lambda_b^0$ . It should be noted that the  $\Lambda_b^0 \rightarrow (p/\Lambda_c^+) \mu \nu$  decay rates peak at high  $q^2$ , which facilitates both lattice QCD calculations and experimental measurements.

The form factors for  $\Lambda_b^0$  decays have been studied with lattice QCD [181]. Based on these results the differential rates for both  $\Lambda_b^0 \rightarrow \Lambda_c^+ \mu \bar{\nu}$  as well as for  $\Lambda_b^0 \rightarrow p \mu \bar{\nu}$  can be predicted in the full phase space. In particular, for the experimentally interesting region they find the ratio of decay rates to be [181]

$$\frac{\mathcal{B}(\Lambda_b^0 \rightarrow p \mu \bar{\nu})_{q^2 > 15 \text{ GeV}^2}}{\mathcal{B}(\Lambda_b^0 \rightarrow \Lambda_c^+ \mu \bar{\nu})_{q^2 > 7 \text{ GeV}^2}} = (1.471 \pm 0.095 \pm 0.109) \left| \frac{V_{ub}}{V_{cb}} \right|^2 \quad (75.48)$$

where the first uncertainty is statistical and the second, systematic.

##### 75.4.2 Measurements at LHCb

The LHCb experiment has measured the branching fractions of the semileptonic decays  $\Lambda_b^0 \rightarrow \Lambda_c^+ \mu \bar{\nu}$  and  $\Lambda_b^0 \rightarrow p \mu \bar{\nu}$ , from which they determine  $|V_{ub}|/|V_{cb}|$ . This is the first such determination at a hadron collider, the first to use a  $b$  baryon decay, and the first observation of  $\Lambda_b^0 \rightarrow p \mu \bar{\nu}$ . Excellent vertex resolution allows the calculation of the transverse momentum  $p_\perp$  of the  $p\mu$  pair relative to the  $\Lambda_b^0$  flight direction. The corrected mass,  $m_{\text{corr}} = \sqrt{p_\perp^2 + m_{p\mu}^2} + p_\perp$ , peaks at the  $\Lambda_b^0$  mass for signal decays and provides good discrimination against background combinations. The topologically similar decay  $\Lambda_b^0 \rightarrow \Lambda_c^+ \mu \bar{\nu}$  is also measured, which eliminates the need to know the production cross-section or absolute efficiencies. Using vertex and  $\Lambda_b^0$  mass constraints,  $q^2$  can be determined up to a two-fold ambiguity. The LHCb analysis requires both solutions to be in the high  $q^2$  region to minimise contamination from the low  $q^2$  region. Their result [182], rescaled [5] to take into account the recent branching fraction measurement [183]  $\mathcal{B}(\Lambda_c^+ \rightarrow p K^- \pi^+) = (6.28 \pm 0.32)\%$ , is

$$\frac{\mathcal{B}(\Lambda_b^0 \rightarrow p \mu \bar{\nu})_{q^2 > 15 \text{ GeV}^2}}{\mathcal{B}(\Lambda_b^0 \rightarrow \Lambda_c^+ \mu \bar{\nu})_{q^2 > 7 \text{ GeV}^2}} = (0.92 \pm 0.04 \pm 0.07) \times 10^{-2} \quad (75.49)$$

The largest systematic uncertainty is from the measured  $\mathcal{B}(\Lambda_c^+ \rightarrow p K^- \pi^+)$ ; uncertainties due to trigger, tracking and the  $\Lambda_c^+$  selection efficiency are each about 3%.

A recent LHCb analysis [184] measures the normalized  $q^2$  spectrum and finds good agreement with the shape calculated with lattice QCD [181].

##### 75.4.3 The ratio $|V_{ub}|/|V_{cb}|$

The ratio of matrix elements,  $|V_{ub}|/|V_{cb}|$ , is often required when testing the compatibility of a set of measurements with theoretical predictions. It can be determined from the ratio of branching

fractions measured by the LHCb experiment, quoted in the previous section. It can also be calculated based on the  $|V_{ub}|$  and  $|V_{cb}|$  values quoted earlier in this review.

As previously noted, the decay rate for  $\Lambda_b^0 \rightarrow p\mu\bar{\nu}$  peaks at high  $q^2$  where the calculation of the associated form factors using lattice QCD is under good control. Using the measured ratio from Eq. (75.49) along with the calculations of Ref. [181] results in [5]

$$|V_{ub}|/|V_{cb}| = 0.079 \pm 0.004 \pm 0.004 \quad (\text{LHCb}). \quad (75.50)$$

where the first uncertainty is experimental and the second is from the LQCD calculation.

Given the similarities in the theoretical frameworks used for charmed and charmless decays, we choose to quote the ratio  $|V_{ub}|/|V_{cb}|$  separately for inclusive and exclusive  $B$  decays, as discussed earlier:

$$|V_{ub}|/|V_{cb}| = 0.101 \pm 0.007 \quad (\text{inclusive}), \quad (75.51)$$

$$|V_{ub}|/|V_{cb}| = 0.094 \pm 0.005 \quad (\text{exclusive}). \quad (75.52)$$

The respective determinations of  $|V_{ub}|$  and  $|V_{cb}|$  are taken to be uncorrelated in the ratio, although there could be some small cancellations of the uncertainties in both the experimental and theoretical input. We average the mesonic decay values, along with the baryonic result in Eq. (75.50), weighting by relative errors. The average has  $p(\chi^2) = 4\%$ , so we scale the uncertainty by a factor  $\sqrt{\chi^2/2} = 1.8$  to find

$$|V_{ub}|/|V_{cb}| = 0.091 \pm 0.006 \quad (\text{average}). \quad (75.53)$$

## 75.5 Semitaucic decays

*Summary:* Semileptonic decays to third-generation leptons provide sensitivity to non-Standard Model amplitudes, such as from a charged Higgs boson [185–188] and from leptoquarks [189–195]. The ratios of branching fractions of semileptonic decays involving tau leptons to those involving  $\ell = e/\mu$ ,  $R(D^{(*)}) \equiv \mathcal{B}(\bar{B} \rightarrow D^{(*)}\tau\bar{\nu}_\tau)/\mathcal{B}(\bar{B} \rightarrow D^{(*)}\ell\bar{\nu}_\ell)$ , are predicted with good precision in the Standard Model [42, 43, 47, 196, 197]. For  $R(D)$  and  $R(D^*)$  we use the values obtained in [198]

$$\begin{aligned} R(D)^{\text{SM}} &= 0.297 \pm 0.003, \\ R(D^*)^{\text{SM}} &= 0.252 \pm 0.003. \end{aligned} \quad (75.54)$$

Measurements [199–207] of these ratios yield higher values; averaging  $B$ -tagged measurements of  $R(D)$  and  $R(D^*)$  at the  $\Upsilon(4S)$  and the LHCb measurements of  $R(D^*)$  yields [208]

$$\begin{aligned} R(D)^{\text{meas}} &= 0.340 \pm 0.027 \pm 0.013, \\ R(D^*)^{\text{meas}} &= 0.295 \pm 0.011 \pm 0.008, \end{aligned} \quad (75.55)$$

with a linear correlation of  $-0.38$ . These values exceed Standard Model predictions by  $1.4\sigma$  and  $2.5\sigma$ , respectively. A variety of new physics models have been proposed, see eg. [185–195] to explain this excess. Most models proposed to explain the semitaucic decay excesses tend to, but not always have very little impact on semileptonic decays involving muons or electrons, so they do not significantly modify the  $|V_{ub}|$  or  $|V_{cb}|$  determinations discussed previously in this review. Lepton flavour universality in the ratio of electron and muon modes has been confirmed in a direct ratio measurement,  $\mathcal{B}(\bar{B} \rightarrow D^{(*)}e\bar{\nu}_e)/\mathcal{B}(\bar{B} \rightarrow D^{(*)}e\bar{\nu}_\mu) = 1.01 \pm 0.03$ , from Belle [40]. The uncertainty is dominated by lepton identification uncertainties that do not cancel in the ratio.

### 75.5.1 Sensitivity of $\bar{B} \rightarrow D^{(*)}\tau\bar{\nu}_\tau$ to additional amplitudes

In addition to the helicity amplitudes present for decays to  $e\bar{\nu}_e$  and  $\mu\bar{\nu}_\mu$ , decays proceeding through  $\tau\bar{\nu}_\tau$  include a scalar amplitude  $H_s$ . The differential decay rate is given by [209]

$$\begin{aligned} \frac{d\Gamma}{dq^2} &= \frac{G_F^2 |V_{cb}|^2 |\mathbf{p}_{D^{(*)}}^*|^2}{96\pi^3 m_B^2} \left( 1 - \frac{m_\tau^2}{q^2} \right)^2 \\ &\left[ (|H_+|^2 + |H_-|^2 + |H_0|^2) \left( 1 + \frac{m_\tau^2}{2q^2} \right) + \frac{3m_\tau^2}{2q^2} |H_s|^2 \right], \end{aligned} \quad (75.56)$$

where  $|\mathbf{p}_{D^{(*)}}^*|$  is the 3-momentum of the  $D^{(*)}$  in the  $\bar{B}$  rest frame and the helicity amplitudes  $H$  depend on the four-momentum transfer  $q^2$ . All four helicity amplitudes contribute to  $\bar{B} \rightarrow D^*\tau\bar{\nu}_\tau$ , while only  $H_0$  and  $H_s$  contribute to  $\bar{B} \rightarrow D\tau\bar{\nu}_\tau$ ; as a result, new physics contributions can produce larger effects in the latter mode. Semi-leptonic  $B$  decays into a  $\tau$  lepton provide a stringent test of the two-Higgs doublet model of type II (2HD-MII), i.e. where the two Higgs doublets couple separately to up- and down-type quarks. The distinct feature of the 2HDMII is that the contributions of the charged Higgs scalars scale as  $m_\tau^2/m_{H^\pm}^2$ , since the couplings to the charged Higgs particles are proportional to the mass of the lepton. As a consequence, one may expect visible effects in decays into a  $\tau$ , but only small effects for decays into  $e$  and  $\mu$ . The present data rule out the 2HDMII, see below.

### 75.5.2 Measurement of $R(D^{(*)})$

$\bar{B} \rightarrow D^{(*)}\tau\bar{\nu}_\tau$  decays have been studied at the  $\Upsilon(4S)$  resonance and in  $pp$  collisions. At the  $\Upsilon(4S)$ , the majority of experimental measurements are based on signatures that consist of a  $D$  or  $D^*$  meson, an electron or muon (denoted here by  $\ell$ ) from the decay  $\tau \rightarrow \ell\nu_\tau\bar{\nu}_\ell$ , a fully-reconstructed decay of the second  $B$  meson in the event, and multiple missing neutrinos. One analysis reconstructs the  $\tau$  in a hadronic mode. The analyses that use hadronic  $B$  tags separate signal decays from  $\bar{B} \rightarrow D^{(*)}\ell\bar{\nu}_\ell$  decays using the lepton momentum and the measured missing mass squared; decays with only a single missing neutrino peak sharply at zero in this variable, while the signal is spread out to positive values. When a semileptonic  $B$  tag is used, the discrimination between signal and  $\bar{B} \rightarrow D^{(*)}\ell\bar{\nu}_\ell$  decays comes from the calorimeter energy that is unassociated with any particle used in the reconstruction of the  $B$  meson candidates, the measured missing mass squared and the cosine of the angle between the  $D^*\ell$  system and its parent  $B$  meson, which is calculated under the assumption that only one particle (a neutrino) is missing. In both these approaches, background from  $\bar{B} \rightarrow D^{**}\ell\bar{\nu}_\ell$  decays with one or more unreconstructed particles is challenging to separate from signal, as is background from  $\bar{B} \rightarrow D^{(*)}H_c X$  (where  $H_c$  is a hadron containing a  $\bar{c}$  quark) decays. The leading sources of systematic uncertainty are due to the limited size of simulation samples used in constructing the PDFs, the composition of the  $D^{**}$  states, efficiency corrections, and cross-feed (swapping soft particles between the signal and tag  $B$ ).

The most recent measurement from Belle [205] uses semileptonic  $B$  tags and leptonic  $\tau$  decays to simultaneously measure  $R(D^*)$  and  $R(D)$ . The measurement provides the single most precise determination of these ratios, combining results from charged and neutral  $B$  decays, and is compatible with the standard model expectation within  $1\sigma$ .

In addition to the ratio measurements, the Belle experiment has recently performed polarization measurements of the  $\tau$  [204] and  $D^*$  [210] respectively. The  $\tau$  polarization measurement uses hadronic  $B$  tags and  $\tau^-$  decays to  $\pi^- \nu_\tau$  or  $\rho^- \nu_\tau$ . The main discriminant variables are the measured missing mass squared and the unassociated calorimeter energy. This measurement provides the first determination of the  $\tau$  polarization in the  $\bar{B} \rightarrow D^*\tau\bar{\nu}_\tau$  decay,  $\mathcal{P}(D^*) = -0.38 \pm 0.51_{-0.16}^{+0.21}$ , compatible with the standard model expectation [20],  $-0.476_{-0.034}^{+0.037}$ .

The main uncertainties on the  $R(D^*)$  measurement come from the composition of the hadronic  $B$  background and from modeling of semileptonic  $B$  decays and mis-reconstructed  $D^*$  mesons. The  $D^*$  polarization measurement uses an inclusive tag approach based on Refs. [211, 212], and reconstructs the  $\tau$  decays in  $\ell\nu_\tau\bar{\nu}_\ell$  and  $\pi^+\bar{\nu}_\tau$  channels. The main discriminant variables are  $X_{\text{miss}}$ , a quantity that approximates missing mass but does not depend on tag  $B$  reconstruction, the visible energy of the event, and the beam-energy constrained mass,  $M_{\text{bc}}$ , of the inclusively reconstructed tag side  $B$ . This measurement provides the first determination of the  $D^*$  longitudinal polarization fraction in the  $\bar{B} \rightarrow D^*\tau\bar{\nu}_\tau$  decay,  $\mathcal{F}_L(D^*) = -0.38 \pm 0.60_{-0.04}^{+0.08}$ , compatible with the standard model expectation [213] within  $1.7\sigma$ .

The LHCb experiment has studied the decay  $\bar{B} \rightarrow D^{*+}\tau\bar{\nu}_\tau$  with  $D^{*+} \rightarrow D^0\pi^+$ ,  $D^0 \rightarrow K^-\pi^+$  and  $\tau \rightarrow \mu\nu_\tau\bar{\nu}_\mu$  in  $pp$  collisions. Their analysis [206] takes advantage of the measurable

flight lengths of  $b$  and  $c$  hadrons and  $\tau$  leptons. A multivariate discriminant is used to select decays where no additional charged particles are consistent with coming from the signal decay vertices. The separation between the primary and  $B$  decay vertices is used to calculate the momentum of the  $B$  decay products transverse to the  $B$  flight direction. The longitudinal component of the  $B$  momentum can be estimated based on the visible decay products; this allows a determination of the  $B$  rest frame, with modest resolution, and enables the calculation of the same discrimination variables available at the  $e^+e^- B$  factories. The (rest frame) muon energy, missing mass-squared and  $q^2$  are used in a 3- $d$  fit. The most recent LHCb result [214] on  $R(D^*)$  uses three-prong  $\tau$  decays that take advantage of their excellent vertex resolution to isolate the  $\tau$  decay from hadronic background. A 3- $d$  fit is performed to determine the signal yield, based on the  $\tau\nu_\tau$  pair  $q^2$ , the  $\tau$  lifetime, as well as a boosted decision tree classifier based on isolation, invariant mass and flight distance information. The leading sources of systematic uncertainty are due to the size of the simulation sample used in constructing the fit templates, uncertainties in modelling the background from hadronic  $\bar{B} \rightarrow D^{(*)}H_c X$  decays, as well as reconstruction and trigger effects. The result is normalized to  $B^0 \rightarrow D^{*-}\pi^+\pi^-\pi^+$  and found to be  $1\sigma$  from the standard model expectation (using the expectation value quoted here). An analogous measurement of  $B_c \rightarrow J/\psi\tau\bar{\nu}_\tau$  was performed by the LHCb measurement [215], in leptonic  $\tau$  decays. The result,  $R(J/\psi) = 0.71 \pm 0.17 \pm 0.18$ , while relatively high is compatible within  $2\sigma$  of the standard model. Systematic uncertainties are dominated by form factors, as  $B_c$  decays are relatively unexplored.

Measurements from BABAR [199–201], Belle [202–205] and LHCb [206, 214] result in values for  $R(D)$  and  $R(D^*)$  that exceed Standard Model predictions. Table 75.2 lists these values and their average. The simultaneous measurements of  $R(D)$  and  $R(D^*)$  have linear correlation coefficients of  $-0.27$  (BABAR [200, 201]),  $-0.49$  (Belle hadronic tag [202]) and  $-0.51$  (Belle semileptonic tag [205]); the  $R(D)$  and  $R(D^*)$  averages have a correlation of  $-0.38$ . Two early untagged Belle measurements [211, 212] are subject to larger systematic uncertainties, with a breakdown of the respective contributions that is inconsistent with the more recent determinations, hence they cannot be reliably combined in the average. All three experiments assume the Standard Model kinematic distributions for  $\bar{B} \rightarrow D^{(*)}\tau\bar{\nu}_\tau$  in their determinations of the branching fraction ratios.

**Table 75.2:** Measurements of  $R(D)$  and  $R(D^*)$ , their correlations,  $\rho$ , and the combined averages [208].

	$R(D) \times 10^2$	$R(D^*) \times 10^2$	$\rho$
BABAR [200, 201]	$B^0, B^+$ $44.0 \pm 5.8 \pm 4.2$	$33.2 \pm 2.4 \pm 1.8$	$-0.27$
Belle [202]	$B^0, B^+$ $37.5 \pm 6.4 \pm 2.6$	$29.3 \pm 3.8 \pm 1.5$	$-0.49$
Belle [204, 216]	$B^0, B^+$	$27.0 \pm 3.5 \pm \begin{smallmatrix} 2.8 \\ 2.5 \end{smallmatrix}$	
Belle [205]	$B^0, B^+$ $30.7 \pm 3.7 \pm 1.6$	$28.3 \pm 1.8 \pm 1.4$	$-0.51$
LHCb [206]	$B^0$	$33.6 \pm 2.7 \pm 3.0$	
LHCb [214]	$B^0$	$28.0 \pm 1.8 \pm 2.9$	
Average	$B^0, B^+$ $34.0 \pm 2.7 \pm 1.3$	$29.5 \pm 1.1 \pm 0.8$	$-0.38$

The measurement combination in the  $R(D) - R(D^*)$  plane is shown in Fig. 75.1, compared with an arithmetic average of predictions from Refs. [47, 217, 218]. The figure is taken from Ref. [5]. The tension between the SM prediction and the measurements is at the level of  $1.4\sigma$  ( $R(D)$ ) and  $2.5\sigma$  ( $R(D^*)$ ); if one considers these deviations together the significance rises to  $3.1\sigma$ . This motivates speculation on possible new physics contributions, although this discrepancy has reduced with respect to previous editions of the RPP due to the results reported in Refs. [205, 214, 216]. There is some tension in the combination coming from the BABAR measurement, the only measurement to claim a deviation from the SM of more than  $3\sigma$ , although the  $p$ -value of the full combination is an acceptable 27%.

The current discussion of  $R(D)$  and  $R(D^*)$  may be embedded in the theoretical analysis of the other anomalies that have been

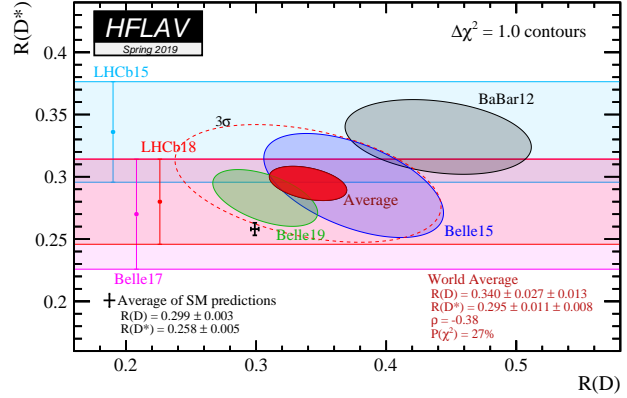


Figure 75.1: Measurements of  $R(D)$  and  $R(D^*)$  and their two-dimensional average compared with the average predictions for  $R(D)$  and  $R(D^*)$ . Contours correspond to  $\Delta\chi^2 = 1$  i.e., 68% CL for the bands and 39% CL for the ellipses. The prediction and the experimental average deviate from each other by  $3.08\sigma$ . The dashed ellipse corresponds to a  $3\sigma$  contour (99.73% CL).

observed in semileptonic FCNC ( $b \rightarrow s\ell\ell$ ) transitions. More sophisticated approaches fit the data to a general effective Hamiltonian. Matching this effective Hamiltonian to simplified models, the current situation of the anomalies seems to be compatible with scenarios with an additional  $Z'$  or a leptoquark scenario, see eg. [189–195].

## 75.6 Conclusion

The study of semileptonic  $B$  meson decays continues to be an active area for both theory and experiment. The application of HQE calculations to inclusive decays is mature, and fits to moments of  $\bar{B} \rightarrow X_c\ell\bar{\nu}_\ell$  decays provide precise values for  $|V_{cb}|$  and, in conjunction with input on  $m_c$  or from  $B \rightarrow X_s\gamma$  decays, provide precise and consistent values for  $m_b$ .

The determination of  $|V_{ub}|$  from inclusive  $\bar{B} \rightarrow X_u\ell\bar{\nu}_\ell$  decays is based on multiple calculational approaches and independent measurements over a variety of kinematic regions, all of which provide consistent results. Further progress in this area is possible, but will require better theoretical control over higher-order terms, improved experimental knowledge of the  $\bar{B} \rightarrow X_c\ell\bar{\nu}_\ell$  background and improvements to the modeling of the  $\bar{B} \rightarrow X_u\ell\bar{\nu}_\ell$  signal distributions.

In both  $b \rightarrow u$  and  $b \rightarrow c$  exclusive channels there has been significant recent progress in lattice-QCD calculations, resulting in improved precision on both  $|V_{ub}|$  and  $|V_{cb}|$ . These calculations now provide information on the form factors well away from the high  $q^2$  region, allowing better use of experimental data. For  $|V_{cb}|$  recent measurements have provided binned data for fitting form factors with reduced model dependence.

The values from the inclusive and exclusive determinations of  $|V_{cb}|$  and  $|V_{ub}|$  are only marginally consistent. This is a long-standing puzzle, and the measurement of  $|V_{ub}|/|V_{cb}|$  from LHCb based on  $A_b^0$  decays does not simplify the picture.

Both  $|V_{cb}|$  and  $|V_{ub}|$  are indispensable inputs into unitarity triangle fits. In particular, knowing  $|V_{ub}|$  with good precision allows a test of CKM unitarity in a most direct way, by comparing the length of the  $|V_{ub}|$  side of the unitarity triangle with the measurement of  $\sin(2\beta)$ . This comparison of a “tree” process ( $b \rightarrow u$ ) with a “loop-induced” process ( $B^0 - \bar{B}^0$  mixing) provides sensitivity to possible contributions from new physics.

The observation of semileptonic decays into  $\tau$  leptons has opened a new window to the physics of the third generation. The measurements indicate a tension between the data and the Standard Model prediction, which could be a hint for new physics, manifesting itself as a violation of lepton universality beyond the standard-model couplings to the Higgs. It should be noted that none of the most recent measurements alone claim evidence for a deviation from the Standard Model. Combining the data of the semitaonic decays with the anomalies observed in the FCNC

$b \rightarrow s\ell\ell$  transitions allows an interpretation in terms of additional  $Z'$  or in terms of additional leptoquarks, but the current data does not allow us to draw a definite conclusion.

The authors would like to acknowledge helpful input from C. Bozzi, M. Rotondo, and C. Schwanda, P. Gambino, Z. Ligeti, F. Bernlochner, S. Stone, S. Meinel, G. Wormser, and D. Robinson.

### References

- [1] C. Patrignani *et al.* (Particle Data Group), *Chin. Phys.* **C40**, 10, 100001 (2016).
- [2] See “Heavy-Quark and Soft-Collinear Effective Theory” by C.W. Bauer and M. Neubert in this *Review*.
- [3] See “Lattice Quantum Chromodynamics” by S. Hashimoto, J. Laiho, and S.R. Sharpe in this *Review*.
- [4] See “Production and Decay of  $b$ -Flavored Hadrons” by P. Eerola, M. Kreps and Y. Kwon in this *Review*.
- [5] Y. S. Amhis *et al.* (HFLAV) (2019), [arXiv:1909.12524].
- [6] N. Isgur and M. B. Wise, *Phys. Lett.* **B232**, 113 (1989); N. Isgur and M. B. Wise, *Phys. Lett.* **B237**, 527 (1990).
- [7] M. A. Shifman and M. B. Voloshin, *Sov. J. Nucl. Phys.* **47**, 511 (1988), [*Yad. Fiz.*47,801(1988)].
- [8] M. E. Luke, *Phys. Lett.* **B252**, 447 (1990).
- [9] A. V. Manohar and M. B. Wise, *Camb. Monogr. Part. Phys. Nucl. Phys. Cosmol.* **10**, 1 (2000).
- [10] H. Georgi, *Phys. Lett.* **B240**, 447 (1990).
- [11] A. F. Falk *et al.*, *Nucl. Phys.* **B343**, 1 (1990).
- [12] E. Eichten and B. R. Hill, *Phys. Lett.* **B234**, 511 (1990).
- [13] A. Sirlin, *Nucl. Phys.* **B196**, 83 (1982).
- [14] J. A. Bailey *et al.* (Fermilab Lattice, MILC), *Phys. Rev.* **D89**, 11, 114504 (2014), [arXiv:1403.0635].
- [15] C. G. Boyd, B. Grinstein and R. F. Lebed, *Phys. Rev. Lett.* **74**, 4603 (1995), [hep-ph/9412324].
- [16] C. G. Boyd, B. Grinstein and R. F. Lebed, *Phys. Rev.* **D56**, 6895 (1997), [hep-ph/9705252].
- [17] B. Grinstein and A. Kobach, *Phys. Lett.* **B771**, 359 (2017), [arXiv:1703.08170].
- [18] I. Caprini, L. Lellouch and M. Neubert, *Nucl. Phys.* **B530**, 153 (1998), [hep-ph/9712417].
- [19] D. Bigi, P. Gambino and S. Schacht, *Phys. Lett.* **B769**, 441 (2017), [arXiv:1703.06124].
- [20] P. Gambino, M. Jung and S. Schacht, *Phys. Lett.* **B795**, 386 (2019), [arXiv:1905.08209].
- [21] F. U. Bernlochner, Z. Ligeti and D. J. Robinson, *Phys. Rev.* **D100**, 1, 013005 (2019), [arXiv:1902.09553].
- [22] F. U. Bernlochner *et al.*, *Phys. Rev.* **D96**, 9, 091503 (2017), [arXiv:1708.07134].
- [23] A. Czarnecki and K. Melnikov, *Nucl. Phys.* **B505**, 65 (1997), [hep-ph/9703277].
- [24] J. Harrison, C. Davies and M. Wingate (HPQCD), *Phys. Rev.* **D97**, 5, 054502 (2018), [arXiv:1711.11013].
- [25] S. Aoki *et al.* (Flavour Lattice Averaging Group) (2019), [arXiv:1902.08191].
- [26] I. I. Y. Bigi *et al.*, *Phys. Rev.* **D52**, 196 (1995), [hep-ph/9405410].
- [27] A. Kapustin *et al.*, *Phys. Lett.* **B375**, 327 (1996), [hep-ph/9602262].
- [28] P. Gambino, T. Mannel and N. Uraltsev, *Phys. Rev.* **D81**, 113002 (2010), [arXiv:1004.2859].
- [29] P. Gambino, T. Mannel and N. Uraltsev, *JHEP* **10**, 169 (2012), [arXiv:1206.2296].
- [30] D. Buskulic *et al.* (ALEPH), *Phys. Lett.* **B395**, 373 (1997).
- [31] G. Abbiendi *et al.* (OPAL), *Phys. Lett.* **B482**, 15 (2000), [hep-ex/0003013].
- [32] P. Abreu *et al.* (DELPHI), *Phys. Lett.* **B510**, 55 (2001), [hep-ex/0104026].
- [33] J. Abdallah *et al.* (DELPHI), *Eur. Phys. J.* **C33**, 213 (2004), [hep-ex/0401023].
- [34] N. E. Adam *et al.* (CLEO), *Phys. Rev.* **D67**, 032001 (2003), [hep-ex/0210040].
- [35] B. Aubert *et al.* (BaBar), *Phys. Rev.* **D77**, 032002 (2008), [arXiv:0705.4008].
- [36] B. Aubert *et al.* (BaBar), *Phys. Rev. Lett.* **100**, 231803 (2008), [arXiv:0712.3493].
- [37] B. Aubert *et al.* (BaBar), *Phys. Rev.* **D79**, 012002 (2009), [arXiv:0809.0828].
- [38] W. Dungen *et al.* (Belle), *Phys. Rev.* **D82**, 112007 (2010), [arXiv:1010.5620].
- [39] A. Abdesselam *et al.* (Belle) (2017), [arXiv:1702.01521].
- [40] A. Abdesselam *et al.* (Belle) (2018), [arXiv:1809.03290].
- [41] J. P. Lees *et al.* (BaBar), *Phys. Rev. Lett.* **123**, 091801 (2019), [arXiv:1903.10002].
- [42] J. A. Bailey *et al.* (MILC), *Phys. Rev.* **D92**, 3, 034506 (2015), [arXiv:1503.07237].
- [43] H. Na *et al.* (HPQCD), *Phys. Rev.* **D92**, 5, 054510 (2015), [Erratum: *Phys. Rev.*D93,no.11,119906(2016)], [arXiv:1505.03925].
- [44] C. Bourrely, I. Caprini and L. Lellouch, *Phys. Rev.* **D79**, 013008 (2009), [Erratum: *Phys. Rev.*D82,099902(2010)], [arXiv:0807.2722].
- [45] B. Aubert *et al.* (BaBar), *Phys. Rev. Lett.* **104**, 011802 (2010), [arXiv:0904.4063].
- [46] R. Glattauer *et al.* (Belle), *Phys. Rev.* **D93**, 3, 032006 (2016), [arXiv:1510.03657].
- [47] D. Bigi and P. Gambino, *Phys. Rev.* **D94**, 9, 094008 (2016), [arXiv:1606.08030].
- [48] A. V. Manohar and M. B. Wise, *Phys. Rev.* **D49**, 1310 (1994), [hep-ph/9308246].
- [49] I. I. Y. Bigi *et al.*, *Phys. Rev. Lett.* **71**, 496 (1993), [201(1993)], [hep-ph/9304225]; I. I. Y. Bigi *et al.*, *Phys. Lett.* **B323**, 408 (1994), [hep-ph/9311339].
- [50] D. Benson *et al.*, *Nucl. Phys.* **B665**, 367 (2003), [hep-ph/0302262].
- [51] M. Gremm and A. Kapustin, *Phys. Rev.* **D55**, 6924 (1997), [hep-ph/9603448].
- [52] B. M. Dassing, T. Mannel and S. Turczyk, *JHEP* **03**, 087 (2007), [hep-ph/0611168].
- [53] I. I. Bigi, N. Uraltsev and R. Zwicky, *Eur. Phys. J.* **C50**, 539 (2007), [hep-ph/0511158].
- [54] T. Mannel, S. Turczyk and N. Uraltsev, *JHEP* **11**, 109 (2010), [arXiv:1009.4622].
- [55] A. Pak and A. Czarnecki, *Phys. Rev.* **D78**, 114015 (2008), [arXiv:0808.3509].
- [56] S. Biswas and K. Melnikov, *JHEP* **02**, 089 (2010), [arXiv:0911.4142].
- [57] P. Gambino, *JHEP* **09**, 055 (2011), [arXiv:1107.3100].
- [58] P. Gambino and N. Uraltsev, *Eur. Phys. J.* **C34**, 181 (2004), [hep-ph/0401063].
- [59] V. Aquila *et al.*, *Nucl. Phys.* **B719**, 77 (2005), [hep-ph/0503083].
- [60] T. Becher, H. Boos and E. Lunghi, *JHEP* **12**, 062 (2007), [arXiv:0708.0855].
- [61] A. Alberti *et al.*, *Nucl. Phys.* **B870**, 16 (2013), [arXiv:1212.5082].
- [62] A. Alberti, P. Gambino and S. Nandi, *JHEP* **01**, 147 (2014), [arXiv:1311.7381].
- [63] T. Mannel, A. A. Pivovarov and D. Rosenthal, *Phys. Rev.* **D92**, 5, 054025 (2015), [arXiv:1506.08167].

- [64] C. Breidenbach *et al.*, Phys. Rev. **D78**, 014022 (2008), [arXiv:0805.0971].
- [65] I. Bigi *et al.*, JHEP **04**, 073 (2010), [arXiv:0911.3322].
- [66] A. Kobach and S. Pal, Phys. Lett. **B772**, 225 (2017), [arXiv:1704.00008].
- [67] J. Heinonen and T. Mannel, Nucl. Phys. **B889**, 46 (2014), [arXiv:1407.4384].
- [68] P. Gambino, K. J. Healey and S. Turczyk, Phys. Lett. **B763**, 60 (2016), [arXiv:1606.06174].
- [69] T. Mannel and K. K. Vos, JHEP **06**, 115 (2018), [arXiv:1802.09409].
- [70] M. Fael, T. Mannel and K. Keri Vos, JHEP **02**, 177 (2019), [arXiv:1812.07472].
- [71] I. I. Y. Bigi *et al.*, Phys. Rev. **D50**, 2234 (1994), [hep-ph/9402360].
- [72] A. H. Hoang, Z. Ligeti and A. V. Manohar, Phys. Rev. Lett. **82**, 277 (1999), [hep-ph/9809423].
- [73] A. H. Hoang, Z. Ligeti and A. V. Manohar, Phys. Rev. **D59**, 074017 (1999), [hep-ph/9811239].
- [74] A. H. Hoang and T. Teubner, Phys. Rev. **D60**, 114027 (1999), [hep-ph/9904468].
- [75] A. H. Hoang, Phys. Rev. **D61**, 034005 (2000), [hep-ph/9905550].
- [76] S. E. Csorna *et al.* (CLEO), Phys. Rev. **D70**, 032002 (2004), [hep-ex/0403052].
- [77] A. H. Mahmood *et al.* (CLEO), Phys. Rev. **D70**, 032003 (2004), [hep-ex/0403053].
- [78] B. Aubert *et al.* (BaBar), Phys. Rev. **D69**, 111103 (2004), [hep-ex/0403031].
- [79] B. Aubert *et al.* (BaBar), Phys. Rev. **D69**, 111104 (2004), [hep-ex/0403030].
- [80] C. Schwanda *et al.* (Belle), Phys. Rev. **D75**, 032005 (2007), [hep-ex/0611044].
- [81] P. Urquijo *et al.* (Belle), Phys. Rev. **D75**, 032001 (2007), [hep-ex/0610012].
- [82] J. Abdallah *et al.* (DELPHI), Eur. Phys. J. **C45**, 35 (2006), [hep-ex/0510024].
- [83] D. Acosta *et al.* (CDF), Phys. Rev. **D71**, 051103 (2005), [hep-ex/0502003].
- [84] B. Aubert *et al.* (BaBar), Phys. Rev. **D81**, 032003 (2010), [arXiv:0908.0415].
- [85] A. Limosani *et al.* (Belle), Phys. Rev. Lett. **103**, 241801 (2009), [arXiv:0907.1384].
- [86] C. Schwanda *et al.* (Belle), Phys. Rev. **D78**, 032016 (2008), [arXiv:0803.2158].
- [87] B. Aubert *et al.* (BaBar), Phys. Rev. **D72**, 052004 (2005), [hep-ex/0508004].
- [88] B. Aubert *et al.* (BaBar), Phys. Rev. Lett. **97**, 171803 (2006), [hep-ex/0607071].
- [89] S. Chen *et al.* (CLEO), Phys. Rev. Lett. **87**, 251807 (2001), [hep-ex/0108032].
- [90] M. Battaglia *et al.*, eConf **C0304052**, WG102 (2003), [Phys. Lett. **B556**, 41 (2003)], [hep-ph/0210319].
- [91] B. Aubert *et al.* (BaBar), Phys. Rev. Lett. **93**, 011803 (2004), [hep-ex/0404017].
- [92] O. Buchmüller and H. Flächer, hep-ph/0507253 updated in Ref. [219].
- [93] C. W. Bauer *et al.*, Phys. Rev. **D70**, 094017 (2004), updated in Ref. [219], [hep-ph/0408002].
- [94] P. Gambino and C. Schwanda, Phys. Rev. **D89**, 1, 014022 (2014), [arXiv:1307.4551].
- [95] A. Alberti *et al.*, Phys. Rev. Lett. **114**, 6, 061802 (2015), [arXiv:1411.6560].
- [96] M. Antonelli *et al.*, Phys. Rept. **494**, 197 (2010), see section 5.4.2, [arXiv:0907.5386].
- [97] B. Dehnadi *et al.*, JHEP **09**, 103 (2013), [arXiv:1102.2264].
- [98] I. Allison *et al.* (HPQCD), Phys. Rev. **D78**, 054513 (2008), [arXiv:0805.2999].
- [99] K. G. Chetyrkin *et al.*, Phys. Rev. **D80**, 074010 (2009), [arXiv:0907.2110].
- [100] N. Uraltsev, Int. J. Mod. Phys. **A14**, 4641 (1999), [hep-ph/9905520].
- [101] M. Neubert, Phys. Rev. **D49**, 4623 (1994), [hep-ph/9312311]; M. Neubert, Phys. Rev. **D49**, 3392 (1994), [hep-ph/9311325].
- [102] I. I. Y. Bigi *et al.*, Int. J. Mod. Phys. **A9**, 2467 (1994), [hep-ph/9312359].
- [103] C. W. Bauer, M. E. Luke and T. Mannel, Phys. Rev. **D68**, 094001 (2003), [hep-ph/0102089].
- [104] M. Benzke *et al.*, Phys. Rev. Lett. **106**, 141801 (2011), [arXiv:1012.3167].
- [105] A. Gunawardana and G. Paz (2019), [arXiv:1908.02812].
- [106] M. Neubert, Phys. Lett. **B513**, 88 (2001), [hep-ph/0104280].
- [107] M. Neubert, Phys. Lett. **B543**, 269 (2002), [hep-ph/0207002].
- [108] A. K. Leibovich, I. Low and I. Z. Rothstein, Phys. Rev. **D61**, 053006 (2000), [hep-ph/9909404].
- [109] A. K. Leibovich, I. Low and I. Z. Rothstein, Phys. Rev. **D62**, 014010 (2000), [hep-ph/0001028].
- [110] A. K. Leibovich, I. Low and I. Z. Rothstein, Phys. Lett. **B486**, 86 (2000), [hep-ph/0005124].
- [111] A. K. Leibovich, I. Low and I. Z. Rothstein, Phys. Lett. **B513**, 83 (2001), [hep-ph/0105066].
- [112] A. H. Hoang, Z. Ligeti and M. Luke, Phys. Rev. **D71**, 093007 (2005), [hep-ph/0502134].
- [113] B. O. Lange, M. Neubert and G. Paz, JHEP **10**, 084 (2005), [hep-ph/0508178].
- [114] B. O. Lange, JHEP **01**, 104 (2006), [hep-ph/0511098].
- [115] M. Neubert, Phys. Lett. **B612**, 13 (2005), [hep-ph/0412241].
- [116] Z. Ligeti, I. W. Stewart and F. J. Tackmann, Phys. Rev. **D78**, 114014 (2008), [arXiv:0807.1926].
- [117] P. Gambino, K. J. Healey and C. Mondino, Phys. Rev. **D94**, 1, 014031 (2016), [arXiv:1604.07598].
- [118] B. O. Lange, M. Neubert and G. Paz, Phys. Rev. **D72**, 073006 (2005), [hep-ph/0504071].
- [119] P. Gambino *et al.*, JHEP **10**, 058 (2007), [arXiv:0707.2493].
- [120] J. R. Andersen and E. Gardi, JHEP **01**, 097 (2006), [hep-ph/0509360].
- [121] M. Beneke *et al.*, JHEP **06**, 071 (2005), [hep-ph/0411395].
- [122] C. Greub, M. Neubert and B. D. Pecjak, Eur. Phys. J. **C65**, 501 (2010), [arXiv:0909.1609].
- [123] M. Brucherseifer, F. Caola and K. Melnikov, Phys. Lett. **B721**, 107 (2013), [arXiv:1302.0444].
- [124] T. Mannel and S. Recksiegel, Phys. Rev. **D60**, 114040 (1999), [hep-ph/9904475].
- [125] U. Aglietti *et al.*, Eur. Phys. J. **C59**, 831 (2009), [arXiv:0711.0860].
- [126] C. W. Bauer, Z. Ligeti and M. E. Luke, Phys. Rev. **D64**, 113004 (2001), [hep-ph/0107074].
- [127] C. W. Bauer, Z. Ligeti and M. E. Luke, Phys. Lett. **B479**, 395 (2000), [hep-ph/0002161].
- [128] I. I. Y. Bigi and N. G. Uraltsev, Nucl. Phys. **B423**, 33 (1994), [hep-ph/9310285].
- [129] M. B. Voloshin, Phys. Lett. **B515**, 74 (2001), [hep-ph/0106040].

- [130] Z. Ligeti, M. Luke and A. V. Manohar, Phys. Rev. **D82**, 033003 (2010), [arXiv:1003.1351].
- [131] P. Gambino and J. F. Kamenik, Nucl. Phys. **B840**, 424 (2010), [arXiv:1004.0114].
- [132] J. L. Rosner *et al.* (CLEO), Phys. Rev. Lett. **96**, 121801 (2006), [hep-ex/0601027].
- [133] R. Barate *et al.* (ALEPH), Eur. Phys. J. **C6**, 555 (1999).
- [134] M. Acciarri *et al.* (L3), Phys. Lett. **B436**, 174 (1998).
- [135] G. Abbiendi *et al.* (OPAL), Eur. Phys. J. **C21**, 399 (2001), [hep-ex/0107016].
- [136] P. Abreu *et al.* (DELPHI), Phys. Lett. **B478**, 14 (2000), [hep-ex/0105054].
- [137] A. Bornheim *et al.* (CLEO), Phys. Rev. Lett. **88**, 231803 (2002), [hep-ex/0202019].
- [138] A. Limosani *et al.* (Belle), Phys. Lett. **B621**, 28 (2005), [hep-ex/0504046].
- [139] B. Aubert *et al.* (BaBar), Phys. Rev. **D73**, 012006 (2006), [hep-ex/0509040].
- [140] J. P. Lees *et al.* (BaBar), Phys. Rev. **D95**, 7, 072001 (2017), [arXiv:1611.05624].
- [141] B. Aubert *et al.* (BaBar), Phys. Rev. Lett. **95**, 111801 (2005), [Erratum: Phys. Rev. Lett.97,019903(2006)], [hep-ex/0506036].
- [142] R. V. Kowalewski and S. Menke, Phys. Lett. **B541**, 29 (2002), [hep-ex/0205038].
- [143] J. P. Lees *et al.* (BaBar), Phys. Rev. **D86**, 032004 (2012), [arXiv:1112.0702].
- [144] I. Bizjak *et al.* (Belle), Phys. Rev. Lett. **95**, 241801 (2005), [hep-ex/0505088].
- [145] P. Urquijo *et al.* (Belle), Phys. Rev. Lett. **104**, 021801 (2010), [arXiv:0907.0379].
- [146] B. Aubert *et al.* (BaBar), Phys. Rev. Lett. **96**, 221801 (2006), [hep-ex/0601046].
- [147] A. Sibidanov *et al.* (Belle), Phys. Rev. **D88**, 3, 032005 (2013), [arXiv:1306.2781].
- [148] B. Aubert *et al.* (BaBar), Phys. Rev. Lett. **90**, 181801 (2003), [eConfC0304052,WG117(2003)], [hep-ex/0301001].
- [149] T. Hokuue *et al.* (Belle), Phys. Lett. **B648**, 139 (2007), [hep-ex/0604024].
- [150] B. Aubert *et al.* (BaBar), Phys. Rev. **D79**, 052011 (2009), [arXiv:0808.3524].
- [151] J. P. Lees *et al.* (BaBar), Phys. Rev. **D88**, 7, 072006 (2013), [arXiv:1308.2589].
- [152] J. P. Lees *et al.* (BaBar), Phys. Rev. **D87**, 3, 032004 (2013), [Erratum: Phys. Rev.D87,no.9,099904(2013)], [arXiv:1205.6245].
- [153] C. Schwanda *et al.* (Belle), Phys. Rev. Lett. **93**, 131803 (2004), [hep-ex/0402023].
- [154] N. E. Adam *et al.* (CLEO), Phys. Rev. Lett. **99**, 041802 (2007), [hep-ex/0703041].
- [155] S. B. Athar *et al.* (CLEO), Phys. Rev. **D68**, 072003 (2003), superceded by Ref. [156], [hep-ex/0304019].
- [156] R. Gray *et al.* (CLEO), Phys. Rev. **D76**, 012007 (2007), [Addendum: Phys. Rev.D76,no.3,039901(2007)], [hep-ex/0703042].
- [157] P. del Amo Sanchez *et al.* (BaBar), Phys. Rev. **D83**, 032007 (2011), supercedes Ref. [158], [arXiv:1005.3288].
- [158] B. Aubert *et al.* (BaBar), Phys. Rev. **D72**, 051102 (2005), [hep-ex/0507003].
- [159] P. del Amo Sanchez *et al.* (BaBar), Phys. Rev. **D83**, 052011 (2011), updated in Ref. [160], [arXiv:1010.0987].
- [160] J. P. Lees *et al.* (BaBar), Phys. Rev. **D86**, 092004 (2012), [arXiv:1208.1253].
- [161] J. A. Bailey *et al.* (Fermilab Lattice, MILC), Phys. Rev. **D92**, 1, 014024 (2015), [arXiv:1503.07839].
- [162] A. Bazavov *et al.* (Fermilab Lattice, MILC), Phys. Rev. **D100**, 3, 034501 (2019), [arXiv:1901.02561].
- [163] C. M. Bouchard *et al.*, Phys. Rev. **D90**, 054506 (2014), [arXiv:1406.2279].
- [164] B. Colquhoun *et al.*, Phys. Rev. **D93**, 3, 034502 (2016), [arXiv:1510.07446].
- [165] J. M. Flynn *et al.*, Phys. Rev. **D91**, 7, 074510 (2015), [arXiv:1501.05373].
- [166] T. Becher and R. J. Hill, Phys. Lett. **B633**, 61 (2006), [hep-ph/0509090].
- [167] M. C. Arnesen *et al.*, Phys. Rev. Lett. **95**, 071802 (2005), [hep-ph/0504209].
- [168] M. A. Shifman, A. I. Vainshtein and V. I. Zakharov, Nucl. Phys. **B147**, 385 (1979); M. A. Shifman, A. I. Vainshtein and V. I. Zakharov, Nucl. Phys. **B147**, 448 (1979).
- [169] P. Ball and R. Zwicky, Phys. Rev. **D71**, 014015 (2005), [hep-ph/0406232].
- [170] G. Duplancic *et al.*, JHEP **04**, 014 (2008), [arXiv:0801.1796].
- [171] A. Bharucha, JHEP **05**, 092 (2012), [arXiv:1203.1359].
- [172] A. V. Rusov, Eur. Phys. J. **C77**, 7, 442 (2017), [arXiv:1705.01929].
- [173] I. Sentitemsu Imsong *et al.*, JHEP **02**, 126 (2015), [arXiv:1409.7816].
- [174] H. Ha *et al.* (Belle), Phys. Rev. **D83**, 071101 (2011), [arXiv:1012.0090].
- [175] B. Aubert *et al.* (BaBar), Phys. Rev. Lett. **101**, 081801 (2008), [arXiv:0805.2408].
- [176] W. S. Brower and H. P. Paar, Nucl. Instrum. Meth. **A421**, 411 (1999), [hep-ex/9710029].
- [177] P. Ball, eConf **C070512**, 016 (2007), [arXiv:0705.2290].
- [178] J. M. Flynn and J. Nieves, Phys. Lett. **B649**, 269 (2007), [hep-ph/0703284].
- [179] S. Aoki *et al.*, Eur. Phys. J. **C77**, 2, 112 (2017), [arXiv:1607.00299].
- [180] T. Feldmann and M. W. Y. Yip, Phys. Rev. **D85**, 014035 (2012), [Erratum: Phys. Rev.D86,079901(2012)], [arXiv:1111.1844].
- [181] W. Detmold, C. Lehner and S. Meinel, Phys. Rev. **D92**, 3, 034503 (2015), [arXiv:1503.01421].
- [182] R. Aaij *et al.* (LHCb), Nature Phys. **11**, 743 (2015), [arXiv:1504.01568].
- [183] M. Ablikim *et al.* (BESIII), Phys. Rev. Lett. **116**, 5, 052001 (2016), [arXiv:1511.08380].
- [184] R. Aaij *et al.* (LHCb), Phys. Rev. **D96**, 11, 112005 (2017), [arXiv:1709.01920].
- [185] M. Tanaka, Z. Phys. **C67**, 321 (1995), [hep-ph/9411405].
- [186] H. Itoh, S. Komine and Y. Okada, Prog. Theor. Phys. **114**, 179 (2005), [hep-ph/0409228].
- [187] U. Nierste, S. Trine and S. Westhoff, Phys. Rev. **D78**, 015006 (2008), [arXiv:0801.4938].
- [188] M. Tanaka and R. Watanabe, Phys. Rev. **D82**, 034027 (2010), [arXiv:1005.4306].
- [189] A. Datta, M. Duraisamy and D. Ghosh, Phys. Rev. **D86**, 034027 (2012), [arXiv:1206.3760].
- [190] D. Bečirević, N. Košnik and A. Tayduganov, Phys. Lett. **B716**, 208 (2012), [arXiv:1206.4977].
- [191] S. Fajfer *et al.*, Phys. Rev. Lett. **109**, 161801 (2012), [arXiv:1206.1872].
- [192] A. Crivellin, C. Greub and A. Kokulu, Phys. Rev. **D86**, 054014 (2012), [arXiv:1206.2634].

- [193] M. Bauer and M. Neubert, Phys. Rev. Lett. **116**, 14, 141802 (2016), [arXiv:1511.01900].
- [194] I. Doršner *et al.*, Phys. Rept. **641**, 1 (2016), [arXiv:1603.04993].
- [195] A. Celis *et al.*, Phys. Lett. **B771**, 168 (2017), [arXiv:1612.07757].
- [196] J. F. Kamenik and F. Mescia, Phys. Rev. **D78**, 014003 (2008), [arXiv:0802.3790].
- [197] S. Fajfer, J. F. Kamenik and I. Nisandzic, Phys. Rev. **D85**, 094025 (2012), [arXiv:1203.2654].
- [198] M. Bordone, M. Jung and D. van Dyk (2019), [arXiv:1908.09398].
- [199] B. Aubert *et al.* (BaBar), Phys. Rev. Lett. **100**, 021801 (2008), [arXiv:0709.1698].
- [200] J. P. Lees *et al.* (BaBar), Phys. Rev. Lett. **109**, 101802 (2012), [arXiv:1205.5442].
- [201] J. P. Lees *et al.* (BaBar), Phys. Rev. **D88**, 7, 072012 (2013), [arXiv:1303.0571].
- [202] M. Huschle *et al.* (Belle), Phys. Rev. **D92**, 7, 072014 (2015), [arXiv:1507.03233].
- [203] Y. Sato *et al.* (Belle), Phys. Rev. **D94**, 7, 072007 (2016), [arXiv:1607.07923].
- [204] S. Hirose *et al.* (Belle), Phys. Rev. Lett. **118**, 21, 211801 (2017), [arXiv:1612.00529].
- [205] G. Caria *et al.* (Belle) (2019), [arXiv:1910.05864].
- [206] R. Aaij *et al.* (LHCb), Phys. Rev. Lett. **115**, 11, 111803 (2015), [Erratum: Phys. Rev. Lett.115,no.15,159901(2015)], [arXiv:1506.08614].
- [207] R. Aaij *et al.* (LHCb), Phys. Rev. Lett. **120**, 17, 171802 (2018), [arXiv:1708.08856].
- [208] <http://www.slac.stanford.edu/xorg/hfag/semi/fpcp17/RDRDs.html>.
- [209] J. G. Korner and G. A. Schuler, Z. Phys. **C46**, 93 (1990).
- [210] A. Abdesselam *et al.* (Belle), in “10th International Workshop on the CKM Unitarity Triangle (CKM 2018) Heidelberg, Germany, September 17-21, 2018,” (2019), [arXiv:1903.03102].
- [211] A. Matyja *et al.* (Belle), Phys. Rev. Lett. **99**, 191807 (2007), [arXiv:0706.4429].
- [212] A. Bozek *et al.* (Belle), Phys. Rev. **D82**, 072005 (2010), [arXiv:1005.2302].
- [213] M. Tanaka and R. Watanabe, Phys. Rev. **D87**, 3, 034028 (2013), [arXiv:1212.1878].
- [214] R. Aaij *et al.* (LHCb), Phys. Rev. **D97**, 7, 072013 (2018), [arXiv:1711.02505].
- [215] R. Aaij *et al.* (LHCb), Phys. Rev. Lett. **120**, 12, 121801 (2018), [arXiv:1711.05623].
- [216] S. Hirose *et al.* (Belle), Phys. Rev. **D97**, 1, 012004 (2018), [arXiv:1709.00129].
- [217] F. U. Bernlochner *et al.*, Phys. Rev. **D95**, 11, 115008 (2017), [erratum: Phys. Rev.D97,no.5,059902(2018)], [arXiv:1703.05330].
- [218] S. Jaiswal, S. Nandi and S. K. Patra, JHEP **12**, 060 (2017), [arXiv:1707.09977].
- [219] Y. Amhis *et al.* (HFLAV), Eur. Phys. J. **C77**, 12, 895 (2017), [arXiv:1612.07233].

## 76. Determination of CKM angles from B hadrons

Written August 2019 by T. Gershon (Warwick U.), M. Kenzie (Warwick U.) and K. Trabelsi (U. Paris-Saclay, IJCLab).

### 76.1 Introduction

The Cabibbo–Kobayashi–Maskawa (CKM) description of quark mixing [1, 2] leads to a number of triangle relations between pairs of CKM matrix elements. One of these,

$$V_{ud}V_{ub}^* + V_{cd}V_{cb}^* + V_{td}V_{tb}^* = 0, \quad (76.1)$$

is of particular interest since (i) all its terms are of comparable magnitude, and (ii) its properties can be measured through studies of oscillations and decays of  $B$  mesons. As the area of this unitary triangle is a measure of the amount of  $CP$  violation in the Standard Model [3], it is of particular interest to determine the values of its angles and to test the consistency of the CKM paradigm with the experimental measurements. The angles are defined as

$$\begin{aligned} \alpha &= \arg \left[ -\frac{V_{td}V_{tb}^*}{V_{ud}V_{ub}^*} \right], & \beta &= \arg \left[ -\frac{V_{cd}V_{cb}^*}{V_{td}V_{tb}^*} \right], \\ \gamma &= \arg \left[ -\frac{V_{ud}V_{ub}^*}{V_{cd}V_{cb}^*} \right], \end{aligned} \quad (76.2)$$

with an alternative notation  $(\phi_2, \phi_1, \phi_3) \equiv (\alpha, \beta, \gamma)$  also widely used in the literature.

In this mini-review, the most precise methods to determine the CKM angles are described, with a particular focus on nontrivial aspects of the combination of results. More detailed discussions of these points can be found in Ref. [4]. A similar mini-review on the side of the unitarity triangle adjacent to the angle  $\gamma$  can be found in Ref. [5]. A detailed overview of the CKM quark-mixing matrix is given in Ref. [6] while  $CP$  violation in the quark sector is discussed in Ref. [7].

### 76.2 $\beta$

The relative weak (*i.e.*  $CP$ -violating) phase between the amplitude for any CKM-favoured  $B^0$  meson decay to a  $CP$  eigenstate and that for the decay following  $B^0$ – $\bar{B}^0$  oscillation is twice the angle  $\beta$ . The decay-time-dependent  $CP$  asymmetry can be expressed as

$$A_{f_{CP}}(t) \equiv \frac{d\Gamma/dt[\bar{B}_{\text{phys}}^0(t) \rightarrow f_{CP}] - d\Gamma/dt[B_{\text{phys}}^0(t) \rightarrow f_{CP}]}{d\Gamma/dt[\bar{B}_{\text{phys}}^0(t) \rightarrow f_{CP}] + d\Gamma/dt[B_{\text{phys}}^0(t) \rightarrow f_{CP}]}, \quad (76.3a)$$

$$= S_f \sin(\Delta m t) - C_f \cos(\Delta m t), \quad (76.3b)$$

where the notation  $B_{\text{phys}}^0(t)$  ( $\bar{B}_{\text{phys}}^0(t)$ ) denotes a neutral  $B$  meson that decays at time  $t$  into the final state  $f_{CP}$ , and is known (“tagged”) at time  $t = 0$  to have flavour content corresponding to  $B^0$  ( $\bar{B}^0$ ). In Eq. (76.3b),  $\Delta m$  denotes the mass difference between the two physical eigenstates of the  $B^0$ – $\bar{B}^0$  system, while the corresponding decay-width difference is assumed to be negligible [8]; moreover  $CPT$  symmetry and the absence of  $CP$  violation in  $B^0$ – $\bar{B}^0$  mixing is assumed throughout this mini-review.

In the general case, one can write

$$S_f \equiv \frac{2\mathcal{I}m(\lambda_f)}{1 + |\lambda_f|^2} \quad \text{and} \quad C_f \equiv \frac{1 - |\lambda_f|^2}{1 + |\lambda_f|^2}, \quad (76.4)$$

where the parameter  $\lambda_f = \frac{\bar{A}_f}{p A_f}$  is defined in terms of  $p$  and  $q$ , which define the flavour content of the mass eigenstates of the  $B^0$ – $\bar{B}^0$  system [8], and the amplitudes  $\bar{A}_f$  ( $A_f$ ) for a  $\bar{B}^0$  ( $B^0$ ) decay to the final state  $f_{CP}$ . In the limit that the decay amplitude is dominated by a CKM-favoured transition, as is the case for  $B^0 \rightarrow J/\psi K_S^0$  decays, one obtains simple relations:  $S_f = -\eta_{CP} \sin(2\beta)$  and  $C_f = 0$ , where  $\eta_{CP}$  is the  $CP$  eigenvalue of the final state [9, 10]. This method has been pursued intensively by experiments. The current world averages, combining results for

several charmonium-kaon final states but dominated by results on  $B^0 \rightarrow J/\psi K_S^0$  ( $CP$  odd) and  $B^0 \rightarrow J/\psi K_L^0$  ( $CP$  even), are [4]

$$-\eta_{CP} S_f = 0.699 \pm 0.017, \quad C_f = -0.005 \pm 0.015. \quad (76.5)$$

Despite the large number of signal events in the data, the dominant uncertainties are still statistical. One important source of potential systematic correlation between results from different experiments is that due to “tag-side interference” [11], which is common to measurements exploiting production through the  $e^+e^- \rightarrow \Upsilon(4S) \rightarrow B^0\bar{B}^0$  process, including the latest results from BaBar [12] and Belle [13]. It does not, however, affect the results from LHCb [14] that have comparable statistical sensitivity. Another common source of systematic uncertainty is due to knowledge of the value of  $\Delta m$ , but since this quantity has been measured precisely [8] the effect remains small.

The interpretation of the value of  $-\eta_{CP} S_f$  from Eq. (76.5) as  $\sin(2\beta)$  assumes negligible contributions from subleading amplitudes with a different weak phase to that of the tree diagram (*i.e.* to that of the CKM matrix elements  $V_{cb}V_{cs}^*$ ). This potential additional contribution is often referred to as “penguin pollution”. All existing data, including the value of  $C_f$  in Eq. (76.5), as well as several explicit calculations [15–18], are consistent with penguin pollution in  $B^0$  meson decays to charmonium-kaon decays being negligible at the current level of precision. Therefore, the value of  $-\eta_{CP} S_f$  is generally converted to  $\sin(2\beta)$  without any correction or additional uncertainty being assigned due to this assumption. This gives [4]

$$\beta = (22.2 \pm 0.7)^\circ, \quad (76.6)$$

where only the solution consistent with the Standard Model is reported (methods to resolve the trigonometric ambiguity in the result are discussed below). It is also possible to use data-driven methods, typically based on flavour symmetries plus some additional assumptions, to constrain the effects of penguin pollution [19–21]. In this case it is necessary to consider each charmonium-kaon final state separately, since the penguin pollution to each may differ. The most common approach [19], which relies on experimental information on  $B^0 \rightarrow J/\psi\pi^0$  decays, currently gives an additional uncertainty on  $\sin(2\beta)$  from  $B^0 \rightarrow J/\psi K_S^0$  of around 0.01.

It is possible to avoid the issue of penguin pollution in the measurement of  $\beta$  by using  $B^0$  meson decays to a charm- and light-meson final state, such as  $D_{CP}\pi^0$  (where  $D_{CP}$  represents a  $D^0$  meson decaying into a  $CP$  eigenstate), instead of the charmonium-kaon final states. These decays do have a CKM-suppressed contribution ( $V_{ub}V_{cd}^*$  instead of  $V_{cb}V_{ud}^*$ ), which can in principle bias the determination of  $\sin(2\beta)$  from  $S_f$ , but this can be calculated and is known to be negligible at current precision. The requirement that the neutral  $D$  meson decays to a final state that is common to both  $D^0$  and  $\bar{D}^0$ , such as the  $CP$ -even eigenstate  $K^+K^-$ , reduces the sample size that is available for analysis. Consequently, the world average [4],  $\sin(2\beta) = 0.71 \pm 0.09$ , with these channels is not as precise as that from the charmonium-kaon states.

Converting experimental results on  $\sin(2\beta)$  into constraints on  $\beta$  leads to a trigonometric ambiguity in the range  $[0^\circ, 180^\circ]$ . This can be resolved with experimental measurements of  $\cos(2\beta)$ , which can be obtained from decay-time-dependent analyses of  $B^0$  meson decays to multibody (non- $CP$ -eigenstate) final states. Among the charmonium-kaon decays, study of  $B^0 \rightarrow J/\psi K^*(892)^0$  with  $K^*(892)^0 \rightarrow K_S^0\pi^0$  is the most promising approach, but due to the limited sample size that has been analysed to date the precision is not sufficient to resolve the ambiguity conclusively. The charm- and light-meson channels such as  $B^0 \rightarrow D\pi^0$  with  $D \rightarrow K_S^0\pi^+\pi^-$  have been shown to provide good statistical power for this purpose, with a joint analysis of BaBar and Belle data giving  $\cos(2\beta) = 0.91 \pm 0.25$  [22, 23], sufficient to rule out the alternative solution for  $\beta$ .

### 76.3 $\alpha$

In the limit that only tree amplitudes contribute to  $B^0$  meson decays to light mesons, such as  $B^0 \rightarrow \pi^+\pi^-$ , then the observables of the decay-time-dependent  $CP$  asymmetry of Eq. (76.3) would allow a straight-forward determination of  $2\alpha$ :  $S_f = +\eta_{CP} \sin(2\alpha)$



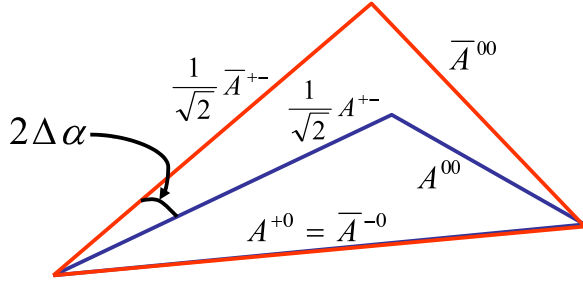


Figure 76.1: Isospin triangles for  $B \rightarrow \pi\pi$  decays, reproduced from Ref. [24]. Here, the relative phase between  $A^{+0}$  and  $\bar{A}^{-0}$  has been rotated away to simplify the picture. The total relative phase probed by  $S_{\pi^+\pi^-}$  is  $\arg\left(\frac{q}{p}\frac{\bar{A}^{+-}}{A^{+-}}\right) = 2\alpha - 2\Delta\alpha$ , including contributions from  $B^0\text{--}\bar{B}^0$  mixing, the tree-level amplitudes and the correction  $\Delta\alpha$ , and exploiting the unitarity requirement  $\alpha + \beta + \gamma = 180^\circ$ .

and  $C_f = 0$ . In general, however, the determination of  $\alpha$  is complicated by the presence of contributions from  $b \rightarrow d(u\bar{u})$  neutral-current penguin transitions, which have a similar level of CKM-suppression as the  $b \rightarrow u(\bar{u}d)$  charged-current tree amplitudes but have a different weak phase. Consequently one obtains instead for  $B^0 \rightarrow \pi^+\pi^-$

$$S_{\pi^+\pi^-} = \sqrt{1 - C_{\pi^+\pi^-}^2} \sin(2\alpha - 2\Delta\alpha), \quad (76.7)$$

where  $\Delta\alpha$  is the *a priori* unknown penguin contribution.

This contribution from the penguin amplitude can be accounted for in an analysis relating the amplitudes for isospin partner decays, *e.g.*  $A^{+-}$  for  $B^0 \rightarrow \pi^+\pi^-$ ,  $A^{+0}$  for  $B^+ \rightarrow \pi^+\pi^0$ ,  $A^{00}$  for  $B^0 \rightarrow \pi^0\pi^0$  decays and  $(\bar{A}^{+-}, \bar{A}^{-0}, \bar{A}^{00})$  for their charge conjugates. The isospin analysis relies on the fact that there is no penguin contribution to  $A^{+0}$  and  $\bar{A}^{-0}$ , because  $\pi^\pm\pi^0$  is a pure isospin-2 state, and the ( $\Delta I = \frac{1}{2}$ ) QCD-penguin amplitudes only contribute to the isospin-0 final state. One therefore obtains the following isospin triangle relations [25]

$$A^{+0} = \frac{1}{\sqrt{2}}A^{+-} + A^{00} \quad \text{and} \quad \bar{A}^{-0} = \frac{1}{\sqrt{2}}\bar{A}^{+-} + \bar{A}^{00}, \quad (76.8)$$

from which it is possible to determine  $\Delta\alpha$ , as shown in Fig. 76.1.

Since the determination of  $\Delta\alpha$  and thus also  $\alpha$  requires construction of amplitude-level relations, it is not appropriate to simply average results of  $\alpha$  from different experiments. Instead, measurements of each of the observable quantities needed to determine  $\alpha$  are input into a combination. For the  $B \rightarrow \pi\pi$  system, the inputs are the branching fractions of  $B^0 \rightarrow \pi^+\pi^-$ ,  $B^+ \rightarrow \pi^+\pi^0$  and  $B^0 \rightarrow \pi^0\pi^0$  decays, the lifetimes of the  $B^+$  and  $B^0$  mesons (which relate the branching fractions to amplitude-level quantities), and the  $S_{\pi^+\pi^-}$ ,  $C_{\pi^+\pi^-}$  and  $C_{\pi^0\pi^0}$  observables. Potential sources of correlation must be taken into account, but these are predominantly systematic in origin and thus have a small effect on the combination, since the measurements are statistically limited. An exception is that the LHCb measurements of  $(S_{\pi^+\pi^-}, C_{\pi^+\pi^-})$  [26] have a significant statistical correlation due to the fact that the time variable of Eq. (76.3) is the difference between production and decay, and hence is in the range  $[0, \infty]$ . This correlation is largely absent for measurements from BaBar [27] and Belle [28], where the difference between the signal and tagging  $B$  meson decay times is measured, and hence  $t \in [-\infty, \infty]$ . The combination itself can be performed with different statistical approaches; the procedure described in detail in Ref. [29], based on a frequentist treatment, is used here. The knowledge of  $C_{\pi^0\pi^0}$  [27, 30] is currently the limiting factor in the precision on  $\alpha$  from the  $B \rightarrow \pi\pi$  system, and is likely to remain so for some time due to the difficulty to reconstruct this final state.

In general, the isospin triangle construction gives a four-fold ambiguity on  $2\Delta\alpha$  (each triangle can face either up or down), leading to an eight-fold ambiguity on  $\alpha$  in the range  $[0^\circ, 180^\circ]$ .

This is reduced if either or both of the triangles are flat, or if the two triangles have sides of identical length. The ambiguities can also be reduced if measurement of the  $S_{\pi^0\pi^0}$  (or equivalent) observable is available, since this can be combined with the corresponding  $\Delta\alpha$  parameter from the right-hand corner of the triangle in Fig. 76.1 to provide an additional constraint. None of these possibilities are realised in the  $B \rightarrow \pi\pi$  system; in particular a decay-time-dependent analysis of  $B^0 \rightarrow \pi^0\pi^0$  is extremely challenging experimentally due to the absence of any charged particle originating from the  $B$  decay position. Nonetheless, solutions consistent with  $\alpha = 0$  can be rejected on physical grounds [24].

The isospin analysis can also be performed with the  $B \rightarrow \rho\rho$  system, which contains two vector particles in the final state and so does not have a fixed  $CP$  eigenvalue. In principle the analysis can be performed separately for each  $\rho\rho$  polarisation state, but in practise it is found that the longitudinal polarisation fraction,  $f_L$ , is close to unity, and hence the final state is approximately  $CP$ -even. Compared to  $B^0 \rightarrow \pi\pi$ , the  $\rho\rho$  modes benefit experimentally from a higher branching fraction and smaller penguin contributions, so that the isospin triangles are flatter, reducing the ambiguities. (The value of  $\Delta\alpha$  in the  $B \rightarrow \rho\rho$  system, obtained from the isospin analysis, has a single solution in  $[0, \pi]$  at  $(3 \pm 5)^\circ$ , while for  $B \rightarrow \pi\pi$  there are two solutions at  $13^\circ$  and  $27^\circ$  with  $\Delta\alpha \in [7, 33]^\circ$  at 68.3% confidence level (CL). The isospin analysis with either final state has an ambiguity under  $\Delta\alpha \leftrightarrow -\Delta\alpha$ .) For the BaBar [31] and Belle [32] experiments, the high branching fraction and smaller penguin contribution compensate for the increased difficulty to reconstruct the  $\rho\rho$  final state relative to  $\pi\pi$ . Moreover, in contrast to  $S_{\pi^0\pi^0}$ , measurement of  $S_{\rho^0\rho^0}$  is possible due to the four charged pion final state (following  $\rho^0 \rightarrow \pi^+\pi^-$  decay), as has been demonstrated by BaBar [33].

In the  $B \rightarrow \rho\pi$  system there are more amplitudes to consider, so that the isospin relation corresponds to a pentagon rather than a triangle and Eq. (76.8) is modified to become

$$\begin{aligned} \sqrt{2}(A^{+0} + A^{0+}) &= A^{+-} + A^{-+} + 2A^{00} \quad \text{and} \\ \sqrt{2}(\bar{A}^{-0} + \bar{A}^{0-}) &= \bar{A}^{+-} + \bar{A}^{-+} + 2\bar{A}^{00}. \end{aligned} \quad (76.9)$$

As in Eq. (76.8), the left-hand sides of these expressions correspond to a pure isospin-2 final state, and therefore the ratio of the right-hand sides gives a pure phase term that, accounting for the  $B^0\text{--}\bar{B}^0$  mixing phase that also contributes to the measured quantities, is  $2\alpha$ . The relative amplitudes for  $B^0$  and  $\bar{B}^0$  decays to  $\rho^+\pi^-$ ,  $\rho^-\pi^+$  and  $\rho^0\pi^0$  can all be determined from a decay-time-dependent analysis of the  $\pi^+\pi^-\pi^0$  Dalitz plot, so that study of this channel alone allows determination of  $\alpha$  [34]. This analysis in principle leads to a single solution for  $\alpha$  in  $[0^\circ, 180^\circ]$ , but the precision of current measurements [35–37] is limited.

The isospin analysis used to determine  $\alpha$  is believed to be valid to high precision, and theoretical uncertainties in the procedure are usually neglected. Nonetheless, it should be noted that the analysis assumes the absence of electroweak penguin amplitudes, which can contribute to  $\Delta I = \frac{3}{2}$  transitions with a different weak phase from that of the tree amplitudes [38, 39]. Moreover, isospin-breaking effects such as  $(\pi^0, \eta, \eta')$  mixing would impact on the relations of Eq. (76.8). A further complication in the  $B \rightarrow \rho\rho$  system is the effect of the non-zero  $\rho$  meson width [40]. Estimates of the size of these effects on the determined value of  $\alpha$  are typically at the  $1^\circ$  level or less [29]. By contrast, methods to determine  $\alpha$  using SU(3) or other flavour symmetries are generally considered to have larger theoretical uncertainties and are not included here.

The world average obtained for the angle  $\alpha$  from isospin analysis of  $B \rightarrow \pi\pi$ ,  $\rho\pi$  and  $\rho\rho$  decays is [4]

$$\alpha = (84.9_{-4.5}^{+5.1})^\circ, \quad (76.10)$$

where the quoted uncertainty is at the 68.3% CL and does not include effects due to isospin-breaking. This world average, together with results split by decay mode, is shown in Fig. 76.2. The combination has a total of 51 experimental inputs from which 24 parameters are determined, and an overall  $\chi^2$  of 16.4, which corresponds to a p-value of 94%. Thus, there is excellent overall consistency between the inputs, despite the tension apparent in

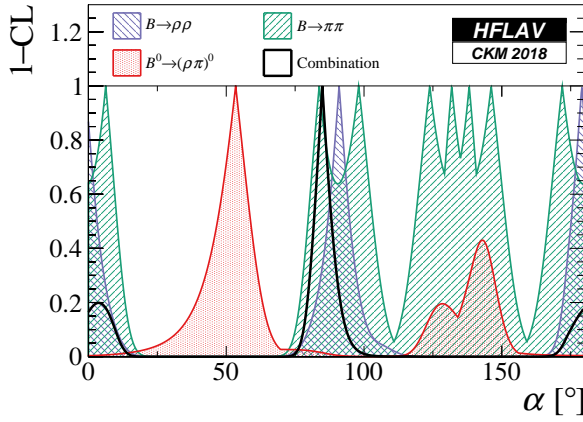


Figure 76.2: World average of  $\alpha$ , as well as contributions from individual modes, in terms of 1-CL.

Fig. 76.2 between the results from  $B^0 \rightarrow (\rho\pi)^0$  and the others. The combination gives a single best-fit for  $\alpha$  in  $[0^\circ, 180^\circ]$ , but an ambiguous solution exists at  $\alpha \Leftrightarrow \alpha + 180^\circ$ . A secondary minimum close to zero is disfavoured [29].

#### 76.4 $\gamma$

The angle  $\gamma$  is the weak phase between Cabibbo-favoured  $b \rightarrow c$  and suppressed  $b \rightarrow u$  quark transitions and can be determined by exploiting interference between them. Explicitly, the ratio of suppressed to favoured amplitudes is parametrised by

$$r_B e^{i(\delta_B \pm \gamma)} = \frac{A_{\text{sup}}}{A_{\text{fav}}}, \quad (76.11)$$

where  $r_B$  is the ratio of amplitude magnitudes,  $\delta_B$  the strong phase difference and the + or - sign depends on whether the transition involves a  $\bar{b}$  or  $b$  quark, respectively. Measurement of  $\gamma$  in this way has negligible theoretical uncertainty in the Standard Model [41], and therefore this approach provides a benchmark against which determinations from other methods, typically involving loop diagrams, can be compared.

Interference between these amplitudes is realised in  $B^+ \rightarrow DK^+$  decays, where  $D$  represents an admixture of  $D^0$  and  $\bar{D}^0$  mesons. The simplest case is that of  $D$  decays to  $CP$ -eigenstates (GLW method [42, 43]), either  $CP$ -even such as  $K^+K^-$  ( $CP+$ ) or  $CP$ -odd such as  $K_S^0\pi^0$  ( $CP-$ ). The normalised decay rate and  $CP$  asymmetry are given by

$$R_{CP\pm} = \frac{\Gamma(B^- \rightarrow D_{CP\pm}K^-) + \Gamma(B^+ \rightarrow D_{CP\pm}K^+)}{\Gamma(B^- \rightarrow D^0K^-) + \Gamma(B^+ \rightarrow \bar{D}^0K^+)} \\ = 1 + r_B^2 \pm 2r_B \cos(\delta_B) \cos(\gamma), \quad (76.12a)$$

$$A_{CP\pm} = \frac{\Gamma(B^- \rightarrow D_{CP\pm}K^-) - \Gamma(B^+ \rightarrow D_{CP\pm}K^+)}{\Gamma(B^- \rightarrow D_{CP\pm}K^-) + \Gamma(B^+ \rightarrow D_{CP\pm}K^+)} \\ = \frac{\pm 2r_B \sin(\delta_B) \sin(\gamma)}{1 + r_B^2 \pm 2r_B \cos(\delta_B) \cos(\gamma)}. \quad (76.12b)$$

These relations assume the absence of direct  $CP$  violation in the charm system; experimentally allowed deviations from this assumption are too small to cause a significant bias on  $\gamma$  [7, 44]. It is convenient to determine the  $R_{CP\pm}$  quantities through a double ratio, normalising to  $B^+ \rightarrow D\pi^+$  decays involving the same final states, since this cancels potential sources of systematic uncertainty due to the branching fractions of the  $D$  decays that are used; small possible effects of  $CP$  violation in  $B^+ \rightarrow D\pi^+$  decays are a source of systematic uncertainty in this procedure. The GLW method can be extended to include final states that are almost  $CP$ -eigenstates [45], as is the case in  $D \rightarrow \pi^+\pi^-\pi^0$  and  $D \rightarrow K^+K^-\pi^0$  decays, via inclusion of a factor encoding the fraction of  $CP$ -even (or  $CP$ -odd) content,  $F_{\pm}$ , which dilutes the sensitivity to  $\gamma$  by reducing the size of the interference terms (the terms linear with  $r_B$ ) in Eq. (76.12).

For other  $D$  decays, the ratio of amplitudes for the  $D^0$  and  $\bar{D}^0$  decays to the final state of interest has to be accounted for in the formalism. The ADS method [46, 47] uses  $D$  decays to final states such as  $K^\mp\pi^\pm$ , which involve interference between Cabibbo-favoured (CF) and doubly-Cabibbo-suppressed (DCS) transitions. The observables in this case are

$$A_{\text{ADS}} = \frac{\Gamma(B^- \rightarrow [K^+\pi^-]_D K^-) - \Gamma(B^+ \rightarrow [K^-\pi^+]_D K^+)}{\Gamma(B^- \rightarrow [K^+\pi^-]_D K^-) + \Gamma(B^+ \rightarrow [K^-\pi^+]_D K^+)} \\ = \frac{2r_B r_D \sin(\delta_B + \delta_D) \sin(\gamma)}{r_B^2 + r_D^2 + 2r_B r_D \cos(\delta_B + \delta_D) \cos(\gamma)}, \quad (76.13a)$$

$$R_{\text{ADS}} = \frac{\Gamma(B^- \rightarrow [K^+\pi^-]_D K^-) + \Gamma(B^+ \rightarrow [K^-\pi^+]_D K^+)}{\Gamma(B^- \rightarrow [K^-\pi^+]_D K^-) + \Gamma(B^+ \rightarrow [K^+\pi^-]_D K^+)} \\ = r_B^2 + r_D^2 + 2r_B r_D \cos(\delta_B + \delta_D) \cos(\gamma), \quad (76.13b)$$

where  $r_D$  and  $\delta_D$  are the amplitude magnitude ratio and strong phase difference between the CF and DCS  $D$  decay. An alternative pair of observables,  $(R_-, R_+)$ , is also sometimes used, where  $R_-$  ( $R_+$ ) is the ratio of decay rates between the suppressed and favoured transitions for  $B^-$  ( $B^+$ ) decays. The  $R_-$  and  $R_+$  observables are statistically independent, while  $A_{\text{ADS}}$  and  $R_{\text{ADS}}$  are not (in particular, the uncertainty on  $A_{\text{ADS}}$  depends on the central value of  $R_{\text{ADS}}$ ). However, the pair  $(R_-, R_+)$  has more correlated sources of systematic uncertainty compared to  $(A_{\text{ADS}}, R_{\text{ADS}})$ . The observables of Eq. (76.13) are therefore usually preferred once a significant signal is established. The ADS method can also be extended to include decays to multibody final states, such as  $D \rightarrow K^\pm\pi^\mp\pi^0$  and  $D \rightarrow K^\pm\pi^\mp\pi^+\pi^-$ , by addition of a coherence factor [48] which appears in the interference terms of Eq. (76.13) and accounts for dilution of the sensitivity due to variation of the decay amplitude across the phase space of the final state. A similar method can be used for singly Cabibbo-suppressed  $D$  decays to non- $CP$  eigenstates such as  $K^*K$  [49].

For  $D$  decays to multibody self-conjugate final states (BPGGSZ method [50, 51]), such as  $D \rightarrow K_S^0\pi^+\pi^-$ , one can write the partial decay rate as a function of the position in the phase space in terms of the ‘‘Cartesian parameters’’  $x_{\pm} + iy_{\pm} = r_B e^{i(\delta_B \pm \gamma)}$ :

$$d\Gamma(B^\pm \rightarrow [K_S^0\pi^+\pi^-]_D K^\pm) = A_{(\mp, \pm)}^2 + r_B^2 A_{(\pm, \mp)}^2 \\ + 2A_{(\pm, \mp)} A_{(\mp, \pm)} [x_{\pm} c_{D(\pm, \mp)} + y_{\pm} s_{D(\pm, \mp)}], \quad (76.14)$$

where the notation  $(+, -)$  is shorthand for the dependence on the Dalitz position - the squared invariant masses of  $K_S^0\pi^+$  and  $K_S^0\pi^-$  combinations, respectively. The quantities  $A_{(+, -)}$  and  $A_{(-, +)}$  represent the magnitudes of the  $D^0$  and  $\bar{D}^0$  decay amplitudes at the Dalitz point  $(+, -)$  and are interchangeable with their  $CP$  conjugate amplitudes because  $CP$  conservation is assumed in the  $D$  decay (i.e.  $A_{(-, +)} = \bar{A}_{(+, -)}$ ). The quantities  $c_{D(\pm, \mp)}$  and  $s_{D(\pm, \mp)}$  are the cosine and sine of the strong phase difference,  $\delta_{D(+, -)} = \arg(\bar{A}_{(+, -)}) - \arg(A_{(+, -)})$ , between the  $\bar{D}^0$  and  $D^0$  amplitudes. These quantities can be determined from an amplitude model, although this leads to a hard-to-quantify systematic uncertainty associated to the composition of the model. An alternative, ‘‘model-independent’’, approach involves dividing the phase space into appropriate bins. In this case, the analysis benefits from external input on the values of  $c_D$  and  $s_D$  integrated over each bin. Measurements of these external parameters have been performed for the  $D \rightarrow K_S^0\pi^+\pi^-$  decay by the CLEO-c collaboration [52, 53] and will be further improved upon by BES-III. The use of common input values for these parameters in model-independent determinations of  $\gamma$  with the BPGGSZ method by different experiments is a source of correlation between experiments that is currently negligible but will become more significant as the available  $B$  meson data samples increase in size.

The discussion above refers to  $B^+ \rightarrow DK^+$  decays, but analogous measurements can be made also for additional channels such as  $B^+ \rightarrow D^*K^+$  (with  $D^* \rightarrow D\pi^0, D\gamma$ ) and  $B^+ \rightarrow DK^{*+}$  (with  $K^{*+} \rightarrow K_S^0\pi^+, K^+\pi^0$ ). In the limit that these can be treated purely as two-body decays, the expressions for  $B^+ \rightarrow DK^+$  are modified only by ensuring the  $r_B$  and  $\delta_B$  parameters are specific to each  $B$  decay. Moreover, for  $B^+ \rightarrow D^*K^+$  decays an

effective shift of the strong phase by  $\pi$  between  $D^* \rightarrow D\pi^0$  and  $D\gamma$  decays [54] has to be taken into account. In case the finite width of the decaying resonance is non-negligible, as is the case for the  $K^*(892)$  state, the sensitivity is diluted by relevant coherence factors,  $\kappa_B$ . For the  $B^0 \rightarrow DK^{*0}$  decay, full amplitude analysis of the  $B^0 \rightarrow DK^+\pi^-$  Dalitz plot provides additional sensitivity compared to the quasi-two-body approach [55, 56].

It is also possible to measure  $\gamma$  using decay-time-dependent analysis of the  $B_s^0$  meson [57]. The weak phase arising in the interference between direct decay of  $B_s^0 \rightarrow D_s^\mp K^\pm$  and decay via mixing is  $(\gamma - 2\beta_s)$ , where  $\beta_s$  is the angle associated with  $B_s^0 \rightarrow J/\psi\phi$  decays in a similar way to the relation between  $\beta$  and  $B^0 \rightarrow J/\psi K_S^0$  decays described in Sec. 76.2. Sufficient information can be obtained from the tagged, decay-time-dependent rates of  $B_s^0 \rightarrow D_s^\mp K^\pm$  decays that this weak phase can be determined, up to an ambiguity, together with the strong phase difference between, and the ratio of the magnitudes of, the suppressed and favoured amplitudes. Since  $\beta_s$  is known to good precision [8], measurements of the decay-time-dependent  $CP$ -asymmetry observables in  $B_s^0 \rightarrow D_s^\mp K^\pm$  decays can be used to infer constraints on  $\gamma$ . Alternatively, if effects of penguin pollution in  $B_s^0 \rightarrow J/\psi\phi$  decays [17, 18] are a concern, as they will become in the future, results from the  $B_s^0 \rightarrow D_s^\mp K^\pm$  mode can be combined with an independent precise measurement of  $\gamma$  to provide a penguin-free determination of  $\beta_s$ .

The average for  $\gamma$  requires a non-trivial combination due the complicated relations between the observables and the physics parameters of interest, such as in Eqs. (76.12), (76.13) and (76.14). Moreover, hadronic parameters such as  $r_B$  and  $\delta_B$  defined in Eq. (76.11) are common to all different  $D$  decay modes (but differ for each  $B$  decay mode). Thus, it is not correct to simply average results for  $\gamma$  obtained by different experiments or in different channels. Instead, measurements of rate asymmetries, rate ratios and the Cartesian parameters are taken as inputs to the combination, from which results are obtained not only for  $\gamma$  but also for the hadronic parameters. The precision to which  $\gamma$  can be measured with a particular  $B$  decay is approximately inversely proportional to the value of  $r_B$ . Thus, results from channels with smaller yields but larger values of  $r_B$ , such as  $B^0 \rightarrow DK^{*0}$  and  $B_s^0 \rightarrow D_s^\mp K^\pm$  ( $r_B \approx 0.3-0.4$ ), can have a significant impact on the world average and are included in the combination. By contrast the  $B^+ \rightarrow D\pi^+$  mode, for which large samples are available but  $r_B \approx 0.005$ , has little impact and is also more sensitive to potential systematic biases; hence it is not included. The sensitivity of the world average at present is dominated by results from  $B^+ \rightarrow DK^+$ , where  $r_B \approx 0.1$ , in particular results with the GLW [58], ADS [59] and BPGGSZ [60–62] methods.

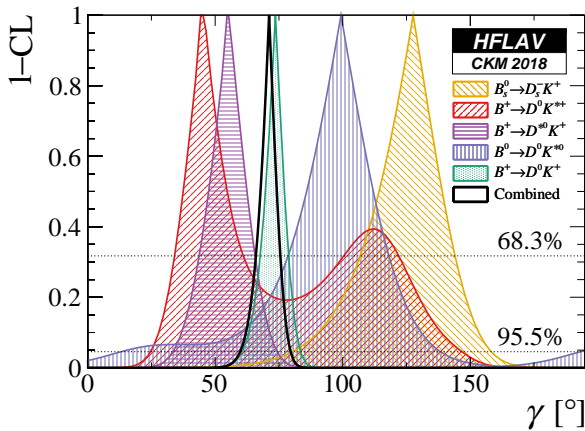


Figure 76.3: World average of  $\gamma \equiv \phi_3$ , as well as contributions from individual modes, in terms of 1–CL.

The world average obtained for the angle  $\gamma$ , obtained by combining results from  $B^+ \rightarrow DK^+$ ,  $D^*K^+$ ,  $DK^{*+}$ ,  $DK^+\pi^+\pi^-$ ,  $B^0 \rightarrow DK^+\pi^-$  and  $B_s^0 \rightarrow D_s^\mp K^\pm$  decays, is [4]

$$\gamma = (72.1_{-4.5}^{+4.1})^\circ, \quad (76.15)$$

where the quoted uncertainty is at the 68.3% CL.

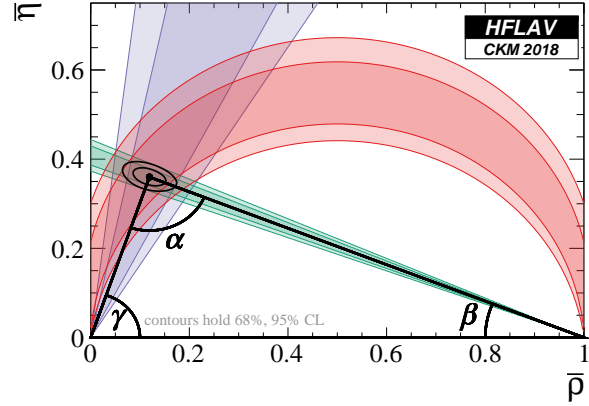


Figure 76.4: Constraints from the measurements of the angles of the CKM unitarity triangle in the  $(\bar{\rho}, \bar{\eta})$  plane.

Effects related to charm and kaon mixing and  $CP$  violation are generally negligible at the current level of precision, in particular for modes with  $r_B \gtrsim 0.1$ . An exception is that a dependence of the selection efficiency on the charm decay time can induce a dependence of the observables on charm mixing parameters [63]. Such effects can be important at hadron collider experiments such as LHCb, but can be corrected for. Interactions of neutral kaons with detector material can also cause a bias in determination of  $\gamma$  from modes with low values of  $r_B$  [64], such as the BPGGSZ method applied to  $B^+ \rightarrow D\pi^+$ , but are negligible in modes with larger  $r_B$  values.

Effects from correlated uncertainties between amplitude models and strong phase differences in charm decays are negligible and are not explicitly accounted for in the combination, nor are effects related to charm and kaon mixing and  $CP$  violation. This world average, together with results split by decay mode, is shown in Fig. 76.3. The combination has a total of 136 experimental inputs from which 29 parameters are determined, an overall  $\chi^2$  of 123.4, which corresponds to a p-value of 13% indicating acceptable agreement between the inputs. The combination gives a single solution for  $\gamma$  in  $[0^\circ, 180^\circ]$ , but an ambiguous solution exists at  $\gamma \Leftrightarrow \gamma + 180^\circ$ .

## 76.5 Summary

Experimental progress has resulted in all three angles of the CKM unitarity triangle being measured with good accuracy, with  $\beta$  known to subdegree precision and both  $\alpha$  and  $\gamma$  known to about  $5^\circ$ . The constraints from these three measurements in the  $(\bar{\rho}, \bar{\eta})$  plane are shown in Fig. 76.4; further discussion and comparison with constraints from independent measurements can be found in Ref. [6]. The determinations of all three angles remain statistically limited, but it will be a challenge for experiments to ensure that this remains the case as the precision improves. Consequently, the correct treatment of sources of correlation between the measurements that go into the world average combinations is becoming increasingly important.

## References

- [1] N. Cabibbo, Phys. Rev. Lett. **10**, 531 (1963).
- [2] M. Kobayashi and T. Maskawa, Prog. Theor. Phys. **49**, 652 (1973).
- [3] C. Jarlskog, Phys. Rev. Lett. **55**, 1039 (1985).
- [4] Y. Amhis *et al.* (HFLAV), Eur. Phys. J. **C77**, 895 (2017), [arXiv:1612.07233].
- [5] See the review on “Semileptonic  $b$ -Hadron Decays, Determination of  $V_{cb}$ ,  $V_{ub}$ ” in this Review.
- [6] See the review on “Cabibbo-Kobayashi-Maskawa Mixing Matrix,” in this Review.
- [7] See the review on “ $CP$  Violation in the Quark Sector,” in this Review.

- [8] See the review on “ $B^0-\bar{B}^0$  Mixing” in this *Review*.
- [9] A. Carter and A. Sanda, Phys. Rev. **D23**, 1567 (1981).
- [10] I. Bigi and A. Sanda, Nucl. Phys. **B193**, 85 (1981).
- [11] O. Long *et al.*, Phys. Rev. **D68**, 034010 (2003), [hep-ex/0303030].
- [12] B. Aubert *et al.* (BaBar), Phys. Rev. **D79**, 072009 (2009), [arXiv:0902.1708].
- [13] I. Adachi *et al.*, Phys. Rev. Lett. **108**, 171802 (2012), [arXiv:1201.4643].
- [14] R. Aaij *et al.* (LHCb), Phys. Rev. Lett. **115**, 031601 (2015), [arXiv:1503.07089].
- [15] H.-n. Li and S. Mishima, JHEP **03**, 009 (2007), [hep-ph/0610120].
- [16] M. Jung, Phys. Rev. **D86**, 053008 (2012), [arXiv:1206.2050].
- [17] K. De Bruyn and R. Fleischer, JHEP **1503**, 145 (2015), [arXiv:1412.6834].
- [18] P. Frings, U. Nierste and M. Wiebusch, Phys. Rev. Lett. **115**, 6, 061802 (2015), [arXiv:1503.00859].
- [19] M. Ciuchini, M. Pierini and L. Silvestrini, Phys. Rev. Lett. **95**, 221804 (2005), [hep-ph/0507290].
- [20] S. Faller *et al.*, Phys. Rev. **D79**, 014030 (2009), [arXiv:0809.0842].
- [21] Z. Ligeti and D. Robinson, Phys. Rev. Lett. **115**, 251801 (2015), [arXiv:1507.06671].
- [22] I. Adachi *et al.* (BaBar, Belle), Phys. Rev. Lett. **121**, 261801 (2018), [arXiv:1804.06152].
- [23] I. Adachi *et al.* (BaBar, Belle), Phys. Rev. **D98**, 112012 (2018), [arXiv:1804.06153].
- [24] M. Antonelli *et al.*, Phys. Rept. **494**, 197 (2010), [arXiv:0907.5386].
- [25] M. Gronau and D. London, Phys. Rev. Lett. **65**, 3381 (1990).
- [26] R. Aaij *et al.* (LHCb), Phys. Rev. **D98**, 032004 (2018), [arXiv:1805.06759].
- [27] J. P. Lees *et al.* (BaBar), Phys. Rev. **D87**, 052009 (2013), [arXiv:1206.3525].
- [28] I. Adachi *et al.* (Belle), Phys. Rev. **D88**, 092003 (2013), [arXiv:1302.0551].
- [29] J. Charles *et al.*, Eur. Phys. J. **C77**, 574 (2017), [arXiv:1705.02981].
- [30] T. Julius *et al.* (Belle), Phys. Rev. **D96**, 032007 (2017), [arXiv:1705.02083].
- [31] B. Aubert *et al.* (BaBar), Phys. Rev. **D76**, 052007 (2007), [arXiv:0705.2157].
- [32] P. Vanhoefer *et al.* (Belle), Phys. Rev. **D93**, 032010 (2016), [Addendum *ibid.* **D94** 099903 (2016)], [arXiv:1510.01245].
- [33] B. Aubert *et al.* (BaBar), Phys. Rev. **D78**, 071104 (2008), [arXiv:0807.4977].
- [34] A. E. Snyder and H. R. Quinn, Phys. Rev. **D48**, 2139 (1993).
- [35] J. P. Lees *et al.* (BaBar), Phys. Rev. **D88**, 012003 (2013), [arXiv:1304.3503].
- [36] A. Kusaka *et al.* (Belle), Phys. Rev. Lett. **98**, 221602 (2007), [hep-ex/0701015].
- [37] A. Kusaka *et al.* (Belle), Phys. Rev. **D77**, 072001 (2008), [arXiv:0710.4974].
- [38] M. Gronau and J. Zupan, Phys. Rev. **D71**, 074017 (2005), [hep-ph/0502139].
- [39] S. Gardner, Phys. Rev. **D72**, 034015 (2005), [hep-ph/0505071].
- [40] A. Falk *et al.*, Phys. Rev. **D69**, 011502 (2004), [hep-ph/0310242].
- [41] J. Brod and J. Zupan, JHEP **01**, 051 (2014), [arXiv:1308.5663].
- [42] M. Gronau and D. London, Phys. Lett. **B253**, 483 (1991).
- [43] M. Gronau and D. Wyler, Phys. Lett. **B265**, 172 (1991).
- [44] See the review on “ $D^0-\bar{D}^0$  Mixing” in this *Review*.
- [45] M. Nayak *et al.*, Phys. Lett. **B740**, 1 (2015), [arXiv:1410.3964].
- [46] D. Atwood, I. Dunietz and A. Soni, Phys. Rev. Lett. **78**, 3257 (1997), [hep-ph/9612433].
- [47] D. Atwood, I. Dunietz and A. Soni, Phys. Rev. **D63**, 036005 (2001), [hep-ph/0008090].
- [48] D. Atwood and A. Soni, Phys. Rev. **D68**, 033003 (2003), [hep-ph/0304085].
- [49] Y. Grossman, Z. Ligeti and A. Soffer, Phys. Rev. **D67**, 071301 (2003), [hep-ph/0210433].
- [50] A. Giri *et al.*, Phys. Rev. **D68**, 054018 (2003), [hep-ph/0303187].
- [51] A. Bondar, *Proceedings of BINP special analysis meeting on Dalitz analysis*, 24-26 Sep. 2002, unpublished.
- [52] R. Briere *et al.* (CLEO), Phys. Rev. **D80**, 032002 (2009), [arXiv:0903.1681].
- [53] J. Libby *et al.* (CLEO), Phys. Rev. **D82**, 112006 (2010), [arXiv:1010.2817].
- [54] A. Bondar and T. Gershon, Phys. Rev. **D70**, 091503 (2004), [hep-ph/0409281].
- [55] T. Gershon, Phys. Rev. **D79**, 051301 (2009), [arXiv:0810.2706].
- [56] T. Gershon and M. Williams, Phys. Rev. **D80**, 092002 (2009), [arXiv:0909.1495].
- [57] R. Aleksan, I. Dunietz and B. Kayser, Z. Phys. **C54**, 653 (1992).
- [58] R. Aaij *et al.* (LHCb), Phys. Lett. **B777**, 16 (2018), [arXiv:1708.06370].
- [59] R. Aaij *et al.* (LHCb), Phys. Lett. **B760**, 117 (2016), [arXiv:1603.08993].
- [60] P. del Amo Sanchez *et al.* (BaBar), Phys. Rev. Lett. **105**, 121801 (2010), [arXiv:1005.1096].
- [61] A. Poluektov *et al.* (Belle), Phys. Rev. **D81**, 112002 (2010), [arXiv:1003.3360].
- [62] R. Aaij *et al.* (LHCb), JHEP **08**, 176 (2018), [Erratum *ibid.* **10**, 107 (2018)], [arXiv:1806.01202].
- [63] M. Rama, Phys. Rev. **D89**, 014021 (2014), [arXiv:1307.4384].
- [64] M. Bjørn and S. Malde, JHEP **07**, 106 (2019), [arXiv:1904.01129].



## 77. Spectroscopy of Mesons Containing Two Heavy Quarks

Revised March 2020 by S. Eidelman (Budker Inst., Novosibirsk; Novosibirsk U.), C. Hanhart (Jülich), J. J. Hernández-Rey (IFIC, Valencia), R.E. Mitchell (Indiana U.), S. Navas (Dp.de Física. U. de Granada) and C. Patrignani (Bologna U.).

A golden age for heavy quarkonium physics dawned at the turn of this century, initiated by the confluence of exciting advances in quantum chromodynamics (QCD) and an explosion of related experimental activity. The subsequent broad spectrum of breakthroughs, surprises, and continuing puzzles had not been anticipated. Since that time CLEO-c, BESIII and the B-factories, recently joined by ATLAS, CMS and LHCb, have continued to make groundbreaking observations. For an extensive presentation of the status of heavy quarkonium physics, the reader is referred to several reviews [1–6]. This note focuses on experimental developments in heavy quarkonium spectroscopy with very few theoretical comments. Possible theoretical interpretations of the states not predicted by the quark model are presented in the minireview on non- $q\bar{q}$  states. Note that in this review we follow the new naming scheme for hadrons (see the review “Naming scheme for hadrons” in the current edition).

This minireview covers the newly discovered states, where “newly” refers to the period since 2002. In earlier versions of this write-up the particles were sorted according to an assumed *conventional* or *unconventional* nature with respect to the quark model. However, since this classification is not always unambiguous, we here follow Ref. [8] and sort the states into three groups, namely states below (*cf.* Table 77.1), near (*cf.* Table 77.2) and above (*cf.* Table 77.3) the lowest open-flavor thresholds.

Table 77.1 lists properties of newly observed heavy quarkonium states located below the lowest open-flavor thresholds. Those are expected to be (at least prominently) conventional quarkonia. The  $h_c(1P)$  is the  $^1P_1$  state of charmonium, singlet partner of the long-known  $\chi_{cJ}$  triplet  $^3P_J$ . The  $\eta_c(2S)$  is the first excited state of the pseudoscalar ground state  $\eta_c(1S)$ , lying just below the mass of its vector counterpart,  $\psi(2S)$ .

Although  $\eta_c(2S)$  measurements began to converge towards a mass and a width some time ago, refinements are still in progress. In particular, Belle [9] has revisited its analysis of  $B \rightarrow K\eta_c(2S)$ ,  $\eta_c(2S) \rightarrow K\bar{K}\pi$  decays with more data and methods that account for interference between the above decay chain, an equivalent one with the  $\eta_c(1S)$  instead, and one with no intermediate resonance. The net effect of this interference is far from trivial; it shifts the apparent mass by  $\sim +10$  MeV and inflates the apparent width by a factor of six. The updated  $\eta_c(2S)$  mass and width are in better accordance with other measurements than the previous treatment [10], which did not include interference. Complementing this measurement in  $B$ -decay, BaBar [11] updated their previous [12]  $\eta_c(2S)$  mass and width measurements in two-photon production, where interference effects, judging from studies of  $\eta_c(1S)$ , appear to be small. In combination, precision on the  $\eta_c(2S)$  mass has improved dramatically. The currently most accurate individual mass measurement is from LHCb using  $B^+ \rightarrow K^+\bar{p}p$  [13].

Belle reported an observation of the  $\psi_2(1D)$  decaying to  $\gamma\chi_{c1}$  with  $J^{PC}$  presumed to be  $2^{--}$  [14]. This state is listed in Table 77.1 as  $\psi_2(3823)$ . Its existence was confirmed with high significance by BESIII [15]. While the negative C-parity is indeed established by its observed decay channel, the assignment of  $J = 2$  was done by matching to the closest quark model state. This assignment therefore requires experimental confirmation.

The  $1^1D_2$  state, or the  $\eta_{c2}(1D)$ , with a mass expected near 3820 MeV, has not been observed yet. Recently Belle performed its search in  $B \rightarrow \eta_{c2}(1D)K(\pi)$  decays in the mass range 3795–3845 MeV and found no signal [16]. Thus, the  $\eta_{c2}(1D)$  remains the only unobserved conventional charmonium state that does not have open-charm decays.

A new  $c\bar{b}$  state was discovered by the ATLAS Collaboration [17]. Its properties are consistent with expectations for the first excited state of the  $B_c^\pm$  meson, the  $B_c^\pm(2S)$ . The real picture appears to be more complicated. The ATLAS state was observed at  $6842 \pm 6$  MeV. Five years later, the CMS collaboration investigated the  $B_c^\pm \pi^+ \pi^-$  invariant mass spectrum and observed two close signals consistent with the  $B_c^{*+}(2S)$  and  $B_c^+(2S)$  states [18]. The two

peaks are well resolved (a significance of 6.5 standard deviations), with a measured mass difference of  $\Delta M = 29.1 \pm 1.5(\text{stat}) \pm 0.7(\text{syst})$  MeV. The mass of the right peak,  $B_c^+(2S)$ , is measured to be  $6871.0 \pm 1.2(\text{stat}) \pm 0.8(\text{syst}) \pm 0.8(B_c^+)$  MeV, where the last term is the uncertainty in the world-average  $B_c^+$  mass. Since the low-energy photon emitted in the  $B_c^{*+} \rightarrow B_c^+ + \gamma$  radiative decay is not reconstructed, the observed  $B_c^{*+}(2S)$  peak has a mass lower than the true value, which remains unknown. Therefore the  $B_c^{*+}(2S)$  does not yet appear in the listings. LHCb confirmed the CMS results and measured masses with higher precision [19]. Their signal corresponding to the  $B_c^{*+}(2S)$  is observed at  $6841.2 \pm 0.6(\text{stat}) \pm 0.1(\text{syst}) \pm 0.8(B_c^+)$  MeV with a significance of 6.3 standard deviations. Also here the low energy photon was not observed. The data also show a hint ( $2.2\sigma$ ) for a second structure consistent with the  $B_c^+(2S)$  with a mass  $31.0 \pm 1.4(\text{stat}) \pm 0.0(\text{syst})$  higher.

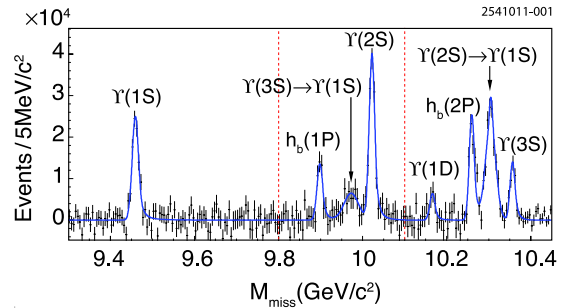


Figure 77.1: From Belle [20], the mass recoiling against  $\pi^+\pi^-$  pairs,  $M_{\text{miss}}$ , in  $e^+e^-$  collision data taken near the peak of the  $\Upsilon(10860)$  (points with error bars). The smooth combinatorial and  $K_S^0 \rightarrow \pi^+\pi^-$  background contributions have been subtracted. The fit to the various labeled signal contributions is overlaid (curve). Adapted from [20] with kind permission, copyright (2011) The American Physical Society.

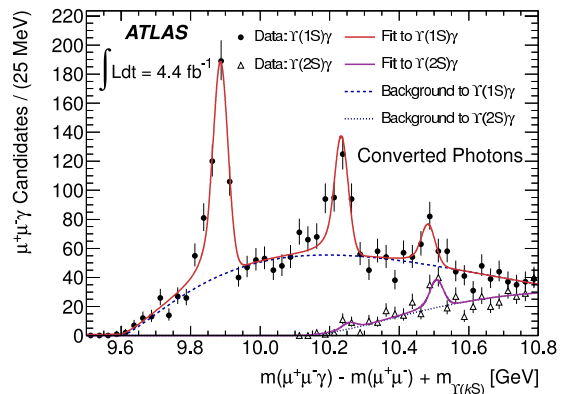


Figure 77.2: From ATLAS [21]  $pp$  collision data (points with error bars) taken at  $\sqrt{s} = 7$  TeV, the effective mass of  $\chi_{bJ}(1P, 2P, 3P) \rightarrow \gamma\Upsilon(1S, 2S)$  candidates in which  $\Upsilon(1S, 2S) \rightarrow \mu^+\mu^-$  and the photon is reconstructed as an  $e^+e^-$  conversion in the tracking system. Fits (smooth curves) show significant signals for each triplet ( $J$ -merged) on top of a smooth background. From [21] with kind permission, copyright (2012) The American Physical Society.

The ground state of bottomonium,  $\eta_b(1S)$ , was confirmed with a second observation of more than  $5\sigma$  significance at Belle. In addition, the same experiment collected strong evidence for the  $\eta_b(2S)$  [22], but it still needs experimental confirmation at the  $5\sigma$  level.

Using dipion transitions from the  $\Upsilon(10860)$  (Fig. 77.1), Belle simultaneously discovered the  $h_b(1P)$ , the bottomonium counterpart of the  $h_c(1P)$ , and the next excited state, the  $h_b(2P)$  [20].

**Table 77.1:** New states below the open-flavor thresholds in the  $c\bar{c}$ ,  $b\bar{c}$ , and  $b\bar{b}$  regions, ordered by mass. Masses  $m$  and widths  $\Gamma$  represent the PDG20 weighted averages with statistical and systematic uncertainties added in quadrature. In the Production column, the state is always denoted by  $X$ . Ellipses (...) indicate inclusively selected event topologies, *i.e.*, additional particles not directly detected by experiment. A question mark (?) indicates an unmeasured value. The Discovery Year column gives the date of the first measurement cited. The Summary Table column indicates whether or not the state appears in the summary tables, usually requiring at least two independent experiments with significance of  $>5\sigma$ . Refer to the particle listings for references and further information.

PDG Name	Former Name(s)	$m$ (MeV)	$\Gamma$ (MeV)	$I^G(J^{PC})$	Production	Decay	Discovery Year	Summary Table
$h_c(1P)$		$3525.38 \pm 0.11$	$0.7 \pm 0.35$	$0^-(1^{+-})$	$\psi(2S) \rightarrow \pi^0 X$ $p\bar{p} \rightarrow X$	$\gamma\eta_c(1S)$ hadrons	2004	YES
$\eta_c(2S)$		$3639.2 \pm 1.2$	$11.3^{+3.2}_{-2.9}$	$0^+(0^{-+})$	$e^+e^- \rightarrow \pi\pi X$ $B \rightarrow KX$	(see listings) $K_S^0 K^- \pi^+$ $\bar{p}p$ hadrons	2002	YES
$\psi_2(3823)$	$X(3823)$	$3822.2 \pm 1.2$	$< 16$	$0^-(2^{--})$	$e^+e^- \rightarrow e^+e^-X$ $e^+e^- \rightarrow J/\psi X$ $B \rightarrow KX$ $e^+e^- \rightarrow \pi^+\pi^-X$	(see listings) $\gamma\chi_{c1}(1P)$	2013	YES
$B_c^+$		$6274.9 \pm 0.8$	?	$0(0^-)$	$\bar{p}p \rightarrow X...$ $pp \rightarrow X...$	$\pi^+ J/\psi$ (see listings)	2007	YES
$B_c^+(2S)$		$6842 \pm 6$	?	$0(0^-)$	$pp \rightarrow X...$	$B_c^+ \pi^+ \pi^-$	2014	NO
$\eta_b(1S)$		$9399.0 \pm 1.3$	$10^{+5}_{-4}$	$0^+(0^{-+})$	$\Upsilon(2S, 3S) \rightarrow \gamma X$ $h_b(1P, 2P) \rightarrow \gamma X$		2008	YES
$h_b(1P)$		$9899.3 \pm 0.8$	?	$0^-(1^{+-})$	$\Upsilon(10860) \rightarrow \pi^+\pi^-X$ $\Upsilon(3S) \rightarrow \pi^0 X$	$\gamma\eta_b(1S)$	2011	YES
$\eta_b(2S)$		$9999.0^{+4.5}_{-4.0}$	$< 24$	$0^+(0^{-+})$	$h_b(2P) \rightarrow \gamma X$	hadrons	2012	NO
$\Upsilon_2(1D)$		$10163.7 \pm 1.4$	?	$0^-(2^{--})$	$\Upsilon(3S) \rightarrow \gamma\gamma X$ $\Upsilon(10860) \rightarrow \pi^+\pi^-X$	$\gamma\gamma\Upsilon(1S)$ $\pi^+\pi^-\Upsilon(1S)$	2004	YES
$h_b(2P)$		$10259.8 \pm 1.2$	?	$0^-(1^{+-})$	$\Upsilon(10860) \rightarrow \pi^+\pi^-X$	$\gamma\eta_b(1S, 2S)$	2011	NO
$\chi_{b1}(3P)$		$10512.1 \pm 2.3$	?	$0^+(1^{++})$	$pp \rightarrow X...$	$\gamma\mu^+\mu^-$	2011	YES

**Table 77.2:** As in Table 77.1, but for new states near the first open-flavor thresholds in the  $c\bar{c}$  and  $b\bar{b}$  regions, ordered by mass. Updated from [7] with kind permission, copyright (2011), Springer, and [8] with kind permission from the authors.

PDG Name	Former Name(s)	$m$ (MeV)	$\Gamma$ (MeV)	$I^G(J^{PC})$	Production	Decay	Discovery Year	Summary Table
$\chi_{c1}(3872)$	$X(3872)$	$3871.69 \pm 0.17$	$< 1.2$	$0^+(1^{++})$	$B \rightarrow KX$ $p\bar{p} \rightarrow X...$ $pp \rightarrow X...$ $e^+e^- \rightarrow \gamma X$	$\pi^+\pi^- J/\psi$ $3\pi J/\psi$ $D^{*0}\bar{D}^0$ $\gamma J/\psi$ $\gamma\psi(2S)$ $\pi^0\chi_{c1}(1P)$	2003	YES
$Z_c(3900)$		$3886.6 \pm 2.4$	$28.2 \pm 2.6$	$1^+(1^{+-})$	$\psi(4260) \rightarrow \pi^- X$ $\psi(4260) \rightarrow \pi^0 X$	$\pi^+ J/\psi$ $\pi^0 J/\psi$ $(D\bar{D}^*)^+$ $(D\bar{D}^*)^0$	2013	YES
$X(4020)$	$Z_c(4020)$	$4024.1 \pm 1.9$	$13 \pm 5$	$1^+(?^{? -})$	$\psi(4260, 4360) \rightarrow \pi^- X$ $\psi(4260, 4360) \rightarrow \pi^0 X$	$\pi^+ h_c$ $\pi^0 h_c$ $(D^*\bar{D}^*)^+$ $(D^*\bar{D}^*)^0$	2013	YES
$Z_b(10610)$		$10607.2 \pm 2.0$	$18.4 \pm 2.4$	$1^+(1^{+-})$	$\Upsilon(10860) \rightarrow \pi^- X$ $\Upsilon(10860) \rightarrow \pi^0 X$	$\pi^+\Upsilon(1S, 2S, 3S)$ $\pi^0\Upsilon(1S, 2S, 3S)$ $\pi^+ h_b(1P, 2P)$ $(B\bar{B}^*)^+$	2011	YES
$Z_b(10650)$		$10652.2 \pm 1.5$	$11.5 \pm 2.2$	$1^+(1^{+-})$	$\Upsilon(10860) \rightarrow \pi^- X$	$\pi^+\Upsilon(1S, 2S, 3S)$ $\pi^+ h_b(1P, 2P)$ $(B^*\bar{B}^*)^+$	2011	YES

**Table 77.3:** As in Table 77.1, but for new states above the first open-flavor thresholds in the  $c\bar{c}$  and  $b\bar{b}$  regions, ordered by mass.

PDG Name	Former Name(s)	$m$ (MeV)	$\Gamma$ (MeV)	$I^G(J^{PC})$	Production	Decay	Discovery Year	Summary Table
$\psi_3$ (3842)		$3842.7 \pm 0.2$	$2.79 \pm 0.6$	$0^+(3^{--})^*$	$pp \rightarrow X\dots$	$D\bar{D}$	2019	NO
$\chi_{c0}$ (3860)		$3862_{-35}^{+48}$	$201_{-106}^{+177}$	$0^+(0^{++})$	$e^+e^- \rightarrow J/\psi X$	$D\bar{D}$	2017	NO
$X$ (3915)	$\chi_{c0}$ (3915), $Y$ (3940)	$3918.4 \pm 1.9$	$20 \pm 5$	$0^+(0/2^{++})$	$B \rightarrow KX$ $e^+e^- \rightarrow e^+e^-X$	$\omega J/\psi$	2004	YES
$\chi_{c2}$ (3930)	$\chi_{c2}$ (2P), $Z$ (3930)	$3927.2 \pm 2.6$	$24 \pm 6$	$0^+(2^{++})$	$e^+e^- \rightarrow e^+e^-X$	$D\bar{D}$	2005	YES
$X$ (3940)		$3942_{-8}^{+9}$	$37_{-17}^{+27}$	$??(???)$	$e^+e^- \rightarrow J/\psi X$	$D\bar{D}^*$	2007	NO
$X$ (4050) $^\pm$	$Z_1$ (4050)	$4051_{-43}^{+24}$	$82_{-28}^{+51}$	$1^-(??^+)$	$B \rightarrow KX$	$\pi^+\chi_{c1}(1P)$	2008	NO
$X$ (4055) $^\pm$	$Z_c$ (4055)	$4054 \pm 3$	$45 \pm 13$	$1^+(??^-)$	$e^+e^- \rightarrow \pi^-X$	$\pi^+\psi(2S)$	2017	NO
$\chi_{c1}$ (4140)	$Y$ (4140)	$4146.8 \pm 2.4$	$22_{-7}^{+8}$	$0^+(1^{++})$	$B^+ \rightarrow K^+X$ $e^+e^- \rightarrow e^+e^-X$	$\phi J/\psi$	2009	YES
$X$ (4160)		$4156_{-25}^{+29}$	$139_{-65}^{+113}$	$??(???)$	$e^+e^- \rightarrow J/\psi X$	$D\bar{D}^*$	2007	NO
$Z_c$ (4200)		$4196_{-32}^{+35}$	$370_{-149}^{+99}$	$1^+(1^{+-})$	$\bar{B}^0 \rightarrow K^-X$	$J/\psi\pi^+$	2014	NO
$\psi$ (4230)	$Y$ (4230)	$4218_{-4}^{+5}$	$59_{-10}^{+12}$	$0^-(1^{--})$	$e^+e^- \rightarrow X$	$\omega\chi_{c0}(1P)$ $\pi^+\pi^-\psi(2S)$ $\pi^+\pi^-h_c(1P)$	2015	YES
$R_{c0}$ (4240)	$Z_c$ (4240)	$4239_{-21}^{+48}$	$220_{-88}^{+118}$	$1^+(0^{--})$	$\bar{B}^0 \rightarrow K^-X$	$\pi^+\psi(2S)$	2014	NO
$X$ (4250) $^\pm$	$Z_2$ (4250)	$4248_{-45}^{+185}$	$177_{-72}^{+321}$	$1^-(??^+)$	$B \rightarrow KX$	$\pi^+\chi_{c1}(1P)$	2008	NO
$\psi$ (4260)	$Y$ (4260)	$4230 \pm 8$	$55 \pm 19$	$0^-(1^{--})$	$e^+e^- \rightarrow X$	$\pi\pi J/\psi$ $\gamma\chi_{c0}(3872)$	2005	NO
$\chi_{c1}$ (4274)	$Y$ (4274)	$4274_{-6}^{+8}$	$49 \pm 12$	$0^+(1^{++})$	$B^+ \rightarrow K^+X$	$\phi J/\psi$	2011	NO
$X$ (4350)		$4350.6_{-5.1}^{+4.6}$	$13.3_{-10.0}^{+18.4}$	$0^+(??^+)$	$e^+e^- \rightarrow e^+e^-X$	$\phi J/\psi$	2009	NO
$\psi$ (4360)	$Y$ (4360)	$4368 \pm 13$	$96 \pm 7$	$0^-(1^{--})$	$e^+e^- \rightarrow X$	$\pi^+\pi^-\psi(2S)$	2007	YES
$\psi$ (4390)	$Y$ (4390)	$4391.5_{-6.9}^{+6.4}$	$139.5_{-20.6}^{+16.2}$	$0^-(1^{--})$	$e^+e^- \rightarrow X$	$\pi^+\pi^-h_c(1P)$	2017	NO
$Z_c$ (4430)		$4478_{-18}^{+15}$	$181 \pm 31$	$1^+(1^{+-})$	$\bar{B}^0 \rightarrow K^-X$	$\pi^+\psi(2S)$ $\pi^+J/\psi$	2007	YES
$\chi_{c0}$ (4500)	$X$ (4500)	$4506_{-19}^{+16}$	$92_{-29}^{+30}$	$0^+(0^{++})$	$B^+ \rightarrow K^+X$	$\phi J/\psi$	2017	NO
$\psi$ (4660)	$Y$ (4660), $X$ (4630)	$4643 \pm 9$	$72 \pm 11$	$0^-(1^{--})$	$e^+e^- \rightarrow X$	$\pi^+\pi^-\psi(2S)$ $A_c^+A_c^-$ $D_s^+D_{s1}(2536)$	2007	YES
$\chi_{c0}$ (4700)	$X$ (4700)	$4704_{-26}^{+17}$	$120_{-45}^{+52}$	$0^+(0^{++})$	$B^+ \rightarrow K^+X$	$\phi J/\psi$	2017	NO
$\Upsilon$ (10753)		$10752.7 \pm 5.9$	$35.5_{-11.8}^{+18.0}$	$0^-(1^{--})$	$e^+e^- \rightarrow X$	$\pi\pi\Upsilon(1S, 2S, 3S)$	2019	NO
$\Upsilon$ (10860)	$\Upsilon$ (5S)	$10889.9_{-2.6}^{+3.2}$	$51_{-7}^{+6}$	$0^-(1^{--})$	$e^+e^- \rightarrow X$	$B_{(s)}^{(*)}\bar{B}_{(s)}^{(*)}(\pi)$ $\pi\pi\Upsilon(1S, 2S, 3S)$ $\pi^+\pi^-h_b(1P, 2P)$ $\eta\Upsilon(1S, 2S)$ $\pi^+\pi^-\Upsilon(1D)$	1985	YES
$\Upsilon$ (11020)	$\Upsilon$ (6S)	$10992.9_{-3.1}^{+10.0}$	$49_{-15}^{+9}$	$0^-(1^{--})$	$e^+e^- \rightarrow X$	$B_{(s)}^{(*)}\bar{B}_{(s)}^{(*)}(\pi)$ $\pi\pi\Upsilon(1S, 2S, 3S)$ $\pi^+\pi^-h_b(1P, 2P)$	1985	YES

\*Quantum numbers fixed from the quark model and need confirmation.

The same analysis also showed the  $\Upsilon_2(1D)$ , the lowest-lying  $D$ -wave triplet of the  $b\bar{b}$  system. The search for the  $h_b(1P)$  was directly inspired by a CLEO result [23], which found a surprisingly copious production of  $e^+e^- \rightarrow \pi^+\pi^-h_c(1P)$  as well as an indication that  $\psi(4230) \rightarrow \pi^+\pi^-h_c(1P)$  occurs at a comparable rate with the signature mode,  $\psi(4230) \rightarrow \pi^+\pi^-J/\psi$ . The presence of  $\Upsilon(nS)$  peaks in Fig. 77.1 at rates two orders of magnitude larger than expected, along with separate studies with exclusive decays  $\Upsilon(nS) \rightarrow \mu^+\mu^-$ , allow precise calibration of the  $\pi^+\pi^-$  recoil mass spectrum and very accurate measurements of  $h_b(1P)$  and  $h_b(2P)$  masses. Both corresponding hyperfine splittings are consistent with zero within an uncertainty of about 1.5 MeV (lowered to  $\pm 1.1$  MeV for  $h_b(1P)$  in Ref. [24]).

We no longer mention a hypothetical  $Y_b(10888)$  state since a new analysis of the  $\Upsilon(10860)$  energy range does not show evidence for an additional state with a mass different from the mass of the  $\Upsilon(10860)$  [25]. After the mass of the  $\eta_b(1S)$  was shifted upwards by about 10 MeV based on the new Belle measurements [22] [26], all of the bottomonium states mentioned above fit into their respective spectroscopies roughly where expected. An independent experimental confirmation of the shifted masses came from the Belle observation of  $\Upsilon(4S) \rightarrow \eta h_b(1P)$  [26].

The  $\chi_{bJ}(nP)$  states have been observed at the LHC by ATLAS [21] and confirmed by D0 [27] for  $n = 1, 2, 3$ , although in each case the three  $J$  states are not distinguished from one another. Events are sought which have both a photon and an  $\Upsilon(1S, 2S) \rightarrow \mu^+\mu^-$  candidate which together form a mass in the  $\chi_b$  region. All three  $J$ -merged peaks are observed with a significance in excess of  $6\sigma$  for both unconverted and converted photons. The mass plot for converted photons, which provide better mass resolution, is shown in Fig. 77.2. This marks the first observation of the  $\chi_{bJ}(3P)$  triplet, quite near the expected mass. A precise confirmation of this result came from LHCb [28].

A large number of states was discovered recently both near and above the lowest open-flavor thresholds. They are displayed in Table 77.2 and Table 77.3, respectively. With the exception of the tensor state located at 3930 MeV, now called  $\chi_{c2}(3930)$ , which has properties consistent with those expected for the  $\chi_{c2}(2P)$ , none of these states can easily be assigned a place in the quark model spectrum of charmonia or bottomonia. At the same time, these states have no universally accepted unconventional interpretation either. The  $\chi_{c1}(3872)$ , also known as  $X(3872)$ , is widely studied and seen in many transitions — *c.f.* Table 77.2. Yet its interpretation demands additional experimental attention: after the quantum numbers were fixed at LHCb [29, 30], the next experimental challenge will be a measurement of its lineshape.

LHCb observed in prompt proton-proton collisions a new narrow charmonium state, the  $X(3842)$  resonance, in the decay modes  $X(3842) \rightarrow D^0\bar{D}^0$  and  $X(3842) \rightarrow D^+D^-$  [31]. The mass and width of this state are measured to be  $(3842.71 \pm 0.16 \pm 0.12)$  MeV and  $(2.79 \pm 0.51 \pm 0.35)$  MeV, respectively. The observed mass and narrow width is consistent with the interpretation of the new state as the unobserved spin-3  $\psi_3(1^3D_3)$  charmonium state. Accordingly the state got the name  $\psi_3(3842)$  in the listings with the remark that the quantum numbers were fixed from the quark model and need to be confirmed.

Another state (referred to here as the  $X(3915)$ ), was discovered at 3915 MeV [32] and from a subsequent measurement its quantum numbers were determined to be  $J^{PC} = 0^{++}$  [33]. This suggests it may be the  $\chi_{c0}(2P)$  quark model state, but this interpretation is not generally accepted [34, 35]. In addition, it was pointed out in Ref. [36] that if the assumption of helicity-2 dominance is abandoned and instead one allows for a sizable helicity-0 component, a  $J^{PC} = 2^{++}$  assignment is possible. This could imply that the state at 3930 MeV (referred to here as the  $\chi_{c2}(3930)$ ) is actually identical to the one at 3915 MeV—but to explain the large helicity-0 component a sizable portion of non- $q\bar{q}$  is necessary [36]. Because of this analysis, the name of the state was changed from  $\chi_{c0}(3915)$  back to  $X(3915)$ . An alternative candidate for the  $\chi_{c0}(2P)$  (referred to here as the  $\chi_{c0}(3860)$ ) was reported in Ref. [37] with properties more consistent with expectation: its mass is close to the potential model expectations, it decays to  $D\bar{D}$ , and the preferred quantum numbers are  $J^{PC} = 0^{++}$  (this hypothesis is

favored over the  $2^{++}$  one with a  $2.5\sigma$  significance).

The  $\psi(4260)$ , also known as  $Y(4260)$ , and the  $\psi(4360)$ , also known as  $Y(4360)$ , are vector states decaying to  $\pi^+\pi^-J/\psi$  and  $\pi^+\pi^-\psi(2S)$ , respectively, yet, unlike most conventional vector charmonia, they do not correspond to enhancements in the  $e^+e^-$  hadronic cross section nor decay to  $D\bar{D}$ . Recently BESIII produced a high-accuracy data set for  $e^+e^- \rightarrow \pi^+\pi^-J/\psi$  [38], demonstrating that the lineshape in this mass range is highly non-trivial. The latter observation was interpreted by the authors as the presence of two states. However, this lineshape is also consistent with other possible interpretations, such as one assuming a molecular structure for the  $\psi(4260)$  [39]. The data of Ref. [38] also called for a significant downward shift of the mass of  $\psi(4260)$  no longer justifying a distinction between  $\psi(4260)$  and  $\psi(4230)$ . The latter was discovered earlier in various decay modes, amongst others  $h_c(1P)\pi\pi$  [40]. The original mass parameter for the  $\psi(4260)$  was the result of a fit to the  $\pi^+\pi^-J/\psi$  cross section using a symmetric Breit-Wigner line shape [41]. Therefore, starting from the 2020 Edition of the Review of Particle Physics, we list the measurement of Ref. [38] under the node  $\psi(4230)$  and promoted the  $\psi(4230)$  to the summary tables to replace the  $\psi(4260)$ . BESIII also observed the  $\chi_{c1}(3872)$ , also known as  $X(3872)$ , in  $e^+e^- \rightarrow \gamma\chi_{c1}(3872)$  in the  $\psi(4230)$  mass range [42], which could allow for additional insight into the structure of both the  $\psi(4230)$  as well as the  $\chi_{c1}(3872)$  (*c.f.* the minireview on non- $q\bar{q}$  states). BESIII also performed a recent study of the process  $e^+e^- \rightarrow \pi^+\pi^-\psi(2S)$  and found evidence for a lower mass state, possibly the  $\psi(4230)$ , in addition to the more dominant  $\psi(4360)$  [43].

Note that the data of Ref. [38] does not show any indication of the  $Y(4008)$  reported by Belle — the data in this region can either be fit with a non-resonant background component or a much wider resonance at lower mass. Also see the analysis of the  $Y(4008)$  region in Ref. [44], where a wide resonance is also extracted.

Another interesting question is whether a heavier  $\pi^+\pi^-\psi(2S)$  state, the  $\psi(4660)$ , discovered by Belle [45, 46] and confirmed by BaBar [47], is identical to the  $\Lambda_c^+\Lambda_c^-$  state observed by Belle with a nearby mass and width [48]. Most probably it is, with  $\Lambda_c^+\Lambda_c^-$  just being one more decay mode of the  $\psi(4660)$  (*c.f.* the minireview on non- $q\bar{q}$  states for more detail). Note that this is the interpretation adopted in the particle listings.

Belle reported the first observation of a vector charmoniumlike state decaying to  $D_s^+D_{s1}(2536)$  with a significance of  $5.9\sigma$  [49]. Its measured mass and width are  $(4625.9_{-6.0}^{+6.2} \pm 0.4)$  MeV and  $(49.8_{-11.5}^{+13.9} \pm 4.0)$  MeV, respectively, consistent with those of  $\psi(4660)$ . Therefore these new data appear now as additional decay mode of  $\psi(4660)$  in the listings.

Based on a full amplitude analysis of  $B^0 \rightarrow K^+\pi^-\psi(2S)$  decays, Belle determined the spin-parity of the  $Z_c(4430)$  to be  $J^P = 1^+$  [50]. From their study of  $B^0 \rightarrow K^+\pi^-J/\psi$  decays, Belle also found evidence for the decay mode  $Z_c(4430) \rightarrow \pi J/\psi$  [51], which has an order of magnitude lower branching fraction than the discovery mode  $Z_c(4430) \rightarrow \pi\psi(2S)$ . In the same analysis, Belle also reported evidence for one more charged state, dubbed  $Z_c(4200)$ , decaying to  $\pi J/\psi$ . The existence of the  $Z_c(4430)$  in  $\pi\psi(2S)$  as well as its quantum number assignments were confirmed at LHCb [52] with much higher statistics. Improved values for the mass and width of the  $Z_c(4430)$  from LHCb are consistent with earlier measurements; the experiment even reports a resonant behavior of the  $Z_c(4430)$  amplitude. The  $Z_c(4430)$  was not confirmed (or excluded) by BaBar [53].

Belle also reported an observation of two charged states decaying to  $\pi\chi_{c1}$  in an analysis of  $B^0 \rightarrow K^+\pi^-\chi_{c1}$  decays [54]. These were originally called the  $Z_1(4050)^\pm$  and the  $Z_2(4250)^\pm$ , but are referred to in Table 77.3 as  $X(4050)^\pm$  and  $X(4250)^\pm$ . These states were also not confirmed by BaBar [55]. Belle observes signals with  $5.0\sigma$  significance for both the  $Z_1(4050)^\pm$  and  $Z_2(4250)^\pm$ , whereas BABAR reports  $1.1\sigma$  and  $2.0\sigma$  effects, respectively, setting upper limits on product branching fractions that are not inconsistent with Belle's measured rates. The situation remains unresolved.

In addition to the  $Z_c$  states discussed above, in 2013 a state named  $Z_c(3900)$  was unearthed in the charmonium region at BESIII [56] and Belle [41]. The corresponding spectrum from BESIII



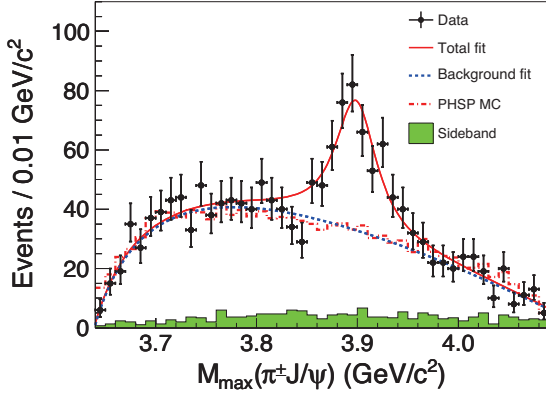


Figure 77.3:  $J/\psi\pi$  invariant mass distributions from BES-III [56]  $e^+e^-$  collision data taken near the peak of the  $Y(4260)$ . Adapted from [56] with kind permission, copyright (2013) The American Physical Society.

is shown in Fig. 77.3. Ref. [57] confirmed this finding and also provided evidence for a neutral partner. A nearby signal was also seen in the  $D\bar{D}^*$  channel [58] whose quantum numbers were fixed to  $1^{+-}$ . BESIII reported its neutral partner in both  $J/\psi\pi^0$  [59] and  $D\bar{D}^*$  [60] decay modes. The masses extracted from these experiments in different decay modes have differences reaching up to  $2\sigma$ . However, since the extraction of the mass and width parameters did not allow for an interference with the background and used Breit-Wigner line shapes, which is not justified near thresholds, there might be some additional systematic uncertainty in the mass values. Therefore in the RPP listings as well as Table 77.2, both structures appear under the name  $Z_c(3900)$ . BESIII also reported an observation of another charged state, the  $X(4020)^\pm$  (originally called  $Z_c(4020)^\pm$ ), in two decay modes —  $h_c\pi^\pm$  [61] and  $(D^*\bar{D}^*)^\pm$  [62]. The neutral partners have also been observed by BESIII in the  $h_c\pi^0$  [63] and  $(D^*\bar{D}^*)^0$  [64] final states. The  $Z_c$  states show some remarkable similarities to the  $Z_b$  states (discussed below), e.g. they decay dominantly to  $D^{(*)}\bar{D}^*$  channels. However, current analyses suggest that the mass of the  $Z_c(3900)$  might be somewhat above the  $D\bar{D}^*$  threshold. If confirmed, this feature would clearly challenge a possible  $D\bar{D}^*$ -molecular interpretation. Finally,  $3.5\sigma$  evidence for one more charged charmoniumlike state at 4055 MeV decaying into  $\psi(2S)\pi^\pm$  was reported by Belle in their analysis of the process  $e^+e^- \rightarrow \psi(2S)\pi^+\pi^-$  [46]. This state was confirmed by BESIII, although there appears to be complications in the Dalitz plot requiring further investigation [43].

The  $Y(4140)$  observed in 2008 by CDF [65] [66] was confirmed at D0 and CMS [67] [68]. However, a second structure, the  $Y(4274)$ , could not be established unambiguously. Neither of the two states was seen in  $B$  decays at Belle [69], LHCb [70] and BaBar [71] or in  $\gamma\gamma$  collisions at Belle [72]. The real breakthrough happened recently when LHCb performed a full amplitude analysis of  $B^+ \rightarrow J/\psi\phi K^+$  with  $J/\psi \rightarrow \mu^+\mu^-$ ,  $\phi \rightarrow K^+K^-$  decays and showed that the data cannot be described in a model that contains only excited kaon states decaying into  $\phi K^+$  [73] [74]. They observe two  $1^{++}$  states with masses close to those originally reported by CDF (the  $\chi_{c1}(4140)$  and  $\chi_{c1}(4274)$ ), but the width of the one at 4140 MeV is much larger. In addition, they find two significant  $0^{++}$  structures at 4500 and 4700 MeV (the  $\chi_{c0}(4500)$  and  $\chi_{c0}(4700)$ ).

New results on the  $\eta_b$ ,  $h_b$ , and  $Z_b$  mostly come from Belle [20, 22], [24–26], [75–81], all from analyses of  $121.4 \text{ fb}^{-1}$  of  $e^+e^-$  collision data collected near the peak of the  $Y(10860)$  resonance as well as from an additional  $25 \text{ fb}^{-1}$  of data collected during the scans of the c.m. energy range 10.63–11.05 GeV. The  $\eta_b$ ,  $h_b$ , and  $Z_b$  appear in the decay chains:  $Y(10860) \rightarrow \pi^- Z_b^+$ ,  $Z_b^+ \rightarrow \pi^+(b\bar{b})$ , and, when the  $b\bar{b}$  forms an  $h_b(1P)$ , frequently decaying as  $h_b(1P) \rightarrow \gamma\eta_b$ .

Belle soon noticed that, for events in the peaks of Fig. 77.1, there seemed to be two intermediate charged states. For exam-

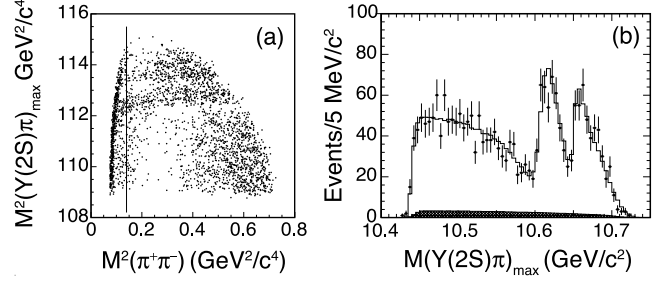


Figure 77.4: From Belle [75]  $e^+e^-$  collision data taken near the peak of the  $Y(10860)$  for events with a  $\pi^+\pi^-$ -missing mass consistent with an  $Y(2S) \rightarrow \mu^+\mu^-$ , (a) the maximum of the two possible single  $\pi^\pm$ -missing-mass-squared combinations vs. the  $\pi^+\pi^-$ -mass-squared; and (b) projection of the maximum of the two possible single  $\pi^\pm$ -missing-mass combinations (*points with error bars*) overlaid with a fit (*curve*). Events to the left of the vertical line in (a) are excluded from amplitude analysis. The hatched histogram in (b) corresponds to the combinatorial background. The two horizontal stripes in (a) and two peaks in (b) correspond to the two  $Z_b$  states. Adapted from [75] with kind permission, copyright (2011) The American Physical Society.

ple, Fig. 77.4 shows a Dalitz plot for events restricted to the  $Y(2S)$  region of  $\pi^+\pi^-$  recoil mass, with  $Y(2S) \rightarrow \mu^+\mu^-$  [75]. The two bands observed in the maximum of the two  $M[\pi^\pm Y(2S)]^2$  values also appear for  $Y(1S)$ ,  $Y(3S)$ ,  $h_b(1P)$ , and  $h_b(2P)$  samples. Belle fits all subsamples to resonant plus non-resonant amplitudes, allowing for interference (notably, between  $\pi^- Z_b^+$  and  $\pi^+ Z_b^-$ ), and finds consistent pairs of  $Z_b$  masses for all bottomonium transitions, and comparable strengths of the two states. A recent angular analysis assigned  $J^P = 1^+$  for both  $Z_b$  states [76], which must also have negative  $G$ -parity. Transitions through  $Z_b$  to the  $h_b(nP)$  saturate the observed  $\pi^+\pi^- h_b(nP)$  cross sections. While the two masses of the  $Z_b$  states as extracted from Breit-Wigner fits for the various channels are just a few MeV above the  $B^*\bar{B}$  and  $B^*\bar{B}^*$  thresholds, respectively, more refined analyses find pole locations right below the corresponding thresholds either on the physical [82] or the unphysical sheet [83]. Regardless of their proximity to the corresponding thresholds, both states predominantly decay into these open-flavor channels [78] [84] with branching fractions that exceed 80% and 70%, respectively, at 90% CL. This feature provides strong evidence for their molecular nature.

Belle reported a new measurement of the  $e^+e^- \rightarrow Y(nS)\pi^+\pi^-$  ( $n = 1, 2, 3$ ) cross sections at energies from 10.52 to 11.02 GeV [85]. They observed with a  $5.2\sigma$  significance a new structure in the energy dependence of the cross sections. If described by a Breit-Wigner function, its mass and width are found to be  $(10752.7 \pm 5.9^{+0.7}_{-1.1}) \text{ MeV}$  and  $(35.5^{+17.6+3.9}_{-11.3-3.3}) \text{ MeV}$ . The new structure could have a resonant origin and correspond to a signal for the not yet observed  $Y(3D)$  state provided  $S-D$  mixing is enhanced, or an exotic state, e.g., a compact tetraquark or hadrobottomonium. It could also be a non-resonant effect due to some complicated rescattering.

## References

- [1] R. F. Lebed, R. E. Mitchell and E. S. Swanson, Prog. Part. Nucl. Phys. **93**, 143 (2017), [arXiv:1610.04528].
- [2] A. Ali, J. S. Lange and S. Stone, Prog. Part. Nucl. Phys. **97**, 123 (2017), [arXiv:1706.00610].
- [3] F.-K. Guo *et al.*, Rev. Mod. Phys. **90**, 1, 015004 (2018), [arXiv:1705.00141].
- [4] S. L. Olsen, T. Skwarnicki and D. Zieminska, Rev. Mod. Phys. **90**, 1, 015003 (2018), [arXiv:1708.04012].
- [5] Y.-R. Liu *et al.*, Prog. Part. Nucl. Phys. **107**, 237 (2019), [arXiv:1903.11976].
- [6] N. Brambilla *et al.* (2019), [arXiv:1907.07583].
- [7] N. Brambilla *et al.*, Eur. Phys. J. **C71**, 1534 (2011), [arXiv:1010.5827].

- [8] N. Brambilla *et al.*, Eur. Phys. J. **C74**, 10, 2981 (2014), [arXiv:1404.3723].
- [9] A. Vinokurova *et al.* (Belle), Phys. Lett. **B706**, 139 (2011), [arXiv:1105.0978].
- [10] S. K. Choi *et al.* (Belle), Phys. Rev. Lett. **89**, 102001 (2002), [Erratum: Phys. Rev. Lett.89,129901(2002)], [hep-ex/0206002].
- [11] P. del Amo Sanchez *et al.* (BaBar), Phys. Rev. **D84**, 012004 (2011), [arXiv:1103.3971].
- [12] B. Aubert *et al.* (BaBar), Phys. Rev. Lett. **92**, 142002 (2004), [hep-ex/0311038].
- [13] R. Aaij *et al.* (LHCb), Phys. Lett. **B769**, 305 (2017), [arXiv:1607.06446].
- [14] V. Bhardwaj *et al.* (Belle), Phys. Rev. Lett. **111**, 3, 032001 (2013), [arXiv:1304.3975].
- [15] M. Ablikim *et al.* (BESIII), Phys. Rev. Lett. **115**, 1, 011803 (2015), [arXiv:1503.08203].
- [16] K. Chilikin *et al.* (Belle) (2020), [arXiv:2003.08335].
- [17] G. Aad *et al.* (ATLAS), Phys. Rev. Lett. **113**, 21, 212004 (2014), [arXiv:1407.1032].
- [18] A. M. Sirunyan *et al.* (CMS), Phys. Rev. Lett. **122**, 13, 132001 (2019), [arXiv:1902.00571].
- [19] R. Aaij *et al.* (LHCb), Phys. Rev. Lett. **122**, 23, 232001 (2019), [arXiv:1904.00081].
- [20] I. Adachi *et al.* (Belle), Phys. Rev. Lett. **108**, 032001 (2012), [arXiv:1103.3419].
- [21] G. Aad *et al.* (ATLAS), Phys. Rev. Lett. **108**, 152001 (2012), [arXiv:1112.5154].
- [22] R. Mizuk *et al.* (Belle), Phys. Rev. Lett. **109**, 232002 (2012), [arXiv:1205.6351].
- [23] T. K. Pedlar *et al.* (CLEO), Phys. Rev. Lett. **107**, 041803 (2011), [arXiv:1104.2025].
- [24] I. Adachi (Belle), in "8th International Workshop On Heavy Quarkonium (QWG2011) Darmstadt, Germany, October 3-7, 2011," (2011), [arXiv:1110.3934].
- [25] D. Santel *et al.* (Belle), Phys. Rev. **D93**, 1, 011101 (2016), [arXiv:1501.01137].
- [26] U. Tamponi *et al.* (Belle), Phys. Rev. Lett. **115**, 14, 142001 (2015), [arXiv:1506.08914].
- [27] V. M. Abazov *et al.* (D0), Phys. Rev. **D86**, 031103 (2012), [arXiv:1203.6034].
- [28] R. Aaij *et al.* (LHCb), JHEP **10**, 088 (2014), [arXiv:1409.1408].
- [29] R. Aaij *et al.* (LHCb), Phys. Rev. Lett. **110**, 222001 (2013), [arXiv:1302.6269].
- [30] R. Aaij *et al.* (LHCb), Phys. Rev. **D92**, 1, 011102 (2015), [arXiv:1504.06339].
- [31] R. Aaij *et al.* (LHCb), JHEP **07**, 035 (2019), [arXiv:1903.12240].
- [32] K. Abe *et al.* (Belle), Phys. Rev. Lett. **94**, 182002 (2005), [hep-ex/0408126].
- [33] J. P. Lees *et al.* (BaBar), Phys. Rev. **D86**, 072002 (2012), [arXiv:1207.2651].
- [34] F.-K. Guo and U.-G. Meissner, Phys. Rev. **D86**, 091501 (2012), [arXiv:1208.1134].
- [35] S. L. Olsen, Phys. Rev. **D91**, 5, 057501 (2015), [arXiv:1410.6534].
- [36] Z.-Y. Zhou, Z. Xiao and H.-Q. Zhou, Phys. Rev. Lett. **115**, 2, 022001 (2015), [arXiv:1501.00879].
- [37] K. Chilikin *et al.* (Belle), Phys. Rev. **D95**, 112003 (2017), [arXiv:1704.01872].
- [38] M. Ablikim *et al.* (BESIII), Phys. Rev. Lett. **118**, 9, 092001 (2017), [arXiv:1611.01317].
- [39] M. Cleven *et al.*, Phys. Rev. **D90**, 7, 074039 (2014), [arXiv:1310.2190].
- [40] M. Ablikim *et al.* (BESIII), Phys. Rev. Lett. **118**, 9, 092002 (2017), [arXiv:1610.07044].
- [41] Z. Q. Liu *et al.* (Belle), Phys. Rev. Lett. **110**, 252002 (2013), [arXiv:1304.0121].
- [42] M. Ablikim *et al.* (BESIII), Phys. Rev. Lett. **112**, 9, 092001 (2014), [arXiv:1310.4101].
- [43] M. Ablikim *et al.* (BESIII), Phys. Rev. **D96**, 3, 032004 (2017), [erratum: Phys. Rev.D99,no.1,019903(2019)], [arXiv:1703.08787].
- [44] X. Y. Gao, C. P. Shen and C. Z. Yuan, Phys. Rev. **D95**, 9, 092007 (2017), [arXiv:1703.10351].
- [45] X. L. Wang *et al.* (Belle), Phys. Rev. Lett. **99**, 142002 (2007), [arXiv:0707.3699].
- [46] X. L. Wang *et al.* (Belle), Phys. Rev. **D91**, 112007 (2015), [arXiv:1410.7641].
- [47] J. P. Lees *et al.* (BaBar), Phys. Rev. **D89**, 11, 111103 (2014), [arXiv:1211.6271].
- [48] G. Pakhlova *et al.* (Belle), Phys. Rev. Lett. **101**, 172001 (2008), [arXiv:0807.4458].
- [49] S. Jia *et al.* (Belle), Phys. Rev. **D100**, 11, 111103 (2019), [arXiv:1911.00671].
- [50] K. Chilikin *et al.* (Belle), Phys. Rev. **D88**, 7, 074026 (2013), [arXiv:1306.4894].
- [51] K. Chilikin *et al.* (Belle), Phys. Rev. **D90**, 11, 112009 (2014), [arXiv:1408.6457].
- [52] R. Aaij *et al.* (LHCb), Phys. Rev. Lett. **112**, 22, 222002 (2014), [arXiv:1404.1903].
- [53] B. Aubert *et al.* (BaBar), Phys. Rev. **D79**, 112001 (2009), [arXiv:0811.0564].
- [54] R. Mizuk *et al.* (Belle), Phys. Rev. **D78**, 072004 (2008), [arXiv:0806.4098].
- [55] J. P. Lees *et al.* (BaBar), Phys. Rev. **D85**, 052003 (2012), [arXiv:1111.5919].
- [56] M. Ablikim *et al.* (BESIII), Phys. Rev. Lett. **110**, 252001 (2013), [arXiv:1303.5949].
- [57] T. Xiao *et al.*, Phys. Lett. **B727**, 366 (2013), [arXiv:1304.3036].
- [58] M. Ablikim *et al.* (BESIII), Phys. Rev. Lett. **112**, 2, 022001 (2014), [arXiv:1310.1163].
- [59] M. Ablikim *et al.* (BESIII), Phys. Rev. Lett. **115**, 11, 112003 (2015), [arXiv:1506.06018].
- [60] M. Ablikim *et al.* (BESIII), Phys. Rev. Lett. **115**, 22, 222002 (2015), [arXiv:1509.05620].
- [61] M. Ablikim *et al.* (BESIII), Phys. Rev. Lett. **111**, 24, 242001 (2013), [arXiv:1309.1896].
- [62] M. Ablikim *et al.* (BESIII), Phys. Rev. Lett. **112**, 13, 132001 (2014), [arXiv:1308.2760].
- [63] M. Ablikim *et al.* (BESIII), Phys. Rev. Lett. **113**, 21, 212002 (2014), [arXiv:1409.6577].
- [64] M. Ablikim *et al.* (BESIII), Phys. Rev. Lett. **115**, 18, 182002 (2015), [arXiv:1507.02404].
- [65] T. Aaltonen *et al.* (CDF), Phys. Rev. Lett. **102**, 242002 (2009), [arXiv:0903.2229].
- [66] T. Aaltonen *et al.* (CDF), Mod. Phys. Lett. **A32**, 26, 1750139 (2017), [arXiv:1101.6058].
- [67] V. M. Abazov *et al.* (D0), Phys. Rev. **D89**, 1, 012004 (2014), [arXiv:1309.6580].
- [68] S. Chatrchyan *et al.* (CMS), Phys. Lett. **B734**, 261 (2014), [arXiv:1309.6920].
- [69] J. Brodzicka, Conf. Proc. **C0908171**, 299 (2009), [299(2009)].

- [70] R. Aaij *et al.* (LHCb), Phys. Rev. **D85**, 091103 (2012), [arXiv:1202.5087].
- [71] J. P. Lees *et al.* (BaBar), Phys. Rev. **D91**, 1, 012003 (2015), [arXiv:1407.7244].
- [72] C. P. Shen *et al.* (Belle), Phys. Rev. Lett. **104**, 112004 (2010), [arXiv:0912.2383].
- [73] R. Aaij *et al.* (LHCb), Phys. Rev. **D95**, 1, 012002 (2017), [arXiv:1606.07898].
- [74] R. Aaij *et al.* (LHCb), Phys. Rev. Lett. **118**, 2, 022003 (2017), [arXiv:1606.07895].
- [75] A. Bondar *et al.* (Belle), Phys. Rev. Lett. **108**, 122001 (2012), [arXiv:1110.2251].
- [76] A. Garmash *et al.* (Belle), Phys. Rev. **D91**, 7, 072003 (2015), [arXiv:1403.0992].
- [77] P. Krokovny *et al.* (Belle), Phys. Rev. **D88**, 5, 052016 (2013), [arXiv:1308.2646].
- [78] I. Adachi *et al.* (Belle) (2012), [arXiv:1209.6450].
- [79] K. F. Chen *et al.* (Belle), Phys. Rev. Lett. **100**, 112001 (2008), [arXiv:0710.2577].
- [80] P. Krokovny (Belle Collab.), talk given at Les Rencontres de Physique de la Vallee d'Aoste, La Thuile, Aosta Valley, Italy, 2012.
- [81] A. Abdesselam *et al.* (Belle), Phys. Rev. Lett. **117**, 14, 142001 (2016), [arXiv:1508.06562].
- [82] M. Cleven *et al.*, Eur. Phys. J. **A47**, 120 (2011), [arXiv:1107.0254].
- [83] F. K. Guo *et al.*, Phys. Rev. **D93**, 7, 074031 (2016), [arXiv:1602.00940].
- [84] A. Garmash *et al.* (Belle), Phys. Rev. Lett. **116**, 21, 212001 (2016), [arXiv:1512.07419].
- [85] R. Mizuk *et al.* (Belle), JHEP **10**, 220 (2019), [arXiv:1905.05521].

## 78. Non- $q\bar{q}$ Mesons

Revised August 2019 by C. Amsler (Stefan Meyer Inst.) and C. Hanhart (Jülich).

The constituent quark model describes the observed meson spectrum as bound  $q\bar{q}$  states grouped into SU(N) flavor multiplets (see the ‘Quark Model’ in this issue of the *Review of Particle Physics*). However, the self coupling of gluons in QCD suggests that additional mesons made of bound gluons (glueballs), or  $q\bar{q}$ -pairs with an excited gluon (hybrids), may exist. Furthermore, multi-quark color singlet states such as  $qq\bar{q}\bar{q}$  (tetraquarks as compact diquark-antidiquark systems and ‘molecular’ bound states of two mesons) or  $qqq\bar{q}\bar{q}$  (six-quark and ‘baryonium’ states of two baryons) have also been predicted.

In recent years experimental evidence for states beyond the quark model has accumulated in the heavy quark sector and elsewhere. We therefore split our review into three parts discussing separately light systems, heavy–light systems and heavy–heavy systems. For a more detailed discussion on exotic mesons we refer to [1] for the light meson sector and [2, 3] for the heavy meson sector. Reviews with main focus on tetraquarks and molecular states are presented in [4] and [5], respectively. For an experimental status with focus on the heavy quark sector see [6].

### 78.1 Light systems

#### 78.1.1 Glueball candidates

Among the signatures naively expected for glueballs are (i) isoscalar states that do not fit into  $q\bar{q}$  nonets, (ii) enhanced production in gluon-rich channels such as central production and radiative  $J/\psi(1S)$  decay, (iii) decay branching fractions incompatible with SU(N) predictions for  $q\bar{q}$  states, and (iv) reduced  $\gamma\gamma$  couplings. However, mixing effects with isoscalar  $q\bar{q}$  mesons [7–15] and decay form factors [16] can obscure these simple signatures.

Lattice calculations, QCD sum rules, flux tube, and constituent glue models agree that the lightest glueballs have quantum numbers  $J^{PC} = 0^{++}$  and  $2^{++}$ . Lattice calculations predict for the ground state ( $0^{++}$ ) a mass around 1600 – 1700 MeV [12, 17–19] with an uncertainty of about 100 MeV, while the first excited state ( $2^{++}$ ) has a mass of about 2300 MeV. Hence, the light glueballs lie in the same mass region as ordinary isoscalar  $q\bar{q}$  states, in the mass range of the  $1^3P_0(0^{++})$ ,  $2^3P_2(2^{++})$ ,  $3^3P_2(2^{++})$ , and  $1^3F_2(2^{++})$   $q\bar{q}$  states. Heavier glueballs with quantum numbers  $0^{-+}$ ,  $2^{-+}$ ,  $1^{+-}$ , ... are predicted above 2500 MeV (in holographic QCD the  $0^{+-}$  being very broad [20] and the  $1^{+-}$  at least as broad as its width [21]), and the lowest exotic ones (with non- $q\bar{q}$  quantum numbers such as  $0^{+-}$  and  $2^{+-}$ ) are expected above 4000 MeV [19]. The lattice calculations were performed so far in the quenched approximation. Thus neither quark loops nor mixing with conventional mesons were included, although quenching effects seem to be small [22]. (For a recent comparison between quenched and unquenched lattice studies see [23].) The mixing of glueballs with nearby  $q\bar{q}$  states of the same quantum numbers should lead to a supernumerary isoscalar state in the SU(3) classification of  $q\bar{q}$  mesons. A lattice study in full QCD (performed at unphysical quark masses corresponding to a pion mass of 400 MeV) did not identify states with sizeable overlap with pure gluonic sources [24, 25].

In the following we focus on glueball candidates in the scalar sector. For the  $2^{++}$  sector we refer to the section on non- $q\bar{q}$  mesons in the 2006 issue of the *Review* [26], and for the  $0^{-+}$  glueball to the note on ‘The Pseudoscalar and Pseudovector Mesons in the 1400 MeV Region’ in the *Meson Listings* of the *Review*.

Five isoscalar resonances are established: the very broad  $f_0(500)$  (or  $\sigma$ ), the  $f_0(980)$ , the broad  $f_0(1370)$ , and the comparatively narrow  $f_0(1500)$  and  $f_0(1710)$ , see the note on ‘Scalar Mesons below 2 GeV’ in the *Meson Listings*, and also [27]. Their isospin  $\frac{1}{2}$  and isovector partners are the  $K_0^*(700)$  (or  $\kappa$ ), the  $K_0^*(1430)$ , the  $a_0(980)$  and the  $a_0(1450)$ . However, none of the proposed  $q\bar{q}$  ordering schemes in scalar multiplets is entirely satisfactory. The  $f_0(1370)$  and  $f_0(1500)$  decay mostly into pions ( $2\pi$  and  $4\pi$ ) while the  $f_0(1710)$  decays mainly into  $K\bar{K}$  final states. Naively, this suggests an  $n\bar{n}$  ( $= u\bar{u} + d\bar{d}$ ) structure for the  $f_0(1370)$  and  $f_0(1500)$ , and  $s\bar{s}$  for the  $f_0(1710)$ . The last state is not observed in  $p\bar{p}$  annihilation [28], as expected from the OZI suppress-

sion for an  $s\bar{s}$  state.

In  $\gamma\gamma$  collisions leading to  $K_S K_S$  [29] and  $K^+ K^-$  [30] a spin-0 signal is observed at the  $f_0(1710)$  mass (together with a dominant spin-2 component), while the  $f_0(1500)$  is not observed in  $\gamma\gamma \rightarrow K\bar{K}$  nor  $\pi^+ \pi^-$  [31]. The  $f_0(1500)$  is also not observed by Belle in  $\gamma\gamma \rightarrow \pi^0 \pi^0$ , although a shoulder is seen which could also be due to the  $f_0(1370)$  [32]. The absence of a signal in the  $\pi\pi$  channel in  $\gamma\gamma$  collisions does not favor an  $n\bar{n}$  interpretation for the  $f_0(1500)$ . The upper limit from  $\pi^+ \pi^-$  excludes a large  $n\bar{n}$  content, and hence points to a mainly  $s\bar{s}$  content [33]. This is in contradiction with the small  $K\bar{K}$  decay branching ratio of the  $f_0(1500)$  [34–36]. This state could be mainly glue due its absence of  $\gamma\gamma$  coupling, while the  $f_0(1710)$  coupling to  $\gamma\gamma$  would be compatible with an  $s\bar{s}$  state. Indeed, Belle finds that in  $\gamma\gamma \rightarrow K_S K_S$  collisions the 1500 MeV region is dominated by the  $f_2'(1525)$ . The  $f_0(1710)$  is also observed but its production  $\times$  decay rate is too large for a glueball [37]. However, the  $\gamma\gamma$  couplings are sensitive to glue mixing with  $q\bar{q}$  [38].

Since the  $f_0(1370)$  does not couple strongly to  $s\bar{s}$  [36], the  $f_0(1370)$  or  $f_0(1500)$  appear to be supernumerary. The narrow width of the  $f_0(1500)$ , and its enhanced production at low transverse momentum transfer in central collisions [39–41] also favor the  $f_0(1500)$  to be non- $q\bar{q}$ . In [7] the ground state scalar nonet is made of the  $a_0(1450)$ ,  $f_0(1370)$ ,  $K_0^*(1430)$ , and  $f_0(1710)$ . The isoscalars  $f_0(1370)$  and  $f_0(1710)$  contain a small fraction of glue, while the  $f_0(1500)$  is mostly gluonic (see also [13]). The light scalars  $f_0(500)$ ,  $f_0(980)$ ,  $a_0(980)$ , and  $K_0^*(700)$  are four-quark states or two-meson resonances, see [1] for a review and [42] which focuses on the  $f_0(500)$ . In the mixing scheme of Ref. [38], which uses central production data from WA102 and the hadronic  $J/\psi$  decay data from BES [43, 44], glue is shared between the  $f_0(1370)$ ,  $f_0(1500)$  and  $f_0(1710)$ . The  $f_0(1370)$  is mainly  $n\bar{n}$ , the  $f_0(1500)$  mainly glue and the  $f_0(1710)$  dominantly  $s\bar{s}$ . This agrees with previous analyses [7, 13], but, as already pointed out, alternative schemes have been proposed [7–15], in particular with the  $f_0(1710)$  as the glueball [45, 46] or the  $f_0(1500)$  as a tetraquark [47].

For a scalar glueball the two-gluon coupling to  $n\bar{n}$  appears to be suppressed by chiral symmetry [48] and therefore  $K\bar{K}$  decay could be enhanced. However,  $K\bar{K}$  is naturally enhanced also in the extended linear sigma model with a dilaton as glueball [45] and in the holographic model of [46]. It was argued that chiral symmetry constraints in a multichannel analysis imply that the  $f_0(1710)$  is an unmixed scalar glueball [49], a view that is challenged in [50].

Different mixing options have been studied in [15]. In the preferred solution the ground state scalar nonet consists of the  $f_0(980)$ ,  $a_0(980)$ ,  $K_0^*(1430)$ ,  $f_0(1500)$  and  $f_0(1710)$ . The  $f_0(980)$  and  $f_0(1500)$  mix similarly to the  $\eta$  and  $\eta'$  in the pseudoscalar nonet, while the  $f_0(1500)$  mixes with a glueball in the 500 – 1000 MeV mass range, which is identified with the  $f_0(500)$  ( $\sigma$ ). A reanalysis of the CERN-Munich data shows no signal for the  $f_0(1370)$  decaying into  $\pi\pi$ , in contrast to [51]. However, in this scheme the  $K_0^*(700)$  ( $\kappa$ ) and the  $a_0(1450)$  are left out (see also our note on ‘Scalar Mesons below 2 GeV’ in the *Meson Listings*). The  $a_0(1450)$  has recently been confirmed by LHCb data in  $D^0 \rightarrow K_S^0 K^\pm \pi^\mp$  [52].

The  $f_0(1370)$  is also not needed in the COMPASS  $\pi^- p \rightarrow \pi^- \pi^- \pi^+ p$  data [53], which questions its mere existence. However, a recent analysis from CLEO-c on  $D^0 \rightarrow \pi^+ \pi^- \pi^+ \pi^-$  decay requires a contribution from  $f_0(500) f_0(1370) \rightarrow 4\pi$  [54].

The Dalitz plots of  $B^\pm \rightarrow \pi^\pm \pi^\pm \pi^\mp$  have been studied by BaBar [55]. A broad  $2\pi$  signal is observed around 1400 MeV which is attributed to the  $f_0(1370)$ , but could also be due to the  $f_0(1500)$ . LHCb has analyzed  $\bar{B}^0$  decay into  $J/\psi \pi^+ \pi^-$  [56]. The fit to the  $\pi\pi$  mass spectrum above  $\sim 1.2$  GeV does not show any significant scalar component. However, the data analysis has been challenged [57]. For  $\bar{B}_s^0 \rightarrow J/\psi \pi^+ \pi^-$  a strong scalar contribution from the  $f_0(1370)$  is found [58]. Following the suggestion in Ref. [15], new data for the same reaction were analyzed by introducing instead the  $f_0(500)$  and  $f_0(1500)$  without any need for the  $f_0(1370)$  [59]. This conclusion does not change when improved theoretical tools, as well as the data from [60] on  $\bar{B}_s^0 \rightarrow J/\psi K\bar{K}$ ,

are employed in the analysis [61].

In  $B^\pm \rightarrow K^\pm K^\pm K^\mp$  both BaBar [62] and Belle [63] observe a strong spin-0 activity in  $K\bar{K}$  around 1550 MeV. The decay  $B \rightarrow J/\psi X$  filters out the  $d\bar{d}$  content of  $X$  while  $B_s^0 \rightarrow J/\psi X$  selects its  $s\bar{s}$  component. These decays may therefore be ideal environments to determine the flavor contents of neutral mesons [64].

The contribution of  $f_0(1500)$  production in (the supposedly gluon rich) radiative  $J/\psi$  decay is not well known. The  $f_0(1500)$  is observed by BESII in  $J/\psi \rightarrow \gamma\pi\pi$  [65] and by BESIII in  $J/\psi \rightarrow \gamma\eta\eta$  [66] with a much smaller rate than for the  $f_0(1710)$ , which speaks against a glueball interpretation for the former. However, the  $f_0(1500)$  mass found by BES is significantly lower than the expected value. The overlap with the  $f_0(1370)$  and  $f_2'(1525)$ , and the statistically limited data sample, prevent a proper  $K$ -matrix analysis to be performed. Hence more data are needed in radiative  $J/\psi$  decay and in  $\gamma\gamma$  collisions to clarify the spectrum of scalar mesons.

### 78.1.2 Tetraquark candidates and molecular bound states

The existence of multi-quark states was suggested a long time ago based on duality arguments [67], see also [68]. The  $a_0(980)$  and  $f_0(980)$  could be tetraquark states [69–71] or  $K\bar{K}$  molecular states [72–74] due to their large branching ratios into  $K\bar{K}$ , in spite of their masses being very close to threshold, leaving very little phase space. For  $q\bar{q}$  states, the expected  $\gamma\gamma$  widths [75, 76] are not significantly larger than for molecular states [75, 77], both predictions being consistent with data. Radiative decays of the  $\phi(1020)$  into  $a_0(980)$  and  $f_0(980)$  were claimed to enable disentangling compact from molecular structures. Interpreting the data from DAΦNE [78, 79] and VEPP-2M [80, 81] along the lines of [82, 83] seems to favor these mesons to be tetraquark states. In Ref. [84] they are made of a four-quark core and a virtual  $K\bar{K}$  cloud at the periphery. This is challenged in [85] which shows that  $\phi$  radiative decay data are consistent with molecular structures of the light scalars. The  $f_0(980)$  is strongly produced in  $D_s^+$  decay [86], which points to a large  $s\bar{s}$  component, assuming Cabibbo-favored  $c \rightarrow s$  decay. However, the mainly  $n\bar{n}$   $f_0(1370)$  is also strongly produced in  $D_s^+$  decay, indicating that other graphs must contribute [87].

Ratios of decay rates of  $B$  and/or  $B_s$  mesons into  $J/\psi f_0(980)$  or  $J/\psi f_0(500)$  were proposed to extract the flavor mixing angle and to probe the tetraquark nature of those mesons within certain models [88, 89]. The phenomenological fits of LHCb, based on an isobar model, do neither allow for a contribution of the  $f_0(980)$  in the  $B \rightarrow J/\psi\pi\pi$  [56] nor for an  $f_0(500)$  in  $B_s \rightarrow J/\psi\pi\pi$  decays [59]. Hence the authors conclude that their data are incompatible at the eight standard deviation level with a model in which the  $f_0(500)$  and  $f_0(980)$  are tetraquarks. They also extract an upper limit for the mixing angle of  $17^\circ$  between the  $f_0(980)$  and the  $f_0(500)$  that would correspond to a substantial  $s\bar{s}$  content in the  $f_0(980)$  [59]. However, in a dispersive analysis [90] of the same data that allows for a model independent inclusion of the hadronic final state interactions, a substantial  $f_0(980)$  contribution is also found in the  $B$ -decays, thus putting into question the conclusions in [59].

COMPASS reports a new  $1^{++}$  isovector meson decaying into  $f_0(980)\pi$ , the  $a_1(1420)$  [91, 92]. The resonance is observed in diffractive dissociation  $\pi^-p \rightarrow \pi^-(\pi^+\pi^-)p$ . Traditionally, the  $1^{++}$  ground state nonet is believed to contain the  $a_1(1260)$ ,  $f_1(1285)$  and  $f_1(1420)$  (see ‘The Pseudoscalar and Pseudovector Mesons in the 1400 MeV Region’ in the *Meson Listings*). A molecular  $K\bar{K}\pi$  structure has been proposed for the  $f_1(1420)$  [93] in view of the proximity of the  $K^*\bar{K}$  threshold. The new  $a_1(1420)$  could also be a molecular state, the isovector partner of the  $f_1(1420)$ . However, according to [94], the  $f_1(1420)$  may not exist, being a manifestation of the  $f_1(1285)$  due to a triangle singularity. Ref. [95] also explains the  $a_1(1420)$  as the signature of the  $a_1(1260)$  distorted by a triangle singularity.

### 78.1.3 Baryonia

Bound states of a baryon and an antibaryon have been predicted in the past [96, 97], but have remained elusive. The  $f_2(1565)$  which is only observed in  $\bar{p}p$  annihilation [98, 99] is a good candidate for a  $2^{++}$   $\bar{p}p$  bound state. Enhancements close to the  $\bar{p}p$  thresh-

old have been reported in  $B^+ \rightarrow K^+\bar{p}p$ ,  $B^0 \rightarrow K_S^0\bar{p}p$  [100, 101],  $\bar{B}^0 \rightarrow D^0\bar{p}p$  [102],  $e^+e^- \rightarrow \bar{p}p$  [103, 104],  $\bar{p}p \rightarrow \pi^+\pi^-$  and  $\bar{p}p \rightarrow e^+e^-$  [105]. The spectacular signal seen in  $J/\psi \rightarrow \gamma\bar{p}p$  [106–108] could be due to a  $0^{-+}$  baryonium [109]. Such a pole is not necessarily a compact  $qqq\bar{q}\bar{q}$  state, but might be generated via non-perturbative nucleon-antinucleon final state interactions [110–113]. Also the structures visible in various data sets for  $e^+e^- \rightarrow n\pi$  [114, 115] near the  $\bar{p}p$  threshold appear to be largely explained by the same nucleon-antinucleon final state interactions [116]. However, other explanations have also been proposed to explain e.g. the signals in  $B \rightarrow \bar{p}pK$ , such as the dynamics of the fragmentation mechanism [101].

The pronounced signal observed by Belle in  $e^+e^- \rightarrow A_c^+ A_c^-$  around  $\sqrt{s} = 4.63$  GeV [117] was argued to be a strong evidence in favor of an interpretation of  $Y(4660)$  as charmed baryonium [118]. However, this picture was challenged in Refs. [119, 120].

### 78.1.4 Hybrid mesons

Hybrids may be viewed as  $q\bar{q}$  mesons with a vibrating gluon flux tube. In contrast to glueballs, they can have isospin 0 or 1. The mass spectrum of hybrids with exotic (non- $q\bar{q}$ ) quantum numbers was predicted in [121], while [122] also deals with non-exotic quantum numbers. The ground-state hybrids with quantum numbers ( $0^{-+}$ ,  $1^{-+}$ ,  $1^{--}$ , and  $2^{-+}$ ) are expected around 1.7 to 1.9 GeV. Lattice calculations predict that the hybrid with exotic quantum numbers  $1^{-+}$  lies at a mass of  $1.9 \pm 0.2$  GeV [123, 124]. Most hybrids are expected to be rather broad, but some can be as narrow as 100 MeV [125]. They prefer to decay into a pair of  $S$ - and  $P$ -wave mesons. The lattice study in [24, 126], based on full QCD with pion masses around 400 MeV, finds that several of the high-lying states observed in their spectrum show significant overlap with gluon rich source terms interpreted as hybrid states. For a recent experimental and theoretical review on hybrid mesons see [127].

A  $J^{PC} = 1^{-+}$  exotic meson, the  $\pi_1(1400)$ , was reported in  $\pi^-p \rightarrow \eta\pi^-p$  [128, 129] and in  $\pi^-p \rightarrow \eta\pi^0 n$  [130]. It was observed as an interference between the angular momentum  $L = 1$  and  $L = 2$   $\eta\pi$  amplitudes, leading to a forward/backward asymmetry in the  $\eta\pi$  angular distribution. This state had been reported earlier in  $\pi^-p$  reactions [131], but ambiguous solutions in the partial wave analysis were pointed out [132, 133]. A resonating  $1^{-+}$  contribution to the  $\eta\pi$   $P$ -wave is also required in the Dalitz plot analysis of  $\bar{p}n$  annihilation into  $\pi^-\pi^0\eta$  [134], and in  $\bar{p}p$  annihilation into  $\pi^0\pi^0\eta$  [135]. Mass and width are consistent with the results of [128].

Another  $1^{-+}$  state, the  $\pi_1(1600)$  decaying into  $\rho\pi$ , was reported by COMPASS with 190 GeV pions hitting a lead target [136]. It was observed earlier in  $\pi^-p$  interactions in the decay modes  $\eta'\pi$  [137],  $f_1(1285)\pi$  [138], and  $\omega\pi\pi$  [139],  $b_1(1235)\pi$ , but not  $\eta\pi$  [140]. A strong enhancement in the  $1^{-+}$   $\eta'\pi$  wave, compared to  $\eta\pi$ , was reported at this mass in [141]. Ref. [142] suggested that a Deck-generated  $\eta\pi$  background from final state rescattering in  $\pi_1(1600)$  decay could mimic  $\pi_1(1400)$ . However, this mechanism is absent in  $\bar{p}p$  annihilation. The  $\eta\pi\pi$  data require  $\pi_1(1400)$  and cannot accommodate a state at 1600 MeV [143]. A coupled channel analysis of the COMPASS data leads to a single pole at 1564 MeV [144].

The flux tube model and the lattice concur to predict a hybrid mass of about 1.9 GeV while the  $\pi_1(1400)$  and  $\pi_1(1600)$  are lighter. As isovectors,  $\pi_1(1400)$  and  $\pi_1(1600)$  cannot be glueballs. The coupling to  $\eta\pi$  of the former points to a four-quark state [145], while the strong  $\eta'\pi$  coupling of the latter is favored for hybrid states [146, 147]. The mass of  $\pi_1(1600)$  is also not far below the lattice prediction.

Evidence for a  $\pi_1(2015)$  has also been reported [138, 139]. Hybrid candidates with  $J^{PC} = 0^{-+}$ ,  $1^{--}$ , and  $2^{-+}$  have also been reported. The  $\pi(1800)$  decays mostly to a pair of  $S$ - and  $P$ -wave mesons [136, 148], in line with expectations for  $0^{-+}$  hybrid mesons. This meson is also somewhat narrow if interpreted as the second radial excitation of the pion. The evidence for  $1^{--}$  hybrids required in  $e^+e^-$  annihilation and in  $\tau$  decays has been discussed in [149]. A candidate for the  $2^{-+}$  hybrid, the  $\eta_2(1870)$ , was reported in  $\gamma\gamma$  interactions [150], in  $\bar{p}p$  annihilation [151], and in central production [152]. The near degeneracy of  $\eta_2(1645)$  and

$\pi_2(1670)$  suggests ideal mixing in the  $2^{-+}$   $q\bar{q}$  nonet, and hence, the second isoscalar should be mainly  $s\bar{s}$ . However,  $\eta_2(1870)$  decays mainly to  $a_2(1320)\pi$  and  $f_2(1270)\pi$  [151], with a relative rate compatible with a hybrid state [122].

## 78.2 Heavy-light systems

Two very narrow states,  $D_{s0}^*(2317)^\pm$  and  $D_{s1}(2460)^\pm$ , were observed at B factories [153, 154]. They lie far below the predicted masses for the two expected broad  $P$ -wave  $c\bar{s}$  mesons. These states have hence been interpreted as four-quark states [155–158] or  $DK$  ( $DK^*$ ) molecules [159–163]. However, strong cusp effects, due to the nearby  $DK$  ( $DK^*$ ) thresholds, could shift their masses downwards and quench the observed widths, an effect similar to that claimed for the  $a_0(980)$  and  $f_0(980)$  mesons, which lie just below  $K\bar{K}$  threshold. A hadronic width of typically 100 keV would be the unequivocal signature for a prominent molecular nature of  $D_{s0}^*(2317)^\pm$  [161–163]. More compact structures typically produce widths below 10 keV [164, 165]. The currently measured upper bound for the width is 3.8 MeV.

It should be stressed that – akin to  $q\bar{q}$  mesons – multi-quark states also appear in multiplets. For example, recent studies [166–168] show that, if  $D_{s0}(2317)$  were of molecular nature, the lowest non-strange scalar  $D$ -state, the  $D_0^*(2300)$ , would also be molecular in nature, with a two-pole structure (the lower one at 2105 MeV and the upper one at 2451 MeV, on different physical sheets, however, see Ref. [166] for details) similar to the  $A(1405)$ , see ‘Pole structure of the  $A(1405)$  region’ in the *Review*. In [167] this assignment is demonstrated to be consistent with recent data from LHCb on  $B^- \rightarrow D^+\pi^-\pi^-$  [169]. Two poles in the non-strange scalar sector are also generated in the tetraquark picture of Ref. [158], but in this work the real parts of the poles are located at 2308 MeV and 2666 MeV, which should be testable experimentally.

## 78.3 Heavy-heavy systems

Several unexpected states have been observed in both charmonium and bottomonium regions. With the discovery of the  $X(3872)$  in  $B^\pm \rightarrow K^\pm X$  ( $X \rightarrow J/\psi \pi^+\pi^-$ ) by Belle [170] in 2003, soon confirmed by BaBar [171], many searches for states beyond the standard quark model were initiated in the charm and in the bottom sectors. For an updated collection of the currently available experimental information on multi-quark states we refer to ‘Spectroscopy of mesons containing two heavy quarks’ in the *Review*. Moreover, in the decay  $A_b^0 \rightarrow J/\psi K^- p$  the LHCb collaboration has recently reported the observation of two new baryons decaying into  $J/\psi p$ , which are candidates for heavy pentaquark states [172]. They are discussed in some depth in ‘Pentaquarks’ in the *Review*.

When restricting ourselves to confirmed states we are faced with several ones that do not seem to fit into the most simple quark models. This is clear for the six established charged states ( $Z_c(3900)^\pm$ ,  $Z_c(4020)^\pm$ <sup>1</sup>,  $Z_c(4200)^\pm$  and  $Z_c(4430)^\pm$  in the charmonium sector, and  $Z_b(10610)^\pm$  and  $Z_b(10650)^\pm$  in the bottomonium sector). The neutral ones ( $\chi_{c1}(3872)$  aka  $X(3872)$ ,  $\psi(4260)$  aka  $Y(4260)$ ,  $\psi(4360)$  aka  $Y(4360)$ ,  $\psi(4660)$  aka  $Y(4660)$ )<sup>2</sup> also challenge the quark models since their masses and decay properties are in conflict with expectations.

The quantum numbers of the  $X(3872)$  have been determined by LHCb to be  $J^{PC} = 1^{++}$ , first by assuming the angular momentum zero between the  $J/\psi$  and the dipion [173] and then by relaxing this constraint [174]. The  $X(3872)$  can hardly be identified with the  $2^3P_1$   $\chi'_{c1}$  since the latter is predicted to lie about 100 MeV higher in mass [175]. Instead, the  $X(3940)$  reported by Belle in  $e^+e^- \rightarrow J/\psi X$ , decaying into  $D^*\bar{D}$  but not into  $D\bar{D}$  [176], and also observed in  $B \rightarrow K(X \rightarrow \omega J/\psi)$  [177] could be the  $\chi'_{c1}$ . The  $2^3P_2$  tensor partner ( $\chi'_{c2}$ ) was reported by Belle at 3931 MeV in  $\gamma\gamma$  interactions [178].

<sup>1</sup>While the  $J^P = 1^+$  quantum numbers are plausible for this state, they are not yet established experimentally. This is why this state appears as  $X(4020)$  in both listings and summary tables.

<sup>2</sup>According to the PDG naming scheme the prime name for these states is the quark model name, here listed first for each state, since it expresses the quantum numbers. However, in what follows we use the names mostly used in the literature to ease notations and to avoid confusion.

The  $X(3872)$  lies within 200 keV of the  $D^0\bar{D}^{*0}$  threshold and therefore the most natural explanation for this state is a  $1^{++}$   $DD^*$  molecule [179], for which strong isospin breaking is predicted [179, 180], since the distance of the pole of the  $X(3872)$  to the  $D^0\bar{D}^{*0}$  threshold is significantly smaller than to the  $D^+D^{*-}$  threshold. Indeed, the comparable rates for  $\omega J/\psi$  and  $\rho^0 J/\psi$  are consistent with an interpretation of  $X(3872)$  as an isoscalar  $DD^*$  molecule when the different widths of the  $\rho$  and  $\omega$  are taken into account [181]. A four-quark state  $c\bar{q}c\bar{q}'$  is also possible [157] but unlikely, since the charged partner of the  $X(3872)$  has not been observed (e.g. not in  $B^- \rightarrow \bar{K}^0 X^-$  nor in  $B^0 \rightarrow K^+ X^-$ , where  $X^- \rightarrow J/\psi \pi^-\pi^0$  [182]) – see [183] for a possible explanation of this non-observation within the tetraquark approach. The claim that  $X(3872)$  must be a compact (tetraquark) state, since it is also produced at very high  $p_T$  in  $\bar{p}p$  collisions [184], was challenged in [185], which stresses the importance of rescattering, see also [186, 187].

A broad structure,  $Y(4260)$ , decaying into  $J/\psi \pi^+\pi^-$  was reported by BaBar in initial state radiation  $e^+e^- \rightarrow \gamma(e^+e^- \rightarrow Y(4260))$  [188]. A measurement with significantly improved statistics was recently reported by BESIII [189]. The Breit-Wigner fit of these data leads to a mass reduction of 40 MeV, but also requires a second state at 4320 MeV. However, the  $D_1\bar{D}$  molecular model for the  $Y(4260)$  [190] is capable to describe the same data with just one single pole [191].

There are no charmonium states expected in this mass region with quantum numbers  $1^{--}$  from quark models using the Cornell type of interaction, although this might not be true for some screened versions thereof – for a recent discussion we refer to Ref. [192]. In addition, a charmonium at this mass should have a significant coupling to  $\bar{D}D$ , a decay channel that is not observed for the  $Y(4260)$ . This state could be a hybrid charmonium with a spin-1  $\bar{c}c$  [193, 194] or a spin-0 [195, 196] core. However, provided that the observation of  $Y(4260)$  decay into  $h_c(1P)\pi\pi$  by BESIII [197] is confirmed, the hybrid hypothesis would be under pressure, since the spin of the heavy quarks (coupled to zero in the  $h_c(1P)$ ) should be conserved in leading order in the expansion in  $(\Lambda_{\text{QCD}}/m_c)$ . (The individual conservation of the heavy quark spin and the total angular momentum of the light quark cloud is a consequence of the heavy-quark spin symmetry, see ‘Heavy-Quark and Soft-Collinear Effective Theory’ in this issue of the *Review*.)

The same criticism applies to the hadrocharmonium interpretation of the  $Y(4260)$ , which describes this state as spin-1 quarkonium surrounded by a light quark cloud [198]. To circumvent the spin-symmetry argument Ref. [199] argues that  $Y(4260)$  and  $Y(4360)$  could be mixtures of two hadrocharmonia with spin-triplet and spin-singlet heavy quark pairs. The same kind of mixing could also operate for a hybrid.

A dominant  $D_1\bar{D}$  component in the  $Y(4260)$  [200] explains naturally why  $Z_c(3900)^\pm$  (interpreted by the authors as a  $\bar{D}D^*$  bound state) is seen in  $Y(4260) \rightarrow \pi^\mp Z_c(3900)^\pm$ . Furthermore, a copious production of  $X(3872)$  in  $Y(4260)$  radiative decays was predicted from the prominent  $D_1\bar{D}$  component of the  $Y(4260)$  [201], which was confirmed by BESIII [202]. The  $Y(4360)$  as a  $D_1\bar{D}^*$  bound state could be the spin partner of the  $Y(4260)$  [203, 204], but a detailed microscopic calculation is still lacking.

The tetraquark picture explains the observed  $Y$  states [205] and is also capable – when including a tailor-made spin-spin interaction [206] – to describe the  $X(3872)$ , both  $Z_c(3900)^\pm$ <sup>0</sup> and  $Z_c(4020)^\pm$  and even the  $Z(4430)^\pm$  confirmed by Belle [207] and LHCb [208]. The latter reference also determined the quantum numbers of this state to  $J^P = 1^+$ . However, the model predicts many additional charged and neutral states which have not yet been discovered. A possible explanation can be found in [183].

Ref. [209] found a sizeable SU(3) flavor octet contribution when analysing the  $\pi\pi$  final state from  $Y(4260) \rightarrow J/\psi \pi^+\pi^-$ , which is consistent with both a molecular and a tetraquark interpretation of  $Y(4260)$ , but at odds with a hybrid or a  $\bar{c}c$  interpretation.

The charged states  $Z_c(3900)^\pm$ , first observed by BESIII [210] and the  $Z_c(4020)^\pm$  [211] decay predominantly into  $\bar{D}D^*$  and  $\bar{D}^*D^*$ , respectively, while  $Z_b(10610)^\pm$ <sup>0</sup> and  $Z_b(10650)^\pm$  [212, 213] decay predominantly into  $\bar{B}B^*$  and  $\bar{B}^*B^*$  [214], respectively, although all of them were discovered in the decay mode heavy

quarkonium plus pion. This suggests that these states are close relatives and their interactions are connected via heavy quark flavor symmetry. A molecular interpretation for the bottomonium states was proposed shortly after the discovery of the  $Z_b^\pm$  states [215] and also shortly after that of the  $Z_c(3900)^\pm$  [200]. However, some of their properties also appear to be consistent with tetraquark structures [216]. If the molecular picture were correct for the  $Z_b$  states, spin symmetry would lead to the existence of spin partner states [217–219], which are still to be found. In Ref. [220] it was shown that the actual pole locations of those partner states would be good probes of the role of the one-pion exchange in the molecular potential, which makes the experimental search for those states even more interesting.

The heaviest confirmed charged state in the charmonium sector is the  $Z(4430)^\pm$  observed by Belle [207]. It is interpreted as hadrocharmonium [198],  $\bar{D}_1 D^*$  molecule [221] as well as tetraquark [206]. Alternatively, in [222, 223] the  $Z(4430)^\pm$  is explained as a cross-channel effect enhanced by a triangle singularity from open charm states. These works were criticised in Ref. [224] where an alternative triangle consisting of a  $K^*$ , a  $\pi$  and the  $Y(4260)$  is proposed to generate the  $Z_c(4430)$ . The Argand diagram shows an anticlockwise circle, in line with the experimental analysis [208], while the one of Ref. [223] shows a clockwise motion. By replacing the  $Y(4260)$  by the  $\psi(3770)$  and changing the  $K^*$  one can also interpret the  $Z_c(4200)$  as a kinematic effect [224].

It should be stressed that the various scenarios, while describing the data, also make decisive predictions, e.g. yet unobserved quantum numbers [205, 225]. The forthcoming data on heavy meson spectroscopy from various facilities should provide a much deeper understanding on how QCD forms matter out of quarks and gluons.

## References

- [1] C. Amsler and N. A. Tornqvist, Phys. Rept. **389**, 61 (2004).
- [2] N. Brambilla *et al.*, Eur. Phys. J. **C71**, 1534 (2011), [arXiv:1010.5827].
- [3] N. Brambilla *et al.* (2019), [arXiv:1907.07583].
- [4] A. Esposito, A. Pilloni and A. D. Polosa, Phys. Rept. **668**, 1 (2017), [arXiv:1611.07920].
- [5] F.-K. Guo *et al.*, Rev. Mod. Phys. **90**, 1, 015004 (2018), [arXiv:1705.00141].
- [6] S. L. Olsen, T. Skwarnicki and D. Zieminska, Rev. Mod. Phys. **90**, 1, 015003 (2018), [arXiv:1708.04012].
- [7] C. Amsler and F. E. Close, Phys. Rev. **D53**, 295 (1996), [hep-ph/9507326].
- [8] N. A. Tornqvist and M. Roos, Phys. Rev. Lett. **76**, 1575 (1996), [hep-ph/9511210].
- [9] A. V. Anisovich, V. V. Anisovich and A. V. Sarantsev, Phys. Lett. **B395**, 123 (1997), [hep-ph/9611333].
- [10] M. Boglione and M. R. Pennington, Phys. Rev. Lett. **79**, 1998 (1997), [hep-ph/9703257].
- [11] P. Minkowski and W. Ochs, Eur. Phys. J. **C9**, 283 (1999), [hep-ph/9811518].
- [12] W.-J. Lee and D. Weingarten, Phys. Rev. **D61**, 014015 (2000), [hep-lat/9910008].
- [13] F. E. Close and A. Kirk, Eur. Phys. J. **C21**, 531 (2001), [hep-ph/0103173].
- [14] H.-Y. Cheng, C.-K. Chua and K.-F. Liu, Phys. Rev. **D74**, 094005 (2006), [hep-ph/0607206].
- [15] W. Ochs, J. Phys. **G40**, 043001 (2013), [arXiv:1301.5183].
- [16] T. Barnes *et al.*, Phys. Rev. **D55**, 4157 (1997), [hep-ph/9609339].
- [17] G. S. Bali *et al.* (UKQCD), Phys. Lett. **B309**, 378 (1993), [hep-lat/9304012].
- [18] C. J. Morningstar and M. J. Peardon, Phys. Rev. **D56**, 4043 (1997), [hep-lat/9704011].
- [19] Y. Chen *et al.*, Phys. Rev. **D73**, 014516 (2006), [hep-lat/0510074].
- [20] J. Leutgeb and A. Rebhan, Phys. Rev. **D101**, 1, 014006 (2020), [arXiv:1909.12352].
- [21] F. Br unner, J. Leutgeb, A. Rebhan, Phys. Lett. **B788**, 431 (2019).
- [22] C. M. Richards *et al.* (UKQCD), Phys. Rev. **D82**, 034501 (2010), [arXiv:1005.2473].
- [23] E. Gregory *et al.*, JHEP **10**, 170 (2012), [arXiv:1208.1858].
- [24] J. J. Dudek *et al.*, Phys. Rev. **D83**, 111502 (2011), [arXiv:1102.4299].
- [25] W. Sun *et al.*, EPJ Web Conf. **175**, 05016 (2018), [arXiv:1711.00711].
- [26] W. M. Yao *et al.* (Particle Data Group), J. Phys. **G33**, 1 (2006).
- [27] C. Amsler, Rev. Mod. Phys. **70**, 1293 (1998), [hep-ex/9708025].
- [28] C. Amsler *et al.* (Crystal Barrel), Eur. Phys. J. **C23**, 29 (2002).
- [29] M. Acciarri *et al.* (L3), Phys. Lett. **B501**, 173 (2001), [hep-ex/0011037].
- [30] K. Abe *et al.* (Belle), Eur. Phys. J. **C32**, 323 (2003), [hep-ex/0309077].
- [31] R. Barate *et al.* (ALEPH), Phys. Lett. **B472**, 189 (2000), [hep-ex/9911022].
- [32] S. Uehara *et al.* (Belle), Phys. Rev. **D78**, 052004 (2008), [arXiv:0805.3387].
- [33] C. Amsler, Phys. Lett. **B541**, 22 (2002), [hep-ph/0206104].
- [34] A. Abele *et al.* (Crystal Barrel), Phys. Lett. **B385**, 425 (1996).
- [35] A. Abele *et al.*, Phys. Rev. **D57**, 3860 (1998).
- [36] D. Barberis *et al.* (WA102), Phys. Lett. **B462**, 462 (1999), [hep-ex/9907055].
- [37] S. Uehara *et al.* (Belle), PTEP **2013**, 12, 123C01 (2013), [arXiv:1307.7457].
- [38] F. E. Close and Q. Zhao, Phys. Rev. **D71**, 094022 (2005), [hep-ph/0504043].
- [39] F. E. Close and A. Kirk, Phys. Lett. **B397**, 333 (1997), [hep-ph/9701222].
- [40] F. E. Close, Phys. Lett. **B419**, 387 (1998), [hep-ph/9710450].
- [41] A. Kirk, Phys. Lett. **B489**, 29 (2000), [hep-ph/0008053].
- [42] J. R. Pelaez, Phys. Rept. **658**, 1 (2016), [arXiv:1510.00653].
- [43] M. Ablikim *et al.* (BES), Phys. Lett. **B603**, 138 (2004), [hep-ex/0409007].
- [44] M. Ablikim *et al.* (BES), Phys. Lett. **B607**, 243 (2005), [hep-ex/0411001].
- [45] S. Janowski, F. Giacosa and D. H. Rischke, Phys. Rev. **D90**, 11, 114005 (2014), [arXiv:1408.4921].
- [46] F. Br enner and A. Rebhan, Phys. Rev. Lett. **115**, 13, 131601 (2015), [arXiv:1504.05815].
- [47] L. Zou *et al.*, Phys. Rev. **D99**, 114024 (2019).
- [48] M. Chanowitz, Phys. Rev. Lett. **95**, 172001 (2005), [hep-ph/0506125].
- [49] M. Albaladejo and J. A. Oller, Phys. Rev. Lett. **101**, 252002 (2008), [arXiv:0801.4929].
- [50] L. S. Geng and E. Oset, Phys. Rev. **D79**, 074009 (2009), [arXiv:0812.1199].
- [51] D. V. Bugg, B. S. Zou and A. V. Sarantsev, Nucl. Phys. **B471**, 59 (1996).
- [52] R. Aaij *et al.* (LHCb), Phys. Rev. **D93**, 5, 052018 (2016), [arXiv:1509.06628].
- [53] C. Adolph *et al.* (COMPASS), Phys. Rev. **D95**, 3, 032004 (2017), [arXiv:1509.00992].
- [54] P. d'Argent *et al.*, JHEP **05**, 143 (2017), [arXiv:1703.08505].



- [55] B. Aubert *et al.* (BaBar), Phys. Rev. **D79**, 072006 (2009), [arXiv:0902.2051].
- [56] R. Aaij *et al.* (LHCb), Phys. Rev. **D90**, 1, 012003 (2014), [arXiv:1404.5673].
- [57] F. E. Close and A. Kirk, Phys. Rev. **D91**, 11, 114015 (2015), [arXiv:1503.06942].
- [58] R. Aaij *et al.* (LHCb), Phys. Rev. **D86**, 052006 (2012), [arXiv:1204.5643].
- [59] R. Aaij *et al.* (LHCb), Phys. Rev. **D89**, 9, 092006 (2014), [arXiv:1402.6248].
- [60] R. Aaij *et al.* (LHCb), JHEP **08**, 037 (2017), [arXiv:1704.08217].
- [61] S. Ropertz, C. Hanhart and B. Kubis, Eur. Phys. J. **C78**, 12, 1000 (2018), [arXiv:1809.06867].
- [62] B. Aubert *et al.* (BaBar), Phys. Rev. **D74**, 032003 (2006), [hep-ex/0605003].
- [63] A. Garmash *et al.* (Belle), Phys. Rev. **D71**, 092003 (2005), [hep-ex/0412066].
- [64] C.-D. Lu *et al.*, Eur. Phys. J. **A49**, 58 (2013), [arXiv:1301.0225].
- [65] M. Ablikim *et al.*, Phys. Lett. **B642**, 441 (2006), [hep-ex/0603048].
- [66] M. Ablikim *et al.* (BESIII), Phys. Rev. **D87**, 9, 092009 (2013), [Erratum: Phys. Rev.D87,no.11,119901(2013)], [arXiv:1301.0053].
- [67] J. L. Rosner, Phys. Rev. Lett. **21**, 950 (1968).
- [68] G. C. Rossi and G. Veneziano, Nucl. Phys. **B123**, 507 (1977).
- [69] R. L. Jaffe, Phys. Rev. **D15**, 281 (1977).
- [70] M. G. Alford and R. L. Jaffe, Nucl. Phys. **B578**, 367 (2000), [hep-lat/0001023].
- [71] G. 't Hooft *et al.*, Phys. Lett. **B662**, 424 (2008), [arXiv:0801.2288].
- [72] J. D. Weinstein and N. Isgur, Phys. Rev. **D41**, 2236 (1990).
- [73] G. Janssen *et al.*, Phys. Rev. **D52**, 2690 (1995), [arXiv:nucl-th/9411021].
- [74] M. P. Locher, V. E. Markushin and H. Q. Zheng, Eur. Phys. J. **C4**, 317 (1998), [hep-ph/9705230].
- [75] J. A. Oller and E. Oset, AIP Conf. Proc. **432**, 1, 413 (1998), [hep-ph/9710557].
- [76] R. Delbourgo, D.-s. Liu and M. D. Scadron, Phys. Lett. **B446**, 332 (1999), [hep-ph/9811474].
- [77] C. Hanhart *et al.*, Phys. Rev. **D75**, 074015 (2007), [hep-ph/0701214].
- [78] A. Aloisio *et al.* (KLOE), Phys. Lett. **B536**, 209 (2002), [hep-ex/0204012].
- [79] A. Aloisio *et al.* (KLOE), Phys. Lett. **B537**, 21 (2002), [hep-ex/0204013].
- [80] R. R. Akhmetshin *et al.* (CMD-2), Phys. Lett. **B462**, 371 (1999), [hep-ex/9907005].
- [81] M. N. Achasov *et al.*, Phys. Lett. **B479**, 53 (2000), [hep-ex/0003031].
- [82] F. E. Close, N. Isgur and S. Kumano, Nucl. Phys. **B389**, 513 (1993), [hep-ph/9301253].
- [83] N. N. Achasov, V. V. Gubin and V. I. Shevchenko, Phys. Rev. **D56**, 203 (1997), [hep-ph/9605245].
- [84] F. E. Close and N. A. Tornqvist, J. Phys. **G28**, R249 (2002), [hep-ph/0204205].
- [85] Yu. S. Kalashnikova *et al.*, Eur. Phys. J. **A24**, 437 (2005), [hep-ph/0412340].
- [86] E. M. Aitala *et al.* (E791), Phys. Rev. Lett. **86**, 765 (2001), [hep-ex/0007027].
- [87] H.-Y. Cheng, Phys. Rev. **D67**, 054021 (2003), [hep-ph/0212361].
- [88] R. Fleischer, R. Knegjens and G. Ricciardi, Eur. Phys. J. **C71**, 1832 (2011), [arXiv:1109.1112].
- [89] S. Stone and L. Zhang, Phys. Rev. Lett. **111**, 6, 062001 (2013), [arXiv:1305.6554].
- [90] J. T. Daub, C. Hanhart and B. Kubis, JHEP **02**, 009 (2016), [arXiv:1508.06841].
- [91] C. Adolph *et al.* (COMPASS), Phys. Rev. Lett. **115**, 8, 082001 (2015), [arXiv:1501.05732].
- [92] M. Aghasyan *et al.* (COMPASS), Phys. Rev. **D98**, 092003 (2018).
- [93] R. S. Longacre, Phys. Rev. **D42**, 874 (1990).
- [94] V. R. Debastiani *et al.*, Phys. Rev. **D 95**, 034015 (2017).
- [95] M. Mikhasenko, B. Ketzner and A. Sarantsev, Phys. Rev. **D91**, 9, 094015 (2015), [arXiv:1501.07023].
- [96] G. C. Rossi and G. Veneziano, Phys. Rep. **63**, 153 (1980).
- [97] L. Montanet, Phys. Rep. **63**, 201 (1980).
- [98] B. May *et al.* (ASTERIX), Z. Phys. **C46**, 203 (1990).
- [99] A. Bertin *et al.* (OBELIX), Phys. Rev. **D57**, 55 (1998).
- [100] K. Abe *et al.* (Belle), Phys. Rev. Lett. **88**, 181803 (2002), [hep-ex/0202017].
- [101] M. Z. Wang *et al.* (Belle), Phys. Lett. **B617**, 141 (2005), [hep-ex/0503047].
- [102] K. Abe *et al.* (Belle), Phys. Rev. Lett. **89**, 151802 (2002), [hep-ex/0205083].
- [103] J. P. Lees *et al.* (BaBar), Phys. Rev. **D87**, 9, 092005 (2013), [arXiv:1302.0055].
- [104] E. P. Solodov *et al.*, EPJ Web Conf. **212**, 07002 (2019).
- [105] G. Bardin *et al.*, Nucl. Phys. **B411**, 3 (1994).
- [106] J. Z. Bai *et al.* (BES), Phys. Rev. Lett. **91**, 022001 (2003), [hep-ex/0303006].
- [107] J. P. Alexander *et al.* (CLEO), Phys. Rev. **D82**, 092002 (2010), [arXiv:1007.2886].
- [108] M. Ablikim *et al.* (BESIII), Phys. Rev. Lett. **108**, 112003 (2012), [arXiv:1112.0942].
- [109] G.-J. Ding and M.-L. Yan, Phys. Rev. **C72**, 015208 (2005), [hep-ph/0502127].
- [110] B. Loiseau and S. Wycech, Phys. Rev. **C72**, 011001 (2005), [hep-ph/0501112].
- [111] A. Sibirtsev *et al.*, Phys. Rev. **D71**, 054010 (2005), [hep-ph/0411386].
- [112] X.-W. Kang, J. Haidenbauer and U.-G. Meissner, JHEP **02**, 113 (2014), [arXiv:1311.1658].
- [113] X.-W. Kang, J. Haidenbauer and U.-G. Meissner, Phys. Rev. **D91**, 7, 074003 (2015), [arXiv:1502.00880].
- [114] B. Aubert *et al.* (BaBar), Phys. Rev. **D76**, 092005 (2007), [Erratum: Phys. Rev.D77,119902(2008)], [arXiv:0708.2461].
- [115] R. R. Akhmetshin *et al.* (CMD-3), Phys. Lett. **B723**, 82 (2013), [arXiv:1302.0053].
- [116] J. Haidenbauer, X. W. Kang and U. G. Meissner, Nucl. Phys. **A929**, 102 (2014), [arXiv:1405.1628].
- [117] G. Pakhlova *et al.* (Belle), Phys. Rev. Lett. **101**, 172001 (2008), [arXiv:0807.4458].
- [118] G. Cotugno *et al.*, Phys. Rev. Lett. **104**, 132005 (2010), [arXiv:0911.2178].
- [119] F.-K. Guo *et al.*, Phys. Rev. **D82**, 094008 (2010), [arXiv:1005.2055].
- [120] L.-Y. Dai, J. Haidenbauer and U. G. Meissner, Phys. Rev. **D96**, 11, 116001 (2017), [arXiv:1710.03142].
- [121] N. Isgur, R. Kokoski and J. Paton, Phys. Rev. Lett. **54**, 869 (1985), [AIP Conf. Proc.132,242(1985)].
- [122] F. E. Close and P. R. Page, Nucl. Phys. **B443**, 233 (1995), [hep-ph/9411301].



- [123] P. Lacock *et al.* (UKQCD), Phys. Lett. **B401**, 308 (1997), [hep-lat/9611011].
- [124] C. W. Bernard *et al.* (MILC), Phys. Rev. **D56**, 7039 (1997), [hep-lat/9707008].
- [125] P. R. Page, E. S. Swanson and A. P. Szczepaniak, Phys. Rev. **D59**, 034016 (1999), [hep-ph/9808346].
- [126] J. J. Dudek *et al.* (Hadron Spectrum), Phys. Rev. **D88**, 9, 094505 (2013), [arXiv:1309.2608].
- [127] C. A. Meyer and E. S. Swanson, Prog. Part. Nucl. Phys. **82**, 21 (2015), [arXiv:1502.07276].
- [128] D. R. Thompson *et al.* (E852), Phys. Rev. Lett. **79**, 1630 (1997), [hep-ex/9705011].
- [129] S. U. Chung *et al.* (E852), Phys. Rev. **D60**, 092001 (1999), [hep-ex/9902003].
- [130] G. S. Adams *et al.* (E862), Phys. Lett. **B657**, 27 (2007), [hep-ex/0612062].
- [131] D. Alde *et al.* (IHEP-Brussels-Los Alamos-Annecy(LAPP)), Phys. Lett. **B205**, 397 (1988).
- [132] Yu. D. Prokoshkin and S. A. Sadovsky, Phys. Atom. Nucl. **58**, 606 (1995), [Yad. Fiz.58N4,662(1995)].
- [133] Yu. D. Prokoshkin and S. A. Sadovsky, Phys. Atom. Nucl. **58**, 853 (1995), [Yad. Fiz.58,921(1995)].
- [134] A. Abele *et al.* (Crystal Barrel), Phys. Lett. **B423**, 175 (1998).
- [135] A. Abele *et al.* (Crystal Barrel), Phys. Lett. **B446**, 349 (1999).
- [136] M. Alekseev *et al.* (COMPASS), Phys. Rev. Lett. **104**, 241803 (2010), [arXiv:0910.5842].
- [137] E. I. Ivanov *et al.* (E852), Phys. Rev. Lett. **86**, 3977 (2001), [hep-ex/0101058].
- [138] J. Kuhn *et al.* (E852), Phys. Lett. **B595**, 109 (2004), [hep-ex/0401004].
- [139] M. Lu *et al.* (E852), Phys. Rev. Lett. **94**, 032002 (2005), [hep-ex/0405044].
- [140] Yu.P. Gouz *et al.*, Proc. XXVI Int. Conf. on HEP, Dallas (1992).
- [141] G. M. Beladidze *et al.* (VES), Phys. Lett. **B313**, 276 (1993).
- [142] A. Donnachie and P. R. Page, Phys. Rev. **D58**, 114012 (1998), [hep-ph/9808225].
- [143] W. Dunnweber (Crystal Barrel), Nucl. Phys. **A663**, 592 (2000).
- [144] A. Rodas *et al.*, Phys. Rev. Lett. **122**, 042002 (2019).
- [145] S. U. Chung, E. Klempt and J. G. Korner, Eur. Phys. J. **A15**, 539 (2002), [hep-ph/0211100].
- [146] F. E. Close and H. J. Lipkin, Phys. Lett. **B196**, 245 (1987).
- [147] F. Iddir and A. S. Safir, Phys. Lett. **B507**, 183 (2001), [hep-ph/0010121].
- [148] D. V. Amelin *et al.* (VES), Phys. Lett. **B356**, 595 (1995).
- [149] A. Donnachie and Yu. S. Kalashnikova, Phys. Rev. **D60**, 114011 (1999), [hep-ph/9901334].
- [150] K. Karch *et al.* (Crystal Ball), Z. Phys. **C54**, 33 (1992).
- [151] J. Adomeit *et al.* (Crystal Barrel), Z. Phys. **C71**, 227 (1996).
- [152] D. Barberis *et al.* (WA102), Phys. Lett. **B413**, 217 (1997), [hep-ex/9707021].
- [153] B. Aubert *et al.* (BaBar), Phys. Rev. Lett. **90**, 242001 (2003), [hep-ex/0304021].
- [154] D. Besson *et al.* (CLEO), Phys. Rev. **D68**, 032002 (2003), [Erratum: Phys. Rev. D75,119908(2007)], [hep-ex/0305100].
- [155] H.-Y. Cheng and W.-S. Hou, Phys. Lett. **B566**, 193 (2003), [hep-ph/0305038].
- [156] K. Terasaki, Phys. Rev. **D68**, 011501 (2003), [hep-ph/0305213].
- [157] L. Maiani *et al.*, Phys. Rev. **D71**, 014028 (2005), [hep-ph/0412098].
- [158] V. Dmitrasinovic, Phys. Rev. Lett. **94**, 162002 (2005).
- [159] T. Barnes, F. E. Close and H. J. Lipkin, Phys. Rev. **D68**, 054006 (2003), [hep-ph/0305025].
- [160] E. E. Kolomeitsev and M. F. M. Lutz, Phys. Lett. **B582**, 39 (2004), [hep-ph/0307133].
- [161] A. Faessler *et al.*, Phys. Rev. **D76**, 014005 (2007), [arXiv:0705.0254].
- [162] M. F. M. Lutz and M. Soyeur, Nucl. Phys. **A813**, 14 (2008), [arXiv:0710.1545].
- [163] L. Liu *et al.*, Phys. Rev. **D87**, 1, 014508 (2013), [arXiv:1208.4535].
- [164] S. Godfrey, Phys. Lett. **B568**, 254 (2003), [hep-ph/0305122].
- [165] P. Colangelo and F. De Fazio, Phys. Lett. **B570**, 180 (2003), [hep-ph/0305140].
- [166] M. Albaladejo *et al.*, Phys. Lett. **B767**, 465 (2017), [arXiv:1610.06727].
- [167] M.-L. Du *et al.*, Phys. Rev. **D98**, 9, 094018 (2018), [arXiv:1712.07957].
- [168] X.-Y. Guo, Y. Heo and M. F. M. Lutz, Phys. Rev. **D98**, 1, 014510 (2018), [arXiv:1801.10122].
- [169] R. Aaij *et al.* (LHCb), Phys. Rev. **D94**, 7, 072001 (2016), [arXiv:1608.01289].
- [170] S. K. Choi *et al.* (Belle), Phys. Rev. Lett. **91**, 262001 (2003), [hep-ex/0309032].
- [171] B. Aubert *et al.* (BaBar), Phys. Rev. **D71**, 071103 (2005), [hep-ex/0406022].
- [172] R. Aaij *et al.* (LHCb), Phys. Rev. Lett. **115**, 072001 (2015), [arXiv:1507.03414].
- [173] R. Aaij *et al.* (LHCb), Phys. Rev. Lett. **110**, 222001 (2013), [arXiv:1302.6269].
- [174] R. Aaij *et al.* (LHCb), Phys. Rev. **D92**, 1, 011102 (2015), [arXiv:1504.06339].
- [175] T. Barnes and S. Godfrey, Phys. Rev. **D69**, 054008 (2004), [hep-ph/0311162].
- [176] K. Abe *et al.* (Belle), Phys. Rev. Lett. **98**, 082001 (2007), [hep-ex/0507019].
- [177] K. Abe *et al.* (Belle), Phys. Rev. Lett. **94**, 182002 (2005), [hep-ex/0408126].
- [178] S. Uehara *et al.* (Belle), Phys. Rev. Lett. **96**, 082003 (2006), [hep-ex/0512035].
- [179] N. A. Tornqvist, Phys. Lett. **B590**, 209 (2004), [hep-ph/0402237].
- [180] E. S. Swanson, Phys. Lett. **B588**, 189 (2004), [hep-ph/0311229].
- [181] D. Gamermann and E. Oset, Phys. Rev. **D80**, 014003 (2009), [arXiv:0905.0402].
- [182] B. Aubert *et al.* (BaBar), Phys. Rev. **D71**, 031501 (2005), [hep-ex/0412051].
- [183] L. Maiani, A. D. Polosa and V. Riquer, Phys. Lett. **B778**, 247 (2018), [arXiv:1712.05296].
- [184] C. Bignamini *et al.*, Phys. Rev. Lett. **103**, 162001 (2009), [arXiv:0906.0882].
- [185] P. Artoisenet and E. Braaten, Phys. Rev. **D81**, 114018 (2010), [arXiv:0911.2016].
- [186] F.-K. Guo *et al.*, JHEP **05**, 138 (2014), [arXiv:1403.4032].
- [187] M. Albaladejo *et al.*, Chin. Phys. **C41**, 12, 121001 (2017), [arXiv:1709.09101].
- [188] B. Aubert *et al.* (BaBar), Phys. Rev. Lett. **95**, 142001 (2005), [hep-ex/0506081].
- [189] M. Ablikim *et al.* (BESIII), Phys. Rev. Lett. **118**, 9, 092001 (2017), [arXiv:1611.01317].

- [190] M. Cleven *et al.*, Phys. Rev. **D90**, 7, 074039 (2014), [arXiv:1310.2190].
- [191] C. Hanhart, Int. J. Mod. Phys. Conf. Ser. **46**, 1860004 (2018), [arXiv:1712.01136].
- [192] C. Hanhart and E. Klempt (2019), [arXiv:1906.11971].
- [193] F. E. Close and P. R. Page, Phys. Lett. **B628**, 215 (2005), [hep-ph/0507199].
- [194] M. Berwein *et al.*, Phys. Rev. **D92**, 11, 114019 (2015), [arXiv:1510.04299].
- [195] E. Kou and O. Pene, Phys. Lett. **B631**, 164 (2005), [hep-ph/0507119].
- [196] Yu. S. Kalashnikova and A. V. Nefediev, Phys. Rev. **D77**, 054025 (2008), [arXiv:0801.2036].
- [197] M. Ablikim *et al.* (BESIII), Phys. Rev. Lett. **111**, 24, 242001 (2013), [arXiv:1309.1896].
- [198] M. B. Voloshin, Prog. Part. Nucl. Phys. **61**, 455 (2008), [arXiv:0711.4556].
- [199] X. Li and M. B. Voloshin, Mod. Phys. Lett. **A29**, 12, 1450060 (2014), [arXiv:1309.1681].
- [200] Q. Wang, C. Hanhart and Q. Zhao, Phys. Rev. Lett. **111**, 13, 132003 (2013), [arXiv:1303.6355].
- [201] F.-K. Guo *et al.*, Phys. Lett. **B725**, 127 (2013), [arXiv:1306.3096].
- [202] M. Ablikim *et al.* (BESIII), Phys. Rev. Lett. **112**, 9, 092001 (2014), [arXiv:1310.4101].
- [203] Q. Wang *et al.*, Phys. Rev. **D89**, 3, 034001 (2014), [arXiv:1309.4303].
- [204] V. Baru *et al.*, Phys. Rev. **D91**, 3, 034002 (2015), [arXiv:1501.02924].
- [205] A. Ali *et al.*, Eur. Phys. J. **C78**, 1, 29 (2018), [arXiv:1708.04650].
- [206] L. Maiani *et al.*, Phys. Rev. **D89**, 114010 (2014), [arXiv:1405.1551].
- [207] K. Chilikin *et al.* (Belle), Phys. Rev. **D88**, 7, 074026 (2013), [arXiv:1306.4894].
- [208] R. Aaij *et al.* (LHCb), Phys. Rev. Lett. **112**, 22, 222002 (2014), [arXiv:1404.1903].
- [209] Y.-H. Chen *et al.*, Phys. Rev. **D99**, 7, 074016 (2019), [arXiv:1902.10957].
- [210] M. Ablikim *et al.* (BESIII), Phys. Rev. Lett. **110**, 252001 (2013), [arXiv:1303.5949].
- [211] M. Ablikim *et al.* (BESIII), Phys. Rev. Lett. **112**, 2, 022001 (2014), [arXiv:1310.1163].
- [212] P. Krokovny *et al.* (Belle), Phys. Rev. **D88**, 5, 052016 (2013), [arXiv:1308.2646].
- [213] A. Bondar *et al.* (Belle), Phys. Rev. Lett. **108**, 122001 (2012), [arXiv:1110.2251].
- [214] A. Garmash *et al.* (Belle), Phys. Rev. Lett. **116**, 21, 212001 (2016), [arXiv:1512.07419].
- [215] A. E. Bondar *et al.*, Phys. Rev. **D84**, 054010 (2011), [arXiv:1105.4473].
- [216] A. Ali *et al.*, Phys. Rev. **D91**, 1, 017502 (2015), [arXiv:1412.2049].
- [217] M. B. Voloshin, Phys. Rev. **D84**, 031502 (2011), [arXiv:1105.5829].
- [218] T. Mehen and J. W. Powell, Phys. Rev. **D84**, 114013 (2011), [arXiv:1109.3479].
- [219] V. Baru *et al.*, JHEP **06**, 158 (2017), [arXiv:1704.07332].
- [220] V. Baru *et al.*, Phys. Rev. **D99**, 9, 094013 (2019), [arXiv:1901.10319].
- [221] T. Branz, T. Gutsche and V. E. Lyubovitskij, Phys. Rev. **D82**, 054025 (2010), [arXiv:1005.3168].
- [222] P. Pakhlov, Phys. Lett. **B702**, 139 (2011), [arXiv:1105.2945].
- [223] P. Pakhlov and T. Uglov, Phys. Lett. **B748**, 183 (2015), [arXiv:1408.5295].
- [224] S. X. Nakamura and K. Tsushima, Phys. Rev. **D100**, 5, 051502 (2019), [arXiv:1901.07385].
- [225] M. Cleven *et al.*, Phys. Rev. **D92**, 1, 014005 (2015), [arXiv:1505.01771].

## 79. Baryon Decay Parameters

Written 1996 by E.D. Commins (University of California, Berkeley).

### 79.1. Baryon semileptonic decays

The typical spin-1/2 baryon semileptonic decay is described by a matrix element, the hadronic part of which may be written as:

$$\bar{B}_f \left[ f_1(q^2)\gamma_\lambda + i f_2(q^2)\sigma_{\lambda\mu}q^\mu + g_1(q^2)\gamma_\lambda\gamma_5 + g_3(q^2)\gamma_5q_\lambda \right] B_i . \quad (79.1)$$

Here  $B_i$  and  $\bar{B}_f$  are spinors describing the initial and final baryons, and  $q = p_i - p_f$ , while the terms in  $f_1$ ,  $f_2$ ,  $g_1$ , and  $g_3$  account for vector, induced tensor (“weak magnetism”), axial vector, and induced pseudoscalar contributions [1]. Second-class current contributions are ignored here. In the limit of zero momentum transfer,  $f_1$  reduces to the vector coupling constant  $g_V$ , and  $g_1$  reduces to the axial-vector coupling constant  $g_A$ . The latter coefficients are related by Cabibbo’s theory [2], generalized to six quarks (and three mixing angles) by Kobayashi and Maskawa [3]. The  $g_3$  term is negligible for transitions in which an  $e^\pm$  is emitted, and gives a very small correction, which can be estimated by PCAC [4], for  $\mu^\pm$  modes. Recoil effects include weak magnetism, and are taken into account adequately by considering terms of first order in

$$\delta = \frac{m_i - m_f}{m_i + m_f} , \quad (79.2)$$

where  $m_i$  and  $m_f$  are the masses of the initial and final baryons.

The experimental quantities of interest are the total decay rate, the lepton-neutrino angular correlation, the asymmetry coefficients in the decay of a polarized initial baryon, and the polarization of the decay baryon in its own rest frame for an unpolarized initial baryon. Formulae for these quantities are derived by standard means [5] and are analogous to formulae for nuclear beta decay [6]. We use the notation of Ref. 6 in the Listings for neutron beta decay. For comparison with experiments at higher  $q^2$ , it is necessary to modify the form factors at  $q^2 = 0$  by a “dipole”  $q^2$  dependence, and for high-precision comparisons to apply appropriate radiative corrections [7].

The ratio  $g_A/g_V$  may be written as

$$g_A/g_V = |g_A/g_V| e^{i\phi_{AV}} . \quad (79.3)$$

The presence of a “triple correlation” term in the transition probability, proportional to  $\text{Im}(g_A/g_V)$  and of the form

$$\boldsymbol{\sigma}_i \cdot (\mathbf{p}_\ell \times \mathbf{p}_\nu) \quad (79.4)$$

for initial baryon polarization or

$$\boldsymbol{\sigma}_f \cdot (\mathbf{p}_\ell \times \mathbf{p}_\nu) \quad (79.5)$$

for final baryon polarization, would indicate failure of time-reversal invariance. The phase angle  $\phi$  has been measured precisely only in neutron decay (and in  $^{19}\text{Ne}$  nuclear beta decay), and the results are consistent with  $T$  invariance.

### 79.2. Hyperon nonleptonic decays

The amplitude for a spin-1/2 hyperon decaying into a spin-1/2 baryon and a spin-0 meson may be written in the form

$$M = G_F m_\pi^2 \cdot \bar{B}_f (A - B\gamma_5) B_i , \quad (79.6)$$

where  $A$  and  $B$  are constants [1]. The transition rate is proportional to

$$R = 1 + \gamma \hat{\boldsymbol{\omega}}_f \cdot \hat{\boldsymbol{\omega}}_i + (1 - \gamma)(\hat{\boldsymbol{\omega}}_f \cdot \hat{\mathbf{n}})(\hat{\boldsymbol{\omega}}_i \cdot \hat{\mathbf{n}}) + \alpha(\hat{\boldsymbol{\omega}}_f \cdot \hat{\mathbf{n}} + \hat{\boldsymbol{\omega}}_i \cdot \hat{\mathbf{n}}) + \beta \hat{\mathbf{n}} \cdot (\hat{\boldsymbol{\omega}}_f \times \hat{\boldsymbol{\omega}}_i) , \quad (79.7)$$

where  $\hat{\mathbf{n}}$  is a unit vector in the direction of the final baryon momentum, and  $\hat{\boldsymbol{\omega}}_i$  and  $\hat{\boldsymbol{\omega}}_f$  are unit vectors in the directions of the initial and final baryon spins. (The sign of the last term in the above equation

was incorrect in our 1988 and 1990 editions.) The parameters  $\alpha$ ,  $\beta$ , and  $\gamma$  are defined as

$$\begin{aligned} \alpha &= 2 \text{Re}(s^*p)/(|s|^2 + |p|^2) , \\ \beta &= 2 \text{Im}(s^*p)/(|s|^2 + |p|^2) , \\ \gamma &= (|s|^2 - |p|^2)/(|s|^2 + |p|^2) , \end{aligned} \quad (79.8)$$

where  $s = A$  and  $p = |\mathbf{p}_f| B/(E_f + m_f)$ ; here  $E_f$  and  $\mathbf{p}_f$  are the energy and momentum of the final baryon. The parameters  $\alpha$ ,  $\beta$ , and  $\gamma$  satisfy

$$\alpha^2 + \beta^2 + \gamma^2 = 1 . \quad (79.9)$$

If the hyperon polarization is  $\mathbf{P}_Y$ , the polarization  $\mathbf{P}_B$  of the decay baryons is

$$\mathbf{P}_B = \frac{(\alpha + \mathbf{P}_Y \cdot \hat{\mathbf{n}})\hat{\mathbf{n}} + \beta(\mathbf{P}_Y \times \hat{\mathbf{n}}) + \gamma\hat{\mathbf{n}} \times (\mathbf{P}_Y \times \hat{\mathbf{n}})}{1 + \alpha\mathbf{P}_Y \cdot \hat{\mathbf{n}}} . \quad (79.10)$$

Here  $\mathbf{P}_B$  is defined in the rest system of the baryon, obtained by a Lorentz transformation along  $\hat{\mathbf{n}}$  from the hyperon rest frame, in which  $\hat{\mathbf{n}}$  and  $\mathbf{P}_Y$  are defined.

An additional useful parameter  $\phi$  is defined by

$$\beta = (1 - \alpha^2)^{1/2} \sin\phi . \quad (79.11)$$

In the Listings, we compile  $\alpha$  and  $\phi$  for each decay, since these quantities are most closely related to experiment and are essentially uncorrelated. When necessary, we have changed the signs of reported values to agree with our sign conventions. In the Baryon Summary Table, we give  $\alpha$ ,  $\phi$ , and  $\Delta$  (defined below) with errors, and also give the value of  $\gamma$  without error.

Time-reversal invariance requires, in the absence of final-state interactions, that  $s$  and  $p$  be relatively real, and therefore that  $\beta = 0$ . However, for the decays discussed here, the final-state interaction is strong. Thus

$$s = |s| e^{i\delta_s} \text{ and } p = |p| e^{i\delta_p} , \quad (79.12)$$

where  $\delta_s$  and  $\delta_p$  are the pion-baryon  $s$ - and  $p$ -wave strong interaction phase shifts. We then have

$$\beta = \frac{-2|s||p|}{|s|^2 + |p|^2} \sin(\delta_s - \delta_p) . \quad (79.13)$$

One also defines  $\Delta = -\tan^{-1}(\beta/\alpha)$ . If  $T$  invariance holds,  $\Delta = \delta_s - \delta_p$ . For  $\Lambda \rightarrow p\pi^-$  decay, the value of  $\Delta$  may be compared with the  $s$ - and  $p$ -wave phase shifts in low-energy  $\pi^-p$  scattering, and the results are consistent with  $T$  invariance.

See also the note on “Radiative Hyperon Decays” in this *Review*.

### References:

1. E.D. Commins and P.H. Bucksbaum, *Weak Interactions of Leptons and Quarks* (Cambridge University Press, Cambridge, England, 1983).
2. N. Cabibbo, Phys. Rev. Lett. **10**, 531 (1963).
3. M. Kobayashi and T. Maskawa, Prog. Theor. Phys. **49**, 652 (1973).
4. M.L. Goldberger and S.B. Treiman, Phys. Rev. **111**, 354 (1958).
5. P.H. Frampton and W.K. Tung, Phys. Rev. **D3**, 1114 (1971).
6. J.D. Jackson, S.B. Treiman, and H.W. Wyld, Jr., Phys. Rev. **106**, 517 (1957), and Nucl. Phys. **4**, 206 (1957).
7. Y. Yokoo, S. Suzuki, and M. Morita, Prog. Theor. Phys. **50**, 1894 (1973).

## 80. *N* and $\Delta$ Resonances

Revised July 2019 by V. Burkert (Jefferson Lab), E. Klempt (University of Bonn), U. Thoma (University of Bonn), L. Tiator (University of Mainz), and R.L. Workman (George Washington University).

### 80.1. Introduction

The excited states of the nucleon have been studied in a large number of formation and production experiments. Until recently, the Breit-Wigner masses and widths, the pole positions, and the elasticities of the *N* and  $\Delta$  resonances in the Baryon Summary Table came largely from partial-wave analyses of  $\pi N$  total, elastic, and charge-exchange scattering data. The most comprehensive analyses were carried out by the Karlsruhe-Helsinki (KH80) [1], Carnegie Mellon-Berkeley (CMB80) [2], and George Washington U (GWU) [3] groups. Partial-wave analyses have also been performed on much smaller  $\pi N$  reaction data sets to get  $\eta N$ ,  $K\Lambda$ , and  $K\Sigma$  branching fractions (see the Listings for references). Other branching fractions come from analyses of  $\pi N \rightarrow \pi\pi N$  data.

In recent years, a large amount of data on photoproduction of many final states has been accumulated, and these data are beginning to tell us much about the properties of baryon resonances. A survey of data on photoproduction can be found in the proceedings of recent conferences [4] and workshops [5], and in recent reviews [6,7].

### 80.2. Naming scheme for baryon resonances

In the past, when nearly all resonance information came from elastic  $\pi N$  scattering, it was common to label resonances with the incoming partial wave  $L_{2I,2J}$ , as in  $\Delta(1232)P_{33}$  and  $N(1680)F_{15}$ . However, most recent information has come from  $\gamma N$  experiments. Therefore, we have replaced  $L_{2I,2J}$  with the spin-parity  $J^P$  of the state, as in  $\Delta(1232)3/2^+$  and  $N(1680)5/2^+$ ; this name gives intrinsic properties of the resonance that are independent of the specific particles and reactions used to study them. This applies equally to all baryons, including  $\Xi$  resonances and charm baryons that are not produced in formation experiments. We do not, however, attach the mass or spin-parity to the names of the ground-state (“stable”) baryons  $N, \Lambda, \Sigma, \Xi, \Omega, \Lambda_c, \dots$ .

### 80.3. Using the *N* and $\Delta$ listings

Tables 80.1 and 80.2 list all the *N* and  $\Delta$  entries in the Baryon Listings and give our evaluation of the overall status and the status channel by channel. Only the established resonances (overall status 3 or 4 stars) are promoted to the Baryon Summary Table. We long ago omitted from the Listings information from old analyses, prior to KH80 and CMB80, which can be found in earlier editions. A rather complete survey of older results was given in our 1982 edition [8].

As a rule, we award an overall status \*\*\*\* or \*\*\* only to those resonances which are derived from analyses of data sets that include precision differential cross sections and polarization observables, and are confirmed by independent analyses. All other signals are given \*\* or \* status. New results that are not accompanied by proper error evaluation are less valuable for evaluating star ratings. The following criteria are guidelines for future error analysis.

1. Uncertainties in resonance parameters: The publication should have a detailed discussion on how the uncertainties of parameters were estimated. This requires that the error estimates go beyond the simple fit error as e.g. given by MINUIT, and the robustness of the results should be demonstrated.

2. Fit quality: Concrete measures for the fit quality should be provided. The reduced global  $\chi^2$  value of the fit, while useful, is insufficient. Other possibilities include quoting variations of local  $\chi^2$  values in kinematic regions where evidence for new resonances, or significantly improved information on resonance parameters, is claimed.

3. Weight factors in observables: Analyses sometimes use weight factors for certain data sets to either increase or reduce their impact on the results. This has been particularly important when polarization observables are involved, which often are sensitive to

resonance amplitudes through interferences, but usually have much poorer statistics than differential cross section data. To evaluate sensitivities, the resulting resonance parameters should be checked against variations of the specific weight factors.

Claims of evidence for new baryon states must be based on a sufficiently complete set of partial waves in the fit. The robustness of signals must be demonstrated, e.g. by examining the effect of higher partial waves in the fit.

### 80.4. Properties of resonances

Resonances are defined by poles of the *S*-matrix, whether in scattering, production or decay matrix elements. These are poles in the complex plane in *s*, as discussed in the new review on *Resonances*. As is traditional, we quote here the pole positions in the complex energy  $w = \sqrt{s}$  plane. Crucially, the position of the pole of the *S*-matrix is independent of the process, and the production and decay properties factorize. This is the rationale for listing the pole position first for each resonance. These key properties of the *S*-matrix pole are in contrast to other quantities related to resonance phenomena, such as Breit-Wigner parameters or any *K*-matrix pole. Breit-Wigner parameters depend on the formalism used, such as angular-momentum barrier factors, or cut-off parameters, and the assumed or modeled background. However, the accurate determination of pole parameters from the analysis of data on the real energy axis is not necessarily simple, or even straightforward. It requires the implementation of the correct analytic structure of the relevant (often coupled) channels.

In principle, there are two ways to extract pole parameters from experimental data: (i) analytic continuation of theoretical single- or multi-channel models into the complex energy plane or (ii) local expansions of the partial-wave *T*-matrix amplitudes in the complex energy plane in the vicinity of a pole.

At present, poles are usually extracted using the first method [9–14], but considerable effort has been put into the development of alternate approaches, such as the speed plot [15], time delay [16], N/D method [17], regularization procedure [18], or Padé approximation [19].

Methods of the second type are based on the idea to use first or higher-order derivatives in energy to reduce the importance of, or totally eliminate, the background contribution. One either has to model the background contribution and introduce model dependence, or one is faced with numerical derivatives of single-energy data. In both cases, one reaches almost unsurmountable difficulties.

An alternate way to extract pole parameters from partial waves has been proposed by introducing a Laurent+Pietarinen (L+P) expansion [20–22]

$$T(W) = \sum_{i=1}^N \frac{Res_i}{W - W_i} + \sum_{j=1}^M \sum_{n=0}^{n_{max}} c_n^j \left( \frac{\alpha_j - \sqrt{x_j - W}}{\alpha_j + \sqrt{x_j - W}} \right)^n, \quad (1)$$

where  $T(W)$  is a given partial wave amplitude,  $W_i$  and  $Res_i$  are the *N* complex pole positions and residues. The background is parameterized with *M* Pietarinen functions, where  $\alpha_j$  are positive range parameters and  $x_j$  are real or complex branch points;  $c_n^j$  are real expansion coefficients.

The main idea of this procedure is to find the simplest analytic function, with well-defined poles and cuts, regardless of whether they are generated by a theoretical model or some energy-independent procedure. Instead of searching for the function which reproduces the input amplitudes over the complete complex energy plane, on all Riemann sheets, a representation is searched only in a limited complex energy range, near the real axis, which is defined by the radius of

Table 80.1. The status of the *N* resonances and their decays. Sub-threshold decay modes are omitted. Only resonances with an overall status of \*\*\* or \*\*\*\* are included in the main Baryon Summary Table.

Particle $J^P$	overall	Status as seen in									
		$N\gamma$	$N\pi$	$\Delta\pi$	$N\sigma$	$N\eta$	$\Lambda K$	$\Sigma K$	$N\rho$	$N\omega$	$N\eta'$
<i>N</i> 1/2 <sup>+</sup> ****											
<i>N</i> (1440)1/2 <sup>+</sup> ****	****	*****									
<i>N</i> (1520)3/2 <sup>-</sup> ****	****	*****				****					
<i>N</i> (1535)1/2 <sup>-</sup> ****	****	*****	*			****					
<i>N</i> (1650)1/2 <sup>-</sup> ****	****	*****	*			****					
<i>N</i> (1675)5/2 <sup>-</sup> ****	****	*****	*	*		*					
<i>N</i> (1680)5/2 <sup>+</sup> ****	****	*****	*	*		*					
<i>N</i> (1700)3/2 <sup>-</sup> ***	**	***	***	*	*				*		
<i>N</i> (1710)1/2 <sup>+</sup> ****	****	*****				***	**	*	*	*	
<i>N</i> (1720)3/2 <sup>+</sup> ****	****	*****	*	*		*****	*	*	*	*	
<i>N</i> (1860)5/2 <sup>+</sup> **	*	**	*	*		*					
<i>N</i> (1875)3/2 <sup>-</sup> ***	**	**	*	**	*	*	*	*	*	*	
<i>N</i> (1880)1/2 <sup>+</sup> ***	**	*	**	*	*	**	**		**		
<i>N</i> (1895)1/2 <sup>-</sup> ****	****	*	*	*	*****	**	*	*	*	****	
<i>N</i> (1900)3/2 <sup>+</sup> ****	****	**	**	*	*	**	**	*	*	**	
<i>N</i> (1990)7/2 <sup>+</sup> **	**	**			*	*	*				
<i>N</i> (2000)5/2 <sup>+</sup> **	**	*	**	*	*				*		
<i>N</i> (2040)3/2 <sup>+</sup> *		*									
<i>N</i> (2060)5/2 <sup>-</sup> ***	***	**	*	*	*	*	*	*	*	*	
<i>N</i> (2100)1/2 <sup>+</sup> ***	**	***	**	**	*	*		*	*	**	
<i>N</i> (2120)3/2 <sup>-</sup> ***	***	**	**	**	*	**	*	*	*	*	
<i>N</i> (2190)7/2 <sup>-</sup> ****	****	*****	*	*	*	**	*	*	*	*	
<i>N</i> (2220)9/2 <sup>+</sup> ****	**	****			*	*	*				
<i>N</i> (2250)9/2 <sup>-</sup> ****	**	****			*	*	*				
<i>N</i> (2300)1/2 <sup>+</sup> **		**									
<i>N</i> (2570)5/2 <sup>-</sup> **		**									
<i>N</i> (2600)11/2 <sup>-</sup> ***		***									
<i>N</i> (2700)13/2 <sup>+</sup> **		**									

\*\*\*\* Existence is certain.  
 \*\*\* Existence is very likely.  
 \*\* Evidence of existence is fair.  
 \* Evidence of existence is poor.

convergence of the Laurent decomposition, and which contains the input amplitudes. All details are found in Ref. [21]. Applications of the method can be found in [20–27].

### 80.5. Photoproduction

A new approach to the nucleon excitation spectrum is provided by dedicated facilities at the Universities of Bonn, Grenoble, and Mainz, and at the national laboratories Jefferson Lab in the US and SPring-8 in Japan. High-precision cross sections and polarization observables for the photoproduction of pseudoscalar mesons provide a data set that is approaching a “complete experiment,” one that fully constrains the four complex amplitudes describing the spin-structure of the reaction [28]. A large number of photoproduction reactions has been studied.

In pseudoscalar meson photoproduction, the four independent helicity amplitudes can be expressed in terms of the four CGLN [29] amplitudes allowed by Lorentz and gauge invariance. These amplitudes can be expanded in a series of electric and magnetic multipoles. Except for  $J = 1/2$ , one electric and one magnetic multipole contributes to each  $J^P$  combination.

Table 80.2. The status of the  $\Delta$  resonances and their decays. Sub-threshold decay modes are omitted. Only resonances with an overall status of \*\*\* or \*\*\*\* are included in the main Baryon Summary Table.

Particle $J^P$	overall	Status as seen in					
		$N\gamma$	$N\pi$	$\Delta\pi$	$\Sigma K$	$N\rho$	$\Delta\eta$
$\Delta$ (1232)3/2 <sup>+</sup> ****	****	****	****				
$\Delta$ (1600)3/2 <sup>+</sup> ****	****	****	***	****			
$\Delta$ (1620)1/2 <sup>-</sup> ****	****	****	****	****			
$\Delta$ (1700)3/2 <sup>-</sup> ****	****	****	****	****	*		
$\Delta$ (1750)1/2 <sup>+</sup> *	*	*	*		*		
$\Delta$ (1900)1/2 <sup>-</sup> ***	***	***	***	*	**	*	
$\Delta$ (1905)5/2 <sup>+</sup> ****	****	****	****	**	*	*	**
$\Delta$ (1910)1/2 <sup>+</sup> ****	****	***	****	**	**		*
$\Delta$ (1920)3/2 <sup>+</sup> ***	***	***	***	***	**		**
$\Delta$ (1930)5/2 <sup>-</sup> ***	*	*	***	*	*		
$\Delta$ (1940)3/2 <sup>-</sup> **	*	**	*				*
$\Delta$ (1950)7/2 <sup>+</sup> ****	****	****	****	**	***		
$\Delta$ (2000)5/2 <sup>+</sup> **	*	**	*		*		*
$\Delta$ (2150)1/2 <sup>-</sup> *	*	*					
$\Delta$ (2200)7/2 <sup>-</sup> ***	***	***	**	***	**		
$\Delta$ (2300)9/2 <sup>+</sup> **	**	**	**				
$\Delta$ (2350)5/2 <sup>-</sup> *	*	*					
$\Delta$ (2390)7/2 <sup>+</sup> *	*	*					
$\Delta$ (2400)9/2 <sup>-</sup> **	**	**	**				
$\Delta$ (2420)11/2 <sup>+</sup> ****	*	****					
$\Delta$ (2750)13/2 <sup>-</sup> **	**	**					
$\Delta$ (2950)15/2 <sup>+</sup> **	**	**					

\*\*\*\* Existence is certain.  
 \*\*\* Existence is very likely.  
 \*\* Evidence of existence is fair.  
 \* Evidence of existence is poor.

For a given state, these two amplitudes determine the resonance photo-decay helicity amplitudes  $A_{1/2}$  and  $A_{3/2}$ . As described below, this resonance extraction has been carried out either assuming a Breit-Wigner resonance or at the pole.

If a Breit-Wigner parametrization is used, the  $N\gamma$  partial width,  $\Gamma_\gamma$ , is given in terms of the helicity amplitudes  $A_{1/2}$  and  $A_{3/2}$  by

$$\Gamma_\gamma = \frac{k_{\text{BW}}^2}{\pi} \frac{2m_N}{(2J+1)m_{\text{BW}}} \left( |A_{1/2}|^2 + |A_{3/2}|^2 \right). \quad (2)$$

Here  $m_N$  and  $m_{\text{BW}}$  are the nucleon and resonance masses,  $J$  is the resonance spin, and  $k_{\text{BW}}$  is the photon c.m. decay momentum. Most earlier analyses have provided these real quantities  $A_{1/2}$  and  $A_{3/2}$ .

More recent studies have quoted related complex quantities, evaluated at the T-matrix pole. These complex helicity amplitudes,  $\tilde{A}_{1/2}$  and  $\tilde{A}_{3/2}$ , can be cast onto the form

$$\tilde{A}_h = \sqrt{\frac{\pi(2J+1)w_{\text{pole}}}{m_N k_{\text{pole}}^2}} \frac{\text{Res}(T_h(\gamma N \rightarrow N b))}{\sqrt{\text{Res}(T(N b \rightarrow N b))}} \quad (3)$$

where the residues (*Res*) are evaluated at the pole position,  $w_{\text{pole}}$ , and  $k_{\text{pole}}^2 = (w_{\text{pole}}^2 - m_N^2)^2 / 4w_{\text{pole}}^2$  [30]. For Breit-Wigner amplitudes,  $w_{\text{pole}} = m_{\text{BW}}$  and  $\tilde{A}_h = A_h$ . Similar relations for the photo and electro couplings at the pole position can be found in [31,32].

The determination of eight real numbers from four complex amplitudes (with one overall phase undetermined) requires at least seven independent measurements. At least one further measurement is required to resolve discrete ambiguities that result from the fact that data are proportional to squared amplitudes. Photon beams and

nucleon targets can be polarized (with linear or circular polarization  $P_{\perp}$ ,  $P_{\odot}$  and  $\vec{T}$ , respectively); the recoil polarization of the outgoing baryon  $\vec{R}$  can be measured. The experiments can be divided into three classes: (1) the beam and target are polarized (BT); (2) the beam is polarized and the recoil baryon polarization is measured (BR); (3) the target is polarized and the recoil polarization is measured (TR). Different sign conventions are used in the literature, as summarized in [33].

One of the best studied reactions is  $\gamma p \rightarrow \Lambda K^+$ . Published data include differential cross sections, the beam asymmetry  $\Sigma$ , the target asymmetry  $T$ , the recoil polarization  $P$ , and the BR double-polarization variables  $C_{x'}$ ,  $C_{z'}$ ,  $O_{x'}$ , and  $O_{z'}$ . For the photoproduction of pions and etas, off proton and neutron targets, differential cross sections, single- and double-polarization asymmetries have been measured, mainly for pions.

## 80.6. Electroproduction

Electroproduction of mesons provides information on the internal structure of resonances. The helicity amplitudes are functions of the (squared) momentum transfer  $Q^2 = -(e - e')^2$ , where  $e$  and  $e'$  are the 4-momenta of the incident and scattered electron, and a third amplitude,  $S_{1/2}$ , measures the resonance response to the longitudinal component of the virtual photon. Most data stem from the reactions  $e^- p \rightarrow e^- n \pi^+$  and  $e^- p \rightarrow e^- p \pi^0$  but also the reactions  $e^- p \rightarrow e^- p \eta$ ,  $e^- p \rightarrow e^- p \pi^+ \pi^-$ , and  $e^- p \rightarrow e^- \Lambda(\Sigma^0) K^+$  have been studied. The data and their interpretation are reviewed in Refs. [34,35].

The transition to the  $\Delta(1232)3/2^+$  is often quantified in terms of the magnetic dipole transition moment  $M_{1+}$  (or the magnetic transition form factor  $G_{M,Ash}^*(Q^2)$ ) [36], and the electric and scalar quadrupole transition moments  $E_{1+}$  and  $S_{1+}$ . Figure 80.1 shows the strength of the  $p \rightarrow \Delta^+$  transition plotted versus the photon virtuality  $Q^2$ . At  $Q^2 = 0$ ,  $M_{1+}$  dominates the resonance transition strength. The two amplitudes  $E_{1+}$  and  $S_{1+}$  imply a quadrupole deformation of the transition to the lowest excited state. The magnitude of  $R_{EM} = E_{1+}/M_{1+}$  remains nearly constant, while the magnitude of  $R_{SM} = S_{1+}/M_{1+}$  increases rapidly up to 25% at the highest  $Q^2$  value.

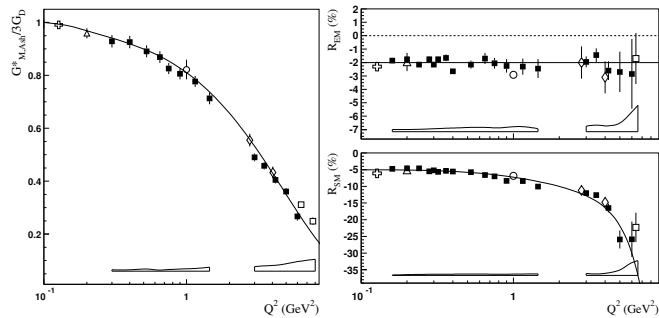


**Figure 80.1:** Left: The magnetic transition form factor for the  $\gamma^* p \rightarrow \Delta^+(1232)$  transition versus the photon virtuality  $Q^2$ . Right: The electric and scalar quadrupole ratios  $R_{EM}$  and  $R_{SM}$ . The different symbols are results from different experiments at JLab (squares, diamonds, circle) and MAMI (triangle, cross). The boxes near the horizontal axis indicate model uncertainties of the squares. Curves to guide the eyes.

Figure 80.2 shows the transverse and scalar helicity amplitudes for the  $N(1440)1/2^+$ ,  $N(1520)3/2^-$ , and  $N(1535)1/2^-$  resonances from JLab [34]. Similar results have been achieved at Mainz [35]. For the states  $N(1440)1/2^+$  and  $N(1520)3/2^-$ , helicity amplitudes and  $\pi\Delta$  and  $\rho p$  decays were determined at JLab in an analysis of  $\pi^+ \pi^- p$  electroproduction [37]. The data show distinctly different  $Q^2$  dependencies that indicate different internal structures.

The  $N(1520)3/2^-$  helicity amplitudes reveal the dominance of its three-quark nature: the  $A_{3/2}$  amplitude is large at the photon point and decreases rapidly  $\sim Q^{-5}$  with increasing  $Q^2$ ;  $A_{1/2}$  is small at the

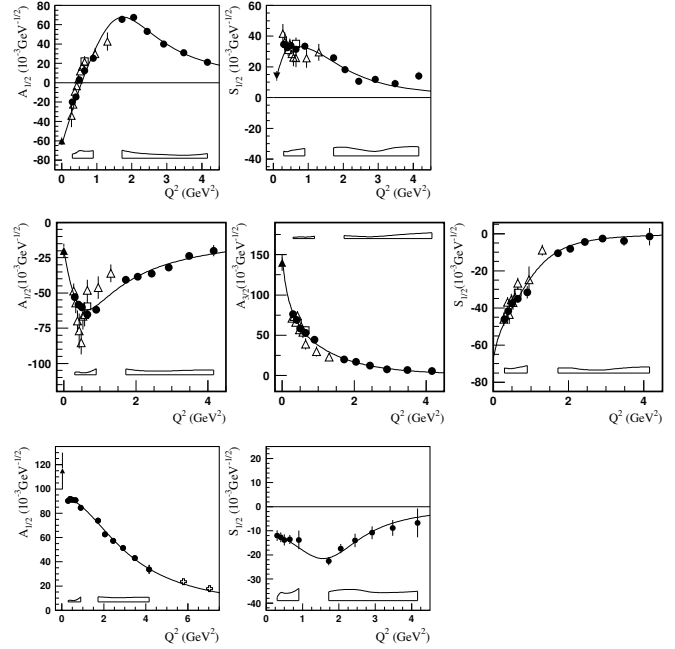


**Figure 80.2:** Transverse and scalar (longitudinal) helicity amplitudes for  $\gamma p \rightarrow N(1440)1/2^+$  (top),  $\gamma p \rightarrow N(1520)3/2^-$  (center), and  $\gamma p \rightarrow N(1535)1/2^-$  (bottom) as extracted from the JLab/CLAS data in  $n\pi^+$  production (full circles), MAMI/A1 data in  $p\pi^0$  production (full down triangle), in  $p\pi^+\pi^-$  (open triangles), and combined single and double pion production (open squares). The solid triangle is the PDG 2014 value at  $Q^2 = 0$ . The open boxes are the model uncertainties of the full circles.

photon point, increases rapidly with  $Q^2$  and then falls off with  $\sim Q^{-3}$ . Quantitative agreement with the data is, however, achieved only when meson cloud effects are included.

At high  $Q^2$ , both amplitudes for  $N(1440)1/2^+$  are qualitatively described by light front quark models [38]: at short distances the resonance behaves as expected from a radial excitation of the nucleon. On the other hand,  $A_{1/2}$  changes sign at about  $0.6\text{GeV}^2$ . This remarkable behavior has not been observed before for any nucleon form factor or transition amplitude. Obviously, an important change in the structure occurs when the resonance is probed as a function of  $Q^2$ .

The  $Q^2$  dependence of  $A_{1/2}$  of the  $N(1535)1/2^-$  resonance exhibits the expected  $Q^{-3}$  dependence, except for small  $Q^2$  values where meson cloud effects set in.

Figure 80.3 shows the transverse and scalar amplitudes for three states in the 3rd nucleon resonance region, the  $\Delta(1620)1/2^-$ , the  $N(1675)5/2^-$  and  $N(1680)5/2^+$ . The latter two states have nearly degenerate masses and are parity partners. In the quark model picture, the transverse amplitudes for  $N(1675)5/2^-$  on the proton are suppressed due to the Moorhouse selection rule, allowing for a quantitative evaluation of the meson-baryon contributions. The data show significant meson-baryon strength in the  $A_{1/2}$  amplitude even at quite high  $Q^2$ , while  $A_{3/2}$  drops much faster with  $Q^2$ .  $N(1680)5/2^+$  shows qualitatively the features predicted in constituent quark models, a dominant  $A_{3/2}$  at the real photon point that drops rapidly with increasing  $Q^2$ , while  $A_{1/2}$  becomes the dominant contribution at high  $Q^2$ , indicating a switch of the helicity structure in the resonance transition at short distances.

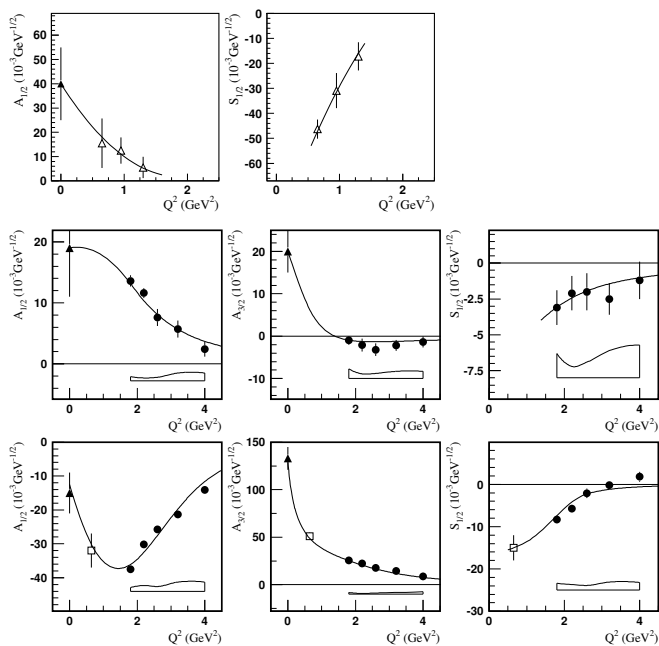


**Figure 80.3:** Transverse and scalar helicity amplitudes for  $\gamma p \rightarrow \Delta(1620)1/2^-$  (top),  $\gamma p \rightarrow N(1675)5/2^-$  (center), and  $\gamma p \rightarrow N(1680)5/2^+$  (bottom) as extracted from the JLab/CLAS data in  $n\pi^+$  production (full circles),  $p\pi^+\pi^-$  (open triangles), combined single and double pion production (open square). The solid triangle is the 2014 PDG value at  $Q^2 = 0$ . The open boxes are the model uncertainties of the full circles. The curves are to guide the eye.

### 80.7. Partial wave analyses

Several PWA groups are now actively involved in the analysis of the new data. The GWU group maintains a nearly complete database covering reactions from  $\pi N$  and  $KN$  elastic scattering to  $\gamma N \rightarrow N\pi$ ,  $N\eta$ , and  $N\eta'$ . It is presently the only group determining  $\pi N$  elastic amplitudes from scattering data in sliced energy bins. Given the high-precision of photoproduction data already or soon to be collected, the spectrum of  $N$  and  $\Delta$  resonances will in the near future be better known.

Fits to the data are performed by various groups with the aim to understand the reaction dynamics and to identify  $N$  and  $\Delta$  resonances. For practical reasons, approximations have to be made. We mention several analyses here: (1) The Mainz unitary isobar model [39] focuses on the correct treatment of the low-energy domain. Resonances are added to the unitary amplitude as a sum of Breit-Wigner amplitudes. This model also obtains resonance transition form factors and helicity amplitudes from electroproduction [35]. (2) For  $N\pi$  electroproduction, the Yerevan/JLab group uses both the unitary isobar model and the dispersion relation approach developed in [38]. A phenomenological model was developed to extract resonance couplings and partial decay widths from exclusive  $\pi^+\pi^-p$  electroproduction [37]. (3) Multichannel analyses using K-matrix parameterizations derive background terms from a chiral Lagrangian - providing a microscopical description of the background - (Giessen [40,41]) or from phenomenology (KSU [42,43], Bonn-Gatchina [44]). (4) Several groups (EBAC-Jlab [45,46], ANL-Osaka [47], Dubna-Mainz-Taipeh [48], Bonn-Jülich [49,50,51], Valencia [52]) use dynamical reaction models, driven by chiral Lagrangians, which take dispersive parts of intermediate states into account. Several other groups have made important contributions. The Giessen group pioneered multichannel analyses of large data sets on pion- and photo-induced reactions [40,41]. The Bonn-Gatchina group included recent high-statistics data and reported systematic searches for new baryon resonances in all relevant partial waves. A summary of their results can be found in [44].

### References:

- G. Höhler, Pion-Nucleon Scattering, Landolt-Börnstein Vol. I/9b2 (1983), ed. H. Schopper, Springer Verlag.
- R.E. Cutkosky *et al.*, Baryon 1980, *IV International Conference on Baryon Resonances*, Toronto, ed. N. Isgur, p. 19.
- R.A. Arndt *et al.*, Phys. Rev. **C74**, 045205 (2006).
- “Hadron 2011: 14th International Conference on Hadron Spectroscopy”, München, Germany, June, 13 - 17, 2011, published in eConf.
- “NSTAR 2013: 9th International Workshop on the Physics of Excited Nucleons”, 27-30 May 2013, Peñíscola, Spain.
- E. Klempt and J.M. Richard, Rev. Mod. Phys. **82**, 1095 (2010).
- V. Credé and W. Roberts, Rept. on Prog. in Phys. **76**, 076301 (2013).
- M. Roos *et al.*, Phys. Lett. **B111**, 1 (1982).
- M. Döring, C. Hanhart, F. Huang, S. Krewald, and U.-G. Meissner, Nucl. Phys. **A829**, 170 (2009), and references therein.
- N. Suzuki, B. Juliá-Díaz, H. Kamano, T.-S. H. Lee, A. Matsuyama, and T. Sato, Phys. Rev. Lett. **104**, 042302 (2010); H. Kamano, T.-S. H. Lee, A. Matsuyama, T. Sato, N. Suzuki, Phys. Rev. **C80**, 025207 (2009), and references therein.
- R. E. Cutkosky, C. P. Forsyth, R. E. Hendrick, and R. L. Kelly, Phys. Rev. **D20**, 2839 (1979).
- R. A. Arndt, W. J. Briscoe, I. I. Strakovsky, R. L. Workman, and M. M. Pavan, Phys. Rev. **C69**, 035213 (2004)..
- M. Batinić, I. Šlaus, A. Švarc, and B. M. K. Nefkens, Phys. Rev. **C51**, 2310 (1995); M. Batinić *et al.*, Phys. Scr. **58**, 15 (1998).
- A. V. Anisovich, R. Beck, E. Klempt, V. A. Nikonov, A. V. Sarantsev, U. Thoma, Eur. Phys. J. **A48**, 15 (2012), and references therein.
- G. Höhler,  $\pi N$  Newsletter **9**, 1 (1993).
- N. G. Kelkar, M. Nowakowski, Phys. Rev. **A78**, 012709 (2008), and references therein.
- G. F. Chew and S. Mandelstam, Phys. Rev. **119**, 467 (1960).
- S. Ceci, J. Stahov, A. Švarc, S. Watson, and B. Zauner, Phys. Rev. **D77**, 116007 (2008).
- P. Masjuan, J. J. Sanz-Cillero, Eur. Phys. J. **C73**, 2594 (2013).
- A. Švarc, M. Hadžimehmedović, H. Osmanović, J. Stahov, L. Tiator, and R. L. Workman, Phys. Rev. **C88**, 035206 (2013).
- A. Švarc, M. Hadžimehmedović, R. Omerović, H. Osmanović, and J. Stahov, Phys. Rev. **C89**, 045205 (2014).
- A. Švarc, M. Hadžimehmedović, H. Osmanović, J. Stahov, L. Tiator, and R. L. Workman, Phys. Lett. **B 755**, 452 (2016).
- A. Švarc, M. Hadžimehmedović, H. Osmanović, J. Stahov, L. Tiator, and R. L. Workman, Phys. Rev. **C89**, 065208 (2014).
- A. Švarc, M. Hadžimehmedović, H. Osmanović, J. Stahov, and R. L. Workman, Phys. Rev. **C91**, 015207 (2015).
- L. Tiator, M. Döring, R. L. Workman, M. Hadžimehmedović, R. Omerović, H. Osmanović, J. Stahov, and A. Švarc, Phys. Rev. **C94**, 065204 (2016).
- A. V. Anisovich *et al.*, Eur. Phys. J. **A53**, 242 (2017).
- A. V. Anisovich *et al.*, Phys. Rev. Lett. **119**, 062004 (2017).
- C. G. Fasano *et al.*, Phys. Rev. **C46**, 2430 (1992).
- G.F. Chew *et al.*, Phys. Rev. **106**, 1345 (1957).
- R.L. Workman, L. Tiator, and A. Sarantsev, Phys. Rev. **C87**, 068201 (2013).
- N. Suzuki, T. Sato, and T.-S.H. Lee, Phys. Rev. **C82**, 045206 (2010).
- H. Kamano, Phys. Rev. **C88**, 045203 (2013).
- A.M. Sandorfi *et al.*, AIP Conf. Proc. **1432**, 219 (2012).
- I. G. Aznauryan and V. D. Burkert, Prog. in Part. Nucl. Phys. **67**, 1 (2012).
- L. Tiator *et al.*, Eur. Phys. J. ST **198**, 141 (2011); S. Štajner *et al.*, Phys. Rev. Lett. **119**, 022001 (2017).
- W.W. Ash, Phys. Lett. **B24**, 165 (1967).
- V.I. Moiseev *et al.* [CLAS Collab.], Phys. Rev. **C86**, 035203 (2012).
- I.G. Aznauryan, Phys. Rev. **C67**, 015209 (2003).
- D. Drechsel, S.S. Kamalov, and L. Tiator, Eur. Phys. J. **A34**, 69 (2007).
- G. Penner and U. Mosel, Phys. Rev. **C66**, 055211 (2002).

41. G. Penner and U. Mosel, Phys. Rev. **C66**, 055212 (2002).
42. D.M. Manley and E.M. Saleski, Phys. Rev. **D45**, 4002 (1992).
43. M. Shrestha and D.M. Manley, Phys. Rev. **C86**, 055203 (2012).
44. A.V. Anisovich *et al.*, Eur. Phys. J. **A48**, 15 (2012).
45. A. Matsuyama, T. Sato, and T.-S.H. Lee, Phys. Reports **439**, 193 (2007).
46. T. Sato and T.-S.H. Lee, J. Phys. **G36**, 073001 (2009).
47. H. Kamano *et al.*, Phys. Rev. **C88**, 035209 (2013).
48. G.Y. Chen *et al.*, Phys. Rev. **C76**, 035206 (2007).
49. M. Döring *et al.*, Phys. Lett. **B681**, 26 (2009).
50. M. Döring *et al.*, Nucl. Phys. **A829**, 170 (2009).
51. D. Rönchen *et al.*, Eur. Phys. J. **A49**, 44 (2013).
52. S. Sarkar, E. Oset, and M.J. Vicente Vacas, Nucl. Phys. **A750**, 294 (2005) [Erratum-ibid. **A780**, 78 (2006)].



## 81. Baryon Magnetic Moments

Written 1994 by C.G. Wohl (LBNL).

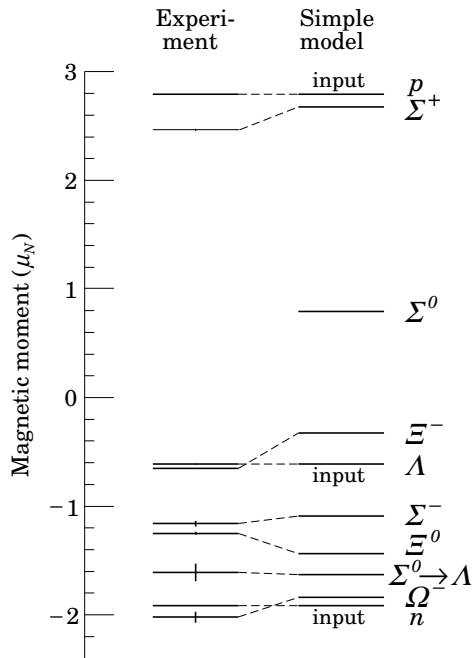
The figure below shows the measured magnetic moments of the stable baryons. It also shows the predictions of the simplest quark model, using the measured  $p$ ,  $n$ , and  $\Lambda$  moments as input. In this model, the moments are [1]

$$\begin{aligned} \mu_p &= (4\mu_u - \mu_d)/3 & \mu_n &= (4\mu_d - \mu_u)/3 \\ \mu_{\Sigma^+} &= (4\mu_u - \mu_s)/3 & \mu_{\Sigma^-} &= (4\mu_d - \mu_s)/3 \\ \mu_{\Xi^0} &= (4\mu_s - \mu_u)/3 & \mu_{\Xi^-} &= (4\mu_s - \mu_d)/3 \\ \mu_\Lambda &= \mu_s & \mu_{\Sigma^0} &= (2\mu_u + 2\mu_d - \mu_s)/3 \\ & & \mu_{\Omega^-} &= 3\mu_s \end{aligned}$$

and the  $\Sigma^0 \rightarrow \Lambda$  transition moment is

$$\mu_{\Sigma^0\Lambda} = (\mu_d - \mu_u)/\sqrt{3}.$$

The quark moments that result from this model are  $\mu_u = +1.852\mu_N$ ,  $\mu_d = -0.972\mu_N$ , and  $\mu_s = -0.613\mu_N$ . The corresponding effective quark masses, taking the quarks to be Dirac point particles, where  $\mu = q\hbar/2m$ , are 338, 322, and 510 MeV. As the figure shows, the model gives a good first approximation to the experimental moments. For efforts to make a better model, we refer to the literature [2].



## References:

- See, for example, D.H. Perkins, *Introduction to High Energy Physics* (Addison-Wesley, Reading, MA, 1987), or D. Griffiths, *Introduction to Elementary Particles* (Harper & Row, New York, 1987).
- See, for example, J. Franklin, Phys. Rev. **D29**, 2648 (1984); H.J. Lipkin, Nucl. Phys. **B241**, 477 (1984); K. Suzuki, H. Kumagai, and Y. Tanaka, Europhys. Lett. **2**, 109 (1986); S.K. Gupta and S.B. Khadkikar, Phys. Rev. **D36**, 307 (1987); M.I. Krivoruchenko, Sov. J. Nucl. Phys. **45**, 109 (1987); L. Brekke and J.L. Rosner, Comm. Nucl. Part. Phys. **18**, 83 (1988); K.-T. Chao, Phys. Rev. **D41**, 920 (1990) and references cited therein; Also, see references cited in discussions of results in the experimental papers..

82.  $\Lambda$  and  $\Sigma$  Resonances

Written December 2019 by V. Burkert (Jefferson Lab), E. Klempt (Bonn U.), U. Thoma (Bonn U.), L. Tiator (KPH, JGU Mainz) and R.L. Workman (George Washington U.).

## 82.1 Introduction

For several decades, there has been very little new experimental data bearing on the properties of  $\Lambda$  and  $\Sigma$  resonances. An exception was the study at JLab of the reactions  $\gamma p \rightarrow K^+ \Sigma^\pm \pi^\mp$  and  $\gamma p \rightarrow K^+ \Sigma^0 \pi^0$  [1], which established

the spin and parity of the  $\Lambda(1405)$  [2]. There was also from BNL new data on the very low energy region of  $K^-p$  scattering [3–7]. Otherwise, the field is starved for data. Recent analyses (see below) have improved what we know about the *properties* of the known  $\Lambda$  and  $\Sigma$  resonances, but the *established* resonances are exactly the same ones that were in our 1984 edition [8]. The 1990 Review [9] gave a full report of the status then, and included Argand plots from the partial-wave analyses. The 2018 Review [10] has a short survey of the 1670 MeV region, which may in fact include three or four states – the well-established  $J^P = \Sigma(1670)3/2^-$ , the probable  $\Sigma(1660)1/2^+$ , and “bumps” at 1670 and 1690 MeV.

In the last few years, four groups have re-analyzed  $K^-p$  reactions using fuller collections of the old data. These analyses make an update of the status of the  $\Lambda$  and  $\Sigma$  resonances appropriate. Although they have not established any new resonances, they have provided at least some evidence for new states and have given a better understanding of the old ones.

Table I is our evaluation of the status, both over-all and channel by channel, of each  $\Lambda$  and  $\Sigma$  resonance in the Particle Listings. In making these evaluations, we considered, in addition to the four analyses just discussed, the ratings that predated them. The ratings use a 1- to 4-star system. The main Summary Table includes only established states with an overall status of 3 or 4 stars; as has already been noted, they are the same thirteen  $\Lambda$  and eight  $\Sigma$  resonances (above  $\Sigma(1385)3/2^+$ ) that have long been in the Table. In addition, there are four 1-star and four 2-star  $\Lambda$ 's, and four 1-star and six 2-star  $\Sigma$ 's in the Particle Listings.

## 82.2 New analyses

The new analysis progress was pioneered by the Kent group which collected a large fraction of the available data and performed a comprehensive partial wave analysis [11, 12].  $K^-p$  scattering into a pseudoscalar meson and an octet baryon is governed by two complex amplitudes; hence four quantities need to be measured to construct fully the amplitudes (up to an arbitrary phase per energy and angular bin). Discussions of complete experiments also generally assume perfect data (no experimental errors); realistic errors further complicate the task of amplitude extraction. Here, the available data are limited to the differential cross section and the target or hyperon recoil polarization  $P$  and partial-wave amplitudes are required. The authors of Ref. [11] overcame this difficulty by using start values for the partial wave amplitudes determined in [13] and/or from an energy-dependent fit and by freezing or releasing sets of amplitudes. The resulting amplitudes were fitted with a unitary multichannel parameterization [12].

The JPAC group presented a coupled-channel fit to the  $\bar{K}N$  partial waves derived by the Kent group [14]. The JPAC approach was based on the  $K$ -matrix formalism. Special attention was paid to the analytical properties of the amplitudes determined by the square-root unitary branch points and the continuation to the complex angular momentum plane. The fit described the Kent partial waves reasonably well. However, when observables were calculated from their partial-wave amplitudes, significant discrepancies became apparent. The results were therefore not included in the RPP.

The ANL-Osaka group derived the energy-dependent amplitudes in fits to a large subset of the data collected in Ref. [11] and further data sets described in Ref. [15]. Their fits were based on a phenomenological SU(3) Lagrangian [15]. The two models agree on the leading contributions but differ significantly in cases with weaker candidates [16].

**Table 82.1:** The status of the  $\Lambda$  resonances. Only those with an overall status of \*\*\* or \*\*\*\* are included in the main Baryon Summary Table.

Particle	$J^P$	Overall status	Status as seen in –		
			$N\bar{K}$	$\Sigma\pi$	Other channels
$\Lambda(1116)$	$1/2^+$	****			$N\pi$ (weakly)
$\Lambda(1380)$	$1/2^-$	**	**	**	
$\Lambda(1405)$	$1/2^-$	****	****	****	
$\Lambda(1520)$	$3/2^-$	****	****	****	$\Lambda\pi\pi, \Lambda\gamma$
$\Lambda(1600)$	$1/2^+$	***	***	***	$\Lambda\pi\pi, \Sigma(1385)\pi$
$\Lambda(1670)$	$1/2^-$	****	****	****	$\Lambda\eta$
$\Lambda(1690)$	$3/2^-$	****	****	***	$\Lambda\pi\pi, \Sigma(1385)\pi$
$\Lambda(1710)$	$1/2^+$	**	**	*	
$\Lambda(1800)$	$1/2^-$	****	**	**	$\Lambda\pi\pi, \Sigma(1385)\pi, N\bar{K}^*$
$\Lambda(1810)$	$1/2^+$	**	**	**	$N\bar{K}_2^*$
$\Lambda(1820)$	$5/2^+$	****	****	****	$\Sigma(1385)\pi$
$\Lambda(1830)$	$5/2^-$	****	****	****	$\Sigma(1385)\pi$
$\Lambda(1890)$	$3/2^+$	****	****	**	$\Sigma(1385)\pi, N\bar{K}^*$
$\Lambda(2000)$	$1/2^-$	*	*	*	
$\Lambda(2050)$	$3/2^-$	*	*	*	$\Sigma(1385)\pi$
$\Lambda(2070)$	$3/2^+$	**	*	*	$\Sigma(1385)\pi$
$\Lambda(2080)$	$5/2^-$	**	**	*	$\Sigma(1385)\pi$
$\Lambda(2085)$	$7/2^+$	*	*	*	$\Sigma(1385)\pi$
$\Lambda(2100)$	$7/2^-$	****	****	**	$\Sigma(1385)\pi$
$\Lambda(2110)$	$5/2^+$	***	***	**	$\Lambda\omega, N\bar{K}^*$
$\Lambda(2325)$	$3/2^-$	*	*	*	$\Lambda\omega$
$\Lambda(2350)$	$9/2^+$	***	***	*	

**Table 82.2:** The status of the  $\Sigma$  resonances. Only those with an overall status of \*\*\* or \*\*\*\* are included in the main Baryon Summary Table.

Particle	$J^P$	Overall status	Status as seen in –		
			$N\bar{K}$	$\Lambda\pi$	$\Sigma\pi$
$\Sigma(1193)$	$1/2^+$	****			$N\pi$ (weakly)
$\Sigma(1385)$	$3/2^+$	****		****	****
$\Sigma(1620)$	$1/2^-$	**	**	*	**
$\Sigma(1660)$	$1/2^+$	***	***	***	***
$\Sigma(1670)$	$3/2^-$	****	****	****	****
$\Sigma(1730)$	$3/2^+$	*	*	*	*
$\Sigma(1750)$	$1/2^-$	***	***	**	***
$\Sigma(1775)$	$5/2^-$	****	****	****	**
$\Sigma(1880)$	$1/2^+$	**	**	*	
$\Sigma(1950)$	$1/2^-$	**	***	*	**
$\Sigma(1915)$	$5/2^+$	****	***	***	***
$\Sigma(1920)$	$3/2^-$	***	*	**	***
$\Sigma(1940)$	$3/2^+$	**	**	*	
$\Sigma(2010)$	$3/2^-$	*	*	*	
$\Sigma(2030)$	$7/2^+$	****	****	****	**
$\Sigma(2070)$	$5/2^+$	*	*	*	
$\Sigma(2080)$	$3/2^+$	**	**	*	
$\Sigma(2100)$	$7/2^-$	*	*	*	
$\Sigma(2110)$	$1/2^-$	**	***	***	**
$\Sigma(2160)$	$1/2^-$	*	*	*	*
$\Sigma(2230)$	$3/2^+$	**	**	*	*
$\Sigma(2250)$		***	***	*	*

The Bonn-Gatchina (BnGa) group added further (old) data to those analyzed in Ref. [11]. The data set was fitted in a modified  $K$ -matrix approach and the resulting amplitudes were compared with those from Refs. [11, 15]. New resonances were found; all resonances were tested for their statistical significance. Additional states with any set of quantum numbers were tested and were found to produce only small improvements in the fit [17]. In Ref. [18], properties of the full set of contributing hyperons were reported.

The star ratings of  $\Lambda$  and  $\Sigma$  resonances given in our earlier editions, and the new results from the Kent, ANL-Osaka and BnGa groups were used to update the star rating of the hyperon resonances. In [18], the overall star rating is directly estimated, for [12] we estimate the overall star rating from the branching-ratio errors. In [16], two solutions are given but no uncertainties for branching ratios. We call a resonance *seen* when it is seen in both solutions with similar properties.

We decided to remove the twelve so-called *bumps*, one 2-star resonance,  $\Sigma(1580)3/2^-$ , and three 1-star resonances  $\Sigma(1770)1/2^+$ ,  $\Sigma(1840)3/2^+$  and  $\Sigma(2000)1/2^-$ , which were not confirmed in any of the four modern analyses. Apart from  $\Lambda(1380)1/2^-$ , four further new resonances were included in the Listings:  $\Lambda(2070)3/2^+$  and  $\Lambda(2080)5/2^-$  with two stars,  $\Sigma(2010)3/2^-$  and  $\Sigma(2160)1/2^-$  with one star.

### 82.3 Sign conventions for resonance couplings

In terms of the isospin-0 and isospin-1 elastic scattering amplitudes  $A_0$  and  $A_1$ , the amplitude for  $K^-p \rightarrow \bar{K}^0 n$  scattering is  $\pm(A_1 - A_0)/2$ , where the sign depends on conventions used in conjunction with the Clebsch-Gordan coefficients (such as, is the baryon or the meson the “first” particle). If this reaction is partial-wave analyzed and if the overall phase is chosen so that, say, the  $\Sigma(1775)D_{15}$  amplitude at resonance points along the positive imaginary axis (points “up”), then any  $\Sigma$  at resonance will point “up” and any  $\Lambda$  at resonance will point “down” (along the negative imaginary axis). Thus the phase at resonance determines the isospin. The above ignores background amplitudes in the resonating partial waves.

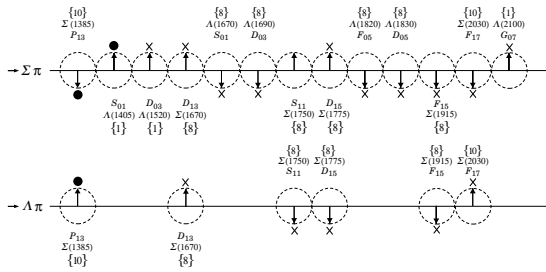


Figure 82.1: The signs of the imaginary parts of resonating amplitudes in the  $\bar{K}N \rightarrow \Lambda\pi$  and  $\Sigma\pi$  channels. The signs of the  $\Sigma(1385)$  and  $\Lambda(1405)$ , marked with a  $\bullet$ , are set by convention, and then the others are determined relative to them. The signs required by the SU(3) assignments of the resonances are shown with an arrow, and the experimentally determined signs are shown with an  $\times$ .

That is the basic idea. In a similar but somewhat more complicated way, the phases of the  $\bar{K}N \rightarrow \Lambda\pi$  and  $\bar{K}N \rightarrow \Sigma\pi$  amplitudes for a resonating wave help determine the SU(3) multiplet to which the resonance belongs. Again, a convention has to be adopted for some overall arbitrary phases: which way is “up”? Our convention is that of Levi-Setti [19] and is shown in Fig. 82.1, which also compares experimental results with theoretical predictions for the signs of several resonances. In the Listings, a + or – sign in front of a measurement of an inelastic resonance coupling indicates the sign (the *absence* of a sign means that the sign is not determined, *not* that it is positive). Also other decay modes can be used to assign a hyperon to a SU(3) multiplet [20, 21]. Modern analyses determine properties of resonances at the pole position. In these analyses, the + or – sign is replaced by a phase. Background amplitudes can lead to significant phase shifts, and an additional phase shift due to rescattering is admitted in some analyses. Three  $\Lambda$  spin doublets can be identified as belonging to SU(3) singlets: the well-known ( $\Lambda(1405)1/2^-$ ,  $\Lambda(1520)3/2^-$ ), the ( $\Lambda(2080)5/2^-$ ,  $\Lambda(2100)7/2^-$ ), and ( $\Lambda(2070)3/2^+$ ,  $\Lambda(2110)5/2^+$ ).

### 82.4 The $\Lambda(1405)$

In coupled-channels calculations based on the chiral SU(3) effective field theory, the strongly attractive forces between  $N\bar{K}$

and  $\Sigma\pi$  generate five poles, one SU(3) singlet pole, two  $\Lambda$  octet poles and two octet  $\Sigma$  poles (see Section 100). At least three of them are seen in the 1300 to 1500 MeV mass range. The appearance of two  $\Lambda$  poles in this mass range, a narrow SU(3) octet at  $\sim 1420$  MeV and a wider SU(3) singlet at  $\sim 1380$  MeV, was unexpected. This approach has been pursued by a number of groups; for a summary of the results see our Review 100, “Pole Structure of the  $\Lambda(1405)$  Region”. In the Listings, we have introduced the  $\Lambda(1380)$  as a new candidate resonance (with two stars), named in accordance with its approximate pole position. The second SU(3) octet  $\Lambda$  state is the well-known  $\Lambda(1670)$ . The masses of the two associated  $\Sigma$  states are uncertain so far, and no new entries are introduced in the Listings.

In traditional approaches only one resonance was seen, the narrow state at 1405 MeV. It was reported to be the SU(3) singlet state a long time ago in Ref. [22], in contrast to the findings based on coupled-channels calculations within chiral SU(3) effective field theories and in agreement with the quark-model expectations. A recent analysis using a modified  $K$ -matrix approach found only one resonance, with a pole at  $(1422 \pm 3)$  MeV [23]. Its SU(3) structure was found to be consistent with a singlet state. In the Listings, the  $\Lambda(1405)$  has been retained with its traditional name. In quark models, this state is identified with the SU(3) singlet state, the two  $\Lambda$  octet states with  $\Lambda(1670)$  and  $\Lambda(1800)$ , and the two  $\Sigma$  states with  $\Sigma(1620)$  and  $\Sigma(1750)$ .

### 82.5 Errors on masses and widths

The errors quoted on resonance parameters from partial-wave analyses are often only statistical, and the parameters can change by more than these errors when a different parametrization of the waves is used. Furthermore, the different analyses use more or less the same data, so it is not really appropriate to treat the different determinations of the resonance parameters as independent or to average them together. In any case, the spread of the masses, widths, and branching fractions from the different analyses is certainly a better indication of the uncertainties than are the quoted errors. In the Listings, we usually give a range reflecting the spread of the values rather than a particular value with error.

### 82.6 Production experiments

Partial-wave analyses of course separate partial waves, whereas a peak in a cross section or an invariant mass distribution usually cannot be disentangled from background and analyzed for its quantum numbers; and more than one resonance may be contributing to the peak. The  $\Sigma(1385)$  and  $\Lambda(1405)$  lie below the  $\bar{K}N$  threshold and nearly everything about  $\Sigma(1385)$  is learned from production experiments. Our knowledge on  $\Lambda(1405)$  benefits greatly from photoproduction of the three  $\Sigma\pi$  charge states [1, 2] and from the precise measurement of the energy shift and width of the kaonic hydrogen atom [24].

Production and formation experiments agree quite well in the case of  $\Lambda(1520)$  and results have been combined. Above this mass, no new results on peak hunting have been reported for about 40 years. For these early results, we refer the reader to our earlier editions. In photoproduction with energetic photons [25, 26] or at LHCb [27], hyperons are produced abundantly. So far, no attempt has been made to extract hyperon properties from these data. New data on hyperon spectroscopy can be expected from J-PARC [28], JLAB [29], and the forthcoming PANDA experiment [30].

### References

- [1] K. Moriya *et al.* (CLAS), Phys. Rev. **C87**, 3, 035206 (2013), [arXiv:1301.5000].
- [2] K. Moriya *et al.* (CLAS), Phys. Rev. Lett. **112**, 8, 082004 (2014), [arXiv:1402.2296].
- [3] A. Starostin *et al.* (Crystal Ball), Phys. Rev. **C64**, 055205 (2001).
- [4] S. Prakhov *et al.*, Phys. Rev. **C69**, 042202 (2004).
- [5] S. Prakhov *et al.* (Crystal Ball), Phys. Rev. **C70**, 034605 (2004).

- [6] R. Manweiler *et al.*, Phys. Rev. **C77**, 015205 (2008).
- [7] S. Prakhov *et al.*, Phys. Rev. **C80**, 025204 (2009), [arXiv:0812.1888].
- [8] C. G. Wohl *et al.* (Particle Data Group), Rev. Mod. Phys. **56**, S1 (1984).
- [9] J. J. Hernandez *et al.* (Particle Data Group), Phys. Lett. **B239**, 1 (1990), [Erratum: Phys. Lett.B253,524(1991)].
- [10] M. Tanabashi *et al.* (Particle Data Group), Phys. Rev. **D98**, 3, 030001 (2018).
- [11] H. Zhang *et al.*, Phys. Rev. **C88**, 3, 035204 (2013), [arXiv:1305.3598].
- [12] H. Zhang *et al.*, Phys. Rev. **C88**, 3, 035205 (2013), [arXiv:1305.4575].
- [13] J. Tulpan, Kent State University, 3, 035205 (2008), [arXiv:1305.4575].
- [14] C. Fernandez-Ramirez *et al.*, Phys. Rev. **D93**, 3, 034029 (2016), [arXiv:1510.07065].
- [15] H. Kamano *et al.*, Phys. Rev. **C90**, 6, 065204 (2014), [arXiv:1407.6839].
- [16] H. Kamano *et al.*, Phys. Rev. **C92**, 2, 025205 (2015), [Erratum: Phys. Rev.C95,no.4,049903(2017)], [arXiv:1506.01768].
- [17] M. Matveev *et al.*, Eur. Phys. J. **A55**, 10, 179 (2019), [arXiv:1907.03645].
- [18] A. V. Sarantsev *et al.*, Eur. Phys. J. **A55**, 10, 180 (2019), [arXiv:1907.13387].
- [19] R. Levi Setti, Conf. Proc. **C690625**, 339 (1969).
- [20] V. Guzey and M. V. Polyakov, Annalen Phys. **13**, 673 (2004).
- [21] V. Guzey and M. V. Polyakov (2005), [hep-ph/0512355].
- [22] R. D. Tripp *et al.*, Phys. Rev. Lett. **21**, 1721 (1968).
- [23] A. V. Anisovich *et al.* (2019), [arXiv:1905.05456].
- [24] M. Bazzi *et al.* (SIDDHARTA), Phys. Lett. **B704**, 113 (2011), [arXiv:1105.3090].
- [25] K. Moriya *et al.* (CLAS), Phys. Rev. **C88**, 045201 (2013), [Addendum: Phys. Rev.C88,no.4,049902(2013)], [arXiv:1305.6776].
- [26] B. Dey *et al.* (CLAS), Phys. Rev. **C89**, 5, 055208 (2014), [Addendum: Phys. Rev.C90,no.1,019901(2014)], [arXiv:1403.2110].
- [27] R. Aaij *et al.* (LHCb), Phys. Rev. Lett. **115**, 072001 (2015), [arXiv:1507.03414].
- [28] K. Hicks and H. Sako (Crystall Ball), Proposal for J-PARC E45 **C70**, 034605 (2013).
- [29] S. Adhikari *et al.* (Crystall Ball), Proposal for JLAB PAC47 **C70**, 034605 (2019).
- [30] F. Iazzi (PANDA), AIP Conf. Proc. **1743**, 1, 050006 (2016).

83. Pole Structure of the  $\Lambda(1405)$  Region

Written August 2019 by Ulf-G. Meißner (Bonn Univ. / FZ Jülich) and Tetsuo Hyodo (Tokyo Metropolitan Univ.).

The  $\Lambda(1405)$  resonance emerges in the meson-baryon scattering amplitude with the strangeness  $S = -1$  and isospin  $I = 0$ . It is the archetype of what is called a dynamically generated resonance, as pioneered by Dalitz and Tuan [1]. The most powerful and systematic approach for the low-energy regime of the strong interactions is chiral perturbation theory (ChPT), see e.g. Ref. 2. A perturbative calculation is, however, not applicable to this sector because of the existence of the  $\Lambda(1405)$  just below the  $\bar{K}N$  threshold. In this case, ChPT has to be combined with a non-perturbative resummation technique, just as in the case of the nuclear forces. By solving the Lippmann-Schwinger equation with the interaction kernel determined by ChPT and using a particular regularization, in Ref. 3 a successful description of the low-energy  $K^-p$  scattering data as well as the mass distribution of the  $\Lambda(1405)$  was achieved (for further developments, see Ref. 4 and references therein).

The study of the pole structure was initiated by Ref. 5, which finds two poles of the scattering amplitude in the complex energy plane between the  $\bar{K}N$  and  $\pi\Sigma$  thresholds. The spectrum in experiments exhibits one effective resonance shape, while the existence of two poles results in the reaction-dependent lineshape [6]. The origin of this two-pole structure is attributed to the two attractive channels of the leading order interaction in the SU(3) basis (singlet and octet) [6] and in the isospin basis ( $\bar{K}N$  and  $\pi\Sigma$ ) [7]. It is remarkable that the sign and the strength of the leading order interaction is determined by a low-energy theorem of chiral symmetry, i.e. the so-called Weinberg-Tomozawa term. The two-pole nature of the  $\Lambda(1405)$  is qualitatively different from the case of the N(1440) resonance. Two poles of the N(1440) appear on different Riemann sheets of the complex energy plane separated by the  $\pi\Delta$  branch point. These poles reflect a single state, with a nearby pole and a more distant shadow pole. In contrast, the two poles in the  $\Lambda(1405)$  region on the same Riemann sheet (where  $\pi\Sigma$  channels are unphysical and all other channels physical, correspondingly to the one, connected to the real axis between the  $\pi\Sigma$  and  $\bar{K}N$  thresholds) are generated from two attractive forces mentioned above [6,7].

Recently, various new experimental results on the  $\Lambda(1405)$  have become available [4]. Among these, the most striking measurement is the precise determination of the energy shift and width of kaonic hydrogen by the SIDDHARTA collaboration [8,9], which provides a quantitative and stringent constraint on the  $K^-p$  amplitude at threshold through the improved Deser formula [10]. Systematic studies with error analyses based on the next-to-leading order ChPT interaction including the SIDDHARTA constraint have been performed by various groups [11–15]. All these studies confirm that the new kaonic hydrogen data are compatible with the scattering data above threshold.

The results of the pole positions of  $\Lambda(1405)$  in the various approaches are summarized in Table 83.1. We may regard the difference among the calculations as a systematic error, which stems from the various approximations of the Bethe-Salpeter equation, the fitting procedure, and also the inclusion of SU(3) breaking effects such as the choice of the various meson decay constants, and so on. A detailed comparison of the various approaches that enter the table is given in Ref. 16. A recent analysis including also the  $J^P = 1/2^+$  P-wave contribution (and also an explicit  $\Sigma(1385)$   $3/2^+$  state) gives results consistent with the findings reported above, with the pole positions at  $(1364 - i43)$  MeV and  $(1430 - i15)$  MeV, respectively [17].

The main component for the  $\Lambda(1405)$  is the pole 1, whose position converges within a relatively small region near the  $\bar{K}N$  threshold. On the other hand, the position of the pole 2 shows a sizeable scatter. Detailed studies of the  $\pi\Sigma$  spectrum in various reaction processes, together with the precise experimental lineshape (see e.g. the recent precise photoproduction data from the LEPS collaboration [18] and from the CLAS collaboration [19,20], electroproduction data from the CLAS collaboration [21], and proton-proton collision data from COSY [22] and the HADES collaboration [23]), will shed light on the position of the second pole. The  $\pi\Sigma$  spectra from the CLAS data are analyzed in Ref. 24 and Ref. 15. It was shown in Ref. 15 that

several solutions, which agree with the scattering data, are ruled out if confronted with the recent CLAS data. The remaining solutions are collected as solution #2 and solution #4 in Table 83.1. The HADES data are analyzed in Ref. 25 and Ref. 26. Although the result of the pole found in Ref. 25 is not compatible with other results, the authors of Ref. 26 invoke the anomalous triangle singularity mechanism to argue that the invariant mass distribution of the  $\pi\Sigma$  system is found at lower masses than in other reactions. It is thus desirable to perform more comprehensive analyses of  $\pi\Sigma$  spectra together with the systematic error analysis of the scattering data.

**Table 83.1:** Comparison of the pole positions of  $\Lambda(1405)$  in the complex energy plane from next-to-leading order chiral unitary coupled-channel approaches including the SIDDHARTA constraint. The lower two results also include the CLAS photoproduction data.

approach	pole 1 [MeV]	pole 2 [MeV]
Refs. 11,12, NLO	$1424^{+7}_{-23} - i 26^{+3}_{-14}$	$1381^{+18}_{-6} - i 81^{+19}_{-8}$
Ref. 14, Fit II	$1421^{+3}_{-2} - i 19^{+8}_{-5}$	$1388^{+9}_{-9} - i 114^{+24}_{-25}$
Ref. 15, solution #2	$1434^{+2}_{-2} - i 10^{+2}_{-1}$	$1330^{+4}_{-5} - i 56^{+17}_{-11}$
Ref. 15, solution #4	$1429^{+8}_{-7} - i 12^{+2}_{-3}$	$1325^{+15}_{-15} - i 90^{+12}_{-18}$

## References:

1. R.H. Dalitz, S.F. Tuan Phys. Rev. Lett. **2**, 425 (1959).
2. V. Bernard *et al.*, Int. J. Mod. Phys. **E4**, 193 (1995).
3. N. Kaiser *et al.*, Nucl. Phys. **A594**, 325 (1995).
4. T. Hyodo, D. Jido, Prog. in Part. Nucl. Phys. **67**, 55 (2012).
5. J.A. Oller, U.-G. Meißner, Phys. Lett. **B500**, 263 (2001).
6. D. Jido *et al.*, Nucl. Phys. **A725**, 181 (2003).
7. T. Hyodo, W. Weise, Phys. Rev. **C77**, 035204 (2008).
8. M. Bazzi *et al.*, Phys. Lett. **B704**, 113 (2011).
9. M. Bazzi *et al.*, Nucl. Phys. **A881**, 88 (2012).
10. U.-G. Meißner *et al.*, Eur. Phys. J. **C35**, 349 (2004).
11. Y. Ikeda *et al.*, Phys. Lett. **B706**, 63 (2011).
12. Y. Ikeda *et al.*, Nucl. Phys. **A881**, 98 (2012).
13. M. Mai, U.-G. Meißner, Nucl. Phys. **A900**, 51 (2013).
14. Z.-H. Guo, J. Oller, Phys. Rev. **C87**, 035202 (2013).
15. M. Mai, U.-G. Meißner, Eur. Phys. J. **A51**, 30 (2015).
16. A. Cieply *et al.*, Nucl. Phys. **A954**, 17 (2016).
17. D. Sadasivan *et al.*, Phys. Lett. **B789**, 329 (2019).
18. M. Niiyama *et al.*, Phys. Rev. **C78**, 035202 (2008).
19. K. Moriya *et al.*, Phys. Rev. **C87**, 035206 (2013).
20. K. Moriya *et al.*, Phys. Rev. Lett. **112**, 082004 (2014).
21. H.Y. Lu *et al.*, Phys. Rev. **C88**, 045202 (2013).
22. I. Zychor *et al.*, Phys. Lett. **B660**, 167 (2008).
23. G. Agakishiev *et al.*, Phys. Rev. **C87**, 025201 (2013).
24. L. Roca, E. Oset, Phys. Rev. **C87**, 055201 (2013).
25. M. Hassanvand *et al.*, Phys. Rev. **C87**, 055202 (2013).
26. M. Bayar *et al.*, Phys. Rev. **C97**, 035203 (2018).

## 84. Charmed Baryons

Revised in part June 2020 by D.J. Robinson (LBNL).

## 84.1 Spectrum

Similar to the light baryons, the naming convention for charmed baryon base symbols is determined by their isospin,  $I$ , and charm-strangeness,  $C+S$ , quantum numbers: In particular,  $\Lambda_c$ ,  $\Sigma_c$ ,  $\Xi_{c,cc}$  and  $\Omega_{c,cc,ccc}$  with  $I(C+S) = 0(1), 1(1), 1/2(2)$  and  $0(3)$ , respectively. While this review considers only the charmed baryons, approximate heavy quark flavor symmetry implies the spectroscopy of the bottom baryons is expected to be similar, up to corrections

of order  $\Lambda_{\text{QCD}}/m_{c,b}$ .

Figure 84.1(a) shows the spectrum of the singly-charmed baryons: There are now 36 such established states. In the quark model picture (see the *Quark Model* review), states consistent with all singly-charmed ground-state (zero angular momentum, or  $S$ -wave, state) baryons have been discovered, along with many excited states. The  $\Lambda_c(2860)$  and the five heaviest  $\Omega_c^0$ 's are recent, intriguing discoveries. The spin-parity quantum numbers of the latter are currently unknown, but one may speculate they correspond to the five  $ssc$  excited baryons in a  $P$ -wave state, although other interpretations are also possible and plausible.

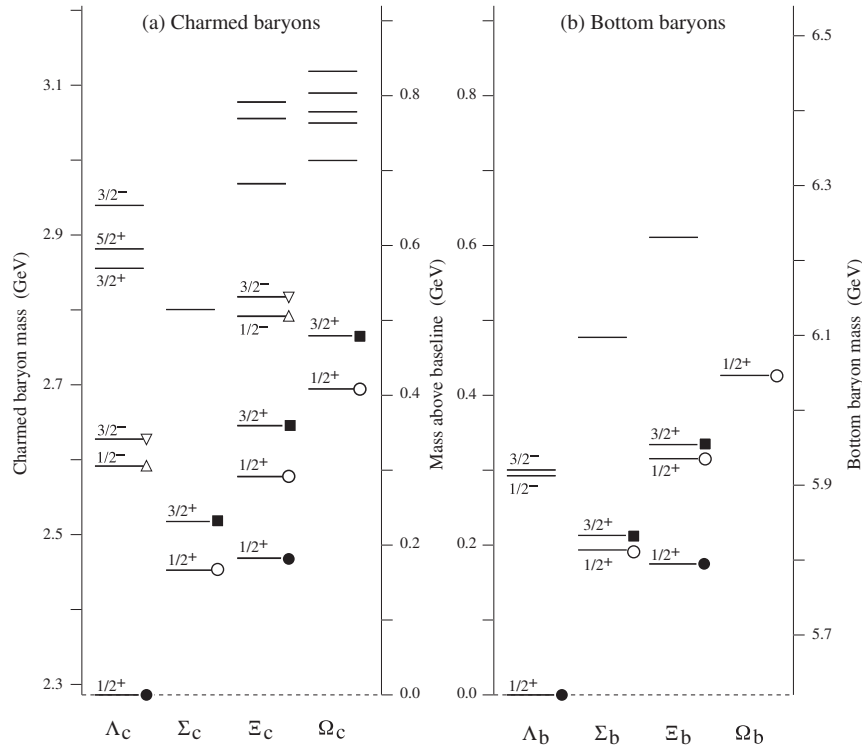


Figure 84.1: (a) The spectrum of established singly-charmed baryons, with their  $J^P$  assignments (where known). In accordance with their isospin, the  $\Sigma_c$  ( $\Xi_c$ ) lines each correspond to three (two) charged or neutral states that are nearly degenerate, with the exception of the upper two  $\Xi_c$  lines for which only the charged state has been found. Unique flavor  $SU(3)$  representations are shown by various filled and open symbols: The three  $J^P = 3/2^+$  ( $J^P = 1/2^+$ ) lines marked with a filled square (open circle) fill a ground-state **6** of flavor  $SU(3)$ ; the two  $J^P = 1/2^+$  ( $1/2^-$  and  $3/2^-$ ) lines marked by a filled circle (open triangles) fill a ground-state (excited-state)  **$\bar{3}$** . Fig 84.1(b) shows a similar spectrum for several known bottom baryons.

## 84.2 Flavor symmetry

Just as for the light mesons and baryons, approximate flavor  $SU(3)$  symmetry of the light quarks – the  $u$ ,  $d$ , and  $s$  – is expected to relate matrix elements of charmed baryons belonging to the same multiplet, up to corrections of order  $(m_s - m_d)/\Lambda_{\text{QCD}} \sim 20\%$ . (Similarly, isospin relations should hold to the percent level.) This includes Gell-Mann-Okubo mass relations – a set of linear combinations of masses that must vanish up to higher-order  $SU(3)$ -breaking corrections – as well as similar relations between matrix elements for charmed baryon multibody decays. These relations may be constructed order-by-order in the appropriate symmetry-breaking parameters.

For singly-charmed baryons with valence quarks  $q_1 q_2 c$ , the flavor  $SU(3)$  tensor product of the two light quarks  $\mathbf{3} \times \mathbf{3} = \mathbf{6} + \bar{\mathbf{3}}$ . For ground-state baryons, the overall antisymmetry of baryon wavefunction requires the light diquark to either form a spin-0 color antitriplet, antisymmetric under the interchange of the two light quark flavors – i.e. the  $\bar{\mathbf{3}}$  – or a spin-1 color antitriplet that is symmetric under this interchange – i.e. the  $\mathbf{6}$ . The spin-0  $\bar{\mathbf{3}}$  can only combine with the charm quark to form  $J^P = 1/2^+$  states, while the spin-1  $\mathbf{6}$  can combine to form states either  $J^P = 1/2^+$  or  $J^P = 3/2^+$ . States consistent with the corresponding  $\bar{\mathbf{3}}$  and

two  $\mathbf{6}$   $SU(3)$  representations are denoted in Figure 84.1 by filled circles, open circles and filled squares, respectively. In Fig. 84.2 we show the explicit contents of the  $\bar{\mathbf{3}}$  and  $\mathbf{6}$  ground-state representations. The singly-charmed baryons within each multiplet obey isospin and  $SU(3)$  mass relations at the expected orders.

Excited singly-charmed baryon states may arise as higher orbital angular momentum states. For instance, for such a baryon in a  $P$ -wave state, the allowed spin-flavor representations for the light diquark are either a spin-1  $\bar{\mathbf{3}}$  or a spin-0  $\mathbf{6}$ . Combined with the charm quark, the  $\bar{\mathbf{3}}$  can then generate  $J^P = 1/2^-, 3/2^-$  or  $5/2^-$  states: States consistent with the  $1/2^-$  and  $3/2^-$   $\bar{\mathbf{3}}$  representations are indicated in Figure 84.1 by open triangles. (One might speculate that the  $J^P = 5/2^-$   $\bar{\mathbf{3}}$  could be composed of the claimed  $\Lambda_c(2765)$  – not shown in the figure – and the  $\Xi_c(2930)$ .) Note that excited states might also arise from hadronic ‘molecule’ or pentaquark type states,  $\sim qq\bar{q}c$ , which may generate baryons in higher  $SU(3)$  representations.

To extend this discussion to doubly or triply charmed baryons, or charmless baryons, it is convenient to embed the baryons into flavor  $SU(4)$ , in which  $u$ ,  $d$ ,  $s$  and  $c$  transform as a  $\mathbf{4}$ . Flavor  $SU(4)$  is heavily broken, and is not a good approximate symmetry of QCD. However, under the decomposition  $SU(4) \rightarrow SU(3) \times$

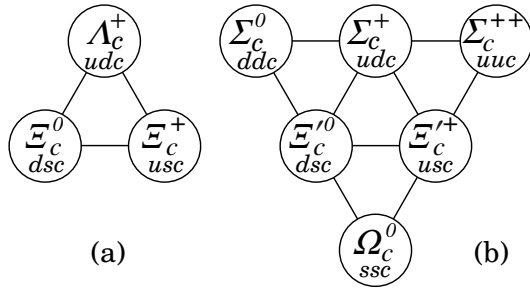


Figure 84.2: The  $SU(3)$   $\bar{\mathbf{3}}$  (a) and  $\mathbf{6}$  (b) ground-state  $J^P = 1/2^+$  representations. The  $\mathbf{6}$  ground-state with  $J^P = 3/2^+$  is identical in structure to the right-hand figure.

$U(1)_{\text{charm}}$ , it does provide a useful bookkeeping scheme for the various flavor  $SU(3)$  multiplets with different numbers of valence charm quarks.

For instance, for charmed baryons with three quarks, the tensor product  $\mathbf{4} \times \mathbf{4} \times \mathbf{4} = \mathbf{20}_S + \mathbf{20}_M + \mathbf{20}_M + \bar{\mathbf{4}}$ .<sup>1</sup> The spin-flavor representation of a ground-state baryon must be fully symmetric, so that ground-state baryons may belong to the  $\mathbf{20}_S$  and a single combination of the two  $\mathbf{20}_M$ 's, with spin and parity  $J^P = 3/2^+$  and  $J^P = 1/2^+$ , respectively. The  $\bar{\mathbf{4}}$ , however, is fully antisymmetric in flavor indices, and one cannot form the required fully antisymmetrized spin state from three quarks each with two possible spin configurations. This can be also understood directly in terms of the  $SU(8)$  contracted spin-flavor group: The only fully symmetric irreducible representation contained in  $\mathbf{8} \times \mathbf{8} \times \mathbf{8}$  is the  $\mathbf{120}$ , which contains a  $(\mathbf{20}_S, \mathbf{4})$  and a  $(\mathbf{20}_M, \mathbf{2})$  with respect to  $SU(4) \times SU(2)_{\text{spin}}$ .

The decompositions  $\mathbf{20}_S \rightarrow \mathbf{10}_0 + \mathbf{6}_1 + \bar{\mathbf{3}}_2 + \mathbf{1}_3$  and  $\mathbf{20}_M \rightarrow \mathbf{8}_0 + \mathbf{6}_1 + \bar{\mathbf{3}}_1 + \mathbf{3}_2$ , where the subscript indicates charm number, indicates the expected flavor  $SU(3)$  multiplets for each value of charm number in the ground-state baryons. Fig. 84.3(a) shows the  $\mathbf{20}_S$  representation, in which each charm number layer in the decomposition to  $SU(3) \times U(1)_{\text{charm}}$  is shaded in yellow. The bot-

tom  $c = 0$  level is the  $J^P = 3/2^+$  flavor  $SU(3)$  baryon decuplet containing the  $\Delta(1232)$ . Fig. 84.3(b) shows the  $\mathbf{20}_M$  representation, whose bottom  $c = 0$  level is the  $1/2^+$   $SU(3)$  light baryon octet, containing the nucleons.

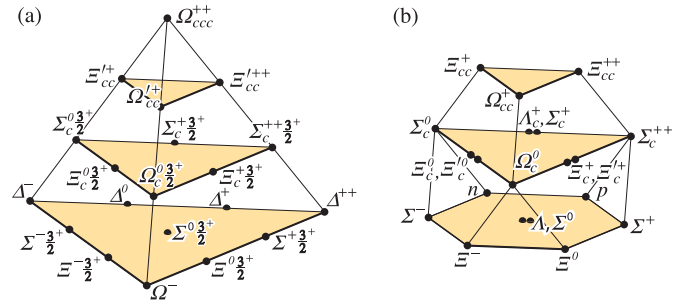


Figure 84.3: (a) The  $J^P = 3/2^+$  flavor  $SU(4)$  ground-state charmed baryons in the  $\mathbf{20}_S$ , with the flavor  $SU(3)$  baryon decuplet on the lowest level. (b) The  $J^P = 1/2^+$  ground-state charmed baryons in the  $\mathbf{20}_M$ -plet with the flavor  $SU(3)$  baryon octet on the lowest level. In some conventions, the states with a “ $\frac{3}{2}^+$ ” label are instead denoted with a \* superscript to distinguish them from the  $J^P = 1/2^+$  states.

Of the doubly charmed baryons, only the  $\Xi_{cc}^{++}$  has been discovered, though its spin-parity is unknown. For excited baryons in, e.g., a  $P$ -wave state, the same contracted spin-flavor analysis implies that there are excited baryon states in, e.g., a  $\mathbf{20}_M$  with  $J^P = 1/2^-$  or a  $\bar{\mathbf{4}}$  with  $J^P = 3/2^-$ , which together fill the fully antisymmetric  $\mathbf{56}$  of  $SU(8)$ . The  $\bar{\mathbf{4}}$  decomposes into  $\bar{\mathbf{3}}_1 + \mathbf{1}_0$ , consistent with the  $3/2^-$  singly-charmed  $\bar{\mathbf{3}}$ 's denoted by open triangles in Fig. 84.1(a). Just as for flavor  $SU(3)$ , excited state  $\mathbf{20}_{S,M}$  and  $\bar{\mathbf{4}}$  representations may also arise with other spin-parity assignments, and higher representations may also be present.

**References**

[1] R. Slansky, Phys. Rept. **79**, 1 (1981).

<sup>1</sup> More generally, for  $SU(N)$ ,  $N \times N \times N = [N(N+1)(N+2)/6] + 2 \times [N(N^2-1)/3] + [N(N-1)(N-2)/6]$ . The  $\mathbf{20}_S$ ,  $\mathbf{20}_M$  and  $\bar{\mathbf{4}}$  correspond to the representations with Dynkin labels  $(3, 0, 0)$ ,  $(1, 1, 0)$  and  $(0, 0, 1)$ , respectively. See Ref. [1] for a review.



## 85. Pentaquarks

Revised September 2019 by M. Karliner (Tel Aviv U.) and T. Skwarnicki (Syracuse U.).

Experimental searches for pentaquark hadrons comprised of light flavors have a long and vivid history. No undisputed candidates have been found in 50 years. The first wave of observations of pentaquark candidates containing a strange antiquark occurred in the early seventies, see e.g. a review in the 1976 edition of Particle Data Group listings for  $Z_0(1780)$ ,  $Z_0(1865)$  and  $Z_1(1900)$  [1]. The last mention of these candidates can be found in the 1992 edition [2] with the perhaps prophetic comment “the results permit no definite conclusion - the same story for 20 years. [...] The skepticism about baryons not made of three quarks, and lack of any experimental activity in this area, make it likely that another 20 years will pass before the issue is decided.” A decade later, a second wave of observations occurred, possibly motivated by specific theoretical predictions for their existence [3–5]. The evidence for pentaquarks was based on observations of peaks in the invariant mass distributions of their decay products. More data, or more sensitive experiments did not confirm these claims [6]. In the last mention of the best known candidate from that period,  $\Theta(1540)^+$ , the 2006 Particle Data Group listing [7] included a statement: “The conclusion that pentaquarks in general, and that  $\Theta^+$ , in particular, do not exist, appears compelling.” which well reflected the prevailing mood in the particle physics community until a study of  $\Lambda_b^0 \rightarrow J/\psi p K^-$  ( $J/\psi \rightarrow \mu^+ \mu^-$ ) decays by LHCb [8] (charge conjugate modes are implied). From an analysis of 3 fb $^{-1}$  Run 1 data at 7 and 8 TeV at the LHC, the LHCb collaboration reported a significant  $J/\psi p$  structure in  $\Lambda_b^0 \rightarrow J/\psi p K^-$  decays [8]. The exotic character of this structure, with the minimal quark content of  $uudc\bar{c}$ , was demonstrated in a nearly model-independent way in Ref. [9], where it was shown that the  $J/\psi p$  mass ( $m_{J/\psi p}$ ) peak near 4450 MeV was too narrow to be accounted for by  $\Lambda^* \rightarrow p K^-$  reflections ( $\Lambda^*$  denotes a generic  $\Lambda$  excitation), reinforcing the results from the earlier model-dependent six-dimensional amplitude analysis of invariant masses and decay angles describing the  $\Lambda_b^0$  decay in the same data [8]. Even though not apparent from the  $m_{J/\psi p}$  distribution, the amplitude analysis also required a second broad  $J/\psi p$  state to obtain a good description of the data, which peaked at  $4380 \pm 8 \pm 29$  MeV with a width of  $205 \pm 18 \pm 86$  MeV and a fit fraction of  $(8.4 \pm 0.7 \pm 4.2)\%$ .

The LHCb 6 fb $^{-1}$  Run 2 LHC data at 13 TeV, together with the improvements in the data selection for both runs, resulted in a nine-fold increase in the number of reconstructed  $\Lambda_b^0 \rightarrow J/\psi p K^-$  decays [10]. When fit with the same six-dimensional amplitude model, the enlarged data sample gives consistent results for the  $P_c(4450)^+$  and  $P_c(4380)^+$  parameters, corroborating the compatibility of the data samples. However, the two-state interpretation of the data is contradicted by the observation of new narrow  $J/\psi p$  structures which are too faint to have been significant in the Run 1 data analysis. Second horizontal band is observed in the Dalitz plot (Fig. 85.1) near 4312 MeV in the  $J/\psi p$  mass. The 4450 MeV structure also appears to consist of two narrower peaks at 4440 and 4457 MeV. Performing a rigorous six-dimensional amplitude analysis of these faint  $J/\psi p$  structures is challenging and has not been accomplished yet. Fortunately, the newly observed peaks are so narrow that it is not necessary to construct an amplitude model to prove that these states are not artifacts of interfering  $\Lambda^*$  resonances, as was previously demonstrated in Ref. [9]. Their masses and widths have been characterized by the LHCb (see Table 85.1) from one-dimensional fits to  $J/\psi p$  mass distributions, with different levels of suppression of the  $\Lambda^*$  contributions, which peak at the lower  $p K^-$  masses (Fig. 85.1). Such analysis is not sensitive to any broad  $J/\psi p$  contributions like  $P_c(4380)^+$ . The histograms analyzed by the LHCb are available in tabular form at <https://www.hepdata.net/record/89271>.

The fit chosen by the LHCb for the central mass and width values is displayed in Fig. 85.2. The  $P_c(4312)^+$  state peaks right below the  $\Sigma_c^+ \bar{D}^0$  threshold and has statistical significance over  $7.6\sigma$ . The  $P_c(4457)^+$  state peaks right below the  $\Sigma_c^+ \bar{D}^{*0}$  threshold, while the  $P_c(4440)^+$  state peaks about 20 MeV below it. The significance of the two-peak versus one-peak hypothesis for the 4450 MeV structure is over  $5.4\sigma$ , rendering the single peak in-

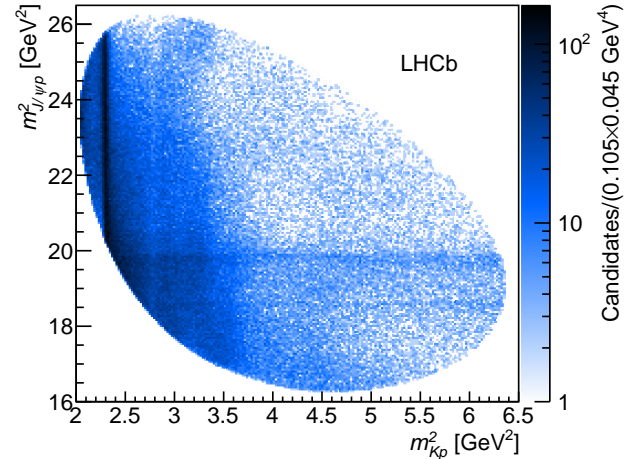


Figure 85.1: Dalitz plot distributions for  $\Lambda_b^0 \rightarrow J/\psi p K^-$  decays as observed by LHCb.

terpretation of this region obsolete. The six-dimensional amplitude analysis reported in Ref. [8], which provided evidence for the  $P_c(4380)^+$  state, is obsolete since it used the single  $P_c(4450)^+$  state and it lacked the  $P_c(4312)^+$  state. Therefore, the previously reported evidence for the  $P_c(4380)^+$  state is weakened, but not contradicted, since the new one-dimensional analysis by LHCb is not sensitive to wide  $P_c^+$  states. Even if this state exists, any preferences for its quantum numbers [8], which were reported without statistical or systematic significances, are even more uncertain now. An in-depth discussion of the relevant issues is provided in Supplemental Material of Ref. [10]. The LHCb results from the six-dimensional amplitude analysis of the Cabibbo suppressed channel  $\Lambda_b^0 \rightarrow J/\psi p \pi^-$  [11], which contain a statistically marginal evidence for the sum of the  $P_c^+$  and the  $Z_c(4200)^-$  contributions, took extensive input from Ref. [8], and should be treated with caution until the both amplitude analyses are completed on the enlarged data sets.

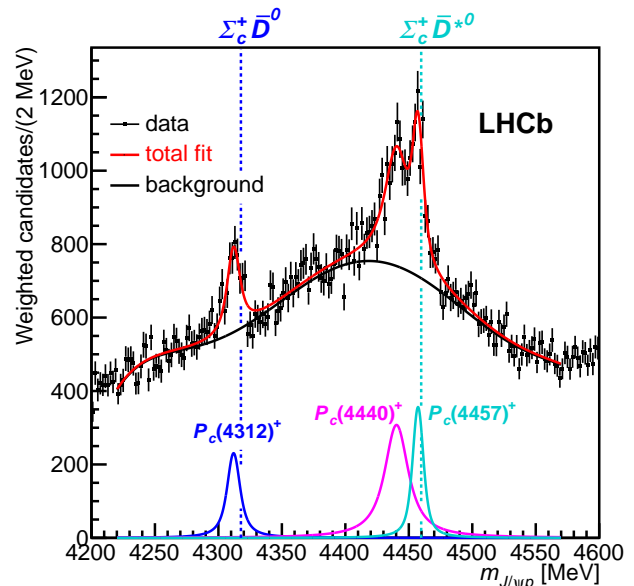


Figure 85.2: Fit to the  $J/\psi p$  mass distribution, in which events were weighted to suppress  $\Lambda^* \rightarrow p K^-$  backgrounds, of three Breit-Wigner functions and a sixth-order polynomial background. This fit was used to determine the central values of the masses and widths of the  $P_c^+$  states reported by LHCb. The mass thresholds for the  $\Sigma_c^+ \bar{D}^0$  and  $\Sigma_c^+ \bar{D}^{*0}$  final states are superimposed.

While  $\Sigma_c \bar{D}^{(*)}$  states had been predicted [12–15] before the first



**Table 85.1:** Summary of the narrow  $P_c^+$  properties, interpreted as Breit-Wigner resonances. The central values are based on the fit displayed in Fig. 85.2.

State	$M$ [MeV]	$\Gamma$ [MeV] (95% CL)	$\mathcal{R}$ [%]
$P_c(4312)^+$	$4311.9 \pm 0.7^{+6.8}_{-0.6}$	$9.8 \pm 2.7^{+3.7}_{-4.5} (< 27)$	$0.30 \pm 0.07^{+0.34}_{-0.09}$
$P_c(4440)^+$	$4440.3 \pm 1.3^{+4.1}_{-4.7}$	$20.6 \pm 4.9^{+8.7}_{-10.1} (< 49)$	$1.11 \pm 0.33^{+0.22}_{-0.10}$
$P_c(4457)^+$	$4457.3 \pm 0.6^{+4.1}_{-1.7}$	$6.4 \pm 2.0^{+5.7}_{-1.9} (< 20)$	$0.53 \pm 0.16^{+0.15}_{-0.13}$

LHCb results [8], after these results became known, many theoretical groups interpreted the  $P_c(4450)^+$  and  $P_c(4380)^+$  states in terms of diquarks and triquarks as building blocks of a compact pentaquark [16–22], or even of states below the lowest threshold for spontaneous dissociation [23]. In the first implementation of this approach [16], the pentaquark mass splitting was generated mostly by the change of angular momentum between the sub-components ( $L$ ) from zero to one, which would also make the heavier state narrower and of opposite parity. Explicit modeling of multi-quark systems [24] questions if centrifugal barrier factor provides enough width suppression via spatial separation of  $c$  and  $\bar{c}$  quarks at these masses, as the phase space for  $J/\psi p$  decay is very large (more than 400 MeV). Also, the observed mass splitting was too small to be only due to the mechanism proposed in Ref. [16] and required fine-tuning of such models. A variation of this model, in which the heavy ( $cu$ ) diquark couples with heavy  $\bar{c}$  to form colored triquark attracting the light diquark ( $ud$ ), has been re-implemented for the narrow  $P_c^+$  states [25]. In this model, the  $P_c(4440)^+$  and  $P_c(4457)^+$  states are accommodated via spin-orbit interactions for the  $L = 1$  states, while the  $P_c(4312)^+$  is one of the  $L = 0$  states. However, the mass prediction for the latter is off by  $(-72 \pm 29)$  MeV [25]. This work has recently been extended to  $SU(3)_F$  [26]. The width dilemma becomes more severe in view of the narrow widths of the newly observed states (Table 85.1), especially for the  $L = 0$   $P_c(4312)^+$  state, and requires a different origin of potential barrier between  $c$  and  $\bar{c}$  than angular momentum [25, 27], which remains a subject of theoretical controversy.

More effective width suppression mechanism is offered by a loosely bound charmed baryon-anticharmed meson molecular model, in which  $c$  and  $\bar{c}$  can be separated by much larger distances, resulting in a smaller probability of them getting close enough to each other in order to make a  $J/\psi$ . Since molecular binding energy cannot be large, such molecules are in  $S$ -wave and their masses must be near the sum of the baryon and meson masses [15]. The mass coincidence of the  $P_c(4312)^+$  and of  $P_c(4457)^+$  states, with the two related thresholds,  $\Sigma_c^+ \bar{D}^0$  and  $\Sigma_c^+ \bar{D}^{*0}$ , provides very strong experimental evidence in favor of this interpretation. Given how close  $P_c(4312)^+$  is to the  $\Sigma_c^+ \bar{D}^0$  threshold, it might be a virtual rather than a bound state [28]. It is worth stressing that other baryon-meson combinations,  $\Lambda_c^{(*)+} \bar{D}^{(*)0}$  and  $\chi_{cJ} p$  are not expected to bind [12, 29]. Since the spins of  $\Sigma_c^+$  and of  $\bar{D}^{*0}$  can be combined in two different ways, the third narrow  $P_c(4440)^+$  peak also finds natural explanation in this model, and cannot be a virtual state since it is sufficiently below the  $\Sigma_c^+ \bar{D}^{*0}$  threshold. Additional states at, or below, the  $\Sigma_c^{*+} \bar{D}$  and  $\Sigma_c^{*+} \bar{D}^*$  thresholds, are expected [30–32]. Since  $\Sigma_c^{*+}$  width is likely around 15 MeV [33], more than the width of either  $P_c(4312)^+$  or  $P_c(4457)^+$ , it is important to keep in mind that a molecule's width cannot be smaller than the sum of its constituents' widths [34–36]. For a recent review on hadronic molecules, see [37].

It is useful to consider the  $P_c(4312)^+$ ,  $P_c(4440)^+$  and  $P_c(4457)^+$  narrow pentaquarks together with several analogous exotic states with hidden charm and bottom in the meson sector. This provides additional significant motivation for the molecular model. At least five exotic mesons are close to thresholds of two heavy-light mesons:  $X(3872)$  [38–41],  $Z_b(10610)$  and  $Z_b(10650)$  in the bottomonium sector [42–46] and  $Z_c(3900)$  [47–51] and  $Z_c(4020/4025)$  [52–54] in the charmonium sector (see Table II in Ref. [55]; for reviews of experimental information see Ref. [56, 57], as well as *Spectroscopy of Mesons Containing Two Heavy Quarks and Non- $q\bar{q}$  Mesons* in Ref. [33]). These states share several important features: a) their masses are near thresholds and their

spin and parity correspond to  $S$ -wave combination of the two mesons; b) they are very narrow, despite very large phase space for decay into quarkonium + pion(s); c) the branching fractions for “fall apart” mode into two mesons are much larger than branching fractions for decay into quarkonium and pion(s). So far, there is no experimental evidence for states at two pseudoscalar thresholds ( $D\bar{D}$  and  $B\bar{B}$ ), implying that pseudoscalar exchange is essential for binding in meson-meson systems.

The above provide a strong hint that these states are deuteron-like loosely bound states of two heavy mesons [58–66]. It is then natural to conjecture that similar bound states might exist of two heavy baryons [67, 68], or a meson and a baryon or a baryon and an antibaryon, leading to a rather accurate prediction of the  $P_c(4457)^+$  mass as  $3/2^- \Sigma_c \bar{D}^*$  molecule (the mass threshold is 4462.4 MeV) [15, 55], following similar predictions obtained in a wider framework of doubly heavy baryon-meson hadronic molecules, which might include mixtures of various two-hadron states [12–14, 29]. However, single pion exchange is not possible in  $\Sigma_c^+ \bar{D}^0$  system, thus the existence of  $P_c(4312)^+$  points to importance of vector or two-pion exchanges in baryon-meson molecules. Two-pion exchange in  $D\bar{D}$  system is highly suppressed, because the intermediate state is  $D^* \bar{D}^*$ , which is 282 MeV heavier than  $D\bar{D}$ . On the other hand, there is little suppression in the  $\Sigma_c \bar{D}$  system, because the dominant intermediate state is  $\Lambda_c \bar{D}^*$  which is just 25 MeV lighter than  $\Sigma_c \bar{D}$  [69]. In a generic hadronic molecule it is essential that the two hadrons are heavy, in order to minimize the repulsive kinetic energy [67, 68, 70].

Following the initial LHCb discovery [8], several groups carried out a detailed analysis of the  $P_c^+$  states as hadronic molecules [71–80] followed by further analysis [32, 81–105] after the updated LHCb results [10]. Very recently partial widths of all the allowed decay channels for the  $P_c$  states have been estimated within the molecular picture [106]. The most striking result is that  $P_c(4312)$  decays are totally dominated by the  $\bar{D}^* \Lambda_c$  channel. This channel is also expected to be very prominent in decays of  $P_c(4440)$  and  $P_c(4457)$ .

The  $P_c$  states have also been interpreted as so called hadro-charmonium [107], a bound state of relatively compact charmonium states with light hadronic matter. It was proposed that  $P_c(4440)^+$  and  $P_c(4457)^+$  are spin-split  $\psi(2S)p$  bound states with  $J^P = \frac{1}{2}^-$  and  $\frac{3}{2}^-$ , while  $P_c(4312)^+$  is a  $\chi_{c0} p$  bound state with  $J^P = \frac{1}{2}^+$  [108]. While very interesting from theoretical point of view, it is not at all clear why the binding energies between charmonia and the nucleon should conspire to produce states so close to the  $\Sigma_c \bar{D}$  and  $\Sigma_c \bar{D}^*$  thresholds. Moreover, the predicted widths of  $P_c(4440)^+$  and  $P_c(4457)^+$  are too big by a factor  $\sim 2$ -3. One should also keep in mind that the molecular and hadro-charmonium pictures provide opposite predictions for the parity of  $P_c(4312)^+$ . In principle LHCb can check the spin and parity through partial wave analysis, but at present it is not known if systematic uncertainties can be sufficiently reduced to make such an analysis conclusive.

Shortly after the initial experimental discovery it was conjectured that the  $P_c(4450)^+$  could be due to coincidence with the  $\chi_{c1} p$  threshold, at which peaking can be induced via so called triangle singularity [109–112]. These explanations are no longer popular, since the  $P_c(4440)^+$  mass is not at any threshold and the  $P_c(4312)^+$  and  $P_c(4457)^+$  peak slightly below the  $\Sigma_c^+ \bar{D}^0$  and  $\Sigma_c^+ \bar{D}^{*0}$  thresholds. The  $P_c(4457)^+$  mass is exactly at  $\Lambda_c^{*+} \bar{D}^0$  thresholds, but the LHCb has demonstrated that the observed peaking is narrower in the data than expected from the triangle-diagram when a realistic width of the excited  $D_s^-$  state exchanged

in the triangle is used (Supplemental Material in Ref. [10]).

More extensive pre-2019 reviews of some of the theoretical issues can be found in Refs. [113,114]. Two recent relevant reviews are Refs. [115,116].

So far the  $P_c^+$  states have been observed by only one experiment in only one channel. It is essential to explore other possible experimental channels, such as  $P_c \rightarrow \Lambda_c \bar{D}^{(*)}$ ,  $\eta_c p$ . These channels are however much more experimentally challenging than  $P_c \rightarrow J/\psi p$ . Proposals have also been made to search for heavy pentaquarks in photo-production [117–124]. Ref. [125] discusses photoproduction within the string-junction physical picture of the pentaquarks. Photoproduction is also related to recent work on  $J/\psi(\eta_c)N$  scattering on the lattice [126] and on computation of  $J/\psi(\eta_c)N$  and  $\Upsilon(\eta_b)N$  cross sections [127]. In addition, pentaquark production has been discussed in the context of antiproton-deuteron collisions [128], of heavy ion collisions at LHC [129], in  $pA$  collisions [130] and in pion-induced processes [131–133]. Recently, the GlueX Collaboration reported negative search results for the  $P_c^+$  states in photo-production at JLAB [134]. Within the large experimental errors and considerable theoretical model dependence these results do not contradict the molecular interpretations of the narrow  $P_c^+$  states. It was recently suggested to determine the pentaquark photo-couplings and branching ratios by measuring the polarization transfer between the incident photon and the outgoing proton in the exclusive photo-production of  $J/\psi$  near threshold [135].

### References

- [1] T. G. Trippe *et al.* (Particle Data Group), *Rev. Mod. Phys.* **48**, S1 (1976), [Erratum: *Rev. Mod. Phys.* **48**, 497 (1976)].
- [2] K. Hikasa *et al.* (Particle Data Group), *Phys. Rev.* **D45**, S1 (1992), [Erratum: *Phys. Rev.* **D46**, 5210 (1992)].
- [3] M. Praszalowicz, *Skyrmions and Anomalies, p.112*, M. Jezabek Ed., World Scientific Publishing (1987), ISBN 9971503506.
- [4] D. Diakonov, V. Petrov and M. V. Polyakov, *Z. Phys.* **A359**, 305 (1997), [hep-ph/9703373].
- [5] H. Weigel, *Eur. Phys. J.* **A2**, 391 (1998), [hep-ph/9804260].
- [6] K. H. Hicks, *Eur. Phys. J.* **H37**, 1 (2012).
- [7] W. M. Yao *et al.* (Particle Data Group), *J. Phys.* **G33**, 1 (2006).
- [8] R. Aaij *et al.* (LHCb), *Phys. Rev. Lett.* **115**, 072001 (2015), [arXiv:1507.03414].
- [9] R. Aaij *et al.* (LHCb), *Phys. Rev. Lett.* **117**, 8, 082002 (2016), [arXiv:1604.05708].
- [10] R. Aaij *et al.* (LHCb), *Phys. Rev. Lett.* **122**, 22, 222001 (2019), [arXiv:1904.03947].
- [11] R. Aaij *et al.* (LHCb), *Phys. Rev. Lett.* **117**, 8, 082003 (2016), [Addendum: *Phys. Rev. Lett.* **118**, 119901 (2017)], [arXiv:1606.06999].
- [12] Z.-C. Yang *et al.*, *Chin. Phys.* **C36**, 6 (2012), [arXiv:1105.2901].
- [13] J.-J. Wu *et al.*, *Phys. Rev. Lett.* **105**, 232001 (2010), [arXiv:1007.0573].
- [14] J.-J. Wu, T. S. H. Lee and B. S. Zou, *Phys. Rev.* **C85**, 044002 (2012), [arXiv:1202.1036].
- [15] M. Karliner and J. L. Rosner, *Phys. Rev. Lett.* **115**, 12, 122001 (2015), [arXiv:1506.06386].
- [16] L. Maiani, A. D. Polosa and V. Riquer, *Phys. Lett.* **B749**, 289 (2015), [arXiv:1507.04980].
- [17] R. F. Lebed, *Phys. Lett.* **B749**, 454 (2015), [arXiv:1507.05867].
- [18] V. V. Anisovich *et al.* (2015), [arXiv:1507.07652].
- [19] G.-N. Li, X.-G. He and M. He, *JHEP* **12**, 128 (2015), [arXiv:1507.08252].
- [20] R. Ghosh, A. Bhattacharya and B. Chakrabarti (2015), [arXiv:1508.00356].
- [21] Z.-G. Wang, *Eur. Phys. J.* **C76**, 2, 70 (2016), [arXiv:1508.01468].
- [22] R. Zhu and C.-F. Qiao, *Phys. Lett.* **B756**, 259 (2016), [arXiv:1510.08693].
- [23] J. M. Richard, A. Valcarce and J. Vijande, *Phys. Lett.* **B774**, 710 (2017), [arXiv:1710.08239].
- [24] E. Hiyama *et al.*, *Phys. Rev.* **C98**, 4, 045208 (2018), [arXiv:1803.11369].
- [25] A. Ali and A. Y. Parkhomenko, *Phys. Lett.* **B793**, 365 (2019), [arXiv:1904.00446].
- [26] A. Ali *et al.* (2019), [arXiv:1907.06507].
- [27] L. Maiani, A. D. Polosa and V. Riquer, *Phys. Lett.* **B778**, 247 (2018), [arXiv:1712.05296].
- [28] C. Fernandez-Ramirez *et al.* (JPAC), *Phys. Rev. Lett.* **123**, 9, 092001 (2019), [arXiv:1904.10021].
- [29] W. L. Wang *et al.*, *Phys. Rev.* **C84**, 015203 (2011), [arXiv:1101.0453].
- [30] C. W. Xiao, J. Nieves and E. Oset, *Phys. Rev.* **D88**, 056012 (2013), [arXiv:1304.5368].
- [31] C. W. Xiao, J. Nieves and E. Oset, *Phys. Rev.* **D100**, 1, 014021 (2019), [arXiv:1904.01296].
- [32] M.-Z. Liu *et al.*, *Phys. Rev. Lett.* **122**, 24, 242001 (2019), [arXiv:1903.11560].
- [33] M. Tanabashi *et al.* (Particle Data Group), *Phys. Rev.* **D98**, 3, 030001 (2018).
- [34] C. Hanhart, Yu. S. Kalashnikova and A. V. Nefediev, *Phys. Rev.* **D81**, 094028 (2010), [arXiv:1002.4097].
- [35] A. A. Filin *et al.*, *Phys. Rev. Lett.* **105**, 019101 (2010), [arXiv:1004.4789].
- [36] F.-K. Guo and U.-G. Meissner, *Phys. Rev.* **D84**, 014013 (2011), [arXiv:1102.3536].
- [37] F.-K. Guo *et al.*, *Rev. Mod. Phys.* **90**, 1, 015004 (2018), [arXiv:1705.00141].
- [38] S. K. Choi *et al.* (Belle), *Phys. Rev. Lett.* **91**, 262001 (2003), [hep-ex/0309032].
- [39] D. Acosta *et al.* (CDF), *Phys. Rev. Lett.* **93**, 072001 (2004), [hep-ex/0312021].
- [40] B. Aubert *et al.* (BaBar), *Phys. Rev.* **D71**, 071103 (2005), [hep-ex/0406022].
- [41] V. M. Abazov *et al.* (D0), *Phys. Rev. Lett.* **93**, 162002 (2004), [hep-ex/0405004].
- [42] M. Karliner and H. J. Lipkin (2008), [arXiv:0802.0649].
- [43] K. F. Chen *et al.* (Belle), *Phys. Rev. Lett.* **100**, 112001 (2008), [arXiv:0710.2577].
- [44] A. Bondar *et al.* (Belle), *Phys. Rev. Lett.* **108**, 122001 (2012), [arXiv:1110.2251].
- [45] P. Krokovny *et al.* (Belle), *Phys. Rev.* **D88**, 5, 052016 (2013), [arXiv:1308.2646].
- [46] A. Garmash *et al.* (Belle), *Phys. Rev.* **D91**, 7, 072003 (2015), [arXiv:1403.0992].
- [47] M. Ablikim *et al.* (BESIII), *Phys. Rev. Lett.* **110**, 252001 (2013), [arXiv:1303.5949].
- [48] Z. Q. Liu *et al.* (Belle), *Phys. Rev. Lett.* **110**, 252002 (2013), [arXiv:1304.0121].
- [49] T. Xiao *et al.*, *Phys. Lett.* **B727**, 366 (2013), [arXiv:1304.3036].
- [50] M. Ablikim *et al.* (BESIII), *Phys. Rev. Lett.* **112**, 2, 022001 (2014), [arXiv:1310.1163].
- [51] M. Ablikim *et al.* (BESIII), *Phys. Rev. Lett.* **115**, 11, 112003 (2015), [arXiv:1506.06018].
- [52] M. Ablikim *et al.* (BESIII), *Phys. Rev. Lett.* **111**, 24, 242001 (2013), [arXiv:1309.1896].
- [53] M. Ablikim *et al.* (BESIII), *Phys. Rev. Lett.* **113**, 21, 212002 (2014), [arXiv:1409.6577].

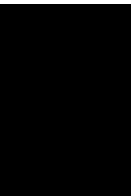
- [54] M. Ablikim *et al.* (BESIII), Phys. Rev. Lett. **112**, 13, 132001 (2014), [arXiv:1308.2760].
- [55] M. Karliner, Acta Phys. Polon. **B47**, 117 (2016).
- [56] M. Karliner, J. L. Rosner and T. Skwarnicki, Ann. Rev. Nucl. Part. Sci. **68**, 17 (2018), [arXiv:1711.10626].
- [57] S. L. Olsen, T. Skwarnicki and D. Zieminska, Rev. Mod. Phys. **90**, 1, 015003 (2018), [arXiv:1708.04012].
- [58] M. B. Voloshin and L. B. Okun, JETP Lett. **23**, 333 (1976), [Pisma Zh. Eksp. Teor. Fiz.23,369(1976)].
- [59] A. De Rujula, H. Georgi and S. Glashow, Phys. Rev. Lett. **38**, 317 (1977).
- [60] N. A. Tornqvist, Phys. Rev. Lett. **67**, 556 (1991).
- [61] N. A. Tornqvist, Z. Phys. **C61**, 525 (1994), [hep-ph/9310247].
- [62] N. A. Tornqvist, Phys. Lett. **B590**, 209 (2004), [hep-ph/0402237].
- [63] C. E. Thomas and F. E. Close, Phys. Rev. **D78**, 034007 (2008), [arXiv:0805.3653].
- [64] M. Suzuki, Phys. Rev. **D72**, 114013 (2005), [hep-ph/0508258].
- [65] S. Fleming *et al.*, Phys. Rev. **D76**, 034006 (2007), [hep-ph/0703168].
- [66] T. E. O. Ericson and G. Karl, Phys. Lett. **B309**, 426 (1993).
- [67] M. Karliner, H. J. Lipkin and N. A. Tornqvist, in “Proceedings, 14th International Conference on Hadron spectroscopy (Hadron 2011),” (2011), [arXiv:1109.3472], URL <http://inspirehep.net/record/927616/files/arXiv:1109.3472.pdf>.
- [68] M. Karliner, H. J. Lipkin and N. A. Tornqvist, Nucl. Phys. Proc. Suppl. **225-227**, 102 (2012).
- [69] M. Karliner, “Open Questions in Heavy Exotics,” invited talk at *Bled 2019* Mini-Workshop, Bled, Slovenia, July 15-19, 2019, [http://www-f1.ijs.si/Bled2019/Karliner\\_Bled2019.pdf](http://www-f1.ijs.si/Bled2019/Karliner_Bled2019.pdf) ; M. Karliner and J. L. Rosner, in preparation.
- [70] X.-Q. Li and X. Liu, Eur. Phys. J. **C74**, 12, 3198 (2014), [arXiv:1409.3332].
- [71] R. Chen *et al.*, Phys. Rev. Lett. **115**, 13, 132002 (2015), [arXiv:1507.03704].
- [72] H.-X. Chen *et al.*, Phys. Rev. Lett. **115**, 17, 172001 (2015), [arXiv:1507.03717].
- [73] L. Roca, J. Nieves and E. Oset, Phys. Rev. **D92**, 9, 094003 (2015), [arXiv:1507.04249].
- [74] J. He, Phys. Lett. **B753**, 547 (2016), [arXiv:1507.05200].
- [75] H. Huang *et al.*, Eur. Phys. J. **C76**, 11, 624 (2016), [arXiv:1510.04648].
- [76] L. Roca and E. Oset, Eur. Phys. J. **C76**, 11, 591 (2016), [arXiv:1602.06791].
- [77] Q.-F. Lü and Y.-B. Dong, Phys. Rev. **D93**, 7, 074020 (2016), [arXiv:1603.00559].
- [78] Y. Shimizu, D. Suenaga and M. Harada, Phys. Rev. **D93**, 11, 114003 (2016), [arXiv:1603.02376].
- [79] C.-W. Shen *et al.*, Nucl. Phys. **A954**, 393 (2016), [arXiv:1603.04672].
- [80] Y. Yamaguchi *et al.*, Phys. Rev. **D96**, 11, 114031 (2017), [arXiv:1709.00819].
- [81] J. F. Giron, R. F. Lebed and C. T. Peterson, JHEP **05**, 061 (2019), [arXiv:1903.04551].
- [82] R. Chen *et al.*, Phys. Rev. **D100**, 1, 011502 (2019), [arXiv:1903.11013].
- [83] F.-K. Guo *et al.*, Phys. Rev. **D99**, 9, 091501 (2019), [arXiv:1903.11503].
- [84] J. He, Eur. Phys. J. **C79**, 5, 393 (2019), [arXiv:1903.11872].
- [85] H. Huang, J. He and J. Ping (2019), [arXiv:1904.00221].
- [86] Y. Shimizu, Y. Yamaguchi and M. Harada (2019), [arXiv:1904.00587].
- [87] Z.-H. Guo and J. A. Oller, Phys. Lett. **B793**, 144 (2019), [arXiv:1904.00851].
- [88] C.-J. Xiao *et al.*, Phys. Rev. **D100**, 1, 014022 (2019), [arXiv:1904.00872].
- [89] Z.-G. Wang (2019), [arXiv:1905.02892].
- [90] L. Meng *et al.*, Phys. Rev. **D100**, 1, 014031 (2019), [arXiv:1905.04113].
- [91] F. Giannuzzi, Phys. Rev. **D99**, 9, 094006 (2019), [arXiv:1903.04430].
- [92] Q. Wu and D.-Y. Chen (2019), [arXiv:1906.02480].
- [93] C.-W. Shen, J.-J. Wu and B.-S. Zou, Phys. Rev. **D100**, 5, 056006 (2019), [arXiv:1906.03896].
- [94] F. Stancu (2019), [arXiv:1902.07101].
- [95] C. W. Xiao, J. Nieves and E. Oset (2019), [arXiv:1906.09010].
- [96] M. B. Voloshin, Phys. Rev. **D100**, 3, 034020 (2019), [arXiv:1907.01476].
- [97] S. Sakai, H.-J. Jing and F.-K. Guo (2019), [arXiv:1907.03414].
- [98] Z.-G. Wang and X. Wang (2019), [arXiv:1907.04582].
- [99] Y. Yamaguchi *et al.* (2019), [arXiv:1907.04684].
- [100] Y.-J. Xu *et al.* (2019), [arXiv:1907.05097].
- [101] M. Pavon Valderrama (2019), [arXiv:1907.05294].
- [102] F.-Z. Peng *et al.* (2019), [arXiv:1907.05322].
- [103] M.-Z. Liu *et al.* (2019), [arXiv:1907.06093].
- [104] Y.-W. Pan *et al.* (2019), [arXiv:1907.11220].
- [105] T. J. Burns and E. S. Swanson (2019), [arXiv:1908.03528].
- [106] Y.-H. Lin and B.-S. Zou, Phys. Rev. **D100**, 5, 056005 (2019), [arXiv:1908.05309].
- [107] S. Dubynskiy and M. B. Voloshin, Phys. Lett. **B666**, 344 (2008), [arXiv:0803.2224].
- [108] M. I. Eides, V. Y. Petrov and M. V. Polyakov (2019), [arXiv:1904.11616].
- [109] F.-K. Guo *et al.*, Phys. Rev. **D92**, 7, 071502 (2015), [arXiv:1507.04950].
- [110] U.-G. Meissner and J. A. Oller, Phys. Lett. **B751**, 59 (2015), [arXiv:1507.07478].
- [111] X.-H. Liu, Q. Wang and Q. Zhao, Phys. Lett. **B757**, 231 (2016), [arXiv:1507.05359].
- [112] M. Mikhasenko (2015), [arXiv:1507.06552].
- [113] T. J. Burns, Eur. Phys. J. **A51**, 11, 152 (2015), [arXiv:1509.02460].
- [114] H.-X. Chen *et al.*, Phys. Rept. **639**, 1 (2016), [arXiv:1601.02092].
- [115] Y.-R. Liu *et al.*, Prog. Part. Nucl. Phys. **107**, 237 (2019), [arXiv:1903.11976].
- [116] N. Brambilla *et al.* (2019), [arXiv:1907.07583].
- [117] Y. Huang *et al.*, J. Phys. **G41**, 11, 115004 (2014), [arXiv:1305.4434].
- [118] Q. Wang, X.-H. Liu and Q. Zhao, Phys. Rev. **D92**, 034022 (2015), [arXiv:1508.00339].
- [119] V. Kubarovsky and M. B. Voloshin, Phys. Rev. **D92**, 3, 031502 (2015), [arXiv:1508.00888].
- [120] M. Karliner and J. L. Rosner, Phys. Lett. **B752**, 329 (2016), [arXiv:1508.01496].
- [121] A. N. Hiller Blin *et al.*, Phys. Rev. **D94**, 3, 034002 (2016), [arXiv:1606.08912].
- [122] X. Cao and J.-p. Dai, Phys. Rev. **D100**, 5, 054033 (2019), [arXiv:1904.06015].

- [123] X.-Y. Wang, X.-R. Chen and J. He, Phys. Rev. **D99**, 11, 114007 (2019), [arXiv:1904.11706].
- [124] J.-J. Wu, T. S. H. Lee and B.-S. Zou, Phys. Rev. **C100**, 3, 035206 (2019), [arXiv:1906.05375].
- [125] G. C. Rossi and G. Veneziano (2019), [arXiv:1909.01753].
- [126] U. Skerbis and S. Prelovsek, Phys. Rev. **D99**, 9, 094505 (2019), [arXiv:1811.02285].
- [127] C. W. Xiao and U. G. Meissner, Phys. Rev. **D92**, 11, 114002 (2015), [arXiv:1508.00924].
- [128] M. B. Voloshin, Phys. Rev. **D99**, 9, 093003 (2019), [arXiv:1903.04422].
- [129] R.-Q. Wang *et al.*, Phys. Rev. **C94**, 4, 044913 (2016), [arXiv:1601.02835].
- [130] I. Schmidt and M. Siddikov, Phys. Rev. **D93**, 9, 094005 (2016), [arXiv:1601.05621].
- [131] Q.-F. Lü *et al.*, Phys. Rev. **D93**, 3, 034009 (2016), [arXiv:1510.06271].
- [132] X.-H. Liu and M. Oka, Nucl. Phys. **A954**, 352 (2016), [arXiv:1602.07069].
- [133] X.-Y. Wang *et al.*, Phys. Lett. **B797**, 134862 (2019), [arXiv:1906.04044].
- [134] A. Ali *et al.* (GlueX), Phys. Rev. Lett. **123**, 7, 072001 (2019), [arXiv:1905.10811].
- [135] D. Winney *et al.* (JPAC), Phys. Rev. **D100**, 3, 034019 (2019), [arXiv:1907.09393].



## Hypothetical Particles and Concepts

86. Extra dimensions (rev.) . . . . .	889
87. $W'$ -boson searches (rev.) . . . . .	897
88. $Z'$ -boson searches (rev.) . . . . .	900
89. Supersymmetry: theory (rev.) . . . . .	905
90. Supersymmetry: experiment (rev.) . . . . .	923
91. Axions and other similar particles (rev.) . . . . .	939
92. Quark and lepton compositeness, searches for (rev.) . . . . .	953
93. Dynamical electroweak symmetry breaking: implications of the $H(0)$ (rev.) . . . . .	958
94. Grand unified theories (rev.) . . . . .	971
95. Leptoquarks (rev.) . . . . .	986
96. Magnetic monopoles (rev.) . . . . .	989





## 86. Extra Dimensions

Revised August 2019 by Y. Gershtein (Rutgers U.) and A. Pomarol (U. Autònoma de Barcelona; IFAE).

### 86.1 Introduction

Proposals for a spacetime with more than three spatial dimensions date back to the 1920s, mainly through the work of Kaluza and Klein, in an attempt to unify the forces of nature [1]. Although their initial idea failed, the formalism that they and others developed is still useful nowadays. Around 1980, string theory proposed again to enlarge the number of space dimensions, this time as a requirement for describing a consistent theory of quantum gravity. The extra dimensions were supposed to be compactified at a scale close to the Planck scale, and thus not testable experimentally in the near future.

A different approach was given by Arkani-Hamed, Dimopoulos, and Dvali (ADD) in their seminal paper in 1998 [2], where they showed that the weakness of gravity could be explained by postulating two or more extra dimensions in which only gravity could propagate. The size of these extra dimensions should range between roughly a millimeter and  $\sim 1/\text{TeV}$ , leading to possible observable consequences in current and future experiments. A year later, Randall and Sundrum (RS) [3] found a new possibility using a warped geometry, postulating a five-dimensional Anti-de Sitter (AdS) spacetime with a compactification scale of order  $1/\text{TeV}$ . The origin of the smallness of the electroweak scale versus the Planck scale was explained by the gravitational redshift factor present in the warped AdS metric. As in the ADD model, originally only gravity was assumed to propagate in the extra dimensions, although it was soon clear that this was not necessary in warped extra-dimensions and also the SM gauge fields [4, 5] and SM fermions [6, 7] could propagate in the five-dimensional spacetime.

The physics of warped extra-dimensional models has an alternative interpretation by means of the AdS/CFT correspondence [8–10]. Models with warped extra dimensions are related to four-dimensional strongly-interacting theories, allowing an understanding of the properties of five-dimensional fields as those of four-dimensional composite states [11]. This approach has opened new directions for tackling outstanding questions in particle physics, such as the flavor problem, grand unification, and the origin of electroweak symmetry breaking or supersymmetry breaking.

#### 86.1.1 Experimental Constraints

Constraints on extra-dimensional models arise from astrophysical and cosmological considerations, tabletop experiments exploring gravity at sub-mm distances, and collider experiments. Collider limits on extra-dimensional models are dominated by LHC results, which can be found on the public WWW pages of ATLAS [12] and CMS [13]. This review includes the most recent limits, most of which are published results based on 36  $\text{fb}^{-1}$  LHC data collected in 2015–16 at a center-of-mass energy of 13 TeV and legacy results from 20  $\text{fb}^{-1}$  of 8 TeV data collected in Run 1. In addition, there are a few published and preliminary results based on the full Run 2 datasets. For most of the models, Run 2 results surpass the sensitivity of Run 1, even in the cases when the integrated luminosity is smaller.

#### 86.1.2 Kaluza-Klein Theories

Field theories with compact extra dimensions can be written as theories in ordinary four dimensions (4D) by performing a Kaluza-Klein (KK) reduction. As an illustration, consider a simple example, namely a field theory of a complex scalar in flat five-dimensional (5D) spacetime. The action will be given by <sup>1</sup>

$$S_5 = - \int d^4x dy M_5 \left[ |\partial_\mu \phi|^2 + |\partial_y \phi|^2 + \lambda_5 |\phi|^4 \right], \quad (86.1)$$

where  $y$  refers to the extra (fifth) dimension. A universal scale  $M_5$  has been extracted in front of the action in order to keep the

5D field with the same mass-dimension as in 4D. This theory is perturbative for energies  $E \lesssim \ell_5 M_5 / \lambda_5$  where  $\ell_5 = 24\pi^3$  [14].

Let us now consider that the fifth dimension is compact with the topology of a circle  $S^1$  of radius  $R$ , which corresponds to the identification of  $y$  with  $y + 2\pi R$ . In such a case, the 5D complex scalar field can be expanded in a Fourier series:

$$\phi(x, y) = \frac{1}{\sqrt{2\pi R M_5}} \sum_{n=-\infty}^{\infty} e^{iny/R} \phi^{(n)}(x), \quad (86.2)$$

that, inserted in Eq. (86.1) and integrating over  $y$ , gives

$$S_5 = S_4^{(0)} + S_4^{(n)}, \quad (86.3)$$

where

$$S_4^{(0)} = - \int d^4x \left[ |\partial_\mu \phi^{(0)}|^2 + \lambda_4 |\phi^{(0)}|^4 \right], \quad (86.4)$$

and,

$$S_4^{(n)} = - \int d^4x \sum_{n \neq 0} \left[ |\partial_\mu \phi^{(n)}|^2 + \left(\frac{n}{R}\right)^2 |\phi^{(n)}|^2 \right] + \text{quartic interactions}. \quad (86.5)$$

The  $n = 0$  mode self-coupling is given by

$$\lambda_4 = \frac{\lambda_5}{2\pi R M_5}. \quad (86.6)$$

The above action corresponds to a 4D theory with a massless scalar  $\phi^{(0)}$ , referred to as the zero mode, and an infinite tower of massive modes  $\phi^{(n)}$  with  $n > 0$ , known as KK modes. The KK reduction thus allows a treatment of 5D theories as 4D field theories with an infinite number of fields. At energies smaller than  $1/R$ , the KK modes can be neglected, leaving the zero-mode action of Eq. (86.4). The strength of the interaction of the zero-mode, given by Eq. (86.6), decreases as  $R$  increases. Thus, for a large extra dimension  $R \gg 1/M_5$ , the massless scalar is very weakly coupled.

### 86.2 Large Extra Dimensions for Gravity

#### 86.2.1 The ADD Scenario

The ADD scenario [2, 15] (for a review see, for example, [16]) assumes a  $D = 4 + \delta$  dimensional spacetime, with  $\delta$  compactified spatial dimensions. The apparent weakness of gravity arises since it propagates in the higher-dimensional space. The SM is assumed to be localized in a 4D subspace, a 3-brane, as can be found in certain string theory constructions [17, 18]. Gravity is described by the Einstein-Hilbert action in  $D = 4 + \delta$  spacetime dimensions

$$S_D = - \frac{\bar{M}_D^{2+\delta}}{2} \int d^4x d^\delta y \sqrt{-g} \mathcal{R} + \int d^4x \sqrt{-g_{\text{ind}}} \mathcal{L}_{\text{SM}}, \quad (86.7)$$

where  $x$  labels the ordinary four coordinates,  $y$  the  $\delta$  extra coordinates,  $g$  refers to the determinant of the  $D$ -dimensional metric whose Ricci scalar is defined by  $\mathcal{R}$ , and  $\bar{M}_D$  is called the reduced Planck scale of the  $D$ -dimensional theory. In the second term of Eq. (86.7), which gives the gravitational interactions of SM fields, the  $D$ -dimensional metric reduces to the induced metric on the 3-brane where the SM fields propagate. The extra dimensions are assumed to be flat and compactified in a volume  $V_\delta$ . As an example, consider a toroidal compactification of equal radii  $R$  and volume  $V_\delta = (2\pi R)^\delta$ . After a KK reduction, one finds that the fields that couple to the SM are the spin-2 gravitational field  $G_{\mu\nu}(x, y)$  and a tower of spin-1 KK graviscalars [19]. The graviscalars, however, only couple to SM fields through the trace of the energy-momentum tensor, resulting in weaker couplings to the SM fields. The Fourier expansion of the spin-2 field is given by

$$G_{\mu\nu}(x, y) = G_{\mu\nu}^{(0)}(x) + \frac{1}{\sqrt{V_\delta}} \sum_{\vec{n} \neq 0} e^{i\vec{n} \cdot \vec{y}/R} G_{\mu\nu}^{(\vec{n})}(x), \quad (86.8)$$

<sup>1</sup>Our convention for the metric is  $\eta_{MN} = \text{Diag}(-1, 1, 1, 1, 1)$ .



where  $\vec{y} = (y_1, y_2, \dots, y_\delta)$  are the extra-dimensional coordinates and  $\vec{n} = (n_1, n_2, \dots, n_\delta)$ . Eq. (86.8) contains a massless state, the 4D graviton  $G_{\mu\nu}^{(0)}$ , and its KK tower  $G_{\mu\nu}^{(\vec{n})}$  with masses  $m_{\vec{n}}^2 = |\vec{n}|^2/R^2$ . At energies below  $1/R$  the action is that of the zero mode

$$S_4^{(0)} = -\frac{\bar{M}_D^{2+\delta}}{2} \int d^4x V_\delta \sqrt{-g^{(0)}} \mathcal{R}^{(0)} + \int d^4x \sqrt{-g_{\text{ind}}^{(0)}} \mathcal{L}_{\text{SM}}, \tag{86.9}$$

where we can identify the 4D reduced Planck mass,  $M_P \equiv 1/\sqrt{8\pi G_N} \simeq 2.4 \times 10^{18}$  GeV, as a function of the  $D$ -dimensional parameters:

$$M_P^2 = V^\delta \bar{M}_D^{2+\delta} \equiv R^\delta M_D^{2+\delta}. \tag{86.10}$$

Fixing  $M_D$  at around the electroweak scale  $M_D \sim \text{TeV}$  to avoid introducing a new mass scale in the model, Eq. (86.10) gives a prediction for  $R$ :

$$\delta = 1, 2, \dots, 6 \rightarrow R \sim 10^9 \text{ km}, 0.5 \text{ mm}, \dots, 0.1 \text{ MeV}^{-1}. \tag{86.11}$$

The option  $\delta = 1$  is clearly ruled out, as it leads to modifications of Newton’s law at solar system distances. However this is not the case for  $\delta \geq 2$ , and possible observable consequences can be sought in present and future experiments.

Consistency of the model requires a stabilization mechanism for the radii of the extra dimensions, to the values shown in Eq. (86.11). The fact that we need  $R \gg 1/M_D$  leads to a new hierarchy problem, the solution of which might require imposing supersymmetry in the extra-dimensional bulk (for the case of two extra dimensions see for example [20]).

**86.2.2 Tests of the Gravitational Force Law at Sub-mm Distances**

The KK modes of the graviton give rise to deviations from Newton’s law of gravitation for distances  $\lesssim R$ . Such deviations are usually parametrized by a modified Newtonian potential of the form

$$V(r) = -G_N \frac{m_1 m_2}{r} [1 + \alpha e^{-r/\lambda}]. \tag{86.12}$$

For a 2-torus compactification,  $\alpha = 16/3$  and  $\lambda = R$ . Searches for deviations from Newton’s law of gravitation have been performed in several experiments. Refs. [21–23] give the present constraints:  $R < 37\mu\text{m}$  at 95% CL for  $\delta = 2$ , corresponding to  $M_D > 3.6$  TeV.

**86.2.3 Astrophysical and Cosmological Constraints**

The light KK gravitons could be copiously produced in stars, carrying away energy. Ensuring that the graviton luminosity is low enough to preserve the agreement of stellar models with observations provides powerful bounds on the scale  $M_D$ . The most stringent bound arises from supernova SN1987A, giving  $M_D > 27$  (2.4) TeV for  $\delta = 2$  (3) [24]. After a supernova explosion, most of the KK gravitons stay gravitationally trapped in the remnant neutron star. The requirement that neutron stars are not excessively heated by KK decays into photons leads to  $M_D > 1700$  (76) TeV for  $\delta = 2$  (3) [25].

Cosmological constraints are also quite stringent [26]. To avoid overclosure of the universe by relic gravitons one needs  $M_D > 7$  TeV for  $\delta = 2$ . Relic KK gravitons decaying into photons contribute to the cosmic diffuse gamma radiation, from which one can derive the bound  $M_D > 100$  TeV for  $\delta = 2$ .

We must mention however that bounds coming from the decays of KK gravitons into photons can be reduced if we assume that KK gravitons decay mainly into other non-SM states. This could happen, for example, if there were other 3-branes with hidden sectors residing on them [15].

**86.2.4 Collider Signals**

**86.2.4.1 Graviton and Other Particle Production**

Although each KK graviton has a purely gravitational coupling, suppressed by  $1/M_P$ , inclusive processes in which one sums over the almost continuous spectrum of available gravitons have cross sections suppressed only by powers of  $M_D$ . Processes involving gravitons are therefore detectable in collider experiments if  $M_D \sim \text{TeV}$ . A number of experimental searches for evidence of large extra dimensions have been performed at colliders, and interpreted in the context of the ADD model.

One signature arises from direct graviton emission. By making a derivative expansion of Einstein gravity, one can construct an effective theory, valid for energies much lower than  $M_D$ , and use it to make predictions for graviton-emission processes at colliders [19, 27, 28]. Gravitons produced in the final state would escape detection, giving rise to missing transverse energy ( $\cancel{E}_T$ ). The results quoted below are 95% CL lower limits on  $M_D$  for a range of values of  $\delta$  between 2 and 6, with more stringent limits corresponding to lower  $\delta$  values.

At hadron colliders, experimentally sensitive channels include the jet ( $j$ ) +  $\cancel{E}_T$  and  $\gamma$  +  $\cancel{E}_T$  final states. CMS (ATLAS)  $j$  +  $\cancel{E}_T$  results with  $36 \text{ fb}^{-1}$  of 13 TeV data provide limits of  $M_D > 5.3$ – $9.9$  TeV [29] ( $M_D > 4.8$ – $7.7$  TeV [30]). For these analyses, both experiments are assuming leading order (LO) cross sections. Since the effective theory is only valid for energies much less than  $M_D$ , the results are quoted for the full space, and include the information that suppressing the graviton cross section by a factor  $M_D^4/\hat{s}^2$  for  $\sqrt{\hat{s}} > M_D$ , where  $\sqrt{\hat{s}}$  is the parton-level center-of-mass energy of the hard collision, weakens the limits on  $M_D$  by a negligible amount for  $\delta = 2$  ( $\sim 3\%$  for  $\delta = 6$ ). Less stringent limits are obtained by CMS [31] from analysis of  $36 \text{ fb}^{-1}$  of 13 TeV data in the  $\gamma$  +  $\cancel{E}_T$  final state. The analogous ATLAS search [32] has comparable sensitivity but does not quote ADD interpretation of the results.

In models in which the ADD scenario is embedded in a string theory at the TeV scale [18], we expect the string scale  $M_s$  to be smaller than  $M_D$ , and therefore expect production of string resonances at the LHC [33]. A Run 2 result from CMS analyzing the dijet invariant mass distribution for  $36 \text{ fb}^{-1}$  of 13 TeV data excludes string resonances that decay predominantly to  $q+g$  with masses below 7.7 TeV [34]. ATLAS dijet analysis [35] provides their results in the context of model-independent limits on the cross section times acceptance for generic resonances of a variety of possible widths.

**86.2.4.2 Virtual graviton effects**

One can also search for virtual graviton effects, the calculation of which however depends on the ultraviolet cut-off of the theory and is therefore very model dependent. In the literature, several different formulations exist [19, 28, 36] for the dimension-eight operator for gravity exchange at tree level:

$$\mathcal{L}_8 = \pm \frac{4}{M_{TT}^4} \left( T_{\mu\nu} T^{\mu\nu} - \frac{1}{\delta + 2} T_\mu^\mu T_\nu^\nu \right), \tag{86.13}$$

where  $T_{\mu\nu}$  is the energy-momentum tensor and  $M_{TT}$  is related to  $M_D$  by some model-dependent coefficient [37]. The relations with the parametrizations of Refs. [36] and [19] are, respectively,  $M_{TT} = M_S$  and  $M_{TT} = (2/\pi)^{1/4} A_T$ . The experimental results below are given as 95% CL lower limits on  $M_{TT}$ , including in some cases the possibility of both constructive or destructive interference, depending on the sign chosen in Eq. (9).

The most stringent limits arise from LHC analyses of the dijet angular distribution. Using  $35.9 \text{ fb}^{-1}$  of 13 TeV data, CMS [38] obtains results that correspond to an approximate limit of  $M_{TT} > 9.1$  TeV.

The next most restrictive results come from the analyses of diphoton ( $M_{TT} > 6.1$  TeV from ATLAS [39] and  $M_{TT} > 7.0$  TeV from CMS [40]) and dilepton mass spectra ( $M_{TT} > 6.1$  TeV from CMS [41]). The complete Run 2 ( $139 \text{ fb}^{-1}$ ) analysis of ATLAS di-lepton data [42] does not quote the limits on ADD.

At the one-loop level, gravitons can also generate dimension-six operators with coefficients that are also model dependent. Experimental bounds on these operators can also give stringent constraints on  $M_D$  [37].

**86.2.4.3 Black Hole Production**

The physics at energies  $\sqrt{s} \sim M_D$  is sensitive to the details of the unknown quantum theory of gravity. Nevertheless, in the transplanckian regime,  $\sqrt{s} \gg M_D$ , one can rely on a semiclassical description of gravity to obtain predictions. An interesting feature of transplanckian physics is the creation of black holes [43, 44] (for a review see, for example, [45]). A black hole is expected to be formed in a collision in which the impact parameter is smaller

than the Schwarzschild radius [46]:

$$R_S = \frac{1}{M_D} \left[ \frac{2^\delta \pi^{(\delta-3)/2}}{\delta+2} \Gamma\left(\frac{\delta+3}{2}\right) \frac{M_{BH}}{M_D} \right]^{1/(\delta+1)}, \quad (86.14)$$

where  $M_{BH}$  is the mass of the black hole, which would roughly correspond to the total energy in the collision. The cross section for black hole production can be estimated to be of the same order as the geometric area  $\sigma \sim \pi R_S^2$ . For  $M_D \sim \text{TeV}$ , this gives a production of  $\sim 10^7$  black holes at the  $\sqrt{s} = 14$  TeV LHC with an integrated luminosity of  $30 \text{ fb}^{-1}$  [43, 44]. A black hole would provide a striking experimental signature since it is expected to thermally radiate with a Hawking temperature  $T_H = (\delta+1)/(4\pi R_S)$ , and therefore would evaporate democratically into all SM states. Nevertheless, given the present constraints on  $M_D$ , the LHC will not be able to reach energies much above  $M_D$ . This implies that predictions based on the semiclassical approximation could receive sizable modifications from model-dependent quantum-gravity effects.

The most stringent limits on microscopic black holes arise from LHC searches which observed no excesses above the SM background in high-multiplicity final states. The results are usually quoted as model-independent limits on the cross section for new physics in the final state and kinematic region analyzed. These results can then be used to provide constraints of models of low-scale gravity and weakly-coupled string theory. In addition, limits are sometimes quoted on particular implementations of models, which are used as benchmarks to illustrate the sensitivity.

A CMS analysis [47] of multi-object final states using  $36 \text{ fb}^{-1}$  of 13 TeV data, excludes semiclassical black holes below masses of up to 10.1 TeV for  $M_D = 2$  TeV and  $\delta = 6$ . Analogous Run 2 ATLAS analysis [48], using  $3.0 \text{ fb}^{-1}$  of 13 TeV data, excludes black hole masses up to 9.0–9.7 TeV, depending on  $M_D$ , for  $\delta = 6$ . Another ATLAS search [49] for an excess of events with multiple high transverse momentum objects, including charged leptons and jets, using  $3.2 \text{ fb}^{-1}$  of 13 TeV data, excludes semiclassical black holes below masses of  $\sim 8.7$  TeV for  $M_D = 2$  TeV and  $\delta = 6$ .

A complementary approach is to look for jet extinction at high transverse momenta, as we expect hard short distance scattering processes to be highly suppressed at energies above  $M_D$  [50]. The CMS analysis [51] of inclusive jet  $p_T$  spectrum in  $10.7 \text{ fb}^{-1}$  of 8 TeV data set a lower limit of 3.3 TeV on the extinction mass scale.

For black hole masses near  $M_D$ , the semi-classical approximation is not valid, and one could instead expect quantum black holes (QBH) that decay primarily into two-body final states [52]. LHC Run 2 results at 13 TeV provide lower limits on QBH masses of order 2.3–9.0 TeV, depending on the details of the model. Searches that consider interpretations in terms of QBH limits include the CMS multi-object analysis [53], ATLAS dijet analysis [35], and different flavor di-lepton analyses at CMS ( $e\mu$ ,  $36 \text{ fb}^{-1}$  at 13 TeV [54]) and ATLAS ( $e\mu$ ,  $e\tau$ ,  $\mu\tau$ ,  $36.1 \text{ fb}^{-1}$  at 13 TeV [55]).

In weakly-coupled string models the semiclassical description of gravity fails in the energy range between  $M_s$  and  $M_s/g_s^2$  where stringy effects are important. In this regime one expects, instead of black holes, the formation of string balls, made of highly excited long strings, that could be copiously produced at the LHC for  $M_s \sim \text{TeV}$  [56], and would evaporate thermally at the Hagedorn temperature giving rise to high-multiplicity events. The same analyses used to search for black holes can be interpreted in the context of string balls. For example, for the case of  $\delta = 6$  with  $M_s = M_D/1.26 = 3$  TeV, the ATLAS multiple high transverse momentum object analysis [48] excludes string balls with masses below 6.5 to 9.0 TeV for values of  $0.2 < g_s < 0.8$ . The CMS multi-object analysis [47] studies string ball production in two scenarios, both assuming  $\delta = 6$ . For the constant  $g_s = 0.2$  and  $1 < M_s < 3.5$  TeV the string ball masses below 7.2 to 9.4 TeV are excluded, while at constant  $M_s = 3.6$  TeV and  $0.2 < g_s < 0.4$  masses below 7.2 to 8.1 TeV are excluded.

## 86.3 TeV-Scale Extra Dimensions

### 86.3.1 Warped Extra Dimensions

The RS model [3] is the most attractive setup of warped extra dimensions at the TeV scale, since it provides an alternative solution to the hierarchy problem. The RS model is based on a 5D theory with the extra dimension compactified in an orbifold,  $S^1/Z_2$ , a circle  $S^1$  with the extra identification of  $y$  with  $-y$ . This corresponds to the segment  $y \in [0, \pi R]$ , a manifold with boundaries at  $y = 0$  and  $y = \pi R$ . Let us now assume that this 5D theory has a cosmological constant in the bulk  $\Lambda$ , and on the two boundaries  $\Lambda_0$  and  $\Lambda_{\pi R}$ :

$$S_5 = - \int d^4x dy \left\{ \sqrt{-g} \left[ \frac{1}{2} M_5^3 \mathcal{R} + \Lambda \right] + \sqrt{-g_0} \delta(y) \Lambda_0 + \sqrt{-g_{\pi R}} \delta(y - \pi R) \Lambda_{\pi R} \right\}, \quad (86.15)$$

where  $g_0$  and  $g_{\pi R}$  are the values of the determinant of the induced metric on the two respective boundaries. Einstein's equations can be solved, giving in this case the metric

$$ds^2 = a(y)^2 dx^\mu dx^\nu \eta_{\mu\nu} + dy^2, \quad a(y) = e^{-ky}, \quad (86.16)$$

where  $k = \sqrt{-\Lambda/6M_5^3}$ . Consistency of the solution requires  $\Lambda_0 = -\Lambda_{\pi R} = -\Lambda/k$ . The metric in Eq. (86.16) corresponds to a 5D AdS space. The factor  $a(y)$  is called the ‘‘warp’’ factor and determines how 4D scales change as a function of the position in the extra dimension. In particular, this implies that energy scales for 4D fields localized at the boundary at  $y = \pi R$  are redshifted by a factor  $e^{-k\pi R}$  with respect to those localized at  $y = 0$ . For this reason, the boundaries at  $y = 0$  and  $y = \pi R$  are usually referred to as the ultraviolet (UV) and infrared (IR) boundaries, respectively.

As in the ADD case, we can perform a KK reduction and obtain the low-energy effective theory of the 4D massless graviton. In this case we obtain

$$M_P^2 = \int_0^{\pi R} dy e^{-2ky} M_5^3 = \frac{M_5^3}{2k} (1 - e^{-2k\pi R}). \quad (86.17)$$

Taking  $M_5 \sim k \sim M_P$ , we can generate an IR-boundary scale of order  $ke^{-k\pi R} \sim \text{TeV}$  for an extra dimension of radius  $R \simeq 11/k$ . Mechanisms to stabilize  $R$  to this value have been proposed [57, 58] that, contrary to the ADD case, do not require introducing any new small or large parameter. Therefore a natural solution to the hierarchy problem can be achieved in this framework if the Higgs field, whose vacuum expectation value (VEV) is responsible for electroweak symmetry breaking, is localized at the IR-boundary where the effective mass scales are of order TeV. The radion field is generically heavy in models with a stabilized  $R$ . Nevertheless, it has been recently discussed that under some conditions a naturally light radion can arise [59–62]. In these cases the radion is identified with the dilaton, the Goldstone boson associated to the spontaneous breaking of scale invariance, and its mass can be naturally below  $ke^{-k\pi R} \sim \text{TeV}$ . Collider bounds on the radion mass and couplings can be found in [63–65].

In the RS model [3], all the SM fields were assumed to be localized on the IR-boundary. Nevertheless, for the hierarchy problem, only the Higgs field has to be localized there. SM gauge bosons and fermions can propagate in the 5D bulk [4–7] (for a review see, for example, [66, 67]). By performing a KK reduction from the 5D action of a gauge boson, we find [4, 5]

$$\frac{1}{g_4^2} = \int_0^{\pi R} dy \frac{1}{g_5^2} = \frac{\pi R}{g_5^2}, \quad (86.18)$$

where  $g_D$  ( $D = 4, 5$ ) is the gauge coupling in  $D$ -dimensions. Therefore the 4D gauge couplings can be of order one, as is the case of the SM, if one demands  $g_5^2 \sim \pi R$ . Using  $kR \sim 10$  and  $g_4 \sim 0.5$ , one obtains the 5D gauge coupling

$$g_5 \sim 4/\sqrt{k}. \quad (86.19)$$

Boundary kinetic terms for the gauge bosons can modify this relation, allowing for larger values of  $g_5\sqrt{k}$ .

Fermions propagating in a warped extra dimension have 4D massless zero-modes with wavefunctions which vary as  $f_0 \sim \exp[(1/2 - c_f)ky]$ , where  $c_fk$  is their 5D mass [7,68]. Depending on the free parameter  $c_fk$ , fermions can be localized either towards the UV-boundary ( $c_f > 1/2$ ) or IR-boundary ( $c_f < 1/2$ ). Since the Higgs boson is localized on the IR-boundary, one can generate exponentially suppressed Yukawa couplings by having the fermion zero-modes localized towards the UV-boundary, generating naturally the light SM fermion spectrum [7]. A large overlap with the wavefunction of the Higgs is needed for the top quark, in order to generate its large mass, thus requiring it to be localized towards the IR-boundary. In conclusion, the large mass hierarchies present in the SM fermion spectrum can be easily obtained in warped models via suitable choices of the order-one parameters  $c_f$  [69]. In these scenarios, deviations in flavor physics from the SM predictions are expected to arise from flavor-changing KK gluon couplings [70], putting certain constraints on the parameters of the models and predicting new physics effects to be observed in  $B$ -physics processes (see, for example, [71,72]).

The masses of the KK states can also be calculated. One finds [7]

$$m_n \simeq \left( n + \frac{\alpha}{2} - \frac{1}{4} \right) \pi k e^{-\pi k R}, \quad (86.20)$$

where  $n = 1, 2, \dots$  and  $\alpha = \{c_f - 1/2, 0, 1\}$  for KK fermions, KK gauge bosons and KK gravitons, respectively. Their masses are of order  $ke^{-\pi k R} \sim \text{TeV}$  (for this reason we refer to these scenarios as TeV-scale extra dimensions). The first KK state of the gauge bosons would be the lightest, while gravitons are expected to be the heaviest.

### 86.3.1.1 Models of Electroweak Symmetry Breaking

Theories in warped extra dimensions can be used to implement symmetry breaking at low energies by boundary conditions (for a review see, for example, [73]). For example, for a  $U(1)$  gauge symmetry in the 5D bulk, this can be easily achieved by imposing a Dirichlet boundary condition on the IR-boundary for the gauge-boson field,  $A_\mu|_{y=\pi R} = 0$ . This makes the zero-mode gauge boson get a mass, given by  $m_A = g_4 \sqrt{2k/g_5^2} e^{-\pi k R}$ . A very different situation occurs if the Dirichlet boundary condition is imposed on the UV-boundary,  $A_\mu|_{y=0} = 0$ . In this case the zero-mode gauge boson disappears from the spectrum. Finally, if a Dirichlet boundary condition is imposed on the two boundaries, one obtains a massless 4D scalar corresponding to the fifth component of the 5D gauge boson,  $A_5$ . Thus, different scenarios can be implemented by appropriately choosing the 5D bulk gauge symmetry,  $\mathcal{G}_5$ , and the symmetries to which it reduces on the UV and IR-boundary,  $\mathcal{H}_{UV}$  and  $\mathcal{H}_{IR}$ , respectively. In all cases the KK spectrum comes in representations of the group  $\mathcal{G}_5$ .

Among the most interesting scenarios are those called gauge-Higgs unified models, where the Higgs boson appears as the fifth component of a 5D gauge boson,  $A_5$ . The Higgs mass is protected by the 5D gauge invariance and can only get a nonzero value from non-local one-loop effects [74]. To guarantee the relation  $M_W^2 \simeq M_Z^2 \cos^2 \theta_W$ , a custodial  $SU(2)_V$  symmetry is needed in the bulk and IR-boundary [75]. The simplest realization [76,77] has

$$\begin{aligned} \mathcal{G}_5 &= SU(3)_c \times SO(5) \times U(1)_X, \\ \mathcal{H}_{IR} &= SU(3)_c \times SO(4) \times U(1)_X, \\ \mathcal{H}_{UV} &= G_{SM}. \end{aligned}$$

The Higgs boson gets a potential at the one-loop level that triggers a VEV, breaking the electroweak symmetry. In these models there is a light Higgs boson whose mass can be around 125 GeV, as required by the discovered Higgs boson [78]. This state, as will be explained in Sec. 86.3.2, behaves as a composite pseudo-Goldstone boson with couplings that deviate from the SM Higgs [79]. The present experimental determination of the Higgs couplings at the LHC, that agrees with the SM predictions, put important constraints on these scenarios [78]. The lightest KK modes of the model are color fermions with charges  $Q = -1/3, 2/3$  and  $5/3$  [80].

### 86.3.1.2 Constraints from Electroweak Precision Tests

Models in which the SM gauge bosons propagate in 1/TeV-sized extra dimensions give generically large corrections to electroweak observables. When the SM fermions are confined on a boundary these corrections are universal and can be parametrized by four quantities:  $\widehat{S}$ ,  $\widehat{T}$ ,  $W$  and  $Y$ , as defined in Ref. [81]. For warped models, where the 5D gauge coupling of Eq. (86.19) is large, the most relevant parameter is  $\widehat{T}$ , which gives the bound  $m_{KK} \gtrsim 10 \text{ TeV}$  [66]. When a custodial symmetry is imposed [75], the main constraint comes from the  $\widehat{S}$  parameter, requiring  $m_{KK} \gtrsim 3 \text{ TeV}$ , independent of the value of  $g_5$ . Corrections to the  $Zb_L\bar{b}_L$  coupling can also be important [66], especially in warped models for electroweak symmetry breaking as the ones described above.

### 86.3.1.3 Kaluza-Klein Searches

The main prediction of 1/TeV-sized extra dimensions is the presence of a discretized KK spectrum, with masses around the TeV scale, associated with the SM fields that propagate in the extra dimension.

In the RS model [3], only gravity propagates in the 5D bulk. Experimental searches have been performed for the lightest KK graviton through its decay to a variety of SM particle-antiparticle pairs. The results are usually interpreted in the plane of the dimensionless coupling  $k/M_P$  versus  $m_1$ , where  $M_P$  is the reduced Planck mass defined previously and  $m_1$  is the mass of the lightest KK excitation of the graviton. Since the AdS curvature  $\sim k$  cannot exceed the cut-off scale of the model, which is estimated to be  $\ell_5^{1/3} M_5$  [37], one must demand  $k \ll \sqrt{2\ell_5} M_P$ .

The most stringent limits currently arise from LHC searches for resonances in the dilepton and diphoton final states, using 13 TeV collisions. Best sensitivities are obtained in the  $\gamma\gamma$  final state, which is quite powerful since it has a branching fraction twice that of any individual lepton flavor. The CMS analysis [40] of 36 fb $^{-1}$  of 13 TeV data excludes KK gravitons below 2.3 to 4.6 TeV, depending on the value of the coupling  $k/M_P$ , which is varied between 0.01 and 0.2, while ATLAS [39] provides a lower limit on the KK graviton mass of 4.1 TeV for the coupling parameter 0.1. The CMS [82] dilepton analyses, combining results from the  $ee$  and  $\mu\mu$  channels, exclude KK gravitons with masses below 4.25 TeV for coupling parameter 0.1. The ATLAS [42] analysis of 139fb $^{-1}$  of Run 2 data does not include a RS KK graviton interpretation of the results. Less stringent limits on the KK graviton mass come from analyses of the dijet [34],  $HH$  [83,84], and  $VV$  [85,86] final states, where  $V$  can represent either a  $W$  or  $Z$  boson.

In warped extra-dimensional models in which the SM fields propagate in the 5D bulk, the couplings of the KK graviton to  $ee/\mu\mu/\gamma\gamma$  are suppressed [87], and the above bounds do not apply. Furthermore, the KK graviton is the heaviest KK state (see Eq. (86.20)), and therefore experimental searches for KK gauge bosons and fermions are more appropriate discovery channels in these scenarios. For the scenarios discussed above in which only the Higgs boson and the top quark are localized close to the IR-boundary, the KK gauge bosons mainly decay into top quarks, longitudinal  $W/Z$  bosons, and Higgs bosons. Couplings to light SM fermions are suppressed by a factor  $g/\sqrt{g_5^2 k} \sim 0.2$  [7] for the value of Eq. (86.19) that is considered from now on. Searches have been made for evidence of the lightest KK excitation of the gluon, through its decay to  $t\bar{t}$  pairs. The searches take into account the natural KK gluon width, which is typically  $\sim 15\%$  of its mass. The decay of a heavy particle to  $t\bar{t}$  would tend to produce highly boosted top (anti-)quarks in the final state. Products of the subsequent top decays would therefore tend to be close to each other in the detector. In the case of  $t \rightarrow Wb \rightarrow jjb$  decays, the three jets could overlap one another and not be individually reconstructed with the standard jet algorithms, while  $t \rightarrow Wb \rightarrow \ell\nu b$  decays could result in the lepton failing standard isolation requirements due to its proximity to the  $b$ -jet; in both cases, the efficiency for properly reconstructing the final state would fall as the mass of the original particle increases. To avoid the loss in sensitivity which would result, a number of techniques, known generally as “top quark tagging”, have been developed to reconstruct and identify highly boosted top quarks, for example by using a single “wide” jet to contain all the decay products of a hadronic top decay. The

large backgrounds from QCD jets can then be reduced by requiring the “jet mass” be consistent with that of a top quark, and also by examining the substructure of the wide jet for indication that it resulted from the hadronic decay of a top quark. These techniques are key to extending to very high masses the range of accessible resonances decaying to  $t\bar{t}$  pairs. The CMS analysis [88] of  $36\text{ fb}^{-1}$  of 13 TeV data combines di-lepton, lepton-plus-jet, and all-hadronic  $t\bar{t}$  decays and excludes KK gluons with masses below 4.55 TeV. ATLAS uses all-hadronic [89] and lepton-plus-jet [90] final states to exclude KK gluons up to 3.4 and 3.8 TeV respectively with  $36\text{ fb}^{-1}$  of 13 TeV data. The results are not directly comparable between the two LHC experiments, since they employ in their respective analyses different implementations of the theoretical model. For masses between 3 and 5 TeV, the cross-section limits are around 20 fb for CMS and 30 fb for ATLAS.

A gauge boson KK excitation could be also sought through its decay to longitudinal  $W/Z$  bosons. Recent analyses from  $36\text{ fb}^{-1}$  of 13 TeV data by ATLAS [91] and CMS [92] searching for heavy vector resonances decaying to a  $W$  or  $Z$  boson and a Higgs in the  $q\bar{q}b\bar{b}$  final state have set a lower limit on the mass of these KK of  $\sim 2.5$  TeV (warped models are equivalent to the Model B considered in the analyses with  $g_V \sim g_5\sqrt{k}$ ). The decay to a pair of intermediate vector bosons has also been exploited to search for KK gravitons in models in which the SM fields propagate in the 5D bulk. The analyses typically reconstruct hadronic  $W/Z$  decays using variants of the boosted techniques mentioned previously. An ATLAS analysis [85] combines leptonic and hadronic final states from the KK graviton decay  $G^* \rightarrow VV$ , where  $V$  can represent either a  $W$  or  $Z$  boson, exclude KK gravitons with masses below 2.3 TeV, for a value of  $k/M_P = 1$ . CMS  $VV$  analysis [93] also provides cross section limits in the context of bulk gravitons; however, a maximum value of  $k/M_P = 0.5$  is presented, for which no mass exclusion is possible using the  $36\text{ fb}^{-1}$  of 13 TeV data.

The lightest KK states are, in certain models, the partners of the top quark. For example, in 5D composite Higgs models these are colored states with charges  $Q = -1/3, 2/3$  and  $5/3$  (arising from  $SU(2)_L$  doublets with  $Y = 7/6, 1/6$ ), and masses expected to be below the TeV [80]. They can be either singly or pair-produced, and mainly decay into a combination of  $W/Z$  with top/bottom quarks [94–97]. An exhaustive review of these searches can be found in Ref. [98]. Of particular note, the  $Q = 5/3$  state decays mainly into  $W^+t \rightarrow W^+W^+b$ , giving a pair of same-sign leptons in the final state. An analysis by ATLAS [99] searching in the lepton-plus-jets final state for evidence of pair production of the  $Q = 5/3$  state provides a lower mass limit of 1.25 TeV. A CMS analysis [100] searching for pair production of the  $Q = 5/3$  state using both lepton-plus-jets and same sign lepton final states excludes masses below 1.3 TeV. Both LHC experiments have searched for pair production of vector-like quarks  $T$  and  $B$  of charges  $Q = 2/3$  and  $-1/3$  respectively, assuming the allowable decays are  $T \rightarrow Wb/Zt/Ht$  and  $B \rightarrow Wt/Zb/Hb$ . In each case, it is assumed the branching fractions of the three decay modes sum to unity, but the individual branching fractions, which are model-dependent, are allowed to vary within this constraint. Both ATLAS [101] and CMS [102–104] obtain lower limits on the mass of the  $T$  and  $B$  vector-like quarks up to 1.3 TeV.

Recent analyses from ATLAS [105] and CMS [106] also search for a single top partner production, the cross section for which is model-dependent [107] but does not carry the kinematic penalty for producing two heavy objects.

### 86.3.2 Connection with Strongly Coupled Models via the AdS/CFT Correspondence

The AdS/CFT correspondence [8] provides a connection between warped extra-dimensional models and strongly-coupled theories in ordinary 4D. Although the exact connection is only known for certain cases, the AdS/CFT techniques have been very useful to obtain, at the qualitative level, a 4D holographic description of the various phenomena in warped extra-dimensional models [11].

The connection goes as follows. The physics of the bulk AdS<sub>5</sub> models can be interpreted as that of a 4D conformal field theory (CFT) which is strongly coupled. The extra-dimensional coordinate  $y$  plays the role of the renormalization scale  $\mu$  of the CFT by means of the identification  $\mu \equiv ke^{-ky}$ . Therefore the

UV-boundary corresponds in the CFT to a UV cut-off scale at  $A_{UV} = k \sim M_P$ , breaking explicitly conformal invariance, while the IR-boundary can be interpreted as a spontaneous breaking of the conformal symmetry at energies  $ke^{-k\pi R} \sim \text{TeV}$ . Fields localized on the UV-boundary are elementary fields external to the CFT, while fields localized on the IR-boundary and KK states correspond to composite resonances of the CFT. Furthermore, local gauge symmetries in the 5D models,  $\mathcal{G}_5$ , correspond to global symmetries of the CFT, while the UV-boundary symmetry can be interpreted as a gauging of the subgroup  $\mathcal{H}_{UV}$  of  $\mathcal{G}_5$  in the CFT. Breaking gauge symmetries by IR-boundary conditions corresponds to the spontaneous breaking  $\mathcal{G}_5 \rightarrow \mathcal{H}_{IR}$  in the CFT at energies  $\sim ke^{-k\pi R}$ . Using this correspondence one can easily derive the 4D massless spectrum of the compactified AdS<sub>5</sub> models. One also has the identification  $k^3/M_5^3 \approx 16\pi^2/N^2$  and  $g_5^2k \approx 16\pi^2/N^r$  ( $r = 1$  or  $2$  for CFT fields in the fundamental or adjoint representation of the gauge group), where  $N$  plays the role of the number of colors of the CFT. Therefore the weak-coupling limit in AdS<sub>5</sub> corresponds to a large- $N$  expansion in the CFT.

Following the above AdS/CFT dictionary one can understand the RS solution to the hierarchy problem from a 4D viewpoint. The equivalent 4D model is a CFT with a TeV mass gap and a Higgs boson emerging as a composite state. In the particular case where the Higgs is the fifth-component of the gauge-boson,  $A_5$  [108], this corresponds to models, similar to those proposed in Ref. [109,110], where the Higgs is a composite pseudo-Goldstone boson arising from the spontaneous breaking  $\mathcal{G}_5 \rightarrow \mathcal{H}_{IR}$  in the CFT. The AdS/CFT dictionary tells us that KK states must behave as composite resonances. For example, if the SM gauge bosons propagate in the 5D bulk, the lowest KK  $SU(2)_L$ -gauge boson must have properties similar to those of the Techni-rho  $\rho_T$  [98] with a coupling to longitudinal  $W/Z$  bosons given by  $g_5\sqrt{k} \approx g_{\rho T}$ , while the coupling to elementary fermions is  $g^2/\sqrt{g_5^2k} \approx g^2F_{\rho T}/M_{\rho T}$ .

Fermions in compactified AdS<sub>5</sub> also have a simple 4D holographic interpretation. The 4D massless mode described in Sec. 86.3.1 corresponds to an external fermion  $\psi_i$  linearly coupled to a fermionic CFT operator  $\mathcal{O}_i$ :  $\mathcal{L}_{\text{int}} = \lambda_i\bar{\psi}_i\mathcal{O}_i + h.c.$ . The dimension of the operator  $\mathcal{O}_i$  is related to the 5D fermion mass according to  $\text{Dim}[\mathcal{O}_i] = |c_f + 1/2| - 1$ . Therefore, by varying  $c_f$  one varies  $\text{Dim}[\mathcal{O}_i]$ , making the coupling  $\lambda_i$  irrelevant ( $c_f > 1/2$ ), marginal ( $c_f = 1/2$ ) or relevant ( $c_f < 1/2$ ). When irrelevant, the coupling is exponentially suppressed at low energies, and then the coupling of  $\psi_i$  to the CFT (and eventually to the composite Higgs) is very small. When relevant, the coupling grows in the IR and become as large as  $g_5$  (in units of  $k$ ), meaning that the fermion is as strongly coupled as the CFT states [76]. In this latter case  $\psi_i$  behaves as a composite fermion.

### 86.3.3 Flat Extra Dimensions

Models with quantum gravity at the TeV scale, as in the ADD scenario, can have extra (flat) dimensions of  $1/\text{TeV}$  size, as happens in string scenarios (see, for example, [111]). All SM fields may propagate in these extra dimensions, leading to the possibility of observing their corresponding KK states.

A simple example is to assume that the SM gauge bosons propagate in a flat five-dimensional orbifold  $S^1/Z_2$  of radius  $R$ , with the fermions localized on a 4D boundary. The KK gauge bosons behave as sequential SM gauge bosons with a coupling to fermions enhanced by a factor  $\sqrt{2}$  [111]. The experimental limits on such sequential gauge bosons could therefore be recast as limits on KK gauge bosons. Such an interpretation of the ATLAS 7 TeV dilepton analysis [112] yielded the bound  $1/R > 4.16$  TeV, while a CMS 8 TeV search with a lepton and missing transverse energy in the final state [113] give  $1/R > 3.4$  TeV. Indirect bounds from LEP2 require however  $1/R \gtrsim 6$  TeV [81,114], a bound that can considerably improve in the future by high-energy measurements of the dilepton invariant mass spectrum from Drell-Yan processes at the LHC [115]. More recent LHC limits on leptonically decaying gauge bosons [42, 82, 116, 117] are not interpreted as bounds on  $1/R$  by the collaborations, but the published results allow for independent derivation of such bound.

An alternative scenario, known as Universal Extra Dimensions

(UED) [118] (for a review see, for example, [119]), assumes that all SM fields propagate universally in a flat orbifold  $S^1/Z_2$  with an extra  $Z_2$  parity, called KK-parity, that interchanges the two boundaries. In this case, the lowest KK state is stable and is a Dark Matter candidate. At colliders, the KK particles would have to be created in pairs, and would then cascade decay to the lightest KK particle, which would be stable and escape detection. The UED mass-spectrum depends not only on the extra-dimensional radius  $R$ , but also on the cut-off of the 5D theory  $\Lambda$ , since quantum corrections sensitive to  $\Lambda R$  induce mass-splittings between the KK states. Experimental signatures, such as jets or leptons and  $\cancel{E}_T$ , would be similar to those of typical  $R$ -parity conserving SUSY searches. An interpretation of the recent LHC experimental SUSY searches for UED models has been presented in Refs. [120,121]. A lower bound  $1/R > 1.4\text{--}1.5$  TeV was derived for  $\Lambda R \sim 5\text{--}35$  [120].

Finally, realistic models of electroweak symmetry breaking can also be constructed with flat extra spatial dimensions, similarly to those in the warped case, requiring, however, the presence of sizeable boundary kinetic terms [122]. There is also the possibility of breaking supersymmetry by boundary conditions [123]. Models of this type could explain naturally the presence of a Higgs boson lighter than  $M_D \sim \text{TeV}$  (see, for example, [124–126]).

### References

- [1] For a comprehensive collection of the original papers see, “Modern Kaluza-Klein Theories”, edited by T. Appelquist *et al.*, Addison-Wesley (1987).
- [2] N. Arkani-Hamed, S. Dimopoulos and G. Dvali, Phys. Lett. **B429**, 263 (1998), [hep-ph/9803315].
- [3] L. Randall and R. Sundrum, Phys. Rev. Lett. **83**, 3370 (1999), [hep-ph/9905221].
- [4] H. Davoudiasl, J. L. Hewett and T. G. Rizzo, Phys. Lett. **B473**, 43 (2000), [hep-ph/9911262].
- [5] A. Pomarol, Phys. Lett. **B486**, 153 (2000), [hep-ph/9911294].
- [6] S. Chang *et al.*, Phys. Rev. **D62**, 084025 (2000), [hep-ph/9912498].
- [7] T. Gherghetta and A. Pomarol, Nucl. Phys. **B586**, 141 (2000), [hep-ph/0003129].
- [8] J. M. Maldacena, Int. J. Theor. Phys. **38**, 1113 (1999), [Adv. Theor. Math. Phys.2,231(1998)], [hep-th/9711200].
- [9] E. Witten, Adv. Theor. Math. Phys. **2**, 253 (1998), [hep-th/9802150].
- [10] S. S. Gubser, I. R. Klebanov and A. M. Polyakov, Phys. Lett. **B428**, 105 (1998), [hep-th/9802109].
- [11] N. Arkani-Hamed, M. Porrati and L. Randall, JHEP **08**, 017 (2001), [hep-th/0012148].
- [12] ATLAS public results are available on WWW at <https://twiki.cern.ch/twiki/bin/view/AtlasPublic>.
- [13] CMS public results are available on WWW at <https://cms-results.web.cern.ch/cms-results/public-results/publications>.
- [14] Z. Chacko, M. A. Luty and E. Ponton, JHEP **07**, 036 (2000), [hep-ph/9909248].
- [15] N. Arkani-Hamed, S. Dimopoulos and G. R. Dvali, Phys. Rev. **D59**, 086004 (1999), [hep-ph/9807344].
- [16] R. Rattazzi, hep-ph/0607055 (2006); I. Antoniadis, Yellow report CERN-2002-002 (2002).
- [17] J. D. Lykken, Phys. Rev. **D54**, R3693 (1996), [hep-th/9603133].
- [18] I. Antoniadis *et al.*, Phys. Lett. **B436**, 257 (1998), [hep-ph/9804398].
- [19] G. F. Giudice, R. Rattazzi and J. D. Wells, Nucl. Phys. **B544**, 3 (1999), [hep-ph/9811291].
- [20] N. Arkani-Hamed *et al.*, Phys. Rev. **D62**, 105002 (2000), [hep-ph/9912453].
- [21] E. G. Adelberger *et al.*, Prog. Part. Nucl. Phys. **62**, 102 (2009).
- [22] J. Murata and S. Tanaka, Class. Quant. Grav. **32**, 3, 033001 (2015), [arXiv:1408.3588].
- [23] W.-H. Tan *et al.*, Phys. Rev. Lett. **116**, 13, 131101 (2016).
- [24] C. Hanhart *et al.*, Phys. Lett. **B509**, 1 (2001), [arXiv:astro-ph/0102063].
- [25] S. Hannestad and G. G. Raffelt, Phys. Rev. **D67**, 125008 (2003), [Erratum: Phys. Rev.D69,029901(2004)], [hep-ph/0304029].
- [26] L. J. Hall and D. Tucker-Smith, Phys. Rev. **D60**, 085008 (1999), [hep-ph/9904267].
- [27] E. A. Mirabelli, M. Perelstein and M. E. Peskin, Phys. Rev. Lett. **82**, 2236 (1999), [hep-ph/9811337].
- [28] T. Han, J. D. Lykken and R.-J. Zhang, Phys. Rev. **D59**, 105006 (1999), [hep-ph/9811350].
- [29] A. M. Sirunyan *et al.* (CMS), Phys. Rev. **D97**, 9, 092005 (2018), [arXiv:1712.02345].
- [30] M. Aaboud *et al.* (ATLAS), JHEP **01**, 126 (2018), [arXiv:1711.03301].
- [31] A. M. Sirunyan *et al.* (CMS), JHEP **02**, 074 (2019), [arXiv:1810.00196].
- [32] M. Aaboud *et al.* (ATLAS), Eur. Phys. J. **C77**, 6, 393 (2017), [arXiv:1704.03848].
- [33] S. Cullen, M. Perelstein and M. E. Peskin, Phys. Rev. **D62**, 055012 (2000), [hep-ph/0001166].
- [34] A. M. Sirunyan *et al.* (CMS), JHEP **08**, 130 (2018), [arXiv:1806.00843].
- [35] M. Aaboud *et al.* (ATLAS), Phys. Rev. **D96**, 5, 052004 (2017), [arXiv:1703.09127].
- [36] J. L. Hewett, Phys. Rev. Lett. **82**, 4765 (1999), [hep-ph/9811356].
- [37] G. F. Giudice and A. Strumia, Nucl. Phys. **B663**, 377 (2003), [hep-ph/0301232].
- [38] A. M. Sirunyan *et al.* (CMS), Eur. Phys. J. **C78**, 9, 789 (2018), [arXiv:1803.08030].
- [39] M. Aaboud *et al.* (ATLAS), Phys. Lett. **B775**, 105 (2017), [arXiv:1707.04147].
- [40] A. M. Sirunyan *et al.* (CMS), Phys. Rev. **D98**, 9, 092001 (2018), [arXiv:1809.00327].
- [41] A. M. Sirunyan *et al.* (CMS), JHEP **04**, 114 (2019), [arXiv:1812.10443].
- [42] G. Aad *et al.* (ATLAS), Phys. Lett. **B796**, 68 (2019), [arXiv:1903.06248].
- [43] S. B. Giddings and S. D. Thomas, Phys. Rev. **D65**, 056010 (2002), [hep-ph/0106219].
- [44] S. Dimopoulos and G. L. Landsberg, Phys. Rev. Lett. **87**, 161602 (2001), [hep-ph/0106295].
- [45] P. Kanti, Int. J. Mod. Phys. **A19**, 4899 (2004), [hep-ph/0402168].
- [46] R. C. Myers and M. J. Perry, Annals Phys. **172**, 304 (1986).
- [47] A. M. Sirunyan *et al.* (CMS), JHEP **11**, 042 (2018), [arXiv:1805.06013].
- [48] G. Aad *et al.* (ATLAS), JHEP **03**, 026 (2016), [arXiv:1512.02586].
- [49] M. Aaboud *et al.* (ATLAS), Phys. Lett. **B760**, 520 (2016), [arXiv:1606.02265].
- [50] C. Kilic *et al.*, Phys. Rev. **D89**, 1, 016003 (2014), [arXiv:1207.3525].
- [51] V. Khachatryan *et al.* (CMS), Phys. Rev. **D90**, 3, 032005 (2014), [arXiv:1405.7653].
- [52] P. Meade and L. Randall, JHEP **05**, 003 (2008), [arXiv:0708.3017].
- [53] A. M. Sirunyan *et al.* (CMS), Phys. Lett. **B774**, 279 (2017), [arXiv:1705.01403].

- [54] A. M. Sirunyan *et al.* (CMS), JHEP **04**, 073 (2018), [arXiv:1802.01122].
- [55] M. Aaboud *et al.* (ATLAS), Phys. Rev. **D98**, 9, 092008 (2018), [arXiv:1807.06573].
- [56] S. Dimopoulos and R. Emparan, Phys. Lett. **B526**, 393 (2002), [hep-ph/0108060].
- [57] W. D. Goldberger and M. B. Wise, Phys. Rev. Lett. **83**, 4922 (1999), [hep-ph/9907447].
- [58] J. Garriga and A. Pomarol, Phys. Lett. **B560**, 91 (2003), [hep-th/0212227].
- [59] See talk by R. Rattazzi at Planck 2010, CERN.
- [60] B. Bellazzini *et al.*, Eur. Phys. J. **C74**, 2790 (2014), [arXiv:1305.3919].
- [61] F. Coradeschi *et al.*, JHEP **11**, 057 (2013), [arXiv:1306.4601].
- [62] E. Megias and O. Pujolas, JHEP **08**, 081 (2014), [arXiv:1401.4998].
- [63] K. Blum *et al.*, JHEP **03**, 099 (2015), [arXiv:1410.1873].
- [64] A. Efrati *et al.*, Phys. Rev. **D91**, 5, 055034 (2015), [arXiv:1410.2225].
- [65] F. Abu-Ajamieh, J. S. Lee and J. Terning, JHEP **10**, 050 (2018), [arXiv:1711.02697].
- [66] E. P. H. Davoudiasl, S. Gopalakrishna and J. Santiago, New J. Phys. **12**, 075011 (2010), [arXiv:0908.1968].
- [67] T. Gherghetta, in “Physics of the large and the small, TASI 09, proceedings of the Theoretical Advanced Study Institute in Elementary Particle Physics, Boulder, Colorado, USA, 1-26 June 2009,” 165–232 (2011), [arXiv:1008.2570].
- [68] Y. Grossman and M. Neubert, Phys. Lett. **B474**, 361 (2000), [hep-ph/9912408].
- [69] S. J. Huber and Q. Shafi, Phys. Lett. **B498**, 256 (2001), [hep-ph/0010195].
- [70] A. Delgado, A. Pomarol and M. Quiros, JHEP **01**, 030 (2000), [hep-ph/9911252].
- [71] K. Agashe, G. Perez and A. Soni, Phys. Rev. **D71**, 016002 (2005), [hep-ph/0408134].
- [72] M. Bauer *et al.*, JHEP **09**, 017 (2010), [arXiv:0912.1625].
- [73] A. Pomarol, Int. J. Mod. Phys. **A24**, 61 (2009), [In *Kane, Gordon (ed.) et al.: Perspectives on LHC physics*, 259(2008)].
- [74] Y. Hosotani, Phys. Lett. **126B**, 309 (1983).
- [75] K. Agashe *et al.*, JHEP **08**, 050 (2003), [hep-ph/0308036].
- [76] K. Agashe, R. Contino and A. Pomarol, Nucl. Phys. **B719**, 165 (2005), [hep-ph/0412089].
- [77] For a review see, for example, R. Contino, arXiv:1005.4269.
- [78] See, for example, PDG review of Higgs boson in this *Review*.
- [79] G. F. Giudice *et al.*, JHEP **06**, 045 (2007), [hep-ph/0703164].
- [80] R. Contino, L. Da Rold and A. Pomarol, Phys. Rev. **D75**, 055014 (2007), [hep-ph/0612048].
- [81] R. Barbieri *et al.*, Nucl. Phys. **B703**, 127 (2004), [hep-ph/0405040].
- [82] A. M. Sirunyan *et al.* (CMS), JHEP **06**, 120 (2018), [arXiv:1803.06292].
- [83] A. M. Sirunyan *et al.* (CMS), Phys. Rev. Lett. **122**, 12, 121803 (2019), [arXiv:1811.09689].
- [84] M. Aaboud *et al.* (ATLAS), JHEP **01**, 030 (2019), [arXiv:1804.06174].
- [85] M. Aaboud *et al.* (ATLAS), Phys. Rev. **D98**, 5, 052008 (2018), [arXiv:1808.02380].
- [86] A. M. Sirunyan *et al.* (CMS) (2019), [arXiv:1906.05977].
- [87] K. Agashe *et al.*, Phys. Rev. **D76**, 036006 (2007), [hep-ph/0701186].
- [88] A. M. Sirunyan *et al.* (CMS), JHEP **04**, 031 (2019), [arXiv:1810.05905].
- [89] M. Aaboud *et al.* (ATLAS), Phys. Rev. **D99**, 9, 092004 (2019), [arXiv:1902.10077].
- [90] M. Aaboud *et al.* (ATLAS), Eur. Phys. J. **C78**, 7, 565 (2018), [arXiv:1804.10823].
- [91] M. Aaboud *et al.* (ATLAS), Phys. Lett. **B774**, 494 (2017), [arXiv:1707.06958].
- [92] A. M. Sirunyan *et al.* (CMS), Eur. Phys. J. **C77**, 9, 636 (2017), [arXiv:1707.01303].
- [93] A. M. Sirunyan *et al.* (CMS) (2019), [arXiv:1906.00057].
- [94] R. Contino and G. Servant, JHEP **06**, 026 (2008), [arXiv:0801.1679].
- [95] J. A. Aguilar-Saavedra, JHEP **11**, 030 (2009), [arXiv:0907.3155].
- [96] J. Mrazek and A. Wulzer, Phys. Rev. **D81**, 075006 (2010), [arXiv:0909.3977].
- [97] G. Dissertori *et al.*, JHEP **09**, 019 (2010), [arXiv:1005.4414].
- [98] See, for example, PDG review of Technicolor searches in this volume.
- [99] M. Aaboud *et al.* (ATLAS), JHEP **10**, 141 (2017), [arXiv:1707.03347].
- [100] A. M. Sirunyan *et al.* (CMS), JHEP **03**, 082 (2019), [arXiv:1810.03188].
- [101] M. Aaboud *et al.* (ATLAS), Phys. Rev. Lett. **121**, 21, 211801 (2018), [arXiv:1808.02343].
- [102] A. M. Sirunyan *et al.* (CMS), Phys. Lett. **B779**, 82 (2018), [arXiv:1710.01539].
- [103] A. M. Sirunyan *et al.* (CMS), JHEP **08**, 177 (2018), [arXiv:1805.04758].
- [104] A. M. Sirunyan *et al.* (CMS), Eur. Phys. J. **C79**, 4, 364 (2019), [arXiv:1812.09768].
- [105] M. Aaboud *et al.* (ATLAS), JHEP **05**, 164 (2019), [arXiv:1812.07343].
- [106] A. M. Sirunyan *et al.* (CMS), Phys. Lett. **B781**, 574 (2018), [arXiv:1708.01062].
- [107] A. De Simone *et al.*, JHEP **04**, 004 (2013), [arXiv:1211.5663].
- [108] R. Contino, Y. Nomura and A. Pomarol, Nucl. Phys. **B671**, 148 (2003), [hep-ph/0306259].
- [109] H. Georgi, D. B. Kaplan and P. Galison, Phys. Lett. **143B**, 152 (1984).
- [110] D. B. Kaplan and H. Georgi, Phys. Lett. **136B**, 183 (1984).
- [111] I. Antoniadis and K. Benakli, Int. J. Mod. Phys. **A15**, 4237 (2000), [hep-ph/0007226].
- [112] G. Aad *et al.* (ATLAS), JHEP **11**, 138 (2012), [arXiv:1209.2535].
- [113] V. Khachatryan *et al.* (CMS), Phys. Rev. **D91**, 9, 092005 (2015), [arXiv:1408.2745].
- [114] K. Cheung and G. L. Landsberg, Phys. Rev. **D65**, 076003 (2002), [hep-ph/0110346].
- [115] M. Farina *et al.*, Phys. Lett. **B772**, 210 (2017), [arXiv:1609.08157].
- [116] G. Aad *et al.* (ATLAS) (2019), [arXiv:1906.05609].
- [117] A. M. Sirunyan *et al.* (CMS), JHEP **06**, 128 (2018), [arXiv:1803.11133].
- [118] T. Appelquist, H.-C. Cheng and B. A. Dobrescu, Phys. Rev. **D64**, 035002 (2001), [hep-ph/0012100].
- [119] A. Datta, K. Kong and K. T. Matchev, New J. Phys. **12**, 075017 (2010), [arXiv:1002.4624].
- [120] N. Deutschmann, T. Flacke and J. S. Kim, Phys. Lett. **B771**, 515 (2017), [arXiv:1702.00410].
- [121] J. Beuria *et al.*, Comput. Phys. Commun. **226**, 187 (2018), [arXiv:1702.00413].

- [122] G. Panico, M. Safari and M. Serone, JHEP **02**, 103 (2011), [arXiv:1012.2875].
- [123] J. Scherk and J. H. Schwarz, Phys. Lett. **82B**, 60 (1979).
- [124] A. Pomarol and M. Quiros, Phys. Lett. **B438**, 255 (1998), [hep-ph/9806263].
- [125] I. Antoniadis *et al.*, Nucl. Phys. **B544**, 503 (1999), [hep-ph/9810410].
- [126] R. Barbieri, L. J. Hall and Y. Nomura, Phys. Rev. **D63**, 105007 (2001), [hep-ph/0011311].

## 87. $W'$ -Boson Searches

Revised November, 2019 by B.A. Dobrescu (Fermilab) and S. Willocq (U. Massachusetts).

The  $W'$  boson is a massive hypothetical particle of spin 1 and electric charge  $\pm 1$ , which is a color singlet and is predicted in various extensions of the Standard Model (SM).

### 87.1 $W'$ couplings to quarks and leptons

The Lagrangian terms describing the couplings of a  $W'^+$  boson to fermions are given by

$$\frac{W'^+_\mu}{\sqrt{2}} \left[ \bar{u}_i (C_{q_{ij}}^R P_R + C_{q_{ij}}^L P_L) \gamma^\mu d_j + \bar{\nu}_i (C_{\ell_{ij}}^R P_R + C_{\ell_{ij}}^L P_L) \gamma^\mu e_j \right]. \quad (87.1)$$

Here,  $u, d, \nu$ , and  $e$  are the SM fermions in the mass eigenstate basis,  $i, j = 1, 2, 3$  label the fermion generation, and  $P_{R,L} = (1 \pm \gamma_5)/2$ . The coefficients  $C_{q_{ij}}^L, C_{q_{ij}}^R, C_{\ell_{ij}}^L$ , and  $C_{\ell_{ij}}^R$  are complex dimensionless parameters. If  $C_{\ell_{ij}}^R \neq 0$ , then the  $i$ th generation includes a right-handed neutrino. Using this notation, the SM  $W$  couplings are  $C_q^L = g V_{\text{CKM}}, C_\ell^L = g \approx 0.63$  and  $C_\ell^R = C_\ell^R = 0$ .

Unitarity considerations imply that the  $W'$  boson is associated with a spontaneously-broken gauge symmetry. This is true even when it is a composite particle (*e.g.*  $\rho^\pm$ -like bound states [1]) if its mass is much smaller than the compositeness scale, or a Kaluza-Klein mode in theories where the  $W$  boson propagates in extra dimensions [2]. The simplest extension of the electroweak gauge group that includes a  $W'$  boson is  $SU(2)_1 \times SU(2)_2 \times U(1)$ , but larger groups are encountered in some theories. A generic property of these gauge theories is that they also include a  $Z'$  boson [3]; the  $W'$ -to- $Z'$  mass ratio is often a free parameter.

A tree-level mass mixing may be induced between the electrically-charged gauge bosons. Upon diagonalization of their mass matrix, the  $W$ -to- $Z$  mass ratio and the couplings of the observed  $W$  boson are shifted from the SM values. Their measurements imply that the mixing angle,  $\theta_+$ , between the gauge eigenstates must be smaller than about  $10^{-2}$ . In certain theories the mixing is negligible (*e.g.*, due to a new parity [4]), even when the  $W'$  mass is near the electroweak scale. Note that  $SU(2)$  gauge invariance suppresses the kinetic mixing between the  $W$  and  $W'$  bosons (in contrast to the case of a  $Z'$  boson [3]).

The  $W'$  coupling to  $WZ$  is fixed by Lorentz and gauge invariances, and to leading order in  $\theta_+$  is given by [5]

$$\frac{g \theta_+ i}{\cos \theta_W} \left[ W'^+_\mu (W^-_\nu Z^{\nu\mu} + Z_\nu W^{-\mu\nu}) + Z^\nu W^{-\mu} W'^+_{\nu\mu} \right] + \text{H.c.}, \quad (87.2)$$

where  $W^{\mu\nu} \equiv \partial^\mu W^\nu - \partial^\nu W^\mu$ , etc. The  $\theta_W$  dependence shown here corrects the one given in Ref. [6], which has been referred to as the Extended Gauge Model by the experimental collaborations. The  $W'$  coupling to  $Wh^0$ , where  $h^0$  is the SM Higgs boson, is

$$-\xi_h g_{W'} M_W W'^+_\mu W^{\mu-} h^0 + \text{H.c.}, \quad (87.3)$$

where  $g_{W'}$  is the gauge coupling of the  $W'$  boson, and the coefficient  $\xi_h$  satisfies  $\xi_h \leq 1$  in simple Higgs sectors [5].

In models based on the “left-right symmetric” gauge group [7],  $SU(2)_L \times SU(2)_R \times U(1)_{B-L}$ , the SM fermions that couple to the  $W$  boson transform as doublets under  $SU(2)_L$  while the other fermions transform as doublets under  $SU(2)_R$ . Consequently, the  $W'$  boson couples primarily to right-handed fermions; its coupling to left-handed fermions arises due to the  $\theta_+$  mixing, so that  $C_q^L$  is proportional to the CKM matrix and its elements are much smaller than the diagonal elements of  $C_q^R$ . Generically,  $C_q^R$  does not need to be proportional to  $V_{\text{CKM}}$ .

There are many other models based on the  $SU(2)_1 \times SU(2)_2 \times U(1)$  gauge symmetry. In the “alternate left-right” model [8], all the couplings shown in Eq. (87.1) vanish, but there are some new fermions such that the  $W'$  boson couples to pairs involving a SM fermion and a new fermion. In the “unified SM” [9], the left-handed quarks are doublets under one  $SU(2)$ , and the left-handed leptons are doublets under a different  $SU(2)$ , leading to a mostly leptophobic  $W'$  boson:  $C_{\ell_{ij}}^L \ll C_{q_{ij}}^L$  and  $C_{\ell_{ij}}^R = C_{q_{ij}}^R = 0$ . Fermions of different generations may also transform

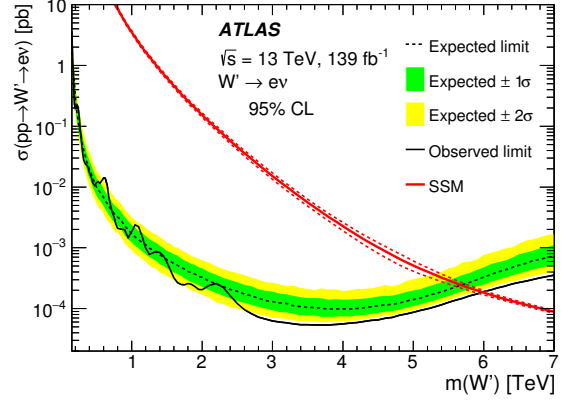


Figure 87.1: Upper limit on  $\sigma(pp \rightarrow W'X) B(W' \rightarrow e\nu)$  from ATLAS [12]. The red line shows the theoretical prediction in the Sequential SM.

as doublets under different  $SU(2)$  gauge groups [10]. In particular, the couplings to third generation quarks may be enhanced [11].

It is also possible that the  $W'$  couplings to SM fermions are highly suppressed. For example, if the quarks and leptons are singlets under one  $SU(2)$  [13], then the couplings are proportional to the tiny mixing angle  $\theta_+$ . Similar suppressions may arise if some vectorlike fermions mix with the SM fermions [14].

Gauge groups that embed the electroweak symmetry, such as  $SU(3)_W \times U(1)$  or  $SU(4)_W \times U(1)$ , also include one or more  $W'$  bosons [15].

### 87.2 Collider searches

At LEP-II,  $W'$  bosons could have been produced in pairs via their photon and  $Z$  couplings. The production cross section is large enough to rule out  $M_{W'} < \sqrt{s}/2 \approx 105$  GeV for most patterns of decay modes.

At hadron colliders,  $W'$  bosons can be detected through resonant pair production of fermions ( $f$  and  $f'$ ) or electroweak bosons with a net electric charge equal to  $\pm 1$ . When  $W'$  has a width much smaller than its mass ( $M_{W'}/\Gamma_{W'} \lesssim 7\%$ ), the contribution of the  $s$ -channel  $W'$  exchange to the total rate for  $pp \rightarrow f f' X$ , where  $X$  is any final state, may be approximated by the branching fraction  $B(W' \rightarrow f f')$  times the production cross section

$$\sigma(pp \rightarrow W'X) \simeq \frac{\pi}{6s} \sum_{i,j} [(C_{q_{ij}}^L)^2 + (C_{q_{ij}}^R)^2] w_{ij} (M_{W'}^2/s, M_{W'}). \quad (87.4)$$

The functions  $w_{ij}$  include the information about proton structure, and are given to leading order in  $\alpha_s$  by

$$w_{ij}(z, \mu) = \int_z^1 \frac{dx}{x} \left[ u_i(x, \mu) \bar{d}_j\left(\frac{z}{x}, \mu\right) + \bar{u}_i(x, \mu) d_j\left(\frac{z}{x}, \mu\right) \right], \quad (87.5)$$

where  $u_i(x, \mu)$  and  $d_i(x, \mu)$  are the parton distributions inside the proton at the factorization scale  $\mu$  and parton momentum fraction  $x$  for the up- and down-type quarks of the  $i$ th generation, respectively. QCD corrections to  $W'$  production are sizable (they also include quark-gluon initial states), but preserve the above factorization of couplings at next-to-leading order [16].

The most commonly studied  $W'$  signal consists of a high-momentum electron or muon and large missing transverse momentum. The signal transverse mass distribution forms a Jacobian peak with its endpoint at  $M_{W'}$  (see Fig. 1 (top) of Ref. [12]). Given that the branching fractions for  $W' \rightarrow e\nu$  and  $W' \rightarrow \mu\nu$  could be very different, the results in these channels should be presented separately. Searches in these channels often implicitly assume that the left-handed couplings vanish (no interference between  $W$  and  $W'$ ), and that the right-handed neutrino is light compared to the  $W'$  boson and escapes the detector. An example of parameter values that satisfy these assumptions is  $C_q^R = g V_{\text{CKM}}, C_\ell^R = g, C_q^L = C_\ell^L = 0$ , which define a model that



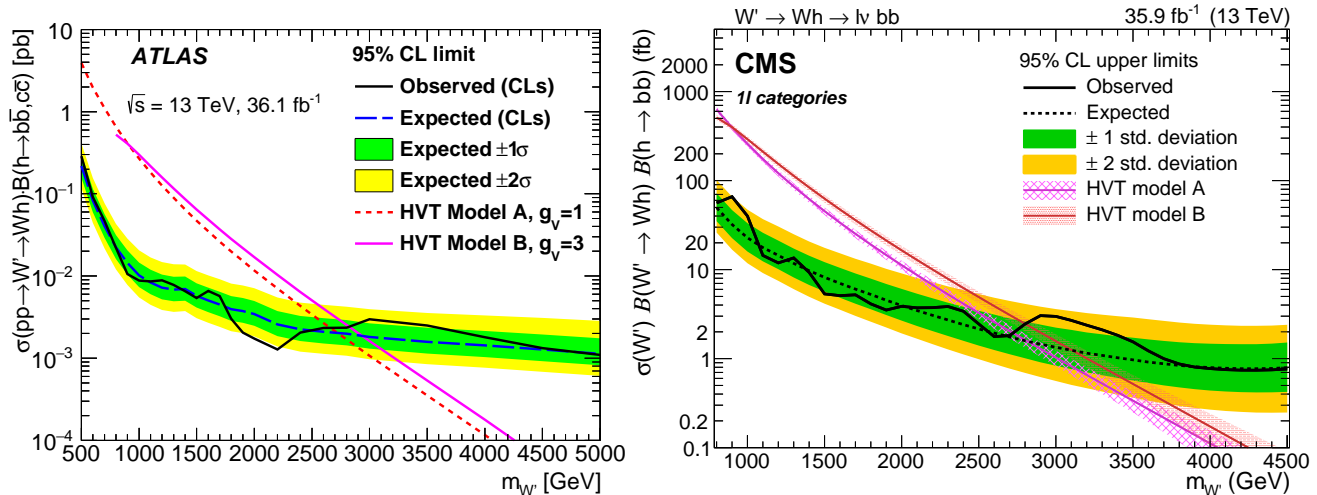


Figure 87.2: Upper limits on  $W'$  production cross section times branching fraction into a  $W$  and a SM Higgs boson decaying into heavy-flavor quarks, from ATLAS [17] (left) and CMS [18] (right).

preserves lepton universality and predicts the same total cross section as the Sequential SM used in many  $W'$  searches. However, if a  $W'$  boson were discovered and the final state fermions have left-handed helicity, then the effects of  $W - W'$  interference could be observed [19], providing information about the  $W'$  couplings. The effects of the  $W'$  width on interference are discussed in [20].

In the  $e\nu$  channel, the ATLAS and CMS collaborations set limits on the  $W'$  production cross section times branching fraction (and thus indirectly on the  $W'$  couplings). These limits are set for  $M_{W'}$  in the 0.15 – 7 TeV range and are based on 36–139  $\text{fb}^{-1}$  at  $\sqrt{s} = 13$  TeV [12, 21], as shown in Fig. 87.1 for the most stringent limits. ATLAS sets the strongest mass limit  $M_{W'} > 6.0$  TeV in the Sequential SM (all limits in this mini-review are at the 95% CL). The coupling limits are much weaker for  $M_{W'} < 150$  GeV, a range last explored with the Tevatron at  $\sqrt{s} = 1.8$  TeV [22].

In the  $\mu\nu$  channel, ATLAS and CMS set rate limits for  $M_{W'}$  in the 0.15–7 TeV range from the same analyses as mentioned above, with the strongest mass lower limit of 5.1 TeV in the Sequential SM set by ATLAS [12] using 139  $\text{fb}^{-1}$  of  $\sqrt{s} = 13$  TeV data. When combined with the  $e\nu$  channel assuming lepton universality, the upper limit on the  $\sqrt{s} = 13$  TeV cross section times branching fraction to  $\ell\nu$  varies between 0.05 and 2.1 fb for  $M_{W'}$  values in the range between 1 and 6 TeV [12]. Only weak limits on  $W' \rightarrow \mu\nu$  exist for  $M_{W'} < 150$  GeV [23]. Note that masses of the order of the electroweak scale are interesting from a theory point of view, while lepton universality does not necessarily apply to a  $W'$  boson.

Dedicated searches for  $W' \rightarrow \tau\nu$  have been performed by CMS at 8 TeV [24] and both ATLAS and CMS with 36  $\text{fb}^{-1}$  at 13 TeV [25, 26]. Limits are set on  $\sigma \cdot B$  for  $M_{W'}$  between 0.4 and 4 TeV for the former and between 0.4 and 5.6 TeV for the latter. A mass lower limit of 4.0 TeV is set in the Sequential SM and the upper limit on the cross section times branching fraction to  $\tau\nu$  at 13 TeV varies between 1.7 and 12 fb for  $M_{W'}$  values in the range between 1 and 5 TeV [26].

The  $W'$  decay into a charged lepton and a right-handed neutrino,  $\nu_R$ , may also be followed by the  $\nu_R$  decay through a virtual  $W'$  boson into a charged lepton and two quark jets. The CMS [27] and ATLAS [28] searches in the  $eejj$  and  $\mu\mu jj$  channels have set limits on the cross section times branching fraction as a function of the  $\nu_R$  mass or of  $M_{W'}$ . No requirement is placed on the charge of the lepton pair. A related  $W'$  search in the  $\tau\tau jj$  channel with hadronic  $\tau$  decays was also performed by CMS [29].

The  $t\bar{b}$  channel is particularly important because a  $W'$  boson that couples only to right-handed fermions cannot decay to leptons when the right-handed neutrinos are heavier than  $M_{W'}$ . Additional motivations are provided by a  $W'$  boson with enhanced couplings to the third generation [11], and by a leptophobic  $W'$  boson. The usual signature consists of a leptonically-decaying  $W$  boson and two  $b$ -jets. Recent studies have also incorporated

the fully hadronic decay channel for  $M_{W'} \gg m_t$  with the use of jet substructure techniques to tag highly boosted top-jets. For a detailed discussion of this channel, see Ref. [30].

Searches for dijet resonances may be used to set limits on  $W' \rightarrow q\bar{q}'$ . ATLAS [31] and CMS [32] provide similar coverage in the  $\sim 1.5 - 8.0$  TeV mass range with 139 and 137  $\text{fb}^{-1}$  of data, respectively, collected at  $\sqrt{s} = 13$  TeV. Interpretation in terms of  $W'$  decays with 139  $\text{fb}^{-1}$  of 13 TeV data yields a  $W'$  mass lower limit of 4.0 TeV in the Sequential SM [31]. For masses in the range  $\sim 0.5 - 1.5$  TeV, analyses based on jets reconstructed on-line provide the best sensitivity because they circumvent trigger bandwidth limitations [33, 34]. For  $W'$  masses below  $\sim 0.5$  TeV, the best limits are set in novel analyses exploiting boosted technologies and initial state radiation [35–38]. Cross-section limits for  $W'$  masses below  $\sim 1.5$  TeV can be derived from the dijet limits on  $Z'$  bosons summarized in Ref. [3].

In some theories [4] the  $W'$  couplings to SM fermions are suppressed by discrete symmetries.  $W'$  production then occurs in pairs, through a photon or  $Z$  boson. The decay modes are model-dependent and often involve other new particles. The ensuing collider signals arise from cascade decays and typically include missing transverse momentum.

Searches for  $WZ$  resonances at the LHC [30] have focused on the process  $pp \rightarrow W' \rightarrow WZ$  with the production mainly from  $u\bar{d} \rightarrow W'$  assuming SM-like couplings to quarks. ATLAS and CMS have set the upper limits on the  $W'WZ$  coupling for  $M_{W'}$  in the 0.2 – 5.0 TeV range with a combination of fully leptonic, semi-leptonic and fully hadronic channels with  $\sim 36 \text{fb}^{-1}$  at 13 TeV [39, 40] (see also Ref. [30]). The strongest lower limits on the  $W'$  mass are set by ATLAS [41] and CMS [42] at 13 TeV with 139  $\text{fb}^{-1}$  and 77  $\text{fb}^{-1}$ , respectively, in the  $WZ \rightarrow (jj)(jj)$  final state, where the parentheses represent a resonance. The lower limit on  $M_{W'}$  is 3.4 TeV in the context of the Heavy Vector Triplet (HVT) weakly-coupled scenario A [43]. A fermiophobic  $W'$  boson that couples to  $WZ$  may be produced at hadron colliders in association with a  $Z$  boson, or via  $WZ$  fusion. This would give rise to  $(WZ)Z$  and  $(WZ)jj$  final states [44].

$W'$  bosons have also been searched for in final states with a  $W$  boson and a SM Higgs boson in the channels  $W \rightarrow \ell\nu$  or  $W \rightarrow q\bar{q}'$  and  $h^0 \rightarrow b\bar{b}$  by ATLAS [17, 45] and CMS [18, 46] with 36  $\text{fb}^{-1}$  at  $\sqrt{s} = 13$  TeV. Cross-section limits are set for  $W'$  masses in the range between 0.5 and 5.0 TeV. The ATLAS and CMS 13 TeV analyses both set the most stringent lower limit on the mass:  $M_{W'} > 2.7$  TeV for the HVT weakly-coupled scenario A, as shown in Fig. 87.2.

### 87.3 Low-energy constraints

The properties of  $W'$  bosons are also constrained by measurements of processes at energies much below  $M_{W'}$ . The bounds on

$W - W'$  mixing [47] are mostly due to the change in  $W$  properties compared to the SM. Limits on deviations in the  $ZWW$  couplings provide a leading constraint for fermiophobic  $W'$  bosons [14].

Constraints arising from low-energy effects of  $W'$  exchange are strongly model-dependent. If the  $W'$  couplings to quarks are not suppressed, then box diagrams involving a  $W$  and a  $W'$  boson contribute to neutral meson-mixing. In the case of  $W'$  couplings to right-handed quarks as in the left-right symmetric model, the limit from  $K_L - K_S$  mixing is severe:  $M_{W'} > 2.9$  TeV for  $C_q^R = gV_{CKM}$  [48]. However, if no correlation between the  $W'$  and  $W$  couplings is assumed, then the limit on  $M_{W'}$  may be significantly relaxed [49].

$W'$  exchange also contributes at tree level to various low-energy processes. In particular, it would impact the measurement of the Fermi constant  $G_F$  in muon decay, which in turn would change the predictions of many other electroweak processes. A recent test of parity violation in polarized muon decay [50] has set limits of about 600 GeV on  $M_{W'}$ , assuming  $W'$  couplings to right-handed leptons as in left-right symmetric models and a light  $\nu_R$ . There are also  $W'$  contributions to the neutron electric dipole moment,  $\beta$  decays, and other processes [47].

If right-handed neutrinos have Majorana masses, then there are tree-level contributions to neutrinoless double-beta decay, and a limit on  $M_{W'}$  versus the  $\nu_R$  mass may be derived [51]. For  $\nu_R$  masses below a few GeV, the  $W'$  boson contributes to leptonic and semileptonic  $B$  meson decays, so that limits may be placed on various combinations of  $W'$  parameters [49]. For  $\nu_R$  masses below  $\sim 30$  MeV, the most stringent constraints on  $M_{W'}$  are due to the limits on  $\nu_R$  emission from supernovae.

### References

- [1] M. Bando, T. Kugo and K. Yamawaki, Phys. Rept. **164**, 217 (1988).
- [2] H.-C. Cheng *et al.*, Phys. Rev. **D64**, 065007 (2001), [hep-th/0104179].
- [3] See the Section on “ $Z'$ -boson searches” in this *Review*.
- [4] H.-C. Cheng and I. Low, JHEP **09**, 051 (2003), [hep-ph/0308199].
- [5] B. A. Dobrescu and Z. Liu, JHEP **10**, 118 (2015), [arXiv:1507.01923].
- [6] G. Altarelli, B. Mele and M. Ruiz-Altaba, Z. Phys. **C45**, 109 (1989), [Erratum: Z. Phys. **C47**, 676 (1990)].
- [7] R. N. Mohapatra and J. C. Pati, Phys. Rev. **D11**, 566 (1975).
- [8] K. S. Babu, X.-G. He and E. Ma, Phys. Rev. **D36**, 878 (1987).
- [9] H. Georgi, E. E. Jenkins and E. H. Simmons, Nucl. Phys. **B331**, 541 (1990).
- [10] X.-y. Li and E. Ma, J. Phys. **G19**, 1265 (1993), [hep-ph/9208210].
- [11] D. J. Muller and S. Nandi, Phys. Lett. **B383**, 345 (1996), [hep-ph/9602390].
- [12] G. Aad *et al.* (ATLAS), Phys. Rev. **D100**, 052013 (2019), [arXiv:1906.05609].
- [13] A. Donini *et al.*, Nucl. Phys. **B507**, 51 (1997), [hep-ph/9705450].
- [14] R. S. Chivukula *et al.*, Phys. Rev. **D74**, 075011 (2006), [hep-ph/0607124].
- [15] F. Pisano and V. Pleitez, Phys. Rev. **D46**, 410 (1992), [hep-ph/9206242].
- [16] Z. Sullivan, Phys. Rev. **D66**, 075011 (2002), [hep-ph/0207290].
- [17] M. Aaboud *et al.* (ATLAS), JHEP **03**, 174 (2018), [Erratum: JHEP **11**, 051 (2018)], [arXiv:1712.06518].
- [18] A. M. Sirunyan *et al.* (CMS), JHEP **11**, 172 (2018), [arXiv:1807.02826].
- [19] T. G. Rizzo, JHEP **05**, 037 (2007), [arXiv:0704.0235].
- [20] E. Accomando *et al.*, Phys. Rev. **D85**, 115017 (2012), [arXiv:1110.0713].
- [21] A. M. Sirunyan *et al.* (CMS), JHEP **06**, 128 (2018), [arXiv:1803.11133].
- [22] F. Abe *et al.* (CDF), Phys. Rev. Lett. **74**, 2900 (1995).
- [23] F. Abe *et al.* (CDF), Phys. Rev. Lett. **67**, 2609 (1991).
- [24] V. Khachatryan *et al.* (CMS), Phys. Lett. **B755**, 196 (2016), [arXiv:1508.04308].
- [25] M. Aaboud *et al.* (ATLAS), Phys. Rev. Lett. **120**, 161802 (2018), [arXiv:1801.06992].
- [26] A. M. Sirunyan *et al.* (CMS), Phys. Lett. **B792**, 107 (2019), [arXiv:1807.11421].
- [27] A. M. Sirunyan *et al.* (CMS), JHEP **05**, 148 (2018), [arXiv:1803.11116].
- [28] M. Aaboud *et al.* (ATLAS), Submitted to: Phys. Lett. (2019), [arXiv:1904.12679].
- [29] A. M. Sirunyan *et al.* (CMS), JHEP **03**, 170 (2019), [arXiv:1811.00806].
- [30] K.M. Black *et al.*, “Dynamical electroweak symmetry breaking” in this *Review*.
- [31] G. Aad *et al.* (ATLAS) (2019), [arXiv:1910.08447].
- [32] CMS Collab., CMS PAS EXO-19-012, Jul. 2019.
- [33] M. Aaboud *et al.* (ATLAS), Phys. Rev. Lett. **121**, 081801 (2018), [arXiv:1804.03496].
- [34] A. M. Sirunyan *et al.* (CMS), JHEP **08**, 130 (2018), [arXiv:1806.00843].
- [35] M. Aaboud *et al.* (ATLAS), Phys. Lett. **B788**, 316 (2019), [arXiv:1801.08769].
- [36] M. Aaboud *et al.* (ATLAS), Phys. Lett. **B795**, 56 (2019), [arXiv:1901.10917].
- [37] A. M. Sirunyan *et al.* (CMS) (2019), [arXiv:1909.04114].
- [38] A. M. Sirunyan *et al.* (CMS) (2019), [arXiv:1905.10331].
- [39] M. Aaboud *et al.* (ATLAS), Phys. Rev. **D98**, 052008 (2018), [arXiv:1808.02380].
- [40] A. M. Sirunyan *et al.* (CMS), Phys. Lett. **B798**, 134952 (2019), [arXiv:1906.00057].
- [41] G. Aad *et al.* (ATLAS), JHEP **09**, 091 (2019), [arXiv:1906.08589].
- [42] A. M. Sirunyan *et al.* (CMS) (2019), [arXiv:1906.05977].
- [43] D. Pappadopulo *et al.*, JHEP **09**, 060 (2014), [arXiv:1402.4431].
- [44] H.-J. He *et al.*, Phys. Rev. **D78**, 031701 (2008), [arXiv:0708.2588].
- [45] M. Aaboud *et al.* (ATLAS), Phys. Lett. **B774**, 494 (2017), [arXiv:1707.06958].
- [46] A. M. Sirunyan *et al.* (CMS), Eur. Phys. J. **C77**, 636 (2017), [arXiv:1707.01303].
- [47] See the particle listings for  $W'$  in this *Review*.
- [48] Y. Zhang *et al.*, Phys. Rev. **D76**, 091301 (2007), [arXiv:0704.1662].
- [49] P. Langacker and S. U. Sankar, Phys. Rev. **D40**, 1569 (1989).
- [50] J. F. Bueno *et al.* (TWIST), Phys. Rev. **D84**, 032005 (2011), [arXiv:1104.3632].
- [51] See Fig. 5 of G. Prezeau, M. Ramsey-Musolf, and P. Vogel, Phys. Rev. D **68**, 034016 (2003).

## 88. $Z'$ -Boson Searches

Revised October, 2019 by B.A. Dobrescu (Fermilab) and S. Willocq (U. Massachusetts).

The  $Z'$  boson is a massive, electrically-neutral and color-singlet hypothetical particle of spin 1. This particle is predicted in many extensions of the Standard Model (SM) and has been the object of extensive phenomenological studies [1].

### 88.1 $Z'$ boson couplings

The couplings of a  $Z'$  boson to the first-generation fermions are given by

$$Z'_\mu \left( g_u^L \bar{u}_L \gamma^\mu u_L + g_d^L \bar{d}_L \gamma^\mu d_L + g_u^R \bar{u}_R \gamma^\mu u_R + g_d^R \bar{d}_R \gamma^\mu d_R + g_\nu^L \bar{\nu}_L \gamma^\mu \nu_L + g_e^L \bar{e}_L \gamma^\mu e_L + g_e^R \bar{e}_R \gamma^\mu e_R \right), \quad (88.1)$$

where  $u, d, \nu, e$  are the quark and lepton fields in the mass eigenstate basis, and the coefficients  $g_u^L, g_d^L, g_u^R, g_d^R, g_\nu^L, g_e^L, g_e^R$  are real dimensionless parameters. If the  $Z'$  couplings to quarks and leptons are generation-independent, then these seven parameters describe the couplings of the  $Z'$  boson to all SM fermions. More generally, however, the  $Z'$  couplings to fermions are generation-dependent, in which case Eq. (88.1) may be written with generation indices  $i, j = 1, 2, 3$  labeling the quark and lepton fields, and with the seven coefficients promoted to  $3 \times 3$  Hermitian matrices (e.g.,  $g_{ij}^L, \bar{e}_L^i \gamma^\mu e_L^j$ , where  $e_L^i$  is the left-handed muon, etc.).

The parameters describing the  $Z'$  boson interactions with quarks and leptons are subject to some theoretical constraints. Quantum field theories that include a heavy spin-1 particle are well behaved at high energies only if that particle is a gauge boson associated with a spontaneously broken gauge symmetry. Quantum effects preserve the gauge symmetry only if the couplings of the gauge boson to fermions satisfy the anomaly equations [2]. Furthermore, the fermion charges under the new gauge symmetry are constrained by the requirement that the quarks and leptons get masses from gauge-invariant interactions with the Higgs fields.

The relation between the couplings displayed in Eq. (88.1) and the gauge charges  $z_{fi}^L$  and  $z_{fi}^R$  of the fermions  $f = u, d, \nu, e$  involves the unitary  $3 \times 3$  matrices  $V_f^L$  and  $V_f^R$  that transform the gauge eigenstate fermions  $f_L^i$  and  $f_R^i$ , respectively, into the mass eigenstates. The  $Z'$  couplings also depend on the mixings of the new gauge boson in the gauge eigenstate basis ( $\tilde{Z}'_\mu$ ). The main ones are a kinetic mixing  $(-\chi/2)B^{\mu\nu}\tilde{Z}'_{\mu\nu}$  with the hypercharge gauge boson  $B^\mu$  ( $\chi$  is a dimensionless parameter), and a mass mixing  $\delta M^2 \tilde{Z}'^\mu \tilde{Z}'_\mu$  with the linear combination ( $\tilde{Z}_\mu$ ) of neutral bosons that couples as the SM  $Z$  boson [3]. Since both the kinetic and mass mixings shift the mass and couplings of the  $Z$  boson, electroweak measurements impose upper limits on  $\chi$  and  $\delta M^2/(M_{Z'}^2 - M_Z^2)$  of the order of  $10^{-3}$  [4]. Keeping only linear terms in these two small quantities, the couplings of the mass-eigenstate  $Z'$  boson are given by

$$g_{fij}^L = g_z V_{fii'}^L z_{f'i'}^L (V_f^L)_{i'j}^\dagger + \frac{e}{c_W} \left( \frac{s_W \chi M_{Z'}^2 + \delta M^2}{2s_W (M_{Z'}^2 - M_Z^2)} \sigma_f^3 - \epsilon Q_f \right), \quad (88.2)$$

$$g_{fij}^R = g_z V_{fii'}^R z_{f'i'}^R (V_f^R)_{i'j}^\dagger - \frac{e}{c_W} \epsilon Q_f, \quad (88.3)$$

where  $g_z$  is the new gauge coupling,  $Q_f$  is the electric charge of  $f$ ,  $e$  is the electromagnetic gauge coupling,  $s_W$  and  $c_W$  are the sine and cosine of the weak mixing angle,  $\sigma_f^3 = +1$  for  $f = u, \nu$  and  $\sigma_f^3 = -1$  for  $f = d, e$ , and

$$\epsilon = \frac{\chi (M_{Z'}^2 - c_W^2 M_Z^2) + s_W \delta M^2}{M_{Z'}^2 - M_Z^2}. \quad (88.4)$$

The interaction of the  $Z'$  boson with a pair of  $W$  bosons has

the form

$$\begin{aligned} & [i (W_\mu^- Z'_\nu - W_\nu^- Z'_\mu) \partial^\mu W^{+\nu} + \text{H.c.}] \\ & + i (W_\mu^+ W_\nu^- - W_\nu^+ W_\mu^-) \partial^\mu Z'^\nu \end{aligned} \quad (88.5)$$

with a coefficient of order  $M_W^2/M_{Z'}^2$ , [5]. The  $Z'$  also couples to one SM Higgs boson and one  $Z$  boson,  $Z'_\mu Z^\mu h^0$ , with a coefficient of order  $M_Z$ .

### 88.2 $Z'$ models

A simple origin of a  $Z'$  boson is a new  $U(1)'$  gauge symmetry. In that case, the matrixial equalities  $z_u^L = z_d^L$  and  $z_\nu^L = z_e^L$  are required by the SM  $SU(2)_W$  gauge symmetry. Given that the  $U(1)'$  interaction is not asymptotically free, the theory may be well-behaved at high energies (e.g., by embedding  $U(1)'$  in a non-Abelian gauge group) only if the charges are commensurate numbers, i.e. any ratio of charges is a rational number. Satisfying the anomaly equations with rational numbers is highly nontrivial, and typically new fermions charged under  $U(1)'$  are necessary.

If the couplings are generation-independent ( $V_f^{L,R}$  are then unit matrices in Eq. (88.2)) and the mixings of  $\tilde{Z}'$  are negligible, then there are five commensurate couplings:  $g_u^R, g_d^R, g_e^R, g_q^L$  ( $q = u$  or  $d$ ),  $g_l^L$  ( $l = \nu$  or  $e$ ). Four sets of charges are displayed in Table 88.1, each of them spanned by a free parameter  $x$  [6]. The first set, labelled  $B - xL$ , has charges proportional to the baryon number minus  $x$  times the lepton number. These charges allow all SM Yukawa couplings to a Higgs doublet which is neutral under  $U(1)_{B-xL}$ , so that there is no tree-level  $\tilde{Z} - \tilde{Z}'$  mixing. For  $x = 1$  one recovers the  $U(1)_{B-L}$  group, which is non-anomalous in the presence of one “right-handed neutrino” (a chiral fermion that is a singlet under the SM gauge group) per generation. For  $x \neq 1$ , it is necessary to include some fermions that are vectorlike (i.e. their mass terms are gauge invariant) with respect to the electroweak gauge group and chiral with respect to  $U(1)_{B-xL}$ . In the particular cases  $x = 0$  or  $x \gg 1$ , the  $Z'$  is leptophobic or quark-phobic, respectively.

The second set,  $U(1)_{10+x5}$ , has charges that commute with the representations of the  $SU(5)$  grand unified group. Here  $x$  is related to the mixing angle between the two  $U(1)$  bosons encountered in the  $E_6 \rightarrow SU(5) \times U(1) \times U(1)$  symmetry breaking patterns of grand unified theories [1, 9]. With these charges, two Higgs doublets are typically required to generate masses for both up- and down- type fermions. This set leads to  $\tilde{Z} - \tilde{Z}'$  mass mixing at tree level, such that for a  $Z'$  mass close to the electroweak scale, the measurements at the  $Z$ -pole require some fine tuning between the charges and VEVs of the two Higgs doublets. Vectorlike fermions charged under the electroweak gauge group and also carrying color are required (except for  $x = -3$ ) to make this set anomaly free. The particular cases  $x = -3, 1, -1/2$  are usually labelled  $U(1)_\chi, U(1)_\psi$ , and  $U(1)_\eta$ , respectively. Under the third set,  $U(1)_{d-xu}$ , the weak-doublet quarks are neutral, and the ratio of  $u_R$  and  $d_R$  charges is  $-x$ . For  $x = 1$ , this is the “right-handed” group  $U(1)_R$ . For  $x = 0$ , the charges are those of the  $E_6$ -inspired  $U(1)_I$  group, which requires new quarks and leptons. Other generation-independent sets of  $U(1)'$  charges are given in [10].

In the absence of new fermions charged under the SM group, the most general generation-independent charge assignment is  $U(1)_{q+Xu}$ , which is a linear combination of hypercharge and  $B-L$ . Many other anomaly-free solutions exist if generation-dependent charges are allowed. An example is  $B - xL_e - yL_\mu + (y-3)L_\tau$ , with  $x, y$  free parameters. This allows all fermion masses to be generated by Yukawa couplings to a single Higgs doublet, without inducing tree-level flavor-changing neutral current (FCNC) processes. There are also lepton-flavor dependent charges that allow neutrino masses to arise only from operators of high dimensionality [11].

If the  $SU(2)_W$ -doublet quarks have generation-dependent  $U(1)'$  charges, then the mass eigenstate quarks have flavor off-diagonal couplings to the  $Z'$  boson (see Eq. (88.1), and note that  $V_u^L (V_d^L)^\dagger$

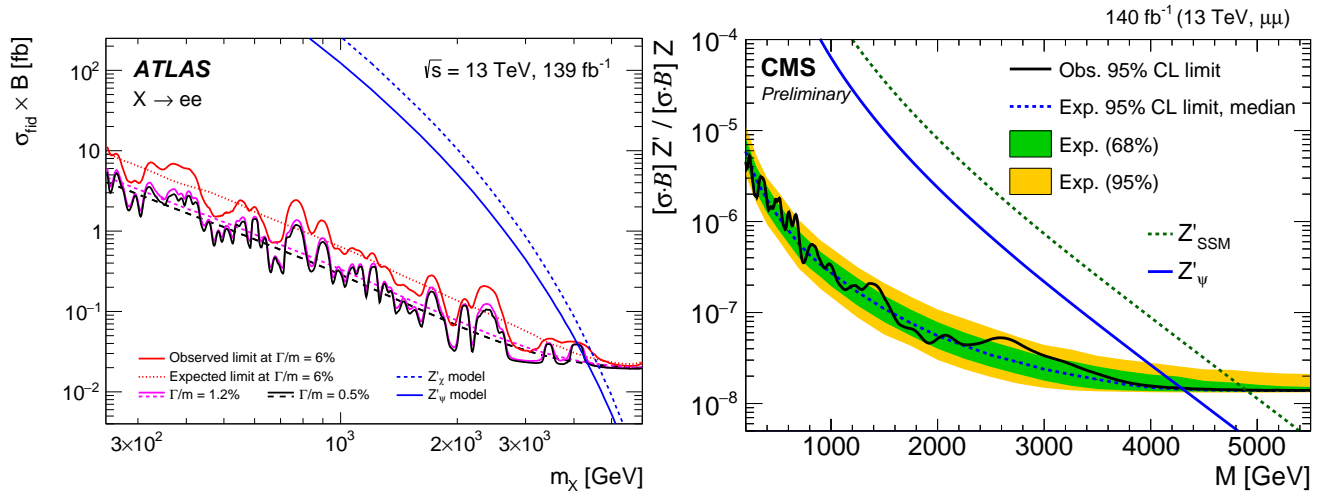


Figure 88.1: Upper limits on the cross section for  $Z'$  production times the branching fraction for  $Z' \rightarrow e^+e^-$  (left panel, set by ATLAS [7]) or  $Z' \rightarrow \mu^+\mu^-$  (right panel, set by CMS [8]) as a function of  $M_{Z'}$ . The lines labelled by  $Z'_\psi$  and  $Z'_\chi$  are theoretical predictions for the  $U(1)_{10+x5}$  models in Table 88.1 with  $x = -3$  and  $x = +1$ , respectively, for  $g_z$  fixed by an  $E_6$  unification condition. The  $Z'_{\text{SSM}}$  line corresponds to  $Z'$  couplings equal to those of the  $Z$  boson.

**Table 88.1:** Examples of generation-independent  $U(1)'$  charges for quarks and leptons. The parameter  $x$  is an arbitrary rational number. Gauge anomaly cancellation requires certain new fermions [6].

fermion	$U(1)_{B-xL}$	$U(1)_{10+x5}$	$U(1)_{d-xu}$	$U(1)_{q+xu}$
$(u_L, d_L)$	1/3	1/3	0	1/3
$u_R$	1/3	-1/3	-x/3	x/3
$d_R$	1/3	-x/3	1/3	(2-x)/3
$(\nu_L, e_L)$	-x	x/3	(-1+x)/3	-1
$e_R$	-x	-1/3	x/3	-(2+x)/3

is the CKM matrix). These are severely constrained by measurements of FCNC processes, which in this case are mediated at tree-level by  $Z'$  boson exchange [12]. The constraints are relaxed if the first and second generation charges are the same, although they are increasingly tightened by the measurements of  $B$  meson properties [13]. If only the  $SU(2)_W$ -singlet quarks have generation-dependent  $U(1)'$  charges, there is more freedom in adjusting the flavor off-diagonal couplings because the  $V_{u,d}^R$  matrices are not observable in the SM.

The anomaly equations for  $U(1)'$  could be circumvented only if there is an axion with certain dimension-5 couplings to the gauge bosons. However, such a scenario violates unitarity unless the quantum field theory description breaks down at a scale near  $M_{Z'}$  [14].

$Z'$  bosons may also arise from larger gauge groups. These may extend the electroweak group, as in  $SU(2) \times SU(2) \times U(1)$ , or may embed the electroweak group, as in  $SU(3)_W \times U(1)$  [15]. If the larger group is spontaneously broken down to  $SU(2)_W \times U(1)_Y \times U(1)'$  at a scale  $v_* \gg M_{Z'}/g_z$ , then the above discussion applies up to corrections of order  $M_{Z'}^2/(g_z v_*)^2$ . For  $v_* \sim M_{Z'}/g_z$ , additional gauge bosons have masses comparable to  $M_{Z'}$ , including at least a  $W'$  boson [15]. If the larger gauge group breaks together with the electroweak symmetry directly to the electromagnetic  $U(1)_{\text{em}}$ , then the left-handed fermion charges are no longer correlated ( $z_u^L \neq z_d^L$ ,  $z_\nu^L \neq z_e^L$ ) and a  $Z'W^+W^-$  coupling is induced.

If the electroweak gauge bosons propagate in extra dimensions, then their Kaluza-Klein (KK) excitations include a series of  $Z'$  boson pairs. Each of these pairs can be associated with a different  $SU(2) \times U(1)$  gauge group in four dimensions. The properties of the KK particles depend strongly on the extra-dimensional theory [16]. For example, in universal extra dimensions there is a parity

that forces all couplings of Eq. (88.1) to vanish in the case of the lightest KK bosons, while allowing couplings to pairs of fermions involving a SM and a heavy vectorlike fermion. There are also 4-dimensional gauge theories (e.g. little Higgs with  $T$  parity) with  $Z'$  bosons exhibiting similar properties. By contrast, in a warped extra dimension, the couplings of Eq. (88.1) may be sizable even when SM fields propagate along the extra dimension.

$Z'$  bosons may also be composite particles. For example, in confining gauge theories [17], the  $\rho$ -like bound state is a spin-1 boson that may be interpreted as arising from a spontaneously broken gauge symmetry [18].

### 88.3 Non-resonant $Z'$ signatures at colliders

In the presence of the couplings shown in Eq. (88.1), the  $Z'$  boson may be produced in the  $s$ -channel at colliders, and would decay to pairs of fermions. The decay width into a pair of electrons is given by

$$\Gamma(Z' \rightarrow e^+e^-) \simeq \left[ (g_e^L)^2 + (g_e^R)^2 \right] \frac{M_{Z'}}{24\pi}, \quad (88.6)$$

where small corrections from electroweak loops are not included. The decay width into  $q\bar{q}$  is similar, except for an additional color factor of 3, QCD radiative corrections, and fermion mass corrections. Thus, one may compute the  $Z'$  branching fractions in terms of the couplings of Eq. (88.1). However, other decay channels, such as  $WW$  or a pair of new particles, could have large widths and need to be added to the total decay width.

As mentioned above, there are theories in which the  $Z'$  couplings are controlled by a discrete symmetry that forbids decays into a pair of SM particles. Typically, such theories involve several new particles, which may be produced only in pairs and undergo cascade decays through  $Z'$  bosons, leading to signals involving missing (transverse) momentum. Given that the cascade decays depend on the properties of new particles other than the  $Z'$  boson, this case is not discussed further here.

The  $Z'$  contribution to the cross sections for  $e^+e^- \rightarrow f\bar{f}$  proceeds through an  $s$ -channel  $Z'$  exchange (when  $f = e$ , there are also  $t$ - and  $u$ -channel exchanges). For  $M_{Z'} < \sqrt{s}$ , the  $Z'$  appears as an  $f\bar{f}$  resonance in the radiative return process where photon emission tunes the effective center-of-mass energy to  $M_{Z'}$ . The agreement between the LEP-II measurements and the SM predictions implies that either the  $Z'$  couplings are smaller than or of order  $10^{-2}$ , or else  $M_{Z'}$  is above 209 GeV, the maximum energy of LEP-II. In the latter case, the  $Z'$  exchange may be approximated

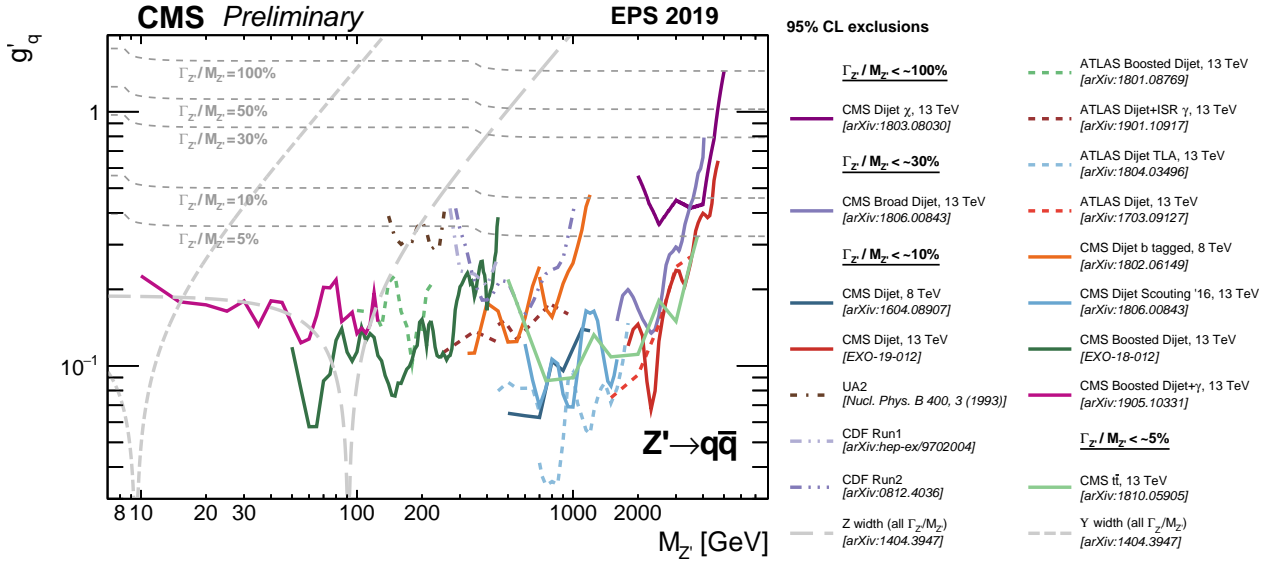


Figure 88.2: Upper limits on the  $Z'$  coupling to quarks as a function of  $M_{Z'}$  based on various searches performed by the ATLAS, CMS, CDF, and UA2 experiments [19].

up to corrections of order  $s/M_{Z'}^2$ , by the contact interactions

$$\frac{g_z^2}{M_{Z'}^2 - s} \left[ \bar{e} \gamma^\mu (z_e^L P_L + z_e^R P_R) e \right] \left[ \bar{f} \gamma^\mu (z_f^L P_L + z_f^R P_R) f \right], \quad (88.7)$$

where  $P_{L,R}$  are chirality projection operators, and the relation between  $Z'$  couplings and charges (see Eq. (88.2) in the limit where the mass and kinetic mixings are neglected) is used, assuming generation-independent charges. The four LEP collaborations have set limits on the coefficients of such operators for all possible chiral structures and for various combinations of fermions [20]. Thus, one may derive bounds on  $(M_{Z'}/g_z) |z_e^L z_f^L|^{-1/2}$  and the analogous combinations of  $LR$ ,  $RL$  and  $RR$  charges, which are typically on the order of a few TeV. LEP-II limits were derived [6] on the four sets of charges shown in Table 88.1.

Somewhat stronger bounds can be set on  $M_{Z'}/g_z$  for specific sets of  $Z'$  couplings if the effects of several operators (88.7) are combined. Dedicated analyses by the LEP collaborations have set limits on  $Z'$  bosons for particular values of the gauge coupling (see section 3.5 of Ref. [20]). For example,  $M_{Z_{SSM}} > 1.76$  TeV for a “sequential”  $Z'$  of same couplings as the SM  $Z$  boson, while  $M_{Z_\chi} > 0.785$  TeV for the  $Z'$  associated with  $U(1)_\chi$  assuming a unification condition for the gauge coupling.

#### 88.4 Searches at hadron colliders

$Z'$  bosons with couplings to quarks (see Eq. (88.1)) may be produced at hadron colliders in the  $s$ -channel and would show up as resonances in the invariant mass distribution of the decay products. The cross section for producing a  $Z'$  boson at the LHC, which then decays to some  $f\bar{f}$  final state, takes the form [21]

$$\sigma(pp \rightarrow Z' X \rightarrow f\bar{f} X) \simeq \frac{\pi}{6s} \sum_q c_q^f w_q(s, M_{Z'}^2) \quad (88.8)$$

for flavor-diagonal couplings to quarks. Here, we have neglected the interference with the SM contribution to  $f\bar{f}$  production, which is a good approximation for a narrow  $Z'$  resonance (deviations from the narrow width approximation are discussed in Ref. [22]). The coefficients

$$c_q^f = \left[ (g_q^L)^2 + (g_q^R)^2 \right] B(Z' \rightarrow f\bar{f}) \quad (88.9)$$

contain all the dependence on the  $Z'$  couplings, while the functions  $w_q$  include all the information about parton distributions and QCD corrections [6, 10]. This factorization holds exactly to

NLO and the deviations from it induced at NNLO are very small. Note that the  $w_u$  and  $w_d$  functions are substantially larger than the  $w_q$  functions for the other quarks. Eq. (88.8) also applies to the Tevatron, except for changing the  $pp$  initial state to  $p\bar{p}$ , which implies that the  $w_q(s, M_{Z'}^2)$  functions are replaced by some other functions  $\bar{w}_q((1.96 \text{ TeV})^2, M_{Z'}^2)$ .

It is common to present results of  $Z'$  searches as limits on the cross section versus  $M_{Z'}$  (see for example Fig. 88.1).

An alternative is to plot exclusion curves for fixed  $M_{Z'}$  values in the  $c_u^f - c_d^f$  planes, allowing a simple derivation of the mass limit within any  $Z'$  model. CMS upper limits in the  $c_\ell^u - c_\ell^d$  plane ( $\ell = e$  or  $\mu$ ) for different  $M_{Z'}$  are shown in Ref. [23] (for Tevatron limits, see Refs. [10, 24]).

The discovery of a dilepton resonance at the LHC would determine the  $Z'$  mass and width. A measurement of the total cross section would define a band in the  $c_\ell^u - c_\ell^d$  plane. Angular distributions can be used to measure several combinations of  $Z'$  parameters (angular distributions were used in Ref. [25] to improve the Tevatron sensitivity). Even though the original quark direction in a  $pp$  collider is unknown, the leptonic forward-backward asymmetry  $A_{FB}^\ell$  can be extracted from the kinematics of the dilepton system, and is sensitive to parity-violating couplings. A fit to the  $Z'$  rapidity distribution can distinguish between the couplings to up and down quarks. These measurements, combined with off-peak observables, have the potential to differentiate among various  $Z'$  models [26]. In some cases,  $A_{FB}^\ell$  may provide discovery sensitivity that is competitive with the mass distribution [27]. The spin of the  $Z'$  boson may be determined from angular distributions [28].

Searches for  $Z'$  decays into  $e^+e^-$  and  $\mu^+\mu^-$  by the ATLAS and CMS collaborations [7, 8] have set 95% C.L. upper cross-section limits as low as 0.02 fb (see Fig. 88.1), with the mass lower limits in specific models as high as 4.9 TeV in a single channel. Cross section limits in the dimuon channel for low mass regions, below 200 GeV but not near the  $Z$  mass, have been set at the LHC by CMS [29] and LHCb [30] (and also in  $e^+e^-$  collisions by BaBar [31], assuming a dark photon, *i.e.*, a  $Z'$  boson whose couplings arise only from the kinetic mixing with the hypercharge gauge boson).

In the case of final states with tau-leptons, the mass lower limits obtained at 13 TeV are as high as  $\sim 2.4$  TeV for the  $\tau^+\tau^-$  [32] decay in the case of a sequential  $Z'$ . Limits in the flavor-violating leptonic final states have also been reported by ATLAS [33] and CMS [34] at 13 TeV, for resonances in the  $e^\pm\mu^\mp$ ,  $e^\pm\tau^\mp$  and  $\mu^\pm\tau^\mp$  channels.

Final states with higher background,  $t\bar{t}$ ,  $b\bar{b}$  and  $jj$ , are also important as they probe various combinations of  $Z'$  couplings to



quarks, see Ref. [35] for further discussion. Besides the improved sensitivity at masses of several TeV, the LHC searches in the dijet channel have been also extended to masses as low as 10 GeV, through the use of new techniques involving boosted topologies and initial state radiation [36]. Limits from such  $Z'$  searches in hadronic final states are summarized in Fig. 88.2.

$Z'$  decays to  $Zh^0$  with  $Z \rightarrow \ell^+\ell^-$ ,  $\nu\bar{\nu}$  or  $q\bar{q}$  and  $h^0 \rightarrow b\bar{b}$  have been studied by ATLAS [37, 38] and CMS [39, 40] using 13 TeV data. The most stringent constraint is set in the fully hadronic channel, with a mass lower limit of 2.65 TeV in the context of the Heavy Vector Triplet (HVT) model weakly-coupled scenario A [41].

Searches for a  $Z'$  boson lighter than the SM  $Z$  and which couples to leptons have been performed in the 4-lepton final state. CMS [42] focused on the  $Z$  decays into a muon pair followed by the radiation of a  $Z'$  boson which decays itself into a muon pair. ATLAS [43] considered the  $h^0 \rightarrow ZZ'$  and  $h^0 \rightarrow Z'Z'$  processes followed by the leptonic decays of both  $Z$  and  $Z'$ .

The  $pp \rightarrow Z'X \rightarrow W^+W^-X$  process has also been searched for at the LHC. The channel where the  $Z'$  boson is produced through its couplings to quarks, and the  $W$  bosons decay hadronically, has been explored using boosted techniques to analyze the 13 TeV data [44, 45] with a mass lower limit of 2.9 TeV in the HVT model A. The  $Z'$  boson may also be produced through its couplings to  $W$  bosons [46], which has been explored by ATLAS with the use of forward jets consistent with a vector boson fusion event topology.

At the Tevatron, the CDF and DØ collaborations have searched for  $Z'$  bosons in the  $e^+e^-$  [47],  $\mu^+\mu^-$  [48],  $e^\pm\mu^\mp$  [49],  $\tau^+\tau^-$  [50],  $t\bar{t}$  [51],  $jj$  [52] and  $W^+W^-$  [53] final states. These limits have been mostly superseded by the LHC results.

### 88.5 Low-energy constraints

$Z'$  boson properties are also constrained by a variety of low-energy experiments [54]. Polarized electron-nucleon scattering and atomic parity violation are sensitive to electron-quark contact interactions, which get contributions from  $Z'$  exchange that can be expressed in terms of the couplings introduced in Eq. (88.1) and  $M'_{Z'}$ . Further corrections to the electron-quark contact interactions are induced in the presence of  $\tilde{Z}-\tilde{Z}'$  mixing because of the shifts in the  $Z$  couplings to quarks and leptons [3]. Deep-inelastic neutrino-nucleon scattering is similarly affected by  $Z'$  bosons. Other low-energy observables are discussed in [4]. Viable models with  $Z'$  bosons much lighter than the  $Z$  boson have been constructed, despite many additional experimental constraints [55].

In some models, the lower limits on  $M_{Z'}$  set by low-energy data are above 1 TeV. For example,  $M_{Z'_\chi} > 1.1$  TeV and  $M_{Z'_\eta} > 0.43$  TeV assuming that the Higgs sectors consist of electroweak doublets and singlets only [4], while the gauge coupling is fixed by an  $SO(10)$  unification condition for  $U(1)_\chi$  and  $U(1)_\eta$ . For more general models, see [1, 6, 56]. The mass bounds from direct searches at the LHC [7, 8] exceed the electroweak constraints by a factor of three or more for the models mentioned here. This conclusion could change if the collider bounds are weakened by exotic decay channels [57].

Although the LHC data are most constraining for many  $Z'$  models, one should be careful in assessing the relative reach of various experiments given the freedom in  $Z'$  couplings. For example, a  $Z'$  coupled to  $B-yL_\mu+(y-3)L_\tau$  has implications for the muon  $g-2$ , neutrino oscillations or  $\tau$  decays, and would be hard to see in processes involving first-generation fermions. Moreover, the combination of LHC searches and low-energy measurements could allow a precise determination of the  $Z'$  parameters [58].

#### References

[1] A. Leike, Phys. Rept. **317**, 143 (1999), [hep-ph/9805494].  
 [2] T. P. Cheng and L. F. Li, *Gauge Theory of Elementary Particle Physics* (1984), ISBN 9780198519614.  
 [3] K. S. Babu, C. F. Kolda and J. March-Russell, Phys. Rev. **D57**, 6788 (1998), [hep-ph/9710441].  
 [4] J. Erler *et al.*, JHEP **08**, 017 (2009), [arXiv:0906.2435].  
 [5] B. A. Dobrescu and P. J. Fox, JHEP **05**, 047 (2016), [arXiv:1511.02148].

[6] M. Carena *et al.*, Phys. Rev. **D70**, 093009 (2004), [hep-ph/0408098].  
 [7] G. Aad *et al.* (ATLAS), Phys. Lett. **B796**, 68 (2019), [arXiv:1903.06248].  
 [8] CMS Collab., PAS EXO-19-019, Aug. 2019.  
 [9] F. Del Aguila, M. Cvetič and P. Langacker, Phys. Rev. **D52**, 37 (1995), [hep-ph/9501390].  
 [10] E. Accomando *et al.*, Phys. Rev. **D83**, 075012 (2011), [arXiv:1010.6058].  
 [11] M.-C. Chen, A. de Gouvea and B. A. Dobrescu, Phys. Rev. **D75**, 055009 (2007), [hep-ph/0612017].  
 [12] P. Langacker and M. Plumacher, Phys. Rev. **D62**, 013006 (2000), [hep-ph/0001204].  
 [13] A. J. Buras, F. De Fazio and J. Girrbach, JHEP **02**, 116 (2013), [arXiv:1211.1896].  
 [14] L. E. Ibanez and G. G. Ross, Phys. Lett. **B332**, 100 (1994), [hep-ph/9403338].  
 [15] See the Section on “ $W'$  searches” in this *Review*.  
 [16] J. Parsons and A. Pomarol, “Extra dimensions” in this *Review*.  
 [17] K.M. Black *et al.*, “Dynamical electroweak symmetry breaking” in this *Review*.  
 [18] M. Bando, T. Kugo and K. Yamawaki, Phys. Rept. **164**, 217 (1988).  
 [19] CMS Collab., <https://twiki.cern.ch/twiki/bin/view/CMSPublic/SummaryPlotsEXO13TeV>.  
 [20] S. Schael *et al.* (ALEPH, DELPHI, L3, OPAL, LEP Electroweak), Phys. Rept. **532**, 119 (2013), [arXiv:1302.3415].  
 [21] G. Paz and J. Roy, Phys. Rev. **D97**, 075025 (2018), [arXiv:1711.02655].  
 [22] E. Accomando *et al.*, JHEP **10**, 153 (2013), [arXiv:1304.6700].  
 [23] V. Khachatryan *et al.* (CMS), JHEP **04**, 025 (2015), [arXiv:1412.6302].  
 [24] A. Abulencia *et al.* (CDF), Phys. Rev. Lett. **95**, 252001 (2005), [hep-ex/0507104].  
 [25] A. Abulencia *et al.* (CDF), Phys. Rev. Lett. **96**, 211801 (2006), [hep-ex/0602045].  
 [26] F. Petriello and S. Quackenbush, Phys. Rev. **D77**, 115004 (2008), [arXiv:0801.4389].  
 [27] E. Accomando *et al.*, JHEP **01**, 127 (2016), [arXiv:1503.02672].  
 [28] P. Osland *et al.*, Phys. Rev. **D79**, 115021 (2009), [arXiv:0904.4857].  
 [29] CMS Collab., PAS EXO-19-018, Aug. 2019.  
 [30] R. Aaij *et al.* (LHCb), Phys. Rev. Lett. **120**, 061801 (2018), [arXiv:1710.02867].  
 [31] J. P. Lees *et al.* (BaBar), Phys. Rev. Lett. **113**, 201801 (2014), [arXiv:1406.2980].  
 [32] M. Aaboud *et al.* (ATLAS), JHEP **01**, 055 (2018), [arXiv:1709.07242].  
 [33] M. Aaboud *et al.* (ATLAS), Phys. Rev. **D98**, 092008 (2018), [arXiv:1807.06573].  
 [34] A. M. Sirunyan *et al.* (CMS), JHEP **04**, 073 (2018), [arXiv:1802.01122].  
 [35] See the Section on “Dynamical Electroweak Symmetry Breaking” in this *Review*.  
 [36] A. M. Sirunyan *et al.* (CMS) (2019), [arXiv:1905.10331].  
 [37] M. Aaboud *et al.* (ATLAS), Phys. Lett. **B774**, 494 (2017), [arXiv:1707.06958].  
 [38] M. Aaboud *et al.* (ATLAS), JHEP **03**, 174 (2018), [Erratum: JHEP **11**, 051 (2018)], [arXiv:1712.06518].  
 [39] A. M. Sirunyan *et al.* (CMS), JHEP **11**, 172 (2018), [arXiv:1807.02826].

- [40] A. M. Sirunyan *et al.* (CMS), Eur. Phys. J. **C77**, 636 (2017), [arXiv:1707.01303].
- [41] D. Pappadopulo *et al.*, JHEP **09**, 060 (2014), [arXiv:1402.4431].
- [42] A. M. Sirunyan *et al.* (CMS), Phys. Lett. **B792**, 345 (2019), [arXiv:1808.03684].
- [43] M. Aaboud *et al.* (ATLAS), JHEP **06**, 166 (2018), [arXiv:1802.03388].
- [44] G. Aad *et al.* (ATLAS), JHEP **09**, 091 (2019), [arXiv:1906.08589].
- [45] A. M. Sirunyan *et al.* (CMS) (2019), [arXiv:1906.05977].
- [46] H.-J. He *et al.*, Phys. Rev. **D78**, 031701 (2008), [arXiv:0708.2588].
- [47] V. M. Abazov *et al.* (D0), Phys. Lett. **B695**, 88 (2011), [arXiv:1008.2023].
- [48] T. Aaltonen *et al.* (CDF), Phys. Rev. Lett. **106**, 121801 (2011), [arXiv:1101.4578].
- [49] A. Abulencia *et al.* (CDF), Phys. Rev. Lett. **96**, 211802 (2006), [hep-ex/0603006].
- [50] D. Acosta *et al.* (CDF), Phys. Rev. Lett. **95**, 131801 (2005), [hep-ex/0506034].
- [51] T. Aaltonen *et al.* (CDF), Phys. Rev. **D84**, 072004 (2011), [arXiv:1107.5063].
- [52] T. Aaltonen *et al.* (CDF), Phys. Rev. **D79**, 112002 (2009), [arXiv:0812.4036].
- [53] T. Aaltonen *et al.* (CDF), Phys. Rev. Lett. **104**, 241801 (2010), [arXiv:1004.4946].
- [54] V. D. Barger *et al.*, Phys. Rev. **D57**, 391 (1998), [hep-ph/9707412].
- [55] R. Harnik, J. Kopp and P. A. N. Machado, JCAP **1207**, 026 (2012), [arXiv:1202.6073].
- [56] E. Rojas and J. Erler, JHEP **10**, 063 (2015), [arXiv:1505.03208].
- [57] J. Kang and P. Langacker, Phys. Rev. **D71**, 035014 (2005), [hep-ph/0412190].
- [58] Y. Li, F. Petriello and S. Quackenbush, Phys. Rev. **D80**, 055018 (2009), [arXiv:0906.4132].

## 89. Supersymmetry, Part I (Theory)

Revised August 2019 by B.C. Allanach (DAMTP, Cambridge U.) and H.E. Haber (UC Santa Cruz).

89.1	Introduction . . . . .	905
89.2	Structure of the MSSM . . . . .	905
89.2.1	R-parity and the lightest supersymmetric particle . . . . .	906
89.2.2	The goldstino and gravitino . . . . .	906
89.2.3	Hidden sectors and the structure of SUSY breaking . . . . .	907
89.2.4	SUSY and extra dimensions . . . . .	907
89.2.5	Split-SUSY . . . . .	907
89.3	Parameters of the MSSM . . . . .	908
89.3.1	The SUSY-conserving parameters . . . . .	908
89.3.2	The SUSY-breaking parameters . . . . .	908
89.3.3	MSSM-124 . . . . .	908
89.4	The supersymmetric-particle spectrum . . . . .	908
89.4.1	The charginos and neutralinos . . . . .	909
89.4.2	The squarks and sleptons . . . . .	909
89.5	The supersymmetric Higgs sector . . . . .	910
89.5.1	The tree-level Higgs sector . . . . .	910
89.5.2	The radiatively-corrected Higgs sector . . . . .	910
89.6	Restricting the MSSM parameter freedom . . . . .	911
89.6.1	Gaugino mass relations . . . . .	911
89.6.2	Constrained versions of the MSSM: mSUGRA, CMSSM, etc. . . . .	911
89.6.3	Gauge-mediated SUSY breaking . . . . .	912
89.6.4	The phenomenological MSSM . . . . .	913
89.6.5	Simplified models . . . . .	913
89.7	Experimental data confronts the MSSM . . . . .	913
89.7.1	Naturalness constraints and the little hierarchy . . . . .	913
89.7.2	Constraints from virtual exchange of supersymmetric particles . . . . .	914
89.8	Massive neutrinos in weak-scale SUSY . . . . .	915
89.8.1	The supersymmetric seesaw . . . . .	915
89.8.2	R-parity-violating SUSY . . . . .	915
89.9	Extensions beyond the MSSM . . . . .	916

## 89.1 Introduction

Supersymmetry (SUSY) is a generalization of the space-time symmetries of quantum field theory that transforms fermions into bosons and vice versa [1]. The existence of such a non-trivial extension of the Poincaré symmetry of ordinary quantum field theory was initially surprising, and its form is highly constrained by theoretical principles [2]. SUSY also provides a framework for the unification of particle physics and gravity [3–6] at the Planck energy scale,  $M_P \sim 10^{19}$  GeV, where the gravitational interactions become comparable in strength to the gauge interactions. Moreover, supersymmetry can stabilize the hierarchy between the energy scale that characterizes electroweak symmetry breaking,  $M_{EW} \sim 100$  GeV, and the Planck scale [7–10] against large radiative corrections. The stability of this large gauge hierarchy with respect to radiative quantum corrections is not possible to maintain in the Standard Model (SM) without an unnatural fine-tuning of the parameters of the fundamental theory at the Planck scale. In contrast, in a supersymmetric extension of the SM, it is possible to maintain the gauge hierarchy while providing a natural framework for elementary scalar fields.

If supersymmetry were an exact symmetry of nature, then particles and their superpartners, which differ in spin by half a unit, would be degenerate in mass. Since superpartners have not (yet) been observed, supersymmetry must be a broken symmetry. Nevertheless, the stability of the gauge hierarchy can still be maintained if the SUSY breaking is soft [11, 12], and the corresponding SUSY-breaking mass parameters are no larger than a few TeV. Whether this is still plausible in light of recent SUSY searches at the LHC (see Sec. 90) will be discussed in Sec. 89.7.

In particular, soft-SUSY-breaking terms of the Lagrangian involve combinations of fields with total mass dimension of three or

less, with some restrictions on the dimension-three terms as elucidated in Ref. [11]. The impact of the soft terms becomes negligible at energy scales much larger than the size of the SUSY-breaking masses. Thus, a theory of weak-scale supersymmetry, where the effective scale of supersymmetry breaking is tied to the scale of electroweak symmetry breaking, provides a natural framework for the origin and the stability of the gauge hierarchy [7–10].

At present, there is no unambiguous experimental evidence for the breakdown of the SM at or below the TeV scale. The expectations for new TeV-scale physics beyond the SM are based primarily on three theoretical arguments. First, in a theory with an elementary scalar field of mass  $m$  and interaction strength  $\lambda$  (e.g., a quartic scalar self-coupling, the square of a gauge coupling or the square of a Yukawa coupling), the stability with respect to quantum corrections requires the existence of an energy cutoff roughly of order  $(16\pi^2/\lambda)^{1/2}m$ , beyond which new physics must enter [13]. A significantly larger energy cutoff would require an unnatural fine-tuning of parameters that govern the effective low-energy theory. Applying this argument to the SM leads to an expectation of new physics at the TeV scale [10].

Second, the unification of the three SM gauge couplings at a very high energy close to the Planck scale is possible if new physics beyond the SM (which modifies the running of the gauge couplings above the electroweak scale) is present. The minimal supersymmetric extension of the SM, where superpartner masses lie below a few TeV, provides an example of successful gauge coupling unification [14].

Third, the existence of dark matter that makes up approximately one quarter of the energy density of the universe, cannot be explained within the SM of particle physics [15]. Remarkably, a stable weakly-interacting massive particle (WIMP) whose mass and interaction rate are governed by new physics associated with the TeV-scale can be consistent with the observed density of dark matter (this is the so-called WIMP miracle, which is reviewed in Ref. [16]). The lightest supersymmetric particle, if stable, is a promising (although not the unique) candidate for the dark matter [17–21]. Further aspects of dark matter can be found in Sec. 27.

## 89.2 Structure of the MSSM

The minimal supersymmetric extension of the SM (MSSM) consists of the fields of the two-Higgs-doublet extension of the SM and the corresponding superpartners [22, 23]. A particle and its superpartner together form a supermultiplet. The corresponding field content of the supermultiplets of the MSSM and their gauge quantum numbers are shown in Table 89.1. The electric charge  $Q = T_3 + \frac{1}{2}Y$  is determined in terms of the third component of the weak isospin ( $T_3$ ) and the U(1) weak hypercharge ( $Y$ ).

The gauge supermultiplets consist of the gluons and their gluino fermionic superpartners and the SU(2)×U(1) gauge bosons and their gaugino fermionic superpartners. The matter supermultiplets consist of three generations of left-handed quarks and leptons and their scalar superpartners (squarks and sleptons, collectively referred to as sfermions), and the corresponding antiparticles. The Higgs supermultiplets consist of two complex Higgs doublets, their higgsino fermionic superpartners, and the corresponding antiparticles. The enlarged Higgs sector of the MSSM constitutes the minimal structure needed to guarantee the cancellation of gauge anomalies [25] generated by the higgsino superpartners that can appear as internal lines in triangle diagrams with three external electroweak gauge bosons. Moreover, without a second Higgs doublet, one cannot generate mass for both “up”-type and “down”-type quarks (and charged leptons) in a way consistent with the underlying SUSY [26–28].

In the most elegant treatment of SUSY, spacetime is extended to superspace which consists of the spacetime coordinates and new anticommuting fermionic coordinates  $\theta$  and  $\theta^\dagger$  [29, 30]. Each supermultiplet is represented by a superfield that is a function of the superspace coordinates. The fields of a given supermultiplet (which are functions of the spacetime coordinates) are coefficients of the  $\theta$  and  $\theta^\dagger$  expansion of the corresponding superfield.

Vector superfields contain the gauge boson fields and their gaugino partners. Chiral superfields contain the spin-0 and spin-1/2



**Table 89.1:** The fields of the MSSM and their  $SU(3)\times SU(2)\times U(1)$  quantum numbers are listed. For simplicity, only one generation of quarks and leptons is exhibited. For each lepton, quark, and Higgs supermultiplet (each denoted by a hatted upper-case letter), there is a corresponding antiparticle multiplet of charge-conjugated fermions and their associated scalar partners [24].

Field Content of the MSSM						
Super-multiplets	Super-field	Bosonic fields	Fermionic partners	SU(3)	SU(2)	U(1)
gluon/gluino	$\hat{V}_8$	$g$	$\tilde{g}$	8	1	0
gauge boson/	$\hat{V}$	$W^\pm, W^0$	$\tilde{W}^\pm, \tilde{W}^0$	1	3	0
gaugino	$\hat{V}'$	$B$	$\tilde{B}$	1	1	0
slepton/	$\hat{L}$	$(\tilde{\nu}_L, \tilde{e}_L^-)$	$(\nu, e^-)_L$	1	2	-1
lepton	$\hat{E}^c$	$\tilde{e}_R^+$	$e_L^c$	1	1	2
squark/	$\hat{Q}$	$(\tilde{u}_L, \tilde{d}_L)$	$(u, d)_L$	3	2	1/3
quark	$\hat{U}^c$	$\tilde{u}_R^*$	$u_L^c$	$\bar{3}$	1	-4/3
	$\hat{D}^c$	$\tilde{d}_R^*$	$d_L^c$	$\bar{3}$	1	2/3
Higgs/	$\hat{H}_d$	$(H_d^0, H_d^-)$	$(\tilde{H}_d^0, \tilde{H}_d^-)$	1	2	-1
higgsino	$\hat{H}_u$	$(H_u^+, H_u^0)$	$(\tilde{H}_u^+, \tilde{H}_u^0)$	1	2	1

fields of the matter or Higgs supermultiplets. A general supersymmetric Lagrangian is determined by three functions of the chiral superfields [4]: the superpotential, the Kähler potential, and the gauge kinetic function (which can be appropriately generalized to accommodate higher derivative terms [31]). Minimal forms for the Kähler potential and gauge kinetic function, which generate canonical kinetic energy terms for all the fields, are required for renormalizable globally supersymmetric theories. A renormalizable superpotential, which is at most cubic in the chiral superfields, yields supersymmetric Yukawa couplings and mass terms. A combination of gauge invariance and SUSY produces couplings of gaugino fields to matter (or Higgs) fields and their corresponding superpartners. The (renormalizable) MSSM Lagrangian is then constructed by including all possible supersymmetric interaction terms (of dimension four or less) that satisfy  $SU(3)\times SU(2)\times U(1)$  gauge invariance and  $B-L$  conservation (where  $B$  = baryon number and  $L$  = lepton number). Finally, the most general soft-supersymmetry-breaking terms consistent with these symmetries are added [11, 12, 32].

Although the MSSM is the focus of much of this review, there is some motivation for considering non-minimal supersymmetric extensions of the SM. For example, extra structure is needed to generate non-zero neutrino masses as discussed in Sec. 89.8. In addition, in order to address some theoretical issues and tensions associated with the MSSM, it has been fruitful to introduce one additional singlet Higgs superfield. The resulting next-to-minimal supersymmetric extension of the Standard Model (NMSSM) [33] is considered further in Sec. 89.4–89.7 and 89.9. Finally, one is always free to add additional fields to the SM along with the corresponding superpartners. However, only certain choices for the new fields (*e.g.*, the addition of complete  $SU(5)$  multiplets) will preserve the successful gauge coupling unification of the MSSM. Some examples will be briefly mentioned in Sec. 89.9.

### 89.2.1 $R$ -parity and the lightest supersymmetric particle

The (renormalizable) SM Lagrangian possesses an accidental global  $B-L$  symmetry due to the fact that  $B$  and  $L$ -violating operators composed of SM fields must have dimension  $d = 5$  or larger [34]. Consequently,  $B$  and  $L$ -violating effects are suppressed by  $(M_{EW}/M)^{d-4}$ , where  $M$  is the characteristic mass scale of the physics that generates the corresponding higher dimensional operators. Indeed, values of  $M$  of order the grand unification scale or larger yield the observed (approximate) stability of the proton and suppression of neutrino masses. Unfortunately, these results are not guaranteed in a generic supersymmetric extension of the SM. For example, it is possible to construct gauge invariant supersymmetric dimension-four  $B$  and  $L$ -violating operators made up of fields of SM particles and their superpartners. Such operators, if present in the theory, could yield a proton decay rate many orders of magnitude larger than the current experimental bound. It is for this reason that  $B-L$  conservation is imposed on the supersymmetric Lagrangian when defining the MSSM, which

is sufficient for eliminating all  $B$  and  $L$ -violating operators of dimension  $d \leq 4$ .

As a consequence of the  $B-L$  symmetry, the MSSM possesses a multiplicative  $R$ -parity invariance, where  $R = (-1)^{3(B-L)+2S}$  for a particle of spin  $S$  [35]. This implies that all the particles of the SM have even  $R$ -parity, whereas the corresponding superpartners have odd  $R$ -parity. The conservation of  $R$ -parity in scattering and decay processes has a critical impact on supersymmetric phenomenology. For example, any initial state in a scattering experiment will involve ordinary ( $R$ -even) particles. Consequently, it follows that supersymmetric particles must be produced in pairs. In general, these particles are highly unstable and decay into lighter states. Moreover,  $R$ -parity invariance also implies that the lightest supersymmetric particle (LSP) is absolutely stable, and must eventually be produced at the end of a decay chain initiated by the decay of a heavy unstable supersymmetric particle.

In order to be consistent with cosmological constraints, a stable LSP is almost certainly electrically and color neutral [19]. Consequently, the LSP in an  $R$ -parity-conserving theory is weakly interacting with ordinary matter, *i.e.*, it behaves like a stable heavy neutrino and will escape collider detectors without being directly observed. Thus, the canonical signature for conventional  $R$ -parity-conserving supersymmetric theories is missing (transverse) momentum, due to the escape of the LSP. Moreover, as noted in Sec. 89.1 and reviewed in Refs. [20] and [21], the stability of the LSP in  $R$ -parity-conserving SUSY makes it a promising candidate for dark matter.

The possibility of relaxing the  $R$ -parity invariance of the MSSM (which would generate new  $B$  and/or  $L$ -violating interactions) will be addressed in Sec. 89.8.2.

### 89.2.2 The goldstino and gravitino

In the MSSM, SUSY breaking is accomplished by including the most general renormalizable soft-SUSY-breaking terms consistent with the  $SU(3)\times SU(2)\times U(1)$  gauge symmetry and  $R$ -parity invariance. These terms parameterize our ignorance of the fundamental mechanism of supersymmetry breaking. If supersymmetry breaking occurs spontaneously, then a massless Goldstone fermion called the goldstino ( $\tilde{G}_{1/2}$ ) must exist. The goldstino would then be the LSP, and could play an important role in supersymmetric phenomenology [36].

However, the goldstino degrees of freedom are physical only in models of spontaneously-broken global SUSY. If SUSY is a local symmetry, then the theory must incorporate gravity; the resulting theory is called supergravity [5, 37]. In models of spontaneously-broken supergravity, the goldstino is “absorbed” by the gravitino ( $\tilde{G}$ ), the spin-3/2 superpartner of the graviton, via the super-Higgs mechanism [38]. Consequently, the goldstino is removed from the physical spectrum and the gravitino acquires a mass (denoted by  $m_{3/2}$ ). If  $m_{3/2}$  is smaller than the mass of the lightest superpartner of the SM particles, then the gravitino is the LSP.

In processes with center-of-mass energy  $E \gg m_{3/2}$ , one can

employ the goldstino–gravitino equivalence theorem [39], which implies that the interactions of the helicity  $\pm\frac{1}{2}$  gravitino (whose properties approximate those of the goldstino) dominate those of the helicity  $\pm\frac{3}{2}$  gravitino. The interactions of gravitinos with other light fields can be described by a low-energy effective Lagrangian that is determined by fundamental principles [40].

### 89.2.3 Hidden sectors and the structure of SUSY breaking

It is very difficult (perhaps impossible) to construct a realistic model of spontaneously-broken weak-scale supersymmetry where the supersymmetry breaking arises solely as a consequence of the interactions of the particles of the MSSM. A more successful scheme posits a theory with at least two distinct sectors: a visible sector consisting of the particles of the MSSM [32] and a sector where SUSY breaking is generated. It is often (but not always) assumed that particles of the hidden sector are neutral with respect to the SM gauge group. The effects of the hidden sector supersymmetry breaking are then transmitted to the MSSM by some mechanism (often involving the mediation by particles that comprise an additional messenger sector). Two theoretical scenarios that exhibit this structure are gravity-mediated and gauge-mediated SUSY breaking.

Supergravity models provide a natural mechanism for transmitting the SUSY breaking of the hidden sector to the particle spectrum of the MSSM. In models of gravity-mediated supersymmetry breaking, gravity is the messenger of supersymmetry breaking [41–45]. More precisely, supersymmetry breaking is mediated by effects of gravitational strength (suppressed by inverse powers of the Planck mass). The soft-SUSY-breaking parameters with dimensions of mass arise as model-dependent multiples of the gravitino mass  $m_{3/2}$ . In this scenario,  $m_{3/2}$  is of order the electroweak-symmetry-breaking scale, while the gravitino couplings are roughly gravitational in strength [3, 46]. However, such a gravitino typically plays no direct role in supersymmetric phenomenology at colliders (except perhaps indirectly in the case where the gravitino is the LSP [47]).

Under certain theoretical assumptions on the structure of the Kähler potential (the so-called sequestered form introduced in Ref. [48]), SUSY breaking is due entirely to the super-conformal (super-Weyl) anomaly, which is common to all supergravity models [48]. In particular, gaugino masses are radiatively generated at one-loop, and squark and slepton squared-mass matrices are flavor-diagonal. In sequestered scenarios, sfermion squared-masses arise at two-loops, which implies that gluino and sfermion masses are of the same order of magnitude. This approach is called anomaly-mediated SUSY breaking (AMSB). Indeed, anomaly mediation is more generic than originally conceived, and provides a ubiquitous source of SUSY breaking [49]. However in the simplest formulation of AMSB as applied to the MSSM, the squared-masses of the sleptons are negative (known as the tachyonic slepton problem). It may be possible to cure this otherwise fatal flaw in non-minimal extensions of the MSSM [50]. Alternatively, one can assert that anomaly mediation is not the sole source of SUSY breaking in the sfermion sector. In non-sequestered scenarios, sfermion squared-masses can arise at tree-level, in which case squark masses would be parametrically larger than the loop-suppressed gaugino masses [51].

In gauge-mediated supersymmetry breaking (GMSB), gauge forces transmit the supersymmetry breaking to the MSSM. A typical structure of such models involves a hidden sector where SUSY is broken, a messenger sector consisting of particles (messengers) with nontrivial  $SU(3)\times SU(2)\times U(1)$  quantum numbers, and the visible sector consisting of the fields of the MSSM [52–55]. The direct coupling of the messengers to the hidden sector generates a supersymmetry-breaking spectrum in the messenger sector. Supersymmetry breaking is then transmitted to the MSSM via the virtual exchange of the messenger fields. In models of direct gauge mediation, there is no separate hidden sector. In particular, the sector in which the SUSY breaking originates includes fields that carry nontrivial SM quantum numbers, which allows for the direct transmission of SUSY breaking to the MSSM [56].

In models of gauge-mediated SUSY breaking, the gravitino is the LSP [17], as its mass can range from a few eV (in the case of low SUSY breaking scales) up to a few GeV (in the case of high

SUSY breaking scales). In particular, the gravitino is a potential dark matter candidate (for a review and guide to the literature, see Ref. [21]). Big bang nucleosynthesis (see Section 24) also provides some interesting constraints on the gravitino and the properties of the next-to-lightest supersymmetric particle that decays into the gravitino LSP [57]. The couplings of the helicity  $\pm\frac{1}{2}$  components of  $\tilde{G}$  to the particles of the MSSM (which approximate those of the goldstino as previously noted in Sec. 89.2.2) are significantly stronger than gravitational strength and amenable to experimental collider analyses.

The concept of a hidden sector is more general than SUSY. Hidden valley models [58] posit the existence of a hidden sector of new particles and interactions that are very weakly coupled to particles of the SM. The impact of a hidden valley on supersymmetric phenomenology at colliders can be significant if the LSP lies in the hidden sector [59].

### 89.2.4 SUSY and extra dimensions

Approaches to SUSY breaking have also been developed in the context of theories in which the number of spatial dimensions is greater than three. In particular, a number of SUSY-breaking mechanisms have been proposed that are inherently extra-dimensional [60]. The size of the extra dimensions can be significantly larger than  $M_{\text{P}}^{-1}$ ; in some cases of order  $(\text{TeV})^{-1}$  or even larger (see, e.g., Sec. 86 or Ref. [61]).

For example, in one approach the fields of the MSSM live on some brane (a lower-dimensional manifold embedded in a higher-dimensional spacetime), while the sector of the theory that breaks SUSY lives on a second spatially-separated brane. Two examples of this approach are AMSB [48] and gaugino-mediated SUSY breaking [62]. In both cases, SUSY breaking is transmitted through fields that live in the bulk (the higher-dimensional space between the two branes). This setup has some features in common with both gravity-mediated and gauge-mediated SUSY breaking (e.g., a hidden and visible sector and messengers).

Since a higher dimensional theory must be compactified to four spacetime dimensions, one can also generate a source of SUSY breaking by employing boundary conditions on the compactified space that distinguish between fermions and bosons. This is the so-called Scherk-Schwarz mechanism [63]. The phenomenology of such models can be strikingly different from that of the usual MSSM [64].

### 89.2.5 Split-SUSY

If SUSY is not connected with the origin of the electroweak scale, it may still be possible that some remnant of the superparticle spectrum survives down to the TeV-scale or below. This is the idea of split-SUSY [65, 66], in which scalar superpartners of the quarks and leptons are significantly heavier (perhaps by many orders of magnitude) than 1 TeV, whereas the fermionic superpartners of the gauge and Higgs bosons have masses on the order of 1 TeV or below. With the exception of a single light neutral scalar whose properties are practically indistinguishable from those of the SM Higgs boson, all other Higgs bosons are also assumed to be very heavy. Among the supersymmetric particles, only the fermionic superpartners may be kinematically accessible at the LHC.

In models of split SUSY, the top squark masses cannot be arbitrarily large, as these parameters enter in the radiative corrections to the mass of the observed Higgs boson [67, 68]. In the MSSM, a Higgs boson mass of 125 GeV (see Sec. 11) implies an upper bound on the top squark mass scale in the range of 10 to  $10^8$  TeV [69–71], depending on the value of the ratio of the two neutral Higgs field vacuum expectation values, although this mass range can be somewhat extended by varying other relevant MSSM parameters. In some approaches, gaugino masses are one-loop suppressed relative to the sfermion masses, corresponding to the so-called mini-split SUSY spectrum [68, 72]. The higgsino mass scale may or may not be likewise suppressed depending on the details of the model [73].

The SUSY breaking required to produce such a split-SUSY spectrum would destabilize the gauge hierarchy, and thus would not provide an explanation for the scale of electroweak symmetry breaking. Nevertheless, models of split-SUSY can account for the dark matter (which is assumed to be the LSP gaugino or higgsino)

and gauge coupling unification, thereby preserving two of the desirable features of weak-scale SUSY. Finally, as a consequence of the very large squark and slepton masses, neutral flavor changing and CP-violating effects, which can be problematic in models with TeV-scale SUSY-breaking masses, are sufficiently reduced to avoid conflict with experimental observations.

### 89.3 Parameters of the MSSM

The parameters of the MSSM are conveniently described by considering separately the supersymmetry-conserving and the supersymmetry-breaking sectors. A careful discussion of the conventions used here in defining the tree-level MSSM parameters can be found in Refs. [74, 75]. For simplicity, consider first the case of one generation of quarks, leptons, and their scalar superpartners.

#### 89.3.1 The SUSY-conserving parameters

The parameters of the supersymmetry-conserving sector consist of: (i) gauge couplings,  $g_s$ ,  $g$ , and  $g'$ , corresponding to the SM gauge group  $SU(3) \times SU(2) \times U(1)$  respectively; (ii) a supersymmetry-conserving higgsino mass parameter  $\mu$ ; and (iii) Higgs-fermion Yukawa couplings,  $\lambda_u$ ,  $\lambda_d$ , and  $\lambda_e$ , of one generation of left- and right-handed quarks and leptons, and their superpartners to the Higgs bosons and higgsinos. Because there is no right-handed neutrino/sneutrino in the MSSM as defined here, a Yukawa coupling  $\lambda_\nu$  is not included. The complex  $\mu$  parameter and Yukawa couplings enter via the most general renormalizable R-parity-conserving superpotential,

$$W = \lambda_d \hat{H}_d \hat{Q} \hat{D}^c - \lambda_u \hat{H}_u \hat{Q} \hat{U}^c + \lambda_e \hat{H}_d \hat{L} \hat{E}^c + \mu \hat{H}_u \hat{H}_d, \quad (89.1)$$

where the superfields are defined in Table 1 and the gauge group indices are suppressed.

#### 89.3.2 The SUSY-breaking parameters

The supersymmetry-breaking sector contains the following sets of parameters: (i) three complex gaugino Majorana mass parameters,  $M_3$ ,  $M_2$ , and  $M_1$ , associated with the  $SU(3)$ ,  $SU(2)$ , and  $U(1)$  subgroups of the SM; (ii) five sfermion squared-mass parameters,  $M_Q^2$ ,  $M_U^2$ ,  $M_D^2$ ,  $M_L^2$ , and  $M_E^2$ , corresponding to the five electroweak gauge multiplets, *i.e.*, superpartners of the left-handed fields  $(u, d)_L$ ,  $u_L^c$ ,  $d_L^c$ ,  $(\nu, e^-)_L$ , and  $e_L^c$ , where the superscript  $c$  indicates a charge-conjugated fermion field [24]; and (iii) three Higgs-squark-squark and Higgs-slepton-slepton trilinear interaction terms, with complex coefficients  $T_U \equiv \lambda_u A_U$ ,  $T_D \equiv \lambda_d A_D$ , and  $T_E \equiv \lambda_e A_E$  (which define the “ $A$ -parameters”). The notation  $T_U$ ,  $T_D$  and  $T_E$  is employed in Ref. [75]. It is conventional to separate out the factors of the Yukawa couplings in defining the  $A$ -parameters (originally motivated by a simple class of gravity-mediated SUSY-breaking models [3, 6]). If the  $A$ -parameters are parametrically of the same order (or smaller) relative to other SUSY-breaking mass parameters, then only the third generation  $A$ -parameters are phenomenologically relevant.

Finally, we have (iv) two real squared-mass parameters,  $m_1^2$  and  $m_2^2$  (also called  $m_{H_d}^2$  and  $m_{H_u}^2$ , respectively, in the literature), and one complex squared-mass parameter,  $m_{12}^2 \equiv \mu B$  (the latter defines the “ $B$ -parameter”), which appear in the MSSM tree-level scalar Higgs potential [28],

$$V = (m_1^2 + |\mu|^2) H_d^\dagger H_d + (m_2^2 + |\mu|^2) H_u^\dagger H_u + (m_{12}^2 H_u H_d + \text{h.c.}) + \frac{1}{8} (g^2 + g'^2) (H_d^\dagger H_d - H_u^\dagger H_u)^2 + \frac{1}{2} g^2 |H_d^\dagger H_u|^2, \quad (89.2)$$

where the  $SU(2)$ -invariant combination,  $H_u H_d \equiv H_u^+ H_d^- - H_u^0 H_d^0$ . Note that the quartic Higgs couplings are related to the gauge couplings  $g$  and  $g'$  as a consequence of SUSY. The breaking of the  $SU(2) \times U(1)$  electroweak symmetry group to  $U(1)_{EM}$  is only possible after incorporating the SUSY-breaking Higgs squared-mass parameters  $m_1^2$ ,  $m_2^2$  (which can be negative) and  $m_{12}^2$ . After minimizing the Higgs scalar potential, these three squared-mass parameters can be re-expressed in terms of the two Higgs vacuum expectation values,  $\langle H_d^0 \rangle \equiv v_d/\sqrt{2}$  and  $\langle H_u^0 \rangle \equiv v_u/\sqrt{2}$ , and the CP-odd Higgs mass  $m_A$  [cf. Eqs. (89.4) and (89.5) below]. One is always free to re-phase the Higgs doublet fields such that  $v_d$  and

$v_u$  (also called  $v_1$  and  $v_2$ , respectively, in the literature) are both real and positive.

The quantity,  $v_d^2 + v_u^2 = 4m_W^2/g^2 = (2G_F^2)^{-1/2} \simeq (246 \text{ GeV})^2$ , is fixed by the Fermi constant,  $G_F$ , whereas the ratio

$$\tan \beta = v_u/v_d \quad (89.3)$$

is a free parameter such that  $0 < \beta < \pi/2$ . By employing the tree-level conditions resulting from the minimization of the scalar potential, one can eliminate the diagonal and off-diagonal Higgs squared-masses in favor of  $m_Z^2 = \frac{1}{4}(g^2 + g'^2)(v_d^2 + v_u^2)$ , the CP-odd Higgs mass  $m_A$  and the parameter  $\tan \beta$ ,

$$\sin 2\beta = \frac{2m_{12}^2}{m_1^2 + m_2^2 + 2|\mu|^2} = \frac{2m_{12}^2}{m_A^2}, \quad (89.4)$$

$$\frac{1}{2} m_Z^2 = -|\mu|^2 + \frac{m_1^2 - m_2^2 \tan^2 \beta}{\tan^2 \beta - 1}. \quad (89.5)$$

One must also guard against the existence of charge and/or color breaking global minima due to non-zero vacuum expectation values for the squark and charged slepton fields. This possibility can be avoided if the  $A$ -parameters are not unduly large [42, 76, 77]. Additional constraints must also be respected to avoid the possibility of directions in scalar field space in which the full tree-level scalar potential can become unbounded from below [77].

Note that SUSY-breaking mass terms for the fermionic superpartners of scalar fields and non-holomorphic trilinear scalar interactions (*i.e.*, interactions that mix scalar fields and their complex conjugates) have not been included above in the soft-SUSY-breaking sector. These terms can potentially destabilize the gauge hierarchy [11] in models with a gauge-singlet superfield. The latter is not present in the MSSM; hence as noted in Ref. [12], these so-called non-standard soft-SUSY-breaking terms are benign. The phenomenological impact of non-holomorphic soft SUSY-breaking terms has been reconsidered in Refs. [78–80]. However, in the most common approaches to constructing a fundamental theory of SUSY-breaking, the coefficients of these terms (which have dimensions of mass) are significantly suppressed compared to the TeV-scale [81]. Consequently, we follow the usual approach and omit these terms from further consideration.

#### 89.3.3 MSSM-124

The total number of independent physical parameters that define the MSSM (in its most general form) is quite large, primarily due to the soft-supersymmetry-breaking sector. In particular, in the case of three generations of quarks, leptons, and their superpartners,  $M_Q^2$ ,  $M_U^2$ ,  $M_D^2$ ,  $M_L^2$ , and  $M_E^2$  are hermitian  $3 \times 3$  matrices, and  $A_U$ ,  $A_D$ , and  $A_E$  are complex  $3 \times 3$  matrices. In addition,  $M_1$ ,  $M_2$ ,  $M_3$ ,  $B$ , and  $\mu$  are in general complex parameters. Finally, as in the SM, the Higgs-fermion Yukawa couplings,  $\lambda_f$  ( $f = u, d$ , and  $e$ ), are complex  $3 \times 3$  matrices that are related to the quark and lepton mass matrices via:  $M_f = \lambda_f v_f/\sqrt{2}$ , where  $v_e \equiv v_d$  [with  $v_u$  and  $v_d$  as defined above Eq. (89.3)].

However, not all these parameters are physical. Some of the MSSM parameters can be eliminated by expressing interaction eigenstates in terms of the mass eigenstates, with an appropriate redefinition of the MSSM fields to remove unphysical degrees of freedom. The analysis of Ref. [82] shows that the MSSM possesses 124 independent real degrees of freedom. Of these, 18 correspond to SM parameters (including the QCD vacuum angle  $\theta_{QCD}$ ), one corresponds to a Higgs sector parameter (the analogue of the SM Higgs mass), and 105 are genuinely new parameters of the model. The latter include: five real parameters and three CP-violating phases in the gaugino/higgsino sector, 21 squark and slepton (sfermion) masses, 36 real mixing angles to define the sfermion mass eigenstates, and 40 CP-violating phases that can appear in sfermion interactions. The most general R-parity-conserving minimal supersymmetric extension of the SM (without additional theoretical assumptions) will be denoted henceforth as MSSM-124 [83].

### 89.4 The supersymmetric-particle spectrum

The supersymmetric particles (sparticles) differ in spin by half a unit from their SM partners. The superpartners of the gauge and

Higgs bosons are fermions, whose names are obtained by appending “ino” to the end of the corresponding SM particle name. The gluino is the color-octet Majorana fermion partner of the gluon with mass  $M_{\tilde{g}} = |M_3|$ . The superpartners of the electroweak gauge and Higgs bosons (the gauginos and higgsinos) can mix due to  $SU(2) \times U(1)$  breaking effects. As a result, the physical states of definite mass are model-dependent linear combinations of the charged or neutral gauginos and higgsinos, called charginos and neutralinos, respectively (sometimes collectively called electroweakinos). The neutralinos are Majorana fermions, which can lead to some distinctive phenomenological signatures [84,85]. The superpartners of the quarks and leptons are spin-zero bosons: the squarks, charged sleptons, and sneutrinos, respectively. A complete set of Feynman rules for the sparticles of the MSSM can be found in Ref. [86]. The MSSM Feynman rules also are implicitly contained in a number of amplitude generation and Feynman diagram software packages (see *e.g.*, Refs. [87–89]).

It should be noted that all mass formulae quoted below in this Section are tree-level results. Radiative loop corrections will modify these results and must be included in any precision study of supersymmetric phenomenology [90]. Beyond tree level, the definition of the supersymmetric parameters becomes convention-dependent. For example, one can define physical couplings or running couplings, which differ beyond the tree level. This provides a challenge to any effort that attempts to extract supersymmetric parameters from data. The SUSY Les Houches Accord (SLHA) [75,91] has been adopted, which establishes a set of conventions for specifying generic file structures for supersymmetric model specifications and input parameters, supersymmetric mass and coupling spectra, and decay tables. These provide a universal interface between spectrum calculation programs, decay packages, and high energy physics event generators.

#### 89.4.1 The charginos and neutralinos

The mixing of the charged gauginos ( $\tilde{W}^\pm$ ) and charged higgsinos ( $\tilde{H}_u^\pm$  and  $\tilde{H}_d^\pm$ ) is described (at tree-level) by a  $2 \times 2$  complex mass matrix [92,93],

$$M_C \equiv \begin{pmatrix} M_2 & \frac{1}{\sqrt{2}} g v_u \\ \frac{1}{\sqrt{2}} g v_d & \mu \end{pmatrix}. \quad (89.6)$$

To determine the physical chargino states and their masses, one must perform a singular value decomposition [94,95] of the complex matrix  $M_C$ :

$$U^* M_C V^{-1} = \text{diag}(M_{\tilde{\chi}_1^\pm}, M_{\tilde{\chi}_2^\pm}), \quad (89.7)$$

where  $U$  and  $V$  are unitary matrices, and the right-hand side of Eq. (89.7) is the diagonal matrix of (real non-negative) chargino masses. The physical chargino states are denoted by  $\tilde{\chi}_1^\pm$  and  $\tilde{\chi}_2^\pm$ . These are linear combinations of the charged gaugino and higgsino states determined by the matrix elements of  $U$  and  $V$  [92,93]. The chargino masses correspond to the singular values [94] of  $M_C$ , *i.e.*, the positive square roots of the eigenvalues of  $M_C^\dagger M_C$ :

$$M_{\tilde{\chi}_1^\pm, \tilde{\chi}_2^\pm}^2 = \frac{1}{2} \left\{ |\mu|^2 + |M_2|^2 + 2m_W^2 \mp \sqrt{(|\mu|^2 + |M_2|^2 + 2m_W^2)^2 - 4|\mu M_2 - m_W^2 \sin 2\beta|^2} \right\}, \quad (89.8)$$

where the states are ordered such that  $M_{\tilde{\chi}_1^\pm} \leq M_{\tilde{\chi}_2^\pm}$ . The relative phase of  $\mu$  and  $M_2$  is physical and potentially observable. The mixing of the neutral gauginos ( $\tilde{B}$  and  $\tilde{W}^0$ ) and neutral higgsinos ( $\tilde{H}_d^0$  and  $\tilde{H}_u^0$ ) is described (at tree-level) by a  $4 \times 4$  complex symmetric mass matrix [92,93],

$$M_N \equiv \begin{pmatrix} M_1 & 0 & -\frac{1}{2} g' v_d & \frac{1}{2} g' v_u \\ 0 & M_2 & \frac{1}{2} g' v_d & -\frac{1}{2} g' v_u \\ -\frac{1}{2} g' v_d & \frac{1}{2} g' v_d & 0 & -\mu \\ \frac{1}{2} g' v_u & -\frac{1}{2} g' v_u & -\mu & 0 \end{pmatrix}. \quad (89.9)$$

To determine the physical neutralino states and their masses, one must perform an Autonne-Takagi factorization [94,96] (also called Takagi diagonalization [95,97]) of the complex symmetric matrix  $M_N$ :

$$W^T M_N W = \text{diag}(M_{\tilde{\chi}_1^0}, M_{\tilde{\chi}_2^0}, M_{\tilde{\chi}_3^0}, M_{\tilde{\chi}_4^0}), \quad (89.10)$$

where  $W$  is a unitary matrix and the right-hand side of Eq. (89.10) is the diagonal matrix of (real non-negative) neutralino masses. The physical neutralino states are denoted by  $\tilde{\chi}_i^0$  ( $i = 1, \dots, 4$ ), where the states are ordered such that  $M_{\tilde{\chi}_1^0} \leq M_{\tilde{\chi}_2^0} \leq M_{\tilde{\chi}_3^0} \leq M_{\tilde{\chi}_4^0}$ . The  $\tilde{\chi}_i^0$  are the linear combinations of the neutral gaugino and higgsino states determined by the matrix elements of  $W$  (which is denoted by  $N^{-1}$  in Ref. [92]). The neutralino masses correspond to the singular values of  $M_N$ , *i.e.*, the positive square roots of the eigenvalues of  $M_N^\dagger M_N$ . Exact formulae for these masses can be found in Refs. [98] and [99]. A numerical algorithm for determining the mixing matrix  $W$  has been given in Ref. [100].

If a chargino or neutralino state approximates a particular gaugino or higgsino state, it is convenient to employ the corresponding nomenclature. Specifically, if  $|M_1|$  and  $|M_2|$  are small compared to  $m_Z$  and  $|\mu|$ , then the lightest neutralino  $\tilde{\chi}_1^0$  would be nearly a pure photino,  $\tilde{\gamma}$ , the superpartner of the photon. If  $|M_1|$  and  $m_Z$  are small compared to  $|M_2|$  and  $|\mu|$ , then the lightest neutralino would be nearly a pure bino,  $\tilde{B}$ , the superpartner of the weak hypercharge gauge boson. If  $|M_2|$  and  $m_Z$  are small compared to  $|M_1|$  and  $|\mu|$ , then the lightest chargino pair and neutralino would constitute a triplet of roughly mass-degenerate pure winos,  $\tilde{W}^\pm$ , and  $\tilde{W}^0$ , the superpartners of the weak  $SU(2)$  gauge bosons. Finally, if  $|\mu|$  and  $m_Z$  are small compared to  $|M_1|$  and  $|M_2|$ , then the lightest chargino pair and neutralino would be nearly pure higgsino states, the superpartners of the Higgs bosons. Each of the above cases leads to a strikingly different phenomenology.

In the NMSSM, an additional Higgs singlet superfield is added to the MSSM. This superfield comprises two real Higgs scalar degrees of freedom and an associated neutral higgsino degree of freedom. Consequently, there are five neutralino mass eigenstates that are obtained by a Takagi-diagonalization of the  $5 \times 5$  neutralino mass matrix. In many cases, the fifth neutralino state is dominated by its  $SU(2) \times U(1)$  singlet component, and thus is very weakly coupled to the SM particles and their superpartners.

#### 89.4.2 The squarks and sleptons

For a given Dirac fermion  $f$ , there are two superpartners,  $\tilde{f}_L$  and  $\tilde{f}_R$ , where the  $L$  and  $R$  subscripts simply identify the scalar partners that are related by SUSY to the left-handed and right-handed fermions,  $f_{L,R} \equiv \frac{1}{2}(1 \mp \gamma_5)f$ , respectively. (There is no  $\tilde{\nu}_R$  in the MSSM.) However,  $\tilde{f}_L$ - $\tilde{f}_R$  mixing is possible, in which case  $\tilde{f}_L$  and  $\tilde{f}_R$  are not mass eigenstates. For three generations of squarks, one must diagonalize  $6 \times 6$  matrices corresponding to the basis  $(\tilde{q}_{iL}, \tilde{q}_{iR})$ , where  $i = 1, 2, 3$  are the generation labels. For simplicity, only the one-generation case is illustrated in detail below. (The effects of second and third generation squark mixing can be significant and are treated in Ref. [101].)

Using the notation of the third family, the one-generation tree-level squark squared-mass matrix is given by [102],

$$\mathcal{M}^2 = \begin{pmatrix} M_Q^2 + m_q^2 + L_q & m_q X_q^* \\ m_q X_q & M_R^2 + m_q^2 + R_q \end{pmatrix}, \quad (89.11)$$

where

$$X_q \equiv A_q - \mu^* (\cot \beta)^{2T_{3q}}, \quad (89.12)$$

and  $T_{3q} = \frac{1}{2} [-\frac{1}{2}]$  for  $q = t$  [b]. The diagonal squared-masses are governed by soft-SUSY-breaking squared-masses  $M_Q^2$  and  $M_R^2 \equiv M_D^2$  [for  $q = t$  [b]], the corresponding quark masses  $m_t$  [m<sub>b</sub>] and the electroweak correction terms:

$$\begin{aligned} L_q &\equiv (T_{3q} - e_q \sin^2 \theta_W) m_Z^2 \cos 2\beta, \\ R_q &\equiv e_q \sin^2 \theta_W m_Z^2 \cos 2\beta, \end{aligned} \quad (89.13)$$

where  $\epsilon_q = \frac{2}{3} [-\frac{1}{3}]$  for  $q = t [b]$ . The off-diagonal squark squared-masses are proportional to the corresponding quark masses and depend on  $\tan\beta$ , the soft-SUSY-breaking  $A$ -parameters and the higgsino mass parameter  $\mu$ . Assuming that the  $A$ -parameters are parametrically of the same order (or smaller) relative to other SUSY-breaking mass parameters, it then follows that the first and second generation  $\tilde{q}_L\text{-}\tilde{q}_R$  mixing is smaller than that of the third generation where mixing can be enhanced by factors of  $m_t$  and  $m_b \tan\beta$ .

In the case of third generation  $\tilde{q}_L\text{-}\tilde{q}_R$  mixing, the mass eigenstates (usually denoted by  $\tilde{q}_1$  and  $\tilde{q}_2$ , with  $m_{\tilde{q}_1} < m_{\tilde{q}_2}$ ) are determined by diagonalizing the  $2 \times 2$  matrix  $\mathcal{M}^2$  given by Eq. (89.11). The corresponding squared-masses and mixing angle are given by [102]:

$$m_{\tilde{q}_{1,2}}^2 = \frac{1}{2} \left[ \text{Tr} \mathcal{M}^2 \mp \sqrt{(\text{Tr} \mathcal{M}^2)^2 - 4 \det \mathcal{M}^2} \right],$$

$$\sin 2\theta_{\tilde{q}} = \frac{2m_q |X_q|}{m_{\tilde{q}_2}^2 - m_{\tilde{q}_1}^2}.$$
(89.14)

The one-generation results above also apply to the charged sleptons, with the obvious substitutions:  $q \rightarrow \ell$  with  $T_{3\ell} = -\frac{1}{2}$  and  $e_\ell = -1$ , and the replacement of the SUSY-breaking parameters:  $M_Q^2 \rightarrow M_L^2$ ,  $M_D^2 \rightarrow M_E^2$ , and  $A_q \rightarrow A_\tau$ . For the neutral sleptons,  $\tilde{\nu}_R$  does not exist in the MSSM, so  $\tilde{\nu}_L$  is a mass eigenstate.

In the case of three generations, the SUSY-breaking scalar-squared masses  $[M_Q^2, M_U^2, M_D^2, M_L^2, \text{ and } M_E^2]$  and the  $A$ -parameters  $[A_U, A_D, \text{ and } A_E]$  are now  $3 \times 3$  matrices as noted in Sec. 89.3.3. The diagonalization of the  $6 \times 6$  squark mass matrices yields  $\tilde{f}_{iL}\text{-}\tilde{f}_{jR}$  mixing. In practice, since the  $\tilde{f}_L\text{-}\tilde{f}_R$  mixing is appreciable only for the third generation, this additional complication can often be neglected (although see Ref. [101] for examples in which the mixing between the second and third generation squarks is relevant).

### 89.5 The supersymmetric Higgs sector

Consider first the MSSM Higgs sector [27, 28, 103]. Despite the large number of potential  $CP$ -violating phases among the MSSM-124 parameters, the tree-level MSSM Higgs potential given by Eq. (89.2) is automatically  $CP$ -conserving. This follows from the fact that the only potentially complex parameter ( $m_{12}^2$ ) of the MSSM Higgs potential can be chosen real and positive by rephasing the Higgs fields, in which case  $\tan\beta$  is a real positive parameter. Consequently, the physical neutral Higgs scalars are  $CP$ -eigenstates (at tree-level). The MSSM Higgs sector contains five physical spin-zero particles: a charged Higgs boson pair ( $H^\pm$ ), two  $CP$ -even neutral Higgs bosons (denoted by  $h^0$  and  $H^0$  where  $m_h < m_H$ ), and one  $CP$ -odd neutral Higgs boson ( $A^0$ ). The discovery of a SM-like Higgs boson at the LHC with a mass of 125 GeV (see Sec. 11) strongly suggests that this state should be identified with  $h^0$ , although the possibility that the 125 GeV state should be identified with  $H^0$  cannot yet be completely ruled out [104].

In the NMSSM [33], the scalar component of the singlet Higgs superfield adds two additional neutral states to the Higgs sector. In this model, the tree-level Higgs sector can exhibit explicit  $CP$ -violation. If  $CP$  is conserved, then the two extra neutral scalar states are  $CP$ -even and  $CP$ -odd, respectively. These states can potentially mix with the neutral Higgs states of the MSSM. If scalar states exist that are dominantly singlet, then they are weakly coupled to SM gauge bosons and fermions through their small mixing with the MSSM Higgs scalars. Consequently, it is possible that one (or both) of the singlet-dominated states is considerably lighter than the Higgs boson that was observed at the LHC.

#### 89.5.1 The tree-level Higgs sector

The tree-level properties of the Higgs sector are determined by the Higgs potential given by Eq. (89.2). The quartic interaction terms are manifestly supersymmetric (although these are modified by SUSY-breaking effects at the loop level). In general, the quartic couplings arise from two sources: (i) the supersymmetric generalization of the scalar potential (the so-called “ $F$ -terms”), and

(ii) interaction terms related by SUSY to the coupling of the scalar fields and the gauge fields, whose coefficients are proportional to the corresponding gauge couplings (the so-called “ $D$ -terms”).

In the MSSM,  $F$ -term contributions to the quartic Higgs self-couplings are absent. As a result, the strengths of the MSSM quartic Higgs interactions are fixed in terms of the gauge couplings, as noted below Eq. (89.2). Consequently, all the tree-level MSSM Higgs-sector parameters depend only on two quantities:  $\tan\beta$  [defined in Eq. (89.3)] and one Higgs mass usually taken to be  $m_A$ . From these two quantities, one can predict the values of the remaining Higgs boson masses, an angle  $\alpha$  that measures the mixture of the hypercharge  $\pm 1$  scalar fields,  $H_u^0$  and  $H_d^0$ , in the physical  $CP$ -even neutral scalars, and the Higgs boson self-couplings. Moreover, the tree-level mass of the lighter  $CP$ -even Higgs boson is bounded,  $m_h \leq m_Z |\cos 2\beta| \leq m_Z$  [27, 28]. This bound can be substantially modified when radiative corrections are included, as discussed in Sec. 89.5.2.

In the NMSSM, the superpotential contains a trilinear term that couples the two  $Y = \pm 1$  Higgs doublet superfields and the singlet Higgs superfield. The coefficient of this term is denoted by  $\lambda$ . Consequently, the tree-level bound for the mass of the lightest  $CP$ -even MSSM Higgs boson is modified [105],

$$m_h^2 \leq m_Z^2 \cos^2 2\beta + \frac{1}{2} \lambda^2 v^2 \sin^2 2\beta,$$
(89.15)

where  $v \equiv (v_u^2 + v_d^2)^{1/2} = 246$  GeV. If one demands that  $\lambda$  should stay finite after renormalization-group evolution up to the Planck scale, then  $\lambda$  is constrained to lie below about 0.7–0.8 at the electroweak scale [33] (although larger values of  $\lambda$  have also been considered [106]).

The tree-level Higgs-quark and Higgs-lepton interactions of the MSSM are governed by the Yukawa couplings defined by the superpotential given in Eq. (89.1). In particular, the Higgs sector of the MSSM is a Type-II two-Higgs doublet model [107], in which one Higgs doublet ( $H_d$ ) couples exclusively to the right-handed down-type quark (or lepton) fields and the second Higgs doublet ( $H_u$ ) couples exclusively to the right-handed up-type quark fields. Consequently, the diagonalization of the fermion mass matrices simultaneously diagonalizes the matrix Yukawa couplings, resulting in flavor-diagonal tree-level couplings of the neutral Higgs bosons  $h^0$ ,  $H^0$  and  $A^0$  to quark and lepton pairs.

#### 89.5.2 The radiatively-corrected Higgs sector

When radiative corrections are incorporated, additional parameters of the supersymmetric model enter via virtual supersymmetric particles that appear in loops. The impact of these corrections can be significant [108]. The qualitative behavior of these radiative corrections can be most easily seen in the large top-squark mass limit, where in addition, both the splitting of the two diagonal entries and the off-diagonal entries of the top-squark squared-mass matrix [Eq. (89.11)] are small in comparison to the geometric mean of the two top-squark squared-masses,  $M_S^2 \equiv M_{t_1} M_{t_2}$ . In this case (assuming  $m_A > m_Z$ ), the predicted upper bound for  $m_h$  is approximately given by

$$m_h^2 \lesssim m_Z^2 \cos^2 2\beta + \frac{3g^2 m_t^4}{8\pi^2 m_W^2} \left[ \ln \left( \frac{M_S^2}{m_t^2} \right) + \frac{X_t^2}{M_S^2} \left( 1 - \frac{X_t^2}{12M_S^2} \right) \right],$$
(89.16)

where  $X_t \equiv A_t - \mu \cot\beta$  [cf. Eq. (89.12)] is proportional to the off-diagonal entry of the top-squark squared-mass matrix (where for simplicity,  $A_t$  and  $\mu$  are taken to be real). The Higgs mass upper limit specified by Eq. (89.16) is saturated when  $\tan\beta$  is large (*i.e.*,  $\cos^2 2\beta \sim 1$ ) and  $X_t = \sqrt{6} M_S$ , which defines the so-called maximal mixing scenario.

A more complete treatment of the radiative corrections shows that Eq. (89.16) somewhat overestimates the true upper bound of  $m_h$ . These more refined computations, which incorporate renormalization group improvement, the two loop and the leading three-loop contributions, yield  $m_h \lesssim 135$  GeV in the region of large  $\tan\beta$  (with an accuracy of a few GeV) for  $m_t = 175$  GeV and  $M_S \lesssim 2$  TeV [109].

In addition, one-loop radiative corrections can introduce  $CP$ -violating effects in the Higgs sector that depend on some of

the  $CP$ -violating phases among the MSSM-124 parameters [110]. This phenomenon is most easily understood in a scenario where  $m_A \ll M_S$  (i.e., all five physical Higgs states are significantly lighter than the SUSY breaking scale). In this case, one can integrate out the heavy superpartners to obtain a low-energy effective theory with two Higgs doublets. The resulting effective two-Higgs doublet model will now contain all possible Higgs self-interaction terms (both  $CP$ -conserving and  $CP$ -violating) and Higgs-fermion interactions (beyond those of Type-II) that are consistent with electroweak gauge invariance [111].

In the NMSSM, the dominant radiative correction to Eq. (89.15) is the same as the one given in Eq. (89.16). However, in contrast to the MSSM, one does not need as large a boost from the radiative corrections to achieve a Higgs mass of 125 GeV in certain regimes of the NMSSM parameter space (e.g.,  $\tan\beta \sim 2$  and  $\lambda \sim 0.7$  [112]).

## 89.6 Restricting the MSSM parameter freedom

In Sections 89.4 and 89.5, we surveyed the parameters that comprise the MSSM-124. However, without additional restrictions on the choice of parameters, a generic parameter set within the MSSM-124 framework is not phenomenologically viable. In particular, a generic point of the MSSM-124 parameter space exhibits: (i) no conservation of the separate lepton numbers  $L_e, L_\mu,$  and  $L_\tau$ ; (ii) unsuppressed flavor-changing neutral currents (FCNCs); and (iii) new sources of  $CP$  violation that are inconsistent with the experimental bounds.

For example, the MSSM contains many new sources of  $CP$  violation [113]. Indeed, for TeV-scale sfermion and gaugino masses, some combinations of the complex phases of the gaugino-mass parameters, the  $A$ -parameters, and  $\mu$  must be less than about  $10^{-2}$ – $10^{-3}$  to avoid generating electric dipole moments for the neutron, electron, and atoms [114–116] in conflict with observed data [117]. The rarity of FCNCs [118–120] places additional constraints on the off-diagonal matrix elements of the squark and slepton soft-SUSY-breaking squared-masses and  $A$ -parameters (see Sec. 89.3.3).

The MSSM-124 is also theoretically incomplete as it provides no explanation for the fundamental origin of the supersymmetry-breaking parameters. The successful unification of the SM gauge couplings at very high energies close to the Planck scale [8, 66, 121–123] suggests that the high-energy structure of the theory may be considerably simpler than its low-energy realization. In a top-down approach, the dynamics that governs the more fundamental theory at high energies is used to derive the effective broken-supersymmetric theory at the TeV scale. A suitable choice for the high energy dynamics is one that yields a TeV-scale theory that satisfies all relevant phenomenological constraints.

In this Section, we examine a number of theoretical frameworks that potentially yield phenomenologically viable regions of the MSSM-124 parameter space. The resulting supersymmetric particle spectrum is then a function of a relatively small number of input parameters. This is accomplished by imposing a simple structure on the soft SUSY-breaking parameters at a common high-energy scale  $M_X$  (typically chosen to be the Planck scale,  $M_P$ , the grand unification scale,  $M_{\text{GUT}}$ , or the messenger scale,  $M_{\text{mess}}$ ). These serve as initial conditions for the MSSM renormalization group equations (RGEs), which are given in the two-loop approximation in Ref. [124] (an automated program to compute RGEs for the MSSM and other models of new physics beyond the SM has been developed in Ref. [125]). Solving these equations numerically, one can then derive the low-energy MSSM parameters relevant for phenomenology. A number of software packages exist that numerically calculate the spectrum of supersymmetric particles, consistent with theoretical conditions on SUSY breaking at high energies and some experimental data at low energies [126].

Examples of this scenario are provided by models of gravity-mediated, anomaly mediated and gauge-mediated SUSY breaking, to be discussed in more detail below. In some of these approaches, one of the diagonal Higgs squared-mass parameters is driven negative by renormalization group evolution [127]. In such models, electroweak symmetry breaking is generated radiatively, and the resulting electroweak symmetry-breaking scale is intimately tied to the scale of low-energy SUSY breaking.

### 89.6.1 Gaugino mass relations

One prediction of many supersymmetric grand unified models is the unification of the (tree-level) gaugino mass parameters at some high-energy scale,  $M_X$ ,

$$M_1(M_X) = M_2(M_X) = M_3(M_X) = m_{1/2}. \quad (89.17)$$

Due to renormalization group running, in the one-loop approximation the effective low-energy gaugino mass parameters (at the electroweak scale) are related,

$$M_3 = (g_s^2/g^2)M_2 \simeq 3.5M_2, \quad M_1 = (5g'^2/3g^2)M_2 \simeq 0.5M_2. \quad (89.18)$$

Eq. (89.18) can arise more generally in gauge-mediated SUSY-breaking models where the gaugino masses are generated at the messenger scale  $M_{\text{mess}}$  (which typically lies significantly below the unification scale where the gauge couplings unify). In this case, the gaugino mass parameters are proportional to the corresponding squared gauge couplings at the messenger scale.

When Eq. (89.18) is satisfied, the chargino and neutralino masses and mixing angles depend only on three unknown parameters: the gluino mass,  $\mu$ , and  $\tan\beta$ . It then follows that the lightest neutralino must be heavier than 46 GeV due to the non-observation of charginos at LEP [128]. If in addition  $|\mu| \gg |M_1| \gtrsim m_Z$ , then the lightest neutralino is nearly a pure bino, an assumption often made in supersymmetric particle searches at colliders. Although Eq. (89.18) is often assumed in many phenomenological studies, a truly model-independent approach would take the gaugino mass parameters,  $M_i$ , to be independent parameters to be determined by experiment. Indeed, an approximately massless neutralino *cannot* be ruled out at present by a model-independent analysis [129].

It is possible that the tree-level masses for the gauginos are zero. In this case, the gaugino mass parameters arise at one-loop and do not satisfy Eq. (89.18). For example, the gaugino masses in AMSB models arise entirely from a model-independent contribution derived from the super-conformal anomaly [48, 130]. In this case, Eq. (89.18) is replaced (in the one-loop approximation) by:

$$M_i \simeq \frac{b_i g_i^2}{16\pi^2} m_{3/2}, \quad (89.19)$$

where  $m_{3/2}$  is the gravitino mass and the  $b_i$  are the coefficients of the MSSM gauge beta-functions corresponding to the corresponding  $U(1)$ ,  $SU(2)$ , and  $SU(3)$  gauge groups,  $(b_1, b_2, b_3) = (\frac{33}{5}, 1, -3)$ . Eq. (89.19) yields  $M_1 \simeq 2.8M_2$  and  $M_3 \simeq -8.3M_2$ , which implies that the lightest chargino pair and neutralino comprise a nearly mass-degenerate triplet of winos,  $\tilde{W}^\pm, \tilde{W}^0$  (cf. Table 1), over most of the MSSM parameter space. For example, if  $|\mu| \gg m_Z, |M_2|$ , then Eq. (89.19) implies that  $M_{\tilde{\chi}^\pm} \simeq M_{\tilde{\chi}_1^0} \simeq M_2$  [131]. Alternatively, one can construct an AMSB model where  $|\mu|, m_Z \ll M_2$ , which yields an LSP that is an approximate higgsino state [132]. In both cases, the corresponding supersymmetric phenomenology differs significantly from the standard phenomenology based on Eq. (89.18) [133, 134].

Finally, it should be noted that the unification of gaugino masses (and scalar masses) can be accidental. In particular, the energy scale where unification takes place may not be directly related to any physical scale. One version of this phenomenon has been called mirage unification and can occur in certain theories of fundamental SUSY breaking [135].

### 89.6.2 Constrained versions of the MSSM: $mSUGRA$ , $CMSSM$ , etc.

In the minimal supergravity ( $mSUGRA$ ) framework [3–6, 41–43], a form of the Kähler potential is employed that yields minimal kinetic energy terms for the MSSM fields [45]. As a result, the soft supersymmetry-breaking parameters at the high-energy scale  $M_X$  take a particularly simple form in which the scalar squared-masses

and the  $A$ -parameters are flavor-diagonal and universal [43]:

$$\begin{aligned} M_Q^2(M_X) &= M_U^2(M_X) = M_D^2(M_X) = m_0^2 \mathbf{1}, \\ M_L^2(M_X) &= M_E^2(M_X) = m_0^2 \mathbf{1}, \\ m_1^2(M_X) &= m_2^2(M_X) = m_0^2, \\ A_U(M_X) &= A_D(M_X) = A_E(M_X) = A_0 \mathbf{1}, \end{aligned} \tag{89.20}$$

where  $\mathbf{1}$  is a  $3 \times 3$  identity matrix in generation space. As in the SM, this approach exhibits minimal flavor violation [136, 137], whose unique source is the nontrivial flavor structure of the Higgs-fermion Yukawa couplings. The gaugino masses are also unified according to Eq. (89.17).

Renormalization group evolution is then used to derive the values of the supersymmetric parameters at the low-energy (electroweak) scale. For example, to compute squark masses, one should use the low-energy values for  $M_Q^2$ ,  $M_U^2$ , and  $M_D^2$  in Eq. (89.11). Through the renormalization group running with boundary conditions specified in Eq. (89.18) and Eq. (89.20), one can show that the low-energy values of  $M_Q^2$ ,  $M_U^2$ , and  $M_D^2$  depend primarily on  $m_0^2$  and  $m_{1/2}^2$ . A number of useful approximate analytic expressions for superpartner masses in terms of the mSUGRA parameters can be found in Ref. [138].

In the mSUGRA approach, four flavors of squarks (with two squark eigenstates per flavor) are nearly mass-degenerate. If  $\tan \beta$  is not very large,  $\tilde{b}_R$  is also approximately degenerate in mass with the first two generations of squarks. The  $\tilde{b}_L$  mass and the diagonal  $t_L$  and  $t_R$  masses are typically reduced relative to the common squark mass of the first two generations. In addition, there are six flavors of nearly mass-degenerate sleptons (with two slepton eigenstates per flavor for the charged sleptons and one per flavor for the sneutrinos); the sleptons are expected to be somewhat lighter than the mass-degenerate squarks. As noted below Eq. (89.11), third-generation squark masses and tau-slepton masses are sensitive to the strength of the respective  $\tilde{f}_L$ - $\tilde{f}_R$  mixing. The LSP is typically the lightest neutralino,  $\tilde{\chi}_1^0$ , which is dominated by its bino component. Regions of the mSUGRA parameter space in which the LSP is electrically charged do exist but are not phenomenologically viable [19].

One can count the number of independent parameters in the mSUGRA framework. In addition to 18 SM parameters (excluding the Higgs mass), one must specify  $m_0$ ,  $m_{1/2}$ ,  $A_0$ , the Planck-scale values for  $\mu$  and  $B$ -parameters (denoted by  $\mu_0$  and  $B_0$ ), and the gravitino mass  $m_{3/2}$ . Without additional model assumptions,  $m_{3/2}$  is independent of the parameters that govern the mass spectrum of the superpartners of the SM [43]. In principle,  $A_0$ ,  $B_0$ ,  $\mu_0$ , and  $m_{3/2}$  can be complex, although in the mSUGRA approach, these parameters are taken (arbitrarily) to be real.

As previously noted, renormalization group evolution is used to compute the low-energy values of the mSUGRA parameters, which then fixes all the parameters of the low-energy MSSM. In particular, the two Higgs vacuum expectation values (or equivalently,  $m_Z$  and  $\tan \beta$ ) can be expressed as a function of the Planck-scale supergravity parameters. The most common procedure is to remove  $\mu_0$  and  $B_0$  in favor of  $m_Z$  and  $\tan \beta$  [the sign of  $\mu_0$ , denoted  $\text{sgn}(\mu_0)$  below, is not fixed in this process]. In this case, the MSSM spectrum and its interaction strengths are determined by five parameters:

$$m_0, A_0, m_{1/2}, \tan \beta, \text{ and } \text{sgn}(\mu_0), \tag{89.21}$$

and an independent gravitino mass  $m_{3/2}$  (in addition to the 18 parameters of the SM). In Ref. [139], this framework was dubbed the constrained minimal supersymmetric extension of the SM (CMSSM).

In the early literature, additional conditions were obtained by assuming a simplified form for the hidden sector that provides the fundamental source of SUSY breaking. Two additional relations emerged among the mSUGRA parameters [41, 45]:  $B_0 = A_0 - m_0$  and  $m_{3/2} = m_0$ . These relations characterize a theory that was called minimal supergravity when first proposed. In the subsequent literature, it has been more common to omit these extra

conditions in defining the mSUGRA model (in which case the mSUGRA model and the CMSSM are synonymous). The authors of Ref. [140] advocate restoring the original nomenclature in which the mSUGRA model is defined with the extra conditions as originally proposed. Additional mSUGRA variations can also be considered where different relations among the CMSSM parameters are imposed.

One can also relax the universality of scalar masses by decoupling the squared-masses of the Higgs bosons and the squarks/sleptons. This leads to the non-universal Higgs mass models (NUHMs), thereby adding one or two new parameters to the CMSSM depending on whether the diagonal Higgs scalar squared-mass parameters ( $m_1^2$  and  $m_2^2$ ) are set equal (NUHM1 [141]) or taken to be independent (NUHM2 [142]) at the high energy scale  $M_X^2$ . Clearly, this modification preserves the minimal flavor violation of the mSUGRA approach. Nevertheless, the mSUGRA approach and its NUHM generalizations are probably too simplistic. Theoretical considerations suggest that the universality of Planck-scale soft SUSY-breaking parameters is not generic [143]. In particular, effective operators at the Planck scale exist that do not respect flavor universality, and it is difficult to find a theoretical principle that would forbid them.

In the framework of supergravity, if anomaly mediation is the sole source of SUSY breaking, then the gaugino mass parameters, diagonal scalar squared-mass parameters, and the SUSY-breaking trilinear scalar interaction terms (proportional to  $\lambda_f A_F$ ) are determined in terms of the beta functions of the gauge and Yukawa couplings and the anomalous dimensions of the squark and slepton fields [48, 130, 134]. As noted in Sec. 89.2.3, this approach yields tachyonic sleptons in the MSSM unless additional sources of SUSY breaking are present. In the minimal AMSB (mAMSB) scenario, a universal squared-mass parameter,  $m_0^2$ , is added to the AMSB expressions for the diagonal scalar squared-masses [134]. Thus, the mAMSB spectrum and its interaction strengths are determined by four parameters,  $m_0^2$ ,  $m_{3/2}$ ,  $\tan \beta$  and  $\text{sgn}(\mu_0)$ .

The mAMSB scenario appears to be ruled out based on the observed value of the Higgs boson mass, assuming an upper limit on  $M_S$  of a few TeV, since the mAMSB constraint on  $A_F$  implies that the maximal mixing scenario cannot be achieved [cf. Eq. (89.16)]. Indeed, under the stated assumptions, the mAMSB Higgs mass upper bound lies below the observed Higgs mass value [144]. Thus within the AMSB scenario, either an additional SUSY-breaking contribution to  $\lambda_f A_F$  and/or new ingredients beyond the MSSM are required.

### 89.6.3 Gauge-mediated SUSY breaking

In contrast to models of gravity-mediated SUSY breaking, the flavor universality of the fundamental soft SUSY-breaking squark and slepton squared-mass parameters is guaranteed in gauge-mediated SUSY breaking (GMSB) because the supersymmetry breaking is communicated to the sector of MSSM fields via gauge interactions [53, 55]. In GMSB models, the mass scale of the messenger sector (or its equivalent) is sufficiently below the Planck scale such that the additional SUSY-breaking effects mediated by supergravity can be neglected.

In the minimal GMSB approach, there is one effective mass scale,  $\Lambda$ , that determines all low-energy scalar and gaugino mass parameters through loop effects, while the resulting  $A$ -parameters are suppressed. In order that the resulting superpartner masses be of order 1 TeV, one must have  $\Lambda \sim \mathcal{O}(100 \text{ TeV})$ . The origin of the  $\mu$  and  $B$ -parameters is model-dependent, and lies somewhat outside the ansatz of gauge-mediated SUSY breaking [145].

The simplest GMSB models appear to be ruled out based on the observed value of the Higgs boson mass. Due to suppressed  $A$  parameters, it is difficult to boost the contributions of the radiative corrections in Eq. (89.16) to obtain a Higgs mass as large as 125 GeV. However, this conflict can be alleviated in more complicated GMSB models [146]. To analyze these generalized GMSB models, it has been especially fruitful to develop model-independent techniques that encompass all known GMSB models [147]. These techniques are well-suited for a comprehensive analysis [148] of the phenomenological profile of gauge-mediated SUSY breaking.

The gravitino is the LSP in GMSB models, as noted in Sec. 89.2.3. As a result, the next-to-lightest supersymmetric par-

title (NLSP) now plays a crucial role in the phenomenology of supersymmetric particle production and decays. Note that unlike the LSP, the NLSP can be charged. In GMSB models, the most likely candidates for the NLSP are  $\tilde{\chi}_1^0$  and  $\tilde{\tau}_R^\pm$ . The NLSP will decay into its superpartner plus a gravitino (e.g.,  $\tilde{\chi}_1^0 \rightarrow \gamma\tilde{G}$ ,  $\tilde{\chi}_1^0 \rightarrow Z\tilde{G}$ ,  $\tilde{\chi}_1^0 \rightarrow h^0\tilde{G}$  or  $\tilde{\tau}_1^\pm \rightarrow \tau^\pm\tilde{G}$ ), with lifetimes and branching ratios that depend on the model parameters. There are also GMSB scenarios in which there are several nearly degenerate co-NLSP's, any one of which can be produced at the penultimate step of a supersymmetric decay chain [149]. For example, in the slepton co-NLSP case, all three right-handed sleptons are close enough in mass and thus can each play the role of the NLSP.

Different choices for the identity of the NLSP and its decay rate lead to a variety of distinctive supersymmetric phenomenologies [55,150]. For example, a long-lived  $\tilde{\chi}_1^0$ -NLSP that decays outside collider detectors leads to supersymmetric decay chains with missing energy in association with leptons and/or hadronic jets (this case is indistinguishable from the standard phenomenology of the  $\tilde{\chi}_1^0$ -LSP). On the other hand, if  $\tilde{\chi}_1^0 \rightarrow \gamma\tilde{G}$  is the dominant decay mode, and the decay occurs inside the detector, then nearly all supersymmetric particle decay chains would contain a photon. In contrast, in the case of a  $\tilde{\tau}_1^\pm$ -NLSP, the  $\tilde{\tau}_1^\pm$  would either be long-lived or would decay inside the detector into a  $\tau$ -lepton plus missing energy.

A number of attempts have been made to address the origins of the  $\mu$  and  $B$ -parameters in GMSB models based on the field content of the MSSM (see, e.g., Refs. [145,151]). An alternative approach is to consider GMSB models based on the NMSSM [152]. The vacuum expectation value of the additional singlet Higgs superfield can be used to generate effective  $\mu$  and  $B$ -parameters [153]. Such models provide an alternative GMSB framework for achieving a Higgs mass of 125 GeV, while still being consistent with LHC bounds on supersymmetric particle masses [154].

### 89.6.4 The phenomenological MSSM

Of course, any of the theoretical assumptions described in the previous three subsections must be tested experimentally and could turn out to be wrong. To facilitate the exploration of MSSM phenomena in a more model-independent way while respecting the constraints noted at the beginning of this Section, the phenomenological MSSM (pMSSM) has been introduced [155].

The pMSSM is governed by 19 independent real supersymmetric parameters: the three gaugino mass parameters  $M_1$ ,  $M_2$  and  $M_3$ , the Higgs sector parameters  $m_A$  and  $\tan\beta$ , the Higgsino mass parameter  $\mu$ , five sfermion squared-mass parameters for the degenerate first and second generations ( $M_{\tilde{Q}}^2$ ,  $M_{\tilde{U}}^2$ ,  $M_{\tilde{D}}^2$ ,  $M_{\tilde{L}}^2$  and  $M_{\tilde{E}}^2$ ), the five corresponding sfermion squared-mass parameters for the third generation, and three third-generation  $A$ -parameters ( $A_t$ ,  $A_b$  and  $A_\tau$ ). The first and second generation  $A$ -parameters are typically neglected in pMSSM studies, as their phenomenological consequences are negligible in most applications (one counterexample is the  $A_\mu$  dependence of the anomalous magnetic moment of the muon, which can be as significant as other contributions due to superpartner mediated radiative corrections [156]). Since its initial proposal, the pMSSM approach has been extended to include CP-violating SUSY-breaking parameters in Ref. [157].

A comprehensive study of the 19-parameter pMSSM is computationally expensive. This is somewhat ameliorated in Ref. [158], where the number of pMSSM parameters is reduced to ten by assuming one common squark squared-mass parameter for the first two generations, a second common squark squared-mass parameter for the third generation, a common slepton squared-mass parameter and a common third generation  $A$  parameter. Applications of the pMSSM approach to supersymmetric particle searches, and a discussion of the implications for past and future LHC and dark matter studies can be found in Refs. [158–160].

### 89.6.5 Simplified models

As Sec. 90 demonstrates, experiments present their searches for supersymmetric particles primarily in terms of simplified models. Simplified models for supersymmetric searches [161] are defined mostly by the empirical objects and kinematic variables involved

in the search. Their interpretation by the experimental collaboration usually involves only a small number of supersymmetric particles (often two or three). Other supersymmetric particles are assumed to play no role (this may happen by virtue of them being too heavy to be produced). Experimental bounds from non-observation of a signal are usually presented in terms of the physical masses of the supersymmetric particles involved. Bounds may be presented on the relevant supersymmetric particle masses assuming a 100% branching ratio for a certain decay, or as an upper bound on signal production cross-section times branching ratio as a function of the relevant supersymmetric particle masses.

For example, consider a search for hadronic jets plus missing transverse momentum. One can match such a search to the simplified model of squark pair production followed by the subsequent decay of each squark into a quark (which appears as a jet) and a neutralino LSP that produces the missing transverse momentum, i.e.  $\tilde{q}\tilde{q} \rightarrow (q\tilde{\chi}_1^0)(q\tilde{\chi}_1^0)$ . Excluded regions resulting from the non-observation of a signal may be exhibited in the squark mass versus LSP mass plane.

Simplified models have the advantage that one makes fewer assumptions, compared to more complete supersymmetric models, where the larger number of free parameters makes it difficult to present excluded regions in any generality. It is hoped that simplified models may be a reasonable approximation over sizeable regions of parameter space of more complete models, within which the simplified model is embedded. On the other hand, as stressed in Sec. 90, simplified models have the disadvantage that the presentation of negative search limits tends to be overly strong when compared to the more complete models, particularly if 100% branching ratios are assumed. A contrast between supersymmetric particle search limits in the context of simplified models and the corresponding constraints obtained in the more complete pMSSM is provided in Ref. [162]. As long as one is able to dispel undue pessimism, simplified models remain an efficient vehicle for organizing and presenting the results of supersymmetric particle searches.

## 89.7 Experimental data confronts the MSSM

At present, there is no direct evidence for weak-scale SUSY from the data analyzed by the LHC experiments. Recent LHC data have been effectively employed in ruling out the existence of colored supersymmetric particles (primarily the gluino and the first generation of squarks) with masses below about 2 TeV (see Sec. 90). The precise mass limits are model dependent. For example, as Sec. 90 demonstrates, regions of the pMSSM parameter space can be identified in which lighter squarks and gluinos below 1 TeV cannot be definitely ruled out. Additional constraints arise from limits on the contributions of virtual supersymmetric particle exchange to a variety of SM processes [118–120].

In light of these negative results, one must confront the tension that exists between the theoretical expectations for the magnitude of the SUSY-breaking parameters and the non-observation of supersymmetric phenomena at colliders.

### 89.7.1 Naturalness constraints and the little hierarchy

In Sec. 89.1, weak-scale SUSY was motivated as a natural solution to the hierarchy problem, which could provide an understanding of the origin of the electroweak symmetry-breaking scale without a significant fine-tuning of the fundamental parameters that govern the MSSM. In this context, the weak scale soft supersymmetry-breaking masses must be generally of the order of 1 TeV or below [163]. This requirement is most easily seen in the determination of  $m_Z$  by the scalar potential minimum condition. In light of Eq. (89.5), to avoid the fine-tuning of MSSM parameters, the soft SUSY-breaking squared-masses  $m_1^2$  and  $m_2^2$  and the higgsino squared-mass  $|\mu|^2$  should all be roughly of  $\mathcal{O}(m_Z^2)$ . Many authors have proposed quantitative measures of fine-tuning [163–167]. One of the simplest measures is the one advocated by Barbieri and Giudice [163] (which was also introduced previously in Ref. [164]),

$$\Delta_i \equiv \left| \frac{\partial \ln m_Z^2}{\partial \ln p_i} \right|, \quad \Delta \equiv \max \Delta_i, \quad (89.22)$$



where the  $p_i$  are the MSSM parameters at the high-energy scale  $M_X$ , which are set by the fundamental SUSY-breaking dynamics. The theory is more fine-tuned as  $\Delta$  becomes larger. However, different measures of fine-tuning yield quantitatively different results; in particular, calculating minimal fine-tuning based on the high-scale parameters [as defined in Eq. (89.22)] yields a difference by a factor  $\sim 10$  to fine-tuning based on TeV-scale parameters [168, 169].

One can apply the fine-tuning measure to any explicit model of SUSY breaking. For example, in the approaches discussed in Sec. 89.6, the  $p_i$  are parameters of the model at the energy scale  $M_X$  where the soft SUSY-breaking operators are generated by the dynamics of SUSY breaking. Renormalization group evolution then determines the values of the parameters appearing in Eq. (89.5) at the electroweak scale. In this way,  $\Delta$  is sensitive to all the SUSY-breaking parameters of the model (see e.g. Ref. [170]). It should be noted that the computation of  $\Delta$  is often based on Eq. (89.5), which is a tree-level condition. For example, an analysis in Ref. [80] shows that the fine tuning measure can be reduced by as much as a factor of two when loop corrections are included [171].

As anticipated, there is a tension between the present experimental lower limits on the masses of colored supersymmetric particles [172, 173] and the expectation that supersymmetry-breaking is associated with the electroweak symmetry-breaking scale. Moreover, this tension is exacerbated [174] by the observed value of the Higgs mass ( $m_h \simeq 125$  GeV), which is not far from the MSSM upper bound ( $m_h \lesssim 135$  GeV) [which depends on the top-squark mass and mixing as noted in Sec. 89.5.2]. If  $M_{\text{SUSY}}$  characterizes the scale of supersymmetric particle masses, then one would crudely expect  $\Delta \sim M_{\text{SUSY}}^2/m_Z^2$ . For example, if  $M_{\text{SUSY}} \sim 1$  TeV then one expects a  $\Delta^{-1} \sim 1\%$  fine-tuning of the MSSM parameters to achieve the observed value of  $m_Z$ . This separation of the electroweak symmetry-breaking and SUSY-breaking scales is an example of the little hierarchy problem [175, 176].

The fine-tuning parameter  $\Delta$  can depend quite sensitively on the structure of the SUSY-breaking dynamics, such as the value of  $M_X$  and relations among SUSY-breaking parameters in the fundamental high energy theory [177]. For example, in so-called focus point SUSY models [166, 178], all squark masses can be as heavy as 5 TeV *without* significant fine-tuning. This can be attributed to a focusing behavior of the renormalization group evolution when certain relations hold among the high-energy values of the scalar squared-mass SUSY-breaking parameters. Although the focus point region of the CMSSM still yields an uncomfortably high value of  $\Delta$  due to the observed Higgs mass of 125 GeV, one can achieve moderate values of  $\Delta$  in models with NUHM2 boundary conditions for the scalar masses [174].

Among the colored superpartners, the third generation squarks typically have the most significant impact on the naturalness constraints [179], while their masses are the least constrained by the LHC data. Hence, in the absence of any relation between third generation squarks and those of the first two generations, the naturalness constraints due to present LHC data can be considerably weaker than those obtained in the CMSSM. Indeed, models with first and second generation squark masses in the multi-TeV range do not necessarily require significant fine tuning. Such models have the added benefit that undesirable FCNCs mediated by squark exchange are naturally suppressed [180]. Other MSSM mass spectra that are compatible with moderate fine tuning have been considered in Refs. [177] and [181].

The lower bounds on squark and gluino masses may not be as large as suggested by the experimental analyses based on the CMSSM or simplified models. For example, mass bounds for the gluino and the first and second generation squarks based on the CMSSM can often be evaded in alternative or extended MSSM models, e.g., compressed SUSY [182] and stealth SUSY [183]. Moreover, the experimental upper limits for the third generation squark masses (which have a more direct impact on the fine-tuning measure) are weaker than the corresponding mass limits for other colored supersymmetric states.

Among the uncolored superpartners, the higgsinos are typically the most impacted by the naturalness constraints. Eq. (89.5) sug-

gests that the masses of the two neutral higgsinos and charged higgsino pair (which are governed by  $|\mu|$ ) should not be significantly larger than  $m_Z$  to avoid an unnatural fine-tuning of the supersymmetric parameters, which would imply the existence of light higgsinos (whose masses are not well constrained, as they are difficult to detect directly at the LHC due to their soft decay products). Nevertheless, it may be possible to avoid the conclusion that  $\mu \sim \mathcal{O}(m_Z)$  if additional correlations among the SUSY breaking mass parameters and  $\mu$  are present. Such a scenario can be realized in models in which the boundary conditions for SUSY breaking are generated by approximately conformal strong dynamics. For example, in the so-called scalar-sequestering model of Ref. [184], values of  $|\mu| > 1$  TeV can be achieved while naturally maintaining the observed value of  $m_Z$ .

Finally, one can also consider extensions of the MSSM in which the degree of fine-tuning is relaxed. For example, it has already been noted in Sec. 89.5 that it is possible to accommodate the observed Higgs mass more easily in the NMSSM due to contributions to  $m_h^2$  proportional to the parameter  $\lambda^2$ . This means that we do not have to rely on a large contribution from the radiative corrections to boost the Higgs mass sufficiently above its tree-level bound. This allows for smaller top squark masses, which are more consistent with the demands of naturalness. The reduction of the fine-tuning in various NMSSM models was initially advocated in Ref. [185], and subsequently treated in more detail in Refs. [106, 186]. Naturalness can also be relaxed in extended supersymmetric models with vector-like quarks [187] and in gauge extensions of the MSSM [188].

The experimental absence of any new physics beyond the Standard Model at the LHC suggests that the principle of naturalness is presently under significant stress [189]. Nevertheless, one must be very cautious when drawing conclusions about the viability of weak-scale SUSY to explain the origin of electroweak symmetry breaking, since different measures of fine-tuning noted above can lead to different assessments [168, 169]. Moreover, the maximal value of  $\Delta$  that determines whether weak-scale SUSY is a fine-tuned model (should it be  $\Delta \sim 10^?$   $100^?$   $1000^?$ ) is ultimately subjective. Thus, it is premature to conclude that weak-scale SUSY is on the verge of exclusion. However, it might be possible to sharpen the upper bounds on superpartner masses based on naturalness arguments, which ultimately will either confirm or refute the weak scale SUSY hypothesis [190]. Of course, if evidence for supersymmetric phenomena in the multi-TeV regime were to be established at a future collider facility (with an energy reach beyond the LHC [191]), it would be viewed as a spectacularly successful explanation of the large gauge hierarchy between the (multi)-TeV scale and Planck scale. In this case, the remaining little hierarchy, characterized by the somewhat large value of the fine-tuning parameter  $\Delta$  discussed above, would be regarded as a less pressing issue.

### 89.7.2 Constraints from virtual exchange of supersymmetric particles

There are a number of low-energy measurements that are sensitive to the effects of new physics through indirect searches via supersymmetric loop effects. For example, the virtual exchange of supersymmetric particles can contribute to the muon anomalous magnetic moment,  $a_\mu \equiv \frac{1}{2}(g-2)_\mu$ , as reviewed in Ref. [192]. The SM prediction for  $a_\mu$  exhibits a deviation in the range of  $3-4\sigma$  from the experimentally observed value [193]. This discrepancy is difficult to accommodate in the constrained SUSY models of Sec. 89.6.2 and 89.6.3 given the present sparticle mass bounds [173]. Nevertheless, there are regions of the more general pMSSM parameter space that are consistent with the observed value of  $a_\mu$  [194]. An updated value of the fine structure constant has resulted in a new SM prediction [195] for the electron anomalous magnetic moment  $a_e$  which is  $2.4\sigma$  above the measurement [196]. Indeed, it is possible within the pMSSM to find allowed parameter space regions where the observed values of  $a_\mu$  and  $a_e$  are simultaneously accommodated [197].

The rare inclusive decay  $b \rightarrow s\gamma$  also provides a sensitive probe to the virtual effects of new physics beyond the SM. The experimental measurements of  $B \rightarrow X_s + \gamma$  [198] are in agreement with the theoretical SM predictions of Ref. [199]. Since supersymmet-

ric loop corrections can contribute an observable shift from the SM predictions, the absence of any significant deviation places useful constraints on the MSSM parameter space [200].

The rare decays  $B_s \rightarrow \mu^+ \mu^-$  and  $B_d \rightarrow \mu^+ \mu^-$  are especially sensitive to supersymmetric loop effects, with some loop contributions scaling as  $\tan^6 \beta$  when  $\tan \beta \gg 1$  [201]. At present, a combination of the measurements of these rare decay modes [202] are in slight tension at the  $2\sigma$  level [203] with the predicted SM rates [204]. Such a tension can be resolved by the aforementioned supersymmetric loop effects [201].

The decays  $B^\pm \rightarrow \tau^\pm \nu_\tau$  and  $B \rightarrow D^{(*)} \tau^- \bar{\nu}_\tau$  are noteworthy, since in models with extended Higgs sectors such as the MSSM, these processes possess tree-level charged Higgs exchange contributions that can compete with the dominant  $W$ -exchange. As Section 71 shows, experimental measurements of  $B^\pm \rightarrow \tau^\pm \nu_\tau$  are currently consistent with SM expectations [205]. The BaBar Collaboration measured values of the rates for  $\bar{B} \rightarrow D \tau^- \bar{\nu}_\tau$  and  $\bar{B} \rightarrow D^* \tau^- \bar{\nu}_\tau$  [206] that showed a combined  $3.4\sigma$  discrepancy from the SM predictions, which was also not compatible with the Type-II Higgs Yukawa couplings employed by the MSSM. Some subsequent measurements of the LHCb and Belle Collaborations [207] were consistent with the BaBar measurements, although more recent Belle measurements using a semi-leptonic tag are more consistent with SM expectations [208]. The combined difference between the measured and expected values of the  $\bar{B} \rightarrow D \tau^- \bar{\nu}_\tau$  and  $\bar{B} \rightarrow D^* \tau^- \bar{\nu}_\tau$  decay rates relative to the corresponding SM values has a significance of about three standard deviations [209]. There are a number of additional anomalies in  $B$  decay data that have recently attracted some attention, although at present the observed deviations from SM expectations are mostly at the level of about two to three standard deviations (see, *e.g.*, Ref. [203]).

In summary, although there are a few hints of possible deviations from the SM in  $B$  decays, none of the discrepancies by themselves are significant enough to conclusively imply the existence of new physics beyond the SM. The absence of definitive evidence for deviations in various  $B$ -physics observables from their SM predictions places useful constraints on the MSSM parameter space [120,172,210]. In contrast, if one or more of the  $B$  anomalies referred to above were to be experimentally confirmed, it would require require significant modifications to the supersymmetric models treated in this review.

Finally, we note that the constraints from precision electroweak observables (see Sec. 10) and measurements of the  $\epsilon'/\epsilon$  anomaly [211], if it persists [212], in the Kaon system are easily accommodated in models of TeV-scale SUSY [213,214]. Thus, robust regions of the MSSM parameter space, compatible with the results of direct and indirect searches for SUSY, remain viable.

## 89.8 Massive neutrinos in weak-scale SUSY

In the minimal SM and its supersymmetric extension, there are no right-handed neutrinos, and Majorana mass terms for the left-handed neutrinos are absent. However, given the overwhelming evidence for neutrino masses and mixing (see Sec. 14 and Ref. [215]), any viable model of fundamental particles must provide a mechanism for generating neutrino masses [216]. In extended supersymmetric models, various mechanisms exist for producing massive neutrinos [217]. Although one can devise models for generating massive Dirac neutrinos [218], the most common approaches for incorporating neutrino masses are based on  $L$ -violating supersymmetric extensions of the MSSM, which generate massive Majorana neutrinos. Two classes of  $L$ -violating supersymmetric models will now be considered.

### 89.8.1 The supersymmetric seesaw

Neutrino masses can be incorporated into the SM by introducing  $SU(3) \times SU(2) \times U(1)$  singlet right-handed neutrinos ( $\nu_R$ ) whose mass parameters are very large, typically near the grand unification scale. In addition, one must also include a standard Yukawa couplings between the lepton doublets, the Higgs doublet, and  $\nu_R$ . The Higgs vacuum expectation value then induces an off-diagonal  $\nu_L - \nu_R$  mass on the order of the electroweak scale. Diagonalizing the neutrino mass matrix (in the three-generation model) yields three superheavy neutrino states, and three very

light neutrino states that are identified with the light neutrinos observed in nature. This is the seesaw mechanism [219].

It is straightforward to construct a supersymmetric generalization of the seesaw model of neutrino masses [220,221] by promoting the right-handed neutrino field to a superfield  $\hat{N}^c = (\tilde{\nu}_R; \nu_R)$ . Integrating out the heavy right-handed neutrino supermultiplet yields a new term in the superpotential [cf. Eq. (89.1)] of the form

$$W_{\text{seesaw}} = \frac{f}{M_R} (\hat{H}_U \hat{L}) (\hat{H}_U \hat{L}), \quad (89.23)$$

where  $M_R$  is the mass scale of the right-handed neutrino sector and  $f$  is a dimensionless constant. Note that lepton number is broken by two units, which implies that R-parity is conserved. The supersymmetric analogue of the Majorana neutrino mass term in the sneutrino sector leads to sneutrino-antisneutrino mixing phenomena [221,222].

The SUSY Les Houches Accords [75,91], mentioned at the end of the introduction to Sec. 89.4, have been extended to the supersymmetric seesaw (and other extensions of the MSSM) in Ref. [223].

### 89.8.2 R-parity-violating SUSY

It is possible to incorporate massive neutrinos in renormalizable supersymmetric models while retaining the minimal particle content of the MSSM by relaxing the assumption of R-parity invariance. The most general R-parity-violating (RPV) model involving the MSSM spectrum introduces many new parameters to both the SUSY-conserving and the SUSY-breaking sectors [75,224]. Each new interaction term violates either  $B$  or  $L$  conservation. For example, starting from the MSSM superpotential given in Eq. (89.1) [suitably generalized to three generations of quarks, leptons and their superpartners], consider the effect of adding the following new terms:

$$W_{\text{RPV}} = (\lambda_L)_{pmn} \hat{L}_p \hat{L}_m \hat{E}_n^c + (\lambda'_L)_{pmn} \hat{L}_p \hat{Q}_m \hat{D}_n^c + (\lambda_B)_{pmn} \hat{U}_p^c \hat{D}_m^c \hat{D}_n^c + (\mu_L)_p \hat{H}_u \hat{L}_p, \quad (89.24)$$

where  $p$ ,  $m$ , and  $n$  are generation indices, and gauge group indices are suppressed. Eq. (89.24) yields new scalar-fermion Yukawa couplings consisting of all possible combinations involving two SM fermions and one scalar superpartner.

Note that the term in Eq. (89.24) proportional to  $\lambda_B$  violates  $B$ , while the other three terms violate  $L$ . The  $L$ -violating term in Eq. (89.24) proportional to  $\mu_L$  is the RPV generalization of the  $\mu \hat{H}_u \hat{H}_d$  term of the MSSM superpotential, in which the  $Y = -1$  Higgs/higgsino supermultiplet  $\hat{H}_d$  is replaced by the slepton/lepton supermultiplet  $\hat{L}_p$ .

Phenomenological constraints derived from data on various low-energy  $B$ - and  $L$ -violating processes can be used to establish limits on each of the coefficients  $(\lambda_L)_{pmn}$ ,  $(\lambda'_L)_{pmn}$ , and  $(\lambda_B)_{pmn}$  taken one at a time [224,225]. If more than one coefficient is simultaneously non-zero, then the limits are in general more complicated [226]. All possible RPV terms cannot be simultaneously present and unsuppressed; otherwise the proton decay rate would be many orders of magnitude larger than the present experimental bound. One way to avoid proton decay is to impose  $B$  or  $L$  invariance (either one alone would suffice). Otherwise, one must accept the requirement that certain RPV coefficients must be extremely suppressed.

One particularly interesting class of RPV models is one in which  $B$  is conserved, but  $L$  is violated. It is possible to enforce baryon number conservation (and the stability of the proton), while allowing for lepton-number-violating interactions by imposing a discrete  $\mathbf{Z}_3$  baryon triality symmetry on the low-energy theory [227], in place of the standard  $\mathbf{Z}_2$  R-parity. Since the distinction between the Higgs and matter supermultiplets is lost in RPV models where  $L$  is violated, the mixing of sleptons and Higgs bosons, the mixing of neutrinos and neutralinos, and the mixing of charged leptons and charginos are now possible, leading to more complicated mass matrices and mass eigenstates than in the MSSM. The treatment of neutrino masses and mixing in this framework can be found, *e.g.*, in Ref. [228].

Alternatively, one can consider imposing a lepton parity such that all lepton superfields are odd [227, 229]. In this case, only the  $B$ -violating term in Eq. (89.24) survives, and  $L$  is conserved. Models of this type have been considered in Ref. [230]. Since  $L$  is conserved in these models, the mixing of the lepton and Higgs superfields is forbidden. Moreover, neutrino masses (and mixing) are not generated if lepton parity is an exact symmetry. However, one expects that lepton parity cannot be exact due to quantum gravity effects. Remarkably, the standard  $\mathbf{Z}_2$  R-parity and the  $\mathbf{Z}_3$  baryon triality are stable with respect to quantum gravity effects, as they can be identified as residual discrete symmetries that arise from spontaneously broken non-anomalous gauge symmetries [227].

The symmetries employed above to either remove or suppress R-parity violating operators were flavour independent. In contrast, there exist a number of motivated scenarios based on flavor symmetries that can also yield the suppression as required by the experimental data (e.g., see Ref. [231]).

The supersymmetric phenomenology of the RPV models exhibits features that are distinct from that of the MSSM [224]. The LSP is no longer stable, which implies that not all supersymmetric decay chains must yield missing-energy events at colliders. A comprehensive examination of the phenomenology of the MSSM extended by a single R-parity violating coupling at the unification scale and its implications for LHC searches has been given in Ref. [232]. As an example, the sparticle mass bounds obtained in searches for R-parity-conserving SUSY can be considerably relaxed in certain RPV models due to the absence of large missing transverse momentum signatures [233]. This can alleviate some of the tension with naturalness discussed in Sec. 89.7.1.

Nevertheless, the loss of the missing-energy signature is often compensated by other striking signals (which depend on which R-parity-violating parameters are dominant). For example, supersymmetric particles in RPV models can be singly produced (in contrast to R-parity-conserving models where supersymmetric particles must be produced in pairs). The phenomenology of pair-produced supersymmetric particles is also modified in RPV models due to new decay chains not present in R-parity-conserving SUSY models [224].

In RPV models with lepton number violation (these include weak-scale SUSY models with baryon triality mentioned above), both  $\Delta L = 1$  and  $\Delta L = 2$  phenomena are allowed, leading to neutrino masses and mixing [234], neutrinoless double-beta decay [235], sneutrino-antisneutrino mixing [236], and resonant  $s$ -channel production of sneutrinos in  $e^+e^-$  collisions [237] and charged sleptons in  $p\bar{p}$  and  $pp$  collisions [238].

### 89.9 Extensions beyond the MSSM

Extensions of the MSSM have been proposed to solve a variety of theoretical problems. One such problem involves the  $\mu$  parameter of the MSSM. Although  $\mu$  is a SUSY-preserving parameter, it must be of order the effective SUSY-breaking scale of the MSSM to yield a consistent supersymmetric phenomenology [239]. Any natural solution to the so-called  $\mu$ -problem must incorporate a symmetry that enforces  $\mu = 0$  and a small symmetry-breaking parameter that generates a value of  $\mu$  that is not parametrically larger than the effective SUSY-breaking scale [240]. A number of proposed mechanisms in the literature (e.g., see Refs. [239–241]) provide concrete examples of a natural solution to the  $\mu$ -problem of the MSSM.

In extensions of the MSSM, new compelling solutions to the  $\mu$ -problem are possible. For example, one can replace  $\mu$  by the vacuum expectation value of a new  $SU(3) \times SU(2) \times U(1)$  singlet scalar field. This is the NMSSM, which yields phenomena that were briefly discussed in Sections 89.4–89.7. The NMSSM superpotential consists only of trilinear terms whose coefficients are dimensionless. There are some advantages to extending the NMSSM further to the USSM [97] by adding a new broken  $U(1)$  gauge symmetry [242], under which the singlet field is charged.

Alternatively, one can consider a generalized version of the NMSSM (called the GNMSSM in Ref. [186]), where all possible renormalizable terms in the superpotential are allowed, which yields new supersymmetric mass terms (analogous to the  $\mu$  term of the MSSM). A discussion of the parameters of the GNMSSM

can be found in Ref. [75]. Although the GNMSSM does not solve the  $\mu$ -problem, it does exhibit regions of parameter space in which the degree of fine-tuning is relaxed, as discussed in Sec. 89.7.1.

The generation of the  $\mu$  term may be connected with the solution to the strong CP problem [243]. Models of this type, which include new gauge singlet fields that are charged under the Peccei-Quinn (PQ) symmetry [244], were first proposed in Ref. [239]. The breaking of the PQ symmetry is thus intimately tied to SUSY breaking, while naturally yielding a value of  $\mu$  that is of order the electroweak symmetry breaking scale [245].

It is also possible to add higher dimensional Higgs multiplets, such as Higgs triplet superfields [246], provided a custodial-symmetric model (in which the  $\rho$ -parameter of precision electroweak physics is close to 1, see Sec. 10) can be formulated. Such models can provide a rich phenomenology of new signals for future LHC studies.

All supersymmetric models discussed so far in this review possess self-conjugate fermions—the Majorana gluinos and neutralinos. However, it is possible to add additional chiral superfields in the adjoint representation. The spin-1/2 components of these new superfields can pair up with the gauginos to form Dirac gauginos [247, 248]. Such states appear in models of so-called supersoft SUSY breaking [249], in some generalized GMSB models [250] and in R-symmetric SUSY [251, 252]. Such approaches often lead to improved naturalness and/or significantly relaxed flavor constraints. The implications of models of Dirac gauginos on the observed Higgs boson mass and its properties are addressed in Ref. [253].

For completeness, we briefly note other MSSM extensions considered in the literature. These include an enlarged electroweak gauge group beyond  $SU(2) \times U(1)$  [254]; and/or the addition of new (possibly exotic) matter supermultiplets such as vector-like fermions and their superpartners [187, 255].

### References

- [1] *The Supersymmetric World—The Beginnings of the Theory*, World Scientific, Singapore (2000), edited by G. Kane and M. Shifman, contains an early history of supersymmetry and a guide to the original literature.
- [2] R. Haag, J. T. Lopuszanski and M. Sohnius, Nucl. Phys. **B88**, 257 (1975); S. R. Coleman and J. Mandula, Phys. Rev. **159**, 1251 (1967).
- [3] H. P. Nilles, Phys. Rept. **110**, 1 (1984).
- [4] S. Weinberg, *The Quantum Theory of Fields, Volume III: Supersymmetry* (Cambridge University Press, Cambridge, UK, 2000).
- [5] P. Nath, *Supersymmetry, Supergravity, and Unification* (Cambridge University Press, Cambridge, UK, 2017).
- [6] S. P. Martin *A Supersymmetry Primer*, [hep-ph/9709356].
- [7] E. Witten, Nucl. Phys. **B188**, 513 (1981).
- [8] S. Dimopoulos and H. Georgi, Nucl. Phys. **B193**, 150 (1981).
- [9] N. Sakai, Z. Phys. **C11**, 153 (1981).
- [10] L. Susskind, Phys. Rept. **104**, 181 (1984).
- [11] L. Girardello and M. T. Grisaru, Nucl. Phys. **B194**, 65 (1982).
- [12] L. J. Hall and L. Randall, Phys. Rev. Lett. **65**, 2939 (1990); I. Jack and D. R. T. Jones, Phys. Lett. **B457**, 101 (1999), [hep-ph/9903365].
- [13] V. F. Weisskopf, Phys. Rev. **56**, 72 (1939).
- [14] See e.g., N. Polonsky, *Supersymmetry: Structure and phenomena. Extensions of the standard model*, Lect. Notes Phys. **M68**, 1 (2001).
- [15] G. Bertone, D. Hooper and J. Silk, Phys. Rept. **405**, 279 (2005), [hep-ph/0404175].
- [16] D. Hooper, “TASI 2008 Lectures on Dark Matter,” in *The Dawn of the LHC Era, Proceedings of the 2008 Theoretical and Advanced Study Institute in Elementary Particle Physics*, Boulder, Colorado, 2–27 June 2008, edited by Tao Han (World Scientific, Singapore, 2009).

- [17] H. Pagels and J. R. Primack, *Phys. Rev. Lett.* **48**, 223 (1982).
- [18] H. Goldberg, *Phys. Rev. Lett.* **50**, 1419 (1983).
- [19] J. R. Ellis *et al.*, *Nucl. Phys.* **B238**, 453 (1984).
- [20] G. Jungman, M. Kamionkowski, and K. Griest, *Phys. Reports* **267**, 195 (1996).
- [21] F. D. Steffen, *Eur. Phys. J.* **C59**, 557 (2009), [arXiv:0811.3347].
- [22] H. E. Haber and G. L. Kane, *Phys. Rept.* **117**, 75 (1985).
- [23] M. Drees, R. Godbole, and P. Roy, *Theory and Phenomenology of Sparticles* (World Scientific, Singapore, 2005); H. Baer and X. Tata, *Weak Scale Supersymmetry: from Superfields to Scattering Events* (Cambridge University Press, Cambridge, UK, 2006); I.J.R. Aitchison, *Supersymmetry in Particle Physics: an elementary introduction* (Cambridge University Press, Cambridge, UK, 2007).
- [24] Our notation for the charge-conjugated fields follows the notation of P. Langacker, *The Standard Model and Beyond*, 2nd edition (CRC Press, Boca Raton, FL, 2017).
- [25] H. Georgi and S. L. Glashow, *Phys. Rev.* **D6**, 429 (1972).
- [26] P. Fayet, *Nucl. Phys.* **B90**, 104 (1975).
- [27] K. Inoue *et al.*, *Prog. Theor. Phys.* **67**, 1889 (1982).
- [28] J. F. Gunion and H. E. Haber, *Nucl. Phys.* **B272**, 1 (1986), [Erratum: **B402**, 567 (1993)].
- [29] A. Salam and J. A. Strathdee, *Nucl. Phys.* **B76**, 477 (1974).
- [30] J. Wess and J. Bagger, *Supersymmetry and Supergravity* (Princeton University Press, Princeton, NJ, 1992).
- [31] I. L. Buchbinder, S. Kuzenko and Z. Yarevskaya, *Nucl. Phys.* **B411**, 665 (1994); I. Antoniadis, E. Dudas and D. M. Ghilencea, *JHEP* **03**, 045 (2008), [arXiv:0708.0383].
- [32] D. J. H. Chung *et al.*, *Phys. Rept.* **407**, 1 (2005), [hep-ph/0312378].
- [33] J. R. Ellis *et al.*, *Phys. Rev.* **D39**, 844 (1989); U. Ellwanger and C. Hugonie, *Eur. Phys. J.* **C25**, 297 (2002), [hep-ph/9909260]; U. Ellwanger, C. Hugonie and A. M. Teixeira, *Phys. Rept.* **496**, 1 (2010), [arXiv:0910.1785]; M. Maniatis, *Int. J. Mod. Phys.* **A25**, 3505 (2010), [arXiv:0906.0777].
- [34] S. Weinberg, *Phys. Rev. Lett.* **43**, 1566 (1979); S. Weinberg, *Phys. Rev.* **D22**, 1694 (1980); F. Wilczek and A. Zee, *Phys. Rev. Lett.* **43**, 1571 (1979); H. A. Weldon and A. Zee, *Nucl. Phys.* **B173**, 269 (1980).
- [35] P. Fayet, *Phys. Lett.* **69B**, 489 (1977); G. R. Farrar and P. Fayet, *Phys. Lett.* **76B**, 575 (1978).
- [36] P. Fayet, *Phys. Lett.* **84B**, 421 (1979); P. Fayet, *Phys. Lett.* **86B**, 272 (1979).
- [37] D.Z. Freedman and A. Van Proeyen, *Supergravity* (Cambridge University Press, Cambridge, UK, 2012); M. Rausch de Traubenberg and M. Valenzuela, *A Supergravity Primer* (World Scientific, Singapore, 2020).
- [38] S. Deser and B. Zumino, *Phys. Rev. Lett.* **38**, 1433 (1977); E. Cremmer *et al.*, *Phys. Lett.* **79B**, 231 (1978).
- [39] R. Casalbuoni *et al.*, *Phys. Lett.* **B215**, 313 (1988); R. Casalbuoni *et al.*, *Phys. Rev.* **D39**, 2281 (1989); A. L. Maroto and J. R. Pelaez, *Phys. Rev.* **D62**, 023518 (2000), [hep-ph/9912212].
- [40] Z. Komargodski and N. Seiberg, *JHEP* **09**, 066 (2009), [arXiv:0907.2441]; I. Antoniadis *et al.*, *Theor. Math. Phys.* **170**, 26 (2012), [Teor. Mat. Fiz. **170**, 34 (2012)].
- [41] A.H. Chamseddine, R. Arnowitt, and P. Nath, *Phys. Rev. Lett.* **49**, 970 (1982); R. Barbieri, S. Ferrara and C. A. Savoy, *Phys. Lett.* **119B**, 343 (1982); L. E. Ibanez, *Nucl. Phys.* **B218**, 514 (1983); H. P. Nilles, M. Srednicki and D. Wyler, *Phys. Lett.* **120B**, 346 (1983); H. P. Nilles, M. Srednicki and D. Wyler, *Phys. Lett.* **124B**, 337 (1983); E. Cremmer, P. Fayet and L. Girardello, *Phys. Lett.* **122B**, 41 (1983); N. Ohta, *Prog. Theor. Phys.* **70**, 542 (1983).
- [42] L. Alvarez-Gaumé, J. Polchinski, and M.B. Wise, *Nucl. Phys.* **B221**, 495 (1983).
- [43] L. J. Hall, J. D. Lykken and S. Weinberg, *Phys. Rev.* **D27**, 2359 (1983).
- [44] S. K. Soni and H. A. Weldon, *Phys. Lett.* **126B**, 215 (1983); Y. Kawamura, H. Murayama and M. Yamaguchi, *Phys. Rev.* **D51**, 1337 (1995), [hep-ph/9406245].
- [45] See, *e.g.*, A. Brignole, L.E. Ibáñez, and C. Muñoz, in *Perspectives on Supersymmetry II*, edited by G.L. Kane (World Scientific, Singapore, 2010) pp. 244–268.
- [46] A. B. Lahanas and D. V. Nanopoulos, *Phys. Rept.* **145**, 1 (1987).
- [47] J. L. Feng, A. Rajaraman and F. Takayama, *Phys. Rev. Lett.* **91**, 011302 (2003), [hep-ph/0302215]; J. L. Feng, A. Rajaraman and F. Takayama, *Phys. Rev.* **D68**, 063504 (2003), [hep-ph/0306024]; J. L. Feng, A. Rajaraman and F. Takayama, *Int. J. Mod. Phys.* **D13**, 2355 (2004), [hep-th/0405248].
- [48] L. Randall and R. Sundrum, *Nucl. Phys.* **B557**, 79 (1999), [hep-th/9810155].
- [49] F. D’Eramo, J. Thaler and Z. Thomas, *JHEP* **06**, 151 (2012), [arXiv:1202.1280]; F. D’Eramo, J. Thaler and Z. Thomas, *JHEP* **09**, 125 (2013), [arXiv:1307.3251]; S. P. de Alwis, *Phys. Rev.* **D77**, 105020 (2008), [arXiv:0801.0578]; S. P. de Alwis, *JHEP* **01**, 006 (2013), [arXiv:1206.6775]; K. Harigaya and M. Ibe, *Phys. Rev.* **D90**, 085028 (2014), [arXiv:1409.5029].
- [50] I. Jack, D. R. T. Jones and R. Wild, *Phys. Lett.* **B535**, 193 (2002), [hep-ph/0202101]; B. Murakami and J. D. Wells, *Phys. Rev.* **D68**, 035006 (2003), [hep-ph/0302209]; R. Kitano, G. D. Kribs and H. Murayama, *Phys. Rev.* **D70**, 035001 (2004), [hep-ph/0402215]; R. Hodgson *et al.*, *Nucl. Phys.* **B728**, 192 (2005), [hep-ph/0507193]; D. R. T. Jones and G. G. Ross, *Phys. Lett.* **B642**, 540 (2006), [hep-ph/0609210].
- [51] S. Asai *et al.*, *Phys. Lett.* **B653**, 81 (2007), [arXiv:0705.3086].
- [52] M. Dine, W. Fischler and M. Srednicki, *Nucl. Phys.* **B189**, 575 (1981); S. Dimopoulos and S. Raby, *Nucl. Phys.* **B192**, 353 (1981); S. Dimopoulos and S. Raby, *Nucl. Phys.* **B219**, 479 (1983); M. Dine and W. Fischler, *Phys. Lett.* **110B**, 227 (1982); C. R. Nappi and B. A. Ovrut, *Phys. Lett.* **113B**, 175 (1982); L. Alvarez-Gaume, M. Claudson and M. B. Wise, *Nucl. Phys.* **B207**, 96 (1982).
- [53] M. Dine and A. E. Nelson, *Phys. Rev.* **D48**, 1277 (1993), [hep-ph/9303230]; M. Dine, A. E. Nelson and Y. Shirman, *Phys. Rev.* **D51**, 1362 (1995), [hep-ph/9408384].
- [54] M. Dine *et al.*, *Phys. Rev.* **D53**, 2658 (1996), [hep-ph/9507378].
- [55] G. F. Giudice and R. Rattazzi, *Phys. Rept.* **322**, 419 (1999), [hep-ph/9801271].
- [56] E. Poppitz and S. P. Trivedi, *Phys. Rev.* **D55**, 5508 (1997), [hep-ph/9609529]; H. Murayama, *Phys. Rev. Lett.* **79**, 18 (1997), [hep-ph/9705271]; M. A. Luty and J. Terning, *Phys. Rev.* **D57**, 6799 (1998), [hep-ph/9709306]; K. Agashe, *Phys. Lett.* **B435**, 83 (1998), [hep-ph/9804450]; N. Arkani-Hamed, J. March-Russell and H. Murayama, *Nucl. Phys.* **B509**, 3 (1998), [hep-ph/9701286]; C. Csaki, Y. Shirman and J. Terning, *JHEP* **05**, 099 (2007), [hep-ph/0612241]; M. Ibe and R. Kitano, *Phys. Rev.* **D77**, 075003 (2008), [arXiv:0711.0416].
- [57] M. Kawasaki *et al.*, *Phys. Rev.* **D78**, 065011 (2008), [arXiv:0804.3745].
- [58] M. J. Strassler and K. M. Zurek, *Phys. Lett.* **B651**, 374 (2007), [hep-ph/0604261]; T. Han *et al.*, *JHEP* **07**, 008 (2008), [arXiv:0712.2041].
- [59] M. J. Strassler [hep-ph/0607160]; K. M. Zurek, *Phys. Rev.* **D79**, 115002 (2009), [arXiv:0811.4429].

- [60] See *e.g.*, M. Quiros, in *Particle Physics and Cosmology: The Quest for Physics Beyond the Standard Model(s), Proceedings of the 2002 Theoretical Advanced Study Institute in Elementary Particle Physics (TASI 2002)*, edited by H.E. Haber and A.E. Nelson (World Scientific, Singapore, 2004) pp. 549–601; C. Csaki, in *ibid.*, pp. 605–698.
- [61] V.A. Rubakov, *Sov. Phys. Usp.* **44**, 871 (2001); J. L. Hewett and M. Spiropulu, *Ann. Rev. Nucl. Part. Sci.* **52**, 397 (2002), [hep-ph/0205106].
- [62] Z. Chacko, M. A. Luty and E. Ponton, *JHEP* **07**, 036 (2000), [hep-ph/9909248]; D. E. Kaplan, G. D. Kribs and M. Schmaltz, *Phys. Rev.* **D62**, 035010 (2000), [hep-ph/9911293]; Z. Chacko *et al.*, *JHEP* **01**, 003 (2000), [hep-ph/9911323].
- [63] J. Scherk and J. H. Schwarz, *Phys. Lett.* **82B**, 60 (1979); J. Scherk and J. H. Schwarz, *Nucl. Phys.* **B153**, 61 (1979).
- [64] R. Barbieri, L. J. Hall and Y. Nomura, *Phys. Rev.* **D66**, 045025 (2002), [hep-ph/0106190]; R. Barbieri, L. J. Hall and Y. Nomura, *Nucl. Phys.* **B624**, 63 (2002), [hep-th/0107004]; I. Garcia Garcia, K. Howe and J. March-Russell, *JHEP* **12**, 005 (2015), [arXiv:1510.07045].
- [65] J. D. Wells, in “11th International Conference on Supersymmetry and the Unification of Fundamental Interactions (SUSY 2003) Tucson, Arizona, June 5-10, 2003,” (2003), [hep-ph/0306127]; J. D. Wells, *Phys. Rev.* **D71**, 015013 (2005), [hep-ph/0411041].
- [66] N. Arkani-Hamed and S. Dimopoulos, *JHEP* **06**, 073 (2005), [hep-th/0405159]; G. F. Giudice and A. Romanino, *Nucl. Phys.* **B699**, 65 (2004), [Erratum: **B706**, 487 (2005)], [hep-ph/0406088].
- [67] G. F. Giudice and A. Strumia, *Nucl. Phys.* **B858**, 63 (2012), [arXiv:1108.6077].
- [68] A. Arvanitaki *et al.*, *JHEP* **02**, 126 (2013), [arXiv:1210.0555]; N. Arkani-Hamed *et al.* (2012), [arXiv:1212.6971].
- [69] E. Bagnaschi *et al.*, *JHEP* **09**, 092 (2014), [arXiv:1407.4081].
- [70] J. Pardo Vega and G. Villadoro, *JHEP* **07**, 159 (2015), [arXiv:1504.05200].
- [71] B. C. Allanach and A. Voigt, *Eur. Phys. J.* **C78**, 573 (2018), [arXiv:1804.09410].
- [72] Y. Kahn, M. McCullough and J. Thaler, *JHEP* **11**, 161 (2013), [arXiv:1308.3490].
- [73] L. J. Hall and Y. Nomura, *JHEP* **01**, 082 (2012), [arXiv:1111.4519]; M. Ibe and T. T. Yanagida, *Phys. Lett.* **B709**, 374 (2012), [arXiv:1112.2462].
- [74] H. E. Haber and L. Stephenson Haskins (2018), *Supersymmetric Theory and Models*, in *Anticipating the Next Discoveries in Particle Physics*, Proceedings of the 2016 Theoretical Advanced Study Institute in Elementary Particle Physics, edited by Rouven Essig and Ian Low (World Scientific, Singapore, 2018) pp. 355–499, [arXiv:1712.05926].
- [75] B. C. Allanach *et al.*, *Comput. Phys. Commun.* **180**, 8 (2009), [arXiv:0801.0045].
- [76] J. M. Frere, D. R. T. Jones and S. Raby, *Nucl. Phys.* **B222**, 11 (1983); J. P. Derendinger and C. A. Savoy, *Nucl. Phys.* **B237**, 307 (1984); J. F. Gunion, H. E. Haber and M. Sher, *Nucl. Phys.* **B306**, 1 (1988); D. Chowdhury *et al.*, *JHEP* **02**, 110 (2014), [Erratum: **03**, 149 (2018)], [arXiv:1310.1932]; W. G. Hollik, *JHEP* **08**, 126 (2016), [arXiv:1606.08356].
- [77] J. A. Casas, A. Lleyda and C. Munoz, *Nucl. Phys.* **B471**, 3 (1996), [hep-ph/9507294].
- [78] C. S. Ün *et al.*, *Phys. Rev.* **D91**, 105033 (2015), [arXiv:1412.1440].
- [79] G. G. Ross, K. Schmidt-Hoberg and F. Staub, *Phys. Lett.* **B759**, 110 (2016), [arXiv:1603.09347].
- [80] G. G. Ross, K. Schmidt-Hoberg and F. Staub, *JHEP* **03**, 021 (2017), [arXiv:1701.03480].
- [81] S. P. Martin, *Phys. Rev.* **D61**, 035004 (2000), [hep-ph/9907550].
- [82] S. Dimopoulos and D. W. Sutter, *Nucl. Phys.* **B452**, 496 (1995), [hep-ph/9504415]; D.W. Sutter, Stanford Ph. D. thesis, arXiv:hep-ph/9704390.
- [83] H.E. Haber, *Nucl. Phys. B (Proc. Suppl.)* **62A-C**, 469 (1998).
- [84] R. M. Barnett, J. F. Gunion and H. E. Haber, *Phys. Lett.* **B315**, 349 (1993), [hep-ph/9306204]; H. Baer, X. Tata and J. Woodside, *Phys. Rev.* **D41**, 906 (1990).
- [85] S. M. Bilenky, N. P. Nedelcheva and E. K. Khristova, *Phys. Lett.* **161B**, 397 (1985); S. M. Bilenky, E. K. Khristova and N. P. Nedelcheva, *Bulg. J. Phys.* **13**, 283 (1986).
- [86] J. Rosiek, *Phys. Rev.* **D41**, 3464 (1990).
- [87] J. Alwall *et al.*, *JHEP* **09**, 028 (2007), [arXiv:0706.2334].
- [88] T. Hahn, *Comput. Phys. Commun.* **140**, 418 (2001), [hep-ph/0012260].
- [89] A. Pukhov *et al.*, INP MSU report 98-41/542 (arXiv:hep-ph/9908288); E. Boos *et al.* [CompHEP Collab.], *Nucl. Instrum. Methods* **A534**, 50 (2004); CompHEP webpage, <https://theory.sinp.msu.ru/dokuwiki/doku.php/comphep/news>.
- [90] D. M. Pierce *et al.*, *Nucl. Phys.* **B491**, 3 (1997), [hep-ph/9606211].
- [91] P. Z. Skands *et al.*, *JHEP* **07**, 036 (2004), [hep-ph/0311123].
- [92] For further details, see *e.g.*, Appendix C of Ref. [22] and Appendix A of Ref. [28].
- [93] J. L. Kneur and G. Moultaka, *Phys. Rev.* **D59**, 015005 (1999), [hep-ph/9807336].
- [94] R.A. Horn and C.R. Johnson, *Matrix Analysis*, 2nd Edition (Cambridge University Press, Cambridge, UK, 2003).
- [95] H. K. Dreiner, H. E. Haber and S. P. Martin, *Phys. Rept.* **494**, 1 (2010), [arXiv:0812.1594].
- [96] L. Autonne, *Annals de l'Université de Lyon, Nouvelle Série I, Fasc.* **38**, 1 (1915); T. Takagi, *Japan J. Math.* **1**, 83 (1925).
- [97] S. Y. Choi *et al.*, *Nucl. Phys.* **B778**, 85 (2007), [hep-ph/0612218].
- [98] S. Y. Choi *et al.*, *Eur. Phys. J.* **C22**, 563 (2001), [Addendum: *Eur. Phys. J.* **C23**, 769 (2002)], [hep-ph/0108117].
- [99] M. M. El Kheishen, A. A. Aboshousha and A. A. Shafik, *Phys. Rev.* **D45**, 4345 (1992).
- [100] T. Hahn (2006), [arXiv:physics/0607103].
- [101] K.-i. Hikasa and M. Kobayashi, *Phys. Rev.* **D36**, 724 (1987); F. Gabbiani and A. Masiero, *Nucl. Phys.* **B322**, 235 (1989); P. Brax and C. A. Savoy, *Nucl. Phys.* **B447**, 227 (1995), [hep-ph/9503306].
- [102] J. R. Ellis and S. Rudaz, *Phys. Lett.* **128B**, 248 (1983); F. Browning, D. Chang and W.-Y. Keung, *Phys. Rev.* **D64**, 015010 (2001), [hep-ph/0012258]; A. Bartl *et al.*, *Phys. Lett.* **B573**, 153 (2003), [hep-ph/0307317]; A. Bartl *et al.*, *Phys. Rev.* **D70**, 035003 (2004), [hep-ph/0311338].
- [103] J.F. Gunion *et al.*, *The Higgs Hunter's Guide* (Westview Press, Boulder, CO, 2000); M. Carena and H. E. Haber, *Prog. Part. Nucl. Phys.* **50**, 63 (2003), [hep-ph/0208209]; A. Djouadi, *Phys. Rept.* **459**, 1 (2008), [hep-ph/0503173].
- [104] E. Bagnaschi *et al.*, *Eur. Phys. J.* **C79**, 617 (2019), [arXiv:1808.07542].
- [105] H. E. Haber and M. Sher, *Phys. Rev.* **D35**, 2206 (1987).
- [106] L. J. Hall, D. Pinner and J. T. Ruderman, *JHEP* **04**, 131 (2012), [arXiv:1112.2703].
- [107] L. J. Hall and M. B. Wise, *Nucl. Phys.* **B187**, 397 (1981).
- [108] H. E. Haber and R. Hempfling, *Phys. Rev. Lett.* **66**, 1815 (1991); Y. Okada, M. Yamaguchi and T. Yanagida, *Prog. Theor. Phys.* **85**, 1 (1991); J. R. Ellis, G. Ridolfi and F. Zwirner, *Phys. Lett.* **B257**, 83 (1991).

- [109] P. Draper and H. Rzehak, Phys. Rept. **619**, 1 (2016), [arXiv:1601.01890].
- [110] A. Pilaftsis and C. E. M. Wagner, Nucl. Phys. **B553**, 3 (1999), [hep-ph/9902371]; D. A. Demir, Phys. Rev. **D60**, 055006 (1999), [hep-ph/9901389]; S. Y. Choi, M. Drees and J. S. Lee, Phys. Lett. **B481**, 57 (2000), [hep-ph/0002287]; M. Carena *et al.*, Nucl. Phys. **B586**, 92 (2000), [hep-ph/0003180]; M. Carena *et al.*, Phys. Lett. **B495**, 155 (2000), [hep-ph/0009212]; M. Carena *et al.*, Nucl. Phys. **B625**, 345 (2002), [hep-ph/0111245]; M. Frank *et al.*, JHEP **02**, 047 (2007), [hep-ph/0611326]; S. Heinemeyer *et al.*, Phys. Lett. **B652**, 300 (2007), [arXiv:0705.0746].
- [111] H. E. Haber and J. D. Mason, Phys. Rev. **D77**, 115011 (2008), [arXiv:0711.2890].
- [112] M. Carena *et al.*, Phys. Rev. **D93**, 035013 (2016), [arXiv:1510.09137].
- [113] S. Khalil, Int. J. Mod. Phys. **A18**, 1697 (2003), [hep-ph/0212050].
- [114] W. Fischler, S. Paban and S. D. Thomas, Phys. Lett. **B289**, 373 (1992), [hep-ph/9205233].
- [115] A. Masiero and L. Silvestrini, in *Perspectives on Supersymmetry*, edited by G.L. Kane (World Scientific, Singapore, 1998) pp. 423–441.
- [116] M. Pospelov and A. Ritz, Annals Phys. **318**, 119 (2005), [hep-ph/0504231].
- [117] J. M. Pendlebury *et al.*, Phys. Rev. **D92**, 092003 (2015), [arXiv:1509.04411]; V. Andreev *et al.* (ACME Collaboration), Nature **562**, 7727, 355 (2018).
- [118] F. Gabbiani *et al.*, Nucl. Phys. **B477**, 321 (1996), [hep-ph/9604387].
- [119] M. J. Ramsey-Musolf and S. Su, Phys. Rept. **456**, 1 (2008), [hep-ph/0612057].
- [120] M. Carena, A. Menon and C. E. M. Wagner, Phys. Rev. **D79**, 075025 (2009), [arXiv:0812.3594].
- [121] M. B. Einhorn and D. R. T. Jones, Nucl. Phys. **B196**, 475 (1982).
- [122] W. J. Marciano and G. Senjanovic, Phys. Rev. **D25**, 3092 (1982).
- [123] R.N. Mohapatra, *Unification and Supersymmetry*, Third Edition (Springer Science, New York, 2003).
- [124] S. P. Martin and M. T. Vaughn, Phys. Rev. **D50**, 2282 (1994), [Erratum: Phys. Rev. **D78**, 039903 (2008)], [hep-ph/9311340]; R. M. Fonseca *et al.*, Nucl. Phys. **B854**, 28 (2012), [arXiv:1107.2670]; F. Staub, Comput. Phys. Commun. **182**, 808 (2011), [arXiv:1002.0840].
- [125] F. Staub, Comput. Phys. Commun. **185**, 1773 (2014), [arXiv:1309.7223]; F. Staub, Adv. High Energy Phys. **2015**, 840780 (2015), [arXiv:1503.04200]; The SARAH homepage is <https://sarah.hepforge.org/>.
- [126] B. C. Allanach, Comput. Phys. Commun. **143**, 305 (2002), [hep-ph/0104145]; The SOFTSUSY homepage is <http://softsusy.hepforge.org/>; A. Djouadi, J.-L. Kneur and G. Moultaka, Comput. Phys. Commun. **176**, 426 (2007), [hep-ph/0211331]; The Suspect homepage is <http://suspect.in2p3.fr/>; F. E. Paige *et al.* (2003), [hep-ph/0312045]; Isajet may be obtained from <http://www.nhn.ou.edu/~isajet/>; W. Porod, Comput. Phys. Commun. **153**, 275 (2003), [hep-ph/0301101]; Spheno may be obtained from <https://spheno.hepforge.org/>; P. Athron *et al.*, Comput. Phys. Commun. **190**, 139 (2015), [arXiv:1406.2319]; The FlexibleSUSY homepage is <https://flexiblesusy.hepforge.org/>.
- [127] L. E. Ibanez and G. G. Ross, Phys. Lett. **110B**, 215 (1982).
- [128] J. Abdallah *et al.* (DELPHI Collaboration), Eur. Phys. J. **C31**, 421 (2003), [hep-ex/0311019].
- [129] H. K. Dreiner *et al.*, Eur. Phys. J. **C62**, 547 (2009), [arXiv:0901.3485].
- [130] G. F. Giudice *et al.*, JHEP **12**, 027 (1998), [hep-ph/9810442]; A. Pomarol and R. Rattazzi, JHEP **05**, 013 (1999), [hep-ph/9903448]; D.-W. Jung and J. Y. Lee, JHEP **03**, 123 (2009), [arXiv:0902.0464].
- [131] J. F. Gunion and H. E. Haber, Phys. Rev. **D37**, 2515 (1988); S. Y. Choi, M. Drees and B. Gaissmaier, Phys. Rev. **D70**, 014010 (2004), [hep-ph/0403054].
- [132] H. Baer, V. Barger and D. Sengupta, Phys. Rev. **D98**, 015039 (2018), [arXiv:1801.09730].
- [133] J. L. Feng *et al.*, Phys. Rev. Lett. **83**, 1731 (1999), [hep-ph/9904250]; J. F. Gunion and S. Mrenna, Phys. Rev. **D62**, 015002 (2000), [hep-ph/9906270].
- [134] T. Gherghetta, G. F. Giudice and J. D. Wells, Nucl. Phys. **B559**, 27 (1999), [hep-ph/9904378].
- [135] M. Endo, M. Yamaguchi and K. Yoshioka, Phys. Rev. **D72**, 015004 (2005), [hep-ph/0504036]; K. Choi, K. S. Jeong and K.-i. Okumura, JHEP **09**, 039 (2005), [hep-ph/0504037]; O. Loaiza-Brito *et al.*, AIP Conf. Proc. **805**, 198 (2005), [hep-th/0509158].
- [136] See *e.g.*, G. D'Ambrosio *et al.*, Nucl. Phys. **B645**, 155 (2002).
- [137] C. Smith, Acta Phys. Polon. Supp. **3**, 53 (2010), [arXiv:0909.4444].
- [138] M. Drees and S.P. Martin, in *Electroweak Symmetry Breaking and New Physics at the TeV Scale*, edited by T. Barklow *et al.* (World Scientific, Singapore, 1996) pp. 146–215.
- [139] G. L. Kane *et al.*, Phys. Rev. **D49**, 6173 (1994), [hep-ph/9312272].
- [140] J. R. Ellis *et al.*, Phys. Lett. **B573**, 162 (2003), [hep-ph/0305212]; J. R. Ellis *et al.*, Phys. Rev. **D70**, 055005 (2004), [hep-ph/0405110].
- [141] H. Baer *et al.*, Phys. Rev. **D71**, 095008 (2005), [hep-ph/0412059].
- [142] V. Berezhinsky *et al.*, Astropart. Phys. **5**, 1 (1996), [hep-ph/9508249]; J. R. Ellis *et al.*, Nucl. Phys. **B652**, 259 (2003), [hep-ph/0210205].
- [143] L. E. Ibanez and D. Lust, Nucl. Phys. **B382**, 305 (1992), [hep-th/9202046]; B. de Carlos, J. A. Casas and C. Munoz, Phys. Lett. **B299**, 234 (1993), [hep-ph/9211266]; V. S. Kaplunovsky and J. Louis, Phys. Lett. **B306**, 269 (1993), [hep-th/9303040]; A. Brignole, L. E. Ibanez and C. Munoz, Nucl. Phys. **B422**, 125 (1994), [Erratum: **B436**, 747 (1995)], [hep-ph/9308271].
- [144] A. Arbey *et al.*, Phys. Rev. **D87**, 115020 (2013), [arXiv:1304.0381].
- [145] G. R. Dvali, G. F. Giudice and A. Pomarol, Nucl. Phys. **B478**, 31 (1996), [hep-ph/9603238].
- [146] P. Draper *et al.*, Phys. Rev. **D85**, 095007 (2012), [arXiv:1112.3068].
- [147] P. Meade, N. Seiberg and D. Shih, Prog. Theor. Phys. Suppl. **177**, 143 (2009), [arXiv:0801.3278]; M. Buican *et al.*, JHEP **03**, 016 (2009), [arXiv:0812.3668].
- [148] A. Rajaraman *et al.*, Phys. Lett. **B678**, 367 (2009), [arXiv:0903.0668]; L. M. Carpenter *et al.*, Phys. Rev. **D79**, 035002 (2009), [arXiv:0805.2944].
- [149] S. Ambrosanio, G. D. Kribs and S. P. Martin, Nucl. Phys. **B516**, 55 (1998), [hep-ph/9710217].
- [150] For a review and guide to the literature, see J.F. Gunion and H.E. Haber, in *Perspectives on Supersymmetry II*, edited by G.L. Kane (World Scientific, Singapore, 2010) pp. 420–445.
- [151] T. S. Roy and M. Schmaltz, Phys. Rev. **D77**, 095008 (2008), [arXiv:0708.3593].
- [152] A. de Gouvea, A. Friedland and H. Murayama, Phys. Rev. **D57**, 5676 (1998), [hep-ph/9711264].

- [153] T. Han, D. Marfatia and R.-J. Zhang, Phys. Rev. **D61**, 013007 (2000), [hep-ph/9906508]; Z. Chacko and E. Ponton, Phys. Rev. **D66**, 095004 (2002), [hep-ph/0112190]; A. Delgado, G. F. Giudice and P. Slavich, Phys. Lett. **B653**, 424 (2007), [arXiv:0706.3873]; T. Liu and C. E. M. Wagner, JHEP **06**, 073 (2008), [arXiv:0803.2895].
- [154] B. Allanach *et al.*, Phys. Rev. **D92**, 015006 (2015), [arXiv:1502.05836].
- [155] A. Djouadi, J.L. Kneur, and G. Moultaka, Comp. Phys. Comm. **176**, 426 (2007); C. F. Berger *et al.*, JHEP **02**, 023 (2009), [arXiv:0812.0980].
- [156] S. P. Martin and J. D. Wells, Phys. Rev. **D64**, 035003 (2001), [hep-ph/0103067].
- [157] J. Berger *et al.*, Phys. Rev. **D93**, 035017 (2016), [arXiv:1510.08840].
- [158] K. J. de Vries *et al.*, Eur. Phys. J. **C75**, 422 (2015), [arXiv:1504.03260].
- [159] M. Cahill-Rowley *et al.*, Phys. Rev. **D90**, 095017 (2014), [arXiv:1407.7021]; M. Cahill-Rowley *et al.*, Phys. Rev. **D91**, 055011 (2015), [arXiv:1405.6716]; A. Barr and J. Liu, Eur. Phys. J. **C77**, 202 (2017), [arXiv:1608.05379].
- [160] G. Bertone *et al.*, JCAP **1604**, 037 (2016), [arXiv:1507.07008].
- [161] N. Arkani-Hamed *et al.* (2007), [hep-ph/0703088]; J. Alwall *et al.*, Phys. Rev. **D79**, 015005 (2009), [arXiv:0809.3264]; J. Alwall, P. Schuster and N. Toro, Phys. Rev. **D79**, 075020 (2009), [arXiv:0810.3921]; D. S. M. Alves, E. Izaguirre and J. G. Wacker, Phys. Lett. **B702**, 64 (2011), [arXiv:1008.0407]; D. S. M. Alves, E. Izaguirre and J. G. Wacker, JHEP **10**, 012 (2011), [arXiv:1102.5338]; D. Alves (LHC New Physics Working Group), J. Phys. **G39**, 105005 (2012), [arXiv:1105.2838].
- [162] F. Ambrogio *et al.*, Eur. Phys. J. **C78**, 215 (2018), [arXiv:1707.09036].
- [163] R. Barbieri and G.F. Giudice, Nucl. Phys. **B305**, 63 (1988).
- [164] J. R. Ellis *et al.*, Mod. Phys. Lett. **A1**, 57 (1986).
- [165] G. W. Anderson and D. J. Castano, Phys. Lett. **B347**, 300 (1995), [hep-ph/9409419]; G. W. Anderson and D. J. Castano, Phys. Rev. **D52**, 1693 (1995), [hep-ph/9412322]; G. W. Anderson and D. J. Castano, Phys. Rev. **D53**, 2403 (1996), [hep-ph/9509212]; P. Athron and D. J. Miller, Phys. Rev. **D76**, 075010 (2007), [arXiv:0705.2241]; M. E. Cabrera, J. A. Casas and R. Ruiz de Austri, JHEP **03**, 075 (2009), [arXiv:0812.0536]; H. Baer *et al.*, Phys. Rev. Lett. **109**, 161802 (2012), [arXiv:1207.3343].
- [166] J. L. Feng, K. T. Matchev and T. Moroi, Phys. Rev. **D61**, 075005 (2000), [hep-ph/9909334].
- [167] D. M. Ghilencea and G. G. Ross, Nucl. Phys. **B868**, 65 (2013), [arXiv:1208.0837].
- [168] H. Baer, V. Barger and D. Mickelson, Phys. Rev. **D88**, 095013 (2013), [arXiv:1309.2984].
- [169] M. van Beekveld, S. Caron and R. Ruiz de Austri, JHEP **01**, 147 (2020), [arXiv:1906.10706].
- [170] G. L. Kane and S. F. King, Phys. Lett. **B451**, 113 (1999), [hep-ph/9810374]; M. Bastero-Gil, G. L. Kane and S. F. King, Phys. Lett. **B474**, 103 (2000), [hep-ph/9910506]; J. A. Casas, J. R. Espinosa and I. Hidalgo, JHEP **01**, 008 (2004), [hep-ph/0310137]; H. Abe, T. Kobayashi and Y. Omura, Phys. Rev. **D76**, 015002 (2007), [hep-ph/0703044]; R. Essig and J.-F. Fortin, JHEP **04**, 073 (2008), [arXiv:0709.0980].
- [171] B. de Carlos and J. A. Casas, Phys. Lett. **B309**, 320 (1993), [hep-ph/9303291]; S. Cassel, D. M. Ghilencea and G. G. Ross, Nucl. Phys. **B825**, 203 (2010), [arXiv:0903.1115]; S. Cassel, D. M. Ghilencea and G. G. Ross, Nucl. Phys. **B835**, 110 (2010), [arXiv:1001.3884].
- [172] O. Buchmueller *et al.*, Eur. Phys. J. **C74**, 6, 2922 (2014), [arXiv:1312.5250].
- [173] P. Bechtle *et al.*, Eur. Phys. J. **C76**, 96 (2016), [arXiv:1508.05951].
- [174] H. Baer *et al.*, Phys. Rev. **D89**, 115019 (2014), [arXiv:1404.2277].
- [175] R. Barbieri and A. Strumia, in “4th Rencontres du Vietnam: Physics at Extreme Energies (Particle Physics and Astrophysics) Hanoi, Vietnam, July 19-25, 2000,” (2000), [hep-ph/0007265].
- [176] L. Giusti, A. Romanino and A. Strumia, Nucl. Phys. **B550**, 3 (1999), [hep-ph/9811386]; H.-C. Cheng and I. Low, JHEP **09**, 051 (2003), [hep-ph/0308199]; H.-C. Cheng and I. Low, JHEP **08**, 061 (2004), [hep-ph/0405243]; R. Harnik *et al.*, Phys. Rev. **D70**, 015002 (2004), [hep-ph/0311349].
- [177] H. Baer *et al.*, Phys. Rev. **D87**, 035017 (2013), [arXiv:1210.3019]; H. Baer *et al.*, Phys. Rev. **D87**, 115028 (2013), [arXiv:1212.2655]; J. L. Feng, Ann. Rev. Nucl. Part. Sci. **63**, 351 (2013), [arXiv:1302.6587].
- [178] J. L. Feng, K. T. Matchev and T. Moroi, Phys. Rev. Lett. **84**, 2322 (2000), [hep-ph/9908309]; J. L. Feng and F. Wilczek, Phys. Lett. **B631**, 170 (2005), [hep-ph/0507032]; D. Horton and G. G. Ross, Nucl. Phys. **B830**, 221 (2010), [arXiv:0908.0857].
- [179] M. Drees, Phys. Rev. **D33**, 1468 (1986); S. Dimopoulos and G. F. Giudice, Phys. Lett. **B357**, 573 (1995), [hep-ph/9507282]; A. Pomarol and D. Tommasini, Nucl. Phys. **B466**, 3 (1996), [hep-ph/9507462].
- [180] M. Dine, A. Kagan and S. Samuel, Phys. Lett. **B243**, 250 (1990); A. G. Cohen, D. B. Kaplan and A. E. Nelson, Phys. Lett. **B388**, 588 (1996), [hep-ph/9607394].
- [181] C. Brust *et al.*, JHEP **03**, 103 (2012), [arXiv:1110.6670].
- [182] S. P. Martin, Phys. Rev. **D75**, 115005 (2007), [hep-ph/0703097]; S. P. Martin, Phys. Rev. **D78**, 055019 (2008), [arXiv:0807.2820].
- [183] J. Fan, M. Reece and J. T. Ruderman, JHEP **11**, 012 (2011), [arXiv:1105.5135]; J. Fan, M. Reece and J. T. Ruderman, JHEP **07**, 196 (2012), [arXiv:1201.4875].
- [184] H. Murayama, Y. Nomura and D. Poland, Phys. Rev. **D77**, 015005 (2008), [arXiv:0709.0775]; G. Perez, T. S. Roy and M. Schmaltz, Phys. Rev. **D79**, 095016 (2009), [arXiv:0811.3206].
- [185] R. Dermisek and J. F. Gunion, Phys. Rev. Lett. **95**, 041801 (2005), [hep-ph/0502105]; Phys. Rev. **D75**, 095019 (2007); R. Dermisek and J. F. Gunion, Phys. Rev. **D76**, 095006 (2007), [arXiv:0705.4387].
- [186] G. G. Ross and K. Schmidt-Hoberg, Nucl. Phys. **B862**, 710 (2012), [arXiv:1108.1284]; G. G. Ross, K. Schmidt-Hoberg and F. Staub, JHEP **08**, 074 (2012), [arXiv:1205.1509]; A. Kaminska, G. G. Ross and K. Schmidt-Hoberg, JHEP **11**, 209 (2013), [arXiv:1308.4168].
- [187] S. P. Martin and J. D. Wells, Phys. Rev. **D86**, 035017 (2012), [arXiv:1206.2956].
- [188] B. Bellazzini *et al.*, Phys. Rev. **D79**, 095003 (2009), [arXiv:0902.0015].
- [189] M. Dine, Ann. Rev. Nucl. Part. Sci. **65**, 43 (2015), [arXiv:1501.01035].
- [190] H. Baer, V. Barger and M. Savoy, Phys. Rev. **D93**, 035016 (2016), [arXiv:1509.02929].
- [191] M.L. Mangano, editor, *Physics at the FCC-hh, a 100 TeV pp collider*, CERN Yellow Report, CERN-2017-003-M (2017).
- [192] D. Stockinger, J. Phys. **G34**, R45 (2007), [hep-ph/0609168]; P. Athron *et al.*, Eur. Phys. J. **C76**, 62 (2016), [arXiv:1510.08071].
- [193] F. Jegerlehner, Acta Phys. Polon. **B49**, 1157 (2018), [arXiv:1804.07409]; M. Davier *et al.*, Eur. Phys. J. **C80**, 3, 241 (2020), [arXiv:1908.00921].



- [194] M. Ibe, T. T. Yanagida and N. Yokozaki, *JHEP* **08**, 067 (2013), [arXiv:1303.6995].
- [195] R. H. Parker *et al.*, *Science* **360**, 191 (2018), [arXiv:1812.04130].
- [196] D. Hanneke, S. Fogwell and G. Gabrielse, *Phys. Rev. Lett.* **100**, 120801 (2008), [arXiv:0801.1134].
- [197] B. Dutta and Y. Mimura, *Phys. Lett.* **B790**, 563 (2019), [arXiv:1811.10209]; M. Endo and W. Yin, *JHEP* **08**, 122 (2019), [arXiv:1906.08768]; M. Badziak and K. Sakurai, *JHEP* **10**, 024 (2019), [arXiv:1908.03607].
- [198] A. Limosani *et al.* (Belle Collaboration), *Phys. Rev. Lett.* **103**, 241801 (2009), [arXiv:0907.1384]; J. P. Lees *et al.* (BaBar Collaboration), *Phys. Rev. Lett.* **109**, 191801 (2012), [arXiv:1207.2690]; J. P. Lees *et al.* (BaBar Collaboration), *Phys. Rev.* **D86**, 112008 (2012), [arXiv:1207.5772].
- [199] M. Misiak *et al.*, *Phys. Rev. Lett.* **114**, 221801 (2015), [arXiv:1503.01789]; M. Czakon *et al.*, *JHEP* **04**, 168 (2015), [arXiv:1503.01791].
- [200] H. Baer and M. Brhlik, *Phys. Rev.* **D55**, 3201 (1997), [hep-ph/9610224]; M. Ciuchini *et al.*, *Phys. Rev.* **D67**, 075016 (2003), [Erratum: **D68**, 079901 (2003)], [hep-ph/0212397]; T. Hurth, *Rev. Mod. Phys.* **75**, 1159 (2003), [hep-ph/0212304]; F. Mahmoudi, *JHEP* **12**, 026 (2007), [arXiv:0710.3791]; K. A. Olive and L. Velasco-Sevilla, *JHEP* **05**, 052 (2008), [arXiv:0801.0428].
- [201] S. R. Choudhury and N. Gaur, *Phys. Lett.* **B451**, 86 (1999), [hep-ph/9810307]; K. S. Babu and C. F. Kolda, *Phys. Rev. Lett.* **84**, 228 (2000), [hep-ph/9909476]; G. Isidori and A. Retico, *JHEP* **11**, 001 (2001), [hep-ph/0110121]; G. Isidori and A. Retico, *JHEP* **09**, 063 (2002), [hep-ph/0208159].
- [202] S. Chatrchyan *et al.* (CMS Collaboration), *Phys. Rev. Lett.* **111**, 101804 (2013), [arXiv:1307.5025]; V. Khachatryan *et al.* (CMS and LHCb Collaborations), *Nature* **522**, 68 (2015), [arXiv:1411.4413]; M. Aaboud *et al.* (ATLAS Collaboration), *JHEP* **04**, 098 (2019), [arXiv:1812.03017]; R. Aaij *et al.* (LHCb Collaboration), *Phys. Rev. Lett.* **118**, 191801 (2017), [arXiv:1703.05747].
- [203] J. Aebischer *et al.*, *Eur. Phys. J. C* **80**, 3, 252 (2020), [arXiv:1903.10434].
- [204] C. Bobeth *et al.*, *Phys. Rev. Lett.* **112**, 101801 (2014), [arXiv:1311.0903].
- [205] M. Bona *et al.* (UTfit Collaboration), *Phys. Lett.* **B687**, 61 (2010), [arXiv:0908.3470].
- [206] J. P. Lees *et al.* (BaBar Collaboration), *Phys. Rev. Lett.* **109**, 101802 (2012), [arXiv:1205.5442]; J. P. Lees *et al.* (BaBar Collaboration), *Phys. Rev.* **D88**, 072012 (2013), [arXiv:1303.0571].
- [207] R. Aaij *et al.* (LHCb Collaboration), *Phys. Rev. Lett.* **115**, 111803 (2015), [Erratum: **115**, 159901 (2015)], [arXiv:1506.08614]; R. Aaij *et al.* (LHCb Collaboration), *Phys. Rev. Lett.* **120**, 171802 (2018), [arXiv:1708.08856]; M. Huschle *et al.* (Belle Collaboration), *Phys. Rev.* **D92**, 072014 (2015), [arXiv:1507.03233]; Y. Sato *et al.* (Belle Collaboration), *Phys. Rev.* **D94**, 072007 (2016), [arXiv:1607.07923]; S. Hirose *et al.* (Belle Collaboration), *Phys. Rev. Lett.* **118**, 211801 (2017), [arXiv:1612.00529]; S. Hirose *et al.* (Belle Collaboration), *Phys. Rev.* **D97**, 012004 (2018), [arXiv:1709.00129].
- [208] G. Caria *et al.* (Belle Collaboration), *Phys. Rev. Lett.* **124**, 16, 161803 (2020), [arXiv:1910.05864].
- [209] S. Klaver (LHCb Collaboration), in "Proceedings of the 17th Conference on Flavor Physics and CP Violation (FPCP 2019) Victoria, BC, Canada, May 6-10, 2019," (2019), [arXiv:1907.01500].
- [210] F. Mahmoudi, S. Neshatpour and J. Orloff, *JHEP* **08**, 092 (2012), [arXiv:1205.1845]; A. Arbey *et al.*, *JHEP* **11**, 132 (2017), [arXiv:1707.00426].
- [211] A. J. Buras, *Acta Phys. Polon.* **B49**, 1043 (2018), [arXiv:1805.11096].
- [212] V. Cirigliano *et al.*, *JHEP* **02**, 032 (2020), [arXiv:1911.01359].
- [213] J. R. Ellis *et al.*, *JHEP* **08**, 083 (2007), [arXiv:0706.0652]; S. Heinemeyer *et al.*, *JHEP* **08**, 087 (2008), [arXiv:0805.2359]; G.-C. Cho *et al.*, *JHEP* **11**, 068 (2011), [arXiv:1104.1769]; E. Bagnaschi *et al.*, *Eur. Phys. J.* **C78**, 256 (2018), [arXiv:1710.11091].
- [214] A. J. Buras *et al.*, *Nucl. Phys.* **B592**, 55 (2001), [hep-ph/0007313].
- [215] I. Esteban *et al.*, *JHEP* **01**, 106 (2019), [arXiv:1811.05487].
- [216] K. Zuber, *Phys. Rept.* **305**, 295 (1998), [hep-ph/9811267]; S. F. King, *J. Phys.* **G42**, 123001 (2015), [arXiv:1510.02091]; S. F. King, *Prog. Part. Nucl. Phys.* **94**, 217 (2017), [arXiv:1701.04413].
- [217] For a review of neutrino masses in supersymmetry, see *e.g.*, B. Mukhopadhyaya, *Proc. Indian National Science Academy* **A70**, 239 (2004); M. Hirsch and J. W. F. Valle, *New J. Phys.* **6**, 76 (2004), [hep-ph/0405015].
- [218] F. Borzumati and Y. Nomura, *Phys. Rev.* **D64**, 053005 (2001), [hep-ph/0007018].
- [219] P. Minkowski, *Phys. Lett.* **67B**, 421 (1977); M. Gell-Mann, P. Ramond, and R. Slansky, in *Supergravity*, edited by D. Freedman and P. van Nieuwenhuizen (North Holland, Amsterdam, 1979) p. 315; T. Yanagida, *Prog. Theor. Phys.* **64**, 1103 (1980); R. N. Mohapatra and G. Senjanovic, *Phys. Rev. Lett.* **44**, 912 (1980); R. N. Mohapatra and G. Senjanovic, *Phys. Rev.* **D23**, 165 (1981).
- [220] J. Hisano *et al.*, *Phys. Lett.* **B357**, 579 (1995), [hep-ph/9501407]; J. Hisano *et al.*, *Phys. Rev.* **D53**, 2442 (1996), [hep-ph/9510309]; J. A. Casas and A. Ibarra, *Nucl. Phys.* **B618**, 171 (2001), [hep-ph/0103065]; J. R. Ellis *et al.*, *Phys. Rev.* **D66**, 115013 (2002), [hep-ph/0206110]; A. Masiero, S. K. Vempati and O. Vives, *New J. Phys.* **6**, 202 (2004), [hep-ph/0407325]; E. Arganda *et al.*, *Phys. Rev.* **D71**, 035011 (2005), [hep-ph/0407302]; F. R. Joaquim and A. Rossi, *Phys. Rev. Lett.* **97**, 181801 (2006), [hep-ph/0604083]; J. R. Ellis and O. Lebedev, *Phys. Lett.* **B653**, 411 (2007), [arXiv:0707.3419].
- [221] Y. Grossman and H. E. Haber, *Phys. Rev. Lett.* **78**, 3438 (1997), [hep-ph/9702421]; A. Dedes, H. E. Haber and J. Rosiek, *JHEP* **11**, 059 (2007), [arXiv:0707.3718].
- [222] M. Hirsch, H. V. Klapdor-Kleingrothaus and S. G. Kovalenko, *Phys. Lett.* **B398**, 311 (1997), [hep-ph/9701253]; L. J. Hall, T. Moroi and H. Murayama, *Phys. Lett.* **B424**, 305 (1998), [hep-ph/9712515]; K. Choi, K. Hwang and W. Y. Song, *Phys. Rev. Lett.* **88**, 141801 (2002), [hep-ph/0108028]; T. Honkavaara, K. Huitu and S. Roy, *Phys. Rev.* **D73**, 055011 (2006), [hep-ph/0512277].
- [223] L. Basso *et al.*, *Comput. Phys. Commun.* **184**, 698 (2013), [arXiv:1206.4563].
- [224] M. Chemtob, *Prog. Part. Nucl. Phys.* **54**, 71 (2005), [hep-ph/0406029]; R. Barbier *et al.*, *Phys. Rept.* **420**, 1 (2005), [hep-ph/0406039].
- [225] H. Dreiner, in *Perspectives on Supersymmetry II*, edited by G.L. Kane (World Scientific, Singapore, 2010) pp. 565–583.
- [226] B. C. Allanach, A. Dedes and H. K. Dreiner, *Phys. Rev.* **D60**, 075014 (1999), [hep-ph/9906209].
- [227] L. E. Ibanez and G. G. Ross, *Nucl. Phys.* **B368**, 3 (1992); L. E. Ibanez, *Nucl. Phys.* **B398**, 301 (1993), [hep-ph/9210211].
- [228] A. Dedes, S. Rimmer and J. Rosiek, *JHEP* **08**, 005 (2006), [hep-ph/0603225]; B. C. Allanach and C. H. Kom, *JHEP* **04**, 081 (2008), [arXiv:0712.0852]; H. K. Dreiner *et al.*, *Phys. Rev.* **D84**, 113005 (2011), [arXiv:1106.4338].
- [229] H. K. Dreiner, C. Luhn and M. Thormeier, *Phys. Rev.* **D73**, 075007 (2006), [hep-ph/0512163].



- [230] K. Tamvakis, Phys. Lett. **B382**, 251 (1996), [hep-ph/9604343]; G. Eyal and Y. Nir, JHEP **06**, 024 (1999), [hep-ph/9904473]; A. Florez *et al.*, Phys. Rev. **D87**, 095010 (2013), [arXiv:1303.0278].
- [231] C. Csaki, Y. Grossman and B. Heidenreich, Phys. Rev. **D85**, 095009 (2012), [arXiv:1111.1239].
- [232] D. Dercks *et al.*, Eur. Phys. J. **C77**, 856 (2017), [arXiv:1706.09418].
- [233] B. C. Allanach and B. Gripaios, JHEP **05**, 062 (2012), [arXiv:1202.6616]; M. Asano, K. Rolbiecki and K. Sakurai, JHEP **01**, 128 (2013), [arXiv:1209.5778]; N. Chamoun *et al.*, JHEP **08**, 142 (2014), [arXiv:1407.2248].
- [234] J. C. Romao, Nucl. Phys. Proc. Suppl. **81**, 231 (2000), [hep-ph/9907466]; Y. Grossman and S. Rakshit, Phys. Rev. **D69**, 093002 (2004), [hep-ph/0311310].
- [235] R. N. Mohapatra, Phys. Rev. **D34**, 3457 (1986); K. S. Babu and R. N. Mohapatra, Phys. Rev. Lett. **75**, 2276 (1995), [hep-ph/9506354]; M. Hirsch, H. V. Klapdor-Kleingrothaus and S. G. Kovalenko, Phys. Rev. Lett. **75**, 17 (1995); M. Hirsch, H. V. Klapdor-Kleingrothaus and S. G. Kovalenko, Phys. Rev. **D53**, 1329 (1996), [hep-ph/9502385].
- [236] Y. Grossman and H. E. Haber, Phys. Rev. **D59**, 093008 (1999), [hep-ph/9810536].
- [237] S. Dimopoulos and L. J. Hall, Phys. Lett. **B207**, 210 (1988); J. Kalinowski *et al.*, Phys. Lett. **B406**, 314 (1997), [hep-ph/9703436]; J. Erler, J. L. Feng and N. Polonsky, Phys. Rev. Lett. **78**, 3063 (1997), [hep-ph/9612397].
- [238] H. K. Dreiner, P. Richardson and M. H. Seymour, Phys. Rev. **D63**, 055008 (2001), [hep-ph/0007228].
- [239] J. E. Kim and H. P. Nilles, Phys. Lett. **138B**, 150 (1984).
- [240] J. E. Kim and H. P. Nilles, Mod. Phys. Lett. **A9**, 3575 (1994), [hep-ph/9406296].
- [241] G. F. Giudice and A. Masiero, Phys. Lett. **B206**, 480 (1988); J. A. Casas and C. Munoz, Phys. Lett. **B306**, 288 (1993), [hep-ph/9302227]; K. J. Bae *et al.*, Phys. Rev. **D99**, 115027 (2019), [arXiv:1902.10748].
- [242] M. Cvetič *et al.*, Phys. Rev. **D56**, 2861 (1997), [Erratum: **D58**, 119905 (1998)], [hep-ph/9703317].
- [243] R. D. Peccei, Lect. Notes Phys. **741**, 3 (2008), [hep-ph/0607268].
- [244] R. D. Peccei and H. R. Quinn, Phys. Rev. Lett. **38**, 1440 (1977); R. D. Peccei and H. R. Quinn, Phys. Rev. **D16**, 1791 (1977).
- [245] H. Murayama, H. Suzuki and T. Yanagida, Phys. Lett. **B291**, 418 (1992); T. Gherghetta and G. L. Kane, Phys. Lett. **B354**, 300 (1995), [hep-ph/9504420]; K. J. Bae, H. Baer and H. Serce, Phys. Rev. **D91**, 1, 015003 (2015), [arXiv:1410.7500]; H. Baer, V. Barger and D. Sengupta, Phys. Lett. **B790**, 58 (2019), [arXiv:1810.03713].
- [246] A. Delgado, G. Nardini and M. Quiros, Phys. Rev. **D86**, 115010 (2012), [arXiv:1207.6596].
- [247] P. Fayet, Phys. Lett. **78B**, 417 (1978).
- [248] K. Benakli, Fortsch. Phys. **59**, 1079 (2011), [arXiv:1106.1649].
- [249] P. J. Fox, A. E. Nelson and N. Weiner, JHEP **08**, 035 (2002), [hep-ph/0206096].
- [250] K. Benakli and M. D. Goodsell, Nucl. Phys. **B816**, 185 (2009), [arXiv:0811.4409]; K. Benakli and M. D. Goodsell, Nucl. Phys. **B840**, 1 (2010), [arXiv:1003.4957].
- [251] U. Sarkar and R. Adhikari, Phys. Rev. **D55**, 3836 (1997), [hep-ph/9608209]; R. Fok *et al.*, Phys. Rev. **D87**, 055018 (2013), [arXiv:1208.2784].
- [252] G. D. Kribs, E. Poppitz and N. Weiner, Phys. Rev. **D78**, 055010 (2008), [arXiv:0712.2039].
- [253] K. Benakli, M. D. Goodsell and F. Staub, JHEP **06**, 073 (2013), [arXiv:1211.0552].
- [254] J. L. Hewett and T. G. Rizzo, Phys. Rept. **183**, 193 (1989).
- [255] S. F. King, S. Moretti and R. Nevzorov, Phys. Lett. **B634**, 278 (2006), [hep-ph/0511256]; S. F. King, S. Moretti and R. Nevzorov, Phys. Rev. **D73**, 035009 (2006), [hep-ph/0510419].

## 90. Supersymmetry, Part II (Experiment)

Revised September 2019 by O. Buchmuller (Imperial Coll. London) and P. de Jong (NIKHEF).

### 90.1 Introduction

Supersymmetry (SUSY), a transformation relating fermions to bosons and vice versa [1–9] is one of the most compelling possible extensions of the Standard Model of particle physics (SM).

On theoretical grounds SUSY is motivated as a generalization of space-time symmetries. A low-energy realization of SUSY, *i.e.*, SUSY at the TeV scale, is, however, not a necessary consequence. Instead, low-energy SUSY is motivated by the possible cancellation of quadratic divergences in radiative corrections to the Higgs boson mass [10–15]. Furthermore, it is intriguing that a weakly interacting, (meta)stable supersymmetric particle might make up some or all of the dark matter in the universe [16–18]. In addition, SUSY predicts that gauge couplings, as measured experimentally at the electroweak scale, unify at an energy scale  $\mathcal{O}(10^{16})$  GeV (“GUT scale”) near the Planck scale [19–24].

In the minimal supersymmetric extension to the Standard Model, the so called MSSM [11,25,26], a supersymmetry transformation relates every chiral fermion and gauge boson in the SM to a supersymmetric partner with half a unit of spin difference, but otherwise with the same properties (such as mass) and quantum numbers. These are the “sfermions”: squarks ( $\tilde{q}$ ) and sleptons ( $\tilde{\ell}$ ,  $\tilde{\nu}$ ), and the “gauginos”. The MSSM Higgs sector contains two doublets, for up-type quarks and for down-type quarks and charged leptons respectively. After electroweak symmetry breaking, five Higgs bosons arise, of which two are charged. The supersymmetric partners of the Higgs doublets are known as “higgsinos.” The weak gauginos and higgsinos mix, giving rise to charged mass eigenstates called “charginos” ( $\tilde{\chi}^{\pm}$ ), and neutral mass eigenstates called “neutralinos” ( $\tilde{\chi}^0$ ). The SUSY partners of the gluons are known as “gluinos” ( $\tilde{g}$ ). The fact that such particles are not yet observed leads to the conclusion that, if supersymmetry is realized, it is a broken symmetry. A description of SUSY in the form of an effective Lagrangian with only “soft” SUSY breaking terms and SUSY masses at the TeV scale maintains the cancellation of quadratic divergences of soft SUSY breaking scalar mass squared parameters.

The phenomenology of SUSY is to a large extent determined by the SUSY breaking mechanism and the SUSY breaking scale. This determines the SUSY particle masses, the mass hierarchy, the field contents of physical particles, and their decay modes. In addition, phenomenology crucially depends on whether the multiplicative quantum number of R-parity [26],  $R = (-1)^{3(B-L)+2S}$ , where  $B$  and  $L$  are baryon and lepton numbers and  $S$  is the spin, is conserved or violated. If R-parity is conserved, SUSY particles (sparticles), which have odd R-parity, are produced in pairs and the decays of each SUSY particle must involve an odd number of lighter SUSY particles. The lightest SUSY particle (LSP) is then stable and often assumed to be a weakly interacting massive particle (WIMP). If R-parity is violated, new terms  $\lambda_{ijk}$ ,  $\lambda'_{ijk}$  and  $\lambda''_{ijk}$  appear in the superpotential, where  $ijk$  are generation indices;  $\lambda$ -type couplings appear between lepton superfields only,  $\lambda'$ -type are between quark superfields only, and  $\lambda''$ -type couplings connect the two. R-parity violation implies lepton and/or baryon number violation. More details of the theoretical framework of SUSY are discussed elsewhere in this volume [27].

Today, low-energy data from flavor physics experiments, high-precision electroweak observables as well as astrophysical data impose strong constraints on the allowed SUSY parameter space. Recent examples of such data include measurements of the rare B-meson decay  $B_s \rightarrow \mu^+ \mu^-$  [28,29], measurements of the anomalous magnetic moment of the muon [30], and accurate determinations of the cosmological dark matter relic density constraint [31,32].

These indirect constraints are often more sensitive to higher SUSY mass scales than experiments searching for direct sparticle production at colliders, but the interpretation of these results is often strongly model dependent. In contrast, direct searches for sparticle production at collider experiments are less subject to interpretation ambiguities and therefore they play a crucial role in the search for SUSY.

The discovery of a Higgs boson with a mass around 125 GeV imposes constraints on SUSY models, which are discussed elsewhere [27,33].

In this review we limit ourselves to direct searches, covering data analyses at LEP, HERA, the Tevatron and the LHC, with emphasis on the latter. For more details on LEP and Tevatron constraints, see earlier PDG reviews [34].

### 90.2 Experimental search program

The electron-positron collider LEP was operational at CERN between 1989 and 2000. In the initial phase, center-of-mass energies around the  $Z$ -peak were probed, but after 1995 the LEP experiments collected a significant amount of luminosity at higher center-of-mass energies, some  $235 \text{ pb}^{-1}$  per experiment at  $\sqrt{s} \geq 204 \text{ GeV}$ , with a maximum  $\sqrt{s}$  of 209 GeV.

Searches for new physics at  $e^+e^-$  colliders benefit from the clean experimental environment and the fact that momentum balance can be measured not only in the plane transverse to the beam, but also in the direction along the beam (up to the beam pipe holes), defined as the longitudinal direction. Searches at LEP are dominated by the data samples taken at the highest center-of-mass energies.

Constraints on SUSY have been set by the CDF and D0 experiments at the Tevatron, a proton-antiproton collider at a center-of-mass energy of up to 1.96 TeV. CDF and D0 collected integrated luminosities between 10 and  $11 \text{ fb}^{-1}$  each up to the end of collider operations in 2011.

The electron-proton collider HERA provided collisions to the H1 and ZEUS experiments between 1992 and 2007, at a center-of-mass energy up to 318 GeV. A total integrated luminosity of approximately  $0.5 \text{ fb}^{-1}$  was collected by each experiment. Since at HERA baryons collide with leptons, SUSY searches at HERA typically look for R-parity violating production of single SUSY particles.

The Large Hadron Collider (LHC) at CERN started proton-proton operation at a center-of-mass energy of 7 TeV in 2010. By the end of 2011 the experiments ATLAS and CMS had collected about  $5 \text{ fb}^{-1}$  of integrated luminosity each, and the LHCb experiment had collected approximately  $1 \text{ fb}^{-1}$ . In 2012, the LHC operated at a center-of-mass energy of 8 TeV, and ATLAS and CMS collected approximately  $20 \text{ fb}^{-1}$  each, whereas LHCb collected  $2 \text{ fb}^{-1}$ . In 2015, the LHC started Run 2, with a center-of-mass energy of 13 TeV. At the end of Run 2 in November 2018, ATLAS and CMS had both collected approximately  $140 \text{ fb}^{-1}$ , and LHCb had collected almost  $6 \text{ fb}^{-1}$ .

Proton-(anti)proton colliders produce interactions at higher center-of-mass energies than those available at LEP, and cross sections of QCD-mediated processes are larger, which is reflected in the higher sensitivity for SUSY particles carrying color charge: squarks and gluinos. Large background contributions from Standard Model processes, however, pose challenges to the trigger and analysis. Such backgrounds are dominated by multijet production processes, including, particularly at the LHC, those of top quark production, as well as jet production in association with vector bosons. The proton momentum is shared between its parton constituents, and in each collision only a fraction of the total center-of-mass energy is available in the hard parton-parton scattering. Since the parton momenta in the longitudinal direction are not known on an event-by-event basis, use of momentum conservation constraints in an analysis is restricted to the transverse plane, leading to the definition of transverse variables, such as the missing transverse momentum, and the transverse mass. Proton-proton collisions at the LHC differ from proton-antiproton collisions at the Tevatron in the sense that there are no valence anti-quarks in the proton, and that gluon-initiated processes play a more dominant role. The increased center-of-mass energy of the LHC compared to the Tevatron, as well as the increase at the LHC between Run 1 and Run 2, significantly extends the kinematic reach for SUSY searches. This is reflected foremost in the sensitivity for squarks and gluinos, but also for other SUSY particles.

The main production mechanisms of massive colored sparticles at hadron colliders are squark-squark, squark-gluino and gluino-

gluino production; when “squark” is used “antisquark” is also implied. Assuming R-parity conservation, the typical SUSY search signature at hadron colliders contains high- $p_T$  jets, which are produced in the decay chains of heavy squarks and gluinos, and significant missing momentum originating from the two LSPs produced at the end of the decay chain, which escape experimental detection. Standard Model backgrounds with missing transverse momentum include leptonic  $W/Z$ -boson decays, heavy-flavor decays to neutrinos, and multijet events that may be affected by instrumental effects such as jet mismeasurement.

Selection variables designed to separate the SUSY signal from the Standard Model backgrounds include  $H_T$ ,  $E_T^{\text{miss}}$ , and  $m_{\text{eff}}$ . The quantities  $H_T$  and  $E_T^{\text{miss}}$  refer to the measured transverse energy and the missing transverse momentum in the event, respectively. They are usually defined as the scalar sum of the transverse jet momenta or calorimeter clusters transverse energies measured in the event ( $H_T$ ), or the magnitude ( $E_T^{\text{miss}}$ ) of the negative vector sum of transverse momenta of reconstructed objects like jets and leptons in the event ( $\vec{p}_T^{\text{miss}}$ ). The quantity  $m_{\text{eff}}$  is referred to as the effective mass of the event and is defined as  $m_{\text{eff}} = H_T + E_T^{\text{miss}}$ . The peak of the  $m_{\text{eff}}$  distribution for SUSY signal events correlates with the SUSY mass scale, in particular with the mass difference between the primary produced SUSY particle and the LSP [35], whereas the Standard Model backgrounds dominate at low  $m_{\text{eff}}$ . Additional reduction of multijet backgrounds can be achieved by demanding isolated leptons or photons in the final states; in such events the lepton or photon transverse momentum may be added to  $H_T$  or  $m_{\text{eff}}$  for further signal-background separation.

At the LHC, alternative approaches have been developed to increase the sensitivity to pair production of heavy sparticles with TeV-scale masses focusing on the kinematics of their decays, and to further suppress the background from multijet production. Prominent examples of these new approaches are searches using the  $\alpha_T$  [36–40], *razor* [41], *stransverse mass* ( $m_{T2}$ ) [42], and *contransverse mass* ( $m_{CT}$ ) [43] variables. Recently, the topological event reconstruction methods have expanded with the *super-razor* [44] and *recursive jigsaw reconstruction* [45] techniques. Furthermore, frequently the searches for massive SUSY particles attempt to identify their decay into top quarks or vector bosons, which are themselves unstable. If these are produced with a significant boost, jets from their decay will typically overlap, and such topologies are searched for with *jet-substructure* [46] techniques.

### 90.3 Interpretation of results

Since the mechanism by which SUSY is broken is unknown, a general approach to SUSY via the most general soft SUSY breaking Lagrangian adds a significant number of new free parameters. For the minimal supersymmetric standard model, MSSM, *i.e.*, the model with the minimal particle content, these comprise 105 new real degrees of freedom. A phenomenological analysis of SUSY searches leaving all these parameters free is not feasible. For the practical interpretation of SUSY searches at colliders several approaches are taken to reduce the number of free parameters.

One approach is to assume a SUSY breaking mechanism and lower the number of free parameters through the assumption of additional constraints. Before the start of the LHC, interpretations of experimental results were predominately performed in constrained models of gravity mediated [50, 51], gauge-mediated [52–54], and anomaly mediated [55, 56] SUSY breaking. The most popular model was the constrained MSSM (CMSSM) [50, 57, 58], which in the literature is also referred to as minimal supergravity, or MSUGRA.

These constrained SUSY models are theoretically well motivated and provide a rich spectrum of experimental signatures. However, with universality relations imposed on the soft SUSY breaking parameters, they do not cover all possible kinematic signatures and mass relations of SUSY. In such scenarios the squarks are often nearly degenerate in mass, in particular for the first and second generation. The exclusion of parameter space in the CMSSM and in CMSSM-inspired models is mainly driven by first and second generation squark production together with gluino production. As shown in Fig. 90.1 [47–49] these processes possess

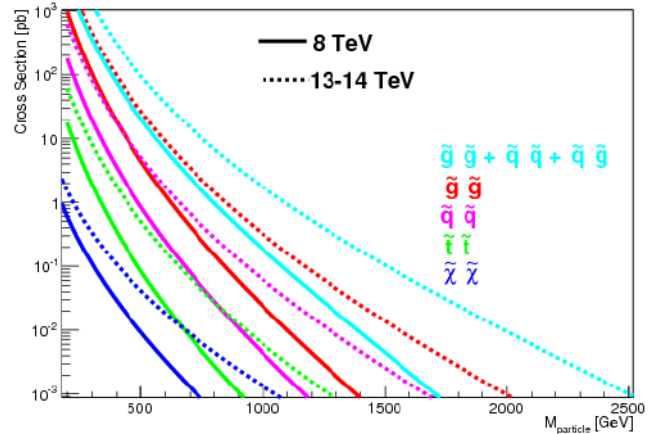


Figure 90.1: Cross sections for pair production of different sparticles as a function of their mass at the LHC for a center-of-mass energy of 8 TeV (solid curves) and 13–14 TeV (dotted curves), taken from Ref. [47]. Typically the production cross section of colored squarks and gluinos, calculated with NLL-FAST [48] at  $\sqrt{s} = 8$  and 13 TeV, is several orders of magnitude larger than the one for electroweak gauginos, calculated with Prospino [49] at  $\sqrt{s} = 8$  and 14 TeV for higgsino-like neutralinos. Except for the explicitly shown pair production of stops, production cross sections for squarks assumes mass degeneracy of left- and right-handed  $u$ ,  $d$ ,  $s$ ,  $c$  and  $b$  squarks.

the largest production cross sections in proton-proton collisions, and thus the LHC searches typically provide the tightest mass limits on these colored sparticles. This, however, implies that the allowed parameter space of constrained SUSY models today has been restrained significantly by searches from ATLAS and CMS. Furthermore, confronting the remaining allowed parameter space with other collider and non-collider measurements, which are directly or indirectly sensitive to contributions from SUSY, the overall compatibility of these models with all data is significantly worse than in the pre-LHC era (see section II.8 for further discussion), indicating that very constrained models like the CMSSM are no longer good benchmark scenarios to solely characterize the results of SUSY searches at the LHC.

For these reasons, an effort has been made to complement the traditional constrained models with more flexible approaches.

One approach to study a broader and more comprehensive subset of the MSSM is via the phenomenological-MSSM, or pMSSM [59–61]. It is derived from the MSSM, using experimental data to eliminate parameters that are free in principle but have already been highly constrained by measurements of *e.g.*, flavor mixing and CP-violation. This effective approach reduces the number of free parameters in the MSSM to typically 19 or even less, making it a practical compromise between the full MSSM and highly constrained models such as the CMSSM.

Even less dependent on fundamental assumptions are interpretations in terms of so-called simplified models [62–65]. Such models assume a limited set of SUSY particle production and decay modes and leave open the possibility to vary masses and other parameters freely. Therefore, simplified models enable comprehensive studies of individual SUSY topologies, and are useful for optimization of the experimental searches over a wide parameter space without limitations on fundamental kinematic properties such as masses, production cross sections, and decay modes.

As a consequence, ATLAS and CMS have adopted simplified models as the primary framework to provide interpretations of their searches. In addition to using simplified models that describe prompt decays of SUSY particles, the experiments are now also focusing more on the use of simplified models that allow for decays of long-lived SUSY particles as they can arise in different SUSY scenarios (see Section 90.7 for further discussion). Today, almost every individual search provides interpretations of their results in one or even several simplified models that are characteristic of

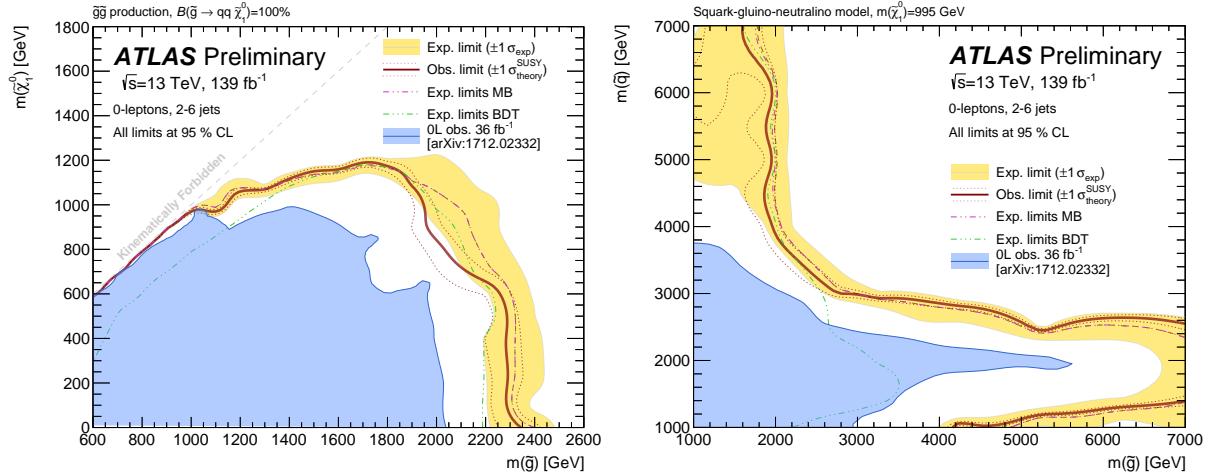


Figure 90.2: Left: lower mass limits, at 95% C.L., on gluino pair production and decay in a simplified model with  $\tilde{g} \rightarrow q\bar{q}\tilde{\chi}_1^0$ . Right: 95% C.L. mass limits on gluinos and squarks assuming gluino and squark production, and  $m_{\tilde{\chi}_1^0} = 995$  GeV. Results of the ATLAS collaboration.

SUSY topologies probed by the analysis.

However, while these models are very convenient for the interpretation of individual SUSY production and decay topologies, care must be taken when applying these limits to more complex SUSY spectra. Therefore, in practice, simplified model limits are often used as an approximation of the constraints that can be placed on sparticle masses in more complex SUSY spectra. Yet, depending on the assumed SUSY spectrum, the sparticle of interest, and the considered simplified model limit, this approximation can lead to a significant mistake, typically an overestimation, in the assumed constraint on the sparticle mass (see for example [66]). Only on a case-by-case basis can it be determined whether the limit of a given simplified model represents a good approximation of the true underlying constraint that can be applied on a sparticle mass in a complex SUSY spectrum. In the following, we will point out explicitly the assumptions that have entered the limits when quoting interpretations from simplified models.

This review covers results up to September 2019 and since none of the searches performed so far have shown significant excess above the SM background prediction, the interpretation of the presented results are exclusion limits on SUSY parameter space. Unless stated differently, all quoted exclusion limits are at 95% confidence level.

#### 90.4 Exclusion limits on gluino and squark masses

Gluinos and squarks are the SUSY partners of gluons and quarks, and thus carry color charge. Limits on squark masses of the order 100 GeV have been set by the LEP experiments [67], in the decay to quark plus neutralino, and for a mass difference between squark and quark plus neutralino of typically at least a few GeV. However, due to the colored production of these particles at hadron colliders (see e.g. Fig. 90.1), hadron collider experiments are able to set much tighter mass limits.

Pair production of these massive colored sparticles at hadron colliders usually involve both the s-channel and t-channel parton-parton interactions. Since there is a negligible amount of bottom and top quark content in the proton, top- and bottom squark production proceeds through s-channel diagrams only. In the past, experimental analyses of squark and/or gluino production typically assumed the first and second generation squarks to be approximately degenerate in mass. However, in order to have even less model dependent interpretations of the searches, the experiments have started to also provide simplified model limits on individual first or second generation squarks.

Assuming R-parity conservation and assuming gluinos to be heavier than squarks, squarks will predominantly decay to a quark and a neutralino or chargino, if kinematically allowed. The de-

cay may involve the lightest neutralino (typically the LSP) or chargino, but, depending on the masses and couplings of the gauginos, may involve heavier neutralinos or charginos. For pair production of first and second generation squarks, the simplest decay modes involve two jets and missing momentum, with potential extra jets stemming from initial state or final state radiation (ISR/FSR) or from decay modes with longer decay chains (cascades). Similarly, gluino pair production leads to four jets and missing momentum, and possibly additional jets from ISR/FSR or cascades. Associated production of a gluino and a (anti-)squark is also possible, in particular if squarks and gluinos have similar masses, typically leading to three or more jets in the final state. In cascades, isolated photons or leptons may appear from the decays of sparticles such as neutralinos or charginos. Final states are thus characterized by significant missing transverse momentum, and at least two, and possibly many more high  $p_T$  jets, which can be accompanied by one or more isolated objects like photons or leptons, including  $\tau$  leptons, in the final state. Table 90.1 shows a schematic overview of characteristic final state signatures of gluino and squark production for different mass hierarchy hypotheses and assuming decays involving the lightest neutralino.

**Table 90.1:** Typical search signatures at hadron colliders for direct gluino and first- and second-generation squark production assuming different mass hierarchies.

Mass Hierarchy	Main Production	Dominant Decay	Typical Signature
$m_{\tilde{q}} \ll m_{\tilde{g}}$	$\tilde{q}\tilde{q}, \tilde{q}\tilde{q}$	$\tilde{q} \rightarrow q\tilde{\chi}_1^0$	$\geq 2$ jets + $E_T^{\text{miss}}$ + X
$m_{\tilde{q}} \approx m_{\tilde{g}}$	$\tilde{q}\tilde{q}, \tilde{q}\tilde{g}$	$\tilde{q} \rightarrow q\tilde{\chi}_1^0$ $\tilde{g} \rightarrow q\tilde{q}\tilde{\chi}_1^0$	$\geq 3$ jets + $E_T^{\text{miss}}$ + X
$m_{\tilde{q}} \gg m_{\tilde{g}}$	$\tilde{g}\tilde{g}$	$\tilde{g} \rightarrow q\tilde{q}\tilde{\chi}_1^0$	$\geq 4$ jets + $E_T^{\text{miss}}$ + X

##### 90.4.1 Exclusion limits on the gluino mass

Limits set by the Tevatron experiments on the gluino mass assume the framework of the CMSSM, with  $\tan\beta = 5$  (CDF) or  $\tan\beta = 3$  (D0), where  $\tan\beta$  is the ratio of vacuum expectation values of the Higgs fields for up-type and down-type fermions. Furthermore,  $A_0 = 0$  and  $\mu < 0$  is assumed, and the resulting lower mass limits are about 310 GeV for all squark masses, or 390 GeV for the case  $m_{\tilde{q}} = m_{\tilde{g}}$  [68, 69]. These limits have been superseded by those provided by ATLAS and CMS, and the tightest constraints have been set with up to approximately  $140 \text{ fb}^{-1}$  of data recorded at the LHC at a center-of-mass energy of 13 TeV.

Limits on the gluino mass have been established in the framework of simplified models. Assuming only gluino pair production, in particular three primary decay chains of the gluino have been

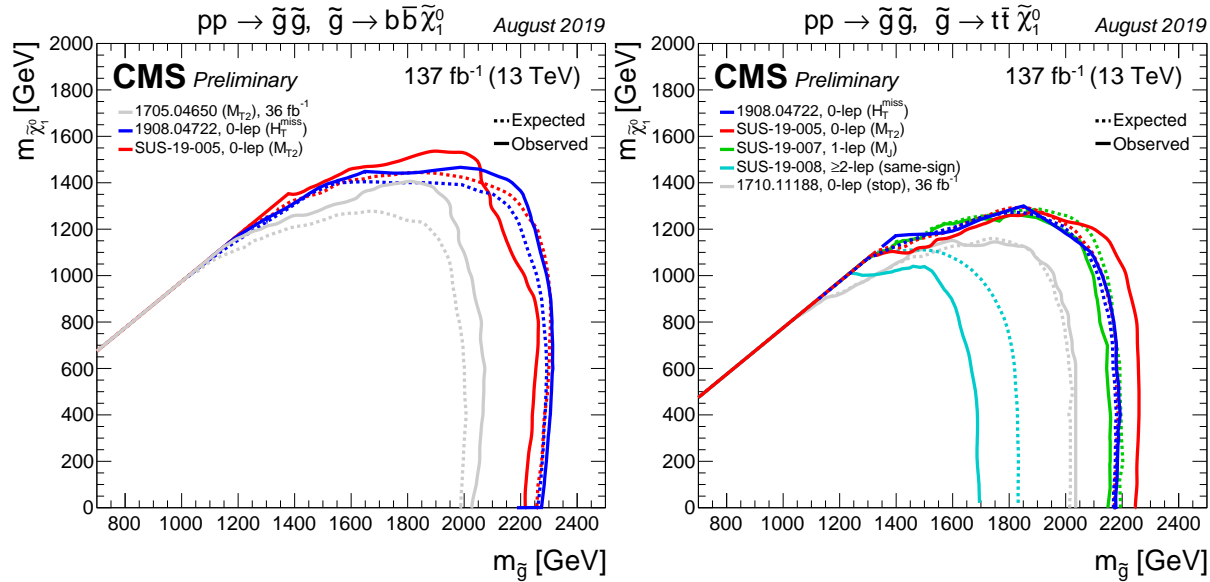


Figure 90.3: Lower mass limits, at 95% C.L., on gluino pair production for various decay chains in the framework of simplified models. Left:  $\tilde{g} \rightarrow b\bar{b}\tilde{\chi}_1^0$ . Right:  $\tilde{g} \rightarrow t\bar{t}\tilde{\chi}_1^0$ . Results of the CMS collaboration.

considered by the LHC experiments for interpretations of their search results. The first decay chain  $\tilde{g} \rightarrow q\bar{q}\tilde{\chi}_1^0$  assumes gluino mediated production of first and second generation squarks (on-shell or off-shell) which leads to four light flavor quarks in the final state. Therefore, inclusive all-hadronic analyses searching for multijet plus  $E_T^{\text{miss}}$  final states are utilized to put limits on this simplified model. These limits are derived as a function of the gluino and neutralino (LSP) mass. As shown in Fig. 90.2 (left), using the cross section from next-to-leading order QCD corrections and the resummation of soft gluon emission at next-to-leading-logarithmic accuracy as reference [48], the ATLAS collaboration [70] excludes in this simplified model gluino masses below approximately 2.3 TeV, for a massless neutralino. In scenarios where neutralinos are not very light, the efficiency of the analyses is reduced by the fact that jets are less energetic, and there is less missing transverse momentum in the event. This leads to weaker limits when the mass difference  $\Delta m = m_{\tilde{g}} - m_{\tilde{\chi}_1^0}$  is reduced. For example, for neutralino masses above about 1.2 TeV no limit on the gluino mass can be set for this decay chain. Therefore, limits on gluino masses are strongly affected by the assumption of the neutralino mass. Similar results for this simplified model have been obtained by CMS [71].

The second important decay chain of the gluino considered for interpretation in a simplified model is  $\tilde{g} \rightarrow b\bar{b}\tilde{\chi}_1^0$ . Here the decay is mediated via bottom squarks and thus leads to four jets from  $b$  quarks and  $E_T^{\text{miss}}$  in the final state. Also for this topology inclusive all-hadronic searches provide the highest sensitivity. However, with four  $b$  quarks in the final state, the use of secondary vertex reconstruction for the identification of jets originating from  $b$  quarks provides a powerful handle on the SM background. Therefore, in addition to a multijet plus  $E_T^{\text{miss}}$  signature these searches also require several jets to be tagged as  $b$ -jets. As shown in Fig. 90.3 (left), for this simplified model CMS [71] excludes gluino masses below  $\approx 2.3$  TeV for a massless neutralino, while for neutralino masses above  $\approx 1.5$  TeV no limit on the gluino mass can be set. Comparable limits for this simplified model are provided by searches from ATLAS [72].

Gluino decays are not limited to first and second generation squarks or bottom squarks; if kinematically allowed, decays to top squarks via  $\tilde{g} \rightarrow t\bar{t}$  are also possible. This leads to a “four tops” final state  $ttt\tilde{\chi}_1^0$  and defines the third important simplified model,  $\tilde{g} \rightarrow t\bar{t}\tilde{\chi}_1^0$ , characterizing gluino pair production. The topology of this decay is very rich in different experimental signatures: as many as four isolated leptons, four  $b$ -jets, several light flavor quark jets, and significant missing momentum from the neu-

trinos in the  $W$  decay and from the two neutralinos. As shown in Fig. 90.3 (right), the CMS search based on the  $m_{T2}$  variable [73] rules out gluinos with masses below  $\approx 2.25$  TeV for massless neutralinos in this model. For neutralino masses above  $\approx 1.3$  TeV, no limit can be placed on the gluino mass. The ATLAS multiple  $b$ -jets search [72] obtains similar limits.

The ATLAS collaboration also provides limits in a pMSSM-inspired model with only gluinos and first and second generation squarks, and a bino-like  $\tilde{\chi}_1^0$  [70]. As shown in Fig. 90.2 (right), assuming  $m_{\tilde{\chi}_1^0} = 995$  GeV, gluinos with masses below  $\approx 1.6$  TeV are excluded for any squark mass. For  $m_{\tilde{q}} \approx m_{\tilde{g}}$ , the mass exclusion is about 3.0 TeV. The dependence of these limits on  $m_{\tilde{\chi}_1^0}$  is illustrated in Ref. [70]. For massless  $\tilde{\chi}_1^0$ , gluino masses below 2.2 TeV are excluded for all squark masses.

R-parity violating gluino decays are searched for in a number of final states. Searches in multilepton final states set lower mass limits of 1 to 1.4 TeV, depending on neutralino mass and lepton flavor, on decays mediated by  $\lambda$  and  $\lambda'$  couplings [74–78], assuming prompt decays. Searches for displaced vertices are sensitive to non-prompt decays [79–82]. Multijet final states have been used to search for fully hadronic gluino decays involving  $\lambda''$ , by CDF [83], ATLAS [79, 84–86] and CMS [87–89]. Lower gluino mass limits range between 600 and 2000 GeV depending on neutralino mass and flavor content of the final state.

#### 90.4.2 Exclusion limits on squark masses

Limits on first and second generation squark masses set by the Tevatron experiments assume the CMSSM, and amount to lower limits of about 380 GeV for all gluino masses, or 390 GeV for the case  $m_{\tilde{q}} = m_{\tilde{g}}$  [68, 69].

At the LHC, limits on squark masses have been set using up to approximately  $140 \text{ fb}^{-1}$  of data at 13 TeV. Interpretations in simplified models typically characterize squark pair production with only one decay chain of  $\tilde{q} \rightarrow q\tilde{\chi}_1^0$ . Here it is assumed that the left and right-handed  $\tilde{u}$ ,  $\tilde{d}$ ,  $\tilde{s}$  and  $\tilde{c}$  squarks are degenerate in mass. Furthermore, it is assumed that the mass of the gluino is very high and thus contributions of the corresponding  $t$ -channel diagrams to squark pair production are negligible. Therefore, the total production cross section for this simplified model is eight times the production cross section of an individual squark (e.g.  $\tilde{u}_L$ ). Under these assumptions, ATLAS obtains a lower squark mass limit of  $\approx 1.9$  TeV for light neutralinos [70], as shown in Fig. 90.4 (left). The effects of heavy neutralinos on squark limits are similar to those discussed in the gluino case (see Section 90.4.1), and only for neutralino masses below  $\approx 800$  GeV can any squark masses



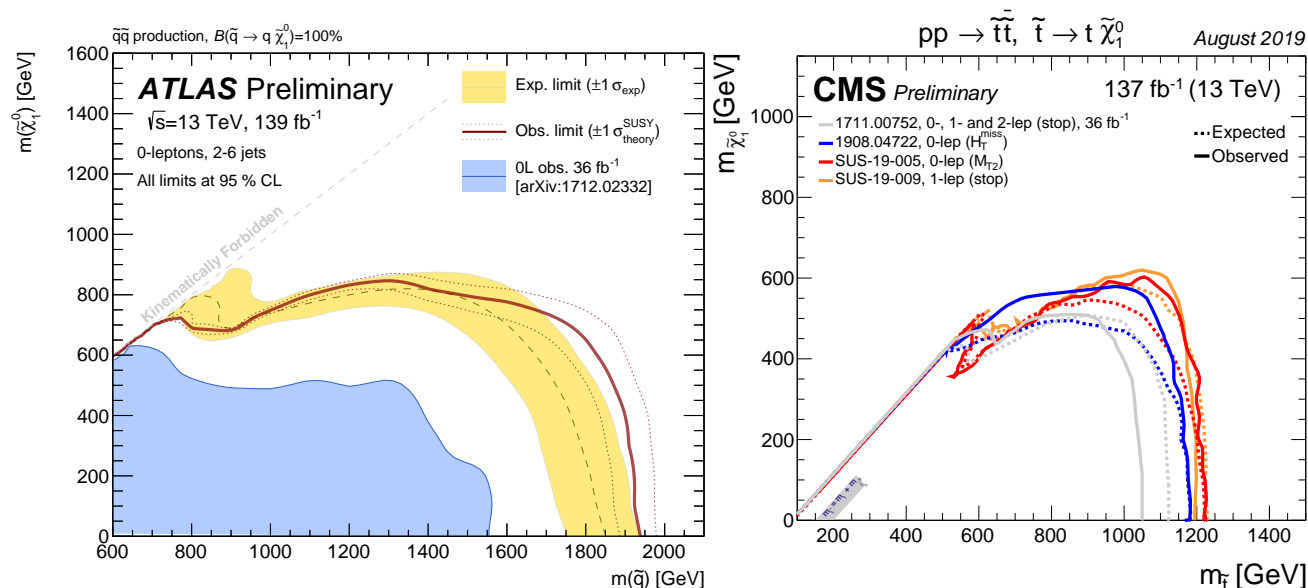


Figure 90.4: Left: 95% C.L. exclusion contours in the squark-neutralino mass plane defined in the framework of simplified models assuming a single decay chain of  $\tilde{q} \rightarrow q\tilde{\chi}_1^0$ , obtained by ATLAS. Right: the 95% C.L. exclusion contours in the stop-neutralino mass plane defined in the framework of a simplified model assuming a single decay chain of  $\tilde{t} \rightarrow t\tilde{\chi}_1^0$  as obtained by CMS.

be excluded.

For the same analysis ATLAS also provides an interpretation of their search result in the aforementioned pMSSM-inspired model with only gluinos and first and second generation squarks, and a bino-like  $\tilde{\chi}_1^0$  [70], as shown in Fig. 90.2 (right). In this model, squark production can take place with non-decoupled gluinos, enhancing the squark production cross section through gluino exchange diagrams.

If the assumption of mass degenerate first and second generation squarks is dropped and only the production of a single light squark is assumed, the limits weaken significantly. For example, the CMS limit on degenerate squarks of 1750 GeV for light neutralinos drops to  $\approx 1300$  GeV for pair production of a single light squark, and for neutralinos heavier than  $\approx 600$  GeV no squark mass limit can be placed [73]. It should be noted that this limit is not a result of a simple scaling of the above mentioned mass limits assuming eightfold mass degeneracy but it also takes into account that for an eight times lower production cross section the analyses must probe kinematic regions of phase space that are closer to the ones of SM background production. Since signal acceptance and the ratio of expected signal to SM background events of the analyses are typically worse in this region of phase space not only the 1/8 reduction in production cross section but also a worse analysis sensitivity are responsible for the much weaker limit on single squark pair production.

For single light squarks ATLAS also reports results of a dedicated search for pair production of scalar partners of charm quarks [90]. Assuming that the scalar-charm state exclusively decays into a charm quark and a neutralino, scalar-charm masses up to 800 GeV are excluded for neutralino masses below 260 GeV.

Besides placing stringent limits on first and second generation squark masses, the LHC experiments also search for the production of third generation squarks. SUSY at the TeV-scale is often motivated by naturalness arguments, most notably as a solution to cancel quadratic divergences in radiative corrections to the Higgs boson mass. In this context, the most relevant terms for SUSY phenomenology arise from the interplay between the masses of the third generation squarks and the Yukawa coupling of the top quark to the Higgs boson. This motivates a potential constraint on the masses of the top squarks and the left-handed bottom squark. Due to the large top quark mass, significant mixing between  $\tilde{t}_L$  and  $\tilde{t}_R$  is expected, leading to a lighter mass state  $\tilde{t}_1$  and a heavier mass state  $\tilde{t}_2$ . In the MSSM, the lightest top squark ( $\tilde{t}_1$ ) can be the lightest squark.

Bottom squarks are expected to decay predominantly to  $b\tilde{\chi}_1^0$  giving rise to the characteristic multi  $b$ -jet and  $E_{\text{T}}^{\text{miss}}$  signature. Direct production of bottom squark pairs has been searched for at the Tevatron and at the LHC. Limits from the Tevatron are  $m_{\tilde{b}} > 247$  GeV for a massless neutralino [91] [92]. The LHC experiments have surpassed these limits, and the latest results are based on up to 140 fb $^{-1}$  of data collected at  $\sqrt{s} = 13$  TeV. CMS has set a lower limit of  $m_{\tilde{b}} > \approx 1250$  GeV for massless neutralinos in this model [73]. For  $m_{\tilde{\chi}_1^0} \approx 700$  GeV or higher no limit can be placed on direct bottom squark pair production in this simplified model. Limits from ATLAS are comparable [93]. Further bottom squark decay modes have also been searched for by ATLAS [94,95] and CMS [71,76,96].

The top squark decay modes depend on the SUSY mass spectrum, and on the  $\tilde{t}_L$ - $\tilde{t}_R$  mixture of the top squark mass eigenstate. If kinematically allowed, the two-body decays  $\tilde{t} \rightarrow t\tilde{\chi}_1^0$  (which requires  $m_{\tilde{t}} - m_{\tilde{\chi}_1^0} > m_t$ ) and  $\tilde{t} \rightarrow b\tilde{\chi}_1^\pm$  (which requires  $m_{\tilde{t}} - m_{\tilde{\chi}_1^\pm} > m_b$ ) are expected to dominate. If not, the top squark decay may proceed either via the two-body decay  $\tilde{t} \rightarrow c\tilde{\chi}_1^0$  or through  $\tilde{t} \rightarrow bf\tilde{f}'\tilde{\chi}_1^0$  (where  $f$  and  $\tilde{f}'$  denote a fermion-antifermion pair with appropriate quantum numbers). For  $m_{\tilde{t}} - m_{\tilde{\chi}_1^0} > m_b$  the latter decay chain represents a four-body decay with a  $W$  boson, charged Higgs  $H$ , slepton  $\tilde{\ell}$ , or light flavor squark  $\tilde{q}$ , exchange. If the exchanged  $W$  boson and/or sleptons are kinematically allowed to be on-shell ( $(m_{\tilde{t}} - m_{\tilde{\chi}_1^\pm}) > (m_b + m_W)$  and/or  $(m_{\tilde{t}} - m_{\tilde{\chi}_1^\pm}) > m_b$ ), the three-body decays  $\tilde{t} \rightarrow Wb\tilde{\chi}_1^0$  and/or  $\tilde{t} \rightarrow b\tilde{\ell}\tilde{\chi}_1^0$  will become dominant. For further discussion on top squark decays see for example Ref. [97].

Limits from LEP on the  $\tilde{t}_1$  mass are  $m_{\tilde{t}} > 96$  GeV in the charm plus neutralino final state, and  $> 93$  GeV in the lepton,  $b$ -quark and sneutrino final state [67].

The Tevatron experiments have performed a number of searches for top squarks, often assuming direct pair production. In the  $b\tilde{\nu}$  decay channel, and assuming a 100% branching fraction, limits are set as  $m_{\tilde{t}} > 210$  GeV for  $m_{\tilde{\nu}} < 110$  GeV and  $m_{\tilde{t}} - m_{\tilde{\nu}} > 30$  GeV, or  $m_{\tilde{t}} > 235$  GeV for  $m_{\tilde{\nu}} < 50$  GeV [98] [99]. In the  $\tilde{t} \rightarrow c\tilde{\chi}_1^0$  decay mode, a top squark with a mass below 180 GeV is excluded for a neutralino lighter than 95 GeV [100] [101]. In both analyses, no limits on the top squark can be set for heavy sneutrinos or neutralinos. In the  $\tilde{t} \rightarrow b\tilde{\chi}_1^\pm$  decay channel, searches for a relatively light top squark have been performed in the dilepton final state [102] [103]. The CDF experiment sets limits in the  $\tilde{t} - \tilde{\chi}_1^0$

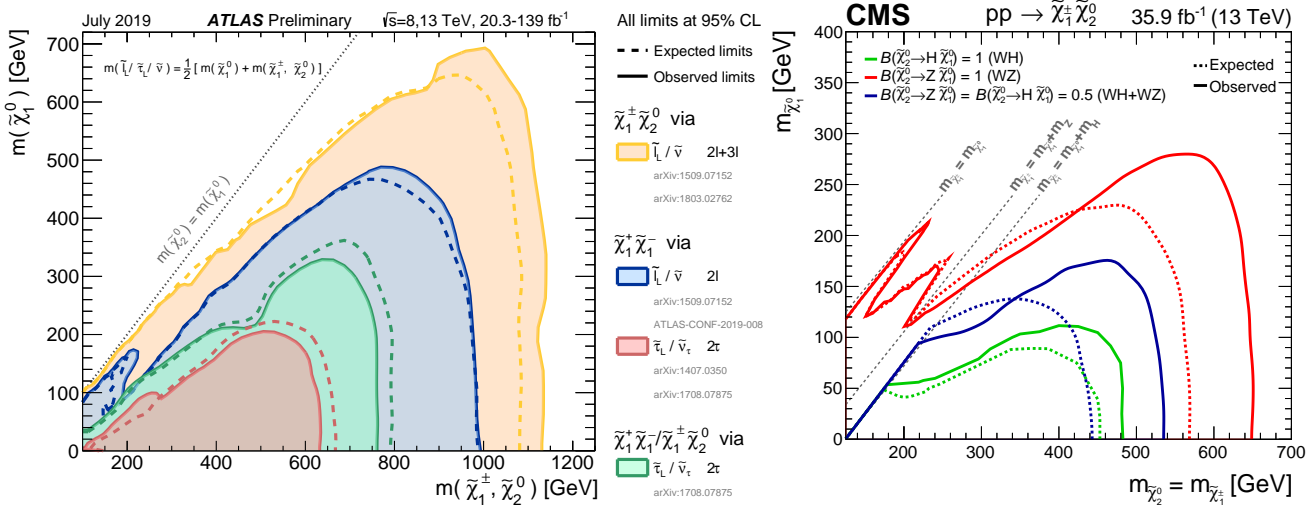


Figure 90.5: LHC exclusion limits on chargino and neutralino masses in a number of simplified models. Left: limits on chargino and neutralino masses for pair production of charginos, pair production of heavier neutralinos, or pair production of chargino and neutralino, under the assumption of light sleptons mediating the decays. Right: limits on chargino and neutralino masses for pair production of chargino and neutralino, under the assumption of decoupled sleptons, and chargino/neutralino decay through  $W^*$ ,  $Z^*$  or  $H$ .

mass plane for various branching fractions of the chargino decay to leptons and for two values of  $m_{\tilde{\chi}_1^\pm}$ . For  $m_{\tilde{\chi}_1^\pm} = 105.8$  GeV and  $m_{\tilde{\chi}_1^0} = 47.6$  GeV, top squarks between 128 and 135 GeV are excluded for  $W$ -like leptonic branching fractions of the chargino.

The LHC experiments have improved these limits substantially. As shown in the right plot of Fig. 90.4, limits on the top squark mass assuming a simplified model with a single decay chain of  $\tilde{t} \rightarrow t\tilde{\chi}_1^0$  now surpass 1 TeV. The most important searches for this top squark decay topology are dedicated searches requiring zero or one isolated lepton, modest  $E_T^{\text{miss}}$ , and four or more jets out of which at least one jet must be reconstructed as a  $b$ -jet [71, 73, 104–106]. For example, CMS excludes top squarks with masses below about 1200 GeV in this model for massless neutralinos, while for  $m_{\tilde{\chi}_1^0} > 600$  GeV no limits can be provided.

Assuming that the top squark decay exclusively proceeds via the chargino mediated decay chain  $\tilde{t} \rightarrow b\tilde{\chi}_1^\pm, \tilde{\chi}_1^\pm \rightarrow W^{\pm(*)}\tilde{\chi}_1^0$  yields stop mass exclusion limits that vary strongly with the assumptions made on the  $\tilde{t} - \tilde{\chi}_1^\pm - \tilde{\chi}_1^0$  mass hierarchy. For example, for  $m_{\tilde{\chi}_1^\pm} = (m_{\tilde{t}} + m_{\tilde{\chi}_1^0})/2$ , a stop mass below  $\approx 1150$  GeV for a light  $\tilde{\chi}_1^0$  is excluded, while no limit can be placed for  $m_{\tilde{\chi}_1^0} > 550$  GeV [104]. These limits, however, can weaken significantly when other assumptions about the mass hierarchy or the decay of the charginos are imposed [104, 106–108].

If the decays  $\tilde{t} \rightarrow t\tilde{\chi}_1^0$  and  $\tilde{t} \rightarrow b\tilde{\chi}_1^\pm, \tilde{\chi}_1^\pm \rightarrow W^{\pm(*)}\tilde{\chi}_1^0$  are kinematically forbidden, the decay chains  $\tilde{t} \rightarrow Wb\tilde{\chi}_1^0$  and  $\tilde{t} \rightarrow c\tilde{\chi}_1^0$  can become important. The one-lepton ATLAS search provides for the kinematic region  $m_{\tilde{t}} - m_{\tilde{\chi}_1^\pm} > m_b + m_W$  lower limits on the top squark mass of  $\approx 700$  GeV for a neutralino lighter than  $\approx 570$  GeV [109]. Other analyses with zero, one or two leptons also target this kinematic region [105, 106, 110–114].

For the kinematic region in which even the production of real  $W$  bosons is not allowed, ATLAS and CMS improve the Tevatron limit on  $\tilde{t} \rightarrow c\tilde{\chi}_1^0$  substantially. Based on a monojet analysis [115] ATLAS excludes top squark masses below  $m_{\tilde{\chi}_1^0} \approx 450$  GeV along the kinematic boundary for the  $\tilde{t} \rightarrow c\tilde{\chi}_1^0$  decay. A dedicated analysis for  $\tilde{t} \rightarrow c\tilde{\chi}_1^0$  excludes stop masses below 500 GeV for  $m_{\tilde{\chi}_1^0}$  below 420 GeV [90]. The CMS collaboration uses the hadronic searches [111, 113] to place constraints on this particular stop decay and excludes  $m_{\tilde{t}} \approx 550$  GeV for  $m_{\tilde{\chi}_1^0}$  below 450 GeV. The exclusion at  $m_{\tilde{t}} \approx m_{\tilde{\chi}_1^0}$  is also about 550 GeV.

The other decay chain relevant in this phase region is  $\tilde{t} \rightarrow$

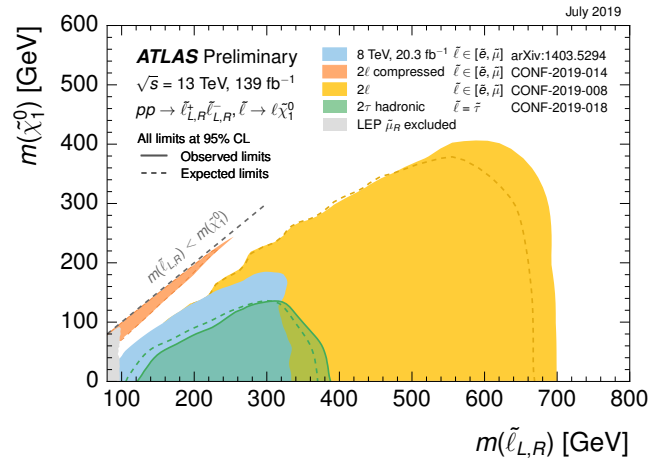


Figure 90.6: LHC exclusion limits on slepton (selectron and smuon) masses, assuming equal masses of selectrons and smuons, degeneracy of  $\tilde{\ell}_L$  and  $\tilde{\ell}_R$ , and a 100% branching fraction for  $\tilde{\ell} \rightarrow \ell\tilde{\chi}_1^0$ .

$bf\tilde{f}'\tilde{\chi}_1^0$ . Here the ATLAS one-lepton [106] and two-lepton [110] searches exclude up to  $m_{\tilde{t}} \approx 440$  GeV for  $m_{\tilde{\chi}_1^0}$  below 340 GeV, while the monojet analysis [115] excludes at the kinematic boundary top squarks below 400 GeV. As for the  $\tilde{t} \rightarrow c\tilde{\chi}_1^0$  decay, CMS uses the zero-lepton searches [111, 113] to also place constraints on  $\tilde{t} \rightarrow bf\tilde{f}'\tilde{\chi}_1^0$ . Also in this case CMS excludes  $m_{\tilde{t}} \approx 550$  GeV for  $m_{\tilde{\chi}_1^0}$  below 450 GeV.

In general, the variety of top squark decay chains in the phase space region where  $\tilde{t} \rightarrow t\tilde{\chi}_1^0$  is kinematically forbidden represents a challenge for the experimental search program and more data and refined analyses will be required to further improve the sensitivity in this difficult but important region of SUSY parameter space.

R-parity violating production of single squarks via a  $\lambda'$ -type coupling has been studied at HERA. In such models, a lower limit on the squark mass of the order of 275 GeV has been set for electromagnetic-strength-like couplings  $\lambda' = 0.3$  [116]. At the LHC, both prompt [75, 78, 117] and non-prompt [80, 118] R-parity violating squark decays have been searched for, but no signal was found. Squark mass limits are very model-dependent.

R-parity violating production of single top squarks has been

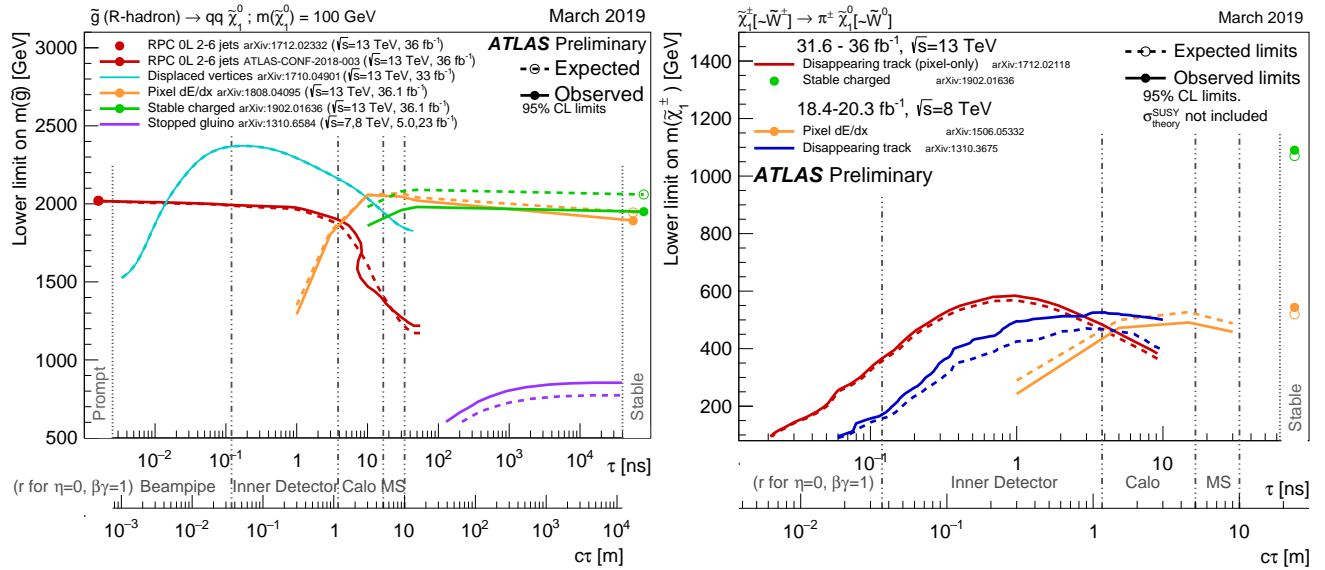


Figure 90.7: Limits at 95% C.L. on the gluino mass in R-hadron models (left), and on the chargino mass in a model where the wino-like chargino is almost degenerate with the LSP (right), as a function of gluino or chargino lifetime, as obtained by ATLAS.

searched for at LEP, HERA, and the Tevatron. For example, an analysis from the ZEUS collaboration [119] makes an interpretation of its search result assuming top squarks to be produced via a  $\lambda'$  coupling and decay either to  $b\tilde{\chi}_1^\pm$  or R-parity-violating to a lepton and a jet. Limits are set on  $\lambda'_{131}$  as a function of the top squark mass in an MSSM framework with gaugino mass unification at the GUT scale.

The search for top squark pair production in the context of R-parity violating supersymmetry has now also become a focus point for searches at the LHC. CMS and ATLAS have performed searches for top squarks using a variety of multilepton final states [75, 120]. The  $\lambda'$ -mediated top squark decay  $\tilde{t} \rightarrow b\ell$  has been studied by ATLAS for prompt decays [121], and by ATLAS and CMS for non-prompt decays [122–124], setting limits up to 1.4–1.6 TeV in simplified models for this mode. CMS also searched for the  $\lambda'$ -mediated decay  $\tilde{t} \rightarrow b\ell qq$ , setting lower stop mass limits of 890 GeV ( $e$ ) or 1000 GeV ( $\mu$ ) [125]. The fully hadronic R-parity violating top squark decays  $\tilde{t} \rightarrow bs$ ,  $\tilde{t} \rightarrow ds$ , and  $\tilde{t} \rightarrow bd$ , involving  $\lambda''$ , have been searched for by ATLAS [75, 79, 94, 126], and CMS [127, 128], and lower top squark mass limits up to 610 GeV were set.

It should be noted that limits discussed in this section belong to different top and bottom squark decay channels, different particle mass hierarchies, and different simplified decay scenarios. Therefore, care must be taken when interpreting these limits in the context of more complete SUSY models.

#### 90.4.3 Summary of exclusion limits on squarks and gluinos assuming R-Parity conservation

A summary of the most important squark and gluino mass limits for different interpretation approaches assuming R-parity conservation is shown in Table 90.2.

For gluino masses rather similar limits of about 2.3 TeV are obtained from different model assumptions, indicating that the LHC is indeed probing direct gluino production at the TeV scale and beyond. However, for neutralino masses above approximately 1 to 1.4 TeV, in the best case scenarios, ATLAS and CMS searches do not place any limits on the gluino mass.

Limits on direct squark production, on the other hand, depend strongly on the chosen model. Especially for direct production of top squarks there are still large regions in parameter space where masses below 1 TeV cannot be excluded. This is also true for first and second generation squarks when only one single squark is considered. Furthermore, for neutralino masses above  $\approx 500$  GeV no limits on any direct squark production scenario are placed by the LHC.

## 90.5 Exclusion limits on the masses of charginos and neutralinos

Charginos and neutralinos result from mixing of the charged wino and higgsino states, and the neutral bino, wino and higgsino states, respectively. The mixing is determined by a limited number of parameters. For charginos these are the wino mass parameter  $M_2$ , the higgsino mass parameter  $\mu$ , and  $\tan\beta$ , and for neutralinos these are the same parameters plus the bino mass parameter  $M_1$ . If any of the parameters  $M_1$ ,  $M_2$  or  $\mu$  happened to be substantially smaller than the others, the chargino/neutralino composition would be dominated by specific states, which are referred to as bino-like ( $M_1 \ll M_2, \mu$ ), wino-like ( $M_2 \ll M_1, \mu$ ), or higgsino-like ( $\mu \ll M_1, M_2$ ). If gaugino mass unification at the GUT scale is assumed, a relation between  $M_1$  and  $M_2$  at the electroweak scale follows:  $M_1 = 5/3 \tan^2\theta_W M_2 \approx 0.5M_2$ , with  $\theta_W$  the weak mixing angle. Charginos and neutralinos carry no color charge.

### 90.5.1 Exclusion limits on chargino masses

If kinematically allowed, two body decay modes such as  $\tilde{\chi}^\pm \rightarrow \tilde{f}\tilde{f}'$  (including  $\ell\tilde{\nu}$  and  $\tilde{\ell}\nu$ ) are dominant. If not, three body decays  $\tilde{\chi}^\pm \rightarrow f\tilde{f}'\tilde{\chi}^0$ , mediated through virtual  $W$  bosons or sfermions, become dominant. If sfermions are heavy, the  $W$  mediation dominates, and  $f\tilde{f}'$  are distributed with branching fractions similar to  $W$  decay products (barring phase space effects for small mass gaps between  $\tilde{\chi}^\pm$  and  $\tilde{\chi}^0$ ). If, on the other hand, sleptons are light enough to play a significant role in the decay, leptonic final states will be enhanced.

At LEP, charginos have been searched for in fully-hadronic, semi-leptonic and fully leptonic decay modes [129] [130]. A general lower limit on the lightest chargino mass of 103.5 GeV is derived, except in corners of phase space with low electron sneutrino mass, where destructive interference in chargino production, or two-body decay modes, play a role. The limit is also affected if the mass difference between  $\tilde{\chi}_1^\pm$  and  $\tilde{\chi}_1^0$  is small; dedicated searches for such scenarios set a lower limit of 92 GeV.

At the Tevatron, charginos have been searched for via associated production of  $\tilde{\chi}_1^\pm\tilde{\chi}_2^0$  [131] [132]. Decay modes involving multilepton final states provide the best discrimination against the large multijet background. Analyses have looked for at least three charged isolated leptons, for two leptons with missing transverse momentum, or for two leptons with the same charge. Depending on the  $(\tilde{\chi}_1^\pm - \tilde{\chi}_1^0)$  and/or  $(\tilde{\chi}_2^0 - \tilde{\chi}_1^0)$  mass differences, leptons may be soft.

At the LHC, the search strategy is similar to that at the Teva-



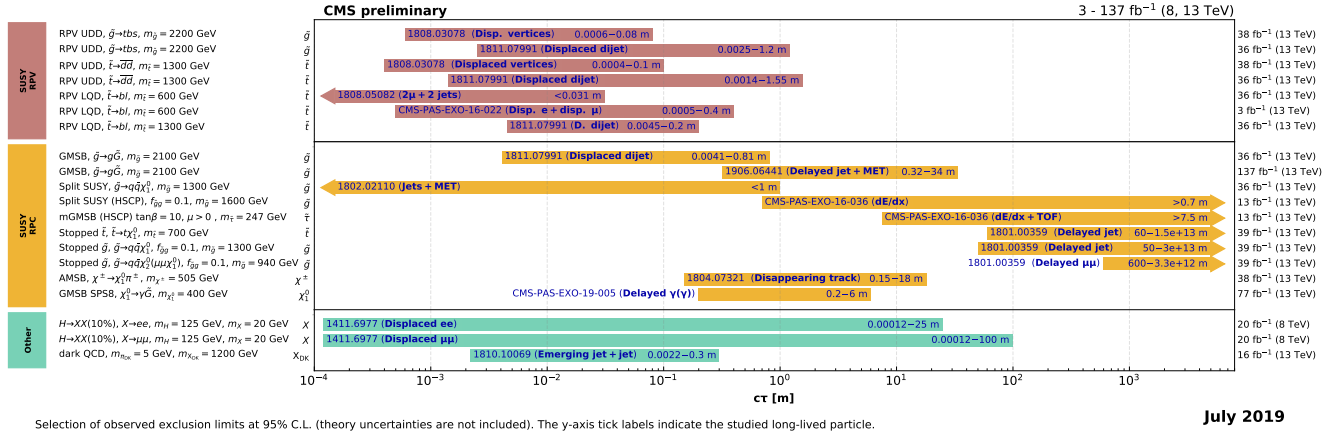


Figure 90.8: Excluded regions, at 95% C.L., in the lifetimes of long-lived particles in several models, as obtained by CMS.

**Table 90.2:** Summary of squark mass and gluino mass limits using different interpretation approaches assuming R-parity conservation. Masses in this table are provided in GeV. Further details about the assumptions and analyses from which these limits are obtained are discussed in the corresponding sections of the text.

Model	Assumption	$m_{\tilde{q}}$	$m_{\tilde{g}}$
Simplified model $\tilde{g}\tilde{q}, \tilde{g}\tilde{\bar{q}}$	$m_{\tilde{\chi}_1^0} = 0, m_{\tilde{q}} \approx m_{\tilde{g}}$	$\approx 3000$	$\approx 3000$
	$m_{\tilde{\chi}_1^0} = 0, \text{ all } m_{\tilde{q}}$	-	$\approx 2200$
	$m_{\tilde{\chi}_1^0} = 0, \text{ all } m_{\tilde{g}}$	$\approx 2600$	-
Simplified models $\tilde{g}\tilde{g}$			
$\tilde{g} \rightarrow q\tilde{q}\tilde{\chi}_1^0$	$m_{\tilde{\chi}_1^0} = 0$	-	$\approx 2300$
	$m_{\tilde{\chi}_1^0} > \approx 1200$	-	no limit
$\tilde{g} \rightarrow b\tilde{b}\tilde{\chi}_1^0$	$m_{\tilde{\chi}_1^0} = 0$	-	$\approx 2300$
	$m_{\tilde{\chi}_1^0} > \approx 1500$	-	no limit
$\tilde{g} \rightarrow t\tilde{t}\tilde{\chi}_1^0$	$m_{\tilde{\chi}_1^0} = 0$	-	$\approx 2250$
	$m_{\tilde{\chi}_1^0} > \approx 1300$	-	no limit
Simplified models $\tilde{q}\tilde{q}$			
$\tilde{q} \rightarrow q\tilde{\chi}_1^0$	$m_{\tilde{\chi}_1^0} = 0$	$\approx 1900$	-
	$m_{\tilde{\chi}_1^0} > \approx 800$	no limit	-
$\tilde{u}_L \rightarrow q\tilde{\chi}_1^0$	$m_{\tilde{\chi}_1^0} = 0$	$\approx 1300$	-
	$m_{\tilde{\chi}_1^0} > \approx 600$	no limit	-
$\tilde{b} \rightarrow b\tilde{\chi}_1^0$	$m_{\tilde{\chi}_1^0} = 0$	$\approx 1250$	-
	$m_{\tilde{\chi}_1^0} > \approx 700$	no limit	-
$\tilde{t} \rightarrow t\tilde{\chi}_1^0$	$m_{\tilde{\chi}_1^0} = 0$	$\approx 1200$	-
	$m_{\tilde{\chi}_1^0} > \approx 600$	no limit	-
$\tilde{t} \rightarrow b\tilde{\chi}_1^\pm$	$m_{\tilde{\chi}_1^0} = 0$	$\approx 1150$	-
	$m_{\tilde{\chi}_1^0} > \approx 550$	no limit	-
$(m_{\tilde{\chi}_1^\pm} = (m_{\tilde{t}} - m_{\tilde{\chi}_1^0})/2)$	$m_{\tilde{\chi}_1^0} < \approx 570$	$\approx 700$	-
$(m_W < m_{\tilde{t}} - m_{\tilde{\chi}_1^0} < m_t)$	$\tilde{t} \rightarrow Wb\tilde{\chi}_1^0$	$m_{\tilde{\chi}_1^0} < \approx 450$	$\approx 550$
	$\tilde{t} \rightarrow c\tilde{\chi}_1^0$	$m_{\tilde{t}} \approx m_{\tilde{\chi}_1^0}$	$\approx 550$
	$\tilde{t} \rightarrow bff'\tilde{\chi}_1^0$	$m_{\tilde{\chi}_1^0} < \approx 450$	$\approx 550$
	$m_{\tilde{t}} \approx m_{\tilde{\chi}_1^0}$	$\approx 550$	-
$(m_{\tilde{t}} - m_{\tilde{\chi}_1^0} < m_W)$			

tron. As shown in Fig. 90.1, the cross section of pair production of electroweak gauginos at the LHC, for masses of several hundreds of GeV, is at least two orders of magnitude smaller than for colored SUSY particles (e.g. top squark pair production). For this reason a large data sample is required to improve the sensitivity

of LEP and Tevatron searches for direct chargino/neutralino production. With the full LHC Run 1 and Run 2 data sets, ATLAS and CMS have surpassed the limits from LEP and Tevatron in regions of SUSY parameter space.

Chargino pair production is searched for in the dilepton plus missing momentum final state. In a simplified model interpretation of the results, assuming mediation of the chargino decay by light sleptons ( $\tilde{e}$  and  $\tilde{\mu}$ ), ATLAS [133] and CMS [134] set limits on the chargino mass up to 1 TeV for massless LSPs, but no limits on the chargino mass can be set for  $\tilde{\chi}_1^0$  heavier than 480 GeV. Limits are fairly robust against variation of the slepton mass, unless the mass gap between chargino and slepton becomes small. For decays mediated through  $\tilde{\tau}$  or  $\tilde{\nu}_\tau$ , limits of 630 GeV are set by ATLAS [135] for LSPs not heavier than 200 GeV. The CMS experiment provides similar limits [136]. ATLAS also sets limits on charginos decaying via a  $W$  boson [133]: chargino masses below 420 GeV are excluded for massless LSPs, but no limits are set for LSPs heavier than 120 GeV.

The trilepton plus missing momentum final state is used to set limits on  $\tilde{\chi}_1^\pm \tilde{\chi}_2^0$  production, assuming wino-like  $\tilde{\chi}_1^\pm$  and bino-like  $\tilde{\chi}_2^0$ , and  $m_{\tilde{\chi}_1^\pm} = m_{\tilde{\chi}_2^0}$ , leaving  $m_{\tilde{\chi}_1^\pm}$  and  $m_{\tilde{\chi}_1^0}$  free. Again, the branching fraction of leptonic final states is determined by the slepton masses. If the decay is predominantly mediated by a light  $\tilde{\ell}_L$ , i.e.  $\tilde{\ell}_R$  is assumed to be heavy, the three charged-lepton flavors will be produced in equal amounts. It is assumed that  $\tilde{\ell}_L$  and sneutrino masses are equal, and diagrams with sneutrinos are included. In this scenario, ATLAS [137] and CMS [138] exclude chargino masses below 1140 GeV for massless LSPs; no limits are set for LSP masses above 700 GeV. If the decay is dominated by a light  $\tilde{\ell}_R$ , the chargino cannot be a pure wino but needs to have a large higgsino component, preferring the decays to tau leptons. Limits are set in various scenarios. If, like for  $\tilde{\ell}_L$ , a flavor-democratic scenario is assumed, CMS sets limits of 1060 GeV on the chargino mass for massless LSPs, but under the assumption that both  $\tilde{\chi}_1^\pm$  and  $\tilde{\chi}_2^0$  decay leads to tau leptons in the final state, the chargino mass limit deteriorates to 620 GeV for massless LSPs [138]. ATLAS assumes a simplified model in which staus are significantly lighter than the other sleptons in order to search for a similar multi-tau final state, and sets a lower limit on the chargino mass of 760 GeV in this model [135]. The CMS experiment provides similar limits [136].

If sleptons are heavy, the chargino is assumed to decay to a  $W$  boson plus LSP, and the  $\tilde{\chi}_2^0$  into  $Z$  plus LSP or  $H$  plus LSP. In the  $WZ$  channel, ATLAS [137, 139] and CMS [140] limits on the chargino mass reach 650 GeV for massless LSPs, but no limits are set for LSPs heavier than 300 GeV. In the  $WH$  channel, for  $m_H = 125$  GeV and using various Higgs decay modes, ATLAS [141–143] and CMS [140] set lower limits on the chargino mass up to 740 GeV for massless LSPs, but vanish for LSP masses above 240 GeV.

The results on electroweak gaugino searches interpreted in sim-

plified models are summarized in Fig. 90.5 for the two cases of light or decoupled sleptons. For both cases, ATLAS and CMS have comparable limits.

In both the wino region (a characteristic of anomaly-mediated SUSY breaking models) and the higgsino region of the MSSM, the mass splitting between  $\tilde{\chi}_1^\pm$  and  $\tilde{\chi}_1^0$  is small. The chargino decay products are very soft and may escape detection. These compressed spectra are hard to detect, and have triggered dedicated search strategies. ATLAS has performed a search for charginos and neutralinos in a compressed mass spectrum using initial state radiation [144]. For wino-like charginos, assuming degenerate  $\tilde{\chi}_1^\pm$  and  $\tilde{\chi}_2^0$ , exclusion contours in the chargino-mass versus  $\Delta m(\tilde{\chi}_1^\pm - \tilde{\chi}_1^0)$  plane are derived. As an example, such charginos are excluded below 200 GeV for  $\Delta m(\tilde{\chi}_1^\pm - \tilde{\chi}_1^0) = 10$  GeV. CMS has searched for chargino-pair production through vector-boson-fusion [145], also targetting compressed mass spectra. Assuming degenerate  $\tilde{\chi}_1^\pm$  and  $\tilde{\chi}_2^0$ , charginos with a mass below 112 GeV are excluded for  $\Delta m(\tilde{\chi}_1^\pm - \tilde{\chi}_1^0) = 1$  GeV. CMS has published further searches for such compressed spectra with soft leptons [146] or a soft tau lepton [147].

### 90.5.2 Exclusion limits on neutralino masses

In a considerable part of the MSSM parameter space, and in particular when demanding that the LSP carries no electric or color charge, the lightest neutralino  $\tilde{\chi}_1^0$  is the LSP. If R-parity is conserved, such a  $\tilde{\chi}_1^0$  is stable. Since it is weakly interacting, it will typically escape detectors unseen. Limits on the invisible width of the  $Z$  boson apply to neutralinos with a mass below 45.5 GeV, but depend on the  $Z$ -neutralino coupling. Such a coupling could be small or even absent; in such a scenario there is no general lower limit on the mass of the lightest neutralino [148]. In models with gaugino mass unification and sfermion mass unification at the GUT scale, a lower limit on the neutralino mass is derived from limits from direct searches, notably for charginos and sleptons, and amounts to 47 GeV [149]. Assuming a constrained model like the CMSSM, this limit increases to 50 GeV at LEP; however the strong constraints now set by the LHC increase such CMSSM-derived  $\tilde{\chi}_1^0$  mass limits to well above 200 GeV [150–152].

In gauge-mediated SUSY breaking models (GMSB), the LSP is typically a gravitino, and the phenomenology is determined by the nature of the next-to-lightest supersymmetric particle (NLSP). A NLSP neutralino will decay to a gravitino and a SM particle whose nature is determined by the neutralino composition. Final states with two high  $p_T$  photons and missing momentum are searched for, and interpreted in gauge mediation models with bino-like neutralinos [153–158].

Assuming the production of at least two neutralinos per event, neutralinos with large non-bino components can also be searched for by their decay in final states with missing momentum plus any two bosons out of the collection  $\gamma, Z, H$ . A number of searches at the LHC have tried to cover the rich phenomenology of the various  $Z$  and  $H$  decay modes [74, 96, 138, 140, 142, 156, 159–165].

Heavier neutralinos, in particular  $\tilde{\chi}_2^0$ , have been searched for in their decays to the lightest neutralino plus a  $\gamma$ , a  $Z$  boson or a Higgs boson. Limits on electroweak production of  $\tilde{\chi}_2^0$  plus  $\tilde{\chi}_1^\pm$  from trilepton analyses have been discussed in the section on charginos; the assumption of equal mass of  $\tilde{\chi}_2^0$  and  $\tilde{\chi}_1^\pm$  make the limits on chargino masses apply to  $\tilde{\chi}_2^0$  as well. Multilepton analyses have also been used to set limits on  $\tilde{\chi}_2^0\tilde{\chi}_3^0$  production; assuming equal mass and decay through light sleptons, limits are set up to 680 GeV for massless LSPs [166]. Again, compressed spectra with small mass differences between the heavier neutralinos and the LSP form the most challenging region.

In  $\tilde{\chi}_2^0$  decays to  $\tilde{\chi}_1^0$  and a lepton pair, the lepton pair invariant mass distribution may show a structure that can be used to measure the  $\tilde{\chi}_2^0 - \tilde{\chi}_1^0$  mass difference in case of a signal [35]. This structure, however, can also be used in the search strategy itself, as demonstrated by ATLAS [167, 168] and CMS [96, 169].

In models with R-parity violation, the lightest neutralino can decay even if it is the lightest supersymmetric particle. If the decay involves a non-zero  $\lambda$  coupling, the final state will be a

**Table 90.3:** Summary of weak gaugino mass limits in simplified models, assuming R-parity conservation. Masses in the table are provided in GeV. Further details about assumptions and analyses from which these limits are obtained are discussed in the text.

Assumption	$m_\chi$
$\tilde{\chi}_1^\pm$ , all $\Delta m(\tilde{\chi}_1^\pm, \tilde{\chi}_1^0)$	> 92
$\tilde{\chi}_1^\pm$ $\Delta m > 5$ , $m_{\tilde{\nu}} > 300$	> 103.5
$\tilde{\chi}_1^\pm$ , $m_{(\tilde{\ell}, \tilde{\nu})} = (m_{\tilde{\chi}_1^\pm} + m_{\tilde{\chi}_1^0})/2$	
$m_{\tilde{\chi}_1^0} \approx 0$	> 1000
$\tilde{\chi}_1^\pm$ , $m_{\tilde{\chi}_1^0} > 480$	no LHC limit
$\tilde{\chi}_1^\pm$ , $m_{\tilde{\ell}} > m_{\tilde{\chi}_1^\pm}$	
$m_{\tilde{\chi}_1^0} \approx 0$	> 420
$\tilde{\chi}_1^\pm$ , $m_{\tilde{\chi}_1^0} > 120$	no LHC limit
$m_{\tilde{\chi}_1^\pm} = m_{\tilde{\chi}_2^0}$ , $m_{\tilde{\ell}_L} = (m_{\tilde{\chi}_1^\pm} + m_{\tilde{\chi}_1^0})/2$	
$m_{\tilde{\chi}_1^0} \approx 0$	> 1140
$m_{\tilde{\chi}_1^0} > 700$	no LHC limit
$m_{\tilde{\chi}_1^\pm} = m_{\tilde{\chi}_2^0}$ , $m_{\tilde{\ell}_R} = (m_{\tilde{\chi}_1^\pm} + m_{\tilde{\chi}_1^0})/2$	flavor-democratic
$m_{\tilde{\chi}_1^0} \approx 0$	> 1060
$m_{\tilde{\chi}_1^0} > 600$	no LHC limit
$m_{\tilde{\chi}_1^\pm} = m_{\tilde{\chi}_2^0}$ , $m_{\tilde{\tau}} = (m_{\tilde{\chi}_1^\pm} + m_{\tilde{\chi}_1^0})/2$	$\tilde{\tau}$ -dominated
$m_{\tilde{\chi}_1^0} \approx 0$	> 620
$m_{\tilde{\chi}_1^0} > 260$	no LHC limit
$m_{\tilde{\chi}_1^\pm} = m_{\tilde{\chi}_2^0}$ , $m_{\tilde{\ell}} > m_{\tilde{\chi}_1^\pm}$ , $\text{BF}(WZ) = 1$	
$m_{\tilde{\chi}_1^0} \approx 0$	> 650
$m_{\tilde{\chi}_1^0} > 300$	no LHC limit
$m_{\tilde{\chi}_1^\pm} = m_{\tilde{\chi}_2^0}$ , $m_{\tilde{\ell}} > m_{\tilde{\chi}_1^\pm}$ , $\text{BF}(WH) = 1$	
$m_{\tilde{\chi}_1^0} \approx 0$	> 740
$m_{\tilde{\chi}_1^0} > 240$	no LHC limit

multi-lepton one. Searches for events with four or more isolated charged leptons by ATLAS [74] and CMS [78] are interpreted in such models. With very small coupling values, the neutralino would be long-lived, leading to lepton pairs with a displaced vertex, which have also been searched for [118, 124, 170].

Various searches, including searches for multi-lepton and lepton plus jets events, and searches for events with a displaced hadronic vertex, with or without a matched lepton, are interpreted in a model with R-parity violating neutralino decays involving a non-zero  $\lambda'$  coupling [75, 80, 86, 171]. Neutralino decays involving non-zero  $\lambda''$  lead to fully hadronic final states, and searches for multi-jet events and jet-pair resonances are used to set limits, typically on the production of colored particles like top squarks or gluinos, which are assumed to be the primary produced sparticles in these interpretations, as discussed earlier [79, 84, 86].

The limits on weak gauginos in simplified models are summarized in Table 90.3. Interpretations of the search results outside simplified models, such as in the phenomenological MSSM [172–176], show that the simplified model limits must be interpreted with care. Electroweak gauginos in models that are compatible with the relic density of dark matter in the universe, for example, have particularly tuned mixing parameters and mass spectra, which are not always captured by the simplified models used.

## 90.6 Exclusion limits on slepton masses

In models with slepton and gaugino mass unification at the GUT scale, the right-handed slepton,  $\tilde{\ell}_R$ , is expected to be lighter than the left-handed slepton,  $\tilde{\ell}_L$ . For tau sleptons there may be considerable mixing between the L and R states, leading to a significant mass difference between the lighter  $\tilde{\tau}_1$  and the heavier  $\tilde{\tau}_2$ .

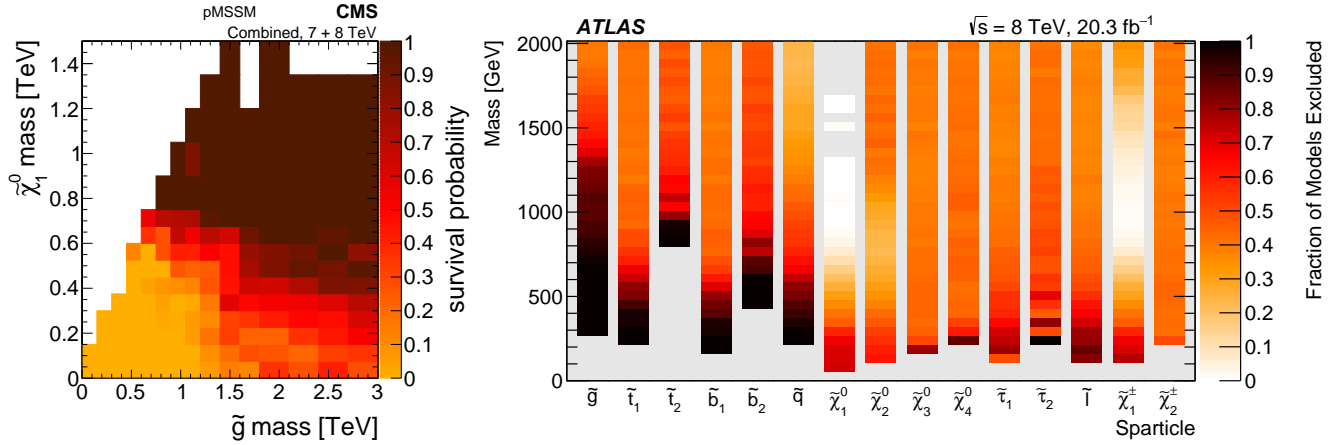


Figure 90.9: The plot on the left shows the survival probability of a pMSSM parameter space model in the gluino-neutralino mass plane after the application of the relevant CMS search results. The plot on the right shows a graphical representation of the ATLAS exclusion power in a pMSSM model. Each vertical bar is a one-dimensional projection of the fraction of models points excluded for each sparticle by ATLAS analyses. The experimental results are obtained from data taken at  $\sqrt{s} = 7$  and 8 TeV.

### 90.6.1 Exclusion limits on the masses of charged sleptons

The most model-independent searches for selectrons, smuons and staus originate from the LEP experiments [177]. Smuon production only takes place via s-channel  $\gamma^*/Z$  exchange. Search results are often quoted for  $\tilde{\mu}_R$ , since it is typically lighter than  $\tilde{\mu}_L$  and has a weaker coupling to the Z boson; limits are therefore conservative. Decays are expected to be dominated by  $\tilde{\mu}_R \rightarrow \mu \tilde{\chi}_1^0$ , leading to two non-back-to-back muons and missing momentum. Slepton mass limits are calculated in the MSSM under the assumption of gaugino mass unification at the GUT scale, and depend on the mass difference between the smuon and  $\tilde{\chi}_1^0$ . A  $\tilde{\mu}_R$  with a mass below 94 GeV is excluded for  $m_{\tilde{\mu}_R} - m_{\tilde{\chi}_1^0} > 10$  GeV. The selectron case is similar to the smuon case, except that an additional production mechanism is provided by t-channel neutralino exchange. The  $\tilde{e}_R$  lower mass limit is 100 GeV for  $m_{\tilde{\chi}_1^0} < 85$  GeV. Due to the t-channel neutralino exchange,  $\tilde{e}_R \tilde{e}_L$  pair production was possible at LEP, and a lower limit of 73 GeV was set on the selectron mass regardless of the neutralino mass by scanning over MSSM parameter space [178]. The potentially large mixing between  $\tilde{\tau}_L$  and  $\tilde{\tau}_R$  not only makes the  $\tilde{\tau}_1$  light, but can also make its coupling to the Z boson small. LEP lower limits on the  $\tilde{\tau}$  mass range between 87 and 93 GeV depending on the  $\tilde{\chi}_1^0$  mass, for  $m_{\tilde{\tau}} - m_{\tilde{\chi}_1^0} > 7$  GeV [177].

At the LHC, pair production of sleptons is not only heavily suppressed with respect to pair production of colored SUSY particles but the cross section is also almost two orders of magnitude smaller than the one of pair production of charginos and neutralinos. With the full data sets of Run 1 and Run 2, however, ATLAS and CMS have surpassed the sensitivity of the LEP analyses under certain assumptions.

**Table 90.4:** Summary of slepton mass limits from LEP and LHC, assuming R-parity conservation and 100% branching fraction for  $\tilde{\ell} \rightarrow \ell \tilde{\chi}_1^0$ . Masses in this table are provided in GeV.

Assumption	$m_{\tilde{\ell}}$
$\tilde{\mu}_R, \Delta m(\tilde{\mu}_R, \tilde{\chi}_1^0) > 10$	> 94
$\tilde{e}_R, \Delta m(\tilde{e}_R, \tilde{\chi}_1^0) > 10$	> 94
$\tilde{e}_R, \text{any } \Delta m$	> 73
$\tilde{\tau}_R, \Delta m(\tilde{\tau}_R, \tilde{\chi}_1^0) > 7$	> 87
$\tilde{\nu}_e, \Delta m(\tilde{e}_R, \tilde{\chi}_1^0) > 10$	> 94
$m_{\tilde{e}_{L,R}} = m_{\tilde{\mu}_{L,R}}, m_{\tilde{\chi}_1^0} \approx 0$	> 700
$m_{\tilde{\chi}_1^0} \approx 400$	no LHC limit
$m_{\tilde{\tau}_L} = m_{\tilde{\tau}_R}, m_{\tilde{\chi}_1^0} \approx 0$	> 390
$m_{\tilde{\chi}_1^0} \approx 130$	no LHC limit

ATLAS and CMS have searched for direct production of selectron pairs and smuon pairs at the LHC, with each slepton decaying to its corresponding SM partner lepton and the  $\tilde{\chi}_1^0$  LSP. In simplified models, ATLAS [133] and CMS [179] set lower mass limits on sleptons of 700 GeV for degenerate  $\tilde{\ell}_L$  and  $\tilde{\ell}_R$ , for a massless  $\tilde{\chi}_1^0$  and assuming equal selectron and smuon masses, as shown in Fig. 90.6. The limits deteriorate with increasing  $\tilde{\chi}_1^0$  mass due to decreasing missing momentum and lepton momentum. As a consequence, no limits are set for  $\tilde{\chi}_1^0$  masses above 400 GeV. Limits are also derived without the assumption of slepton mass degeneracy [133, 179]. A dedicated search for sleptons with small mass difference between  $\tilde{\ell}$  and  $\tilde{\chi}_1^0$  is performed by ATLAS [144] demanding the presence of ISR jets.

ATLAS and CMS have also searched for  $\tilde{\tau}$ -pair production. In simplified models, ATLAS excludes  $\tilde{\tau}$  masses between 120 and 390 GeV assuming light  $\tilde{\chi}_1^0$ , combining the production of degenerate left- and right-handed  $\tilde{\tau}$ s [180]. The CMS analysis [181] covers lower masses and closes the mass gap with LEP. No limits are set for  $\tilde{\chi}_1^0$  masses above 130 GeV.

In gauge-mediated SUSY breaking models, sleptons can be (co-)NLSPs, *i.e.*, the next-to-lightest SUSY particles and almost degenerate in mass, decaying to a lepton and a gravitino. This decay can either be prompt, or the slepton can have a non-zero lifetime. Combining several analyses, lower mass limits on  $\tilde{\mu}_R$  of 96.3 GeV and on  $\tilde{e}_R$  of 66 GeV are set for all slepton lifetimes at LEP [182]. In a considerable part of parameter space in these models, the  $\tilde{\tau}$  is the NLSP. The LEP experiments have set lower limits on the mass of such a  $\tilde{\tau}$  between 87 and 97 GeV, depending on the  $\tilde{\tau}$  lifetime. ATLAS and CMS have searched for final states with  $\tau$ s, jets and missing transverse momentum, and has interpreted the results in GMSB models setting limits on the model parameters [183, 184]. CMS has interpreted a multilepton analysis in terms of limits on gauge mediation models with slepton NLSP [185]. CDF has put limits on gauge mediation models at high  $\tan \beta$  and slepton NLSP using an analysis searching for like-charge light leptons and taus [186].

Limits also exist on sleptons in R-parity violating models, both from LEP and the Tevatron experiments. From LEP, lower limits on  $\tilde{\mu}_R$  and  $\tilde{e}_R$  masses in such models are 97 GeV, and the limits on the stau mass are very close: 96 GeV [187]. CMS has searched for resonant smuon production in a modified CMSSM scenario [188], putting limits on  $\lambda_{211}^2$  as a function of  $m_0, m_{1/2}$ .

### 90.6.2 Exclusion limits on sneutrino masses

The invisible width of the Z boson puts a lower limit on the sneutrino mass of about 45 GeV. Tighter limits are derived from other searches, notably for gauginos and sleptons, under the assumption of gaugino and sfermion mass universality at the GUT scale, and amount to approximately 94 GeV in the MSSM [189].

It is possible that the lightest sneutrino is the LSP; however, a left-handed sneutrino LSP is ruled out as a cold dark matter candidate [190, 191].

Production of pairs of sneutrinos in R-parity violating models has been searched for at LEP [187]. Assuming fully leptonic decays via  $\lambda$ -type couplings, lower mass limits between 85 and 100 GeV are set. At the Tevatron [192, 193] and at the LHC [188, 194–196], searches have focused on scenarios with resonant production of a sneutrino, decaying to  $e\mu$ ,  $\mu\tau$  and  $e\tau$  final states. No signal has been seen, and limits have been set on sneutrino masses as a function of the value of relevant RPV couplings. As an example, the LHC experiments exclude a resonant tau sneutrino with a mass below 2.3 TeV for  $\lambda_{312} = \lambda_{321} > 0.07$  and  $\lambda'_{311} > 0.11$ .

The limits on sleptons in simplified models are summarized in Table 90.4.

### 90.7 Exclusion limits on long-lived sparticles

Long-lived sparticles arise in many different SUSY models. In particular in co-annihilation scenarios, where the NLSP and LSP are nearly mass-degenerate, this is rather common in order to obtain the correct Dark Matter relic density. Prominent examples are scenarios featuring stau co-annihilation, or models of SUSY breaking, e.g. minimal anomaly-mediated SUSY breaking (AMSB), in which the appropriate Dark Matter density is obtained by co-annihilation of the LSP with an almost degenerate long-lived wino. However, in general, also other sparticles can be long-lived and it is desirable to establish a comprehensive search program for these special long-lived cases, which lead to distinct experimental search signatures, including displaced vertices or disappearing tracks, etc.

Past experiments have performed dedicated searches for long-lived SUSY signatures, but given the absence of any experimental evidence for SUSY so far, more effort and focus has gone into such searches at the LHC recently. As for the interpretation of more standard searches for e.g. R-parity conserving SUSY, simplified models are also a convenient tool to benchmark long-lived scenarios (see e.g. [197, 198]).

If the decay of gluinos is suppressed, for example if squark masses are high, gluinos may live longer than typical hadronization times. It is expected that such gluinos will hadronize to long-living strongly interacting particles known as R-hadrons. In particular, if the suppression of the gluino decay is strong, as in the case that the squark masses are much higher than the TeV scale, these R-hadrons can be (semi-)stable in collider timescales. Searches for such R-hadrons exploit the typical signature of stable charged massive particles in the detector. R-hadrons decaying in the detector are searched for using  $dE/dx$  measurements and searches for displaced vertices. As shown in the left plot of Fig. 90.7, the ATLAS experiment excludes semi-stable gluino R-hadrons with masses below 1.9 – 2.3 TeV for all lifetimes in a simplified model where such gluinos always form R-hadrons, and decay into jets and a light neutralino, by combining a number of analyses [79, 199–201]. A combination of CMS searches for long-lived particles, as shown in Fig. 90.8, reaches similar limits [82, 202–204].

Alternatively, since such R-hadrons are strongly interacting, they may be stopped in the calorimeter or in other material, and decay later into energetic jets. These decays are searched for by identifying the jets [205–207] or muons [207] outside the time window associated with bunch-bunch collisions. As shown in Fig. 90.8, the CMS collaboration sets limits on such stopped R-hadrons over 13 orders of magnitude in gluino lifetime, up to masses of 1390 GeV [207].

Top squarks can also be long-lived and hadronize to a R-hadron, for example in the scenario where the top squark is the next-to-lightest SUSY particle (NLSP), with a small mass difference to the LSP. Searches for massive stable charged particles are sensitive to such top squarks. Tevatron limits are approximately  $m_{\tilde{t}} > 300$  GeV [208, 209]. ATLAS sets a limit of 1340 GeV on such top squarks [200], the CMS limits are comparable [204].

In addition to colored sparticles, also sparticles like charginos may be long-lived, especially in scenarios with compressed mass spectra. Charginos decaying in the detectors away from the pri-

mary vertex could lead to signatures such as kinked-tracks, or apparently disappearing tracks, since, for example, the pion in  $\tilde{\chi}_1^\pm \rightarrow \pi^\pm \tilde{\chi}_1^0$  might be too soft to be reconstructed. At the LHC, searches have been performed for such disappearing tracks, and interpreted within anomaly-mediated SUSY breaking models [210–212]. The right plot of Fig. 90.7 shows constraints for different ATLAS searches on the chargino mass-vs-lifetime plane for an AMSB model ( $\tan\beta = 5$ ,  $\mu > 0$ ) in which a wino-like  $\tilde{\chi}^\pm$  decays to a soft pion and an almost mass-degenerated wino-like  $\tilde{\chi}_1^0$  [200, 201, 211, 212]. For a similar model, CMS excludes  $c\tau$  values between 0.15 and 18 m for a chargino mass of 505 GeV [210], see Fig. 90.8. Charginos with a lifetime longer than the time needed to pass through the detector appear as charged stable massive particles. Limits have been derived by the LEP experiments [213], by D0 at the Tevatron [209], and by the LHC experiments [200, 214], and such charginos with mass below 1090 GeV are excluded.

In gauge mediation models, NLSP neutralino decays need not be prompt, and experiments have searched for late decays with photons in the final state. CDF have searched for delayed  $\tilde{\chi}_1^0 \rightarrow \gamma\tilde{G}$  decays using the timing of photon signals in the calorimeter [215]. CMS has used the same technique at the LHC [216]. Results are given as exclusion contours in the neutralino mass versus lifetime plane, and for example in a GMSB model with a neutralino mass of 300 GeV,  $c\tau$  values between 10 and 2000 cm are excluded [216]. D0 has looked at the direction of showers in the electromagnetic calorimeter with a similar goal [217], and ATLAS has searched for photon candidates that do not point back to the primary vertex, as well as for delayed photons [218].

Charged slepton decays may be kinematically suppressed, for example in the scenario of a NLSP slepton with a very small mass difference to the LSP. Such a slepton may appear to be a stable charged massive particle. Interpretation of searches at LEP for such signatures within GMSB models with stau NLSP or slepton co-NLSP exclude masses up to 99 GeV [213]. Searches of stable charged particles at the Tevatron [208, 209] and at the LHC [200, 204] are also interpreted in terms of limits on stable charged sleptons. The limits obtained at the LHC exclude stable staus with masses below 430 GeV when produced directly in pairs, and below 660 GeV when staus are produced both directly and indirectly in the decay of other particles in a GMSB model.

### 90.8 Global interpretations

Apart from the interpretation of direct searches for sparticle production at colliders in terms of limits on masses of individual SUSY particles, model-dependent interpretations of allowed SUSY parameter space are derived from global SUSY fits. Typically these fits combine the results from collider experiments with indirect constraints on SUSY as obtained from low-energy experiments, flavor physics, high-precision electroweak results, and astrophysical data.

In the pre-LHC era these fits were mainly dominated by indirect constraints. Even for very constrained models like the CMSSM, the allowed parameter space, in terms of squark and gluino masses, ranged from several hundreds of GeV to a few TeV. Furthermore, these global fits indicated that squarks and gluino masses in the range of 500 to 1000 GeV were the preferred region of parameter space, although values as high as few TeV were allowed with lower probabilities [219–226].

With ATLAS and CMS now probing mass scales around 1 TeV and beyond, the importance of the direct searches for global analyses of allowed SUSY parameter space has increased. For example, imposing the new experimental limits on constrained supergravity models pushes the most likely values of first generation squark and gluino masses significantly beyond 2 TeV, typically resulting in overall values of fit quality much worse than those in the pre-LHC era [150–152, 174, 227–234]. Also the measured value of  $m_h$  pushes the sparticle masses upwards. Although these constrained models are not yet ruled out, the extended experimental limits impose very tight constraints on the allowed parameter space.

For this reason, the emphasis of global SUSY fits has shifted towards less-constrained SUSY models. Especially interpretations in the pMSSM [172–176, 214, 227] but also in simplified models have been useful to generalize SUSY searches, for example to re-

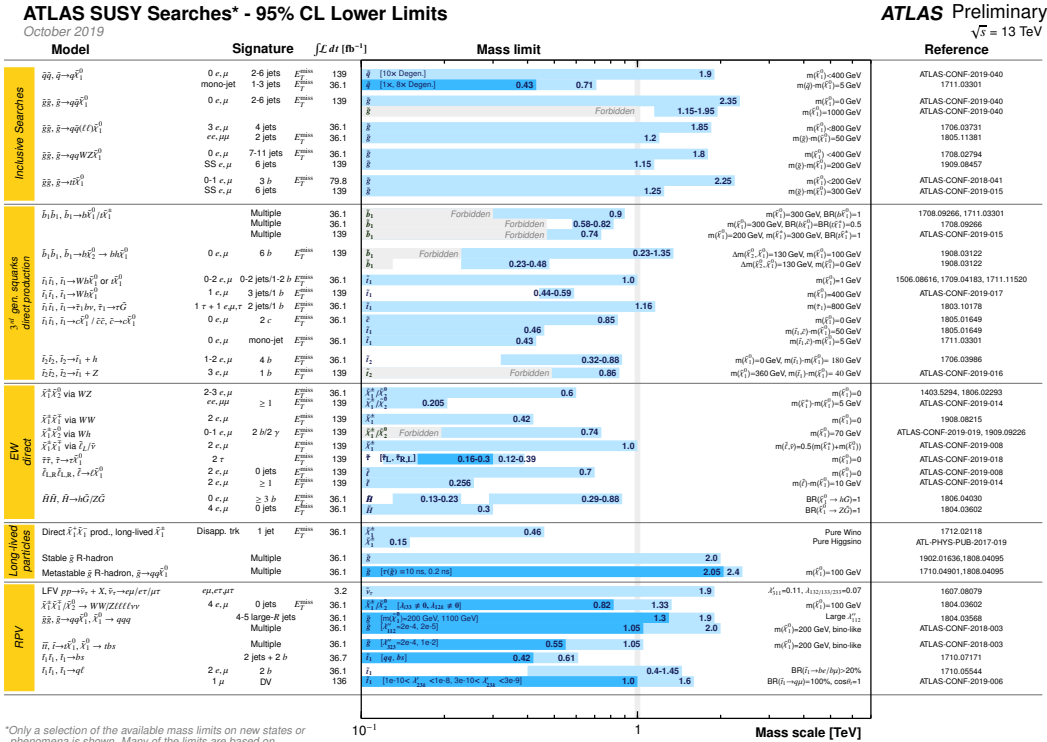


Figure 90.10: Overview of the current landscape of SUSY searches at the LHC. The plot shows exclusion mass limits of ATLAS for different searches and interpretation assumptions. The corresponding results of the CMS experiment are similar.

design experimental analyses in order to increase their sensitivity for compressed spectra, where the mass of the LSP is much closer to squark and gluino masses than predicted, for example, by the CMSSM. As shown in Table 90.2, for neutralino masses above 0.5 – 1 TeV the current set of ATLAS and CMS searches, interpreted in simplified models, cannot exclude the existence of squarks or gluinos with masses only marginally above the neutralino mass. However, as these exclusion limits are defined in the context of simplified models, they are only valid for the assumptions in which these models are defined.

As an alternative approach, both ATLAS [172] and CMS [173] have performed an analysis of the impact of their searches on the parameter space of the pMSSM. Fig. 90.9 shows graphically the LHC exclusion power in the pMSSM based on searches performed at  $\sqrt{s} = 7$  and 8 TeV. The plot on the left shows the survival probability in the gluino-neutralino mass plane, which is a measure of the parameter space that remains after inclusion of the relevant CMS search results. As can be seen, gluino masses below about 1.2 TeV are almost fully excluded. This result agrees well with the typical exclusion obtained at 8 TeV in simplified models for gluino production. However, as shown in the right plot of Fig. 90.9, when a similar analysis for other sparticles is performed it becomes apparent that exclusions on the pMSSM parameter can be significantly less stringent than simplified model limits might suggest. This is especially apparent for the electroweak sector, where even at rather low masses several of the pMSSM test points still survive the constraint of ATLAS searches at  $\sqrt{s} = 7$  and 8 TeV. This again indicates that care must be taken when interpreting results from the LHC searches and there are still several scenarios where sparticles below the 1 TeV scale are not excluded, even when considering the most recent results at  $\sqrt{s} = 13$  TeV.

Furthermore, the discovery of a Higgs boson with a mass around 125 GeV has triggered many studies regarding the compatibility of SUSY parameter space with this new particle. Much of it is still work in progress and it will be interesting to see how the interplay between the results from direct SUSY searches and more precise measurements of the properties of the Higgs boson will unfold in the future.

### 90.9 Summary and Outlook

The absence of any observation of new phenomena at the first run of the LHC at  $\sqrt{s} = 7/8$  TeV, and after the second run at  $\sqrt{s} = 13$  TeV, place significant constraints on SUSY parameter space. Today, inclusive searches probe production of gluinos at about 2.3 TeV, first and second generation squarks in the range of about 1 to 1.9 TeV, third generation squarks at scales around 600 GeV to 1.2 TeV, electroweak gauginos at scales around 400 – 1100 GeV, and sleptons around 700 GeV. However, depending on the assumptions made on the underlying SUSY spectrum these limits can also weaken considerably.

With the LHC having reached almost its maximum energy of about  $\sqrt{s} = 14$  TeV, future sensitivity improvement will have to originate from more data, the improvement of experimental analysis techniques and the focus of special signatures like the one arising in long-lived sparticle decays. Therefore, it is expected that the current landscape of SUSY searches and corresponding exclusion limits at the LHC, as, for example, shown in Fig. 90.10 from the ATLAS experiment [235] (CMS results are similar [236]), will not change as rapidly anymore as it did in the past, when the LHC underwent several successive increases of collision energy.

The interpretation of results at the LHC has moved away from constrained models like the CMSSM towards a large set of simplified models, or the pMSSM. On the one hand this move is because the LHC limits have put constrained models like the CMSSM under severe pressure, while on the other hand simplified models leave more freedom to vary parameters and form a better representation of the underlying sensitivity of analyses. However, these interpretations in simplified models do not come without a price: the decomposition of a potentially complicated reality in a limited set of individual decay chains can be significantly incomplete. Therefore, quoted limits in simplified models are only valid under the explicit assumptions made in these models. The recent addition of more comprehensive interpretations in the pMSSM will complement those derived from simplified models and, thus, will enable an even more refined understanding of the probed SUSY parameter space.

In this context, the limit range of 1.5 – 2.3 TeV on generic



colored SUSY particles only holds for light neutralinos, in the R-parity conserving MSSM. Limits on third generation squarks and electroweak gauginos also only hold for light neutralinos, and under specific assumptions for decay modes and slepton masses.

The next LHC runs at  $\sqrt{s} = 13$  or 14 TeV with significantly larger integrated luminosities (notably the High-Luminosity LHC), will provide a large data sample for future SUSY searches. As mentioned above, the improvement in sensitivity will largely have to come from a larger data set, and evolution of trigger and analysis techniques, since there will be no significant energy increase at the LHC anymore. Although the sensitivity for colored sparticles will increase somewhat as well, the expanded data set will be particularly beneficial for electroweak gaugino searches, and for the more difficult final states presented by compressed particle spectra, stealth SUSY, long-lived sparticles, or R-parity violating scenarios.

### References

- [1] H. Miyazawa, Prog. Theor. Phys. **36**, 6, 1266 (1966).
- [2] Yu. A. Golfand and E. P. Likhtman, JETP Lett. **13**, 323 (1971), [Pisma Zh. Eksp. Teor. Fiz.13,452(1971)].
- [3] J.-L. Gervais and B. Sakita, Nucl. Phys. **B34**, 632 (1971).
- [4] D. V. Volkov and V. P. Akulov, Phys. Lett. **46B**, 109 (1973).
- [5] J. Wess and B. Zumino, Phys. Lett. **49B**, 52 (1974).
- [6] J. Wess and B. Zumino, Nucl. Phys. **B70**, 39 (1974).
- [7] A. Salam and J. A. Strathdee, Nucl. Phys. **B76**, 477 (1974).
- [8] H. P. Nilles, Phys. Rept. **110**, 1 (1984).
- [9] H. E. Haber and G. L. Kane, Phys. Rept. **117**, 75 (1985).
- [10] E. Witten, Nucl. Phys. **B188**, 513 (1981).
- [11] S. Dimopoulos and H. Georgi, Nucl. Phys. **B193**, 150 (1981).
- [12] M. Dine, W. Fischler and M. Srednicki, Nucl. Phys. **B189**, 575 (1981).
- [13] S. Dimopoulos and S. Raby, Nucl. Phys. **B192**, 353 (1981).
- [14] N. Sakai, Z. Phys. **C11**, 153 (1981).
- [15] R. K. Kaul and P. Majumdar, Nucl. Phys. **B199**, 36 (1982).
- [16] H. Goldberg, Phys. Rev. Lett. **50**, 1419 (1983).
- [17] J. R. Ellis *et al.*, Nucl. Phys. **B238**, 453 (1984).
- [18] G. Jungman, M. Kamionkowski and K. Griest, Phys. Rept. **267**, 195 (1996), [hep-ph/9506380].
- [19] S. Dimopoulos, S. Raby and F. Wilczek, Phys. Rev. **D24**, 1681 (1981).
- [20] W. J. Marciano and G. Senjanovic, Phys. Rev. **D25**, 3092 (1982).
- [21] M. B. Einhorn and D. R. T. Jones, Nucl. Phys. **B196**, 475 (1982).
- [22] L. E. Ibanez and G. G. Ross, Phys. Lett. **105B**, 439 (1981).
- [23] U. Amaldi, W. de Boer and H. Furstenau, Phys. Lett. **B260**, 447 (1991).
- [24] P. Langacker and N. Polonsky, Phys. Rev. **D52**, 3081 (1995), [hep-ph/9503214].
- [25] P. Fayet, Phys. Lett. **64B**, 159 (1976).
- [26] G. R. Farrar and P. Fayet, Phys. Lett. **76B**, 575 (1978).
- [27] B.C. Allanach and H.E. Haber, *Supersymmetry, Part I (Theory)*, in this Review.
- [28] V. Khachatryan *et al.* (CMS, LHCb), Nature **522**, 68 (2015), [arXiv:1411.4413].
- [29] R. Aaij *et al.* (LHCb), Phys. Rev. Lett. **118**, 19, 191801 (2017), [arXiv:1703.05747].
- [30] A. Höcker and W.J. Marciano, *Muon Anomalous Magnetic Moment*, in this Review.
- [31] G. Hinshaw *et al.* (WMAP), Astrophys. J. Suppl. **208**, 19 (2013), [arXiv:1212.5226].
- [32] Planck Collab., Astron. & Astrophys. **594**, A13 (2016).
- [33] M. Carena *et al.*, *Status of Higgs Boson Physics*, in this Review.
- [34] K. Nakamura *et al.* (Particle Data Group), J. Phys. **G37**, 075021 (2010).
- [35] I. Hinchliffe *et al.*, Phys. Rev. **D55**, 5520 (1997), [hep-ph/9610544].
- [36] L. Randall and D. Tucker-Smith, Phys. Rev. Lett. **101**, 221803 (2008), [arXiv:0806.1049].
- [37] V. Khachatryan *et al.* (CMS), Phys. Lett. **B698**, 196 (2011), [arXiv:1101.1628].
- [38] S. Chatrchyan *et al.* (CMS), Phys. Rev. Lett. **107**, 221804 (2011), [arXiv:1109.2352].
- [39] S. Chatrchyan *et al.* (CMS), JHEP **01**, 077 (2013), [arXiv:1210.8115].
- [40] S. Chatrchyan *et al.* (CMS), Eur. Phys. J. **C73**, 9, 2568 (2013), [arXiv:1303.2985].
- [41] S. Chatrchyan *et al.* (CMS), Phys. Rev. **D85**, 012004 (2012), [arXiv:1107.1279].
- [42] C. G. Lester and D. J. Summers, Phys. Lett. **B463**, 99 (1999), [hep-ph/9906349].
- [43] D. R. Tovey, JHEP **04**, 034 (2008), [arXiv:0802.2879].
- [44] M. R. Buckley *et al.*, Phys. Rev. **D89**, 5, 055020 (2014), [arXiv:1310.4827].
- [45] P. Jackson, C. Rogan and M. Santoni, Phys. Rev. **D95**, 3, 035031 (2017), [arXiv:1607.08307].
- [46] J. M. Butterworth *et al.*, Phys. Rev. Lett. **100**, 242001 (2008), [arXiv:0802.2470].
- [47] E. Halkiadakis, G. Redlinger and D. Shih, Ann. Rev. Nucl. Part. Sci. **64**, 319 (2014), [arXiv:1411.1427].
- [48] W. Beenakker *et al.*, Int. J. Mod. Phys. **A26**, 2637 (2011), [arXiv:1105.1110].
- [49] W. Beenakker *et al.*, Nucl. Phys. **B492**, 51 (1997), [hep-ph/9610490].
- [50] A.H. Chamseddine, R. Arnowitt, and P. Nath, Phys. Rev. Lett. **49**, 970 (1982).
- [51] E. Cremmer *et al.*, Nucl. Phys. **B212**, 413 (1983).
- [52] P. Fayet, Phys. Lett. **70B**, 461 (1977).
- [53] M. Dine, A. E. Nelson and Y. Shirman, Phys. Rev. **D51**, 1362 (1995), [hep-ph/9408384].
- [54] P. Meade, N. Seiberg and D. Shih, Prog. Theor. Phys. Suppl. **177**, 143 (2009), [arXiv:0801.3278].
- [55] G. F. Giudice *et al.*, JHEP **12**, 027 (1998), [hep-ph/9810442].
- [56] L. Randall and R. Sundrum, Nucl. Phys. **B557**, 79 (1999), [hep-th/9810155].
- [57] R. L. Arnowitt and P. Nath, Phys. Rev. Lett. **69**, 725 (1992).
- [58] G. L. Kane *et al.*, Phys. Rev. **D49**, 6173 (1994), [hep-ph/9312272].
- [59] A. Djouadi, J.-L. Kneur and G. Moutaka, Comput. Phys. Commun. **176**, 426 (2007), [hep-ph/0211331].
- [60] C. F. Berger *et al.*, JHEP **02**, 023 (2009), [arXiv:0812.0980].
- [61] H. Baer *et al.*, in “Workshop on Physics at Current Accelerators and the Supercollider Argonne, Illinois, June 2-5, 1993,” 0703-720 (1993), [hep-ph/9305342], URL [http://lss.fnal.gov/cgi-bin/find\\_paper.pl?other/ssc/sscl-preprint-441](http://lss.fnal.gov/cgi-bin/find_paper.pl?other/ssc/sscl-preprint-441).
- [62] R. M. Barnett, H. E. Haber and G. L. Kane, Nucl. Phys. **B267**, 625 (1986).
- [63] H. Baer, D. Karatas and X. Tata, Phys. Lett. **B183**, 220 (1987).
- [64] J. Alwall, P. Schuster and N. Toro, Phys. Rev. **D79**, 075020 (2009), [arXiv:0810.3921].
- [65] J. Alwall *et al.*, Phys. Rev. **D79**, 015005 (2009), [arXiv:0809.3264].

- [66] O. Buchmueller and J. Marrouche, *Int. J. Mod. Phys. A* **29**, 06, 1450032 (2014), [arXiv:1304.2185].
- [67] LEP2 SUSY Working Group, ALEPH, DELPHI, L3 and OPAL experiments, note LEPSUSYWG/04-02.1, <http://lepsusy.web.cern.ch/lepsusy>.
- [68] T. Aaltonen *et al.* (CDF), *Phys. Rev. Lett.* **102**, 121801 (2009), [arXiv:0811.2512].
- [69] V. M. Abazov *et al.* (D0), *Phys. Lett.* **B660**, 449 (2008), [arXiv:0712.3805].
- [70] ATLAS Collab., ATLAS-CONF-2019-040 (2019).
- [71] A. M. Sirunyan *et al.* (CMS) (2019), [arXiv:1908.04722].
- [72] ATLAS Collab., ATLAS-CONF-2018-041 (2018).
- [73] A. M. Sirunyan *et al.* (CMS) (2019), [arXiv:1909.03460].
- [74] M. Aaboud *et al.* (ATLAS), *Phys. Rev.* **D98**, 3, 032009 (2018), [arXiv:1804.03602].
- [75] M. Aaboud *et al.* (ATLAS), *JHEP* **09**, 084 (2017), [arXiv:1706.03731].
- [76] CMS Collab., CMS-PAS-SUS-19-008 (2019).
- [77] V. Khachatryan *et al.* (CMS), *Phys. Rev.* **D94**, 11, 112009 (2016), [arXiv:1606.08076].
- [78] CMS Collab., CMS-PAS-SUS-13-010 (2013).
- [79] ATLAS Collab., ATLAS-CONF-2018-003 (2018).
- [80] G. Aad *et al.* (ATLAS), *Phys. Rev.* **D92**, 7, 072004 (2015), [arXiv:1504.05162].
- [81] A. M. Sirunyan *et al.* (CMS), *Phys. Rev.* **D98**, 9, 092011 (2018), [arXiv:1808.03078].
- [82] A. M. Sirunyan *et al.* (CMS), *Phys. Rev.* **D99**, 3, 032011 (2019), [arXiv:1811.07991].
- [83] T. Aaltonen *et al.* (CDF), *Phys. Rev. Lett.* **107**, 042001 (2011), [arXiv:1105.2815].
- [84] M. Aaboud *et al.* (ATLAS), *Phys. Lett.* **B785**, 136 (2018), [arXiv:1804.03568].
- [85] ATLAS Collab., ATLAS-CONF-2016-057 (2016).
- [86] M. Aaboud *et al.* (ATLAS), *JHEP* **09**, 088 (2017), [arXiv:1704.08493].
- [87] A. M. Sirunyan *et al.* (CMS), *Phys. Lett.* **B783**, 114 (2018), [arXiv:1712.08920].
- [88] S. Chatrchyan *et al.* (CMS), *Phys. Lett.* **B730**, 193 (2014), [arXiv:1311.1799].
- [89] V. Khachatryan *et al.* (CMS), *Phys. Lett.* **B770**, 257 (2017), [arXiv:1608.01224].
- [90] M. Aaboud *et al.* (ATLAS), *JHEP* **09**, 050 (2018), [arXiv:1805.01649].
- [91] T. Aaltonen *et al.* (CDF), *Phys. Rev. Lett.* **105**, 081802 (2010), [arXiv:1005.3600].
- [92] V. M. Abazov *et al.* (D0), *Phys. Lett.* **B693**, 95 (2010), [arXiv:1005.2222].
- [93] M. Aaboud *et al.* (ATLAS), *JHEP* **11**, 195 (2017), [arXiv:1708.09266].
- [94] G. Aad *et al.* (ATLAS) (2019), [arXiv:1909.08457].
- [95] G. Aad *et al.* (ATLAS) (2019), [arXiv:1908.03122].
- [96] A. M. Sirunyan *et al.* (CMS), *JHEP* **03**, 076 (2018), [arXiv:1709.08908].
- [97] C. Boehm, A. Djouadi and Y. Mambrini, *Phys. Rev.* **D61**, 095006 (2000), [hep-ph/9907428].
- [98] T. Aaltonen *et al.* (CDF), *Phys. Rev.* **D82**, 092001 (2010), [arXiv:1009.0266].
- [99] V. M. Abazov *et al.* (D0), *Phys. Lett.* **B696**, 321 (2011), [arXiv:1009.5950].
- [100] T. Aaltonen *et al.* (CDF), *JHEP* **10**, 158 (2012), [arXiv:1203.4171].
- [101] V. M. Abazov *et al.* (D0), *Phys. Lett.* **B665**, 1 (2008), [arXiv:0803.2263].
- [102] T. Aaltonen *et al.* (CDF), *Phys. Rev. Lett.* **104**, 251801 (2010), [arXiv:0912.1308].
- [103] V. M. Abazov *et al.* (D0), *Phys. Lett.* **B674**, 4 (2009), [arXiv:0901.1063].
- [104] CMS Collab., CMS-PAS-SUS-19-009 (2019).
- [105] M. Aaboud *et al.* (ATLAS), *JHEP* **12**, 085 (2017), [arXiv:1709.04183].
- [106] M. Aaboud *et al.* (ATLAS), *JHEP* **06**, 108 (2018), [arXiv:1711.11520].
- [107] M. Aaboud *et al.* (ATLAS), *Phys. Rev.* **D98**, 3, 032008 (2018), [arXiv:1803.10178].
- [108] CMS Collab., CMS-PAS-SUS-19-003 (2019).
- [109] ATLAS Collab., ATLAS-CONF-2019-017 (2019).
- [110] M. Aaboud *et al.* (ATLAS), *Eur. Phys. J.* **C77**, 12, 898 (2017), [arXiv:1708.03247].
- [111] A. M. Sirunyan *et al.* (CMS), *Eur. Phys. J.* **C77**, 10, 710 (2017), [arXiv:1705.04650].
- [112] A. M. Sirunyan *et al.* (CMS), *Phys. Rev.* **D96**, 3, 032003 (2017), [arXiv:1704.07781].
- [113] A. M. Sirunyan *et al.* (CMS), *JHEP* **10**, 005 (2017), [arXiv:1707.03316].
- [114] A. M. Sirunyan *et al.* (CMS), *JHEP* **10**, 019 (2017), [arXiv:1706.04402].
- [115] M. Aaboud *et al.* (ATLAS), *JHEP* **01**, 126 (2018), [arXiv:1711.03301].
- [116] F. D. Aaron *et al.* (H1), *Eur. Phys. J.* **C71**, 1572 (2011), [arXiv:1011.6359].
- [117] ATLAS Collab., ATLAS-CONF-2015-018 (2015).
- [118] V. Khachatryan *et al.* (CMS), *Phys. Rev.* **D91**, 5, 052012 (2015), [arXiv:1411.6977].
- [119] S. Chekanov *et al.* (ZEUS), *Eur. Phys. J.* **C50**, 269 (2007), [hep-ex/0611018].
- [120] S. Chatrchyan *et al.* (CMS), *Phys. Rev. Lett.* **111**, 22, 221801 (2013), [arXiv:1306.6643].
- [121] M. Aaboud *et al.* (ATLAS), *Phys. Rev.* **D97**, 3, 032003 (2018), [arXiv:1710.05544].
- [122] ATLAS Collab., ATLAS-CONF-2019-006 (2019).
- [123] A. M. Sirunyan *et al.* (CMS), *Phys. Rev.* **D99**, 3, 032014 (2019), [arXiv:1808.05082].
- [124] CMS Collab., CMS-PAS-EXO-16-022 (2016).
- [125] V. Khachatryan *et al.* (CMS), *Phys. Lett.* **B760**, 178 (2016), [arXiv:1602.04334].
- [126] M. Aaboud *et al.* (ATLAS), *Eur. Phys. J.* **C78**, 3, 250 (2018), [arXiv:1710.07171].
- [127] V. Khachatryan *et al.* (CMS), *Phys. Rev.* **D95**, 1, 012009 (2017), [arXiv:1610.05133].
- [128] V. Khachatryan *et al.* (CMS), *Phys. Lett.* **B747**, 98 (2015), [arXiv:1412.7706].
- [129] LEP2 SUSY Working Group, ALEPH, DELPHI, L3 and OPAL experiments, note LEPSUSYWG/01-03.1, <http://lepsusy.web.cern.ch/lepsusy>.
- [130] LEP2 SUSY Working Group, ALEPH, DELPHI, L3 and OPAL experiments, note LEPSUSYWG/02-04.1, <http://lepsusy.web.cern.ch/lepsusy>.
- [131] CDF Collab., CDF Note 10636 (2011).
- [132] V. M. Abazov *et al.* (D0), *Phys. Lett.* **B680**, 34 (2009), [arXiv:0901.0646].
- [133] G. Aad *et al.* (ATLAS) (2019), [arXiv:1908.08215].
- [134] A. M. Sirunyan *et al.* (CMS), *JHEP* **11**, 079 (2018), [arXiv:1807.07799].
- [135] M. Aaboud *et al.* (ATLAS), *Eur. Phys. J.* **C78**, 2, 154 (2018), [arXiv:1708.07875].

- [136] A. M. Sirunyan *et al.* (CMS), JHEP **11**, 151 (2018), [arXiv:1807.02048].
- [137] M. Aaboud *et al.* (ATLAS), Eur. Phys. J. **C78**, 12, 995 (2018), [arXiv:1803.02762].
- [138] A. M. Sirunyan *et al.* (CMS), JHEP **03**, 166 (2018), [arXiv:1709.05406].
- [139] M. Aaboud *et al.* (ATLAS), Phys. Rev. **D98**, 9, 092012 (2018), [arXiv:1806.02293].
- [140] A. M. Sirunyan *et al.* (CMS), JHEP **03**, 160 (2018), [arXiv:1801.03957].
- [141] M. Aaboud *et al.* (ATLAS), Phys. Rev. **D100**, 1, 012006 (2019), [arXiv:1812.09432].
- [142] ATLAS Collab., ATLAS-CONF-2019-019 (2019).
- [143] G. Aad *et al.* (ATLAS) (2019), [arXiv:1909.09226].
- [144] ATLAS Collab., ATLAS-CONF-2019-014 (2019).
- [145] A. M. Sirunyan *et al.* (CMS), JHEP **08**, 150 (2019), [arXiv:1905.13059].
- [146] A. M. Sirunyan *et al.* (CMS), Phys. Lett. **B782**, 440 (2018), [arXiv:1801.01846].
- [147] A. M. Sirunyan *et al.* (CMS) (2019), [arXiv:1910.01185].
- [148] H. K. Dreiner *et al.*, Eur. Phys. J. **C62**, 547 (2009), [arXiv:0901.3485].
- [149] LEP2 SUSY Working Group, ALEPH, DELPHI, L3 and OPAL experiments, note LEPSUSYWG/04-07.1, <http://lepsusy.web.cern.ch/lepsusy>.
- [150] O. Buchmueller *et al.*, Eur. Phys. J. **C74**, 6, 2922 (2014), [arXiv:1312.5250].
- [151] C. Strege *et al.*, JCAP **1304**, 013 (2013), [arXiv:1212.2636].
- [152] A. Fowlie *et al.*, Phys. Rev. **D86**, 075010 (2012), [arXiv:1206.0264].
- [153] LEP2 SUSY Working Group, ALEPH, DELPHI, L3 and OPAL experiments, note LEPSUSYWG/04-09.1, <http://lepsusy.web.cern.ch/lepsusy>.
- [154] T. Aaltonen *et al.* (CDF), Phys. Rev. Lett. **104**, 011801 (2010), [arXiv:0910.3606].
- [155] V. M. Abazov *et al.* (D0), Phys. Rev. Lett. **105**, 221802 (2010), [arXiv:1008.2133].
- [156] M. Aaboud *et al.* (ATLAS), Phys. Rev. **D97**, 9, 092006 (2018), [arXiv:1802.03158].
- [157] A. M. Sirunyan *et al.* (CMS), JHEP **06**, 143 (2019), [arXiv:1903.07070].
- [158] A. M. Sirunyan *et al.* (CMS) (2019), [arXiv:1907.00857].
- [159] M. Aaboud *et al.* (ATLAS), Phys. Rev. **D98**, 9, 092002 (2018), [arXiv:1806.04030].
- [160] M. Aaboud *et al.* (ATLAS), Phys. Rev. **D99**, 1, 012001 (2019), [arXiv:1808.03057].
- [161] A. M. Sirunyan *et al.* (CMS), Eur. Phys. J. **C79**, 5, 444 (2019), [arXiv:1901.06726].
- [162] A. M. Sirunyan *et al.* (CMS), JHEP **01**, 154 (2019), [arXiv:1812.04066].
- [163] A. M. Sirunyan *et al.* (CMS), Phys. Lett. **B780**, 118 (2018), [arXiv:1711.08008].
- [164] A. M. Sirunyan *et al.* (CMS), Phys. Rev. **D97**, 3, 032007 (2018), [arXiv:1709.04896].
- [165] A. M. Sirunyan *et al.* (CMS), Phys. Lett. **B779**, 166 (2018), [arXiv:1709.00384].
- [166] G. Aad *et al.* (ATLAS), Phys. Rev. **D93**, 5, 052002 (2016), [arXiv:1509.07152].
- [167] M. Aaboud *et al.* (ATLAS), Eur. Phys. J. **C78**, 8, 625 (2018), [arXiv:1805.11381].
- [168] M. Aaboud *et al.* (ATLAS), Eur. Phys. J. **C77**, 3, 144 (2017), [arXiv:1611.05791].
- [169] C. P. Herzog and M. Spillane, JHEP **04**, 124 (2016), [arXiv:1506.06757].
- [170] G. Aad *et al.* (ATLAS) (2019), [arXiv:1907.10037].
- [171] V. Khachatryan *et al.* (CMS), Phys. Rev. **D91**, 1, 012007 (2015), [arXiv:1411.6530].
- [172] G. Aad *et al.* (ATLAS), JHEP **10**, 134 (2015), [arXiv:1508.06608].
- [173] V. Khachatryan *et al.* (CMS), JHEP **10**, 129 (2016), [arXiv:1606.03577].
- [174] P. Athron *et al.* (GAMBIT), Eur. Phys. J. **C77**, 12, 879 (2017), [arXiv:1705.07917].
- [175] K. J. de Vries *et al.*, Eur. Phys. J. **C75**, 9, 422 (2015), [arXiv:1504.03260].
- [176] C. Strege *et al.*, JHEP **09**, 081 (2014), [arXiv:1405.0622].
- [177] LEP2 SUSY Working Group, ALEPH, DELPHI, L3 and OPAL experiments, note LEPSUSYWG/04-01.1, <http://lepsusy.web.cern.ch/lepsusy>.
- [178] A. Heister *et al.* (ALEPH), Phys. Lett. **B544**, 73 (2002), [hep-ex/0207056].
- [179] A. M. Sirunyan *et al.* (CMS), Phys. Lett. **B790**, 140 (2019), [arXiv:1806.05264].
- [180] ATLAS Collab., ATLAS-CONF-2019-018 (2019).
- [181] A. M. Sirunyan *et al.* (CMS) (2019), [arXiv:1907.13179].
- [182] LEP2 SUSY Working Group, ALEPH, DELPHI, L3 and OPAL experiments, note LEPSUSYWG/02-09.2, <http://lepsusy.web.cern.ch/lepsusy>.
- [183] M. Aaboud *et al.* (ATLAS), Phys. Rev. **D99**, 1, 012009 (2019), [arXiv:1808.06358].
- [184] S. Chatrchyan *et al.* (CMS), Eur. Phys. J. **C73**, 2493 (2013), [arXiv:1301.3792].
- [185] S. Chatrchyan *et al.* (CMS), Phys. Rev. **D90**, 032006 (2014), [arXiv:1404.5801].
- [186] T. Aaltonen *et al.* (CDF), Phys. Rev. Lett. **110**, 20, 201802 (2013), [arXiv:1302.4491].
- [187] LEP2 SUSY Working Group, ALEPH, DELPHI, L3 and OPAL experiments, note LEPSUSYWG/02-10.1, <http://lepsusy.web.cern.ch/lepsusy>.
- [188] A. M. Sirunyan *et al.* (CMS), Eur. Phys. J. **C79**, 4, 305 (2019), [arXiv:1811.09760].
- [189] DELPHI Collab., Eur. Phys. J. **C31**, 412 (2003).
- [190] T. Falk, K. A. Olive and M. Srednicki, Phys. Lett. **B339**, 248 (1994), [hep-ph/9409270].
- [191] C. Arina and N. Fornengo, JHEP **11**, 029 (2007), [arXiv:0709.4477].
- [192] T. Aaltonen *et al.* (CDF), Phys. Rev. Lett. **105**, 191801 (2010), [arXiv:1004.3042].
- [193] V. M. Abazov *et al.* (D0), Phys. Rev. Lett. **105**, 191802 (2010), [arXiv:1007.4835].
- [194] G. Aad *et al.* (ATLAS), Phys. Rev. Lett. **115**, 3, 031801 (2015), [arXiv:1503.04430].
- [195] M. Aaboud *et al.* (ATLAS), Eur. Phys. J. **C76**, 10, 541 (2016), [arXiv:1607.08079].
- [196] V. Khachatryan *et al.* (CMS), Eur. Phys. J. **C76**, 6, 317 (2016), [arXiv:1604.05239].
- [197] O. Buchmueller *et al.*, JHEP **09**, 076 (2017), [arXiv:1704.06515].
- [198] V. V. Khoze, A. D. Plascencia and K. Sakurai, JHEP **06**, 041 (2017), [arXiv:1702.00750].
- [199] M. Aaboud *et al.* (ATLAS), Phys. Rev. **D97**, 5, 052012 (2018), [arXiv:1710.04901].
- [200] M. Aaboud *et al.* (ATLAS), Phys. Rev. **D99**, 9, 092007 (2019), [arXiv:1902.01636].
- [201] G. Aad *et al.* (ATLAS), Eur. Phys. J. **C75**, 9, 407 (2015), [arXiv:1506.05332].
- [202] A. M. Sirunyan *et al.* (CMS), Phys. Lett. **B797**, 134876 (2019), [arXiv:1906.06441].



- [203] A. M. Sirunyan *et al.* (CMS), JHEP **05**, 025 (2018), [arXiv:1802.02110].
- [204] CMS Collab., CMS-PAS-EXO-16-036 (2016).
- [205] V. M. Abazov *et al.* (D0), Phys. Rev. Lett. **99**, 131801 (2007), [arXiv:0705.0306].
- [206] G. Aad *et al.* (ATLAS), Phys. Rev. **D88**, 11, 112003 (2013), [arXiv:1310.6584].
- [207] A. M. Sirunyan *et al.* (CMS), JHEP **05**, 127 (2018), [arXiv:1801.00359].
- [208] T. Aaltonen *et al.* (CDF), Phys. Rev. Lett. **103**, 021802 (2009), [arXiv:0902.1266].
- [209] V. M. Abazov *et al.* (D0), Phys. Rev. **D87**, 5, 052011 (2013), [arXiv:1211.2466].
- [210] A. M. Sirunyan *et al.* (CMS), JHEP **08**, 016 (2018), [arXiv:1804.07321].
- [211] M. Aaboud *et al.* (ATLAS), JHEP **06**, 022 (2018), [arXiv:1712.02118].
- [212] G. Aad *et al.* (ATLAS), Phys. Rev. **D88**, 11, 112006 (2013), [arXiv:1310.3675].
- [213] LEP2 SUSY Working Group, ALEPH, DELPHI, L3 and OPAL experiments, note LEPSUSYWG/02-05.1, <http://lepsusy.web.cern.ch/lepsusy>.
- [214] V. Khachatryan *et al.* (CMS), Eur. Phys. J. **C75**, 7, 325 (2015), [arXiv:1502.02522].
- [215] T. Aaltonen *et al.* (CDF), Phys. Rev. **D88**, 3, 031103 (2013), [arXiv:1307.0474].
- [216] A. M. Sirunyan *et al.* (CMS) (2019), [arXiv:1909.06166].
- [217] V. M. Abazov *et al.* (D0), Phys. Rev. Lett. **101**, 111802 (2008), [arXiv:0806.2223].
- [218] G. Aad *et al.* (ATLAS), Phys. Rev. **D90**, 11, 112005 (2014), [arXiv:1409.5542].
- [219] O. Buchmueller *et al.*, Eur. Phys. J. **C71**, 1722 (2011), [arXiv:1106.2529].
- [220] E. A. Baltz and P. Gondolo, JHEP **10**, 052 (2004), [hep-ph/0407039].
- [221] B. C. Allanach and C. G. Lester, Phys. Rev. **D73**, 015013 (2006), [hep-ph/0507283].
- [222] R. Ruiz de Austri, R. Trotta and L. Roszkowski, JHEP **05**, 002 (2006), [hep-ph/0602028].
- [223] R. Lafaye *et al.*, Eur. Phys. J. **C54**, 617 (2008), [arXiv:0709.3985].
- [224] M. Shaposhnikov, JHEP **08**, 008 (2008), [arXiv:0804.4542].
- [225] R. Trotta *et al.*, JHEP **12**, 024 (2008), [arXiv:0809.3792].
- [226] P. Bechtle *et al.*, Eur. Phys. J. **C66**, 215 (2010), [arXiv:0907.2589].
- [227] E. Bagnaschi *et al.*, Eur. Phys. J. C **78**, 256, 1 (2018).
- [228] J. Costa *et al.*, Eur. Phys. J. C **78**, 158, 1 (2018).
- [229] E. Bagnaschi *et al.*, Eur. Phys. J. **C77**, 4, 268 (2017), [arXiv:1612.05210].
- [230] E. Bagnaschi *et al.*, Eur. Phys. J. **C77**, 2, 104 (2017), [arXiv:1610.10084].
- [231] L. A. Harland-Lang, V. A. Khoze and M. G. Ryskin, Eur. Phys. J. **C76**, 1, 9 (2016), [arXiv:1508.02718].
- [232] E. A. Bagnaschi *et al.*, Eur. Phys. J. **C75**, 500 (2015), [arXiv:1508.01173].
- [233] O. Buchmueller *et al.*, Eur. Phys. J. **C74**, 12, 3212 (2014), [arXiv:1408.4060].
- [234] M. Citron *et al.*, Phys. Rev. **D87**, 3, 036012 (2013), [arXiv:1212.2886].
- [235] Supersymmetry Physics Results, ATLAS experiment, <http://twiki.cern.ch/twiki/bin/view/AtlasPublic/SupersymmetryPublicResults/>.
- [236] Supersymmetry Physics Results, CMS experiment, <http://cms-results.web.cern.ch/cms-results/public-results/publications/SUS/index.html>.

## 91. Axions and Other Similar Particles

Revised October 2019 by A. Ringwald (DESY, Hamburg), L.J. Rosenberg (U. Washington) and G. Rybka (U. Washington).

### 91.1 Introduction

In this section, we list coupling-strength and mass limits for light neutral scalar or pseudoscalar bosons that couple weakly to normal matter and radiation. Such bosons may arise from the spontaneous breaking of a global U(1) symmetry, resulting in a massless Nambu-Goldstone (NG) boson. If there is a small explicit symmetry breaking, either already in the Lagrangian or due to quantum effects such as anomalies, the boson acquires a mass and is called a pseudo-NG boson. Typical examples are axions ( $A^0$ ) [1–4] and majorons [5], associated, respectively, with a spontaneously broken Peccei-Quinn and lepton-number symmetry.

A common feature of these light bosons  $\phi$  is that their coupling to Standard-Model particles is suppressed by the energy scale that characterizes the symmetry breaking, *i.e.*, the decay constant  $f$ . The interaction Lagrangian is

$$\mathcal{L} = f^{-1} J^\mu \partial_\mu \phi, \quad (91.1)$$

where  $J^\mu$  is the Noether current of the spontaneously broken global symmetry. If  $f$  is very large, these new particles interact very weakly. Detecting them would provide a window to physics far beyond what can be probed at accelerators.

Axions are of particular interest because the Peccei-Quinn (PQ) mechanism remains perhaps the most credible scheme to preserve CP-symmetry in QCD. Moreover, the cold dark matter (CDM) of the universe may well consist of axions and they are searched for in dedicated experiments with a realistic chance of discovery.

Originally it was assumed that the PQ scale  $f_A$  was related to the electroweak symmetry-breaking scale  $v_{EW} = (\sqrt{2}G_F)^{-1/2} = 247$  GeV. However, the associated “standard” and “variant” axions were quickly excluded—we refer to the Listings for detailed limits. Here we focus on “invisible axions” with  $f_A \gg v_{EW}$  as the main possibility.

Axions have a characteristic two-photon vertex, inherited from their mixing with  $\pi^0$  and  $\eta$ . This coupling allows for the main search strategy based on axion-photon conversion in external magnetic fields [6], an effect that also can be of astrophysical interest. While for axions the product “ $A\gamma\gamma$  interaction strength  $\times$  mass” is essentially fixed by the corresponding  $\pi^0$  properties, one may consider a more general class of axion-like particles (ALPs) where the two parameters (coupling and mass) are independent. A number of experiments explore this more general parameter space. ALPs populating the latter are predicted to arise generically, in addition to the axion, in low-energy effective field theories emerging from string theory [7–14]. The latter often contain also very light Abelian vector bosons under which the Standard-Model particles are not charged: so-called hidden-sector photons, dark photons or paraphotons. They share a number of phenomenological features with the axion and ALPs, notably the possibility of hidden photon to photon conversion. Their physics cases and the current constraints are compiled in Refs. [15–17].

### 91.2 Theory

#### 91.2.1 Peccei-Quinn mechanism and axions

The QCD Lagrangian includes a CP-violating term  $\mathcal{L}_\Theta = -\bar{\Theta}(\alpha_s/8\pi)G^{\mu\nu a}\tilde{G}_{\mu\nu}^a$ , where  $-\pi \leq \bar{\Theta} \leq +\pi$  is the effective  $\Theta$  parameter after diagonalizing quark masses,  $G_{\mu\nu}^a$  is the color field strength tensor, and  $\tilde{G}^{a,\mu\nu} \equiv \epsilon^{\mu\nu\lambda\rho}G_{\lambda\rho}^a/2$ , with  $\epsilon^{0123} = 1$ , its dual. Limits on the neutron electric dipole moment [18] imply  $|\bar{\Theta}| \lesssim 10^{-10}$  even though  $\bar{\Theta} = \mathcal{O}(1)$  is otherwise completely satisfactory. The spontaneously broken global Peccei-Quinn symmetry U(1)<sub>PQ</sub> was introduced to solve this “strong CP problem” [1, 2], the axion being the pseudo-NG boson of U(1)<sub>PQ</sub> [3, 4]. This symmetry is broken due to the axion’s anomalous triangle coupling to gluons,

$$\mathcal{L} = \left(\frac{\phi_A}{f_A} - \bar{\Theta}\right) \frac{\alpha_s}{8\pi} G^{\mu\nu a} \tilde{G}_{\mu\nu}^a, \quad (91.2)$$

where  $\phi_A$  is the axion field and  $f_A$  the axion decay constant. Color anomaly factors have been absorbed in the normalization of  $f_A$  which is defined by this Lagrangian. Thus normalized,  $f_A$

is the quantity that enters all low-energy phenomena [19]. Non-perturbative topological fluctuations of the gluon fields in QCD induce a potential for  $\phi_A$  whose minimum is at  $\phi_A = \bar{\Theta} f_A$ , thereby canceling the  $\bar{\Theta}$  term in the QCD Lagrangian and thus restoring CP symmetry.

The resulting axion mass, in units of the PQ scale  $f_A$ , is identical to the square root of the topological susceptibility in QCD,  $m_A f_A = \sqrt{\chi}$ . The latter can be evaluated further [20, 21], exploiting the chiral limit (masses of up and down quarks much smaller than the scale of QCD), yielding  $m_A f_A = \sqrt{\chi} \approx f_\pi m_\pi$ , where  $m_\pi = 135$  MeV and  $f_\pi \approx 92$  MeV. In more detail one finds, to next-to-next-to-leading order in chiral perturbation theory [22],

$$m_A = 5.691(51) \left(\frac{10^9 \text{ GeV}}{f_A}\right) \text{meV}. \quad (91.3)$$

A direct calculation of the topological susceptibility via QCD lattice simulations finds almost the same central value, albeit with an about five times larger error bar [23].

Axions with  $f_A \gg v_{EW}$  evade all current experimental limits. One generic class of models invokes “hadronic axions” where new heavy quarks carry U(1)<sub>PQ</sub> charges, leaving ordinary quarks and leptons without tree-level axion couplings. The archetype is the KSVZ model [24], where in addition the heavy new quarks are electrically neutral. Another generic class requires at least two Higgs doublets and ordinary quarks and leptons carry PQ charges, the archetype being the DFSZ model [25]. All of these models contain at least one electroweak singlet scalar that acquires a vacuum expectation value and thereby breaks the PQ symmetry. The KSVZ and DFSZ models are frequently used as benchmark examples, but other models exist where both heavy quarks and Higgs doublets carry PQ charges. In supersymmetric models, the axion is part of a supermultiplet and thus inevitably accompanied by a spin-0 saxion and a spin-1 axino, which both also have couplings suppressed by  $f_A$  and are expected to have large masses due to supersymmetry breaking [26].

#### 91.2.2 Model-dependent axion couplings

Although the generic axion interactions scale approximately with  $f_\pi/f_A$  from the corresponding  $\pi^0$  couplings, there are non-negligible model-dependent factors and uncertainties. The axion’s two-photon interaction plays a key role for many searches,

$$\mathcal{L}_{A\gamma\gamma} = -\frac{g_{A\gamma\gamma}}{4} F_{\mu\nu} \tilde{F}^{\mu\nu} \phi_A = g_{A\gamma\gamma} \mathbf{E} \cdot \mathbf{B} \phi_A, \quad (91.4)$$

where  $F$  is the electromagnetic field-strength tensor and  $\tilde{F}^{\mu\nu} \equiv \epsilon^{\mu\nu\lambda\rho} F_{\lambda\rho}/2$ , with  $\epsilon^{0123} = 1$ , its dual. The coupling constant is [27]

$$g_{A\gamma\gamma} = \frac{\alpha}{2\pi f_A} \left(\frac{E}{N} - 1.92(4)\right) = \left(0.203(3) \frac{E}{N} - 0.39(1)\right) \frac{m_A}{\text{GeV}^2}, \quad (91.5)$$

where  $E$  and  $N$  are the electromagnetic and color anomalies of the axial current associated with the axion. In grand unified models, and notably for DFSZ [25],  $E/N = 8/3$ , whereas for KSVZ [24]  $E/N = 0$  if the electric charge of the new heavy quark is taken to vanish. In general, a broad range of  $E/N$  values is possible [28, 29], as indicated by the diagonal yellow band in Fig. 91.1. However, this band still does not exhaust all the possibilities. In fact, there exist classes of QCD axion models whose photon couplings populate the entire still allowed region above the yellow band in Fig. 91.1, motivating axion search efforts over a wide range of masses and couplings [30, 31].

The two-photon decay width is

$$\Gamma_{A \rightarrow \gamma\gamma} = \frac{g_{A\gamma\gamma}^2 m_A^3}{64\pi} = 1.1 \times 10^{-24} \text{ s}^{-1} \left(\frac{m_A}{\text{eV}}\right)^5. \quad (91.6)$$

The second expression uses Eq. (91.5) with  $E/N = 0$ . Axions decay faster than the age of the universe if  $m_A \gtrsim 20$  eV. The interaction with fermions  $f$  has derivative form and is invariant under a shift  $\phi_A \rightarrow \phi_A + \phi_0$  as behaves a NG boson,

$$\mathcal{L}_{Aff} = \frac{C_f}{2f_A} \bar{\Psi}_f \gamma^\mu \gamma_5 \Psi_f \partial_\mu \phi_A. \quad (91.7)$$

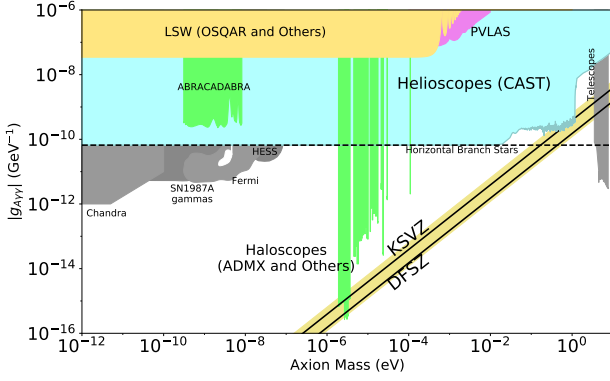


Figure 91.1: Exclusion plot for ALPs as described in the text.

Here,  $\Psi_f$  is the fermion field,  $m_f$  its mass, and  $C_f$  a model-dependent coefficient. The dimensionless combination  $g_{Aff} \equiv C_f m_f / f_A$  plays the role of a Yukawa coupling and  $\alpha_{Aff} \equiv g_{Aff}^2 / 4\pi$  of a “fine-structure constant.” The often-used pseudoscalar form  $\mathcal{L}_{Aff} = -i(C_f m_f / f_A) \bar{\Psi}_f \gamma_5 \Psi_f \phi_A$  need not be equivalent to the appropriate derivative structure, for example when two NG bosons are attached to one fermion line as in axion emission by nucleon bremsstrahlung [32].

In the DFSZ model [25], the tree-level coupling coefficient to electrons is [33]

$$C_e = \frac{\sin^2 \beta}{3}, \quad (91.8)$$

where  $\tan \beta$  is the ratio of the vacuum expectation values of the two Higgs doublets giving masses to the up- and down-type quarks, respectively:  $\tan \beta = v_u / v_d$ .

For nucleons,  $C_{p,n}$  have been determined as [27]

$$\begin{aligned} C_p &= -0.47(3) + 0.88(3)C_u - 0.39(2)C_d - 0.038(5)C_s \\ &\quad - 0.012(5)C_c - 0.009(2)C_b - 0.0035(4)C_t, \\ C_n &= -0.02(3) + 0.88(3)C_d - 0.39(2)C_u - 0.038(5)C_s \\ &\quad - 0.012(5)C_c - 0.009(2)C_b - 0.0035(4)C_t, \end{aligned} \quad (91.9)$$

in terms of the corresponding model-dependent quark couplings  $C_q$ ,  $q = u, d, s, c, b, t$ .

For hadronic axions with  $C_q = 0$ ,  $C_n$  is compatible with zero whereas  $C_p$  does not vanish. In the DFSZ model, on the other hand,  $C_u = C_c = C_t = \frac{1}{3} \cos^2 \beta$  and  $C_d = C_s = C_b = \frac{1}{3} \sin^2 \beta$ , and  $C_p$  and  $C_n$ , as functions of  $\beta$ ,

$$\begin{aligned} C_p &= -0.435 \sin^2 \beta + (-0.182 \pm 0.025), \\ C_n &= 0.414 \sin^2 \beta + (-0.160 \pm 0.025), \end{aligned} \quad (91.10)$$

do not vanish simultaneously.

The axion-pion interaction is given by the Lagrangian [34]

$$\mathcal{L}_{A\pi} = \frac{C_{A\pi}}{f_\pi f_A} (\pi^0 \pi^+ \partial_\mu \pi^- + \pi^0 \pi^- \partial_\mu \pi^+ - 2\pi^+ \pi^- \partial_\mu \pi^0) \partial_\mu \phi_A, \quad (91.11)$$

where  $C_{A\pi} = (1-z)/[3(1+z)]$  in hadronic models, with  $0.38 < z = m_u / m_d < 0.58$  [35, 36]. The chiral symmetry-breaking Lagrangian provides an additional term  $\mathcal{L}'_{A\pi} \propto (m_\pi^2 / f_\pi f_A) (\pi^0 \pi^0 + 2\pi^- \pi^+) \pi^0 \phi_A$ . For hadronic axions it vanishes identically, in contrast to the DFSZ model (Roberto Peccei, private communication).

## 91.3 Laboratory Searches

### 91.3.1 Light shining through walls

Searching for “invisible axions” is extremely challenging due to its extraordinarily feeble coupling to normal matter and radiation. Currently, the most promising approaches rely on the axion-two-photon interaction, allowing for axion-photon conversion in external electric or magnetic fields [6]. For the Coulomb field of a charged particle, the conversion is best viewed as a scattering process,  $\gamma + Ze \leftrightarrow Ze + A$ , called Primakoff effect [37].

In the other extreme of a macroscopic field, usually a large-scale  $B$ -field, the momentum transfer is small, the interaction is coherent over a large distance, and the conversion is best viewed as an axion-photon oscillation phenomenon in analogy to neutrino flavor oscillations [38].

Photons propagating through a transverse magnetic field, with incident  $\mathbf{E}_\gamma$  and magnetic field  $\mathbf{B}$  parallel, may convert into axions. For  $m_A^2 L / 2\omega \ll 2\pi$ , where  $L$  is the length of the  $B$  field region and  $\omega$  the photon energy, the resultant axion beam is coherent with the incident photon beam and the conversion probability is  $\Pi \sim (1/4)(g_{A\gamma\gamma} B L)^2$ . A practical realization uses a laser beam propagating down the bore of a superconducting dipole magnet (like the bending magnets in high-energy accelerators). If another magnet is in line with the first, but shielded by an optical barrier, then photons may be regenerated from the pure axion beam [39, 40]. The overall probability is  $P(\gamma \rightarrow A \rightarrow \gamma) = \Pi^2$ .

The first such Light-Shining-through-Walls (LSW) experiment was performed by the BFRT collaboration. It utilized two magnets of length  $L = 4.4$  m and  $B = 3.7$  T and found  $|g_{A\gamma\gamma}| < 6.7 \times 10^{-7} \text{ GeV}^{-1}$  at 95% CL for  $m_A < 1$  meV [41]. More recently, several such experiments were performed (see Listings) [42–48]. The current best limit,  $|g_{A\gamma\gamma}| < 3.5 \times 10^{-8} \text{ GeV}^{-1}$  at 95% CL for  $m_A \lesssim 0.3$  meV (see Fig. 91.1), has been achieved by the OSQAR (Optical Search for QED Vacuum Birefringence, Axions, and Photon Regeneration) experiment, which exploited two 9 T LHC dipole magnets and an 18.5 W continuous wave laser emitting at the wavelength of 532 nm [48]. Some of these experiments have also reported limits for scalar bosons where the photon  $\mathbf{E}_\gamma$  must be chosen perpendicular to the magnetic field  $\mathbf{B}$ .

The concept of resonantly enhanced photon regeneration may open unexplored regions of coupling strength [49, 50]. In this scheme, both the production and detection magnets are within Fabry-Perot optical cavities and actively locked in frequency. The  $\gamma \rightarrow A \rightarrow \gamma$  rate is enhanced by a factor  $\mathcal{F}\mathcal{F}'/\pi^2$  relative to a single-pass experiment, where  $\mathcal{F}$  and  $\mathcal{F}'$  are the finesses of the two cavities. The resonant enhancement could be of order  $10^{(10-12)}$ , improving the  $g_{A\gamma\gamma}$  sensitivity by  $10^{(2.5-3)}$ . The experiment ALPS II (Any Light Particle Search II) is based on this concept and aims at an improvement of the current laboratory bound on  $g_{A\gamma\gamma}$  by a factor  $\sim 10^3$  in the year 2020 [51].

Resonantly enhanced photon regeneration has already been exploited in experiments searching for ‘radiowaves shining through a shielding’ [52–55]. For  $m_A \lesssim 10^{-5}$  eV, the upper bound on  $g_{A\gamma\gamma}$  established by the CROWS (CERN Resonant Weakly Interacting sub-eV Particle Search) experiment [56] is slightly less stringent than the one set by OSQAR.

### 91.3.2 Photon polarization

An alternative to regenerating the lost photons is to use the beam itself to detect conversion: the polarization of light propagating through a transverse  $B$  field suffers dichroism and birefringence [57]. Dichroism: The  $E_{\parallel}$  component, but not  $E_{\perp}$ , is depleted by axion production, causing a small rotation of linearly polarized light. For  $m_A^2 L / 2\omega \ll 2\pi$ , the effect is independent of  $m_A$ . For heavier axions, it oscillates and diminishes as  $m_A$  increases, and it vanishes for  $m_A > \omega$ . Birefringence: This effect occurs because there is mixing of virtual axions in the  $E_{\parallel}$  state, but not for  $E_{\perp}$ . Hence, linearly polarized light will develop elliptical polarization. Higher-order QED also induces vacuum magnetic birefringence (VMB). A search for these effects was performed in the same dipole magnets of the BFRT experiment mentioned before [58]. The dichroic rotation gave a stronger limit than the ellipticity rotation:  $|g_{A\gamma\gamma}| < 3.6 \times 10^{-7} \text{ GeV}^{-1}$  at 95% CL, for  $m_A < 5 \times 10^{-4}$  eV. The ellipticity limits are better at higher masses, as they fall off smoothly and do not terminate at  $m_A$ .

In 2006, the PVLAS collaboration reported a signature of magnetically induced vacuum dichroism that could be interpreted as the effect of a pseudoscalar with  $m_A = 1\text{--}1.5$  meV and  $|g_{A\gamma\gamma}| = (1.6\text{--}5) \times 10^{-6} \text{ GeV}^{-1}$  [59]. Later, it turned out that these findings are due to instrumental artifacts [60]. This particle interpretation is also excluded by the above photon regeneration searches that were inspired by the original PVLAS result. The fourth generation setup of the PVLAS experiment has published results on searches for VMB (see Fig. 91.1) and dichroism [61].

The bounds from the non-observation of the latter on  $g_{A\gamma\gamma}$  are slightly weaker than the ones from OSQAR.

### 91.3.3 Long-range forces

New bosons would mediate long-range forces, which are severely constrained by “fifth force” experiments [62]. Those looking for new mass-spin couplings provide significant constraints on pseudoscalar bosons [63]. Presently, the most restrictive limits are obtained from combining long-range force measurements with stellar cooling arguments [64]. For the moment, any of these limits are far from realistic values expected for axions. Still, these efforts provide constraints on more general low-mass bosons.

In Ref. [65], a method was proposed that can extend the search for axion-mediated spin-dependent forces by several orders of magnitude. By combining techniques used in nuclear magnetic resonance and short-distance tests of gravity, this method appears to be sensitive to axions in the  $\mu\text{eV} - \text{meV}$  mass range, independent of the cosmic axion abundance, if axions have a CP-violating interaction with nuclei as large as the current experimental bound on the electric dipole moment of the neutron allows. Experimental tests to demonstrate the requirements of ARIADNE (Axion Resonant InterAction DetectioN Experiment) are under way [66].

## 91.4 Axions from Astrophysical Sources

### 91.4.1 Stellar energy-loss limits

Low-mass weakly-interacting particles (neutrinos, gravitons, axions, baryonic or leptonic gauge bosons, *etc.*) are produced in hot astrophysical plasmas, and can thus transport energy out of stars. The coupling strength of these particles with normal matter and radiation is bounded by the constraint that stellar lifetimes or energy-loss rates are not in conflict with observation [67, 68].

We begin this discussion with our Sun and concentrate on hadronic axions. They are produced predominantly by the Primakoff process  $\gamma + Ze \rightarrow Ze + A$ . Integrating over a standard solar model yields the axion luminosity [69]

$$L_A = g_{10}^2 \times 1.85 \times 10^{-3} L_\odot, \quad (91.12)$$

where  $g_{10} = |g_{A\gamma\gamma}| \times 10^{10} \text{ GeV}$ . The maximum of the spectrum is at 3.0 keV, the average at 4.2 keV, and the number flux at Earth is  $g_{10}^2 \times 3.75 \times 10^{11} \text{ cm}^{-2} \text{ s}^{-1}$ . The solar photon luminosity is fixed, so energy losses due to the Primakoff process require enhanced nuclear energy production and thus enhanced neutrino fluxes. The all-flavor measurements by SNO (Solar Neutrino Observatory), together with a standard solar model, imply  $L_A \lesssim 0.10 L_\odot$ , corresponding to  $g_{10} \lesssim 7$  [70], mildly superseding a similar limit from helioseismology [71]. In Ref. [72], this limit was improved to  $g_{10} < 4.1$  (at  $3\sigma$ ), exploiting a new statistical analysis that combined helioseismology (sound speed, surface helium and convective radius) and solar neutrino observations, including theoretical and observational errors, and accounting for tensions between input parameters of solar models, in particular the solar element abundances.

A more restrictive limit derives from globular-cluster (GC) stars that allow for detailed tests of stellar-evolution theory. The stars on the horizontal branch (HB) in the color-magnitude diagram have reached helium burning with a core-averaged energy release of about  $80 \text{ erg g}^{-1} \text{ s}^{-1}$ , compared to Primakoff axion losses of  $g_{10}^2 30 \text{ erg g}^{-1} \text{ s}^{-1}$ . The accelerated consumption of helium reduces the HB lifetime by about  $80/(80+30 g_{10}^2)$ . Number counts of HB stars in a large sample of 39 Galactic GCs compared with the number of red giants (that are not much affected by Primakoff losses) give a weak indication of non-standard losses which may be accounted by Primakoff-like axion emission, if the photon coupling is in the range  $|g_{A\gamma\gamma}| = (2.9 \pm 1.8) \times 10^{-11} \text{ GeV}^{-1}$  [73, 74]. Still, the upper bound found in this analysis,

$$|g_{A\gamma\gamma}| < 6.6 \times 10^{-11} \text{ GeV}^{-1} \quad (95\% \text{ CL}), \quad (91.13)$$

represents the strongest limit on  $g_{A\gamma\gamma}$  for a wide mass range, see Fig. 91.1. The conservative constraint, Eq. (91.13), on  $g_{A\gamma\gamma}$  may be translated to  $f_A > 3.4 \times 10^7 \text{ GeV}$  ( $m_A < 0.2 \text{ eV}$ ), using  $E/N = 0$  as in the KSVZ model, or to  $f_A > 1.3 \times 10^7 \text{ GeV}$  ( $m_A < 0.5 \text{ eV}$ ), for the DFSZ axion model, with  $E/N = 8/3$ , see Fig. 91.1.

If axions couple directly to electrons, the dominant emission processes are atomic axio-recombination and axio-deexcitation, axio-bremsstrahlung in electron-ion or electron-electron collisions, and Compton scattering [75]. Stars in the red giant (RG) branch of the color-magnitude diagram of GCs are particularly sensitive to these processes. In fact, they would lead to an extension of the latter to larger brightness. Reference [76] provided high-precision photometry for the Galactic globular cluster M5 (NGC 5904), allowing for a detailed comparison between the observed tip of the RG branch with predictions based on state-of-the-art stellar evolution theory. It was found that, within the uncertainties, the observed and predicted tip of the RG branch brightness agree reasonably well, leading to the bound

$$|g_{Aee}| < 4.3 \times 10^{-13} \quad (95\% \text{ CL}), \quad (91.14)$$

implying an upper bound on the axion mass in the DFSZ model,

$$m_A \sin^2 \beta < 15 \text{ meV} \quad (95\% \text{ CL}), \quad (91.15)$$

see Fig. 91.2 (left panel). Intriguingly, the agreement would improve with a small amount of extra cooling that slightly postpones helium ignition, preferring an electron coupling around  $|g_{Aee}| \sim 1.9 \times 10^{-13}$ , corresponding to  $m_A \sin^2 \beta \sim 7 \text{ meV}$ .

Bremsstrahlung is also efficient in white dwarfs (WDs), where the Primakoff and Compton processes are suppressed by the large plasma frequency. A comparison of the predicted and observed luminosity function of WDs can be used to put limits on  $|g_{Aee}|$  [78]. A recent analysis, based on detailed WD cooling treatment and new data on the WD luminosity function (WDLF) of the Galactic Disk, found that electron couplings above  $|g_{Aee}| \gtrsim 3 \times 10^{-13}$ , corresponding to a DFSZ axion mass  $m_A \sin^2 \beta \gtrsim 10 \text{ meV}$ , are disfavoured [79], see Fig. 91.2 (left panel). Lower couplings cannot be discarded from the current knowledge of the WDLF of the Galactic Disk. On the contrary, features in some WDLFs can be interpreted as suggestions for electron couplings in the range  $7.2 \times 10^{-14} \lesssim |g_{Aee}| \lesssim 2.2 \times 10^{-13}$ , corresponding to  $2.5 \text{ meV} \lesssim m_A \sin^2 \beta \lesssim 7.5 \text{ meV}$  [79, 80]. This hypothesis will be further scrutinized by the Large Synoptic Survey Telescope (LSST) which is expected to increase the sample of WDs in the Galactic halo to hundreds of thousands [81]. This will allow for the determination of independent WDLFs from different Galactic populations, greatly reducing the uncertainties related to star formation histories. For pulsationally unstable WDs (ZZ Ceti stars), the period decrease  $\dot{P}/P$  is a measure of the cooling speed. The corresponding observations of the pulsating WDs G117-B15A and R548 imply additional cooling that can be interpreted also in terms of similar axion losses [82, 83].

Recently, it has been pointed out that the hints of excessive cooling of WDs, RGs and HB stars can be explained at one stroke by an ALP coupling to electrons and photons, with couplings  $|g_{Aee}| \sim 1.5 \times 10^{-13}$  and  $|g_{A\gamma\gamma}| \sim 1.4 \times 10^{-11} \text{ GeV}^{-1}$ , respectively [84, 85]. Intriguingly, good fits to the data can be obtained employing the DFSZ axion with a mass in the range  $4 \text{ meV} \lesssim m_A \lesssim 250 \text{ meV}$  [84].

Similar constraints derive from the measured duration of the neutrino signal of the supernova SN 1987A. Numerical simulations for a variety of cases, including axions and Kaluza-Klein gravitons, reveal that the energy-loss rate of a nuclear medium at the density  $3 \times 10^{14} \text{ g cm}^{-3}$  and temperature 30 MeV should not exceed about  $1 \times 10^{19} \text{ erg g}^{-1} \text{ s}^{-1}$  [86]. The energy-loss rate from nucleon bremsstrahlung,  $N+N \rightarrow N+N+A$ , is  $(C_N/2f_A)^2 (T^4/\pi^2 m_N) F$ . Here  $F$  is a numerical factor that represents an integral over the dynamical spin-density structure function because axions couple to the nucleon spin. For realistic conditions, even after considerable effort, one is limited to a heuristic estimate leading to  $F \approx 1$  [68]. The SN 1987A limits are of particular interest for hadronic axions where the bounds on  $|g_{Aee}|$  are moot. Using a proton fraction of 0.3,  $g_{Ann} = 0$ ,  $F = 1$ , and  $T = 30 \text{ MeV}$ , one finds  $f_A \gtrsim 4 \times 10^8 \text{ GeV}$  and  $m_A \lesssim 16 \text{ meV}$  [68], see Fig. 91.2 (right panel). A more detailed numerical calculation [87] with state of the art SN models, again assuming  $g_{Ann} = 0$ , found that a coupling larger than  $|g_{App}| \gtrsim 6 \times 10^{-10}$ , would shorten significantly the timescale of the neutrino emission. This result is, not surprisingly, rather close to the estimate in Ref. [68]. Improving the

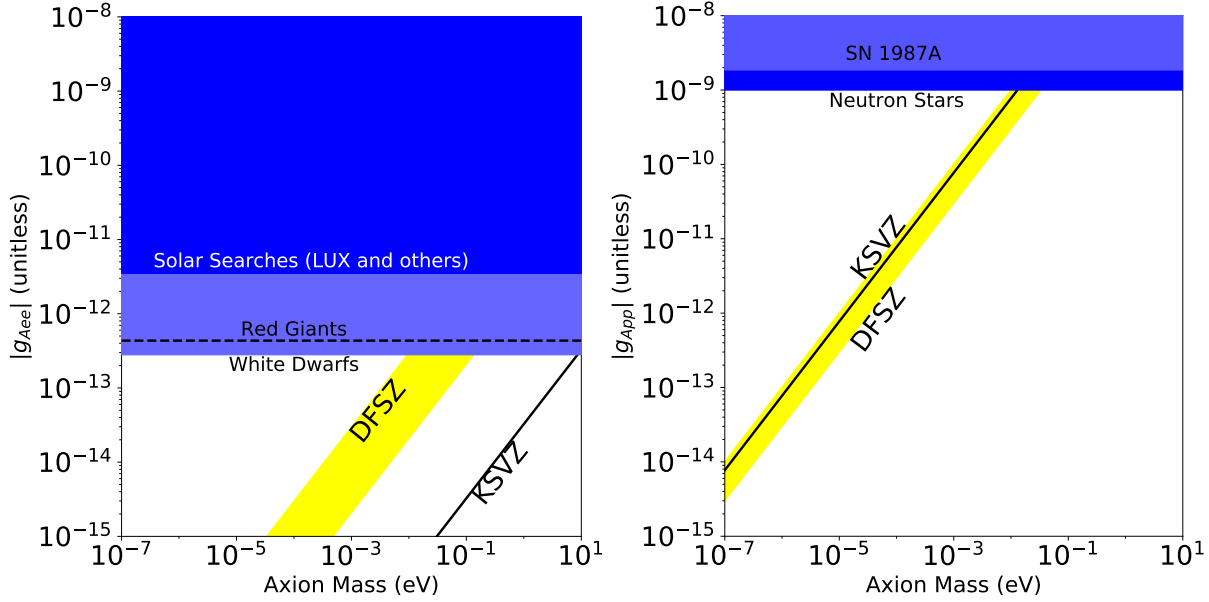


Figure 91.2: Exclusion plots for ALPs as described in the text. For the DFSZ range we have taken into account the constraint  $0.28 \lesssim \tan \beta \lesssim 140$  [77] arising from the requirement of perturbative unitarity of the Yukawa couplings of Standard Model fermions.

calculation of axion emission via nucleon-nucleon bremsstrahlung beyond the basic one-pion exchange approximation appears to loosen the bound [88, 89]. The latter analysis finds a reduction of the axion emissivity by an order of magnitude if one takes into account the non-vanishing mass of the exchanged pion, the contribution from two-pion exchange, effective in-medium nucleon masses and multiple nucleon scattering, leading to a looser bound (Maurizio Giannotti and Alessandro Mirizzi, private communication)

$$g_{Ann}^2 + 0.29 g_{App}^2 + 0.27 g_{Ann} g_{App} < 3.25 \times 10^{-18}. \quad (91.16)$$

However, with the present understanding of SNe (current lack of self-consistent 3D SN simulations) and the sparse data from SN 1987A, the constraint on the axion-nucleon couplings from SN 1987A should be considered more as indicative than as a sharp bound [87].

If axions interact sufficiently strongly they are trapped. Only about three orders of magnitude in  $g_{ANN}$  or  $m_A$  are excluded. For even larger couplings, the axion flux would have been negligible, yet it would have triggered additional events in the detectors, excluding a further range [90]. A possible gap between these two SN 1987A arguments was discussed as the “hadronic axion window” under the assumption that  $g_{A\gamma\gamma}$  was anomalously small [91]. This range is now excluded by hot dark matter (HDM) bounds (see below).

There is another hint for excessive stellar energy losses from the neutron star (NS) in the supernova remnant Cassiopeia A (Cas A): its surface temperature measured over 10 years reveals an unusually fast cooling rate. This rapid cooling of the Cas A NS may be explained by NS minimal cooling with neutron superfluidity and proton superconductivity [92, 93]. The rapid cooling may also arise from a phase transition of the neutron condensate into a multicomponent state [94]. Recently, Ref. [95] analyzed Cas A NS cooling in the presence of axion emission and obtained

$$g_{App}^2 + 1.6g_{Ann}^2 < 1 \times 10^{-18}, \quad (91.17)$$

which is comparable to the SN 1987A bound. Refs. [96] put a more conservative bound without an attempt to fit a transient behavior of Cas A,

$$g_{App}^2 < (1 - 6) \times 10^{-17} \text{ (or } f_A > (5 - 10) \times 10^7 \text{ GeV)}, \quad (91.18)$$

from the temperatures of Cas A and other NSs. The Cas A NS cooling may also be interpreted as a hint for extra cooling caused

by the emission of axions from the breaking and re-formation of neutron triplet Cooper pairs [97], requiring a coupling to the neutron of

$$g_{Ann}^2 = (1.4 \pm 0.5) \times 10^{-19}, \quad (91.19)$$

corresponding to an axion mass

$$m_A = (2.3 \pm 0.4) \text{ meV}/C_n. \quad (91.20)$$

On the other hand, Ref. [98] considered another hot young NS in the supernova remnant HESS J1731-347. Its high temperature implies that all the neutrino emission processes except neutron-neutron bremsstrahlung must be strongly suppressed, which can be realized with a negligible neutron triplet gap and a large proton singlet gap. In this setup, the bremsstrahlung from neutrons is the dominant channel for axion emission, from which one obtains a limit

$$g_{Ann}^2 < 7.7 \times 10^{-20}, \quad (91.21)$$

see Fig. 91.3 (left panel).

Finally, let us note that if the interpretation of the various hints for additional cooling of stars reported in this section in terms of emission of axions with  $m_A \sim \text{meV}$  were correct, SNe would lose a large fraction of their energy as axions. This would lead to a diffuse SN axion background in the universe with an energy density comparable to the extra-galactic background light [99]. However, there is no apparent way of detecting it or the axion burst from the next nearby SN. On the other hand, neutrino detectors such as IceCube, Super-Kamiokande or a future mega-ton water Cherenkov detector will probe exactly the mass region of interest by measuring the neutrino pulse duration of the next galactic SN [87].

#### 91.4.2 Searches for solar axions and ALPs

Instead of using stellar energy losses to derive axion limits, one can also search directly for these fluxes, notably from the Sun. The main focus has been on ALPs with a two-photon vertex. They are produced by the Primakoff process with a flux given by Eq. (91.12) and an average energy of 4.2 keV, and can be detected at Earth with the reverse process in a macroscopic  $B$ -field (“axion helioscope”) [6]. In order to extend the sensitivity in mass towards larger values, one can endow the photon with an effective mass in a gas,  $m_\gamma = \omega_{\text{plas}}$ , thus matching the axion and photon dispersion relations [100].

An early implementation of these ideas used a conventional dipole magnet, with a conversion volume of variable-pressure gas with a xenon proportional chamber as x-ray detector [101]. The

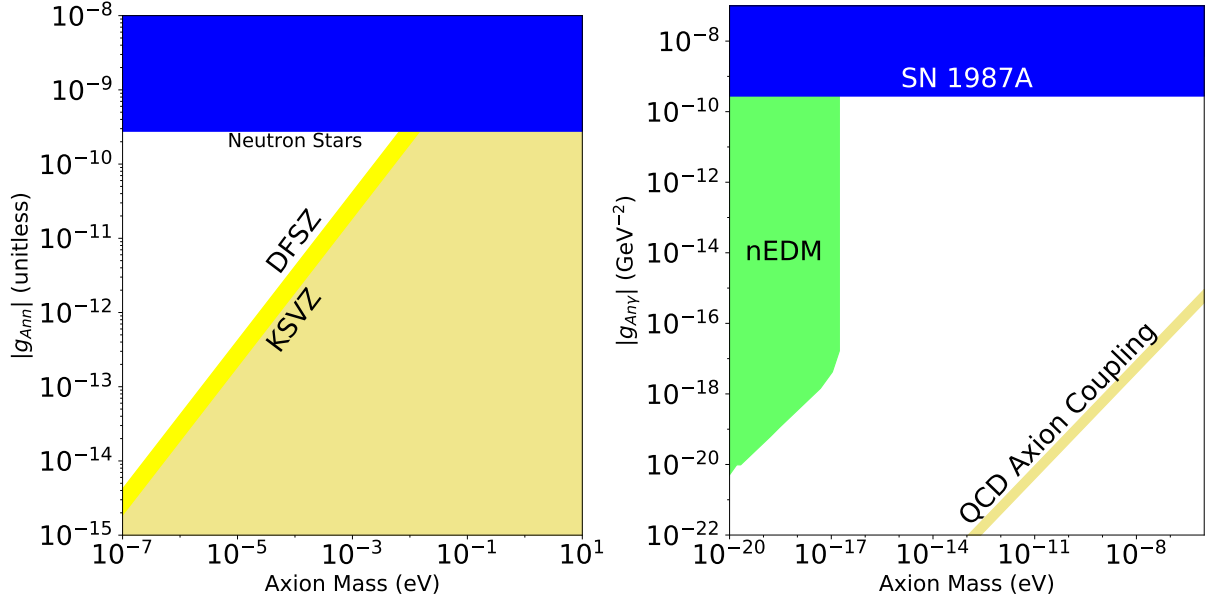


Figure 91.3: Exclusion plots for ALPs as described in the text.

conversion magnet was fixed in orientation and collected data for about 1000 s/day. Axions were excluded for  $|g_{A\gamma\gamma}| < 3.6 \times 10^{-9} \text{ GeV}^{-1}$  for  $m_A < 0.03 \text{ eV}$ , and  $|g_{A\gamma\gamma}| < 7.7 \times 10^{-9} \text{ GeV}^{-1}$  for  $0.03 < m_A < 0.11 \text{ eV}$  at 95% CL.

Later, the Tokyo axion helioscope used a superconducting magnet on a tracking mount, viewing the Sun continuously. They reported  $|g_{A\gamma\gamma}| < 6 \times 10^{-10} \text{ GeV}^{-1}$  for  $m_A < 0.3 \text{ eV}$  [102]. This experiment was recommissioned and a similar limit for masses around 1 eV was reported [103].

The most recent helioscope CAST (CERN Axion Solar Telescope) uses a decommissioned LHC dipole magnet on a tracking mount. The hardware includes grazing-incidence x-ray optics with solid-state x-ray detectors, as well as novel x-ray Micromegas position-sensitive gaseous detectors. Exploiting a IAXO (see below) pathfinder system, CAST has established the limit

$$|g_{A\gamma\gamma}| < 6.6 \times 10^{-11} \text{ GeV}^{-1} \quad (95\% \text{ CL}), \quad (91.22)$$

for  $m_A < 0.02 \text{ eV}$  [104]. To cover larger masses, the magnet bores are filled with a gas at varying pressure. The runs with  $^4\text{He}$  cover masses up to about 0.4 eV [105], providing the  $^4\text{He}$  limits shown in Fig. 91.1. To cover yet larger masses,  $^3\text{He}$  was used to achieve a larger pressure at cryogenic temperatures. Limits up to 1.17 eV allowed CAST to “cross the axion line” for the KSVZ model [106], see Fig. 91.1.

Going to yet larger masses in a helioscope search is not well motivated because of the cosmic HDM bound of  $m_A \lesssim 1 \text{ eV}$  (see below). Sensitivity to significantly smaller values of  $g_{A\gamma\gamma}$  can be achieved with a next-generation axion helioscope with a much larger magnetic-field cross section. Realistic design options for this “International Axion Observatory” (IAXO) have been studied in some detail [107] and its physics potential has been reviewed recently [108]. Such a next-generation axion helioscope may also push the sensitivity in the product of couplings to photons and to electrons,  $g_{A\gamma\gamma}g_{Aee}$ , into a range beyond stellar energy-loss limits and test the hypothesis that WD, RG, and HB cooling is dominated by axion emission [84, 109]. As a first step towards IAXO, an intermediate experimental stage called BabyIAXO is currently under preparation at DESY (for a short introduction, see Ref. [108]).

Other Primakoff searches for solar axions and ALPs have been carried out using crystal detectors, exploiting the coherent conversion of axions into photons when the axion angle of incidence satisfies a Bragg condition with a crystal plane [110]. However, none of these limits is more restrictive than the one derived from the constraint on the solar axion luminosity ( $L_A \lesssim 0.10 L_\odot$ ) discussed earlier.

Another idea is to look at the Sun with an x-ray satellite when the Earth is in between. Solar axions and ALPs would convert in the Earth magnetic field on the far side and could be detected [111]. The sensitivity to  $g_{A\gamma\gamma}$  could be comparable to CAST, but only for much smaller  $m_A$ . Deep solar x-ray measurements with existing satellites, using the solar magnetosphere as conversion region, have reported preliminary limits on  $g_{A\gamma\gamma}$  [112].

Direct detection experiments searching for dark matter (DM) consisting of weakly interacting massive particles, such as EDELWEISS-II, LUX, and XENON100, have also the capability to search for solar axions and ALPs [113, 114]. Recently, the LUX experiment [114] has put a bound on the axion-electron coupling constant by exploiting the axio-electric effect in liquid xenon,

$$|g_{Aee}| < 3.5 \times 10^{-12} \quad (90\% \text{ CL}), \quad (91.23)$$

excluding the DFSZ model with  $m_A \sin^2 \beta > 0.12 \text{ eV}$ , cf. see Fig. 91.2 (left panel). However, as obvious from the same figure, this technique has not reached the sensitivity of energy-loss considerations in stars (RGs and WDs).

### 91.4.3 Conversion of astrophysical photon fluxes

Large-scale  $B$  fields exist in astrophysics that can induce axion-photon oscillations. In practical cases,  $B$  is much smaller than in the laboratory, whereas the conversion region  $L$  is much larger. Therefore, while the product  $BL$  can be large, realistic sensitivities are usually restricted to very low-mass particles, far away from the “axion band” in a plot like Fig. 91.1.

One example is SN 1987A, which would have emitted a burst of ALPs due to the Primakoff production in its core. They would have partially converted into  $\gamma$ -rays in the galactic  $B$ -field. The lack of a gamma-ray signal in the GRS instrument of the SMM satellite in coincidence with the observation of the neutrinos emitted from SN 1987A therefore provides a strong bound on their coupling to photons [115]. This bound has been revisited and the underlying physics has been brought to the current state-of-the-art, as far as modelling of the supernova and the Milky-Way magnetic field are concerned, resulting in the limit [116]

$$|g_{A\gamma\gamma}| < 5.3 \times 10^{-12} \text{ GeV}^{-1}, \text{ for } m_A \lesssim 4.4 \times 10^{-10} \text{ eV}, \quad (91.24)$$

see Fig. 91.1. Magnetically induced oscillations between photons and ALPs can modify the photon fluxes from distant sources in various ways, featuring (i) frequency-dependent dimming, (ii) modified polarization, and (iii) avoiding absorption by propagation in the form of axions.

For example, dimming of SNe Ia could influence the interpretation in terms of cosmic acceleration [117], although it has become



clear that photon-ALP conversion could only be a subdominant effect [118]. Searches for linearly polarised emission from magnetised white dwarfs [119] and changes of the linear polarisation from radio galaxies (see, e.g., Ref. [120]) provide limits close to  $g_{A\gamma\gamma} \sim 10^{-11} \text{ GeV}^{-1}$ , for masses  $m_A \lesssim 10^{-7} \text{ eV}$  and  $m_A \lesssim 10^{-15} \text{ eV}$ , respectively, albeit with uncertainties related to the underlying assumptions. Even stronger limits,  $g_{A\gamma\gamma} \lesssim 2 \times 10^{-13} \text{ GeV}^{-1}$ , for  $m_A \lesssim 10^{-14} \text{ eV}$ , have been obtained by exploiting high-precision measurements of quasar polarisations [121].

Remarkably, it appears that the universe could be too transparent to TeV  $\gamma$ -rays that should be absorbed by pair production on the extra-galactic background light [122–126]. The situation is not conclusive at present [127–129], but the possible role of photon-ALP oscillations in TeV  $\gamma$ -ray astronomy is tantalizing [130]. Fortunately, the region in ALP parameter space,  $g_{A\gamma\gamma} \sim 10^{-12} - 10^{-10} \text{ GeV}^{-1}$  for  $m_A \lesssim 10^{-7} \text{ eV}$  [131], required to explain the anomalous TeV transparency of the universe, could be conceivably probed by the next generation of laboratory experiments (ALPS II) and helioscopes (IAXO) mentioned above. This parameter region can also be probed by searching for an irregular behavior of the gamma ray spectrum of distant active galactic nuclei (AGN), expected to arise from photon-ALP mixing in a limited energy range. The H.E.S.S. collaboration has set a limit of  $|g_{A\gamma\gamma}| \lesssim 2.1 \times 10^{-11} \text{ GeV}^{-1}$ , for  $1.5 \times 10^{-8} \text{ eV} \lesssim m_A \lesssim 6.0 \times 10^{-8} \text{ eV}$ , from the non-observation of an irregular behavior of the spectrum of the AGN PKS 2155-304 [132], see Fig. 91.1. The Fermi-LAT collaboration has put an even more stringent limit on the ALP-photon coupling [133] from observations of the gamma ray spectrum of NGC 1275, the central galaxy of the Perseus cluster, see Fig. 91.1. A similar analysis has been carried out in Ref. [134] using Fermi-LAT data of PKS 2155-304.

Evidence for spectral irregularities has been reported in Galactic sources, such as pulsars and supernova remnants, and has been interpreted as hints for ALPs [135, 136]. However, the inferred ALP parameters are in tension with the CAST helioscope bounds. It should also be noted that the high signal-to-noise spectra of Galactic gamma-ray sources are dominated by uncertainties of the instrumental systematics rather than statistical errors. Furthermore, it has been shown that additional care has to be taken when deriving confidence intervals on ALP parameters based on Wilks' theorem [137], since it has been shown that it does not apply for testing the ALP hypothesis [133].

At smaller masses,  $m_A \lesssim 10^{-12} \text{ eV}$ , galaxy clusters become highly efficient at interconverting ALPs and photons at x-ray energies. Constraints on spectral irregularities in the spectra of luminous x-ray sources (Hydra A, M87, NGC 1275, NGC 3862, Seyfert galaxy 2E3140; taken by Chandra and XMM-Newton) located in or behind galaxy clusters then lead to stringent upper limits on the ALP-photon coupling [138–143]. In this type of studies, the uncertainty in the cluster magnetic field needs to be taken into account. This typically leads to a range of limits on the ALP-photon coupling that depend on the modelling assumptions. Reference [143] recently performed the most sensitive x-ray searches for ALPs to date by employing Chandra's High-Energy Transmission Gratings that allow for an unsurpassed spectral resolution. New observations of the AGN NGC 1275 then led to the bound

$$|g_{A\gamma\gamma}| < 8 \times 10^{-13} \text{ GeV}^{-1} \quad (99.7\% \text{ CL}) \quad (91.25)$$

for light ALPs, see Fig. 91.1.

#### 91.4.4 Superradiance of black holes

Light bosonic fields such as axions or ALPs can affect the dynamics and gravitational wave emission of rapidly rotating astrophysical black holes through the superradiance mechanism. When their Compton wavelength is of order of the black hole size, they form gravitational bound states around the black hole. Their occupation number grows exponentially by extracting energy and angular momentum from the black hole, forming a coherent axion or ALP bound state emitting gravitational waves. When accretion cannot replenish the spin of the black hole, superradiance dominates the black hole spin evolution; this is true for both su-

permassive and stellar mass black holes. The existence of destabilizing light bosonic fields thus leads to gaps in the mass vs. spin plot of rotating black holes. Stellar black hole spin measurements – exploiting well-studied binaries and two independent techniques – exclude a mass range  $6 \times 10^{-13} \text{ eV} < m_A < 2 \times 10^{-11} \text{ eV}$  at  $2\sigma$ , which for the axion excludes  $3 \times 10^{17} \text{ GeV} < f_A < 1 \times 10^{19} \text{ GeV}$  [11, 144, 145]. These bounds apply when gravitational interactions dominate over the axion self-interaction, which is true for the QCD axion in this mass range. Long lasting, monochromatic gravitational wave signals, which can be distinguished from ordinary astrophysical sources by their clustering in a narrow frequency range, are expected to be produced by axions or ALPs annihilating to gravitons. Gravitational waves could also be sourced by axions/ALPs transitioning between gravitationally bound levels. Accordingly, the gravitational wave detector Advanced LIGO should be sensitive to the axion in the  $m_A \lesssim 10^{-10} \text{ eV}$  region. LIGO measurements of black hole spins in binary merger events could also provide statistical evidence for the presence of an axion [146, 147]. Similar signatures could arise for supermassive black holes for particle with masses  $\lesssim 10^{-15} \text{ eV}$ . Gravitational waves from such sources could be detected at lower-frequency observatories such as LISA.

## 91.5 Cosmic Axions

### 91.5.1 Cosmic axion populations

In the early universe, axions are produced by processes involving quarks and gluons [148]. After color confinement, the dominant thermalization process is  $\pi + \pi \leftrightarrow \pi + A$  [34]. The resulting axion population would contribute an HDM component in analogy to massive neutrinos. Cosmological precision data provide restrictive constraints on a possible HDM fraction that translate into  $m_A \lesssim 1 \text{ eV}$  [149], but in detail depend on the used data set and assumed cosmological model. In the future, data from a EUCLID-like survey combined with Planck CMB data can detect HDM axions with a mass  $m_A \gtrsim 0.15 \text{ eV}$  at very high significance [150].

For  $m_A \gtrsim 20 \text{ eV}$ , axions decay fast on a cosmic time scale, removing the axion population while injecting photons. This excess radiation provides additional limits up to very large axion masses [151]. An anomalously small  $g_{A\gamma\gamma}$  provides no loophole because suppressing decays leads to thermal axions overdominating the mass density of the universe.

The main cosmological interest in axions derives from their possible role as CDM. In addition to thermal processes, axions are abundantly produced by the vacuum re-alignment (VR) mechanism [152].

The axion DM abundance crucially depends on the cosmological history. Let us first consider the so called *pre-inflationary PQ symmetry breaking scenario*, in which the PQ symmetry is broken before and during inflation and not restored afterwards. After the breakdown of the PQ symmetry, the axion field relaxes somewhere in the bottom of the “wine-bottle-bottom” potential. Near the QCD epoch, topological fluctuations of the gluon fields such as instantons explicitly break the PQ symmetry. This tilting of the “wine-bottle-bottom” drives the axion field toward the CP-conserving minimum, thereby exciting coherent oscillations of the axion field that ultimately represent a condensate of CDM. The fractional cosmic mass density in this homogeneous field mode, created by the VR mechanism, is [23, 153–155],

$$\begin{aligned} \Omega_A^{\text{VR}} h^2 &\approx 0.12 \left( \frac{f_A}{9 \times 10^{11} \text{ GeV}} \right)^{1.165} F \Theta_i^2 \\ &\approx 0.12 \left( \frac{6 \mu\text{eV}}{m_A} \right)^{1.165} F \Theta_i^2, \end{aligned} \quad (91.26)$$

where  $h$  is the present-day Hubble expansion parameter in units of  $100 \text{ km s}^{-1} \text{ Mpc}^{-1}$ , and  $-\pi \leq \Theta_i \leq \pi$  is the initial “misalignment angle” relative to the CP-conserving position attained in the causally connected region which evolved into today's observable universe.  $F = F(\Theta_i, f_A)$  is a factor accounting for anharmonicities in the axion potential. For  $F \Theta_i^2 = \mathcal{O}(1)$ ,  $m_A$  should be above  $\sim 6 \mu\text{eV}$  in order that the cosmic axion density does not exceed the observed CDM density,  $\Omega_{\text{CDM}} h^2 = 0.12$ . However, much smaller

axion masses (much higher PQ scales) are still possible if the initial value  $\Theta_i$  just happens to be small enough in today's observable universe ("anthropic axion window" [156]). In this cosmological scenario, however, quantum fluctuations of the axion field during inflation are expected to lead to isocurvature density fluctuations which get imprinted to the temperature fluctuations of the CMB [157, 158]. Their non-observation puts severe constraints on the Hubble expansion rate  $H_I$  during inflation [159–163], which read, in the simplest cosmological inflationary scenario,

$$H_I \lesssim 5.7 \times 10^8 \text{ GeV} \left( \frac{5 \text{ neV}}{m_a} \right)^{0.4175}, \quad (91.27)$$

if axions represent all of DM.

In the *post-inflationary PQ symmetry breaking scenario*, on the other hand,  $\Theta_i$  will take on different values in different patches of the present universe. The average contribution is [23, 153–155]

$$\Omega_A^{\text{VR}} h^2 \approx 0.12 \left( \frac{30 \text{ } \mu\text{eV}}{m_A} \right)^{1.165}. \quad (91.28)$$

The decay of cosmic strings and domain walls gives rise to a further population of CDM axions, whose abundance suffers from significant uncertainties [154, 155, 164–172] which arise from the difficulty in understanding the energy loss process of topological defects and the generated axion spectrum in a quantitative way. In fact, in the present state-of-the-art it is still possible that the CDM contribution from the decay of topological defects is subdominant or overwhelmingly large in comparison to the one from the VR mechanism. Correspondingly, the plausible range of axion masses providing all of CDM in scenarios with postinflationary PQ symmetry breaking is still rather large, namely

$$m_A \approx 25 \text{ } \mu\text{eV} - 4.4 \text{ meV}, \quad (91.29)$$

for models with short-lived (requiring unit color anomaly  $N = 1$ ) domain walls, such as the KSVZ model. For models with long-lived ( $N > 1$ ) domain walls, such as an accidental DFSZ model [173], where the PQ symmetry is broken by higher dimensional Planck suppressed operators, the mass is predicted to be significantly higher [168, 173, 174],

$$m_A \approx (0.58 - 130) \text{ meV}. \quad (91.30)$$

However, the upper part of the predicted range is in conflict with stellar energy-loss limits on the axion, cf. Fig. 91.2 (right panel) and Fig. 91.3 (left panel).

In this post-inflationary PQ symmetry breakdown scenario, the spatial axion density variations are large at the QCD transition and they are not erased by free streaming. Gravitationally bound "axion miniclusters" form before and around matter-radiation equality [175–177]. A significant fraction of CDM axions can reside in these bound objects [171, 178]. Remarkably, the minicluster fraction can be bounded by gravitational lensing [179–181].

In the above predictions of the fractional cosmic mass density in axions, the exponent, 1.165, arises from the non-trivial temperature dependence of the topological susceptibility  $\chi(T) = m_A^2(T) f_A^2$  at temperatures slightly above the QCD quark-hadron phase transition. Lattice QCD calculations of this exponent [23, 182–186], but also Ref. [187], found it to be remarkably close to the prediction of the dilute instanton gas approximation [188] which was previously exploited. Therefore, the state-of-the-art prediction of the axion mass relevant for DM for a fixed initial misalignment angle  $\Theta_i$  differs from the previous prediction by just a factor of order one.

The non-thermal production mechanisms attributed to axions are generic to light bosonic weakly interacting particles such as ALPs [189]. The relic abundance is set by the epoch when the axion mass becomes significant,  $3H(t) \approx m_A(t)$ , and ALP field oscillations begin. For ALPs to contribute to the DM density this epoch must precede that of matter radiation equality. For a temperature independent ALP mass this leads to the bound:

$$m_A \gtrsim 7 \times 10^{-28} \text{ eV} \left( \frac{\Omega_m h^2}{0.15} \right)^{1/2} \left( \frac{1 + z_{\text{eq}}}{3.4 \times 10^3} \right)^{3/2}. \quad (91.31)$$

ALPs lighter than this bound are allowed if their cosmic energy density is small, but they are quite distinct from other forms of DM [190]. Ignoring anharmonicities in the ALP potential, and taking the ALP mass to be temperature independent, the relic density in DM ALPs due to the VR mechanism is given by

$$\Omega_{\text{ALP}}^{\text{VR}} h^2 = 0.12 \left( \frac{m_A}{4.7 \times 10^{-19} \text{ eV}} \right)^{1/2} \left( \frac{f_A}{10^{16} \text{ GeV}} \right)^2 \times \left( \frac{\Omega_m h^2}{0.15} \right)^{3/4} \left( \frac{1 + z_{\text{eq}}}{3.4 \times 10^3} \right)^{-3/4} \Theta_i^2. \quad (91.32)$$

An ALP decay constant near the GUT scale gives the correct relic abundance for *ultralight ALPs* (ULAs), which we now define. Extended discussions of ULAs can be found in Refs. [191, 192].

The standard CDM model treats DM as a distribution of cold, collisionless particles interacting only via gravity. Below the Compton wavelength,  $\lambda_c = 2\pi/m_A$ , the particle description of ALPs breaks down. For large occupation numbers we can model ALPs below the Compton wavelength as a coherent classical field. Taking as a reference length scale the Earth radius,  $R_{\oplus} = 6371 \text{ km}$ , we define ULAs to be those axions with  $\lambda_c > R_{\oplus}$ , leading to the defining bound

$$m_{\text{ULA}} < 2 \times 10^{-13} \text{ eV}. \quad (91.33)$$

ULAs encompass the entire Earth in a single coherent field. The coherence time of the ULA field on Earth can be estimated from the crossing time of the de Broglie wavelength at the virial velocity in the Milky Way,  $\tau_{\text{coh}} \sim 1/m_{\text{ULA}} v_{\text{vir}}^2$ .

We notice that by the definition, Eq. (91.33), an ultralight QCD axion must have a super-Planckian decay constant,  $f_A > 3 \times 10^{19} \text{ GeV}$  and would require fine tuning of  $\theta_i$  to provide the relic abundance. Natural models for ULAs can be found in string and M-theory compactifications [7–14], in field theory with accidental symmetries [193], or new hidden strongly coupled sectors [194].

In addition to the gravitational potential energy, the ULA field also carries gradient energy. On scales where the gradient energy is non-negligible, ULAs acquire an effective pressure and do not behave as CDM. The gradient energy opposes gravitational collapse, leading to a Jeans scale below which perturbations are stable [195]. The Jeans scale suppresses linear cosmological structure formation relative to CDM [196]. The Jeans scale at matter-radiation equality in the case that ULAs make up all of CDM is:

$$k_{\text{J,eq}} = 8.7 \text{ Mpc}^{-1} \left( \frac{1 + z_{\text{eq}}}{3.4 \times 10^3} \right)^{-1/4} \left( \frac{\Omega_{\text{ALP}}^{\text{VR}}}{0.12} \right)^{1/4} \times \left( \frac{m_{\text{ULA}}}{10^{-22} \text{ eV}} \right)^{1/2}. \quad (91.34)$$

On non-linear scales the gradient energy leads to the existence of a class of pseudo-solitons known as oscillatons, or axion stars [197].

Cosmological and astrophysical observations are consistent with the CDM model, and departures from it are only allowed on the scales of the smallest observed DM structures with  $M \sim 10^{6-8} M_{\odot}$ . The CMB power spectrum and galaxy auto-correlation power spectrum limit the ULA mass to  $m_{\text{ULA}} > 10^{-24} \text{ eV}$  from linear theory of structure formation [190, 198]. Analytic models [199] and  $N$ -body simulations [200] for non-linear structures show that halo formation is suppressed in ULA models relative to CDM. This leads to constraints on the ULA mass of  $m_{\text{ULA}} > 10^{-22} \text{ eV}$  from observations of high- $z$  galaxies [200, 201], and  $m_{\text{ULA}} > 10^{-21} \text{ eV}$  from the Lyman-alpha forest flux power spectrum [202]. Including the effects of anharmonicities on structure formation with ALPs can weaken these bounds if the misalignment angle  $\Theta_i \approx \pi$  [203]. Cosmological simulations that treat gradient energy in the ULA field beyond the  $N$ -body approximation have just recently become available [204, 205], and show, among other things, evidence for the formation of axion stars in the centres of ULA halos (various consequences of axion stars are considered in Refs. [206]). These central axion stars have been conjectured to play a role in the apparently cored density



profiles of dwarf spheroidal galaxies, and other central galactic regions [204, 207–209]. However, the relationship between the halo mass and the axion star mass [210] leads to problems with this scenario in some galaxies [211–213]. It should be emphasised that many of the conclusions about the role of ULA axion stars in galactic dynamics are based on use of simulation results that do not contain baryons (however, see Ref. [214]), and feedback [215] could be important.

Inside DM halos the axion gradient energy causes coherence on the de Broglie wavelength and fluctuations on the coherence time [204, 216]. These fluctuations can be thought of as short-lived quasiparticles and lead to relaxation processes that can be described statistically [192, 217] (this relaxation processes also leads to the gravitational condensation of axion stars [218]). The typical relaxation time is:

$$t \sim 10^{10} \text{ years} \left( \frac{m_{\text{ULA}}}{10^{-22} \text{ eV}} \right)^3 \left( \frac{v}{100 \text{ km s}^{-1}} \right)^2 \left( \frac{r}{5 \text{ kpc}} \right)^4, \quad (91.35)$$

where  $v$  and  $r$  are the velocity and radius of the orbit in the host DM halo.

Relaxation processes such as these are not observed in galaxies, though there are some circumstances where they may be desirable [192]. An absence of observed relaxation can be used to set limits on the ULA mass. An absence of observed Milky Way disk thickening excludes  $m_{\text{ULA}} > 0.6 \times 10^{-22} \text{ eV}$  [219], while stellar streams give the stronger bound  $m_{\text{ULA}} > 1.5 \times 10^{-22} \text{ eV}$  [220]. The survival of the old star cluster in Eridanus II [221] excludes the range of masses  $10^{-21} \text{ eV} \lesssim m_{\text{ULA}} \lesssim 10^{-19} \text{ eV}$  [222]. As in the case of ULA axion stars, current constraints from heating do not fully account for the possible role of baryons.

Finally, one should note that the beyond-CDM physics of ULAs (Jeans scale, relaxation, axion star formation) of course also applies to the QCD axion on smaller length scales. This is of particular interest inside axion miniclusters [175, 176, 218, 223].

### 91.5.2 Telescope searches

The two-photon decay is extremely slow for axions with masses in the CDM regime, but could be detectable for eV masses. The signature would be a quasi-monochromatic emission line from galaxies and galaxy clusters. The expected optical line intensity for DFSZ axions is similar to the continuum night emission. An early search in three rich Abell clusters [224] and a recent search in two rich Abell clusters [225] exclude the ‘‘Telescope’’ range in Fig. 91.1. Of course, axions in this mass range would anyway provide an excessive hot DM contribution.

Very low-mass axions in halos produce a weak quasi-monochromatic radio line. Virial velocities in undisrupted dwarf galaxies are very low, and the axion decay line would therefore be extremely narrow. A search with the Haystack radio telescope on three nearby dwarf galaxies provided a limit  $|g_{A\gamma\gamma}| < 1.0 \times 10^{-9} \text{ GeV}^{-1}$  at 96% CL for  $298 < m_A < 363 \mu\text{eV}$  [226]. However, this combination of  $m_A$  and  $g_{A\gamma\gamma}$  does not exclude plausible axion models.

A monochromatic signal is also produced in the conversion of DM axions in the background of slowly varying galactic  $B$ -fields [227]. The signal is, however, sensitive to magnetic field power on the scale of the axion mass [228]. Present and future radio telescopes appear to be able to probe ALP DM in the mass range  $0.1 - 100 \mu\text{eV}$  for couplings  $g_{A\gamma\gamma} \gtrsim 10^{-13} \text{ GeV}^{-1}$  [228] – unfortunately not reaching down to the benchmark QCD axion sensitivity.

Resonant conversion of QCD axion DM in neutron star magnetospheres may give a detectable signal from individual neutron stars for axion masses in the  $\mu\text{eV}$  range [229]. Furthermore, stimulated ALP decays in high radiation environments may be detectable, by next-generation radio telescopes such as the Square Kilometer Array, down to  $g_{A\gamma\gamma} \gtrsim 10^{-11} \text{ GeV}^{-1}$ , for masses between  $\mu\text{eV}$  and  $0.1 \text{ meV}$  [230].

Photon propagation on an ULA DM background can induce birefringence that can be compared with upper limits from the CMB [231] and may also be probed with other sources such as pulsars [232].

### 91.5.3 Microwave cavity experiments

In a big part of the plausible  $m_A$  range for CDM, galactic halo axions may be detected by their resonant conversion into a quasi-monochromatic microwave signal in a high-Q electromagnetic cavity permeated by a strong static  $B$  field [6, 233, 234]. The cavity frequency is tunable, and the signal is maximized when the frequency is the total axion energy, rest mass plus kinetic energy, of  $\nu = (m_A/2\pi) [1 + \mathcal{O}(10^{-6})]$ , the width above the rest mass representing the virial distribution in the galaxy. The frequency spectrum may also contain finer structure from axions more recently fallen into the galactic potential and not yet completely virialized [235, 236].

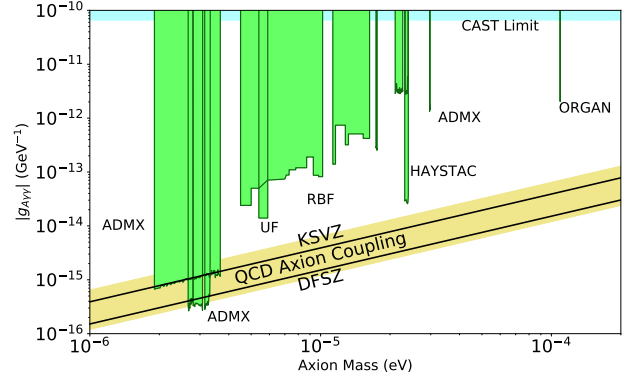


Figure 91.4: Exclusion plot for ALPs as described in the text.

The feasibility of this technique was established in early experiments (RBF and UF) of relatively small sensitive volume,  $\mathcal{O}(1)$  liter), with HFET-based amplifiers, setting limits in the range  $4.5 < m_A < 16.3 \mu\text{eV}$  [237], but lacking by 2–3 orders of magnitude the sensitivity required to detect realistic axions, see Fig. 91.4. Later, ADMX ( $B \sim 8 \text{ T}$ ,  $V \sim 200$  liters) has achieved sensitivity to KSVZ axions, assuming they saturate the local DM density and are well virialized, over the mass range  $1.9 - 3.3 \mu\text{eV}$  [238]. Should halo axions have a significant component not yet virialized, ADMX is sensitive to DFSZ axions over the entire mass range [239]. The corresponding 90% CL exclusion regions shown in Fig. 91.4 are normalized to an assumed local CDM density of  $7.5 \times 10^{-25} \text{ g cm}^{-3}$  ( $450 \text{ MeV cm}^{-3}$ ). More recently, the ADMX experiment commissioned an upgrade [240] that replaces the microwave HFET amplifiers by near quantum-limited low-noise dc SQUID microwave amplifiers [241]. It has reached an unprecedented axion DM sensitivity in the mass range between  $2.66$  and  $3.31 \mu\text{eV}$  [242, 243], down to the DFSZ benchmark axion-photon coupling, see Fig. 91.4. This apparatus is also sensitive to other hypothetical light bosons, such as hidden photons or chameleons, over a limited parameter space [189, 244, 245]. ADMX has also done a testbed experiment to probe higher masses. This experiment lives inside of and operates in tandem with the main ADMX experiment, searches in three widely spaced frequency ranges (4202–4249 MHz, 5086–5799 MHz and 7173–7203 MHz), uses both the  $\text{TM}_{010}$  and  $\text{TM}_{020}$  cavity modes, and demonstrates the successful use of a piezoelectric actuator for cavity tuning [246]. Recently, the HAYSTAC experiment reported on first results from a new microwave cavity search for DM axions with masses above  $20 \mu\text{eV}$ . They exclude axions with two-photon coupling  $|g_{A\gamma\gamma}| \gtrsim 2 \times 10^{-14} \text{ GeV}^{-1}$  over the range  $23.15 \mu\text{eV} < m_A < 24.0 \mu\text{eV}$  [247, 248], a factor of 2.7 above the KSVZ benchmark, see Fig. 91.4. Exploiting a Josephson parametric amplifier, this experiment has demonstrated total noise approaching the standard quantum limit for the first time in an axion search. A Rydberg atom single-photon detector [249], like any photon counter, can in principle evade the standard quantum limit for coherent photon detection. The ORGAN experiment is designed to probe axions in the mass range  $60 \mu\text{eV} < m_A < 210 \mu\text{eV}$ . In a pathfinding run, it has set the limit  $|g_{A\gamma\gamma}| < 2 \times 10^{-12} \text{ GeV}^{-1}$  at  $110 \mu\text{eV}$ , in a span of  $2.5 \text{ neV}$  [250]. There are further microwave cavity axion DM experiments recently in operation (CULTASK [251]), under construction (RADES [252]) or proposed (KLASH [253]).

### 91.5.4 New concepts for axion DM direct detection

Other new concepts for searching for axion DM are also being investigated. An alternative to the microwave cavity technique is based on a novel detector architecture consisting of an open, Fabry-Perot resonator and a series of current-carrying wire planes [254]. The Orpheus detector has demonstrated this new technique, excluding DM ALPs with masses between 68.2 and 76.5  $\mu\text{eV}$  and axion-photon couplings greater than  $4 \times 10^{-7} \text{ GeV}^{-1}$ . This technique may be able to probe DM axions in the mass range from 40 to 700  $\mu\text{eV}$ . Another detector concept exploits the fact that a magnetized mirror would radiate photons in the background of axion DM, which could be collected like in a dish antenna [255]. Searches for hidden photon DM exploiting this technique are already underway [256]. The proposed MADMAX experiment will place a stack of dielectric layers in a magnetic field in order to resonantly enhance the photon signal, aiming a sensitivity to probe the mass range  $40 \mu\text{eV} \lesssim m_A \lesssim 200 \mu\text{eV}$  [257, 258]. Optical dielectric haloscopes with single photon signal detection have been proposed to search for axions in the 50 meV – 10 eV mass range [259]. Absorption of axions on molecular transitions can be sensitive to the axion pseudoscalar coupling  $g_{ANN}$  to nucleons or the pseudoscalar coupling  $g_{Aee}$  to electrons in the 0.5 – 20 eV range [260]. Another proposed axion DM search method sensitive in the 100  $\mu\text{eV}$  mass range is to cool a kilogram-sized sample to mK temperatures and count axion induced atomic transitions using laser techniques [261].

The oscillating galactic DM axion field induces oscillating nuclear electric dipole moments (EDMs) [262],

$$d_N(t) = g_{AN\gamma} \sqrt{2\rho_{\text{ADM}}} \cos(m_A t) / m_A, \quad (91.36)$$

where  $g_{AN\gamma}$  is the coupling of the axion to the nucleon EDM operator,

$$\mathcal{L}_A \supset -\frac{i}{2} g_{AN\gamma} A \bar{\Psi}_N \sigma_{\mu\nu} \gamma_5 \Psi_N F^{\mu\nu}. \quad (91.37)$$

For the QCD axion, this coupling is predicted as [263]

$$\begin{aligned} g_{AN\gamma} = -g_{Ap\gamma} &= (3.7 \pm 1.5) \times 10^{-3} \left( \frac{1}{f_A} \right) \frac{1}{\text{GeV}} = \\ &= (6.5 \pm 2.6) \times 10^{-13} \left( \frac{m_A}{\text{meV}} \right) \frac{1}{\text{GeV}^2} \end{aligned} \quad (91.38)$$

and plotted as a yellow diagonal band in Fig. 91.3 (right panel). An analysis of the ratio of spin-precession frequencies of stored ultracold neutrons and  $^{199}\text{Hg}$  atoms measured by neutron EDM experiments for an axion-induced oscillating neutron EDM revealed no signal consistent with axion DM, excluding a sizeable region of parameter space in the mass region  $10^{-24} \text{ eV} \leq m_A \leq 10^{-17} \text{ eV}$  [264], which surpass the limits on anomalous energy loss of SN 1987A [262] by more than seven orders of magnitude, but are still a few orders of magnitude above the QCD axion expectations, see Fig. 91.3 (right panel). The oscillating EDMs cause also the precession of nuclear spins in a nucleon spin polarized sample in the presence of an electric field. The resulting transverse magnetization can be searched for by exploiting magnetic-resonance (MR) techniques, which are most sensitive in the range of low oscillation frequencies corresponding to sub-neV axion masses. The aim of the corresponding Cosmic Axion Spin Precession Experiment (CASPER) [265] is to probe axion DM in the anthropic window,  $f_A \gtrsim 10^{15} \text{ GeV}$  ( $m_A \lesssim \text{neV}$ ), motivated from Grand Unification [266–269]. Sub- $\mu\text{eV}$  ALP masses can also be probed by using the storage ring EDM method proposed in Ref. [270] which exploits a combination of B and E-fields to produce a resonance between the  $g - 2$  spin precession frequency and the DM ALP field oscillation frequency. This method, however, does not reach the sensitivity to probe the QCD axion prediction for  $g_{AN\gamma}$ .

In the intermediate mass region,  $\text{neV} \lesssim m_A \lesssim 0.1 \mu\text{eV}$ , one may exploit a cooled LC circuit and precision magnetometry to search for the oscillating electric current induced by DM axions in a strong magnetic field [271]. A similar approach is followed by the proposed ABRACADABRA [272] and DM-Radio Pathfinder [273] experiments. Recently, ABRACADABRA-10 cm – a small-scale prototype for a future detector that could be sensitive to the QCD

axion – established upper limits on the axion-photon coupling in the mass range  $3.1 \times 10^{-10} \text{ eV} - 8.3 \times 10^{-9} \text{ eV}$  [274], which are, however, not competitive yet with other limits in this mass range, see Fig. 91.1.

An eventually non-zero axion electron coupling  $g_{Aee}$  will lead to an electron spin precession about the axion DM wind [275]. The QUAX (QUAerere AXions) experiment aims at exploiting MR inside a magnetized material [276]. Because of the higher Larmor frequency of the electron, it is sensitive in the classic window.

### 91.6 Conclusions

There is a strengthening physics case for very weakly coupled light particles beyond the Standard Model. The elegant solution of the strong CP problem proposed by Peccei and Quinn yields a particularly strong motivation for the axion. In many theoretically appealing ultraviolet completions of the Standard Model axions and ALPs occur automatically. Moreover, they are natural CDM candidates. Perhaps the first hints of their existence have already been seen in the anomalous excessive cooling of stars and the anomalous transparency of the Universe for VHE gamma rays. Interestingly, a significant portion of previously unexplored, but phenomenologically very interesting and theoretically very well motivated axion and ALP parameter space can be tackled in the foreseeable future by a number of terrestrial experiments searching for axion/ALP DM, for solar axions/ALPs, and for light apparently shining through a wall.

### References

- [1] R. D. Peccei and H. R. Quinn, Phys. Rev. Lett. **38**, 1440 (1977).
- [2] R. D. Peccei and H. R. Quinn, Phys. Rev. **D16**, 1791 (1977).
- [3] S. Weinberg, Phys. Rev. Lett. **40**, 223 (1978).
- [4] F. Wilczek, Phys. Rev. Lett. **40**, 279 (1978).
- [5] Y. Chikashige, R.N. Mohapatra, and R.D. Peccei, Phys. Lett. **B98**, 265 (1981); G. B. Gelmini and M. Roncadelli, Phys. Lett. **99B**, 411 (1981).
- [6] P. Sikivie, Phys. Rev. Lett. **51**, 1415 (1983) and Erratum *ibid.*, **52**, 695 (1984).
- [7] E. Witten, Phys. Lett. **149B**, 351 (1984).
- [8] J. P. Conlon, JHEP **05**, 078 (2006), [hep-th/0602233].
- [9] P. Svrcek and E. Witten, JHEP **06**, 051 (2006), [hep-th/0605206].
- [10] K.-S. Choi *et al.*, Phys. Lett. **B675**, 381 (2009), [arXiv:0902.3070].
- [11] A. Arvanitaki *et al.*, Phys. Rev. **D81**, 123530 (2010), [arXiv:0905.4720].
- [12] B. S. Acharya, K. Bobkov and P. Kumar, JHEP **11**, 105 (2010), [arXiv:1004.5138].
- [13] M. Cicoli, M. Goodsell and A. Ringwald, JHEP **10**, 146 (2012), [arXiv:1206.0819].
- [14] J. Halverson, C. Long and P. Nath, Phys. Rev. **D96**, 5, 056025 (2017), [arXiv:1703.07779].
- [15] J. Jaeckel and A. Ringwald, Ann. Rev. Nucl. Part. Sci. **60**, 405 (2010), [arXiv:1002.0329].
- [16] A. Ringwald, Phys. Dark Univ. **1**, 116 (2012), [arXiv:1210.5081].
- [17] J. Jaeckel, Frascati Phys. Ser. **56**, 172 (2012), [arXiv:1303.1821].
- [18] C. A. Baker *et al.*, Phys. Rev. Lett. **97**, 131801 (2006), [hep-ex/0602020].
- [19] H. Georgi, D. B. Kaplan and L. Randall, Phys. Lett. **169B**, 73 (1986).
- [20] R. J. Crewther, Phys. Lett. **70B**, 349 (1977).
- [21] P. Di Vecchia and G. Veneziano, Nucl. Phys. **B171**, 253 (1980).
- [22] M. Gorghetto and G. Villadoro, JHEP **03**, 033 (2019), [arXiv:1812.01008].

- [23] S. Borsanyi *et al.*, Nature **539**, 7627, 69 (2016), [arXiv:1606.07494].
- [24] J. E. Kim, Phys. Rev. Lett. **43**, 103 (1979); M. A. Shifman, A. I. Vainshtein and V. I. Zakharov, Nucl. Phys. **B166**, 493 (1980).
- [25] M. Dine, W. Fischler and M. Srednicki, Phys. Lett. **104B**, 199 (1981); A. R. Zhitnitsky, Sov. J. Nucl. Phys. **31**, 260 (1980), [Yad. Fiz.31,497(1980)].
- [26] J. E. Kim and G. Carosi, Rev. Mod. Phys. **82**, 557 (2010), [arXiv:0807.3125].
- [27] G. Grilli di Cortona *et al.*, JHEP **01**, 034 (2016), [arXiv:1511.02867].
- [28] J. E. Kim, Phys. Rev. **D58**, 055006 (1998), [hep-ph/9802220].
- [29] L. Di Luzio, F. Mescia and E. Nardi, Phys. Rev. Lett. **118**, 3, 031801 (2017), [arXiv:1610.07593]; L. Di Luzio, F. Mescia and E. Nardi, Phys. Rev. **D96**, 7, 075003 (2017), [arXiv:1705.05370].
- [30] M. Farina *et al.*, JHEP **01**, 095 (2017), [arXiv:1611.09855].
- [31] P. Agrawal *et al.*, JHEP **02**, 006 (2018), [arXiv:1709.06085].
- [32] G. Raffelt and D. Seckel, Phys. Rev. Lett. **60**, 1793 (1988); M. Carena and R. D. Peccei, Phys. Rev. **D40**, 652 (1989); K. Choi, K. Kang and J. E. Kim, Phys. Rev. Lett. **62**, 849 (1989).
- [33] M. Srednicki, Nucl. Phys. **B260**, 689 (1985).
- [34] S. Chang and K. Choi, Phys. Lett. **B316**, 51 (1993), [hep-ph/9306216].
- [35] H. Leutwyler, Phys. Lett. **B378**, 313 (1996), [hep-ph/9602366].
- [36] C. Patrignani *et al.* (Particle Data Group), Chin. Phys. **C40**, 10, 100001 (2016).
- [37] D. A. Dicus *et al.*, Phys. Rev. **D18**, 1829 (1978).
- [38] G. Raffelt and L. Stodolsky, Phys. Rev. **D37**, 1237 (1988).
- [39] A. A. Anselm, Yad. Fiz. **42**, 1480 (1985).
- [40] K. van Bibber *et al.*, Phys. Rev. Lett. **59**, 759 (1987).
- [41] G. Ruoso *et al.*, Z. Phys. **C56**, 505 (1992); R. Cameron *et al.*, Phys. Rev. **D47**, 3707 (1993).
- [42] M. Fouche *et al.*, Phys. Rev. **D78**, 032013 (2008), [arXiv:0808.2800].
- [43] P. Pagnat *et al.* (OSQAR), Phys. Rev. **D78**, 092003 (2008), [arXiv:0712.3362].
- [44] A. S. Chou *et al.* (GammeV (T-969)), Phys. Rev. Lett. **100**, 080402 (2008), [arXiv:0710.3783].
- [45] A. Afanasev *et al.*, Phys. Rev. Lett. **101**, 120401 (2008), [arXiv:0806.2631].
- [46] K. Ehret *et al.* (ALPS), Phys. Lett. **B689**, 149 (2010), [arXiv:1004.1313].
- [47] P. Pagnat *et al.* (OSQAR), Eur. Phys. J. **C74**, 8, 3027 (2014), [arXiv:1306.0443].
- [48] R. Ballou *et al.* (OSQAR), Phys. Rev. **D92**, 9, 092002 (2015), [arXiv:1506.08082].
- [49] F. Hoogeveen and T. Ziegenhagen, Nucl. Phys. **B358**, 3 (1991).
- [50] P. Sikivie, D. B. Tanner and K. van Bibber, Phys. Rev. Lett. **98**, 172002 (2007), [hep-ph/0701198]; G. Mueller *et al.*, Phys. Rev. **D80**, 072004 (2009), [arXiv:0907.5387].
- [51] R. Baehre *et al.* (ALPS Collab.), JINST **1308**, T09001 (2013).
- [52] F. Hoogeveen, Phys. Lett. **B288**, 195 (1992).
- [53] J. Jaeckel and A. Ringwald, Phys. Lett. **B659**, 509 (2008), [arXiv:0707.2063].
- [54] F. Caspers, J. Jaeckel and A. Ringwald, JINST **4**, P11013 (2009), [arXiv:0908.0759].
- [55] R. Povey, J. Hartnett and M. Tobar, Phys. Rev. **D82**, 052003 (2010), [arXiv:1003.0964].
- [56] M. Betz *et al.*, Phys. Rev. **D88**, 7, 075014 (2013), [arXiv:1310.8098].
- [57] L. Maiani, R. Petronzio and E. Zavattini, Phys. Lett. **B175**, 359 (1986).
- [58] Y. Semertzidis *et al.*, Phys. Rev. Lett. **64**, 2988 (1990).
- [59] E. Zavattini *et al.* (PVLAS), Phys. Rev. Lett. **96**, 110406 (2006), [Erratum: Phys. Rev. Lett.99,129901(2007)], [hep-ex/0507107].
- [60] E. Zavattini *et al.* (PVLAS), Phys. Rev. **D77**, 032006 (2008), [arXiv:0706.3419].
- [61] F. Della Valle *et al.*, Eur. Phys. J. **C76**, 1, 24 (2016), [arXiv:1510.08052].
- [62] E. Fischbach and C. Talmadge, Nature **356**, 207 (1992).
- [63] J. E. Moody and F. Wilczek, Phys. Rev. **D30**, 130 (1984); A. N. Youdin *et al.*, Phys. Rev. Lett. **77**, 2170 (1996); W.-T. Ni *et al.*, Phys. Rev. Lett. **82**, 2439 (1999); D. F. Phillips *et al.*, Phys. Rev. **D63**, 111101 (2001), [arXiv:physics/0008230]; B. R. Heckel *et al.*, Phys. Rev. Lett. **97**, 021603 (2006), [hep-ph/0606218]; S. A. Hoedl *et al.*, Phys. Rev. Lett. **106**, 041801 (2011).
- [64] G. Raffelt, Phys. Rev. **D86**, 015001 (2012), [arXiv:1205.1776].
- [65] A. Arvanitaki and A. A. Geraci, Phys. Rev. Lett. **113**, 16, 161801 (2014), [arXiv:1403.1290].
- [66] A. A. Geraci *et al.* (ARIADNE), Springer Proc. Phys. **211**, 151 (2018), [arXiv:1710.05413].
- [67] M. S. Turner, Phys. Rept. **197**, 67 (1990).
- [68] G. G. Raffelt, Lect. Notes Phys. **741**, 51 (2008), [51(2006)], [hep-ph/0611350].
- [69] S. Andriamonje *et al.* (CAST), JCAP **0704**, 010 (2007), [hep-ex/0702006].
- [70] P. Gondolo and G. G. Raffelt, Phys. Rev. **D79**, 107301 (2009), [arXiv:0807.2926].
- [71] H. Schlattl, A. Weiss and G. Raffelt, Astropart. Phys. **10**, 353 (1999), [hep-ph/9807476].
- [72] N. Vinyoles *et al.*, JCAP **1510**, 10, 015 (2015), [arXiv:1501.01639].
- [73] A. Ayala *et al.*, Phys. Rev. Lett. **113**, 19, 191302 (2014), [arXiv:1406.6053].
- [74] O. Straniero *et al.*, in "Proceedings, 11th Patras Workshop on Axions, WIMPs and WISPs (Axion-WIMP 2015): Zaragoza, Spain, June 22-26, 2015," 77–81 (2015).
- [75] J. Redondo, JCAP **1312**, 008 (2013), [arXiv:1310.0823].
- [76] N. Viaux *et al.*, Phys. Rev. Lett. **111**, 231301 (2013), [arXiv:1311.1669].
- [77] C.-Y. Chen and S. Dawson, Phys. Rev. **D87**, 055016 (2013), [arXiv:1301.0309].
- [78] G. G. Raffelt, Phys. Lett. **166B**, 402 (1986); S. I. Blinnikov and N. V. Dunina-Barkovskaya, Mon. Not. Roy. Astron. Soc. **266**, 289 (1994).
- [79] M. M. Miller Bertolami *et al.*, JCAP **1410**, 10, 069 (2014), [arXiv:1406.7712].
- [80] J. Isern *et al.*, Astrophys. J. **682**, L109 (2008), [arXiv:0806.2807]; J. Isern *et al.*, J. Phys. Conf. Ser. **172**, 012005 (2009), [arXiv:0812.3043].
- [81] A. Drlica-Wagner *et al.* (LSST Dark Matter Group) (2019), [arXiv:1902.01055].
- [82] J. Isern *et al.*, Astron. & Astrophys. **512**, A86 (2010); A. H. Corsico *et al.*, Mon. Not. Roy. Astron. Soc. **424**, 2792 (2012), [arXiv:1205.6180]; A. H. Corsico *et al.*, JCAP **1212**, 010 (2012), [arXiv:1211.3389].
- [83] A. H. Córscico *et al.* (2019), [arXiv:1907.00115].

- [84] M. Giannotti *et al.*, JCAP **1710**, 10, 010 (2017), [arXiv:1708.02111].
- [85] M. Giannotti *et al.*, JCAP **1605**, 05, 057 (2016), [arXiv:1512.08108].
- [86] G.G. Raffelt, *Stars as Laboratories for Fundamental Physics*, (Univ. of Chicago Press, Chicago, 1996).
- [87] T. Fischer *et al.*, Phys. Rev. **D94**, 8, 085012 (2016), [arXiv:1605.08780].
- [88] J. H. Chang, R. Essig and S. D. McDermott, JHEP **09**, 051 (2018), [arXiv:1803.00993].
- [89] P. Carena *et al.* (2019), [arXiv:1906.11844].
- [90] J. Engel, D. Seckel and A. C. Hayes, Phys. Rev. Lett. **65**, 960 (1990).
- [91] T. Moroi and H. Murayama, Phys. Lett. **B440**, 69 (1998), [hep-ph/9804291].
- [92] D. Page *et al.*, Phys. Rev. Lett. **106**, 081101 (2011), [arXiv:1011.6142].
- [93] P. S. Shternin *et al.*, Mon. Not. Roy. Astron. Soc. **412**, L108 (2011), [arXiv:1012.0045].
- [94] L. B. Leinson, Phys. Lett. **B741**, 87 (2015), [arXiv:1411.6833].
- [95] K. Hamaguchi *et al.*, Phys. Rev. **D98**, 10, 103015 (2018), [arXiv:1806.07151].
- [96] J. Keller and A. Sedrakian, Nucl. Phys. **A897**, 62 (2013), [arXiv:1205.6940]; A. Sedrakian, Phys. Rev. **D93**, 6, 065044 (2016), [arXiv:1512.07828].
- [97] L. B. Leinson, JCAP **1408**, 031 (2014), [arXiv:1405.6873].
- [98] M. V. Beznogov *et al.*, Phys. Rev. **C98**, 3, 035802 (2018), [arXiv:1806.07991].
- [99] G. G. Raffelt, J. Redondo and N. Viaux Maira, Phys. Rev. **D84**, 103008 (2011), [arXiv:1110.6397].
- [100] K. van Bibber *et al.*, Phys. Rev. **D39**, 2089 (1989).
- [101] D. M. Lazarus *et al.*, Phys. Rev. Lett. **69**, 2333 (1992).
- [102] S. Moriyama *et al.*, Phys. Lett. **B434**, 147 (1998), [hep-ex/9805026]; Y. Inoue *et al.*, Phys. Lett. **B536**, 18 (2002), [arXiv:astro-ph/0204388].
- [103] Y. Inoue *et al.*, Phys. Lett. **B668**, 93 (2008), [arXiv:0806.2230].
- [104] V. Anastassopoulos *et al.* (CAST), Nature Phys. **13**, 584 (2017), [arXiv:1705.02290].
- [105] E. Arik *et al.* (CAST), JCAP **0902**, 008 (2009), [arXiv:0810.4482].
- [106] S. Aune *et al.* (CAST), Phys. Rev. Lett. **107**, 261302 (2011), [arXiv:1106.3919]; M. Arik *et al.* (CAST), Phys. Rev. Lett. **112**, 9, 091302 (2014), [arXiv:1307.1985]; M. Arik *et al.* (CAST), Phys. Rev. **D92**, 2, 021101 (2015), [arXiv:1503.00610].
- [107] E. Armengaud *et al.*, JINST **9**, T05002 (2014), [arXiv:1401.3233].
- [108] E. Armengaud *et al.* (IAXO), JCAP **1906**, 06, 047 (2019), [arXiv:1904.09155].
- [109] K. Barth *et al.*, JCAP **1305**, 010 (2013), [arXiv:1302.6283].
- [110] F. T. Avignone, III *et al.* (SOLAX), Phys. Rev. Lett. **81**, 5068 (1998), [arXiv:astro-ph/9708008]; S. Cebrian *et al.*, Astropart. Phys. **10**, 397 (1999), [arXiv:astro-ph/9811359]; A. Morales *et al.* (COSME), Astropart. Phys. **16**, 325 (2002), [hep-ex/0101037]; R. Bernabei *et al.*, Phys. Lett. **B515**, 6 (2001); Z. Ahmed *et al.* (CDMS), Phys. Rev. Lett. **103**, 141802 (2009), [arXiv:0902.4693].
- [111] H. Davoudiasl and P. Huber, Phys. Rev. Lett. **97**, 141302 (2006), [hep-ph/0509293].
- [112] H. S. Hudson *et al.*, ASP Conf. Ser. **455**, 25 (2012), [arXiv:1201.4607].
- [113] E. Armengaud *et al.*, JCAP **1311**, 067 (2013), [arXiv:1307.1488]; E. Aprile *et al.* (XENON100), Phys. Rev. **D90**, 6, 062009 (2014), [Erratum: Phys. Rev. D95, no.2, 029904 (2017)], [arXiv:1404.1455].
- [114] D. S. Akerib *et al.* (LUX), Phys. Rev. Lett. **118**, 26, 261301 (2017), [arXiv:1704.02297].
- [115] J. W. Brockway, E. D. Carlson and G. G. Raffelt, Phys. Lett. **B383**, 439 (1996), [arXiv:astro-ph/9605197]; J. A. Grifols, E. Masso and R. Toldra, Phys. Rev. Lett. **77**, 2372 (1996), [arXiv:astro-ph/9606028].
- [116] A. Payez *et al.*, JCAP **1502**, 02, 006 (2015), [arXiv:1410.3747].
- [117] C. Csaki, N. Kaloper and J. Terning, Phys. Rev. Lett. **88**, 161302 (2002), [hep-ph/0111311].
- [118] A. Mirizzi, G.G. Raffelt, and P.D. Serpico, Lect. Notes Phys. **741**, 115 (2008).
- [119] R. Gill and J. S. Heyl, Phys. Rev. **D84**, 085001 (2011), [arXiv:1105.2083].
- [120] D. Horns *et al.*, Phys. Rev. **D85**, 085021 (2012), [arXiv:1203.2184].
- [121] A. Payez, J. R. Cudell and D. Hutsemekers, JCAP **1207**, 041 (2012), [arXiv:1204.6187].
- [122] A. Dominguez, M. A. Sanchez-Conde and F. Prada, JCAP **1111**, 020 (2011), [arXiv:1106.1860].
- [123] W. Essey and A. Kusenko, Astrophys. J. **751**, L11 (2012), [arXiv:1111.0815].
- [124] D. Horns and M. Meyer, JCAP **1202**, 033 (2012), [arXiv:1201.4711].
- [125] G. I. Rubtsov and S. V. Troitsky, JETP Lett. **100**, 6, 355 (2014), [Pisma Zh. Eksp. Teor. Fiz.100,no.6,397(2014)], [arXiv:1406.0239].
- [126] K. Kohri and H. Kodama, Phys. Rev. **D96**, 5, 051701 (2017), [arXiv:1704.05189].
- [127] D. A. Sanchez, S. Fegan and B. Giebels, Astron. Astrophys. **554**, A75 (2013), [arXiv:1303.5923].
- [128] J. Biteau and D. A. Williams, Astrophys. J. **812**, 1, 60 (2015), [arXiv:1502.04166].
- [129] A. Domínguez and M. Ajello, Astrophys. J. **813**, 2, L34 (2015), [arXiv:1510.07913].
- [130] A. De Angelis, G. Galanti and M. Roncadelli, Phys. Rev. **D84**, 105030 (2011), [Erratum: Phys. Rev. D87, no.10, 109903 (2013)], [arXiv:1106.1132]; M. Simet, D. Hooper and P. D. Serpico, Phys. Rev. **D77**, 063001 (2008), [arXiv:0712.2825]; M. A. Sanchez-Conde *et al.*, Phys. Rev. **D79**, 123511 (2009), [arXiv:0905.3270].
- [131] M. Meyer, D. Horns and M. Raue, Phys. Rev. **D87**, 3, 035027 (2013), [arXiv:1302.1208].
- [132] A. Abramowski *et al.* (H.E.S.S.), Phys. Rev. **D88**, 10, 102003 (2013), [arXiv:1311.3148].
- [133] M. Ajello *et al.* (Fermi-LAT), Phys. Rev. Lett. **116**, 16, 161101 (2016), [arXiv:1603.06978].
- [134] C. Zhang *et al.*, Phys. Rev. **D97**, 6, 063009 (2018), [arXiv:1802.08420].
- [135] Z.-Q. Xia *et al.*, Phys. Rev. **D97**, 6, 063003 (2018), [arXiv:1801.01646].
- [136] J. Majumdar, F. Calore and D. Horns, JCAP **1804**, 04, 048 (2018), [arXiv:1801.08813].
- [137] S. S. Wilks, Annals Math. Statist. **9**, 1, 60 (1938).
- [138] D. Wouters and P. Brun, Astrophys. J. **772**, 44 (2013), [arXiv:1304.0989].
- [139] M. Berg *et al.*, Astrophys. J. **847**, 2, 101 (2017), [arXiv:1605.01043].
- [140] M. C. D. Marsh *et al.*, JCAP **1712**, 12, 036 (2017), [arXiv:1703.07354].

- [141] J. P. Conlon *et al.*, JCAP **1707**, 07, 005 (2017), [arXiv:1704.05256].
- [142] L. Chen and J. P. Conlon, Mon. Not. Roy. Astron. Soc. **479**, 2, 2243 (2018), [arXiv:1712.08313].
- [143] C. S. Reynolds *et al.* (2019), [arXiv:1907.05475].
- [144] A. Arvanitaki and S. Dubovsky, Phys. Rev. **D83**, 044026 (2011), [arXiv:1004.3558].
- [145] A. Arvanitaki, M. Baryakhtar and X. Huang, Phys. Rev. **D91**, 8, 084011 (2015), [arXiv:1411.2263].
- [146] A. Arvanitaki *et al.*, Phys. Rev. **D95**, 4, 043001 (2017), [arXiv:1604.03958].
- [147] K. K. Y. Ng *et al.* (2019), [arXiv:1908.02312].
- [148] M. S. Turner, Phys. Rev. Lett. **59**, 2489 (1987), [Erratum: Phys. Rev. Lett. **60**, 1101(1988)]; E. Masso, F. Rota and G. Zsembinszki, Phys. Rev. **D66**, 023004 (2002), [hep-ph/0203221]; P. Graf and F. D. Steffen, Phys. Rev. **D83**, 075011 (2011), [arXiv:1008.4528].
- [149] S. Hannestad *et al.*, JCAP **1008**, 001 (2010), [arXiv:1004.0695]; M. Archidiacono *et al.*, JCAP **1310**, 020 (2013), [arXiv:1307.0615]; E. Di Valentino *et al.*, Phys. Lett. **B752**, 182 (2016), [arXiv:1507.08665].
- [150] M. Archidiacono *et al.*, JCAP **1505**, 05, 050 (2015), [arXiv:1502.03325].
- [151] E. Masso and R. Toldra, Phys. Rev. **D55**, 7967 (1997), [hep-ph/9702275]; D. Cadamuro and J. Redondo, JCAP **1202**, 032 (2012), [arXiv:1110.2895].
- [152] J. Preskill, M. B. Wise and F. Wilczek, Phys. Lett. **B120**, 127 (1983); L. F. Abbott and P. Sikivie, Phys. Lett. **B120**, 133 (1983); M. Dine and W. Fischler, Phys. Lett. **B120**, 137 (1983).
- [153] K. J. Bae, J.-H. Huh and J. E. Kim, JCAP **0809**, 005 (2008), [arXiv:0806.0497].
- [154] O. Wantz and E. P. S. Shellard, Phys. Rev. **D82**, 123508 (2010), [arXiv:0910.1066].
- [155] G. Ballesteros *et al.*, JCAP **1708**, 08, 001 (2017), [arXiv:1610.01639].
- [156] M. Tegmark *et al.*, Phys. Rev. **D73**, 023505 (2006), [arXiv:astro-ph/0511774].
- [157] A. D. Linde, Phys. Lett. **158B**, 375 (1985).
- [158] D. Seckel and M. S. Turner, Phys. Rev. **D32**, 3178 (1985).
- [159] M. Beltran, J. Garcia-Bellido and J. Lesgourgues, Phys. Rev. **D75**, 103507 (2007), [hep-ph/0606107].
- [160] M. P. Hertzberg, M. Tegmark and F. Wilczek, Phys. Rev. **D78**, 083507 (2008), [arXiv:0807.1726].
- [161] J. Hamann *et al.*, JCAP **0906**, 022 (2009), [arXiv:0904.0647].
- [162] P. A. R. Ade *et al.* (Planck), Astron. Astrophys. **571**, A22 (2014), [arXiv:1303.5082].
- [163] P. A. R. Ade *et al.* (Planck), Astron. Astrophys. **594**, A20 (2016), [arXiv:1502.02114].
- [164] S. Chang, C. Hagmann and P. Sikivie, Phys. Rev. **D59**, 023505 (1999), [hep-ph/9807374].
- [165] C. Hagmann, S. Chang and P. Sikivie, Phys. Rev. **D63**, 125018 (2001), [hep-ph/0012361].
- [166] T. Hiramatsu *et al.*, Phys. Rev. **D83**, 123531 (2011), [arXiv:1012.5502].
- [167] T. Hiramatsu *et al.*, Phys. Rev. **D85**, 105020 (2012), [Erratum: Phys. Rev. **D86**, 089902(2012)], [arXiv:1202.5851].
- [168] M. Kawasaki, K. Saikawa and T. Sekiguchi, Phys. Rev. **D91**, 6, 065014 (2015), [arXiv:1412.0789].
- [169] V. B. Klaer and G. D. Moore, JCAP **1711**, 11, 049 (2017), [arXiv:1708.07521].
- [170] M. Gorghetto, E. Hardy and G. Villadoro, JHEP **07**, 151 (2018), [arXiv:1806.04677].
- [171] M. Buschmann, J. W. Foster and B. R. Safdi (2019), [arXiv:1906.00967].
- [172] M. Hindmarsh *et al.* (2019), [arXiv:1908.03522].
- [173] A. Ringwald and K. Saikawa, Phys. Rev. **D93**, 8, 085031 (2016), [Addendum: Phys. Rev. **D94**, no.4, 049908(2016)], [arXiv:1512.06436].
- [174] T. Hiramatsu *et al.*, JCAP **1301**, 001 (2013), [arXiv:1207.3166].
- [175] C. J. Hogan and M. J. Rees, Phys. Lett. **B205**, 228 (1988).
- [176] E. W. Kolb and I. I. Tkachev, Phys. Rev. Lett. **71**, 3051 (1993), [hep-ph/9303313].
- [177] K. M. Zurek, C. J. Hogan and T. R. Quinn, Phys. Rev. **D75**, 043511 (2007), [arXiv:astro-ph/0607341].
- [178] A. Vaquero, J. Redondo and J. Stadler (2018), [JCAP1904,no.04,012(2019)], [arXiv:1809.09241].
- [179] E. W. Kolb and I. I. Tkachev, Astrophys. J. **460**, L25 (1996), [arXiv:astro-ph/9510043].
- [180] M. Fairbairn, D. J. E. Marsh and J. Quevillon, Phys. Rev. Lett. **119**, 2, 021101 (2017), [arXiv:1701.04787].
- [181] A. Katz *et al.*, JCAP **1812**, 005 (2018), [arXiv:1807.11495].
- [182] E. Berkowitz, M. I. Buchoff and E. Rinaldi, Phys. Rev. **D92**, 3, 034507 (2015), [arXiv:1505.07455].
- [183] S. Borsanyi *et al.*, Phys. Lett. **B752**, 175 (2016), [arXiv:1508.06917].
- [184] R. Kitano and N. Yamada, JHEP **10**, 136 (2015), [arXiv:1506.00370].
- [185] P. Petreczky, H.-P. Schadler and S. Sharma, Phys. Lett. **B762**, 498 (2016), [arXiv:1606.03145].
- [186] Y. Taniguchi *et al.*, Phys. Rev. **D95**, 5, 054502 (2017), [arXiv:1611.02411].
- [187] M. Dine *et al.*, Phys. Rev. **D96**, 9, 095001 (2017), [arXiv:1705.00676].
- [188] R. D. Pisarski and L. G. Yaffe, Phys. Lett. **97B**, 110 (1980).
- [189] P. Arias *et al.*, JCAP **1206**, 013 (2012), [arXiv:1201.5902].
- [190] R. Hlozek *et al.*, Phys. Rev. **D91**, 10, 103512 (2015), [arXiv:1410.2896].
- [191] D. J. E. Marsh, Phys. Rept. **643**, 1 (2016), [arXiv:1510.07633].
- [192] L. Hui *et al.*, Phys. Rev. **D95**, 4, 043541 (2017), [arXiv:1610.08297].
- [193] A. G. Dias *et al.*, JHEP **06**, 037 (2014), [arXiv:1403.5760]; J. E. Kim and D. J. E. Marsh, Phys. Rev. **D93**, 2, 025027 (2016), [arXiv:1510.01701].
- [194] H. Davoudiasl and C. W. Murphy, Phys. Rev. Lett. **118**, 14, 141801 (2017), [arXiv:1701.01136].
- [195] M. Khlopov, B. A. Malomed and I. B. Zeldovich, Mon. Not. Roy. Astron. Soc. **215**, 575 (1985).
- [196] W. Hu, R. Barkana and A. Gruzinov, Phys. Rev. Lett. **85**, 1158 (2000), [arXiv:astro-ph/0003365]; L. Amendola and R. Barbieri, Phys. Lett. **B642**, 192 (2006), [hep-ph/0509257]; D. J. E. Marsh and P. G. Ferreira, Phys. Rev. **D82**, 103528 (2010), [arXiv:1009.3501].
- [197] E. Seidel and W. M. Suen, Phys. Rev. Lett. **66**, 1659 (1991).
- [198] R. Hlozek, D. J. E. Marsh and D. Grin, Mon. Not. Roy. Astron. Soc. **476**, 3, 3063 (2018), [arXiv:1708.05681].
- [199] D. J. E. Marsh and J. Silk, Mon. Not. Roy. Astron. Soc. **437**, 3, 2652 (2014), [arXiv:1307.1705].
- [200] H.-Y. Schive *et al.*, Astrophys. J. **818**, 1, 89 (2016), [arXiv:1508.04621].
- [201] B. Bozek *et al.*, Mon. Not. Roy. Astron. Soc. **450**, 1, 209 (2015), [arXiv:1409.3544]; P. S. Corasaniti *et al.*, Phys. Rev. **D95**, 8, 083512 (2017), [arXiv:1611.05892].

- [202] E. Armengaud *et al.*, *Mon. Not. Roy. Astron. Soc.* **471**, 4, 4606 (2017), [arXiv:1703.09126]; V. Iršič *et al.*, *Phys. Rev. Lett.* **119**, 3, 031302 (2017), [arXiv:1703.04683]; T. Kobayashi *et al.*, *Phys. Rev.* **D96**, 12, 123514 (2017), [arXiv:1708.00015].
- [203] H.-Y. Schive and T. Chiueh, *Mon. Not. Roy. Astron. Soc.* **473**, 1, L36 (2018), [arXiv:1706.03723].
- [204] H.-Y. Schive, T. Chiueh and T. Broadhurst, *Nature Phys.* **10**, 496 (2014), [arXiv:1406.6586].
- [205] B. Schwabe, J. C. Niemeyer and J. F. Engels, *Phys. Rev.* **D94**, 4, 043513 (2016), [arXiv:1606.05151]; J. Veltmaat and J. C. Niemeyer, *Phys. Rev.* **D94**, 12, 123523 (2016), [arXiv:1608.00802]; P. Mocz *et al.*, *Mon. Not. Roy. Astron. Soc.* **471**, 4, 4559 (2017), [arXiv:1705.05845].
- [206] D. G. Levkov, A. G. Panin and I. I. Tkachev, *Phys. Rev. Lett.* **118**, 011301 (2017); T. Helfer *et al.*, *JCAP* **1703**, 03, 055 (2017), [arXiv:1609.04724].
- [207] D. J. E. Marsh and A.-R. Pop, *Mon. Not. Roy. Astron. Soc.* **451**, 3, 2479 (2015), [arXiv:1502.03456]; S.-R. Chen, H.-Y. Schive and T. Chiueh, *Mon. Not. Roy. Astron. Soc.* **468**, 2, 1338 (2017), [arXiv:1606.09030]; A. X. González-Morales *et al.*, *Mon. Not. Roy. Astron. Soc.* **472**, 2, 1346 (2017), [arXiv:1609.05856].
- [208] I. De Martino *et al.* (2018), [arXiv:1807.08153].
- [209] T. Broadhurst *et al.* (2019), [arXiv:1902.10488].
- [210] H.-Y. Schive *et al.*, *Phys. Rev. Lett.* **113**, 26, 261302 (2014), [arXiv:1407.7762].
- [211] V. H. Robles, J. S. Bullock and M. Boylan-Kolchin, *Mon. Not. Roy. Astron. Soc.* **483**, 1, 289 (2019), [arXiv:1807.06018].
- [212] V. Desjacques and A. Nusser (2019), [arXiv:1905.03450].
- [213] M. Safarzadeh and D. N. Spergel (2019), [arXiv:1906.11848].
- [214] J. H. H. Chan *et al.*, *Mon. Not. R. Astron. Soc.* **478**, 2686 (2018), [arXiv:1712.01947].
- [215] A. Pontzen and F. Governato, *Nature* **506**, 171 (2014), [arXiv:1402.1764].
- [216] J. Veltmaat, J. C. Niemeyer and B. Schwabe, *Phys. Rev.* **D98**, 4, 043509 (2018), [arXiv:1804.09647].
- [217] B. Bar-Or, J.-B. Fouvry and S. Tremaine, *Astrophys. J.* **871**, 1, 28 (2019), [arXiv:1809.07673].
- [218] D. G. Levkov, A. G. Panin and I. I. Tkachev, *Phys. Rev. Lett.* **121**, 15, 151301 (2018), [arXiv:1804.05857].
- [219] B. V. Church, P. Mocz and J. P. Ostriker, *Mon. Not. R. Astron. Soc.* **485**, 2861 (2019), [arXiv:1809.04744].
- [220] N. C. Amorisco and A. Loeb (2018), [arXiv:1808.00464].
- [221] T. S. Li *et al.* (DES), *Astrophys. J.* **838**, 1, 8 (2017), [arXiv:1611.05052].
- [222] D. J. E. Marsh and J. C. Niemeyer, *Phys. Rev. Lett.* **123**, 5, 051103 (2019), [arXiv:1810.08543].
- [223] B. Eggemeier and J. C. Niemeyer (2019), [arXiv:1906.01348].
- [224] M. A. Bershad, M. T. Ressel and M. S. Turner, *Phys. Rev. Lett.* **66**, 1398 (1991); M. T. Ressel, *Phys. Rev.* **D44**, 3001 (1991).
- [225] D. Grin *et al.*, *Phys. Rev.* **D75**, 105018 (2007), [arXiv:astro-ph/0611502].
- [226] B. D. Blout *et al.*, *Astrophys. J.* **546**, 825 (2001), [arXiv:astro-ph/0006310].
- [227] K. Kelley and P. J. Quinn, *Astrophys. J.* **845**, 1, L4 (2017), [arXiv:1708.01399].
- [228] G. Sigl, *Phys. Rev.* **D96**, 10, 103014 (2017), [arXiv:1708.08908].
- [229] A. Hook *et al.*, *Phys. Rev. Lett.* **121**, 24, 241102 (2018), [arXiv:1804.03145].
- [230] A. Caputo *et al.*, *JCAP* **1903**, 03, 027 (2019), [arXiv:1811.08436].
- [231] M. A. Fedderke, P. W. Graham and S. Rajendran, *Phys. Rev.* **D100**, 1, 015040 (2019), [arXiv:1903.02666].
- [232] T. Liu, G. Smoot and Y. Zhao (2019), [arXiv:1901.10981].
- [233] P. Sikivie, *Phys. Rev.* **D32**, 2988 (1985), [Erratum: *Phys. Rev.* **D36**, 974 (1987)].
- [234] R. Bradley *et al.*, *Rev. Mod. Phys.* **75**, 777 (2003).
- [235] P. Sikivie and J. R. Ipser, *Phys. Lett.* **B291**, 288 (1992).
- [236] P. Sikivie, I. I. Tkachev and Y. Wang, *Phys. Rev. Lett.* **75**, 2911 (1995), [arXiv:astro-ph/9504052].
- [237] S. De Panfilis *et al.*, *Phys. Rev. Lett.* **59**, 839 (1987); W. Wuensch *et al.*, *Phys. Rev.* **D40**, 3153 (1989); C. Hagmann *et al.*, *Phys. Rev.* **D42**, 1297 (1990).
- [238] S. J. Asztalos *et al.* (ADMX), *Phys. Rev.* **D69**, 011101 (2004), [arXiv:astro-ph/0310042].
- [239] L. Duffy *et al.*, *Phys. Rev. Lett.* **95**, 091304 (2005), [arXiv:astro-ph/0505237]; J. Hoskins *et al.*, *Phys. Rev.* **D84**, 121302 (2011), [arXiv:1109.4128].
- [240] S. J. Asztalos *et al.* (ADMX), *Phys. Rev. Lett.* **104**, 041301 (2010), [arXiv:0910.5914].
- [241] S. J. Asztalos *et al.* (ADMX), *Nucl. Instrum. Meth.* **A656**, 39 (2011), [arXiv:1105.4203].
- [242] N. Du *et al.* (ADMX), *Phys. Rev. Lett.* **120**, 15, 151301 (2018), [arXiv:1804.05750].
- [243] T. Braine *et al.* (ADMX) (2019), [arXiv:1910.08638].
- [244] G. Rybka *et al.* (ADMX), *Phys. Rev. Lett.* **105**, 051801 (2010), [arXiv:1004.5160].
- [245] A. Wagner *et al.* (ADMX), *Phys. Rev. Lett.* **105**, 171801 (2010), [arXiv:1007.3766].
- [246] C. Boutan *et al.* (ADMX), *Phys. Rev. Lett.* **121**, 26, 261302 (2018), [arXiv:1901.00920].
- [247] B. M. Brubaker *et al.*, *Phys. Rev. Lett.* **118**, 6, 061302 (2017), [arXiv:1610.02580].
- [248] L. Zhong *et al.* (HAYSTAC), *Phys. Rev.* **D97**, 9, 092001 (2018), [arXiv:1803.03690].
- [249] I. Ogawa, S. Matsuki and K. Yamamoto, *Phys. Rev.* **D53**, R1740 (1996).
- [250] B. T. McAllister *et al.*, *Phys. Dark Univ.* **18**, 67 (2017), [arXiv:1706.00209].
- [251] W. Chung, *PoS CORFU2015*, 047 (2016).
- [252] A. A. Melcon *et al.* (RADES), *JCAP* **1805**, 05, 040 (2018), [arXiv:1803.01243].
- [253] D. Alesini *et al.* (KLASH) (2017), [arXiv:1707.06010].
- [254] G. Rybka *et al.*, *Phys. Rev.* **D91**, 1, 011701 (2015), [arXiv:1403.3121].
- [255] D. Horns *et al.*, *JCAP* **1304**, 016 (2013), [arXiv:1212.2970].
- [256] J. Suzuki *et al.*, *JCAP* **1509**, 09, 042 (2015), [arXiv:1504.00118].
- [257] A. Caldwell *et al.* (MADMAX Working Group), *Phys. Rev. Lett.* **118**, 9, 091801 (2017), [arXiv:1611.05865].
- [258] P. Brun *et al.* (MADMAX), *Eur. Phys. J.* **C79**, 3, 186 (2019), [arXiv:1901.07401].
- [259] M. Baryakhtar, J. Huang and R. Lasenby, *Phys. Rev.* **D98**, 3, 035006 (2018), [arXiv:1803.11455].
- [260] A. Arvanitaki, S. Dimopoulos and K. Van Tilburg, *Phys. Rev.* **X8**, 4, 041001 (2018), [arXiv:1709.05354].
- [261] P. Sikivie, *Phys. Rev. Lett.* **113**, 20, 201301 (2014), [arXiv:1409.2806].
- [262] P. W. Graham and S. Rajendran, *Phys. Rev.* **D88**, 035023 (2013), [arXiv:1306.6088].
- [263] M. Pospelov and A. Ritz, *Nucl. Phys.* **B573**, 177 (2000), [hep-ph/9908508].

- [264] C. Abel *et al.*, Phys. Rev. **X7**, 4, 041034 (2017), [arXiv:1708.06367].
- [265] D. Budker *et al.*, Phys. Rev. **X4**, 2, 021030 (2014), [arXiv:1306.6089].
- [266] M. B. Wise, H. Georgi and S. L. Glashow, Phys. Rev. Lett. **47**, 402 (1981).
- [267] A. Ernst, A. Ringwald and C. Tamarit, JHEP **02**, 103 (2018), [arXiv:1801.04906].
- [268] L. Di Luzio, A. Ringwald and C. Tamarit, Phys. Rev. **D98**, 9, 095011 (2018), [arXiv:1807.09769].
- [269] P. Fileviez Perez, C. Murgui and A. D. Plascencia (2019), [arXiv:1908.01772].
- [270] S. P. Chang *et al.*, Phys. Rev. **D99**, 8, 083002 (2019), [arXiv:1710.05271].
- [271] P. Sikivie, N. Sullivan, and D. B. Tanner, Phys. Rev. Lett. **112**, 131301 (2014).
- [272] Y. Kahn, B. R. Safdi and J. Thaler, Phys. Rev. Lett. **117**, 14, 141801 (2016), [arXiv:1602.01086].
- [273] M. Silva-Feaver *et al.*, IEEE Trans. Appl. Supercond. **27**, 4, 1400204 (2017), [arXiv:1610.09344].
- [274] J. L. Ouellet *et al.* (ABRACADABRA), Phys. Rev. Lett. **122**, 12, 121802 (2019), [arXiv:1810.12257].
- [275] L. Krauss *et al.*, Phys. Rev. Lett. **55**, 1797 (1985).
- [276] R. Barbieri *et al.*, Phys. Dark Univ. **15**, 135 (2017).



## 92. Searches for Quark and Lepton Compositeness

Revised 2019 by K. Hikasa (Tohoku University), M. Tanabashi (Nagoya University), K. Terashi (ICEPP, University of Tokyo), and N. Varelas (University of Illinois at Chicago)

### 92.1. Limits on contact interactions

If quarks and leptons are made of constituents, then at the scale of constituent binding energies (compositeness scale) there should appear new interactions among them. At energies much below the compositeness scale ( $\Lambda$ ), these interactions are suppressed by inverse powers of  $\Lambda$ . The dominant effect of the compositeness of fermion  $\psi$  should come from the lowest dimensional interactions with four fermions (contact terms), whose most general flavor-diagonal color-singlet chirally invariant form reads [1,2]

$$\mathcal{L} = \mathcal{L}_{LL} + \mathcal{L}_{RR} + \mathcal{L}_{LR} + \mathcal{L}_{RL},$$

with

$$\begin{aligned} \mathcal{L}_{LL} &= \frac{g_{\text{contact}}^2}{2\Lambda^2} \sum_{i,j} \eta_{LL}^{ij} (\bar{\psi}_L^i \gamma_\mu \psi_L^i) (\bar{\psi}_L^j \gamma^\mu \psi_L^j), \\ \mathcal{L}_{RR} &= \frac{g_{\text{contact}}^2}{2\Lambda^2} \sum_{i,j} \eta_{RR}^{ij} (\bar{\psi}_R^i \gamma_\mu \psi_R^i) (\bar{\psi}_R^j \gamma^\mu \psi_R^j), \\ \mathcal{L}_{LR} &= \frac{g_{\text{contact}}^2}{2\Lambda^2} \sum_{i,j} \eta_{LR}^{ij} (\bar{\psi}_L^i \gamma_\mu \psi_L^i) (\bar{\psi}_R^j \gamma^\mu \psi_R^j), \\ \mathcal{L}_{RL} &= \frac{g_{\text{contact}}^2}{2\Lambda^2} \sum_{i,j} \eta_{RL}^{ij} (\bar{\psi}_R^i \gamma_\mu \psi_R^i) (\bar{\psi}_L^j \gamma^\mu \psi_L^j), \end{aligned} \quad (92.1)$$

where  $i, j$  are the indices of fermion species. Color and other indices are suppressed in Eq. (92.1). Chiral invariance provides a natural explanation why quark and lepton masses are much smaller than their inverse size  $\Lambda$ . Note  $\eta_{\alpha\beta}^{ij} = \eta_{\beta\alpha}^{ji}$ , therefore, in order to specify the contact interaction among the same fermion species  $i = j$ , it is enough to use  $\eta_{LL}$ ,  $\eta_{RR}$  and  $\eta_{LR}$ . We will suppress the indices of fermion species hereafter. We may determine the scale  $\Lambda$  unambiguously by using the above form of the effective interactions; the conventional method [1] is to fix its scale by setting  $g_{\text{contact}}^2/4\pi = g_{\text{contact}}^2(\Lambda)/4\pi = 1$  for the new strong interaction coupling and by setting the largest magnitude of the coefficients  $\eta_{\alpha\beta}$  to be unity. In the following, we denote

$$\begin{aligned} \Lambda &= \Lambda_{LL}^\pm \text{ for } (\eta_{LL}, \eta_{RR}, \eta_{LR}) = (\pm 1, 0, 0), \\ \Lambda &= \Lambda_{RR}^\pm \text{ for } (\eta_{LL}, \eta_{RR}, \eta_{LR}) = (0, \pm 1, 0), \\ \Lambda &= \Lambda_{VV}^\pm \text{ for } (\eta_{LL}, \eta_{RR}, \eta_{LR}) = (\pm 1, \pm 1, \pm 1), \\ \Lambda &= \Lambda_{AA}^\pm \text{ for } (\eta_{LL}, \eta_{RR}, \eta_{LR}) = (\pm 1, \pm 1, \mp 1), \\ \Lambda &= \Lambda_{V-A}^\pm \text{ for } (\eta_{LL}, \eta_{RR}, \eta_{LR}) = (0, 0, \pm 1). \end{aligned} \quad (92.2)$$

Such interactions can arise by interchanging constituents (when the fermions have common constituents), and/or by exchanging the binding quanta (whenever binding quanta couple to constituents of both particles).

Fermion scattering amplitude induced from the contact interaction in Eq. (92.1) interferes with the Standard Model (SM) amplitude destructively or constructively [2]. The sign of interference depends on the sign of  $\eta_{\alpha\beta}$  ( $\alpha, \beta = L, R$ ). For instance, in the parton level  $qq \rightarrow qq$  scattering cross section in the  $\Lambda_{LL}^\pm$  model, the contact interaction amplitude and the SM gluon exchange amplitude interfere destructively for  $\eta_{LL} = +1$ , while they interfere constructively for  $\eta_{LL} = -1$ . In models of quark compositeness, the quark scattering cross sections induced from the contact interactions receive sizable QCD radiative corrections. Ref. 3 provides the exact next-to-leading order (NLO) QCD corrections to the contact interaction induced quark scattering cross sections.

Over the last three decades experiments at the CERN SpS [4,5], the Fermilab Tevatron [6,7], and the CERN LHC [8–12] have searched for quark contact interactions, characterized by the four-fermion effective Lagrangian in Eq. (92.1), using jet final states. These searches have been performed primarily by studying the angular distribution of the two highest transverse momentum,  $p_T$ , jets (dijets), and the inclusive jet  $p_T$  spectrum. The variable  $\chi = \exp(|(y_1 - y_2)|)$  is used to measure the dijet angular distribution, where  $y_1$  and  $y_2$  are the rapidities of the two jets with the highest transverse momenta. For collinear massless parton scattering,  $\chi$  is related to the polar scattering angle  $\theta^*$  in the partonic center-of-mass frame by  $\chi = (1 + |\cos\theta^*|)/(1 - |\cos\theta^*|)$ . The choice of  $\chi$  is motivated by the fact that the angular distribution for Rutherford scattering, which is proportional to  $1/(1 - \cos\theta^*)^2$ , is independent of  $\chi$ . In perturbative QCD the  $\chi$  distributions are relatively uniform and only mildly modified by higher-order QCD or electroweak corrections. Signatures of quark contact interactions exhibit more isotropic angular distribution than QCD and they can be identified as an excess at low values of  $\chi$ . In the inclusive jet cross section measurement, quark contact interaction effects are searched for as deviations from the predictions of perturbative QCD in the tails of the high- $p_T$  jet spectrum [11].

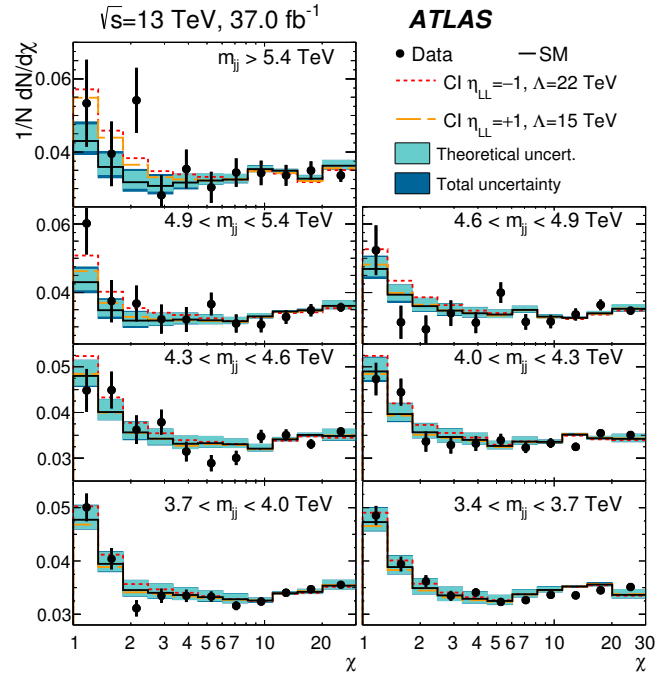


**Figure 92.1:** Normalized dijet angular distributions in several dijet mass ( $m_{jj}$ ) ranges. The data distributions are compared to PYTHIA8 predictions with NLO and electroweak corrections applied (solid line) and with the predictions including a contact interaction (CI) term in which only left-handed quarks participate of compositeness scale  $\Lambda_{LL}^+ = 15$  TeV (dashed line) and  $\Lambda_{LL}^- = 22$  TeV (dotted line). The theoretical uncertainties and the total theoretical and experimental uncertainties in the predictions are displayed as shaded bands around the SM prediction. Figure adopted from Ref. 9.

Recent results from the LHC, using data collected at proton-proton center-of-mass energy of  $\sqrt{s} = 13$  TeV, extend previous limits on quark contact interactions. Figure 92.1 shows the normalized dijet angular distributions for several dijet mass ranges measured in ATLAS [9] at  $\sqrt{s} = 13$  TeV. The data distributions are compared with SM predictions, estimated using PYTHIA8 [13] with GEANT4-based [14] ATLAS detector simulation and corrected to NLO QCD calculation provided by NLO Jet++ [15] including electroweak corrections [16], and with predictions including a contact interaction term in which only



left-handed quarks participate at compositeness scale  $\Lambda_{LL}^+ = 15$  TeV ( $\Lambda_{LL}^- = 22$  TeV) with destructive (constructive) interference. Over a wide range of  $\chi$  and dijet mass the data are well described by the SM predictions. Using the dijet angular distributions measured at high dijet masses and  $\sqrt{s} = 13$  TeV, the ATLAS [9] and CMS [12] Collaborations have set 95% confidence level (C.L.) lower limits on the contact interaction scale  $\Lambda$ , ranging from 9.2 to 29.5 TeV for different quark contact interaction models that correspond to various combinations of  $(\eta_{LL}, \eta_{RR}, \eta_{LR})$ , as summarized in Figure 92.2. The contact interaction scale limits extracted using the dijet angular distributions include the exact NLO QCD corrections to dijet production induced by contact interactions [3]. In proton-proton collisions, the  $\Lambda_{LL}^\pm$  and  $\Lambda_{RR}^\pm$  contact interaction models result in identical tree-level cross sections and NLO QCD corrections and yield the same exclusion limits. For  $\Lambda_{VV}^\pm$  and  $\Lambda_{AA}^\pm$ , the contact interaction predictions are identical at tree level, but exhibit different NLO QCD corrections and yield different exclusion limits.

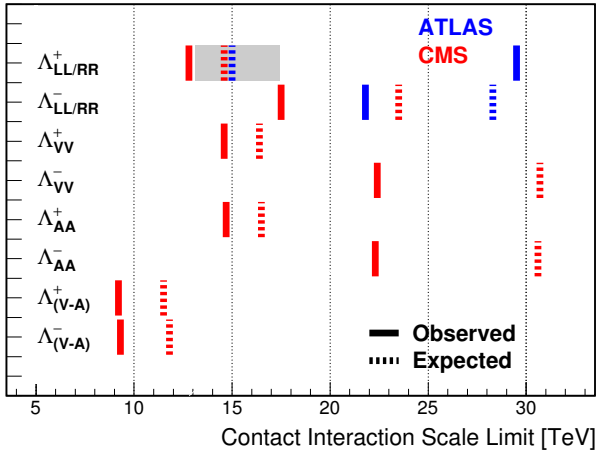


**Figure 92.2:** Observed (solid lines) and expected (dashed lines) 95% C.L. lower limits on the contact interaction scale  $\Lambda$  for different contact interaction models from ATLAS [9] and CMS [12] using the dijet angular distributions. The contact interaction models used for the dijet angular distributions include the exact NLO QCD corrections to dijet production. The shaded band for the  $\Lambda_{LL/RR}^+$  model indicates the range of contact interaction scale that was not excluded in ATLAS [9] due to statistical fluctuation of observed data.

If leptons ( $l$ ) and quarks ( $q$ ) are composite with common constituents, the interaction of these constituents will manifest itself in the form of a  $llqq$ -type four-fermion contact interaction Lagrangian at energies below the compositeness scale  $\Lambda$ . The  $llqq$  terms in the contact interaction Lagrangian can be expressed as

$$\begin{aligned}\mathcal{L}_{LL} &= \frac{g_{\text{contact}}^2}{\Lambda^2} \sum_{i,j} \eta_{LL}^{ij} (\bar{q}_L^i \gamma_\mu q_L^i) (\bar{l}_L^j \gamma^\mu l_L^j), \\ \mathcal{L}_{RR} &= \frac{g_{\text{contact}}^2}{\Lambda^2} \sum_{i,j} \eta_{RR}^{ij} (\bar{q}_R^i \gamma_\mu q_R^i) (\bar{l}_R^j \gamma^\mu l_R^j), \\ \mathcal{L}_{LR} &= \frac{g_{\text{contact}}^2}{\Lambda^2} \sum_{i,j} \eta_{LR}^{ij} (\bar{q}_L^i \gamma_\mu q_L^i) (\bar{l}_R^j \gamma^\mu l_R^j), \\ \mathcal{L}_{RL} &= \frac{g_{\text{contact}}^2}{\Lambda^2} \sum_{i,j} \eta_{RL}^{ij} (\bar{q}_R^i \gamma_\mu q_R^i) (\bar{l}_L^j \gamma^\mu l_L^j).\end{aligned}\quad (92.3)$$

Searches on quark-lepton compositeness have been reported from experiments at LEP [17–20], HERA [21,22], the Tevatron [23,24], and recently from the ATLAS [25,26] and CMS [27–29] experiments at

the LHC. The most stringent searches for  $llqq$  contact interactions are performed by the LHC experiments using high-mass oppositely-charged lepton pairs produced through the  $q\bar{q} \rightarrow l^+l^-$  Drell-Yan process. The contact interaction amplitude of the  $u\bar{u} \rightarrow l^+l^-$  process ( $l = e$  or  $\mu$ ) interferes with the corresponding SM amplitude constructively (destructively) for  $\eta_{\alpha\beta}^{ul} = -1$  ( $\eta_{\alpha\beta}^{ul} = +1$ ). The ATLAS Collaboration has extracted limits on the  $llqq$  contact interaction at  $\sqrt{s} = 13$  TeV for the right-right ( $\eta_{RR} = \pm 1$ ,  $\eta_{LL} = \eta_{LR} = \eta_{RL} = 0$ ), left-left ( $\eta_{LL} = \pm 1$ ,  $\eta_{RR} = \eta_{LR} = \eta_{RL} = 0$ ), and left-right ( $\eta_{LR} = \eta_{RL} = \pm 1$ ,  $\eta_{RR} = \eta_{LL} = 0$ ) models. Combining the dielectron and dimuon channels, the 95% C.L. lower limits on the  $llqq$  contact interaction scale  $\Lambda$  are 35 TeV (28 TeV) for the right-right model, 40 TeV (25 TeV) for the left-left model, and 36 TeV (28 TeV) for the left-right model, each with constructive (destructive) interference [26]. The CMS Collaboration, using a  $36 \text{ fb}^{-1}$  dataset at 13 TeV, has set 95% C.L. exclusion limits on the  $llqq$  contact interaction scale that range from  $\Lambda_{LL} > 20$  TeV for the destructive interference to  $\Lambda_{RR} > 32$  TeV for the constructive interference, for the left-left and the right-right models, respectively [29].

Note that the contact interactions arising from the compositeness of quarks and leptons in Eq. (92.1) can also be regarded as a part of more general dimension six operators in the context of low energy standard model effective theory. For a complete list of these dimension six operators, see [30,31].

Interactions of hypothetical dark matter candidate particles with SM particles through mediators can also be described as contact interactions at low energy. See “Searches for WIMPs and Other Particles” in this volume for limits on the interactions involving dark matter candidate particles.

## 92.2. Limits on excited fermions

Another typical consequence of compositeness is the appearance of excited leptons and quarks ( $l^*$  and  $q^*$ ). Phenomenologically, an excited lepton is defined to be a heavy lepton which shares a leptonic quantum number with one of the existing leptons (an excited quark is defined similarly). For example, an excited electron  $e^*$  is characterized by a nonzero transition-magnetic coupling with electrons. Smallness of the lepton mass and the success of QED prediction for  $g - 2$  suggest chirality conservation, *i.e.*, an excited lepton should not couple to both left- and right-handed components of the corresponding lepton [32–34].

Excited leptons may be classified by  $SU(2) \times U(1)$  quantum numbers. Typical examples are:

1. Sequential type

$$\begin{pmatrix} \nu^* \\ l^* \end{pmatrix}_L, \quad [\nu_R^*], \quad l_R^*.$$

$\nu_R^*$  is necessary unless  $\nu^*$  has a Majorana mass.

2. Mirror type

$$[\nu_L^*], \quad l_L^*, \quad \begin{pmatrix} \nu^* \\ l^* \end{pmatrix}_R.$$

3. Homodoublet type

$$\begin{pmatrix} \nu^* \\ l^* \end{pmatrix}_L, \quad \begin{pmatrix} \nu^* \\ l^* \end{pmatrix}_R.$$

Similar classification can be made for excited quarks.

Excited fermions can be pair produced via their minimal gauge couplings. The couplings of excited leptons with  $Z$  are given by

$$\begin{aligned}& \frac{e}{2 \sin \theta_W \cos \theta_W} (-1 + 2 \sin^2 \theta_W) \bar{l}^* \gamma^\mu l^* Z_\mu \\ & + \frac{e}{2 \sin \theta_W \cos \theta_W} \bar{\nu}^* \gamma^\mu \nu^* Z_\mu\end{aligned}$$

in the homodoublet model. The corresponding couplings of excited quarks can be easily obtained. Although form factor effects can be present for the gauge couplings at  $q^2 \neq 0$ , they are usually neglected.

Excited fermions may also be produced via the contact interactions with ordinary quarks and leptons [35]

$$\mathcal{L} = \frac{g_{\text{contact}}^2}{\Lambda^2} [\eta'_{LL}(\bar{\psi}_L \gamma_\mu \psi_L)(\bar{\psi}_L^* \gamma^\mu \psi_L^*) + (\eta''_{LL}(\bar{\psi}_L \gamma_\mu \psi_L)(\bar{\psi}_L^* \gamma^\mu \psi_L) + \text{h.c.}) + \dots]. \quad (92.4)$$

Again, the coefficient is conventionally taken  $g_{\text{contact}}^2 = 4\pi$ . It is widely assumed  $\eta'_{LL} = \eta''_{LL} = 1$ ,  $\eta'_{LR} = \eta''_{LR} = \eta'_{RL} = \eta''_{RL} = \eta'_{RR} = \eta''_{RR} = 0$  in experimental analyses for simplicity.

In addition, transition-magnetic type couplings with a gauge boson are expected. These couplings can be generally parameterized as follows:

$$\begin{aligned} \mathcal{L} = & \frac{\lambda_\gamma^{(\psi^*)} e}{2m_{\psi^*}} \bar{\psi}^* \sigma^{\mu\nu} (\eta_L \frac{1-\gamma_5}{2} + \eta_R \frac{1+\gamma_5}{2}) \psi F_{\mu\nu} \\ & + \frac{\lambda_Z^{(\psi^*)} e}{2m_{\psi^*}} \bar{\psi}^* \sigma^{\mu\nu} (\eta_L \frac{1-\gamma_5}{2} + \eta_R \frac{1+\gamma_5}{2}) \psi Z_{\mu\nu} \\ & + \frac{\lambda_W^{(l^*)} g}{2m_{l^*}} \bar{l}^* \sigma^{\mu\nu} \frac{1-\gamma_5}{2} \nu W_{\mu\nu} \\ & + \frac{\lambda_W^{(\nu^*)} g}{2m_{\nu^*}} \bar{\nu}^* \sigma^{\mu\nu} (\eta_L \frac{1-\gamma_5}{2} + \eta_R \frac{1+\gamma_5}{2}) l W_{\mu\nu}^\dagger \\ & + \text{h.c.}, \end{aligned} \quad (92.5)$$

where  $g = e/\sin\theta_W$ ,  $\psi = \nu$  or  $l$ ,  $F_{\mu\nu} = \partial_\mu A_\nu - \partial_\nu A_\mu$  is the photon field strength,  $Z_{\mu\nu} = \partial_\mu Z_\nu - \partial_\nu Z_\mu$ , etc.. The normalization of the coupling is chosen such that

$$\max(|\eta_L|, |\eta_R|) = 1.$$

Chirality conservation requires

$$\eta_L \eta_R = 0. \quad (92.6)$$

These couplings in Eq. (92.5) can arise from  $SU(2) \times U(1)$ -invariant higher-dimensional interactions. A well-studied model is the interaction of homodoublet type  $l^*$  with the Lagrangian (see [36,37])

$$\mathcal{L} = \frac{1}{2\Lambda} \bar{L}^* \sigma^{\mu\nu} (g f \frac{\tau^a}{2} W_{\mu\nu}^a + g' f' Y B_{\mu\nu}) \frac{1-\gamma_5}{2} L + \text{h.c.}, \quad (92.7)$$

where  $L$  denotes the lepton doublet  $(\nu, l)$ ,  $\Lambda$  is the compositeness scale,  $g, g'$  are  $SU(2)$  and  $U(1)_Y$  gauge couplings, and  $W_{\mu\nu}^a$  and  $B_{\mu\nu}$  are the field strengths for  $SU(2)$  and  $U(1)_Y$  gauge fields. These couplings satisfy the relation

$$\lambda_W = -\sqrt{2} \sin^2 \theta_W (\lambda_Z \cot \theta_W + \lambda_\gamma), \quad (92.8)$$

with  $\lambda_{W,Z,\gamma}$  being defined in Eq. (92.5) with  $\lambda_{W,Z,\gamma} = \lambda_{W,Z,\gamma}^{(e^*)}$  or  $\lambda_{W,Z,\gamma} = \lambda_{W,Z,\gamma}^{(\nu^*)}$ . Here  $(\eta_L, \eta_R) = (1, 0)$  is assumed. It should be noted that the electromagnetic radiative decay of  $l^*$  ( $\nu^*$ ) is forbidden if  $f = -f'$  ( $f = f'$ ).

Additional coupling with gluons is possible for excited quarks:

$$\begin{aligned} \mathcal{L} = & \frac{1}{2\Lambda} \bar{Q}^* \sigma^{\mu\nu} \left( g_s f_s \frac{\lambda^a}{2} G_{\mu\nu}^a + g f \frac{\tau^a}{2} W_{\mu\nu}^a + g' f' Y B_{\mu\nu} \right) \\ & \times \frac{1-\gamma_5}{2} Q + \text{h.c.}, \end{aligned} \quad (92.9)$$

where  $Q$  denotes a quark doublet,  $g_s$  is the QCD gauge coupling, and  $G_{\mu\nu}^a$  the gluon field strength.

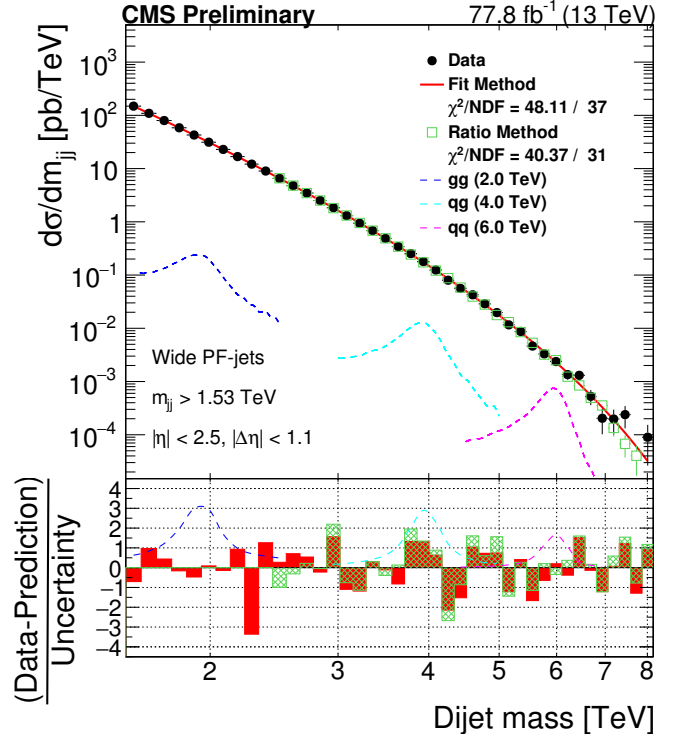


**Figure 92.3:** Dijet mass distribution measured by CMS using wide jets reconstructed from two highest transverse momentum jets by adding nearby jets within  $\Delta R = \sqrt{\Delta\eta^2 + \Delta\phi^2} < 1.1$ . The data distribution is compared to a fit representing a smooth background spectrum (solid curve). The excited quark signal with mass of 4.0 TeV (labeled as  $q\bar{q}$ ) is shown together with other benchmark signals. Shown at the bottom panel is the difference between the data and the fitted parametrization divided by the statistical uncertainty of the data. Figure adopted from Ref. 62.

If leptons are made of color triplet and antitriplet constituents, we may expect their color-octet partners. Transitions between the octet leptons ( $l_8$ ) and the ordinary lepton ( $l$ ) may take place via the dimension-five interactions

$$\mathcal{L} = \frac{1}{2\Lambda} \sum_l \{ \bar{l}_8^\alpha g_S F_{\mu\nu}^\alpha \sigma^{\mu\nu} (\eta_L l_L + \eta_R l_R) + \text{h.c.} \} \quad (92.10)$$

where the summation is over charged leptons and neutrinos. The leptonic chiral invariance implies  $\eta_L \eta_R = 0$  as before.

Searches for the excited quarks and leptons have been performed over the last decades in experiments at the LEP [38–41], HERA [42,43], Tevatron [44,45], and LHC [46–71]. Most stringent constraints, which are described below at 95% confidence level, come from the LHC experiments.

The signature of excited quarks  $q^*$  at hadron colliders is characterized by a narrow resonant peak in the reconstructed invariant mass distribution of the  $q^*$  decay products. The decays via the transition-magnetic type operator in Eq. (92.9) are considered for excited quarks in LHC searches, and the final states to search for are dijet ( $q\bar{q}$ ) [46, 47, 59–62] or a jet in association with a photon ( $q\gamma$ ) [48, 49, 63, 64] or a weak gauge boson ( $qW, qZ$ ) [65, 66]. All analyses consider only spin-1/2 excited states of first generation quarks ( $u^*, d^*$ ) with degenerate masses, expected to be predominantly produced in proton-proton collisions except for the excited  $b$  quark searches described below. Only the minimal gauge interactions and the transition-magnetic couplings with the form given in Eq. (92.9) are considered in the production process, and hence the contact interactions in Eq. (92.4) are not considered. The compositeness scale  $\Lambda$  is taken to be the same as the excited quark mass  $m_{q^*}$ . The transition-magnetic coupling coefficients  $f_s, f$  and  $f'$  are assumed to be equal to 1 (denoted by  $f$ ).

With proton-proton collision data recorded at  $\sqrt{s} = 13$  TeV at the LHC, the excited quark masses are excluded in dijet resonance searches up to 6.7 TeV in ATLAS using  $140 \text{ fb}^{-1}$  [47] and 6.0 TeV in CMS using  $77.8 \text{ fb}^{-1}$  [62]. Figure 92.3 shows the dijet mass distribution measured in CMS [62] by using the two highest  $p_T$  jets reconstructed with the anti- $k_T$  algorithm [72] of a distance parameter of 0.4, and by combining nearby jets within  $\Delta R = \sqrt{\Delta\eta^2 + \Delta\phi^2} < 1.1$  around the leading two jets. The measured dijet mass spectrum is compared to a fit with smoothly falling background shape (solid curve) to look for a narrow resonance; an excited quark signal with mass of 4.0 TeV is shown in the figure (denoted by  $qg$ ) as one of the benchmark signals considered in the analysis.

The photon + jet resonance searches, targeting excited quarks decaying into a quark and a photon ( $q^* \rightarrow q + \gamma$ ), have excluded  $q^*$  masses up to 5.3 TeV in ATLAS [49] and 5.5 TeV in CMS [64] using collision data at  $\sqrt{s} = 13$  TeV. The  $W/Z$  boson + jet final states are examined to look for the  $q^* \rightarrow q + W$  and  $q + Z$  signal in CMS [66], exploiting jet substructure technique designed to provide sensitivity for highly-boosted hadronically decaying  $W$  and  $Z$  bosons. The lower mass limit of 5.0 (4.8) TeV is obtained from the  $W + \text{jet}$  ( $Z + \text{jet}$ ) search using dataset recorded at  $\sqrt{s} = 13$  TeV.

The excited  $b$  quarks ( $b^*$ ) are also considered in the present searches at the LHC. Assuming the similar production processes to the first-generation excited quarks, the  $b^*$  has been searched for in final states containing at least one jet identified as originating from a  $b$  quark ( $b$ -tagging). The searches using two jets including at least one  $b$ -tagged jet have been performed at 8 and 13 TeV [50, 51, 60], resulting in  $b^*$  lower mass limits of 2.6 TeV in ATLAS using  $36.1 \text{ fb}^{-1}$  at  $\sqrt{s} = 13$  TeV [50] and 1.6 TeV in CMS using  $19.7 \text{ fb}^{-1}$  at  $\sqrt{s} = 8$  TeV [60]. The CMS Collaboration also performed a search for  $b^* \rightarrow b + \gamma$  in events with a  $b$ -tagged jet in association with a photon using data at  $\sqrt{s} = 13$  TeV [64], and excluded  $b^*$  masses up to 1.8 TeV. Excited  $b$  quarks with charged-current decay into a  $W$ -boson and a top quark ( $b^* \rightarrow t + W$ ) were looked for in both ATLAS and CMS using the full 8 TeV data [52, 67]. ATLAS excluded  $b^*$  masses below 1.5 TeV for the  $b^*$  with left- and right-handed couplings [52] while CMS excluded the masses below 1.39(1.43) TeV for the left(right)-handed couplings [67].

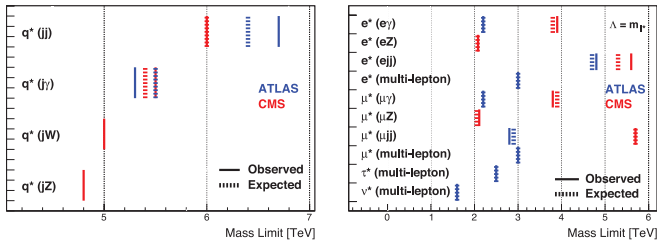


**Figure 92.4:** 95% C.L. lower mass limits for the excited quarks (left) and excited leptons (right) at ATLAS [47,49,55–57] and CMS [62,64,66] [69–71] experiments. Shown are the most stringent limits for each final state (denoted in parentheses) of the excited fermions from both experiments. Only first generation quarks ( $u, d$ ) with transition-magnetic type interactions with  $f_s = f = f' = 1$  are considered for the excited quarks. The excited lepton limits are given for the production via contact interactions with  $\Lambda = m_{l^*}$ .

Searches for excited leptons  $l^*$  are also performed at the LHC using proton-proton collision data recorded at  $\sqrt{s} = 7$  and 8 TeV [54–58, 68, 69] as well as at 13 TeV [70]. Considering single  $l^*$  production in contact interactions (Eq. (92.4)) and electromagnetic radiative decay to a SM lepton and a photon ( $l^* \rightarrow l + \gamma$  where  $l = e, \mu$ ), the excited electron and muon masses are excluded for  $\Lambda = m_{l^*}$  up to 3.9 and 3.8 TeV, respectively, using  $35.9 \text{ fb}^{-1}$  at  $\sqrt{s} = 13$  TeV in CMS [70] and 2.2 TeV using  $13 \text{ fb}^{-1}$  at  $\sqrt{s} = 8$  TeV in ATLAS [55].

With the full  $20.3 \text{ fb}^{-1}$  data at  $\sqrt{s} = 8$  TeV, the inclusive search on multi-lepton signatures with 3 or more charged leptons

in ATLAS [56] further constrains the excited charged leptons and neutrinos. Considering both the transition-magnetic (Eq. (92.7)) and contact interaction (Eq. (92.4)) processes, the lower mass limits for the  $e^*$ ,  $\mu^*$ ,  $\tau^*$  and  $\nu_i^*$  (for every excited neutrino flavor) are obtained to be 3.0, 3.0, 2.5 and 1.6 TeV, respectively, for  $\Lambda = m_{e^*}$ ,  $m_{\mu^*}$ ,  $m_{\tau^*}$  and  $m_{\nu_i^*}$ . The rate of pair-produced excited leptons is independent of  $\Lambda$  for the minimal gauge interaction processes, and it allows to improve search sensitivity with multi-lepton signatures at high  $\Lambda$ , especially for excited neutrinos because the predominant  $\nu_i^* \rightarrow l + W$  decays result in a higher acceptance for  $\geq 3$  charged lepton final states.

Both ATLAS and CMS Collaborations performed searches for singly produced excited leptons. The single excited leptons, both produced and decayed in contact interaction processes (Eq. (92.4)), were searched for in CMS using  $77.4 \text{ fb}^{-1}$  at 13 TeV [71] and in ATLAS using  $20.3 \text{ fb}^{-1}$  at 8 TeV [57] using the final states with two leptons and two jets ( $q\bar{q} \rightarrow ll^* \rightarrow llq\bar{q}$ ). The CMS search [71] considered both excited electrons and excited muons, using the invariant mass of the combination of the two leptons and two jets as a discriminating variable to separate signal from background. The ATLAS search [57] considered only excited muons. The single excited electrons, produced in contact interactions and decayed either in contact interaction or charged-current processes, were considered in ATLAS using  $36.1 \text{ fb}^{-1}$  at 13 TeV [58] in the final states with two electrons and two jets ( $q\bar{q} \rightarrow ee^* \rightarrow eeq\bar{q}$ ) or an electron, missing transverse momentum and a hadronically decaying  $W$ -boson candidate ( $q\bar{q} \rightarrow ee^* \rightarrow e\nu W$ ). The excited electron (muon) mass was excluded up to 5.6 (5.7) TeV in CMS [71] at  $\Lambda = m_{e^*}$  ( $\Lambda = m_{\mu^*}$ ), which is the best limit to date on the excited electrons (muons).

The CMS Collaboration also performed an excited lepton search in the final states containing a  $Z$  boson [69], probing the excited leptons produced in contact interactions and decayed in neutral-current processes ( $l^* \rightarrow l + Z$ ) with  $f = f' = 1$  or  $f = -f' = 1$ . The leptonic and hadronic decays of  $Z$  bosons have been considered in the search, and the most stringent limits are obtained from the hadronic  $Z$  decay to be 2.08 (2.34) TeV and 2.11 (2.37) TeV for the  $e^*$  and  $\mu^*$ , respectively, with  $f = f' = 1$  ( $f = -f' = 1$ ) at  $\Lambda = m_{l^*}$ .

Figure 92.4 summarizes the most stringent 95% C.L. lower mass limits for excited quarks and leptons obtained from the LHC experiments.

## References:

1. E.J. Eichten, K.D. Lane, and M.E. Peskin, Phys. Rev. Lett. **50**, 811 (1983).
2. E.J. Eichten *et al.*, Rev. Mod. Phys. **56**, 579 (1984); Erratum *ibid.* **58**, 1065 (1986).
3. J. Gao *et al.*, Phys. Rev. Lett. **106**, 142001 (2011).
4. G. Arnison *et al.* [UA1 Collab.], Phys. Lett. **B177**, 244 (1986).
5. J.A. Appel *et al.* [UA2 Collab.], Phys. Lett. **B160**, 349 (1985).
6. F. Abe *et al.* [CDF Collab.], Phys. Rev. Lett. **62**, 613 (1989); F. Abe *et al.* [CDF Collab.], Phys. Rev. Lett. **69**, 2896 (1992); F. Abe *et al.* [CDF Collab.], Phys. Rev. Lett. **77**, 5336 (1996); F. Abe *et al.* [CDF Collab.], Erratum Phys. Rev. Lett. **78**, 4307 (1997).
7. B. Abbott *et al.* [DØ Collab.], Phys. Rev. Lett. **80**, 666 (1998); B. Abbott *et al.* [DØ Collab.], Phys. Rev. Lett. **82**, 2457 (1999); B. Abbott *et al.* [DØ Collab.], Phys. Rev. **D62**, 031101 (2000); B. Abbott *et al.* [DØ Collab.], Phys. Rev. **D64**, 032003 (2001); B. Abbott *et al.* [DØ Collab.], Phys. Rev. Lett. **103**, 191803 (2009).
8. G. Aad *et al.* [ATLAS Collab.], Phys. Lett. **B694**, 327 (2011); G. Aad *et al.* [ATLAS Collab.], New J. Phys. **13**, 053044 (2011); G. Aad *et al.* [ATLAS Collab.], JHEP **01**, 029 (2013); G. Aad *et al.* [ATLAS Collab.], Phys. Rev. Lett. **114**, 221802 (2015); G. Aad *et al.* [ATLAS Collab.], Phys. Lett. **B754**, 302 (2016).
9. G. Aad *et al.* [ATLAS Collab.], Phys. Rev. **D96**, 052004 (2017).
10. V. Khachatryan *et al.* [CMS Collab.], Phys. Rev. Lett. **105**, 262001 (2010); V. Khachatryan *et al.* [CMS Collab.], Phys. Rev. Lett. **106**, 201804 (2011); S. Chatrchyan *et al.* [CMS Collab.], JHEP **1205**, 055 (2012);

- V. Khachatryan *et al.* [CMS Collab.], Phys. Lett. **B746**, 79 (2015);  
A.M. Sirunyan *et al.* [CMS Collab.], JHEP **07**, 013 (2017).
11. S. Chatrchyan *et al.* [CMS Collab.], Phys. Rev. **D87**, 052017 (2013).
  12. A.M. Sirunyan *et al.* [CMS Collab.], Eur. Phys. J. **C78**, 789 (2018).
  13. T. Sjöstrand, S. Mrenna, and P. Skands, Comp. Phys. Comm. **178**, 852 (2008).
  14. S. Agostinelli *et al.* [GEANT4 Collab.], GEANT4: a simulation toolkit, Nucl. Instrum. Methods **A506**, 250 (2003).
  15. Z. Nagy, Phys. Rev. Lett. **88**, 122003 (2002);  
Z. Nagy, Phys. Rev. **D68**, 094002, (2003).
  16. S. Dittmaier, A. Huss, and C. Speckner, JHEP **1211**, 095 (2012).
  17. S. Schael *et al.* [ALEPH Collab.], Eur. Phys. J. **C49**, 411 (2007).
  18. J. Abdallah *et al.* [DELPHI Collab.], Eur. Phys. J. **C45**, 589 (2006).
  19. M. Acciarri *et al.* [L3 Collab.], Phys. Lett. **B489**, 81 (2000).
  20. K. Ackerstaff *et al.* [OPAL Collab.], Phys. Lett. **B391**, 221 (1997);  
G. Abbiendi *et al.* [OPAL Collab.], Eur. Phys. J. **C33**, 173 (2004).
  21. F.D. Aaron *et al.* [H1 Collab.], Phys. Lett. **B705**, 52 (2011).
  22. S. Chekanov *et al.* [ZEUS Collab.], Phys. Lett. **B591**, 23 (2004).
  23. F. Abe *et al.* [CDF Collab.], Phys. Rev. Lett. **68**, 1463 (1992);  
F. Abe *et al.* [CDF Collab.], Phys. Rev. Lett. **79**, 2198 (1997);  
T. Affolder *et al.* [CDF Collab.], Phys. Rev. Lett. **87**, 231803 (2001);  
A. Abulencia *et al.* [CDF Collab.], Phys. Rev. Lett. **96**, 211801 (2006).
  24. B. Abbott *et al.* [DØ Collab.], Phys. Rev. Lett. **82**, 4769 (1999).
  25. G. Aad *et al.* [ATLAS Collab.], Phys. Rev. **D84**, 011101 (2011);  
G. Aad *et al.* [ATLAS Collab.], Phys. Lett. **B712**, 40 (2012);  
G. Aad *et al.* [ATLAS Collab.], Phys. Rev. **D87**, 015010 (2013);  
G. Aad *et al.* [ATLAS Collab.], Eur. Phys. J. **C74**, 3134 (2014);  
M. Aaboud *et al.* [ATLAS Collab.], Phys. Lett. **B761**, 372 (2016).
  26. M. Aaboud *et al.* [ATLAS Collab.], JHEP **10**, 182 (2017).
  27. S. Chatrchyan *et al.* [CMS Collab.], Phys. Rev. **D87**, 032001 (2013).
  28. V. Khachatryan *et al.* [CMS Collab.], JHEP **04**, 025 (2015).
  29. A.M. Sirunyan *et al.* [CMS Collab.], JHEP **04**, 114 (2019).
  30. W. Buchmuller and D. Wyler, Nucl. Phys. **B268**, 621 (1986).
  31. B. Grzadkowski *et al.*, JHEP **1010**, 085 (2010).
  32. F.M. Renard, Phys. Lett. **B116**, 264 (1982).
  33. F. del Aguila, A. Mendez, and R. Pascual, Phys. Lett. **B140**, 431 (1984).
  34. M. Suzuki, Phys. Lett. **B143**, 237 (1984).
  35. U. Baur, M. Spira, and P.M. Zerwas, Phys. Rev. **D42**, 815 (1990).
  36. K. Hagiwara, D. Zeppenfeld, and S. Komamiya, Z. Phys. **C29**, 115 (1985).
  37. N. Cabibbo, L. Maiani, and Y. Srivastava, Phys. Lett. **B139**, 459 (1984).
  38. D. Decamp *et al.* [ALEPH Collab.], Phys. Reports **216**, 253 (1992);  
P. Barate *et al.* [ALEPH Collab.], Eur. Phys. J. **C4**, 571 (1998).
  39. P. Abreu *et al.* [DELPHI Collab.], Nucl. Phys. **B367**, 511 (1991);  
J. Abdallah *et al.* [DELPHI Collab.], Eur. Phys. J. **C37**, 405 (2004).
  40. O. Adriani *et al.* [L3 Collab.], Phys. Reports **236**, 1 (1993);  
P. Achard *et al.* [L3 Collab.], Phys. Lett. **B531**, 28 (2002);  
P. Achard *et al.* [L3 Collab.], Phys. Lett. **B568**, 23 (2003).
  41. G. Abbiendi *et al.* [OPAL Collab.], Phys. Lett. **B544**, 57 (2002);  
G. Abbiendi *et al.* [OPAL Collab.], Phys. Lett. **B602**, 167 (2004).
  42. C. Adloff *et al.* [H1 Collab.], Phys. Lett. **B525**, 9 (2002);  
F.D. Aaron *et al.* [H1 Collab.], Phys. Lett. **B663**, 382 (2008);  
F.D. Aaron *et al.* [H1 Collab.], Phys. Lett. **B666**, 131 (2008).
  43. S. Chekanov *et al.* [ZEUS Collab.], Phys. Lett. **B549**, 32 (2002).
  44. D. Acosta *et al.* [CDF Collab.], Phys. Rev. Lett. **94**, 101802 (2005);  
A. Abulencia *et al.* [CDF Collab.], Phys. Rev. Lett. **97**, 191802 (2006);  
T. Aaltonen *et al.* [CDF Collab.], Phys. Rev. **D79**, 112002 (2009).
  45. V.M. Abazov *et al.* [DØ Collab.], Phys. Rev. **D73**, 111102 (2006);  
V.M. Abazov *et al.* [DØ Collab.], Phys. Rev. **D77**, 091102 (2008);  
V.M. Abazov *et al.* [DØ Collab.], Phys. Rev. Lett. **103**, 191803 (2009).
  46. G. Aad *et al.* [ATLAS Collab.], Phys. Lett. **B708**, 37 (2012);  
G. Aad *et al.* [ATLAS Collab.], JHEP **1301**, 29 (2013);  
G. Aad *et al.* [ATLAS Collab.], Phys. Rev. **D91**, 052007 (2015);  
G. Aad *et al.* [ATLAS Collab.], Phys. Lett. **B754**, 302 (2016);  
M. Aaboud *et al.* [ATLAS Collab.], Phys. Rev. **D96**, 052004 (2017).
  47. ATLAS Collaboration, ATLAS-CONF-2019-007 (2019).
  48. G. Aad *et al.* [ATLAS Collab.], Phys. Rev. Lett. **108**, 211802 (2012);  
G. Aad *et al.* [ATLAS Collab.], Phys. Lett. **B728**, 562 (2014);  
G. Aad *et al.* [ATLAS Collab.], JHEP **1603**, 41 (2016).
  49. M. Aaboud *et al.* [ATLAS Collab.], Eur. Phys. J. **C78**, 102 (2018).
  50. M. Aaboud *et al.* [ATLAS Collab.], Phys. Rev. **D98**, 032016 (2018).
  51. M. Aaboud *et al.* [ATLAS Collab.], Phys. Lett. **B759**, 229 (2016).
  52. G. Aad *et al.* [ATLAS Collab.], JHEP **1602**, 110 (2016).
  53. G. Aad *et al.* [ATLAS Collab.], Phys. Lett. **B721**, 171 (2013).
  54. G. Aad *et al.* [ATLAS Collab.], Phys. Rev. **D85**, 072003 (2012).
  55. G. Aad *et al.* [ATLAS Collab.], New J. Phys. **15**, 093011 (2013).
  56. G. Aad *et al.* [ATLAS Collab.], JHEP **1508**, 138 (2015).
  57. G. Aad *et al.* [ATLAS Collab.], New J. Phys. **18**, 073021 (2016).
  58. M. Aaboud *et al.* [ATLAS Collab.], Eur. Phys. J. **C79**, 803 (2019).
  59. S. Chatrchyan *et al.* [CMS Collab.], Phys. Lett. **B704**, 123 (2011);  
S. Chatrchyan *et al.* [CMS Collab.], JHEP **1301**, 13 (2013);  
S. Chatrchyan *et al.* [CMS Collab.], Phys. Rev. **D87**, 114015 (2013).
  60. V. Khachatryan *et al.* [CMS Collab.], Phys. Rev. **D91**, 052009 (2015).
  61. V. Khachatryan *et al.* [CMS Collab.], Phys. Rev. Lett. **116**, 071801 (2016);  
V. Khachatryan *et al.* [CMS Collab.], Phys. Rev. Lett. **117**, 031802 (2016);  
A.M. Sirunyan *et al.* [CMS Collab.], Phys. Lett. **B769**, 520 (2017);  
A.M. Sirunyan *et al.* [CMS Collab.], JHEP **1808**, 130 (2018).
  62. CMS Collaboration, CMS-PAS-EXO-17-026 (2018).
  63. V. Khachatryan *et al.* [CMS Collab.], Phys. Lett. **B738**, 274 (2014).
  64. A.M. Sirunyan *et al.* [CMS Collab.], Phys. Lett. **B781**, 390 (2018).
  65. S. Chatrchyan *et al.* [CMS Collab.], Phys. Lett. **B722**, 28 (2013);  
S. Chatrchyan *et al.* [CMS Collab.], Phys. Lett. **B723**, 280 (2013);  
V. Khachatryan *et al.* [CMS Collab.], JHEP **1408**, 173 (2014).
  66. A.M. Sirunyan *et al.* [CMS Collab.], Phys. Rev. **D97**, 072006 (2018).
  67. V. Khachatryan *et al.* [CMS Collab.], JHEP **1601**, 166 (2016).
  68. S. Chatrchyan *et al.* [CMS Collab.], Phys. Lett. **B704**, 143 (2011);  
S. Chatrchyan *et al.* [CMS Collab.], Phys. Lett. **B720**, 309 (2013).
  69. V. Khachatryan *et al.* [CMS Collab.], JHEP **1603**, 125 (2016).
  70. A.M. Sirunyan *et al.* [CMS Collab.], JHEP **1904**, 015 (2019).
  71. CMS Collaboration, CMS-PAS-EXO-18-013 (2019).
  72. M. Cacciari, G.P. Salam, and G. Soyez, JHEP **0804**, 063 (2008).
  73. T. Sjöstrand *et al.*, Comp. Phys. Comm. **135**, 238 (2001).

## 93. Dynamical Electroweak Symmetry Breaking: Implications of the $H^0$

Revised August 2019 by K.M. Black (Wisconsin U.), R.Sekhar Chivukula (UC San Diego) and M. Narain (Brown U.).

### 93.1 Introduction and Phenomenology

In theories of dynamical electroweak symmetry breaking, the electroweak interactions are broken to electromagnetism by the vacuum expectation value of a composite operator, typically a fermion bilinear. In these theories, the longitudinal components of the massive weak bosons are identified with composite Nambu-Goldstone bosons arising from dynamical symmetry breaking in a strongly-coupled extension of the standard model. Viable theories of dynamical electroweak symmetry breaking must also explain (or at least accommodate) the presence of an additional composite scalar state to be identified with the  $H^0$  scalar boson [1,2] – a state unlike any other observed previously.

Theories of dynamical electroweak symmetry breaking can be classified by the nature of the composite singlet state to be associated with the  $H^0$  and the corresponding dimensional scales  $f$ , the analog of the pion decay-constant in QCD, and  $\Lambda$ , the scale of the underlying strong dynamics.<sup>1</sup> Of particular importance is the ratio  $v/f$ , where  $v^2 = 1/(\sqrt{2}G_F) \approx (246 \text{ GeV})^2$ , since this ratio measures the expected size of the deviations of the couplings of a composite Higgs boson from those expected in the standard model. The basic possibilities, and the additional states that they predict, are described below.

#### 93.1.1 Technicolor, $v/f \simeq 1$ , $\Lambda \simeq 1 \text{ TeV}$

Technicolor models [7–9] provided the first examples of theories of dynamical electroweak symmetry breaking. These theories incorporate a new asymptotically free gauge theory (“technicolor”) and additional massless fermions (“technifermions” transforming under a vectorial representation of the gauge group). The global chiral symmetry of the fermions is spontaneously broken by the formation of a technifermion condensate, just as the approximate chiral symmetry in QCD is broken down to isospin by the formation of a quark condensate. The  $SU(2)_W \times U(1)_Y$  interactions are embedded in the global technifermion chiral symmetries in such a way that the only unbroken gauge symmetry after chiral symmetry breaking is  $U(1)_{em}$ .<sup>2</sup> The theories naturally provide the Nambu-Goldstone bosons “eaten” by the  $W$  and  $Z$  boson. There would also typically be additional heavy states (e.g. vector mesons, analogous to the  $\rho$  and  $\omega$  mesons in QCD) with TeV masses [13,14], and the  $WW$  and  $ZZ$  scattering amplitudes would be expected to be strong at energies of order 1 TeV.

There are various possibilities for the scalar  $H^0$  in technicolor models. First, the  $H^0$  could be identified as a singlet scalar resonance, analogous to the  $\sigma$  particle expected in pion-scattering in QCD [15,16]. Alternatively, the  $H^0$  could be identified as a dilaton, a (pseudo-)Goldstone boson of scale invariance in theories of “walking technicolor” [17–21].<sup>3</sup> Finally, the  $H^0$  could be identified as an additional isosinglet state if the chiral symmetry breaking pattern of the technicolor theory provides for such a state.<sup>4</sup> In all of these cases, however, one expects large deviations in the couplings of this particle from those of the standard model Higgs boson. Since the couplings observed for the  $H^0$  approximate those of the Higgs boson to the 10% level, models of this kind are very highly constrained.

<sup>1</sup>In a strongly interacting theory “Naive Dimensional Analysis” [3,4] implies that, in the absence of fine-tuning,  $\Lambda \simeq g^* f$  where  $g^* \simeq 4\pi$  is the typical size of a strong coupling in the low-energy theory [5,6]. This estimate is modified in the presence of multiple flavors or colors [7].

<sup>2</sup>For a review of technicolor models, see [10–12].

<sup>3</sup>If both the electroweak symmetry and the approximate scale symmetry are broken only by electroweak doublet condensate(s), then the decay-constants for scale and electroweak symmetry breaking may be approximately equal – differing only by terms formally proportional to the amount of explicit scale-symmetry breaking.

<sup>4</sup>In this case, however, the coupling strength of the singlet state to  $WW$  and  $ZZ$  pairs would be comparable to the couplings to gluon and photon pairs, and these would all arise from loop-level couplings in the underlying technicolor theory [22].

#### 93.1.2 The Higgs doublet as a pseudo-Nambu-Goldstone Boson, $v/f < 1$ , $\Lambda > 1 \text{ TeV}$

In technicolor models, the symmetry-breaking properties of the underlying strong dynamics necessarily breaks the electroweak gauge symmetries. An alternative possibility is that the underlying strong dynamics itself does not break the electroweak interactions, and that the entire quartet of bosons in the Higgs doublet (including the state associated with the  $H^0$ ) are composite (pseudo-) Nambu-Goldstone particles [23,24]. In this case, the underlying dynamics can occur at energies exceeding 1 TeV and additional interactions with the top-quark mass generating sector (and possibly with additional weakly-coupled gauge bosons) cause the vacuum energy to be minimized when the composite Higgs doublet gains a vacuum expectation value [25,26]. In these theories, the couplings of the remaining singlet scalar state would naturally be equal to that of the standard model Higgs boson up to corrections of order  $(v/f)^2$  and, therefore, constraints on the size of deviations of the  $H^0$  couplings from that of the standard model Higgs [27] give rise to lower bounds on the scales  $f$  and  $\Lambda$ .<sup>5</sup>

The electroweak gauge interactions, as well as the interactions responsible for the top-quark mass, explicitly break the chiral symmetries of the composite Higgs model and lead generically to sizable corrections to the mass-squared of the Higgs-doublet – the so-called “Little Hierarchy Problem” [28]. “Little Higgs” theories [29–32] are examples of composite Higgs models in which the (collective) symmetry-breaking structure is selected so as to suppress these contributions to the Higgs mass-squared.

Composite Higgs models typically require a larger global symmetry of the underlying theory, and hence additional relatively light (compared to  $\Lambda$ ) scalar particles, extra electroweak vector bosons (e.g. an additional  $SU(2) \times U(1)$  gauge group), and vector-like partners of the top-quark of charge  $+2/3$  and possibly also  $+5/3$  [33]. In addition to these states, one would expect the underlying dynamics to yield additional scalar and vector resonances with masses of order  $\Lambda$ . If the theory respects a custodial symmetry [34], the couplings of these additional states to the electroweak and Higgs boson will be related – and, for example, one might expect a charged vector resonance to have similar branching ratios to  $WZ$  and  $WH$ . Different composite Higgs models utilize different mechanisms for arranging for the hierarchy of scales  $v < f$  and arranging for a scalar Higgs self-coupling small enough to produce an  $H^0$  of mass of order 125 GeV, for a review see [35]. If the additional states in these models carry color, they can provide additional contributions to Higgs production via gluon fusion [36]. The extent to which Higgs production at the LHC conforms with standard model predictions provides additional constraints (typically lower bounds on the masses of the additional colored states of order 0.7 TeV) on these models.

In addition, if the larger symmetry of the underlying composite Higgs theory does not commute with the standard model gauge group, then the additional states found in those models – especially those related to the top-quark, which tend to have the largest couplings to the electroweak sector – may be *colorless*. For example, in twin Higgs models [37], the top-partners carry no standard model charges. The phenomenology of the additional states in twin Higgs theories is rather different, since lacking color the production of these particles at the LHC will be suppressed – and, their decays may occur only via the electroweak symmetry breaking sector, leading to their being long-lived.

#### 93.1.3 Top-Condensate, Top-Color, Top-Seesaw and related theories, $v/f < 1$ , $\Lambda > 1 \text{ TeV}$

A final alternative is to consider a strongly interacting theory with a high (compared to a TeV) underlying dynamical scale that would naturally break the electroweak interactions, but whose

<sup>5</sup>In these models  $v/f$  is an adjustable parameter, and in the limit  $v/f \rightarrow 1$  they reduce, essentially, to the technicolor models discussed in the previous subsection. Our discussion here is consistent with that given there, since we expect corrections to the SM Higgs couplings to be large for  $v/f \simeq 1$ . Current measurements constrain the couplings of the  $H^0$  to equal those predicted for the Higgs in the standard model to about the 10% level [27], suggesting that  $f$  must have values of order a TeV or higher and, therefore, a dynamical scale  $\Lambda$  of at least several TeV.



strength is adjusted (“fine-tuned”) to produce electroweak symmetry breaking at 1 TeV. This alternative is possible if the electroweak (quantum) phase transition is continuous (second order) in the strength of the strong dynamics [38]. If the fine tuning can be achieved, the underlying strong interactions will produce a light composite Higgs bound state with couplings equal to that of the standard model Higgs boson up to corrections of order  $(1 \text{ TeV}/\Lambda)^2$ . As in theories in which electroweak symmetry breaking occurs through vacuum alignment, therefore, constraints on the size of deviations of the  $H^0$  couplings from that of the standard model Higgs give rise to lower bounds on the scale  $\Lambda$ . Formally, in the limit  $\Lambda \rightarrow \infty$  (a limit which requires arbitrarily fine adjustment of the strength of the high-energy interactions), these theories are equivalent to a theory with a fundamental Higgs boson – and the fine adjustment of the coupling strength is a manifestation of the hierarchy problem of theories with a fundamental scalar particle.

In many of these theories the top-quark itself interacts strongly (at high energies), potentially through an extended color gauge sector [39, 39–43]. In these theories, top-quark condensation (or the condensation of an admixture of the top with additional vector-like quarks) is responsible for electroweak symmetry breaking, and the  $H^0$  is identified with a bound state involving the third generation of quarks. These theories typically include an extra set of massive color-octet vector bosons (top-gluons), and an extra  $U(1)$  interaction (giving rise to a top-color  $Z'$ ) which couple preferentially to the third generation and whose masses define the scale  $\Lambda$  of the underlying physics.

#### 93.1.4 Flavor

In addition to the electroweak symmetry breaking dynamics described above, which gives rise to the masses of the  $W$  and  $Z$  particles, additional interactions must be introduced to produce the masses of the standard model fermions. Two general avenues have been suggested for these new interactions. In “extended technicolor” (ETC) theories [44, 45], the gauge interactions in the underlying strongly interacting theory are extended to incorporate flavor. This extended gauge symmetry is broken down (possibly sequentially, at several different mass scales) to the residual strong interaction responsible for electroweak symmetry breaking. The massive gauge-bosons corresponding to the broken symmetries then mediate interactions between mass operators for the quarks/leptons and the corresponding bilinears of the strongly-interacting fermions, giving rise to the masses of the ordinary fermions after electroweak symmetry breaking.

In the case of “partial compositeness” [46], the additional flavor-dependent interactions arise from mixing between the ordinary quarks and leptons and massive composite fermions in the strongly-interacting underlying theory. Theories incorporating partial compositeness include additional vector-like partners of the ordinary quarks and leptons, typically with masses of order a TeV or less.

In both cases, the effects of flavor interactions on the electroweak properties of the ordinary quarks and leptons are likely to be most pronounced in the third generation of fermions.<sup>6</sup> The additional particles present in these theories, especially the additional scalars, often couple more strongly to heavier fermions.

Moreover, since the flavor interactions must give rise to quark mixing, we expect that a generic theory of this kind could give rise to large flavor-changing neutral-currents [45]. In ETC theories, these constraints are typically somewhat relaxed if the theory incorporates approximate generational flavor symmetries [47], the theory has a slowly running coupling constant or “walks” [17–21], or if  $\Lambda > 1 \text{ TeV}$  [48]. In theories of partial compositeness, the masses of the ordinary fermions depend on the scaling-dimension of the operators corresponding to the composite fermions with which they mix. This leads to a new mechanism for generating the mass-hierarchy of the observed quarks and leptons that, potentially, ameliorates flavor-changing neutral current problems and can provide new contributions to the composite Higgs poten-

tial which allow for  $v/f < 1$  [49–53].

Alternatively, one can assume that the underlying flavor dynamics respect flavor symmetries (“minimal” [54, 55] or “next-to-minimal” [56] flavor violation) that suppress flavor-changing neutral currents in the two light generations. Additional considerations apply when extending these arguments to potential explanation of neutrino masses (see, for example, [57, 58]).

Since the underlying high-energy dynamics in these theories are strongly coupled, there are no reliable calculation techniques that can be applied to analyze their properties. Instead, most phenomenological studies depend on the construction of a “low-energy” effective theory describing additional scalar, fermion, or vector boson degrees of freedom, which incorporates the relevant symmetries and, when available, dynamical principles. In some cases, motivated by the AdS/CFT correspondence [59], the strongly-interacting theories described above have been investigated by analyzing a dual compactified five-dimensional gauge theory. In these cases, the AdS/CFT “dictionary” is used to map the features of the underlying strongly coupled high-energy dynamics onto the low-energy weakly coupled dual theory [60].

More recently, progress has been made in investigating strongly-coupled models using lattice gauge theory [61]. These calculations offer the prospect of establishing which strongly coupled theories of electroweak symmetry breaking have a particle with properties consistent with those observed for the  $H^0$  – and for establishing concrete predictions for these theories at the LHC [62].

## 93.2 Experimental Searches

As discussed above, the extent to which the couplings of the  $H^0$  conform to the expectations for a standard model Higgs boson constrains the viability of each of these models. Measurements of the  $H^0$  couplings, and their interpretation in terms of effective field theory, are summarized in the  $H^0$  review in this volume. In what follows, we will focus on searches for the additional particles that might be expected to accompany the singlet scalar: extra scalars, fermions, and vector bosons. In some cases, detailed model-specific searches have been made for the particles described above (though generally not yet taking account of the demonstrated existence of the  $H^0$  boson).

In most cases, however, generic searches (e.g. for extra  $W'$  or  $Z'$  particles, extra scalars in the context of multi-Higgs models, or for fourth-generation quarks) are quoted that can be used – when appropriately translated – to derive bounds on a specific model of interest.

The mass scale of the new particles implied by the interpretations of the low mass of  $H^0$  discussed above, and existing studies from the Tevatron and lower-energy colliders, suggests that only the Large Hadron Collider has any real sensitivity. A number of analyses already carried out by ATLAS and CMS use relevant final states and might have been expected to observe a deviation from standard model expectations – in no case so far has any such deviation been reported. The detailed implications of these searches in various model frameworks are described below.

Except where otherwise noted, all limits in this section are quoted at a confidence level of 95%. The searches at  $\sqrt{s} = 8 \text{ TeV}$  (Run 1) are based on  $20.3 \text{ fb}^{-1}$  of data recorded by ATLAS, and an integrated luminosity of  $19.7 \text{ fb}^{-1}$  analyzed by CMS. The datasets collected at  $\sqrt{s} = 13 \text{ TeV}$  during Run 2 of the LHC since 2015 are based on analyses with varied integrated luminosities ranging from  $\sim 2\text{--}140 \text{ fb}^{-1}$ .

### 93.2.1 Searches for $Z'$ or $W'$ Bosons

Massive vector bosons or particles with similar decay channels would be expected to arise in Little Higgs theories, in theories of Technicolor, or models involving a dilaton, adjusted to produce a light Higgs boson, consistent with the observed  $H^0$ . These particles would be expected to decay to pairs of vector bosons, or to third generation quarks, or to leptons. The generic searches for  $W'$  and  $Z'$  vector bosons listed below can, therefore, be used to constrain models incorporating a composite Higgs-like boson.

A general review of searches for  $Z'$  and  $W'$  bosons is also included in this volume [63, 64]. In the context of the dynamical electroweak symmetry breaking models, we emphasize their decays to third generation fermions by including a detailed overview,

<sup>6</sup>Indeed, from this point of view, the vector-like partners of the top-quark in top-seesaw and little Higgs models can be viewed as incorporating partial compositeness to explain the origin of the top quark’s large mass.

while also briefly summarizing the other searches.

#### $Z' \rightarrow \ell\ell$ :

ATLAS [65] and CMS [66] have both searched for  $Z'$  production with  $Z' \rightarrow ee$  or  $\mu\mu$ . No deviation from the standard model prediction was seen in the dielectron and dimuon invariant mass spectra, by either the ATLAS or the CMS analysis, and lower limits on possible  $Z'$  boson masses were set. A  $Z'_{\text{SSM}}$  with couplings equal to the standard model  $Z'$  (a “sequential standard model”  $Z'$ ) and a mass below 5.1 TeV was excluded by ATLAS, while CMS set a lower mass limit of 5.15 TeV. The experiments also place limits on the parameters of extra dimension models and in the case of ATLAS on the parameters of a minimal walking technicolor model [17–21], consistent with a 125 GeV Higgs boson [67]. For a general review of searches in these channels see the PDG review of Z prime in this volume [63].

In addition, both experiments have also searched for  $Z'$  decaying to a ditau final state [68, 69]. An excess in  $\tau^+\tau^-$  could have interesting implications for models in which lepton universality is not a requirement and enhanced couplings to the third generation are allowed. This analysis led to lower limits on the mass of a  $Z'_{\text{SSM}}$  of 2.4 and 2.1 TeV from ATLAS and CMS respectively.

#### $Z' \rightarrow q\bar{q}$ :

The ability to relatively cleanly select  $t\bar{t}$  pairs at the LHC together with the existence of enhanced couplings to the third generation in many models makes it worthwhile to search for new particles decaying in this channel. Both ATLAS [70] and CMS [71] have carried out searches for new particles decaying into  $t\bar{t}$ .

Both the ATLAS and CMS collaborations searched for  $t\bar{t}$  in the all hadronic mode [72] [73] in both the resolved and boosted regions. No evidence of resonance production were seen and limits were produced for various models including the  $Z'$  boson in topcolor-assisted technicolor which excludes masses less than 3.1 to 3.6 TeV (ATLAS) depending on the details of the model and 3.3, 5.25, and 6.65 TeV for widths of 1, 10 and 30 percent relative to the mass of the resonance.

ATLAS also presented results on the lepton plus jets final state, where the top quark pair decays as  $t\bar{t} \rightarrow WbWb$  with one W boson decaying leptonically and the other hadronically; CMS used final states where both, one or neither W decays leptonically and then combined the results. The  $t\bar{t}$  invariant mass spectrum was analyzed for any excess, and no evidence for any resonance was seen. ATLAS excluded a narrow ( $\Gamma/m = 1.2\%$ ) leptophobic topcolor  $Z'$  boson with masses between 0.7 and 2.1 TeV and with  $\Gamma/m = 3\%$  between 0.7 and 3.2 TeV. CMS set limits on leptophobic  $Z'$  bosons for three different assumed widths  $\Gamma/m = 1.0\%$ ,  $\Gamma/m = 10.0\%$ , and  $\Gamma/m = 30.0\%$  of 3.9 TeV to 4.0 TeV and exclude RS KK gluons up to 3.3 TeV.

Both ATLAS [74] and CMS [75] have also searched for resonances decaying into  $q\bar{q}$ ,  $qg$  or  $gg$  using the dijet invariant mass spectrum. Excited quarks are excluded up to masses of 6.7 TeV and model-independent upper limits on cross sections with a gaussian signal shape were set. CMS excluded string resonances with masses below 7.9 TeV, scalar diquarks below 7.5 TeV, axigluons and colorons below 6.6 TeV, excited quarks below 6.3 TeV, color-octet scalars below 3.7 TeV,  $W'$  bosons below 3.6 TeV,  $Z'$  bosons with SM-like couplings below 2.9 TeV and between 3.1 TeV and 3.3 TeV, Randall–Sundrum Gravitons below 2.6 TeV.

#### $W' \rightarrow \ell\nu$ :

Both LHC experiments have also searched for massive charged vector bosons. In this section we include a summary of the results, with emphasis on final states with third generation fermions, while the details on other decays are discussed in the mini-review of  $W'$  [64]. ATLAS searched for a heavy  $W'$  decaying to  $e\nu$  or  $\mu\nu$  and find no excess over the standard model expectation. A sequential standard model (SSM)  $W'$  boson (assuming zero branching ratio to  $WZ$ ) with mass less than 7 TeV was excluded [76] using 139 fb $^{-1}$  dataset at  $\sqrt{s} = 13$  TeV, as well as setting model independent cross-section limits as a function of mass. Based on a smaller dataset, the CMS experiment excluded a SSM  $W'$  boson with mass up to 4.1 TeV [77] and presented the upper limits on the production of generic  $W'$  bosons decaying into this final state using a model-independent approach.

CMS [78] has carried out a complementary search in the  $\tau\nu$  final state. As noted above, such searches place limits on models with enhanced couplings to the third generation. No excess was observed and limits between 2.0 and 2.7 TeV were set on the mass of a  $W'$  decaying preferentially to the third generation; a  $W'$  with universal fermion couplings was also excluded for masses less than 2.7 TeV.

#### $W' \rightarrow t\bar{b}$ :

Heavy new gauge bosons can couple to left-handed fermions like the SM  $W$  boson or to right-handed fermions.  $W'$  bosons that couple only to right-handed fermions ( $W'_R$ ) may not have leptonic decay modes, depending on the mass of the right-handed neutrino. For these  $W'$  bosons, the  $t\bar{b}$  ( $\bar{t}b + \bar{t}b$ ) decay mode is especially important because in many models the  $W'$  boson is expected to have enhanced couplings to the third generation of quarks relative to those in the first and second generations. It is also the hadronic decay mode with the best signal-to-background. ATLAS and CMS have performed searches for  $W'$  bosons via the  $W' \rightarrow t\bar{b}$  decay channel in the lepton+jets and all-hadronic final state.

The CMS lepton+jets search [79–82],  $W' \rightarrow t\bar{b} \rightarrow Wbb \rightarrow \ell\nu b\bar{b}$ , proceeded via selecting events with an isolated lepton (electron or muon), and at least two jets, one of which is identified to originate from a b-quark. The mass of the  $W'$  boson ( $M_{t\bar{b}}$ ) was reconstructed using the four-momentum vectors of the final state objects ( $b\bar{b}\ell\nu$ ). The distribution of  $M_{t\bar{b}}$  is used as the search discriminant. A search [82] using 35.9 fb $^{-1}$  of data, collected at  $\sqrt{s} = 13$  TeV, led to an exclusion of  $W'_R$  bosons with masses below 3.4 TeV (3.6 TeV) if  $M_{W'_R} \gg M_{\nu_R}$  ( $M_{W'_R} < M_{\nu_R}$ ), where  $M_{\nu_R}$  is the mass of the right-handed neutrino.

The CMS search for  $W' \rightarrow t\bar{b}$  decays using the all-hadronic final state focused on  $W'$  masses above 1 TeV [81]. In this region, the top quark gets a large Lorentz boost and hence the three hadronic products from its decay merge into a single large-radius jet. Techniques which rely on substructure information of the jets [83] are employed to identify boosted all hadronic W boson and top quark jets and compute the mass of the jet.  $W'$  candidate mass was computed from back-to-back boosted top-tagged jet and a low mass b-tagged jet. From this all-hadronic search,  $W'$  bosons were excluded for masses up to 2.02 TeV.

ATLAS has searched for  $W'_R$  bosons in the  $t\bar{b}$  final state both for lepton+jets [84] and all-hadronic [85] decays of the top. No significant deviations from the standard model were seen in either analysis and limits were set on the  $W' \rightarrow t\bar{b}$  cross section times branching ratio and  $W'$  bosons with purely right-handed couplings to fermions were excluded for masses below 3.15 TeV when the two channels are combined.

In addition, the above studies also provided upper limits on the  $W'$  effective couplings to right- and left-handed fermions. In Fig. 93.1 (bottom) the upper limits on  $W'$  couplings normalized to the SM W boson couplings derived by ATLAS [86] are shown. The top panel of Fig. 93.1 shows the upper limits for arbitrary combinations of left- and right-handed couplings of the  $W'$  boson to fermions set using a model independent approach by CMS [82].

### 93.2.2 Searches for Resonances decaying to Vector Bosons and/or Higgs Bosons

Both the ATLAS and CMS experiments have used the data collected at  $\sqrt{s} = 13$  TeV to search for resonances decaying to pairs of bosons. Overall no significant excesses were seen in the full datasets that were analyzed and the results are interpreted in models with heavy vector triplets (HVT) [87], models with strong gravity and extra spatial dimensions, as well as setting model independent limits as a function of mass. For a full review of models including extra spatial dimensions including the interpretation of many of these results in that context please see the review of extra dimensions in this volume [60].

Utilizing data collected at  $\sqrt{s} = 13$  TeV, ATLAS [88] and CMS [89], have both looked for a resonant state decaying into VV (with  $V = W$  or  $Z$ ), VH (with H representing the SM Higgs boson), and HH. Both collaborations have analyzed bosonic decay modes. ATLAS searches in the  $qqqq$ ,  $\nu\nu qq$ ,  $\nu\nu qq$ ,  $llqq$ ,  $l\nu l\nu$ ,  $ll\nu l$ ,  $ll\nu l$ ,  $llll$ ,  $qqbb$   $\nu\nu bb$ ,  $l\nu bb$ , and  $llbb$  final states and combined the results

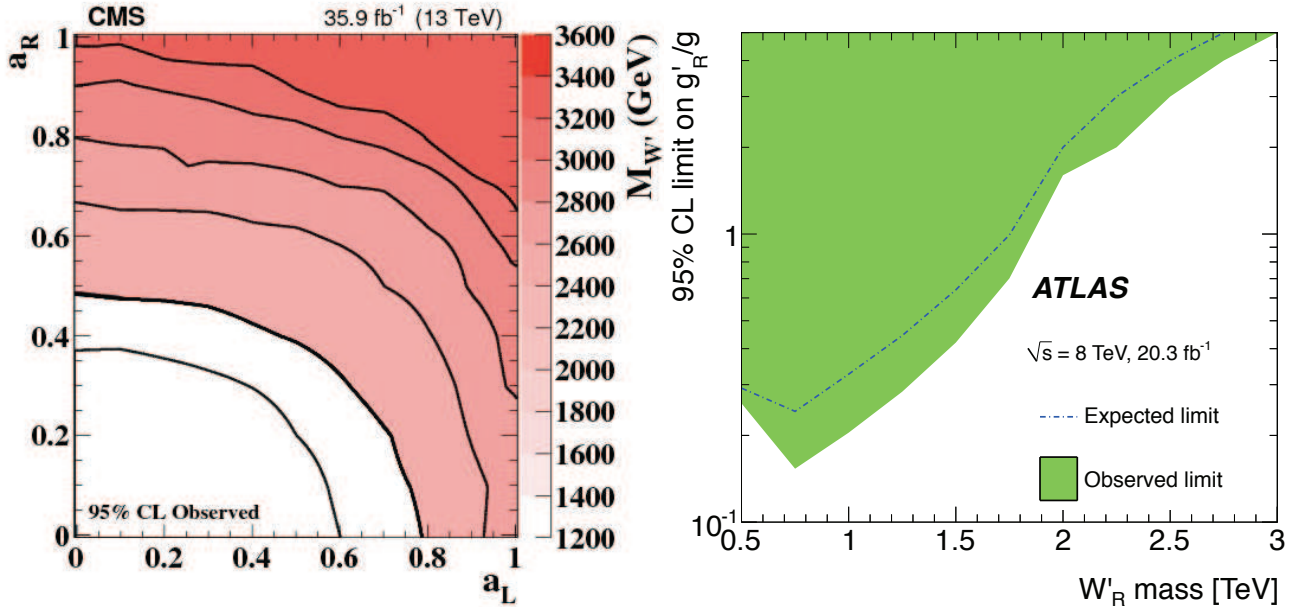


Figure 93.1: Left panel: Observed limits on the  $W'$  boson mass as function of the left-handed ( $a_L$ ) and right-handed ( $a_R$ ) couplings. Black lines represent contours of equal  $W'$  boson mass [82]. Right panel: Observed and expected regions, on the  $g'/g$  vs mass of the  $W'$  boson plane, that are excluded at 95% CL, for right-handed  $W'$  bosons [86].

(separately within each experiment). While CMS analyzes the  $qqqq$ ,  $\nu\nu qq$ ,  $lvqq$ ,  $llqq$ ,  $ll\nu\nu$ ,  $\nu\nu bb$ ,  $lvbb$ ,  $llbb$ ,  $bbbb$ ,  $\tau\tau bb$ , and  $qq\tau\tau$  final states.

The combined limits are expressed both as limits on the cross-section as a function resonance mass as well as constraints on the coupling of the heavy boson triplet to quarks, leptons, and the Higgs boson.

#### $X \rightarrow WZ$ :

ATLAS searches for new heavy resonances decaying into  $WZ$  in the channels  $WZ \rightarrow qqqq$  [90],  $lvqq$  [91], and  $lvll$  [92]. In the fully leptonic channel, the invariant mass of the  $WZ$  pair is obtained by considering all possible four lepton permutations in each event. The dominant background is Standard Model continuum  $WZ$  production,  $ZZ$  production where one lepton is not identified or falls outside the detector acceptance, and top quark plus vector boson production. No resonant production is seen in data and lower limits on the mass of a HVT decaying into  $WZ$  are set at 2260 (2460) GeV assuming a coupling constant of  $g_V = 1$  ( $g_V = 3$ ). In the  $WZ \rightarrow lvqq$  mode, ATLAS searches in both the cases that the quarks are observed as individual jets (resolved) and where they merge into one jet in the detector (boosted) which probe the low and high  $p_T$  regime of the  $Z$  boson. No significant excess is seen in either channel and combined lower mass limits are placed at 2900 (3000) GeV for  $g_V = 1$  ( $g_V = 3$ ) in the HVT model. In the all hadronic decay mode, ATLAS searches for two high  $p_T$  hadronically decaying vector bosons looking for a resonant structure. No excess is seen and limits are placed excluding 1200-3000 (1200-3300) GeV for  $g_V = 1$  ( $g_V = 3$ ) in the HVT model.

The CMS collaboration searches for  $VV \rightarrow qqqq$  [93] in the large R dijet search. The  $W$  and  $Z$  boson are identified through the mass of the large R jet and substructure variables. No excess is seen and limits are set for charged HVT bosons with masses lower than 3200 (3800) GeV for  $g_V = 1$  ( $g_V = 3$ ). Cross-section limits as function of mass are reported for the charged spin-1 resonance interpretation and are placed at 44.4 fb at 1.4 TeV to 0.7 pb at 4 TeV. In the  $\nu\nu qq$  final state [94], the CMS collaboration searches for a charged spin 1 resonance decaying into a  $VZ$  final state with a  $Z$  boson decaying into a pair of neutrinos and the other boson decaying into two collimated quarks reconstructed as a large R-jet. The transverse mass of the  $VZ$  candidate is reconstructed and utilized to search for evidence of resonant  $VZ$  production. No excess is seen and lower mass limits are placed on the charged resonance at 3100 (3400) GeV for  $g_V = 1$  ( $g_V = 3$ ).

In the  $2l2q$  final state, the CMS collaboration searches for a heavy resonance decaying into  $ZV$  [95] looking for events with one large R-jet consistent with the hadronic decay of a vector boson and a  $Z$  boson reconstructed in the charged lepton decay channel ( $e$  or  $\mu$ ). Limits are set for a HVT  $W'$  with a lower mass of 2270 (2330) for  $g_V = 1$  ( $g_V = 3$ ).

#### $X \rightarrow WW$ :

The ATLAS collaboration searches for a new heavy resonance decaying into  $WW$  in the channels  $WW \rightarrow qqqq$  [90],  $lvqq$  [91], and  $lv\nu\nu$  [96]. In the case where both  $W$ 's decay leptonically, ATLAS utilizes the transverse of the two lepton and two neutrino final state and searches for an excess in this distribution between 200 GeV and 5 TeV. No excess is seen and the mass of a HVT is excluded below 1300 GeV. Further vector boson fusion is also considered and cross-section limits as a function of mass are placed ranging from 1.3 pb to 0.006 pb at 200 GeV to 3 TeV, respectively. In the  $lvqq$  mode, ATLAS completed a companion analysis to the  $WZ \rightarrow$  analysis discussed above and places lower mass limits of 2850 (3150) GeV for  $g_V = 1$  ( $g_V = 3$ ) in the HVT model. ATLAS also interprets the all hadronic mode analysis in the hypothesis that  $WW \rightarrow qqqq$  and places limits on a HVT boson decaying into  $WW$  in the all hadronic mode between 1200 to 2200 (1200 to 2800) GeV for  $g_V = 1$  ( $g_V = 3$ ).

The CMS collaboration searches for  $VV \rightarrow qqqq$  [93] in the large R dijet search. The  $W$  and  $Z$  boson are identified through the mass of the large R jet and substructure variables. No excess is seen and limits are set for charged HVT bosons with masses lower than 2700 (2800) GeV for  $g_V = 1$  ( $g_V = 3$ ). Cross-section limits as function of mass are reported for the uncharged spin-1 resonance interpretation and are placed at 41.6 fb at 1.4 TeV to 0.6 pb at 4 TeV.

#### $X \rightarrow VH$ :

The ATLAS Collaboration searches for a new heavy resonance decaying into  $WH$  and  $ZH$  in the  $qbb$  ( $WH$  and  $ZH$ ) [97],  $lvbb$  ( $WH$ ),  $\nu\nu bb$  ( $ZH$ ),  $llbb$  ( $ZH$ ) [98]. In the all hadronic mode, ATLAS searches for boosted  $VH$  production looking for two large R jets where the larger invariant mass large R jet is interpreted as the Higgs boson decay products while the lesser the hadronically decaying vector boson requiring  $b$  tagging on the Higgs boson subjects. The invariant mass is reconstructed and a search is done for resonant production of  $ZH$ . None is found and limits from



1100 to 2500 (1300 to 3800 GeV) are placed for  $g_V = 1$  ( $g_V = 3$ ). ATLAS also searches for  $ZH$  where the  $W$  or  $Z$  boson decays into  $\nu\nu$ ,  $l\nu$ , and  $ll$ . The analysis searches for both resolved and merged (boosted)  $b$  jets from the decay of the Higgs boson as well as defining signal regions based on the number of reconstructed charged leptons (0,1,or 2). In the dilepton channel the invariant mass is explicitly reconstructed of the entire diboson system, the single lepton channel reconstructs the diboson final state constraining the lepton and missing transverse momentum utilizing the known  $W$  boson mass, while the 0 charged lepton channel reconstructs the transverse mass of the diboson system. No excess is seen in any channel and limits on the production of a HVT are placed at 2800 GeV (2930 GeV for  $g_V = 1$  ( $g_V = 3$ )).

The CMS Collaboration searches for a heavy resonance decaying into  $VH$  [99] searching for resonances decaying into a Higgs boson and either a hadronically decaying  $W$  or  $Z$  boson. The search identifies events with two large- $R$  jets using substructure variables and requires one large- $R$  jets is tagged with a pair of  $b$ -hadrons clustered in a single jet. The invariant mass of the  $VH$  bosons is reconstructed and evidence for resonance production is sought. No excess is seen and limits are placed. With  $g_V = 1$  (3) a narrow  $W'$  resonance with  $m_{W'} < 2470(3150)$  GeV and  $m_{Z'} < 1150(1190)$  GeV. Summary of Searches with Diboson Final States:

Both ATLAS [88] and CMS [89] provide plots summarizing the various searches results and limits combining. The results are shown in the context of HVT models and models of strong gravity with extra spatial dimensions. No excess is seen in any search and limits on the 4.3 (4.5) TeV (ATLAS) and (CMS). Inclusion of decays directly to fermions increase these limits to 5.3 (5.5) TeV and 5.0 (5.2) TeV from the ATLAS and CMS combinations, respectively. Both collaborations also place varying limits on the coupling strength as a function of HVT boson mass as well.

### 93.2.3 Vector-like third generation quarks

Vector-like quarks (VLQ) have non-chiral couplings to  $W$  bosons, i.e. their left- and right-handed components couple in the same way. They therefore have vectorial couplings to  $W$  bosons. Vector-like quarks arise in Little Higgs theories, top-coloron-models, and theories of a composite Higgs boson with partial compositeness. In the following, the notation  $T$  quark refers to a vector-like quark with charge  $2/3$  and the notation  $B$  quark refers to a vector-like quark with charge  $-1/3$ , the same charges as the SM top and  $b$  quarks respectively. The exotic vector-like quarks  $X_{5/3}$  and  $Y_{-4/3}$  have charges  $5/3$ , and  $-4/3$  respectively. Vector-like quarks couple with SM quarks with Yukawa interactions and may exist as  $SU(2)$  singlets ( $T$ , and  $B$ ), doublets  $[(X_{5/3}, T), (T, B), (B, Y_{-4/3})]$ , or triplets  $[(X_{5/3}, T, B), (T, B, Y_{-4/3})]$ . At the LHC, VLQs can be pair produced via the dominant gluon-gluon fusion. VLQs can also be produced singly by their electroweak effective couplings to a weak boson and a standard model quark. Single production rate is expected to dominate over the rate of pair production at large VLQ masses.  $T$  quarks can decay to  $bW$ ,  $tZ$ , or  $tH^0$ . Weak isospin singlets are expected to decay to all three final states with (asymptotic) branching fractions of 50%, 25%, 25%, respectively. Weak isospin doublets are expected to decay exclusively to  $tZ$  and to  $tH^0$  [100] with equal branching ratios. Analogously,  $B$  quarks can decay to  $tW$ ,  $bZ$ , or  $bH^0$ . The  $Y_{-4/3}$  and  $X_{5/3}$  quarks decay exclusively to  $bW$  and to  $tW$ . While these are taken as the benchmark scenarios, other representations are possible and hence the final results are interpreted for many allowed branching fraction combinations.

Given the multiple decay modes of the VLQs, the final state signatures of both pair produced and the singly produced VLQs are fairly rich with leptons, jets,  $b$  jets, and missing energy. Depending on the mass of the VLQ, the top quarks and  $W/Z/H^0$  bosons may be Lorentz boosted and identified using jet substructure techniques. Thus the searches are performed using lepton+jets signatures, multi-lepton and all-hadronic decays. In addition,  $T$  or  $B$  quarks with their antiparticles can result in events with same-sign leptons, for example if the decay  $T \rightarrow tH \rightarrow bWW^+W^-$  is present, followed by leptonic decays of two same-sign  $W$  bosons. In the following subsections, while we describe the searches for each of the decay modes of the VLQs, the same analysis can be

re-interpreted to obtain the sensitivity to a combination with varied branching fractions to the different decay modes.

In the following sections, the results obtained for  $T$  ( $B$ ) quarks assuming 100% branching ratio to  $Wb$  ( $Wt$ ) are also applicable to heavy vector-like  $Y_{-4/3}$  ( $X_{5/3}$ ) with charge  $4/3$  ( $5/3$ ).

#### 93.2.3.1 Searches for $T$ quarks that decay to $W$ , $Z$ and $H^0$ bosons

##### $T/Y \rightarrow bW$ :

CMS has searched for pair production of heavy  $T$  quarks that decay exclusively to  $bW$  [101–103]. The analysis selected events with exactly one charged lepton, assuming that the  $W$  boson from the second  $T$  quark decays hadronically. Under this hypothesis, a 2-constraint kinematic fit can be performed to reconstruct the mass of the  $T$  quark as a narrow mass peak with a mass resolution of around 7%. In Refs. [102] and [103], the two-dimensional distribution of reconstructed mass vs  $S_T$  was used to test for the signal, where  $S_T$  is the scalar sum of the missing  $p_T$  and the transverse momenta of the lepton and the leading four jets. This analysis, when combined with the search in the fully hadronic final state [104] excluded new quarks that decay 100% to  $bW$  for masses below 0.89 TeV [103]. At times the hadronically-decaying  $W$  boson is produced with a large Lorentz boost, leading to the  $W$  decay products merged into a large-radius jet. Algorithms such as jet pruning [105] were used to remove contributions from soft, wide angle radiation, from large-radius jets, leading to better discrimination between QCD jets and those arising from decays of the heavy particles. If the mass of the boosted jet was compatible with the  $W$  boson mass, then the  $W$  boson candidate jet and its subjects were used in the kinematic reconstruction of the  $T$  quark. No excess over standard model backgrounds was observed. Upper limits on the production cross section as a function of the mass of  $T$  quarks were measured. By comparing them with the predicted cross section for vector like quark pair production, the strong pair production of  $T$  quarks was excluded for masses below 1.30 TeV (1.28 TeV expected) [101].

Another “cut-based” search for pair produced  $T$  quarks in the all-hadronic final state targeting the  $Wb$  decay mode [106], relies on mass reconstruction of two highest  $p_T$   $Wb$  combinations using boosted  $W$  boson candidates with  $p_T > 200$  GeV and  $b$ -tagged jets.  $H_T$  is used as the signal discriminator, with selected events divided into nine categories based on the multiplicity of  $W$  and  $b$  jets in the event. From this search  $T$  quarks with pure  $Wb$  decays are excluded for masses below 1.04 TeV (1.07 TeV expected).

An analogous search has been carried out by ATLAS [107, 108] for the pair production of heavy  $T$  quarks. It used the lepton+jets final state with an isolated electron or muon and at least four jets, including a  $b$  jet and required reconstruction of the  $T$  quark mass. Given the mass range of the  $T$  quark being explored was from a 0.4 TeV to a couple of TeV, the  $W$  boson from the  $T$  quark may fall in two categories: those with a high boost leading to merged decay products, and others where the two jets from the  $W$  boson were resolved. In addition, the selection was optimized to require large angular separation between the high  $p_T$   $W$  bosons and the  $b$  jets.

The  $T \rightarrow Wb$  candidates were constructed from both the leptonically and hadronically decaying  $W$  bosons by pairing them with the two highest  $p_T$   $b$ -tagged jets in the event. The pairing of  $b$  jets with  $W$  bosons which minimizes the difference between the masses of leptonically decaying  $T$  ( $m_{lep}(T)$ ) and the hadronic  $T$  ( $m_{had}(T)$ ) was chosen. Finally,  $m_{lep}(T)$  was used as the discriminating variable in a signal region defined by high  $S'_T$  (here  $S'_T$  is defined as the scalar sum of the missing  $p_T$ , the  $p_T$  of the lepton and jets) and the opening angle between the lepton and the neutrino ( $\Delta R(e, \nu)$ ). With the  $36.1 \text{ fb}^{-1}$  data collected during Run 2 at  $\sqrt{s} = 13$  TeV, assuming 100% branching ratio to the  $Wb$  decay, the observed lower limit on the  $T$  mass was 1.35 TeV, and in the  $SU(2)$  singlet scenario, the lower mass limit was obtained to be 1.17 TeV [107].

A targeted search for a  $T$  quark, produced singly in association with a light flavor quark and a  $b$  quark and decaying into  $bW$ , was carried out by CMS at  $\sqrt{s}=13$  TeV and a dataset corresponding to  $2.3 \text{ fb}^{-1}$  [109]. The analysis used lepton+jets events, with at least

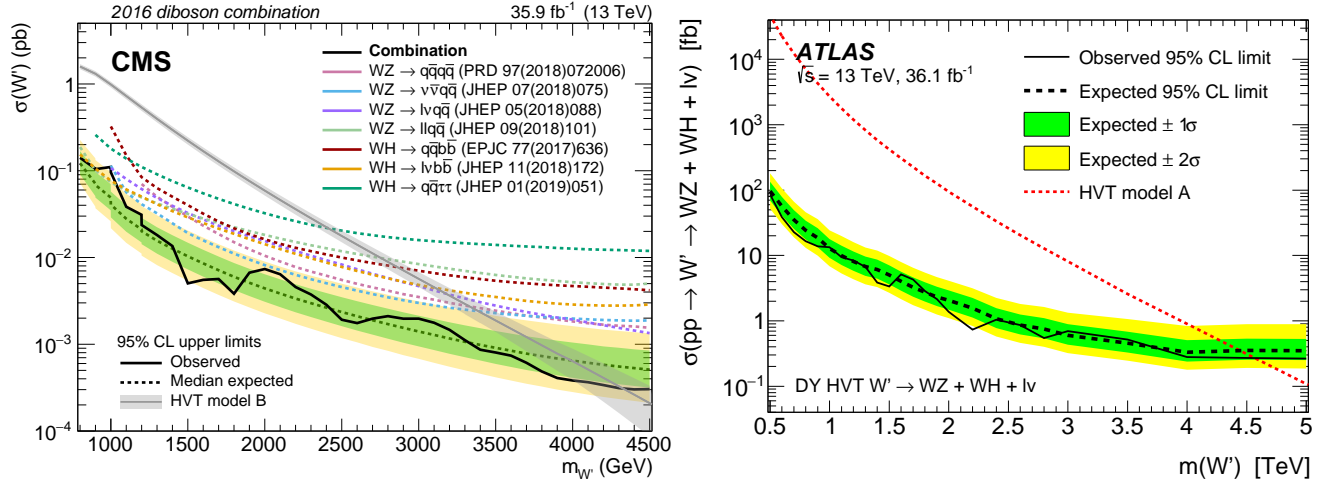


Figure 93.2: Left panel: Observed limits from  $W'$  to diboson from CMS [89]. Right panel: Observed limits from  $W'$  to diboson decays from ATLAS [88].

one b-tagged jet with large transverse momentum, and a jet in the forward  $\eta$  region. Selected events were required to have  $S_T'' > 500$  GeV, where  $S_T''$  is defined as the scalar sum of the transverse momenta of the lepton, the leading central jet, and the missing transverse momentum. The invariant mass of the  $T$  candidate was used as the discriminating variable and was reconstructed using the four-vectors of the leptonically decaying  $W$  boson and the leading central jet. No excess over the standard model prediction was observed. As the VLQ width is proportional to the square of the coupling, upper limits were set on the production cross section assuming a narrow width VLQ with coupling greater than 0.5. For  $Y/T$  quarks with a coupling of 0.5 and a 100% branching fraction for the decay to  $bW$  the excluded masses were in the range from 0.85 to 1.40 TeV [109]. A similar search [110, 111] performed by ATLAS singly produced  $T$  or  $Y_{-4/3}$  quark decaying to  $Wb$  using a dataset corresponding to  $36.1 \text{ fb}^{-1}$ . The search was performed using lepton+jets events with a high  $p_T$  b-tagged jet, and at least one forward jet. The reconstructed mass of the  $T/Y_{-4/3}$  quark, was used as the discriminating variable and showed no excess above the expectation from SM. Interference effects with the SM background are included in the study. This search led to 95% CL upper limits on the mixing angle  $|\sin(\theta_L)|$  ( $C_L^{Wb}$ ) in the range of 0.18–0.35 (0.25–0.49) for singlet  $T$  quark mass between 0.8–1.2 TeV. This search also provided limits as a function of the  $Y_{-4/3}$  quark mass, on the coupling of the  $Y_{-4/3}$  quark to  $bW$ , and the mixing parameter  $|\sin\theta_R|$  ( $C_R^{Wb}$ ) for a  $(B, Y_{-4/3})$  doublet model [110]. For VLQ masses between 0.08–1.8 TeV, the limits on  $|\sin(\theta_R)|$  ( $C_R^{Wb}$ ) is in the range 0.17–0.55 (0.24–0.77), where limits on  $|\sin\theta_R|$  are around 0.18–0.19 and below the constraints from electroweak precision observables for  $Y_{-4/3}$  quark mass between 0.9–1.25 TeV. For  $Y_{-4/3}$  quark in the triplets  $(T, B, Y_{-4/3})$ , limits on  $|\sin(\theta_L)|$  ( $C_L^{Wb}$ ) are between 0.16–0.39 (0.31–0.78) for masses between 0.8 GeV–1.6 TeV [110].

#### $T \rightarrow tH^0$ :

ATLAS has performed a search for  $T\bar{T}$  production with  $T \rightarrow tH^0$  [108, 112]. Given the dominant decay mode  $H^0 \rightarrow b\bar{b}$ , these events are characterized by a large number of jets, many of which are b jets. Thus the event selection required one isolated electron or muon and high jet multiplicity (including b-tagged jets). The sample is categorized by the jet multiplicity (5 and  $\geq 6$  jets in the 1-lepton channel; 6 and  $\geq 7$  jets in the 0-lepton channel), b tag multiplicity (2, 3 and  $\geq 4$ ) and mass-tagged jet multiplicity (0, 1 and  $\geq 2$ ). The distribution of  $m_{\text{eff}}$ , defined as the scalar sum of the lepton and jet  $p_T$  and the missing  $E_T$ , for each category were used as the discriminant for the final signal and background separation. No excess of events were found. Weak isospin doublet  $T$  quarks were excluded below 1.16 TeV.

A search by ATLAS for pair produced VLQs with an all-hadronic final state signature yields an exclusion of pure decays

$T \rightarrow tH^0$  upto a  $T$  quark mass of 1.01 TeV [113]. This analysis used a deep neural network technique to identify jets originating from boosted bosons and top-quarks and described further in subsection 93.2.3.2.

The CMS search for  $T\bar{T}$  production, with  $T \rightarrow tH^0$  decays has been performed in both lepton+jets, multilepton and all-hadronic final states. The lepton+jets analysis [114] emphasizes the presence of large number of b-tagged jets, and combined with other kinematic variables in a Boosted Decision Tree (BDT) for enhancing signal to background discrimination. The multilepton analysis [114] was optimized for the presence of b jets and the large hadronic activity. For  $\mathcal{B}(T \rightarrow Wb) = 1$ , the combined lepton+jets and multilepton analyses led to a lower limit on  $T$  quark masses of 0.71 TeV. A search for  $T \rightarrow tH^0$  in all-hadronic decays [115], optimized for a high mass  $T$  quark, and based on identifying boosted top quark jets has been carried out by CMS. This search aimed to resolve subjects within the jets arising from boosted top quark decays, including b tagging of the subjects. A likelihood discriminator was defined based on the distributions of  $H_T$ , and the invariant mass of the two b jets in the events for signal and background. No excess above background expectations was observed. Assuming 100% branching ratio for  $T \rightarrow tH^0$ , this analysis led to a lower limit of 0.75 TeV on the mass of the  $T$  quark.

Searches for  $T$  quarks at  $\sqrt{s}=13$  TeV, based on a  $2.6 \text{ fb}^{-1}$  dataset [116] have been performed by CMS using the lepton+jets final state. This search has been optimized for high mass  $T$  quarks by exploiting techniques to identify  $W$  or Higgs bosons decaying hadronically with large transverse momenta. The boosted  $W$  channel excluded  $T$  quarks decaying only to  $bW$  with masses below 0.91 TeV, and the boosted  $tH$  channel excluded  $T$  quarks decaying only to  $tH$  for masses below 0.89 TeV.

A CMS search for  $T \rightarrow tH^0$  with  $H^0 \rightarrow \gamma\gamma$  decays has been performed [117] in pair production of  $T$  quarks. To identify the Higgs boson produced in the decay of the heavy  $T$  quark, and the subsequent  $H^0 \rightarrow \gamma\gamma$  decay, the analysis focused on identification of two photons in events with one or more high  $p_T$  lepton+jets or events with no leptons and large hadronic activity. A search for a resonance in the invariant mass distribution of the two photons in events with large hadronic activity defined by the  $H_T$  variable showed no excess above the prediction from standard model processes. The analysis resulted in exclusion of  $T$  quark masses below 0.54 TeV.

A search for electroweak single production of  $T$  quark decaying to  $tH^0$  using boosted topologies in fully hadronic [118] and lepton+jets [119] in the final states has been performed by CMS. The electroweak couplings of the  $T$  quarks to the SM third generation quarks are highly model dependent and hence these couplings determine the rates of the single  $T$  quark production. In both analyses,  $T$  quark candidate invariant mass was reconstructed using the

Implications of the  $H^0$ 

boosted Higgs boson jets and the top quark. Higgs boson jets were identified using jet substructure techniques and subjet  $b$  tagging. For the lepton+jets analysis the top quark was reconstructed from the leptonically decaying  $W$  and the  $b$  jet, while in the all-hadronic analysis the top quark jet was tagged using substructure analysis. There was no excess of events observed above background. Exclusion limits on the product of the production cross section and the branching fraction ( $\sigma(pp \rightarrow Tqt/b) \times \mathcal{B}(T \rightarrow tH^0)$ ) were derived for the  $T$  quark masses in the range 0.70–1.8 TeV. From the lepton+jets analysis, for a mass of 1.0 TeV, values of ( $\sigma(pp \rightarrow Tqt/b) \times \mathcal{B}(T \rightarrow tH^0)$ ) greater than 0.8 and 0.7 pb were excluded assuming left- and right-handed coupling of the  $T$  quark to standard model fermions, respectively [119]. For the all-hadronic analysis, upper limits between 0.31 and 0.93 pb were obtained on ( $\sigma(pp \rightarrow Tqt/b) \times \mathcal{B}(T \rightarrow tH^0)$ ) for  $T$  quark masses in the range 1.0–1.8 TeV [118].

 $T \rightarrow tZ$ :

Both ATLAS and CMS searched for  $T$  quarks that decay exclusively into  $tZ$  in pp collisions at  $\sqrt{s} = 13$  TeV. No excesses were found in either search.

ATLAS performed a search [120] for optimized pair production of vector-like top quarks decaying into  $tZ$  where the  $Z$  boson subsequently decays into neutrino pairs utilizing  $36.1 \text{ fb}^{-1}$  of data. The search selected events with one lepton, multiple jets, and significant missing transverse momentum. No significant excesses were found and lower limits on the mass of a vector like top quark were placed, excluding masses below 0.87 TeV (weak-isospin singlet), 1.05 TeV (weak-isospin doublet), and 1.16 TeV (pure  $tZ$  mode).

Another search by ATLAS for pair produced  $T$  decaying to  $tZ$  has been carried out by reconstructing the high transverse momentum  $Z$  boson from a pair of opposite-sign same-flavor lepton, using events with two or three charged leptons [121]. The final analysis is based on three final signatures. In the trilepton events, at least one  $b$ -tagged jet is required and  $S_T$  is used as the discriminating variable. In events with two leptons, at least 2  $b$  jets are requested and those with zero or one high  $p_T$  top-tagged jet, use  $H_T$  as the discriminator. The second dilepton analysis with two top-tagged high  $p_T$  jets focuses on hadronically decaying heavy resonances and the invariant mass of the  $Z$  boson and the highest  $p_T$   $b$ -tagged jet if found to be a good discriminating variable. No excess was observed over the background expectations. The combined analysis yields a lower limit on  $T$  quark mass of 1.03 TeV (1.21 TeV) in the singlet (doublet) model or 100% branching ratio for  $T \rightarrow tZ$  a lower limit on the  $T$  quark mass of 1.34 TeV is obtained.

ATLAS has subsequently carried out a search [122] for singly produced  $T$  quark decaying to  $tZ$  where the  $Z$  boson decays into neutrino pairs. The search is carried out using  $36.1 \text{ fb}^{-1}$  of data in events with two different final state signatures: one with jets, and significant missing  $p_T$  (0L) and the other with single lepton, jets and missing  $p_T$  (1L). Events are divided into signal and dedicated  $W$ +jets and  $t\bar{t}$  background control regions. The sensitivity to  $T$  quark signal is extracted using distributions of missing  $p_T$  for 1L and the distributions of transverse mass  $T$  quark constructed from missing  $p_T$  and the high  $p_T$  large-radius top-tagged jet for 0L analysis. The is no excess found over the expected background and lower limits on the production of  $T$  singlets is obtained as a function of the left- and right-handed couplings  $c_{L,W}$  and  $c_{R,W}$  to top quarks and  $W$  bosons, where  $c_W$  above 0.7 are excluded for  $T$  quark mass of 1.4 TeV. The limits on  $c_W$  are also recasted into expected and observed 95% CL upper limits for the mixing angle ( $\theta_L$ ) of a singlet  $T$  with the top quark.

CMS searched [123] for single production of  $T$  quarks decaying into  $tZ$  with the  $Z$  boson decaying to pairs of charged leptons (electrons and muons) and the top quark decaying hadronically using  $35.9 \text{ fb}^{-1}$  of data. Limits were placed on  $T$  quarks with masses between 0.7 and 1.7 TeV excluding the product of cross section and branching fraction above values of 0.27 to 0.04 pb. Additionally, limits on the product of cross section and branching fractions for a  $Z'$  boson decaying into  $tZ$  were set between 0.13 and 0.06 pb for  $Z'$  boson masses in the range from 1.5 to 2.5 TeV.

Similar searches by ATLAS for singly produced  $T$  decaying to

$Zt$  have been performed in final state signatures with two or three charged leptons [121]. The analysis relies on tagging  $b$  jets and high  $p_T$  large-radius jets originating from top-quarks. Additional selections are devised to reduce the contributions from pair production of  $T$  quarks. For events with dilepton analysis, the discriminating variable is the mass of the  $T$  quark formed using the invariant mass of the  $Z$  boson candidate and the highest  $p_T$  top-tagged jet, while for the trilepton analysis, the variable  $S_T$  is used to search for an excess of data over the expected SM background. No excess above the SM expectations is observed. The two final states (dilepton and trileptons) are combined to obtain the final results. For the coupling parameter  $\kappa_T$  between 0.1–1.6, the 95% CL upper limits on the production cross section times branching fraction into  $Zt$  is between 0.16–0.18 (0.03–0.05) pb at  $T$  quark mass of 0.7 (2) TeV.

Combination of  $T \rightarrow bW/tZ/tH^0$ :

Most of the analyses described above targeted an individual decay mode of the  $T$  quark, with 100% branching ratio to either  $bW$ ,  $tZ$  or  $tH^0$  and were optimized accordingly. However, they have varied sensitivity to all three decay modes and the results can be interpreted as a function of branching ratios to each of the three decay modes, with the total adding up to unity ( $\mathcal{B}(tH) + \mathcal{B}(tZ) + \mathcal{B}(Wb) = 1$ ).

Combinations of analyses have been performed by both ATLAS and CMS. The limits set by ATLAS searches in  $W(\ell\nu)b = X$ ,  $H(bb)b + X$ ,  $Z(\ell\bar{\nu})$ ,  $Z(\ell\ell)t/b + X$ , dileptons with same-sign charge, trileptons, all-hadronic final states have been combined and the results obtained for various sets of branching fractions for  $T$  quark decays to  $bW$ ,  $tH^0$  and  $tZ$  are shown in Fig. 93.3 (left). In the combined analysis, ATLAS sets lower  $T$  quarks mass limit of 1.31 TeV for all possible values of the branching fractions to the three decay modes [107, 120, 124]. In Fig. 93.3, exclusion is shown in the plane of  $\mathcal{B}(T \rightarrow Ht)$  versus  $\mathcal{B}(T \rightarrow Wb)$ , for different values of the  $T$  quark mass. The default branching ratio values for the weak-isospin singlet and doublet cases are also shown in Fig. 93.3 as yellow circle and star symbols respectively. Assuming a weak isospin ( $T, B$ ) doublet and  $|V_{Tb}| \ll |V_{tB}|$ ,  $T$  quark mass below 1.37 TeV is excluded.

CMS analysis for pair production of  $T$ , combined three channels with lepton final states: single lepton, two leptons with the same sign of the electric charge (SS), or at least three leptons (trilepton) [125]. For various combinations of branching fractions for  $T$  quark decays to  $bW$ ,  $tH^0$  and  $tZ$ , the combined results exclude  $T$  quarks with masses below 1.14–1.3 TeV and are shown in Figure 93.3 (right). Single lepton events are classified into 16 signal categories and 6 background control regions based on multiplicity of  $b$ -tagged, high  $p_T$   $H^0$  and  $W$ -tagged jets. The discriminating variables are  $H_T$  for  $H^0$ -tagged and the minimum invariant mass constructed from the lepton and the  $b$  jet,  $\min[M_{l\bar{b}}]$ , for zero  $H^0$ -tagged events. For the same-sign dilepton and trilepton analyses, the non-prompt backgrounds due to misidentified jets and leptons are derived from data control regions. In the trilepton analysis the  $S_T$  variable is used as the signal discriminator binned in four categories based on the lepton flavor combinations ( $eee$ ,  $e\mu\mu$ ,  $e\mu\mu$ ,  $\mu\mu\mu$ ). The single lepton analysis is most sensitive for  $tHbW$  and  $WbWb$  decay modes, within the the SS dilepton analysis  $tHtH$  and  $tHtZ$  have the best efficiency and for trileptons the  $tZtZ$  and  $tHtZ$  decays modes have the highest efficiency. CMS excludes singlet (doublet)  $T$  quark masses below 1.2 (1.28) TeV. Masses below 800 GeV were excluded in previous searches. For  $T$  quark masses in the range 0.8–1.8 TeV, cross sections smaller than 30.4–9.4 fb (21.2–6.1 fb) are excluded for the singlet (doublet) scenario.

Another inclusive search for pair produced  $T$  in all-hadronic final state [106] has been performed by CMS using the boosted event shape tagger (BEST) neural network technique to classify jets in six categories  $W$ ,  $Z$ ,  $H^0$ ,  $t$ ,  $b$ , and light. This search does not focus on a given VLQ mode, but on various combinations of the boson and quark jets in the final state. Anti- $k_T$  jets with a distance parameter of 0.8 are used. The BEST NN algorithm simultaneously classifies jets according to heavy object type. For each of the six particle hypothesis, it boosts each jet constituent into corresponding frame along jet momentum direction, and cal-

culates event shape and angular variables in the boosted frame, with the expectation that when boosting to the correct rest frame, jet constituents will be isotropic and show the expected N-prong structure of the decaying object in its rest frame. A neural network is trained using the event shape and angular variables in the boosted frame to classify jets according to one of those six possibilities ( $W, Z, H, t, b$ , or light). The analysis bins the events into 126 categories depending on the number of  $W, Z, H, t, b$ , or light jets in the final state with a maximum of four such objects. For each category  $H_T^{\text{AK8}}$ , the scalar sum of  $p_T$  of all AK8 jets, is used as the signal discriminator. A scan over a combination of various branching fractions is also performed. This search excludes  $T$  quark masses in the range 0.74–1.37 TeV for the  $tH$  decay mode in the NN analysis.

An inclusive search for VLQs has been carried out by CMS targeted at heavy  $T$  quarks decaying to any combination of  $bW, tZ$ , or  $tH^0$  is described in [114]. Selected events have at least one isolated charged lepton. Events were categorized according to number and flavour of the leptons, the number of jets, and the presence of hadronic vector boson and top quark decays that are merged into a single jet. The use of jet substructure to identify hadronic decays significantly increases the acceptance for high  $T$  quark masses. No excess above standard model backgrounds was observed. Limits on the pair production cross section of the new quarks are set, combining all event categories, for all combinations of branching fractions into the three final states. For  $T$  quarks that exclusively decay to  $bW/tZ/tH^0$ , masses below 0.70/0.78/0.71 TeV are excluded.

### 93.2.3.2 Searches for $B$ quarks that decay to $W, Z$ and $H^0$ bosons

ATLAS and CMS have performed searches for pair production of heavy  $B$  quarks which subsequently decay to  $Wt, bZ$  or  $bH^0$ . The searches have been carried out in final states with single leptons, dileptons (with same charge or opposite charge), multileptons, as well as in fully hadronic final states.

#### $B \rightarrow bH^0 X$ :

Using  $36.1 \text{ fb}^{-1}$  of data, ATLAS has performed a search for pair produced VLQs with all-hadronic final state signature [113]. While this analysis provides exclusion limits for all third generation VLQs, it provides the strongest results for  $B \rightarrow bH^0$  decay mode and excludes pure  $B \rightarrow bH^0$  decays for  $B$  masses up to 1.01 TeV. The limits are also casted as a two-dimensional plane of branching ratio values of  $B \rightarrow bH^0$  vs.  $B \rightarrow Wb$ . This analysis required the presence of high  $p_T$  jets and multiple  $b$  tags. It used a multi-class DNN to classify jets arising from  $W, Z, H^0$  bosons and top-quarks. In addition, the matrix element method is used to compute the likelihood for the event to arise from a particular VLQ final state and used to construct the final discriminator. To increase the performance sensitivity, processes with the same number of top quarks,  $W/Z$  bosons, and  $H^0$  Higgs bosons are combined into a single hypothesis.

#### $B \rightarrow WtX$ :

A search for  $B \rightarrow tW$  in  $B$  pair produced events has been performed by the ATLAS experiment [107] using lepton+jets events with one hadronically decaying  $W$  and one leptonically decaying  $W$  utilizing  $36.1 \text{ fb}^{-1}$  of data at  $\sqrt{s} = 13 \text{ TeV}$ . The search was optimized for  $T$  production decaying into  $Wb$ . Since the analysis was optimized for  $T \rightarrow Wb$  rather than  $Wt$  decays the analysis does not reconstruct the full  $B$  mass. As discussed earlier, the hadronically and leptonically decaying heavy quarks were required to have similar reconstructed masses (within 300 GeV). The interpretation of the  $T \rightarrow Wb$  in the context of  $B \rightarrow tW$  production led to the exclusion of heavy  $B$  like VLQs for masses less than 1.25 TeV and 1.08 TeV, assuming a 100% branching fraction to  $tW$  or SU(2) singlet  $B$  scenario, respectively.

A similar search by CMS [126], using  $19.8 \text{ fb}^{-1}$  of  $\sqrt{s} = 8 \text{ TeV}$  data, selected events with one lepton and four or more jets, with at least one  $b$ -tagged jet, significant missing  $p_T$ , and further categorizes them based on the number of jets tagged as arising from the decay of boosted  $W, Z$  or  $H^0$  bosons. The  $S_T$  distributions of the events in different categories showed no excess of events

above the expected background and yielded a lower limit on the  $B$  quark mass of 0.73 TeV for  $BR(B \rightarrow Wt) = 1$ .

CMS [116] also searched for pair production of both  $TT$  and  $BB$  with collisions from  $2.5 \text{ fb}^{-1}$  of  $\sqrt{s} = 13 \text{ TeV}$  data. The analysis searches for events with one high  $p_T$  lepton, multiple jets, and highly boosted  $W$  or Higgs bosons decaying hadronically. The analysis focuses on pair production and selects events with either a boosted  $W$  or Higgs candidate and then proceeds to search for anomalous production in excess of standard model production. Seeing no significant excesses CMS then proceeded to set limits in many different interpretations. The strongest was from the the  $B \rightarrow Wt$  interpretation leading to excluding heavy vector-like  $B$  quark less than 0.73 TeV.

The all-hadronic inclusive analysis [106] performed by CMS using the BEST NN technique to classify  $W/Z/H^0/t/b$  light jets also gives exclusion limits on  $B$  quark production for various combinations of branching fractions for decays to  $tW, bZ, bH^0$ . By considering categories based on various combinations of the boson and quark jets in the final state it excludes  $B$  quarks with masses up to 1230 GeV, for  $B$  decays to  $tW$  with a 100% branching fraction.

Electroweak production of single heavy  $B+b$  productions has been studied by CMS in the decay to  $tW$  with lepton+jets final state [127]. Single lepton events with hadronic jets, including a forward jet, missing  $p_T$  are selected and divided into 10 different categories based on lepton flavor ( $e/\mu$ ), top-tagged,  $W$ -tagged, and 0/1/2  $b$ -tagged jets.  $B$  quark mass  $m_{reco}$  is fully reconstructed from lepton, jets, and missing  $p_T$ , where the neutrino four-momentum is computed using the missing  $p_T$  and the  $W$  mass constraint (assuming massless  $\nu$ ). For events within top-tagged category, the high  $p_T$  top-tagged hadronic jet and the leptonically decaying  $W$  boson is used to compute  $m_{reco}$ . The  $m_{reco}$  distribution is used as the signal discriminator. In the absence of an excess over the expected SM background, the exclusion limits on the production cross section is for  $B$  quark masses between 0.7-2 TeV varies between 0.3 to 0.03 pb. In addition,  $B$  quarks with left-handed couplings and a relative width of 10, 20, and 30% are excluded for masses below 1.49, 1.59, and 1.66 TeV respectively.

#### $B \rightarrow bZX$ :

A search by CMS [128] for the pair-production of a heavy  $B$  quark and its antiparticle has been performed, where one the heavy  $B$  quark decays to  $bZ$ . Events with a  $Z$  boson decaying to  $e^+e^-$  or  $\mu^+\mu^-$  and at least one  $b$  jet are selected. The signal from  $B \rightarrow bZ$  decays are expected to appear as a local enhancement in the  $bZ$  mass distribution. No such enhancement was found and  $B$  quarks that decay 100% into  $bZ$  are excluded below 0.70 TeV. This analysis also set upper limits on the branching fraction for  $B \rightarrow bZ$  decays of 30-100% in the  $B$  quark mass range 0.45-0.70 TeV. A complementary search has been carried out by ATLAS for new heavy quarks decaying into a  $Z$  boson and a  $b$ -quark [129]. Selected dilepton events contain a high transverse momentum  $Z$  boson that decays leptonically, together with two  $b$  jets. If the dilepton events have an extra lepton in addition to those from the  $Z$  boson, then only one  $b$ -jet is required. No significant excess of events above the standard model expectation was observed, and mass limits were set depending on the assumed branching ratios, as shown in Fig. 93.4. In a weak-isospin singlet scenario, a  $B$  quark with mass lower than 0.65 TeV was excluded, while for a particular weak-isospin doublet scenario, a  $B$  quark with mass lower than 0.73 TeV was ruled out.

ATLAS has searched for the electroweak production of single  $B$  quarks, which is accompanied by a  $b$  jet and a light jet [129]. The dilepton selection for double  $B$  production was modified for the single  $B$  production study by requiring the presence of an additional energetic jet in the forward region. An upper limit of 200 fb was obtained for the process  $\sigma(pp \rightarrow B\bar{b}q) \times B(B \rightarrow Zb)$  with a heavy  $B$  quark mass at 0.70 TeV. This search indicated that the electroweak mixing parameter  $X_{Bb}$  below 0.5 is neither expected or observed to be excluded for any values of  $B$  quark mass.

#### Combination of $B \rightarrow tW/bZ/bH^0$ :

The ATLAS experiment has combined the various analyses tar-

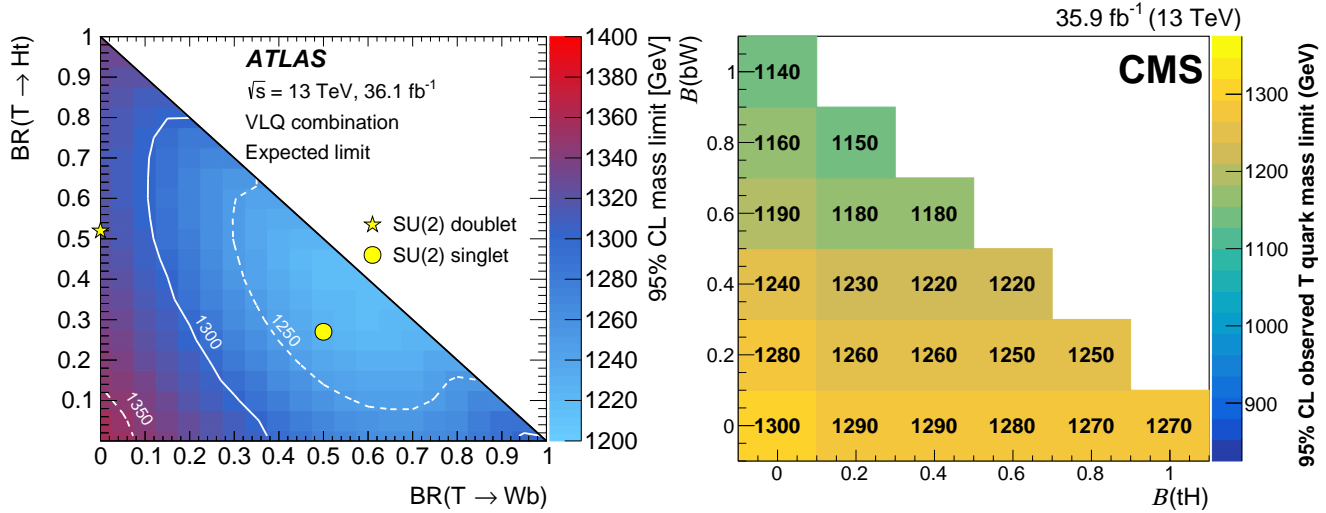


Figure 93.3: Left panel: observed limits on the mass of the  $T$  quark in the plane of  $\mathcal{B}(T \rightarrow tH^0)$  versus  $\mathcal{B}(T \rightarrow bW)$  from a combination [124] of all ATLAS searches for  $TT$  production. The markers indicate the default branching ratios for the SU(2) singlet and doublet scenarios. Right panel: the observed lower limits on the  $T$  quark mass (in GeV), from CMS searches after combining all lepton channels [125], for various branching fraction scenarios.  $\mathcal{B}(T \rightarrow Wb) + \mathcal{B}(T \rightarrow tZ) + \mathcal{B}(T \rightarrow tH^0) = 1$  is assumed.

geted for specific decay modes to obtain the most sensitive limits on the pair production of  $B$  quarks [107, 108, 124]. Various searches ( $W(\ell\nu)t + X$ ,  $Z(\ell\ell)t/b + X$ , same sign charge dilepton events, trilepton events, and all-hadronic) are combined to obtain lower limits on the mass of the  $B$  quark in the plane of  $BR(B \rightarrow Wt)$  vs  $BR(B \rightarrow bH)$ . The searches were optimized for 100% branching fractions and hence are most sensitive at large  $BR(B \rightarrow Wt)$ , and also at large  $BR(B \rightarrow bH^0)$ . For all possible values of branching ratios in the three decay modes  $tW$ ,  $bZ$ , or  $bH^0$ , the lower limits on the  $B$  quark mass was found to be 1.03 TeV and shown in Fig. 93.4 (left) as a function of both  $B$  mass and branching ratio.

CMS combined three channels with lepton final states: single lepton, two leptons with the same sign of the electric charge (SS), or at least three leptons (trilepton) [125]. For various combinations of branching fractions for  $B$  quark decays to  $tW$ ,  $bH^0$  and  $bZ$ , the combined results exclude  $b$  quarks with masses below 0.91–1.24 TeV and are shown in Figure 93.4 (right) the details are provided earlier in subsection 93.2.3.1. The single lepton analysis is most sensitive for  $tHbW$  and  $WbWb$  decay modes, within the the SS dilepton analysis  $tHtH$  and  $tHtZ$  have the best efficiency and for trileptons the  $tZtZ$  and  $tHtZ$  decays modes have the highest efficiency. CMS excludes singlet (doublet)  $B$  quark masses below 1.17 (0.94) TeV. Masses below 800 GeV were excluded in previous searches. For  $B$  quark masses in the range 0.8–1.8 TeV, cross sections smaller than 40.6–9.4 fb (101–49.0 fb) are excluded for the singlet (doublet) scenario.

### 93.2.3.3 Searches for top-partner quark $X_{5/3}$

Searches for a heavy top vector-like quark  $X_{5/3}$ , with exotic charge  $\pm 5/3$ , such as that proposed in Refs. [131, 132], have been performed by both ATLAS and CMS [107, 133].

The analyses assumed pair-production or single-production of  $X_{5/3}$  with  $X_{5/3}$  decaying with 100% branching fraction to  $tW$ . Searches for  $X_{5/3}$  have been performed using two final state signatures: same-sign leptons and lepton+jets.

The analysis based on searching for same-sign leptons, from the two  $W$  bosons from one of the  $X_{5/3}$ , has smaller backgrounds compared to the lepton+jets signature. Requiring same-sign leptons eliminates most of the standard model background processes, leaving those with smaller cross sections:  $t\bar{t}$ ,  $W$ ,  $t\bar{t}Z$ ,  $WWW$ , and same-sign  $WW$ . In addition, backgrounds from instrumental effects due to charge misidentification were considered. Assuming pair production of  $X_{5/3}$ , the analyses by CMS using  $H_T$  as the discriminating variable restrict the  $X_{5/3}$  mass to be higher than 1.16 (1.10) TeV for a right (left) handed chirality particle [133–135]. The limits obtained by ATLAS, by classifying the signal region by

number of  $b$  jets,  $H_T$ , and missing  $p_T$  in the event, corresponded to a lower mass limit on  $X_{5/3}$  of 1.19 TeV [136, 137].

Searches for  $X_{5/3}$  using leptons+jets final state signatures are based on either full or partial reconstruction of the  $T$  mass from the lepton, jets (including  $b$  jets) and missing  $p_T$ . The CMS search [133, 138] also utilized jet substructure techniques to identify boosted  $X_{5/3}$  topologies. The discriminating variable used was the mass constructed from the lepton and  $b$ -tagged jet,  $M_{(\ell,b)}$ , which corresponds to the visible mass of leptonically decaying top quark. To optimize the search sensitivity, the events were further separated into categories based on lepton flavor ( $e$ ,  $\mu$ ), the number of  $b$ -tagged jets, the number of  $W$ -tagged jets, and the number of  $t$ -tagged jets. In the absence of a signal, the CMS analysis excluded  $X_{5/3}$  quark masses with right-handed (left-handed) couplings below 1.32 (1.30) TeV [138]. Combining the lepton+jets with the same-sign leptons analyses leads to a slight improvement and excludes  $X_{5/3}$  quark masses with right-handed (left-handed) couplings below 1.33 (1.30) TeV.

The ATLAS lepton+jets search for  $X_{5/3}$  utilized events with high  $p_T$   $W$  bosons and  $b$  jets. The search described earlier for  $T$  pair production, with  $T \rightarrow Wb$  decays, can be reinterpreted as a search for  $X \rightarrow tW$ . This analysis excluded  $X_{5/3}$  with masses below 1.25 TeV [107].

The single  $X_{5/3}$  production cross section depends on the coupling constant  $\lambda$  of the  $tWX$  vertex. ATLAS has performed an analysis of same-sign dileptons which includes both the single and pair production. This analysis led to a lower limit on the mass of the  $X_{5/3}$  of 0.75 TeV for both values of  $\lambda = 0.5$  and 1.0 [139].

Single heavy  $X_{5/3}+t$  production has been studied by CMS in the decay to  $tW$  with lepton+jets final state [127]. The description of the analysis is provided earlier in the discussion of  $B \rightarrow WtX$  decays, where the reconstructed mass of  $X_{5/3}$ ,  $m_{reco}$  distribution is used as the signal discriminator. In the absence of a excess over the expected SM background, the exclusion limits on the production cross section is for  $X_{5/3}$  quark masses between 0.7–2 TeV varies between 0.3 to 0.03 pb, depending on the width of  $X_{5/3}$  between 1–10%. In addition,  $X_{5/3}$  quarks with left-handed couplings and a relative width of 10, 20, and 30% are excluded for masses below 0.92, 1.3, and 1.45 TeV respectively.

### 93.2.4 Heavy resonances decaying to VLQ

CMS has performed search for VLQ production in the decay of massive resonances such as  $Z'$  and  $W'$  bosons.

$Z' \rightarrow tT$ : Specifically searches are presented by CMS in Refs. [140] and [141] for massive spin-1  $Z'$  resonances decaying to a top quark and heavy VLQ top quark partner  $T$ . The results of this search for a heavy spin-1 resonance are interpreted in the



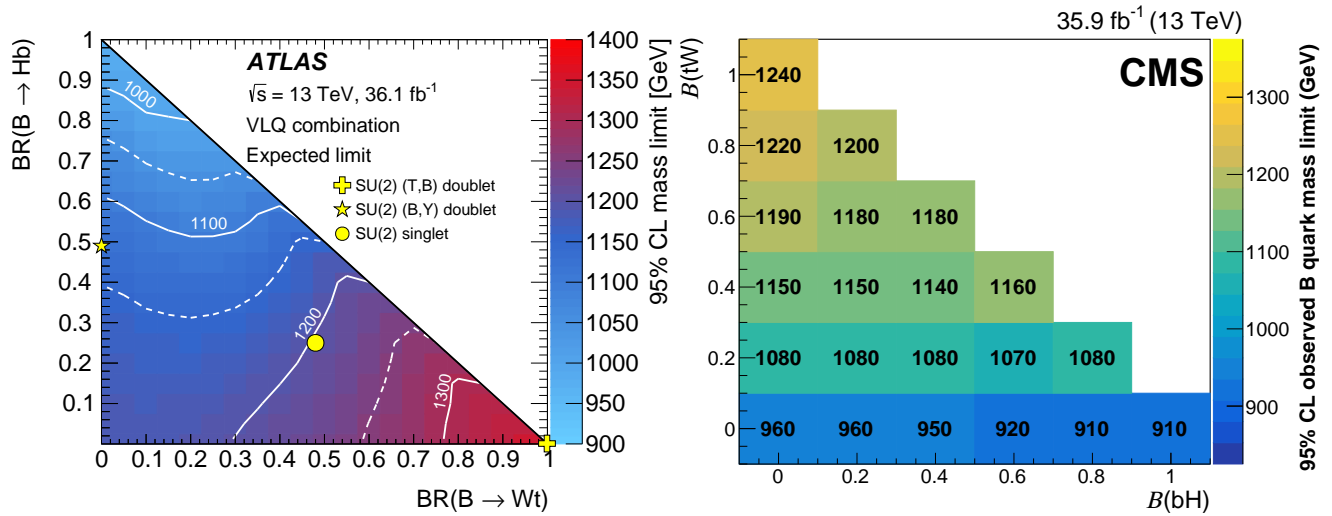


Figure 93.4: Observed limits on the mass of the  $B$  quark in the plane of  $BR(B \rightarrow bH^0)$  versus  $BR(B \rightarrow tW)$  from ATLAS searches [124] on the left panel, and CMS searches [125] on the right panel, for  $BB$  production.  $B(B \rightarrow \mathcal{H}) + B(B \rightarrow \mathcal{Z}) + B(B \rightarrow \mathcal{W}) = 1$  is assumed. The yellow markers indicate the branching ratios for the SU(2) singlet and doublet scenarios.

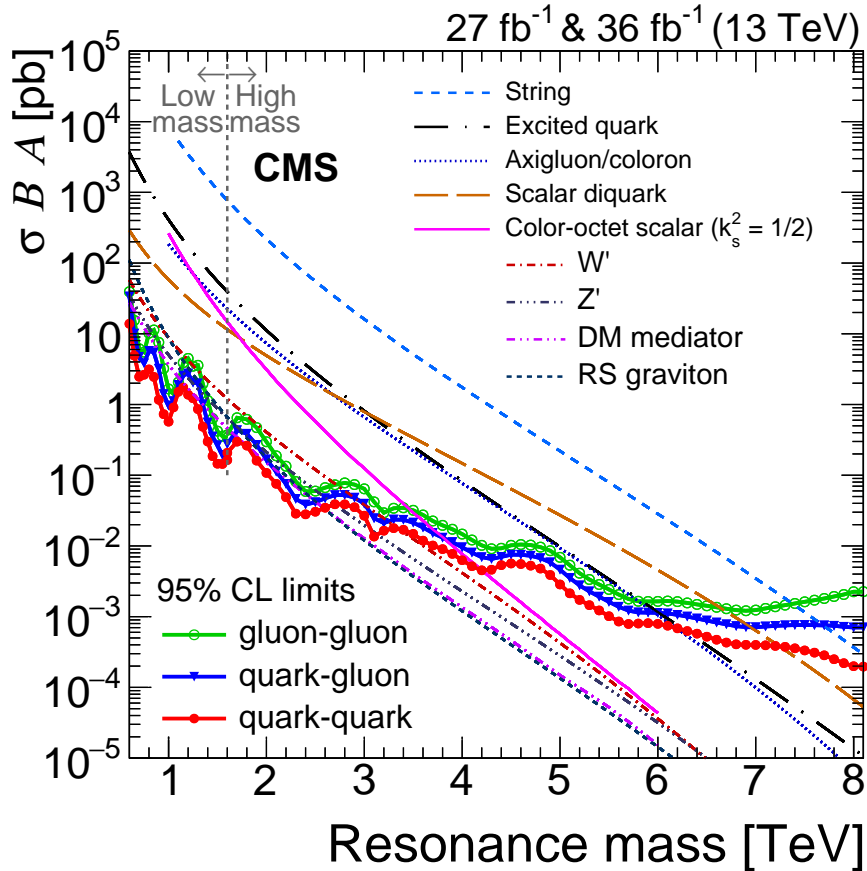


Figure 93.5: Observed 95% C.L. limits on  $\sigma \times B \times A$  for string resonances, excited quarks, axigluons, colorons, E6 diquarks, s8 resonances,  $W'$  and  $Z'$  bosons, and Randall-Sundrum Gravitons  $g_{KK}$  from [130].

context of two different models. In the  $G^*$  model which predicts ten VLQs ( $T, B, \tilde{T}, \tilde{B}, T_{5/3}, T_{2/3}, T', B', B_{-1/3}, B_{-4/3}$ ) with the mass relationship  $M(T_{5/3}) = M(T_{2/3}) = M(T)\cos(\phi_L)$ . For the benchmark scenario [142],  $\cos(\phi_L) = 0.84$  and the branching fractions  $T \rightarrow tH^0, tZ, Wb$  are 0.25, 0.25 and 0.5 respectively. The  $\rho^0$  model predicts a multiple of four new VLQs  $T, B, X_{2/3}, X_{5/3}$ , and in the benchmark scenario [143], the branching fractions  $T \rightarrow tH^0, tZ, Wb$  are 0.5, 0.5 and 0 respectively.

Two of the three different decays of the  $Z' \rightarrow tT$  with  $T \rightarrow$

$tH^0, tZ, Wb$  are characterized by the presence of two top quark decays and a boson ( $H^0/Z$ ). A search [141] by CMS, optimized for  $T \rightarrow tH/Zt$  decays is carried out in the lepton+jets final state using a dataset corresponding to an integrated luminosity of  $35.9 \text{ fb}^{-1}$ . Jet substructure techniques are used to identify (or tag) the high  $p_T$  large-radius jets originating from  $H^0, Z$  bosons and merged top quarks. The mass of the  $Z'$  boson is used as the signal discriminator and constructed using  $H^0$  or  $Z$ -tagged dijet, the hadronic and leptonic top quark four vectors. For the

leptonic top quark reconstruction ( $t \rightarrow b\ell\nu_\ell$ ), the neutrino four vector is obtained from the event missing  $p_T$  using the  $W$  boson mass constraint. While the high  $p_T$  hadronic top quark jets from decays of massive  $Z'$  bosons are mostly merged and identified by top tagging techniques, those from  $T$  decays maybe resolved. The reconstructed  $Z'$  candidate events are classified into six different categories requiring the presence of either  $H^0$ -tagged jet with 2 b-tagged subjets or one b-tagged subjet or a  $Z$ -tagged boson, each with either zero or one top-tagged jet. This search does not observe any significant deviation in data over the expectation from standard model backgrounds. Within the context of the  $G^*$  model, for a  $T$  mass of 1.2 (1.5), this search excludes  $G^*$  [142] resonances with masses between 1.5–2.3 (2.0–2.4) TeV.

The search in the all-hadronic final state is based on a  $2.6 \text{ fb}^{-1}$  dataset [140], and optimized for  $T \rightarrow Wb$  decays. Jet substructure techniques are deployed for tagging jets from high  $p_T$   $W$  boson and top quarks. Events are categorized into two groups based on the presence of b-tagged subjet in the top-tagged jet. Multijet background estimation is challenging and determined using sidebands defined by inverting the b tagging requirement. Upper limits on cross section for  $Z' \rightarrow tT$  are obtained in the range of 0.13–10 pb. With additional data, this search has the potential to exclude scenarios in composite Higgs and extra dimension models.

$W' \rightarrow Tb/Bt$ :  $W'$  bosons are predicted to decay to VLQ third generation partners  $T$ ,  $B$  quarks within composite Higgs and warped extra dimensional models [144]. In the benchmark scenarios of this framework,  $W'$  decays to  $Tb$  or  $Bt$  are equally distributed and the subsequent VLQ decays  $T \rightarrow tH$  and  $B \rightarrow bH^0$  each are assumed to have a branching fraction of 0.5. The search for  $W' \rightarrow Tb/bH^0 \rightarrow tbH^0$  is performed using a sample of  $35.9 \text{ fb}^{-1}$  by CMS [145] in the final state with all-hadronic decays of both the Higgs boson ( $H^0 \rightarrow b\bar{b}$ ) and the top quark. Both the  $H^0$  boson and the top quark are expected to be boosted in the decay of a heavy  $W'$ , and hence jet substructure techniques, including subjet b-tagging and double b-tagging are deployed to identify the  $H^0$ -tagged and the top-tagged jets. The three particle mass  $m_{tbH^0}$ , is used as the signal discriminant to observe the  $W'$  resonance. There is no excess observed in data above the expected SM background. This search excludes  $W'$  production cross section above 0.01–0.43 pb for masses between 1.5–4.0 TeV.

### 93.2.5 Colorons and Colored Scalars

These particles are associated with top-condensate and top-seesaw models, which involve an enlarged color gauge group. The new particles decay to dijets,  $t\bar{t}$ , and  $b\bar{b}$ .

Direct searches for colorons, color-octet scalars and other heavy objects decaying to  $q\bar{q}$ ,  $qg$ ,  $qg$ , or  $gg$  has been performed using LHC data from pp collisions at  $\sqrt{s} = 7, 8$  and 13 TeV. Based on the analysis of dijet events from a data sample corresponding to a luminosity of  $19.6 \text{ fb}^{-1}$ , at  $\sqrt{s} = 8$  TeV the CMS experiment excluded pair production of colorons with mass between 1.20–3.60 and 3.90–4.08 TeV [146]. Analyses of inclusive 8- and 10-jet final states with low missing transverse momentum by CMS [147], set limits in several benchmark models. Colorons (axigluons) with masses between 0.6 and 0.75 (up to 1.15) TeV were excluded, and gluinos in R-parity violating supersymmetric scenarios were ruled out from 0.6 up to 1.1 TeV.

A search for pair-produced colorons based on an integrated luminosity of  $5.0 \text{ fb}^{-1}$  at  $\sqrt{s} = 7$  TeV by CMS excluded colorons with masses between 0.25 TeV and 0.74 TeV, assuming colorons decay 100% into  $q\bar{q}$  [148]. This analysis was based on events with at least four jets and two dijet combinations with similar dijet mass. Color-octet scalars (s8) with masses between 1.20–2.79 TeV were excluded by CMS [146], and below 2.7 TeV by ATLAS [149].

These studies have now been extended to take advantage of the increased center-of-mass energy during Run 2 of the LHC. Using the  $35.9 \text{ fb}^{-1}$  of data collected at  $\sqrt{s} = 13$  TeV, searches for narrow resonances have been performed by CMS. An analysis of the dijet invariant mass spectrum formed using wide jets [130, 150, 151], separated by  $\Delta\eta_{jj} \leq 1.3$ , led to limits on new particles decaying to parton pairs ( $q\bar{q}$ ,  $qg$ ,  $gg$ ). Specific exclusions on the masses of colorons and color-octet scalars were obtained and are shown in Fig. 93.5. Exclusions have been obtained for axigluons and

colorons below 6.1 TeV, and color-octet scalars below 3.4 TeV.

## 93.3 Conclusions

As the above analyses have demonstrated, there is already substantial sensitivity to possible new particles predicted to accompany the  $H^0$  in dynamical frameworks of electroweak symmetry breaking. No significant hints of any deviations from the standard model have been observed, and limits typically at the scale of a few hundred GeV to a few TeV are set.

Given the need to better understand the  $H^0$  and to determine in detail how it behaves, such analyses continue to be a major theme of Run 2 the LHC, and we look forward to increased sensitivity as a result of the higher luminosity at the increased center of mass energy of collisions.

## References

- [1] G. Aad *et al.* (ATLAS), Phys. Lett. **B716**, 1 (2012), [arXiv:1207.7214].
- [2] S. Chatrchyan *et al.* (CMS), Phys. Lett. **B716**, 30 (2012), [arXiv:1207.7235].
- [3] S. Weinberg, Physica **A96**, 1-2, 327 (1979).
- [4] A. Manohar and H. Georgi, Nucl. Phys. **B234**, 189 (1984).
- [5] H. Georgi, Nucl. Phys. **B266**, 274 (1986).
- [6] R. S. Chivukula, in “Flavor physics for the millennium. Proceedings, Theoretical Advanced Study Institute in elementary particle physics, TASI 2000, Boulder, USA, June 4-30, 2000,” 731–772 (2000), [hep-ph/0011264].
- [7] R. S. Chivukula, M. J. Dugan and M. Golden, Phys. Rev. **D47**, 2930 (1993), [hep-ph/9206222].
- [8] S. Weinberg, Phys. Rev. **D13**, 974 (1976), [Addendum: Phys. Rev. **D19**, 1277(1979)].
- [9] L. Susskind, Phys. Rev. **D20**, 2619 (1979).
- [10] K. Lane (2002), [hep-ph/0202255].
- [11] C. T. Hill and E. H. Simmons, Phys. Rept. **381**, 235 (2003), [Erratum: Phys. Rept. **390**, 553(2004)], [hep-ph/0203079].
- [12] R. Shrock, in “The origin of mass and strong coupling gauge theories. Proceedings, 5th International Workshop, SCGT’06, Nagoya, Japan November 21-24, 2006,” 227–241 (2007), [hep-ph/0703050].
- [13] E. Eichten *et al.*, Rev. Mod. Phys. **56**, 579 (1984), [Addendum: Rev. Mod. Phys. **58**, 1065(1986)].
- [14] E. Eichten *et al.*, Phys. Rev. **D34**, 1547 (1986).
- [15] R. S. Chivukula and V. Koulovassilopoulos, Phys. Lett. **B309**, 371 (1993), [hep-ph/9304293].
- [16] R. Foadi, M. T. Frandsen and F. Sannino, Phys. Rev. **D87**, 9, 095001 (2013), [arXiv:1211.1083].
- [17] B. Holdom, Phys. Lett. **150B**, 301 (1985).
- [18] K. Yamawaki, M. Bando, and K.-i. Matumoto, Phys. Rev. Lett. **56**, 1335 (1986).
- [19] T. W. Appelquist, D. Karabali and L. C. R. Wijewardhana, Phys. Rev. Lett. **57**, 957 (1986).
- [20] T. Appelquist and L. C. R. Wijewardhana, Phys. Rev. **D35**, 774 (1987).
- [21] T. Appelquist and L. C. R. Wijewardhana, Phys. Rev. **D36**, 568 (1987).
- [22] E. Eichten, K. Lane and A. Martin (2012), [arXiv:1210.5462].
- [23] D. B. Kaplan and H. Georgi, Phys. Lett. **136B**, 183 (1984).
- [24] D. B. Kaplan, H. Georgi and S. Dimopoulos, Phys. Lett. **136B**, 187 (1984).
- [25] M. E. Peskin, Nucl. Phys. **B175**, 197 (1980).
- [26] J. Preskill, Nucl. Phys. **B177**, 21 (1981).
- [27] See “Status of Higgs Boson Physics” review in this volume.
- [28] R. Barbieri and A. Strumia, in “4th Rencontres du Vietnam: Physics at Extreme Energies (Particle Physics and Astrophysics) Hanoi, Vietnam, July 19-25, 2000,” (2000), [hep-ph/0007265].

- [29] N. Arkani-Hamed, A. G. Cohen and H. Georgi, Phys. Lett. **B513**, 232 (2001), [hep-ph/0105239].
- [30] N. Arkani-Hamed *et al.*, JHEP **08**, 020 (2002), [hep-ph/0202089].
- [31] N. Arkani-Hamed *et al.*, JHEP **07**, 034 (2002), [hep-ph/0206021].
- [32] M. Schmaltz and D. Tucker-Smith, Ann. Rev. Nucl. Part. Sci. **55**, 229 (2005), [hep-ph/0502182].
- [33] K. Agashe *et al.*, Phys. Lett. **B641**, 62 (2006), [hep-ph/0605341].
- [34] P. Sikivie *et al.*, Nucl. Phys. **B173**, 189 (1980).
- [35] B. Bellazzini, C. Csáki and J. Serra, Eur. Phys. J. **C74**, 5, 2766 (2014), [arXiv:1401.2457].
- [36] R. Essig *et al.*, JHEP **09**, 085 (2017), [arXiv:1707.03399].
- [37] Z. Chacko, H.-S. Goh and R. Harnik, Phys. Rev. Lett. **96**, 231802 (2006), [hep-ph/0506256].
- [38] R. S. Chivukula, A. G. Cohen and K. D. Lane, Nucl. Phys. **B343**, 554 (1990).
- [39] V. A. Miransky, M. Tanabashi and K. Yamawaki, Mod. Phys. Lett. **A4**, 1043 (1989).
- [40] W. A. Bardeen, C. T. Hill and M. Lindner, Phys. Rev. **D41**, 1647 (1990).
- [41] C. T. Hill, Phys. Lett. **B266**, 419 (1991).
- [42] B. A. Dobrescu and C. T. Hill, Phys. Rev. Lett. **81**, 2634 (1998), [hep-ph/9712319].
- [43] R. S. Chivukula *et al.*, Phys. Rev. **D59**, 075003 (1999), [hep-ph/9809470].
- [44] S. Dimopoulos and L. Susskind, Nucl. Phys. **B155**, 237 (1979), [2,930(1979)].
- [45] E. Eichten and K. D. Lane, Phys. Lett. **90B**, 125 (1980).
- [46] D. B. Kaplan, Nucl. Phys. **B365**, 259 (1991).
- [47] T. Appelquist, M. Piai and R. Shrock, Phys. Rev. **D69**, 015002 (2004), [hep-ph/0308061].
- [48] R.S. Chivukula, B.A. Dobrescu, and E.H. Simmons, Phys. Lett. **B401**, 74 (1997).
- [49] Y. Grossman and M. Neubert, Phys. Lett. **B474**, 361 (2000), [hep-ph/9912408].
- [50] S. J. Huber and Q. Shafi, Phys. Lett. **B498**, 256 (2001), [hep-ph/0010195].
- [51] T. Gherghetta and A. Pomarol, Nucl. Phys. **B586**, 141 (2000), [hep-ph/0003129].
- [52] K. Agashe, R. Contino and A. Pomarol, Nucl. Phys. **B719**, 165 (2005), [hep-ph/0412089].
- [53] G. F. Giudice *et al.*, JHEP **06**, 045 (2007), [hep-ph/0703164].
- [54] R. S. Chivukula and H. Georgi, Phys. Lett. **B188**, 99 (1987).
- [55] G. D'Ambrosio *et al.*, Nucl. Phys. **B645**, 155 (2002), [hep-ph/0207036].
- [56] K. Agashe *et al.* (2005), [hep-ph/0509117].
- [57] T. Appelquist and R. Shrock, Phys. Lett. **B548**, 204 (2002), [hep-ph/0204141].
- [58] K. Sakai, Nucl. Phys. **B867**, 429 (2013), [arXiv:1207.4057].
- [59] J. M. Maldacena, Int. J. Theor. Phys. **38**, 1113 (1999), [Adv. Theor. Math. Phys.2,231(1998)], [hep-th/9711200].
- [60] For a review, see C. Csaki, J. Hubisz, and P. Meade, hep-ph/0510275 (2005), and “Extra Dimensions” review in this volume.
- [61] C. Pica, PoS **LATTICE2016**, 015 (2016), [arXiv:1701.07782].
- [62] T. Appelquist *et al.*, Phys. Rev. **D93**, 11, 114514 (2016), [arXiv:1601.04027].
- [63] PDG review of Zprime boson in this volume.
- [64] PDG review of Wprime boson in this volume.
- [65] M. Aaboud *et al.* (ATLAS), Phys. Lett. **B**, 68 (2019), [arXiv:1903.06248].
- [66] CMS Collaboration, Technical Report CMS-PAS-EXO-19-019, CERN, Geneva (2019), URL <http://cds.cern.ch/record/2684757>.
- [67] G. Aad *et al.* (ATLAS), Phys. Rev. **D90**, 5, 052005 (2014), [arXiv:1405.4123].
- [68] M. Aaboud *et al.* (ATLAS), JHEP **01**, 055 (2018), [arXiv:1709.07242].
- [69] CMS Collaboration, JHEP **0217**, 48 (2017).
- [70] ATLAS Collaboration, ATLAS-CONF-2016-014 (2016).
- [71] CMS Collaboration, JHEP **0717**, 001 (2016).
- [72] M. Aaboud *et al.* (ATLAS), Phys. Rev. D. **99**, 092004 (2019), [arXiv:1902.10077].
- [73] A. M. Sirunyan *et al.* (CMS), JHEP **04**, 031 (2019), [arXiv:1810.05905].
- [74] ATLAS Collaboration, ATLAS-CONF-2019-007 (2019).
- [75] CMS Collaboration, CMS-PAS-EXO-19-012 (2019).
- [76] M. Aaboud *et al.* (ATLAS), Accepted by Phys. Rev. [arXiv:1906.05609].
- [77] V. Khachatryan *et al.* (CMS), Phys. Lett. **B770**, 278 (2017), [arXiv:1612.09274].
- [78] V. Khachatryan *et al.* (CMS), Phys. Lett. **B755**, 196 (2016), [arXiv:1508.04308].
- [79] S. Chatrchyan *et al.* (CMS), JHEP **05**, 108 (2014), [arXiv:1402.2176].
- [80] V. Khachatryan *et al.* (CMS), JHEP **02**, 122 (2016), [arXiv:1509.06051].
- [81] A. M. Sirunyan *et al.* (CMS), JHEP **08**, 029 (2017), [arXiv:1706.04260].
- [82] A. M. Sirunyan *et al.* (CMS), Phys. Lett. **B777**, 39 (2018), [arXiv:1708.08539].
- [83] CMS Collaboration, Technical Report CMS-PAS-JME-15-002, CERN, Geneva (2016), URL <http://cds.cern.ch/record/2126325>.
- [84] G. Aad *et al.* (ATLAS), Phys. Lett. **B788**, 347 (2019), [arXiv:1807.10473].
- [85] G. Aad *et al.* (ATLAS), Eur. Phys. J. **C75**, 4, 165 (2015), [arXiv:1408.0886].
- [86] G. Aad *et al.* (ATLAS), Phys. Lett. **B743**, 235 (2015), [arXiv:1410.4103].
- [87] D. Pappadopulo *et al.*, JHEP **09**, 060 (2014), [arXiv:1402.4431].
- [88] M. Aaboud *et al.* (ATLAS), Phys. Rev. **D98**, 5, 052008 (2018), [arXiv:1601.04027].
- [89] A. M. Sirunyan *et al.* (CMS), Phys. Lett. **B798**, 134952 (2019), [arXiv:1906.00057].
- [90] M. Aaboud *et al.* (ATLAS), Phys. Lett. **B**, 91 (2017), [arXiv:1708.04445].
- [91] M. Aaboud *et al.* (ATLAS), JHEP **03**, 042 (2018), [arXiv:1710.07235].
- [92] M. Aaboud *et al.* (ATLAS), Phys. Lett. **B**, 68 (2018), [arXiv:1806.10532].
- [93] A. M. Sirunyan *et al.* (CMS), Phys. Rev. **D97**, 072006, [arXiv:1708.05379].
- [94] A. M. Sirunyan *et al.* (CMS), JHEP **07**, 075, [arXiv:1802.09407].
- [95] A. M. Sirunyan *et al.* (CMS), JHEP **09**, 101, [arXiv:1803.10093].
- [96] M. Aaboud *et al.* (ATLAS), Eur. Phys. J. **C**, 78 (2017), [arXiv:1710.01123].
- [97] M. Aaboud *et al.* (ATLAS), Phys. Lett. **B**, 774 (2017), [arXiv:1707.06858].



- [98] M. Aaboud *et al.* (ATLAS), JHEP **B**, 174 (2018), [arXiv:1712.06518].
- [99] A. M. Sirunyan *et al.* (CMS), Eur. Phys. J. **C**, 636, [arXiv:1707.01303].
- [100] F. del Aguila *et al.*, Nucl. Phys. **B334**, 1 (1990).
- [101] A. M. Sirunyan *et al.* (CMS), Phys. Lett. **B779**, 82 (2018), [arXiv:1710.01539].
- [102] CMS Collaboration, Technical report (2014).
- [103] V. Khachatryan *et al.* (CMS), Phys. Rev. **D93**, 1, 012003 (2016), [arXiv:1509.04177].
- [104] CMS Collaboration, Technical report (2012).
- [105] S. D. Ellis, C. K. Vermilion and J. R. Walsh, Phys. Rev. **D80**, 051501 (2009), [arXiv:0903.5081].
- [106] A. M. Sirunyan *et al.* (CMS) (2019), [arXiv:1906.11903].
- [107] M. Aaboud *et al.* (ATLAS), JHEP **10**, 141 (2017), [arXiv:1707.03347].
- [108] G. Aad *et al.* (ATLAS), JHEP **08**, 105 (2015), [arXiv:1505.04306].
- [109] A. M. Sirunyan *et al.* (CMS), Phys. Lett. **B772**, 634 (2017), [arXiv:1701.08328].
- [110] M. Aaboud *et al.* (ATLAS), JHEP **05**, 164 (2019), [arXiv:1812.07343].
- [111] G. Aad *et al.* (ATLAS), Eur. Phys. J. **C76**, 8, 442 (2016), [arXiv:1602.05606].
- [112] ATLAS collaboration (ATLAS), Technical report (2016).
- [113] M. Aaboud *et al.* (ATLAS), Phys. Rev. **D98**, 9, 092005 (2018), [arXiv:1808.01771].
- [114] S. Chatrchyan *et al.* (CMS), Phys. Lett. **B729**, 149 (2014), [arXiv:1311.7667].
- [115] V. Khachatryan *et al.* (CMS), JHEP **06**, 080 (2015), [arXiv:1503.01952].
- [116] A. M. Sirunyan *et al.* (CMS), JHEP **11**, 085 (2017), [arXiv:1706.03408].
- [117] CMS Collaboration, [cds.cern.ch/record/1709129](https://cds.cern.ch/record/1709129) (2014).
- [118] A. M. Sirunyan *et al.* (CMS), JHEP **04**, 136 (2017), [arXiv:1612.05336].
- [119] V. Khachatryan *et al.* (CMS), Phys. Lett. **B771**, 80 (2017), [arXiv:1612.00999].
- [120] M. Aaboud *et al.* (ATLAS), JHEP **08**, 052 (2017), [arXiv:1705.10751].
- [121] M. Aaboud *et al.* (ATLAS), Phys. Rev. **D98**, 11, 112010 (2018), [arXiv:1806.10555].
- [122] M. Aaboud *et al.* (ATLAS), JHEP **05**, 041 (2019), [arXiv:1812.09743].
- [123] A. M. Sirunyan *et al.* (CMS), Phys. Lett. **B781**, 574 (2018), [arXiv:1708.01062].
- [124] M. Aaboud *et al.* (ATLAS), Phys. Rev. Lett. **121**, 21, 211801 (2018), [arXiv:1808.02343].
- [125] A. M. Sirunyan *et al.* (CMS), JHEP **08**, 177 (2018), [arXiv:1805.04758].
- [126] CMS Collaboration, Technical report (2012).
- [127] A. M. Sirunyan *et al.* (CMS), Eur. Phys. J. **C79**, 90 (2019), [arXiv:1809.08597].
- [128] V. Khachatryan *et al.* (CMS), Phys. Rev. **D93**, 11, 112009 (2016), [arXiv:1507.07129].
- [129] G. Aad *et al.* (ATLAS), JHEP **11**, 104 (2014), [arXiv:1409.5500].
- [130] A. M. Sirunyan *et al.* (CMS), JHEP **08**, 130 (2018), [arXiv:1806.00843].
- [131] R. Contino and G. Servant, JHEP **06**, 026 (2008), [arXiv:0801.1679].
- [132] J. Mrazek and A. Wulzer, Phys. Rev. **D81**, 075006 (2010), [arXiv:0909.3977].
- [133] A. M. Sirunyan *et al.* (CMS), JHEP **08**, 073 (2017), [arXiv:1705.10967].
- [134] CMS Collaboration, Technical report (2017).
- [135] S. Chatrchyan *et al.* (CMS), Phys. Rev. Lett. **112**, 17, 171801 (2014), [arXiv:1312.2391].
- [136] M. Aaboud *et al.* (ATLAS), JHEP **12**, 039 (2018), [arXiv:1807.11883].
- [137] G. Aad *et al.* (ATLAS), Phys. Rev. **D91**, 11, 112011 (2015), [arXiv:1503.05425].
- [138] A. M. Sirunyan *et al.* (CMS), JHEP **03**, 082 (2019), [arXiv:1810.03188].
- [139] G. Aad *et al.* (ATLAS), JHEP **10**, 150 (2015), [arXiv:1504.04605].
- [140] A. M. Sirunyan *et al.* (CMS), JHEP **09**, 053 (2017), [arXiv:1703.06352].
- [141] A. M. Sirunyan *et al.* (CMS), Eur. Phys. J. **C79**, 3, 208 (2019), [arXiv:1812.06489].
- [142] C. Bini, R. Contino and N. Vignaroli, JHEP **01**, 157 (2012), [arXiv:1110.6058].
- [143] D. Greco and D. Liu, JHEP **12**, 126 (2014), [arXiv:1410.2883].
- [144] N. Vignaroli, Phys. Rev. **D89**, 9, 095027 (2014), [arXiv:1404.5558].
- [145] A. M. Sirunyan *et al.* (CMS), JHEP **03**, 127 (2019), [arXiv:1811.07010].
- [146] V. Khachatryan *et al.* (CMS), Phys. Rev. **D91**, 5, 052009 (2015), [arXiv:1501.04198].
- [147] V. Khachatryan *et al.* (CMS), Phys. Lett. **B770**, 257 (2017), [arXiv:1608.01224].
- [148] S. Chatrchyan *et al.* (CMS), Phys. Rev. Lett. **110**, 14, 141802 (2013), [arXiv:1302.0531].
- [149] G. Aad *et al.* (ATLAS), Phys. Rev. **D91**, 5, 052007 (2015), [arXiv:1407.1376].
- [150] A. M. Sirunyan *et al.* (CMS), Phys. Lett. **B769**, 520 (2017), [Erratum: Phys. Lett. **B772**, 882 (2017)], [arXiv:1611.03568].
- [151] CMS Collaboration, Technical report (2015).

## 94. Grand Unified Theories

Revised August 2019 by A. Hebecker (Heidelberg U.) and J. Hisano (KMI, Nagoya U.).

### 94.1 The standard model

The Standard Model (SM) may be defined as the renormalizable field theory with gauge group  $G_{SM} = SU(3)_C \times SU(2)_L \times U(1)_Y$ , with 3 generations of fermions in the representation

$$(3, 2)_{1/3} + (\bar{3}, 1)_{-4/3} + (\bar{3}, 1)_{2/3} + (1, 2)_{-1} + (1, 1)_2, \quad (94.1)$$

and a scalar Higgs doublet  $H$  transforming as  $(1, 2)_1$ . Here and below we use boldface numbers to specify the dimension of representations of non-Abelian groups (in this case fundamental and antifundamental) and lower indices for  $U(1)$  charges. The fields of Eq. (94.1) should also be familiar as  $[Q, u^c, d^c, L, e^c]$ , with  $Q = (u, d)$  and  $L = (\nu, e)$  being the quark and lepton  $SU(2)$ -doublets and  $u^c, d^c, e^c$  charge conjugate  $SU(2)$ -singlets.<sup>1</sup> Especially after the discovery of the Higgs, this model is remarkably complete and consistent with almost all experimental data.

A notable exception are neutrino masses, which are known to be non-zero but are absent in the SM even after the Higgs acquires its vacuum expectation value (VEV). The minimalist attitude is to allow for the dimension-five operator  $(HL)^2$  [1], which induces (Majorana) neutrino masses. In the seesaw mechanism [2–4] this operator is generated by integrating out heavy singlet fermions (right-handed (r.h.) neutrinos). Alternatively, neutrinos can have Dirac masses if light singlet neutrinos are added to the SM spectrum.

Conceptual problems of the SM include the absence of a Dark Matter candidate, of a mechanism for generating the baryon asymmetry of the universe, and of any reason for the observed smallness of the  $\theta$  parameter of QCD ( $\theta_{QCD}$ ). In addition, the apparently rather complex group-theoretic data of Eq. (94.1) remains unexplained. Together with the abundance of seemingly arbitrary coupling constants, this disfavors the SM as a candidate fundamental theory, even before quantum gravity problems arise at energies near the Planck mass  $M_P$ .

To be precise, there are 19 SM parameters which have to be fitted to data: Three gauge couplings<sup>2</sup>  $g_3, g_2$  and  $g_1$ , 13 parameters associated with the Yukawa couplings (9 charged fermion masses, three mixing angles and one CP phase in the CKM matrix.), the Higgs mass and quartic coupling, and  $\theta_{QCD}$ . In addition, Majorana neutrinos introduce 3 more masses and 6 mixing angles and phases. As we will see, the paradigm of grand unification addresses mainly the group theoretic data of Eq. (94.1) and the values of the three gauge couplings. In many concrete realizations, it then impacts also the other mentioned issues of the SM, such as the family structure and fermion mass hierarchy.

More specifically, after precision measurements of the Weinberg angle  $\theta_W$  in the LEP experiments, supersymmetric GUTs (SUSY GUTs) have become the leading candidates in the search for ‘Physics beyond the SM’. Supersymmetry (SUSY) is a symmetry between bosons and fermions which requires the addition of superpartners to the SM spectrum. If SUSY is motivated as a solution to the gauge hierarchy problem (i.e. to the naturalness or fine-tuning problem of the electroweak scale) [5], superpartners have to be present near the weak scale. SUSY GUTs [6] then lead to the prediction of  $\theta_W$ , in good agreement with subsequent observations [7]. However, the non-discovery of new particles at the LHC puts into question the presence of new physics at the TeV scale in general and in particular of low-scale supersymmetry. Still, SUSY may be present just outside the presently explored energy domain.

The measured Higgs mass (125 GeV) is in principle consistent with this picture, assuming superpartners in the region of roughly 10 TeV. Such heavy superpartners then induce radiative corrections raising the Higgs mass above the  $Z$  boson mass  $m_Z$  [8, 9]. However, from the vantage point of the hierarchy problem, heavy

superpartners are problematic: They also contribute to SUSY-breaking Higgs mass parameters and thereby to the Higgs potential, tending to raise the  $Z$  mass. As a result, the incarnation of SUSY in terms of the minimal supersymmetric SM (MSSM) is becoming questionable. Turning the logic around, one may say that compared to expectations based on the MSSM with superpartner masses below about 1 TeV, the measured Higgs mass value of 125 GeV is somewhat too high [10]. Independently, the LHC has disfavored light colored superpartners (which does not imply that *all* superpartners are heavy). These facts represent new hints for future work on SUSY GUTs or on GUTs without TeV-scale supersymmetry.

### 94.2 Basic group theory and charge quantization

#### 94.2.1 $SU(4)_C \times SU(2)_L \times SU(2)_R$

Historically, the first attempt at unification was the Pati-Salam model with gauge group  $G_{PS} = SU(4)_C \times SU(2)_L \times SU(2)_R$  [11]. It unifies SM fermions in the sense that one generation (plus an extra SM singlet) now comes from the  $(4, 2, 1) + (\bar{4}, 1, 2)$  of  $G_{PS}$ . This is easy to verify from the breaking pattern  $SU(4)_C \rightarrow SU(3)_C \times U(1)_{B-L}$  together with the identification of SM hypercharge as a linear combination between  $B-L$  (baryon minus lepton number) and the  $T_3$  generator of  $SU(2)_R$ . This model explains charge quantization, that is, why all electric charges are integer multiples of some smallest charge in the SM. Concretely, the  $4$  and  $\bar{4}$  of  $SU(4)_C$  identify lepton number as the 4th colour and the tracelessness of the diagonal generator implies that quark charges are expressed in terms of  $1/N_c$  fractions of lepton charges. However,  $G_{PS}$  is not simple (containing three simple factors), and thus it does not predict gauge coupling unification.

#### 94.2.2 $SU(5)$

Since  $G_{SM}$  has rank four (two for  $SU(3)_C$  and one for  $SU(2)_L$  and  $U(1)_Y$ , respectively), the rank-four group  $SU(5)$  is the minimal choice for unification in a simple group [12]. The three SM gauge coupling constants derive from a universal coupling  $\alpha_G$  at the GUT scale  $M_G$ . Explicitly embedding  $G_{SM}$  in  $SU(5)$  is straightforward, with  $SU(3)_C$  and  $SU(2)_L$  corresponding e.g. to the upper-left  $3 \times 3$  and lower-right  $2 \times 2$  blocks, respectively, in traceless  $5 \times 5$  matrices for  $SU(5)$  generators of the fundamental representation. The  $U(1)_Y$  corresponds to matrices generated by  $\text{diag}(-2/3, -2/3, -2/3, 1, 1)$  and hence commutes with  $SU(3)_C \times SU(2)_L \subset SU(5)$ . It is then easy to derive how one SM generation precisely comes from the  $\mathbf{10} + \bar{\mathbf{5}}$  of  $SU(5)$  (where  $\mathbf{10}$  is the antisymmetric rank-2 tensor):

$$\mathbf{10} : \begin{pmatrix} 0 & u_b^c & -u_g^c & u_r & d_r \\ -u_b^c & 0 & u_r^c & u_g & d_g \\ u_g^c & -u_r^c & 0 & u_b & d_b \\ -u_r & -u_g & -u_b & 0 & e^c \\ -d_r & -d_g & -d_b & -e^c & 0 \end{pmatrix} \quad \text{and} \quad \bar{\mathbf{5}} : \begin{pmatrix} d_r^c \\ d_g^c \\ d_b^c \\ e \\ -\nu_e \end{pmatrix}. \quad (94.2)$$

In addition to charge quantisation this structure explains why the l.h. quark and lepton states fall in  $SU(2)_L$  doublets while the r.h. states are singlets.

Since  $SU(5)$  has 24 generators,  $SU(5)$  GUTs have 12 new gauge bosons known as  $X$  bosons (or  $X/Y$  bosons) in addition to the SM.  $X$  bosons form an  $SU(3)_C$ -triplet and  $SU(2)_L$ -doublet. Their interaction connects quarks and leptons such that baryon and lepton numbers are not conserved and nucleon decay is predicted. Furthermore,  $U(1)_Y$  hypercharge is automatically quantized since it is embedded in  $SU(5)$ .

In order to break the electroweak symmetry at the weak scale and give mass to quarks and leptons, Higgs doublets are needed. In the minimal  $SU(5)$  model, they can sit in either a  $\mathbf{5}_H$  or  $\bar{\mathbf{5}}_H$ . The three additional states are referred to as color-triplet Higgs scalars. Their couplings also violate baryon and lepton numbers, inducing nucleon decay. In order not to violently disagree with the non-observation of nucleon decay, the triplet mass must be greater than  $\sim 10^{11}$  GeV [13]. Moreover, in SUSY GUTs [6], in order to cancel anomalies as well as give mass to both up and down quarks, both Higgs multiplets  $\mathbf{5}_H$  and  $\bar{\mathbf{5}}_H$  are required. As we shall discuss later, nucleon decay now constrains the Higgs triplets to have

<sup>1</sup> In our convention the electric charge is  $Q = T_3 + Y/2$  and all our spinor fields are left-handed (l.h.).

<sup>2</sup> Equivalently, the  $SU(2)_L$  and  $U(1)_Y$  couplings are denoted as  $g = g_2$  and  $g' = \sqrt{3/5} g_1$ . One also uses  $\alpha_s = \alpha_3 = (g_3^2/4\pi)$ ,  $\alpha_{EM} = (e^2/4\pi)$  with  $e = g \sin \theta_W$  and  $\sin^2 \theta_W = (g')^2/(g^2 + (g')^2)$ .

mass significantly greater than  $M_G$  in the minimal SUSY  $SU(5)$  GUT since integrating out the Higgs triplets generates dimension-five baryon-number-violating operators [14]. The mass splitting between doublet and triplet in the  $\mathbf{5}_H$  (and  $\bar{\mathbf{5}}_H$ ) comes from their interaction with the  $SU(5)$  breaking sector.

94.2.3  $SO(10)$

While  $SU(5)$  allows for the minimal GUT models, unification is not complete: Two independent representations,  $\mathbf{10}$  and  $\bar{\mathbf{5}}$ , are required for one SM generation. A further representation, an  $SU(5)$  singlet, has to be added to serve as r.h. neutrino in the seesaw mechanism. In this case, the r.h. neutrino masses are not necessarily related to the GUT scale. By contrast, a single  $\mathbf{16}$ -dimensional spinor representation of  $SO(10)$  accommodates a full SM generation together with an extra singlet, potentially providing a r.h. neutrino [15]. This is most easily understood from the breaking pattern  $SO(10) \rightarrow SU(5) \times U(1)_X$  and the associated branching rule<sup>3</sup>  $\mathbf{16} = \mathbf{10}_{-1} + \bar{\mathbf{5}}_3 + \mathbf{1}_{-4}$ . Here the indices refer to charges under the  $U(1)_X$  subgroup, which is orthogonal to  $SU(5)$  and reflects the fact that  $SO(10)$  has rank five. From the above, it is easy to see that  $U(1)_X$  charges can be given as  $2Y - 5(B - L)$ . Intriguingly, all representations of  $SO(10)$  are anomaly free in four dimensions (4d). Thus, the absence of anomalies in an  $SU(5)$ -GUT or a SM generation can be viewed as deriving from this feature.

We now describe in more detail how one family of quarks and leptons appears in the  $\mathbf{16}$ . To understand this, recall that the  $\Gamma$ -matrices of the 10d Clifford algebra give rise to five independent, anticommuting ‘creation-annihilation’ operators  $\Gamma^{a\pm} = (\Gamma^{2a-1} \pm i\Gamma^{2a})/2$  with  $a = 1, \dots, 5$ . These correspond to five fermionic harmonic oscillators or “spin” 1/2 systems. The 32-dimensional tensor product of those is reducible since the 10d rotation generators  $M_{mn} = -i[\Gamma^m, \Gamma^n]/4$  ( $m, n = 1, \dots, 10$ ) always flip an even number of “spins”. This gives rise to the  $\mathbf{16}$  as displayed in Table 94.1. Next, one also recalls that the natural embedding of  $SU(5)$  in  $SO(10)$  relies on ‘pairing up’ the 10 real dimensions to produce 5 complex dimensions,  $\mathbb{R}^{10} \equiv \mathbb{C}^5$ , similarly to the pairing up of  $\Gamma^m$ s used above. This makes it clear how to associate one  $|\pm\rangle$  system to each complex dimension of  $SU(5)$ , which explains the labeling of the “spin” columns in Table 94.1: The first three and last two “spins” correspond to  $SU(3)_C$  and  $SU(2)_L$ , respectively. In fact, an  $SU(3)_C$  rotation just raises one color index and lowers another, changing colors  $\{r, g, b\}$ , or changes relative phases between the three spin states. Similarly, an  $SU(2)_L$  rotation raises one weak index and lowers another, thereby flipping the weak isospin from up to down or vice versa, or changes the relative phase between the two spin states. In this representation  $U(1)_Y$  hypercharge is simply given by  $Y = -2/3(\sum \text{color spins}) + (\sum \text{weak spins})$ .  $SU(5)$  rotations corresponding to  $X$  bosons then raise (or lower) a color index, while at the same time lowering (or raising) a weak index. It is easy to see that such rotations can mix the states  $\{Q, u^c, e^c\}$  and  $\{d^c, L\}$  among themselves and  $\nu^c$  is a singlet. Since  $SO(10)$  has 45 generators, additional 21 gauge bosons are introduced including the  $U(1)_X$  above. The 20 new  $SO(10)$  rotations not in  $SU(5)$  are then given by either raising any two spins or lowering them. With these rotations,  $\mathbf{1}$  and  $\bar{\mathbf{5}}$  are connected with  $\mathbf{10}$ . The last  $SO(10)$  rotation changes phases of states with weight  $2(\sum \text{color spins}) + 2(\sum \text{weak spins})$ , which corresponds to  $U(1)_X$ .

$SO(10)$  has two inequivalent maximal subgroups and hence breaking patterns,  $SO(10) \rightarrow SU(5) \times U(1)_X$  and  $SO(10) \rightarrow SU(4)_C \times SU(2)_L \times SU(2)_R$ . In the first case, one can carry on breaking to  $G_{SM} \subset SU(5)$  precisely as in the minimal  $SU(5)$  case above. Alternatively, one can identify  $U(1)_Y$  as an appropriate linear combination of  $U(1)_X$  and the  $U(1)$  factor from  $SU(5)$ , leading to the so-called flipped  $SU(5)$  [17] as an intermediate step in breaking  $SO(10)$  to  $G_{SM}$ . In the second case, we have an intermediate Pati-Salam model thanks to the branching rule  $\mathbf{16} = (\mathbf{4}, \mathbf{2}, \mathbf{1}) + (\bar{\mathbf{4}}, \mathbf{1}, \mathbf{2})$ . Finally,  $SO(10)$  can break directly to the SM at  $M_G$ . Gauge coupling unification remains intact in

Table 94.1: Quantum numbers of  $\mathbf{16}$ -dimensional representation of  $SO(10)$ .

state	Y	Color	Weak	$SU(5)$	$SO(10)$
$\nu^c$	0	---	--	<b>1</b>	<b>16</b>
$e^c$	2	---	++	<b>10</b>	
$u_r$	1/3	+--	-+		
$d_r$	1/3	+--	+-		
$u_g$	1/3	-+-	-+		
$d_g$	1/3	-+-	+-		
$u_b$	1/3	--+	-+		
$d_b$	1/3	--+	+-		
$u_r^c$	-4/3	-++	--		
$u_g^c$	-4/3	-++	--		
$u_b^c$	-4/3	-++	--		
$d_r^c$	2/3	-++	++		
$d_g^c$	2/3	-++	++		
$d_b^c$	2/3	-++	++		
$\nu$	-1	+++	-+		
$e$	-1	+++	+-		

the case of this ‘direct’ breaking and for the breaking pattern  $SO(10) \rightarrow SU(5) \rightarrow G_{SM}$  (with  $SU(5)$  broken at  $M_G$ ). In the case of intermediate-scale Pati-Salam or flipped  $SU(5)$  models, gauge coupling predictions are modified. The Higgs multiplets in the minimal  $SO(10)$  come from the fundamental representation,  $\mathbf{10}_H = \mathbf{5}_H + \bar{\mathbf{5}}_H$ . Note, only in  $SO(10)$  does the representation type distinguish SM matter from Higgs fields.

94.2.4 Beyond  $SO(10)$

Finally, larger symmetry groups can be considered. For example, the exceptional group  $E_6$  has maximal subgroup  $SO(10) \times U(1)$  [18]. Its fundamental representation branches as  $\mathbf{27} = \mathbf{16}_1 + \mathbf{10}_{-2} + \mathbf{1}_4$ . Another maximal subgroup is  $SU(3)_C \times SU(3)_L \times SU(3)_R \subset E_6$  with branching rule  $\mathbf{27} = (\mathbf{3}, \mathbf{3}, \mathbf{1}) + (\bar{\mathbf{3}}, \mathbf{1}, \bar{\mathbf{3}}) + (\mathbf{1}, \bar{\mathbf{3}}, \bar{\mathbf{3}})$ . Independently of any underlying  $E_6$ , the group  $[SU(3)]^3$  with additional permutation symmetry  $Z_3$  interchanging the three factors can be considered. This is known as “trification” [19]. The  $E_6 \rightarrow [SU(3)]^3$  breaking pattern has been used in phenomenological analyses of the heterotic string [20]. However, in larger symmetry groups, such as  $E_6$ ,  $SU(6)$ , etc., there are now many more states which have not been observed and must be removed from the effective low-energy theory.

Intriguingly, the logic by which  $G_{SM}$  is a maximal subgroup of  $SU(5)$ , which together with  $U(1)_X$  is a maximal subgroup of  $SO(10)$ , continues in a very elegant and systematic way up to the largest exceptional group. The resulting famous breaking chain  $E_8 \rightarrow E_7 \rightarrow E_6 \rightarrow SO(10) \rightarrow SU(5) \rightarrow G_{SM}$  together with the special role played by  $E_8$  in group and in string theory is a tantalizing hint at deeper structures. However, since all representations of  $E_8$  and  $E_7$  are real and can not lead to 4d chiral fermions, this is necessarily outside the 4d GUT framework.

94.3 GUT breaking and doublet-triplet splitting

In the standard, 4d field-theoretic approach to GUTs, the unified gauge group is broken spontaneously by an appropriate GUT Higgs sector. Scalar potentials (or superpotentials in SUSY GUTs) exist whose vacua spontaneously break  $SU(5)$  or  $SO(10)$ . While these potentials are ad hoc (just like the Higgs potential in the SM), the most naive expectation is that all their dimensional parameters are  $O(M_G)$ . In the simplest case of  $SU(5)$ , the  $\mathbf{24}$  (adjoint) GUT Higgs develops a VEV along the  $G_{SM}$ -singlet direction as  $\langle \Phi \rangle \propto \text{diag}(-2/3, -2/3, -2/3, 1, 1)$ . In order for  $SO(10)$  to break to  $SU(5)$ , the  $\mathbf{16}$  or  $\mathbf{126}$ , which have a  $G_{SM}$ -singlet with non-zero  $U(1)_X$  charge, get a VEV.

The masses of doublet and triplet in the  $\mathbf{5}_H$  (and  $\bar{\mathbf{5}}_H$ ) generically split due to their coupling to the GUT Higgs. In addition, both the doublet and the triplet masses also get an equal contribution from an  $SU(5)$ -invariant GUT-scale mass term. Without any further structure, an extreme fine-tuning between two large effects is then necessary to keep the doublet mass at the electroweak scale. Supersymmetry plays an important role in for-

<sup>3</sup> Useful references on group theory in the present context include [16] and refs. therein.

bidding large radiative correction to the doublet mass due to the non-renormalization theorem [5]. However, even in this case we have to fine tune parameters at tree level. This is the doublet-triplet splitting problem which, in the SUSY context, is clearly related the  $\mu$ -term problem of the MSSM (the smallness of the coefficient of  $\mu H_u H_d$ ).

Several mechanisms for natural doublet-triplet splitting have been suggested under the assumption of supersymmetry, such as the sliding singlet [21], missing partner [22], missing VEV [23], and pseudo-Nambu-Goldstone boson mechanisms [24]. Particular examples of the missing partner mechanism for  $SU(5)$  [25], the missing VEV mechanism for  $SO(10)$  [26, 27] and the pseudo-Nambu-Goldstone boson mechanism for  $SU(6)$  [28] have been shown to be consistent with gauge coupling unification and nucleon decay. From the GUT-scale perspective, one is satisfied if the triplets are naturally heavy and the doublets are massless ( $\mu \simeq 0$ ). There are also several mechanisms for resolving the subsequent issue of why  $\mu$  is of order the SUSY breaking scale [29].<sup>4</sup> For a review of the  $\mu$  problem and some suggested solutions in SUSY GUTs and string theory, see [30–33] and references therein.

In general, GUT-breaking sectors successfully resolving the doublet-triplet splitting problem, dynamically stabilizing all GUT-scale VEVs and allowing for realistic neutrino masses and Yukawa couplings (including the GUT-symmetry violation in the latter) require a number of ingredients. However, for validity of the effective theory, introduction of higher or many representations is limited, otherwise a Landau pole may appear below the Planck scale. In addition, GUTs are only effective theories below the Planck scale in the 4d field-theoretic approach. Since  $M_G$  is close to this scale, the effects of higher-dimension operators are not obviously negligible. In particular, operators including the GUT-breaking Higgs may affect low-energy predictions, such as quark and lepton masses.

Thus, especially in the context of GUT breaking and doublet-triplet splitting, models beyond 4d field theory appear attractive. While this is mainly the subject of the next section, some advantages can already be noted: In models with extra dimensions, in particular string constructions, GUT breaking may occur due to boundary conditions in the compactified dimensions [34–37]. No complicated GUT breaking sector is then required. Moreover, boundary conditions can give mass only to the triplet, leaving the doublet massless. This is similar to the ‘missing partner mechanism’ since the effective mass term does not ‘pair up’ the triplets from  $\mathbf{5}_H$  and  $\bar{\mathbf{5}}_H$  but rather each of them with further fields which are automatically present in the higher-dimensional theory. This can eliminate dimension-five nucleon decay (cf. Sec. 94.6).

#### 94.4 String-theoretic and higher-dimensional unified models

As noted earlier, the GUT scale is dangerously close to the scale of quantum gravity. It may hence be necessary to discuss unified models of particle physics in the latter, more ambitious context. Among the models of quantum gravity, superstring or M-theory stands out as the best-studied and technically most developed proposal, possessing in particular a high level of internal, mathematical consistency. For our purposes, it is sufficient to know that five 10d and one 11d low-energy effective supergravity theories arise in this setting (cf. [38] and refs. therein).

Grand unification is realized most naturally in the context of the two ‘heterotic’ theories with gauge groups  $E_8 \times E_8$  and  $SO(32)$ , respectively [36, 39] (see [40] for some of the more recent results). Justified in part by the intriguing breaking path  $E_8 \rightarrow \dots \rightarrow G_{SM}$  mentioned above, the focus has historically largely been on  $E_8 \times E_8$ . To describe particle physics, solutions of the 10d theory with geometry  $\mathbb{R}^{1,3} \times M_6$  are considered, where  $M_6$  is a Calabi-Yau (CY) 3-fold (with 6 real dimensions) [36]. The background solution involves expectation values of higher-dimensional components of the  $E_8 \times E_8$  gauge fields. This includes

both Wilson lines [34] and non-vanishing field-strength and leads, in general, to a reduced gauge symmetry and to chirality in the resulting 4d effective theory. The 4d fermions arise from 10d gauginos.

Given an appropriate embedding<sup>5</sup> of  $G_{SM}$  in  $E_8 \times E_8$ , gauge coupling unification is automatic at leading order. Corrections arise mainly through (string)-loop effects and are similar to the familiar field-theory thresholds of 4d GUTs<sup>6</sup> [41]. Thus, one may say that coupling unification is a generic prediction in spite of the complete absence<sup>7</sup> of a 4d GUT at any energy scale. This absence is both an advantage and a weakness. On the up side, GUT breaking and doublet-triplet splitting [43] are more naturally realized and dimension-five nucleon decay is relatively easy to avoid. On the down side, there is no reason to expect full GUT representations in the matter sector and flavor model building is much less tied to the GUT structure than in 4d.

Let us pause to explain the beautiful idea behind the advertised solution of the doublet-triplet splitting problem: One starts with a simply connected CY  $X$  and mods out the action of a discrete group  $G$  (say  $\mathbb{Z}_2$ ). In the absence of fixed points,  $X/G$  is smooth and has a non-contractible 1-cycle. Furthermore, let  $G$  also act on the gauge bundle, according to an embedding  $G \rightarrow E_8$ . Now the parallel transport around the 1-cycle is tied to a gauge rotation (one says a non-trivial Wilson-line is present). Moreover, this Wilson line can not be continuously turned off since, e.g. in the case of  $\mathbb{Z}_2$ , its square is the unit element of the group. The induced ‘Wilson-line breaking’, which comes on top of the breaking by non-zero field strengths, may remove certain sub-representations (e.g. the triplet of  $SU(5) \rightarrow G_{SM}$ ) while keeping others exactly massless. A simpler and, due to fixed points, singular version of this will appear below in the context of orbifold GUTs.

One technical problem of heterotic constructions is the dependence on the numerous size and shape parameters of  $M_6$  (the so-called moduli), the stabilization of which is poorly understood (see [44] for recent developments). Another is the sheer mathematical complexity of the analysis, involving in particular the study of (non-Abelian) gauge-bundles on CY spaces [45] (see however [46]).

An interesting aspect of heterotic string constructions is represented by orbifold models [35]. Here the internal space is given by a six-torus, modded out by a discrete symmetry group (e.g.  $T^6/\mathbb{Z}_n$ ). More recent progress is reported in [47, 48], including in particular the systematic exploration of the phenomenological advantages of so-called ‘non-prime’ (referring to  $n$ ) orbifolds. The symmetry breaking to  $G_{SM}$  as well as the survival of Higgs doublets without triplet partners is ensured by the appropriate embedding of the discrete orbifold group in  $E_8 \times E_8$ . String theory on such spaces, which are locally flat but include singularities, is much more calculable than in the CY case. The orbifold geometries can be viewed as singular limits of CYs.

An even simpler approach to unified models, which includes many of the advantages of full-fledged string constructions, is provided by Orbifold GUTs [37]. These are (mostly) 5d or 6d SUSY field theories with unified gauge group (e.g.  $SU(5)$  or  $SO(10)$ ), broken in the process of compactifying to 4d. To give a particularly simple example, consider  $SU(5)$  on  $\mathbb{R}^{1,3} \times S^1/(\mathbb{Z}_2 \times \mathbb{Z}'_2)$ . Here the compact space is an interval of length  $\pi R/2$  and the embedding of  $\mathbb{Z}'_2$  in the hypercharge direction of  $SU(5)$  realizes the breaking to  $G_{SM}$ . Concretely, 5d  $X$  bosons are given Dirichlet BCs at one endpoint of the interval and thus have no Kaluza-Klein (KK) zero mode. Their lightest modes have mass  $\sim 1/R$ , making the KK-scale the effective GUT scale. As an implication, the boundary theory has no  $SU(5)$  invariance. Nevertheless, since the  $SU(5)$ -symmetric 5d bulk dominates 4d gauge couplings, unification remains a prediction. Many other features but also problems

<sup>4</sup> The solution of [29] relies on the absence of the fundamental superpotential term  $\mu H_u H_d$  (or  $\mu \mathbf{5}_H \bar{\mathbf{5}}_H$ ). This can be ensured either by a discrete  $R$  symmetry or by a  $U(1)_R$ . The latter clashes with typical superpotentials for the GUT breaking sector. However, higher-dimensional or stringy GUTs, where the triplet Higgs is simply projected out, can be consistent with the  $U(1)_R$  symmetry.

<sup>5</sup> All embeddings of  $G_{SM}$  in one  $E_8$  factor which are consistent with a breaking-pattern  $E_8 \rightarrow SU(5) \rightarrow G_{SM}$  are suitable (cf. for example the natural breaking chain from  $E_8$  to  $G_{SM}$  through maximal subgroups mentioned at the end of Sect. 94.3). Other embeddings can change the ratios between the three resulting  $G_{SM}$  couplings at the GUT scale by group-theoretic factors. Crucially, due to the single 10d gauge coupling, no continuous tuning is possible.

<sup>6</sup> Field-theory thresholds of 4d GUTs are discussed in 94.5.

<sup>7</sup> See however [42].

of 4d GUTs can be circumvented, especially doublet-triplet splitting is easily realized.

With the advent of the string-theory ‘flux landscape’ [49], which is best understood in 10d type-IIB supergravity, the focus in string model building has shifted to this framework. While type II string theories have no gauge group in 10d, brane-stacks support gauge dynamics. A particularly appealing setting (see e.g. [50]) is provided by type IIB models with D7 branes (defining 8d submanifolds). However, in the  $SO(10)$  context the  $\mathbf{16}$  is not available and, for  $SU(5)$ , the top-Yukawa coupling vanishes at leading order [51]. As a crucial insight, this can be overcome on the non-perturbative branch of type IIB, also known as F-theory [52, 53]. This setting allows for more general branes, thus avoiding constraints of the  $Dp$ -brane framework. GUT breaking can be realized using hypercharge flux (the VEV of the  $U(1)_Y$  field strength), an option not available in heterotic models. The whole framework combines the advantages of the heterotic or higher-dimensional unification approach with the more recent progress in understanding moduli stabilization. It thus represents at this moment the most active and promising branch of theory-driven GUT model building (see e.g. [54] and refs. therein).

As a result of the flux-breaking, a characteristic ‘type IIB’ or ‘F-theoretic’ tree-level correction to gauge unification arises [55]. The fact that this correction can be rather significant numerically is occasionally held against the framework of F-theory GUTs. However, at a parametric level, this correction nevertheless behaves like a 4d threshold, i.e., it provides  $\mathcal{O}(1)$  additive contributions to the inverse 4d gauge couplings  $\alpha_i^{-1}(M_G)$ .

A final important issue in string GUTs is the so-called string-scale/GUT-scale problem [56]. It arises since, in heterotic compactifications, the Planck scale and the high-scale value of the gauge coupling unambiguously fix the string-scale to about  $10^{18}$  GeV. As the compactification radius  $R$  is raised above the string length, the GUT scale (identified with  $1/R$ ) goes down and the string coupling goes up. Within the domain of perturbative string theory, a gap of about a factor  $\sim 20$  remains between the lowest GUT scale achievable in this way and the phenomenological goal of  $2 \times 10^{16}$  GeV. The situation can be improved by venturing into the non-perturbative regime [56], by considering ‘anisotropic’ geometries with hierarchically different radii  $R$  [56, 57] or by including GUT scale threshold corrections [58, 59].

In F-theory GUTs, the situation is dramatically improved since the gauge theory lives only in four out of the six compact dimensions. This allows for models with a ‘decoupling limit’, where the GUT scale is parametrically below the Planck scale [53]. However, moduli stabilization may not be without problems in such constructions, in part due to a tension between the required large volume and the desirable low SUSY breaking scale.

### 94.5 Gauge coupling unification

The quantitative unification of the three SM gauge couplings at the energy scale  $M_G$  is one of the cornerstones of the GUT paradigm. It is obviously of direct phenomenological relevance. Gauge coupling unification is well understood in the framework of effective field theory (EFT) [60]. In the simplest case, the relevant EFT at energies  $\mu \gg M_G$  has a unified gauge symmetry (say  $SU(5)$  for definiteness) and a single running gauge coupling  $\alpha_G(\mu)$ . At energies  $\mu \ll M_G$ , states with mass  $\sim M_G$  (such as  $X$  bosons, GUT Higgs, color-triplet Higgs) have to be integrated out. The EFT now has three independent couplings and SM (or SUSY SM) matter content. One-loop renormalization group equations readily allow for an extrapolation to the weak scale,

$$\alpha_i^{-1}(m_Z) = \alpha_G^{-1}(M_G) + \frac{b_i}{2\pi} \log\left(\frac{M_G}{m_Z}\right) + \delta_i, \quad (94.3)$$

( $i = 1, 2, 3$ ). Here we defined  $\delta_i$  to absorb all sub-leading effects, such as threshold corrections at or near the weak scale (e.g. from superpartners and the additional Higgs bosons in the case of the MSSM) and at the GUT scale, and also higher-order corrections. We will discuss them momentarily.

It is apparent from Eq. (94.3) that the three low-scale couplings can be very different. This is due to the large energy range  $m_Z \ll \mu \ll M_G$  and the non-universal  $\beta$ -function coefficients

( $b_i^{\text{SM}} = \{41/10, -19/6, -7\}$  or  $b_i^{\text{MSSM}} = \{33/5, 1, -3\}$ ). Incomplete GUT multiplets, such as gauge and Higgs bosons in the SM and also their superpartners and the additional Higgs bosons in the MSSM, contribute to the differences between the  $\beta$  functions. Inverting the argument, one expects that extrapolating the measured couplings to the high scale, we find quantitative unification at  $\mu \sim M_G$ . While this fails in the SM, it works intriguingly well in the MSSM (cf. Fig. 94.1).

The three equations contained in Eq. (94.3) can be used to determine the three ‘unknowns’  $\alpha_3(m_Z)$ ,  $\alpha_G(M_G)$  and  $M_G$ , assuming that all other parameters entering the equations are given. Focusing on the SUSY case and using the  $\overline{\text{MS}}$  coupling constants  $\alpha_{\text{EM}}^{-1}(m_Z)$  and  $\sin^2 \theta_W(m_Z)$  from [62],

$$\alpha_{\text{EM}}^{-1}(m_Z) = 127.955 \pm 0.010, \quad (94.4)$$

$$\sin^2 \theta_W(m_Z) = 0.23122 \pm 0.00003, \quad (94.5)$$

as input, one determines  $\alpha_{1,2}^{-1}(m_Z)$ , which then gives

$$\alpha_G^{-1}(M_G) \simeq 24.3 \quad \text{and} \quad M_G \simeq 2 \times 10^{16} \text{ GeV}. \quad (94.6)$$

Here we have set  $\delta_i = 0$  for simplicity. Crucially, one in addition obtains a prediction for the low-energy observable  $\alpha_3$ ,

$$\alpha_3^{-1}(m_Z) = -\frac{5}{7}\alpha_1^{-1}(m_Z) + \frac{12}{7}\alpha_2^{-1}(m_Z) + \Delta_3, \quad (94.7)$$

where

$$\Delta_3 = \frac{5}{7}\delta_1 - \frac{12}{7}\delta_2 + \delta_3. \quad (94.8)$$

Here we followed the elegant formulation in Ref. [63] of the classical analyses of [7]. Of course, it is a matter of convention which of the three low-energy gauge coupling parameters one ‘predicts’ and indeed, early works on the subject discussed the prediction of  $\sin^2 \theta_W$  in terms of  $\alpha_{\text{EM}}$  and  $\alpha_3$  [64, 65].

Remarkably, the leading order result (i.e. Eq. (94.7) with  $\delta_i = 0$ ) is in excellent agreement with experiments [62]:

$$\alpha_3^{\text{LO}}(m_Z) = 0.117 \quad \text{vs.} \quad \alpha_3^{\text{EXP}}(m_Z) = 0.1181 \pm 0.0011. \quad (94.9)$$

However, this near perfection is to some extent accidental. To see this, we now discuss the various contributions to the  $\delta_i$  (and hence to  $\Delta_3$ ).

The two-loop running correction from the gauge sector  $\Delta_3^{(2)}$  and the low-scale threshold correction  $\Delta_3^{(l)}$  from superpartners can be summarized as [63]

$$\Delta_3^{(2)} \simeq -0.82 \quad \text{and} \quad \Delta_3^{(l)} \simeq \frac{19}{28\pi} \log\left(\frac{m_{\text{SUSY}}}{m_Z}\right). \quad (94.10)$$

The relevant scale  $m_{\text{SUSY}}$  can be estimated as [66]

$$m_{\text{SUSY}} \rightarrow m_H^{3/19} m_{\tilde{H}}^{12/19} m_{\tilde{W}}^{4/19} \times \left(\frac{m_{\tilde{W}}}{m_{\tilde{g}}}\right)^{28/19} \left(\frac{m_{\tilde{t}}}{m_{\tilde{q}}}\right)^{3/19}, \quad (94.11)$$

where  $m_H$  stands for the masses of non-SM Higgs states and superpartner masses are given in self-evident notation. Detailed analyses including the above effects are best done using appropriate software packages, such as SOFTSUSY [61] (or alternatively SuSpect [67] or SPheno [68]). See also [61] for references to the underlying theoretical two-loop analyses.

To get a very rough feeling for these effects, let us assume that all superpartners are degenerate at  $m_{\text{SUSY}} = 1$  TeV, except for heavier gluinos:  $m_{\tilde{W}}/m_{\tilde{g}} \simeq 1/3$ . This gives  $\Delta_3^{(l)} \simeq -0.35 + 0.22 \ln(m_{\text{SUSY}}/m_Z) \simeq 0.18$ . The resulting prediction of  $\alpha_3(m_Z) \simeq 0.126$  significantly upsets the perfect one-loop agreement found earlier. Before discussing this issue further, it is useful to introduce yet another important type of correction, the high or GUT scale thresholds.

To discuss high scale thresholds, let us set all other corrections to zero for the moment and write down a version of Eq. (94.3)

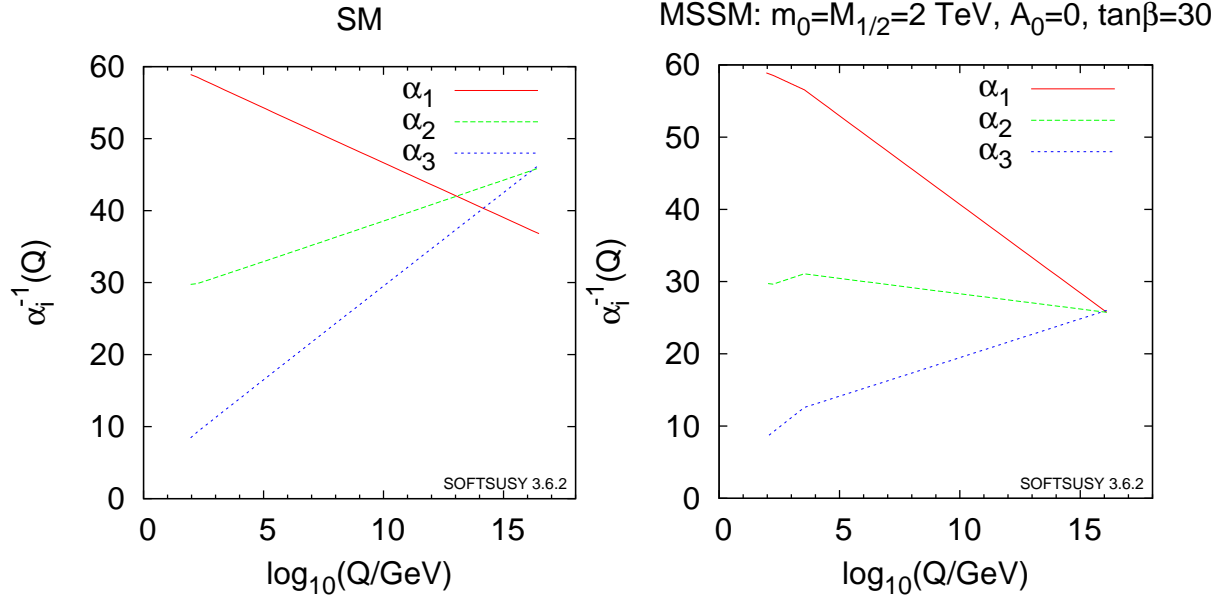


Figure 94.1: Running couplings in SM and MSSM using two-loop RG evolution. The SUSY threshold at 2 TeV is clearly visible on the MSSM side. (We thank Ben Allanach for providing the plots created using SOFTSUSY [61].)

that captures the running near and above the GUT scale more correctly. The threshold correction at one-loop level can be evaluated accurately by the simple step-function approximation for the  $\beta$  functions in the  $\overline{\text{DR}}$  scheme<sup>8</sup> [72],

$$\alpha_i^{-1}(m_Z) = \alpha_G^{-1}(\mu) + \frac{1}{2\pi} \left[ b_i \ln \frac{\mu}{m_Z} + b_i^C \ln \frac{\mu}{M_C} + b_i^X \ln \frac{\mu}{M_X} + b_i^\Phi \ln \frac{\mu}{M_\Phi} \right]. \quad (94.12)$$

Here we started the running at some scale  $\mu \gg M_G$ , including the contribution of the minimal set of states relevant for the transition from the high-scale  $SU(5)$  model to the MSSM. These are the color-triplet Higgs multiplets with mass  $M_C$ , massive vector multiplets of  $X$ -bosons with mass  $M_X$  (including GUT Higgs degrees of freedom), and the remaining GUT-Higgs fields and superpartners with mass  $M_\Phi$ . The coefficients  $b_i^{C,X,\Phi}$  can be found in Ref. [73]. Crucially, the  $b_i$  in Eq. (94.12) conspire to make the running GUT-universal at high scales, such that the resulting prediction for  $\alpha_3$  does not depend on the value of  $\mu$ .

To relate this to our previous discussion, we can, for example, define  $M_G \equiv M_X$  and then choose  $\mu = M_G$  in Eq. (94.12). This gives the high-scale threshold corrections

$$\delta_i^{(h)} = \frac{1}{2\pi} \left[ b_i^C \ln \frac{M_G}{M_C} + b_i^\Phi \ln \frac{M_G}{M_\Phi} \right], \quad (94.13)$$

and a corresponding correction  $\Delta_3^{(h)}$ . To get some intuition for the magnitude, one can furthermore assume  $M_\Phi = M_G$ , finding (with  $b_i^C = \{2/5, 0, 1\}$ )

$$\Delta_3^{(h)} = \frac{9}{14\pi} \ln \left( \frac{M_G}{M_C} \right). \quad (94.14)$$

To obtain the desired effect of  $-\Delta_3^{(2)} - \Delta_3^{(l)} \simeq +0.64$ , the triplet Higgs would have to be by about a factor 20 lighter than the GUT scale. While this is ruled out by nucleon decay in the minimal model [74] as will be discussed Sec. 94.6, it is also clear that threshold corrections of this order of magnitude can, in general, be realized with a certain amount of GUT-scale model building, e.g. in specific  $SU(5)$  [25] or  $SO(10)$  [26,27] constructions. Corrections

<sup>8</sup>The  $\overline{\text{DR}}$  scheme is frequently used in a supersymmetric regularization [69]. The renormalization transformation of the gauge coupling constants from  $\overline{\text{MS}}$  to  $\overline{\text{DR}}$  scheme is given in Ref. [70]. For an alternative treatment using holomorphic gauge couplings and NSVZ  $\beta$ -functions see e.g. [71].

can also be much larger or of different sign if, as is required in many fully realistic 4d GUT models, many additional (and in particular higher) representations are introduced. Thus, there is considerable model building freedom. Nevertheless, a significant constraint from getting the right GUT threshold corrections while keeping the triplet Higgs heavy remains.

The above analysis implicitly assumes universal soft SUSY breaking masses at the GUT scale, which directly affect the spectrum of SUSY particles at the weak scale. In the simplest case we have a universal gaugino mass  $M_{1/2}$ , a universal mass for squarks and sleptons  $m_{16}$  and a universal Higgs mass  $m_{10}$ , as motivated by  $SO(10)$ . In some cases, threshold corrections to gauge coupling unification can be exchanged for threshold corrections to soft SUSY parameters (see [75] and refs. therein). For example, if gaugino masses were not unified at  $M_G$  and, in particular, gluinos were lighter than winos at the weak scale (cf. Eq. (94.11)), then it is possible that, due to weak scale threshold corrections, a much smaller or even slightly negative threshold correction at the GUT scale would be consistent with gauge coupling unification [76].

It is also noteworthy that perfect unification can be realized without significant GUT-scale corrections, simply by slightly raising the (universal) SUSY breaking scale. In this case the dark matter abundance produced by thermal processes in the early universe (if the lightest neutralino is the dark matter particle) is too high. However, even if the gaugino mass in the MSSM is about 1 TeV to explain the dark matter abundance, if the Higgsino and the non-SM Higgs boson masses are about 10-100 TeV, the effective SUSY scale can be raised [77]. This setup is realized in split SUSY [78] or the pure gravity mediation model [79] based on anomaly mediation [80]. Since the squarks and sleptons are much heavier than the gaugino masses in those setups, a gauge hierarchy problem is reintroduced. The facts that no superpartners have so far been seen at the LHC and that the observed Higgs mass favors heavier stop masses than about 1 TeV force one to accept a certain amount of fine-tuning anyway.

For non-SUSY GUTs or GUTs with a very high SUSY breaking scale to fit the data, new light states in incomplete GUT multiplets or multiple GUT breaking scales are required. For example, non-SUSY models  $SO(10) \rightarrow SU(4)_C \times SU(2)_L \times SU(2)_R \rightarrow \text{SM}$ , with the second breaking scale of order an intermediate scale, determined by light neutrino masses using the see-saw mechanism, can fit the low-energy data for gauge couplings [81] and at the same time survive nucleon decay bounds [82]. Alternatively, one can appeal to string-theoretic corrections discussed in Sec. 94.4 to compensate for a high SUSY breaking scale. This has, for ex-

ample, been concretely analyzed in the context of F-theory GUTs in [83]. Similarly, one may even wonder whether particularly large GUT threshold corrections could be sufficient to ensure non-SUSY precision unification. Notice here that the gauge coupling unification predicts just one parameter. When introducing new states, typically one can fit the data by choice of their masses. This is not the case in SUSY GUTs with low-scale SUSY breaking scale where the masses are constrained by fine tuning.

In 5d or 6d orbifold GUTs, certain ‘‘GUT scale’’ threshold corrections come from the Kaluza-Klein modes between the compactification scale,  $M_c \sim 1/R$ , and the effective cutoff scale  $M_*$ . In string theory, this cutoff scale is the string scale. Gauge coupling unification at two loops then constrains the values of  $M_c$  and  $M_*$ .<sup>9</sup> Often, one finds  $M_c$  to be lower than the 4d GUT scale. Since the  $X$ -bosons, responsible for nucleon decay, get mass at the compactification scale, this has significant consequences for nucleon decay.

Finally, it has been shown that non-supersymmetric GUTs in warped 5d orbifolds can be consistent with gauge coupling unification. This assumes (in 4d language) that the r.h. top quark and the Higgs doublets are composite-like objects with a compositeness scale in the TeV range [85].

### 94.6 Nucleon decay

Quarks and leptons are indistinguishable in any 4d GUT, and both the baryon ( $B$ ) and lepton number ( $L$ ) are not conserved. This leads to baryon-number-violating nucleon decay. In addition to baryon-number violation, lepton-number violation is also required for nucleon decay since, in the SM, leptons are the only free fermions which are lighter than nucleons. The lowest-dimension operators relevant for nucleon decay are  $(B+L)$  violating dimension-six four-fermion-terms in the SM, and all baryon-violating operators with dimension less than seven preserve  $(B-L)$  [1, 86].

In  $SU(5)$  GUTs, the dimension-six operators are induced by  $X$  boson exchange. These operators are suppressed by  $(1/M_X^2)$  ( $M_X$  is the  $X$  boson mass), and the nucleon lifetime is given by  $\tau_N \propto M_X^4/(\alpha_G^2 m_p^5)$  ( $m_p$  is proton mass). The dominant decay mode of the proton (and the baryon-violating decay mode of the neutron), via  $X$  boson exchange, is  $p \rightarrow e^+ \pi^0$  ( $n \rightarrow e^+ \pi^-$ ). In any simple gauge symmetry, with one universal GUT coupling  $\alpha_G$  and scale  $M_X$ , the nucleon lifetime from gauge boson exchange is calculable. Hence, the GUT scale may be directly observed via the extremely rare decay of the nucleon. Experimental searches for nucleon decay began with the Kolar Gold Mine, Homestake, Soudan, NUSEX, Frejus, HPW, IMB, and Kamiokande detectors [64]. The present experimental bounds on the modes come from Super-Kamiokande. With 306 kton-years of data they find  $\tau_p/\text{Br}(p \rightarrow e^+ \pi^0) > 1.67 \times 10^{34}$  years at 90% CL [87]. In addition, Hyper-Kamiokande [88] is planned to reach to  $\tau_p/\text{Br}(p \rightarrow e^+ \pi^0) \sim 10^{35}$  years. The hadronic matrix elements for baryon-number-violating operators are evaluated with lattice QCD simulations [89]. In SUSY  $SU(5)$  GUTs, the lower bound on the  $X$  boson mass from null results in nucleon decay searches is approaching  $10^{16}$  GeV [90], which is close to the GUT scale suggested by gauge coupling unification. On the other hand, the prediction for nucleon decay in non-SUSY GUTs is hard to quantify. The reason is that gauge couplings do not unify with just the SM particle content. Once extra states or large thresholds are included to ensure precision unification, a certain range of unification scales is allowed.

In SUSY GUTs there are additional sources for baryon and/or lepton-number violation – dimension-four and five operators [14]. These arise since, in the SUSY SM, quarks and leptons have scalar partners (squarks and sleptons). Although our notation does not change, when discussing SUSY models our fields are chiral superfields and both fermionic and bosonic matter is implicitly represented by those. In this language, baryon- and/or lepton-number-violating dimension-four and five operators are given as so-called  $F$  terms of products of chiral superfields, which con-

tain two fermionic components and the rest scalars or products of scalars. Within the context of  $SU(5)$  the dimension-four and five operators have the form

$$(10 \bar{5} \bar{5}) \supset (u^c d^c d^c) + (Q L d^c) + (e^c L L),$$

$$(10 10 10 \bar{5}) \supset (Q Q Q L) + (u^c u^c d^c e^c) + B\text{- and }L\text{-conserving terms},$$

respectively.

The dimension-four operators in  $(10 \bar{5} \bar{5})$  violate either baryon number or lepton number. The nucleon lifetime is extremely short if both types of dimension-four operators are present in the SUSY SM since squark or slepton exchange induces the dangerous dimension-six SM operators. Even in the case that they violate baryon number or lepton number only but not both, they are constrained by various phenomena [91]. For example, the primordial baryon number in the universe is washed out unless the dimensionless coupling constants are less than  $10^{-7}$ . Both types of operators can be eliminated by requiring  $R$  parity, which distinguishes Higgs from ordinary matter multiplets.  $R$  parity [92] or its cousin, matter parity [6, 93], act as  $F \rightarrow -F$ ,  $H \rightarrow H$  with  $F = \{10, \bar{5}\}$ ,  $H = \{\bar{5}_H, 5_H\}$  in  $SU(5)$ .<sup>10</sup> In  $SU(5)$ , the Higgs multiplet  $\bar{5}_H$  and the matter multiplets  $\bar{5}$  have identical gauge quantum numbers. In  $E_6$ , Higgs and matter multiplets could be unified within the fundamental  $27$  representation. Only in  $SO(10)$  are Higgs and matter multiplets distinguished by their gauge quantum numbers. The  $Z_4$  center of  $SO(10)$  distinguishes  $10_s$  from  $16_s$  and can be associated with  $R$  parity [94].

The baryon-number violating dimension-five operators have a dimensionful coupling. They are generated by integrating out the color-triplet Higgs with GUT-scale mass in SUSY GUTs such that the coefficient is suppressed by  $1/M_G$ . Note that both triplet Higgsinos (due to their fermionic nature) and Higgs scalars (due to their mass-enhanced trilinear coupling with matter) contribute to the operators. The dimension-five operators include squarks and/or sleptons. To allow for nucleon decay, these must be converted to light quarks or leptons by exchange of a gaugino or Higgsino in the SUSY SM. The nucleon lifetime is proportional to  $M_G^2 m_{\text{SUSY}}^2/m_p^5$ , where  $m_{\text{SUSY}}$  is the SUSY breaking scale. Thus, dimension-five operators may predict a shorter nucleon lifetime than dimension-six operators. Unless accidental cancellations are present, the dominant decay modes from dimension-five operators include a  $K$  meson, such as  $p \rightarrow K^+ \bar{\nu}$  ( $n \rightarrow K^0 \bar{\nu}$ ). This is due to a simple symmetry argument: The operators are given as  $(Q_i Q_j Q_k L_l)$  and  $(u_i^c u_j^c d_k^c e_l^c)$ , where  $i, j, k, l (= 1, 2, 3)$  are family indices and color and weak indices are implicit. They must be invariant under  $SU(3)_C$  and  $SU(2)_L$  so that their color and weak doublet indices must be anti-symmetrized. Since these operators are given by bosonic superfields, they must be totally symmetric under interchange of all indices. Thus the first operator vanishes for  $i = j = k$  and the second vanishes for  $i = j$ . Hence a second or third generation member exists in the dominant modes of nucleon decay unless these modes are accidentally suppressed [93].

The Super-Kamiokande bounds on the proton lifetime severely constrain the dimension-five operators. With 306 kton-years of data they find  $\tau_p/\text{Br}(p \rightarrow K^+ \bar{\nu}) > 6.61 \times 10^{33}$  years at 90% CL [87]. In the minimal SUSY  $SU(5)$ ,  $\tau_p/\text{Br}(p \rightarrow K^+ \bar{\nu})$  is smaller than about  $10^{31}$  years if the triplet Higgs mass is  $10^{16}$  GeV and  $m_{\text{SUSY}} = 1$  TeV [95]. The triplet Higgs mass bound from nucleon decay is then in conflict with gauge coupling unification so that this model is considered to be ruled out [74].

Since nucleon decay induced by the triplet Higgs is a severe problem in SUSY GUTs, various proposals for its suppression have been made. First, some accidental symmetry or accidental structure in non-minimal Higgs sectors in  $SU(5)$  or  $SO(10)$  theories may suppress the dimension-five operators [22, 26, 27, 96].

<sup>9</sup> It is interesting to note that a ratio  $M_*/M_c \sim 100$ , needed for gauge coupling unification to work in orbifold GUTs, is typically the maximum value for this ratio consistent with perturbativity [84].

<sup>10</sup> This forbids the dimension-four operator  $(10 \bar{5} \bar{5})$ , but allows the Yukawa couplings for quark and lepton masses of the form  $(10 \bar{5} \bar{5}_H)$  and  $(10 10 \bar{5}_H)$ . It also forbids the dimension-three, lepton-number-violating operator  $(\bar{5} 5_H) \supset (L H_u)$  as well as the dimension-five, baryon-number-violating operator  $(10 10 10 \bar{5}_H) \supset (Q Q Q H_d) + \dots$



Symmetries to suppress the dimension-five operators are typically broken by the VEVs responsible for the color-triplet Higgs masses. Consequently the dimension-five operators are generically generated via the triplet Higgs exchange in SUSY  $SU(5)$  GUTs, as mentioned above. In other words, the nucleon decay is suppressed if the Higgs triplets in  $\bar{\mathbf{5}}_H$  and  $\mathbf{5}_H$  do not have a common mass term but, instead, their mass terms involve partners from other  $SU(5)$  multiplets. Second, the SUSY breaking scale may be around  $\mathcal{O}(10\text{--}100)$  TeV in order to explain the observed Higgs boson mass at the LHC. In this case, nucleon decay is automatically suppressed [78, 97, 98]. Third, accidental cancellations among diagrams due to a fine-tuned structure of squark and slepton flavor mixing might suppress nucleon decay [99]. Last, we have also implicitly assumed a hierarchical structure for Yukawa matrices in the analysis. It is however possible to fine-tune a hierarchical structure for quarks and leptons which baffles the family structure so that the nucleon decay is suppressed [100]. The upper bound on the proton lifetime from some of these theories is approximately a factor of 10 above the experimental bounds. Future experiments with larger neutrino detectors, such as JUNO [101], Hyper-Kamiokande [88] and DUNE [102], are planned and will have higher sensitivities to nucleon decay.

Are there ways to avoid the stringent predictions for proton decay discussed above? Orbifold GUTs and string theories, see Sec. 94.4, contain grand unified symmetries realized in higher dimensions. In the process of compactification and GUT symmetry breaking, the triplet Higgs states may be removed (projected out of the massless sector of the theory). In such models, the nucleon decay due to dimension-five operators can be severely suppressed or eliminated completely. However, nucleon decay due to dimension-six operators may be enhanced, since the gauge-bosons mediating proton decay obtain mass at the compactification scale,  $M_c$ , which is typically less than the 4d GUT scale (cf. Sec. 94.5). Alternatively, the same projections which eliminate the triplet Higgs may rearrange the quark and lepton states such that the massless states of one family come from different higher-dimensional GUT multiplets. This can suppress or completely eliminate even dimension-six proton decay. Thus, enhancement or suppression of dimension-six proton decay is model-dependent. In some complete 5d orbifold GUT models [63, 103] the lifetime for the decay  $\tau_p/\text{Br}(p \rightarrow e^+\pi^0)$  can be near the bound of  $1 \times 10^{34}$  years with, however, large model-dependence and/or theoretical uncertainties. In other cases, the modes  $p \rightarrow K^+\bar{\nu}$  and  $p \rightarrow K^0\mu^+$  may be dominant [63]. Thus, interestingly, the observation of nucleon decay may distinguish string or higher-dimensional GUTs from 4d ones.

In orbifold GUTs or string theory, new discrete symmetries consistent with SUSY GUTs can forbid all dimension-three and four baryon- and lepton-number-violating operators. Even the  $\mu$  term and dimension-five baryon- and lepton-number-violating operators can be forbidden to all orders in perturbation theory [33]. The  $\mu$  term and dimension-five baryon- and lepton-number-violating operators may then be generated, albeit sufficiently suppressed, via non-perturbative effects. The simplest example of this is a  $Z_4^R$  symmetry which is the unique discrete  $R$  symmetry consistent with  $SO(10)$  [33]. Even though it forbids the dimension-five proton decay operator to the desired level, it allows the required dimension-five neutrino mass term. In this case, proton decay is dominated by dimension-six operators, leading to decays such as  $p \rightarrow e^+\pi^0$ .

## 94.7 Yukawa coupling unification

In the SM, masses and mixings for quarks and leptons come from the Yukawa couplings with the Higgs doublet, but the values of these couplings remain a mystery. GUTs provide at least a partial understanding since each generation is embedded in unified multiplet(s). Specifically, since quarks and leptons are two sides of the same coin, the GUT symmetry relates the Yukawa couplings (and hence the masses) of quarks and leptons.

In  $SU(5)$ , there are two types of independent renormalizable Yukawa interactions given by  $\lambda_{ij}(\mathbf{10}_i \mathbf{10}_j \mathbf{5}_H) + \lambda'_{ij}(\mathbf{10}_i \bar{\mathbf{5}}_j \bar{\mathbf{5}}_H)$ . These contain the SM interactions  $\lambda_{ij}(Q_i u_j^c H_u) + \lambda'_{ij}(Q_i d_j^c H_d + e_i^c L_j H_d)$ . Here  $i, j (= 1, 2, 3)$

are, as before, family indices. Hence, at the GUT scale we have tree-level relations between Yukawa coupling constants for charged lepton and down quark masses, such as  $\lambda_b = \lambda_\tau$  in which  $\lambda_{b/\tau}$  are the bottom quark /  $\tau$  lepton Yukawa coupling constants [104, 105]. In  $SO(10)$ , there is only one type of independent renormalizable Yukawa interaction given by  $\lambda_{ij}(\mathbf{16}_i \mathbf{16}_j \mathbf{10}_H)$ , leading to relations among all Yukawa coupling constants and quark and lepton masses within one generation [106, 107] (such as  $\lambda_t = \lambda_b = \lambda_\tau$ , with  $\lambda_t$  the top quark Yukawa coupling constant).

In addition to gauge coupling unification, the ratio of bottom quark and  $\tau$  lepton mass has been a central target in the study of GUTs since it was found that this ratio was almost consistent with observations after including the QCD correction [104]. Today the quark masses and the gauge coupling constants are known precisely such that, as discussed below, the ratio of bottom quark and  $\tau$  lepton mass has become a target of precision analyses in the GUT context.

### 94.7.1 The third generation, $b\text{--}\tau$ or $t\text{--}b\text{--}\tau$ unification

Third generation Yukawa couplings are larger than those of the first two generations. Hence, the fermion mass relations predicted from renormalizable GUT interactions which we introduced above are expected to be more reliable. In order to compare them with data, we have to include the radiative correction to these relations from the RG evolution between GUT and fermion mass scale, from integrating out heavy particles at the GUT scale, and from weak scale thresholds.

Since testing Yukawa coupling unification is only possible in models with successful gauge coupling unification, we here focus on SUSY GUTs. In the MSSM, top and bottom quark and  $\tau$  lepton masses are related to the Yukawa coupling constants at the scale  $m_Z$  as

$$\begin{aligned} m_t(m_Z) &= \lambda_t(m_Z) v_u(1 + \delta m_t/m_t), \\ m_{b/\tau}(m_Z) &= \lambda_{b/\tau}(m_Z) v_d(1 + \delta m_{b/\tau}/m_{b/\tau}), \end{aligned}$$

where  $\langle H_u^0 \rangle \equiv v_u = \sin\beta v/\sqrt{2}$ ,  $\langle H_d^0 \rangle \equiv v_d = \cos\beta v/\sqrt{2}$ ,  $v_u/v_d \equiv \tan\beta$  and  $v \sim 246$  GeV is fixed by the Fermi constant,  $G_\mu$ . Here,  $\delta m_f/m_f$  ( $f = t, b, \tau$ ) represents the threshold correction due to integrating out SUSY partners. For the bottom quark mass, it is found [108] that the dominant corrections come from the gluino-sbottom and from the Higgsino-stop loops,

$$\begin{aligned} \left(\frac{\delta m_b}{m_b}\right)_{g_3} &\sim \frac{g_3^2}{6\pi^2} \frac{m_{\tilde{g}}\mu}{m_{\text{SUSY}}^2} \tan\beta \quad \text{and} \\ \left(\frac{\delta m_b}{m_b}\right)_{\lambda_t} &\sim \frac{\lambda_t^2}{16\pi^2} \frac{A_t\mu}{m_{\text{SUSY}}^2} \tan\beta, \end{aligned} \quad (94.16)$$

where  $m_{\tilde{g}}$ ,  $\mu$ , and  $A_t$  stand for gluino and Higgsino masses and trilinear stop coupling, respectively. Note that Eq. (94.16) only illustrates the structure of the corrections – non-trivial functional dependences on several soft parameters  $\sim m_{\text{SUSY}}$  have been suppressed. For the full one-loop correction to the bottom quark mass see, for example, Ref. [109].

Note also that the corrections do not go to zero as SUSY particles become much heavier than  $m_Z$ . They may change the bottom quark mass at the  $\mathcal{O}(10)\%$  level for  $\tan\beta = \mathcal{O}(10)$ . The total effect is sensitive to the relative phase between gluino and Higgsino masses since  $A_t \sim -m_{\tilde{g}}$  due to the infrared fixed point nature of the RG equation for  $A_t$  [110] in settings where SUSY breaking terms come from Planck scale dynamics, such as gravity mediation. The  $\tau$  lepton mass also receives a similar correction, though only at the few % level. The top quark mass correction, not being proportional to  $\tan\beta$ , is at most 10% [111].

Including one loop threshold corrections at  $m_Z$  and additional RG running, one finds the top, bottom and  $\tau$  pole masses. In SUSY GUTs,  $b\text{--}\tau$  unification has two possible solutions with  $\tan\beta \sim 1$  or  $\mathcal{O}(10)$ . The small  $\tan\beta$  solution may be realized in the MSSM if superpartner masses are  $\mathcal{O}(10)$  TeV, as suggested by the observed Higgs mass [97]. The large  $\tan\beta$  limit such as  $\tan\beta \sim 40\text{--}50$  overlaps the  $SO(10)$  symmetry relation [111, 112]. When  $\tan\beta$  is large, there are significant threshold corrections to



down quark masses as mentioned above, and Yukawa unification is only consistent with low-energy data in a restricted region of SUSY parameter space, with important consequences for SUSY searches [111, 113]. More recent analyses of Yukawa unification after LHC Run-I are found in Ref. [114].

Gauge coupling unification is also successful in the scenario of split supersymmetry [78], in which squarks and sleptons have mass at a scale  $\tilde{m} \gg m_Z$ , while gauginos and/or Higgsinos have masses of order the weak scale. Unification of  $b$ - $\tau$  Yukawa couplings requires  $\tan\beta$  to be fine-tuned close to 1 [97]. If by contrast,  $\tan\beta \gtrsim 1.5$ ,  $b$ - $\tau$  Yukawa unification only works for  $\tilde{m} \lesssim 10^4$  GeV. This is because the effective theory between the gaugino mass scale and  $\tilde{m}$  includes only one Higgs doublet, as in the standard model. As a result, the large top quark Yukawa coupling tends to increase the ratio  $\lambda_b/\lambda_\tau$  due to the vertex correction, which is absent in supersymmetric theories, as one runs down in energy below  $\tilde{m}$ . This is opposite to what happens in the MSSM where the large top quark Yukawa coupling lowers the ratio  $\lambda_b/\lambda_\tau$  [105].

**94.7.2 Beyond leading order: three-family models**

Simple Yukawa unification is not possible for the first two generations. Indeed, the simplest implementation of  $SU(5)$  implies  $\lambda_s = \lambda_\mu$ ,  $\lambda_d = \lambda_e$  and hence  $\lambda_s/\lambda_d = \lambda_\mu/\lambda_e$ . This is an RG-invariant relation which extrapolates to  $m_s/m_d = m_\mu/m_e$  at the weak scale, in serious disagreement with data ( $m_s/m_d \sim 20$  and  $m_\mu/m_e \sim 200$ ). An elegant solution to this problem was given by Georgi and Jarlskog [115] (for a recent analysis in the SUSY context see [116]).

More generally, we have to recall that in all of the previous discussion of Yukawa couplings, we assumed renormalizable interactions as well as the minimal matter and Higgs content. Since the GUT scale is close to the Planck scale, higher-dimension operators involving the GUT-breaking Higgs may modify the predictions, especially for lower generations. An example is provided by the operators  $\mathbf{10} \bar{\mathbf{5}} \bar{\mathbf{5}}_H \mathbf{24}_H$  with  $\mathbf{24}_H$  the GUT-breaking Higgs of  $SU(5)$ . We can fit parameters to the observed fermion masses with these operators, though some fine-tuning is introduced in doing so. The SM Higgs doublet may come in part from higher representations of the GUT group. For example, the  $\mathbf{45}$  of  $SU(5)$  includes an  $SU(2)_L$  doublet with appropriate  $U(1)_Y$  charge [115]. This  $\mathbf{45}$  can, in turn, come from the  $\mathbf{120}$  or  $\mathbf{126}$  of  $SO(10)$  after its breaking to  $SU(5)$  [117, 118]. These fields may also have renormalizable couplings with quarks and leptons. The relations among the Yukawa coupling constants in the SM are modified if the SM Higgs doublet is a linear combination of several such doublets from different  $SU(5)$  multiplets. Finally, the SM fermions may not be embedded in GUT multiplets in the minimal way. Indeed, if all quarks and leptons are embedded in  $\mathbf{16}$ s of  $SO(10)$ , the renormalizable interactions with  $\mathbf{10}_H$  cannot explain the observed CKM mixing angles. This situation improves when extra matter multiplets, such as  $\mathbf{10}$ , are introduced: After  $U(1)_X$ , which distinguishes the  $\bar{\mathbf{5}}$ s coming from the  $\mathbf{16}$  and the  $\mathbf{10}$  of  $SO(10)$ , is broken (e.g. by a VEV of  $\mathbf{16}_H$  or  $\mathbf{126}_H$ ), the r.h. down quarks and l.h. leptons in the SM can be linear combinations of components in  $\mathbf{16}$ s and  $\mathbf{10}$ s. As a result,  $\lambda \neq \lambda'$  in  $SU(5)$  [119].

To construct realistic three-family models, some or all of the above effects can be used. Even so, to achieve significant predictions for fermion masses and mixing angles grand unification alone is not sufficient. Other ingredients, for example additional global family symmetries are needed (in particular, non-Abelian symmetries can strongly reduce the number of free parameters). These family symmetries constrain the set of effective higher-dimensional fermion mass operators discussed above. In addition, sequential breaking of the family symmetry can be correlated with the hierarchy of fermion masses [120]. One simple, widely known idea in this context is to ensure that each  $\mathbf{10}_i$  enters Yukawa interactions together with a suppression factor  $e^{3-i}$  ( $\epsilon$  being a small parameter). This way one automatically generates a stronger hierarchy in up-type quark Yukawas as compared to down-type quark and lepton Yukawas and no hierarchy for neutrinos, which agrees with observations at the  $\mathcal{O}(1)$ -level. Three-family models exist which fit all the data, including neutrino masses and mixing [27, 121].

Finally, a particularly ambitious variant of unification is to re-

quire that the fermions of all three generations come from a single representation of a large gauge group. A somewhat weaker assumption is that the flavor group (e.g.  $SU(3)$ ) unifies with the SM gauge group in a simple gauge group at some energy scale  $M \geq M_G$ . Early work on such ‘flavor-unified GUTs’, see e.g. [119, 122], has been reviewed in [123, 124]. For a selection of more recent papers see [125]. In such settings, Yukawa couplings are generally determined by gauge couplings together with symmetry breaking VEVs. This is reminiscent of heterotic string GUTs, where all couplings come from the 10d gauge coupling. However, while the  $E_8 \rightarrow SU(3) \times E_6$  branching rule  $\mathbf{248} = (\mathbf{8}, \mathbf{1}) + (\mathbf{1}, \mathbf{78}) + (\mathbf{3}, \mathbf{27}) + (\bar{\mathbf{3}}, \mathbf{27})$  looks very suggestive in this context, the way in which most modern heterotic models arrive at three generations is actually more complicated.

**94.8 Neutrino masses**

We see from atmospheric and solar neutrino oscillation observations, along with long baseline accelerator and reactor experiments, that neutrinos have finite masses. By adding three ‘sterile’ neutrinos  $\nu_i^c$  with Yukawa couplings  $\lambda_{\nu,ij} (\nu_i^c L_j H_u)$  ( $i, j = 1, 2, 3$ ), one easily obtains three massive Dirac neutrinos with mass  $m_\nu = \lambda_\nu v_u$ , analogously to quark and charged lepton masses. However, in order to obtain a  $\tau$  neutrino with mass of order 0.1 eV, one requires the exceedingly small coupling ratio  $\lambda_{\nu\tau}/\lambda_\tau \lesssim 10^{-10}$ . By contrast, in GUTs the seesaw mechanism *naturally* explains such tiny neutrino masses as follows [2–4]: The sterile neutrinos have no SM gauge quantum numbers so that there is no symmetry other than global lepton number which forbids the Majorana mass term  $\frac{1}{2} M_{ij} \nu_i^c \nu_j^c$ . Note also that sterile neutrinos can be identified with the r.h. neutrinos necessarily contained in complete families of  $SO(10)$  or Pati-Salam models. Since the Majorana mass term violates  $U(1)_X$  in  $SO(10)$ , one might expect  $M_{ij} \sim M_G$ . The heavy sterile neutrinos can be integrated out, defining an effective low-energy theory with only three light active Majorana neutrinos with the effective dimension-five operator

$$- \mathcal{L}_{eff} = \frac{1}{2} c_{ij} (L_i H_u) (L_j H_u), \tag{94.17}$$

where  $c = \lambda_\nu^T M^{-1} \lambda_\nu$ . This then leads to a  $3 \times 3$  Majorana neutrino mass matrix  $m = m_\nu^T M^{-1} m_\nu$ .

The seesaw mechanism implemented by r.h. neutrinos is sometimes called the type-I seesaw model. There are variant models in which the dimension-five operator for neutrino masses is induced in different ways: In the type-II model, an  $SU(2)_L$  triplet Higgs boson  $\Sigma$  is introduced to have couplings  $\Sigma L^2$  and also  $\Sigma H_u^2$  [117, 126]. In the type-III model, an  $SU(2)_L$  triplet of fermions  $\tilde{\Sigma}$  with a Yukawa coupling  $\tilde{\Sigma} L H_u$  is introduced [127]. In these models, the dimension-five operator is induced by integrating out the triplet Higgs boson or fermions. Such models can also be implemented in GUTs by introducing Higgs bosons in the  $\mathbf{15}$  or fermions in the  $\mathbf{24}$  in  $SU(5)$  GUTs or the  $\mathbf{126}$  in  $SO(10)$  GUTs. Notice that the gauge non-singlet fields in the type-II and III models have masses at the intermediate scale. Thus, gauge coupling unification is not automatic if these variant mechanisms are implemented in SUSY GUTs.

Atmospheric neutrino oscillations discovered by Super-Kamiokande [128] require neutrino masses with  $\Delta m_\nu^2 \sim 2.5 \times 10^{-3}$  eV<sup>2</sup> with maximal mixing [62], in the simplest scenario of two neutrino dominance. With hierarchical neutrino masses this implies  $m_{\nu\tau} = \sqrt{\Delta m_\nu^2} \sim 0.05$  eV. Next, we can try to relate the neutrino Yukawa coupling to the top quark Yukawa coupling,  $\lambda_{\nu\tau} = \lambda_t$  at the GUT scale, as in  $SO(10)$  or  $SU(4) \times SU(2)_L \times SU(2)_R$  models. This gives  $M \sim 10^{14}$  GeV, which is remarkably close to the GUT scale.

Neutrinos pose a special problem for GUTs. The question is why the quark mixing angles in the CKM matrix are small while there are two large lepton mixing angles in the PMNS matrix. Global fits of neutrino masses and mixing angles can, for example, be found in Refs. [129] and [130]. For SUSY GUT models which fit quark and lepton masses, see Ref. [131] for reviews. Finally, for a compilation of the range of SUSY GUT predictions for neutrino mixing, see [132].

## 94.9 Selected topics

### 94.9.1 Global symmetries

As we discussed, global symmetries are frequently introduced to control higher-dimension operators in GUT models. This is particularly important in the context of nucleon decay but also plays a role in GUT-based flavor model building and cosmological applications, such as baryogenesis and inflation. However, we should note that appealing to global symmetries to suppress specific interactions may not be as straightforward as it naively seems. Indeed, there are two possibilities: On the one hand, the relevant symmetry might be gauged at a higher scale. Effects of the VEVs responsible for the spontaneous breaking are then in principle dangerous and need to be quantified. On the other hand, the symmetry might be truly only global. This must e.g. be the case for anomalous symmetries, which are then also violated by field-theoretic non-perturbative effects. The latter can in principle be exponentially small. It is, however, widely believed that global symmetries are always broken in quantum gravity (see e.g. [133]). One then needs to understand which power or functional form the Planck scale suppression of the relevant interaction has. For example, dimension-five baryon number violating operators suppressed by just one unit of the Planck or string scale are completely excluded.

In view of the above, it is also useful to recall that in string models 4d global symmetries generally originate in higher-dimensional gauge symmetries [38, 134]. Here ‘global’ implies that the gauge boson has acquired a Stückelberg-mass. This is a necessity in the anomalous case (Green-Schwarz mechanism [135]) but can also happen to non-anomalous symmetries. One expects no symmetry violation beyond the well-understood non-perturbative effects. Discrete symmetries arise as subgroups of continuous gauge symmetries, such as  $\mathbb{Z}_N \subset U(1)$ . In particular, non-anomalous subgroups of Stückelberg-massive  $U(1)$ s represent unbroken discrete gauge symmetries and as such are non-perturbatively exact (see e.g. [136]). Of course, such discrete gauge symmetries may also arise as remnants of continuous gauge symmetries after conventional 4d spontaneous breaking.

### 94.9.2 Anomaly constraints vs. GUT paradigm

As emphasized at the very beginning, the fact that the SM fermions of one generation fill out the  $\mathbf{10} + \bar{\mathbf{5}}$  of  $SU(5)$  appears to provide overwhelming evidence for some form of GUT embedding. However, one should be aware that a counterargument can be made which is related to the issue of ‘charge quantization by anomaly cancellation’ (see [137, 138] for some early papers and [139] for a more detailed reference list): Imagine we only knew that the low-energy gauge group were  $G_{SM}$  and the matter content included the  $(\mathbf{3}, \mathbf{2})_Y$ , i.e. a ‘quark doublet’ with  $U(1)$ -charge  $Y$ . One can then ask which possibilities exist of adding further matter to ensure the cancellation of all triangle anomalies. It turns out that this problem has only three different, minimal<sup>11</sup> solutions [138]. One of those is precisely a single SM generation, with the apparent ‘ $SU(5)$ -ness’ emerging accidentally. Thus, if one randomly picks models from the set of consistent gauge theories, preconditioning on  $G_{SM}$  and  $(\mathbf{3}, \mathbf{2})_Y$ , one may easily end up with ‘ $\mathbf{10} + \bar{\mathbf{5}}$ ’ of an  $SU(5)$  that is in no way dynamically present. This is precisely what happens in the context of non-GUT string model building [140].

### 94.9.3 Magnetic monopoles

In the broken phase of a GUT there are typically localized classical solutions carrying magnetic charge under an unbroken  $U(1)$  symmetry [141]. These magnetic monopoles with mass of order  $M_G/\alpha_G$  can be produced during a possible GUT phase transition in the early universe. The flux of magnetic monopoles is experimentally found to be less than  $\sim 10^{-16} \text{ cm}^{-2} \text{ s}^{-1} \text{ sr}^{-1}$  [142]. Many more are however predicted, hence the GUT monopole problem. In fact, one of the original motivations for inflation was to solve the monopole problem by exponential expansion after the GUT phase transition [143] and hence dilution of the

monopole density. Other possible solutions to the monopole problem include: sweeping them away by domain walls [144],  $U(1)$  electromagnetic symmetry breaking at high temperature [145] or GUT symmetry non-restoration [146]. Parenthetically, it was also shown that GUT monopoles can catalyze nucleon decay [147]. A significantly stronger bound on the monopole flux can then be obtained by considering X-ray emission from radio pulsars due to monopole capture and the subsequent nucleon decay catalysis [148].

Note that the present upper bound on the inflationary vacuum energy density is very close to the GUT scale,  $V_{inf}^{1/4} = (1.88 \times 10^{16} \text{ GeV}) \times (r/0.10)^{1/4}$ , with the scalar-to-tensor ratio constrained to  $r < 0.07$  [149]. This guarantees that reheating does not lead to temperatures above  $M_G$  and hence the monopole problem is solved by inflation (unless  $M_G$  is unexpectedly low).

### 94.9.4 Flavor violation

Yukawa interactions of GUT-scale particles with quarks and leptons may leave imprints on the flavor violation induced by SUSY breaking parameters [150]. To understand this, focus first on the MSSM with universal Planck-scale boundary conditions (as e.g. in gravity mediation). Working in a basis where up-quark and lepton Yukawas are diagonal, one finds that the large top-quark Yukawa coupling reduces the l.h. squark mass squareds in the third generation radiatively. It turns out that only the l.h. down-type squark mass matrix has sizable off-diagonal terms in the flavor basis after CKM-rotation. However, in GUTs the color-triplet Higgs has flavor violating interactions from the Yukawa coupling  $\lambda_{ij}(\mathbf{10}_i \mathbf{10}_j \mathbf{5}_H)$ , such that flavor-violating r.h. slepton mass terms are radiatively generated in addition [151]. In  $SU(5)$  extension of the type-I seesaw model, where r.h. neutrinos are introduced as  $SU(5)$  singlets with interactions  $\lambda''_{ij}(\mathbf{1}_i \bar{\mathbf{5}}_j \mathbf{5}_H)$ , the doublet and color-triplet Higgses acquire another type of Yukawa coupling, respectively. They then radiatively generate flavor-violating l.h. slepton [152] and r.h. down squark masses [153]. These flavor-violating SUSY breaking terms induce new contributions to FCNC processes in quark and lepton sectors, such as  $\mu \rightarrow e\gamma$  and  $K^0-\bar{K}^0$  and  $B^0-\bar{B}^0$  mixing. Note that even if the SUSY breaking terms are generated at  $M_G$ , the r.h. neutrino Yukawa coupling may induce sizable flavor violation in l.h. slepton masses due to the running between  $M_G$  and the right-handed-neutrino mass scale.

EDMs are also induced when both l.h. and r.h. squarks/sleptons have flavor-violating mass terms with relative phases, as discussed for  $SO(10)$  in [154] or for  $SU(5)$  with r.h. neutrinos in [155]. Thus, such low-energy observables constrain GUT-scale interactions.

### 94.9.5 From GUT baryogenesis to leptogenesis and B/L-violating transitions

During inflation, any conserved quantum number is extremely diluted. Thus, one expects the observed baryon asymmetry of the universe to originate at reheating or in the subsequent cosmological evolution. In detail, the situation is slightly more involved: Both baryon number  $B$  and lepton number  $L$  are global symmetries of the SM. However,  $(B+L)$  is anomalous and violated by thermal fluctuations in the early universe, via so-called sphaleron processes. Moreover, it is violated in GUT models, as is most apparent in proton decay. By contrast,  $(B-L)$  is anomaly free and preserved by both the SM as well as  $SU(5)$  or  $SO(10)$  gauge interactions.

Now, the old idea of GUT baryogenesis [156, 157] is to generate a  $(B+L)$  and hence a baryon asymmetry by the out-of-equilibrium decay of the color-triplet Higgs. However such an asymmetry, generated at GUT temperatures, is washed out by sphalerons<sup>12</sup>. This can be overcome [159] using lepton-number violating interaction of neutrinos to create a  $(B-L)$  from the  $(B+L)$  asymmetry, before sphaleron processes become sufficiently fast at  $T < 10^{12}$  GeV. This  $(B-L)$  asymmetry can then survive the subsequent sphaleron dominated phase. Note that this does not work in the minimal SUSY GUT setting, with the triplet Higgs above the

<sup>11</sup> Adding extra vector-like sets of fields, e.g. two fermions which only transform under  $U(1)$  and have charges  $Y$  and  $-Y$ , is considered to violate minimality.

<sup>12</sup> To be precise, if lepton flavor numbers  $L_i$  ( $i = 1-3$ ) are nonzero and  $(L_i - L_j) \neq 0$  ( $i \neq j$ ), one may obtain nonzero values for  $B$  and  $L$  even if  $(B-L) = 0$  [158].

GUT scale. The reason is that a correspondingly high reheating temperature would be required which, as explained above, is ruled out by Planck data.

However, the most widely accepted simple way out of the dilemma is to directly generate a net  $(B-L)$  asymmetry dynamically in the early universe, also using r.h. neutrinos. Indeed, we have seen that neutrino oscillations suggest a new scale of physics of order  $10^{14}$  GeV. This scale is associated with heavy Majorana neutrinos in the seesaw mechanism. If in the early universe, the decay of the heavy neutrinos is out of equilibrium and violates both lepton number and CP, then a net lepton number may be generated. This lepton number will then be partially converted into baryon number via electroweak processes [160]. This mechanism is called leptogenesis.

If the three heavy Majorana neutrino masses are hierarchical, the net lepton number is produced by decay of the lightest one, and it is proportional to the CP asymmetry in the decay. The CP asymmetry is bounded from above, and the lightest neutrino mass is required to be larger than  $10^9$  GeV in order to explain the observed baryon asymmetry [161]. This implies that the reheating temperature after inflation should be larger than  $10^9$  GeV so that the heavy neutrinos are thermally produced<sup>13</sup>. In supersymmetric models, there is a tension between leptogenesis and Big Bang Nucleosynthesis (BBN) if gravitinos decay in the BBN era. The gravitino problem gives a constraint on the reheating temperature  $\lesssim 10^{6-10}$  GeV though the precise value depends on the SUSY breaking parameters [163]. Recent reviews of leptogenesis can be found in Ref. [164].

One of the important tests of leptogenesis are searches for neutrinoless double- $\beta$  ( $0\nu\beta\beta$ ) decays<sup>14</sup>. In a  $0\nu\beta\beta$  decay, only two electrons but no (anti-)neutrinos are emitted by the decaying nucleus. This is in contrast to ordinary double- $\beta$  decay. Thus,  $0\nu\beta\beta$  decays are lepton-number-violating with  $\Delta L = 2$ . At the nucleon level, this is described by dimension-nine effective operators for  $nn \rightarrow ppee$ . These operators may in turn come from SM operators of with dimension less than nine, in combination with SM weak interactions. The lowest one is the dimension-five operator generating the Majorana neutrino mass terms (Eq. (94.17)). Thus, if the lepton-number violating effective interactions come from physics at energies much above the weak scale, the  $0\nu\beta\beta$  decay rates are proportional to the Majorana neutrino masses. The latest experimental results are reviewed in [62]. For recent studies of the  $0\nu\beta\beta$  decay including SM operators up to mass dimension nine, see [165] and refs. therein.

In addition to  $L$ -violation, one can consider  $(B-L)$  and  $B$  violating phenomena. They are interesting in their own right and may also be relevant to baryogenesis. The relevant operators have higher mass dimension than the familiar dimension-six  $(B+L)$ -violating operators (cf. Sec. 94.6). They may be predicted in  $SO(10)$  GUTs with an intermediate scale, at which baryogenesis is realized, such as in [166]. First, one may have nucleon decays with  $\Delta(B-L) = 2$ , such as  $n \rightarrow e^-\pi^+$ . This is induced by dimension-seven effective operators in the SM, which are suppressed by the SM Higgs VEV or derivatives. Second, there are neutron-antineutron ( $n-\bar{n}$ ) oscillations, which are induced by  $\Delta B = 2$  dimension-nine effective operators in the SM. The upper bound on the mean time for  $n-\bar{n}$  transitions is directly derived using free neutrons [167]. It is also constrained from the lower limit on the lifetime for neutrons bound in  $^{16}O$ , derived by Super-Kamiokande [168]. Their results are very similar. Super-Kamiokande also searches for dinucleon decays with  $\Delta B = 2$ , such as  $pp \rightarrow \pi^+\pi^+$  and  $nn \rightarrow \pi^+\pi^-$  [169].

## 94.10 Conclusion

Most conservatively, grand unification means that (some of) the SM gauge interactions of  $U(1)_Y$ ,  $SU(2)_L$  and  $SU(3)_C$  become

<sup>13</sup> This constraint may be avoided in resonant leptogenesis [162], in which the right-handed neutrinos are required to be almost degenerate in mass.

<sup>14</sup> Another important test of leptogenesis would be the observation of CP violation in neutrino oscillations. Strictly speaking, the CP phase in the PMNS matrix does not contribute to  $\epsilon_1$  in the seesaw model. Nevertheless, the observation of CP violation in neutrino oscillations would suggest that the seesaw mechanism is associated with a large CP violation, similarly to the quark sector.

part of a larger, unifying gauge symmetry at a high energy scale. In most models, especially in the simplest and most appealing variants of  $SU(5)$  and  $SO(10)$  unification, the statement is much stronger: One expects the three gauge couplings to unify (up to small threshold corrections) at a unique scale,  $M_G$ , and the proton to be unstable due to exchange of gauge bosons of the larger symmetry group. Supersymmetric grand unified theories provide, by far, the most predictive and economical framework allowing for perturbative unification. Many more details than could be discussed in the present article can be found in some of the classic reviews [123,170] and the two books [171] (see also [172] for two recent overviews).

Thus, the three classical pillars of GUTs are gauge coupling unification at  $M_G \sim 2 \times 10^{16}$  GeV, low-energy supersymmetry (with a large SUSY desert), and nucleon decay. The first of these may be viewed as predicting the value of the strong coupling – a prediction which has already been verified (see Fig. 94.1). Numerically, this prediction remains intact even if SUSY partner masses are somewhat above the weak scale. However, at the conceptual level a continuously increasing lower bound on the SUSY scale is nevertheless problematic for the GUT paradigm: Indeed, if the independent, gauge-hierarchy-based motivation for SUSY is completely abandoned, the SUSY scale and hence  $\alpha_3$  become simply free parameters and the first two pillars crumble. Thus, it is important to keep pushing bounds on proton decay which, although again not completely universal in all GUT constructions, is arguably a more generic part of the GUT paradigm than low-energy SUSY.

Whether or not Yukawa couplings unify is more model dependent. However, irrespective of possible (partial) Yukawa unification, there certainly exists a very interesting and potentially fruitful interplay between flavor model building and grand unification. Especially in the neutrino sector this is strongly influenced by the developing experimental situation.

Another phenomenological signature of grand unification is the strength of the direct coupling of the QCD axion to photons, relative to its coupling to gluons. It is quantified by the predicted anomaly ratio  $E/N = 8/3$  (see [173,174]). This arises in field-theoretic axion models consistent with GUT symmetry (such as DFSZ [175]) and in string-theoretic GUTs [174,176]. In the latter, the axion does not come from the phase of a complex scalar but is a fundamental shift-symmetric real field, coupling through a higher-dimension operator directly to the product of the GUT field-strength and its dual.

It is probably fair to say that, due to limitations of the 4d approach, including especially remaining ambiguities (free parameters or ad hoc assumptions) in models of flavor and GUT breaking, the string theoretic approach has become more important in GUT model building. In this framework, challenges include learning how to deal with the many vacua of the ‘landscape’ as well as, for each vacuum, developing the tools for reliably calculating detailed, phenomenological observables. Finally, due to limitations of space, the present article has barely touched on the interesting cosmological implications of GUTs. They may become more important in the future, especially in the case that a high inflationary energy scale is established observationally.

## References

- [1] S. Weinberg, Phys. Rev. Lett. **43**, 1566 (1979).
- [2] P. Minkowski, Phys. Lett. **67B**, 421 (1977).
- [3] T. Yanagida, in *Proceedings of the Workshop on the Unified Theory and the Baryon Number of the Universe*, eds. O. Sawada and A. Sugamoto, KEK report No. 79-18, Tsukuba, Japan, 1979; S. Glashow, Quarks and leptons, published in *Proceedings of the Cargèse Lectures*, M. Levy (ed.), Plenum Press, New York, (1980); M. Gell-Mann, P. Ramond and R. Slansky, in *Supergravity*, ed. P. van Nieuwenhuizen *et al.*, North-Holland, Amsterdam, (1979), p. 315 [arXiv:1306.4669].
- [4] F. Wilczek, eConf **C790823**, 437 (1979); E. Witten, Phys. Lett. **91B**, 81 (1980); R. N. Mohapatra and G. Senjanovic, Phys. Rev. Lett. **44**, 912 (1980), [231(1979)].

- [5] G. 't Hooft, NATO Sci. Ser. B **59**, 135 (1980); M. J. G. Veltman, Acta Phys. Polon. **B12**, 437 (1981); L. Maiani, Gif-sur-Yvette Summer School on Particle Physics, 11th, Gif-sur-Yvette, France, 1979 (Inst. Nat. Phys. Nucl. Phys. Particules, Paris, 1979); E. Witten, Nucl. Phys. **B188**, 513 (1981).
- [6] S. Dimopoulos, S. Raby and F. Wilczek, Phys. Rev. **D24**, 1681 (1981); S. Dimopoulos and H. Georgi, Nucl. Phys. **B193**, 150 (1981); L. E. Ibanez and G. G. Ross, Phys. Lett. **105B**, 439 (1981); N. Sakai, Z. Phys. **C11**, 153 (1981); M. B. Einhorn and D. R. T. Jones, Nucl. Phys. **B196**, 475 (1982); W. J. Marciano and G. Senjanovic, Phys. Rev. **D25**, 3092 (1982).
- [7] U. Amaldi, W. de Boer and H. Furstenau, Phys. Lett. **B260**, 447 (1991); J. R. Ellis, S. Kelley and D. V. Nanopoulos, Phys. Lett. **B260**, 131 (1991); P. Langacker and M.-x. Luo, Phys. Rev. **D44**, 817 (1991); C. Giunti, C.W. Kim and U.W. Lee, Mod. Phys. Lett. **A6**, 1745 (1991); P. Langacker and N. Polonsky, Phys. Rev. **D47**, 4028 (1993), [hep-ph/9210235]; M. Carena, S. Pokorski and C. E. M. Wagner, Nucl. Phys. **B406**, 59 (1993), [hep-ph/9303202]; See also the review by S. Dimopoulos, S.A. Raby and F. Wilczek, Physics Today, p. 25 October (1991).
- [8] Y. Okada, M. Yamaguchi and T. Yanagida, Prog. Theor. Phys. **85**, 1 (1991); J. R. Ellis, G. Ridolfi and F. Zwirner, Phys. Lett. **B257**, 83 (1991); H. E. Haber and R. Hempfling, Phys. Rev. Lett. **66**, 1815 (1991).
- [9] M. Carena *et al.*, Phys. Lett. **B355**, 209 (1995), [hep-ph/9504316]; G. Degrandi *et al.*, Eur. Phys. J. **C28**, 133 (2003), [hep-ph/0212020]; P. Kant *et al.*, JHEP **08**, 104 (2010), [arXiv:1005.5709].
- [10] J. L. Feng *et al.*, Phys. Rev. Lett. **111**, 131802 (2013), [arXiv:1306.2318]; S. Heinemeyer (2014), [arXiv:1405.3781]; P. Draper and H. Rzehak, Phys. Rept. **619**, 1 (2016), [arXiv:1601.01890].
- [11] J. C. Pati and A. Salam, Phys. Rev. **D8**, 1240 (1973); For more discussion on the standard charge assignments in this formalism, see A. Davidson, Phys. Rev. **D20**, 776 (1979) and R.N. Mohapatra and R.E. Marshak, Phys. Lett. **B91**, 222 (1980); see also J. C. Pati, Int. J. Mod. Phys. A **32**, 1741013 (2017), arXiv:1706.09531 for a recent account.
- [12] H. Georgi and S. L. Glashow, Phys. Rev. Lett. **32**, 438 (1974).
- [13] J. R. Ellis, M. K. Gaillard and D. V. Nanopoulos, Phys. Lett. **80B**, 360 (1979), [Erratum: Phys. Lett. **82B**, 464 (1979)]; E. Golowich, Phys. Rev. **D24**, 2899 (1981).
- [14] S. Weinberg, Phys. Rev. **D26**, 287 (1982); N. Sakai and T. Yanagida, Nucl. Phys. **B197**, 533 (1982).
- [15] H. Georgi, Particles and Fields, *Proceedings of the APS Div. of Particles and Fields*, ed. C. Carlson, p. 575 (1975); H. Fritzsch and P. Minkowski, Annals Phys. **93**, 193 (1975).
- [16] R. Slansky, Phys. Rept. **79**, 1 (1981); H. Georgi, Front. Phys. **54**, 1 (1982); R. Feger and T. W. Kephart, Comput. Phys. Commun. **192**, 166 (2015), [arXiv:1206.6379]; N. Yamatsu, PTEP **2016**, 4, 043B02 (2016), [arXiv:1512.05559].
- [17] S. M. Barr, Phys. Lett. **112B**, 219 (1982); J. P. Derendinger, J. E. Kim and D. V. Nanopoulos, Phys. Lett. **139B**, 170 (1984); I. Antoniadis *et al.*, Phys. Lett. **B194**, 231 (1987); I. Antoniadis *et al.*, Phys. Lett. **B231**, 65 (1989).
- [18] F. Gursev, P. Ramond and P. Sikivie, Phys. Lett. **60B**, 177 (1976).
- [19] A. de Rujula, H. Georgi and S. L. Glashow, *5th Workshop on Grand Unification*, ed. K. Kang, H. Fried and P. Frampton, World Scientific, Singapore (1984), p. 88; See also earlier paper by Y. Achiman and B. Stech, p. 303, "New Phenomena in Lepton-Hadron Physics," ed. D.E.C. Fries and J. Wess, Plenum, NY (1979).
- [20] B. R. Greene *et al.*, Nucl. Phys. **B278**, 667 (1986); B. R. Greene *et al.*, Nucl. Phys. **B292**, 606 (1987); B. R. Greene, C. A. Lutken and G. G. Ross, Nucl. Phys. **B325**, 101 (1989); J. E. Kim, Phys. Lett. **B591**, 119 (2004), [hep-ph/0403196].
- [21] E. Witten, Phys. Lett. **105B**, 267 (1981).
- [22] A. Masiero *et al.*, Phys. Lett. **115B**, 380 (1982); B. Grinstein, Nucl. Phys. **B206**, 387 (1982).
- [23] S. Dimopoulos and F. Wilczek, *Proceedings Erice Summer School*, ed. A. Zichichi (1981); M. Srednicki, Nucl. Phys. **B202**, 327 (1982).
- [24] K. Inoue, A. Kakuto and H. Takano, Prog. Theor. Phys. **75**, 664 (1986).
- [25] Y. Yamada, Z. Phys. **C60**, 83 (1993); J. Hisano *et al.*, Phys. Lett. **B342**, 138 (1995), [hep-ph/9406417]; G. Altarelli, F. Feruglio and I. Masina, JHEP **11**, 040 (2000), [hep-ph/0007254].
- [26] K. S. Babu and S. M. Barr, Phys. Rev. **D48**, 5354 (1993), [hep-ph/9306242]; K. S. Babu and S. M. Barr, Phys. Rev. **D50**, 3529 (1994), [hep-ph/9402291]; K. S. Babu, J. C. Pati and Z. Tavartkiladze, JHEP **06**, 084 (2010), [arXiv:1003.2625].
- [27] K. S. Babu and R. N. Mohapatra, Phys. Rev. Lett. **74**, 2418 (1995), [hep-ph/9410326]; V. Lucas and S. Raby, Phys. Rev. **D54**, 2261 (1996), [hep-ph/9601303]; T. Blazek *et al.*, Phys. Rev. **D56**, 6919 (1997), [hep-ph/9611217]; S. M. Barr and S. Raby, Phys. Rev. Lett. **79**, 4748 (1997), [hep-ph/9705366]; K. S. Babu, J. C. Pati and F. Wilczek, Nucl. Phys. **B566**, 33 (2000), [hep-ph/9812538]; R. Dermisek, A. Mafi and S. Raby, Phys. Rev. **D63**, 035001 (2001), [hep-ph/0007213].
- [28] R. Barbieri, G. R. Dvali and A. Strumia, Nucl. Phys. **B391**, 487 (1993); Z. Berezhiani, C. Csaki and L. Randall, Nucl. Phys. **B444**, 61 (1995), [hep-ph/9501336]; Q. Shafi and Z. Tavartkiladze, Phys. Lett. **B522**, 102 (2001), [hep-ph/0105140].
- [29] G. F. Giudice and A. Masiero, Phys. Lett. **B206**, 480 (1988); J. E. Kim and H. P. Nilles, Mod. Phys. Lett. **A9**, 3575 (1994), [hep-ph/9406296].
- [30] L. Randall and C. Csaki, in "Supersymmetry and unification of fundamental interactions. Proceedings, International Workshop, SUSY 95, Palaiseau, France, May 15-19, 1995," 99-109 (1995), [235(1995)], [hep-ph/9508208].
- [31] E. Witten, in "Supersymmetry and unification of fundamental interactions. Proceedings, 10th International Conference, SUSY'02, Hamburg, Germany, June 17-23, 2002," 472-491 (2001), [hep-ph/0201018], URL [http://www-library.desy.de/preparch/desy/proc/proc02-02/Proceedings/susy02/special/hertz\\_pr.ps](http://www-library.desy.de/preparch/desy/proc/proc02-02/Proceedings/susy02/special/hertz_pr.ps); M. Dine, Y. Nir and Y. Shadmi, Phys. Rev. **D66**, 115001 (2002), [hep-ph/0206268].
- [32] A. Hebecker, J. March-Russell and R. Ziegler, JHEP **08**, 064 (2009), [arXiv:0801.4101]; F. Brummer *et al.*, JHEP **08**, 011 (2009), [arXiv:0906.2957]; F. Brummer *et al.*, JHEP **04**, 006 (2010), [arXiv:1003.0084].
- [33] H. M. Lee *et al.*, Phys. Lett. **B694**, 491 (2011), [arXiv:1009.0905]; R. Kappl *et al.*, Nucl. Phys. **B847**, 325 (2011), [arXiv:1012.4574]; H. M. Lee *et al.*, Nucl. Phys. **B850**, 1 (2011), [arXiv:1102.3595].
- [34] Y. Hosotani, Phys. Lett. **126B**, 309 (1983).
- [35] L. J. Dixon *et al.*, Nucl. Phys. **B261**, 678 (1985), [678(1985)]; L. J. Dixon *et al.*, Nucl. Phys. **B274**, 285 (1986); L. E. Ibanez, H. P. Nilles and F. Quevedo, Phys. Lett. **B187**, 25 (1987); L. E. Ibanez *et al.*, Phys. Lett. **B191**, 282 (1987).
- [36] P. Candelas *et al.*, Nucl. Phys. **B258**, 46 (1985).
- [37] Y. Kawamura, Prog. Theor. Phys. **103**, 613 (2000), [hep-ph/9902423]; Y. Kawamura, Prog. Theor. Phys. **105**, 999 (2001), [hep-ph/0012125]; G. Altarelli and F. Feruglio, Phys. Lett. **B511**, 257 (2001), [hep-ph/0102301];

- L. J. Hall and Y. Nomura, *Phys. Rev.* **D64**, 055003 (2001), [hep-ph/0103125]; A. Hebecker and J. March-Russell, *Nucl. Phys.* **B613**, 3 (2001), [hep-ph/0106166]; T. Asaka, W. Buchmuller and L. Covi, *Phys. Lett.* **B523**, 199 (2001), [hep-ph/0108021]; L. J. Hall *et al.*, *Phys. Rev.* **D65**, 035008 (2002), [hep-ph/0108071]; R. Dermisek and A. Mafi, *Phys. Rev.* **D65**, 055002 (2002), [hep-ph/0108139]; H. D. Kim and S. Raby, *JHEP* **01**, 056 (2003), [hep-ph/0212348].
- [38] L.E. Ibanez and A.M. Uranga, “String theory and particle physics: An introduction to string phenomenology,” Cambridge University Press 2012; K.-S. Choi and J. E. Kim, *Lect. Notes Phys.* **696**, 1 (2006); R. Blumenhagen *et al.*, *Phys. Rept.* **445**, 1 (2007), [hep-th/0610327].
- [39] D. J. Gross *et al.*, *Phys. Rev. Lett.* **54**, 502 (1985).
- [40] V. Braun *et al.*, *JHEP* **05**, 043 (2006), [hep-th/0512177]; V. Bouchard and R. Donagi, *Phys. Lett.* **B633**, 783 (2006), [hep-th/0512149]; L. B. Anderson *et al.*, *Phys. Rev.* **D84**, 106005 (2011), [arXiv:1106.4804].
- [41] L. J. Dixon, V. Kaplunovsky and J. Louis, *Nucl. Phys.* **B355**, 649 (1991).
- [42] G. Aldazabal *et al.*, *Nucl. Phys.* **B452**, 3 (1995), [hep-th/9410206]; Z. Kakushadze *et al.*, *Int. J. Mod. Phys.* **A13**, 2551 (1998), [hep-th/9710149].
- [43] E. Witten, *Nucl. Phys.* **B258**, 75 (1985).
- [44] S. Gukov *et al.*, *Phys. Rev.* **D69**, 086008 (2004), [hep-th/0310159]; G. Curio, A. Krause and D. Lust, *Fortsch. Phys.* **54**, 225 (2006), [hep-th/0502168]; L. B. Anderson *et al.*, *Phys. Rev.* **D83**, 106011 (2011), [arXiv:1102.0011].
- [45] R. Friedman, J. Morgan and E. Witten, *Commun. Math. Phys.* **187**, 679 (1997), [hep-th/9701162].
- [46] R. Blumenhagen, G. Honecker and T. Weigand, *JHEP* **08**, 009 (2005), [hep-th/0507041]; L. B. Anderson *et al.*, *JHEP* **01**, 047 (2014), [arXiv:1307.4787].
- [47] T. Kobayashi, S. Raby and R.-J. Zhang, *Phys. Lett.* **B593**, 262 (2004), [hep-ph/0403065].
- [48] S. Forste *et al.*, *Phys. Rev.* **D70**, 106008 (2004), [hep-th/0406208]; T. Kobayashi, S. Raby and R.-J. Zhang, *Nucl. Phys.* **B704**, 3 (2005), [hep-ph/0409098]; W. Buchmuller *et al.*, *Nucl. Phys.* **B712**, 139 (2005), [hep-ph/0412318]; W. Buchmuller *et al.*, *Phys. Rev. Lett.* **96**, 121602 (2006), [hep-ph/0511035]; W. Buchmuller *et al.*, *Nucl. Phys.* **B785**, 149 (2007), [hep-th/0606187]; O. Lebedev *et al.*, *Phys. Lett.* **B645**, 88 (2007), [hep-th/0611095]; J. E. Kim, J.-H. Kim and B. Kyae, *JHEP* **06**, 034 (2007), [hep-ph/0702278]; O. Lebedev *et al.*, *Phys. Rev.* **D77**, 046013 (2008), [arXiv:0708.2691].
- [49] S. B. Giddings, S. Kachru and J. Polchinski, *Phys. Rev.* **D66**, 106006 (2002), [hep-th/0105097]; S. Kachru *et al.*, *Phys. Rev.* **D68**, 046005 (2003), [hep-th/0301240].
- [50] R. Blumenhagen *et al.*, *Nucl. Phys.* **B815**, 1 (2009), [arXiv:0811.2936].
- [51] R. Blumenhagen *et al.*, *Nucl. Phys.* **B616**, 3 (2001), [hep-th/0107138].
- [52] R. Donagi and M. Wijnholt, *Adv. Theor. Math. Phys.* **15**, 5, 1237 (2011), [arXiv:0802.2969].
- [53] C. Beasley, J. J. Heckman and C. Vafa, *JHEP* **01**, 058 (2009), [arXiv:0802.3391]; C. Beasley, J. J. Heckman and C. Vafa, *JHEP* **01**, 059 (2009), [arXiv:0806.0102].
- [54] T. Weigand, *Class. Quant. Grav.* **27**, 214004 (2010), [arXiv:1009.3497]; J. J. Heckman, *Ann. Rev. Nucl. Part. Sci.* **60**, 237 (2010), [arXiv:1001.0577]; M. Cvetič, I. Garcia-Etxebarria and J. Halverson, *JHEP* **01**, 073 (2011), [arXiv:1003.5337]; A. Maharana and E. Palti, *Int. J. Mod. Phys.* **A28**, 1330005 (2013), [arXiv:1212.0555]; S. Krippendorf, S. Schafer-Nameki and J.-M. Wong, *JHEP* **11**, 008 (2015), [arXiv:1507.05961].
- [55] R. Donagi and M. Wijnholt, *Adv. Theor. Math. Phys.* **15**, 6, 1523 (2011), [arXiv:0808.2223]; R. Blumenhagen, *Phys. Rev. Lett.* **102**, 071601 (2009), [arXiv:0812.0248]; K.-S. Choi and J. E. Kim, *Phys. Rev.* **D83**, 065016 (2011), [arXiv:1012.0847]; C. Mayrhofer, E. Palti and T. Weigand, *JHEP* **09**, 082 (2013), [arXiv:1303.3589]; G. K. Leontaris and Q. Shafi, *Phys. Rev.* **D96**, 6, 066023 (2017), [arXiv:1706.08372].
- [56] E. Witten, *Nucl. Phys.* **B471**, 135 (1996), [hep-th/9602070].
- [57] A. Hebecker and M. Trapletti, *Nucl. Phys.* **B713**, 173 (2005), [hep-th/0411131].
- [58] B. Dundee and S. Raby (2008), [arXiv:0808.0992].
- [59] G. G. Ross (2004), [hep-ph/0411057].
- [60] H. Georgi, H. R. Quinn and S. Weinberg, *Phys. Rev. Lett.* **33**, 451 (1974); S. Weinberg, *Phys. Lett.* **91B**, 51 (1980); L. J. Hall, *Nucl. Phys.* **B178**, 75 (1981).
- [61] B. C. Allanach, *Comput. Phys. Commun.* **143**, 305 (2002), [hep-ph/0104145].
- [62] M. Tanabashi *et al.* (Particle Data Group), *Phys. Rev.* **D98**, 3, 030001 (2018).
- [63] M. L. Alciati *et al.*, *JHEP* **03**, 054 (2005), [hep-ph/0501086].
- [64] See talks on proposed and running nucleon decay experiments, and theoretical talks by P. Langacker, p. 131, and W.J. Marciano and A. Sirlin, p. 151, in *The Second Workshop on Grand Unification*, eds. J.P. Leveille *et al.*, Birkhäuser, Boston (1981).
- [65] W.J. Marciano, p. 190, *Eighth Workshop on Grand Unification*, ed. K. Wali, World Scientific Publishing Co., Singapore (1987).
- [66] M.S. Carena *et al.*, in Ref. [7].
- [67] A. Djouadi, J.-L. Kneur and G. Moultaka, *Comput. Phys. Commun.* **176**, 426 (2007), [hep-ph/0211331].
- [68] W. Porod and F. Staub, *Comput. Phys. Commun.* **183**, 2458 (2012), [arXiv:1104.1573].
- [69] W. Siegel, *Phys. Lett.* **94B**, 37 (1980).
- [70] I. Antoniadis, C. Kounnas, and R. Lacaze, *Nucl. Phys.* **B221**, 377 (1983).
- [71] M. A. Shifman, *Int. J. Mod. Phys.* **A11**, 5761 (1996), [hep-ph/9606281]; N. Arkani-Hamed and H. Murayama, *JHEP* **06**, 030 (2000), [hep-th/9707133]; I. Jack, D. R. T. Jones and A. Pickering, *Phys. Lett.* **B435**, 61 (1998), [hep-ph/9805482].
- [72] M.B. Einhorn and D.R.T. Jones in Ref. [6]; I. Antoniadis, C. Kounnas and K. Tamvakis, *Phys. Lett.* **119B**, 377 (1982).
- [73] J. Hisano, H. Murayama and T. Yanagida, *Phys. Rev. Lett.* **69**, 1014 (1992); J. Hisano, H. Murayama and T. Yanagida, *Nucl. Phys.* **B402**, 46 (1993), [hep-ph/9207279].
- [74] H. Murayama and A. Pierce, *Phys. Rev.* **D65**, 055009 (2002), [hep-ph/0108104].
- [75] G. Anderson *et al.*, eConf **C960625**, SUP107 (1996) [hep-ph/9609457].
- [76] L. Roszkowski and M. A. Shifman, *Phys. Rev.* **D53**, 404 (1996), [hep-ph/9503358]; S. Raby, M. Ratz and K. Schmidt-Hoberg, *Phys. Lett.* **B687**, 342 (2010), [arXiv:0911.4249].
- [77] J. Hisano, T. Kuwahara and N. Nagata, *Phys. Lett.* **B723**, 324 (2013), [arXiv:1304.0343].
- [78] N. Arkani-Hamed, A. Delgado and G. F. Giudice, *Nucl. Phys.* **B741**, 108 (2006), [hep-ph/0601041].
- [79] M. Ibe, T. Moroi and T. T. Yanagida, *Phys. Lett.* **B644**, 355 (2007), [hep-ph/0610277].
- [80] G. F. Giudice *et al.*, *JHEP* **12**, 027 (1998), [hep-ph/9810442]; L. Randall and R. Sundrum, *Nucl. Phys.* **B557**, 79 (1999), [hep-th/9810155].
- [81] R. N. Mohapatra and M. K. Parida, *Phys. Rev.* **D47**, 264 (1993), [hep-ph/9204234].

- [82] D.-G. Lee *et al.*, Phys. Rev. **D51**, 229 (1995), [hep-ph/9404238].
- [83] L. E. Ibanez *et al.*, JHEP **07**, 195 (2012), [arXiv:1206.2655].
- [84] K. R. Dienes, E. Dudas and T. Gherghetta, Phys. Rev. Lett. **91**, 061601 (2003), [hep-th/0210294].
- [85] K. Agashe, R. Contino and R. Sundrum, Phys. Rev. Lett. **95**, 171804 (2005), [hep-ph/0502222].
- [86] F. Wilczek and A. Zee, Phys. Rev. Lett. **43**, 1571 (1979).
- [87] K. Abe *et al.* (Super-Kamiokande), Phys. Rev. **D95**, 1, 012004 (2017), [arXiv:1610.03597]; S. Mine (Super Kamiokande), J. Phys. Conf. Ser. **718**, 6, 062044 (2016).
- [88] K. Abe *et al.* (Hyper-Kamiokande) (2018), [arXiv:1805.04163].
- [89] Y. Aoki *et al.*, Phys. Rev. **D96**, 1, 014506 (2017), [arXiv:1705.01338].
- [90] J. Hisano, T. Kuhahara and Y. Omura, Nucl. Phys. **B898**, 1 (2015), [Erratum: Nucl. Phys. B907,476(2016)], [arXiv:1503.08561].
- [91] R. Barbier *et al.*, Phys. Rept. **420**, 1 (2005), [hep-ph/0406039]; F. Domingo *et al.*, JHEP **02**, 066 (2019), [arXiv:1810.08228].
- [92] G. R. Farrar and P. Fayet, Phys. Lett. **76B**, 575 (1978).
- [93] S. Dimopoulos, S. Raby and F. Wilczek, Phys. Lett. **112B**, 133 (1982); J. R. Ellis, D. V. Nanopoulos and S. Rudaz, Nucl. Phys. **B202**, 43 (1982).
- [94] C. S. Aulakh *et al.*, Nucl. Phys. **B597**, 89 (2001), [hep-ph/0004031].
- [95] T. Goto and T. Nihei, Phys. Rev. **D59**, 115009 (1999), [hep-ph/9808255].
- [96] G. D. Coughlan *et al.*, Phys. Lett. **160B**, 249 (1985); J. L. Chkareuli and I. G. Gogoladze, Phys. Rev. **D58**, 055011 (1998), [hep-ph/9803335].
- [97] G. F. Giudice and A. Romanino, Nucl. Phys. **B699**, 65 (2004), [Erratum: Nucl. Phys. B706,487(2005)], [hep-ph/0406088].
- [98] J. Hisano *et al.*, JHEP **07**, 038 (2013), [arXiv:1304.3651].
- [99] B. Bajc, P. Fileviez Perez and G. Senjanovic, Phys. Rev. **D66**, 075005 (2002), [hep-ph/0204311].
- [100] K.-S. Choi, Phys. Lett. **B668**, 392 (2008), [arXiv:0807.2766].
- [101] F. An *et al.* (JUNO), J. Phys. **G43**, 3, 030401 (2016), [arXiv:1507.05613].
- [102] R. Acciarri *et al.* (DUNE) (2015), [arXiv:1512.06148].
- [103] L. J. Hall and Y. Nomura, Phys. Rev. **D66**, 075004 (2002), [hep-ph/0205067]; H. D. Kim, S. Raby and L. Schradin, JHEP **05**, 036 (2005), [hep-ph/0411328].
- [104] M.S. Chanowitz, J.R. Ellis and M.K. Gaillard, Nucl. Phys. **B128**, 506 (1977); A. J. Buras *et al.*, Nucl. Phys. **B135**, 66 (1978).
- [105] K. Inoue *et al.*, Prog. Theor. Phys. **67**, 1889 (1982); L. E. Ibanez and C. Lopez, Nucl. Phys. **B233**, 511 (1984).
- [106] H. Georgi and D. V. Nanopoulos, Nucl. Phys. **B159**, 16 (1979); J. A. Harvey, P. Ramond and D. B. Reiss, Phys. Lett. **92B**, 309 (1980); J. A. Harvey, D. B. Reiss and P. Ramond, Nucl. Phys. **B199**, 223 (1982).
- [107] T. Banks, Nucl. Phys. **B303**, 172 (1988); M. Olechowski and S. Pokorski, Phys. Lett. **B214**, 393 (1988); S. Pokorski, Nucl. Phys. Proc. Suppl. **13**, 606 (1990); B. Ananthanarayan, G. Lazarides and Q. Shafi, Phys. Rev. **D44**, 1613 (1991); Q. Shafi and B. Ananthanarayan, ICTP Summer School lectures (1991); S. Dimopoulos, L. J. Hall and S. Raby, Phys. Rev. Lett. **68**, 1984 (1992); S. Dimopoulos, L. J. Hall and S. Raby, Phys. Rev. **D45**, 4192 (1992); G. W. Anderson *et al.*, Phys. Rev. **D47**, R3702 (1993), [hep-ph/9209250]; B. Ananthanarayan, G. Lazarides and Q. Shafi, Phys. Lett. **B300**, 245 (1993); G. Anderson *et al.*, Phys. Rev. **D49**, 3660 (1994), [hep-ph/9308333]; B. Ananthanarayan, Q. Shafi and X. M. Wang, Phys. Rev. **D50**, 5980 (1994), [hep-ph/9311225].
- [108] L. J. Hall, R. Rattazzi and U. Sarid, Phys. Rev. **D50**, 7048 (1994), [hep-ph/9306309]; M. Carena *et al.*, Nucl. Phys. **B426**, 269 (1994), [hep-ph/9402253].
- [109] A. Anandakrishnan, B. C. Bryant and S. Raby, JHEP **05**, 088 (2015), [arXiv:1411.7035].
- [110] M. Lanzagorta and G. G. Ross, Phys. Lett. **B364**, 163 (1995), [hep-ph/9507366].
- [111] K. Tobe and J. D. Wells, Nucl. Phys. **B663**, 123 (2003), [hep-ph/0301015].
- [112] G. Ross and M. Serna, Phys. Lett. **B664**, 97 (2008), [arXiv:0704.1248].
- [113] T. Blazek, R. Dermisek and S. Raby, Phys. Rev. Lett. **88**, 111804 (2002), [hep-ph/0107097]; T. Blazek, R. Dermisek and S. Raby, Phys. Rev. **D65**, 115004 (2002), [hep-ph/0201081]; D. Auto *et al.*, JHEP **06**, 023 (2003), [hep-ph/0302155]; R. Dermisek *et al.*, JHEP **04**, 037 (2003), [hep-ph/0304101]; R. Dermisek *et al.*, JHEP **09**, 029 (2005), [hep-ph/0507233].
- [114] A. Anandakrishnan, S. Raby and A. Wingerter, Phys. Rev. **D87**, 5, 055005 (2013), [arXiv:1212.0542]; M. Adeel Ajaib *et al.*, JHEP **07**, 139 (2013), [arXiv:1303.6964]; Z. Poh and S. Raby, Phys. Rev. **D92**, 1, 015017 (2015), [arXiv:1505.00264]; M. Badziak, M. Olechowski and S. Pokorski, JHEP **10**, 088 (2013), [arXiv:1307.7999].
- [115] H. Georgi and C. Jarlskog, Phys. Lett. **86B**, 297 (1979).
- [116] S. Antusch and M. Spinrath, Phys. Rev. **D79**, 095004 (2009), [arXiv:0902.4644].
- [117] G. Lazarides, Q. Shafi and C. Wetterich, Nucl. Phys. **B181**, 287 (1981).
- [118] T. E. Clark, T.-K. Kuo and N. Nakagawa, Phys. Lett. **115B**, 26 (1982); K. S. Babu and R. N. Mohapatra, Phys. Rev. Lett. **70**, 2845 (1993), [hep-ph/9209215].
- [119] R. Barbieri and D. V. Nanopoulos, Phys. Lett. **91B**, 369 (1980).
- [120] C. D. Froggatt and H. B. Nielsen, Nucl. Phys. **B147**, 277 (1979).
- [121] R. Barbieri *et al.*, Nucl. Phys. **B493**, 3 (1997), [hep-ph/9610449]; T. Blazek, S. Raby and K. Tobe, Phys. Rev. **D60**, 113001 (1999), [hep-ph/9903340]; T. Blazek, S. Raby and K. Tobe, Phys. Rev. **D62**, 055001 (2000), [hep-ph/9912482]; Q. Shafi and Z. Tavartkiladze, Phys. Lett. **B487**, 145 (2000), [hep-ph/9910314]; C. H. Albright and S. M. Barr, Phys. Rev. Lett. **85**, 244 (2000), [hep-ph/0002155]; Z. Berezhiani and A. Rossi, Nucl. Phys. **B594**, 113 (2001), [hep-ph/0003084]; C. H. Albright and S. M. Barr, Phys. Rev. **D64**, 073010 (2001), [hep-ph/0104294]; M.-C. Chen and K. T. Mahanthappa, Int. J. Mod. Phys. **A18**, 5819 (2003), [hep-ph/0305088]; R. Dermisek and S. Raby, Phys. Lett. **B622**, 327 (2005), [hep-ph/0507045].
- [122] H. Georgi, Nucl. Phys. **B156**, 126 (1979); P. H. Frampton, Phys. Lett. **88B**, 299 (1979); P. Frampton and S. Nandi, Phys. Rev. Lett. **43**, 1460 (1979); J.E. Kim, Phys. Rev. Lett. **45**, 1916 (1980), Phys. Rev. **D23**, 2706 (1981) and Phys. Rev. **D26**, 674 (1982); Y. Fujimoto, Phys. Rev. **D26**, 3183 (1982).
- [123] P. Langacker, Phys. Rept. **72**, 185 (1981).
- [124] H. Georgi, Conf. Proc. C **820726**, 705 (1982).
- [125] S. M. Barr, Phys. Rev. **D78**, 055008 (2008), [arXiv:0805.4808]; Y. Goto, Y. Kawamura and T. Miura, Phys. Rev. **D88**, 5, 055016 (2013), [arXiv:1307.2631]; J. E. Kim, JHEP **06**, 114 (2015), [arXiv:1503.03104]; C.H. Albright, R.P. Feger and T.W. Kephart, arXiv:1601.07523; M. Reig, J. W. F. Valle, C. A. Vaquera-Araujo and F. Wilczek, arXiv:1706.03116.

- [126] M. Magg and C. Wetterich, Phys. Lett. **94B**, 61 (1980); J. Schechter and J. W. F. Valle, Phys. Rev. **D22**, 2227 (1980); R. N. Mohapatra and G. Senjanovic, Phys. Rev. **D23**, 165 (1981); G. B. Gelmini and M. Roncadelli, Phys. Lett. **99B**, 411 (1981).
- [127] R. Foot *et al.*, Z. Phys. **C44**, 441 (1989).
- [128] Y. Fukuda *et al.* (Super-Kamiokande), Phys. Rev. Lett. **81**, 1562 (1998), [hep-ex/9807003].
- [129] G. L. Fogli *et al.*, Phys. Rev. **D84**, 053007 (2011), [arXiv:1106.6028].
- [130] T. Schwetz, M. Tortola and J. W. F. Valle, New J. Phys. **13**, 109401 (2011), [arXiv:1108.1376].
- [131] G. Altarelli, Soryushiron Kenkyu Electron. **116**, A29 (2008), [arXiv:0711.0161]; S. F. King and C. Luhn, Rept. Prog. Phys. **76**, 056201 (2013), [arXiv:1301.1340].
- [132] C. H. Albright and M.-C. Chen, Phys. Rev. **D74**, 113006 (2006), [hep-ph/0608137].
- [133] R. Kallosh *et al.*, Phys. Rev. **D52**, 912 (1995), [hep-th/9502069].
- [134] H. Ruegg and M. Ruiz-Altaba, Int. J. Mod. Phys. **A19**, 3265 (2004), [hep-th/0304245].
- [135] M. B. Green and J. H. Schwarz, Phys. Lett. **149B**, 117 (1984).
- [136] L. E. Ibanez and G. G. Ross, Nucl. Phys. **B368**, 3 (1992); M. Berasaluce-Gonzalez *et al.*, JHEP **12**, 113 (2011), [arXiv:1106.4169].
- [137] N.G. Deshpande, OITS-107; C. Q. Geng and R. E. Marshak, Phys. Rev. **D39**, 693 (1989); A. Font, L. E. Ibanez and F. Quevedo, Phys. Lett. **B228**, 79 (1989); K. S. Babu and R. N. Mohapatra, Phys. Rev. Lett. **63**, 938 (1989).
- [138] R. Foot *et al.*, Phys. Rev. **D39**, 3411 (1989).
- [139] M. Nowakowski and A. Pilaftsis, Phys. Rev. **D48**, 259 (1993), [hep-ph/9304312].
- [140] T. P. T. Dijkstra, L. R. Huiszoon and A. N. Schellekens, Phys. Lett. **B609**, 408 (2005), [hep-th/0403196]; F. Gmeiner *et al.*, JHEP **01**, 004 (2006), [hep-th/0510170]; B. Gato-Rivera and A. N. Schellekens, Nucl. Phys. **B883**, 529 (2014), [arXiv:1401.1782].
- [141] G. 't Hooft, Nucl. Phys. **B79**, 276 (1974) A.M. Polyakov, Pis'ma Zh. Eksp. Teor. Fiz. **20**, 430 (1974) [Sov. Phys. JETP Lett. **20**, 194 (1974)]; For a pedagogical introduction, see S. Coleman, in *Aspects of Symmetry*, Selected Erice Lectures, Cambridge University Press, Cambridge, (1985), and P. Goddard and D. Olive, Rept. on Prog. in Phys. **41**, 1357 (1978).
- [142] M. Ambrosio *et al.* (MACRO), Eur. Phys. J. **C25**, 511 (2002), [hep-ex/0207020]; S. Balestra *et al.* (2011), [arXiv:1105.5587]; L. Patrizii and M. Spurio, Ann. Rev. Nucl. Part. Sci. **65**, 279 (2015), [arXiv:1510.07125].
- [143] For a review, see A.D. Linde, *Particle Physics and Inflationary Cosmology*, Harwood Academic, Switzerland (1990).
- [144] G. R. Dvali, H. Liu and T. Vachaspati, Phys. Rev. Lett. **80**, 2281 (1998), [hep-ph/9710301].
- [145] P. Langacker and S.-Y. Pi, Phys. Rev. Lett. **45**, 1 (1980).
- [146] G. R. Dvali, A. Melfo and G. Senjanovic, Phys. Rev. Lett. **75**, 4559 (1995), [hep-ph/9507230].
- [147] V. Rubakov, Nucl. Phys. **B203**, 311 (1982) and Institute of Nuclear Research Report No. P-0211, Moscow (1981), unpublished; C. G. Callan, Jr., Phys. Rev. **D26**, 2058 (1982); F. Wilczek, Phys. Rev. Lett. **48**, 1146 (1982); S. Dawson and A. N. Schellekens, Phys. Rev. **D27**, 2119 (1983).
- [148] K. Freese, M. S. Turner and D. N. Schramm, Phys. Rev. Lett. **51**, 1625 (1983).
- [149] P. A. R. Ade *et al.* (BICEP2, Keck Array), Phys. Rev. Lett. **116**, 031302 (2016), [arXiv:1510.09217]; N. Aghanim *et al.* (Planck) (2018), [arXiv:1807.06209].
- [150] L. J. Hall, V. A. Kostelecky and S. Raby, Nucl. Phys. **B267**, 415 (1986).
- [151] R. Barbieri and L. J. Hall, Phys. Lett. **B338**, 212 (1994), [hep-ph/9408406]; R. Barbieri, L. J. Hall and A. Strumia, Nucl. Phys. **B445**, 219 (1995), [hep-ph/9501334].
- [152] F. Borzumati and A. Masiero, Phys. Rev. Lett. **57**, 961 (1986); J. Hisano *et al.*, Phys. Lett. **B357**, 579 (1995), [hep-ph/9501407]; J. Hisano *et al.*, Phys. Rev. **D53**, 2442 (1996), [hep-ph/9510309]; J. Hisano and D. Nomura, Phys. Rev. **D59**, 116005 (1999), [hep-ph/9810479].
- [153] T. Moroi, JHEP **03**, 019 (2000), [hep-ph/0002208]; D. Chang, A. Masiero and H. Murayama, Phys. Rev. **D67**, 075013 (2003), [hep-ph/0205111].
- [154] S. Dimopoulos and L. J. Hall, Phys. Lett. **B344**, 185 (1995), [hep-ph/9411273].
- [155] J. Hisano *et al.*, Phys. Lett. **B604**, 216 (2004), [hep-ph/0407169].
- [156] A. Yu. Ignatiev *et al.*, Phys. Lett. **76B**, 436 (1978); M. Yoshimura, Phys. Rev. Lett. **41**, 281 (1978), [Erratum: Phys. Rev. Lett. **42**, 746 (1979)].
- [157] D. Toussaint *et al.*, Phys. Rev. **D19**, 1036 (1979); S. Weinberg, Phys. Rev. Lett. **42**, 850 (1979); M. Yoshimura, Phys. Lett. **88B**, 294 (1979); S. M. Barr, G. Segre and H. A. Weldon, Phys. Rev. **D20**, 2494 (1979); D. V. Nanopoulos and S. Weinberg, Phys. Rev. **D20**, 2484 (1979); A. Yildiz and P. H. Cox, Phys. Rev. **D21**, 906 (1980).
- [158] H. K. Dreiner and G. G. Ross, Nucl. Phys. **B410**, 188 (1993), [hep-ph/9207221].
- [159] M. Fukugita and T. Yanagida, Phys. Rev. Lett. **89**, 131602 (2002), [hep-ph/0203194].
- [160] M. Fukugita and T. Yanagida, Phys. Lett. **B174**, 45 (1986).
- [161] S. Davidson and A. Ibarra, Phys. Lett. **B535**, 25 (2002), [hep-ph/0202239]; K. Hamaguchi, H. Murayama and T. Yanagida, Phys. Rev. **D65**, 043512 (2002), [hep-ph/0109030].
- [162] A. Pilaftsis and T. E. J. Underwood, Phys. Rev. **D72**, 113001 (2005), [hep-ph/0506107].
- [163] M. Kawasaki *et al.*, Phys. Rev. **D78**, 065011 (2008), [arXiv:0804.3745].
- [164] W. Buchmuller, R. D. Peccei and T. Yanagida, Ann. Rev. Nucl. Part. Sci. **55**, 311 (2005), [hep-ph/0502169]; C. S. Fong, E. Nardi and A. Riotto, Adv. High Energy Phys. **2012**, 158303 (2012), [arXiv:1301.3062].
- [165] V. Cirigliano *et al.*, JHEP **12**, 097 (2018), [arXiv:1806.02780].
- [166] K. S. Babu and R. N. Mohapatra, Phys. Rev. **D86**, 035018 (2012), [arXiv:1203.5544]; K. S. Babu and R. N. Mohapatra, Phys. Lett. **B715**, 328 (2012), [arXiv:1206.5701]; K. S. Babu and R. N. Mohapatra, Phys. Rev. Lett. **109**, 091803 (2012), [arXiv:1207.5771].
- [167] M. Baldo-Ceolin *et al.*, Z. Phys. **C63**, 409 (1994).
- [168] K. Abe *et al.* (Super-Kamiokande), Phys. Rev. **D91**, 072006 (2015), [arXiv:1109.4227].
- [169] J. Gustafson *et al.* (Super-Kamiokande), Phys. Rev. **D91**, 7, 072009 (2015), [arXiv:1504.01041].
- [170] K. R. Dienes, Phys. Rept. **287**, 447 (1997), [hep-th/9602045]; P. Nath and P. Fileviez Perez, Phys. Rept. **441**, 191 (2007), [hep-ph/0601023].
- [171] G.G. Ross, "Grand Unified Theories", Benjamin/Cummings, 1984.; S. Raby, Lect. Notes Phys. **939**, 1 (2017).
- [172] P. Nath, Int. J. Mod. Phys. **A33**, 20, 1830017 (2018), [arXiv:1807.05302]; D. Croon *et al.*, Front.in Phys. **7**, 76 (2019), [arXiv:1903.04977].
- [173] A. Ringwald, L.J. Rosenberg and G. Rybka, Review of 'Axions and other Similar Particles' in Ref. [62].

- [174] P. Svrcek and E. Witten, JHEP **06**, 051 (2006), [hep-th/0605206].
- [175] M. Dine, W. Fischler and M. Srednicki, Phys. Lett. **104B**, 199 (1981); A. R. Zhitnitsky, Sov. J. Nucl. Phys. **31**, 260 (1980), [Yad. Fiz.31,497(1980)].
- [176] J. P. Conlon, JHEP **05**, 078 (2006), [hep-th/0602233].



## 95. Leptoquarks

Updated August 2019 by S. Rolli (US Department of Energy) and M. Tanabashi (Nagoya U.)

Leptoquarks are hypothetical particles carrying both baryon number (B) and lepton number (L). The possible quantum numbers of leptoquark states can be restricted by assuming that their direct interactions with the ordinary standard model (SM) fermions are dimensionless and invariant under the SM gauge group. Table 95.1 shows the list of all possible quantum numbers with this assumption [1]. The columns of  $SU(3)_C$ ,  $SU(2)_W$ , and  $U(1)_Y$  in Table 95.1 indicate the QCD representation, the weak isospin representation, and the weak hypercharge, respectively. The spin of a leptoquark state is taken to be 1 (vector leptoquark) or 0 (scalar leptoquark).

**Table 95.1:** Possible leptoquarks and their quantum numbers.

Spin	$3B + L$	$SU(3)_c$	$SU(2)_W$	$U(1)_Y$	Allowed coupling
0	-2	$\bar{3}$	1	1/3	$\bar{q}_L^c \ell_L$ or $\bar{u}_R^c e_R$
0	-2	$\bar{3}$	1	4/3	$\bar{d}_R^c e_R$
0	-2	$\bar{3}$	3	1/3	$\bar{q}_L^c \ell_L$
1	-2	$\bar{3}$	2	5/6	$\bar{q}_L^c \gamma^\mu e_R$ or $\bar{d}_R^c \gamma^\mu \ell_L$
1	-2	$\bar{3}$	2	-1/6	$\bar{u}_R^c \gamma^\mu \ell_L$
0	0	3	2	7/6	$\bar{q}_L e_R$ or $\bar{u}_R \ell_L$
0	0	3	2	1/6	$\bar{d}_R \ell_L$
1	0	3	1	2/3	$\bar{q}_L \gamma^\mu \ell_L$ or $\bar{d}_R \gamma^\mu e_R$
1	0	3	1	5/3	$\bar{u}_R \gamma^\mu e_R$
1	0	3	3	2/3	$\bar{q}_L \gamma^\mu \ell_L$

If we do not require leptoquark states to couple directly with SM fermions, different assignments of quantum numbers become possible [2,3].

Leptoquark states are expected to exist in various extensions of the SM. The Pati-Salam model [4] is an example predicting the existence of a leptoquark state. Leptoquark states also exist in grand unification theories based on  $SU(5)$  [5],  $SO(10)$  [6], which includes Pati-Salam color  $SU(4)$ , and larger gauge groups. Scalar quarks in supersymmetric models with R-parity violation may also have leptoquark-type Yukawa couplings. The bounds on the leptoquark states can therefore be applied to constrain R-parity-violating supersymmetric models. Scalar leptoquarks are expected to exist at the TeV scale in extended technicolor models [7,8] where leptoquark states appear as the bound states of techni-fermions. Compositeness of quarks and leptons also provides examples of models which may have light leptoquark states [9].

Bounds on leptoquark states are obtained both directly and indirectly. Direct limits are from their production cross sections at colliders, while indirect limits are calculated from bounds on leptoquark-induced four-fermion interactions, which are obtained from low-energy experiments, or from collider experiments below threshold. These four-fermion interactions often cause lepton-flavor non-universalities in heavy quark decays. Anomalies observed recently in the  $R_K$  and  $R_D$  ratios [10,11] in the semi-leptonic  $B$  decays may be explained in models with TeV scale leptoquarks.

If a leptoquark couples to quarks (leptons) belonging to more than a single generation in the mass eigenbasis, it can induce four-fermion interactions causing flavor-changing neutral currents (lepton-family-number violations). The quantum number assignment of Table 1 allows several leptoquark states to couple to both left- and right-handed quarks simultaneously. Such leptoquark states are called non-chiral and may cause four-fermion interactions affecting the  $(\pi \rightarrow e\nu)/(\pi \rightarrow \mu\nu)$  ratio [12]. Non-chiral scalar leptoquarks also contribute to the muon anomalous magnetic moment [13,14]. Since indirect limits provide more stringent constraints on these types of leptoquarks, it is often assumed that a leptoquark state couples only to a single generation of quarks and a single generation of leptons in a chiral interaction, for which indirect limits become much weaker.

Additionally, this assumption gives strong constraints on models of leptoquarks.

Refs. [15,16,17] give extensive lists of the bounds on the leptoquark-induced four-fermion interactions. For the isoscalar scalar and vector leptoquarks  $S_0$  and  $V_0$ , for example, which couple with the first- (second-) generation left-handed quark, and the first-generation left-handed lepton, the bounds  $\lambda^2 < 0.07 \times (M_{LQ}/1 \text{ TeV})^2$  for  $S_0$ , and  $\lambda^2 < 0.4 \times (M_{LQ}/1 \text{ TeV})^2$  for  $V_0$  ( $\lambda^2 < 0.7 \times (M_{LQ}/1 \text{ TeV})^2$  for  $S_0$ , and  $\lambda^2 < 0.5 \times (M_{LQ}/1 \text{ TeV})^2$  for  $V_0$ ) with  $\lambda$  being the leptoquark coupling strength, can be derived from the limits listed in Ref. [17]. The  $e^+e^-$  experiments are sensitive to the indirect effects coming from  $t$ - and  $u$ -channel exchanges of leptoquarks in the  $e^+e^- \rightarrow q\bar{q}$  process. The HERA experiments give bounds on the leptoquark-induced four-fermion interaction. For detailed bounds obtained in this way, see the Boson Particle Listings for “Indirect Limits for Leptoquarks” and its references.

Collider experiments provide direct limits on the leptoquark states through limits on the pair- and single-production cross sections. The leading-order cross sections of the parton processes

$$\begin{aligned}
 q + \bar{q} &\rightarrow LQ + \bar{LQ} \\
 g + g &\rightarrow LQ + \bar{LQ} \\
 e + q &\rightarrow LQ
 \end{aligned}
 \tag{95.1}$$

may be written as [21]

$$\begin{aligned}
 \hat{\sigma}_{LO} [q\bar{q} \rightarrow LQ + \bar{LQ}] &= \frac{2\alpha_s^2 \pi}{27\hat{s}} \beta^3, \\
 \hat{\sigma}_{LO} [gg \rightarrow LQ + \bar{LQ}] &= \frac{\alpha_s^2 \pi}{96\hat{s}} \\
 &\times \left[ \beta(41 - 31\beta^2) + (18\beta^2 - \beta^4 - 17) \log \frac{1+\beta}{1-\beta} \right], \\
 \hat{\sigma}_{LO} [eq \rightarrow LQ] &= \frac{\pi\lambda^2}{4} \delta(\hat{s} - M_{LQ}^2)
 \end{aligned}
 \tag{95.2}$$

for a scalar leptoquark. Here  $\sqrt{\hat{s}}$  is the invariant energy of the parton subprocess, and  $\beta \equiv \sqrt{1 - 4M_{LQ}^2/\hat{s}}$ . The leptoquark Yukawa coupling is given by  $\lambda$ . Leptoquarks are also produced singly at hadron colliders through  $g + q \rightarrow LQ + \ell$  [22], which allows extending to higher masses the collider reach in the leptoquark search [23], depending on the leptoquark Yukawa coupling. See also Ref. [24] for a comprehensive review on the leptoquark phenomenology in precision experiments and particle colliders.

Leptoquark states which couple only to left- or right-handed quarks are called chiral leptoquarks. Leptoquark states which couple only to the first (second, third) generation are referred as the first- (second-, third-) generation leptoquarks.

The LHC, Tevatron and LEP experiments have been searching for pair production of the leptoquark states, which arises from the leptoquark gauge interaction. Due to the typical decay of the leptoquark into charged and neutral leptons and quarks, the searches are carried on in signatures including high  $P_T$  charged leptons, high  $E_T$  jets and large missing transverse energy. Additionally searches for pair produced LQs are often organized by the decay mode of the pair of LQs, via the decay parameter  $\beta$ , which represents the branching fraction into a charge lepton vs a neutrino:  $\beta = 1$  for both LQs decaying into a charged lepton,  $\beta = 0.5$  for one LQ decaying into a charged lepton and one into a neutrino. The gauge couplings of a scalar leptoquark are determined uniquely according to its quantum numbers in Table 95.1. Since all of the leptoquark states belong to color-triplet representation, the scalar leptoquark pair-production cross section at the Tevatron and LHC can be determined solely as a function of the leptoquark mass without making further assumptions. This is in contrast to the indirect or single-production limits, which give constraints in the leptoquark mass-coupling plane.

Older results from the Tevatron run can be found here: [26], [27], [28] and [29].

Since the previous version of this review, both ATLAS and CMS have updated their results concerning searches for first, second, and third generation LQs and leptoquark states which couple only with the  $i$ -th generation quarks and the  $j$ -th generation leptons ( $i \neq j$ ) without causing conflicts with severe indirect constraints. The datasets were almost all collected at center of mass energy of 13 TeV and corresponding to the latest integrated luminosity collected before the shutdown of the LHC occurring in 2019 and 2020.

It is worthy to note that organizing LQs by flavor quantum number first before organizing them by gauge quantum number is becoming more common and advantageous because it relates more closely to some of the experimental searches being performed. The traditional nomenclature for 1st, 2nd, and 3rd generation LQ encourages only looking for the diagonal elements in a flavor matrix of possibilities, which has been the traditional experimental search strategy.

Current results extend previous mass limits for scalar leptoquarks to  $> 1435$  GeV (first generation, CMS,  $\beta = 1, \sqrt{s} = 13$  TeV) and  $> 1270$  GeV (first generation, CMS,  $\beta = 0.5, \sqrt{s} = 13$  TeV) [30];  $> 1400$  GeV (first generation, ATLAS,  $\beta = 1, \sqrt{s} = 13$  TeV) and  $> 1290$  GeV (first generation, ATLAS,  $\beta = 0.5, \sqrt{s} = 13$  TeV) [31];  $> 1530$  GeV (second generation, CMS,  $\beta = 1, \sqrt{s} = 13$  TeV) and  $> 1285$  GeV (second generation, CMS,  $\beta = 0.5, \sqrt{s} = 13$  TeV) [32]; and  $> 1560$  GeV (second generation, ATLAS,  $\beta = 1, \sqrt{s} = 13$  TeV) and  $> 1230$  GeV (second generation, ATLAS,  $\beta = 0.5, \sqrt{s} = 13$  TeV) [31]. All limits are presented at 95% C.L.

As for third generation leptoquarks, CMS results are the following: 1) assuming that all leptoquarks decay to a top quark and a  $\tau$  lepton, the existence of pair produced, third-generation leptoquark up to a mass of 900 GeV ( $\beta = 1, 13$  TeV) is excluded at 95% confidence level [33]; 2) assuming that all leptoquarks decay to a bottom quark and a  $\tau$  lepton, the existence of pair produced, third-generation leptoquark up to a mass of 1020 GeV ( $\beta = 1, 13$  TeV) is excluded at 95% confidence level [34]; 3) assuming that all leptoquarks decay to a bottom quark and a  $\tau$  neutrino, the existence of pair produced, third-generation leptoquark up to a mass of 450 GeV ( $\beta = 0, 7$  TeV) is excluded at 95% confidence level [35]. In a recent paper [36], the ATLAS collaboration has limits on pair production of third generation scalar leptoquarks where all possible decays of the leptoquark into a quark ( $t, b$ ) and a lepton ( $\tau, \nu$ ) of the third generation are considered. The limits are presented as a function of the leptoquark mass and the branching ratio into charged leptons for leptoquark of up-type ( $LQ_3^{up} \rightarrow \tau\nu/b\tau$ ) and down-type ( $LQ_3^d \rightarrow b\nu/t\tau$ ); many results are re-interpretation of previously published ATLAS searches. The collaboration finds that masses below 800 GeV are excluded for both  $LQ_3^u$  and  $LQ_3^d$  independently of the branching ratio, with masses below about 1 TeV being excluded for the limiting cases of branching ratios equal to zero or unity.

It is also possible to consider leptoquark states which couple only with the  $i$ -th generation quarks and the  $j$ -th generation leptons ( $i \neq j$ ) without causing conflicts with severe indirect constraints. Such couplings have received renewed attention because they may provide an explanation to anomalies in rare  $B - meson$  decays and the anomalous magnetic moment of the muon. See Ref. [37], [38] and [39] and references therein for collider search strategies and limits on the pair production cross sections of this class of leptoquark states. In this framework, a novel CMS result [40] presents a non-traditional search for pair production of LQs coupled to a top quark and a muon. As no deviation from the standard model prediction was observed, scalar LQs decaying exclusively into  $top - \mu$  are excluded up to masses of 1420 GeV.

The magnetic-dipole-type and the electric-quadrupole-type interactions of a vector leptoquark are not determined even if we fix its gauge quantum numbers as listed in the Table 95.1 [41]. The production of vector leptoquarks depends in general on additional assumptions, where the leptoquark couplings and their pair production cross sections are enhanced relative to the scalar leptoquark contributions. The most stringent limits on vector LQ production are now from CMS [42] where previous searches for squarks and gluinos have been reinterpreted to constrain models of leptoquark production. LQ masses below 1530 GeV are excluded assuming the Yang-Mills case with coupling  $\kappa = 1$ , or 1115 GeV in the minimal coupling case

where  $\kappa = 0$ , placing the most stringent constraint to date from pair production of vector LQs.

The leptoquark pair-production cross sections in  $e^+e^-$  collisions depend on the leptoquark  $SU(2) \times U(1)$  quantum numbers and Yukawa coupling with electron [43].

Searches for first generation leptoquark singly produced were performed by the HERA experiments. Since the leptoquark single-production cross section depends on its Yukawa coupling, the leptoquark mass limits from HERA are usually displayed in the mass-coupling plane. For leptoquark Yukawa coupling  $\lambda = 0.1$ , early ZEUS Collaboration bounds on the first-generation leptoquarks range from 248 to 290 GeV, depending on the leptoquark species [45]. The ZEUS Collaboration has recently released a new paper [46] where data corresponding to a luminosity of around  $1 \text{ fb}^{-1}$  have been used in the framework of  $eeqq$  contact interactions (CI) to set limits on possible high-energy contributions beyond the Standard Model to electron-quark scattering. The analysis of the  $ep$  data has been based on simultaneous fits of parton distribution functions including contributions of Contact Interaction (CI) couplings to  $ep$  scattering. Several general CI models and scenarios with heavy leptoquarks were considered. As unambiguous deviations from the SM cannot be established, limits for CI compositeness scales and LQ mass scales were set that are in the TeV range. The H1 Collaboration has a comprehensive summary of searches for first generation leptoquarks using the full data sample collected in  $ep$  collisions at HERA ( $446 \text{ pb}^{-1}$ ). No evidence of production of leptoquarks was observed in final states with a large transverse momentum electron or large missing transverse momentum. For a coupling strength  $\lambda = 0.3$ , first generation leptoquarks with masses up to 800 GeV are excluded at 95% C.L. [48].

At the LHC, the CMS collaboration performed searches for single production of first and second generation leptoquarks [49], which is complementary to the HERA searches in the high  $\lambda$  region (for coupling strength  $\lambda = 1.0$ , first generation leptoquarks are excluded for masses up to 1.73 TeV and second generation leptoquark are excluded up to masses of 530 GeV). CMS also recently searched for third generation LQ decaying into  $\tau$  and *bottom* in [50]. Assuming unit Yukawa coupling ( $\lambda$ ), a third generation scalar leptoquark is excluded for masses below 740 GeV. Limits are also set on  $\lambda$  of the hypothesized leptoquark as a function of its mass. Above  $\lambda = 1.4$ , the results provide the best upper limit on the mass of a third-generation scalar leptoquark decaying to a  $\tau$  lepton and a bottom quark.

Searches for LQ will continue with more LHC data, particularly in light of the renewed interest in this type of particle to explain violation of lepton flavor universality and other anomalies, which point to explanations laying outside the Standard Model.

## References:

1. W. Buchmüller, R. Rückl, and D. Wyler, Phys. Lett. **B191**, 442 (1987).
2. K.S. Babu, C.F. Kolda, and J. March-Russell, Phys. Lett. **B408**, 261 (1997).
3. J.L. Hewett and T.G. Rizzo, Phys. Rev. **D58**, 055005 (1998).
4. J.C. Pati and A. Salam, Phys. Rev. **D10**, 275 (1974).
5. H. Georgi and S.L. Glashow, Phys. Rev. Lett. **32**, 438 (1974).
6. H. Georgi, AIP Conf. Proc. **23**, 575 (1975);  
H. Fritzsch and P. Minkowski, Ann. Phys. **93**, 193 (1975).
7. For a review, see, E. Farhi and L. Susskind, Phys. Reports **74**, 277 (1981).
8. K. Lane and M. Ramana, Phys. Rev. **D44**, 2678 (1991).
9. See, for example, B. Schrepf and F. Schrepf, Phys. Lett. **153B**, 101 (1985).
10. R. Aaij *et al.* [LHCb Collab.], Phys. Rev. Lett. **113**, 151601 (2014);  
R. Aaij *et al.* [LHCb Collab.], JHEP **08**, 055 (2017);  
R. Aaij *et al.* [LHCb Collab.], Phys. Rev. Lett. **122**, 191801 (2019).
11. Y. Amhis *et al.*, [HFLAV Collab.], Eur. Phys. J. **C77**, 895 (2017), updated results and plots available at [hf.lav.web.cern.ch/](http://hf.lav.web.cern.ch/).
12. O. Shanker, Nucl. Phys. **B204**, 375, (1982).

13. U. Mahanta, Eur. Phys. J. **C21**, 171 (2001) [Phys. Lett. **B515**, 111 (2001)].
14. K. Cheung, Phys. Rev. **D64**, 033001 (2001).
15. S. Davidson, D.C. Bailey, and B.A. Campbell, Z. Phys. **C61**, 613 (1994).
16. M. Leurer, Phys. Rev. **D49**, 333 (1994); Phys. Rev. **D50**, 536 (1994).
17. M. Carpentier and S. Davidson, Eur. Phys. J. **C70**, 1071 (2010).
18. A. Falkowski, M. González-Alonso and K. Mimouni, JHEP **08**, 123 (2017).
19. S. Davidson and A. Saporta, Phys. Rev. **D99**, 015032 (2019).
20. M. Chala, J. Santiago and M. Spannowsky, JHEP **04**, 014 (2019).
21. T. Plehn *et al.*, Z. Phys. **C74**, 611 (1997); M. Kramer *et al.*, Phys. Rev. Lett. **79**, 341 (1997); and references therein.
22. J.L. Hewett and S. Pakvasa, Phys. Rev. **D37**, 3165 (1988); O.J.P. Eboli and A.V. Olinto, Phys. Rev. **D38**, 3461 (1988); A. Dobado, M.J. Herrero, and C. Muñoz, Phys. Lett. **207B**, 97 (1988); V.D. Barger *et al.*, Phys. Lett. **B220**, 464 (1989); M. De Montigny and L. Marleau, Phys. Rev. **D40**, 2869 (1989) [Erratum-*ibid.* **D56**, 3156 (1997)].
23. A. Belyaev *et al.*, JHEP **0509**, 005 (2005).
24. I. Doršner *et al.*, Phys. Reports **641**, 1 (2016).
25. D. Acosta *et al.* [CDF Collab.], Phys. Rev. **D72**, 051107 (2005).
26. V.M. Abazov *et al.* [DØCollab.], Phys. Lett. **B681**, 224 (2009).
27. A. Abulencia *et al.* [CDF Collab.], Phys. Rev. **D73**, 051102 (2006).
28. V.M. Abazov *et al.* [DØCollab.], Phys. Lett. **B671**, 224 (2009).
29. V. Abazov *et al.* [DØCollab.], Phys. Lett. **B693**, 95 (2010).
30. [CMS Collab.], Phys. Rev. **D99**, 052002 (2019).
31. [ATLAS Collab.], Eur. Phys. J. **C79**, 733 (2019).
32. [CMS Collab.], Phys. Rev. **D99**, 032014 (2019).
33. [CMS Collab.], Eur. Phys. J. **C78**, 707 (2018).
34. [CMS Collab.], JHEP **03**, 170 (2019).
35. [CMS Collab.], JHEP **1212**, 055 (2012).
36. [ATLAS Collab.], JHEP **06**, 144 (2019).
37. B. Diaz, M. Schmaltz, and Y. M. Zhong, JHEP **10**, 097 (2017).
38. M. Schmaltz, and Y. M. Zhong, JHEP **01**, 132 (2019).
39. D. Muller, EPJ Web Conf. **179**, 01015 (2018)..
40. [CMS Collab.] Phys. Rev. Lett. **121**, 241802 (2018).
41. J. Blümlein, E. Boos, and A. Kryukov, Z. Phys. **C76**, 137 (1997).
42. [CMS Collab.] Phys. Rev. **D98**, 032005 (2018).
43. J. Blümlein and R. Ruckl, Phys. Lett. **B304**, 337 (1993).
44. G. Abbiendi *et al.* [OPAL Collab.], Eur. Phys. J. **C31**, 281 (2003).
45. S. Chekanov *et al.* [ZEUS Collab.], Phys. Rev. **D68**, 052004 (2003).
46. H. Abramowicz *et al.* [ZEUS Collab.], Phys. Rev. **D99**, 092006 (2019).
47. A. Aktas *et al.* [H1 Collab.], Phys. Lett. **B629**, 9 (2005).
48. F.D. Aaron *et al.* [H1 Collab.], Phys. Lett. **B704**, 388 (2011).
49. V. Khachatryan *et al.* [CMS Collab.], Phys. Rev. **D93**, 032005 (2016).
50. [CMS Collab.] JHEP **07**, 115 (2018).

## 96. Magnetic Monopoles

Revised August 2019 by D. Milstead (Stockholm U.) and E.J. Weinberg (Columbia U.).

### 96.1 Theory of magnetic monopoles

The symmetry between electric and magnetic fields in the source-free Maxwell's equations naturally suggests that electric charges might have magnetic counterparts, known as magnetic monopoles. Although the greatest interest has been in the super-massive monopoles that are a firm prediction of all grand unified theories, one cannot exclude the possibility of lighter monopoles.

In either case, the magnetic charge is constrained by a quantization condition first found by Dirac [1]. Consider a monopole with magnetic charge  $Q_M$  and a Coulomb magnetic field

$$\mathbf{B} = \frac{Q_M}{4\pi} \frac{\hat{\mathbf{r}}}{r^2}. \quad (96.1)$$

Any vector potential  $\mathbf{A}$  whose curl is equal to  $\mathbf{B}$  must be singular along some line running from the origin to spatial infinity. This Dirac string singularity could potentially be detected through the extra phase that the wavefunction of a particle with electric charge  $Q_E$  would acquire if it moved along a loop encircling the string. For the string to be unobservable, this phase must be a multiple of  $2\pi$ . Requiring that this be the case for any pair of electric and magnetic charges gives the condition that all charges be integer multiples of minimum charges  $Q_E^{\min}$  and  $Q_M^{\min}$  obeying

$$Q_E^{\min} Q_M^{\min} = 2\pi. \quad (96.2)$$

(For monopoles which also carry an electric charge, called dyons [2], the quantization conditions on their electric charges can be modified. However, the constraints on magnetic charges, as well as those on all purely electric particles, will be unchanged.)

Another way to understand this result is to note that the conserved orbital angular momentum of a point electric charge moving in the field of a magnetic monopole has an additional component, with

$$\mathbf{L} = m\mathbf{r} \times \mathbf{v} - 4\pi Q_E Q_M \hat{\mathbf{r}} \quad (96.3)$$

Requiring the radial component of  $\mathbf{L}$  to be quantized in half-integer units yields Eq. 96.1.

If there are unbroken gauge symmetries in addition to the U(1) of electromagnetism, the above analysis must be modified [3] [4]. For example, a monopole could have both a U(1) magnetic charge and a color magnetic charge. The latter could combine with the color charge of a quark to give an additional contribution to the phase factor associated with a loop around the Dirac string, so that the U(1) charge could be the Dirac charge  $Q_M^D \equiv 2\pi/e$ , the result that would be obtained by substituting the electron charge into Eq. (96.1). On the other hand, for monopoles without color-magnetic charge, one would simply insert the quark electric charges into Eq. 96.1 and conclude that  $Q_M$  must be a multiple of  $6\pi/e$ .

The prediction of GUT monopoles arises from the work of 't Hooft [5] and Polyakov [6], who showed that certain spontaneously broken gauge theories have nonsingular classical solutions that lead to magnetic monopoles in the quantum theory. The simplest example occurs in a theory where the vacuum expectation value of a triplet Higgs field  $\mathbf{CE}$  breaks an SU(2) gauge symmetry down to the U(1) of electromagnetism and gives a mass  $M_V$  to two of the gauge bosons. In order to have finite energy,  $\mathbf{CE}$  must approach a vacuum value at infinity. However, there is a continuous family of possible vacua, since the scalar field potential determines only the magnitude  $v$  of  $\langle \mathbf{CE} \rangle$ , but not its orientation in the internal SU(2) space. In the monopole solution, the direction of  $\mathbf{CE}$  in internal space is correlated with the position in physical space; *i.e.*,  $\phi^a \sim v\hat{r}^a$ . The stability of the solution follows from the fact that this twisting Higgs field cannot be smoothly deformed to a spatially uniform vacuum configuration. Reducing the energetic cost of the spatial variation of  $\mathbf{CE}$  requires a nonzero gauge potential, which turns out to yield the magnetic field corresponding to a charge  $Q_M = 4\pi/e$ . Numerical solution of the classical field equations shows that the mass of this monopole is

$$M_{\text{mon}} \sim \frac{4\pi M_V}{e^2}. \quad (96.4)$$

The essential ingredient here was the fact that the Higgs fields at spatial infinity could be arranged in a topologically nontrivial configuration. A discussion of the general conditions under which this is possible is beyond the scope of this review, so we restrict ourselves to the two phenomenologically most important cases.

The first is the standard electroweak theory, with SU(2)  $\times$  U(1) broken to U(1). There are no topologically nontrivial configurations of the Higgs field, and hence no topologically stable monopole solutions.

The second is when any simple Lie group is broken to a subgroup with a U(1) factor, a case that includes all grand unified theories. The monopole mass is determined by the mass scale of the symmetry breaking that allows nontrivial topology. For example, an SU(5) model with

$$\text{SU}(5) \xrightarrow{M_X} \text{SU}(3) \times \text{SU}(2) \times \text{U}(1) \xrightarrow{M_W} \text{SU}(3) \times \text{U}(1) \quad (96.5)$$

has a monopole [7] with  $Q_M = 2\pi/e$  and mass

$$M_{\text{mon}} \sim \frac{4\pi M_X}{g^2}, \quad (96.6)$$

where  $g$  is the SU(5) gauge coupling. For a unification scale of  $10^{16}$  GeV, these monopoles would have a mass  $M_{\text{mon}} \sim 10^{17} - 10^{18}$  GeV.

In theories with several stages of symmetry breaking, monopoles of different mass scales can arise. In an SO(10) theory with

$$\text{SO}(10) \xrightarrow{M_1} \text{SU}(4) \times \text{SU}(2) \times \text{SU}(2) \xrightarrow{M_2} \text{SU}(3) \times \text{SU}(2) \times \text{U}(1) \quad (96.7)$$

there is monopole with  $Q_M = 2\pi/e$  and mass  $\sim 4\pi M_1/g^2$  and a much lighter monopole with  $Q_M = 4\pi/e$  and mass  $\sim 4\pi M_2/g^2$  [8].

The central core of a GUT monopole contains the fields of the superheavy gauge bosons that mediate baryon number violation, so one might expect that baryon number conservation could be violated in baryon-monopole scattering. The surprising feature, pointed out by Callan [9] and Rubakov [10], is that these processes are not suppressed by powers of the gauge boson mass. Instead, the cross-sections for catalysis processes such as  $p + \text{monopole} \rightarrow e^+ + \pi^0 + \text{monopole}$  are essentially geometric; *i.e.*,  $\sigma_{\Delta B} \beta \sim 10^{-27} \text{ cm}^2$ , where  $\beta = v/c$ . Note, however, that this catalysis is model-dependent and is not even a universal property of all GUT monopoles.

### 96.2 Production and Annihilation

GUT monopoles are far too massive to be produced in any foreseeable accelerator. However, they could have been produced in the early universe as topological defects arising via the Kibble mechanism [11] in a symmetry-breaking phase transition. Estimates of the initial monopole abundance, and of the degree to which it can be reduced by monopole-antimonopole annihilation, predict a present-day monopole abundance that exceeds by many orders of magnitude the astrophysical and experimental bounds described below [12]. Cosmological inflation and other proposed solutions to this primordial monopole problem generically lead to present-day abundances exponentially smaller than could be plausibly detected, although potentially observable abundances can be obtained in scenarios with carefully tuned parameters.

If monopoles light enough to be produced at colliders exist, one would expect that these could be produced by analogs of the electromagnetic processes that produce pairs of electrically charged particles. Because of the large size of the magnetic charge, this is a strong coupling problem for which perturbation theory cannot be trusted. Indeed, the problem of obtaining reliable quantitative estimates of the production cross-sections remains an open one, on which there is no clear consensus.

### 96.3 Astrophysical and Cosmological Bounds

If there were no galactic magnetic field, one would expect monopoles in the galaxy to have typical velocities of the order of  $10^{-3}c$ , comparable to the virial velocity in the galaxy (relevant if the monopoles cluster with the galaxy) and the peculiar velocity of the galaxy with respect to the CMB rest frame (relevant

if the monopoles are not bound to the galaxy). This situation is modified by the existence of a galactic magnetic field  $B \sim 3\mu\text{G}$ . A monopole with the Dirac charge and mass  $M$  would be accelerated by this field to a velocity

$$v_{\text{mag}} \sim \begin{cases} c, & M \lesssim 10^{11} \text{ GeV}, \\ 10^{-3} c \left( \frac{10^{17} \text{ GeV}}{M} \right)^{1/2}, & M \gtrsim 10^{11} \text{ GeV}. \end{cases} \quad (96.8)$$

Accelerating these monopoles drains energy from the magnetic field. Parker [13] obtained an upper bound on the flux of monopoles in the galaxy by requiring that the rate of this energy loss be small compared to the time scale on which the galactic field can be regenerated. With reasonable choices for the astrophysical parameters (see Ref. [14] for details), this Parker bound is

$$F < \begin{cases} 10^{-15} \text{ cm}^{-2} \text{ sr}^{-1} \text{ sec}^{-1}, & M \lesssim 10^{17} \text{ GeV}, \\ 10^{-15} \left( \frac{M}{10^{17} \text{ GeV}} \right) \text{ cm}^{-2} \text{ sr}^{-1} \text{ sec}^{-1}, & M \gtrsim 10^{17} \text{ GeV}. \end{cases} \quad (96.9)$$

Applying similar arguments to an earlier seed field that was the progenitor of the current galactic field leads to a tighter bound [15],

$$F < \left[ \frac{M}{10^{17} \text{ GeV}} + (3 \times 10^{-6}) \right] 10^{-16} \text{ cm}^{-2} \text{ sr}^{-1} \text{ sec}^{-1}. \quad (96.10)$$

Considering magnetic fields in galactic clusters gives a bound [16] which, although less secure, is about three orders of magnitude lower than the Parker bound.

A flux bound can also be inferred from the total mass of monopoles in the universe. If the monopole mass density is a fraction  $\Omega_M$  of the critical density, and the monopoles were uniformly distributed throughout the universe, there would be a monopole flux

$$F_{\text{uniform}} = 1.3 \times 10^{-16} \Omega_M \left( \frac{10^{17} \text{ GeV}}{M} \right) \left( \frac{v}{10^{-3} c} \right) \text{ cm}^{-2} \text{ sr}^{-1} \text{ sec}^{-1}. \quad (96.11)$$

If we assume that  $\Omega_M \sim 0.1$ , this gives a stronger constraint than the Parker bound for  $M \sim 10^{15}$  GeV. However, monopoles with masses  $\sim 10^{17}$  GeV are not ejected by the galactic field and can be gravitationally bound to the galaxy. In this case their flux within the galaxy is increased by about five orders of magnitude for a given value of  $\Omega_M$ , and the mass density bound only becomes stronger than the Parker bound for  $M \sim 10^{18}$  GeV.

A much more stringent flux bound applies to GUT monopoles that catalyze baryon number violation. The essential idea is that compact astrophysical objects would capture monopoles at a rate proportional to the galactic flux. These monopoles would then catalyze proton decay, with the energy released in the decay leading to an observable increase in the luminosity of the object. A variety of bounds, based on neutron stars [17–21], white dwarfs [22], and Jovian planets [23] have been obtained. These depend in the obvious manner on the catalysis cross section, but also on the details of the astrophysical scenarios; *e.g.*, on how much the accumulated density is reduced by monopole-antimonopole annihilation, and on whether monopoles accumulated in the progenitor star survive its collapse to a white dwarf or neutron star. The bounds obtained in this manner lie in the range

$$F \left( \frac{\sigma_{\Delta B \beta}}{10^{-27} \text{ cm}^2} \right) \sim (10^{-18} - 10^{-29}) \text{ cm}^{-2} \text{ sr}^{-1} \text{ sec}^{-1}. \quad (96.12)$$

It is important to remember that not all GUT monopoles catalyze baryon number nonconservation. In particular, the intermediate mass monopoles that arise in some GUTs at later stages of symmetry-breaking are examples of theoretically motivated monopoles that are exempt from the bound of the above equation.

## 96.4 Searches for Magnetic Monopoles

To date there have been no confirmed observations of exotic particles possessing magnetic charge. Precision measurements of the properties of known particles have led to tight limits on the values of magnetic charge they may possess. Using the induction method (see below), the electron’s magnetic charge has been found to be  $Q_e^m < 10^{-24} Q_M^D$  [24] (where  $Q_M^D$  is the Dirac charge). Furthermore, measurements of the anomalous magnetic moment of the muon have been used to place a model dependent lower limit of 120 GeV on the monopole mass<sup>1</sup> [25]. Nevertheless, guided mainly by Dirac’s argument and the predicted existence of monopoles from spontaneous symmetry breaking mechanisms, searches have been routinely made for monopoles produced at accelerators, in cosmic rays, and bound in matter [26]. Although the resultant limits from such searches are usually made under the assumption of a particle possessing only magnetic charge, most of the searches are also sensitive to dyons.

## 96.5 Search Techniques

Search strategies are determined by the expected interactions of monopoles as they pass through matter. These would give rise to a number of striking characteristic signatures. Since a complete description of monopole search techniques falls outside of the scope of this minireview, only the most common methods are described below. More comprehensive descriptions of search techniques can be found in Refs. [27] [28].

The induction method exploits the long-ranged electromagnetic interaction of the monopole with the quantum state of a superconducting ring which would lead to a monopole which passes through such a ring inducing a permanent current. The induction technique typically uses Superconducting Quantum Interference Devices (SQUID) technology for detection and is employed for searches for monopoles in cosmic rays and matter. Another approach is to exploit the electromagnetic energy loss of monopoles. Monopoles with Dirac charge would typically lose energy at a rate which is several thousand times larger than that expected from particles possessing the elementary electric charge. Consequently, scintillators, gas chambers and nuclear track detectors (NTDs) have been used in cosmic ray and collider experiments. A further approach, which has been used at colliders, is to search for particles describing a non-helical path in a uniform magnetic field.

### 96.5.1 Searches for Monopoles Bound in Matter

Monopoles have been sought in a range of bulk materials which it is assumed would have absorbed incident cosmic ray monopoles over a long exposure time of order million years. Materials which have been studied include moon rock, meteorites, manganese modules, and sea water [29, 30]. A stringent upper limit on the monopoles per nucleon ratio of  $\sim 10^{-29}$  has been obtained [30].

### 96.5.2 Searches in Cosmic Rays

Direct searches for monopoles in cosmic rays refer to those experiments in which the passage of the monopole is measured by an active detector. Searches made assuming a catalysis processes in which GUT monopoles could induce nucleon decay are discussed in the next section. To interpret the results of the non-catalysis searches, the cross section for the catalysis process is typically either set to zero [31] or assigned a modest value (1mb) [32].

Although early cosmic ray searches using the induction technique [33] and NTDs [34] observed monopole candidates, none of these apparent observations have been confirmed. Recent experiments have typically employed large scale detectors. The MACRO experiment at the Gran Sasso underground laboratory comprised three different types of detector: liquid scintillator, limited stream tubes, and NTDs, which provided a total acceptance of  $\sim 10000\text{m}^2$  for an isotropic flux. As shown in Fig. 96.1, this experiment has so far provided the most extensive  $\beta$ -dependent flux limits for GUT monopoles with Dirac charge [32]. Also shown are limits from an experiment at the OHYA mine in Japan [31], which used a  $2000\text{m}^2$  array of NTDs.

In Fig. 96.1, upper flux limits are also shown as a function of mass for monopole speed  $\beta > 0.05$ . In addition to MACRO

<sup>1</sup> Where no ambiguity is likely to arise, a reference to a monopole implies a particle possessing Dirac charge.

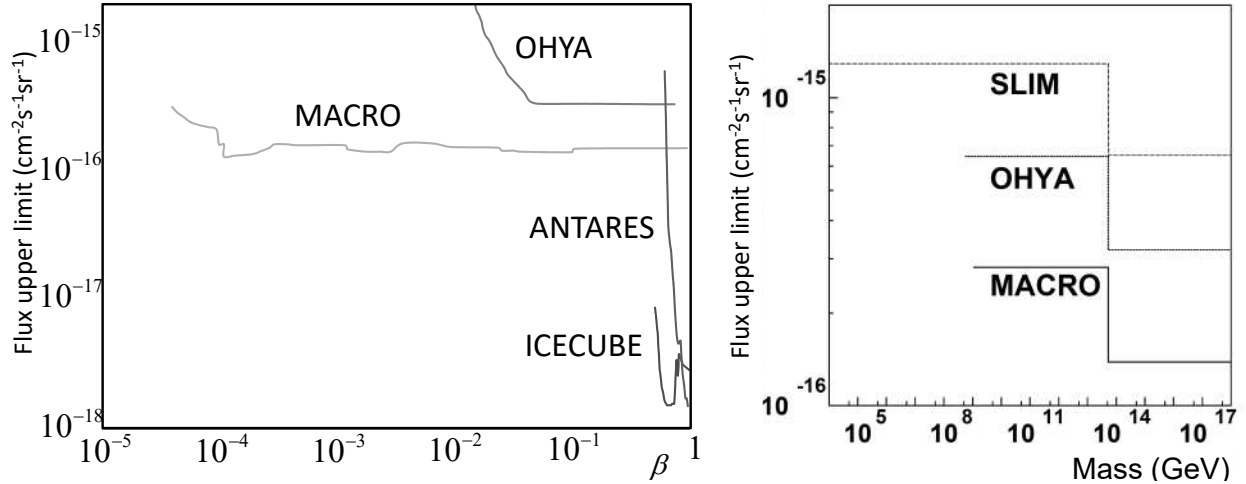


Figure 96.1: Upper flux limits for (left) GUT monopoles as a function of  $\beta$  (right) Monopoles as a function of mass for  $\beta > 0.05$ .

and OYHA flux limits, results from the SLIM [35] high-altitude experiment are shown. The SLIM experiment provided a good sensitivity to intermediate mass monopoles ( $10^5 \lesssim M \lesssim 10^{12}$  GeV). In addition to the results shown in Fig. 96.1, limits as low as  $\sim 1.5 \times 10^{-18} \text{ cm}^{-2} \text{ s}^{-1} \text{ sr}^{-1}$  were obtained for monopoles with  $\beta > 0.51$  and  $\beta > 0.6$  by the IceCube [36] and Antares [37] experiments, respectively. Stringent constraints on the flux of ultra-relativistic monopoles have been obtained at the Pierre Auger Observatory [38] which was sensitive to monopoles with  $\gamma$  values ranging from  $10^9$  to  $10^{12}$ , leading to flux limits in the range  $10^{-15} - 2.5 \times 10^{-21} \text{ cm}^{-2} \text{ s}^{-1} \text{ sr}^{-1}$ . The RICE [39] and ANITA-II experiments [40] at the South Pole have also sought ultra-relativistic monopoles with  $\gamma$  values of  $10^7 \lesssim \gamma \lesssim 10^{12}$  and  $10^9 \lesssim \gamma \lesssim 10^{13}$ , respectively, and which produced flux limits as low as  $2.5 \times 10^{-21} \text{ cm}^{-2} \text{ s}^{-1} \text{ sr}^{-1}$ .

### 96.5.3 Searches via the Catalysis of Nucleon-Decay

Searches have been performed for evidence of the catalysed decay of a nucleon by a monopole, as predicted by the Callan-Rubakov mechanism. The searches are thus sensitive to the assumed value of the catalysis decay cross section. Searches have been made with the Soudan [41] and Macro [42] experiments, using tracking detectors. Searches at IMB [43], the underwater Lake Baikal experiment [44] and the The IceCube experiment [45] which exploit the Cerenkov effect have also been made. The resulting  $\beta$ -dependent flux limits from these experiments typically vary between  $\sim 10^{-18}$  and  $\sim 10^{-14} \text{ cm}^{-2} \text{ s}^{-1} \text{ sr}^{-1}$ . A recent search for low energy neutrinos (assumed to be produced from induced proton decay in the sun) was made at Super-Kamiokande [46]. A model- and  $\beta$ -dependent of limit of  $6.3 \times 10^{-24} (\frac{\beta}{10^{-3}})^2 \text{ cm}^{-2} \text{ sr}^{-1} \text{ s}^{-1}$  was obtained.

### 96.5.4 Searches at Colliders

Searches have been performed at hadron-hadron, electron-positron and lepton-hadron experiments. Collider searches can be broadly classed as being direct or indirect. In a direct search, evidence of the passage of a monopole through material, such as a charged particle track, is sought. In indirect searches, virtual monopole processes are assumed to influence the production rates of certain final states.

#### 96.5.4.1 Direct Searches at Colliders

Collider experiments typically express their results in terms of upper limits on a production cross section and/or monopole mass. To calculate these limits, ansatzes are used to model the kinematics of monopole-antimonopole pair production processes since perturbative field theory cannot be used to calculate the rate and kinematic properties of produced monopoles. Limits therefore suffer from a degree of model-dependence, implying that a comparison between the results of different experiments can be problematic, in particular when this concerns excluded mass re-

gions. A conservative approach with as little model-dependence as possible is thus to present representative values of the upper cross-section limits as a function of one half the centre-of-mass energy of the collisions, as shown in Fig. 96.2 for recent results from high energy colliders.

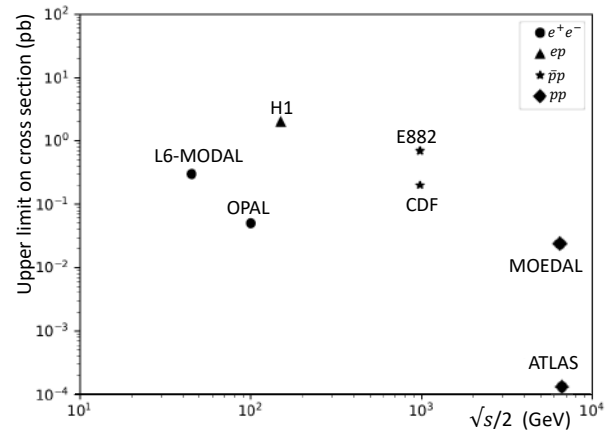


Figure 96.2: Upper limits on the production cross sections of monopoles from various collider-based experiments.

Searches for monopoles produced at the highest available energies in hadron-hadron collisions were made in  $pp$  collisions at the LHC by the ATLAS [47, 48] and MoEDAL [49, 50] experiments. The experiments looked for highly ionising particles leaving characteristic energy deposition profiles and stopped monopoles with the induction method, respectively. The charge-dependent mass limits extend up to around 4 TeV. The ATLAS work considers monopoles with  $0.5Q_M^D$  and  $2Q_M^D$  while MoEDAL quotes limits for monopoles with charges from  $Q_M^D$  to  $5Q_M^D$ . MoEDAL considered monopole-pair production via photon fusion along with, as is commonly used in hadron-hadron collisions, Drell-Yan processes [51]. Tevatron searches have also been carried out by the CDF [52] and E882 [53] experiments. The CDF experiment used a dedicated time-of-flight system whereas the E882 experiment employed the induction technique to search for stopped monopoles in discarded detector material which had been part of the CDF and D0 detectors using periods of luminosity. Earlier searches at the Tevatron, such as [54], used NTDs and were based on comparatively modest amounts of integrated luminosity. Lower energy hadron-hadron experiments have employed a variety of search techniques including plastic track detectors [55] and searches for trapped monopoles [56].

The only LEP-2 search was made by OPAL [57] which quoted

cross section limits for the production of monopoles possessing masses up to around 103 GeV. At LEP-1, searches were made with NTDs deployed around an interaction region. This allowed a range of charges to be sought for masses up to  $\sim 45$  GeV. The L6-MODAL experiment [58] gave limits for monopoles with charges in the range  $0.9Q_M^D$  and  $3.6Q_M^D$ , whilst an earlier search by the MODAL experiment was sensitive to monopoles with charges as low as  $0.1Q_M^D$  [59]. The deployment of NTDs around the beam interaction point was also used at earlier  $e^+e^-$  colliders such as KEK [60] and PETRA [61]. Searches at  $e^+e^-$  facilities have also been made for particles following non-helical trajectories [62] [63].

There has so far been one search for monopole production in lepton-hadron scattering. Using the induction method, monopoles were sought which could have stopped in the aluminium beampipe which had been used by the H1 experiment at HERA [64]. Cross section limits were set for monopoles with charges in the range  $Q_M^D - 6Q_M^D$  for masses up to around 140 GeV.

#### 96.5.4.2 Indirect Searches at Colliders

It has been proposed that virtual monopoles can mediate processes which give rise to multi-photon final-states [65] [66]. Photon-based searches were made by the D0 [67] and L3 [68] experiments. The D0 work led to spin-dependent lower mass limits of between 610 and 1580 GeV, while L3 reported a lower mass limit of 510 GeV. However, it should be stressed that uncertainties on the theoretical calculations which were used to derive these limits are difficult to estimate.

#### References

- [1] P. A. M. Dirac, Proc. Roy. Soc. Lond. **A133**, 821, 60 (1931).
- [2] J. S. Schwinger, Science **165**, 757 (1969).
- [3] F. Englert and P. Windey, Phys. Rev. **D14**, 2728 (1976).
- [4] P. Goddard, J. Nuyts and D. I. Olive, Nucl. Phys. **B125**, 1 (1977).
- [5] G. 't Hooft, Nucl. Phys. **B79**, 276 (1974).
- [6] A. M. Polyakov, JETP Lett. **20**, 194 (1974).
- [7] C. P. Dokos and T. N. Tomaras, Phys. Rev. **D21**, 2940 (1980).
- [8] G. Lazarides and Q. Shafi, Phys. Lett. **94B**, 149 (1980).
- [9] C. G. Callan, Jr., Phys. Rev. **D26**, 2058 (1982).
- [10] V. A. Rubakov, Nucl. Phys. **B203**, 311 (1982).
- [11] T. W. B. Kibble, J. Phys. **A9**, 1387 (1976).
- [12] J. Preskill, Phys. Rev. Lett. **43**, 1365 (1979).
- [13] E. N. Parker, Astrophys. J. **160**, 383 (1970).
- [14] M. S. Turner, E. N. Parker and T. J. Bogdan, Phys. Rev. **D26**, 1296 (1982).
- [15] F. C. Adams *et al.*, Phys. Rev. Lett. **70**, 2511 (1993).
- [16] Y. Rephaeli and M. S. Turner, Phys. Lett. **121B**, 115 (1983).
- [17] E. W. Kolb, S. A. Colgate and J. A. Harvey, Phys. Rev. Lett. **49**, 1373 (1982).
- [18] S. Dimopoulos, J. Preskill and F. Wilczek, Phys. Lett. **119B**, 320 (1982).
- [19] K. Freese, M. S. Turner and D. N. Schramm, Phys. Rev. Lett. **51**, 1625 (1983).
- [20] E. W. Kolb and M. S. Turner, Astrophys. J. **286**, 702 (1984).
- [21] J. A. Harvey, Nucl. Phys. **B236**, 255 (1984).
- [22] K. Freese and E. Krasteva, Phys. Rev. **D59**, 063007 (1999), [arXiv:astro-ph/9804148].
- [23] J. Arafune, M. Fukugita and S. Yanagita, Phys. Rev. **D32**, 2586 (1985).
- [24] L. L. Vant-Hull, Phys. Rev. **173**, 1412 (1968).
- [25] S. Graf, A. Schaefer and W. Greiner, Phys. Lett. **B262**, 463 (1991).
- [26] Review of Particle Physics 2020 (*this paper*), listing on *Searches for Magnetic Monopoles*.
- [27] L. Patrizii and M. Spurio, Ann. Rev. Nucl. Part. Sci. **65**, 279 (2015), [arXiv:1510.07125].
- [28] M. Fairbairn *et al.*, Phys. Rept. **438**, 1 (2007), [hep-ph/0611040].
- [29] J. M. Kovalik and J. L. Kirschvink, Phys. Rev. **A33**, 1183 (1986).
- [30] H. Jeon and M. J. Longo, Phys. Rev. Lett. **75**, 1443 (1995), [Erratum: Phys. Rev. Lett. 76,159(1996)], [hep-ex/9508003].
- [31] S. Orito *et al.*, Phys. Rev. Lett. **66**, 1951 (1991).
- [32] M. Ambrosio *et al.* (MACRO), Eur. Phys. J. **C25**, 511 (2002), [hep-ex/0207020].
- [33] B. Cabrera, Phys. Rev. Lett. **48**, 1378 (1982).
- [34] P. B. Price *et al.*, Phys. Rev. Lett. **35**, 487 (1975).
- [35] S. Balestra *et al.*, Eur. Phys. J. **C55**, 57 (2008), [arXiv:0801.4913].
- [36] M. G. Aartsen *et al.* (IceCube), Eur. Phys. J. **C76**, 3, 133 (2016), [arXiv:1511.01350].
- [37] A. Albert *et al.* (ANTARES), JHEP **07**, 054 (2017), [arXiv:1703.00424].
- [38] A. Aab *et al.* (Pierre Auger), Phys. Rev. **D94**, 8, 082002 (2016), [arXiv:1609.04451].
- [39] D. P. Hogan *et al.*, Phys. Rev. **D78**, 075031 (2008), [arXiv:0806.2129].
- [40] M. Detrixhe *et al.* (ANITA-II), Phys. Rev. **D83**, 023513 (2011), [arXiv:1008.1282].
- [41] J.E. Bartelt *et al.*, Phys. Rev. **D36**, 1990 (1987) [Erratum-ibid. **D40**, 1701 (1989)].
- [42] M. Ambrosio *et al.* (MACRO), Eur. Phys. J. **C26**, 163 (2002), [hep-ex/0207024].
- [43] R. Becker-Szendy *et al.*, Phys. Rev. **D49**, 2169 (1994).
- [44] V. A. Balkanov *et al.* (Baikal), Prog. Part. Nucl. Phys. **40**, 391 (1998), [arXiv:astro-ph/9801044].
- [45] M. G. Aartsen *et al.* (IceCube), Eur. Phys. J. **C74**, 7, 2938 (2014), [Erratum: Eur. Phys. J. C79,no.2,124(2019)], [arXiv:1402.3460].
- [46] K. Ueno *et al.* (Super-Kamiokande), Astropart. Phys. **36**, 131 (2012), [arXiv:1203.0940].
- [47] G. Aad *et al.* (ATLAS), Phys. Rev. **D93**, 5, 052009 (2016), [arXiv:1509.08059].
- [48] G. Aad *et al.* (ATLAS) (2019), [arXiv:1905.10130].
- [49] B. Acharya *et al.* (MoEDAL), Phys. Rev. Lett. **118**, 6, 061801 (2017), [arXiv:1611.06817].
- [50] B. Acharya *et al.* (MoEDAL), Phys. Rev. Lett. **123**, 2, 021802 (2019), [arXiv:1903.08491].
- [51] S. Baines *et al.*, Eur. Phys. J. **C78**, 11, 966 (2018), [Erratum: Eur. Phys. J. C79,no.2,166(2019)], [arXiv:1808.08942].
- [52] A. Abulencia *et al.* (CDF), Phys. Rev. Lett. **96**, 201801 (2006), [hep-ex/0509015].
- [53] G. R. Kalbfleisch *et al.*, Phys. Rev. **D69**, 052002 (2004), [hep-ex/0306045].
- [54] P. B. Price, G.-X. Ren and K. Kinoshita, Phys. Rev. Lett. **59**, 2523 (1987).
- [55] B. Aubert *et al.*, Phys. Lett. **120B**, 465 (1983).
- [56] R. A. Carrigan, F. A. Nezzrick and B. P. Strauss, Phys. Rev. **D8**, 3717 (1973).
- [57] G. Abbiendi *et al.* (OPAL), Phys. Lett. **B663**, 37 (2008), [arXiv:0707.0404].
- [58] J. L. Pinfold *et al.*, Phys. Lett. **B316**, 407 (1993).
- [59] K. Kinoshita *et al.*, Phys. Rev. **D46**, R881 (1992).
- [60] K. Kinoshita *et al.*, Phys. Lett. **B228**, 543 (1989).
- [61] P. Musset, M. Price and E. Lohrmann, Phys. Lett. **128B**, 333 (1983).
- [62] T. Gentile *et al.* (CLEO), Phys. Rev. **D35**, 1081 (1987).
- [63] W. Braunschweig *et al.* (TASSO), Z. Phys. **C38**, 543 (1988).

- [64] A. Aktas *et al.* (H1), *Eur. Phys. J.* **C41**, 133 (2005), [hep-ex/0501039].
- [65] A. De Rujula, *Nucl. Phys.* **B435**, 257 (1995), [hep-th/9405191].
- [66] I. F. Ginzburg and A. Schiller, *Phys. Rev.* **D60**, 075016 (1999), [hep-ph/9903314].
- [67] B. Abbott *et al.* (D0), *Phys. Rev. Lett.* **81**, 524 (1998), [hep-ex/9803023].
- [68] M. Acciarri *et al.* (L3), *Phys. Lett.* **B345**, 609 (1995).





## VOLUME II: TABLE OF CONTENTS

## PARTICLE LISTINGS\*

<b>Illustrative key and abbreviations</b>	999
<b>Gauge and Higgs bosons</b>	
( $\gamma$ , gluon, graviton, $W$ , $Z$ , Higgs, Axions)	1013
<b>Leptons</b>	
( $e$ , $\mu$ , $\tau$ , Heavy-charged lepton searches, Neutrino properties, Number of neutrino types Double- $\beta$ decay, Neutrino mixing, Heavy-neutral lepton searches)	1101
<b>Quarks</b>	
( $u$ , $d$ , $s$ , $c$ , $b$ , $t$ , $b'$ , $t'$ ( $4^{th}$ gen.), Free quarks)	1173
<b>Mesons</b>	
Light unflavored ( $\pi$ , $\rho$ , $a$ , $b$ ) ( $\eta$ , $\omega$ , $f$ , $\phi$ , $h$ )	1209
Other light unflavored	1332
Strange ( $K$ , $K^*$ )	1337
Charmed ( $D$ , $D^*$ )	1391
Charmed, strange ( $D_s$ , $D_s^*$ , $D_{sJ}$ )	1448
Bottom ( $B$ , $V_{cb}/V_{ub}$ , $B^*$ , $B_J^*$ )	1465
Bottom, strange ( $B_s$ , $B_s^*$ , $B_{sJ}^*$ )	1640
Bottom, charmed ( $B_c$ )	1664
$c\bar{c}$ ( $\eta_c$ , $J/\psi(1S)$ , $\chi_c$ , $h_c$ , $\psi$ )	1668
$b\bar{b}$ ( $\eta_b$ , $\Upsilon$ , $\chi_b$ , $h_b$ )	1782
<b>Baryons</b>	
$N$	1825
$\Delta$	1878
$\Lambda$	1902
$\Sigma$	1927
$\Xi$	1959
$\Omega$	1971
Charmed ( $\Lambda_c$ , $\Sigma_c$ , $\Xi_c$ , $\Omega_c$ )	1974
Doubly charmed ( $\Xi_{cc}$ )	1996
Bottom ( $\Lambda_b$ , $\Sigma_b$ , $\Xi_b$ , $\Omega_b$ , $b$ -baryon admixture)	1997
Exotic baryons ( $P_c$ pentaquarks)	2014
<b>Searches not in Other Sections</b>	
Magnetic monopole searches	2017
Supersymmetric particle searches	2019
Technicolor	2062
Searches for quark and lepton compositeness	2063
Extra dimensions	2067
WIMP and dark matter searches	2073
Other particle searches	2085

\*The divider sheets give more detailed indices for each main section of the Particle Listings.



## INTRODUCTION TO THE PARTICLE LISTINGS

Illustrative key . . . . .	999
Abbreviations . . . . .	1000



# Illustrative Key to the Particle Listings

Name of particle. "Old" name used before 1986 renaming scheme also given if different. See the section "Naming Scheme for Hadrons" for details.

**$a_0(1200)$**

$$I^G(J^{PC}) = 1^-(0^{++})$$

Particle quantum numbers (where known).

OMITTED FROM SUMMARY TABLE  
Evidence not compelling, may be a kinematic effect.

Indicates particle omitted from Particle Physics Summary Table, implying particle's existence is not confirmed.

Quantity tabulated below.

### $a_0(1200)$ MASS

Top line gives our best value (and error) of quantity tabulated here, based on weighted average of measurements used. Could also be from fit, best limit, estimate, or other evaluation. See next page for details.

VALUE (MeV)	EVTS	DOCUMENT ID	TECN	CHG	COMMENT
<b>1206 ± 7 OUR AVERAGE</b>					
1210 ± 8 ± 9	3000	FENNER 87	MMS	-	3.5 $\pi^- p$
1198 ± 10		PIERCE 83	ASPK	+	2.1 $K^- p$
1216 ± 11 ± 9	1500	MERRILL 81	HBC	0	3.2 $K^- p$
• • • We do not use the following data for averages, fits, limits, etc. • • •					
1192 ± 16		200 LYNCH 81	HBC	±	2.7 $\pi^- p$
1 Systematic error was added quadratically by us in our 1986 edition.					

General comments on particle.

"Document id" for this result; full reference given below.

Measurement technique. (See abbreviations on next page.)

Footnote number linking measurement to text of footnote.

### $a_0(1200)$ WIDTH

Number of events above background.

Measured value used in averages, fits, limits, etc.

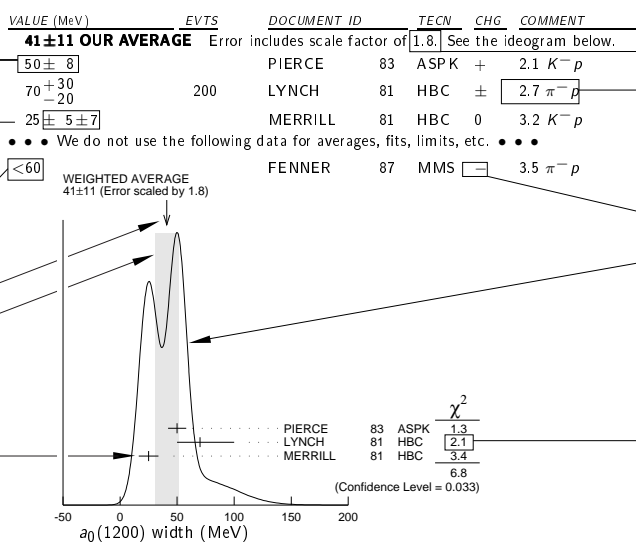
Error in measured value (often statistical only; followed by systematic if separately known; the two are combined in quadrature for averaging and fitting.)

Measured value *not* used in averages, fits, limits, etc. See the Introductory Text for explanations.

Arrow points to weighted average.

Shaded pattern extends  $\pm 1\sigma$  (scaled by "scale factor" S) from weighted average.

Value and error for each experiment.



Scale factor > 1 indicates possibly inconsistent data.

Reaction producing particle, or general comments.

"Change bar" indicates result added or changed since previous edition.

Charge(s) of particle(s) detected.

Ideogram to display possibly inconsistent data. Curve is sum of Gaussians, one for each experiment (area of Gaussian = 1/error; width of Gaussian =  $\pm$ error). See Introductory Text for discussion.

Contribution of experiment to  $\chi^2$  (if no entry present, experiment not used in calculating  $\chi^2$  or scale factor because of very large error).

### $a_0(1200)$ DECAY MODES

Partial decay mode (labeled by  $\Gamma_i$ ).

Mode	Fraction ( $\Gamma_i/\Gamma$ )	Scale factor/ Confidence level
$\Gamma_1$ $3\pi$	(65.2 ± 1.3) %	S=1.7
$\Gamma_2$ $K\bar{K}$	(34.8 ± 1.3) %	S=1.7
$\Gamma_3$ $\eta\pi^\pm$	< 5 × 10 <sup>-4</sup>	CL=95%

Our best value for branching fraction as determined from data averaging, fitting, evaluating, limit selection, etc. This list is basically a compact summary of results in the Branching Ratio section below.

### $a_0(1200)$ BRANCHING RATIOS

Branching ratio.

Our best value (and error) of quantity tabulated, as determined from constrained fit (using *all significant* measured branching ratios for this particle).

Weighted average of measurements of this ratio only.

Footnote (referring to LYNCH 81).

Confidence level for measured upper limit.

References, ordered inversely by year, then author.

"Document id" used on data entries above.

Journal, report, preprint, etc. (See abbreviations on next page.)

VALUE	DOCUMENT ID	TECN	CHG	COMMENT	$\Gamma_1/\Gamma$	
<b>0.652 ± 0.013 OUR FIT</b>				Error includes scale factor of 1.7.		
<b>0.643 ± 0.010 OUR AVERAGE</b>						
0.64 ± 0.01	PIERCE 83	ASPK	+	2.1 $K^- p$		
0.74 ± 0.06	MERRILL 81	HBC	0	3.2 $K^- p$		
• • • We do not use the following data for averages, fits, limits, etc. • • •						
0.48 ± 0.15	<sup>2</sup> LYNCH 81	HBC	±	2.7 $\pi^- p$		
<sup>2</sup> Data has questionable background subtraction.						
<b><math>\Gamma(K\bar{K})/\Gamma_{total}</math></b>					$\Gamma_2/\Gamma$	
VALUE	DOCUMENT ID	TECN	CHG	COMMENT		
<b>0.348 ± 0.013 OUR FIT</b>				Error includes scale factor of 1.7.		
<b>0.35 ± 0.05</b>	PIERCE 83	ASPK	+	2.1 $K^- p$		
<b><math>\Gamma(K\bar{K})/\Gamma(3\pi)</math></b>					$\Gamma_2/\Gamma_1$	
VALUE	DOCUMENT ID	TECN	CHG	COMMENT		
<b>0.535 ± 0.030 OUR FIT</b>				Error includes scale factor of 1.7.		
<b>0.50 ± 0.03</b>	MERRILL 81	HBC	0	3.2 $K^- p$		
<b><math>\Gamma(\eta(\text{neutral decay})\pi^\pm)/\Gamma_{total}</math></b>					<b>0.71 <math>\Gamma_3/\Gamma</math></b>	
VALUE (units 10 <sup>-4</sup> )	CL%	DOCUMENT ID	TECN	CHG	COMMENT	
<b>&lt;3.5</b>	95	PIERCE 83	ASPK	+	2.1 $K^- p$	

Branching ratio in terms of partial decay mode(s)  $\Gamma_i$  above.

### $a_0(1200)$ REFERENCES

FENNER 87	PRL 55 14	H. Fenner et al.	(SLAC)
PIERCE 83	PL 123B 230	J.H. PIERCE	(FNAL) JUP
LYNCH 81	PR D24 610	G.R. Lynch et al.	(CLEO Collab.)
MERRILL 81	PRL 47 143	D.W. Merrill et al.	(SACL, CERN)

Partial list of author(s) in addition to first author.

Quantum number determinations in this reference.

Institution(s) of author(s). (See abbreviations on next page.)

# Abbreviations Used in the Particle Listings

## Indicator of Procedure Used to Obtain Our Result

OUR AVERAGE	From a weighted average of selected data.
OUR FIT	From a constrained or overdetermined multiparameter fit of selected data.
OUR EVALUATION	Not from a direct measurement, but evaluated from measurements of other quantities.
OUR ESTIMATE	Based on the observed range of the data. Not from a formal statistical procedure.
OUR LIMIT	For special cases where the limit is evaluated by us from measured ratios or other data. Not from a direct measurement.

## Measurement Techniques

(i.e., Detectors and Methods of Analysis)

A1	A1 Collaboration at MAMI
A2MM	A2 spectrometer at the Mainz Microtron, MAMI
ABRA	ABRACADABRA QCD axion dark matter search
ACCM	ACCMOR Collaboration
ADMX	Axion Dark Matter Experiment
AEMS	Argonne effective mass spectrometer
ALEP	ALEPH – CERN LEP detector
ALPS	Photon regeneration experiment
AMND	AMANDA South Pole neutrino detector
AMY	AMY detector at KEK-TRISTAN
ANAI	Direct DM detection exp. with NaI at Canfranc Underground Lab, Spain
ANIT	Antarctic Impulsive Transient Antenna balloon mission
ANTR	ANTARES underwater neutrino telescope in the Western Mediterranean Sea
APEX	FNAL APEX Collab.
ARG	ARGUS detector at DORIS
ARGD	Fit to semicircular amplitude path on Argand diagram
ASP	Anomalous single-photon detector
ASPK	Automatic spark chambers
ASTE	ASTERIX detector at LEAR
ASTR	Astronomy
ATLS	ATLAS detector at CERN LHC
AUGE	Pierre Auger Observatory
AURG	Resonant-mass gravitational wave AURIGA detector
B787	BNL experiment 787 detector
B791	BNL experiment 791 detector
B845	BNL experiment 845 detector
B852	BNL E-852
B865	BNL E865 detector
B871	BNL experiment 871 detector
B949	BNL E949 detector at AGS
BABR	BaBar Collab.
BAIK	Lake Baikal neutrino telescope
BAKS	Baksan underground scintillation telescope
BC	Bubble chamber
BDMP	Beam dump
BEAT	CERN BEATRICE Collab.
BEBC	Big European bubble chamber at CERN
BELL	Belle Collab.
BES	BES Beijing Spectrometer at Beijing Electron-Positron Collider
BES2	BES Beijing Spectrometer at Beijing Electron-Positron Collider
BES3	BES Beijing Spectrometer at Beijing Electron-Positron Collider
BIS2	BIS-2 spectrometer at Serpukhov
BKEI	BENKEI spectrometer system at KEK Proton Synchrotron
BOLO	Bolometer, a cryogenic thermal detector
BONA	Bonanza nonmagnetic detector at DORIS
BORX	BOREXINO
BPWA	Barrelet-zero partial-wave analysis
C100	COSINE-100 experiment in South Korea
CALO	Calorimeter
CAST	CAST experiment at CERN
CBAL	Crystal Ball detector at SLAC-SPEAR or DORIS
CBAR	Crystal Barrel detector at CERN-LEAR
CBOX	Crystal Box at LAMPF
CBTP	CBELSA/TAPS Collaboration
CC	Cloud chamber
CCFR	Columbia-Chicago-Fermilab-Rochester detector
CDEX	China Dark Matter Experiment
CDF	Collider detector at Fermilab
CDF2	CDF-II Collab.
CDHS	CDHS neutrino detector at CERN
CDM2	CDMS II, Cryogenic Dark Matter Search at Soudan Underground Lab.

CDMS	CDMS Collaboration
CELL	CELLO detector at DESY
CGNT	CoGeNT dark matter search experiment
CHER	Cherenkov detector
CHM2	CHARM-II neutrino detector (glass) at CERN
CHOZ	Nuclear Power Station near Chooz, France
CHRM	CHARM neutrino detector (marble) at CERN
CHRS	CHORUS Collaboration – CERN SPS
CIB	Cosmic Infrared Background
CIBS	CERN-IHEP boson spectrometer
CLAS	Jefferson CLAS Collab.
CLE2	CLEO II detector at CESR
CLE3	CLEO III detector at CESR
CLEC	CLEO-c detector at CESR
CLEO	Cornell magnetic detector at CESR
CMB	Cosmic Microwave Background
CMD	Cryogenic magnetic detector at VEPP-2M, Novosibirsk
CMD2	Cryogenic magnetic detector 2 at VEPP-2M, Novosibirsk
CMD3	Cryogenic magnetic detector 3 at VEPP-2000, Novosibirsk
CMS	CMS detector at CERN LHC
CNTR	Counters
COMB	Combined analysis of data from independent experiments.
COMP	COMPASS experiment at the CERN SPS
COSM	Cosmology and astrophysics
COSY	COSY-TOF Collaboration
COUP	COUPP (the Chicagoland Observatory for Underground Particle Physics) Collab.
CPLR	CLEAR Collaboration
CRBT	Crystal Ball and TAPS detector at MAMI
CRES	CRESST cryogenic detector
CRYB	Crystal Ball at BNL
CRYM	Crystal Ball detector at Mainz Microtron MAMI
CSB2	Columbia U. - Stony Brook BGO calorimeter inserted in NaI array
CSME	COSME Collaboration
CUOR	CUORICINO experiment at Gran Sasso Laboratory.
CUSB	Columbia U. - Stony Brook segmented NaI detector at CESR
D0	D0 detector at Fermilab Tevatron Collider
DAMA	DAMA, dark matter detector at Gran Sasso National Lab.
DASP	DESY double-arm spectrometer
DAYA	Daya Bay Collaboration
DBC	Deuterium bubble chamber
DCHZ	Double Chooz Collaboration
DEAP	DEAP-3600 DM search with argon at SNOLAB
DISP	Graviton mass measurement based on dispersion measure
DLCO	DELCO detector at SLAC-SPEAR or SLAC-PEP
DLPH	DELPHI detector at LEP
DM1	Magnetic detector no. 1 at Orsay DCI collider
DM2	Magnetic detector no. 2 at Orsay DCI collider
DMIC	DAMIC Dark Matter in CCD experiment at Fermilab
DMTP	Dark Matter Time Projection Chamber (DMTPC) directional detection experiment
DONU	DONUT Collab.
DPWA	Energy-dependent partial-wave analysis
DRFT	Directional dark matter detector at Boulby Underground Science Facility
DS50	DarkSide-50 Liquid Argon TPC at Gran Sasso National Laboratory
E137	SLAC E137 beam-dump experiment
E621	Fermilab E621 detector
E653	Fermilab E653 detector
E665	Fermilab E665 detector
E687	Fermilab E687 detector
E691	Fermilab E691 detector
E705	Fermilab E705 Spectrometer-Calorimeter
E731	Fermilab E731 Spectrometer-Calorimeter
E756	Fermilab E756 detector
E760	Fermilab E760 detector
E761	Fermilab E761 detector
E771	Fermilab E771 detector
E773	Fermilab E773 Spectrometer-Calorimeter
E789	Fermilab E789 detector
E791	Fermilab E791 detector
E799	Fermilab E799 Spectrometer-Calorimeter
E835	Fermilab E835 detector
EDE2	EDELWEISS II dark matter search Collaboration
EDE3	EDELWEISS III dark matter search Collaboration
EDEL	EDELWEISS dark matter search Collaboration
EHS	Four-pi detector at CERN

## Abbreviations Used in the Particle Listings

ELEC	Electronic combination	KOLR	Kolar Gold Field underground detector
EMC	European muon collaboration detector at CERN	KOTO	KOTO experiment with $K_L^0$ beam at J-PARC
EMUL	Emulsions	KTEV	KTeV Collaboration
ESR	Electron spin resonance spectroscopy	L3	L3 detector at LEP
FAST	Fiber Active Scintillator Target detector at PSI	LASR	Laser
FBC	Freon bubble chamber	LASS	Large-angle superconducting solenoid spectrometer at SLAC
FENI	FENICE (at the ADONE collider of Frascati)	LATT	Lattice calculations
FIT	Fit to previously existing data	LEBC	Little European bubble chamber at CERN
FLAT	Large Area Telescope onboard the Fermi Gamma-Ray Space Telescope (Fermi-LAT)	LEGS	BNL LEGS Collab.
FMPS	Fermilab Multiparticle Spectrometer	LENA	Nonmagnetic lead-glass NaI detector at DORIS
FOCS	FNAL E831 FOCUS Collab.	LEP	From combination of all 4 LEP experiments: ALEPH, DELPHI, L3, OPAL
FRAB	ADONE $B\bar{B}$ group detector	LEPS	Low-Energy Pion Spectrometer at the Paul Scherrer Institute
FRAG	ADONE $\gamma\gamma$ group detector	LGW	Lead Glass Wall collaboration at SPEAR/SLAC
FRAM	ADONE MEA group detector	LHC	Combined analysis of LHC experiments
FREJ	FREJUS Collaboration – modular flash chamber detector (calorimeter)	LHCB	LHCb detector at CERN LHC
GA24	Hodoscope Cherenkov $\gamma$ calorimeter (IHEP GAMS-2000) (CERN GAMS-4000)	L+P	Multichannel L + P model fit
GALX	GALLEX solar neutrino detector in the Gran Sasso Underground Lab.	LSD	Mont Blanc liquid scintillator detector
GAM2	IHEP hodoscope Cherenkov $\gamma$ calorimeter GAMS-2000	LSND	Liquid Scintillator Neutrino Detector
GAM4	CERN hodoscope Cherenkov $\gamma$ calorimeter GAMS-4000	LSW	Light Shining through a Wall
GAMS	IHEP hodoscope Cherenkov $\gamma$ calorimeter GAMS-4 $\pi$	LUX	Large Underground Xenon experiment at SURF
GNO	Gallium Neutrino Observatory in the Gran Sasso Underground Lab.	MAC	MAC detector at PEP/SLAC
GOLI	CERN Goliath spectrometer	MAJD	Majorana Demonstrator experiment at SURF
GRAL	GRAAL Collaboration	MBNE	Fermilab MiniBooNE neutrino experiment
H1	H1 detector at DESY/HERA	MBR	Molecular beam resonance technique
HAWC	High Altitude Water Cherenkov Observatory experiment at Sierra Negra, Mexico	MCRO	MACRO detector in Gran Sasso
HBC	Hydrogen bubble chamber	MD1	Magnetic detector at VEPP-4, Novosibirsk
HDBC	Hydrogen and deuterium bubble chambers	MDRP	Millikan drop measurement
HDES	HADES Collaboration at GSI in Darmstadt	MEG	Muon to electron conversion detector at PSI
HDMO	Heidelberg-Moscow Experiment	MGFL	MAGIC and Fermi-LAT Collaborations
HDMS	Heidelberg Dark Matter Search Experiment	MGIC	MAGIC Telescopes gamma-ray observatory
HEBC	Helium bubble chamber	MICA	Underground mica deposits
HEPT	Helium proportional tubes	MICR	MICROSCOPE satellite test of weak equivalence principle
HERA	H1 and ZEUS Collaborations at DESY/HERA	MINS	Fermilab MINOS experiment
HERB	HERA-B detector at DESY/HERA	MIRA	MIRABELLE Liquid-hydrogen bubble chamber
HERM	HERMES detector at DESY/HERA	MLEV	Magnetic levitation
HESS	High Energy Stereoscopic System gamma-ray instrument	MLS	Modified Laurent Series
HFS	Hyperfine structure	MMS	Missing mass spectrometer
HLBC	Heavy-liquid bubble chamber	MOED	MoEDAL magnetic monopoles search experiment at LHC
HOME	Homestake underground scintillation detector	MPS	Multiparticle spectrometer at BNL
HPGE	High-purity Germanium detector	MPS2	Multiparticle spectrometer upgrade at BNL
HPS	Heavy Photon Search experiment at JLAB	MPSF	Multiparticle spectrometer at Fermilab
HPW	Harvard-Pennsylvania-Wisconsin detector	MPWA	Model-dependent partial-wave analysis
HRS	SLAC high-resolution spectrometer	MRK1	SLAC Mark-I detector
HYBR	Hybrid: bubble chamber + electronics	MRK2	SLAC Mark-II detector
HYCP	HyperCP Collab. (FNAL E-871)	MRK3	SLAC Mark-III detector
HYST	HAYSTAC axion search experiment	MRKJ	Mark-J detector at DESY
IACT	Imaging Air Cherenkov Telescope	MRS	Magnetic resonance spectrometer
ICAR	ICARUS experiment at Gran Sasso Laboratory.	MUG2	Muon ( $g-2$ )
ICCB	IceCube neutrino detector at South Pole	MWPC	Multi-Wire Proportional Chamber
IGEX	IGEX Collab.	NA14	CERN NA14
IMB	Irvine-Michigan-Brookhaven underground Cherenkov detector	NA31	CERN NA31 Spectrometer-Calorimeter
IMB3	Irvine-Michigan-Brookhaven underground Cherenkov detector	NA32	CERN NA32 Spectrometer
INDU	Magnetic induction	NA48	CERN NA48 Collaboration
IPWA	Energy-independent partial-wave analysis	NA49	CERN NA49 Collaboration
ISTR	IHEP ISTR+ spectrometer-calorimeter	NA60	CERN NA60 Collaboration
JADE	JADE detector at DESY	NA62	CERN NA62 Experiment
JPAC	Joint Physics Analysis Center (JPAC) Collaboration	NA64	CERN SPS NA64 Experiment
K246	KEK E246 detector with polarimeter	NAGE	NEWAGE, New generation WIMP-search experiment with advanced gaseous tracking
K2K	KEK to Super-Kamiokande	NAIA	NAIAD (NaI Advanced Detector) dark matter search experiment
K391	KEK E391a detector	ND	NaI detector at VEPP-2M, Novosibirsk
K470	KEK-E470 Stopping K detector	NEOS	NEOS Collaboration
KAM2	KAMIOKANDE-II underground Cherenkov detector	NEWS	NEWS-G direct dark matter search at LSM
KAMI	KAMIOKANDE underground Cherenkov detector	NICE	Serpukhov nonmagnetic precision spectrometer
KAR2	KARMEN2 calorimeter at the ISIS neutron spallation source at Rutherford	NMR	Nuclear magnetic resonance
KARM	KARMEN calorimeter at the ISIS neutron spallation source at Rutherford	NOMD	NOMAD Collaboration, CERN SPS
KEDR	detector operating at VEPP-4M collider (Novosibirsk)	NOVA	NOvA experiment with Fermilab's NuMI neutrino beam
KIMS	Korea Invisible Mass Search experiment at YangYang, Korea	NTEV	NuTeV Collab. at Fermilab
KLND	KamLand Collab. (Japan)	nTRV	neutron Time-Reversal Violation
KLOE	KLOE detector at DAFNE (the Frascati e+e- collider Italy)	NUSX	Mont Blanc NUSEX underground detector
		OBLX	OBELIX detector at LEAR
		OKA	OKA collaboration at U70 accelerator in Protvino, Russia
		OLYA	Detector at VEPP-2M and VEPP-4, Novosibirsk
		OMEG	CERN OMEGA spectrometer
		OPAL	OPAL detector at LEP
		OPER	OPERA experiment with emulsion tracking at Gran Sasso



# Abbreviations Used in the Particle Listings

OSPK Optical spark chamber  
 PIBE The PIBETA detector at the Paul Scherrer Institute (PSI), Switzerland.  
 PICA PICASSO dark matter search experiment  
 PICO PICO bubble chamber experiment in SNOLAB underground laboratory  
 PIE3  $\pi$ E3 beam-line of Paul Scherrer Institute  
 PLAS Plastic detector  
 PLUT DESY PLUTO detector  
 PMLA PAMELA space spectrometer on Resurs-DK1 satellite  
 PNDX PandaX dual-phase liquid xenon dark matter experiment at Jin-Ping  
 PPTA Parkes Pulsar Timing Array  
 PRMX The PRIMEX detector in Hall B at TJNAF  
 PWA Partial-wave analysis  
 QUAX QUAX axion search experiment  
 RDK2 NIST rare radioactive decay experiment  
 REDE Resonance depolarization  
 RENO RENO Collaboration  
 RICE Radio Ice Cherenkov Experiment  
 RVUE Review of previous data  
 SAGE US - Russian Gallium Experiment  
 SCDM SuperCDMS experiment at Soudan Underground Lab.  
 SELX FNAL SELEX Collab.  
 SENS Sub-Electron-Noise Skipper CCD Experimental Instrument (SENSEI)  
 SFM CERN split-field magnet  
 SHF SLAC Hybrid Facility Photon Collaboration  
 SHUK SHUKET: search for U(1) dark matter with an electromagnetic telescope  
 SIGM Serpukhov CERN-IHEP magnetic spectrometer (SIGMA)  
 SILI Silicon detector  
 SIMP SIMPLE, dark matter detector at Laboratori Nazionali del Sud  
 SKAM Super-Kamiokande Collab.  
 SLAX Solar Axion Experiment in Canfranc Underground Laboratory  
 SLD SLC Large Detector for  $e^+e^-$  colliding beams at SLAC  
 SMPL SIMPLE, Superheated Instrument for Massive Particle Experiments  
 SND Novosibirisk Spherical neutral detector at VEPP-2M  
 SNDR SINDRUM spectrometer at PSI  
 SNO SNO Collaboration (Sudbury Neutrino Observatory)  
 SNO+ SNO+ Collaboration (Sudbury Neutrino Observatory)  
 SOU2 Soudan 2 underground detector  
 SOUD Soudan underground detector  
 SPEC Spectrometer  
 SPED From maximum of speed plot or resonant amplitude  
 SPHR Bonn SAPHIR Collab.  
 SPNX SPHINX spectrometer at IHEP accelerator  
 SPRK Spark chamber  
 SQID SQUID device  
 STRC Streamer chamber  
 SVD2 SVD-2 experiment at IHEP, Protvino  
 T2K T2K Collaboration  
 TASS DESY TASSO detector  
 TEVA Combined analysis of CDF and  $D\bar{0}$  experiments  
 TEXO TEXONO Collab., ultra low energy Ge detector at Kuo-Sheng Laboratory  
 THEO Theoretical or heavily model-dependent result  
 TNF TNF-IHEP facility at 70 GeV IHEP accelerator  
 TOF Time-of-flight  
 TOPZ TOPAZ detector at KEK-TRISTAN  
 TPC TPC detector at PEP/SLAC  
 TPS Tagged photon spectrometer at Fermilab  
 TRAP Penning trap  
 TWST TWIST spectrometer at TRIUMF  
 UA1 UA1 detector at CERN  
 UA2 UA2 detector at CERN  
 UA5 UA5 detector at CERN  
 UCNA UCNA collaboration using polarized ultracold neutrons at LANSCE  
 UKDM UK Dark Matter Collab.  
 VES Vertex Spectrometer Facility at 70 GeV IHEP accelerator  
 VLBI Very Long Baseline Interferometer  
 VNS VENUS detector at KEK-TRISTAN  
 VRTS Very Energetic Radiation Imaging Telescope Array System (VERITAS)  
 WA75 CERN WA75 experiment  
 WA82 CERN WA82 experiment

WA89 CERN WA89 experiment  
 WARP Liquid argon detector for CDM searches at Gran Sasso  
 WASA WASA detector at CELSIUS, Uppsala and at COSY, Juelich  
 WDMX WISP Dark Matter eXperiment (WISPDIMX) for direct hidden photon search  
 WIRE Wire chamber  
 X100 XENON100 dark matter search experiment at Gran Sasso National Laboratory  
 XE10 XENON10 experiment at Gran Sasso National Laboratory  
 XE1T XENON1T dark matter search experiment at Gran Sasso National Laboratory  
 XEBC Xenon bubble chamber  
 XMAS XMASS, liquid xenon scintillation detector at Kamioka Observatory  
 YUKA Graviton mass measurement based on Yukawa potential  
 ZEP2 ZEPLIN-II dark matter detector  
 ZEP3 ZEPLIN-III dark matter detector at Palmer Underground Lab.  
 ZEPL ZEPLIN-I galactic dark matter detector  
 ZEUS ZEUS detector at DESY/HERA

## Conferences

Conferences are generally referred to by the location at which they were held (e.g., HAMBURG, TORONTO, CORNELL, BRIGHTON, etc.).

## Journals

AA Astronomy and Astrophysics  
 ADVP Advances in Physics  
 AFIS Anales de Fisica  
 AJP American Journal of Physics  
 AL Astronomy Letters  
 ANP Annals of Physics  
 ANPL Annals of Physics (Leipzig)  
 ANYAS Annals of the New York Academy of Sciences  
 AP Atomic Physics  
 APAH Acta Physica Academiae Scientiarum Hungaricae  
 APJ Astrophysical Journal  
 APJS Astrophysical Journal Suppl.  
 APP Acta Physica Polonica  
 APS Acta Physica Slovaca  
 ARNPS Annual Review of Nuclear and Particle Science  
 ARNS Annual Review of Nuclear Science  
 ASP Astroparticle Physics  
 AST American Statistician  
 BAPS Bulletin of the American Physical Society  
 BASUP Bulletin of the Academy of Science, USSR (Physics)  
 CJNP Chinese Journal of Nuclear Physics  
 CJP Canadian Journal of Physics  
 CNPP Comments on Nuclear and Particle Physics  
 CP Chinese Physics  
 CPC Chinese Physics C  
 CTP Communications in Theoretical Physics  
 CZJP Czechoslovak Journal of Physics  
 DANS Doklady Akademii nauk SSSR  
 DP Doklady Physics (Magazine)  
 EPJ The European Physical Journal  
 EPL Europhysics Letters  
 FECAY Fizika Elementarnykh Chastits i Atomnogo Yadra  
 HADJ Hadronic Journal  
 IJMP International Journal of Modern Physics  
 JAP Journal of Applied Physics  
 JCAP Journal of Cosmology and Astroparticle Physics  
 JETP English Translation of Soviet Physics ZETF  
 JETPL English Translation of Soviet Physics ZETF Letters  
 JHEP Journal of High Energy Physics  
 JINR Joint Inst. for Nuclear Research  
 JINRRC JINR Rapid Communications  
 JP Journal of Physics  
 JPA Journal of Physics, A  
 JPB Journal of Physics, B  
 JPCRD Journal of Physical and Chemical Reference Data  
 JPCS Journal of Physics: Conference Series  
 JPG Journal of Physics, G  
 JPSJ Journal of the Physical Society of Japan  
 LNC Lettere Nuovo Cimento  
 MNRAS Monthly Notices of the Royal Astronomical Society  
 MPL Modern Physics Letters

## Abbreviations Used in the Particle Listings

NAST	New Astronomy		AMES	<b>Ames Lab.</b>	Ames, IA, USA
NAT	Nature		AMHT	<b>Amherst College</b>	Amherst, MA, USA
NATC	Nature Communications (NCAOBW)		AMST	Univ. van <b>Amsterdam</b>	GL Amsterdam, The Netherlands
NATP	Nature Physics				
NC	Nuovo Cimento		ANIK	<b>NIKHEF</b>	<b>Amsterdam</b> , The Netherlands
NIM	Nuclear Instruments and Methods		ANKA	<b>Middle East Technical Univ.</b> ; Dept. of Physics; Experimental HEP Lab	Ankara, Turkey
NJP	New Journal of Physics				
NP	Nuclear Physics		ANL	<b>Argonne National Lab.</b> ; High Energy Physics Division, Bldg. 362; Physics Division, Bldg. 203	Argonne, IL, USA
NPBPS	Nuclear Physics B Proceedings Supplement		ANSM	<b>St. Anselm Coll.</b>	Manchester, NH, USA
NPPP	Nuclear and Particle Physics Proceedings		AQUI	Univ. di <b>LAquila</b>	<b>Aquila</b> , Italy
PAN	Physics of Atomic Nuclei (formerly SJNP)		ARCBO	<b>Arecibo Observatory</b>	Arecibo, PR, USA
PD	Physics Doklady (Magazine)		ARIZ	Univ. of <b>Arizona</b>	Tucson, AZ, USA
PDAT	Physik Daten		ARZS	<b>Arizona State Univ.</b>	Tempe, AZ, USA
PL	Physics Letters		ASCI	Russian Academy of Sciences	<b>Moscow</b> , Russian Federation
PN	Particles and Nuclei		AST	<b>Accademia Sinica</b>	Nankang, Taipei, Taiwan
PPCF	Plasma Physics and Controlled Fusion		ATEN	NCSR " <b>Demokritos</b> "	<b>Aghia Paraskevi</b> , Greece
PPN	Physics of Particles and Nuclei (formerly SJPN)		ATHU	Univ. of <b>Athens</b>	Athens, Greece
PPNL	Physics of Particles and Nuclei Letters		AUCK	Univ. of <b>Auckland</b>	Auckland, New Zealand
PPNP	Progress in Particles and Nuclear Physics		BAKU	<b>Natl. Azerbaijan Academy of Sciences</b> , Inst. of Physics	<b>Baku</b> , Azerbaijan
PPSL	Proc. of the Physical Society of London				
PR	Physical Review		BANG	Indian Inst. of Science	<b>Bangalore</b> , India
PRAM	Pramana		BANGB	<b>Bangabasi College</b>	Calcutta, India
PRL	Physical Review Letters		BARC	Univ. Autónoma de <b>Barcelona</b> ; Dept. de Física	Bellaterra (Barcelona), Spain
PRPL	Physics Reports (Physics Letters C)		BARCE	Univ. Autónoma de <b>Barcelona</b> ; Inst. de Física de Altas Energías	Bellaterra (Barcelona), Spain
PRSE	Proc. of the Royal Society of Edinburgh		BARI	Univ. e del Politecnico di <b>Bari</b>	Bari, Italy
PRSL	Proc. of the Royal Society of London, Section A		BART	Univ. of <b>Delaware</b> ; <b>Bartol</b> Research Inst.	Newark, DE, USA
PS	Physica Scripta		BASL	Inst. für Physik der Univ. <b>Basel</b>	Basel, Switzerland
PTEP	Progress of Theoretical and Experimental Physics		BAYR	Univ. <b>Bayreuth</b>	Bayreuth, Germany
PTP	Progress of Theoretical Physics		BCEN	Centre d'Etudes Nucleaires de <b>Bordeaux-Gradignan</b>	Gradignan, France
PTPS	Progress of Theoretical Physics Supplement		BCIP	Natl. Inst. for Physics & Nuclear Eng. "Horia Hulubei" ( <b>IFIN-HH</b> )	<b>Bucharest-Magurele</b> , Romania
PTRSL	Phil. Trans. Royal Society of London				
RA	Radiochimica Acta		BELJ	<b>Beijing Univ.</b>	Beijing, China
RMP	Reviews of Modern Physics		BELJT	<b>Inst. of Theoretical Physics</b>	<b>Beijing</b> , China
RNC	La Rivista del Nuovo Cimento		BELG	Inter-University Inst. for High Energies (ULB-VUB)	<b>Brussel</b> , Belgium
RPP	Reports on Progress in Physics		BELL	AT & T <b>Bell Labs</b>	Murray Hill, NJ, USA
RRP	Revue Roumaine de Physique		BERG	Univ. of <b>Bergen</b>	Bergen, Norway
SCI	Science		BERL	<b>DESY</b> , Deutsches Elektronen-Synchrotron	<b>Zeuthen</b> , Germany
SJNP	Soviet Journal of Nuclear Physics		BERN	Univ. of <b>Berne</b>	Berne, Switzerland
SJPN	Soviet Journal of Particles and Nuclei		BGNA	Univ. di <b>Bologna</b> , & <b>INFN</b> , Sezione di Bologna; Via Irnerio, 46, I-40126 Bologna; Viale C. Berti Pichat, n. 6/2	Bologna, Italy
SPD	Soviet Physics Doklady (Magazine)		BHAB	<b>Bhabha Atomic Research Center</b>	Trombay, Bombay, India
SPU	Soviet Physics - Uspekhi		BHEP	<b>Inst. of High Energy Physics</b>	<b>Beijing</b> , China
UFN	Usp. Fiz. Nauk - Russian version of SPU		BIEL	Univ. <b>Bielefeld</b>	Bielefeld, Germany
YAF	Yadernaya Fizika		BING	<b>SUNY at Binghamton</b>	Binghamton, NY, USA
ZETF	Zhurnal Eksperimental'noi i Teoreticheskoi Fiziki		BIRK	<b>Birkbeck College</b> , Univ. of London	London, United Kingdom
ZETFP	Zhurnal Eksperimental'noi i Teoreticheskoi Fiziki, Pis'ma v Redakts		BIRM	Univ. of <b>Birmingham</b>	Edgbaston, Birmingham, United Kingdom
ZNAT	Zeitschrift für Naturforschung		BLSU	<b>Bloomsburg Univ.</b>	Bloomsburg, PA, USA
ZPHY	Zeitschrift für Physik		BNL	<b>Brookhaven National Lab.</b>	Upton, NY, USA
<b>Institutions</b>			BOCH	<b>Ruhr Univ. Bochum</b>	Bochum, Germany
AACH	Phys. Inst. der Techn. Hochschule <b>Aachen</b> (Historical, use for general Inst. der Techn. Hochschule)	Aachen, Germany	BOHR	<b>Niels Bohr Inst.</b>	Copenhagen Ø, Denmark
AACH1	I Phys. Inst. B, RWTH <b>Aachen</b>	Aachen, Germany	BOIS	<b>Boise State Univ.</b>	Boise, ID, USA
AACH3	III Phys. Inst. A, RWTH <b>Aachen Univ.</b>	Aachen, Germany	BOMB	Univ. of <b>Bombay</b>	Bombay, India
AACHT	Inst. für Theoretische Teilchenphysik & Kosmologie, RWTH <b>Aachen</b>	Aachen, Germany	BONN	<b>Univ. of Bonn</b>	Bonn, Germany
AARH	Univ. of <b>Aarhus</b>	Aarhus C, Denmark	BORD	Centre d'Etudes Nucléaires de <b>Bordeaux Gradignan (CENBG)</b>	Gradignan, France
ABO	<b>Åbo Akademi Univ.</b>	Turku, Finland	BOSE	S.N. <b>Bose National Centre for Basis Sciences</b>	Calcutta, India
ADEL	<b>Adelphi Univ.</b>	Garden City, NY, USA			
ADLD	The Univ. of <b>Adelaide</b>	Adelaide, SA, Australia			
AERE	Atomic Energy Research Estab.	Didcot, United Kingdom			
AFRR	<b>Armed Forces Radiobiology Res. Inst.</b>	Bethesda, MD, USA			
AHMED	Physical Research Lab.	<b>Ahmedabad</b> , Gujarat, India			
AICH	<b>Aichi Univ.</b> of Education	Aichi, Japan			
AKIT	<b>Akita Univ.</b>	Akita, Japan			
ALAH	Univ. of <b>Alabama (Huntsville)</b>	Huntsville, AL, USA			
ALAT	Univ. of <b>Alabama (Tuscaloosa)</b>	Tuscaloosa, AL, USA			
ALBA	<b>SUNY at Albany</b>	Albany, NY, USA			
ALBE	Univ. of <b>Alberta</b>	Edmonton, AB, Canada			

## Abbreviations Used in the Particle Listings

BOSK	“ <b>Rudjer Bošković</b> ” Inst.	Zagreb, Croatia	COLO	Univ. of <b>Colorado</b>	Boulder, CO, USA
BOST	<b>Boston</b> Univ.	Boston, MA, USA	COLU	<b>Columbia</b> Univ.	New York, NY, USA
BRAN	<b>Brandeis</b> Univ.	Waltham, MA, USA	CONC	<b>Concordia</b> University	Montreal, PQ, Canada
BRCO	Univ. of <b>British Columbia</b>	Vancouver, BC, Canada	CORN	<b>Cornell</b> Univ.	Ithaca, NY, USA
BRIS	Univ. of <b>Bristol</b>	Bristol, United Kingdom	COSU	<b>Colorado State</b> Univ.	Fort Collins, CO, USA
BROW	<b>Brown</b> Univ.	Providence, RI, USA	CPPM	Centre National de la Recherche Scientifique, Lu- miny	<b>Marseille</b> , France
BRUN	<b>Brunel</b> Univ.	Uxbridge, Middlesex, United Kingdom	CRAC	Henryk Niewodniczański Inst. of Nuclear Physics	<b>Kraków</b> , Poland
BRUX	Univ. Libre de <b>Bruxelles</b> ; Physique des Particules Elémentaires	Bruxelles, Belgium	CRNL	<b>Chalk River</b> Labs.	Chalk River, ON, Canada
BRUXT	Univ. Libre de <b>Bruxelles</b> ; Physique Théorique	Bruxelles, Belgium	CSOK	<b>Oklahoma Central State</b> Univ.	Edmond, OK, USA
BUCH	Univ. of <b>Bucharest</b>	Bucharest-Magurele, Romania	CST	Univ. of <b>Science and Tech-</b> <b>nology</b> of China	<b>Hefei</b> , Anhui 230026, China
BUDA	<b>Wigner</b> Research Centre for Physics	<b>Budapest</b> , Hungary	CSULB	<b>California State Univ.</b>	Long Beach, CA, USA
BUFF	<b>SUNY at Buffalo</b>	Buffalo, NY, USA	CSUS	<b>California State Univ.</b>	Sacramento, CA, USA
BURE	Inst. des Hautes Etudes Scien- tifiques	<b>Bures-sur-Yvette</b> , France	CUNY	<b>City College of New York</b>	New York, NY, USA
CAEN	Lab. de Physique Corpuscu- laire, <b>ENSICAEN</b>	<b>Caen</b> , France	CURCP	<b>Univ. Pierre et Marie</b> <b>Curie</b> (Paris VI), LCP	Paris, France
CAGL	Univ. degli Studi di <b>Cagliari</b>	Monserato (CA), Italy	CURIN	<b>Univ. Pierre et Marie</b> <b>Curie</b> (Paris VI), LPNHE	Paris, France
CAIR	<b>Cairo</b> University	Orman, Giza, Cairo, Egypt	CURIT	<b>Univ. Pierre et Marie</b> <b>Curie</b> (Paris VI), LPTHE	Paris, France
CAIW	<b>Carnegie Inst.</b> of Washing- ton	Washington, DC, USA	DALH	<b>Dalhousie</b> Univ.	Halifax, NS, Canada
CALB	Univ. della <b>Calabria</b>	Cosenza, Italy	DALI	<b>Dalian</b> Univ. of Tech.	Dalian, China
CALC	Univ. of <b>Calcutta</b>	Calcutta, India	DARE	<b>Daresbury</b> Lab	Cheshire, United Kingdom
CAMB	<b>DAMTP</b>	Cambridge, United Kingdom	DARM	Tech. Hochschule <b>Darmstadt</b>	Darmstadt, Germany
CAMP	Univ. Estadual de <b>Campinas</b> (UNICAMP)	<b>Campinas</b> , SP, Brazil	DELA	Univ. of <b>Delaware</b> ; Dept. of Physics & Astronomy	Newark, DE, USA
CANB	<b>Australian National Univ.</b>	Canberra, ACT, Australia	DELH	Univ. of <b>Delhi</b>	Delhi, India
CANTB	Inst. de Física de Cantabria (CSIC–Univ. <b>Cantabria</b> )	Santander, Spain	DESY	<b>DESY</b> , Deutsches Elektronen-Synchrotron	<b>Hamburg</b> , Germany
CAPE	University of <b>Cape Town</b>	Rondebosch, Cape Town, South Africa	DFAB	Escuela de Ingenieros	<b>Bilbao</b> , Spain
CARA	Univ. Central de <b>Venezuela</b>	Caracas, Venezuela	DOE	<b>Department of Energy</b>	Washington, DC, USA
CARL	<b>Carleton</b> Univ.	Ottawa, ON, Canada	DORT	Technische Univ. <b>Dortmund</b>	Dortmund, Germany
CARLC	<b>Carleton</b> College	Northfield, MN, USA	DUKE	<b>Duke</b> Univ.	Durham, NC, USA
CASE	<b>Case</b> Western Reserve Univ.	Cleveland, OH, USA	DURH	Univ. of <b>Durham</b>	Durham, United Kingdom
CAST	<b>China</b> Center of Advanced Science and Technology	Beijing, China	DUUC	<b>University College</b> Dublin	Dublin, Ireland
CATA	Univ. di <b>Catania</b>	Catania, Italy	EDIN	Univ. of <b>Edinburgh</b>	Edinburgh, United Kingdom
CATH	<b>Catholic</b> Univ. of America	Washington, DC, USA	EFI	Univ. of Chicago, <b>The En-</b> <b>rico Fermi Inst.</b>	<b>Chicago</b> , IL, USA
CAVE	<b>Cavendish</b> Lab.	Cambridge, United Kingdom	ELMT	<b>Elmhurst</b> College	Elmhurst, IL, USA
CBNM	CBNM	<b>Geel</b> , Belgium	ENSP	<b>l’Ecole Normale</b> <b>Supérieure</b>	<b>Paris</b> , France
CBPF	Centro Brasileiro de Pesquisas Físicas – <b>BIB/CDI/CBPF</b>	<b>Rio de Janeiro</b> , RJ, Brazil	EOTV	<b>Eötvös</b> University	Budapest, Hungary
CCAC	<b>Allegheny</b> College	Meadville, PA, USA	EPOL	<b>École Polytechnique</b>	<b>Palaiseau</b> , France
CDEF	<b>Univ. Paris VII, Denis</b> <b>Diderot</b>	Paris, France	ERLA	Univ. <b>Erlangen-Nurnberg</b>	Erlangen, Germany
CEA	Cambridge Electron Accelera- tor (Historical in <i>Review</i> )	<b>Cambridge, MA</b> , USA	ETH	<b>Univ. Zürich</b>	Zürich, Switzerland
CEADE	Center for Apl. Studies for Nuclear Physics	Havana, Cuba	FERR	Univ. di <b>Ferrara</b>	Ferrara, Italy
CEBAF	<b>Jefferson Lab—Thomas</b> <b>Jefferson National Accel-</b> <b>erator Facility</b>	<b>Newport News</b> , VA, USA	FIRZ	Univ. degli Studi di <b>Firenze</b>	Sesto Fiorentino, Italy
CENG	Centre d’Etudes Nucleaires	<b>Grenoble</b> , France	FISK	<b>Fisk</b> Univ.	Nashville, TN, USA
CERN	<b>CERN</b> , European Organiza- tion for Nuclear Research	Genève, Switzerland	FLOR	Univ. of <b>Florida</b>	Gainesville, FL, USA
CFPA	Univ. of <b>California, (Berke-</b> <b>ley)</b>	Berkeley, CA, USA	FNAL	<b>Fermilab</b>	Batavia, IL, USA
CHIC	Univ. of <b>Chicago</b>	Chicago, IL, USA	FOM	<b>FOM</b> , Stichting voor Funda- menteel Onderzoek der Ma- terie	<b>JP Utrecht</b> , The Netherlands
CIAE	<b>State Nuclear Power Re-</b> <b>search Inst.</b>	<b>Beijing</b> , China	FRAN	<b>Frankfurt Inst. for Ad-</b> <b>vanced Studies (FIAS)</b>	Frankfurt am Main, Germany
CINC	Univ. of <b>Cincinnati</b>	Cincinnati, OH, USA	FRAS	Lab. Nazionali di <b>Frascati</b> dell’ <b>INFN</b>	Frascati (Roma), Italy
CINV	<b>CINVESTAV-IPN</b> Centro de Investigacion y de Estudios Avanzados del IPN	<b>México</b> , DF, Mexico	FREIB	<b>Albert-Ludwigs</b> Univ.	<b>Freiburg</b> , Germany
CIT	<b>California Inst. of Tech.</b>	Pasadena, CA, USA	FREIE	<b>Freie Univ. Berlin</b>	Berlin, Germany
CLER	Univ. de <b>Clermont-Ferrand</b>	Aubière, France	FRIB	Univ. de <b>Fribourg</b>	Fribourg, Switzerland
CLEV	<b>Cleveland State</b> Univ.	Cleveland, OH, USA	FSU	<b>Florida State Univ.</b> ; High Energy Physics	Tallahassee, FL, USA
CMNS	<b>Comenius</b> Univ. (FMFI UK)	<b>Bratislava</b> , Slovakia	FSUSC	<b>Florida State Univ.</b> ; SCS (School of Computational Science)	Tallahassee, FL, USA
CMU	<b>Carnegie Mellon</b> Univ.	Pittsburgh, PA, USA	FUKI	<b>Fukui</b> Univ.	Fukui, Japan
CNEA	<b>Comisión Nacional de En-</b> <b>ergía Atómica</b>	Buenos Aires, Argentina	FUKU	<b>Fukushima</b> Univ.	Fukushima, Japan
CNRC	Centre for Research in Partic- le Physics	Ottawa, ON, Canada	GENO	Univ. di <b>Genova</b>	Genova, Italy
COIM	Univ. de Coimbra	<b>Coimbra</b> , Portugal	GEOR	<b>E. Andronikashvili Inst. of</b> <b>Physics</b>	Tbilisi, Republic of Georgia
			GESC	<b>General Electric Co.</b>	Schenectady, NY, USA
			GEVA	Univ. de <b>Genève</b>	Genève, Switzerland
			GIES	Univ. <b>Giessen</b>	Giessen, Germany
			GIFU	<b>Gifu</b> Univ.	Gifu, Japan

## Abbreviations Used in the Particle Listings

GLAS	Univ. of <b>Glasgow</b>	Glasgow, United Kingdom	IOFF	A.F. <b>Ioffe</b> Phys. Tech. Inst.	St. <b>Petersburg</b> , Russian Federation
GMAS	<b>George Mason</b> Univ.	Fairfax, VA, USA	IOWA	Univ. of <b>Iowa</b>	Iowa City, IA, USA
GOET	Univ. <b>Göttingen</b>	Göttingen, Germany	IPN	<b>IPN</b> , Inst. de Phys. Nucl.	<b>Orsay</b> , France
GOML	<b>Gomel State</b> Univ.	Gomel, Belarus	IPNP	Univ. Pierre et Marie Curie ( <b>Paris VI</b> )	Paris, France
GRAN	Univ. de <b>Granada</b>	Granada, Spain	IRAD	Inst. du Radium (Historical)	<b>Paris</b> , France
GRAZ	Univ. <b>Graz</b>	Graz, Austria	ISNG	Lab. de Physique Subatomique et de Cosmologie ( <b>LPSC</b> )	<b>Grenoble</b> , France
GRON	Univ. of <b>Groningen</b>	Groningen, The Netherlands	ISU	<b>Iowa State</b> Univ.	Ames, IA, USA
GSCO	<b>Geological Survey of Canada</b>	Ottawa, ON, Canada	ISUT	Isfahan University of Technology	Isfahan, Iran
GSI	GSI Helmholtzzentrum für Schwerionenforschung GmbH	<b>Darmstadt</b> , Germany	ITEP	<b>ITEP</b> , Inst. of Theor. and Exp. Physics	<b>Moscow</b> , Russian Federation
GUAN	Univ. de <b>Guanajuato</b>	León, Gto., Mexico	ITHA	<b>Ithaca</b> College	Ithaca, NY, USA
GUEL	Univ. of <b>Guelph</b>	Guelph, ON, Canada	IUPU	<b>Indiana</b> Univ., <b>Purdue</b> Univ. <b>Indianapolis</b>	Indianapolis, IN, USA
GWU	<b>George Washington</b> Univ.	Washington, DC, USA	JADA	<b>Jadavpur</b> Univ.	Calcutta, India
HAHN	<b>Hahn-Meitner</b> Inst. Berlin GmbH	Berlin, Germany	JAGL	<b>Jagiellonian</b> Univ.	Kraków, Poland
HAIF	<b>Technion</b> – Israel Inst. of Tech.	Technion, Haifa, Israel	JHU	<b>Johns Hopkins</b> Univ.	Baltimore, MD, USA
HAMB	Univ. <b>Hamburg</b>	Hamburg, Germany	JINR	<b>JINR</b> , Joint Inst. for Nucl. Research	<b>Dubna</b> , Russian Federation
HANN	Univ. <b>Hannover</b>	Hannover, Germany	JULI	Forschungszentrum <b>Jülich</b>	Jülich, Germany
HARC	<b>Houston Advanced Research Ctr.</b>	The Woodlands, TX, USA	JYV	Univ. of <b>Jyväskylä</b>	Jyväskylä, Finland
HARV	<b>Harvard</b> Univ.	Cambridge, MA, USA	KAGO	Univ. of <b>Kagoshima</b>	Kagoshima-shi, Japan
HARV	<b>Harvard</b> Univ. (LPPC)	Cambridge, MA, USA	KAIST	<b>Korea</b> Advanced Inst. of Science and Technology	Yusung ku, Daejeon, Republic of Korea
HAWA	Univ. of <b>Hawai'i</b>	Honolulu, HI, USA	KANP	Indian Inst. of Tech.	<b>Kanpur</b> , UT, India
HEBR	<b>Hebrew</b> Univ.	Jerusalem, Israel	KANS	Univ. of <b>Kansas</b>	Lawrence, KS, USA
HEID	Univ. <b>Heidelberg</b> ; (unspecified division) (Historical in <i>Review</i> )	Heidelberg, Germany	KARL	Univ. <b>Karlsruhe</b> (Historical in <i>Review</i> )	Karlsruhe, Germany
HEIDH	Ruprecht-Karls Univ. <b>Heidelberg</b>	Heidelberg, Germany	KARLE	<b>Karlsruhe</b> Inst. of Technology (KIT); Inst. for Experimental Nuclear Physics	Karlsruhe, Germany
HEIDP	Univ. <b>Heidelberg</b> ; Physics Inst.	Heidelberg, Germany	KARLK	<b>Karlsruhe</b> Inst. of Technology (KIT)	Eggenstein-Leopoldshafen, Germany
HEIDT	Ruprecht-Karls-Univ. <b>Heidelberg</b>	Heidelberg, Germany	KARLT	<b>Karlsruhe</b> Inst. of Technology (KIT); Inst. for Theoretical Physics	Karlsruhe, Germany
HELS	Univ. of <b>Helsinki</b>	University of Helsinki, Finland	KAZA	<b>Kazakh</b> Inst. of High Energy Physics	Alma Ata, Kazakhstan
HINR	Inst. of Nuclear Research ( <b>ATOMKI</b> )	<b>Debrecen</b> , Hungary	KEK	<b>KEK</b> , High Energy Accelerator Research Organization	Ibaraki-ken, Japan
HIRO	<b>Hiroshima</b> Univ.	Higashi-Hiroshima, Japan	KENT	Univ. of <b>Kent</b>	Canterbury, United Kingdom
HOUS	Univ. of <b>Houston</b>	Houston, TX, USA	KEYN	<b>Open</b> Univ.	Milton Keynes, United Kingdom
HPC	<b>Hewlett-Packard</b> Corp.	Cupertino, CA, USA	KFTI	<b>Kharkov</b> Inst. of Physics and Tech. (NSC KIPT)	Kharkov, Ukraine
HSCA	<b>Harvard-Smithsonian</b> Center for Astrophysics	Cambridge, MA, USA	KIAE	<b>Kurchatov</b> Inst.	<b>Moscow</b> , Russian Federation
HYDER	Indian Inst. of Technology	Hyderabad, India	KIAM	<b>Keldysh</b> Inst. of Applied Math., Acad. Sci., Russia	<b>Moscow</b> , Russian Federation
IAS	<b>Inst. for Advanced Study</b>	Princeton, NJ, USA	KIDR	<b>Vinča Inst. of Nuclear Sciences</b>	Belgrade, Serbia
IASD	<b>Dublin</b> Inst. for Advanced Studies	Dublin, Ireland	KIEV	<b>Institute for Nuclear Research</b>	<b>Kyiv</b> , Ukraine
IBAR	<b>Ibaraki</b> Univ.	Ibaraki, Japan	KINK	<b>Kinki</b> Univ.	Osaka, Japan
IBM	<b>IBM</b> Corp.	Palo Alto, CA, USA	KNTY	Univ. of <b>Kentucky</b>	Lexington, KY, USA
IBMY	<b>IBM</b>	Yorktown Heights, NY, USA	KOBE	<b>Kobe</b> Univ.	Kobe, Japan
IBS	Inst. for <b>Boson Studies</b>	Pasadena, CA, USA	KOMAB	Univ. of <b>Tokyo</b> , <b>Komaba</b>	Tokyo, Japan
ICEPP	The Univ. of <b>Tokyo</b>	Tokyo, Japan	KONAN	<b>Konan</b> Univ.	Kobe, Japan
ICRR	Univ. of <b>Tokyo</b>	Chiba, Japan	KOSI	Inst. of Experimental Physics SAS	<b>Košice</b> , Slovakia
ICTP	<b>Abdus Salam</b> International Centre for Theoretical Physics	<b>Trieste</b> , Italy	KYOT	<b>Kyoto</b> Univ.; Dept. of Physics, Graduate School of Science	Kyoto, Japan
IFIC	<b>IFIC</b> (Instituto de Física Corpuscular)	<b>Paterna (Valencia)</b> , Spain	KYOTU	<b>Kyoto</b> Univ.; <b>Yukawa</b> Inst. for Theor. Physics	Kyoto, Japan
IFRJ	Univ. Federal do <b>Rio de Janeiro</b>	Rio de Janeiro, RJ, Brazil	KYUN	<b>Kyungpook</b> National Univ.	Daegu, Republic of Korea
IIT	<b>Illinois Inst. of Tech.</b>	Chicago, IL, USA	KYUSH	<b>Kyushu</b> Univ.; Elementary Particle Theory Group; Exp. Particle Physics Group; Research Center for Advanced Particle Physics	Fukuoka, Japan
ITI	Indian Inst. of Tech. (of IIT Indore)	Simrol, Indore, India	LALO	<b>LAL</b> , Laboratoire de l'Accélérateur Linéaire	<b>Orsay</b> , France
ILL	Univ. of <b>Illinois at Urbana-Champaign</b>	Urbana, IL, USA	LANC	<b>Lancaster</b> Univ.	Lancaster, United Kingdom
ILLC	Univ. of <b>Illinois at Chicago</b>	Chicago, IL, USA	LANL	<b>Los Alamos National Lab.</b> (LANL)	Los Alamos, NM, USA
ILLG	Inst. <b>Laue-Langevin</b>	Grenoble, France	LAPL	Univ. Nacional de <b>La Plata</b>	La Plata, Argentina
IND	<b>Indiana</b> Univ.	Bloomington, IN, USA			
INEL	E G and G <b>Idaho</b> , Inc.	Idaho Falls, ID, USA			
INFN	Ist. Nazionale di Fisica Nucleare (Generic INFN, unknown location)	Various places, Italy			
INNS	Univ. of <b>Innsbruck</b>	<b>Innsbruck</b> , Austria			
INPK	Henryk Niewodniczański Inst. of Nuclear Physics	<b>Kraków</b> , Poland			
INRM	<b>INR</b> , Inst. for Nucl. Research	<b>Moscow</b> , Russian Federation			
INUS	<b>KEK</b> , High Energy Accelerator Research Organization	Tokyo, Japan			
IOAN	Univ. of <b>Ioannina</b>	Ioannina, Greece			

## Abbreviations Used in the Particle Listings

LAPP	<b>LAPP</b> , Lab. d'Annecy-le-Vieux de Phys. des Particules	<b>Annecy-le-Vieux</b> , France	MICH	Univ. of <b>Michigan</b>	Ann Arbor, MI, USA
LASL	U.C. <b>Los Alamos Scientific Lab.</b> (Old name for LANL)	Los Alamos, NM, USA	MILA	Univ. di <b>Milano</b>	Milano, Italy
LATV	<b>Latvian State Univ.</b>	Riga, Latvia	MILAI	<b>INFN</b> , Sez. di <b>Milano</b>	Milano, Italy
LAUS	EPFL <b>Lausanne</b>	Lausanne, Switzerland	MINN	Univ. of <b>Minnesota</b>	Minneapolis, MN, USA
LAVL	Univ. <b>Laval</b>	Quebec, QC, Canada	MIPT	Moscow Institute of Physics and Technology	Moscow, Russian Federation
LBL	<b>Lawrence Berkeley National Lab.</b>	Berkeley, CA, USA	MISS	Univ. of <b>Mississippi</b>	University, MS, USA
LCGT	Univ. di <b>Torino</b>	Turin, Italy	MISSR	Univ. of <b>Missouri</b>	Rolla, MO, USA
LEBD	<b>Lebedev Physical Inst.</b>	<b>Moscow</b> , Russian Federation	MIT	<b>MIT Massachusetts Inst. of Technology</b>	Cambridge, MA, USA
LECE	Univ. di <b>Lecce</b>	Lecce, Italy	MIU	<b>Maharishi International Univ.</b>	Fairfield, IA, USA
LEED	Univ. of <b>Leeds</b>	Leeds, United Kingdom	MIYA	<b>Miyazaki Univ.</b>	Miyazaki-shi, Japan
LEGN	Lab. Naz. di <b>Legnaro</b>	<b>Legnaro</b> , Italy	MONP	Univ. de <b>Montpellier II</b>	Montpellier, France
LEHI	<b>Lehigh Univ.</b>	Bethlehem, PA, USA	MONS	Univ. of <b>Mons</b>	<b>Mons</b> , Belgium
LEHM	<b>Lehman College of CUNY</b>	Bronx, NY, USA	MONT	Univ. de <b>Montréal</b> ; Pavillon René-J.-A.-Lévesque	Montréal, PQ, Canada
LEID	Univ. <b>Leiden</b>	Leiden, The Netherlands	MONTC	Univ. de <b>Montréal</b> ; Centre de recherches mathématiques	Montréal, PQ, Canada
LEMO	<b>Le Moyne Coll.</b>	Syracuse, NY, USA	MOSU	<b>Skobeltsyn Inst. of Nuclear Physics</b> , Lomonosov Moscow State Univ.; Experimental HEP Division; Theoretical HEP Division	<b>Moscow</b> , Russian Federation
LENSU	<b>Saint-Petersburg State Univ.</b>	<b>St. Petersburg</b> , Russian Federation	MPCM	Max Planck Inst. für Chemie	<b>Mainz</b> , Germany
LEUV	Katholieke Univ. <b>Leuven</b>	Leuven, Belgium	MPEI	<b>Moscow Physical Engineering Inst.</b>	Moscow, Russian Federation
LIEG	Univ. de <b>Liège</b>	Liège, Belgium	MPIG	<b>Max-Planck-Institute für Astrophysik</b>	Garching, Germany
LINZ	Univ. <b>Linz</b>	Linz, Austria	MPIH	<b>Max-Planck-Inst. für Kernphysik</b>	<b>Heidelberg</b> , Germany
LISB	Inst. Nacional de Investigacion Cientifica	<b>Lisboa CODEX</b> , Portugal	MPIM	<b>Max-Planck-Inst. für Physik</b>	<b>München</b> , Germany
LISBT	Centro de Física Teórica de Partículas ( <b>CFTP</b> )	<b>Lisboa</b> , Portugal	MSST	Mississippi State University	Mississippi State, MS, USA
LIVP	Univ. of <b>Liverpool</b>	Liverpool, United Kingdom	MSU	<b>Michigan State Univ.</b>	East Lansing, MI, USA
LLL	<b>Lawrence Livermore Lab.</b> (Old name for LLNL)	Livermore, CA, USA	MTHO	<b>Mount Holyoke College</b>	South Hadley, MA, USA
LLNL	<b>Lawrence Livermore National Lab.</b>	Livermore, CA, USA	MULH	Centre Univ. du <b>Haut-Rhin</b>	Mulhouse, France
LNUDA		Dalian, China	MUNI	<b>Ludwig-Maximilians-Univ. München</b>	Garching, Germany
LOCK	<b>Lockheed Palo Alto Res. Lab</b>	Palo Alto, CA, USA	MUNT	Tech. Univ. <b>München</b>	Garching, Germany
LOIC	<b>Imperial College of Science Tech. &amp; Medicine</b>	London, United Kingdom	MURA	<b>Midwestern Univ. Research Assoc.</b> (Historical in <i>Review</i> )	Stroughton, WI, USA
LOKC	Univ. of <b>London</b> , King's College	London, United Kingdom	MURC	Univ. of Murcia	Murcia, Spain
LOQM	Queen Mary, Univ. of <b>London</b>	London, United Kingdom	NAAS	North Americal Aviation Science Center (Historical in <i>Review</i> )	Thousand Oaks, CA, USA
LOUC	<b>University College London</b>	London, United Kingdom	NAGO	<b>Nagoya Univ.</b>	Nagoya, Japan
LOUV	Univ. Catholique de <b>Louvain</b>	Louvain-la-Neuve, Belgium	NANJ	<b>Nanjing Univ.</b>	Nanjing, China
LOWC	<b>Westfield College</b> (Historical, see LOQM (Queen Mary and Westfield joined))	London, United Kingdom	NAPL	Univ. di <b>Napoli</b> "Federico II"	Napoli, Italy
LRL	U.C. Lawrence Radiation Lab. (Old name for LBL)	<b>Berkeley</b> , CA, USA	NASA	<b>NASA</b>	Greenbelt, MD, USA
LSU	<b>Louisiana State Univ.</b>	Baton Rouge, LA, USA	NBS	U.S. <b>National Bureau of Standards</b> (Old name for NIST)	Gaithersburg, MD, USA
LUND	<b>Fysiska Institutionen</b>	<b>Lund</b> , Sweden	NBSB	<b>National Inst. Standards Tech.</b>	Boulder, CO, USA
LUND	<b>Lund Univ.</b>	Lund, Sweden	NCAR	<b>National Center for Atmospheric Research</b>	Boulder, CO, USA
LYON	Institute de Physique Nucléaire de <b>Lyon (IPN)</b>	Villeurbanne, France	NCSU	<b>North Carolina State Univ.</b>	<b>Raleigh</b> , NC, USA
MADE	<b>UAM/CSIC</b> , Inst. de Física Teórica	<b>Madrid</b> , Cantoblanco, Spain	NDAM	Univ. of <b>Notre Dame</b>	Notre Dame, IN, USA
MADR	<b>C.I.E.M.A.T</b>	<b>Madrid</b> , Spain	NEAS	<b>Northeastern Univ.</b>	Boston, MA, USA
MADRA	Univ. of <b>Madras</b>	Madras, India	NEBR	Univ. of <b>Nebraska</b>	Lincoln, NE, USA
MADU	Univ. Autónoma de <b>Madrid</b>	Cantoblanco, Madrid, Spain	NEUC	Univ. de <b>Neuchâtel</b>	Neuchâtel, Switzerland
MANI	Univ. of <b>Manitoba</b>	Winnipeg, MB, Canada	NICEA	Univ. de <b>Nice</b>	Nice, France
MANZ	<b>Johannes-Gutenberg-Univ.</b> ; Inst. für Kernphysik, J.-J.-Becher-Weg 45; Inst. für Physik, Staudingerweg 7	<b>Mainz</b> , Germany	NICEO	Observatoire de <b>Nice</b>	Nice, France
MARB	Univ. <b>Marburg</b>	Marburg, Germany	NIHO	<b>Nihon Univ.</b>	Tokyo, Japan
MARS	Centre de Physique des Particules de <b>Marseille</b>	Marseille, France	NIIG	<b>Niigata Univ.</b>	Niigata, Japan
MASA	Univ. of <b>Massachusetts</b> Amherst	<b>Amherst</b> , MA, USA	NIJM	<b>Radboud Univ. Nijmegen</b>	AJ <b>Nijmegen</b> , The Netherlands
MASB	Univ. of <b>Massachusetts</b> Boston	<b>Boston</b> , MA, USA	NIRS	Nat. Inst. Radiological Sciences	<b>Chiba</b> , Japan
MASD	Univ. of <b>Massachusetts</b> Dartmouth	North <b>Dartmouth</b> , MA, USA	NIST	<b>National Institute of Standards &amp; Technology</b>	Gaithersburg, MD, USA
MCGI	<b>McGill Univ.</b>	Montreal, QC, Canada	NIU	<b>Northern Illinois Univ.</b>	De Kalb, IL, USA
MCHS	Univ. of <b>Manchester</b>	Manchester, United Kingdom	NMSU	<b>New Mexico State Univ.</b> ; Dept. of Physics, MSC 3D; Part. & Nucl. Phys. Group, Box 30001/Dept.	Las Cruces, NM, USA
MCMS	<b>McMaster Univ.</b>	Hamilton, ON, Canada	NORD	<b>Nordita</b>	Stockholm, Sweden
MEHTA	<b>Harish-Chandra Research Inst.</b>	Allahabad, India	NOTT	Univ. of <b>Nottingham</b>	Nottingham, United Kingdom
MEIS	<b>Meisei Univ.</b>	Tokyo, Japan			
MELB	Univ. of <b>Melbourne</b>	Victoria, Australia			
MEUD	Observatoire de <b>Meudon</b>	Meudon, France			

## Abbreviations Used in the Particle Listings

NOVM	Inst. of Mathematics	<b>Novosibirsk</b> , Russian Federation	RHEL	<b>Rutherford High Energy Lab</b> (Old name for RAL)	Chilton, Didcot, Oxon., United Kingdom
NOVO	BINP, <b>Budker Inst.</b> of Nuclear Physics	<b>Novosibirsk</b> , Russian Federation	RICE	<b>Rice Univ.</b>	Houston, TX, USA
NPOL	Polytechnic of <b>North London</b>	London, United Kingdom	RIKEN	<b>Riken Nishina Center</b> for Accelerator-Based Science	Saitama, Japan
NRL	<b>Naval Research Lab</b>	Washington, DC, USA	RIKK	<b>Rikkyo Univ.</b>	Tokyo, Japan
NSF	<b>National Science Foundation</b>	Arlington, VA, USA	RIS	<b>Rowland Inst.</b> for Science	Cambridge, MA, USA
NTHU	<b>National Tsing Hua Univ.</b>	Hsinchu, Taiwan	RISC	<b>Rockwell International</b>	Thousand Oaks, CA, USA
NTUA	<b>National Tech. Univ. of Athens</b>	Athens, Greece	RISL	<b>Universities Research Reactor</b>	<b>Risley</b> , Warrington, United Kingdom
NWES	<b>Northwestern Univ.</b>	Evanston, IL, USA	RISO	<b>Riso National Laboratory</b>	Roskilde, Denmark
NYU	<b>New York Univ.</b>	New York, NY, USA	RITS	Royal Inst. of Technology ( <b>KTH</b> )	<b>Stockholm</b> , Sweden
OBER	<b>Oberlin College</b>	Oberlin, OH, USA	RL	<b>Rutherford High Energy Lab</b> (Old name for RAL)	Chilton, Didcot, Oxon., United Kingdom
OCH	<b>Ochanomizu Univ.</b>	Tokyo, Japan	RMCS	<b>Royal Military Coll.</b> of Science	Swindon, Wilts., United Kingdom
OHIO	<b>Ohio Univ.</b>	Athens, OH, USA	ROCH	Univ. of <b>Rochester</b>	Rochester, NY, USA
OKAY	<b>Okayama Univ.</b>	Okayama, Japan	ROCK	<b>Rockefeller Univ.</b>	New York, NY, USA
OKLA	Univ. of <b>Oklahoma</b>	Norman, OK, USA	ROMA	Univ. di <b>Roma</b> (Historical)	<b>Roma</b> , Italy
OKSU	<b>Oklahoma State Univ.</b>	Stillwater, OK, USA	ROMA2	Univ. di <b>Roma</b> , "Tor Vergata"	Roma, Italy
OREG	Univ. of <b>Oregon</b> ; Inst. of Theoretical Science; U.O. Center for High Energy Physics	Eugene, OR, USA	ROMA3	<b>INFN, Sez. di Roma Tre</b>	<b>Roma</b> , Italy
ORNL	<b>Oak Ridge National Laboratory</b>	Oak Ridge, TN, USA	ROMAI	<b>INFN, Sez. di Roma</b>	Roma, Italy
ORSAY	Univ. de <b>Paris Sud 11</b>	<b>Orsay CEDEX</b> , France	ROSE	<b>Rose-Hulman Inst.</b> of Technology	Terre Haute, IN, USA
ORST	<b>Oregon State Univ.</b>	Corvallis, OR, USA	RPI	<b>Rensselaer Polytechnic Inst.</b>	Troy, NY, USA
OSAK	<b>Osaka Univ.</b>	Osaka, Japan	RUTG	<b>Rutgers</b> , the State Univ. of New Jersey	Piscataway, NJ, USA
OSKC	<b>Osaka City Univ.</b>	Osaka, Japan	S0GA	<b>Sogang University</b>	Seoul, Republic of Korea
OSLO	Univ. of <b>Oslo</b>	Oslo, Norway	SACL	<b>CEA Saclay</b> , IRFU	Gif-sur-Yvette, France
OSU	<b>Ohio State Univ.</b>	Columbus, OH, USA	SACL5	<b>CEA Saclay – IPhT</b>	Gif-sur-Yvette, France
OTTA	Univ. of <b>Ottawa</b>	Ottawa, ON, Canada	SACL6	<b>CEA Saclay</b> (Essonne)	Gif-sur-Yvette, France
OXF	University of <b>Oxford</b>	Oxford, United Kingdom	SAGA	<b>Saga Univ.</b>	Saga-shi, Japan
OXFTP	Univ. of <b>Oxford</b>	Oxford, United Kingdom	SAHA	<b>Saha Inst.</b> of Nuclear Physics	Bidhan Nagar, Calcutta, India
PADO	Univ. degli Studi di <b>Padova</b>	Padova, Italy	SANG	<b>Kyoto Sangyo Univ.</b>	Kyoto-shi, Japan
PARIN	<b>LPNHE, IN<sup>2</sup>P<sup>3</sup>/CNRS</b>	Paris, France	SANI	Ist. Superiore di Sanità	<b>Roma</b> , Italy
PARIS	Univ. de Paris (Historical)	<b>Paris</b> , France	SASK	Univ. of <b>Saskatchewan</b>	Saskatoon, SK, Canada
PARIT	<b>Univ. Paris VII, LPTHE</b>	Paris, France	SASSO	Lab. Naz. <b>Gran Sasso</b> dell'INFN	<b>Assergi</b> (AQ), Italy
PARM	<b>INFN</b> , Gruppo Collegato di <b>Parma</b>	Parma, Italy	SAVO	Univ. de <b>Savoie</b>	Chambery, France
PAST	Institut <b>Pasteur</b>	<b>Paris</b> , France	SBER	<b>California State Univ.</b>	<b>San Bernardino</b> , CA, USA
PATR	Univ. of <b>Patras</b>	Patras, Greece	SCHAF	W.J. <b>Schafer Assoc.</b>	Livermore, DA, USA
PAVI	Univ. di <b>Pavia</b>	Pavia, Italy	SCIT	<b>Science Univ. of Tokyo</b>	Tokyo, Japan
PAVII	<b>INFN, Sez. di Pavia</b>	<b>Pavia</b> , Italy	SCOT	<b>Scottish Univ. Research and Reactor Ctr.</b>	Glasgow, United Kingdom
PENN	Univ. of <b>Pennsylvania</b>	Philadelphia, PA, USA	SCUC	Univ. of <b>South Carolina</b>	Columbia, SC, USA
PGIA	<b>INFN</b> , Sezione di <b>Perugia</b>	Perugia, Italy	SEAT	<b>Seattle Pacific Coll.</b>	Seattle, WA, USA
PISA	Univ. di <b>Pisa</b>	Pisa, Italy	SEIB	Austrian Research Center, <b>Seibersdorf LTD.</b>	Seibersdorf, Austria
PISAI	<b>INFN, Sez. di Pisa</b>	Pisa, Italy	SEOU	<b>Korea Univ.</b> ; Dept. of Physics; HEP Group	Seoul, Republic of Korea
PITT	Univ. of <b>Pittsburgh</b>	Pittsburgh, PA, USA	SEOUL	<b>Seoul National Univ.</b> ; Center for Theoretical Physics; Dept. of Physics & Astronomy, Coll. of Natural Sciences	Seoul, Republic of Korea
PLAT	<b>SUNY at Plattsburgh</b>	Plattsburgh, NY, USA	SERP	<b>IHEP</b> , Inst. for High Energy Physics	Protvino, Russian Federation
PLRM	Univ. di <b>Palermo</b>	Palermo, Italy	SETO	<b>Seton Hall Univ.</b>	South Orange, NJ, USA
PNL	<b>Battelle Memorial Inst.</b>	Richland, WA, USA	SFLA	Univ. of <b>South Florida</b>	Tampa, FL, USA
PNPI	<b>Petersburg Nuclear Physics Inst.</b> of Russian Academy of Sciences	Gatchina, Russian Federation	SFRA	<b>Simon Fraser University</b>	Burnaby, BC, Canada
PPA	Princeton-Penn. Proton Accelerator (Historical in <i>Review</i> )	Princeton, NJ, USA	SFSU	<b>California State Univ.</b>	<b>San Francisco</b> , CA, USA
PRAG	Inst. of Physics, <b>ASCR</b>	<b>Prague</b> , Czech Republic	SHAMS	<b>Ain Shams University</b>	Abbassia, Cairo, Egypt
PRIN	<b>Princeton Univ.</b>	Princeton, NJ, USA	SHDN	<b>Shandong Univ.</b>	Jinan, Shandong, China
PSI	Paul Scherrer Inst.	<b>Villigen PSI</b> , Switzerland	SHEF	Univ. of <b>Sheffield</b>	Sheffield, United Kingdom
PSLL	<b>Physical Science Lab</b>	Las Cruces, NM, USA	SHMP	Univ. of <b>Southampton</b>	Southampton, United Kingdom
PSU	<b>Penn State Univ.</b>	University Park, PA, USA	SHRZ	<b>Shiraz Univ.</b>	Shiraz, Iran
PUCB	<b>Pontificia Univ. Católica do Rio de Janeiro</b>	Rio de Janeiro, RJ, Brazil	SIEG	Univ. of <b>Siegen</b>	Siegen, Germany
PUEB	Univ. Autonoma de <b>Puebla</b>	<b>Puebla</b> , Pue, Mexico	SILES	Univ. of <b>Silesia</b>	Katowice, Poland
PURD	<b>Purdue Univ.</b>	West Lafayette, IN, USA	SIN	Swiss Inst. of Nuclear Research (Old name for VILL)	<b>Villigen</b> , Switzerland
QUKI	<b>Queen's Univ.</b>	Kingston, ON, Canada	SING	<b>National Univ.</b> of Singapore	Kent Ridge, Singapore
RAL	<b>STFC Rutherford Appleton Lab.</b>	Chilton, Didcot, Oxfordshire, United Kingdom	SISSA	Scuola Internazionale Superiore di Studi Avanzati	<b>Trieste</b> , Italy
REGE	Univ. <b>Regensburg</b>	Regensburg, Germany	SLAC	<b>SLAC National Accelerator Laboratory</b>	Menlo Park, CA, USA
REHO	<b>Weizmann Inst.</b> of Science	Rehovot, Israel	SLOV	Inst. of Physics, Slovak Acad. of Sciences	<b>Bratislava 45</b> , Slovakia
REZ	Nuclear Physics Inst. <b>AVČR</b>	<b>Řež</b> , Czech Republic			
RGSUL	Univ. Federal do <b>Rio Grande do Sul</b> (UFRGS)	Porto Alegre, RS, Brazil			
RHBL	<b>Royal Holloway, Univ. of London</b>	Egham, Surrey, United Kingdom			

## Abbreviations Used in the Particle Listings

SMU	<b>Southern Methodist Univ.</b>	Dallas, TX, USA	TUZL	<b>Tuzla Univ.</b>	Tuzla, Argentina
SNSP	<b>Scuola Normale Superiore</b>	Pisa, Italy	UBA	Univ. de <b>Buenos Aires</b>	Buenos Aires, Argentina
SOFI	Inst. for Nuclear Research and Nuclear Energy	<b>Sofia</b> , Bulgaria	UCB	Univ. of <b>California (Berkeley)</b>	Berkeley, CA, USA
SOFU	Univ. of <b>Sofia</b> "St. Kliment Ohridski"	Sofia, Bulgaria	UCD	Univ. of <b>California (Davis)</b>	Davis, CA, USA
SORB	Sorbonne Université	Paris, France	UCI	Univ. of <b>California (Irvine)</b>	Irvine, CA, USA
SPAUL	Univ. de <b>São Paulo</b>	São Paulo, SP, Brazil	UCLA	Univ. of <b>California (Los Angeles)</b>	Los Angeles, CA, USA
SPIFT	Inst. de Física Teórica ( <b>IFT</b> )	<b>São Paulo</b> , SP, Brazil	UCND	<b>Union Carbide Corp.</b>	Oak Ridge, TN, USA
SSL	Univ. of <b>California (Berkeley)</b>	Berkeley, CA, USA	UCR	Univ. of <b>California (Riverside)</b>	Riverside, CA, USA
STAN	<b>Stanford Univ.</b>	Stanford, CA, USA	UCSB	Univ. of <b>California (Santa Barbara)</b> ; Physics Dept., High Energy Physics Experiment	Santa Barbara, CA, USA
STEV	<b>Stevens Inst. of Tech.</b>	Hoboken, NJ, USA	UCSBT	Univ. of <b>California (Santa Barbara)</b> ; Kavli Inst. for Theoretical Physics	Santa Barbara, CA, USA
STFN	<b>Jožef Stefan Institute</b>	<b>Ljubljana</b> , Slovenia	UCSC	Univ. of <b>California (Santa Cruz)</b>	Santa Cruz, CA, USA
STLO	<b>St. Louis Univ.</b>	St. Louis, MO, USA	UCSD	Univ. of <b>California (San Diego)</b>	La Jolla, CA, USA
STOH	<b>Stockholm Univ.</b>	Stockholm, Sweden	UGAZ	Univ. of <b>Gaziantep</b>	Gaziantep, Turkey
STON	<b>SUNY at Stony Brook</b>	Stony Brook, NY, USA	UMD	Univ. of <b>Maryland</b>	College Park, MD, USA
STRB	Inst. Pluridisciplinaire Hubert Curien ( <b>CNRS</b> )	<b>Strasbourg</b> , France	UNAM	Univ. Nac. Autónoma de México ( <b>UNAM</b> )	México, DF, Mexico
STUT	Univ. <b>Stuttgart</b>	Stuttgart, Germany	UNAM	Univ. Nacional Autónoma de México ( <b>UNAM</b> )	México, DF, Mexico
STUTM	Max-Planck-Inst.	<b>Stuttgart</b> , Germany	UNC	Univ. of <b>North Carolina</b>	Greensboro, NC, USA
SUGI	<b>Sugiyama Jogakuen Univ.</b>	Aichi, Japan	UNCCH	Univ. of <b>North Carolina at Chapel Hill</b>	Chapel Hill, NC, USA
SUNG	<b>Sungkyunkwan Univ.</b>	Suwon, Republic of Korea	UNCS	<b>Union College</b>	Schenectady, NY, USA
SURR	Univ. of <b>Surrey</b>	Guildford, Surrey, United Kingdom	UNESP	<b>UNESP</b>	Botucatu, Brazil
SUSS	Univ. of <b>Sussex</b>	Brighton, United Kingdom	UNH	Univ. of <b>New Hampshire</b>	Durham, NH, USA
SVR	<b>Savannah River Labs.</b>	Aiken, SC, USA	UNM	Univ. of <b>New Mexico</b>	Albuquerque, NM, USA
SYDN	Univ. of <b>Sydney</b>	Sydney, NSW, Australia	UOEH	Univ. of Occupational and Environmental Health	<b>Kitakyushu</b> , Japan
SYRA	<b>Syracuse Univ.</b>	Syracuse, NY, USA	UPNJ	<b>Uppsala College</b>	East Orange, NJ, USA
TAJK	Acad. Sci., Tadjik SSR	<b>Dushanbe</b> , Tadjikistan	UPPS	<b>Uppsala Univ.</b>	<b>Uppsala</b> , Sweden
TAMU	<b>Texas A&amp;M Univ.</b>	College Station, TX, USA	UPR	Univ. of <b>Puerto Rico</b>	<b>San Juan</b> , PR, USA
TATA	<b>Tata Inst. of Fundamental Research</b>	Bombay, India	URI	Univ. of <b>Rhode Island</b>	Kingston, RI, USA
TBIL	<b>Tbilisi State University</b>	Tbilisi, Republic of Georgia	USC	Univ. of <b>Southern California</b>	Los Angeles, CA, USA
TELA	<b>Tel-Aviv Univ.</b>	Tel Aviv, Israel	USF	Univ. of <b>San Francisco</b>	San Francisco, CA, USA
TELE	<b>Teledyne Brown Engineering</b>	Huntsville, AL, USA	UTAH	Univ. of <b>Utah</b>	Salt Lake City, UT, USA
TEMP	<b>Temple Univ.</b>	Philadelphia, PA, USA	UTRE	Univ. of <b>Utrecht</b>	Utrecht, The Netherlands
TENN	Univ. of <b>Tennessee</b>	Knoxville, TN, USA	UTRO	<b>Norwegian Univ. of Science &amp; Technology</b>	Trondheim, Norway
TEXA	Univ. of <b>Texas at Austin</b>	Austin, TX, USA	UVA	Univ. of <b>Virginia</b>	Charlottesville, VA, USA
TGAK	<b>Tokyo Gakugei Univ.</b>	Tokyo, Japan	UZINR	Acad. Sci., <b>Ukrainian SSR</b>	<b>Uzhgorod</b> , Ukraine
TGU	<b>Tohoku Gakuin Univ.</b>	Miyagi, Japan	VALE	Univ. de <b>Valencia</b>	Burjassot, <b>Valencia</b> , Spain
THES	Aristotle Univ. of <b>Thessaloniki (ATh)</b>	Thessaloniki, Greece	VALP	<b>Valparaiso Univ.</b>	Valparaiso, IN, USA
TINT	<b>Tokyo Inst. of Technology</b>	Tokyo, Japan	VAND	<b>Vanderbilt Univ.</b>	Nashville, TN, USA
TISA	<b>Sagamihara Inst. of Space &amp; Astronautical Sci.</b>	Kanagawa, Japan	VASS	<b>Vassar College</b>	Poughkeepsie, NY, USA
TMSK	<b>Tomsk Polytechnic Univ.</b>	<b>Tomsk</b> , Russian Federation	VICT	Univ. of <b>Victoria</b>	Victoria, BC, Canada
TMTC	<b>Tokyo Metropolitan Coll. Tech.</b>	Tokyo, Japan	VIEN	Inst. für Hochenergiephysik (HEPHY)	<b>Vienna</b> , Austria
TMU	<b>Tokyo Metropolitan Univ.</b>	Tokyo, Japan	VILL	<b>ETH Zürich</b>	Zürich, Switzerland
TNTO	Univ. of <b>Toronto</b>	Toronto, ON, Canada	VPI	<b>Virginia Tech.</b>	Blacksburg, VA, USA
TOHO	<b>Toho Univ.</b>	Chiba, Japan	VRIJ	<b>Vrije Univ.</b>	HV <b>Amsterdam</b> , The Netherlands
TOHOK	<b>Tohoku Univ.</b>	Sendai, Japan	WABRNE	Eidgenössisches Amt für Messwesen	<b>Waber</b> , Switzerland
TOKA	<b>Tokai Univ.</b>	Shimizu, Japan	WARS	Univ. of <b>Warsaw</b>	Warsaw, Poland
TOKAH	<b>Tokai Univ.</b>	Hiratsuka, Japan	WASCR	<b>Waseda Univ.</b> ; Cosmic Ray Division	Tokyo, Japan
TOKMS	Univ. of <b>Tokyo</b> ; Meson Science Laboratory	Tokyo, Japan	WASH	Univ. of <b>Washington</b> ; Elem. Particle Experiment (EPE); Particle Astrophysics (PA)	Seattle, WA, USA
TOKU	Univ. of <b>Tokushima</b>	Tokushima-shi, Japan	WASU	<b>Waseda Univ.</b> ; Dept. of Physics, High Energy Physics Group	Tokyo, Japan
TOKY	Univ. of <b>Tokyo</b> ; High-Energy Physics Theory Group	Tokyo, Japan	WAYN	<b>Wayne State Univ.</b>	Detroit, MI, USA
TOKYC	Univ. of <b>Tokyo</b> ; Dept. of Chemistry	Tokyo, Japan	WESL	<b>Wesleyan Univ.</b>	Middletown, CT, USA
TORI	Univ. degli Studi di <b>Torino</b>	Torino, Italy	WIEN	Univ. <b>Wien</b>	Vienna, Austria
TPTI	<b>Uzbek Academy of Sciences</b>	<b>Tashkent</b> , Republic of Uzbekistan	WILL	Coll. of <b>William and Mary</b>	Williamsburg, VA, USA
TRIN	Trinity College <b>Dublin</b>	Dublin, Ireland	WINR	National Centre for Nuclear Research	<b>Warsaw</b> , Poland
TRIU	<b>TRIUMF</b>	Vancouver, BC, Canada	WISC	Univ. of <b>Wisconsin</b>	Madison, WI, USA
TRST	Univ. di <b>Trieste</b>	Trieste, Italy			
TRSTI	<b>INFN, Sez. di Trieste</b>	Trieste, Italy			
TRSTT	Univ. degli Studi di <b>Trieste</b>	Trieste, Italy			
TSUK	Univ. of <b>Tsukuba</b>	Ibaraki-ken, Japan			
TTAM	<b>Tamagawa Univ.</b>	Tokyo, Japan			
TUAT	<b>Tokyo Univ. of Agriculture Tech.</b>	Tokyo, Japan			
TUBIN	Univ. <b>Tübingen</b>	Tübingen, Germany			
TUFTS	<b>Tufts Univ.</b>	Medford, MA, USA			
TUW	<b>Technische Univ. Wien</b>	Vienna, Austria			

## Abbreviations Used in the Particle Listings

WITW	Univ. of the <b>Witwatersrand</b>	Wits, South Africa	YERE	<b>Yerevan</b> Physics Inst.	Yerevan, Armenia
WMIU	<b>Western Michigan</b> Univ.	Kalamazoo, MI, USA	YOKO	<b>Yokohama National</b> Univ.	Yokohama-shi, Japan
WONT	The Univ. of <b>Western Ontario</b>	London, ON, Canada	YORKC	<b>York</b> Univ.	Toronto, Canada
WOOD	<b>Woodstock</b> College (No longer in existence)	Woodstock, MD, USA	ZAGR	<b>Zagreb</b> Univ.	Zagreb, Croatia
WUPP	<b>Bergische</b> Univ. Wuppertal	<b>Wuppertal</b> , Germany	ZARA	Univ. de <b>Zaragoza</b>	Zaragoza, Spain
WURZ	Univ. <b>Würzburg</b>	Würzburg, Germany	ZEEM	Univ. van <b>Amsterdam</b>	TV Amsterdam, The Netherlands
WUSL	<b>Washington</b> Univ.	St. Louis, MO, USA	ZHON	<b>Zhongshan</b> (Sun Yat-Sen) Univ.	Guangzhou, China
WYOM	Univ. of <b>Wyoming</b>	Laramie, WY, USA	ZHZH	<b>Zhengzhou</b> Univ.	Zhengzhou, Henan, China
YALE	<b>Yale</b> Univ.	New Haven, CT, USA	ZURI	Univ. <b>Zürich</b>	Zürich, Switzerland
YARO	<b>Yaroslavl</b> State Univ.	Yaroslavl, Russian Federation			
YCC	<b>Yokohama</b> Coll. of Commerce	Yokohama, Japan			





## GAUGE AND HIGGS BOSONS

$\gamma$ . . . . .	1013
$g$ (gluon) . . . . .	1014
graviton . . . . .	1014
$W$ . . . . .	1014
$Z$ . . . . .	1026
$H^0$ . . . . .	1046
Neutral Higgs Bosons, Searches for . . . . .	1056
Charged Higgs Bosons ( $H^\pm$ and $H^{\pm\pm}$ ), Searches for . . . . .	1065
New Heavy Bosons . . . . .	1068
Axions ( $A^0$ ) and Other Very Light Bosons . . . . .	1084

### Notes in the Listings

Extraction of triple gauge couplings (TGC's) (rev.) . . . . .	1017
Anomalous $ZZ\gamma$ , $Z\gamma\gamma$ , and $ZZV$ couplings . . . . .	1042
Anomalous $W/Z$ quartic couplings (rev.) . . . . .	1043

### Related Reviews in Volume 1

53. Mass and width of the $W$ boson (rev.) . . . . .	715
54. $Z$ boson (rev.) . . . . .	717



**GAUGE AND HIGGS BOSONS**

**γ (photon)**

$$I(J^{PC}) = 0,1(1^{- -})$$

**γ MASS**

Results prior to 2008 are critiqued in GOLDHABER 10. All experimental results published prior to 2005 are summarized in detail by TU 05.

The following conversions are useful:  $1 \text{ eV} = 1.783 \times 10^{-33} \text{ g} = 1.957 \times 10^{-6} m_e$ ;  $\chi_C = (1.973 \times 10^{-7} \text{ m})(1 \text{ eV}/m_\gamma)$ .

VALUE (eV)	CL%	DOCUMENT ID	COMMENT
<b>&lt;1 × 10<sup>-18</sup></b>		1 RYUTOV 07	MHD of solar wind
••• We do not use the following data for averages, fits, limits, etc. •••			
<2.2 × 10 <sup>-14</sup>		2 BONETTI 17	Fast Radio Bursts, FRB 121102
<1.8 × 10 <sup>-14</sup>		3 BONETTI 16	Fast Radio Bursts, FRB 150418
<1.9 × 10 <sup>-15</sup>		4 RETINO 16	Ampere's Law in solar wind
<2.3 × 10 <sup>-9</sup>	95	5 EGOROV 14	Lensed quasar position
		6 ACCIOLY 10	Anomalous magn. mom.
<1 × 10 <sup>-26</sup>		7 ADELBERGER 07A	Proca galactic field
no limit feasible		7 ADELBERGER 07A	γ as Higgs particle
<1 × 10 <sup>-19</sup>		8 TU 06	Torque on rotating magnetized toroid
<1.4 × 10 <sup>-7</sup>		ACCIOLY 04	Dispersion of GHz radio waves by sun
<2 × 10 <sup>-16</sup>		9 FULLEKRUG 04	Speed of 5-50 Hz radiation in atmosphere
<7 × 10 <sup>-19</sup>		10 LUO 03	Torque on rotating magnetized toroid
<1 × 10 <sup>-17</sup>		11 LAKES 98	Torque on toroid balance
<6 × 10 <sup>-17</sup>		12 RYUTOV 97	MHD of solar wind
<8 × 10 <sup>-16</sup>	90	13 FISCHBACH 94	Earth magnetic field
<5 × 10 <sup>-13</sup>		14 CHERNIKOV 92	Ampere's Law null test
<1.5 × 10 <sup>-9</sup>	90	15 RYAN 85	Coulomb's Law null test
<3 × 10 <sup>-27</sup>		16 CHIBISOV 76	Galactic magnetic field
<6 × 10 <sup>-16</sup>	99.7	17 DAVIS 75	Jupiter's magnetic field
<7.3 × 10 <sup>-16</sup>		HOLLWEG 74	Alfvén waves
<6 × 10 <sup>-17</sup>		18 FRANKEN 71	Low freq. res. circuit
<2.4 × 10 <sup>-13</sup>		19 KROLL 71A	Dispersion in atmosphere
<1 × 10 <sup>-14</sup>		20 WILLIAMS 71	Tests Coulomb's Law
<2.3 × 10 <sup>-15</sup>		GOLDHABER 68	Satellite data

- RYUTOV 07 extends the method of RYUTOV 97 to the radius of Pluto's orbit.
- BONETTI 17 uses frequency-dependent time delays of repeating FRB with well-determined redshift, assuming the DM is caused by expected dispersion in IGM. There are several uncertainties, leading to mass limit  $2.2 \times 10^{-14} \text{ eV}$ .
- BONETTI 16 uses frequency-dependent time delays of FRB, assuming the DM is caused by expected dispersion in IGM. There are several uncertainties, leading to mass limit  $1.8 \times 10^{-14} \text{ eV}$ , if indeed the FRB is at the initially reported redshift.
- RETINO 16 looks for deviations from Ampere's law in the solar wind, using Cluster four spacecraft data. Authors quote a range of limits from  $1.9 \times 10^{-15} \text{ eV}$  to  $7.9 \times 10^{-14} \text{ eV}$  depending on the assumptions of the vector potential from the interplanetary magnetic field.
- EGOROV 14 studies chromatic dispersion of lensed quasar positions ("gravitational rainbows") that could be produced by any of several mechanisms, among them via photon mass. Limit not competitive but obtained on cosmological distance scales.
- ACCIOLY 10 limits come from possible alterations of anomalous magnetic moment of electron and gravitational deflection of electromagnetic radiation. Reported limits are not "claimed" by the authors and in any case are not competitive.
- When trying to measure  $m$  one must distinguish between measurements performed on large and small scales. If the photon acquires mass by the Higgs mechanism, the large-scale behavior of the photon might be effectively Maxwellian. If, on the other hand, one postulates the Proca regime for all scales, the very existence of the galactic field implies  $m < 10^{-26} \text{ eV}$ , as correctly calculated by YAMAGUCHI 59 and CHIBISOV 76.
- TU 06 continues the work of LUO 03, with extended LAKES 98 method, reporting the improved limit  $\mu^2 A = (0.7 \pm 1.7) \times 10^{-13} \text{ T/m}$  if  $A = 0.2 \mu\text{G}$  out to  $4 \times 10^{22} \text{ m}$ . Reported result  $\mu = (0.9 \pm 1.5) \times 10^{-52} \text{ g}$  reduces to the frequentist mass limit  $1.2 \times 10^{-19} \text{ eV}$  (FELDMAN 98).
- FULLEKRUG 04 adopted KROLL 71A method with newer and better Schumann resonance data. Result questionable because assumed frequency shift with photon mass is assumed to be linear. It is quadratic according to theorem by GOLDHABER 71B, KROLL 71, and PARK 71.
- LUO 03 extends LAKES 98 technique to set a limit on  $\mu^2 A$ , where  $\mu^{-1}$  is the Compton wavelength  $\chi_C$  of the massive photon and  $A$  is the ambient vector potential. The important departure is that the apparatus rotates, removing sensitivity to the direction of  $A$ . They take  $A = 10^{12} \text{ Tm}$ , due to "cluster level fields." But see comment of GOLDHABER 03 and reply by LUO 03B.
- LAKES 98 reports limits on torque on a toroid Cavendish balance, obtaining a limit on  $\mu^2 A < 2 \times 10^{-9} \text{ Tm}^2/\text{m}^2$  via the Maxwell-Proca equations, where  $\mu^{-1}$  is the characteristic length associated with the photon mass and  $A$  is the ambient vector potential in the Lorentz gauge. Assuming  $A \approx 1 \times 10^{12} \text{ Tm}$  due to cluster fields he obtains  $\mu^{-1} > 2 \times 10^{10} \text{ m}$ , corresponding to  $\mu < 1 \times 10^{-17} \text{ eV}$ . A more conservative limit, using  $A \approx (1 \mu\text{G})(600 \text{ pc})$  based on the galactic field, is  $\mu^{-1} > 1 \times 10^9 \text{ m}$  or  $\mu < 2 \times 10^{-16} \text{ eV}$ .
- RYUTOV 97 uses a magnetohydrodynamics argument concerning survival of the Sun's field to the radius of the Earth's orbit. "To reconcile observations to theory, one has to

- reduce [the photon mass] by approximately an order of magnitude compared with" per DAVIS 75. "Secure limit, best by this method" (per GOLDHABER 10).
- FISCHBACH 94 analysis is based on terrestrial magnetic fields; approach analogous to DAVIS 75. Similar result based on a much smaller planet probably follows from more precise  $B$  field mapping. "Secure limit, best by this method" (per GOLDHABER 10).
  - CHERNIKOV 92, motivated by possibility that photon exhibits mass only below some unknown critical temperature, searches for departure from Ampere's Law at 1.24 K. See also RYAN 85.
  - RYAN 85, motivated by possibility that photon exhibits mass only below some unknown critical temperature, sets mass limit at  $< (1.5 \pm 1.4) \times 10^{-42} \text{ g}$  based on Coulomb's Law departure limit at 1.36 K. We report the result as frequentist 90% CL (FELDMAN 98).
  - CHIBISOV 76 depends in critical way on assumptions such as applicability of virial theorem. Some of the arguments given only in unpublished references.
  - DAVIS 75 analysis of Pioneer-10 data on Jupiter's magnetic field. "Secure limit, best by this method" (per GOLDHABER 10).
  - FRANKEN 71 method is of dubious validity (KROLL 71A, JACKSON 99, GOLDHABER 10, and references therein).
  - KROLL 71A used low frequency Schumann resonances in cavity between the conducting earth and resistive ionosphere, overcoming objections to resonant-cavity methods (JACKSON 99, GOLDHABER 10, and references therein). "Secure limit, best by this method" (per GOLDHABER 10).
  - WILLIAMS 71 is landmark test of Coulomb's law. "Secure limit, best by this method" (per GOLDHABER 10).

**γ CHARGE**

OKUN 06 has argued that schemes in which all photons are charged are inconsistent. He says that if a neutral photon is also admitted to avoid this problem, then other problems emerge, such as those connected with the emission and absorption of charged photons by charged particles. He concludes that in the absence of a self-consistent phenomenological basis, interpretation of experimental data is at best difficult.

VALUE (e)	CHARGE	DOCUMENT ID	TECN	COMMENT
<b>&lt;1 × 10<sup>-46</sup></b>	<b>mixed</b>	1 ALTSCHUL 07B	VLBI	Aharonov-Bohm effect
<b>&lt;1 × 10<sup>-35</sup></b>	<b>single</b>	2 CAPRINI 05	CMB	Isotropy constraint
••• We do not use the following data for averages, fits, limits, etc. •••				
<1 × 10 <sup>-32</sup>	single	1 ALTSCHUL 07B	VLBI	Aharonov-Bohm effect
<3 × 10 <sup>-33</sup>	mixed	3 KOBYCHEV 05	VLBI	Smear as function of B-E <sub>γ</sub>
<4 × 10 <sup>-31</sup>	single	3 KOBYCHEV 05	VLBI	Deflection as function of B-E <sub>γ</sub>
<8.5 × 10 <sup>-17</sup>		4 SEMERTZIDIS 03		Laser light deflection in B-field
<3 × 10 <sup>-28</sup>	single	5 SIVARAM 95	CMB	For $\Omega_M = 0.3, h^2 = 0.5$
<5 × 10 <sup>-30</sup>		6 RAFFELT 94	TOF	Pulsar $t_1 - t_2$
<2 × 10 <sup>-28</sup>		7 COCCONI 92		VLBA radio telescope resolution
<2 × 10 <sup>-32</sup>		COCCONI 88	TOF	Pulsar $t_1 - t_2$ TOF

- ALTSCHUL 07B looks for Aharonov-Bohm phase shift in addition to geometric phase shift in radio interference fringes (VSOP mission).
- CAPRINI 05 uses isotropy of the cosmic microwave background to place stringent limits on possible charge asymmetry of the Universe. Charge limits are set on the photon, neutrino, and dark matter particles. Valid if charge asymmetries produced by different particles are not anticorrelated.
- KOBYCHEV 05 considers a variety of observable effects of photon charge for extragalactic compact radio sources. Best limits if source observed through a foreground cluster of galaxies.
- SEMERTZIDIS 03 reports the first laboratory limit on the photon charge in the last 30 years. Straightforward improvements in the apparatus could attain a sensitivity of  $10^{-20} \text{ e}$ .
- SIVARAM 95 requires that CMB photon charge density not overwhelm gravity. Result scales as  $\Omega_M h^2$ .
- RAFFELT 94 notes that COCCONI 88 neglects the fact that the time delay due to dispersion by free electrons in the interstellar medium has the same photon energy dependence as that due to bending of a charged photon in the magnetic field. His limit is based on the assumption that the entire observed dispersion is due to photon charge. It is a factor of 200 less stringent than the COCCONI 88 limit.
- See COCCONI 92 for less stringent limits in other frequency ranges. Also see RAFFELT 94 note.

**γ REFERENCES**

BONETTI 17	PL B768 326	L. Bonetti et al.	(ORLEANS, CERN)
BONETTI 16	PL B757 548	L. Bonetti et al.	
RETINO 16	ASP 82 49	A. Retino, A.D.A.M. Spallicci, A. Vaivads (CURCP+)	
EGOROV 14	MNRAS 437 L90	P. Egorov et al.	(MOSU, MIPT, INRM)
ACCIOLY 10	PR D82 065026	A. Accioly, J. Helayel-Neto, E. Scatena (LABEX+)	
GOLDHABER 10	RMP 82 939	A.S. Goldhaber, M.M. Nieto (STON, LANL)	
ADELBERGER 07A	PRL 98 010402	E. Adelberger, G. Dvali, A. Gruzinov (WASH, NYU)	
ALTSCHUL 07B	PRL 98 261801	B. Altschul (IND)	
Also	ASP 29 230	B. Altschul (SUC)	
RYUTOV 07	PPCF 49 B429	D.D. Ryutov	(LLNL)
OKUN 06	APP B37 555	L.B. Okun	(ITEP)
TU 06	PL A352 267	L.-C. Tu et al.	
CAPRINI 05	JCAP 0502 006	C. Caprini, P.G. Ferreira (GEVA, OXFTP)	
KOBYCHEV 05	AL 31 147	V.V. Kobychiev, S.B. Popov (KIEV, PADO)	
TU 05	RPP 68 77	L.-C. Tu, J. Luo, G.T. Gillies	
ACCIOLY 04	PR D69 107501	A. Accioly, R. Paszko	
FULLEKRUG 04	PRL 93 043901	M. Fullekrug	
GOLDHABER 03	PRL 91 149101	A.S. Goldhaber, M.M. Nieto	
LUO 03	PRL 90 081801	J. Luo et al.	
LUO 03B	PRL 91 149102	J. Luo et al.	
SEMERTZIDIS 03	PR D67 017701	Y.K. Semertzidis, G.T. Danby, D.M. Lazarus	
JACKSON 99	Classical Electrodynamics (3rd ed., J. Wiley and Sons (1999))	J.D. Jackson	
FELDMAN 98	PR D57 3873	G.J. Feldman, R.D. Cousins	
LAKES 98	PRL 80 1826	R. Lakes	(WISC)
RYUTOV 97	PPCF 39 A73	D.D. Ryutov	(LLNL)

# Gauge & Higgs Boson Particle Listings

## $\gamma, g, \text{graviton}, W$

SIVARAM	95	AJP 63 473	C. Sivaram	(BANG)
FISCHBACH	94	PRL 73 514	E. Fischbach <i>et al.</i>	(PURD, JHU+)
RAFFELT	94	PR D50 7729	G. Raffelt	(MPIM)
CHERNIKOV	92	PRL 68 3383	M.A. Chernikov <i>et al.</i>	(ETH)
Also		PRL 69 2999 (erratum)	M.A. Chernikov <i>et al.</i>	(ETH)
COCCONI	92	AJP 60 750	G. Cocconi	(CERN)
COCCONI	88	PL B206 705	G. Cocconi	(CERN)
RYAN	85	PR D32 802	J.J. Ryan, F. Accetta, R.H. Austin	(PRIN)
CHIBISOV	76	SPU 19 524	G.V. Chibisov	(LEBD)
		Translated from UFN 119 551.		
DAVIS	75	PRL 35 1402	L. Davis, A.S. Goldhaber, M.M. Nieto	(CIT, STON+)
HOLLWEG	74	PRL 32 961	J.V. Hollweg	(NCAR)
FRANKEN	71	PRL 26 115	P.A. Franken, G.W. Ampulski	(MICH)
GOLDHABER	71B	RMP 43 277	A.S. Goldhaber, M.M. Nieto	(STON, BOHR, UCSB)
KROLL	71	PRL 26 1395	N.M. Kroll	(SLAC)
KROLL	71A	PRL 27 340	N.M. Kroll	(SLAC)
PARK	71	PRL 26 1393	D. Park, E.R. Williams	(WISC)
WILLIAMS	71	PRL 26 721	E.R. Williams, J.E. Faller, H.A. Hill	(WESL)
GOLDHABER	68	PRL 21 567	A.S. Goldhaber, M.M. Nieto	(STON)
YAMAGUCHI	59	PTPS 11 37	Y. Yamaguchi	

### $g$ or gluon

$$I(J^P) = 0(1^-)$$

SU(3) color octet

Mass  $m = 0$ . Theoretical value. A mass as large as a few MeV may not be precluded, see YNDURAIN 95.

VALUE	DOCUMENT ID	TECN	COMMENT
••• We do not use the following data for averages, fits, limits, etc. •••			
	ABREU 92E	DLPH	Spin 1, not 0
	ALEXANDER 91H	OPAL	Spin 1, not 0
	BEHREND 82D	CELL	Spin 1, not 0
	BERGER 80D	PLUT	Spin 1, not 0
	BRANDELIK 80C	TASS	Spin 1, not 0

### gluon REFERENCES

YNDURAIN 95	PL B345 524	F.J. Yndurain	(MADU)
ABREU 92E	PL B274 490	P. Abreu <i>et al.</i>	(DELPHI Collab.)
ALEXANDER 91H	ZPHY C52 543	G. Alexander <i>et al.</i>	(OPAL Collab.)
BEHREND 82D	PL B110 329	H.J. Behrend <i>et al.</i>	(CELLO Collab.)
BERGER 80D	PL B97 459	C. Berger <i>et al.</i>	(PLUTO Collab.)
BRANDELIK 80C	PL B97 453	R. Brandelik <i>et al.</i>	(TASSO Collab.)

### graviton

$$J = 2$$

### graviton MASS

Van Dam and Veltman (VANDAM 70), Iwasaki (IWASAKI 70), and Zakharov (ZAKHAROV 70) almost simultaneously showed that "... there is a discrete difference between the theory with zero-mass and a theory with finite mass, no matter how small as compared to all external momenta." The resolution of this "vDVZ discontinuity" has to do with whether the linear approximation is valid. De Rham *et al.* (DE-RHAM 11) have shown that nonlinear effects not captured in their linear treatment can give rise to a screening mechanism, allowing for massive gravity theories. See also GOLDHABER 10 and DE-RHAM 17 and references therein. Experimental limits have been set based on a Yukawa potential or signal dispersion.  $h_0$  is the Hubble constant in units of  $100 \text{ km s}^{-1} \text{ Mpc}^{-1}$ .

The following conversions are useful:  $1 \text{ eV} = 1.783 \times 10^{-33} g = 1.957 \times 10^{-6} m_e$ ;  $\chi_C = (1.973 \times 10^{-7} \text{ m}) \times (1 \text{ eV}/m_e)$ .

VALUE (eV)	DOCUMENT ID	TECN	COMMENT
$< 6 \times 10^{-32}$	1 CHOUDHURY 04	YUKA	Weak gravitational lensing
••• We do not use the following data for averages, fits, limits, etc. •••			
$< 6.8 \times 10^{-23}$	BERNUS 19	YUKA	Planetary ephemeris INPOP17b
$< 1.4 \times 10^{-29}$	2 DESAI 18	YUKA	Gal cluster Abell 1689
$< 5 \times 10^{-30}$	3 GUPTA 18	YUKA	SPT-SZ
$< 3 \times 10^{-30}$	3 GUPTA 18	YUKA	Planck all-sky SZ
$< 1.3 \times 10^{-29}$	3 GUPTA 18	YUKA	redMaPPer SDSS-DR8
$< 6 \times 10^{-30}$	4 RANA 18	YUKA	Weak lensing in massive clusters
$< 8 \times 10^{-30}$	5 RANA 18	YUKA	SZ effect in massive clusters
$< 7 \times 10^{-23}$	6 ABBOTT 17	DISP	Combined dispersion limit from three BH mergers
$< 1.2 \times 10^{-22}$	6 ABBOTT 16	DISP	Combined dispersion limit from two BH mergers
$< 2.9 \times 10^{-21}$	7 ZAKHAROV 16	YUKA	S2 star orbit
$< 5 \times 10^{-23}$	8 BRITO 13		Spinning black holes bounds
$< 4 \times 10^{-25}$	9 BASKARAN 08		Graviton phase velocity fluctuations
$< 6 \times 10^{-32}$	10 GRUZINOV 05	YUKA	Solar System observations
$< 9.0 \times 10^{-34}$	11 GERSHTEIN 04		From $\Omega_{tot}$ value assuming RTG
$> 6 \times 10^{-34}$	12 DVALI 03		Horizon scales
$< 8 \times 10^{-20}$	13,14 FINN 02	DISP	Binary pulsar orbital period decrease
	14,15 DAMOUR 91		Binary pulsar PSR 1913+16
$< 7 \times 10^{-23}$	TALMADGE 88	YUKA	Solar system planetary astrometric data
$< 2 \times 10^{-29} h_0^{-1}$	GOLDHABER 74		Rich clusters
$< 7 \times 10^{-28}$	HARE 73		Galaxy
$< 8 \times 10^4$	HARE 73		$2\gamma$ decay

- CHOUDHURY 04 concludes from a study of weak-lensing data that masses heavier than about the inverse of 100 Mpc seem to be ruled out if the gravitation field has the Yukawa form.
- DESAI 18 limit based on dynamical mass models of galaxy cluster Abell 1689.
- GUPTA 18 obtains graviton mass limits using stacked clusters from 3 disparate surveys.
- RANA 18 limit, 68% CL, obtained using weak lensing mass profiles out to the radius at which the cluster density falls to 200 times the critical density of the Universe. Limit is based on the fractional change between Newtonian and Yukawa accelerations for the 50 most massive galaxy clusters in the Local Cluster Substructure Survey. Limits for other CL's and other density cuts are also given.
- RANA 18 limit, 68% CL, obtained using mass measurements via the SZ effect out to the radius at which the cluster density falls to 500 times the critical density of the Universe for 182 optically confirmed galaxy clusters in an Altacama Cosmology Telescope survey. Limits for other CL's and other density cuts are also given.
- ABBOTT 16 and ABBOTT 17 assumed a dispersion relation for gravitational waves modified relative to GR.
- ZAKHAROV 16 constrains range of Yukawa gravity interaction from S2 star orbit about black hole at Galactic center. The limit is  $< 2.9 \times 10^{-21} \text{ eV}$  for  $\delta = 100$ .
- BRITO 13 explore massive graviton (spin-2) fluctuations around rotating black holes.
- BASKARAN 08 consider fluctuations in pulsar timing due to photon interactions ("surfing") with background gravitational waves.
- GRUZINOV 05 uses the DGP model (DVALI 00) showing that non-perturbative effects restore continuity with Einstein's equations as the graviton mass approaches 0, then bases his limit on Solar System observations.
- GERSHTEIN 04 use non-Einstein field relativistic theory of gravity (RTG), with a massive graviton, to obtain the 95% CL mass limit implied by the value of  $\Omega_{tot} = 1.02 \pm 0.02$  current at the time of publication.
- DVALI 03 suggest scale of horizon distance via DGP model (DVALI 00). For a horizon distance of  $3 \times 10^{26} \text{ m}$  (about age of Universe/ $c$ ; GOLDHABER 10) this graviton mass limit is implied.
- FINN 02 analyze the orbital decay rates of PSR B1913+16 and PSR B1534+12 with a possible graviton mass as a parameter. The combined frequentist mass limit is at 90% CL.
- As of 2014, limits on  $dP/dt$  are now about 0.1% (see T. Damour, "Experimental tests of gravitational theory," in this Review).
- DAMOUR 91 is an analysis of the orbital period change in binary pulsar PSR 1913+16, and confirms the general relativity prediction to 0.8%. "The theoretical importance of the [rate of orbital period decay] measurement has long been recognized as a direct confirmation that the gravitational interaction propagates with velocity  $c$  (which is the immediate cause of the appearance of a damping force in the binary pulsar system) and thereby as a test of the existence of gravitational radiation and of its quadrupolar nature." TAYLOR 93 adds that orbital parameter studies now agree with general relativity to 0.5%, and set limits on the level of scalar contribution in the context of a family of tensor [spin 2]-biscalar theories.

### graviton REFERENCES

BERNUS 19	PRL 123 161103	L. Bernus <i>et al.</i>	
DESAI 18	PL B778 325	S. Desai	(HYDER)
GUPTA 18	ANP 399 85	S. Gupta, S. Desai	
RANA 18	PL B781 220	A. Rana <i>et al.</i>	(DELHI)
ABBOTT 17	PRL 118 221101	B.P. Abbott <i>et al.</i>	(LIGO and Virgo Collabs.)
DE-RHAM 17	RMP 89 025004	C. de Rham <i>et al.</i>	
ABBOTT 16	PRL 116 061102	B.P. Abbott <i>et al.</i>	(LIGO and Virgo Collabs.)
ZAKHAROV 16	JCAP 1605 045	A.F. Zakharov <i>et al.</i>	
BRITO 13	PR D88 023514	R. Brito, V. Cardoso, P. Pani	(LISB, MISS, HSCA+)
DE-RHAM 11	PRL 106 231101	C. de Rham, G. Gabadadze, A.J. Tolley	
GOLDHABER 10	RMP 82 939	A.S. Goldhaber, M.M. Nieto	(STON, LANL)
BASKARAN 08	PR D78 044018	D. Baskaran <i>et al.</i>	
GRUZINOV 05	NAST 10 311	A. Gruzinov	(NYU)
CHOUDHURY 04	ASP 21 559	S.R. Choudhury <i>et al.</i>	(DELPHI, MELB)
GERSHTEIN 04	PAN 67 1596	S.S. Gershtein <i>et al.</i>	(SERP)
DVALI 03	Translated from YAF 67 1618.	G.R. Dvali, A. Gruzinov, M. Zaldarriaga	(NYU)
FINN 02	PR D65 044022	L.S. Finn, P.J. Sutton	
DVALI 00	PL B485 208	G.R. Dvali, G. Gabadadze, M. Porrati	(NYU)
TAYLOR 93	NAT 355 132	J.N. Taylor <i>et al.</i>	(PRIN, ARCO, BURE+)
DAMOUR 91	APJ 366 501	T. Damour, J.H. Taylor	(BURE, MEUD, PRIN)
TALMADGE 88	PRL 61 1159	C. Talmadge <i>et al.</i>	(JPL)
GOLDHABER 74	PR D9 1119	A.S. Goldhaber, M.M. Nieto	(LANL, STON)
HARE 73	CJP 51 431	M.G. Hare	(SASK)
IWASAKI 70	PR D2 2255	Y. Iwasaki	
VANDAM 70	NP B22 397	H. van Dam, M. Veltman	(UTRE)
ZAKHAROV 70	JETPL 12 312	V.I. Zakharov <i>et al.</i>	

### $W$

$$J = 1$$

See the related review(s):  
Mass and Width of the  $W$  Boson

### $W$ MASS

The  $W$ -mass listed here corresponds to the mass parameter in a Breit-Wigner distribution with mass-dependent width. To obtain the world average, common systematic uncertainties between experiments are properly taken into account. The LEP-2 average  $W$  mass based on published results is  $80.376 \pm 0.033 \text{ GeV}$  [SCHAEL 13a]. The combined Tevatron data yields an average  $W$  mass of  $80.387 \pm 0.016 \text{ GeV}$  [AALTONEN 13n]. A combination of the LEP average with this Tevatron average and the ATLAS value [AABOUD 18j], assuming a common systematic error of 7 MeV between the latter two [Jens Erler, 52nd Rencontres de Moriond

EW, March 2017], the world average  $W$  mass of  $80.379 \pm 0.012$  GeV is obtained. OUR FIT quotes this value for the  $W$  mass.

VALUE (GeV)	EVTS	DOCUMENT ID	TECN	COMMENT
<b>80.379 ± 0.012 OUR FIT</b>				
80.370 ± 0.007 ± 0.017	13.7M	<sup>1</sup> AABOUD	18J ATLS	$E_{cm}^{pp} = 7$ TeV
80.375 ± 0.023	2177k	<sup>2</sup> ABAZOV	14N D0	$E_{cm}^{pp} = 1.96$ TeV
80.387 ± 0.019	1095k	<sup>3</sup> AALTONEN	12E CDF	$E_{cm}^{pp} = 1.96$ TeV
80.336 ± 0.055 ± 0.039	10.3k	<sup>4</sup> ABDALLAH	08A DLPH	$E_{cm}^{ee} = 161-209$ GeV
80.415 ± 0.042 ± 0.031	11830	<sup>5</sup> ABBIENDI	06 OPAL	$E_{cm}^{ee} = 170-209$ GeV
80.270 ± 0.046 ± 0.031	9909	<sup>6</sup> ACHARD	06 L3	$E_{cm}^{ee} = 161-209$ GeV
80.440 ± 0.043 ± 0.027	8692	<sup>7</sup> SCHAEEL	06 ALEP	$E_{cm}^{ee} = 161-209$ GeV
80.483 ± 0.084	49247	<sup>8</sup> ABAZOV	02D D0	$E_{cm}^{pp} = 1.8$ TeV
80.433 ± 0.079	53841	<sup>9</sup> AFFOLDER	01E CDF	$E_{cm}^{pp} = 1.8$ TeV
• • • We do not use the following data for averages, fits, limits, etc. • • •				
80.520 ± 0.115		<sup>10</sup> ANDREEV	18A H1	$e^\pm p$
80.367 ± 0.026	1677k	<sup>11</sup> ABAZOV	12F D0	$E_{cm}^{pp} = 1.96$ TeV
80.401 ± 0.043	500k	<sup>12</sup> ABAZOV	09AB D0	$E_{cm}^{pp} = 1.96$ TeV
80.413 ± 0.034 ± 0.034	115k	<sup>13</sup> AALTONEN	07F CDF	$E_{cm}^{pp} = 1.96$ TeV
82.87 ± 1.82 ± $\begin{smallmatrix} +0.30 \\ -0.16 \end{smallmatrix}$	1500	<sup>14</sup> AKTAS	06 H1	$e^\pm p \rightarrow \mathcal{T}_e(\nu_e)X$ , $\sqrt{s} \approx 300$ GeV
80.3 ± 2.1 ± 1.2 ± 1.0	645	<sup>15</sup> CHEKANOV	02C ZEUS	$e^- p \rightarrow \nu_e X$ , $\sqrt{s} = 318$ GeV
81.4 + $\begin{smallmatrix} +2.7 \\ -2.6 \end{smallmatrix}$ ± 2.0 + $\begin{smallmatrix} +3.3 \\ -3.0 \end{smallmatrix}$	1086	<sup>16</sup> BREITWEG	00D ZEUS	$e^+ p \rightarrow \mathcal{T}_e X$ , $\sqrt{s} \approx 300$ GeV
80.84 ± 0.22 ± 0.83	2065	<sup>17</sup> ALITTI	92B UA2	See $W/Z$ ratio below
80.79 ± 0.31 ± 0.84		<sup>18</sup> ALITTI	90B UA2	$E_{cm}^{pp} = 546,630$ GeV
80.0 ± 3.3 ± 2.4	22	<sup>19</sup> ABE	89I CDF	$E_{cm}^{pp} = 1.8$ TeV
82.7 ± 1.0 ± 2.7	149	<sup>20</sup> ALBAJAR	89 UA1	$E_{cm}^{pp} = 546,630$ GeV
81.8 ± $\begin{smallmatrix} +6.0 \\ -5.3 \end{smallmatrix}$ ± 2.6	46	<sup>21</sup> ALBAJAR	89 UA1	$E_{cm}^{pp} = 546,630$ GeV
89 ± 3 ± 6	32	<sup>22</sup> ALBAJAR	89 UA1	$E_{cm}^{pp} = 546,630$ GeV
81. ± 5.	6	ARNISON	83 UA1	$E_{cm}^{ee} = 546$ GeV
80. ± $\begin{smallmatrix} +10. \\ -6. \end{smallmatrix}$	4	BANNER	83B UA2	Repl. by ALITTI 90B

- AABOUD 18J select  $4.61M W^+ \rightarrow \mu^+ \nu_\mu$ ,  $3.40M W^+ \rightarrow e^+ \nu_e$ ,  $3.23M W^- \rightarrow \mu^- \bar{\nu}_\mu$  and  $2.49M W^- \rightarrow e^- \bar{\nu}_e$  events in  $4.6 \text{ fb}^{-1} pp$  data at 7 TeV. The  $W$  mass is determined using the transverse mass and transverse lepton momentum distributions, accounting for correlations. The systematic error includes 0.011 GeV experimental and 0.014 GeV modelling uncertainties.
- ABAZOV 14N is a combination of ABABOV 09AB and ABABOV 12F, also giving more details on the analysis.
- AALTONEN 12E select  $470k W \rightarrow e \nu$  decays and  $625k W \rightarrow \mu \nu$  decays in  $2.2 \text{ fb}^{-1}$  of Run-II data. The mass is determined using the transverse mass, transverse lepton momentum and transverse missing energy distributions, accounting for correlations. This result supersedes AALTONEN 07F. AALTONEN 14D gives more details on the procedures followed by the authors.
- ABDALLAH 08A use direct reconstruction of the kinematics of  $W^+ W^- \rightarrow q \bar{q} \ell \nu$  and  $W^+ W^- \rightarrow q \bar{q} q \bar{q}$  events for energies 172 GeV and above. The  $W$  mass was also extracted from the dependence of the  $WW$  cross section close to the production threshold and combined appropriately to obtain the final result. The systematic error includes  $\pm 0.025$  GeV due to final state interactions and  $\pm 0.009$  GeV due to LEP energy uncertainty.
- ABBIENDI 06 use direct reconstruction of the kinematics of  $W^+ W^- \rightarrow q \bar{q} \ell \nu \ell$  and  $W^+ W^- \rightarrow q \bar{q} q \bar{q}$  events. The result quoted here is obtained combining this mass value with the results using  $W^+ W^- \rightarrow \ell \nu \ell \ell \nu \ell$  events in the energy range 183–207 GeV (ABBIENDI 03C) and the dependence of the  $WW$  production cross-section on  $m_{WW}$  at threshold. The systematic error includes  $\pm 0.009$  GeV due to the uncertainty on the LEP beam energy.
- ACHARD 06 use direct reconstruction of the kinematics of  $W^+ W^- \rightarrow q \bar{q} \ell \nu \ell$  and  $W^+ W^- \rightarrow q \bar{q} q \bar{q}$  events in the C.M. energy range 189–209 GeV. The result quoted here is obtained combining this mass value with the results obtained from a direct  $W$  mass reconstruction at 172 and 183 GeV and with those from the dependence of the  $WW$  production cross-section on  $m_{WW}$  at 161 and 172 GeV (ACCIARRI 99).
- SCHAEEL 06 use direct reconstruction of the kinematics of  $W^+ W^- \rightarrow q \bar{q} \ell \nu \ell$  and  $W^+ W^- \rightarrow q \bar{q} q \bar{q}$  events in the C.M. energy range 183–209 GeV. The result quoted here is obtained combining this mass value with those obtained from the dependence of the  $W$  pair production cross-section on  $m_{WW}$  at 161 and 172 GeV (BARATE 97 and BARATE 97s respectively). The systematic error includes  $\pm 0.009$  GeV due to possible effects of final state interactions in the  $q \bar{q} q \bar{q}$  channel and  $\pm 0.009$  GeV due to the uncertainty on the LEP beam energy.
- ABAZOV 02D improve the measurement of the  $W$ -boson mass including  $W \rightarrow e \nu_e$  events in which the electron is close to a boundary of a central electromagnetic calorimeter module. Properly combining the results obtained by fitting  $m_T(W)$ ,  $p_T(e)$ , and  $p_T(\nu)$ , this sample provides a mass value of  $80.574 \pm 0.045$  GeV. The value reported here is a combination of this measurement with all previous DØ  $W$ -boson mass measurements.
- AFFOLDER 01E fit the transverse mass spectrum of 30115  $W \rightarrow e \nu_e$  events ( $M_{WW} = 80.473 \pm 0.065 \pm 0.092$  GeV) and of 14740  $W \rightarrow \mu \nu_\mu$  events ( $M_{WW} = 80.465 \pm 0.100 \pm 0.103$  GeV) obtained in the run IB (1994–95). Combining the electron and muon results, accounting for correlated uncertainties, yields  $M_{WW} = 80.470 \pm 0.089$  GeV. They combine this value with their measurement of ABE 95P reported in run IA (1992–93) to obtain the quoted value.
- ANDREEV 18A obtain this result in a combined electroweak and QCD analysis using all deep-inelastic  $e^+ p$  and  $e^- p$  neutral current and charged current scattering cross sections published by the H1 Collaboration, including data with longitudinally polarized lepton beams.

- ABAZOV 12F select  $1677k W \rightarrow e \nu$  decays in  $4.3 \text{ fb}^{-1}$  of Run-II data. The mass is determined using the transverse mass and transverse lepton momentum distributions, accounting for correlations.
- ABAZOV 09AB study the transverse mass, transverse electron momentum, and transverse missing energy in a sample of 0.5 million  $W \rightarrow e \nu$  decays selected in Run-II data. The quoted result combines all three methods, accounting for correlations.
- AALTONEN 07F obtain high purity  $W \rightarrow e \nu_e$  and  $W \rightarrow \mu \nu_\mu$  candidate samples totaling 63,964 and 51,128 events respectively. The  $W$  mass value quoted above is derived by simultaneously fitting the transverse mass and the lepton, and neutrino  $p_T$  distributions.
- AKTAS 06 fit the  $Q^2$  dependence ( $300 < Q^2 < 30,000 \text{ GeV}^2$ ) of the charged-current differential cross section with a propagator mass. The first error is experimental and the second corresponds to uncertainties due to input parameters and model assumptions.
- CHEKANOV 02c fit the  $Q^2$  dependence ( $200 < Q^2 < 60000 \text{ GeV}^2$ ) of the charged-current differential cross sections with a propagator mass fit. The last error is due to the uncertainty on the probability density functions.
- BREITWEG 00D fit the  $Q^2$  dependence ( $200 < Q^2 < 22500 \text{ GeV}^2$ ) of the charged-current differential cross sections with a propagator mass fit. The last error is due to the uncertainty on the probability density functions.
- ALITTI 92B result has two contributions to the systematic error ( $\pm 0.83$ ); one ( $\pm 0.81$ ) cancels in  $m_{W/m_Z}$  and one ( $\pm 0.17$ ) is noncancelling. These were added in quadrature. We choose the ALITTI 92B value without using the LEP  $m_Z$  value, because we perform our own combined fit.
- There are two contributions to the systematic error ( $\pm 0.84$ ): one ( $\pm 0.81$ ) which cancels in  $m_{W/m_Z}$  and one ( $\pm 0.21$ ) which is non-cancelling. These were added in quadrature.
- ABE 89I systematic error dominated by the uncertainty in the absolute energy scale.
- ALBAJAR 89 result is from a total sample of 299  $W \rightarrow e \nu$  events.
- ALBAJAR 89 result is from a total sample of 67  $W \rightarrow \mu \nu$  events.
- ALBAJAR 89 result is from  $W \rightarrow \tau \nu$  events.

W/Z MASS RATIO

VALUE	EVTS	DOCUMENT ID	TECN	COMMENT
<b>0.88147 ± 0.00013</b>		<sup>1</sup> PDG	19	
• • • We do not use the following data for averages, fits, limits, etc. • • •				
0.8821 ± 0.0011 ± 0.0008	28323	<sup>2</sup> ABBOTT	98N D0	$E_{cm}^{pp} = 1.8$ TeV
0.88114 ± 0.00154 ± 0.00252	5982	<sup>3</sup> ABBOTT	98P D0	$E_{cm}^{pp} = 1.8$ TeV
0.8813 ± 0.0036 ± 0.0019	156	<sup>4</sup> ALITTI	92B UA2	$E_{cm}^{pp} = 630$ GeV

- This value was obtained using the world average values of  $m_Z$  and  $m_W$  as listed in these listings.
- ABBOTT 98N obtain this from a study of 28323  $W \rightarrow e \nu_e$  and 3294  $Z \rightarrow e^+ e^-$  decays. Of this latter sample, 2179 events are used to calibrate the electron energy scale.
- ABBOTT 98P obtain this from a study of 5982  $W \rightarrow e \nu_e$  events. The systematic error includes an uncertainty of  $\pm 0.00175$  due to the electron energy scale.
- Scale error cancels in this ratio.

$m_Z - m_W$

VALUE (GeV)	DOCUMENT ID	TECN	COMMENT
<b>10.809 ± 0.012</b>	<sup>1</sup> PDG	19	
• • • We do not use the following data for averages, fits, limits, etc. • • •			
10.4 ± 1.4 ± 0.8	ALBAJAR	89 UA1	$E_{cm}^{pp} = 546,630$ GeV
11.3 ± 1.3 ± 0.9	ANSARI	87 UA2	$E_{cm}^{pp} = 546,630$ GeV

- This value was obtained using the world average values of  $m_Z$  and  $m_W$  as listed in these listings.

$m_{W^+} - m_{W^-}$

Test of CPT invariance.

VALUE (GeV)	EVTS	DOCUMENT ID	TECN	COMMENT
<b>-0.029 ± 0.028 OUR AVERAGE</b>				
-0.029 ± 0.013 ± 0.025	13.7M	<sup>1</sup> AABOUD	18J ATLS	$E_{cm}^{pp} = 7$ TeV
-0.19 ± 0.58	1722	ABE	90G CDF	$E_{cm}^{pp} = 1.8$ TeV

- AABOUD 18J select  $4.61M W^+ \rightarrow \mu^+ \nu_\mu$ ,  $3.40M W^+ \rightarrow e^+ \nu_e$ ,  $3.23M W^- \rightarrow \mu^- \bar{\nu}_\mu$  and  $2.49M W^- \rightarrow e^- \bar{\nu}_e$  events in  $4.6 \text{ fb}^{-1} pp$  data at 7 TeV. The  $W$  mass is determined using the transverse mass and transverse lepton momentum distributions, accounting for correlations. The systematic error includes 0.007 GeV experimental and 0.024 GeV modelling uncertainties.

W WIDTH

The  $W$  width listed here corresponds to the width parameter in a Breit-Wigner distribution with mass-dependent width. To obtain the world average, common systematic uncertainties between experiments are properly taken into account. The LEP-2 average  $W$  width based on published results is  $2.195 \pm 0.083$  GeV [SCHAEEL 13A]. The combined Tevatron data yields an average  $W$  width of  $2.046 \pm 0.049$  GeV [FERMILAB-TM-2460-E].

OUR FIT uses these average LEP and Tevatron width values and combines them assuming no correlations.

VALUE (GeV)	EVTS	DOCUMENT ID	TECN	COMMENT
<b>2.085 ± 0.042 OUR FIT</b>				
2.028 ± 0.072	5272	<sup>1</sup> ABABOV	09AK D0	$E_{cm}^{pp} = 1.96$ GeV
2.032 ± 0.045 ± 0.057	6055	<sup>2</sup> AALTONEN	08B CDF	$E_{cm}^{pp} = 1.96$ TeV
2.404 ± 0.140 ± 0.101	10.3k	<sup>3</sup> ABDALLAH	08A DLPH	$E_{cm}^{ee} = 183-209$ GeV
1.996 ± 0.096 ± 0.102	10729	<sup>4</sup> ABBIENDI	06 OPAL	$E_{cm}^{ee} = 170-209$ GeV

# Gauge & Higgs Boson Particle Listings

## W

2.18 ± 0.11 ± 0.09	9795	<sup>5</sup> ACHARD	06 L3	$E_{cm}^{ee} = 172\text{--}209$ GeV
2.14 ± 0.09 ± 0.06	8717	<sup>6</sup> SCHAEEL	06 ALEP	$E_{cm}^{ee} = 183\text{--}209$ GeV
2.23 $^{+0.15}_{-0.14}$ ± 0.10	294	<sup>7</sup> ABAZOV	02E D0	$E_{cm}^{pp} = 1.8$ TeV
2.05 ± 0.10 ± 0.08	662	<sup>8</sup> AFFOLDER	00M CDF	$E_{cm}^{pp} = 1.8$ TeV
• • • We do not use the following data for averages, fits, limits, etc. • • •				
2.152 ± 0.066	79176	<sup>9</sup> ABBOTT	00B D0	Extracted value
2.064 ± 0.060 ± 0.059		<sup>10</sup> ABE	95W CDF	Extracted value
2.10 $^{+0.14}_{-0.13}$ ± 0.09	3559	<sup>11</sup> ALITTI	92 UA2	Extracted value
2.18 $^{+0.26}_{-0.24}$ ± 0.04		<sup>12</sup> ALBAJAR	91 UA1	Extracted value

- ABAZOV 09AK obtain this result fitting the high-end tail (100–200 GeV) of the transverse mass spectrum in  $W \rightarrow e\nu$  decays.
- AALTONEN 08B obtain this result fitting the high-end tail (90–200 GeV) of the transverse mass spectrum in semileptonic  $W \rightarrow e\nu_e$  and  $W \rightarrow \mu\nu_\mu$  decays.
- ABDALLAH 08A use direct reconstruction of the kinematics of  $W^+ W^- \rightarrow q\bar{q}\ell\nu$  and  $W^+ W^- \rightarrow q\bar{q}q\bar{q}$  events. The systematic error includes ±0.065 GeV due to final state interactions.
- ABBIENDI 06 use direct reconstruction of the kinematics of  $W^+ W^- \rightarrow q\bar{q}\ell\nu_\ell$  and  $W^+ W^- \rightarrow q\bar{q}q\bar{q}$  events. The systematic error includes ±0.003 GeV due to the uncertainty on the LEP beam energy.
- ACHARD 06 use direct reconstruction of the kinematics of  $W^+ W^- \rightarrow q\bar{q}\ell\nu_\ell$  and  $W^+ W^- \rightarrow q\bar{q}q\bar{q}$  events in the C.M. energy range 189–209 GeV. The result quoted here is obtained combining this value of the width with the result obtained from a direct  $W$  mass reconstruction at 172 and 183 GeV (ACCIARRI 99).
- SCHAEEL 06 use direct reconstruction of the kinematics of  $W^+ W^- \rightarrow q\bar{q}\ell\nu_\ell$  and  $W^+ W^- \rightarrow q\bar{q}q\bar{q}$  events. The systematic error includes ±0.05 GeV due to possible effects of final state interactions in the  $q\bar{q}q\bar{q}$  channel and ±0.01 GeV due to the uncertainty on the LEP beam energy.
- ABAZOV 02E obtain this result fitting the high-end tail (90–200 GeV) of the transverse-mass spectrum in semileptonic  $W \rightarrow e\nu_e$  decays.
- AFFOLDER 00M fit the high transverse mass (100–200 GeV)  $W \rightarrow e\nu_e$  and  $W \rightarrow \mu\nu_\mu$  events to obtain  $\Gamma(W) = 2.04 \pm 0.11$  (stat) ± 0.09 (syst) GeV. This is combined with the earlier CDF measurement (ABE 95C) to obtain the quoted result.
- ABBOTT 00B measure  $R = 10.43 \pm 0.27$  for the  $W \rightarrow e\nu_e$  decay channel. They use the SM theoretical predictions for  $\sigma(W)/\sigma(Z)$  and  $\Gamma(W \rightarrow e\nu_e)$  and the world average for  $B(Z \rightarrow e e)$ . The value quoted here is obtained combining this result (2.169 ± 0.070 GeV) with that of ABBOTT 99H.
- ABE 95W measured  $R = 10.90 \pm 0.32 \pm 0.29$ . They use  $m_W = 80.23 \pm 0.18$  GeV,  $\sigma(W)/\sigma(Z) = 3.35 \pm 0.03$ ,  $\Gamma(W \rightarrow e\nu) = 225.9 \pm 0.9$  MeV,  $\Gamma(Z \rightarrow e^+ e^-) = 83.98 \pm 0.18$  MeV, and  $\Gamma(Z) = 2.4969 \pm 0.0038$  GeV.
- ALITTI 92 measured  $R = 10.4^{+0.7}_{-0.6} \pm 0.3$ . The values of  $\sigma(Z)$  and  $\sigma(W)$  come from  $O(\alpha_s^2)$  calculations using  $m_W = 80.14 \pm 0.27$  GeV, and  $m_Z = 91.175 \pm 0.021$  GeV along with the corresponding value of  $\sin^2\theta_W = 0.2274$ . They use  $\sigma(W)/\sigma(Z) = 3.26 \pm 0.07 \pm 0.05$  and  $\Gamma(Z) = 2.487 \pm 0.010$  GeV.
- ALBAJAR 91 measured  $R = 9.5^{+1.1}_{-1.0}$  (stat. + syst.).  $\sigma(W)/\sigma(Z)$  is calculated in QCD at the parton level using  $m_W = 80.18 \pm 0.28$  GeV and  $m_Z = 91.172 \pm 0.031$  GeV along with  $\sin^2\theta_W = 0.2322 \pm 0.0014$ . They use  $\sigma(W)/\sigma(Z) = 3.23 \pm 0.05$  and  $\Gamma(Z) = 2.498 \pm 0.020$  GeV. This measurement is obtained combining both the electron and muon channels.

### W+ DECAY MODES

$W^-$  modes are charge conjugates of the modes below.

Mode	Fraction ( $\Gamma_i/\Gamma$ )	Confidence level
$\Gamma_1$ $\ell^+ \nu$	[a] (10.86 ± 0.09) %	
$\Gamma_2$ $e^+ \nu$	(10.71 ± 0.16) %	
$\Gamma_3$ $\mu^+ \nu$	(10.63 ± 0.15) %	
$\Gamma_4$ $\tau^+ \nu$	(11.38 ± 0.21) %	
$\Gamma_5$ hadrons	(67.41 ± 0.27) %	
$\Gamma_6$ $\pi^+ \gamma$	< 7 × 10 <sup>-6</sup>	95%
$\Gamma_7$ $D_s^+ \gamma$	< 1.3 × 10 <sup>-3</sup>	95%
$\Gamma_8$ $cX$	(33.3 ± 2.6) %	
$\Gamma_9$ $c\bar{s}$	(31 $^{+13}_{-11}$ ) %	
$\Gamma_{10}$ invisible	[b] ( 1.4 ± 2.9 ) %	
$\Gamma_{11}$ $\pi^+ \pi^+ \pi^-$	< 1.01 × 10 <sup>-6</sup>	95%

[a]  $\ell$  indicates each type of lepton ( $e$ ,  $\mu$ , and  $\tau$ ), not sum over them.

[b] This represents the width for the decay of the  $W$  boson into a charged particle with momentum below detectability,  $p < 200$  MeV.

### W PARTIAL WIDTHS

$\Gamma$ (invisible)	$\Gamma_{10}$		
This represents the width for the decay of the $W$ boson into a charged particle with momentum below detectability, $p < 200$ MeV.			
VALUE (MeV)	DOCUMENT ID	TECN	COMMENT
<b>30<sup>+52</sup><sub>-48</sub> ± 33</b>	<sup>1</sup> BARATE	99I ALEP	$E_{cm}^{ee} = 161+172+183$ GeV
• • • We do not use the following data for averages, fits, limits, etc. • • •			
	<sup>2</sup> BARATE	99L ALEP	$E_{cm}^{ee} = 161+172+183$ GeV

- BARATE 99I measure this quantity using the dependence of the total cross section  $\sigma_W W$  upon a change in the total width. The fit is performed to the  $W W$  measured cross sections at 161, 172, and 183 GeV. This partial width is < 139 MeV at 95%CL.
- BARATE 99L use  $W$ -pair production to search for effectively invisible  $W$  decays, tagging with the decay of the other  $W$  boson to Standard Model particles. The partial width for effectively invisible decay is < 27 MeV at 95%CL.

### W BRANCHING RATIOS

Overall fits are performed to determine the branching ratios of the  $W$  boson. Averages on  $W \rightarrow e\nu$ ,  $W \rightarrow \mu\nu$ , and  $W \rightarrow \tau\nu$ , and their correlations are obtained by combining results from the four LEP experiments properly taking into account the common systematic uncertainties and their correlations [SCHAEEL 13A]. A first fit determines the three individual leptonic branching ratios  $B(W \rightarrow e\nu)$ ,  $B(W \rightarrow \mu\nu)$ , and  $B(W \rightarrow \tau\nu)$ . This fit has a  $\chi^2 = 6.3$  for 9 degrees of freedom. The correlation coefficients between the branching fractions are 0.14 ( $e-\mu$ ), -0.20 ( $e-\tau$ ), -0.12 ( $\mu-\tau$ ). A second fit assumes lepton universality and determines the leptonic branching ratio  $B(W \rightarrow \ell\nu)$  and the hadronic branching ratio is derived as  $B(W \rightarrow \text{hadrons}) = 1 - 3 B(W \rightarrow \ell\nu)$ . This fit has a  $\chi^2 = 15.4$  for 11 degrees of freedom.

$\Gamma(\ell^+ \nu)/\Gamma_{\text{total}}$   $\ell$  indicates average over  $e$ ,  $\mu$ , and  $\tau$  modes, not sum over modes.  $\Gamma_1/\Gamma$

VALUE (units 10 <sup>-2</sup> )	EVTs	DOCUMENT ID	TECN	COMMENT
<b>10.86 ± 0.09 OUR FIT</b>				
10.86 ± 0.12 ± 0.08	16438	ABBIENDI	07A OPAL	$E_{cm}^{ee} = 161\text{--}209$ GeV
10.85 ± 0.14 ± 0.08	13600	ABDALLAH	04G DLPH	$E_{cm}^{ee} = 161\text{--}209$ GeV
10.83 ± 0.14 ± 0.10	11246	ACHARD	04J L3	$E_{cm}^{ee} = 161\text{--}209$ GeV
10.96 ± 0.12 ± 0.05	16116	SCHAEEL	04A ALEP	$E_{cm}^{ee} = 183\text{--}209$ GeV
• • • We do not use the following data for averages, fits, limits, etc. • • •				
11.02 ± 0.52	11858	<sup>1</sup> ABBOTT	99H D0	$E_{cm}^{pp} = 1.8$ TeV
10.4 ± 0.8	3642	<sup>2</sup> ABE	92I CDF	$E_{cm}^{pp} = 1.8$ TeV

- ABBOTT 99H measure  $R \equiv [\sigma_W B(W \rightarrow \ell\nu_\ell)]/[\sigma_Z B(Z \rightarrow \ell\ell)] = 10.90 \pm 0.52$  combining electron and muon channels. They use  $m_W = 80.39 \pm 0.06$  GeV and the SM theoretical predictions for  $\sigma(W)/\sigma(Z)$  and  $B(Z \rightarrow \ell\ell)$ .
- 1216 ± 38  $^{+27}_{-31}$   $W \rightarrow \mu\nu$  events from ABE 92I and 2426  $W \rightarrow e\nu$  events of ABE 91C. ABE 92I give the inverse quantity as 9.6 ± 0.7 and we have inverted.

$\Gamma(e^+ \nu)/\Gamma_{\text{total}}$   $\Gamma_2/\Gamma$

VALUE (units 10 <sup>-2</sup> )	EVTs	DOCUMENT ID	TECN	COMMENT
<b>10.71 ± 0.16 OUR FIT</b>				
10.71 ± 0.25 ± 0.11	2374	ABBIENDI	07A OPAL	$E_{cm}^{ee} = 161\text{--}209$ GeV
10.55 ± 0.31 ± 0.14	1804	ABDALLAH	04G DLPH	$E_{cm}^{ee} = 161\text{--}209$ GeV
10.78 ± 0.29 ± 0.13	1576	ACHARD	04J L3	$E_{cm}^{ee} = 161\text{--}209$ GeV
10.78 ± 0.27 ± 0.10	2142	SCHAEEL	04A ALEP	$E_{cm}^{ee} = 183\text{--}209$ GeV
• • • We do not use the following data for averages, fits, limits, etc. • • •				
10.61 ± 0.28		<sup>1</sup> ABAZOV	04D TEVA	$E_{cm}^{pp} = 1.8$ TeV

- ABAZOV 04D take into account all correlations to properly combine the CDF (ABE 95W) and DØ (ABBOTT 00B) measurements of the ratio  $R$  in the electron channel. The ratio  $R$  is defined as  $[\sigma_W \cdot B(W \rightarrow e\nu_e)] / [\sigma_Z \cdot B(Z \rightarrow e e)]$ . The combination gives  $R^{\text{TeVatron}} = 10.59 \pm 0.23$ .  $\sigma_W / \sigma_Z$  is calculated at next-to-next-to-leading order (3.360 ± 0.051). The branching fraction  $B(Z \rightarrow e e)$  is taken from this Review as (3.363 ± 0.004) %.

$\Gamma(\mu^+ \nu)/\Gamma_{\text{total}}$   $\Gamma_3/\Gamma$

VALUE (units 10 <sup>-2</sup> )	EVTs	DOCUMENT ID	TECN	COMMENT
<b>10.63 ± 0.15 OUR FIT</b>				
10.78 ± 0.24 ± 0.10	2397	ABBIENDI	07A OPAL	$E_{cm}^{ee} = 161\text{--}209$ GeV
10.65 ± 0.26 ± 0.08	1998	ABDALLAH	04G DLPH	$E_{cm}^{ee} = 161\text{--}209$ GeV
10.03 ± 0.29 ± 0.12	1423	ACHARD	04J L3	$E_{cm}^{ee} = 161\text{--}209$ GeV
10.87 ± 0.25 ± 0.08	2216	SCHAEEL	04A ALEP	$E_{cm}^{ee} = 183\text{--}209$ GeV

$\Gamma(\mu^+ \nu)/\Gamma(e^+ \nu)$   $\Gamma_3/\Gamma_2$

VALUE	EVTs	DOCUMENT ID	TECN	COMMENT
<b>0.996 ± 0.008 OUR AVERAGE</b>				
1.003 ± 0.010		<sup>1</sup> AABOUD	17Q ATLS	$E_{cm}^{pp} = 7$ TeV
0.980 ± 0.018		<sup>2</sup> AAIJ	16AJ LHCB	$E_{cm}^{pp} = 8$ TeV
0.993 ± 0.019		SCHAEEL	13A LEP	$E_{cm}^{ee} = 130\text{--}209$ GeV
0.89 ± 0.10	13k	<sup>3</sup> ABACHI	95D D0	$E_{cm}^{pp} = 1.8$ TeV
1.02 ± 0.08	1216	<sup>4</sup> ABE	92I CDF	$E_{cm}^{pp} = 1.8$ TeV
1.00 ± 0.14 ± 0.08	67	ALBAJAR	89 UA1	$E_{cm}^{pp} = 546,630$ GeV
• • • We do not use the following data for averages, fits, limits, etc. • • •				
1.24 $^{+0.6}_{-0.4}$	14	ARNISON	84D UA1	Repl. by ALBAJAR 89

- AABOUD 17Q make a precise determination of  $W \rightarrow e\nu$  and  $W \rightarrow \mu\nu$  production in the following fiducial phase space: lepton pseudo-rapidity range  $|\eta| < 2.5$ , lepton and neutrino transverse momenta larger than 25 GeV each, and  $W$  transverse mass larger than 25 GeV. They determine the ratio of the  $W$  branching fractions  $B(W \rightarrow e\nu)/B(W \rightarrow \mu\nu) = 0.9967 \pm 0.0004 \pm 0.0101 = 0.997 \pm 0.010$ .

See key on page 999

## Gauge &amp; Higgs Boson Particle Listings

W

<sup>2</sup> AAIJ 16AJ make precise measurements of forward  $W \rightarrow e\nu$  and  $W \rightarrow \mu\nu$  production in proton-proton collisions at 8 TeV and determine the ratio of the  $W$  branching fractions  $B(W \rightarrow e\nu)/B(W \rightarrow \mu\nu) = 1.020 \pm 0.002 \pm 0.019$ .

<sup>3</sup> ABACHI 95D obtain this result from the measured  $\sigma_W B(W \rightarrow \mu\nu) = 2.09 \pm 0.23 \pm 0.11$  nb and  $\sigma_W B(W \rightarrow e\nu) = 2.36 \pm 0.07 \pm 0.13$  nb in which the first error is the combined statistical and systematic uncertainty, the second reflects the uncertainty in the luminosity.

<sup>4</sup> ABE 92I obtain  $\sigma_W B(W \rightarrow \mu\nu) = 2.21 \pm 0.07 \pm 0.21$  and combine with ABE 91C  $\sigma_W B(W \rightarrow e\nu)$  to give a ratio of the couplings from which we derive this measurement.

$\Gamma(\tau^+\nu)/\Gamma_{\text{total}}$		$\Gamma_4/\Gamma$			
VALUE (units $10^{-2}$ )	EVTS	DOCUMENT ID	TECN	COMMENT	
<b>11.38 ± 0.21 OUR FIT</b>					
11.14 ± 0.31 ± 0.17	2177	ABBIENDI	07A OPAL	$E_{\text{cm}}^{\text{e}e} = 161\text{--}209$ GeV	
11.46 ± 0.39 ± 0.19	2034	ABDALLAH	04G DLPH	$E_{\text{cm}}^{\text{e}e} = 161\text{--}209$ GeV	
11.89 ± 0.40 ± 0.20	1375	ACHARD	04J L3	$E_{\text{cm}}^{\text{e}e} = 161\text{--}209$ GeV	
11.25 ± 0.32 ± 0.20	2070	SCHAEEL	04A ALEP	$E_{\text{cm}}^{\text{e}e} = 183\text{--}209$ GeV	

$\Gamma(\tau^+\nu)/\Gamma(e^+\nu)$		$\Gamma_4/\Gamma_2$			
VALUE	EVTS	DOCUMENT ID	TECN	COMMENT	
<b>1.043 ± 0.024 OUR AVERAGE</b>					
1.063 ± 0.027		SCHAEEL	13A LEP	$E_{\text{cm}}^{\text{e}e} = 130\text{--}209$ GeV	
0.961 ± 0.061	980	<sup>1</sup> ABBOTT	00D D0	$E_{\text{cm}}^{\text{p}p} = 1.8$ TeV	
0.94 ± 0.14	179	<sup>2</sup> ABE	92E CDF	$E_{\text{cm}}^{\text{p}p} = 1.8$ TeV	
1.04 ± 0.08 ± 0.08	754	<sup>3</sup> ALITTI	92F UA2	$E_{\text{cm}}^{\text{p}p} = 630$ GeV	
1.02 ± 0.20 ± 0.12	32	ALBAJAR	89 UA1	$E_{\text{cm}}^{\text{p}p} = 546, 630$ GeV	
• • • We do not use the following data for averages, fits, limits, etc. • • •					
0.995 ± 0.112 ± 0.083	198	ALITTI	91c UA2	Repl. by ALITTI 92F	
1.02 ± 0.20 ± 0.10	32	ALBAJAR	87 UA1	Repl. by ALBAJAR 89	

<sup>1</sup> ABBOTT 00D measure  $\sigma_W \times B(W \rightarrow \tau\nu_\tau) = 2.22 \pm 0.09 \pm 0.10 \pm 0.10$  nb. Using the ABBOTT 00B result  $\sigma_W \times B(W \rightarrow e\nu_e) = 2.31 \pm 0.01 \pm 0.05 \pm 0.10$  nb, they quote the ratio of the couplings from which we derive this measurement.

<sup>2</sup> ABE 92E use two procedures for selecting  $W \rightarrow \tau\nu_\tau$  events. The missing  $E_T$  trigger leads to 132 ± 14 ± 8 events and the  $\tau$  trigger to 47 ± 9 ± 4 events. Proper statistical and systematic correlations are taken into account to arrive at  $\sigma_B(W \rightarrow \tau\nu) = 2.05 \pm 0.27$  nb. Combined with ABE 91C result on  $\sigma_B(W \rightarrow e\nu)$ , ABE 92E quote a ratio of the couplings from which we derive this measurement.

<sup>3</sup> This measurement is derived by us from the ratio of the couplings of ALITTI 92F.

$\Gamma(\tau^+\nu)/\Gamma(\mu^+\nu)$		$\Gamma_4/\Gamma_3$			
VALUE		DOCUMENT ID	TECN	COMMENT	
<b>1.070 ± 0.026</b>		SCHAEEL	13A LEP	$E_{\text{cm}}^{\text{e}e} = 130\text{--}209$ GeV	

$\Gamma(\text{hadrons})/\Gamma_{\text{total}}$		$\Gamma_5/\Gamma$			
VALUE (units $10^{-2}$ )	EVTS	DOCUMENT ID	TECN	COMMENT	
<b>67.41 ± 0.27 OUR FIT</b>					
67.41 ± 0.37 ± 0.23	16438	ABBIENDI	07A OPAL	$E_{\text{cm}}^{\text{e}e} = 161\text{--}209$ GeV	
67.45 ± 0.41 ± 0.24	13600	ABDALLAH	04G DLPH	$E_{\text{cm}}^{\text{e}e} = 161\text{--}209$ GeV	
67.50 ± 0.42 ± 0.30	11246	ACHARD	04J L3	$E_{\text{cm}}^{\text{e}e} = 161\text{--}209$ GeV	
67.13 ± 0.37 ± 0.15	16116	SCHAEEL	04A ALEP	$E_{\text{cm}}^{\text{e}e} = 183\text{--}209$ GeV	

$\Gamma(\pi^+\gamma)/\Gamma(e^+\nu)$		$\Gamma_6/\Gamma_2$			
VALUE	CL%	DOCUMENT ID	TECN	COMMENT	
<b>&lt; 6.4 × 10<sup>-5</sup></b>	95	AALTONEN	12W CDF	$E_{\text{cm}}^{\text{p}p} = 1.96$ TeV	
< 7 × 10 <sup>-4</sup>	95	ABE	98H CDF	$E_{\text{cm}}^{\text{p}p} = 1.8$ TeV	
< 4.9 × 10 <sup>-3</sup>	95	<sup>1</sup> ALITTI	92D UA2	$E_{\text{cm}}^{\text{p}p} = 630$ GeV	
< 58 × 10 <sup>-3</sup>	95	<sup>2</sup> ALBAJAR	90 UA1	$E_{\text{cm}}^{\text{p}p} = 546, 630$ GeV	

<sup>1</sup> ALITTI 92D limit is  $3.8 \times 10^{-3}$  at 90%CL.

<sup>2</sup> ALBAJAR 90 obtain < 0.048 at 90%CL.

$\Gamma(D_s^+\gamma)/\Gamma(e^+\nu)$		$\Gamma_7/\Gamma_2$			
VALUE	CL%	DOCUMENT ID	TECN	COMMENT	
<b>&lt; 1.2 × 10<sup>-2</sup></b>	95	ABE	98P CDF	$E_{\text{cm}}^{\text{p}p} = 1.8$ TeV	

$\Gamma(cX)/\Gamma(\text{hadrons})$		$\Gamma_8/\Gamma_5$			
VALUE	EVTS	DOCUMENT ID	TECN	COMMENT	
<b>0.49 ± 0.04 OUR AVERAGE</b>					
0.481 ± 0.042 ± 0.032	3005	<sup>1</sup> ABBIENDI	00V OPAL	$E_{\text{cm}}^{\text{e}e} = 183 + 189$ GeV	
0.51 ± 0.05 ± 0.03	746	<sup>2</sup> BARATE	99M ALEP	$E_{\text{cm}}^{\text{e}e} = 172 + 183$ GeV	

<sup>1</sup> ABBIENDI 00V tag  $W \rightarrow cX$  decays using measured jet properties, lifetime information, and leptons produced in charm decays. From this result, and using the additional measurements of  $\Gamma(W)$  and  $B(W \rightarrow \text{hadrons})$ ,  $|V_{cs}|$  is determined to be  $0.969 \pm 0.045 \pm 0.036$ .

<sup>2</sup> BARATE 99M tag  $c$  jets using a neural network algorithm. From this measurement  $|V_{cs}|$  is determined to be  $1.00 \pm 0.11 \pm 0.07$ .

$\Gamma(\pi^+\pi^+\pi^-)/\Gamma_{\text{total}}$		$\Gamma_{11}/\Gamma$			
VALUE (units $10^{-6}$ )	CL%	DOCUMENT ID	TECN	COMMENT	
<b>&lt; 1.01</b>	95	<sup>1</sup> SIRUNYAN	19BG CMS	$E_{\text{cm}}^{\text{p}p} = 13$ TeV	

<sup>1</sup> SIRUNYAN 19BG search for the rare decay of a  $W$  boson into three charged pions. Three pion candidates are required in each event, with transverse momentum larger than 35 GeV, 35 GeV, 18 GeV, respectively, while the transverse momentum of the three-pion system is required to be larger than 40 GeV. Analyzing the three-pion invariant mass, no excess is observed in the  $W$  mass region, leading to the 95% C.L. upper limit on the branching fraction.

$R_{cs} = \Gamma(c\bar{s})/\Gamma(\text{hadrons})$		$\Gamma_9/\Gamma_5$			
VALUE		DOCUMENT ID	TECN	COMMENT	
<b>0.46<sup>+0.18</sup><sub>-0.14</sub> ± 0.07</b>		<sup>1</sup> ABREU	98N DLPH	$E_{\text{cm}}^{\text{e}e} = 161 + 172$ GeV	

<sup>1</sup> ABREU 98N tag  $c$  and  $s$  jets by identifying a charged kaon as the highest momentum particle in a hadronic jet. They also use a lifetime tag to independently identify a  $c$  jet, based on the impact parameter distribution of charged particles in a jet. From this measurement  $|V_{cs}|$  is determined to be  $0.94<sup>+0.32</sup><sub>-0.26</sub> ± 0.13$ .

## AVERAGE PARTICLE MULTIPLICITIES IN HADRONIC W DECAY

Summed over particle and antiparticle, when appropriate.

$\langle N_{\pi^\pm} \rangle$					
VALUE		DOCUMENT ID	TECN	COMMENT	
<b>15.70 ± 0.35</b>		<sup>1</sup> ABREU,P	00F DLPH	$E_{\text{cm}}^{\text{e}e} = 189$ GeV	

<sup>1</sup> ABREU,P 00F measure  $\langle N_{\pi^\pm} \rangle = 31.65 \pm 0.48 \pm 0.76$  and  $15.51 \pm 0.38 \pm 0.40$  in the fully hadronic and semileptonic final states respectively. The value quoted is a weighted average without assuming any correlations.

$\langle N_{K^\pm} \rangle$					
VALUE		DOCUMENT ID	TECN	COMMENT	
<b>2.20 ± 0.19</b>		<sup>1</sup> ABREU,P	00F DLPH	$E_{\text{cm}}^{\text{e}e} = 189$ GeV	

<sup>1</sup> ABREU,P 00F measure  $\langle N_{K^\pm} \rangle = 4.38 \pm 0.42 \pm 0.12$  and  $2.23 \pm 0.32 \pm 0.17$  in the fully hadronic and semileptonic final states respectively. The value quoted is a weighted average without assuming any correlations.

$\langle N_p \rangle$					
VALUE		DOCUMENT ID	TECN	COMMENT	
<b>0.92 ± 0.14</b>		<sup>1</sup> ABREU,P	00F DLPH	$E_{\text{cm}}^{\text{e}e} = 189$ GeV	

<sup>1</sup> ABREU,P 00F measure  $\langle N_p \rangle = 1.82 \pm 0.29 \pm 0.16$  and  $0.94 \pm 0.23 \pm 0.06$  in the fully hadronic and semileptonic final states respectively. The value quoted is a weighted average without assuming any correlations.

$\langle N_{\text{charged}} \rangle$					
VALUE		DOCUMENT ID	TECN	COMMENT	
<b>19.39 ± 0.08 OUR AVERAGE</b>					
19.38 ± 0.05 ± 0.08		<sup>1</sup> ABBIENDI	06A OPAL	$E_{\text{cm}}^{\text{e}e} = 189\text{--}209$ GeV	
19.44 ± 0.17		<sup>2</sup> ABREU,P	00F DLPH	$E_{\text{cm}}^{\text{e}e} = 183 + 189$ GeV	
19.3 ± 0.3 ± 0.3		<sup>3</sup> ABBIENDI	99N OPAL	$E_{\text{cm}}^{\text{e}e} = 183$ GeV	
19.23 ± 0.74		<sup>4</sup> ABREU	98C DLPH	$E_{\text{cm}}^{\text{e}e} = 172$ GeV	

<sup>1</sup> ABBIENDI 06A measure  $\langle N_{\text{charged}} \rangle = 38.74 \pm 0.12 \pm 0.26$  when both  $W$  bosons decay hadronically and  $\langle N_{\text{charged}} \rangle = 19.39 \pm 0.11 \pm 0.09$  when one  $W$  boson decays semileptonically. The value quoted here is obtained under the assumption that there is no color reconnection between  $W$  bosons; the value is a weighted average taking into account correlations in the systematic uncertainties.

<sup>2</sup> ABREU,P 00F measure  $\langle N_{\text{charged}} \rangle = 39.12 \pm 0.33 \pm 0.36$  and  $38.11 \pm 0.57 \pm 0.44$  in the fully hadronic final states at 189 and 183 GeV respectively, and  $\langle N_{\text{charged}} \rangle = 19.49 \pm 0.31 \pm 0.27$  and  $19.78 \pm 0.49 \pm 0.43$  in the semileptonic final states. The value quoted is a weighted average without assuming any correlations.

<sup>3</sup> ABBIENDI 99N use the final states  $W^+ W^- \rightarrow q\bar{q}l\bar{l}$  to derive this value.

<sup>4</sup> ABREU 98C combine results from both the fully hadronic as well semileptonic  $WW$  final states after demonstrating that the  $W$  decay charged multiplicity is independent of the topology within errors.

## TRIPLE GAUGE COUPLINGS (TGC'S)

Revised April 2017 by M.W. Grunewald (U. College Dublin) and A. Gurtu (Formerly Tata Inst.).

Fourteen independent couplings, seven each for  $ZWW$  and  $\gamma WW$ , completely describe the  $VWW$  vertices within the most general framework of the electroweak Standard Model (SM) consistent with Lorentz invariance and U(1) gauge invariance. Of each of the seven TGCs, three conserve  $C$  and  $P$  individually, three violate  $CP$ , and one violates  $C$  and  $P$  individually while conserving  $CP$ . Assumption of  $C$  and  $P$  conservation and electromagnetic gauge invariance reduces the number of independent  $VWW$  couplings to five: one common set [1,2]



# Gauge & Higgs Boson Particle Listings

## W

is  $(\kappa_\gamma, \kappa_Z, \lambda_\gamma, \lambda_Z, g_1^Z)$ , where  $\kappa_\gamma = \kappa_Z = g_1^Z = 1$  and  $\lambda_\gamma = \lambda_Z = 0$  in the Standard Model at tree level. The parameters  $\kappa_Z$  and  $\lambda_Z$  are related to the other three due to constraints of gauge invariance as follows:  $\kappa_Z = g_1^Z - (\kappa_\gamma - 1) \tan^2 \theta_W$  and  $\lambda_Z = \lambda_\gamma$ , where  $\theta_W$  is the weak mixing angle. The  $W$  magnetic dipole moment,  $\mu_W$ , and the  $W$  electric quadrupole moment,  $q_W$ , are expressed as  $\mu_W = e(1 + \kappa_\gamma + \lambda_\gamma)/2M_W$  and  $q_W = -e(\kappa_\gamma - \lambda_\gamma)/M_W^2$ .

Precision measurements of suitable observables at LEP1 has already led to an exploration of much of the TGC parameter space. At LEP2, the  $VWW$  coupling arises in  $W$ -pair production via  $s$ -channel exchange, or in single  $W$  production via the radiation of a virtual photon off the incident  $e^+$  or  $e^-$ . At the Tevatron and the LHC, hard-photon bremsstrahlung off a produced  $W$  or  $Z$  signals the presence of a triple-gauge vertex. In order to extract the value of one TGC, the others are generally kept fixed to their SM values. While most analyses use the above gauge constraints in the extraction of TGCs, one analysis of  $W$ -pair events also determines the real and imaginary parts of all 14 couplings using unconstrained single-parameter fits [3]. The results are consistent. Some experiments have determined limits on the couplings under various non-LEP scenarios and assuming different values of the form factor  $\Lambda$ , where the coupling parameters are scaled by  $1/(1 + s/\Lambda^2)^2$ . For practical reasons it is not possible to quote all such determinations in the listings. For that the individual papers may be consulted. Recently, EFT-inspired sets of couplings [4,5], such as  $c_{WWW}/\Lambda^2, c_W/\Lambda^2, c_B/\Lambda^2$  which are linearly related to the couplings discussed above, are also determined by the LHC experiments.

### References

1. K. Hagiwara *et al.*, Nucl. Phys. **B282**, 253 (1987).
2. G. Gounaris *et al.*, CERN 96-01 p. 525.
3. S. Schael *et al.* (ALEPH Collab.), Phys. Lett. **B614**, 7 (2005).
4. K. Hagiwara *et al.*, Phys. Rev. **D48**, 2182 (1993).
5. C. Degrande *et al.*, Annals Phys. **335** (2013) 21-32.

$g_1^Z$

OUR FIT below is taken from [SCHAE1 13A].

VALUE	EVTS	DOCUMENT ID	TECN	COMMENT
<b><math>0.984^{+0.018}_{-0.020}</math></b>				<b>OUR FIT</b>
$0.975^{+0.033}_{-0.030}$	7872	1 ABDALLAH	10 DLPH	$E_{cm}^{pp} = 189-209$ GeV
$1.001 \pm 0.027 \pm 0.013$	9310	2 SCHAE1	05A ALEP	$E_{cm}^{ee} = 183-209$ GeV
$0.987^{+0.034}_{-0.033}$	9800	3 ABBIENDI	04D OPAL	$E_{cm}^{ee} = 183-209$ GeV
$0.966^{+0.034}_{-0.032} \pm 0.015$	8325	4 ACHARD	04D L3	$E_{cm}^{ee} = 161-209$ GeV
• • • We do not use the following data for averages, fits, limits, etc. • • •				
		5 SIRUNYAN	19CL CMS	$E_{cm}^{pp} = 13$ TeV
		6 SIRUNYAN	18BZ CMS	$E_{cm}^{pp} = 13$ TeV
		7 AABOUD	17s ATLS	$E_{cm}^{pp} = 7+8$ TeV
		8 AABOUD	17u ATLS	$E_{cm}^{pp} = 8$ TeV
		9 KHACHATRY...	17o CMS	$E_{cm}^{pp} = 8$ TeV
		10 SIRUNYAN	17x CMS	$E_{cm}^{pp} = 8$ TeV
		11 AAD	16AR ATLS	$E_{cm}^{pp} = 8$ TeV
		12 AAD	16P ATLS	$E_{cm}^{pp} = 8$ TeV
		13 AAD	14Y ATLS	$E_{cm}^{pp} = 8$ TeV
		14 AAD	13AL ATLS	$E_{cm}^{pp} = 7$ TeV

		15 CHATRCHYAN	13BF CMS	$E_{cm}^{pp} = 7$ TeV
		16 AAD	12CD ATLS	$E_{cm}^{pp} = 7$ TeV
		17 AALTONEN	12AC CDF	$E_{cm}^{pp} = 1.96$ TeV
		18 ABAZOV	12AG D0	$E_{cm}^{pp} = 1.96$ TeV
		34 19 ABAZOV	11 D0	$E_{cm}^{pp} = 1.96$ TeV
		334 20 AALTONEN	10K CDF	$E_{cm}^{pp} = 1.96$ TeV
$1.04 \pm 0.09$		21 ABAZOV	09AD D0	$E_{cm}^{pp} = 1.96$ TeV
		22 ABAZOV	09AJ D0	$E_{cm}^{pp} = 1.96$ TeV
$1.07^{+0.08}_{-0.12}$	1880	23 ABDALLAH	08c DLPH	Superseded by ABDAL-LAH 10
		13 24 ABAZOV	07Z D0	$E_{cm}^{pp} = 1.96$ TeV
		2.3 25 ABAZOV	05s D0	$E_{cm}^{pp} = 1.96$ TeV
$0.98 \pm 0.07 \pm 0.01$	2114	26 ABREU	01i DLPH	$E_{cm}^{ee} = 183+189$ GeV
		331 27 ABBOTT	99i D0	$E_{cm}^{pp} = 1.8$ TeV

1 ABDALLAH 10 use data on the final states  $e^+e^- \rightarrow jj\ell\nu, jjjj, jjX, \ell X$ , at center-of-mass energies between 189-209 GeV at LEP2, where  $j = \text{jet}$ ,  $\ell = \text{lepton}$ , and  $X$  represents missing momentum. The fit is carried out keeping all other parameters fixed at their SM values.

2 SCHAE1 05A study single-photon, single- $W$ , and  $WW$ -pair production from 183 to 209 GeV. The result quoted here is derived from the  $WW$ -pair production sample. Each parameter is determined from a single-parameter fit in which the other parameters assume their Standard Model values.

3 ABBIENDI 04D combine results from  $W^+W^-$  in all decay channels. Only  $CP$ -conserving couplings are considered and each parameter is determined from a single-parameter fit in which the other parameters assume their Standard Model values. The 95% confidence interval is  $0.923 < g_1^Z < 1.054$ .

4 ACHARD 04b study  $WW$ -pair production, single- $W$  production and single-photon production with missing energy from 189 to 209 GeV. The result quoted here is obtained from the  $WW$ -pair production sample including data from 161 to 183 GeV, ACCIARRI 99q. Each parameter is determined from a single-parameter fit in which the other parameters assume their Standard Model values.

5 SIRUNYAN 19CL study  $WW$  and  $WZ$  production in lepton + jet events, with one  $W$  boson decaying leptonically (electron or muon), and another  $W$  or  $Z$  boson decaying hadronically, reconstructed as a single massive large-radius jet. In the electron channel 2,456 (2,235) events are selected in the  $WW(WZ)$  category, while in the muon channel 3,996 (3,572) events are selected in the  $WW(WZ)$  category. Analysing the di-boson invariant mass distribution, the following 95% C.L. limit is obtained:  $0.9939 < g_1^Z < 1.0074$ .

6 SIRUNYAN 18BZ study  $pp \rightarrow Z$  jet jet events at 13 TeV where  $Z \rightarrow e^+e^-/\mu^+\mu^-$ . Isolated electrons and muons are selected with  $p_T$  of the leading/sub-leading lepton  $> 30/20$  GeV and  $|\eta| < 2.4$ , with the di-lepton invariant mass within 15 GeV of the  $Z$  mass. The two highest  $p_T$  jets are selected with  $p_T$  of the leading/sub-leading jet  $> 50/30$  GeV respectively and dijet invariant mass  $> 200$  GeV. Templates in the transverse momentum of the  $Z$  are utilized to set limits on the triple gauge couplings in the EFT and the LEP parametrizations. The following 95% C.L. limit is obtained:  $0.965 < g_1^Z < 1.042$ .

7 AABOUD 17s analyze electroweak production of a  $W$  boson in association with two jets at high dijet invariant mass, with the  $W$  boson decaying to electron or muon plus neutrino. In the signal region of dijet mass larger than 1 TeV and leading-jet transverse momentum larger than 600 GeV, 30 events are observed in the data with  $39 \pm 4$  events expected in the Standard Model, yielding the following limit at 95% CL for the form factor cut-off scale  $\Lambda_{FF} \rightarrow \infty$ :  $0.87 < g_1^Z < 1.12$ .

8 AABOUD 17u analyze production of  $WW$  or  $WZ$  boson pairs with one  $W$  boson decaying to electron or muon plus neutrino, and the other  $W$  or  $Z$  boson decaying hadronically. The hadronic decay system is reconstructed as either a resolved two-jet system or as a single large jet. Analysing the transverse momentum distribution of the hadronic system above 100 GeV yields the following limit at 95% CL for the form factor cut-off scale  $\Lambda_{FF} \rightarrow \infty$ :  $0.979 < g_1^Z < 1.024$ .

9 KHACHATRYAN 17o analyse  $WZ$  production where each boson decays into electrons or muons. Events are required to have a tri-lepton invariant mass larger than 100 GeV, with one of the lepton pairs having an invariant mass within 20 GeV of the  $Z$  boson mass. The  $Z$  transverse momentum spectrum is analyzed to set a 95% C.L. limit of:  $0.982 < g_1^Z < 1.035$ .

10 SIRUNYAN 17x study  $pp \rightarrow WW/WZ \rightarrow \ell\nu q\bar{q}$  production at 8 TeV where  $\ell$  is an electron or muon with  $p_T > 30$  or 25 GeV respectively. Suitable cuts are put on the  $p_T$  of the dijet system and the missing  $E_T$  of the event yielding a total of 285 and 204  $WV$  events observed in the electron and muon channels. The following 95% C.L. limit is obtained:  $0.9913 < g_1^Z < 1.024$ .

11 AAD 16AR study  $WW$  production in  $pp$  collisions and select 6636  $WW$  candidates in decay modes with electrons or muons with an expected background of  $1546 \pm 157$  events. Assuming the LEP formulation and setting the form-factor  $\Lambda$  to infinity, a fit to the transverse momentum distribution of the leading charged lepton, leads to a 95% C.L. range of  $0.984 < g_1^Z < 1.027$ .

12 AAD 16P study  $WZ$  production in  $pp$  collisions and select 2091  $WZ$  candidates in 4 decay modes with electrons and muons, with an expected background of  $1825 \pm 7$  events. Analysing the  $WZ$  transverse momentum distribution, the resulting 95% C.L. limit is:  $0.981 < g_1^Z < 1.029$ .

13 AAD 14Y determine the electroweak  $Z$ -dijet cross section in 8 TeV  $pp$  collisions.  $Z \rightarrow ee$  and  $Z \rightarrow \mu\mu$  decays are selected with the di-lepton  $p_T > 20$  GeV and mass in the 81-101 GeV range. Minimum two jets are required with  $p_T > 55$  and 45 GeV and no additional jets with  $p_T > 25$  GeV in the rapidity interval between them. The normalized  $p_T$  balance between the  $Z$  and the two jets is required to be  $< 0.15$ . This leads to a selection of 900 events with dijet mass  $> 1$  TeV. The number of signal and background events expected is 261 and 592 respectively. A Poisson likelihood method is used on an event by event basis to obtain the 95% CL limit  $0.5 < g_1^Z < 1.26$  for a form factor value  $\Lambda = \infty$ .

14 AAD 13AL study  $WW$  production in  $pp$  collisions and select 1325  $WW$  candidates in decay modes with electrons or muons with an expected background of  $369 \pm 61$  events. Assuming the LEP formulation and setting the form-factor  $\Lambda = \text{infinity}$ , a fit to the

- transverse momentum distribution of the leading charged lepton, leads to a 95% C.L. range of  $0.961 < g_1^Z < 1.052$ . Supersedes AAD 12Ac.
- 15 CHATRCHYAN 13BF determine the  $W^+ W^-$  production cross section using unlike sign di-lepton ( $e$  or  $\mu$ ) events with high  $p_T$ . The leptons have  $p_T > 20$  GeV/c and are isolated. 1134 candidate events are observed with an expected SM background of  $247 \pm 34$ . The  $p_T$  distribution of the leading lepton is fitted to obtain 95% C.L. limits of  $0.905 \leq g_1^Z \leq 1.095$ .
- 16 AAD 12CD study  $WZ$  production in  $pp$  collisions and select 317  $WZ$  candidates in three  $\ell\nu$  decay modes with an expected background of  $68.0 \pm 10.0$  events. The resulting 95% C.L. range is:  $0.943 < g_1^Z < 1.093$ . Supersedes AAD 12v.
- 17 AALTONEN 12AC study  $WZ$  production in  $p\bar{p}$  collisions and select 63  $WZ$  candidates in three  $\ell\nu$  decay modes with an expected background of  $7.9 \pm 1.0$  events. Based on the cross section and shape of the  $Z$  transverse momentum spectrum, the following 95% C.L. range is reported:  $0.92 < g_1^Z < 1.20$  for a form factor of  $\Lambda = 2$  TeV.
- 18 ABZOV 12AG combine new results with already published results on  $W\gamma, WW$  and  $WZ$  production in order to determine the couplings with increased precision, superseding ABZOV 08R, ABZOV 11AC, ABZOV 09AJ, ABZOV 09AD. The 68% C.L. result for a formfactor cutoff of  $\Lambda = 2$  TeV is  $g_1^Z = 1.022^{+0.032}_{-0.030}$ .
- 19 ABZOV 11 study the  $p\bar{p} \rightarrow 3\ell\nu$  process arising in  $WZ$  production. They observe 34  $WZ$  candidates with an estimated background of 6 events. An analysis of the  $p_T$  spectrum of the  $Z$  boson leads to a 95% C.L. limit of  $0.944 < g_1^Z < 1.154$ , for a form factor  $\Lambda = 2$  TeV.
- 20 AALTONEN 10K study  $p\bar{p} \rightarrow W^+ W^-$  with  $W \rightarrow e/\mu\nu$ . The  $p_T$  of the leading (second) lepton is required to be  $> 20$  (10) GeV. The final number of events selected is 654 of which  $320 \pm 47$  are estimated to be background. The 95% C.L. interval is  $0.76 < g_1^Z < 1.34$  for  $\Lambda = 1.5$  TeV and  $0.78 < g_1^Z < 1.30$  for  $\Lambda = 2$  TeV.
- 21 ABZOV 09AD study the  $p\bar{p} \rightarrow \ell\nu 2jet$  process arising in  $WW$  and  $WZ$  production. They select 12,473 (14,392) events in the electron (muon) channel with an expected di-boson signal of 436 (527) events. The results on the anomalous couplings are derived from an analysis of the  $p_T$  spectrum of the 2-jet system and quoted at 68% C.L. and for a form factor of 2 TeV. This measurement is not used for obtaining the mean as it is for a specific form factor. The 95% confidence interval is  $0.88 < g_1^Z < 1.20$ .
- 22 ABZOV 09AJ study the  $p\bar{p} \rightarrow 2\ell 2\nu$  process arising in  $WW$  production. They select 100 events with an expected  $WW$  signal of 65 events. An analysis of the  $p_T$  spectrum of the two charged leptons leads to 95% C.L. limits of  $0.86 < g_1^Z < 1.3$ , for a form factor  $\Lambda = 2$  TeV.
- 23 ABDALLAH 08c determine this triple gauge coupling from the measurement of the spin density matrix elements in  $e^+ e^- \rightarrow W^+ W^- \rightarrow (qq)(\ell\nu)$ , where  $\ell = e$  or  $\mu$ . Values of all other couplings are fixed to their standard model values.
- 24 ABZOV 07z set limits on anomalous TGCs using the measured cross section and  $p_T(Z)$  distribution in  $WZ$  production with both the  $W$  and the  $Z$  decaying leptonically into electrons and muons. Setting the other couplings to their standard model values, the 95% C.L. limit for a form factor scale  $\Lambda = 2$  TeV is  $0.86 < g_1^Z < 1.35$ .
- 25 ABZOV 05s study  $p\bar{p} \rightarrow WZ$  production with a subsequent trilepton decay to  $\ell\nu\ell'\bar{\ell}'$  ( $\ell$  and  $\ell' = e$  or  $\mu$ ). Three events (estimated background  $0.71 \pm 0.08$  events) with  $WZ$  decay characteristics are observed from which they derive limits on the anomalous  $WWZ$  couplings. The 95% CL limit for a form factor scale  $\Lambda = 1.5$  TeV is  $0.51 < g_1^Z < 1.66$ , fixing  $\lambda_Z$  and  $\kappa_Z$  to their Standard Model values.
- 26 ABREU 01i combine results from  $e^+ e^-$  interactions at 189 GeV leading to  $W^+ W^-$  and  $W\nu_e$  final states with results from ABREU 99L at 183 GeV. The 95% confidence interval is  $0.84 < g_1^Z < 1.13$ .
- 27 ABBOTT 99i perform a simultaneous fit to the  $W\gamma, WW \rightarrow$  dilepton,  $WW/WZ \rightarrow e\nu jj, WW/WZ \rightarrow \mu\nu jj$ , and  $WZ \rightarrow$  trilepton data samples. For  $\Lambda = 2.0$  TeV, the 95%CL limits are  $0.63 < g_1^Z < 1.57$ , fixing  $\lambda_Z$  and  $\kappa_Z$  to their Standard Model values, and assuming Standard Model values for the  $WW\gamma$  couplings.

$\kappa_\gamma$  OUR FIT below is taken from [SCHAEEL 13A].

VALUE	EVTS	DOCUMENT ID	TECN	COMMENT
<b>0.982±0.042 OUR FIT</b>				
$1.024^{+0.077}_{-0.081}$	7872	1 ABDALLAH	10 DLPH	$E_{cm}^{pp} = 189-209$ GeV
$0.971 \pm 0.055 \pm 0.030$	10689	2 SCHAEEL	05A ALEP	$E_{cm}^{pp} = 183-209$ GeV
$0.88^{+0.09}_{-0.08}$	9800	3 ABBIENDI	04D OPAL	$E_{cm}^{pp} = 183-209$ GeV
$1.013^{+0.067}_{-0.064} \pm 0.026$	10575	4 ACHARD	04D L3	$E_{cm}^{pp} = 161-209$ GeV
• • • We do not use the following data for averages, fits, limits, etc. • • •				
		5 AABOUD	17U ATLS	$E_{cm}^{pp} = 8$ TeV
		6 SIRUNYAN	17X CMS	$E_{cm}^{pp} = 8$ TeV
		7 CHATRCHYAN14AB	CMS	$E_{cm}^{pp} = 7$ TeV
		8 AAD	13AN ATLS	$E_{cm}^{pp} = 7$ TeV
		9 CHATRCHYAN13BF	CMS	$E_{cm}^{pp} = 7$ TeV
		10 ABZOV	12AG D0	$E_{cm}^{pp} = 1.96$ TeV
		11 ABZOV	11AC D0	$E_{cm}^{pp} = 1.96$ TeV
		12 CHATRCHYAN11M	CMS	$E_{cm}^{pp} = 7$ TeV
	334	13 AALTONEN	10K CDF	$E_{cm}^{pp} = 1.96$ TeV
	53	14 AARON	09B H1	$E_{cm}^{pp} = 0.3$ TeV
		15 ABZOV	09AD D0	$E_{cm}^{pp} = 1.96$ TeV
		16 ABZOV	09AJ D0	$E_{cm}^{pp} = 1.96$ TeV
		17 ABZOV	08R D0	$E_{cm}^{pp} = 1.96$ TeV
$1.07^{+0.26}_{-0.29}$				

- 0.68  $^{+0.17}_{-0.15}$  1880 18 ABDALLAH 08c DLPH Superseded by ABDALLAH 10
- 1617 19 AALTONEN 07L CDF  $E_{cm}^{pp} = 1.96$  GeV
- 17 20 ABZOV 06H D0  $E_{cm}^{pp} = 1.96$  TeV
- 141 21 ABZOV 05J D0  $E_{cm}^{pp} = 1.96$  TeV
- 1.25  $^{+0.21}_{-0.20} \pm 0.06$  2298 22 ABREU 01i DLPH  $E_{cm}^{pp} = 183+189$  GeV
- 23 BREITWEG 00 ZEUS  $e^+ p \rightarrow e^+ W^\pm X$ ,  $\sqrt{s} \approx 300$  GeV
- 0.92  $\pm 0.34$  331 24 ABBOTT 99i D0  $E_{cm}^{pp} = 1.8$  TeV
- 1 ABDALLAH 10 use data on the final states  $e^+ e^- \rightarrow jj\ell\nu, jjjj, jjX, \ell X$ , at center-of-mass energies between 189-209 GeV at LEP2, where  $j = jet, \ell = lepton$ , and  $X$  represents missing momentum. The fit is carried out keeping all other parameters fixed at their SM values.
- 2 SCHAEEL 05A study single-photon, single- $W$ , and  $WW$ -pair production from 183 to 209 GeV. Each parameter is determined from a single-parameter fit in which the other parameters assume their Standard Model values.
- 3 ABBIENDI 04d combine results from  $W^+ W^-$  in all decay channels. Only  $CP$ -conserving couplings are considered and each parameter is determined from a single-parameter fit in which the other parameters assume their Standard Model values. The 95% confidence interval is  $0.73 < \kappa_\gamma < 1.07$ .
- 4 ACHARD 04d study  $WW$ -pair production, single- $W$  production and single-photon production with missing energy from 189 to 209 GeV. The result quoted here is obtained including data from 161 to 183 GeV, ACCIARRI 99q. Each parameter is determined from a single-parameter fit in which the other parameters assume their Standard Model values.
- 5 AABOUD 17U analyze production of  $WW$  or  $WZ$  boson pairs with one  $W$  boson decaying to electron or muon plus neutrino, and the other  $W$  or  $Z$  boson decaying hadronically. The hadronic decay system is reconstructed as either a resolved two-jet system or as a single large jet. Analysing the transverse momentum distribution of the hadronic system above 100 GeV yields the following limit at 95% CL for the form factor cut-off scale  $\Lambda_{FF} \rightarrow \infty$ :  $0.939 < \kappa_\gamma < 1.064$ .
- 6 SIRUNYAN 17x study  $pp \rightarrow WW/WZ \rightarrow \ell\nu q\bar{q}$  production at 8 TeV where  $\ell$  is an electron or muon with  $p_T > 30$  or 25 GeV respectively. Suitable cuts are put on the  $p_T$  of the dijet system and the missing  $E_T$  of the event yielding a total of 285 and 204  $WV$  events observed in the electron and muon channels. The following 95% C.L. limit is obtained:  $0.956 < \kappa_\gamma < 1.063$ .
- 7 CHATRCHYAN 14AB measure  $W\gamma$  production cross section for  $p_T^\gamma > 15$  GeV and  $R(\ell\gamma) > 0.7$ , which is the separation between the  $\gamma$  and the final state charged lepton ( $e$  or  $\mu$ ) in the azimuthal angle-pseudorapidity ( $\phi - \eta$ ) plane. After background subtraction the number of  $e\nu\gamma$  and  $\mu\nu\gamma$  events is determined to be  $3200 \pm 325$  and  $4970 \pm 543$  respectively, compatible with expectations from the SM. This leads to a 95% CL limit of  $0.62 < \kappa_\gamma < 1.29$ , assuming other parameters have SM values.
- 8 AAD 13AN study  $W\gamma$  production in  $pp$  collisions. In events with no additional jet, 4449 (6578)  $W$  decays to electron (muon) are selected, with an expected background of  $1662 \pm 262$  ( $2538 \pm 362$ ) events. Analysing the photon  $p_T$  spectrum above 100 GeV yields a 95% C.L. limit of  $0.59 < \kappa_\gamma < 1.46$ . Supersedes AAD 12Bx.
- 9 CHATRCHYAN 13BF determine the  $W^+ W^-$  production cross section using unlike sign di-lepton ( $e$  or  $\mu$ ) events with high  $p_T$ . The leptons have  $p_T > 20$  GeV/c and are isolated. 1134 candidate events are observed with an expected SM background of  $247 \pm 34$ . The  $p_T$  distribution of the leading lepton is fitted to obtain 95% C.L. limits of  $0.79 \leq \kappa_\gamma \leq 1.22$ .
- 10 ABZOV 12AG combine new results with already published results on  $W\gamma, WW$  and  $WZ$  production in order to determine the couplings with increased precision, superseding ABZOV 08R, ABZOV 11AC, ABZOV 09AJ, ABZOV 09AD. The 68% C.L. result for a formfactor cutoff of  $\Lambda = 2$  TeV is  $\kappa_\gamma = 1.048^{+0.106}_{-0.105}$ .
- 11 ABZOV 11AC study  $W\gamma$  production in  $p\bar{p}$  collisions at 1.96 TeV, with the  $W$  decay products containing an electron or a muon. They select 196 (363) events in the electron (muon) mode, with a SM expectation of 190 (372) events. A likelihood fit to the photon  $E_T$  spectrum above 15 GeV yields at 95% C.L. the result:  $0.6 < \kappa_\gamma < 1.4$  for a formfactor  $\Lambda = 2$  TeV.
- 12 CHATRCHYAN 11M study  $W\gamma$  production in  $pp$  collisions at  $\sqrt{s} = 7$  TeV using 36  $pb^{-1}$   $pp$  data with the  $W$  decaying to electron and muon. The total cross section is measured for photon transverse energy  $E_T^\gamma > 10$  GeV and spatial separation from charged leptons in the plane of pseudo rapidity and azimuthal angle  $\Delta R(\ell, \gamma) > 0.7$ . The number of candidate (background) events is 452 ( $228 \pm 21$ ) for the electron channel and 520 ( $277 \pm 25$ ) for the muon channel. Setting other couplings to their standard model value, they derive a 95% CL limit of  $-0.11 < \kappa_\gamma < 2.04$ .
- 13 AALTONEN 10K study  $p\bar{p} \rightarrow W^+ W^-$  with  $W \rightarrow e/\mu\nu$ . The  $p_T$  of the leading (second) lepton is required to be  $> 20$  (10) GeV. The final number of events selected is 654 of which  $320 \pm 47$  are estimated to be background. The 95% C.L. interval is  $0.37 < \kappa_\gamma < 1.72$  for  $\Lambda = 1.5$  TeV and  $0.43 < \kappa_\gamma < 1.65$  for  $\Lambda = 2$  TeV.
- 14 AARON 09B study single- $W$  production in  $ep$  collisions at 0.3 TeV C.M. energy. They select 53  $W \rightarrow e/\mu$  events with a standard model expectation of  $54.1 \pm 7.4$  events. Fitting the transverse momentum spectrum of the hadronic recoil system they obtain a 95% C.L. limit of  $-3.7 < \kappa_\gamma < -1.5$  or  $0.3 < \kappa_\gamma < 1.5$ , where the ambiguity is due to the quadratic dependence of the cross section to the coupling parameter.
- 15 ABZOV 09AD study the  $p\bar{p} \rightarrow \ell\nu 2jet$  process arising in  $WW$  and  $WZ$  production. They select 12,473 (14,392) events in the electron (muon) channel with an expected di-boson signal of 436 (527) events. The results on the anomalous couplings are derived from an analysis of the  $p_T$  spectrum of the 2-jet system and quoted at 68% C.L. and for a form factor of 2 TeV. This measurement is not used for obtaining the mean as it is for a specific form factor. The 95% confidence interval is  $0.56 < \kappa_\gamma < 1.55$ .
- 16 ABZOV 09AJ study the  $p\bar{p} \rightarrow 2\ell 2\nu$  process arising in  $WW$  production. They select 100 events with an expected  $WW$  signal of 65 events. An analysis of the  $p_T$  spectrum of the two charged leptons leads to 95% C.L. limits of  $0.46 < \kappa_\gamma < 1.83$ , for a form factor  $\Lambda = 2$  TeV.
- 17 ABZOV 08R use 0.7  $fb^{-1}$   $p\bar{p}$  data at  $\sqrt{s} = 1.96$  TeV to select 263  $W\gamma + X$  events, of which 187 constitute signal, with the  $W$  decaying into an electron or a muon, which is required to be well separated from a photon with  $E_T > 9$  GeV. A likelihood fit to the photon  $E_T$  spectrum yields a 95% CL limit  $0.49 < \kappa_\gamma < 1.51$  with other couplings fixed to their Standard Model values.

## Gauge &amp; Higgs Boson Particle Listings

## W

- <sup>18</sup> ABDALLAH 08c determine this triple gauge coupling from the measurement of the spin density matrix elements in  $e^+e^- \rightarrow W^+W^- \rightarrow (qq)(\ell\nu)$ , where  $\ell = e$  or  $\mu$ . Values of all other couplings are fixed to their standard model values.
- <sup>19</sup> AALTONEN 07L set limits on anomalous TGCs using the  $p_T(W)$  distribution in  $WW$  and  $WZ$  production with the  $W$  decaying to an electron or muon and the  $Z$  to 2 jets. Setting other couplings to their standard model value, the 95% C.L. limits are  $0.54 < \kappa_\gamma < 1.39$  for a form factor scale  $\Lambda = 1.5$  TeV.
- <sup>20</sup> ABAZOV 06H study  $\bar{p}p \rightarrow WW$  production with a subsequent decay  $WW \rightarrow e^+\nu_e e^- \bar{\nu}_e$ ,  $WW \rightarrow e^\pm \nu_e \mu^\mp \nu_\mu$  or  $WW \rightarrow \mu^\pm \nu_\mu \mu^\mp \bar{\nu}_\mu$ . The 95% C.L. limit for a form factor scale  $\Lambda = 1$  TeV is  $-0.05 < \kappa_\gamma < 2.29$ , fixing  $\lambda_\gamma = 0$ . With the assumption that the  $WW\gamma$  and  $WWZ$  couplings are equal the 95% C.L. one-dimensional limit ( $\Lambda = 2$  TeV) is  $0.68 < \kappa < 1.45$ .
- <sup>21</sup> ABAZOV 05J perform a likelihood fit to the photon  $E_T$  spectrum of  $W\gamma + X$  events, where the  $W$  decays to an electron or muon which is required to be well separated from the photon. For  $\Lambda = 2.0$  TeV the 95% CL limits are  $0.12 < \kappa_\gamma < 1.96$ . In the fit  $\lambda_\gamma$  is kept fixed to its Standard Model value.
- <sup>22</sup> ABREU 01i combine results from  $e^+e^-$  interactions at 189 GeV leading to  $W^+W^-$ ,  $W\nu_e$ , and  $\nu\bar{\nu}\gamma$  final states with results from ABREU 99L at 183 GeV. The 95% confidence interval is  $0.87 < \kappa_\gamma < 1.68$ .
- <sup>23</sup> BREITWEG 00 search for  $W$  production in events with large hadronic  $p_T$ . For  $p_T > 20$  GeV, the upper limit on the cross section gives the 95% CL limit  $-3.7 < \kappa_\gamma < 2.5$  (for  $\lambda_\gamma = 0$ ).
- <sup>24</sup> ABBOTT 99i perform a simultaneous fit to the  $W\gamma$ ,  $WW \rightarrow$  dilepton,  $WW/WZ \rightarrow e\nu jj$ ,  $WW/WZ \rightarrow \mu\nu jj$ , and  $WZ \rightarrow$  trilepton data samples. For  $\Lambda = 2.0$  TeV, the 95% CL limits are  $0.75 < \kappa_\gamma < 1.39$ .

$\lambda_\gamma$   
OUR FIT below is taken from [SCHAEEL 13A].

VALUE	EVTS	DOCUMENT ID	TECN	COMMENT
<b>-0.022 ± 0.019 OUR FIT</b>				
0.002 ± 0.035	7872	1 ABDALLAH	10 DLPH	$E_{cm}^{ee} = 189-209$ GeV
-0.012 ± 0.027 ± 0.011	10689	2 SCHAEEL	05A ALEP	$E_{cm}^{ee} = 183-209$ GeV
-0.060 + 0.034 -0.033	9800	3 ABBIENDI	04D OPAL	$E_{cm}^{ee} = 183-209$ GeV
-0.021 + 0.035 -0.034 ± 0.017	10575	4 ACHARD	04D L3	$E_{cm}^{ee} = 161-209$ GeV
• • • We do not use the following data for averages, fits, limits, etc. • • •				
		5 CHATRCHYAN14AB	CMS	$E_{cm}^{pp} = 7$ TeV
		6 AAD	13AN ATLS	$E_{cm}^{pp} = 7$ TeV
		7 ABAZOV	12AG D0	$E_{cm}^{pp} = 1.96$ TeV
		8 ABAZOV	11AC D0	$E_{cm}^{pp} = 1.96$ TeV
		9 CHATRCHYAN11M	CMS	$E_{cm}^{pp} = 7$ TeV
	53	10 AARON	09B H1	$E_{cm}^{ep} = 0.3$ TeV
0.00 ± 0.06		11 ABAZOV	09AD D0	$E_{cm}^{pp} = 1.96$ TeV
		12 ABAZOV	09AJ D0	$E_{cm}^{pp} = 1.96$ TeV
		13 ABAZOV	08R D0	$E_{cm}^{pp} = 1.96$ TeV
0.16 + 0.12 -0.13	1880	14 ABDALLAH	08c DLPH	Superseded by ABDAL-LAH 10
	1617	15 AALTONEN	07L CDF	$E_{cm}^{pp} = 1.96$ GeV
	17	16 ABAZOV	06H D0	$E_{cm}^{pp} = 1.96$ TeV
	141	17 ABAZOV	05J D0	$E_{cm}^{pp} = 1.96$ TeV
0.05 ± 0.09 ± 0.01	2298	18 ABREU	01i DLPH	$E_{cm}^{ee} = 183+189$ GeV
		19 BREITWEG	00 ZEUS	$e^+p \rightarrow e^+W^\pm X$ , $\sqrt{s} \approx 300$ GeV
0.00 + 0.10 -0.09	331	20 ABBOTT	99i D0	$E_{cm}^{pp} = 1.8$ TeV

- <sup>1</sup> ABDALLAH 10 use data on the final states  $e^+e^- \rightarrow jj\ell\nu$ ,  $jjjj$ ,  $jjX$ ,  $\ell X$ , at center-of-mass energies between 189–209 GeV at LEP2, where  $j =$  jet,  $\ell =$  lepton, and  $X$  represents missing momentum. The fit is carried out keeping all other parameters fixed at their SM values.
- <sup>2</sup> SCHAEEL 05A study single-photon, single- $W$ , and  $WW$ -pair production from 183 to 209 GeV. Each parameter is determined from a single-parameter fit in which the other parameters assume their Standard Model values.
- <sup>3</sup> ABBIENDI 04d combine results from  $W^+W^-$  in all decay channels. Only  $CP$ -conserving couplings are considered and each parameter is determined from a single-parameter fit in which the other parameters assume their Standard Model values. The 95% confidence interval is  $-0.13 < \lambda_\gamma < 0.01$ .
- <sup>4</sup> ACHARD 04b study  $WW$ -pair production, single- $W$  production and single-photon production with missing energy from 189 to 209 GeV. The result quoted here is obtained including data from 161 to 183 GeV, ACCIARRI 99q. Each parameter is determined from a single-parameter fit in which the other parameters assume their Standard Model values.
- <sup>5</sup> CHATRCHYAN 14AB measure  $W\gamma$  production cross section for  $p_T^\gamma > 15$  GeV and  $R(\ell\gamma) > 0.7$ , which is the separation between the  $\gamma$  and the final state charged lepton ( $e$  or  $\mu$ ) in the azimuthal angle-pseudorapidity ( $\phi - \eta$ ) plane. After background subtraction the number of  $e\nu\gamma$  and  $\mu\nu\gamma$  events is determined to be  $3200 \pm 325$  and  $4970 \pm 543$  respectively, compatible with expectations from the SM. This leads to a 95% CL limit of  $-0.050 < \lambda_\gamma < 0.037$ , assuming all other parameters have SM values.
- <sup>6</sup> AAD 13AN study  $W\gamma$  production in  $pp$  collisions. In events with no additional jet, 4449 (6578)  $W$  decays to electron (muon) are selected, with an expected background of  $1662 \pm 262$  (2538  $\pm$  362) events. Analysing the photon  $p_T$  spectrum above 100 GeV yields a 95% C.L. limit of  $-0.065 < \lambda_\gamma < 0.061$ . Supersedes AAD 12bx.
- <sup>7</sup> ABAZOV 12AG combine new results with already published results on  $W\gamma$ ,  $WW$  and  $WZ$  production in order to determine the couplings with increased precision, superseding ABAZOV 08R, ABAZOV 11AC, ABAZOV 09AJ, ABAZOV 09AD. The 68% C.L. result for a formfactor cutoff of  $\Lambda = 2$  TeV is  $\lambda_\gamma = 0.007^{+0.021}_{-0.022}$ .

- <sup>8</sup> ABAZOV 11AC study  $W\gamma$  production in  $p\bar{p}$  collisions at 1.96 TeV, with the  $W$  decay products containing an electron or a muon. They select 196 (363) events in the electron (muon) mode, with a SM expectation of 190 (372) events. A likelihood fit to the photon  $E_T$  spectrum above 15 GeV yields at 95% C.L. the result:  $-0.08 < \lambda_\gamma < 0.07$  for a formfactor  $\Lambda = 2$  TeV.
- <sup>9</sup> CHATRCHYAN 11M study  $W\gamma$  production in  $pp$  collisions at  $\sqrt{s} = 7$  TeV using 36 pb<sup>-1</sup>  $pp$  data with the  $W$  decaying to electron and muon. The total cross section is measured for photon transverse energy  $E_T^\gamma > 10$  GeV and spatial separation from charged leptons in the plane of pseudo rapidity and azimuthal angle  $\Delta R(\ell, \gamma) > 0.7$ . The number of candidate (background) events is 452 (228  $\pm$  21) for the electron channel and 520 (277  $\pm$  25) for the muon channel. Setting other couplings to their standard model value, they derive a 95% CL limit of  $-0.18 < \lambda_\gamma < 0.17$ .
- <sup>10</sup> AARON 09B study single- $W$  production in  $e p$  collisions at 0.3 TeV C.M. energy. They select 53  $W \rightarrow e/\mu$  events with a standard model expectation of  $54.1 \pm 7.4$  events. Fitting the transverse momentum spectrum of the hadronic recoil system they obtain a 95% C.L. limit of  $-2.5 < \lambda_\gamma < 2.5$ .
- <sup>11</sup> ABAZOV 09AD study the  $p\bar{p} \rightarrow \ell\nu$  2jet process arising in  $WW$  and  $WZ$  production. They select 12,473 (14,392) events in the electron (muon) channel with an expected di-boson signal of 436 (527) events. The results on the anomalous couplings are derived from an analysis of the  $p_T$  spectrum of the 2-jet system and quoted at 68% C.L. and for a form factor of 2 TeV. This measurement is not used for obtaining the mean as it is for a specific form factor. The 95% confidence interval is  $-0.10 < \lambda_\gamma < 0.11$ .
- <sup>12</sup> ABAZOV 09AJ study the  $p\bar{p} \rightarrow 2\ell\nu$  process arising in  $WW$  production. They select 100 events with an expected  $WW$  signal of 65 events. An analysis of the  $p_T$  spectrum of the two charged leptons leads to 95% C.L. limits of  $-0.14 < \lambda_\gamma < 0.18$ , for a form factor  $\Lambda = 2$  TeV.
- <sup>13</sup> ABAZOV 08R use 0.7 fb<sup>-1</sup>  $p\bar{p}$  data at  $\sqrt{s} = 1.96$  TeV to select 263  $W\gamma + X$  events, of which 187 constitute signal, with the  $W$  decaying into an electron or a muon, which is required to be well separated from a photon with  $E_T > 9$  GeV. A likelihood fit to the photon  $E_T$  spectrum yields a 95% CL limit  $-0.12 < \lambda_\gamma < 0.13$  with other couplings fixed to their Standard Model values.
- <sup>14</sup> ABDALLAH 08c determine this triple gauge coupling from the measurement of the spin density matrix elements in  $e^+e^- \rightarrow W^+W^- \rightarrow (qq)(\ell\nu)$ , where  $\ell = e$  or  $\mu$ . Values of all other couplings are fixed to their standard model values.
- <sup>15</sup> AALTONEN 07L set limits on anomalous TGCs using the  $p_T(W)$  distribution in  $WW$  and  $WZ$  production with the  $W$  decaying to an electron or muon and the  $Z$  to 2 jets. Setting other couplings to their standard model value, the 95% C.L. limits are  $-0.18 < \lambda_\gamma < 0.17$  for a form factor scale  $\Lambda = 1.5$  TeV.
- <sup>16</sup> ABAZOV 06H study  $\bar{p}p \rightarrow WW$  production with a subsequent decay  $WW \rightarrow e^+\nu_e e^- \bar{\nu}_e$ ,  $WW \rightarrow e^\pm \nu_e \mu^\mp \nu_\mu$  or  $WW \rightarrow \mu^\pm \nu_\mu \mu^\mp \bar{\nu}_\mu$ . The 95% C.L. limit for a form factor scale  $\Lambda = 1$  TeV is  $-0.29 < \lambda < 0.30$ . With the assumption that the  $WW\gamma$  and  $WWZ$  couplings are equal the 95% C.L. one-dimensional limit ( $\Lambda = 2$  TeV) is  $-0.29 < \lambda < 0.30$ .
- <sup>17</sup> ABAZOV 05J perform a likelihood fit to the photon  $E_T$  spectrum of  $W\gamma + X$  events, where the  $W$  decays to an electron or muon which is required to be well separated from the photon. For  $\Lambda = 2.0$  TeV the 95% CL limits are  $-0.20 < \lambda_\gamma < 0.20$ . In the fit  $\kappa_\gamma$  is kept fixed to its Standard Model value.
- <sup>18</sup> ABREU 01i combine results from  $e^+e^-$  interactions at 189 GeV leading to  $W^+W^-$ ,  $W\nu_e$ , and  $\nu\bar{\nu}\gamma$  final states with results from ABREU 99L at 183 GeV. The 95% confidence interval is  $-0.11 < \lambda_\gamma < 0.23$ .
- <sup>19</sup> BREITWEG 00 search for  $W$  production in events with large hadronic  $p_T$ . For  $p_T > 20$  GeV, the upper limit on the cross section gives the 95% CL limit  $-3.2 < \lambda_\gamma < 3.2$  for  $\kappa_\gamma$  fixed to its Standard Model value.
- <sup>20</sup> ABBOTT 99i perform a simultaneous fit to the  $W\gamma$ ,  $WW \rightarrow$  dilepton,  $WW/WZ \rightarrow e\nu jj$ ,  $WW/WZ \rightarrow \mu\nu jj$ , and  $WZ \rightarrow$  trilepton data samples. For  $\Lambda = 2.0$  TeV, the 95% CL limits are  $-0.18 < \lambda_\gamma < 0.19$ .

$\kappa_Z$   
This coupling is  $CP$ -conserving ( $C$  and  $P$ -separately conserving).

VALUE	EVTS	DOCUMENT ID	TECN	COMMENT
<b>0.924 + 0.059 ± 0.024</b> <b>-0.056 ± 0.024</b>	7171	1 ACHARD	04D L3	$E_{cm}^{ee} = 189-209$ GeV
• • • We do not use the following data for averages, fits, limits, etc. • • •				
		2 SIRUNYAN	19CL CMS	$E_{cm}^{pp} = 13$ TeV
		3 AABOUD	17s ATLS	$E_{cm}^{pp} = 7+8$ TeV
		4 KHACHATRY...17o	CMS	$E_{cm}^{pp} = 8$ TeV
		5 AAD	16AR ATLS	$E_{cm}^{pp} = 8$ TeV
		6 AAD	16P ATLS	$E_{cm}^{pp} = 8$ TeV
		7 AAD	13AL ATLS	$E_{cm}^{pp} = 7$ TeV
		8 AAD	12CD ATLS	$E_{cm}^{pp} = 7$ TeV
		9 AALTONEN	12AC CDF	$E_{cm}^{pp} = 1.96$ TeV
	34	10 ABAZOV	11 D0	$E_{cm}^{pp} = 1.96$ TeV
	17	11 ABAZOV	06H D0	$E_{cm}^{pp} = 1.96$ TeV
	2.3	12 ABAZOV	05s D0	$E_{cm}^{pp} = 1.96$ TeV

- <sup>1</sup> ACHARD 04b study  $WW$ -pair production, single- $W$  production and single-photon production with missing energy from 189 to 209 GeV. The result quoted here is obtained using the  $WW$ -pair production sample. Each parameter is determined from a single-parameter fit in which the other parameters assume their Standard Model values.
- <sup>2</sup> SIRUNYAN 19CL study  $WW$  and  $WZ$  production in lepton + jet events, with one  $W$  boson decaying leptonically (electron or muon), and another  $W$  or  $Z$  boson decaying hadronically, reconstructed as a single massive large-radius jet. In the electron channel 2,456 (2,235) events are selected in the  $WW(WZ)$  category, while in the muon channel 3,996 (3,572) events are selected in the  $WW(WZ)$  category. Analysing the di-boson invariant mass distribution, the following 95% C.L. limit is obtained:  $0.9921 < \kappa_Z < 1.0082$ .
- <sup>3</sup> AABOUD 17s analyze electroweak production of a  $W$  boson in association with two jets at high dijet invariant mass, with the  $W$  boson decaying to electron or muon plus neutrino. In the signal region of dijet mass larger than 1 TeV and leading-jet transverse

- momentum larger than 600 GeV, 30 events are observed in the data with  $39 \pm 4$  events expected in the Standard Model, yielding the following limit at 95% CL for the form factor cut-off scale  $\Lambda_{FF} \rightarrow \infty$ :  $0.85 < \kappa_Z < 1.16$ .
- 4 KHACHATRYAN 17o analyse  $WZ$  production where each boson decays into electrons or muons. Events are required to have a tri-lepton invariant mass larger than 100 GeV, with one of the lepton pairs having an invariant mass within 20 GeV of the  $Z$  boson mass. The  $Z$  transverse momentum spectrum is analyzed to set a 95% C.L. limit of:  $0.79 < \kappa_Z < 1.25$ .
  - 5 AAD 16AR study  $WW$  production in  $pp$  collisions and select 6636  $WW$  candidates in decay modes with electrons or muons with an expected background of  $1546 \pm 157$  events. Assuming the LEP formulation and setting the form-factor  $\Lambda$  to infinity, a fit to the transverse momentum distribution of the leading charged lepton, leads to a 95% C.L. range of  $0.975 < \kappa_Z < 1.020$ .
  - 6 AAD 16P study  $WZ$  production in  $pp$  collisions and select 2091  $WZ$  candidates in 4 decay modes with electrons and muons, with an expected background of  $1825 \pm 7$  events. Analyzing the  $WZ$  transverse momentum distribution, the resulting 95% C.L. limit is:  $0.81 < \kappa_Z < 1.30$ .
  - 7 AAD 13AL study  $WW$  production in  $pp$  collisions and select 1325  $WW$  candidates in decay modes with electrons or muons with an expected background of  $369 \pm 61$  events. Assuming the LEP formulation and setting the form-factor  $\Lambda = \infty$ , a fit to the transverse momentum distribution of the leading charged lepton, leads to a 95% C.L. range of  $0.957 < \kappa_Z < 1.043$ . Supersedes AAD 12AC.
  - 8 AAD 12CD study  $WZ$  production in  $pp$  collisions and select 317  $WZ$  candidates in three  $\ell\nu$  decay modes with an expected background of  $68.0 \pm 10.0$  events. The resulting 95% C.L. range is:  $0.63 < \kappa_Z < 1.57$ . Supersedes AAD 12V.
  - 9 AALTONEN 12AC study  $WZ$  production in  $p\bar{p}$  collisions and select 63  $WZ$  candidates in three  $\ell\nu$  decay modes with an expected background of  $7.9 \pm 1.0$  events. Based on the cross section and shape of the  $Z$  transverse momentum spectrum, the following 95% C.L. range is reported:  $0.61 < \kappa_Z < 1.90$  for a form factor of  $\Lambda = 2$  TeV.
  - 10 ABAZOV 11 study the  $p\bar{p} \rightarrow 3\ell\nu$  process arising in  $WZ$  production. They observe 34  $WZ$  candidates with an estimated background of 6 events. An analysis of the  $p_T$  spectrum of the  $Z$  boson leads to a 95% C.L. limit of  $0.600 < \kappa_Z < 1.675$ , for a form factor  $\Lambda = 2$  TeV.
  - 11 ABAZOV 06H study  $p\bar{p} \rightarrow WW$  production with a subsequent decay  $WW \rightarrow e^+ \nu_e e^- \bar{\nu}_e$ ,  $WW \rightarrow e^\pm \nu_e \mu^\mp \nu_\mu$  or  $WW \rightarrow \mu^+ \nu_\mu \mu^- \bar{\nu}_\mu$ . The 95% C.L. limit for a form factor scale  $\Lambda = 2$  TeV is  $0.55 < \kappa_Z < 1.55$ , fixing  $\lambda_Z = 0$ . With the assumption that the  $WW\gamma$  and  $WWZ$  couplings are equal the 95% C.L. one-dimensional limit ( $\Lambda = 2$  TeV) is  $0.68 < \kappa < 1.45$ .
  - 12 ABAZOV 05s study  $p\bar{p} \rightarrow WZ$  production with a subsequent trilepton decay to  $\ell\nu\ell'\bar{\ell}'$  ( $\ell$  and  $\ell' = e$  or  $\mu$ ). Three events (estimated background  $0.71 \pm 0.08$  events) with  $WZ$  decay characteristics are observed from which they derive limits on the anomalous  $WWZ$  couplings. The 95% CL limit for a form factor scale  $\Lambda = 1$  TeV is  $-1.0 < \kappa_Z < 3.4$ , fixing  $\lambda_Z$  and  $g_1^Z$  to their Standard Model values.

$\lambda_Z$  This coupling is CP-conserving (C- and P- separately conserving).

VALUE	EVTS	DOCUMENT ID	TECN	COMMENT
$-0.088 \pm 0.060$ $-0.057 \pm 0.023$	7171	1 ACHARD	04D L3	$E_{cm}^{ee} = 189-209$ GeV
••• We do not use the following data for averages, fits, limits, etc. •••				
		2 SIRUNYAN	19CL CMS	$E_{cm}^{pp} = 13$ TeV
		3 SIRUNYAN	18BZ CMS	$E_{cm}^{pp} = 13$ TeV
		4 ABOUD	17S ATLS	$E_{cm}^{pp} = 7+8$ TeV
		5 ABOUD	17U ATLS	$E_{cm}^{pp} = 8$ TeV
		6 KHACHATRYAN 17O	CMS	$E_{cm}^{pp} = 8$ TeV
		7 SIRUNYAN	17X CMS	$E_{cm}^{pp} = 8$ TeV
		8 AAD	16AR ATLS	$E_{cm}^{pp} = 8$ TeV
		9 AAD	16P ATLS	$E_{cm}^{pp} = 8$ TeV
		10 AAD	14Y ATLS	$E_{cm}^{pp} = 8$ TeV
		11 AAD	13AL ATLS	$E_{cm}^{pp} = 7$ TeV
		12 CHATRCHYAN 13BF	CMS	$E_{cm}^{pp} = 7$ TeV
		13 AAD	12CD ATLS	$E_{cm}^{pp} = 7$ TeV
		14 AALTONEN	12AC CDF	$E_{cm}^{pp} = 1.96$ TeV
	34	15 ABAZOV	11 D0	$E_{cm}^{pp} = 1.96$ TeV
	334	16 AALTONEN	10K CDF	$E_{cm}^{pp} = 1.96$ TeV
	13	17 ABAZOV	07Z D0	$E_{cm}^{pp} = 1.96$ TeV
	17	18 ABAZOV	06H D0	$E_{cm}^{pp} = 1.96$ TeV
	2.3	19 ABAZOV	05S D0	$E_{cm}^{pp} = 1.96$ TeV

- 1 ACHARD 04D study  $WW$ -pair production, single- $W$  production and single-photon production with missing energy from 189 to 209 GeV. The result quoted here is obtained using the  $WW$ -pair production sample. Each parameter is determined from a single-parameter fit in which the other parameters assume their Standard Model values.
- 2 SIRUNYAN 19CL study  $WW$  and  $WZ$  production in lepton + jet events, with one  $W$  boson decaying leptonically (electron or muon), and another  $W$  or  $Z$  boson decaying hadronically, reconstructed as a single massive large-radius jet. In the electron channel 2,456 (2,235) events are selected in the  $W(W)WZ$  category, while in the muon channel 3,996 (3,572) events are selected in the  $W(W)WZ$  category. Analysing the di-boson invariant mass distribution, the following 95% C.L. limit is obtained:  $-0.0065 < \lambda_Z < 0.0066$ .
- 3 SIRUNYAN 18BZ study  $pp \rightarrow Z$  jet jet events at 13 TeV where  $Z \rightarrow e^+ e^- / \mu^+ \mu^-$ . Isolated electrons and muons are selected with  $p_T$  of the leading/sub-leading lepton  $> 30/20$  GeV and  $|\eta| < 2.4$ , with the di-lepton invariant mass within 15 GeV of the  $Z$  mass. The two highest  $p_T$  jets are selected with  $p_T$  of the leading/sub-leading jet  $> 50/30$  GeV respectively and dijet invariant mass  $> 200$  GeV. Templates in the transverse momentum of the  $Z$  are utilized to set limits on the triple gauge couplings in the EFT and the LEP parametrizations. The following 95% C.L. limit is obtained  $-0.010 < \lambda_Z < 0.010$ .

- 4 ABOUD 17S analyze electroweak production of a  $W$  boson in association with two jets at high dijet invariant mass, with the  $W$  boson decaying to electron or muon plus neutrino. In the signal region of dijet mass larger than 1 TeV and leading-jet transverse momentum larger than 600 GeV, 30 events are observed in the data with  $39 \pm 4$  events expected in the Standard Model, yielding the following limit at 95% CL for the form factor cut-off scale  $\Lambda_{FF} \rightarrow \infty$ :  $-0.053 < \lambda_Z < 0.042$ .
- 5 ABOUD 17U analyze production of  $WW$  or  $WZ$  boson pairs with one  $W$  boson decaying to electron or muon plus neutrino, and the other  $W$  or  $Z$  boson decaying hadronically. The hadronic decay system is reconstructed as either a resolved two-jet system or as a single large jet. Analysing the transverse momentum distribution of the hadronic system above 100 GeV yields the following limit at 95% CL for the form factor cut-off scale  $\Lambda_{FF} \rightarrow \infty$ :  $-0.013 < \lambda_Z < 0.013$ .
- 6 KHACHATRYAN 17o analyse  $WZ$  production where each boson decays into electrons or muons. Events are required to have a tri-lepton invariant mass larger than 100 GeV, with one of the lepton pairs having an invariant mass within 20 GeV of the  $Z$  boson mass. The  $Z$  transverse momentum spectrum is analyzed to set a 95% C.L. limit of:  $-0.018 < \lambda_Z < 0.016$ .
- 7 SIRUNYAN 17X study  $pp \rightarrow WW/WZ \rightarrow \ell\nu q\bar{q}$  production at 8 TeV where  $\ell$  is an electron or muon with  $p_T > 30$  or 25 GeV respectively. Suitable cuts are put on the  $p_T$  of the dijet system and the missing  $E_T$  of the event yielding a total of 285 and 204  $WW$  events observed in the electron and muon channels. The following 95% C.L. limit is obtained:  $-0.011 < \lambda_Z < 0.011$ .
- 8 AAD 16AR study  $WW$  production in  $pp$  collisions and select 6636  $WW$  candidates in decay modes with electrons or muons with an expected background of  $1546 \pm 157$  events. Assuming the LEP formulation and setting the form-factor  $\Lambda$  to infinity, a fit to the transverse momentum distribution of the leading charged lepton, leads to a 95% C.L. range of  $-0.019 < \lambda_Z < 0.019$ .
- 9 AAD 16P study  $WZ$  production in  $pp$  collisions and select 2091  $WZ$  candidates in 4 decay modes with electrons and muons, with an expected background of  $1825 \pm 7$  events. Analyzing the  $WZ$  transverse momentum distribution, the resulting 95% C.L. limit is:  $-0.016 < \lambda_Z < 0.016$ .
- 10 AAD 14Y determine the electroweak  $Z$ -dijet cross section in 8 TeV  $pp$  collisions.  $Z \rightarrow ee$  and  $Z \rightarrow \mu\mu$  decays are selected with the di-lepton  $p_T > 20$  GeV and mass in the 81-101 GeV range. Minimum two jets are required with  $p_T > 55$  and 45 GeV and no additional jets with  $p_T > 25$  GeV in the rapidity interval between them. The normalized  $p_T$  balance between the  $Z$  and the two jets is required to be  $< 0.15$ . This leads to a selection of 900 events with dijet mass  $> 1$  TeV. The number of signal and background events expected is 261 and 592 respectively. A Poisson likelihood method is used on an event by event basis to obtain the 95% CL limit  $-0.15 < \lambda_Z < 0.13$  for a form factor value  $\Lambda = \infty$ .
- 11 AAD 13AL study  $WW$  production in  $pp$  collisions and select 1325  $WW$  candidates in decay modes with electrons or muons with an expected background of  $369 \pm 61$  events. Assuming the LEP formulation and setting the form-factor  $\Lambda = \infty$ , a fit to the transverse momentum distribution of the leading charged lepton, leads to a 95% C.L. range of  $-0.062 < \lambda_Z < 0.059$ . Supersedes AAD 12AC.
- 12 CHATRCHYAN 13BF determine the  $W^+W^-$  production cross section using unlike sign di-lepton ( $e$  or  $\mu$ ) events with high  $p_T$ . The leptons have  $p_T > 20$  GeV/c and are isolated. 1134 candidate events are observed with an expected SM background of 247  $\pm 34$ . The  $p_T$  distribution of the leading lepton is fitted to obtain 95% C.L. limits of  $-0.048 < \lambda_Z < 0.048$ .
- 13 AAD 12CD study  $WZ$  production in  $pp$  collisions and select 317  $WZ$  candidates in three  $\ell\nu$  decay modes with an expected background of  $68.0 \pm 10.0$  events. The resulting 95% C.L. range is:  $-0.046 < \lambda_Z < 0.047$ . Supersedes AAD 12V.
- 14 AALTONEN 12AC study  $WZ$  production in  $p\bar{p}$  collisions and select 63  $WZ$  candidates in three  $\ell\nu$  decay modes with an expected background of  $7.9 \pm 1.0$  events. Based on the cross section and shape of the  $Z$  transverse momentum spectrum, the following 95% C.L. range is reported:  $-0.08 < \lambda_Z < 0.10$  for a form factor of  $\Lambda = 2$  TeV.
- 15 ABAZOV 11 study the  $p\bar{p} \rightarrow 3\ell\nu$  process arising in  $WZ$  production. They observe 34  $WZ$  candidates with an estimated background of 6 events. An analysis of the  $p_T$  spectrum of the  $Z$  boson leads to a 95% C.L. limit of  $-0.077 < \lambda_Z < 0.093$ , for a form factor  $\Lambda = 2$  TeV.
- 16 AALTONEN 10K study  $p\bar{p} \rightarrow W^+W^-$  with  $W \rightarrow e/\mu\nu$ . The  $p_T$  of the leading (second) lepton is required to be  $> 20$  (10) GeV. The final number of events selected is 654 of which 320  $\pm 47$  are estimated to be background. The 95% C.L. interval is  $-0.16 < \lambda_Z < 0.16$  for  $\Lambda = 1.5$  TeV and  $-0.14 < \lambda_Z < 0.15$  for  $\Lambda = 2$  TeV.
- 17 ABAZOV 07Z set limits on anomalous TGCs using the measured cross section and  $p_T(Z)$  distribution in  $WZ$  production with both the  $W$  and the  $Z$  decaying leptonically into electrons and muons. Setting the other couplings to their standard model values, the 95% C.L. limit for a form factor scale  $\Lambda = 2$  TeV is  $-0.17 < \lambda_Z < 0.21$ .
- 18 ABAZOV 06H study  $p\bar{p} \rightarrow WW$  production with a subsequent decay  $WW \rightarrow e^+ \nu_e e^- \bar{\nu}_e$ ,  $WW \rightarrow e^\pm \nu_e \mu^\mp \nu_\mu$  or  $WW \rightarrow \mu^+ \nu_\mu \mu^- \bar{\nu}_\mu$ . The 95% C.L. limit for a form factor scale  $\Lambda = 2$  TeV is  $-0.39 < \lambda_Z < 0.39$ , fixing  $\kappa_{\mathcal{P}} = 1$ . With the assumption that the  $WW\gamma$  and  $WWZ$  couplings are equal the 95% C.L. one-dimensional limit ( $\Lambda = 2$  TeV) is  $-0.29 < \lambda < 0.30$ .
- 19 ABAZOV 05s study  $p\bar{p} \rightarrow WZ$  production with a subsequent trilepton decay to  $\ell\nu\ell'\bar{\ell}'$  ( $\ell$  and  $\ell' = e$  or  $\mu$ ). Three events (estimated background  $0.71 \pm 0.08$  events) with  $WZ$  decay characteristics are observed from which they derive limits on the anomalous  $WWZ$  couplings. The 95% CL limit for a form factor scale  $\Lambda = 1.5$  TeV is  $-0.48 < \lambda_Z < 0.48$ , fixing  $g_1^Z$  and  $\kappa_Z$  to their Standard Model values.

$\kappa_Z$  This coupling is CP-conserving but C- and P-violating.

VALUE	EVTS	DOCUMENT ID	TECN	COMMENT
$-0.07 \pm 0.09$ OUR AVERAGE		Error includes scale factor of 1.1.		
$-0.04 \pm 0.13$ $-0.12$	9800	1 ABBIENDI	04D OPAL	$E_{cm}^{ee} = 183-209$ GeV
$0.00 \pm 0.13 \pm 0.05$	7171	2 ACHARD	04D L3	$E_{cm}^{ee} = 189-209$ GeV
$-0.44 \pm 0.23$ $-0.22 \pm 0.12$	1154	3 ACCIARRI	99Q L3	$E_{cm}^{ee} = 161+172+183$ GeV
••• We do not use the following data for averages, fits, limits, etc. •••				
$-0.31 \pm 0.23$		4 EBOLI	00 THES	LEP1, SLC+ Tevatron

## Gauge &amp; Higgs Boson Particle Listings

## W

<sup>1</sup> ABBIENDI 04d combine results from  $W^+W^-$  in all decay channels. Only  $CP$ -conserving couplings are considered and each parameter is determined from a single-parameter fit in which the other parameters assume their Standard Model values. The 95% confidence interval is  $-0.28 < g_5^Z < +0.21$ .

<sup>2</sup> ACHARD 04d study  $WW$ -pair production, single- $W$  production and single-photon production with missing energy from 189 to 209 GeV. The result quoted here is obtained using the  $WW$ -pair production sample. Each parameter is determined from a single-parameter fit in which the other parameters assume their Standard Model values.

<sup>3</sup> ACCIARRI 99q study  $W$ -pair, single- $W$ , and single photon events.

<sup>4</sup> EBOL 00 extract this indirect value of the coupling studying the non-universal one-loop contributions to the experimental value of the  $Z \rightarrow b\bar{b}$  width ( $\Lambda=1$  TeV is assumed).

 $g_4^Z$ 

This coupling is  $CP$ -violating ( $C$ -violating and  $P$ -conserving).

VALUE	EVTS	DOCUMENT ID	TECN	COMMENT
<b><math>-0.30 \pm 0.17</math> OUR AVERAGE</b>				
$-0.39^{+0.19}_{-0.20}$	1880	1 ABDALLAH	08c DLPH	$E_{cm}^{ee} = 189-209$ GeV
$-0.02^{+0.32}_{-0.33}$	1065	2 ABBIENDI	01H OPAL	$E_{cm}^{ee} = 189$ GeV

<sup>1</sup> ABDALLAH 08c determine this triple gauge coupling from the measurement of the spin density matrix elements in  $e^+e^- \rightarrow W^+W^- \rightarrow (qq)(\ell\nu)$ , where  $\ell = e$  or  $\mu$ . Values of all other couplings are fixed to their standard model values.

<sup>2</sup> ABBIENDI 01H study  $W$ -pair events, with one leptonically and one hadronically decaying  $W$ . The coupling is extracted using information from the  $W$  production angle together with decay angles from the leptonically decaying  $W$ .

 $\tilde{\kappa}_Z$ 

This coupling is  $CP$ -violating ( $C$ -conserving and  $P$ -violating).

VALUE	EVTS	DOCUMENT ID	TECN	COMMENT
<b><math>-0.12^{+0.06}_{-0.04}</math> OUR AVERAGE</b>				
$-0.09^{+0.08}_{-0.05}$	1880	1 ABDALLAH	08c DLPH	$E_{cm}^{ee} = 189-209$ GeV
$-0.20^{+0.10}_{-0.07}$	1065	2 ABBIENDI	01H OPAL	$E_{cm}^{ee} = 189$ GeV
• • • We do not use the following data for averages, fits, limits, etc. • • •				
		3 AABOUD	17s ATLS	$E_{cm}^{pp} = 7+8$ TeV
		4 BLINOV	11 LEP	$E_{cm}^{ee} = 183-207$ GeV

<sup>1</sup> ABDALLAH 08c determine this triple gauge coupling from the measurement of the spin density matrix elements in  $e^+e^- \rightarrow W^+W^- \rightarrow (qq)(\ell\nu)$ , where  $\ell = e$  or  $\mu$ . Values of all other couplings are fixed to their standard model values.

<sup>2</sup> ABBIENDI 01H study  $W$ -pair events, with one leptonically and one hadronically decaying  $W$ . The coupling is extracted using information from the  $W$  production angle together with decay angles from the leptonically decaying  $W$ .

<sup>3</sup> AABOUD 17s analyze electroweak production of a  $W$  boson in association with two jets at high dijet invariant mass, with the  $W$  boson decaying to electron or muon plus neutrino. In the signal region of dijet mass larger than 1 TeV and leading-jet transverse momentum larger than 600 GeV, 30 events are observed in the data with  $39 \pm 4$  events expected in the Standard Model, yielding the following limit at 95% CL for the form factor cut-off scale  $A_{FF} \rightarrow \infty$ :  $-0.56 < \tilde{\kappa}_Z < 0.56$ .

<sup>4</sup> BLINOV 11 use the LEP-average  $e^+e^- \rightarrow W^+W^-$  cross section data for  $\sqrt{s} = 183-207$  GeV to determine an upper limit on the TGC  $\tilde{\kappa}_Z$ . The average values of the cross sections as well as their correlation matrix, and standard model expectations of the cross sections are taken from the LEPEWVG note hep-ex/0612034. At 95% confidence level  $|\tilde{\kappa}_Z| < 0.13$ .

 $\tilde{\lambda}_Z$ 

This coupling is  $CP$ -violating ( $C$ -conserving and  $P$ -violating).

VALUE	EVTS	DOCUMENT ID	TECN	COMMENT
<b><math>-0.09 \pm 0.07</math> OUR AVERAGE</b>				
$-0.08 \pm 0.07$	1880	1 ABDALLAH	08c DLPH	$E_{cm}^{ee} = 189-209$ GeV
$-0.18^{+0.24}_{-0.16}$	1065	2 ABBIENDI	01H OPAL	$E_{cm}^{ee} = 189$ GeV
• • • We do not use the following data for averages, fits, limits, etc. • • •				
		3 AABOUD	17s ATLS	$E_{cm}^{pp} = 7+8$ TeV
		4 BLINOV	11 LEP	$E_{cm}^{ee} = 183-207$ GeV

<sup>1</sup> ABDALLAH 08c determine this triple gauge coupling from the measurement of the spin density matrix elements in  $e^+e^- \rightarrow W^+W^- \rightarrow (qq)(\ell\nu)$ , where  $\ell = e$  or  $\mu$ . Values of all other couplings are fixed to their standard model values.

<sup>2</sup> ABBIENDI 01H study  $W$ -pair events, with one leptonically and one hadronically decaying  $W$ . The coupling is extracted using information from the  $W$  production angle together with decay angles from the leptonically decaying  $W$ .

<sup>3</sup> AABOUD 17s analyze electroweak production of a  $W$  boson in association with two jets at high dijet invariant mass, with the  $W$  boson decaying to electron or muon plus neutrino. In the signal region of dijet mass larger than 1 TeV and leading-jet transverse momentum larger than 600 GeV, 30 events are observed in the data with  $39 \pm 4$  events expected in the Standard Model, yielding the following limit at 95% CL for the form factor cut-off scale  $A_{FF} \rightarrow \infty$ :  $-0.047 < \tilde{\lambda}_Z < 0.046$ .

<sup>4</sup> BLINOV 11 use the LEP-average  $e^+e^- \rightarrow W^+W^-$  cross section data for  $\sqrt{s} = 183-207$  GeV to determine an upper limit on the TGC  $\tilde{\lambda}_Z$ . The average values of the cross sections as well as their correlation matrix, and standard model expectations of the cross sections are taken from the LEPEWVG note hep-ex/0612034. At 95% confidence level  $|\tilde{\lambda}_Z| < 0.31$ .

of these moments and additional references can be found in HAGIWARA 87 and BAUR 88. The parameter  $\Lambda$  appearing in the theoretical limits below is a regularization cutoff which roughly corresponds to the energy scale where the structure of the  $W$  boson becomes manifest.

VALUE ( $\epsilon/2m_W$ )	EVTS	DOCUMENT ID	TECN	COMMENT
$2.22^{+0.20}_{-0.19}$	2298	1 ABREU	01i DLPH	$E_{cm}^{ee} = 183+189$ GeV
• • • We do not use the following data for averages, fits, limits, etc. • • •				
		2 ABE	95G CDF	
		3 ALITTI	92C UA2	
		4 SAMUEL	92 THEO	
		5 SAMUEL	91 THEO	
		6 GRIFOLS	88 THEO	
		7 GROTC	87 THEO	
		8 VANDERBIJ	87 THEO	
		9 GRAU	85 THEO	
		10 SUZUKI	85 THEO	
		11 HERZOG	84 THEO	

<sup>1</sup> ABREU 01i combine results from  $e^+e^-$  interactions at 189 GeV leading to  $W^+W^-$ ,  $W e \nu_e$ , and  $\nu \bar{\nu} \gamma$  final states with results from ABREU 99L at 183 GeV to determine  $\Delta g_5^Z$ ,  $\Delta \kappa_\gamma$ , and  $\lambda_\gamma$ .  $\Delta \kappa_\gamma$  and  $\lambda_\gamma$  are simultaneously floated in the fit to determine  $\mu W$ .

<sup>2</sup> ABE 95G report  $-1.3 < \kappa < 3.2$  for  $\lambda=0$  and  $-0.7 < \lambda < 0.7$  for  $\kappa=1$  in  $p\bar{p} \rightarrow e \nu_e \gamma X$  and  $\mu \nu_\mu \gamma X$  at  $\sqrt{s} = 1.8$  TeV.

<sup>3</sup> ALITTI 92C measure  $\kappa = 1^{+2.6}_{-2.9}$  and  $\lambda = 0^{+1.7}_{-1.8}$  in  $p\bar{p} \rightarrow e \nu \gamma + X$  at  $\sqrt{s} = 630$  GeV. At 95%CL they report  $-3.5 < \kappa < 5.9$  and  $-3.6 < \lambda < 3.5$ .

<sup>4</sup> SAMUEL 92 use preliminary CDF and UA2 data and find  $-2.4 < \kappa < 3.7$  at 96%CL and  $-3.1 < \kappa < 4.2$  at 95%CL respectively. They use data for  $W\gamma$  production and radiative  $W$  decay.

<sup>5</sup> SAMUEL 91 use preliminary CDF data for  $p\bar{p} \rightarrow W\gamma X$  to obtain  $-11.3 \leq \Delta \kappa \leq 10.9$ . Note that their  $\kappa = 1 - \Delta \kappa$ .

<sup>6</sup> GRIFOLS 88 uses deviation from  $\rho$  parameter to set limit  $\Delta \kappa \lesssim 65 (M_W^2/\Lambda^2)$ .

<sup>7</sup> GROTC 87 finds the limit  $-37 < \Delta \kappa < 73.5$  (90% CL) from the experimental limits on  $e^+e^- \rightarrow \nu \bar{\nu} \gamma$  assuming three neutrino generations and  $-19.5 < \Delta \kappa < 56$  for four generations. Note their  $\Delta \kappa$  has the opposite sign as our definition.

<sup>8</sup> VANDERBIJ 87 uses existing limits to the photon structure to obtain  $|\Delta \kappa| < 33 (m_W/\Lambda)$ . In addition VANDERBIJ 87 discusses problems with using the  $\rho$  parameter of the Standard Model to determine  $\Delta \kappa$ .

<sup>9</sup> GRAU 85 uses the muon anomaly to derive a coupled limit on the anomalous magnetic dipole and electric quadrupole ( $\lambda$ ) moments  $1.05 > \Delta \kappa \ln(\Lambda/m_W) + \lambda/2 > -2.77$ . In the Standard Model  $\lambda = 0$ .

<sup>10</sup> SUZUKI 85 uses partial-wave unitarity at high energies to obtain  $|\Delta \kappa| \lesssim 190 (m_W/\Lambda)^2$ . From the anomalous magnetic moment of the muon, SUZUKI 85 obtains  $|\Delta \kappa| \lesssim 2.2/\ln(\Lambda/m_W)$ . Finally SUZUKI 85 uses deviations from the  $\rho$  parameter and obtains a very qualitative, order-of-magnitude limit  $|\Delta \kappa| \lesssim 150 (m_W/\Lambda)^4$  if  $|\Delta \kappa| \ll 1$ .

<sup>11</sup> HERZOG 84 consider the contribution of  $W$ -boson to muon magnetic moment including anomalous coupling of  $WW\gamma$ . Obtain a limit  $-1 < \Delta \kappa < 3$  for  $\Lambda \gtrsim 1$  TeV.

 $c_{WW}/\Lambda^2, c_W/\Lambda^2, c_B/\Lambda^2$ 

These couplings are used in EFT-based approaches to anomalous couplings. They are linearly related to the couplings discussed above.

VALUE	DOCUMENT ID	TECN	COMMENT
• • • We do not use the following data for averages, fits, limits, etc. • • •			
	1 AABOUD	19BA ATLS	$E_{cm}^{pp} = 13$ TeV
	2 SIRUNYAN	19AD CMS	$E_{cm}^{pp} = 13$ TeV
	3 SIRUNYAN	19CL CMS	$E_{cm}^{pp} = 13$ TeV
	4 AABOUD	18Q ATLS	$E_{cm}^{pp} = 13$ TeV
	5 SIRUNYAN	18BZ CMS	$E_{cm}^{pp} = 13$ TeV
	6 AABOUD	17s ATLS	$E_{cm}^{pp} = 7+8$ TeV
	7 AABOUD	17U ATLS	$E_{cm}^{pp} = 8$ TeV
	8 KHACHATRY..17O	CMS	$E_{cm}^{pp} = 8$ TeV
	9 SIRUNYAN	17X CMS	$E_{cm}^{pp} = 8$ TeV
	10 AAD	16AR ATLS	$E_{cm}^{pp} = 8$ TeV
	11 AAD	16P ATLS	$E_{cm}^{pp} = 8$ TeV
	12 KHACHATRY..16BI	CMS	$E_{cm}^{pp} = 8$ TeV

<sup>1</sup> AABOUD 19BA study  $WW$  production in decay modes with an electron and a muon. The charged leptons are each required to have a transverse momentum larger than 27 GeV and rapidity less than 2.5. The electron-muon system is required to have a mass larger than 55 GeV and a transverse momentum larger than 30 GeV. The missing transverse energy must be larger than 20 GeV. Events containing a jet with transverse momentum exceeding 35 GeV and rapidity smaller than 4.5 are rejected. A total of 12,659 events are selected in the data, with an expected background of  $4240 \pm 477$  events. Analysing the transverse momentum spectrum of the leading charged lepton, the following 95% C.L. limits are derived in units of  $\text{TeV}^{-2}$ :  $-3.4 < c_{WW}/\Lambda^2 < 3.3$ ,  $-7.4 < c_W/\Lambda^2 < 4.1$ ,  $-21 < c_B/\Lambda^2 < 18$ ,  $-1.6 < c_{\overline{W}W}/\Lambda^2 < 1.6$ ,  $-76 < c_{\overline{W}W}/\Lambda^2 < 76$ .

## W ANOMALOUS MAGNETIC MOMENT

The full magnetic moment is given by  $\mu_W = e(1+\kappa+\lambda)/2m_W$ . In the Standard Model, at tree level,  $\kappa=1$  and  $\lambda=0$ . Some papers have defined  $\Delta \kappa = 1-\kappa$  and assume that  $\lambda=0$ . Note that the electric quadrupole moment is given by  $-e(\kappa-\lambda)/m_W^2$ . A description of the parameterization

- <sup>2</sup> SIRUNYAN 19AD study inclusive  $WZ$  production, with  $W$  and  $Z$  decaying to electrons or muons. The leading (subleading) charged lepton candidate from the  $Z$  boson decay is required to have a transverse momentum larger than 25 GeV (10 GeV). The charged lepton candidate from the  $W$  boson decay is required to have a transverse momentum larger than 25 GeV. The invariant mass of the two leptons from  $Z$  decay is required to be within 15 GeV of the  $Z$  mass, while the invariant mass of the tri-lepton system is required to exceed 100 GeV. A total of 3,831 tri-lepton events are observed, with a fitted SM  $WZ$  signal of  $3166 \pm 62$  events and a fitted background of  $666 \pm 45$  events. The approximated  $WZ$  invariant mass distribution is analyzed to set 95% C.L. limits as follows:  $-4.1 < c_{WW}/\Lambda^2 < 1.1$ ,  $-2.0 < c_{WWW}/\Lambda^2 < 2.1$ ,  $-100 < c_B/\Lambda^2 < 160$ , in units of  $\text{TeV}^{-2}$ .
- <sup>3</sup> SIRUNYAN 19cl study  $WW$  and  $WZ$  production in lepton + jet events, with one  $W$  boson decaying leptonically (electron or muon), and another  $W$  or  $Z$  boson decaying hadronically, reconstructed as a single massive large-radius jet. In the electron channel 2,456 (2,235) events are selected in the  $W(W/Z)$  category, while in the muon channel 3,996 (3,572) events are selected in the  $W(W/Z)$  category. Analysing the di-boson invariant mass distribution, the following 95% C.L. limits are obtained in units of  $\text{TeV}^{-2}$ :  $-1.58 < c_{WWW}/\Lambda^2 < 1.59$ ,  $-2.00 < c_W/\Lambda^2 < 2.65$ ,  $-8.78 < c_B/\Lambda^2 < 8.54$ .
- <sup>4</sup> AABOUD 18q study  $pp \rightarrow ZZ$  events at  $\sqrt{s} = 13$  TeV with  $Z \rightarrow e^+e^-$  or  $Z \rightarrow \mu^+\mu^-$ . The number of events observed in the  $4e$ ,  $2e2\mu$ , and  $4\mu$  channels is 249, 465, and 303 respectively. Analysing the  $p_T$  spectrum of the leading  $Z$  boson, the following the following 95% C.L. limits are derived in units of  $\text{TeV}^{-4}$ :  $-5.9 < c_{\tilde{B}W}/\Lambda^4 < 5.9$ ,  $-3.0 < c_{WW}/\Lambda^4 < 3.0$ ,  $-3.3 < c_{BW}/\Lambda^4 < 3.3$ ,  $-2.7 < c_{BB}/\Lambda^4 < 2.8$ .
- <sup>5</sup> SIRUNYAN 18bz study  $pp \rightarrow Z$  jet events at 13 TeV where  $Z \rightarrow e^+e^-/\mu^+\mu^-$ . Isolated electrons and muons are selected with  $p_T$  of the leading/sub-leading lepton  $> 30/20$  GeV and  $|\eta| < 2.4$ , with the di-lepton invariant mass within 15 GeV of the  $Z$  mass. The two highest  $p_T$  jets are selected with  $p_T$  of the leading/sub-leading jet  $> 50/30$  GeV respectively and dijet invariant mass  $> 200$  GeV. Templates in the transverse momentum of the  $Z$  are utilized to set limits on the triple gauge couplings in the EFT and the LEP parametrizations. The following 95% C.L. limits are obtained in units of  $\text{TeV}^{-2}$ :  $-2.6 < c_{WWW}/\Lambda^2 < 2.6$  and  $-8.4 < c_W/\Lambda^2 < 10.1$ .
- <sup>6</sup> AABOUD 17s analyze electroweak production of a  $W$  boson in association with two jets at high dijet invariant mass, with the  $W$  boson decaying to electron or muon plus neutrino. In the signal region of dijet mass larger than 1 TeV and leading-jet transverse momentum larger than 600 GeV, 30 events are observed in the data with  $39 \pm 4$  events expected in the Standard Model, yielding the following limits at 95% CL for the form factor cut-off scale  $\Lambda_{FF} \rightarrow \infty$ :  $-33 < c_{WW}/\Lambda^2 < 30$ ,  $-170 < c_B/\Lambda^2 < 160$ ,  $-13 < c_{WWW}/\Lambda^2 < 9$ ,  $-580 < c_{\tilde{W}W}/\Lambda^2 < 580$ ,  $-11 < c_{\tilde{W}W}/\Lambda^2 < 11$ , in units of  $\text{TeV}^{-2}$ .
- <sup>7</sup> AABOUD 17u analyze production of  $WW$  or  $WZ$  boson pairs with one  $W$  boson decaying to electron or muon plus neutrino, and the other  $W$  or  $Z$  boson decaying hadronically. The hadronic decay system is reconstructed as either a resolved two-jet system or as a single large jet. Analysing the transverse momentum distribution of the hadronic system above 100 GeV yields the following limits at 95% CL for the form factor cut-off scale  $\Lambda_{FF} \rightarrow \infty$ :  $-3.1 < c_{WWW}/\Lambda^2 < 3.1$ ,  $-19 < c_B/\Lambda^2 < 20$ ,  $-5.1 < c_W/\Lambda^2 < 5.8$ , in units of  $\text{TeV}^{-2}$ .
- <sup>8</sup> KHACHATRYAN 17o analyse  $WZ$  production where each boson decays into electrons or muons. Events are required to have a tri-lepton invariant mass larger than 100 GeV, with one of the lepton pairs having an invariant mass within 20 GeV of the  $Z$  boson mass. The  $Z$  transverse momentum spectrum is analyzed to set 95% C.L. limits of:  $-260 < c_B/\Lambda^2 < 210$ ,  $-4.2 < c_W/\Lambda^2 < 8.0$ ,  $-4.6 < c_{WWW}/\Lambda^2 < 4.2$ , in units of  $\text{TeV}^{-2}$ .
- <sup>9</sup> SIRUNYAN 17x study  $pp \rightarrow WW/WZ \rightarrow \ell\nu q\bar{q}$  production at 8 TeV where  $\ell$  is an electron or muon with  $p_T > 30$  or 25 GeV respectively. Suitable cuts are put on the  $p_T$  of the dijet system and the missing  $E_T$  of the event yielding a total of 285 and 204  $WV$  events observed in the electron and muon channels. The following 95% C.L. limits in units of  $\text{TeV}^{-2}$  are obtained:  $-2.7 < c_{WWW}/\Lambda^2 < 2.7$ ,  $-14 < c_B/\Lambda^2 < 17$ ,  $-2.0 < c_W/\Lambda^2 < 5.7$ .
- <sup>10</sup> AAD 16AR study  $WW$  production in  $pp$  collisions and select 6636  $WW$  candidates in decay modes with electrons or muons with an expected background of  $1546 \pm 157$  events. Assuming an EFT formulation, a fit to the transverse momentum distribution of the leading charged lepton, leads to 95% C.L. ranges of:  $-4.61 < c_{WWW}/\Lambda^2 < 4.60$ ,  $-5.87 < c_W/\Lambda^2 < 10.54$  and  $-20.9 < c_B/\Lambda^2 < 26.3$ , in units of  $\text{TeV}^{-2}$ .
- <sup>11</sup> AAD 16P study  $WZ$  production in  $pp$  collisions and select 2091  $WZ$  candidates in 4 decay modes with electrons and muons, with an expected background of  $1825 \pm 7$  events. Analysing the  $WZ$  transverse momentum distribution, the resulting 95% C.L. limits are:  $-3.9 < c_{WWW}/\Lambda^2 < 4.0$ ,  $-4.3 < c_W/\Lambda^2 < 6.8$ , and  $-320 < c_B/\Lambda^2 < 210$ , in units of  $\text{TeV}^{-2}$ .
- <sup>12</sup> KHACHATRYAN 16Bi determine the  $W^+W^-$  production cross section using unlike sign di-lepton ( $e$  or  $\mu$ ) events with high  $p_T$ . The leptons have  $p_T > 20$  GeV/ $c$  and are isolated. Events are required to have no jets above  $p_T$  of 30 GeV/ $c$ . 4847 (2233) events are selected with different (same) flavor leptons, with an expected total background of  $1179 \pm 123$  (643  $\pm$  73) events. Analysing the di-lepton invariant mass spectrum, the following values are obtained:  $c_{WWW}/\Lambda^2 = 0.1 \pm 3.2$ ,  $c_W/\Lambda^2 = -3.6^{+5.0}_{-4.5}$  and  $c_B/\Lambda^2 = -3.2^{+15.0}_{-14.5}$ , in units of  $\text{TeV}^{-2}$ . The limits at 95% C.L. are:  $-5.7 < c_{WWW}/\Lambda^2 < 5.9$ ,  $-11.4 < c_W/\Lambda^2 < 5.4$  and  $-29.2 < c_B/\Lambda^2 < 23.9$ , in units of  $\text{TeV}^{-2}$ .

### ANOMALOUS W/Z QUARTIC COUPLINGS

Revised November 2015 by M.W. Grunewald (U. College Dublin) and A. Gurtu (Formerly Tata Inst.).

Quartic couplings,  $WWZZ$ ,  $WWZ\gamma$ ,  $WW\gamma\gamma$ , and  $ZZ\gamma\gamma$ , were studied at LEP and Tevatron at energies at which the Standard Model predicts negligible contributions to multiboson production. Thus, to parametrize limits on these couplings, an

effective theory approach is adopted which supplements the Standard Model Lagrangian with higher dimensional operators which include quartic couplings. The LEP collaborations chose the lowers dimensional representation of operators (dimension 6) which presumes the  $SU(2) \times U(1)$  gauge symmetry is broken by means other than the conventional Higgs scalar doublet [1–3]. In this representation possible quartic couplings,  $a_0, a_c, a_n$ , are expressed in terms of the following dimension-6 operators [1,2];

$$\begin{aligned} L_6^0 &= -\frac{e^2}{16\Lambda^2} a_0 F^{\mu\nu} F_{\mu\nu} \vec{W}^\alpha \cdot \vec{W}_\alpha \\ L_6^c &= -\frac{e^2}{16\Lambda^2} a_c F^{\mu\alpha} F_{\mu\beta} \vec{W}^\beta \cdot \vec{W}_\alpha \\ L_6^n &= -i\frac{e^2}{16\Lambda^2} a_n \epsilon_{ijk} W_{\mu\alpha}^{(i)} W_\nu^{(j)} W^{(k)\alpha} F^{\mu\nu} \\ \tilde{L}_6^0 &= -\frac{e^2}{16\Lambda^2} \tilde{a}_0 F^{\mu\nu} \tilde{F}_{\mu\nu} \vec{W}^\alpha \cdot \vec{W}_\alpha \\ \tilde{L}_6^n &= -i\frac{e^2}{16\Lambda^2} \tilde{a}_n \epsilon_{ijk} W_{\mu\alpha}^{(i)} W_\nu^{(j)} W^{(k)\alpha} \tilde{F}^{\mu\nu} \end{aligned}$$

where  $F, W$  are photon and  $W$  fields,  $L_6^0$  and  $L_6^c$  conserve  $C, P$  separately ( $\tilde{L}_6^0$  conserves only  $C$ ) and generate anomalous  $W^+W^-\gamma\gamma$  and  $ZZ\gamma\gamma$  couplings,  $L_6^n$  violates  $CP$  ( $\tilde{L}_6^n$  violates both  $C$  and  $P$ ) and generates an anomalous  $W^+W^-Z\gamma$  coupling, and  $\Lambda$  is an energy scale for new physics. For the  $ZZ\gamma\gamma$  coupling the  $CP$ -violating term represented by  $L_6^n$  does not contribute. These couplings are assumed to be real and to vanish at tree level in the Standard Model.

Within the same framework as above, a more recent description of the quartic couplings [3] treats the anomalous parts of the  $WW\gamma\gamma$  and  $ZZ\gamma\gamma$  couplings separately, leading to two sets parametrized as  $a_0^V/\Lambda^2$  and  $a_c^V/\Lambda^2$ , where  $V = W$  or  $Z$ .

With the discovery of a Higgs at the LHC in 2012, it is then useful to go to the next higher dimensional representation (dimension 8 operators) in which the gauge symmetry is broken by the conventional Higgs scalar doublet [3,4]. There are 14 operators which can contribute to the anomalous quartic coupling signal. Some of the operators have analogues in the dimension 6 scheme. The CMS collaboration, [5], have used this parametrization, in which the connections between the two schemes are also summarized:

$$\begin{aligned} \mathcal{L}_{AQGC} &= -\frac{e^2 a_0^W}{8 \Lambda^2} F_{\mu\nu} F^{\mu\nu} W^{+a} W_a^- \\ &\quad -\frac{e^2 a_c^W}{16 \Lambda^2} F_{\mu\nu} F^{\mu\alpha} (W^{+\nu} W_a^- + W^{-\nu} W_a^+) \\ &\quad -e^2 g^2 \frac{\kappa_0^W}{\Lambda^2} F_{\mu\nu} Z^{\mu\nu} W^{+a} W_a^- \\ &\quad -\frac{e^2 g^2 \kappa_c^W}{2 \Lambda^2} F_{\mu\nu} Z^{\mu\alpha} (W^{+\nu} W_a^- + W^{-\nu} W_a^+) \\ &\quad + \frac{f_{T,0}}{\Lambda^4} Tr[\widehat{W}_{\mu\nu} \widehat{W}^{\mu\nu}] \times Tr[\widehat{W}_{\alpha\beta} \widehat{W}^{\alpha\beta}] \end{aligned}$$

The energy scale of possible new physics is  $\Lambda$ , and  $g = e/\sin(\theta_W)$ ,  $e$  being the unit electric charge and  $\theta_W$  the Weinberg angle. The field tensors are described in [3,4].

The two dimension 6 operators  $a_0^W/\Lambda^2$  and  $a_c^W/\Lambda^2$  are associated with the  $WW\gamma\gamma$  vertex. Among dimension 8 operators,  $\kappa_0^W/\Lambda^2$  and  $\kappa_c^W/\Lambda^2$  are associated with the  $WWZ\gamma$  vertex, whereas the parameter  $f_{T,0}/\Lambda^4$  contributes to both vertices. There is a relationship between these two dimension 6 parameters and the dimension 8 parameters  $f_{M,i}/\Lambda^4$  as follows [3]:

$$\frac{a_0^W}{\Lambda^2} = -\frac{4M_W^2 f_{M,0}}{g^2 \Lambda^4} - \frac{8M_W^2 f_{M,2}}{g'^2 \Lambda^4}$$

$$\frac{a_c^W}{\Lambda^2} = -\frac{4M_W^2 f_{M,1}}{g^2 \Lambda^4} - \frac{8M_W^2 f_{M,3}}{g'^2 \Lambda^4}$$

where  $g' = e/\cos(\theta_W)$  and  $M_W$  is the invariant mass of the  $W$  boson. This relation provides a translation between limits on dimension 6 operators  $a_{0,c}^W$  and  $f_{M,j}/\Lambda^4$ . It is further required [4] that  $f_{M,0} = 2f_{M,2}$  and  $f_{M,1} = 2f_{M,3}$  which suppresses contributions to the  $WWZ\gamma$  vertex. The complete set of Lagrangian contributions as presented in [4] corresponds to 19 anomalous couplings in total –  $f_{S,i}$ ,  $i = 1, 2$ ,  $f_{M,i}$ ,  $i = 0, \dots, 8$  and  $f_{T,i}$ ,  $i = 0, \dots, 9$  – each scaled by  $1/\Lambda^4$ .

The ATLAS collaboration [6], on the other hand, follows a K-matrix driven approach of Ref. 7 in which the anomalous couplings can be expressed in terms of two parameters  $\alpha_4$  and  $\alpha_5$ , which account for all BSM effects.

It is the early stages in the determination of quartic couplings by the LHC experiments. It is hoped that the two collaborations, ATLAS and CMS, will agree to use at least one common set of parameters to express these limits to enable the reader to make a comparison and allow for a possible LHC combination.

## References

1. G. Belanger and F. Boudjema, Phys. Lett. **B288**, 201 (1992).
2. J.W. Stirling and A. Werthenbach, Eur. Phys. J. **C14**, 103 (2000);  
J.W. Stirling and A. Werthenbach, Phys. Lett. **B466**, 369 (1999);  
A. Denner *et al.*, Eur. Phys. J. **C20**, 201 (2001);  
G. Montagna *et al.*, Phys. Lett. **B515**, 197 (2001).
3. G. Belanger *et al.*, Eur. Phys. J. **C13**, 283 (2000).
4. O.J.P. Éboli, M.C. Gonzalez-Garcia, and S.M. Lietti, Phys. Rev. **D69**, 095005 (2004);  
O.J.P. Éboli, M.C. Gonzalez-Garcia, and J.K. Mizukoshi, Phys. Rev. **D77**, 073005 (2006).
5. S. Chatrchyan *et al.*, Phys. Rev. **D90**, 032008 (2014);  
S. Chatrchyan *et al.*, Phys. Rev. Lett. **114**, 051801 (2015).
6. G. Aad *et al.*, Phys. Rev. Lett. **113**, 141803 (2014).
7. A. Albateanu, W. Killian, and J. Reuter, JHEP **0811**, 010 (2008).

$a_0/\Lambda^2$ ,  $a_c/\Lambda^2$ ,  $a_n/\Lambda^2$ ,  $\kappa_0^W/\Lambda^2$ ,  $\kappa_c^W/\Lambda^2$ ,  $f_{T,0}/\Lambda^4$ ,  $f_{M,i}/\Lambda^4$ ,  $\alpha_4$ ,  $\alpha_5$ ,  
 $F_{S,i}/\Lambda^4$ ,  $F_{M,i}/\Lambda^4$ ,  $F_{T,i}/\Lambda^4$

Anomalous  $W$  quartic couplings are measured by the experiments at LEP, the Tevatron, and the LHC. Some of the recent results from the Tevatron and LHC experiments individually surpass the combined LEP-2 results in precision (see below). As discussed in the review on the “Anomalous  $W/Z$  quartic couplings (QGCS),” the measurements are typically done using different operator expansions which then do not allow the results to be compared and averaged. At least one common framework should be agreed upon for the use in the future publications by the experiments.

Some publications from LHC experiments derive limits for various assumed values of the form-factor cutoff  $\Lambda_{FF}$ . The values quoted below are for  $\Lambda_{FF} \rightarrow \infty$ .

VALUE	DOCUMENT ID	TECN	COMMENT
••• We do not use the following data for averages, fits, limits, etc. •••			
	1 SIRUNYAN	19BM CMS	$E_{cm}^{pp} = 13$ TeV
	2 SIRUNYAN	19BP CMS	$E_{cm}^{pp} = 13$ TeV
	3 SIRUNYAN	19CQ CMS	$E_{cm}^{pp} = 13$ TeV

4 SIRUNYAN	18CC CMS	$E_{cm}^{pp} = 13$ TeV
5 AABOUD	17AA ATLS	$E_{cm}^{pp} = 8$ TeV
6 AABOUD	17AG ATLS	$E_{cm}^{pp} = 8$ TeV
7 AABOUD	17D ATLS	$E_{cm}^{pp} = 8$ TeV
8 AABOUD	17J ATLS	$E_{cm}^{pp} = 8$ TeV
9 AABOUD	17M ATLS	$E_{cm}^{pp} = 8$ TeV
10 KHACHATRYAN	17AA CMS	$E_{cm}^{pp} = 8$ TeV
11 KHACHATRYAN	17M CMS	$E_{cm}^{pp} = 8$ TeV
12 SIRUNYAN	17AD CMS	$E_{cm}^{pp} = 13$ TeV
13 SIRUNYAN	17AR CMS	$E_{cm}^{pp} = 8$ TeV
14 AABOUD	16E ATLS	$E_{cm}^{pp} = 8$ TeV
15 AAD	16Q ATLS	$E_{cm}^{pp} = 8$ TeV
16 KHACHATRYAN	16AX CMS	$E_{cm}^{pp} = 8$ TeV
17 AAD	15N ATLS	$E_{cm}^{pp} = 8$ TeV
18 KHACHATRYAN	15D CMS	$E_{cm}^{pp} = 8$ TeV
19 AAD	14AM ATLS	
20 CHATRCHYAN	14Q CMS	
21 ABZOV	13D D0	
22 CHATRCHYAN	13AA CMS	
23 ABBIENDI	04B OPAL	
24 ABBIENDI	04L OPAL	
25 HEISTER	04A ALEP	
26 ABDALLAH	03I DLPH	
27 ACHARD	02F L3	

<sup>1</sup> SIRUNYAN 19BM search for the final state  $W^+W^-W^\pm$  using  $W$  decays to electrons or muons. Two event samples are considered, events with three leptons, or events with two oppositely charged leptons accompanied by two jets. In a kinematic region selected to enhance the effect of anomalous couplings, no events are selected in the data, and 95% C.L. upper limits are obtained as follows:  $-1.2 < f_{T,0}/\Lambda^4 < 1.2$ ,  $-3.3 < f_{T,1}/\Lambda^4 < 3.3$ ,  $-2.7 < f_{T,2}/\Lambda^4 < 2.6$ , in units of  $\text{TeV}^{-4}$  and without application of a form factor.

<sup>2</sup> SIRUNYAN 19BP study  $WZ$  plus 2 jets production, using  $W$  and  $Z$  decay channels with electrons or muons. In the data, 75 events are selected, with a fitted SM signal of  $15.1 \pm 1.6$  events and a fitted background of  $62.4 \pm 2.8$  events. The transverse mass distribution of the  $WZ$  system is analyzed to set the following limits at 95% C.L., in units of  $\text{TeV}^{-4}$ :  $-9.15 < f_{M,0}/\Lambda^4 < 9.15$ ,  $-9.15 < f_{M,1}/\Lambda^4 < 9.45$ ,  $-26.5 < f_{S,0}/\Lambda^4 < 27.5$ ,  $-41.2 < f_{S,1}/\Lambda^4 < 42.8$ ,  $-0.75 < f_{T,0}/\Lambda^4 < 0.81$ ,  $-0.49 < f_{T,1}/\Lambda^4 < 0.55$ ,  $-1.49 < f_{T,2}/\Lambda^4 < 1.85$ .

<sup>3</sup> SIRUNYAN 19CQ search for anomalous electroweak production of vector boson pairs in association with two jets. Events are selected by requiring two jets with a large invariant mass and rapidity separation, one or two leptons (electrons or muons), and a  $W$  or  $Z$  boson decaying hadronically. In the  $WV$  ( $ZV$ ) channel, 347 (47) events are selected in the data, with a total expected background of  $352 \pm 19$  ( $50.3 \pm 5.8$ ) events. Analysing the mass distribution of the  $WV$  or  $ZV$  system, the following 95% C.L. limits are obtained:  $-2.7 < f_{S,0}/\Lambda^4 < 2.7$ ,  $-3.4 < f_{S,1}/\Lambda^4 < 3.4$ ,  $-0.69 < f_{M,0}/\Lambda^4 < 0.70$ ,  $-2.0 < f_{M,1}/\Lambda^4 < 2.1$ ,  $-1.3 < f_{M,6}/\Lambda^4 < 1.3$ ,  $-3.4 < f_{M,7}/\Lambda^4 < 3.4$ ,  $-0.12 < f_{T,0}/\Lambda^4 < 0.11$ ,  $-0.12 < f_{T,1}/\Lambda^4 < 0.13$ ,  $-0.28 < f_{T,2}/\Lambda^4 < 0.28$ , in units of  $\text{TeV}^{-4}$ .

<sup>4</sup> SIRUNYAN 18CC study  $pp$  collisions at  $\sqrt{s} = 13$  TeV leading to a pair of same-sign  $W$  pairs decaying leptonically ( $e$  or  $\mu$ ) associated with a pair of jets. Isolated leptons with  $p_T > 25$  (20) GeV for the leading (trailing) lepton, with  $|\eta| < 2.5$  (2.4) for  $e$  ( $\mu$ ) and jets with  $p_T > 30$  GeV,  $|\eta| < 5.0$ ,  $|\Delta\eta_{jj}| > 2.5$  and  $m_{jj} > 500$  GeV is required. Further cuts are applied to minimize  $Z \rightarrow ee$  events, non-prompt leptons and hadronically decaying taus. The number of selected events is 201, with an expected SM signal of  $66.9 \pm 2.4$  and background of  $138 \pm 13$  events. Analysing the dilepton invariant mass spectrum the following 95% C.L. limits are derived:  $-7.7 < f_{S,0}/\Lambda^4 < 7.7$ ,  $-21.6 < f_{S,1}/\Lambda^4 < 21.8$ ,  $-6.0 < f_{M,0}/\Lambda^4 < 5.9$ ,  $-8.7 < f_{M,1}/\Lambda^4 < 9.1$ ,  $-11.9 < f_{M,6}/\Lambda^4 < 11.8$ ,  $-13.3 < f_{M,7}/\Lambda^4 < 12.9$ ,  $-0.62 < f_{T,0}/\Lambda^4 < 0.65$ ,  $-0.28 < f_{T,1}/\Lambda^4 < 0.31$ ,  $-0.89 < f_{T,2}/\Lambda^4 < 1.02$ .

<sup>5</sup> AABOUD 17AA analyze  $W^\pm W^\pm$  production in association with two jets and  $W$  decay modes with electrons or muons. In the kinematic region of VBS the effect of anomalous QGCs is enhanced by requiring the transverse mass of the  $WW$  system to be larger than 400 GeV. In the data, 8 events are selected with a total background expected from SM processes of  $3.8 \pm 0.6$  events. Assuming the other QGC coupling to have the SM value of zero, the observed event yield is used to determine 95% CL limits on the QGCs:  $-0.14 < \alpha_4 < 0.15$  and  $-0.22 < \alpha_5 < 0.22$ . Supersedes AAD 14AM.

<sup>6</sup> AABOUD 17AG determine the  $WV\gamma$  and  $WZ\gamma$  cross sections in 8 TeV  $pp$  interactions by studying the final states  $e\nu\mu\nu\gamma$  and  $e\nu jj\gamma$  or  $\mu\nu jj\gamma$ . Upper limits on the production cross sections are derived in a fiducial region optimized for BSM physics. These are used to derive the following 95% C.L. upper limits for quartic couplings assuming the form scale factor,  $\Lambda_{FF} = \infty$  (all in units of  $10^3 \text{TeV}^{-4}$ ):  $-0.3 < f_{M,0}/\Lambda^4 < 0.3$ ,  $-0.5 < f_{M,1}/\Lambda^4 < 0.5$ ,  $-1.8 < f_{M,2}/\Lambda^4 < 1.8$ ,  $-1.1 < f_{M,4}/\Lambda^4 < 1.1$ ,  $-1.7 < f_{M,5}/\Lambda^4 < 1.7$ ,  $-0.6 < f_{M,6}/\Lambda^4 < 0.6$ ,  $-1.1 < f_{M,7}/\Lambda^4 < 1.1$ ,  $-0.1 < f_{T,0}/\Lambda^4 < 0.1$ ,  $-0.2 < f_{T,1}/\Lambda^4 < 0.2$ ,  $-0.4 < f_{T,4}/\Lambda^4 < 0.4$ ,  $-1.5 < f_{T,5}/\Lambda^4 < 1.6$ ,  $-1.9 < f_{T,6}/\Lambda^4 < 1.9$ ,  $-4.3 < f_{T,7}/\Lambda^4 < 4.3$ .

<sup>7</sup> AABOUD 17D analyze electroweak diboson ( $WV$ ,  $V = W, Z$ ) production in association with a high-mass dijet system. In the data, 32 events are selected with an expected total background of  $32 \pm 12$  events. Analysing the transverse mass distribution of the  $WV$  system, the following limits are set at 95% C.L.:  $-0.024 < \alpha_4 < 0.030$  and  $-0.028 < \alpha_5 < 0.033$ .

- <sup>8</sup> AABOUD 17J analyze the  $Z\gamma$  production in association with a high-mass dijet system, with the Z boson decaying into a pair of electrons, muons, or neutrinos. In the charged lepton (neutrino) channel, events are selected with a dijet mass larger than 500 (600) GeV and a transverse photon energy larger than 250 (150) GeV, with 2 (4) events selected in the data and  $0.30 \pm 0.08$  ( $1.6 \pm 0.5$ ) expected background events. The observed event yield is used to determine 95% CL limits as follows:  $-4.1 \times 10^3 < f_{T,9}/\Lambda^4 < 4.2 \times 10^3$ ,  $-1.9 \times 10^3 < f_{T,8}/\Lambda^4 < 2.1 \times 10^3$ ,  $-1.9 \times 10^1 < f_{T,0}/\Lambda^4 < 1.6 \times 10^1$ ,  $-1.6 \times 10^2 < f_{M,0}/\Lambda^4 < 1.8 \times 10^2$ ,  $-3.5 \times 10^2 < f_{M,1}/\Lambda^4 < 3.4 \times 10^2$ ,  $-8.9 \times 10^2 < f_{M,2}/\Lambda^4 < 8.9 \times 10^2$ ,  $-1.7 \times 10^3 < f_{M,3}/\Lambda^4 < 1.7 \times 10^3$ , in units of  $\text{TeV}^{-4}$  and without application of a form factor.
- <sup>9</sup> AABOUD 17M analyze tri-boson  $W^\pm W^\pm W^\mp$  production in decay channels with three charged leptons or two like-sign charged leptons with two jets, where the lepton can be an electron or muon. In the data, 24 tri-lepton events and 21 di-lepton plus jets events are selected, compared to a total event yield expected in the SM of  $30.8 \pm 3.0$  and  $21.9 \pm 2.0$ , respectively. Analysing the tri-lepton transverse mass or the transverse momentum sum of the two leptons, two jets and the missing transverse energy, the following limits at 95% CL are derived for the form factor cut-off scale  $\Lambda_{FF} \rightarrow \infty$ :  $-0.13 < f_{S,0}/\Lambda^4 < 0.18$ ,  $-0.21 < f_{S,1}/\Lambda^4 < 0.27$ , in units of  $10^4 \text{ TeV}^{-4}$ , which are converted into the following limits:  $-0.49 < \alpha_4 < 0.75$  and  $-0.48 < \alpha_5 < 0.62$ .
- <sup>10</sup> KHACHATRYAN 17AA analyse electroweak production of  $Z\gamma$  in association with two hadronic jets, with the Z boson decaying to electron or muon pairs. Events with photon transverse momentum larger than 60 GeV and di-jet invariant mass larger than 400 GeV are selected. The  $Z\gamma$  invariant mass spectrum is analysed to set 95% C.L. limits as follows:  $-71 < f_{M,0}/\Lambda^4 < 75$ ,  $-190 < f_{M,1}/\Lambda^4 < 182$ ,  $-32 < f_{M,2}/\Lambda^4 < 31$ ,  $-58 < f_{M,3}/\Lambda^4 < 59$ ,  $-3.8 < f_{T,0}/\Lambda^4 < 3.4$ ,  $-4.4 < f_{T,1}/\Lambda^4 < 4.4$ ,  $-9.9 < f_{T,2}/\Lambda^4 < 9.0$ ,  $-1.8 < f_{T,8}/\Lambda^4 < 1.8$ ,  $-4.0 < f_{T,9}/\Lambda^4 < 4.0$ , in units of  $\text{TeV}^{-4}$  and without application of a form factor.
- <sup>11</sup> KHACHATRYAN 17M analyse electroweak production of  $W\gamma$  in association with two hadronic jets, with the W boson decaying to electrons or muons. Events with photon transverse momentum larger than 200 GeV and di-jet invariant mass larger than 200 GeV are selected. The W transverse momentum spectrum is analysed to set 95% C.L. limits as follows:  $-77 < f_{M,0}/\Lambda^4 < 74$ ,  $-125 < f_{M,1}/\Lambda^4 < 129$ ,  $-26 < f_{M,2}/\Lambda^4 < 26$ ,  $-43 < f_{M,3}/\Lambda^4 < 44$ ,  $-40 < f_{M,4}/\Lambda^4 < 40$ ,  $-65 < f_{M,5}/\Lambda^4 < 65$ ,  $-129 < f_{M,6}/\Lambda^4 < 129$ ,  $-164 < f_{M,7}/\Lambda^4 < 162$ ,  $-5.4 < f_{T,0}/\Lambda^4 < 5.6$ ,  $-3.7 < f_{T,1}/\Lambda^4 < 4.0$ ,  $-11 < f_{T,2}/\Lambda^4 < 12$ ,  $-3.8 < f_{T,5}/\Lambda^4 < 3.8$ ,  $-2.8 < f_{T,6}/\Lambda^4 < 3.0$ ,  $-7.3 < f_{T,7}/\Lambda^4 < 7.7$ , in units of  $\text{TeV}^{-4}$  and without application of a form factor.
- <sup>12</sup> SIRUNYAN 17AD study  $pp$  collisions at  $\sqrt{s} = 13 \text{ TeV}$  to determine the cross section of  $ZZjj$  with the Z decaying to  $ee$  or  $\mu\mu$ . The ZZ mass distribution is used to set upper limits on the anomalous quartic couplings. The 95% upper limits for the relevant quartic couplings in units of  $\text{TeV}^{-4}$  are:  $-0.46 < f_{T,0}/\Lambda^4 < 0.44$ ,  $-0.61 < f_{T,1}/\Lambda^4 < 0.61$ ,  $-1.2 < f_{T,2}/\Lambda^4 < 1.2$ ,  $-0.84 < f_{T,8}/\Lambda^4 < 0.84$ ,  $-1.8 < f_{T,9}/\Lambda^4 < 1.8$ .
- <sup>13</sup> SIRUNYAN 17AR study  $pp$  collisions at  $\sqrt{s} = 8 \text{ TeV}$  to determine the cross section of  $pp \rightarrow W\gamma\gamma$  and  $pp \rightarrow Z\gamma\gamma$  where  $W \rightarrow \ell\nu$  and  $Z \rightarrow \ell^+\ell^-$ ,  $\ell$  being an electron or a muon. The number of W events in the e and  $\mu$  channels is 63 and 108 respectively, and the number of Z events in the e and  $\mu$  channels is 117 and 141. To increase sensitivity, the transverse momentum of the leading photon is required to be larger than 70 GeV. The 95% C.L. upper limits in units of  $\text{TeV}^{-4}$  are  $-701 < f_{M,2}/\Lambda^4 < 683$ ,  $-1170 < f_{M,3}/\Lambda^4 < 1220$ ,  $-33.5 < f_{T,0}/\Lambda^4 < 34.0$ ,  $-44.3 < f_{T,1}/\Lambda^4 < 44.8$ ,  $-93.8 < f_{T,2}/\Lambda^4 < 93.2$ .
- <sup>14</sup> AABOUD 16E study  $WW$  production in two-photon mediated  $pp$  collisions at 8 TeV where the W boson decays into an electron or muon, probing the  $\gamma\gamma WW$  vertex for anomalous quartic gauge couplings. The lepton  $p_T$  is required to be larger than 30 GeV. Limits on anomalous couplings are determined from events with  $p_T$  larger than 120 GeV where the aQGC effect is enhanced and the SM background reduced; in the data corresponding to an integrated luminosity of  $20.2\text{fb}^{-1}$ , 1 event is selected with an expected SM background of  $0.37 \pm 0.13$  events. The 95% C.L. limits without a form-factor cutoff ( $\Lambda_{\text{cutoff}} \rightarrow \infty$ ) are as follows:  $-1.7 < a_0^W/\Lambda^2 < 1.7$  and  $-6.4 < a_C^W/\Lambda^2 < 6.3$  in units of  $10^{-6} \text{ GeV}^{-2}$ . In terms of another set of variables:  $-6.6 < f_{M,0}/\Lambda^4 < 6.6$  and  $-24 < f_{M,1}/\Lambda^4 < 25$  in units of  $10^{-11} \text{ GeV}^{-4}$ .
- <sup>15</sup> AAD 16Q study  $Z\gamma\gamma$  production in  $pp$  collisions. In events with no additional jets, 29 (22) Z decays to electron (muon) pairs are selected, with an expected background of  $3.3 \pm 1.1$  ( $6.5 \pm 2.0$ ) events, as well as 19 Z decays to neutrino pairs with an expected background of  $8.3 \pm 4.4$  events. Analysing the photon transverse momentum distribution for  $m_{\gamma\gamma}$  above 200 GeV (300 GeV) for lepton (neutrino) events, yields the 95% C.L. limits:  $-1.6 \times 10^4 < f_{M,2}/\Lambda^4 < 1.6 \times 10^4$ ,  $-2.9 \times 10^4 < f_{M,3}/\Lambda^4 < 2.7 \times 10^4$ ,  $-0.86 \times 10^2 < f_{T,0}/\Lambda^4 < 1.03 \times 10^2$ ,  $-0.69 \times 10^3 < f_{T,5}/\Lambda^4 < 0.68 \times 10^3$ ,  $-0.74 \times 10^4 < f_{T,9}/\Lambda^4 < 0.74 \times 10^4$  in units of  $\text{TeV}^{-4}$  and without application of a form factor  $\Lambda_{FF}$ .
- <sup>16</sup> KHACHATRYAN 16AX searches for anomalous  $WW\gamma\gamma$  quartic gauge couplings in the two-photon-mediated process  $pp \rightarrow ppWW$ , assuming the  $WW\gamma$  triple gauge boson couplings to be at their Standard Model values. 13 events containing an  $e^\pm\mu^\mp$  pair with  $p_T(e, \mu) > 30 \text{ GeV}$  are selected in a total luminosity of  $19.7 \text{ fb}^{-1}$ , with an expected  $\gamma\gamma$  to  $WW$  signal of  $5.3 \pm 0.1$  events and an expected background of  $3.9 \pm 0.5$  events. When combining with the data collected at 7 TeV (KHACHATRYAN 13AA), and not assuming a form factor, the following 1-parameter limits at 95% C.L. are obtained from the  $p_T(e, \mu)$  spectrum:  $|a_0^W/\Lambda^2| < 1.1 \times 10^{-6} \text{ GeV}^{-2}$  ( $a_C^W = 0$ ), and  $|a_C^W/\Lambda^2| < 4.1 \times 10^{-6} \text{ GeV}^{-2}$  ( $a_0^W = 0$ ). In terms of another set of variables:  $|f_{M,0}/\Lambda^4| < 4.2 \times 10^{-12} \text{ GeV}^{-4}$ ,  $|f_{M,1}/\Lambda^4| < 16 \times 10^{-12} \text{ GeV}^{-4}$ ,  $|f_{M,2}/\Lambda^4| < 2.1 \times 10^{-12} \text{ GeV}^{-4}$ ,  $|f_{M,3}/\Lambda^4| < 7.8 \times 10^{-12} \text{ GeV}^{-4}$ .
- <sup>17</sup> AAD 15N study  $W\gamma\gamma$  events in 8 TeV  $pp$  interactions, where the W decays into an electron or a muon. The events are characterized by an isolated lepton, a missing transverse energy due to the decay neutrino, and two isolated photons, with the  $p_T$  of the lepton and the photons being  $> 20 \text{ GeV}$ . The number of candidate events observed in the
- electron channel for  $N(\text{jet}) \geq 0$  and  $N(\text{jet}) = 0$  is 47 and 15, the corresponding numbers for the muon channel being 110 and 53. The backgrounds expected are  $30.2 \pm 7.4$ ,  $8.7 \pm 3.0$ ,  $52.1 \pm 12.2$ , and  $24.4 \pm 8.3$  respectively. The 95% C.L. limits on the values of the parameters  $f_{T,0}/\Lambda^4$ ,  $f_{M,2}/\Lambda^4$  and  $f_{M,3}/\Lambda^4$  are  $-0.9$ – $0.9 \times 10^2$ ,  $-0.8$ – $0.8 \times 10^4$ , and  $-1.5$ – $1.4 \times 10^4$  respectively, without application of a form factor  $\Lambda_{FF}$ .
- <sup>18</sup> KHACHATRYAN 15D study vector-boson-scattering tagged by two jets, requiring two same-sign charged leptons arising from  $W^\pm W^\pm$  production and decay. The two jets must have a transverse momentum larger than 30 GeV, while the leptons, electrons or muons, must have a transverse momentum  $> 20 \text{ GeV}$ . The dijet mass is required to be  $> 500 \text{ GeV}$ , the dilepton mass  $> 50 \text{ GeV}$ , with additional requirement of differing from the Z mass by  $> 15 \text{ GeV}$ . In the two categories  $W^+W^+$  and  $W^-W^-$ , 10 and 2 data events are observed in a data sample corresponding to an integrated luminosity of  $19.4 \text{ fb}^{-1}$ , with an expected background of  $3.1 \pm 0.6$  and  $2.6 \pm 0.5$  events. Analysing the distribution of the dilepton invariant mass, the following limits at 95% C.L. are obtained, in units of  $\text{TeV}^{-4}$ :  $-38 < f_{S,0}/\Lambda^4 < 40$ ,  $-118 < f_{S,1}/\Lambda^4 < 120$ ,  $-33 < f_{M,0}/\Lambda^4 < 32$ ,  $-44 < f_{M,1}/\Lambda^4 < 47$ ,  $-65 < f_{M,6}/\Lambda^4 < 63$ ,  $-70 < f_{M,7}/\Lambda^4 < 66$ ,  $-4.2 < f_{T,0}/\Lambda^4 < 4.6$ ,  $-1.9 < f_{T,1}/\Lambda^4 < 2.2$ ,  $-5.2 < f_{T,2}/\Lambda^4 < 6.4$ .
- <sup>19</sup> AAD 14AM analyze electroweak production of  $WW$  jet jet same-charge diboson plus two jets production, with the W bosons decaying to electron or muon, to study the quartic  $WWWW$  coupling. In a kinematic region enhancing the electroweak production over the strong production, 34 events are observed in the data while  $29.8 \pm 2.4$  events are expected with a background of  $15.9 \pm 1.9$  events. Assuming the other QGC coupling to have the SM value of zero, the observed event yield is used to determine 95% CL limits on the quartic gauge couplings:  $-0.14 < \alpha_4 < 0.16$  and  $-0.23 < \alpha_5 < 0.24$ .
- <sup>20</sup> CHATRCHYAN 14Q study  $WV\gamma$  production in 8 TeV  $pp$  collisions, in the single lepton final state, with  $W \rightarrow \ell\nu$ ,  $Z \rightarrow \text{dijet}$  or  $W \rightarrow \ell\nu$ ,  $W \rightarrow \text{dijet}$ , the dijet mass resolution precluding differentiation between the W and Z.  $p_T$  and pseudo-rapidity cuts are put on the lepton, the photon and the two jets to minimize backgrounds. The dijet mass is required to be between 70–100 GeV and  $|\Delta\eta_{jj}| < 1.4$ . The selected number of muon (electron) events are 183 (139), with SM expectation being  $194.2 \pm 11.5$  ( $147.9 \pm 10.7$ ) including signal and background. The photon  $E_T$  distribution is used to set limits on the anomalous quartic couplings. The following 95% CL limits are deduced (all in units of  $\text{TeV}^{-2}$  or  $\text{TeV}^{-4}$ ):  $-21 < a_0^W/\Lambda^2 < 20$ ,  $-34 < a_C^W/\Lambda^2 < 32$ ,  $-12 < \kappa_0^W/\Lambda^2 < 10$  and  $-18 < \kappa_C^W/\Lambda^2 < 17$ ; and  $-25 < f_{T,0}/\Lambda^4 < 24 \text{ TeV}^{-4}$ .
- <sup>21</sup> ABAZOV 13D searches for anomalous  $WW\gamma\gamma$  quartic gauge couplings in the two-photon-mediated process  $pp \rightarrow ppWW$ , assuming the  $WW\gamma$  triple gauge boson couplings to be at their Standard Model values. 946 events containing an  $e^+e^-$  pair with missing energy are selected in a total luminosity of  $9.7 \text{ fb}^{-1}$ , with an expectation of  $983 \pm 108$  events from Standard-Model processes. The following 1-parameter limits at 95% CL are obtained:  $|a_0^W/\Lambda^2| < 4.3 \times 10^{-4} \text{ GeV}^{-2}$  ( $a_C^W = 0$ ),  $|a_C^W/\Lambda^2| < 1.5 \times 10^{-3} \text{ GeV}^{-2}$  ( $a_0^W = 0$ ).
- <sup>22</sup> CHATRCHYAN 13AA searches for anomalous  $WW\gamma\gamma$  quartic gauge couplings in the two-photon-mediated process  $pp \rightarrow ppWW$ , assuming the  $WW\gamma$  triple gauge boson couplings to be at their Standard Model values. 2 events containing an  $e^\pm\mu^\mp$  pair with  $p_T(e, \mu) > 30 \text{ GeV}$  are selected in a total luminosity of  $5.05 \text{ fb}^{-1}$ , with an expected  $ppWW$  signal of  $2.2 \pm 0.4$  events and an expected background of  $0.84 \pm 0.15$  events. The following 1-parameter limits at 95% CL are obtained from the  $p_T(e, \mu)$  spectrum:  $|a_0^W/\Lambda^2| < 4.0 \times 10^{-6} \text{ GeV}^{-2}$  ( $a_C^W = 0$ ),  $|a_C^W/\Lambda^2| < 1.5 \times 10^{-5} \text{ GeV}^{-2}$  ( $a_0^W = 0$ ).
- <sup>23</sup> ABBIENDI 04B select  $187 e^+e^- \rightarrow W^+W^-\gamma$  events in the C.M. energy range 180–209 GeV, where  $E_\gamma > 2.5 \text{ GeV}$ , the photon has a polar angle  $|\cos\theta_\gamma| < 0.975$  and is well isolated from the nearest jet and charged lepton, and the effective masses of both fermion-antifermion systems agree with the W mass within  $3\Gamma_W$ . The measured differential cross section as a function of the photon energy and photon polar angle is used to extract the 95% CL limits:  $-0.020 \text{ GeV}^{-2} < a_0/\Lambda^2 < 0.020 \text{ GeV}^{-2}$ ,  $-0.053 \text{ GeV}^{-2} < a_C/\Lambda^2 < 0.037 \text{ GeV}^{-2}$  and  $-0.16 \text{ GeV}^{-2} < a_n/\Lambda^2 < 0.15 \text{ GeV}^{-2}$ .
- <sup>24</sup> ABBIENDI 04L select  $20 e^+e^- \rightarrow \nu\bar{\nu}\gamma$  acoplanar events in the energy range 180–209 GeV and  $176 e^+e^- \rightarrow q\bar{q}\gamma\gamma$  events in the energy range 130–209 GeV. These samples are used to constrain possible anomalous  $W^+W^-\gamma\gamma$  and  $ZZ\gamma\gamma$  quartic couplings. Further combining with the  $W^+W^-\gamma$  sample of ABBIENDI 04B the following one-parameter 95% CL limits are obtained:  $-0.007 < a_0^Z/\Lambda^2 < 0.023 \text{ GeV}^{-2}$ ,  $-0.029 < a_C^Z/\Lambda^2 < 0.029 \text{ GeV}^{-2}$ ,  $-0.020 < a_0^W/\Lambda^2 < 0.020 \text{ GeV}^{-2}$ ,  $-0.052 < a_C^W/\Lambda^2 < 0.037 \text{ GeV}^{-2}$ .
- <sup>25</sup> In the CM energy range 183 to 209 GeV HEISTER 04A select  $30 e^+e^- \rightarrow \nu\bar{\nu}\gamma\gamma$  events with two acoplanar, high energy and high transverse momentum photons. The photon-photon acoplanarity is required to be  $> 5^\circ$ ,  $E_\gamma/\sqrt{s} > 0.025$  (the more energetic photon having energy  $> 0.2\sqrt{s}$ ),  $p_{T,\gamma}/E_{\text{beam}} > 0.05$  and  $|\cos\theta_\gamma| < 0.94$ . A likelihood fit to the photon energy and recoil missing mass yields the following one-parameter 95% CL limits:  $-0.012 < a_0^Z/\Lambda^2 < 0.019 \text{ GeV}^{-2}$ ,  $-0.041 < a_C^Z/\Lambda^2 < 0.044 \text{ GeV}^{-2}$ ,  $-0.060 < a_0^W/\Lambda^2 < 0.055 \text{ GeV}^{-2}$ ,  $-0.099 < a_C^W/\Lambda^2 < 0.093 \text{ GeV}^{-2}$ .
- <sup>26</sup> ABDALLAH 03I select  $122 e^+e^- \rightarrow W^+W^-\gamma$  events in the C.M. energy range 189–209 GeV, where  $E_\gamma > 5 \text{ GeV}$ , the photon has a polar angle  $|\cos\theta_\gamma| < 0.95$  and is well isolated from the nearest charged fermion. A fit to the photon energy spectra yields  $a_C/\Lambda^2 = 0.000 \pm 0.019 \text{ GeV}^{-2}$ ,  $a_0/\Lambda^2 = -0.004 \pm 0.018 \text{ GeV}^{-2}$ ,  $\bar{a}_0/\Lambda^2 = -0.007 \pm 0.019 \text{ GeV}^{-2}$ ,  $\bar{a}_n/\Lambda^2 = -0.09 \pm 0.16 \text{ GeV}^{-2}$ , and  $\bar{a}_n/\Lambda^2 = +0.05 \pm 0.07 \text{ GeV}^{-2}$ , keeping the other parameters fixed to their Standard Model values (0). The 95% CL limits are:  $-0.063 \text{ GeV}^{-2} < a_C/\Lambda^2 < +0.032 \text{ GeV}^{-2}$ ,  $-0.020 \text{ GeV}^{-2} < a_0/\Lambda^2 < +0.020 \text{ GeV}^{-2}$ ,  $-0.020 \text{ GeV}^{-2} < \bar{a}_0/\Lambda^2 < +0.020 \text{ GeV}^{-2}$ ,  $-0.18 \text{ GeV}^{-2} < \bar{a}_n/\Lambda^2 < +0.14 \text{ GeV}^{-2}$ ,  $-0.16 \text{ GeV}^{-2} < \bar{a}_n/\Lambda^2 < +0.17 \text{ GeV}^{-2}$ .
- <sup>27</sup> ACHARD 02F select  $86 e^+e^- \rightarrow W^+W^-\gamma$  events at 192–207 GeV, where  $E_\gamma > 5 \text{ GeV}$  and the photon is well isolated. They also select 43 acoplanar  $e^+e^- \rightarrow \nu\bar{\nu}\gamma\gamma$  events in this energy range, where the photon energies are  $> 5 \text{ GeV}$  and  $> 1 \text{ GeV}$  and the photon polar angles are between  $14^\circ$  and  $166^\circ$ . All these 43 events are in the recoil mass region corresponding to the Z (75–110 GeV). Using the shape and normalization of the photon spectra in the  $W^+W^-\gamma$  events, and combining with the 42 event sample from





• • • We do not use the following data for averages, fits, limits, etc. • • •

91.084 ± 0.107		5	ANDREEV	18A	H1	$e^\pm \rho$
91.1872 ± 0.0033		6	ABBIENDI	04G	OPAL	$E_{cm}^{ee} = \text{LEP1} + 130\text{--}209 \text{ GeV}$
91.272 ± 0.032 ± 0.033		7	ACHARD	04c	L3	$E_{cm}^{ee} = 183\text{--}209 \text{ GeV}$
91.1875 ± 0.0039	3.97M	8	ACCIARRI	00Q	L3	$E_{cm}^{ee} = \text{LEP1} + 130\text{--}189 \text{ GeV}$
91.151 ± 0.008		9	MIYABAYASHI	95	TOPZ	$E_{cm}^{ee} = 57.8 \text{ GeV}$
91.74 ± 0.28 ± 0.93	156	10	ALITTI	92B	UA2	$E_{cm}^{pp} = 630 \text{ GeV}$
90.9 ± 0.3 ± 0.2	188	11	ABE	89c	CDF	$E_{cm}^{pp} = 1.8 \text{ TeV}$
91.14 ± 0.12	480	12	ABRAMS	89B	MRK2	$E_{cm}^{ee} = 89\text{--}93 \text{ GeV}$
93.1 ± 1.0 ± 3.0	24	13	ALBAJAR	89	UA1	$E_{cm}^{pp} = 546,630 \text{ GeV}$

- ABBIENDI 01A error includes approximately 2.3 MeV due to statistics and 1.8 MeV due to LEP energy uncertainty.
- The error includes 1.6 MeV due to LEP energy uncertainty.
- The error includes 1.8 MeV due to LEP energy uncertainty.
- BARATE 00c error includes approximately 2.4 MeV due to statistics, 0.2 MeV due to experimental systematics, and 1.7 MeV due to LEP energy uncertainty.
- ANDREEV 18A obtain this result in a combined electroweak and QCD analysis using all deep-inelastic  $e^+p$  and  $e^-p$  neutral current and charged current scattering cross sections published by the H1 Collaboration, including data with longitudinally polarized lepton beams.
- ABBIENDI 04G obtain this result using the S-matrix formalism for a combined fit to their cross section and asymmetry data at the Z peak and their data at 130–209 GeV. The authors have corrected the measurement for the 34 MeV shift with respect to the Breit-Wigner fits.
- ACHARD 04c select  $e^+e^- \rightarrow Z\gamma$  events with hard initial-state radiation. Z decays to  $q\bar{q}$  and muon pairs are considered. The fit results obtained in the two samples are found consistent to each other and combined considering the uncertainty due to ISR modelling as fully correlated.
- ACCIARRI 00q interpret the s-dependence of the cross sections and lepton forward-backward asymmetries in the framework of the S-matrix formalism. They fit to their cross section and asymmetry data at high energies, using the results of S-matrix fits to Z-peak data (ACCIARRI 00c) as constraints. The 130–189 GeV data constrains the  $\gamma/Z$  interference term. The authors have corrected the measurement for the 34.1 MeV shift with respect to the Breit-Wigner fits. The error contains a contribution of  $\pm 2.3 \text{ MeV}$  due to the uncertainty on the  $\gamma Z$  interference.
- MIYABAYASHI 95 combine their low energy total hadronic cross-section measurement with the ACTON 93D data and perform a fit using an S-matrix formalism. As expected, this result is below the mass values obtained with the standard Breit-Wigner parametrization.
- Enters fit through  $W/Z$  mass ratio given in the W Particle Listings. The ALITTI 92B systematic error ( $\pm 0.93$ ) has two contributions: one ( $\pm 0.92$ ) cancels in  $m_W/m_Z$  and one ( $\pm 0.12$ ) is noncancelling. These were added in quadrature.
- First error of ABE 89 is combination of statistical and systematic contributions; second is mass scale uncertainty.
- ABRAMS 89B uncertainty includes 35 MeV due to the absolute energy measurement.
- ALBAJAR 89 result is from a total sample of  $33 Z \rightarrow e^+e^-$  events.

Z WIDTH

OUR FIT is obtained using the fit procedure and correlations as determined by the LEP Electroweak Working Group (see the note "The Z boson" and ref. LEP-SLC 06).

VALUE (GeV)	EVTS	DOCUMENT ID	TECN	COMMENT
<b>2.4952 ± 0.0023 OUR FIT</b>				
2.4948 ± 0.0041	4.57M	1 ABBIENDI	01A OPAL	$E_{cm}^{ee} = 88\text{--}94 \text{ GeV}$
2.4876 ± 0.0041	4.08M	2 ABREU	00F DLPH	$E_{cm}^{ee} = 88\text{--}94 \text{ GeV}$
2.5024 ± 0.0042	3.96M	3 ACCIARRI	00C L3	$E_{cm}^{ee} = 88\text{--}94 \text{ GeV}$
2.4951 ± 0.0043	4.57M	4 BARATE	00C ALEP	$E_{cm}^{ee} = 88\text{--}94 \text{ GeV}$
• • • We do not use the following data for averages, fits, limits, etc. • • •				
2.4943 ± 0.0041		5 ABBIENDI	04G OPAL	$E_{cm}^{ee} = \text{LEP1} + 130\text{--}209 \text{ GeV}$
2.5025 ± 0.0041	3.97M	6 ACCIARRI	00Q L3	$E_{cm}^{ee} = \text{LEP1} + 130\text{--}189 \text{ GeV}$
2.50 ± 0.21 ± 0.06		7 ABREU	96R DLPH	$E_{cm}^{ee} = 91.2 \text{ GeV}$
3.8 ± 0.8 ± 1.0	188	8 ABE	89c CDF	$E_{cm}^{pp} = 1.8 \text{ TeV}$
2.42 $\begin{smallmatrix} +0.45 \\ -0.35 \end{smallmatrix}$ ± 1.0	480	9 ABRAMS	89B MRK2	$E_{cm}^{ee} = 89\text{--}93 \text{ GeV}$
2.7 $\begin{smallmatrix} +1.2 \\ -1.0 \end{smallmatrix}$ ± 1.3	24	10 ALBAJAR	89 UA1	$E_{cm}^{pp} = 546,630 \text{ GeV}$
2.7 ± 2.0 ± 1.0	25	11 ANSARI	87 UA2	$E_{cm}^{pp} = 546,630 \text{ GeV}$

- ABBIENDI 01A error includes approximately 3.6 MeV due to statistics, 1 MeV due to event selection systematics, and 1.3 MeV due to LEP energy uncertainty.
- The error includes 1.2 MeV due to LEP energy uncertainty.
- The error includes 1.3 MeV due to LEP energy uncertainty.
- BARATE 00c error includes approximately 3.8 MeV due to statistics, 0.9 MeV due to experimental systematics, and 1.3 MeV due to LEP energy uncertainty.
- ABBIENDI 04G obtain this result using the S-matrix formalism for a combined fit to their cross section and asymmetry data at the Z peak and their data at 130–209 GeV. The authors have corrected the measurement for the 1 MeV shift with respect to the Breit-Wigner fits.
- ACCIARRI 00q interpret the s-dependence of the cross sections and lepton forward-backward asymmetries in the framework of the S-matrix formalism. They fit to their cross section and asymmetry data at high energies, using the results of S-matrix fits to Z-peak data (ACCIARRI 00c) as constraints. The 130–189 GeV data constrains the  $\gamma/Z$  interference term. The authors have corrected the measurement for the 0.9 MeV shift with respect to the Breit-Wigner fits.

- ABREU 96R obtain this value from a study of the interference between initial and final state radiation in the process  $e^+e^- \rightarrow Z \rightarrow \mu^+\mu^-$ .
- ABRAMS 89B uncertainty includes 50 MeV due to the miniSAM background subtraction error.
- ALBAJAR 89 result is from a total sample of  $33 Z \rightarrow e^+e^-$  events.
- Quoted values of ANSARI 87 are from direct fit. Ratio of Z and W production gives either  $\Gamma(Z) < (1.09 \pm 0.07) \times \Gamma(W)$ , CL = 90% or  $\Gamma(Z) = (0.82^{+0.19}_{-0.14} \pm 0.06) \times \Gamma(W)$ . Assuming Standard-Model value  $\Gamma(W) = 2.65 \text{ GeV}$  then gives  $\Gamma(Z) < 2.89 \pm 0.19$  or  $= 2.17^{+0.50}_{-0.37} \pm 0.16$ .

Z DECAY MODES

Mode	Fraction ( $\Gamma_i/\Gamma$ )	Scale factor / Confidence level
Γ <sub>1</sub> $e^+e^-$	[a] ( 3.3632 ± 0.0042 ) %	
Γ <sub>2</sub> $\mu^+\mu^-$	[a] ( 3.3662 ± 0.0066 ) %	
Γ <sub>3</sub> $\tau^+\tau^-$	[a] ( 3.3696 ± 0.0083 ) %	
Γ <sub>4</sub> $\ell^+\ell^-$	[a,b] ( 3.3658 ± 0.0023 ) %	
Γ <sub>5</sub> $\mu^+\mu^-\mu^+\mu^-$		
Γ <sub>6</sub> $\ell^+\ell^-\ell^+\ell^-$		
Γ <sub>7</sub> invisible	[c] ( 4.63 ± 0.21 ) × 10 <sup>-6</sup>	
Γ <sub>8</sub> hadrons	[a] ( 69.911 ± 0.056 ) %	
Γ <sub>9</sub> $(u\bar{u} + c\bar{c})/2$	( 11.6 ± 0.6 ) %	
Γ <sub>10</sub> $(d\bar{d} + s\bar{s} + b\bar{b})/3$	( 15.6 ± 0.4 ) %	
Γ <sub>11</sub> $c\bar{c}$	( 12.03 ± 0.21 ) %	
Γ <sub>12</sub> $b\bar{b}$	( 15.12 ± 0.05 ) %	
Γ <sub>13</sub> $b\bar{b}b\bar{b}$	( 3.6 ± 1.3 ) × 10 <sup>-4</sup>	
Γ <sub>14</sub> $ggg$	< 1.1 %	CL=95%
Γ <sub>15</sub> $\pi^0\gamma$	< 2.01 × 10 <sup>-5</sup>	CL=95%
Γ <sub>16</sub> $\eta\gamma$	< 5.1 × 10 <sup>-5</sup>	CL=95%
Γ <sub>17</sub> $\rho^0\gamma$	< 2.5 × 10 <sup>-5</sup>	CL=95%
Γ <sub>18</sub> $\omega\gamma$	< 6.5 × 10 <sup>-4</sup>	CL=95%
Γ <sub>19</sub> $\eta'(958)\gamma$	< 4.2 × 10 <sup>-5</sup>	CL=95%
Γ <sub>20</sub> $\phi\gamma$	< 9 × 10 <sup>-7</sup>	CL=95%
Γ <sub>21</sub> $\gamma\gamma$	< 1.46 × 10 <sup>-5</sup>	CL=95%
Γ <sub>22</sub> $\pi^0\pi^0$	< 1.52 × 10 <sup>-5</sup>	CL=95%
Γ <sub>23</sub> $\gamma\gamma\gamma$	< 2.2 × 10 <sup>-6</sup>	CL=95%
Γ <sub>24</sub> $\pi^\pm W^\mp$	[d] < 7 × 10 <sup>-5</sup>	CL=95%
Γ <sub>25</sub> $\rho^\pm W^\mp$	[d] < 8.3 × 10 <sup>-5</sup>	CL=95%
Γ <sub>26</sub> $J/\psi(1S)X$	( 3.51 $\begin{smallmatrix} +0.23 \\ -0.25 \end{smallmatrix}$ ) × 10 <sup>-3</sup>	S=1.1
Γ <sub>27</sub> $J/\psi(1S)\gamma$	< 1.4 × 10 <sup>-6</sup>	CL=95%
Γ <sub>28</sub> $\psi(2S)X$	( 1.60 ± 0.29 ) × 10 <sup>-3</sup>	
Γ <sub>29</sub> $\psi(2S)\gamma$	< 4.5 × 10 <sup>-6</sup>	CL=95%
Γ <sub>30</sub> $J/\psi(1S)\ell^+\ell^-$		
Γ <sub>31</sub> $J/\psi(1S)J/\psi(1S)$	< 2.2 × 10 <sup>-6</sup>	CL=95%
Γ <sub>32</sub> $\chi_{c1}(1P)X$	( 2.9 ± 0.7 ) × 10 <sup>-3</sup>	
Γ <sub>33</sub> $\chi_{c2}(1P)X$	< 3.2 × 10 <sup>-3</sup>	CL=90%
Γ <sub>34</sub> $\Upsilon(1S)X + \Upsilon(2S)X + \Upsilon(3S)X$	( 1.0 ± 0.5 ) × 10 <sup>-4</sup>	
Γ <sub>35</sub> $\Upsilon(1S)X$	< 3.4 × 10 <sup>-6</sup>	CL=95%
Γ <sub>36</sub> $\Upsilon(1S)\gamma$	< 2.8 × 10 <sup>-6</sup>	CL=95%
Γ <sub>37</sub> $\Upsilon(2S)X$	< 6.5 × 10 <sup>-6</sup>	CL=95%
Γ <sub>38</sub> $\Upsilon(2S)\gamma$	< 1.7 × 10 <sup>-6</sup>	CL=95%
Γ <sub>39</sub> $\Upsilon(3S)X$	< 5.4 × 10 <sup>-6</sup>	CL=95%
Γ <sub>40</sub> $\Upsilon(3S)\gamma$	< 4.8 × 10 <sup>-6</sup>	CL=95%
Γ <sub>41</sub> $\Upsilon(1,2,3S)\Upsilon(1,2,3S)$	< 1.5 × 10 <sup>-6</sup>	CL=95%
Γ <sub>42</sub> $(D^0/\bar{D}^0)X$	( 20.7 ± 2.0 ) %	
Γ <sub>43</sub> $D^\pm X$	( 12.2 ± 1.7 ) %	
Γ <sub>44</sub> $D^*(2010)^\pm X$	[d] ( 11.4 ± 1.3 ) %	
Γ <sub>45</sub> $D_{s1}(2536)^\pm X$	( 3.6 ± 0.8 ) × 10 <sup>-3</sup>	
Γ <sub>46</sub> $D_{sJ}(2573)^\pm X$	( 5.8 ± 2.2 ) × 10 <sup>-3</sup>	
Γ <sub>47</sub> $D^{*'}(2629)^\pm X$	searched for	
Γ <sub>48</sub> $BX$		
Γ <sub>49</sub> $B^*X$		
Γ <sub>50</sub> $B^+X$	[e] ( 6.08 ± 0.13 ) %	
Γ <sub>51</sub> $B_s^0X$	[e] ( 1.59 ± 0.13 ) %	
Γ <sub>52</sub> $B_c^\pm X$	searched for	
Γ <sub>53</sub> $\Lambda_c^+ X$	( 1.54 ± 0.33 ) %	
Γ <sub>54</sub> $\Xi_c^0 X$	seen	
Γ <sub>55</sub> $\Xi_b X$	seen	
Γ <sub>56</sub> $b$ -baryon X	[e] ( 1.38 ± 0.22 ) %	
Γ <sub>57</sub> anomalous $\gamma$ + hadrons	[f] < 3.2 × 10 <sup>-3</sup>	CL=95%
Γ <sub>58</sub> $e^+e^- \gamma$	[f] < 5.2 × 10 <sup>-4</sup>	CL=95%
Γ <sub>59</sub> $\mu^+\mu^- \gamma$	[f] < 5.6 × 10 <sup>-4</sup>	CL=95%
Γ <sub>60</sub> $\tau^+\tau^- \gamma$	[f] < 7.3 × 10 <sup>-4</sup>	CL=95%
Γ <sub>61</sub> $\ell^+\ell^- \gamma\gamma$	[g] < 6.8 × 10 <sup>-6</sup>	CL=95%

## Gauge &amp; Higgs Boson Particle Listings

## Z

$\Gamma_{62}$	$q\bar{q}\gamma\gamma$		$[g] < 5.5$	$\times 10^{-6}$	CL=95%
$\Gamma_{63}$	$\nu\bar{\nu}\gamma\gamma$		$[g] < 3.1$	$\times 10^{-6}$	CL=95%
$\Gamma_{64}$	$e^{\pm}\mu^{\mp}$	LF	$[d] < 7.5$	$\times 10^{-7}$	CL=95%
$\Gamma_{65}$	$e^{\pm}\tau^{\mp}$	LF	$[d] < 9.8$	$\times 10^{-6}$	CL=95%
$\Gamma_{66}$	$\mu^{\pm}\tau^{\mp}$	LF	$[d] < 1.2$	$\times 10^{-5}$	CL=95%
$\Gamma_{67}$	$\rho e$	L,B	$< 1.8$	$\times 10^{-6}$	CL=95%
$\Gamma_{68}$	$\rho\mu$	L,B	$< 1.8$	$\times 10^{-6}$	CL=95%

[a] This parameter is not directly used in the overall fit but is derived using the fit results; see the note "The Z boson" and ref. LEP-SLC 06 (Physics Reports (Physics Letters C) **427** 257 (2006)).

[b]  $\ell$  indicates each type of lepton ( $e$ ,  $\mu$ , and  $\tau$ ), not sum over them.

[c] Here  $\ell$  indicates  $e$  or  $\mu$ .

[d] The value is for the sum of the charge states or particle/antiparticle states indicated.

[e] This value is updated using the product of (i) the  $Z \rightarrow b\bar{b}$  fraction from this listing and (ii) the  $b$ -hadron fraction in an unbiased sample of weakly decaying  $b$ -hadrons produced in Z-decays provided by the Heavy Flavor Averaging Group (HFLAV, [http://www.slac.stanford.edu/xorg/hflav/osc/PDG\\_2009/#FRACZ](http://www.slac.stanford.edu/xorg/hflav/osc/PDG_2009/#FRACZ)).

[f] See the Particle Listings below for the  $\gamma$  energy range used in this measurement.

[g] For  $m_{\gamma\gamma} = (60 \pm 5)$  GeV.

## Z PARTIAL WIDTHS

$\Gamma(e^+e^-)$   $\Gamma_1$   
For the LEP experiments, this parameter is not directly used in the overall fit but is derived using the fit results; see the note "The Z boson" and ref. LEP-SLC 06.

VALUE (MeV)	EVTS	DOCUMENT ID	TECN	COMMENT
<b>83.91 ± 0.12 OUR FIT</b>				
83.66 ± 0.20	137.0K	ABBIENDI	01A OPAL	$E_{cm}^{ee} = 88-94$ GeV
83.54 ± 0.27	117.8k	ABREU	00F DLPH	$E_{cm}^{ee} = 88-94$ GeV
84.16 ± 0.22	124.4k	ACCIARRI	00c L3	$E_{cm}^{ee} = 88-94$ GeV
83.88 ± 0.19		BARATE	00c ALEP	$E_{cm}^{ee} = 88-94$ GeV
82.89 ± 1.20 ± 0.89		<sup>1</sup> ABE	95J SLD	$E_{cm}^{ee} = 91.31$ GeV

<sup>1</sup> ABE 95J obtain this measurement from Bhabha events in a restricted fiducial region to improve systematics. They use the values 91.187 and 2.489 GeV for the Z mass and total decay width to extract this partial width.

$\Gamma(\mu^+\mu^-)$   $\Gamma_2$   
This parameter is not directly used in the overall fit but is derived using the fit results; see the note "The Z boson" and ref. LEP-SLC 06.

VALUE (MeV)	EVTS	DOCUMENT ID	TECN	COMMENT
<b>83.99 ± 0.18 OUR FIT</b>				
84.03 ± 0.30	182.8K	ABBIENDI	01A OPAL	$E_{cm}^{ee} = 88-94$ GeV
84.48 ± 0.40	157.6k	ABREU	00F DLPH	$E_{cm}^{ee} = 88-94$ GeV
83.95 ± 0.44	113.4k	ACCIARRI	00c L3	$E_{cm}^{ee} = 88-94$ GeV
84.02 ± 0.28		BARATE	00c ALEP	$E_{cm}^{ee} = 88-94$ GeV

$\Gamma(\tau^+\tau^-)$   $\Gamma_3$   
This parameter is not directly used in the overall fit but is derived using the fit results; see the note "The Z boson" and ref. LEP-SLC 06.

VALUE (MeV)	EVTS	DOCUMENT ID	TECN	COMMENT
<b>84.08 ± 0.22 OUR FIT</b>				
83.94 ± 0.41	151.5K	ABBIENDI	01A OPAL	$E_{cm}^{ee} = 88-94$ GeV
83.71 ± 0.58	104.0k	ABREU	00F DLPH	$E_{cm}^{ee} = 88-94$ GeV
84.23 ± 0.58	103.0k	ACCIARRI	00c L3	$E_{cm}^{ee} = 88-94$ GeV
84.38 ± 0.31		BARATE	00c ALEP	$E_{cm}^{ee} = 88-94$ GeV

$\Gamma(\ell^+\ell^-)$   $\Gamma_4$   
 $\ell$  indicates each type of lepton ( $e$ ,  $\mu$ , and  $\tau$ ), not sum over them.

In our fit  $\Gamma(\ell^+\ell^-)$  is defined as the partial Z width for the decay into a pair of massless charged leptons. This parameter is not directly used in the 5-parameter fit assuming lepton universality but is derived using the fit results. See the note "The Z boson" and ref. LEP-SLC 06.

VALUE (MeV)	EVTS	DOCUMENT ID	TECN	COMMENT
<b>83.984 ± 0.086 OUR FIT</b>				
83.82 ± 0.15	471.3K	ABBIENDI	01A OPAL	$E_{cm}^{ee} = 88-94$ GeV
83.85 ± 0.17	379.4k	ABREU	00F DLPH	$E_{cm}^{ee} = 88-94$ GeV
84.14 ± 0.17	340.8k	ACCIARRI	00c L3	$E_{cm}^{ee} = 88-94$ GeV
84.02 ± 0.15	500k	BARATE	00c ALEP	$E_{cm}^{ee} = 88-94$ GeV

$\Gamma(\text{invisible})$   $\Gamma_7$   
We use only direct measurements of the invisible partial width using the single photon channel to obtain the average value quoted below. OUR FIT value is obtained as a difference between the total and the observed partial widths assuming lepton universality.

VALUE (MeV)	EVTS	DOCUMENT ID	TECN	COMMENT
<b>499.0 ± 1.5 OUR FIT</b>				
<b>503 ± 16 OUR AVERAGE</b>	Error includes scale factor of 1.2.			
498 ± 12 ± 12	1791	ACCIARRI	98G L3	$E_{cm}^{ee} = 88-94$ GeV
539 ± 26 ± 17	410	AKERS	95c OPAL	$E_{cm}^{ee} = 88-94$ GeV
450 ± 34 ± 34	258	BUSKULIC	93L ALEP	$E_{cm}^{ee} = 88-94$ GeV
540 ± 80 ± 40	52	ADEVA	92 L3	$E_{cm}^{ee} = 88-94$ GeV
• • •	We do not use the following data for averages, fits, limits, etc. • • •			
498.1 ± 2.6		<sup>1</sup> ABBIENDI	01A OPAL	$E_{cm}^{ee} = 88-94$ GeV
498.1 ± 3.2		<sup>1</sup> ABREU	00F DLPH	$E_{cm}^{ee} = 88-94$ GeV
499.1 ± 2.9		<sup>1</sup> ACCIARRI	00c L3	$E_{cm}^{ee} = 88-94$ GeV
499.1 ± 2.5		<sup>1</sup> BARATE	00c ALEP	$E_{cm}^{ee} = 88-94$ GeV

<sup>1</sup> This is an indirect determination of  $\Gamma(\text{invisible})$  from a fit to the visible Z decay modes.

$\Gamma(\text{hadrons})$   $\Gamma_8$   
This parameter is not directly used in the 5-parameter fit assuming lepton universality, but is derived using the fit results. See the note "The Z boson" and ref. LEP-SLC 06.

VALUE (MeV)	EVTS	DOCUMENT ID	TECN	COMMENT
<b>1744.4 ± 2.0 OUR FIT</b>				
1745.4 ± 3.5	4.10M	ABBIENDI	01A OPAL	$E_{cm}^{ee} = 88-94$ GeV
1738.1 ± 4.0	3.70M	ABREU	00F DLPH	$E_{cm}^{ee} = 88-94$ GeV
1751.1 ± 3.8	3.54M	ACCIARRI	00c L3	$E_{cm}^{ee} = 88-94$ GeV
1744.0 ± 3.4	4.07M	BARATE	00c ALEP	$E_{cm}^{ee} = 88-94$ GeV

## Z BRANCHING RATIOS

OUR FIT is obtained using the fit procedure and correlations as determined by the LEP Electroweak Working Group (see the note "The Z boson" and ref. LEP-SLC 06).

VALUE	DOCUMENT ID	TECN	COMMENT	$\Gamma_2/\Gamma_1$
<b>1.0001 ± 0.0024 OUR AVERAGE</b>				
0.9974 ± 0.0050	<sup>1</sup> AABOUD	17Q ATLS	$E_{cm}^{pp} = 7$ TeV	
1.0009 ± 0.0028	<sup>2</sup> LEP-SLC	06	$E_{cm}^{ee} = 88-94$ GeV	

<sup>1</sup> AABOUD 17Q make a precise determination of  $Z \rightarrow ee$  and  $Z \rightarrow \mu\mu$  production in the lepton pseudo-rapidity range  $|\eta| < 2.5$  and determine the ratio of the Z branching fractions  $B(Z \rightarrow ee)/B(Z \rightarrow \mu\mu) = 1.0026 \pm 0.0013 \pm 0.0048 = 1.0026 \pm 0.0050$ .

<sup>2</sup> This parameter is not directly used in the overall fit but is derived using the fit results; see the note "The Z boson" and ref. LEP-SLC 06.

VALUE	DOCUMENT ID	TECN	COMMENT	$\Gamma_3/\Gamma_1$
<b>1.0020 ± 0.0032 OUR AVERAGE</b>				
1.02 ± 0.06	<sup>1</sup> AAIJ	18AR LHCB	$E_{cm}^{pp} = 8$ TeV	
1.0019 ± 0.0032	<sup>2</sup> LEP-SLC	06	$E_{cm}^{ee} = 88-94$ GeV	

<sup>1</sup> AAIJ 18AR obtain the result from the ratio of the measured  $pp \rightarrow Z + X$  cross sections in the corresponding Z decay channels.

<sup>2</sup> This parameter is not directly used in the overall fit but is derived using the fit results; see the note "The Z boson" and ref. LEP-SLC 06.

VALUE	DOCUMENT ID	TECN	COMMENT	$\Gamma_3/\Gamma_2$
<b>1.0010 ± 0.0026 OUR AVERAGE</b>				
1.01 ± 0.05	<sup>1</sup> AAIJ	18AR LHCB	$E_{cm}^{pp} = 8$ TeV	
1.0010 ± 0.0026	<sup>2</sup> LEP-SLC	06	$E_{cm}^{ee} = 88-94$ GeV	

<sup>1</sup> AAIJ 18AR obtain the result from the ratio of the measured  $pp \rightarrow Z + X$  cross sections in the corresponding Z decay channels.

<sup>2</sup> This parameter is not directly used in the overall fit but is derived using the fit results; see the note "The Z boson" and ref. LEP-SLC 06.

VALUE (units $10^{-6}$ )	EVTS	DOCUMENT ID	TECN	COMMENT	$\Gamma_6/\Gamma_{\text{total}}$
<b>4.63 ± 0.21 OUR AVERAGE</b>					
4.70 ± 0.32 ± 0.25		<sup>1</sup> AABOUD	19N ATLS	$E_{cm}^{pp} = 13$ TeV	
4.83 <sup>+0.23+0.35</sup> <sub>-0.22-0.32</sub>	509	<sup>2</sup> SIRUNYAN	18BT CMS	$E_{cm}^{pp} = 13$ TeV	
4.9 <sup>+0.8+0.4</sup> <sub>-0.7-0.2</sub>	39	<sup>3</sup> KHACHATRY...	16cc CMS	$E_{cm}^{pp} = 13$ TeV	
4.31 ± 0.34 ± 0.17	172	AAD	14N ATLS	$E_{cm}^{pp} = 7, 8$ TeV	
4.6 <sup>+1.0</sup> <sub>-0.9</sub> ± 0.2	28	<sup>4</sup> CHATRCHYAN12BN	CMS	$E_{cm}^{pp} = 7$ TeV	

Here  $\ell$  indicates either  $e$  or  $\mu$ . The branching fractions in this note are given within the phase-space defined by the requirements that (i) the 4-lepton invariant mass is between 80 GeV and 100 GeV, and (ii) any opposite-sign same-flavor lepton pair has a di-lepton invariant mass larger than 4 GeV.

- <sup>1</sup> AABOUD 19N reports  $(4.70 \pm 0.32 \pm 0.21 \pm 0.14) \times 10^{-6}$ , where the uncertainties are statistical, systematic, and luminosity. We have combined the latter two in quadrature.
- <sup>2</sup> SIRUNYAN 18BT report the  $Z \rightarrow 4\ell$  branching fraction =  $(4.83^{+0.23+0.32}_{-0.22-0.29} \pm 0.08 \pm 0.12) \times 10^{-6}$ , where the uncertainties are statistical, systematic, due to theory, and luminosity. The last three have been added in quadrature to obtain the total systematic error.
- <sup>3</sup> KHACHATRYAN 16CC reports  $(4.9^{+0.8+0.3+0.2+0.1}_{-0.7-0.2-0.1-0.1}) \times 10^{-6}$  value, where the uncertainties are statistical, systematic, theory, and due to luminosity. We have combined uncertainties in quadrature.
- <sup>4</sup> CHATRCHYAN 12BN reports  $(4.2^{+0.9}_{-0.8} \pm 0.2) \times 10^{-6}$  value. Their result (both central value and uncertainties) is scaled up by 10% to account for the different phase-space definition used here (see RAINBOLT 19).

**$\Gamma(\text{hadrons})/\Gamma(e^+e^-)$   $\Gamma_8/\Gamma_1$**

VALUE	EVTS	DOCUMENT ID	TECN	COMMENT
<b>20.804 ± 0.050 OUR FIT</b>				
20.902 ± 0.084	137.0K	<sup>1</sup> ABBIENDI	01A OPAL	$E_{cm}^{ee} = 88-94$ GeV
20.88 ± 0.12	117.8k	ABREU	00F DLPH	$E_{cm}^{ee} = 88-94$ GeV
20.816 ± 0.089	124.4k	ACCIARRI	00C L3	$E_{cm}^{ee} = 88-94$ GeV
20.677 ± 0.075		<sup>2</sup> BARATE	00C ALEP	$E_{cm}^{ee} = 88-94$ GeV
27.0 $\pm_{-8.8}^{+11.7}$	12	<sup>3</sup> ABRAMS	89D MRK2	$E_{cm}^{ee} = 89-93$ GeV

- • • We do not use the following data for averages, fits, limits, etc. • • •
- <sup>1</sup> ABBIENDI 01A error includes approximately 0.067 due to statistics, 0.040 due to event selection systematics, 0.027 due to the theoretical uncertainty in  $t$ -channel prediction, and 0.014 due to LEP energy uncertainty.
- <sup>2</sup> BARATE 00C error includes approximately 0.062 due to statistics, 0.033 due to experimental systematics, and 0.026 due to the theoretical uncertainty in  $t$ -channel prediction.
- <sup>3</sup> ABRAMS 89D have included both statistical and systematic uncertainties in their quoted errors.

**$\Gamma(\text{hadrons})/\Gamma(\mu^+\mu^-)$   $\Gamma_8/\Gamma_2$**

OUR FIT is obtained using the fit procedure and correlations as determined by the LEP Electroweak Working Group (see the note "The Z boson" and ref. LEP-SLC 06).

VALUE	EVTS	DOCUMENT ID	TECN	COMMENT
<b>20.785 ± 0.033 OUR FIT</b>				
20.811 ± 0.058	182.8K	<sup>1</sup> ABBIENDI	01A OPAL	$E_{cm}^{ee} = 88-94$ GeV
20.65 ± 0.08	157.6k	ABREU	00F DLPH	$E_{cm}^{ee} = 88-94$ GeV
20.861 ± 0.097	113.4k	ACCIARRI	00C L3	$E_{cm}^{ee} = 88-94$ GeV
20.799 ± 0.056		<sup>2</sup> BARATE	00C ALEP	$E_{cm}^{ee} = 88-94$ GeV
18.9 $\pm_{-5.3}^{+7.1}$	13	<sup>3</sup> ABRAMS	89D MRK2	$E_{cm}^{ee} = 89-93$ GeV

- • • We do not use the following data for averages, fits, limits, etc. • • •
- <sup>1</sup> ABBIENDI 01A error includes approximately 0.050 due to statistics and 0.027 due to event selection systematics.
- <sup>2</sup> BARATE 00C error includes approximately 0.053 due to statistics and 0.021 due to experimental systematics.
- <sup>3</sup> ABRAMS 89D have included both statistical and systematic uncertainties in their quoted errors.

**$\Gamma(\text{hadrons})/\Gamma(\tau^+\tau^-)$   $\Gamma_8/\Gamma_3$**

OUR FIT is obtained using the fit procedure and correlations as determined by the LEP Electroweak Working Group (see the note "The Z boson" and ref. LEP-SLC 06).

VALUE	EVTS	DOCUMENT ID	TECN	COMMENT
<b>20.764 ± 0.045 OUR FIT</b>				
20.832 ± 0.091	151.5K	<sup>1</sup> ABBIENDI	01A OPAL	$E_{cm}^{ee} = 88-94$ GeV
20.84 ± 0.13	104.0k	ABREU	00F DLPH	$E_{cm}^{ee} = 88-94$ GeV
20.792 ± 0.133	103.0k	ACCIARRI	00C L3	$E_{cm}^{ee} = 88-94$ GeV
20.707 ± 0.062		<sup>2</sup> BARATE	00C ALEP	$E_{cm}^{ee} = 88-94$ GeV
15.2 $\pm_{-3.9}^{+4.8}$	21	<sup>3</sup> ABRAMS	89D MRK2	$E_{cm}^{ee} = 89-93$ GeV

- • • We do not use the following data for averages, fits, limits, etc. • • •
- <sup>1</sup> ABBIENDI 01A error includes approximately 0.055 due to statistics and 0.071 due to event selection systematics.
- <sup>2</sup> BARATE 00C error includes approximately 0.054 due to statistics and 0.033 due to experimental systematics.
- <sup>3</sup> ABRAMS 89D have included both statistical and systematic uncertainties in their quoted errors.

**$\Gamma(\text{hadrons})/\Gamma(\ell^+\ell^-)$   $\Gamma_8/\Gamma_4$**

$\ell$  indicates each type of lepton ( $e$ ,  $\mu$ , and  $\tau$ ), not sum over them.

Our fit result is obtained requiring lepton universality.

VALUE	EVTS	DOCUMENT ID	TECN	COMMENT
<b>20.767 ± 0.025 OUR FIT</b>				
20.823 ± 0.044	471.3K	<sup>1</sup> ABBIENDI	01A OPAL	$E_{cm}^{ee} = 88-94$ GeV
20.730 ± 0.060	379.4k	ABREU	00F DLPH	$E_{cm}^{ee} = 88-94$ GeV
20.810 ± 0.060	340.8k	ACCIARRI	00C L3	$E_{cm}^{ee} = 88-94$ GeV
20.725 ± 0.039	500k	<sup>2</sup> BARATE	00C ALEP	$E_{cm}^{ee} = 88-94$ GeV
18.9 $\pm_{-3.2}^{+3.6}$	46	ABRAMS	89B MRK2	$E_{cm}^{ee} = 89-93$ GeV

- • • We do not use the following data for averages, fits, limits, etc. • • •
- <sup>1</sup> ABBIENDI 01A error includes approximately 0.034 due to statistics and 0.027 due to event selection systematics.
- <sup>2</sup> BARATE 00C error includes approximately 0.033 due to statistics, 0.020 due to experimental systematics, and 0.005 due to the theoretical uncertainty in  $t$ -channel prediction.

**$\Gamma((u\bar{u} + c\bar{c})/2)/\Gamma(\text{hadrons})$   $\Gamma_9/\Gamma_8$**

This quantity is the branching ratio of  $Z \rightarrow$  "up-type" quarks to  $Z \rightarrow$  hadrons. Except ACKERSTAFF 97T the values of  $Z \rightarrow$  "up-type" and  $Z \rightarrow$  "down-type" branchings are extracted from measurements of  $\Gamma(\text{hadrons})$ , and  $\Gamma(Z \rightarrow \gamma + \text{jets})$  where  $\gamma$  is a high-energy ( $>5$  or 7 GeV) isolated photon. As the experiments use different procedures and slightly different values of  $M_Z$ ,  $\Gamma(\text{hadrons})$  and  $\alpha_s$  in their extraction procedures, our average has to be taken with caution.

VALUE	DOCUMENT ID	TECN	COMMENT
<b>0.166 ± 0.009 OUR AVERAGE</b>			
0.172 $\pm_{-0.010}^{+0.011}$	<sup>1</sup> ABBIENDI	04E OPAL	$E_{cm}^{ee} = 91.2$ GeV
0.160 ± 0.019 ± 0.019	<sup>2</sup> ACKERSTAFF	97T OPAL	$E_{cm}^{ee} = 88-94$ GeV
0.137 $\pm_{-0.054}^{+0.038}$	<sup>3</sup> ABREU	95X DLPH	$E_{cm}^{ee} = 88-94$ GeV
0.137 ± 0.033	<sup>4</sup> ADRIANI	93 L3	$E_{cm}^{ee} = 91.2$ GeV

- <sup>1</sup> ABBIENDI 04E select photons with energy  $> 7$  GeV and use  $\Gamma(\text{hadrons}) = 1744.4 \pm 2.0$  MeV and  $\alpha_s = 0.1172 \pm 0.002$  to obtain  $\Gamma_u = 300^{+19}_{-18}$  MeV.
- <sup>2</sup> ACKERSTAFF 97T measure  $\Gamma_{u\bar{u}}/\Gamma_{d\bar{d}+u\bar{u}+s\bar{s}} = 0.258 \pm 0.031 \pm 0.032$ . To obtain this branching ratio authors use  $R_c + R_b = 0.380 \pm 0.010$ . This measurement is fully negatively correlated with the measurement of  $\Gamma_{d\bar{d},s\bar{s}}/\Gamma_{d\bar{d}+u\bar{u}+s\bar{s}}$  given in the next data block.
- <sup>3</sup> ABREU 95X use  $M_Z = 91.187 \pm 0.009$  GeV,  $\Gamma(\text{hadrons}) = 1725 \pm 12$  MeV and  $\alpha_s = 0.123 \pm 0.005$ . To obtain this branching ratio we divide their value of  $C_{2/3} = 0.91 \pm 0.25_{-0.36}$  by their value of  $(3C_{1/3} + 2C_{2/3}) = 6.66 \pm 0.05$ .
- <sup>4</sup> ADRIANI 93 use  $M_Z = 91.181 \pm 0.022$  GeV,  $\Gamma(\text{hadrons}) = 1742 \pm 19$  MeV and  $\alpha_s = 0.125 \pm 0.009$ . To obtain this branching ratio we divide their value of  $C_{2/3} = 0.92 \pm 0.22$  by their value of  $(3C_{1/3} + 2C_{2/3}) = 6.720 \pm 0.076$ .

**$\Gamma((d\bar{d} + s\bar{s} + b\bar{b})/3)/\Gamma(\text{hadrons})$   $\Gamma_{10}/\Gamma_8$**

This quantity is the branching ratio of  $Z \rightarrow$  "down-type" quarks to  $Z \rightarrow$  hadrons. Except ACKERSTAFF 97T the values of  $Z \rightarrow$  "up-type" and  $Z \rightarrow$  "down-type" branchings are extracted from measurements of  $\Gamma(\text{hadrons})$ , and  $\Gamma(Z \rightarrow \gamma + \text{jets})$  where  $\gamma$  is a high-energy ( $>5$  or 7 GeV) isolated photon. As the experiments use different procedures and slightly different values of  $M_Z$ ,  $\Gamma(\text{hadrons})$  and  $\alpha_s$  in their extraction procedures, our average has to be taken with caution.

VALUE	DOCUMENT ID	TECN	COMMENT
<b>0.223 ± 0.006 OUR AVERAGE</b>			
0.218 ± 0.007	<sup>1</sup> ABBIENDI	04E OPAL	$E_{cm}^{ee} = 91.2$ GeV
0.230 ± 0.010 ± 0.010	<sup>2</sup> ACKERSTAFF	97T OPAL	$E_{cm}^{ee} = 88-94$ GeV
0.243 $\pm_{-0.026}^{+0.036}$	<sup>3</sup> ABREU	95X DLPH	$E_{cm}^{ee} = 88-94$ GeV
0.243 ± 0.022	<sup>4</sup> ADRIANI	93 L3	$E_{cm}^{ee} = 91.2$ GeV

- <sup>1</sup> ABBIENDI 04E select photons with energy  $> 7$  GeV and use  $\Gamma(\text{hadrons}) = 1744.4 \pm 2.0$  MeV and  $\alpha_s = 0.1172 \pm 0.002$  to obtain  $\Gamma_d = 381 \pm 12$  MeV.
- <sup>2</sup> ACKERSTAFF 97T measure  $\Gamma_{d\bar{d},s\bar{s}}/\Gamma_{d\bar{d}+u\bar{u}+s\bar{s}} = 0.371 \pm 0.016 \pm 0.016$ . To obtain this branching ratio authors use  $R_c + R_b = 0.380 \pm 0.010$ . This measurement is fully negatively correlated with the measurement of  $\Gamma_{u\bar{u}}/\Gamma_{d\bar{d}+u\bar{u}+s\bar{s}}$  presented in the previous data block.
- <sup>3</sup> ABREU 95X use  $M_Z = 91.187 \pm 0.009$  GeV,  $\Gamma(\text{hadrons}) = 1725 \pm 12$  MeV and  $\alpha_s = 0.123 \pm 0.005$ . To obtain this branching ratio we divide their value of  $C_{1/3} = 1.62 \pm 0.24_{-0.17}$  by their value of  $(3C_{1/3} + 2C_{2/3}) = 6.66 \pm 0.05$ .
- <sup>4</sup> ADRIANI 93 use  $M_Z = 91.181 \pm 0.022$  GeV,  $\Gamma(\text{hadrons}) = 1742 \pm 19$  MeV and  $\alpha_s = 0.125 \pm 0.009$ . To obtain this branching ratio we divide their value of  $C_{1/3} = 1.63 \pm 0.15$  by their value of  $(3C_{1/3} + 2C_{2/3}) = 6.720 \pm 0.076$ .

**$R_c = \Gamma(c\bar{c})/\Gamma(\text{hadrons})$   $\Gamma_{11}/\Gamma_8$**

OUR FIT is obtained by a simultaneous fit to several  $c$ - and  $b$ -quark measurements as explained in the note "The Z boson" and ref. LEP-SLC 06.

The Standard Model predicts  $R_c = 0.1723$  for  $m_t = 174.3$  GeV and  $M_H = 150$  GeV.

VALUE	DOCUMENT ID	TECN	COMMENT
<b>0.1721 ± 0.0030 OUR FIT</b>			
0.1744 ± 0.0031 ± 0.0021	<sup>1</sup> ABE	05F SLD	$E_{cm}^{ee} = 91.28$ GeV
0.1665 ± 0.0051 ± 0.0081	<sup>2</sup> ABREU	00 DLPH	$E_{cm}^{ee} = 88-94$ GeV
0.1698 ± 0.0069	<sup>3</sup> BARATE	00B ALEP	$E_{cm}^{ee} = 88-94$ GeV
0.180 ± 0.011 ± 0.013	<sup>4</sup> ACKERSTAFF	98E OPAL	$E_{cm}^{ee} = 88-94$ GeV
0.167 ± 0.011 ± 0.012	<sup>5</sup> ALEXANDER	96R OPAL	$E_{cm}^{ee} = 88-94$ GeV
0.1623 ± 0.0085 ± 0.0209	<sup>6</sup> ABREU	95D DLPH	$E_{cm}^{ee} = 88-94$ GeV

- • • We do not use the following data for averages, fits, limits, etc. • • •
- <sup>1</sup> ABE 05F use hadronic Z decays collected during 1996-98 to obtain an enriched sample of  $c\bar{c}$  events using a double tag method. The single  $c$ -tag is obtained with a neural network trained to perform flavor discrimination using as input several signatures (corrected secondary vertex mass, vertex decay length, multiplicity and total momentum of the hemisphere). A multitag approach is used, defining 4 regions of the output value of the neural network and  $R_c$  is extracted from a simultaneous fit to the count rates of the 4 different tags. The quoted systematic error includes an uncertainty of  $\pm 0.0006$  due to the uncertainty on  $R_b$ .
- <sup>2</sup> ABREU 00 obtain this result properly combining the measurement from the  $D^{*+}$  production rate ( $R_c = 0.1610 \pm 0.0104 \pm 0.0077 \pm 0.0043$  (BR)) with that from the overall charm counting ( $R_c = 0.1692 \pm 0.0047 \pm 0.0063 \pm 0.0074$  (BR)) in  $c\bar{c}$  events. The systematic error includes an uncertainty of  $\pm 0.0054$  due to the uncertainty on the charmed hadron branching fractions.
- <sup>3</sup> BARATE 00B use exclusive decay modes to independently determine the quantities  $R_c \times f(c \rightarrow X)$ ,  $X = D^0, D^+, D_s^+, \text{ and } \Lambda_c$ . Estimating  $R_c \times f(c \rightarrow \Xi_c / \Omega_c) = 0.0034$ , they simply sum over all the charm decays to obtain  $R_c = 0.1738 \pm 0.0047 \pm 0.0088 \pm$

## Gauge &amp; Higgs Boson Particle Listings

## Z

0.0075(BR). This is combined with all previous ALEPH measurements (BARATE 98T and BUSKULIC 94G,  $R_C = 0.1681 \pm 0.0054 \pm 0.0062$ ) to obtain the quoted value.

<sup>4</sup>ACKERSTAFF 98E use an inclusive/exclusive double tag. In one jet  $D^{*\pm}$  mesons are exclusively reconstructed in several decay channels and in the opposite jet a slow pion (opposite charge inclusive  $D^{*\pm}$ ) tag is used. The  $b$  content of this sample is measured by the simultaneous detection of a lepton in one jet and an inclusively reconstructed  $D^{*\pm}$  meson in the opposite jet. The systematic error includes an uncertainty of  $\pm 0.006$  due to the external branching ratios.

<sup>5</sup>ALEXANDER 96R obtain this value via direct charm counting, summing the partial contributions from  $D^0$ ,  $D^+$ ,  $D_S^+$ , and  $\Lambda_C^+$ , and assuming that strange-charmed baryons account for the 15% of the  $\Lambda_C^+$  production. An uncertainty of  $\pm 0.005$  due to the uncertainties in the charm hadron branching ratios is included in the overall systematics.

<sup>6</sup>ABREU 95D perform a maximum likelihood fit to the combined  $p$  and  $p_T$  distributions of single and dilepton samples. The second error includes an uncertainty of  $\pm 0.0124$  due to models and branching ratios.

### $R_b = \Gamma(b\bar{b})/\Gamma(\text{hadrons})$ $\Gamma_{12}/\Gamma_8$

OUR FIT is obtained by a simultaneous fit to several  $c$ - and  $b$ -quark measurements as explained in the note "The Z boson" and ref. LEP-SLC 06.

The Standard Model predicts  $R_b = 0.21581$  for  $m_t = 174.3$  GeV and  $M_H = 150$  GeV.

VALUE	DOCUMENT ID	TECN	COMMENT
<b>0.21629 ± 0.00066 OUR FIT</b>			
0.21594 ± 0.00094 ± 0.00075	<sup>1</sup> ABE	05F SLD	$E_{cm}^{ee} = 91.28$ GeV
0.2174 ± 0.0015 ± 0.0028	<sup>2</sup> ACCIARRI	00 L3	$E_{cm}^{ee} = 89-93$ GeV
0.2178 ± 0.0011 ± 0.0013	<sup>3</sup> ABBIENDI	99B OPAL	$E_{cm}^{ee} = 88-94$ GeV
0.21634 ± 0.00067 ± 0.00060	<sup>4</sup> ABREU	99B DLPH	$E_{cm}^{ee} = 88-94$ GeV
0.2159 ± 0.0009 ± 0.0011	<sup>5</sup> BARATE	97F ALEP	$E_{cm}^{ee} = 88-94$ GeV
• • • We do not use the following data for averages, fits, limits, etc. • • •			
0.2145 ± 0.0089 ± 0.0067	<sup>6</sup> ABREU	95D DLPH	$E_{cm}^{ee} = 88-94$ GeV
0.219 ± 0.006 ± 0.005	<sup>7</sup> BUSKULIC	94G ALEP	$E_{cm}^{ee} = 88-94$ GeV
0.251 ± 0.049 ± 0.030	<sup>8</sup> JACOBSEN	91 MRK2	$E_{cm}^{ee} = 91$ GeV

<sup>1</sup>ABE 05F use hadronic Z decays collected during 1996-98 to obtain an enriched sample of  $b\bar{b}$  events using a double tag method. The single b-tag is obtained with a neural network trained to perform flavor discrimination using as input several signatures (corrected secondary vertex mass, vertex decay length, multiplicity and total momentum of the hemisphere; the key tag is obtained requiring the secondary vertex corrected mass to be above the  $D$ -meson mass). ABE 05F obtain  $R_b = 0.21604 \pm 0.00098 \pm 0.00074$  where the systematic error includes an uncertainty of  $\pm 0.00012$  due to the uncertainty on  $R_C$ . The value reported here is obtained properly combining with ABE 98D. The quoted systematic error includes an uncertainty of  $\pm 0.00012$  due to the uncertainty on  $R_C$ .

<sup>2</sup>ACCIARRI 00 obtain this result using a double-tagging technique, with a high  $p_T$  lepton tag and an impact parameter tag in opposite hemispheres.

<sup>3</sup>ABBIENDI 99B tag  $Z \rightarrow b\bar{b}$  decays using leptons and/or separated decay vertices. The b-tagging efficiency is measured directly from the data using a double-tagging technique.

<sup>4</sup>ABREU 99B obtain this result combining in a multivariate analysis several tagging methods (impact parameter and secondary vertex reconstruction, complemented by event shape variables). For  $R_C$  different from its Standard Model value of 0.172,  $R_b$  varies as  $-0.024 \times (R_C - 0.172)$ .

<sup>5</sup>BARATE 97F combine the lifetime-mass hemisphere tag (BARATE 97E) with event shape information and lepton tag to identify  $Z \rightarrow b\bar{b}$  candidates. They further use  $c$ - and  $u$   $d$ -selection tags to identify the background. For  $R_C$  different from its Standard Model value of 0.172,  $R_b$  varies as  $-0.019 \times (R_C - 0.172)$ .

<sup>6</sup>ABREU 95D perform a maximum likelihood fit to the combined  $p$  and  $p_T$  distributions of single and dilepton samples. The second error includes an uncertainty of  $\pm 0.0023$  due to models and branching ratios.

<sup>7</sup>BUSKULIC 94G perform a simultaneous fit to the  $p$  and  $p_T$  spectra of both single and dilepton events.

<sup>8</sup>JACOBSEN 91 tagged  $b\bar{b}$  events by requiring coincidence of  $\geq 3$  tracks with significant impact parameters using vertex detector. Systematic error includes lifetime and decay uncertainties ( $\pm 0.014$ ).

### $\Gamma(b\bar{b}b\bar{b})/\Gamma(\text{hadrons})$ $\Gamma_{13}/\Gamma_8$

VALUE (units $10^{-4}$ )	DOCUMENT ID	TECN	COMMENT
<b>5.2 ± 1.9 OUR AVERAGE</b>			
3.6 ± 1.7 ± 2.7	<sup>1</sup> ABBIENDI	01G OPAL	$E_{cm}^{ee} = 88-94$ GeV
6.0 ± 1.9 ± 1.4	<sup>2</sup> ABREU	99u DLPH	$E_{cm}^{ee} = 88-94$ GeV

<sup>1</sup>ABBIENDI 01G use a sample of four-jet events from hadronic Z decays. To enhance the  $b\bar{b}b\bar{b}$  signal, at least three of the four jets are required to have a significantly detached secondary vertex.

<sup>2</sup>ABREU 99u force hadronic Z decays into 3jets to use all the available phase space and require a b tag for every jet. This decay mode includes primary and secondary 4b production, e.g. from gluon splitting to  $b\bar{b}$ .

### $\Gamma(ggg)/\Gamma(\text{hadrons})$ $\Gamma_{14}/\Gamma_8$

VALUE	CL%	DOCUMENT ID	TECN	COMMENT
<b>&lt;1.6 × 10<sup>-2</sup></b>	95	<sup>1</sup> ABREU	96S DLPH	$E_{cm}^{ee} = 88-94$ GeV

<sup>1</sup>This branching ratio is slightly dependent on the jet-finder algorithm. The value we quote is obtained using the JADE algorithm, while using the DURHAM algorithm ABREU 96S obtain an upper limit of  $1.5 \times 10^{-2}$ .

### $\Gamma(\pi^0\gamma)/\Gamma_{\text{total}}$ $\Gamma_{15}/\Gamma$

VALUE	CL%	DOCUMENT ID	TECN	COMMENT
<b>&lt;2.01 × 10<sup>-5</sup></b>	95	AALTONEN	14E CDF	$E_{cm}^{pp} = 1.96$ TeV
<5.2 × 10 <sup>-5</sup>	95	<sup>1</sup> ACCIARRI	95G L3	$E_{cm}^{ee} = 88-94$ GeV
<5.5 × 10 <sup>-5</sup>	95	ABREU	94B DLPH	$E_{cm}^{ee} = 88-94$ GeV
<2.1 × 10 <sup>-4</sup>	95	DECAMP	92 ALEP	$E_{cm}^{ee} = 88-94$ GeV
<1.4 × 10 <sup>-4</sup>	95	AKRAWY	91F OPAL	$E_{cm}^{ee} = 88-94$ GeV

<sup>1</sup>This limit is for both decay modes  $Z \rightarrow \pi^0\gamma/\gamma\gamma$  which are indistinguishable in ACCIARRI 95G.

### $\Gamma(\eta\gamma)/\Gamma_{\text{total}}$ $\Gamma_{16}/\Gamma$

VALUE	CL%	DOCUMENT ID	TECN	COMMENT
<7.6 × 10 <sup>-5</sup>	95	ACCIARRI	95G L3	$E_{cm}^{ee} = 88-94$ GeV
<8.0 × 10 <sup>-5</sup>	95	ABREU	94B DLPH	$E_{cm}^{ee} = 88-94$ GeV
<b>&lt;5.1 × 10<sup>-5</sup></b>	95	DECAMP	92 ALEP	$E_{cm}^{ee} = 88-94$ GeV
<2.0 × 10 <sup>-4</sup>	95	AKRAWY	91F OPAL	$E_{cm}^{ee} = 88-94$ GeV

### $\Gamma(\rho^0\gamma)/\Gamma_{\text{total}}$ $\Gamma_{17}/\Gamma$

VALUE	CL%	EVTS	DOCUMENT ID	TECN	COMMENT
<b>&lt;2.5 × 10<sup>-5</sup></b>	95	12.5k	<sup>1</sup> AABOUD	18AU ATLS	$E_{cm}^{pp} = 13$ TeV

<sup>1</sup>AABOUD 18AU search for the  $Z \rightarrow \rho\gamma$  decay mode where the  $\rho$  is identified through its decay  $\rho \rightarrow \pi^+\pi^-$ . In the data corresponding to  $32.3 \text{ fb}^{-1}$ , 12,583 events are selected for  $635 < m(\pi^+\pi^-) < 915$  MeV.

### $\Gamma(\omega\gamma)/\Gamma_{\text{total}}$ $\Gamma_{18}/\Gamma$

VALUE	CL%	DOCUMENT ID	TECN	COMMENT
<b>&lt;6.5 × 10<sup>-4</sup></b>	95	ABREU	94B DLPH	$E_{cm}^{ee} = 88-94$ GeV

### $\Gamma(\eta'(958)\gamma)/\Gamma_{\text{total}}$ $\Gamma_{19}/\Gamma$

VALUE	CL%	DOCUMENT ID	TECN	COMMENT
<b>&lt;4.2 × 10<sup>-5</sup></b>	95	DECAMP	92 ALEP	$E_{cm}^{ee} = 88-94$ GeV

### $\Gamma(\phi\gamma)/\Gamma_{\text{total}}$ $\Gamma_{20}/\Gamma$

VALUE	CL%	EVTS	DOCUMENT ID	TECN	COMMENT
<b>&lt;9 × 10<sup>-7</sup></b>	95	3.3k	<sup>1</sup> AABOUD	18AU ATLS	$E_{cm}^{pp} = 13$ TeV

• • • We do not use the following data for averages, fits, limits, etc. • • •

<8.3 × 10<sup>-6</sup> 95 1.0k <sup>2</sup>AABOUD 16k ATLS  $E_{cm}^{pp} = 13$  TeV

<sup>1</sup>AABOUD 18AU search for the  $Z \rightarrow \phi\gamma$  decay mode where the  $\phi$  is identified through its decay  $\phi \rightarrow K^+K^-$ . In the data corresponding to  $32.3 \text{ fb}^{-1}$ , 3,364 events are selected for  $1012 < m(K^+K^-) < 1028$  MeV.

<sup>2</sup>AABOUD 16k search for the  $Z \rightarrow \phi\gamma$  decay mode where the  $\phi$  is identified through its decay into  $K^+K^-$ . In the data corresponding to a total luminosity of  $2.7 \text{ fb}^{-1}$ , 1065 events are selected and their  $K^+K^-\gamma$  invariant mass spectrum is analyzed.

### $\Gamma(\gamma\gamma)/\Gamma_{\text{total}}$ $\Gamma_{21}/\Gamma$

This decay would violate the Landau-Yang theorem.

VALUE	CL%	DOCUMENT ID	TECN	COMMENT
<b>&lt;1.46 × 10<sup>-5</sup></b>	95	AALTONEN	14E CDF	$E_{cm}^{pp} = 1.96$ TeV
<5.2 × 10 <sup>-5</sup>	95	<sup>1</sup> ACCIARRI	95G L3	$E_{cm}^{ee} = 88-94$ GeV
<5.5 × 10 <sup>-5</sup>	95	ABREU	94B DLPH	$E_{cm}^{ee} = 88-94$ GeV
<1.4 × 10 <sup>-4</sup>	95	AKRAWY	91F OPAL	$E_{cm}^{ee} = 88-94$ GeV

<sup>1</sup>This limit is for both decay modes  $Z \rightarrow \pi^0\gamma/\gamma\gamma$  which are indistinguishable in ACCIARRI 95G.

### $\Gamma(\pi^0\pi^0)/\Gamma_{\text{total}}$ $\Gamma_{22}/\Gamma$

VALUE	CL%	DOCUMENT ID	TECN	COMMENT
<b>&lt;1.52 × 10<sup>-5</sup></b>	95	AALTONEN	14E CDF	$E_{cm}^{pp} = 1.96$ TeV

### $\Gamma(\gamma\gamma\gamma)/\Gamma_{\text{total}}$ $\Gamma_{23}/\Gamma$

VALUE	CL%	DOCUMENT ID	TECN	COMMENT
<b>&lt;2.2 × 10<sup>-6</sup></b>	95	AAD	16L ATLS	$E_{cm}^{pp} = 8$ TeV

• • • We do not use the following data for averages, fits, limits, etc. • • •

<1.0 × 10<sup>-5</sup> 95 <sup>1</sup> ACCIARRI 95c L3  $E_{cm}^{ee} = 88-94$  GeV

<1.7 × 10<sup>-5</sup> 95 <sup>1</sup> ABREU 94B DLPH  $E_{cm}^{ee} = 88-94$  GeV

<6.6 × 10<sup>-5</sup> 95 AKRAWY 91F OPAL  $E_{cm}^{ee} = 88-94$  GeV

<sup>1</sup>Limit derived in the context of composite Z model.

### $\Gamma(\pi^\pm W^\mp)/\Gamma_{\text{total}}$ $\Gamma_{24}/\Gamma$

The value is for the sum of the charge states indicated.

VALUE	CL%	DOCUMENT ID	TECN	COMMENT
<b>&lt;7 × 10<sup>-5</sup></b>	95	DECAMP	92 ALEP	$E_{cm}^{ee} = 88-94$ GeV

### $\Gamma(\rho^\pm W^\mp)/\Gamma_{\text{total}}$ $\Gamma_{25}/\Gamma$

The value is for the sum of the charge states indicated.

VALUE	CL%	DOCUMENT ID	TECN	COMMENT
<b>&lt;8.3 × 10<sup>-5</sup></b>	95	DECAMP	92 ALEP	$E_{cm}^{ee} = 88-94$ GeV

$\Gamma(J/\psi(1S)X)/\Gamma_{\text{total}}$   $\Gamma_{26}/\Gamma$ 

VALUE (units $10^{-3}$ )	EVTS	DOCUMENT ID	TECN	COMMENT
<b><math>3.51^{+0.23}_{-0.25}</math> OUR AVERAGE</b>				Error includes scale factor of 1.1.
$3.21 \pm 0.21^{+0.19}_{-0.28}$	553	<sup>1</sup> ACCIARRI	99F L3	$E_{\text{cm}}^{pp} = 88\text{--}94$ GeV
$3.9 \pm 0.2 \pm 0.3$	511	<sup>2</sup> ALEXANDER	96B OPAL	$E_{\text{cm}}^{pp} = 88\text{--}94$ GeV
$3.73 \pm 0.39 \pm 0.36$	153	<sup>3</sup> ABREU	94P DLPH	$E_{\text{cm}}^{pp} = 88\text{--}94$ GeV

<sup>1</sup> ACCIARRI 99F combine  $\mu^+\mu^-$  and  $e^+e^- J/\psi(1S)$  decay channels. The branching ratio for prompt  $J/\psi(1S)$  production is measured to be  $(2.1 \pm 0.6 \pm 0.4^{+0.4}_{-0.2}(\text{theor.})) \times 10^{-4}$ .

<sup>2</sup> ALEXANDER 96B identify  $J/\psi(1S)$  from the decays into lepton pairs.  $(4.8 \pm 2.4)\%$  of this branching ratio is due to prompt  $J/\psi(1S)$  production (ALEXANDER 96N).

<sup>3</sup> Combining  $\mu^+\mu^-$  and  $e^+e^-$  channels and taking into account the common systematic errors.  $(7.7^{+6.3}_{-5.4})\%$  of this branching ratio is due to prompt  $J/\psi(1S)$  production.

 $\Gamma(J/\psi(1S)\gamma)/\Gamma_{\text{total}}$   $\Gamma_{27}/\Gamma$ 

VALUE	CL%	DOCUMENT ID	TECN	COMMENT
<b><math>&lt;1.4 \times 10^{-6}</math></b>	95	<sup>1</sup> SIRUNYAN	19AJ CMS	$E_{\text{cm}}^{pp} = 13$ TeV
$<2.3 \times 10^{-6}$	95	<sup>2</sup> AABOUD	18BL ATLS	$E_{\text{cm}}^{pp} = 13$ TeV
$<2.6 \times 10^{-6}$	95	<sup>3</sup> AAD	15I ATLS	$E_{\text{cm}}^{pp} = 8$ TeV

<sup>1</sup> SIRUNYAN 19AJ study  $Z \rightarrow J/\psi\gamma$  with  $J/\psi \rightarrow \mu^+\mu^-$ . Candidate events are selected by requiring a pair of oppositely charged muons and a well isolated photon. The leading (subleading) muon is required to have a transverse momentum larger than 20 GeV (4 GeV), while the photon must have a transverse energy larger than 33 GeV. Requiring the invariant mass of the  $\mu\mu$  ( $\mu\mu\gamma$ ) system in the range 3.0 to 3.2 (81 to 101) GeV, selects 183 data events which is consistent with the expected background. The 95% C.L. limit on the Z branching fraction is obtained assuming the  $J/\psi$  to be unpolarized.

<sup>2</sup> AABOUD 18BL study  $Z \rightarrow J/\psi\gamma$  in 13 TeV  $pp$  interactions. Two triggers were used: isolated photon of  $p_T > 35(25)$  GeV and a muon with  $p_T > 18(24)$  GeV. The  $J/\psi$  is detected via its dimuon decay and it is required that the azimuthal angle between the photon and the  $J/\psi$  in the plane transverse to the beam direction is  $> \pi/2$ . The number of observed/expected background events is 92/89  $\pm 6$  in the dimuon mass range 2.9–3.3 GeV leading to the quoted 95% C.L. limit.

<sup>3</sup> AAD 15I use events with the highest  $p_T$  muon in the pair required to have  $p_T > 20$  GeV, the dimuon mass required to be within 0.2 GeV of the  $J/\psi(1S)$  mass and its transverse momentum required to be  $> 36$  GeV. The photon is also required to have its  $p_T > 36$  GeV.

 $\Gamma(\psi(2S)X)/\Gamma_{\text{total}}$   $\Gamma_{28}/\Gamma$ 

VALUE (units $10^{-3}$ )	EVTS	DOCUMENT ID	TECN	COMMENT
<b><math>1.60 \pm 0.29</math> OUR AVERAGE</b>				
$1.6 \pm 0.5 \pm 0.3$	39	<sup>1</sup> ACCIARRI	97J L3	$E_{\text{cm}}^{pp} = 88\text{--}94$ GeV
$1.6 \pm 0.3 \pm 0.2$	46.9	<sup>2</sup> ALEXANDER	96B OPAL	$E_{\text{cm}}^{pp} = 88\text{--}94$ GeV
$1.60 \pm 0.73 \pm 0.33$	5.4	<sup>3</sup> ABREU	94P DLPH	$E_{\text{cm}}^{pp} = 88\text{--}94$ GeV

<sup>1</sup> ACCIARRI 97J measure this branching ratio via the decay channel  $\psi(2S) \rightarrow \ell^+\ell^-$  ( $\ell = \mu, e$ ).

<sup>2</sup> ALEXANDER 96B measure this branching ratio via the decay channel  $\psi(2S) \rightarrow J/\psi\pi^+\pi^-$ , with  $J/\psi \rightarrow \ell^+\ell^-$ .

<sup>3</sup> ABREU 94P measure this branching ratio via decay channel  $\psi(2S) \rightarrow J/\psi\pi^+\pi^-$ , with  $J/\psi \rightarrow \mu^+\mu^-$ .

 $\Gamma(\psi(2S)\gamma)/\Gamma_{\text{total}}$   $\Gamma_{29}/\Gamma$ 

VALUE	CL%	DOCUMENT ID	TECN	COMMENT
<b><math>&lt;4.5 \times 10^{-6}</math></b>	95	<sup>1</sup> AABOUD	18BL ATLS	$E_{\text{cm}}^{pp} = 13$ TeV

<sup>1</sup> AABOUD 18BL study  $Z \rightarrow \psi(2S)\gamma$  in 13 TeV  $pp$  interactions. Two triggers were used: isolated photon of  $p_T > 35(25)$  GeV and a muon with  $p_T > 18(24)$  GeV. The  $\psi(2S)$  is detected via its dimuon decay and it is required that the azimuthal angle between the photon and the  $\psi(2S)$  in the plane transverse to the beam direction is  $> \pi/2$ . The number of observed/expected background events is 43/42  $\pm 5$  in the dimuon mass range 3.5–3.9 GeV leading to the quoted 95% C.L. limit.

 $\Gamma(J/\psi(1S)\ell^+\ell^-)/\Gamma(\mu^+\mu^-\mu^+\mu^-)$   $\Gamma_{30}/\Gamma_5$ 

VALUE	DOCUMENT ID	TECN	COMMENT
<b><math>0.67 \pm 0.18 \pm 0.05</math></b>	<sup>1</sup> SIRUNYAN	18DZ CMS	$pp$ at 13 TeV

<sup>1</sup> SIRUNYAN 18DZ observe the decay  $Z \rightarrow \Psi\ell^+\ell^-$  in  $pp$  collisions at  $\sqrt{s} = 13$  TeV, where  $\Psi$  includes  $J/\psi$  as well as  $\psi(2S) \rightarrow J/\psi X$ , and  $\ell^+\ell^-$  represents an electron or muon pair while the  $J/\psi$  is detected via its  $\mu^+\mu^-$  decay channel. To reduce systematic errors they determine the ratio of the branching fraction of this decay to that of  $Z \rightarrow \mu^+\mu^- \mu^+\mu^-$  within phase-space cuts imposed on lepton transverse momentum and pseudo rapidity, dilepton invariant mass, and  $J/\psi$  transverse momentum. The number of selected  $\Psi\mu^+\mu^-$  ( $\Psi e^+e^-$ ) candidate events is 29 (18). Analyzing the  $\mu^+\mu^-$  and  $\mu^+\mu^- \ell^+\ell^-$  invariant mass distributions, a yield of  $13.0 \pm 3.9$  ( $11.2 \pm 3.4$ ) events for the  $\Psi\mu^+\mu^-$  ( $\Psi e^+e^-$ ) mode is obtained. The ratio of the branching fractions is determined as  $0.67 \pm 0.18 \pm 0.05$  within the selected phase-space cuts. Assuming extrapolation to full phase space cancels in the ratio, and using their measured value of  $B(Z \rightarrow \mu^+\mu^- \mu^+\mu^-) = (1.20 \pm 0.08) \times 10^{-6}$ , they estimate  $B(Z \rightarrow J/\psi\ell^+\ell^-) = 8 \times 10^{-7}$ .

 $\Gamma(J/\psi(1S)J/\psi(1S))/\Gamma_{\text{total}}$   $\Gamma_{31}/\Gamma$ 

VALUE	CL%	EVTS	DOCUMENT ID	TECN	COMMENT
<b><math>&lt;2.2 \times 10^{-6}</math></b>	95	189	<sup>1</sup> SIRUNYAN	19BR CMS	$E_{\text{cm}}^{pp} = 13$ TeV

<sup>1</sup> SIRUNYAN 19BR search for Z decays to a pair of  $J/\psi$  mesons in the channel  $J/\psi \rightarrow \mu^+\mu^-$ . The invariant masses of the higher/lower- $p_T$   $J/\psi$  candidates have to be within 0.1/0.15 GeV of the nominal  $J/\psi$  mass. A total of 189 events are selected in the 40–140 GeV 4-muon invariant mass range. An un-binned extended maximum likelihood fits leads to the 95% C.L. upper limit, obtained assuming the  $J/\psi$  mesons to be unpolarised.

 $\Gamma(\chi_{c1}(1P)X)/\Gamma_{\text{total}}$   $\Gamma_{32}/\Gamma$ 

VALUE (units $10^{-3}$ )	EVTS	DOCUMENT ID	TECN	COMMENT
<b><math>2.9 \pm 0.7</math> OUR AVERAGE</b>				
$2.7 \pm 0.6 \pm 0.5$	33	<sup>1</sup> ACCIARRI	97J L3	$E_{\text{cm}}^{pp} = 88\text{--}94$ GeV
$5.0 \pm 2.1^{+1.5}_{-0.9}$	6.4	<sup>2</sup> ABREU	94P DLPH	$E_{\text{cm}}^{pp} = 88\text{--}94$ GeV

<sup>1</sup> ACCIARRI 97J measure this branching ratio via the decay channel  $\chi_{c1} \rightarrow J/\psi + \gamma$ , with  $J/\psi \rightarrow \ell^+\ell^-$  ( $\ell = \mu, e$ ). The  $M(\ell^+\ell^-\gamma) - M(\ell^+\ell^-)$  mass difference spectrum is fitted with two gaussian shapes for  $\chi_{c1}$  and  $\chi_{c2}$ .

<sup>2</sup> This branching ratio is measured via the decay channel  $\chi_{c1} \rightarrow J/\psi + \gamma$ , with  $J/\psi \rightarrow \mu^+\mu^-$ .

 $\Gamma(\chi_{c2}(1P)X)/\Gamma_{\text{total}}$   $\Gamma_{33}/\Gamma$ 

VALUE	CL%	DOCUMENT ID	TECN	COMMENT
<b><math>&lt;3.2 \times 10^{-3}</math></b>	90	<sup>1</sup> ACCIARRI	97J L3	$E_{\text{cm}}^{pp} = 88\text{--}94$ GeV

<sup>1</sup> ACCIARRI 97J derive this limit via the decay channel  $\chi_{c2} \rightarrow J/\psi + \gamma$ , with  $J/\psi \rightarrow \ell^+\ell^-$  ( $\ell = \mu, e$ ). The  $M(\ell^+\ell^-\gamma) - M(\ell^+\ell^-)$  mass difference spectrum is fitted with two gaussian shapes for  $\chi_{c1}$  and  $\chi_{c2}$ .

 $\Gamma(\Upsilon(1S)X + \Upsilon(2S)X + \Upsilon(3S)X)/\Gamma_{\text{total}}$   $\Gamma_{34}/\Gamma = (\Gamma_{35} + \Gamma_{37} + \Gamma_{39})/\Gamma$ 

VALUE (units $10^{-4}$ )	EVTS	DOCUMENT ID	TECN	COMMENT
<b><math>1.0 \pm 0.4 \pm 0.22</math></b>	6.4	<sup>1</sup> ALEXANDER	96F OPAL	$E_{\text{cm}}^{pp} = 88\text{--}94$ GeV

<sup>1</sup> ALEXANDER 96F identify the  $\Upsilon$  (which refers to any of the three lowest bound states) through its decay into  $e^+e^-$  and  $\mu^+\mu^-$ . The systematic error includes an uncertainty of  $\pm 0.2$  due to the production mechanism.

 $\Gamma(\Upsilon(1S)X)/\Gamma_{\text{total}}$   $\Gamma_{35}/\Gamma$ 

VALUE	CL%	DOCUMENT ID	TECN	COMMENT
<b><math>&lt;3.4 \times 10^{-6}</math></b>	95	<sup>1</sup> AAD	15I ATLS	$E_{\text{cm}}^{pp} = 8$ TeV
$<4.4 \times 10^{-5}$	95	<sup>2</sup> ACCIARRI	99F L3	$E_{\text{cm}}^{pp} = 88\text{--}94$ GeV

<sup>1</sup> AAD 15I use events with the highest  $p_T$  muon in the pair required to have  $p_T > 20$  GeV, the dimuon mass required to be in the range 8–12 GeV and its transverse momentum required to be  $> 36$  GeV. The photon is also required to have its  $p_T > 36$  GeV.

<sup>2</sup> ACCIARRI 99F search for  $\Upsilon(1S)$  through its decay into  $\ell^+\ell^-$  ( $\ell = e$  or  $\mu$ ).

 $\Gamma(\Upsilon(1S)\gamma)/\Gamma_{\text{total}}$   $\Gamma_{36}/\Gamma$ 

VALUE	CL%	DOCUMENT ID	TECN	COMMENT
<b><math>&lt;2.8 \times 10^{-6}</math></b>	95	<sup>1</sup> AABOUD	18BL ATLS	$E_{\text{cm}}^{pp} = 13$ TeV

<sup>1</sup> AABOUD 18BL study  $Z \rightarrow \Upsilon(1S)\gamma$  in 13 TeV  $pp$  interactions. Two triggers were used: isolated photon of  $p_T > 35(25)$  GeV and a muon with  $p_T > 18(24)$  GeV. The  $\Upsilon(1S)$  is detected via its dimuon decay and it is required that the azimuthal angle between the photon and the  $\Upsilon(1S)$  in the plane transverse to the beam direction is  $> \pi/2$ . The number of observed/expected background events is 115/126  $\pm 8$  in the dimuon mass range 9.0–10.0 GeV leading to the quoted 95% C.L. limit.

 $\Gamma(\Upsilon(2S)X)/\Gamma_{\text{total}}$   $\Gamma_{37}/\Gamma$ 

VALUE	CL%	DOCUMENT ID	TECN	COMMENT
<b><math>&lt; 6.5 \times 10^{-6}</math></b>	95	<sup>1</sup> AAD	15I ATLS	$E_{\text{cm}}^{pp} = 8$ TeV
$<13.9 \times 10^{-5}$	95	<sup>2</sup> ACCIARRI	97R L3	$E_{\text{cm}}^{pp} = 88\text{--}94$ GeV

<sup>1</sup> AAD 15I use events with the highest  $p_T$  muon in the pair required to have  $p_T > 20$  GeV, the dimuon mass required to be in the range 8–12 GeV and its transverse momentum required to be  $> 36$  GeV. The photon is also required to have its  $p_T > 36$  GeV.

<sup>2</sup> ACCIARRI 97R search for  $\Upsilon(2S)$  through its decay into  $\ell^+\ell^-$  ( $\ell = e$  or  $\mu$ ).

 $\Gamma(\Upsilon(2S)\gamma)/\Gamma_{\text{total}}$   $\Gamma_{38}/\Gamma$ 

VALUE	CL%	DOCUMENT ID	TECN	COMMENT
<b><math>&lt;1.7 \times 10^{-6}</math></b>	95	<sup>1</sup> AABOUD	18BL ATLS	$E_{\text{cm}}^{pp} = 13$ TeV

<sup>1</sup> AABOUD 18BL study  $Z \rightarrow \Upsilon(2S)\gamma$  in 13 TeV  $pp$  interactions. Two triggers were used: isolated photon of  $p_T > 35(25)$  GeV and a muon with  $p_T > 18(24)$  GeV. The  $\Upsilon(2S)$  is detected via its dimuon decay and it is required that the azimuthal angle between the photon and the  $\Upsilon(2S)$  in the plane transverse to the beam direction is  $> \pi/2$ . The number of observed/expected background events is 106/121  $\pm 8$  in the dimuon mass range 9.5–10.5 GeV leading to the quoted 95% C.L. limit.

 $\Gamma(\Upsilon(3S)X)/\Gamma_{\text{total}}$   $\Gamma_{39}/\Gamma$ 

VALUE	CL%	DOCUMENT ID	TECN	COMMENT
<b><math>&lt;5.4 \times 10^{-6}</math></b>	95	<sup>1</sup> AAD	15I ATLS	$E_{\text{cm}}^{pp} = 8$ TeV
$<9.4 \times 10^{-5}$	95	<sup>2</sup> ACCIARRI	97R L3	$E_{\text{cm}}^{pp} = 88\text{--}94$ GeV

<sup>1</sup> AAD 15I use events with the highest  $p_T$  muon in the pair required to have  $p_T > 20$  GeV, the dimuon mass required to be in the range 8–12 GeV and its transverse momentum required to be  $> 36$  GeV. The photon is also required to have its  $p_T > 36$  GeV.

<sup>2</sup> ACCIARRI 97R search for  $\Upsilon(3S)$  through its decay into  $\ell^+\ell^-$  ( $\ell = e$  or  $\mu$ ).

# Gauge & Higgs Boson Particle Listings

## Z

### $\Gamma(\mathcal{T}(3S)\gamma)/\Gamma_{\text{total}}$

VALUE	CL%	DOCUMENT ID	TECN	COMMENT
$<4.8 \times 10^{-6}$	95	<sup>1</sup> AABOUD	18BL ATLS	$E_{\text{cm}}^{pp} = 13 \text{ TeV}$

<sup>1</sup> AABOUD 18BL study  $Z \rightarrow \mathcal{T}(3S)\gamma$  in 13 TeV  $pp$  interactions. Two triggers were used: isolated photon of  $p_T > 35(25) \text{ GeV}$  and a muon with  $p_T > 18(24) \text{ GeV}$ . The  $\mathcal{T}(3S)$  is detected via its dimuon decay and it is required that the azimuthal angle between the photon and the  $\mathcal{T}(3S)$  in the plane transverse to the beam direction is  $> \pi/2$ . The number of observed/expected background events is  $112/113 \pm 8$  in the dimuon mass range  $10.0\text{--}11.0 \text{ GeV}$  leading to the quoted 95% C.L. limit.

### $\Gamma(\mathcal{T}(1, 2, 3S) \mathcal{T}(1, 2, 3S))/\Gamma_{\text{total}}$

VALUE	CL%	EVTS	DOCUMENT ID	TECN	COMMENT
$<1.5 \times 10^{-6}$	95	106	<sup>1</sup> SIRUNYAN	19BR CMS	$E_{\text{cm}}^{pp} = 13 \text{ TeV}$

<sup>1</sup> SIRUNYAN 19BR search for  $Z$  decays to a pair of  $\mathcal{T}$  mesons in the channel  $\mathcal{T} \rightarrow \mu^+ \mu^-$ . The invariant mass of the  $\mathcal{T}$  candidates has to be in the range of 8.5 to 11 GeV. A total of 106 events are selected in the 20–140 GeV 4-muon invariant mass range. An un-binned extended maximum likelihood fit leads to the 95% C.L. upper limit, obtained assuming the  $\mathcal{T}$  mesons to be unpolarised.

### $\Gamma((D^0/\bar{D}^0)X)/\Gamma(\text{hadrons})$

VALUE	EVTS	DOCUMENT ID	TECN	COMMENT
$0.296 \pm 0.019 \pm 0.021$	369	<sup>1</sup> ABREU	93I	$E_{\text{cm}}^{ee} = 88\text{--}94 \text{ GeV}$

<sup>1</sup> The  $(D^0/\bar{D}^0)$  states in ABREU 93I are detected by the  $K\pi$  decay mode. This is a corrected result (see the erratum of ABREU 93I).

### $\Gamma(D^{\pm}X)/\Gamma(\text{hadrons})$

VALUE	EVTS	DOCUMENT ID	TECN	COMMENT
$0.174 \pm 0.016 \pm 0.018$	539	<sup>1</sup> ABREU	93I	$E_{\text{cm}}^{ee} = 88\text{--}94 \text{ GeV}$

<sup>1</sup> The  $D^{\pm}$  states in ABREU 93I are detected by the  $K\pi\pi$  decay mode. This is a corrected result (see the erratum of ABREU 93I).

### $\Gamma(D^*(2010)^{\pm}X)/\Gamma(\text{hadrons})$

VALUE	EVTS	DOCUMENT ID	TECN	COMMENT
$0.163 \pm 0.019$ OUR AVERAGE	Error includes scale factor of 1.3.			
$0.155 \pm 0.010 \pm 0.013$	358	<sup>1</sup> ABREU	93I	$E_{\text{cm}}^{ee} = 88\text{--}94 \text{ GeV}$
$0.21 \pm 0.04$	362	<sup>2</sup> DECAMP	91J	$E_{\text{cm}}^{ee} = 88\text{--}94 \text{ GeV}$

<sup>1</sup>  $D^*(2010)^{\pm}$  in ABREU 93I are reconstructed from  $D^0\pi^{\pm}$ , with  $D^0 \rightarrow K^-\pi^+$ . The new CLEO II measurement of  $B(D^{*\pm} \rightarrow D^0\pi^{\pm}) = (68.1 \pm 1.6)\%$  is used. This is a corrected result (see the erratum of ABREU 93I).

<sup>2</sup> DECAMP 91J report  $B(D^*(2010)^+ \rightarrow D^0\pi^+) B(D^0 \rightarrow K^-\pi^+) \Gamma(D^*(2010)^{\pm}X)/\Gamma(\text{hadrons}) = (5.11 \pm 0.34) \times 10^{-3}$ . They obtained the above number assuming  $B(D^0 \rightarrow K^-\pi^+) = (3.62 \pm 0.34 \pm 0.44)\%$  and  $B(D^*(2010)^+ \rightarrow D^0\pi^+) = (55 \pm 4)\%$ . We have rescaled their original result of  $0.26 \pm 0.05$  taking into account the new CLEO II branching ratio  $B(D^*(2010)^+ \rightarrow D^0\pi^+) = (68.1 \pm 1.6)\%$ .

### $\Gamma(D_{s1}(2536)^{\pm}X)/\Gamma(\text{hadrons})$

VALUE (%)	EVTS	DOCUMENT ID	TECN	COMMENT
$0.52 \pm 0.09 \pm 0.06$	92	<sup>1</sup> HEISTER	02B ALEP	$E_{\text{cm}}^{ee} = 88\text{--}94 \text{ GeV}$

<sup>1</sup> HEISTER 02B reconstruct this meson in the decay modes  $D_{s1}(2536)^{\pm} \rightarrow D^{\pm}K^0$  and  $D_{s1}(2536)^{\pm} \rightarrow D^*0K^{\pm}$ . The quoted branching ratio assumes that the decay width of the  $D_{s1}(2536)$  is saturated by the two measured decay modes.

### $\Gamma(D_{sJ}(2573)^{\pm}X)/\Gamma(\text{hadrons})$

VALUE (%)	EVTS	DOCUMENT ID	TECN	COMMENT
$0.83 \pm 0.29 \pm 0.07$ $0.13$	64	<sup>1</sup> HEISTER	02B ALEP	$E_{\text{cm}}^{ee} = 88\text{--}94 \text{ GeV}$

<sup>1</sup> HEISTER 02B reconstruct this meson in the decay mode  $D_{s2}^*(2573)^{\pm} \rightarrow D^0K^{\pm}$ . The quoted branching ratio assumes that the detected decay mode represents 45% of the full decay width.

### $\Gamma(D^{*'}(2629)^{\pm}X)/\Gamma(\text{hadrons})$

VALUE	EVTS	DOCUMENT ID	TECN	COMMENT
searched for		<sup>1</sup> ABBIENDI	01N OPAL	$E_{\text{cm}}^{ee} = 88\text{--}94 \text{ GeV}$

<sup>1</sup> ABBIENDI 01N searched for the decay mode  $D^{*'}(2629)^{\pm} \rightarrow D^{*\pm}\pi^+\pi^-$  with  $D^{*+} \rightarrow D^0\pi^+$ , and  $D^0 \rightarrow K^-\pi^+$ . They quote a 95% CL limit for  $Z \rightarrow D^{*'}(2629)^{\pm} \times B(D^{*'}(2629)^+ \rightarrow D^{*+}\pi^+\pi^-) < 3.1 \times 10^{-3}$ .

### $\Gamma(B^*X)/[\Gamma(BX) + \Gamma(B^*X)]$

VALUE	EVTS	DOCUMENT ID	TECN	COMMENT
$0.75 \pm 0.04$ OUR AVERAGE				
$0.760 \pm 0.036 \pm 0.083$		<sup>1</sup> ACKERSTAFF	97M OPAL	$E_{\text{cm}}^{ee} = 88\text{--}94 \text{ GeV}$
$0.771 \pm 0.026 \pm 0.070$		<sup>2</sup> BUSKULIC	96D ALEP	$E_{\text{cm}}^{ee} = 88\text{--}94 \text{ GeV}$
$0.72 \pm 0.03 \pm 0.06$		<sup>3</sup> ABREU	95R DLPH	$E_{\text{cm}}^{ee} = 88\text{--}94 \text{ GeV}$
$0.76 \pm 0.08 \pm 0.06$	1378	<sup>4</sup> ACCIARRI	95B L3	$E_{\text{cm}}^{ee} = 88\text{--}94 \text{ GeV}$

As the experiments assume different values of the  $b$ -baryon contribution, our average should be taken with caution.

<sup>1</sup> ACKERSTAFF 97M use an inclusive  $B$  reconstruction method and assume a  $(13.2 \pm 4.1)\%$   $b$ -baryon contribution. The value refers to a  $b$ -flavored meson mixture of  $B_u, B_d$ , and  $B_s$ .

<sup>2</sup> BUSKULIC 96D use an inclusive reconstruction of  $B$  hadrons and assume a  $(12.2 \pm 4.3)\%$   $b$ -baryon contribution. The value refers to a  $b$ -flavored mixture of  $B_u, B_d$ , and  $B_s$ .

<sup>3</sup> ABREU 95R use an inclusive  $B$ -reconstruction method and assume a  $(10 \pm 4)\%$   $b$ -baryon contribution. The value refers to a  $b$ -flavored meson mixture of  $B_u, B_d$ , and  $B_s$ .

<sup>4</sup> ACCIARRI 95B assume a 9.4%  $b$ -baryon contribution. The value refers to a  $b$ -flavored mixture of  $B_u, B_d$ , and  $B_s$ .

### $\Gamma(B^+X)/\Gamma(\text{hadrons})$

VALUE	DOCUMENT ID	TECN	COMMENT
$0.0869 \pm 0.0019$ OUR EVALUATION			
$0.0887 \pm 0.0030$	<sup>1</sup> ABDALLAH	03k DLPH	$E_{\text{cm}}^{ee} = 88\text{--}94 \text{ GeV}$

<sup>1</sup> ABDALLAH 03k measure the production fraction of  $B^+$  mesons in hadronic  $Z$  decays  $f(B^+) = (40.99 \pm 0.82 \pm 1.11)\%$ . The value quoted here is obtained multiplying this production fraction by our value of  $R_b = \Gamma(\bar{b}b)/\Gamma(\text{hadrons})$ .

### $\Gamma(B_s^0X)/\Gamma(\text{hadrons})$

VALUE	DOCUMENT ID	TECN	COMMENT
$0.0227 \pm 0.0019$ OUR EVALUATION			
seen	<sup>1</sup> ABREU	92M DLPH	$E_{\text{cm}}^{ee} = 88\text{--}94 \text{ GeV}$
seen	<sup>2</sup> ACTON	92N OPAL	$E_{\text{cm}}^{ee} = 88\text{--}94 \text{ GeV}$
seen	<sup>3</sup> BUSKULIC	92E ALEP	$E_{\text{cm}}^{ee} = 88\text{--}94 \text{ GeV}$

<sup>1</sup> ABREU 92M reported value is  $\Gamma(B_s^0X) \times B(B_s^0 \rightarrow D_s \mu \nu \mu X) \times B(D_s \rightarrow \phi \pi)/\Gamma(\text{hadrons}) = (18 \pm 8) \times 10^{-5}$ .

<sup>2</sup> ACTON 92N find evidence for  $B_s^0$  production using  $D_s\text{--}\ell$  correlations, with  $D_s^+ \rightarrow \phi \pi^+$  and  $K^*(892)K^+$ . Assuming  $R_b$  from the Standard Model and averaging over the  $e$  and  $\mu$  channels, authors measure the product branching fraction to be  $f(\bar{b} \rightarrow B_s^0) \times B(B_s^0 \rightarrow D_s^- \ell^+ \nu_\ell X) \times B(D_s^- \rightarrow \phi \pi^-) = (3.9 \pm 1.1 \pm 0.8) \times 10^{-4}$ .

<sup>3</sup> BUSKULIC 92E find evidence for  $B_s^0$  production using  $D_s\text{--}\ell$  correlations, with  $D_s^+ \rightarrow \phi \pi^+$  and  $K^*(892)K^+$ . Using  $B(D_s^+ \rightarrow \phi \pi^+) = (2.7 \pm 0.7)\%$  and summing up the  $e$  and  $\mu$  channels, the weighted average product branching fraction is measured to be  $f(\bar{b} \rightarrow B_s^0) \times B(B_s^0 \rightarrow D_s^- \ell^+ \nu_\ell X) = 0.040 \pm 0.011 \pm 0.012$ .

### $\Gamma(B_c^+X)/\Gamma(\text{hadrons})$

VALUE	DOCUMENT ID	TECN	COMMENT
searched for	<sup>1</sup> ACKERSTAFF	98O OPAL	$E_{\text{cm}}^{ee} = 88\text{--}94 \text{ GeV}$
searched for	<sup>2</sup> ABREU	97E DLPH	$E_{\text{cm}}^{ee} = 88\text{--}94 \text{ GeV}$
searched for	<sup>3</sup> BARATE	97H ALEP	$E_{\text{cm}}^{ee} = 88\text{--}94 \text{ GeV}$

<sup>1</sup> ACKERSTAFF 98O searched for the decay modes  $B_c \rightarrow J/\psi \pi^+, J/\psi a_1^+,$  and  $J/\psi \ell^+ \nu_\ell$ , with  $J/\psi \rightarrow \ell^+ \ell^-, \ell = e, \mu$ . The number of candidates (background) for the three decay modes is  $2(0.63 \pm 0.2), 0(1.10 \pm 0.22),$  and  $1(0.82 \pm 0.19)$  respectively. Interpreting the  $2B_c \rightarrow J/\psi \pi^+$  candidates as signal, they report  $\Gamma(B_c^+X) \times B(B_c \rightarrow J/\psi \pi^+)/\Gamma(\text{hadrons}) = (3.8 \pm 5.0 \pm 0.5) \times 10^{-5}$ . Interpreted as background, the 90% CL bounds are  $\Gamma(B_c^+X) \times B(B_c \rightarrow J/\psi \pi^+)/\Gamma(\text{hadrons}) < 1.06 \times 10^{-4}, \Gamma(B_c^+X) \times B(B_c \rightarrow J/\psi a_1^+)/\Gamma(\text{hadrons}) < 5.29 \times 10^{-4}, \Gamma(B_c^+X) \times B(B_c \rightarrow J/\psi \ell^+ \nu_\ell)/\Gamma(\text{hadrons}) < 6.96 \times 10^{-5}$ .

<sup>2</sup> ABREU 97E searched for the decay modes  $B_c \rightarrow J/\psi \pi^+, J/\psi \ell^+ \nu_\ell,$  and  $J/\psi(3\pi^+)$ , with  $J/\psi \rightarrow \ell^+ \ell^-, \ell = e, \mu$ . The number of candidates (background) for the three decay modes is  $1(1.7), 0(0.3),$  and  $1(2.3)$  respectively. They report the following 90% CL limits:  $\Gamma(B_c^+X) \times B(B_c \rightarrow J/\psi \pi^+)/\Gamma(\text{hadrons}) < (1.05\text{--}0.84) \times 10^{-4}, \Gamma(B_c^+X) \times B(B_c \rightarrow J/\psi \ell^+ \nu_\ell)/\Gamma(\text{hadrons}) < (5.8\text{--}5.0) \times 10^{-5}, \Gamma(B_c^+X) \times B(B_c \rightarrow J/\psi(3\pi^+))/\Gamma(\text{hadrons}) < 1.75 \times 10^{-4}$ , where the ranges are due to the predicted  $B_c$  lifetime (0.4–1.4) ps.

<sup>3</sup> BARATE 97H searched for the decay modes  $B_c \rightarrow J/\psi \pi^+$  and  $J/\psi \ell^+ \nu_\ell$  with  $J/\psi \rightarrow \ell^+ \ell^-, \ell = e, \mu$ . The number of candidates (background) for the two decay modes is  $0(0.44)$  and  $2(0.81)$  respectively. They report the following 90% CL limits:  $\Gamma(B_c^+X) \times B(B_c \rightarrow J/\psi \pi^+)/\Gamma(\text{hadrons}) < 3.6 \times 10^{-5}$  and  $\Gamma(B_c^+X) \times B(B_c \rightarrow J/\psi \ell^+ \nu_\ell)/\Gamma(\text{hadrons}) < 5.2 \times 10^{-5}$ .

### $\Gamma(A_c^+X)/\Gamma(\text{hadrons})$

VALUE	DOCUMENT ID	TECN	COMMENT
$0.022 \pm 0.005$ OUR AVERAGE			
$0.024 \pm 0.003 \pm 0.006$	<sup>1</sup> ALEXANDER	96R OPAL	$E_{\text{cm}}^{ee} = 88\text{--}94 \text{ GeV}$
$0.021 \pm 0.005 \pm 0.005$	<sup>2</sup> BUSKULIC	96Y ALEP	$E_{\text{cm}}^{ee} = 88\text{--}94 \text{ GeV}$

<sup>1</sup> ALEXANDER 96R measure  $R_b \times f(b \rightarrow \Lambda_c^+ X) \times B(\Lambda_c^+ \rightarrow p K^- \pi^+) = (0.122 \pm 0.023 \pm 0.010)\%$  in hadronic Z decays; the value quoted here is obtained using our best value  $B(\Lambda_c^+ \rightarrow p K^- \pi^+) = (5.0 \pm 1.3)\%$ . The first error is the total experiment's error and the second error is the systematic error due to the branching fraction uncertainty.

<sup>2</sup> BUSKULIC 96V obtain the production fraction of  $\Lambda_c^+$  baryons in hadronic Z decays  $f(b \rightarrow \Lambda_c^+ X) = 0.110 \pm 0.014 \pm 0.006$  using  $B(\Lambda_c^+ \rightarrow p K^- \pi^+) = (4.4 \pm 0.6)\%$ ; we have rescaled using our best value  $B(\Lambda_c^+ \rightarrow p K^- \pi^+) = (5.0 \pm 1.3)\%$  obtaining  $f(b \rightarrow \Lambda_c^+ X) = 0.097 \pm 0.013 \pm 0.025$  where the first error is their total experiment's error and the second error is the systematic error due to the branching fraction uncertainty. The value quoted here is obtained multiplying this production fraction by our value of  $R_b = \Gamma(b\bar{b})/\Gamma(\text{hadrons})$ .

$\Gamma(\Xi_c^0 X)/\Gamma(\text{hadrons})$   $\Gamma_{54}/\Gamma_8$

••• We do not use the following data for averages, fits, limits, etc. •••  
seen <sup>1</sup> ABDALLAH 05c DLPH  $E_{cm}^{ee} = 88-94$  GeV

<sup>1</sup> ABDALLAH 05c searched for the charmed strange baryon  $\Xi_c^0$  in the decay channel  $\Xi_c^0 \rightarrow \Xi^- \pi^+$  ( $\Xi^- \rightarrow \Lambda \pi^-$ ). The production rate is measured to be  $f_{\Xi_c^0}^b \times B(\Xi_c^0 \rightarrow \Xi^- \pi^+) = (4.7 \pm 1.4 \pm 1.1) \times 10^{-4}$  per hadronic Z decay.

$\Gamma(\Xi_b X)/\Gamma(\text{hadrons})$   $\Gamma_{55}/\Gamma_8$

Here  $\Xi_b$  is used as a notation for the strange b-baryon states  $\Xi_b^-$  and  $\Xi_b^0$ .  
••• We do not use the following data for averages, fits, limits, etc. •••

seen <sup>1</sup> ABDALLAH 05c DLPH  $E_{cm}^{ee} = 88-94$  GeV  
seen <sup>2</sup> BUSKULIC 96T ALEP  $E_{cm}^{ee} = 88-94$  GeV  
seen <sup>3</sup> ABREU 95v DLPH  $E_{cm}^{ee} = 88-94$  GeV

<sup>1</sup> ABDALLAH 05c searched for the beauty strange baryon  $\Xi_b$  in the inclusive semileptonic decay channel  $\Xi_b \rightarrow \Xi^- \ell^+ \nu_\ell X$ . Evidence for the  $\Xi_b$  production is seen from the observation of  $\Xi^\mp$  production accompanied by a lepton of the same sign. From the excess of "right-sign" pairs  $\Xi^\mp \ell^\mp$  compared to "wrong-sign" pairs  $\Xi^\mp \ell^\pm$  the production rate is measured to be  $B(b \rightarrow \Xi_b) \times B(\Xi_b \rightarrow \Xi^- \ell^+ X) = (3.0 \pm 1.0 \pm 0.3) \times 10^{-4}$  per lepton species, averaged over electrons and muons.

<sup>2</sup> BUSKULIC 96T investigate  $\Xi$ -lepton correlations and find a significant excess of "right-sign" pairs  $\Xi^\mp \ell^\mp$  compared to "wrong-sign" pairs  $\Xi^\mp \ell^\pm$ . This excess is interpreted as evidence for  $\Xi_b$  semileptonic decay. The measured product branching ratio is  $B(b \rightarrow \Xi_b) \times B(\Xi_b \rightarrow X_c X \ell^+ \nu_\ell) \times B(X_c \rightarrow \Xi^- X') = (5.4 \pm 1.1 \pm 0.8) \times 10^{-4}$  per lepton species, averaged over electrons and muons, with  $X_c$  a charmed baryon.

<sup>3</sup> ABREU 95v observe an excess of "right-sign" pairs  $\Xi^\mp \ell^\mp$  compared to "wrong-sign" pairs  $\Xi^\mp \ell^\pm$  in jets: this excess is interpreted as evidence for the beauty strange baryon  $\Xi_b$  production, with  $\Xi_b \rightarrow \Xi^- \ell^+ \nu_\ell X$ . They find that the probability for this signal to come from non b-baryon decays is less than  $5 \times 10^{-4}$  and that  $\Lambda_b$  decays can account for less than 10% of these events. The  $\Xi_b$  production rate is then measured to be  $B(b \rightarrow \Xi_b) \times B(\Xi_b \rightarrow \Xi^- \ell^+ X) = (5.9 \pm 2.1 \pm 1.0) \times 10^{-4}$  per lepton species, averaged over electrons and muons.

$\Gamma(b\text{-baryon } X)/\Gamma(\text{hadrons})$   $\Gamma_{56}/\Gamma_8$

"OUR EVALUATION" is obtained using our current values for  $f(b \rightarrow b\text{-baryon})$  and  $R_b = \Gamma(b\bar{b})/\Gamma(\text{hadrons})$ . We calculate  $\Gamma(b\text{-baryon } X)/\Gamma(\text{hadrons}) = R_b \times f(b \rightarrow b\text{-baryon})$ . The decay fraction ( $f(b \rightarrow b\text{-baryon})$ ) was provided by the Heavy Flavor Averaging Group (<https://inflav.web.cern.ch/>).

VALUE DOCUMENT ID TECN COMMENT  
**0.0197 ± 0.0032 OUR EVALUATION**  
**0.0221 ± 0.0015 ± 0.0058** <sup>1</sup> BARATE 98v ALEP  $E_{cm}^{ee} = 88-94$  GeV

<sup>1</sup> BARATE 98v use the overall number of identified protons in b-hadron decays to measure  $f(b \rightarrow b\text{-baryon}) = 0.102 \pm 0.007 \pm 0.027$ . They assume  $BR(b\text{-baryon} \rightarrow p X) = (58 \pm 6)\%$  and  $BR(B_s^0 \rightarrow p X) = (8.0 \pm 4.0)\%$ . The value quoted here is obtained multiplying this production fraction by our value of  $R_b = \Gamma(b\bar{b})/\Gamma(\text{hadrons})$ .

$\Gamma(\text{anomalous } \gamma + \text{hadrons})/\Gamma_{\text{total}}$   $\Gamma_{57}/\Gamma$

Limits on additional sources of prompt photons beyond expectations for final-state bremsstrahlung.

VALUE CL% DOCUMENT ID TECN COMMENT  
**<3.2 × 10<sup>-3</sup>** 95 <sup>1</sup> AKRAWY 90J OPAL  $E_{cm}^{ee} = 88-94$  GeV

<sup>1</sup> AKRAWY 90J report  $\Gamma(\gamma X) < 8.2$  MeV at 95%CL. They assume a three-body  $\gamma q \bar{q}$  distribution and use  $E(\gamma) > 10$  GeV.

$\Gamma(e^+ e^- \gamma)/\Gamma_{\text{total}}$   $\Gamma_{58}/\Gamma$

VALUE CL% DOCUMENT ID TECN COMMENT  
**<5.2 × 10<sup>-4</sup>** 95 <sup>1</sup> ACTON 91B OPAL  $E_{cm}^{ee} = 91.2$  GeV

<sup>1</sup> ACTON 91B looked for isolated photons with  $E > 2\%$  of beam energy ( $> 0.9$  GeV).

$\Gamma(\mu^+ \mu^- \gamma)/\Gamma_{\text{total}}$   $\Gamma_{59}/\Gamma$

VALUE CL% DOCUMENT ID TECN COMMENT  
**<5.6 × 10<sup>-4</sup>** 95 <sup>1</sup> ACTON 91B OPAL  $E_{cm}^{ee} = 91.2$  GeV

<sup>1</sup> ACTON 91B looked for isolated photons with  $E > 2\%$  of beam energy ( $> 0.9$  GeV).

$\Gamma(\tau^+ \tau^- \gamma)/\Gamma_{\text{total}}$   $\Gamma_{60}/\Gamma$

VALUE CL% DOCUMENT ID TECN COMMENT  
**<7.3 × 10<sup>-4</sup>** 95 <sup>1</sup> ACTON 91B OPAL  $E_{cm}^{ee} = 91.2$  GeV

<sup>1</sup> ACTON 91B looked for isolated photons with  $E > 2\%$  of beam energy ( $> 0.9$  GeV).

$\Gamma(\ell^+ \ell^- \gamma \gamma)/\Gamma_{\text{total}}$   $\Gamma_{61}/\Gamma$

The value is the sum over  $\ell = e, \mu, \tau$ .  
VALUE CL% DOCUMENT ID TECN COMMENT  
**<6.8 × 10<sup>-6</sup>** 95 <sup>1</sup> ACTON 93E OPAL  $E_{cm}^{ee} = 88-94$  GeV

<sup>1</sup> For  $m_{\gamma\gamma} = 60 \pm 5$  GeV.

$\Gamma(q \bar{q} \gamma \gamma)/\Gamma_{\text{total}}$   $\Gamma_{62}/\Gamma$

VALUE CL% DOCUMENT ID TECN COMMENT  
**<5.5 × 10<sup>-6</sup>** 95 <sup>1</sup> ACTON 93E OPAL  $E_{cm}^{ee} = 88-94$  GeV

<sup>1</sup> For  $m_{\gamma\gamma} = 60 \pm 5$  GeV.

$\Gamma(\nu \bar{\nu} \gamma \gamma)/\Gamma_{\text{total}}$   $\Gamma_{63}/\Gamma$

VALUE CL% DOCUMENT ID TECN COMMENT  
**<3.1 × 10<sup>-6</sup>** 95 <sup>1</sup> ACTON 93E OPAL  $E_{cm}^{ee} = 88-94$  GeV

<sup>1</sup> For  $m_{\gamma\gamma} = 60 \pm 5$  GeV.

$\Gamma(e^\pm \mu^\mp)/\Gamma_{\text{total}}$   $\Gamma_{64}/\Gamma$

Test of lepton family number conservation. The value is for the sum of the charge states indicated.

VALUE CL% DOCUMENT ID TECN COMMENT  
**<7.5 × 10<sup>-7</sup>** 95 AAD 14AU ATLS  $E_{cm}^{pp} = 8$  TeV  
**<2.5 × 10<sup>-6</sup>** 95 ABREU 97c DLPH  $E_{cm}^{ee} = 88-94$  GeV  
**<1.7 × 10<sup>-6</sup>** 95 AKERS 95w OPAL  $E_{cm}^{ee} = 88-94$  GeV  
**<0.6 × 10<sup>-5</sup>** 95 ADRIANI 93i L3  $E_{cm}^{ee} = 88-94$  GeV  
**<2.6 × 10<sup>-5</sup>** 95 DECAMP 92 ALEP  $E_{cm}^{ee} = 88-94$  GeV

$\Gamma(e^\pm \mu^\mp)/\Gamma(e^+ e^-)$   $\Gamma_{64}/\Gamma_1$

Test of lepton family number conservation. The value is for the sum of the charge states indicated.

VALUE CL% DOCUMENT ID TECN COMMENT  
**<0.07** 90 ALBAJAR 89 UA1  $E_{cm}^{pp} = 546,630$  GeV

$\Gamma(e^\pm \tau^\mp)/\Gamma_{\text{total}}$   $\Gamma_{65}/\Gamma$

Test of lepton family number conservation. The value is for the sum of the charge states indicated.

VALUE CL% DOCUMENT ID TECN COMMENT  
**<5.8 × 10<sup>-5</sup>** 95 AABOUD 18CN ATLS  $E_{cm}^{pp} = 13$  TeV  
**<2.2 × 10<sup>-5</sup>** 95 ABREU 97c DLPH  $E_{cm}^{ee} = 88-94$  GeV  
**<9.8 × 10<sup>-6</sup>** 95 AKERS 95w OPAL  $E_{cm}^{ee} = 88-94$  GeV  
**<1.3 × 10<sup>-5</sup>** 95 ADRIANI 93i L3  $E_{cm}^{ee} = 88-94$  GeV  
**<1.2 × 10<sup>-4</sup>** 95 DECAMP 92 ALEP  $E_{cm}^{ee} = 88-94$  GeV

$\Gamma(\mu^\pm \tau^\mp)/\Gamma_{\text{total}}$   $\Gamma_{66}/\Gamma$

Test of lepton family number conservation. The value is for the sum of the charge states indicated.

VALUE CL% DOCUMENT ID TECN COMMENT  
**<1.3 × 10<sup>-5</sup>** 95 AABOUD 18CN ATLS  $E_{cm}^{pp} = 8, 13$  TeV  
**<1.2 × 10<sup>-5</sup>** 95 ABREU 97c DLPH  $E_{cm}^{ee} = 88-94$  GeV  
**<1.7 × 10<sup>-5</sup>** 95 AKERS 95w OPAL  $E_{cm}^{ee} = 88-94$  GeV  
**<1.9 × 10<sup>-5</sup>** 95 ADRIANI 93i L3  $E_{cm}^{ee} = 88-94$  GeV  
**<1.0 × 10<sup>-4</sup>** 95 DECAMP 92 ALEP  $E_{cm}^{ee} = 88-94$  GeV

$\Gamma(p e)/\Gamma_{\text{total}}$   $\Gamma_{67}/\Gamma$

Test of baryon number and lepton number conservations. Charge conjugate states are implied.

VALUE CL% DOCUMENT ID TECN COMMENT  
**<1.8 × 10<sup>-6</sup>** 95 <sup>1</sup> ABBIENDI 99i OPAL  $E_{cm}^{ee} = 88-94$  GeV

<sup>1</sup> ABBIENDI 99i give the 95%CL limit on the partial width  $\Gamma(Z^0 \rightarrow p e) < 4.6$  KeV and we have transformed it into a branching ratio.

$\Gamma(p \mu)/\Gamma_{\text{total}}$   $\Gamma_{68}/\Gamma$

Test of baryon number and lepton number conservations. Charge conjugate states are implied.

VALUE CL% DOCUMENT ID TECN COMMENT  
**<1.8 × 10<sup>-6</sup>** 95 <sup>1</sup> ABBIENDI 99i OPAL  $E_{cm}^{ee} = 88-94$  GeV

<sup>1</sup> ABBIENDI 99i give the 95%CL limit on the partial width  $\Gamma(Z^0 \rightarrow p \mu) < 4.4$  KeV and we have transformed it into a branching ratio.

AVERAGE PARTICLE MULTIPLICITIES IN HADRONIC Z DECAY

Summed over particle and antiparticle, when appropriate.

$\langle N_\gamma \rangle$   
VALUE DOCUMENT ID TECN COMMENT  
**20.97 ± 0.02 ± 1.15** ACKERSTAFF 98A OPAL  $E_{cm}^{ee} = 91.2$  GeV

$\langle N_{\pi^\pm} \rangle$   
VALUE DOCUMENT ID TECN COMMENT  
**17.03 ± 0.16 OUR AVERAGE**  
17.007 ± 0.209 ABE 04c SLD  $E_{cm}^{ee} = 91.2$  GeV  
17.26 ± 0.10 ± 0.88 ABREU 98L DLPH  $E_{cm}^{ee} = 91.2$  GeV  
17.04 ± 0.31 BARATE 98v ALEP  $E_{cm}^{ee} = 91.2$  GeV  
17.05 ± 0.43 AKERS 94P OPAL  $E_{cm}^{ee} = 91.2$  GeV



# Gauge & Higgs Boson Particle Listings

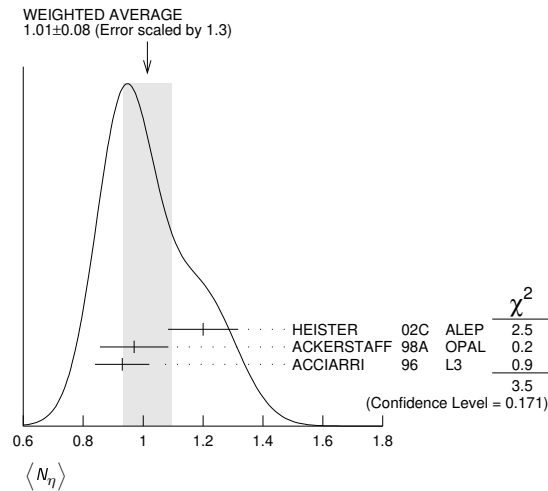
## Z

### $\langle N_{\pi^0} \rangle$

VALUE	DOCUMENT ID	TECN	COMMENT
<b>9.76 ± 0.26 OUR AVERAGE</b>			
9.55 ± 0.06 ± 0.75	ACKERSTAFF 98A	OPAL	$E_{cm}^{ee} = 91.2$ GeV
9.63 ± 0.13 ± 0.63	BARATE 97J	ALEP	$E_{cm}^{ee} = 91.2$ GeV
9.90 ± 0.02 ± 0.33	ACCIARRI 96	L3	$E_{cm}^{ee} = 91.2$ GeV
9.2 ± 0.2 ± 1.0	ADAM 96	DLPH	$E_{cm}^{ee} = 91.2$ GeV

### $\langle N_{\eta} \rangle$

VALUE	DOCUMENT ID	TECN	COMMENT
<b>1.01 ± 0.08 OUR AVERAGE</b>			Error includes scale factor of 1.3. See the ideogram below.
1.20 ± 0.04 ± 0.11	HEISTER 02c	ALEP	$E_{cm}^{ee} = 91.2$ GeV
0.97 ± 0.03 ± 0.11	ACKERSTAFF 98A	OPAL	$E_{cm}^{ee} = 91.2$ GeV
0.93 ± 0.01 ± 0.09	ACCIARRI 96	L3	$E_{cm}^{ee} = 91.2$ GeV



### $\langle N_{\rho^\pm} \rangle$

VALUE	DOCUMENT ID	TECN	COMMENT
<b>2.57 ± 0.15 OUR AVERAGE</b>			
2.59 ± 0.03 ± 0.16	<sup>1</sup> BEDDALL 09	ALEPH archive,	$E_{cm}^{ee} = 91.2$ GeV
2.40 ± 0.06 ± 0.43	ACKERSTAFF 98A	OPAL	$E_{cm}^{ee} = 91.2$ GeV

<sup>1</sup>BEDDALL 09 analyse 3.2 million hadronic Z decays as archived by ALEPH collaboration and report a value of  $2.59 \pm 0.03 \pm 0.15 \pm 0.04$ . The first error is statistical, the second systematic, and the third arises from extrapolation to full phase space. We combine the systematic errors in quadrature.

### $\langle N_{\rho^0} \rangle$

VALUE	DOCUMENT ID	TECN	COMMENT
<b>1.24 ± 0.10 OUR AVERAGE</b>			Error includes scale factor of 1.1.
1.19 ± 0.10	ABREU 99J	DLPH	$E_{cm}^{ee} = 91.2$ GeV
1.45 ± 0.06 ± 0.20	BUSKULIC 96H	ALEP	$E_{cm}^{ee} = 91.2$ GeV

### $\langle N_{\omega} \rangle$

VALUE	DOCUMENT ID	TECN	COMMENT
<b>1.02 ± 0.06 OUR AVERAGE</b>			
1.00 ± 0.03 ± 0.06	HEISTER 02c	ALEP	$E_{cm}^{ee} = 91.2$ GeV
1.04 ± 0.04 ± 0.14	ACKERSTAFF 98A	OPAL	$E_{cm}^{ee} = 91.2$ GeV
1.17 ± 0.09 ± 0.15	ACCIARRI 97D	L3	$E_{cm}^{ee} = 91.2$ GeV

### $\langle N_{\eta'} \rangle$

VALUE	DOCUMENT ID	TECN	COMMENT
<b>0.17 ± 0.05 OUR AVERAGE</b>			Error includes scale factor of 2.4.
0.14 ± 0.01 ± 0.02	ACKERSTAFF 98A	OPAL	$E_{cm}^{ee} = 91.2$ GeV
0.25 ± 0.04	<sup>1</sup> ACCIARRI 97D	L3	$E_{cm}^{ee} = 91.2$ GeV

• • • We do not use the following data for averages, fits, limits, etc. • • •  
 0.068 ± 0.018 ± 0.016 <sup>2</sup>BUSKULIC 92D ALEP  $E_{cm}^{ee} = 91.2$  GeV  
<sup>1</sup>ACCIARRI 97D obtain this value averaging over the two decay channels  $\eta' \rightarrow \pi^+ \pi^- \eta$  and  $\eta' \rightarrow \rho^0 \gamma$ .  
<sup>2</sup>BUSKULIC 92D obtain this value for  $x > 0.1$ .

### $\langle N_{f_0(980)} \rangle$

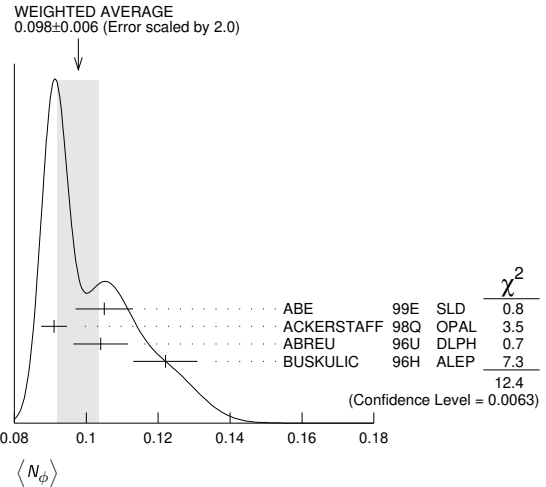
VALUE	DOCUMENT ID	TECN	COMMENT
<b>0.147 ± 0.011 OUR AVERAGE</b>			
0.164 ± 0.021	ABREU 99J	DLPH	$E_{cm}^{ee} = 91.2$ GeV
0.141 ± 0.007 ± 0.011	ACKERSTAFF 98Q	OPAL	$E_{cm}^{ee} = 91.2$ GeV

### $\langle N_{\pi_0(980)^\pm} \rangle$

VALUE	DOCUMENT ID	TECN	COMMENT
<b>0.27 ± 0.04 ± 0.10</b>	ACKERSTAFF 98A	OPAL	$E_{cm}^{ee} = 91.2$ GeV

### $\langle N_{\phi} \rangle$

VALUE	DOCUMENT ID	TECN	COMMENT
<b>0.098 ± 0.006 OUR AVERAGE</b>			Error includes scale factor of 2.0. See the ideogram below.
0.105 ± 0.008	ABE 99E	SLD	$E_{cm}^{ee} = 91.2$ GeV
0.091 ± 0.002 ± 0.003	ACKERSTAFF 98Q	OPAL	$E_{cm}^{ee} = 91.2$ GeV
0.104 ± 0.003 ± 0.007	ABREU 96U	DLPH	$E_{cm}^{ee} = 91.2$ GeV
0.122 ± 0.004 ± 0.008	BUSKULIC 96H	ALEP	$E_{cm}^{ee} = 91.2$ GeV



### $\langle N_{f_1(1270)} \rangle$

VALUE	DOCUMENT ID	TECN	COMMENT
<b>0.169 ± 0.025 OUR AVERAGE</b>			Error includes scale factor of 1.4.
0.214 ± 0.038	ABREU 99J	DLPH	$E_{cm}^{ee} = 91.2$ GeV
0.155 ± 0.011 ± 0.018	ACKERSTAFF 98Q	OPAL	$E_{cm}^{ee} = 91.2$ GeV

### $\langle N_{f_1(1285)} \rangle$

VALUE	DOCUMENT ID	TECN	COMMENT
<b>0.165 ± 0.051</b>	<sup>1</sup> ABDALLAH 03H	DLPH	$E_{cm}^{ee} = 91.2$ GeV

<sup>1</sup>ABDALLAH 03H assume a  $K\bar{K}\pi$  branching ratio of  $(9.0 \pm 0.4)\%$ .

### $\langle N_{f_1(1420)} \rangle$

VALUE	DOCUMENT ID	TECN	COMMENT
<b>0.056 ± 0.012</b>	<sup>1</sup> ABDALLAH 03H	DLPH	$E_{cm}^{ee} = 91.2$ GeV

<sup>1</sup>ABDALLAH 03H assume a  $K\bar{K}\pi$  branching ratio of 100%.

### $\langle N_{f_2'(1525)} \rangle$

VALUE	DOCUMENT ID	TECN	COMMENT
<b>0.012 ± 0.006</b>	ABREU 99J	DLPH	$E_{cm}^{ee} = 91.2$ GeV

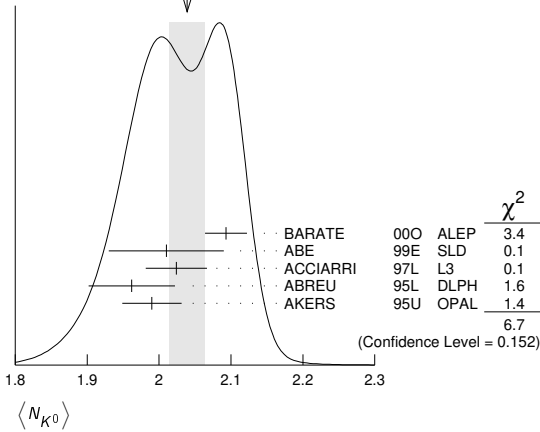
### $\langle N_{K^\pm} \rangle$

VALUE	DOCUMENT ID	TECN	COMMENT
<b>2.24 ± 0.04 OUR AVERAGE</b>			
2.203 ± 0.071	ABE 04c	SLD	$E_{cm}^{ee} = 91.2$ GeV
2.21 ± 0.05 ± 0.05	ABREU 98L	DLPH	$E_{cm}^{ee} = 91.2$ GeV
2.26 ± 0.12	BARATE 98v	ALEP	$E_{cm}^{ee} = 91.2$ GeV
2.42 ± 0.13	AKERS 94P	OPAL	$E_{cm}^{ee} = 91.2$ GeV

### $\langle N_{K^0} \rangle$

VALUE	DOCUMENT ID	TECN	COMMENT
<b>2.039 ± 0.025 OUR AVERAGE</b>			Error includes scale factor of 1.3. See the ideogram below.
2.093 ± 0.004 ± 0.029	BARATE 00o	ALEP	$E_{cm}^{ee} = 91.2$ GeV
2.01 ± 0.08	ABE 99E	SLD	$E_{cm}^{ee} = 91.2$ GeV
2.024 ± 0.006 ± 0.042	ACCIARRI 97L	L3	$E_{cm}^{ee} = 91.2$ GeV
1.962 ± 0.022 ± 0.056	ABREU 95L	DLPH	$E_{cm}^{ee} = 91.2$ GeV
1.99 ± 0.01 ± 0.04	AKERS 95U	OPAL	$E_{cm}^{ee} = 91.2$ GeV

WEIGHTED AVERAGE  
2.039±0.025 (Error scaled by 1.3)



$\langle N_{K^*(892)\pm} \rangle$

VALUE	DOCUMENT ID	TECN	COMMENT
<b>0.72 ± 0.05 OUR AVERAGE</b>			
0.712 ± 0.031 ± 0.059	ABREU 95L	DLPH	$E_{cm}^{ee} = 91.2$ GeV
0.72 ± 0.02 ± 0.08	ACTON 93	OPAL	$E_{cm}^{ee} = 91.2$ GeV

$\langle N_{K^*(892)^0} \rangle$

VALUE	DOCUMENT ID	TECN	COMMENT
<b>0.739 ± 0.022 OUR AVERAGE</b>			
0.707 ± 0.041	ABE 99E	SLD	$E_{cm}^{ee} = 91.2$ GeV
0.74 ± 0.02 ± 0.02	ACKERSTAFF 97S	OPAL	$E_{cm}^{ee} = 91.2$ GeV
0.77 ± 0.02 ± 0.07	ABREU 96U	DLPH	$E_{cm}^{ee} = 91.2$ GeV
0.83 ± 0.01 ± 0.09	BUSKULIC 96H	ALEP	$E_{cm}^{ee} = 91.2$ GeV
0.97 ± 0.18 ± 0.31	ABREU 93	DLPH	$E_{cm}^{ee} = 91.2$ GeV

$\langle N_{K_2^*(1430)} \rangle$

VALUE	DOCUMENT ID	TECN	COMMENT
<b>0.073 ± 0.023</b>	ABREU 99J	DLPH	$E_{cm}^{ee} = 91.2$ GeV
0.19 ± 0.04 ± 0.06	<sup>1</sup> AKERS 95X	OPAL	$E_{cm}^{ee} = 91.2$ GeV

• • • We do not use the following data for averages, fits, limits, etc. • • •

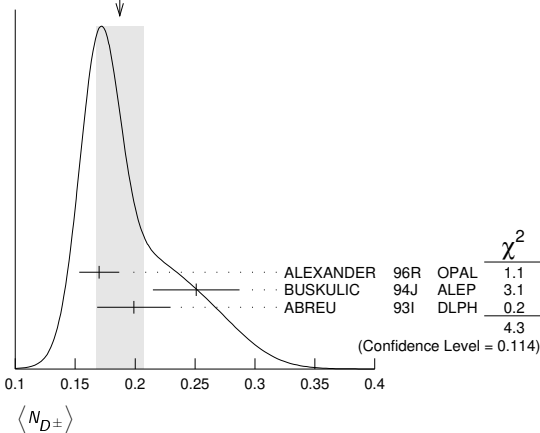
<sup>1</sup> AKERS 95X obtain this value for  $x < 0.3$ .

$\langle N_{D^\pm} \rangle$

VALUE	DOCUMENT ID	TECN	COMMENT
<b>0.187 ± 0.020 OUR AVERAGE</b>			Error includes scale factor of 1.5. See the ideogram below.
0.170 ± 0.009 ± 0.014	ALEXANDER 96R	OPAL	$E_{cm}^{ee} = 91.2$ GeV
0.251 ± 0.026 ± 0.025	BUSKULIC 94J	ALEP	$E_{cm}^{ee} = 91.2$ GeV
0.199 ± 0.019 ± 0.024	<sup>1</sup> ABREU 93I	DLPH	$E_{cm}^{ee} = 91.2$ GeV

<sup>1</sup> See ABREU 95 (erratum).

WEIGHTED AVERAGE  
0.187±0.020 (Error scaled by 1.5)



$\langle N_{D^0} \rangle$

VALUE	DOCUMENT ID	TECN	COMMENT
<b>0.462 ± 0.026 OUR AVERAGE</b>			
0.465 ± 0.017 ± 0.027	ALEXANDER 96R	OPAL	$E_{cm}^{ee} = 91.2$ GeV
0.518 ± 0.052 ± 0.035	BUSKULIC 94J	ALEP	$E_{cm}^{ee} = 91.2$ GeV
0.403 ± 0.038 ± 0.044	<sup>1</sup> ABREU 93I	DLPH	$E_{cm}^{ee} = 91.2$ GeV

<sup>1</sup> See ABREU 95 (erratum).

$\langle N_{D_s^\pm} \rangle$

VALUE	DOCUMENT ID	TECN	COMMENT
<b>0.183 ± 0.010 ± 0.018</b>	ALEXANDER 96R	OPAL	$E_{cm}^{ee} = 91.2$ GeV

$\langle N_{D^*(2010)\pm} \rangle$

VALUE	DOCUMENT ID	TECN	COMMENT
<b>0.183 ± 0.008 OUR AVERAGE</b>			
0.1854 ± 0.0041 ± 0.0091	<sup>1</sup> ACKERSTAFF 98E	OPAL	$E_{cm}^{ee} = 91.2$ GeV
0.187 ± 0.015 ± 0.013	BUSKULIC 94J	ALEP	$E_{cm}^{ee} = 91.2$ GeV
0.171 ± 0.012 ± 0.016	<sup>2</sup> ABREU 93I	DLPH	$E_{cm}^{ee} = 91.2$ GeV

<sup>1</sup> ACKERSTAFF 98E systematic error includes an uncertainty of ± 0.0069 due to the branching ratios  $B(D^{*+} \rightarrow D^0 \pi^+) = 0.683 \pm 0.014$  and  $B(D^0 \rightarrow K^- \pi^+) = 0.0383 \pm 0.0012$ .

<sup>2</sup> See ABREU 95 (erratum).

$\langle N_{D_{s1}(2536)^+} \rangle$

VALUE (units 10 <sup>-3</sup> )	DOCUMENT ID	TECN	COMMENT
<b>2.9<sup>+0.7</sup><sub>-0.6</sub> ± 0.2</b>	<sup>1</sup> ACKERSTAFF 97W	OPAL	$E_{cm}^{ee} = 91.2$ GeV

• • • We do not use the following data for averages, fits, limits, etc. • • •

<sup>1</sup> ACKERSTAFF 97W obtain this value for  $x > 0.6$  and with the assumption that its decay width is saturated by the  $D^* K$  final states.

$\langle N_{B^*} \rangle$

VALUE	DOCUMENT ID	TECN	COMMENT
<b>0.28 ± 0.01 ± 0.03</b>	<sup>1</sup> ABREU 95R	DLPH	$E_{cm}^{ee} = 91.2$ GeV

<sup>1</sup> ABREU 95R quote this value for a flavor-averaged excited state.

$\langle N_{J/\psi(1S)} \rangle$

VALUE	DOCUMENT ID	TECN	COMMENT
<b>0.0056 ± 0.0003 ± 0.0004</b>	<sup>1</sup> ALEXANDER 96B	OPAL	$E_{cm}^{ee} = 91.2$ GeV

<sup>1</sup> ALEXANDER 96B identify  $J/\psi(1S)$  from the decays into lepton pairs.

$\langle N_{\psi(2S)} \rangle$

VALUE	DOCUMENT ID	TECN	COMMENT
<b>0.0023 ± 0.0004 ± 0.0003</b>	ALEXANDER 96B	OPAL	$E_{cm}^{ee} = 91.2$ GeV

$\langle N_p \rangle$

VALUE	DOCUMENT ID	TECN	COMMENT
<b>1.046 ± 0.026 OUR AVERAGE</b>			
1.054 ± 0.035	ABE 04C	SLD	$E_{cm}^{ee} = 91.2$ GeV
1.08 ± 0.04 ± 0.03	ABREU 98L	DLPH	$E_{cm}^{ee} = 91.2$ GeV
1.00 ± 0.07	BARATE 98V	ALEP	$E_{cm}^{ee} = 91.2$ GeV
0.92 ± 0.11	AKERS 94P	OPAL	$E_{cm}^{ee} = 91.2$ GeV

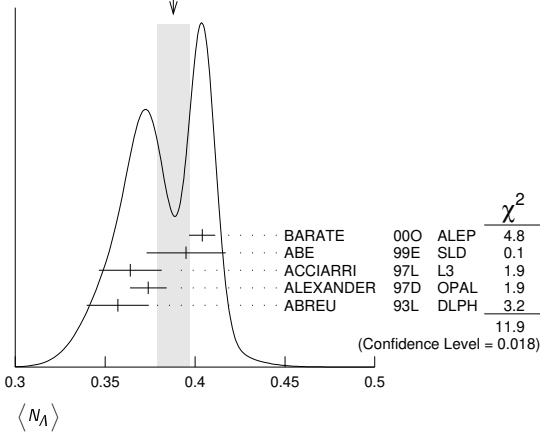
$\langle N_{\Delta(1232)^{++}} \rangle$

VALUE	DOCUMENT ID	TECN	COMMENT
<b>0.087 ± 0.033 OUR AVERAGE</b>			Error includes scale factor of 2.4.
0.079 ± 0.009 ± 0.011	ABREU 95W	DLPH	$E_{cm}^{ee} = 91.2$ GeV
0.22 ± 0.04 ± 0.04	ALEXANDER 95D	OPAL	$E_{cm}^{ee} = 91.2$ GeV

$\langle N_\Lambda \rangle$

VALUE	DOCUMENT ID	TECN	COMMENT
<b>0.388 ± 0.009 OUR AVERAGE</b>			Error includes scale factor of 1.7. See the ideogram below.
0.404 ± 0.002 ± 0.007	BARATE 00O	ALEP	$E_{cm}^{ee} = 91.2$ GeV
0.395 ± 0.022	ABE 99E	SLD	$E_{cm}^{ee} = 91.2$ GeV
0.364 ± 0.004 ± 0.017	ACCIARRI 97L	L3	$E_{cm}^{ee} = 91.2$ GeV
0.374 ± 0.002 ± 0.010	ALEXANDER 97D	OPAL	$E_{cm}^{ee} = 91.2$ GeV
0.357 ± 0.003 ± 0.017	ABREU 93L	DLPH	$E_{cm}^{ee} = 91.2$ GeV

WEIGHTED AVERAGE  
0.388±0.009 (Error scaled by 1.7)



$\langle N_{\Lambda(1520)} \rangle$

VALUE	DOCUMENT ID	TECN	COMMENT
<b>0.0224 ± 0.0027 OUR AVERAGE</b>			
0.029 ± 0.005 ± 0.005	ABREU	00P	DLPH $E_{cm}^{ee} = 91.2$ GeV
0.0213 ± 0.0021 ± 0.0019	ALEXANDER	97D	OPAL $E_{cm}^{ee} = 91.2$ GeV

$\langle N_{\Sigma^+} \rangle$

VALUE	DOCUMENT ID	TECN	COMMENT
<b>0.107 ± 0.010 OUR AVERAGE</b>			
0.114 ± 0.011 ± 0.009	ACCIARRI	00J	L3 $E_{cm}^{ee} = 91.2$ GeV
0.099 ± 0.008 ± 0.013	ALEXANDER	97E	OPAL $E_{cm}^{ee} = 91.2$ GeV

$\langle N_{\Sigma^-} \rangle$

VALUE	DOCUMENT ID	TECN	COMMENT
<b>0.082 ± 0.007 OUR AVERAGE</b>			
0.081 ± 0.002 ± 0.010	ABREU	00P	DLPH $E_{cm}^{ee} = 91.2$ GeV
0.083 ± 0.006 ± 0.009	ALEXANDER	97E	OPAL $E_{cm}^{ee} = 91.2$ GeV

$\langle N_{\Sigma^+ + \Sigma^-} \rangle$

VALUE	DOCUMENT ID	TECN	COMMENT
<b>0.181 ± 0.018 OUR AVERAGE</b>			
0.182 ± 0.010 ± 0.016	<sup>1</sup> ALEXANDER	97E	OPAL $E_{cm}^{ee} = 91.2$ GeV
0.170 ± 0.014 ± 0.061	ABREU	95O	DLPH $E_{cm}^{ee} = 91.2$ GeV

<sup>1</sup> We have combined the values of  $\langle N_{\Sigma^+} \rangle$  and  $\langle N_{\Sigma^-} \rangle$  from ALEXANDER 97E adding the statistical and systematic errors of the two final states separately in quadrature. If isospin symmetry is assumed this value becomes  $0.174 \pm 0.010 \pm 0.015$ .

$\langle N_{\Sigma^0} \rangle$

VALUE	DOCUMENT ID	TECN	COMMENT
<b>0.076 ± 0.010 OUR AVERAGE</b>			
0.095 ± 0.015 ± 0.013	ACCIARRI	00J	L3 $E_{cm}^{ee} = 91.2$ GeV
0.071 ± 0.012 ± 0.013	ALEXANDER	97E	OPAL $E_{cm}^{ee} = 91.2$ GeV
0.070 ± 0.010 ± 0.010	ADAM	96B	DLPH $E_{cm}^{ee} = 91.2$ GeV

$\langle N_{(\Sigma^+ + \Sigma^- + \Sigma^0)/3} \rangle$

VALUE	DOCUMENT ID	TECN	COMMENT
<b>0.084 ± 0.005 ± 0.008</b>			
	ALEXANDER	97E	OPAL $E_{cm}^{ee} = 91.2$ GeV

$\langle N_{\Sigma(1385)^+} \rangle$

VALUE	DOCUMENT ID	TECN	COMMENT
<b>0.0239 ± 0.0009 ± 0.0012</b>			
	ALEXANDER	97D	OPAL $E_{cm}^{ee} = 91.2$ GeV

$\langle N_{\Sigma(1385)^-} \rangle$

VALUE	DOCUMENT ID	TECN	COMMENT
<b>0.0240 ± 0.0010 ± 0.0014</b>			
	ALEXANDER	97D	OPAL $E_{cm}^{ee} = 91.2$ GeV

$\langle N_{\Sigma(1385)^+ + \Sigma(1385)^-} \rangle$

VALUE	DOCUMENT ID	TECN	COMMENT
<b>0.046 ± 0.004 OUR AVERAGE</b>			
0.0479 ± 0.0013 ± 0.0026	ALEXANDER	97D	OPAL $E_{cm}^{ee} = 91.2$ GeV
0.0382 ± 0.0028 ± 0.0045	ABREU	95O	DLPH $E_{cm}^{ee} = 91.2$ GeV

Error includes scale factor of 1.6.

$\langle N_{\Xi^-} \rangle$

VALUE	DOCUMENT ID	TECN	COMMENT
<b>0.0258 ± 0.0009 OUR AVERAGE</b>			
0.0247 ± 0.0009 ± 0.0025	ABDALLAH	06E	DLPH $E_{cm}^{ee} = 91.2$ GeV
0.0259 ± 0.0004 ± 0.0009	ALEXANDER	97D	OPAL $E_{cm}^{ee} = 91.2$ GeV

$\langle N_{\Xi(1530)^0} \rangle$

VALUE	DOCUMENT ID	TECN	COMMENT
<b>0.0059 ± 0.0011 OUR AVERAGE</b>			Error includes scale factor of 2.3.
0.0045 ± 0.0005 ± 0.0006	ABDALLAH	05C	DLPH $E_{cm}^{ee} = 91.2$ GeV
0.0068 ± 0.0005 ± 0.0004	ALEXANDER	97D	OPAL $E_{cm}^{ee} = 91.2$ GeV

$\langle N_{\Omega^-} \rangle$

VALUE	DOCUMENT ID	TECN	COMMENT
<b>0.00164 ± 0.00028 OUR AVERAGE</b>			
0.0018 ± 0.0003 ± 0.0002	ALEXANDER	97D	OPAL $E_{cm}^{ee} = 91.2$ GeV
0.0014 ± 0.0002 ± 0.0004	ADAM	96B	DLPH $E_{cm}^{ee} = 91.2$ GeV

$\langle N_{\Lambda_c^+} \rangle$

VALUE	DOCUMENT ID	TECN	COMMENT
<b>0.078 ± 0.012 ± 0.012</b>			
	ALEXANDER	96R	OPAL $E_{cm}^{ee} = 91.2$ GeV

$\langle N_D \rangle$

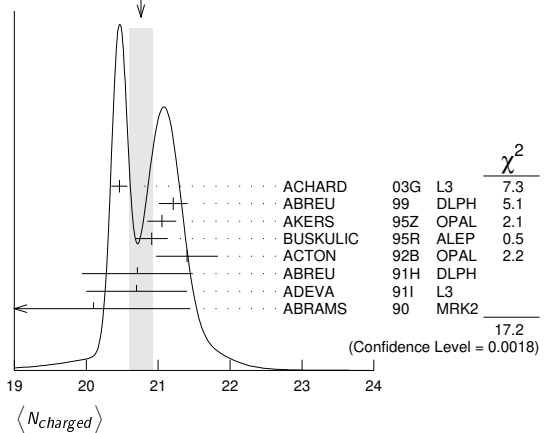
VALUE (units $10^{-6}$ )	DOCUMENT ID	TECN	COMMENT
<b>5.9 ± 1.8 ± 0.5</b>			
	<sup>1</sup> SCHAEEL	06A	ALEP $E_{cm}^{ee} = 91.2$ GeV

<sup>1</sup> SCHAEEL 06A obtain this anti-deuteron production rate per hadronic Z decay in the anti-deuteron momentum range from 0.62 to 1.03 GeV/c.

$\langle N_{\text{charged}} \rangle$

VALUE	DOCUMENT ID	TECN	COMMENT
<b>20.76 ± 0.16 OUR AVERAGE</b>			Error includes scale factor of 2.1. See the ideogram below.
20.46 ± 0.01 ± 0.11	ACHARD	03G	L3 $E_{cm}^{ee} = 91.2$ GeV
21.21 ± 0.01 ± 0.20	ABREU	99	DLPH $E_{cm}^{ee} = 91.2$ GeV
21.05 ± 0.20	AKERS	95Z	OPAL $E_{cm}^{ee} = 91.2$ GeV
20.91 ± 0.03 ± 0.22	BUSKULIC	95R	ALEP $E_{cm}^{ee} = 91.2$ GeV
21.40 ± 0.43	ACTON	92B	OPAL $E_{cm}^{ee} = 91.2$ GeV
20.71 ± 0.04 ± 0.77	ABREU	91H	DLPH $E_{cm}^{ee} = 91.2$ GeV
20.7 ± 0.7	ADEVA	91I	L3 $E_{cm}^{ee} = 91.2$ GeV
20.1 ± 1.0 ± 0.9	ABRAMS	90	MRK2 $E_{cm}^{ee} = 91.1$ GeV

WEIGHTED AVERAGE  
20.76±0.16 (Error scaled by 2.1)



Z HADRONIC POLE CROSS SECTION

OUR FIT is obtained using the fit procedure and correlations as determined by the LEP Electroweak Working Group (see the note "The Z boson" and ref. LEP-SLC 06). This quantity is defined as

$$\sigma_h^0 = \frac{12\pi}{M_Z^2} \frac{\Gamma(e^+e^-)\Gamma(\text{hadrons})}{\Gamma_Z^2}$$

It is one of the parameters used in the Z lineshape fit.

VALUE (nb)	EVTS	DOCUMENT ID	TECN	COMMENT
<b>41.541 ± 0.037 OUR FIT</b>				
41.501 ± 0.055	4.10M	<sup>1</sup> ABBIENDI	01A	OPAL $E_{cm}^{ee} = 88-94$ GeV
41.578 ± 0.069	3.70M	ABREU	00F	DLPH $E_{cm}^{ee} = 88-94$ GeV
41.535 ± 0.055	3.54M	ACCIARRI	00C	L3 $E_{cm}^{ee} = 88-94$ GeV
41.559 ± 0.058	4.07M	<sup>2</sup> BARATE	00C	ALEP $E_{cm}^{ee} = 88-94$ GeV
42 ± 4	450	ABRAMS	89B	MRK2 $E_{cm}^{ee} = 89.2-93.0$ GeV

<sup>1</sup> ABBIENDI 01A error includes approximately 0.031 due to statistics, 0.033 due to event selection systematics, 0.029 due to uncertainty in luminosity measurement, and 0.011 due to LEP energy uncertainty.

<sup>2</sup> BARATE 00C error includes approximately 0.030 due to statistics, 0.026 due to experimental systematics, and 0.025 due to uncertainty in luminosity measurement.

Z VECTOR COUPLINGS

These quantities are the effective vector couplings of the Z to charged leptons and quarks. Their magnitude is derived from a measurement of the Z lineshape and the forward-backward lepton asymmetries as a function of energy around the Z mass. The relative sign among the vector to axial-vector couplings is obtained from a measurement of the Z asymmetry parameters,  $A_e$ ,  $A_\mu$ , and  $A_\tau$ . By convention the sign of  $g_A^e$  is fixed to be negative (and opposite to that of  $g^{V_e}$  obtained using  $\nu_e$  scattering measurements). For the light quarks, the sign of the couplings is assigned consistently with this assumption. The LEP/SLD-based fit values quoted below correspond to global nine- or five-parameter fits to lineshape, lepton forward-backward asymmetry, and  $A_e$ ,  $A_\mu$ , and  $A_\tau$  measurements. See the note "The Z boson" and ref. LEP-SLC 06 for details. Where  $p\bar{p}$  and  $e\bar{p}$  data is quoted, OUR FIT value corresponds to a weighted average of this with the LEP/SLD fit result.

VALUE	EVTS	DOCUMENT ID	TECN	COMMENT
<b>-0.03817 ± 0.00047 OUR FIT</b>				
-0.058 ± 0.016 ± 0.007	5026	1 ACOSTA	05M CDF	$E_{cm}^{p\bar{p}} = 1.96$ TeV
-0.0346 ± 0.0023	137.0K	2 ABBIENDI	01o OPAL	$E_{cm}^{ee} = 88-94$ GeV
-0.0412 ± 0.0027	124.4k	3 ACCIARRI	00c L3	$E_{cm}^{ee} = 88-94$ GeV
-0.0400 ± 0.0037		BARATE	00c ALEP	$E_{cm}^{ee} = 88-94$ GeV
-0.0414 ± 0.0020		4 ABE	95J SLD	$E_{cm}^{ee} = 91.31$ GeV

- ACOSTA 05M determine the forward-backward asymmetry of  $e^+e^-$  pairs produced via  $q\bar{q} \rightarrow Z/\gamma^* \rightarrow e^+e^-$  in 15 M( $e^+e^-$ ) effective mass bins ranging from 40 GeV to 600 GeV. These results are used to obtain the vector and axial-vector couplings of the Z to  $e^+e^-$ , assuming the quark couplings are as predicted by the standard model. Higher order radiative corrections have not been taken into account.
- ABBIENDI 01o use their measurement of the  $\tau$  polarization in addition to the lineshape and forward-backward lepton asymmetries.
- ACCIARRI 00c use their measurement of the  $\tau$  polarization in addition to forward-backward lepton asymmetries.
- ABE 95J obtain this result combining polarized Bhabha results with the  $A_{LR}$  measurement of ABE 94c. The Bhabha results alone give  $-0.0507 \pm 0.0096 \pm 0.0020$ .

VALUE	EVTS	DOCUMENT ID	TECN	COMMENT
<b>-0.0367 ± 0.0023 OUR FIT</b>				
-0.0388 ± 0.0060 ± 0.0064	182.8K	1 ABBIENDI	01o OPAL	$E_{cm}^{ee} = 88-94$ GeV
-0.0386 ± 0.0073	113.4k	2 ACCIARRI	00c L3	$E_{cm}^{ee} = 88-94$ GeV
-0.0362 ± 0.0061		BARATE	00c ALEP	$E_{cm}^{ee} = 88-94$ GeV
-0.0413 ± 0.0060	66143	3 ABBIENDI	01k OPAL	$E_{cm}^{ee} = 89-93$ GeV

- • • We do not use the following data for averages, fits, limits, etc. • • •
- ABBIENDI 01o use their measurement of the  $\tau$  polarization in addition to the lineshape and forward-backward lepton asymmetries.
  - ACCIARRI 00c use their measurement of the  $\tau$  polarization in addition to forward-backward lepton asymmetries.
  - ABBIENDI 01k obtain this from an angular analysis of the muon pair asymmetry which takes into account effects of initial state radiation on an event by event basis and of initial-final state interference.

VALUE	EVTS	DOCUMENT ID	TECN	COMMENT
<b>-0.0366 ± 0.0010 OUR FIT</b>				
-0.0365 ± 0.0023	151.5K	1 ABBIENDI	01o OPAL	$E_{cm}^{ee} = 88-94$ GeV
-0.0384 ± 0.0026	103.0k	2 ACCIARRI	00c L3	$E_{cm}^{ee} = 88-94$ GeV
-0.0361 ± 0.0068		BARATE	00c ALEP	$E_{cm}^{ee} = 88-94$ GeV

- ABBIENDI 01o use their measurement of the  $\tau$  polarization in addition to the lineshape and forward-backward lepton asymmetries.
- ACCIARRI 00c use their measurement of the  $\tau$  polarization in addition to forward-backward lepton asymmetries.

VALUE	EVTS	DOCUMENT ID	TECN	COMMENT
<b>-0.03783 ± 0.00041 OUR FIT</b>				
-0.0358 ± 0.0014	471.3K	1 ABBIENDI	01o OPAL	$E_{cm}^{ee} = 88-94$ GeV
-0.0397 ± 0.0020	379.4k	2 ABREU	00f DLPH	$E_{cm}^{ee} = 88-94$ GeV
-0.0397 ± 0.0017	340.8k	3 ACCIARRI	00c L3	$E_{cm}^{ee} = 88-94$ GeV
-0.0383 ± 0.0018	500k	BARATE	00c ALEP	$E_{cm}^{ee} = 88-94$ GeV

- ABBIENDI 01o use their measurement of the  $\tau$  polarization in addition to the lineshape and forward-backward lepton asymmetries.
- Using forward-backward lepton asymmetries.
- ACCIARRI 00c use their measurement of the  $\tau$  polarization in addition to forward-backward lepton asymmetries.

VALUE	EVTS	DOCUMENT ID	TECN	COMMENT
<b>0.266 ± 0.034 OUR AVERAGE</b>				
0.270 ± 0.037		1 ANDREEV	18A H1	$e^\pm p$
0.201 ± 0.112	156k	2 ABAZOV	11D D0	$E_{cm}^{p\bar{p}} = 1.97$ TeV
0.24 ± 0.28 ± 0.11		3 LEP-SLC	06	$E_{cm}^{ee} = 88-94$ GeV
0.399 ± 0.152 ± 0.188	5026	4 ACOSTA	05M CDF	$E_{cm}^{p\bar{p}} = 1.96$ TeV

• • • We do not use the following data for averages, fits, limits, etc. • • •

0.14 ± 0.09 ± 0.09		5 ABRAMOWICZ16A	ZEUS	
0.144 ± 0.066 ± 0.058		6 ABT	16	
0.27 ± 0.13	1500	7 AKTAS	06 H1	$e^\pm p \rightarrow \mathcal{P}_e(\nu_e)X$ , $\sqrt{s} \approx 300$ GeV

- ANDREEV 18A obtain this result in a combined electroweak and QCD analysis using all deep-inelastic  $e^+p$  and  $e^-p$  neutral current and charged current scattering cross sections published by the H1 Collaboration, including data with longitudinally polarized lepton beams.
- ABAZOV 11D study  $p\bar{p} \rightarrow Z/\gamma^* e^+e^-$  events using 5 fb<sup>-1</sup> data at  $\sqrt{s} = 1.96$  TeV. The candidate events are selected by requiring two isolated electromagnetic showers with  $E_T > 25$  GeV, at least one electron in the central region and the di-electron mass in the range 50–1000 GeV. From the forward-backward asymmetry, determined as a function of the di-electron mass, they derive the axial and vector couplings of the  $u$ - and  $d$ -quarks and the value of  $\sin^2\theta_{eff}^l = 0.2309 \pm 0.0008(\text{stat}) \pm 0.0006(\text{syst})$ .
- LEP-SLC 06 is a combination of the results from LEP and SLC experiments using light quark tagging.  $s$ - and  $d$ -quark couplings are assumed to be identical.
- ACOSTA 05M determine the forward-backward asymmetry of  $e^+e^-$  pairs produced via  $q\bar{q} \rightarrow Z/\gamma^* \rightarrow e^+e^-$  in 15 M( $e^+e^-$ ) effective mass bins ranging from 40 GeV to 600 GeV. These results are used to obtain the vector and axial-vector couplings of the Z to the light quarks, assuming the electron couplings are as predicted by the Standard Model. Higher order radiative corrections have not been taken into account.
- ABRAMOWICZ 16A determine the Z<sup>0</sup> couplings to  $u$ - and  $d$ -quarks using the ZEUS polarised data from Run II together with the unpolarised data from both ZEUS and H1 Collaborations for Run I and unpolarised H1 data from Run II.
- ABT 16 determine the Z<sup>0</sup> couplings to  $u$ - and  $d$ -quarks using the same techniques and data as ABRAMOWICZ 16A but additionally use the published H1 polarised data.
- AKTAS 06 fit the neutral current ( $1.5 \leq Q^2 \leq 30,000$  GeV<sup>2</sup>) and charged current ( $1.5 \leq Q^2 \leq 15,000$  GeV<sup>2</sup>) differential cross sections. In the determination of the  $u$ -quark couplings the electron and  $d$ -quark couplings are fixed to their standard model values.

VALUE	EVTS	DOCUMENT ID	TECN	COMMENT
<b>-0.38 ± 0.04 ± 0.05 OUR AVERAGE</b>				
-0.488 ± 0.092		1 ANDREEV	18A H1	$e^\pm p$
-0.351 ± 0.251	156k	2 ABAZOV	11D D0	$E_{cm}^{p\bar{p}} = 1.97$ TeV
-0.33 ± 0.05 ± 0.07		3 LEP-SLC	06	$E_{cm}^{ee} = 88-94$ GeV
-0.226 ± 0.635 ± 0.290 ± 0.090	5026	4 ACOSTA	05M CDF	$E_{cm}^{p\bar{p}} = 1.96$ TeV

• • • We do not use the following data for averages, fits, limits, etc. • • •

-0.41 ± 0.25 ± 0.20		5 ABRAMOWICZ16A	ZEUS	
-0.503 ± 0.171 ± 0.103		6 ABT	16	
-0.33 ± 0.33	1500	7 AKTAS	06 H1	$e^\pm p \rightarrow \mathcal{P}_e(\nu_e)X$ , $\sqrt{s} \approx 300$ GeV

- ANDREEV 18A obtain this result in a combined electroweak and QCD analysis using all deep-inelastic  $e^+p$  and  $e^-p$  neutral current and charged current scattering cross sections published by the H1 Collaboration, including data with longitudinally polarized lepton beams.
- ABAZOV 11D study  $p\bar{p} \rightarrow Z/\gamma^* e^+e^-$  events using 5 fb<sup>-1</sup> data at  $\sqrt{s} = 1.96$  TeV. The candidate events are selected by requiring two isolated electromagnetic showers with  $E_T > 25$  GeV, at least one electron in the central region and the di-electron mass in the range 50–1000 GeV. From the forward-backward asymmetry, determined as a function of the di-electron mass, they derive the axial and vector couplings of the  $u$ - and  $d$ -quarks and the value of  $\sin^2\theta_{eff}^l = 0.2309 \pm 0.0008(\text{stat}) \pm 0.0006(\text{syst})$ .
- LEP-SLC 06 is a combination of the results from LEP and SLC experiments using light quark tagging.  $s$ - and  $d$ -quark couplings are assumed to be identical.
- ACOSTA 05M determine the forward-backward asymmetry of  $e^+e^-$  pairs produced via  $q\bar{q} \rightarrow Z/\gamma^* \rightarrow e^+e^-$  in 15 M( $e^+e^-$ ) effective mass bins ranging from 40 GeV to 600 GeV. These results are used to obtain the vector and axial-vector couplings of the Z to the light quarks, assuming the electron couplings are as predicted by the Standard Model. Higher order radiative corrections have not been taken into account.
- ABRAMOWICZ 16A determine the Z<sup>0</sup> couplings to  $u$ - and  $d$ -quarks using the ZEUS polarised data from Run II together with the unpolarised data from both ZEUS and H1 Collaborations for Run I and unpolarised H1 data from Run II.
- ABT 16 determine the Z<sup>0</sup> couplings to  $u$ - and  $d$ -quarks using the same techniques and data as ABRAMOWICZ 16A but additionally use the published H1 polarised data.
- AKTAS 06 fit the neutral current ( $1.5 \leq Q^2 \leq 30,000$  GeV<sup>2</sup>) and charged current ( $1.5 \leq Q^2 \leq 15,000$  GeV<sup>2</sup>) differential cross sections. In the determination of the  $d$ -quark couplings the electron and  $u$ -quark couplings are fixed to their standard model values.

Z AXIAL-VECTOR COUPLINGS

These quantities are the effective axial-vector couplings of the Z to charged leptons and quarks. Their magnitude is derived from a measurement of the Z lineshape and the forward-backward lepton asymmetries as a function of energy around the Z mass. The relative sign among the vector to axial-vector couplings is obtained from a measurement of the Z asymmetry parameters,  $A_e$ ,  $A_\mu$ , and  $A_\tau$ . By convention the sign of  $g_A^e$  is fixed to be negative (and opposite to that of  $g^{V_e}$  obtained using  $\nu_e$  scattering measurements). For the light quarks, the sign of the couplings is assigned consistently with this assumption. The LEP/SLD-based fit values quoted below correspond to global nine- or five-parameter fits to lineshape, lepton forward-backward asymmetry, and  $A_e$ ,  $A_\mu$ , and  $A_\tau$  measurements. See

## Gauge &amp; Higgs Boson Particle Listings

## Z

the note "The Z boson" and ref. LEP-SLC 06 for details. Where  $p\bar{p}$  and  $ep$  data is quoted, OUR FIT value corresponds to a weighted average of this with the LEP/SLD fit result.

 $g_A^e$ 

VALUE	EVTS	DOCUMENT ID	TECN	COMMENT
<b>-0.50111 ± 0.00035 OUR FIT</b>				
-0.528 ± 0.123 ± 0.059	5026	1 ACOSTA	05M CDF	$E_{cm}^{p\bar{p}} = 1.96$ TeV
-0.50062 ± 0.00062	137.0K	2 ABBIENDI	01o OPAL	$E_{cm}^{ee} = 88-94$ GeV
-0.5015 ± 0.0007	124.4k	3 ACCIARRI	00c L3	$E_{cm}^{ee} = 88-94$ GeV
-0.50166 ± 0.00057		BARATE	00c ALEP	$E_{cm}^{ee} = 88-94$ GeV
-0.4977 ± 0.0045		4 ABE	95J SLD	$E_{cm}^{ee} = 91.31$ GeV

- ACOSTA 05M determine the forward-backward asymmetry of  $e^+e^-$  pairs produced via  $q\bar{q} \rightarrow Z/\gamma^* \rightarrow e^+e^-$  in 15 M( $e^+e^-$ ) effective mass bins ranging from 40 GeV to 600 GeV. These results are used to obtain the vector and axial-vector couplings of the Z to  $e^+e^-$ , assuming the quark couplings are as predicted by the standard model. Higher order radiative corrections have not been taken into account.
- ABBIENDI 01o use their measurement of the  $\tau$  polarization in addition to the lineshape and forward-backward lepton asymmetries.
- ACCIARRI 00c use their measurement of the  $\tau$  polarization in addition to forward-backward lepton asymmetries.
- ABE 95J obtain this result combining polarized Bhabha results with the  $A_{FB}$  measurement of ABE 94c. The Bhabha results alone give  $-0.4968 \pm 0.0039 \pm 0.0027$ .

 $g_A^\mu$ 

VALUE	EVTS	DOCUMENT ID	TECN	COMMENT
<b>-0.50120 ± 0.00054 OUR FIT</b>				
-0.50117 ± 0.00099	182.8K	1 ABBIENDI	01o OPAL	$E_{cm}^{ee} = 88-94$ GeV
-0.5009 ± 0.0014	113.4k	2 ACCIARRI	00c L3	$E_{cm}^{ee} = 88-94$ GeV
-0.50046 ± 0.00093		BARATE	00c ALEP	$E_{cm}^{ee} = 88-94$ GeV
• • • We do not use the following data for averages, fits, limits, etc. • • •				
-0.520 ± 0.015	66143	3 ABBIENDI	01k OPAL	$E_{cm}^{ee} = 89-93$ GeV

- ABBIENDI 01o use their measurement of the  $\tau$  polarization in addition to the lineshape and forward-backward lepton asymmetries.
- ACCIARRI 00c use their measurement of the  $\tau$  polarization in addition to forward-backward lepton asymmetries.
- ABBIENDI 01k obtain this from an angular analysis of the muon pair asymmetry which takes into account effects of initial state radiation on an event by event basis and of initial-final state interference.

 $g_A^\tau$ 

VALUE	EVTS	DOCUMENT ID	TECN	COMMENT
<b>-0.50204 ± 0.00064 OUR FIT</b>				
-0.50165 ± 0.00124	151.5K	1 ABBIENDI	01o OPAL	$E_{cm}^{ee} = 88-94$ GeV
-0.5023 ± 0.0017	103.0K	2 ACCIARRI	00c L3	$E_{cm}^{ee} = 88-94$ GeV
-0.50216 ± 0.00100		BARATE	00c ALEP	$E_{cm}^{ee} = 88-94$ GeV

- ABBIENDI 01o use their measurement of the  $\tau$  polarization in addition to the lineshape and forward-backward lepton asymmetries.
- ACCIARRI 00c use their measurement of the  $\tau$  polarization in addition to forward-backward lepton asymmetries.

 $g_A^l$ 

VALUE	EVTS	DOCUMENT ID	TECN	COMMENT
<b>-0.50123 ± 0.00026 OUR FIT</b>				
-0.50089 ± 0.00045	471.3K	1 ABBIENDI	01o OPAL	$E_{cm}^{ee} = 88-94$ GeV
-0.5007 ± 0.0005	379.4k	ABREU	00f DLPH	$E_{cm}^{ee} = 88-94$ GeV
-0.50153 ± 0.00053	340.8k	2 ACCIARRI	00c L3	$E_{cm}^{ee} = 88-94$ GeV
-0.50150 ± 0.00046	500k	BARATE	00c ALEP	$E_{cm}^{ee} = 88-94$ GeV

- ABBIENDI 01o use their measurement of the  $\tau$  polarization in addition to the lineshape and forward-backward lepton asymmetries.
- ACCIARRI 00c use their measurement of the  $\tau$  polarization in addition to forward-backward lepton asymmetries.

 $g_A^u$ 

VALUE	EVTS	DOCUMENT ID	TECN	COMMENT
<b>0.519 ± 0.028 OUR AVERAGE</b>				
0.548 ± 0.036		1 ANDREEV	18A H1	$e^\pm p$
0.501 ± 0.110	156k	2 ABAZOV	11D D0	$E_{cm}^{p\bar{p}} = 1.97$ TeV
0.47 ± 0.05 -0.33		3 LEP-SLC	06	$E_{cm}^{ee} = 88-94$ GeV
0.441 ± 0.207 -0.173 ± 0.067	5026	4 ACOSTA	05M CDF	$E_{cm}^{p\bar{p}} = 1.96$ TeV
• • • We do not use the following data for averages, fits, limits, etc. • • •				
0.50 ± 0.12 -0.05		5 ABRAMOWICZ16A	ZEUS	
0.532 ± 0.107 -0.063		6 ABT	16	
0.57 ± 0.08	1500	7 AKTAS	06 H1	$e^\pm p \rightarrow \bar{\nu}_e(\nu_e)X$ , $\sqrt{s} \approx 300$ GeV

VALUE	EVTS	DOCUMENT ID	TECN	COMMENT
<b>0.519 ± 0.028 OUR AVERAGE</b>				
0.548 ± 0.036		1 ANDREEV	18A H1	$e^\pm p$
0.501 ± 0.110	156k	2 ABAZOV	11D D0	$E_{cm}^{p\bar{p}} = 1.97$ TeV
0.47 ± 0.05 -0.33		3 LEP-SLC	06	$E_{cm}^{ee} = 88-94$ GeV
0.441 ± 0.207 -0.173 ± 0.067	5026	4 ACOSTA	05M CDF	$E_{cm}^{p\bar{p}} = 1.96$ TeV
• • • We do not use the following data for averages, fits, limits, etc. • • •				
0.50 ± 0.12 -0.05		5 ABRAMOWICZ16A	ZEUS	
0.532 ± 0.107 -0.063		6 ABT	16	
0.57 ± 0.08	1500	7 AKTAS	06 H1	$e^\pm p \rightarrow \bar{\nu}_e(\nu_e)X$ , $\sqrt{s} \approx 300$ GeV

- ANDREEV 18A obtain this result in a combined electroweak and QCD analysis using all deep-inelastic  $e^+p$  and  $e^-p$  neutral current and charged current scattering cross sections published by the H1 Collaboration, including data with longitudinally polarized lepton beams.
- ABAZOV 11D study  $p\bar{p} \rightarrow Z/\gamma^* e^+e^-$  events using 5 fb<sup>-1</sup> data at  $\sqrt{s} = 1.96$  TeV. The candidate events are selected by requiring two isolated electromagnetic showers with  $E_T > 25$  GeV, at least one electron in the central region and the di-electron mass in the range 50–1000 GeV. From the forward-backward asymmetry, determined as a function of the di-electron mass, they derive the axial and vector couplings of the  $u$ - and  $d$ -quarks and the value of  $\sin^2\theta_{eff}^l = 0.2309 \pm 0.0008(\text{stat}) \pm 0.0006(\text{syst})$ .
- LEP-SLC 06 is a combination of the results from LEP and SLC experiments using light quark tagging.  $s$ - and  $d$ -quark couplings are assumed to be identical.
- ACOSTA 05M determine the forward-backward asymmetry of  $e^+e^-$  pairs produced via  $q\bar{q} \rightarrow Z/\gamma^* \rightarrow e^+e^-$  in 15 M( $e^+e^-$ ) effective mass bins ranging from 40 GeV to 600 GeV. These results are used to obtain the vector and axial-vector couplings of the Z to the light quarks, assuming the electron couplings are as predicted by the Standard Model. Higher order radiative corrections have not been taken into account.
- ABRAMOWICZ 16A determine the  $Z^0$  couplings to  $u$ - and  $d$ -quarks using the ZEUS polarised data from Run II together with the unpolarised data from both ZEUS and H1 Collaborations for Run I and unpolarised H1 data from Run II.
- ABT 16 determine the  $Z^0$  couplings to  $u$ - and  $d$ -quarks using the same techniques and data as ABRAMOWICZ 16A but additionally use the published H1 polarised data.
- AKTAS 06 fit the neutral current ( $1.5 \leq Q^2 \leq 30,000$  GeV<sup>2</sup>) and charged current ( $1.5 \leq Q^2 \leq 15,000$  GeV<sup>2</sup>) differential cross sections. In the determination of the  $u$ -quark couplings the electron and  $d$ -quark couplings are fixed to their standard model values.

 $g_A^d$ 

VALUE	EVTS	DOCUMENT ID	TECN	COMMENT
<b>-0.527 ± 0.040 OUR AVERAGE</b>				
-0.619 ± 0.108		1 ANDREEV	18A H1	$e^\pm p$
-0.497 ± 0.165	156k	2 ABAZOV	11D D0	$E_{cm}^{p\bar{p}} = 1.97$ TeV
-0.52 ± 0.05 -0.03		3 LEP-SLC	06	$E_{cm}^{ee} = 88-94$ GeV
-0.016 ± 0.346 -0.536 ± 0.091	5026	4 ACOSTA	05M CDF	$E_{cm}^{p\bar{p}} = 1.96$ TeV
• • • We do not use the following data for averages, fits, limits, etc. • • •				
-0.56 ± 0.41 -0.15		5 ABRAMOWICZ16A	ZEUS	
-0.409 ± 0.373 -0.213		6 ABT	16	
-0.80 ± 0.24	1500	7 AKTAS	06 H1	$e^\pm p \rightarrow \bar{\nu}_e(\nu_e)X$ , $\sqrt{s} \approx 300$ GeV

- ANDREEV 18A obtain this result in a combined electroweak and QCD analysis using all deep-inelastic  $e^+p$  and  $e^-p$  neutral current and charged current scattering cross sections published by the H1 Collaboration, including data with longitudinally polarized lepton beams.
- ABAZOV 11D study  $p\bar{p} \rightarrow Z/\gamma^* e^+e^-$  events using 5 fb<sup>-1</sup> data at  $\sqrt{s} = 1.96$  TeV. The candidate events are selected by requiring two isolated electromagnetic showers with  $E_T > 25$  GeV, at least one electron in the central region and the di-electron mass in the range 50–1000 GeV. From the forward-backward asymmetry, determined as a function of the di-electron mass, they derive the axial and vector couplings of the  $u$ - and  $d$ -quarks and the value of  $\sin^2\theta_{eff}^l = 0.2309 \pm 0.0008(\text{stat}) \pm 0.0006(\text{syst})$ .
- LEP-SLC 06 is a combination of the results from LEP and SLC experiments using light quark tagging.  $s$ - and  $d$ -quark couplings are assumed to be identical.
- ACOSTA 05M determine the forward-backward asymmetry of  $e^+e^-$  pairs produced via  $q\bar{q} \rightarrow Z/\gamma^* \rightarrow e^+e^-$  in 15 M( $e^+e^-$ ) effective mass bins ranging from 40 GeV to 600 GeV. These results are used to obtain the vector and axial-vector couplings of the Z to the light quarks, assuming the electron couplings are as predicted by the Standard Model. Higher order radiative corrections have not been taken into account.
- ABRAMOWICZ 16A determine the  $Z^0$  couplings to  $u$ - and  $d$ -quarks using the ZEUS polarised data from Run II together with the unpolarised data from both ZEUS and H1 Collaborations for Run I and unpolarised H1 data from Run II.
- ABT 16 determine the  $Z^0$  couplings to  $u$ - and  $d$ -quarks using the same techniques and data as ABRAMOWICZ 16A but additionally use the published H1 polarised data.
- AKTAS 06 fit the neutral current ( $1.5 \leq Q^2 \leq 30,000$  GeV<sup>2</sup>) and charged current ( $1.5 \leq Q^2 \leq 15,000$  GeV<sup>2</sup>) differential cross sections. In the determination of the  $d$ -quark couplings the electron and  $u$ -quark couplings are fixed to their standard model values.

## Z COUPLINGS TO NEUTRAL LEPTONS

Averaging over neutrino species, the invisible Z decay width determines the effective neutrino coupling  $g^{\nu e}$ . For  $g^{\nu e}$  and  $g^{\nu \mu}$ ,  $\nu_e e$  and  $\nu_\mu e$  scattering results are combined with  $g_A^e$  and  $g_V^e$  measurements at the Z mass to obtain  $g^{\nu e}$  and  $g^{\nu \mu}$  following NOVIKOV 93c.

 $g^{\nu e}$ 

VALUE	DOCUMENT ID	COMMENT
<b>0.50076 ± 0.00076</b>	1 LEP-SLC 06	$E_{cm}^{ee} = 88-94$ GeV

- From invisible Z-decay width.

 $g^{\nu \mu}$ 

VALUE	DOCUMENT ID	TECN	COMMENT
<b>0.528 ± 0.085</b>	1 VILAIN 94	CHM2	From $\nu_\mu e$ and $\nu_e e$ scattering

- VILAIN 94 derive this value from their value of  $g^{\nu \mu}$  and their ratio  $g^{\nu e}/g^{\nu \mu} = 1.05 \pm 0.15$ .

$g^{\nu\mu}$	VALUE	DOCUMENT ID	TECN	COMMENT
	<b>0.502 ± 0.017</b>	1 VILAIN	94 CHM2	From $\nu_\mu e$ scattering

<sup>1</sup> VILAIN 94 derive this value from their measurement of the couplings  $g_A^{\nu\mu} = -0.503 \pm 0.017$  and  $g_V^{\nu\mu} = -0.035 \pm 0.017$  obtained from  $\nu_\mu e$  scattering. We have re-evaluated this value using the current PDG values for  $g_A^e$  and  $g_V^e$ .

**Z ASYMMETRY PARAMETERS**

For each fermion-antifermion pair coupling to the Z these quantities are defined as

$$A_f = \frac{2g_V^f g_A^f}{(g_V^f)^2 + (g_A^f)^2}$$

where  $g_V^f$  and  $g_A^f$  are the effective vector and axial-vector couplings. For their relation to the various lepton asymmetries see the note "The Z boson" and ref. LEP-SLC 06.

**A<sub>e</sub>** Using polarized beams, this quantity can also be measured as  $(\sigma_L - \sigma_R) / (\sigma_L + \sigma_R)$ , where  $\sigma_L$  and  $\sigma_R$  are the  $e^+e^-$  production cross sections for Z bosons produced with left-handed and right-handed electrons respectively.

VALUE	EVTS	DOCUMENT ID	TECN	COMMENT
<b>0.1515 ± 0.0019 OUR AVERAGE</b>				
0.1454 ± 0.0108 ± 0.0036	144810	<sup>1</sup> ABBIENDI	01o OPAL	$E_{cm}^{ee} = 88-94$ GeV
0.1516 ± 0.0021	559000	<sup>2</sup> ABE	01B SLD	$E_{cm}^{ee} = 91.24$ GeV
0.1504 ± 0.0068 ± 0.0008		<sup>3</sup> HEISTER	01 ALEP	$E_{cm}^{ee} = 88-94$ GeV
0.1382 ± 0.0116 ± 0.0005	105000	<sup>4</sup> ABREU	00E DLPH	$E_{cm}^{ee} = 88-94$ GeV
0.1678 ± 0.0127 ± 0.0030	137092	<sup>5</sup> ACCIARRI	98H L3	$E_{cm}^{ee} = 88-94$ GeV
0.162 ± 0.041 ± 0.014	89838	<sup>6</sup> ABE	97 SLD	$E_{cm}^{ee} = 91.27$ GeV
0.202 ± 0.038 ± 0.008		<sup>7</sup> ABE	95J SLD	$E_{cm}^{ee} = 91.31$ GeV

- <sup>1</sup> ABBIENDI 01o fit for  $A_e$  and  $A_\tau$  from measurements of the  $\tau$  polarization at varying  $\tau$  production angles. The correlation between  $A_e$  and  $A_\tau$  is less than 0.03.
- <sup>2</sup> ABE 01B use the left-right production and left-right forward-backward decay asymmetries in leptonic Z decays to obtain a value of  $0.1544 \pm 0.0060$ . This is combined with left-right production asymmetry measurement using hadronic Z decays (ABE 00B) to obtain the quoted value.
- <sup>3</sup> HEISTER 01 obtain this result fitting the  $\tau$  polarization as a function of the polar production angle of the  $\tau$ .
- <sup>4</sup> ABREU 00E obtain this result fitting the  $\tau$  polarization as a function of the polar  $\tau$  production angle. This measurement is a combination of different analyses (exclusive  $\tau$  decay modes, inclusive hadronic 1-prong reconstruction, and a neural network analysis).
- <sup>5</sup> Derived from the measurement of forward-backward  $\tau$  polarization asymmetry.
- <sup>6</sup> ABE 97 obtain this result from a measurement of the observed left-right charge asymmetry,  $A_{LR}^{Obs} = 0.225 \pm 0.056 \pm 0.019$ , in hadronic Z decays. If they combine this value of  $A_{LR}^{Obs}$  with their earlier measurement of  $A_{LR}^{Obs}$  they determine  $A_e$  to be  $0.1574 \pm 0.0197 \pm 0.0067$  independent of the beam polarization.
- <sup>7</sup> ABE 95J obtain this result from polarized Bhabha scattering.

**A <sub>$\mu$</sub>**  This quantity is directly extracted from a measurement of the left-right forward-backward asymmetry in  $\mu^+\mu^-$  production at SLC using a polarized electron beam. This double asymmetry eliminates the dependence on the Z-e-e coupling parameter  $A_e$ .

VALUE	EVTS	DOCUMENT ID	TECN	COMMENT
<b>0.142 ± 0.015</b>	16844	<sup>1</sup> ABE	01B SLD	$E_{cm}^{ee} = 91.24$ GeV
• • • We do not use the following data for averages, fits, limits, etc. • • •				
0.153 ± 0.012	1.7M	<sup>2</sup> AAD	15BT ATLS	$E_{cm}^{pp} = 7$ TeV

- <sup>1</sup> ABE 01B obtain this direct measurement using the left-right production and left-right forward-backward polar angle asymmetries in  $\mu^+\mu^-$  decays of the Z boson obtained with a polarized electron beam.
- <sup>2</sup> AAD 15BT study  $pp \rightarrow Z \rightarrow \ell^+\ell^-$  events where  $\ell$  is an electron or a muon in the dilepton mass region 70–1000 GeV. The background in the Z peak region is estimated to be < 1% for the muon channel. The muon asymmetry parameter is derived from the measured forward-backward asymmetry assuming the value of the quark asymmetry parameter from the SM. For this reason it is not used in the average.

**A <sub>$\tau$</sub>**  The LEP Collaborations derive this quantity from the measurement of the  $\tau$  polarization in  $Z \rightarrow \tau^+\tau^-$ . The SLD Collaboration directly extracts this quantity from its measured left-right forward-backward asymmetry in  $Z \rightarrow \tau^+\tau^-$  produced using a polarized  $e^-$  beam. This double asymmetry eliminates the dependence on the Z-e-e coupling parameter  $A_e$ .

VALUE	EVTS	DOCUMENT ID	TECN	COMMENT
<b>0.143 ± 0.004 OUR AVERAGE</b>				
0.1456 ± 0.0076 ± 0.0057	144810	<sup>1</sup> ABBIENDI	01o OPAL	$E_{cm}^{ee} = 88-94$ GeV
0.136 ± 0.015	16083	<sup>2</sup> ABE	01B SLD	$E_{cm}^{ee} = 91.24$ GeV
0.1451 ± 0.0052 ± 0.0029		<sup>3</sup> HEISTER	01 ALEP	$E_{cm}^{ee} = 88-94$ GeV
0.1359 ± 0.0079 ± 0.0055	105000	<sup>4</sup> ABREU	00E DLPH	$E_{cm}^{ee} = 88-94$ GeV
0.1476 ± 0.0088 ± 0.0062	137092	ACCIARRI	98H L3	$E_{cm}^{ee} = 88-94$ GeV

- <sup>1</sup> ABBIENDI 01o fit for  $A_e$  and  $A_\tau$  from measurements of the  $\tau$  polarization at varying  $\tau$  production angles. The correlation between  $A_e$  and  $A_\tau$  is less than 0.03.
- <sup>2</sup> ABE 01B obtain this direct measurement using the left-right production and left-right forward-backward polar angle asymmetries in  $\tau^+\tau^-$  decays of the Z boson obtained with a polarized electron beam.
- <sup>3</sup> HEISTER 01 obtain this result fitting the  $\tau$  polarization as a function of the polar production angle of the  $\tau$ .
- <sup>4</sup> ABREU 00E obtain this result fitting the  $\tau$  polarization as a function of the polar  $\tau$  production angle. This measurement is a combination of different analyses (exclusive  $\tau$  decay modes, inclusive hadronic 1-prong reconstruction, and a neural network analysis).

**A<sub>S</sub>** The SLD Collaboration directly extracts this quantity by a simultaneous fit to four measured s-quark polar angle distributions corresponding to two states of  $e^-$  polarization (positive and negative) and to the  $K^+K^-$  and  $K^\pm K_S^0$  strange particle tagging modes in the hadronic final states.

VALUE	EVTS	DOCUMENT ID	TECN	COMMENT
<b>0.895 ± 0.066 ± 0.062</b>	2870	<sup>1</sup> ABE	00D SLD	$E_{cm}^{ee} = 91.2$ GeV

<sup>1</sup> ABE 00D tag  $Z \rightarrow s\bar{s}$  events by an absence of B or D hadrons and the presence in each hemisphere of a high momentum  $K^\pm$  or  $K_S^0$ .

**A<sub>C</sub>** This quantity is directly extracted from a measurement of the left-right forward-backward asymmetry in  $c\bar{c}$  production at SLC using polarized electron beam. This double asymmetry eliminates the dependence on the Z-e-e coupling parameter  $A_e$ . OUR FIT is obtained by a simultaneous fit to several c- and b-quark measurements as explained in the note "The Z boson" and ref. LEP-SLC 06.

VALUE	EVTS	DOCUMENT ID	TECN	COMMENT
<b>0.670 ± 0.027 OUR FIT</b>				
0.6712 ± 0.0224 ± 0.0157		<sup>1</sup> ABE	05 SLD	$E_{cm}^{ee} = 91.24$ GeV
• • • We do not use the following data for averages, fits, limits, etc. • • •				
0.583 ± 0.055 ± 0.055		<sup>2</sup> ABE	02G SLD	$E_{cm}^{ee} = 91.24$ GeV
0.688 ± 0.041		<sup>3</sup> ABE	01c SLD	$E_{cm}^{ee} = 91.25$ GeV

- <sup>1</sup> ABE 05 use hadronic Z decays collected during 1996–98 to obtain an enriched sample of  $c\bar{c}$  events tagging on the invariant mass of reconstructed secondary decay vertices. The charge of the underlying c-quark is obtained with an algorithm that takes into account the net charge of the vertex as well as the charge of tracks emanating from the vertex and identified as kaons. This yields (9970 events)  $A_C = 0.6747 \pm 0.0290 \pm 0.0233$ . Taking into account all correlations with earlier results reported in ABE 02G and ABE 01C, they obtain the quoted overall SLD result.
- <sup>2</sup> ABE 02G tag b and c quarks through their semileptonic decays into electrons and muons. A maximum likelihood fit is performed to extract simultaneously  $A_b$  and  $A_c$ .
- <sup>3</sup> ABE 01c tag  $Z \rightarrow c\bar{c}$  events using two techniques: exclusive reconstruction of  $D^{*+}, D^+$  and  $D^0$  mesons and the soft pion tag for  $D^{*+} \rightarrow D^0\pi^+$ . The large background from D mesons produced in  $b\bar{b}$  events is separated efficiently from the signal using precision vertex information. When combining the  $A_C$  values from these two samples, care is taken to avoid double counting of events common to the two samples, and common systematic errors are properly taken into account.

**A<sub>b</sub>** This quantity is directly extracted from a measurement of the left-right forward-backward asymmetry in  $b\bar{b}$  production at SLC using polarized electron beam. This double asymmetry eliminates the dependence on the Z-e-e coupling parameter  $A_e$ . OUR FIT is obtained by a simultaneous fit to several c- and b-quark measurements as explained in the note "The Z boson" and ref. LEP-SLC 06.

VALUE	EVTS	DOCUMENT ID	TECN	COMMENT
<b>0.923 ± 0.020 OUR FIT</b>				
0.9170 ± 0.0147 ± 0.0145		<sup>1</sup> ABE	05 SLD	$E_{cm}^{ee} = 91.24$ GeV
• • • We do not use the following data for averages, fits, limits, etc. • • •				
0.907 ± 0.020 ± 0.024	48028	<sup>2</sup> ABE	03F SLD	$E_{cm}^{ee} = 91.24$ GeV
0.919 ± 0.030 ± 0.024		<sup>3</sup> ABE	02G SLD	$E_{cm}^{ee} = 91.24$ GeV
0.855 ± 0.088 ± 0.102	7473	<sup>4</sup> ABE	99L SLD	$E_{cm}^{ee} = 91.27$ GeV

- <sup>1</sup> ABE 05 use hadronic Z decays collected during 1996–98 to obtain an enriched sample of  $b\bar{b}$  events tagging on the invariant mass of reconstructed secondary decay vertices. The charge of the underlying b-quark is obtained with an algorithm that takes into account the net charge of the vertex as well as the charge of tracks emanating from the vertex and identified as kaons. This yields (25917 events)  $A_b = 0.9173 \pm 0.0184 \pm 0.0173$ . Taking into account all correlations with earlier results reported in ABE 03F, ABE 02G and ABE 99L, they obtain the quoted overall SLD result.
- <sup>2</sup> ABE 03F obtain an enriched sample of  $b\bar{b}$  events tagging on the invariant mass of a 3-dimensional topologically reconstructed secondary decay. The charge of the underlying b quark is obtained using a self-calibrating track-charge method. For the 1996–1998 data sample they measure  $A_b = 0.906 \pm 0.022 \pm 0.023$ . The value quoted here is obtained combining the above with the result of ABE 98L (1993–1995 data sample).
- <sup>3</sup> ABE 02G tag b and c quarks through their semileptonic decays into electrons and muons. A maximum likelihood fit is performed to extract simultaneously  $A_b$  and  $A_c$ .
- <sup>4</sup> ABE 99L obtain an enriched sample of  $b\bar{b}$  events tagging with an inclusive vertex mass cut. For distinguishing b and  $\bar{b}$  quarks they use the charge of identified  $K^\pm$ .

**TRANSVERSE SPIN CORRELATIONS IN  $Z \rightarrow \tau^+\tau^-$**

The correlations between the transverse spin components of  $\tau^+\tau^-$  produced in Z decays may be expressed in terms of the vector and axial-vector couplings:

$$C_{TT} = \frac{|g_A^\tau|^2 - |g_V^\tau|^2}{|g_A^\tau|^2 + |g_V^\tau|^2}$$

## Gauge &amp; Higgs Boson Particle Listings

## Z

$$C_{TN} = -2 \frac{|g_A^\tau| |g_V^\tau|}{|g_A^\tau|^2 + |g_V^\tau|^2} \sin(\Phi_{g_V^\tau} - \Phi_{g_A^\tau})$$

$C_{TT}$  refers to the transverse-transverse (within the collision plane) spin correlation and  $C_{TN}$  refers to the transverse-normal (to the collision plane) spin correlation.

The longitudinal  $\tau$  polarization  $P_\tau$  ( $= -A_\tau$ ) is given by:

$$P_\tau = -2 \frac{|g_A^\tau| |g_V^\tau|}{|g_A^\tau|^2 + |g_V^\tau|^2} \cos(\Phi_{g_V^\tau} - \Phi_{g_A^\tau})$$

Here  $\Phi$  is the phase and the phase difference  $\Phi_{g_V^\tau} - \Phi_{g_A^\tau}$  can be obtained using both the measurements of  $C_{TN}$  and  $P_\tau$ .

 $C_{TT}$ 

VALUE	EVTS	DOCUMENT ID	TECN	COMMENT
<b>1.01 ± 0.12 OUR AVERAGE</b>				
$0.87 \pm 0.20^{+0.10}_{-0.12}$	9.1k	ABREU	97G DLPH	$E_{cm}^{ee} = 91.2$ GeV
$1.06 \pm 0.13 \pm 0.05$	120k	BARATE	97D ALEP	$E_{cm}^{ee} = 91.2$ GeV

 $C_{TN}$ 

VALUE	EVTS	DOCUMENT ID	TECN	COMMENT
<b>0.08 ± 0.13 ± 0.04</b>				
	120k	1 BARATE	97D ALEP	$E_{cm}^{ee} = 91.2$ GeV

<sup>1</sup> BARATE 97D combine their value of  $C_{TN}$  with the world average  $P_\tau = -0.140 \pm 0.007$  to obtain  $\tan(\Phi_{g_V^\tau} - \Phi_{g_A^\tau}) = -0.57 \pm 0.97$ .

FORWARD-BACKWARD  $e^+e^- \rightarrow f\bar{f}$  CHARGE ASYMMETRIES

These asymmetries are experimentally determined by tagging the respective lepton or quark flavor in  $e^+e^-$  interactions. Details of heavy flavor ( $c$ - or  $b$ -quark) tagging at LEP are described in the note on "The Z boson" and ref. LEP-SLC 06. The Standard Model predictions for LEP data have been (re)computed using the ZFITTER package (version 6.36) with input parameters  $M_Z = 91.187$  GeV,  $M_{top} = 174.3$  GeV,  $M_{Higgs} = 150$  GeV,  $\alpha_s = 0.119$ ,  $\alpha^{(5)}(M_Z) = 1/128.877$  and the Fermi constant  $G_F = 1.16637 \times 10^{-5} \text{ GeV}^{-2}$  (see the note on "The Z boson" for references). For non-LEP data the Standard Model predictions are as given by the authors of the respective publications.

 $A_{FB}^{(0,e)}$  CHARGE ASYMMETRY IN  $e^+e^- \rightarrow e^+e^-$ 

OUR FIT is obtained using the fit procedure and correlations as determined by the LEP Electroweak Working Group (see the note "The Z boson" and ref. LEP-SLC 06). For the Z peak, we report the pole asymmetry defined by  $(3/4)A_e^2$  as determined by the nine-parameter fit to cross-section and lepton forward-backward asymmetry data.

ASYMMETRY (%)	STD. MODEL	$\sqrt{s}$ (GeV)	DOCUMENT ID	TECN
<b>1.45 ± 0.25 OUR FIT</b>				
$0.89 \pm 0.44$	1.57	91.2	<sup>1</sup> ABBIENDI	01A OPAL
$1.71 \pm 0.49$	1.57	91.2	ABREU	00F DLPH
$1.06 \pm 0.58$	1.57	91.2	ACCIARRI	00C L3
$1.88 \pm 0.34$	1.57	91.2	<sup>2</sup> BARATE	00C ALEP

<sup>1</sup> ABBIENDI 01A error includes approximately 0.38 due to statistics, 0.16 due to event selection systematics, and 0.18 due to the theoretical uncertainty in  $t$ -channel prediction.  
<sup>2</sup> BARATE 00C error includes approximately 0.31 due to statistics, 0.06 due to experimental systematics, and 0.13 due to the theoretical uncertainty in  $t$ -channel prediction.

 $A_{FB}^{(0,\mu)}$  CHARGE ASYMMETRY IN  $e^+e^- \rightarrow \mu^+\mu^-$ 

OUR FIT is obtained using the fit procedure and correlations as determined by the LEP Electroweak Working Group (see the note "The Z boson" and ref. LEP-SLC 06). For the Z peak, we report the pole asymmetry defined by  $(3/4)A_e A_\mu$  as determined by the nine-parameter fit to cross-section and lepton forward-backward asymmetry data.

ASYMMETRY (%)	STD. MODEL	$\sqrt{s}$ (GeV)	DOCUMENT ID	TECN
<b>1.69 ± 0.13 OUR FIT</b>				
$1.59 \pm 0.23$	1.57	91.2	<sup>1</sup> ABBIENDI	01A OPAL
$1.65 \pm 0.25$	1.57	91.2	ABREU	00F DLPH
$1.88 \pm 0.33$	1.57	91.2	ACCIARRI	00C L3
$1.71 \pm 0.24$	1.57	91.2	<sup>2</sup> BARATE	00C ALEP

• • • We do not use the following data for averages, fits, limits, etc. • • •

$9 \pm 30$	-1.3	20	<sup>3</sup> ABREU	95M DLPH
$7 \pm 26$	-8.3	40	<sup>3</sup> ABREU	95M DLPH
$-11 \pm 33$	-24.1	57	<sup>3</sup> ABREU	95M DLPH
$-62 \pm 17$	-44.6	69	<sup>3</sup> ABREU	95M DLPH
$-56 \pm 10$	-63.5	79	<sup>3</sup> ABREU	95M DLPH
$-13 \pm 5$	-34.4	87.5	<sup>3</sup> ABREU	95M DLPH
$-29.0 \pm 5.0^{+0.5}_{-4.8}$	-32.1	56.9	<sup>4</sup> ABE	90I VNS
$-9.9 \pm 1.5 \pm 0.5$	-9.2	35	HEGNER	90 JADE
$0.05 \pm 0.22$	0.026	91.14	<sup>5</sup> ABRAMS	89D MRK2
$-43.4 \pm 17.0$	-24.9	52.0	<sup>6</sup> BACALA	89 AMY
$-11.0 \pm 16.5$	-29.4	55.0	<sup>6</sup> BACALA	89 AMY

$-30.0 \pm 12.4$	-31.2	56.0	<sup>6</sup> BACALA	89 AMY
$-46.2 \pm 14.9$	-33.0	57.0	<sup>6</sup> BACALA	89 AMY
$-29 \pm 13$	-25.9	53.3	ADACHI	88C TOPZ
$+5.3 \pm 5.0 \pm 0.5$	-1.2	14.0	ADEVA	88 MRKJ
$-10.4 \pm 1.3 \pm 0.5$	-8.6	34.8	ADEVA	88 MRKJ
$-12.3 \pm 5.3 \pm 0.5$	-10.7	38.3	ADEVA	88 MRKJ
$-15.6 \pm 3.0 \pm 0.5$	-14.9	43.8	ADEVA	88 MRKJ
$-1.0 \pm 6.0$	-1.2	13.9	BRAUNSCH...	88D TASS
$-9.1 \pm 2.3 \pm 0.5$	-8.6	34.5	BRAUNSCH...	88D TASS
$-10.6 \pm 2.2^{+2.2}_{-2.3}$	-8.9	35.0	BRAUNSCH...	88D TASS
$-17.6 \pm 4.4^{+4.3}_{-4.3}$	-15.2	43.6	BRAUNSCH...	88D TASS
$-4.8 \pm 6.5 \pm 1.0$	-11.5	39	BEHREND	87C CELL
$-18.8 \pm 4.5 \pm 1.0$	-15.5	44	BEHREND	87C CELL
$+2.7 \pm 4.9$	-1.2	13.9	BARTEL	86C JADE
$-11.1 \pm 1.8 \pm 1.0$	-8.6	34.4	BARTEL	86C JADE
$-17.3 \pm 4.8 \pm 1.0$	-13.7	41.5	BARTEL	86C JADE
$-22.8 \pm 5.1 \pm 1.0$	-16.6	44.8	BARTEL	86C JADE
$-6.3 \pm 0.8 \pm 0.2$	-6.3	29	ASH	85 MAC
$-4.9 \pm 1.5 \pm 0.5$	-5.9	29	DERRICK	85 HRS
$-7.1 \pm 1.7$	-5.7	29	LEVI	83 MRK2
$-16.1 \pm 3.2$	-9.2	34.2	BRANDELIK	82C TASS

<sup>1</sup> ABBIENDI 01A error is almost entirely on account of statistics.

<sup>2</sup> BARATE 00C error is almost entirely on account of statistics.

<sup>3</sup> ABREU 95M perform this measurement using radiative muon-pair events associated with high-energy isolated photons.

<sup>4</sup> ABE 90I measurements in the range  $50 \leq \sqrt{s} \leq 60.8$  GeV.

<sup>5</sup> ABRAMS 89D asymmetry includes both  $9 \mu^+ \mu^-$  and  $15 \tau^+ \tau^-$  events.

<sup>6</sup> BACALA 89 systematic error is about 5%.

 $A_{FB}^{(0,\tau)}$  CHARGE ASYMMETRY IN  $e^+e^- \rightarrow \tau^+\tau^-$ 

OUR FIT is obtained using the fit procedure and correlations as determined by the LEP Electroweak Working Group (see the note "The Z boson" and ref. LEP-SLC 06). For the Z peak, we report the pole asymmetry defined by  $(3/4)A_e A_\tau$  as determined by the nine-parameter fit to cross-section and lepton forward-backward asymmetry data.

ASYMMETRY (%)	STD. MODEL	$\sqrt{s}$ (GeV)	DOCUMENT ID	TECN
<b>1.88 ± 0.17 OUR FIT</b>				
$1.45 \pm 0.30$	1.57	91.2	<sup>1</sup> ABBIENDI	01A OPAL
$2.41 \pm 0.37$	1.57	91.2	ABREU	00F DLPH
$2.60 \pm 0.47$	1.57	91.2	ACCIARRI	00C L3
$1.70 \pm 0.28$	1.57	91.2	<sup>2</sup> BARATE	00C ALEP

• • • We do not use the following data for averages, fits, limits, etc. • • •

$-32.8 \pm 6.4^{+6.2}_{-6.2}$	-32.1	56.9	<sup>3</sup> ABE	90I VNS
$-8.1 \pm 2.0 \pm 0.6$	-9.2	35	HEGNER	90 JADE
$-18.4 \pm 19.2$	-24.9	52.0	<sup>4</sup> BACALA	89 AMY
$-17.7 \pm 26.1$	-29.4	55.0	<sup>4</sup> BACALA	89 AMY
$-45.9 \pm 16.6$	-31.2	56.0	<sup>4</sup> BACALA	89 AMY
$-49.5 \pm 18.0$	-33.0	57.0	<sup>4</sup> BACALA	89 AMY
$-20 \pm 14$	-25.9	53.3	ADACHI	88C TOPZ
$-10.6 \pm 3.1 \pm 1.5$	-8.5	34.7	ADEVA	88 MRKJ
$-8.5 \pm 6.6 \pm 1.5$	-15.4	43.8	ADEVA	88 MRKJ
$-6.0 \pm 2.5 \pm 1.0$	8.8	34.6	BARTEL	85F JADE
$-11.8 \pm 4.6 \pm 1.0$	14.8	43.0	BARTEL	85F JADE
$-5.5 \pm 1.2 \pm 0.5$	-0.063	29.0	FERNANDEZ	85 MAC
$-4.2 \pm 2.0$	0.057	29	LEVI	83 MRK2
$-10.3 \pm 5.2$	-9.2	34.2	BEHREND	82 CELL
$-0.4 \pm 6.6$	-9.1	34.2	BRANDELIK	82C TASS

<sup>1</sup> ABBIENDI 01A error includes approximately 0.26 due to statistics and 0.14 due to event selection systematics.

<sup>2</sup> BARATE 00C error includes approximately 0.26 due to statistics and 0.11 due to experimental systematics.

<sup>3</sup> ABE 90I measurements in the range  $50 \leq \sqrt{s} \leq 60.8$  GeV.

<sup>4</sup> BACALA 89 systematic error is about 5%.

 $A_{FB}^{(0,\ell)}$  CHARGE ASYMMETRY IN  $e^+e^- \rightarrow \ell^+\ell^-$ 

For the Z peak, we report the pole asymmetry defined by  $(3/4)A_e^2$  as determined by the five-parameter fit to cross-section and lepton forward-backward asymmetry data assuming lepton universality. For details see the note "The Z boson" and ref. LEP-SLC 06.

ASYMMETRY (%)	STD. MODEL	$\sqrt{s}$ (GeV)	DOCUMENT ID	TECN
<b>1.71 ± 0.10 OUR FIT</b>				
$1.45 \pm 0.17$	1.57	91.2	<sup>1</sup> ABBIENDI	01A OPAL
$1.87 \pm 0.19$	1.57	91.2	ABREU	00F DLPH
$1.92 \pm 0.24$	1.57	91.2	ACCIARRI	00C L3
$1.73 \pm 0.16$	1.57	91.2	<sup>2</sup> BARATE	00C ALEP

<sup>1</sup> ABBIENDI 01A error includes approximately 0.15 due to statistics, 0.06 due to event selection systematics, and 0.03 due to the theoretical uncertainty in  $t$ -channel prediction.

<sup>2</sup> BARATE 00C error includes approximately 0.15 due to statistics, 0.04 due to experimental systematics, and 0.02 due to the theoretical uncertainty in  $t$ -channel prediction.

$A_{FB}^{(0,u)}$  CHARGE ASYMMETRY IN  $e^+ e^- \rightarrow u\bar{u}$

ASYMMETRY (%)	STD. MODEL	$\sqrt{s}$ (GeV)	DOCUMENT ID	TECN
<b>4.0 ± 6.7 ± 2.8</b>	<b>7.2</b>	<b>91.2</b>	<sup>1</sup> ACKERSTAFF 97T	OPAL

<sup>1</sup> ACKERSTAFF 97T measure the forward-backward asymmetry of various fast hadrons made of light quarks. Then using SU(2) isospin symmetry and flavor independence for down and strange quarks authors solve for the different quark types.

$A_{FB}^{(0,s)}$  CHARGE ASYMMETRY IN  $e^+ e^- \rightarrow s\bar{s}$

The s-quark asymmetry is derived from measurements of the forward-backward asymmetry of fast hadrons containing an s quark.

ASYMMETRY (%)	STD. MODEL	$\sqrt{s}$ (GeV)	DOCUMENT ID	TECN
<b>9.8 ± 1.1 OUR AVERAGE</b>				
10.08 ± 1.13 ± 0.40	10.1	91.2	<sup>1</sup> ABREU 00B	DLPH
6.8 ± 3.5 ± 1.1	10.1	91.2	<sup>2</sup> ACKERSTAFF 97T	OPAL

<sup>1</sup> ABREU 00B tag the presence of an s quark requiring a high-momentum-identified charged kaon. The s-quark pole asymmetry is extracted from the charged-kaon asymmetry taking the expected d- and u-quark asymmetries from the Standard Model and using the measured values for the c- and b-quark asymmetries.  
<sup>2</sup> ACKERSTAFF 97T measure the forward-backward asymmetry of various fast hadrons made of light quarks. Then using SU(2) isospin symmetry and flavor independence for down and strange quarks authors solve for the different quark types. The value reported here corresponds then to the forward-backward asymmetry for "down-type" quarks.

$A_{FB}^{(0,c)}$  CHARGE ASYMMETRY IN  $e^+ e^- \rightarrow c\bar{c}$

OUR FIT, which is obtained by a simultaneous fit to several c- and b-quark measurements as explained in the note "The Z boson" and ref. LEP-SLC 06, refers to the Z pole asymmetry. The experimental values, on the other hand, correspond to the measurements carried out at the respective energies.

ASYMMETRY (%)	STD. MODEL	$\sqrt{s}$ (GeV)	DOCUMENT ID	TECN
<b>7.07 ± 0.35 OUR FIT</b>				
6.31 ± 0.93 ± 0.65	6.35	91.26	<sup>1</sup> ABDALLAH 04F	DLPH
5.68 ± 0.54 ± 0.39	6.3	91.25	<sup>2</sup> ABBIENDI 03P	OPAL
6.45 ± 0.57 ± 0.37	6.10	91.21	<sup>3</sup> HEISTER 02H	ALEP
6.59 ± 0.94 ± 0.35	6.2	91.235	<sup>4</sup> ABREU 99Y	DLPH
6.3 ± 0.9 ± 0.3	6.1	91.22	<sup>5</sup> BARATE 98O	ALEP
6.3 ± 1.2 ± 0.6	6.1	91.22	<sup>6</sup> ALEXANDER 97C	OPAL
8.3 ± 3.8 ± 2.7	6.2	91.24	<sup>7</sup> ADRIANI 92D	L3
• • • We do not use the following data for averages, fits, limits, etc. • • •				
3.1 ± 3.5 ± 0.5	-3.5	89.43	<sup>1</sup> ABDALLAH 04F	DLPH
11.0 ± 2.8 ± 0.7	12.3	92.99	<sup>1</sup> ABDALLAH 04F	DLPH
-6.8 ± 2.5 ± 0.9	-3.0	89.51	<sup>2</sup> ABBIENDI 03P	OPAL
14.6 ± 2.0 ± 0.8	12.2	92.95	<sup>2</sup> ABBIENDI 03P	OPAL
-12.4 ± 15.9 ± 2.0	-9.6	88.38	<sup>3</sup> HEISTER 02H	ALEP
-2.3 ± 2.6 ± 0.2	-3.8	89.38	<sup>3</sup> HEISTER 02H	ALEP
-0.3 ± 8.3 ± 0.6	0.9	90.21	<sup>3</sup> HEISTER 02H	ALEP
10.6 ± 7.7 ± 0.7	9.6	92.05	<sup>3</sup> HEISTER 02H	ALEP
11.9 ± 2.1 ± 0.6	12.2	92.94	<sup>3</sup> HEISTER 02H	ALEP
12.1 ± 11.0 ± 1.0	14.2	93.90	<sup>3</sup> HEISTER 02H	ALEP
-4.96 ± 3.68 ± 0.53	-3.5	89.434	<sup>4</sup> ABREU 99Y	DLPH
11.80 ± 3.18 ± 0.62	12.3	92.990	<sup>4</sup> ABREU 99Y	DLPH
-1.0 ± 4.3 ± 1.0	-3.9	89.37	<sup>5</sup> BARATE 98O	ALEP
11.0 ± 3.3 ± 0.8	12.3	92.96	<sup>5</sup> BARATE 98O	ALEP
3.9 ± 5.1 ± 0.9	-3.4	89.45	<sup>6</sup> ALEXANDER 97C	OPAL
15.8 ± 4.1 ± 1.1	12.4	93.00	<sup>6</sup> ALEXANDER 97C	OPAL
-12.9 ± 7.8 ± 5.5	-13.6	35	BEHREND 90D	CELL
7.7 ± 13.4 ± 5.0	-22.1	43	BEHREND 90D	CELL
-12.8 ± 4.4 ± 4.1	-13.6	35	ELSEN 90	JADE
-10.9 ± 12.9 ± 4.6	-23.2	44	ELSEN 90	JADE
-14.9 ± 6.7	-13.3	35	OULD-SAADA 89	JADE

<sup>1</sup> ABDALLAH 04F tag b- and c-quarks using semileptonic decays combined with charge flow information from the hemisphere opposite to the lepton. Enriched samples of c $\bar{c}$  and b $\bar{b}$  events are obtained using lifetime information.  
<sup>2</sup> ABBIENDI 03P tag heavy flavors using events with one or two identified leptons. This allows the simultaneous fitting of the b and c quark forward-backward asymmetries as well as the average B<sup>0</sup>-B<sup>0</sup> mixing.  
<sup>3</sup> HEISTER 02H measure simultaneously b and c quark forward-backward asymmetries using their semileptonic decays to tag the quark charge. The flavor separation is obtained with a discriminating multivariate analysis.  
<sup>4</sup> ABREU 99Y tag Z → b $\bar{b}$  and Z → c $\bar{c}$  events by an exclusive reconstruction of several D meson decay modes (D<sup>\*+</sup>, D<sup>0</sup>, and D<sup>+</sup> with their charge-conjugate states).  
<sup>5</sup> BARATE 98O tag Z → c $\bar{c}$  events requiring the presence of high-momentum reconstructed D<sup>\*+</sup>, D<sup>+</sup>, or D<sup>0</sup> mesons.  
<sup>6</sup> ALEXANDER 97C identify the b and c events using a D/D\* tag.  
<sup>7</sup> ADRIANI 92D use both electron and muon semileptonic decays.

on the other hand, correspond to the measurements carried out at the respective energies.

ASYMMETRY (%)	STD. MODEL	$\sqrt{s}$ (GeV)	DOCUMENT ID	TECN
<b>9.92 ± 0.16 OUR FIT</b>				
9.58 ± 0.32 ± 0.14	9.68	91.231	<sup>1</sup> ABDALLAH 05	DLPH
10.04 ± 0.56 ± 0.25	9.69	91.26	<sup>2</sup> ABDALLAH 04F	DLPH
9.72 ± 0.42 ± 0.15	9.67	91.25	<sup>3</sup> ABBIENDI 03P	OPAL
9.77 ± 0.36 ± 0.18	9.69	91.26	<sup>4</sup> ABBIENDI 02I	OPAL
9.52 ± 0.41 ± 0.17	9.59	91.21	<sup>5</sup> HEISTER 02H	ALEP
10.00 ± 0.27 ± 0.11	9.63	91.232	<sup>6</sup> HEISTER 01D	ALEP
7.62 ± 1.94 ± 0.85	9.64	91.235	<sup>7</sup> ABREU 99Y	DLPH
9.60 ± 0.66 ± 0.33	9.69	91.26	<sup>8</sup> ACCIARRI 99D	L3
9.31 ± 1.01 ± 0.55	9.65	91.24	<sup>9</sup> ACCIARRI 98U	L3
9.4 ± 2.7 ± 2.2	9.61	91.22	<sup>10</sup> ALEXANDER 97C	OPAL

• • • We do not use the following data for averages, fits, limits, etc. • • •

6.37 ± 1.43 ± 0.17	5.8	89.449	<sup>1</sup> ABDALLAH 05	DLPH
10.41 ± 1.15 ± 0.24	12.1	92.990	<sup>1</sup> ABDALLAH 05	DLPH
6.7 ± 2.2 ± 0.2	5.7	89.43	<sup>2</sup> ABDALLAH 04F	DLPH
11.2 ± 1.8 ± 0.2	12.1	92.99	<sup>2</sup> ABDALLAH 04F	DLPH
4.7 ± 1.8 ± 0.1	5.9	89.51	<sup>3</sup> ABBIENDI 03P	OPAL
10.3 ± 1.5 ± 0.2	12.0	92.95	<sup>3</sup> ABBIENDI 03P	OPAL
5.82 ± 1.53 ± 0.12	5.9	89.50	<sup>4</sup> ABBIENDI 02I	OPAL
12.21 ± 1.23 ± 0.25	12.0	92.91	<sup>4</sup> ABBIENDI 02I	OPAL
-13.1 ± 13.5 ± 1.0	3.2	88.38	<sup>5</sup> HEISTER 02H	ALEP
5.5 ± 1.9 ± 0.1	5.6	89.38	<sup>5</sup> HEISTER 02H	ALEP
-0.4 ± 6.7 ± 0.8	7.5	90.21	<sup>5</sup> HEISTER 02H	ALEP
11.1 ± 6.4 ± 0.5	11.0	92.05	<sup>5</sup> HEISTER 02H	ALEP
10.4 ± 1.5 ± 0.3	12.0	92.94	<sup>5</sup> HEISTER 02H	ALEP
13.8 ± 9.3 ± 1.1	12.9	93.90	<sup>5</sup> HEISTER 02H	ALEP
4.36 ± 1.19 ± 0.11	5.8	89.472	<sup>6</sup> HEISTER 01D	ALEP
11.72 ± 0.97 ± 0.11	12.0	92.950	<sup>6</sup> HEISTER 01D	ALEP
5.67 ± 7.56 ± 1.17	5.7	89.434	<sup>7</sup> ABREU 99Y	DLPH
8.82 ± 6.33 ± 1.22	12.1	92.990	<sup>7</sup> ABREU 99Y	DLPH
6.11 ± 2.93 ± 0.43	5.9	89.50	<sup>8</sup> ACCIARRI 99D	L3
13.71 ± 2.40 ± 0.44	12.2	93.10	<sup>8</sup> ACCIARRI 99D	L3
4.95 ± 5.23 ± 0.40	5.8	89.45	<sup>9</sup> ACCIARRI 98U	L3
11.37 ± 3.99 ± 0.65	12.1	92.99	<sup>9</sup> ACCIARRI 98U	L3
-8.6 ± 10.8 ± 2.9	5.8	89.45	<sup>10</sup> ALEXANDER 97C	OPAL
-2.1 ± 9.0 ± 2.6	12.1	93.00	<sup>10</sup> ALEXANDER 97C	OPAL
-71 ± 34 ± 7	-58	58.3	SHIMONAKA 91	TOPZ
-22.2 ± 7.7 ± 3.5	-26.0	35	BEHREND 90D	CELL
-49.1 ± 16.0 ± 5.0	-39.7	43	BEHREND 90D	CELL
-28 ± 11	-23	35	BRAUNSCH... 90	TASS
-16.6 ± 7.7 ± 4.8	-24.3	35	ELSEN 90	JADE
-33.6 ± 22.2 ± 5.2	-39.9	44	ELSEN 90	JADE
3.4 ± 7.0 ± 3.5	-16.0	29.0	BAND 89	MAC
-72 ± 28 ± 13	-56	55.2	SAGAWA 89	AMY

<sup>1</sup> ABDALLAH 05 obtain an enriched samples of b $\bar{b}$  events using lifetime information. The quark (or antiquark) charge is determined with a neural network using the secondary vertex charge, the jet charge and particle identification.  
<sup>2</sup> ABDALLAH 04F tag b- and c-quarks using semileptonic decays combined with charge flow information from the hemisphere opposite to the lepton. Enriched samples of c $\bar{c}$  and b $\bar{b}$  events are obtained using lifetime information.  
<sup>3</sup> ABBIENDI 03P tag heavy flavors using events with one or two identified leptons. This allows the simultaneous fitting of the b and c quark forward-backward asymmetries as well as the average B<sup>0</sup>-B<sup>0</sup> mixing.  
<sup>4</sup> ABBIENDI 02I tag Z<sup>0</sup> → b $\bar{b}$  decays using a combination of secondary vertex and lepton tags. The sign of the b-quark charge is determined using an inclusive tag based on jet, vertex, and kaon charges.  
<sup>5</sup> HEISTER 02H measure simultaneously b and c quark forward-backward asymmetries using their semileptonic decays to tag the quark charge. The flavor separation is obtained with a discriminating multivariate analysis.  
<sup>6</sup> HEISTER 01D tag Z → b $\bar{b}$  events using the impact parameters of charged tracks complemented with information from displaced vertices, event shape variables, and lepton identification. The b-quark direction and charge is determined using the hemisphere charge method along with information from fast kaon tagging and charge estimators of primary and secondary vertices. The change in the quoted value due to variation of A<sub>FB</sub><sup>c</sup> and R<sub>b</sub> is given as +0.103 (A<sub>FB</sub><sup>c</sup> - 0.0651) - 0.440 (R<sub>b</sub> - 0.21585).  
<sup>7</sup> ABREU 99Y tag Z → b $\bar{b}$  and Z → c $\bar{c}$  events by an exclusive reconstruction of several D meson decay modes (D<sup>\*+</sup>, D<sup>0</sup>, and D<sup>+</sup> with their charge-conjugate states).  
<sup>8</sup> ACCIARRI 99D tag Z → b $\bar{b}$  events using high p and p $\bar{p}$  leptons. The analysis determines simultaneously a mixing parameter  $\chi_b = 0.1192 \pm 0.0068 \pm 0.0051$  which is used to correct the observed asymmetry.  
<sup>9</sup> ACCIARRI 98U tag Z → b $\bar{b}$  events using lifetime and measure the jet charge using the hemisphere charge.  
<sup>10</sup> ALEXANDER 97C identify the b and c events using a D/D\* tag.

CHARGE ASYMMETRY IN  $e^+ e^- \rightarrow q\bar{q}$

Summed over five lighter flavors.

Experimental and Standard Model values are somewhat event-selection dependent. Standard Model expectations contain some assumptions on B<sup>0</sup>-B<sup>0</sup> mixing and on other electroweak parameters.

$A_{FB}^{(0,b)}$  CHARGE ASYMMETRY IN  $e^+ e^- \rightarrow b\bar{b}$

OUR FIT, which is obtained by a simultaneous fit to several c- and b-quark measurements as explained in the note "The Z boson" and ref. LEP-SLC 06, refers to the Z pole asymmetry. The experimental values,



ASYMMETRY (%)	STD. MODEL	$\sqrt{s}$ (GeV)	DOCUMENT ID	TECN
• • • We do not use the following data for averages, fits, limits, etc. • • •				
- 0.76 ± 0.12 ± 0.15		91.2	<sup>1</sup> ABREU 92l	DLPH
4.0 ± 0.4 ± 0.63	4.0	91.3	<sup>2</sup> ACTON 92L	OPAL
9.1 ± 1.4 ± 1.6	9.0	57.9	ADACHI 91	TOPZ
- 0.84 ± 0.15 ± 0.04		91	DECAMP 91B	ALEP
8.3 ± 2.9 ± 1.9	8.7	56.6	STUART 90	AMY
11.4 ± 2.2 ± 2.1	8.7	57.6	ABE 89L	VNS
6.0 ± 1.3	5.0	34.8	GREENSHAW 89	JADE
8.2 ± 2.9	8.5	43.6	GREENSHAW 89	JADE

<sup>1</sup> ABREU 92l has 0.14 systematic error due to uncertainty of quark fragmentation.

<sup>2</sup> ACTON 92L use the weight function method on 259k selected  $Z \rightarrow$  hadrons events.

The systematic error includes a contribution of 0.2 due to  $B^0\bar{B}^0$  mixing effect, 0.4 due to Monte Carlo (MC) fragmentation uncertainties and 0.3 due to MC statistics. ACTON 92L derive a value of  $\sin^2\theta_{\text{eff}}^W$  to be  $0.2321 \pm 0.0017 \pm 0.0028$ .

### CHARGE ASYMMETRY IN $p\bar{p} \rightarrow Z \rightarrow e^+e^-$

ASYMMETRY (%)	STD. MODEL	$\sqrt{s}$ (GeV)	DOCUMENT ID	TECN
• • • We do not use the following data for averages, fits, limits, etc. • • •				
5.2 ± 5.9 ± 0.4		91	ABE 91E	CDF

### ANOMALOUS $ZZ\gamma$ , $Z\gamma\gamma$ , AND $ZZV$ COUPLINGS

Revised September 2013 by M.W. Gr unewald (U. College Dublin and U. Ghent) and A. Gurtu (Formerly Tata Inst.).

In on-shell  $Z\gamma$  production, deviations from the Standard Model for the  $Z\gamma\gamma^*$  and  $Z\gamma Z^*$  couplings may be described in terms of eight parameters,  $h_i^V$  ( $i = 1, 4; V = \gamma, Z$ ) [1]. The parameters  $h_i^\gamma$  describe the  $Z\gamma\gamma^*$  couplings and the parameters  $h_i^Z$  the  $Z\gamma Z^*$  couplings. In this formalism  $h_1^V$  and  $h_2^V$  lead to  $CP$ -violating and  $h_3^V$  and  $h_4^V$  to  $CP$ -conserving effects. All these anomalous contributions to the cross section increase rapidly with center-of-mass energy. In order to ensure unitarity, these parameters are usually described by a form-factor representation,  $h_i^V(s) = h_{i0}^V/(1 + s/\Lambda^2)^n$ , where  $\Lambda$  is the energy scale for the manifestation of a new phenomenon and  $n$  is a sufficiently large power. By convention one uses  $n = 3$  for  $h_{1,3}^V$  and  $n = 4$  for  $h_{2,4}^V$ . Usually limits on  $h_i^V$ 's are put assuming some value of  $\Lambda$ , sometimes  $\infty$ .

In on-shell  $ZZ$  production, deviations from the Standard Model for the  $ZZ\gamma^*$  and  $ZZZ^*$  couplings may be described by means of four anomalous couplings  $f_i^V$  ( $i = 4, 5; V = \gamma, Z$ ) [2]. As above, the parameters  $f_i^\gamma$  describe the  $ZZ\gamma^*$  couplings and the parameters  $f_i^Z$  the  $ZZZ^*$  couplings. The anomalous couplings  $f_5^V$  lead to violation of  $C$  and  $P$  symmetries while  $f_4^V$  introduces  $CP$  violation. Also here, formfactors depending on a scale  $\Lambda$  are used.

All these couplings  $h_i^V$  and  $f_i^V$  are zero at tree level in the Standard Model; they are measured in  $e^+e^-$ ,  $p\bar{p}$  and  $pp$  collisions at LEP, Tevatron and LHC.

### References

- U. Baur and E.L. Berger, Phys. Rev. **D47**, 4889 (1993).
- K. Hagiwara *et al.*, Nucl. Phys. **B282**, 253 (1987).

### $h_i^V$

Combining the LEP-2 results taking into account the correlations, the following 95% CL limits are derived [SCHAEL 13A]:

$$\begin{aligned} -0.12 < h_1^\gamma < +0.11, & \quad -0.07 < h_2^\gamma < +0.07, \\ -0.19 < h_3^\gamma < +0.06, & \quad -0.04 < h_4^\gamma < +0.13, \\ -0.05 < h_1^Z < +0.05, & \quad -0.04 < h_2^Z < +0.02, \\ -0.05 < h_3^Z < +0.00, & \quad +0.01 < h_4^Z < +0.05. \end{aligned}$$

Some of the recent results from the Tevatron and LHC experiments individually surpass the combined LEP-2 results in precision (see below).

VALUE	DOCUMENT ID	TECN	COMMENT
• • • We do not use the following data for averages, fits, limits, etc. • • •			
<sup>1</sup> AAD 16Q	ATLS	$E_{\text{cm}}^{pp} = 8$ TeV	
<sup>2</sup> KHACHATRYAN 16AE	CMS	$E_{\text{cm}}^{pp} = 8$ TeV	
<sup>3</sup> KHACHATRYAN 15AC	CMS	$E_{\text{cm}}^{pp} = 8$ TeV	
<sup>4</sup> CHATRCHYAN 14AB	CMS	$E_{\text{cm}}^{pp} = 7$ TeV	
<sup>5</sup> AAD 13AN	ATLS	$E_{\text{cm}}^{pp} = 7$ TeV	
<sup>6</sup> CHATRCHYAN 13BI	CMS	$E_{\text{cm}}^{pp} = 7$ TeV	
<sup>7</sup> ABAZOV 12S	D0	$E_{\text{cm}}^{pp} = 1.96$ TeV	
<sup>8</sup> AALTONEN 11S	CDF	$E_{\text{cm}}^{pp} = 1.96$ TeV	
<sup>9</sup> CHATRCHYAN 11M	CMS	$E_{\text{cm}}^{pp} = 7$ TeV	
<sup>10</sup> ABAZOV 09L	D0	$E_{\text{cm}}^{pp} = 1.96$ TeV	
<sup>11</sup> ABAZOV 07M	D0	$E_{\text{cm}}^{pp} = 1.96$ TeV	
<sup>12</sup> ABDALLAH 07C	DLPH	$E_{\text{cm}}^{ee} = 183\text{--}208$ GeV	
<sup>13</sup> ACHARD 04H	L3	$E_{\text{cm}}^{ee} = 183\text{--}208$ GeV	
<sup>14</sup> ABBIENDI, G 00C	OPAL	$E_{\text{cm}}^{ee} = 189$ GeV	
<sup>15</sup> ABBOTT 98M	D0	$E_{\text{cm}}^{pp} = 1.8$ TeV	
<sup>16</sup> ABREU 98K	DLPH	$E_{\text{cm}}^{ee} = 161, 172$ GeV	

<sup>1</sup> AAD 16Q study  $Z\gamma$  production in  $pp$  collisions. In events with no additional jets, 10268 (12738)  $Z$  decays to electron (muon) pairs are selected, with an expected background of  $1291 \pm 340$  ( $1537 \pm 408$ ) events, as well as 1039  $Z$  decays to neutrino pairs with an expected background of  $450 \pm 96$  events. Analyzing the photon transverse momentum distribution above 250 GeV (400 GeV) for lepton (neutrino) events, yields the 95% C.L. limits:  $-7.8 \times 10^{-4} < h_3^Z < 8.6 \times 10^{-4}$ ,  $-3.0 \times 10^{-6} < h_4^Z < 2.9 \times 10^{-6}$ ,  $-9.5 \times 10^{-4} < h_3^\gamma < 9.9 \times 10^{-4}$ ,  $-3.2 \times 10^{-6} < h_4^\gamma < 3.2 \times 10^{-6}$ .

<sup>2</sup> KHACHATRYAN 16AE determine the  $Z\gamma \rightarrow \nu\bar{\nu}\gamma$  cross section by selecting events with a photon of  $E_T > 145$  GeV and  $\cancel{E}_T > 140$  GeV. 630 candidate events are observed with an expected SM background of  $269 \pm 26$ . The  $E_T$  spectrum of the photon is used to set 95% C.L. limits as follows:  $-1.5 \times 10^{-3} < h_3^Z < 1.6 \times 10^{-3}$ ,  $-3.9 \times 10^{-6} < h_4^Z < 4.5 \times 10^{-6}$ ,  $-1.1 \times 10^{-3} < h_3^\gamma < 0.9 \times 10^{-3}$ ,  $-3.8 \times 10^{-6} < h_4^\gamma < 4.3 \times 10^{-6}$ .

<sup>3</sup> KHACHATRYAN 15AC study  $Z\gamma$  events in 8 TeV  $pp$  interactions, where the  $Z$  decays into 2 same-flavor, opposite sign leptons ( $e$  or  $\mu$ ) and a photon with  $p_T > 15$  GeV. The  $p_T$  of a lepton is required to be  $> 20$  GeV/ $c$ , their effective mass  $> 50$  GeV, and the photon should have a separation  $\Delta R > 0.7$  with each lepton. The observed  $p_T$  distribution of the photons is used to extract the 95% C.L. limits:  $-3.8 \times 10^{-3} < h_3^Z < 3.7 \times 10^{-3}$ ,  $-3.1 \times 10^{-5} < h_4^Z < 3.0 \times 10^{-5}$ ,  $-4.6 \times 10^{-3} < h_3^\gamma < 4.6 \times 10^{-3}$ ,  $-3.6 \times 10^{-5} < h_4^\gamma < 3.5 \times 10^{-5}$ .

<sup>4</sup> CHATRCHYAN 14AB measure  $Z\gamma$  production cross section for  $p_T^\gamma > 15$  GeV and  $R(\ell\gamma) > 0.7$ , which is the separation between the  $\gamma$  and the final state charged lepton ( $e$  or  $\mu$ ) in the azimuthal angle-pseudorapidity ( $\phi - \eta$ ) plane. The di-lepton mass is required to be  $> 50$  GeV. After background subtraction the number of  $e\bar{e}\gamma$  and  $\mu\bar{\mu}\gamma$  events is determined to be  $3160 \pm 120$  and  $5030 \pm 233$  respectively, compatible with expectations from the SM. This leads to a 95% CL limits of  $-1 \times 10^{-2} < h_3^\gamma < 1 \times 10^{-2}$ ,  $-9 \times 10^{-5} < h_4^\gamma < 9 \times 10^{-5}$ ,  $-9 \times 10^{-3} < h_3^Z < 9 \times 10^{-3}$ ,  $-8 \times 10^{-5} < h_4^Z < 8 \times 10^{-5}$ , assuming  $h_1^V$  and  $h_2^V$  have SM values,  $V = \gamma$  or  $Z$ .

<sup>5</sup> AAD 13AN study  $Z\gamma$  production in  $pp$  collisions. In events with no additional jet, 1417 (2031)  $Z$  decays to electron (muon) pairs are selected, with an expected background of  $156 \pm 54$  ( $244 \pm 64$ ) events, as well as 662  $Z$  decays to neutrino pairs with an expected background of  $302 \pm 42$  events. Analysing the photon  $p_T$  spectrum above 100 GeV yields the 95% C.L. limits:  $-0.013 < h_3^Z < 0.014$ ,  $-8.7 \times 10^{-5} < h_4^Z < 8.7 \times 10^{-5}$ ,  $-0.015 < h_3^\gamma < 0.016$ ,  $-9.4 \times 10^{-5} < h_4^\gamma < 9.2 \times 10^{-5}$ . Supersedes AAD 12BX.

<sup>6</sup> CHATRCHYAN 13BI determine the  $Z\gamma \rightarrow \nu\bar{\nu}\gamma$  cross section by selecting events with a photon of  $E_T > 145$  GeV and a  $\cancel{E}_T > 130$  GeV. 73 candidate events are observed with an expected SM background of  $30.2 \pm 6.5$ . The  $E_T$  spectrum of the photon is used to set 95% C.L. limits as follows:  $|h_3^Z| < 2.7 \times 10^{-3}$ ,  $|h_4^Z| < 1.3 \times 10^{-5}$ ,  $|h_3^\gamma| < 2.9 \times 10^{-3}$ ,  $|h_4^\gamma| < 1.5 \times 10^{-5}$ .

<sup>7</sup> ABAZOV 12S study  $Z\gamma$  production in  $p\bar{p}$  collisions at  $\sqrt{s} = 1.96$  TeV using  $6.2 \text{ fb}^{-1}$  of data where the  $Z$  decays to electron (muon) pairs and the photon has at least 10 GeV of transverse momentum. In data, 304 (308) di-electron (di-muon) events are observed with an expected background of  $255 \pm 16$  ( $285 \pm 24$ ) events. Based on the photon  $p_T$  spectrum, and including also earlier data and the  $Z \rightarrow \nu\bar{\nu}$  decay mode (from ABAZOV 09L), the following 95% C.L. limits are reported:  $|h_{03}^Z| < 0.026$ ,  $|h_{04}^Z| < 0.0013$ ,  $|h_{03}^\gamma| < 0.027$ ,  $|h_{04}^\gamma| < 0.0014$  for a form factor scale of  $\Lambda = 1.5$  TeV.

<sup>8</sup> AALTONEN 11S study  $Z\gamma$  events in  $p\bar{p}$  interactions at  $\sqrt{s} = 1.96$  TeV with integrated luminosity  $5.1 \text{ fb}^{-1}$  for  $Z \rightarrow e^+e^-/\mu^+\mu^-$  and  $4.9 \text{ fb}^{-1}$  for  $Z \rightarrow \nu\bar{\nu}$ . For the charged lepton case, the two leptons must be of the same flavor with the transverse momentum/energy of one  $> 20$  GeV and the other  $> 10$  GeV. The isolated photon must have  $E_T > 50$  GeV. They observe 91 events with  $87.2 \pm 7.8$  events expected from standard model processes. For the  $\nu\bar{\nu}$  case they require solitary photons with  $E_T > 25$  GeV and missing  $E_T > 25$  GeV and observe 85 events with standard model expectation of  $85.9 \pm 5.6$  events. Taking the form factor  $\Lambda = 1.5$  TeV they derive 95% C.L. limits as  $|h_{3,4}^Z| < 0.022$  and  $|h_{3,4}^\gamma| < 0.0009$ .

<sup>9</sup> CHATRCHYAN 11M study  $Z\gamma$  production in  $pp$  collisions at  $\sqrt{s} = 7$  TeV using  $36 \text{ pb}^{-1}$   $pp$  data, where the  $Z$  decays to  $e^+e^-$  or  $\mu^+\mu^-$ . The total cross sections are measured for photon transverse energy  $E_T^\gamma > 10$  GeV and spatial separation from charged leptons in the plane of pseudo rapidity and azimuthal angle  $\Delta R(\ell, \gamma) > 0.7$  with

- the dilepton invariant mass requirement of  $M_{\ell\ell} > 50$  GeV. The number of  $e^+e^- \gamma$  and  $\mu^+\mu^- \gamma$  candidates is 81 and 90 with estimated backgrounds of  $20.5 \pm 2.5$  and  $27.3 \pm 3.2$  events respectively. The 95% CL limits for  $ZZ\gamma$  couplings are  $-0.05 < h_3^Z < 0.06$  and  $-0.0005 < h_4^Z < 0.0005$ , and for  $Z\gamma\gamma$  couplings are  $-0.07 < h_3^\gamma < 0.07$  and  $-0.0005 < h_4^\gamma < 0.0006$ .
- <sup>10</sup> ABZOV 09L study  $Z\gamma, Z \rightarrow \nu\bar{\nu}$  production in  $p\bar{p}$  collisions at 1.96 TeV C.M. energy. They select 51 events with a photon of transverse energy  $E_T$  larger than 90 GeV, with an expected background of 17 events. Based on the photon  $E_T$  spectrum and including also Z decays to charged leptons (from ABZOV 07M), the following 95% CL limits are reported:  $|h_{30}^\gamma| < 0.033, |h_{40}^\gamma| < 0.0017, |h_{30}^Z| < 0.033, |h_{40}^Z| < 0.0017$ .
- <sup>11</sup> ABZOV 07M use 968  $p\bar{p} \rightarrow e^+e^-/\mu^+\mu^- \gamma X$  candidates, at 1.96 TeV center of mass energy, to tag  $p\bar{p} \rightarrow Z\gamma$  events by requiring  $E_T(\gamma) > 7$  GeV, lepton-gamma separation  $\Delta R_{\ell\gamma} > 0.7$ , and di-lepton invariant mass  $> 30$  GeV. The cross section is in agreement with the SM prediction. Using these  $Z\gamma$  events they obtain 95% C.L. limits on each  $h_i^V$ , keeping all others fixed at their SM values. They report:  $-0.083 < h_{30}^Z < 0.082, -0.0053 < h_{40}^Z < 0.0054, -0.085 < h_{30}^\gamma < 0.084, -0.0053 < h_{40}^\gamma < 0.0054$ , for the form factor scale  $\Lambda = 1.2$  TeV.
- <sup>12</sup> Using data collected at  $\sqrt{s} = 183\text{--}208$ , ABDALLAH 07c select 1,877  $e^+e^- \rightarrow Z\gamma$  events with  $Z \rightarrow q\bar{q}$  or  $\nu\bar{\nu}$ , 171  $e^+e^- \rightarrow ZZ$  events with  $Z \rightarrow q\bar{q}$  or lepton pair (except an explicit  $\tau$  pair), and 74  $e^+e^- \rightarrow Z\gamma^*$  events with a  $q\bar{q}\mu^+\mu^-$  or  $q\bar{q}e^+e^-$  signature, to derive 95% CL limits on  $h_i^V$ . Each limit is derived with other parameters set to zero. They report:  $-0.23 < h_1^Z < 0.23, -0.30 < h_2^Z < 0.16, -0.14 < h_1^\gamma < 0.14, -0.049 < h_2^\gamma < 0.044$ .
- <sup>13</sup> ACHARD 04H select 3515  $e^+e^- \rightarrow Z\gamma$  events with  $Z \rightarrow q\bar{q}$  or  $\nu\bar{\nu}$  at  $\sqrt{s} = 189\text{--}209$  GeV to derive 95% CL limits on  $h_i^V$ . For deriving each limit the other parameters are fixed at zero. They report:  $-0.153 < h_1^Z < 0.141, -0.087 < h_2^Z < 0.079, -0.220 < h_3^Z < 0.112, -0.068 < h_4^Z < 0.148, -0.057 < h_1^\gamma < 0.057, -0.050 < h_2^\gamma < 0.023, -0.059 < h_3^\gamma < 0.004, -0.004 < h_4^\gamma < 0.024$ .
- <sup>14</sup> ABBIENDI, G 00c study  $e^+e^- \rightarrow Z\gamma$  events (with  $Z \rightarrow q\bar{q}$  and  $Z \rightarrow \nu\bar{\nu}$ ) at 189 GeV to obtain the central values (and 95% CL limits) of these couplings:  $h_1^Z = 0.000 \pm 0.100$  ( $-0.190, 0.190$ ),  $h_2^Z = 0.000 \pm 0.068$  ( $-0.128, 0.128$ ),  $h_3^Z = -0.074 \pm_{-0.103}^{+0.102}$  ( $-0.269, 0.119$ ),  $h_4^Z = 0.046 \pm 0.068$  ( $-0.084, 0.175$ ),  $h_1^\gamma = 0.000 \pm 0.061$  ( $-0.115, 0.115$ ),  $h_2^\gamma = 0.000 \pm 0.041$  ( $-0.077, 0.077$ ),  $h_3^\gamma = -0.080 \pm_{-0.041}^{+0.039}$  ( $-0.164, -0.006$ ),  $h_4^\gamma = 0.064 \pm_{-0.030}^{+0.033}$  ( $+0.007, +0.134$ ). The results are derived assuming that only one coupling at a time is different from zero.
- <sup>15</sup> ABBOTT 98M study  $p\bar{p} \rightarrow Z\gamma + X$ , with  $Z \rightarrow e^+e^-, \mu^+\mu^-, \nu\bar{\nu}$  at 1.8 TeV, to obtain 95% CL limits at  $\Lambda = 750$  GeV:  $|h_{30}^Z| < 0.36, |h_{40}^Z| < 0.05$  (keeping  $h_i^Z = 0$ ), and  $|h_{30}^\gamma| < 0.37, |h_{40}^\gamma| < 0.05$  (keeping  $h_i^\gamma = 0$ ). Limits on the CP-violating couplings are  $|h_{10}^Z| < 0.36, |h_{20}^Z| < 0.05$  (keeping  $h_i^Z = 0$ ), and  $|h_{10}^\gamma| < 0.37, |h_{20}^\gamma| < 0.05$  (keeping  $h_i^\gamma = 0$ ).
- <sup>16</sup> ABREU 98k determine a 95% CL upper limit on  $\sigma(e^+e^- \rightarrow \gamma + \text{invisible particles}) < 2.5$  pb using 161 and 172 GeV data. This is used to set 95% CL limits on  $|h_{30}^\gamma| < 0.8$  and  $|h_{50}^Z| < 1.3$ , derived at a scale  $\Lambda = 1$  TeV and with  $n = 3$  in the form factor representation.
- $f_i^V$**   
Combining the LEP-2 results taking into account the correlations, the following 95% CL limits are derived [SCHAEEL 13A]:
- $$-0.28 < f_4^Z < +0.32, \quad -0.34 < f_5^Z < +0.35,$$
- $$-0.17 < f_4^\gamma < +0.19, \quad -0.35 < f_5^\gamma < +0.32.$$
- Some of the recent results from the Tevatron and LHC experiments individually surpass the combined LEP-2 results in precision (see below).
- | VALUE | DOCUMENT ID   | TECN      | COMMENT                             |
|-------|---|-----------|-------------------------------------|
| • • • | We do not use the following data for averages, fits, limits, etc. | • • •     |                                     |
| 1     | AABOUD  | 19AY ATLS | $E_{cm}^{pp} = 13$ TeV              |
| 2     | AABOUD  | 18Q ATLS  | $E_{cm}^{pp} = 13$ TeV              |
| 3     | SIRUNYAN  | 18BT CMS  | $E_{cm}^{pp} = 13$ TeV              |
| 4     | KHACHATRYAN...15B   | CMS       | $E_{cm}^{pp} = 8$ TeV               |
| 5     | KHACHATRYAN...15Bc  | CMS       | $E_{cm}^{pp} = 7, 8$ TeV            |
| 6     | AAD   | 13z ATLS  | $E_{cm}^{pp} = 7$ TeV               |
| 7     | CHATRCHYAN13B   | CMS       | $E_{cm}^{pp} = 7$ TeV               |
| 8     | SCHAEEL   | 09 ALEP   | $E_{cm}^{ee} = 192\text{--}209$ GeV |
| 9     | ABAZOV  | 08k D0    | $E_{cm}^{pp} = 1.96$ TeV            |
| 10    | ABDALLAH  | 07c DLPH  | $E_{cm}^{ee} = 183\text{--}208$ GeV |
| 11    | ABBIENDI  | 04c OPAL  |                                     |
| 12    | ACHARD  | 03D L3    |                                     |
- <sup>1</sup> AABOUD 19AY study ZZ production in the  $\ell\ell\nu\nu$  decay channel. Events with a pair of isolated high-transverse momentum charged leptons (electron pairs or muon pairs), and with large missing energy, are selected. In the data, 371 (416) di-electron (di-muon) events are found, with a total expected background of  $128 \pm 8$  ( $143 \pm 8$ ) events. Analysing the transverse momentum distribution of the charged dilepton system above 150 GeV, the following 95% C.L. limits are derived in units of  $10^{-3}$ :  $-1.2 < f_4^Z < 1.2, -1.0 < f_4^\gamma < 1.0, -1.2 < f_5^Z < 1.2, -1.0 < f_5^\gamma < 1.0$ .
- <sup>2</sup> AABOUD 18Q study  $pp \rightarrow ZZ$  events at  $\sqrt{s} = 13$  TeV with  $Z \rightarrow e^+e^-$  or  $Z \rightarrow \mu^+\mu^-$ . The number of events observed in the  $4e, 2e2\mu$ , and  $4\mu$  channels is 249, 465, and 303 respectively. Analysing the  $p_T$  spectrum of the leading Z boson, the following the following 95% C.L. limits are derived in units of  $10^{-4}$ :  $-1.8 < f_4^Z < 1.8, -1.5 < f_4^\gamma < 1.5, -1.8 < f_5^Z < 1.8, -1.5 < f_5^\gamma < 1.5$ .
- <sup>3</sup> SIRUNYAN 18BT study  $ppZZ$  events at  $\sqrt{s} = 13$  TeV with  $Z \rightarrow e^+e^-$  or  $Z \rightarrow \mu^+\mu^-$ . The number of events observed in the  $4e, 2e2\mu$ , and  $4\mu$  channels is 220, 543 and 335 respectively. Analysing the 4-lepton invariant mass spectrum, the following 95% C.L. limits are derived in units of  $10^{-3}$ :  $-1.2 < f_4^Z < 1.3, -1.2 < f_4^\gamma < 1.0, -1.2 < f_5^Z < 1.3, -1.0 < f_5^\gamma < 1.3$ .
- <sup>4</sup> KHACHATRYAN 15B study ZZ production in 8 TeV pp collisions. In the decay modes  $ZZ \rightarrow 4e, 4\mu, 2e2\mu, 54, 75, 148$  events are observed, with an expected background of  $2.2 \pm 0.9, 1.2 \pm 0.6$ , and  $2.4 \pm 1.0$  events, respectively. Analysing the 4-lepton invariant mass spectrum in the range from 110 GeV to 1200 GeV, the following 95% C.L. limits are obtained:  $|f_4^Z| < 0.004, |f_5^Z| < 0.004, |f_4^\gamma| < 0.005, |f_5^\gamma| < 0.005$ .
- <sup>5</sup> KHACHATRYAN 15Bc use the cross section measurement of the final state  $pp \rightarrow ZZ \rightarrow 2\ell 2\ell'$  ( $\ell$  being an electron or a muon) at 7 and 8 TeV to put limits on these triple gauge couplings. Effective mass of the charged lepton pair is required to be in the range 83.5–98.5 GeV and the dilepton  $p_T > 45$  GeV. The reduced missing  $E_T$  is required to be  $> 65$  GeV, which takes into account the fake missing  $E_T$  due to detector effects. The numbers of  $e^+e^-$  and  $\mu^+\mu^-$  events selected are 35 and 40 at 7 TeV and 176 and 271 at 8 TeV respectively. The production cross sections so obtained are in agreement with SM predictions. The following 95% C.L. limits are set:  $-0.0028 < f_4^Z < 0.0032, -0.0037 < f_4^\gamma < 0.0033, -0.0029 < f_5^Z < 0.0031, -0.0033 < f_5^\gamma < 0.0037$ . Combining with previous results (KHACHATRYAN 15B and CHATRCHYAN 13B) which include 7 TeV and 8 TeV data on the final states  $pp \rightarrow ZZ \rightarrow 2\ell 2\ell'$  where  $\ell$  and  $\ell'$  are an electron or a muon, the best limits are  $-0.0022 < f_4^Z < 0.0026, -0.0029 < f_4^\gamma < 0.0026, -0.0023 < f_5^Z < 0.0023, -0.0026 < f_5^\gamma < 0.0027$ .
- <sup>6</sup> AAD 13z study ZZ production in pp collisions at  $\sqrt{s} = 7$  TeV. In the  $ZZ \rightarrow \ell^+\ell^-\ell'^+\ell'^-$  final state they observe a total of 66 events with an expected background of  $0.9 \pm 1.3$ . In the  $ZZ \rightarrow \ell^+\ell^-\nu\nu$  final state they observe a total of 87 events with an expected background of  $46.9 \pm 5.2$ . The limits on anomalous TGCs are determined using the observed and expected numbers of these ZZ events binned in  $p_T^Z$ . The 95% C.L. are as follows: for form factor scale  $\Lambda = \infty, -0.015 < f_4^Z < 0.015, -0.013 < f_4^\gamma < 0.013, -0.016 < f_5^Z < 0.015, -0.013 < f_5^\gamma < 0.013$ ; for form factor scale  $\Lambda = 3$  TeV,  $-0.022 < f_4^Z < 0.023, -0.019 < f_4^\gamma < 0.019, -0.023 < f_5^Z < 0.023, -0.020 < f_5^\gamma < 0.019$ .
- <sup>7</sup> CHATRCHYAN 13B study ZZ production in pp collisions and select 54 ZZ candidates in the Z decay channel with electrons or muons with an expected background of  $1.4 \pm 0.5$  events. The resulting 95% C.L. ranges are:  $-0.013 < f_4^Z < 0.015, -0.011 < f_4^\gamma < 0.012, -0.014 < f_5^Z < 0.014, -0.012 < f_5^\gamma < 0.012$ .
- <sup>8</sup> Using data collected in the center of mass energy range 192–209 GeV, SCHAEEL 09 select 318  $e^+e^- \rightarrow ZZ$  events with 319.4 expected from the standard model. Using this data they derive the following 95% CL limits:  $-0.321 < f_4^Z < 0.318, -0.534 < f_4^\gamma < 0.534, -0.724 < f_5^Z < 0.733, -1.194 < f_5^\gamma < 1.190$ .
- <sup>9</sup> ABZOV 08k search for ZZ and  $Z\gamma^*$  events with  $1\text{fb}^{-1} p\bar{p}$  data at  $\sqrt{s} = 1.96$  TeV in  $(e\ell)(e\ell), (\mu\mu)(\mu\mu), (e\ell)(\mu\mu)$  final states requiring the lepton pair masses to be  $> 30$  GeV. They observe 1 event, which is consistent with an expected signal of  $1.71 \pm 0.15$  events and a background of  $0.13 \pm 0.03$  events. From this they derive the following limits, for a form factor ( $\Lambda$ ) value of 1.2 TeV:  $-0.28 < f_{40}^Z < 0.28, -0.31 < f_{50}^Z < 0.29, -0.26 < f_{40}^\gamma < 0.26, -0.30 < f_{50}^\gamma < 0.28$ .
- <sup>10</sup> Using data collected at  $\sqrt{s} = 183\text{--}208$  GeV, ABDALLAH 07c select 171  $e^+e^- \rightarrow ZZ$  events with  $Z \rightarrow q\bar{q}$  or lepton pair (except an explicit  $\tau$  pair), and 74  $e^+e^- \rightarrow Z\gamma^*$  events with a  $q\bar{q}\mu^+\mu^-$  or  $q\bar{q}e^+e^-$  signature, to derive 95% CL limits on  $f_i^V$ . Each limit is derived with other parameters set to zero. They report:  $-0.40 < f_4^Z < 0.42, -0.38 < f_5^Z < 0.62, -0.23 < f_4^\gamma < 0.25, -0.52 < f_5^\gamma < 0.48$ .
- <sup>11</sup> ABBIENDI 04c study ZZ production in  $e^+e^-$  collisions in the C.M. energy range 190–209 GeV. They select 340 events with an expected background of 180 events. Including the ABBIENDI 00N data at 183 and 189 GeV (118 events with an expected background of 65 events) they report the following 95% CL limits:  $-0.45 < f_4^Z < 0.58, -0.94 < f_5^Z < 0.25, -0.32 < f_4^\gamma < 0.33, \text{ and } -0.71 < f_5^\gamma < 0.59$ .
- <sup>12</sup> ACHARD 03D study Z-boson pair production in  $e^+e^-$  collisions in the C.M. energy range 200–209 GeV. They select 549 events with an expected background of 432 events. Including the ACCIARRI 99G and ACCIARRI 99O data (183 and 189 GeV respectively, 286 events with an expected background of 241 events) and the 192–202 GeV ACCIARRI 011 results (656 events, expected background of 512 events), they report the following 95% CL limits:  $-0.48 \leq f_4^Z \leq 0.46, -0.36 \leq f_5^Z \leq 1.03, -0.28 \leq f_4^\gamma \leq 0.28, \text{ and } -0.40 \leq f_5^\gamma \leq 0.47$ .

## ANOMALOUS W/Z QUARTIC COUPLINGS

Revised November 2015 by M.W. Grunewald (U. College Dublin) and A. Gurtu (Formerly Tata Inst.).

Quartic couplings,  $WWZZ, WWZ\gamma, WW\gamma\gamma$ , and  $ZZ\gamma\gamma$ , were studied at LEP and Tevatron at energies at which the Standard Model predicts negligible contributions to multiboson production. Thus, to parametrize limits on these couplings, an

effective theory approach is adopted which supplements the Standard Model Lagrangian with higher dimensional operators which include quartic couplings. The LEP collaborations chose the lower dimensional representation of operators (dimension 6) which presumes the  $SU(2) \times U(1)$  gauge symmetry is broken by means other than the conventional Higgs scalar doublet [1–3]. In this representation possible quartic couplings,  $a_0, a_c, a_n$ , are expressed in terms of the following dimension-6 operators [1,2];

$$\begin{aligned} L_6^0 &= -\frac{e^2}{16\Lambda^2} a_0 F^{\mu\nu} F_{\mu\nu} \vec{W}^\alpha \cdot \vec{W}_\alpha \\ L_6^c &= -\frac{e^2}{16\Lambda^2} a_c F^{\mu\alpha} F_{\mu\beta} \vec{W}^\beta \cdot \vec{W}_\alpha \\ L_6^n &= -i\frac{e^2}{16\Lambda^2} a_n \epsilon_{ijk} W_{\mu\alpha}^{(i)} W_\nu^{(j)} W^{(k)\alpha} F^{\mu\nu} \\ \tilde{L}_6^0 &= -\frac{e^2}{16\Lambda^2} \tilde{a}_0 F^{\mu\nu} \tilde{F}_{\mu\nu} \vec{W}^\alpha \cdot \vec{W}_\alpha \\ \tilde{L}_6^n &= -i\frac{e^2}{16\Lambda^2} \tilde{a}_n \epsilon_{ijk} W_{\mu\alpha}^{(i)} W_\nu^{(j)} W^{(k)\alpha} \tilde{F}^{\mu\nu} \end{aligned}$$

where  $F, W$  are photon and  $W$  fields,  $L_6^0$  and  $L_6^c$  conserve  $C, P$  separately ( $\tilde{L}_6^0$  conserves only  $C$ ) and generate anomalous  $W^+W^-\gamma\gamma$  and  $ZZ\gamma\gamma$  couplings,  $L_6^n$  violates  $CP$  ( $\tilde{L}_6^n$  violates both  $C$  and  $P$ ) and generates an anomalous  $W^+W^-Z\gamma$  coupling, and  $\Lambda$  is an energy scale for new physics. For the  $ZZ\gamma\gamma$  coupling the  $CP$ -violating term represented by  $L_6^n$  does not contribute. These couplings are assumed to be real and to vanish at tree level in the Standard Model.

Within the same framework as above, a more recent description of the quartic couplings [3] treats the anomalous parts of the  $WW\gamma\gamma$  and  $ZZ\gamma\gamma$  couplings separately, leading to two sets parametrized as  $a_0^V/\Lambda^2$  and  $a_c^V/\Lambda^2$ , where  $V = W$  or  $Z$ .

With the discovery of a Higgs at the LHC in 2012, it is then useful to go to the next higher dimensional representation (dimension 8 operators) in which the gauge symmetry is broken by the conventional Higgs scalar doublet [3,4]. There are 14 operators which can contribute to the anomalous quartic coupling signal. Some of the operators have analogues in the dimension 6 scheme. The CMS collaboration, [5], have used this parametrization, in which the connections between the two schemes are also summarized:

$$\begin{aligned} \mathcal{L}_{AQGC} &= -\frac{e^2 a_0^W}{8 \Lambda^2} F_{\mu\nu} F^{\mu\nu} W^{+\alpha} W_a^- \\ &\quad -\frac{e^2 a_c^W}{16 \Lambda^2} F_{\mu\nu} F^{\mu\alpha} (W^{+\nu} W_a^- + W^{-\nu} W_a^+) \\ &\quad -e^2 g^2 \frac{\kappa_0^W}{\Lambda^2} F_{\mu\nu} Z^{\mu\nu} W^{+\alpha} W_a^- \\ &\quad -\frac{e^2 g^2 \kappa_c^W}{2 \Lambda^2} F_{\mu\nu} Z^{\mu\alpha} (W^{+\nu} W_a^- + W^{-\nu} W_a^+) \\ &\quad + \frac{f_{T,0}}{\Lambda^4} Tr[\widehat{W}_{\mu\nu} \widehat{W}^{\mu\nu}] \times Tr[\widehat{W}_{\alpha\beta} \widehat{W}^{\alpha\beta}] \end{aligned}$$

The energy scale of possible new physics is  $\Lambda$ , and  $g = e/\sin(\theta_W)$ ,  $e$  being the unit electric charge and  $\theta_W$  the Weinberg angle. The field tensors are described in [3,4].

The two dimension 6 operators  $a_0^W/\Lambda^2$  and  $a_c^W/\Lambda^2$  are associated with the  $WW\gamma\gamma$  vertex. Among dimension 8 operators,  $\kappa_0^W/\Lambda^2$  and  $\kappa_c^W/\Lambda^2$  are associated with the  $WWZ\gamma$  vertex, whereas the parameter  $f_{T,0}/\Lambda^4$  contributes to both vertices. There is a relationship between these two dimension 6 parameters and the dimension 8 parameters  $f_{M,i}/\Lambda^4$  as follows [3]:

$$\frac{a_0^W}{\Lambda^2} = -\frac{4M_W^2}{g^2} \frac{f_{M,0}}{\Lambda^4} - \frac{8M_W^2}{g'^2} \frac{f_{M,2}}{\Lambda^4}$$

$$\frac{a_c^W}{\Lambda^2} = -\frac{4M_W^2}{g^2} \frac{f_{M,1}}{\Lambda^4} - \frac{8M_W^2}{g'^2} \frac{f_{M,3}}{\Lambda^4}$$

where  $g' = e/\cos(\theta_W)$  and  $M_W$  is the invariant mass of the  $W$  boson. This relation provides a translation between limits on dimension 6 operators  $a_{0,c}^W$  and  $f_{M,j}/\Lambda^4$ . It is further required [4] that  $f_{M,0} = 2f_{M,2}$  and  $f_{M,1} = 2f_{M,3}$  which suppresses contributions to the  $WWZ\gamma$  vertex. The complete set of Lagrangian contributions as presented in [4] corresponds to 19 anomalous couplings in total –  $f_{S,i}$ ,  $i = 1, 2$ ,  $f_{M,i}$ ,  $i = 0, \dots, 8$  and  $f_{T,i}$ ,  $i = 0, \dots, 9$  – each scaled by  $1/\Lambda^4$ .

The ATLAS collaboration [6], on the other hand, follows a K-matrix driven approach of Ref. 7 in which the anomalous couplings can be expressed in terms of two parameters  $\alpha_4$  and  $\alpha_5$ , which account for all BSM effects.

It is the early stages in the determination of quartic couplings by the LHC experiments. It is hoped that the two collaborations, ATLAS and CMS, will agree to use at least one common set of parameters to express these limits to enable the reader to make a comparison and allow for a possible LHC combination.

## References

- G. Belanger and F. Boudjema, Phys. Lett. **B288**, 201 (1992).
- J.W. Stirling and A. Werthenbach, Eur. Phys. J. **C14**, 103 (2000);  
J.W. Stirling and A. Werthenbach, Phys. Lett. **B466**, 369 (1999);  
A. Denner *et al.*, Eur. Phys. J. **C20**, 201 (2001);  
G. Montagna *et al.*, Phys. Lett. **B515**, 197 (2001).
- G. Belanger *et al.*, Eur. Phys. J. **C13**, 283 (2000).
- O.J.P. Éboli, M.C. Gonzalez-Garcia, and S.M. Lietti, Phys. Rev. **D69**, 095005 (2004);  
O.J.P. Éboli, M.C. Gonzalez-Garcia, and J.K. Mizukoshi, Phys. Rev. **D77**, 073005 (2006).
- S. Chatrchyan *et al.*, Phys. Rev. **D90**, 032008 (2014);  
S. Chatrchyan *et al.*, Phys. Rev. Lett. **114**, 051801 (2015).
- G. Aad *et al.*, Phys. Rev. Lett. **113**, 141803 (2014).
- A. Albateanu, W. Killian, and J. Reuter, JHEP **0811**, 010 (2008).

## $a_0/\Lambda^2, a_c/\Lambda^2$

Combining published and unpublished preliminary LEP results the following 95% CL intervals for the QGCs associated with the  $ZZ\gamma\gamma$  vertex are derived (CERN-PH-EP/2005-051 or hep-ex/0511027):

$$\begin{aligned} -0.008 < a_0^Z/\Lambda^2 < +0.021 \\ -0.029 < a_c^Z/\Lambda^2 < +0.039 \end{aligned}$$

Anomalous Z quartic couplings have also been measured by the Tevatron and LHC experiments. As discussed in the review on "Anomalous W/Z quartic couplings," the coupling parameters in the Anomalous QGC Lagrangian may relate to processes involving only the  $W$  or only to the  $Z$  or to both. Thus, results on all other AQGCs are reported together in the  $W$  listings.

VALUE	DOCUMENT ID	TECN
•••	We do not use the following data for averages, fits, limits, etc. •••	
1	ABBIENDI	04L OPAL
2	HEISTER	04A ALEP
3	ACHARD	02G L3

- 1** ABBIENDI 04L select  $20 e^+ e^- \rightarrow \nu \bar{\nu} \gamma \gamma$  acoplanar events in the energy range 180–209 GeV and  $176 e^+ e^- \rightarrow q \bar{q} \gamma \gamma$  events in the energy range 130–209 GeV. These samples are used to constrain possible anomalous  $W^+ W^- \gamma \gamma$  and  $Z Z \gamma \gamma$  quartic couplings. Further combining with the  $W^+ W^- \gamma$  sample of ABBIENDI 04B the following one-parameter 95% CL limits are obtained:  $-0.007 < a_0^Z/\Lambda^2 < 0.023 \text{ GeV}^{-2}$ ,  $-0.029 < a_0^W/\Lambda^2 < 0.029 \text{ GeV}^{-2}$ ,  $-0.020 < a_0^W/\Lambda^2 < 0.020 \text{ GeV}^{-2}$ ,  $-0.052 < a_C^W/\Lambda^2 < 0.037 \text{ GeV}^{-2}$ .
- 2** In the CM energy range 183 to 209 GeV HEISTER 04A select  $30 e^+ e^- \rightarrow \nu \bar{\nu} \gamma \gamma$  events with two acoplanar, high energy and high transverse momentum photons. The photon-photon acoplanarity is required to be  $> 5^\circ$ ,  $E_\gamma/\sqrt{s} > 0.025$  (the more energetic photon having energy  $> 0.2 \sqrt{s}$ ),  $p_{T\gamma}/E_{\text{beam}} > 0.05$  and  $|\cos \theta_\gamma| < 0.94$ . A likelihood fit to the photon energy and recoil missing mass yields the following one-parameter 95% CL limits:  $-0.012 < a_0^Z/\Lambda^2 < 0.019 \text{ GeV}^{-2}$ ,  $-0.041 < a_C^Z/\Lambda^2 < 0.044 \text{ GeV}^{-2}$ ,  $-0.060 < a_0^W/\Lambda^2 < 0.055 \text{ GeV}^{-2}$ ,  $-0.099 < a_C^W/\Lambda^2 < 0.093 \text{ GeV}^{-2}$ .
- 3** ACHARD 02c study  $e^+ e^- \rightarrow Z \gamma \gamma \rightarrow q \bar{q} \gamma \gamma$  events using data at center-of-mass energies from 200 to 209 GeV. The photons are required to be isolated, each with energy  $> 5 \text{ GeV}$  and  $|\cos \theta| < 0.97$ , and the di-jet invariant mass to be compatible with that of the Z boson (74–111 GeV). Cuts on Z velocity ( $\beta < 0.73$ ) and on the energy of the most energetic photon reduce the backgrounds due to non-resonant production of the  $q \bar{q} \gamma \gamma$  state and due to ISR respectively, yielding a total of 40 candidate events of which 8.6 are expected to be due to background. The energy spectra of the least energetic photon are fitted for all ten center-of-mass energy values from 130 GeV to 209 GeV (as obtained adding to the present analysis 130–202 GeV data of ACCIARRI 01E, for a total of 137 events with an expected background of 34.1 events) to obtain the fitted values  $a_0/\Lambda^2 = 0.00 \pm 0.02 \text{ GeV}^{-2}$  and  $a_C/\Lambda^2 = 0.03 \pm 0.01 \text{ GeV}^{-2}$ , where the other parameter is kept fixed to its Standard Model value (0). A simultaneous fit to both parameters yields the 95% CL limits  $-0.02 \text{ GeV}^{-2} < a_0/\Lambda^2 < 0.03 \text{ GeV}^{-2}$  and  $-0.07 \text{ GeV}^{-2} < a_C/\Lambda^2 < 0.05 \text{ GeV}^{-2}$ .

Z REFERENCES

AABOUD 19AY JHEP 1910 127  
AABOUD 19N JHEP 1904 048  
RAINBOLT 19 PR D99 013004  
SIRUNYAN 19AJ EPJ C79 94  
SIRUNYAN 19BR PL B797 134811  
AABOUD 18AL JHEP 1807 127  
AABOUD 18BL PL B786 134  
AABOUD 18CM PR D98 092010  
AABOUD 18Q PR D97 032005  
AAJ 18AR JHEP 1809 159  
ANDREEV 18A EPJ C78 777  
SIRUNYAN 18BT EPJ C78 165  
SIRUNYAN 18DZ PRL 121 141801  
AABOUD 17Q EPJ C77 367  
AABOUD 16K PRL 117 111802  
AAD 16L EPJ C76 210  
AAD 16Q PR D93 112002  
ABRAMOWICZ 16A PR D93 02002  
ABT 16 PR D94 052007  
KHACHATRYAN 16AC PL B760 448  
KHACHATRYAN 16CC PL B763 280  
AAD 15B JHEP 1509 049  
AAD 15I PRL 114 121801  
KHACHATRYAN 15AC JHEP 1504 164  
KHACHATRYAN 15BC PL B740 250  
KHACHATRYAN 15BC EPJ C75 511  
AAD 14AU PR D90 072010  
AAD 14N PRL 112 231806  
AALTONEN 14E PRL 112 111803  
CHATRCHYAN 14AB PR D89 092005  
AAD 13AN PR D87 112003  
Also PR D91 119901 (erratum)  
AAD 13Z JHEP 1303 128  
CHATRCHYAN 13B JHEP 1301 063  
CHATRCHYAN 13BI JHEP 1310 164  
SCHAE 13A PRPL 532 119  
AAD 12XB PL B717 49  
ABAZOV 12S PR D85 052001  
ALATONEN 12BM JHEP 1212 034  
AALTONEN 11S PRL 107 051802  
ABAZOV 11D PR D84 012007  
CHATRCHYAN 11M PL B701 535  
ABAZOV 09L PRL 102 201802  
BEDDALL 09 PL B670 300  
SCHAE 09 JHEP 0904 124  
ABAZOV 08K PRL 100 131801  
ABAZOV 07M PL B653 378  
ABDALLAH 07C EPJ C51 525  
ABDALLAH 06E PL B639 179  
AKTAS 06 PL B632 35  
LEP-SLC 06 PRL 427 257  
SCHAE 06A PL B639 192  
ABDALLAH 05 EPJ C40 1  
ABDALLAH 05C EPJ C44 299  
ABE 05 PRL 94 091801  
ABE 05F PR D71 112004  
ACOSTA 05M PR D71 052002  
ABBIENDI 04B PL B580 17  
ABBIENDI 04C EPJ C32 303  
ABBIENDI 04E PL B586 167  
ABBIENDI 04G EPJ C33 173  
ABBIENDI 04L PR D70 032005  
ABDALLAH 04F EPJ C34 109  
ABE 04C PR D69 072003  
ACHARD 04C PL B585 42  
ACHARD 04H PL B597 119  
HEISTER 04A PL B602 31  
ABBIENDI 03P PL B577 18  
ABDALLAH 03H PL B569 129  
ABDALLAH 03K PL B576 29  
ABE 03F PRL 90 141804  
ACHARD 03D PL B572 133  
ACHARD 03G PL B577 109  
ABBIENDI 02I PL B548 29  
ABE 02G PRL 88 151801  
ACHARD 02G PL B540 43  
HEISTER 02B PL B526 34  
HEISTER 02C PL B528 19

HEISTER 02H EPJ C24 177  
ABBIENDI 01A EPJ C19 587  
ABBIENDI 01G EPJ C18 447  
ABBIENDI 01K PL B516 1  
ABBIENDI 01N EPJ C20 445  
ABBIENDI 01O EPJ C21 1  
ABE 01B PRL 86 1162  
ABE 01C PR D63 032005  
ACCIARRI 01E PL B505 47  
ACCIARRI 01I PL B497 23  
HEISTER 01I EPJ C20 401  
HEISTER 01D EPJ C22 201  
ABBIENDI 00N PL B476 256  
ABBIENDI,G 00C EPJ C17 553  
ABE 00B PRL 84 5945  
ABE 00D PRL 85 5059  
ABREU 00 EPJ C12 225  
ABREU 00B EPJ C14 613  
ABREU 00E EPJ C14 585  
ABREU 00F EPJ C16 371  
ABREU 00P PL B475 429  
ACCIARRI 00 EPJ C13 47  
ACCIARRI 00C EPJ C16 1  
ACCIARRI 00Q PL B479 79  
ACCIARRI 00J PL B489 93  
BARATE 00 EPJ C16 597  
BARATE 00C EPJ C14 1  
BARATE 00O EPJ C16 613  
ABBIENDI 99B EPJ C8 217  
ABBIENDI 99I PL B447 157  
ABE 99L PR D59 052001  
ABE 99R PRL 83 1902  
ABREU 99 EPJ C6 19  
ABREU 99B EPJ C10 415  
ABREU 99J PL B449 364  
ABREU 99U PL B462 425  
ABREU 99Y EPJ C10 219  
ACCIARRI 99D PL B448 152  
ACCIARRI 99F PL B453 94  
ACCIARRI 99G PL B450 281  
ACCIARRI 99O PL B465 363  
ABBOTT 98M PR D55 0817  
ABE 98D PRL 80 660  
ABE 98I PRL 81 942  
ABREU 98K PL B423 194  
ABREU 98L EPJ C5 585  
ACCIARRI 98G PL B431 199  
ACCIARRI 98H PL B429 387  
ACCIARRI 98U PL B439 225  
ACKERSTAFF 98A EPJ C5 411  
ACKERSTAFF 98E EPJ C1 439  
ACKERSTAFF 98O PL B420 157  
ACKERSTAFF 98Q EPJ C4 19  
BARATE 98M PL B434 415  
BARATE 98T EPJ C4 557  
BARATE 98V EPJ C5 205  
ABE 97 PRL 78 17  
ABREU 97C ZPHY C73 243  
ABREU 97E PL B398 207  
ABREU 97F PL B404 194  
ACCIARRI 97D PL B393 465  
ACCIARRI 97J PL B407 351  
ACCIARRI 97L PL B407 389  
ACCIARRI 97R PL B413 167  
ACKERSTAFF 97M ZPHY C74 413  
ACKERSTAFF 97S PL B412 210  
ACKERSTAFF 97T ZPHY C76 387  
ACKERSTAFF 97W ZPHY C76 425  
ALEXANDER 97C ZPHY C73 379  
ALEXANDER 97D ZPHY C73 569  
ALEXANDER 97E ZPHY C73 587  
BARATE 97E PL B405 191  
BARATE 97F PL B401 150  
BARATE 97G PL B401 163  
BARATE 97H PL B404 213  
BARATE 97J ZPHY C74 451  
ABREU 96R ZPHY C72 31  
ABREU 96S PL B389 405  
ABREU 96U ZPHY C73 61  
ACCIARRI 96 PL B371 126  
ADAM 96 ZPHY C69 561  
ADAM 96B ZPHY C70 371  
ALEXANDER 96B ZPHY C70 197  
ALEXANDER 96F PL B370 185  
ALEXANDER 96N PL B384 343  
ALEXANDER 96R ZPHY C72 1  
BUSKULIC 96D ZPHY C69 393  
BUSKULIC 96H ZPHY C69 379  
BUSKULIC 96T PL B384 449  
BUSKULIC 96Y PL B388 648  
ABE 95J PRL 74 2880  
ABREU 95 ZPHY C65 709 (erratum)  
ABREU 95D ZPHY C66 323  
ABREU 95M ZPHY C65 587  
ABREU 95P ZPHY C65 603  
ABREU 95Q ZPHY C67 543  
ABREU 95R ZPHY C68 353  
ABREU 95V ZPHY C68 541  
ABREU 95W PL B361 207  
ABREU 95X ZPHY C69 1  
ACCIARRI 95B PL B345 589  
ACCIARRI 95C PL B345 609  
ACCIARRI 95G PL B353 136  
AKERS 95C ZPHY C65 47  
AKERS 95U ZPHY C67 389  
AKERS 95V ZPHY C67 555  
AKERS 95Z ZPHY C68 203  
ALEXANDER 95D PL B358 162  
BUSKULIC 95R ZPHY C69 15  
MIYABAYASHI 95 PL B347 171  
ABE 94C PRL 73 25  
ABREU 94B PL B327 386  
ABREU 94P PL B341 109  
AKERS 94 ZPHY C63 181  
BUSKULIC 94G ZPHY C62 179  
BUSKULIC 94J ZPHY C62 1  
VILAIN 94 PL B320 203  
ABREU 93Z ZPHY C68 206  
ABREU 93I ZPHY C59 533  
Also ZPHY C65 709 (erratum)  
ABREU 93L PL B318 249

Downloaded from https://academic.oup.com/ptep/article/2020/08/083C01/5891211 by guest on 12 November 2020

# Gauge & Higgs Boson Particle Listings

## Z, H<sup>0</sup>

ACTON	93	PL B305 407	P.D. Acton <i>et al.</i>	(OPAL Collab.)
ACTON	93D	ZPHY C58 219	P.D. Acton <i>et al.</i>	(OPAL Collab.)
ACTON	93E	PL B311 391	P.D. Acton <i>et al.</i>	(OPAL Collab.)
ADRIANI	93	PL B301 136	O. Adriani <i>et al.</i>	(L3 Collab.)
ADRIANI	93I	PL B316 427	O. Adriani <i>et al.</i>	(L3 Collab.)
BUSKULIC	93L	PL B313 520	D. Buskulic <i>et al.</i>	(ALEPH Collab.)
NOVIKOV	93C	PL B298 453	V.A. Novikov, L.B. Okun, M.I. Vysotsky	(DELPHI Collab.)
ABREU	92I	PL B277 371	P. Abreu <i>et al.</i>	(DELPHI Collab.)
ABREU	92M	PL B289 199	P. Abreu <i>et al.</i>	(DELPHI Collab.)
ACTON	92B	ZPHY C53 539	D.P. Acton <i>et al.</i>	(OPAL Collab.)
ACTON	92L	PL B294 436	P.D. Acton <i>et al.</i>	(OPAL Collab.)
ACTON	92N	PL B295 357	P.D. Acton <i>et al.</i>	(OPAL Collab.)
ADEVA	92	PL B275 209	B. Adeva <i>et al.</i>	(L3 Collab.)
ADRIANI	92D	PL B292 454	O. Adriani <i>et al.</i>	(L3 Collab.)
ALITTI	92B	PL B276 354	J. Alitti <i>et al.</i>	(UA2 Collab.)
BUSKULIC	92D	PL B292 210	D. Buskulic <i>et al.</i>	(ALEPH Collab.)
BUSKULIC	92E	PL B294 145	D. Buskulic <i>et al.</i>	(ALEPH Collab.)
DECAMP	92	PRL 216 253	D. Decamp <i>et al.</i>	(CDF Collab.)
ABE	91E	PRL 67 3502	F. Abe <i>et al.</i>	(CDF Collab.)
ABREU	91H	ZPHY C59 185	F. Abreu <i>et al.</i>	(DELPHI Collab.)
ACTON	91B	PL B273 338	D.P. Acton <i>et al.</i>	(OPAL Collab.)
ADACHI	91	PL B255 613	I. Adachi <i>et al.</i>	(TOPAZ Collab.)
ADEVA	91I	PL B259 199	B. Adeva <i>et al.</i>	(L3 Collab.)
AKRAWY	91F	PL B257 531	M.Z. Akrawy <i>et al.</i>	(OPAL Collab.)
DECAMP	91B	PL B259 377	D. Decamp <i>et al.</i>	(ALEPH Collab.)
DECAMP	91J	PL B266 218	D. Decamp <i>et al.</i>	(ALEPH Collab.)
JACOBSEN	91	PRL 67 3347	R.G. Jacobsen <i>et al.</i>	(Mark II Collab.)
SHIMONAKA	91	PL B268 457	A. Shimonaka <i>et al.</i>	(TOPAZ Collab.)
ABE	90I	ZPHY C48 13	K. Abe <i>et al.</i>	(VENUS Collab.)
ABRAMS	90	PRL 64 1334	G.S. Abrams <i>et al.</i>	(Mark II Collab.)
AKRAWY	90J	PL B246 205	M.Z. Akrawy <i>et al.</i>	(OPAL Collab.)
BEHREND	90D	ZPHY C47 333	H.J. Behrend <i>et al.</i>	(CELLO Collab.)
BRUNSCHEWIG	90	ZPHY C48 433	W. Brunschweig <i>et al.</i>	(TASSO Collab.)
ELSEN	90	ZPHY C46 349	E. Elsen <i>et al.</i>	(JADE Collab.)
HEGNER	90	ZPHY C46 547	S. Hegner <i>et al.</i>	(JADE Collab.)
STUART	90	PRL 64 983	D. Stuart <i>et al.</i>	(AMY Collab.)
ABE	89	PRL 62 613	F. Abe <i>et al.</i>	(CDF Collab.)
ABE	89C	PRL 63 720	F. Abe <i>et al.</i>	(CDF Collab.)
ABE	89L	PL B232 425	K. Abe <i>et al.</i>	(VENUS Collab.)
ABRAMS	89B	PRL 63 2173	G.S. Abrams <i>et al.</i>	(Mark II Collab.)
ABRAMS	89D	PRL 63 2780	G.S. Abrams <i>et al.</i>	(Mark II Collab.)
ALBAJAR	89	ZPHY C44 15	C. Albajar <i>et al.</i>	(UA1 Collab.)
BACALA	89	PL B218 112	A. Bacala <i>et al.</i>	(AMY Collab.)
BAND	89	PL B218 369	H.R. Band <i>et al.</i>	(MAC Collab.)
GREENSHAW	89	ZPHY C42 1	T. Greenshaw <i>et al.</i>	(JADE Collab.)
OULD-SAAD	89	ZPHY C44 567	F. Ould-Saada <i>et al.</i>	(JADE Collab.)
SAGAWA	89	PRL 63 2341	H. Sagawa <i>et al.</i>	(AMY Collab.)
ADACHI	88C	PL B208 319	I. Adachi <i>et al.</i>	(TOPAZ Collab.)
ADEVA	88	PL D38 2665	B. Adeva <i>et al.</i>	(Mark-J Collab.)
BRUNSCHEWIG	88D	ZPHY C40 163	W. Brunschweig <i>et al.</i>	(TASSO Collab.)
ANSARI	87	PL B186 440	R. Ansari <i>et al.</i>	(UA2 Collab.)
BEHREND	87C	PL B191 209	H.J. Behrend <i>et al.</i>	(CELLO Collab.)
BARTEL	86C	ZPHY C30 371	W. Bartel <i>et al.</i>	(JADE Collab.)
Also	Also	ZPHY C26 507	W. Bartel <i>et al.</i>	(JADE Collab.)
Also	Also	PL 108B 140	W. Bartel <i>et al.</i>	(JADE Collab.)
ASH	85	PRL 55 1831	W.W. Ash <i>et al.</i>	(MAC Collab.)
BARTEL	85F	PL 161B 188	W. Bartel <i>et al.</i>	(JADE Collab.)
DERRICK	85	PR D31 2352	M. Derrick <i>et al.</i>	(HRS Collab.)
FERNANDEZ	85	PRL 54 1624	E. Fernandez <i>et al.</i>	(MAC Collab.)
LEVI	83	PRL 51 1941	M.E. Levi <i>et al.</i>	(Mark II Collab.)
BEHREND	82	PL 114B 282	H.J. Behrend <i>et al.</i>	(CELLO Collab.)
BRANDELIC	82C	PL 110B 173	R. Brandelic <i>et al.</i>	(TASSO Collab.)

124.51 ± 0.52 ± 0.06	<sup>8</sup> AAD	14W ATLS	$pp, 7, 8 \text{ TeV}, ZZ^* \rightarrow 4\ell$
125.6 ± 0.4 ± 0.2	<sup>9</sup> CHATRCHYAN 14AA	CMS	$pp, 7, 8 \text{ TeV}, ZZ^* \rightarrow 4\ell$
122 ± 7	<sup>10</sup> CHATRCHYAN 14K	CMS	$pp, 7, 8 \text{ TeV}, \tau\tau$
124.70 ± 0.31 ± 0.15	<sup>11</sup> KHACHATRYAN...14P	CMS	$pp, 7, 8 \text{ TeV}, \gamma\gamma$
125.5 ± 0.2 ± 0.5 ± 0.6	<sup>1,12</sup> AAD	13AK ATLS	$pp, 7, 8 \text{ TeV}$
126.8 ± 0.2 ± 0.7	<sup>12</sup> AAD	13AK ATLS	$pp, 7, 8 \text{ TeV}, \gamma\gamma$
124.3 + 0.6 + 0.5 - 0.5 - 0.3	<sup>12</sup> AAD	13AK ATLS	$pp, 7, 8 \text{ TeV}, ZZ^* \rightarrow 4\ell$
125.8 ± 0.4 ± 0.4	<sup>1,13</sup> CHATRCHYAN 13J	CMS	$pp, 7, 8 \text{ TeV}$
126.2 ± 0.6 ± 0.2	<sup>13</sup> CHATRCHYAN 13J	CMS	$pp, 7, 8 \text{ TeV}, ZZ^* \rightarrow 4\ell$
126.0 ± 0.4 ± 0.4	<sup>1,14</sup> AAD	12AI ATLS	$pp, 7, 8 \text{ TeV}$
125.3 ± 0.4 ± 0.5	<sup>1,15</sup> CHATRCHYAN 12N	CMS	$pp, 7, 8 \text{ TeV}$

- <sup>1</sup> Combined value from  $\gamma\gamma$  and  $ZZ^* \rightarrow 4\ell$  final states.
- <sup>2</sup> SIRUNYAN 17AV use 35.9 fb<sup>-1</sup> of  $pp$  collisions at  $E_{\text{cm}} = 13 \text{ TeV}$  with  $H^0 \rightarrow ZZ^* \rightarrow 4\ell$  where  $\ell = e, \mu$ .
- <sup>3</sup> ATLAS and CMS data are fitted simultaneously.
- <sup>4</sup> AABOUD 18BM use 36.1 fb<sup>-1</sup> of  $pp$  collisions at  $E_{\text{cm}} = 13 \text{ TeV}$  with  $H^0 \rightarrow ZZ^* \rightarrow 4\ell$  where  $\ell = e, \mu$ .
- <sup>5</sup> AABOUD 18BM use 36.1 fb<sup>-1</sup> of  $pp$  collisions at  $E_{\text{cm}} = 13 \text{ TeV}$  with  $H^0 \rightarrow \gamma\gamma$ .
- <sup>6</sup> AABOUD 18BM combine 13 TeV results with 7 and 8 TeV results. Other combined results are summarized in their Fig. 4.
- <sup>7</sup> KHACHATRYAN 15AM use up to 5.1 fb<sup>-1</sup> of  $pp$  collisions at  $E_{\text{cm}} = 7 \text{ TeV}$  and up to 19.7 fb<sup>-1</sup> at  $E_{\text{cm}} = 8 \text{ TeV}$ .
- <sup>8</sup> AAD 14W use 4.5 fb<sup>-1</sup> of  $pp$  collisions at  $E_{\text{cm}} = 7 \text{ TeV}$  and 20.3 fb<sup>-1</sup> at 8 TeV.
- <sup>9</sup> CHATRCHYAN 14AA use 5.1 fb<sup>-1</sup> of  $pp$  collisions at  $E_{\text{cm}} = 7 \text{ TeV}$  and 19.7 fb<sup>-1</sup> at  $E_{\text{cm}} = 8 \text{ TeV}$ .
- <sup>10</sup> CHATRCHYAN 14K use 4.9 fb<sup>-1</sup> of  $pp$  collisions at  $E_{\text{cm}} = 7 \text{ TeV}$  and 19.7 fb<sup>-1</sup> at  $E_{\text{cm}} = 8 \text{ TeV}$ .
- <sup>11</sup> KHACHATRYAN 14P use 5.1 fb<sup>-1</sup> of  $pp$  collisions at  $E_{\text{cm}} = 7 \text{ TeV}$  and 19.7 fb<sup>-1</sup> at  $E_{\text{cm}} = 8 \text{ TeV}$ .
- <sup>12</sup> AAD 13AK use 4.7 fb<sup>-1</sup> of  $pp$  collisions at  $E_{\text{cm}} = 7 \text{ TeV}$  and 20.7 fb<sup>-1</sup> at  $E_{\text{cm}} = 8 \text{ TeV}$ . Superseded by AAD 14W.
- <sup>13</sup> CHATRCHYAN 13J use 5.1 fb<sup>-1</sup> of  $pp$  collisions at  $E_{\text{cm}} = 7 \text{ TeV}$  and 12.2 fb<sup>-1</sup> at  $E_{\text{cm}} = 8 \text{ TeV}$ .
- <sup>14</sup> AAD 12AI obtain results based on 4.6–4.8 fb<sup>-1</sup> of  $pp$  collisions at  $E_{\text{cm}} = 7 \text{ TeV}$  and 5.8–5.9 fb<sup>-1</sup> at  $E_{\text{cm}} = 8 \text{ TeV}$ . An excess of events over background with a local significance of 5.9  $\sigma$  is observed at  $m_{H^0} = 126 \text{ GeV}$ . See also AAD 12DA.
- <sup>15</sup> CHATRCHYAN 12N obtain results based on 4.9–5.1 fb<sup>-1</sup> of  $pp$  collisions at  $E_{\text{cm}} = 7 \text{ TeV}$  and 5.1–5.3 fb<sup>-1</sup> at  $E_{\text{cm}} = 8 \text{ TeV}$ . An excess of events over background with a local significance of 5.0  $\sigma$  is observed at about  $m_{H^0} = 125 \text{ GeV}$ . See also CHATRCHYAN 12BY and CHATRCHYAN 13J.

## H<sup>0</sup> SPIN AND CP PROPERTIES

The observation of the signal in the  $\gamma\gamma$  final state rules out the possibility that the discovered particle has spin 1, as a consequence of the Landau-Yang theorem. This argument relies on the assumptions that the decaying particle is an on-shell resonance and that the decay products are indeed two photons rather than two pairs of boosted photons, which each could in principle be misidentified as a single photon.

Concerning distinguishing the spin 0 hypothesis from a spin 2 hypothesis, some care has to be taken in modelling the latter in order to ensure that the discriminating power is actually based on the spin properties rather than on unphysical behavior that may affect the model of the spin 2 state.

Under the assumption that the observed signal consists of a single state rather than an overlap of more than one resonance, it is sufficient to discriminate between distinct hypotheses in the spin analyses. On the other hand, the determination of the CP properties is in general much more difficult since in principle the observed state could consist of any admixture of CP-even and CP-odd components. As a first step, the compatibility of the data with distinct hypotheses of pure CP-even and pure CP-odd states with different spin assignments has been investigated. In order to treat the case of a possible mixing of different CP states, certain cross section ratios are considered. Those cross section ratios need to be distinguished from the amount of mixing between a CP-even and a CP-odd state, as the cross section ratios depend in addition also on the coupling strengths of the CP-even and CP-odd components to the involved particles. A small relative coupling implies a small sensitivity of the corresponding cross section ratio to effects of CP mixing.

VALUE	DOCUMENT ID	TECN	COMMENT
••• We do not use the following data for averages, fits, limits, etc. •••			
	<sup>1</sup> SIRUNYAN	19bL CMS	$pp, 7, 8, 13 \text{ TeV}, ZZ^*/Z\tau \rightarrow 4\ell$
	<sup>2</sup> SIRUNYAN	19bZ CMS	$pp \rightarrow H^0 + 2\text{jets} (\text{VBF}, \text{ggF}, V, H), H^0 \rightarrow \tau\tau, 13 \text{ TeV}$
	<sup>3</sup> AABOUD	18AJ ATLS	$H^0 \rightarrow ZZ^* \rightarrow 4\ell (\ell = e, \mu), 13\text{TeV}$
	<sup>4</sup> SIRUNYAN	17AM CMS	$pp \rightarrow H^0 + \geq 2\ell, H^0 \rightarrow 4\ell (\ell = e, \mu)$
	<sup>5</sup> AAD	16 ATLS	$H^0 \rightarrow \gamma\gamma$
	<sup>6</sup> AAD	16bL ATLS	$pp \rightarrow H^0 jjX (\text{VBF}), H^0 \rightarrow \tau\tau, 8 \text{ TeV}$
	<sup>7</sup> KHACHATRYAN...16AB	CMS	$pp \rightarrow WH^0, ZH^0, H^0 \rightarrow b\bar{b}, 8 \text{ TeV}$
	<sup>8</sup> AAD	15AX ATLS	$H^0 \rightarrow WW^*$
	<sup>9</sup> AAD	15CI ATLS	$H^0 \rightarrow ZZ^*, WW^*, \gamma\gamma$
	<sup>10</sup> AALTONEN	15 TEVA	$p\bar{p} \rightarrow WH^0, ZH^0, H^0 \rightarrow b\bar{b}$
	<sup>11</sup> AALTONEN	15B CDF	$p\bar{p} \rightarrow WH^0, ZH^0, H^0 \rightarrow b\bar{b}$
	<sup>12</sup> KHACHATRYAN...15Y	CMS	$H^0 \rightarrow 4\ell, WW^*, \gamma\gamma$
	<sup>13</sup> ABAZOV	14F D0	$p\bar{p} \rightarrow WH^0, ZH^0, H^0 \rightarrow b\bar{b}$
	<sup>14</sup> CHATRCHYAN 14AA	CMS	$H^0 \rightarrow ZZ^*$
	<sup>15</sup> CHATRCHYAN 14G	CMS	$H^0 \rightarrow WW^*$
	<sup>16</sup> KHACHATRYAN...14P	CMS	$H^0 \rightarrow \gamma\gamma$
	<sup>17</sup> AAD	13AJ ATLS	$H^0 \rightarrow \gamma\gamma, ZZ^* \rightarrow 4\ell, WW^* \rightarrow \ell\nu\ell\nu$
	<sup>18</sup> CHATRCHYAN 13J	CMS	$H^0 \rightarrow ZZ^* \rightarrow 4\ell$

## H<sup>0</sup>

$$J = 0$$

In the following  $H^0$  refers to the signal that has been discovered in the Higgs searches. Whereas the observed signal is labeled as a spin 0 particle and is called a Higgs Boson, the detailed properties of  $H^0$  and its role in the context of electroweak symmetry breaking need to be further clarified. These issues are addressed by the measurements listed below.

Concerning mass limits and cross section limits that have been obtained in the searches for neutral and charged Higgs bosons, see the sections “Searches for Neutral Higgs Bosons” and “Searches for Charged Higgs Bosons ( $H^\pm$  and  $H^{\pm\pm}$ )”, respectively.

### H<sup>0</sup> MASS

VALUE (GeV)	DOCUMENT ID	TECN	COMMENT
<b>125.10 ± 0.14 OUR AVERAGE</b>			
124.86 ± 0.27	<sup>1</sup> AABOUD	18BM ATLS	$pp, 13 \text{ TeV}, 36.1 \text{ fb}^{-1}, \gamma\gamma, ZZ^* \rightarrow 4\ell$
125.26 ± 0.20 ± 0.08	<sup>2</sup> SIRUNYAN	17AV CMS	$pp, 13 \text{ TeV}, ZZ^* \rightarrow 4\ell$
125.09 ± 0.21 ± 0.11	<sup>1,3</sup> AAD	15B LHC	$pp, 7, 8 \text{ TeV}$
••• We do not use the following data for averages, fits, limits, etc. •••			
124.79 ± 0.37	<sup>4</sup> AABOUD	18BM ATLS	$pp, 13 \text{ TeV}, 36.1 \text{ fb}^{-1}, ZZ^* \rightarrow 4\ell$
124.93 ± 0.40	<sup>5</sup> AABOUD	18BM ATLS	$pp, 13 \text{ TeV}, 36.1 \text{ fb}^{-1}, \gamma\gamma$
124.97 ± 0.24	<sup>1,6</sup> AABOUD	18BM ATLS	$pp, 7, 8, 13 \text{ TeV}, \gamma\gamma, ZZ^* \rightarrow 4\ell$
125.07 ± 0.25 ± 0.14	<sup>3</sup> AAD	15B LHC	$pp, 7, 8 \text{ TeV}, \gamma\gamma$
125.15 ± 0.37 ± 0.15	<sup>3</sup> AAD	15B LHC	$pp, 7, 8 \text{ TeV}, ZZ^* \rightarrow 4\ell$
126.02 ± 0.43 ± 0.27	AAD	15B ATLS	$pp, 7, 8 \text{ TeV}, \gamma\gamma$
124.51 ± 0.52 ± 0.04	AAD	15B ATLS	$pp, 7, 8 \text{ TeV}, ZZ^* \rightarrow 4\ell$
125.59 ± 0.42 ± 0.17	AAD	15B CMS	$pp, 7, 8 \text{ TeV}, ZZ^* \rightarrow 4\ell$
125.02 ± 0.26 ± 0.14 ± 0.27 ± 0.15	<sup>7</sup> KHACHATRYAN...15AM	CMS	$pp, 7, 8 \text{ TeV}$
125.36 ± 0.37 ± 0.18	<sup>1,8</sup> AAD	14W ATLS	$pp, 7, 8 \text{ TeV}$
125.98 ± 0.42 ± 0.28	<sup>8</sup> AAD	14W ATLS	$pp, 7, 8 \text{ TeV}, \gamma\gamma$

- <sup>1</sup> SIRUNYAN 19BL measure the anomalous  $HVV$  couplings from on-shell and off-shell production in the  $4\ell$  final state. Data of  $80.2 \text{ fb}^{-1}$  at 13 TeV,  $19.7 \text{ fb}^{-1}$  at 8 TeV, and  $5.1 \text{ fb}^{-1}$  at 7 TeV are used. See their Tables VI and VII for anomalous  $HVV$  couplings of  $CP$ -violating and  $CP$ -conserving parameters with on- and off-shells.
- <sup>2</sup> SIRUNYAN 19BZ constrain anomalous  $HVV$  couplings of the Higgs boson with data of  $35.9 \text{ fb}^{-1}$  at  $E_{\text{cm}} = 13 \text{ TeV}$  using Higgs boson candidates with two jets produced in VBF, ggF, and  $VH$  that decay to  $\tau\tau$ . See their Table 2 and Fig. 10, which show 68% CL and 95% CL intervals. Combining those with the  $H^0 \rightarrow 4\ell$  (SIRUNYAN 19BL, on-shell scenario), results shown in their Tables 3, 4, and Fig. 11 are obtained. A  $CP$ -violating parameter is set to be  $f_{a3}\cos(\phi_{a3}) = (0.00 \pm 0.27) \times 10^{-3}$  and  $CP$ -conserving parameters are  $f_{a2}\cos(\phi_{a2}) = (0.06 \pm 1.04) \times 10^{-3}$ ,  $f_{\Lambda 1}\cos(\phi_{\Lambda 1}) = (0.00 \pm 0.53) \times 10^{-3}$ , and  $f_{\Lambda 1}^{\prime}\cos(\phi_{\Lambda 1}^{\prime}) = (0.0 \pm 1.1) \times 10^{-3}$ .
- <sup>3</sup> AABOUD 18AJ study the tensor structure of the Higgs boson couplings using an effective Lagrangian using  $36.1 \text{ fb}^{-1}$  of  $pp$  collision data at  $E_{\text{cm}} = 13 \text{ TeV}$ . Constraints are set on the non-Standard-Model  $CP$ -even and  $CP$ -odd couplings to  $Z$  bosons and on the  $CP$ -odd coupling to gluons. See their Figs. 9 and 10, and Tables 10 and 11.
- <sup>4</sup> SIRUNYAN 17AM constrain anomalous couplings of the Higgs boson with  $5.1 \text{ fb}^{-1}$  of  $pp$  collisions at  $E_{\text{cm}} = 7 \text{ TeV}$ ,  $19.7 \text{ fb}^{-1}$  at  $E_{\text{cm}} = 8 \text{ TeV}$ , and  $38.6 \text{ fb}^{-1}$  at  $E_{\text{cm}} = 13 \text{ TeV}$ . See their Table 3 and Fig. 3, which show 68% CL and 95% CL intervals. A  $CP$  violation parameter  $f_{a3}$  is set to be  $f_{a3}\cos(\phi_{a3}) = [-0.38, 0.46]$  at 95% CL ( $\phi_{a3} = 0$  or  $\pi$ ).
- <sup>5</sup> AAD 16 study  $H^0 \rightarrow \gamma\gamma$  with an effective Lagrangian including  $CP$  even and odd terms in  $20.3 \text{ fb}^{-1}$  of  $pp$  collisions at  $E_{\text{cm}} = 8 \text{ TeV}$ . The data is consistent with the expectations for the Higgs boson of the Standard Model. Limits on anomalous couplings are also given.
- <sup>6</sup> AAD 16BL study VBF  $H^0 \rightarrow \tau\tau$  with an effective Lagrangian including a  $CP$  odd term in  $20.3 \text{ fb}^{-1}$  of  $pp$  collisions at  $E_{\text{cm}} = 8 \text{ TeV}$ . The measurement is consistent with the expectation of the Standard Model. The  $CP$ -mixing parameter  $\bar{d}$  (a dimensionless coupling  $\bar{d} = -(m_W^2/\Lambda^2)f_{\bar{d}WW}$ ) is constrained to the interval of  $(-0.11, 0.05)$  at 68% CL under the assumption of  $\bar{d} = \bar{d}_B$ .
- <sup>7</sup> KHACHATRYAN 16AB search for anomalous pseudoscalar couplings of the Higgs boson to  $W$  and  $Z$  with  $18.9 \text{ fb}^{-1}$  of  $pp$  collisions at  $E_{\text{cm}} = 8 \text{ TeV}$ . See their Table 5 and Figs 5 and 6 for limits on possible anomalous pseudoscalar coupling parameters.
- <sup>8</sup> AAD 15AX compare the  $J^{CP} = 0^+$  Standard Model assignment with other  $J^{CP}$  hypotheses in  $20.3 \text{ fb}^{-1}$  of  $pp$  collisions at  $E_{\text{cm}} = 8 \text{ TeV}$ , using the process  $H^0 \rightarrow WW^* \rightarrow e\nu\mu\nu$ .  $2^+$  hypotheses are excluded at 84.5–99.4%CL,  $0^-$  at 96.5%CL,  $0^+$  (field strength coupling) at 70.8%CL. See their Fig. 19 for limits on possible  $CP$  mixture parameters.
- <sup>9</sup> AAD 15CI compare the  $J^{CP} = 0^+$  Standard Model assignment with other  $J^{CP}$  hypotheses in  $4.5 \text{ fb}^{-1}$  of  $pp$  collisions at  $E_{\text{cm}} = 7 \text{ TeV}$  and  $20.3 \text{ fb}^{-1}$  at  $E_{\text{cm}} = 8 \text{ TeV}$ , using the processes  $H^0 \rightarrow ZZ^* \rightarrow 4\ell$ ,  $H^0 \rightarrow \gamma\gamma$  and combine with AAD 15AX data.  $0^+$  (field strength coupling),  $0^-$  and several  $2^+$  hypotheses are excluded at more than 99.9% CL. See their Tables 7–9 for limits on possible  $CP$  mixture parameters.
- <sup>10</sup> AALTONEN 15 combine AALTONEN 15B and ABAZOV 14F data. An upper limit of 0.36 of the Standard Model production rate at 95% CL is obtained both for a  $0^-$  and a  $2^+$  state. Assuming the SM event rate, the  $J^{CP} = 0^-$  ( $2^+$ ) hypothesis is excluded at the  $5.0\sigma$  ( $4.9\sigma$ ) level.
- <sup>11</sup> AALTONEN 15B compare the  $J^{CP} = 0^+$  Standard Model assignment with other  $J^{CP}$  hypotheses in  $9.45 \text{ fb}^{-1}$  of  $p\bar{p}$  collisions at  $E_{\text{cm}} = 1.96 \text{ TeV}$ , using the processes  $ZH^0 \rightarrow \ell\ell b\bar{b}$ ,  $WH^0 \rightarrow \ell\nu b\bar{b}$ , and  $ZH^0 \rightarrow \nu\nu b\bar{b}$ . Bounds on the production rates of  $0^-$  and  $2^+$  (graviton-like) states are set, see their tables II and III.
- <sup>12</sup> KHACHATRYAN 15Y compare the  $J^{CP} = 0^+$  Standard Model assignment with other  $J^{CP}$  hypotheses in up to  $5.1 \text{ fb}^{-1}$  of  $pp$  collisions at  $E_{\text{cm}} = 7 \text{ TeV}$  and up to  $19.7 \text{ fb}^{-1}$  at  $E_{\text{cm}} = 8 \text{ TeV}$ , using the processes  $H^0 \rightarrow 4\ell$ ,  $H^0 \rightarrow WW^*$ , and  $H^0 \rightarrow \gamma\gamma$ .  $0^-$  is excluded at 99.98% CL, and several  $2^+$  hypotheses are excluded at more than 99% CL. Spin 1 models are excluded at more than 99.999% CL in  $ZZ^*$  and  $WW^*$  modes. Limits on anomalous couplings and several cross section fractions, treating the case of  $CP$ -mixed states, are also given.
- <sup>13</sup> ABAZOV 14F compare the  $J^{CP} = 0^+$  Standard Model assignment with  $J^{CP} = 0^-$  and  $2^+$  (graviton-like coupling) hypotheses in up to  $9.7 \text{ fb}^{-1}$  of  $p\bar{p}$  collisions at  $E_{\text{cm}} = 1.96 \text{ TeV}$ . They use kinematic correlations between the decay products of the vector boson and the Higgs boson in the final states  $ZH \rightarrow \ell\ell b\bar{b}$ ,  $WH \rightarrow \ell\nu b\bar{b}$ , and  $ZH \rightarrow \nu\nu b\bar{b}$ . The  $0^-$  ( $2^+$ ) hypothesis is excluded at 97.6% CL (99.0% CL). In order to treat the case of a possible mixture of a  $0^+$  state with another  $J^{CP}$  state, the cross section fractions  $f_X = \sigma_X/(\sigma_{0^+} + \sigma_X)$  are considered, where  $X = 0^-, 2^+$ . Values for  $f_{0^-}$  ( $f_{2^+}$ ) above 0.80 (0.67) are excluded at 95% CL under the assumption that the total cross section is that of the SM Higgs boson.
- <sup>14</sup> CHATRCHYAN 14AA compare the  $J^{CP} = 0^+$  Standard Model assignment with various  $J^{CP}$  hypotheses in  $5.1 \text{ fb}^{-1}$  of  $pp$  collisions at  $E_{\text{cm}} = 7 \text{ TeV}$  and  $19.7 \text{ fb}^{-1}$  at  $E_{\text{cm}} = 8 \text{ TeV}$ .  $J^{CP} = 0^-$  and  $1^{\pm}$  hypotheses are excluded at 99% CL, and several  $J = 2$  hypotheses are excluded at 95% CL. In order to treat the case of a possible mixture of a  $0^+$  state with another  $J^{CP}$  state, the cross section fraction  $f_{a3} = |a_3|^2 \sigma_3 / (|a_1|^2 \sigma_1 + |a_2|^2 \sigma_2 + |a_3|^2 \sigma_3)$  is considered, where the case  $a_3 = 1$ ,  $a_1 = a_2 = 0$  corresponds to a pure  $CP$ -odd state. Assuming  $a_2 = 0$ , a value for  $f_{a3}$  above 0.51 is excluded at 95% CL.
- <sup>15</sup> CHATRCHYAN 14G compare the  $J^{CP} = 0^+$  Standard Model assignment with  $J^{CP} = 0^-$  and  $2^+$  (graviton-like coupling) hypotheses in  $4.9 \text{ fb}^{-1}$  of  $pp$  collisions at  $E_{\text{cm}} = 7 \text{ TeV}$  and  $19.4 \text{ fb}^{-1}$  at  $E_{\text{cm}} = 8 \text{ TeV}$ . Varying the fraction of the production of the  $2^+$  state via  $g\bar{g}$  and  $q\bar{q}$ ,  $2^+$  hypotheses are disfavored at CL between 83.7 and 99.8%. The  $0^-$  hypothesis is disfavored against  $0^+$  at the 65.3% CL.
- <sup>16</sup> KHACHATRYAN 14P compare the  $J^{CP} = 0^+$  Standard Model assignment with a  $2^+$  (graviton-like coupling) hypothesis in  $5.1 \text{ fb}^{-1}$  of  $pp$  collisions at  $E_{\text{cm}} = 7 \text{ TeV}$  and  $19.7 \text{ fb}^{-1}$  at  $E_{\text{cm}} = 8 \text{ TeV}$ . Varying the fraction of the production of the  $2^+$  state via  $g\bar{g}$  and  $q\bar{q}$ ,  $2^+$  hypotheses are disfavored at CL between 71 and 94%.
- <sup>17</sup> AAD 13AJ compare the spin 0,  $CP$ -even hypothesis with specific alternative hypotheses of spin 0,  $CP$ -odd, spin 1,  $CP$ -even and  $CP$ -odd, and spin 2,  $CP$ -even models using the

Higgs boson decays  $H \rightarrow \gamma\gamma$ ,  $H \rightarrow ZZ^* \rightarrow 4\ell$  and  $H \rightarrow WW^* \rightarrow \ell\nu\ell\nu$  and combinations thereof. The data are compatible with the spin 0,  $CP$ -even hypothesis, while all other tested hypotheses are excluded at confidence levels above 97.8%.

- <sup>18</sup> CHATRCHYAN 13J study angular distributions of the lepton pairs in the  $ZZ^*$  channel where both  $Z$  bosons decay to  $e$  or  $\mu$  pairs. Under the assumption that the observed particle has spin 0, the data are found to be consistent with the pure  $CP$ -even hypothesis, while the pure  $CP$ -odd hypothesis is disfavored.

## $H^0$ DECAY WIDTH

The total decay width for a light Higgs boson with a mass in the observed range is not expected to be directly observable at the LHC. For the case of the Standard Model the prediction for the total width is about 4 MeV, which is three orders of magnitude smaller than the experimental mass resolution. There is no indication from the results observed so far that the natural width is broadened by new physics effects to such an extent that it could be directly observable. Furthermore, as all LHC Higgs channels rely on the identification of Higgs decay products, the total Higgs width cannot be measured indirectly without additional assumptions. The different dependence of on-peak and off-peak contributions on the total width in Higgs decays to  $ZZ^*$  and interference effects between signal and background in Higgs decays to  $\gamma\gamma$  can provide additional information in this context. Constraints on the total width from the combination of on-peak and off-peak contributions in Higgs decays to  $ZZ^*$  rely on the assumption of equal on- and off-shell effective couplings. Without an experimental determination of the total width or further theoretical assumptions, only ratios of couplings can be determined at the LHC rather than absolute values of couplings.

VALUE (GeV)	CL%	DOCUMENT ID	TECN	COMMENT
<b>0.0032</b>	<b>0.0028</b>	1	SIRUNYAN 19BL CMS	$pp, 7, 8, 13 \text{ TeV}, ZZ^*/ZZ \rightarrow 4\ell$
<b>&lt;0.0144</b>	95	2	AABOUD 18BP ATLS	$pp, 13 \text{ TeV}, ZZ \rightarrow 4\ell, 2\ell 2\nu$
<b>&lt;1.10</b>	95	3	SIRUNYAN 17AV CMS	$pp, 13 \text{ TeV}, ZZ^* \rightarrow 4\ell$
<b>&lt;0.013</b>	95	4	KHACHATRYAN...16BA CMS	$pp, 7, 8 \text{ TeV}, ZZ^*, WW^*$
<b>&lt;1.7</b>	95	5	KHACHATRYAN...15AM CMS	$pp, 7, 8 \text{ TeV}$
<b>&gt; 3.5 × 10<sup>-12</sup></b>	95	6	KHACHATRYAN...15BA CMS	$pp, 7, 8 \text{ TeV}, \text{flight distance}$
<b>&lt;5.0</b>	95	7	AAD 14W ATLS	$pp, 7, 8 \text{ TeV}, \gamma\gamma$
<b>&lt;2.6</b>	95	7	AAD 14W ATLS	$pp, 7, 8 \text{ TeV}, ZZ^* \rightarrow 4\ell$
• • • We do not use the following data for averages, fits, limits, etc. • • •				
<0.026	95	8	KHACHATRYAN...16BA CMS	$pp, 7, 8 \text{ TeV}, WW^*$
<0.0227	95	9	AAD 15BE ATLS	$pp, 8 \text{ TeV}, ZZ^*, WW^*$
<0.046	95	10	KHACHATRYAN...15BA CMS	$pp, 7, 8 \text{ TeV}, ZZ^* \rightarrow 4\ell$
<3.4	95	11	CHATRCHYAN14AA CMS	$pp, 7, 8 \text{ TeV}, ZZ^* \rightarrow 4\ell$
<0.022	95	12	KHACHATRYAN...14D CMS	$pp, 7, 8 \text{ TeV}, ZZ^*$
<2.4	95	13	KHACHATRYAN...14P CMS	$pp, 7, 8 \text{ TeV}, \gamma\gamma$

- <sup>1</sup> SIRUNYAN 19BL measure the width and anomalous  $HVV$  couplings from on-shell and off-shell production in the  $4\ell$  final state. Data of  $80.2 \text{ fb}^{-1}$  at 13 TeV,  $19.7 \text{ fb}^{-1}$  at 8 TeV, and  $5.1 \text{ fb}^{-1}$  at 7 TeV are used. The total width for the SM-like couplings is measured to be also  $[0.08, 9.16]$  MeV with 95% CL, assuming SM-like couplings for on- and off-shells (see their Table VIII). Constraints on the total width for anomalous  $HVV$  interaction cases are found in their Table IX. See their Table X for the Higgs boson signal strength in the off-shell region.
- <sup>2</sup> AABOUD 18BP use  $36.1 \text{ fb}^{-1}$  at  $E_{\text{cm}} = 13 \text{ TeV}$ . An observed upper limit on the off-shell Higgs signal strength of 3.8 is obtained at 95% CL using off-shell Higgs boson production in the  $ZZ \rightarrow 4\ell$  and  $ZZ \rightarrow 2\ell 2\nu$  decay channels ( $\ell = e, \mu$ ). Combining with the on-shell signal strength measurements, the quoted upper limit on the Higgs boson total width is obtained, assuming the ratios of the relevant Higgs-boson couplings to the SM predictions are constant with energy from on-shell production to the high-mass range.
- <sup>3</sup> SIRUNYAN 17AV obtain an upper limit on the width from the  $m_{4\ell}$  distribution in  $ZZ^* \rightarrow 4\ell$  ( $\ell = e, \mu$ ) decays. Data of  $35.9 \text{ fb}^{-1}$   $pp$  collisions at  $E_{\text{cm}} = 13 \text{ TeV}$  is used. The expected limit is 1.60 GeV.
- <sup>4</sup> KHACHATRYAN 16BA combine the  $WW^*$  result with  $ZZ^*$  results of KHACHATRYAN 15BA and KHACHATRYAN 14D.
- <sup>5</sup> KHACHATRYAN 15AM combine  $\gamma\gamma$  and  $ZZ^* \rightarrow 4\ell$  results. The expected limit is 2.3 GeV.
- <sup>6</sup> KHACHATRYAN 15BA derive a lower limit on the total width from an upper limit on the decay flight distance  $\tau < 1.9 \times 10^{-13} \text{ s}$ .  $5.1 \text{ fb}^{-1}$  of  $pp$  collisions at  $E_{\text{cm}} = 7 \text{ TeV}$  and  $19.7 \text{ fb}^{-1}$  at  $E_{\text{cm}} = 8 \text{ TeV}$  are used.
- <sup>7</sup> AAD 14W use  $4.5 \text{ fb}^{-1}$  of  $pp$  collisions at  $E_{\text{cm}} = 7 \text{ TeV}$  and  $20.3 \text{ fb}^{-1}$  at 8 TeV. The expected limit is 6.2 GeV.
- <sup>8</sup> KHACHATRYAN 16BA derive constraints on the total width from comparing  $WW^*$  production via on-shell and off-shell  $H^0$  using  $4.9 \text{ fb}^{-1}$  of  $pp$  collisions at  $E_{\text{cm}} = 7 \text{ TeV}$  and  $19.4 \text{ fb}^{-1}$  at 8 TeV.
- <sup>9</sup> AAD 15BE derive constraints on the total width from comparing  $ZZ^*$  and  $WW^*$  production via on-shell and off-shell  $H^0$  using  $20.3 \text{ fb}^{-1}$  of  $pp$  collisions at  $E_{\text{cm}} = 8 \text{ TeV}$ . The K factor for the background processes is assumed to be equal to that for the signal.
- <sup>10</sup> KHACHATRYAN 15BA derive constraints on the total width from comparing  $ZZ^*$  production via on-shell and off-shell  $H^0$  with an unconstrained anomalous coupling.  $4\ell$  final states in  $5.1 \text{ fb}^{-1}$  of  $pp$  collisions at  $E_{\text{cm}} = 7 \text{ TeV}$  and  $19.7 \text{ fb}^{-1}$  at  $E_{\text{cm}} = 8 \text{ TeV}$  are used.
- <sup>11</sup> CHATRCHYAN 14AA use  $5.1 \text{ fb}^{-1}$  of  $pp$  collisions at  $E_{\text{cm}} = 7 \text{ TeV}$  and  $19.7 \text{ fb}^{-1}$  at  $E_{\text{cm}} = 8 \text{ TeV}$ . The expected limit is 2.8 GeV.
- <sup>12</sup> KHACHATRYAN 14D derive constraints on the total width from comparing  $ZZ^*$  production via on-shell and off-shell  $H^0$ .  $4\ell$  and  $\ell\nu\nu\ell$  final states in  $5.1 \text{ fb}^{-1}$  of  $pp$  collisions at  $E_{\text{cm}} = 7 \text{ TeV}$  and  $19.7 \text{ fb}^{-1}$  at  $E_{\text{cm}} = 8 \text{ TeV}$  are used.
- <sup>13</sup> KHACHATRYAN 14P use  $5.1 \text{ fb}^{-1}$  of  $pp$  collisions at  $E_{\text{cm}} = 7 \text{ TeV}$  and  $19.7 \text{ fb}^{-1}$  at  $E_{\text{cm}} = 8 \text{ TeV}$ . The expected limit is 3.1 GeV.

## Gauge &amp; Higgs Boson Particle Listings

 $H^0$  $H^0$  DECAY MODES

Mode	Fraction ( $\Gamma_i/\Gamma$ )	Confidence level
$\Gamma_1$ $W W^*$		
$\Gamma_2$ $Z Z^*$		
$\Gamma_3$ $\gamma\gamma$		
$\Gamma_4$ $b\bar{b}$		
$\Gamma_5$ $e^+e^-$	$<3.6 \times 10^{-4}$	95%
$\Gamma_6$ $\mu^+\mu^-$		
$\Gamma_7$ $\tau^+\tau^-$		
$\Gamma_8$ $Z\gamma$		
$\Gamma_9$ $\gamma^*\gamma$		
$\Gamma_{10}$ $J/\psi\gamma$	$<3.5 \times 10^{-4}$	95%
$\Gamma_{11}$ $J/\psi J/\psi$	$<1.8 \times 10^{-3}$	95%
$\Gamma_{12}$ $\psi(2S)\gamma$	$<2.0 \times 10^{-3}$	95%
$\Gamma_{13}$ $\Upsilon(1S)\gamma$	$<4.9 \times 10^{-4}$	95%
$\Gamma_{14}$ $\Upsilon(2S)\gamma$	$<5.9 \times 10^{-4}$	95%
$\Gamma_{15}$ $\Upsilon(3S)\gamma$	$<5.7 \times 10^{-4}$	95%
$\Gamma_{16}$ $\Upsilon(nS)\Upsilon(mS)$	$<1.4 \times 10^{-3}$	95%
$\Gamma_{17}$ $\rho(770)\gamma$	$<8.8 \times 10^{-4}$	95%
$\Gamma_{18}$ $\phi(1020)\gamma$	$<4.8 \times 10^{-4}$	95%
$\Gamma_{19}$ $e\mu$	LF $<6.1 \times 10^{-5}$	95%
$\Gamma_{20}$ $e\tau$	LF $<4.7 \times 10^{-3}$	95%
$\Gamma_{21}$ $\mu\tau$	LF $<2.5 \times 10^{-3}$	95%
$\Gamma_{22}$ invisible		
$\Gamma_{23}$ $\gamma$ invisible	$<4.6\%$	95%

 $H^0$  BRANCHING RATIOS $\Gamma(e^+e^-)/\Gamma_{\text{total}}$   $\Gamma_5/\Gamma$ 

VALUE	CL%	DOCUMENT ID	TECN	COMMENT
$<3.6 \times 10^{-4}$	95	<sup>1</sup> AAD	20F ATLS	$pp$ , 13 TeV
•••				We do not use the following data for averages, fits, limits, etc. •••
$<1.9 \times 10^{-3}$	95	<sup>2</sup> KHACHATRYAN...15H	CMS	$pp$ , 7, 8 TeV
<sup>1</sup> AAD 20F use 139 fb <sup>-1</sup> of $pp$ collisions at $E_{\text{cm}} = 13$ TeV. The best-fit value of the $H^0 \rightarrow ee$ branching fraction is $(0.0 \pm 1.7 \pm 0.6) \times 10^{-4}$ for $m_{H^0} = 125$ GeV.				
<sup>2</sup> KHACHATRYAN 15H use 5.0 fb <sup>-1</sup> of $pp$ collisions at $E_{\text{cm}} = 7$ TeV and 19.7 fb <sup>-1</sup> at 8 TeV.				

 $\Gamma(J/\psi\gamma)/\Gamma_{\text{total}}$   $\Gamma_{10}/\Gamma$ 

VALUE	CL%	DOCUMENT ID	TECN	COMMENT
$<7.6 \times 10^{-4}$	95	<sup>1</sup> SIRUNYAN	19AJ CMS	13 TeV, 35.9 fb <sup>-1</sup>
$<3.5 \times 10^{-4}$	95	<sup>2</sup> AABOUD	18BL ATLS	13 TeV, 36.1 fb <sup>-1</sup>
•••				We do not use the following data for averages, fits, limits, etc. •••
$<1.5 \times 10^{-3}$	95	<sup>3</sup> KHACHATRYAN...16B	CMS	8 TeV
$<1.5 \times 10^{-3}$	95	<sup>4</sup> AAD	15I ATLS	8 TeV
<sup>1</sup> SIRUNYAN 19AJ search for $H^0 \rightarrow J/\psi\gamma, J/\psi \rightarrow \mu^+\mu^-$ with 35.9 fb <sup>-1</sup> of $pp$ collision data at $E_{\text{cm}} = 13$ TeV. The upper limit corresponds to 260 times the SM prediction and by combining the KHACHATRYAN 16B, it is 220 times the SM prediction.				
<sup>2</sup> AABOUD 18BL search for $H^0 \rightarrow J/\psi\gamma, J/\psi \rightarrow \mu^+\mu^-$ with 36.1 fb <sup>-1</sup> of $pp$ collision data at $E_{\text{cm}} = 13$ TeV.				
<sup>3</sup> KHACHATRYAN 16B use 19.7 fb <sup>-1</sup> of $pp$ collision data at 8 TeV.				
<sup>4</sup> AAD 15I use 19.7 fb <sup>-1</sup> of $pp$ collision data at 8 TeV.				

 $\Gamma(J/\psi J/\psi)/\Gamma_{\text{total}}$   $\Gamma_{11}/\Gamma$ 

VALUE	CL%	DOCUMENT ID	TECN	COMMENT
$<1.8 \times 10^{-3}$	95	<sup>1</sup> SIRUNYAN	19BR CMS	$pp$ at 13 TeV
<sup>1</sup> SIRUNYAN 19BR search for $H^0 \rightarrow J/\psi J/\psi, J/\psi \rightarrow \mu^+\mu^-$ with 37.5 fb <sup>-1</sup> of $pp$ collision data at $E_{\text{cm}} = 13$ TeV. $J/\psi$ s from the Higgs decay are assumed to be unpolarized. For fully longitudinal (transverse) polarized $J/\psi$ s, limits change by $-22\%$ ( $+10\%$ ).				

 $\Gamma(\psi(2S)\gamma)/\Gamma_{\text{total}}$   $\Gamma_{12}/\Gamma$ 

VALUE	CL%	DOCUMENT ID	TECN	COMMENT
$<2.0 \times 10^{-3}$	95	<sup>1</sup> AABOUD	18BL ATLS	13 TeV, 36.1 fb <sup>-1</sup>
<sup>1</sup> AABOUD 18BL search for $H^0 \rightarrow \psi(2S)\gamma, \psi(2S) \rightarrow \mu^+\mu^-$ with 36.1 fb <sup>-1</sup> of $pp$ collision data at $E_{\text{cm}} = 13$ TeV.				

 $\Gamma(\Upsilon(1S)\gamma)/\Gamma_{\text{total}}$   $\Gamma_{13}/\Gamma$ 

VALUE	CL%	DOCUMENT ID	TECN	COMMENT
$<4.9 \times 10^{-4}$	95	<sup>1</sup> AABOUD	18BL ATLS	13 TeV, 36.1 fb <sup>-1</sup>
•••				We do not use the following data for averages, fits, limits, etc. •••
$<1.3 \times 10^{-3}$	95	<sup>2</sup> AAD	15I ATLS	8 TeV
<sup>1</sup> AABOUD 18BL search for $H^0 \rightarrow \Upsilon(1S)\gamma, \Upsilon(1S) \rightarrow \mu^+\mu^-$ with 36.1 fb <sup>-1</sup> of $pp$ collision data at $E_{\text{cm}} = 13$ TeV.				
<sup>2</sup> AAD 15I use 19.7 fb <sup>-1</sup> of $pp$ collision data at 8 TeV.				

 $\Gamma(\Upsilon(2S)\gamma)/\Gamma_{\text{total}}$   $\Gamma_{14}/\Gamma$ 

VALUE	CL%	DOCUMENT ID	TECN	COMMENT
$<5.9 \times 10^{-4}$	95	<sup>1</sup> AABOUD	18BL ATLS	13 TeV, 36.1 fb <sup>-1</sup>
•••				We do not use the following data for averages, fits, limits, etc. •••
$<1.9 \times 10^{-3}$	95	<sup>2</sup> AAD	15I ATLS	8 TeV
<sup>1</sup> AABOUD 18BL search for $H^0 \rightarrow \Upsilon(2S)\gamma, \Upsilon(2S) \rightarrow \mu^+\mu^-$ with 36.1 fb <sup>-1</sup> of $pp$ collision data at $E_{\text{cm}} = 13$ TeV.				
<sup>2</sup> AAD 15I use 19.7 fb <sup>-1</sup> of $pp$ collision data at 8 TeV.				

 $\Gamma(\Upsilon(3S)\gamma)/\Gamma_{\text{total}}$   $\Gamma_{15}/\Gamma$ 

VALUE	CL%	DOCUMENT ID	TECN	COMMENT
$<5.7 \times 10^{-4}$	95	<sup>1</sup> AABOUD	18BL ATLS	13 TeV, 36.1 fb <sup>-1</sup>
•••				We do not use the following data for averages, fits, limits, etc. •••
$<1.3 \times 10^{-3}$	95	<sup>2</sup> AAD	15I ATLS	8 TeV
<sup>1</sup> AABOUD 18BL search for $H^0 \rightarrow \Upsilon(3S)\gamma, \Upsilon(3S) \rightarrow \mu^+\mu^-$ with 36.1 fb <sup>-1</sup> of $pp$ collision data at $E_{\text{cm}} = 13$ TeV.				
<sup>2</sup> AAD 15I use 19.7 fb <sup>-1</sup> of $pp$ collision data at 8 TeV.				

 $\Gamma(\Upsilon(nS)\Upsilon(mS))/\Gamma_{\text{total}}$   $\Gamma_{16}/\Gamma$ 

VALUE	CL%	DOCUMENT ID	TECN	COMMENT
$<1.4 \times 10^{-3}$	95	<sup>1</sup> SIRUNYAN	19BR CMS	$pp$ at 13 TeV
<sup>1</sup> SIRUNYAN 19BR search for $H^0 \rightarrow \Upsilon(nS)\Upsilon(mS)$ with $\Upsilon(nS), \Upsilon(mS) \rightarrow \mu^+\mu^-$ ( $n, m = 1, 2, 3$ ) for 37.5 fb <sup>-1</sup> of $pp$ collision data at $E_{\text{cm}} = 13$ TeV. $\Upsilon$ s from the Higgs decay are assumed to be unpolarized. For fully longitudinal (transverse) polarized $\Upsilon$ s, limits change by $-22\%$ ( $+10\%$ ). The three $\Upsilon$ states selected in a mass range of 8.5–11 GeV are not distinguished.				

 $\Gamma(\rho(770)\gamma)/\Gamma_{\text{total}}$   $\Gamma_{17}/\Gamma$ 

VALUE	CL%	DOCUMENT ID	TECN	COMMENT
$<8.8 \times 10^{-4}$	95	<sup>1</sup> AABOUD	18AU ATLS	$pp$ , 13 TeV
<sup>1</sup> AABOUD 18AU use 35.6 fb <sup>-1</sup> of $pp$ collision data at 13 TeV.				

 $\Gamma(\phi(1020)\gamma)/\Gamma_{\text{total}}$   $\Gamma_{18}/\Gamma$ 

VALUE	CL%	DOCUMENT ID	TECN	COMMENT
$<4.8 \times 10^{-4}$	95	<sup>1</sup> AABOUD	18AU ATLS	$pp$ , 13 TeV
•••				We do not use the following data for averages, fits, limits, etc. •••
$<1.4 \times 10^{-3}$	95	<sup>2</sup> AABOUD	16K ATLS	$pp$ , 13 TeV
<sup>1</sup> AABOUD 18AU use 35.6 fb <sup>-1</sup> of $pp$ collision data at 13 TeV.				
<sup>2</sup> AABOUD 16K use 2.7 fb <sup>-1</sup> of $pp$ collision data at 13 TeV.				

 $\Gamma(e\mu)/\Gamma_{\text{total}}$   $\Gamma_{19}/\Gamma$ 

VALUE	CL%	DOCUMENT ID	TECN	COMMENT
$<6.1 \times 10^{-5}$	95	<sup>1</sup> AAD	20F ATLS	$pp$ , 13 TeV
•••				We do not use the following data for averages, fits, limits, etc. •••
$<3.5 \times 10^{-4}$	95	<sup>2</sup> KHACHATRYAN...16CD	CMS	$pp$ , 8 TeV
<sup>1</sup> AAD 20F use 139 fb <sup>-1</sup> of $pp$ collisions at $E_{\text{cm}} = 13$ TeV. The best-fit value of the $H^0 \rightarrow e\mu$ branching fraction is $(0.4 \pm 2.9 \pm 0.3) \times 10^{-5}$ for $m_{H^0} = 125$ GeV.				
<sup>2</sup> KHACHATRYAN 16CD search for $H^0 \rightarrow e\mu$ in 19.7 fb <sup>-1</sup> of $pp$ collisions at $E_{\text{cm}} = 8$ TeV. The limit constrains the $Y_{e\mu}$ Yukawa coupling to $\sqrt{ Y_{e\mu} ^2 +  Y_{\mu e} ^2} < 5.4 \times 10^{-4}$ at 95% CL (see their Fig. 6).				

 $\Gamma(e\tau)/\Gamma_{\text{total}}$   $\Gamma_{20}/\Gamma$ 

VALUE	CL%	DOCUMENT ID	TECN	COMMENT
$<4.7 \times 10^{-3}$	95	<sup>1</sup> AAD	20A ATLS	$pp$ , 13 TeV
•••				We do not use the following data for averages, fits, limits, etc. •••
$<6.1 \times 10^{-3}$	95	<sup>2</sup> SIRUNYAN	18BH CMS	$pp$ , 13 TeV
$<1.04 \times 10^{-2}$	95	<sup>3</sup> AAD	17 ATLS	$pp$ , 8 TeV
$<6.9 \times 10^{-3}$	95	<sup>4</sup> KHACHATRYAN...16CD	CMS	$pp$ , 8 TeV
<sup>1</sup> AAD 20A search for $H^0 \rightarrow e\tau$ in 36.1 fb <sup>-1</sup> of $pp$ collisions at $E_{\text{cm}} = 13$ TeV. The limit constrains the $Y_{e\tau}$ Yukawa coupling to $\sqrt{ Y_{e\tau} ^2 +  Y_{\tau e} ^2} < 2.0 \times 10^{-3}$ at 95% CL (see their Fig. 5).				
<sup>2</sup> SIRUNYAN 18BH search for $H^0 \rightarrow e\tau$ in 35.9 fb <sup>-1</sup> of $pp$ collisions at $E_{\text{cm}} = 13$ TeV. The limit constrains the $Y_{e\tau}$ Yukawa coupling to $\sqrt{ Y_{e\tau} ^2 +  Y_{\tau e} ^2} < 2.26 \times 10^{-3}$ at 95% CL (see their Fig. 10).				
<sup>3</sup> AAD 17 search for $H^0 \rightarrow e\tau$ in 20.3 fb <sup>-1</sup> of $pp$ collisions at $E_{\text{cm}} = 8$ TeV.				
<sup>4</sup> KHACHATRYAN 16CD search for $H^0 \rightarrow e\tau$ in 19.7 fb <sup>-1</sup> of $pp$ collisions at $E_{\text{cm}} = 8$ TeV. The limit constrains the $Y_{e\tau}$ Yukawa coupling to $\sqrt{ Y_{e\tau} ^2 +  Y_{\tau e} ^2} < 2.4 \times 10^{-3}$ at 95% CL (see their Fig. 6).				

 $\Gamma(\mu\tau)/\Gamma_{\text{total}}$   $\Gamma_{21}/\Gamma$ 

VALUE	CL%	DOCUMENT ID	TECN	COMMENT
$<2.5 \times 10^{-3}$	95	<sup>1</sup> SIRUNYAN	18BH CMS	$pp$ , 13 TeV
•••				We do not use the following data for averages, fits, limits, etc. •••
$<2.8 \times 10^{-3}$	95	<sup>2</sup> AAD	20A ATLS	$pp$ , 13 TeV
$<0.26$	95	<sup>3</sup> AAIJ	18AMLHCB	$pp$ , 8 TeV
$<1.43 \times 10^{-2}$	95	<sup>4</sup> AAD	17 ATLS	$pp$ , 8 TeV
$<1.51 \times 10^{-2}$	95	<sup>5</sup> KHACHATRYAN...15Q	CMS	$pp$ , 8 TeV

- 1 SIRUNYAN 18BH search for  $H^0 \rightarrow \mu\tau$  in 35.9 fb<sup>-1</sup> of  $pp$  collisions at  $E_{cm} = 13$  TeV. The limit constrains the  $Y_{\mu\tau}$  Yukawa coupling to  $\sqrt{|Y_{\mu\tau}|^2 + |Y_{\tau\mu}|^2} < 1.43 \times 10^{-3}$  at 95% CL (see their Fig. 10).
- 2 AAD 20A search for  $H^0 \rightarrow \mu\tau$  in 36.1 fb<sup>-1</sup> of  $pp$  collisions at  $E_{cm} = 13$  TeV. The limit constrains the  $Y_{\mu\tau}$  Yukawa coupling to  $\sqrt{|Y_{\mu\tau}|^2 + |Y_{\tau\mu}|^2} < 1.5 \times 10^{-3}$  at 95% CL (see their Fig. 5).
- 3 AAIJ 18AM search for  $H^0 \rightarrow \mu\tau$  in 2.0 fb<sup>-1</sup> of  $pp$  collisions at  $E_{cm} = 8$  TeV. The limit constrains the  $Y_{\mu\tau}$  Yukawa coupling to  $\sqrt{|Y_{\mu\tau}|^2 + |Y_{\tau\mu}|^2} < 1.7 \times 10^{-2}$  at 95% CL assuming SM production cross sections.
- 4 AAD 17 search for  $H^0 \rightarrow \mu\tau$  in 20.3 fb<sup>-1</sup> of  $pp$  collisions at  $E_{cm} = 8$  TeV.
- 5 KHACHATRYAN 15Q search for  $H^0 \rightarrow \mu\tau$  with  $\tau$  decaying electronically or hadronically in 19.7 fb<sup>-1</sup> of  $pp$  collisions at  $E_{cm} = 8$  TeV. The fit gives  $B(H^0 \rightarrow \mu\tau) = (0.84_{-0.39}^{+0.37})\%$  with a significance of 2.4  $\sigma$ .

$\Gamma(\text{invisible})/\Gamma_{\text{total}}$		$\Gamma_{22}/\Gamma$			
VALUE	CL%	DOCUMENT ID	TECN	COMMENT	
<0.26	95	1 AABOUD	19AL ATLS	$pp, 7, 8, 13$ TeV, $H \rightarrow \text{inv}$	
<0.19	95	2 SIRUNYAN	19Bo CMS	$pp, 7, 8, 13$ TeV	
• • • We do not use the following data for averages, fits, limits, etc. • • •					
<0.37	95	3 AABOUD	19AI ATLS	$pp \rightarrow qqH^0X, H^0 \rightarrow \text{inv}, 13$ TeV	
<0.38	95	4 AABOUD	19AL ATLS	$pp, 13$ TeV, $H \rightarrow \text{inv}$	
<0.22	95	5 SIRUNYAN	19AT CMS	$pp, 13$ TeV, $H \rightarrow \text{inv}$	
<0.33	95	6 SIRUNYAN	19Bo CMS	$pp \rightarrow qqH^0X, H^0 \rightarrow \text{inv}, 13$ TeV	
<0.26	95	7 SIRUNYAN	19Bo CMS	$pp, 13$ TeV	
<0.67	95	8 AABOUD	18 ATLS	$pp \rightarrow H^0ZX, H^0 \rightarrow \text{inv}, 13$ TeV	
<0.83	95	9 AABOUD	18CA ATLS	$pp \rightarrow H^0W/Z, W/Z \rightarrow jj, 13$ TeV	
<0.40	95	10 SIRUNYAN	18BV CMS	$pp \rightarrow Z(\ell\ell)H^0, H^0 \rightarrow \text{inv}, 13$ TeV	
<0.53	95	11 SIRUNYAN	18s CMS	$pp, 13$ TeV, jet or $V(\rightarrow q\bar{q}), H^0 \rightarrow \text{inv}$	
<0.46	95	12 AABOUD	17BD ATLS	$pp \rightarrow gH^0X, qqH^0X, H^0 \rightarrow \text{inv}, 13$ TeV	
<0.24	95	13 KHACHATRY..17F	CMS	$pp, 7, 8, 13$ TeV	
<0.28	95	14 AAD	16AF ATLS	$pp \rightarrow qqH^0X, 8$ TeV	
<0.34	95	15 AAD	16AN LHC	$pp, 7, 8$ TeV	
<0.78	95	16 AAD	15BD ATLS	$pp \rightarrow H^0W/ZX, 8$ TeV	
<0.25	95	17 AAD	15CX ATLS	$pp, 7, 8$ TeV, $H \rightarrow \text{inv}$	
<0.75	95	18 AAD	14O ATLS	$pp \rightarrow H^0ZX, 7, 8$ TeV	
<0.58	95	19 CHATRCHYAN14B	CMS	$pp \rightarrow H^0ZX, qqH^0X$	
<0.81	95	20 CHATRCHYAN14B	CMS	$pp \rightarrow H^0ZX, 7, 8$ TeV	
<0.65	95	21 CHATRCHYAN14B	CMS	$pp \rightarrow qqH^0X, 8$ TeV	

- 1 AABOUD 19AL combine results of 7, 8 (AAD 15CX), and 13 TeV for  $H^0$  decaying to invisible final states.
- 2 SIRUNYAN 19Bo combine 13 TeV 35.9 fb<sup>-1</sup> results with 7, 8, 13 TeV (KHACHATRYAN 17F) for  $H^0$  decaying to invisible final states. The quoted limit on the branching ratio is given for  $m_{H^0} = 125.09$  GeV and assumes the Standard Model production rates. The branching ratio is obtained to be  $0.05 \pm 0.03$  (stat)  $\pm 0.07$  (syst).
- 3 AABOUD 19AI search for  $pp \rightarrow qqH^0X$  (VBF) with  $H^0$  decaying to invisible final states using 36.1 fb<sup>-1</sup> of data. The quoted limit on the branching ratio is given for  $m_{H^0} = 125$  GeV and assumes the Standard Model rates for VBF and gluon-fusion production.
- 4 AABOUD 19AL combine results of  $H^0$  decaying to invisible final states with VBF(AABOUD 19AI),  $ZH$ , and  $WH$  productions (AABOUD 18, AABOUD 18CA), which use 36.1 fb<sup>-1</sup> of data at 13 TeV. The quoted limit is given for  $m_{H^0} = 125$  GeV and assumes the Standard Model rates for gluon fusion, VBF,  $ZH$ , and  $WH$  productions.
- 5 SIRUNYAN 19AT perform a combined fit with visible decay using 35.9 fb<sup>-1</sup> of data at 13 TeV.
- 6 SIRUNYAN 19Bo search for  $pp \rightarrow qqH^0X$  (VBF) with  $H^0$  decaying to invisible final states using 35.9 fb<sup>-1</sup> of data. The quoted limit on the branching ratio is given for  $m_{H^0} = 125.09$  GeV and assumes the Standard Model production rates.
- 7 SIRUNYAN 19Bo combine the VBF channel with results of other 13 TeV analyses: SIRUNYAN 18BV and SIRUNYAN 18s. The quoted limit on the branching ratio is given for  $m_{H^0} = 125.09$  GeV and assumes the Standard Model production rates.
- 8 AABOUD 18 search for  $pp \rightarrow H^0ZX, Z \rightarrow ee, \mu\mu$  with  $H^0$  decaying to invisible final states in 36.1 fb<sup>-1</sup> at  $E_{cm} = 13$  TeV. The quoted limit on the branching ratio is given for  $m_{H^0} = 125$  GeV and assumes the Standard Model rate for  $H^0Z$  production.
- 9 AABOUD 18CA search for  $H^0$  decaying to invisible final states using  $WH, ZH$  and  $ZH$  productions, where  $W$  and  $Z$  hadronically decay. The data of 36.1 fb<sup>-1</sup> at  $E_{cm} = 13$  TeV is used. The quoted limit assumes SM production cross sections with combining the contributions from  $WH, ZH, ggF$  and VBF production modes.
- 10 SIRUNYAN 18BV search for  $H^0$  decaying to invisible final states associated with a  $Z, Z \rightarrow \ell\ell$  using 35.9 fb<sup>-1</sup> at 13 TeV. The limit is obtained for  $m_{H^0} = 125$  GeV and assuming the SM  $ZH^0$  production cross section.
- 11 SIRUNYAN 18s search for  $H^0$  decaying to invisible final states associated with an energetic jet or a  $V, V \rightarrow q\bar{q}$  using 35.9 fb<sup>-1</sup> at 13 TeV.
- 12 AABOUD 17BD search for  $H^0$  decaying to invisible final states with  $\geq 1$  jet and VBF events using 3.2 fb<sup>-1</sup> of  $pp$  collisions at  $E_{cm} = 13$  TeV. A cross-section ratio  $R^{\text{miss}}$  is used in the measurement. The quoted limit is given for  $m_{H^0} = 125$  GeV.
- 13 KHACHATRYAN 17F search for  $H^0$  decaying to invisible final states with gluon fusion, VBF,  $ZH$ , and  $WH$  productions using 2.3 fb<sup>-1</sup> of  $pp$  collisions at  $E_{cm} = 13$  TeV, 19.7 fb<sup>-1</sup> at 8 TeV, and 5.1 fb<sup>-1</sup> at 7 TeV. The quoted limit is given for  $m_{H^0} =$

- 125 GeV and assumes the Standard Model rates for gluon fusion, VBF,  $ZH$ , and  $WH$  productions.
- 14 AAD 16AF search for  $pp \rightarrow qqH^0X$  (VBF) with  $H^0$  decaying to invisible final states in 20.3 fb<sup>-1</sup> at  $E_{cm} = 8$  TeV. The quoted limit on the branching ratio is given for  $m_{H^0} = 125$  GeV and assumes the Standard Model rates for VBF and gluon-fusion production.
- 15 AAD 16AN perform fits to the ATLAS and CMS data at  $E_{cm} = 7$  and 8 TeV. The branching fraction of decays into BSM particles that are invisible or into undetected decay modes is measured for  $m_{H^0} = 125.09$  GeV.
- 16 AAD 15BD search for  $pp \rightarrow H^0WX$  and  $pp \rightarrow H^0ZX$  with  $W$  or  $Z$  decaying hadronically and  $H^0$  decaying to invisible final states using data at  $E_{cm} = 8$  TeV. The quoted limit is given for  $m_{H^0} = 125$  GeV, assumes the Standard Model rates for the production processes and is based on a combination of the contributions from  $H^0W, H^0Z$  and the gluon-fusion process.
- 17 AAD 15CX search for  $H^0$  decaying to invisible final states with VBF,  $ZH$ , and  $WH$  productions using 20.3 fb<sup>-1</sup> at 8 TeV, and 4.7 fb<sup>-1</sup> at 7 TeV. The quoted limit is given for  $m_{H^0} = 125.36$  GeV and assumes the Standard Model rates for gluon fusion, VBF,  $ZH$ , and  $WH$  productions. The upper limit is improved to 0.23 by adding the measured visible decay rates.
- 18 AAD 14O search for  $pp \rightarrow H^0ZX, Z \rightarrow \ell\ell$ , with  $H^0$  decaying to invisible final states in 4.5 fb<sup>-1</sup> at  $E_{cm} = 7$  TeV and 20.3 fb<sup>-1</sup> at  $E_{cm} = 8$  TeV. The quoted limit on the branching ratio is given for  $m_{H^0} = 125.5$  GeV and assumes the Standard Model rate for  $H^0Z$  production.
- 19 CHATRCHYAN 14B search for  $pp \rightarrow H^0ZX, Z \rightarrow \ell\ell$  and  $Z \rightarrow b\bar{b}$ , and also  $pp \rightarrow qqH^0X$  with  $H^0$  decaying to invisible final states using data at  $E_{cm} = 7$  and 8 TeV. The quoted limit on the branching ratio is obtained from a combination of the limits from  $H^0Z$  and  $qqH^0X$ . It is given for  $m_{H^0} = 125$  GeV and assumes the Standard Model rates for the two production processes.
- 20 CHATRCHYAN 14B search for  $pp \rightarrow H^0ZX$  with  $H^0$  decaying to invisible final states and  $Z \rightarrow \ell\ell$  in 4.9 fb<sup>-1</sup> at  $E_{cm} = 7$  TeV and 19.7 fb<sup>-1</sup> at  $E_{cm} = 8$  TeV, and also with  $Z \rightarrow b\bar{b}$  in 18.9 fb<sup>-1</sup> at  $E_{cm} = 8$  TeV. The quoted limit on the branching ratio is given for  $m_{H^0} = 125$  GeV and assumes the Standard Model rate for  $H^0Z$  production.
- 21 CHATRCHYAN 14B search for  $pp \rightarrow qqH^0X$  (vector boson fusion) with  $H^0$  decaying to invisible final states in 19.5 fb<sup>-1</sup> at  $E_{cm} = 8$  TeV. The quoted limit on the branching ratio is given for  $m_{H^0} = 125$  GeV and assumes the Standard Model rate for  $qqH^0X$  production.

$\Gamma(\gamma\text{invisible})/\Gamma_{\text{total}}$		$\Gamma_{23}/\Gamma$			
VALUE	CL%	DOCUMENT ID	TECN	COMMENT	
<0.046	95	1 SIRUNYAN	19CG CMS	$pp \rightarrow H^0Z, H^0 \rightarrow \gamma\text{invisible}, Z \rightarrow \ell\ell, 13$ TeV	
1 SIRUNYAN 19CG search for $pp \rightarrow H^0Z, Z \rightarrow ee, \mu\mu$ with $H^0$ decaying to invisible final states plus a $\gamma$ in 137 fb <sup>-1</sup> at $E_{cm} = 13$ TeV. The quoted limit on the branching ratio is given for $m_{H^0} = 125$ GeV assuming the Standard Model rate for $H^0Z$ production and is obtained in the context of a theoretical model, where the undetected (invisible) is massless.					

**$H^0$  SIGNAL STRENGTHS IN DIFFERENT CHANNELS**

The  $H^0$  signal strength in a particular final state  $xx$  is given by the cross section times branching ratio in this channel normalized to the Standard Model (SM) value,  $\sigma \cdot B(H^0 \rightarrow xx) / (\sigma \cdot B(H^0 \rightarrow xx))_{\text{SM}}$ , for the specified mass value of  $H^0$ . For the SM predictions, see DITTMAYER 11, DITTMAYER 12, and HEINEMEYER 13A. Results for fiducial and differential cross sections are also listed below.

Combined Final States		DOCUMENT ID	TECN	COMMENT
<b>1.13 ± 0.06 OUR AVERAGE</b>				
1.11 +0.09 -0.08		1 AAD	20 ATLS	$pp, 13$ TeV
1.17 ± 0.10		2 SIRUNYAN	19AT CMS	$pp, 13$ TeV
1.09 ± 0.07 ± 0.04 ± 0.03 +0.07 -0.06		3,4 AAD	16AN LHC	$pp, 7, 8$ TeV
1.44 +0.59 -0.56		5 AALTONEN	13M TEVA	$p\bar{p} \rightarrow H^0X, 1.96$ TeV
• • • We do not use the following data for averages, fits, limits, etc. • • •				
1.20 ± 0.10 ± 0.06 ± 0.04 +0.08 -0.07		4 AAD	16AN ATLS	$pp, 7, 8$ TeV
0.97 ± 0.09 ± 0.05 +0.04 +0.07 -0.03 -0.06		4 AAD	16AN CMS	$pp, 7, 8$ TeV
1.18 ± 0.10 ± 0.07 +0.08 -0.07		7 AAD	16K ATLS	$pp, 7, 8$ TeV
0.75 +0.28 +0.13 +0.08 -0.26 -0.11 -0.05		7 AAD	16K ATLS	$pp, 7$ TeV
1.28 ± 0.11 ± 0.08 +0.10 -0.07 -0.08		7 AAD	16K ATLS	$pp, 8$ TeV
		8 AAD	15P ATLS	$pp, 8$ TeV, cross section
1.00 ± 0.09 ± 0.07 +0.08 -0.07		9 KHACHATRY...15AM	CMS	$pp, 7, 8$ TeV
1.33 +0.14 -0.10 ± 0.15		10 AAD	13AK ATLS	$pp, 7$ and 8 TeV
1.54 +0.77 -0.73		11 AALTONEN	13L CDF	$p\bar{p} \rightarrow H^0X, 1.96$ TeV
1.40 +0.92 -0.88		12 ABAZOV	13L D0	$p\bar{p} \rightarrow H^0X, 1.96$ TeV
1.4 ± 0.3		13 AAD	12AI ATLS	$pp \rightarrow H^0X, 7, 8$ TeV
1.2 ± 0.4		13 AAD	12AI ATLS	$pp \rightarrow H^0X, 7$ TeV
1.5 ± 0.4		13 AAD	12AI ATLS	$pp \rightarrow H^0X, 8$ TeV
0.87 ± 0.23		14 CHATRCHYAN12N	CMS	$pp \rightarrow H^0X, 7, 8$ TeV



## Gauge &amp; Higgs Boson Particle Listings

 $H^0$ 

- <sup>1</sup> AAD 20 combine results of up to  $79.8 \text{ fb}^{-1}$  of data at  $E_{\text{cm}} = 13 \text{ TeV}$ , assuming  $m_{H^0} = 125.09 \text{ GeV}$ :  $\gamma\gamma$ ,  $ZZ^*$ ,  $WW^*$ ,  $\tau\tau$ ,  $b\bar{b}$ ,  $\mu\mu$ , invisible, and off-shell analyses (see their Table I). The signal strengths for individual production processes are  $1.04 \pm 0.09$  for gluon fusion,  $1.21^{+0.24}_{-0.22}$  for vector boson fusion,  $1.30^{+0.40}_{-0.38}$  for  $WH^0$  production,  $1.05^{+0.31}_{-0.29}$  for  $ZH^0$  production, and  $1.21^{+0.26}_{-0.24}$  for  $t\bar{t}H^0 + tH^0$  production (see their Fig. 2 and Table IV). Several results with the simplified template cross section and  $\kappa$ -frameworks are presented: see their Figs. 9–11, Figs 20, 21 and Table VIII for stage-1 simplified template cross sections, their Figs. 12–17 and Tables X–XII for the  $\kappa$ -framework.
- <sup>2</sup> SIRUNYAN 19AT combine results of  $35.9 \text{ fb}^{-1}$  of data at  $E_{\text{cm}} = 13 \text{ TeV}$ , assuming  $m_{H^0} = 125.09 \text{ GeV}$ . The signal strengths for individual production processes are  $1.22^{+0.14}_{-0.12}$  for gluon fusion,  $0.73^{+0.30}_{-0.27}$  for vector boson fusion,  $2.18^{+0.58}_{-0.55}$  for  $WH^0$  production,  $0.87^{+0.44}_{-0.42}$  for  $ZH^0$  production, and  $1.18^{+0.30}_{-0.27}$  for  $t\bar{t}H^0$  production. Several results with the simplified template cross section and  $\kappa$ -frameworks are presented: see their Fig. 8 and Table 5 for stage-0 simplified template cross sections, their Figs. 9–18 and Tables 7–11 for the  $\kappa$ -framework.
- <sup>3</sup> AAD 16AN perform fits to the ATLAS and CMS data at  $E_{\text{cm}} = 7$  and  $8 \text{ TeV}$ . The signal strengths for individual production processes are  $1.03^{+0.16}_{-0.14}$  for gluon fusion,  $1.18^{+0.25}_{-0.23}$  for vector boson fusion,  $0.89^{+0.40}_{-0.38}$  for  $WH^0$  production,  $0.79^{+0.38}_{-0.36}$  for  $ZH^0$  production, and  $2.3^{+0.7}_{-0.6}$  for  $t\bar{t}H^0$  production.
- <sup>4</sup> AAD 16AN: The uncertainties represent statistics, experimental systematics, theory systematics on the background, and theory systematics on the signal. The quoted signal strengths are given for  $m_{H^0} = 125.09 \text{ GeV}$ . In the fit, relative branching ratios and relative production cross sections are fixed to those in the Standard Model.
- <sup>5</sup> AALTONEN 13M combine all Tevatron data from the CDF and D0 Collaborations with up to  $10.0 \text{ fb}^{-1}$  and  $9.7 \text{ fb}^{-1}$ , respectively, of  $p\bar{p}$  collisions at  $E_{\text{cm}} = 1.96 \text{ TeV}$ . The quoted signal strength is given for  $m_{H^0} = 125 \text{ GeV}$ .
- <sup>6</sup> SIRUNYAN 19BA measure differential cross sections for the Higgs boson transverse momentum, the number of jets, the rapidity of the Higgs boson and the transverse momentum of the leading jet using  $35.9 \text{ fb}^{-1}$  of data at  $E_{\text{cm}} = 13 \text{ TeV}$  with  $H^0 \rightarrow \gamma\gamma$ ,  $H^0 \rightarrow ZZ^*$ , and  $H^0 \rightarrow b\bar{b}$ . The total cross section for Higgs boson production is measured to be  $61.1 \pm 6.0 \pm 3.7 \text{ pb}$  using  $H^0 \rightarrow \gamma\gamma$  and  $H^0 \rightarrow ZZ^*$  channels. Several coupling measurements in the  $\kappa$ -framework are performed.
- <sup>7</sup> AAD 16K use up to  $4.7 \text{ fb}^{-1}$  of  $pp$  collisions at  $E_{\text{cm}} = 7 \text{ TeV}$  and up to  $20.3 \text{ fb}^{-1}$  at  $E_{\text{cm}} = 8 \text{ TeV}$ . The third uncertainty in the measurement is theory systematics. The signal strengths for individual production modes are  $1.23 \pm 0.14^{+0.09}_{-0.08}$  for gluon fusion,  $1.23^{+0.28}_{-0.27} + 0.13^{+0.11}_{-0.09}$  for vector boson fusion,  $0.80^{+0.31}_{-0.30} \pm 0.17^{+0.10}_{-0.05}$  for  $W/ZH^0$  production, and  $1.81^{+0.52}_{-0.50} + 0.58^{+0.31}_{-0.55} - 0.12^{+0.12}_{-0.05}$  for  $t\bar{t}H^0$  production. The quoted signal strengths are given for  $m_{H^0} = 125.36 \text{ GeV}$ .
- <sup>8</sup> AAD 15P measure total and differential cross sections of the process  $pp \rightarrow H^0 X$  at  $E_{\text{cm}} = 8 \text{ TeV}$  with  $20.3 \text{ fb}^{-1}$ .  $\gamma\gamma$  and  $4\ell$  final states are used.  $\sigma(pp \rightarrow H^0 X) = 33.0 \pm 5.3 \pm 1.6 \text{ pb}$  is given. See their Figs. 2 and 3 for data on differential cross sections.
- <sup>9</sup> KHACHATRYAN 15AM use up to  $5.1 \text{ fb}^{-1}$  of  $pp$  collisions at  $E_{\text{cm}} = 7 \text{ TeV}$  and up to  $19.7 \text{ fb}^{-1}$  at  $E_{\text{cm}} = 8 \text{ TeV}$ . The third uncertainty in the measurement is theory systematics. Fits to each production mode give the value of  $0.85^{+0.19}_{-0.16}$  for gluon fusion,  $1.16^{+0.37}_{-0.34}$  for vector boson fusion,  $0.92^{+0.38}_{-0.36}$  for  $WH^0$ ,  $ZH^0$  production, and  $2.90^{+1.08}_{-0.94}$  for  $t\bar{t}H^0$  production.
- <sup>10</sup> AAD 13AK use  $4.7 \text{ fb}^{-1}$  of  $pp$  collisions at  $E_{\text{cm}} = 7 \text{ TeV}$  and  $20.7 \text{ fb}^{-1}$  at  $E_{\text{cm}} = 8 \text{ TeV}$ . The combined signal strength is based on the  $\gamma\gamma$ ,  $ZZ^* \rightarrow 4\ell$ , and  $WW^* \rightarrow \ell\nu\ell\nu$  channels. The quoted signal strength is given for  $m_{H^0} = 125.5 \text{ GeV}$ . Reported statistical error value modified following private communication with the experiment.
- <sup>11</sup> AALTONEN 13L combine all CDF results with  $9.45\text{--}10.0 \text{ fb}^{-1}$  of  $p\bar{p}$  collisions at  $E_{\text{cm}} = 1.96 \text{ TeV}$ . The quoted signal strength is given for  $m_{H^0} = 125 \text{ GeV}$ .
- <sup>12</sup> ABAZOV 13L combine all D0 results with up to  $9.7 \text{ fb}^{-1}$  of  $p\bar{p}$  collisions at  $E_{\text{cm}} = 1.96 \text{ TeV}$ . The quoted signal strength is given for  $m_{H^0} = 125 \text{ GeV}$ .
- <sup>13</sup> AAD 12AI obtain results based on  $4.6\text{--}4.8 \text{ fb}^{-1}$  of  $pp$  collisions at  $E_{\text{cm}} = 7 \text{ TeV}$  and  $5.8\text{--}5.9 \text{ fb}^{-1}$  at  $E_{\text{cm}} = 8 \text{ TeV}$ . An excess of events over background with a local significance of  $5.9 \sigma$  is observed at  $m_{H^0} = 126 \text{ GeV}$ . The quoted signal strengths are given for  $m_{H^0} = 126 \text{ GeV}$ . See also AAD 12DA.
- <sup>14</sup> CHATRCHYAN 12N obtain results based on  $4.9\text{--}5.1 \text{ fb}^{-1}$  of  $pp$  collisions at  $E_{\text{cm}} = 7 \text{ TeV}$  and  $5.1\text{--}5.3 \text{ fb}^{-1}$  at  $E_{\text{cm}} = 8 \text{ TeV}$ . An excess of events over background with a local significance of  $5.0 \sigma$  is observed at about  $m_{H^0} = 125 \text{ GeV}$ . The combined signal strength is based on the  $\gamma\gamma$ ,  $ZZ^*$ ,  $WW^*$ ,  $\tau^+\tau^-$ , and  $b\bar{b}$  channels. The quoted signal strength is given for  $m_{H^0} = 125.5 \text{ GeV}$ . See also CHATRCHYAN 13Y.

**WW\* Final State**

VALUE	DOCUMENT ID	TECN	COMMENT
<b>1.19±0.12 OUR AVERAGE</b>			
$1.28^{+0.17}_{-0.16}$	1	SIRUNYAN 19AT CMS	$pp$ , 13 TeV
$1.09^{+0.18}_{-0.16}$	2,3	AAD 16AN LHC	$pp$ , 7, 8 TeV
$0.94^{+0.85}_{-0.83}$	4	AALTONEN 13M TEVA	$p\bar{p} \rightarrow H^0 X$ , 1.96 TeV
••• We do not use the following data for averages, fits, limits, etc. •••			
	5	AABOUD 19F ATLS	$pp$ , 13 TeV, cross sections
$2.5^{+0.9}_{-0.8}$	6	AAD 19A ATLS	$pp \rightarrow H^0 W/H^0 Z$ , $H^0 \rightarrow WW^*$ , 13 TeV

$1.28^{+0.18}_{-0.17}$	7	SIRUNYAN 19AX CMS	$pp$ , 13 TeV
$1.22^{+0.23}_{-0.21}$	3	AAD 16AN ATLS	$pp$ , 7, 8 TeV
$0.90^{+0.23}_{-0.21}$	3	AAD 16AN CMS	$pp$ , 7, 8 TeV
	8	AAD 16AO ATLS	$pp$ , 8 TeV, cross sections
$1.18 \pm 0.16^{+0.17}_{-0.14}$	9	AAD 16K ATLS	$pp$ , 7, 8 TeV
$1.09^{+0.16}_{-0.15} + 0.17^{+0.17}_{-0.14}$	10	AAD 15AA ATLS	$pp$ , 7, 8 TeV
$3.0^{+1.3}_{-1.1} + 1.0^{+1.0}_{-0.7}$	11	AAD 15AQ ATLS	$pp \rightarrow H^0 W/ZX$ , 7, 8 TeV
$1.16^{+0.16}_{-0.15} + 0.18^{+0.18}_{-0.15}$	12	AAD 15AQ ATLS	$pp$ , 7, 8 TeV
$0.72 \pm 0.12 \pm 0.10^{+0.12}_{-0.10}$	13	CHATRCHYAN 14G CMS	$pp$ , 7, 8 TeV
$0.99^{+0.31}_{-0.28}$	14	AAD 13AK ATLS	$pp$ , 7 and 8 TeV
$0.00^{+1.78}_{-0.00}$	15	AALTONEN 13L CDF	$p\bar{p} \rightarrow H^0 X$ , 1.96 TeV
$1.90^{+1.63}_{-1.52}$	16	ABAZOV 13L D0	$p\bar{p} \rightarrow H^0 X$ , 1.96 TeV
$1.3 \pm 0.5$	17	AAD 12AI ATLS	$pp \rightarrow H^0 X$ , 7, 8 TeV
$0.5 \pm 0.6$	17	AAD 12AI ATLS	$pp \rightarrow H^0 X$ , 7 TeV
$1.9 \pm 0.7$	17	AAD 12AI ATLS	$pp \rightarrow H^0 X$ , 8 TeV
$0.60^{+0.42}_{-0.37}$	18	CHATRCHYAN 12N CMS	$pp \rightarrow H^0 X$ , 7, 8 TeV

- <sup>1</sup> SIRUNYAN 19AT perform a combine fit to  $35.9 \text{ fb}^{-1}$  of data at  $E_{\text{cm}} = 13 \text{ TeV}$ .
- <sup>2</sup> AAD 16AN perform fits to the ATLAS and CMS data at  $E_{\text{cm}} = 7$  and  $8 \text{ TeV}$ . The signal strengths for individual production processes are  $0.84 \pm 0.17$  for gluon fusion,  $1.2 \pm 0.4$  for vector boson fusion,  $1.6^{+1.2}_{-1.0}$  for  $WH^0$  production,  $5.9^{+2.8}_{-2.2}$  for  $ZH^0$  production, and  $5.0^{+1.8}_{-1.7}$  for  $t\bar{t}H^0$  production.
- <sup>3</sup> AAD 16AN: In the fit, relative production cross sections are fixed to those in the Standard Model. The quoted signal strength is given for  $m_{H^0} = 125.09 \text{ GeV}$ .
- <sup>4</sup> AALTONEN 13M combine all Tevatron data from the CDF and D0 Collaborations with up to  $10.0 \text{ fb}^{-1}$  and  $9.7 \text{ fb}^{-1}$ , respectively, of  $p\bar{p}$  collisions at  $E_{\text{cm}} = 1.96 \text{ TeV}$ . The quoted signal strength is given for  $m_{H^0} = 125 \text{ GeV}$ .
- <sup>5</sup> AABOUD 19F measure cross-sections times the  $H^0 \rightarrow WW^*$  branching fraction in the  $H^0 \rightarrow WW^* \rightarrow e\nu\mu\nu$  channel using  $36.1 \text{ fb}^{-1}$  of  $pp$  collisions at  $E_{\text{cm}} = 13 \text{ TeV}$ :  $\sigma_{ggF} \times B(H^0 \rightarrow WW^*) = 11.4^{+1.2}_{-1.1} + 1.8^{+1.8}_{-1.7} \text{ pb}$  and  $\sigma_{VBF} \times B(H^0 \rightarrow WW^*) = 0.50^{+0.24}_{-0.22} \pm 0.17 \text{ pb}$ .
- <sup>6</sup> AAD 19A use  $36.1 \text{ fb}^{-1}$  data at  $13 \text{ TeV}$ . The cross section times branching fraction values are measured to be  $0.67^{+0.31}_{-0.27} + 0.18^{+0.18}_{-0.14} \text{ pb}$  for  $WH^0$ ,  $H^0 \rightarrow WW^*$  and  $0.54^{+0.31}_{-0.24} + 0.15^{+0.15}_{-0.07} \text{ pb}$  for  $ZH^0$ ,  $H^0 \rightarrow WW^*$ .
- <sup>7</sup> SIRUNYAN 19AX measure the signal strengths, cross sections and so on using gluon fusion, VBF and  $VH^0$  production processes with  $35.9 \text{ fb}^{-1}$  of data. The quoted signal strength is given for  $m_{H^0} = 125.09 \text{ GeV}$ . Signal strengths for each production process is found in their Fig. 9. Measured cross sections and ratios to the SM predictions in the stage-0 simplified template cross section framework are shown in their Fig. 10.  $\kappa_F = 1.52^{+0.48}_{-0.41}$  and  $\kappa_V = 1.10 \pm 0.08$  are obtained (see their Fig. 11 (right)).
- <sup>8</sup> AAD 16AO measure fiducial total and differential cross sections of gluon fusion process at  $E_{\text{cm}} = 8 \text{ TeV}$  with  $20.3 \text{ fb}^{-1}$  using  $H^0 \rightarrow WW^* \rightarrow e\nu\mu\nu$ . The measured fiducial total cross section is  $36.0 \pm 9.7 \text{ fb}$  in their fiducial region (Table 7). See their Fig. 6 for fiducial differential cross sections. The results are given for  $m_{H^0} = 125 \text{ GeV}$ .
- <sup>9</sup> AAD 16K use up to  $4.7 \text{ fb}^{-1}$  of  $pp$  collisions at  $E_{\text{cm}} = 7 \text{ TeV}$  and up to  $20.3 \text{ fb}^{-1}$  at  $E_{\text{cm}} = 8 \text{ TeV}$ . The quoted signal strength is given for  $m_{H^0} = 125.36 \text{ GeV}$ .
- <sup>10</sup> AAD 15AA use  $4.5 \text{ fb}^{-1}$  of  $pp$  collisions at  $E_{\text{cm}} = 7 \text{ TeV}$  and  $20.3 \text{ fb}^{-1}$  at  $E_{\text{cm}} = 8 \text{ TeV}$ . The signal strength for the gluon fusion and vector boson fusion mode is  $1.02 \pm 0.19^{+0.22}_{-0.18}$  and  $1.27^{+0.44}_{-0.40} + 0.30^{+0.30}_{-0.21}$ , respectively. The quoted signal strengths are given for  $m_{H^0} = 125.36 \text{ GeV}$ .
- <sup>11</sup> AAD 15AQ use  $4.5 \text{ fb}^{-1}$  of  $pp$  collisions at  $E_{\text{cm}} = 7 \text{ TeV}$  and  $20.3 \text{ fb}^{-1}$  at  $E_{\text{cm}} = 8 \text{ TeV}$ . The quoted signal strength is given for  $m_{H^0} = 125.36 \text{ GeV}$ .
- <sup>12</sup> AAD 15AQ combine their result on  $W/ZH^0$  production with the results of AAD 15AA (gluon fusion and vector boson fusion, slightly updated). The quoted signal strength is given for  $m_{H^0} = 125.36 \text{ GeV}$ .
- <sup>13</sup> CHATRCHYAN 14G use  $4.9 \text{ fb}^{-1}$  of  $pp$  collisions at  $E_{\text{cm}} = 7 \text{ TeV}$  and  $19.4 \text{ fb}^{-1}$  at  $E_{\text{cm}} = 8 \text{ TeV}$ . The last uncertainty in the measurement is theory systematics. The quoted signal strength is given for  $m_{H^0} = 125.6 \text{ GeV}$ .
- <sup>14</sup> AAD 13AK use  $4.7 \text{ fb}^{-1}$  of  $pp$  collisions at  $E_{\text{cm}} = 7 \text{ TeV}$  and  $20.7 \text{ fb}^{-1}$  at  $E_{\text{cm}} = 8 \text{ TeV}$ . The quoted signal strength is given for  $m_{H^0} = 125.5 \text{ GeV}$ . Superseded by AAD 15AA.
- <sup>15</sup> AALTONEN 13L combine all CDF results with  $9.45\text{--}10.0 \text{ fb}^{-1}$  of  $p\bar{p}$  collisions at  $E_{\text{cm}} = 1.96 \text{ TeV}$ . The quoted signal strength is given for  $m_{H^0} = 125 \text{ GeV}$ .
- <sup>16</sup> ABAZOV 13L combine all D0 results with up to  $9.7 \text{ fb}^{-1}$  of  $p\bar{p}$  collisions at  $E_{\text{cm}} = 1.96 \text{ TeV}$ . The quoted signal strength is given for  $m_{H^0} = 125 \text{ GeV}$ .
- <sup>17</sup> AAD 12AI obtain results based on  $4.7 \text{ fb}^{-1}$  of  $pp$  collisions at  $E_{\text{cm}} = 7 \text{ TeV}$  and  $5.8 \text{ fb}^{-1}$  at  $E_{\text{cm}} = 8 \text{ TeV}$ . The quoted signal strengths are given for  $m_{H^0} = 126 \text{ GeV}$ . See also AAD 12DA.
- <sup>18</sup> CHATRCHYAN 12N obtain results based on  $4.9 \text{ fb}^{-1}$  of  $pp$  collisions at  $E_{\text{cm}} = 7 \text{ TeV}$  and  $5.1 \text{ fb}^{-1}$  at  $E_{\text{cm}} = 8 \text{ TeV}$ . The quoted signal strength is given for  $m_{H^0} = 125.5 \text{ GeV}$ . See also CHATRCHYAN 13Y.

**Z Z\* Final State**

VALUE	CL%	DOCUMENT ID	TECN	COMMENT
<b>1.20<sup>+0.12</sup><sub>-0.11</sub></b>		<b>OUR AVERAGE</b>		
1.06 <sup>+0.19</sup> <sub>-0.17</sub>		1 SIRUNYAN	19AT CMS	$pp$ , 13 TeV
1.28 <sup>+0.21</sup> <sub>-0.19</sub>		2 AABOUD	18AJ ATLS	$pp$ , 13 TeV
1.29 <sup>+0.26</sup> <sub>-0.23</sub>		3,4 AAD	16AN LHC	$pp$ , 7, 8 TeV
• • • We do not use the following data for averages, fits, limits, etc. • • •				
<6.5	95	5 AABOUD	19N ATLS	$pp$ , 13 TeV, off-shell
<3.8	95	6 AABOUD	18BP ATLS	$pp$ , 13 TeV, off-shell
1.05 <sup>+0.15+0.11</sup> <sub>-0.14-0.09</sub>		7 SIRUNYAN	17AV CMS	$pp$ , 13 TeV
1.52 <sup>+0.40</sup> <sub>-0.34</sub>		4 AAD	16AN ATLS	$pp$ , 7, 8 TeV
1.04 <sup>+0.32</sup> <sub>-0.26</sub>		4 AAD	16AN CMS	$pp$ , 7, 8 TeV
1.46 <sup>+0.35+0.19</sup> <sub>-0.31-0.13</sub>		8 AAD	16K ATLS	$pp$ , 7, 8 TeV
		9 KHACHATRYAN	16AR CMS	$pp$ , 7, 8 TeV cross sections
1.44 <sup>+0.34+0.21</sup> <sub>-0.31-0.11</sub>		10 AAD	15F ATLS	$pp \rightarrow H^0 X$ , 7, 8 TeV
		11 AAD	14AR ATLS	$pp$ , 8 TeV, differential cross section
0.93 <sup>+0.26+0.13</sup> <sub>-0.23-0.09</sub>		12 CHATRCHYAN	14AA CMS	$pp$ , 7, 8 TeV
1.43 <sup>+0.40</sup> <sub>-0.35</sub>		13 AAD	13AK ATLS	$pp$ , 7 and 8 TeV
0.80 <sup>+0.35</sup> <sub>-0.28</sub>		14 CHATRCHYAN	13J CMS	$pp \rightarrow H^0 X$ , 7, 8 TeV
1.2 $\pm$ 0.6		15 AAD	12AI ATLS	$pp \rightarrow H^0 X$ , 7, 8 TeV
1.4 $\pm$ 1.1		15 AAD	12AI ATLS	$pp \rightarrow H^0 X$ , 7 TeV
1.1 $\pm$ 0.8		15 AAD	12AI ATLS	$pp \rightarrow H^0 X$ , 8 TeV
0.73 <sup>+0.45</sup> <sub>-0.33</sub>		16 CHATRCHYAN	12N CMS	$pp \rightarrow H^0 X$ , 7, 8 TeV

- 1 SIRUNYAN 19AT perform a combine fit to 35.9 fb<sup>-1</sup> of data at  $E_{cm} = 13$  TeV.
- 2 AABOUD 18AJ perform analyses using  $H^0 \rightarrow ZZ^* \rightarrow 4\ell$  ( $\ell = e, \mu$ ) with data of 36.1 fb<sup>-1</sup> at  $E_{cm} = 13$  TeV. Results are given for  $m_{H^0} = 125.09$  GeV. The inclusive cross section times branching ratio for  $H^0 \rightarrow ZZ^*$  decay ( $|\eta(H^0)| < 2.5$ ) is measured to be  $1.73^{+0.26}_{-0.24}$  pb (with  $1.34^{+0.09}_{-0.09}$  pb expected in the SM).
- 3 AAD 16AN perform fits to the ATLAS and CMS data at  $E_{cm} = 7$  and 8 TeV. The signal strengths for individual production processes are  $1.13^{+0.34}_{-0.31}$  for gluon fusion and  $0.1^{+1.1}_{-0.6}$  for vector boson fusion.
- 4 AAD 16AN: In the fit, relative production cross sections are fixed to those in the Standard Model. The quoted signal strength is given for  $m_{H^0} = 125.09$  GeV.
- 5 AABOUD 19N measure the spectrum of the four-lepton invariant mass  $m_{4\ell}$  ( $\ell = e$  or  $\mu$ ) using 36.1 fb<sup>-1</sup> of data at  $E_{cm} = 13$  TeV. The quoted signal strength upper limit is obtained from 180 GeV <  $m_{4\ell}$  < 1200 GeV.
- 6 AABOUD 18BP measure an off-shell Higgs boson production using  $ZZ \rightarrow 4\ell$  and  $ZZ \rightarrow 2\ell 2\nu$  ( $\ell = e, \mu$ ) decay channels with 36.1 fb<sup>-1</sup> of data at  $E_{cm} = 13$  TeV. The quoted signal strength upper limit is obtained from a combination of these two channels, where 220 GeV <  $m_{4\ell}$  < 2000 GeV for  $ZZ \rightarrow 4\ell$  and 250 GeV <  $m_{\ell\ell}^{ZZ} < 2000$  GeV for  $ZZ \rightarrow 2\ell 2\nu$  ( $m_{\ell\ell}^{ZZ}$  is defined in their Section 5). See their Table 2 for each measurement.
- 7 SIRUNYAN 17AV use 35.9 fb<sup>-1</sup> of  $pp$  collisions at  $E_{cm} = 13$  TeV. The quoted signal strength, obtained from the analysis of  $H^0 \rightarrow ZZ^* \rightarrow 4\ell$  ( $\ell = e, \mu$ ) decays, is given for  $m_{H^0} = 125.09$  GeV. The signal strengths for different production modes are given in their Table 3. The fiducial and differential cross sections are shown in their Fig. 10.
- 8 AAD 16K use up to 4.7 fb<sup>-1</sup> of  $pp$  collisions at  $E_{cm} = 7$  TeV and up to 20.3 fb<sup>-1</sup> at  $E_{cm} = 8$  TeV. The quoted signal strength is given for  $m_{H^0} = 125.36$  GeV.
- 9 KHACHATRYAN 16AR use data of 5.1 fb<sup>-1</sup> at  $E_{cm} = 7$  TeV and 19.7 fb<sup>-1</sup> at 8 TeV. The fiducial cross sections for the production of 4 leptons via  $H^0 \rightarrow 4\ell$  decays are measured to be  $0.56^{+0.67+0.21}_{-0.44-0.06}$  fb at 7 TeV and  $1.11^{+0.41+0.14}_{-0.35-0.10}$  fb at 8 TeV in their fiducial region (Table 2). The differential cross sections at  $E_{cm} = 8$  TeV are also shown in Figs. 4 and 5. The results are given for  $m_{H^0} = 125$  GeV.
- 10 AAD 15F use 4.5 fb<sup>-1</sup> of  $pp$  collisions at  $E_{cm} = 7$  TeV and 20.3 fb<sup>-1</sup> at  $E_{cm} = 8$  TeV. The quoted signal strength is given for  $m_{H^0} = 125.36$  GeV. The signal strength for the gluon fusion production mode is  $1.66^{+0.45+0.25}_{-0.41-0.15}$ , while the signal strength for the vector boson fusion production mode is  $0.26^{+1.60+0.36}_{-0.91-0.23}$ .
- 11 AAD 14AR measure the cross section for  $pp \rightarrow H^0 X$ ,  $H^0 \rightarrow ZZ^*$  using 20.3 fb<sup>-1</sup> at  $E_{cm} = 8$  TeV. They give  $\sigma \cdot B = 2.11^{+0.53}_{-0.47} \pm 0.08$  fb in their fiducial region, where  $1.30 \pm 0.13$  fb is expected in the Standard Model for  $m_{H^0} = 125.4$  GeV. Various differential cross sections are also given, which are in agreement with the Standard Model expectations.
- 12 CHATRCHYAN 14AA use 5.1 fb<sup>-1</sup> of  $pp$  collisions at  $E_{cm} = 7$  TeV and 19.7 fb<sup>-1</sup> at  $E_{cm} = 8$  TeV. The quoted signal strength is given for  $m_{H^0} = 125.6$  GeV. The signal strength for the gluon fusion and  $t\bar{t}H$  production mode is  $0.80^{+0.46}_{-0.36}$ , while the signal strength for the vector boson fusion and  $WH^0$ ,  $ZH^0$  production mode is  $1.7^{+2.2}_{-2.1}$ .
- 13 AAD 13AK use 4.7 fb<sup>-1</sup> of  $pp$  collisions at  $E_{cm} = 7$  TeV and 20.7 fb<sup>-1</sup> at  $E_{cm} = 8$  TeV. The quoted signal strength is given for  $m_{H^0} = 125.5$  GeV.
- 14 CHATRCHYAN 13J obtain results based on  $ZZ \rightarrow 4\ell$  final states in 5.1 fb<sup>-1</sup> of  $pp$  collisions at  $E_{cm} = 7$  TeV and 12.2 fb<sup>-1</sup> at  $E_{cm} = 8$  TeV. The quoted signal strength is given for  $m_{H^0} = 125.8$  GeV. Superseded by CHATRCHYAN 14AA.

- 15 AAD 12AI obtain results based on 4.7–4.8 fb<sup>-1</sup> of  $pp$  collisions at  $E_{cm} = 7$  TeV and 5.8 fb<sup>-1</sup> at  $E_{cm} = 8$  TeV. The quoted signal strengths are given for  $m_{H^0} = 126$  GeV. See also AAD 12DA.

- 16 CHATRCHYAN 12N obtain results based on 4.9–5.1 fb<sup>-1</sup> of  $pp$  collisions at  $E_{cm} = 7$  TeV and 5.1–5.3 fb<sup>-1</sup> at  $E_{cm} = 8$  TeV. An excess of events over background with a local significance of 5.0  $\sigma$  is observed at about  $m_{H^0} = 125$  GeV. The quoted signal strengths are given for  $m_{H^0} = 125.5$  GeV. See also CHATRCHYAN 12BY and CHATRCHYAN 13Y.

 **$\gamma\gamma$  Final State**

VALUE	DOCUMENT ID	TECN	COMMENT
<b>1.11<sup>+0.10</sup><sub>-0.09</sub></b>	<b>OUR AVERAGE</b>		
1.20 <sup>+0.18</sup> <sub>-0.14</sub>	1 SIRUNYAN	19AT CMS	$pp$ , 13 TeV
0.99 <sup>+0.15</sup> <sub>-0.14</sub>	2 AABOUD	18BO ATLS	$pp$ , 13 TeV, 36.1 fb <sup>-1</sup>
1.14 <sup>+0.19</sup> <sub>-0.18</sub>	3,4 AAD	16AN LHC	$pp$ , 7, 8 TeV
5.97 <sup>+3.39</sup> <sub>-3.12</sub>	5 AALTONEN	13M TEVA	$p\bar{p} \rightarrow H^0 X$ , 1.96 TeV
• • • We do not use the following data for averages, fits, limits, etc. • • •			
1.18 <sup>+0.17</sup> <sub>-0.14</sub>	6 SIRUNYAN	19L CMS	$pp$ , 13 TeV, diff. x-section
	7 SIRUNYAN	18DS CMS	$pp$ , $H^0 \rightarrow \gamma\gamma$ , 13 TeV, floated $m_{H^0}$
1.14 <sup>+0.27</sup> <sub>-0.25</sub>	4 AAD	16AN ATLS	$pp$ , 7, 8 TeV
1.11 <sup>+0.25</sup> <sub>-0.23</sub>	4 AAD	16AN CMS	$pp$ , 7, 8 TeV
	8 KHACHATRYAN	16G CMS	$pp$ , 8 TeV, diff. x-section
1.17 $\pm$ 0.23 <sup>+0.10+0.12</sup> <sub>-0.08-0.08</sub>	9 AAD	14BC ATLS	$pp \rightarrow H^0 X$ , 7, 8 TeV
	10 AAD	14BJ ATLS	$pp$ , 8 TeV, diff. x-section
1.14 $\pm$ 0.21 <sup>+0.09+0.13</sup> <sub>-0.05-0.09</sub>	11 KHACHATRYAN	14P CMS	$pp$ , 7, 8 TeV
1.55 <sup>+0.33</sup> <sub>-0.28</sub>	12 AAD	13AK ATLS	$pp$ , 7 and 8 TeV
7.81 <sup>+4.61</sup> <sub>-4.42</sub>	13 AALTONEN	13L CDF	$p\bar{p} \rightarrow H^0 X$ , 1.96 TeV
4.20 <sup>+4.60</sup> <sub>-4.20</sub>	14 ABAZOV	13L D0	$p\bar{p} \rightarrow H^0 X$ , 1.96 TeV
1.8 $\pm$ 0.5	15 AAD	12AI ATLS	$pp \rightarrow H^0 X$ , 7, 8 TeV
2.2 $\pm$ 0.7	15 AAD	12AI ATLS	$pp \rightarrow H^0 X$ , 7 TeV
1.5 $\pm$ 0.6	15 AAD	12AI ATLS	$pp \rightarrow H^0 X$ , 8 TeV
1.54 <sup>+0.46</sup> <sub>-0.42</sub>	16 CHATRCHYAN	12N CMS	$pp \rightarrow H^0 X$ , 7, 8 TeV

- 1 SIRUNYAN 19AT perform a combine fit to 35.9 fb<sup>-1</sup> of data at  $E_{cm} = 13$  TeV.
- 2 AABOUD 18BO use 36.1 fb<sup>-1</sup> of  $pp$  collisions at  $E_{cm} = 13$  TeV. The signal strengths for the individual production modes are:  $0.81^{+0.19}_{-0.18}$  for gluon fusion,  $2.0^{+0.6}_{-0.5}$  for vector boson fusion,  $0.7^{+0.9}_{-0.8}$  for  $VH^0$  production ( $V = W, Z$ ), and  $0.5 \pm 0.6$  for  $t\bar{t}H^0$  and  $tH^0$  production. Other measurements of cross sections and couplings are summarized in their Section 10. The quoted values are given for  $m_{H^0} = 125.09$  GeV.
- 3 AAD 16AN perform fits to the ATLAS and CMS data at  $E_{cm} = 7$  and 8 TeV. The signal strengths for individual production processes are  $1.10^{+0.23}_{-0.22}$  for gluon fusion,  $1.3 \pm 0.5$  for vector boson fusion,  $0.5^{+1.3}_{-1.2}$  for  $WH^0$  production,  $0.5^{+3.0}_{-2.5}$  for  $ZH^0$  production, and  $2.2^{+1.6}_{-1.3}$  for  $t\bar{t}H^0$  production.
- 4 AAD 16AN: In the fit, relative production cross sections are fixed to those in the Standard Model. The quoted signal strength is given for  $m_{H^0} = 125.09$  GeV.
- 5 AALTONEN 13M combine all Tevatron data from the CDF and D0 Collaborations with up to 10.0 fb<sup>-1</sup> and 9.7 fb<sup>-1</sup>, respectively, of  $p\bar{p}$  collisions at  $E_{cm} = 1.96$  TeV. The quoted signal strength is given for  $m_{H^0} = 125$  GeV.
- 6 SIRUNYAN 19L measure fiducial and differential cross sections of the process  $pp \rightarrow H^0 \rightarrow \gamma\gamma$  at  $E_{cm} = 13$  TeV with 35.9 fb<sup>-1</sup>. See their Figs. 4–11.
- 7 SIRUNYAN 18DS use 35.9 fb<sup>-1</sup> of  $pp \rightarrow H^0$  collisions with  $H^0 \rightarrow \gamma\gamma$  at  $E_{cm} = 13$  TeV. The Higgs mass is floated in the measurement of a signal strength. The result is  $1.18^{+0.12}_{-0.11}$  (stat.)  $\pm 0.09$  (syst.)  $\pm 0.07$  (theory), which is largely insensitive to the Higgs mass around 125 GeV.
- 8 KHACHATRYAN 16G measure fiducial and differential cross sections of the process  $pp \rightarrow H^0 X$ ,  $H^0 \rightarrow \gamma\gamma$  at  $E_{cm} = 8$  TeV with 19.7 fb<sup>-1</sup>. See their Figs. 4–6 and Table 1 for data.
- 9 AAD 14BC use 4.5 fb<sup>-1</sup> of  $pp$  collisions at  $E_{cm} = 7$  TeV and 20.3 fb<sup>-1</sup> at  $E_{cm} = 8$  TeV. The last uncertainty in the measurement is theory systematics. The quoted signal strength is given for  $m_{H^0} = 125.4$  GeV. The signal strengths for the individual production modes are:  $1.32 \pm 0.38$  for gluon fusion,  $0.8 \pm 0.7$  for vector boson fusion,  $1.0 \pm 1.6$  for  $WH^0$  production,  $0.1^{+3.7}_{-0.1}$  for  $ZH^0$  production, and  $1.6^{+2.7}_{-1.8}$  for  $t\bar{t}H^0$  production.
- 10 AAD 14BJ measure fiducial and differential cross sections of the process  $pp \rightarrow H^0 X$ ,  $H^0 \rightarrow \gamma\gamma$  at  $E_{cm} = 8$  TeV with 20.3 fb<sup>-1</sup>. See their Table 3 and Figs. 3–12 for data.
- 11 KHACHATRYAN 14P use 5.1 fb<sup>-1</sup> of  $pp$  collisions at  $E_{cm} = 7$  TeV and 19.7 fb<sup>-1</sup> at  $E_{cm} = 8$  TeV. The last uncertainty in the measurement is theory systematics. The quoted signal strength is given for  $m_{H^0} = 124.7$  GeV. The signal strength for the gluon fusion and  $t\bar{t}H$  production mode is  $1.13^{+0.37}_{-0.31}$ , while the signal strength for the vector boson fusion and  $WH^0$ ,  $ZH^0$  production mode is  $1.16^{+0.63}_{-0.58}$ .
- 12 AAD 13AK use 4.7 fb<sup>-1</sup> of  $pp$  collisions at  $E_{cm} = 7$  TeV and 20.7 fb<sup>-1</sup> at  $E_{cm} = 8$  TeV. The quoted signal strength is given for  $m_{H^0} = 125.5$  GeV.
- 13 AALTONEN 13L combine all CDF results with 9.45–10.0 fb<sup>-1</sup> of  $p\bar{p}$  collisions at  $E_{cm} = 1.96$  TeV. The quoted signal strength is given for  $m_{H^0} = 125$  GeV.

## Gauge &amp; Higgs Boson Particle Listings

 $H^0$ 

- <sup>14</sup> ABAZOV 13L combine all D0 results with up to  $9.7 \text{ fb}^{-1}$  of  $p\bar{p}$  collisions at  $E_{\text{cm}} = 1.96 \text{ TeV}$ . The quoted signal strength is given for  $m_{H^0} = 125 \text{ GeV}$ .
- <sup>15</sup> AAD 12A1 obtain results based on  $4.8 \text{ fb}^{-1}$  of  $pp$  collisions at  $E_{\text{cm}} = 7 \text{ TeV}$  and  $5.9 \text{ fb}^{-1}$  at  $E_{\text{cm}} = 8 \text{ TeV}$ . The quoted signal strengths are given for  $m_{H^0} = 126 \text{ GeV}$ . See also AAD 12DA.
- <sup>16</sup> CHATRCHYAN 12N obtain results based on  $5.1 \text{ fb}^{-1}$  of  $pp$  collisions at  $E_{\text{cm}} = 7 \text{ TeV}$  and  $5.3 \text{ fb}^{-1}$  at  $E_{\text{cm}} = 8 \text{ TeV}$ . The quoted signal strength is given for  $m_{H^0} = 125.5 \text{ GeV}$ . See also CHATRCHYAN 13Y.

 $c\bar{c}$  Final State

VALUE	CL%	DOCUMENT ID	TECN	COMMENT
<b>&lt;110</b>	95	<sup>1</sup> AABOUD	18M ATLS	$pp$ , 13 TeV

- <sup>1</sup> AABOUD 18M use  $36.1 \text{ fb}^{-1}$  at of  $pp$  collisions at  $E_{\text{cm}} = 13 \text{ TeV}$ . The upper limit on  $\sigma(pp \rightarrow ZH^0) \cdot B(H^0 \rightarrow c\bar{c})$  is  $2.7 \text{ pb}$  at 95% CL. The quoted values are given for  $m_{H^0} = 125 \text{ GeV}$ .

 $b\bar{b}$  Final State

VALUE	DOCUMENT ID	TECN	COMMENT
<b>1.04 ± 0.13 OUR AVERAGE</b>			
$1.12 \pm 0.29$	<sup>1</sup> SIRUNYAN	19AT CMS	$pp$ , 13 TeV
$1.16^{+0.27}_{-0.25}$	<sup>2</sup> AABOUD	18BN ATLS	$pp \rightarrow H^0 W/H^0 Z, H^0 \rightarrow b\bar{b}$ , 13 TeV, 79.8 $\text{fb}^{-1}$
$1.06 \pm 0.26$	<sup>3</sup> SIRUNYAN	18DB CMS	$pp \rightarrow H^0 W/H^0 Z, H^0 \rightarrow b\bar{b}$ , 13 TeV, 77.2 $\text{fb}^{-1}$
$0.70^{+0.29}_{-0.27}$	<sup>4,5</sup> AAD	16AN LHC	$pp$ , 7, 8 TeV
$1.59^{+0.69}_{-0.72}$	<sup>6</sup> AALTONEN	13M TEVA	$p\bar{p} \rightarrow H^0 X$ , 1.96 TeV
$0.98^{+0.22}_{-0.21}$	<sup>7</sup> AABOUD	19U ATLS	$pp \rightarrow VH^0, H^0 \rightarrow b\bar{b}$ , 13 TeV, cross sections
$1.01 \pm 0.20$	<sup>8</sup> AABOUD	18BN ATLS	$pp \rightarrow H^0 W/H^0 Z, H^0 \rightarrow b\bar{b}$ , 7, 8, 13 TeV
$2.5^{+1.4}_{-1.3}$	<sup>9,10,11</sup> AABOUD	18BN ATLS	$pp \rightarrow H^0 X, \text{ggF}, VBF, VH^0, t\bar{t}H^0$ , 7, 8, 13 TeV
$3.0^{+1.7}_{-1.6}$	<sup>10,12</sup> AABOUD	18BQ ATLS	$pp \rightarrow H^0 X, VBF$ , 13 TeV
$1.19^{+0.40}_{-0.38}$	<sup>13</sup> AALTONEN	18C CDF	$p\bar{p} \rightarrow H^0 X$ , 1.96 TeV
$1.06^{+0.31}_{-0.29}$	<sup>14</sup> SIRUNYAN	18AE CMS	$pp \rightarrow H^0 W/H^0 Z, H^0 \rightarrow b\bar{b}$ , 13 TeV
$1.01 \pm 0.22$	<sup>15</sup> SIRUNYAN	18AE CMS	$pp \rightarrow H^0 W/H^0 Z, H^0 \rightarrow b\bar{b}$ , 7, 8, 13 TeV
$1.04 \pm 0.20$	<sup>16</sup> SIRUNYAN	18DB CMS	$pp \rightarrow H^0 W/H^0 Z, H^0 \rightarrow b\bar{b}$ , 7, 8, 13 TeV
$2.3^{+1.8}_{-1.6}$	<sup>17</sup> SIRUNYAN	18DB CMS	$pp \rightarrow H^0 X, \text{ggF}, VBF, VH^0, t\bar{t}H^0$ , 7, 8, 13 TeV
$1.20^{+0.24+0.34}_{-0.23-0.28}$	<sup>18</sup> SIRUNYAN	18E CMS	$pp \rightarrow H^0 X$ , boosted, 13 TeV
$0.90 \pm 0.18^{+0.21}_{-0.19}$	<sup>19</sup> AABOUD	17BA ATLS	$pp \rightarrow H^0 W/ZX, H^0 \rightarrow b\bar{b}$ , 13 TeV, 36.1 $\text{fb}^{-1}$
$-0.8 \pm 1.3^{+1.8}_{-1.9}$	<sup>20</sup> AABOUD	17BA ATLS	$pp \rightarrow H^0 W/ZX, H^0 \rightarrow b\bar{b}$ , 7, 8, 13 TeV
$0.62 \pm 0.37$	<sup>21</sup> AABOUD	16X ATLS	$pp \rightarrow H^0 X, VBF$ , 8 TeV
$0.81^{+0.45}_{-0.43}$	<sup>5</sup> AAD	16AN ATLS	$pp$ , 7, 8 TeV
$0.63^{+0.31+0.24}_{-0.30-0.23}$	<sup>5</sup> AAD	16AN CMS	$pp$ , 7, 8 TeV
$0.52 \pm 0.32 \pm 0.24$	<sup>22</sup> AAD	16K ATLS	$pp$ , 7, 8 TeV
$2.8^{+1.6}_{-1.4}$	<sup>23</sup> AAD	15G ATLS	$pp \rightarrow H^0 W/ZX$ , 7, 8 TeV
$1.03^{+0.44}_{-0.42}$	<sup>24</sup> KHACHATRYAN..15Z	CMS	$pp \rightarrow H^0 X, VBF$ , 8 TeV
$1.0 \pm 0.5$	<sup>25</sup> KHACHATRYAN..15Z	CMS	$pp$ , 8 TeV, combined
$1.72^{+0.92}_{-0.87}$	<sup>26</sup> CHATRCHYAN14A1	CMS	$pp \rightarrow H^0 W/ZX$ , 7, 8 TeV
$1.23^{+1.24}_{-1.17}$	<sup>27</sup> AALTONEN	13L CDF	$p\bar{p} \rightarrow H^0 X$ , 1.96 TeV
$0.5 \pm 2.2$	<sup>28</sup> ABAZOV	13L D0	$p\bar{p} \rightarrow H^0 X$ , 1.96 TeV
$0.48^{+0.81}_{-0.70}$	<sup>29</sup> AAD	12A1 ATLS	$pp \rightarrow H^0 W/ZX$ , 7 TeV
	<sup>30</sup> AALTONEN	12T TEVA	$p\bar{p} \rightarrow H^0 W/ZX$ , 1.96 TeV
	<sup>31</sup> CHATRCHYAN12N	CMS	$pp \rightarrow H^0 W/ZX$ , 7, 8 TeV

- <sup>1</sup> SIRUNYAN 19AT perform a combine fit to  $35.9 \text{ fb}^{-1}$  of data at  $E_{\text{cm}} = 13 \text{ TeV}$ .
- <sup>2</sup> AABOUD 18BN search for  $VH^0, H^0 \rightarrow b\bar{b}$  ( $V = W, Z$ ) using  $79.8 \text{ fb}^{-1}$  of  $pp$  collision data at  $E_{\text{cm}} = 13 \text{ TeV}$ . The quoted signal strength corresponds to a significance of 4.9 standard deviations and is given for  $m_{H^0} = 125 \text{ GeV}$ .
- <sup>3</sup> SIRUNYAN 18DB search for  $VH^0, H^0 \rightarrow b\bar{b}$  ( $V = W, Z$ ) using  $77.2 \text{ fb}^{-1}$  of  $pp$  collision data at  $E_{\text{cm}} = 13 \text{ TeV}$ . The quoted signal strength corresponds to a significance of 4.4 standard deviations and is given for  $m_{H^0} = 125.09 \text{ GeV}$ .
- <sup>4</sup> AAD 16AN perform fits to the ATLAS and CMS data at  $E_{\text{cm}} = 7$  and  $8 \text{ TeV}$ . The signal strengths for individual production processes are  $1.0 \pm 0.5$  for  $WH^0$  production,  $0.4 \pm 0.4$  for  $ZH^0$  production, and  $1.1 \pm 1.0$  for  $t\bar{t}H^0$  production.
- <sup>5</sup> AAD 16AN: In the fit, relative production cross sections are fixed to those in the Standard Model. The quoted signal strength is given for  $m_{H^0} = 125.09 \text{ GeV}$ .

- <sup>6</sup> AALTONEN 13M combine all Tevatron data from the CDF and D0 Collaborations with up to  $10.0 \text{ fb}^{-1}$  and  $9.7 \text{ fb}^{-1}$ , respectively, of  $p\bar{p}$  collisions at  $E_{\text{cm}} = 1.96 \text{ TeV}$ . The quoted signal strength is given for  $m_{H^0} = 125 \text{ GeV}$ .
- <sup>7</sup> AABOUD 19U measure cross sections of  $pp \rightarrow VH^0, H^0 \rightarrow b\bar{b}$  production as a function of the gauge boson transverse momentum using data of  $79.8 \text{ fb}^{-1}$ . The kinematic fiducial volumes used is based on the simplified template cross section framework (reduced stage-1). See their Table 3 and Fig. 3.
- <sup>8</sup> AABOUD 18BN combine results of  $79.8 \text{ fb}^{-1}$  at  $E_{\text{cm}} = 13 \text{ TeV}$  with results of  $VH^0$  at  $E_{\text{cm}} = 7$  and  $8 \text{ TeV}$ .
- <sup>9</sup> AABOUD 18BN combine results of  $VH^0$  at  $E_{\text{cm}} = 7, 8$  and  $13 \text{ TeV}$  with results of VBF (+gluon fusion) and  $t\bar{t}H^0$  at  $E_{\text{cm}} = 7, 8$ , and  $13 \text{ TeV}$  to perform a search for the  $H^0 \rightarrow b\bar{b}$  decay. The quoted signal strength assumes a SM production strength and corresponds to a significance of 5.4 standard deviations.
- <sup>10</sup> AABOUD 18BQ search for  $H^0 \rightarrow b\bar{b}$  produced through vector-boson fusion (VBF) and VBF+ $\gamma$  with  $30.6 \text{ fb}^{-1}$   $pp$  collision data at  $E_{\text{cm}} = 13 \text{ TeV}$ . The quoted signal strength is given for  $m_{H^0} = 125 \text{ GeV}$ .
- <sup>11</sup> The signal strength is measured including all production modes (VBF, ggF,  $VH^0, t\bar{t}H^0$ ).
- <sup>12</sup> The signal strength is measured for VBF-only and others (ggF,  $VH^0, t\bar{t}H^0$ ) are constrained to Standard Model expectations with uncertainties described in their Section VIII B.
- <sup>13</sup> AALTONEN 18C use  $5.4 \text{ fb}^{-1}$  of  $p\bar{p}$  collisions at  $E_{\text{cm}} = 1.96 \text{ TeV}$ . The upper limit at 95% CL on  $p\bar{p} \rightarrow H^0 \rightarrow b\bar{b}$  is 33 times the SM prediction, which corresponds to a cross section of  $40.6 \text{ pb}$ .
- <sup>14</sup> SIRUNYAN 18AE use  $35.9 \text{ fb}^{-1}$  of  $pp$  collision data at  $E_{\text{cm}} = 13 \text{ TeV}$ . The quoted signal strength corresponds to 3.3 standard deviations and is given for  $m_{H^0} = 125.09 \text{ GeV}$ .
- <sup>15</sup> SIRUNYAN 18AE combine the result of  $35.9 \text{ fb}^{-1}$  at  $E_{\text{cm}} = 13 \text{ TeV}$  with the results obtained from data of up to  $5.1 \text{ fb}^{-1}$  at  $E_{\text{cm}} = 7 \text{ TeV}$  and up to  $18.9 \text{ fb}^{-1}$  at  $E_{\text{cm}} = 8 \text{ TeV}$  (CHATRCHYAN 14A1 and KHACHATRYAN 15Z). The quoted signal strength corresponds to 3.8 standard deviations and is given for  $m_{H^0} = 125.09 \text{ GeV}$ .
- <sup>16</sup> SIRUNYAN 18DB combine the result of  $77.2 \text{ fb}^{-1}$  at  $E_{\text{cm}} = 13 \text{ TeV}$  with the results obtained from data of up to  $5.1 \text{ fb}^{-1}$  at  $E_{\text{cm}} = 7 \text{ TeV}$  and up to  $18.9 \text{ fb}^{-1}$  at  $E_{\text{cm}} = 8 \text{ TeV}$ . The quoted signal strength corresponds to a significance of 4.8 standard deviations and is given for  $m_{H^0} = 125.09 \text{ GeV}$ .
- <sup>17</sup> SIRUNYAN 18DB combine results of  $77.2 \text{ fb}^{-1}$  at  $E_{\text{cm}} = 13 \text{ TeV}$  with results of gluon fusion (ggF), VBF and  $t\bar{t}H^0$  at  $E_{\text{cm}} = 7 \text{ TeV}$ ,  $8 \text{ TeV}$  and  $13 \text{ TeV}$  to perform a search for the  $H^0 \rightarrow b\bar{b}$  decay. The quoted signal strength assumes a SM production strength and corresponds to a significance of 5.6 standard deviations and is given for  $m_{H^0} = 125.09 \text{ GeV}$ .
- <sup>18</sup> SIRUNYAN 18E use  $35.9 \text{ fb}^{-1}$  at  $E_{\text{cm}} = 13 \text{ TeV}$ . The quoted signal strength is given for  $m_{H^0} = 125 \text{ GeV}$ . They measure  $\sigma \cdot B$  for gluon fusion production of  $H^0 \rightarrow b\bar{b}$  with  $p_T > 450 \text{ GeV}$ ,  $|\eta| < 2.5$  to be  $74 \pm 48^{+17}_{-10} \text{ fb}$ .
- <sup>19</sup> AABOUD 17BA use  $36.1 \text{ fb}^{-1}$  at  $E_{\text{cm}} = 13 \text{ TeV}$ . The quoted signal strength is given for  $m_{H^0} = 125 \text{ GeV}$ . They give  $\sigma(WH) \cdot B(H^0 \rightarrow b\bar{b}) = 1.08^{+0.54}_{-0.47} \text{ pb}$  and  $\sigma(ZH) \cdot B(H^0 \rightarrow b\bar{b}) = 0.57^{+0.26}_{-0.23} \text{ pb}$ .
- <sup>20</sup> AABOUD 17BA combine 7, 8 and 13 TeV analyses. The quoted signal strength is given for  $m_{H^0} = 125 \text{ GeV}$ .
- <sup>21</sup> AABOUD 16X search for vector-boson fusion production of  $H^0$  decaying to  $b\bar{b}$  in  $20.2 \text{ fb}^{-1}$  of  $pp$  collisions at  $E_{\text{cm}} = 8 \text{ TeV}$ . The quoted signal strength is given for  $m_{H^0} = 125 \text{ GeV}$ .
- <sup>22</sup> AAD 16K use up to  $4.7 \text{ fb}^{-1}$  of  $pp$  collisions at  $E_{\text{cm}} = 7 \text{ TeV}$  and up to  $20.3 \text{ fb}^{-1}$  at  $E_{\text{cm}} = 8 \text{ TeV}$ . The quoted signal strength is given for  $m_{H^0} = 125.36 \text{ GeV}$ .
- <sup>23</sup> AAD 15G use  $4.7 \text{ fb}^{-1}$  of  $pp$  collisions at  $E_{\text{cm}} = 7 \text{ TeV}$  and  $20.3 \text{ fb}^{-1}$  at  $E_{\text{cm}} = 8 \text{ TeV}$ . The quoted signal strength is given for  $m_{H^0} = 125.36 \text{ GeV}$ .
- <sup>24</sup> KHACHATRYAN 15Z search for vector-boson fusion production of  $H^0$  decaying to  $b\bar{b}$  in up to  $19.8 \text{ fb}^{-1}$  of  $pp$  collisions at  $E_{\text{cm}} = 8 \text{ TeV}$ . The quoted signal strength is given for  $m_{H^0} = 125 \text{ GeV}$ .
- <sup>25</sup> KHACHATRYAN 15Z combined vector boson fusion,  $WH^0, ZH^0$  production, and  $t\bar{t}H^0$  production results. The quoted signal strength is given for  $m_{H^0} = 125 \text{ GeV}$ .
- <sup>26</sup> CHATRCHYAN 14A1 use up to  $5.1 \text{ fb}^{-1}$  of  $pp$  collisions at  $E_{\text{cm}} = 7 \text{ TeV}$  and up to  $18.9 \text{ fb}^{-1}$  at  $E_{\text{cm}} = 8 \text{ TeV}$ . The quoted signal strength is given for  $m_{H^0} = 125 \text{ GeV}$ . See also CHATRCHYAN 14A1.
- <sup>27</sup> AALTONEN 13L combine all CDF results with  $9.45\text{--}10.0 \text{ fb}^{-1}$  of  $p\bar{p}$  collisions at  $E_{\text{cm}} = 1.96 \text{ TeV}$ . The quoted signal strength is given for  $m_{H^0} = 125 \text{ GeV}$ .
- <sup>28</sup> ABAZOV 13L combine all D0 results with up to  $9.7 \text{ fb}^{-1}$  of  $p\bar{p}$  collisions at  $E_{\text{cm}} = 1.96 \text{ TeV}$ . The quoted signal strength is given for  $m_{H^0} = 125 \text{ GeV}$ .
- <sup>29</sup> AAD 12A1 obtain results based on  $4.6\text{--}4.8 \text{ fb}^{-1}$  of  $pp$  collisions at  $E_{\text{cm}} = 7 \text{ TeV}$ . The quoted signal strengths are given in their Fig. 10 for  $m_{H^0} = 126 \text{ GeV}$ . See also Fig. 13 of AAD 12DA.
- <sup>30</sup> AALTONEN 12T combine AALTONEN 12Q, AALTONEN 12R, AALTONEN 12S, ABAZOV 12P, ABAZOV 12P, and ABAZOV 12K. An excess of events over background is observed which is most significant in the region  $m_{H^0} = 120\text{--}135 \text{ GeV}$ , with a local significance of up to  $3.3 \sigma$ . The local significance at  $m_{H^0} = 125 \text{ GeV}$  is  $2.8 \sigma$ , which corresponds to  $(\sigma(H^0 W) + \sigma(H^0 Z)) \cdot B(H^0 \rightarrow b\bar{b}) = (0.23^{+0.09}_{-0.08}) \text{ pb}$ , compared to the Standard Model expectation at  $m_{H^0} = 125 \text{ GeV}$  of  $0.12 \pm 0.01 \text{ pb}$ . Superseded by AALTONEN 13M.
- <sup>31</sup> CHATRCHYAN 12N obtain results based on  $5.0 \text{ fb}^{-1}$  of  $pp$  collisions at  $E_{\text{cm}} = 7 \text{ TeV}$  and  $5.1 \text{ fb}^{-1}$  at  $E_{\text{cm}} = 8 \text{ TeV}$ . The quoted signal strength is given for  $m_{H^0} = 125.5 \text{ GeV}$ . See also CHATRCHYAN 13Y.

$\mu^+ \mu^-$  Final State

VALUE	CL%	DOCUMENT ID	TECN	COMMENT
<b>0.6 ± 0.8</b>				<b>OUR AVERAGE</b>
1.0 ± 1.0 ± 0.1		1 SIRUNYAN	19E CMS	$pp$ , 7, 8, 13 TeV
-0.1 ± 1.4		2 AABOUD	17Y ATLS	$pp$ , 7, 8, 13 TeV
• • • We do not use the following data for averages, fits, limits, etc. • • •				
0.68 <sup>+1.25</sup> <sub>-1.24</sub>		3 SIRUNYAN	19AT CMS	$pp$ , 13 TeV
0.7 ± 1.0 <sup>+0.2</sup> <sub>-0.1</sub>		1 SIRUNYAN	19E CMS	$pp$ , 13 TeV, 35.9 fb <sup>-1</sup>
-0.1 ± 1.5		2 AABOUD	17Y ATLS	$pp$ , 13 TeV
0.1 ± 2.5		4 AAD	16AN LHC	$pp$ , 7, 8 TeV
-0.6 ± 3.6		4 AAD	16AN ATLS	$pp$ , 7, 8 TeV
0.9 ± 3.6 <sub>-3.5</sub>		4 AAD	16AN CMS	$pp$ , 7, 8 TeV
< 7.4	95	5 KHACHATRYAN...15H	CMS	$pp \rightarrow H^0 X$ , 7, 8 TeV
< 7.0	95	6 AAD	14AS ATLS	$pp \rightarrow H^0 X$ , 7, 8 TeV
1 SIRUNYAN 19E search for $H^0 \rightarrow \mu^+ \mu^-$ using 35.9 fb <sup>-1</sup> of $pp$ collisions at $E_{cm} = 13$ TeV and combine with results of 7 TeV (5.0 fb <sup>-1</sup> ) and 8 TeV (19.7 fb <sup>-1</sup> ). The upper limit at 95% CL on the signal strength is 2.9, which corresponds to the SM Higgs boson branching fraction to a muon pair of $6.4 \times 10^{-4}$ .				
2 AABOUD 17Y use 36.1 fb <sup>-1</sup> of $pp$ collisions at $E_{cm} = 13$ TeV, 20.3 fb <sup>-1</sup> at 8 TeV and 4.5 fb <sup>-1</sup> at 7 TeV. The quoted signal strength is given for $m_{H^0} = 125$ GeV.				
3 SIRUNYAN 19AT perform a combine fit to 35.9 fb <sup>-1</sup> of data at $E_{cm} = 13$ TeV.				
4 AAD 16AN: In the fit, relative production cross sections are fixed to those in the Standard Model. The quoted signal strength is given for $m_{H^0} = 125.09$ GeV.				
5 KHACHATRYAN 15H use 5.0 fb <sup>-1</sup> of $pp$ collisions at $E_{cm} = 7$ TeV and 19.7 fb <sup>-1</sup> at 8 TeV. The quoted signal strength is given for $m_{H^0} = 125$ GeV.				
6 AAD 14AS search for $H^0 \rightarrow \mu^+ \mu^-$ in 4.5 fb <sup>-1</sup> of $pp$ collisions at $E_{cm} = 7$ TeV and 20.3 fb <sup>-1</sup> at $E_{cm} = 8$ TeV. The quoted signal strength is given for $m_{H^0} = 125.5$ GeV.				

 $\tau^+ \tau^-$  Final State

VALUE	CL%	DOCUMENT ID	TECN	COMMENT
<b>1.15 ± 0.16</b>				<b>OUR AVERAGE</b>
1.09 <sup>+0.18</sup> <sub>-0.17</sub> + 0.26 <sup>+0.16</sup> <sub>-0.22</sub> - 0.11		1 AABOUD	19AQ ATLS	$pp$ , 13 TeV, $H \rightarrow \tau\tau$
1.24 <sup>+0.29</sup> <sub>-0.27</sub>		2 SIRUNYAN	19AF CMS	$pp$ , 13 TeV
1.11 <sup>+0.24</sup> <sub>-0.22</sub>		3,4 AAD	16AN LHC	$pp$ , 7, 8 TeV
1.68 <sup>+2.28</sup> <sub>-1.68</sub>		5 AALTONEN	13M TEVA	$p\bar{p} \rightarrow H^0 X$ , 1.96 TeV
• • • We do not use the following data for averages, fits, limits, etc. • • •				
2.5 <sup>+1.4</sup> <sub>-1.3</sub>		6 SIRUNYAN	19AF CMS	$pp \rightarrow H^0 W/H^0 Z$ , $H^0 \rightarrow \tau\tau$ , 13 TeV
1.02 <sup>+0.26</sup> <sub>-0.24</sub>		7 SIRUNYAN	19AT CMS	$pp$ , 13 TeV
1.09 <sup>+0.27</sup> <sub>-0.26</sub>		8 SIRUNYAN	18Y CMS	$pp$ , 13 TeV
0.98 ± 0.18		9 SIRUNYAN	18Y CMS	$pp$ , 7, 8, 13 TeV
2.3 ± 1.6		10 AAD	16AC ATLS	$pp \rightarrow H^0 W/ZX$ , 8 TeV
1.41 <sup>+0.40</sup> <sub>-0.36</sub>		4 AAD	16AN ATLS	$pp$ , 7, 8 TeV
0.88 <sup>+0.30</sup> <sub>-0.28</sub>		4 AAD	16AN CMS	$pp$ , 7, 8 TeV
1.44 <sup>+0.30</sup> <sub>-0.29</sub> - 0.23		11 AAD	16K ATLS	$pp$ , 7, 8 TeV
1.43 <sup>+0.27</sup> <sub>-0.26</sub> ± 0.09		12 AAD	15AH ATLS	$pp \rightarrow H^0 X$ , 7, 8 TeV
0.78 ± 0.27		13 CHATRCHYAN 14K	CMS	$pp \rightarrow H^0 X$ , 7, 8 TeV
0.00 <sup>+8.44</sup> <sub>-0.00</sub>		14 AALTONEN	13L DDF	$p\bar{p} \rightarrow H^0 X$ , 1.96 TeV
3.96 <sup>+4.11</sup> <sub>-3.38</sub>		15 ABAZOV	13L DDF	$p\bar{p} \rightarrow H^0 X$ , 1.96 TeV
0.4 <sup>+1.6</sup> <sub>-2.0</sub>		16 AAD	12AI ATLS	$pp \rightarrow H^0 X$ , 7 TeV
0.00 <sup>+0.76</sup> <sub>-0.74</sub>		17 CHATRCHYAN 12N	CMS	$pp \rightarrow H^0 X$ , 7, 8 TeV
1 AABOUD 19AQ use 36.1 fb <sup>-1</sup> of data. The first, second and third quoted errors are statistical, experimental systematic and theory systematic uncertainties, respectively. The quoted signal strength is given for $m_{H^0} = 125$ GeV and corresponds to 4.4 standard deviations. Combining with 7 TeV and 8 TeV results (AAD 15AH), the observed significance is 6.4 standard deviations. The cross sections in the $H^0 \rightarrow \tau\tau$ decay channel ( $m_{H^0} = 125$ GeV) are measured to $3.77^{+0.60}_{-0.59}$ (stat) $\pm 0.87$ (syst) pb for the inclusive, $0.28 \pm 0.09^{+0.11}_{-0.09}$ pb for VBF, and $3.1 \pm 1.0^{+1.6}_{-1.3}$ pb for gluon-fusion production. See their Table XI for the cross sections in the framework of simplified template cross sections.				
2 SIRUNYAN 19AF use 35.9 fb <sup>-1</sup> of data. $H^0 W/Z$ channels are added with a few updates on gluon fusion and vector boson fusion with respect to SIRUNYAN 18Y. The quoted signal strength is given for $m_{H^0} = 125$ GeV and corresponds to 5.5 standard deviations. The signal strengths for the individual production modes are: $1.12^{+0.53}_{-0.50}$ for gluon fusion, $1.13^{+0.45}_{-0.42}$ for vector boson fusion, $3.39^{+1.68}_{-1.54}$ for $WH^0$ and $1.23^{+1.62}_{-1.35}$ for $ZH^0$ . See their Fig. 7 for other couplings ( $\kappa_V, \kappa_f$ ).				
3 AAD 16AN perform fits to the ATLAS and CMS data at $E_{cm} = 7$ and 8 TeV. The signal strengths for individual production processes are $1.0 \pm 0.6$ for gluon fusion, $1.3 \pm 0.4$ for vector boson fusion, $-1.4 \pm 1.4$ for $WH^0$ production, $2.2^{+2.2}_{-1.8}$ for $ZH^0$ production, and $-1.9^{+3.7}_{-3.3}$ for $t\bar{t}H^0$ production.				

- 4 AAD 16AN: In the fit, relative production cross sections are fixed to those in the Standard Model. The quoted signal strength is given for  $m_{H^0} = 125.09$  GeV.
- 5 AALTONEN 13M combine all Tevatron data from the CDF and D0 Collaborations with up to 10.0 fb<sup>-1</sup> and 9.7 fb<sup>-1</sup>, respectively, of  $p\bar{p}$  collisions at  $E_{cm} = 1.96$  TeV. The quoted signal strength is given for  $m_{H^0} = 125$  GeV.
- 6 SIRUNYAN 19AF use 35.9 fb<sup>-1</sup> of data. The quoted signal strength is given for  $m_{H^0} = 125$  GeV and corresponds to 2.3 standard deviations.
- 7 SIRUNYAN 19AT perform a combine fit to 35.9 fb<sup>-1</sup> of data at  $E_{cm} = 13$  TeV. This combination is based on SIRUNYAN 18Y.
- 8 SIRUNYAN 18Y use 35.9 fb<sup>-1</sup> of  $pp$  collisions at  $E_{cm} = 13$  TeV. The quoted signal strength is given for  $m_{H^0} = 125.09$  GeV and corresponds to 4.9 standard deviations.
- 9 SIRUNYAN 18Y combine the result of 35.9 fb<sup>-1</sup> at  $E_{cm} = 13$  TeV with the results obtained from data of 4.9 fb<sup>-1</sup> at  $E_{cm} = 7$  TeV and 19.7 fb<sup>-1</sup> at  $E_{cm} = 8$  TeV (KHACHATRYAN 15AM). The quoted signal strength is given for  $m_{H^0} = 125.09$  GeV and corresponds to 5.9 standard deviations.
- 10 AAD 16AC measure the signal strength with  $pp \rightarrow H^0 W/ZX$  processes using 20.3 fb<sup>-1</sup> of  $E_{cm} = 8$  TeV. The quoted signal strength is given for  $m_{H^0} = 125$  GeV.
- 11 AAD 16K use up to 4.7 fb<sup>-1</sup> of  $pp$  collisions at  $E_{cm} = 7$  TeV and up to 20.3 fb<sup>-1</sup> at  $E_{cm} = 8$  TeV. The quoted signal strength is given for  $m_{H^0} = 125.36$  GeV.
- 12 AAD 15AH use 4.5 fb<sup>-1</sup> of  $pp$  collisions at  $E_{cm} = 7$  TeV and 20.3 fb<sup>-1</sup> at  $E_{cm} = 8$  TeV. The third uncertainty in the measurement is theory systematics. The signal strength for the gluon fusion mode is  $2.0 \pm 0.8^{+1.2}_{-0.8} \pm 0.3$  and that for vector boson fusion and  $W/ZH^0$  production modes is  $1.24^{+0.49+0.31}_{-0.45-0.29} \pm 0.08$ . The quoted signal strength is given for  $m_{H^0} = 125.36$  GeV.
- 13 CHATRCHYAN 14K use 4.9 fb<sup>-1</sup> of  $pp$  collisions at  $E_{cm} = 7$  TeV and 19.7 fb<sup>-1</sup> at  $E_{cm} = 8$  TeV. The quoted signal strength is given for  $m_{H^0} = 125$  GeV. See also CHATRCHYAN 14AJ.
- 14 AALTONEN 13L combine all CDF results with 9.45–10.0 fb<sup>-1</sup> of  $p\bar{p}$  collisions at  $E_{cm} = 1.96$  TeV. The quoted signal strength is given for  $m_{H^0} = 125$  GeV.
- 15 ABAZOV 13L combine all D0 results with up to 9.7 fb<sup>-1</sup> of  $p\bar{p}$  collisions at  $E_{cm} = 1.96$  TeV. The quoted signal strength is given for  $m_{H^0} = 125$  GeV.
- 16 AAD 12AI obtain results based on 4.7 fb<sup>-1</sup> of  $pp$  collisions at  $E_{cm} = 7$  TeV. The quoted signal strengths are given in their Fig. 10 for  $m_{H^0} = 126$  GeV. See also Fig. 13 of AAD 12DA.
- 17 CHATRCHYAN 12N obtain results based on 4.9 fb<sup>-1</sup> of  $pp$  collisions at  $E_{cm} = 7$  TeV and 5.1 fb<sup>-1</sup> at  $E_{cm} = 8$  TeV. The quoted signal strength is given for  $m_{H^0} = 125.5$  GeV. See also CHATRCHYAN 13Y.

 $Z\gamma$  Final State

VALUE	CL%	DOCUMENT ID	TECN	COMMENT
<b>&lt; 6.6</b>	95	1 AABOUD	17AW ATLS	$pp \rightarrow H^0 X$ , 13 TeV
• • • We do not use the following data for averages, fits, limits, etc. • • •				
< 7.4	95	2 SIRUNYAN	18DQ CMS	$pp \rightarrow H^0 X$ , 13 TeV, $H^0 \rightarrow Z\gamma$
< 11	95	3 AAD	14I ATLS	$pp \rightarrow H^0 X$ , 7, 8 TeV
< 9.5	95	4 CHATRCHYAN 13BK	CMS	$pp \rightarrow H^0 X$ , 7, 8 TeV
1 AABOUD 17AW search for $H^0 \rightarrow Z\gamma, Z \rightarrow ee, \mu\mu$ in 36.1 fb <sup>-1</sup> of $pp$ collisions at $E_{cm} = 13$ TeV. The quoted signal strength is given for $m_{H^0} = 125.09$ GeV. The upper limit on the branching ratio of $H^0 \rightarrow Z\gamma$ is 1.0% at 95% CL assuming the SM Higgs boson production.				
2 SIRUNYAN 18DQ search for $H^0 \rightarrow Z\gamma, Z \rightarrow ee, \mu\mu$ in 35.9 fb <sup>-1</sup> of $pp$ collisions at $E_{cm} = 13$ TeV. The quoted signal strength (see their Figs. 6 and 7) is given for $m_{H^0} = 125$ GeV.				
3 AAD 14I search for $H^0 \rightarrow Z\gamma \rightarrow \ell\ell\gamma$ in 4.5 fb <sup>-1</sup> of $pp$ collisions at $E_{cm} = 7$ TeV and 20.3 fb <sup>-1</sup> at $E_{cm} = 8$ TeV. The quoted signal strength is given for $m_{H^0} = 125.5$ GeV.				
4 CHATRCHYAN 13BK search for $H^0 \rightarrow Z\gamma \rightarrow \ell\ell\gamma$ in 5.0 fb <sup>-1</sup> of $pp$ collisions at $E_{cm} = 7$ TeV and 19.6 fb <sup>-1</sup> at $E_{cm} = 8$ TeV. A limit on cross section times branching ratio which corresponds to (4–25) times the expected Standard Model cross section is given in the range $m_{H^0} = 120$ –160 GeV at 95% CL. The quoted limit is given for $m_{H^0} = 125$ GeV, where 10 is expected for no signal.				

 $\gamma^* \gamma$  Final State

VALUE	CL%	DOCUMENT ID	TECN	COMMENT
• • • We do not use the following data for averages, fits, limits, etc. • • •				
< 4.0	95	1 SIRUNYAN	18DQ CMS	$pp \rightarrow H^0 X$ , 13 TeV, $H^0 \rightarrow \gamma^* \gamma$
< 6.7	95	2 KHACHATRYAN...16B	CMS	$pp$ , 8 TeV, $e e \gamma, \mu \mu \gamma$
1 SIRUNYAN 18DQ search for $H^0 \rightarrow \gamma^* \gamma, \gamma^* \rightarrow \mu\mu$ in 35.9 fb <sup>-1</sup> of $pp$ collisions at $E_{cm} = 13$ TeV. The mass of $\gamma^*$ is smaller than 50 GeV except in $J/\psi$ and $\Upsilon$ mass regions. The quoted signal strength (see their Figs. 6 and 7) is given for $m_{H^0} = 125$ GeV.				
2 KHACHATRYAN 16B search for $H^0 \rightarrow \gamma^* \gamma \rightarrow e^+ e^- \gamma$ and $\mu^+ \mu^- \gamma$ (with $m(e^+ e^-) < 3.5$ GeV and $m(\mu^+ \mu^-) < 20$ GeV) in 19.7 fb <sup>-1</sup> of $pp$ collisions at $E_{cm} = 8$ TeV. See their Fig. 6 for limits on individual channels.				

## Higgs Yukawa couplings

## top Yukawa coupling

VALUE	CL%	DOCUMENT ID	TECN	COMMENT
<b>&lt; 1.7</b>	95	1 SIRUNYAN	20c CMS	$pp$ , 13 TeV
• • • We do not use the following data for averages, fits, limits, etc. • • •				
< 1.67	95	2 SIRUNYAN	19BY CMS	$pp$ , 13 TeV
< 2.1	95	3 SIRUNYAN	18BU CMS	$pp$ , 13 TeV

## Gauge &amp; Higgs Boson Particle Listings

 $H^0$ 

- 1 SIRUNYAN 20c search for the production of four top quarks with same-sign and multilepton final states with  $137 \text{ fb}^{-1}$   $pp$  collision data at  $E_{\text{cm}} = 13 \text{ TeV}$ . The results constrain the ratio of the top quark Yukawa coupling  $y_t$  to its Standard Model by comparing to the central value of a theoretical prediction (see their Refs. [1-2]), yielding  $|y_t/y_t^{\text{SM}}| < 1.7$  at 95% CL. See their Fig. 5.
- 2 SIRUNYAN 19bY measure the top quark Yukawa coupling from  $t\bar{t}$  kinematic distributions, the invariant mass of the top quark pair and the rapidity difference between  $t$  and  $\bar{t}$ , in the  $\ell$ -jets final state with  $35.8 \text{ fb}^{-1}$   $pp$  collision data at  $E_{\text{cm}} = 13 \text{ TeV}$ . The results constrain the ratio of the top quark Yukawa coupling to its Standard Model to be  $1.07^{+0.34}_{-0.43}$  with an upper limit of 1.67 at 95% CL (see their Table III).
- 3 SIRUNYAN 18bU search for the production of four top quarks with same-sign and multilepton final states with  $35.9 \text{ fb}^{-1}$   $pp$  collision data at  $E_{\text{cm}} = 13 \text{ TeV}$ . The results constrain the ratio of the top quark Yukawa coupling  $y_t$  to its Standard Model by comparing to the central value of a theoretical prediction (see their Ref. [16]), yielding  $|y_t/y_t^{\text{SM}}| < 2.1$  at 95% CL.

OTHER  $H^0$  PRODUCTION PROPERTIES $t\bar{t}H^0$  Production

Signal strength relative to the Standard Model cross section.

VALUE	CL%	DOCUMENT ID	TECN	COMMENT
<b>1.28 ± 0.20 OUR AVERAGE</b>				
1.2 ± 0.3		1 AABOUD	18Ac ATLS	$pp, 13 \text{ TeV}, H^0 \rightarrow b\bar{b}, \tau\tau, \gamma\gamma, WW^*, ZZ^*$
1.26 <sup>+0.31</sup> <sub>-0.26</sub>		2 SIRUNYAN	18L CMS	$pp, 7, 8, 13 \text{ TeV}, H^0 \rightarrow b\bar{b}, \tau\tau, \gamma\gamma, WW^*, ZZ^*$
1.9 <sup>+0.8</sup> <sub>-0.7</sub>		3 AAD	16AN ATLS	$pp, 7, 8 \text{ TeV}$
• • • We do not use the following data for averages, fits, limits, etc. • • •				
0.72 ± 0.24 ± 0.38		4 SIRUNYAN	19R CMS	$pp, 13 \text{ TeV}, H^0 \rightarrow b\bar{b}$
1.6 <sup>+0.5</sup> <sub>-0.4</sub>		5 AABOUD	18Ac ATLS	$pp, 13 \text{ TeV}, H^0 \rightarrow \tau\tau, WW^*, ZZ^*$
		6 AABOUD	18Bk ATLS	$pp, 13 \text{ TeV}, H^0 \rightarrow b\bar{b}, \tau\tau, \gamma\gamma, WW^*, ZZ^*$
0.84 <sup>+0.64</sup> <sub>-0.61</sub>		7 AABOUD	18T ATLS	$pp, 13 \text{ TeV}, H^0 \rightarrow b\bar{b}$
0.9 ± 1.5		8 SIRUNYAN	18Bd CMS	$pp, 13 \text{ TeV}, H^0 \rightarrow b\bar{b}$
1.23 <sup>+0.45</sup> <sub>-0.43</sub>		9 SIRUNYAN	18Bq CMS	$pp, 13 \text{ TeV}, H^0 \rightarrow \tau\tau, WW^*, ZZ^*$
1.7 ± 0.8		10 AAD	16AL ATLS	$pp, 7, 8 \text{ TeV}, H^0 \rightarrow b\bar{b}, \tau\tau, \gamma\gamma, WW^*, \text{ and } ZZ^*$
2.3 <sup>+0.7</sup> <sub>-0.6</sub>		3.11 AAD	16AN LHC	$pp, 7, 8 \text{ TeV}$
2.9 <sup>+1.0</sup> <sub>-0.9</sub>		3 AAD	16AN CMS	$pp, 7, 8 \text{ TeV}$
1.81 <sup>+0.52+0.58+0.31</sup> <sub>-0.50-0.55-0.12</sub>		12 AAD	16K ATLS	$pp, 7, 8 \text{ TeV}$
1.4 <sup>+2.1</sup> <sub>-1.4</sub> <sup>+0.6</sup> <sub>-0.3</sub>		13 AAD	15 ATLS	$pp, 7, 8 \text{ TeV}$
1.5 ± 1.1		14 AAD	15Bc ATLS	$pp, 8 \text{ TeV}$
2.1 <sup>+1.4</sup> <sub>-1.2</sub>		15 AAD	15T ATLS	$pp, 8 \text{ TeV}$
1.2 <sup>+1.6</sup> <sub>-1.5</sub>		16 KHACHATRYAN...15AN	CMS	$pp, 8 \text{ TeV}$
2.8 <sup>+1.0</sup> <sub>-0.9</sub>		17 KHACHATRYAN...14H	CMS	$pp, 7, 8 \text{ TeV}$
9.49 <sup>+6.60</sup> <sub>-6.28</sub>		18 AALTONEN	13L CDF	$p\bar{p}, 1.96 \text{ TeV}$
< 5.8	95	19 CHATRCHYAN 13x	CMS	$pp, 7, 8 \text{ TeV}, H^0 \rightarrow b\bar{b}$

- 1 AABOUD 18Ac combine results of  $t\bar{t}H^0, H^0 \rightarrow \tau\tau, WW^*(\rightarrow \ell\nu\nu, \ell\nu q\bar{q}), ZZ^*(\rightarrow \ell\nu\nu, \ell q\bar{q})$  with results of  $t\bar{t}H^0, H^0 \rightarrow b\bar{b}$  (AABOUD 18T),  $\gamma\gamma$  (AABOUD 18Bo),  $ZZ^*(\rightarrow 4\ell)$  (AABOUD 18Aj) in  $36.1 \text{ fb}^{-1}$  of  $pp$  collisions at  $E_{\text{cm}} = 13 \text{ TeV}$ . The quoted signal strength is given for  $m_{H^0} = 125 \text{ GeV}$ . See their Table 14.
- 2 SIRUNYAN 18L use up to 5.1, 19.7 and  $35.9 \text{ fb}^{-1}$  of  $pp$  collisions at  $E_{\text{cm}} = 7, 8,$  and  $13 \text{ TeV}$ , respectively. The quoted signal strength corresponds to a significance of 5.2 standard deviations and is given for  $m_{H^0} = 125.09 \text{ GeV}$ .  $H^0$  decay channels of  $WW^*, ZZ^*, \gamma\gamma, \tau\tau,$  and  $b\bar{b}$  are used. See their Table 1 and Fig. 2 for results on individual channels.
- 3 AAD 16AN: In the fit, relative branching ratios are fixed to those in the Standard Model. The quoted signal strength is given for  $m_{H^0} = 125.09 \text{ GeV}$ .
- 4 SIRUNYAN 19R search for  $t\bar{t}H^0$  production with  $H^0$  decaying to  $b\bar{b}$  in  $35.9 \text{ fb}^{-1}$  of data at  $E_{\text{cm}} = 13 \text{ TeV}$ . The quoted signal strength is given for  $m_{H^0} = 125 \text{ GeV}$ .
- 5 AABOUD 18Ac search for  $t\bar{t}H^0$  production with  $H^0$  decaying to  $\tau\tau, WW^*(\rightarrow \ell\nu\nu, \ell\nu q\bar{q}), ZZ^*(\rightarrow \ell\nu\nu, \ell q\bar{q})$  in  $36.1 \text{ fb}^{-1}$  of  $pp$  collisions at  $E_{\text{cm}} = 13 \text{ TeV}$ . The quoted signal strength is given for  $m_{H^0} = 125 \text{ GeV}$ . See their Table 13 and Fig. 13.
- 6 AABOUD 18Bk use  $79.8 \text{ fb}^{-1}$  data for  $t\bar{t}H^0$  production with  $H^0 \rightarrow \gamma\gamma$  and  $ZZ^* \rightarrow 4\ell$  ( $\ell = e, \mu$ ) and  $36.1 \text{ fb}^{-1}$  for other decay channels at  $E_{\text{cm}} = 13 \text{ TeV}$ . A significance of 5.8 standard deviations is observed for  $m_{H^0} = 125.09 \text{ GeV}$  and its signal strength without the uncertainty of the  $t\bar{t}H^0$  cross section is  $1.32^{+0.28}_{-0.26}$ . Combining with results of 7 and 8 TeV (AAD 16K), the significance is 6.3 standard deviations. Assuming Standard Model branching fractions, the total  $t\bar{t}H^0$  production cross section at 13 TeV is measured to be  $670 \pm 90^{+110}_{-100} \text{ fb}$ .

- 7 AABOUD 18T search for  $t\bar{t}H^0$  production with  $H^0$  decaying to  $b\bar{b}$  in  $36.1 \text{ fb}^{-1}$  of  $pp$  collisions at  $E_{\text{cm}} = 13 \text{ TeV}$ . The quoted signal strength is given for  $m_{H^0} = 125 \text{ GeV}$ .
- 8 SIRUNYAN 18Bd search for  $t\bar{t}H^0, H^0 \rightarrow b\bar{b}$  in the all-jet final state with  $35.9 \text{ fb}^{-1}$   $pp$  collision data at  $E_{\text{cm}} = 13 \text{ TeV}$ . The quoted signal strength is given for  $m_{H^0} = 125 \text{ GeV}$ .
- 9 SIRUNYAN 18Bq search for  $t\bar{t}H^0$  in final states with electrons, muons and hadronically decaying  $\tau$  leptons ( $H^0 \rightarrow WW^*, ZZ^*, \tau\tau$ ) with  $35.9 \text{ fb}^{-1}$  of  $pp$  collision data at  $E_{\text{cm}} = 13 \text{ TeV}$ . The quoted signal strength corresponds to a significance of 3.2 standard deviations and is given for  $m_{H^0} = 125 \text{ GeV}$ .
- 10 AAD 16AL search for  $t\bar{t}H^0$  production with  $H^0$  decaying to  $\gamma\gamma$  in  $4.5 \text{ fb}^{-1}$  of  $pp$  collisions at  $E_{\text{cm}} = 7 \text{ TeV}$  and  $b\bar{b}, \tau\tau, \gamma\gamma, WW^*,$  and  $ZZ^*$  in  $20.3 \text{ fb}^{-1}$  at  $E_{\text{cm}} = 8 \text{ TeV}$ . The quoted signal strength is given for  $m_{H^0} = 125 \text{ GeV}$ . This paper combines the results of previous papers, and the new result of this paper only is:  $\mu = 1.6 \pm 2.6$ .
- 11 AAD 16AN perform fits to the ATLAS and CMS data at  $E_{\text{cm}} = 7$  and  $8 \text{ TeV}$ .
- 12 AAD 16K use up to  $4.7 \text{ fb}^{-1}$  of  $pp$  collisions at  $E_{\text{cm}} = 7 \text{ TeV}$  and up to  $20.3 \text{ fb}^{-1}$  at  $E_{\text{cm}} = 8 \text{ TeV}$ . The third uncertainty in the measurement is theory systematics. The quoted signal strength is given for  $m_{H^0} = 125.36 \text{ GeV}$ .
- 13 AAD 15 search for  $t\bar{t}H^0$  production with  $H^0$  decaying to  $\gamma\gamma$  in  $4.5 \text{ fb}^{-1}$  of  $pp$  collisions at  $E_{\text{cm}} = 7 \text{ TeV}$  and  $20.3 \text{ fb}^{-1}$  at  $E_{\text{cm}} = 8 \text{ TeV}$ . The quoted result on the signal strength is equivalent to an upper limit of 6.7 at 95% CL and is given for  $m_{H^0} = 125.4 \text{ GeV}$ .
- 14 AAD 15Bc search for  $t\bar{t}H^0$  production with  $H^0$  decaying to  $b\bar{b}$  in  $20.3 \text{ fb}^{-1}$  of  $pp$  collisions at  $E_{\text{cm}} = 8 \text{ TeV}$ . The corresponding upper limit is 3.4 at 95% CL. The quoted signal strength is given for  $m_{H^0} = 125 \text{ GeV}$ .
- 15 AAD 15T search for  $t\bar{t}H^0$  production with  $H^0$  resulting in multilepton final states (mainly from  $WW^*, \tau\tau, ZZ^*$ ) in  $20.3 \text{ fb}^{-1}$  of  $pp$  collisions at  $E_{\text{cm}} = 8 \text{ TeV}$ . The quoted result on the signal strength is given for  $m_{H^0} = 125 \text{ GeV}$  and corresponds to an upper limit of 4.7 at 95% CL. The data sample is independent from AAD 15 and AAD 15Bc.
- 16 KHACHATRYAN 15AN search for  $t\bar{t}H^0$  production with  $H^0$  decaying to  $b\bar{b}$  in  $19.5 \text{ fb}^{-1}$  of  $pp$  collisions at  $E_{\text{cm}} = 8 \text{ TeV}$ . The quoted result on the signal strength is equivalent to an upper limit of 4.2 at 95% CL and is given for  $m_{H^0} = 125 \text{ GeV}$ .
- 17 KHACHATRYAN 14H search for  $t\bar{t}H^0$  production with  $H^0$  decaying to  $b\bar{b}, \tau\tau, \gamma\gamma, WW^*,$  and  $ZZ^*$ , in  $5.1 \text{ fb}^{-1}$  of  $pp$  collisions at  $E_{\text{cm}} = 7 \text{ TeV}$  and  $19.7 \text{ fb}^{-1}$  at  $E_{\text{cm}} = 8 \text{ TeV}$ . The quoted signal strength is given for  $m_{H^0} = 125.6 \text{ GeV}$ .
- 18 AALTONEN 13L combine all CDF results with  $9.45\text{--}10.0 \text{ fb}^{-1}$  of  $p\bar{p}$  collisions at  $E_{\text{cm}} = 1.96 \text{ TeV}$ . The quoted signal strength is given for  $m_{H^0} = 125 \text{ GeV}$ .
- 19 CHATRCHYAN 13x search for  $t\bar{t}H^0$  production followed by  $H^0 \rightarrow b\bar{b}$ , one top decaying to  $\ell\nu$  and the other to either  $\ell\nu$  or  $q\bar{q}$  in  $5.0 \text{ fb}^{-1}$  and  $5.1 \text{ fb}^{-1}$  of  $pp$  collisions at  $E_{\text{cm}} = 7$  and  $8 \text{ TeV}$ . A limit on cross section times branching ratio which corresponds to  $(4.0\text{--}8.6)$  times the expected Standard Model cross section is given for  $m_{H^0} = 110\text{--}140 \text{ GeV}$  at 95% CL. The quoted limit is given for  $m_{H^0} = 125 \text{ GeV}$ , where 5.2 is expected for no signal.

 $H^0H^0$  ProductionThe 95% CL limits are for the cross section (CS) and Higgs self coupling ( $\kappa_\lambda$ ) scaling factors both relative to the SM predictions.

CS	$\kappa_\lambda$	CL%	DOCUMENT ID	TECN	COMMENT
• • • We do not use the following data for averages, fits, limits, etc. • • •					
< 6.9	-5.0 to 12.0	95	1 AAD	20c ATLS	13 TeV, $b\bar{b}\gamma\gamma, b\bar{b}\tau\tau, b\bar{b}b\bar{b}, b\bar{b}WW^*, WW^*\gamma\gamma, WW^*WW^*$
< 40		95	2 AAD	20E ATLS	13 TeV, $H^0H^0 \rightarrow b\bar{b}\ell\nu\ell\nu$
< 12.9		95	3 AABOUD	19A ATLS	13 TeV, $b\bar{b}b\bar{b}$
< 300		95	4 AABOUD	19O ATLS	13 TeV, $b\bar{b}WW^*$
< 160		95	5 AABOUD	19T ATLS	13 TeV, $WW^*WW^*$
< 24	-11 to 17	95	6 SIRUNYAN	19A CMS	13 TeV, $\gamma\gamma b\bar{b}$
< 75		95	7 SIRUNYAN	19AB CMS	13 TeV, $b\bar{b}b\bar{b}$
< 22.2	-11.8 to 18.8	95	8 SIRUNYAN	19BE CMS	13 TeV, $b\bar{b}\gamma\gamma, b\bar{b}\tau\tau, b\bar{b}b\bar{b}, b\bar{b}WW^*, b\bar{b}ZZ^*$
< 179		95	9 SIRUNYAN	19H CMS	13 TeV, $b\bar{b}b\bar{b}$
< 230		95	10 AABOUD	18Bu ATLS	13 TeV, $\gamma\gamma WW^*$
< 12.7		95	11 AABOUD	18Cq ATLS	13 TeV, $b\bar{b}\tau\tau$
< 22	-8.2 to 13.2	95	12 AABOUD	18Cw ATLS	13 TeV, $\gamma\gamma b\bar{b}$
< 30		95	13 SIRUNYAN	18A CMS	13 TeV, $b\bar{b}\tau\tau$
< 79		95	14 SIRUNYAN	18F CMS	13 TeV, $b\bar{b}\ell\nu\ell\nu$
< 43		95	15 SIRUNYAN	17CN CMS	8 TeV, $b\bar{b}\tau\tau, \gamma\gamma b\bar{b}, b\bar{b}b\bar{b}$
< 108		95	16 AABOUD	16i ATLS	13 TeV, $b\bar{b}b\bar{b}$
< 74		95	17 KHACHATRYAN...16Bq	CMS	8 TeV, $\gamma\gamma b\bar{b}$
< 70		95	18 AAD	15CE ATLS	8 TeV, $b\bar{b}b\bar{b}, b\bar{b}\tau\tau, \gamma\gamma b\bar{b}, \gamma\gamma WW$

- 1 AAD 20c combine results of up to  $36.1 \text{ fb}^{-1}$  data at  $E_{\text{cm}} = 13 \text{ TeV}$  for  $pp \rightarrow H^0H^0 \rightarrow b\bar{b}\gamma\gamma, b\bar{b}\tau\tau, b\bar{b}b\bar{b}, b\bar{b}WW^*, WW^*\gamma\gamma, WW^*WW^*$  (AABOUD 18Cw, AABOUD 18Cq, AABOUD 19A, AABOUD 19O, AABOUD 18Bu, and AABOUD 19T).
- 2 AAD 20e search non-resonant for  $H^0H^0$  production using  $H^0H^0 \rightarrow b\bar{b}\ell\nu\ell\nu$ , where one of the Higgs bosons decays to  $b\bar{b}$  and the other decays to either  $WW^*, ZZ^*,$  or  $\tau\tau$ , with data of  $139 \text{ fb}^{-1}$  at  $E_{\text{cm}} = 13 \text{ TeV}$ . The upper limit on the  $pp \rightarrow H^0H^0$  production cross section at 95% CL is measured to be 1.2 pb, which corresponds to about 40 times the SM prediction.
- 3 AABOUD 19A search for  $H^0H^0$  production using  $H^0H^0 \rightarrow b\bar{b}b\bar{b}$  with data of  $36.1 \text{ fb}^{-1}$  at  $E_{\text{cm}} = 13 \text{ TeV}$ . The upper limit on the  $pp \rightarrow H^0H^0 \rightarrow b\bar{b}b\bar{b}$  production cross section at 95% is measured to be 147 fb, which corresponds to about 12.9 times the SM prediction.



## Gauge &amp; Higgs Boson Particle Listings

 $H^0$ , Neutral Higgs Bosons, Searches for

Author	Year	Ref	Journal	Collab
SIRUNYAN	17CN	PR D96	072004	(CMS Collab.)
AABOUD	16I	PR D94	052002	(ATLAS Collab.)
AABOUD	16K	PRL 117	111802	(ATLAS Collab.)
AABOUD	16X	JHEP	1611 112	(ATLAS Collab.)
AAD	16	PL B753	69	(ATLAS Collab.)
AAD	16AC	PR D93	092005	(ATLAS Collab.)
AAD	16AF	JHEP	1601 172	(ATLAS Collab.)
AAD	16AL	JHEP	1605 160	(ATLAS Collab.)
AAD	16AN	JHEP	1608 045	(ATLAS and CMS Collabs.)
AAD	16AO	JHEP	1608 104	(ATLAS Collab.)
AAD	16BL	EPJ C76	658	(ATLAS Collab.)
AAD	16K	EPJ C76	6	(ATLAS Collab.)
KHACHATRYAN	16AB	PL B759	672	(CMS Collab.)
KHACHATRYAN	16AR	JHEP	1604 005	(CMS Collab.)
KHACHATRYAN	16AU	JHEP	1606 177	(CMS Collab.)
KHACHATRYAN	16B	PL B753	341	(CMS Collab.)
KHACHATRYAN	16BA	JHEP	1609 051	(CMS Collab.)
KHACHATRYAN	16BQ	PR D94	052012	(CMS Collab.)
KHACHATRYAN	16CD	PL B763	472	(CMS Collab.)
KHACHATRYAN	16G	EPJ C76	13	(CMS Collab.)
AAD	15	PL B740	222	(ATLAS Collab.)
AAD	15AA	PR D92	012006	(ATLAS Collab.)
AAD	15AH	JHEP	1504 117	(ATLAS Collab.)
AAD	15AQ	JHEP	1508 137	(ATLAS Collab.)
AAD	15AX	EPJ C75	231	(ATLAS Collab.)
AAD	15B	PRL 114	191803	(ATLAS and CMS Collabs.)
AAD	15BC	EPJ C75	349	(ATLAS Collab.)
AAD	15BD	EPJ C75	337	(ATLAS Collab.)
AAD	15BE	EPJ C75	335	(ATLAS Collab.)
AAD	15CE	PR D92	092004	(ATLAS Collab.)
AAD	15CI	EPJ C76	476	(ATLAS Collab.)
AAD	Also	EPJ C76	152 (err.)	(ATLAS Collab.)
AAD	15CX	JHEP	1511 206	(ATLAS Collab.)
AAD	15F	PR D91	012006	(ATLAS Collab.)
AAD	15G	JHEP	1501 069	(ATLAS Collab.)
AAD	15I	PRL 114	121801	(ATLAS Collab.)
AAD	15P	PRL 115	091801	(ATLAS Collab.)
AAD	15T	PL B749	519	(ATLAS Collab.)
AALTONEN	15	PRL 114	151802	(CDF and DO Collabs.)
AALTONEN	15B	PRL 114	141802	(CDF Collab.)
KHACHATRYAN	15AM	EPJ C75	212	(CMS Collab.)
KHACHATRYAN	15AN	EPJ C75	251	(CMS Collab.)
KHACHATRYAN	15BA	PR D92	072010	(CMS Collab.)
KHACHATRYAN	15H	PL B744	184	(CMS Collab.)
KHACHATRYAN	15J	PL B749	337	(CMS Collab.)
KHACHATRYAN	15K	PR D92	012004	(CMS Collab.)
KHACHATRYAN	15L	PR D92	032008	(CMS Collab.)
AAD	14AR	PL B738	234	(ATLAS Collab.)
AAD	14AS	PL B738	68	(ATLAS Collab.)
AAD	14BC	PR D90	112015	(ATLAS Collab.)
AAD	14BJ	JHEP	1409 112	(ATLAS Collab.)
AAD	14J	PL B732	8	(ATLAS Collab.)
AAD	14O	PRL 112	201802	(ATLAS Collab.)
AAD	14W	PR D90	052004	(ATLAS Collab.)
ABAZOV	14F	PRL 113	161802	(DO Collab.)
CHATRCHYAN	14AA	PR D89	092007	(CMS Collab.)
CHATRCHYAN	14AI	PR D89	012003	(CMS Collab.)
CHATRCHYAN	14AJ	NATP 10	557	(CMS Collab.)
CHATRCHYAN	14B	EPJ C74	2980	(CMS Collab.)
CHATRCHYAN	14G	JHEP	1401 096	(CMS Collab.)
CHATRCHYAN	14K	JHEP	1405 104	(CMS Collab.)
KHACHATRYAN	14D	PL B736	64	(CMS Collab.)
KHACHATRYAN	14H	JHEP	1409 087	(CMS Collab.)
KHACHATRYAN	14P	EPJ C74	3076	(CMS Collab.)
AAD	13AJ	PL B726	120	(ATLAS Collab.)
AAD	13AK	PL B726	88	(ATLAS Collab.)
AAD	Also	PL B734	406 (err.)	(ATLAS Collab.)
AALTONEN	13L	PR D88	052013	(CDF Collab.)
AALTONEN	13M	PR D88	052014	(CDF and DO Collabs.)
ABAZOV	13L	PR D88	052011	(DO Collab.)
CHATRCHYAN	13BK	PL B726	587	(CMS Collab.)
CHATRCHYAN	13J	PRL 110	081803	(CMS Collab.)
CHATRCHYAN	13X	JHEP	1305 145	(CMS Collab.)
CHATRCHYAN	13Y	JHEP	1306 081	(CMS Collab.)
HEINEMEYER	13A	arXiv:1307.1347		(LHC Higgs CS Working Group)
AAD	12AI	PL B716	1	(ATLAS Collab.)
AAD	12DA	SCI 338	1576	(ATLAS Collab.)
AALTONEN	12Q	PRL 109	111803	(CDF Collab.)
AALTONEN	12R	PRL 109	111804	(CDF Collab.)
AALTONEN	12S	PRL 109	111805	(CDF Collab.)
AALTONEN	12T	PRL 109	071804	(CDF and DO Collabs.)
ABAZOV	12K	PL B716	285	(DO Collab.)
ABAZOV	12O	PRL 109	121803	(DO Collab.)
ABAZOV	12P	PRL 109	121804	(DO Collab.)
CHATRCHYAN	12BY	SCI 338	1569	(CMS Collab.)
CHATRCHYAN	12N	PL B716	30	(CMS Collab.)
DIETMAIER	12	arXiv:1201.3084		(LHC Higgs CS Working Group)
DIETMAIER	11	arXiv:1101.0593		(LHC Higgs CS Working Group)

## Neutral Higgs Bosons, Searches for

## CONTENTS:

- Mass Limits for Neutral Higgs Bosons in Supersymmetric Models
  - Mass Limits for heavy neutral Higgs bosons ( $H_2^0, A^0$ ) in the MSSM
  - Mass Limits for  $H_1^0$  (Higgs Boson) in Supersymmetric Models
- Mass Limits for Neutral Higgs Bosons in Extended Higgs Models
  - Mass Limits in General two-Higgs-doublet Models
  - Mass Limits for  $H^0$  with Vanishing Yukawa Couplings
  - Mass Limits for  $H^0$  Decaying to Invisible Final States
  - Mass Limits for Light  $A^0$
  - Other Mass Limits
- Searches for a Higgs Boson with Standard Model Couplings
  - Direct Mass Limits for  $H^0$
  - Indirect Mass Limits for  $H^0$  from Electroweak Analysis

## MASS LIMITS FOR NEUTRAL HIGGS BOSONS IN SUPERSYMMETRIC MODELS

The minimal supersymmetric model has two complex doublets of Higgs bosons. The resulting physical states are two scalars [ $H_1^0$  and  $H_2^0$ ], where we define  $m_{H_1^0} < m_{H_2^0}$ , a pseudoscalar ( $A^0$ ), and a charged Higgs pair ( $H^\pm$ ).  $H_1^0$  and  $H_2^0$  are also called  $h$  and  $H$  in the literature. There are two free parameters in the Higgs sector which can be chosen to be  $m_{A^0}$  and  $\tan\beta = v_2/v_1$ , the ratio of vacuum expectation values of the two Higgs doublets. Tree-level Higgs masses are constrained by the model to be  $m_{H_1^0} \leq m_Z$ ,  $m_{H_2^0} \geq m_Z$ ,  $m_{A^0} \geq m_{H^0}$ , and  $m_{H^\pm} \geq m_W$ . However, as described in the review on "Status of Higgs Boson Physics" in this Volume these relations are violated by radiative corrections.

The observed signal at about 125 GeV, see section "H<sup>0</sup>", can be interpreted as one of the neutral Higgs bosons of supersymmetric models. Unless otherwise noted, we identify the lighter scalar  $H_1^0$  with the Higgs discovered at 125 GeV at the LHC (AAD 12AI, CHATRCHYAN 12N).

Unless otherwise noted, the experiments in  $e^+e^-$  collisions search for the processes  $e^+e^- \rightarrow H_1^0 Z^0$  in the channels used for the Standard Model Higgs searches and  $e^+e^- \rightarrow H_2^0 A^0$  in the final states  $b\bar{b}b\bar{b}$  and  $b\bar{b}\tau^+\tau^-$ . Unless otherwise stated, the following results assume no invisible  $H_1^0$  or  $A^0$  decays. Unless otherwise noted, the results are given in the  $m_h^{max}$  scenario, CARENA 13.

In  $p\bar{p}$  and  $pp$  collisions the experiments search for a variety of processes, as explicitly specified for each entry. Limits on the  $A^0$  mass arise from these direct searches, as well as from the relations valid in the minimal supersymmetric model between  $m_{A^0}$  and  $m_{H_1^0}$ . As discussed in the review on "Status of Higgs Boson Physics" in this Volume, these relations depend, via potentially large radiative corrections, on the mass of the  $t$  quark and on the supersymmetric parameters, in particular those of the stop sector. These indirect limits are weaker for larger  $t$  and  $\bar{t}$  masses. To include the radiative corrections to the Higgs masses, unless otherwise stated, the listed papers use theoretical predictions incorporating two-loop corrections, and the results are given for the  $m_h^{mod+}$  benchmark scenario, see CARENA 13.

Mass Limits for heavy neutral Higgs bosons ( $H_2^0, A^0$ ) in the MSSM

The limits rely on  $pp \rightarrow H_2^0/A^0 \rightarrow \tau^+\tau^-$  and assume that  $H_2^0$  and  $A^0$  are (sufficiently) mass degenerate. The limits depend on  $\tan\beta$ .

VALUE (GeV)	CL%	DOCUMENT ID	TECN	COMMENT
> 377	95	1 AABOUD	18G ATLS	$\tan\beta = 10$ GeV
> 863	95	1 AABOUD	18G ATLS	$\tan\beta = 20$ GeV
>1157	95	1 AABOUD	18G ATLS	$\tan\beta = 30$ GeV
>1328	95	1 AABOUD	18G ATLS	$\tan\beta = 40$ GeV
>1483	95	1 AABOUD	18G ATLS	$\tan\beta = 50$ GeV
>1613	95	1 AABOUD	18G ATLS	$\tan\beta = 60$ GeV
> 389	95	2 SIRUNYAN	18CX CMS	$\tan\beta = 10$ GeV
> 832	95	2 SIRUNYAN	18CX CMS	$\tan\beta = 20$ GeV
>1148	95	2 SIRUNYAN	18CX CMS	$\tan\beta = 30$ GeV
>1341	95	2 SIRUNYAN	18CX CMS	$\tan\beta = 40$ GeV
>1496	95	2 SIRUNYAN	18CX CMS	$\tan\beta = 50$ GeV
>1613	95	2 SIRUNYAN	18CX CMS	$\tan\beta = 60$ GeV

• • • We do not use the following data for averages, fits, limits, etc. • • •

3 AAD	20 ATLS	$H^0$ properties
4 AAD	20C ATLS	$H_2^0 \rightarrow H^0 H^0$
5 SIRUNYAN	19CR CMS	$H_2^0/A^0 \rightarrow \mu^+\mu^-$
6 SIRUNYAN	18A CMS	$H_2^0 \rightarrow H^0 H^0$
7 SIRUNYAN	18BP CMS	$pp \rightarrow H_2^0/A^0 + b + X$ , $H_2^0/A^0 \rightarrow b\bar{b}$
8 AABOUD	16AA ATLS	$A^0 \rightarrow \tau^+\tau^-$
9 KHACHATRYAN	16A CMS	$H_{1,2}^0/A^0 \rightarrow \mu^+\mu^-$
10 KHACHATRYAN	16P CMS	$H_2^0 \rightarrow H^0 H^0, A^0 \rightarrow Z H^0$
11 KHACHATRYAN	15AY CMS	$pp \rightarrow H_{1,2}^0/A^0 + b + X$ , $H_{1,2}^0/A^0 \rightarrow b\bar{b}$
12 AAD	14AW ATLS	$pp \rightarrow H_{1,2}^0/A^0 + X$ , $H_{1,2}^0/A^0 \rightarrow \tau\tau$
13 KHACHATRYAN	14M CMS	$pp \rightarrow H_{1,2}^0/A^0 + X$ , $H_{1,2}^0/A^0 \rightarrow \tau\tau$
14 AAD	13o ATLS	$pp \rightarrow H_{1,2}^0/A^0 + X$ , $H_{1,2}^0/A^0 \rightarrow \tau^+\tau^-$
15 AAIJ	13T LHCB	$pp \rightarrow H_{1,2}^0/A^0 + X$ , $H_{1,2}^0/A^0 \rightarrow \tau^+\tau^-$
16 CHATRCHYAN	13AG CMS	$pp \rightarrow H_{1,2}^0/A^0 + b + X$ , $H_{1,2}^0/A^0 \rightarrow b\bar{b}$
17 AALTONEN	12AQ TEVA	$p\bar{p} \rightarrow H_{1,2}^0/A^0 + b + X$ , $H_{1,2}^0/A^0 \rightarrow b\bar{b}$

	18	AALTONEN	12X	CDF	$p\bar{p} \rightarrow H_{1,2}^0/A^0 + b + X,$ $H_{1,2}^0/A^0 \rightarrow b\bar{b}$		
	19	ABAZOV	12G	D0	$p\bar{p} \rightarrow H_{1,2}^0/A^0 + X,$ $H_{1,2}^0/A^0 \rightarrow \tau^+\tau^-$		
	20	CHATRCHYAN	12K	CMS	$pp \rightarrow H_{1,2}^0/A^0 + X,$ $H_{1,2}^0/A^0 \rightarrow \tau^+\tau^-$		
	21	ABAZOV	11K	D0	$p\bar{p} \rightarrow H_{1,2}^0/A^0 + b + X,$ $H_{1,2}^0/A^0 \rightarrow b\bar{b}$		
	22	ABAZOV	11W	D0	$p\bar{p} \rightarrow H_{1,2}^0/A^0 + b + X,$ $H_{1,2}^0/A^0 \rightarrow \tau^+\tau^-$		
	23	AALTONEN	09AR	CDF	$p\bar{p} \rightarrow H_{1,2}^0/A^0 + X,$ $H_{1,2}^0/A^0 \rightarrow \tau^+\tau^-$		
>	90.4	24	ABDALLAH	08B	DLPH	$E_{cm} \leq 209$ GeV	
>	93.4	95	25	SCHAEEL	06B	LEP	$E_{cm} \leq 209$ GeV
		26	ACOSTA	05Q	CDF	$p\bar{p} \rightarrow H_{1,2}^0/A^0 + X$	
>	85.0	95	27,28	ABBIENDI	04M	OPAL	$E_{cm} \leq 209$ GeV
		29	ABBIENDI	03G	OPAL	$H_1^0 \rightarrow A^0 A^0$	
>	86.5	95	27,30	ACHARD	02H	L3	$E_{cm} \leq 209$ GeV, $\tan\beta > 0.4$
		31	AKERROYD	02	RVUE		
>	90.1	95	27,32	HEISTER	02	ALEP	$E_{cm} \leq 209$ GeV, $\tan\beta > 0.5$
		1	ABOUD	18G	search for production of $H_{2,3}^0/A^0 \rightarrow \tau^+\tau^-$ by gluon fusion and $b$ -associated production in $36.1 \text{ fb}^{-1}$ of $pp$ collisions at $E_{cm} = 13$ TeV. See their Fig. 10 for excluded regions in the $m_{A^0} - \tan\beta$ plane in several MSSM scenarios.		
		2	SIRUNYAN	18CX	search for production of $H_{1,2}^0/A^0 \rightarrow \tau^+\tau^-$ by gluon fusion and $b$ -associated production in $35.9 \text{ fb}^{-1}$ of $pp$ collisions at $E_{cm} = 13$ TeV. See their Fig. 9 for excluded regions in the $m_{A^0} - \tan\beta$ plane in several MSSM scenarios.		
		3	AAD	20	combine measurements of $H^0$ production and decay using data taken in years 2015–2017 (up to $79.8 \text{ fb}^{-1}$ ) of $pp$ collisions at $E_{cm} = 13$ TeV. See their Fig. 19 for excluded region in the hMSSM parameter space.		
		4	AAD	20C	combine searches for a scalar resonance decaying to $H^0 H^0$ in $36.1 \text{ fb}^{-1}$ of $pp$ collisions at $E_{cm} = 13$ TeV from ABOUD 19A, ABOUD 19O, ABOUD 18CQ, ABOUD 19T, ABOUD 18CW, and ABOUD 18BU. See their Fig. 7(b) for the excluded region in the hMSSM parameter space.		
		5	SIRUNYAN	19CR	search for production of $H_{2,3}^0/A^0$ in gluon fusion and in association with a $b\bar{b}$ pair, decaying to $\mu^+\mu^-$ in $35.9 \text{ fb}^{-1}$ of $pp$ collisions at $E_{cm} = 13$ TeV. See their Fig. 5 for the excluded region in the MSSM parameter space in the $m_h^{\text{mod}+}$ and hMSSM scenarios.		
		6	SIRUNYAN	18A	search for production of a scalar resonance decaying to $H^0 H^0 \rightarrow b\bar{b}\tau^+\tau^-$ in $35.9 \text{ fb}^{-1}$ of $pp$ collisions at $E_{cm} = 13$ TeV. See their Fig. 5 (lower) for excluded regions in the $m_{A^0} - \tan\beta$ plane in the hMSSM scenario.		
		7	SIRUNYAN	18BP	search for production of $H_{2,3}^0/A^0 \rightarrow b\bar{b}$ by $b$ -associated production in $35.7 \text{ fb}^{-1}$ of $pp$ collisions at $E_{cm} = 13$ TeV. See their Fig. 6 for the limits on cross section times branching ratio for $m_{H_{2,3}^0}, m_{A^0} = 0.3\text{--}1.3$ TeV, and Fig. 7 for excluded regions in the $m_{A^0} - \tan\beta$ plane in several MSSM scenarios.		
		8	ABOUD	16AA	search for production of a Higgs boson in gluon fusion and in association with a $b\bar{b}$ pair followed by the decay $A^0 \rightarrow \tau^+\tau^-$ in $3.2 \text{ fb}^{-1}$ of $pp$ collisions at $E_{cm} = 13$ TeV. See their Fig. 5(a, b) for limits on cross section times branching ratio for $m_{A^0} = 200\text{--}1200$ GeV, and Fig. 5(c, d) for the excluded region in the MSSM parameter space in the $m_h^{\text{mod}+}$ and hMSSM scenarios.		
		9	KHACHATRYAN	16A	search for production of a Higgs boson in gluon fusion and in association with a $b\bar{b}$ pair followed by the decay $H_{1,2}^0/A^0 \rightarrow \mu^+\mu^-$ in $5.1 \text{ fb}^{-1}$ of $pp$ collisions at $E_{cm} = 7$ TeV and $19.3 \text{ fb}^{-1}$ at $E_{cm} = 8$ TeV. See their Fig. 7 for the excluded region in the MSSM parameter space in the $m_h^{\text{mod}+}$ benchmark scenario and Fig. 9 for limits on cross section times branching ratio.		
		10	KHACHATRYAN	16P	search for gluon fusion production of an $H_{2,3}^0$ decaying to $H^0 H^0 \rightarrow b\bar{b}\tau^+\tau^-$ and an $A^0$ decaying to $ZH^0 \rightarrow \ell^+\ell^-\tau^+\tau^-$ in $19.7 \text{ fb}^{-1}$ of $pp$ collisions at $E_{cm} = 8$ TeV. See their Fig. 12 for excluded region in the $\tan\beta - \cos(\beta - \alpha)$ plane for $m_{H_{2,3}^0} = m_{A^0} = 300$ GeV.		
		11	KHACHATRYAN	15AY	search for production of a Higgs boson in association with a $b$ quark in the decay $H_{1,2}^0/A^0 \rightarrow b\bar{b}$ in $19.7 \text{ fb}^{-1}$ of $pp$ collisions at $E_{cm} = 8$ TeV and combine with CHATRCHYAN 13AG 7 TeV data. See their Fig. 6 for the limits on cross section times branching ratio for $m_{A^0} = 100\text{--}900$ GeV and Figs. 7–9 for the excluded region in the MSSM parameter space in various benchmark scenarios.		
		12	AAD	14AW	search for production of a Higgs boson followed by the decay $H_{1,2}^0/A^0 \rightarrow \tau^+\tau^-$ in $19.5\text{--}20.3 \text{ fb}^{-1}$ of $pp$ collisions at $E_{cm} = 8$ TeV. See their Fig. 11 for the limits on cross section times branching ratio and their Figs. 9 and 10 for the excluded region in the MSSM parameter space. For $m_{A^0} = 140$ GeV, the region $\tan\beta > 5.4$ is excluded at 95% CL in the $m_h^{\text{max}}$ scenario.		
		13	KHACHATRYAN	14M	search for production of a Higgs boson in gluon fusion and in association with a $b$ quark followed by the decay $H_{1,2}^0/A^0 \rightarrow \tau^+\tau^-$ in $4.9 \text{ fb}^{-1}$ of $pp$ collisions at $E_{cm} = 7$ TeV and $19.7 \text{ fb}^{-1}$ at $E_{cm} = 8$ TeV. See their Figs. 7 and 8 for one- and two-dimensional limits on cross section times branching ratio and their Figs. 5 and 6 for the excluded region in the MSSM parameter space. For $m_{A^0} = 140$ GeV, the region $\tan\beta > 3.8$ is excluded at 95% CL in the $m_h^{\text{max}}$ scenario.		
		14	AAD	13O	search for production of a Higgs boson in the decay $H_{1,2}^0/A^0 \rightarrow \tau^+\tau^-$ and $\mu^+\mu^-$ with $4.7\text{--}4.8 \text{ fb}^{-1}$ of $pp$ collisions at $E_{cm} = 7$ TeV. See their Fig. 6 for the excluded region in the MSSM parameter space and their Fig. 7 for the limits on cross		

section times branching ratio. For  $m_{A^0} = 110\text{--}170$  GeV,  $\tan\beta \gtrsim 10$  is excluded, and for  $\tan\beta = 50$ ,  $m_{A^0}$  below 470 GeV is excluded at 95% CL in the  $m_h^{\text{max}}$  scenario.

- 15 AAIJ 13T search for production of a Higgs boson in the forward region in the decay  $H_{1,2}^0/A^0 \rightarrow \tau^+\tau^-$  in  $1.0 \text{ fb}^{-1}$  of  $pp$  collisions at  $E_{cm} = 7$  TeV. See their Fig. 2 for the limits on cross section times branching ratio and the excluded region in the MSSM parameter space.
- 16 CHATRCHYAN 13AG search for production of a Higgs boson in association with a  $b$  quark in the decay  $H_{1,2}^0/A^0 \rightarrow b\bar{b}$  in  $2.7\text{--}4.8 \text{ fb}^{-1}$  of  $pp$  collisions at  $E_{cm} = 7$  TeV. See their Fig. 6 for the excluded region in the MSSM parameter space and Fig. 5 for the limits on cross section times branching ratio. For  $m_{A^0} = 90\text{--}350$  GeV, upper bounds on  $\tan\beta$  of 18–42 at 95% CL are obtained in the  $m_h^{\text{max}}$  scenario with  $\mu = +200$  GeV.
- 17 AALTONEN 12AQ combine AALTONEN 12X and ABAZOV 11K. See their Table I and Fig. 1 for the limit on cross section times branching ratio and Fig. 2 for the excluded region in the MSSM parameter space.
- 18 AALTONEN 12X search for associated production of a Higgs boson and a  $b$  quark in the decay  $H_{1,2}^0/A^0 \rightarrow b\bar{b}$ , with  $2.6 \text{ fb}^{-1}$  of  $p\bar{p}$  collisions at  $E_{cm} = 1.96$  TeV. See their Table III and Fig. 15 for the limit on cross section times branching ratio and Figs. 17, 18 for the excluded region in the MSSM parameter space.
- 19 ABAZOV 12G search for production of a Higgs boson in the decay  $H_{1,2}^0/A^0 \rightarrow \tau^+\tau^-$  with  $7.3 \text{ fb}^{-1}$  of  $p\bar{p}$  collisions at  $E_{cm} = 1.96$  TeV and combine with ABAZOV 11W and ABAZOV 11K. See their Figs. 4, 5, and 6 for the excluded region in the MSSM parameter space. For  $m_{A^0} = 90\text{--}180$  GeV,  $\tan\beta \gtrsim 30$  is excluded at 95% CL in the  $m_h^{\text{max}}$  scenario.
- 20 CHATRCHYAN 12K search for production of a Higgs boson in the decay  $H_{1,2}^0/A^0 \rightarrow \tau^+\tau^-$  with  $4.6 \text{ fb}^{-1}$  of  $pp$  collisions at  $E_{cm} = 7$  TeV. See their Fig. 3 and Table 4 for the excluded region in the MSSM parameter space. For  $m_{A^0} = 160$  GeV, the region  $\tan\beta > 7.1$  is excluded at 95% CL in the  $m_h^{\text{max}}$  scenario. Superseded by KHACHATRYAN 14M.
- 21 ABAZOV 11K search for associated production of a Higgs boson and a  $b$  quark, followed by the decay  $H_{1,2}^0/A^0 \rightarrow b\bar{b}$ , in  $5.2 \text{ fb}^{-1}$  of  $p\bar{p}$  collisions at  $E_{cm} = 1.96$  TeV. See their Fig. 5/Table 2 for the limit on cross section times branching ratio and Fig. 6 for the excluded region in the MSSM parameter space for  $\mu = -200$  GeV.
- 22 ABAZOV 11W search for associated production of a Higgs boson and a  $b$  quark, followed by the decay  $H_{1,2}^0/A^0 \rightarrow \tau\tau$ , in  $7.3 \text{ fb}^{-1}$  of  $p\bar{p}$  collisions at  $E_{cm} = 1.96$  TeV. See their Fig. 2 for the limit on cross section times branching ratio and for the excluded region in the MSSM parameter space.
- 23 AALTONEN 09AR search for Higgs bosons decaying to  $\tau^+\tau^-$  in two doublet models in  $1.8 \text{ fb}^{-1}$  of  $p\bar{p}$  collisions at  $E_{cm} = 1.96$  TeV. See their Fig. 2 for the limit on  $\sigma \cdot B(H_{1,2}^0/A^0 \rightarrow \tau^+\tau^-)$  for different Higgs masses, and see their Fig. 3 for the excluded region in the MSSM parameter space.
- 24 ABDALLAH 08B give limits in eight  $CP$ -conserving benchmark scenarios and some  $CP$ -violating scenarios. See paper for excluded regions for each scenario. Supersedes ABDALLAH 04.
- 25 SCHAEEL 06B make a combined analysis of the LEP data. The quoted limit is for the  $m_h^{\text{max}}$  scenario with  $m_t = 174.3$  GeV. In the  $CP$ -violating CPX scenario no lower bound on  $m_{H_1^0}$  can be set at 95% CL. See paper for excluded regions in various scenarios. See Figs. 2–6 and Tabs. 14–21 for limits on  $\sigma(ZH^0) \cdot B(H^0 \rightarrow b\bar{b}, \tau^+\tau^-)$  and  $\sigma(H_1^0 H_2^0) \cdot B(H_1^0 H_2^0 \rightarrow b\bar{b}, \tau^+\tau^-)$ .
- 26 ACOSTA 05Q search for  $H_{1,2}^0/A^0$  production in  $p\bar{p}$  collisions at  $E_{cm} = 1.8$  TeV with  $H_{1,2}^0/A^0 \rightarrow \tau^+\tau^-$ . At  $m_{A^0} = 100$  GeV, the obtained cross section upper limit is above theoretical expectation.
- 27 Search for  $e^+e^- \rightarrow H_{1,2}^0/A^0$  in the final states  $b\bar{b}b\bar{b}$  and  $b\bar{b}\tau^+\tau^-$ , and  $e^+e^- \rightarrow H_{1,2}^0 Z$ . Universal scalar mass of 1 TeV,  $SU(2)$  gaugino mass of 200 GeV, and  $\mu = -200$  GeV are assumed, and two-loop radiative corrections incorporated. The limits hold for  $m_t = 175$  GeV, and for the  $m_h^{\text{max}}$  scenario.
- 28 ABBIENDI 04M exclude  $0.7 < \tan\beta < 1.9$ , assuming  $m_t = 174.3$  GeV. Limits for other MSSM benchmark scenarios, as well as for  $CP$  violating cases, are also given.
- 29 ABBIENDI 03G search for  $e^+e^- \rightarrow H_{1,2}^0/A^0$  followed by  $H_{1,2}^0/A^0 \rightarrow A^0 A^0, A^0 \rightarrow c\bar{c}, gg$ , or  $\tau^+\tau^-$ . In the no-mixing scenario, the region  $m_{H_1^0} = 45\text{--}85$  GeV and  $m_{A^0} = 2\text{--}9.5$  GeV is excluded at 95% CL.
- 30 ACHARD 02H also search for the final state  $H_{1,2}^0 Z \rightarrow 2A^0 q\bar{q}, A^0 \rightarrow q\bar{q}$ . In addition, the MSSM parameter set in the “large- $\mu$ ” and “no-mixing” scenarios are examined.
- 31 AKEROYD 02 examine the possibility of a light  $A^0$  with  $\tan\beta < 1$ . Electroweak measurements are found to be inconsistent with such a scenario.
- 32 HEISTER 02 excludes the range  $0.7 < \tan\beta < 2.3$ . A wider range is excluded with different stop mixing assumptions. Updates BARATE 01C.

### Mass Limits for $H_1^0$ (Higgs Boson) in Supersymmetric Models

VALUE (GeV)	CL%	DOCUMENT ID	TECN	COMMENT
>89.7		1	ABDALLAH	08B DLPH $E_{cm} \leq 209$ GeV
>92.8	95	2	SCHAEEL	06B LEP $E_{cm} \leq 209$ GeV
>84.5	95	3,4	ABBIENDI	04M OPAL $E_{cm} \leq 209$ GeV
>86.0	95	3,5	ACHARD	02H L3 $E_{cm} \leq 209$ GeV, $\tan\beta > 0.4$
>89.8	95	3,6	HEISTER	02 ALEP $E_{cm} \leq 209$ GeV, $\tan\beta > 0.5$

- We do not use the following data for averages, fits, limits, etc. •••
- 7 AALTONEN 12AQ TEVA  $p\bar{p} \rightarrow H_{1,2}^0/A^0 + b + X,$   
 $H_{1,2}^0/A^0 \rightarrow b\bar{b}$

1 ABDALLAH 08B give limits in eight  $CP$ -conserving benchmark scenarios and some  $CP$ -violating scenarios. See paper for excluded regions for each scenario. Supersedes ABDALLAH 04.

2 SCHAEEL 06B make a combined analysis of the LEP data. The quoted limit is for the  $m_h^{\text{max}}$  scenario with  $m_t = 174.3$  GeV. In the  $CP$ -violating CPX scenario no lower bound



# Gauge & Higgs Boson Particle Listings

## Neutral Higgs Bosons, Searches for

on  $m_{H_1^0}$  can be set at 95% CL. See paper for excluded regions in various scenarios. See

Figs. 2–6 and Tabs. 14–21 for limits on  $\sigma(ZH^0) \cdot \mathcal{B}(H^0 \rightarrow b\bar{b}, \tau^+\tau^-)$  and  $\sigma(H_1^0 H_2^0) \cdot \mathcal{B}(H_1^0, H_2^0 \rightarrow b\bar{b}, \tau^+\tau^-)$ .

<sup>3</sup> Search for  $e^+e^- \rightarrow H_1^0 A^0$  in the final states  $b\bar{b}b\bar{b}$  and  $b\bar{b}\tau^+\tau^-$ , and  $e^+e^- \rightarrow H_1^0 Z$ . Universal scalar mass of 1 TeV, SU(2) gaugino mass of 200 GeV, and  $\mu = -200$  GeV are assumed, and two-loop radiative corrections incorporated. The limits hold for  $m_t = 175$  GeV, and for the  $m_h^{\text{max}}$  scenario.

<sup>4</sup> ABBIENDI 04M exclude  $0.7 < \tan\beta < 1.9$ , assuming  $m_t = 174.3$  GeV. Limits for other MSSM benchmark scenarios, as well as for CP violating cases, are also given.

<sup>5</sup> ACHARD 02H also search for the final state  $H_1^0 Z \rightarrow 2A^0 q\bar{q}$ ,  $A^0 \rightarrow q\bar{q}$ . In addition, the MSSM parameter set in the “large- $\mu$ ” and “no-mixing” scenarios are examined.

<sup>6</sup> HEISTER 02 excludes the range  $0.7 < \tan\beta < 2.3$ . A wider range is excluded with different stop mixing assumptions. Updates BARATE 01c.

<sup>7</sup> AALTONEN 12A0 combine AALTONEN 12x and ABAZOV 11k. See their Table I and Fig. 1 for the limit on cross section times branching ratio and Fig. 2 for the excluded region in the MSSM parameter space.

### MASS LIMITS FOR NEUTRAL HIGGS BOSONS IN EXTENDED HIGGS MODELS

This Section covers models which do not fit into either the Standard Model or its simplest minimal Supersymmetric extension (MSSM), leading to anomalous production rates, or nonstandard final states and branching ratios. In particular, this Section covers limits which may apply to generic two-Higgs-doublet models (2HDM), or to special regions of the MSSM parameter space where decays to invisible particles or to photon pairs are dominant (see the review on “Status of Higgs Boson Physics”). Concerning the mass limits for  $H^0$  and  $A^0$  listed below, see the footnotes or the comment lines for details on the nature of the models to which the limits apply.

The observed signal at about 125 GeV, see section “ $H^0$ ”, can be interpreted as one of the neutral Higgs bosons of an extended Higgs sector.

#### Mass Limits in General two-Higgs-doublet Models

VALUE (GeV)	CL%	DOCUMENT ID	TECN	COMMENT
• • •				We do not use the following data for averages, fits, limits, etc. • • •
		1 AAD 20 ATLS	$H^0$	properties
		2 SIRUNYAN 19AE CMS	$A^0 \rightarrow \tau^+\tau^-$	
		3 SIRUNYAN 19AV CMS	$A^0 \rightarrow ZH^0$	
		4 AABOUD 18AH ATLS	$A^0 \rightarrow ZH_2^0$	
		5 AABOUD 18AI ATLS	$A^0 \rightarrow ZH^0$	
		6 AABOUD 18BF ATLS	$H_2^0 \rightarrow ZZ$	
		7 AABOUD 18CE ATLS	$pp \rightarrow H_2^0/A^0 t\bar{t}$ , $H_2^0/A^0 \rightarrow t\bar{t}$	
		8 HALLER 18 RVUE	global fits	
		9 SIRUNYAN 18BP CMS	$pp \rightarrow H_2^0/A^0 + b + X$ , $H_2^0/A^0 \rightarrow b\bar{b}$	
		10 SIRUNYAN 18ED CMS	$A^0 \rightarrow ZH^0$	
		11 AABOUD 17AN ATLS	$H_2^0, A^0 \rightarrow t\bar{t}$	
		12 SIRUNYAN 17AX CMS	$A^0 b\bar{b}, A^0 \rightarrow \mu^+\mu^-$	
		13 AAD 16AX ATLS	$H_2^0 \rightarrow ZZ$	
		14 KHACHATRYAN 16P CMS	$H_2^0 \rightarrow H^0 H^0, A^0 \rightarrow ZH^0$	
		15 KHACHATRYAN 16W CMS	$A^0 b\bar{b}, A^0 \rightarrow \tau^+\tau^-$	
		16 KHACHATRYAN 16Z CMS	$H_2^0 \rightarrow ZA^0$ or $A^0 \rightarrow ZH_2^0$	
		17 AAD 15BK ATLS	$H_2^0 \rightarrow H^0 H^0$	
		18 AAD 15S ATLS	$A^0 \rightarrow ZH^0$	
		19 KHACHATRYAN 15BB CMS	$H_2^0, A^0 \rightarrow \gamma\gamma$	
		20 KHACHATRYAN 15N CMS	$A^0 \rightarrow ZH^0$	
		21 AAD 14M ATLS	$H_2^0 \rightarrow H^\pm W^\mp \rightarrow H^0 W^\pm W^\mp, H^0 \rightarrow b\bar{b}$	
		22 KHACHATRYAN 14Q CMS	$H_2^0 \rightarrow H^0 H^0, A^0 \rightarrow ZH^0$	
		23 AALTONEN 09AR CDF	$p\bar{p} \rightarrow H_{1,2}^0/A^0 + X$ , $H_{1,2}^0/A^0 \rightarrow \tau^+\tau^-$	
none 1–55	95	24 ABBIENDI 05A OPAL	$H_1^0$ , Type II model	
>110.6	95	25 ABDALLAH 05D DLPH	$H^0 \rightarrow 2$ jets	
		26 ABDALLAH 04O DLPH	$Z \rightarrow t\bar{t}H$	
		27 ABDALLAH 04O DLPH	$e^+e^- \rightarrow H^0 Z, H^0 A^0$	
		28 ABBIENDI 02D OPAL	$e^+e^- \rightarrow b\bar{b}H$	
none 1–44	95	29 ABBIENDI 01E OPAL	$H_1^0$ , Type-II model	
> 68.0	95	30 ABBIENDI 99E OPAL	$\tan\beta > 1$	
		31 ABREU 95H DLPH	$Z \rightarrow H^0 Z^*, H^0 A^0$	
		32 PICH 92 RVUE	Very light Higgs	

<sup>1</sup> AAD 20 combine measurements on  $H^0$  production and decay using data taken in years 2015–2017 (up to  $79.8 \text{ fb}^{-1}$ ) of  $pp$  collisions at  $E_{\text{cm}} = 13$  TeV. See their Fig. 18 for excluded regions in various 2HDMs.

<sup>2</sup> SIRUNYAN 19AE search for a pseudoscalar resonance produced in association with a  $b\bar{b}$  pair, decaying to  $\tau^+\tau^-$  in  $35.9 \text{ fb}^{-1}$  of  $pp$  collisions at  $E_{\text{cm}} = 13$  TeV. See their Fig. 4 for cross section limits for  $m_{A^0} = 25\text{--}70$  GeV and comparison with some representative 2HDMs.

<sup>3</sup> SIRUNYAN 19AV search for a scalar resonance produced by gluon fusion or  $b$  associated production, decaying to  $ZH^0 \rightarrow \ell^+\ell^- b\bar{b}$  ( $\ell = e, \mu$ ) or  $\nu\bar{\nu}b\bar{b}$  in  $35.9 \text{ fb}^{-1}$  of  $pp$  collisions at  $E_{\text{cm}} = 13$  TeV. See their Figs. 6 and 7 for excluded regions in the parameter space of various 2HDMs.

<sup>4</sup> AABOUD 18AH search for production of an  $A^0$  in gluon-gluon fusion and in association with a  $b\bar{b}$ , decaying to  $ZH_2^0 \rightarrow \ell^+\ell^- b\bar{b}$  in  $36.1 \text{ fb}^{-1}$  of  $pp$  collisions at  $E_{\text{cm}} = 13$  TeV. See their Fig. 6 for excluded regions in the parameter space of various 2HDMs.

<sup>5</sup> AABOUD 18AI search for production of an  $A^0$  in gluon-gluon fusion and in association with a  $b\bar{b}$ , decaying to  $ZH^0$  in the final states  $\nu\bar{\nu}b\bar{b}$  and  $\ell^+\ell^- b\bar{b}$  in  $36.1 \text{ fb}^{-1}$  of  $pp$  collisions at  $E_{\text{cm}} = 13$  TeV. See their Figs. 7 and 8 for excluded regions in the parameter space in various 2HDMs.

<sup>6</sup> AABOUD 18BF search for production of a heavy  $H_2^0$  state decaying to  $ZZ$  in the final states  $\ell^+\ell^- \ell^+\ell^-$  and  $\ell^+\ell^- \nu\bar{\nu}$  in  $36.1 \text{ fb}^{-1}$  of  $pp$  collisions at  $E_{\text{cm}} = 13$  TeV. See their Figs. 8 and 9 for excluded parameter regions in 2HDM Type I and II.

<sup>7</sup> AABOUD 18CE search for the process  $pp \rightarrow H_2^0/A^0 t\bar{t}$  followed by the decay  $H_2^0/A^0 \rightarrow t\bar{t}$  in  $36.1 \text{ fb}^{-1}$  of  $pp$  collisions at  $E_{\text{cm}} = 13$  TeV. See their Fig. 12 for limits on cross section times branching ratio, and for lower limits on  $\tan\beta$  for  $m_{H_2^0}, m_{A^0} = 0.4\text{--}1.0$  TeV in the 2HDM type II.

<sup>8</sup> HALLER 18 perform global fits in the framework of two-Higgs-doublet models (type I, II, lepton specific, flipped). See their Fig. 8 for extended parameter regions from fits to LHC  $H^0$  measurements, Fig. 9 bottom and charm decays, Fig. 10 muon anomalous magnetic moment, Fig. 11 electroweak precision data, and Fig. 12 by combination of all data.

<sup>9</sup> SIRUNYAN 18BP search for production of  $H_2^0/A^0 \rightarrow b\bar{b}$  by  $b$ -associated production in  $35.7 \text{ fb}^{-1}$  of  $pp$  collisions at  $E_{\text{cm}} = 13$  TeV. See their Fig. 6 for the limits on cross section times branching ratio for  $m_{H_2^0}, m_{A^0} = 0.3\text{--}1.3$  TeV, and Figs. 8 and 9 for excluded regions in the parameter space of type-II and flipped 2HDMs.

<sup>10</sup> SIRUNYAN 18ED search for production of an  $A^0$  in gluon-gluon fusion and in association with a  $b\bar{b}$ , decaying to  $ZH^0$  in the final states  $\nu\bar{\nu}b\bar{b}$  or  $\ell^+\ell^- b\bar{b}$  in  $35.9 \text{ fb}^{-1}$  of  $pp$  collisions at  $E_{\text{cm}} = 13$  TeV. See their Fig. 9 for excluded regions in the parameter space in Type I and II 2HDMs.

<sup>11</sup> AABOUD 17AN search for production of a heavy  $H_2^0$  and/or  $A^0$  decaying to  $t\bar{t}$  in  $20.3 \text{ fb}^{-1}$  of  $pp$  collisions at  $E_{\text{cm}} = 8$  TeV. See their Fig. 3 and Table III for excluded parameter regions in Type II Two-Higgs-Doublet-Models.

<sup>12</sup> SIRUNYAN 17AX search for  $A^0 b\bar{b}$  production followed by the decay  $A^0 \rightarrow \mu^+\mu^-$  in  $19.7 \text{ fb}^{-1}$  of  $pp$  collisions at  $E_{\text{cm}} = 8$  TeV. Limits are set in the range  $m_{A^0} = 25\text{--}60$  GeV. See their Fig. 5 for upper limits on  $\sigma(A^0 b\bar{b}) \cdot \mathcal{B}(A^0 \rightarrow \mu^+\mu^-)$ .

<sup>13</sup> AAD 16AX search for production of a heavy  $H^0$  state decaying to  $ZZ$  in the final states  $\ell^+\ell^- \ell^+\ell^-$ ,  $\ell^+\ell^- \nu\bar{\nu}$ ,  $\ell^+\ell^- q\bar{q}$ , and  $\nu\bar{\nu}q\bar{q}$  in  $20.3 \text{ fb}^{-1}$  of  $pp$  collisions at  $E_{\text{cm}} = 8$  TeV. See their Figs. 13 and 14 for excluded parameter regions in Type I and II models.

<sup>14</sup> KHACHATRYAN 16P search for gluon fusion production of an  $H_2^0$  decaying to  $H^0 H^0 \rightarrow b\bar{b}\tau^+\tau^-$  and an  $A^0$  decaying to  $ZH^0 \rightarrow \ell^+\ell^- \tau^+\tau^-$  in  $19.7 \text{ fb}^{-1}$  of  $pp$  collisions at  $E_{\text{cm}} = 8$  TeV. See their Fig. 11 for limits on  $\tan\beta$  for  $m_{A^0} = 230\text{--}350$  GeV.

<sup>15</sup> KHACHATRYAN 16W search for  $A^0 b\bar{b}$  production followed by the decay  $A^0 \rightarrow \tau^+\tau^-$  in  $19.7 \text{ fb}^{-1}$  of  $pp$  collisions at  $E_{\text{cm}} = 8$  TeV. See their Fig. 3 for upper limits on  $\sigma(A^0 b\bar{b}) \cdot \mathcal{B}(A^0 \rightarrow \tau^+\tau^-)$ .

<sup>16</sup> KHACHATRYAN 16Z search for  $H_2^0 \rightarrow ZA^0$  followed by  $A^0 \rightarrow b\bar{b}$  or  $\tau^+\tau^-$ , and  $A^0 \rightarrow ZH_2^0$  followed by  $H_2^0 \rightarrow b\bar{b}$  or  $\tau^+\tau^-$ , in  $19.8 \text{ fb}^{-1}$  of  $pp$  collisions at  $E_{\text{cm}} = 8$  TeV. See their Fig. 4 for cross section limits and Fig. 5 for excluded region in the parameter space.

<sup>17</sup> AAD 15BK search for production of a heavy  $H_2^0$  decaying to  $H^0 H^0$  in the final state  $b\bar{b}b\bar{b}$  in  $19.5 \text{ fb}^{-1}$  of  $pp$  collisions at  $E_{\text{cm}} = 8$  TeV. See their Figs. 15–18 for excluded regions in the parameter space.

<sup>18</sup> AAD 15S search for production of  $A^0$  decaying to  $ZH^0 \rightarrow \ell^+\ell^- b\bar{b}$ ,  $\nu\bar{\nu}b\bar{b}$  and  $\ell^+\ell^- \tau^+\tau^-$  in  $20.3 \text{ fb}^{-1}$  of  $pp$  collisions at  $E_{\text{cm}} = 8$  TeV. See their Figs. 4 and 5 for excluded regions in the parameter space.

<sup>19</sup> KHACHATRYAN 15BB search for  $H_2^0, A^0 \rightarrow \gamma\gamma$  in  $19.7 \text{ fb}^{-1}$  of  $pp$  collisions at  $E_{\text{cm}} = 8$  TeV. See their Fig. 10 for excluded regions in the two-Higgs-doublet model parameter space.

<sup>20</sup> KHACHATRYAN 15N search for production of  $A^0$  decaying to  $ZH^0 \rightarrow \ell^+\ell^- b\bar{b}$  in  $19.7 \text{ fb}^{-1}$  of  $pp$  collisions at  $E_{\text{cm}} = 8$  TeV. See their Fig. 5 for excluded regions in the  $\tan\beta - \cos(\beta - \alpha)$  plane for  $m_{A^0} = 300$  GeV.

<sup>21</sup> AAD 14M search for the decay cascade  $H_2^0 \rightarrow H^\pm W^\mp \rightarrow H^0 W^\pm W^\mp, H^0$  decaying to  $b\bar{b}$  in  $20.3 \text{ fb}^{-1}$  of  $pp$  collisions at  $E_{\text{cm}} = 8$  TeV. See their Table IV for limits in a two-Higgs-doublet model for  $m_{H_2^0} = 325\text{--}1025$  GeV and  $m_{H^\pm} = 225\text{--}825$  GeV.

<sup>22</sup> KHACHATRYAN 14Q search for  $H_2^0 \rightarrow H^0 H^0$  and  $A^0 \rightarrow ZH^0$  in  $19.5 \text{ fb}^{-1}$  of  $pp$  collisions at  $E_{\text{cm}} = 8$  TeV. See their Figs. 4 and 5 for limits on cross section times branching ratio for  $m_{H_2^0, A^0} = 260\text{--}360$  GeV and their Figs. 7–9 for limits in two-Higgs-doublet models.

<sup>23</sup> AALTONEN 09AR search for Higgs bosons decaying to  $\tau^+\tau^-$  in two doublet models in  $1.8 \text{ fb}^{-1}$  of  $p\bar{p}$  collisions at  $E_{\text{cm}} = 1.96$  TeV. See their Fig. 2 for the limit on  $\sigma \cdot \mathcal{B}(H_{1,2}^0/A^0 \rightarrow \tau^+\tau^-)$  for different Higgs masses, and see their Fig. 3 for the excluded region in the MSSM parameter space.

<sup>24</sup> ABBIENDI 05A search for  $e^+e^- \rightarrow H_1^0 A^0$  in general Type-II two-doublet models, with decays  $H_1^0, A^0 \rightarrow q\bar{q}, gg, \tau^+\tau^-$ , and  $H_1^0 \rightarrow A^0 A^0$ .

<sup>25</sup> ABDALLAH 05D search for  $e^+e^- \rightarrow H^0 Z$  and  $H^0 A^0$  with  $H^0, A^0$  decaying to two jets of any flavor including  $gg$ . The limit is for SM  $H^0 Z$  production cross section with  $\mathcal{B}(H^0 \rightarrow jj) = 1$ .

<sup>26</sup> ABDALLAH 04O search for  $Z \rightarrow b\bar{b}H^0, b\bar{b}A^0, \tau^+\tau^- H^0$  and  $\tau^+\tau^- A^0$  in the final states  $4b, b\bar{b}\tau^+\tau^-$ , and  $4\tau$ . See paper for limits on Yukawa couplings.

<sup>27</sup> ABDALLAH 04O search for  $e^+e^- \rightarrow H^0 Z$  and  $H^0 A^0$ , with  $H^0, A^0$  decaying to  $b\bar{b}, \tau^+\tau^-$ , or  $H^0 \rightarrow A^0 A^0$  at  $E_{\text{cm}} = 189\text{--}208$  GeV. See paper for limits on couplings.

<sup>28</sup> ABBIENDI 02D search for  $Z \rightarrow b\bar{b}H^0$  and  $b\bar{b}A^0$  with  $H_{1,2}^0/A^0 \rightarrow \tau^+\tau^-$ , in the range  $4 < m_H < 12$  GeV. See their Fig. 8 for limits on the Yukawa coupling.

See key on page 999

# Gauge & Higgs Boson Particle Listings

## Neutral Higgs Bosons, Searches for

- 29 ABBIENDI 01E search for neutral Higgs bosons in general Type-II two-doublet models, at  $E_{\text{cm}} \leq 189$  GeV. In addition to usual final states, the decays  $H_1^0, A^0 \rightarrow q\bar{q}, gg$  are searched for. See their Figs. 15, 16 for excluded regions.
- 30 ABBIENDI 99E search for  $e^+e^- \rightarrow H^0 A^0$  and  $H^0 Z$  at  $E_{\text{cm}} = 183$  GeV. The limit is with  $m_H = m_A$  in general two Higgs-doublet models. See their Fig. 18 for the exclusion limit in the  $m_H - m_A$  plane. Updates the results of ACKERSTAFF 98s.
- 31 See Fig. 4 of ABREU 95H for the excluded region in the  $m_{H^0} - m_{A^0}$  plane for general two-doublet models. For  $\tan\beta > 1$ , the region  $m_{H^0} + m_{A^0} \lesssim 87$  GeV,  $m_{H^0} < 47$  GeV is excluded at 95% CL.
- 32 PICH 92 analyse  $H^0$  with  $m_{H^0} < 2m_\mu$  in general two-doublet models. Excluded regions in the space of mass-mixing angles from LEP, beam dump, and  $\pi^\pm, \eta$  rare decays are shown in Figs. 3, 4. The considered mass region is not totally excluded.

### Mass Limits for $H^0$ with Vanishing Yukawa Couplings

These limits assume that  $H^0$  couples to gauge bosons with the same strength as the Standard Model Higgs boson, but has no coupling to quarks and leptons (this is often referred to as “fermiophobic”).

VALUE (GeV)	CL%	DOCUMENT ID	TECN	COMMENT
• • •		We do not use the following data for averages, fits, limits, etc. • • •		
none 100–113	95	1 AALTONEN	13K CDF	$H^0 \rightarrow WW^*$
none 100–116	95	2 AALTONEN	13L CDF	$H^0 \rightarrow \gamma\gamma, WW^*, ZZ^*$
none 100–113	95	3 AALTONEN	13M TEVA	$H^0 \rightarrow \gamma\gamma, WW^*, ZZ^*$
none 100–114	95	4 ABAZOV	13G D0	$H^0 \rightarrow WW^*$
none 100–114	95	5 ABAZOV	13H D0	$H^0 \rightarrow \gamma\gamma$
none 100–114	95	6 ABAZOV	13I D0	$H^0 \rightarrow WW^*$
none 100–114	95	7 ABAZOV	13J D0	$H^0 \rightarrow WW^*, ZZ^*$
none 100–114	95	8 ABAZOV	13L D0	$H^0 \rightarrow \gamma\gamma, WW^*, ZZ^*$
none 110–147	95	9 CHATRCHYAN	13AL CMS	$H^0 \rightarrow \gamma\gamma$
none 110–118, 119.5–121	95	10 AAD	12N ATLS	$H^0 \rightarrow \gamma\gamma$
none 100–114	95	11 AALTONEN	12AN CDF	$H^0 \rightarrow \gamma\gamma$
none 110–194	95	12 CHATRCHYAN	12AO CMS	$H^0 \rightarrow \gamma\gamma, WW^*, ZZ^*$
none 70–106	95	13 AALTONEN	09AB CDF	$H^0 \rightarrow \gamma\gamma$
none 70–100	95	14 ABAZOV	08U D0	$H^0 \rightarrow \gamma\gamma$
>105.8	95	15 SCHAEEL	07 ALEP	$e^+e^- \rightarrow H^0 Z, H^0 \rightarrow WW^*$
>104.1	95	16,17 ABDALLAH	04L DLPH	$e^+e^- \rightarrow H^0 Z, H^0 \rightarrow \gamma\gamma$
>107	95	18 ACHARD	03C L3	$H^0 \rightarrow WW^*, ZZ^*, \gamma\gamma$
>105.5	95	16,19 ABBIENDI	02F OPAL	$H^0 \rightarrow \gamma\gamma$
>105.4	95	20 ACHARD	02C L3	$H^0 \rightarrow \gamma\gamma$
none 60–82	95	21 AFFOLDER	01H CDF	$p\bar{p} \rightarrow H^0 W/Z, H^0 \rightarrow \gamma\gamma$
> 94.9	95	22 ACCIARRI	00s L3	$e^+e^- \rightarrow H^0 Z, H^0 \rightarrow \gamma\gamma$
>100.7	95	23 BARATE	00L ALEP	$e^+e^- \rightarrow H^0 Z, H^0 \rightarrow \gamma\gamma$
> 96.2	95	24 ABBIENDI	99O OPAL	$e^+e^- \rightarrow H^0 Z, H^0 \rightarrow \gamma\gamma$
> 78.5	95	25 ABBOTT	99B D0	$p\bar{p} \rightarrow H^0 W/Z, H^0 \rightarrow \gamma\gamma$
		26 ABREU	99P DLPH	$e^+e^- \rightarrow H^0 \gamma$ and/or $H^0 \rightarrow \gamma\gamma$

- 1 AALTONEN 13K search for  $H^0 \rightarrow WW^*$  in  $9.7 \text{ fb}^{-1}$  of  $p\bar{p}$  collisions at  $E_{\text{cm}} = 1.96$  TeV. A limit on cross section times branching ratio which corresponds to (1.3–6.6) times the expected cross section is given in the range  $m_{H^0} = 110\text{--}200$  GeV at 95% CL.
- 2 AALTONEN 13L combine all CDF searches with  $9.45\text{--}10.0 \text{ fb}^{-1}$  of  $p\bar{p}$  collisions at  $E_{\text{cm}} = 1.96$  TeV.
- 3 AALTONEN 13M combine all Tevatron data from the CDF and D0 Collaborations of  $p\bar{p}$  collisions at  $E_{\text{cm}} = 1.96$  TeV.
- 4 ABAZOV 13G search for  $H^0 \rightarrow WW^*$  in  $9.7 \text{ fb}^{-1}$  of  $p\bar{p}$  collisions at  $E_{\text{cm}} = 1.96$  TeV. A limit on cross section times branching ratio which corresponds to (2–9) times the expected cross section is given for  $m_{H^0} = 100\text{--}200$  GeV at 95% CL.
- 5 ABAZOV 13H search for  $H^0 \rightarrow \gamma\gamma$  in  $9.6 \text{ fb}^{-1}$  of  $p\bar{p}$  collisions at  $E_{\text{cm}} = 1.96$  TeV.
- 6 ABAZOV 13I search for  $H^0$  production in the final state with one lepton and two or more jets plus missing  $E_T$  in  $9.7 \text{ fb}^{-1}$  of  $p\bar{p}$  collisions at  $E_{\text{cm}} = 1.96$  TeV. The search is sensitive to  $WH^0, ZH^0$  and vector-boson fusion Higgs production with  $H^0 \rightarrow WW^*$ . A limit on cross section times branching ratio which corresponds to (8–30) times the expected cross section is given in the range  $m_{H^0} = 100\text{--}200$  GeV at 95% CL.
- 7 ABAZOV 13J search for  $H^0$  production in the final states  $e e \mu, e \mu \mu, \mu \tau \tau$ , and  $e^\pm \mu^\pm$  in  $8.6\text{--}9.7 \text{ fb}^{-1}$  of  $p\bar{p}$  collisions at  $E_{\text{cm}} = 1.96$  TeV. The search is sensitive to  $WH^0, ZH^0$  production with  $H^0 \rightarrow WW^*, ZZ^*$ , decaying to leptonic final states. A limit on cross section times branching ratio which corresponds to (2.4–13.0) times the expected cross section is given in the range  $m_{H^0} = 100\text{--}200$  GeV at 95% CL.
- 8 ABAZOV 13L combine all D0 results with up to  $9.7 \text{ fb}^{-1}$  of  $p\bar{p}$  collisions at  $E_{\text{cm}} = 1.96$  TeV.
- 9 CHATRCHYAN 13AL search for  $H^0 \rightarrow \gamma\gamma$  in  $5.1 \text{ fb}^{-1}$  and  $5.3 \text{ fb}^{-1}$  of  $pp$  collisions at  $E_{\text{cm}} = 7$  and 8 TeV.
- 10 AAD 12N search for  $H^0 \rightarrow \gamma\gamma$  with  $4.9 \text{ fb}^{-1}$  of  $pp$  collisions at  $E_{\text{cm}} = 7$  TeV in the mass range  $m_{H^0} = 110\text{--}150$  GeV.
- 11 AALTONEN 12AN search for  $H^0 \rightarrow \gamma\gamma$  with  $10 \text{ fb}^{-1}$  of  $p\bar{p}$  collisions at  $E_{\text{cm}} = 1.96$  TeV in the mass range  $m_{H^0} = 100\text{--}150$  GeV.
- 12 CHATRCHYAN 12AO use data from CHATRCHYAN 12G, CHATRCHYAN 12E, CHATRCHYAN 12H, CHATRCHYAN 12I, CHATRCHYAN 12D, and CHATRCHYAN 12C.
- 13 AALTONEN 09AB search for  $H^0 \rightarrow \gamma\gamma$  in  $3.0 \text{ fb}^{-1}$  of  $p\bar{p}$  collisions at  $E_{\text{cm}} = 1.96$  TeV in the mass range  $m_{H^0} = 70\text{--}150$  GeV. Associated  $H^0 W, H^0 Z$  production and  $WW, ZZ$  fusion are considered.
- 14 ABAZOV 08U search for  $H^0 \rightarrow \gamma\gamma$  in  $p\bar{p}$  collisions at  $E_{\text{cm}} = 1.96$  TeV in the mass range  $m_{H^0} = 70\text{--}150$  GeV. Associated  $H^0 W, H^0 Z$  production and  $WW, ZZ$  fusion are considered. See their Tab. 1 for the limit on  $\sigma \cdot \text{B}(H^0 \rightarrow \gamma\gamma)$ , and see their Fig. 3 for the excluded region in the  $m_{H^0} - \text{B}(H^0 \rightarrow \gamma\gamma)$  plane.

- 15 SCHAEEL 07 search for Higgs bosons in association with a fermion pair and decaying to  $WW^*$ . The limit is from this search and HEISTER 02L for a  $H^0$  with SM production cross section.
- 16 Search for associated production of a  $\gamma\gamma$  resonance with a Z boson, followed by  $Z \rightarrow q\bar{q}, \ell^+ \ell^-$ , or  $\nu\bar{\nu}$ , at  $E_{\text{cm}} \leq 209$  GeV. The limit is for a  $H^0$  with SM production cross section.
- 17 Updates ABREU 01F.
- 18 ACHARD 03C search for  $e^+e^- \rightarrow ZH^0$  followed by  $H^0 \rightarrow WW^*$  or  $ZZ^*$  at  $E_{\text{cm}} = 200\text{--}209$  GeV and combine with the ACHARD 02c result. The limit is for a  $H^0$  with SM production cross section. For  $\text{B}(H^0 \rightarrow WW^*) + \text{B}(H^0 \rightarrow ZZ^*) = 1$ ,  $m_{H^0} > 108.1$  GeV is obtained. See Fig. 6 for the limits under different BR assumptions.
- 19 For  $\text{B}(H^0 \rightarrow \gamma\gamma) = 1$ ,  $m_{H^0} > 117$  GeV is obtained.
- 20 ACHARD 02c search for associated production of a  $\gamma\gamma$  resonance with a Z boson, followed by  $Z \rightarrow q\bar{q}, \ell^+ \ell^-$ , or  $\nu\bar{\nu}$ , at  $E_{\text{cm}} \leq 209$  GeV. The limit is for a  $H^0$  with SM production cross section. For  $\text{B}(H^0 \rightarrow \gamma\gamma) = 1$ ,  $m_{H^0} > 114$  GeV is obtained.
- 21 AFFOLDER 01H search for associated production of a  $\gamma\gamma$  resonance and a W or Z (tagged by two jets, an isolated lepton, or missing  $E_T$ ). The limit assumes Standard Model values for the production cross section and for the couplings of the  $H^0$  to W and Z bosons. See their Fig. 11 for limits with  $\text{B}(H^0 \rightarrow \gamma\gamma) < 1$ .
- 22 ACCIARRI 00s search for associated production of a  $\gamma\gamma$  resonance with a  $q\bar{q}, \nu\bar{\nu}$ , or  $\ell^+ \ell^-$  pair in  $e^+e^-$  collisions at  $E_{\text{cm}} = 189$  GeV. The limit is for a  $H^0$  with SM production cross section. For  $\text{B}(H^0 \rightarrow \gamma\gamma) = 1$ ,  $m_{H^0} > 98$  GeV is obtained. See their Fig. 5 for limits on  $\text{B}(H^0 \rightarrow \gamma\gamma) \cdot \sigma(e^+e^- \rightarrow H^0 \gamma) / \sigma(e^+e^- \rightarrow H^0 \gamma)$  (SM).
- 23 BARATE 00L search for associated production of a  $\gamma\gamma$  resonance with a  $q\bar{q}, \nu\bar{\nu}$ , or  $\ell^+ \ell^-$  pair in  $e^+e^-$  collisions at  $E_{\text{cm}} = 88\text{--}202$  GeV. The limit is for a  $H^0$  with SM production cross section. For  $\text{B}(H^0 \rightarrow \gamma\gamma) = 1$ ,  $m_{H^0} > 109$  GeV is obtained. See their Fig. 3 for limits on  $\text{B}(H^0 \rightarrow \gamma\gamma) \cdot \sigma(e^+e^- \rightarrow H^0 \gamma) / \sigma(e^+e^- \rightarrow H^0 \gamma)$  (SM).
- 24 ABBIENDI 99O search for associated production of a  $\gamma\gamma$  resonance with a  $q\bar{q}, \nu\bar{\nu}$ , or  $\ell^+ \ell^-$  pair in  $e^+e^-$  collisions at 189 GeV. The limit is for a  $H^0$  with SM production cross section. See their Fig. 4 for limits on  $\sigma(e^+e^- \rightarrow H^0 Z^0) \times \text{B}(H^0 \rightarrow \gamma\gamma) \times \text{B}(X^0 \rightarrow \gamma\gamma)$  for various masses. Updates the results of ACKERSTAFF 98Y.
- 25 ABBOTT 99B search for associated production of a  $\gamma\gamma$  resonance and a dijet pair. The limit assumes Standard Model values for the production cross section and for the couplings of the  $H^0$  to W and Z bosons. Limits in the range of  $\sigma(H^0 + Z/W) \cdot \text{B}(H^0 \rightarrow \gamma\gamma) = 0.80\text{--}0.34$  pb are obtained in the mass range  $m_{H^0} = 65\text{--}150$  GeV.
- 26 ABREU 99P search for  $e^+e^- \rightarrow H^0 \gamma$  with  $H^0 \rightarrow b\bar{b}$  or  $\gamma\gamma$ , and  $e^+e^- \rightarrow H^0 q\bar{q}$  with  $H^0 \rightarrow \gamma\gamma$ . See their Fig. 4 for limits on  $\sigma \times \text{B}$ . Explicit limits within an effective interaction framework are also given.

### Mass Limits for $H^0$ Decaying to Invisible Final States

These limits are for a neutral scalar  $H^0$  which predominantly decays to invisible final states. Standard Model values are assumed for the couplings of  $H^0$  to ordinary particles unless otherwise stated.

VALUE (GeV)	CL%	DOCUMENT ID	TECN	COMMENT
• • •		We do not use the following data for averages, fits, limits, etc. • • •		
>108.2	95	1 AABOUD	19AI ATLS	$W W/Z$ fusion
>112.3	95	2 AAD	15BD ATLS	$p\bar{p} \rightarrow H^0 WX, H^0 ZX$
>112.1	95	3 AAD	15BH ATLS	jet + missing $E_T$
>114.1	95	4 AAD	14BA ATLS	secondary vertex
>106.4	95	5 AAD	14O ATLS	$p\bar{p} \rightarrow H^0 ZX$
> 89.2	95	6 CHATRCHYAN	14B CMS	$p\bar{p} \rightarrow H^0 ZX, qqH^0 X$
		7 AAD	13AG ATLS	secondary vertex
		8 AAD	13AT ATLS	electron jets
		9 CHATRCHYAN	13BI CMS	
		10 AAD	12AQ ATLS	secondary vertex
		11 AALTONEN	12AB CDF	secondary vertex
		12 AALTONEN	12U CDF	secondary vertex
		13 ABBIENDI	10 OPAL	
		14 ABBIENDI	07 OPAL	large width
		15 ACHARD	05 L3	
		15 ABDALLAH	04B DLPH	
		15 HEISTER	02 ALEP	$E_{\text{cm}} \leq 209$ GeV
		15 BARATE	01C ALEP	$E_{\text{cm}} \leq 202$ GeV
		16 ACCIARRI	00M L3	

- 1 AABOUD 19AI search for  $H_{1,2}^0$  production by vector boson fusion and decay to invisible final states in  $36.1 \text{ fb}^{-1}$  of  $pp$  collisions at  $E_{\text{cm}} = 13$  TeV. See their Fig. 6(b) for limits on cross section times branching ratios for  $m_{H_{1,2}^0} = 0.1\text{--}3$  TeV.
- 2 AAD 15BD search for  $p\bar{p} \rightarrow H^0 WX$  and  $p\bar{p} \rightarrow H^0 ZX$  with W or Z decaying hadronically and  $H^0$  decaying to invisible final states in  $20.3 \text{ fb}^{-1}$  at  $E_{\text{cm}} = 8$  TeV. See their Fig. 6 for a limit on the cross section times branching ratio for  $m_{H^0} = 115\text{--}300$  GeV.
- 3 AAD 15BH search for events with a jet and missing  $E_T$  in  $20.3 \text{ fb}^{-1}$  of  $pp$  collisions at  $E_{\text{cm}} = 8$  TeV. Limits on  $\sigma(H^0) \text{B}(H^0 \rightarrow \text{invisible}) < (44\text{--}10)$  pb (95%CL) is given for  $m_{H^0} = 115\text{--}300$  GeV.
- 4 AAD 14BA search for  $H^0$  production in the decay mode  $H^0 \rightarrow X^0 X^0$ , where  $X^0$  is a long-lived particle which decays to collimated pairs of  $e^+e^-, \mu^+\mu^-,$  or  $\pi^+\pi^-$  plus invisible particles, in  $20.3 \text{ fb}^{-1}$  of  $pp$  collisions at  $E_{\text{cm}} = 8$  TeV. See their Figs. 15 and 16 for limits on cross section times branching ratio.
- 5 AAD 14O search for  $p\bar{p} \rightarrow H^0 ZX, Z \rightarrow \ell\ell$ , with  $H^0$  decaying to invisible final states in  $4.5 \text{ fb}^{-1}$  at  $E_{\text{cm}} = 7$  TeV and  $20.3 \text{ fb}^{-1}$  at  $E_{\text{cm}} = 8$  TeV. See their Fig. 3 for a limit on the cross section times branching ratio for  $m_{H^0} = 110\text{--}400$  GeV.
- 6 CHATRCHYAN 14B search for  $p\bar{p} \rightarrow H^0 ZX, Z \rightarrow \ell\ell$  and  $Z \rightarrow b\bar{b}$ , and also  $p\bar{p} \rightarrow qqH^0 X$  with  $H^0$  decaying to invisible final states using data at  $E_{\text{cm}} = 7$  and 8 TeV. See their Figs. 10, 11 for limits on the cross section times branching ratio for  $m_{H^0} = 100\text{--}400$  GeV.

# Gauge & Higgs Boson Particle Listings

## Neutral Higgs Bosons, Searches for

- 7 AAD 13AG search for  $H^0$  production in the decay mode  $H^0 \rightarrow X^0 X^0$ , where  $X^0$  is a long-lived particle which decays to  $\mu^+ \mu^- X^0$ , in  $1.9 \text{ fb}^{-1}$  of  $pp$  collisions at  $E_{\text{cm}} = 7 \text{ TeV}$ . See their Fig. 7 for limits on cross section times branching ratio.
- 8 AAD 13AT search for  $H^0$  production in the decay  $H^0 \rightarrow X^0 X^0$ , where  $X^0$  eventually decays to clusters of collimated  $e^+ e^-$  pairs, in  $2.04 \text{ fb}^{-1}$  of  $pp$  collisions at  $E_{\text{cm}} = 7 \text{ TeV}$ . See their Fig. 3 for limits on cross section times branching ratio.
- 9 CHATRCHYAN 13BJ search for  $H^0$  production in the decay chain  $H^0 \rightarrow X^0 X^0, X^0 \rightarrow \mu^+ \mu^- X^0$  in  $5.3 \text{ fb}^{-1}$  of  $pp$  collisions at  $E_{\text{cm}} = 7 \text{ TeV}$ . See their Fig. 2 for limits on cross section times branching ratio.
- 10 AAD 12AQ search for  $H^0$  production in the decay mode  $H^0 \rightarrow X^0 X^0$ , where  $X^0$  is a long-lived particle which decays mainly to  $b\bar{b}$  in the muon detector, in  $1.94 \text{ fb}^{-1}$  of  $pp$  collisions at  $E_{\text{cm}} = 7 \text{ TeV}$ . See their Fig. 3 for limits on cross section times branching ratio for  $m_{H^0} = 120, 140 \text{ GeV}$ ,  $m_{X^0} = 20, 40 \text{ GeV}$  in the  $c\tau$  range of 0.5–35 m.
- 11 AALTONEN 12AB search for  $H^0$  production in the decay  $H^0 \rightarrow X^0 X^0$ , where  $X^0$  eventually decays to clusters of collimated  $\ell^+ \ell^-$  pairs, in  $5.1 \text{ fb}^{-1}$  of  $p\bar{p}$  collisions at  $E_{\text{cm}} = 1.96 \text{ TeV}$ . Cross section limits are provided for a benchmark MSSM model incorporating the parameters given in Table VI.
- 12 AALTONEN 12U search for  $H^0$  production in the decay mode  $H^0 \rightarrow X^0 X^0$ , where  $X^0$  is a long-lived particle with  $c\tau \approx 1 \text{ cm}$  which decays mainly to  $b\bar{b}$ , in  $3.2 \text{ fb}^{-1}$  of  $p\bar{p}$  collisions at  $E_{\text{cm}} = 1.96 \text{ TeV}$ . See their Figs. 9 and 10 for limits on cross section times branching ratio for  $m_{H^0} = (130\text{--}170) \text{ GeV}$ ,  $m_{X^0} = 20, 40 \text{ GeV}$ .
- 13 ABBIENDI 10 search for  $e^+ e^- \rightarrow H^0 Z$  with  $H^0$  decaying invisibly. The limit assumes SM production cross section and  $B(H^0 \rightarrow \text{invisible}) = 1$ .
- 14 ABBIENDI 07 search for  $e^+ e^- \rightarrow H^0 Z$  with  $Z \rightarrow q\bar{q}$  and  $H^0$  decaying to invisible final states. The  $H^0$  width is varied between 1 GeV and 3 TeV. A limit  $\sigma \cdot B(H^0 \rightarrow \text{invisible}) < (0.07\text{--}0.57) \text{ pb}$  (95%CL) is obtained at  $E_{\text{cm}} = 206 \text{ GeV}$  for  $m_{H^0} = 60\text{--}114 \text{ GeV}$ .
- 15 Search for  $e^+ e^- \rightarrow H^0 Z$  with  $H^0$  decaying invisibly. The limit assumes SM production cross section and  $B(H^0 \rightarrow \text{invisible}) = 1$ .
- 16 ACCIARRI 00M search for  $e^+ e^- \rightarrow ZH^0$  with  $H^0$  decaying invisibly at  $E_{\text{cm}} = 183\text{--}189 \text{ GeV}$ . The limit assumes SM production cross section and  $B(H^0 \rightarrow \text{invisible}) = 1$ . See their Fig. 6 for limits for smaller branching ratios.

### Mass Limits for Light $A^0$

These limits are for a pseudoscalar  $A^0$  in the mass range below  $\mathcal{O}(10) \text{ GeV}$ .

VALUE (GeV)	DOCUMENT ID	TECN	COMMENT
• • • We do not use the following data for averages, fits, limits, etc. • • •			
1	AABOUD 18AP ATLS	$H^0 \rightarrow A^0 A^0$	
2	KHACHATRYAN...17AZ CMS	$H^0 \rightarrow A^0 A^0$	
3	ABLIKIM 16E BES3	$J/\psi \rightarrow A^0 \gamma$	
4	KHACHATRYAN...16F CMS	$H^0 \rightarrow A^0 A^0$	
5	LEES 15H BABR	$\Upsilon(1S) \rightarrow A^0 \gamma$	
6	LEES 13C BABR	$\Upsilon(1S) \rightarrow A^0 \gamma$	
7	LEES 13L BABR	$\Upsilon(1S) \rightarrow A^0 \gamma$	
8	LEES 13R BABR	$\Upsilon(1S) \rightarrow A^0 \gamma$	
9	ABLIKIM 12E BES3	$J/\psi \rightarrow A^0 \gamma$	
10	CHATRCHYAN 12V CMS	$A^0 \rightarrow \mu^+ \mu^-$	
11	AALTONEN 11P CDF	$t \rightarrow bH^+, H^+ \rightarrow W^+ A^0$	
12,13	ABOUZAID 11A KTEV	$K_L \rightarrow \pi^0 \pi^0 A^0, A^0 \rightarrow \mu^+ \mu^-$	
14	DEL-AMO-SANCHEZ...11J BABR	$\Upsilon(1S) \rightarrow A^0 \gamma$	
15	LEES 11H BABR	$\Upsilon(2S, 3S) \rightarrow A^0 \gamma$	
16	ANDREAS 10 RVUE		
13,17	HYUN 10 BELL	$B^0 \rightarrow K^{*0} A^0, A^0 \rightarrow \mu^+ \mu^-$	
13,18	HYUN 10 BELL	$B^0 \rightarrow \rho^0 A^0, A^0 \rightarrow \mu^+ \mu^-$	
19	AUBERT 09P BABR	$\Upsilon(3S) \rightarrow A^0 \gamma$	
20	AUBERT 09Z BABR	$\Upsilon(2S) \rightarrow A^0 \gamma$	
21	AUBERT 09Z BABR	$\Upsilon(3S) \rightarrow A^0 \gamma$	
13,22	TUNG 09 K391	$K_L \rightarrow \pi^0 \pi^0 A^0, A^0 \rightarrow \gamma \gamma$	
23	LOVE 08 CLEO	$\Upsilon(1S) \rightarrow A^0 \gamma$	
24	BESSION 07 CLEO	$\Upsilon(1S) \rightarrow \eta_b \gamma$	
25	PARK 05 HYCP	$\Sigma^+ \rightarrow p A^0, A^0 \rightarrow \mu^+ \mu^-$	
26	BALEST 95 CLE2	$\Upsilon(1S) \rightarrow A^0 \gamma$	
27	ANTREASIAN 90C CBAL	$\Upsilon(1S) \rightarrow A^0 \gamma$	

- 1 AABOUD 18AP search for the decay  $H^0 \rightarrow A^0 A^0 \rightarrow \mu^+ \mu^- \mu^+ \mu^-$  in  $36.1 \text{ fb}^{-1}$  of  $pp$  collisions at  $E_{\text{cm}} = 13 \text{ TeV}$ . See their Fig. 10(b) for limits on  $B(H^0 \rightarrow A^0 A^0)$  in the range  $m_{A^0} = 1\text{--}2.5, 4.5\text{--}8 \text{ GeV}$ , assuming a type-II two-doublet plus singlet model with  $\tan(\beta) = 5$ .
- 2 KHACHATRYAN 17AZ search for the decay  $H^0 \rightarrow A^0 A^0 \rightarrow \tau^+ \tau^- \tau^+ \tau^-$ ,  $\mu^+ \mu^- b\bar{b}$ , and  $\mu^+ \mu^- \tau^+ \tau^-$  in  $19.7 \text{ fb}^{-1}$  of  $pp$  collisions at  $E_{\text{cm}} = 8 \text{ TeV}$ . See their Figs. 4, 5, and 6 for cross section limits in the range  $m_{A^0} = 5\text{--}62.5 \text{ GeV}$ . See also their Figs. 7, 8, and 9 for interpretation of the data in terms of models with two Higgs doublets and a singlet.
- 3 ABLIKIM 16E search for the process  $J/\psi \rightarrow A^0 \gamma$  with  $A^0$  decaying to  $\mu^+ \mu^-$  and give limits on  $B(J/\psi \rightarrow A^0 \gamma) \cdot B(A^0 \rightarrow \mu^+ \mu^-)$  in the range  $2.8 \times 10^{-8}\text{--}5.0 \times 10^{-6}$  (90% CL) for  $0.212 \leq m_{A^0} \leq 3.0 \text{ GeV}$ . See their Fig. 5.
- 4 KHACHATRYAN 16F search for the decay  $H^0 \rightarrow A^0 A^0 \rightarrow \tau^+ \tau^- \tau^+ \tau^-$  in  $19.7 \text{ fb}^{-1}$  of  $pp$  collisions at  $E_{\text{cm}} = 8 \text{ TeV}$ . See their Fig. 8 for cross section limits for  $m_{A^0} = 4\text{--}8 \text{ GeV}$ .
- 5 LEES 15H search for the process  $\Upsilon(2S) \rightarrow \Upsilon(1S) \pi^+ \pi^- \rightarrow A^0 \gamma \pi^+ \pi^-$  with  $A^0$  decaying to  $c\bar{c}$  and give limits on  $B(\Upsilon(1S) \rightarrow A^0 \gamma) \cdot B(A^0 \rightarrow c\bar{c})$  in the range  $7.4 \times 10^{-5}\text{--}2.4 \times 10^{-3}$  (90% CL) for  $4.00 \leq m_{A^0} \leq 8.95$  and  $9.10 \leq m_{A^0} \leq 9.25 \text{ GeV}$ . See their Fig. 6.
- 6 LEES 13C search for the process  $\Upsilon(2S, 3S) \rightarrow \Upsilon(1S) \pi^+ \pi^- \rightarrow A^0 \gamma \pi^+ \pi^-$  with  $A^0$  decaying to  $\mu^+ \mu^-$  and give limits on  $B(\Upsilon(1S) \rightarrow A^0 \gamma) \cdot B(A^0 \rightarrow \mu^+ \mu^-)$  in the range  $(0.3\text{--}9.7) \times 10^{-6}$  (90% CL) for  $0.212 \leq m_{A^0} \leq 9.20 \text{ GeV}$ . See their Fig. 5(e) for limits on the  $b\text{--}A^0$  Yukawa coupling derived by combining this result with AUBERT 09Z.
- 7 LEES 13L search for the process  $\Upsilon(2S) \rightarrow \Upsilon(1S) \pi^+ \pi^- \rightarrow A^0 \gamma \pi^+ \pi^-$  with  $A^0$  decaying to  $g\bar{g}$  or  $s\bar{s}$  and give limits on  $B(\Upsilon(1S) \rightarrow A^0 \gamma) \cdot B(A^0 \rightarrow g\bar{g})$  between  $1 \times 10^{-6}$  and  $2 \times 10^{-2}$  (90% CL) for  $0.5 \leq m_{A^0} \leq 9.0 \text{ GeV}$ , and  $B(\Upsilon(1S) \rightarrow A^0 \gamma) \cdot B(A^0 \rightarrow s\bar{s})$  between  $4 \times 10^{-6}$  and  $1 \times 10^{-3}$  (90%CL) for  $1.5 \leq m_{A^0} \leq 9.0 \text{ GeV}$ . See their Fig. 4.
- 8 LEES 13R search for the process  $\Upsilon(2S) \rightarrow \Upsilon(1S) \pi^+ \pi^- \rightarrow A^0 \gamma \pi^+ \pi^-$  with  $A^0$  decaying to  $\tau^+ \tau^-$  and give limits on  $B(\Upsilon(1S) \rightarrow A^0 \gamma) \cdot B(A^0 \rightarrow \tau^+ \tau^-)$  in the range  $0.9\text{--}13 \times 10^{-5}$  (90% CL) for  $3.6 \leq m_{A^0} \leq 9.2 \text{ GeV}$ . See their Fig. 4 for limits on the  $b\text{--}A^0$  Yukawa coupling derived by combining this result with AUBERT 09P.
- 9 ABLIKIM 12 searches for the process  $\psi(3686) \rightarrow \pi \pi J/\psi, J/\psi \rightarrow A^0 \gamma$  with  $A^0$  decaying to  $\mu^+ \mu^-$ . It gives mass dependent limits on  $B(J/\psi \rightarrow A^0 \gamma) \cdot B(A^0 \rightarrow \mu^+ \mu^-)$  in the range  $4 \times 10^{-7}\text{--}2.1 \times 10^{-5}$  (90% C.L.) for  $0.212 \leq m_{A^0} \leq 3.0 \text{ GeV}$ . See their Fig. 2.
- 10 CHATRCHYAN 12V search for  $A^0$  production in the decay  $A^0 \rightarrow \mu^+ \mu^-$  with  $1.3 \text{ fb}^{-1}$  of  $pp$  collisions at  $E_{\text{cm}} = 7 \text{ TeV}$ . A limit on  $\sigma(A^0) \cdot B(A^0 \rightarrow \mu^+ \mu^-)$  in the range  $(1.5\text{--}7.5) \text{ pb}$  is given for  $m_{A^0} = (5.5\text{--}8.7)$  and  $(11.5\text{--}14) \text{ GeV}$  at 95% CL.
- 11 AALTONEN 11P search in  $2.7 \text{ fb}^{-1}$  of  $p\bar{p}$  collisions at  $E_{\text{cm}} = 1.96 \text{ TeV}$  for the decay chain  $t \rightarrow bH^+, H^+ \rightarrow W^+ A^0, A^0 \rightarrow \tau^+ \tau^-$  with  $m_{A^0}$  between 4 and 9 GeV. See their Fig. 4 for limits on  $B(t \rightarrow bH^+)$  for  $90 < m_{H^+} < 160 \text{ GeV}$ .
- 12 ABOUZAID 11A search for the decay chain  $K_L \rightarrow \pi^0 \pi^0 A^0, A^0 \rightarrow \mu^+ \mu^-$  and give a limit  $B(K_L \rightarrow \pi^0 \pi^0 A^0) \cdot B(A^0 \rightarrow \mu^+ \mu^-) < 1.0 \times 10^{-10}$  at 90% CL for  $m_{A^0} = 214.3 \text{ MeV}$ .
- 13 The search was motivated by PARK 05.
- 14 DEL-AMO-SANCHEZ 11J search for the process  $\Upsilon(2S) \rightarrow \Upsilon(1S) \pi^+ \pi^- \rightarrow A^0 \gamma \pi^+ \pi^-$  with  $A^0$  decaying to invisible final states. They give limits on  $B(\Upsilon(1S) \rightarrow A^0 \gamma) \cdot B(A^0 \rightarrow \text{invisible})$  in the range  $(1.9\text{--}4.5) \times 10^{-6}$  (90% CL) for  $0 \leq m_{A^0} \leq 8.0 \text{ GeV}$ , and  $(2.7\text{--}37) \times 10^{-6}$  for  $8.0 \leq m_{A^0} \leq 9.2 \text{ GeV}$ .
- 15 LEES 11H search for the process  $\Upsilon(2S, 3S) \rightarrow A^0 \gamma$  with  $A^0$  decaying hadronically and give limits on  $B(\Upsilon(2S, 3S) \rightarrow A^0 \gamma) \cdot B(A^0 \rightarrow \text{hadrons})$  in the range  $1 \times 10^{-6}\text{--}8 \times 10^{-5}$  (90% CL) for  $0.3 < m_{A^0} < 7 \text{ GeV}$ . The decay rates for  $\Upsilon(2S)$  and  $\Upsilon(3S)$  are assumed to be equal up to the phase space factor. See their Fig. 5.
- 16 ANDREAS 10 analyze constraints from rare decays and other processes on a light  $A^0$  with  $m_{A^0} < 2m_\mu$  and give limits on its coupling to fermions at the level of  $10^{-4}$  times the Standard Model value.
- 17 HYUN 10 search for the decay chain  $B^0 \rightarrow K^{*0} A^0, A^0 \rightarrow \mu^+ \mu^-$  and give a limit on  $B(B^0 \rightarrow K^{*0} A^0) \cdot B(A^0 \rightarrow \mu^+ \mu^-)$  in the range  $(2.26\text{--}5.53) \times 10^{-8}$  at 90%CL for  $m_{A^0} = 212\text{--}300 \text{ MeV}$ . The limit for  $m_{A^0} = 214.3 \text{ MeV}$  is  $2.26 \times 10^{-8}$ .
- 18 HYUN 10 search for the decay chain  $B^0 \rightarrow \rho^0 A^0, A^0 \rightarrow \mu^+ \mu^-$  and give a limit on  $B(B^0 \rightarrow \rho^0 A^0) \cdot B(A^0 \rightarrow \mu^+ \mu^-)$  in the range  $(1.73\text{--}4.51) \times 10^{-8}$  at 90%CL for  $m_{A^0} = 212\text{--}300 \text{ MeV}$ . The limit for  $m_{A^0} = 214.3 \text{ MeV}$  is  $1.73 \times 10^{-8}$ .
- 19 AUBERT 09P search for the process  $\Upsilon(3S) \rightarrow A^0 \gamma$  with  $A^0 \rightarrow \tau^+ \tau^-$  for  $4.03 < m_{A^0} < 9.52$  and  $9.61 < m_{A^0} < 10.10 \text{ GeV}$ , and give limits on  $B(\Upsilon(3S) \rightarrow A^0 \gamma) \cdot B(A^0 \rightarrow \tau^+ \tau^-)$  in the range  $(1.5\text{--}16) \times 10^{-5}$  (90% CL).
- 20 AUBERT 09Z search for the process  $\Upsilon(2S) \rightarrow A^0 \gamma$  with  $A^0 \rightarrow \mu^+ \mu^-$  for  $0.212 < m_{A^0} < 9.3 \text{ GeV}$  and give limits on  $B(\Upsilon(2S) \rightarrow A^0 \gamma) \cdot B(A^0 \rightarrow \mu^+ \mu^-)$  in the range  $(0.3\text{--}8) \times 10^{-6}$  (90% CL).
- 21 AUBERT 09Z search for the process  $\Upsilon(3S) \rightarrow A^0 \gamma$  with  $A^0 \rightarrow \mu^+ \mu^-$  for  $0.212 < m_{A^0} < 9.3 \text{ GeV}$  and give limits on  $B(\Upsilon(3S) \rightarrow A^0 \gamma) \cdot B(A^0 \rightarrow \mu^+ \mu^-)$  in the range  $(0.3\text{--}5) \times 10^{-6}$  (90% CL).
- 22 TUNG 09 search for the decay chain  $K_L \rightarrow \pi^0 \pi^0 A^0, A^0 \rightarrow \gamma \gamma$  and give a limit on  $B(K_L \rightarrow \pi^0 \pi^0 A^0) \cdot B(A^0 \rightarrow \gamma \gamma)$  in the range  $(2.4\text{--}10.7) \times 10^{-7}$  at 90%CL for  $m_{A^0} = 194.3\text{--}219.3 \text{ MeV}$ . The limit for  $m_{A^0} = 214.3 \text{ MeV}$  is  $2.4 \times 10^{-7}$ .
- 23 LOVE 08 search for the process  $\Upsilon(1S) \rightarrow A^0 \gamma$  with  $A^0 \rightarrow \mu^+ \mu^-$  (for  $m_{A^0} < 2m_\tau$ ) and  $A^0 \rightarrow \tau^+ \tau^-$ . Limits on  $B(\Upsilon(1S) \rightarrow A^0 \gamma) \cdot B(A^0 \rightarrow \ell^+ \ell^-)$  in the range  $10^{-6}\text{--}10^{-4}$  (90% CL) are given.
- 24 BESSION 07 give a limit  $B(\Upsilon(1S) \rightarrow \eta_b \gamma) \cdot B(\eta_b \rightarrow \tau^+ \tau^-) < 0.27\%$  (95% CL), which constrains a possible  $A^0$  exchange contribution to the  $\eta_b$  decay.
- 25 PARK 05 found three candidate events for  $\Sigma^+ \rightarrow p \mu^+ \mu^-$  in the HyperCP experiment. Due to a narrow spread in dimuon mass, they hypothesize the events as a possible signal of a new boson. It can be interpreted as a neutral particle with  $m_{A^0} = 214.3 \pm 0.5 \text{ MeV}$  and the branching fraction  $B(\Sigma^+ \rightarrow p A^0) \cdot B(A^0 \rightarrow \mu^+ \mu^-) = (3.1^{+2.4}_{-1.9} \pm 1.5) \times 10^{-8}$ .
- 26 BALEST 95 give limits  $B(\Upsilon(1S) \rightarrow A^0 \gamma) \cdot 1.5 \times 10^{-5}$  at 90% CL for  $m_{A^0} < 5 \text{ GeV}$ . The limit becomes  $< 10^{-4}$  for  $m_{A^0} < 7.7 \text{ GeV}$ .
- 27 ANTREASIAN 90C give limits  $B(\Upsilon(1S) \rightarrow A^0 \gamma) \cdot 5.6 \times 10^{-5}$  at 90% CL for  $m_{A^0} < 7.2 \text{ GeV}$ .  $A^0$  is assumed not to decay in the detector.

### Other Mass Limits

We use a symbol  $H_1^0$  if mass  $< 125 \text{ GeV}$  or  $H_2^0$  if mass  $> 125 \text{ GeV}$ . The notation  $H^0$  is reserved for the 125 GeV particle.

VALUE (GeV)	CL%	DOCUMENT ID	TECN	COMMENT
• • • We do not use the following data for averages, fits, limits, etc. • • •				
1	AAD	20C ATLS	$H_2^0 \rightarrow H^0 H^0$	
2	SIRUNYAN	20 CMS	$H^0 \rightarrow A^0 A^0$	
3	AABOUD	19A ATLS	$H_2^0 \rightarrow H^0 H^0$	
4	AABOUD	19AG ATLS	$H^0 \rightarrow A^0 A^0$	
5	AABOUD	19O ATLS	$H_2^0 \rightarrow H^0 H^0$	
6	AABOUD	19T ATLS	$H_2^0 \rightarrow H^0 H^0$	
7	AABOUD	19V ATLS	two doublet + pseudoscalar model	
8	AABOUD	19Y ATLS	$H_2^0 \rightarrow \mu^+ \mu^-$	

# Gauge & Higgs Boson Particle Listings

## Neutral Higgs Bosons, Searches for

9	AALTONEN	19	CDF	$H_{1,2}^0 \rightarrow b\bar{b}$
10	SIRUNYAN	19	CMS	$H_2^0 \rightarrow H^0 H^0$
11	SIRUNYAN	19AE	CMS	$A_2^0 \rightarrow \tau^+ \tau^-$
12	SIRUNYAN	19AN	CMS	$A_2^0 \rightarrow H^0 A_1^0$
13	SIRUNYAN	19AV	CMS	$A_2^0 \rightarrow Z H^0$
14	SIRUNYAN	19B	CMS	$H_{1,2}^0/A^0 \rightarrow b\bar{b}$
15	SIRUNYAN	19BB	CMS	$H_1^0 \rightarrow \gamma\gamma$
16	SIRUNYAN	19BD	CMS	$H^0 \rightarrow A^0 A^0$
17	SIRUNYAN	19BE	CMS	$H_2^0 \rightarrow H^0 H^0$
18	SIRUNYAN	19BQ	CMS	$H_{1,2}^0 \rightarrow A^0 A^0$
19	SIRUNYAN	19CR	CMS	$H_2^0/A^0 \rightarrow \mu^+ \mu^-$
20	SIRUNYAN	19H	CMS	$H_2^0 \rightarrow H^0 H^0$
21	AABOUD	18AA	ATLS	$H_2^0 \rightarrow Z\gamma$
22	AABOUD	18AG	ATLS	$H_2^0 \rightarrow A^0 A^0$
23	AABOUD	18AH	ATLS	$A^0 \rightarrow Z H_2^0$
24	AABOUD	18AI	ATLS	$A^0 \rightarrow Z H_1^0$
25	AABOUD	18BF	ATLS	$H_2^0 \rightarrow ZZ$
26	AABOUD	18BU	ATLS	$H_2^0 \rightarrow H^0 H^0$
27	AABOUD	18BX	ATLS	$H_2^0 \rightarrow A^0 A^0$
28	AABOUD	18CQ	ATLS	$H_2^0 \rightarrow H^0 H^0$
29	AABOUD	18F	ATLS	$H_2^0 \rightarrow W^+ W^-, ZZ$
30	AAIJ	18AMLHCB		$H_{1,2}^0 \rightarrow \mu\tau$
31	AAIJ	18AQ	LHCB	$A^0 \rightarrow \mu^+ \mu^-$
32	AAIJ	18AQ	LHCB	$H^0 \rightarrow A^0 A^0, A^0 \rightarrow \mu^+ \mu^-$
33	SIRUNYAN	18AF	CMS	$H_2^0 \rightarrow H^0 H^0$
34	SIRUNYAN	18BA	CMS	$H_2^0 \rightarrow ZZ$
35	SIRUNYAN	18CW	CMS	$H_2^0 \rightarrow H^0 H^0$
36	SIRUNYAN	18DK	CMS	$H_2^0 \rightarrow Z\gamma$
37	SIRUNYAN	18DT	CMS	$H^0 \rightarrow A^0 A^0$
38	SIRUNYAN	18DU	CMS	$H_2^0 \rightarrow \gamma\gamma$
39	SIRUNYAN	18ED	CMS	$A^0 \rightarrow Z H^0$
40	SIRUNYAN	18EE	CMS	$H^0 \rightarrow A^0 A^0$
41	SIRUNYAN	18F	CMS	$pp, 13 \text{ TeV}, H_2^0 \rightarrow H^0 H^0$
42	AABOUD	17	ATLS	$H_2^0 \rightarrow Z\gamma$
43	AABOUD	17AW	ATLS	$H_2^0 \rightarrow Z\gamma$
44	KHACHATRY...	17AZ	CMS	$H^0 \rightarrow A^0 A^0$
45	KHACHATRY...	17D	CMS	$pp, 8, 13 \text{ TeV}, H_2^0 \rightarrow Z\gamma$
46	KHACHATRY...	17R	CMS	$H_2^0 \rightarrow \gamma\gamma$
47	SIRUNYAN	17CN	CMS	$pp, 8 \text{ TeV}, H_2^0 \rightarrow H^0 H^0$
48	SIRUNYAN	17Y	CMS	$pp, 8, 13 \text{ TeV}, H_2^0 \rightarrow Z\gamma$
49	AABOUD	16AB	ATLS	$H^0 \rightarrow A^0 A^0$
50	AABOUD	16AE	ATLS	$H_2^0 \rightarrow W^+ W^-, ZZ$
51	AABOUD	16H	ATLS	$H_2^0 \rightarrow \gamma\gamma$
52	AABOUD	16I	ATLS	$H_2^0 \rightarrow H^0 H^0$
53	AAD	16AX	ATLS	$H^0 \rightarrow ZZ$
54	AAD	16C	ATLS	$H^0 \rightarrow W^+ W^-$
55	AAD	16L	ATLS	$H^0 \rightarrow A^0 A^0$
56	AAD	16L	ATLS	$H_2^0 \rightarrow A^0 A^0$
57	AALTONEN	16C	CDF	$H_1^0 H^\pm \rightarrow H_1^0 H_1^0 W^*$ , $H_1^0 \rightarrow \gamma\gamma$
58	KHACHATRY...	16BG	CMS	$H_2^0 \rightarrow H^0 H^0$
59	KHACHATRY...	16BQ	CMS	$pp, 8 \text{ TeV}, H_2^0 \rightarrow H^0 H^0$
60	KHACHATRY...	16F	CMS	$H^0 \rightarrow H_1^0 H_1^0$
61	KHACHATRY...	16M	CMS	$H_2^0 \rightarrow \gamma\gamma$
62	KHACHATRY...	16P	CMS	$H_2^0 \rightarrow H^0 H^0$
63	KHACHATRY...	16P	CMS	$A^0 \rightarrow Z H^0$
64	AAD	15BK	ATLS	$H_2^0 \rightarrow H^0 H^0$
65	AAD	15BZ	ATLS	$H^0 \rightarrow A^0 A^0$
66	AAD	15BZ	ATLS	$H_2^0 \rightarrow A^0 A^0$
67	AAD	15CE	ATLS	$H_2^0 \rightarrow H^0 H^0$
68	AAD	15H	ATLS	$H_2^0 \rightarrow H^0 H^0$
69	AAD	15S	ATLS	$A^0 \rightarrow Z H^0$
70	KHACHATRY...	15AW	CMS	$H_2^0 \rightarrow W^+ W^-, ZZ$
71	KHACHATRY...	15BB	CMS	$H^0 \rightarrow \gamma\gamma$
72	KHACHATRY...	15N	CMS	$A^0 \rightarrow Z H^0$
73	KHACHATRY...	15O	CMS	$A^0 \rightarrow Z H^0$
74	KHACHATRY...	15R	CMS	$H_2^0 \rightarrow H^0 H^0$
75	AAD	14AP	ATLS	$H^0 \rightarrow \gamma\gamma$
76	AAD	14M	ATLS	$H_2^0 \rightarrow H^\pm W^\mp \rightarrow H^0 W^\pm W^\mp, H^0 \rightarrow b\bar{b}$
77	CHATRCHYAN14G	CMS		$H^0 \rightarrow WW^*$
78	KHACHATRY...	14P	CMS	$H^0 \rightarrow \gamma\gamma$
79	AALTONEN	13P	CDF	$H^0 \rightarrow H^\pm W^\mp \rightarrow H^0 W^\pm W^\mp$
80	CHATRCHYAN13BJ	CMS		$H^0 \rightarrow A^0 A^0$

81	AALTONEN	11P	CDF	$t \rightarrow bH^+, H^+ \rightarrow W^+ A^0$
82	ABBIENDI	10	OPAL	$H^0 \rightarrow \tilde{\chi}_1^0 \tilde{\chi}_2^0$
83	SCHAELE	10	ALEP	$H^0 \rightarrow A^0 A^0$
84	ABAZOV	09V	D0	$H^0 \rightarrow A^0 A^0$
85	ABBIENDI	05A	OPAL	$A^0$ , Type II model
86	ABBIENDI	04K	OPAL	$H^0 \rightarrow 2 \text{ jets}$
87	ABDALLAH	04	DLPH	$H^0 VV$ couplings
88	ACHARD	04B	L3	$H^0 \rightarrow 2 \text{ jets}$
89	ACHARD	04F	L3	Anomalous coupling
90	ABBIENDI	03F	OPAL	$e^+ e^- \rightarrow H^0 Z, H^0 \rightarrow \text{any}$
91	ABBIENDI	03G	OPAL	$H^0 \rightarrow A^0 A^0$
92,93	HEISTER	02L	ALEP	$H^0 \rightarrow \gamma\gamma$
94	HEISTER	02M	ALEP	$H^0 \rightarrow 2 \text{ jets or } \tau^+ \tau^-$
95	ABBIENDI	01E	OPAL	$A^0$ , Type-II model
96	ACCIARRI	00R	L3	$e^+ e^- \rightarrow H^0 \gamma$ and/or $H^0 \rightarrow \gamma\gamma$
97	ACCIARRI	00R	L3	$e^+ e^- \rightarrow e^+ e^- H^0$
98	GONZALEZ...	98B	RVUE	Anomalous coupling
99	KRAWCZYK	97	RVUE	$(g-2)_\mu$
100	ALEXANDER	96H	OPAL	$Z \rightarrow H^0 \gamma$

- AAD 20c combine searches for a scalar resonance decaying to  $H^0 H^0$  in  $36.1 \text{ fb}^{-1}$  of  $pp$  collisions at  $E_{\text{cm}} = 13 \text{ TeV}$  from AABOUD 19A, AABOUD 19O, AABOUD 18CQ, AABOUD 19T, AABOUD 18CW, and AABOUD 18BU. See their Fig. 5(a) for limits on cross section times branching ratio for  $m_{H_2^0} = 0.26\text{--}3 \text{ TeV}$ .
- SIRUNYAN 20 search for the decay  $H^0 \rightarrow A^0 A^0 \rightarrow \tau^+ \tau^- \tau^+ \tau^-$  or  $\tau^+ \tau^- \mu^+ \mu^-$  in  $35.9 \text{ fb}^{-1}$  of  $pp$  collisions at  $E_{\text{cm}} = 13 \text{ TeV}$ . See their Fig. 10 for limits on the product of production cross section (normalized to the SM) and branching ratios in the range  $m_{A^0} = 4\text{--}15 \text{ GeV}$ .
- AABOUD 19A search for a narrow scalar resonance decaying to  $H^0 H^0 \rightarrow b\bar{b}b\bar{b}$  in  $27.5\text{--}36.1 \text{ fb}^{-1}$  of  $pp$  collisions at  $E_{\text{cm}} = 13 \text{ TeV}$ . See their Fig. 9(a) for limits on cross section times branching ratios for  $m_{H_2^0} = 0.26\text{--}3 \text{ TeV}$ .
- AABOUD 19AG search for the decay  $H^0 \rightarrow A^0 A^0 \rightarrow \mu^+ \mu^- b\bar{b}$  in  $36.7 \text{ fb}^{-1}$  of  $pp$  collisions at  $E_{\text{cm}} = 13 \text{ TeV}$ . See their Fig. 6 (a) for limits on the product of production cross section (normalized to the SM) and branching ratios in the range  $m_{A^0} = 20\text{--}60 \text{ GeV}$ .
- AABOUD 19O search for a scalar resonance decaying to  $H^0 H^0 \rightarrow b\bar{b}WW^*$  in  $36.1 \text{ fb}^{-1}$  of  $pp$  collisions at  $E_{\text{cm}} = 13 \text{ TeV}$ . See their Fig. 12 (left) for limits on cross section times branching ratio for  $m_{H_2^0} = 0.5\text{--}3 \text{ TeV}$ .
- AABOUD 19T search for a scalar resonance decaying to  $H^0 H^0 \rightarrow WW^* WW^*$  in  $36.1 \text{ fb}^{-1}$  of  $pp$  collisions at  $E_{\text{cm}} = 13 \text{ TeV}$ . See their Fig. 3 for limits on cross section times branching ratio for  $m_{H_2^0} = 260\text{--}500 \text{ GeV}$ , assuming SM decay rates for the  $H^0$ .
- AABOUD 19V combine published ATLAS data to constrain two-Higgs-doublet plus singlet pseudoscalar model with  $A_1^0$  decaying to invisible final states. See their Fig. 19 for excluded parameter regions.
- AABOUD 19Y search for a narrow scalar resonance produced by gluon fusion or  $b$  associated production, decaying to  $\mu^+ \mu^-$  in  $36.1 \text{ fb}^{-1}$  of  $pp$  collisions at  $E_{\text{cm}} = 13 \text{ TeV}$ . See their Figs. 4 and 5(a) for cross section limits for  $m_{H_2^0} = 0.2\text{--}1.0 \text{ TeV}$ .
- AALTONEN 19 search for  $b$  associated production of a scalar particle decaying to  $b\bar{b}$  in  $5.4 \text{ fb}^{-1}$  of  $p\bar{p}$  collisions at  $E_{\text{cm}} = 1.96 \text{ TeV}$ . See their Fig. 3 for limits on cross section times branching ratio for  $m_{H_{1,2}^0} = 100\text{--}300 \text{ GeV}$ .
- SIRUNYAN 19 search for a narrow scalar resonance decaying to  $H^0 H^0 \rightarrow \gamma\gamma b\bar{b}$  in  $35.9 \text{ fb}^{-1}$  of  $pp$  collisions at  $E_{\text{cm}} = 13 \text{ TeV}$ . See their Fig. 9 (left) for limits on cross section times branching ratios for  $m_{H_2^0} = 260\text{--}900 \text{ GeV}$ .
- SIRUNYAN 19AE search for a scalar resonance produced in association with a  $b\bar{b}$  pair, decaying to  $\tau^+ \tau^-$  in  $35.9 \text{ fb}^{-1}$  of  $pp$  collisions at  $E_{\text{cm}} = 13 \text{ TeV}$ . See their Fig. 4 for cross section limits for  $m_{A^0} = 25\text{--}70 \text{ GeV}$ .
- SIRUNYAN 19AN search for production of  $A_2^0$  decaying to  $H^0 A_1^0$  followed by  $H^0 \rightarrow b\bar{b}, A_1^0 \rightarrow \text{invisible}$  in  $35.9 \text{ fb}^{-1}$  of  $pp$  collisions at  $E_{\text{cm}} = 13 \text{ TeV}$ , in the mass range  $m_{A_2^0} = 0.2\text{--}1.6 \text{ TeV}$ ,  $m_{A_1^0} = 0.15\text{--}0.5 \text{ TeV}$ . See their Fig. 6 for limits in terms of two-Higgs-doublet plus singlet pseudoscalar model.
- SIRUNYAN 19AV search for a scalar resonance produced by gluon fusion or  $b$ -associated production, decaying to  $Z H^0 \rightarrow \ell^+ \ell^- b\bar{b}$  ( $\ell = e, \mu$ ) or  $\nu\bar{\nu}b\bar{b}$  in  $35.9 \text{ fb}^{-1}$  of  $pp$  collisions at  $E_{\text{cm}} = 13 \text{ TeV}$ . See their Fig. 5 for cross section limits for  $m_{A^0} = 0.22\text{--}1.0 \text{ TeV}$ .
- SIRUNYAN 19B search for gluon fusion production of narrow scalar resonance with large transverse momentum, decaying to  $b\bar{b}$ , in  $35.9 \text{ fb}^{-1}$  of  $pp$  collisions at  $E_{\text{cm}} = 13 \text{ TeV}$ . See their Figs. 7 and 8 for limits on cross section times branching ratio for the resonance mass of  $50\text{--}350 \text{ GeV}$ .
- SIRUNYAN 19BB search for the decay  $H_1^0 \rightarrow \gamma\gamma$  in  $19.7 \text{ fb}^{-1}$  of  $pp$  collisions at  $E_{\text{cm}} = 8 \text{ TeV}$  and  $35.9 \text{ fb}^{-1}$  at  $E_{\text{cm}} = 13 \text{ TeV}$ . See their Figs. 4–6 for limits on cross section times branching ratio for  $m_{H_1^0} = 80\text{--}110 \text{ GeV}$  (some results in Fig. 5 for  $m_{H_1^0} = 70\text{--}110 \text{ GeV}$ ).
- SIRUNYAN 19BD search for the decay  $H^0 \rightarrow A^0 A^0 \rightarrow \mu^+ \mu^- b\bar{b}$  in  $35.9 \text{ fb}^{-1}$  of  $pp$  collisions at  $E_{\text{cm}} = 13 \text{ TeV}$ . See their Fig. 5 for limits on the product of cross section times branching ratios in the range  $m_{A^0} = 20\text{--}62.5 \text{ GeV}$ . See also their Figs. 6 and 7 for interpretation of the data in terms of models with two Higgs doublets and a singlet.
- SIRUNYAN 19BE combine searches for  $H_2^0 \rightarrow H^0 H^0$  in  $35.9 \text{ fb}^{-1}$  of  $pp$  collisions at  $E_{\text{cm}} = 13 \text{ TeV}$  in various  $H^0$  decay modes, from SIRUNYAN 18A, SIRUNYAN 18AF, SIRUNYAN 18CW, SIRUNYAN 19, and SIRUNYAN 19H. See their Fig. 3 for limits on cross section times branching ratios for  $m_{H_2^0} = 0.25\text{--}3 \text{ TeV}$ .

# Gauge & Higgs Boson Particle Listings

## Neutral Higgs Bosons, Searches for

- 18 SIRUNYAN 19BQ search for production of  $H_{1,2}^0$  decaying to  $A^0 A^0 \rightarrow \mu^+ \mu^- \mu^+ \mu^-$  in 35.9 fb<sup>-1</sup> of  $pp$  collisions at  $E_{\text{cm}} = 13$  TeV. See their Fig. 2 for limits on cross section times branching ratio for  $m_{H_{1,2}^0} = 90\text{--}150$  GeV,  $m_{A^0} = 0.25\text{--}3.55$  GeV.
- 19 SIRUNYAN 19CR search for production of  $H_{2,3}^0/A^0$  in gluon fusion and in association with a  $b\bar{b}$  pair, decaying to  $\mu^+ \mu^-$  in 35.9 fb<sup>-1</sup> of  $pp$  collisions at  $E_{\text{cm}} = 13$  TeV. See their Fig. 6 for limits on cross section times branching ratio.
- 20 SIRUNYAN 19H search for a narrow scalar resonance decaying to  $H^0 H^0 \rightarrow b\bar{b}b\bar{b}$  in 35.9 fb<sup>-1</sup> of  $pp$  collisions at  $E_{\text{cm}} = 13$  TeV, where one  $b\bar{b}$  pair is resolved and the other not. Limits on cross section times branching ratios for  $m_{H_{2,3}^0} = 0.75\text{--}1.6$  TeV are obtained and combined with data from SIRUNYAN 18AF. See their Fig. 5 (right).
- 21 AABOUD 18AA search for production of a scalar resonance decaying to  $Z\gamma$ , with  $Z$  decaying hadronically, in 36.1 fb<sup>-1</sup> of  $pp$  collisions at  $E_{\text{cm}} = 13$  TeV. See their Fig. 8(a) for limits on cross section times branching ratio for  $m_{H_{2,3}^0} = 1.0\text{--}6.8$  TeV.
- 22 AABOUD 18AG search for the decay  $H^0 \rightarrow A^0 A^0 \rightarrow \gamma\gamma gg$  in 36.7 fb<sup>-1</sup> of  $pp$  collisions at  $E_{\text{cm}} = 13$  TeV. See their Fig. 2 and Table 6 for cross section limits in the range  $m_{A^0} = 20\text{--}60$  GeV.
- 23 AABOUD 18AH search for production of an  $A^0$  in gluon-gluon fusion and in association with a  $b\bar{b}$ , decaying to  $ZH_{2,3}^0 \rightarrow \ell^+ \ell^- b\bar{b}$  in 36.1 fb<sup>-1</sup> of  $pp$  collisions at  $E_{\text{cm}} = 13$  TeV. See their Fig. 5 for cross section limits for  $m_{A^0} = 230\text{--}800$  GeV and  $m_{H_{2,3}^0} = 130\text{--}700$  GeV.
- 24 AABOUD 18AI search for production of an  $A^0$  in gluon-gluon fusion and in association with a  $b\bar{b}$ , decaying to  $ZH^0$  in the final states  $\nu\bar{\nu}b\bar{b}$  and  $\ell^+ \ell^- b\bar{b}$  in 36.1 fb<sup>-1</sup> of  $pp$  collisions at  $E_{\text{cm}} = 13$  TeV. See their Fig. 6 for cross section limits for  $m_{A^0} = 0.2\text{--}2$  TeV. See also AABOUD 18CC.
- 25 AABOUD 18BF search for production of a heavy  $H_{2,3}^0$  state decaying to  $ZZ$  in the final states  $\ell^+ \ell^- \ell^+ \ell^-$  and  $\ell^+ \ell^- \nu\bar{\nu}$  in 36.1 fb<sup>-1</sup> of  $pp$  collisions at  $E_{\text{cm}} = 13$  TeV. See their Fig. 6 for upper limits on cross section times branching ratio for  $m_{H_{2,3}^0} = 0.2\text{--}1.2$  TeV assuming ggF or VBF with the NWA. See their Fig. 7 for upper limits on cross section times branching ratio for  $m_{H_{2,3}^0} = 0.4\text{--}1.0$  TeV assuming ggF, and with several assumptions on its width.
- 26 AABOUD 18BU search for a narrow scalar resonance decaying to  $H^0 H^0 \rightarrow \gamma\gamma WW^*$  in 36.1 fb<sup>-1</sup> of  $pp$  collisions at  $E_{\text{cm}} = 13$  TeV. See their Fig. 4 for limits on cross section times branching ratios for  $m_{H_{2,3}^0} = 260\text{--}500$  GeV.
- 27 AABOUD 18BX search for associated production of  $WH^0$  or  $ZH^0$  followed by the decay  $H^0 \rightarrow A^0 A^0 \rightarrow b\bar{b}b\bar{b}$  in 36.1 fb<sup>-1</sup> of  $pp$  collisions at  $E_{\text{cm}} = 13$  TeV. See their Fig. 9 for limits on cross section times branching ratios for  $m_{A^0} = 20\text{--}60$  GeV. See also their Fig. 10 for the dependence of the limit on  $A^0$  lifetime.
- 28 AABOUD 18CQ search for a narrow scalar resonance decaying to  $H^0 H^0 \rightarrow b\bar{b}\tau^+ \tau^-$  in 36.1 fb<sup>-1</sup> of  $pp$  collisions at  $E_{\text{cm}} = 13$  TeV. See their Fig. 2 (above) for limits on cross section times branching ratios for  $m_{H_{2,3}^0} = 260\text{--}1000$  GeV.
- 29 AABOUD 18F search for production of a narrow scalar resonance decaying to  $W^+ W^-$  and  $ZZ$ , followed by hadronic decays of  $W$  and  $Z$ , in 36.7 fb<sup>-1</sup> of  $pp$  collisions at  $E_{\text{cm}} = 13$  TeV. See their Fig. 5(c) for limits on cross section times branching ratio for  $m_{H_{2,3}^0} = 1.2\text{--}3.0$  TeV.
- 30 AAIJ 18AM search for gluon-fusion production of  $H_{1,2}^0$  decaying to  $\mu\tau$  in 2 fb<sup>-1</sup> of  $pp$  collisions at  $E_{\text{cm}} = 8$  TeV. See their Fig. 2 for limits on cross section times branching ratio for  $m_{H_{1,2}^0} = 45\text{--}195$  GeV.
- 31 AAIJ 18AQ search for gluon-fusion production of a scalar particle  $A^0$  decaying to  $\mu^+ \mu^-$  in 1.99 fb<sup>-1</sup> of  $pp$  collisions at  $E_{\text{cm}} = 8$  TeV and 0.98 fb<sup>-1</sup> at  $E_{\text{cm}} = 7$  TeV. See their Fig. 4 for limits on cross section times branching ratio for  $m_{A^0} = 5.5\text{--}15$  GeV (using the  $E_{\text{cm}} = 8$  TeV data set).
- 32 AAIJ 18AQ search for the decay  $H^0 \rightarrow A^0 A^0$ , with one of the  $A^0$  decaying to  $\mu^+ \mu^-$ , in 1.99 fb<sup>-1</sup> of  $pp$  collisions at  $E_{\text{cm}} = 8$  TeV and 0.98 fb<sup>-1</sup> at  $E_{\text{cm}} = 7$  TeV. See their Fig. 5 (right) for limits on the product of branching ratios for  $m_{A^0} = 5.5\text{--}15$  GeV (using the  $E_{\text{cm}} = 8$  TeV data set).
- 33 SIRUNYAN 18AF search for a narrow scalar resonance decaying to  $H^0 H^0 \rightarrow b\bar{b}b\bar{b}$  in 35.9 fb<sup>-1</sup> of  $pp$  collisions at  $E_{\text{cm}} = 13$  TeV, where both  $b\bar{b}$  pairs are not resolved. See their Fig. 9 for limits on cross section times branching ratios for  $m_{H_{2,3}^0} = 0.75\text{--}3$  TeV.
- 34 SIRUNYAN 18BA search for production of a heavy  $H_{2,3}^0$  state decaying to  $ZZ$  in the final states  $\ell^+ \ell^- \ell^+ \ell^-$ ,  $\ell^+ \ell^- q\bar{q}$ , and  $\ell^+ \ell^- \nu\bar{\nu}$  in 35.9 fb<sup>-1</sup> of  $pp$  collisions at  $E_{\text{cm}} = 13$  TeV. See their Figs. 10 and 11 for upper limits on cross section times branching ratio for  $m_{H_{2,3}^0} = 0.13\text{--}3$  TeV with several assumptions on its width and on the fraction of Vector-Boson-Fusion of the total production cross section.
- 35 SIRUNYAN 18CW search for a narrow scalar resonance decaying to  $H^0 H^0 \rightarrow b\bar{b}b\bar{b}$  in 35.9 fb<sup>-1</sup> of  $pp$  collisions at  $E_{\text{cm}} = 13$  TeV, where both  $b\bar{b}$  pairs are resolved. See their Fig. 9 for limits on cross section times branching ratios for  $m_{H_{2,3}^0} = 260\text{--}1200$  GeV.
- 36 SIRUNYAN 18DK search for production of a scalar resonance decaying to  $Z\gamma$ , with  $Z$  decaying to  $\ell^+ \ell^-$  or hadronically, in 35.9 fb<sup>-1</sup> of  $pp$  collisions at  $E_{\text{cm}} = 13$  TeV. See their Fig. 7 for limits on cross section times branching ratio for  $m_{H_{2,3}^0} = 0.35\text{--}4$  TeV for different assumptions on the width of the resonance.
- 37 SIRUNYAN 18DT search for the decay  $H^0 \rightarrow A^0 A^0 \rightarrow \tau^+ \tau^- b\bar{b}$  in 35.9 fb<sup>-1</sup> of  $pp$  collisions at  $E_{\text{cm}} = 13$  TeV. See their Fig. 7 for limits on the product of branching ratios in the range  $m_{A^0} = 15\text{--}60$  GeV. See also their Fig. 8 for interpretation of the data in terms of models with two Higgs doublets and a singlet.
- 38 SIRUNYAN 18DU search for production of a narrow scalar resonance decaying to  $\gamma\gamma$  in 35.9 fb<sup>-1</sup> (taken in 2016) of  $pp$  collisions at  $E_{\text{cm}} = 13$  TeV. See their Fig. 3 (right) for limits on cross section times branching ratio for  $m_{H_{2,3}^0} = 0.5\text{--}5$  TeV for several values of its width-to-mass ratio.
- 39 SIRUNYAN 18ED search for production of an  $A^0$  in gluon-gluon fusion and in association with a  $b\bar{b}$ , decaying to  $ZH^0$  in the final states  $\nu\bar{\nu}b\bar{b}$  or  $\ell^+ \ell^- b\bar{b}$  in 35.9 fb<sup>-1</sup> of  $pp$  collisions at  $E_{\text{cm}} = 13$  TeV. See their Fig. 8 for cross section limits for  $m_{A^0} = 0.8\text{--}2$  TeV.
- 40 SIRUNYAN 18EE search for the decay  $H^0 \rightarrow A^0 A^0 \rightarrow \mu^+ \mu^- \tau^+ \tau^-$  in 35.9 fb<sup>-1</sup> of  $pp$  collisions at  $E_{\text{cm}} = 13$  TeV. See their Fig. 4 for limits on the product of branching ratios in the range  $m_{A^0} = 15\text{--}62.5$  GeV, normalized to the SM production cross section. See also their Fig. 5 for interpretation of the data in terms of models with two Higgs doublets and a singlet.
- 41 SIRUNYAN 18F search for a narrow scalar resonance decaying to  $H^0 H^0 \rightarrow WWb\bar{b}$  or  $ZZb\bar{b}$  in the final state  $\ell\ell\nu\nu b\bar{b}$  in 35.9 fb<sup>-1</sup> of  $pp$  collisions at  $E_{\text{cm}} = 13$  TeV. See their Fig. 7 for limits on cross section times branching ratios for  $m_{H_{2,3}^0} = 250\text{--}900$  GeV.
- 42 AABOUD 17 search for production of a scalar resonance decaying to  $Z\gamma$  in 3.2 fb<sup>-1</sup> of  $pp$  collisions at  $E_{\text{cm}} = 13$  TeV. See their Fig. 4 for the limits on cross section times branching ratio for  $m_{H_{2,3}^0} = 0.25\text{--}3.0$  TeV.
- 43 AABOUD 17AW search for production of a scalar resonance decaying to  $Z\gamma$  in 36.1 fb<sup>-1</sup> of  $pp$  collisions at  $E_{\text{cm}} = 13$  TeV. See their Fig. 7 for limits on cross section times branching ratio for  $m_{H_{2,3}^0} = 0.25\text{--}2.4$  TeV.
- 44 KHACHATRYAN 17AZ search for the decay  $H^0 \rightarrow A^0 A^0 \rightarrow \tau^+ \tau^- \tau^+ \tau^-$ ,  $\mu^+ \mu^- b\bar{b}$ , and  $\mu^+ \mu^- \tau^+ \tau^-$  in 19.7 fb<sup>-1</sup> of  $pp$  collisions at  $E_{\text{cm}} = 8$  TeV. See their Figs. 4, 5, and 6 for cross section limits in the range  $m_{A^0} = 5\text{--}62.5$  GeV. See also their Figs. 7, 8, and 9 for interpretation of the data in terms of models with two Higgs doublets and a singlet.
- 45 KHACHATRYAN 17D search for production of a scalar resonance decaying to  $Z\gamma$  in 19.7 fb<sup>-1</sup> of  $pp$  collisions at  $E_{\text{cm}} = 8$  TeV and 2.7 fb<sup>-1</sup> at  $E_{\text{cm}} = 13$  TeV. See their Figs. 3 and 4 for the limits on cross section times branching ratio for  $m_{H_{2,3}^0} = 0.2\text{--}2.0$  TeV.
- 46 KHACHATRYAN 17R search for production of a narrow scalar resonance decaying to  $\gamma\gamma$  in 12.9 fb<sup>-1</sup> (taken in 2016) of  $pp$  collisions at  $E_{\text{cm}} = 13$  TeV. See their Fig. 2 for limits on cross section times branching ratio for  $m_{H_{2,3}^0} = 0.5\text{--}4.5$  TeV for several values of its width-to-mass ratio. Limits from combination with KHACHATRYAN 16M are shown in their Figs. 4 and 6.
- 47 SIRUNYAN 17CN search for a narrow scalar resonance decaying to  $H^0 H^0 \rightarrow b\bar{b}\tau^+ \tau^-$  in 18.3 fb<sup>-1</sup> of  $pp$  collisions at  $E_{\text{cm}} = 8$  TeV. See their Fig. 5 (above) and Table II for limits on the cross section times branching ratios for  $m_{H_{2,3}^0} = 0.3\text{--}1$  TeV, and Fig. 6 (above) and Table III for the corresponding limits by combining with data from KHACHATRYAN 16BQ and KHACHATRYAN 15R.
- 48 SIRUNYAN 17Y search for production of a scalar resonance decaying to  $Z\gamma$  in 19.7 fb<sup>-1</sup> of  $pp$  collisions at  $E_{\text{cm}} = 8$  TeV and 2.7 fb<sup>-1</sup> at  $E_{\text{cm}} = 13$  TeV. See their Figs. 3, 4 and Table 3 for limits on cross section times branching ratio for  $m_{H_{2,3}^0} = 0.7\text{--}3.0$  TeV, and Fig. 5 for the corresponding limits for  $m_{H_{2,3}^0} = 0.2\text{--}3.0$  TeV from combination with KHACHATRYAN 17D data.
- 49 AABOUD 16AB search for associated production of  $WH^0$  with the decay  $H^0 \rightarrow A^0 A^0 \rightarrow b\bar{b}b\bar{b}$  in 3.2 fb<sup>-1</sup> of  $pp$  collisions at  $E_{\text{cm}} = 13$  TeV. See their Fig. 8 for limits on cross section times branching ratios for  $m_{A^0} = 20\text{--}60$  GeV.
- 50 AABOUD 16AE search for production of a narrow scalar resonance decaying to  $W^+ W^-$  and  $ZZ$  in 3.2 fb<sup>-1</sup> of  $pp$  collisions at  $E_{\text{cm}} = 13$  TeV. See their Fig. 4 for limits on cross section times branching ratio for  $m_{H_{2,3}^0} = 0.5\text{--}3$  TeV.
- 51 AABOUD 16H search for production of a scalar resonance decaying to  $\gamma\gamma$  in 3.2 fb<sup>-1</sup> of  $pp$  collisions at  $E_{\text{cm}} = 13$  TeV. See their Fig. 12 for limits on cross section times branching ratio for  $m_{H_{2,3}^0} = 0.2\text{--}2$  TeV with different assumptions on the width.
- 52 AABOUD 16I search for a narrow scalar resonance decaying to  $H^0 H^0 \rightarrow b\bar{b}b\bar{b}$  in 3.2 fb<sup>-1</sup> of  $pp$  collisions at  $E_{\text{cm}} = 13$  TeV. See their Fig. 10(c) for limits on cross section times branching ratios for  $m_{H_{2,3}^0} = 0.5\text{--}3$  TeV.
- 53 AAD 16AX search for production of a heavy  $H^0$  state decaying to  $ZZ$  in the final states  $\ell^+ \ell^- \ell^+ \ell^-$ ,  $\ell^+ \ell^- \nu\bar{\nu}$ ,  $\ell^+ \ell^- q\bar{q}$ , and  $\nu\bar{\nu}q\bar{q}$  in 20.3 fb<sup>-1</sup> of  $pp$  collisions at  $E_{\text{cm}} = 8$  TeV. See their Fig. 12 for upper limits on  $\sigma(H^0) B(H^0 \rightarrow ZZ)$  for  $m_{H^0}$  ranging from 140 GeV to 1000 GeV.
- 54 AAD 16C search for production of a heavy  $H^0$  state decaying to  $W^+ W^-$  in the final states  $\ell\nu\ell\nu$  and  $\ell\nu q\bar{q}$  in 20.3 fb<sup>-1</sup> of  $pp$  collisions at  $E_{\text{cm}} = 8$  TeV. See their Figs. 12, 13, and 16 for upper limits on  $\sigma(H^0) B(H^0 \rightarrow W^+ W^-)$  for  $m_{H^0}$  ranging from 300 GeV to 1000 or 1500 GeV with various assumptions on the total width of  $H^0$ .
- 55 AAD 16L search for the decay  $H^0 \rightarrow A^0 A^0 \rightarrow \gamma\gamma\gamma\gamma$  in 20.3 fb<sup>-1</sup> of  $pp$  collisions at  $E_{\text{cm}} = 8$  TeV. See their Fig. 4 (upper right) for limits on cross section times branching ratios (normalized to the SM  $H^0$  cross section) for  $m_{A^0} = 10\text{--}60$  GeV.
- 56 AAD 16L search for the decay  $H_{2,3}^0 \rightarrow A^0 A^0 \rightarrow \gamma\gamma\gamma\gamma$  in 20.3 fb<sup>-1</sup> of  $pp$  collisions at  $E_{\text{cm}} = 8$  TeV. See their Fig. 4 (lower right) for limits on cross section times branching ratios for  $m_{H_{2,3}^0} = 600$  GeV and  $m_{A^0} = 10\text{--}245$  GeV, and Table 5 for limits for  $m_{H_{2,3}^0} = 300$  and 900 GeV.
- 57 AALTONEN 16C search for electroweak associated production of  $H_{1,2}^0 H^\pm$  followed by the decays  $H^\pm \rightarrow H_{1,2}^0 W^*$ ,  $H_{1,2}^0 \rightarrow \gamma\gamma$  for  $m_{H_{1,2}^0} = 10\text{--}105$  GeV and  $m_{H^\pm} = 30\text{--}300$  GeV. See their Fig. 3 for excluded parameter region in a two-doublet model in which  $H_{1,2}^0$  has no direct decay to fermions.
- 58 KHACHATRYAN 16BG search for a narrow scalar resonance decaying to  $H^0 H^0 \rightarrow b\bar{b}b\bar{b}$  in 19.7 fb<sup>-1</sup> of  $pp$  collisions at  $E_{\text{cm}} = 8$  TeV. See their Fig. 6 for limits on the cross section times branching ratios for  $m_{H_{2,3}^0} = 1.15\text{--}3$  TeV.
- 59 KHACHATRYAN 16BQ search for a resonance decaying to  $H^0 H^0 \rightarrow \gamma\gamma b\bar{b}$  in 19.7 fb<sup>-1</sup> of  $pp$  collisions at  $E_{\text{cm}} = 8$  TeV. See their Fig. 9 for limits on the cross section times branching ratios for  $m_{H_{2,3}^0} = 0.26\text{--}1.1$  TeV.
- 60 KHACHATRYAN 16F search for the decay  $H^0 \rightarrow H_{1,2}^0 H_{1,2}^0 \rightarrow \tau^+ \tau^- \tau^+ \tau^-$  in 19.7 fb<sup>-1</sup> of  $pp$  collisions at  $E_{\text{cm}} = 8$  TeV. See their Fig. 8 for cross section limits for  $m_{H_{1,2}^0} = 4\text{--}8$  GeV.

See key on page 999

# Gauge & Higgs Boson Particle Listings

## Neutral Higgs Bosons, Searches for

- 61 KHACHATRYAN 16M search for production of a narrow resonance decaying to  $\gamma\gamma$  in  $19.7 \text{ fb}^{-1}$  of  $pp$  collisions at  $E_{\text{cm}} = 8 \text{ TeV}$  and  $3.3 \text{ fb}^{-1}$  at  $E_{\text{cm}} = 13 \text{ TeV}$ . See their Fig. 3 (top) for limits on cross section times branching ratio for  $m_{H_2^0} = 0.5\text{--}4 \text{ TeV}$ .
- 62 KHACHATRYAN 16P search for gluon fusion production of an  $H_2^0$  decaying to  $H^0 H^0 \rightarrow b\bar{b}\tau^+\tau^-$  in  $19.7 \text{ fb}^{-1}$  of  $pp$  collisions at  $E_{\text{cm}} = 8 \text{ TeV}$ . See their Fig. 8 (lower right) for cross section limits for  $m_{H_2^0} = 260\text{--}350 \text{ GeV}$ .
- 63 KHACHATRYAN 16P search for gluon fusion production of an  $A^0$  decaying to  $ZH^0 \rightarrow \ell^+\ell^-\tau^+\tau^-$  in  $19.7 \text{ fb}^{-1}$  of  $pp$  collisions at  $E_{\text{cm}} = 8 \text{ TeV}$ . See their Fig. 10 for cross section limits for  $m_{H_2^0} = 220\text{--}350 \text{ GeV}$ .
- 64 AAD 15BK search for production of a heavy  $H_2^0$  decaying to  $H^0 H^0$  in the final state  $b\bar{b}\tau^+\tau^-$  in  $19.5 \text{ fb}^{-1}$  of  $pp$  collisions at  $E_{\text{cm}} = 8 \text{ TeV}$ . See their Fig. 14(c) for  $\sigma(H_2^0) B(H_2^0 \rightarrow H^0 H^0)$  for  $m_{H_2^0} = 500\text{--}1500 \text{ GeV}$  with  $\Gamma_{H_2^0} = 1 \text{ GeV}$ .
- 65 AAD 15BZ search for the decay  $H^0 \rightarrow A^0 A^0 \rightarrow \mu^+\mu^-\tau^+\tau^-$  ( $m_{H^0} = 125 \text{ GeV}$ ) in  $20.3 \text{ fb}^{-1}$  of  $pp$  collisions at  $E_{\text{cm}} = 8 \text{ TeV}$ . See their Fig. 6 for limits on cross section times branching ratio for  $m_{A^0} = 3.7\text{--}50 \text{ GeV}$ .
- 66 AAD 15BZ search for a state  $H_2^0$  via the decay  $H_2^0 \rightarrow A^0 A^0 \rightarrow \mu^+\mu^-\tau^+\tau^-$  in  $20.3 \text{ fb}^{-1}$  of  $pp$  collisions at  $E_{\text{cm}} = 8 \text{ TeV}$ . See their Fig. 6 for limits on cross section times branching ratio for  $m_{H_2^0} = 100\text{--}500 \text{ GeV}$  and  $m_{A^0} = 5 \text{ GeV}$ .
- 67 AAD 15CE search for production of a heavy  $H_2^0$  decaying to  $H^0 H^0$  in the final states  $b\bar{b}\tau^+\tau^-$  and  $\gamma\gamma WW^*$  in  $20.3 \text{ fb}^{-1}$  of  $pp$  collisions at  $E_{\text{cm}} = 8 \text{ TeV}$  and combine with data from AAD 15H and AAD 15BK. A limit  $\sigma(H_2^0) B(H_2^0 \rightarrow H^0 H^0) < 2.1\text{--}0.011 \text{ pb}$  (95% CL) is given for  $m_{H_2^0} = 260\text{--}1000 \text{ GeV}$ . See their Fig. 6.
- 68 AAD 15H search for production of a heavy  $H_2^0$  decaying to  $H^0 H^0$  in the final state  $\gamma\gamma b\bar{b}$  in  $20.3 \text{ fb}^{-1}$  of  $pp$  collisions at  $E_{\text{cm}} = 8 \text{ TeV}$ . A limit of  $\sigma(H_2^0) B(H_2^0 \rightarrow H^0 H^0) < 3.5\text{--}0.7 \text{ pb}$  is given for  $m_{H_2^0} = 260\text{--}500 \text{ GeV}$  at 95% CL. See their Fig. 3.
- 69 AAD 15S search for production of  $A^0$  decaying to  $ZH^0 \rightarrow \ell^+\ell^-b\bar{b}, \nu\bar{\nu}b\bar{b}$  and  $\ell^+\ell^-\tau^+\tau^-$  in  $20.3 \text{ fb}^{-1}$  of  $pp$  collisions at  $E_{\text{cm}} = 8 \text{ TeV}$ . See their Fig. 3 for cross section limits for  $m_{A^0} = 200\text{--}1000 \text{ GeV}$ .
- 70 KHACHATRYAN 15AW search for production of a heavy state  $H_2^0$  of an electroweak singlet extension of the Standard Model via the decays of  $H_2^0$  to  $W^+W^-$  and  $ZZ$  in up to  $5.1 \text{ fb}^{-1}$  of  $pp$  collisions at  $E_{\text{cm}} = 7 \text{ TeV}$  and up to  $19.7 \text{ fb}^{-1}$  at  $E_{\text{cm}} = 8 \text{ TeV}$  in the range  $m_{H_2^0} = 145\text{--}1000 \text{ GeV}$ . See their Figs. 8 and 9 for limits in the parameter space of the model.
- 71 KHACHATRYAN 15BB search for production of a resonance  $H^0$  decaying to  $\gamma\gamma$  in  $19.7 \text{ fb}^{-1}$  of  $pp$  collisions at  $E_{\text{cm}} = 8 \text{ TeV}$ . See their Fig. 7 for limits on cross section times branching ratio for  $m_{H^0} = 150\text{--}850 \text{ GeV}$ .
- 72 KHACHATRYAN 15N search for production of  $A^0$  decaying to  $ZH^0 \rightarrow \ell^+\ell^-b\bar{b}$  in  $19.7 \text{ fb}^{-1}$  of  $pp$  collisions at  $E_{\text{cm}} = 8 \text{ TeV}$ . See their Fig. 3 for limits on cross section times branching ratios for  $m_{A^0} = 225\text{--}600 \text{ GeV}$ .
- 73 KHACHATRYAN 15O search for production of a high-mass narrow resonance  $A^0$  decaying to  $ZH^0 \rightarrow q\bar{q}\tau^+\tau^-$  in  $19.7 \text{ fb}^{-1}$  of  $pp$  collisions at  $E_{\text{cm}} = 8 \text{ TeV}$ . See their Fig. 6 for limits on cross section times branching ratios for  $m_{A^0} = 800\text{--}2500 \text{ GeV}$ .
- 74 KHACHATRYAN 15R search for a narrow scalar resonance decaying to  $H^0 H^0 \rightarrow b\bar{b}b\bar{b}$  in  $17.9 \text{ fb}^{-1}$  of  $pp$  collisions at  $E_{\text{cm}} = 8 \text{ TeV}$ . See their Fig. 5 (top) for limits on cross section times branching ratios for  $m_{H_2^0} = 0.27\text{--}1.1 \text{ TeV}$ .
- 75 AAD 14AP search for a second  $H^0$  state decaying to  $\gamma\gamma$  in addition to the state at about  $125 \text{ GeV}$  in  $20.3 \text{ fb}^{-1}$  of  $pp$  collisions at  $E_{\text{cm}} = 8 \text{ TeV}$ . See their Fig. 4 for limits on cross section times branching ratio for  $m_{H^0} = 65\text{--}600 \text{ GeV}$ .
- 76 AAD 14M search for the decay cascade  $H_2^0 \rightarrow H^\pm W^\mp \rightarrow H^0 W^\pm W^\mp, H^0$  decaying to  $b\bar{b}$  in  $20.3 \text{ fb}^{-1}$  of  $pp$  collisions at  $E_{\text{cm}} = 8 \text{ TeV}$ . See their Table III for limits on cross section times branching ratio for  $m_{H_2^0} = 325\text{--}1025 \text{ GeV}$  and  $m_{H^\pm} = 225\text{--}925 \text{ GeV}$ .
- 77 CHATRYAN 14G search for a second  $H^0$  state decaying to  $WW^{(*)}$  in addition to the observed signal at about  $125 \text{ GeV}$  using  $4.9 \text{ fb}^{-1}$  of  $pp$  collisions at  $E_{\text{cm}} = 7 \text{ TeV}$  and  $19.4 \text{ fb}^{-1}$  at  $E_{\text{cm}} = 8 \text{ TeV}$ . See their Fig. 21 (right) for cross section limits in the mass range  $110\text{--}600 \text{ GeV}$ .
- 78 KHACHATRYAN 14P search for a second  $H^0$  state decaying to  $\gamma\gamma$  in addition to the observed signal at about  $125 \text{ GeV}$  using  $5.1 \text{ fb}^{-1}$  of  $pp$  collisions at  $E_{\text{cm}} = 7 \text{ TeV}$  and  $19.7 \text{ fb}^{-1}$  at  $E_{\text{cm}} = 8 \text{ TeV}$ . See their Figs. 27 and 28 for cross section limits in the mass range  $110\text{--}150 \text{ GeV}$ .
- 79 AALTONEN 13P search for production of a heavy Higgs boson  $H^0$  that decays into a charged Higgs boson  $H^\pm$  and a lighter Higgs boson  $H^0$  via the decay chain  $H^0 \rightarrow H^\pm W^\mp, H^\pm \rightarrow W^\pm H^0, H^0 \rightarrow b\bar{b}$  in the final state  $\ell\nu$  plus 4 jets in  $8.7 \text{ fb}^{-1}$  of  $p\bar{p}$  collisions at  $E_{\text{cm}} = 1.96 \text{ TeV}$ . See their Fig. 4 for limits on cross section times branching ratio in the  $m_{H^\pm}\text{--}m_{H^0}$  plane for  $m_{H^0} = 126 \text{ GeV}$ .
- 80 CHATRYAN 13BJ search for  $H^0$  production in the decay chain  $H^0 \rightarrow A^0 A^0, A^0 \rightarrow \mu^+\mu^-$  in  $5.3 \text{ fb}^{-1}$  of  $pp$  collisions at  $E_{\text{cm}} = 7 \text{ TeV}$ . See their Fig. 2 for limits on cross section times branching ratio.
- 81 AALTONEN 11P search in  $2.7 \text{ fb}^{-1}$  of  $p\bar{p}$  collisions at  $E_{\text{cm}} = 1.96 \text{ TeV}$  for the decay chain  $t \rightarrow bH^+, H^+ \rightarrow W^+ A^0, A^0 \rightarrow \tau^+\tau^-$  with  $m_{A^0}$  between 4 and 9 GeV. See their Fig. 4 for limits on  $B(t \rightarrow bH^+)$  for  $90 < m_{H^\pm} < 160 \text{ GeV}$ .
- 82 ABBIENDI 10 search for  $e^+e^- \rightarrow ZH^0$  with the decay chain  $H^0 \rightarrow \tilde{\chi}_1^0 \tilde{\chi}_2^0, \tilde{\chi}_2^0 \rightarrow \tilde{\chi}_1^0 + (\gamma \text{ or } Z^*)$ , when  $\tilde{\chi}_1^0$  and  $\tilde{\chi}_2^0$  are nearly degenerate. For a mass difference of 2 (4) GeV, a lower limit on  $m_{H^0}$  of 108.4 (107.0) GeV (95% CL) is obtained for SM  $ZH^0$  cross section and  $B(H^0 \rightarrow \tilde{\chi}_1^0 \tilde{\chi}_2^0) = 1$ .
- 83 SCHAE 10 search for the process  $e^+e^- \rightarrow H^0 Z$  followed by the decay chain  $H^0 \rightarrow A^0 A^0 \rightarrow \tau^+\tau^-\tau^+\tau^-$  with  $Z \rightarrow \ell^+\ell^-, \nu\bar{\nu}$  at  $E_{\text{cm}} = 183\text{--}209 \text{ GeV}$ . For a  $H^0 Z Z$  coupling equal to the SM value,  $B(H^0 \rightarrow A^0 A^0) = B(A^0 \rightarrow \tau^+\tau^-) = 1$ , and  $m_{A^0} = 4\text{--}10 \text{ GeV}$ ,  $m_{H^0}$  up to  $107 \text{ GeV}$  is excluded at 95% CL.
- 84 ABAZOV 09v search for  $H^0$  production followed by the decay chain  $H^0 \rightarrow A^0 A^0 \rightarrow \mu^+\mu^-\mu^+\mu^-$  or  $\mu^+\mu^-\tau^+\tau^-$  in  $4.2 \text{ fb}^{-1}$  of  $p\bar{p}$  collisions at  $E_{\text{cm}} = 1.96 \text{ TeV}$ . See their Fig. 3 for limits on  $\sigma(H^0) B(H^0 \rightarrow A^0 A^0)$  for  $m_{A^0} = 3.6\text{--}19 \text{ GeV}$ .
- 85 ABBIENDI 05A search for  $e^+e^- \rightarrow H_1^0 A^0$  in general Type-II two-doublet models, with decays  $H_1^0, A^0 \rightarrow q\bar{q}, gg, \tau^+\tau^-$ , and  $H_1^0 \rightarrow A^0 A^0$ .
- 86 ABBIENDI 04k search for  $e^+e^- \rightarrow H^0 Z$  with  $H^0$  decaying to two jets of any flavor including  $gg$ . The limit is for SM production cross section with  $B(H^0 \rightarrow jj) = 1$ .
- 87 ABDALLAH 04 consider the full combined LEP and LEP2 datasets to set limits on the Higgs coupling to  $W$  or  $Z$  bosons, assuming SM decays of the Higgs. Results in Fig. 26.
- 88 ACHARD 04B search for  $e^+e^- \rightarrow H^0 Z$  with  $H^0$  decaying to  $b\bar{b}, c\bar{c}$ , or  $gg$ . The limit is for SM production cross section with  $B(H^0 \rightarrow jj) = 1$ .
- 89 ACHARD 04F search for  $H^0$  with anomalous coupling to gauge boson pairs in the processes  $e^+e^- \rightarrow H^0 \gamma, e^+e^- H^0, H^0 Z$  with decays  $H^0 \rightarrow f\bar{f}, \gamma\gamma, Z\gamma$ , and  $W^* W^*$  at  $E_{\text{cm}} = 189\text{--}209 \text{ GeV}$ . See paper for limits.
- 90 ABBIENDI 03f search for  $H^0 \rightarrow$  anything in  $e^+e^- \rightarrow H^0 Z$ , using the recoil mass spectrum of  $Z \rightarrow e^+e^-$  or  $\mu^+\mu^-$ . In addition, it searched for  $Z \rightarrow \nu\bar{\nu}$  and  $H^0 \rightarrow e^+e^-$  or photons. Scenarios with large width or continuum  $H^0$  mass distribution are considered. See their Figs. 11–14 for the results.
- 91 ABBIENDI 03G search for  $e^+e^- \rightarrow H_1^0 Z$  followed by  $H_1^0 \rightarrow A^0 A^0, A^0 \rightarrow c\bar{c}, gg$ , or  $\tau^+\tau^-$  in the region  $m_{H_1^0} = 45\text{--}86 \text{ GeV}$  and  $m_{A^0} = 2\text{--}11 \text{ GeV}$ . See their Fig. 7 for the limits.
- 92 Search for associated production of a  $\gamma\gamma$  resonance with a  $Z$  boson, followed by  $Z \rightarrow q\bar{q}, \ell^+\ell^-, \nu\bar{\nu}$ , at  $E_{\text{cm}} \leq 209 \text{ GeV}$ . The limit is for a  $H^0$  with SM production cross section and  $B(H^0 \rightarrow f\bar{f})=0$  for all fermions  $f$ .
- 93 For  $B(H^0 \rightarrow \gamma\gamma)=1, m_{H^0} > 113.1 \text{ GeV}$  is obtained.
- 94 HEISTER 02M search for  $e^+e^- \rightarrow H^0 Z$ , assuming that  $H^0$  decays to  $q\bar{q}, gg$ , or  $\tau^+\tau^-$  only. The limit assumes SM production cross section.
- 95 ABBIENDI 01E search for neutral Higgs bosons in general Type-II two-doublet models, at  $E_{\text{cm}} \leq 189 \text{ GeV}$ . In addition to usual final states, the decays  $H_1^0, A^0 \rightarrow q\bar{q}, gg$  are searched for. See their Figs. 15,16 for excluded regions.
- 96 ACCIARRI 00R search for  $e^+e^- \rightarrow H^0 \gamma$  with  $H^0 \rightarrow b\bar{b}, Z\gamma$ , or  $\gamma\gamma$ . See their Fig. 3 for limits on  $\sigma\text{--}B$ . Explicit limits within an effective interaction framework are also given, for which the Standard Model Higgs search results are used in addition.
- 97 ACCIARRI 00R search for the two-photon type processes  $e^+e^- \rightarrow e^+e^- H^0$  with  $H^0 \rightarrow b\bar{b}$  or  $\gamma\gamma$ . See their Fig. 4 for limits on  $\Gamma(H^0 \rightarrow \gamma\gamma) \cdot B(H^0 \rightarrow \gamma\gamma \text{ or } b\bar{b})$  for  $m_{H^0} = 70\text{--}170 \text{ GeV}$ .
- 98 GONZALEZ-GARCIA 98B use  $D\bar{0}$  limit for  $\gamma\gamma$  events with missing  $E_T$  in  $p\bar{p}$  collisions (ABBOTT 98) to constrain possible  $ZH$  or  $WH$  production followed by unconventional  $H \rightarrow \gamma\gamma$  decay which is induced by higher-dimensional operators. See their Figs. 1 and 2 for limits on the anomalous couplings.
- 99 KRAWCZYK 97 analyse the muon anomalous magnetic moment in a two-doublet Higgs model (with type II Yukawa couplings) assuming no  $H_1^0 Z Z$  coupling and obtain  $m_{H_1^0} \gtrsim 5 \text{ GeV}$  or  $m_{A^0} \gtrsim 5 \text{ GeV}$  for  $\tan\beta > 50$ . Other Higgs bosons are assumed to be much heavier.
- 100 ALEXANDER 96H give  $B(Z \rightarrow H^0 \gamma) \times B(H^0 \rightarrow q\bar{q}) < 1\text{--}4 \times 10^{-5}$  (95%CL) and  $B(Z \rightarrow H^0 \gamma) \times B(H^0 \rightarrow b\bar{b}) < 0.7\text{--}2 \times 10^{-5}$  (95%CL) in the range  $20 < m_{H^0} < 80 \text{ GeV}$ .

### SEARCHES FOR A HIGGS BOSON WITH STANDARD MODEL COUPLINGS

These listings are based on experimental searches for a scalar boson whose couplings to  $W, Z$  and fermions are precisely those of the Higgs boson predicted by the three-generation Standard Model with the minimal Higgs sector.

For a review and a bibliography, see the review on "Status of Higgs Boson Physics."

### Indirect Mass Limits for $H^0$ from Electroweak Analysis

The mass limits shown below apply to a Higgs boson  $H^0$  with Standard Model couplings whose mass is a priori unknown.

For limits obtained before the direct measurement of the top quark mass, see the 1996 (Physical Review D54 1 (1996)) Edition of this Review. Other studies based on data available prior to 1996 can be found in the 1998 Edition (The European Physical Journal C 3 1 (1998)) of this Review.

VALUE (GeV)	DOCUMENT ID	TECN
$90^{+21}_{-18}$	1 HALLER	18 RVUE
$91^{+30}_{-23}$	2 BAAK	12 RVUE
$94^{+25}_{-22}$	3 BAAK	12A RVUE
$91^{+31}_{-24}$	4 ERLER	10A RVUE
$129^{+74}_{-49}$	5 LEP-SLC	06 RVUE

••• We do not use the following data for averages, fits, limits, etc. •••

Gauge & Higgs Boson Particle Listings
Neutral Higgs Bosons, Searches for

- 1 HALLER 18 make Standard Model fits to Z and neutral current parameters, m\_t, m\_W, and Gamma\_W measurements available in 2018.
2 BAAK 12 make Standard Model fits to Z and neutral current parameters, m\_t, m\_W, and Gamma\_W measurements available in 2010.
3 BAAK 12A make Standard Model fits to Z and neutral current parameters, m\_t, m\_W, and Gamma\_W measurements available in 2012.
4 ERLER 10A makes Standard Model fits to Z and neutral current parameters, m\_t, m\_W measurements available in 2009.
5 LEP-SLC 06 make Standard Model fits to Z parameters from LEP/SLC and m\_t, m\_W, and Gamma\_W measurements available in 2005.

SEARCHES FOR NEUTRAL HIGGS BOSONS REFERENCES

AAD 20 PR D101 012002
AAD 20C PL B800 135103
SIRUNYAN 20 PL B800 135087
AABOUD 19A JHEP 1901 030
AABOUD 19AG PL B790 1
AABOUD 19AI PL B793 499
AABOUD 19J JHEP 1904 492
AABOUD 19T JHEP 1905 124
AABOUD 19V JHEP 1905 142
AABOUD 19Y JHEP 1907 117
AALTONEN 19 PR D99 052001
SIRUNYAN 19 PL B788 7
SIRUNYAN 19AE JHEP 1905 210
SIRUNYAN 19AN EPJ C79 280
SIRUNYAN 19AV EPJ C79 564
SIRUNYAN 19B PR D99 012005
SIRUNYAN 19BB PL B793 320
SIRUNYAN 19BD PL B795 398
SIRUNYAN 19BE PRL 122 121803
SIRUNYAN 19CF PL B796 131
SIRUNYAN 19CR PL B798 134992
SIRUNYAN 19H JHEP 1901 040
AABOUD 18AA PR D98 032015
AABOUD 18AG PL B782 750
AABOUD 18AH PL B783 392
AABOUD 18AI JHEP 1803 174
Also JHEP 1811 0511 (erratum)
AABOUD 18AP JHEP 1806 166
AABOUD 18BF EPJ C78 293
AABOUD 18BU EPJ C78 1007
AABOUD 18BX JHEP 1810 031
AABOUD 18CC JHEP 1811 0511 (erratum)
AABOUD 18CE JHEP 1812 039
AABOUD 18CQ PRL 121 191801
AABOUD 18CW JHEP 1811 040
AABOUD 18F PL B777 91
AABOUD 18G JHEP 1801 055
AAJ 18AM EPJ C78 1008
AAJ 18AQ JHEP 1809 147
HALLER 18 EPJ C78 675
SIRUNYAN 18A PL B778 101
SIRUNYAN 18AF PL B781 244
SIRUNYAN 18BA JHEP 1806 127
Also JHEP 1903 128 (erratum)
SIRUNYAN 18BP JHEP 1808 113
SIRUNYAN 18CW JHEP 1808 152
SIRUNYAN 18CX JHEP 1809 007
SIRUNYAN 18DK JHEP 1809 148
SIRUNYAN 18DT PL B785 462
SIRUNYAN 18DU PR D98 092001
SIRUNYAN 18ED JHEP 1811 172
SIRUNYAN 18EE JHEP 1811 078
SIRUNYAN 18F JHEP 1801 054
AABOUD 17 PL B764 11
AABOUD 17AN PRL 119 191803
AABOUD 17AW JHEP 1710 112
KHACHATRYAN... 17AZ JHEP 1710 076
KHACHATRYAN... 17D JHEP 1701 076
KHACHATRYAN... 17R PL B767 147
SIRUNYAN 17AX JHEP 1711 010
SIRUNYAN 17CN PR D96 072004
SIRUNYAN 17Y PL B772 363
AABOUD 16AA EPJ C76 585
AABOUD 16AB EPJ C76 605
AABOUD 16AE JHEP 1609 173
AABOUD 16H JHEP 1609 001
AABOUD 16I PR D94 052002
AAD 16AX EPJ C76 45
AAD 16C JHEP 1601 032
AAD 16L EPJ C76 210
AALTONEN 16C PR D93 112010
ABLIKIM 16E PR D93 052005
KHACHATRYAN... 16A PL B752 221
KHACHATRYAN... 16BG EPJ C76 371
KHACHATRYAN... 16BQ PR D94 052012
KHACHATRYAN... 16F JHEP 1601 079
KHACHATRYAN... 16M PRL 117 051802
KHACHATRYAN... 16P PL B755 217
KHACHATRYAN... 16W PL B758 296
KHACHATRYAN... 16Z PL B759 369
AAD 15BD EPJ C75 337
AAD 15BH EPJ C75 299
Also EPJ C75 408 (erratum)
AAD 15BK EPJ C75 412
AAD 15BZ PR D92 052002
AAD 15CE PR D92 092004
AAD 15H PRL 114 081802
AAD 15S PRL B744 163
KHACHATRYAN... 15AW JHEP 1510 144
KHACHATRYAN... 15AY JHEP 1511 071
KHACHATRYAN... 15B PL B750 494
KHACHATRYAN... 15BN PL B748 221

PL B748 255
KHACHATRYAN... 15R PL B749 560
LEES 15R PR D91 071102
AAD 14AP PRL 113 171801
AAD 14AW JHEP 1411 056
AAD 14BA JHEP 1411 088
AAD 14M PR D89 032002
AAD 14Q PRL 112 201802
CHATRCHYAN 14B EPJ C74 2980
CHATRCHYAN 14G JHEP 1401 096
KHACHATRYAN... 14M JHEP 1410 160
KHACHATRYAN... 14P EPJ C74 3076
KHACHATRYAN... 14Q PR D90 112013
AAD 13AG PL B721 32
AAD 13AT NJP 15 043009
AAD 13O JHEP 1302 095
AAJ 13T JHEP 1305 132
AALTONEN 13K PR D88 052012
AALTONEN 13L PR D88 052013
AALTONEN 13M PR D88 052014
AALTONEN 13P PRL 110 121801
ABAZOV 13G PR D88 052006
ABAZOV 13H PR D88 052007
ABAZOV 13J PR D88 052008
ABAZOV 13I PR D88 052009
ABAZOV 13L PR D88 052011
CARENA 13 EPJ C73 2552
CHATRCHYAN 13AG PL B722 207
CHATRCHYAN 13BJ PL B726 564
CHATRCHYAN 13C PR D87 031102
LEES 13L PR D88 031701
LEES 13R PR D88 071102
AAD 12AI PL B716 1
AAD 12AQ PRL 108 251801
AAD 12N EPJ C72 2157
AALTONEN 12AB PR D85 092001
AALTONEN 12AN PL B717 173
AALTONEN 12AQ PR D86 091101
AALTONEN 12Q PR D85 012007
AALTONEN 12X PR D85 032005
ABAZOV 12G PL B710 569
ABLIKIM 12 PR D85 092012
BAAK 12 EPJ C72 2003
BAAK 12A EPJ C72 2205
CHATRCHYAN 12AO JHEP 1209 111
CHATRCHYAN 12C JHEP 1203 081
CHATRCHYAN 12D JHEP 1204 036
CHATRCHYAN 12E PL B710 91
CHATRCHYAN 12G PL B710 403
CHATRCHYAN 12H PRL 108 111804
CHATRCHYAN 12I JHEP 1203 040
CHATRCHYAN 12K PL B713 68
CHATRCHYAN 12N PL B716 30
CHATRCHYAN 12V PRL 109 121801
AALTONEN 11P PRL 107 031801
ABAZOV 11K PL B698 97
ABAZOV 11W PRL 107 121801
ABOUBAZID 11A PRL 107 201803
DEL-AMO-SALAS... 11J PRL 107 021804
LEES 11H PRL 107 221803
ABBIENDI 10 PL B682 381
ANDREAS 10 JHEP 1008 003
ERLER 10A PR D83 05101
HYUN 10 PRL 105 091801
SCHAEF 10 JHEP 1005 049
AALTONEN 09AB PRL 103 061803
AALTONEN 09AR PRL 103 201801
ABAZOV 09V PRL 103 061801
AUBERT 09P PRL 103 181801
AUBERT 09Z PRL 103 081803
TUNG 09 PR 102 051802
ABAZOV 08U PRL 101 051801
ABDALLAH 08B EPJ C54 1
Also EPJ C61 165 (erratum)
W. Love et al. (CLEO Collab.)
G. Abbiendi et al. (OPAL Collab.)
D. Besson et al. (CLEO Collab.)
S. Schael et al. (ALEPH Collab.)
ALEPH, DELPHI, L3, OPAL, SLD and working groups
S. Schael et al. (LEP Collab.)
G. Abbiendi et al. (OPAL Collab.)
J. Abdallah et al. (DELPHI Collab.)
P. Achard et al. (L3 Collab.)
O. Acosta et al. (CDF Collab.)
H. Park et al. (FNAL Hyperion Collab.)
G. Abbiendi et al. (OPAL Collab.)
G. Abbiendi et al. (OPAL Collab.)
J. Abdallah et al. (DELPHI Collab.)
J. Abdallah et al. (DELPHI Collab.)
J. Abdallah et al. (DELPHI Collab.)
P. Achard et al. (L3 Collab.)
P. Achard et al. (L3 Collab.)
G. Abbiendi et al. (OPAL Collab.)
G. Abbiendi et al. (OPAL Collab.)
P. Achard et al. (L3 Collab.)
P. Achard et al. (L3 Collab.)
A.G. Akeroyd et al.
A. Heister et al. (ALEPH Collab.)
A. Heister et al. (ALEPH Collab.)
A. Heister et al. (ALEPH Collab.)
G. Abbiendi et al. (OPAL Collab.)
P. Abreu et al. (DELPHI Collab.)
T. Affolder et al. (CDF Collab.)
R. Barate et al. (ALEPH Collab.)
M. Acciarri et al. (L3 Collab.)
M. Acciarri et al. (L3 Collab.)
R. Barate et al. (ALEPH Collab.)
G. Abbiendi et al. (OPAL Collab.)
G. Abbiendi et al. (OPAL Collab.)
M. Abbott et al. (DO Collab.)
P. Abreu et al. (DELPHI Collab.)
M. Abbott et al. (DO Collab.)
K. Ackerstaff et al. (CDF Collab.)
K. Ackerstaff et al. (CDF Collab.)
M.C. Gonzalez-Garcia, S.M. Lletti, S.F. Novaes

Downloaded from https://academic.oup.com/ptep/article/2020/8/083C01/5891211 by guest on 12 November 2020

See key on page 999

Gauge & Higgs Boson Particle Listings

Neutral Higgs Bosons, Searches for, Charged Higgs Bosons ( $H^\pm$  and  $H^{\pm\pm}$ ), Searches for

PDG 98	EPJ C3 1	C. Caso <i>et al.</i>	(PDG Collab.)
KRAWCZYK 97	PR D55 6968	M. Krawczyk, J. Zochowski	(Warsaw)
ALEXANDER 96H	ZPHY C71 1	G. Alexander <i>et al.</i>	(OPAL Collab.)
PDG 96	PR D54 1	R. M. Barnett <i>et al.</i>	(PDG Collab.)
ABREU 95H	ZPHY C67 69	P. Abreu <i>et al.</i>	(DELPHI Collab.)
BALEST 95	PR D51 2053	R. Balest <i>et al.</i>	(CLEO Collab.)
PICH 92	NP B388 31	A. Pich, J. Prades, P. Yepes	(CERN, CPPM)
ANTREASANYAN 90C	PL B251 204	D. Antreasyan <i>et al.</i>	(Crystal Ball Collab.)

**Charged Higgs Bosons ( $H^\pm$  and  $H^{\pm\pm}$ ), Searches for**

**CONTENTS:**

- $H^\pm$  (charged Higgs) mass limits for  $m_{H^\pm} < m(\text{top})$
- $H^\pm$  (charged Higgs) mass limits for  $m_{H^\pm} > m(\text{top})$
- $H^{\pm\pm}$  (doubly-charged Higgs boson) mass limits
  - Limits for  $H^{\pm\pm}$  with  $T_3 = \pm 1$
  - Limits for  $H^{\pm\pm}$  with  $T_3 = 0$

**$H^\pm$  (charged Higgs) mass limits for  $m_{H^\pm} < m(\text{top})$**

Unless otherwise stated, LEP limits assume  $B(H^+ \rightarrow \tau^+ \nu) + B(H^+ \rightarrow c\bar{s}) = 1$ , and hold for all values of  $B(H^+ \rightarrow \tau^+ \nu_\tau)$ , and assume  $H^+$  weak isospin of  $T_3 = +1/2$ . In the following,  $\tan\beta$  is the ratio of the two vacuum expectation values in two-doublet models (2HDM).

The limits are also applicable to point-like technipions. For a discussion of techniparticles, see the Review of Dynamical Electroweak Symmetry Breaking in this Review.

Limits obtained at the LHC are given in the  $m_h^{\text{mod-}}$  benchmark scenario, see CARENA 13, and hold for all  $\tan\beta$  values.

For limits obtained in hadronic collisions before the observation of the top quark, and based on the top mass values inconsistent with the current measurements, see the 1996 (Physical Review D54 1 (1996)) Edition of this Review.

Searches in  $e^+e^-$  collisions at and above the  $Z$  pole have conclusively ruled out the existence of a charged Higgs in the region  $m_{H^\pm} \lesssim 45$  GeV, and are meanwhile superseded by the searches in higher energy  $e^+e^-$  collisions at LEP. Results that are by now obsolete are therefore not included in this compilation, and can be found in a previous Edition (The European Physical Journal C15 1 (2000)) of this Review.

In the following, and unless otherwise stated, results from the LEP experiments (ALEPH, DELPHI, L3, and OPAL) are assumed to derive from the study of the  $e^+e^- \rightarrow H^\pm H^\mp$  process. Limits from  $b \rightarrow s\gamma$  decays are usually stronger in generic 2HDM models than in Supersymmetric models.

VALUE (GeV)	CL%	DOCUMENT ID	TECN	COMMENT
none 80-140	95	1 AAD 15AF ATLS	$t \rightarrow bH^+$	
none 80-155	95	2 KHACHATRYAN...15AX CMS	$t \rightarrow bH^+, H^+ \rightarrow \tau^+ \nu$	
> 80	95	3 LEP 13 LEP	$e^+e^- \rightarrow H^+H^-, E_{\text{cm}} \leq 209\text{GeV}$	
> 76.3	95	4 ABBIENDI 12 OPAL	$e^+e^- \rightarrow H^+H^-, E_{\text{cm}} \leq 209\text{GeV}$	
> 74.4	95	ABDALLAH 04i DLPH	$E_{\text{cm}} \leq 209\text{ GeV}$	
> 76.5	95	ACHARD 03e L3	$E_{\text{cm}} \leq 209\text{ GeV}$	
> 79.3	95	HEISTER 02P ALEP	$E_{\text{cm}} \leq 209\text{ GeV}$	
• • • We do not use the following data for averages, fits, limits, etc. • • •				
		5 SIRUNYAN 19AH CMS	$H^+ \rightarrow \tau^+ \nu$	
		6 SIRUNYAN 19BP CMS	$H^+ \rightarrow W^+ Z$	
		7 SIRUNYAN 19CC CMS	$t \rightarrow bH^+, H^+ \rightarrow W^+ A^0, A^0 \rightarrow \mu^+ \mu^-$	
		8 SIRUNYAN 19CQ CMS	$H^+ \rightarrow W^+ Z$	
		9 AABOUD 18BWATLS	$\bar{t}bH^+$ or $t \rightarrow bH^+, H^+ \rightarrow \tau^+ \nu$	
		10 AABOUD 18CD ATLS	$\bar{t}bH^+, H^+ \rightarrow t\bar{b}$	
		11 AABOUD 18CH ATLS	$H^\pm \rightarrow W^\pm Z$	
		12 HALLER 18 RVUE	$b \rightarrow s\gamma$	
		13 SIRUNYAN 18DO CMS	$t \rightarrow bH^+, H^+ \rightarrow c\bar{b}$	
		14 MISIAK 17 RVUE	$b \rightarrow s(d)\gamma$	
		15 SIRUNYAN 17AE CMS	$H^\pm \rightarrow W^\pm Z$	
		16 AABOUD 16A ATLS	$t(b) H^+, H^+ \rightarrow \tau^+ \nu$	
		17 AAD 16AJ ATLS	$t(b) H^+, H^+ \rightarrow t\bar{b}$	
		18 AAD 16AJ ATLS	$qq \rightarrow H^+, H^+ \rightarrow t\bar{b}$	
		19 AAD 15AF ATLS	$tH^\pm$	
		20 AAD 15M ATLS	$H^\pm \rightarrow W^\pm Z$	
		21 KHACHATRYAN...15AX CMS	$tH^+, H^+ \rightarrow t\bar{b}$	
		22 KHACHATRYAN...15AX CMS	$tH^\pm, H^\pm \rightarrow \tau^\pm \nu$	
		23 KHACHATRYAN...15BF CMS	$t \rightarrow bH^+, H^+ \rightarrow c\bar{s}$	
		24 AAD 14M ATLS	$H_2^0 \rightarrow H^\pm W^\mp \rightarrow H^0 W^\pm W^\mp, H^0 \rightarrow b\bar{b}$	
		25 AALTONEN 14A CDF	$t \rightarrow b\tau\nu$	
		26 AAD 13AC ATLS	$t \rightarrow bH^+$	

>316	95	27 AAD 13v ATLS	$t \rightarrow bH^+, \text{lepton non-universality}$
		28 AAD 12BH ATLS	$t \rightarrow bH^+$
		29 CHATRCHYAN 12AA CMS	$t \rightarrow bH^+$
		30 AALTONEN 11P CDF	$t \rightarrow bH^+, H^+ \rightarrow W^+ A^0$
		31 DESCHAMPS 10 RVUE	Type II, flavor physics data
		32 AALTONEN 09AJ OPAL	$t \rightarrow bH^+$
		33 ABAZOV 09AC D0	$t \rightarrow bH^+$
		34 ABAZOV 09AG D0	$t \rightarrow bH^+$
		35 ABAZOV 09AI D0	$t \rightarrow bH^+$
		36 ABAZOV 09P D0	$H^+ \rightarrow t\bar{b}$
		37 ABULENCIA 06E CDF	$t \rightarrow bH^+$
> 92.0	95	ABBIENDI 04 OPAL	$B(\tau\nu) = 1$
> 76.7	95	38 ABDALLAH 04i DLPH	Type I
		39 ABBIENDI 03 OPAL	$\tau \rightarrow \mu\bar{\nu}\nu, e\bar{\nu}\nu$
		40 ABAZOV 02B D0	$t \rightarrow bH^+, H \rightarrow \tau\nu$
		41 BORZUMATI 02 RVUE	
		42 ABBIENDI 01q OPAL	$B \rightarrow \tau\nu_\mu X$
		43 BARATE 01E ALEP	$B \rightarrow \tau\nu_\tau$
>315	99	44 GAMBINO 01 RVUE	$b \rightarrow s\gamma$
		45 AFFOLDER 00i CDF	$t \rightarrow bH^+, H \rightarrow \tau\nu$
> 59.5	95	ABBIENDI 99E OPAL	$E_{\text{cm}} \leq 183\text{ GeV}$
		46 ABBOTT 99E D0	$t \rightarrow bH^+$
		47 ACKERSTAFF 99D OPAL	$\tau \rightarrow e\nu\nu, \mu\nu\nu$
		48 ACCIARRI 97F L3	$B \rightarrow \tau\nu_\tau$
		49 AMMAR 97B CLEO	$\tau \rightarrow \mu\nu\nu$
		50 COARASA 97 RVUE	$B \rightarrow \tau\nu_\mu X$
		51 GUCHAIT 97 RVUE	$t \rightarrow bH^+, H \rightarrow \tau\nu$
		52 MANGANO 97 RVUE	$B_{u(c)} \rightarrow \tau\nu_\tau$
		53 STAHL 97 RVUE	$\tau \rightarrow \mu\nu\nu$
>244	95	54 ALAM 95 CLE2	$b \rightarrow s\gamma$
		55 BUSKULIC 95 ALEP	$b \rightarrow \tau\nu_\tau X$

- 1 AAD 15AF search for  $t\bar{t}$  production followed by  $t \rightarrow bH^+, H^+ \rightarrow \tau^+ \nu$  in 19.5 fb<sup>-1</sup> of  $pp$  collisions at  $E_{\text{cm}} = 8$  TeV. Upper limits on  $B(t \rightarrow bH^+) B(H^+ \rightarrow \tau\nu)$  between  $2.3 \times 10^{-3}$  and  $1.3 \times 10^{-2}$  (95% CL) are given for  $m_{H^\pm} = 80\text{-}160$  GeV. See their Fig. 8 for the excluded regions in different benchmark scenarios of the MSSM. The region  $m_{H^\pm} < 140$  GeV is excluded for  $\tan\beta > 1$  in the considered scenarios.
- 2 KHACHATRYAN 15AX search for  $t\bar{t}$  production followed by  $t \rightarrow bH^+, H^+ \rightarrow \tau^+ \nu$  in 19.7 fb<sup>-1</sup> of  $pp$  collisions at  $E_{\text{cm}} = 8$  TeV. Upper limits on  $B(t \rightarrow bH^+) B(H^+ \rightarrow \tau\nu)$  between  $1.2 \times 10^{-2}$  and  $1.5 \times 10^{-3}$  (95% CL) are given for  $m_{H^\pm} = 80\text{-}160$  GeV. See their Fig. 11 for the excluded regions in different benchmark scenarios of the MSSM. The region  $m_{H^\pm} < 155$  GeV is excluded for  $\tan\beta > 1$  in the considered scenarios.
- 3 LEP 13 give a limit that refers to the Type II scenario. The limit for  $B(H^+ \rightarrow \tau\nu) = 1$  is 94 GeV (95% CL), and for  $B(H^+ \rightarrow c\bar{s}) = 1$  the region below 80.5 as well as the region 83-88 GeV is excluded (95% CL). LEP 13 also search for the decay mode  $H^+ \rightarrow A^0 W^+$  with  $A^0 \rightarrow b\bar{b}$ , which is not negligible in Type I models. The limit in Type I models is 72.5 GeV (95% CL) if  $m_{A^0} > 12$  GeV.
- 4 ABBIENDI 12 also search for the decay mode  $H^+ \rightarrow A^0 W^+$  with  $A^0 \rightarrow b\bar{b}$ .
- 5 SIRUNYAN 19AH search for  $H^+$  in the decay of a pair-produced  $t$  quark, or in associated  $tbH^+$  or nonresonant  $b\bar{b}H^+ W^-$  production, followed by  $H^+ \rightarrow \tau^+ \nu$ , in 35.9 fb<sup>-1</sup> of  $pp$  collisions at  $E_{\text{cm}} = 13$  TeV. Upper limits on cross section times branching ratio between 6 pb and 5 fb (95% CL) are given for  $m_{H^\pm} = 80\text{-}3000$  GeV (including the non-resonant production near the top quark mass), see their Fig. 6 (left). See their Fig. 6 (right) for the excluded regions in the  $m_h^{\text{mod-}}$  scenario of the MSSM.
- 6 SIRUNYAN 19BP search for vector boson fusion production of  $H^+$  decaying to  $H^+ \rightarrow W^+ Z \rightarrow \ell^+ \nu \ell^+ \ell^-$  in 35.9 fb<sup>-1</sup> of  $pp$  collisions at  $E_{\text{cm}} = 13$  TeV. See their Fig. 7 for limits on cross section times branching ratio for  $m_{H^\pm} = 0.3\text{-}2.0$  TeV, and also for limits on the triplet vacuum expectation value fraction in the Georgi-Machacek model.
- 7 SIRUNYAN 19CC search for  $t \rightarrow bH^+$  from pair produced top quarks, with the decay chain  $H^+ \rightarrow W^+ A^0, A^0 \rightarrow \mu^+ \mu^-$  in 35.9 fb<sup>-1</sup> of  $pp$  collisions at  $E_{\text{cm}} = 13$  TeV. See their Fig. 2 for limits on the product of branching ratios for  $m_{A^0} = 15\text{-}75$  GeV.
- 8 SIRUNYAN 19CQ search for vector boson fusion production of  $H^+$  decaying to  $H^+ \rightarrow W^+ Z \rightarrow \ell^+ \nu q\bar{q}$  or  $q\bar{q}\ell^+ \ell^-$  in 35.9 fb<sup>-1</sup> of  $pp$  collisions at  $E_{\text{cm}} = 13$  TeV. See their Fig. 5 for limits on cross section times branching ratio for  $m_{H^\pm} = 0.6\text{-}2.0$  TeV, and also for limits on the triplet vacuum expectation value fraction in the Georgi-Machacek model.
- 9 AABOUD 18BW search for  $\bar{t}bH^+$  associated production or the decay  $t \rightarrow bH^+$ , followed by  $H^+ \rightarrow \tau^+ \nu$ , in 36.1 fb<sup>-1</sup> of  $pp$  collisions at  $E_{\text{cm}} = 13$  TeV. See their Fig. 8(a) for upper limits on cross section times branching ratio for  $m_{H^\pm} = 90\text{-}2000$  GeV, and Fig. 8(b) for limits on  $B(t \rightarrow bH^+) B(H^+ \rightarrow \tau^+ \nu)$  for  $m_{H^\pm} = 90\text{-}160$  GeV. See also their Fig. 9 for the excluded region in the hMSSM parameter space.
- 10 AABOUD 18CD search for  $\bar{t}bH^+$  associated production followed by  $H^+ \rightarrow t\bar{b}$  in 36.1 fb<sup>-1</sup> of  $pp$  collisions at  $E_{\text{cm}} = 13$  TeV. See their Fig. 8 for upper limits on cross section times branching ratio for  $m_{H^\pm} = 0.2\text{-}2$  TeV. See also their Fig. 9 for the excluded region in the parameter space of the  $m_h^{\text{mod-}}$  and hMSSM scenarios of the MSSM. The theory predictions overlaid to the experimental limits to determine the excluded  $m_{H^\pm}$  range are shown without their respective uncertainty band.
- 11 AABOUD 18CH search for vector boson fusion production of  $H^\pm$  decaying to  $H^\pm \rightarrow W^\pm Z \rightarrow \ell^\pm \nu \ell^\pm \ell^-$  in 36.1 fb<sup>-1</sup> of  $pp$  collisions at  $E_{\text{cm}} = 13$  TeV. See their Fig. 7 for limits on cross section times branching ratio for  $m_{H^\pm} = 0.2\text{-}0.9$  TeV, and also for limits on the triplet vacuum expectation value fraction in the Georgi-Machacek model.
- 12 HALLER 18 give 95% CL lower limits on  $m_{H^\pm}$  of 590 GeV in type II two Higgs doublet model from combined data (including an unpublished BELLE result) for  $(b \rightarrow s\gamma)$ .



# Gauge & Higgs Boson Particle Listings

## Charged Higgs Bosons ( $H^\pm$ and $H^{\pm\pm}$ ), Searches for

- 13 SIRUNYAN 18D search for  $t\bar{t}$  production followed by  $t \rightarrow bH^+$ ,  $H^+ \rightarrow c\bar{b}$  in  $19.7 \text{ fb}^{-1}$  of  $pp$  collisions at  $E_{\text{cm}} = 8 \text{ TeV}$ . See their Fig. 3 for upper limits on  $B(t \rightarrow bH^+)$  for  $m_{H^+} = 90\text{--}150 \text{ GeV}$  assuming that  $B(H^+ \rightarrow c\bar{b}) = 1$  and  $B(t \rightarrow bH^+) + B(t \rightarrow bW^+) = 1$ .
- 14 MISIAK 17 give 95% CL lower limits on  $m_{H^+}$  between 570 and 800 GeV in type II two Higgs doublet model from combined data (including an unpublished BELLE result) for  $B(b \rightarrow s(d)\gamma)$ .
- 15 SIRUNYAN 17AE search for vector boson fusion production of  $H^\pm$  decaying to  $H^\pm \rightarrow W^\pm Z \rightarrow \ell^\pm \nu \ell^+ \ell^-$  in  $15.2 \text{ fb}^{-1}$  of  $pp$  collisions at  $E_{\text{cm}} = 13 \text{ TeV}$ . See their Fig. 3 for limits on cross section times branching ratio for  $m_{H^\pm} = 0.2\text{--}2.0 \text{ TeV}$ , and also for limits on the triplet vacuum expectation value fraction in the Georgi-Machacek model.
- 16 AABOUD 16A search for  $t(b) H^\pm$  associated production followed by  $H^\pm \rightarrow \tau^\pm \nu$  in  $3.2 \text{ fb}^{-1}$  of  $pp$  collisions at  $E_{\text{cm}} = 13 \text{ TeV}$ . Upper limits on  $\sigma(t(b) H^\pm) B(H^\pm \rightarrow \tau \nu)$  between 1.9 pb and 15 fb (95% CL) are given for  $m_{H^\pm} = 200\text{--}2000 \text{ GeV}$ , see their Fig. 6. See their Fig. 7 for the excluded regions in the hMSSM scenario.
- 17 AAD 16AJ search for  $t(b) H^\pm$  associated production followed by  $H^\pm \rightarrow tb$  in  $20.3 \text{ fb}^{-1}$  of  $pp$  collisions at  $E_{\text{cm}} = 8 \text{ TeV}$ . See their Fig. 6 for upper limits on  $\sigma(t(b) H^\pm) B(H^\pm \rightarrow tb)$  for  $m_{H^\pm} = 200\text{--}600 \text{ GeV}$ .
- 18 AAD 16AJ search for  $H^\pm$  production from quark-antiquark annihilation, followed by  $H^\pm \rightarrow tb$ , in  $20.3 \text{ fb}^{-1}$  of  $pp$  collisions at  $E_{\text{cm}} = 8 \text{ TeV}$ . See their Fig. 10 for upper limits on  $\sigma(H^\pm) B(H^\pm \rightarrow tb)$  for  $m_{H^\pm} = 400\text{--}3000 \text{ GeV}$ .
- 19 AAD 15AF search for  $tH^\pm$  associated production followed by  $H^\pm \rightarrow \tau^\pm \nu$  in  $19.5 \text{ fb}^{-1}$  of  $pp$  collisions at  $E_{\text{cm}} = 8 \text{ TeV}$ . Upper limits on  $\sigma(tH^\pm) B(H^\pm \rightarrow \tau \nu)$  between 760 and 4.5 fb (95% CL) are given for  $m_{H^\pm} = 180\text{--}1000 \text{ GeV}$ . See their Fig. 8 for the excluded regions in different benchmark scenarios of the MSSM.
- 20 AAD 15M search for vector boson fusion production of  $H^\pm$  decaying to  $H^\pm \rightarrow W^\pm Z \rightarrow q\bar{q}\ell^+\ell^-$  in  $20.3 \text{ fb}^{-1}$  of  $pp$  collisions at  $E_{\text{cm}} = 8 \text{ TeV}$ . See their Fig. 2 for limits on cross section times branching ratio for  $m_{H^\pm} = 200\text{--}1000 \text{ GeV}$ , and Fig. 3 for limits on the triplet vacuum expectation value fraction in the Georgi-Machacek model.
- 21 KHACHATRYAN 15AX search for  $tH^\pm$  associated production followed by  $H^\pm \rightarrow tb$  in  $19.7 \text{ fb}^{-1}$  of  $pp$  collisions at  $E_{\text{cm}} = 8 \text{ TeV}$ . Upper limits on  $\sigma(tH^\pm) B(H^\pm \rightarrow t\bar{b})$  between 2.0 and 0.13 pb (95% CL) are given for  $m_{H^\pm} = 180\text{--}600 \text{ GeV}$ . See their Fig. 11 for the excluded regions in different benchmark scenarios of the MSSM.
- 22 KHACHATRYAN 15AX search for  $tH^\pm$  associated production followed by  $H^\pm \rightarrow \tau^\pm \nu$  in  $19.7 \text{ fb}^{-1}$  of  $pp$  collisions at  $E_{\text{cm}} = 8 \text{ TeV}$ . Upper limits on  $\sigma(tH^\pm) B(H^\pm \rightarrow \tau \nu)$  between 380 and 25 fb (95% CL) are given for  $m_{H^\pm} = 180\text{--}600 \text{ GeV}$ . See their Fig. 11 for the excluded regions in different benchmark scenarios of the MSSM.
- 23 KHACHATRYAN 15BF search for  $t\bar{t}$  production followed by  $t \rightarrow bH^+$ ,  $H^+ \rightarrow c\bar{s}$  in  $19.7 \text{ fb}^{-1}$  of  $pp$  collisions at  $E_{\text{cm}} = 8 \text{ TeV}$ . Upper limits on  $B(t \rightarrow bH^+) B(H^+ \rightarrow c\bar{s})$  between  $1.2 \times 10^{-2}$  and  $6.5 \times 10^{-2}$  (95% CL) are given for  $m_{H^+} = 90\text{--}160 \text{ GeV}$ .
- 24 AAD 14M search for the decay cascade  $H_2^0 \rightarrow H^\pm W^\mp \rightarrow H^0 W^\pm W^\mp$ ,  $H^0$  decaying to  $b\bar{b}$  in  $20.3 \text{ fb}^{-1}$  of  $pp$  collisions at  $E_{\text{cm}} = 8 \text{ TeV}$ . See their Table III for limits on cross section times branching ratio for  $m_{H_2^0} = 325\text{--}1025 \text{ GeV}$  and  $m_{H^\pm} = 225\text{--}925 \text{ GeV}$ .
- 25 AALTONEN 14A measure  $B(t \rightarrow b\tau\nu) = 0.096 \pm 0.028$  using  $9 \text{ fb}^{-1}$  of  $p\bar{p}$  collisions at  $E_{\text{cm}} = 1.96 \text{ TeV}$ . For  $m_{H^\pm} = 80\text{--}140 \text{ GeV}$ , this measured value is translated to a limit  $B(t \rightarrow bH^+) < 0.059$  at 95% CL assuming  $B(H^+ \rightarrow \tau^+\nu) = 1$ .
- 26 AAD 13AC search for  $t\bar{t}$  production followed by  $t \rightarrow bH^+$ ,  $H^+ \rightarrow c\bar{s}$  (flavor unidentified) in  $4.7 \text{ fb}^{-1}$  of  $pp$  collisions at  $E_{\text{cm}} = 7 \text{ TeV}$ . Upper limits on  $B(t \rightarrow bH^+) B(H^+ \rightarrow c\bar{s})$  between 0.05 and 0.01 (95% CL) are given for  $m_{H^\pm} = 90\text{--}150 \text{ GeV}$  and  $B(H^+ \rightarrow c\bar{s}) = 1$ .
- 27 AAD 13V search for  $t\bar{t}$  production followed by  $t \rightarrow bH^+$ ,  $H^+ \rightarrow \tau^+\nu$  through violation of lepton universality with  $4.6 \text{ fb}^{-1}$  of  $pp$  collisions at  $E_{\text{cm}} = 7 \text{ TeV}$ . Upper limits on  $B(t \rightarrow bH^+) B(H^+ \rightarrow \tau^+\nu) = 1$ . By combining with AAD 12BH, the limits improve to 0.008 to 0.034 for  $m_{H^\pm} = 90\text{--}160 \text{ GeV}$ . See their Fig. 7 for the excluded region in the  $m_{H^\pm}^{\text{max}}$  scenario of the MSSM.
- 28 AAD 12BH search for  $t\bar{t}$  production followed by  $t \rightarrow bH^+$ ,  $H^+ \rightarrow \tau^+\nu$  with  $4.6 \text{ fb}^{-1}$  of  $pp$  collisions at  $E_{\text{cm}} = 7 \text{ TeV}$ . Upper limits on  $B(t \rightarrow bH^+) B(H^+ \rightarrow \tau^+\nu) = 1$  (95% CL) are given for  $m_{H^\pm} = 90\text{--}160 \text{ GeV}$  and  $B(H^+ \rightarrow \tau^+\nu) = 1$ . See their Fig. 8 for the excluded region in the  $m_{H^\pm}^{\text{max}}$  scenario of the MSSM.
- 29 CHATRCHYAN 12AA search for  $t\bar{t}$  production followed by  $t \rightarrow bH^+$ ,  $H^+ \rightarrow \tau^+\nu$  with  $2 \text{ fb}^{-1}$  of  $pp$  collisions at  $E_{\text{cm}} = 7 \text{ TeV}$ . Upper limits on  $B(t \rightarrow bH^+) B(H^+ \rightarrow \tau^+\nu) = 1$  (95% CL) are given for  $m_{H^\pm} = 80\text{--}160 \text{ GeV}$  and  $B(H^+ \rightarrow \tau^+\nu) = 1$ .
- 30 AALTONEN 11P search in  $2.7 \text{ fb}^{-1}$  of  $p\bar{p}$  collisions at  $E_{\text{cm}} = 1.96 \text{ TeV}$  for the decay chain  $t \rightarrow bH^+$ ,  $H^+ \rightarrow W^+ A^0$ ,  $A^0 \rightarrow \tau^+ \tau^-$  with  $m_{A^0}$  between 4 and 9 GeV. See their Fig. 4 for limits on  $B(t \rightarrow bH^+) B(H^+ \rightarrow \tau^+ \tau^-)$  for  $90 < m_{H^\pm} < 160 \text{ GeV}$ .
- 31 DESCHAMPS 10 make Type II two Higgs doublet model fits to weak leptonic and semileptonic decays,  $b \rightarrow s\gamma$ ,  $B_s$  mixings, and  $Z \rightarrow b\bar{b}$ . The limit holds irrespective of  $\tan\beta$ .
- 32 AALTONEN 09AJ search for  $t \rightarrow bH^+$ ,  $H^+ \rightarrow c\bar{s}$  in  $t\bar{t}$  events in  $2.2 \text{ fb}^{-1}$  of  $p\bar{p}$  collisions at  $E_{\text{cm}} = 1.96 \text{ TeV}$ . Upper limits on  $B(t \rightarrow bH^+) B(H^+ \rightarrow c\bar{s})$  between 0.08 and 0.32 (95% CL) are given for  $m_{H^\pm} = 60\text{--}150 \text{ GeV}$  and  $B(H^+ \rightarrow c\bar{s}) = 1$ .
- 33 ABZOV 09AC search for  $t \rightarrow bH^+$ ,  $H^+ \rightarrow \tau^+\nu$  in  $t\bar{t}$  events in  $0.9 \text{ fb}^{-1}$  of  $p\bar{p}$  collisions at  $E_{\text{cm}} = 1.96 \text{ TeV}$ . Upper limits on  $B(t \rightarrow bH^+) B(H^+ \rightarrow \tau^+\nu) = 1$  (95% CL) are given for  $m_{H^\pm} = 80\text{--}155 \text{ GeV}$  and  $B(H^+ \rightarrow \tau^+\nu) = 1$ . See their Fig. 4 for an excluded region in a MSSM scenario.
- 34 ABZOV 09AG measure  $t\bar{t}$  cross sections in final states with  $\ell$  + jets ( $\ell = e, \mu$ ),  $\ell\ell$ , and  $\tau\ell$  in  $1 \text{ fb}^{-1}$  of  $p\bar{p}$  collisions at  $E_{\text{cm}} = 1.96 \text{ TeV}$ , which constrains possible  $t \rightarrow bH^+$  branching fractions. Upper limits (95% CL) on  $B(t \rightarrow bH^+) B(H^+ \rightarrow \tau^+\nu) = 1$  ( $B(H^+ \rightarrow c\bar{s}) = 1$ ) for  $m_{H^\pm} = 80\text{--}155 \text{ GeV}$ .
- 35 ABZOV 09AI search for  $t \rightarrow bH^+$  in  $t\bar{t}$  events in  $1 \text{ fb}^{-1}$  of  $p\bar{p}$  collisions at  $E_{\text{cm}} = 1.96 \text{ TeV}$ . Final states with  $\ell$  + jets ( $\ell = e, \mu$ ),  $\ell\ell$ , and  $\tau\ell$  are examined. Upper limits on  $B(t \rightarrow bH^+) B(H^+ \rightarrow \tau^+\nu) = 1$  ( $B(H^+ \rightarrow c\bar{s}) = 1$ ) for  $m_{H^\pm} = 80\text{--}155 \text{ GeV}$ . A simultaneous extraction of  $B(t \rightarrow bH^+)$  and the  $t\bar{t}$  cross section is performed, yielding a limit on  $B(t \rightarrow bH^+)$  between 0.12 and 0.26 for  $m_{H^\pm} = 80\text{--}155 \text{ GeV}$ . See their Figs. 5–8 for excluded regions in several MSSM scenarios.
- 36 ABZOV 09P search for  $H^\pm$  production by  $q\bar{q}'$  annihilation followed by  $H^\pm \rightarrow t\bar{b}$  decay in  $0.9 \text{ fb}^{-1}$  of  $p\bar{p}$  collisions at  $E_{\text{cm}} = 1.96 \text{ TeV}$ . Cross section limits in several two-doublet models are given for  $m_{H^\pm} = 180\text{--}300 \text{ GeV}$ . A region with  $20 \lesssim \tan\beta \lesssim 70$  is excluded (95% CL) for  $180 \text{ GeV} \lesssim m_{H^\pm} \lesssim 184 \text{ GeV}$  in type-I models.
- 37 ABULENCIA 06E search for associated  $H^0 W$  production in  $p\bar{p}$  collisions at  $E_{\text{cm}} = 1.96 \text{ TeV}$ . A fit is made for  $t\bar{t}$  production processes in dilepton, lepton + jets, and lepton +  $\tau$  final states, with the decays  $t \rightarrow W^+ b$  and  $t \rightarrow H^+ b$  followed by  $H^+ \rightarrow \tau^+ \nu$ ,  $c\bar{s}$ ,  $t^* \bar{b}$ , or  $W^+ H^0$ . Within the MSSM the search is sensitive to the region  $\tan\beta < 1$  or  $> 30$  in the mass range  $m_{H^\pm} = 80\text{--}160 \text{ GeV}$ . See Fig. 2 for the excluded region in a certain MSSM scenario.
- 38 ABDALLAH 04I search for  $e^+ e^- \rightarrow H^\pm H^\mp$  with  $H^\pm$  decaying to  $\tau\nu$ ,  $c\bar{s}$ , or  $W^* A^0$  in Type-I two-Higgs-doublet models.
- 39 ABBIENDI 03 give a limit  $m_{H^\pm} > 1.28 \tan\beta \text{ GeV}$  (95% CL) in Type II two-doublet models.
- 40 ABZOV 02B search for a charged Higgs boson in top decays with  $H^+ \rightarrow \tau^+ \nu$  at  $E_{\text{cm}} = 1.8 \text{ TeV}$ . For  $m_{H^+} = 75 \text{ GeV}$ , the region  $\tan\beta > 32.0$  is excluded at 95% CL. The excluded mass region extends to over 140 GeV for  $\tan\beta$  values above 100.
- 41 BORZUMATI 02 point out that the decay modes such as  $b\bar{b} W$ ,  $A^0 W$ , and supersymmetric ones can have substantial branching fractions in the mass range explored at LEP II and Tevatron.
- 42 ABBIENDI 01Q give a limit  $\tan\beta/m_{H^\pm} < 0.53 \text{ GeV}^{-1}$  (95% CL) in Type II two-doublet models.
- 43 BARATE 01E give a limit  $\tan\beta/m_{H^\pm} < 0.40 \text{ GeV}^{-1}$  (90% CL) in Type II two-doublet models. An independent measurement of  $B \rightarrow \tau\nu X$  gives  $\tan\beta/m_{H^\pm} < 0.49 \text{ GeV}^{-1}$  (90% CL).
- 44 GAMBINO 01 use the world average data in the summer of 2001  $B(b \rightarrow s\gamma) = (3.23 \pm 0.42) \times 10^{-4}$ . The limit applies for Type-II two-doublet models.
- 45 AFFOLDER 00I search for a charged Higgs boson in top decays with  $H^+ \rightarrow \tau^+ \nu$  in  $p\bar{p}$  collisions at  $E_{\text{cm}} = 1.8 \text{ TeV}$ . The excluded mass region extends to over 120 GeV for  $\tan\beta$  values above 100 and  $B(\tau\nu) = 1$ . If  $B(t \rightarrow bH^+) \gtrsim 0.6$ ,  $m_{H^+}$  up to 160 GeV is excluded. Updates ABE 97L.
- 46 ABBOTT 99E search for a charged Higgs boson in top decays in  $p\bar{p}$  collisions at  $E_{\text{cm}} = 1.8 \text{ TeV}$ , by comparing the observed  $t\bar{t}$  cross section (extracted from the data assuming the dominant decay  $t \rightarrow bW^+$ ) with theoretical expectation. The search is sensitive to regions of the domains  $\tan\beta \lesssim 1$ ,  $50 < m_{H^\pm} (\text{GeV}) \lesssim 120$  and  $\tan\beta \gtrsim 40$ ,  $50 < m_{H^\pm} (\text{GeV}) \lesssim 160$ . See Fig. 3 for the details of the excluded region.
- 47 ACKERSTAFF 99D measure the Michel parameters  $\rho$ ,  $\xi$ ,  $\eta$ , and  $\xi\delta$  in leptonic  $\tau$  decays from  $Z \rightarrow \tau\tau$ . Assuming  $e\text{--}\mu$  universality, the limit  $m_{H^\pm} > 0.97 \tan\beta \text{ GeV}$  (95% CL) is obtained for two-doublet models in which only one doublet couples to leptons.
- 48 ACCIARRI 97F give a limit  $m_{H^\pm} > 2.6 \tan\beta \text{ GeV}$  (90% CL) from their limit on the exclusive  $B \rightarrow \tau\nu X$  branching ratio.
- 49 AMMAR 97B measure the Michel parameter  $\rho$  from  $\tau \rightarrow e\nu\nu$  decays and assumes  $e/\mu$  universality to extract the Michel  $\eta$  parameter from  $\tau \rightarrow \mu\nu\nu$  decays. The measurement is translated to a lower limit on  $m_{H^\pm}$  in a two-doublet model  $m_{H^\pm} > 0.97 \tan\beta \text{ GeV}$  (90% CL).
- 50 COARASA 97 reanalyzed the constraint on the  $(m_{H^\pm}, \tan\beta)$  plane derived from the inclusive  $B \rightarrow \tau\nu X$  branching ratio in GROSSMAN 95B and BUSKULIC 95. They show that the constraint is quite sensitive to supersymmetric one-loop effects.
- 51 GUCHAIT 97 studies the constraints on  $m_{H^\pm}$  set by Tevatron data on  $\ell\tau$  final states in  $t\bar{t} \rightarrow (Wb)(Hb)$ ,  $W \rightarrow \ell\nu$ ,  $H \rightarrow \tau\nu$ . See Fig. 2 for the excluded region.
- 52 MANGANO 97 reconsiders the limit in ACCIARRI 97F including the effect of the potentially large  $B_c \rightarrow \tau\nu$  background to  $B_u \rightarrow \tau\nu$  decays. Stronger limits are obtained.
- 53 STAHL 97 fit  $\tau$  lifetime, leptonic branching ratios, and the Michel parameters and derive limit  $m_{H^\pm} > 1.5 \tan\beta \text{ GeV}$  (90% CL) for a two-doublet model. See also STAHL 94.
- 54 ALAM 95 measure the inclusive  $b \rightarrow s\gamma$  branching ratio at  $\mathcal{T}(45)$  and give  $B(b \rightarrow s\gamma) < 4.2 \times 10^{-4}$  (95% CL), which translates to the limit  $m_{H^\pm} > [244 + 63/(\tan\beta)]^{1.3}$  GeV in the Type II two-doublet model. Light supersymmetric particles can invalidate this bound.
- 55 BUSKULIC 95 give a limit  $m_{H^\pm} > 1.9 \tan\beta \text{ GeV}$  (90% CL) for Type-II models from  $b \rightarrow \tau\nu X$  branching ratio, as proposed in GROSSMAN 94.

### $H^\pm$ (charged Higgs) mass limits for $m_{H^\pm} > m(\text{top})$

Limits obtained at the LHC are given in the  $m_{H^\pm}^{\text{mod-}}$  benchmark scenario, see CARENA 13, and depend on the  $\tan\beta$  values.

VALUE (GeV)	CL%	DOCUMENT ID	TECN	COMMENT
> 181	95	1 AABOUD	18BWATLS	$\tan\beta = 10$
> 249	95	1 AABOUD	18BWATLS	$\tan\beta = 20$
> 390	95	1 AABOUD	18BWATLS	$\tan\beta = 30$
> 894	95	1 AABOUD	18BWATLS	$\tan\beta = 40$
> 1017	95	1 AABOUD	18BWATLS	$\tan\beta = 50$
> 1103	95	1 AABOUD	18BWATLS	$\tan\beta = 60$

1 AABOUD 18Bw search for  $\bar{t}bH^+$  associated production in  $36.1 \text{ fb}^{-1}$  of  $pp$  collisions at  $E_{\text{cm}} = 13 \text{ TeV}$ . See also their Fig. 9 for the excluded region in the hMSSM parameter space.

See key on page 999

Gauge & Higgs Boson Particle Listings  
Charged Higgs Bosons ( $H^\pm$  and  $H^{\pm\pm}$ ), Searches for **$H^{\pm\pm}$  (doubly-charged Higgs boson) mass limits**

This section covers searches for a doubly-charged Higgs boson with couplings to lepton pairs. Its weak isospin  $T_3$  is thus restricted to two possibilities depending on lepton chiralities:  $T_3(H^{\pm\pm}) = \pm 1$ , with the coupling  $g_{\ell\ell}$  to  $\ell_L^- \ell_L^-$  and  $\ell_R^+ \ell_R^+$  ("left-handed") and  $T_3(H^{\pm\pm}) = 0$ , with the coupling to  $\ell_R^- \ell_R^-$  and  $\ell_L^+ \ell_L^+$  ("right-handed"). These Higgs bosons appear in some left-right symmetric models based on the gauge group  $SU(2)_L \times SU(2)_R \times U(1)$ , the type-II seesaw model, and the Zee-Babu model. The two cases are listed separately in the following. Unless noted, one of the lepton flavor combinations is assumed to be dominant in the decay.

**Limits for  $H^{\pm\pm}$  with  $T_3 = \pm 1$** 

VALUE (GeV)	CL%	DOCUMENT ID	TECN	COMMENT
>220	95	1 AABOUD	19K ATLS	$W^\pm W^\pm$
>768	95	2 AABOUD	188C ATLS	$e e$
>846	95	2 AABOUD	188C ATLS	$\mu \mu$
>468	95	3 AAD	15AG ATLS	$e \mu$
>400	95	4 AAD	15AP ATLS	$e \tau$
>400	95	4 AAD	15AP ATLS	$\mu \tau$
>169	95	5 CHATRCHYAN12AU	CMS	$\tau \tau$
>300	95	5 CHATRCHYAN12AU	CMS	$\mu \tau$
>293	95	5 CHATRCHYAN12AU	CMS	$e \tau$
>395	95	5 CHATRCHYAN12AU	CMS	$\mu \mu$
>391	95	5 CHATRCHYAN12AU	CMS	$e \mu$
>382	95	5 CHATRCHYAN12AU	CMS	$e e$
> 98.1	95	6 ABDALLAH	03 DLPH	$\tau \tau$
> 99.0	95	7 ABBIENDI	02C OPAL	$\tau \tau$
•••				We do not use the following data for averages, fits, limits, etc. •••
		8 SIRUNYAN	19CQ CMS	$W^\pm W^\pm$
		9 SIRUNYAN	18CC CMS	$W^\pm W^\pm$
>551	95	3 AAD	15AG ATLS	$e e$
>516	95	3 AAD	15AG ATLS	$\mu \mu$
		10 KANEMURA	15 RVUE	$W^{(*)\pm} W^{(*)\pm}$
		11 KHACHATRYAN	15D CMS	$W^\pm W^\pm$
		12 KANEMURA	14 RVUE	$W^{(*)\pm} W^{(*)\pm}$
>330	95	13 AAD	13Y ATLS	$\mu \mu$
>237	95	13 AAD	13Y ATLS	$\mu \tau$
>355	95	14 AAD	12AY ATLS	$\mu \mu$
>398	95	15 AAD	12CQ ATLS	$\mu \mu$
>375	95	15 AAD	12CQ ATLS	$e \mu$
>409	95	15 AAD	12CQ ATLS	$e e$
>128	95	16 ABAZOV	12A D0	$\tau \tau$
>144	95	16 ABAZOV	12A D0	$\mu \tau$
>245	95	17 AALTONEN	11AF CDF	$\mu \mu$
>210	95	17 AALTONEN	11AF CDF	$e \mu$
>225	95	17 AALTONEN	11AF CDF	$e e$
>114	95	18 AALTONEN	08AA CDF	$e \tau$
>112	95	18 AALTONEN	08AA CDF	$\mu \tau$
>168	95	19 ABAZOV	08V D0	$\mu \mu$
		20 AKTAS	06A H1	single $H^{\pm\pm}$
>133	95	21 ACOSTA	05L CDF	stable
>118.4	95	22 ABAZOV	04E D0	$\mu \mu$
		23 ABBIENDI	03Q OPAL	$E_{cm} \leq 209$ GeV, single $H^{\pm\pm}$
		24 GORDEEV	97 SPEC	muonium conversion
		25 ASAKA	95 THEO	
> 45.6	95	26 ACTON	92M OPAL	
> 30.4	95	27 ACTON	92M OPAL	
none 6.5–36.6	95	28 SWARTZ	90 MRK2	

1 AABOUD 19K search for pair production of  $H^{++}H^{--}$  followed by the decay  $H^{\pm\pm} \rightarrow W^\pm W^\pm$  in  $36.1 \text{ fb}^{-1}$  of  $pp$  collisions at  $E_{cm} = 13$  TeV. The search is interpreted in a doublet-triplet extension of the scalar sector with a vev of 0.1 GeV, leading to  $B(H^{\pm\pm} \rightarrow W^\pm W^\pm) = 1$ . See their Fig. 5 for limits on the cross section for  $m_{H^{++}}$  between 200 and 700 GeV.

2 See their Figs. 11(b) and 13 for limits with smaller branching ratios.

3 AAD 15AG search for  $H^{++}H^{--}$  production in  $20.3 \text{ fb}^{-1}$  of  $pp$  collisions at  $E_{cm} = 8$  TeV. The limit assumes 100% branching ratio to the specified final state. See their Fig. 5 for limits for arbitrary branching ratios.

4 AAD 15AP search for  $H^{++}H^{--}$  production in  $20.3 \text{ fb}^{-1}$  of  $pp$  collisions at  $E_{cm} = 8$  TeV. The limit assumes 100% branching ratio to the specified final state.

5 CHATRCHYAN 12AU search for  $H^{++}H^{--}$  production with  $4.9 \text{ fb}^{-1}$  of  $pp$  collisions at  $E_{cm} = 7$  TeV. The limit assumes 100% branching ratio to the specified final state. See their Table 6 for limits including associated  $H^{++}H^-$  production or assuming different scenarios.

6 ABDALLAH 03 search for  $H^{++}H^{--}$  pair production either followed by  $H^{++} \rightarrow \tau^+ \tau^+$ , or decaying outside the detector.

7 ABBIENDI 02C searches for pair production of  $H^{++}H^{--}$ , with  $H^{\pm\pm} \rightarrow \ell^\pm \ell^\pm (\ell, \ell' = e, \mu, \tau)$ . The limit holds for  $\ell = \ell' = \tau$ , and becomes stronger for other combinations of leptonic final states. To ensure the decay within the detector, the limit only applies for  $g(H\ell\ell) \gtrsim 10^{-7}$ .

8 SIRUNYAN 19CQ search for  $H^{\pm\pm}$  production by vector boson fusion followed by the decay  $H^{\pm\pm} \rightarrow W^\pm W^\pm \rightarrow qq\ell\nu$  in  $35.9 \text{ fb}^{-1}$  of  $pp$  collisions at  $E_{cm} = 13$  TeV. See their Fig. 5 for limits on cross section times branching ratio for  $m_{H^{\pm\pm}}$  between 0.6 and 2 TeV.

9 SIRUNYAN 18CC search for  $H^{\pm\pm}$  production by vector boson fusion followed by the decay  $H^{\pm\pm} \rightarrow W^\pm W^\pm$  in  $35.9 \text{ fb}^{-1}$  of  $pp$  collisions at  $E_{cm} = 13$  TeV. See their Fig. 3 for limits on cross section times branching ratio for  $m_{H^{\pm\pm}}$  between 200 and 1000 GeV.

10 KANEMURA 15 examine the case where  $H^{++}$  decays preferentially to  $W^{(*)} W^{(*)}$  and estimate that a lower mass limit of  $\sim 84$  GeV can be derived from the same-sign dilepton data of AAD 15AG if  $H^{++}$  decays with 100% branching ratio to  $W^{(*)} W^{(*)}$ .

11 KHACHATRYAN 15D search for  $H^{\pm\pm}$  production by vector boson fusion followed by the decay  $H^{\pm\pm} \rightarrow W^\pm W^\pm$  in  $19.4 \text{ fb}^{-1}$  of  $pp$  collisions at  $E_{cm} = 8$  TeV. See their Fig. 4 for limits on cross section times branching ratio for  $m_{H^{++}}$  between 160 and 800 GeV.

12 KANEMURA 14 examine the case where  $H^{++}$  decays preferentially to  $W^{(*)} W^{(*)}$  and estimate that a lower mass limit of  $\sim 60$  GeV can be derived from the same-sign dilepton data of AAD 12CQ.

13 AAD 13Y search for  $H^{++}H^{--}$  production in a generic search of events with three charged leptons in  $4.6 \text{ fb}^{-1}$  of  $pp$  collisions at  $E_{cm} = 7$  TeV. The limit assumes 100% branching ratio to the specified final state.

14 AAD 12AY search for  $H^{++}H^{--}$  production with  $1.6 \text{ fb}^{-1}$  of  $pp$  collisions at  $E_{cm} = 7$  TeV. The limit assumes 100% branching ratio to the specified final state.

15 AAD 12CQ search for  $H^{++}H^{--}$  production with  $4.7 \text{ fb}^{-1}$  of  $pp$  collisions at  $E_{cm} = 7$  TeV. The limit assumes 100% branching ratio to the specified final state. See their Table 1 for limits assuming smaller branching ratios.

16 ABAZOV 12A search for  $H^{++}H^{--}$  production in  $7.0 \text{ fb}^{-1}$  of  $p\bar{p}$  collisions at  $E_{cm} = 1.96$  TeV.

17 AALTONEN 11AF search for  $H^{++}H^{--}$  production in  $6.1 \text{ fb}^{-1}$  of  $p\bar{p}$  collisions at  $E_{cm} = 1.96$  TeV.

18 AALTONEN 08AA search for  $H^{++}H^{--}$  production in  $p\bar{p}$  collisions at  $E_{cm} = 1.96$  TeV. The limit assumes 100% branching ratio to the specified final state.

19 ABAZOV 08V search for  $H^{++}H^{--}$  production in  $p\bar{p}$  collisions at  $E_{cm} = 1.96$  TeV. The limit is for  $B(H \rightarrow \mu\mu) = 1$ . The limit is updated in ABAZOV 12A.

20 AKTAS 06A search for single  $H^{\pm\pm}$  production in  $ep$  collisions at HERA. Assuming that  $H^{++}$  only couples to  $e^+ \mu^+$  with  $g_{e\mu} = 0.3$  (electromagnetic strength), a limit  $m_{H^{++}} > 141$  GeV (95% CL) is derived. For the case where  $H^{++}$  couples to  $e\tau$  only the limit is 112 GeV.

21 ACOSTA 05L search for  $H^{++}H^{--}$  pair production in  $p\bar{p}$  collisions. The limit is valid for  $g_{\ell\ell} \leq 10^{-8}$  so that the Higgs decays outside the detector.

22 ABAZOV 04E search for  $H^{++}H^{--}$  pair production in  $H^{\pm\pm} \rightarrow \mu^\pm \mu^\pm$ . The limit is valid for  $g_{\mu\mu} \gtrsim 10^{-7}$ .

23 ABBIENDI 03Q searches for single  $H^{\pm\pm}$  via direct production in  $e^+ e^- \rightarrow e^\mp e^\mp H^{\pm\pm}$ , and via  $t$ -channel exchange in  $e^+ e^- \rightarrow e^+ e^-$ . In the direct case, and assuming  $B(H^{\pm\pm} \rightarrow \ell^\pm \ell^\pm) = 1$ , a 95% CL limit on  $h_{ee} < 0.071$  is set for  $m_{H^{\pm\pm}} \leq 160$  GeV (see Fig. 6). In the second case, indirect limits on  $h_{ee}$  are set for  $m_{H^{\pm\pm}} < 2$  TeV (see Fig. 8).

24 GORDEEV 97 search for muonium-antimuonium conversion and find  $G_{M\bar{M}}/G_F < 0.14$  (90% CL), where  $G_{M\bar{M}}$  is the lepton-flavor violating effective four-fermion coupling. This limit may be converted to  $m_{H^{++}} > 210$  GeV if the Yukawa couplings of  $H^{++}$  to  $ee$  and  $\mu\mu$  are as large as the weak gauge coupling. For similar limits on muonium-antimuonium conversion, see the muon Particle Listings.

25 ASAKA 95 point out that  $H^{++}$  decays dominantly to four fermions in a large region of parameter space where the limit of ACTON 92M from the search of dilepton modes does not apply.

26 ACTON 92M limit assumes  $H^{\pm\pm} \rightarrow \ell^\pm \ell^\pm$  or  $H^{\pm\pm}$  does not decay in the detector. Thus the region  $g_{\ell\ell} \approx 10^{-7}$  is not excluded.

27 ACTON 92M from  $\Delta\Gamma_Z < 40$  MeV.

28 SWARTZ 90 assume  $H^{\pm\pm} \rightarrow \ell^\pm \ell^\pm$  (any flavor). The limits are valid for the Higgs-lepton coupling  $g(H\ell\ell) \gtrsim 7.4 \times 10^{-7} [m_{H^\pm}/\text{GeV}]^{1/2}$ . The limits improve somewhat for  $ee$  and  $\mu\mu$  decay modes.

**Limits for  $H^{\pm\pm}$  with  $T_3 = 0$** 

VALUE (GeV)	CL%	DOCUMENT ID	TECN	COMMENT
> 58	95	1 AABOUD	188C ATLS	$e e$
>723	95	1 AABOUD	188C ATLS	$\mu \mu$
>402	95	2 AAD	15AG ATLS	$e \mu$
>290	95	3 AAD	15AP ATLS	$e \tau$
>290	95	3 AAD	15AP ATLS	$\mu \tau$
> 97.3	95	4 ABDALLAH	03 DLPH	$\tau \tau$
> 97.3	95	5 ACHARD	03F L3	$\tau \tau$
> 98.5	95	6 ABBIENDI	02C OPAL	$\tau \tau$
•••				We do not use the following data for averages, fits, limits, etc. •••
>374	95	2 AAD	15AG ATLS	$e e$
>438	95	2 AAD	15AG ATLS	$\mu \mu$
>251	95	7 AAD	12AY ATLS	$\mu \mu$
>306	95	8 AAD	12CQ ATLS	$\mu \mu$
>310	95	8 AAD	12CQ ATLS	$e \mu$
>322	95	8 AAD	12CQ ATLS	$e e$
>113	95	9 ABAZOV	12A D0	$\mu \tau$
>205	95	10 AALTONEN	11AF CDF	$\mu \mu$
>190	95	10 AALTONEN	11AF CDF	$e \mu$
>205	95	10 AALTONEN	11AF CDF	$e e$
>145	95	11 ABAZOV	08V D0	$\mu \mu$
		12 AKTAS	06A H1	single $H^{\pm\pm}$
>109	95	13 ACOSTA	05L CDF	stable
> 98.2	95	14 ABAZOV	04E D0	$\mu \mu$
		15 ABBIENDI	03Q OPAL	$E_{cm} \leq 209$ GeV, single $H^{\pm\pm}$
		16 GORDEEV	97 SPEC	muonium conversion
> 45.6	95	17 ACTON	92M OPAL	
> 25.5	95	18 ACTON	92M OPAL	
none 7.3–34.3	95	19 SWARTZ	90 MRK2	

# Gauge & Higgs Boson Particle Listings

## Charged Higgs Bosons ( $H^\pm$ and $H^{\pm\pm}$ ), Searches for, New Heavy Bosons

- See their Figs. 12(b) and 14 for limits with smaller branching ratios.
- AAD 15AG search for  $H^{++}H^{--}$  production in  $20.3\text{ fb}^{-1}$  of  $pp$  collisions at  $E_{\text{cm}} = 8$  TeV. The limit assumes 100% branching ratio to the specified final state. See their Fig. 5 for limits for arbitrary branching ratios.
- AAD 15AP search for  $H^{++}H^{--}$  production in  $20.3\text{ fb}^{-1}$  of  $pp$  collisions at  $E_{\text{cm}} = 8$  TeV. The limit assumes 100% branching ratio to the specified final state.
- ABDALLAH 03 search for  $H^{++}H^{--}$  pair production either followed by  $H^{++} \rightarrow \tau^+ \tau^+$ , or decaying outside the detector.
- ACHARD 03F search for  $e^+e^- \rightarrow H^{\pm\pm}H^{--}$  with  $H^{\pm\pm} \rightarrow \ell^\pm \ell^\pm$ . The limit holds for  $\ell = \ell' = \tau$ , and slightly different limits apply for other flavor combinations. The limit is valid for  $g_{\ell\ell} \gtrsim 10^{-7}$ .
- ABBIENDI 02c searches for pair production of  $H^{++}H^{--}$ , with  $H^{\pm\pm} \rightarrow \ell^\pm \ell^\pm (\ell, \ell' = e, \mu, \tau)$ , the limit holds for  $\ell = \ell' = \tau$ , and becomes stronger for other combinations of leptonic final states. To ensure the decay within the detector, the limit only applies for  $g(H\ell\ell) \gtrsim 10^{-7}$ .
- AAD 12AY search for  $H^{++}H^{--}$  production with  $1.6\text{ fb}^{-1}$  of  $pp$  collisions at  $E_{\text{cm}} = 7$  TeV. The limit assumes 100% branching ratio to the specified final state.
- AAD 12CQ search for  $H^{++}H^{--}$  production with  $4.7\text{ fb}^{-1}$  of  $pp$  collisions at  $E_{\text{cm}} = 7$  TeV. The limit assumes 100% branching ratio to the specified final state. See their Table 1 for limits assuming smaller branching ratios.
- ABAZOV 12A search for  $H^{++}H^{--}$  production in  $7.0\text{ fb}^{-1}$  of  $p\bar{p}$  collisions at  $E_{\text{cm}} = 1.96$  TeV.
- AALTONEN 11AF search for  $H^{++}H^{--}$  production in  $6.1\text{ fb}^{-1}$  of  $p\bar{p}$  collisions at  $E_{\text{cm}} = 1.96$  TeV.
- ABAZOV 08v search for  $H^{++}H^{--}$  production in  $p\bar{p}$  collisions at  $E_{\text{cm}} = 1.96$  TeV. The limit is for  $B(H \rightarrow \mu\mu) = 1$ . The limit is updated in ABAZOV 12A.
- AKTAS 06A search for single  $H^{\pm\pm}$  production in  $ep$  collisions at HERA. Assuming that  $H^{++}$  only couples to  $e^+ \mu^+$  with  $g_{e\mu} = 0.3$  (electromagnetic strength), a limit  $m_{H^{++}} > 141$  GeV (95% CL) is derived. For the case where  $H^{++}$  couples to  $e\tau$  only the limit is 112 GeV.
- ACOSTA 05L search for  $H^{++}H^{--}$  pair production in  $p\bar{p}$  collisions. The limit is valid for  $g_{\ell\ell} < 10^{-8}$  so that the Higgs decays outside the detector.
- ABAZOV 04E search for  $H^{++}H^{--}$  pair production in  $H^{\pm\pm} \rightarrow \mu^\pm \mu^\pm$ . The limit is valid for  $g_{\mu\mu} \gtrsim 10^{-7}$ .
- ABBIENDI 03Q searches for single  $H^{\pm\pm}$  via direct production in  $e^+e^- \rightarrow e^\mp e^\mp H^{\pm\pm}$ , and via  $t$ -channel exchange in  $e^+e^- \rightarrow e^+e^-$ . In the direct case, and assuming  $B(H^{\pm\pm} \rightarrow \ell^\pm \ell^\pm) = 1$ , a 95% CL limit on  $h_{ee} < 0.071$  is set for  $m_{H^{\pm\pm}} < 160$  GeV (see Fig. 6). In the second case, indirect limits on  $h_{ee}$  are set for  $m_{H^{\pm\pm}} < 2$  TeV (see Fig. 8).
- GORDEEV 97 search for muonium-antimuonium conversion and find  $G_{MM}/G_F < 0.14$  (90% CL), where  $G_{MM}$  is the lepton-flavor violating effective four-fermion coupling. This limit may be converted to  $m_{H^{++}} > 210$  GeV if the Yukawa couplings of  $H^{++}$  to  $ee$  and  $\mu\mu$  are as large as the weak gauge coupling. For similar limits on muonium-antimuonium conversion, see the muon Particle Listings.
- ACTON 92M limit assumes  $H^{\pm\pm} \rightarrow \ell^\pm \ell^\pm$  or  $H^{\pm\pm}$  does not decay in the detector. Thus the region  $g_{\ell\ell} \approx 10^{-7}$  is not excluded.
- ACTON 92M from  $\Delta\Gamma_Z < 40$  MeV.
- SWARTZ 90 assume  $H^{\pm\pm} \rightarrow \ell^\pm \ell^\pm$  (any flavor). The limits are valid for the Higgs-lepton coupling  $g(H\ell\ell) \gtrsim 7.4 \times 10^{-7} [m_H/\text{GeV}]^{1/2}$ . The limits improve somewhat for  $ee$  and  $\mu\mu$  decay modes.

### $H^\pm$ and $H^{\pm\pm}$ REFERENCES

ABOUD	19K	EPJ C79 58	M. Aaboud et al.	(ATLAS Collab.)
SIRUNYAN	19AH	JHEP 1907 142	A.M. Sirunyan et al.	(CMS Collab.)
SIRUNYAN	19BP	PL B795 281	A.M. Sirunyan et al.	(CMS Collab.)
SIRUNYAN	19CC	PRL 123 131802	A.M. Sirunyan et al.	(CMS Collab.)
SIRUNYAN	19CQ	PL B798 134985	A.M. Sirunyan et al.	(CMS Collab.)
ABOUD	18BC	EPJ C78 199	M. Aaboud et al.	(ATLAS Collab.)
ABOUD	18BW	JHEP 1809 139	M. Aaboud et al.	(ATLAS Collab.)
ABOUD	18CD	JHEP 1811 085	M. Aaboud et al.	(ATLAS Collab.)
ABOUD	18CH	PL B787 68	M. Aaboud et al.	(ATLAS Collab.)
HALLER	18	EPJ C78 675	J. Haller et al.	(Glitter Group)
SIRUNYAN	18CC	PRL 120 081801	A.M. Sirunyan et al.	(CMS Collab.)
SIRUNYAN	18DO	JHEP 1811 115	A.M. Sirunyan et al.	(CMS Collab.)
MISIJK	17	EPJ C77 201	M. Misiajk, M. Steinhauser	(ATLAS Collab.)
SIRUNYAN	17AE	PRL 119 141802	A.M. Sirunyan et al.	(CMS Collab.)
ABOUD	16A	PL B759 555	M. Aaboud et al.	(ATLAS Collab.)
AAD	16AJ	JHEP 1603 127	G. Aad et al.	(ATLAS Collab.)
AAD	15AF	JHEP 1503 088	G. Aad et al.	(ATLAS Collab.)
AAD	15AG	JHEP 1503 041	G. Aad et al.	(ATLAS Collab.)
AAD	15AP	JHEP 1508 138	G. Aad et al.	(ATLAS Collab.)
AAD	15M	PRL 114 231801	G. Aad et al.	(ATLAS Collab.)
KANEMURA	15	PTEP 2015 051B02	S. Kanemura et al.	(CMS Collab.)
KHACHATRYAN	15AX	JHEP 1511 018	V. Khachatryan et al.	(CMS Collab.)
KHACHATRYAN	15BF	JHEP 1512 178	V. Khachatryan et al.	(CMS Collab.)
KHACHATRYAN	15D	PRL 114 051801	V. Khachatryan et al.	(ATLAS Collab.)
AAD	14M	PR D89 032002	G. Aad et al.	(ATLAS Collab.)
AALTONEN	14A	PR D89 091101	T. Aaltonen et al.	(CDF Collab.)
KANEMURA	14	PR D90 115018	S. Kanemura et al.	(ATLAS Collab.)
AAD	13AC	EPJ C73 2465	G. Aad et al.	(ATLAS Collab.)
AAD	13V	JHEP 1303 076	G. Aad et al.	(ATLAS Collab.)
AAD	13Y	PR D87 052002	G. Aad et al.	(ATLAS Collab.)
CARENA	13	EPJ C73 2552	M. Carena et al.	(ALEPH, DELPHI, L3, OPAL, LEP)
LEP	13	EPJ C73 2463	LEP Collabs.	(ALEPH, DELPHI, L3, OPAL, LEP)
AAD	12AY	PR D85 032004	G. Aad et al.	(ATLAS Collab.)
AAD	12BH	JHEP 1206 039	G. Aad et al.	(ATLAS Collab.)
AAD	12CQ	EPJ C72 2244	G. Aad et al.	(ATLAS Collab.)
AAD	12CY	JHEP 1212 007	G. Aad et al.	(ATLAS Collab.)
ABAZOV	12A	PRL 108 021801	V.M. Abazov et al.	(DO Collab.)
ABBIENDI	12	EPJ C72 2076	G. Abbiendi et al.	(OPAL Collab.)
CHATRCHYAN	12AA	JHEP 1207 143	S. Chatrchyan et al.	(CMS Collab.)
CHATRCHYAN	12AU	EPJ C72 2189	S. Chatrchyan et al.	(CMS Collab.)
AALTONEN	11AF	PRL 107 181801	T. Aaltonen et al.	(CDF Collab.)
AALTONEN	11P	PRL 107 031801	T. Aaltonen et al.	(CDF Collab.)
DESCHAMPS	10	PR D82 073012	O. Deschamps et al.	(CLER, ORSAY, LAPP)
AALTONEN	09AJ	PRL 103 101803	T. Aaltonen et al.	(CDF Collab.)
ABAZOV	09AC	PR D80 051107	V.M. Abazov et al.	(DO Collab.)
ABAZOV	09AG	PR D80 071102	V.M. Abazov et al.	(DO Collab.)

ABAZOV	09AI	PL B682 278	V.M. Abazov et al.	(DO Collab.)
ABAZOV	09P	PRL 102 191802	V.M. Abazov et al.	(DO Collab.)
AALTONEN	08AA	PRL 101 121801	T. Aaltonen et al.	(CDF Collab.)
ABAZOV	08V	PRL 101 071803	V.M. Abazov et al.	(DO Collab.)
ABULENCIA	06E	PRL 96 042003	A. Abulencia et al.	(CDF Collab.)
AKTAS	06A	PL B638 432	A. Aktas et al.	(HI Collab.)
ACOSTA	05L	PRL 95 071801	D. Acosta et al.	(CDF Collab.)
ABAZOV	04E	PRL 93 141801	V.M. Abazov et al.	(DO Collab.)
ABBIENDI	04	EPJ C32 453	G. Abbiendi et al.	(OPAL Collab.)
ABDALLAH	04I	EPJ C34 399	J. Abdallah et al.	(DELPHI Collab.)
ABBIENDI	03Q	PL B551 35	G. Abbiendi et al.	(OPAL Collab.)
ABBIENDI	03P	PL B577 93	G. Abbiendi et al.	(OPAL Collab.)
ABDALLAH	03E	PL B552 127	J. Abdallah et al.	(DELPHI Collab.)
ACHARD	03E	PL B575 208	P. Achard et al.	(L3 Collab.)
ACHARD	03F	PL B576 18	P. Achard et al.	(L3 Collab.)
ABAZOV	02B	PRL 88 151803	V.M. Abazov et al.	(DO Collab.)
ABBIENDI	02C	PL B526 221	G. Abbiendi et al.	(OPAL Collab.)
BORZUMATI	02	PL B549 170	F.M. Borzumati, A. Djouadi	(OPAL Collab.)
HEISTER	02P	PL B543 1	A. Heister et al.	(ALEPH Collab.)
ABBIENDI	01Q	PL B520 1	G. Abbiendi et al.	(OPAL Collab.)
BARATE	01E	EPJ C19 213	R. Barate et al.	(ALEPH Collab.)
GAMBINO	01	NP B611 338	P. Gambino, M. Misiajk	(ALEPH Collab.)
AFFOLDER	00I	PR D62 012004	T. Affolder et al.	(CDF Collab.)
PDG	00	EPJ C15 1	D.E. Groom et al.	(PDG Collab.)
ABBIENDI	99E	EPJ C7 407	G. Abbiendi et al.	(OPAL Collab.)
ABBOTT	99E	PRL 82 4975	B. Abbott et al.	(DO Collab.)
ACKERSTAFF	99D	EPJ C8 3	K. Ackerstaff et al.	(OPAL Collab.)
ABE	97L	PRL 79 357	F. Abe et al.	(CDF Collab.)
ACCIARRI	97F	PL B396 327	M. Acciarri et al.	(L3 Collab.)
AMMAR	97B	PRL 78 4686	R. Ammar et al.	(CLEO Collab.)
COARASA	97B	PL B406 337	J.A. Coarasa, R.A. Jimenez, J. Sola	(CLEO Collab.)
GORDEEV	97	PAN 60 1164	V.A. Gordeev et al.	(PNPI)
GUCHAIT	97	PR D55 7263	M. Guchait, D.P. Roy	(TATA)
MANGANO	97	PL B410 299	M. Mangano, S. Slabospitsky	(TATA)
STAHL	97	ZPHY C74 73	A. Stahl, H. Voss	(BONN)
PDG	96	PR D54 1	R. M. Barnett et al.	(PDG Collab.)
ALAM	95	PRL 74 2895	M.S. Alam et al.	(CLEO Collab.)
ASAKA	95	PL B345 36	T. Asaka, K.I. Hikasa	(TOHOK)
BUSKULIC	95	PL B343 444	D. Buskulic et al.	(ALEPH Collab.)
GROSSMAN	95B	PL B357 520	Y. Grossman, H. Haber, Y. Nir	(ALEPH Collab.)
GROSSMAN	94	PL B332 373	Y. Grossman, Z. Ligeti	(ALEPH Collab.)
STAHL	94	PL B324 121	A. Stahl	(BONN)
ACTON	92M	PL B295 347	P.D. Acton et al.	(OPAL Collab.)
SWARTZ	90	PRL 64 2877	M.L. Swartz et al.	(Mark II Collab.)

## New Heavy Bosons ( $W'$ , $Z'$ , leptoquarks, etc.), Searches for

We list here various limits on charged and neutral heavy vector bosons (other than  $W$ 's and  $Z$ 's), heavy scalar bosons (other than Higgs bosons), vector or scalar leptoquarks, and axiglions. The latest unpublished results are described in "W' Searches" and "Z' Searches" reviews. For recent searches on scalar bosons which could be identified as Higgs bosons, see the listings in the Higgs boson section.

### CONTENTS:

Mass Limits for $W'$ (Heavy Charged Vector Boson Other Than $W$ ) in Hadron Collider Experiments
$W_R$ (Right-Handed $W$ Boson) Mass Limits
Limit on $W_L$ - $W_R$ Mixing Angle $\zeta$
Mass Limits for $Z'$ (Heavy Neutral Vector Boson Other Than $Z$ )
– Limits for $Z'_{SM}$
– Limits for $Z'_{LR}$
– Limits for $Z'_{\nu}$
– Limits for $Z'_{\eta}$
– Limits for other $Z'$
– Searches for $Z'$ with Lepton-Flavor-Violating decays
Indirect Constraints on Kaluza-Klein Gauge Bosons
Mass Limits for Leptoquarks from Pair Production
Mass Limits for Leptoquarks from Single Production
Indirect Limits for Leptoquarks
Mass Limits for Diquarks
Mass Limits for $g_A$ (axigluon) and Other Color-Octet Gauge Bosons
Mass Limits for Color-Octet Scalar Bosons
$X^0$ (Heavy Boson) Searches in $Z$ Decays
Mass Limits for a Heavy Neutral Boson Coupling to $e^+e^-$
Search for $X^0$ Resonance in $e^+e^-$ Collisions
Search for $X^0$ Resonance in $ep$ Collisions
Search for $X^0$ Resonance in Two-Photon Process
Search for $X^0$ Resonance in $e^+e^- \rightarrow X^0\gamma$
Search for $X^0$ Resonance in $Z \rightarrow f\bar{f}X^0$
Search for $X^0$ Resonance in $W$ or $Z$ final state
Search for $X^0$ Resonance in Quarkonium Decays

See the related review(s):

[W'-Boson Searches](#)

**MASS LIMITS FOR  $W'$  (HEAVY CHARGED VECTOR BOSON OTHER THAN  $W$ ) IN HADRON COLLIDER EXPERIMENTS**

Couplings of  $W'$  to quarks and leptons are taken to be identical with those of  $W$ . The following limits are obtained from  $p\bar{p}$  or  $pp \rightarrow W'X$  with  $W'$  decaying to the mode indicated in the comments. New decay channels (e.g.,  $W' \rightarrow WZ$ ) are assumed to

See key on page 999

# Gauge & Higgs Boson Particle Listings

## New Heavy Bosons

be suppressed. The most recent preliminary results can be found in the "W'-boson searches" review above.

VALUE (GeV)	CL%	DOCUMENT ID	TECN	COMMENT
<b>&gt;5200 (CL = 95%) OUR LIMIT</b>				
none 500-3250	95	1 AABOUD 19B ATLS	W' → Nℓ → ℓℓj	
>6000	95	2 AABOUD 19E ATLS	W' → tb	
none 1300-3600	95	3 AAD 19C ATLS	W' → eν, μν	
none 400-4000	95	4 AAD 19D ATLS	W' → WZ	
>4300	95	5 SIRUNYAN 19AY CMS	W' → τν	
>2600	95	6 SIRUNYAN 19CP CMS	W' → WZ, WH, ℓν	
none 1000-3000	95	7 SIRUNYAN 19I CMS	W' → WH	
none 500-2820	95	8 AABOUD 18AF ATLS	W' → tb	
none 300-3000	95	9 AABOUD 18AI ATLS	W' → WH	
none 800-3200	95	10 AABOUD 18AK ATLS	W' → WZ	
>5100	95	11 AABOUD 18AL ATLS	W' → WZ	
none 250-2460	95	12 AABOUD 18BG ATLS	W' → eν, μν	
none 1200-3300	95	13 AABOUD 18CH ATLS	W' → WZ	
none 500-3700	95	14 AABOUD 18F ATLS	W' → WZ	
none 1000-3600	95	15 AABOUD 18K ATLS	W' → τν	
none 1000-3050	95	16 SIRUNYAN 18 CMS	W' → tb	
none 1000-5200	95	17 SIRUNYAN 18AX CMS	W' → WZ	
none 1000-3400	95	18 SIRUNYAN 18AZ CMS	W' → eν, μν	
none 600-3300	95	19 SIRUNYAN 18BK CMS	W' → WZ	
none 900-4400	95	20 SIRUNYAN 18BO CMS	W' → q̄q̄	
none 800-2330	95	21 SIRUNYAN 18CV CMS	W' → Nℓ → ℓℓj	
>2800	95	22 SIRUNYAN 18DJ CMS	W' → WZ	
none 1200-3200, 3300-3600	95	23 SIRUNYAN 18ED CMS	W' → WH	
>3600	95	24 SIRUNYAN 18P CMS	W' → WZ	
none 1100-2500	95	25 AABOUD 17AK ATLS	W' → q̄q̄	
>2220	95	26 AABOUD 17AO ATLS	W' → WH	
>2300	95	27 AABOUD 17B ATLS	W' → WH	
none 600-2700	95	28 KHACHATRY...17J CMS	W' → Nτ → ττjj	
>4100	95	29 KHACHATRY...17W CMS	W' → q̄q̄	
>2200	95	30 KHACHATRY...17Z CMS	W' → eν, μν	
>2300	95	31 SIRUNYAN 17A CMS	W' → WZ	
>2900	95	32 SIRUNYAN 17AK CMS	W' → WZ, WH	
>2600	95	33 SIRUNYAN 17H CMS	W' → τN	
>2450	95	34 SIRUNYAN 17I CMS	W' → tb	
none 2780-3150	95	35 SIRUNYAN 17R CMS	W' → WH	
>2600	95	36 SIRUNYAN 17S CMS	W' → WH	
>4070	95	37 AABOUD 16AE ATLS	W' → WZ	
>1810	95	38 AABOUD 16V ATLS	W' → eν, μν	
>2600	95	39 AAD 16R ATLS	W' → WZ	
>2150	95	40 AAD 16S ATLS	W' → q̄q̄	
none 1000-1600	95	41 KHACHATRY...16AO CMS	W' → tb	
none 800-1500	95	42 KHACHATRY...16AP CMS	W' → WH	
none 1500-2600	95	43 KHACHATRY...16BD CMS	W' → WH → b̄b̄ℓν	
none 500-1600	95	44 KHACHATRY...16K CMS	W' → q̄q̄	
none 300-2700	95	45 KHACHATRY...16L CMS	W' → q̄q̄	
none 400-1590	95	46 KHACHATRY...16O CMS	W' → τν	
none 1500-1760	95	47 AAD 15AU ATLS	W' → WZ	
none 300-1490	95	48 AAD 15AV ATLS	W' → tb	
none 1300-1500	95	49 AAD 15AZ ATLS	W' → WZ	
none 500-1920	95	50 AAD 15CP ATLS	W' → WZ	
none 800-2450	95	51 AAD 15R ATLS	W' → tb	
>1470	95	52 AAD 15V ATLS	W' → q̄q̄	
>3710	95	53 KHACHATRY...15C CMS	W' → WZ	
none 1000-3010	95	54 KHACHATRY...15T CMS	W' → eν, μν	
		55 KHACHATRY...14O CMS	W' → Nℓ → ℓℓj	
		56 AABOUD 19BB ATLS	W' → Nℓ → jℓℓ	
		57 SIRUNYAN 19V CMS	W' → Bt, Tb	
		58 AABOUD 18AA ATLS	W' → Wγ	
		59 AABOUD 18AD ATLS	W' → HX	
>4500	95	60 AABOUD 18AJ ATLS	W' → WZ, WH, ℓν	
		61 KHACHATRY...17U CMS	W' → WH	
		62 AAD 15BB ATLS	W' → WH	
none 300-880	95	63 AALTONEN 15c CDF	W' → tb	
none 1200-1900 and 2000-2200	95	64 KHACHATRY...15V CMS	W' → q̄q̄	
>3240	95	AAD 14AI ATLS	W' → eν, μν	
none 200-1520	95	AAD 14AT ATLS	W' → Wγ	
none 1000-1700	95	AAD 14S ATLS	W' → WZ	
		65 KHACHATRY...14 CMS	W' → WZ	
		66 KHACHATRY...14A CMS	W' → WZ	
none 500-950	95	67 KHACHATRY...13A CMS	W' → WZ	
none 1100-1680	95	AAD 13D ATLS	W' → q̄q̄	
none 1000-1920	95	CHATRCHYAN13A CMS	W' → q̄q̄	
		68 CHATRCHYAN13AJ CMS	W' → WZ	
		69 CHATRCHYAN13AQ CMS	W' → WZ	
>2900	95	70 CHATRCHYAN13E CMS	W' → eν, μν	
none 800-1510	95	71 CHATRCHYAN13I CMS	W' → tb	
none 700-940	95	72 CHATRCHYAN13U CMS	W' → WZ	
none 700-1130	95	73 AAD 12AV ATLS	W' → tb	

• • • We do not use the following data for averages, fits, limits, etc. • • •

none 200-760	95	74 AAD 12BB ATLS	W' → WZ
		75 AAD 12CK ATLS	W' → Tq
>2550	95	76 AAD 12CR ATLS	W' → eν, μν
		77 AAD 12M ATLS	W' → Nℓ → ℓℓjj
		78 AALTONEN 12N CDF	W' → Tq
none 200-1143	95	79 CHATRCHYAN12AF CMS	W' → WZ
		80 CHATRCHYAN12AR CMS	W' → Tq
		81 CHATRCHYAN12BG CMS	W' → Nℓ → ℓℓjj
>1120	95	AALTONEN 11c CDF	W' → eν
none 180-690	95	82 ABZOV 11H D0	W' → WZ
none 600-863	95	83 ABZOV 11L D0	W' → tb
none 285-516	95	84 AALTONEN 10N CDF	W' → WZ
none 280-840	95	85 AALTONEN 09AC CDF	W' → q̄q̄
>1000	95	ABZOV 08c D0	W' → eν
none 300-800	95	ABZOV 04c D0	W' → q̄q̄
none 225-536	95	86 ACOSTA 03B CDF	W' → tb
none 200-480	95	87 AFFOLDER 02c CDF	W' → WZ
> 786	95	88 AFFOLDER 01I CDF	W' → eν, μν
none 300-420	95	89 ABE 97G CDF	W' → q̄q̄
> 720	95	90 ABACHI 96c D0	W' → eν
> 610	95	91 ABACHI 95E D0	W' → eν, τν
none 260-600	95	RIZZO 93 RVUE	W' → q̄q̄

- AABOUD 19B search for right-handed  $W_R$  in  $pp$  collisions at  $\sqrt{s} = 13$  TeV.  $W_R$  is assumed to decay into  $\ell$  and hypothetical heavy neutrino  $N$ , with  $N$  decaying to  $\ell j j$ . See their Figs. 7 and 8 for excluded regions in  $M_{W'} - M_N$  plane.
- AABOUD 19E search for right-handed  $W'$  in  $pp$  collisions at  $\sqrt{s} = 13$  TeV. See their Fig. 8 for limit on  $\sigma \cdot B$ .
- AAD 19c search for  $W'$  with SM-like couplings in  $pp$  collisions at  $\sqrt{s} = 13$  TeV. Bosonic decays and  $W - W'$  interference are neglected. The limits on  $e$  and  $\mu$  separately are 6.0 and 5.1 TeV respectively. See their Fig. 2 for limits on  $\sigma \cdot B$ .
- AAD 19d search for resonances decaying to  $WZ$  in  $pp$  collisions at  $\sqrt{s} = 13$  TeV. The quoted limit is for heavy-vector-triplet  $W'$  with  $g_V = 3$ . The limit becomes  $M_{W'} > 3400$  GeV for  $g_V = 1$ . If we assume  $M_{W'} = M_{Z'}$ , the limit increases  $M_{W'} > 3800$  GeV and  $M_{W'} > 3500$  GeV for  $g_V = 3$  and  $g_V = 1$ , respectively. See their Fig. 9 for limits on  $\sigma \cdot B$ .
- SIRUNYAN 19ay limits shown for  $W'$  with SM-like coupling using  $pp$  collisions at  $\sqrt{s} = 13$  TeV.  $W - W'$  interference and bosonic decays of  $W'$  are not included. See their Fig. 5 for limits on  $\sigma \cdot B$ . Limits in the context of a nonuniversal gauge interaction are shown in Fig. 7. Model independent limits on  $\sigma B A \epsilon$  can be seen in Fig. 8.
- SIRUNYAN 19cp present a statistical combinations of searches for  $W'$  decaying to pairs of bosons or leptons in  $pp$  collisions at  $\sqrt{s} = 13$  TeV. The quoted limit is for heavy-vector-triplet  $W'$  with  $g_V = 3$ . If we assume  $M_{W'} = M_{Z'}$ , the limit becomes  $M_{W'} > 4500$  GeV for  $g_V = 3$  and  $M_{W'} > 5000$  GeV for  $g_V = 1$ . See their Figs. 2 and 3 for limits on  $\sigma \cdot B$ .
- SIRUNYAN 19i search for resonances decaying to  $HW$  in  $pp$  collisions at  $\sqrt{s} = 13$  TeV. The quoted limit is for heavy-vector-triplet  $W'$  with  $g_V = 3$ . The limit becomes  $M_{W'} > 2800$  GeV if we assume  $M_{W'} = M_{Z'}$ .
- AABOUD 18af give the limit above for right-handed  $W'$  using  $pp$  collisions at  $\sqrt{s} = 13$  TeV. These limits also exclude  $W$  bosons with left-handed couplings with masses below 2.9 TeV, at the 95% confidence level.  $W' \rightarrow \ell \nu_R$  is assumed to be forbidden. See their Fig.5 for limits on  $\sigma \cdot B$  for both cases of left- and right-handed  $W'$ .
- AABOUD 18ai search for resonances decaying to  $HW$  in  $pp$  collisions at  $\sqrt{s} = 13$  TeV. The quoted limit is for heavy-vector-triplet  $W'$  with  $g_V = 3$ . The limit becomes  $M_{W'} > 2670$  GeV for  $g_V = 1$ . If we assume  $M_{W'} = M_{Z'}$ , the limit increases  $M_{W'} > 2930$  GeV and  $M_{W'} > 2800$  GeV for  $g_V = 3$  and  $g_V = 1$ , respectively. See their Fig. 5 for limits on  $\sigma \cdot B$ .
- AABOUD 18ak search for resonances decaying to  $WZ$  in  $pp$  collisions at  $\sqrt{s} = 13$  TeV. The limit quoted above is for heavy-vector-triplet  $W'$  with  $g_V = 3$ . The limit becomes  $M_{W'} > 2800$  GeV for  $g_V = 1$ .
- AABOUD 18al search for resonances decaying to  $WZ$  in  $pp$  collisions at  $\sqrt{s} = 13$  TeV. The limit quoted above is for heavy-vector-triplet  $W'$  with  $g_V = 3$ . The limit becomes  $M_{W'} > 2900$  GeV for  $g_V = 1$ .
- AABOUD 18bg limit is for  $W'$  with SM-like couplings using  $pp$  collisions at  $\sqrt{s} = 13$  TeV. Bosonic decays of  $W'$  and  $W - W'$  interference are neglected. See Fig. 2 for limits on  $\sigma \cdot B$ .
- AABOUD 18ch search for resonances decaying to  $WZ$  in  $pp$  collisions at  $\sqrt{s} = 13$  TeV. The limit quoted above is for heavy-vector-triplet  $W'$  with  $g_V = 3$ . The limit becomes  $M_{W'} > 2260$  GeV for  $g_V = 1$ .
- AABOUD 18f search for resonances decaying to  $WZ$  in  $pp$  collisions at  $\sqrt{s} = 13$  TeV. The quoted limit is for heavy-vector-triplet  $W'$  with  $g_V = 3$ . The limit becomes  $M_{W'} > 3000$  GeV for  $g_V = 1$ . If we assume  $M_{Z'} = M_{W'}$ , the limit increases  $M_{W'} > 3500$  GeV and  $M_{W'} > 3100$  GeV for  $g_V = 3$  and  $g_V = 1$ , respectively. See their Fig.5 for limits on  $\sigma \cdot B$ .
- AABOUD 18k limit is for  $W'$  with SM-like coupling using  $pp$  collisions at  $\sqrt{s} = 13$  TeV.  $W - W'$  interference and bosonic decays of  $W'$  are not included. See their Fig. 4 for limit on  $\sigma \cdot B$ .
- SIRUNYAN 18 limit is for right-handed  $W'$  using  $pp$  collisions at  $\sqrt{s} = 13$  TeV.  $W' \rightarrow \ell \nu_R$  decay is assumed to be forbidden. The limit becomes  $M_{W'} > 3.4$  TeV if  $M_{\nu_R} \ll M_{W'}$ . See their Fig. 5 for exclusion limits on  $W'$  models having both left- and right-handed couplings.
- SIRUNYAN 18ax search for resonances decaying to  $WZ$  in  $pp$  collisions at  $\sqrt{s} = 13$  TeV. The quoted limit is for heavy-vector-triplet  $W'$  with  $g_V = 3$ . See their Fig.6 for limits on  $\sigma \cdot B$ .
- SIRUNYAN 18az limit is derived for  $W'$  with SM-like coupling using  $pp$  collisions at  $\sqrt{s} = 13$  TeV. No interference with SM  $W$  process is considered. The bosonic decays are assumed to be negligible. See their Fig.6 for limits on  $\sigma \cdot B$ .

- 19 SIRUNYAN 18BK search for resonances decaying to  $WZ$  in  $pp$  collisions at  $\sqrt{s} = 13$  TeV. The limit quoted above is for heavy-vector-triplet  $W'$  with  $g_V = 3$ . The limit becomes  $M_{W'} > 3100$  GeV for  $g_V = 1$ .
- 20 SIRUNYAN 18BO limit is for  $W'$  with SM-like coupling using  $pp$  collisions at  $\sqrt{s} = 13$  TeV.
- 21 SIRUNYAN 18CV search for right-handed  $W_R$  in  $pp$  collisions at  $\sqrt{s} = 13$  TeV.  $W_R$  is assumed to decay into  $\ell$  and hypothetical heavy neutrino  $N$ , with  $N$  decaying to  $\ell j$ . The quoted limit is for  $M_N = M_{W_R}/2$ . See their Fig. 6 for excluded regions in the  $M_{W_R} - M_N$  plane.
- 22 SIRUNYAN 18DJ search for resonances decaying to  $WZ$  in  $pp$  collisions at  $\sqrt{s} = 13$  TeV. The limit quoted above is for heavy-vector-triplet  $W'$  with  $g_V = 3$ . The limit becomes  $M_{W'} > 2270$  GeV for  $g_V = 1$ .
- 23 SIRUNYAN 18ED search for resonances decaying to  $HW$  in  $pp$  collisions at  $\sqrt{s} = 13$  TeV. The limit above is for heavy-vector-triplet  $W'$  with  $g_V = 3$ . If we assume  $M_{W'} = M_{Z'}$ , the limit increases  $M_{W'} > 2900$  GeV and  $M_{W'} > 2800$  GeV for  $g_V = 3$  and  $g_V = 1$ , respectively.
- 24 SIRUNYAN 18P give this limit for a heavy-vector-triplet  $W'$  with  $g_V = 3$ . If they assume  $M_{Z'} = M_{W'}$ , the limit increases to  $M_{W'} > 3800$  GeV.
- 25 AABOUD 17AK search for a new resonance decaying to dijets in  $pp$  collisions at  $\sqrt{s} = 13$  TeV. The limit above is for a  $W'$  boson having axial-vector SM couplings and decaying to quarks with 75% branching fraction.
- 26 AABOUD 17AO search for resonances decaying to  $HW$  in  $pp$  collisions at  $\sqrt{s} = 13$  TeV. The limit quoted above is for a  $W'$  in the heavy-vector-triplet model with  $g_V = 3$ . See their Fig.4 for limits on  $\sigma \cdot B$ .
- 27 AABOUD 17B search for resonances decaying to  $HW$  ( $H \rightarrow b\bar{b}, c\bar{c}; W \rightarrow \ell\nu$ ) in  $pp$  collisions at  $\sqrt{s} = 13$  TeV. The quoted limit is for heavy-vector-triplet  $W'$  with  $g_V = 3$ . The limit becomes  $M_{W'} > 1750$  GeV for  $g_V = 1$ . If we assume  $M_{W'} = M_{Z'}$ , the limit increases  $M_{W'} > 2310$  GeV and  $M_{W'} > 1730$  GeV for  $g_V = 3$  and  $g_V = 1$ , respectively. See their Fig.3 for limits on  $\sigma \cdot B$ .
- 28 KHACHATRYAN 17J search for right-handed  $W_R$  in  $pp$  collisions at  $\sqrt{s} = 13$  TeV.  $W_R$  is assumed to decay into  $\tau$  and hypothetical heavy neutrino  $N_\tau$ , with  $N_\tau$  decaying into  $\tau j$ . The quoted limit is for  $M_{N_\tau} = M_{W_R}/2$ . The limit becomes  $M_{W_R} > 2350$  GeV (1630 GeV) for  $M_{W_R}/M_{N_\tau} = 0.8$  (0.2). See their Fig. 4 for excluded regions in the  $M_{W_R} - M_{N_\tau}$  plane.
- 29 KHACHATRYAN 17W search for resonances decaying to dijets in  $pp$  collisions at  $\sqrt{s} = 13$  TeV.
- 30 KHACHATRYAN 17Z limit is for  $W'$  with SM-like coupling using  $pp$  collisions at  $\sqrt{s} = 13$  TeV. The bosonic decays of  $W'$  and the interference with SM  $W$  process are neglected.
- 31 SIRUNYAN 17A search for resonances decaying to  $WZ$  with  $WZ \rightarrow \ell\nu q\bar{q}, q\bar{q}q\bar{q}$  in  $pp$  collisions at  $\sqrt{s} = 13$  TeV. The quoted limit is for heavy-vector-triplet  $W'$  with  $g_V = 3$ . The limit becomes  $M_{W'} > 2000$  GeV for  $g_V = 1$ . If we assume  $M_{Z'} = M_{W'}$ , the limit increases  $M_{W'} > 2400$  GeV and  $M_{W'} > 2300$  GeV for  $g_V = 3$  and  $g_V = 1$ , respectively. See their Fig.6 for limits on  $\sigma \cdot B$ .
- 32 SIRUNYAN 17AK search for resonances decaying to  $WZ$  or  $HW$  in  $pp$  collisions at  $\sqrt{s} = 8$  and 13 TeV. The quoted limit is for heavy-vector-triplet  $W'$  with  $g_V = 3$ . The limit becomes  $M_{W'} > 2300$  GeV for  $g_V = 1$ . If we assume  $M_{W'} = M_{Z'}$ , the limit increases  $M_{W'} > 2400$  GeV for both  $g_V = 3$  and  $g_V = 1$ . See their Fig.1 and 2 for limits on  $\sigma \cdot B$ .
- 33 SIRUNYAN 17H search for right-handed  $W'$  in  $pp$  collisions at  $\sqrt{s} = 13$  TeV.  $W'$  is assumed to decay into  $\tau$  and a heavy neutrino  $N$ , with  $N$  decaying to  $\tau q\bar{q}$ . The limit above assumes  $M_N = M_{W'}/2$ .
- 34 SIRUNYAN 17I limit is for a right-handed  $W'$  using  $pp$  collisions at  $\sqrt{s} = 13$  TeV. The limit becomes  $M_{W'} > 2400$  GeV for  $M_{\nu R} \ll M_{W'}$ .
- 35 SIRUNYAN 17R search for resonances decaying to  $HW$  in  $pp$  collisions at  $\sqrt{s} = 13$  TeV. The quoted limit is for heavy-vector-triplet  $W'$  with  $g_V = 3$ . Mass regions  $M_{W'} < 2370$  GeV and  $2870 < M_{W'} < 2970$  GeV are excluded for  $g_V = 1$ . If we assume  $M_{Z'} = M_{W'}$ , the excluded mass regions are  $1000 < M_{W'} < 2500$  GeV and  $2760 < M_{W'} < 3300$  GeV for  $g_V = 3$ ;  $1000 < M_{W'} < 2430$  GeV and  $2810 < M_{W'} < 3130$  GeV for  $g_V = 1$ . See their Fig.5 for limits on  $\sigma \cdot B$ .
- 36 AABOUD 16AE search for resonances decaying to  $VV$  ( $V = W$  or  $Z$ ) in  $pp$  collisions at  $\sqrt{s} = 13$  TeV. Results from  $\nu\nu q\bar{q}, \nu\ell q\bar{q}, \ell\ell q\bar{q}$  and  $qqq$  final states are combined. The quoted limit is for a heavy-vector-triplet  $W'$  with  $g_V = 3$  and  $M_{W'} = M_{Z'}$ .
- 37 AABOUD 16V limit is for  $W'$  with SM-like coupling using  $pp$  collisions at  $\sqrt{s} = 13$  TeV. The bosonic decays of  $W'$  and the interference with SM  $W$  process are neglected.
- 38 AAD 16R search for  $W' \rightarrow WZ$  in  $pp$  collisions at  $\sqrt{s} = 8$  TeV.  $\ell\nu\ell'\ell', \ell\ell q\bar{q}, \ell\nu q\bar{q}$ , and all hadronic channels are combined. The quoted limit assumes  $g_{W'WZ}/g_{WWZ} = (M_W/M_{W'})^2$ .
- 39 AAD 16S search for a new resonance decaying to dijets in  $pp$  collisions at  $\sqrt{s} = 13$  TeV. The limit quoted above is for a  $W'$  having SM-like couplings to quarks.
- 40 KHACHATRYAN 16AO limit is for a SM-like right-handed  $W'$  using  $pp$  collisions at  $\sqrt{s} = 8$  TeV. The quoted limit combines  $t \rightarrow qq\bar{b}$  and  $t \rightarrow \ell\nu b$  events.
- 41 KHACHATRYAN 16AP search for a resonance decaying to  $HW$  in  $pp$  collisions at  $\sqrt{s} = 8$  TeV. Both  $H$  and  $W$  are assumed to decay to fat jets. The quoted limit is for heavy-vector-triplet  $W'$  with  $g_V = 3$ .
- 42 KHACHATRYAN 16BD search for resonance decaying to  $HW$  in  $pp$  collisions at  $\sqrt{s} = 8$  TeV. The quoted limit is for heavy-vector-triplet (HVT)  $W'$  with  $g_V = 3$ . The HVT model  $m_{W'} = m_{Z'} > 1.8$  TeV is also obtained by combining  $W'/Z' \rightarrow WH/ZH \rightarrow \ell\nu b\bar{b}, q\bar{q}\tau\tau, q\bar{q}b\bar{b}$ , and  $qqqqqq$  channels.
- 43 KHACHATRYAN 16K search for resonances decaying to dijets in  $pp$  collisions at  $\sqrt{s} = 13$  TeV.
- 44 KHACHATRYAN 16L search for resonances decaying to dijets in  $pp$  collisions at  $\sqrt{s} = 8$  TeV with the data scouting technique, increasing the sensitivity to the low mass resonances.
- 45 KHACHATRYAN 16O limit is for  $W'$  having universal couplings. Interferences with the SM amplitudes are assumed to be absent.
- 46 AAD 15AU search for  $W'$  decaying into the  $WZ$  final state with  $W \rightarrow q\bar{q}'$ ,  $Z \rightarrow \ell^+\ell^-$  using  $pp$  collisions at  $\sqrt{s} = 8$  TeV. The quoted limit assumes  $g_{W'WZ}/g_{WWZ} = (M_W/M_{W'})^2$ .
- 47 AAD 15AV limit is for a SM like right-handed  $W'$  using  $pp$  collisions at  $\sqrt{s} = 8$  TeV.  $W' \rightarrow \ell\nu$  decay is assumed to be forbidden.
- 48 AAD 15AZ search for  $W'$  decaying into the  $WZ$  final state with  $W \rightarrow \ell\nu$ ,  $Z \rightarrow q\bar{q}$  using  $pp$  collisions at  $\sqrt{s} = 8$  TeV. The quoted limit assumes  $g_{W'WZ}/g_{WWZ} = (M_W/M_{W'})^2$ .
- 49 AAD 15CP search for  $W'$  decaying into the  $WZ$  final state with  $W \rightarrow q\bar{q}$ ,  $Z \rightarrow q\bar{q}$  using  $pp$  collisions at  $\sqrt{s} = 8$  TeV. The quoted limit assumes  $g_{W'WZ}/g_{WWZ} = (M_W/M_{W'})^2$ .
- 50 AAD 15R limit is for a SM like right-handed  $W'$  using  $pp$  collisions at  $\sqrt{s} = 8$  TeV.  $W' \rightarrow \ell\nu$  decay is assumed to be forbidden.
- 51 AAD 15V search for new resonance decaying to dijets in  $pp$  collisions at  $\sqrt{s} = 8$  TeV.
- 52 KHACHATRYAN 15C search for  $W'$  decaying via  $WZ$  to fully leptonic final states using  $pp$  collisions at  $\sqrt{s}=8$  TeV. The quoted limit assumes  $g_{W'WZ}/g_{WWZ} = M_{W'} M_Z/M_{Z'}^2$ .
- 53 KHACHATRYAN 15T limit is for  $W'$  with SM-like coupling which interferes the SM  $W$  boson constructively using  $pp$  collisions at  $\sqrt{s} = 8$  TeV. For  $W'$  without interference, the limit becomes  $> 3280$  GeV.
- 54 KHACHATRYAN 14O search for right-handed  $W_R$  in  $pp$  collisions at  $\sqrt{s} = 8$  TeV.  $W_R$  is assumed to decay into  $\ell$  and hypothetical heavy neutrino  $N$ , with  $N$  decaying into  $\ell j$ . The quoted limit is for  $M_{\nu eR} = M_{\nu \mu R} = M_{W_R}/2$ . See their Fig. 3 and Fig. 5 for excluded regions in the  $M_{W_R} - M_\nu$  plane.
- 55 AABOUD 19BB search for right handed  $W_R$  in  $pp$  collisions at  $\sqrt{s} = 13$  TeV.  $W_R$  is assumed to decay into  $\ell$  and a boosted hypothetical heavy neutrino  $N$ , with  $N$  decaying to  $\ell$  and a large radius jet  $j = q\bar{q}$ . See their Fig. 7 for excluded regions in  $M_{W_R} - M_N$  plane.
- 56 SIRUNYAN 19V search for a new resonance decaying to a top quark and a heavy vector-like bottom partner  $B$  decaying to  $Hb$  (or a bottom quark and a heavy vector-like top partner  $T$  decaying to  $Ht$ ) in  $pp$  collisions at  $\sqrt{s} = 13$  TeV. See their Fig. 8 for limits on  $\sigma \cdot B$ .
- 57 AABOUD 18AA search for a narrow charged vector boson decaying to  $W\gamma$ . See their Fig. 9 for the exclusion limit in  $M_{W'} - \sigma B$  plane.
- 58 AABOUD 18AD search for resonances decaying to  $HX$  ( $H \rightarrow b\bar{b}$ ,  $X \rightarrow q\bar{q}'$ ) in  $pp$  collisions at  $\sqrt{s} = 13$  TeV. See their Figs. 3-5 for limits on  $\sigma \cdot B$ .
- 59 AABOUD 18CJ search for heavy-vector-triplet  $W'$  in  $pp$  collisions at  $\sqrt{s} = 13$  TeV. The limit quoted above is for model with  $g_V = 3$  assuming  $M_{W'} = M_{Z'}$ . The limit becomes  $M_{W'} > 5500$  GeV for model with  $g_V = 1$ .
- 60 KHACHATRYAN 17U search for resonances decaying to  $HW$  ( $H \rightarrow b\bar{b}$ ;  $W \rightarrow \ell\nu$ ) in  $pp$  collisions at  $\sqrt{s} = 13$  TeV. The limit on the heavy-vector-triplet model is  $M_{Z'} = M_{W'} > 2$  TeV for  $g_V = 3$ , in which constraints from the  $Z' \rightarrow HZ$  ( $H \rightarrow b\bar{b}$ ;  $Z \rightarrow \ell^+\ell^-, \nu\bar{\nu}$ ) are combined. See their Fig.3 and Fig.4 for limits on  $\sigma \cdot B$ .
- 61 AAD 15BB search for  $W'$  decaying into  $WH$  with  $W \rightarrow \ell\nu$ ,  $H \rightarrow b\bar{b}$ . See their Fig. 4 for the exclusion limits in the heavy vector triplet benchmark model parameter space.
- 62 AALTONEN 15C limit is for a SM-like right-handed  $W'$  assuming  $W' \rightarrow \ell\nu$  decays are forbidden, using  $p\bar{p}$  collisions at  $\sqrt{s}=1.96$  TeV. See their Fig. 3 for limit on  $g_{W'}/g_W$ .
- 63 KHACHATRYAN 15V search new resonance decaying to dijets in  $pp$  collisions at  $\sqrt{s} = 8$  TeV.
- 64 AAD 14AT search for a narrow charged vector boson decaying to  $W\gamma$ . See their Fig. 3a for the exclusion limit in  $m_{W'} - \sigma B$  plane.
- 65 AAD 14S search for  $W'$  decaying into the  $WZ$  final state with  $W \rightarrow \ell\nu$ ,  $Z \rightarrow \ell\ell$  using  $pp$  collisions at  $\sqrt{s}=8$  TeV. The quoted limit assumes  $g_{W'WZ}/g_{WWZ} = (M_W/M_{W'})^2$ .
- 66 KHACHATRYAN 14 search for  $W'$  decaying into  $WZ$  final state with  $W \rightarrow q\bar{q}$ ,  $Z \rightarrow q\bar{q}$  using  $pp$  collisions at  $\sqrt{s}=8$  TeV. The quoted limit assumes  $g_{W'WZ}/g_{WWZ} = (M_W/M_{W'})^2$ .
- 67 KHACHATRYAN 14A search for  $W'$  decaying into the  $WZ$  final state with  $W \rightarrow \ell\nu$ ,  $Z \rightarrow q\bar{q}$ , or  $W \rightarrow q\bar{q}$ ,  $Z \rightarrow \ell\ell$ .  $pp$  collisions data at  $\sqrt{s}=8$  TeV are used for the search. See their Fig. 13 for the exclusion limit on the number of events in the mass-width plane.
- 68 AAD 13AO search for  $W'$  decaying into the  $WZ$  final state with  $W \rightarrow \ell\nu$ ,  $Z \rightarrow 2j$  using  $pp$  collisions at  $\sqrt{s}=7$  TeV. The quoted limit assumes  $g_{W'WZ}/g_{WWZ} = (M_W/M_{W'})^2$ .
- 69 CHATRYAN 13AJ search for resonances decaying to  $WZ$  pair, using the hadronic decay modes of  $W$  and  $Z$ , in  $pp$  collisions at  $\sqrt{s}=7$  TeV. See their Fig. 7 for the limit on the cross section.
- 70 CHATRYAN 13AQ limit is for  $W'$  with SM-like coupling which interferes with the SM  $W$  boson using  $pp$  collisions at  $\sqrt{s}=7$  TeV.
- 71 CHATRYAN 13E limit is for  $W'$  with SM-like coupling which interferes with the SM  $W$  boson using  $pp$  collisions at  $\sqrt{s}=7$  TeV. For  $W'$  with right-handed coupling, the bound becomes  $>1850$  GeV ( $>1910$  GeV) if  $W'$  decays to both leptons and quarks (only to quarks). If both left- and right-handed couplings are present, the limit becomes  $>1640$  GeV.
- 72 CHATRYAN 13U search for  $W'$  decaying to the  $WZ$  final state, with  $W$  decaying into jets, in  $pp$  collisions at  $\sqrt{s}=7$  TeV. The quoted limit assumes  $g_{W'WZ}/g_{WWZ} = (M_W/M_{W'})^2$ .
- 73 The AAD 12AV quoted limit is for a SM-like right-handed  $W'$  using  $pp$  collisions at  $\sqrt{s}=7$  TeV.  $W' \rightarrow \ell\nu$  decay is assumed to be forbidden.
- 74 AAD 12BB use  $pp$  collisions data at  $\sqrt{s}=7$  TeV. The quoted limit assumes  $g_{W'WZ}/g_{WWZ} = (M_W/M_{W'})^2$ .
- 75 AAD 12CK search for  $pp \rightarrow tW'$ ,  $W' \rightarrow \bar{T}q$  events in  $pp$  collisions. See their Fig. 5 for the limit on  $\sigma \cdot B$ .
- 76 AAD 12CR use  $pp$  collisions at  $\sqrt{s}=7$  TeV.

See key on page 999

# Gauge & Higgs Boson Particle Listings

## New Heavy Bosons

- 77 AAD 12M search for right-handed  $W_R$  in  $pp$  collisions at  $\sqrt{s} = 7$  TeV.  $W_R$  is assumed to decay into  $\ell$  and hypothetical heavy neutrino  $N$ , with  $N$  decaying into  $\ell jj$ . See their Fig. 4 for the limit in the  $m_N - m_{W_R}$  plane.
- 78 AALTONEN 12N search for  $p\bar{p} \rightarrow t W', W' \rightarrow \bar{t} d$  events in  $p\bar{p}$  collisions. See their Fig. 3 for the limit on  $\sigma \cdot B$ .
- 79 CHATRCHYAN 12AR search for  $pp \rightarrow t W', W' \rightarrow \bar{t} d$  events in  $pp$  collisions. See their Fig. 2 for the limit on  $\sigma \cdot B$ .
- 80 CHATRCHYAN 12BG search for right-handed  $W_R$  in  $pp$  collisions  $\sqrt{s} = 7$  TeV.  $W_R$  is assumed to decay into  $\ell$  and hypothetical heavy neutrino  $N$ , with  $N$  decaying into  $\ell jj$ . See their Fig. 3 for the limit in the  $m_N - m_{W_R}$  plane.
- 81 ABAZOV 11H use data from  $p\bar{p}$  collisions at  $\sqrt{s}=1.96$  TeV. The quoted limit is obtained assuming  $W' W Z$  coupling strength is the same as the ordinary  $W W Z$  coupling strength in the Standard Model.
- 82 ABAZOV 11L limit is for  $W'$  with SM-like coupling which interferes with the SM  $W$  boson, using  $p\bar{p}$  collisions at  $\sqrt{s}=1.96$  TeV. For  $W'$  with right-handed coupling, the bound becomes  $>885$  GeV ( $>890$  GeV) if  $W'$  decays to both leptons and quarks (only to quarks). If both left- and right-handed couplings present, the limit becomes  $>916$  GeV.
- 83 AALTONEN 10N use  $p\bar{p}$  collision data at  $\sqrt{s}=1.96$  TeV. The quoted limit assumes  $g_{W' W Z} / g_{W W Z} = (M_{W'} / M_W)^2$ . See their Fig. 4 for limits in mass-coupling plane.
- 84 AALTONEN 09AC search for new particle decaying to dijets using  $p\bar{p}$  collisions at  $\sqrt{s}=1.96$  TeV.
- 85 The ACOSTA 03B quoted limit is for  $M_{W'} \gg M_{\nu_R}$ , using  $p\bar{p}$  collisions at  $\sqrt{s}=1.8$  TeV. For  $M_{W'} < M_{\nu_R}$ ,  $M_{W'}$  between 225 and 566 GeV is excluded.
- 86 The quoted limit is obtained assuming  $W' W Z$  coupling strength is the same as the ordinary  $W W Z$  coupling strength in the Standard Model, using  $p\bar{p}$  collisions at  $\sqrt{s}=1.8$  TeV. See their Fig. 2 for the limits on the production cross sections as a function of the  $W'$  width.
- 87 AFFOLDER 01i combine a new bound on  $W' \rightarrow e \nu$  of 754 GeV, using  $p\bar{p}$  collisions at  $\sqrt{s}=1.8$  TeV, with the bound of ABE 00 on  $W' \rightarrow \mu \nu$  to obtain quoted bound.
- 88 ABE 97G search for new particle decaying to dijets using  $p\bar{p}$  collisions at  $\sqrt{s}=1.8$  TeV.
- 89 For bounds on  $W_R$  with nonzero right-handed mass, see Fig. 5 from ABACHI 96c.
- 90 ABACHI 95E assume that the decay  $W' \rightarrow W Z$  is suppressed and that the neutrino from  $W'$  decay is stable and has a mass significantly less  $m_{W'}$ .
- 91 RIZZO 93 analyses CDF limit on possible two-jet resonances. The limit is sensitive to the inclusion of the assumed  $K$  factor.

### $W_R$ (Right-Handed $W$ Boson) MASS LIMITS

Assuming a light right-handed neutrino, except for BEALL 82, LANGACKER 89b, and COLANGELO 91.  $g_R = g_L$  assumed. [Limits in the section MASS LIMITS for  $W'$  below are also valid for  $W_R$  if  $m_{\nu_R} \ll m_{W_R}$ .] Some limits assume manifest left-right symmetry, i.e., the equality of left- and right Cabibbo-Kobayashi-Maskawa matrices. For a comprehensive review, see LANGACKER 89b. Limits on the  $W_L - W_R$  mixing angle  $\zeta$  are found in the next section. Values in brackets are from cosmological and astrophysical considerations and assume a light right-handed neutrino.

VALUE (GeV)	CL%	DOCUMENT ID	TECN	COMMENT
> 5.92	90	1 BUENO 11	TWST	$\mu$ decay
> 715	90	2 CZAKON 99	RVUE	Electroweak
• • • We do not use the following data for averages, fits, limits, etc. • • •				
> 235	90	3 PRIEELS 14	PIE3	$\mu$ decay
> 245	90	4 WAUTERS 10	CNTR	$^{60}\text{Co}$ $\beta$ decay
> 2500	90	5 ZHANG 08	THEO	$m_{K_L^0} - m_{K_S^0}$
> 180	90	6 MELCONIAN 07	CNTR	$^{37}\text{K}$ $\beta^+$ decay
> 290.7	90	7 SCHUMANN 07	CNTR	Polarized neutron decay
[> 3300]	95	8 CYBURT 05	COSM	Nucleosynthesis; light $\nu_R$
> 310	90	9 THOMAS 01	CNTR	$\beta^+$ decay
> 137	95	10 ACKERSTAFF 99D	OPAL	$\tau$ decay
> 1400	68	11 BARENBOIM 98	RVUE	Electroweak, $Z-Z'$ mixing
> 549	68	12 BARENBOIM 97	RVUE	$\mu$ decay
> 220	95	13 STAHL 97	RVUE	$\tau$ decay
> 220	90	14 ALLET 96	CNTR	$\beta^+$ decay
> 281	90	15 KUZNETSOV 95	CNTR	Polarized neutron decay
> 282	90	16 KUZNETSOV 94b	CNTR	Polarized neutron decay
> 439	90	17 BHATTACH... 93	RVUE	$Z-Z'$ mixing
> 250	90	18 SEVERIJNS 93	CNTR	$\beta^+$ decay
		19 IMAZATO 92	CNTR	$K^+$ decay
> 475	90	20 POLAK 92b	RVUE	$\mu$ decay
> 240	90	21 AQUINO 91	RVUE	Neutron decay
> 496	90	21 AQUINO 91	RVUE	Neutron and muon decay
> 700	90	22 COLANGELO 91	THEO	$m_{K_L^0} - m_{K_S^0}$
> 477	90	23 POLAK 91	RVUE	$\mu$ decay
[none 540-23000]		24 BARBIERI 89b	ASTR	SN 1987A; light $\nu_R$
> 300	90	25 LANGACKER 89b	RVUE	General
> 160	90	26 BALKE 88	CNTR	$\mu \rightarrow e \nu \bar{\nu}$
> 406	90	27 JODIDIO 86	ELEC	Any $\zeta$
> 482	90	27 JODIDIO 86	ELEC	$\zeta = 0$
> 800	90	MOHAPATRA 86	RVUE	$\text{SU}(2)_L \times \text{SU}(2)_R \times \text{U}(1)$
> 400	95	28 STOKER 85	ELEC	Any $\zeta$
> 475	95	28 STOKER 85	ELEC	$\zeta < 0.041$
		29 BERGSMA 83	CHRM	$\nu_\mu e \rightarrow \mu \nu_e$
> 380	90	30 CARR 83	ELEC	$\mu^+$ decay
> 1600		31 BEALL 82	THEO	$m_{K_L^0} - m_{K_S^0}$

1 The quoted limit is for manifest left-right symmetric model.

2 CZAKON 99 perform a simultaneous fit to charged and neutral sectors.

- 3 PRIEELS 14 limit is from  $\mu^+ \rightarrow e^+ \nu \bar{\nu}$  decay parameter  $\xi''$ , which is determined by the positron polarization measurement.
- 4 WAUTERS 10 limit is from a measurement of the asymmetry parameter of polarized  $^{60}\text{Co}$   $\beta$  decays. The listed limit assumes no mixing.
- 5 ZHANG 08 limit uses a lattice QCD calculation of the relevant hadronic matrix elements, while BEALL 82 limit used the vacuum saturation approximation.
- 6 MELCONIAN 07 measure the neutrino angular asymmetry in  $\beta^+$ -decays of polarized  $^{37}\text{K}$ , stored in a magneto-optical trap. Result is consistent with SM prediction and does not constrain the  $W_L - W_R$  mixing angle appreciably.
- 7 SCHUMANN 07 limit is from measurements of the asymmetry  $\langle \bar{p}_\nu \cdot \sigma_n \rangle$  in the  $\beta$  decay of polarized neutrons. Zero mixing is assumed.
- 8 CYBURT 05 limit follows by requiring that three light  $\nu_R$ 's decouple when  $T_{dec} > 140$  MeV. For different  $T_{dec}$ , the bound becomes  $M_{W_R} > 3.3 \text{ TeV} (T_{dec} / 140 \text{ MeV})^{3/4}$ .
- 9 THOMAS 01 limit is from measurement of  $\beta^+$  polarization in decay of polarized  $^{12}\text{N}$ . The listed limit assumes no mixing.
- 10 ACKERSTAFF 99D limit is from  $\tau$  decay parameters. Limit increase to 145 GeV for zero mixing.
- 11 BARENBOIM 98 assumes minimal left-right model with Higgs of  $\text{SU}(2)_R$  in  $\text{SU}(2)_L$  doublet. For Higgs in  $\text{SU}(2)_L$  triplet,  $m_{W_R} > 1100$  GeV. Bound calculated from effect of corresponding  $Z_{LR}$  on electroweak data through  $Z-Z_{LR}$  mixing.
- 12 The quoted limit is from  $\mu$  decay parameters. BARENBOIM 97 also evaluate limit from  $K_L - K_S$  mass difference.
- 13 STAHL 97 limit is from fit to  $\tau$ -decay parameters.
- 14 ALLET 96 measured polarization-asymmetry correlation in  $^{12}\text{N}$   $\beta^+$  decay. The listed limit assumes zero  $L-R$  mixing.
- 15 KUZNETSOV 95 limit is from measurements of the asymmetry  $\langle \bar{p}_\nu \cdot \sigma_n \rangle$  in the  $\beta$  decay of polarized neutrons. Zero mixing assumed. See also KUZNETSOV 94b.
- 16 KUZNETSOV 94b limit is from measurements of the asymmetry  $\langle \bar{p}_\nu \cdot \sigma_n \rangle$  in the  $\beta$  decay of polarized neutrons. Zero mixing assumed.
- 17 BHATTACHARYYA 93 uses  $Z-Z'$  mixing limit from LEP '90 data, assuming a specific Higgs sector of  $\text{SU}(2)_L \times \text{SU}(2)_R \times \text{U}(1)$  gauge model. The limit is for  $m_t = 200$  GeV and slightly improves for smaller  $m_t$ .
- 18 SEVERIJNS 93 measured polarization-asymmetry correlation in  $^{107}\text{In}$   $\beta^+$  decay. The listed limit assumes zero  $L-R$  mixing. Value quoted here is from SEVERIJNS 94 erratum.
- 19 IMAZATO 92 measure positron asymmetry in  $K^+ \rightarrow \mu^+ \nu_\mu$  decay and obtain  $\xi_{P,\mu} > 0.990$  (90% CL). If  $W_R$  couples to  $u\bar{s}$  with full weak strength ( $V_{us}^R = 1$ ), the result corresponds to  $m_{W_R} > 653$  GeV. See their Fig. 4 for  $m_{W_R}$  limits for general  $|V_{us}^R|^2 = 1 - |V_{ud}^R|^2$ .
- 20 POLAK 92b limit is from fit to muon decay parameters and is essentially determined by JODIDIO 86 data assuming  $\zeta=0$ . Supersedes POLAK 91.
- 21 AQUINO 91 limits obtained from neutron lifetime and asymmetries together with unitarity of the CKM matrix. Manifest left-right symmetry assumed. Stronger of the two limits also includes muon decay results.
- 22 COLANGELO 91 limit uses hadronic matrix elements evaluated by QCD sum rule and is less restrictive than BEALL 82 limit which uses vacuum saturation approximation. Manifest left-right symmetry assumed.
- 23 POLAK 91 limit is from fit to muon decay parameters and is essentially determined by JODIDIO 86 data assuming  $\zeta=0$ . Superseded by POLAK 92b.
- 24 BARBIERI 89b limit holds for  $m_{\nu_R} \leq 10$  MeV.
- 25 LANGACKER 89b limit is for any  $\nu_R$  mass (either Dirac or Majorana) and for a general class of right-handed quark mixing matrices.
- 26 BALKE 88 limit is for  $m_{\nu_{eR}} = 0$  and  $m_{\nu_{\mu R}} \leq 50$  MeV. Limits come from precise measurements of the muon decay asymmetry as a function of the positron energy.
- 27 JODIDIO 86 is the same TRIUMF experiment as STOKER 85 (and CARR 83); however, it uses a different technique. The results given here are combined results of the two techniques. The technique here involves precise measurement of the end-point  $e^+$  spectrum in the decay of the highly polarized  $\mu^+$ .
- 28 STOKER 85 is same TRIUMF experiment as CARR 83. Here they measure the decay  $e^+$  spectrum asymmetry above 46 MeV/c using a muon-spin-rotation technique. Assumed a light right-handed neutrino. Quoted limits are from combining with CARR 83.
- 29 BERGSMA 83 set limit  $m_{W_2} / m_{W_1} > 1.9$  at CL = 90%.
- 30 CARR 83 is TRIUMF experiment with a highly polarized  $\mu^+$  beam. Looked for deviation from  $V-A$  at the high momentum end of the decay  $e^+$  energy spectrum. Limit from previous world-average muon polarization parameter is  $m_{W_R} > 240$  GeV. Assumes a light right-handed neutrino.
- 31 BEALL 82 limit is obtained assuming that  $W_R$  contribution to  $K_L^0 - K_S^0$  mass difference is smaller than the standard one, neglecting the top quark contributions. Manifest left-right symmetry assumed.

### Limit on $W_L - W_R$ Mixing Angle $\zeta$

Lighter mass eigenstate  $W_1 = W_L \cos \zeta - W_R \sin \zeta$ . Light  $\nu_R$  assumed unless noted. Values in brackets are from cosmological and astrophysical considerations.

VALUE	CL%	DOCUMENT ID	TECN	COMMENT
• • • We do not use the following data for averages, fits, limits, etc. • • •				
-0.020 to 0.017	90	BUENO 11	TWST	$\mu \rightarrow e \nu \bar{\nu}$
< 0.022	90	MACDONALD 08	TWST	$\mu \rightarrow e \nu \bar{\nu}$
< 0.12	95	1 ACKERSTAFF 99D	OPAL	$\tau$ decay
< 0.013	90	2 CZAKON 99	RVUE	Electroweak
< 0.0333	90	3 BARENBOIM 97	RVUE	$\mu$ decay
< 0.04	90	4 MISHRA 92	CCFR	$\nu N$ scattering
-0.0006 to 0.0028	90	5 AQUINO 91	RVUE	
[none 0.00001-0.02]		6 BARBIERI 89b	ASTR	SN 1987A
< 0.040	90	7 JODIDIO 86	ELEC	$\mu$ decay
-0.056 to 0.040	90	7 JODIDIO 86	ELEC	$\mu$ decay

## Gauge &amp; Higgs Boson Particle Listings

## New Heavy Bosons

- <sup>1</sup> ACKERSTAFF 99D limit is from  $\tau$  decay parameters.  
<sup>2</sup> CZAKON 99 perform a simultaneous fit to charged and neutral sectors.  
<sup>3</sup> The quoted limit is from  $\mu$  decay parameters. BARENBOIM 97 also evaluate limit from  $K_L - K_S$  mass difference.  
<sup>4</sup> MISHRA 92 limit is from the absence of extra large- $x$ , large- $y$   $\bar{\nu}_\mu N \rightarrow \bar{\nu}_\mu X$  events at Tevatron, assuming left-handed  $\nu$  and right-handed  $\bar{\nu}$  in the neutrino beam. The result gives  $\zeta^2(1-2m_{W_1}^2/m_{W_2}^2) < 0.0015$ . The limit is independent of  $\nu_{R^1}$  mass.  
<sup>5</sup> AQUINO 91 limits obtained from neutron lifetime and asymmetries together with unitarity of the CKM matrix. Manifest left-right asymmetry is assumed.  
<sup>6</sup> BARBIERI 89B limit holds for  $m_{\nu_R} \leq 10$  MeV.  
<sup>7</sup> First JODIDIO 86 result assumes  $m_{W_R} = \infty$ , second is for unconstrained  $m_{W_R}$ .

- <sup>9</sup> KHACHATRYAN 17W search for resonances decaying to dijets in  $pp$  collisions at  $\sqrt{s} = 13$  TeV.  
<sup>10</sup> AABOUD 16U search for resonances decaying to  $\ell^+ \ell^-$  in  $pp$  collisions at  $\sqrt{s} = 13$  TeV.  
<sup>11</sup> KHACHATRYAN 15AE search for resonances decaying to  $e^+ e^-, \mu^+ \mu^-$  in  $pp$  collisions at  $\sqrt{s} = 8$  TeV.  
<sup>12</sup> KHACHATRYAN 15V search for resonances decaying to dijets in  $pp$  collisions at  $\sqrt{s} = 8$  TeV.  
<sup>13</sup> AAD 14V search for resonances decaying to  $e^+ e^-, \mu^+ \mu^-$  in  $pp$  collisions at  $\sqrt{s} = 8$  TeV.  
<sup>14</sup> BOBOVNIKOV 18 use the ATLAS limits on  $\sigma(pp \rightarrow Z')B(Z' \rightarrow W^+ W^-)$  to constrain the  $Z-Z'$  mixing parameter  $\xi$ . See their Fig. 11 for limits in  $M_{Z'} - \xi$  plane.  
<sup>15</sup> AABOUD 16AA search for resonances decaying to  $\tau^+ \tau^-$  in  $pp$  collisions at  $\sqrt{s} = 13$  TeV.  
<sup>16</sup> AAD 15AM search for resonances decaying to  $\tau^+ \tau^-$  in  $pp$  collisions at  $\sqrt{s} = 8$  TeV.  
<sup>17</sup> AAD 13S search for resonances decaying to  $\tau^+ \tau^-$  in  $pp$  collisions at  $\sqrt{s} = 7$  TeV.  
<sup>18</sup> CHATRCHYAN 13A use  $pp$  collisions at  $\sqrt{s} = 7$  TeV.  
<sup>19</sup> CHATRCHYAN 13AF search for resonances decaying to  $e^+ e^-, \mu^+ \mu^-$  in  $pp$  collisions at  $\sqrt{s} = 7$  TeV and 8 TeV.  
<sup>20</sup> AAD 12CC search for resonances decaying to  $e^+ e^-, \mu^+ \mu^-$  in  $pp$  collisions at  $\sqrt{s} = 7$  TeV.  
<sup>21</sup> CHATRCHYAN 12O search for resonances decaying to  $\tau^+ \tau^-$  in  $pp$  collisions at  $\sqrt{s} = 7$  TeV.  
<sup>22</sup> AALTONEN 11I search for resonances decaying to  $\mu^+ \mu^-$  in  $p\bar{p}$  collisions at  $\sqrt{s} = 1.96$  TeV.  
<sup>23</sup> ABZOV 11A, AALTONEN 09T, AALTONEN 07H, and ABULENCIA 06L search for resonances decaying to  $e^+ e^-$  in  $p\bar{p}$  collisions at  $\sqrt{s} = 1.96$  TeV.  
<sup>24</sup> The quoted limit assumes  $g_{WWZ'}/g_{WWZ} = (M_W/M_{Z'})^2$ . See their Fig. 4 for limits in mass-coupling plane.  
<sup>25</sup> AALTONEN 09AC search for new particle decaying to dijets.  
<sup>26</sup> ERLER 09 give 95% CL limit on the  $Z-Z'$  mixing  $-0.0026 < \theta < 0.0006$ .  
<sup>27</sup> ABDALLAH 06c use data  $\sqrt{s} = 130-207$  GeV.  
<sup>28</sup> ACOSTA 05R search for resonances decaying to tau lepton pairs in  $p\bar{p}$  collisions at  $\sqrt{s} = 1.96$  TeV.  
<sup>29</sup> ABBIENDI 04c give 95% CL limit on  $Z-Z'$  mixing  $-0.00422 < \theta < 0.00091$ .  $\sqrt{s} = 91$  to 207 GeV.  
<sup>30</sup> ABZOV 01B search for resonances in  $p\bar{p} \rightarrow e^+ e^-$  at  $\sqrt{s} = 1.8$  TeV. They find  $\sigma \cdot B(Z' \rightarrow ee) < 0.06$  pb for  $M_{Z'} > 500$  GeV.  
<sup>31</sup> CHEUNG 01B limit is derived from bounds on contact interactions in a global electroweak analysis.  
<sup>32</sup> ABREU 00s uses LEP data at  $\sqrt{s} = 90$  to 189 GeV.  
<sup>33</sup> BARATE 00i search for deviations in cross section and asymmetries in  $e^+ e^- \rightarrow$  fermions at  $\sqrt{s} = 90$  to 183 GeV. Assume  $\theta = 0$ . Bounds in the mass-mixing plane are shown in their Figure 18.  
<sup>34</sup> ERLER 99 give 90%CL limit on the  $Z-Z'$  mixing  $-0.0041 < \theta < 0.0003$ .  $\rho_0 = 1$  is assumed.  
<sup>35</sup> ABE 97s find  $\sigma(Z') \times B(e^+ e^-, \mu^+ \mu^-) < 40$  fb for  $M_{Z'} > 600$  GeV at  $\sqrt{s} = 1.8$  TeV.  
<sup>36</sup> VILAIN 94B assume  $m_t = 150$  GeV.  
<sup>37</sup> ALITTI 93 search for resonances in the two-jet invariant mass. The limit assumes  $B(Z' \rightarrow q\bar{q}) = 0.7$ . See their Fig. 5 for limits in the  $m_{Z'} - B(q\bar{q})$  plane.  
<sup>38</sup> RIZZO 93 analyses CDF limit on possible two-jet resonances.  
<sup>39</sup> ABE 90f use data for  $R, R_{\ell\ell}$ , and  $A_{\ell\ell}$ . They fix  $m_W = 80.49 \pm 0.43 \pm 0.24$  GeV and  $m_Z = 91.13 \pm 0.03$  GeV.

## See the related review(s):

 $Z'$ -Boson SearchesMASS LIMITS for  $Z'$  (Heavy Neutral Vector Boson Other Than  $Z$ )Limits for  $Z'_{SM}$ 

$Z'_{SM}$  is assumed to have couplings with quarks and leptons which are identical to those of  $Z$ , and decays only to known fermions. The most recent preliminary results can be found in the " $Z'$ -boson searches" review above.

VALUE (GeV)	CL%	DOCUMENT ID	TECN	COMMENT
none 250-5100	95	1 AAD	19L ATLS	$pp; Z'_{SM} \rightarrow e^+ e^-, \mu^+ \mu^-$
none 600-2000	95	2 AABOUD	18AB ATLS	$pp; Z'_{SM} \rightarrow b\bar{b}$
>2420	95	3 AABOUD	18G ATLS	$pp; Z'_{SM} \rightarrow \tau^+ \tau^-$
none 200-4500	95	4 SIRUNYAN	18BB CMS	$pp; Z'_{SM} \rightarrow e^+ e^-, \mu^+ \mu^-$
none 600-2700	95	5 SIRUNYAN	18B0 CMS	$pp; Z'_{SM} \rightarrow q\bar{q}$
>4500	95	6 AABOUD	17AT ATLS	$pp; Z'_{SM} \rightarrow e^+ e^-, \mu^+ \mu^-$
>2100	95	7 KHACHATRYAN	17H CMS	$pp; Z'_{SM} \rightarrow \tau^+ \tau^-$
>3370	95	8 KHACHATRYAN	17T CMS	$pp; Z'_{SM} \rightarrow e^+ e^-, \mu^+ \mu^-$
none 600-2100, 2300-2600	95	9 KHACHATRYAN	17W CMS	$pp; Z'_{SM} \rightarrow q\bar{q}$
>3360	95	10 AABOUD	16U ATLS	$pp; Z'_{SM} \rightarrow e^+ e^-, \mu^+ \mu^-$
>2900	95	11 KHACHATRYAN	15AE CMS	$pp; Z'_{SM} \rightarrow e^+ e^-, \mu^+ \mu^-$
none 1200-1700	95	12 KHACHATRYAN	15V CMS	$pp; Z'_{SM} \rightarrow q\bar{q}$
>2900	95	13 AAD	14V ATLS	$pp; Z'_{SM} \rightarrow e^+ e^-, \mu^+ \mu^-$
• • • We do not use the following data for averages, fits, limits, etc. • • •				
>1900	95	14 BOBOVNIKOV	18 RVUE	$pp; Z'_{SM} \rightarrow W^+ W^-$
>2020	95	15 AABOUD	16AA ATLS	$pp; Z'_{SM} \rightarrow \tau^+ \tau^-$
>1400	95	16 AAD	15AM ATLS	$pp; Z'_{SM} \rightarrow \tau^+ \tau^-$
>1470	95	17 AAD	13S ATLS	$pp; Z'_{SM} \rightarrow \tau^+ \tau^-$
>2590	95	18 CHATRCHYAN	13A CMS	$pp; Z'_{SM} \rightarrow q\bar{q}$
>2220	95	19 CHATRCHYAN	13AF CMS	$pp; Z'_{SM} \rightarrow e^+ e^-, \mu^+ \mu^-$
>1400	95	20 AAD	12CC ATLS	$pp; Z'_{SM} \rightarrow e^+ e^-, \mu^+ \mu^-$
>1071	95	21 CHATRCHYAN	12O CMS	$pp; Z'_{SM} \rightarrow \tau^+ \tau^-$
>1023	95	22 AALTONEN	11I CDF	$p\bar{p}; Z'_{SM} \rightarrow \mu^+ \mu^-$
none 247-544	95	23 ABZOV	11A D0	$p\bar{p}; Z'_{SM} \rightarrow e^+ e^-$
none 320-740	95	24 AALTONEN	10N CDF	$Z' \rightarrow WW$
> 963	95	25 AALTONEN	09AC CDF	$Z' \rightarrow q\bar{q}$
>1403	95	26 AALTONEN	09T CDF	$p\bar{p}; Z'_{SM} \rightarrow e^+ e^-$
>1305	95	27 ERLER	09 RVUE	Electroweak
> 399	95	28 ABDALLAH	06C DLPH	$e^+ e^-$
none 400-640	95	29 ACOSTA	05R CDF	$p\bar{p}; Z'_{SM} \rightarrow \tau^+ \tau^-$
>1018	95	30 ABZOV	04C D0	$p\bar{p}; Z'_{SM} \rightarrow q\bar{q}$
> 670	95	31 ABBIENDI	04G OPAL	$e^+ e^-$
>1500	95	32 ABZOV	01B D0	$p\bar{p}; Z'_{SM} \rightarrow e^+ e^-$
> 710	95	33 CHEUNG	01B RVUE	Electroweak
> 898	95	34 ABREU	00s DLPH	$e^+ e^-$
> 809	95	35 BARATE	00i ALEP	$e^+ e^-$
> 690	95	36 ERLER	99 RVUE	Electroweak
> 398	95	37 ABE	97s CDF	$p\bar{p}; Z'_{SM} \rightarrow e^+ e^-, \mu^+ \mu^-$
> 237	90	38 VILAIN	94B CHM2	$\nu_\mu e \rightarrow \nu_\mu e$ and $\bar{\nu}_\mu e \rightarrow \bar{\nu}_\mu e$
none 260-600	95	39 ALITTI	93 UA2	$p\bar{p}; Z'_{SM} \rightarrow q\bar{q}$
> 426	90	40 RIZZO	93 RVUE	$p\bar{p}; Z'_{SM} \rightarrow q\bar{q}$
		41 ABE	90F VNS	$e^+ e^-$

- <sup>1</sup> AAD 19L search for resonances decaying to  $\ell^+ \ell^-$  in  $pp$  collisions at  $\sqrt{s} = 13$  TeV.  
<sup>2</sup> AABOUD 18AB search for resonances decaying to  $b\bar{b}$  in  $pp$  collisions at  $\sqrt{s} = 13$  TeV.  
<sup>3</sup> AABOUD 18G search for resonances decaying to  $\tau^+ \tau^-$  in  $pp$  collisions at  $\sqrt{s} = 13$  TeV.  
<sup>4</sup> SIRUNYAN 18BB search for resonances decaying to  $\ell^+ \ell^-$  in  $pp$  collisions at  $\sqrt{s} = 13$  TeV. See their Fig. 5 for limits on the  $Z'$  coupling strengths with light quarks.  
<sup>5</sup> SIRUNYAN 18B0 search for resonances decaying to dijets in  $pp$  collisions at  $\sqrt{s} = 13$  TeV.  
<sup>6</sup> AABOUD 17AT search for resonances decaying to  $\ell^+ \ell^-$  in  $pp$  collisions at  $\sqrt{s} = 13$  TeV.  
<sup>7</sup> KHACHATRYAN 17H search for resonances decaying to  $\tau^+ \tau^-$  in  $pp$  collisions at  $\sqrt{s} = 13$  TeV.  
<sup>8</sup> KHACHATRYAN 17T search for resonances decaying to  $e^+ e^-, \mu^+ \mu^-$  in  $pp$  collisions at  $\sqrt{s} = 8, 13$  TeV.

Limits for  $Z'_{LR}$ 

$Z'_{LR}$  is the extra neutral boson in left-right symmetric models.  $g_L = g_R$  is assumed unless noted. Values in parentheses assume stronger constraint on the Higgs sector, usually motivated by specific left-right symmetric models (see the Note on the  $W'$ ). Values in brackets are from cosmological and astrophysical considerations and assume a light right-handed neutrino. Direct search bounds assume decays to Standard Model fermions only, unless noted.

VALUE (GeV)	CL%	DOCUMENT ID	TECN	COMMENT
>1162	95	1 DEL-AGUILA	10 RVUE	Electroweak
> 630	95	2 ABE	97s CDF	$p\bar{p}; Z'_{LR} \rightarrow e^+ e^-, \mu^+ \mu^-$
• • • We do not use the following data for averages, fits, limits, etc. • • •				
> 998	95	3 BOBOVNIKOV	18 RVUE	$pp; Z'_{LR} \rightarrow W^+ W^-$
> 600	95	4 ERLER	09 RVUE	Electroweak
> 455	95	5 SCHAEEL	07A ALEP	$e^+ e^-$
> 518	95	6 ABDALLAH	06C DLPH	$e^+ e^-$
> 860	95	7 ABBIENDI	04G OPAL	$e^+ e^-$
> 380	95	8 CHEUNG	01B RVUE	Electroweak
> 436	95	9 ABREU	00s DLPH	$e^+ e^-$
> 550	95	10 BARATE	00i ALEP	Repl. by SCHAEEL 07A
(> 1205)	90	11 CHAY	00 RVUE	Electroweak
> 564	95	12 ERLER	00 RVUE	Cs
(> 1673)	95	13 ERLER	99 RVUE	Electroweak
(> 1700)	68	14 BARENBOIM	98 RVUE	Electroweak
> 244	95	15 CONRAD	98 RVUE	$\nu_\mu N$ scattering
> 253	95	16 VILAIN	94B CHM2	$\nu_\mu e \rightarrow \nu_\mu e$ and $\bar{\nu}_\mu e \rightarrow \bar{\nu}_\mu e$
none 200-600	95	17 RIZZO	93 RVUE	$p\bar{p}; Z'_{LR} \rightarrow q\bar{q}$
[> 2000]		18 WALKER	91 COSM	Nucleosynthesis; light $\nu_R$
none 200-500		19 GRIFOLS	90 ASTR	SN 1987A; light $\nu_R$
none 350-2400		20 BARBIERI	89B ASTR	SN 1987A; light $\nu_R$

- 1 DEL-AGUILA 10 give 95% CL limit on the Z-Z' mixing  $-0.0012 < \theta < 0.0004$ .
- 2 ABE 97s find  $\sigma(Z') \times B(e^+ e^-, \mu^+ \mu^-) < 40 \text{ fb}$  for  $m_{Z'} > 600 \text{ GeV}$  at  $\sqrt{s} = 1.8 \text{ TeV}$ .
- 3 BOBOVNIKOV 18 use the ATLAS limits on  $\sigma(pp \rightarrow Z') \cdot B(Z' \rightarrow W^+ W^-)$  to constrain the Z-Z' mixing parameter  $\xi$ . See their Fig. 10 for limits in  $M_{Z'} - \xi$  plane.
- 4 ERLER 09 give 95% CL limit on the Z-Z' mixing  $-0.0013 < \theta < 0.0006$ .
- 5 ABDALLAH 06c give 95% CL limit  $|\theta| < 0.0028$ . See their Fig. 14 for limit contours in the mass-mixing plane.
- 6 ABBIENDI 04g give 95% CL limit on Z-Z' mixing  $-0.00098 < \theta < 0.00190$ . See their Fig. 20 for the limit contour in the mass-mixing plane.  $\sqrt{s} = 91$  to 207 GeV.
- 7 CHEUNG 01b limit is derived from bounds on contact interactions in a global electroweak analysis.
- 8 ABREU 00s give 95% CL limit on Z-Z' mixing  $|\theta| < 0.0018$ . See their Fig. 6 for the limit contour in the mass-mixing plane.  $\sqrt{s} = 90$  to 189 GeV.
- 9 BARATE 00i search for deviations in cross section and asymmetries in  $e^+ e^- \rightarrow$  fermions at  $\sqrt{s} = 90$  to 183 GeV. Assume  $\theta = 0$ . Bounds in the mass-mixing plane are shown in their Figure 18.
- 10 CHAY 00 also find  $-0.0003 < \theta < 0.0019$ . For  $g_R$  free,  $m_{Z'} > 430 \text{ GeV}$ .
- 11 ERLER 00 discuss the possibility that a discrepancy between the observed and predicted values of  $Q_{WV}(Cs)$  is due to the exchange of Z'. The data are better described in a certain class of the Z' models including  $Z'_{LR}$  and  $Z'_\chi$ .
- 12 CASALBUONI 99 discuss the discrepancy between the observed and predicted values of  $Q_{WV}(Cs)$ . It is shown that the data are better described in a class of models including the  $Z'_{LR}$  model.
- 13 CZAKON 99 perform a simultaneous fit to charged and neutral sectors. Assumes manifest left-right symmetric model. Finds  $|\theta| < 0.0042$ .
- 14 ERLER 99 give 90% CL limit on the Z-Z' mixing  $-0.0009 < \theta < 0.0017$ .
- 15 ERLER 99 assumes 2 Higgs doublets, transforming as 10 of SO(10), embedded in  $E_6$ .
- 16 BARENBOIM 98 also gives 68% CL limits on the Z-Z' mixing  $-0.0005 < \theta < 0.0033$ . Assumes Higgs sector of minimal left-right model.
- 17 CONRAD 98 limit is from measurements at CCFR, assuming no Z-Z' mixing.
- 18 VILAIN 94b assume  $m_t = 150 \text{ GeV}$  and  $\theta = 0$ . See Fig. 2 for limit contours in the mass-mixing plane.
- 19 RIZZO 93 analyses CDF limit on possible two-jet resonances.
- 20 GRIFOLS 90 limit holds for  $m_{\nu_R} \lesssim 1 \text{ MeV}$ . A specific Higgs sector is assumed. See also GRIFOLS 90d, RIZZO 91.
- 21 BARBIERI 89b limit holds for  $m_{\nu_R} \lesssim 10 \text{ MeV}$ . Bounds depend on assumed supernova core temperature.

**Limits for  $Z'_\chi$**

$Z'_\chi$  is the extra neutral boson in  $\text{SU}(5) \times \text{U}(1)_\chi \rightarrow \text{SU}(3) \times \text{U}(1)_Y$ ,  $g_\chi = e/\cos\theta_W$  is assumed unless otherwise stated. We list limits with the assumption  $\rho = 1$  but with no further constraints on the Higgs sector. Values in parentheses assume stronger constraint on the Higgs sector motivated by superstring models. Values in brackets are from cosmological and astrophysical considerations and assume a light right-handed neutrino.

VALUE (GeV)	CL%	DOCUMENT ID	TECN	COMMENT
none 250-4800	95	1 AAD	19L ATLS	$pp; Z'_\chi \rightarrow e^+ e^-, \mu^+ \mu^-$
<b>&gt;4100</b>	95	2 AABOUD	17AT ATLS	$pp; Z'_\chi \rightarrow e^+ e^-, \mu^+ \mu^-$
••• We do not use the following data for averages, fits, limits, etc. •••				
>3050	95	3 BOBOVNIKOV 18	RVUE	$pp, Z'_\chi \rightarrow W^+ W^-$
>2620	95	4 AABOUD	16u ATLS	$pp; Z'_\chi \rightarrow e^+ e^-, \mu^+ \mu^-$
>1970	95	5 AAD	14v ATLS	$pp, Z'_\chi \rightarrow e^+ e^-, \mu^+ \mu^-$
>930	95	6 AAD	12cc ATLS	$pp, Z'_\chi \rightarrow e^+ e^-, \mu^+ \mu^-$
>903	95	7 AALTONEN	11i CDF	$p\bar{p}; Z'_\chi \rightarrow \mu^+ \mu^-$
>903	95	8 ABAZOV	11A D0	$p\bar{p}; Z'_\chi \rightarrow e^+ e^-$
>1022	95	9 DEL-AGUILA	10 RVUE	Electroweak
>862	95	8 AALTONEN	09T CDF	$p\bar{p}; Z'_\chi \rightarrow e^+ e^-$
>892	95	10 AALTONEN	09v CDF	Repl. by AALTONEN 11i
>1141	95	11 ERLER	09 RVUE	Electroweak
>822	95	8 AALTONEN	07H CDF	Repl. by AALTONEN 09T
>680	95	SCHAEEL	07A ALEP	$e^+ e^-$
>545	95	12 ABDALLAH	06c DLPH	$e^+ e^-$
>740	95	8 ABULENCIA	06L CDF	Repl. by AALTONEN 07H
>690	95	13 ABULENCIA	05A CDF	$p\bar{p}; Z'_\chi \rightarrow e^+ e^-, \mu^+ \mu^-$
>781	95	14 ABBIENDI	04g OPAL	$e^+ e^-$
>2100	95	15 BARGER	03b COSM	Nucleosynthesis; light $\nu_R$
>680	95	16 CHEUNG	01b RVUE	Electroweak
>440	95	17 ABREU	00s DLPH	$e^+ e^-$
>533	95	18 BARATE	00i ALEP	Repl. by SCHAEEL 07A
>554	95	19 CHO	00 RVUE	Electroweak
		20 ERLER	00 RVUE	Cs
		21 ROSNER	00 RVUE	Cs
>545	95	22 ERLER	99 RVUE	Electroweak
(> 1368)	95	23 ERLER	99 RVUE	Electroweak
>215	95	24 CONRAD	98 RVUE	$\nu_\mu N$ scattering
>595	95	25 ABE	97s CDF	$p\bar{p}; Z'_\chi \rightarrow e^+ e^-, \mu^+ \mu^-$
>190	95	26 ARIMA	97 VNS	Bhabha scattering
>262	95	27 VILAIN	94b CHM2	$\nu_\mu e \rightarrow \nu_\mu e; \bar{\nu}_\mu e \rightarrow \bar{\nu}_\mu e$
[>1470]		28 FARAGGI	91 COSM	Nucleosynthesis; light $\nu_R$
>231	90	29 ABE	90F VNS	$e^+ e^-$
[> 1140]		30 GONZALEZ...	90d COSM	Nucleosynthesis; light $\nu_R$
[> 2100]		31 GRIFOLS	90 ASTR	SN 1987A; light $\nu_R$

- 1 AAD 19L search for resonances decaying to  $\ell^+ \ell^-$  in  $pp$  collisions at  $\sqrt{s} = 13 \text{ TeV}$ .
- 2 AABOUD 17AT search for resonances decaying to  $\ell^+ \ell^-$  in  $pp$  collisions at  $\sqrt{s} = 13 \text{ TeV}$ .
- 3 BOBOVNIKOV 18 use the ATLAS limits on  $\sigma(pp \rightarrow Z') \cdot B(Z' \rightarrow W^+ W^-)$  to constrain the Z-Z' mixing parameter  $\xi$ . See their Fig. 9 for limits in  $M_{Z'} - \xi$  plane.
- 4 AABOUD 16u search for resonances decaying to  $\ell^+ \ell^-$  in  $pp$  collisions at  $\sqrt{s} = 13 \text{ TeV}$ .
- 5 AAD 14v search for resonances decaying to  $e^+ e^-, \mu^+ \mu^-$  in  $pp$  collisions at  $\sqrt{s} = 8 \text{ TeV}$ .
- 6 AAD 12cc search for resonances decaying to  $e^+ e^-, \mu^+ \mu^-$  in  $pp$  collisions at  $\sqrt{s} = 7 \text{ TeV}$ .
- 7 AALTONEN 11i search for resonances decaying to  $\mu^+ \mu^-$  in  $p\bar{p}$  collisions at  $\sqrt{s} = 1.96 \text{ TeV}$ .
- 8 ABIZONI 11A, AALTONEN 09T, AALTONEN 07H, and ABULENCIA 06L search for resonances decaying to  $e^+ e^-$  in  $p\bar{p}$  collisions at  $\sqrt{s} = 1.96 \text{ TeV}$ .
- 9 DEL-AGUILA 10 give 95% CL limit on the Z-Z' mixing  $-0.0011 < \theta < 0.0007$ .
- 10 AALTONEN 09v search for resonances decaying to  $\mu^+ \mu^-$  in  $p\bar{p}$  collisions at  $\sqrt{s} = 1.96 \text{ TeV}$ .
- 11 ERLER 09 give 95% CL limit on the Z-Z' mixing  $-0.0016 < \theta < 0.0006$ .
- 12 ABDALLAH 06c give 95% CL limit  $|\theta| < 0.0031$ . See their Fig. 14 for limit contours in the mass-mixing plane.
- 13 ABULENCIA 05A search for resonances decaying to electron or muon pairs in  $p\bar{p}$  collisions at  $\sqrt{s} = 1.96 \text{ TeV}$ .
- 14 ABBIENDI 04g give 95% CL limit on Z-Z' mixing  $-0.00099 < \theta < 0.00194$ . See their Fig. 20 for the limit contour in the mass-mixing plane.  $\sqrt{s} = 91$  to 207 GeV.
- 15 BARGER 03b limit is from the nucleosynthesis bound on the effective number of light neutrino  $\delta N_\nu < 1$ . The quark-hadron transition temperature  $T_C = 150 \text{ MeV}$  is assumed. The limit with  $T_C = 400 \text{ MeV}$  is  $>4300 \text{ GeV}$ .
- 16 CHEUNG 01b limit is derived from bounds on contact interactions in a global electroweak analysis.
- 17 ABREU 00s give 95% CL limit on Z-Z' mixing  $|\theta| < 0.0017$ . See their Fig. 6 for the limit contour in the mass-mixing plane.  $\sqrt{s} = 90$  to 189 GeV.
- 18 BARATE 00i search for deviations in cross section and asymmetries in  $e^+ e^- \rightarrow$  fermions at  $\sqrt{s} = 90$  to 183 GeV. Assume  $\theta = 0$ . Bounds in the mass-mixing plane are shown in their Figure 18.
- 19 CHO 00 use various electroweak data to constrain Z' models assuming  $m_H = 100 \text{ GeV}$ . See Fig. 3 for limits in the mass-mixing plane.
- 20 ERLER 00 discuss the possibility that a discrepancy between the observed and predicted values of  $Q_{WV}(Cs)$  is due to the exchange of Z'. The data are better described in a certain class of the Z' models including  $Z'_{LR}$  and  $Z'_\chi$ .
- 21 ROSNER 00 discusses the possibility that a discrepancy between the observed and predicted values of  $Q_{WV}(Cs)$  is due to the exchange of Z'. The data are better described in a certain class of the Z' models including  $Z'_\chi$ .
- 22 ERLER 99 give 90% CL limit on the Z-Z' mixing  $-0.0020 < \theta < 0.0015$ .
- 23 ERLER 99 assumes 2 Higgs doublets, transforming as 10 of SO(10), embedded in  $E_6$ .
- 24 CONRAD 98 limit is from measurements at CCFR, assuming no Z-Z' mixing.
- 25 ABE 97s find  $\sigma(Z') \times B(e^+ e^-, \mu^+ \mu^-) < 40 \text{ fb}$  for  $m_{Z'} > 600 \text{ GeV}$  at  $\sqrt{s} = 1.8 \text{ TeV}$ .
- 26 Z-Z' mixing is assumed to be zero.  $\sqrt{s} = 57.77 \text{ GeV}$ .
- 27 VILAIN 94b assume  $m_t = 150 \text{ GeV}$  and  $\theta = 0$ . See Fig. 2 for limit contours in the mass-mixing plane.
- 28 FARAGGI 91 limit assumes the nucleosynthesis bound on the effective number of neutrinos  $\Delta N_\nu < 0.5$  and is valid for  $m_{\nu_R} < 1 \text{ MeV}$ .
- 29 ABE 90f use data for  $R, R_{\ell\ell}$ , and  $A_{\ell\ell}$ . ABE 90f fix  $m_W = 80.49 \pm 0.43 \pm 0.24 \text{ GeV}$  and  $m_Z = 91.13 \pm 0.03 \text{ GeV}$ .
- 30 Assumes the nucleosynthesis bound on the effective number of light neutrinos ( $\delta N_\nu < 1$ ) and that  $\nu_R$  is light ( $\lesssim 1 \text{ MeV}$ ).
- 31 GRIFOLS 90 limit holds for  $m_{\nu_R} \lesssim 1 \text{ MeV}$ . See also GRIFOLS 90d, RIZZO 91.

**Limits for  $Z'_\psi$**

$Z'_\psi$  is the extra neutral boson in  $E_6 \rightarrow \text{SO}(10) \times \text{U}(1)_\psi$ ,  $g_\psi = e/\cos\theta_W$  is assumed unless otherwise stated. We list limits with the assumption  $\rho = 1$  but with no further constraints on the Higgs sector. Values in brackets are from cosmological and astrophysical considerations and assume a light right-handed neutrino.

VALUE (GeV)	CL%	DOCUMENT ID	TECN	COMMENT
<b>&gt;3900 (CL = 95%) OUR LIMIT</b>				
none 250-4500	95	1 AAD	19L ATLS	$pp; Z'_\psi \rightarrow e^+ e^-, \mu^+ \mu^-$
<b>none 200-3900</b>	95	2 SIRUNYAN	18BB CMS	$pp; Z'_\psi \rightarrow e^+ e^-, \mu^+ \mu^-$
>3800	95	3 AABOUD	17AT ATLS	$pp; Z'_\psi \rightarrow e^+ e^-, \mu^+ \mu^-$
>2820	95	4 KHACHATRY...17T	CMS	$pp; Z'_\psi \rightarrow e^+ e^-, \mu^+ \mu^-$
>1100	95	5 CHATRCHYAN 12o	CMS	$pp, Z'_\psi \rightarrow \tau^+ \tau^-$
••• We do not use the following data for averages, fits, limits, etc. •••				
>2740	95	6 BOBOVNIKOV 18	RVUE	$pp, Z'_\psi \rightarrow W^+ W^-$
>2570	95	7 AABOUD	16u ATLS	$pp; Z'_\psi \rightarrow e^+ e^-, \mu^+ \mu^-$
>2510	95	8 KHACHATRY...15AE	CMS	$pp; Z'_\psi \rightarrow e^+ e^-, \mu^+ \mu^-$
>2510	95	9 AAD	14v ATLS	$pp, Z'_\psi \rightarrow e^+ e^-, \mu^+ \mu^-$
>2260	95	10 CHATRCHYAN 13AF	CMS	$pp, Z'_\psi \rightarrow e^+ e^-, \mu^+ \mu^-$
>1790	95	11 AAD	12cc ATLS	$pp, Z'_\psi \rightarrow e^+ e^-, \mu^+ \mu^-$
>2000	95	12 CHATRCHYAN 12M	CMS	Repl. by CHATRCHYAN 13AF
>917	95	13 AALTONEN	11i CDF	$p\bar{p}; Z'_\psi \rightarrow \mu^+ \mu^-$
>891	95	14 ABAZOV	11A D0	$p\bar{p}; Z'_\psi \rightarrow e^+ e^-$
>476	95	15 DEL-AGUILA	10 RVUE	Electroweak
>851	95	14 AALTONEN	09T CDF	$p\bar{p}; Z'_\psi \rightarrow e^+ e^-$
>878	95	16 AALTONEN	09v CDF	Repl. by AALTONEN 11i
>147	95	17 ERLER	09 RVUE	Electroweak



# Gauge & Higgs Boson Particle Listings

## New Heavy Bosons

> 822	95	14	AALTONEN	07H	CDF	Repl. by AALTONEN 09T
> 410	95		SCHAEEL	07A	ALEP	$e^+e^-$
> 475	95		ABDALLAH	06C	DLPH	$e^+e^-$
> 725		14	ABULENCIA	06L	CDF	Repl. by AALTONEN 07H
> 675	95	19	ABULENCIA	05A	CDF	Repl. by AALTONEN 11i and AALTONEN 09T
> 366	95	20	ABBIENDI	04G	OPAL	$e^+e^-$
> 600		21	BARGER	03B	COSM	Nucleosynthesis; light $\nu_R$
> 350	95	22	ABREU	00S	DLPH	$e^+e^-$
> 294	95	23	BARATE	00i	ALEP	Repl. by SCHAEEL 07A
> 137	95	24	CHO	00	RVUE	Electroweak
> 146	95	25	ERLER	99	RVUE	Electroweak
> 54	95	26	CONRAD	98	RVUE	$\nu_\mu N$ scattering
> 590	95	27	ABE	97S	CDF	$p\bar{p}; Z'_\psi \rightarrow e^+e^-, \mu^+\mu^-$
> 135	95	28	VILAIN	94B	CHM2	$\nu_\mu e \rightarrow \nu_\mu e; \bar{\nu}_\mu e \rightarrow \bar{\nu}_\mu e$
> 105	90	29	ABE	90F	VNS	$e^+e^-$
[> 160]		30	GONZALEZ...	90D	COSM	Nucleosynthesis; light $\nu_R$
[> 2000]		31	GRIFOLS	90D	ASTR	SN 1987A; light $\nu_R$

- AAD 19L search for resonances decaying to  $\ell^+\ell^-$  in  $pp$  collisions at  $\sqrt{s} = 13$  TeV.
- SIRUNYAN 18BB search for resonances decaying to  $\ell^+\ell^-$  in  $pp$  collisions at  $\sqrt{s} = 13$  TeV.
- AABOUD 17AT search for resonances decaying to  $\ell^+\ell^-$  in  $pp$  collisions at  $\sqrt{s} = 13$  TeV.
- KHACHATRYAN 17T search for resonances decaying to  $e^+e^-, \mu^+\mu^-$  in  $pp$  collisions at  $\sqrt{s} = 8, 13$  TeV.
- CHATRCHYAN 12O search for resonances decaying to  $\tau^+\tau^-$  in  $pp$  collisions at  $\sqrt{s} = 7$  TeV.
- BOBOVNIKOV 18 use the ATLAS limits on  $\sigma(pp \rightarrow Z')B(Z' \rightarrow W^+W^-)$  to constrain the  $Z$ - $Z'$  mixing parameter  $\xi$ . See their Fig. 10 for limits in  $M_{Z'}-\xi$  plane.
- AABOUD 16U search for resonances decaying to  $\ell^+\ell^-$  in  $pp$  collisions at  $\sqrt{s} = 13$  TeV.
- KHACHATRYAN 15AE search for resonances decaying to  $e^+e^-, \mu^+\mu^-$  in  $pp$  collisions at  $\sqrt{s} = 8$  TeV.
- AAD 14V search for resonances decaying to  $e^+e^-, \mu^+\mu^-$  in  $pp$  collisions at  $\sqrt{s} = 8$  TeV.
- CHATRCHYAN 13AF search for resonances decaying to  $e^+e^-, \mu^+\mu^-$  in  $pp$  collisions at  $\sqrt{s} = 7$  TeV and 8 TeV.
- AAD 12CC search for resonances decaying to  $e^+e^-, \mu^+\mu^-$  in  $pp$  collisions at  $\sqrt{s} = 7$  TeV.
- CHATRCHYAN 12M search for resonances decaying to  $e^+e^-$  or  $\mu^+\mu^-$  in  $pp$  collisions at  $\sqrt{s} = 7$  TeV.
- AALTONEN 11i search for resonances decaying to  $\mu^+\mu^-$  in  $p\bar{p}$  collisions at  $\sqrt{s} = 1.96$  TeV.
- ABAZOV 11A, AALTONEN 09T, AALTONEN 07H, and ABULENCIA 06L search for resonances decaying to  $e^+e^-$  in  $p\bar{p}$  collisions at  $\sqrt{s} = 1.96$  TeV.
- DEL-AGUILA 10 give 95% CL limit on the  $Z$ - $Z'$  mixing  $-0.0019 < \theta < 0.0007$ .
- AALTONEN 09V search for resonances decaying to  $\mu^+\mu^-$  in  $p\bar{p}$  collisions at  $\sqrt{s} = 1.96$  TeV.
- ERLER 09 give 95% CL limit on the  $Z$ - $Z'$  mixing  $-0.0018 < \theta < 0.0009$ .
- ABDALLAH 06C give 95% CL limit  $|\theta| < 0.0027$ . See their Fig. 14 for limit contours in the mass-mixing plane.
- ABULENCIA 05A search for resonances decaying to electron or muon pairs in  $p\bar{p}$  collisions at  $\sqrt{s} = 1.96$  TeV.
- ABBIENDI 04G give 95% CL limit on  $Z$ - $Z'$  mixing  $-0.00129 < \theta < 0.00258$ . See their Fig. 20 for the limit contour in the mass-mixing plane.  $\sqrt{s} = 91$  to 207 GeV.
- BARGER 03B limit is from the nucleosynthesis bound on the effective number of light neutrino  $\delta N_\nu < 1$ . The quark-hadron transition temperature  $T_C = 150$  MeV is assumed. The limit with  $T_C = 400$  MeV is  $> 1100$  GeV.
- ABREU 00S give 95% CL limit on  $Z$ - $Z'$  mixing  $|\theta| < 0.0018$ . See their Fig. 6 for the limit contour in the mass-mixing plane.  $\sqrt{s} = 90$  to 189 GeV.
- BARATE 00i search for deviations in cross section and asymmetries in  $e^+e^- \rightarrow$  fermions at  $\sqrt{s} = 90$  to 183 GeV. Assume  $\theta = 0$ . Bounds in the mass-mixing plane are shown in their Figure 18.
- CHO 00 use various electroweak data to constrain  $Z'$  models assuming  $m_H = 100$  GeV. See Fig. 3 for limits in the mass-mixing plane.
- ERLER 99 give 90% CL limit on the  $Z$ - $Z'$  mixing  $-0.0013 < \theta < 0.0024$ .
- CONRAD 98 limit is from measurements at CCFR, assuming no  $Z$ - $Z'$  mixing.
- ABE 97S find  $\sigma(Z') \times B(e^+e^-, \mu^+\mu^-) < 40$  fb for  $m_{Z'} > 600$  GeV at  $\sqrt{s} = 1.8$  TeV.
- VILAIN 94B assume  $m_t = 150$  GeV and  $\theta = 0$ . See Fig. 2 for limit contours in the mass-mixing plane.
- ABE 90F use data for  $R, R_{\ell\ell}$ , and  $A_{\ell\ell}$ . ABE 90F fix  $m_W = 80.49 \pm 0.43 \pm 0.24$  GeV and  $m_Z = 91.13 \pm 0.03$  GeV.
- Assumes the nucleosynthesis bound on the effective number of light neutrinos ( $\delta N_\nu < 1$ ) and that  $\nu_R$  is light ( $\lesssim 1$  MeV).
- GRIFOLS 90D limit holds for  $m_{\nu_R} \lesssim 1$  MeV. See also RIZZO 91.

### Limits for $Z_\eta$

$Z_\eta$  is the extra neutral boson in  $E_6$  models, corresponding to  $Q_\eta = \sqrt{3/8} Q_X - \sqrt{5/8} Q_\psi$ .  $g_\eta = e/\cos\theta_W$  is assumed unless otherwise stated. We list limits with the assumption  $\rho = 1$  but with no further constraints on the Higgs sector. Values in parentheses assume stronger constraint on the Higgs sector motivated by superstring models. Values in brackets are from cosmological and astrophysical considerations and assume a light right-handed neutrino.

VALUE (GeV)	CL%	DOCUMENT ID	TECN	COMMENT
>3900	95	1 AABOUD	17AT ATLS	$p\bar{p}; Z'_\eta \rightarrow e^+e^-, \mu^+\mu^-$

• • • We do not use the following data for averages, fits, limits, etc. • • •

>2810	95	2	BOBOVNIKOV	18	RVUE	$p\bar{p}; Z'_\eta \rightarrow W^+W^-$
>1870	95	3	AABOUD	16U	ATLS	$p\bar{p}; Z'_\eta \rightarrow e^+e^-, \mu^+\mu^-$
> 938	95	4	AAD	12CC	ATLS	$p\bar{p}; Z'_\eta \rightarrow e^+e^-, \mu^+\mu^-$
> 923	95	5	AALTONEN	11i	CDF	$p\bar{p}; Z'_\eta \rightarrow \mu^+\mu^-$
> 488	95	6	ABAZOV	11A	D0	$p\bar{p}; Z'_\eta \rightarrow e^+e^-$
> 877	95	7	DEL-AGUILA	10	RVUE	Electroweak
> 904	95	8	AALTONEN	09T	CDF	$p\bar{p}; Z'_\eta \rightarrow e^+e^-$
> 427	95	9	ERLER	09	RVUE	Electroweak
> 891	95	10	AALTONEN	07H	CDF	Repl. by AALTONEN 11i
> 350	95	11	SCHAEEL	07A	ALEP	$e^+e^-$
> 360	95	12	ABDALLAH	06C	DLPH	$e^+e^-$
> 745	95	13	ABULENCIA	06L	CDF	Repl. by AALTONEN 07H
> 720	95	14	ABULENCIA	05A	CDF	Repl. by AALTONEN 11i and AALTONEN 09T
> 515	95	15	ABBIENDI	04G	OPAL	$e^+e^-$
>1600		16	BARGER	03B	COSM	Nucleosynthesis; light $\nu_R$
> 310	95	17	ABREU	00S	DLPH	$e^+e^-$
> 329	95	18	BARATE	00i	ALEP	Repl. by SCHAEEL 07A
> 619	95	19	CHO	00	RVUE	Electroweak
> 365	95	20	ERLER	99	RVUE	Electroweak
> 87	95	21	CONRAD	98	RVUE	$\nu_\mu N$ scattering
> 620	95	22	ABE	97S	CDF	$p\bar{p}; Z'_\eta \rightarrow e^+e^-, \mu^+\mu^-$
> 100	95	23	VILAIN	94B	CHM2	$\nu_\mu e \rightarrow \nu_\mu e; \bar{\nu}_\mu e \rightarrow \bar{\nu}_\mu e$
> 125	90	24	ABE	90F	VNS	$e^+e^-$
[> 820]		25	GONZALEZ...	90D	COSM	Nucleosynthesis; light $\nu_R$
[> 3300]		26	GRIFOLS	90	ASTR	SN 1987A; light $\nu_R$
[> 1040]		27	LOPEZ	90	COSM	Nucleosynthesis; light $\nu_R$

- AABOUD 17AT search for resonances decaying to  $\ell^+\ell^-$  in  $pp$  collisions at  $\sqrt{s} = 13$  TeV.
- BOBOVNIKOV 18 use the ATLAS limits on  $\sigma(pp \rightarrow Z')B(Z' \rightarrow W^+W^-)$  to constrain the  $Z$ - $Z'$  mixing parameter  $\xi$ . See their Fig. 9 for limits in  $M_{Z'}-\xi$  plane.
- AABOUD 16U search for resonances decaying to  $\ell^+\ell^-$  in  $pp$  collisions at  $\sqrt{s} = 13$  TeV.
- AAD 12CC search for resonances decaying to  $e^+e^-, \mu^+\mu^-$  in  $pp$  collisions at  $\sqrt{s} = 7$  TeV.
- AALTONEN 11i search for resonances decaying to  $\mu^+\mu^-$  in  $p\bar{p}$  collisions at  $\sqrt{s} = 1.96$  TeV.
- ABAZOV 11A, AALTONEN 09T, AALTONEN 07H, and ABULENCIA 06L search for resonances decaying to  $e^+e^-$  in  $p\bar{p}$  collisions at  $\sqrt{s} = 1.96$  TeV.
- DEL-AGUILA 10 give 95% CL limit on the  $Z$ - $Z'$  mixing  $-0.0023 < \theta < 0.0027$ .
- AALTONEN 09V search for resonances decaying to  $\mu^+\mu^-$  in  $p\bar{p}$  collisions at  $\sqrt{s} = 1.96$  TeV.
- ERLER 09 give 95% CL limit on the  $Z$ - $Z'$  mixing  $-0.0047 < \theta < 0.0021$ .
- ABDALLAH 06C give 95% CL limit  $|\theta| < 0.0092$ . See their Fig. 14 for limit contours in the mass-mixing plane.
- ABULENCIA 05A search for resonances decaying to electron or muon pairs in  $p\bar{p}$  collisions at  $\sqrt{s} = 1.96$  TeV.
- ABBIENDI 04G give 95% CL limit on  $Z$ - $Z'$  mixing  $-0.00447 < \theta < 0.00331$ . See their Fig. 20 for the limit contour in the mass-mixing plane.  $\sqrt{s} = 91$  to 207 GeV.
- BARGER 03B limit is from the nucleosynthesis bound on the effective number of light neutrino  $\delta N_\nu < 1$ . The quark-hadron transition temperature  $T_C = 150$  MeV is assumed. The limit with  $T_C = 400$  MeV is  $> 3300$  GeV.
- ABREU 00S give 95% CL limit on  $Z$ - $Z'$  mixing  $|\theta| < 0.0024$ . See their Fig. 6 for the limit contour in the mass-mixing plane.  $\sqrt{s} = 90$  to 189 GeV.
- BARATE 00i search for deviations in cross section and asymmetries in  $e^+e^- \rightarrow$  fermions at  $\sqrt{s} = 90$  to 183 GeV. Assume  $\theta = 0$ . Bounds in the mass-mixing plane are shown in their Figure 18.
- CHO 00 use various electroweak data to constrain  $Z'$  models assuming  $m_H = 100$  GeV. See Fig. 3 for limits in the mass-mixing plane.
- ERLER 99 give 90% CL limit on the  $Z$ - $Z'$  mixing  $-0.0062 < \theta < 0.0011$ .
- CONRAD 98 limit is from measurements at CCFR, assuming no  $Z$ - $Z'$  mixing.
- ABE 97S find  $\sigma(Z') \times B(e^+e^-, \mu^+\mu^-) < 40$  fb for  $m_{Z'} > 600$  GeV at  $\sqrt{s} = 1.8$  TeV.
- VILAIN 94B assume  $m_t = 150$  GeV and  $\theta = 0$ . See Fig. 2 for limit contours in the mass-mixing plane.
- ABE 90F use data for  $R, R_{\ell\ell}$ , and  $A_{\ell\ell}$ . ABE 90F fix  $m_W = 80.49 \pm 0.43 \pm 0.24$  GeV and  $m_Z = 91.13 \pm 0.03$  GeV.
- These authors claim that the nucleosynthesis bound on the effective number of light neutrinos ( $\delta N_\nu < 1$ ) constrains  $Z'$  masses if  $\nu_R$  is light ( $\lesssim 1$  MeV).
- GRIFOLS 90 limit holds for  $m_{\nu_R} \lesssim 1$  MeV. See also GRIFOLS 90D, RIZZO 91.

### Limits for other $Z'$

VALUE (GeV)	CL%	DOCUMENT ID	TECN	COMMENT
none 580-3100	95	1 AABOUD	19AS ATLS	$Z' \rightarrow t\bar{t}$
none 1300-3100	95	2 AAD	19D ATLS	$Z' \rightarrow WW$
>3800	95	3 SIRUNYAN	19AA CMS	$Z' \rightarrow t\bar{t}$
>3700	95	4 SIRUNYAN	19CP CMS	$Z' \rightarrow WW, HZ, \ell^+\ell^-$
>1800	95	5 SIRUNYAN	19I CMS	$Z' \rightarrow HZ$
none 600-2100	95	6 AABOUD	18AB ATLS	$Z' \rightarrow b\bar{b}$
none 500-2830	95	7 AABOUD	18AI ATLS	$Z' \rightarrow HZ$
none 300-3000	95	8 AABOUD	18AK ATLS	$Z' \rightarrow WW$
>1300	95	9 AABOUD	18B ATLS	$Z' \rightarrow WW$
none 400-3000	95	10 AABOUD	18BI ATLS	$Z' \rightarrow t\bar{t}$
none 1200-2800	95	11 AABOUD	18F ATLS	$Z' \rightarrow WW$
>2300	95	12 SIRUNYAN	18ED CMS	$Z' \rightarrow HZ$

See key on page 999

Gauge & Higgs Boson Particle Listings  
New Heavy Bosons

none 1200–2700	95	13	SIRUNYAN	18P	CMS	$Z' \rightarrow WW$
>2900	95	14	AABOUD	17AK	ATLS	$Z' \rightarrow q\bar{q}$
none 1100–2600	95	15	AABOUD	17AO	ATLS	$Z' \rightarrow HZ$
>2300	95	16	SIRUNYAN	17AK	CMS	$Z' \rightarrow WW, HZ$
>2500	95	17	SIRUNYAN	17Q	CMS	$Z' \rightarrow t\bar{t}$
>1190	95	18	SIRUNYAN	17R	CMS	$Z' \rightarrow HZ$
none 1210–2260	95	18	SIRUNYAN	17R	CMS	$Z' \rightarrow HZ$
•••						We do not use the following data for averages, fits, limits, etc. •••
		19	AABOUD	19AJ	ATLS	$Z' \rightarrow q\bar{q}$
		20	AABOUD	19D	ATLS	$Z' \rightarrow q\bar{q}$
		21	AABOUD	19V	ATLS	DM simplified $Z'$
		22	AAD	19L	ATLS	$Z' \rightarrow e^+e^-, \mu^+\mu^-$
		23	LONG	19	RVUE	Electroweak
		24	PANDEY	19	RVUE	neutrino NSI
		25	SIRUNYAN	19AL	CMS	$Z' \rightarrow tT, T \rightarrow Ht, Zt, Wb$
		26	SIRUNYAN	19AN	CMS	DM simplified $Z'$
		27	SIRUNYAN	19CB	CMS	$Z' \rightarrow q\bar{q}$
		28	SIRUNYAN	19CD	CMS	$Z' \rightarrow q\bar{q}$
		29	SIRUNYAN	19D	CMS	$Z' \rightarrow H\gamma$
		30	AABOUD	18AA	ATLS	$Z' \rightarrow H\gamma$
>4500	95	31	AABOUD	18CJ	ATLS	$Z' \rightarrow WW, HZ, \ell^+\ell^-$
		32	AABOUD	18N	ATLS	$Z' \rightarrow q\bar{q}$
		33	AAIJ	18AQ	LHCB	$Z' \rightarrow \mu^+\mu^-$
		34	SIRUNYAN	18DR	CMS	$Z' \rightarrow \mu^+\mu^-$
		35	SIRUNYAN	18G	CMS	$Z' \rightarrow q\bar{q}$
		36	SIRUNYAN	18I	CMS	$Z' \rightarrow b\bar{b}$
>1580	95	37	AABOUD	17B	ATLS	$Z' \rightarrow HZ$
		38	KHACHATRY...	17AX	CMS	$Z' \rightarrow \ell\ell\ell$
		39	KHACHATRY...	17U	CMS	$Z' \rightarrow HZ$
>1700	95	40	SIRUNYAN	17A	CMS	$Z' \rightarrow WW$
		41	SIRUNYAN	17AP	CMS	$Z' \rightarrow HA$
		42	SIRUNYAN	17T	CMS	$Z' \rightarrow q\bar{q}$
		43	SIRUNYAN	17V	CMS	$Z' \rightarrow Tt$
none 1100–1500	95	44	AABOUD	16	ATLS	$Z' \rightarrow b\bar{b}$
		45	AAD	16L	ATLS	$Z' \rightarrow a\gamma, a \rightarrow \gamma\gamma$
none 1500–2600	95	46	AAD	16S	ATLS	$Z' \rightarrow q\bar{q}$
none 1000–1100, none 1300–1500	95	47	KHACHATRY...	16AP	CMS	$Z' \rightarrow HZ$
>2400	95	48	KHACHATRY...	16E	CMS	$Z' \rightarrow t\bar{t}$
		49	AAD	15AO	ATLS	$Z' \rightarrow t\bar{t}$
		50	AAD	15AT	ATLS	monotop
		51	AAD	15CD	ATLS	$H \rightarrow ZZ', Z'Z'; Z' \rightarrow \ell^+\ell^-$
		52	KHACHATRY...	15F	CMS	monotop
		53	KHACHATRY...	15O	CMS	$Z' \rightarrow HZ$
		54	AAD	14AT	ATLS	$Z' \rightarrow Z\gamma$
		55	KHACHATRY...	14A	CMS	$Z' \rightarrow VV$
		56	MARTINEZ	14	RVUE	Electroweak
none 500–1740	95	57	AAD	13AQ	ATLS	$Z' \rightarrow t\bar{t}$
>1320 or 1000–1280	95	58	AAD	13G	ATLS	$Z' \rightarrow t\bar{t}$
> 915	95	58	AALTONEN	13A	CDF	$Z' \rightarrow t\bar{t}$
>1300	95	59	CHATRCHYAN	13AP	CMS	$Z' \rightarrow t\bar{t}$
>2100	95	58	CHATRCHYAN	13BM	CMS	$Z' \rightarrow t\bar{t}$
		60	AAD	12BV	ATLS	$Z' \rightarrow t\bar{t}$
		61	AAD	12K	ATLS	$Z' \rightarrow t\bar{t}$
		62	AALTONEN	12AR	CDF	Chromophilic
		63	AALTONEN	12N	CDF	$Z' \rightarrow \bar{t}u$
> 835	95	64	ABAZOV	12R	D0	$Z' \rightarrow t\bar{t}$
		65	CHATRCHYAN	12AI	CMS	$Z' \rightarrow t\bar{t}$
		66	CHATRCHYAN	12AQ	CMS	$Z' \rightarrow t\bar{t}$
>1490	95	58	CHATRCHYAN	12BL	CMS	$Z' \rightarrow t\bar{t}$
		67	AALTONEN	11AD	CDF	$Z' \rightarrow t\bar{t}$
		68	AALTONEN	11AE	CDF	$Z' \rightarrow t\bar{t}$
		69	CHATRCHYAN	11O	CMS	$pp \rightarrow tt$
		70	AALTONEN	08D	CDF	$Z' \rightarrow t\bar{t}$
		70	AALTONEN	08Y	CDF	$Z' \rightarrow t\bar{t}$
		70	ABAZOV	08AA	D0	$Z' \rightarrow t\bar{t}$
		71	ABAZOV	04A	D0	Repl. by ABAZOV 08AA
		72	BARGER	03B	COSM	Nucleosynthesis; light $\nu_R$
		73	CHO	00	RVUE	$E_6$ -motivated
		74	CHO	98	RVUE	$E_6$ -motivated
		75	ABE	97G	CDF	$Z' \rightarrow q\bar{q}$

<sup>1</sup> AABOUD 19As search for a resonance decaying to  $t\bar{t}$  in  $pp$  collisions at  $\sqrt{s} = 13$  TeV. The quoted limit is for a top-color  $Z'$  with  $\Gamma_{Z'}/M_{Z'} = 0.01$ . Limits are also set on  $Z'$  masses in simplified Dark Matter models.

<sup>2</sup> AAD 19D search for resonances decaying to  $WW$  in  $pp$  collisions at  $\sqrt{s} = 13$  TeV. The quoted limit is for heavy-vector-triplet  $Z'$  with  $g_V = 3$ . The limit becomes  $M_{Z'} > 2900$  GeV for  $g_V = 1$ . If we assume  $M_{Z'} = M_{W'}$ , the limit increases  $M_{Z'} > 3800$  GeV and  $M_{Z'} > 3500$  GeV for  $g_V = 3$  and  $g_V = 1$ , respectively. See their Fig. 9 for limits on  $\sigma \cdot B$ .

<sup>3</sup> SIRUNYAN 19AA search for a resonance decaying to  $t\bar{t}$  in  $pp$  collisions at  $\sqrt{s} = 13$  TeV. The quoted limit is for a leptophobic top-color  $Z'$  with  $\Gamma_{Z'}/M_{Z'} = 0.01$ .

<sup>4</sup> SIRUNYAN 19CP present a statistical combinations of searches for  $Z'$  decaying to pairs of bosons or leptons in  $pp$  collisions at  $\sqrt{s} = 13$  TeV. The quoted limit is for heavy-vector-triplet  $Z'$  with  $g_V = 3$ . If we assume  $M_{Z'} = M_{W'}$ , the limit becomes  $M_{Z'} > 4500$  GeV for  $g_V = 3$  and  $M_{Z'} > 5000$  GeV for  $g_V = 1$ . See their Figs. 2 and 3 for limits on  $\sigma \cdot B$ .

<sup>5</sup> SIRUNYAN 19I search for resonances decaying to  $ZW$  in  $pp$  collisions at  $\sqrt{s} = 13$  TeV. The quoted limit is for heavy-vector-triplet  $Z'$  with  $g_V = 3$ . The limit becomes  $M_{Z'} > 2800$  GeV if we assume  $M_{Z'} = M_{W'}$ .

<sup>6</sup> AABOUD 18AB search for resonances decaying to  $b\bar{b}$  in  $pp$  collisions at  $\sqrt{s} = 13$  TeV. The limit quoted above is for a leptophobic  $Z'$  with SM-like couplings to quarks. See their Fig. 6 for limits on  $\sigma \cdot B$ .

<sup>7</sup> AABOUD 18AI search for resonances decaying to  $HZ$  in  $pp$  collisions at  $\sqrt{s} = 13$  TeV. The quoted limit is for heavy-vector-triplet  $Z'$  with  $g_V = 3$ . The limit becomes  $M_{Z'} > 2650$  GeV for  $g_V = 1$ . If we assume  $M_{W'} = M_{Z'}$ , the limit increases  $M_{Z'} > 2930$  GeV and  $M_{Z'} > 2800$  GeV for  $g_V = 3$  and  $g_V = 1$ , respectively. See their Fig. 5 for limits on  $\sigma \cdot B$ .

<sup>8</sup> AABOUD 18AK search for resonances decaying to  $WW$  in  $pp$  collisions at  $\sqrt{s} = 13$  TeV. The limit quoted above is for heavy-vector-triplet  $Z'$  with  $g_V = 3$ . The limit becomes  $M_{Z'} > 2750$  GeV for  $g_V = 1$ .

<sup>9</sup> AABOUD 18B search for resonances decaying to  $WW$  in  $pp$  collisions at  $\sqrt{s} = 13$  TeV. The quoted limit is for heavy-vector-triplet  $Z'$  with  $g_V = 1$ . See their Fig.11 for limits on  $\sigma \cdot B$ .

<sup>10</sup> AABOUD 18BI search for a resonance decaying to  $t\bar{t}$  in  $pp$  collisions at  $\sqrt{s} = 13$  TeV. The quoted limit is for a top-color assisted TC  $Z'$  with  $\Gamma_{Z'}/M_{Z'} = 0.01$ . The limits for wider resonances are available. See their Fig. 14 for limits on  $\sigma \cdot B$ .

<sup>11</sup> AABOUD 18F search for resonances decaying to  $WW$  in  $pp$  collisions at  $\sqrt{s} = 13$  TeV. The quoted limit is for heavy-vector-triplet  $Z'$  with  $g_V = 3$ . The limit becomes  $M_{Z'} > 2200$  GeV for  $g_V = 1$ . If we assume  $M_{Z'} = M_{W'}$ , the limit increases  $M_{Z'} > 3500$  GeV and  $M_{Z'} > 3100$  GeV for  $g_V = 3$  and  $g_V = 1$ , respectively. See their Fig.5 for limits on  $\sigma \cdot B$ .

<sup>12</sup> SIRUNYAN 18ED search for resonances decaying to  $HZ$  in  $pp$  collisions at  $\sqrt{s} = 13$  TeV. The limit above is for heavy-vector-triplet  $Z'$  with  $g_V = 3$ . If we assume  $M_{Z'} = M_{W'}$ , the limit increases  $M_{Z'} > 2900$  GeV and  $M_{Z'} > 2800$  GeV for  $g_V = 3$  and  $g_V = 1$ , respectively.

<sup>13</sup> SIRUNYAN 18P give this limit for a heavy-vector-triplet  $Z'$  with  $g_V = 3$ . If they assume  $M_{Z'} = M_{W'}$ , the limit increases to  $M_{Z'} > 3800$  GeV.

<sup>14</sup> AABOUD 17AK search for a new resonance decaying to dijets in  $pp$  collisions at  $\sqrt{s} = 13$  TeV. The limit quoted above is for a leptophobic  $Z'$  boson having axial-vector coupling strength with quarks  $g_q = 0.2$ . The limit is 2100 GeV if  $g_q = 0.1$ .

<sup>15</sup> AABOUD 17AO search for resonances decaying to  $HZ$  in  $pp$  collisions at  $\sqrt{s} = 13$  TeV. The limit quoted above is for a  $Z'$  in the heavy-vector-triplet model with  $g_V = 3$ . See their Fig.4 for limits on  $\sigma \cdot B$ .

<sup>16</sup> SIRUNYAN 17AK search for resonances decaying to  $WW$  or  $HZ$  in  $pp$  collisions at  $\sqrt{s} = 8$  and 13 TeV. The quoted limit is for heavy-vector-triplet  $Z'$  with  $g_V = 3$ . The limit becomes  $M_{Z'} > 2200$  GeV for  $g_V = 1$ . If we assume  $M_{Z'} = M_{W'}$ , the limit increases  $M_{Z'} > 2400$  GeV for both  $g_V = 3$  and  $g_V = 1$ . See their Fig.1 and 2 for limits on  $\sigma \cdot B$ .

<sup>17</sup> SIRUNYAN 17Q search for a resonance decaying to  $t\bar{t}$  in  $pp$  collisions at  $\sqrt{s} = 13$  TeV. The limit quoted above is for a resonance with relative width  $\Gamma_{Z'}/M_{Z'} = 0.01$ . Limits for wider resonances are available. See their Fig.6 for limits on  $\sigma \cdot B$ .

<sup>18</sup> SIRUNYAN 17R search for resonances decaying to  $HZ$  in  $pp$  collisions at  $\sqrt{s} = 13$  TeV. The quoted limit is for heavy-vector-triplet  $Z'$  with  $g_V = 3$ . Mass regions  $M_{Z'} < 1150$  GeV and  $1250$  GeV  $< M_{Z'} < 1670$  GeV are excluded for  $g_V = 1$ . If we assume  $M_{Z'} = M_{W'}$ , the excluded mass regions are  $1000 < M_{Z'} < 2500$  GeV and  $2760 < M_{Z'} < 3300$  GeV for  $g_V = 3$ ;  $1000 < M_{Z'} < 2430$  GeV and  $2810 < M_{Z'} < 3130$  GeV for  $g_V = 1$ . See their Fig.5 for limits on  $\sigma \cdot B$ .

<sup>19</sup> AABOUD 19AJ search in  $pp$  collisions at  $\sqrt{s} = 13$  TeV for a new resonance decaying to  $q\bar{q}$  and produced in association with a high  $p_T$  photon. For a leptophobic axial-vector  $Z'$  in the mass region  $250$  GeV  $< M_{Z'} < 950$  GeV, the  $Z'$  coupling with quarks  $g_q$  is constrained below 0.18. See their Fig.2 for limits in  $M_{Z'} - g_q$  plane.

<sup>20</sup> AABOUD 19D search in  $pp$  collisions at  $\sqrt{s} = 13$  TeV for a new resonance decaying to  $q\bar{q}$  and produced in association with a high- $p_T$  photon or jet. For a leptophobic axial-vector  $Z'$  in the mass region  $100$  GeV  $< M_{Z'} < 220$  GeV, the  $Z'$  coupling with quarks  $g_q$  is constrained below 0.23. See their Fig. 6 for limits in  $M_{Z'} - g_q$  plane.

<sup>21</sup> AABOUD 19V search for Dark Matter simplified  $Z'$  decaying invisibly or decaying to fermion pair in  $pp$  collisions at  $\sqrt{s} = 13$  TeV.

<sup>22</sup> AAD 19L search for resonances decaying to  $\ell^+\ell^-$  in  $pp$  collisions at  $\sqrt{s} = 13$  TeV. See their Fig. 4 for limits in the heavy vector triplet model couplings.

<sup>23</sup> LONG 19 uses the weak charge data of Cesium and proton to constrain mass of  $Z'$  in the 3–3.1 models.

<sup>24</sup> PANDEY 19 obtain limits on  $Z'$  induced neutrino non-standard interaction (NSI) parameter  $\epsilon$  from LHC and IceCube data. See their Fig.2 for limits in  $M_{Z'} - \epsilon$  plane, where  $\epsilon = g_q g_V v^2 / (2 M_{Z'}^2)$ .

<sup>25</sup> SIRUNYAN 19AL search for a new resonance decaying to a top quark and a heavy vector-like top partner in  $pp$  collisions at  $\sqrt{s} = 13$  TeV. See their Fig. 8 for limits on  $Z'$  production cross section.

<sup>26</sup> SIRUNYAN 19AN search for a Dark Matter (DM) simplified model  $Z'$  decaying to  $H$  DM in  $pp$  collisions at  $\sqrt{s} = 13$  TeV. See their Fig. 7 for limits on the signal strength modifiers.

<sup>27</sup> SIRUNYAN 19CB search in  $pp$  collisions at  $\sqrt{s} = 13$  TeV for a new resonance decaying to  $q\bar{q}$ . For a leptophobic  $Z'$  in the mass region 50–300 GeV, the  $Z'$  coupling with quarks  $g'_q$  is constrained below 0.2. See their Figs. 4 and 5 for limits on  $g'_q$  in the mass range  $50 < M_{Z'} < 450$  GeV.

<sup>28</sup> SIRUNYAN 19CD search in  $pp$  collisions at  $\sqrt{s} = 13$  TeV for a leptophobic  $Z'$  produced in association of high  $p_T$  ISR photon and decaying to  $q\bar{q}$ . See their Fig. 2 for limits on the  $Z'$  coupling strength  $g'_q$  to  $q\bar{q}$  in the mass range between 10 and 125 GeV.

# Gauge & Higgs Boson Particle Listings

## New Heavy Bosons

- 29 SIRUNYAN 19D search for a narrow neutral vector resonance decaying to  $H\gamma$ . See their Fig. 3 for exclusion limit in  $M_{Z'}$  -  $\sigma \cdot B$  plane. Upper limits on the production of  $H\gamma$  resonances are set as a function of the resonance mass in the range of 720–3250 GeV.
- 30 AABOUD 18AA search for a narrow neutral vector boson decaying to  $H\gamma$ . See their Fig. 10 for the exclusion limit in  $M_{Z'}$  -  $\sigma \cdot B$  plane.
- 31 AABOUD 18CJ search for heavy-vector-triplet  $Z'$  in  $pp$  collisions at  $\sqrt{s} = 13$  TeV. The limit quoted above is for model with  $g_V = 3$  assuming  $M_{Z'} = M_{W'}$ . The limit becomes  $M_{Z'} > 5500$  GeV for model with  $g_V = 1$ .
- 32 AABOUD 18N search for a narrow resonance decaying to  $q\bar{q}$  in  $pp$  collisions at  $\sqrt{s} = 13$  TeV using trigger level analysis to improve the low mass region sensitivity. See their Fig. 5 for limits in the mass-coupling plane in the  $Z'$  mass range 450–1800 GeV.
- 33 AAIJ 18AQ search for spin-0 and spin-1 resonances decaying to  $\mu^+\mu^-$  in  $pp$  collisions at  $\sqrt{s} = 7$  and 8 TeV in the mass region near 10 GeV. See their Figs. 4 and 5 for limits on  $\sigma \cdot B$ .
- 34 SIRUNYAN 18DR searches for  $\mu^+\mu^-$  resonances produced in association with  $b$ -jets in the  $pp$  collision data with  $\sqrt{s} = 8$  TeV and 13 TeV. An excess of events near  $m_{\mu\mu} = 28$  GeV is observed in the 8 TeV data. See their Fig. 3 for the measured fiducial signal cross sections at  $\sqrt{s} = 8$  TeV and the 95% CL upper limits at  $\sqrt{s} = 13$  TeV.
- 35 SIRUNYAN 18E search for a new resonance decaying to dijets in  $pp$  collisions at  $\sqrt{s} = 13$  TeV in the mass range 50–300 GeV. See their Fig.7 for limits in the mass-coupling plane.
- 36 SIRUNYAN 18I search for a narrow resonance decaying to  $b\bar{b}$  in  $pp$  collisions at  $\sqrt{s} = 8$  TeV using dedicated  $b$ -tagged dijet triggers to improve the sensitivity in the low mass region. See their Fig. 3 for limits on  $\sigma \cdot B$  in the  $Z'$  mass range 325–1200 GeV.
- 37 AABOUD 17B search for resonances decaying to  $HZ$  ( $H \rightarrow b\bar{b}, c\bar{c}, Z \rightarrow \ell^+\ell^-, \nu\bar{\nu}$ ) in  $pp$  collisions at  $\sqrt{s} = 13$  TeV. The quoted limit is for heavy-vector-triplet  $Z'$  with  $g_V = 3$ . The limit becomes  $M_{Z'} > 1490$  GeV for  $g_V = 1$ . If we assume  $M_{Z'} = M_{W'}$ , the limit increases  $M_{Z'} > 2310$  GeV and  $M_{Z'} > 1730$  GeV for  $g_V = 3$  and  $g_V = 1$ , respectively. See their Fig.3 for limits on  $\sigma \cdot B$ .
- 38 KHACHATRYAN 17AX search for lepto-phobic resonances decaying to four leptons in  $pp$  collisions at  $\sqrt{s} = 8$  TeV.
- 39 KHACHATRYAN 17U search for resonances decaying to  $HZ$  ( $H \rightarrow b\bar{b}, c\bar{c}, Z \rightarrow \ell^+\ell^-, \nu\bar{\nu}$ ) in  $pp$  collisions at  $\sqrt{s} = 13$  TeV. The limit on the heavy-vector-triplet model is  $M_{Z'} = M_{W'} > 2$  TeV for  $g_V = 3$ , in which constraints from the  $W' \rightarrow HW$  ( $H \rightarrow b\bar{b}, W \rightarrow \ell\nu$ ) are combined. See their Fig.3 and Fig.4 for limits on  $\sigma \cdot B$ .
- 40 SIRUNYAN 17A search for resonances decaying to  $WW$  with  $WW \rightarrow \ell\nu q\bar{q}, q\bar{q}q\bar{q}$  in  $pp$  collisions at  $\sqrt{s} = 13$  TeV. The quoted limit is for heavy-vector-triplet  $Z'$  with  $g_V = 3$ . The limit becomes  $M_{Z'} > 1600$  GeV for  $g_V = 1$ . If we assume  $M_{Z'} = M_{W'}$ , the limit increases  $M_{Z'} > 2400$  GeV and  $M_{Z'} > 2300$  GeV for  $g_V = 3$  and  $g_V = 1$ , respectively. See their Fig.6 for limits on  $\sigma \cdot B$ .
- 41 SIRUNYAN 17AP search for resonances decaying into a SM-like Higgs scalar  $H$  and a light pseudo scalar  $A$ .  $A$  is assumed to decay invisibly. See their Fig.9 for limits on  $\sigma \cdot B$ .
- 42 SIRUNYAN 17T search for a new resonance decaying to dijets in  $pp$  collisions at  $\sqrt{s} = 13$  TeV in the mass range 100–300 GeV. See their Fig.3 for limits in the mass-coupling plane.
- 43 SIRUNYAN 17V search for a new resonance decaying to a top quark and a heavy vector-like top partner  $T$  in  $pp$  collisions at  $\sqrt{s} = 13$  TeV. See their table 5 for limits on the  $Z'$  production cross section for various values of  $M_{Z'}$  and  $M_T$  in the range of  $M_{Z'} = 1500$ –2500 GeV and  $M_T = 700$ –1500 GeV.
- 44 AABOUD 16 search for a narrow resonance decaying into  $b\bar{b}$  in  $pp$  collisions at  $\sqrt{s} = 13$  TeV. The limit quoted above is for a leptophobic  $Z'$  with SM-like couplings to quarks. See their Fig.6 for limits on  $\sigma \cdot B$ .
- 45 AAD 16L search for  $Z' \rightarrow a\gamma, a \rightarrow \gamma\gamma$  in  $pp$  collisions at  $\sqrt{s} = 8$  TeV. See their Table 6 for limits on  $\sigma \cdot B$ .
- 46 AAD 16S search for a new resonance decaying to dijets in  $pp$  collisions at  $\sqrt{s} = 13$  TeV. The limit quoted above is for a leptophobic  $Z'$  having coupling strength with quark  $g_q = 0.3$  and is taken from their Figure 3.
- 47 KHACHATRYAN 16AP search for a resonance decaying to  $HZ$  in  $pp$  collisions at  $\sqrt{s} = 8$  TeV. Both  $H$  and  $Z'$  are assumed to decay to fat jets. The quoted limit is for heavy-vector-triplet  $Z'$  with  $g_V = 3$ .
- 48 KHACHATRYAN 16E search for a leptophobic top-color  $Z'$  decaying to  $t\bar{t}$  using  $pp$  collisions at  $\sqrt{s} = 8$  TeV. The quoted limit assumes that  $\Gamma_{Z'}/M_{Z'} = 0.012$ . Also  $m_{Z'} < 2.9$  TeV is excluded for wider topcolor  $Z'$  with  $\Gamma_{Z'}/M_{Z'} = 0.1$ .
- 49 AAD 15A search for narrow resonance decaying to  $t\bar{t}$  using  $pp$  collisions at  $\sqrt{s} = 8$  TeV. See Fig. 11 for limit on  $\sigma \cdot B$ .
- 50 AAD 15AT search for monoton production plus large missing  $E_T$  events in  $pp$  collisions at  $\sqrt{s} = 8$  TeV and give constraints on a  $Z'$  model having  $Z'u\bar{t}$  coupling.  $Z'$  is assumed to decay invisibly. See their Fig. 6 for limits on  $\sigma \cdot B$ .
- 51 AAD 15CD search for decays of Higgs bosons to  $4\ell$  states via  $Z'$  bosons,  $H \rightarrow Z'Z' \rightarrow 4\ell$  or  $H \rightarrow Z'Z' \rightarrow 4\ell$ . See Fig. 5 for the limit on the signal strength of the  $H \rightarrow Z'Z' \rightarrow 4\ell$  process and Fig. 16 for the limit on  $H \rightarrow Z'Z' \rightarrow 4\ell$ .
- 52 KHACHATRYAN 15F search for monoton production plus large missing  $E_T$  events in  $pp$  collisions at  $\sqrt{s} = 8$  TeV and give constraints on a  $Z'$  model having  $Z'u\bar{t}$  coupling.  $Z'$  is assumed to decay invisibly. See Fig. 3 for limits on  $\sigma \cdot B$ .
- 53 KHACHATRYAN 15O search for narrow  $Z'$  resonance decaying to  $ZH$  in  $pp$  collisions at  $\sqrt{s} = 8$  TeV. See their Fig. 6 for limit on  $\sigma \cdot B$ .
- 54 AAD 14AT search for a narrow neutral vector boson decaying to  $Z\gamma$ . See their Fig. 3b for the exclusion limit in  $M_{Z'} - \sigma \cdot B$  plane.
- 55 KHACHATRYAN 14A search for new resonance in the  $WW$  ( $\ell\nu q\bar{q}$ ) and the  $ZZ$  ( $\ell\ell q\bar{q}$ ) channels using  $pp$  collisions at  $\sqrt{s}=8$  TeV. See their Fig.13 for the exclusion limit on the number of events in the mass-width plane.
- 56 MARTINEZ 14 use various electroweak data to constrain the  $Z'$  boson in the 3-3-1 models.
- 57 AAD 13AQ search for a leptophobic top-color  $Z'$  decaying to  $t\bar{t}$ . The quoted limit assumes that  $\Gamma_{Z'}/M_{Z'} = 0.012$ .
- 58 CHATRCHYAN 13BM search for top-color  $Z'$  decaying to  $t\bar{t}$  using  $pp$  collisions at  $\sqrt{s}=8$  TeV. The quoted limit is for  $\Gamma_{Z'}/M_{Z'} = 0.012$ .
- 59 CHATRCHYAN 13AP search for top-color leptophobic  $Z'$  decaying to  $t\bar{t}$  using  $pp$  collisions at  $\sqrt{s}=7$  TeV. The quoted limit is for  $\Gamma_{Z'}/M_{Z'} = 0.012$ .

- 60 AAD 12BV search for narrow resonance decaying to  $t\bar{t}$  using  $pp$  collisions at  $\sqrt{s}=7$  TeV. See their Fig. 7 for limit on  $\sigma \cdot B$ .
- 61 AAD 12K search for narrow resonance decaying to  $t\bar{t}$  using  $pp$  collisions at  $\sqrt{s}=7$  TeV. See their Fig. 5 for limit on  $\sigma \cdot B$ .
- 62 AALTONEN 12AR search for chromophilic  $Z'$  in  $p\bar{p}$  collisions at  $\sqrt{s} = 1.96$  TeV. See their Fig. 5 for limit on  $\sigma \cdot B$ .
- 63 AALTONEN 12N search for  $p\bar{p} \rightarrow tZ', Z' \rightarrow T\bar{u}$  events in  $p\bar{p}$  collisions. See their Fig. 3 for the limit on  $\sigma \cdot B$ .
- 64 ABASOV 12R search for top-color  $Z'$  boson decaying exclusively to  $t\bar{t}$ . The quoted limit is for  $\Gamma_{Z'}/M_{Z'} = 0.012$ .
- 65 CHATRCHYAN 12AI search for  $pp \rightarrow tt$  events and give constraints on a  $Z'$  model having  $Z'\bar{t}t$  coupling. See their Fig. 4 for the limit in mass-coupling plane.
- 66 Search for resonance decaying to  $t\bar{t}$ . See their Fig. 6 for limit on  $\sigma \cdot B$ .
- 67 Search for narrow resonance decaying to  $t\bar{t}$ . See their Fig. 4 for limit on  $\sigma \cdot B$ .
- 68 Search for narrow resonance decaying to  $t\bar{t}$ . See their Fig. 3 for limit on  $\sigma \cdot B$ .
- 69 CHATRCHYAN 11O search for same-sign top production in  $pp$  collisions induced by a hypothetical FCNC  $Z'$  at  $\sqrt{s} = 7$  TeV. See their Fig. 3 for limit in mass-coupling plane.
- 70 Search for narrow resonance decaying to  $t\bar{t}$ . See their Fig. 3 for limit on  $\sigma \cdot B$ .
- 71 Search for narrow resonance decaying to  $t\bar{t}$ . See their Fig. 2 for limit on  $\sigma \cdot B$ .
- 72 BARGER 03b use the nucleosynthesis bound on the effective number of light neutrino  $\delta N_{\nu}$ . See their Figs.4–5 for limits in general  $E_6$  motivated models.
- 73 CHO 00 use various electroweak data to constrain  $Z'$  models assuming  $m_H=100$  GeV. See Fig. 2 for limits in general  $E_6$ -motivated models.
- 74 CHO 98 study constraints on four-Fermi contact interactions obtained from low-energy electroweak experiments, assuming no  $Z$ - $Z'$  mixing.
- 75 Search for  $Z'$  decaying to dijets at  $\sqrt{s}=1.8$  TeV. For  $Z'$  with electromagnetic strength coupling, no bound is obtained.

### Searches for $Z'$ with Lepton-Flavor-Violating decays

The following limits are obtained from  $p\bar{p}$  or  $pp \rightarrow Z'X$  with  $Z'$  decaying to the mode indicated in the comments.

VALUE	DOCUMENT ID	TECN	COMMENT
• • •	We do not use the following data for averages, fits, limits, etc. • • •		
1	AABOUD 18CMATLS	18CMATLS	$Z' \rightarrow e\mu, e\tau, \mu\tau$
2	SIRUNYAN 18AT CMS	18AT CMS	$Z' \rightarrow e\mu$
3	AABOUD 16P ATLS	16P ATLS	$Z' \rightarrow e\mu, e\tau, \mu\tau$
4	KHACHATRYAN 16BE CMS	16BE CMS	$Z' \rightarrow e\mu$
5	AAD 15O ATLS	15O ATLS	$Z' \rightarrow e\mu, e\tau, \mu\tau$
6	AAD 11H ATLS	11H ATLS	$Z' \rightarrow e\mu$
7	AAD 11Z ATLS	11Z ATLS	$Z' \rightarrow e\mu$
8	ABULENCIA 06M CDF	06M CDF	$Z' \rightarrow e\mu$

- 1 AABOUD 18CM search for a new particle with lepton-flavor violating decay in  $pp$  collisions at  $\sqrt{s} = 13$  TeV. See their Figs. 4, 5, and 6 for limits on  $\sigma \cdot B$ .
- 2 SIRUNYAN 18AT search for a narrow resonance  $Z'$  decaying into  $e\mu$  in  $pp$  collisions at  $\sqrt{s} = 13$  TeV. See their Fig.5 for limit on  $\sigma \cdot B$  in the range of  $600 \text{ GeV} < M_{Z'} < 5000$  GeV.
- 3 AABOUD 16P search for new particle with lepton flavor violating decay in  $pp$  collisions at  $\sqrt{s} = 13$  TeV. See their Figs.2, 3, and 4 for limits on  $\sigma \cdot B$ .
- 4 KHACHATRYAN 16BE search for new particle  $Z'$  with lepton flavor violating decay in  $pp$  collisions at  $\sqrt{s} = 8$  TeV in the range of  $200 \text{ GeV} < M_{Z'} < 2000$  GeV. See their Fig.4 for limits on  $\sigma \cdot B$  and their Table 5 for bounds on various masses.
- 5 AAD 15O search for new particle  $Z'$  with lepton flavor violating decay in  $pp$  collisions at  $\sqrt{s} = 8$  TeV in the range of  $500 \text{ GeV} < M_{Z'} < 3000$  GeV. See their Fig. 2 for limits on  $\sigma \cdot B$ .
- 6 AAD 11H search for new particle  $Z'$  with lepton flavor violating decay in  $pp$  collisions at  $\sqrt{s} = 7$  TeV in the range of  $700 \text{ GeV} < M_{Z'} < 1000$  GeV. See their Fig. 3 for limits on  $\sigma \cdot B$ .
- 7 AAD 11Z search for new particle  $Z'$  with lepton flavor violating decay in  $pp$  collisions at  $\sqrt{s} = 7$  TeV in the range  $700 \text{ GeV} < M_{Z'} < 2000$  GeV. See their Fig. 3 for limits on  $\sigma \cdot B$ .
- 8 ABULENCIA 06M search for new particle  $Z'$  with lepton flavor violating decay in  $p\bar{p}$  collisions at  $\sqrt{s} = 1.96$  TeV in the range of  $100 \text{ GeV} < M_{Z'} < 800$  GeV. See their Fig. 4 for limits in the mass-coupling plane.

### Indirect Constraints on Kaluza-Klein Gauge Bosons

Bounds on a Kaluza-Klein excitation of the  $Z$  boson or photon in  $d=1$  extra dimension. These bounds can also be interpreted as a lower bound on  $1/R$ , the size of the extra dimension. Unless otherwise stated, bounds assume all fermions live on a single brane and all gauge fields occupy the  $4+d$ -dimensional bulk. See also the section on "Extra Dimensions" in the "Searches" Listings in this Review.

VALUE (TeV)	CL%	DOCUMENT ID	TECN	COMMENT
• • •	We do not use the following data for averages, fits, limits, etc. • • •			
> 4.7		1 MUECK 02	RVUE	Electroweak
> 3.3	95	2 CORNET 00	RVUE	$e\nu qq'$
>5000		3 DELGADO 00	RVUE	$e_K$
> 2.6	95	4 DELGADO 00	RVUE	Electroweak
> 3.3	95	5 RIZZO 00	RVUE	Electroweak
> 2.9	95	6 MARCIANO 99	RVUE	Electroweak
> 2.5	95	7 MASIP 99	RVUE	Electroweak
> 1.6	90	8 NATH 99	RVUE	Electroweak
> 3.4	95	9 STRUMIA 99	RVUE	Electroweak

- 1 MUECK 02 limit is  $2\sigma$  and is from global electroweak fit ignoring correlations among observables. Higgs is assumed to be confined on the brane and its mass is fixed. For scenarios of bulk Higgs, of brane-SU(2)<sub>L</sub>, bulk-U(1)<sub>Y</sub>, and of bulk-SU(2)<sub>L</sub>, brane-U(1)<sub>Y</sub>, the corresponding limits are > 4.6 TeV, > 4.3 TeV and > 3.0 TeV, respectively.
- 2 Bound is derived from limits on  $e\nu qq'$  contact interaction, using data from HERA and the Tevatron.

See key on page 999

# Gauge & Higgs Boson Particle Listings

## New Heavy Bosons

- <sup>3</sup> Bound holds only if first two generations of quarks lives on separate branes. If quark mixing is not complex, then bound lowers to 400 TeV from  $\Delta m_K$ .
- <sup>4</sup> See Figs. 1 and 2 of DELGADO 00 for several model variations. Special boundary conditions can be found which permit KK states down to 950 GeV and that agree with the measurement of  $Q_{WW}(Cs)$ . Quoted bound assumes all Higgs bosons confined to brane; placing one Higgs doublet in the bulk lowers bound to 2.3 TeV.
- <sup>5</sup> Bound is derived from global electroweak analysis assuming the Higgs field is trapped on the matter brane. If the Higgs propagates in the bulk, the bound increases to 3.8 TeV.
- <sup>6</sup> Bound is derived from global electroweak analysis but considering only presence of the KK  $W$  bosons.
- <sup>7</sup> Global electroweak analysis used to obtain bound independent of position of Higgs on brane or in bulk.
- <sup>8</sup> Bounds from effect of KK states on  $G_F$ ,  $\alpha$ ,  $M_{WW}$ , and  $M_Z$ . Hard cutoff at string scale determined using gauge coupling unification. Limits for  $d=2,3,4$  rise to 3.5, 5.7, and 7.8 TeV.
- <sup>9</sup> Bound obtained for Higgs confined to the matter brane with  $m_H=500$  GeV. For Higgs in the bulk, the bound increases to 3.5 TeV.

### See the related review(s): Leptoquarks

#### MASS LIMITS for Leptoquarks from Pair Production

These limits rely only on the color or electroweak charge of the leptoquark.

VALUE (GeV)	CL%	DOCUMENT ID	TECN	COMMENT
>1185	95	1 SIRUNYAN 20A	CMS	Scalar LQ. $B(\nu b) = 1$
>1140	95	2 SIRUNYAN 20A	CMS	Scalar LQ. $B(\nu t) = 1$
>1140	95	3 SIRUNYAN 20A	CMS	Scalar LQ. $B(\nu q) = 1$ with $q = u, d, s, c$
>1925	95	4 SIRUNYAN 20A	CMS	Vector LQ. $\kappa = 1$ . $B(\nu b) = 1$
>1825	95	5 SIRUNYAN 20A	CMS	Vector LQ. $\kappa = 1$ . $B(\nu t) = 1$
>1980	95	6 SIRUNYAN 20A	CMS	Vector LQ. $\kappa = 1$ . $B(\nu q) = 1$ with $q = u, d, s, c$
>1400	95	7 AABOUD 19AX	ATLS	Scalar LQ. $B(e q) = 1$
>1560	95	8 AABOUD 19AX	ATLS	Scalar LQ. $B(\mu q) = 1$
>1000	95	9 AABOUD 19X	ATLS	Scalar LQ. $B(\tau \nu) = 1$
>1030	95	10 AABOUD 19X	ATLS	Scalar LQ. $B(b \tau) = 1$
> 970	95	11 AABOUD 19X	ATLS	Scalar LQ. $B(b \nu) = 1$
> 920	95	12 AABOUD 19X	ATLS	Scalar LQ. $B(\tau \tau) = 1$
>1530	95	13 SIRUNYAN 19BI	CMS	Scalar LQ. $B(\mu q)+B(\nu q) = 1$
>1435	95	14 SIRUNYAN 19BJ	CMS	Scalar LQ. $B(e q)+B(\nu q) = 1$
>1020	95	15 SIRUNYAN 19Y	CMS	Scalar LQ. $B(\tau b) = 1$
none 300-900	95	16 SIRUNYAN 18CZ	CMS	Scalar LQ. $B(\tau t) = 1$
>1420	95	17 SIRUNYAN 18EC	CMS	Scalar LQ. $B(\mu t) = 1$
>1190	95	18 SIRUNYAN 18EC	CMS	Vector LQ. $\mu, \tau, \tau, \nu b$
>1100	95	19 SIRUNYAN 18U	CMS	Scalar LQ. $B(\nu b) = 1$
> 980	95	20 SIRUNYAN 18U	CMS	Scalar LQ. $B(\nu q) = 1$ with $q = u, d, s, c$
>1020	95	21 SIRUNYAN 18U	CMS	Scalar LQ. $B(\nu t) = 1$
>1810	95	22 SIRUNYAN 18U	CMS	Vector LQ. $\kappa=1$ . $LQ \rightarrow b \nu$
>1790	95	23 SIRUNYAN 18U	CMS	Vector LQ. $\kappa=1$ . $LQ \rightarrow q \nu$ with $q = u, d, s, c$
>1780	95	24 SIRUNYAN 18U	CMS	Vector LQ. $\kappa=1$ . $LQ \rightarrow t \nu$
> 740	95	25 KHACHATRY...17J	CMS	Scalar LQ. $B(\tau b) = 1$
> 850	95	26 SIRUNYAN 17H	CMS	Scalar LQ. $B(\tau b) = 1$
>1050	95	27 AAD 16G	ATLS	Scalar LQ. $B(e q) = 1$
>1000	95	28 AAD 16G	ATLS	Scalar LQ. $B(\mu q) = 1$
> 625	95	29 AAD 16G	ATLS	Scalar LQ. $B(\nu b) = 1$
none 200-640	95	30 AAD 16G	ATLS	Scalar LQ. $B(\nu t) = 1$
>1010	95	31 KHACHATRY...16AF	CMS	Scalar LQ. $B(e q) = 1$
>1080	95	32 KHACHATRY...16AF	CMS	Scalar LQ. $B(\mu q) = 1$
> 685	95	33 KHACHATRY...15AJ	CMS	Scalar LQ. $B(\tau t) = 1$
> 740	95	34 KHACHATRY...14T	CMS	Scalar LQ. $B(\tau b) = 1$
••• We do not use the following data for averages, fits, limits, etc. •••				
> 534	95	35 SIRUNYAN 19bc	CMS	Scalar LQ ( $\rightarrow \mu q$ ) LQ ( $\rightarrow X + DM$ )
> 525	95	36 AAD 13AE	ATLS	Third generation
> 660	95	37 CHATRCHYAN 13M	CMS	Third generation
> 685	95	38 AAD 12H	ATLS	First generation
> 830	95	39 AAD 12o	ATLS	Second generation
> 840	95	40 CHATRCHYAN 12AG	CMS	First generation
> 450	95	41 CHATRCHYAN 12AG	CMS	Second generation
> 376	95	42 CHATRCHYAN 12Bo	CMS	Third generation
> 422	95	43 AAD 11D	ATLS	Superseded by AAD 12H
> 326	95	44 AAD 11D	ATLS	Superseded by AAD 12o
> 339	95	45 ABAZOV 11V	D0	First generation
> 384	95	46 CHATRCHYAN 11N	CMS	Superseded by CHATRCHYAN 12AG
> 394	95	47 KHACHATRY...11D	CMS	Superseded by CHATRCHYAN 12AG
> 247	95	48 KHACHATRY...11E	CMS	Superseded by CHATRCHYAN 12AG
> 316	95	49 ABAZOV 10L	D0	Third generation
> 299	95	50 ABAZOV 09 D0	D0	Second generation
> 153	95	51 ABAZOV 09AF	D0	Superseded by ABAZOV 11V
> 205	95	52 AALTONEN 08P	CDF	Third generation
> 210	95	53 AALTONEN 08Z	CDF	Third generation
> 229	95	54 ABAZOV 08AD	D0	All generations
> 251	95	55 ABAZOV 08AN	D0	Third generation
> 136	95	56 ABAZOV 07J	D0	Superseded by ABAZOV 10L
> 226	95	57 ABAZOV 06A	D0	Superseded by ABAZOV 09
	95	58 ABAZOV 06L	D0	Superseded by ABAZOV 08AD
	95	59 ABULENCIA 06T	CDF	Second generation

> 256	95	59 ABAZOV 05H	D0	First generation
> 117	95	54 ACOSTA 05I	CDF	First generation
> 236	95	60 ACOSTA 05P	CDF	First generation
> 99	95	61 ABBIENDI 03R	OPAL	First generation
> 100	95	61 ABBIENDI 03R	OPAL	Second generation
> 98	95	61 ABBIENDI 03R	OPAL	Third generation
> 98	95	62 ABAZOV 02	D0	All generations
> 225	95	63 ABAZOV 01D	D0	First generation
> 85.8	95	64 ABBIENDI 00M	OPAL	Superseded by ABBIENDI 03R
> 85.5	95	64 ABBIENDI 00M	OPAL	Superseded by ABBIENDI 03R
> 82.7	95	64 ABBIENDI 00M	OPAL	Superseded by ABBIENDI 03R
> 200	95	65 ABBOTT 00C	D0	Second generation
> 123	95	66 AFFOLDER 00K	CDF	Second generation
> 148	95	67 AFFOLDER 00K	CDF	Third generation
> 160	95	68 ABBOTT 99J	D0	Second generation
> 225	95	69 ABBOTT 98E	D0	First generation
> 94	95	70 ABBOTT 98J	D0	Third generation
> 202	95	71 ABE 98S	CDF	Second generation
> 242	95	72 GROSS-PILCH.98		First generation
> 99	95	73 ABE 97F	CDF	Third generation
> 213	95	74 ABE 97X	CDF	First generation
> 45.5	95	75,76 ABREU 93J	DLPH	First + second generation
> 44.4	95	77 ADRIANI 93M	L3	First generation
> 44.5	95	77 ADRIANI 93M	L3	Second generation
> 45	95	77 DECAMP 92	ALEP	Third generation
none 8.9-22.6	95	78 KIM 90	AMY	First generation
none 10.2-23.2	95	78 KIM 90	AMY	Second generation
none 5-20.8	95	79 BARTEL 87B	JADE	
none 7-20.5	95	80 BEHREND 86B	CELL	

- 1 SIRUNYAN 20A search for scalar and vector leptoquarks decaying to  $t\nu, b\nu$ , and  $q\nu$  ( $q = u, d, s, c$ ). The limit quoted above assumes scalar leptoquark with  $B(\nu b) = 1$ .
- 2 SIRUNYAN 20A search for scalar and vector leptoquarks decaying to  $t\nu, b\nu$ , and  $q\nu$  ( $q = u, d, s, c$ ). The limit quoted above assumes scalar leptoquark with  $B(\nu t) = 1$ .
- 3 SIRUNYAN 20A search for scalar and vector leptoquarks decaying to  $t\nu, b\nu$ , and  $q\nu$  ( $q = u, d, s, c$ ). The limit quoted above assumes scalar leptoquark with  $B(\nu q) = 1$ .
- 4 SIRUNYAN 20A search for scalar and vector leptoquarks decaying to  $t\nu, b\nu$ , and  $q\nu$  ( $q = u, d, s, c$ ). The limit quoted above assumes vector leptoquark with  $B(\nu b) = 1$  and  $\kappa = 1$ . If we assume  $\kappa = 0$ , the limit becomes  $M_{LQ} > 1560$  GeV.
- 5 SIRUNYAN 20A search for scalar and vector leptoquarks decaying to  $t\nu, b\nu$ , and  $q\nu$  ( $q = u, d, s, c$ ). The limit quoted above assumes vector leptoquark with  $B(\nu t) = 1$  and  $\kappa = 1$ . If we assume  $\kappa = 0$ , the limit becomes  $M_{LQ} > 1475$  GeV.
- 6 SIRUNYAN 20A search for scalar and vector leptoquarks decaying to  $t\nu, b\nu$ , and  $q\nu$  ( $q = u, d, s, c$ ). The limit quoted above assumes vector leptoquark with  $B(\nu q) = 1$  and  $\kappa = 1$ . If we assume  $\kappa = 0$ , the limit becomes  $M_{LQ} > 1560$  GeV.
- 7 AABOUD 19AX search for leptoquarks using  $e\bar{e}jj$  events in  $pp$  collisions at  $\sqrt{s} = 13$  TeV. The limit above assumes  $B(eq) = 1$ .
- 8 AABOUD 19AX search for leptoquarks using  $\mu\mu jj$  events in  $pp$  collisions at  $\sqrt{s} = 13$  TeV. The limit above assumes  $B(\mu q) = 1$ .
- 9 AABOUD 19X search for scalar leptoquarks decaying to  $t\nu$  in  $pp$  collisions at  $\sqrt{s} = 13$  TeV.
- 10 AABOUD 19X search for scalar leptoquarks decaying to  $b\tau$  in  $pp$  collisions at  $\sqrt{s} = 13$  TeV.
- 11 AABOUD 19X search for scalar leptoquarks decaying to  $b\nu$  in  $pp$  collisions at  $\sqrt{s} = 13$  TeV.
- 12 AABOUD 19X search for scalar leptoquarks decaying to  $\tau\tau$  in  $pp$  collisions at  $\sqrt{s} = 13$  TeV.
- 13 SIRUNYAN 19BI search for a pair of scalar leptoquarks decaying to  $\mu\mu jj$  and  $\mu\nu jj$  final states in  $pp$  collisions at  $\sqrt{s} = 13$  TeV. Limits are shown as a function of  $\beta$  where  $\beta$  is the branching fraction to a muon and a quark. For  $\beta = 1.0$  (0.5) LQ masses up to 1530 (1285) GeV are excluded. See Fig. 9 for exclusion limits in the plane of  $\beta$  and LQ mass.
- 14 SIRUNYAN 19BJ search for a pair of scalar leptoquarks decaying to  $e\bar{e}jj$  and  $e\nu jj$  final states in  $pp$  collisions at  $\sqrt{s} = 13$  TeV. Limits are shown as a function of the branching fraction  $\beta$  to an electron and a quark. For  $\beta = 1.0$  (0.5) LQ masses up to 1435 (1270) GeV are excluded. See Fig. 9 for exclusion limits in the plane of  $\beta$  and LQ mass.
- 15 SIRUNYAN 19Y search for a pair of third generation scalar leptoquarks, each decaying to  $\tau$  and a jet. Assuming  $B(\tau b) = 1$ , leptoquark masses below 1.02 TeV are excluded.
- 16 SIRUNYAN 18CZ search for scalar leptoquarks decaying to  $\tau t$  in  $pp$  collisions at  $\sqrt{s} = 13$  TeV. The limit above assumes  $B(\tau t) = 1$ .
- 17 SIRUNYAN 18EC set limits for scalar and vector leptoquarks decaying to  $\mu t, \tau t$ , and  $\nu b$ . The limit quoted above assumes scalar leptoquark with  $B(\mu t) = 1$ .
- 18 SIRUNYAN 18EC set limits for scalar and vector leptoquarks decaying to  $\mu t, \tau t$ , and  $\nu b$ . The limit quoted above assumes vector leptoquark with all possible combinations of branching fractions to  $\mu t, \tau t$ , and  $\nu b$ .
- 19 SIRUNYAN 18U set limits for scalar and vector leptoquarks decaying to  $t\nu, b\nu$ , and  $q\nu$ . The limit quoted above assumes scalar leptoquark with  $B(b\nu) = 1$ . Vector leptoquarks with  $\kappa = 1$  are excluded below masses of 1810 GeV.
- 20 SIRUNYAN 18U set limits for scalar and vector leptoquarks decaying to  $t\nu, b\nu$ , and  $q\nu$ . The limit quoted above assumes scalar leptoquark with  $B(q\nu) = 1$ . Vector leptoquarks with  $\kappa = 1$  are excluded below masses of 1790 GeV.
- 21 SIRUNYAN 18U set limits for scalar and vector leptoquarks decaying to  $t\nu, b\nu$ , and  $q\nu$ . The limit quoted above assumes scalar leptoquark with  $B(\nu t) = 1$ . Vector leptoquarks with  $\kappa = 1$  are excluded below masses of 1780 GeV.
- 22 SIRUNYAN 18U set limits for scalar and vector leptoquarks decaying to  $t\nu, b\nu$ , and  $q\nu$ .  $\kappa = 1$  and  $LQ \rightarrow b\nu$  are assumed.
- 23 SIRUNYAN 18U set limits for scalar and vector leptoquarks decaying to  $t\nu, b\nu$ , and  $q\nu$ .  $\kappa = 1$  and  $LQ \rightarrow q\nu$  with  $q = u, d, s, c$  are assumed.
- 24 SIRUNYAN 18U set limits for scalar and vector leptoquarks decaying to  $t\nu, b\nu$ , and  $q\nu$ .  $\kappa = 1$  and  $LQ \rightarrow t\nu$  are assumed.
- 25 KHACHATRYAN 17J search for scalar leptoquarks decaying to  $\tau b$  using  $pp$  collisions at  $\sqrt{s} = 13$  TeV. The limit above assumes  $B(\tau b) = 1$ .
- 26 SIRUNYAN 17H search for scalar leptoquarks using  $\tau\tau bb$  events in  $pp$  collisions at  $\sqrt{s} = 8$  TeV. The limit above assumes  $B(\tau b) = 1$ .

# Gauge & Higgs Boson Particle Listings

## New Heavy Bosons

- 27 AAD 16G search for scalar leptoquarks using  $eejj$  events in collisions at  $\sqrt{s} = 8$  TeV. The limit above assumes  $B(eq) = 1$ .
- 28 AAD 16G search for scalar leptoquarks using  $\mu\mu jj$  events in collisions at  $\sqrt{s} = 8$  TeV. The limit above assumes  $B(\mu q) = 1$ .
- 29 AAD 16G search for scalar leptoquarks decaying to  $b\nu$ . The limit above assumes  $B(b\nu) = 1$ .
- 30 AAD 16G search for scalar leptoquarks decaying to  $t\nu$ . The limit above assumes  $B(t\nu) = 1$ .
- 31 KHACHATRYAN 16AF search for scalar leptoquarks using  $eejj$  and  $e\nu jj$  events in  $pp$  collisions at  $\sqrt{s} = 8$  TeV. The limit above assumes  $B(eq) = 1$ . For  $B(eq) = 0.5$ , the limit becomes 850 GeV.
- 32 KHACHATRYAN 16AF search for scalar leptoquarks using  $\mu\mu jj$  and  $\mu\nu jj$  events in  $pp$  collisions at  $\sqrt{s} = 8$  TeV. The limit above assumes  $B(\mu q) = 1$ . For  $B(\mu q) = 0.5$ , the limit becomes 760 GeV.
- 33 KHACHATRYAN 15AJ search for scalar leptoquarks using  $\tau\tau tt$  events in  $pp$  collisions at  $\sqrt{s} = 8$  TeV. The limit above assumes  $B(\tau t) = 1$ .
- 34 KHACHATRYAN 14T search for scalar leptoquarks decaying to  $\tau b$  using  $pp$  collisions at  $\sqrt{s} = 8$  TeV. The limit above assumes  $B(\tau b) = 1$ . See their Fig. 5 for the exclusion limit as function of  $B(\tau b)$ .
- 35 SIRUNYAN 19bc search for scalar leptoquark (LQ) pair production in  $pp$  collisions at  $\sqrt{s} = 13$  TeV. One LQ is assumed to decay to  $\mu q$ , while the other decays to dark matter pair and SM particles. See their Fig. 4 for limits in  $M_{LQ} - M_{DM}$  plane.
- 36 AAD 13AE search for scalar leptoquarks using  $\tau\tau bb$  events in  $pp$  collisions at  $E_{cm} = 7$  TeV. The limit above assumes  $B(\tau b) = 1$ .
- 37 CHATRCHYAN 13M search for scalar and vector leptoquarks decaying to  $\tau b$  in  $pp$  collisions at  $E_{cm} = 7$  TeV. The limit above is for scalar leptoquarks with  $B(\tau b) = 1$ .
- 38 AAD 12H search for scalar leptoquarks using  $eejj$  and  $e\nu jj$  events in  $pp$  collisions at  $E_{cm} = 7$  TeV. The limit above assumes  $B(eq) = 1$ . For  $B(eq) = 0.5$ , the limit becomes 607 GeV.
- 39 AAD 12o search for scalar leptoquarks using  $\mu\mu jj$  and  $\mu\nu jj$  events in  $pp$  collisions at  $E_{cm} = 7$  TeV. The limit above assumes  $B(\mu q) = 1$ . For  $B(\mu q) = 0.5$ , the limit becomes 594 GeV.
- 40 CHATRCHYAN 12AG search for scalar leptoquarks using  $eejj$  and  $e\nu jj$  events in  $pp$  collisions at  $E_{cm} = 7$  TeV. The limit above assumes  $B(eq) = 1$ . For  $B(eq) = 0.5$ , the limit becomes 640 GeV.
- 41 CHATRCHYAN 12AG search for scalar leptoquarks using  $\mu\mu jj$  and  $\mu\nu jj$  events in  $pp$  collisions at  $E_{cm} = 7$  TeV. The limit above assumes  $B(\mu q) = 1$ . For  $B(\mu q) = 0.5$ , the limit becomes 650 GeV.
- 42 CHATRCHYAN 12Bo search for scalar leptoquarks decaying to  $\nu b$  in  $pp$  collisions at  $\sqrt{s} = 7$  TeV. The limit above assumes  $B(\nu b) = 1$ .
- 43 AAD 11b search for scalar leptoquarks using  $eejj$  and  $e\nu jj$  events in  $pp$  collisions at  $E_{cm} = 7$  TeV. The limit above assumes  $B(eq) = 1$ . For  $B(eq) = 0.5$ , the limit becomes 319 GeV.
- 44 AAD 11b search for scalar leptoquarks using  $\mu\mu jj$  and  $\mu\nu jj$  events in  $pp$  collisions at  $E_{cm} = 7$  TeV. The limit above assumes  $B(\mu q) = 1$ . For  $B(\mu q) = 0.5$ , the limit becomes 362 GeV.
- 45 ABYZOV 11v search for scalar leptoquarks using  $e\nu jj$  events in  $p\bar{p}$  collisions at  $E_{cm} = 1.96$  TeV. The limit above assumes  $B(eq) = 0.5$ .
- 46 CHATRCHYAN 11N search for scalar leptoquarks using  $e\nu jj$  events in  $pp$  collisions at  $E_{cm} = 7$  TeV. The limit above assumes  $B(eq) = 0.5$ .
- 47 KHACHATRYAN 11D search for scalar leptoquarks using  $eejj$  events in  $pp$  collisions at  $E_{cm} = 7$  TeV. The limit above assumes  $B(eq) = 1$ .
- 48 KHACHATRYAN 11E search for scalar leptoquarks using  $\mu\mu jj$  events in  $pp$  collisions at  $E_{cm} = 7$  TeV. The limit above assumes  $B(\mu q) = 1$ .
- 49 ABYZOV 10L search for pair productions of scalar leptoquark state decaying to  $\nu b$  in  $p\bar{p}$  collisions at  $E_{cm} = 1.96$  TeV. The limit above assumes  $B(\nu b) = 1$ .
- 50 ABYZOV 09 search for scalar leptoquarks using  $\mu\mu jj$  and  $\mu\nu jj$  events in  $p\bar{p}$  collisions at  $E_{cm} = 1.96$  TeV. The limit above assumes  $B(\mu q) = 1$ . For  $B(\mu q) = 0.5$ , the limit becomes 270 GeV.
- 51 ABYZOV 09AF search for scalar leptoquarks using  $eejj$  and  $e\nu jj$  events in  $p\bar{p}$  collisions at  $E_{cm} = 1.96$  TeV. The limit above assumes  $B(eq) = 1$ . For  $B(eq) = 0.5$  the bound becomes 284 GeV.
- 52 AALTONEN 08P search for vector leptoquarks using  $\tau^+\tau^-b\bar{b}$  events in  $p\bar{p}$  collisions at  $E_{cm} = 1.96$  TeV. Assuming Yang-Mills (minimal) couplings, the mass limit is  $>317$  GeV (251 GeV) at 95% CL for  $B(\tau b) = 1$ .
- 53 Search for pair production of scalar leptoquark state decaying to  $\tau b$  in  $p\bar{p}$  collisions at  $E_{cm} = 1.96$  TeV. The limit above assumes  $B(\tau b) = 1$ .
- 54 Search for scalar leptoquarks using  $\nu\nu jj$  events in  $p\bar{p}$  collisions at  $E_{cm} = 1.96$  TeV. The limit above assumes  $B(\nu q) = 1$ .
- 55 ABYZOV 07J search for pair productions of scalar leptoquark state decaying to  $\nu b$  in  $p\bar{p}$  collisions at  $E_{cm} = 1.96$  TeV. The limit above assumes  $B(\nu b) = 1$ .
- 56 ABYZOV 06A search for scalar leptoquarks using  $\mu\mu jj$  events in  $p\bar{p}$  collisions at  $E_{cm} = 1.8$  TeV and 1.96 TeV. The limit above assumes  $B(\mu q) = 1$ . For  $B(\mu q) = 0.5$ , the limit becomes 204 GeV.
- 57 ABYZOV 06L search for scalar leptoquarks using  $\nu\nu jj$  events in  $p\bar{p}$  collisions at  $E_{cm} = 1.8$  TeV and at 1.96 TeV. The limit above assumes  $B(\nu q) = 1$ .
- 58 ABULENCA 06T search for scalar leptoquarks using  $\mu\mu jj$ ,  $\mu\nu jj$ , and  $\nu\nu jj$  events in  $p\bar{p}$  collisions at  $E_{cm} = 1.96$  TeV. The quoted limit assumes  $B(\mu q) = 1$ . For  $B(\mu q) = 0.5$  or 0.1, the bound becomes 208 GeV or 143 GeV, respectively. See their Fig. 4 for the exclusion limit as a function of  $B(\mu q)$ .
- 59 ABYZOV 05H search for scalar leptoquarks using  $eejj$  and  $e\nu jj$  events in  $p\bar{p}$  collisions at  $E_{cm} = 1.8$  TeV and 1.96 TeV. The limit above assumes  $B(eq) = 1$ . For  $B(eq) = 0.5$  the bound becomes 234 GeV.
- 60 ACOSTA 05P search for scalar leptoquarks using  $eejj$ ,  $e\nu jj$  events in  $p\bar{p}$  collisions at  $E_{cm} = 1.96$  TeV. The limit above assumes  $B(eq) = 1$ . For  $B(eq) = 0.5$  and 0.1, the bound becomes 205 GeV and 145 GeV, respectively.
- 61 ABBIENDI 03R search for scalar/vector leptoquarks in  $e^+e^-$  collisions at  $\sqrt{s} = 189-209$  GeV. The quoted limits are for charge  $-4/3$  isospin 0 scalar-leptoquark with  $B(\ell q) = 1$ . See their table 12 for other cases.
- 62 ABYZOV 02 search for scalar leptoquarks using  $\nu\nu jj$  events in  $p\bar{p}$  collisions at  $E_{cm} = 1.8$  TeV. The bound holds for all leptoquark generations. Vector leptoquarks are likewise constrained to lie above 200 GeV.
- 63 ABYZOV 01d search for scalar leptoquarks using  $e\nu jj$ ,  $eejj$ , and  $\nu\nu jj$  events in  $p\bar{p}$  collisions at  $E_{cm} = 1.8$  TeV. The limit above assumes  $B(eq) = 1$ . For  $B(eq) = 0.5$  and 0, the bound becomes 204 and 79 GeV, respectively. Bounds for vector leptoquarks are also given. Supersedes ABBOTT 98E.
- 64 ABBIENDI 00M search for scalar/vector leptoquarks in  $e^+e^-$  collisions at  $\sqrt{s} = 183$  GeV. The quoted limits are for charge  $-4/3$  isospin 0 scalar-leptoquarks with  $B(\ell q) = 1$ . See their Table 8 and Figs. 6-9 for other cases.
- 65 ABBOTT 00c search for scalar leptoquarks using  $\mu\mu jj$ ,  $\mu\nu jj$ , and  $\nu\nu jj$  events in  $p\bar{p}$  collisions at  $E_{cm} = 1.8$  TeV. The limit above assumes  $B(\mu q) = 1$ . For  $B(\mu q) = 0.5$  and 0, the bound becomes 180 and 79 GeV respectively. Bounds for vector leptoquarks are also given.
- 66 AFFOLDER 00k search for scalar leptoquark using  $\nu\nu cc$  events in  $p\bar{p}$  collisions at  $E_{cm} = 1.8$  TeV. The quoted limit assumes  $B(\nu c) = 1$ . Bounds for vector leptoquarks are also given.
- 67 AFFOLDER 00k search for scalar leptoquark using  $\nu\nu bb$  events in  $p\bar{p}$  collisions at  $E_{cm} = 1.8$  TeV. The quoted limit assumes  $B(\nu b) = 1$ . Bounds for vector leptoquarks are also given.
- 68 ABBOTT 99j search for leptoquarks using  $\mu\nu jj$  events in  $p\bar{p}$  collisions at  $E_{cm} = 1.8$  TeV. The quoted limit is for a scalar leptoquark with  $B(\nu b) = 1$ .
- 69 ABBOTT 98E search for scalar leptoquarks using  $e\nu jj$ ,  $eejj$ , and  $\nu\nu jj$  events in  $p\bar{p}$  collisions at  $E_{cm} = 1.8$  TeV. The limit above assumes  $B(eq) = 1$ . For  $B(eq) = 0.5$  and 0, the bound becomes 204 and 79 GeV, respectively.
- 70 ABBOTT 98j search for charge  $-1/3$  third generation scalar and vector leptoquarks in  $p\bar{p}$  collisions at  $E_{cm} = 1.8$  TeV. The quoted limit is for scalar leptoquark with  $B(\nu b) = 1$ .
- 71 ABE 98s search for scalar leptoquarks using  $\mu\mu jj$  events in  $p\bar{p}$  collisions at  $E_{cm} = 1.8$  TeV. The limit is for  $B(\mu q) = 1$ . For  $B(\mu q) = B(\nu q) = 0.5$ , the limit is  $> 160$  GeV.
- 72 GROSS-PILCHER 98 is the combined limit of the CDF and DØ Collaborations as determined by a joint CDF/DØ working group and reported in this FINAL Technical Memo. Original data published in ABE 97x and ABBOTT 98E.
- 73 ABE 97f search for third generation scalar and vector leptoquarks in  $p\bar{p}$  collisions at  $E_{cm} = 1.8$  TeV. The quoted limit is for scalar leptoquark with  $B(\tau b) = 1$ .
- 74 ABE 97x search for scalar leptoquarks using  $eejj$  events in  $p\bar{p}$  collisions at  $E_{cm} = 1.8$  TeV. The limit is for  $B(eq) = 1$ .
- 75 Limit is for charge  $-1/3$  isospin-0 leptoquark with  $B(\ell q) = 2/3$ .
- 76 First and second generation leptoquarks are assumed to be degenerate. The limit is slightly lower for each generation.
- 77 Limits are for charge  $-1/3$ , isospin-0 scalar leptoquarks decaying to  $\ell^- q$  or  $\nu q$  with any branching ratio. See paper for limits for other charge-isospin assignments of leptoquarks.
- 78 KIM 90 assume pair production of charge 2/3 scalar-leptoquark via photon exchange. The decay of the first (second) generation leptoquark is assumed to be any mixture of  $d e^+$  and  $u \bar{\nu}$  ( $s \mu^+$  and  $c \bar{\nu}$ ). See paper for limits for specific branching ratios.
- 79 BARTEL 87B limit is valid when a pair of charge 2/3 spinless leptoquarks X is produced with point coupling, and when they decay under the constraint  $B(X \rightarrow c \bar{\nu}_\mu) + B(X \rightarrow s \mu^+) = 1$ .
- 80 BEHREND 86B assumed that a charge 2/3 spinless leptoquark,  $\chi$ , decays either into  $s \mu^+$  or  $c \bar{\nu}$ :  $B(\chi \rightarrow s \mu^+) + B(\chi \rightarrow c \bar{\nu}) = 1$ .

### MASS LIMITS for Leptoquarks from Single Production

These limits depend on the  $q$ - $\ell$ -leptoquark coupling  $g_{LQ}$ . It is often assumed that  $g_{LQ}^2/4\pi = 1/137$ . Limits shown are for a scalar, weak isoscalar, charge  $-1/3$  leptoquark.

VALUE (GeV)	CL%	DOCUMENT ID	TECN	COMMENT
<b>none 150-740</b>	95	1 SIRUNYAN 18BJ CMS		Third generation
<b>&gt;1755</b>	95	2 KHACHATRY..16AG CMS		First generation
<b>&gt; 660</b>	95	3 KHACHATRY..16AG CMS		Second generation
<b>&gt; 304</b>	95	4 ABRAMOWICZ12A ZEUS		First generation
<b>&gt; 73</b>	95	5 ABREU 93J DLPH		Second generation
••• We do not use the following data for averages, fits, limits, etc. •••				
6 DEY	16	ICCB		$\nu q \rightarrow LQ \rightarrow \nu q$
7 AARON	11A	H1		Lepton-flavor violation
8 AARON	11B	H1		First generation
9 ABYZOV	07E	D0		Second generation
10 AKTAS	05B	H1		First generation
11 CHEKANOV	05A	ZEUS		Lepton-flavor violation
12 CHEKANOV	03B	ZEUS		First generation
13 ABBIENDI	02b	OPAL		First generation
14 CHEKANOV	02	ZEUS		Repl. by CHEKANOV 05A
15 ADLOFF	01C	H1		First generation
16 BREITWEG	01	ZEUS		First generation
17 BREITWEG	00E	ZEUS		First generation
18 ABREU	99G	DLPH		First generation
19 ADLOFF	99	H1		First generation
20 DERRICK	97	ZEUS		Lepton-flavor violation
21 DERRICK	93	ZEUS		First generation

- 1 SIRUNYAN 18BJ search for single production of charge 2/3 scalar leptoquarks decaying to  $\tau b$  in  $pp$  collisions at  $\sqrt{s} = 13$  TeV. The limit above assumes  $B(\tau b) = 1$  and the leptoquark coupling strength  $\lambda = 1$ .
- 2 KHACHATRYAN 16AG search for single production of charge  $\pm 1/3$  scalar leptoquarks using  $eejj$  events in  $pp$  collisions at  $\sqrt{s} = 8$  TeV. The limit above assumes  $B(eq) = 1$  and the leptoquark coupling strength  $\lambda = 1$ .
- 3 KHACHATRYAN 16AG search for single production of charge  $\pm 1/3$  scalar leptoquarks using  $\mu\mu jj$  events in  $pp$  collisions at  $\sqrt{s} = 8$  TeV. The limit above assumes  $B(\mu q) = 1$  and the leptoquark coupling strength  $\lambda = 1$ .
- 4 ABRAMOWICZ 12A limit is for a scalar, weak isoscalar, charge  $-1/3$  leptoquark coupled with  $e_R$ . See their Figs. 12-17 and Table 4 for states with different quantum numbers.
- 5 Limit from single production in Z decay. The limit is for a leptoquark coupling of electromagnetic strength and assumes  $B(\ell q) = 2/3$ . The limit is 77 GeV if first and second leptoquarks are degenerate.
- 6 DEY 16 use the 2010-2012 IceCube PeV energy data set to constrain the leptoquark production cross section through the  $\nu q \rightarrow LQ \rightarrow \nu q$  process. See their Figure 4 for the exclusion limit in the mass-coupling plane.
- 7 AARON 11A search for various leptoquarks with lepton-flavor violating couplings. See their Figs. 2-3 and Tables 1-4 for detailed limits.

See key on page 999

# Gauge & Higgs Boson Particle Listings

## New Heavy Bosons

- <sup>8</sup> The quoted limit is for a scalar, weak isoscalar, charge  $-1/3$  leptoquark coupled with  $e_R$ . See their Figs. 3–5 for limits on states with different quantum numbers.
- <sup>9</sup> ABAZOV 07E search for leptoquark single production through  $qg$  fusion process in  $p\bar{p}$  collisions. See their Fig. 4 for exclusion plot in mass-coupling plane.
- <sup>10</sup> AKTAS 05B limit is for a scalar, weak isoscalar, charge  $-1/3$  leptoquark coupled with  $e_R$ . See their Fig. 3 for limits on states with different quantum numbers.
- <sup>11</sup> CHEKANOV 05 search for various leptoquarks with lepton-flavor violating couplings. See their Figs.6–10 and Tables 1–8 for detailed limits.
- <sup>12</sup> CHEKANOV 03B limit is for a scalar, weak isoscalar, charge  $-1/3$  leptoquark coupled with  $e_R$ . See their Figs. 11–12 and Table 5 for limits on states with different quantum numbers.
- <sup>13</sup> For limits on states with different quantum numbers and the limits in the mass-coupling plane, see their Fig. 4 and Fig. 5.
- <sup>14</sup> CHEKANOV 02 search for various leptoquarks with lepton-flavor violating couplings. See their Figs. 6–7 and Tables 5–6 for detailed limits.
- <sup>15</sup> For limits on states with different quantum numbers and the limits in the mass-coupling plane, see their Fig. 3.
- <sup>16</sup> See their Fig. 14 for limits in the mass-coupling plane.
- <sup>17</sup> BREITWEG 00E search for  $F=0$  leptoquarks in  $e^+p$  collisions. For limits in mass-coupling plane, see their Fig. 11.
- <sup>18</sup> ABREU 99G limit obtained from process  $e\gamma \rightarrow LQ+q$ . For limits on vector and scalar states with different quantum numbers and the limits in the coupling-mass plane, see their Fig. 4 and Table 2.
- <sup>19</sup> For limits on states with different quantum numbers and the limits in the mass-coupling plane, see their Fig. 13 and Fig. 14. ADLOFF 99 also search for leptoquarks with lepton-flavor violating couplings. ADLOFF 99 supersedes AID 96B.
- <sup>20</sup> DERRICK 97 search for various leptoquarks with lepton-flavor violating couplings. See their Figs. 5–8 and Table 1 for detailed limits.
- <sup>21</sup> DERRICK 93 search for single leptoquark production in  $ep$  collisions with the decay  $e q$  and  $\nu q$ . The limit is for leptoquark coupling of electromagnetic strength and assumes  $B(eq) = B(\nu q) = 1/2$ . The limit for  $B(eq) = 1$  is 176 GeV. For limits on states with different quantum numbers, see their Table 3.

- <sup>3</sup> ZHANG 18A give bounds on leptoquark induced four-fermion interactions from  $D \rightarrow K\ell\nu$ . The authors inform us that the shape parameter of the vector form factor in both the abstract and the conclusions of ZHANG 18A should be  $r_{+1} = 2.16 \pm 0.07$  rather than  $\pm 0.007$ . The numbers listed in their Table 7 are correct.
- <sup>4</sup> BARRANCO 16 give bounds on leptoquark induced four-fermion interactions from  $D \rightarrow K\ell\nu$  and  $D_S \rightarrow \ell\nu$ .
- <sup>5</sup> KUMAR 16 gives bound on SU(2) singlet scalar leptoquark with charge  $-1/3$  from  $K^0 - \bar{K}^0$  mixing,  $K \rightarrow \pi\nu\bar{\nu}$ ,  $K_L^0 \rightarrow \mu^+\mu^-$ , and  $K_L^0 \rightarrow \mu^\pm e^\mp$  decays.
- <sup>6</sup> BESSAA 15 obtain limit on leptoquark induced four-fermion interactions from the ATLAS and CMS limit on the  $\bar{q}q\bar{e}e$  contact interactions.
- <sup>7</sup> SAHOV 15A obtain limit on leptoquark induced four-fermion interactions from  $B_{s,d} \rightarrow \mu^+\mu^-$  for  $\lambda \simeq O(1)$ .
- <sup>8</sup> SAKAKI 13 explain the  $B \rightarrow D^{(*)}\tau\bar{\nu}$  anomaly using Wilson coefficients of leptoquark-induced four-fermion operators.
- <sup>9</sup> KOSNIK 12 obtains limits on leptoquark induced four-fermion interactions from  $b \rightarrow s\ell^+\ell^-$  decays.
- <sup>10</sup> AARON 11c limit is for weak isotriplet spin-0 leptoquark at strong coupling  $\lambda = \sqrt{4\pi}$ . For the limits of leptoquarks with different quantum numbers, see their Table 3. Limits are derived from bounds of  $eq$  contact interactions.
- <sup>11</sup> DORSNER 11 give bounds on scalar, weak singlet, charge  $4/3$  leptoquark from  $K, B, \tau$  decays, meson mixings,  $LFV, g-2$  and  $Z \rightarrow b\bar{b}$ .
- <sup>12</sup> AKTAS 07A search for lepton-flavor violation in  $ep$  collision. See their Tables 4–7 for limits on lepton-flavor violating four-fermion interactions induced by various leptoquarks.
- <sup>13</sup> SCHAEEL 07A limit is for the weak-isoscalar spin-0 left-handed leptoquark with the coupling of electromagnetic strength. For the limits of leptoquarks with different quantum numbers, see their Table 35.
- <sup>14</sup> SMIRNOV 07 obtains mass limits for the vector and scalar chiral leptoquark states from  $K \rightarrow e\mu, B \rightarrow e\tau$  decays.
- <sup>15</sup> CHEKANOV 05 search for various leptoquarks with lepton-flavor violating couplings. See their Figs.6–10 and Tables 1–8 for detailed limits.
- <sup>16</sup> ADLOFF 03 limit is for the weak isotriplet spin-0 leptoquark at strong coupling  $\lambda = \sqrt{4\pi}$ . For the limits of leptoquarks with different quantum numbers, see their Table 3. Limits are derived from bounds on  $e^\pm q$  contact interactions.
- <sup>17</sup> The bound is derived from  $B(B^0 \rightarrow e^\pm\mu^\mp) < 1.7 \times 10^{-7}$ .
- <sup>18</sup> CHEKANOV 02 search for lepton-flavor violation in  $ep$  collisions. See their Tables 1–4 for limits on lepton-flavor violating and four-fermion interactions induced by various leptoquarks.
- <sup>19</sup> CHEUNG 01B quoted limit is for a scalar, weak isoscalar, charge  $-1/3$  leptoquark with a coupling of electromagnetic strength. The limit is derived from bounds on contact interactions in a global electroweak analysis. For the limits of leptoquarks with different quantum numbers, see Table 5.
- <sup>20</sup> ACCIARRI 00P limit is for the weak isoscalar spin-0 leptoquark with the coupling of electromagnetic strength. For the limits of leptoquarks with different quantum numbers, see their Table 4.
- <sup>21</sup> ADLOFF 00 limit is for the weak isotriplet spin-0 leptoquark at strong coupling,  $\lambda = \sqrt{4\pi}$ . For the limits of leptoquarks with different quantum numbers, see their Table 2. ADLOFF 00 limits are from the  $Q^2$  spectrum measurement of  $e^+p \rightarrow e^+X$ .
- <sup>22</sup> BARATE 00i search for deviations in cross section and jet-charge asymmetry in  $e^+e^- \rightarrow q\bar{q}$  due to  $t$ -channel exchange of a leptoquark at  $\sqrt{s}=130$  to 183 GeV. Limits for other scalar and vector leptoquarks are also given in their Table 22.
- <sup>23</sup> BARGER 00 explain the deviation of atomic parity violation in cesium atoms from prediction is explained by scalar leptoquark exchange.
- <sup>24</sup> GABRIELLI 00 calculate various process with lepton flavor violation in leptoquark models.
- <sup>25</sup> ZARNECKI 00 limit is derived from data of HERA, LEP, and Tevatron and from various low-energy data including atomic parity violation. Leptoquark coupling with electromagnetic strength is assumed.
- <sup>26</sup> ABBIENDI 99 limits are from  $e^+e^- \rightarrow q\bar{q}$  cross section at 130–136, 161–172, 183 GeV. See their Fig. 8 and Fig. 9 for limits in mass-coupling plane.
- <sup>27</sup> ABE 98v quoted limit is from  $B(B_S \rightarrow e^\pm\mu^\mp) < 8.2 \times 10^{-6}$ . ABE 98v also obtain a similar limit on  $M_{LQ} > 20.4$  TeV from  $B(B_{d,s} \rightarrow e^\pm\mu^\mp) < 4.5 \times 10^{-6}$ . Both bounds assume the non-canonical association of the  $b$  quark with electrons or muons under SU(4).
- <sup>28</sup> ACCIARRI 98j limit is from  $e^+e^- \rightarrow q\bar{q}$  cross section at  $\sqrt{s}=130$ –172 GeV which can be affected by the  $t$ - and  $u$ -channel exchanges of leptoquarks. See their Fig. 4 and Fig. 5 for limits in the mass-coupling plane.
- <sup>29</sup> ACKERSTAFF 98v limits are from  $e^+e^- \rightarrow q\bar{q}$  and  $e^+e^- \rightarrow b\bar{b}$  cross sections at  $\sqrt{s} = 130$ –172 GeV, which can be affected by the  $t$ - and  $u$ -channel exchanges of leptoquarks. See their Fig. 21 and Fig. 22 for limits of leptoquarks in mass-coupling plane.
- <sup>30</sup> DEANDREA 97 limit is for  $\bar{R}_2$  leptoquark obtained from atomic parity violation (APV). The coupling of leptoquark is assumed to be electromagnetic strength. See Table 2 for limits of the four-fermion interactions induced by various scalar leptoquark exchange. DEANDREA 97 combines APV limit and limits from Tevatron and HERA. See Fig. 1–4 for combined limits of leptoquark in mass-coupling plane.
- <sup>31</sup> DERRICK 97 search for lepton-flavor violation in  $ep$  collision. See their Tables 2–5 for limits on lepton-flavor violating four-fermion interactions induced by various leptoquarks.
- <sup>32</sup> GROSSMAN 97 estimate the upper bounds on the branching fraction  $B \rightarrow \tau^+\tau^- (X)$  from the absence of the  $B$  decay with large missing energy. These bounds can be used to constrain leptoquark induced four-fermion interactions.
- <sup>33</sup> JADACH 97 limit is from  $e^+e^- \rightarrow q\bar{q}$  cross section at  $\sqrt{s}=172.3$  GeV which can be affected by the  $t$ - and  $u$ -channel exchanges of leptoquarks. See their Fig. 1 for limits on vector leptoquarks in mass-coupling plane.
- <sup>34</sup> KUZNETSOV 95b use  $\pi, K, B, \tau$  decays and  $\mu e$  conversion and give a list of bounds on the leptoquark mass and the fermion mixing matrix in the Pati-Salam model. The quoted limit is from  $K_L \rightarrow \mu e$  decay assuming zero mixing.
- <sup>35</sup> MIZUKOSHI 95 calculate the one-loop radiative correction to the Z-physics parameters in various scalar leptoquark models. See their Fig. 4 for the exclusion plot of third generation leptoquark models in mass-coupling plane.
- <sup>36</sup> BHATTACHARYYA 94 limit is from one-loop radiative correction to the leptonic decay width of the Z.  $m_H=250$  GeV,  $\alpha_S(m_Z)=0.12$ ,  $m_t=180$  GeV, and the electroweak strength of leptoquark coupling are assumed. For leptoquark coupled to  $\bar{t}_L t_R, \bar{\nu}_L \tau_R$ , and  $\bar{\nu}_L \tau$ , see Fig. 2 in BHATTACHARYYA 94b erratum and Fig. 3.
- <sup>37</sup> DAVIDSON 94 gives an extensive list of the bounds on leptoquark-induced four-fermion interactions from  $\pi, K, D, B, \mu, \tau$  decays and meson mixings, etc. See Table 15 of DAVIDSON 94 for detail.

### Indirect Limits for Leptoquarks

VALUE (TeV)	CL%	DOCUMENT ID	TECN	COMMENT		
• • • We do not use the following data for averages, fits, limits, etc. • • •						
> 3.1	95	1	ABRAMOWICZ19	ZEUS	First generation	
		2	MANDAL	19	RVUE	$\tau, \mu, e, K$
		3	ZHANG	18A	RVUE	$D$ decays
		4	BARRANCO	16	RVUE	$D$ decays
		5	KUMAR	16	RVUE	neutral $K$ mixing, rare $K$ decays
		6	BESSAA	15	RVUE	$q\bar{q} \rightarrow e^+e^-$
		7	SAHOV	15A	RVUE	$B_{s,d} \rightarrow \mu^+\mu^-$
> 14	95	8	SAKAKI	13	RVUE	$B \rightarrow D^{(*)}\tau\bar{\nu}, B \rightarrow X_S\nu\bar{\nu}$
		9	KOSNIK	12	RVUE	$b \rightarrow s\ell^+\ell^-$
		10	AARON	11c	H1	First generation
> 2.5	95	11	DORSNER	11	RVUE	scalar, weak singlet, charge $4/3$
		12	AKTAS	07A	H1	Lepton-flavor violation
		13	SCHAEEL	07A	ALEP	$e^+e^- \rightarrow q\bar{q}$
> 0.49	95	14	SMIRNOV	07	RVUE	$K \rightarrow e\mu, B \rightarrow e\tau$
		15	CHEKANOV	05A	ZEUS	Lepton-flavor violation
		16	ADLOFF	03	H1	First generation
> 1.7	96	17	CHANG	03	BELL	Pati-Salam type
		18	CHEKANOV	02	ZEUS	Repl. by CHEKANOV 05A
> 46	90	19	CHEUNG	01B	RVUE	First generation
		20	ACCIARRI	00P	L3	$e^+e^- \rightarrow q\bar{q}$
> 1.7	95	21	ADLOFF	00	H1	First generation
		22	BARATE	00i	ALEP	Repl. by SCHAEEL 07A
> 0.39	95	23	BARGER	00	RVUE	Cs
		24	GABRIELLI	00	RVUE	Lepton flavor violation
> 1.5	95	25	ZARNECKI	00	RVUE	$S_1$ leptoquark
		26	ABBIENDI	99	OPAL	
> 0.2	95	27	ABE	98v	CDF	$B_S \rightarrow e^\pm\mu^\mp$ , Pati-Salam type
		28	ACCIARRI	98j	L3	$e^+e^- \rightarrow q\bar{q}$
> 19.3	95	29	ACKERSTAFF	98v	OPAL	$e^+e^- \rightarrow q\bar{q}, e^+e^- \rightarrow b\bar{b}$
		30	DEANDREA	97	RVUE	$\bar{R}_2$ leptoquark
> 0.74	95	31	DERRICK	97	ZEUS	Lepton-flavor violation
		32	GROSSMAN	97	RVUE	$B \rightarrow \tau^+\tau^- (X)$
> 1.7	95	33	JADACH	97	RVUE	$e^+e^- \rightarrow q\bar{q}$
		34	KUZNETSOV	95b	RVUE	Pati-Salam type
> 0.3	95	35	MIZUKOSHI	95	RVUE	Third generation scalar leptoquark
		36	BHATTACH...	94	RVUE	Spin-0 leptoquark coupled to $\bar{\nu}_R t_L$
> 18	95	37	DAVIDSON	94	RVUE	
		38	KUZNETSOV	94	RVUE	Pati-Salam type
> 0.43	95	39	LEURER	94	RVUE	First generation spin-1 leptoquark
		39	LEURER	94b	RVUE	First generation spin-0 leptoquark
> 0.44	95	40	MAHANTA	94	RVUE	$P$ and $T$ violation
		41	SHANKER	82	RVUE	Nonchiral spin-0 leptoquark
> 1	95	41	SHANKER	82	RVUE	Nonchiral spin-1 leptoquark

- <sup>1</sup> ABRAMOWICZ 19 obtain a limit on  $\lambda/M_{LQ} > 1.16$  TeV $^{-1}$  for weak isotriplet spin-0 leptoquark  $S_L^+$ . We obtain the limit quoted above by converting the limit on  $\lambda/M_{LQ}$  for  $S_L^+$  assuming  $\lambda = \sqrt{4\pi}$ . See their Table 5 for the limits of leptoquarks with different quantum numbers. These limits are derived from bounds of  $eq$  contact interactions.
- <sup>2</sup> MANDAL 19 give bounds on leptoquarks from  $\tau$ -decays, leptonic dipole moments, lepton-flavor-violating processes, and  $K$  decays.

# Gauge & Higgs Boson Particle Listings

## New Heavy Bosons

- <sup>38</sup> KUZNETSOV 94 gives mixing independent bound of the Pati-Salam leptoquark from the cosmological limit on  $\pi^0 \rightarrow \nu\bar{\nu}$ .
- <sup>39</sup> LEURER 94, LEURER 94B limits are obtained from atomic parity violation and apply to any chiral leptoquark which couples to the first generation with electromagnetic strength. For a nonchiral leptoquark, universality in  $\pi_{\ell 2}$  decay provides a much more stringent bound.
- <sup>40</sup> MAHANTA 94 gives bounds of  $P$ - and  $T$ -violating scalar-leptoquark couplings from atomic and molecular experiments.
- <sup>41</sup> From  $(\pi \rightarrow e\nu)/(\pi \rightarrow \mu\nu)$  ratio. SHANKER 82 assumes the leptoquark induced four-fermion coupling  $4g^2/M^2 (\bar{\nu}_e \ell u_R) (\bar{\ell} \ell e_R)$  with  $g=0.004$  for spin-0 leptoquark and  $g^2/M^2 (\bar{\nu}_e \ell u_L) (\bar{\ell} \ell e_R)$  with  $g \approx 0.6$  for spin-1 leptoquark.

### MASS LIMITS for Diquarks

VALUE (GeV)	CL%	DOCUMENT ID	TECN	COMMENT
<b>&gt;6000 (CL = 95%) OUR LIMIT</b>				
none 600–7200	95	1 SIRUNYAN 18B0 CMS	$E_6$	diquark
none 600–6900	95	2 KHACHATRYAN...17W CMS	$E_6$	diquark
none 1500–6000	95	3 KHACHATRYAN...16K CMS	$E_6$	diquark
none 500–1600	95	4 KHACHATRYAN...16L CMS	$E_6$	diquark
none 1200–4700	95	5 KHACHATRYAN...15V CMS	$E_6$	diquark
• • • We do not use the following data for averages, fits, limits, etc. • • •				
>3750	95	6 CHATRCHYAN 13A CMS	$E_6$	diquark
none 1000–4280	95	7 CHATRCHYAN 13AS CMS	Superseded by KHACHATRYAN 15V	
>3520	95	8 CHATRCHYAN 11Y CMS	Superseded by CHATRCHYAN 13A	
none 970–1080, 1450–1600	95	9 KHACHATRYAN...10 CMS	Superseded by CHATRCHYAN 13A	
none 290–630	95	10 AALTONEN 09AC CDF	$E_6$	diquark
none 290–420	95	11 ABE 97G CDF	$E_6$	diquark
none 15–31.7	95	12 ABREU 94O DLPH	SUSY $E_6$	diquark

- <sup>1</sup> SIRUNYAN 18B0 search for resonances decaying to dijets in  $pp$  collisions at  $\sqrt{s} = 13$  TeV.
- <sup>2</sup> KHACHATRYAN 17W search for resonances decaying to dijets in  $pp$  collisions at  $\sqrt{s} = 13$  TeV.
- <sup>3</sup> KHACHATRYAN 16K search for resonances decaying to dijets in  $pp$  collisions at  $\sqrt{s} = 13$  TeV.
- <sup>4</sup> KHACHATRYAN 16L search for resonances decaying to dijets in  $pp$  collisions at  $\sqrt{s} = 8$  TeV with the data scouting technique, increasing the sensitivity to the low mass resonances.
- <sup>5</sup> KHACHATRYAN 15V search for resonances decaying to dijets in  $pp$  collisions at  $\sqrt{s} = 8$  TeV.
- <sup>6</sup> CHATRCHYAN 13A search for new resonance decaying to dijets in  $pp$  collisions at  $\sqrt{s} = 7$  TeV.
- <sup>7</sup> CHATRCHYAN 13AS search for new resonance decaying to dijets in  $pp$  collisions at  $\sqrt{s} = 8$  TeV.
- <sup>8</sup> CHATRCHYAN 11Y search for new resonance decaying to dijets in  $pp$  collisions at  $\sqrt{s} = 7$  TeV.
- <sup>9</sup> KHACHATRYAN 10 search for new resonance decaying to dijets in  $pp$  collisions at  $\sqrt{s} = 7$  TeV.
- <sup>10</sup> AALTONEN 09AC search for new narrow resonance decaying to dijets.
- <sup>11</sup> ABE 97G search for new particle decaying to dijets.
- <sup>12</sup> ABREU 94O limit is from  $e^+e^- \rightarrow \tau\bar{\tau}c s$ . Range extends up to 43 GeV if diquarks are degenerate in mass.

### MASS LIMITS for $g_A$ (axigluon) and Other Color-Octet Gauge Bosons

Axigluons are massive color-octet gauge bosons in chiral color models and have axial-vector coupling to quarks with the same coupling strength as gluons.

VALUE (GeV)	CL%	DOCUMENT ID	TECN	COMMENT
<b>&gt;6100 (CL = 95%) OUR LIMIT</b>				
none 600–6100	95	1 SIRUNYAN 18B0 CMS	$pp \rightarrow g_A X, g_A \rightarrow 2j$	
none 600–5500	95	2 KHACHATRYAN...17W CMS	$pp \rightarrow g_A X, g_A \rightarrow 2j$	
none 1500–5100	95	3 KHACHATRYAN...16K CMS	$pp \rightarrow g_A X, g_A \rightarrow 2j$	
none 500–1600	95	4 KHACHATRYAN...16L CMS	$pp \rightarrow g_A X, g_A \rightarrow 2j$	
none 1300–3600	95	5 KHACHATRYAN...15V CMS	$pp \rightarrow g_A X, g_A \rightarrow 2j$	
• • • We do not use the following data for averages, fits, limits, etc. • • •				
>2800	95	6 KHACHATRYAN...17Y CMS	$pp \rightarrow g_A g_A \rightarrow 8j$	
		7 AAD 16W ATLS	$pp \rightarrow g_A X, g_A \rightarrow b\bar{b}b\bar{b}$	
		8 KHACHATRYAN...16E CMS	$pp \rightarrow g_{KK} X, g_{KK} \rightarrow t\bar{t}$	
		9 KHACHATRYAN...15AV CMS	$pp \rightarrow \theta^0 \theta^0 \rightarrow b\bar{b}Zg$	
		10 AALTONEN 13R CDF	$p\bar{p} \rightarrow g_A X, g_A \rightarrow \sigma\sigma, \sigma \rightarrow 2j$	
>3360	95	11 CHATRCHYAN 13A CMS	$pp \rightarrow g_A X, g_A \rightarrow 2j$	
none 1000–3270	95	12 CHATRCHYAN 13AS CMS	Superseded by KHACHATRYAN 15V	
none 250–740	95	13 CHATRCHYAN 13AU CMS	$pp \rightarrow 2g_A X, g_A \rightarrow 2j$	
> 775	95	14 ABAZOV 12R D0	$p\bar{p} \rightarrow g_A X, g_A \rightarrow t\bar{t}$	
>2470	95	15 CHATRCHYAN 11Y CMS	Superseded by CHATRCHYAN 13A	
none 1470–1520	95	16 AALTONEN 10L CDF	$p\bar{p} \rightarrow g_A X, g_A \rightarrow t\bar{t}$	
		17 KHACHATRYAN...10 CMS	Superseded by CHATRCHYAN 13A	
none 260–1250	95	18 AALTONEN 09AC CDF	$p\bar{p} \rightarrow g_A X, g_A \rightarrow 2j$	
> 910	95	19 CHOUDHURY 07 RVUE	$p\bar{p} \rightarrow t\bar{t}X$	
> 365	95	20 DONCHESKI 98 RVUE	$\Gamma(Z \rightarrow \text{hadron})$	

none 200–980	95	21 ABE 97G CDF	$p\bar{p} \rightarrow g_A X, g_A \rightarrow 2j$
none 200–870	95	22 ABE 95N CDF	$p\bar{p} \rightarrow g_A X, g_A \rightarrow q\bar{q}$
none 240–640	95	23 ABE 93G CDF	$p\bar{p} \rightarrow g_A X, g_A \rightarrow 2j$
> 50	95	24 CUYPERS 91 RVUE	$\sigma(e^+e^- \rightarrow \text{hadrons})$
none 120–210	95	25 ABE 90H CDF	$p\bar{p} \rightarrow g_A X, g_A \rightarrow 2j$
> 29		26 ROBINETT 89 THEO	Partial-wave unitarity
none 150–310	95	27 ALBAJAR 88B UA1	$p\bar{p} \rightarrow g_A X, g_A \rightarrow 2j$
> 20		BERGSTROM 88 RVUE	$p\bar{p} \rightarrow TX$ via $g_A g$
> 9		28 CUYPERS 88 RVUE	$T$ decay
> 25		29 DONCHESKI 88B RVUE	$T$ decay

- <sup>1</sup> SIRUNYAN 18B0 search for resonances decaying to dijets in  $pp$  collisions at  $\sqrt{s} = 13$  TeV.
- <sup>2</sup> KHACHATRYAN 17W search for resonances decaying to dijets in  $pp$  collisions at  $\sqrt{s} = 13$  TeV.
- <sup>3</sup> KHACHATRYAN 16K search for resonances decaying to dijets in  $pp$  collisions at  $\sqrt{s} = 13$  TeV.
- <sup>4</sup> KHACHATRYAN 16L search for resonances decaying to dijets in  $pp$  collisions at  $\sqrt{s} = 8$  TeV with the data scouting technique, increasing the sensitivity to the low mass resonances.
- <sup>5</sup> KHACHATRYAN 15V search for resonances decaying to dijets in  $pp$  collisions at  $\sqrt{s} = 8$  TeV.
- <sup>6</sup> KHACHATRYAN 17Y search for pair production of color-octet gauge boson  $g_A$  each decaying to  $4j$  in  $pp$  collisions at  $\sqrt{s} = 8$  TeV.
- <sup>7</sup> AAD 16W search for a new resonance decaying to a pair of  $b$  and  $B_H$  in  $pp$  collisions at  $\sqrt{s} = 8$  TeV. The vector-like quark  $B_H$  is assumed to decay to  $bH$ . See their Fig. 3 and Fig. 4 for limits on  $\sigma \cdot B$ .
- <sup>8</sup> KHACHATRYAN 16E search for KK gluon decaying to  $t\bar{t}$  in  $pp$  collisions at  $\sqrt{s} = 8$  TeV.
- <sup>9</sup> KHACHATRYAN 15AV search for pair productions of neutral color-octet weak-triplet scalar particles ( $\theta^0$ ), decaying to  $b\bar{b}$ ,  $Zg$  or  $\gamma g$ , in  $pp$  collisions at  $\sqrt{s} = 8$  TeV. The  $\theta^0$  particle is often predicted in coloron ( $G'$ , color-octet gauge boson) models and appear in the  $pp$  collisions through  $G' \rightarrow \theta^0 \theta^0$  decays. Assuming  $B(\theta^0 \rightarrow b\bar{b}) = 0.5$ , they give limits  $m_{\theta^0} > 623$  GeV (426 GeV) for  $m_{G'} = 2.3 m_{\theta^0}$  ( $m_{G'} = 5 m_{\theta^0}$ ).
- <sup>10</sup> AALTONEN 13R search for new resonance decaying to  $\sigma\sigma$ , with hypothetical strongly interacting  $\sigma$  particle subsequently decaying to 2 jets, in  $p\bar{p}$  collisions at  $\sqrt{s} = 1.96$  TeV, using data corresponding to an integrated luminosity of 6.6 fb<sup>-1</sup>. For 50 GeV  $< m_\sigma < m_{g_A}/2$ , axigluons in mass range 150–400 GeV are excluded.
- <sup>11</sup> CHATRCHYAN 13A search for new resonance decaying to dijets in  $pp$  collisions at  $\sqrt{s} = 7$  TeV.
- <sup>12</sup> CHATRCHYAN 13AS search for new resonance decaying to dijets in  $pp$  collisions at  $\sqrt{s} = 8$  TeV.
- <sup>13</sup> CHATRCHYAN 13AU search for the pair produced color-octet vector bosons decaying to  $q\bar{q}$  pairs in  $pp$  collisions. The quoted limit is for  $B(g_A \rightarrow q\bar{q}) = 1$ .
- <sup>14</sup> ABAZOV 12R search for massive color octet vector particle decaying to  $t\bar{t}$ . The quoted limit assumes  $g_A$  couplings with light quarks are suppressed by 0.2.
- <sup>15</sup> CHATRCHYAN 11Y search for new resonance decaying to dijets in  $pp$  collisions at  $\sqrt{s} = 7$  TeV.
- <sup>16</sup> AALTONEN 10L search for massive color octet non-chiral vector particle decaying into  $t\bar{t}$  pair with mass in the range 400 GeV  $< M < 800$  GeV. See their Fig. 6 for limit in the mass-coupling plane.
- <sup>17</sup> KHACHATRYAN 10 search for new resonance decaying to dijets in  $pp$  collisions at  $\sqrt{s} = 7$  TeV.
- <sup>18</sup> AALTONEN 09AC search for new narrow resonance decaying to dijets.
- <sup>19</sup> CHOUDHURY 07 limit is from the  $t\bar{t}$  production cross section measured at CDF.
- <sup>20</sup> DONCHESKI 98 compare  $\alpha_s$  derived from low-energy data and that from  $\Gamma(Z \rightarrow \text{hadrons})/\Gamma(Z \rightarrow \text{leptons})$ .
- <sup>21</sup> ABE 97G search for new particle decaying to dijets.
- <sup>22</sup> ABE 95N assume axigluons decaying to quarks in the Standard Model only.
- <sup>23</sup> ABE 93G assume  $\Gamma(g_A) = N\alpha_s m_{g_A}/6$  with  $N = 10$ .
- <sup>24</sup> CUYPERS 91 compare  $\alpha_s$  measured in  $T$  decay and that from  $R$  at PEP/PETRA energies.
- <sup>25</sup> ABE 90H assumes  $\Gamma(g_A) = N\alpha_s m_{g_A}/6$  with  $N = 5$  ( $\Gamma(g_A) = 0.09 m_{g_A}$ ). For  $N = 10$ , the excluded region is reduced to 120–150 GeV.
- <sup>26</sup> ROBINETT 89 result demands partial-wave unitarity of  $J = 0$   $t\bar{t} \rightarrow t\bar{t}$  scattering amplitude and derives a limit  $m_{g_A} > 0.5 m_t$ . Assumes  $m_t > 56$  GeV.
- <sup>27</sup> ALBAJAR 88B result is from the nonobservation of a peak in two-jet invariant mass distribution.  $\Gamma(g_A) < 0.4 m_{g_A}$  assumed. See also BAGGER 88.
- <sup>28</sup> CUYPERS 88 requires  $\Gamma(T \rightarrow g g_A) < \Gamma(T \rightarrow g g g)$ . A similar result is obtained by DONCHESKI 88.
- <sup>29</sup> DONCHESKI 88B requires  $\Gamma(T \rightarrow g q\bar{q})/\Gamma(T \rightarrow g g g) < 0.25$ , where the former decay proceeds via axigluon exchange. A more conservative estimate of  $< 0.5$  leads to  $m_{g_A} > 21$  GeV.

### MASS LIMITS for Color-Octet Scalar Bosons

VALUE (GeV)	CL%	DOCUMENT ID	TECN	COMMENT
• • • We do not use the following data for averages, fits, limits, etc. • • •				
none 600–3400	95	1 SIRUNYAN 18B0 CMS	$pp \rightarrow S_8 X, S_8 \rightarrow g g$	
		2 KHACHATRYAN...15AV CMS	$pp \rightarrow \theta^0 \theta^0 \rightarrow b\bar{b}Zg$	
none 150–287	95	3 AAD 13K ATLS	$pp \rightarrow S_8 S_8 X, S_8 \rightarrow 2j$	
		1 SIRUNYAN 18B0	search for color octet scalar boson produced through gluon fusion process in $pp$ collisions at $\sqrt{s} = 13$ TeV. The limit above assumes $S_{8gg}$ coupling $k_s^2 = 1/2$ .	
		2 KHACHATRYAN 15AV	search for pair productions of neutral color-octet weak-triplet scalar particles ( $\theta^0$ ), decaying to $b\bar{b}$ , $Zg$ or $\gamma g$ , in $pp$ collisions at $\sqrt{s} = 8$ TeV. The $\theta^0$ particle is often predicted in coloron ( $G'$ , color-octet gauge boson) models and appear in the $pp$ collisions through $G' \rightarrow \theta^0 \theta^0$ decays. Assuming $B(\theta^0 \rightarrow b\bar{b}) = 0.5$ , they give limits $m_{\theta^0} > 623$ GeV (426 GeV) for $m_{G'} = 2.3 m_{\theta^0}$ ( $m_{G'} = 5 m_{\theta^0}$ ).	

See key on page 999

# Gauge & Higgs Boson Particle Listings

## New Heavy Bosons

<sup>3</sup>AAD 13k search for pair production of color-octet scalar particles in  $pp$  collisions at  $\sqrt{s} = 7$  TeV. Cross section limits are interpreted as mass limits on scalar partners of a Dirac gluino.

### $X^0$ (Heavy Boson) Searches in Z Decays

Searches for radiative transition of Z to a lighter spin-0 state  $X^0$  decaying to hadrons, a lepton pair, a photon pair, or invisible particles as shown in the comments. The limits are for the product of branching ratios.

VALUE	CL%	DOCUMENT ID	TECN	COMMENT
• • • We do not use the following data for averages, fits, limits, etc. • • •				
		1 RAINBOLT 19	RVUE	$X^0 \rightarrow \ell^+ \ell^-$
		2 SIRUNYAN 19AZ	CMS	$X^0 \rightarrow \mu^+ \mu^-$
		3 BARATE 98U	ALEP	$X^0 \rightarrow \ell \bar{\ell}, q \bar{q}, gg, \gamma\gamma, \nu\bar{\nu}$
		4 ACCIARRI 97Q	L3	$X^0 \rightarrow$ invisible particle(s)
		5 ACTON 93E	OPAL	$X^0 \rightarrow \gamma\gamma$
		6 ABREU 92D	DLPH	$X^0 \rightarrow$ hadrons
		7 ADRIANI 92F	L3	$X^0 \rightarrow$ hadrons
		8 ACTON 91	OPAL	$X^0 \rightarrow$ anything
		9 ACTON 91B	OPAL	$X^0 \rightarrow e^+ e^-$
$<1.1 \times 10^{-4}$	95	9 ACTON 91B	OPAL	$X^0 \rightarrow \mu^+ \mu^-$
$<9 \times 10^{-5}$	95	9 ACTON 91B	OPAL	$X^0 \rightarrow \tau^+ \tau^-$
$<1.1 \times 10^{-4}$	95	9 ACTON 91B	OPAL	$X^0 \rightarrow e^+ e^-$
$<2.8 \times 10^{-4}$	95	10 ADEVA 91D	L3	$X^0 \rightarrow e^+ e^-$
$<2.3 \times 10^{-4}$	95	10 ADEVA 91D	L3	$X^0 \rightarrow \mu^+ \mu^-$
$<4.7 \times 10^{-4}$	95	11 ADEVA 91D	L3	$X^0 \rightarrow$ hadrons
$<8 \times 10^{-4}$	95	12 AKRAWY 90J	OPAL	$X^0 \rightarrow$ hadrons

- RAINBOLT 19 limits are from  $B(Z \rightarrow \ell^+ \ell^- \ell^+ \ell^-)$ . See their Figs. 5 and 6 for limits in mass-coupling plane.
- SIRUNYAN 19AZ search for  $pp \rightarrow Z \rightarrow X^0 \mu^+ \mu^- \rightarrow \mu^+ \mu^- \mu^+ \mu^-$  events in  $pp$  collisions at  $\sqrt{s} = 13$  TeV. See their Fig. 5 for limits on  $\sigma(pp \rightarrow X^0 \mu^+ \mu^-) \cdot B(X^0 \rightarrow \mu^+ \mu^-)$ .
- BARATE 98U obtain limits on  $B(Z \rightarrow \gamma X^0) \cdot B(X^0 \rightarrow \ell \bar{\ell}, q \bar{q}, gg, \gamma\gamma, \nu\bar{\nu})$ . See their Fig. 17.
- See Fig. 4 of ACCIARRI 97Q for the upper limit on  $B(Z \rightarrow \gamma X^0; E_\gamma > E_{\min})$  as a function of  $E_{\min}$ .
- ACTON 93E give  $\sigma(e^+ e^- \rightarrow X^0 \gamma) \cdot B(X^0 \rightarrow \gamma\gamma) < 0.4$  pb (95%CL) for  $m_{X^0} = 60 \pm 2.5$  GeV. If the process occurs via s-channel  $\gamma$  exchange, the limit translates to  $\Gamma(X^0) \cdot B(X^0 \rightarrow \gamma\gamma)^2 < 20$  MeV for  $m_{X^0} = 60 \pm 1$  GeV.
- ABREU 92D give  $\sigma_Z \cdot B(Z \rightarrow \gamma X^0) \cdot B(X^0 \rightarrow \text{hadrons}) < (3-10)$  pb for  $m_{X^0} = 10-78$  GeV. A very similar limit is obtained for spin-1  $X^0$ .
- ADRIANI 92F search for isolated  $\gamma$  in hadronic Z decays. The limit  $\sigma_Z \cdot B(Z \rightarrow \gamma X^0) \cdot B(X^0 \rightarrow \text{hadrons}) < (2-10)$  pb (95%CL) is given for  $m_{X^0} = 25-85$  GeV.
- ACTON 91 searches for  $Z \rightarrow Z^* X^0, Z^* \rightarrow e^+ e^-, \mu^+ \mu^-,$  or  $\nu\bar{\nu}$ . Excludes any new scalar  $X^0$  with  $m_{X^0} < 9.5$  GeV/c if it has the same coupling to  $ZZ^*$  as the MSM Higgs boson.
- ACTON 91B limits are for  $m_{X^0} = 60-85$  GeV.
- ADEVA 91D limits are for  $m_{X^0} = 30-89$  GeV.
- ADEVA 91D limits are for  $m_{X^0} = 30-86$  GeV.
- AKRAWY 90J give  $\Gamma(Z \rightarrow \gamma X^0) \cdot B(X^0 \rightarrow \text{hadrons}) < 1.9$  MeV (95%CL) for  $m_{X^0} = 32-80$  GeV. We divide by  $\Gamma(Z) = 2.5$  GeV to get product of branching ratios. For nonresonant transitions, the limit is  $B(Z \rightarrow \gamma q \bar{q}) < 8.2$  MeV assuming three-body phase space distribution.

### MASS LIMITS for a Heavy Neutral Boson Coupling to $e^+ e^-$

VALUE (GeV)	CL%	DOCUMENT ID	TECN	COMMENT
• • • We do not use the following data for averages, fits, limits, etc. • • •				
none 55-61		1 ODAKA 89	VNS	$\Gamma(X^0 \rightarrow e^+ e^-) \cdot B(X^0 \rightarrow \text{had.}) \gtrsim 0.2$ MeV
$>45$	95	2 DERRICK 86	HRS	$\Gamma(X^0 \rightarrow e^+ e^-) = 6$ MeV
$>46.6$	95	3 ADEVA 85	MRKJ	$\Gamma(X^0 \rightarrow e^+ e^-) = 10$ keV
$>48$	95	3 ADEVA 85	MRKJ	$\Gamma(X^0 \rightarrow e^+ e^-) = 4$ MeV
		4 BERGER 85B	PLUT	
none 39.8-45.5		5 ADEVA 84	MRKJ	$\Gamma(X^0 \rightarrow e^+ e^-) = 10$ keV
$>47.8$	95	5 ADEVA 84	MRKJ	$\Gamma(X^0 \rightarrow e^+ e^-) = 4$ MeV
none 39.8-45.2		5 BEHREND 84c	CELL	
$>47$	95	5 BEHREND 84c	CELL	$\Gamma(X^0 \rightarrow e^+ e^-) = 4$ MeV

- ODAKA 89 looked for a narrow or wide scalar resonance in  $e^+ e^- \rightarrow$  hadrons at  $E_{cm} = 55.0-60.8$  GeV.
- DERRICK 86 found no deviation from the Standard Model Bhabha scattering at  $E_{cm} = 29$  GeV and set limits on the possible scalar boson  $e^+ e^-$  coupling. See their figure 4 for excluded region in the  $\Gamma(X^0 \rightarrow e^+ e^-) \cdot m_{X^0}$  plane. Electronic chiral invariance requires a parity doublet of  $X^0$ , in which case the limit applies for  $\Gamma(X^0 \rightarrow e^+ e^-) = 3$  MeV.
- ADEVA 85 first limit is from  $2\gamma, \mu^+ \mu^-,$  hadrons assuming  $X^0$  is a scalar. Second limit is from  $e^+ e^-$  channel.  $E_{cm} = 40-47$  GeV. Supersedes ADEVA 84.
- BERGER 85B looked for effect of spin-0 boson exchange in  $e^+ e^- \rightarrow e^+ e^-$  and  $\mu^+ \mu^-$  at  $E_{cm} = 34.7$  GeV. See Fig. 5 for excluded region in the  $m_{X^0} - \Gamma(X^0)$  plane.
- ADEVA 84 and BEHREND 84c have  $E_{cm} = 39.8-45.5$  GeV. MARK-J searched  $X^0$  in  $e^+ e^- \rightarrow$  hadrons,  $2\gamma, \mu^+ \mu^-, e^+ e^-$  and CELLO in the same channels plus  $\tau$  pair. No narrow or broad  $X^0$  is found in the energy range. They also searched for the effect of  $X^0$  with  $m_X > E_{cm}$ . The second limits are from Bhabha data and for spin-0 singlet.

The same limits apply for  $\Gamma(X^0 \rightarrow e^+ e^-) = 2$  MeV if  $X^0$  is a spin-0 doublet. The second limit of BEHREND 84c was read off from their figure 2. The original papers also list limits in other channels.

### Search for $X^0$ Resonance in $e^+ e^-$ Collisions

The limit is for  $\Gamma(X^0 \rightarrow e^+ e^-) \cdot B(X^0 \rightarrow f)$ , where  $f$  is the specified final state. Spin 0 is assumed for  $X^0$ .

VALUE (keV)	CL%	DOCUMENT ID	TECN	COMMENT
• • • We do not use the following data for averages, fits, limits, etc. • • •				
$<10^3$	95	1 ABE 93c	VNS	$\Gamma(ee)$
$<(0.4-10)$	95	2 ABE 93c	VNS	$f = \gamma\gamma$
$<(0.3-5)$	95	3,4 ABE 93d	TOPZ	$f = \gamma\gamma$
$<(2-12)$	95	3,4 ABE 93d	TOPZ	$f = \text{hadrons}$
$<(4-200)$	95	4,5 ABE 93d	TOPZ	$f = ee$
$<(0.1-6)$	95	4,5 ABE 93d	TOPZ	$f = \mu\mu$
$<(0.5-8)$	90	6 STERNER 93	AMY	$f = \gamma\gamma$

- Limit is for  $\Gamma(X^0 \rightarrow e^+ e^-) m_{X^0} = 56-63.5$  GeV for  $\Gamma(X^0) = 0.5$  GeV.
- Limit is for  $m_{X^0} = 56-61.5$  GeV and is valid for  $\Gamma(X^0) \ll 100$  MeV. See their Fig. 5 for limits for  $\Gamma = 1, 2$  GeV.
- Limit is for  $m_{X^0} = 57.2-60$  GeV.
- Limit is valid for  $\Gamma(X^0) \ll 100$  MeV. See paper for limits for  $\Gamma = 1$  GeV and those for  $J = 2$  resonances.
- Limit is for  $m_{X^0} = 56.6-60$  GeV.
- STERNER 93 limit is for  $m_{X^0} = 57-59.6$  GeV and is valid for  $\Gamma(X^0) < 100$  MeV. See their Fig. 2 for limits for  $\Gamma = 1, 3$  GeV.

### Search for $X^0$ Resonance in $ep$ Collisions

VALUE	DOCUMENT ID	TECN	COMMENT
• • • We do not use the following data for averages, fits, limits, etc. • • •			
	1 CHEKANOV 02B	ZEUS	$X \rightarrow jj$

- CHEKANOV 02B search for photoproduction of X decaying into dijets in  $ep$  collisions. See their Fig. 5 for the limit on the photoproduction cross section.

### Search for $X^0$ Resonance in $e^+ e^- \rightarrow X^0 \gamma$

VALUE (GeV)	DOCUMENT ID	TECN	COMMENT
• • • We do not use the following data for averages, fits, limits, etc. • • •			
	1 ABBIENDI 03d	OPAL	$X^0 \rightarrow \gamma\gamma$
	2 ABREU 00z	DLPH	$X^0$ decaying invisibly
	3 ADAM 96c	DLPH	$X^0$ decaying invisibly

- ABBIENDI 03d measure the  $e^+ e^- \rightarrow \gamma\gamma\gamma$  cross section at  $\sqrt{s}=181-209$  GeV. The upper bound on the production cross section,  $\sigma(e^+ e^- \rightarrow X^0 \gamma)$  times the branching ratio for  $X^0 \rightarrow \gamma\gamma$ , is less than 0.03 pb at 95%CL for  $X^0$  masses between 20 and 180 GeV. See their Fig. 9b for the limits in the mass-cross section plane.
- ABREU 00z is from the single photon cross section at  $\sqrt{s}=183, 189$  GeV. The production cross section upper limit is less than 0.3 pb for  $X^0$  mass between 40 and 160 GeV. See their Fig. 4 for the limit in mass-cross section plane.
- ADAM 96c is from the single photon production cross at  $\sqrt{s}=130, 136$  GeV. The upper bound is less than 3 pb for  $X^0$  masses between 60 and 130 GeV. See their Fig. 5 for the exact bound on the cross section  $\sigma(e^+ e^- \rightarrow \gamma X^0)$ .

### Search for $X^0$ Resonance in $Z \rightarrow f \bar{f} X^0$

The limit is for  $B(Z \rightarrow f \bar{f} X^0) \cdot B(X^0 \rightarrow F)$  where  $f$  is a fermion and  $F$  is the specified final state. Spin 0 is assumed for  $X^0$ .

VALUE	CL%	DOCUMENT ID	TECN	COMMENT
• • • We do not use the following data for averages, fits, limits, etc. • • •				
$<3.7 \times 10^{-6}$	95	1 ABREU 96T	DLPH	$f=e, \mu, \tau; F=\gamma\gamma$
		2 ABREU 96T	DLPH	$f=\nu; F=\gamma\gamma$
		3 ABREU 96T	DLPH	$f=q; F=\gamma\gamma$
$<6.8 \times 10^{-6}$	95	2 ACTON 93E	OPAL	$f=e, \mu, \tau; F=\gamma\gamma$
$<5.5 \times 10^{-6}$	95	2 ACTON 93E	OPAL	$f=q; F=\gamma\gamma$
$<3.1 \times 10^{-6}$	95	2 ACTON 93E	OPAL	$f=\nu; F=\gamma\gamma$
$<6.5 \times 10^{-6}$	95	2 ACTON 93E	OPAL	$f=e, \mu; F=\ell \bar{\ell}, q \bar{q}, \nu\bar{\nu}$
$<7.1 \times 10^{-6}$	95	2 BUSKULIC 93F	ALEP	$f=e, \mu; F=\ell \bar{\ell}, q \bar{q}, \nu\bar{\nu}$
		4 ADRIANI 92F	L3	$f=q; F=\gamma\gamma$

- ABREU 96T obtain limit as a function of  $m_{X^0}$ . See their Fig. 6.
- Limit is for  $m_{X^0}$  around 60 GeV.
- ABREU 96T obtain limit as a function of  $m_{X^0}$ . See their Fig. 15.
- ADRIANI 92F give  $\sigma_Z \cdot B(Z \rightarrow q \bar{q} X^0) \cdot B(X^0 \rightarrow \gamma\gamma) < (0.75-1.5)$  pb (95%CL) for  $m_{X^0} = 10-70$  GeV. The limit is 1 pb at 60 GeV.

### Search for $X^0$ Resonance in $W X^0$ final state

VALUE (MeV)	DOCUMENT ID	TECN	COMMENT
• • • We do not use the following data for averages, fits, limits, etc. • • •			
	1 AALTONEN 13AA	CDF	$X^0 \rightarrow jj$
	2 CHATRCHYAN 12BR	CMS	$X^0 \rightarrow jj$
	3 ABAZOV 11i	D0	$X^0 \rightarrow jj$
	4 ABE 97W	CDF	$X^0 \rightarrow b \bar{b}$





See key on page 999

Gauge & Higgs Boson Particle Listings  
New Heavy Bosons

Table listing particle data including names like AALTONEN, ABZOV, ABRAMOWICZ, etc., and their associated codes and references.

Downloaded from https://academic.oup.com/ptep/article/2020/8/083C01/5891211 by guest on 12 November 2020

# Gauge & Higgs Boson Particle Listings

## New Heavy Bosons, Axions ( $A^0$ ) and Other Very Light Bosons

BARTEL	87B	ZPHY C36 15	W. Bartel et al.	(JADE Collab.)
BEHREND	86B	PL B178 452	H.J. Behrend et al.	(CELLO Collab.)
DERRICK	86	PL 166B 463	M. Derrick et al.	(HRS Collab.)
Also		PR D34 3286	M. Derrick et al.	(HRS Collab.)
JODIDIO	86	PR D34 1967	A. Jodidio et al.	(LBL, NWES, TRIU)
Also		PR D37 237 (erratum)	A. Jodidio et al.	(LBL, NWES, TRIU)
MOHAPATRA	86	PR D34 909	R.N. Mohapatra	(UMD)
ADEVA	85	PL 152B 439	B. Adeva et al.	(Mark-J Collab.)
BERGER	85B	ZPHY C27 341	C. Berger et al.	(PLUTO Collab.)
STOKER	85	PRL 54 1887	D.P. Stoker et al.	(LBL, NWES, TRIU)
ADEVA	84	PRL 53 134	B. Adeva et al.	(Mark-J Collab.)
BEHREND	84C	PL 140B 130	H.J. Behrend et al.	(CELLO Collab.)
BERGSMMA	83	PL 122B 465	F. Bergsma et al.	(CHARM Collab.)
CARR	83	PRL 51 627	J. Carr et al.	(LBL, NWES, TRIU)
BEALL	82	PRL 48 848	G. Beall, M. Bander, A. Soni	(UCI, UCLA)
SHANKER	82	NP B204 375	O. Shanker	(TRIUM)

### Axions ( $A^0$ ) and Other Very Light Bosons, Searches for

See the related review(s):  
[Axions and Other Similar Particles](#)

### $A^0$ (Axion) MASS LIMITS from Astrophysics and Cosmology

These bounds depend on model-dependent assumptions (i.e. — on a combination of axion parameters).

VALUE (MeV)	DOCUMENT ID	TECN	COMMENT
>0.2	BARROSO 82	ASTR	Standard Axion
>0.25	1 RAFFELT 82	ASTR	Standard Axion
>0.2	2 DICUS 78C	ASTR	Standard Axion
	MIKAEELIAN 78	ASTR	Stellar emission
>0.3	2 SATO 78	ASTR	Standard Axion
>0.2	VYSOTSKII 78	ASTR	Standard Axion

1 Lower bound from 5.5 MeV  $\gamma$ -ray line from the sun.  
2 Lower bound from requiring the red giants' stellar evolution not be disrupted by axion emission.

### $A^0$ (Axion) and Other Light Boson ( $X^0$ ) Searches in Hadron Decays

Limits are for branching ratios.

VALUE	CL%	DOCUMENT ID	TECN	COMMENT
<2 $\times 10^{-10}$	95	1 AAIJ 17AQ	LHCB	$B^+ \rightarrow K^+ X^0 (X^0 \rightarrow \mu^+ \mu^-)$
<3.7 $\times 10^{-8}$	90	2 AHN 17	KOTO	$K_L^0 \rightarrow \pi^0 X^0, m_{X^0} = 135 \text{ MeV}$
<6 $\times 10^{-11}$	90	3 BATLEY 17	NA48	$K^\pm \rightarrow \pi^\pm X^0 (X^0 \rightarrow \mu^+ \mu^-)$
		4 WON 16	BELL	$\eta \rightarrow \gamma X^0 (X^0 \rightarrow \pi^+ \pi^-)$
<1 $\times 10^{-9}$	95	5 AAIJ 15AZ	LHCB	$B^0 \rightarrow K^{*0} X^0 (X^0 \rightarrow \mu^+ \mu^-)$
<1.5 $\times 10^{-6}$	90	6 ADLARSON 13	WASA	$\pi^0 \rightarrow \gamma X^0 (X^0 \rightarrow e^+ e^-), m_{X^0} = 100 \text{ MeV}$
<2 $\times 10^{-8}$	90	7 BABUSCI 13B	KLOE	$\phi \rightarrow \eta X^0 (X^0 \rightarrow e^+ e^-)$
		8 ARCHILLI 12A	KLOE	$\phi \rightarrow \eta X^0, X^0 \rightarrow e^+ e^-$
<2 $\times 10^{-15}$	90	9 GNINENKO 12A	BDMP	$\pi^0 \rightarrow \gamma X^0 (X^0 \rightarrow \pi^+ \pi^-)$
<3 $\times 10^{-14}$	90	10 GNINENKO 12B	BDMP	$\eta(\eta') \rightarrow \gamma X^0 (X^0 \rightarrow e^+ e^-)$
<7 $\times 10^{-10}$	90	11 ADLER 04	B787	$K^+ \rightarrow \pi^+ X^0$
<7.3 $\times 10^{-11}$	90	12 ANISIMOVSK. 04	B949	$K^+ \rightarrow \pi^+ X^0$
<4.5 $\times 10^{-11}$	90	13 ADLER 02C	B787	$K^+ \rightarrow \pi^+ X^0$
<4 $\times 10^{-5}$	90	14 ADLER 01	B787	$K^+ \rightarrow \pi^+ \pi^0 A^0$
<4.9 $\times 10^{-5}$	90	AMMAR 01B	CLEO	$B^\pm \rightarrow \pi^\pm (K^\pm) X^0$
<5.3 $\times 10^{-5}$	90	AMMAR 01B	CLEO	$B^0 \rightarrow K_S^0 X^0$
<3.3 $\times 10^{-5}$	90	15 ALTEGOER 98	NOMD	$\pi^0 \rightarrow \gamma X^0, m_{X^0} < 120 \text{ MeV}$
<5.0 $\times 10^{-8}$	90	16 KITCHING 97	B787	$K^+ \rightarrow \pi^+ X^0 (X^0 \rightarrow \gamma \gamma)$
<5.2 $\times 10^{-10}$	90	17 ADLER 96	B787	$K^+ \rightarrow \pi^+ X^0$
<2.8 $\times 10^{-4}$	90	18 AMSLER 96B	CBAR	$\pi^0 \rightarrow \gamma X^0, m_{X^0} < 65 \text{ MeV}$
<3 $\times 10^{-4}$	90	18 AMSLER 96B	CBAR	$\eta \rightarrow \gamma X^0, m_{X^0} = 50\text{--}200 \text{ MeV}$
<4 $\times 10^{-5}$	90	18 AMSLER 96B	CBAR	$\eta' \rightarrow \gamma X^0, m_{X^0} = 50\text{--}925 \text{ MeV}$
<6 $\times 10^{-5}$	90	18 AMSLER 94B	CBAR	$\pi^0 \rightarrow \gamma X^0, m_{X^0} = 65\text{--}125 \text{ MeV}$
<6 $\times 10^{-5}$	90	18 AMSLER 94B	CBAR	$\eta \rightarrow \gamma X^0, m_{X^0} = 200\text{--}525 \text{ MeV}$
<7 $\times 10^{-3}$	90	19 MEIJERDREES 94	CNTR	$\pi^0 \rightarrow \gamma X^0, m_{X^0} = 25 \text{ MeV}$
<2 $\times 10^{-3}$	90	19 MEIJERDREES 94	CNTR	$\pi^0 \rightarrow \gamma X^0, m_{X^0} = 100 \text{ MeV}$
<2 $\times 10^{-7}$	90	20 ATIYA 93B	B787	Sup. by ADLER 04
<3 $\times 10^{-13}$	90	21 NG 93	COSM	$\pi^0 \rightarrow \gamma X^0$
<1.1 $\times 10^{-8}$	90	22 ALLIEGRO 92	SPEC	$K^+ \rightarrow \pi^+ X^0 (X^0 \rightarrow e^+ e^-)$
<5 $\times 10^{-4}$	90	23 ATIYA 92	B787	$\pi^0 \rightarrow \gamma X^0$
<1 $\times 10^{-12}$	95	24 BARABASH 92	BDMP	$\pi^\pm \rightarrow e^\pm \nu X^0 (X^0 \rightarrow e^+ e^-, \gamma \gamma), m_{X^0} = 8 \text{ MeV}$
<1 $\times 10^{-12}$	95	25 BARABASH 92	BDMP	$K^\pm \rightarrow \pi^\pm X^0 (X^0 \rightarrow e^+ e^-, \gamma \gamma), m_{X^0} = 10 \text{ MeV}$
<1 $\times 10^{-11}$	95	26 BARABASH 92	BDMP	$K_L^0 \rightarrow \pi^0 X^0 (X^0 \rightarrow e^+ e^-, \gamma \gamma), m_{X^0} = 10 \text{ MeV}$
<1 $\times 10^{-14}$	95	27 BARABASH 92	BDMP	$\eta' \rightarrow \eta X^0 (X^0 \rightarrow e^+ e^-, \gamma \gamma), m_{X^0} = 10 \text{ MeV}$

<4 $\times 10^{-6}$	90	28 MEIJERDREES 92	SPEC	$\pi^0 \rightarrow \gamma X^0 (X^0 \rightarrow e^+ e^-), m_{X^0} = 100 \text{ MeV}$
<1 $\times 10^{-7}$	90	29 ATIYA 90B	B787	Sup. by KITCHING 97
<1.3 $\times 10^{-8}$	90	30 KORENCHENKO...	87	SPEC $\pi^+ \rightarrow e^+ \nu A^0 (A^0 \rightarrow e^+ e^-)$
<1 $\times 10^{-9}$	90	31 EICHLER 86	SPEC	Stopped $\pi^+ \rightarrow e^+ \nu A^0$
<2 $\times 10^{-5}$	90	32 YAMAZAKI 84	SPEC	For $160 < m < 260 \text{ MeV}$
<(1.5-4) $\times 10^{-6}$	90	32 YAMAZAKI 84	SPEC	$K$ decay, $m_{X^0} \ll 100 \text{ MeV}$
		33 ASANO 82	CNTR	Stopped $K^+ \rightarrow \pi^+ X^0$
		34 ASANO 81B	CNTR	Stopped $K^+ \rightarrow \pi^+ X^0$
		35 ZHITNITSKII 79		Heavy axion

1 The limit is for  $\tau_{X^0} = 10 \text{ ps}$ . See their Fig. 4 for limits in the range of  $m_{X^0} = 250\text{--}4700 \text{ MeV}$  and  $\tau_{X^0} = 0.1\text{--}1000 \text{ ps}$ .

2 The limit as a function of  $m_{X^0}$  from 0 to 250 MeV is provided in their Fig. 5.

3 The limit is for  $m_{X^0} = 216 \text{ MeV}$  and  $\tau_{X^0} \leq 10 \text{ ps}$ . See their Fig. 4(c) for limits in the range of  $m_{X^0} = 211\text{--}354 \text{ MeV}$  and longer lifetimes.

4 WON 16 look for a vector boson coupled to baryon number. Derived limits on  $\alpha' < 10^{-3}\text{--}10^{-2}$  for  $m_{X^0} = 290\text{--}520 \text{ MeV}$  at 95% CL. See their Fig. 4 for mass-dependent limits.

5 The limit is for  $\tau_{X^0} = 10 \text{ ps}$  and  $m_{X^0} = 214\text{--}4350 \text{ MeV}$ . See their Fig. 4 for mass- and lifetime-dependent limits.

6 Limits between  $2.0 \times 10^{-5}$  and  $1.5 \times 10^{-6}$  are obtained for  $m_{X^0} = 20\text{--}100 \text{ MeV}$  (see their Fig. 8). Angular momentum conservation requires that  $X^0$  has spin  $\geq 1$ .

7 The limit is for  $B(\phi \rightarrow \eta X^0) \cdot B(X^0 \rightarrow e^+ e^-)$  and applies to  $m_{X^0} = 410 \text{ MeV}$ . It is derived by analyzing  $\eta \rightarrow \pi^0 \pi^0 \pi^0$  and  $\pi^- \pi^+ \pi^0$ . Limits between  $1 \times 10^{-6}$  and  $2 \times 10^{-8}$  are obtained for  $m_{X^0} \leq 450 \text{ MeV}$  (see their Fig. 6).

8 ARCHILLI 12 analyzed  $\eta \rightarrow \pi^+ \pi^- \pi^0$  decays. Derived limits on  $\alpha'/\alpha < 2 \times 10^{-5}$  for  $m_{X^0} = 50\text{--}420 \text{ MeV}$  at 90% CL. See their Fig. 8 for mass-dependent limits.

9 This limit is for  $B(\pi^0 \rightarrow \gamma X^0) \cdot B(X^0 \rightarrow e^+ e^-)$  and applies for  $m_{X^0} = 90 \text{ MeV}$  and  $\tau_{X^0} \approx 1 \times 10^{-8} \text{ sec}$ . Limits between  $10^{-8}$  and  $2 \times 10^{-15}$  are obtained for  $m_{X^0} = 3\text{--}120 \text{ MeV}$  and  $\tau_{X^0} = 1 \times 10^{-11}\text{--}1 \text{ sec}$ . See their Fig. 3 for limits at different masses and lifetimes.

10 This limit is for  $B(\eta \rightarrow \gamma X^0) \cdot B(X^0 \rightarrow e^+ e^-)$  and applies for  $m_{X^0} = 100 \text{ MeV}$  and  $\tau_{X^0} \approx 6 \times 10^{-9} \text{ sec}$ . Limits between  $10^{-5}$  and  $3 \times 10^{-14}$  are obtained for  $m_{X^0} \lesssim 550 \text{ MeV}$  and  $\tau_{X^0} = 10^{-10}\text{--}10 \text{ sec}$ . See their Fig. 5 for limits at different mass and lifetime and for  $\eta'$  decays.

11 This limit applies for a mass near 180 MeV. For other masses in the range  $m_{X^0} = 150\text{--}250 \text{ MeV}$  the limit is less restrictive, but still improves ADLER 02c and ATIYA 93b.

12 ANISIMOVSKY 04 bound is for  $m_{X^0} = 0$ .

13 ADLER 02c bound is for  $m_{X^0} < 60 \text{ MeV}$ . See Fig. 2 for limits at higher masses.

14 The quoted limit is for  $m_{X^0} = 0\text{--}80 \text{ MeV}$ . See their Fig. 5 for the limit at higher mass. The branching fraction limit assumes pure phase space decay distributions.

15 ALTEGOER 98 looked for  $X^0$  from  $\pi^0$  decay which penetrate the shielding and convert to  $\pi^0$  in the external Coulomb field of a nucleus.

16 KITCHING 97 limit is for  $B(K^+ \rightarrow \pi^+ X^0) \cdot B(X^0 \rightarrow \gamma \gamma)$  and applies for  $m_{X^0} \approx 50 \text{ MeV}$ ,  $\tau_{X^0} < 10^{-10} \text{ s}$ . Limits are provided for  $0 < m_{X^0} < 100 \text{ MeV}$ ,  $\tau_{X^0} < 10^{-8} \text{ s}$ .

17 ADLER 96 looked for a peak in missing-mass distribution. This work is an update of ATIYA 93. The limit is for massless stable  $X^0$  particles and extends to  $m_{X^0} = 80 \text{ MeV}$  at the same level. See paper for dependence on finite lifetime.

18 AMSLER 94b and AMSLER 96b looked for a peak in missing-mass distribution.

19 The MEIJERDREES 94 limit is based on inclusive photon spectrum and is independent of  $X^0$  decay modes. It applies to  $\tau(X^0) > 10^{-23} \text{ sec}$ .

20 ATIYA 93b looked for a peak in missing mass distribution. The bound applies for stable  $X^0$  of  $m_{X^0} = 150\text{--}250 \text{ MeV}$ , and the limit becomes stronger ( $10^{-8}$ ) for  $m_{X^0} = 180\text{--}240 \text{ MeV}$ .

21 NG 93 studied the production of  $X^0$  via  $\gamma \gamma \rightarrow \pi^0 \rightarrow \gamma X^0$  in the early universe at  $T \approx 1 \text{ MeV}$ . The bound on extra neutrinos from nucleosynthesis  $\Delta N_\nu < 0.3$  (WALKER 91) is employed. It applies to  $m_{X^0} \ll 1 \text{ MeV}$  in order to be relativistic down to nucleosynthesis temperature. See paper for heavier  $X^0$ .

22 ALLIEGRO 92 limit applies for  $m_{X^0} = 150\text{--}340 \text{ MeV}$  and is the branching ratio times the decay probability. Limit is  $< 1.5 \times 10^{-8}$  at 99% CL.

23 ATIYA 92 looked for a peak in missing mass distribution. The limit applies to  $m_{X^0} = 0\text{--}130 \text{ MeV}$  in the narrow resonance limit. See paper for the dependence on the lifetime. Covariance requires  $X^0$  to be a vector particle.

24 BARABASH 92 is a beam dump experiment that searched for a light Higgs. Limits between  $1 \times 10^{-12}$  and  $1 \times 10^{-7}$  are obtained for  $3 < m_{X^0} < 40 \text{ MeV}$ .

25 Limits between  $1 \times 10^{-12}$  and 1 are obtained for  $4 < m_{X^0} < 69 \text{ MeV}$ .

26 Limits between  $1 \times 10^{-11}$  and  $5 \times 10^{-3}$  are obtained for  $4 < m_{X^0} < 63 \text{ MeV}$ .

27 Limits between  $1 \times 10^{-14}$  and 1 are obtained for  $3 < m_{X^0} < 82 \text{ MeV}$ .

28 MEIJERDREES 92 limit applies for  $\tau_{X^0} = 10^{-23}\text{--}10^{-11} \text{ sec}$ . Limits between  $2 \times 10^{-4}$  and  $4 \times 10^{-6}$  are obtained for  $m_{X^0} = 25\text{--}120 \text{ MeV}$ . Angular momentum conservation requires that  $X^0$  has spin  $\geq 1$ .

29 ATIYA 90b limit is for  $B(K^+ \rightarrow \pi^+ X^0) \cdot B(X^0 \rightarrow \gamma \gamma)$  and applies for  $m_{X^0} = 50 \text{ MeV}$ ,  $\tau_{X^0} < 10^{-10} \text{ s}$ . Limits are also provided for  $0 < m_{X^0} < 100 \text{ MeV}$ ,  $\tau_{X^0} < 10^{-8} \text{ s}$ .

30 KORENCHENKO 87 limit assumes  $m_{A^0} = 1.7 \text{ MeV}$ ,  $\tau_{A^0} \lesssim 10^{-12} \text{ s}$ , and  $B(A^0 \rightarrow e^+ e^-) = 1$ .

31 EICHLER 86 looked for  $\pi^+ \rightarrow e^+ \nu A^0$  followed by  $A^0 \rightarrow e^+ e^-$ . Limits on the branching fraction depend on the mass and and lifetime of  $A^0$ . The quoted limits are valid when  $\tau(A^0) \gtrsim 3 \times 10^{-10} \text{ s}$  if the decays are kinematically allowed.

See key on page 999

# Gauge & Higgs Boson Particle Listings

## Axions ( $A^0$ ) and Other Very Light Bosons

- <sup>32</sup> YAMAZAKI 84 looked for a discrete line in  $K^+ \rightarrow \pi^+ X$ . Sensitive to wide mass range (5–300 MeV), independent of whether X decays promptly or not.
- <sup>33</sup> ASANO 82 at KEK set limits for  $B(K^+ \rightarrow \pi^+ X^0)$  for  $m_{X^0} < 100$  MeV as  $BR < 4. \times 10^{-8}$  for  $\tau(X^0 \rightarrow n\gamma's) > 1. \times 10^{-9}$  s,  $BR < 1.4 \times 10^{-6}$  for  $\tau < 1. \times 10^{-9}$  s.
- <sup>34</sup> ASANO 81B is KEK experiment. Set  $B(K^+ \rightarrow \pi^+ X^0) < 3.8 \times 10^{-8}$  at CL = 90%.
- <sup>35</sup> ZHITNITSKII 79 argue that a heavy axion predicted by YANG 78 ( $3 < m < 40$  MeV) contradicts experimental muon anomalous magnetic moments.

### $A^0$ (Axion) Searches in Quarkonium Decays

Decay or transition of quarkonium. Limits are for branching ratio.

VALUE	CL%	DOCUMENT ID	TECN	COMMENT
• • • We do not use the following data for averages, fits, limits, etc. • • •				
$< 2.8 \times 10^{-8}$	90	1 ABLIKIM 16E	BES3	$J/\psi \rightarrow A^0 \gamma (A^0 \rightarrow \mu^+ \mu^-)$
$< 4 \times 10^{-7}$	90	2 ABLIKIM 12	BES3	$J/\psi \rightarrow A^0 \gamma (A^0 \rightarrow \mu^+ \mu^-)$
$< 4.0 \times 10^{-5}$	90	3 ANTREASYAN 90c	CBAL	$\Upsilon(1S) \rightarrow A^0 \gamma$
$< 5 \times 10^{-5}$	90	4 DRUZHININ 87	ND	$\phi \rightarrow A^0 \gamma (A^0 \rightarrow e^+ e^-)$
$< 2 \times 10^{-3}$	90	5 DRUZHININ 87	ND	$\phi \rightarrow A^0 \gamma (A^0 \rightarrow \gamma \gamma)$
$< 7 \times 10^{-6}$	90	6 DRUZHININ 87	ND	$\phi \rightarrow A^0 \gamma (A^0 \rightarrow \text{missing})$
$< 1.4 \times 10^{-5}$	90	7 EDWARDS 82	CBAL	$J/\psi \rightarrow A^0 \gamma$
1 ABLIKIM 16E limits between $2.8\text{--}495.3 \times 10^{-8}$ were obtained for $0.212 \text{ GeV} < m_{A^0} < 3.0$ GeV. See their Fig. 5 for mass-dependent limits.				
2 ABLIKIM 12 derived limits between $4 \times 10^{-7}\text{--}2.1 \times 10^{-5}$ for $0.212 \text{ GeV} < m_{A^0} < 3.0$ GeV. See their Fig. 2(c) for mass-dependent limits.				
3 ANTREASYAN 90c assume that $A^0$ does not decay in the detector.				
4 The first DRUZHININ 87 limit is valid when $\tau_{A^0}/m_{A^0} < 3 \times 10^{-13}$ s/MeV and $m_{A^0} < 20$ MeV.				
5 The second DRUZHININ 87 limit is valid when $\tau_{A^0}/m_{A^0} < 5 \times 10^{-13}$ s/MeV and $m_{A^0} < 20$ MeV.				
6 The third DRUZHININ 87 limit is valid when $\tau_{A^0}/m_{A^0} > 7 \times 10^{-12}$ s/MeV and $m_{A^0} < 200$ MeV.				
7 EDWARDS 82 looked for $J/\psi \rightarrow \gamma A^0$ decays by looking for events with a single $\gamma$ [of energy $\sim 1/2$ the $J/\psi(1S)$ mass], plus nothing else in the detector. The limit is inconsistent with the axion interpretation of the FAISSNER 81B result.				

### $A^0$ (Axion) Searches in Positronium Decays

Decay or transition of positronium. Limits are for branching ratio.

VALUE	CL%	DOCUMENT ID	TECN	COMMENT
• • • We do not use the following data for averages, fits, limits, etc. • • •				
$< 4.4 \times 10^{-5}$	90	1 BADERT... 02	CNTR	$\alpha\text{-Ps} \rightarrow \gamma X_1 X_2, m_{X_1} + m_{X_2} \leq 900 \text{ keV}$
$< 2 \times 10^{-4}$	90	MAENO 95	CNTR	$\alpha\text{-Ps} \rightarrow A^0 \gamma, m_{A^0} = 850\text{--}1013 \text{ keV}$
$< 3.0 \times 10^{-4}$	90	2 ASAI 94	CNTR	$\alpha\text{-Ps} \rightarrow A^0 \gamma, m_{A^0} = 30\text{--}500 \text{ keV}$
$< 2.8 \times 10^{-5}$	90	3 AKOPYAN 91	CNTR	$\alpha\text{-Ps} \rightarrow A^0 \gamma (A^0 \rightarrow \gamma \gamma), m_{A^0} < 30 \text{ keV}$
$< 1.1 \times 10^{-6}$	90	4 ASAI 91	CNTR	$\alpha\text{-Ps} \rightarrow A^0 \gamma, m_{A^0} < 800 \text{ keV}$
$< 3.8 \times 10^{-4}$	90	GNINENKO 90	CNTR	$\alpha\text{-Ps} \rightarrow A^0 \gamma, m_{A^0} < 30 \text{ keV}$
$< (1\text{--}5) \times 10^{-4}$	95	5 TSUCHIYAKI 90	CNTR	$\alpha\text{-Ps} \rightarrow A^0 \gamma, m_{A^0} = 300\text{--}900 \text{ keV}$
$< 6.4 \times 10^{-5}$	90	6 ORITO 89	CNTR	$\alpha\text{-Ps} \rightarrow A^0 \gamma, m_{A^0} < 30 \text{ keV}$
		7 AMALDI 85	CNTR	Ortho-positronium
		8 CARBONI 83	CNTR	Ortho-positronium
1 BADERTSCHER 02 looked for a three-body decay of ortho-positronium into a photon and two penetrating (neutral or milli-charged) particles.				
2 The ASAI 94 limit is based on inclusive photon spectrum and is independent of $A^0$ decay modes.				
3 The AKOPYAN 91 limit applies for a short-lived $A^0$ with $\tau_{A^0} < 10^{-13} m_{A^0}$ [keV] s.				
4 ASAI 91 limit translates to $g_{A^0 e^+ e^-}^2 / 4\pi < 1.1 \times 10^{-11}$ (90% CL) for $m_{A^0} < 800$ keV.				
5 The TSUCHIYAKI 90 limit is based on inclusive photon spectrum and is independent of $A^0$ decay modes.				
6 ORITO 89 limit translates to $g_{A^0 e^+ e^-}^2 / 4\pi < 6.2 \times 10^{-10}$ . Somewhat more sensitive limits are obtained for larger $m_{A^0}$ : $B < 7.6 \times 10^{-6}$ at 100 keV.				
7 AMALDI 85 set limits $B(A^0 \gamma) / B(\gamma \gamma \gamma) < (1\text{--}5) \times 10^{-6}$ for $m_{A^0} = 900\text{--}100$ keV which are about 1/10 of the CARBONI 83 limits.				
8 CARBONI 83 looked for ortho-positronium $\rightarrow A^0 \gamma$ . Set limit for $A^0$ electron coupling squared, $(g_{e e A^0})^2 / (4\pi) < 6. \times 10^{-10}\text{--}7. \times 10^{-9}$ for $m_{A^0}$ from 150–900 keV (CL = 99.7%). This is about 1/10 of the bound from $g\text{--}2$ experiments.				

### $A^0$ (Axion) Search in Photoproduction

VALUE	DOCUMENT ID	COMMENT
• • • We do not use the following data for averages, fits, limits, etc. • • •		
	1 BASSOMPIERRE... 95	$m_{A^0} = 1.8 \pm 0.2 \text{ MeV}$
1 BASSOMPIERRE 95 is an extension of BASSOMPIERRE 93. They looked for a peak in the invariant mass of $e^+ e^-$ pairs in the region $m_{e^+ e^-} = 1.8 \pm 0.2 \text{ MeV}$ . They obtained bounds on the production rate $A^0$ for $\tau(A^0) = 10^{-18}\text{--}10^{-9}$ sec. They also found an excess of events in the range $m_{e^+ e^-} = 2.1\text{--}3.5 \text{ MeV}$ .		

### $A^0$ (Axion) Production in Hadron Collisions

Limits are for  $\sigma(A^0) / \sigma(\pi^0)$ .

VALUE	CL%	EVENTS	DOCUMENT ID	TECN	COMMENT
• • • We do not use the following data for averages, fits, limits, etc. • • •					
			1 SIRUNYAN 19BQ	CMS	$X^0 \rightarrow \mu^+ \mu^-$
			2 JAIN 07	CNTR	$A^0 \rightarrow e^+ e^-$
			3 AHMAD 97	SPEC	$e^+$ production
			4 LEINBERGER 97	SPEC	$A^0 \rightarrow e^+ e^-$
			5 GANZ 96	SPEC	$A^0 \rightarrow e^+ e^-$
			6 KAMEL 96	EMUL	$^{32}\text{S}$ emulsion, $A^0 \rightarrow e^+ e^-$
			7 BLUEMLEIN 92	BDMP	$A^0 N_Z \rightarrow \ell^+ \ell^- N_Z$
			8 MEIJERDREES 92	SPEC	$\pi^- p \rightarrow n A^0, A^0 \rightarrow e^+ e^-$
			9 BLUEMLEIN 91	BDMP	$A^0 \rightarrow e^+ e^-, 2\gamma$
			10 FAISSNER 89	OSPCK	Beam dump, $A^0 \rightarrow e^+ e^-$
			11 DEBOER 88	RVUE	$A^0 \rightarrow e^+ e^-$
			12 EL-NADI 88	EMUL	$A^0 \rightarrow e^+ e^-$
			13 FAISSNER 88	OSPCK	Beam dump, $A^0 \rightarrow 2\gamma$
			14 BADIER 86	BDMP	$A^0 \rightarrow e^+ e^-$
			15 BERGSMA 85	CHRM	CERN beam dump
			15 BERGSMA 85	CHRM	CERN beam dump
			16 FAISSNER 83	OSPCK	Beam dump, $A^0 \rightarrow 2\gamma$
			17 FAISSNER 83B	RVUE	LAMPF beam dump
			18 FRANK 83B	RVUE	LAMPF beam dump
			19 HOFFMAN 83	CNTR	$\pi p \rightarrow n A^0 (A^0 \rightarrow e^+ e^-)$
			20 FETSCHER 82	RVUE	See FAISSNER 81B
			21 FAISSNER 81	OSPCK	CERN PS $\nu$ wideband
			22 FAISSNER 81B	OSPCK	Beam dump, $A^0 \rightarrow 2\gamma$
			23 KIM 81	OSPCK	26 GeV $pN \rightarrow A^0 X$
			24 FAISSNER 80	OSPCK	Beam dump, $A^0 \rightarrow e^+ e^-$
$< 2. \times 10^{-11}$	90	0	25 JACQUES 80	HLBC	28 GeV protons
$< 1. \times 10^{-13}$	90	0	25 JACQUES 80	HLBC	Beam dump
			26 SOUKAS 80	CALO	28 GeV $p$ beam dump
			27 BECHIS 79	CNTR	
			28 COTEUS 79	OSPCK	Beam dump
			29 DISHAW 79	CALO	400 GeV $pp$
			30 ALIBRAN 78	HYBR	Beam dump
			31 ASRATYAN 78B	CALO	Beam dump
			30 BELLOTTI 78	HLBC	Beam dump
			30 BELLOTTI 78	HLBC	$m_{A^0} = 1.5 \text{ MeV}$
			30 BELLOTTI 78	HLBC	$m_{A^0} = 1 \text{ MeV}$
			31 BOSETTI 78B	HYBR	Beam dump
			32 DONNELLY 78		
			33 HANSL 78D	WIRE	Beam dump
			34 MICELMAC... 78		
			34 VYSOTSKII 78		
1 SIRUNYAN 19BQ look for the pair production of a new light boson decaying into a pair of muons, and set limits on the product of the production cross section times branching fraction to dimuons squared times acceptance over a range of $m_{X^0} = 0.25\text{--}8.5$ GeV. See the right panel of their Fig. 1 for mass-dependent limits.					
2 JAIN 07 claims evidence for $A^0 \rightarrow e^+ e^-$ produced in 207Pb collision on nuclear emulsion (Ag/Br) for $m(A^0) = 7 \pm 1$ or $19 \pm 1$ MeV and $\tau(A^0) \leq 10^{-13}$ s.					
3 AHMAD 97 reports a result of APEX Collaboration which studied positron production in $^{238}\text{U} + ^{232}\text{Ta}$ and $^{238}\text{U} + ^{181}\text{Ta}$ collisions, without requiring a coincident electron. No narrow lines were found for $250 < E_{e^+} < 750$ keV.					
4 LEINBERGER 97 (ORANGE Collaboration) at GSI looked for a narrow sum-energy $e^+ e^-$ line at $\sim 635$ keV in $^{238}\text{U} + ^{181}\text{Ta}$ collision. Limits on the production probability for a narrow sum-energy $e^+ e^-$ line are set. See their Table 2.					
5 GANZ 96 (EPOS II Collaboration) has placed upper bounds on the production cross section of $e^+ e^-$ pairs from $^{238}\text{U} + ^{181}\text{Ta}$ and $^{238}\text{U} + ^{232}\text{Th}$ collisions at GSI. See Table 2 for limits both for back-to-back and isotropic configurations of $e^+ e^-$ pairs. These limits rule out the existence of peaks in the $e^+ e^-$ sum-energy distribution, reported by an earlier version of this experiment.					
6 KAMEL 96 looked for $e^+ e^-$ pairs from the collision of $^{32}\text{S}$ (200 GeV/nucleon) and emulsion. No evidence of mass peaks is found in the region of sensitivity $m_{e e} > 2 \text{ MeV}$ .					
7 BLUEMLEIN 92 is a proton beam dump experiment at Serpukhov with a secondary target to induce Bethe-Heitler production of $e^+ e^-$ or $\mu^+ \mu^-$ from the produce $A^0$ . See Fig. 5 for the excluded region in $m_{A^0}$ - $x$ plane. For the standard axion, $0.3 < x < 25$ is excluded at 95% CL. If combined with BLUEMLEIN 91, $0.008 < x < 32$ is excluded.					
8 MEIJERDREES 92 give $\Gamma(\pi^- p \rightarrow n A^0) \cdot B(A^0 \rightarrow e^+ e^-) / \Gamma(\pi^- p \rightarrow \text{all}) < 10^{-5}$ (90% CL) for $m_{A^0} = 100$ MeV, $\tau_{A^0} = 10^{-11}\text{--}10^{-23}$ sec. Limits ranging from $2.5 \times 10^{-3}$ to $10^{-7}$ are given for $m_{A^0} = 25\text{--}136$ MeV.					
9 BLUEMLEIN 91 is a proton beam dump experiment at Serpukhov. No candidate event for $A^0 \rightarrow e^+ e^-, 2\gamma$ are found. Fig. 6 gives the excluded region in $m_{A^0}$ - $x$ plane ( $x = \tan\beta = v_2/v_1$ ). Standard axion is excluded for $0.2 < m_{A^0} < 3.2$ MeV for most $x > 1$ , $0.2\text{--}11$ MeV for most $x < 1$ .					
10 FAISSNER 89 searched for $A^0 \rightarrow e^+ e^-$ in a proton beam dump experiment at SIN. No excess of events was observed over the background. A standard axion with mass $2m_e\text{--}20$ MeV is excluded. Lower limit on $f_{A^0}$ of $\approx 10^4$ GeV is given for $m_{A^0} = 2m_e\text{--}20$ MeV.					
11 DEBOER 88 reanalyze EL-NADI 88 data and claim evidence for three distinct states with mass $\sim 1.1, \sim 2.1$ , and $\sim 9$ MeV, lifetimes $10^{-16}\text{--}10^{-15}$ s decaying to $e^+ e^-$					

# Gauge & Higgs Boson Particle Listings

## Axions ( $A^0$ ) and Other Very Light Bosons

- and note the similarity of the data with those of a cosmic-ray experiment by Bristol group (B. M. Anand, Proc. of the Royal Society of London, Section A **A22** 183 (1953)). For a criticism see PERKINS 89, who suggests that the events are compatible with  $\pi^0$  Dalitz decay. DEBOER 89B is a reply which contests the criticism.
- EL-NADI 88 claim the existence of a neutral particle decaying into  $e^+e^-$  with mass  $1.60 \pm 0.59$  MeV, lifetime  $(0.15 \pm 0.01) \times 10^{-14}$  s, which is produced in heavy ion interactions with emulsion nuclei at  $\sim 4$  GeV/c/nucleon.
  - FAISSNER 88 is a proton beam dump experiment at SIN. They found no candidate event for  $A^0 \rightarrow \gamma\gamma$ . A standard axion decaying to  $2\gamma$  is excluded except for a region  $x \approx 1$ . Lower limit on  $f_{A^0}$  of  $10^2$ – $10^3$  GeV is given for  $m_{A^0} = 0.1$ –1 MeV.
  - BADIER 86 did not find long-lived  $A^0$  in 300 GeV  $\pi^-$  Beam Dump Experiment that decays into  $e^+e^-$  in the mass range  $m_{A^0} = (20$ – $200)$  MeV, which excludes the  $A^0$  decay constant  $f(A^0)$  in the interval (60–600) GeV. See their figure 6 for excluded region on  $f(A^0)$ – $m_{A^0}$  plane.
  - BERGSMÄ 85 look for  $A^0 \rightarrow 2\gamma, e^+e^-, \mu^+\mu^-$ . First limit above is for  $m_{A^0} = 1$  MeV; second is for 200 MeV. See their figure 4 for excluded region on  $f_{A^0}$ – $m_{A^0}$  plane, where  $f_{A^0}$  is  $A^0$  decay constant. For Peccei-Quinn PECEI 77  $A^0, m_{A^0} < 180$  keV and  $\tau > 0.037$  s. (CL = 90%). For the axion of FAISSNER 81B at 250 keV, BERGSMÄ 85 expect 15 events but observe zero.
  - FAISSNER 83 observed 19  $1\text{-}\gamma$  and 12  $2\text{-}\gamma$  events where a background of 4.8 and 2.3 respectively is expected. A small-angle peak is observed even if iron wall is set in front of the decay region.
  - FAISSNER 83B extrapolate SIN  $\gamma$  signal to LAMPF  $\nu$  experimental condition. Resulting 370  $\gamma$ 's are not at variance with LAMPF upper limit of 450  $\gamma$ 's. Derived from LAMPF limit that  $[d\sigma(A^0)/d\omega \text{ at } 90^\circ] m_{A^0} / \tau_{A^0} < 14 \times 10^{-35} \text{ cm}^2 \text{ sr}^{-1} \text{ MeV ms}^{-1}$ . See comment on FRANK 83B.
  - FRANK 83B stress the importance of LAMPF data bins with negative net signal. By statistical analysis say that LAMPF and SIN-A0 are at variance when extrapolation by phase-space model is done. They find LAMPF upper limit is 248 not 450  $\gamma$ 's. See comment on FAISSNER 83B.
  - HOFFMAN 83 set CL = 90% limit  $d\sigma/dt B(e^+e^-) < 3.5 \times 10^{-32} \text{ cm}^2/\text{GeV}^2$  for  $140 < m_{A^0} < 160$  MeV. Limit assumes  $\tau(A^0) < 10^{-9}$  s.
  - FETSCHER 82 reanalyzes SIN beam-dump data of FAISSNER 81. Claims no evidence for axion since  $2\text{-}\gamma$  peak rate remarkably decreases if iron wall is set in front of the decay region.
  - FAISSNER 81 see excess  $\mu e$  events. Suggest axion interactions.
  - FAISSNER 81B is SIN 590 MeV proton beam dump. Observed  $14.5 \pm 5.0$  events of  $2\gamma$  decay of long-lived neutral penetrating particle with  $m_{2\gamma} \lesssim 1$  MeV. Axion interpretation with  $\eta$ - $A^0$  mixing gives  $m_{A^0} = 250 \pm 25$  keV,  $\tau_{(2\gamma)} = (7.3 \pm 3.7) \times 10^{-3}$  s from above rate. See critical remarks below in comments of FETSCHER 82, FAISSNER 83, FAISSNER 83B, FRANK 83B, and BERGSMÄ 85. Also see in the next subsection ALEKSEEV 82B, CAVIGNAC 83, and ANANEV 85.
  - KIM 81 analyzed 8 candidates for  $A^0 \rightarrow 2\gamma$  obtained by Aachen-Padova experiment at CERN with 26 GeV protons on Be. Estimated axion mass is about 300 keV and lifetime is  $(0.86$ – $5.6) \times 10^{-3}$  s depending on models. Faisner (private communication), says axion production underestimated and mass overestimated. Correct value around 200 keV.
  - FAISSNER 80 is SIN beam dump experiment with 590 MeV protons looking for  $A^0 \rightarrow e^+e^-$  decay. Assuming  $A^0/\pi^0 = 5.5 \times 10^{-7}$ , obtained decay rate limit  $20/(A^0 \text{ mass}) \text{ MeV/s}$  (CL = 90%), which is about  $10^{-7}$  below theory and interpreted as upper limit to  $m_{A^0} < 2m_{e^-}$ .
  - JACQUES 80 is a BNL beam dump experiment. First limit above comes from nonobservation of excess neutral-current-type events  $[\sigma(\text{production})\sigma(\text{interaction}) < 7. \times 10^{-68} \text{ cm}^4, \text{ CL} = 90\%]$ . Second limit is from nonobservation of axion decays into  $2\gamma$ 's or  $e^+e^-$ , and for axion mass a few MeV.
  - SOUKAS 80 at BNL observed no excess of neutral-current-type events in beam dump.
  - BECHIS 79 looked for the axion production in low energy electron Bremsstrahlung and the subsequent decay into either  $2\gamma$  or  $e^+e^-$ . No signal found. CL = 90% limits for model parameter(s) are given.
  - COTEUS 79 is a beam dump experiment at BNL.
  - DISHAW 79 is a calorimetric experiment and looks for low energy tail of energy distributions due to energy lost to weakly interacting particles.
  - BELLOTTI 78 first value comes from search for  $A^0 \rightarrow e^+e^-$ . Second value comes from search for  $A^0 \rightarrow 2\gamma$ , assuming mass  $< 2m_{e^-}$ . For any mass satisfying this, limit is above value  $\times (\text{mass}^{-4})$ . Third value uses data of PL 60B 401 and quotes  $\sigma(\text{production})\sigma(\text{interaction}) < 10^{-67} \text{ cm}^4$ .
  - BOSETTI 78B quotes  $\sigma(\text{production})\sigma(\text{interaction}) < 2. \times 10^{-67} \text{ cm}^4$ .
  - DONNELLY 78 examines data from reactor neutrino experiments of REINES 76 and GURR 74 as well as SLAC beam dump experiment. Evidence is negative.
  - MICELMACHER 78 finds no evidence of axion existence in reactor experiments of REINES 76 and GURR 74. (See reference under DONNELLY 78 below).
  - VYSOTSKI 78 derived lower limit for the axion mass 25 keV from luminosity of the sun and 200 keV from red supergiants.

### $A^0$ (Axion) Searches in Reactor Experiments

VALUE	DOCUMENT ID	TECN	COMMENT
• • • We do not use the following data for averages, fits, limits, etc. • • •			
1	CHANG 07		Primakoff or Compton
2	ALTMANN 95	CNTR	Reactor; $A^0 \rightarrow e^+e^-$
3	KETOV 86	SPEC	Reactor; $A^0 \rightarrow \gamma\gamma$
4	KOCH 86	SPEC	Reactor; $A^0 \rightarrow \gamma\gamma$
5	DATAR 82	CNTR	Light water reactor
6	VUILLEUMIER 81	CNTR	Reactor; $A^0 \rightarrow 2\gamma$

- CHANG 07 looked for monochromatic photons from Primakoff or Compton conversion of axions from the Kuo-Sheng reactor due to axion coupling to photon or electron, respectively. The search places model-independent limits on the products  $G_{A\gamma\gamma}G_{ANN}$  and  $G_{Aee}G_{ANN}$  for  $m(A^0)$  less than the MeV range.
- ALTMANN 95 looked for  $A^0$  decaying into  $e^+e^-$  from the Bugey5 nuclear reactor. They obtain an upper limit on the  $A^0$  production rate of  $\omega(A^0)/\omega(\gamma) \times B(A^0 \rightarrow e^+e^-) < 10^{-16}$  for  $m_{A^0} = 1.5$  MeV at 90% CL. The limit is weaker for heavier  $A^0$ . In the case of a standard axion, this limit excludes a mass in the range  $2m_e < m_{A^0} < 4.8$  MeV at 90% CL. See Fig. 5 of their paper for exclusion limits of axion-like resonances  $Z^0$  in the  $(m_{X^0}, f_{X^0})$  plane.
- KETOV 86 searched for  $A^0$  at the Rovno nuclear power plant. They found an upper limit on the  $A^0$  production probability of  $0.8 [100 \text{ keV}/m_{A^0}]^6 \times 10^{-6}$  per fission. In the standard axion model, this corresponds to  $m_{A^0} > 150$  keV. Not valid for  $m_{A^0} \gtrsim 1$  MeV.
- KOCH 86 searched for  $A^0 \rightarrow \gamma\gamma$  at nuclear power reactor Biblis A. They found an upper limit on the  $A^0$  production rate of  $\omega(A^0)/\omega(\gamma(M1)) < 1.5 \times 10^{-10}$  (CL=95%). Standard axion with  $m_{A^0} = 250$  keV gives  $10^{-5}$  for the ratio. Not valid for  $m_{A^0} > 1022$  keV.
- DATAR 82 looked for  $A^0 \rightarrow 2\gamma$  in neutron capture ( $np \rightarrow dA^0$ ) at Tarapur 500 MW reactor. Sensitive to sum of  $l = 0$  and  $l = 1$  amplitudes. With ZEHNDER 81 [ $(l = 0) - (l = 1)$ ] result, assert nonexistence of standard  $A^0$ .
- VUILLEUMIER 81 is at Grenoble reactor. Set limit  $m_{A^0} < 280$  keV.

### $A^0$ (Axion) and Other Light Boson ( $X^0$ ) Searches in Nuclear Transitions

VALUE	CL%	DOCUMENT ID	TECN	COMMENT
• • • We do not use the following data for averages, fits, limits, etc. • • •				
$< 8.5 \times 10^{-6}$	90	1 DERBIN 02	CNTR	$^{125m}\text{Te}$ decay
		2 DEBOER 97C	RVUE	M1 transitions
$< 5.5 \times 10^{-10}$	95	3 TSUNODA 95	CNTR	$^{252}\text{Cf}$ fission, $A^0 \rightarrow e e$
$< 1.2 \times 10^{-6}$	95	4 MINOWA 93	CNTR	$^{139}\text{La}^* \rightarrow ^{139}\text{La} A^0$
$< 2 \times 10^{-4}$	90	5 HICKS 92	CNTR	$^{35}\text{S}$ decay, $A^0 \rightarrow \gamma\gamma$
$< 1.5 \times 10^{-9}$	95	6 ASANUMA 90	CNTR	$^{241}\text{Am}$ decay
$< (0.4\text{--}10) \times 10^{-3}$	95	7 DEBOER 90	CNTR	$^8\text{Be}^* \rightarrow ^8\text{Be} A^0, A^0 \rightarrow e^+e^-, ^{16}\text{O}^* \rightarrow ^{16}\text{O} X^0,$
$< (0.2\text{--}1) \times 10^{-3}$	90	8 BINI 89	CNTR	$X^0 \rightarrow e^+e^-, \text{Cu}^* \rightarrow \text{Cu} A^0 (A^0 \rightarrow 2\gamma, A^0 e \rightarrow \gamma e, A^0 Z \rightarrow \gamma Z)$
$< 1.5 \times 10^{-4}$	90	10 DATAR 88	CNTR	$^{12}\text{C}^* \rightarrow ^{12}\text{C} A^0,$
$< 5 \times 10^{-3}$	90	11 DEBOER 88c	CNTR	$^{16}\text{O}^* \rightarrow e^+e^-, X^0 \rightarrow e^+e^-,$
$< 3.4 \times 10^{-5}$	95	12 DOEHNER 88	SPEC	$^2\text{H}^*, A^0 \rightarrow e^+e^-$
$< 4 \times 10^{-4}$	95	13 SAVAGE 88	CNTR	Nuclear decay (isovector)
$< 3 \times 10^{-3}$	95	13 SAVAGE 88	CNTR	Nuclear decay (isoscalar)
$< 10.6 \times 10^{-2}$	90	14 HALLIN 86	SPEC	$^6\text{Li}$ isovector decay
$< 10.8$	90	14 HALLIN 86	SPEC	$^{10}\text{B}$ isoscalar decays
$< 2.2$	90	14 HALLIN 86	SPEC	$^{14}\text{N}$ isoscalar decays
$< 4 \times 10^{-4}$	90	15 SAVAGE 86B	CNTR	$^{14}\text{N}^*$
		16 ANANEV 85	CNTR	$\text{Li}^*, \text{deut}^* A^0 \rightarrow 2\gamma$
		17 CAVIGNAC 83	CNTR	$^{97}\text{Nb}^*, \text{deut}^* \text{ transition } A^0 \rightarrow 2\gamma$
		18 ALEKSEEV 82B	CNTR	$\text{Li}^*, \text{deut}^* \text{ transition } A^0 \rightarrow 2\gamma$
		19 LEHMANN 82	CNTR	$\text{Cu}^* \rightarrow \text{Cu} A^0 (A^0 \rightarrow 2\gamma)$
		20 ZEHNDER 82	CNTR	$\text{Li}^*, \text{Nb}^* \text{ decay, } n\text{-capt.}$
		21 ZEHNDER 81	CNTR	$\text{Ba}^* \rightarrow \text{Ba} A^0 (A^0 \rightarrow 2\gamma)$
		22 CALAPRICE 79		Carbon

- DERBIN 02 looked for the axion emission in an M1 transition in  $^{125m}\text{Te}$  decay. They looked for a possible presence of a shifted energy spectrum in gamma rays due to the undetected axion.
- DEBOER 97C reanalyzed the existent data on Nuclear M1 transitions and find that a 9 MeV boson decaying into  $e^+e^-$  would explain the excess of events with large opening angles. See also DEBOER 01 for follow-up experiments.
- TSUNODA 95 looked for axion emission when  $^{252}\text{Cf}$  undergoes a spontaneous fission, with the axion decaying into  $e^+e^-$ . The bound is for  $m_{A^0} = 40$  MeV. It improves to  $2.5 \times 10^{-5}$  for  $m_{A^0} = 200$  MeV.
- MINOWA 93 studied chain process,  $^{139}\text{Ce} \rightarrow ^{139}\text{La}^*$  by electron capture and M1 transition of  $^{139}\text{La}^*$  to the ground state. It does not assume decay modes of  $A^0$ . The bound applies for  $m_{A^0} < 166$  keV.
- HICKS 92 bound is applicable for  $\tau_{X^0} < 4 \times 10^{-11}$  sec.
- THE ASANUMA 90 limit is for the branching fraction of  $X^0$  emission per  $^{241}\text{Am}$   $\alpha$  decay and valid for  $\tau_{X^0} < 3 \times 10^{-11}$  s.
- THE DEBOER 90 limit is for the branching ratio  $^8\text{Be}^* (18.15 \text{ MeV}, 1^+) \rightarrow ^8\text{Be} A^0, A^0 \rightarrow e^+e^-$  for the mass range  $m_{A^0} = 4$ –15 MeV.
- THE BINI 89 limit is for the branching fraction of  $^{16}\text{O}^* (6.05 \text{ MeV}, 0^+) \rightarrow ^{16}\text{O} X^0, X^0 \rightarrow e^+e^-$  for  $m_{X^0} = 1.5$ –3.1 MeV.  $\tau_{X^0} \lesssim 10^{-11}$  s is assumed. The spin-parity of  $X$  is restricted to  $0^+$  or  $1^-$ .
- AVIGNONE 88 looked for the 1115 keV transition  $\text{C}^* \rightarrow \text{Cu} A^0$ , either from  $A^0 \rightarrow 2\gamma$  in-flight decay or from the secondary  $A^0$  interactions by Compton and by Primakoff processes. Limits for axion parameters are obtained for  $m_{A^0} < 1.1$  MeV.

# Gauge & Higgs Boson Particle Listings

## Axions ( $A^0$ ) and Other Very Light Bosons

- <sup>10</sup>DATAR 88 rule out light pseudoscalar particle emission through its decay  $A^0 \rightarrow e^+e^-$  in the mass range 1.02–2.5 MeV and lifetime range  $10^{-13}$ – $10^{-8}$  s. The above limit is for  $\tau = 5 \times 10^{-13}$  s and  $m = 1.7$  MeV; see the paper for the  $\tau$ - $m$  dependence of the limit.
- <sup>11</sup>The limit is for the branching fraction of  $^{16}\text{O}^*(6.05 \text{ MeV}, 0^+) \rightarrow ^{16}\text{O}X^0$ ,  $X^0 \rightarrow e^+e^-$  against internal pair conversion for  $m_{X^0} = 1.7$  MeV and  $\tau_{X^0} < 10^{-11}$  s. Similar limits are obtained for  $m_{X^0} = 1.3$ – $3.2$  MeV. The spin parity of  $X^0$  must be either  $0^+$  or  $1^-$ . The limit at 1.7 MeV is translated into a limit for the  $X^0$ -nucleon coupling constant:  $g_{X^0 NN}^2/4\pi < 2.3 \times 10^{-9}$ .
- <sup>12</sup>The DOEHNER 88 limit is for  $m_{A^0} = 1.7$  MeV,  $\tau(A^0) < 10^{-10}$  s. Limits less than  $10^{-4}$  are obtained for  $m_{A^0} = 1.2$ – $2.2$  MeV.
- <sup>13</sup>SAVAGE 88 looked for  $A^0$  that decays into  $e^+e^-$  in the decay of the 9.17 MeV  $J^P = 2^+$  state in  $^{14}\text{N}$ , 17.64 MeV state  $J^P = 1^+$  in  $^8\text{Be}$ , and the 18.15 MeV state  $J^P = 1^+$  in  $^8\text{Be}$ . This experiment constrains the isovector coupling of  $A^0$  to hadrons, if  $m_{A^0} = (1.1 \rightarrow 2.2)$  MeV and the isoscalar coupling of  $A^0$  to hadrons, if  $m_{A^0} = (1.1 \rightarrow 2.6)$  MeV. Both limits are valid only if  $\tau(A^0) \lesssim 1 \times 10^{-11}$  s.
- <sup>14</sup>Limits are for  $\Gamma(A^0(1.8 \text{ MeV}))/\Gamma(\pi\text{M}1)$ ; i.e., for 1.8 MeV axion emission normalized to the rate for internal emission of  $e^+e^-$  pairs. Valid for  $\tau_{A^0} < 2 \times 10^{-11}$  s.  $^6\text{Li}$  isovector decay data strongly disfavor PECCCI 86 model I, whereas the  $^{10}\text{B}$  and  $^{14}\text{N}$  isoscalar decay data strongly reject PECCCI 86 model II and III.
- <sup>15</sup>SAVAGE 86b looked for  $A^0$  that decays into  $e^+e^-$  in the decay of the 9.17 MeV  $J^P = 2^+$  state in  $^{14}\text{N}$ . Limit on the branching fraction is valid if  $\tau_{A^0} \lesssim 1 \times 10^{-11}$  s for  $m_{A^0} = (1.1$ – $1.7)$  MeV. This experiment constrains the iso-vector coupling of  $A^0$  to hadrons.
- <sup>16</sup>ANANEV 85 with IBR-2 pulsed reactor exclude standard  $A^0$  at CL = 95% masses below 470 keV ( $\text{Li}^*$  decay) and below  $2m_e$  for deuterium\* decay.
- <sup>17</sup>CAVAIGNAC 83 at Bugey reactor exclude axion at any  $m_{97\text{Nb}^*}$  decay and axion with  $m_{A^0}$  between 275 and 288 keV (deuteron\* decay).
- <sup>18</sup>ALEKSEEV 82 with IBR-2 pulsed reactor exclude standard  $A^0$  at CL = 95% mass-ranges  $m_{A^0} < 400$  keV ( $\text{Li}^*$  decay) and 330 keV  $< m_{A^0} < 2.2$  MeV. (deuteron\* decay).
- <sup>19</sup>LEHMANN 82 obtained  $A^0 \rightarrow 2\gamma$  rate  $< 6.2 \times 10^{-5}/\text{s}$  (CL = 95%) excluding  $m_{A^0}$  between 100 and 1000 keV.
- <sup>20</sup>ZEHNDER 82 used Gogsen 2.8GW light-water reactor to check  $A^0$  production. No  $2\gamma$  peak in  $\text{Li}^*$ ,  $\text{Nb}^*$  decay (both single  $p$  transition) nor in  $n$  capture (combined with previous  $\text{Ba}^*$  negative result) rules out standard  $A^0$ . Set limit  $m_{A^0} < 60$  keV for any  $A^0$ .
- <sup>21</sup>ZEHNDER 81 looked for  $\text{Ba}^* \rightarrow A^0\text{Ba}$  transition with  $A^0 \rightarrow 2\gamma$ . Obtained  $2\gamma$  coincidence rate  $< 2.2 \times 10^{-5}/\text{s}$  (CL = 95%) excluding  $m_{A^0} > 160$  keV (or 200 keV depending on Higgs mixing). However, see BARROSO 81.
- <sup>22</sup>CALAPRICE 79 saw no axion emission from excited states of carbon. Sensitive to axion mass between 1 and 15 MeV.

### $A^0$ (Axion) Limits from Its Electron Coupling

Limits are for  $\tau(A^0 \rightarrow e^+e^-)$ .

VALUE (s)	CL%	DOCUMENT ID	TECN	COMMENT
••• We do not use the following data for averages, fits, limits, etc. •••				
none $4 \times 10^{-16}$ – $4.5 \times 10^{-12}$	90	1 BROSS	91 BDMP $eN \rightarrow eA^0N$ ( $A^0 \rightarrow ee$ )	
		2 GUO	90 BDMP $eN \rightarrow eA^0N$ ( $A^0 \rightarrow ee$ )	
		3 BJORKEN	88 CALO $A \rightarrow e^+e^-$ or $2\gamma$	
		4 BLINOV	88 MD1 $ee \rightarrow eeA^0$ ( $A^0 \rightarrow ee$ )	
none $1 \times 10^{-14}$ – $1 \times 10^{-10}$	90	5 RIORDAN	87 BDMP $eN \rightarrow eA^0N$ ( $A^0 \rightarrow ee$ )	
none $1 \times 10^{-14}$ – $1 \times 10^{-11}$	90	6 BROWN	86 BDMP $eN \rightarrow eA^0N$ ( $A^0 \rightarrow ee$ )	
none $6 \times 10^{-14}$ – $9 \times 10^{-11}$	95	7 DAVIER	86 BDMP $eN \rightarrow eA^0N$ ( $A^0 \rightarrow ee$ )	
none $3 \times 10^{-13}$ – $1 \times 10^{-7}$	90	8 KONAKA	86 BDMP $eN \rightarrow eA^0N$ ( $A^0 \rightarrow ee$ )	

- <sup>1</sup>The listed BROSS 91 limit is for  $m_{A^0} = 1.14$  MeV.  $B(A^0 \rightarrow e^+e^-) = 1$  assumed. Excluded domain in the  $\tau_{A^0}$ - $m_{A^0}$  plane extends up to  $m_{A^0} \approx 7$  MeV (see Fig. 5). Combining with electron  $g$ -2 constraint, axions coupling only to  $e^+e^-$  ruled out for  $m_{A^0} < 4.8$  MeV (90% CL).
- <sup>2</sup>GUO 90 use the same apparatus as BROWN 86 and improve the previous limit in the shorter lifetime region. Combined with  $g$ -2 constraint, axions coupling only to  $e^+e^-$  are ruled out for  $m_{A^0} < 2.7$  MeV (90% CL).
- <sup>3</sup>BJORKEN 88 reports limits on axion parameters ( $f_A, m_A, \tau_A$ ) for  $m_{A^0} < 200$  MeV from electron beam-dump experiment with production via Primakoff photoproduction, bremsstrahlung from electrons, and resonant annihilation of positrons on atomic electrons.
- <sup>4</sup>BLINOV 88 assume zero spin,  $m = 1.8$  MeV and lifetime  $< 5 \times 10^{-12}$  s and find  $\Gamma(A^0 \rightarrow \gamma\gamma)B(A^0 \rightarrow e^+e^-) < 2$  eV (CL=90%).
- <sup>5</sup>Assumes  $A^0\gamma\gamma$  coupling is small and hence Primakoff production is small. Their figure 2 shows limits on axions for  $m_{A^0} < 15$  MeV.
- <sup>6</sup>Uses electrons in hadronic showers from an incident 800 GeV proton beam. Limits for  $m_{A^0} < 15$  MeV are shown in their figure 3.
- <sup>7</sup> $m_{A^0} = 1.8$  MeV assumed. The excluded domain in the  $\tau_{A^0}$ - $m_{A^0}$  plane extends up to  $m_{A^0} \approx 14$  MeV, see their figure 4.
- <sup>8</sup>The limits are obtained from their figure 3. Also given is the limit on the  $A^0\gamma\gamma$ - $A^0e^+e^-$  coupling plane by assuming Primakoff production.

### Search for $A^0$ (Axion) Resonance in Bhabha Scattering

The limit is for  $\Gamma(A^0)[B(A^0 \rightarrow e^+e^-)]^2$ .

VALUE ( $10^{-3}$ eV)	CL%	DOCUMENT ID	TECN	COMMENT
••• We do not use the following data for averages, fits, limits, etc. •••				
$< 1.3$	97	1 HALLIN	92 CNTR	$m_{A^0} = 1.75$ – $1.88$ MeV
none 0.0016–0.47	90	2 HENDERSON	92c CNTR	$m_{A^0} = 1.5$ – $1.86$ MeV
$< 2.0$	90	3 WU	92 CNTR	$m_{A^0} = 1.56$ – $1.86$ MeV
$< 0.013$	95	TSERTOS	91 CNTR	$m_{A^0} = 1.832$ MeV
none 0.19–3.3	95	4 WIDMANN	91 CNTR	$m_{A^0} = 1.78$ – $1.92$ MeV
$< 5$	97	BAUER	90 CNTR	$m_{A^0} = 1.832$ MeV
none 0.09–1.5	95	5 JUDGE	90 CNTR	$m_{A^0} = 1.832$ MeV, $m_{A^0}^{\text{elastic}}$
$< 1.9$	97	6 TSERTOS	89 CNTR	$m_{A^0} = 1.82$ MeV
$<(10-40)$	97	6 TSERTOS	89 CNTR	$m_{A^0} = 1.51$ – $1.65$ MeV
$<(1-2.5)$	97	6 TSERTOS	89 CNTR	$m_{A^0} = 1.80$ – $1.86$ MeV
$< 31$	95	LORENZ	88 CNTR	$m_{A^0} = 1.646$ MeV
$< 94$	95	LORENZ	88 CNTR	$m_{A^0} = 1.726$ MeV
$< 23$	95	LORENZ	88 CNTR	$m_{A^0} = 1.782$ MeV
$< 19$	95	LORENZ	88 CNTR	$m_{A^0} = 1.837$ MeV
$< 3.8$	97	7 TSERTOS	88 CNTR	$m_{A^0} = 1.832$ MeV
		8 VANKLINKEN	88 CNTR	
		9 MAIER	87 CNTR	
$< 2500$	90	MILLS	87 CNTR	$m_{A^0} = 1.8$ MeV
		10 VONWIMMER	87 CNTR	

- <sup>1</sup>HALLIN 92 quote limits on lifetime,  $8 \times 10^{-14}$ – $5 \times 10^{-13}$  sec depending on mass, assuming  $B(A^0 \rightarrow e^+e^-) = 100\%$ . They say that TSERTOS 91 overestimated their sensitivity by a factor of 3.
- <sup>2</sup>HENDERSON 92c exclude axion with lifetime  $\tau_{A^0} = 1.4 \times 10^{-12}$ – $4.0 \times 10^{-10}$  s, assuming  $B(A^0 \rightarrow e^+e^-) = 100\%$ . HENDERSON 92c also exclude a vector boson with  $\tau = 1.4 \times 10^{-12}$ – $6.0 \times 10^{-10}$  s.
- <sup>3</sup>WU 92 quote limits on lifetime  $> 3.3 \times 10^{-13}$  s assuming  $B(A^0 \rightarrow e^+e^-) = 100\%$ . They say that TSERTOS 89 overestimate the limit by a factor of  $\pi/2$ . WU 92 also quote a bound for vector boson,  $\tau > 8.2 \times 10^{-13}$  s.
- <sup>4</sup>WIDMANN 91 bound applies exclusively to the case  $B(A^0 \rightarrow e^+e^-) = 1$ , since the detection efficiency varies substantially as  $\Gamma(A^0)_{\text{total}}$  changes. See their Fig. 6.
- <sup>5</sup>JUDGE 90 excludes an elastic pseudoscalar  $e^+e^-$  resonance for  $4.5 \times 10^{-13}$  s  $< \tau(A^0) < 7.5 \times 10^{-12}$  s (95% CL) at  $m_{A^0} = 1.832$  MeV. Comparable limits can be set for  $m_{A^0} = 1.776$ – $1.856$  MeV.
- <sup>6</sup>See also TSERTOS 88b in references.
- <sup>7</sup>The upper limit listed in TSERTOS 88 is too large by a factor of 4. See TSERTOS 88b, footnote 3.
- <sup>8</sup>VANKLINKEN 88 looked for relatively long-lived resonance ( $\tau = 10^{-10}$ – $10^{-12}$  s). The sensitivity is not sufficient to exclude such a narrow resonance.
- <sup>9</sup>MAIER 87 obtained limits  $R\Gamma \lesssim 60$  eV (100 eV) at  $m_{A^0} \approx 1.64$  MeV (1.83 MeV) for energy resolution  $\Delta E_{\text{cm}} \approx 3$  keV, where  $R$  is the resonance cross section normalized to that of Bhabha scattering, and  $\Gamma = \Gamma_{e^+e^-}^2/\Gamma_{\text{total}}$ . For a discussion implying that  $\Delta E_{\text{cm}} \approx 10$  keV, see TSERTOS 89.
- <sup>10</sup>VONWIMMERSPERG 87 measured Bhabha scattering for  $E_{\text{cm}} = 1.37$ – $1.86$  MeV and found a possible peak at 1.73 with  $\int \sigma dE_{\text{cm}} = 14.5 \pm 6.8$  keV·b. For a comment and a reply, see VANKLINKEN 88b and VONWIMMERSPERG 88. Also see CONNELL 88.

### Search for $A^0$ (Axion) Resonance in $e^+e^- \rightarrow \gamma\gamma$

The limit is for  $\Gamma(A^0 \rightarrow e^+e^-)\Gamma(A^0 \rightarrow \gamma\gamma)/\Gamma_{\text{total}}$

VALUE ( $10^{-3}$ eV)	CL%	DOCUMENT ID	TECN	COMMENT
••• We do not use the following data for averages, fits, limits, etc. •••				
$< 0.18$	95	VO	94 CNTR	$m_{A^0} = 1.1$ MeV
$< 1.5$	95	VO	94 CNTR	$m_{A^0} = 1.4$ MeV
$< 12$	95	VO	94 CNTR	$m_{A^0} = 1.7$ MeV
$< 6.6$	95	1 TRZASKA	91 CNTR	$m_{A^0} = 1.8$ MeV
$< 4.4$	95	WIDMANN	91 CNTR	$m_{A^0} = 1.78$ – $1.92$ MeV
		2 FOX	89 CNTR	
$< 0.11$	95	3 MINOWA	89 CNTR	$m_{A^0} = 1.062$ MeV
$< 33$	97	CONNELL	88 CNTR	$m_{A^0} = 1.580$ MeV
$< 42$	97	CONNELL	88 CNTR	$m_{A^0} = 1.642$ MeV
$< 73$	97	CONNELL	88 CNTR	$m_{A^0} = 1.782$ MeV
$< 79$	97	CONNELL	88 CNTR	$m_{A^0} = 1.832$ MeV

- <sup>1</sup>TRZASKA 91 also give limits in the range  $(6.6$ – $30) \times 10^{-3}$  eV (95% CL) for  $m_{A^0} = 1.6$ – $2.0$  MeV.
- <sup>2</sup>FOX 89 measured positron annihilation with an electron in the source material into two photons and found no signal at 1.062 MeV ( $< 9 \times 10^{-5}$  of two-photon annihilation at rest).
- <sup>3</sup>Similar limits are obtained for  $m_{A^0} = 1.045$ – $1.085$  MeV.

### Search for $X^0$ (Light Boson) Resonance in $e^+e^- \rightarrow \gamma\gamma\gamma$

The limit is for  $\Gamma(X^0 \rightarrow e^+e^-)\Gamma(X^0 \rightarrow \gamma\gamma\gamma)/\Gamma_{\text{total}}$ . C invariance forbids spin-0  $X^0$  coupling to both  $e^+e^-$  and  $\gamma\gamma\gamma$ .

VALUE ( $10^{-3}$ eV)	CL%	DOCUMENT ID	TECN	COMMENT
••• We do not use the following data for averages, fits, limits, etc. •••				

# Gauge & Higgs Boson Particle Listings

## Axions ( $A^0$ ) and Other Very Light Bosons

< 0.2	95	1 VO	94 CNTR	$m_{X^0}=1.1-1.9$ MeV
< 1.0	95	2 VO	94 CNTR	$m_{X^0}=1.1$ MeV
< 2.5	95	2 VO	94 CNTR	$m_{X^0}=1.4$ MeV
<120	95	2 VO	94 CNTR	$m_{X^0}=1.7$ MeV
< 3.8	95	3 SKALSEY	92 CNTR	$m_{X^0}=1.5$ MeV

<sup>1</sup> VO 94 looked for  $X^0 \rightarrow \gamma\gamma\gamma$  decaying at rest. The precise limits depend on  $m_{X^0}$ . See Fig. 2(b) in paper.

<sup>2</sup> VO 94 looked for  $X^0 \rightarrow \gamma\gamma\gamma$  decaying in flight.

<sup>3</sup> SKALSEY 92 also give limits 4.3 for  $m_{X^0}=1.54$  and 7.5 for 1.64 MeV. The spin of  $X^0$  is assumed to be one.

### Light Boson ( $X^0$ ) Search in Nonresonant $e^+e^-$ Annihilation at Rest

Limits are for the ratio of  $n\gamma + X^0$  production relative to  $\gamma\gamma$ .

VALUE (units $10^{-6}$ )	CL%	DOCUMENT ID	TECN	COMMENT
< 4.2	90	1 MITSUI	96 CNTR	$\gamma X^0$
< 4	68	2 SKALSEY	95 CNTR	$\gamma X^0$
<40	68	3 SKALSEY	95 RVUE	$\gamma X^0$
< 0.18	90	4 ADACHI	94 CNTR	$\gamma\gamma X^0, X^0 \rightarrow \gamma\gamma$
< 0.26	90	5 ADACHI	94 CNTR	$\gamma\gamma X^0, X^0 \rightarrow \gamma\gamma$
< 0.33	90	6 ADACHI	94 CNTR	$\gamma\gamma X^0, X^0 \rightarrow \gamma\gamma\gamma$

<sup>1</sup> MITSUI 96 looked for a monochromatic  $\gamma$ . The bound applies for a vector  $X^0$  with  $C=-1$  and  $m_{X^0} < 200$  keV. They derive an upper bound on  $eX^0$  coupling and hence on the branching ratio  $B(\rho\text{-Ps} \rightarrow \gamma\gamma X^0) < 6.2 \times 10^{-6}$ . The bounds weaken for heavier  $X^0$ .

<sup>2</sup> SKALSEY 95 looked for a monochromatic  $\gamma$  without an accompanying  $\gamma$  in  $e^+e^-$  annihilation. The bound applies for scalar and vector  $X^0$  with  $C=-1$  and  $m_{X^0} = 100-1000$  keV.

<sup>3</sup> SKALSEY 95 reinterpreted the bound on  $\gamma A^0$  decay of  $\rho$ -Ps by ASA1 91 where 3% of delayed annihilations are not from  $^3S_1$  states. The bound applies for scalar and vector  $X^0$  with  $C=-1$  and  $m_{X^0} = 0-800$  keV.

<sup>4</sup> ADACHI 94 looked for a peak in the  $\gamma\gamma$  invariant mass distribution in  $\gamma\gamma\gamma\gamma$  production from  $e^+e^-$  annihilation. The bound applies for  $m_{X^0} = 70-800$  keV.

<sup>5</sup> ADACHI 94 looked for a peak in the missing-mass distribution in  $\gamma\gamma$  channel, using  $\gamma\gamma\gamma\gamma$  production from  $e^+e^-$  annihilation. The bound applies for  $m_{X^0} < 800$  keV.

<sup>6</sup> ADACHI 94 looked for a peak in the missing mass distribution in  $\gamma\gamma\gamma$  channel, using  $\gamma\gamma\gamma\gamma$  production from  $e^+e^-$  annihilation. The bound applies for  $m_{X^0} = 200-900$  keV.

### Searches for Goldstone Bosons ( $X^0$ )

(Including Horizontal Bosons and Majorons.) Limits are for branching ratios.

VALUE	CL%	DOCUMENT ID	TECN	COMMENT
<9 $\times 10^{-6}$	90	1 BAYES	15 TWST	$\mu^+ \rightarrow e^+ X^0$ , Familon
		2 LATTANZI	13 COSM	Majoron dark matter decay
		3 LESSA	07 RVUE	Meson, $\ell$ decays to Majoron
		4 DIAZ	98 THEO	$H^0 \rightarrow X^0 X^0, A^0 \rightarrow X^0 X^0 X^0$ , Majoron
		5 BOBRAKOV	91	Electron quasi-magnetic interaction
<3.3 $\times 10^{-2}$	95	6 ALBRECHT	90E ARG	$\tau \rightarrow \mu X^0$ , Familon
<1.8 $\times 10^{-2}$	95	6 ALBRECHT	90E ARG	$\tau \rightarrow e X^0$ , Familon
<6.4 $\times 10^{-9}$	90	7 ATIYA	90 B787	$K^+ \rightarrow \pi^+ X^0$ , Familon
<1.4 $\times 10^{-5}$	90	8 BALKE	88 CNTR	$\mu^+ \rightarrow e^+ X^0$ , Familon
<1.1 $\times 10^{-9}$	90	9 BOLTON	88 CBOX	$\mu^+ \rightarrow e^+ \gamma X^0$ , Familon
		10 CHANDA	88 ASTR	Sun, Majoron
		11 CHOI	88 ASTR	Majoron, SN 1987A
<5 $\times 10^{-6}$	90	12 PICCIOTTO	88 CNTR	$\pi \rightarrow e\nu X^0$ , Majoron
<1.3 $\times 10^{-9}$	90	13 GOLDMAN	87 CNTR	$\mu \rightarrow e\gamma X^0$ , Familon
<3 $\times 10^{-4}$	90	14 BRYMAN	86E RVUE	$\mu \rightarrow e X^0$ , Familon
<1 $\times 10^{-10}$	90	15 EICHLER	86 SPEC	$\mu^+ \rightarrow e^+ X^0$ , Familon
<2.6 $\times 10^{-6}$	90	16 JODIDIO	86 SPEC	$\mu^+ \rightarrow e^+ X^0$ , Familon
		17 BALTRUSAITIS	85 MRK3	$\tau \rightarrow \ell X^0$ , Familon
		18 DICUS	83 COSM	$\nu(\text{hvy}) \rightarrow \nu(\text{light}) X^0$

<sup>1</sup> BAYES 15 limits are the average over  $m_{X^0} = 13-80$  MeV for the isotropic decay distribution of positrons. See their Fig. 4 and Table II for the mass-dependent limits as well as the dependence on the decay anisotropy. In particular, they find a limit  $< 58 \times 10^{-6}$  at 90% CL for massless familons and for the same asymmetry as normal muon decay, a case not covered by JODIDIO 86.

<sup>2</sup> LATTANZI 13 use WMAP 9 year data as well as X-ray and  $\gamma$ -ray observations to derive limits on decaying majoron dark matter. A limit on the decay width  $\Gamma(X^0 \rightarrow \nu\bar{\nu}) < 6.4 \times 10^{-19} \text{ s}^{-1}$  at 95% CL is found if majorons make up all of the dark matter.

<sup>3</sup> LESSA 07 consider decays of the form Meson  $\rightarrow \ell\nu$  Majoron and  $\ell \rightarrow \ell'\nu\bar{\nu}$  Majoron and use existing data to derive limits on the neutrino-Majoron Yukawa couplings  $g_{\alpha\beta}$  ( $\alpha, \beta = e, \mu, \tau$ ). Their best limits are  $|g_{e\alpha}|^2 < 5.5 \times 10^{-6}$ ,  $|g_{\mu\alpha}|^2 < 4.5 \times 10^{-5}$ ,  $|g_{\tau\alpha}|^2 < 5.5 \times 10^{-2}$  at CL = 90%.

<sup>4</sup> DIAZ 98 studied models of spontaneously broken lepton number with both singlet and triplet Higgses. They obtain limits on the parameter space from invisible decay  $Z \rightarrow H^0 A^0 \rightarrow X^0 X^0 X^0 X^0$  and  $e^+e^- \rightarrow Z H^0$  with  $H^0 \rightarrow X^0 X^0$ .

<sup>5</sup> BOBRAKOV 91 searched for anomalous magnetic interactions between polarized electrons expected from the exchange of a massless pseudoscalar boson (arion). A limit

$x_e^2 < 2 \times 10^{-4}$  (95%CL) is found for the effective anomalous magneton parametrized as  $x_e(G_F/8\pi\sqrt{2})^{1/2}$ .

<sup>6</sup> ALBRECHT 90E limits are for  $B(\tau \rightarrow \ell X^0)/B(\tau \rightarrow \ell\nu\bar{\nu})$ . Valid for  $m_{X^0} < 100$  MeV. The limits rise to 7.1% (for  $\mu$ ), 5.0% (for  $e$ ) for  $m_{X^0} = 500$  MeV.

<sup>7</sup> ATIYA 90 limit is for  $m_{X^0} = 0$ . The limit  $B < 1 \times 10^{-8}$  holds for  $m_{X^0} < 95$  MeV.

For the reduction of the limit due to finite lifetime of  $X^0$ , see their Fig. 3.

<sup>8</sup> BALKE 88 limits are for  $B(\mu^+ \rightarrow e^+ X^0)$ . Valid for  $m_{X^0} < 80$  MeV and  $\tau_{X^0} > 10^{-8}$  sec.

<sup>9</sup> BOLTON 88 limit corresponds to  $F > 3.1 \times 10^9$  GeV, which does not depend on the chirality property of the coupling.

<sup>10</sup> CHANDA 88 find  $v_T < 10$  MeV for the weak-triplet Higgs vacuum expectation value in Gelmini-Roncadelli model, and  $v_S > 5.8 \times 10^6$  GeV in the singlet Majoron model.

<sup>11</sup> CHOI 88 used the observed neutrino flux from the supernova SN 1987A to exclude the neutrino Majoron Yukawa coupling  $h$  in the range  $2 \times 10^{-5} < h < 3 \times 10^{-4}$  for the interaction  $L_{\text{int}} = \frac{1}{2} i h \bar{\nu}_\nu \gamma_5 \psi_\nu \phi_X$ . For several families of neutrinos, the limit applies for  $(\sum h_i^2)^{1/4}$ .

<sup>12</sup> PICCIOTTO 88 limit applies when  $m_{X^0} < 55$  MeV and  $\tau_{X^0} > 2$  ns, and it decreases to  $4 \times 10^{-7}$  at  $m_{X^0} = 125$  MeV, beyond which no limit is obtained.

<sup>13</sup> GOLDMAN 87 limit corresponds to  $F > 2.9 \times 10^9$  GeV for the family symmetry breaking scale from the Lagrangian  $L_{\text{int}} = (1/F) \bar{\psi}_\mu \gamma^\mu (a + b\gamma_5) \psi_e \theta_\mu \phi_{X^0}$  with  $a^2 + b^2 = 1$ .

This is not as sensitive as the limit  $F > 9.9 \times 10^9$  GeV derived from the search for  $\mu^+ \rightarrow e^+ X^0$  by JODIDIO 86, but does not depend on the chirality property of the coupling.

<sup>14</sup> Limits are for  $\Gamma(\mu \rightarrow e X^0)/\Gamma(\mu \rightarrow e\nu\bar{\nu})$ . Valid when  $m_{X^0} = 0-93.4, 98.1-103.5$  MeV.

<sup>15</sup> EICHLER 86 looked for  $\mu^+ \rightarrow e^+ X^0$  followed by  $X^0 \rightarrow e^+ e^-$ . Limits on the branching fraction depend on the mass and lifetime of  $X^0$ . The quoted limits are valid when  $\tau_{X^0} \lesssim 3 \times 10^{-10}$  s if the decays are kinematically allowed.

<sup>16</sup> JODIDIO 86 corresponds to  $F > 9.9 \times 10^9$  GeV for the family symmetry breaking scale with the parity-conserving effective Lagrangian  $L_{\text{int}} = (1/F) \bar{\psi}_\mu \gamma^\mu \psi_e \theta_\mu \phi_{X^0}$ .

<sup>17</sup> BALTRUSAITIS 85 search for light Goldstone boson ( $X^0$ ) of broken U(1). CL = 95% limits are  $B(\tau \rightarrow \mu^+ X^0)/B(\tau \rightarrow \mu^+ \nu\bar{\nu}) < 0.125$  and  $B(\tau \rightarrow e^+ X^0)/B(\tau \rightarrow e^+ \nu\bar{\nu}) < 0.04$ . Inferred limit for the symmetry breaking scale is  $m > 3000$  TeV.

<sup>18</sup> The primordial heavy neutrino must decay into  $\nu$  and familon,  $f_A$ , early so that the red-shifted decay products are below critical density, see their table. In addition,  $K \rightarrow \pi f_A$  and  $\mu \rightarrow e f_A$  are unseen. Combining these excludes  $m_{\text{heavy}\nu}$  between  $5 \times 10^{-5}$  and  $5 \times 10^{-4}$  MeV ( $\mu$  decay) and  $m_{\text{heavy}\nu}$  between  $5 \times 10^{-5}$  and 0.1 MeV ( $K$ -decay).

### Majoron Searches in Neutrinoless Double $\beta$ Decay

Limits are for the half-life of neutrinoless  $\beta\beta$  decay with a Majoron emission.

No experiment currently claims any such evidence. Only the best or comparable limits for each isotope are reported.

$t_{1/2}(10^{21} \text{ yr})$	CL%	ISOTOPE	TRANSITION	METHOD	DOCUMENT ID
>7200	90	128Te	CNTR		1 BERNATOW... 92
> 4.4	90	100Mo	0 $\nu$ 1 $\chi$	NEMO-3	2 ARNOLD 19
> 37	90	82Se	0 $\nu$ 1 $\chi$	NEMO-3	3 ARNOLD 18
> 420	90	76Ge	0 $\nu$ 1 $\chi$	GERDA	4 AGOSTINI 15A
> 400	90	100Mo	0 $\nu$ 1 $\chi$	NEMO-3	5 ARNOLD 15
>1200	90	136Xe	0 $\nu$ 1 $\chi$	EXO-200	6 ALBERT 14A
>2600	90	136Xe	0 $\nu$ 1 $\chi$	KamLAND-Zen	7 GANDIO 12
> 16	90	130Te	0 $\nu$ 1 $\chi$	NEMO-3	8 ARNOLD 11
> 1.9	90	96Zr	2 $\nu$ 1 $\chi$	NEMO-3	9 ARGYRADES 10
> 1.52	90	150Nd	0 $\nu$ 1 $\chi$	NEMO-3	10 ARGYRADES 09
> 27	90	100Mo	0 $\nu$ 1 $\chi$	NEMO-3	11 ARNOLD 06
> 15	90	82Se	0 $\nu$ 1 $\chi$	NEMO-3	12 ARNOLD 06
> 14	90	100Mo	0 $\nu$ 1 $\chi$	NEMO-3	13 ARNOLD 04
> 12	90	82Se	0 $\nu$ 1 $\chi$	NEMO-3	14 ARNOLD 04
> 2.2	90	130Te	0 $\nu$ 1 $\chi$	Cryog. det.	15 ARNABOLDI 03
> 0.9	90	130Te	0 $\nu$ 2 $\chi$	Cryog. det.	16 ARNABOLDI 03
> 8	90	116Cd	0 $\nu$ 1 $\chi$	CdWO <sub>4</sub> scint.	17 DANEVICH 03
> 0.8	90	116Cd	0 $\nu$ 2 $\chi$	CdWO <sub>4</sub> scint.	18 DANEVICH 03
> 500	90	136Xe	0 $\nu$ 1 $\chi$	Liquid Xe Scint.	19 BERNABEI 02D
> 5.8	90	100Mo	0 $\nu$ 1 $\chi$	ELEGANT V	20 FUSHIMI 02
> 0.32	90	100Mo	0 $\nu$ 1 $\chi$	Liq. Ar ioniz.	21 ASHITKOV 01
> 0.0035	90	160Gd	0 $\nu$ 1 $\chi$	<sup>160</sup> Gd <sub>2</sub> SiO <sub>5</sub> :Ce	22 DANEVICH 01
> 0.013	90	160Gd	0 $\nu$ 2 $\chi$	<sup>160</sup> Gd <sub>2</sub> SiO <sub>5</sub> :Ce	23 DANEVICH 01
> 2.3	90	82Se	0 $\nu$ 1 $\chi$	NEMO 2	24 ARNOLD 00
> 0.31	90	96Zr	0 $\nu$ 1 $\chi$	NEMO 2	25 ARNOLD 00
> 0.63	90	82Se	0 $\nu$ 2 $\chi$	NEMO 2	26 ARNOLD 00
> 0.063	90	96Zr	0 $\nu$ 2 $\chi$	NEMO 2	26 ARNOLD 00
> 0.16	90	100Mo	0 $\nu$ 2 $\chi$	NEMO 2	26 ARNOLD 00
> 2.4	90	82Se	0 $\nu$ 1 $\chi$	NEMO 2	27 ARNOLD 98
> 7.2	90	136Xe	0 $\nu$ 2 $\chi$	TPC	28 LUESCHER 98
> 7.91	90	76Ge	SPEC	SPEC	29 GUENTHER 96
> 17	90	76Ge	CNTR	BECK	30 BECK 93

<sup>1</sup> BERNATOWICZ 92 studied double- $\beta$  decays of <sup>128</sup>Te and <sup>130</sup>Te, and found the ratio  $\tau(130\text{Te})/\tau(128\text{Te}) = (3.52 \pm 0.11) \times 10^{-4}$  in agreement with relatively stable theoretical predictions. The bound is based on the requirement that Majoron-emitting decay cannot be larger than the observed double-beta rate of <sup>128</sup>Te of  $(7.7 \pm 0.4) \times 10^{24}$  year. We calculated 90% CL limit as  $(7.7-1.28 \times 0.4=7.2) \times 10^{24}$ .

See key on page 999

# Gauge & Higgs Boson Particle Listings

## Axions ( $A^0$ ) and Other Very Light Bosons

- 2 ARNOLD 19 uses the NEMO-3 tracking calorimeter to determine limits for the Majoron emitting double beta decay, with spectral index  $n = 3$ . The limit corresponds to the range of the  $g_{ee}$  coupling of 0.013–0.035; depending on the nuclear matrix elements used.
- 3 ARNOLD 18 use the NEMO-3 tracking detector. The limit corresponds to  $\langle g_{ee} \rangle < 3.2\text{--}8.0 \times 10^{-5}$ ; the range corresponds to different nuclear matrix element calculations.
- 4 AGOSTINI 15A analyze a 20.3 kg yr of data set of the GERDA calorimeter to determine  $g_{\nu\chi} < 3.4\text{--}8.7 \times 10^{-5}$  on the Majoron-neutrino coupling constant. The range reflects the spread of the nuclear matrix elements.
- 5 ARNOLD 15 use the NEMO-3 tracking calorimeter with 3.43 kg yr exposure to determine the limit on Majoron emission. The limit corresponds to  $g_{\nu\chi} < 1.6\text{--}3.0 \times 10^{-4}$ . The spread reflects different nuclear matrix elements. Supersedes ARNOLD 06.
- 6 ALBERT 14A utilize 100 kg yr of exposure of the EXO-200 tracking calorimeter to place a limit on the  $g_{\nu\chi} < 0.8\text{--}1.7 \times 10^{-5}$  on the Majoron-neutrino coupling constant. The range reflects the spread of the nuclear matrix elements.
- 7 GANDO 12 use the KamLAND-Zen detector to obtain the limit on the  $0\nu\chi$  decay with Majoron emission. It implies that the coupling constant  $g_{\nu\chi} < 0.8\text{--}1.6 \times 10^{-5}$  depending on the nuclear matrix elements used.
- 8 ARNOLD 11 use the NEMO-3 detector to obtain the reported limit on Majoron emission. It implies that the coupling constant  $g_{\nu\chi} < 0.6\text{--}1.6 \times 10^{-4}$  depending on the nuclear matrix element used. Supersedes ARNOLD 03.
- 9 ARGYRIADES 10 use the NEMO-3 tracking detector and  $^{96}\text{Zr}$  to derive the reported limit. No limit for the Majoron electron coupling is given.
- 10 ARGYRIADES 09 use  $^{150}\text{Nd}$  data taken with the NEMO-3 tracking detector. The reported limit corresponds to  $\langle g_{\nu\chi} \rangle < 1.7\text{--}3.0 \times 10^{-4}$  using a range of nuclear matrix elements that include the effect of nuclear deformation.
- 11 ARNOLD 06 use  $^{100}\text{Mo}$  data taken with the NEMO-3 tracking detector. The reported limit corresponds to  $\langle g_{\nu\chi} \rangle < (0.4\text{--}1.8) \times 10^{-4}$  using a range of matrix element calculations. Superseded by ARNOLD 15.
- 12 NEMO-3 tracking calorimeter is used in ARNOLD 06. Reported half-life limit for  $^{82}\text{Se}$  corresponds to  $\langle g_{\nu\chi} \rangle < (0.66\text{--}1.9) \times 10^{-4}$  using a range of matrix element calculations. Supersedes ARNOLD 04.
- 13 ARNOLD 04 use the NEMO-3 tracking detector. The limit corresponds to  $\langle g_{\nu\chi} \rangle < (0.5\text{--}0.9)10^{-4}$  using the matrix elements of SIMKOVIĆ 99, STOICA 01 and CIVITARESE 03. Superseded by ARNOLD 06.
- 14 ARNOLD 04 use the NEMO-3 tracking detector. The limit corresponds to  $\langle g_{\nu\chi} \rangle < (0.7\text{--}1.6)10^{-4}$  using the matrix elements of SIMKOVIĆ 99, STOICA 01 and CIVITARESE 03.
- 15 Supersedes ALESSANDRELLO 00. Array of  $\text{TeO}_2$  crystals in high resolution cryogenic calorimeter. Some enriched in  $^{130}\text{Te}$ . Derive  $\langle g_{\nu\chi} \rangle < 17\text{--}33 \times 10^{-5}$  depending on matrix element.
- 16 Supersedes ALESSANDRELLO 00. Cryogenic calorimeter search.
- 17 Limit for the  $0\nu\chi$  decay with Majoron emission of  $^{116}\text{Cd}$  using enriched  $\text{CdWO}_4$  scintillators.  $\langle g_{\nu\chi} \rangle < 4.6\text{--}8.1 \times 10^{-5}$  depending on the matrix element. Supersedes DANEVICH 00.
- 18 Limit for the  $0\nu 2\chi$  decay of  $^{116}\text{Cd}$ . Supersedes DANEVICH 00.
- 19 BERNABEI 02b obtain limit for  $0\nu\chi$  decay with Majoron emission of  $^{136}\text{Xe}$  using liquid Xe scintillation detector. They derive  $\langle g_{\nu\chi} \rangle < 2.0\text{--}3.0 \times 10^{-5}$  with several nuclear matrix elements.
- 20 Replaces TANAKA 93. FUSHIMI 02 derive half-life limit for the  $0\nu\chi$  decay by means of tracking calorimeter ELEGANT V. Considering various matrix element calculations, a range of limits for the Majoron-neutrino coupling is given:  $\langle g_{\nu\chi} \rangle < (6.3\text{--}360) \times 10^{-5}$ .
- 21 ASHITKOV 01 result for  $0\nu\chi$  of  $^{100}\text{Mo}$  is less stringent than ARNOLD 00.
- 22 DANEVICH 01 obtain limit for the  $0\nu\chi$  decay with Majoron emission of  $^{160}\text{Gd}$  using  $\text{Gd}_2\text{SiO}_5\text{:Ce}$  crystal scintillators.
- 23 DANEVICH 01 obtain limit for the  $0\nu 2\chi$  decay with 2 Majoron emission of  $^{160}\text{Gd}$ .
- 24 ARNOLD 00 reports limit for the  $0\nu\chi$  decay with Majoron emission derived from tracking calorimeter NEMO 2. Using  $^{82}\text{Se}$  source:  $\langle g_{\nu\chi} \rangle < 1.6 \times 10^{-4}$ . Matrix element from GUENTHER 96.
- 25 Using  $^{96}\text{Zr}$  source:  $\langle g_{\nu\chi} \rangle < 2.6 \times 10^{-4}$ . Matrix element from ARNOLD 99.
- 26 ARNOLD 00 reports limit for the  $0\nu 2\chi$  decay with two Majoron emission derived from tracking calorimeter NEMO 2.
- 27 ARNOLD 98 determine the limit for  $0\nu\chi$  decay with Majoron emission of  $^{82}\text{Se}$  using the NEMO-2 tracking detector. They derive  $\langle g_{\nu\chi} \rangle < 2.3\text{--}4.3 \times 10^{-4}$  with several nuclear matrix elements.
- 28 LUESCHER 98 report a limit for the  $0\nu$  decay with Majoron emission of  $^{136}\text{Xe}$  using Xe TPC. This result is more stringent than BARABASH 89. Using the matrix elements of ENGEL 88, they obtain a limit on  $\langle g_{\nu\chi} \rangle$  of  $2.0 \times 10^{-4}$ .
- 29 See Table 1 in GUENTHER 96 for limits on the Majoron coupling in different models.

< 1.2	95	12 HANNESTAD 07	COSM	K, hot dark matter
< 0.42	95	13 MELCHIORRI 07A	COSM	K, hot dark matter
< 1.05	95	14 HANNESTAD 05A	COSM	K, hot dark matter
3 to 20		15 MOROI 98	COSM	K, hot dark matter
< 0.007		16 BORISOV 97	ASTR	D, neutron star
< 4		17 KACHELRIESS 97	ASTR	D, neutron star cooling
< $(0.5\text{--}6) \times 10^{-3}$		18 KEIL 97	ASTR	SN 1987A
< 0.018		19 RAFFELT 95	ASTR	D, red giant
< 0.010		20 ALTHERR 94	ASTR	D, red giants, white dwarfs
< 0.01		21 CHANG 93	ASTR	K, SN 1987A
< 0.03		WANG 92	ASTR	D, white dwarf
none 3–8		WANG 92C	ASTR	D, C-O burning
< 10		22 BERSHADY 91	ASTR	D, K, intergalactic light
< 1 $\times 10^{-3}$		23 KIM 91C	COSM	D, K, mass density of the universe, super-symmetry
none $10^{-3}\text{--}3$		24 RAFFELT 91B	ASTR	D, K, SN 1987A
< 0.02		25 RESSELL 91	ASTR	K, intergalactic light
< 1 $\times 10^{-3}$		BURROWS 90	ASTR	D, K, SN 1987A
< $(1.4\text{--}10) \times 10^{-3}$		26 ENGEL 90	ASTR	D, K, SN 1987A
< $3.6 \times 10^{-4}$		27 RAFFELT 90D	ASTR	D, red giant
< 12		28 BURROWS 89	ASTR	D, K, SN 1987A
< 1 $\times 10^{-3}$		29 ERICSON 89	ASTR	D, K, SN 1987A
< 0.07		30 MAYLE 89	ASTR	D, K, SN 1987A
< 0.7		CHANDA 88	ASTR	D, Sun
< 2–5		RAFFELT 88	ASTR	D, K, SN 1987A
< 0.01		31 RAFFELT 88B	ASTR	red giant
< 0.06		FRIEMAN 87	ASTR	D, red giant
< 0.7		32 RAFFELT 87	ASTR	K, red giant
< 0.7		TURNER 87	COSM	K, thermal production
< 0.03		33 DEARBORN 86	ASTR	D, red giant
< 1		RAFFELT 86	ASTR	D, red giant
< 0.003–0.02		34 RAFFELT 86	ASTR	K, red giant
> 1 $\times 10^{-5}$		RAFFELT 86B	ASTR	D, white dwarf
> 1 $\times 10^{-5}$		35 KAPLAN 85	ASTR	K, red giant
> 0.04		IWAMOTO 84	ASTR	D, K, neutron star
> 1 $\times 10^{-5}$		ABBOTT 83	COSM	D, K, mass density of the universe
< 0.1		DINE 83	COSM	D, K, mass density of the universe
< 1		ELLIS 83B	ASTR	D, red giant
< 0.07		PRESKILL 83	COSM	D, K, mass density of the universe
		BARROSO 82	ASTR	D, red giant
		36 FUKUGITA 82	ASTR	D, stellar cooling
		FUKUGITA 82B	ASTR	D, red giant

- 1 PALOMBA 19 used the LIGO O2 dataset to derive limits on nearly monochromatic gravitational waves emitted by boson clouds formed around a stellar-mass black hole. They exclude boson masses in a range of  $1.1 \times 10^{-13}$  and  $4 \times 10^{-13}$  eV for high initial black hole spin, and  $1.2 \times 10^{-13}$  and  $1.8 \times 10^{-13}$  eV for moderate spin. See their Figs. 2 and 3 for limits based on various values of black hole initial spin, boson cloud age, and distance.
- 2 CHANG 18 update axion bremsstrahlung emission rates in nucleon-nucleon collisions, shifting the excluded mass range to higher values. They rule out the hadronic axion with mass up to a few hundred eV, closing the hadronic axion window. See their Fig. 11 for results based on several different choices of the temperature and density profile of the proto-neutron star.
- 3 ARCHIDIACONO 13A is analogous to HANNESTAD 05A. The limit is based on the CMB temperature power spectrum of the Planck data, the CMB polarization from the WMAP 9-yr data, the matter power spectrum from SDSS-DR7, and the local Hubble parameter measurement by the Carnegie Hubble program.
- 4 CADAMURO 11 use the deuterium abundance to show that the  $m_{A0}$  range 0.7 eV – 300 keV is excluded for axions, complementing HANNESTAD 10.
- 5 DERBIN 11A look for solar axions produced by Compton and bremsstrahlung processes, in the resonant excitation of  $^{169}\text{Tm}$ , constraining the axion-electron  $\times$  axion nucleon couplings.
- 6 ANDRIAMONJE 10 search for solar axions produced from  $^7\text{Li}$  (478 keV) and  $\text{D}(\rho, \gamma)^3\text{He}$  (5.5 MeV) nuclear transitions. They show limits on the axion-photon coupling for two reference values of the axion-nucleon coupling for  $m_A < 100$  eV.
- 7 This is an update of HANNESTAD 08 including 7 years of WMAP data.
- 8 ANDRIAMONJE 09 look for solar axions produced from the thermally excited 14.4 keV level of  $^{57}\text{Fe}$ . They show limits on the axion-nucleon  $\times$  axion-photon coupling assuming  $m_A < 0.03$  eV.
- 9 DERBIN 09A look for Primakoff-produced solar axions in the resonant excitation of  $^{169}\text{Tm}$ , constraining the axion-photon  $\times$  axion-nucleon couplings.
- 10 KEKEZ 09 look at axio-electric effect of solar axions in HPGe detectors. The one-loop axion-electron coupling for hadronic axions is used.
- 11 This is an update of HANNESTAD 07 including 5 years of WMAP data.
- 12 This is an update of HANNESTAD 05A with new cosmological data, notably WMAP (3 years) and baryon acoustic oscillations (BAO). Lyman- $\alpha$  data are left out, in contrast to HANNESTAD 05A and MELCHIORRI 07A, because it is argued that systematic errors are large. It uses Bayesian statistics and marginalizes over a possible neutrino hot dark matter component.
- 13 MELCHIORRI 07A is analogous to HANNESTAD 05A, with updated cosmological data, notably WMAP (3 years). Uses Bayesian statistics and marginalizes over a possible neutrino hot dark matter component. Leaving out Lyman- $\alpha$  data, a conservative limit is 1.4 eV.
- 14 HANNESTAD 05A puts an upper limit on the mass of hadronic axion because in this mass range it would have been thermalized and contribute to the hot dark matter component of the universe. The limit is based on the CMB anisotropy from WMAP, SDSS large

### Invisible $A^0$ (Axion) MASS LIMITS from Astrophysics and Cosmology

$v_1 = v_2$  is usually assumed ( $v_j =$  vacuum expectation values). For a review of these limits, see RAFFELT 91 and TURNER 90. In the comment lines below, D and K refer to DFSZ and KSVZ axion types, discussed in the above minireview.

VALUE (eV)	CL%	DOCUMENT ID	TECN	COMMENT
•••				We do not use the following data for averages, fits, limits, etc. •••
none $1\text{--}4 \times 10^{-13}$	95	1 PALOMBA 19	ASTR	BH superradiance
< 0.06		2 CHANG 18	ASTR	K, SN 1987A
< 0.67	95	3 ARCHIDIACO...13A	COSM	K, hot dark matter
none $0.7\text{--}3 \times 10^5$		4 CADAMURO 11	COSM	D abundance
<105	90	5 DERBIN 11A	CNTR	D, solar axion
		6 ANDRIAMON...10	CAST	K, solar axions
< 0.72	95	7 HANNESTAD 10	COSM	K, hot dark matter
		8 ANDRIAMON...09	CAST	K, solar axions
<191	90	9 DERBIN 09A	CNTR	K, solar axions
<334	95	10 KEKEZ 09	HPGE	K, solar axions
< 1.02	95	11 HANNESTAD 08	COSM	K, hot dark matter



# Gauge & Higgs Boson Particle Listings

## Axions ( $A^0$ ) and Other Very Light Bosons

- scale structure, Lyman  $\alpha$ , and the prior Hubble parameter from HST Key Project. A  $\chi^2$  statistic is used. Neutrinos are assumed not to contribute to hot dark matter.
- 15 MORIO 98 points out that a KSVZ axion of this mass range (see CHANG 93) can be a viable hot dark matter of Universe, as long as the model-dependent  $g_{A\gamma}$  is accidentally small enough as originally emphasized by KAPLAN 85; see Fig. 1.
- 16 BORISOV 97 bound is on the axion-electron coupling  $g_{ae} < 1 \times 10^{-13}$  from the photo-production of axions off of magnetic fields in the outer layers of neutron stars.
- 17 KACHELRIESS 97 bound is on the axion-electron coupling  $g_{ae} < 1 \times 10^{-10}$  from the production of axions in strongly magnetized neutron stars. The authors also quote a stronger limit,  $g_{ae} < 9 \times 10^{-13}$  which is strongly dependent on the strength of the magnetic field in white dwarfs.
- 18 KEIL 97 uses new measurements of the axial-vector coupling strength of nucleons, as well as a reanalysis of many-body effects and pion-emission processes in the core of the neutron star, to update limits on the invisible-axion mass.
- 19 RAFFELT 95 reexamined the constraints on axion emission from red giants due to the axion-electron coupling. They improve on DEARBORN 86 by taking into proper account degeneracy effects in the bremsstrahlung rate. The limit comes from requiring the red giant core mass at helium ignition not to exceed its standard value by more than 5% (0.025 solar masses).
- 20 ALTHERR 94 bound is on the axion-electron coupling  $g_{ae} < 1.5 \times 10^{-13}$ , from energy loss via axion emission.
- 21 CHANG 93 updates ENGEL 90 bound with the Kaplan-Manohar ambiguity in  $z=m_{A^0}/m_q$  (see the Note on the Quark Masses in the Quark Particle Listings). It leaves the window  $f_A=3 \times 10^5-3 \times 10^6$  GeV open. The constraint from Big-Bang Nucleosynthesis is satisfied in this window as well.
- 22 BERSHADY 91 searched for a line at wave length from 3100–8300 Å expected from 2 $\gamma$  decays of relic thermal axions in intergalactic light of three rich clusters of galaxies.
- 23 KIM 91c argues that the bound from the mass density of the universe will change drastically for the supersymmetric models due to the entropy production of saxion (scalar component in the axionic chiral multiplet) decay. Note that it is an *upperbound* rather than a lowerbound.
- 24 RAFFELT 91b argue that previous SN1987A bounds must be relaxed due to corrections to nucleon bremsstrahlung processes.
- 25 RESSELL 91 uses absence of any intracuster line emission to set limit.
- 26 ENGEL 90 rule out  $10^{-10} \lesssim g_{AN} \lesssim 10^{-3}$ , which for a hadronic axion with EMC motivated axion-nucleon couplings corresponds to  $2.5 \times 10^{-3} \text{ eV} \lesssim m_{A^0} \lesssim 2.5 \times 10^4 \text{ eV}$ . The constraint is loose in the middle of the range, i.e. for  $g_{AN} \sim 10^{-6}$ .
- 27 RAFFELT 90d is a re-analysis of DEARBORN 86.
- 28 The region  $m_{A^0} \gtrsim 2 \text{ eV}$  is also allowed.
- 29 ERICSON 89 considered various nuclear corrections to axion emission in a supernova core, and found a reduction of the previous limit (MAYLE 88) by a large factor.
- 30 MAYLE 89 limit based on naive quark model couplings of axion to nucleons. Limit based on couplings motivated by EMC measurements is 2–4 times weaker. The limit from axion-electron coupling is weak: see HATSUDA 88b.
- 31 RAFFELT 88b derives a limit for the energy generation rate by exotic processes in helium-burning stars  $\epsilon < 100 \text{ erg g}^{-1} \text{ s}^{-1}$ , which gives a firmer basis for the axion limits based on red giant cooling.
- 32 RAFFELT 87 also gives a limit  $g_{A\gamma} < 1 \times 10^{-10} \text{ GeV}^{-1}$ .
- 33 DEARBORN 86 also gives a limit  $g_{A\gamma} < 1.4 \times 10^{-11} \text{ GeV}^{-1}$ .
- 34 RAFFELT 86 gives a limit  $g_{A\gamma} < 1.1 \times 10^{-10} \text{ GeV}^{-1}$  from red giants and  $< 2.4 \times 10^{-9} \text{ GeV}^{-1}$  from the sun.
- 35 KAPLAN 85 says  $m_{A^0} < 23 \text{ eV}$  is allowed for a special choice of model parameters.
- 36 FUKUGITA 82 gives a limit  $g_{A\gamma} < 2.3 \times 10^{-10} \text{ GeV}^{-1}$ .

### Search for Relic Invisible Axions

Limits are for  $[G_{A\gamma\gamma}/m_{A^0}]^2 \rho_A$  where  $G_{A\gamma\gamma}$  denotes the axion two-photon coupling,

$$L_{\text{int}} = -\frac{G_{A\gamma\gamma}}{4} \phi_A F_{\mu\nu} \tilde{F}^{\mu\nu} = G_{A\gamma\gamma} \phi_A \mathbf{E} \cdot \mathbf{B}, \text{ and } \rho_A \text{ is the axion energy density near the earth.}$$

VALUE	CL%	DOCUMENT ID	TECN	COMMENT
$< 2.6 \times 10^{-39}$	95	1 ALESINI 19	QUAX	$m_{A^0} = 37.5 \mu\text{eV}$
$< 6 \times 10^{-5}$		2 FUJITA 19	ASTR	$m_{A^0} < 10^{-21} \text{ eV}$
$< 2 \times 10^{-27}$	95	3 OUELLET 19a	ABRA	$m_{A^0} = 0.31-8.3 \text{ neV}$
$< 7.3 \times 10^{-40}$	90	4 BOUTAN 18	ADMX	$m_{A^0} = 17.38-17.57 \mu\text{eV}$
$< 1.8 \times 10^{-39}$	90	4 BOUTAN 18	ADMX	$m_{A^0} = 21.03-23.98 \mu\text{eV}$
$< 3.4 \times 10^{-39}$	90	4 BOUTAN 18	ADMX	$m_{A^0} = 29.67-29.79 \mu\text{eV}$
$< 1.4 \times 10^{-44}$	90	5 DU 18	ADMX	$m_{A^0} = 2.66-2.81 \mu\text{eV}$
$< 2.87 \times 10^{-42}$	90	6 ZHONG 18	HYST	$m_{A^0} = 23.15-24 \mu\text{eV}$
		7 BRANCA 17	AURG	$m_{S^0} = 3.5-3.9 \text{ peV}$
$< 3 \times 10^{-42}$	90	8 BRUBAKER 17	HYST	$m_{A^0} = 23.55-24.0 \mu\text{eV}$
$< 1.0 \times 10^{-29}$	95	9 CHOI 17		$m_{A^0} = 24.7-29.1 \mu\text{eV}$
$< 8.6 \times 10^{-42}$	90	10 HOSKINS 16	ADMX	$m_{A^0} = 3.36-3.52 \text{ or } 3.55-3.69 \mu\text{eV}$
		11 BECK 13		$m_{A^0} = 0.11 \text{ meV}$
$< 3.5 \times 10^{-43}$		12 HOSKINS 11	ADMX	$m_{A^0} = 3.3-3.69 \times 10^{-6} \text{ eV}$
$< 2.9 \times 10^{-43}$	90	13 ASZTALOS 10	ADMX	$m_{A^0} = 3.34-3.53 \times 10^{-6} \text{ eV}$
$< 1.9 \times 10^{-43}$	97.7	14 DUFFY 06	ADMX	$m_{A^0} = 1.98-2.17 \times 10^{-6} \text{ eV}$
$< 5.5 \times 10^{-43}$	90	15 ASZTALOS 04	ADMX	$m_{A^0} = 1.9-3.3 \times 10^{-6} \text{ eV}$
		16 KIM 98	THEO	
$< 2 \times 10^{-41}$		17 HAGMANN 90	CNTR	$m_{A^0} = (5.4-5.9) 10^{-6} \text{ eV}$
$< 6.3 \times 10^{-42}$	95	18 WUENSCH 89	CNTR	$m_{A^0} = (4.5-10.2) 10^{-6} \text{ eV}$
$< 5.4 \times 10^{-41}$	95	18 WUENSCH 89	CNTR	$m_{A^0} = (11.3-16.3) 10^{-6} \text{ eV}$

- 1 ALESINI 19 used a superconducting resonant cavity made of NbTi to increase the quality factor. The limit applies to a mass range of 0.2 neV around  $m_{A^0} = 37.5 \mu\text{eV}$ .
- 2 FUJITA 19 look for photon birefringence under the oscillating axion background using the polarimetric imaging observation of a protoplanetary disk, AB Aur. See their Fig. 2 for a more conservative limit taking account of possible systematic effects.
- 3 OUELLET 19a look for the axion-induced oscillating magnetic field generated by a toroidal magnetic field. The quoted limit applies at  $m_{A^0} = 8 \text{ neV}$ . See their Fig. 3 for the mass-dependent limits.
- 4 BOUTAN 18 use a small high frequency cavity installed above the main ADMX cavity to look for heavier axion dark matter. See their Fig. 4 for mass-dependent limits.
- 5 DU 18 is analogous to DUFFY 06. They upgraded a dilution refrigerator to reduce the system noise. The quoted limit is around  $m_{A^0} = 2.69 \mu\text{eV}$  for the boosted Maxwellian axion line shape. See Fig. 4 for their mass-dependent limits.
- 6 ZHONG 18 is analogous to BRUBAKER 17. The quoted limit applies at  $m_{A^0} = 23.76 \mu\text{eV}$ . See Fig. 4 for their mass-dependent limits.
- 7 BRANCA 17 look for modulations of the fine-structure constant and the electron mass due to moduli dark matter by using the cryogenic resonant-mass AURIGA detector. The limit on the assumed dilatonic coupling implies  $G_{S\gamma\gamma} < 1.5 \times 10^{-24} \text{ GeV}^{-1}$  for the scalar to two-photon coupling. See Fig. 5 for the mass-dependent limits.
- 8 BRUBAKER 17 used a microwave cavity detector at the Yale Wright Laboratory to search for dark matter axions. See Fig. 3 for the mass-dependent limits.
- 9 CHOI 17 used a microwave cavity detector with toroidal geometry. See Fig. 4 for their mass-dependent limits.
- 10 HOSKINS 16 is analogous to DUFFY 06. See Fig. 12 for mass-dependent limits in terms of the local dark matter density.
- 11 BECK 13 argues that dark-matter axions passing through Earth may generate a small observable signal in resonant S/N/S Josephson junctions. A measurement by HOFFMANN 04 [Physical Review B70 1805 03 (2004)] is interpreted in terms of subdominant dark matter axions with  $m_{A^0} = 0.11 \text{ meV}$ .
- 12 HOSKINS 11 is analogous to DUFFY 06. See Fig. 4 for the mass-dependent limit in terms of the local density.
- 13 ASZTALOS 10 used the upgraded detector of ASZTALOS 04 to search for halo axions. See their Fig. 5 for the  $m_{A^0}$  dependence of the limit.
- 14 DUFFY 06 used the upgraded detector of ASZTALOS 04, while assuming a smaller velocity dispersion than the isothermal model as in Eq. (8) of their paper. See Fig. 10 of their paper on the axion mass dependence of the limit.
- 15 ASZTALOS 04 looked for a conversion of halo axions to microwave photons in magnetic field. At 90% CL, the KSVZ axion cannot have a local halo density more than  $0.45 \text{ GeV/cm}^3$  in the quoted mass range. See Fig. 7 of their paper on the axion mass dependence of the limit.
- 16 KIM 98 calculated the axion-to-photon couplings for various axion models and compared them to the HAGMANN 90 bounds. This analysis demonstrates a strong model dependence of  $G_{A\gamma\gamma}$  and hence the bound from relic axion search.
- 17 HAGMANN 90 experiment is based on the proposal of SIKIVIE 83.
- 18 WUENSCH 89 looks for condensed axions near the earth that could be converted to photons in the presence of an intense electromagnetic field via the Primakoff effect, following the proposal of SIKIVIE 83. The theoretical prediction with  $[G_{A\gamma\gamma}/m_{A^0}]^2 = 2 \times 10^{-14} \text{ MeV}^{-4}$  (the three generation DFSZ model) and  $\rho_A = 300 \text{ MeV/cm}^3$  that makes up galactic halos gives  $(G_{A\gamma\gamma}/m_{A^0})^2 \rho_A = 4 \times 10^{-44}$ . Note that our definition of  $G_{A\gamma\gamma}$  is  $(1/4\pi)$  smaller than that of WUENSCH 89.

### Invisible $A^0$ (Axion) Limits from Photon Coupling

Limits are for the modulus of the axion-two-photon coupling  $G_{A\gamma\gamma}$  defined by

$$L = -G_{A\gamma\gamma} \phi_A \mathbf{E} \cdot \mathbf{B}. \text{ For scalars } S^0 \text{ the limit is on the coupling constant in } L = G_{S\gamma\gamma} \phi_S (\mathbf{E}^2 - \mathbf{B}^2). \text{ The relation between } G_{A\gamma\gamma} \text{ and } m_{A^0} \text{ is not used unless stated otherwise, i.e., many of these bounds apply to low-mass axion-like particles (ALPs), not to QCD axions.}$$

VALUE ( $\text{GeV}^{-1}$ )	CL%	DOCUMENT ID	TECN	COMMENT
$< 1 \times 10^{-3}$	95	1 ALONI 19	PRMX	$m_{A^0} = 0.16 \text{ GeV}$
$< 1.4 \times 10^{-14}$	95	2 CAPUTO 19	ASTR	$m_{A^0} = 5 \times 10^{-24} \text{ eV}$
$< 9.6 \times 10^{-14}$	95	3 FEDDERKE 19	CMB	$m_{A^0} = 10^{-22} \text{ eV}$
$< 7 \times 10^{-13}$	95	4 IVANOV 19	ASTR	$m_{A^0} = 5 \times 10^{-23} \text{ eV}$
$< 4 \times 10^{-11}$	95	5 LIANG 19	ASTR	$m_{A^0} = 1.2 \times 10^{-7} \text{ eV}$
		6 FORTIN 18	ASTR	Axion-like particles
		7 YAMAJI 18	LSW	$m_{A^0} = 46-1020 \text{ eV}$
$< 5.0 \times 10^{-3}$	90	8 ZHANG 18	ASTR	$m_{A^0} = 0.6-4 \text{ neV}$
$< 1 \times 10^{-11}$	99.9	9 ADE 17	CMB	Axion-like particles
$< 6.6 \times 10^{-11}$	95	10 ANASTASSO...17	CAST	$m_{A^0} < 0.02 \text{ eV}$
		11 DOLAN 17	RVUE	Axion-like particles
		12 INADA 17	LSW	$m_{A^0} < 0.1 \text{ eV}$
$< 2.51 \times 10^{-4}$	95	13 KOHRI 17	ASTR	$m_{A^0} = 0.7-50 \text{ neV}$
$> 1.5 \times 10^{-11}$	95	14 MARSH 17	ASTR	$m_{A^0} \leq 10^{-13} \text{ eV}$
$< 2.6 \times 10^{-12}$	95	15 TIWARI 17	COSM	$m_{A^0} \leq 10^{-15} \text{ eV}$
$< 6 \times 10^{-13}$		16 AJELLO 16	ASTR	$m_{A^0} = 0.5-5 \text{ neV}$
$< 5 \times 10^{-12}$	95	17 DELLA-VALLE 16	LASR	$m_{A^0} = 1.3 \text{ meV}$
$< 1.2 \times 10^{-7}$	95	18 DELLA-VALLE 16	LASR	$m_{A^0} < 0.5 \text{ meV}$
$< 7.2 \times 10^{-8}$	95	19 JAECKEL 16	ALPS	$m_{A^0} = 0.1-100 \text{ GeV}$
$< 8 \times 10^{-4}$		20 LEEFER 16		$m_{S^0} < 10^{-18} \text{ eV}$
$< 6 \times 10^{-21}$		21 ANASTASSO...15	CAST	Chameleons
		22 ARIK 15	CAST	$m_{A^0} = 0.39-0.42 \text{ eV}$
$< 1.47 \times 10^{-10}$	95	23 BALLOU 15	LSW	$m_{A^0} < 2 \times 10^{-4} \text{ eV}$
$< 3.5 \times 10^{-8}$	95	24 BRAX 15	ASTR	$m_{S^0} < 4 \times 10^{-12} \text{ eV}$

See key on page 999

Gauge & Higgs Boson Particle Listings  
Axions ( $A^0$ ) and Other Very Light Bosons

$<5.42 \times 10^{-4}$	95	25	HASEBE	15	LASR	$m_{A^0} = 0.15$ eV
		26	MILLEA	15	COSM	Axion-like particles
		27	VANTILBURG	15		Dilaton-like dark matter
$<4.1 \times 10^{-10}$	99.7	28	VINYOLES	15	ASTR	$m_{A^0} = 0.6\text{--}185$ eV
$<3.3 \times 10^{-10}$	95	29	ARIK	14	CAST	$m_{A^0} = 0.64\text{--}1.17$ eV
$<6.6 \times 10^{-11}$	95	30	AYALA	14	ASTR	Globular clusters
$<1.4 \times 10^{-7}$	95	31	DELLA-VALLE	14	LASR	$m_{A^0} = 1$ meV
		32	EJLLI	14	COSM	$m_{A^0} = 2.66\text{--}48.8$ $\mu$ eV
$<8 \times 10^{-8}$	95	33	PUGNAT	14	LSW	$m_{A^0} < 0.3$ meV
$<1 \times 10^{-11}$		34	REESMAN	14	ASTR	$m_{A^0} < 1 \times 10^{-10}$ eV
$<2.1 \times 10^{-11}$	95	35	ABRAMOWSKI13A	13A	IACT	$m_{A^0} = 15\text{--}60$ neV
$<2.15 \times 10^{-9}$	95	36	ARMENGAUD	13	EDEL	$m_{A^0} < 7 \times 10^6$ eV
$<4.5 \times 10^{-8}$	95	37	BETZ	13	LSW	$m_{A^0} = 7.2 \times 10^{-6}$ eV
$<8 \times 10^{-11}$		38	FRIEDLAND	13	ASTR	Red giants
$>2 \times 10^{-11}$		39	MEYER	13	ASTR	$m_{A^0} < 1 \times 10^{-7}$ eV
$<8.3 \times 10^{-12}$	95	40	WOUTERS	13	ASTR	$m_{A^0} < 7 \times 10^{-12}$ eV
		41	CADAMURO	12	COSM	Axion-like particles
$<2.5 \times 10^{-13}$	95	42	PAYEZ	12	ASTR	$m_{A^0} < 4.2 \times 10^{-14}$ eV
$<2.3 \times 10^{-10}$		43	ARIK	11	CAST	$m_{A^0} = 0.39\text{--}0.64$ eV
$<6.5 \times 10^{-8}$	95	44	EHRET	10	ALPS	$m_{A^0} < 0.7$ meV
$<2.4 \times 10^{-9}$	95	45	AHMED	09A	CDMS	$m_{A^0} < 100$ eV
$<1.2\text{--}2.8 \times 10^{-10}$	95	46	ARIK	09	CAST	$m_{A^0} = 0.02\text{--}0.39$ eV
		47	CHOU	09		Chameleons
		48	GONDOLO	09	ASTR	$m_{A^0} < \text{few keV}$
$<7 \times 10^{-10}$		49	AFANA SEV	08		$m_{S^0} < 1$ meV
$<1.3 \times 10^{-6}$	95	50	CHOU	08		$m_{A^0} < 0.5$ meV
$<3.5 \times 10^{-7}$	99.7	51	FOUCHE	08		$m_{A^0} < 1$ meV
$<1.1 \times 10^{-6}$	99.7	52	INOUE	08		$m_{A^0} = 0.84\text{--}1.00$ eV
$<5.6\text{--}13.4 \times 10^{-10}$	95	53	ZAVATTINI	08		$m_{A^0} < 1$ meV
$<5 \times 10^{-7}$		54	ANDRIAMON..07	07	CAST	$m_{A^0} < 0.02$ eV
$<8.8 \times 10^{-11}$	95	55	ROBILLIARD	07		$m_{A^0} < 1$ meV
$<1.25 \times 10^{-6}$	95	56	ZAVATTINI	06		$m_{A^0} = 1\text{--}1.5$ meV
$2\text{--}5 \times 10^{-6}$		57	INOUE	02		$m_{A^0} = 0.05\text{--}0.27$ eV
$<1.1 \times 10^{-9}$	95	58	MORALES	02B		$m_{A^0} < 1$ keV
$<2.78 \times 10^{-9}$	95	59	BERNABEI	01B		$m_{A^0} < 100$ eV
$<1.7 \times 10^{-9}$	95	60	ASTIER	00B	NOMD	$m_{A^0} < 40$ eV
$<1.5 \times 10^{-4}$	90	61	MASSO	00	THEO	induced $\gamma$ coupling
$<2.7 \times 10^{-9}$	95	62	AVIGNONE	98	SLAX	$m_{A^0} < 1$ keV
$<6.0 \times 10^{-10}$	95	63	MORIYAMA	98		$m_{A^0} < 0.03$ eV
$<3.6 \times 10^{-7}$	95	64	CAMERON	93		$m_{A^0} < 10^{-3}$ eV, optical rotation
$<6.7 \times 10^{-7}$	95	65	CAMERON	93		$m_{A^0} < 10^{-3}$ eV, photon regeneration
$<3.6 \times 10^{-9}$	99.7	66	LAZARUS	92		$m_{A^0} < 0.03$ eV
$<7.7 \times 10^{-9}$	99.7	66	LAZARUS	92		$m_{A^0} = 0.03\text{--}0.11$ eV
$<7.7 \times 10^{-7}$	99	67	RUOSO	92		$m_{A^0} < 10^{-3}$ eV
$<2.5 \times 10^{-6}$		68	SEMERTZIDIS	90		$m_{A^0} < 7 \times 10^{-4}$ eV

- 1 ALONI 19 used the data collected by the PRIMEX experiment to derive a limit based on a data-driven method. See their Fig. 2 for mass-dependent limits.
- 2 CAPUTO 19 look for an oscillating variation of the polarization angle of the pulsar J0437-4715, where they assume the local axion energy density  $\rho_A = 0.3$  GeV/cm<sup>3</sup>. See their Fig. 2 for mass-dependent limits for  $5 \times 10^{-24}$  eV  $\leq m_{A^0} \leq 2 \times 10^{-19}$  eV.
- 3 FEDDERKE 19 look for a uniform reduction of the CMB polarization at large scales, which is induced by the oscillating axion background during CMB decoupling. The quoted limit is based on the assumption that axions make up all of the dark matter. See their Fig. 3 for mass-dependent limits for  $m_{A^0} = 10^{-22}\text{--}10^{-19}$  eV.
- 4 IVANOV 19 look for the axion-induced periodic changes in the polarization angle of parsec-scale jets in active galactic nuclei observed by the MOJAVE program, where they use the axion energy density  $\rho_A = 20$  GeV/cm<sup>3</sup>. See their Fig. 6 for mass-dependent limits for  $5 \times 10^{-23}$  eV  $\leq m_{A^0} \leq 1.2 \times 10^{-21}$  eV.
- 5 LIANG 19 look for spectral irregularities in the spectrum of 10 bright H.E.S.S. sources in the Galactic plane, assuming photon-ALP mixing in the Galactic magnetic fields. See their Fig. 2 for mass-dependent limits with different Galactic magnetic field models.
- 6 FORTIN 18 studied the conversion of axion-like particles produced in the core of a magnetar to hard X-rays in the magnetosphere. See their Fig. 5 for mass-dependent limits with different values of the magnetar core temperature.
- 7 YAMAJI 18 search for axions with an x-ray LSW at Spring-8, using the Laue-case conversion in a silicon crystal. They also obtain  $G_{A\gamma\gamma} < 4.2 \times 10^{-3}$  GeV<sup>-1</sup> for  $m_{A^0} < 10$  eV. See their Fig. 5 for mass-dependent limits.
- 8 ZHANG 18 look for spectral irregularities in the spectrum of PKS 2155-304 measured by Fermi-LAT, assuming photon-ALP mixing in the intercluster and Galactic magnetic fields. See their Figs. 2 and 3 for mass-dependent limits with different values of the intercluster magnetic field parameters.
- 9 ADE 17 look for cosmic birefringence from axion-like particles using CMB polarization data taken by the BICEP2 and Keck Array experiments. They set a limit  $G_{A\gamma\gamma} H_I < 7.2 \times 10^{-2}$  at 95%CL for  $m_{A^0} < 10^{-28}$  eV, where  $H_I$  is the Hubble parameter during inflation.
- 10 ANASTASSOPOULOS 17 looked for solar axions by the CAST axion helioscope in the vacuum phase, and supersedes ANDRIAMONJE 07.

- 11 DOLAN 17 update existing limits on  $G_{A\gamma\gamma}$  for axion-like particles. See their Fig. 2 for mass-dependent limits.
- 12 INADA 17 search for axions with an x-ray LSW at Spring-8. See their Fig. 4 for mass-dependent limits.
- 13 KOHRI 17 attributed to axion-photon oscillations the excess of cosmic infrared background observed by the CIBER experiment. See their Fig. 5 for the region preferred by their scenario.
- 14 MARSH 17 is similar to WOUTERS 13, using Chandra observations of M87. See their Fig. 6 for mass-dependent limits.
- 15 TIWARI 17 use observed limits of the cosmic distance-duality relation to constrain the photon-ALP mixing based on 3D simulations of the magnetic field configuration. The quoted value is for the averaged magnetic field of 1nG with a coherent length of 1 Mpc. See their Fig. 5 for mass-dependent limits.
- 16 AJELLO 16 look for irregularities in the energy spectrum of the NGC1275 measured by Fermi LAT, assuming photon-ALP mixing in the intra-cluster and Galactic magnetic fields. See their Fig. 2 for mass-dependent limits.
- 17 DELLA-VALLE 16 look for the birefringence induced by axion-like particles. See their Fig. 14 for mass-dependent limits.
- 18 DELLA-VALLE 16 look for the dichroism induced by axion-like particles. See their Fig. 14 for mass-dependent limits.
- 19 JAECKEL 16 use the LEP data of  $Z \rightarrow 2\gamma$  and  $Z \rightarrow 3\gamma$  to constrain the ALP production via  $e^+e^- \rightarrow Z \rightarrow A^0\gamma$  ( $A^0 \rightarrow \gamma\gamma$ ), assuming the ALP coupling with two hypercharge bosons. See their Fig. 4 for mass-dependent limits.
- 20 LEEFER 16 derived limits by using radio-frequency spectroscopy of dysprosium and atomic clock measurements. See their Fig. 1 for mass-dependent limits as well as limits on Yukawa-type couplings of the scalar to the electron and nucleons.
- 21 ANASTASSOPOULOS 15 search for solar chameleons with CAST and derived limits on the chameleon coupling to photons and matter. See their Fig. 12 for the exclusion region.
- 22 ARIK 15 is analogous to ARIK 09, and search for solar axions for  $m_{A^0}$  around 0.2 and 0.4 eV. See their Figs. 1 and 3 for the mass-dependent limits.
- 23 Based on OSQAR photon regeneration experiment. See their Fig. 6 for mass-dependent limits on scalar and pseudoscalar bosons.
- 24 BRAX 15 derived limits on conformal and disformal couplings of a scalar to photons by searching for a chaotic absorption pattern in the X-ray and UV bands of the Hydra A galaxy cluster and a BL lac object, respectively. See their Fig. 8.
- 25 HASEBE 15 look for an axion via a four-wave mixing process at quasi-parallel colliding laser beams. They also derived limits on a scalar coupling to photons  $G_{S\gamma\gamma} < 2.62 \times 10^{-4}$  GeV<sup>-1</sup> at  $m_{S^0} = 0.15$  eV. See their Figs. 11 and 12 for mass-dependent limits.
- 26 MILLEA 15 is similar to CADAMURO 12, including the Planck data and the latest inferences of primordial deuterium abundance. See their Fig. 3 for mass-dependent limits.
- 27 VANTILBURG 15 look for harmonic variations in the dysprosium transition frequency data, induced by coherent oscillations of the fine-structure constant due to dilaton-like dark matter, and set the limits,  $G_{S\gamma\gamma} < 6 \times 10^{-27}$  GeV<sup>-1</sup> at  $m_{S^0} = 6 \times 10^{-23}$  eV. See their Fig. 4 for mass-dependent limits between  $1 \times 10^{-24} < m_{S^0} < 1 \times 10^{-15}$  eV.
- 28 VINYOLES 15 performed a global fit analysis based on helioseismology and solar neutrino observations. See their Fig. 9.
- 29 ARIK 14 is similar to ARIK 11. See their Fig. 2 for mass-dependent limits.
- 30 AYALA 14 derived the limit from the helium-burning lifetime of horizontal-branch stars based on number counts in globular clusters.
- 31 DELLA-VALLE 14 use the new PVLAS apparatus to set a limit on vacuum magnetic birefringence induced by axion-like particles. See their Fig. 6 for the mass-dependent limits.
- 32 EJLLI 14 set limits on a product of primordial magnetic field and the axion mass using CMB distortion induced by resonant axion production from CMB photons. See their Fig. 1 for limits applying specifically to the DFSZ and KSVZ axion models.
- 33 PUGNAT 14 is analogous to EHRET 10. See their Fig. 5 for mass-dependent limits on scalar and pseudoscalar bosons.
- 34 REESMAN 14 derive limits by requiring effects of axion-photon interconversion on gamma-ray spectra from distant blazars to be no larger than errors in the best-fit optical depth based on a certain extragalactic background light model. See their Fig. 5 for mass-dependent limits.
- 35 ABRAMOWSKI 13A look for irregularities in the energy spectrum of the BL Lac object PKS 2155-304 measured by H.E.S.S. The limits depend on assumed magnetic field around the source. See their Fig. 7 for mass-dependent limits.
- 36 ARMENGAUD 13 is analogous to AVIGNONE 98. See Fig. 6 for the limit.
- 37 BETZ 13 performed a microwave-based light shining through the wall experiment. See their Fig. 13 for mass-dependent limits.
- 38 FRIEDLAND 13 derived the limit by considering blue-loop suppression of the evolution of red giants with 7-12 solar masses.
- 39 MEYER 13 attributed to axion-photon oscillations the observed excess of very high-energy  $\gamma$ -rays with respect to predictions based on extragalactic background light models. See their Fig. 4 for mass-dependent lower limits for various magnetic field configurations.
- 40 WOUTERS 13 look for irregularities in the X-ray spectrum of the Hydra cluster observed by Chandra. See their Fig. 4 for mass-dependent limits.
- 41 CADAMURO 12 derived cosmological limits on  $G_{A\gamma\gamma}$  for axion-like particles. See their Fig. 1 for mass-dependent limits.
- 42 PAYEZ 12 derive limits from polarization measurements of quasar light (see their Fig. 3). The limits depend on assumed magnetic field strength in galaxy clusters. The limits depend on assumed magnetic field and electron density in the local galaxy supercluster.
- 43 ARIK 11 search for solar axions using <sup>3</sup>He buffer gas in CAST, continuing from the <sup>4</sup>He version of ARIK 09. See Fig. 2 for the exact mass-dependent limits.
- 44 ALPS is a photon regeneration experiment. See their Fig. 4 for mass-dependent limits on scalar and pseudoscalar bosons.
- 45 AHMED 09A is analogous to AVIGNONE 98.
- 46 ARIK 09 is the <sup>4</sup>He filling version of the CAST axion helioscope in analogy to INOUE 02 and INOUE 08. See their Fig. 7 for mass-dependent limits.
- 47 CHOU 09 use the GammeV apparatus in the afterglow mode to search for chameleons, (pseudo)scalar bosons with a mass depending on the environment. For pseudoscalars they exclude at 3 $\sigma$  the range  $2.6 \times 10^{-7}$  GeV<sup>-1</sup>  $< G_{A\gamma\gamma} < 4.2 \times 10^{-6}$  GeV<sup>-1</sup> for vacuum  $m_{A^0}$  roughly below 6 meV for density scaling index exceeding 0.8.

# Gauge & Higgs Boson Particle Listings

## Axions ( $A^0$ ) and Other Very Light Bosons

- <sup>48</sup> GONDOLO 09 use the all-flavor measured solar neutrino flux to constrain solar interior temperature and thus energy losses.
- <sup>49</sup> LIPSS photon regeneration experiment, assuming scalar particle  $S^0$ . See Fig. 4 for mass-dependent limits.
- <sup>50</sup> CHOU 08 perform a variable-baseline photon regeneration experiment. See their Fig. 3 for mass-dependent limits. Excludes the PVLAS result of ZAVATTINI 06.
- <sup>51</sup> FOCHE 08 is an update of ROBILLIARD 07. See their Fig. 12 for mass-dependent limits.
- <sup>52</sup> INOUE 08 is an extension of INOUE 02 to larger axion masses, using the Tokyo axion helioscope. See their Fig. 4 for mass-dependent limits.
- <sup>53</sup> ZAVATTINI 08 is an upgrade of ZAVATTINI 06, see their Fig. 8 for mass-dependent limits. They now exclude the parameter range where ZAVATTINI 06 had seen a positive signature.
- <sup>54</sup> ANDRIAMONJE 07 looked for Primakoff conversion of solar axions in 9T superconducting magnet into X-rays. Supersedes ZIOUTAS 05.
- <sup>55</sup> ROBILLIARD 07 perform a photon regeneration experiment with a pulsed laser and pulsed magnetic field. See their Fig. 4 for mass-dependent limits. Excludes the PVLAS result of ZAVATTINI 06 with a CL exceeding 99.9%.
- <sup>56</sup> ZAVATTINI 06 propagate a laser beam in a magnetic field and observe dichroism and birefringence effects that could be attributed to an axion-like particle. This result is now excluded by ROBILLIARD 07, ZAVATTINI 08, and CHOU 08.
- <sup>57</sup> INOUE 02 looked for Primakoff conversion of solar axions in 4T superconducting magnet into X-ray.
- <sup>58</sup> MORALES 02b looked for the coherent conversion of solar axions to photons via the Primakoff effect in Germanium detector.
- <sup>59</sup> BERNABE 01b looked for Primakoff coherent conversion of solar axions into photons via Bragg scattering in NaI crystal in DAMA dark matter detector.
- <sup>60</sup> ASTIER 00b looked for production of axions from the interaction of high-energy photons with the horn magnetic field and their subsequent re-conversion to photons via the interaction with the NOMAD dipole magnetic field.
- <sup>61</sup> MASSO 00 studied limits on axion-proton coupling using the induced axion-photon coupling through the proton loop and CAMERON 93 bound on the axion-photon coupling using optical rotation. They obtained the bound  $g_{p\gamma}^2/4\pi < 1.7 \times 10^{-9}$  for the coupling  $g_{p\gamma}^2 P^0 A$ .
- <sup>62</sup> AVIGNONE 98 result is based on the coherent conversion of solar axions to photons via the Primakoff effect in a single crystal germanium detector.
- <sup>63</sup> Based on the conversion of solar axions to X-rays in a strong laboratory magnetic field.
- <sup>64</sup> Experiment based on proposal by MAIANI 86.
- <sup>65</sup> Experiment based on proposal by VANBIBBER 87.
- <sup>66</sup> LAZARUS 92 experiment is based on proposal found in VANBIBBER 89.
- <sup>67</sup> RUOSO 92 experiment is based on the proposal by VANBIBBER 87.
- <sup>68</sup> SEMERTZIDIS 90 experiment is based on the proposal of MAIANI 86. The limit is obtained by taking the noise amplitude as the upper limit. Limits extend to  $m_{A^0} = 4 \times 10^{-3}$  where  $G_{A\gamma\gamma} < 1 \times 10^{-4} \text{ GeV}^{-1}$ .

### Limit on Invisible $A^0$ (Axion) Electron Coupling

The limit is for  $g_{Aee} \phi_A \bar{\psi}(\gamma_5)\psi$ , or equivalently, the dipole-dipole potential

$$-\frac{g_{Aee}^2}{16\pi m_{A^0}^2} ((\sigma_1 \cdot \sigma_2) - 3(\sigma_1 \cdot \mathbf{n})(\sigma_2 \cdot \mathbf{n}))/r^3 \text{ where } \mathbf{n} = \mathbf{r}/r \text{ and the sign of the potential was corrected based on DAIDO 17.}$$

VALUE	CL%	DOCUMENT ID	TECN	COMMENT
• • • We do not use the following data for averages, fits, limits, etc. • • •				
$<1.7 \times 10^{-11}$	90	1 ADHIKARI 19B	C100	Solar axions
$<2.3 \times 10^{-14}$	90	2 APRILE 19D	XE1T	$m_{A^0} = 0.186\text{--}1 \text{ keV}$
		3 DESSERT 19	ASTR	Magnetic white dwarf
$<2.6 \times 10^{-10}$	95	4 TERRANO 19		Torsion pendulum
$<1.5 \times 10^{-13}$	90	5 ABE 18F	XMAS	$m_{A^0} = 40\text{--}120 \text{ keV}$
$<1.1 \times 10^{-11}$	90	6 ARMENGAUD 18	EDE3	Solar axions
$<4 \times 10^{-13}$	90	7 ARMENGAUD 18	EDE3	$m_{A^0} = 0.8\text{--}500 \text{ keV}$
$<4.9 \times 10^{-10}$	95	8 CRESCINI 18	QUAX	$m_{A^0} = 58 \mu\text{eV}$
		9 FICEK 18	THEO	$m_{A^0} < 10 \text{ keV}$
$<4.5 \times 10^{-13}$	90	10 ABGRALL 17	HPGE	$m_{A^0} = 11.8 \text{ keV}$
$<3.5 \times 10^{-12}$	90	11 AKERIB 17B	LUX	Solar axions
$<4.2 \times 10^{-13}$	90	12 AKERIB 17B	LUX	$m_{A^0} = 1\text{--}16 \text{ keV}$
$<2.3 \times 10^{-13}$	90	13 APRILE 17B	X100	$m_{A^0} = 6 \text{ keV}$
$<4 \times 10^{-4}$	90	14 FICEK 17	THEO	$m_{A^0} < 1 \text{ keV}$
$<4.35 \times 10^{-12}$	90	15 FU 17A	PNDX	Solar axions
$<4.3 \times 10^{-14}$	90	16 FU 17A	PNDX	$m_{A^0} = 2 \text{ keV}$
$<5 \times 10^{-13}$	90	17 LIU 17A	CDEX	$m_{A^0} = 13 \text{ keV}$
$<2.5 \times 10^{-11}$	90	18 LIU 17A	CDEX	Solar axions
$<0.15$	95	19 LUO 17		$m_{A^0} = 300 \text{ eV}$
$<3.3 \times 10^{-13}$	68	20 BATTICH 16	ASTR	White dwarf cooling
$<7 \times 10^{-13}$		21 CORSICO 16	ASTR	White dwarf cooling
$<1.39 \times 10^{-11}$	90	22 YOON 16	KIMS	Solar axions
$<7.4 \times 10^{-9}$	95	23 TERRANO 15		$m_{A^0} < 30 \mu\text{eV}$
$<8 \times 10^{-13}$	90	24 ABE 14F	XMAS	$m_{A^0} = 60 \text{ keV}$
$<7.7 \times 10^{-12}$	90	25 APRILE 14B	X100	Solar axions
		26 APRILE 14B	X100	$m_{A^0} = 5\text{--}7 \text{ keV}$
$< 0.96\text{--}8.2 \times 10^{-8}$	90	27 DERBIN 14	CNTR	$m_{A^0} = 0.1\text{--}1 \text{ MeV}$
$<2.8 \times 10^{-13}$	99	28 MILLER-BER... 14	ASTR	White dwarf cooling
$<5.4 \times 10^{-11}$	90	29 ABE 13D	XMAS	Solar axions
$<1.07 \times 10^{-12}$	90	30 ARMENGAUD 13	EDEL	$m_{A^0} = 12.5 \text{ keV}$
$<2.59 \times 10^{-11}$	90	31 ARMENGAUD 13	EDEL	Solar axions

$< 1.4\text{--}9.7 \times 10^{-7}$	90	32 BARTH 13	CAST	Solar axions
$<1.5 \times 10^{-8}$	68	33 DERBIN 13	CNTR	$m_{A^0} = 0.1\text{--}1 \text{ MeV}$
$<4.3 \times 10^{-13}$	95	34 HECKEL 13		$m_{A^0} \leq 0.1 \mu\text{eV}$
$<7 \times 10^{-13}$	95	35 VIAUX 13A	ASTR	Low-mass red giants
$<2.2 \times 10^{-10}$	90	36 CORSICO 12	ASTR	White dwarf cooling
$<0.02\text{--}1 \times 10^{-10}$	90	37 DERBIN 12	CNTR	Solar axions
$<1.4 \times 10^{-12}$	90	38 AALSETH 11	CNTR	$m_{A^0} = 0.3\text{--}8 \text{ keV}$
$<4 \times 10^{-9}$	66	39 AHMED 09A	CDMS	$m_{A^0} = 2.5 \text{ keV}$
$<2.7 \times 10^{-8}$		40 DAVOUDIASEL 09	ASTR	Earth cooling
		41 NI 94		Induced magnetism
		41 CHUI 93		Induced magnetism
$<3.6 \times 10^{-7}$	66	42 PAN 92		Torsion pendulum
$<2.9 \times 10^{-8}$	95	41 BOBRAKOV 91		Induced magnetism
$<1.9 \times 10^{-6}$	66	43 WINELAND 91	NMR	
$<7 \times 10^{-7}$	66	42 RITTER 90		Torsion pendulum
$<6.6 \times 10^{-8}$	95	41 VOROBYOV 88		Induced magnetism

<sup>1</sup> ADHIKARI 19B is analogous to LIU 17A.

<sup>2</sup> APRILE 19D is analogous to APRILE 17B, but they use only ionization signals. The quoted limit applies to  $m_{A^0} = 0.7 \text{ keV}$ . See their Fig. 5(e) for mass-dependent limits.

<sup>3</sup> DESSERT 19 used the Suzaku observations of a magnetic white dwarf (RE J0317-853) to look for X-ray signatures converted from axions in the surrounding magnetic fields. They obtained the limit,  $g_{Aee} \cdot G_{A\gamma\gamma} < 1.6 \times 10^{-24} \text{ GeV}^{-1}$  at 95%CL for  $m_{A^0} \sim 10^{-5} \text{ eV}$ . See their Fig. 2 for mass-dependent limits.

<sup>4</sup> TERRANO 19 look for the axion-induced oscillating magnetic field acting on the electron spin, using data taken with a rotating torsion pendulum containing polarized electrons. The quoted limit applies to  $m_{A^0} = 10^{-23}\text{--}10^{-18} \text{ eV}$  and assumes a local axion dark matter density,  $\rho_A = 0.45 \text{ GeV}/\text{cm}^3$ . See their Fig. 5 for mass-dependent limits.

<sup>5</sup> ABE 18F is an update of ABE 14F. The quoted limit applies to  $m_{A^0} = 60 \text{ keV}$ . See their Fig. 5 for mass-dependent limits.

<sup>6</sup> ARMENGAUD 18 is analogous to LIU 17A.

<sup>7</sup> ARMENGAUD 18 is analogous to AHMED 09A. See the left panel of Fig. 5 for mass-dependent limits.

<sup>8</sup> CRESCINI 18 look for collective excitations of the electron spins caused by dark matter axions. The quoted limit assumes the local dark matter density,  $\rho_A = 0.45 \text{ GeV}/\text{cm}^3$ .

<sup>9</sup> FICEK 18 use the measurements of the hyperfine structure of antiprotonic helium to constrain a dipole-dipole potential between electron and antiproton. See their Fig. 3 for limits on various spin- and velocity-dependent potentials.

<sup>10</sup> ABGRALL 17 is analogous to AHMED 09A using the MAJORANA DEMONSTRATOR. See their Fig. 2 for limits between  $6 \text{ keV} < m_{A^0} < 97 \text{ keV}$ .

<sup>11</sup> AKERIB 17B is analogous to LIU 17A.

<sup>12</sup> AKERIB 17B is analogous to AHMED 09A. See their Fig. 7 for mass-dependent limits.

<sup>13</sup> APRILE 17B is analogous to AHMED 09A. They found a bug in their code and needed to correct the limits in Fig. 7 of APRILE 14B. See their Fig. 1 for the corrected limits between  $1 \text{ keV} < m_{A^0} < 40 \text{ keV}$ .

<sup>14</sup> FICEK 17 look for spin-dependent interactions between electrons by comparing precision spectroscopic measurements in  $^4\text{He}$  with theoretical calculations. See their Fig. 1 for limits up to  $m_{A^0} = 10 \text{ keV}$ .

<sup>15</sup> FU 17A is analogous to LIU 17A. See their Fig. 3 for mass-dependent limits.

<sup>16</sup> FU 17A is analogous to AHMED 09A. See their Fig. 4 for mass-dependent limits.

<sup>17</sup> LIU 17A is analogous to AHMED 09A. See their Fig. 9 for limits between  $0.25 \text{ keV} < m_{A^0} < 20 \text{ keV}$ .

<sup>18</sup> LIU 17A look for solar axions produced from Compton, bremsstrahlung, atomic-recombination and deexcitation channels, and set a limit for  $m_{A^0} < 1 \text{ keV}$ .

<sup>19</sup> LUO 17 use a recent measurement of the dipole-dipole interaction between two iron atoms at the nanometer scale and set a limit for  $m_{A^0} < 1 \text{ keV}$ . See their Fig. 3 for mass-dependent limits.

<sup>20</sup> BATTICH 16 is analogous to CORSICO 16 and used the pulsating DB white dwarf PG 1351+489.

<sup>21</sup> CORSICO 16 studied the cooling rate of the pulsating DA white dwarf L19-2 based on an asteroseismic model.

<sup>22</sup> YOON 16 look for solar axions with the axio-electric effect in CsI(Tl) crystals and set a limit for  $m_{A^0} < 1 \text{ keV}$ .

<sup>23</sup> TERRANO 15 used a torsion pendulum and rotating attractor with 20-pole electron-spin distributions. See their Fig. 4 for a mass-dependent limit up to  $m_{A^0} = 500 \mu\text{eV}$ .

<sup>24</sup> ABE 14F set limits on the axioelectric effect in the XMAS detector assuming the pseudoscalar constitutes all the local dark matter. See their Fig. 3 for limits between  $m_{A^0} = 40\text{--}120 \text{ keV}$ .

<sup>25</sup> APRILE 14B look for solar axions using the XENON100 detector.

<sup>26</sup> APRILE 14B is analogous to AHMED 09A. Their Fig. 7 was later found to be incorrect due to a bug in their code. See Fig. 1 in APRILE 17B for the corrected limits.

<sup>27</sup> DERBIN 14 is an update of DERBIN 13 with a BGO scintillating bolometer. See their Fig. 3 for mass-dependent limits.

<sup>28</sup> MILLER-BERTOLAMI 14 studied the impact of axion emission on white dwarf cooling in a self-consistent way.

<sup>29</sup> ABE 13D is analogous to DERBIN 12, using the XMAS detector.

<sup>30</sup> ARMENGAUD 13 is similar to AALSETH 11. See their Fig. 10 for limits between  $3 \text{ keV} < m_{A^0} < 100 \text{ keV}$ .

<sup>31</sup> ARMENGAUD 13 is similar to DERBIN 12, and take account of axio-recombination and axio-deexcitation effects. See their Fig. 12 for mass-dependent limits.

<sup>32</sup> BARTH 13 search for solar axions produced by axion-electron coupling, and obtained the limit,  $g_{Aee} \cdot G_{A\gamma\gamma} < 8.1 \times 10^{-23} \text{ GeV}^{-1}$  at 95%CL.

<sup>33</sup> DERBIN 13 looked for  $5.5 \text{ MeV}$  solar axions produced in  $p\bar{d} \rightarrow ^3\text{He} A^0$  in a BGO detector through the axioelectric effect. See their Fig. 4 for mass-dependent limits.

<sup>34</sup> HECKEL 13 studied the influence of 2 or 4 stationary sources each containing  $6.0 \times 10^{24}$  polarized electrons, on a rotating torsion pendulum containing  $9.8 \times 10^{24}$  polarized electrons. See their Fig. 4 for mass-dependent limits.

# Gauge & Higgs Boson Particle Listings

## Axions ( $A^0$ ) and Other Very Light Bosons

35 VIAUX 13A constrain axion emission using the observed brightness of the tip of the red-giant branch in the globular cluster M5.

36 CORSICO 12 attributed the excessive cooling rate of the pulsating white dwarf R548 to emission of axions with  $g_{Aee} \simeq 4.8 \times 10^{-13}$ .

37 DERBIN 12 look for solar axions with the axio-electric effect in a Si(Li) detector. The solar production is based on Compton and bremsstrahlung processes.

38 AALSETH 11 is analogous to AHMED 09A. See their Fig. 4 for mass-dependent limits.

39 AHMED 09A assume keV-mass pseudoscalars are the local dark matter and constrain the axio-electric effect in the CDMS detector. See their Fig. 5 for mass-dependent limits.

40 DAVOUDI ASL 09 use geophysical constraints on Earth cooling by axion emission.

41 These experiments measured induced magnetization of a bulk material by the spin-dependent potential generated from other bulk material with aligned electron spins, where the magnetic field is shielded with superconductor. The sign of the limit set by CHUI 93 is opposite to that of the axion-mediated dipole-dipole potential.

42 These experiments used a torsion pendulum to measure the potential between two bulk matter objects where the spins are polarized but without a net magnetic field in either of them. The limits reflect the corrected sign of the dipole-dipole potential.

43 WINELAND 91 looked for an effect of bulk matter with aligned electron spins on atomic hyperfine splitting using nuclear magnetic resonance.

### Invisible $A^0$ (Axion) Limits from Nucleon Coupling

Limits are for the axion mass in eV.

VALUE (eV)	CL%	DOCUMENT ID	TECN	COMMENT
● ● ● We do not use the following data for averages, fits, limits, etc. ● ● ●				
< 0.03		1 LEINSON 19	ASTR	Neutron star cooling
< $9.6 \times 10^{-3}$	95	2 LLOYD 19	ASTR	$\gamma$ -rays from NS
		3 SMORRA 19	19	$\bar{p}$ g-factor
		4 WU 19	NMR	Axion dark matter
< 65	95	5 AKHMATOV 18	CNTR	Solar axion
< 6.6	90	6 ARMENGAUD 18	EDE3	Solar axion
< 0.085	90	7 BEZNOGOV 18	ASTR	Neutron star cooling
< 12.7	95	8 GAVRILYUK 18	CNTR	Solar axion
< 0.01		9 HAMAGUCHI 18	ASTR	Neutron star cooling
		10 ABEL 17		Neutron EDM
< 93	90	11 ABGRALL 17	HPGE	Solar axion
< 4	90	12 FU 17A	PNDX	Solar axion
		13 KLIMCHITSK...17A		Casimir effect
<177	90	14 LIU 17A	CDEX	Solar axion
< 0.079	95	15 BERENJI 16	ASTR	$\gamma$ -rays from NS
<100	95	16 GAVRILYUK 15	CNTR	Solar axion
		17 KLIMCHITSK...15		Casimir-less
		18 BEZERRA 14		Casimir effect
		19 BEZERRA 14A		Casimir effect
		20 BEZERRA 14B		Casimir effect
		21 BEZERRA 14C		Casimir effect
		22 BLUM 14	COSM	$^4\text{He}$ abundance
		23 LEINSON 14	ASTR	Neutron star cooling
<250	95	24 ALESSANDRIA 13	CNTR	Solar axion
<155	90	25 ARMENGAUD 13	EDEL	Solar axion
< $8.6 \times 10^3$	90	26 BELLINI 12	CNTR	Solar axion
< $1.4 \times 10^4$	90	27 BELLINI 12B	BORX	Solar axion
<145	95	28 DERBIN 11	CNTR	Solar axion
		29 BELLINI 08	CNTR	Solar axion
		30 ADELBERGER 07		Test of Newton's law

1 LEINSON 19 is analogous to BEZNOGOV 18, but estimating the axion luminosity based on the Tolman's analytic solution to the Einstein equations of spherical fluids in hydrostatic equilibrium. The dimensionless axion-neutron coupling is constrained as  $g_{ANN} < 1.0 \times 10^{-10}$ .

2 LLOYD 19 is analogous to BERENJI 16. They highlight that the limit obtained with this technique strongly depends on the assumed NS core temperature.

3 SMORRA 19 look for spin-precession effects from ultra-light axion dark matter in the  $\bar{p}$  spin-flip resonance data. Assuming  $\rho_A = 0.4 \text{ GeV/cm}^3$ , they constrain the dimensionless axion-antiproton coupling as  $g_{A\bar{p}p} < 2-9$  at 95% CL for  $m_{A^0} = 2 \times 10^{-23}-4 \times 10^{-17} \text{ eV}$ . See the right panel of their Fig. 3.

4 WU 19 look for axion-induced time-oscillating features of the NMR spectrum of acetonitrile- $d_3$ . Assuming  $C_p = C_n$  and  $\rho_A = 0.4 \text{ GeV/cm}^3$ , they constrain the dimensionless axion-nucleon coupling as  $g_{ANN} < 6 \times 10^{-5}$  for  $m_{A^0} = 10^{-21}-1.3 \times 10^{-17} \text{ eV}$ . Note that the limits for  $m_{A^0} < 10^{-21} \text{ eV}$  in their Fig. 3(a) should be weaker than those for heavier masses. See ADELBERGER 19 and WU 19c on this issue.

5 AKHMATOV 18 is an update of GAVRILYUK 15.

6 ARMENGAUD 18 is analogous to ALESSANDRIA 13. The quoted limit assumes the DFSZ axion model. See their Fig. 4 for the limit on product of axion couplings to electrons and nucleons.

7 BEZNOGOV 18 constrain the axion-neutron coupling by assuming that thermal evolution of the hot neutron star HESS J1731-347 is dominated by the lowest possible neutrino emission. The quoted limit assumes the KSVZ axion with the effective Peccei-Quinn charge of the neutron  $C_n = -0.02$ . The dimensionless axion-neutron coupling is constrained as  $g_{ANN} < 2.8 \times 10^{-10}$ .

8 GAVRILYUK 18 look for the resonant excitation of  $^{83}\text{Kr}$  (9.4 keV) by solar axions produced via the Primakoff effect. The mass bound assumes  $m_H/m_D = 0.56$  and  $S = 0.5$ .

9 HAMAGUCHI 18 studied the axion emission from the neutron star in Cassiopeia A based on the minimal cooling scenario which explains the observed rapid cooling rate. The quoted limit corresponds to  $f_A > 5 \times 10^8 \text{ GeV}$  obtained for the KSVZ axion with  $C_p = -0.47$  and  $C_n = -0.02$ .

10 ABEL 17 look for a time-oscillating neutron EDM and an axion-wind spin-precession effect respectively induced by axion dark matter couplings to gluons and nucleons. See their Fig. 4 for limits in the range of  $m_{A^0} = 10^{-24}-10^{-17} \text{ eV}$ .

11 ABGRALL 17 limit assumes the hadronic axion model used in ALESSANDRIA 13. See their Fig. 4 for the limit on product of axion couplings to electrons and nucleons.

12 FU 17A look for the 14.4 keV  $^{57}\text{Fe}$  solar axions. The limit assumes the DFSZ axion model. See their Fig. 3 for mass-dependent limits on the axion-electron coupling. Notice that in this figure the DFSZ and KSVZ lines should be interchanged.

13 KLIMCHITSKAYA 17A use the differential measurement of the Casimir force between a Ni-coated sphere and Au and Ni sectors of the structured disc to constrain the axion coupling to nucleons for  $2.61 \text{ meV} < m_{A^0} < 0.9 \text{ eV}$ . See their Figs. 1 and 2 for mass dependent limits.

14 LIU 17 is analogous to ALESSANDRIA 13. The limit assumes the hadronic axion model. See their Fig. 6(b) for the limit on product of axion couplings to electrons and nucleons.

15 BERENJI 16 used the Fermi LAT observations of neutron stars to look for photons from axion decay. They assume the effective Peccei-Quinn charge of the neutron  $C_n = 0.1$  and a neutron-star core temperature of 20 MeV.

16 GAVRILYUK 15 look for solar axions emitted by the M1 transition of  $^{83}\text{Kr}$  (9.4 keV). The mass bound assumes  $m_H/m_D = 0.56$  and  $S = 0.5$ .

17 KLIMCHITSKAYA 15 use the measurement of differential forces between a test mass and rotating source masses of Au and Si to constrain the force due to two-axion exchange for  $1.7 \times 10^{-3} < m_{A^0} < 0.9 \text{ eV}$ . See their Figs. 1 and 2 for mass dependent limits.

18 BEZERRA 14 use the measurement of the thermal Casimir-Polder force between a Bose-Einstein condensate of  $^{87}\text{Rb}$  atoms and a  $\text{SiO}_2$  plate to constrain the force mediated by exchange of two pseudoscalars for  $0.1 \text{ meV} < m_{A^0} < 0.3 \text{ eV}$ . See their Fig. 2 for the mass-dependent limit on pseudoscalar coupling to nucleons.

19 BEZERRA 14A is analogous to BEZERRA 14. They use the measurement of the Casimir pressure between two Au-coated plates to constrain pseudoscalar coupling to nucleons for  $1 \times 10^{-3} \text{ eV} < m_{A^0} < 15 \text{ eV}$ . See their Figs. 1 and 2 for the mass-dependent limit.

20 BEZERRA 14B is analogous to BEZERRA 14. BEZERRA 14B use the measurement of the normal and lateral Casimir forces between sinusoidally corrugated surfaces of a sphere and a plate to constrain pseudoscalar coupling to nucleons for  $1 \text{ eV} < m_{A^0} < 20 \text{ eV}$ . See their Figs. 1-3 for mass-dependent limits.

21 BEZERRA 14C is analogous to BEZERRA 14. They use the measurement of the gradient of the Casimir force between Au- and Ni-coated surfaces of a sphere and a plate to constrain pseudoscalar coupling to nucleons for  $3 \times 10^{-5} \text{ eV} < m_{A^0} < 1 \text{ eV}$ . See their Figs. 1, 3, and 4 for the mass-dependent limits.

22 BLUM 14 studied effects of an oscillating strong CP phase induced by axion dark matter on the primordial  $^4\text{He}$  abundance. See their Fig. 1 for mass-dependent limits.

23 LEINSON 14 attributes the excessive cooling rate of the neutron star in Cassiopeia A to axion emission from the superfluid core, and found  $C_n^2 m_{A^0}^2 \simeq 5.7 \times 10^{-6} \text{ eV}^2$ , where  $C_n$  is the effective Peccei-Quinn charge of the neutron.

24 ALESSANDRIA 13 used the CUORE experiment to look for 14.4 keV solar axions produced from the M1 transition of thermally excited  $^{57}\text{Fe}$  nuclei in the solar core, using the axio-electric effect. The limit assumes the hadronic axion model. See their Fig. 4 for the limit on product of axion couplings to electrons and nucleons.

25 ARMENGAUD 13 is analogous to ALESSANDRIA 13. The limit assumes the hadronic axion model. See their Fig. 8 for the limit on product of axion couplings to electrons and nucleons.

26 BELLINI 12 looked for solar axions emitted by the M1 transition of  $^7\text{Li}^*$  (478 keV) after the electron capture of  $^7\text{Be}$ , using the resonant excitation  $^7\text{Li}$  in the LiF crystal. The mass bound assumes  $m_H/m_D = 0.55$ ,  $m_H/m_S = 0.029$ , and the flavor-singlet axial vector matrix element  $S = 0.4$ .

27 BELLINI 12B looked for 5.5 MeV solar axions produced in the  $pd \rightarrow ^3\text{He} A^0$ . The limit assumes the hadronic axion model. See their Figs. 6 and 7 for mass-dependent limits on product of axion couplings to photons, electrons, and nucleons.

28 DERBIN 11 looked for solar axions emitted by the M1 transition of thermally excited  $^{57}\text{Fe}$  nuclei in the Sun, using their possible resonant capture on  $^{57}\text{Fe}$  in the laboratory. The mass bound assumes  $m_H/m_D = 0.56$  and the flavor-singlet axial vector matrix element  $S = 3F - D \simeq 0.5$ .

29 BELLINI 08 consider solar axions emitted in the M1 transition of  $^7\text{Li}^*$  (478 keV) and look for a peak at 478 keV in the energy spectra of the Counting Test Facility (CTF), a Borexino prototype. For  $m_{A^0} < 450 \text{ keV}$  they find mass-dependent limits on products of axion couplings to photons, electrons, and nucleons.

30 ADELBERGER 07 use precision tests of Newton's law to constrain a force contribution from the exchange of two pseudoscalars. See their Fig. 5 for limits on the pseudoscalar coupling to nucleons, relevant for  $m_{A^0}$  below about 1 meV.

### Axion Limits from T-violating Medium-Range Forces

The limit is for the coupling  $g = g_p g_n$  in a T-violating potential between nucleons or nucleon and electron of the form  $V = \frac{g_p^2}{8\pi m_p} (\boldsymbol{\sigma} \cdot \boldsymbol{r}) \left( \frac{1}{r^2} + \frac{1}{\lambda r} \right) e^{-r/\lambda}$ , where  $g_p$  and  $g_n$  are dimensionless scalar and pseudoscalar coupling constants and  $\lambda = \hbar/(m_A c)$  is the range of the force.

VALUE	DOCUMENT ID	TECN	COMMENT
● ● ● We do not use the following data for averages, fits, limits, etc. ● ● ●			
	1 DZUBA 18	THEO	atomic EDM
	2 STADNIK 18	THEO	atomic and molecular EDMs
	3 CRESCINI 17	SQID	paramagnetic GSO crystal
	4 AFACH 15		ultracold neutrons
	5 STADNIK 15	THEO	nucleon spin contributions for nuclei
	6 TERRANO 15		torsion pendulum
	7 BULATOWICZ 13	NMR	polarized $^{129}\text{Xe}$ and $^{131}\text{Xe}$
	8 CHU 13		polarized $^3\text{He}$
	9 TULLNEY 13	SQID	polarized $^3\text{He}$ and $^{129}\text{Xe}$
	10 RAFFELT 12		stellar energy loss
	11 HOEDL 11		torsion pendulum
	12 PETUKHOV 10		polarized $^3\text{He}$



See key on page 999

## Gauge & Higgs Boson Particle Listings Axions ( $A^0$ ) and Other Very Light Bosons

- <1  $\times 10^{-3}$  90 64 ABRAHAMY... 11  $m_{\gamma'}$  = 175–250 MeV
- <9  $\times 10^{-8}$  95 65 BLUEMLEIN 11 BDMP  $m_{\gamma'}$  = 70 MeV
- <1  $\times 10^{-7}$  66 BJORKEN 09 BDMP  $m_{\gamma'}$  = 2–400 MeV
- <5  $\times 10^{-9}$  67 BJORKEN 09 ASTR  $m_{\gamma'}$  = 2–50 MeV
- 1 AAIJ 20c look for hidden photons produced from the  $pp$  collision in the decay channel  $\gamma' \rightarrow \mu^+ \mu^-$ . For prompt decaying hidden photons, limits at the level of  $10^{-4}$ – $10^{-3}$  are obtained for  $m_{\gamma'} = 0.214$ –30 GeV. See their Fig. 2 for mass-dependent limits.
- 2 AAIJ 20c look for hidden photons produced from the  $pp$  collision in the decay channel  $\gamma' \rightarrow \mu^+ \mu^-$ . For hidden photons with lifetimes of order ps, limits at the level of  $10^{-5}$  are obtained for  $m_{\gamma'} = 218$ –315 MeV. See their Fig. 4 for mass-dependent limits.
- 3 AABOUD 19g look for  $h \rightarrow \gamma' \gamma'$  ( $\gamma' \rightarrow \mu^+ \mu^-$ ) and exclude a kinetic mixing around  $10^{-9}$ – $10^{-8}$  for  $B(h \rightarrow \gamma' \gamma') = 0.01$  and 0.1. See their Fig. 9 for mass-dependent limits.
- 4 ABLIKIM 19A look for  $J/\psi \rightarrow \gamma' \eta$  ( $\gamma' \rightarrow e^+ e^-$ ). Limits between  $6 \times 10^{-3}$  and  $5 \times 10^{-2}$  are obtained (see their Fig. 8).
- 5 ABLIKIM 19H look for  $J/\psi \rightarrow \gamma' \eta'$  ( $\gamma' \rightarrow e^+ e^-$ ). Limits between  $3.4 \times 10^{-3}$  and  $2.6 \times 10^{-2}$  are obtained. See their Fig. 5 for mass-dependent limits.
- 6 AGUILAR-AREVALO 19A look for the absorption signal of hidden photon dark matter by using a CCD. The quoted limit applies to  $m_{\gamma'} = 17$  eV. The local density  $\rho_{\gamma'} = 0.3$  GeV/cm<sup>3</sup> is assumed. See their Fig. 4 for mass-dependent limits.
- 7 APRILE 19D is analogous to ABE 14F. The quoted limit applies to  $m_{\gamma'} = 0.7$  keV. See their Fig. 5(f) for mass-dependent limits.
- 8 BANERJEE 19 is an update of BANERJEE 18A. The quoted limit is at  $m_{\gamma'} = 1$  MeV. See their Fig. 3 for mass-dependent limits.
- 9 BHONAH 19 examine heating of Galactic Center gas clouds by hidden photon dark matter. The quoted limit applies to  $m_{\gamma'} \simeq 10^{-12}$  eV. See their Fig. 2 for mass-dependent limits.
- 10 BRUN 19 is analogous to SUZUKI 15. The limit is derived under an assumption that hidden photons constitute the local dark matter density  $\rho_{\gamma'} = 0.3$  GeV/cm<sup>3</sup>.
- 11 CORTINA-GIL 19 look for an invisible hidden photon in the reaction  $K^+ \rightarrow \pi^+ \pi^0$  ( $\pi^0 \rightarrow \gamma \gamma'$ ). The quoted limit applies to  $m_{\gamma'} = 62.5$ –65 MeV. See their Figs. 6 and 7 for mass-dependent limits.
- 12 DANILOV 19 examined the hidden photon production in nuclear reactors, correctly taking account of the effective photon mass in the reactor and detector. The limit gets weaker for  $m_{\gamma'}$  less than the effective photon mass in proportion to  $1/m_{\gamma'}^2$ . See their Fig. 1 for mass-dependent limits.
- 13 HOCHBERG 19 look for the absorption signal of hidden photon dark matter by using superconducting-nanowire single-photon detectors. The quoted limit applies to  $m_{\gamma'} \simeq 1$  eV. The local density  $\rho_{\gamma'} = 0.3$  GeV/cm<sup>3</sup> is assumed. See their Fig. 4 for mass-dependent limits.
- 14 KOPYLOV 19 look for hidden-photon dark matter using a counter with an aluminum cathode and derive limits assuming it constitute all the local dark matter. The quoted limit applies to  $m_{\gamma'} = 12$  eV. See their Fig. 7 for mass-dependent limits.
- 15 KOVETZ 19 examine heating of the early Universe plasma by hidden photon dark matter, and derive the limits by requiring that the cosmic mean 21 cm brightness temperature relative to the CMB temperature satisfy  $T_{21} > -100$  mK. The quoted limit applies to  $m_{\gamma'} \simeq 2 \times 10^{-14}$  eV. See their Fig. 3 for mass-dependent limits.
- 16 NGUYEN 19 look for hidden photon dark matter with a resonant cavity, and set limits  $\sim 10^{-12}$  for  $m_{\gamma'} = 0.2$ –2.07  $\mu$ eV. The quoted limit applies to  $m_{\gamma'} = 1.3$   $\mu$ eV. The local density  $\rho_{\gamma'} = 0.3$  GeV/cm<sup>3</sup> is assumed. See their Fig. 19 for mass-dependent limits.
- 17 ABE 18f is an update of ABE 14f. The quoted limit applies to  $m_{\gamma'} \simeq 40$  keV. See their Fig. 5 for mass-dependent limits.
- 18 ADRIAN 18 look for a hidden photon resonance in the reaction  $e^- Z \rightarrow e^- Z \gamma'$  ( $\gamma' \rightarrow e^+ e^-$ ). The quoted limit applies to  $m_{\gamma'} = 40$  MeV. See their Fig. 4 for mass-dependent limits.
- 19 ANASTASI 18b look for a hidden photon resonance in the reaction  $e^+ e^- \rightarrow \gamma' \gamma$  ( $\gamma' \rightarrow \mu^+ \mu^-$ ). The quoted limit is obtained by combining the result of ANASTASI 16 and it applies to  $m_{\gamma'} \simeq 519$ –987 MeV. See their Fig. 9 for mass-dependent limits.
- 20 ARMENGAUD 18 is analogous to ABE 14f. The quoted limits applies to  $m_{\gamma'} = 1.6$  keV. See the right panel of Fig. 5 for mass-dependent limits.
- 21 BANERJEE 18 look for hidden photons produced in the reaction  $e^- Z \rightarrow e^- Z \gamma'$  ( $\gamma' \rightarrow e^+ e^-$ ), and exclude  $9.2 \times 10^{-5} \lesssim \chi \lesssim 1 \times 10^{-2}$  for  $m_{\gamma'} = 1$ –23 MeV. They also set a limit on the electron coupling to a 16.7 MeV gauge boson suggested by the ATOMKI (KRASZNAHORKAY 16) experiment. See their Fig. 3 for mass-dependent limits.
- 22 BANERJEE 18A look for invisible decays of hidden photons produced in the reaction  $e^- Z \rightarrow e^- Z \gamma'$ . The quoted limit is at  $m_{\gamma'} = 1$  MeV. See their Fig. 15 for mass-dependent limits.
- 23 KNIRCK 18 is analogous to SUZUKI 15. See their Fig. 5 for mass-dependent limits.
- 24 ABRALL 17 is analogous to ABE 14f using the MAJORANA DEMONSTRATOR. See their Fig. 3 for limits between 6 keV <  $m_{\gamma'} < 97$  keV.
- 25 ABLIKIM 17AA look for  $e^+ e^- \rightarrow \gamma \gamma'$  ( $\gamma' \rightarrow e^+ e^-$  or  $\mu^+ \mu^-$ ). Limits between  $10^{-3}$  and  $10^{-4}$  are obtained (see their Fig. 3).
- 26 ANGLÖHER 17 is analogous to ABE 14f. The quoted limit is at  $m_{\gamma'} = 0.7$  keV. See their Fig. 8 for mass-dependent limits.
- 27 BANERJEE 17 look for invisible decays of hidden photons produced in the reaction  $e^- Z \rightarrow e^- Z \gamma'$ . The quoted limit applies to  $m_{\gamma'} = 2$  MeV. See their Fig. 3 for mass-dependent limits.
- 28 CHANG 17 examine the hidden photon emission from SN1987A, including the effects of finite temperature and density on  $\chi$  and obtain limits  $\chi (m_{\gamma'}/\text{MeV}) \lesssim 3 \times 10^{-9}$  for  $m_{\gamma'} < 15$  MeV and  $\chi \lesssim 10^{-9}$  for  $m_{\gamma'} = 15$ –120 MeV.
- 29 DUBININA 17 look for  $\mu^+ \rightarrow e^+ \bar{\nu}_\mu \nu_e \gamma'$  ( $\gamma' \rightarrow e^+ e^-$ ) in a nuclear photoemulsion. The quoted limit applies to  $m_{\gamma'} = 1.1$  MeV. Limits between  $4.5 \times 10^{-3}$  and  $10^{-2}$  are obtained (see their Fig. 3).
- 30 LEES 17E look for invisible decays of hidden photons produced in the reaction  $e^+ e^- \rightarrow \gamma \gamma'$ . See their Fig. 5 for limits in the mass range  $m_{\gamma'} \leq 8$  GeV.
- 31 AAD 16Ag look for hidden photons promptly decaying into collimated electrons and/or muons, assuming that they are produced in the cascade decays of squarks or the Higgs boson. See their Fig. 10 and Fig.13 for their limits on the cross section times branching fractions.
- 32 ANASTASI 16 look for the decay  $\gamma' \rightarrow \pi^+ \pi^-$  in the reaction  $e^+ e^- \rightarrow \gamma \gamma'$ . Limits between  $4.3 \times 10^{-3}$  and  $4.4 \times 10^{-4}$  are obtained for  $527 < m_{\gamma'} < 987$  MeV (see their Fig. 9).
- 33 KHACHATRYAN 16 look for  $\gamma' \rightarrow \mu^+ \mu^-$  in a dark SUSY scenario where the SM-like Higgs boson decays into a pair of the visible lightest neutralinos with mass 10 GeV, both of which decay into  $\gamma'$  and a hidden neutralino with mass 1 GeV. See the right panel in their Fig. 2.
- 34 AAD 15CD look for  $H \rightarrow Z \gamma' \rightarrow 4\ell$  with the ATLAS detector at LHC and find  $\chi < 4$ – $17 \times 10^{-2}$  for  $m_{\gamma'} = 15$ –55 GeV. See their Fig. 6.
- 35 ADARE 15 look for a hidden photon in  $\pi^0, \eta^0 \rightarrow \gamma e^+ e^-$  at the PHENIX experiment. See their Fig. 4 for mass-dependent limits.
- 36 AN 15A derived limits from the absence of ionization signals in the XENON10 and XENON100 experiments, assuming hidden photons constitute all the local dark matter. Their best limit is  $\chi < 1.3 \times 10^{-15}$  at  $m_{\gamma'} = 18$  eV. See their Fig. 1 for mass-dependent limits.
- 37 ANASTASI 15 look for a production of a hidden photon and a hidden Higgs boson with the KLOE detector at DAΦNE, where the hidden photon decays into a pair of muons and the hidden Higgs boson lighter than  $m_{\gamma'}$  escape detection. See their Figs. 6 and 7 for mass-dependent limits on a product of the hidden fine structure constant and the kinetic mixing.
- 38 ANASTASI 15A look for the decay  $\gamma' \rightarrow e^+ e^-$  in the reaction  $e^+ e^- \rightarrow e^+ e^- \gamma$ . Limits between  $1.7 \times 10^{-3}$  and  $1 \times 10^{-2}$  are obtained for  $m_{\gamma'} = 5$ –320 MeV (see their Fig. 7).
- 39 BATLEY 15A look for  $\pi^0 \rightarrow \gamma \gamma'$  ( $\gamma' \rightarrow e^+ e^-$ ) at the NA48/2 experiment. Limits between  $4.2 \times 10^{-4}$  and  $8.8 \times 10^{-3}$  are obtained for  $m_{\gamma'} = 9$ –120 MeV (see their Fig. 4).
- 40 JAEGLER 15 look for the decay  $\gamma' \rightarrow e^+ e^-, \mu^+ \mu^-,$  or  $\pi^+ \pi^-$  in the dark Higgsstrahlung channel,  $e^+ e^- \rightarrow \gamma' H'$  ( $H' \rightarrow \gamma' \gamma'$ ) at the BELLE experiment. They set limits on a product of the branching fraction and the Born cross section as well as a product of the hidden fine structure constant and the kinetic mixing. See their Figs. 3 and 4.
- 41 KAZANAS 15 set limits by studying the decay of hidden photons  $\gamma' \rightarrow e^+ e^-$  inside and near the progenitor star of SN1987A. See their Fig. 6 for mass-dependent limits.
- 42 SUZUKI 15 looked for hidden-photon dark matter with a dish antenna and derived limits assuming they constitute all the local dark matter. Their limits are  $\chi < 6 \times 10^{-12}$  for  $m_{\gamma'} = 1.9$ –4.3 eV. See their Fig. 7 for mass-dependent limits.
- 43 VINOLES 15 performed a global fit analysis based on helioseismology and solar neutrino observations, and set the limits  $\chi m_{\gamma'} < 1.8 \times 10^{-12}$  eV for  $m_{\gamma'} = 3 \times 10^{-5}$ –8 eV. See their Fig. 11.
- 44 ABE 14f look for the photoelectric-like interaction in the XMASS detector assuming the hidden photon constitutes all the local dark matter. Limits between  $2 \times 10^{-13}$  and  $1 \times 10^{-12}$  are obtained, where the relation  $\chi^2 = \alpha'/\alpha$  is used to translate the original bound on the ratio of the hidden and EM fine-structure constants. See their Fig. 3 for mass-dependent limits.
- 45 AGA KISHIEV 14 look for hidden photons  $\gamma' \rightarrow e^+ e^-$  at the HADES experiment, and set limits on  $\chi$  for  $m_{\gamma'} = 0.02$ –0.6 GeV. See their Fig. 5 for mass-dependent limits.
- 46 BABUSCI 14 look for the decay  $\gamma' \rightarrow \mu^+ \mu^-$  in the reaction  $e^+ e^- \rightarrow \mu^+ \mu^- \gamma$ . Limits between  $4 \times 10^{-3}$  and  $9.0 \times 10^{-4}$  are obtained for  $520$  MeV <  $m_{\gamma'} < 980$  MeV (see their Fig. 7).
- 47 BATELL 14 derived limits from the electron beam dump experiment at SLAC (E-137) by searching for events with recoil electrons by sub-GeV dark matter produced from the decay of the hidden photon. Limits at the level of  $10^{-4}$ – $10^{-1}$  are obtained for  $m_{\gamma'} = 10^{-3}$ –1 GeV, depending on the dark matter mass and the hidden gauge coupling (see their Fig. 2).
- 48 BLUEMLEIN 14 analyzed the beam dump data taken at the U-70 accelerator to look for  $\gamma'$ -bremsstrahlung and the subsequent decay into muon pairs and hadrons. See their Fig. 4 for mass-dependent excluded region.
- 49 FRADETTE 14 studied effects of decay of relic hidden photons on BBN and CMB to set constraints on very small values of the kinetic mixing. See their Figs. 4 and 7 for mass-dependent excluded regions.
- 50 LEES 14I look for hidden photons in the reaction  $e^+ e^- \rightarrow \gamma \gamma'$  ( $\gamma' \rightarrow e^+ e^-, \mu^+ \mu^-$ ). Limits at the level of  $10^{-4}$ – $10^{-3}$  are obtained for  $0.02$  GeV <  $m_{\gamma'} < 10.2$  GeV. See their Fig. 4 for mass-dependent limits.
- 51 MERKEL 14 look for  $\gamma' \rightarrow e^+ e^-$  at the A1 experiment at the Mainz Microtron (MAMI). See their Fig. 3 for mass-dependent limits.
- 52 AN 13B examined the stellar production of hidden photons, correcting an important error of the production rate of the longitudinal mode which now dominates. See their Fig. 2 for mass-dependent limits based on solar energy loss.
- 53 AN 13c use the solar flux of hidden photons to set a limit on the atomic ionization rate in the XENON10 experiment. They find  $\chi m_{\gamma'} < 3 \times 10^{-12}$  eV for  $m_{\gamma'} < 1$  eV. See their Fig. 2 for mass-dependent limits.
- 54 DIAMOND 13 analyzed the beam dump data taken at the SLAC millicharge experiment to constrain a hidden photon invisibly decaying into lighter long-lived particles, which undergo elastic scattering off nuclei in the detector. Limits between  $8 \times 10^{-4}$ – $2 \times 10^{-2}$



See key on page 999

Gauge & Higgs Boson Particle Listings  
Axions (A<sup>0</sup>) and Other Very Light Bosons

Table listing particle experiments and collaborations. Columns include author names (e.g., GANDO, GNINENKO, ASAI), publication details (e.g., PR C86 021601), collaboration names (e.g., KamLAND-Zen, CoGeNT), and associated institutions or locations (e.g., TOKY, BRCO, OREG, TRIU).

Downloaded from https://academic.oup.com/ptep/article/2020/8/083C01/5891211 by guest on 12 November 2020



# Gauge & Higgs Boson Particle Listings

## Axions ( $A^0$ ) and Other Very Light Bosons

MAIER	87	ZPHY A326 527	K. Maier <i>et al.</i>	(STUT, GSI)	DATAR	82	PL 114B 63	V.M. Datar <i>et al.</i>	(BHAB)
MILLS	87	PR D36 707	A.P. Mills, J. Levy	(BELL)	EDWARDS	82	PRL 48 903	C. Edwards <i>et al.</i>	(Crystal Ball Collab.)
RAFFELT	87	PR D36 2211	G.G. Raffelt, D.S.P. Dearborn	(LLL, UCB)	FETSCHER	82	JP G8 L147	W. Fetscher	(ETH)
RIORDAN	87	PRL 59 755	E.M. Riordan <i>et al.</i>	(ROCH, CIT+)	FUKUGITA	82	PRL 48 1522	M. Fukugita, S. Watamura, M. Yoshimura	(KEK)
TURNER	87	PRL 59 2489	M.S. Turner	(FNAL, EFI)	FUKUGITA	82B	PR D26 1840	M. Fukugita, S. Watamura, M. Yoshimura	(KEK)
VANBIBBER	87	PRL 59 759	K. van Bibber <i>et al.</i>	(LLL, CIT, MIT+)	LEHMANN	82	PL 115B 270	P. Lehmann <i>et al.</i>	(SACL)
VONWIMMER	87	PRL 59 266	U. von Wimmersperg <i>et al.</i>	(WITW)	RAFFELT	82	PL 119B 323	G. Raffelt, L. Stodolsky	(MPIM)
BADIER	86	ZPHY C31 21	J. Badier <i>et al.</i>	(NA3 Collab.)	ZEHNDER	82	PL 110B 419	A. Zehnder, K. G��bath��ler, J.L. Vuilleumier	(ETH+)
BROWN	86	PRL 57 2101	C.N. Brown <i>et al.</i>	(FNAL, WASH, KYOT+)	ASANO	81B	PL 107B 159	Y. Asano <i>et al.</i>	(KEK, TOKY, INUS, OSAK)
BRYMAN	86B	PRL 57 2787	D.A. Bryman, E.T.H. Clifford	(TRIUM)	BARROSO	81	PL 106B 91	A. Barroso, N.C. Mukhopadhyay	(SIN)
DAVIER	86	PL B180 295	M. Davier, J. Jeanjean, H. Nguyen Ngoc	(LALO)	FAISSNER	81	ZPHY C10 95	H. Faissner <i>et al.</i>	(AACH3)
DEARBORN	86	PRL 56 26	D.S.P. Dearborn, D.N. Schramm, G. Steigman	(LLL+)	FAISSNER	81B	PL 103B 234	H. Faissner <i>et al.</i>	(AACH3)
EICHLER	86	PL B175 101	R.A. Eichler <i>et al.</i>	(SINDRUM Collab.)	KIM	81	PL 105B 55	B.R. Kim, C. Stamm	(AACH3)
HALLIN	86	PRL 57 2105	A.L. Hallin <i>et al.</i>	(PRIN)	VUILLEUMIER	81	PL 101B 341	J.L. Vuilleumier <i>et al.</i>	(CIT, MUNI)
JODIDIO	86	PR D34 1967	A. Jodidio <i>et al.</i>	(LBL, NWES, TRIU)	ZEHNDER	81	PL 104B 494	A. Zehnder	(ETH)
Also		PR D37 237 (erratum)	A. Jodidio <i>et al.</i>	(LBL, NWES, TRIU)	FAISSNER	80	PL 96B 201	H. Faissner <i>et al.</i>	(AACH3)
KETOV	86	JETPL 44 146	S.N. Ketov <i>et al.</i>	(KIAE)	JACQUES	80	PR D21 1206	P.F. Jacques <i>et al.</i>	(RUTG, STEV, COLU)
		Translated from ZETFP 44 114			SOUKAS	80	PRL 44 564	A. Soukas <i>et al.</i>	(BNL, HARV, ORNL, PENN)
KOCH	86	NC 96A 182	H.R. Koch, O.W.B. Schult	(JULI)	BECHIS	79	PRL 42 1511	D.J. Bechis <i>et al.</i>	(UMD, COLU, AFRR)
KONAKA	86	PRL 57 659	A. Konaka <i>et al.</i>	(KYOT, KEK)	CALAPRICE	79	PR D20 2708	F.P. Calaprice <i>et al.</i>	(PRIN)
MAIANI	86	PL B175 359	L. Maiani, R. Petronzio, E. Zavattini	(CERN)	COTEUS	79	PRL 42 1438	P. Coteus <i>et al.</i>	(COLU, ILL, BNL)
PECCCI	86	PL B172 435	R.D. Peccci, T.T. Wu, T. Yanagida	(DESY)	DISHAW	79	PL 85B 142	J.P. Dishaw <i>et al.</i>	(SLAC, CIT)
RAFFELT	86	PR D33 897	G.G. Raffelt	(MPIM)	ZHITNITSKII	79	SJNP 29 517	A.R. Zhitnitsky, Y.I. Skovpen	(NOVO)
RAFFELT	86B	PL 166B 402	G.G. Raffelt	(MPIM)			Translated from YAF 29 1001		
SAVAGE	86B	PRL 57 178	M.J. Savage <i>et al.</i>	(CIT)	ALIBRAN	78	PL 74B 134	P. Alibrant <i>et al.</i>	(Gargamelle Collab.)
AMALDI	85	PL 153B 444	U. Amaldi <i>et al.</i>	(CERN)	ASRATYAN	78B	PL 79B 497	A.E. Asratyan <i>et al.</i>	(ITEP, SERP)
ANANEV	85	SJNP 41 585	V.D. Ananev <i>et al.</i>	(JINR)	BELLOTTI	78	PL 76B 223	E. Bellotti, E. Fiorini, L. Zanotti	(MILA)
		Translated from YAF 41 912			BOSETTI	78B	PL 74B 143	P.C. Bosetti <i>et al.</i>	(BEBC Collab.)
BALTRUSAITIS	85	PRL 55 1842	R.M. Baltrusaitis <i>et al.</i>	(Mark III Collab.)	DICUS	78C	PR D18 1829	D.A. Dicus <i>et al.</i>	(TEXA, VPI, STAN)
BERGSM��	85	PL 157B 458	F. Bergsma <i>et al.</i>	(CHARM Collab.)	DONNELLY	78	PR D18 1607	T.W. Donnelly <i>et al.</i>	(STAN)
KAPLAN	85	NP B260 215	D.B. Kaplan	(HARV)	Also		PRL 37 315	F. Reines, H.S. Gurr, H.W. Sobel	(UCI)
IWAMOTO	84	PRL 53 1198	N. Iwamoto	(UCSB, WUSL)	Also		PRL 33 179	H.S. Gurr, F. Reines, H.W. Sobel	(UCI)
YAMAZAKI	84	PRL 52 1089	T. Yamazaki <i>et al.</i>	(INUS, KEK)	HANSL	78D	PL 74B 139	T. Hanst <i>et al.</i>	(CDHS Collab.)
ABBOTT	83	PL 120B 133	L.F. Abbott, P. Sikivie	(BRAN, FLOR)	MICELMAC	78	LNC 21 441	G.V. Mitselmakher, B. Pontecorvo	(JINR)
CARBONI	83	PL 123B 349	G. Carboni, W. Dahme	(CERN, MUNI)	MIKAELIAN	78	PR D18 3605	K.O. Mikaelian	(FNAL, NWES)
CAVAIGNAC	83	PL 121B 193	J.F. Cavaignac <i>et al.</i>	(ISNG, LAPP)	SATO	78	PTP 60 1942	K. Sato	(KYOT)
DICUS	83	PR D28 1778	D.A. Dicus, V.L. Teplitz	(TEXA, UMD)	VYSOTSKII	78	JETPL 27 502	M.L. Vysotsky <i>et al.</i>	(ASCI)
DINE	83	PL 120B 137	M. Dine, W. Fischler	(IAS, PENN)			Translated from ZETFP 27 533		
ELLIS	83B	NP B223 252	J. Ellis, K.A. Olive	(CERN)	YANG	78	PRL 41 523	T.C. Yang	(MASA)
FAISSNER	83	PR D28 1198	H. Faissner <i>et al.</i>	(AACH)	PECCEI	77	PR D16 1791	R.D. Peccci, H.R. Quinn	(STAN, SLAC)
FAISSNER	83B	PR D28 1787	H. Faissner <i>et al.</i>	(AACH3)	Also		PRL 38 1440	R.D. Peccci, H.R. Quinn	(STAN, SLAC)
FRANK	83B	PR D28 1790	J.S. Frank <i>et al.</i>	(LANL, YALE, LBL+)	REINES	76	PRL 37 315	F. Reines, H.S. Gurr, H.W. Sobel	(UCI)
HOFFMAN	83	PR D28 660	C.M. Hoffman <i>et al.</i>	(LANL, ARZS)	GURR	74	PRL 33 179	H.S. Gurr, F. Reines, H.W. Sobel	(UCI)
PRESKILL	83	PL 120B 127	J. Preskill, M.B. Wise, F. Wilczek	(HARV, UCSBT)	ANAND	53	PRSL A22 183	B.M. Anand	
SIKIVIE	83	PRL 51 1415	P. Sikivie	(FLOR)					
Also		PRL 52 695 (erratum)	P. Sikivie	(FLOR)					
ALEKSEEV	82	JETP 55 591	E.A. Alekseeva <i>et al.</i>	(KIAE)					
		Translated from ZETFP 82 1007							
ALEKSEEV	82B	JETPL 36 116	G.D. Alekseev <i>et al.</i>	(MOSU, JINR)	SREDNICKI	85	NP B260 689	M. Srednicki	(UCSB)
		Translated from ZETFP 36 94			BARDEEN	78	PL 74B 229	W.A. Bardeen, S.-H.H. Tye	(FNAL)
ASANO	82	PL 113B 195	Y. Asano <i>et al.</i>	(KEK, TOKY, INUS, OSAK)					
BARROSO	82	PL 116B 247	A. Barroso, G.C. Branco	(LIBS)					

### OTHER RELATED PAPERS

SREDNICKI	85	NP B260 689	M. Srednicki	(UCSB)
BARDEEN	78	PL 74B 229	W.A. Bardeen, S.-H.H. Tye	(FNAL)

## LEPTONS

$e$ . . . . .	1101
$\mu$ . . . . .	1102
$\tau$ . . . . .	1106
Heavy Charged Lepton Searches . . . . .	1134
Neutrino Properties . . . . .	1135
Number of Neutrino Types . . . . .	1143
Double- $\beta$ Decay . . . . .	1145
Neutrino Mixing . . . . .	1149
Heavy Neutral Leptons, Searches for . . . . .	1168

### Notes in the Listings

Neutrino properties . . . . .	1135
Sum of neutrino masses (rev.) . . . . .	1138
Number of light neutrino types from collider experiments . . . . .	1143
Neutrinoless double- $\beta$ decay (rev.) . . . . .	1145
Three-neutrino mixing parameters (rev.) . . . . .	1155

### Related Reviews in Volume 1

55. Muon anomalous magnetic moment (rev.) . . . . .	722
56. Muon decay parameters (rev.) . . . . .	725
57. $\tau$ branching fractions (rev.) . . . . .	728
58. $\tau$ -lepton decay parameters . . . . .	731



LEPTONS

e

J = 1/2

e MASS (atomic mass units u)

The primary determination of an electron's mass comes from measuring the ratio of the mass to that of a nucleus, so that the result is obtained in u (atomic mass units). The conversion factor to MeV is more uncertain than the mass of the electron in u; indeed, the recent improvements in the mass determination are not evident when the result is given in MeV. In this datablock we give the result in u, and in the following datablock in MeV.

Table with columns: VALUE (10^-6 u), DOCUMENT ID, TECN, COMMENT. Includes data for MOHR 16, MOHR 12, MOHR 08, MOHR 05, BEIER 02, MOHR 99, FARNHAM 95, COHEN 87.

1 BEIER 02 compares Larmor frequency of the electron bound in a 12C5+ ion with the cyclotron frequency of a single trapped 12C5+ ion. 2 FARNHAM 95 compares cyclotron frequency of trapped electrons with that of a single trapped 12C6+ ion.

e MASS

2010 CODATA (MOHR 12) gives the conversion factor from u (atomic mass units, see the above datablock) to MeV as 931.494 061 (21). Earlier values use the then-current conversion factor. The conversion error dominates the uncertainty of the masses given below.

Table with columns: VALUE (MeV), DOCUMENT ID, TECN, COMMENT. Includes data for MOHR 16, MOHR 12, MOHR 08, MOHR 05, BEIER 02, MOHR 99, FARNHAM 95, COHEN 87, COHEN 73.

1 Converted to MeV using the 1998 CODATA value of the conversion constant, 931.494013 ± 0.000037 MeV/u. 2 BEIER 02 compares Larmor frequency of the electron bound in a 12C5+ ion with the cyclotron frequency of a single trapped 12C5+ ion. 3 FARNHAM 95 compares cyclotron frequency of trapped electrons with that of a single trapped 12C6+ ion.

(me+ - me-) / maverage

A test of CPT invariance.

Table with columns: VALUE, CL%, DOCUMENT ID, TECN, COMMENT. Includes data for FEE 93, DOLGOV 14, CHU 84.

1 FEE 93 value is obtained under the assumption that the positronium Rydberg constant is exactly half the hydrogen one. 2 DOLGOV 14 result is obtained under the assumption that any mass difference between electron and positron would lead to a non-zero photon mass. The PDG 12 limit of 1 x 10^-18 eV on the photon mass is in turn used to derive the value quoted here.

|qe+ + qe-|/e

A test of CPT invariance. See also similar tests involving the proton.

Table with columns: VALUE, DOCUMENT ID, TECN, COMMENT. Includes data for HUGHES 92, SCHAEFER 95, MUELLER 92.

1 HUGHES 92 uses recent measurements of Rydberg-energy and cyclotron-frequency ratios. 2 SCHAEFER 95 removes model dependency of MUELLER 92. 3 MUELLER 92 argues that an inequality of the charge magnitudes would, through higher-order vacuum polarization, contribute to the net charge of atoms.

e MAGNETIC MOMENT ANOMALY

me/μB - 1 = (g-2)/2

Table with columns: VALUE (units 10^-6), DOCUMENT ID, TECN, CHG, COMMENT. Includes data for MOHR 16, MOHR 12, HANNEKE 08, MOHR 08, ODOM 06, MOHR 05, MOHR 99, COHEN 87, VANDYCK 87, VANDYCK 87.

1 MOHR 08 average is dominated by ODOM 06. 2 Superseded by HANNEKE 08 per private communication with Gerald Gabrielse.

(ge+ - ge-) / gaverage

A test of CPT invariance.

Table with columns: VALUE (units 10^-12), CL%, DOCUMENT ID, TECN, COMMENT. Includes data for VANDYCK 87, VASSERMAN 87, SCHWINBERG 81.

1 VANDYCK 87 measured (g-/g+)-1 and we converted it. 2 VASSERMAN 87 measured (g+ - g-)/(g-2). We multiplied by (g-2)/g = 1.2 x 10^-3.

e ELECTRIC DIPOLE MOMENT (d)

A nonzero value is forbidden by both T invariance and P invariance.

Table with columns: VALUE (10^-28 ecm), CL%, DOCUMENT ID, TECN, COMMENT. Includes data for ANDREEV 18, CAIRNCROSS 17, KIM 15, BARON 14, ECKEL 12, HUDSON 11, REGAN 02, COMMINIS 94, ABDULLAH 90, CHO 89, MURTHY 89, LAMOREAUX 87, SANDARS 75, PLAYER 70, WEISSKOPF 68.

1 ANDREEV 18 gives a measurement corresponding to this limit as (4.3 ± 3.1 ± 2.6) x 10^-30 ecm. 2 CAIRNCROSS 17 gives a measurement corresponding to this limit as (0.09 ± 0.77 ± 0.17) x 10^-28 ecm. 3 BARON 14 gives a measurement corresponding to this limit as (-0.21 ± 0.37 ± 0.25) x 10^-28 ecm. 4 ECKEL 12 gives a measurement corresponding to this limit as (-1.07 ± 3.06 ± 1.74) x 10^-25 ecm. 5 HUDSON 11 gives a measurement corresponding to this limit as (-2.4 ± 5.7 ± 1.5) x 10^-28 ecm. 6 ABDULLAH 90, COMMINIS 94, and REGAN 02 use the relativistic enhancement of a valence electron's electric dipole moment in a high-Z atom.

e- MEAN LIFE / BRANCHING FRACTION

A test of charge conservation. See the "Note on Testing Charge Conservation and the Pauli Exclusion Principle" following this section in our 1992 edition (Physical Review D45 S1 (1992), p. VI.10).

Most of these experiments are one of three kinds: Attempts to observe (a) the 255.5 keV gamma ray produced in e- -> nu\_e gamma, (b) the (K) shell xray produced when an electron decays without additional energy deposit, e.g., e- -> nu\_e nu\_e nu\_e ("disappearance" experiments), and (c) nuclear de-excitation gamma rays after the electron disappears from an atomic shell and the nucleus is left in an excited state. The last can include both weak boson and photon mediating processes. We use the best e- -> nu\_e gamma limit for the Summary Tables.

Note that we use the mean life rather than the half life, which is often reported.

e -> nu\_e gamma and astrophysical limits

Table with columns: VALUE (yr), CL%, DOCUMENT ID, TECN, COMMENT. Includes data for AGOSTINI 15B, BORX.

# Lepton Particle Listings

e, μ

- We do not use the following data for averages, fits, limits, etc. •••
- >1.2 × 10<sup>24</sup> 90 ABRALL 17 HPGE electron decay to invisible
- >1.22 × 10<sup>26</sup> 68 1 Klapdor-K... 07 CNTR e<sup>-</sup> → νγ
- >4.6 × 10<sup>26</sup> 90 BACK 02 BORX e<sup>-</sup> → νγ
- >3.4 × 10<sup>26</sup> 68 BELL 00b DAMA e<sup>-</sup> → νγ, liquid Xe
- >3.7 × 10<sup>25</sup> 68 AHARONOV 95b CNTR e<sup>-</sup> → νγ
- >2.35 × 10<sup>25</sup> 68 BALYSH 93 CNTR e<sup>-</sup> → νγ, <sup>76</sup>Ge detector
- >1.5 × 10<sup>25</sup> 68 AVIGNONE 86 CNTR e<sup>-</sup> → νγ
- >1 × 10<sup>39</sup> 2 ORITO 85 ASTR Astrophysical argument
- >3 × 10<sup>23</sup> 68 BELLOTTI 83b CNTR e<sup>-</sup> → νγ

<sup>1</sup>The authors of A. Derbin et al, arXiv:0704.2047v1 argue that this limit is overestimated by at least a factor of 5.  
<sup>2</sup>ORITO 85 assumes that electromagnetic forces extend out to large enough distances and that the age of our galaxy is 10<sup>10</sup> years.

### Disappearance and nuclear-de-excitation experiments

VALUE (yr)	CL%	DOCUMENT ID	TECN	COMMENT
>6.4 × 10 <sup>24</sup>	68	1 BELL 99b	DAMA	De-excitation of <sup>129</sup> Xe

••• We do not use the following data for averages, fits, limits, etc. •••

>4.2 × 10 <sup>24</sup>	68	BELL 99	DAMA	Iodine L-shell disappearance
>2.4 × 10 <sup>23</sup>	90	2 BELL 99d	DAMA	De-excitation of <sup>127</sup> I (in Na)
>4.3 × 10 <sup>23</sup>	68	AHARONOV 95b	CNTR	Ge K-shell disappearance
>2.7 × 10 <sup>23</sup>	68	REUSSER 91	CNTR	Ge K-shell disappearance
>2 × 10 <sup>22</sup>	68	BELLOTTI 83b	CNTR	Ge K-shell disappearance

<sup>1</sup>BELL 99b limit on charge nonconserving e<sup>-</sup> capture involving excitation of the 236.1 keV nuclear state of <sup>129</sup>Xe; the 90% CL limit is 3.7 × 10<sup>24</sup> yr. Less stringent limits for other states are also given.  
<sup>2</sup>BELL 99d limit on charge nonconserving e<sup>-</sup> capture involving excitation of the 57.6 keV nuclear state of <sup>127</sup>I. Less stringent limits for the other states and for the state of <sup>23</sup>Na are also given.

### LIMITS ON LEPTON-FLAVOR VIOLATION IN PRODUCTION

Forbidden by lepton family number conservation.

This section was added for the 2008 edition of this Review and is not complete. For a list of further measurements see references in the papers listed below.

#### σ(e<sup>+</sup>e<sup>-</sup> → e<sup>±</sup>τ<sup>∓</sup>) / σ(e<sup>+</sup>e<sup>-</sup> → μ<sup>±</sup>μ<sup>-</sup>)

VALUE	CL%	DOCUMENT ID	TECN	COMMENT
<8.9 × 10 <sup>-6</sup>	95	AUBERT 07p	BABR	e <sup>+</sup> e <sup>-</sup> at E <sub>cm</sub> = 10.58 GeV

••• We do not use the following data for averages, fits, limits, etc. •••

<1.8 × 10 <sup>-3</sup>	95	GOMEZ-CAD... 91	MRK2	e <sup>+</sup> e <sup>-</sup> at E <sub>cm</sub> = 29 GeV
-------------------------	----	-----------------	------	---

#### σ(e<sup>+</sup>e<sup>-</sup> → μ<sup>±</sup>τ<sup>∓</sup>) / σ(e<sup>+</sup>e<sup>-</sup> → μ<sup>±</sup>μ<sup>-</sup>)

VALUE	CL%	DOCUMENT ID	TECN	COMMENT
<4.0 × 10 <sup>-6</sup>	95	AUBERT 07p	BABR	e <sup>+</sup> e <sup>-</sup> at E <sub>cm</sub> = 10.58 GeV

••• We do not use the following data for averages, fits, limits, etc. •••

<6.1 × 10 <sup>-3</sup>	95	GOMEZ-CAD... 91	MRK2	e <sup>+</sup> e <sup>-</sup> at E <sub>cm</sub> = 29 GeV
-------------------------	----	-----------------	------	---

### e REFERENCES

ANDREEV 18 NAT 562 355 V. Andreev et al. (ACME Collab.)  
 ABRALL 17 PRL 118 161801 N. Abgrall et al. (MAJORANA Collab.)  
 CAIRN CROSS 17 PRL 119 153001 W.B. Cairncross et al. (NIST, COLO)  
 MOHR 16 RMP 88 035009 P.J. Mohr, D.B. Newell, B.N. Taylor (NIST)  
 AGOSTINI 15b PRL 115 231802 M. Agostini et al. (Borexino Collab.)  
 KIM 15 PR D91 102004 Y.J. Kim et al. (IND, YALE, LANL)  
 BARON 14 SCIENCE 343 269 J. Baron et al. (ACME Collab.)  
 DOLGOV 14 PL B732 244 A.D. Dolgov, V.A. Novikov  
 BEIER 12 PRL 109 193003 S. Eckel, A.O. Sushkov, S.K. Lamoreaux (YALE)  
 MOHR 12 RMP 84 1527 P.J. Mohr, B.N. Taylor, D.B. Newell (NIST)  
 PDG 12 PR D86 010001 J. Berlinger et al. (PDG Collab.)  
 HUDSON 11 NAT 473 493 J.J. Hudson et al. (LOIC)  
 HANNEKE 08 PRL 100 120801 D. Hanneke, S. Fogwell, G. Gabrielse (HARV)  
 MOHR 08 RMP 80 633 P.J. Mohr, B.N. Taylor, D.B. Newell (NIST)  
 AUBERT 07p PR D75 031103 B. Aubert et al. (BABAR Collab.)  
 Klapdor-K... 07 PL B644 109 H.V. Klapdor-Kleingrothaus, I.V. Krivosheina, I.V. Titkova  
 ODOM 06 PRL 97 030801 B. Odum et al. (HARV)  
 MOHR 05 RMP 77 1 P.J. Mohr, B.N. Taylor (NIST)  
 BACK 02 PL B525 29 H.O. Back et al. (Borexino/SASSO Collab.)  
 BEIER 02 PRL 88 011603 T. Beier et al.  
 REGAN 02 PRL 88 071805 B.C. Regan et al.  
 BELL 00b PR D61 117301 P. Belli et al. (DAMA Collab.)  
 BELL 99 PL B460 236 P. Belli et al. (DAMA Collab.)  
 BELL 99b PL B465 315 P. Belli et al. (DAMA Collab.)  
 BELL 99d PR C60 065501 P. Belli et al. (DAMA Collab.)  
 MOHR 99 JPCRD 28 1713 P.J. Mohr, B.N. Taylor (NIST)  
 Also RMP 72 351 P.J. Mohr, B.N. Taylor (NIST)  
 AHARONOV 95b PR D52 3785 Y. Aharonov et al. (SCUC, PNL, ZARA+)  
 Also PL B353 168 Y. Aharonov et al. (SCUC, PNL, ZARA+)  
 FARNHAM 95 PRL 75 3598 D.L. Farnham, R.S. van Dyck, P.B. Schwinberg (WASH)  
 SCHAEFER 95 PR A51 838 A. Schaefer, J. Reinhardt (FRAN)  
 COMMINS 94 PR A50 2960 E.D. Commings et al.  
 BALYSH 93 PL B298 278 A. Balysh et al. (KIAE, MPIH, SASSO)  
 FEE 93 PR A48 192 M.S. Fee et al.  
 HUGHES 92 PRL 69 578 R.J. Hughes, B.J. Deutch (LANL, AARH)  
 MUELLER 92 PRL 69 3432 B. Muller, M.H. Thoma (DUKE)  
 PDG 92 PR D45 51 K. Hikasa et al. (KEK, LBL, BOST+)  
 GOMEZ-CAD... 91 PRL 66 1007 J.J. Gomez-Cadenas et al. (SLAC MARK-2 Collab.)  
 REUSSER 91 PL B255 143 D. Reusser et al. (NEUC, CIT, PSI)  
 ABDULLAH 90 PRL 65 2347 K. Abdullah et al. (LBL, UCB)  
 CHO 89 PRL 63 2559 D. Cho, K. Sangster, E.A. Hinds (YALE)  
 MURTHY 89 PRL 63 965 S.A. Murthy et al. (AMHT)  
 COHEN 87 RMP 59 1121 E.R. Cohen, B.N. Taylor (RISC, NBS)

LAMOREAUX 87 PRL 59 2275 S.K. Lamoreaux et al. (WASH)
VANDYCK 87 PRL 59 26 R.S. van Dyck, P.B. Schwinberg, H.G. Dehmelt (WASH)
VASSERMAN 87 PL B198 302 I.B. Vasserma et al. (NOVO)
Also PL B187 172 I.B. Vasserma et al. (NOVO)
AVIGNONE 86 PR D34 97 F.T. Avignone et al. (PNL, SCUC)
ORITO 85 PR 54 2457 S. Orto, M. Yoshimura (TOKY, KEK)
CHU 84 PRL 52 1689 S. Chu, A.P. Mills, J.L. Hall (BELL, NBS, COLO)
BELLOTTI 83b PL 124B 435 E. Bellotti et al. (MILA)
SCHWINBERG 81 PRL 47 1579 P.B. Schwinberg, R.S. van Dyck, H.G. Dehmelt (WASH)
SANDARS 75 PR A11 473 P.G.H. Sandars, D.M. Sternheimer (OXF, BNL)
COHEN 73 JPCRD 2 664 E.R. Cohen, B.N. Taylor (RISC, NBS)
PLAYER 70 JP B3 1620 M.A. Player, P.G.H. Sandars (OXF)
WEISSKOPF 68 PRL 21 1645 M.C. Weisskopf et al. (BRAN)



$$J = \frac{1}{2}$$

### μ MASS (atomic mass units u)

The muon's mass is obtained from the muon-electron mass ratio as determined from the measurement of Zeeman transition frequencies in muonium (μ<sup>+</sup>e<sup>-</sup> atom). Since the electron's mass is most accurately known in u, the muon's mass is also most accurately known in u. The conversion factor to MeV has approximately the same relative uncertainty as the mass of the muon in u. In this datablock we give the result in u, and in the following datablock in MeV.

VALUE (u)	DOCUMENT ID	TECN	COMMENT
0.1134289257 ± 0.0000000025	MOHR 16	RVUE	2014 CODATA value

••• We do not use the following data for averages, fits, limits, etc. •••

0.1134289267 ± 0.0000000029	MOHR 12	RVUE	2010 CODATA value
0.1134289256 ± 0.0000000029	MOHR 08	RVUE	2006 CODATA value
0.1134289264 ± 0.0000000030	MOHR 05	RVUE	2002 CODATA value
0.1134289168 ± 0.0000000034	1 MOHR 99	RVUE	1998 CODATA value
0.113428913 ± 0.0000000017	2 COHEN 87	RVUE	1986 CODATA value

<sup>1</sup>MOHR 99 make use of other 1998 CODATA entries below.  
<sup>2</sup>COHEN 87 make use of other 1986 CODATA entries below.

### μ MASS

2010 CODATA (MOHR 12) gives the conversion factor from u (atomic mass units, see the above datablock) to MeV as 931.494 061 (21). Earlier values use the then-current conversion factor. The conversion error contributes significantly to the uncertainty of the masses given below.

VALUE (MeV)	DOCUMENT ID	TECN	CHG	COMMENT
105.6583745 ± 0.00000024	MOHR 16	RVUE		2014 CODATA value

••• We do not use the following data for averages, fits, limits, etc. •••

105.6583715 ± 0.00000035	MOHR 12	RVUE		2010 CODATA value
105.6583668 ± 0.00000038	MOHR 08	RVUE		2006 CODATA value
105.6583692 ± 0.00000094	MOHR 05	RVUE		2002 CODATA value
105.6583568 ± 0.00000052	MOHR 99	RVUE		1998 CODATA value
105.658353 ± 0.0000016	1 COHEN 87	RVUE		1986 CODATA value
105.658386 ± 0.0000044	2 MARIAM 82	CNTR +		
105.65836 ± 0.00026	3 CROWE 72	CNTR		
105.65865 ± 0.00044	4 CRANE 71	CNTR		

<sup>1</sup>Converted to MeV using the 1998 CODATA value of the conversion constant, 931.494013 ± 0.000037 MeV/u.  
<sup>2</sup>MARIAM 82 give m<sub>μ</sub>/m<sub>e</sub> = 206.768259(62).  
<sup>3</sup>CROWE 72 give m<sub>μ</sub>/m<sub>e</sub> = 206.7682(5).  
<sup>4</sup>CRANE 71 give m<sub>μ</sub>/m<sub>e</sub> = 206.76878(85).

### μ MEAN LIFE τ

Measurements with an error > 0.001 × 10<sup>-6</sup> s have been omitted.

VALUE (10 <sup>-6</sup> s)	DOCUMENT ID	TECN	CHG	COMMENT
2.1969811 ± 0.0000022 OUR AVERAGE				
2.1969803 ± 0.0000021 ± 0.00000071	TISHCHENKO 13	CNTR +		Surface μ <sup>+</sup> at PSI
2.197083 ± 0.000032 ± 0.000015	BARCZYK 08	CNTR +		Muons from π <sup>+</sup> decay at rest
2.197013 ± 0.000021 ± 0.000011	CHITWOOD 07	CNTR +		Surface μ <sup>+</sup> at PSI
2.197078 ± 0.000073	BARDIN 84	CNTR +		
2.197025 ± 0.000155	BARDIN 84	CNTR -		
2.19695 ± 0.000006	GIOVANNETTI 84	CNTR +		
2.19711 ± 0.000008	BALANDIN 74	CNTR +		
2.1973 ± 0.0003	DUCLOS 73	CNTR +		

••• We do not use the following data for averages, fits, limits, etc. •••

2.1969803 ± 0.0000022	WEBBER 11	CNTR +		Surface μ <sup>+</sup> at PSI
-----------------------	-----------	--------	--	-------------------------------

<sup>1</sup>TISHCHENKO 13 uses 1.6 × 10<sup>12</sup> μ<sup>+</sup> events and supersedes WEBBER 11.

### τ<sub>μ<sup>+</sup></sub>/τ<sub>μ<sup>-</sup></sub> MEAN LIFE RATIO

A test of CPT invariance.

VALUE	DOCUMENT ID	TECN	COMMENT
1.000024 ± 0.000078	BARDIN 84	CNTR	

••• We do not use the following data for averages, fits, limits, etc. •••

1.0008 ± 0.0010	BAILEY	79	CNTR	Storage ring
1.000 ± 0.001	MEYER	63	CNTR	Mean life $\mu^+ / \mu^-$

$$(\tau_{\mu^+} - \tau_{\mu^-}) / \tau_{\text{average}}$$

A test of *CPT* invariance. Calculated from the mean-life ratio, above.

VALUE	DOCUMENT ID
$(2 \pm 8) \times 10^{-5}$	OUR EVALUATION

$\mu/p$  MAGNETIC MOMENT RATIO

This ratio is used to obtain a precise value of the muon mass and to reduce experimental muon Larmor frequency measurements to the muon magnetic moment anomaly. Measurements with an error > 0.00001 have been omitted. By convention, the minus sign on this ratio is omitted. CODATA values were fitted using their selection of data, plus other data from multiparameter fits.

VALUE	DOCUMENT ID	TECN	CHG	COMMENT
<b>3.183345142 ± 0.000000071</b>	MOHR	16	RVUE	2014 CODATA value
••• We do not use the following data for averages, fits, limits, etc. •••				
3.183345107 ± 0.000000084	MOHR	12	RVUE	2010 CODATA value
3.183345137 ± 0.000000085	MOHR	08	RVUE	2006 CODATA value
3.183345118 ± 0.000000089	MOHR	05	RVUE	2002 CODATA value
3.18334513 ± 0.000000039	LIU	99	CNTR +	HFS in muonium
3.18334539 ± 0.000000010	MOHR	99	RVUE	1998 CODATA value
3.18334547 ± 0.000000047	COHEN	87	RVUE	1986 CODATA value
3.1833441 ± 0.00000017	KLEMPPT	82	CNTR +	Precession strob
3.1833461 ± 0.00000011	MARIAM	82	CNTR +	HFS splitting
3.1833448 ± 0.00000029	CAMANI	78	CNTR +	See KLEMPPT 82
3.1833403 ± 0.00000044	CASPERSON	77	CNTR +	HFS splitting
3.1833402 ± 0.00000072	COHEN	73	RVUE	1973 CODATA value
3.1833467 ± 0.00000082	CROWE	72	CNTR +	Precession phase

See the related review(s):  
 Muon Anomalous Magnetic Moment

$\mu$  MAGNETIC MOMENT ANOMALY

The parity-violating decay of muons in a storage ring is observed. The difference frequency  $\omega_3$  between the muon spin precession and the orbital angular frequency ( $e/m_\mu c$ )( $B$ ) is measured, as is the free proton NMR frequency  $\omega_p$ , thus determining the ratio  $R = \omega_3/\omega_p$ . Given the magnetic moment ratio  $\lambda = \mu_\mu/\mu_p$  (from hyperfine structure in muonium),  $(g-2)/2 = R/(\lambda-R)$ .

$$\mu_\mu/(e\hbar/2m_\mu) - 1 = (g_\mu - 2)/2$$

VALUE (units $10^{-10}$ )	DOCUMENT ID	TECN	CHG	COMMENT
<b>11659208.9 ± 5.4 ± 3.3</b>	<sup>1</sup> BENNETT	06	MUG2	Average $\mu^+$ and $\mu^-$
••• We do not use the following data for averages, fits, limits, etc. •••				
11659208 ± 6	BENNETT	04	MUG2	Average $\mu^+$ and $\mu^-$
11659214 ± 8 ± 3	BENNETT	04	MUG2 -	Storage ring
11659203 ± 6 ± 5	BENNETT	04	MUG2 +	Storage ring
11659204 ± 7 ± 5	BENNETT	02	MUG2 +	Storage ring
11659202 ± 14 ± 6	BROWN	01	MUG2 +	Storage ring
11659191 ± 59	BROWN	00	MUG2 +	
11659100 ± 110	<sup>2</sup> BAILEY	79	CNTR +	Storage ring
11659360 ± 120	<sup>2</sup> BAILEY	79	CNTR -	Storage ring
11659230 ± 85	<sup>2</sup> BAILEY	79	CNTR ±	Storage ring
11620000 ± 5000	CHARPAK	62	CNTR +	

<sup>1</sup> BENNETT 06 reports  $(g_\mu - 2)/2 = (11659208.0 \pm 5.4 \pm 3.3) \times 10^{-10}$ . We rescaled this value using  $\mu/p$  magnetic moment ratio of 3.183345137(85) from MOHR 08.  
<sup>2</sup> BAILEY 79 values recalculated by HUGHES 99 using the COHEN 87  $\mu/p$  magnetic moment. The improved MOHR 99 value does not change the result.

$$(g_{\mu^+} - g_{\mu^-}) / g_{\text{average}}$$

A test of *CPT* invariance.

VALUE (units $10^{-8}$ )	DOCUMENT ID	TECN
<b>-0.11 ± 0.12</b>	BENNETT	04 MUG2
••• We do not use the following data for averages, fits, limits, etc. •••		
-2.6 ± 1.6	BAILEY	79 CNTR

$\mu$  ELECTRIC DIPOLE MOMENT (d)

A nonzero value is forbidden by both *T* invariance and *P* invariance.

VALUE ( $10^{-19}$ e cm)	CL%	DOCUMENT ID	TECN	CHG	COMMENT
< 1.8	95	<sup>1</sup> BENNETT	09	MUG2 ±	Storage ring

••• We do not use the following data for averages, fits, limits, etc. •••

-0.1 ± 1.0	<sup>2</sup> BENNETT	09	MUG2 +	Storage ring
-0.1 ± 0.7	<sup>3</sup> BENNETT	09	MUG2 -	Storage ring
-3.7 ± 3.4	<sup>4</sup> BAILEY	78	CNTR ±	Storage ring
8.6 ± 4.5	BAILEY	78	CNTR +	Storage ring
0.8 ± 4.3	BAILEY	78	CNTR -	Storage ring

<sup>1</sup> This is the combination of the two BENNETT 09 measurements quoted here separately for  $\mu^+$  and  $\mu^-$ . The result is also presented as a measurement of  $(0.0 \pm 0.9) \times 10^{-19}$  e cm.  
<sup>2</sup> Also reported as the limit of  $|d(\mu^+)| < 2.1 \times 10^{-19}$  e cm at 95% CL.  
<sup>3</sup> Also reported as the limit of  $|d(\mu^-)| < 1.5 \times 10^{-19}$  e cm at 95% CL.  
<sup>4</sup> This is the combination of the two BAILEY 78 results quoted here separately for  $\mu^+$  and  $\mu^-$ . BAILEY 78 uses the convention  $d = 1/2 \cdot (d_{\mu^+} - d_{\mu^-})$  and reports  $3.7 \pm 3.4$ . We convert their result to use the same convention as BENNETT 09.

MUON-ELECTRON CHARGE RATIO ANOMALY  $q_{\mu^+}/q_{e^-} - 1$

VALUE	DOCUMENT ID	TECN	CHG	COMMENT
<b>(1.1 ± 2.1) × 10<sup>-9</sup></b>	<sup>1</sup> MEYER	00	CNTR +	1s-2s muonium interval
••• We do not use the following data for averages, fits, limits, etc. •••				
	<sup>1</sup> MEYER	00		measure the 1s-2s muonium interval, and then interpret the result in terms of muon-electron charge ratio $q_{\mu^+}/q_{e^-}$ .

$\mu^-$  DECAY MODES

$\mu^+$  modes are charge conjugates of the modes below.

Mode	Fraction ( $\Gamma_i/\Gamma$ )	Confidence level
$\Gamma_1$ $e^- \bar{\nu}_e \nu_\mu$	$\approx 100\%$	
$\Gamma_2$ $e^- \bar{\nu}_e \nu_\mu \gamma$	[a] $(6.0 \pm 0.5) \times 10^{-8}$	
$\Gamma_3$ $e^- \bar{\nu}_e \nu_\mu e^+ e^-$	[b] $(3.4 \pm 0.4) \times 10^{-5}$	

Lepton Family number (LF) violating modes

$\Gamma_i$	Mode	LF	Value	%	90%
$\Gamma_4$	$e^- \nu_e \bar{\nu}_\mu$	LF	[c] < 1.2	%	90%
$\Gamma_5$	$e^- \gamma$	LF	< 4.2	$\times 10^{-13}$	90%
$\Gamma_6$	$e^- e^+ e^-$	LF	< 1.0	$\times 10^{-12}$	90%
$\Gamma_7$	$e^- 2\gamma$	LF	< 7.2	$\times 10^{-11}$	90%

[a] This only includes events with energy of  $e > 45$  MeV and energy of  $\gamma > 40$  MeV. Since the  $e^- \bar{\nu}_e \nu_\mu$  and  $e^- \bar{\nu}_e \nu_\mu \gamma$  modes cannot be clearly separated, we regard the latter mode as a subset of the former.

[b] See the Particle Listings below for the energy limits used in this measurement.

[c] A test of additive vs. multiplicative lepton family number conservation.

$\mu^-$  BRANCHING RATIOS

$\Gamma(e^- \bar{\nu}_e \nu_\mu \gamma) / \Gamma_{\text{total}}$	$\Gamma_2/\Gamma$			
<b>VALUE (units <math>10^{-8}</math>)</b>	<b>EVTS</b>	<b>DOCUMENT ID</b>	<b>TECN</b>	<b>COMMENT</b>
<b><math>6.03 \pm 0.14 \pm 0.53</math></b>	13k	<sup>1</sup> BALDINI	16A	SPEC $\gamma$ KE > 40 MeV
••• We do not use the following data for averages, fits, limits, etc. •••				
$(3.3 \pm 1.3) \times 10^{-3}$	862	BOGART	67	CNTR $\gamma$ KE > 14.5 MeV
$(1.4 \pm 0.4) \times 10^{-2}$		CRITTENDEN	61	CNTR $\gamma$ KE > 20 MeV
		CRITTENDEN	61	CNTR $\gamma$ KE > 10 MeV
	27	ASHKIN	59	CNTR

<sup>1</sup> BALDINI 16 measurement refers to  $\mu^+ \rightarrow e^+ \nu \bar{\nu} \gamma$  decay and requires energy of  $e^+ > 45$  MeV and energy  $\gamma > 40$  MeV.

$\Gamma(e^- \bar{\nu}_e \nu_\mu e^+ e^-) / \Gamma_{\text{total}}$	$\Gamma_3/\Gamma$				
<b>VALUE (units <math>10^{-5}</math>)</b>	<b>EVTS</b>	<b>DOCUMENT ID</b>	<b>TECN</b>	<b>CHG</b>	<b>COMMENT</b>
<b><math>3.4 \pm 0.2 \pm 0.3</math></b>	7443	<sup>1</sup> BERTL	85	SPEC +	SINDRUM
••• We do not use the following data for averages, fits, limits, etc. •••					
2.2 ± 1.5	7	<sup>2</sup> CRITTENDEN	61	HLBC +	$E(e^+ e^-) > 10$ MeV
2	1	<sup>3</sup> GUREVICH	60	EMUL +	
1.5 ± 1.0	3	<sup>4</sup> LEE	59	HBC +	

<sup>1</sup> BERTL 85 has transverse momentum cut  $p_T > 17$  MeV/c. Systematic error was increased by us.

<sup>2</sup> CRITTENDEN 61 count only those decays where total energy of either ( $e^+$ ,  $e^-$ ) combination is >10 MeV.

<sup>3</sup> GUREVICH 60 interpret their event as either virtual or real photon conversion.  $e^+$  and  $e^-$  energies not measured.

<sup>4</sup> In the three LEE 59 events, the sum of energies  $E(e^+) + E(e^-) + E(e^+)$  was 51 MeV, 55 MeV, and 33 MeV.

$\Gamma(e^- \nu_e \bar{\nu}_\mu) / \Gamma_{\text{total}}$	$\Gamma_4/\Gamma$				
<b>VALUE</b>	<b>CL%</b>	<b>DOCUMENT ID</b>	<b>TECN</b>	<b>CHG</b>	<b>COMMENT</b>
< 0.012	90	<sup>1</sup> FREEDMAN	93	CNTR +	$\nu$ oscillation search

Forbidden by the additive conservation law for lepton family number. A multiplicative law predicts this branching ratio to be 1/2. For a review see NEMETHY 81.

## Lepton Particle Listings

 $\mu$ 

• • • We do not use the following data for averages, fits, limits, etc. • • •

VALUE	CL%	DOCUMENT ID	TECN	CHG	COMMENT
< 0.018	90	KRAKAUER 91B	CALO	+	
< 0.05	90	<sup>2</sup> BERGSMA 83	CALO		$\bar{\nu}_\mu e \rightarrow \mu^- \bar{\nu}_e$
< 0.09	90	JONKER 80	CALO		See BERGSMA 83
-0.001 ± 0.061		WILLIS 80	CNTR	+	
0.13 ± 0.15		BLIETSCHAU 78	HLBC	±	Avg. of 4 values
< 0.25	90	EICHTEN 73	HLBC	+	

<sup>1</sup> FREEDMAN 93 limit on  $\bar{\nu}_e$  observation is here interpreted as a limit on lepton family number violation.

<sup>2</sup> BERGSMA 83 gives a limit on the inverse muon decay cross-section ratio  $\sigma(\bar{\nu}_\mu e^- \rightarrow \mu^- \bar{\nu}_e) / \sigma(\nu_\mu e^- \rightarrow \mu^- \nu_e)$ , which is essentially equivalent to  $\Gamma(e^- \nu_e \bar{\nu}_\mu) / \Gamma_{\text{total}}$  for small values like that quoted.

$\Gamma(e^- \gamma) / \Gamma_{\text{total}}$   $\Gamma_5 / \Gamma$

Forbidden by lepton family number conservation.

VALUE (units $10^{-11}$ )	CL%	DOCUMENT ID	TECN	CHG	COMMENT
< 0.042	90	BALDINI 16	SPEC	+	MEG at PSI
< 0.057	90	ADAM 13B	SPEC	+	MEG at PSI
< 0.24	90	ADAM 11	SPEC	+	MEG at PSI
< 2.8	90	ADAM 10	SPEC	+	MEG at PSI
< 1.2	90	AHMED 02	SPEC	+	MEGA
< 1.2	90	BROOKS 99	SPEC	+	LAMPF
< 4.9	90	BOLTON 88	CBOX	+	LAMPF
< 100	90	AZUELOS 83	CNTR	+	TRIUMF
< 17	90	KINNISON 82	SPEC	+	LAMPF
< 100	90	SCHAAF 80	ELEC	+	SIN

$\Gamma(e^- e^+ e^-) / \Gamma_{\text{total}}$   $\Gamma_6 / \Gamma$

Forbidden by lepton family number conservation.

VALUE (units $10^{-12}$ )	CL%	DOCUMENT ID	TECN	CHG	COMMENT
< 1.0	90	<sup>1</sup> BELLGARDT 88	SPEC	+	SINDRUM
< 36	90	BARANOV 91	SPEC	+	ARES
< 35	90	BOLTON 88	CBOX	+	LAMPF
< 2.4	90	<sup>1</sup> BERTL 85	SPEC	+	SINDRUM
< 160	90	<sup>1</sup> BERTL 84	SPEC	+	SINDRUM
< 130	90	<sup>1</sup> BOLTON 84	CNTR		LAMPF

<sup>1</sup> These experiments assume a constant matrix element.

$\Gamma(e^- 2\gamma) / \Gamma_{\text{total}}$   $\Gamma_7 / \Gamma$

Forbidden by lepton family number conservation.

VALUE (units $10^{-11}$ )	CL%	DOCUMENT ID	TECN	CHG	COMMENT
< 7.2	90	BOLTON 88	CBOX	+	LAMPF
< 840	90	<sup>1</sup> AZUELOS 83	CNTR	+	TRIUMF
< 5000	90	<sup>2</sup> BOWMAN 78	CNTR		DEPOMMIER 77 data

<sup>1</sup> AZUELOS 83 uses the phase space distribution of BOWMAN 78.

<sup>2</sup> BOWMAN 78 assumes an interaction Lagrangian local on the scale of the inverse  $\mu$  mass.

LIMIT ON  $\mu^- \rightarrow e^-$  CONVERSION

Forbidden by lepton family number conservation.

$\sigma(\mu^- 32S \rightarrow e^- 32S) / \sigma(\mu^- 32S \rightarrow \nu_\mu 32P^*)$

VALUE	CL%	DOCUMENT ID	TECN	COMMENT
< $7 \times 10^{-11}$	90	BADERT...	80	STRC SIN
< $4 \times 10^{-10}$	90	BADERT...	77	STRC SIN

$\sigma(\mu^- Cu \rightarrow e^- Cu) / \sigma(\mu^- Cu \rightarrow \text{capture})$

VALUE	CL%	DOCUMENT ID	TECN	COMMENT
< $1.6 \times 10^{-8}$	90	BRYMAN 72	SPEC	

$\sigma(\mu^- Ti \rightarrow e^- Ti) / \sigma(\mu^- Ti \rightarrow \text{capture})$

VALUE	CL%	DOCUMENT ID	TECN	COMMENT
< $4.3 \times 10^{-12}$	90	<sup>1</sup> DOHMEN 93	SPEC	SINDRUM II
< $4.6 \times 10^{-12}$	90	AHMAD 88	TPC	TRIUMF
< $1.6 \times 10^{-11}$	90	BRYMAN 85	TPC	TRIUMF

<sup>1</sup> DOHMEN 93 assumes  $\mu^- \rightarrow e^-$  conversion leaves the nucleus in its ground state, a process enhanced by coherence and expected to dominate.

$\sigma(\mu^- Pb \rightarrow e^- Pb) / \sigma(\mu^- Pb \rightarrow \text{capture})$

VALUE	CL%	DOCUMENT ID	TECN	COMMENT
< $4.6 \times 10^{-11}$	90	HONECKER 96	SPEC	SINDRUM II
< $4.9 \times 10^{-10}$	90	AHMAD 88	TPC	TRIUMF

$\sigma(\mu^- Au \rightarrow e^- Au) / \sigma(\mu^- Au \rightarrow \text{capture})$

VALUE	CL%	DOCUMENT ID	TECN	CHG	COMMENT
< $7 \times 10^{-13}$	90	BERTL 06	SPEC	-	SINDRUM II

LIMIT ON  $\mu^- \rightarrow e^+$  CONVERSION

Forbidden by total lepton number conservation.

$\sigma(\mu^- 32S \rightarrow e^+ 32Si^*) / \sigma(\mu^- 32S \rightarrow \nu_\mu 32P^*)$

VALUE	CL%	DOCUMENT ID	TECN	COMMENT
< $9 \times 10^{-10}$	90	BADERT...	80	STRC SIN
< $1.5 \times 10^{-9}$	90	BADERT...	78	STRC SIN

$\sigma(\mu^- 127I \rightarrow e^+ 127Sb^*) / \sigma(\mu^- 127I \rightarrow \text{anything})$

VALUE	CL%	DOCUMENT ID	TECN	COMMENT
< $3 \times 10^{-10}$	90	<sup>1</sup> ABELA 80	CNTR	Radiochemical tech.

<sup>1</sup> ABELA 80 is upper limit for  $\mu^- e^+$  conversion leading to particle-stable states of <sup>127</sup>Sb. Limit for total conversion rate is higher by a factor less than 4 (G. Backenstoss, private communication).

$\sigma(\mu^- Cu \rightarrow e^+ Co) / \sigma(\mu^- Cu \rightarrow \nu_\mu Ni)$

VALUE	CL%	DOCUMENT ID	TECN	COMMENT
< $2.6 \times 10^{-8}$	90	BRYMAN 72	SPEC	
< $2.2 \times 10^{-7}$	90	CONFORTO 62	OSPK	

$\sigma(\mu^- Ti \rightarrow e^+ Ca) / \sigma(\mu^- Ti \rightarrow \text{capture})$

VALUE	CL%	EVTS	DOCUMENT ID	TECN	CHG	COMMENT
< $3.6 \times 10^{-11}$	90	1	<sup>1,2</sup> KAULARD 98	SPEC	-	SINDRUM II
< $1.7 \times 10^{-12}$	90	1	<sup>2,3</sup> KAULARD 98	SPEC	-	SINDRUM II
< $4.3 \times 10^{-12}$	90		<sup>3</sup> DOHMEN 93	SPEC		SINDRUM II
< $8.9 \times 10^{-11}$	90		<sup>1</sup> DOHMEN 93	SPEC		SINDRUM II
< $1.7 \times 10^{-10}$	90		<sup>4</sup> AHMAD 88	TPC		TRIUMF

<sup>1</sup> This limit assumes a giant resonance excitation of the daughter Ca nucleus (mean energy and width both 20 MeV).

<sup>2</sup> KAULARD 98 obtained these same limits using the unified classical analysis of FELDMAN 98.

<sup>3</sup> This limit assumes the daughter Ca nucleus is left in the ground state. However, the probability of this is unknown.

<sup>4</sup> Assuming a giant-resonance-excitation model.

LIMIT ON MUONIUM  $\rightarrow$  ANTIMUONIUM CONVERSION

Forbidden by lepton family number conservation.

$R_g = G_C / G_F$

The effective Lagrangian for the  $\mu^+ e^- \rightarrow \mu^- e^+$  conversion is assumed to be

$$\mathcal{L} = 2^{-1/2} G_C [\bar{\nu}_\mu \gamma_\lambda (1 - \gamma_5) \psi_e] [\bar{\psi}_\mu \gamma_\lambda (1 - \gamma_5) \psi_e] + \text{h.c.}$$

The experimental result is then an upper limit on  $G_C / G_F$ , where  $G_F$  is the Fermi coupling constant.

$\sigma(\mu^- 32S \rightarrow e^- 32S) / \sigma(\mu^- 32S \rightarrow \nu_\mu 32P^*)$

VALUE	CL%	EVTS	DOCUMENT ID	TECN	CHG	COMMENT
< 0.0030	90	1	<sup>1</sup> WILLMANN 99	SPEC	+	$\mu^+$ at 26 GeV/c
< 0.14	90	1	<sup>2</sup> GORDEEV 97	SPEC	+	JINR phasotron
< 0.018	90	0	<sup>3</sup> ABELA 96	SPEC	+	$\mu^+$ at 24 MeV
< 6.9	90		NI 93	CBOX		LAMPF
< 0.16	90		MATTHIAS 91	SPEC		LAMPF
< 0.29	90		HUBER 90B	CNTR		TRIUMF
< 20	95		BEER 86	CNTR		TRIUMF
< 42	95		MARSHALL 82	CNTR		

<sup>1</sup> WILLMANN 99 quote both probability  $P_{M\bar{M}} < 8.3 \times 10^{-11}$  at 90%CL in a 0.1 T field and  $R_g = G_C / G_F$ .

<sup>2</sup> GORDEEV 97 quote limits on both  $f = G_{MM} / G_F$  and the probability  $W_{MM} < 4.7 \times 10^{-7}$  (90% CL).

<sup>3</sup> ABELA 96 quote both probability  $P_{M\bar{M}} < 8 \times 10^{-9}$  at 90% CL and  $R_g = G_C / G_F$ .

See the related review(s):

[Muon Decay Parameters](#)

 $\mu$  DECAY PARAMETERS

$\rho$  PARAMETER

(V-A) theory predicts  $\rho = 0.75$ .

VALUE	CL%	EVTS	DOCUMENT ID	TECN	CHG	COMMENT	
<b>0.74979 ± 0.00026 OUR AVERAGE</b>							
0.74977 ± 0.00012 ± 0.00023			<sup>1</sup> BAYES	11	TWST	+	Surface $\mu^+$
0.7518 ± 0.0026			DERENZO	69	RVUE		

- • • We do not use the following data for averages, fits, limits, etc. • • •

0.75014 ± 0.00017 ± 0.00045	2	MACDONALD	08	TWST	+	Surface $\mu^+$	
0.75080 ± 0.00032 ± 0.00100	6G	3	MUSSER	05	TWST	+	Surface $\mu^+$
0.72 ± 0.06 ± 0.08			4	AMORUSO	04	ICAR	Liquid Ar TPC
0.762 ± 0.008	170k		4	FRYBERGER	68	ASPK	+ 25-53 MeV $e^+$
0.760 ± 0.009	280k		4	SHERWOOD	67	ASPK	+ 25-53 MeV $e^+$
0.7503 ± 0.0026	800k		4	PEOPLES	66	ASPK	+ 20-53 MeV $e^+$

- <sup>1</sup> The quoted systematic error includes a contribution of 0.00013 (added in quadrature) from uncertainties on radiative corrections and on the Michel parameter  $\eta$ .
- <sup>2</sup> The quoted systematic error includes a contribution of 0.00011 (added in quadrature) from the dependence on the Michel parameter  $\eta$ .
- <sup>3</sup> The quoted systematic error includes a contribution of 0.00023 (added in quadrature) from the dependence on the Michel parameter  $\eta$ .
- <sup>4</sup>  $\eta$  constrained = 0. These values incorporated into a two parameter fit to  $\rho$  and  $\eta$  by DERENZO 69.

**$\eta$  PARAMETER**

(V-A) theory predicts  $\eta = 0$ .

VALUE	EVTS	DOCUMENT ID	TECN	CHG	COMMENT
<b>0.057 ± 0.034 OUR AVERAGE</b>					
0.071 ± 0.037 ± 0.005	30M	DANNEBERG	05	CNTR	+ 7-53 MeV $e^+$
0.011 ± 0.081 ± 0.026	5.3M	<sup>1</sup> BURKARD	85B	CNTR	+ 9-53 MeV $e^+$
-0.12 ± 0.21	6346	DERENZO	69	HBC	+ 1.6-6.8 MeV $e^+$
-0.0021 ± 0.0070 ± 0.0010	30M	<sup>2</sup> DANNEBERG	05	CNTR	+ 7-53 MeV $e^+$
-0.012 ± 0.015 ± 0.003	5.3M	<sup>2</sup> BURKARD	85B	CNTR	+ 9-53 MeV $e^+$
-0.007 ± 0.013	5.3M	<sup>3</sup> BURKARD	85B	FIT	+ 9-53 MeV $e^+$
-0.7 ± 0.5	170k	<sup>4</sup> FRYBERGER	68	ASPK	+ 25-53 MeV $e^+$
-0.7 ± 0.6	280k	<sup>4</sup> SHERWOOD	67	ASPK	+ 25-53 MeV $e^+$
0.05 ± 0.5	800k	<sup>4</sup> PEOPLES	66	ASPK	+ 20-53 MeV $e^+$
-2.0 ± 0.9	9213	<sup>5</sup> PLANO	60	HBC	+ Whole spectrum

- • • We do not use the following data for averages, fits, limits, etc. • • •
- <sup>1</sup> Previously we used the global fit result from BURKARD 85B in OUR AVERAGE, we now only include their actual measurement.
- <sup>2</sup>  $\alpha = \alpha' = 0$  assumed.
- <sup>3</sup> Global fit to all measured parameters. The fit correlation coefficients are given in BURKARD 85B.
- <sup>4</sup>  $\rho$  constrained = 0.75.
- <sup>5</sup> Two parameter fit to  $\rho$  and  $\eta$ ; PLANO 60 discounts value for  $\eta$ .

**$\delta$  PARAMETER**

(V-A) theory predicts  $\delta = 0.75$ .

VALUE	EVTS	DOCUMENT ID	TECN	CHG	COMMENT
<b>0.75047 ± 0.00034 OUR AVERAGE</b>					
0.75049 ± 0.00021 ± 0.00027		<sup>1</sup> BAYES	11	TWST	+ Surface $\mu^+$
0.7486 ± 0.0026 ± 0.0028		<sup>2</sup> BALKE	88	SPEC	+ Surface $\mu^+$
0.75067 ± 0.00030 ± 0.00067		MACDONALD	08	TWST	+ Surface $\mu^+$
0.74964 ± 0.00066 ± 0.00112	6G	GAPONENKO	05	TWST	+ Surface $\mu^+$
		<sup>3</sup> VOSSLER	69		
0.752 ± 0.009	490k	FRYBERGER	68	ASPK	+ 25-53 MeV $e^+$
0.782 ± 0.031		KRUGER	61		
0.78 ± 0.05	8354	PLANO	60	HBC	+ Whole spectrum

- • • We do not use the following data for averages, fits, limits, etc. • • •
- <sup>1</sup> The quoted systematic error includes a contribution of 0.00006 (added in quadrature) from uncertainties on radiative corrections and on the Michel parameter  $\eta$ .
- <sup>2</sup> BALKE 88 uses  $\rho = 0.752 \pm 0.003$ .
- <sup>3</sup> VOSSLER 69 has measured the asymmetry below 10 MeV. See comments about radiative corrections in VOSSLER 69.

**$(\xi \text{ PARAMETER}) \times (\mu \text{ LONGITUDINAL POLARIZATION})$**

(V-A) theory predicts  $\xi = 1$ , longitudinal polarization = 1.

VALUE	DOCUMENT ID	TECN	CHG	COMMENT
<b>1.0009 ± 0.0016 OUR AVERAGE</b>				
1.00084 ± 0.00029 ± 0.00165 ± 0.00063	BUENO	11	TWST	Surface $\mu^+$ beam
1.0027 ± 0.0079 ± 0.0030	BELTRAMI	87	CNTR	SIN, $\pi$ decay in flight
1.0003 ± 0.0006 ± 0.0038	JAMIESON	06	TWST	+ surface $\mu^+$ beam
1.0013 ± 0.0030 ± 0.0053	<sup>1</sup> IMAZATO	92	SPEC	+ $K^+ \rightarrow \mu^+ \nu_\mu$
0.975 ± 0.015	AKHMANOV	68	EMUL	140 kG
0.975 ± 0.030	GUREVICH	64	EMUL	See AKHMANOV 68
0.903 ± 0.027	<sup>2</sup> ALI-ZADE	61	EMUL	+ 27 kG
0.93 ± 0.06	PLANO	60	HBC	+ 8.8 kG
0.97 ± 0.05	BARDON	59	CNTR	Bromoform target

- <sup>1</sup> The corresponding 90% confidence limit from IMAZATO 92 is  $|\xi P_\mu| > 0.990$ . This measurement is of  $K^+$  decay, not  $\pi^+$  decay, so we do not include it in an average, nor do we yet set up a separate data block for  $K$  results.
- <sup>2</sup> Depolarization by medium not known sufficiently well.

**$\xi \times (\mu \text{ LONGITUDINAL POLARIZATION}) \times \delta / \rho$**

VALUE	CL%	DOCUMENT ID	TECN	CHG	COMMENT
<b>1.00179 ± 0.00156 OUR AVERAGE</b>					
1.00179 ± 0.00156		<sup>1</sup> BAYES	11	TWST	+ Surface $\mu^+$ beam
>0.99682	90	<sup>2</sup> JODIDIO	86	SPEC	+ TRIUMF
>0.9966	90	<sup>3</sup> STOKER	85	SPEC	+ $\mu$ -spin rotation
>0.9959	90	CARR	83	SPEC	+ 11 kG

- • • We do not use the following data for averages, fits, limits, etc. • • •
- <sup>1</sup> BAYES 11 obtains the limit  $> 0.99909$  (90% CL) with the constraint that  $\xi \times (\mu \text{ LONGITUDINAL POLARIZATION}) \times \delta / \rho \leq 1.0$ .
- <sup>2</sup> JODIDIO 86 includes data from CARR 83 and STOKER 85. The value here is from the erratum.
- <sup>3</sup> STOKER 85 find  $(\xi P_\mu \delta / \rho) > 0.9955$  and  $> 0.9966$ , where the first limit is from new  $\mu$  spin-rotation data and the second is from combination with CARR 83 data. In V-A theory,  $(\delta / \rho) = 1.0$ .

**$\xi' = \text{LONGITUDINAL POLARIZATION OF } e^+$**

(V-A) theory predicts the longitudinal polarization =  $\pm 1$  for  $e^\pm$ , respectively. We have flipped the sign for  $e^-$  so our programs can average.

VALUE	EVTS	DOCUMENT ID	TECN	CHG	COMMENT
<b>1.00 ± 0.04 OUR AVERAGE</b>					
0.998 ± 0.045	1M	BURKARD	85	CNTR	+ Bhabha + annihil
0.89 ± 0.28	29k	SCHWARTZ	67	OSPK	- Moller scattering
0.94 ± 0.38		BLOOM	64	CNTR	+ Brems. transmiss.
1.04 ± 0.18		DUCLOS	64	CNTR	+ Bhabha scattering
1.05 ± 0.30		BUHLER	63	CNTR	+ Annihilation

**$\xi''$  PARAMETER**

VALUE	EVTS	DOCUMENT ID	TECN	CHG	COMMENT
<b>0.98 ± 0.04 OUR AVERAGE</b>					
0.981 ± 0.045 ± 0.003	3.87M	PRIEELS	14	CNTR	+ Bhabha + annihil
0.65 ± 0.36	326k	<sup>1</sup> BURKARD	85	CNTR	+ Bhabha + annihil

- <sup>1</sup> BURKARD 85 measure  $(\xi'' - \xi \xi') / \xi$  and set  $\xi = 1$ .

**TRANSVERSE  $e^+$  POLARIZATION IN PLANE OF  $\mu$  SPIN,  $e^+$  MOMENTUM**

VALUE (units $10^{-3}$ )	EVTS	DOCUMENT ID	TECN	CHG	COMMENT
<b>-2 ± 8 OUR AVERAGE</b>					
6.3 ± 7.7 ± 3.4	30M	DANNEBERG	05	CNTR	+ 7-53 MeV $e^+$
16 ± 21 ± 10	5.3M	BURKARD	85B	CNTR	+ Annihil 9-53 MeV

**TRANSVERSE  $e^+$  POLARIZATION NORMAL TO PLANE OF  $\mu$  SPIN,  $e^+$  MOMENTUM**

Zero if  $T$  invariance holds.

VALUE (units $10^{-3}$ )	EVTS	DOCUMENT ID	TECN	CHG	COMMENT
<b>-2 ± 8 OUR AVERAGE</b>					
-3.7 ± 7.7 ± 3.4	30M	DANNEBERG	05	CNTR	+ 7-53 MeV $e^+$
7 ± 22 ± 7	5.3M	BURKARD	85B	CNTR	+ Annihil 9-53 MeV

**$\alpha/A$**

VALUE (units $10^{-3}$ )	EVTS	DOCUMENT ID	TECN	CHG	COMMENT
<b>0.4 ± 4.3</b>					
15 ± 50 ± 14	5.3M	BURKARD	85B	CNTR	+ 9-53 MeV $e^+$

- • • We do not use the following data for averages, fits, limits, etc. • • •
- <sup>1</sup> Global fit to all measured parameters. Correlation coefficients are given in BURKARD 85B.

**$\alpha'/A$**

Zero if  $T$  invariance holds.

VALUE (units $10^{-3}$ )	EVTS	DOCUMENT ID	TECN	CHG	COMMENT
<b>-10 ± 20 OUR AVERAGE</b>					
-3.4 ± 21.3 ± 4.9	30M	DANNEBERG	05	CNTR	+ 7-53 MeV $e^+$
-47 ± 50 ± 14	5.3M	<sup>1</sup> BURKARD	85B	CNTR	+ 9-53 MeV $e^+$
-0.2 ± 4.3		<sup>2</sup> BURKARD	85B	FIT	

- • • We do not use the following data for averages, fits, limits, etc. • • •
- <sup>1</sup> Previously we used the global fit result from BURKARD 85B in OUR AVERAGE, we now only include their actual measurement. BURKARD 85B measure  $e^+$  polarizations  $P_{T1}$  and  $P_{T2}$  versus  $e^+$  energy.
- <sup>2</sup> Global fit to all measured parameters. The fit correlation coefficients are given in BURKARD 85B.

**$\beta/A$**

VALUE (units $10^{-3}$ )	EVTS	DOCUMENT ID	TECN	CHG	COMMENT
<b>3.9 ± 6.2</b>					
2 ± 17 ± 6	5.3M	BURKARD	85B	CNTR	+ 9-53 MeV $e^+$

- • • We do not use the following data for averages, fits, limits, etc. • • •
- <sup>1</sup> Global fit to all measured parameters. The fit correlation coefficients are given in BURKARD 85B.

**$\beta'/A$**

Zero if  $T$  invariance holds.

VALUE (units $10^{-3}$ )	EVTS	DOCUMENT ID	TECN	CHG	COMMENT
<b>2 ± 7 OUR AVERAGE</b>					
-0.5 ± 7.8 ± 1.8	30M	DANNEBERG	05	CNTR	+ 7-53 MeV $e^+$
17 ± 17 ± 6	5.3M	<sup>1</sup> BURKARD	85B	CNTR	+ 9-53 MeV $e^+$
-1.3 ± 3.5 ± 0.6	30M	<sup>2</sup> DANNEBERG	05	CNTR	+ 7-53 MeV $e^+$
1.5 ± 6.3		<sup>3</sup> BURKARD	85B	FIT	

- • • We do not use the following data for averages, fits, limits, etc. • • •
- <sup>1</sup> Previously we used the global fit result from BURKARD 85B in OUR AVERAGE, we now only include their actual measurement. BURKARD 85B measure  $e^+$  polarizations  $P_{T1}$  and  $P_{T2}$  versus  $e^+$  energy.
- <sup>2</sup>  $\alpha = \alpha' = 0$  assumed.
- <sup>3</sup> Global fit to all measured parameters. The fit correlation coefficients are given in BURKARD 85B.





1776.68 ± 0.12 ± 0.41	682k	<sup>2</sup> AUBERT	09AK BABR	423 fb <sup>-1</sup> , E <sub>cm</sub> <sup>ee</sup> =10.6 GeV
1776.81 <sup>+0.25</sup> <sub>-0.23</sub> ± 0.15	81	ANASHIN	07 KEDR	6.7 pb <sup>-1</sup> , E <sub>cm</sub> <sup>ee</sup> =3.54-3.78 GeV
1776.61 ± 0.13 ± 0.35		<sup>2</sup> BELOUS	07 BELL	414 fb <sup>-1</sup> , E <sub>cm</sub> <sup>ee</sup> =10.6 GeV
1775.1 ± 1.6 ± 1.0	13.3k	<sup>3</sup> ABBIENDI	00A OPAL	1990-1995 LEP runs
1778.2 ± 0.8 ± 1.2		ANASTASSOV	97 CLEO	E <sub>cm</sub> <sup>ee</sup> =10.6 GeV
1776.96 <sup>+0.18</sup> <sub>-0.21</sub> ± 0.25 ± 0.17	65	<sup>4</sup> BAI	96 BES	E <sub>cm</sub> <sup>ee</sup> =3.54-3.57 GeV
1776.3 ± 2.4 ± 1.4	11k	<sup>5</sup> ALBRECHT	92M ARG	E <sub>cm</sub> <sup>ee</sup> =9.4-10.6 GeV
1783 <sup>+3</sup> <sub>-4</sub>	692	<sup>6</sup> BACINO	78B DLCO	E <sub>cm</sub> <sup>ee</sup> =3.1-7.4 GeV

••• We do not use the following data for averages, fits, limits, etc. •••  
 1777.8 ± 0.7 ± 1.7 35k <sup>7</sup>BALEST 93 CLEO Repl. by ANASTASSOV 97  
 1776.9<sup>+0.4</sup><sub>-0.5</sub> ± 0.2 14 <sup>8</sup>BAI 92 BES Repl. by BAI 96

- 1 ABLIKIM 14D fit  $\sigma(e^+e^- \rightarrow \tau^+\tau^-)$  at different energies near threshold.
- 2 AUBERT 09AK and BELOUS 07 fit  $\tau$  pseudomass spectrum in  $\tau \rightarrow \pi^+\pi^-\nu_\tau$  decays. Result assumes  $m_{\nu_\tau} = 0$ .
- 3 ABBIENDI 00A fit  $\tau$  pseudomass spectrum in  $\tau \rightarrow \pi^\pm \leq 2\pi^0 \nu_\tau$  and  $\tau \rightarrow \pi^\pm \pi^+ \pi^- \leq 1\pi^0 \nu_\tau$  decays. Result assumes  $m_{\nu_\tau} = 0$ .
- 4 BAI 96 fit  $\sigma(e^+e^- \rightarrow \tau^+\tau^-)$  at different energies near threshold.
- 5 ALBRECHT 92M fit  $\tau$  pseudomass spectrum in  $\tau^- \rightarrow 2\pi^-\pi^+ \nu_\tau$  decays. Result assumes  $m_{\nu_\tau} = 0$ .
- 6 BACINO 78B value comes from  $e^\pm X^\mp$  threshold. Published mass 1782 MeV increased by 1 MeV using the high precision  $\psi(2S)$  mass measurement of ZHOLENTZ 80 to eliminate the absolute SPEAR energy calibration uncertainty.
- 7 BALEST 93 fit spectra of minimum kinematically allowed  $\tau$  mass in events of the type  $e^+e^- \rightarrow \tau^+\tau^- \rightarrow (\pi^+ n\pi^0 \nu_\tau)(\pi^- m\pi^0 \nu_\tau)$ ,  $n \leq 2$ ,  $m \leq 2$ ,  $1 \leq n+m \leq 3$ . If  $m_{\nu_\tau} \neq 0$ , result increases by  $(m_{\nu_\tau}^2/1100)$  MeV.
- 8 BAI 92 fit  $\sigma(e^+e^- \rightarrow \tau^+\tau^-)$  near threshold using  $e\mu$  events.

$(m_{\tau^+} - m_{\tau^-})/m_{\text{average}}$

A test of CPT invariance.

VALUE	CL%	DOCUMENT ID	TECN	COMMENT
<b>&lt;2.8 × 10<sup>-4</sup></b>	90	BELOUS	07 BELL	414 fb <sup>-1</sup> , E <sub>cm</sub> <sup>ee</sup> =10.6 GeV
••• We do not use the following data for averages, fits, limits, etc. •••				
<5.5 × 10 <sup>-4</sup>	90	<sup>1</sup> AUBERT	09AK BABR	423 fb <sup>-1</sup> , E <sub>cm</sub> <sup>ee</sup> =10.6 GeV
<3.0 × 10 <sup>-3</sup>	90	ABBIENDI	00A OPAL	1990-1995 LEP runs
<sup>1</sup> AUBERT 09AK quote both the listed upper limit and $(m_{\tau^+} - m_{\tau^-})/m_{\text{average}} = (-3.4 \pm 1.3 \pm 0.3) \times 10^{-4}$ .				

$\tau$  MEAN LIFE

VALUE (10 <sup>-15</sup> s)	EVTS	DOCUMENT ID	TECN	COMMENT
<b>290.3 ± 0.5 OUR AVERAGE</b>				
290.17 ± 0.53 ± 0.33	1.1M	BELOUS	14 BELL	711 fb <sup>-1</sup> , E <sub>cm</sub> <sup>ee</sup> =10.6 GeV
290.9 ± 1.4 ± 1.0		ABDALLAH	04T DLPH	1991-1995 LEP runs
293.2 ± 2.0 ± 1.5		ACCIARRI	00B L3	1991-1995 LEP runs
290.1 ± 1.5 ± 1.1		BARATE	97R ALEP	1989-1994 LEP runs
289.2 ± 1.7 ± 1.2		ALEXANDER	96E OPAL	1990-1994 LEP runs
289.0 ± 2.8 ± 4.0	57.4k	BALEST	96 CLEO	E <sub>cm</sub> <sup>ee</sup> =10.6 GeV
••• We do not use the following data for averages, fits, limits, etc. •••				
291.2 ± 2.0 ± 1.2		BARATE	97I ALEP	Repl. by BARATE 97R
291.4 ± 3.0		ABREU	96B DLPH	Repl. by ABDALLAH 04T
290.1 ± 4.0	34k	ACCIARRI	96K L3	Repl. by ACCIARRI 00B
297 ± 9 ± 5	1671	ABE	95Y SLD	1992-1993 SLC runs
304 ± 14 ± 7	4100	BATTLE	92 CLEO	E <sub>cm</sub> <sup>ee</sup> =10.6 GeV
301 ± 29	3780	KLEINWORT	89 JADE	E <sub>cm</sub> <sup>ee</sup> =35-46 GeV
288 ± 16 ± 17	807	AMIDEI	88 MRK2	E <sub>cm</sub> <sup>ee</sup> =29 GeV
306 ± 20 ± 14	695	BRAUNSCH...	88C TASS	E <sub>cm</sub> <sup>ee</sup> =36 GeV
299 ± 15 ± 10	1311	ABACHI	87C HRS	E <sub>cm</sub> <sup>ee</sup> =29 GeV
295 ± 14 ± 11	5696	ALBRECHT	87P ARG	E <sub>cm</sub> <sup>ee</sup> =9.3-10.6 GeV
309 ± 17 ± 7	3788	BAND	87B MAC	E <sub>cm</sub> <sup>ee</sup> =29 GeV
325 ± 14 ± 18	8470	BEBEK	87C CLEO	E <sub>cm</sub> <sup>ee</sup> =10.5 GeV
460 ± 190	102	FELDMAN	82 MRK2	E <sub>cm</sub> <sup>ee</sup> =29 GeV

$(\tau_+ - \tau_-)/\tau_{\text{average}}$

Test of CPT invariance.

VALUE	CL%	DOCUMENT ID	TECN	COMMENT
<b>&lt;7.0 × 10<sup>-3</sup></b>	90	<sup>1</sup> BELOUS	14 BELL	711 fb <sup>-1</sup> , E <sub>cm</sub> <sup>ee</sup> =10.6 GeV
<sup>1</sup> BELOUS 14 quote limit on the absolute value of the relative lifetime difference.				

$\tau$  MAGNETIC MOMENT ANOMALY

The  $q^2$  dependence is expected to be small providing no thresholds are nearby.

$\mu_\tau/(e\hbar/2m_\tau) - 1 = (g_\tau - 2)/2$

For a theoretical calculation  $[(g_\tau - 2)/2 = 117721(5) \times 10^{-8}]$ , see EIDELMAN 07.

VALUE	CL%	DOCUMENT ID	TECN	COMMENT
<b>&gt; -0.052 and &lt; 0.013 (CL = 95%) OUR LIMIT</b>				
> -0.052 and < 0.013	95	<sup>1</sup> ABDALLAH	04k DLPH	$e^+e^- \rightarrow e^+e^-\tau^+\tau^-$ at LEP2
••• We do not use the following data for averages, fits, limits, etc. •••				
<0.107	95	<sup>2</sup> ACHARD	04G L3	$e^+e^- \rightarrow e^+e^-\tau^+\tau^-$ at LEP2
> -0.007 and < 0.005	95	<sup>3</sup> GONZALEZ-S.	00 RVUE	$e^+e^- \rightarrow \tau^+\tau^-$ and $W \rightarrow \tau\nu_\tau$
> -0.052 and < 0.058	95	<sup>4</sup> ACCIARRI	98E L3	1991-1995 LEP runs
> -0.068 and < 0.065	95	<sup>5</sup> ACKERSTAFF	98N OPAL	1990-1995 LEP runs
> -0.004 and < 0.006	95	<sup>6</sup> ESCRIBANO	97 RVUE	$Z \rightarrow \tau^+\tau^-$ at LEP
<0.01	95	<sup>7</sup> ESCRIBANO	93 RVUE	$Z \rightarrow \tau^+\tau^-$ at LEP
<0.12	90	GRIFOLS	91 RVUE	$Z \rightarrow \tau\tau\gamma$ at LEP
<0.023	95	<sup>8</sup> SILVERMAN	83 RVUE	$e^+e^- \rightarrow \tau^+\tau^-$ at PETRA

- 1 ABDALLAH 04k limit is derived from  $e^+e^- \rightarrow e^+e^-\tau^+\tau^-$  total cross-section measurements at  $\sqrt{s}$  between 183 and 208 GeV. In addition to the limits, the authors also quote a value of  $-0.018 \pm 0.017$ .
- 2 ACHARD 04G limit is derived from  $e^+e^- \rightarrow e^+e^-\tau^+\tau^-$  total cross-section measurements at  $\sqrt{s}$  between 189 and 206 GeV, and is on the absolute value of the magnetic moment anomaly.
- 3 GONZALEZ-SPRINBERG 00 use data on tau lepton production at LEP1, SLC, and LEP2, and data from colliders and LEP2 to determine limits. Assume imaginary component is zero.
- 4 ACCIARRI 98E use  $Z \rightarrow \tau^+\tau^-\gamma$  events. In addition to the limits, the authors also quote a value of  $0.004 \pm 0.027 \pm 0.023$ .
- 5 ACKERSTAFF 98N use  $Z \rightarrow \tau^+\tau^-\gamma$  events. The limit applies to an average of the form factor for off-shell  $\tau$ 's having  $p^2$  ranging from  $m_\tau^2$  to  $(M_Z - m_\tau)^2$ .
- 6 ESCRIBANO 97 use preliminary experimental results.
- 7 ESCRIBANO 93 limit derived from  $\Gamma(Z \rightarrow \tau^+\tau^-)$ , and is on the absolute value of the magnetic moment anomaly.
- 8 SILVERMAN 83 limit is derived from  $e^+e^- \rightarrow \tau^+\tau^-$  total cross-section measurements for  $q^2$  up to (37 GeV)<sup>2</sup>.

$\tau$  ELECTRIC DIPOLE MOMENT ( $d_\tau$ )

A nonzero value is forbidden by both T invariance and P invariance.

The  $q^2$  dependence is expected to be small providing no thresholds are nearby.

Re( $d_\tau$ )

VALUE (10 <sup>-16</sup> e cm)	CL%	DOCUMENT ID	TECN	COMMENT
<b>- 0.22 to 0.45</b>	95	<sup>1</sup> INAMI	03 BELL	E <sub>cm</sub> <sup>ee</sup> =10.6 GeV
••• We do not use the following data for averages, fits, limits, etc. •••				
< 2.3	90	<sup>2</sup> GROZIN	09A RVUE	From e EDM limit
< 3.7	95	<sup>3</sup> ABDALLAH	04k DLPH	$e^+e^- \rightarrow e^+e^-\tau^+\tau^-$ at LEP2
< 11.4	95	<sup>4</sup> ACHARD	04G L3	$e^+e^- \rightarrow e^+e^-\tau^+\tau^-$ at LEP2
< 4.6	95	<sup>5</sup> ALBRECHT	00 ARG	E <sub>cm</sub> <sup>ee</sup> =10.4 GeV
> -3.1 and < 3.1	95	ACCIARRI	98E L3	1991-1995 LEP runs
> -3.8 and < 3.6	95	<sup>6</sup> ACKERSTAFF	98N OPAL	1990-1995 LEP runs
< 0.11	95	<sup>7,8</sup> ESCRIBANO	97 RVUE	$Z \rightarrow \tau^+\tau^-$ at LEP
< 0.5	95	<sup>9</sup> ESCRIBANO	93 RVUE	$Z \rightarrow \tau^+\tau^-$ at LEP
< 7	90	GRIFOLS	91 RVUE	$Z \rightarrow \tau\tau\gamma$ at LEP
< 1.6	90	DELAGUILA	90 RVUE	$e^+e^- \rightarrow \tau^+\tau^-$ , E <sub>cm</sub> <sup>ee</sup> =35 GeV

- 1 INAMI 03 use  $e^+e^- \rightarrow \tau^+\tau^-$  events.
- 2 GROZIN 09A calculate the contribution to the electron electric dipole moment from the  $\tau$  electric dipole moment appearing in loops, which is  $\Delta d_e = 6.9 \times 10^{-12} d_\tau$ . Dividing the REGAN 02 upper limit  $|d_e| \leq 1.6 \times 10^{-27}$  e cm at CL=90% by  $6.9 \times 10^{-12}$  gives this limit.
- 3 ABDALLAH 04k limit is derived from  $e^+e^- \rightarrow e^+e^-\tau^+\tau^-$  total cross-section measurements at  $\sqrt{s}$  between 183 and 208 GeV and is on the absolute value of  $d_\tau$ .
- 4 ACHARD 04G limit is derived from  $e^+e^- \rightarrow e^+e^-\tau^+\tau^-$  total cross-section measurements at  $\sqrt{s}$  between 189 and 206 GeV, and is on the absolute value of  $d_\tau$ .
- 5 ALBRECHT 00 use  $e^+e^- \rightarrow \tau^+\tau^-$  events. Limit is on the absolute value of Re( $d_\tau$ ).
- 6 ACKERSTAFF 98N use  $Z \rightarrow \tau^+\tau^-\gamma$  events. The limit applies to an average of the form factor for off-shell  $\tau$ 's having  $p^2$  ranging from  $m_\tau^2$  to  $(M_Z - m_\tau)^2$ .
- 7 ESCRIBANO 97 derive the relationship  $|d_\tau| = \cot \theta_W |d_W^W|$  using effective Lagrangian methods, and use a conference result  $|d_W^W| < 5.8 \times 10^{-18}$  e cm at 95% CL (L. Silvestris, ICHEP96) to obtain this result.
- 8 ESCRIBANO 97 use preliminary experimental results.
- 9 ESCRIBANO 93 limit derived from  $\Gamma(Z \rightarrow \tau^+\tau^-)$ , and is on the absolute value of the electric dipole moment.

# Lepton Particle Listings

$\tau$

## Im( $d_\tau$ )

VALUE ( $10^{-16} e cm$ )	CL%	DOCUMENT ID	TECN	COMMENT
-0.25 to 0.008	95	<sup>1</sup> INAMI	03	BELL $E_{cm}^{ee} = 10.6$ GeV
		•••		We do not use the following data for averages, fits, limits, etc. •••
< 1.8	95	<sup>2</sup> ALBRECHT	00	ARG $E_{cm}^{ee} = 10.4$ GeV
		<sup>1</sup> INAMI 03		use $e^+e^- \rightarrow \tau^+\tau^-$ events.
		<sup>2</sup> ALBRECHT 00		use $e^+e^- \rightarrow \tau^+\tau^-$ events. Limit is on the absolute value of Im( $d_\tau$ ).

## $\tau$ WEAK DIPOLE MOMENT ( $d_\tau^W$ )

A nonzero value is forbidden by CP invariance.

The  $q^2$  dependence is expected to be small providing no thresholds are nearby.

## Re( $d_\tau^W$ )

VALUE ( $10^{-17} e cm$ )	CL%	DOCUMENT ID	TECN	COMMENT
<0.50	95	<sup>1</sup> HEISTER	03F	ALEP 1990-1995 LEP runs
		•••		We do not use the following data for averages, fits, limits, etc. •••
<3.0	90	<sup>1</sup> ACCIARRI	98c	L3 1991-1995 LEP runs
<0.56	95	ACKERSTAFF	97L	OPAL 1991-1995 LEP runs
<0.78	95	<sup>2</sup> AKERS	95F	OPAL Repl. by ACKERSTAFF 97L
<1.5	95	<sup>2</sup> BUSKULIC	95c	ALEP Repl. by HEISTER 03F
<7.0	95	<sup>2</sup> ACTON	92F	OPAL Z $\rightarrow \tau^+\tau^-$ at LEP
<3.7	95	<sup>2</sup> BUSKULIC	92J	ALEP Repl. by BUSKULIC 95c
		<sup>1</sup> Limit		is on the absolute value of the real part of the weak dipole moment.
		<sup>2</sup> Limit		is on the absolute value of the real part of the weak dipole moment, and applies for $q^2 = m_Z^2$ .

## Im( $d_\tau^W$ )

VALUE ( $10^{-17} e cm$ )	CL%	DOCUMENT ID	TECN	COMMENT
<1.1	95	<sup>1</sup> HEISTER	03F	ALEP 1990-1995 LEP runs
		•••		We do not use the following data for averages, fits, limits, etc. •••
<1.5	95	ACKERSTAFF	97L	OPAL 1991-1995 LEP runs
<4.5	95	<sup>2</sup> AKERS	95F	OPAL Repl. by ACKERSTAFF 97L
		<sup>1</sup> HEISTER 03F		limit is on the absolute value of the imaginary part of the weak dipole moment.
		<sup>2</sup> Limit		is on the absolute value of the imaginary part of the weak dipole moment, and applies for $q^2 = m_Z^2$ .

## $\tau$ WEAK ANOMALOUS MAGNETIC DIPOLE MOMENT ( $\alpha_\tau^W$ )

Electroweak radiative corrections are expected to contribute at the  $10^{-6}$  level. See BERNABEU 95.

The  $q^2$  dependence is expected to be small providing no thresholds are nearby.

## Re( $\alpha_\tau^W$ )

VALUE	CL%	DOCUMENT ID	TECN	COMMENT
<1.1 $\times 10^{-3}$	95	<sup>1</sup> HEISTER	03F	ALEP 1990-1995 LEP runs
		•••		We do not use the following data for averages, fits, limits, etc. •••
> -0.0024 and < 0.0025	95	<sup>2</sup> GONZALEZ-S.	00	RVUE $e^+e^- \rightarrow \tau^+\tau^-$ and $W \rightarrow \tau\nu_\tau$
<4.5 $\times 10^{-3}$	90	<sup>1</sup> ACCIARRI	98c	L3 1991-1995 LEP runs
		<sup>1</sup> Limit		is on the absolute value of the real part of the weak anomalous magnetic dipole moment.
		<sup>2</sup> GONZALEZ-SPRINBERG	00	use data on tau lepton production at LEP1, SLC, and LEP2, and data from colliders and LEP2 to determine limits. Assume imaginary component is zero.

## Im( $\alpha_\tau^W$ )

VALUE	CL%	DOCUMENT ID	TECN	COMMENT
<2.7 $\times 10^{-3}$	95	<sup>1</sup> HEISTER	03F	ALEP 1990-1995 LEP runs
		•••		We do not use the following data for averages, fits, limits, etc. •••
<9.9 $\times 10^{-3}$	90	<sup>1</sup> ACCIARRI	98c	L3 1991-1995 LEP runs
		<sup>1</sup> Limit		is on the absolute value of the imaginary part of the weak anomalous magnetic dipole moment.

## $\tau^-$ DECAY MODES

$\tau^\pm$  modes are charge conjugates of the modes below. " $h^\pm$ " stands for  $\pi^\pm$  or  $K^\pm$ . " $e^\pm$ " stands for e or  $\mu$ . "Neutrals" stands for  $\gamma$ 's and/or  $\pi^0$ 's.

Mode	Fraction ( $\Gamma_i/\Gamma$ )	Scale factor/ Confidence level
------	--------------------------------	-----------------------------------

### Modes with one charged particle

$\Gamma_1$	particle $^- \geq 0$ neutrals $\geq 0K^0\nu_\tau$ ("1-prong")	(85.24 $\pm$ 0.06) %	
$\Gamma_2$	particle $^- \geq 0$ neutrals $\geq 0K_L^0\nu_\tau$	(84.58 $\pm$ 0.06) %	
$\Gamma_3$	$\mu^- \bar{\nu}_\mu \nu_\tau$	[a] (17.39 $\pm$ 0.04) %	
$\Gamma_4$	$\mu^- \bar{\nu}_\mu \nu_\tau \gamma$	[b] (3.67 $\pm$ 0.08) $\times 10^{-3}$	
$\Gamma_5$	$e^- \bar{\nu}_e \nu_\tau$	[a] (17.82 $\pm$ 0.04) %	
$\Gamma_6$	$e^- \bar{\nu}_e \nu_\tau \gamma$	[b] (1.83 $\pm$ 0.05) %	
$\Gamma_7$	$h^- \geq 0K_L^0 \nu_\tau$	(12.03 $\pm$ 0.05) %	
$\Gamma_8$	$h^- \nu_\tau$	(11.51 $\pm$ 0.05) %	
$\Gamma_9$	$\pi^- \nu_\tau$	[a] (10.82 $\pm$ 0.05) %	
$\Gamma_{10}$	$K^- \nu_\tau$	[a] (6.96 $\pm$ 0.10) $\times 10^{-3}$	
$\Gamma_{11}$	$h^- \geq 1$ neutrals $\nu_\tau$	(37.01 $\pm$ 0.09) %	
$\Gamma_{12}$	$h^- \geq 1\pi^0 \nu_\tau$ (ex. $K^0$ )	(36.51 $\pm$ 0.09) %	
$\Gamma_{13}$	$h^- \pi^0 \nu_\tau$	(25.93 $\pm$ 0.09) %	
$\Gamma_{14}$	$\pi^- \pi^0 \nu_\tau$	[a] (25.49 $\pm$ 0.09) %	
$\Gamma_{15}$	$\pi^- \pi^0$ non- $\rho(770) \nu_\tau$	(3.0 $\pm$ 3.2) $\times 10^{-3}$	
$\Gamma_{16}$	$K^- \pi^0 \nu_\tau$	[a] (4.33 $\pm$ 0.15) $\times 10^{-3}$	
$\Gamma_{17}$	$h^- \geq 2\pi^0 \nu_\tau$	(10.81 $\pm$ 0.09) %	
$\Gamma_{18}$	$h^- 2\pi^0 \nu_\tau$	(9.48 $\pm$ 0.10) %	
$\Gamma_{19}$	$h^- 2\pi^0 \nu_\tau$ (ex. $K^0$ )	(9.32 $\pm$ 0.10) %	
$\Gamma_{20}$	$\pi^- 2\pi^0 \nu_\tau$ (ex. $K^0$ )	[a] (9.26 $\pm$ 0.10) %	
$\Gamma_{21}$	$\pi^- 2\pi^0 \nu_\tau$ (ex. $K^0$ ), scaJar	< 9 $\times 10^{-3}$	CL=95%
$\Gamma_{22}$	$\pi^- 2\pi^0 \nu_\tau$ (ex. $K^0$ ), vector	< 7 $\times 10^{-3}$	CL=95%
$\Gamma_{23}$	$K^- 2\pi^0 \nu_\tau$ (ex. $K^0$ )	[a] (6.5 $\pm$ 2.2) $\times 10^{-4}$	
$\Gamma_{24}$	$h^- \geq 3\pi^0 \nu_\tau$	(1.34 $\pm$ 0.07) %	
$\Gamma_{25}$	$h^- \geq 3\pi^0 \nu_\tau$ (ex. $K^0$ )	(1.25 $\pm$ 0.07) %	
$\Gamma_{26}$	$h^- 3\pi^0 \nu_\tau$	(1.18 $\pm$ 0.07) %	
$\Gamma_{27}$	$\pi^- 3\pi^0 \nu_\tau$ (ex. $K^0$ )	[a] (1.04 $\pm$ 0.07) %	
$\Gamma_{28}$	$K^- 3\pi^0 \nu_\tau$ (ex. $K^0, \eta$ )	[a] (4.8 $\pm$ 2.1) $\times 10^{-4}$	
$\Gamma_{29}$	$h^- 4\pi^0 \nu_\tau$ (ex. $K^0$ )	(1.6 $\pm$ 0.4) $\times 10^{-3}$	
$\Gamma_{30}$	$h^- 4\pi^0 \nu_\tau$ (ex. $K^0, \eta$ )	[a] (1.1 $\pm$ 0.4) $\times 10^{-3}$	
$\Gamma_{31}$	$a_1(1260) \nu_\tau \rightarrow \pi^- \gamma \nu_\tau$	(3.8 $\pm$ 1.5) $\times 10^{-4}$	
$\Gamma_{32}$	$K^- \geq 0\pi^0 \geq 0K^0 \geq 0\gamma \nu_\tau$	(1.552 $\pm$ 0.029) %	
$\Gamma_{33}$	$K^- \geq 1(\pi^0 \text{ or } K^0 \text{ or } \gamma) \nu_\tau$	(8.59 $\pm$ 0.28) $\times 10^{-3}$	

### Modes with $K^0$ 's

$\Gamma_{34}$	$K_S^0$ (particles) $^- \nu_\tau$	(9.43 $\pm$ 0.28) $\times 10^{-3}$	
$\Gamma_{35}$	$h^- K^0 \nu_\tau$	(9.87 $\pm$ 0.14) $\times 10^{-3}$	
$\Gamma_{36}$	$\pi^- K^0 \nu_\tau$	[a] (8.38 $\pm$ 0.14) $\times 10^{-3}$	
$\Gamma_{37}$	$\pi^- K^0$ (non- $K^*(892)^- \nu_\tau$ )	(5.4 $\pm$ 2.1) $\times 10^{-4}$	
$\Gamma_{38}$	$K^- K^0 \nu_\tau$	[a] (1.486 $\pm$ 0.034) $\times 10^{-3}$	
$\Gamma_{39}$	$K^- K^0 \geq 0\pi^0 \nu_\tau$	(2.99 $\pm$ 0.07) $\times 10^{-3}$	
$\Gamma_{40}$	$h^- K^0 \pi^0 \nu_\tau$	(5.32 $\pm$ 0.13) $\times 10^{-3}$	
$\Gamma_{41}$	$\pi^- K^0 \pi^0 \nu_\tau$	[a] (3.82 $\pm$ 0.13) $\times 10^{-3}$	
$\Gamma_{42}$	$\bar{K}^0 \rho^- \nu_\tau$	(2.2 $\pm$ 0.5) $\times 10^{-3}$	
$\Gamma_{43}$	$K^- K^0 \pi^0 \nu_\tau$	[a] (1.50 $\pm$ 0.07) $\times 10^{-3}$	
$\Gamma_{44}$	$\pi^- K^0 \geq 1\pi^0 \nu_\tau$	(4.08 $\pm$ 0.25) $\times 10^{-3}$	
$\Gamma_{45}$	$\pi^- K^0 \pi^0 \pi^0 \nu_\tau$ (ex. $K^0$ )	[a] (2.6 $\pm$ 2.3) $\times 10^{-4}$	
$\Gamma_{46}$	$K^- K^0 \pi^0 \pi^0 \nu_\tau$	< 1.6 $\times 10^{-4}$	CL=95%
$\Gamma_{47}$	$\pi^- K^0 \bar{K}^0 \nu_\tau$	(1.55 $\pm$ 0.24) $\times 10^{-3}$	
$\Gamma_{48}$	$\pi^- K_S^0 K_S^0 \nu_\tau$	[a] (2.35 $\pm$ 0.06) $\times 10^{-4}$	
$\Gamma_{49}$	$\pi^- K_S^0 K_L^0 \nu_\tau$	[a] (1.08 $\pm$ 0.24) $\times 10^{-3}$	
$\Gamma_{50}$	$\pi^- K_L^0 K_L^0 \nu_\tau$	(2.35 $\pm$ 0.06) $\times 10^{-4}$	
$\Gamma_{51}$	$\pi^- K^0 \bar{K}^0 \pi^0 \nu_\tau$	(3.6 $\pm$ 1.2) $\times 10^{-4}$	
$\Gamma_{52}$	$\pi^- K_S^0 K_S^0 \pi^0 \nu_\tau$	[a] (1.82 $\pm$ 0.21) $\times 10^{-5}$	
$\Gamma_{53}$	$K^* K^0 \pi^0 \nu_\tau \rightarrow \pi^- K_S^0 K_S^0 \pi^0 \nu_\tau$	(1.08 $\pm$ 0.21) $\times 10^{-5}$	
$\Gamma_{54}$	$f_1(1285) \pi^- \nu_\tau \rightarrow \pi^- K_S^0 K_S^0 \pi^0 \nu_\tau$	(6.8 $\pm$ 1.5) $\times 10^{-6}$	
$\Gamma_{55}$	$f_1(1420) \pi^- \nu_\tau \rightarrow \pi^- K_S^0 K_S^0 \pi^0 \nu_\tau$	(2.4 $\pm$ 0.8) $\times 10^{-6}$	
$\Gamma_{56}$	$\pi^- K_S^0 K_L^0 \pi^0 \nu_\tau$	[a] (3.2 $\pm$ 1.2) $\times 10^{-4}$	
$\Gamma_{57}$	$\pi^- K_L^0 K_L^0 \pi^0 \nu_\tau$	(1.82 $\pm$ 0.21) $\times 10^{-5}$	
$\Gamma_{58}$	$K^- K^0 K_S^0 \nu_\tau$	< 6.3 $\times 10^{-7}$	CL=90%
$\Gamma_{59}$	$K^- K_S^0 K_S^0 \pi^0 \nu_\tau$	< 4.0 $\times 10^{-7}$	CL=90%
$\Gamma_{60}$	$K^0 h^+ h^- h^- \geq 0$ neutrals $\nu_\tau$	< 1.7 $\times 10^{-3}$	CL=95%
$\Gamma_{61}$	$K^0 h^+ h^- h^- \nu_\tau$	[a] (2.5 $\pm$ 2.0) $\times 10^{-4}$	



Lepton Particle Listings

$\tau$

Lepton Family number (LF), Lepton number (L), or Baryon number (B) violating modes

L means lepton number violation (e.g.  $\tau^- \rightarrow e^+ \pi^- \pi^-$ ). Following common usage, LF means lepton family violation and not lepton number violation (e.g.  $\tau^- \rightarrow e^- \pi^+ \pi^-$ ). B means baryon number violation.

Table with 6 columns: Particle, Mode, LF/B, Value, Power of 10, CL. Lists various particle decays and their constraints.

CONSTRAINED FIT INFORMATION

An overall fit to 87 branching ratios uses 170 measurements and one constraint to determine 46 parameters. The overall fit has a  $\chi^2 = 135$  for 125 degrees of freedom.

The following off-diagonal array elements are the correlation coefficients  $\langle \delta x_i \delta x_j \rangle / (\delta x_i \delta x_j)$ , in percent, from the fit to the branching fractions,  $x_i \equiv \Gamma_i / \Gamma_{total}$ .

Correlation matrix table showing off-diagonal array elements for parameters x5, x9, x10, x14, x16, x20, x23, x27, x28.

[a] Basis mode for the  $\tau$ . [b] See the Particle Listings below for the energy limits used in this measurement.

See key on page 999

Lepton Particle Listings

τ

Table of correlation coefficients for τ branching fractions. Columns are labeled with variables x36 through x119. Values range from -1 to 39.

Table of correlation coefficients for τ branching ratios. Columns are labeled with variables x126 through x185. Values range from -1 to 25.

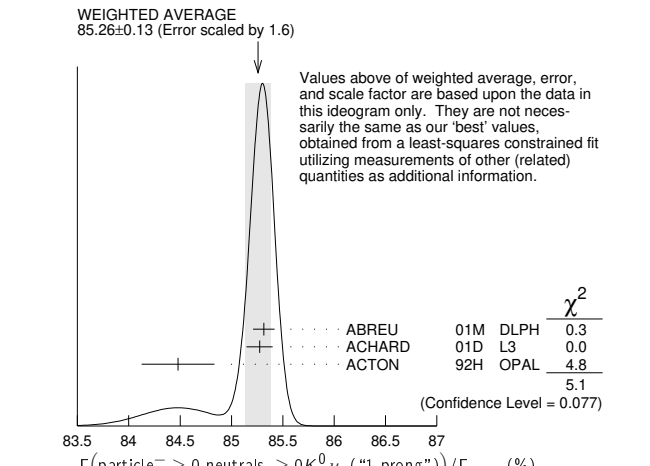
See the related review(s):
τ Branching Fractions

Table with columns: VALUE (%), DOCUMENT ID, TECN, COMMENT. Row: -0.36 ± 0.23 ± 0.11, LEES, 12M BABR, 476 fb^-1 E\_cm^0.6 = 10.6 GeV

τ- BRANCHING RATIOS

Γ (particle- ≥ 0 neutrals ≥ 0 K\_S^0 ν\_τ ("1-prong"))/Γ\_total
The charged particle here can be e, μ, or hadron. In many analyses, the sum of the topological branching fractions (1, 3, and 5 prongs) is constrained to be unity.

Table with columns: VALUE (%), EVTS, DOCUMENT ID, TECN, COMMENT. Row: 85.26 ± 0.13 OUR AVERAGE, Error includes scale factor of 1.6. See the ideogram below.



1 The correlation coefficients between this measurement and the ABREU 01M measure-

Downloaded from https://academic.oup.com/ptep/article/2020/8/083C01/5891211 by guest on 12 November 2020

Lepton Particle Listings

T

ments of B(τ → 3-prong) and B(τ → 5-prong) are -0.98 and -0.08 respectively. 2 The correlation coefficients between this measurement and the ACHARD 01D measurements of B(τ → "3-prong") and B(τ → "5-prong") are -0.978 and -0.082 respectively.

Γ (particle⁻ ≥ 0 neutrals ≥ 0K⁰\_L ν\_τ) / Γ\_total
Table with 4 columns: VALUE (%), EVTS, DOCUMENT ID, TECN, COMMENT. Averages: 84.58 ± 0.06 OUR FIT, 85.1 ± 0.4 OUR AVERAGE.

Table with 4 columns: VALUE (%), EVTS, DOCUMENT ID, TECN, COMMENT. Averages: 84.58 ± 0.06 OUR FIT, 85.1 ± 0.4 OUR AVERAGE.

1 Not independent of ADEVA 91F Γ(h⁻h⁻h⁺ ≥ 0 neutrals ≥ 0K⁰\_L ν\_τ) / Γ\_total value. 2 Not independent of AIHARA 87B Γ(μ⁻ν\_μ ν\_τ) / Γ\_total, Γ(e⁻ν\_e ν\_τ) / Γ\_total, and Γ(h⁻ ≥ 0 neutrals ≥ 0K⁰\_L ν\_τ) / Γ\_total values. 3 Not independent of SCHMIDKE 86 value (also not independent of BURCHAT 87 value for Γ(h⁻h⁻h⁺ ≥ 0 neutrals ≥ 0K⁰\_L ν\_τ) / Γ\_total. 4 Not independent of ALTHOFF 85 Γ(μ⁻ν\_μ ν\_τ) / Γ\_total, Γ(e⁻ν\_e ν\_τ) / Γ\_total, Γ(h⁻ ≥ 0 neutrals ≥ 0K⁰\_L ν\_τ) / Γ\_total, and Γ(h⁻h⁻h⁺ ≥ 0 neutrals ≥ 0K⁰\_L ν\_τ) / Γ\_total values. 5 Not independent of (1-prong + 0π⁰) and (1-prong + ≥ 1π⁰) values.

Γ (μ⁻ν\_μ ν\_τ) / Γ\_total
To minimize the effect of experiments with large systematic errors, we exclude experiments which together would contribute 5% of the weight in the average.

Table with 4 columns: VALUE (%), EVTS, DOCUMENT ID, TECN, COMMENT. Averages: 17.39 ± 0.04 OUR FIT, 17.33 ± 0.05 OUR AVERAGE.

1 See footnote to SCHAEEL 05c Γ(τ⁻ → e⁻ν\_e ν\_τ) / Γ\_total measurement for correlations with other measurements. 2 The correlation coefficient between this measurement and the ACCIARRI 01F measurement of B(τ⁻ → e⁻ν\_e ν\_τ) is 0.08. 3 The correlation coefficients between this measurement and the ANASTASSOV 97 measurements of B(e⁻ν\_e ν\_τ), B(μ⁻ν\_μ ν\_τ) / B(e⁻ν\_e ν\_τ), B(h⁻ν\_τ), and B(h⁻ν\_τ) / B(e⁻ν\_e ν\_τ) are 0.50, 0.58, 0.50, and 0.08 respectively. 4 Not independent of ALBRECHT 92B Γ(μ⁻ν\_μ ν\_τ) / Γ(e⁻ν\_e ν\_τ) and ALBRECHT 93G Γ(μ⁻ν\_μ ν\_τ) × Γ(e⁻ν\_e ν\_τ) / Γ\_total values. 5 Modified using B(e⁻ν\_e ν\_τ) / B("1 prong") and B("1 prong") = 0.855. 6 Error correlated with BALTRUSAITIS 85 e⁻ν μ value.

Γ (μ⁻ν\_μ ν\_τ γ) / Γ\_total
Table with 5 columns: VALUE (%), EVTS, DOCUMENT ID, TECN, COMMENT. Average: 0.367 ± 0.008 OUR AVERAGE.

• • • We do not use the following data for averages, fits, limits, etc. • • • 1 SHIMIZU 18A impose requirements on detected γ's corresponding to a τ-rest-frame energy cutoff E\*\_γ > 10 MeV. 2 LEES 15G impose requirements on detected γ's corresponding to a τ-rest-frame energy cutoff E\*\_γ > 10 MeV. 3 BERGFELD 00 impose requirements on detected γ's corresponding to a τ-rest-frame energy cutoff E\*\_γ > 10 MeV. For E\*\_γ > 20 MeV, they quote (3.04 ± 0.14 ± 0.30) × 10⁻³. 4 ALEXANDER 96S impose requirements on detected γ's corresponding to a τ-rest-frame energy cutoff E\_γ > 20 MeV. 5 WU 90 reports Γ(μ⁻ν\_μ ν\_τ γ) / Γ(μ⁻ν\_μ ν\_τ) = 0.013 ± 0.006, which is converted to Γ(μ⁻ν\_μ ν\_τ γ) / Γ\_total using Γ(μ⁻ν\_μ ν\_τ γ) / Γ\_total = 17.35%. Requirements on detected γ's correspond to a τ rest frame energy cutoff E\_γ > 37 MeV.

Γ (e⁻ν\_e ν\_τ) / Γ\_total
To minimize the effect of experiments with large systematic errors, we exclude experiments which together would contribute 5% of the weight in the average.

Table with 4 columns: VALUE (%), EVTS, DOCUMENT ID, TECN, COMMENT. Averages: 17.82 ± 0.04 OUR FIT, 17.82 ± 0.05 OUR AVERAGE.

1 Correlation matrix for SCHAEEL 05c branching fractions, in percent: (1) Γ(τ⁻ → e⁻ν\_e ν\_τ) / Γ\_total, (2) Γ(τ⁻ → μ⁻ν\_μ ν\_τ) / Γ\_total, (3) Γ(τ⁻ → π⁻ν\_τ) / Γ\_total, (4) Γ(τ⁻ → π⁻π⁰ν\_τ) / Γ\_total, (5) Γ(τ⁻ → π⁻2π⁰ν\_τ (ex. K⁰)) / Γ\_total, (6) Γ(τ⁻ → π⁻3π⁰ν\_τ (ex. K⁰)) / Γ\_total, (7) Γ(τ⁻ → h⁻4π⁰ν\_τ (ex. K⁰, η)) / Γ\_total, (8) Γ(τ⁻ → π⁻π⁺π⁻ν\_τ (ex. K⁰, ω)) / Γ\_total, (9) Γ(τ⁻ → π⁻π⁺π⁻π⁰ν\_τ (ex. K⁰)) / Γ\_total, (10) Γ(τ⁻ → h⁻h⁻h⁺2π⁰ν\_τ (ex. K⁰)) / Γ\_total, (11) Γ(τ⁻ → h⁻h⁻h⁺3π⁰ν\_τ) / Γ\_total, (12) Γ(τ⁻ → 3h⁻2h⁺ν\_τ (ex. K⁰)) / Γ\_total, (13) Γ(τ⁻ → 3h⁻2h⁺π⁰ν\_τ (ex. K⁰)) / Γ\_total.

Correlation matrix table with 13 columns and 13 rows of numerical values.

(9)	-13	-12	-25	-30	4	-2	16	-15				
(10)	0	-2	-23	-14	4	10	13	-6	-17			
(11)	1	0	-5	1	4	6	0	-9	-2	-11		
(12)	0	1	9	4	-8	-4	-6	9	-5	-4	-2	
(13)	1	-4	-3	-5	3	2	-4	-3	-1	4	1	-24

- <sup>2</sup> The correlation coefficient between this measurement and the ACCIARRI 01F measurement of  $B(\tau^- \rightarrow \mu^- \bar{\nu}_\mu \nu_\tau)$  is 0.08.
- <sup>3</sup> The correlation coefficients between this measurement and the ANASTASSOV 97 measurements of  $B(\mu \bar{\nu}_\mu \nu_\tau)$ ,  $B(\mu \bar{\nu}_\mu \nu_\tau)/B(e \bar{\nu}_e \nu_\tau)$ ,  $B(h^- \nu_\tau)$ , and  $B(h^- \nu_\tau)/B(e \bar{\nu}_e \nu_\tau)$  are 0.50, -0.42, 0.48, and -0.39 respectively.
- <sup>4</sup> Not independent of ALBRECHT 92D  $\Gamma(\mu^- \bar{\nu}_\mu \nu_\tau)/\Gamma(e^- \bar{\nu}_e \nu_\tau)$  and ALBRECHT 93G  $\Gamma(\mu^- \bar{\nu}_\mu \nu_\tau) \times \Gamma(e^- \bar{\nu}_e \nu_\tau)/\Gamma_{\text{total}}^2$  values.
- <sup>5</sup> Modified using  $B(e^- \bar{\nu}_e \nu_\tau)/B(\text{"1 prong"})$  and  $B(h^- \nu_\tau)$ , = 0.855.
- <sup>6</sup> Error correlated with BALTRUSAITIS 85  $\Gamma(\mu^- \bar{\nu}_\mu \nu_\tau)/\Gamma_{\text{total}}$ .
- <sup>7</sup> BACINO 78B value comes from fit to events with  $e^\pm$  and one other nonelectron charged prong.

$\Gamma(\mu^- \bar{\nu}_\mu \nu_\tau)/\Gamma(e^- \bar{\nu}_e \nu_\tau)$   $\Gamma_3/\Gamma_5$

Standard Model prediction including mass effects is 0.9726.

VALUE (units $10^{-2}$ )	EVTS	DOCUMENT ID	TECN	COMMENT
<b>97.62 ± 0.28 OUR FIT</b>				
<b>97.9 ± 0.4 OUR AVERAGE</b>				
97.96 ± 0.16 ± 0.36	731k	<sup>1</sup> AUBERT	10F	BABR 467 fb <sup>-1</sup> $E_{\text{cm}}^{\text{ee}} = 10.6$ GeV
97.77 ± 0.63 ± 0.87		<sup>2</sup> ANASTASSOV 97	CLEO	$E_{\text{cm}}^{\text{ee}} = 10.6$ GeV
99.7 ± 3.5 ± 4.0		ALBRECHT 92D	ARG	$E_{\text{cm}}^{\text{ee}} = 9.4\text{--}10.6$ GeV

- <sup>1</sup> Correlation matrix for AUBERT 10F branching fractions:
  - $\Gamma(\tau^- \rightarrow \mu^- \bar{\nu}_\mu \nu_\tau) / \Gamma(\tau^- \rightarrow e^- \bar{\nu}_e \nu_\tau)$
  - $\Gamma(\tau^- \rightarrow \pi^- \nu_\tau) / \Gamma(\tau^- \rightarrow e^- \bar{\nu}_e \nu_\tau)$
  - $\Gamma(\tau^- \rightarrow K^- \nu_\tau) / \Gamma(\tau^- \rightarrow e^- \bar{\nu}_e \nu_\tau)$

(1)	(2)
(2)	0.25
(3)	0.12 0.33

- <sup>2</sup> The correlation coefficients between this measurement and the ANASTASSOV 97 measurements of  $B(\mu \bar{\nu}_\mu \nu_\tau)$ ,  $B(e \bar{\nu}_e \nu_\tau)$ ,  $B(h^- \nu_\tau)$ , and  $B(h^- \nu_\tau)/B(e \bar{\nu}_e \nu_\tau)$  are 0.58, -0.42, 0.07, and 0.45 respectively.

$\Gamma(e^- \bar{\nu}_e \nu_\tau)/\Gamma_{\text{total}}$   $\Gamma_6/\Gamma$

VALUE (%)	EVTS	DOCUMENT ID	TECN	COMMENT
<b>1.83 ± 0.05 OUR AVERAGE</b>				
1.79 ± 0.02 ± 0.10	12K	<sup>1</sup> SHIMIZU	18A	BELL 711 fb <sup>-1</sup> $E_{\text{cm}}^{\text{ee}} = 10.6$ GeV
1.847 ± 0.015 ± 0.052	18k	<sup>2</sup> LEES	15G	BABR 431 fb <sup>-1</sup> $E_{\text{cm}}^{\text{ee}} = 10.6$ GeV
1.75 ± 0.06 ± 0.17		<sup>3</sup> BERGFELD	00	CLEO $E_{\text{cm}}^{\text{ee}} = 10.6$ GeV

- <sup>1</sup> SHIMIZU 18A impose requirements on detected  $\gamma$ 's corresponding to a  $\tau$ -rest-frame energy cutoff  $E_\gamma^* > 10$  MeV.
- <sup>2</sup> LEES 15G impose requirements on detected  $\gamma$ 's corresponding to a  $\tau$ -rest-frame energy cutoff  $E_\gamma^* > 10$  MeV.
- <sup>3</sup> BERGFELD 00 impose requirements on detected  $\gamma$ 's corresponding to a  $\tau$ -rest-frame energy cutoff  $E_\gamma^* > 10$  MeV.

$\Gamma(h^- \geq 0K_L^0 \nu_\tau)/\Gamma_{\text{total}}$   $\Gamma_7/\Gamma$

$\Gamma_7/\Gamma = (\Gamma_9 + \Gamma_{10} + \frac{1}{2}\Gamma_{36} + \frac{1}{2}\Gamma_{38} + \Gamma_{50})/\Gamma$

VALUE (%)	EVTS	DOCUMENT ID	TECN	COMMENT
<b>12.03 ± 0.05 OUR FIT</b>				
<b>12.2 ± 0.4 OUR AVERAGE</b>				
12.47 ± 0.26 ± 0.43	2967	<sup>1</sup> ACCIARRI	95	L3 1992 LEP run
12.4 ± 0.7 ± 0.7	283	<sup>2</sup> ABREU	92N	DLPH 1990 LEP run
12.1 ± 0.7 ± 0.5	309	ALEXANDER	91D	OPAL 1990 LEP run
• • • We use the following data for averages but not for fits. • • •				
11.3 ± 0.5 ± 0.8	798	<sup>3</sup> FORD	87	MAC $E_{\text{cm}}^{\text{ee}} = 29$ GeV
• • • We do not use the following data for averages, fits, limits, etc. • • •				
12.44 ± 0.11 ± 0.11	15k	<sup>4</sup> BUSKULIC	96	ALEP Repl. by SCHAEEL 05c
11.7 ± 0.6 ± 0.8		<sup>5</sup> ALBRECHT	92D	ARG $E_{\text{cm}}^{\text{ee}} = 9.4\text{--}10.6$ GeV
12.98 ± 0.44 ± 0.33		<sup>6</sup> DECAMP	92c	ALEP Repl. by SCHAEEL 05c
12.3 ± 0.9 ± 0.5	1338	BEHREND	90	CELL $E_{\text{cm}}^{\text{ee}} = 35$ GeV
11.1 ± 1.1 ± 1.4		<sup>7</sup> BURCHAT	87D	MRK2 $E_{\text{cm}}^{\text{ee}} = 29$ GeV
12.3 ± 0.6 ± 1.1	328	<sup>8</sup> BARTEL	86D	JADE $E_{\text{cm}}^{\text{ee}} = 34.6$ GeV
13.0 ± 2.0 ± 4.0		BERGER	85	PLUT $E_{\text{cm}}^{\text{ee}} = 34.6$ GeV
11.2 ± 1.7 ± 1.2	34	<sup>9</sup> BEHREND	83c	CELL $E_{\text{cm}}^{\text{ee}} = 34$ GeV

- <sup>1</sup> ACCIARRI 95 with 0.65% added to remove their correction for  $K^*(892)^0$  backgrounds.
- <sup>2</sup> ABREU 92N with 0.5% added to remove their correction for  $K^*(892)^0$  backgrounds.
- <sup>3</sup> FORD 87 result for  $B(\pi^- \nu_\tau)$  with 0.67% added to remove their  $K^-$  correction and adjusted for 1992 B("1 prong").
- <sup>4</sup> BUSKULIC 96 quote  $11.78 \pm 0.11 \pm 0.13$  We add 0.66 to undo their correction for unseen  $K_L^0$  and modify the systematic error accordingly.
- <sup>5</sup> Not independent of ALBRECHT 92D  $\Gamma(\mu^- \bar{\nu}_\mu \nu_\tau)/\Gamma(e^- \bar{\nu}_e \nu_\tau)$ ,  $\Gamma(\mu^- \bar{\nu}_\mu \nu_\tau) \times \Gamma(e^- \bar{\nu}_e \nu_\tau)$ , and  $\Gamma(h^- \geq 0K_L^0 \nu_\tau)/\Gamma(e^- \bar{\nu}_e \nu_\tau)$  values.
- <sup>6</sup> DECAMP 92c quote  $B(h^- \geq 0K_L^0 \nu_\tau) \geq 0(K_S^0 \rightarrow \pi^+ \pi^-) \nu_\tau = 13.32 \pm 0.44 \pm 0.33$ . We subtract 0.35 to correct for their inclusion of the  $K_S^0$  decays.

- <sup>7</sup> BURCHAT 87 with 1.1% added to remove their correction for  $K^-$  and  $K^*(892)^0$  backgrounds.
- <sup>8</sup> BARTEL 86D result for  $B(\pi^- \nu_\tau)$  with 0.59% added to remove their  $K^-$  correction and adjusted for 1992 B("1 prong").
- <sup>9</sup> BEHREND 83c quote  $B(\pi^- \nu_\tau) = 9.9 \pm 1.7 \pm 1.3$  after subtracting  $1.3 \pm 0.5$  to correct for  $B(K^- \nu_\tau)$ .

$\Gamma(h^- \nu_\tau)/\Gamma_{\text{total}}$   $\Gamma_8/\Gamma = (\Gamma_9 + \Gamma_{10})/\Gamma$

VALUE (%)	EVTS	DOCUMENT ID	TECN	COMMENT
<b>11.51 ± 0.05 OUR FIT</b>				
<b>11.63 ± 0.12 OUR AVERAGE</b>				Error includes scale factor of 1.4. See the ideogram below.
11.571 ± 0.120 ± 0.114	19k	<sup>1</sup> ABDALLAH	06A	DLPH 1992-1995 LEP runs
11.98 ± 0.13 ± 0.16		ACKERSTAFF 98M	OPAL	1991-1995 LEP runs
11.52 ± 0.05 ± 0.12		<sup>2</sup> ANASTASSOV 97	CLEO	$E_{\text{cm}}^{\text{ee}} = 10.6$ GeV

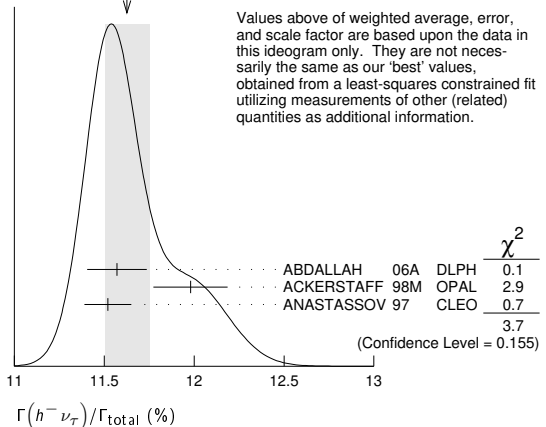
- <sup>1</sup> Correlation matrix for ABDALLAH 06A branching fractions, in percent:

(1)	$\Gamma(\tau^- \rightarrow h^- \nu_\tau)/\Gamma_{\text{total}}$
(2)	$\Gamma(\tau^- \rightarrow h^- \pi^0 \nu_\tau)/\Gamma_{\text{total}}$
(3)	$\Gamma(\tau^- \rightarrow h^- \geq 1\pi^0 \nu_\tau (\text{ex. } K^0))/\Gamma_{\text{total}}$
(4)	$\Gamma(\tau^- \rightarrow h^- 2\pi^0 \nu_\tau (\text{ex. } K^0))/\Gamma_{\text{total}}$
(5)	$\Gamma(\tau^- \rightarrow h^- \geq 3\pi^0 \nu_\tau (\text{ex. } K^0))/\Gamma_{\text{total}}$
(6)	$\Gamma(\tau^- \rightarrow h^- h^- h^+ \nu_\tau (\text{ex. } K^0))/\Gamma_{\text{total}}$
(7)	$\Gamma(\tau^- \rightarrow h^- h^- h^+ \pi^0 \nu_\tau (\text{ex. } K^0))/\Gamma_{\text{total}}$
(8)	$\Gamma(\tau^- \rightarrow h^- h^- h^+ \geq 1\pi^0 \nu_\tau (\text{ex. } K^0))/\Gamma_{\text{total}}$
(9)	$\Gamma(\tau^- \rightarrow h^- h^- h^+ \geq 2\pi^0 \nu_\tau (\text{ex. } K^0))/\Gamma_{\text{total}}$
(10)	$\Gamma(\tau^- \rightarrow 3h^- 2h^+ \nu_\tau (\text{ex. } K^0))/\Gamma_{\text{total}}$
(11)	$\Gamma(\tau^- \rightarrow 3h^- 2h^+ \pi^0 \nu_\tau (\text{ex. } K^0))/\Gamma_{\text{total}}$

(1)	(2)	(3)	(4)	(5)	(6)	(7)	(8)	(9)	(10)	
(2)	-34									
(3)	-47	56								
(4)	6	-66	15							
(5)	-6	38	11	-86						
(6)	-7	-8	15	0	-2					
(7)	-2	-1	-5	-3	3	-53				
(8)	-4	-4	-13	-4	-2	-56	75			
(9)	-1	-1	-4	3	-6	26	-78	-16		
(10)	-1	-1	1	0	0	-2	-3	-1	3	
(11)	0	0	0	0	0	1	0	-5	5	-57

- <sup>2</sup> The correlation coefficients between this measurement and the ANASTASSOV 97 measurements of  $B(\mu \bar{\nu}_\mu \nu_\tau)$ ,  $B(e \bar{\nu}_e \nu_\tau)$ ,  $B(\mu \bar{\nu}_\mu \nu_\tau)/B(e \bar{\nu}_e \nu_\tau)$ , and  $B(h^- \nu_\tau)/B(e \bar{\nu}_e \nu_\tau)$  are 0.50, 0.48, 0.07, and 0.63 respectively.

WEIGHTED AVERAGE  
11.63±0.12 (Error scaled by 1.4)



$\Gamma(h^- \nu_\tau)/\Gamma(e^- \bar{\nu}_e \nu_\tau)$   $\Gamma_8/\Gamma_5 = (\Gamma_9 + \Gamma_{10})/\Gamma_5$

VALUE (units $10^{-2}$ )	EVTS	DOCUMENT ID	TECN	COMMENT
<b>64.62 ± 0.33 OUR FIT</b>				
<b>64.0 ± 0.7 OUR AVERAGE</b>				Error includes scale factor of 1.6.
63.33 ± 0.14 ± 0.61	394k	<sup>1</sup> AUBERT	10F	BABR 467 fb <sup>-1</sup> $E_{\text{cm}}^{\text{ee}} = 10.6$ GeV
64.84 ± 0.41 ± 0.60		<sup>2</sup> ANASTASSOV 97	CLEO	$E_{\text{cm}}^{\text{ee}} = 10.6$ GeV

- <sup>1</sup> Not independent of AUBERT 10F  $\Gamma(\tau^- \rightarrow \pi^- \nu_\tau)/\Gamma(\tau^- \rightarrow e^- \bar{\nu}_e \nu_\tau)$  and  $\Gamma(\tau^- \rightarrow K^- \nu_\tau)/\Gamma(\tau^- \rightarrow e^- \bar{\nu}_e \nu_\tau)$ .
- <sup>2</sup> The correlation coefficients between this measurement and the ANASTASSOV 97 measurements of  $B(\mu \bar{\nu}_\mu \nu_\tau)$ ,  $B(e \bar{\nu}_e \nu_\tau)$ ,  $B(\mu \bar{\nu}_\mu \nu_\tau)/B(e \bar{\nu}_e \nu_\tau)$ , and  $B(h^- \nu_\tau)$  are 0.08, -0.39, 0.45, and 0.63 respectively.



# Lepton Particle Listings

T

$\Gamma(\pi^- \nu_\tau)/\Gamma_{total}$					$\Gamma_9/\Gamma$
VALUE (%)	EVTs	DOCUMENT ID	TECN	COMMENT	
<b>10.82 ± 0.05 OUR FIT</b>					
<b>10.828 ± 0.070 ± 0.078</b>	38k	1 SCHAEL	05c ALEP	1991-1995 LEP runs	
••• We do not use the following data for averages, fits, limits, etc. •••					
11.06 ± 0.11 ± 0.14		2 BUSKULIC	96 ALEP	Repl. by SCHAEL 05c	
11.7 ± 0.4 ± 1.8	1138	BLOCKER	82D MRK2	$E_{cm}^{ee} = 3.5-6.7$ GeV	
1 See footnote to SCHAEL 05c $\Gamma(\tau^- \rightarrow e^- \bar{\nu}_e \nu_\tau)/\Gamma_{total}$ measurement for correlations with other measurements.					
2 Not independent of BUSKULIC 96 B( $h^- \nu_\tau$ ) and B( $K^- \nu_\tau$ ) values.					

$\Gamma(\pi^- \nu_\tau)/\Gamma(e^- \bar{\nu}_e \nu_\tau)$					$\Gamma_9/\Gamma_5$
VALUE (units 10 <sup>-2</sup> )	EVTs	DOCUMENT ID	TECN	COMMENT	
<b>60.71 ± 0.32 OUR FIT</b>					
<b>59.45 ± 0.14 ± 0.61</b>	369k	1 AUBERT	10f BABR	$467 \text{ fb}^{-1} E_{cm}^{ee} = 10.6$ GeV	
1 See footnote to AUBERT 10f $\Gamma(\tau^- \rightarrow \mu^- \bar{\nu}_\mu \nu_\tau)/\Gamma(\tau^- \rightarrow e^- \bar{\nu}_e \nu_\tau)$ for correlations with other measurements.					

$\Gamma(K^- \nu_\tau)/\Gamma_{total}$					$\Gamma_{10}/\Gamma$
VALUE (%)	EVTs	DOCUMENT ID	TECN	COMMENT	
<b>0.696 ± 0.010 OUR FIT</b>					
<b>0.685 ± 0.023 OUR AVERAGE</b>					
0.658 ± 0.027 ± 0.029		1 ABBIENDI	01J OPAL	1990-1995 LEP runs	
0.696 ± 0.025 ± 0.014	2032	BARATE	99k ALEP	1991-1995 LEP runs	
0.85 ± 0.18	27	ABREU	94k DLPH	LEP 1992 Z data	
0.66 ± 0.07 ± 0.09	99	BATTLE	94 CLEO	$E_{cm}^{ee} \approx 10.6$ GeV	
••• We do not use the following data for averages, fits, limits, etc. •••					
0.72 ± 0.04 ± 0.04	728	BUSKULIC	96 ALEP	Repl. by BARATE 99k	
0.59 ± 0.18	16	MILLS	84 DLCO	$E_{cm}^{ee} = 29$ GeV	
1.3 ± 0.5	15	BLOCKER	82b MRK2	$E_{cm}^{ee} = 3.9-6.7$ GeV	
1 The correlation coefficient between this measurement and the ABBIENDI 01J B( $\tau^- \rightarrow K^- \geq 0\pi^0 \geq 0K^0 \geq 0\gamma \nu_\tau$ ) is 0.60.					

$\Gamma(K^- \nu_\tau)/\Gamma(e^- \bar{\nu}_e \nu_\tau)$					$\Gamma_{10}/\Gamma_5$
VALUE (units 10 <sup>-2</sup> )	EVTs	DOCUMENT ID	TECN	COMMENT	
<b>3.91 ± 0.05 OUR FIT</b>					
<b>3.882 ± 0.032 ± 0.057</b>	25k	1 AUBERT	10f BABR	$467 \text{ fb}^{-1} E_{cm}^{ee} = 10.6$ GeV	
1 See footnote to AUBERT 10f $\Gamma(\tau^- \rightarrow \mu^- \bar{\nu}_\mu \nu_\tau)/\Gamma(\tau^- \rightarrow e^- \bar{\nu}_e \nu_\tau)$ for correlations with other measurements.					

$\Gamma(K^- \nu_\tau)/\Gamma(\pi^- \nu_\tau)$					$\Gamma_{10}/\Gamma_9$
VALUE (units 10 <sup>-2</sup> )	EVTs	DOCUMENT ID	TECN	COMMENT	
<b>6.44 ± 0.09 OUR FIT</b>					
<b>6.531 ± 0.056 ± 0.093</b>		1 AUBERT	10f BABR	$467 \text{ fb}^{-1} E_{cm}^{ee} = 10.6$ GeV	
1 Not independent of AUBERT 10f $\Gamma(\tau^- \rightarrow \pi^- \nu_\tau)/\Gamma(\tau^- \rightarrow e^- \bar{\nu}_e \nu_\tau)$ and $\Gamma(\tau^- \rightarrow K^- \nu_\tau)/\Gamma(\tau^- \rightarrow e^- \bar{\nu}_e \nu_\tau)$ .					

$\Gamma(h^- \geq 1 \text{ neutrals } \nu_\tau)/\Gamma_{total}$					$\Gamma_{11}/\Gamma$
VALUE (%)	EVTs	DOCUMENT ID	TECN	COMMENT	
<b>37.01 ± 0.09 OUR FIT</b>					
••• We do not use the following data for averages, fits, limits, etc. •••					
36.14 ± 0.33 ± 0.58		1 AKERS	94E OPAL	1991-1992 LEP runs	
38.4 ± 1.2 ± 1.0		2 BURCHAT	87 MRK2	$E_{cm}^{ee} = 29$ GeV	
42.7 ± 2.0 ± 2.9		BERGER	85 PLUT	$E_{cm}^{ee} = 34.6$ GeV	
1 Not independent of ACKERSTAFF 98M B( $h^- \pi^0 \nu_\tau$ ) and B( $h^- \geq 2\pi^0 \nu_\tau$ ) values.					
2 BURCHAT 87 quote for B( $\pi^{\pm} \geq 1 \text{ neutral } \nu_\tau$ ) = 0.378 ± 0.012 ± 0.010. We add 0.006 to account for contribution from ( $K^* - \nu_\tau$ ) which they fixed at BR = 0.013.					

$\Gamma(h^- \geq 1\pi^0 \nu_\tau \text{ (ex. } K^0))/\Gamma_{total}$					$\Gamma_{12}/\Gamma$
VALUE (%)	EVTs	DOCUMENT ID	TECN	COMMENT	
<b>36.51 ± 0.09 OUR FIT</b>					
<b>36.641 ± 0.155 ± 0.127</b>	45k	1 ABDALLAH	06A DLPH	1992-1995 LEP runs	
1 See footnote to ABDALLAH 06A $\Gamma(\tau^- \rightarrow h^- \nu_\tau)/\Gamma_{total}$ measurement for correlations with other measurements.					

$\Gamma(h^- \pi^0 \nu_\tau)/\Gamma_{total}$					$\Gamma_{13}/\Gamma = (\Gamma_{14} + \Gamma_{16})/\Gamma$
VALUE (%)	EVTs	DOCUMENT ID	TECN	COMMENT	
<b>25.93 ± 0.09 OUR FIT</b>					
<b>25.73 ± 0.16 OUR AVERAGE</b>					
25.67 ± 0.01 ± 0.39	5.4M	FUJIKAWA	08 BELL	$72 \text{ fb}^{-1} E_{cm}^{ee} = 10.6$ GeV	
25.740 ± 0.201 ± 0.138	35k	1 ABDALLAH	06A DLPH	1992-1995 LEP runs	
25.89 ± 0.17 ± 0.29		ACKERSTAFF	98M OPAL	1991-1995 LEP runs	
25.05 ± 0.35 ± 0.50	6613	ACCIARRI	95 L3	1992 LEP run	
25.87 ± 0.12 ± 0.42	51k	2 ARTUSO	94 CLEO	$E_{cm}^{ee} = 10.6$ GeV	

25.76 ± 0.15 ± 0.13	31k	BUSKULIC	96 ALEP	Repl. by SCHAEL 05c	
25.98 ± 0.36 ± 0.52		3 AKERS	94E OPAL	Repl. by ACKERSTAFF 98M	
22.9 ± 0.8 ± 1.3	283	4 ABREU	92N DLPH	$E_{cm}^{ee} = 88.2-94.2$ GeV	
23.1 ± 0.4 ± 0.9	1249	5 ALBRECHT	92Q ARG	$E_{cm}^{ee} = 10$ GeV	
25.02 ± 0.64 ± 0.88	1849	DECAMP	92c ALEP	1989-1990 LEP runs	
22.0 ± 0.8 ± 1.9	779	ANTREASNYAN	91 CBAL	$E_{cm}^{ee} = 9.4-10.6$ GeV	
22.6 ± 1.5 ± 0.7	1101	BEHREND	90 CELL	$E_{cm}^{ee} = 35$ GeV	
23.1 ± 1.9 ± 1.6		BEHREND	84 CELL	$E_{cm}^{ee} = 14, 22$ GeV	

1 See footnote to ABDALLAH 06A  $\Gamma(\tau^- \rightarrow h^- \nu_\tau)/\Gamma_{total}$  measurement for correlations with other measurements.

2 ARTUSO 94 reports the combined result from three independent methods, one of which (23% of the  $\tau^- \rightarrow h^- \pi^0 \nu_\tau$ ) is normalized to the inclusive one-prong branching fraction, taken as 0.854 ± 0.004. Renormalization to the present value causes negligible change.

3 AKERS 94E quote ( $26.25 \pm 0.36 \pm 0.52$ ) × 10<sup>-2</sup>; we subtract 0.27% from their number to correct for  $\tau^- \rightarrow h^- K_L^0 \nu_\tau$ .

4 ABREU 92N with 0.5% added to remove their correction for  $K^*(892)^-$  backgrounds.

5 ALBRECHT 92Q with 0.5% added to remove their correction for  $\tau^- \rightarrow K^*(892)^-$  background.

$\Gamma(\pi^- \pi^0 \nu_\tau)/\Gamma_{total}$					$\Gamma_{14}/\Gamma$
VALUE (%)	EVTs	DOCUMENT ID	TECN	COMMENT	
<b>25.49 ± 0.09 OUR FIT</b>					
<b>25.46 ± 0.12 OUR AVERAGE</b>					
25.471 ± 0.097 ± 0.085	81k	1 SCHAEL	05c ALEP	1991-1995 LEP runs	
••• We use the following data for averages but not for fits. •••					
25.36 ± 0.44		2 ARTUSO	94 CLEO	$E_{cm}^{ee} = 10.6$ GeV	
••• We do not use the following data for averages, fits, limits, etc. •••					
25.30 ± 0.15 ± 0.13		3 BUSKULIC	96 ALEP	Repl. by SCHAEL 05c	
21.5 ± 0.4 ± 1.9	4400	4,5 ALBRECHT	88L ARG	$E_{cm}^{ee} = 10$ GeV	
23.0 ± 1.3 ± 1.7	582	ADLER	87B MRK3	$E_{cm}^{ee} = 3.77$ GeV	
25.8 ± 1.7 ± 2.5		6 BURCHAT	87 MRK2	$E_{cm}^{ee} = 29$ GeV	
22.3 ± 0.6 ± 1.4	629	5 YELTON	86 MRK2	$E_{cm}^{ee} = 29$ GeV	

1 See footnote to SCHAEL 05c  $\Gamma(\tau^- \rightarrow e^- \bar{\nu}_e \nu_\tau)/\Gamma_{total}$  measurement for correlations with other measurements.

2 Not independent of ARTUSO 94 B( $h^- \pi^0 \nu_\tau$ ) and BATTLE 94 B( $K^- \pi^0 \nu_\tau$ ) values.

3 Not independent of BUSKULIC 96 B( $h^- \pi^0 \nu_\tau$ ) and B( $K^- \pi^0 \nu_\tau$ ) values.

4 The authors divide by ( $\Gamma_3 + \Gamma_5 + \Gamma_9 + \Gamma_{10}$ )/ $\Gamma = 0.467$  to obtain this result.

5 Experiment had no hadron identification. Kaon corrections were made, but insufficient information is given to permit their removal.

6 BURCHAT 87 value is not independent of YELTON 86 value. Nonresonant decays included.

$\Gamma(\pi^- \pi^0 \text{ non-}\rho(770) \nu_\tau)/\Gamma_{total}$					$\Gamma_{15}/\Gamma$
VALUE (%)	EVTs	DOCUMENT ID	TECN	COMMENT	
<b>0.3 ± 0.1 ± 0.3</b>					
0.3 ± 0.1 ± 0.3		1 BEHREND	84 CELL	$E_{cm}^{ee} = 14, 22$ GeV	
1 BEHREND 84 assume a flat nonresonant mass distribution down to the $\rho(770)$ mass, using events with mass above 1300 to set the level.					

$\Gamma(K^- \pi^0 \nu_\tau)/\Gamma_{total}$					$\Gamma_{16}/\Gamma$
VALUE (%)	EVTs	DOCUMENT ID	TECN	COMMENT	
<b>0.433 ± 0.015 OUR FIT</b>					
<b>0.426 ± 0.016 OUR AVERAGE</b>					
0.416 ± 0.003 ± 0.018	78k	AUBERT	07AP BABR	$230 \text{ fb}^{-1} E_{cm}^{ee} = 10.6$ GeV	
0.471 ± 0.059 ± 0.023	360	ABBIENDI	04J OPAL	1991-1995 LEP runs	
0.444 ± 0.026 ± 0.024	923	BARATE	99k ALEP	1991-1995 LEP runs	
0.51 ± 0.10 ± 0.07	37	BATTLE	94 CLEO	$E_{cm}^{ee} \approx 10.6$ GeV	
••• We do not use the following data for averages, fits, limits, etc. •••					
0.52 ± 0.04 ± 0.05	395	BUSKULIC	96 ALEP	Repl. by BARATE 99k	

$\Gamma(h^- \geq 2\pi^0 \nu_\tau)/\Gamma_{total}$					$\Gamma_{17}/\Gamma$
VALUE (%)	EVTs	DOCUMENT ID	TECN	COMMENT	
<b>10.81 ± 0.09 OUR FIT</b>					
<b>9.91 ± 0.31 ± 0.27</b>		ACKERSTAFF	98M OPAL	1991-1995 LEP runs	
••• We do not use the following data for averages, fits, limits, etc. •••					
9.89 ± 0.34 ± 0.55		1 AKERS	94E OPAL	Repl. by ACKERSTAFF 98M	
14.0 ± 1.2 ± 0.6	938	2 BEHREND	90 CELL	$E_{cm}^{ee} = 35$ GeV	
12.0 ± 1.4 ± 2.5		3 BURCHAT	87 MRK2	$E_{cm}^{ee} = 29$ GeV	
13.9 ± 2.0 ± 1.9		4 AIHARA	86E TPC	$E_{cm}^{ee} = 29$ GeV	

1 AKERS 94E not independent of AKERS 94E B( $h^- \geq 1\pi^0 \nu_\tau$ ) and B( $h^- \pi^0 \nu_\tau$ ) measurements.

2 No independent of BEHREND 90  $\Gamma(h^- 2\pi^0 \nu_\tau \text{ (exp. } K^0))$  and  $\Gamma(h^- \geq 3\pi^0 \nu_\tau)$ .

3 Error correlated with BURCHAT 87  $\Gamma(\rho^- \nu_e)/\Gamma_{total}$  value.

4 AIHARA 86E (TPC) quote B( $2\pi^0 \pi^- \nu_\tau$ ) + 1.6B( $3\pi^0 \pi^- \nu_\tau$ ) + 1.1B( $\pi^0 \eta \pi^- \nu_\tau$ ).

See key on page 999

Lepton Particle Listings

T

$$\Gamma(h^- 2\pi^0 \nu_\tau)/\Gamma_{\text{total}} \quad \Gamma_{18}/\Gamma$$

$$\Gamma_{18}/\Gamma = (\Gamma_{20} + \Gamma_{23} + 0.15344\Gamma_{36} + 0.15344\Gamma_{38})/\Gamma$$

VALUE (%)	EVTS	DOCUMENT ID	TECN	COMMENT
<b>9.48 ± 0.10 OUR FIT</b>				
• • • We do not use the following data for averages, fits, limits, etc. • • •				
9.48 ± 0.13 ± 0.10	12k	<sup>1</sup> BUSKULIC	96	ALEP Repl. by SCHAELE 05c
<sup>1</sup> BUSKULIC 96 quote 9.29 ± 0.13 ± 0.10. We add 0.19 to undo their correction for $\tau^- \rightarrow h^- K^0 \nu_\tau$ .				

$$\Gamma(h^- 2\pi^0 \nu_\tau (\text{ex. } K^0))/\Gamma_{\text{total}} \quad \Gamma_{19}/\Gamma$$

$$\Gamma_{19}/\Gamma = (\Gamma_{20} + \Gamma_{23})/\Gamma$$

VALUE (%)	EVTS	DOCUMENT ID	TECN	COMMENT
<b>9.32 ± 0.10 OUR FIT</b>				
<b>9.17 ± 0.27 OUR AVERAGE</b>				
9.498 ± 0.320 ± 0.275	9.5k	<sup>1</sup> ABDALLAH	06A	DLPH 1992-1995 LEP runs
8.88 ± 0.37 ± 0.42	1060	ACCIARRI	95	L3 1992 LEP run
• • • We use the following data for averages but not for fits. • • •				
8.96 ± 0.16 ± 0.44		<sup>2</sup> PROCARIO	93	CLEO $E_{\text{cm}}^{\text{ee}} \approx 10.6$ GeV
• • • We do not use the following data for averages, fits, limits, etc. • • •				
10.38 ± 0.66 ± 0.82	809	<sup>3</sup> DECAMP	92c	ALEP Repl. by SCHAELE 05c
5.7 ± 0.5 ± 1.7	133	<sup>4</sup> ANTREASIAN	91	CBAL $E_{\text{cm}}^{\text{ee}} = 9.4-10.6$ GeV
10.0 ± 1.5 ± 1.1	333	<sup>5</sup> BEHREND	90	CELL $E_{\text{cm}}^{\text{ee}} = 35$ GeV
8.7 ± 0.4 ± 1.1	815	<sup>6</sup> BAND	87	MAC $E_{\text{cm}}^{\text{ee}} = 29$ GeV
6.2 ± 0.6 ± 1.2		<sup>7</sup> GAN	87	MRK2 $E_{\text{cm}}^{\text{ee}} = 29$ GeV
6.0 ± 3.0 ± 1.8		BEHREND	84	CELL $E_{\text{cm}}^{\text{ee}} = 14.22$ GeV

<sup>1</sup> See footnote to ABDALLAH 06A  $\Gamma(\tau^- \rightarrow h^- \nu_\tau)/\Gamma_{\text{total}}$  measurement for correlations with other measurements.  
<sup>2</sup> PROCARIO 93 entry is obtained from  $B(h^- 2\pi^0 \nu_\tau)/B(h^- \pi^0 \nu_\tau)$  using ARTUSO 94 result for  $B(h^- \pi^0 \nu_\tau)$ .  
<sup>3</sup> We subtract 0.0015 to account for  $\tau^- \rightarrow K^*(892)^- \nu_\tau$  contribution.  
<sup>4</sup> ANTREASIAN 91 subtract 0.001 to account for the  $\tau^- \rightarrow K^*(892)^- \nu_\tau$  contribution.  
<sup>5</sup> BEHREND 90 subtract 0.002 to account for the  $\tau^- \rightarrow K^*(892)^- \nu_\tau$  contribution.  
<sup>6</sup> BAND 87 assume  $B(\pi^- 3\pi^0 \nu_\tau) = 0.01$  and  $B(\pi^- \pi^0 \eta \nu_\tau) = 0.005$ .  
<sup>7</sup> GAN 87 analysis use photon multiplicity distribution.

$$\Gamma(h^- 2\pi^0 \nu_\tau (\text{ex. } K^0))/\Gamma(h^- \pi^0 \nu_\tau) \quad \Gamma_{19}/\Gamma_{13}$$

$$\Gamma_{19}/\Gamma_{13} = (\Gamma_{20} + \Gamma_{23})/(\Gamma_{14} + \Gamma_{16})$$

VALUE (units $10^{-2}$ )	DOCUMENT ID	TECN	COMMENT
<b>36.0 ± 0.4 OUR FIT</b>			
<b>34.2 ± 0.6 ± 1.6</b>	<sup>1</sup> PROCARIO	93	CLEO $E_{\text{cm}}^{\text{ee}} \approx 10.6$ GeV

<sup>1</sup> PROCARIO 93 quote 0.345 ± 0.006 ± 0.016 after correction for 2 kaon backgrounds assuming  $B(K^* \nu_\tau) = 1.42 \pm 0.18\%$  and  $B(h^- K^0 \pi^0 \nu_\tau) = 0.48 \pm 0.48\%$ . We multiply by 0.990 ± 0.010 to remove these corrections to  $B(h^- \pi^0 \nu_\tau)$ .

$$\Gamma(\pi^- 2\pi^0 \nu_\tau (\text{ex. } K^0))/\Gamma_{\text{total}} \quad \Gamma_{20}/\Gamma$$

VALUE (%)	EVTS	DOCUMENT ID	TECN	COMMENT
<b>9.26 ± 0.10 OUR FIT</b>				
<b>9.239 ± 0.086 ± 0.090</b>	31k	<sup>1</sup> SCHAELE	05c	ALEP 1991-1995 LEP runs
• • • We do not use the following data for averages, fits, limits, etc. • • •				
9.21 ± 0.13 ± 0.11		<sup>2</sup> BUSKULIC	96	ALEP Repl. by SCHAELE 05c

<sup>1</sup> See footnote to SCHAELE 05c  $\Gamma(\tau^- \rightarrow e^- \bar{\nu}_e \nu_\tau)/\Gamma_{\text{total}}$  measurement for correlations with other measurements.  
<sup>2</sup> Not independent of BUSKULIC 96  $B(h^- 2\pi^0 \nu_\tau (\text{ex. } K^0))$  and  $B(K^- 2\pi^0 \nu_\tau (\text{ex. } K^0))$  values.

$$\Gamma(\pi^- 2\pi^0 \nu_\tau (\text{ex. } K^0), \text{scalar})/\Gamma(\pi^- 2\pi^0 \nu_\tau (\text{ex. } K^0)) \quad \Gamma_{21}/\Gamma_{20}$$

VALUE	CL%	DOCUMENT ID	TECN	COMMENT
<b>&lt;0.094</b>	95	<sup>1</sup> BROWDER	00	CLEO 4.7 fb <sup>-1</sup> $E_{\text{cm}}^{\text{ee}} = 10.6$ GeV

<sup>1</sup> Model-independent limit from structure function analysis on contribution to  $B(\tau^- \rightarrow \pi^- 2\pi^0 \nu_\tau (\text{ex. } K^0))$  from scalars.

$$\Gamma(\pi^- 2\pi^0 \nu_\tau (\text{ex. } K^0), \text{vector})/\Gamma(\pi^- 2\pi^0 \nu_\tau (\text{ex. } K^0)) \quad \Gamma_{22}/\Gamma_{20}$$

VALUE	CL%	DOCUMENT ID	TECN	COMMENT
<b>&lt;0.073</b>	95	<sup>1</sup> BROWDER	00	CLEO 4.7 fb <sup>-1</sup> $E_{\text{cm}}^{\text{ee}} = 10.6$ GeV

<sup>1</sup> Model-independent limit from structure function analysis on contribution to  $B(\tau^- \rightarrow \pi^- 2\pi^0 \nu_\tau (\text{ex. } K^0))$  from vectors.

$$\Gamma(K^- 2\pi^0 \nu_\tau (\text{ex. } K^0))/\Gamma_{\text{total}} \quad \Gamma_{23}/\Gamma$$

VALUE (units $10^{-4}$ )	EVTS	DOCUMENT ID	TECN	COMMENT
<b>6.5 ± 2.2 OUR FIT</b>				
<b>5.8 ± 2.4 OUR AVERAGE</b>				
5.6 ± 2.0 ± 1.5	131	BARATE	99K	ALEP 1991-1995 LEP runs
9 ± 10 ± 3	3	<sup>1</sup> BATTLE	94	CLEO $E_{\text{cm}}^{\text{ee}} \approx 10.6$ GeV
• • • We do not use the following data for averages, fits, limits, etc. • • •				
8 ± 2 ± 2	59	BUSKULIC	96	ALEP Repl. by BARATE 99K

<sup>1</sup> BATTLE 94 quote  $(14 \pm 10 \pm 3) \times 10^{-4}$  or  $< 30 \times 10^{-4}$  at 90% CL. We subtract  $(5 \pm 2) \times 10^{-4}$  to account for  $\tau^- \rightarrow K^- (K^0 \rightarrow \pi^0 \pi^0) \nu_\tau$  background.

$$\Gamma(h^- \geq 3\pi^0 \nu_\tau)/\Gamma_{\text{total}} \quad \Gamma_{24}/\Gamma$$

$$\Gamma_{24}/\Gamma = (\Gamma_{27} + \Gamma_{28} + \Gamma_{30} + 0.15344\Gamma_{41} + 0.15344\Gamma_{43} + 0.0942\Gamma_{48} + 0.0942\Gamma_{52} + 0.3268\Gamma_{150} + 0.3268\Gamma_{152} + 0.3268\Gamma_{154} + 0.0501\Gamma_{156})/\Gamma$$

VALUE (%)	EVTS	DOCUMENT ID	TECN	COMMENT
<b>1.34 ± 0.07 OUR FIT</b>				
• • • We do not use the following data for averages, fits, limits, etc. • • •				
1.53 ± 0.40 ± 0.46	186	DECAMP	92c	ALEP Repl. by SCHAELE 05c
3.2 ± 1.0 ± 1.0		BEHREND	90	CELL $E_{\text{cm}}^{\text{ee}} = 35$ GeV

$$\Gamma(h^- \geq 3\pi^0 \nu_\tau (\text{ex. } K^0))/\Gamma_{\text{total}} \quad \Gamma_{25}/\Gamma$$

$$\Gamma_{25}/\Gamma = (\Gamma_{27} + \Gamma_{28} + \Gamma_{30} + 0.3268\Gamma_{150} + 0.3268\Gamma_{152} + 0.3268\Gamma_{154})/\Gamma$$

VALUE (%)	EVTS	DOCUMENT ID	TECN	COMMENT
<b>1.25 ± 0.07 OUR FIT</b>				
<b>1.403 ± 0.214 ± 0.224</b>				
1.1k		<sup>1</sup> ABDALLAH	06A	DLPH 1992-1995 LEP runs
<sup>1</sup> See footnote to ABDALLAH 06A $\Gamma(\tau^- \rightarrow h^- \nu_\tau)/\Gamma_{\text{total}}$ measurement for correlations with other measurements.				

$$\Gamma(h^- 3\pi^0 \nu_\tau)/\Gamma_{\text{total}} \quad \Gamma_{26}/\Gamma$$

$$\Gamma_{26}/\Gamma = (\Gamma_{27} + \Gamma_{28} + 0.15344\Gamma_{41} + 0.15344\Gamma_{43} + 0.3268\Gamma_{152})/\Gamma$$

VALUE (%)	EVTS	DOCUMENT ID	TECN	COMMENT
<b>1.18 ± 0.07 OUR FIT</b>				
<b>1.21 ± 0.17 OUR AVERAGE</b>				
1.70 ± 0.24 ± 0.38	293	ACCIARRI	95	L3 1992 LEP run
• • • We use the following data for averages but not for fits. • • •				
1.15 ± 0.08 ± 0.13		<sup>1</sup> PROCARIO	93	CLEO $E_{\text{cm}}^{\text{ee}} \approx 10.6$ GeV
• • • We do not use the following data for averages, fits, limits, etc. • • •				
1.24 ± 0.09 ± 0.11	2.3k	<sup>2</sup> BUSKULIC	96	ALEP Repl. by SCHAELE 05c
0.0 ± 1.4 ± 1.1		<sup>3</sup> GAN	87	MRK2 $E_{\text{cm}}^{\text{ee}} = 29$ GeV

<sup>1</sup> PROCARIO 93 entry is obtained from  $B(h^- 3\pi^0 \nu_\tau)/B(h^- \pi^0 \nu_\tau)$  using ARTUSO 94 result for  $B(h^- \pi^0 \nu_\tau)$ .  
<sup>2</sup> BUSKULIC 96 quote  $B(h^- 3\pi^0 \nu_\tau (\text{ex. } K^0)) = 1.17 \pm 0.09 \pm 0.11$ . We add 0.07 to remove their correction for  $K^0$  backgrounds.  
<sup>3</sup> Highly correlated with GAN 87  $\Gamma(\pi^- \pi^0 \nu_\tau)/\Gamma_{\text{total}}$  value. Authors quote  $B(\pi^\pm 3\pi^0 \nu_\tau) + 0.67B(\pi^\pm \eta \pi^0 \nu_\tau) = 0.047 \pm 0.010 \pm 0.011$ .

$$\Gamma(h^- 3\pi^0 \nu_\tau)/\Gamma(h^- \pi^0 \nu_\tau) \quad \Gamma_{26}/\Gamma_{13}$$

$$\Gamma_{26}/\Gamma_{13} = (\Gamma_{27} + \Gamma_{28} + 0.15344\Gamma_{41} + 0.15344\Gamma_{43} + 0.3268\Gamma_{152})/(\Gamma_{14} + \Gamma_{16})$$

VALUE (units $10^{-2}$ )	DOCUMENT ID	TECN	COMMENT
<b>4.54 ± 0.28 OUR FIT</b>			
<b>4.4 ± 0.3 ± 0.5</b>	<sup>1</sup> PROCARIO	93	CLEO $E_{\text{cm}}^{\text{ee}} \approx 10.6$ GeV

<sup>1</sup> PROCARIO 93 quote 0.041 ± 0.003 ± 0.005 after correction for 2 kaon backgrounds assuming  $B(K^* \nu_\tau) = 1.42 \pm 0.18\%$  and  $B(h^- K^0 \pi^0 \nu_\tau) = 0.48 \pm 0.48\%$ . We add 0.003 ± 0.003 and multiply the sum by 0.990 ± 0.010 to remove these corrections.

$$\Gamma(\pi^- 3\pi^0 \nu_\tau (\text{ex. } K^0))/\Gamma_{\text{total}} \quad \Gamma_{27}/\Gamma$$

VALUE (%)	EVTS	DOCUMENT ID	TECN	COMMENT
<b>1.04 ± 0.07 OUR FIT</b>				
<b>0.977 ± 0.069 ± 0.058</b>	6.1k	<sup>1</sup> SCHAELE	05c	ALEP 1991-1995 LEP runs

<sup>1</sup> See footnote to SCHAELE 05c  $\Gamma(\tau^- \rightarrow e^- \bar{\nu}_e \nu_\tau)/\Gamma_{\text{total}}$  measurement for correlations with other measurements.

$$\Gamma(K^- 3\pi^0 \nu_\tau (\text{ex. } K^0, \eta))/\Gamma_{\text{total}} \quad \Gamma_{28}/\Gamma$$

VALUE (units $10^{-4}$ )	EVTS	DOCUMENT ID	TECN	COMMENT
<b>4.8 ± 2.1 OUR FIT</b>				
<b>3.7 ± 2.1 ± 1.1</b>	22	BARATE	99K	ALEP 1991-1995 LEP runs
• • • We do not use the following data for averages, fits, limits, etc. • • •				
5 ± 13		<sup>1</sup> BUSKULIC	94E	ALEP Repl. by BARATE 99K

<sup>1</sup> BUSKULIC 94E quote  $B(K^- \geq 0\pi^0 \geq 0K^0 \nu_\tau) - [B(K^- \nu_\tau) + B(K^- \pi^0 \nu_\tau) + B(K^- K^0 \nu_\tau) + B(K^- \pi^0 \pi^0 \nu_\tau) + B(K^- \pi^0 K^0 \nu_\tau)] = (5 \pm 13) \times 10^{-4}$  accounting for common systematic errors in BUSKULIC 94E and BUSKULIC 94F measurements of these modes. We assume  $B(K^- \geq 2K^0 \nu_\tau)$  and  $B(K^- \geq 4\pi^0 \nu_\tau)$  are negligible.

$$\Gamma(h^- 4\pi^0 \nu_\tau (\text{ex. } K^0))/\Gamma_{\text{total}} \quad \Gamma_{29}/\Gamma$$

$$\Gamma_{29}/\Gamma = (\Gamma_{30} + 0.3268\Gamma_{150} + 0.3268\Gamma_{154})/\Gamma$$

VALUE (%)	EVTS	DOCUMENT ID	TECN	COMMENT
<b>0.16 ± 0.04 OUR FIT</b>				
<b>0.16 ± 0.05 ± 0.05</b>		<sup>1</sup> PROCARIO	93	CLEO $E_{\text{cm}}^{\text{ee}} \approx 10.6$ GeV
• • • We do not use the following data for averages, fits, limits, etc. • • •				
0.16 ± 0.04 ± 0.09	232	<sup>2</sup> BUSKULIC	96	ALEP Repl. by SCHAELE 05c

<sup>1</sup> PROCARIO 93 quotes  $B(h^- 4\pi^0 \nu_\tau)/B(h^- \pi^0 \nu_\tau) = 0.006 \pm 0.002 \pm 0.002$ . We multiply by the ARTUSO 94 result for  $B(h^- \pi^0 \nu_\tau)$  to obtain  $B(h^- 4\pi^0 \nu_\tau)$ . PROCARIO 93 assume  $B(h^- \geq 5\pi^0 \nu_\tau)$  is small and do not correct for it.  
<sup>2</sup> BUSKULIC 96 quote result for  $\tau^- \rightarrow h^- \geq 4\pi^0 \nu_\tau$ . We assume  $B(h^- \geq 5\pi^0 \nu_\tau)$  is negligible.

$$\Gamma(h^- 4\pi^0 \nu_\tau (\text{ex. } K^0, \eta))/\Gamma_{\text{total}} \quad \Gamma_{30}/\Gamma$$

VALUE (%)	EVTS	DOCUMENT ID	TECN	COMMENT
<b>0.11 ± 0.04 OUR FIT</b>				
<b>0.112 ± 0.037 ± 0.035</b>	957	<sup>1</sup> SCHAELE	05c	ALEP 1991-1995 LEP runs

<sup>1</sup> See footnote to SCHAELE 05c  $\Gamma(\tau^- \rightarrow e^- \bar{\nu}_e \nu_\tau)/\Gamma_{\text{total}}$  measurement for correlations with other measurements.

# Lepton Particle Listings

$\tau$

## $\Gamma(a_1(1260)\nu_\tau \rightarrow \pi^- \gamma \nu_\tau)/\Gamma_{total}$ $\Gamma_{31}/\Gamma = (0.0021\Gamma_{20} + 0.0021\Gamma_{70})/\Gamma$

The uncertainty on  $\Gamma(\tau^- \rightarrow a_1(1260)\nu_\tau \rightarrow \pi^- \gamma \nu_\tau)/\Gamma_{total}$  is the sum in quadrature of the uncertainty on the fit result for  $\Gamma(\tau^- \rightarrow a_1(1260)\nu_\tau \rightarrow \pi^- \gamma \nu_\tau)/\Gamma_{total}$  and of the uncertainty on  $\Gamma(a_1(1260) \rightarrow \pi\gamma)/\Gamma_{total} = ((2.1 \pm 0.8) \times 10^{-3})$  as reported in SCHAEF 05c, which is the coefficient of the relationship that defines  $\Gamma(\tau^- \rightarrow a_1(1260)\nu_\tau \rightarrow \pi^- \gamma \nu_\tau)/\Gamma_{total}$  in terms of  $\Gamma(\tau^- \rightarrow \pi^- 2\pi^0 \nu_\tau (\text{ex. } K^0))/\Gamma_{total}$  and  $\Gamma(\tau^- \rightarrow \pi^- \pi^+ \pi^- \nu_\tau (\text{ex. } K^0, \omega))/\Gamma_{total}$ .

VALUE (units $10^{-4}$ )	EVTS	DOCUMENT ID	TECN	COMMENT
<b>3.8 ± 1.5 OUR FIT</b>				

## $\Gamma(K^- \geq 0\pi^0 \geq 0K^0 \geq 0\gamma \nu_\tau)/\Gamma_{total}$ $\Gamma_{32}/\Gamma$

$\Gamma_{32}/\Gamma = (\Gamma_{10} + \Gamma_{16} + \Gamma_{23} + \Gamma_{28} + \Gamma_{38} + \Gamma_{43} + 0.7212\Gamma_{152} + 0.1049\Gamma_{170})/\Gamma$

VALUE (%)	EVTS	DOCUMENT ID	TECN	COMMENT
<b>1.552 ± 0.029 OUR FIT</b>				
<b>1.53 ± 0.04 OUR AVERAGE</b>				
1.528 ± 0.039 ± 0.040		1 ABBIENDI 01J OPAL 1990-1995 LEP runs		
1.54 ± 0.24		ABREU 94K DLPH LEP 1992 Z data		
1.70 ± 0.12 ± 0.19	202	2 BATTLE 94 CLEO $E_{cm}^{ee} \approx 10.6$ GeV		

- • • We use the following data for averages but not for fits. • • •
- • • We do not use the following data for averages, fits, limits, etc. • • •
- 1.520 ± 0.040 ± 0.041 4006 3 BARATE 99k ALEP 1991-1995 LEP runs
- 1.70 ± 0.05 ± 0.06 1610 4 BUSKULIC 96 ALEP Repl. by BARATE 99k
- 1.6 ± 0.4 ± 0.2 35 AIHARA 87B TPC  $E_{cm}^{ee} = 29$  GeV
- 1.71 ± 0.29 53 MILLS 84 DLCO  $E_{cm}^{ee} = 29$  GeV

- The correlation coefficient between this measurement and the ABBIENDI 01J  $B(\tau^- \rightarrow K^- \nu_\tau)$  is 0.60.
- BATTLE 94 quote  $1.60 \pm 0.12 \pm 0.19$ . We add  $0.10 \pm 0.02$  to correct for their rejection of  $K_S^0 \rightarrow \pi^+ \pi^-$  decays.
- Not independent of BARATE 99k  $B(K^- \nu_\tau)$ ,  $B(K^- \pi^0 \nu_\tau)$ ,  $B(K^- 2\pi^0 \nu_\tau (\text{ex. } K^0))$ ,  $B(K^- 3\pi^0 \nu_\tau (\text{ex. } K^0))$ ,  $B(K^- K^0 \nu_\tau)$ , and  $B(K^- K^0 \pi^0 \nu_\tau)$  values.
- Not independent of BUSKULIC 96  $B(K^- \nu_\tau)$ ,  $B(K^- \pi^0 \nu_\tau)$ ,  $B(K^- 2\pi^0 \nu_\tau)$ ,  $B(K^- K^0 \nu_\tau)$ , and  $B(K^- K^0 \pi^0 \nu_\tau)$  values.

## $\Gamma(K^- \geq 1(\pi^0 \text{ or } K^0 \text{ or } \gamma) \nu_\tau)/\Gamma_{total}$ $\Gamma_{33}/\Gamma$

$\Gamma_{33}/\Gamma = (\Gamma_{16} + \Gamma_{23} + \Gamma_{28} + \Gamma_{38} + \Gamma_{43} + 0.7212\Gamma_{152} + 0.7212\Gamma_{154} + 0.1049\Gamma_{170})/\Gamma$

VALUE (%)	EVTS	DOCUMENT ID	TECN	COMMENT
<b>0.859 ± 0.028 OUR FIT</b>				
<b>0.86 ± 0.05 OUR AVERAGE</b>				

- • • We use the following data for averages but not for fits. • • •
  - • • We do not use the following data for averages, fits, limits, etc. • • •
  - 0.869 ± 0.031 ± 0.034 1 ABBIENDI 01J OPAL 1990-1995 LEP runs
  - 0.69 ± 0.25 2 ABREU 94K DLPH LEP 1992 Z data
  - 1.2 ± 0.5  $\pm 0.2$  9 AIHARA 87B TPC  $E_{cm}^{ee} = 29$  GeV
- Not independent of ABBIENDI 01J  $B(\tau^- \rightarrow K^- \nu_\tau)$  and  $B(\tau^- \rightarrow K^- \geq 0\pi^0 \geq 0K^0 \geq 0\gamma \nu_\tau)$  values.
  - Not independent of ABREU 94K  $B(K^- \nu_\tau)$  and  $B(K^- \geq 0$  neutrals  $\nu_\tau)$  measurements.

## $\Gamma(K_S^0 (\text{particles})^- \nu_\tau)/\Gamma_{total}$ $\Gamma_{34}/\Gamma$

$\Gamma_{34}/\Gamma = (\frac{1}{2}\Gamma_{36} + \frac{1}{2}\Gamma_{38} + \frac{1}{2}\Gamma_{41} + \frac{1}{2}\Gamma_{43} + \frac{1}{2}\Gamma_{45} + \Gamma_{48} + \Gamma_{49} + \Gamma_{52} + \Gamma_{56} + 0.3606\Gamma_{156} + 0.340\Gamma_{170})/\Gamma$

VALUE (%)	EVTS	DOCUMENT ID	TECN	COMMENT
<b>0.943 ± 0.028 OUR FIT</b>				
<b>0.918 ± 0.015 OUR AVERAGE</b>				
0.970 ± 0.058 ± 0.062	929	BARATE 98E ALEP 1991-1995 LEP runs		
0.97 ± 0.09 ± 0.06	141	AKERS 94G OPAL $E_{cm}^{ee} = 88-94$ GeV		

- • • We use the following data for averages but not for fits. • • •
  - 0.915 ± 0.001 ± 0.015 398k 1 RYU 14 BELL 669 fb<sup>-1</sup>  $E_{cm}^{ee} = 10.6$  GeV
- Not independent of RYU 14 measurements of  $B(\tau^- \rightarrow \pi^- \bar{K}^0 \nu_\tau)$ ,  $B(\tau^- \rightarrow K^- K^0 \nu_\tau)$ ,  $B(\tau^- \rightarrow \pi^- \bar{K}^0 \pi^0 \nu_\tau)$ ,  $B(\tau^- \rightarrow K^- K^0 \pi^0 \nu_\tau)$ ,  $B(\tau^- \rightarrow \pi^- K_S^0 K_S^0 \nu_\tau)$ , and  $B(\tau^- \rightarrow \pi^- K_S^0 K_S^0 \pi^0 \nu_\tau)$ .

## $\Gamma(h^- \bar{K}^0 \nu_\tau)/\Gamma_{total}$ $\Gamma_{35}/\Gamma = (\Gamma_{36} + \Gamma_{38})/\Gamma$

VALUE (%)	EVTS	DOCUMENT ID	TECN	COMMENT
<b>0.987 ± 0.014 OUR FIT</b>				
<b>0.90 ± 0.07 OUR AVERAGE</b>				

- • • We use the following data for averages but not for fits. • • •
  - 0.855 ± 0.036 ± 0.073 1242 COAN 96 CLEO  $E_{cm}^{ee} \approx 10.6$  GeV
  - 1.01 ± 0.11 ± 0.07 555 1 BARATE 98E ALEP 1991-1995 LEP runs
- Not independent of BARATE 98E  $B(\tau^- \rightarrow \pi^- \bar{K}^0 \nu_\tau)$  and  $B(\tau^- \rightarrow K^- K^0 \nu_\tau)$  values.

## $\Gamma(\pi^- \bar{K}^0 \nu_\tau)/\Gamma_{total}$ $\Gamma_{36}/\Gamma$

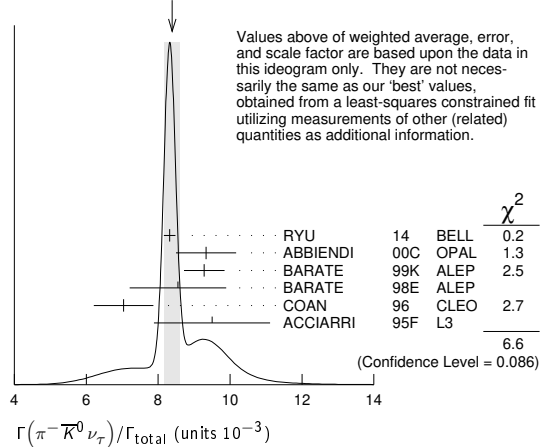
VALUE (units $10^{-3}$ )	EVTS	DOCUMENT ID	TECN	COMMENT
<b>8.38 ± 0.14 OUR FIT</b>				
<b>8.39 ± 0.22 OUR AVERAGE</b>				

- Error includes scale factor of 1.5. See the ideogram below.
- |                    |      |   |  |  |
|--------------------|------|---|--|--|
| 8.32 ± 0.02 ± 0.16 | 158k | 1 RYU 14 BELL 669 fb <sup>-1</sup> $E_{cm}^{ee} = 10.6$ GeV |  |  |
| 9.33 ± 0.68 ± 0.49 | 377  | ABBIENDI 00c OPAL 1991-1995 LEP runs                        |  |  |
| 9.28 ± 0.45 ± 0.34 | 937  | 2 BARATE 99k ALEP 1991-1995 LEP runs                        |  |  |
| 9.5 ± 1.5 ± 0.6    |      | 3 ACCIARRI 95F L3 1991-1993 LEP runs                        |  |  |

- • • We use the following data for averages but not for fits. • • •
- 8.55 ± 1.17 ± 0.66 509 4 BARATE 98E ALEP 1991-1995 LEP runs
- 7.04 ± 0.41 ± 0.72 5 COAN 96 CLEO  $E_{cm}^{ee} \approx 10.6$  GeV

- • • We do not use the following data for averages, fits, limits, etc. • • •
  - 8.08 ± 0.04 ± 0.26 53k EPIFANOV 07 BELL Repl. by RYU 14
  - 7.9 ± 1.0 ± 0.9 98 6 BUSKULIC 96 ALEP Repl. by BARATE 99k
- RYU 14 reconstruct  $K^0$ 's using  $K_S^0 \rightarrow \pi^+ \pi^-$  decays.
  - BARATE 99k measure  $K^0$ 's by detecting  $K_L^0$ 's in their hadron calorimeter.
  - ACCIARRI 95F do not identify  $\pi^-/K^-$  and assume  $B(K^- K^0 \nu_\tau) = (0.29 \pm 0.12)\%$ .
  - BARATE 98E reconstruct  $K^0$ 's using  $K_S^0 \rightarrow \pi^+ \pi^-$  decays. Not independent of BARATE 98E  $B(K^0 \text{ particles}^- \nu_\tau)$  value.
  - Not independent of COAN 96  $B(h^- K^0 \nu_\tau)$  and  $B(K^- K^0 \nu_\tau)$  measurements.
  - BUSKULIC 96 measure  $K^0$ 's by detecting  $K_L^0$ 's in their hadron calorimeter.

WEIGHTED AVERAGE  
8.39 ± 0.22 (Error scaled by 1.5)



## $\Gamma(\pi^- \bar{K}^0 (\text{non-} K^*(892)^- \nu_\tau)/\Gamma_{total}$ $\Gamma_{37}/\Gamma$

VALUE (units $10^{-4}$ )	CL%	DOCUMENT ID	TECN	COMMENT
<b>5.4 ± 2.1</b>				

- • • We do not use the following data for averages, fits, limits, etc. • • •
- <1 95 ACCIARRI 95F L3 1991-1993 LEP runs
- 1 EPIFANOV 07 quote  $B(\tau^- \rightarrow K^*(892)^- \nu_\tau) B(K^*(892)^- \rightarrow K_S^0 \pi^-) / B(\tau^- \rightarrow K_S^0 \pi^- \nu_\tau) = 0.933 \pm 0.027$ . We multiply their  $B(\tau^- \rightarrow \bar{K}^0 \pi^- \nu_\tau)$  by  $[1 - (0.933 \pm 0.027)]$  to obtain this result.

## $\Gamma(K^- K^0 \nu_\tau)/\Gamma_{total}$ $\Gamma_{38}/\Gamma$

VALUE (units $10^{-4}$ )	EVTS	DOCUMENT ID	TECN	COMMENT
<b>14.86 ± 0.34 OUR FIT</b>				
<b>14.83 ± 0.35 OUR AVERAGE</b>				

- |                     |     |   |  |  |
|---------------------|-----|---|--|--|
| 14.78 ± 0.22 ± 0.40 | 29k | 1 LEES 18B BABR 468 fb <sup>-1</sup> $E_{cm}^{ee} = 10.6$ GeV |  |  |
| 14.80 ± 0.14 ± 0.54 | 33k | 2 RYU 14 BELL 669 fb <sup>-1</sup> $E_{cm}^{ee} = 10.6$ GeV   |  |  |
| 16.2 ± 2.1 ± 1.1    | 150 | 3 BARATE 99k ALEP 1991-1995 LEP runs                          |  |  |
| 15.8 ± 4.2 ± 1.7    | 46  | 4 BARATE 98E ALEP 1991-1995 LEP runs                          |  |  |
| 15.1 ± 2.1 ± 2.2    | 111 | COAN 96 CLEO $E_{cm}^{ee} \approx 10.6$ GeV                   |  |  |

- • • We do not use the following data for averages, fits, limits, etc. • • •
  - 26 ± 9 ± 2 13 5 BUSKULIC 96 ALEP Repl. by BARATE 99k
- LEES 18B reconstructs  $K^0$ 's using  $K_S^0 \rightarrow \pi^+ \pi^-$  decays.
  - RYU 14 reconstruct  $K^0$ 's using  $K_S^0 \rightarrow \pi^+ \pi^-$  decays.
  - BARATE 99k measure  $K^0$ 's by detecting  $K_L^0$ 's in their hadron calorimeter.
  - BARATE 98E reconstruct  $K^0$ 's using  $K_S^0 \rightarrow \pi^+ \pi^-$  decays.
  - BUSKULIC 96 measure  $K^0$ 's by detecting  $K_L^0$ 's in their hadron calorimeter.

## $\Gamma(K^- K^0 \geq 0\pi^0 \nu_\tau)/\Gamma_{total}$ $\Gamma_{39}/\Gamma = (\Gamma_{38} + \Gamma_{43})/\Gamma$

VALUE (%)	EVTS	DOCUMENT ID	TECN	COMMENT
<b>0.299 ± 0.007 OUR FIT</b>				
<b>0.330 ± 0.055 ± 0.039</b>				

- |                       |     |                                      |  |  |
|-----------------------|-----|--------------------------------------|--|--|
| 0.330 ± 0.055 ± 0.039 | 124 | ABBIENDI 00c OPAL 1991-1995 LEP runs |  |  |
|-----------------------|-----|--------------------------------------|--|--|

## $\Gamma(h^- \bar{K}^0 \pi^0 \nu_\tau)/\Gamma_{total}$ $\Gamma_{40}/\Gamma = (\Gamma_{41} + \Gamma_{43})/\Gamma$

VALUE (%)	EVTS	DOCUMENT ID	TECN	COMMENT
<b>0.532 ± 0.013 OUR FIT</b>				
<b>0.50 ± 0.06 OUR AVERAGE</b>				

- Error includes scale factor of 1.2.
- |                       |     |   |  |  |
|-----------------------|-----|---|--|--|
| 0.562 ± 0.050 ± 0.048 | 264 | COAN 96 CLEO $E_{cm}^{ee} \approx 10.6$ GeV |  |  |
|-----------------------|-----|---|--|--|
- • • We use the following data for averages but not for fits. • • •
  - 0.446 ± 0.052 ± 0.046 157 1 BARATE 98E ALEP 1991-1995 LEP runs
- Not independent of BARATE 98E  $B(\tau^- \rightarrow \pi^- \bar{K}^0 \pi^0 \nu_\tau)$  and  $B(\tau^- \rightarrow K^- K^0 \pi^0 \nu_\tau)$  values.

$\Gamma(\pi^- \bar{K}^0 \pi^0 \nu_\tau) / \Gamma_{total}$   $\Gamma_{41} / \Gamma$

Table with columns: VALUE (%), EVTS, DOCUMENT ID, TECN, COMMENT. Rows include 0.382 ± 0.013 OUR FIT and 0.383 ± 0.014 OUR AVERAGE with various experiment entries like RYU, BARATE, ACCIARRI.

• • • We use the following data for averages but not for fits. • • •
0.417 ± 0.058 ± 0.044 5 COAN 96 CLEO E\_cm^ee ≈ 10.6 GeV
• • • We do not use the following data for averages, fits, limits, etc. • • •
0.32 ± 0.11 ± 0.05 23 6 BUSKULIC 96 ALEP Repl. by BARATE 99K

$\Gamma(K^0 \rho^- \nu_\tau) / \Gamma_{total}$   $\Gamma_{42} / \Gamma$

Table with columns: VALUE (%), DOCUMENT ID, TECN, COMMENT. Rows include 0.22 ± 0.05 OUR AVERAGE and 0.188 ± 0.054 ± 0.038 with entries BARATE 99K and BARATE 98E.

1 BARATE 99K measure K^0's by detecting K\_L^0's in hadron calorimeter. They determine the K^0 rho^- fraction in pi- to pi- K^0 pi^0 nu\_tau decays to be (0.72 ± 0.12 ± 0.10) and multiply their B(pi- K^0 pi^0 nu\_tau) measurement by this fraction to obtain the quoted result.
2 BARATE 98E reconstruct K^0's using K\_S^0 to pi+ pi- decays. They determine the K^0 rho^- fraction in pi- to pi- K^0 pi^0 nu\_tau decays to be (0.64 ± 0.09 ± 0.10) and multiply their B(pi- K^0 pi^0 nu\_tau) measurement by this fraction to obtain the quoted result.

$\Gamma(K^- K^0 \pi^0 \nu_\tau) / \Gamma_{total}$   $\Gamma_{43} / \Gamma$

Table with columns: VALUE (units 10^-4), EVTS, DOCUMENT ID, TECN, COMMENT. Rows include 15.0 ± 0.7 OUR FIT and 14.9 ± 0.7 OUR AVERAGE with entries RYU, BARATE, COAN, CLEO.

• • • We do not use the following data for averages, fits, limits, etc. • • •
10 ± 5 ± 3 5 4 BUSKULIC 96 ALEP Repl. by BARATE 99K
1 RYU 14 reconstruct K^0's using K\_S^0 to pi+ pi- decays.
2 BARATE 99K measure K^0's by detecting K\_L^0's in their hadron calorimeter.
3 BARATE 98E reconstruct K^0's using K\_S^0 to pi+ pi- decays.
4 BUSKULIC 96 measure K^0's by detecting K\_L^0's in their hadron calorimeter.

$\Gamma(\pi^- \bar{K}^0 \geq 1 \pi^0 \nu_\tau) / \Gamma_{total}$   $\Gamma_{44} / \Gamma = (\Gamma_{41} + \Gamma_{45}) / \Gamma$

Table with columns: VALUE (%), EVTS, DOCUMENT ID, TECN, COMMENT. Rows include 0.408 ± 0.025 OUR FIT and 0.324 ± 0.074 ± 0.066 with entry ABBIENDI.

$\Gamma(\pi^- \bar{K}^0 \pi^0 \pi^0 \nu_\tau (ex. K^0)) / \Gamma_{total}$   $\Gamma_{45} / \Gamma$

Table with columns: VALUE (units 10^-3), CL%, EVTS, DOCUMENT ID, TECN, COMMENT. Rows include 0.26 ± 0.23 OUR FIT and 0.26 ± 0.24 with entry BARATE.

• • • We do not use the following data for averages, fits, limits, etc. • • •
<0.66 95 17 2 BARATE 99K ALEP 1991-1995 LEP runs
0.58 ± 0.33 ± 0.14 5 3 BARATE 98E ALEP 1991-1995 LEP runs

$\Gamma(K^- K^0 \pi^0 \pi^0 \nu_\tau) / \Gamma_{total}$   $\Gamma_{46} / \Gamma$

Table with columns: VALUE, CL%, DOCUMENT ID, TECN, COMMENT. Rows include <0.16 x 10^-3 95 1 BARATE 99R ALEP 1991-1995 LEP runs.

• • • We do not use the following data for averages, fits, limits, etc. • • •
<0.18 x 10^-3 95 2 BARATE 99K ALEP 1991-1995 LEP runs
<0.39 x 10^-3 95 3 BARATE 98E ALEP 1991-1995 LEP runs

$\Gamma(\pi^- K^0 \bar{K}^0 \nu_\tau) / \Gamma_{total}$   $\Gamma_{47} / \Gamma = (\Gamma_{48} + \Gamma_{49} + \Gamma_{50}) / \Gamma$

Table with columns: VALUE (%), EVTS, DOCUMENT ID, TECN, COMMENT. Rows include 0.155 ± 0.024 OUR FIT and 0.153 ± 0.030 ± 0.016 with entry BARATE.

• • • We do not use the following data for averages, fits, limits, etc. • • •
0.31 ± 0.12 ± 0.04 2 ACCIARRI 95F L3 1991-1993 LEP runs
1 BARATE 98E obtain this value by adding twice their B(pi- K\_S^0 K\_L^0 nu\_tau) value to their B(pi- K\_S^0 K\_L^0 nu\_tau) value.
2 ACCIARRI 95F assume B(pi- K\_S^0 K\_S^0 nu) = B(pi- K\_S^0 K\_L^0 nu) = 1/2 B(pi- K\_S^0 K\_L^0 nu).

$\Gamma(\pi^- K_S^0 K_S^0 \nu_\tau) / \Gamma_{total}$   $\Gamma_{48} / \Gamma$

Table with columns: VALUE (units 10^-4), EVTS, DOCUMENT ID, TECN, COMMENT. Rows include 2.35 ± 0.06 OUR FIT and 2.32 ± 0.06 OUR AVERAGE with entries RYU, LEES, BARATE, COAN.

1 The correlation coefficient between this measurement and the LEES 12Y Gamma(pi- to pi- K\_S^0 K\_S^0 pi^0 nu\_tau) / Gamma\_total one is 0.0828.

$\Gamma(\pi^- K_S^0 K_L^0 \nu_\tau) / \Gamma_{total}$   $\Gamma_{49} / \Gamma$

Table with columns: VALUE (units 10^-4), EVTS, DOCUMENT ID, TECN, COMMENT. Rows include 10.8 ± 2.4 OUR FIT and 10.1 ± 2.3 ± 1.3 with entry BARATE.

$\Gamma(\pi^- K_L^0 K_L^0 \nu_\tau) / \Gamma_{total}$   $\Gamma_{50} / \Gamma = \Gamma_{48} / \Gamma$

Table with columns: VALUE (units 10^-4), DOCUMENT ID. Row includes 2.35 ± 0.06 OUR FIT.

$\Gamma(\pi^- K^0 \bar{K}^0 \pi^0 \nu_\tau) / \Gamma_{total}$   $\Gamma_{51} / \Gamma = (\Gamma_{52} + \Gamma_{56} + \Gamma_{57}) / \Gamma$

Table with columns: VALUE (units 10^-4), DOCUMENT ID, TECN, COMMENT. Row includes 3.6 ± 1.2 OUR FIT.

• • • We use the following data for averages but not for fits. • • •
3.1 ± 2.3 1 BARATE 99R ALEP 1991-1995 LEP runs
1 BARATE 99R combine BARATE 98E Gamma(pi- K\_S^0 K\_S^0 pi^0 nu\_tau) / Gamma\_total and Gamma(pi- K\_S^0 K\_L^0 pi^0 nu\_tau) / Gamma\_total measurements to obtain this value.

$\Gamma(\pi^- K_S^0 K_S^0 \pi^0 \nu_\tau) / \Gamma_{total}$   $\Gamma_{52} / \Gamma$

Table with columns: VALUE (units 10^-5), CL% EVTS, DOCUMENT ID, TECN, COMMENT. Rows include 1.82 ± 0.21 OUR FIT and 1.80 ± 0.21 OUR AVERAGE with entries RYU, LEES.

• • • We do not use the following data for averages, fits, limits, etc. • • •
<20 95 BARATE 98E ALEP 1991-1995 LEP runs
1 The correlation coefficient between this measurement and the LEES 12Y Gamma(pi- to pi- K\_S^0 K\_S^0 nu\_tau) / Gamma\_total one is 0.0828.

$\Gamma(K^+ K^0 \pi^0 \nu_\tau \rightarrow \pi^- K_S^0 K_S^0 \pi^0 \nu_\tau) / \Gamma_{total}$   $\Gamma_{53} / \Gamma$

Table with columns: VALUE (units 10^-6), DOCUMENT ID, TECN, COMMENT. Row includes 10.8 ± 1.4 ± 1.5 with entry RYU.

$\Gamma(f_1(1285) \pi^- \nu_\tau \rightarrow \pi^- K_S^0 K_S^0 \pi^0 \nu_\tau) / \Gamma_{total}$   $\Gamma_{54} / \Gamma$

Table with columns: VALUE (units 10^-6), DOCUMENT ID, TECN, COMMENT. Row includes 6.8 ± 1.3 ± 0.7 with entry RYU.

$\Gamma(f_1(1420) \pi^- \nu_\tau \rightarrow \pi^- K_S^0 K_S^0 \pi^0 \nu_\tau) / \Gamma_{total}$   $\Gamma_{55} / \Gamma$

Table with columns: VALUE (units 10^-6), DOCUMENT ID, TECN, COMMENT. Row includes 2.4 ± 0.5 ± 0.6 with entry RYU.

$\Gamma(\pi^- K_S^0 K_L^0 \pi^0 \nu_\tau) / \Gamma_{total}$   $\Gamma_{56} / \Gamma$

Table with columns: VALUE (units 10^-4), EVTS, DOCUMENT ID, TECN, COMMENT. Rows include 3.2 ± 1.2 OUR FIT and 3.1 ± 1.1 ± 0.5 with entry BARATE.

$\Gamma(\pi^- K_L^0 K_L^0 \nu_\tau) / \Gamma_{total}$   $\Gamma_{57} / \Gamma = \Gamma_{52} / \Gamma$

Table with columns: VALUE (units 10^-5), DOCUMENT ID. Row includes 1.82 ± 0.21 OUR FIT.

$\Gamma(K^- K_S^0 K_S^0 \nu_\tau) / \Gamma_{total}$   $\Gamma_{58} / \Gamma$

Table with columns: VALUE, CL%, DOCUMENT ID, TECN, COMMENT. Row includes <6.3 x 10^-7 90 LEES.

$\Gamma(K^- K_S^0 K_S^0 \pi^0 \nu_\tau) / \Gamma_{total}$   $\Gamma_{59} / \Gamma$

Table with columns: VALUE, CL%, DOCUMENT ID, TECN, COMMENT. Row includes <4.0 x 10^-7 90 LEES.

# Lepton Particle Listings

T

### $\Gamma(K^0 h^+ h^- h^- \geq 0 \text{ neutrals } \nu_\tau) / \Gamma_{\text{total}}$ $\Gamma_{60} / \Gamma$

VALUE (%)	CL%	DOCUMENT ID	TECN	COMMENT
<b>&lt;0.17</b>	95	TSCHIRHART 88	HRS	$E_{\text{cm}}^{\text{ee}} = 29$ GeV

●●● We do not use the following data for averages, fits, limits, etc. ●●●

<0.27	90	BELTRAMI 85	HRS	$E_{\text{cm}}^{\text{ee}} = 29$ GeV
-------	----	-------------	-----	--------------------------------------

### $\Gamma(K^0 h^+ h^- h^- \nu_\tau) / \Gamma_{\text{total}}$ $\Gamma_{61} / \Gamma$

VALUE (units $10^{-4}$ )	EVTS	DOCUMENT ID	TECN	COMMENT
--------------------------	------	-------------	------	---------

**2.5 ± 2.0 OUR FIT**  
**2.3 ± 1.9 ± 0.7** 6 <sup>1</sup> BARATE 98E ALEP 1991–1995 LEP runs

<sup>1</sup> BARATE 98E reconstruct  $K^0$ 's using  $K_S^0 \rightarrow \pi^+ \pi^-$  decays.

### $\Gamma(h^- h^- h^+ \geq 0 \text{ neutrals } \geq 0 K^0_L \nu_\tau) / \Gamma_{\text{total}}$ $\Gamma_{62} / \Gamma$

$$\Gamma_{62} / \Gamma = (0.34598\Gamma_{36} + 0.34598\Gamma_{38} + 0.34598\Gamma_{41} + 0.34598\Gamma_{43} + 0.4247\Gamma_{48} + 0.6920\Gamma_{49} + 0.4247\Gamma_{52} + 0.6920\Gamma_{56} + 0.6534\Gamma_{61} + \Gamma_{70} + \Gamma_{78} + \Gamma_{85} + \Gamma_{86} + \Gamma_{97} + \Gamma_{103} + \Gamma_{106} + \Gamma_{107} + 0.2789\Gamma_{150} + 0.2789\Gamma_{152} + 0.2789\Gamma_{154} + 0.2628\Gamma_{156} + 0.7259\Gamma_{170} + 0.9078\Gamma_{178} + 0.9078\Gamma_{179} + 0.9078\Gamma_{180}) / \Gamma$$

VALUE (%)	EVTS	DOCUMENT ID	TECN	COMMENT
-----------	------	-------------	------	---------

**15.20 ± 0.06 OUR FIT**  
**14.8 ± 0.4 OUR AVERAGE**

14.4 ± 0.6 ± 0.3	ADEVA 91F L3 $E_{\text{cm}}^{\text{ee}} = 88.3$ – $94.3$ GeV
15.0 ± 0.4 ± 0.3	BEHREND 89B CELL $E_{\text{cm}}^{\text{ee}} = 14$ – $47$ GeV
15.1 ± 0.8 ± 0.6	AIHARA 87B TPC $E_{\text{cm}}^{\text{ee}} = 29$ GeV

●●● We do not use the following data for averages, fits, limits, etc. ●●●

13.5 ± 0.3 ± 0.3	ABACHI 89B HRS $E_{\text{cm}}^{\text{ee}} = 29$ GeV
12.8 ± 1.0 ± 0.7	<sup>1</sup> BURCHAT 87 MRK2 $E_{\text{cm}}^{\text{ee}} = 29$ GeV
12.1 ± 0.5 ± 1.2	RUCKSTUHL 86 DLCO $E_{\text{cm}}^{\text{ee}} = 29$ GeV
12.8 ± 0.5 ± 0.8	1420 SCHMIDKE 86 MRK2 $E_{\text{cm}}^{\text{ee}} = 29$ GeV
15.3 ± 1.1 $\begin{smallmatrix} +1.3 \\ -1.6 \end{smallmatrix}$	367 ALTHOFF 85 TASS $E_{\text{cm}}^{\text{ee}} = 34.5$ GeV
13.6 ± 0.5 ± 0.8	BARTEL 85F JADE $E_{\text{cm}}^{\text{ee}} = 34.6$ GeV
12.2 ± 1.3 ± 3.9	<sup>2</sup> BERGER 85 PLUT $E_{\text{cm}}^{\text{ee}} = 34.6$ GeV
13.3 ± 0.3 ± 0.6	FERNANDEZ 85 MAC $E_{\text{cm}}^{\text{ee}} = 29$ GeV
24 ± 6	35 BRANDELIK 80 TASS $E_{\text{cm}}^{\text{ee}} = 30$ GeV
32 ± 5	692 <sup>3</sup> BACINO 78B DLCO $E_{\text{cm}}^{\text{ee}} = 3.1$ – $7.4$ GeV
35 ± 11	<sup>3</sup> BRANDELIK 78 DASP Assumes V–A decay
18 ± 6.5	33 <sup>3</sup> JAROS 78 LGW $E_{\text{cm}}^{\text{ee}} > 6$ GeV

- <sup>1</sup> BURCHAT 87 value is not independent of SCHMIDKE 86 value.
- <sup>2</sup> Not independent of BERGER 85  $\Gamma(\mu^- \bar{\nu}_\mu \nu_\tau) / \Gamma_{\text{total}}$ ,  $\Gamma(e^- \bar{\nu}_e \nu_\tau) / \Gamma_{\text{total}}$ ,  $\Gamma(h^- \geq 1 \text{ neutrals } \nu_\tau) / \Gamma_{\text{total}}$ , and  $\Gamma(h^- \geq 0 K^0_L \nu_\tau) / \Gamma_{\text{total}}$ , and therefore not used in the fit.
- <sup>3</sup> Low energy experiments are not in average or fit because the systematic errors in background subtraction are judged to be large.

### $\Gamma(h^- h^- h^+ \geq 0 \text{ neutrals } \nu_\tau \text{ (ex. } K_S^0 \rightarrow \pi^+ \pi^-) \text{ ("3-prong")}) / \Gamma_{\text{total}}$ $\Gamma_{63} / \Gamma$

$$\Gamma_{63} / \Gamma = (\Gamma_{70} + \Gamma_{78} + \Gamma_{85} + \Gamma_{86} + \Gamma_{97} + \Gamma_{103} + \Gamma_{106} + \Gamma_{107} + 0.2789\Gamma_{150} + 0.2789\Gamma_{152} + 0.2789\Gamma_{154} + 0.492\Gamma_{170} + 0.9078\Gamma_{178} + 0.9078\Gamma_{179} + 0.9078\Gamma_{180}) / \Gamma$$

VALUE (%)	EVTS	DOCUMENT ID	TECN	COMMENT
-----------	------	-------------	------	---------

**14.55 ± 0.06 OUR FIT**  
**14.61 ± 0.06 OUR AVERAGE**

14.556 ± 0.105 ± 0.076	<sup>1</sup> ACHARD 01D L3 1992–1995 LEP runs
14.96 ± 0.09 ± 0.22	10.4k AKERS 95Y OPAL 1991–1994 LEP runs

●●● We use the following data for averages but not for fits. ●●●

14.652 ± 0.067 ± 0.086	SCHAEEL 05C ALEP 1991–1995 LEP runs
14.569 ± 0.093 ± 0.048	23k <sup>2</sup> ABREU 01M DLPH 1992–1995 LEP runs
14.22 ± 0.10 ± 0.37	<sup>3</sup> BALEST 95C CLEO $E_{\text{cm}}^{\text{ee}} \approx 10.6$ GeV

●●● We do not use the following data for averages, fits, limits, etc. ●●●

15.26 ± 0.26 ± 0.22	ACTON 92H OPAL Repl. by AKERS 95Y
13.3 ± 0.3 ± 0.8	<sup>4</sup> ALBRECHT 92D ARG $E_{\text{cm}}^{\text{ee}} = 9.4$ – $10.6$ GeV
14.35 $\begin{smallmatrix} +0.40 \\ -0.45 \end{smallmatrix}$ ± 0.24	DECAMP 92C ALEP 1989–1990 LEP runs

- <sup>1</sup> The correlation coefficients between this measurement and the ACHARD 01D measurements of  $B(\tau \rightarrow \text{"1-prong"})$  and  $B(\tau \rightarrow \text{"5-prong"})$  are  $-0.978$  and  $-0.19$  respectively.
- <sup>2</sup> The correlation coefficients between this measurement and the ABREU 01M measurements of  $B(\tau \rightarrow \text{1-prong})$  and  $B(\tau \rightarrow \text{5-prong})$  are  $-0.98$  and  $-0.08$  respectively.
- <sup>3</sup> Not independent of BALEST 95C  $B(h^- h^- h^+ \nu_\tau)$  and  $B(h^- h^- h^+ \pi^0 \nu_\tau)$  values, and BORTOLETTO 93  $B(h^- h^- h^+ 2\pi^0 \nu_\tau) / B(h^- h^- h^+ \geq 0 \text{ neutrals } \nu_\tau)$  value.
- <sup>4</sup> This ALBRECHT 92D value is not independent of their  $\Gamma(\mu^- \bar{\nu}_\mu \nu_\tau) / \Gamma_{\text{total}}$  and  $\Gamma(e^- \bar{\nu}_e \nu_\tau) / \Gamma_{\text{total}}$  value.

### $\Gamma(h^- h^- h^+ \nu_\tau) / \Gamma_{\text{total}}$ $\Gamma_{64} / \Gamma$

$$\Gamma_{64} / \Gamma = (0.34598\Gamma_{36} + 0.34598\Gamma_{38} + \Gamma_{70} + \Gamma_{97} + \Gamma_{106} + 0.492\Gamma_{170} + 0.0153\Gamma_{178} + 0.0153\Gamma_{179}) / \Gamma$$

VALUE (%)	EVTS	DOCUMENT ID	TECN	COMMENT
-----------	------	-------------	------	---------

**9.80 ± 0.05 OUR FIT**

●●● We use the following data for averages but not for fits. ●●●

**7.6 ± 0.1 ± 0.5** 7.5k <sup>1</sup> ALBRECHT 96E ARG  $E_{\text{cm}}^{\text{ee}} = 9.4$ – $10.6$  GeV

●●● We do not use the following data for averages, fits, limits, etc. ●●●

9.92 ± 0.10 ± 0.09	11.2k	<sup>2</sup> BUSKULIC 96 ALEP Repl. by SCHAEEL 05C
9.49 ± 0.36 ± 0.63		DECAMP 92C ALEP Repl. by SCHAEEL 05C
8.7 ± 0.7 ± 0.3	694	<sup>3</sup> BEHREND 90 CELL $E_{\text{cm}}^{\text{ee}} = 35$ GeV
7.0 ± 0.3 ± 0.7	1566	<sup>4</sup> BAND 87 MAC $E_{\text{cm}}^{\text{ee}} = 29$ GeV
6.7 ± 0.8 ± 0.9		<sup>5</sup> BURCHAT 87 MRK2 $E_{\text{cm}}^{\text{ee}} = 29$ GeV
6.4 ± 0.4 ± 0.9		<sup>6</sup> RUCKSTUHL 86 DLCO $E_{\text{cm}}^{\text{ee}} = 29$ GeV
7.8 ± 0.5 ± 0.8	890	SCHMIDKE 86 MRK2 $E_{\text{cm}}^{\text{ee}} = 29$ GeV
8.4 ± 0.4 ± 0.7	1255	<sup>6</sup> FERNANDEZ 85 MAC $E_{\text{cm}}^{\text{ee}} = 29$ GeV
9.7 ± 2.0 ± 1.3		BEHREND 84 CELL $E_{\text{cm}}^{\text{ee}} = 14, 22$ GeV

<sup>1</sup> ALBRECHT 96E not independent of ALBRECHT 93C  $\Gamma(h^- h^- h^+ \nu_\tau \text{ (ex. } K^0)) \times \Gamma(\text{particle}^- \geq 0 \text{ neutrals } \geq 0 K^0_L \nu_\tau) / \Gamma_{\text{total}}$  value.

<sup>2</sup> BUSKULIC 96 quote  $B(h^- h^- h^+ \nu_\tau \text{ (ex. } K^0)) = 9.50 \pm 0.10 \pm 0.11$ . We add 0.42 to remove their  $K^0$  correction and reduce the systematic error accordingly.

<sup>3</sup> BEHREND 90 subtract 0.3% to account for the  $\tau^- \rightarrow K^*(892)^- \nu_\tau$  contribution to measured events.

<sup>4</sup> BAND 87 subtract for charged kaon modes; not independent of FERNANDEZ 85 value.  
<sup>5</sup> BURCHAT 87 value is not independent of SCHMIDKE 86 value.

<sup>6</sup> Value obtained by multiplying paper's  $R = B(h^- h^- h^+ \nu_\tau) / B(3\text{-prong})$  by  $B(3\text{-prong}) = 0.143$  and subtracting 0.3% for  $K^*(892)$  background.

### $\Gamma(h^- h^- h^+ \nu_\tau \text{ (ex. } K^0)) / \Gamma_{\text{total}}$ $\Gamma_{65} / \Gamma$

$$\Gamma_{65} / \Gamma = (\Gamma_{70} + \Gamma_{97} + \Gamma_{106} + 0.492\Gamma_{170} + 0.0153\Gamma_{178} + 0.0153\Gamma_{179}) / \Gamma$$

VALUE (%)	EVTS	DOCUMENT ID	TECN	COMMENT
-----------	------	-------------	------	---------

**9.46 ± 0.05 OUR FIT**  
**9.44 ± 0.14 OUR AVERAGE** Error includes scale factor of 1.4. See the ideogram below.

9.317 ± 0.090 ± 0.082	12.2k	<sup>1</sup> ABDALLAH 06A DLPH 1992–1995 LEP runs
9.51 ± 0.07 ± 0.20	37.7k	BALEST 95C CLEO $E_{\text{cm}}^{\text{ee}} \approx 10.6$ GeV

●●● We use the following data for averages but not for fits. ●●●

9.87 ± 0.10 ± 0.24 <sup>2</sup> AKERS 95Y OPAL 1991–1994 LEP runs

●●● We do not use the following data for averages, fits, limits, etc. ●●●

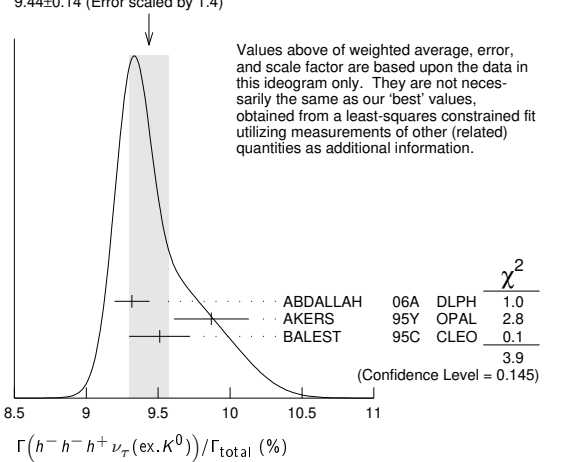
9.50 ± 0.10 ± 0.11 11.2k <sup>3</sup> BUSKULIC 96 ALEP Repl. by SCHAEEL 05C

<sup>1</sup> See footnote to ABDALLAH 06A  $\Gamma(\tau^- \rightarrow h^- \nu_\tau) / \Gamma_{\text{total}}$  measurement for correlations with other measurements.

<sup>2</sup> Not independent of AKERS 95Y  $B(h^- h^- h^+ \geq 0 \text{ neutrals } \nu_\tau \text{ (ex. } K_S^0 \rightarrow \pi^+ \pi^-))$  and  $B(h^- h^- h^+ \nu_\tau \text{ (ex. } K^0)) / B(h^- h^- h^+ \geq 0 \text{ neutrals } \nu_\tau \text{ (ex. } K_S^0 \rightarrow \pi^+ \pi^-))$  values.

<sup>3</sup> Not independent of BUSKULIC 96  $B(h^- h^- h^+ \nu_\tau)$  value.

WEIGHTED AVERAGE  
9.44 ± 0.14 (Error scaled by 1.4)



### $\Gamma(h^- h^- h^+ \nu_\tau \text{ (ex. } K^0)) / \Gamma(h^- h^- h^+ \geq 0 \text{ neutrals } \nu_\tau \text{ (ex. } K_S^0 \rightarrow \pi^+ \pi^-) \text{ ("3-prong")})$ $\Gamma_{65} / \Gamma_{63}$

$$\Gamma_{65} / \Gamma_{63} = (\Gamma_{70} + \Gamma_{97} + \Gamma_{106} + 0.492\Gamma_{170} + 0.0153\Gamma_{178} + 0.0153\Gamma_{179}) / (0.4247\Gamma_{52} + \Gamma_{70} + \Gamma_{78} + \Gamma_{85} + \Gamma_{89} + \Gamma_{97} + \Gamma_{103} + \Gamma_{106} + \Gamma_{107} + 0.2789\Gamma_{150} + 0.2292\Gamma_{151} + 0.2789\Gamma_{152} + 0.2789\Gamma_{154} + 0.1131\Gamma_{156} + 0.3268\Gamma_{160} + 0.492\Gamma_{170} + 0.9078\Gamma_{178} + 0.9078\Gamma_{179} + 0.9078\Gamma_{180} + 0.893\Gamma_{182})$$

VALUE (units $10^{-2}$ )	DOCUMENT ID	TECN	COMMENT
--------------------------	-------------	------	---------

**64.98 ± 0.31 OUR FIT**

**66.0 ± 0.4 ± 1.4** AKERS 95Y OPAL 1991–1994 LEP runs

### $\Gamma(h^- h^- h^+ \nu_\tau \text{ (ex. } K^0, \mu)) / \Gamma_{\text{total}}$ $\Gamma_{66} / \Gamma$

$$\Gamma_{66} / \Gamma = (\Gamma_{70} + \Gamma_{97} + \Gamma_{106} + 0.492\Gamma_{170}) / \Gamma$$

VALUE (%)	DOCUMENT ID
-----------	-------------

**9.43 ± 0.05 OUR FIT**

### $\Gamma(\pi^- \pi^+ \pi^- \nu_\tau) / \Gamma_{\text{total}}$ $\Gamma_{67} / \Gamma = (0.34598\Gamma_{36} + \Gamma_{70} + 0.0153\Gamma_{178}) / \Gamma$

VALUE (%)	DOCUMENT ID
-----------	-------------

**9.31 ± 0.05 OUR FIT**

$\Gamma(\pi^- \pi^+ \pi^- \nu_\tau \text{ (ex. } K^0)) / \Gamma_{\text{total}}$   $\Gamma_{68} / \Gamma = (\Gamma_{70} + 0.0153\Gamma_{178}) / \Gamma$

Table with columns: VALUE (%), EVTS, DOCUMENT ID, TECN, COMMENT. Includes entries for LEE, AUBERT, BRIERE.

1 Quoted statistical error is 0.003%. Correlation matrix for LEE 10 branching fractions: (1)  $\Gamma(\tau^- \rightarrow \pi^- \pi^+ \pi^- \nu_\tau \text{ (ex. } K^0)) / \Gamma_{\text{total}}$  (2)  $\Gamma(\tau^- \rightarrow K^- \pi^+ \pi^- \nu_\tau \text{ (ex. } K^0)) / \Gamma_{\text{total}}$  (3)  $\Gamma(\tau^- \rightarrow K^- K^+ \pi^- \nu_\tau) / \Gamma_{\text{total}}$  (4)  $\Gamma(\tau^- \rightarrow K^- K^+ K^- \nu_\tau) / \Gamma_{\text{total}}$

Table with columns: (1), (2), (3). Values: (1) 0.175, (2) 0.049, (3) 0.080, (4) -0.053, 0.035, -0.008.

2 Correlation matrix for AUBERT 08 branching fractions: (1)  $\Gamma(\tau^- \rightarrow \pi^- \pi^+ \pi^- \nu_\tau \text{ (ex. } K^0)) / \Gamma_{\text{total}}$  (2)  $\Gamma(\tau^- \rightarrow K^- \pi^+ \pi^- \nu_\tau \text{ (ex. } K^0)) / \Gamma_{\text{total}}$  (3)  $\Gamma(\tau^- \rightarrow K^- K^+ \pi^- \nu_\tau) / \Gamma_{\text{total}}$  (4)  $\Gamma(\tau^- \rightarrow K^- K^+ K^- \nu_\tau) / \Gamma_{\text{total}}$

Table with columns: (1), (2), (3). Values: (1) 0.544, (2) 0.390, (3) 0.177, (4) 0.031, 0.093, 0.087.

3 47% correlated with BRIERE 03  $\tau^- \rightarrow K^- \pi^+ \pi^- \nu_\tau$  and 71% correlated with  $\tau^- \rightarrow K^- K^+ \pi^- \nu_\tau$  because of a common 5% normalization error.

$\Gamma(\pi^- \pi^+ \pi^- \nu_\tau \text{ (ex. } K^0, \text{ non-axial vector)}) / \Gamma(\pi^- \pi^+ \pi^- \nu_\tau \text{ (ex. } K^0))$   $\Gamma_{69} / \Gamma_{68}$

Table with columns: VALUE, CL%, DOCUMENT ID, TECN, COMMENT. Value: <0.261, CL%: 95, DOCUMENT ID: 1 ACKERSTAFF 97R OPAL 1992-1994 LEP runs

1 Model-independent limit from structure function analysis on contribution to  $B(\tau^- \rightarrow \pi^- \pi^+ \pi^- \nu_\tau \text{ (ex. } K^0))$  from non-axial vectors.

$\Gamma(\pi^- \pi^+ \pi^- \nu_\tau \text{ (ex. } K^0, \omega)) / \Gamma_{\text{total}}$   $\Gamma_{70} / \Gamma$

Table with columns: VALUE (%), EVTS, DOCUMENT ID, TECN, COMMENT. Value: 9.99 ± 0.05 OUR FIT, 9.041 ± 0.060 ± 0.076, EVTS: 29k, DOCUMENT ID: 1 SCHAEEL 05c ALEP 1991-1995 LEP runs

1 See footnote to SCHAEEL 05c  $\Gamma(\tau^- \rightarrow e^- \bar{\nu}_e \nu_\tau) / \Gamma_{\text{total}}$  measurement for correlations with other measurements.

$\Gamma(h^- h^- h^+ \geq 1 \text{ neutrals } \nu_\tau) / \Gamma_{\text{total}}$   $\Gamma_{71} / \Gamma$

Table with columns: VALUE (%), EVTS, DOCUMENT ID, TECN, COMMENT. Value: 5.29 ± 0.05 OUR FIT, EVTS: 352, DOCUMENT ID: 1 BEHREND 90 CELL  $E_{\text{cm}}^{\text{ee}} = 35 \text{ GeV}$

Table with columns: VALUE (%), EVTS, DOCUMENT ID, TECN, COMMENT. Values: 4.2 ± 0.5 ± 0.9, 6.1 ± 0.8 ± 0.9, 7.6 ± 0.4 ± 0.9, 4.7 ± 0.5 ± 0.8, 5.6 ± 0.4 ± 0.7, 6.2 ± 2.3 ± 1.7

1 BEHREND 90 value is not independent of BEHREND 90  $B(3h\nu_\tau \geq 1 \text{ neutrals}) + B(5\text{-prong})$ . 2 ALBRECHT 87L measure the product of branching ratios  $B(3\pi^\pm \pi^0 \nu_\tau) B((e\bar{\nu}_e \mu\bar{\nu}_\mu \text{ or } \pi^0 \text{ or } K^0 \text{ or } \rho) \nu_\tau) = 0.029$  and use the PDG 86 values for the second branching ratio which sum to 0.69 ± 0.03 to get the quoted value. 3 BURCHAT 87 value is not independent of SCHMIDKE 86 value. 4 Contributions from kaons and from  $>1\pi^0$  are subtracted. Not independent of (3-prong +  $0\pi^0$ ) and (3-prong +  $\geq 0\pi^0$ ) values. 5 Value obtained using paper's  $R = B(h^- h^- h^+ \nu_\tau) / B(3\text{-prong})$  and current  $B(3\text{-prong}) = 0.143$ . 6 Not independent of SCHMIDKE 86  $h^- h^- h^+ \nu_\tau$  and  $h^- h^- h^+ (\geq 0\pi^0) \nu_\tau$  values.

$\Gamma(h^- h^- h^+ \geq 1\pi^0 \nu_\tau \text{ (ex. } K^0)) / \Gamma_{\text{total}}$   $\Gamma_{72} / \Gamma$

Table with columns: VALUE (%), EVTS, DOCUMENT ID, TECN, COMMENT. Value: 5.09 ± 0.05 OUR FIT, 5.10 ± 0.12 OUR AVERAGE, EVTS: 1.3k, DOCUMENT ID: 1 ABDALLAH 06A DLPH 1992-1995 LEP runs

• • • We use the following data for averages but not for fits. • • • 5.106 ± 0.083 ± 0.103 10.1k 1 ABDALLAH 06A DLPH 1992-1995 LEP runs 5.09 ± 0.10 ± 0.23 2 AKERS 95Y OPAL 1991-1994 LEP runs • • • We do not use the following data for averages, fits, limits, etc. • • • 4.95 ± 0.29 ± 0.65 570 DECAMP 92c ALEP Repl. by SCHAEEL 05c

1 See footnote to ABDALLAH 06A  $\Gamma(\tau^- \rightarrow h^- \nu_\tau) / \Gamma_{\text{total}}$  measurement for correlations with other measurements. 2 Not independent of AKERS 95Y  $B(h^- h^- h^+ \geq 0 \text{ neutrals } \nu_\tau \text{ (ex. } K_S^0 \rightarrow \pi^+ \pi^-))$  and  $B(h^- h^- h^+ \geq 0 \text{ neutrals } \nu_\tau \text{ (ex. } K_S^0)) / B(h^- h^- h^+ \geq 0 \text{ neutrals } \nu_\tau \text{ (ex. } K_S^0 \rightarrow \pi^+ \pi^-))$  values.

$\Gamma(h^- h^- h^+ \pi^0 \nu_\tau) / \Gamma_{\text{total}}$   $\Gamma_{73} / \Gamma$

Table with columns: VALUE (%), EVTS, DOCUMENT ID, TECN, COMMENT. Value: 4.76 ± 0.05 OUR FIT, EVTS: 6.1k, DOCUMENT ID: 1 BUSKULIC 96 ALEP Repl. by SCHAEEL 05c

• • • We do not use the following data for averages, fits, limits, etc. • • • 4.45 ± 0.09 ± 0.07 6.1k 1 BUSKULIC 96 quote  $B(h^- h^- h^+ \pi^0 \nu_\tau \text{ (ex. } K^0)) = 4.30 \pm 0.09 \pm 0.09$ . We add 0.15 to remove their  $K^0$  correction and reduce the systematic error accordingly.

$\Gamma(h^- h^- h^+ \pi^0 \nu_\tau \text{ (ex. } K^0)) / \Gamma_{\text{total}}$   $\Gamma_{74} / \Gamma$

Table with columns: VALUE (%), EVTS, DOCUMENT ID, TECN, COMMENT. Value: 4.57 ± 0.05 OUR FIT, 4.45 ± 0.14 OUR AVERAGE, Error includes scale factor of 1.2.

4.545 ± 0.106 ± 0.103 8.9k 1 ABDALLAH 06A DLPH 1992-1995 LEP runs 4.23 ± 0.06 ± 0.22 7.2k BALEST 95c CLEO  $E_{\text{cm}}^{\text{ee}} \approx 10.6 \text{ GeV}$  1 See footnote to ABDALLAH 06A  $\Gamma(\tau^- \rightarrow h^- \nu_\tau) / \Gamma_{\text{total}}$  measurement for correlations with other measurements.

$\Gamma(h^- h^- h^+ \pi^0 \nu_\tau \text{ (ex. } K^0, \omega)) / \Gamma_{\text{total}}$   $\Gamma_{75} / \Gamma = (\Gamma_{78} + \Gamma_{103} + \Gamma_{107} + 0.2292\Gamma_{152}) / \Gamma$

Table with columns: VALUE (%), DOCUMENT ID. Value: 2.79 ± 0.07 OUR FIT, DOCUMENT ID: 1 SCHAEEL 05c ALEP 1991-1995 LEP runs

$\Gamma(\pi^- \pi^+ \pi^- \pi^0 \nu_\tau) / \Gamma_{\text{total}}$   $\Gamma_{76} / \Gamma$

Table with columns: VALUE (%), DOCUMENT ID. Value: 4.62 ± 0.05 OUR FIT, DOCUMENT ID: 1 SCHAEEL 05c ALEP 1991-1995 LEP runs

$\Gamma(\pi^- \pi^+ \pi^- \pi^0 \nu_\tau \text{ (ex. } K^0)) / \Gamma_{\text{total}}$   $\Gamma_{77} / \Gamma = (\Gamma_{78} + 0.893\Gamma_{178} + 0.0153\Gamma_{180}) / \Gamma$

Table with columns: VALUE (%), EVTS, DOCUMENT ID, TECN, COMMENT. Value: 4.49 ± 0.05 OUR FIT, 4.55 ± 0.13 OUR AVERAGE, Error includes scale factor of 1.6.

4.598 ± 0.057 ± 0.064 16k 1 SCHAEEL 05c ALEP 1991-1995 LEP runs 4.19 ± 0.10 ± 0.21 2 EDWARDS 00A CLEO 4.7 fb<sup>-1</sup>  $E_{\text{cm}}^{\text{ee}} = 10.6 \text{ GeV}$  1 SCHAEEL 05c quote (4.590 ± 0.057 ± 0.064)%. We add 0.008% to remove their correction for  $\tau^- \rightarrow \pi^- \pi^0 \omega \nu_\tau \rightarrow \pi^- \pi^0 \pi^+ \pi^- \nu_\tau$  decays. See footnote to SCHAEEL 05c  $\Gamma(\tau^- \rightarrow e^- \bar{\nu}_e \nu_\tau) / \Gamma_{\text{total}}$  measurement for correlations with other measurements. 2 EDWARDS 00A quote (4.19 ± 0.10) × 10<sup>-2</sup> with a 5% systematic error.

$\Gamma(\pi^- \pi^+ \pi^- \pi^0 \nu_\tau \text{ (ex. } K^0, \omega)) / \Gamma_{\text{total}}$   $\Gamma_{78} / \Gamma$

Table with columns: VALUE (%), DOCUMENT ID. Value: 2.74 ± 0.07 OUR FIT, DOCUMENT ID: 1 ALBRECHT 91D ARG  $E_{\text{cm}}^{\text{ee}} = 9.4-10.6 \text{ GeV}$

$\Gamma(h^- \rho \pi^0 \nu_\tau) / \Gamma(h^- h^- h^+ \pi^0 \nu_\tau)$   $\Gamma_{79} / \Gamma_{73}$

Table with columns: VALUE, EVTS, DOCUMENT ID, TECN, COMMENT. Value: 0.30 ± 0.04 ± 0.02, EVTS: 393, DOCUMENT ID: 1 ALBRECHT 91D ARG  $E_{\text{cm}}^{\text{ee}} = 9.4-10.6 \text{ GeV}$

$\Gamma(h^- \rho^+ h^- \nu_\tau) / \Gamma(h^- h^- h^+ \pi^0 \nu_\tau)$   $\Gamma_{80} / \Gamma_{73}$

Table with columns: VALUE, EVTS, DOCUMENT ID, TECN, COMMENT. Value: 0.10 ± 0.03 ± 0.04, EVTS: 142, DOCUMENT ID: 1 ALBRECHT 91D ARG  $E_{\text{cm}}^{\text{ee}} = 9.4-10.6 \text{ GeV}$

$\Gamma(h^- \rho^- h^+ \nu_\tau) / \Gamma(h^- h^- h^+ \pi^0 \nu_\tau)$   $\Gamma_{81} / \Gamma_{73}$

Table with columns: VALUE, EVTS, DOCUMENT ID, TECN, COMMENT. Value: 0.26 ± 0.05 ± 0.01, EVTS: 370, DOCUMENT ID: 1 ALBRECHT 91D ARG  $E_{\text{cm}}^{\text{ee}} = 9.4-10.6 \text{ GeV}$

$\Gamma(h^- h^- h^+ \geq 2\pi^0 \nu_\tau \text{ (ex. } K^0)) / \Gamma_{\text{total}}$   $\Gamma_{82} / \Gamma$

Table with columns: VALUE (%), EVTS, DOCUMENT ID, TECN, COMMENT. Value: 0.517 ± 0.031 OUR FIT, 0.561 ± 0.068 ± 0.095, EVTS: 1.3k, DOCUMENT ID: 1 ABDALLAH 06A DLPH 1992-1995 LEP runs

1 See footnote to ABDALLAH 06A  $\Gamma(\tau^- \rightarrow h^- \nu_\tau) / \Gamma_{\text{total}}$  measurement for correlations with other measurements.

$\Gamma(h^- h^- h^+ 2\pi^0 \nu_\tau) / \Gamma_{\text{total}}$   $\Gamma_{83} / \Gamma$

Table with columns: VALUE (%), DOCUMENT ID. Value: 0.505 ± 0.031 OUR FIT, DOCUMENT ID: 1 ABDALLAH 06A DLPH 1992-1995 LEP runs

# Lepton Particle Listings

$\tau$

$$\Gamma(h^- h^- h^+ 2\pi^0 \nu_\tau (\text{ex. } K^0)) / \Gamma_{\text{total}} \quad \Gamma_{84} / \Gamma$$

$$\Gamma_{84} / \Gamma = (\Gamma_{85} + 0.2292\Gamma_{150} + 0.2292\Gamma_{154} + 0.893\Gamma_{180}) / \Gamma$$

VALUE (%)	EVTS	DOCUMENT ID	TECN	COMMENT
<b>0.495 ± 0.031 OUR FIT</b>				
<b>0.435 ± 0.030 ± 0.035</b>	2.6k	<sup>1</sup> SCHAEL	05c ALEP	1991-1995 LEP runs

• • • We do not use the following data for averages, fits, limits, etc. • • •  
 0.50 ± 0.07 ± 0.07 1.8k BUSKULIC 96 ALEP Repl. by SCHAEL 05c  
<sup>1</sup> SCHAEL 05c quote (0.392 ± 0.030 ± 0.035)%. We add 0.043% to remove their correction for  $\tau^- \rightarrow \pi^- \eta \pi^0 \nu_\tau \rightarrow \pi^- \pi^+ \pi^- 2\pi^0 \nu_\tau$  and  $\tau^- \rightarrow K^*(892)^- \eta \nu_\tau \rightarrow K^- \pi^+ \pi^- 2\pi^0 \nu_\tau$  decays. See footnote to SCHAEL 05c  $\Gamma(\tau^- \rightarrow e^- \bar{\nu}_e \nu_\tau) / \Gamma_{\text{total}}$  measurement for correlations with other measurements.

$$\Gamma(h^- h^- h^+ 2\pi^0 \nu_\tau (\text{ex. } K^0)) / \Gamma(h^- h^- h^+ \geq 0 \text{ neutrals } \nu_\tau) \geq 0 K_{\text{cm}}^0 \nu_\tau \quad \Gamma_{84} / \Gamma_{62}$$

$$\Gamma_{84} / \Gamma_{62} = (\Gamma_{85} + 0.2292\Gamma_{150} + 0.2292\Gamma_{154} + 0.893\Gamma_{180}) / (0.34598\Gamma_{36} + 0.34598\Gamma_{38} + 0.34598\Gamma_{41} + 0.34598\Gamma_{43} + 0.4247\Gamma_{48} + 0.6920\Gamma_{49} + 0.8494\Gamma_{52} + 0.6920\Gamma_{56} + 0.6534\Gamma_{61} + \Gamma_{70} + \Gamma_{78} + \Gamma_{85} + \Gamma_{89} + \Gamma_{97} + \Gamma_{103} + \Gamma_{106} + \Gamma_{107} + 0.2789\Gamma_{150} + 0.2292\Gamma_{151} + 0.2789\Gamma_{152} + 0.2789\Gamma_{154} + 0.3759\Gamma_{156} + 0.3268\Gamma_{160} + 0.7259\Gamma_{170} + 0.9078\Gamma_{178} + 0.9078\Gamma_{179} + 0.9078\Gamma_{180} + 0.893\Gamma_{182})$$

VALUE (units 10 <sup>-2</sup> )	EVTS	DOCUMENT ID	TECN	COMMENT
<b>3.26 ± 0.20 OUR FIT</b>				
<b>3.4 ± 0.2 ± 0.3</b>	668	BORTOLETTO93	CLEO	$E_{\text{cm}}^{ee} \approx 10.6$ GeV

$$\Gamma(h^- h^- h^+ 2\pi^0 \nu_\tau (\text{ex. } K^0, \omega, \eta)) / \Gamma_{\text{total}} \quad \Gamma_{85} / \Gamma$$

VALUE (units 10 <sup>-4</sup> )	DOCUMENT ID	TECN	COMMENT
<b>10 ± 4 OUR FIT</b>			

$$\Gamma(h^- h^- h^+ 3\pi^0 \nu_\tau) / \Gamma_{\text{total}} \quad \Gamma_{86} / \Gamma = (0.4247\Gamma_{52} + \Gamma_{87} + 0.1131\Gamma_{156}) / \Gamma$$

VALUE (units 10 <sup>-4</sup> )	CL%	EVTS	DOCUMENT ID	TECN	COMMENT
<b>2.13 ± 0.30 OUR FIT</b>					
<b>2.2 ± 0.3 ± 0.4</b>		139	ANASTASSOV 01	CLEO	$E_{\text{cm}}^{ee} = 10.6$ GeV

• • • We do not use the following data for averages, fits, limits, etc. • • •  
 < 4.9 95 SCHAEL 05c ALEP 1991-1995 LEP runs  
 2.85 ± 0.56 ± 0.51 57 ANDERSON 97 CLEO Repl. by ANAS-  
 11 ± 4 ± 5 440 <sup>1</sup> BUSKULIC 96 ALEP Repl. by SCHAEL 05c

<sup>1</sup> BUSKULIC 96 state their measurement is for  $B(h^- h^- h^+ \geq 3\pi^0 \nu_\tau)$ . We assume that  $B(h^- h^- h^+ \geq 4\pi^0 \nu_\tau)$  is very small.

$$\Gamma(2\pi^- \pi^+ 3\pi^0 \nu_\tau (\text{ex. } K^0)) / \Gamma_{\text{total}} \quad \Gamma_{87} / \Gamma$$

$$\Gamma_{87} / \Gamma = (\Gamma_{89} + 0.2292\Gamma_{151} + 0.3268\Gamma_{160} + 0.893\Gamma_{182}) / \Gamma$$

VALUE (units 10 <sup>-4</sup> )	DOCUMENT ID	TECN	COMMENT
<b>1.95 ± 0.30 OUR FIT</b>			

• • • We use the following data for averages but not for fits. • • •  
**2.07 ± 0.18 ± 0.37** <sup>1</sup> LEES 12x BABR 468 fb<sup>-1</sup>  $E_{\text{cm}}^{ee} = 10.6$  GeV  
<sup>1</sup> Not independent of LEES 12x  $\Gamma(\tau^- \rightarrow \eta \pi^- \pi^+ \pi^- \nu_\tau (\text{ex. } K^0)) / \Gamma$ ,  $\Gamma(\tau^- \rightarrow \eta \pi^- \pi^0 \pi^0 \nu_\tau) / \Gamma$ ,  $\Gamma(\tau^- \rightarrow \pi^- \omega 2\pi^0 \nu_\tau) / \Gamma$ , and  $\Gamma(\tau^- \rightarrow f_1(1285) \pi^- \nu_\tau \rightarrow \eta \pi^- \pi^+ \pi^- \nu_\tau) / \Gamma$  values.

$$\Gamma(2\pi^- \pi^+ 3\pi^0 \nu_\tau (\text{ex. } K^0, \eta, f_1(1285))) / \Gamma_{\text{total}} \quad \Gamma_{88} / \Gamma$$

VALUE (units 10 <sup>-4</sup> )	DOCUMENT ID	TECN	COMMENT
<b>1.69 ± 0.08 ± 0.43</b>	LEES	12x BABR	468 fb <sup>-1</sup> $E_{\text{cm}}^{ee} = 10.6$ GeV

$$\Gamma(2\pi^- \pi^+ 3\pi^0 \nu_\tau (\text{ex. } K^0, \eta, \omega, f_1(1285))) / \Gamma_{\text{total}} \quad \Gamma_{89} / \Gamma$$

VALUE (units 10 <sup>-5</sup> )	DOCUMENT ID	TECN	COMMENT
<b>1.4 ± 2.7 OUR FIT</b>			
<b>1.0 ± 0.8 ± 3.0</b>	1 LEES	12x BABR	468 fb <sup>-1</sup> $E_{\text{cm}}^{ee} = 10.6$ GeV

<sup>1</sup> LEES 12x measurement corresponds to the lower limit of  $< 5.8 \times 10^{-5}$  at 90% CL.

$$\Gamma(K^- h^+ h^- \geq 0 \text{ neutrals } \nu_\tau) / \Gamma_{\text{total}} \quad \Gamma_{90} / \Gamma$$

$$\Gamma_{90} / \Gamma = (0.34598\Gamma_{38} + 0.34598\Gamma_{43} + \Gamma_{97} + \Gamma_{103} + \Gamma_{106} + \Gamma_{107} + 0.2789\Gamma_{152} + 0.492\Gamma_{170} + 0.9078\Gamma_{179}) / \Gamma$$

VALUE (%)	CL%	DOCUMENT ID	TECN	COMMENT
<b>0.629 ± 0.014 OUR FIT</b>				
<b>&lt; 0.6</b>	90	AIHARA	84c TPC	$E_{\text{cm}}^{ee} = 29$ GeV

$$\Gamma(K^- h^+ \pi^- \nu_\tau (\text{ex. } K^0)) / \Gamma_{\text{total}} \quad \Gamma_{91} / \Gamma = (\Gamma_{97} + \Gamma_{106} + 0.0153\Gamma_{179}) / \Gamma$$

VALUE (%)	DOCUMENT ID	TECN	COMMENT
<b>0.437 ± 0.007 OUR FIT</b>			

$$\Gamma(K^- h^+ \pi^- \nu_\tau (\text{ex. } K^0)) / \Gamma(\pi^- \pi^+ \pi^- \nu_\tau (\text{ex. } K^0)) \quad \Gamma_{91} / \Gamma_{68}$$

$$\Gamma_{91} / \Gamma_{68} = (\Gamma_{97} + \Gamma_{106} + 0.0153\Gamma_{179}) / (\Gamma_{70} + 0.0153\Gamma_{178})$$

VALUE (%)	EVTS	DOCUMENT ID	TECN	COMMENT
<b>4.85 ± 0.08 OUR FIT</b>				
<b>5.44 ± 0.21 ± 0.53</b>	7.9k	RICHICHI	99 CLEO	$E_{\text{cm}}^{ee} = 10.6$ GeV

$$\Gamma(K^- h^+ \pi^- \pi^0 \nu_\tau (\text{ex. } K^0)) / \Gamma_{\text{total}} \quad \Gamma_{92} / \Gamma$$

$$\Gamma_{92} / \Gamma = (\Gamma_{103} + \Gamma_{107} + 0.2292\Gamma_{152} + 0.893\Gamma_{179}) / \Gamma$$

VALUE (units 10 <sup>-4</sup> )	DOCUMENT ID	TECN	COMMENT
<b>8.6 ± 1.2 OUR FIT</b>			

$$\Gamma(K^- h^+ \pi^- \pi^0 \nu_\tau (\text{ex. } K^0)) / \Gamma(\pi^- \pi^+ \pi^- \pi^0 \nu_\tau (\text{ex. } K^0)) \quad \Gamma_{92} / \Gamma_{77}$$

$$\Gamma_{92} / \Gamma_{77} = (\Gamma_{103} + \Gamma_{107} + 0.2292\Gamma_{152} + 0.893\Gamma_{179}) / (\Gamma_{78} + 0.893\Gamma_{178} + 0.0153\Gamma_{180})$$

VALUE (%)	EVTS	DOCUMENT ID	TECN	COMMENT
<b>1.91 ± 0.26 OUR FIT</b>				
<b>2.61 ± 0.45 ± 0.42</b>	719	RICHICHI	99 CLEO	$E_{\text{cm}}^{ee} = 10.6$ GeV

$$\Gamma(K^- \pi^+ \pi^- \geq 0 \text{ neutrals } \nu_\tau) / \Gamma_{\text{total}} \quad \Gamma_{93} / \Gamma$$

$$\Gamma_{93} / \Gamma = (0.34598\Gamma_{38} + 0.34598\Gamma_{43} + \Gamma_{97} + \Gamma_{103} + 0.2789\Gamma_{152} + 0.9078\Gamma_{179}) / \Gamma$$

VALUE (%)	EVTS	DOCUMENT ID	TECN	COMMENT
<b>0.477 ± 0.014 OUR FIT</b>				
<b>0.58 +0.15 -0.13 ± 0.12</b>	20	<sup>1</sup> BAUER	94 TPC	$E_{\text{cm}}^{ee} = 29$ GeV

• • • We do not use the following data for averages, fits, limits, etc. • • •  
 0.22 +0.16 ± 0.05 9 <sup>2</sup> MILLS 85 DLCO  $E_{\text{cm}}^{ee} = 29$  GeV

<sup>1</sup> We multiply 0.58% by 0.20, the relative systematic error quoted by BAUER 94, to obtain the systematic error.  
<sup>2</sup> Error correlated with MILLS 85 ( $K K \pi \nu$ ) value. We multiply 0.22% by 0.23, the relative systematic error quoted by MILLS 85, to obtain the systematic error.

$$\Gamma(K^- \pi^+ \pi^- \geq 0\pi^0 \nu_\tau (\text{ex. } K^0)) / \Gamma_{\text{total}} \quad \Gamma_{94} / \Gamma$$

$$\Gamma_{94} / \Gamma = (\Gamma_{97} + \Gamma_{103} + 0.2292\Gamma_{152} + 0.9078\Gamma_{179}) / \Gamma$$

VALUE (%)	DOCUMENT ID	TECN	COMMENT
<b>0.373 ± 0.013 OUR FIT</b>			
<b>0.30 ± 0.05 OUR AVERAGE</b>			

• • • We use the following data for averages but not for fits. • • •  
 0.343 ± 0.073 ± 0.031 <sup>1</sup> ABBIENDI 00d OPAL 1990-1995 LEP runs  
 0.275 ± 0.064 <sup>1</sup> BARATE 98 ALEP 1991-1995 LEP runs  
<sup>1</sup> Not independent of BARATE 98  $\Gamma(\tau^- \rightarrow K^- \pi^+ \pi^- \nu_\tau) / \Gamma_{\text{total}}$  and  $\Gamma(\tau^- \rightarrow K^- \pi^+ \pi^- \pi^0 \nu_\tau) / \Gamma_{\text{total}}$  values.

$$\Gamma(K^- \pi^+ \pi^- \nu_\tau) / \Gamma_{\text{total}} \quad \Gamma_{95} / \Gamma = (0.34598\Gamma_{38} + \Gamma_{97} + 0.0153\Gamma_{179}) / \Gamma$$

VALUE (%)	DOCUMENT ID	TECN	COMMENT
<b>0.345 ± 0.007 OUR FIT</b>			

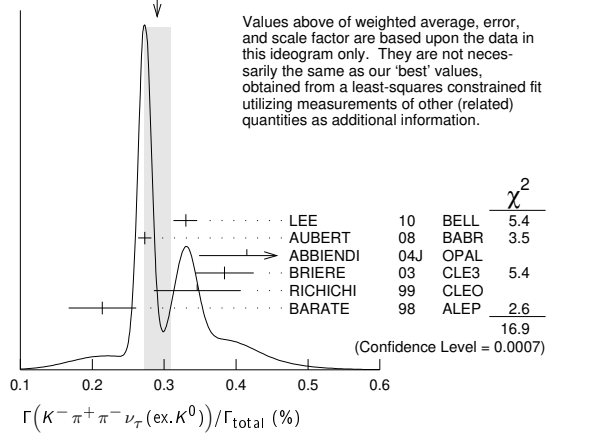
$$\Gamma(K^- \pi^+ \pi^- \nu_\tau (\text{ex. } K^0)) / \Gamma_{\text{total}} \quad \Gamma_{96} / \Gamma = (\Gamma_{97} + 0.0153\Gamma_{179}) / \Gamma$$

VALUE (%)	EVTS	DOCUMENT ID	TECN	COMMENT
<b>0.293 ± 0.007 OUR FIT</b>				
<b>0.290 ± 0.018 OUR AVERAGE</b>				Error includes scale factor of 2.4. See the ideogram below.

0.330 ± 0.001 ± 0.016 -0.017	794k	<sup>1</sup> LEE	10 BELL	666 fb <sup>-1</sup> $E_{\text{cm}}^{ee} = 10.6$ GeV
0.273 ± 0.002 ± 0.009	70k	<sup>2</sup> AUBERT	08 BABR	342 fb <sup>-1</sup> $E_{\text{cm}}^{ee} = 10.6$ GeV
0.415 ± 0.053 ± 0.040	269	ABBIENDI	04J OPAL	1991-1995 LEP runs
0.384 ± 0.014 ± 0.038	3.5k	<sup>3</sup> BRIERE	03 CLE3	$E_{\text{cm}}^{ee} = 10.6$ GeV
0.214 ± 0.037 ± 0.029		BARATE	98 ALEP	1991-1995 LEP runs
• • • We use the following data for averages but not for fits. • • •				
0.346 ± 0.023 ± 0.056	158	<sup>4</sup> RICHICHI	99 CLEO	$E_{\text{cm}}^{ee} = 10.6$ GeV
• • • We do not use the following data for averages, fits, limits, etc. • • •				
0.360 ± 0.082 ± 0.048		ABBIENDI	00d OPAL	1990-1995 LEP runs

<sup>1</sup> See footnote to LEE 10  $\Gamma(\tau^- \rightarrow \pi^- \pi^+ \pi^- \nu_\tau (\text{ex. } K^0)) / \Gamma_{\text{total}}$  measurement for correlations with other measurements. Not independent of LEE 10  $\Gamma(\tau^- \rightarrow K^- \pi^+ \pi^- \nu_\tau (\text{ex. } K^0)) / \Gamma_{\text{total}}$  and  $\Gamma(\tau^- \rightarrow \pi^- \pi^+ \pi^- \nu_\tau (\text{ex. } K^0)) / \Gamma_{\text{total}}$  value.  
<sup>2</sup> See footnote to AUBERT 08  $\Gamma(\tau^- \rightarrow \pi^- \pi^+ \pi^- \nu_\tau (\text{ex. } K^0)) / \Gamma_{\text{total}}$  measurement for correlations with other measurements.  
<sup>3</sup> 47% correlated with BRIERE 03  $\tau^- \rightarrow \pi^- \pi^+ \pi^- \nu_\tau$  and 34% correlated with  $\tau^- \rightarrow K^- K^+ \pi^- \nu_\tau$  because of a common 5% normalization error.  
<sup>4</sup> Not independent of RICHICHI 99  
 $\Gamma(\tau^- \rightarrow K^- h^+ \pi^- \nu_\tau (\text{ex. } K^0)) / \Gamma(\tau^- \rightarrow \pi^- \pi^+ \pi^- \nu_\tau (\text{ex. } K^0))$ ,  $\Gamma(\tau^- \rightarrow K^- K^+ \pi^- \nu_\tau) / \Gamma(\tau^- \rightarrow \pi^- \pi^+ \pi^- \nu_\tau (\text{ex. } K^0))$  and BALEST 95c  $\Gamma(\tau^- \rightarrow h^- h^- h^+ \nu_\tau (\text{ex. } K^0)) / \Gamma_{\text{total}}$  values.

WEIGHTED AVERAGE  
 0.290 ± 0.018 (Error scaled by 2.4)



$$\Gamma(K^- \pi^+ \pi^- \nu_\tau(\text{ex.}K^0))/\Gamma(\pi^- \pi^+ \pi^- \nu_\tau(\text{ex.}K^0)) \quad \Gamma_{96}/\Gamma_{68}$$

$$\Gamma_{96}/\Gamma_{68} = (\Gamma_{97} + 0.0153\Gamma_{179})/(\Gamma_{70} + 0.0153\Gamma_{178})$$

VALUE (units 10 <sup>-2</sup> )	EVTS	DOCUMENT ID	TECN	COMMENT
<b>3.25 ± 0.07 OUR FIT</b>				

• • • We use the following data for averages but not for fits. • • •

**3.92 ± 0.02 ± 0.15** 794k 1 LEE 10 BELL 666 fb<sup>-1</sup> E<sub>cm</sub><sup>ee</sup> = 10.6 GeV

1 Not independent of LEE 10  $\Gamma(\tau^- \rightarrow K^- \pi^+ \pi^- \nu_\tau(\text{ex.}K^0))/\Gamma_{\text{total}}$  and  $\Gamma(\tau^- \rightarrow \pi^- \pi^+ \pi^- \nu_\tau(\text{ex.}K^0))/\Gamma_{\text{total}}$  values.

$$\Gamma(K^- \pi^+ \pi^- \nu_\tau(\text{ex.}K^0, \omega))/\Gamma_{\text{total}} \quad \Gamma_{97}/\Gamma$$

VALUE (units 10 <sup>-3</sup> )	DOCUMENT ID
<b>2.93 ± 0.07 OUR FIT</b>	

$$\Gamma(K^- \rho^0 \nu_\tau \rightarrow K^- \pi^+ \pi^- \nu_\tau)/\Gamma(K^- \pi^+ \pi^- \nu_\tau(\text{ex.}K^0)) \quad \Gamma_{98}/\Gamma_{96}$$

VALUE	DOCUMENT ID	TECN	COMMENT
<b>0.48 ± 0.14 ± 0.10</b>	1 ASNER 00B CLEO	E <sub>cm</sub> <sup>ee</sup> = 10.6 GeV	

• • • We do not use the following data for averages, fits, limits, etc. • • •

0.39 ± 0.14 2 BARATE 99R ALEP 1991-1995 LEP runs

1 ASNER 00B assume  $\tau^- \rightarrow K^- \pi^+ \pi^- \nu_\tau(\text{ex.}K^0)$  decays proceed only through  $K\rho$  and  $K^* \pi$  intermediate states. They assume the resonance structure of  $\tau^- \rightarrow K^- \pi^+ \pi^- \nu_\tau(\text{ex.}K^0)$  decays is dominated by  $K_1(1270)^-$  and  $K_1(1400)^-$  resonances, and assume  $B(K_1(1270) \rightarrow K^*(892)\pi) = (16 \pm 5)\%$ ,  $B(K_1(1270) \rightarrow K\rho) = (42 \pm 6)\%$ , and  $B(K_1(1400) \rightarrow K\rho) = 0$ .

2 BARATE 99R assume  $\tau^- \rightarrow K^- \pi^+ \pi^- \nu_\tau(\text{ex.}K^0)$  decays proceed only through  $K\rho$  and  $K^* \pi$  intermediate states. The quoted error is statistical only.

$$\Gamma(K^- \pi^+ \pi^- \pi^0 \nu_\tau)/\Gamma_{\text{total}} \quad \Gamma_{99}/\Gamma$$

$$\Gamma_{99}/\Gamma = (0.34598\Gamma_{43} + \Gamma_{103} + 0.2292\Gamma_{152} + 0.893\Gamma_{179})/\Gamma$$

VALUE (units 10 <sup>-4</sup> )	DOCUMENT ID
<b>13.1 ± 1.2 OUR FIT</b>	

$$\Gamma(K^- \pi^+ \pi^- \pi^0 \nu_\tau(\text{ex.}K^0))/\Gamma_{\text{total}} \quad \Gamma_{100}/\Gamma$$

$$\Gamma_{100}/\Gamma = (\Gamma_{103} + 0.2292\Gamma_{152} + 0.893\Gamma_{179})/\Gamma$$

VALUE (units 10 <sup>-4</sup> )	CL%	DOCUMENT ID	TECN	COMMENT
<b>7.9 ± 1.2 OUR FIT</b>				
<b>7.3 ± 1.2 OUR AVERAGE</b>				

7.4 ± 0.8 ± 1.1 1 ARMS 05 CLE3 7.6 fb<sup>-1</sup>, E<sub>cm</sub><sup>ee</sup> = 10.6 GeV

6.1 ± 3.9 ± 1.8 BARATE 98 ALEP 1991-1995 LEP runs

• • • We use the following data for averages but not for fits. • • •

7.5 ± 2.6 ± 1.8 2 RICHICHI 99 CLEO E<sub>cm</sub><sup>ee</sup> = 10.6 GeV

• • • We do not use the following data for averages, fits, limits, etc. • • •

<17 95 ABBIENDI 00D OPAL 1990-1995 LEP runs

1 Not independent of ARMS 05  $\Gamma(\tau^- \rightarrow K^- \pi^+ \pi^- \pi^0 \nu_\tau(\text{ex.}K^0, \omega))/\Gamma_{\text{total}}$  and  $\Gamma(\tau^- \rightarrow K^- \omega \nu_\tau)/\Gamma_{\text{total}}$  values.

2 Not independent of RICHICHI 99  $\Gamma(\tau^- \rightarrow K^- h^+ \pi^- \nu_\tau(\text{ex.}K^0))/\Gamma(\tau^- \rightarrow \pi^- \pi^+ \pi^- \nu_\tau(\text{ex.}K^0))$ ,  $\Gamma(\tau^- \rightarrow K^- K^+ \pi^- \nu_\tau)/\Gamma(\tau^- \rightarrow \pi^- \pi^+ \pi^- \nu_\tau(\text{ex.}K^0))$  and BALEST 95c  $\Gamma(\tau^- \rightarrow h^- h^- h^+ \nu_\tau(\text{ex.}K^0))/\Gamma_{\text{total}}$  values.

$$\Gamma(K^- \pi^+ \pi^- \pi^0 \nu_\tau(\text{ex.}K^0, \eta))/\Gamma_{\text{total}} \quad \Gamma_{101}/\Gamma = (\Gamma_{103} + 0.893\Gamma_{179})/\Gamma$$

VALUE (units 10 <sup>-4</sup> )	DOCUMENT ID
<b>7.6 ± 1.2 OUR FIT</b>	

$$\Gamma(K^- \pi^+ \pi^- \pi^0 \nu_\tau(\text{ex.}K^0, \omega))/\Gamma_{\text{total}} \quad \Gamma_{102}/\Gamma$$

VALUE (units 10 <sup>-4</sup> )	EVTS	DOCUMENT ID	TECN	COMMENT
<b>3.7 ± 0.5 ± 0.8</b>	833	ARMS 05 CLE3		7.6 fb <sup>-1</sup> , E <sub>cm</sub> <sup>ee</sup> = 10.6 GeV

$$\Gamma(K^- \pi^+ \pi^- \pi^0 \nu_\tau(\text{ex.}K^0, \omega, \eta))/\Gamma_{\text{total}} \quad \Gamma_{103}/\Gamma$$

VALUE (units 10 <sup>-4</sup> )	DOCUMENT ID
<b>3.9 ± 1.4 OUR FIT</b>	

$$\Gamma(K^- \pi^+ K^- \geq 0 \text{ neut. } \nu_\tau)/\Gamma_{\text{total}} \quad \Gamma_{104}/\Gamma$$

VALUE (%)	CL%	DOCUMENT ID	TECN	COMMENT
<b>&lt;0.09</b>	95	BAUER 94 TPC		E <sub>cm</sub> <sup>ee</sup> = 29 GeV

$$\Gamma(K^- K^+ \pi^- \geq 0 \text{ neut. } \nu_\tau)/\Gamma_{\text{total}} \quad \Gamma_{105}/\Gamma = (\Gamma_{106} + \Gamma_{107})/\Gamma$$

VALUE (%)	EVTS	DOCUMENT ID	TECN	COMMENT
<b>0.1496 ± 0.0033 OUR FIT</b>				
<b>0.203 ± 0.031 OUR AVERAGE</b>				

0.159 ± 0.053 ± 0.020 ABBIENDI 00D OPAL 1990-1995 LEP runs

0.15 ± 0.09 ± 0.03 4 1 BAUER 94 TPC E<sub>cm</sub><sup>ee</sup> = 29 GeV

• • • We use the following data for averages but not for fits. • • •

0.238 ± 0.042 2 BARATE 98 ALEP 1991-1995 LEP runs

1 We multiply 0.15% by 0.20, the relative systematic error quoted by BAUER 94, to obtain the systematic error.

2 Not independent of BARATE 98  $\Gamma(\tau^- \rightarrow K^- K^+ \pi^- \nu_\tau)/\Gamma_{\text{total}}$  and  $\Gamma(\tau^- \rightarrow K^- K^+ \pi^- \pi^0 \nu_\tau)/\Gamma_{\text{total}}$  values.

$$\Gamma(K^- K^+ \pi^- \nu_\tau)/\Gamma_{\text{total}} \quad \Gamma_{106}/\Gamma$$

VALUE (units 10 <sup>-3</sup> )	EVTS	DOCUMENT ID	TECN	COMMENT
<b>1.43 ± 0.07 OUR FIT</b>				
<b>1.43 ± 0.07 OUR AVERAGE</b>				

Error includes scale factor of 2.4. See the ideogram below.

1.55 ± 0.01 ± 0.06 108k 1 LEE 10 BELL 666 fb<sup>-1</sup> E<sub>cm</sub><sup>ee</sup> = 10.6 GeV

1.346 ± 0.010 ± 0.036 18k 2 AUBERT 08 BABR 342 fb<sup>-1</sup> E<sub>cm</sub><sup>ee</sup> = 10.6 GeV

1.55 ± 0.06 ± 0.09 932 3 BRIERE 03 CLE3 E<sub>cm</sub><sup>ee</sup> = 10.6 GeV

1.63 ± 0.21 ± 0.17 BARATE 98 ALEP 1991-1995 LEP runs

• • • We use the following data for averages but not for fits. • • •

0.87 ± 0.56 ± 0.40 ABBIENDI 00D OPAL 1990-1995 LEP runs

1.45 ± 0.13 ± 0.28 2.3k 4 RICHICHI 99 CLEO E<sub>cm</sub><sup>ee</sup> = 10.6 GeV

• • • We do not use the following data for averages, fits, limits, etc. • • •

2.2 ± 1.7 ± 1.1 9 5 MILLS 85 DLCO E<sub>cm</sub><sup>ee</sup> = 29 GeV

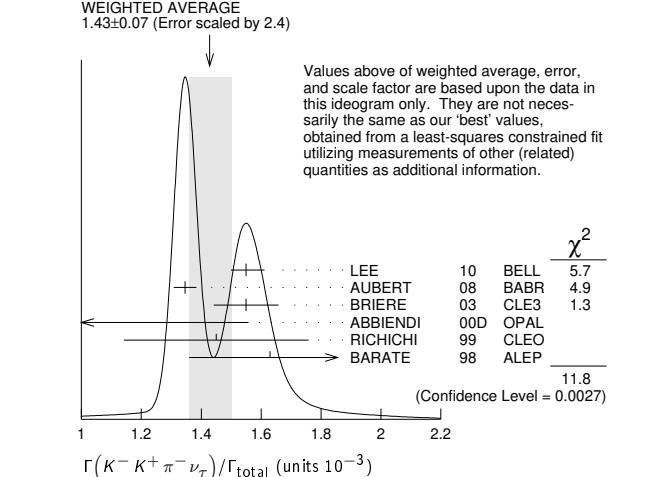
1 See footnote to LEE 10  $\Gamma(\tau^- \rightarrow \pi^- \pi^+ \pi^- \nu_\tau(\text{ex.}K^0))/\Gamma_{\text{total}}$  measurement for correlations with other measurements. Not independent of LEE 10  $\Gamma(\tau^- \rightarrow K^- K^+ \pi^- \nu_\tau)/\Gamma(\tau^- \rightarrow \pi^- \pi^+ \pi^- \nu_\tau(\text{ex.}K^0))$  value.

2 See footnote to AUBERT 08  $\Gamma(\tau^- \rightarrow \pi^- \pi^+ \pi^- \nu_\tau(\text{ex.}K^0))/\Gamma_{\text{total}}$  measurement for correlations with other measurements.

3 71% correlated with BRIERE 03  $\tau^- \rightarrow \pi^- \pi^+ \pi^- \nu_\tau$  and 34% correlated with  $\tau \rightarrow K^- \pi^+ \pi^- \nu_\tau$  because of a common 5% normalization error.

4 Not independent of RICHICHI 99  $\Gamma(\tau^- \rightarrow K^- K^+ \pi^- \nu_\tau)/\Gamma(\tau^- \rightarrow \pi^- \pi^+ \pi^- \nu_\tau(\text{ex.}K^0))$  and BALEST 95c  $\Gamma(\tau^- \rightarrow h^- h^- h^+ \nu_\tau(\text{ex.}K^0))/\Gamma_{\text{total}}$  values.

5 Error correlated with MILLS 85 ( $K \pi \pi^0 \nu$ ) value. We multiply 0.22% by 0.23, the relative systematic error quoted by MILLS 85, to obtain the systematic error.



$$\Gamma(K^- K^+ \pi^- \nu_\tau)/\Gamma(\pi^- \pi^+ \pi^- \nu_\tau(\text{ex.}K^0)) \quad \Gamma_{106}/\Gamma_{68}$$

$$\Gamma_{106}/\Gamma_{68} = \Gamma_{106}/(\Gamma_{70} + 0.0153\Gamma_{178})$$

VALUE (%)	EVTS	DOCUMENT ID	TECN	COMMENT
<b>1.592 ± 0.030 OUR FIT</b>				
<b>1.83 ± 0.05 OUR AVERAGE</b>				

1.60 ± 0.15 ± 0.30 2.3k RICHICHI 99 CLEO E<sub>cm</sub><sup>ee</sup> = 10.6 GeV

• • • We use the following data for averages but not for fits. • • •

1.84 ± 0.01 ± 0.05 108k 1 LEE 10 BELL 666 fb<sup>-1</sup> E<sub>cm</sub><sup>ee</sup> = 10.6 GeV

1 Not independent of LEE 10  $\Gamma(\tau^- \rightarrow K^- K^+ \pi^- \nu_\tau)/\Gamma_{\text{total}}$  and  $\Gamma(\tau^- \rightarrow \pi^- \pi^+ \pi^- \nu_\tau(\text{ex.}K^0))/\Gamma_{\text{total}}$  values.

$$\Gamma(K^- K^+ \pi^- \pi^0 \nu_\tau)/\Gamma_{\text{total}} \quad \Gamma_{107}/\Gamma$$

VALUE (units 10 <sup>-4</sup> )	CL%	EVTS	DOCUMENT ID	TECN	COMMENT
<b>0.61 ± 0.18 OUR FIT</b>					
<b>0.60 ± 0.18 OUR AVERAGE</b>					

0.55 ± 0.14 ± 0.12 48 ARMS 05 CLE3 7.6 fb<sup>-1</sup>, E<sub>cm</sub><sup>ee</sup> = 10.6 GeV

7.5 ± 2.9 ± 1.5 BARATE 98 ALEP 1991-1995 LEP runs

• • • We use the following data for averages but not for fits. • • •

3.3 ± 1.8 ± 0.7 158 1 RICHICHI 99 CLEO E<sub>cm</sub><sup>ee</sup> = 10.6 GeV

• • • We do not use the following data for averages, fits, limits, etc. • • •

<27 95 ABBIENDI 00D OPAL 1990-1995 LEP runs

1 Not independent of RICHICHI 99  $\Gamma(\tau^- \rightarrow K^- K^+ \pi^- \nu_\tau)/\Gamma(\tau^- \rightarrow \pi^- \pi^+ \pi^- \nu_\tau(\text{ex.}K^0))$  and BALEST 95c  $\Gamma(\tau^- \rightarrow h^- h^- h^+ \nu_\tau(\text{ex.}K^0))/\Gamma_{\text{total}}$  values.

$$\Gamma(K^- K^+ \pi^- \pi^0 \nu_\tau)/\Gamma(\pi^- \pi^+ \pi^- \pi^0 \nu_\tau(\text{ex.}K^0)) \quad \Gamma_{107}/\Gamma_{77}$$

$$\Gamma_{107}/\Gamma_{77} = \Gamma_{107}/(\Gamma_{78} + 0.893\Gamma_{178} + 0.0153\Gamma_{180})$$

VALUE (%)	EVTS	DOCUMENT ID	TECN	COMMENT
<b>0.14 ± 0.04 OUR FIT</b>				
<b>0.79 ± 0.44 ± 0.16</b>	158	1 RICHICHI 99 CLEO		E <sub>cm</sub> <sup>ee</sup> = 10.6 GeV

1 RICHICHI 99 also quote a 95%CL upper limit of 0.0157 for this measurement.



Lepton Particle Listings

T

$\Gamma(K^- K^+ K^- \nu_\tau)/\Gamma_{total}$   $\Gamma_{108}/\Gamma = 0.492\Gamma_{170}/\Gamma$

Table with columns: VALUE (units 10^-5), CL%, EVTS, DOCUMENT ID, TECN, COMMENT. Includes entries for LEE, AUBERT, BRIERE, BARATE.

1 See footnote to LEE 10  $\Gamma(\tau^- \rightarrow \pi^- \pi^+ \pi^- \nu_\tau \text{ (ex. } K^0)) / \Gamma_{total}$  measurement for correlations with other measurements. Not independent of LEE 10  $\Gamma(\tau^- \rightarrow K^- K^+ K^- \nu_\tau) / \Gamma(\tau^- \rightarrow \pi^- \pi^+ \pi^- \nu_\tau \text{ (ex. } K^0))$  value.

$\Gamma(K^- K^+ K^- \nu_\tau) / \Gamma(\pi^- \pi^+ \pi^- \nu_\tau \text{ (ex. } K^0))$   $\Gamma_{108}/\Gamma_{68}$

Table with columns: VALUE (units 10^-4), CL%, EVTS, DOCUMENT ID, TECN, COMMENT. Includes entry for LEE.

1 Not independent of LEE 10  $\Gamma(\tau^- \rightarrow K^- K^+ K^- \nu_\tau) / \Gamma_{total}$  and  $\Gamma(\tau^- \rightarrow \pi^- \pi^+ \pi^- \nu_\tau \text{ (ex. } K^0)) / \Gamma_{total}$  values.

$\Gamma(K^- K^+ K^- \nu_\tau \text{ (ex. } \phi)) / \Gamma_{total}$   $\Gamma_{109}/\Gamma$

Table with columns: VALUE, CL%, DOCUMENT ID, TECN, COMMENT. Includes entry for AUBERT.

$\Gamma(K^- K^+ K^- \pi^0 \nu_\tau) / \Gamma_{total}$   $\Gamma_{110}/\Gamma$

Table with columns: VALUE, CL%, DOCUMENT ID, TECN, COMMENT. Includes entry for ARMS.

$\Gamma(\pi^- K^+ \pi^- \geq 0 \text{ neut. } \nu_\tau) / \Gamma_{total}$   $\Gamma_{111}/\Gamma$

Table with columns: VALUE (%), CL%, DOCUMENT ID, TECN, COMMENT. Includes entry for BAUER.

$\Gamma(e^- e^- e^+ \nu_e \nu_\tau) / \Gamma_{total}$   $\Gamma_{112}/\Gamma$

Table with columns: VALUE (units 10^-5), CL%, EVTS, DOCUMENT ID, TECN, COMMENT. Includes entry for ALAM.

$\Gamma(\mu^- e^- e^+ \nu_\mu \nu_\tau) / \Gamma_{total}$   $\Gamma_{113}/\Gamma$

Table with columns: VALUE (units 10^-5), CL%, DOCUMENT ID, TECN, COMMENT. Includes entry for ALAM.

$\Gamma(\pi^- e^- e^+ \nu_\tau) / \Gamma_{total}$   $\Gamma_{114}/\Gamma$

Table with columns: VALUE (units 10^-5), CL%, EVTS, DOCUMENT ID, TECN, COMMENT. Includes entry for JIN.

1 JIN 19 measures  $B(\tau^- \rightarrow \pi^- e^- e^+ \nu_\tau (m_{\pi^- e^- e^+} > 1.05 \text{ GeV}/c^2)) = (5.90 \pm 0.53 \pm 0.86) \times 10^{-6}$ , which is only sensitive to the structure-dependent contribution, and assumes that the decay proceeds with either a pure axial-vector current or a pure vector current to obtain the two respective branching fraction measurements for this mode, which are 100% correlated.

$\Gamma(\pi^- \mu^- \mu^+ \nu_\tau) / \Gamma_{total}$   $\Gamma_{115}/\Gamma$

Table with columns: VALUE, CL%, DOCUMENT ID, TECN, COMMENT. Includes entry for JIN.

$\Gamma(3h^- 2h^+ \geq 0 \text{ neutrals } \nu_\tau \text{ (ex. } K_S^0 \rightarrow \pi^- \pi^+ \text{ ("5-prong"))} / \Gamma_{total}$   $\Gamma_{116}/\Gamma$

Table with columns: VALUE (%), CL%, EVTS, DOCUMENT ID, TECN, COMMENT. Includes entry for ACHARD.

1 ACHARD 01D L3 1992-1995 LEP runs. 2 ABREU 01M DLPH 1992-1995 LEP runs. 3 ACKERSTAFF 99E OPAL 1991-1995 LEP runs. We do not use the following data for averages, fits, limits, etc. ...

Table with columns: VALUE, CL%, EVTS, DOCUMENT ID, TECN, COMMENT. Includes entries for ACTON, DECAMP, BEHREND, BARTEL, BELTRAMI.

Table with columns: VALUE, CL%, EVTS, DOCUMENT ID, TECN, COMMENT. Includes entries for BURCHAT, BEHREND.

1 The correlation coefficients between this measurement and the ACHARD 01D measurements of  $B(\tau \rightarrow \text{"1-prong"})$  and  $B(\tau \rightarrow \text{"3-prong"})$  are -0.082 and -0.19 respectively. 2 The correlation coefficients between this measurement and the ABREU 01M measurements of  $B(\tau \rightarrow \text{1-prong})$  and  $B(\tau \rightarrow \text{3-prong})$  are -0.08 and -0.08 respectively. 3 Not independent of ACKERSTAFF 99E  $B(\tau^- \rightarrow 3h^- 2h^+ \nu_\tau \text{ (ex. } K^0))$  and  $B(\tau^- \rightarrow 3h^- 2h^+ \pi^0 \nu_\tau \text{ (ex. } K^0))$  measurements.

$\Gamma(3h^- 2h^+ \nu_\tau \text{ (ex. } K^0)) / \Gamma_{total}$   $\Gamma_{117}/\Gamma = (\Gamma_{118} + \Gamma_{120} + 0.0153\Gamma_{185}) / \Gamma$

Table with columns: VALUE (units 10^-4), CL%, EVTS, DOCUMENT ID, TECN, COMMENT. Includes entries for ABDALLAH, SCHAEEL, ACKERSTAFF, GIBAUT, ALBRECHT, BYLSMA.

1 See footnote to ABDALLAH 06A  $\Gamma(\tau^- \rightarrow h^- \nu_\tau) / \Gamma_{total}$  measurement for correlations with other measurements. 2 See footnote to SCHAEEL 05C  $\Gamma(\tau^- \rightarrow e^- \bar{\nu}_e \nu_\tau) / \Gamma_{total}$  measurement for correlations with other measurements. 3 The error quoted is statistical only.

Table with columns: VALUE, CL%, DOCUMENT ID, TECN, COMMENT. Includes entry for ABDALLAH.

$\Gamma(3\pi^- 2\pi^+ \nu_\tau \text{ (ex. } K^0, \omega)) / \Gamma_{total}$   $\Gamma_{118}/\Gamma = (\Gamma_{119} + \Gamma_{173}) / \Gamma$

Table with columns: VALUE (units 10^-4), CL%, EVTS, DOCUMENT ID, TECN, COMMENT. Includes entry for LEES.

$\Gamma(3\pi^- 2\pi^+ \nu_\tau \text{ (ex. } K^0, \omega, f_1(1285))) / \Gamma_{total}$   $\Gamma_{119}/\Gamma$

Table with columns: VALUE (units 10^-4), CL%, EVTS, DOCUMENT ID, TECN, COMMENT. Includes entry for LEES.

$\Gamma(K^- 2\pi^- 2\pi^+ \nu_\tau \text{ (ex. } K^0)) / \Gamma_{total}$   $\Gamma_{120}/\Gamma$

Table with columns: VALUE (units 10^-6), CL%, EVTS, DOCUMENT ID, TECN, COMMENT. Includes entry for LEES.

Table with columns: VALUE, CL%, DOCUMENT ID, TECN, COMMENT. Includes entry for LEES.

$\Gamma(K^+ 3\pi^- \pi^+ \nu_\tau) / \Gamma_{total}$   $\Gamma_{121}/\Gamma$

Table with columns: VALUE, CL%, DOCUMENT ID, TECN, COMMENT. Includes entry for LEES.

$\Gamma(K^+ K^- 2\pi^- \pi^+ \nu_\tau) / \Gamma_{total}$   $\Gamma_{122}/\Gamma$

Table with columns: VALUE, CL%, DOCUMENT ID, TECN, COMMENT. Includes entry for LEES.

$\Gamma(3h^- 2h^+ \pi^0 \nu_\tau \text{ (ex. } K^0)) / \Gamma_{total}$   $\Gamma_{123}/\Gamma = (\Gamma_{124} + \Gamma_{127}) / \Gamma$

Table with columns: VALUE (units 10^-4), CL%, EVTS, DOCUMENT ID, TECN, COMMENT. Includes entries for ABDALLAH, SCHAEEL, ANASTASSOV, ACKERSTAFF, BUSKULIC, GIBAUT, BYLSMA, BELTRAMI.

1 See footnote to ABDALLAH 06A  $\Gamma(\tau^- \rightarrow h^- \nu_\tau) / \Gamma_{total}$  measurement for correlations with other measurements. 2 SCHAEEL 05C quote  $(1.4 \pm 0.7 \pm 0.9) \times 10^{-4}$ . We add  $0.7 \times 10^{-4}$  to remove their correction for  $\tau^- \rightarrow \eta \pi^- \pi^+ \pi^- \nu_\tau \rightarrow 3\pi^- 2\pi^+ \pi^0 \nu_\tau$  and  $\tau^- \rightarrow K^*(892)^- \eta \nu_\tau \rightarrow 3\pi^- 2\pi^+ \pi^0 \nu_\tau$  decays. See footnote to SCHAEEL 05C  $\Gamma(\tau^- \rightarrow e^- \bar{\nu}_e \nu_\tau) / \Gamma_{total}$  measurement for correlations with other measurements. 3 The error quoted is statistical only.

$\Gamma(3\pi^- 2\pi^+ \pi^0 \nu_\tau (\text{ex. } K^0))/\Gamma_{\text{total}}$   $\Gamma_{124}/\Gamma$   
 $\Gamma_{124}/\Gamma = (\Gamma_{126} + 0.2292\Gamma_{160} + 0.893\Gamma_{185})/\Gamma$

VALUE (units $10^{-4}$ )	DOCUMENT ID	TECN	COMMENT
<b>1.63 ± 0.11 OUR FIT</b>			
• • • We use the following data for averages but not for fits. • • •			
<b>1.65 ± 0.05 ± 0.09</b>	<sup>1</sup> LEES	12X	BABR 468 fb <sup>-1</sup> $E_{\text{cm}}^{\text{ee}} = 10.6$ GeV
<sup>1</sup> Not independent of LEES 12X measurements of $\Gamma(\tau^- \rightarrow 2\pi^- \pi^+ \omega \nu_\tau (\text{ex. } K^0))/\Gamma$ , $\Gamma(\tau^- \rightarrow \eta \pi^- \pi^+ \pi^- \nu_\tau (\text{ex. } K^0))/\Gamma$ , and $\Gamma(\tau^- \rightarrow 3\pi^- 2\pi^+ \pi^0 \nu_\tau (\text{ex. } K^0, \eta, \omega, f_1(1285)))/\Gamma$ .			

$\Gamma(3\pi^- 2\pi^+ \pi^0 \nu_\tau (\text{ex. } K^0, \eta, f_1(1285)))/\Gamma_{\text{total}}$   $\Gamma_{125}/\Gamma$

VALUE (units $10^{-4}$ )	DOCUMENT ID	TECN	COMMENT
<b>1.11 ± 0.04 ± 0.09</b>	<sup>1</sup> LEES	12X	BABR 468 fb <sup>-1</sup> $E_{\text{cm}}^{\text{ee}} = 10.6$ GeV
<sup>1</sup> Not independent of LEES 12X $\Gamma(\tau^- \rightarrow 2\pi^- \pi^+ \omega \nu_\tau (\text{ex. } K^0))/\Gamma$ and $\Gamma(\tau^- \rightarrow 3\pi^- 2\pi^+ \pi^0 \nu_\tau (\text{ex. } K^0, \eta, \omega, f_1(1285)))/\Gamma$ values.			

$\Gamma(3\pi^- 2\pi^+ \pi^0 \nu_\tau (\text{ex. } K^0, \eta, \omega, f_1(1285)))/\Gamma_{\text{total}}$   $\Gamma_{126}/\Gamma$

VALUE (units $10^{-4}$ )	EVTS	DOCUMENT ID	TECN	COMMENT
<b>0.38 ± 0.09 OUR FIT</b>				
<b>0.36 ± 0.03 ± 0.09</b>	7.3k	LEES	12X	BABR 468 fb <sup>-1</sup> $E_{\text{cm}}^{\text{ee}} = 10.6$ GeV

$\Gamma(K^- 2\pi^- 2\pi^+ \pi^0 \nu_\tau (\text{ex. } K^0))/\Gamma_{\text{total}}$   $\Gamma_{127}/\Gamma$

VALUE (units $10^{-6}$ )	DOCUMENT ID	TECN	COMMENT
<b>1.1 ± 0.6 OUR FIT</b>			
<b>1.1 ± 0.4 ± 0.4</b>	<sup>1</sup> LEES	12X	BABR 468 fb <sup>-1</sup> $E_{\text{cm}}^{\text{ee}} = 10.6$ GeV
<sup>1</sup> LEES 12X measurement corresponds to the lower limit of $< 1.9 \times 10^{-6}$ at 90% CL.			

$\Gamma(K^+ 3\pi^- \pi^+ \pi^0 \nu_\tau)/\Gamma_{\text{total}}$   $\Gamma_{128}/\Gamma$

VALUE	CL%	DOCUMENT ID	TECN	COMMENT
<b><math>&lt; 8 \times 10^{-7}</math></b>	90	LEES	12X	BABR 468 fb <sup>-1</sup> $E_{\text{cm}}^{\text{ee}} = 10.6$ GeV

$\Gamma(3h^- 2h^+ 2\pi^0 \nu_\tau)/\Gamma_{\text{total}}$   $\Gamma_{129}/\Gamma$

VALUE	CL%	DOCUMENT ID	TECN	COMMENT
<b><math>&lt; 3.4 \times 10^{-6}</math></b>	90	AUBERT,B	06	BABR 232 fb <sup>-1</sup> $E_{\text{cm}}^{\text{ee}} = 10.6$ GeV
• • • We do not use the following data for averages, fits, limits, etc. • • •				
<b><math>&lt; 1.1 \times 10^{-4}</math></b>	90	GIBAUT	94B	CLEO $E_{\text{cm}}^{\text{ee}} = 10.6$ GeV

$\Gamma((5\pi^-) - \nu_\tau)/\Gamma_{\text{total}}$   $\Gamma_{130}/\Gamma$   
 $\Gamma_{130}/\Gamma = (\Gamma_{30} + \frac{1}{2}\Gamma_{45} + \Gamma_{48} + \frac{1}{2}\Gamma_{61} + \Gamma_{85} + \Gamma_{117} + 0.5559\Gamma_{150} + 0.893\Gamma_{180})/\Gamma$

VALUE (%)	DOCUMENT ID	TECN	COMMENT
<b>0.78 ± 0.05 OUR FIT</b>			
• • • We use the following data for averages but not for fits. • • •			
<b>0.61 ± 0.06 ± 0.08</b>	<sup>1</sup> GIBAUT	94B	CLEO $E_{\text{cm}}^{\text{ee}} = 10.6$ GeV
<sup>1</sup> Not independent of GIBAUT 94B B(3h <sup>-</sup> 2h <sup>+</sup> $\nu_\tau$ ), PROCARIO 93 B(h <sup>-</sup> 4 $\pi^0$ $\nu_\tau$ ), and BORTOLETTO 93 B(2h <sup>-</sup> h <sup>+</sup> 2 $\pi^0$ $\nu_\tau$ )/B("3prong") measurements. Result is corrected for $\eta$ contributions.			

$\Gamma(4h^- 3h^+ \geq 0 \text{ neutrals } \nu_\tau (\text{"7-prong"}))/\Gamma_{\text{total}}$   $\Gamma_{131}/\Gamma$

VALUE	CL%	DOCUMENT ID	TECN	COMMENT
<b><math>&lt; 3.0 \times 10^{-7}</math></b>	90	AUBERT,B	05F	BABR 232 fb <sup>-1</sup> , $E_{\text{cm}}^{\text{ee}} = 10.6$ GeV
• • • We do not use the following data for averages, fits, limits, etc. • • •				
<b><math>&lt; 1.8 \times 10^{-5}</math></b>	95	ACKERSTAFF	97J	OPAL 1990-1995 LEP runs
<b><math>&lt; 2.4 \times 10^{-6}</math></b>	90	EDWARDS	97B	CLEO $E_{\text{cm}}^{\text{ee}} = 10.6$ GeV
<b><math>&lt; 2.9 \times 10^{-4}</math></b>	90	BYLSMA	87	HRS $E_{\text{cm}}^{\text{ee}} = 29$ GeV

$\Gamma(4h^- 3h^+ \nu_\tau)/\Gamma_{\text{total}}$   $\Gamma_{132}/\Gamma$

VALUE	CL%	DOCUMENT ID	TECN	COMMENT
<b><math>&lt; 4.3 \times 10^{-7}</math></b>	90	AUBERT,B	05F	BABR 232 fb <sup>-1</sup> , $E_{\text{cm}}^{\text{ee}} = 10.6$ GeV

$\Gamma(4h^- 3h^+ \pi^0 \nu_\tau)/\Gamma_{\text{total}}$   $\Gamma_{133}/\Gamma$

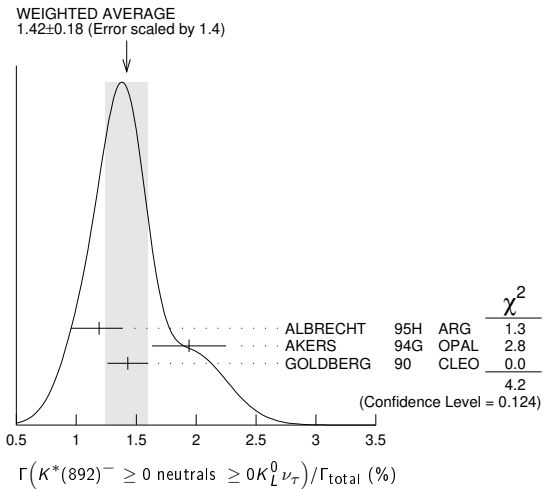
VALUE	CL%	DOCUMENT ID	TECN	COMMENT
<b><math>&lt; 2.5 \times 10^{-7}</math></b>	90	AUBERT,B	05F	BABR 232 fb <sup>-1</sup> , $E_{\text{cm}}^{\text{ee}} = 10.6$ GeV

$\Gamma(X^-(S=-1)\nu_\tau)/\Gamma_{\text{total}}$   $\Gamma_{134}/\Gamma$   
 $\Gamma_{134}/\Gamma = (\Gamma_{10} + \Gamma_{16} + \Gamma_{23} + \Gamma_{28} + \Gamma_{36} + \Gamma_{41} + \Gamma_{45} + \Gamma_{61} + \Gamma_{97} + \Gamma_{103} + \Gamma_{120} + \Gamma_{127} + \Gamma_{152} + \Gamma_{154} + \Gamma_{156} + 0.8312\Gamma_{170} + \Gamma_{179})/\Gamma$

VALUE (%)	DOCUMENT ID	TECN	COMMENT
<b>2.92 ± 0.04 OUR FIT</b>			
• • • We use the following data for averages but not for fits. • • •			
<b>2.87 ± 0.12</b>	<sup>1</sup> BARATE	99R	ALEP 1991-1995 LEP runs
<sup>1</sup> BARATE 99R perform a combined analysis of all ALEPH LEP 1 data on $\tau$ branching fraction measurements for decay modes having total strangeness equal to -1.			

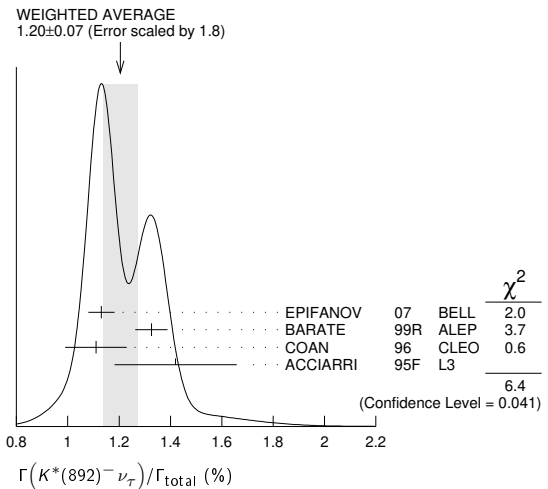
$\Gamma(K^*(892)^- \geq 0 \text{ neutrals } \geq 0 K_L^0 \nu_\tau)/\Gamma_{\text{total}}$   $\Gamma_{135}/\Gamma$

VALUE (%)	EVTS	DOCUMENT ID	TECN	COMMENT
<b>1.42 ± 0.18 OUR AVERAGE</b>				Error includes scale factor of 1.4. See the ideogram below.
1.19 ± 0.15 <sup>+0.13</sup> / <sub>-0.18</sub>	104	ALBRECHT	95H	ARG $E_{\text{cm}}^{\text{ee}} = 9.4-10.6$ GeV
1.94 ± 0.27 ± 0.15	74	<sup>1</sup> AKERS	94G	OPAL $E_{\text{cm}}^{\text{ee}} = 88-94$ GeV
1.43 ± 0.11 ± 0.13	475	<sup>2</sup> GOLDBERG	90	CLEO $E_{\text{cm}}^{\text{ee}} = 9.4-10.9$ GeV
<sup>1</sup> AKERS 94G reject events in which a $K_S^0$ accompanies the $K^*(892)^-$ . We do not correct for them.				
<sup>2</sup> GOLDBERG 90 estimates that 10% of observed $K^*(892)$ are accompanied by a $\pi^0$ .				



$\Gamma(K^*(892)^- \nu_\tau)/\Gamma_{\text{total}}$   $\Gamma_{136}/\Gamma$

VALUE (%)	EVTS	DOCUMENT ID	TECN	COMMENT
<b>1.20 ± 0.07 OUR AVERAGE</b>				Error includes scale factor of 1.8. See the ideogram below.
1.131 ± 0.006 ± 0.051	49k	<sup>1</sup> EPIFANOV	07	BELL 351 fb <sup>-1</sup> $E_{\text{cm}}^{\text{ee}} = 10.6$ GeV
1.326 ± 0.063		BARATE	99R	ALEP 1991-1995 LEP runs
1.11 ± 0.12		<sup>2</sup> COAN	96	CLEO $E_{\text{cm}}^{\text{ee}} \approx 10.6$ GeV
1.42 ± 0.22 ± 0.09		<sup>3</sup> ACCIARRI	95F	L3 1991-1993 LEP runs
• • • We do not use the following data for averages, fits, limits, etc. • • •				
1.39 ± 0.09 ± 0.10		<sup>4</sup> BUSKULIC	96	ALEP Repl. by BARATE 99R
1.45 ± 0.13 ± 0.11	273	<sup>5</sup> BUSKULIC	94F	ALEP Repl. by BUSKULIC 96
1.23 ± 0.21 <sup>+0.11</sup> / <sub>-0.21</sub>	54	<sup>6</sup> ALBRECHT	88L	ARG $E_{\text{cm}}^{\text{ee}} = 10$ GeV
1.9 ± 0.3 ± 0.4	44	<sup>7</sup> TSCHIRHART	88	HRS $E_{\text{cm}}^{\text{ee}} = 29$ GeV
1.5 ± 0.4 ± 0.4	15	<sup>8</sup> AIHARA	87C	TPC $E_{\text{cm}}^{\text{ee}} = 29$ GeV
1.3 ± 0.3 ± 0.3	31	YELTON	86	MRK2 $E_{\text{cm}}^{\text{ee}} = 29$ GeV
1.7 ± 0.7	11	DORFAN	81	MRK2 $E_{\text{cm}}^{\text{ee}} = 4.2-6.7$ GeV



<sup>1</sup> EPIFANOV 07 quote  $B(\tau^- \rightarrow K^*(892)^- \nu_\tau) B(K^*(892)^- \rightarrow K_S^0 \pi^-) = (3.77 \pm 0.02(\text{stat}) \pm 0.12(\text{syst}) \pm 0.12(\text{mod})) \times 10^{-3}$ . We add the systematic and model uncertainties in quadrature and divide by  $B(K^*(892)^- \rightarrow K_S^0 \pi^-) = 0.3333$ .

<sup>2</sup> Not independent of COAN 96 B( $\pi^- \bar{K}^0 \nu_\tau$ ) and BATTLE 94 B( $K^- \pi^0 \nu_\tau$ ) measurements.  $K\pi$  final states are consistent with and assumed to originate from  $K^*(892)^-$  production.

<sup>3</sup> This result is obtained from their B( $\pi^- \bar{K}^0 \nu_\tau$ ) assuming all those decays originate in  $K^*(892)^-$  decays.

# Lepton Particle Listings

$\tau$

- <sup>4</sup> Not independent of BUSKULIC 96 B( $\pi^- \bar{K}^0 \nu_\tau$ ) and B( $K^- \pi^0 \nu_\tau$ ) measurements.
- <sup>5</sup> BUSKULIC 94F obtain this result from BUSKULIC 94F B( $\bar{K}^0 \pi^- \nu_\tau$ ) and BUSKULIC 94E B( $K^- \pi^0 \nu_\tau$ ) assuming all of those decays originate in  $K^*(892)^-$  decays.
- <sup>6</sup> The authors divide by  $\Gamma_2/\Gamma = 0.865$  to obtain this result.
- <sup>7</sup> Not independent of TSCHIRHART 88  $\Gamma(\tau^- \rightarrow h^- \bar{K}^0) \geq 0$  neutrals  $\geq 0 K_L^0 \nu_\tau / \Gamma$ .
- <sup>8</sup> Decay  $\pi^-$  identified in this experiment, is assumed in the others.

$\Gamma(K^*(892)^- \nu_\tau) / \Gamma(\pi^- \pi^0 \nu_\tau)$   $\Gamma_{136} / \Gamma_{14}$

VALUE	DOCUMENT ID	TECN	COMMENT
<b>0.075 ± 0.027</b>	<sup>1</sup> ABREU	94k DLPH	LEP 1992 Z data

<sup>1</sup> ABREU 94k quote B( $\tau^- \rightarrow K^*(892)^- \nu_\tau$ )B( $K^*(892)^- \rightarrow K^- \pi^0$ )/B( $\tau^- \rightarrow \rho^- \nu_\tau$ ) = 0.025 ± 0.009. We divide by B( $K^*(892)^- \rightarrow K^- \pi^0$ ) = 0.333 to obtain this result.

$\Gamma(K^*(892)^- \nu_\tau \rightarrow \pi^- \bar{K}^0 \nu_\tau) / \Gamma(\pi^- \bar{K}^0 \nu_\tau)$   $\Gamma_{137} / \Gamma_{36}$

VALUE	EVTS	DOCUMENT ID	TECN	COMMENT
<b>0.933 ± 0.027</b>	49k	EPIFANOV	07 BELL	351 fb <sup>-1</sup> E <sub>cm</sub> <sup>ee</sup> = 10.6 GeV

$\Gamma(K^*(892)^0 K^- \geq 0 \text{ neutrals } \nu_\tau) / \Gamma_{\text{total}}$   $\Gamma_{138} / \Gamma$

VALUE (%)	EVTS	DOCUMENT ID	TECN	COMMENT
<b>0.32 ± 0.08 ± 0.12</b>	119	GOLDBERG	90 CLEO	E <sub>cm</sub> <sup>ee</sup> = 9.4–10.9 GeV

$\Gamma(K^*(892)^0 K^- \nu_\tau) / \Gamma_{\text{total}}$   $\Gamma_{139} / \Gamma$

VALUE (%)	EVTS	DOCUMENT ID	TECN	COMMENT
<b>0.21 ± 0.04 OUR AVERAGE</b>				
0.213 ± 0.048		<sup>1</sup> BARATE	98 ALEP	1991–1995 LEP runs
0.20 ± 0.05 ± 0.04	47	ALBRECHT	95H ARG	E <sub>cm</sub> <sup>ee</sup> = 9.4–10.6 GeV

<sup>1</sup> BARATE 98 measure the  $K^- (\rho^0 \rightarrow \pi^+ \pi^-)$  fraction in  $\tau^- \rightarrow K^- \pi^+ \pi^- \nu_\tau$  decays to be (35 ± 11)% and derive this result from their measurement of  $\Gamma(\tau^- \rightarrow K^- \pi^+ \pi^- \nu_\tau) / \Gamma_{\text{total}}$  assuming the intermediate states are all  $K^- \rho$  and  $K^- K^*(892)^0$ .

$\Gamma(\bar{K}^*(892)^0 \pi^- \geq 0 \text{ neutrals } \nu_\tau) / \Gamma_{\text{total}}$   $\Gamma_{140} / \Gamma$

VALUE (%)	EVTS	DOCUMENT ID	TECN	COMMENT
<b>0.38 ± 0.11 ± 0.13</b>	105	GOLDBERG	90 CLEO	E <sub>cm</sub> <sup>ee</sup> = 9.4–10.9 GeV

$\Gamma(\bar{K}^*(892)^0 \pi^- \nu_\tau) / \Gamma_{\text{total}}$   $\Gamma_{141} / \Gamma$

VALUE (%)	EVTS	DOCUMENT ID	TECN	COMMENT
<b>0.22 ± 0.05 OUR AVERAGE</b>				
0.209 ± 0.058		<sup>1</sup> BARATE	98 ALEP	1991–1995 LEP runs
0.25 ± 0.10 ± 0.05	27	ALBRECHT	95H ARG	E <sub>cm</sub> <sup>ee</sup> = 9.4–10.6 GeV

<sup>1</sup> BARATE 98 measure the  $K^- K^*(892)^0$  fraction in  $\tau^- \rightarrow K^- K^+ \pi^- \nu_\tau$  decays to be (87 ± 13)% and derive this result from their measurement of  $\Gamma(\tau^- \rightarrow K^- K^+ \pi^- \nu_\tau) / \Gamma_{\text{total}}$ .

$\Gamma((\bar{K}^*(892)^0 \pi^-) \nu_\tau \rightarrow \pi^- \bar{K}^0 \pi^0 \nu_\tau) / \Gamma_{\text{total}}$   $\Gamma_{142} / \Gamma$

VALUE (%)	DOCUMENT ID	TECN	COMMENT
<b>0.10 ± 0.04 OUR AVERAGE</b>			
0.097 ± 0.044 ± 0.036	<sup>1</sup> BARATE	99k ALEP	1991–1995 LEP runs
0.106 ± 0.037 ± 0.032	<sup>2</sup> BARATE	98E ALEP	1991–1995 LEP runs

- <sup>1</sup> BARATE 99k measure  $K^0$ 's by detecting  $K_S^0$ 's in their hadron calorimeter. They determine the  $\bar{K}^0 \rho^-$  fraction in  $\tau^- \rightarrow \pi^- \bar{K}^0 \pi^0 \nu_\tau$  decays to be (0.72 ± 0.12 ± 0.10) and multiply their B( $\pi^- \bar{K}^0 \pi^0 \nu_\tau$ ) measurement by one minus this fraction to obtain the quoted result.
- <sup>2</sup> BARATE 98E reconstruct  $K^0$ 's using  $K_S^0 \rightarrow \pi^+ \pi^-$  decays. They determine the  $\bar{K}^0 \rho^-$  fraction in  $\tau^- \rightarrow \pi^- \bar{K}^0 \pi^0 \nu_\tau$  decays to be (0.64 ± 0.09 ± 0.10) and multiply their B( $\pi^- \bar{K}^0 \pi^0 \nu_\tau$ ) measurement by one minus this fraction to obtain the quoted result.

$\Gamma(K_1(1270)^- \nu_\tau) / \Gamma_{\text{total}}$   $\Gamma_{143} / \Gamma$

VALUE (%)	EVTS	DOCUMENT ID	TECN	COMMENT
<b>0.47 ± 0.11 OUR AVERAGE</b>				
0.48 ± 0.11		BARATE	99R ALEP	1991–1995 LEP runs
0.41 <sup>+0.41</sup> / <sub>-0.35</sub> ± 0.10	5	<sup>1</sup> BAUER	94 TPC	E <sub>cm</sub> <sup>ee</sup> = 29 GeV

<sup>1</sup> We multiply 0.41% by 0.25, the relative systematic error quoted by BAUER 94, to obtain the systematic error.

$\Gamma(K_1(1400)^- \nu_\tau) / \Gamma_{\text{total}}$   $\Gamma_{144} / \Gamma$

VALUE (%)	EVTS	DOCUMENT ID	TECN	COMMENT
<b>0.17 ± 0.26 OUR AVERAGE</b>				Error includes scale factor of 1.7.
0.05 ± 0.17		BARATE	99R ALEP	1991–1995 LEP runs
0.76 <sup>+0.40</sup> / <sub>-0.33</sub> ± 0.20	11	<sup>1</sup> BAUER	94 TPC	E <sub>cm</sub> <sup>ee</sup> = 29 GeV

<sup>1</sup> We multiply 0.76% by 0.25, the relative systematic error quoted by BAUER 94, to obtain the systematic error.

$\Gamma(K_1(1270)^- \nu_\tau) + \Gamma(K_1(1400)^- \nu_\tau) / \Gamma_{\text{total}}$   $(\Gamma_{143} + \Gamma_{144}) / \Gamma$

VALUE (%)	EVTS	DOCUMENT ID	TECN	COMMENT
<b>1.17 <sup>+0.41</sup>/<sub>-0.37</sub> ± 0.29</b>	16	<sup>1</sup> BAUER	94 TPC	E <sub>cm</sub> <sup>ee</sup> = 29 GeV

<sup>1</sup> We multiply 1.17% by 0.25, the relative systematic error quoted by BAUER 94, to obtain the systematic error. Not independent of BAUER 94 B( $K_1(1270)^- \nu_\tau$ ) and BAUER 94 B( $K_1(1400)^- \nu_\tau$ ) measurements.

$\Gamma(K_1(1270)^- \nu_\tau) / [\Gamma(K_1(1270)^- \nu_\tau) + \Gamma(K_1(1400)^- \nu_\tau)]$   $\Gamma_{143} / (\Gamma_{143} + \Gamma_{144})$

VALUE	DOCUMENT ID	TECN	COMMENT
<b>0.69 ± 0.15 OUR AVERAGE</b>			
0.71 ± 0.16 ± 0.11	<sup>1</sup> ABBIENDI	00D OPAL	1990–1995 LEP runs
0.66 ± 0.19 ± 0.13	<sup>2</sup> ASNER	00B CLEO	E <sub>cm</sub> <sup>ee</sup> = 10.6 GeV

<sup>1</sup> ABBIENDI 00D assume the resonance structure of  $\tau^- \rightarrow K^- \pi^+ \pi^- \nu_\tau$  decays is dominated by the  $K_1(1270)^-$  and  $K_1(1400)^-$  resonances.

<sup>2</sup> ASNER 00B assume the resonance structure of  $\tau^- \rightarrow K^- \pi^+ \pi^- \nu_\tau$  (ex.  $K^0$ ) decays is dominated by  $K_1(1270)^-$  and  $K_1(1400)^-$  resonances.

$\Gamma(K^*(1410)^- \nu_\tau) / \Gamma_{\text{total}}$   $\Gamma_{145} / \Gamma$

VALUE (units 10 <sup>-3</sup> )	DOCUMENT ID	TECN	COMMENT
<b>1.5 <sup>+1.4</sup>/<sub>-1.0</sub></b>	BARATE	99R ALEP	1991–1995 LEP runs

$\Gamma(K_0^*(1430)^- \nu_\tau) / \Gamma_{\text{total}}$   $\Gamma_{146} / \Gamma$

VALUE (units 10 <sup>-3</sup> )	CL%	DOCUMENT ID	TECN	COMMENT
<b>&lt; 0.5</b>	95	BARATE	99R ALEP	1991–1995 LEP runs

$\Gamma(K_2^*(1430)^- \nu_\tau) / \Gamma_{\text{total}}$   $\Gamma_{147} / \Gamma$

VALUE (%)	CL%	EVTS	DOCUMENT ID	TECN	COMMENT
<b>&lt; 0.3</b>	95		TSCHIRHART	88 HRS	E <sub>cm</sub> <sup>ee</sup> = 29 GeV

- • • We do not use the following data for averages, fits, limits, etc. • • •
| < 0.33 | 95 | <sup>1</sup> ACCIARRI | 95F L3 | 1991–1993 LEP runs |
| < 0.9 | 95 | DORFAN | 81 MRK2 | E<sub>cm</sub><sup>ee</sup> = 4.2–6.7 GeV |

<sup>1</sup> ACCIARRI 95F quote B( $\tau^- \rightarrow K^*(1430)^- \rightarrow \pi^- \bar{K}^0 \nu_\tau$ ) < 0.11%. We divide by B( $K^*(1430)^- \rightarrow \pi^- \bar{K}^0$ ) = 0.33 to obtain the limit shown.

$\Gamma(a_0(980)^- \geq 0 \text{ neutrals } \nu_\tau) / \Gamma_{\text{total}} \times B(a_0(980)^- \rightarrow K^0 K^-)$   $\Gamma_{148} / \Gamma \times B$

VALUE (units 10 <sup>-4</sup> )	CL%	DOCUMENT ID	TECN	COMMENT
<b>&lt; 2.8</b>	90	GOLDBERG	90 CLEO	E <sub>cm</sub> <sup>ee</sup> = 9.4–10.9 GeV

$\Gamma(\eta \pi^- \nu_\tau) / \Gamma_{\text{total}}$   $\Gamma_{149} / \Gamma$

VALUE (units 10 <sup>-4</sup> )	CL%	EVTS	DOCUMENT ID	TECN	COMMENT
<b>&lt; 0.99</b>	95		<sup>1</sup> DEL-AMO-SA...	11E BABR	470 fb <sup>-1</sup> E <sub>cm</sub> <sup>ee</sup> = 10.6 GeV

- • • We do not use the following data for averages, fits, limits, etc. • • •
| < 6.2 | 95 | BUSKULIC | 97c ALEP | 1991–1994 LEP runs | |
| < 1.4 | 95 | 0 | BARTELT | 96 CLEO | E<sub>cm</sub><sup>ee</sup> ≈ 10.6 GeV |
| < 3.4 | 95 | 0 | ARTUSO | 92 CLEO | E<sub>cm</sub><sup>ee</sup> ≈ 10.6 GeV |
| < 90 | 95 | 0 | ALBRECHT | 88M ARG | E<sub>cm</sub><sup>ee</sup> ≈ 10 GeV |
| < 140 | 90 | 0 | BEHREND | 88 CELL | E<sub>cm</sub><sup>ee</sup> = 14–46.8 GeV |
| < 180 | 95 | 0 | BARINGER | 87 CLEO | E<sub>cm</sub><sup>ee</sup> = 10.5 GeV |
| < 250 | 90 | 0 | COFFMAN | 87 MRK3 | E<sub>cm</sub><sup>ee</sup> = 3.77 GeV |
| 510 ± 100 ± 120 | 65 | DERRICK | 87 HRS | E<sub>cm</sub><sup>ee</sup> = 29 GeV |
| < 100 | 95 | 0 | GAN | 87B MRK2 | E<sub>cm</sub><sup>ee</sup> = 29 GeV |

<sup>1</sup> DEL-AMO-SANCHEZ 11E also quote B( $\tau^- \rightarrow \eta \pi^- \nu_\tau$ ) = (3.4 ± 3.4 ± 2.1) × 10<sup>-5</sup>.

$\Gamma(\eta \pi^- \pi^0 \nu_\tau) / \Gamma_{\text{total}}$   $\Gamma_{150} / \Gamma$

VALUE (units 10 <sup>-3</sup> )	CL%	EVTS	DOCUMENT ID	TECN	COMMENT
<b>1.39 ± 0.07 OUR FIT</b>					
<b>1.38 ± 0.09 OUR AVERAGE</b>					Error includes scale factor of 1.2.
1.35 ± 0.03 ± 0.07	6.0k		INAMI	09 BELL	490 fb <sup>-1</sup> E <sub>cm</sub> <sup>ee</sup> = 10.6 GeV

- 1.8 ± 0.4 ± 0.2
  - 1.7 ± 0.2 ± 0.2
- | DOCUMENT ID | TECN     | COMMENT                                  |
|-------------|----------|--|
| BUSKULIC    | 97c ALEP | 1991–1994 LEP runs                       |
| ARTUSO      | 92 CLEO  | E <sub>cm</sub> <sup>ee</sup> ≈ 10.6 GeV |

- • • We do not use the following data for averages, fits, limits, etc. • • •
| < 11.0 | 95 | ALBRECHT | 88M ARG | E<sub>cm</sub><sup>ee</sup> ≈ 10 GeV |
| < 21.0 | 95 | BARINGER | 87 CLEO | E<sub>cm</sub><sup>ee</sup> = 10.5 GeV |
| 42.0 <sup>+7.0</sup>/<sub>-12.0</sub> ± 16.0 |  | <sup>1</sup> GAN | 87 MRK2 | E<sub>cm</sub><sup>ee</sup> = 29 GeV |

<sup>1</sup> Highly correlated with GAN 87  $\Gamma(\pi^- 3\pi^0 \nu_\tau) / \Gamma(\text{total})$  value.

$\Gamma(\eta \pi^- \pi^0 \pi^0 \nu_\tau) / \Gamma_{\text{total}}$   $\Gamma_{151} / \Gamma$

VALUE (units 10 <sup>-4</sup> )	CL%	EVTS	DOCUMENT ID	TECN	COMMENT
<b>2.0 ± 0.4 OUR FIT</b>					
<b>1.81 ± 0.31 OUR AVERAGE</b>					
2.01 ± 0.34 ± 0.22	381		LEES	12X BABR	468 fb <sup>-1</sup> E <sub>cm</sub> <sup>ee</sup> = 10.6 GeV

- • • We use the following data for averages but not for fits. • • •
| 1.5 ± 0.5 | 30 | <sup>1</sup> ANASTASSOV | 01 CLEO | E<sub>cm</sub><sup>ee</sup> = 10.6 GeV |
- • • We do not use the following data for averages, fits, limits, etc. • • •
| 1.4 ± 0.6 ± 0.3 | 15 | <sup>2</sup> BERGFELD | 97 CLEO | Repl. by ANASTASSOV 01 |
| < 4.3 | 95 | ARTUSO | 92 CLEO | E<sub>cm</sub><sup>ee</sup> ≈ 10.6 GeV |
| < 120 | 95 | ALBRECHT | 88M ARG | E<sub>cm</sub><sup>ee</sup> ≈ 10 GeV |

<sup>1</sup> Weighted average of BERGFELD 97 and ANASTASSOV 01 value of (1.5 ± 0.6 ± 0.3) × 10<sup>-4</sup> obtained using  $\eta$ 's reconstructed from  $\eta \rightarrow \pi^+ \pi^- \pi^0$  decays.

<sup>2</sup> BERGFELD 97 reconstruct  $\eta$ 's using  $\eta \rightarrow \gamma \gamma$  decays.

$\Gamma(\eta K^- \nu_\tau)/\Gamma_{total}$		$\Gamma_{152}/\Gamma$			
VALUE (units $10^{-4}$ )	CL% EVTS	DOCUMENT ID	TECN	COMMENT	
<b>1.55 ± 0.08 OUR FIT</b>					
<b>1.54 ± 0.08 OUR AVERAGE</b>					
1.42 ± 0.11 ± 0.07	690	DEL-AMO-SA..11E	BABR	470 fb <sup>-1</sup> $E_{cm}^{ee} = 10.6$ GeV	
1.58 ± 0.05 ± 0.09	1.6k	INAMI	09	BELL 490 fb <sup>-1</sup> $E_{cm}^{ee} = 10.6$ GeV	
2.9 <sup>+1.3</sup> <sub>-1.2</sub> ± 0.7		BUSKULIC	97c	ALEP 1991-1994 LEP runs	
2.6 ± 0.5 ± 0.5	85	BARTELT	96	CLEO $E_{cm}^{ee} \approx 10.6$ GeV	
• • • We do not use the following data for averages, fits, limits, etc. • • •					
< 4.7	95	ARTUSO	92	CLEO $E_{cm}^{ee} \approx 10.6$ GeV	

$\Gamma(\eta K^*(892)^- \nu_\tau)/\Gamma_{total}$		$\Gamma_{153}/\Gamma$			
VALUE (units $10^{-4}$ )	EVTS	DOCUMENT ID	TECN	COMMENT	
<b>1.38 ± 0.15 OUR AVERAGE</b>					
1.34 ± 0.12 ± 0.09	245	1 INAMI	09	BELL 490 fb <sup>-1</sup> $E_{cm}^{ee} = 10.6$ GeV	
2.90 ± 0.80 ± 0.42	25	BISHAI	99	CLEO $E_{cm}^{ee} = 10.6$ GeV	
1 Not independent of INAMI 09 B( $\tau^- \rightarrow \eta K^- \pi^0 \nu_\tau$ ) and B( $\tau^- \rightarrow \eta \bar{K}^0 \pi^- \nu_\tau$ ) values.					

$\Gamma(\eta K^- \pi^0 \nu_\tau)/\Gamma_{total}$		$\Gamma_{154}/\Gamma$			
VALUE (units $10^{-4}$ )	EVTS	DOCUMENT ID	TECN	COMMENT	
<b>0.48 ± 0.12 OUR FIT</b>					
<b>0.48 ± 0.12 OUR AVERAGE</b>					
0.46 ± 0.11 ± 0.04	270	INAMI	09	BELL 490 fb <sup>-1</sup> $E_{cm}^{ee} = 10.6$ GeV	
1.77 ± 0.56 ± 0.71	36	BISHAI	99	CLEO $E_{cm}^{ee} = 10.6$ GeV	

$\Gamma(\eta K^- \pi^0 (\text{non-}K^*(892)) \nu_\tau)/\Gamma_{total}$		$\Gamma_{155}/\Gamma$			
VALUE	CL%	DOCUMENT ID	TECN	COMMENT	
< 3.5 × 10 <sup>-5</sup>	90	INAMI	09	BELL 490 fb <sup>-1</sup> $E_{cm}^{ee} = 10.6$ GeV	

$\Gamma(\eta \bar{K}^0 \pi^- \nu_\tau)/\Gamma_{total}$		$\Gamma_{156}/\Gamma$			
VALUE (units $10^{-4}$ )	EVTS	DOCUMENT ID	TECN	COMMENT	
<b>0.94 ± 0.15 OUR FIT</b>					
<b>0.93 ± 0.15 OUR AVERAGE</b>					
0.88 ± 0.14 ± 0.06	161	1 INAMI	09	BELL 490 fb <sup>-1</sup> $E_{cm}^{ee} = 10.6$ GeV	
2.20 ± 0.70 ± 0.22	15	2 BISHAI	99	CLEO $E_{cm}^{ee} = 10.6$ GeV	
1 We multiply the INAMI 09 measurement B( $\tau^- \rightarrow \eta K_S^0 \pi^- \nu_\tau$ ) = (0.44 ± 0.07 ± 0.03) × 10 <sup>-4</sup> by 2 to obtain the listed value.					
2 We multiply the BISHAI 99 measurement B( $\tau^- \rightarrow \eta K_S^0 \pi^- \nu_\tau$ ) = (1.10 ± 0.35 ± 0.11) × 10 <sup>-4</sup> by 2 to obtain the listed value.					

$\Gamma(\eta \bar{K}^0 \pi^- \pi^0 \nu_\tau)/\Gamma_{total}$		$\Gamma_{157}/\Gamma$			
VALUE	CL%	DOCUMENT ID	TECN	COMMENT	
< 5.0 × 10 <sup>-5</sup>	90	1 INAMI	09	BELL 490 fb <sup>-1</sup> $E_{cm}^{ee} = 10.6$ GeV	
1 We multiply the INAMI 09 measurement B( $\tau^- \rightarrow \eta K_S^0 \pi^- \pi^0 \nu_\tau$ ) < 2.5 × 10 <sup>-5</sup> by 2 to obtain the listed value.					

$\Gamma(\eta K^- K^0 \nu_\tau)/\Gamma_{total}$		$\Gamma_{158}/\Gamma$			
VALUE	CL%	DOCUMENT ID	TECN	COMMENT	
< 9.0 × 10 <sup>-6</sup>	90	1 INAMI	09	BELL 490 fb <sup>-1</sup> $E_{cm}^{ee} = 10.6$ GeV	
1 We multiply the INAMI 09 measurement B( $\tau^- \rightarrow \eta K^- K_S^0 \nu_\tau$ ) < 4.5 × 10 <sup>-6</sup> by 2 to obtain the listed value.					

$\Gamma(\eta \pi^+ \pi^- \pi^- \geq 0 \text{ neutrals } \nu_\tau)/\Gamma_{total}$		$\Gamma_{159}/\Gamma$			
VALUE (%)	CL%	DOCUMENT ID	TECN	COMMENT	
< 0.3	90	ABACHI	87b	HRS $E_{cm}^{ee} = 29$ GeV	

$\Gamma(\eta \pi^- \pi^+ \pi^- \nu_\tau (\text{ex. } K^0))/\Gamma_{total}$		$\Gamma_{160}/\Gamma$			
VALUE (units $10^{-4}$ )	EVTS	DOCUMENT ID	TECN	COMMENT	
<b>2.20 ± 0.13 OUR FIT</b>					
<b>2.23 ± 0.12 OUR AVERAGE</b>					
2.10 ± 0.09 ± 0.13	2.9k	1 LEES	12x	BABR $\eta \rightarrow \gamma\gamma$	
2.37 ± 0.12 ± 0.18	1.4k	1 LEES	12x	BABR $\eta \rightarrow \pi^+ \pi^- \pi^0$	
2.54 ± 0.27 ± 0.25	315	1 LEES	12x	BABR $\eta \rightarrow 3\pi^0$	
• • • We use the following data for averages but not for fits. • • •					
2.3 ± 0.5	170	2 ANASTASSOV	01	CLEO $E_{cm}^{ee} = 10.6$ GeV	
• • • We do not use the following data for averages, fits, limits, etc. • • •					
1.60 ± 0.05 ± 0.11	1.8 k	AUBERT	08Ae	BABR Repl. by LEES 12x	
3.4 <sup>+0.6</sup> <sub>-0.5</sub> ± 0.6	89	3 BERGFELD	97	CLEO Repl. by ANASTASSOV 01	
1 LEES 12x uses 468 fb <sup>-1</sup> of data taken at $E_{cm}^{ee} = 10.6$ GeV. It gives the average of the three measurements listed here as (2.25 ± 0.07 ± 0.12) × 10 <sup>-4</sup> .					
2 Weighted average of BERGFELD 97 and ANASTASSOV 01 measurements using $\eta$ 's reconstructed from $\eta \rightarrow \pi^+ \pi^- \pi^0$ and $\eta \rightarrow 3\pi^0$ decays.					
3 BERGFELD 97 reconstruct $\eta$ 's using $\eta \rightarrow \gamma\gamma$ and $\eta \rightarrow 3\pi^0$ decays.					

$\Gamma(\eta \pi^- \pi^+ \pi^- \nu_\tau (\text{ex. } K^0, f_1(1285)))/\Gamma_{total}$		$\Gamma_{161}/\Gamma$			
VALUE (units $10^{-4}$ )		DOCUMENT ID	TECN	COMMENT	
<b>0.99 ± 0.09 ± 0.13</b>		1 LEES	12x	BABR 468 fb <sup>-1</sup> $E_{cm}^{ee} = 10.6$ GeV	

1 LEES 12x obtain this result by subtracting their B( $\tau^- \rightarrow f_1(1285) \pi^- \nu_\tau \rightarrow \eta \pi^- \pi^+ \pi^- \nu_\tau$ ) measurement from their B( $\tau^- \rightarrow \eta \pi^- \pi^+ \pi^- \nu_\tau (\text{ex. } K^0)$ ) measurement.

$\Gamma(\eta a_1(1260)^- \nu_\tau \rightarrow \eta \pi^- \rho^0 \nu_\tau)/\Gamma_{total}$		$\Gamma_{162}/\Gamma$			
VALUE	CL%	DOCUMENT ID	TECN	COMMENT	
< 3.9 × 10 <sup>-4</sup>	90	BERGFELD	97	CLEO $E_{cm}^{ee} = 10.6$ GeV	

$\Gamma(\eta \eta \pi^- \nu_\tau)/\Gamma_{total}$		$\Gamma_{163}/\Gamma$			
VALUE	CL%	DOCUMENT ID	TECN	COMMENT	
< 7.4 × 10 <sup>-6</sup>	90	INAMI	09	BELL 490 fb <sup>-1</sup> $E_{cm}^{ee} = 10.6$ GeV	
• • • We do not use the following data for averages, fits, limits, etc. • • •					
< 1.1 × 10 <sup>-4</sup>	95	ARTUSO	92	CLEO $E_{cm}^{ee} \approx 10.6$ GeV	
< 8.3 × 10 <sup>-3</sup>	95	ALBRECHT	88M	ARG $E_{cm}^{ee} \approx 10$ GeV	

$\Gamma(\eta \eta \pi^- \pi^0 \nu_\tau)/\Gamma_{total}$		$\Gamma_{164}/\Gamma$			
VALUE (units $10^{-4}$ )	CL%	DOCUMENT ID	TECN	COMMENT	
< 2.0	95	ARTUSO	92	CLEO $E_{cm}^{ee} \approx 10.6$ GeV	
• • • We do not use the following data for averages, fits, limits, etc. • • •					
< 90	95	ALBRECHT	88M	ARG $E_{cm}^{ee} \approx 10$ GeV	

$\Gamma(\eta \eta K^- \nu_\tau)/\Gamma_{total}$		$\Gamma_{165}/\Gamma$			
VALUE	CL%	DOCUMENT ID	TECN	COMMENT	
< 3.0 × 10 <sup>-6</sup>	90	INAMI	09	BELL 490 fb <sup>-1</sup> $E_{cm}^{ee} = 10.6$ GeV	

$\Gamma(\eta'(958) \pi^- \nu_\tau)/\Gamma_{total}$		$\Gamma_{166}/\Gamma$			
VALUE	CL%	DOCUMENT ID	TECN	COMMENT	
< 4.0 × 10 <sup>-6</sup>	90	LEES	12x	BABR 468 fb <sup>-1</sup> $E_{cm}^{ee} = 10.6$ GeV	
• • • We do not use the following data for averages, fits, limits, etc. • • •					
< 7.2 × 10 <sup>-6</sup>	90	AUBERT	08Ae	BABR 384 fb <sup>-1</sup> $E_{cm}^{ee} = 10.6$ GeV	
< 7.4 × 10 <sup>-5</sup>	90	BERGFELD	97	CLEO $E_{cm}^{ee} = 10.6$ GeV	

$\Gamma(\eta'(958) \pi^- \pi^0 \nu_\tau)/\Gamma_{total}$		$\Gamma_{167}/\Gamma$			
VALUE	CL%	DOCUMENT ID	TECN	COMMENT	
< 1.2 × 10 <sup>-5</sup>	90	LEES	12x	BABR 468 fb <sup>-1</sup> $E_{cm}^{ee} = 10.6$ GeV	
• • • We do not use the following data for averages, fits, limits, etc. • • •					
< 8.0 × 10 <sup>-5</sup>	90	BERGFELD	97	CLEO $E_{cm}^{ee} = 10.6$ GeV	

$\Gamma(\eta'(958) K^- \nu_\tau)/\Gamma_{total}$		$\Gamma_{168}/\Gamma$			
VALUE	CL%	DOCUMENT ID	TECN	COMMENT	
< 2.4 × 10 <sup>-6</sup>	90	LEES	12x	BABR 468 fb <sup>-1</sup> $E_{cm}^{ee} = 10.6$ GeV	

$\Gamma(\phi \pi^- \nu_\tau)/\Gamma_{total}$		$\Gamma_{169}/\Gamma$			
VALUE (units $10^{-5}$ )	CL% EVTS	DOCUMENT ID	TECN	COMMENT	
<b>3.42 ± 0.55 ± 0.25</b>	344	AUBERT	08	BABR 342 fb <sup>-1</sup> $E_{cm}^{ee} = 10.6$ GeV	
• • • We do not use the following data for averages, fits, limits, etc. • • •					
< 20	90	1 AVERY	97	CLEO $E_{cm}^{ee} = 10.6$ GeV	
< 35	90	ALBRECHT	95H	ARG $E_{cm}^{ee} = 9.4$ –10.6 GeV	
1 AVERY 97 limit varies from (1.2–2.0) × 10 <sup>-4</sup> depending on decay model assumptions.					

$\Gamma(\phi K^- \nu_\tau)/\Gamma_{total}$		$\Gamma_{170}/\Gamma$			
VALUE (units $10^{-5}$ )	CL% EVTS	DOCUMENT ID	TECN	COMMENT	
<b>4.4 ± 1.6 OUR FIT</b>					
<b>3.70 ± 0.33 OUR AVERAGE</b> Error includes scale factor of 1.3.					
• • • We use the following data for averages but not for fits. • • •					
3.39 ± 0.20 ± 0.28	274	AUBERT	08	BABR 342 fb <sup>-1</sup> $E_{cm}^{ee} = 10.6$ GeV	
4.05 ± 0.25 ± 0.26	551	INAMI	06	BELL 401 fb <sup>-1</sup> $E_{cm}^{ee} = 10.6$ GeV	
• • • We do not use the following data for averages, fits, limits, etc. • • •					
< 6.7	90	1 AVERY	97	CLEO $E_{cm}^{ee} = 10.6$ GeV	
1 AVERY 97 limit varies from (5.4–6.7) × 10 <sup>-5</sup> depending on decay model assumptions.					

$\Gamma(f_1(1285) \pi^- \nu_\tau)/\Gamma_{total}$		$\Gamma_{171}/\Gamma$			
VALUE (units $10^{-4}$ )	EVTS	DOCUMENT ID	TECN	COMMENT	
<b>3.9 ± 0.5 OUR AVERAGE</b>		Error includes scale factor of 1.9.			
4.73 ± 0.28 ± 0.45	3.7k	1 LEES	12x	BABR 468 fb <sup>-1</sup> $E_{cm}^{ee} = 10.6$ GeV	
3.60 ± 0.18 ± 0.23	2.5k	2 LEES	12x	BABR 468 fb <sup>-1</sup> $E_{cm}^{ee} = 10.6$ GeV	
• • • We do not use the following data for averages, fits, limits, etc. • • •					
3.19 ± 0.18 ± 1.00	1.3 k	3 AUBERT	08Ae	BABR Repl. by LEES 12x	
3.9 ± 0.7 ± 0.5	1.4 k	4 AUBERT,B	05W	BABR Repl. by LEES 12x	
5.8 <sup>+1.4</sup> <sub>-1.3</sub> ± 1.8	54	5 BERGFELD	97	CLEO $E_{cm}^{ee} = 10.6$ GeV	
1 LEES 12x obtain this value by dividing their B( $\tau^- \rightarrow f_1(1285) \pi^- \nu_\tau \rightarrow 3\pi^- 2\pi^+ \nu_\tau$ ) measurement by the PDG 12 value of B( $f_1(1285) \rightarrow 2\pi^+ 2\pi^-$ ) = 0.111 <sup>+0.007</sup> <sub>-0.006</sub>					

# Lepton Particle Listings

$\tau$

<sup>2</sup> LEES 12X obtain this value by dividing their  $B(\tau^- \rightarrow \bar{f}_1(1285)\pi^- \nu_\tau \rightarrow \eta\pi^- \pi^+ \pi^- \nu_\tau)$  measurement by 2/3 of the PDG 12 value of  $B(\bar{f}_1(1285) \rightarrow \eta\pi\pi) = 0.524^{+0.019}_{-0.021}$ .

<sup>3</sup> AUBERT 08AE obtain this value by dividing their  $B(\tau^- \rightarrow \bar{f}_1(1285)\pi^- \nu_\tau \rightarrow \eta\pi^- \pi^+ \pi^- \nu_\tau)$  measurement by the PDG 06 value of  $B(\bar{f}_1(1285) \rightarrow \eta\pi^- \pi^+) = 0.35 \pm 0.11$ . The quote  $(3.19 \pm 0.18 \pm 0.16 \pm 0.99) \times 10^{-4}$  where the final error is due to the uncertainty on  $B(\bar{f}_1(1285) \rightarrow \eta\pi^- \pi^+)$ . We combine the two systematic errors in quadrature.

<sup>4</sup> AUBERT,B 05W use the  $\bar{f}_1(1285) \rightarrow 2\pi^+ 2\pi^-$  decay mode and the PDG 04 value of  $B(\bar{f}_1(1285) \rightarrow 2\pi^+ 2\pi^-) = 0.110^{+0.007}_{-0.006}$ .

<sup>5</sup> BERGFELD 97 use the  $\bar{f}_1(1285) \rightarrow \eta\pi^+ \pi^-$  decay mode.

$\Gamma(\bar{f}_1(1285)\pi^- \nu_\tau \rightarrow \eta\pi^- \pi^+ \pi^- \nu_\tau)/\Gamma_{\text{total}}$		$\Gamma_{172}/\Gamma$		
VALUE (units $10^{-4}$ )	EVTS	DOCUMENT ID	TECN	COMMENT
<b>1.18±0.07 OUR AVERAGE</b> Error includes scale factor of 1.3.				
1.26±0.06±0.06	2.5k	LEES	12X	BABR 468 fb <sup>-1</sup> $E_{\text{cm}}^{\text{e}} = 10.6$ GeV
1.11±0.06±0.05	1.3 k	AUBERT	08AE	BABR 384 fb <sup>-1</sup> , $E_{\text{cm}}^{\text{e}} = 10.6$ GeV

$\Gamma(\bar{f}_1(1285)\pi^- \nu_\tau \rightarrow \eta\pi^- \pi^+ \pi^- \nu_\tau)/\Gamma(\eta\pi^- \pi^+ \pi^- \nu_\tau \text{ (ex. } K^0))$		$\Gamma_{172}/\Gamma_{160}$		
VALUE (%)	EVTS	DOCUMENT ID	TECN	COMMENT
<b>0.69±0.01±0.05</b>				
	1	AUBERT	08AE	BABR 384 fb <sup>-1</sup> , $E_{\text{cm}}^{\text{e}} = 10.6$ GeV
• • • We do not use the following data for averages, fits, limits, etc. • • •				
0.55±0.14		BERGFELD	97	CLEO $E_{\text{cm}}^{\text{e}} = 10.6$ GeV

<sup>1</sup> Not independent of AUBERT 08AE  $B(\tau^- \rightarrow \bar{f}_1(1285)\pi^- \nu_\tau \rightarrow \eta\pi^- \pi^+ \pi^- \nu_\tau)$  and  $B(\tau^- \rightarrow \eta\pi^- \pi^+ \pi^- \nu_\tau \text{ (ex. } K^0))$  values.

$\Gamma(\bar{f}_1(1285)\pi^- \nu_\tau \rightarrow 3\pi^- 2\pi^+ \nu_\tau)/\Gamma_{\text{total}}$		$\Gamma_{173}/\Gamma$		
VALUE (units $10^{-4}$ )	EVTS	DOCUMENT ID	TECN	COMMENT
<b>0.52 ± 0.04 OUR FIT</b>				
0.520±0.031±0.037	3.7k	LEES	12X	BABR 468 fb <sup>-1</sup> $E_{\text{cm}}^{\text{e}} = 10.6$ GeV

$\Gamma(\pi(1300)^- \nu_\tau \rightarrow (\rho\pi)^- \nu_\tau \rightarrow (3\pi)^- \nu_\tau)/\Gamma_{\text{total}}$		$\Gamma_{174}/\Gamma$		
VALUE	CL%	DOCUMENT ID	TECN	COMMENT
<b>&lt;1.0 × 10<sup>-4</sup></b>				
	90	ASNER	00	CLEO $E_{\text{cm}}^{\text{e}} = 10.6$ GeV

$\Gamma(\pi(1300)^- \nu_\tau \rightarrow ((\pi\pi)_{\text{S-wave}} \pi)^- \nu_\tau \rightarrow (3\pi)^- \nu_\tau)/\Gamma_{\text{total}}$		$\Gamma_{175}/\Gamma$		
VALUE	CL%	DOCUMENT ID	TECN	COMMENT
<b>&lt;1.9 × 10<sup>-4</sup></b>				
	90	ASNER	00	CLEO $E_{\text{cm}}^{\text{e}} = 10.6$ GeV

$\Gamma(h^- \omega \geq 0 \text{ neutrals } \nu_\tau)/\Gamma_{\text{total}}$		$\Gamma_{176}/\Gamma$		
VALUE (%)	EVTS	DOCUMENT ID	TECN	COMMENT
<b>2.40±0.08 OUR FIT</b>				
• • • We use the following data for averages but not for fits. • • •				
1.65±0.3 ± 0.2	1513	ALBRECHT	88M	ARG $E_{\text{cm}}^{\text{e}} \approx 10$ GeV

$\Gamma(h^- \omega \nu_\tau)/\Gamma_{\text{total}}$		$\Gamma_{177}/\Gamma = (\Gamma_{178} + \Gamma_{179})/\Gamma$		
VALUE (%)	EVTS	DOCUMENT ID	TECN	COMMENT
<b>1.99±0.06 OUR FIT</b>				
<b>1.92±0.07 OUR AVERAGE</b>				
1.91±0.07±0.06	5803	BUSKULIC	97c	ALEP 1991–1994 LEP runs
1.60±0.27±0.41	139	BARINGER	87	CLEO $E_{\text{cm}}^{\text{e}} = 10.5$ GeV
• • • We use the following data for averages but not for fits. • • •				
1.95±0.07±0.11	2223	<sup>1</sup> BALEST	95c	CLEO $E_{\text{cm}}^{\text{e}} \approx 10.6$ GeV

<sup>1</sup> Not independent of BALEST 95c  $B(\tau^- \rightarrow h^- \omega \nu_\tau)/B(\tau^- \rightarrow h^- h^- h^+ \pi^0 \nu_\tau)$  value.

$[\Gamma(\pi^- \omega \nu_\tau) + \Gamma(K^- \omega \nu_\tau)]/\Gamma(h^- h^- h^+ \pi^0 \nu_\tau \text{ (ex. } K^0))$		$(\Gamma_{178} + \Gamma_{179})/\Gamma_{74}$		
VALUE (units $10^{-2}$ )	EVTS	DOCUMENT ID	TECN	COMMENT
<b>43.5±1.4 OUR FIT</b>				
<b>45.3±1.9 OUR AVERAGE</b>				
43.1±3.3	2350	<sup>1</sup> BUSKULIC	96	ALEP LEP 1991–1993 data
46.4±1.6±1.7	2223	<sup>2</sup> BALEST	95c	CLEO $E_{\text{cm}}^{\text{e}} \approx 10.6$ GeV
• • • We do not use the following data for averages, fits, limits, etc. • • •				
37 ± 5 ± 2	458	<sup>3</sup> ALBRECHT	91D	ARG $E_{\text{cm}}^{\text{e}} = 9.4$ –10.6 GeV

<sup>1</sup> BUSKULIC 96 quote the fraction of  $\tau \rightarrow h^- h^- h^+ \pi^0 \nu_\tau$  (ex.  $K^0$ ) decays which originate in a  $h^- \omega$  final state =  $0.383 \pm 0.029$ . We divide this by the  $\omega(782) \rightarrow \pi^+ \pi^- \pi^0$  branching fraction (0.888).

<sup>2</sup> BALEST 95c quote the fraction of  $\tau^- \rightarrow h^- h^- h^+ \pi^0 \nu_\tau$  (ex.  $K^0$ ) decays which originate in a  $h^- \omega$  final state equals  $0.412 \pm 0.014 \pm 0.015$ . We divide this by the  $\omega(782) \rightarrow \pi^+ \pi^- \pi^0$  branching fraction (0.888).

<sup>3</sup> ALBRECHT 91D quote the fraction of  $\tau^- \rightarrow h^- h^- h^+ \pi^0 \nu_\tau$  decays which originate in a  $\pi^- \omega$  final state equals  $0.33 \pm 0.04 \pm 0.02$ . We divide this by the  $\omega(782) \rightarrow \pi^+ \pi^- \pi^0$  branching fraction (0.888).

$\Gamma(\pi^- \omega \nu_\tau)/\Gamma_{\text{total}}$		$\Gamma_{178}/\Gamma$		
VALUE (%)	EVTS	DOCUMENT ID	TECN	COMMENT
<b>1.95±0.06 OUR FIT</b>				

$\Gamma(K^- \omega \nu_\tau)/\Gamma_{\text{total}}$		$\Gamma_{179}/\Gamma$		
VALUE (units $10^{-4}$ )	EVTS	DOCUMENT ID	TECN	COMMENT
<b>4.1±0.9 OUR FIT</b>				
4.1±0.6±0.7	500	ARMS	05	CLE3 7.6 fb <sup>-1</sup> , $E_{\text{cm}}^{\text{e}} = 10.6$ GeV

$\Gamma(h^- \omega \pi^0 \nu_\tau)/\Gamma_{\text{total}}$		$\Gamma_{180}/\Gamma$		
VALUE (%)	EVTS	DOCUMENT ID	TECN	COMMENT
<b>0.41±0.04 OUR FIT</b>				
0.43±0.06±0.05	7283	BUSKULIC	97c	ALEP 1991–1994 LEP runs

$\Gamma(h^- \omega \pi^0 \nu_\tau)/\Gamma(h^- h^- h^+ \geq 0 \text{ neutrals } \geq 0 K^0 \nu_\tau)$		$\Gamma_{180}/\Gamma_{62}$		
VALUE (%)	EVTS	DOCUMENT ID	TECN	COMMENT
<b>(2.69 ± 0.28) × 10<sup>-2</sup> OUR FIT</b>				
• • • We use the following data for averages but not for fits. • • •				
0.028±0.003±0.003	430	<sup>1</sup> BORTOLETTO	93	CLEO $E_{\text{cm}}^{\text{e}} \approx 10.6$ GeV

<sup>1</sup> Not independent of BORTOLETTO 93  $\Gamma(\tau^- \rightarrow h^- \omega \pi^0 \nu_\tau)/\Gamma(\tau^- \rightarrow h^- h^- h^+ 2\pi^0 \nu_\tau \text{ (ex. } K^0))$  value.

$\Gamma(h^- \omega \pi^0 \nu_\tau)/\Gamma(h^- h^- h^+ 2\pi^0 \nu_\tau \text{ (ex. } K^0))$		$\Gamma_{180}/\Gamma_{84}$		
VALUE (units $10^{-2}$ )	EVTS	DOCUMENT ID	TECN	COMMENT
<b>82±8 OUR FIT</b>				
81±6±6		BORTOLETTO	93	CLEO $E_{\text{cm}}^{\text{e}} \approx 10.6$ GeV

$\Gamma(h^- \omega 2\pi^0 \nu_\tau)/\Gamma_{\text{total}}$		$\Gamma_{181}/\Gamma$		
VALUE (units $10^{-4}$ )	EVTS	DOCUMENT ID	TECN	COMMENT
<b>1.4 ± 0.4 ± 0.3</b>				
1.89 <sup>+0.74</sup> <sub>-0.67</sub> ± 0.40	19	ANDERSON	97	CLEO Repl. by ANASTASSOV 01
• • • We do not use the following data for averages, fits, limits, etc. • • •				

$\Gamma(\pi^- \omega 2\pi^0 \nu_\tau)/\Gamma_{\text{total}}$		$\Gamma_{182}/\Gamma$		
VALUE (units $10^{-4}$ )	EVTS	DOCUMENT ID	TECN	COMMENT
<b>0.72±0.16 OUR FIT</b>				
0.73±0.12±0.12	1.1k	LEES	12X	BABR 468 fb <sup>-1</sup> $E_{\text{cm}}^{\text{e}} = 10.6$ GeV

$\Gamma(h^- 2\omega \nu_\tau)/\Gamma_{\text{total}}$		$\Gamma_{183}/\Gamma$		
VALUE	CL%	DOCUMENT ID	TECN	COMMENT
<b>&lt;5.4 × 10<sup>-7</sup></b>				
	90	AUBERT,B	06	BABR 232 fb <sup>-1</sup> $E_{\text{cm}}^{\text{e}} = 10.6$ GeV

$\Gamma(2h^- h^+ \omega \nu_\tau)/\Gamma_{\text{total}}$		$\Gamma_{184}/\Gamma$		
VALUE (units $10^{-4}$ )	EVTS	DOCUMENT ID	TECN	COMMENT
<b>1.2±0.2±0.1</b>				
	110	ANASTASSOV	01	CLEO $E_{\text{cm}}^{\text{e}} = 10.6$ GeV

$\Gamma(2\pi^- \pi^+ \omega \nu_\tau \text{ (ex. } K^0))/\Gamma_{\text{total}}$		$\Gamma_{185}/\Gamma$		
VALUE (units $10^{-4}$ )	EVTS	DOCUMENT ID	TECN	COMMENT
<b>0.84±0.06 OUR FIT</b>				
0.84±0.04±0.06	2.4k	LEES	12X	BABR 468 fb <sup>-1</sup> $E_{\text{cm}}^{\text{e}} = 10.6$ GeV

$\Gamma(e^- \gamma)/\Gamma_{\text{total}}$		$\Gamma_{186}/\Gamma$		
VALUE	CL%	DOCUMENT ID	TECN	COMMENT
Test of lepton family number conservation.				
<b>&lt;3.3 × 10<sup>-8</sup></b>				
<1.2 × 10 <sup>-7</sup>	90	AUBERT	10B	BABR 516 fb <sup>-1</sup> , $E_{\text{cm}}^{\text{e}} = 10.6$ GeV
• • • We do not use the following data for averages, fits, limits, etc. • • •				
<1.1 × 10 <sup>-7</sup>	90	HAYASAKA	08	BELL 535 fb <sup>-1</sup> , $E_{\text{cm}}^{\text{e}} = 10.6$ GeV
<3.9 × 10 <sup>-7</sup>	90	AUBERT	06c	BABR 232 fb <sup>-1</sup> , $E_{\text{cm}}^{\text{e}} = 10.6$ GeV
<2.7 × 10 <sup>-6</sup>	90	HAYASAKA	05	BELL 86.7 fb <sup>-1</sup> , $E_{\text{cm}}^{\text{e}} = 10.6$ GeV
<1.1 × 10 <sup>-4</sup>	90	EDWARDS	97	CLEO
<1.2 × 10 <sup>-4</sup>	90	ABREU	95u	DLPH 1990–1993 LEP runs
<2.0 × 10 <sup>-4</sup>	90	ALBRECHT	92k	ARG $E_{\text{cm}}^{\text{e}} = 10$ GeV
<6.4 × 10 <sup>-4</sup>	90	KEH	88	CBAL $E_{\text{cm}}^{\text{e}} = 10$ GeV
<6.4 × 10 <sup>-4</sup>	90	HAYES	82	MRK2 $E_{\text{cm}}^{\text{e}} = 3.8$ –6.8 GeV

$\Gamma(\mu^- \gamma)/\Gamma_{\text{total}}$		$\Gamma_{187}/\Gamma$		
VALUE	CL%	DOCUMENT ID	TECN	COMMENT
Test of lepton family number conservation.				
<b>&lt; 4.4 × 10<sup>-8</sup></b>				
< 4.5 × 10 <sup>-8</sup>	90	AUBERT	10B	BABR 516 fb <sup>-1</sup> , $E_{\text{cm}}^{\text{e}} = 10.6$ GeV
• • • We do not use the following data for averages, fits, limits, etc. • • •				
< 6.8 × 10 <sup>-8</sup>	90	HAYASAKA	08	BELL 535 fb <sup>-1</sup> , $E_{\text{cm}}^{\text{e}} = 10.6$ GeV
< 3.1 × 10 <sup>-7</sup>	90	AUBERT,B	05A	BABR 232 fb <sup>-1</sup> , $E_{\text{cm}}^{\text{e}} = 10.6$ GeV
< 1.1 × 10 <sup>-6</sup>	90	ABE	04B	BELL 86.3 fb <sup>-1</sup> , $E_{\text{cm}}^{\text{e}} = 10.6$ GeV
< 3.0 × 10 <sup>-6</sup>	90	AHMED	00	CLEO $E_{\text{cm}}^{\text{e}} = 10.6$ GeV
< 6.2 × 10 <sup>-5</sup>	90	EDWARDS	97	CLEO
< 0.42 × 10 <sup>-5</sup>	90	ABREU	95u	DLPH 1990–1993 LEP runs
< 3.4 × 10 <sup>-5</sup>	90	BEAN	93	CLEO $E_{\text{cm}}^{\text{e}} = 10.6$ GeV
< 5.5 × 10 <sup>-5</sup>	90	ALBRECHT	92k	ARG $E_{\text{cm}}^{\text{e}} = 10$ GeV
< 5.5 × 10 <sup>-5</sup>	90	HAYES	82	MRK2 $E_{\text{cm}}^{\text{e}} = 3.8$ –6.8 GeV

$\Gamma(e^-\pi^0)/\Gamma_{total}$   
Test of lepton family number conservation.  $\Gamma_{188}/\Gamma$

Table with 5 columns: VALUE, CL%, DOCUMENT ID, TECN, COMMENT. Rows include MIYAZAKI 90, AUBERT 07i, ENARI 05, BONVICINI 97, ALBRECHT 92k, KEH 88, HAYES 82.

$\Gamma(\mu^-\pi^0)/\Gamma_{total}$   
Test of lepton family number conservation.  $\Gamma_{189}/\Gamma$

Table with 5 columns: VALUE, CL%, DOCUMENT ID, TECN, COMMENT. Rows include AUBERT 07i, MIYAZAKI 90, ENARI 05, BONVICINI 97, ALBRECHT 92k, HAYES 82.

$\Gamma(e^-K_S^0)/\Gamma_{total}$   
Test of lepton family number conservation.  $\Gamma_{190}/\Gamma$

Table with 5 columns: VALUE, CL%, DOCUMENT ID, TECN, COMMENT. Rows include MIYAZAKI 90, AUBERT 90d, MIYAZAKI 06a, CHEN 02c, HAYES 82.

$\Gamma(\mu^-K_S^0)/\Gamma_{total}$   
Test of lepton family number conservation.  $\Gamma_{191}/\Gamma$

Table with 5 columns: VALUE, CL%, DOCUMENT ID, TECN, COMMENT. Rows include MIYAZAKI 90, AUBERT 90d, MIYAZAKI 06a, CHEN 02c, HAYES 82.

$\Gamma(e^-\eta)/\Gamma_{total}$   
Test of lepton family number conservation.  $\Gamma_{192}/\Gamma$

Table with 5 columns: VALUE, CL%, DOCUMENT ID, TECN, COMMENT. Rows include MIYAZAKI 90, AUBERT 07i, ENARI 05, BONVICINI 97, ALBRECHT 92k, KEH 88.

$\Gamma(\mu^-\eta)/\Gamma_{total}$   
Test of lepton family number conservation.  $\Gamma_{193}/\Gamma$

Table with 5 columns: VALUE, CL%, DOCUMENT ID, TECN, COMMENT. Rows include MIYAZAKI 90, AUBERT 07i, ENARI 05, ENARI 04, BONVICINI 97, ALBRECHT 92k.

$\Gamma(e^-\rho^0)/\Gamma_{total}$   
Test of lepton family number conservation.  $\Gamma_{194}/\Gamma$

Table with 5 columns: VALUE, CL%, DOCUMENT ID, TECN, COMMENT. Rows include MIYAZAKI 90, AUBERT 09w, NISHIO 08, YUSA 06, BLISS 98, BARTELT 94, ALBRECHT 92k, HAYES 82.

$\Gamma(\mu^-\rho^0)/\Gamma_{total}$   
Test of lepton family number conservation.  $\Gamma_{195}/\Gamma$

Table with 5 columns: VALUE, CL%, DOCUMENT ID, TECN, COMMENT. Rows include MIYAZAKI 90, AUBERT 09w, NISHIO 08, YUSA 06, BLISS 98, BARTELT 94, ALBRECHT 92k, HAYES 82.

$\Gamma(e^-\omega)/\Gamma_{total}$   
 $\Gamma_{196}/\Gamma$

Table with 5 columns: VALUE, CL%, DOCUMENT ID, TECN, COMMENT. Rows include MIYAZAKI 90, AUBERT 08k, NISHIO 08.

$\Gamma(\mu^-\omega)/\Gamma_{total}$   
 $\Gamma_{197}/\Gamma$

Table with 5 columns: VALUE, CL%, DOCUMENT ID, TECN, COMMENT. Rows include MIYAZAKI 90, AUBERT 08k, NISHIO 08.

$\Gamma(e^-K^*(892)^0)/\Gamma_{total}$   
Test of lepton family number conservation.  $\Gamma_{198}/\Gamma$

Table with 5 columns: VALUE, CL%, DOCUMENT ID, TECN, COMMENT. Rows include MIYAZAKI 90, AUBERT 09w, NISHIO 08, YUSA 06, BLISS 98, BARTELT 94, ALBRECHT 92k.

$\Gamma(\mu^-K^*(892)^0)/\Gamma_{total}$   
Test of lepton family number conservation.  $\Gamma_{199}/\Gamma$

Table with 5 columns: VALUE, CL%, DOCUMENT ID, TECN, COMMENT. Rows include NISHIO 08, MIYAZAKI 11, AUBERT 09w, ENARI 07, YUSA 06, BLISS 98, BARTELT 94, ALBRECHT 92k.

$\Gamma(e^-K^*(892)^0)/\Gamma_{total}$   
Test of lepton family number conservation.  $\Gamma_{200}/\Gamma$

Table with 5 columns: VALUE, CL%, DOCUMENT ID, TECN, COMMENT. Rows include MIYAZAKI 90, AUBERT 09w, NISHIO 08, YUSA 06, BLISS 98, BARTELT 94.

$\Gamma(\mu^-K^*(892)^0)/\Gamma_{total}$   
Test of lepton family number conservation.  $\Gamma_{201}/\Gamma$

Table with 5 columns: VALUE, CL%, DOCUMENT ID, TECN, COMMENT. Rows include MIYAZAKI 90, AUBERT 09w, NISHIO 08, YUSA 06, BLISS 98, BARTELT 94.

# Lepton Particle Listings

T

### $\Gamma(e^- \eta'(958))/\Gamma_{total}$ $\Gamma_{202}/\Gamma$

VALUE	CL%	DOCUMENT ID	TECN	COMMENT
$< 1.6 \times 10^{-7}$	90	MIYAZAKI	07	BELL 401 fb <sup>-1</sup> , E <sub>cm</sub> <sup>ee</sup> = 10.6 GeV
••• We do not use the following data for averages, fits, limits, etc. •••				
$< 2.4 \times 10^{-7}$	90	AUBERT	07i	BABR 339 fb <sup>-1</sup> , E <sub>cm</sub> <sup>ee</sup> = 10.6 GeV
$< 10. \times 10^{-7}$	90	ENARI	05	BELL 154 fb <sup>-1</sup> , E <sub>cm</sub> <sup>ee</sup> = 10.6 GeV

### $\Gamma(\mu^- \eta(958))/\Gamma_{total}$ $\Gamma_{203}/\Gamma$

VALUE	CL%	DOCUMENT ID	TECN	COMMENT
$< 1.3 \times 10^{-7}$	90	MIYAZAKI	07	BELL 401 fb <sup>-1</sup> , E <sub>cm</sub> <sup>ee</sup> = 10.6 GeV
••• We do not use the following data for averages, fits, limits, etc. •••				
$< 1.4 \times 10^{-7}$	90	AUBERT	07i	BABR 339 fb <sup>-1</sup> , E <sub>cm</sub> <sup>ee</sup> = 10.6 GeV
$< 4.7 \times 10^{-7}$	90	ENARI	05	BELL 154 fb <sup>-1</sup> , E <sub>cm</sub> <sup>ee</sup> = 10.6 GeV

### $\Gamma(e^- f_0(980) \rightarrow e^- \pi^+ \pi^-)/\Gamma_{total}$ $\Gamma_{204}/\Gamma$

VALUE	CL%	DOCUMENT ID	TECN	COMMENT
$< 3.2 \times 10^{-8}$	90	MIYAZAKI	09	BELL 671 fb <sup>-1</sup> E <sub>cm</sub> <sup>ee</sup> = 10.6 GeV

### $\Gamma(\mu^- f_0(980) \rightarrow \mu^- \pi^+ \pi^-)/\Gamma_{total}$ $\Gamma_{205}/\Gamma$

VALUE	CL%	DOCUMENT ID	TECN	COMMENT
$< 3.4 \times 10^{-8}$	90	MIYAZAKI	09	BELL 671 fb <sup>-1</sup> E <sub>cm</sub> <sup>ee</sup> = 10.6 GeV

### $\Gamma(e^- \phi)/\Gamma_{total}$ $\Gamma_{206}/\Gamma$

Test of lepton family number conservation.

VALUE	CL%	DOCUMENT ID	TECN	COMMENT
$< 3.1 \times 10^{-8}$	90	MIYAZAKI	11	BELL 854 fb <sup>-1</sup> E <sub>cm</sub> <sup>ee</sup> = 10.6 GeV
$< 3.1 \times 10^{-8}$	90	AUBERT	09w	BABR 451 fb <sup>-1</sup> E <sub>cm</sub> <sup>ee</sup> = 10.6 GeV
••• We do not use the following data for averages, fits, limits, etc. •••				
$< 7.3 \times 10^{-8}$	90	NISHIO	08	BELL 543 fb <sup>-1</sup> E <sub>cm</sub> <sup>ee</sup> = 10.6 GeV
$< 7.3 \times 10^{-7}$	90	YUSA	06	BELL 158 fb <sup>-1</sup> E <sub>cm</sub> <sup>ee</sup> = 10.6 GeV
$< 6.9 \times 10^{-6}$	90	BLISS	98	CLEO E <sub>cm</sub> <sup>ee</sup> = 10.6 GeV

### $\Gamma(\mu^- \phi)/\Gamma_{total}$ $\Gamma_{207}/\Gamma$

Test of lepton family number conservation.

VALUE	CL%	DOCUMENT ID	TECN	COMMENT
$< 8.4 \times 10^{-8}$	90	MIYAZAKI	11	BELL 854 fb <sup>-1</sup> E <sub>cm</sub> <sup>ee</sup> = 10.6 GeV
••• We do not use the following data for averages, fits, limits, etc. •••				
$< 1.9 \times 10^{-7}$	90	AUBERT	09w	BABR 451 fb <sup>-1</sup> E <sub>cm</sub> <sup>ee</sup> = 10.6 GeV
$< 1.3 \times 10^{-7}$	90	NISHIO	08	BELL 543 fb <sup>-1</sup> E <sub>cm</sub> <sup>ee</sup> = 10.6 GeV
$< 7.7 \times 10^{-7}$	90	YUSA	06	BELL 158 fb <sup>-1</sup> E <sub>cm</sub> <sup>ee</sup> = 10.6 GeV
$< 7.0 \times 10^{-6}$	90	BLISS	98	CLEO E <sub>cm</sub> <sup>ee</sup> = 10.6 GeV

### $\Gamma(e^- e^+ e^-)/\Gamma_{total}$ $\Gamma_{208}/\Gamma$

Test of lepton family number conservation.

VALUE	CL%	DOCUMENT ID	TECN	COMMENT
$< 2.7 \times 10^{-8}$	90	HAYASAKA	10	BELL 782 fb <sup>-1</sup> E <sub>cm</sub> <sup>ee</sup> = 10.6 GeV
••• We do not use the following data for averages, fits, limits, etc. •••				
$< 2.9 \times 10^{-8}$	90	LEES	10A	BABR 468 fb <sup>-1</sup> E <sub>cm</sub> <sup>ee</sup> = 10.6 GeV
$< 3.6 \times 10^{-8}$	90	MIYAZAKI	08	BELL 535 fb <sup>-1</sup> E <sub>cm</sub> <sup>ee</sup> = 10.6 GeV
$< 4.3 \times 10^{-8}$	90	AUBERT	07BK	BABR 376 fb <sup>-1</sup> E <sub>cm</sub> <sup>ee</sup> = 10.6 GeV
$< 2.0 \times 10^{-7}$	90	AUBERT	04J	BABR 91.5 fb <sup>-1</sup> E <sub>cm</sub> <sup>ee</sup> = 10.6 GeV
$< 3.5 \times 10^{-7}$	90	YUSA	04	BELL 87.1 fb <sup>-1</sup> E <sub>cm</sub> <sup>ee</sup> = 10.6 GeV
$< 2.9 \times 10^{-6}$	90	BLISS	98	CLEO E <sub>cm</sub> <sup>ee</sup> = 10.6 GeV
$< 0.33 \times 10^{-5}$	90	<sup>1</sup> BARTELT	94	CLEO Repl. by BLISS 98
$< 1.3 \times 10^{-5}$	90	ALBRECHT	92K	ARG E <sub>cm</sub> <sup>ee</sup> = 10 GeV
$< 2.7 \times 10^{-5}$	90	BOWCOCK	90	CLEO E <sub>cm</sub> <sup>ee</sup> = 10.4-10.9
$< 40 \times 10^{-5}$	90	HAYES	82	MRK2 E <sub>cm</sub> <sup>ee</sup> = 3.8-6.8 GeV

<sup>1</sup> BARTELT 94 assume phase space decays.

### $\Gamma(e^- \mu^+ \mu^-)/\Gamma_{total}$ $\Gamma_{209}/\Gamma$

Test of lepton family number conservation.

VALUE	CL%	DOCUMENT ID	TECN	COMMENT
$< 2.7 \times 10^{-8}$	90	HAYASAKA	10	BELL 782 fb <sup>-1</sup> E <sub>cm</sub> <sup>ee</sup> = 10.6 GeV
••• We do not use the following data for averages, fits, limits, etc. •••				
$< 3.2 \times 10^{-8}$	90	LEES	10A	BABR 468 fb <sup>-1</sup> E <sub>cm</sub> <sup>ee</sup> = 10.6 GeV
$< 4.1 \times 10^{-8}$	90	MIYAZAKI	08	BELL 535 fb <sup>-1</sup> E <sub>cm</sub> <sup>ee</sup> = 10.6 GeV
$< 3.7 \times 10^{-8}$	90	AUBERT	07BK	BABR 376 fb <sup>-1</sup> E <sub>cm</sub> <sup>ee</sup> = 10.6 GeV
$< 3.3 \times 10^{-7}$	90	AUBERT	04J	BABR 91.5 fb <sup>-1</sup> E <sub>cm</sub> <sup>ee</sup> = 10.6 GeV
$< 2.0 \times 10^{-7}$	90	YUSA	04	BELL 87.1 fb <sup>-1</sup> E <sub>cm</sub> <sup>ee</sup> = 10.6 GeV
$< 1.8 \times 10^{-6}$	90	BLISS	98	CLEO E <sub>cm</sub> <sup>ee</sup> = 10.6 GeV
$< 0.36 \times 10^{-5}$	90	<sup>1</sup> BARTELT	94	CLEO Repl. by BLISS 98
$< 1.9 \times 10^{-5}$	90	ALBRECHT	92K	ARG E <sub>cm</sub> <sup>ee</sup> = 10 GeV
$< 2.7 \times 10^{-5}$	90	BOWCOCK	90	CLEO E <sub>cm</sub> <sup>ee</sup> = 10.4-10.9
$< 33 \times 10^{-5}$	90	HAYES	82	MRK2 E <sub>cm</sub> <sup>ee</sup> = 3.8-6.8 GeV

<sup>1</sup> BARTELT 94 assume phase space decays.

### $\Gamma(e^+ \mu^- \mu^-)/\Gamma_{total}$ $\Gamma_{210}/\Gamma$

Test of lepton family number conservation.

VALUE	CL%	DOCUMENT ID	TECN	COMMENT
$< 1.7 \times 10^{-8}$	90	HAYASAKA	10	BELL 782 fb <sup>-1</sup> E <sub>cm</sub> <sup>ee</sup> = 10.6 GeV
••• We do not use the following data for averages, fits, limits, etc. •••				
$< 2.6 \times 10^{-8}$	90	LEES	10A	BABR 468 fb <sup>-1</sup> E <sub>cm</sub> <sup>ee</sup> = 10.6 GeV
$< 2.3 \times 10^{-8}$	90	MIYAZAKI	08	BELL 535 fb <sup>-1</sup> E <sub>cm</sub> <sup>ee</sup> = 10.6 GeV
$< 5.6 \times 10^{-8}$	90	AUBERT	07BK	BABR 376 fb <sup>-1</sup> E <sub>cm</sub> <sup>ee</sup> = 10.6 GeV
$< 1.3 \times 10^{-7}$	90	AUBERT	04J	BABR 91.5 fb <sup>-1</sup> E <sub>cm</sub> <sup>ee</sup> = 10.6 GeV
$< 2.0 \times 10^{-7}$	90	YUSA	04	BELL 87.1 fb <sup>-1</sup> E <sub>cm</sub> <sup>ee</sup> = 10.6 GeV
$< 1.5 \times 10^{-6}$	90	BLISS	98	CLEO E <sub>cm</sub> <sup>ee</sup> = 10.6 GeV
$< 0.35 \times 10^{-5}$	90	<sup>1</sup> BARTELT	94	CLEO Repl. by BLISS 98
$< 1.8 \times 10^{-5}$	90	ALBRECHT	92K	ARG E <sub>cm</sub> <sup>ee</sup> = 10 GeV
$< 1.6 \times 10^{-5}$	90	BOWCOCK	90	CLEO E <sub>cm</sub> <sup>ee</sup> = 10.4-10.9

<sup>1</sup> BARTELT 94 assume phase space decays.

### $\Gamma(\mu^- e^+ e^-)/\Gamma_{total}$ $\Gamma_{211}/\Gamma$

Test of lepton family number conservation.

VALUE	CL%	DOCUMENT ID	TECN	COMMENT
$< 1.8 \times 10^{-8}$	90	HAYASAKA	10	BELL 782 fb <sup>-1</sup> E <sub>cm</sub> <sup>ee</sup> = 10.6 GeV
••• We do not use the following data for averages, fits, limits, etc. •••				
$< 2.2 \times 10^{-8}$	90	LEES	10A	BABR 468 fb <sup>-1</sup> E <sub>cm</sub> <sup>ee</sup> = 10.6 GeV
$< 2.7 \times 10^{-8}$	90	MIYAZAKI	08	BELL 535 fb <sup>-1</sup> E <sub>cm</sub> <sup>ee</sup> = 10.6 GeV
$< 8.0 \times 10^{-8}$	90	AUBERT	07BK	BABR 376 fb <sup>-1</sup> E <sub>cm</sub> <sup>ee</sup> = 10.6 GeV
$< 2.7 \times 10^{-7}$	90	AUBERT	04J	BABR 91.5 fb <sup>-1</sup> E <sub>cm</sub> <sup>ee</sup> = 10.6 GeV
$< 1.9 \times 10^{-7}$	90	YUSA	04	BELL 87.1 fb <sup>-1</sup> E <sub>cm</sub> <sup>ee</sup> = 10.6 GeV
$< 1.7 \times 10^{-6}$	90	BLISS	98	CLEO E <sub>cm</sub> <sup>ee</sup> = 10.6 GeV
$< 0.34 \times 10^{-5}$	90	<sup>1</sup> BARTELT	94	CLEO Repl. by BLISS 98
$< 1.4 \times 10^{-5}$	90	ALBRECHT	92K	ARG E <sub>cm</sub> <sup>ee</sup> = 10 GeV
$< 2.7 \times 10^{-5}$	90	BOWCOCK	90	CLEO E <sub>cm</sub> <sup>ee</sup> = 10.4-10.9
$< 44 \times 10^{-5}$	90	HAYES	82	MRK2 E <sub>cm</sub> <sup>ee</sup> = 3.8-6.8 GeV

<sup>1</sup> BARTELT 94 assume phase space decays.

### $\Gamma(\mu^+ e^- e^-)/\Gamma_{total}$ $\Gamma_{212}/\Gamma$

Test of lepton family number conservation.

VALUE	CL%	DOCUMENT ID	TECN	COMMENT
$< 1.5 \times 10^{-8}$	90	HAYASAKA	10	BELL 782 fb <sup>-1</sup> E <sub>cm</sub> <sup>ee</sup> = 10.6 GeV
••• We do not use the following data for averages, fits, limits, etc. •••				
$< 1.8 \times 10^{-8}$	90	LEES	10A	BABR 468 fb <sup>-1</sup> E <sub>cm</sub> <sup>ee</sup> = 10.6 GeV
$< 2.0 \times 10^{-8}$	90	MIYAZAKI	08	BELL 535 fb <sup>-1</sup> E <sub>cm</sub> <sup>ee</sup> = 10.6 GeV
$< 5.8 \times 10^{-8}$	90	AUBERT	07BK	BABR 376 fb <sup>-1</sup> E <sub>cm</sub> <sup>ee</sup> = 10.6 GeV
$< 1.1 \times 10^{-7}$	90	AUBERT	04J	BABR 91.5 fb <sup>-1</sup> E <sub>cm</sub> <sup>ee</sup> = 10.6 GeV
$< 2.0 \times 10^{-7}$	90	YUSA	04	BELL 87.1 fb <sup>-1</sup> E <sub>cm</sub> <sup>ee</sup> = 10.6 GeV
$< 1.5 \times 10^{-6}$	90	BLISS	98	CLEO E <sub>cm</sub> <sup>ee</sup> = 10.6 GeV
$< 0.34 \times 10^{-5}$	90	<sup>1</sup> BARTELT	94	CLEO Repl. by BLISS 98
$< 1.4 \times 10^{-5}$	90	ALBRECHT	92K	ARG E <sub>cm</sub> <sup>ee</sup> = 10 GeV
$< 1.6 \times 10^{-5}$	90	BOWCOCK	90	CLEO E <sub>cm</sub> <sup>ee</sup> = 10.4-10.9

<sup>1</sup> BARTELT 94 assume phase space decays.

### $\Gamma(\mu^- \mu^+ \mu^-)/\Gamma_{total}$ $\Gamma_{213}/\Gamma$

Test of lepton family number conservation.

VALUE	CL%	DOCUMENT ID	TECN	COMMENT
$< 2.1 \times 10^{-8}$	90	HAYASAKA	10	BELL 782 fb <sup>-1</sup> E <sub>cm</sub> <sup>ee</sup> = 10.6 GeV
••• We do not use the following data for averages, fits, limits, etc. •••				
$< 3.8 \times 10^{-7}$	90	AAD	16BA	ATLS 20.3 fb <sup>-1</sup> $\sqrt{s} = 8$ TeV
$< 4.6 \times 10^{-8}$	90	AAIJ	15A1	LHCB 3.0 fb <sup>-1</sup> $\sqrt{s} = 7, 8$ TeV
$< 8.0 \times 10^{-8}$	90	<sup>1</sup> AAIJ	13AH	LHCB 1.0 fb <sup>-1</sup> $\sqrt{s} = 7$ TeV
$< 3.3 \times 10^{-8}$	90	LEES	10A	BABR 468 fb <sup>-1</sup> E <sub>cm</sub> <sup>ee</sup> = 10.6 GeV
$< 3.2 \times 10^{-8}$	90	MIYAZAKI	08	BELL 535 fb <sup>-1</sup> E <sub>cm</sub> <sup>ee</sup> = 10.6 GeV
$< 5.3 \times 10^{-8}$	90	AUBERT	07BK	BABR 376 fb <sup>-1</sup> E <sub>cm</sub> <sup>ee</sup> = 10.6 GeV
$< 1.9 \times 10^{-7}$	90	AUBERT	04J	BABR 91.5 fb <sup>-1</sup> E <sub>cm</sub> <sup>ee</sup> = 10.6 GeV
$< 2.0 \times 10^{-7}$	90	YUSA	04	BELL 87.1 fb <sup>-1</sup> E <sub>cm</sub> <sup>ee</sup> = 10.6 GeV
$< 1.9 \times 10^{-6}$	90	BLISS	98	CLEO E <sub>cm</sub> <sup>ee</sup> = 10.6 GeV
$< 0.43 \times 10^{-5}$	90	<sup>2</sup> BARTELT	94	CLEO Repl. by BLISS 98
$< 1.9 \times 10^{-5}$	90	ALBRECHT	92K	ARG E <sub>cm</sub> <sup>ee</sup> = 10 GeV
$< 1.7 \times 10^{-5}$	90	BOWCOCK	90	CLEO E <sub>cm</sub> <sup>ee</sup> = 10.4-10.9
$< 49 \times 10^{-5}$	90	HAYES	82	MRK2 E <sub>cm</sub> <sup>ee</sup> = 3.8-6.8 GeV

<sup>1</sup> Repl. by AAIJ 15A1.  
<sup>2</sup> BARTELT 94 assume phase space decays.

### $\Gamma(e^- \pi^+ \pi^-)/\Gamma_{total}$ $\Gamma_{214}/\Gamma$

Test of lepton family number conservation.

VALUE	CL%	DOCUMENT ID	TECN	COMMENT
$< 2.3 \times 10^{-8}$	90	MIYAZAKI	13	BELL 854 fb <sup>-1</sup> E <sub>cm</sub> <sup>ee</sup> = 10.6 GeV

• • • We do not use the following data for averages, fits, limits, etc. • • •

Table with 5 columns: VALUE, CL%, DOCUMENT ID, TECN, COMMENT. Rows include MIYAZAKI, YUSA, AUBERT,BE, BLISS, BARTELT, ALBRECHT, BOWCOCK with various decay rates and references.

<sup>1</sup> BARTELT 94 assume phase space decays.

$\Gamma(e^+ \pi^- \pi^-)/\Gamma_{total}$  Test of lepton number conservation.  $\Gamma_{215}/\Gamma$

Table with 5 columns: VALUE, CL%, DOCUMENT ID, TECN, COMMENT. Rows include MIYAZAKI, YUSA, AUBERT,BE, BLISS, BARTELT, ALBRECHT, BOWCOCK.

<sup>1</sup> BARTELT 94 assume phase space decays.

$\Gamma(\mu^- \pi^+ \pi^-)/\Gamma_{total}$  Test of lepton family number conservation.  $\Gamma_{216}/\Gamma$

Table with 5 columns: VALUE, CL%, DOCUMENT ID, TECN, COMMENT. Rows include MIYAZAKI, YUSA, AUBERT,BE, BLISS, BARTELT, ALBRECHT, BOWCOCK.

<sup>1</sup> BARTELT 94 assume phase space decays.

$\Gamma(\mu^+ \pi^- \pi^-)/\Gamma_{total}$  Test of lepton number conservation.  $\Gamma_{217}/\Gamma$

Table with 5 columns: VALUE, CL%, DOCUMENT ID, TECN, COMMENT. Rows include MIYAZAKI, YUSA, AUBERT,BE, BLISS, BARTELT, ALBRECHT, BOWCOCK.

<sup>1</sup> BARTELT 94 assume phase space decays.

$\Gamma(e^- \pi^+ K^-)/\Gamma_{total}$  Test of lepton family number conservation.  $\Gamma_{218}/\Gamma$

Table with 5 columns: VALUE, CL%, DOCUMENT ID, TECN, COMMENT. Rows include MIYAZAKI, YUSA, AUBERT,BE, BLISS, BARTELT, ALBRECHT, BOWCOCK.

<sup>1</sup> BARTELT 94 assume phase space decays.

$\Gamma(e^- \pi^- K^+)/\Gamma_{total}$  Test of lepton family number conservation.  $\Gamma_{219}/\Gamma$

Table with 5 columns: VALUE, CL%, DOCUMENT ID, TECN, COMMENT. Rows include MIYAZAKI, YUSA, AUBERT,BE, BLISS, BARTELT, BOWCOCK.

<sup>1</sup> BARTELT 94 assume phase space decays.

$\Gamma(e^+ \pi^- K^-)/\Gamma_{total}$  Test of lepton number conservation.  $\Gamma_{220}/\Gamma$

Table with 5 columns: VALUE, CL%, DOCUMENT ID, TECN, COMMENT. Rows include MIYAZAKI, YUSA, AUBERT,BE, BLISS, BARTELT, ALBRECHT, BOWCOCK.

<sup>1</sup> BARTELT 94 assume phase space decays.

$\Gamma(e^- K_S^0 K_S^0)/\Gamma_{total}$  Test of lepton family number conservation.  $\Gamma_{221}/\Gamma$

Table with 5 columns: VALUE, CL%, DOCUMENT ID, TECN, COMMENT. Rows include MIYAZAKI, YUSA, CHEN.

$\Gamma(e^- K^+ K^-)/\Gamma_{total}$  Test of lepton family number conservation.  $\Gamma_{222}/\Gamma$

Table with 5 columns: VALUE, CL%, DOCUMENT ID, TECN, COMMENT. Rows include MIYAZAKI, YUSA, AUBERT,BE, BLISS.

$\Gamma(e^+ K^- K^-)/\Gamma_{total}$  Test of lepton number conservation.  $\Gamma_{223}/\Gamma$

Table with 5 columns: VALUE, CL%, DOCUMENT ID, TECN, COMMENT. Rows include MIYAZAKI, YUSA, AUBERT,BE, BLISS.

$\Gamma(\mu^- \pi^+ K^-)/\Gamma_{total}$  Test of lepton family number conservation.  $\Gamma_{224}/\Gamma$

Table with 5 columns: VALUE, CL%, DOCUMENT ID, TECN, COMMENT. Rows include MIYAZAKI, YUSA, AUBERT,BE, BLISS, BARTELT, ALBRECHT, BOWCOCK.

<sup>1</sup> BARTELT 94 assume phase space decays.

$\Gamma(\mu^- \pi^- K^+)/\Gamma_{total}$  Test of lepton family number conservation.  $\Gamma_{225}/\Gamma$

Table with 5 columns: VALUE, CL%, DOCUMENT ID, TECN, COMMENT. Rows include MIYAZAKI, YUSA, AUBERT,BE, BLISS, BARTELT, BOWCOCK.

<sup>1</sup> BARTELT 94 assume phase space decays.

$\Gamma(\mu^+ \pi^- K^-)/\Gamma_{total}$  Test of lepton number conservation.  $\Gamma_{226}/\Gamma$

Table with 5 columns: VALUE, CL%, DOCUMENT ID, TECN, COMMENT. Rows include MIYAZAKI, YUSA, AUBERT,BE, BLISS, BARTELT, ALBRECHT, BOWCOCK.

<sup>1</sup> BARTELT 94 assume phase space decays.



## Lepton Particle Listings

 $\tau$  $\Gamma(\mu^- K_S^0 K_S^0)/\Gamma_{\text{total}}$   $\Gamma_{227}/\Gamma$ 

VALUE	CL%	DOCUMENT ID	TECN	COMMENT
$<8.0 \times 10^{-8}$	90	MIYAZAKI 10A	BELL	$671 \text{ fb}^{-1}$ , $E_{\text{cm}}^{\text{ee}} = 10.6 \text{ GeV}$
••• We do not use the following data for averages, fits, limits, etc. •••				
$<3.4 \times 10^{-6}$	90	CHEN	02c	CLEO $E_{\text{cm}}^{\text{ee}} = 10.6 \text{ GeV}$

 $\Gamma(\mu^- K^+ K^-)/\Gamma_{\text{total}}$   $\Gamma_{228}/\Gamma$ 

VALUE	CL%	DOCUMENT ID	TECN	COMMENT
$<4.4 \times 10^{-8}$	90	MIYAZAKI 13	BELL	$854 \text{ fb}^{-1}$ , $E_{\text{cm}}^{\text{ee}} = 10.6 \text{ GeV}$
••• We do not use the following data for averages, fits, limits, etc. •••				
$<6.8 \times 10^{-8}$	90	MIYAZAKI 10	BELL	Repl. by MIYAZAKI 13
$<8.0 \times 10^{-7}$	90	YUSA	06	BELL $158 \text{ fb}^{-1}$ , $E_{\text{cm}}^{\text{ee}} = 10.6 \text{ GeV}$
$<2.5 \times 10^{-7}$	90	AUBERT,BE	05D	BABR $221 \text{ fb}^{-1}$ , $E_{\text{cm}}^{\text{ee}} = 10.6 \text{ GeV}$
$<15 \times 10^{-6}$	90	BLISS	98	CLEO $E_{\text{cm}}^{\text{ee}} = 10.6 \text{ GeV}$

 $\Gamma(\mu^+ K^- K^-)/\Gamma_{\text{total}}$   $\Gamma_{229}/\Gamma$ 

VALUE	CL%	DOCUMENT ID	TECN	COMMENT
$<4.7 \times 10^{-8}$	90	MIYAZAKI 13	BELL	$854 \text{ fb}^{-1}$ , $E_{\text{cm}}^{\text{ee}} = 10.6 \text{ GeV}$
••• We do not use the following data for averages, fits, limits, etc. •••				
$<9.6 \times 10^{-8}$	90	MIYAZAKI 10	BELL	Repl. by MIYAZAKI 13
$<4.4 \times 10^{-7}$	90	YUSA	06	BELL $158 \text{ fb}^{-1}$ , $E_{\text{cm}}^{\text{ee}} = 10.6 \text{ GeV}$
$<4.8 \times 10^{-7}$	90	AUBERT,BE	05D	BABR $221 \text{ fb}^{-1}$ , $E_{\text{cm}}^{\text{ee}} = 10.6 \text{ GeV}$
$<6.0 \times 10^{-6}$	90	BLISS	98	CLEO $E_{\text{cm}}^{\text{ee}} = 10.6 \text{ GeV}$

 $\Gamma(e^- \pi^0 \pi^0)/\Gamma_{\text{total}}$   $\Gamma_{230}/\Gamma$ 

VALUE	CL%	DOCUMENT ID	TECN	COMMENT
$<6.5 \times 10^{-6}$	90	BONVICINI 97	CLEO	$E_{\text{cm}}^{\text{ee}} = 10.6 \text{ GeV}$

 $\Gamma(\mu^- \pi^0 \pi^0)/\Gamma_{\text{total}}$   $\Gamma_{231}/\Gamma$ 

VALUE	CL%	DOCUMENT ID	TECN	COMMENT
$<14 \times 10^{-6}$	90	BONVICINI 97	CLEO	$E_{\text{cm}}^{\text{ee}} = 10.6 \text{ GeV}$

 $\Gamma(e^- \eta \eta)/\Gamma_{\text{total}}$   $\Gamma_{232}/\Gamma$ 

VALUE	CL%	DOCUMENT ID	TECN	COMMENT
$<35 \times 10^{-6}$	90	BONVICINI 97	CLEO	$E_{\text{cm}}^{\text{ee}} = 10.6 \text{ GeV}$

 $\Gamma(\mu^- \eta \eta)/\Gamma_{\text{total}}$   $\Gamma_{233}/\Gamma$ 

VALUE	CL%	DOCUMENT ID	TECN	COMMENT
$<60 \times 10^{-6}$	90	BONVICINI 97	CLEO	$E_{\text{cm}}^{\text{ee}} = 10.6 \text{ GeV}$

 $\Gamma(e^- \pi^0 \eta)/\Gamma_{\text{total}}$   $\Gamma_{234}/\Gamma$ 

VALUE	CL%	DOCUMENT ID	TECN	COMMENT
$<24 \times 10^{-6}$	90	BONVICINI 97	CLEO	$E_{\text{cm}}^{\text{ee}} = 10.6 \text{ GeV}$

 $\Gamma(\mu^- \pi^0 \eta)/\Gamma_{\text{total}}$   $\Gamma_{235}/\Gamma$ 

VALUE	CL%	DOCUMENT ID	TECN	COMMENT
$<22 \times 10^{-6}$	90	BONVICINI 97	CLEO	$E_{\text{cm}}^{\text{ee}} = 10.6 \text{ GeV}$

 $\Gamma(\rho \mu^- \mu^-)/\Gamma_{\text{total}}$   $\Gamma_{236}/\Gamma$ 

VALUE	CL%	DOCUMENT ID	TECN	COMMENT
$<4.4 \times 10^{-7}$	90	AAIJ	13AH	LHCb $1.0 \text{ fb}^{-1}$ , $\sqrt{s} = 7 \text{ TeV}$

 $\Gamma(\overline{\rho} \mu^+ \mu^-)/\Gamma_{\text{total}}$   $\Gamma_{237}/\Gamma$ 

VALUE	CL%	DOCUMENT ID	TECN	COMMENT
$<3.3 \times 10^{-7}$	90	AAIJ	13AH	LHCb $1.0 \text{ fb}^{-1}$ , $\sqrt{s} = 7 \text{ TeV}$

 $\Gamma(\overline{\rho} \gamma)/\Gamma_{\text{total}}$   $\Gamma_{238}/\Gamma$ 

VALUE	CL%	DOCUMENT ID	TECN	COMMENT
$<3.5 \times 10^{-6}$	90	GODANG 99	CLEO	$E_{\text{cm}}^{\text{ee}} = 10.6 \text{ GeV}$
••• We do not use the following data for averages, fits, limits, etc. •••				
$<29 \times 10^{-5}$	90	ALBRECHT 92k	ARG	$E_{\text{cm}}^{\text{ee}} = 10 \text{ GeV}$

 $\Gamma(\overline{\rho} \pi^0)/\Gamma_{\text{total}}$   $\Gamma_{239}/\Gamma$ 

VALUE	CL%	DOCUMENT ID	TECN	COMMENT
$<15 \times 10^{-6}$	90	GODANG 99	CLEO	$E_{\text{cm}}^{\text{ee}} = 10.6 \text{ GeV}$
••• We do not use the following data for averages, fits, limits, etc. •••				
$<66 \times 10^{-5}$	90	ALBRECHT 92k	ARG	$E_{\text{cm}}^{\text{ee}} = 10 \text{ GeV}$

 $\Gamma(\overline{\rho} 2\pi^0)/\Gamma_{\text{total}}$   $\Gamma_{240}/\Gamma$ 

VALUE	CL%	DOCUMENT ID	TECN	COMMENT
$<33 \times 10^{-6}$	90	GODANG 99	CLEO	$E_{\text{cm}}^{\text{ee}} = 10.6 \text{ GeV}$

 $\Gamma(\overline{\rho} \eta)/\Gamma_{\text{total}}$   $\Gamma_{241}/\Gamma$ 

VALUE	CL%	DOCUMENT ID	TECN	COMMENT
$<8.9 \times 10^{-6}$	90	GODANG 99	CLEO	$E_{\text{cm}}^{\text{ee}} = 10.6 \text{ GeV}$
••• We do not use the following data for averages, fits, limits, etc. •••				
$<130 \times 10^{-5}$	90	ALBRECHT 92k	ARG	$E_{\text{cm}}^{\text{ee}} = 10 \text{ GeV}$

 $\Gamma(\overline{\rho} \pi^0 \eta)/\Gamma_{\text{total}}$   $\Gamma_{242}/\Gamma$ 

VALUE	CL%	DOCUMENT ID	TECN	COMMENT
$<27 \times 10^{-6}$	90	GODANG 99	CLEO	$E_{\text{cm}}^{\text{ee}} = 10.6 \text{ GeV}$

 $\Gamma(\Lambda \pi^-)/\Gamma_{\text{total}}$   $\Gamma_{243}/\Gamma$ 

VALUE	CL%	DOCUMENT ID	TECN	COMMENT
$<0.72 \times 10^{-7}$	90	MIYAZAKI 06	BELL	$154 \text{ fb}^{-1}$ , $E_{\text{cm}}^{\text{ee}} = 10.6 \text{ GeV}$

 $\Gamma(\overline{\Lambda} \pi^-)/\Gamma_{\text{total}}$   $\Gamma_{244}/\Gamma$ 

VALUE	CL%	DOCUMENT ID	TECN	COMMENT
$<1.4 \times 10^{-7}$	90	MIYAZAKI 06	BELL	$154 \text{ fb}^{-1}$ , $E_{\text{cm}}^{\text{ee}} = 10.6 \text{ GeV}$

 $\Gamma(e^- \text{light boson})/\Gamma(e^- \overline{\nu}_e \nu_\tau)$   $\Gamma_{245}/\Gamma_5$ 

VALUE	CL%	DOCUMENT ID	TECN	COMMENT
$<0.015$	95	1 ALBRECHT 95G	ARG	$E_{\text{cm}}^{\text{ee}} = 9.4\text{--}10.6 \text{ GeV}$
••• We do not use the following data for averages, fits, limits, etc. •••				
$<0.018$	95	2 ALBRECHT 90E	ARG	$E_{\text{cm}}^{\text{ee}} = 9.4\text{--}10.6 \text{ GeV}$
$<0.040$	95	3 BALTRUSAITIS...85	MRK3	$E_{\text{cm}}^{\text{ee}} = 3.77 \text{ GeV}$

1 ALBRECHT 95G limit holds for bosons with mass  $< 0.4 \text{ GeV}$ . The limit rises to 0.036 for a mass of 1.0 GeV, then falls to 0.006 at the upper mass limit of 1.6 GeV.  
 2 ALBRECHT 90E limit applies for spinless boson with mass  $< 100 \text{ MeV}$ , and rises to 0.050 for mass = 500 MeV.  
 3 BALTRUSAITIS 85 limit applies for spinless boson with mass  $< 100 \text{ MeV}$ .

 $\Gamma(\mu^- \text{light boson})/\Gamma(e^- \overline{\nu}_e \nu_\tau)$   $\Gamma_{246}/\Gamma_5$ 

VALUE	CL%	DOCUMENT ID	TECN	COMMENT
$<0.026$	95	1 ALBRECHT 95G	ARG	$E_{\text{cm}}^{\text{ee}} = 9.4\text{--}10.6 \text{ GeV}$
••• We do not use the following data for averages, fits, limits, etc. •••				
$<0.033$	95	2 ALBRECHT 90E	ARG	$E_{\text{cm}}^{\text{ee}} = 9.4\text{--}10.6 \text{ GeV}$
$<0.125$	95	3 BALTRUSAITIS...85	MRK3	$E_{\text{cm}}^{\text{ee}} = 3.77 \text{ GeV}$

1 ALBRECHT 95G limit holds for bosons with mass  $< 1.3 \text{ GeV}$ . The limit rises to 0.034 for a mass of 1.4 GeV, then falls to 0.003 at the upper mass limit of 1.6 GeV.  
 2 ALBRECHT 90E limit applies for spinless boson with mass  $< 100 \text{ MeV}$ , and rises to 0.071 for mass = 500 MeV.  
 3 BALTRUSAITIS 85 limit applies for spinless boson with mass  $< 100 \text{ MeV}$ .

 $\tau$ -DECAY PARAMETERS

See the related review(s):

 $\tau$ -Lepton Decay Parameters $\rho(e \text{ or } \mu)$  PARAMETER(V-A) theory predicts  $\rho = 0.75$ .

VALUE	EVTS	DOCUMENT ID	TECN	COMMENT
<b>0.745 ± 0.008 OUR FIT</b>				
<b>0.749 ± 0.008 OUR AVERAGE</b>				
0.742 ± 0.014 ± 0.006	81k	HEISTER 01E	ALEP	1991–1995 LEP runs
0.775 ± 0.023 ± 0.020	36k	ABREU 00L	DLPH	1992–1995 runs
0.781 ± 0.028 ± 0.018	46k	ACKERSTAFF 99D	OPAL	1990–1995 LEP runs
0.762 ± 0.035	54k	ACCIARRI 98R	L3	1991–1995 LEP runs
0.731 ± 0.031		1 ALBRECHT 98	ARG	$E_{\text{cm}}^{\text{ee}} = 9.5\text{--}10.6 \text{ GeV}$
0.72 ± 0.09 ± 0.03		2 ABE 97O	SLD	1993–1995 SLC runs
0.747 ± 0.010 ± 0.006	55k	ALEXANDER 97F	CLEO	$E_{\text{cm}}^{\text{ee}} = 10.6 \text{ GeV}$
0.79 ± 0.10 ± 0.10	3732	FORD 87B	MAC	$E_{\text{cm}}^{\text{ee}} = 29 \text{ GeV}$
0.71 ± 0.09 ± 0.03	1426	BEHRENDIS 85	CLEO	$e^+ e^-$ near $\Upsilon(4S)$
••• We do not use the following data for averages, fits, limits, etc. •••				
0.735 ± 0.013 ± 0.008	31k	AMMAR 97B	CLEO	Repl. by ALEXANDER 97F
0.794 ± 0.039 ± 0.031	18k	ACCIARRI 96H	L3	Repl. by ACCIARRI 98R
0.732 ± 0.034 ± 0.020	8.2k	3 ALBRECHT 95	ARG	$E_{\text{cm}}^{\text{ee}} = 9.5\text{--}10.6 \text{ GeV}$
0.738 ± 0.038		4 ALBRECHT 95C	ARG	Repl. by ALBRECHT 98
0.751 ± 0.039 ± 0.022		BUSKULIC 95D	ALEP	Repl. by HEISTER 01E
0.742 ± 0.035 ± 0.020	8000	ALBRECHT 90E	ARG	$E_{\text{cm}}^{\text{ee}} = 9.4\text{--}10.6 \text{ GeV}$

1 Combined fit to ARGUS tau decay parameter measurements in ALBRECHT 98, ALBRECHT 95C, ALBRECHT 93G, and ALBRECHT 94E. ALBRECHT 98 use tau pair events of the type  $\tau^- \tau^+ \rightarrow (\ell^- \overline{\nu}_\ell \nu_\tau)(\pi^+ \pi^0 \overline{\nu}_\tau)$ , and their charged conjugates.  
 2 ABE 97O assume  $\eta = 0$  in their fit. Letting  $\eta$  vary in the fit gives a  $\rho$  value of  $0.69 \pm 0.13 \pm 0.05$ .  
 3 Value is from a simultaneous fit for the  $\rho$  and  $\eta$  decay parameters to the lepton energy spectrum. Not independent of ALBRECHT 90E  $\rho(e \text{ or } \mu)$  value which assumes  $\eta = 0$ . Result is strongly correlated with ALBRECHT 95C.  
 4 Combined fit to ARGUS tau decay parameter measurements in ALBRECHT 95C, ALBRECHT 93G, and ALBRECHT 94E.

ρ(e) PARAMETER

(V-A) theory predicts ρ = 0.75.

Table with columns: VALUE, EVTS, DOCUMENT ID, TECN, COMMENT. Rows include HEISTER, ABREU, ACKERSTAFF, ALBRECHT, ABE, ALEXANDER, JANSSSEN, FORD, BEHREND, BACINO.

• • • We do not use the following data for averages, fits, limits, etc. • • •
1 ALBRECHT 98 use tau pair events of the type τ-τ+ → (ℓ-νℓντ)(π+π0ντ), and their charged conjugates.
2 ALBRECHT 95 use tau pair events of the type τ-τ+ → (ℓ-νℓντ)(h+h-h+π0ντ) and their charged conjugates.
3 ALBRECHT 93G use tau pair events of the type τ-τ+ → (μ-νμντ)(e+νeντ) and their charged conjugates.

ρ(μ) PARAMETER

(V-A) theory predicts ρ = 0.75.

Table with columns: VALUE, EVTS, DOCUMENT ID, TECN, COMMENT. Rows include HEISTER, ABREU, ACKERSTAFF, ALBRECHT, ABE, ALEXANDER, ALBRECHT, FORD, BEHREND, AMMAR, BUSKULIC.

1 ALBRECHT 98 use tau pair events of the type τ-τ+ → (ℓ-νℓντ)(π+π0ντ), and their charged conjugates.

ξ(e or μ) PARAMETER

(V-A) theory predicts ξ = 1.

Table with columns: VALUE, EVTS, DOCUMENT ID, TECN, COMMENT. Rows include HEISTER, ABREU, ACKERSTAFF, ACCIARRI, ALBRECHT, ALEXANDER, ACCIARRI, ALBRECHT, BUSKULIC, ALBRECHT.

1 Combined fit to ARGUS tau decay parameter measurements in ALBRECHT 98, ALBRECHT 95C, ALBRECHT 93G, and ALBRECHT 94E. ALBRECHT 98 use tau pair events of the type τ-τ+ → (ℓ-νℓντ)(π+π0ντ), and their charged conjugates.
2 ABE 97o assume η = 0 in their fit. Letting η vary in the fit gives a ξ value of 1.02 ± 0.36 ± 0.05.
3 Combined fit to ARGUS tau decay parameter measurements in ALBRECHT 95C, ALBRECHT 93G, and ALBRECHT 94E. ALBRECHT 95C uses events of the type τ-τ+ → (ℓ-νℓντ)(h+h-h+π0ντ) and their charged conjugates.
4 ALBRECHT 93G measurement determines |ξ| for the case ξ(e) = ξ(μ), but the authors point out that other LEP experiments determine the sign to be positive.

ξ(e) PARAMETER

(V-A) theory predicts ξ = 1.

Table with columns: VALUE, EVTS, DOCUMENT ID, TECN, COMMENT. Rows include HEISTER, ABREU, ACKERSTAFF, ALBRECHT, ABE, ALEXANDER.

• • • We do not use the following data for averages, fits, limits, etc. • • •
1 ALBRECHT 98 use tau pair events of the type τ-τ+ → (ℓ-νℓντ)(π+π0ντ), and their charged conjugates.

ξ(μ) PARAMETER

(V-A) theory predicts ξ = 1.

Table with columns: VALUE, EVTS, DOCUMENT ID, TECN, COMMENT. Rows include HEISTER, ABREU, ACKERSTAFF, ALBRECHT, ABE, ALEXANDER, BUSKULIC.

• • • We do not use the following data for averages, fits, limits, etc. • • •
1 ALBRECHT 98 use tau pair events of the type τ-τ+ → (ℓ-νℓντ)(π+π0ντ), and their charged conjugates.

η(e or μ) PARAMETER

(V-A) theory predicts η = 0.

Table with columns: VALUE, EVTS, DOCUMENT ID, TECN, COMMENT. Rows include HEISTER, ABREU, ACKERSTAFF, ACCIARRI, ABE, AMMAR, ALBRECHT, ACCIARRI, BUSKULIC.

• • • We do not use the following data for averages, fits, limits, etc. • • •
0.25 ± 0.17 ± 0.11 18k ACCIARRI 96H L3 Repl. by ACCIARRI 98R
-0.04 ± 0.15 ± 0.11 BUSKULIC 95D ALEP Repl. by HEISTER 01E

η(μ) PARAMETER

(V-A) theory predicts η = 0.

Table with columns: VALUE, EVTS, DOCUMENT ID, TECN, COMMENT. Rows include HEISTER, ABREU, ABE, AMMAR, ACKERSTAFF, BUSKULIC.

• • • We do not use the following data for averages, fits, limits, etc. • • •
0.010 ± 0.065 ± 0.001 27k 3 ACKERSTAFF 99D OPAL 1990-1995 LEP runs
-0.24 ± 0.23 ± 0.18 BUSKULIC 95D ALEP Repl. by HEISTER 01E
1 Highly correlated (corr. = 0.92) with ABE 97o ρ(μ) measurement.
2 Highly correlated (corr. = 0.949) with AMMAR 97B ρ(μ) value.
3 ACKERSTAFF 99D result is dominated by a constraint on η from the OPAL measurements of the τ lifetime and B(τ- → μ-νμντ) assuming lepton universality for the total coupling strength.

(δξ)(e or μ) PARAMETER

(V-A) theory predicts (δξ) = 0.75.

Table with columns: VALUE, EVTS, DOCUMENT ID, TECN, COMMENT. Rows include HEISTER, ABREU, ACKERSTAFF, ACCIARRI, ALBRECHT, ALEXANDER, ACCIARRI, ALBRECHT, BUSKULIC.

Downloaded from https://academic.oup.com/ptep/article/2020/8/083C01/5891211 by guest on 12 November 2020



REFERENCES

Table with columns for author names, journal abbreviations, volume numbers, page numbers, and years. Includes entries for authors like JIN, LEES, SHIMIZU, AAD, AAU, etc., and journals like PR, EPJ, JHEP, PRL, etc.

Downloaded from https://academic.oup.com/ptep/article/2020/8/083C01/5891211 by guest on 12 November 2020

# Lepton Particle Listings

## $\tau$ , Heavy Charged Lepton Searches

FORD	87	PR D35 408	W.T. Ford <i>et al.</i>	(MAC Collab.)
FORD	87B	PR D36 1971	W.T. Ford <i>et al.</i>	(MAC Collab.)
GAN	87	PRL 59 411	K.K. Gan <i>et al.</i>	(Mark II Collab.)
GAN	87B	PL B197 561	K.K. Gan <i>et al.</i>	(Mark II Collab.)
AIHARA	86E	PRL 57 1836	H. Aihara <i>et al.</i>	(JADE Collab.)
BARTEL	86D	PL B182 216	W. Bartel <i>et al.</i>	(CERN, CIT+)
PDG	86	PL 170B 1	M. Aguilar-Benítez <i>et al.</i>	(DELCO Collab.)
RUCKSTUHL	86	PRL 56 2132	W. Ruckstuhl <i>et al.</i>	(Mark II Collab.)
SCHMIDKE	86	PRL 57 527	W.B. Schmidke <i>et al.</i>	(Mark II Collab.)
YELTON	86	PRL 56 812	J.M. Yelton <i>et al.</i>	(TASSO Collab.)
ALTHOFF	85	ZPHY C26 521	M. Althoff <i>et al.</i>	(MAC Collab.)
ASH	85B	PRL 55 2118	W.W. Ash <i>et al.</i>	(Mark III Collab.)
BALTRUSAITIS...	85	PRL 55 1842	R.M. Baltrusaitis <i>et al.</i>	(JADE Collab.)
BARTEL	85F	PL 161B 188	W. Bartel <i>et al.</i>	(CLEO Collab.)
BEHRENDIS	85	PR D32 2468	S. Behrendis <i>et al.</i>	(HRS Collab.)
BELTRAMI	85	PRL 54 1775	I. Beltrami <i>et al.</i>	(PLUTO Collab.)
BERGER	85	ZPHY C28 1	C. Berger <i>et al.</i>	(MAC Collab.)
BURCHAT	85	PRL 54 2489	P.R. Burchat <i>et al.</i>	(DELCO Collab.)
FERNANDEZ	85	PL 54 1624	E. Fernandez <i>et al.</i>	(DELCO Collab.)
MILLS	85	PRL 54 524	G.B. Mills <i>et al.</i>	(TPC Collab.)
AIHARA	84C	PR D30 2436	H. Aihara <i>et al.</i>	(CELLO Collab.)
BEHREND	84	ZPHY C23 103	H.J. Behrend <i>et al.</i>	(DELCO Collab.)
MILLS	84	PRL 52 1944	G.B. Mills <i>et al.</i>	(CELLO Collab.)
BEHREND	83C	PL 127B 270	H.J. Behrend <i>et al.</i>	(UCI)
SILVERMAN	83	PR D27 1196	D.J. Silverman, G.L. Shaw	(CELLO Collab.)
BEHREND	82	PL 114B 282	H.J. Behrend <i>et al.</i>	(Mark II Collab.)
BLOCKER	82B	PRL 48 1586	C.A. Blocker <i>et al.</i>	(Mark II Collab.)
BLOCKER	82D	PL 109B 119	C.A. Blocker <i>et al.</i>	(Mark II Collab.)
FELDMAN	82	PRL 48 66	G.J. Feldman <i>et al.</i>	(Mark II Collab.)
HAYES	82	PR D25 2869	K.G. Hayes <i>et al.</i>	(PLUTO Collab.)
BERGER	81B	PL 99B 489	C. Berger <i>et al.</i>	(Mark II Collab.)
DORFAN	81	PRL 46 215	J.M. Dorfan <i>et al.</i>	(TASSO Collab.)
BRANDELIK	80	PL 92B 199	R. Brandelik <i>et al.</i>	(NOVO)
ZHOLENTZ	80	PL 96B 214	A.A. Zholents <i>et al.</i>	(NOVO)
Also		SJNP 34 814	A.A. Zholents <i>et al.</i>	(NOVO)
		Translated from YAF 34 1471.		
BACINO	79B	PRL 42 749	W.J. Bacino <i>et al.</i>	(DELCO Collab.)
KIRKBY	79	SLAC-PUB-2419	J. Kirkby	(SLAC)J
		Batavia Lepton Conference.		
BACINO	78B	PRL 41 13	W.J. Bacino <i>et al.</i>	(DELCO Collab.)
Also		Tokyo Conf. 249	J. Kirz	(STON)
Also		PL 96B 214	A.A. Zholents <i>et al.</i>	(NOVO)
BRANDELIK	78	PL 73B 109	R. Brandelik <i>et al.</i>	(DASP Collab.)
FELDMAN	78	Tokyo Conf. 777	G.J. Feldman	(SLAC)J
JAROS	78	PRL 40 1120	J. Jaros <i>et al.</i>	(LGW Collab.)
PERL	75	PRL 35 1489	M.L. Perl <i>et al.</i>	(LBL, SLAC)

### OTHER RELATED PAPERS

DAVIER	06	RMP 78 1043	M. Davier, A. Hocker, Z. Zhang	(LALO, PARIN+)
RAHAL-CAL...	98	IJMP A13 695	G. Rahal-Callot	(ETH)
GENTILE	96	PRPL 274 287	S. Gentile, M. Pohl	(ROMAI, ETH)
WEINSTEIN	93	ARNPS 43 457	A.J. Weinstein, R. Stroynowski	(CIT, SMU)
PERL	92	RPP 55 653	M.L. Perl	(SLAC)
PICH	90	MPL A5 1995	A. Pich	(VALE)
BARISH	88	PRPL 157 1	B.C. Barish, R. Stroynowski	(CIT)
GAN	88	IJMP A3 531	K.K. Gan, M.L. Perl	(SLAC)
HAYES	88	PR D38 3351	K.G. Hayes, M.L. Perl	(SLAC)
PERL	80	ARNPS 30 299	M.L. Perl	(SLAC)

## Heavy Charged Lepton Searches

### Charged Heavy Lepton MASS LIMITS

**Sequential Charged Heavy Lepton ( $L^\pm$ ) MASS LIMITS**  
 These experiments assumed that a fourth generation  $L^\pm$  decayed to a fourth generation  $\nu_L$  (or  $L^0$ ) where  $\nu_L$  was stable, or that  $L^\pm$  decays to a light  $\nu_L$  via mixing.  
 See the "Quark and Lepton Compositeness, Searches for" Listings for limits on radiatively decaying excited leptons, *i.e.*  $\ell^* \rightarrow \ell\gamma$ . See the "WIMPs and other Particle Searches" section for heavy charged particle search limits in which the charged particle could be a lepton.

VALUE (GeV)	CL%	DOCUMENT ID	TECN	COMMENT
>100.8	95	ACHARD 01B L3	L3	Decay to $\nu W$
>101.9	95	ACHARD 01B L3	L3	$m_L - m_{L^0} > 15$ GeV
• • • We do not use the following data for averages, fits, limits, etc. • • •				
> 81.5	95	ACKERSTAFF 98C OPAL	OPAL	Assumed $m_{L^\pm} - m_{L^0} > 8.4$ GeV
> 80.2	95	ACKERSTAFF 98C OPAL	OPAL	$m_{L^0} > m_{L^\pm}$ and $L^\pm \rightarrow \nu W$
< 48 or > 61	95	<sup>1</sup> ACCIARRI 96G L3	L3	
> 63.9	95	ALEXANDER 96P OPAL	OPAL	Decay to massless $\nu$ 's
> 63.5	95	BUSKULIC 96S ALEP	ALEP	$m_L - m_{L^0} > 7$ GeV
> 65	95	BUSKULIC 96S ALEP	ALEP	Decay to massless $\nu$ 's
none 10-225		<sup>2</sup> AHMED 94 CNTR	HI Collab.	at HERA
none 12.6-29.6	95	KIM 91B AMY	AMY	Massless $\nu$ assumed
> 44.3	95	AKRAWY 90G OPAL	OPAL	
none 0.5-1.0	95	<sup>3</sup> RILES 90 MRK2	MRK2	For $(m_{L^0} - m_{L^+}) > 0.25-0.4$ GeV
> 8		<sup>4</sup> STOKER 89 MRK2	MRK2	For $(m_{L^+} - m_{L^0}) = 0.4$ GeV
> 12		<sup>4</sup> STOKER 89 MRK2	MRK2	For $m_{L^0} = 0.9$ GeV
none 18.4-27.6	95	<sup>5</sup> ABE 88 VNS	VNS	
> 25.5	95	<sup>6</sup> ADACHI 88B TOPZ	TOPZ	
none 1.5-22.0	95	BEHREND 88C CELL	CELL	
> 41	90	<sup>7</sup> ALBAJAR 87B UA1	UA1	
> 22.5	95	<sup>8</sup> ADEVA 85 MRKJ	MRKJ	
> 18.0	95	<sup>9</sup> BARTEL 83 JADE	JADE	
none 4-14.5	95	<sup>10</sup> BERGER 81B PLUT	PLUT	
> 15.5	95	<sup>11</sup> BRANDELIK 81 TASS	TASS	
> 13.		<sup>12</sup> AZIMOV 80		
> 16.	95	<sup>13</sup> BARBER 80B CNTR	CNTR	
> 0.490		<sup>14</sup> ROTHER 69 RVUE	RVUE	

- ACCIARRI 96G assumes LEP result that the associated neutral heavy lepton mass  $> 40$  GeV.
- The AHMED 94 limits are from a search for neutral and charged sequential heavy leptons at HERA via the decay channels  $L^- \rightarrow e\gamma$ ,  $L^- \rightarrow \nu W^-$ ,  $L^- \rightarrow eZ$ ; and  $L^0 \rightarrow \nu\gamma$ ,  $L^0 \rightarrow e^- W^+$ ,  $L^- \rightarrow \nu Z$ , where the  $W$  decays to  $\ell\nu_\ell$  or to jets, and  $Z$  decays to  $\ell^+ \ell^-$  or jets.
- RILES 90 limits were the result of a special analysis of the data in the case where the mass difference  $m_{L^-} - m_{L^0}$  was allowed to be quite small, where  $L^0$  denotes the neutrino into which the sequential charged lepton decays. With a slightly reduced  $m_{L^\pm}$  range, the mass difference extends to about 4 GeV.
- STOKER 89 (Mark II at PEP) gives bounds on charged heavy lepton ( $L^+$ ) mass for the generalized case in which the corresponding neutral heavy lepton ( $L^0$ ) in the SU(2) doublet is not of negligible mass.
- ABE 88 search for  $L^+$  and  $L^- \rightarrow$  hadrons looking for acoplanar jets. The bound is valid for  $m_{\nu} < 10$  GeV.
- ADACHI 88B search for hadronic decays giving acoplanar events with large missing energy.  $E_{cm}^{ee} = 52$  GeV.
- Assumes associated neutrino is approximately massless.
- ADEVA 85 analyze one-isolated-muon data and sensitive to  $\tau < 10$  nanosec. Assume B(lepton) = 0.30.  $E_{cm} = 40-47$  GeV.
- BARTEL 83 limit is from PETRA  $e^+e^-$  experiment with average  $E_{cm} = 34.2$  GeV.
- BERGER 81B is DESY DORIS and PETRA experiment. Looking for  $e^+e^- \rightarrow L^+L^-$ .
- BRANDELIK 81 is DESY-PETRA experiment. Looking for  $e^+e^- \rightarrow L^+L^-$ .
- AZIMOV 80 estimated probabilities for  $M+N$  type events in  $e^+e^- \rightarrow L^+L^-$  deducing semi-hadronic decay multiplicities of  $L$  from  $e^+e^-$  annihilation data at  $E_{cm} = (2/3)m_L$ . Obtained above limit comparing these with  $e^+e^-$  data (BRANDELIK 80).
- BARBER 80B looked for  $e^+e^- \rightarrow L^+L^-, L^- \rightarrow \nu L^+ X$  with MARK-J at DESY-PETRA.
- ROTHER 69 examines previous data on  $\mu$  pair production and  $\pi$  and  $K$  decays.

### Stable Charged Heavy Lepton ( $L^\pm$ ) MASS LIMITS

VALUE (GeV)	CL%	DOCUMENT ID	TECN
>102.6	95	ACHARD 01B L3	L3
• • • We do not use the following data for averages, fits, limits, etc. • • •			
> 28.2	95	<sup>15</sup> ADACHI 90c TOPZ	TOPZ
none 18.5-42.8	95	AKRAWY 90f OPAL	OPAL
> 26.5	95	DECAMP 90f ALEP	ALEP
none $m_{\mu} - 36.3$	95	SODERSTROM90 MRK2	MRK2
<sup>15</sup> ADACHI 90c put lower limits on the mass of stable charged particles with electric charge $Q$ satisfying $2/3 < Q/e < 4/3$ and with spin 0 or 1/2. We list here the special case for a stable charged heavy lepton.			

### Charged Long-Lived Heavy Lepton MASS LIMITS

VALUE (GeV)	CL%	DOCUMENT ID	TECN	CHG	COMMENT
• • • We do not use the following data for averages, fits, limits, etc. • • •					
>574	95	CHATRCHYAN13AB CMS	CMS		Leptons singlet model
>102.0	95	ABBIENDI 03L OPAL	OPAL		pair produced in $e^+e^-$
> 0.1		<sup>16</sup> ANSORGE 73B HBC	HBC	-	Long-lived
none 0.55-4.5		<sup>17</sup> BUSHNIN 73 CNTR	CNTR	-	Long-lived
none 0.2-0.92		<sup>18</sup> BARNA 68 CNTR	CNTR	-	Long-lived
none 0.97-1.03		<sup>18</sup> BARNA 68 CNTR	CNTR	-	Long-lived
<sup>16</sup> ANSORGE 73B looks for electron pair production and electron-like Bremsstrahlung.					
<sup>17</sup> BUSHNIN 73 is SERPUKHOV 70 GeV $p$ experiment. Masses assume mean life above $7 \times 10^{-10}$ and $3 \times 10^{-8}$ respectively. Calculated from cross section (see "Charged Quasi-Stable Lepton Production Differential Cross Section" below) and 30 GeV muon pair production data.					
<sup>18</sup> BARNA 68 is SLAC photoproduction experiment.					

### Doubly-Charged Heavy Lepton MASS LIMITS

VALUE (GeV)	CL%	DOCUMENT ID	TECN	CHG
• • • We do not use the following data for averages, fits, limits, etc. • • •				
none 1-9 GeV	90	<sup>19</sup> CLARK 81 SPEC	SPEC	++
<sup>19</sup> CLARK 81 is FNAL experiment with 209 GeV muons. Bounds apply to $\mu_P$ which couples with full weak strength to muon. See also section on "Doubly-Charged Lepton Production Cross Section."				

### Doubly-Charged Lepton Production Cross Section ( $\mu N$ Scattering)

VALUE (cm <sup>2</sup> )	EVTS	DOCUMENT ID	TECN	CHG
• • • We do not use the following data for averages, fits, limits, etc. • • •				
$< 6. \times 10^{-38}$	0	<sup>20</sup> CLARK 81 SPEC	SPEC	++
<sup>20</sup> CLARK 81 is FNAL experiment with 209 GeV muon. Looked for $\mu^+$ nucleon $\rightarrow \bar{P}^0 X$ , $\bar{P}^0 \rightarrow \mu^+ \bar{\nu}_\mu + \bar{p}$ and $\mu^+ n \rightarrow \mu_P^{++} X$ , $\mu_P^{++} \rightarrow 2\mu^+ \nu_\mu$ . Above limits are for $\sigma \times BR$ taken from their mass-dependence plot figure 2.				

### REFERENCES FOR Heavy Charged Lepton Searches

CHATRCHYAN 13AB	JHEP 1307 122	S. Chatrchyan <i>et al.</i>	(CMS Collab.)
ABBIENDI 03L	PL B572 8	G. Abbiendi <i>et al.</i>	(OPAL Collab.)
ACHARD 01B	PL B517 75	P. Achard <i>et al.</i>	(L3 Collab.)
ACKERSTAFF 98C	EJP C1 45	K. Ackerstaff <i>et al.</i>	(OPAL Collab.)
ACCIARRI 96G	PL B377 304	M. Acciarri <i>et al.</i>	(L3 Collab.)
ALEXANDER 96P	PL B385 433	G. Alexander <i>et al.</i>	(OPAL Collab.)
BUSKULIC 96S	PL B384 439	D. Buskulic <i>et al.</i>	(ALEPH Collab.)
AHMED 94	PL B340 205	T. Ahmed <i>et al.</i>	(HI Collab.)

# Lepton Particle Listings

## Heavy Charged Lepton Searches, Neutrino Properties

KIM	91B	UMP A6 2583	G.N. Kim <i>et al.</i>	(AMY Collab.)
ADACHI	90C	PL B244 352	I. Adachi <i>et al.</i>	(TOPAZ Collab.)
AKRAWY	90G	PL B240 250	M.Z. Akrawy <i>et al.</i>	(OPAL Collab.)
AKRAWY	90O	PL B252 290	M.Z. Akrawy <i>et al.</i>	(OPAL Collab.)
DECAMP	90F	PL B236 511	D. Decamp <i>et al.</i>	(ALEPH Collab.)
RILES	90	PR D42 1	K. Riles <i>et al.</i>	(Mark II Collab.)
SODERSTROM	90	PRL 64 2980	E. Soderstrom <i>et al.</i>	(Mark II Collab.)
STOKER	89	PR D39 1811	D.P. Stoker <i>et al.</i>	(Mark II Collab.)
ABE	88	PRL 61 915	K. Abe <i>et al.</i>	(VENUS Collab.)
ADACHI	85B	PR D37 1339	I. Adachi <i>et al.</i>	(TOPAZ Collab.)
BEHREND	85C	ZPHY C41 7	H.J. Behrend <i>et al.</i>	(CELLO Collab.)
ALBAJAR	87B	PL B185 241	C. Albajar <i>et al.</i>	(UA1 Collab.)
ADEVA	85	PL 152B 439	B. Adeva <i>et al.</i>	(Mark-J Collab.)
Also		PRPL 109 131	B. Adeva <i>et al.</i>	(Mark-J Collab.)
BARTEL	83	PL 123B 353	W. Bartel <i>et al.</i>	(JADE Collab.)
BERGER	81B	PL 99B 489	C. Berger <i>et al.</i>	(PLUTO Collab.)
BRANDELIK	81	PL 99B 163	R. Brandelik <i>et al.</i>	(TASSO Collab.)
CLARK	81	PRL 46 299	A.R. Clark <i>et al.</i>	(UCB, LBL, FNAL+)
Also		PR D25 2762	W.H. Smith <i>et al.</i>	(LBL, FNAL, PRIN)
AZIMOV	80	JETPL 32 664	Y.I. Azimov, V.A. Khoze	(PNPI)
Translated from	ZETFP	32 677		
BARBER	80B	PRL 45 1904	D.P. Barber <i>et al.</i>	(Mark-J Collab.)
BRANDELIK	80	PL 92B 199	R. Brandelik <i>et al.</i>	(TASSO Collab.)
ANSORGE	73B	PR D7 26	R.E. Ansorge <i>et al.</i>	(CAVE)
BUSHNIN	73	NP B58 476	Y.B. Bushnin <i>et al.</i>	(SERP)
Also		PL 42B 136	S.V. Golovkin <i>et al.</i>	(SERP)
ROTHE	69	NP B10 241	K.W. Rothe, A.M. Wolsky	(PENN)
BARNA	68	PR 173 1391	A. Barna <i>et al.</i>	(SLAC, STAN)

OTHER RELATED PAPERS

PERL	81	SLAC-PUB-2752	M.L. Perl	(SLAC)
		Physics in Collision Conference.		

### Neutrino Properties

#### NEUTRINO PROPERTIES

Revised August 2019 by P. Vogel (Caltech) and A. Piepke (University of Alabama).

The Neutrino Properties Listings concern measurements of various properties of neutrinos. Nearly all of the measurements, so far only limits, actually concern superpositions of the mass eigenstates  $\nu_i$ , which are in turn related to the weak eigenstates  $\nu_\ell$ , via the neutrino mixing matrix

$$|\nu_\ell\rangle = \sum_i U_{\ell i} |\nu_i\rangle.$$

In the analogous case of quark mixing via the CKM matrix, the smallness of the off-diagonal terms (small mixing angles) permits a “dominant eigenstate” approximation. However, the results of neutrino oscillation searches show that the mixing matrix contains two large mixing angles and a third angle that is not exceedingly small. We cannot therefore associate any particular state  $|\nu_i\rangle$  with any particular lepton label  $e, \mu$  or  $\tau$ . Nevertheless, note that in the standard labeling the  $|\nu_1\rangle$  has the largest  $|\nu_e\rangle$  component ( $\sim 2/3$ ),  $|\nu_2\rangle$  contains  $\sim 1/3$  of the  $|\nu_e\rangle$  component and  $|\nu_3\rangle$  contains only a small  $\sim 2.5\%$   $|\nu_e\rangle$  component.

Neutrinos are produced in weak decays with a definite lepton flavor, and are typically detected by the charged current weak interaction again associated with a specific lepton flavor. Hence, the listings for the neutrino mass that follow are separated into the three associated charged lepton categories. Other properties (mean lifetime, magnetic moment, charge and charge radius) are no longer separated this way. If needed, the associated lepton flavor is reported in the footnotes.

Measured quantities (mass-squared, magnetic moments, mean lifetimes, *etc.*) all depend upon the mixing parameters  $|U_{\ell i}|^2$ , but to some extent also on experimental conditions (e.g., on energy resolution). Many of these observables, in particular

mass-squared, cannot distinguish between Dirac and Majorana neutrinos and are unaffected by  $CP$  phases.

Direct neutrino mass measurements are usually based on the analysis of the kinematics of charged particles (leptons, pions) emitted together with neutrinos (flavor states) in various weak decays. The most sensitive neutrino mass measurement to date, involving electron type antineutrinos, is based on fitting the shape of the beta spectrum. The quantity  $m_{\nu_e}^{2(eff)} = \sum_i |U_{ei}|^2 m_{\nu_i}^2$  is determined or constrained, where the sum is over all mass eigenvalues  $m_{\nu_i}$  that are too close together to be resolved experimentally. (The quantity  $m_{\nu_e}^{eff} \equiv \sqrt{m_{\nu_e}^{2(eff)}}$  is often denoted  $\langle m_\beta \rangle$  in the literature.) If the energy resolution is better than  $\Delta m_{ij}^2 \equiv m_{\nu_i}^2 - m_{\nu_j}^2$ , the corresponding heavier  $m_{\nu_i}$  and mixing parameter could be determined by fitting the resulting spectral anomaly (step or kink).

The dependence of  $m_{\nu_e}$  on the mass of the lightest neutrino is shown in Fig. 14.11 of the *Neutrino Masses, Mixing, and Oscillations* review. In the case of inverted ordering there is a minimum possible value of  $m_{\nu_e}^{eff}$ , approximately  $\sqrt{(\Delta m_{32}^2)} \sim 50$  meV. If  $m_{\nu_e}^{eff}$  is found to be larger than this value, it is impossible, based on this information only, to decide which ordering is realized in nature. On the other hand, if the  $m_{\nu_e}^{eff}$  is less than  $\sim 50$  meV, only the normal mass ordering is possible.

A limit on  $m_{\nu_e}^{2(eff)}$  implies an upper limit on the minimum value  $m_{min}^2$  of  $m_{\nu_i}^2$ , independent of the mixing parameters  $U_{ei}$ :  $m_{min}^2 \leq m_{\nu_e}^{2(eff)}$ . However, if and when the value of  $m_{\nu_e}^{2(eff)}$  is determined then its combination with the results derived from neutrino oscillations that give us the values of the neutrino mass-squared differences  $\Delta m_{ij}^2 \equiv m_i^2 - m_j^2$ , including eventually also their signs, and the mixing parameters  $|U_{ei}|^2$ , the individual neutrino mass squares  $m_{\nu_j}^2 = m_{\nu_e}^{2(eff)} - \sum_i |U_{ei}|^2 \Delta m_{ij}^2$  can be determined.

So far solar, reactor, atmospheric and accelerator neutrino oscillation experiments can be consistently described using three active neutrino flavors, i.e. two mass splittings and three mixing angles. However, several experiments with radioactive sources, reactors, and accelerators imply the possible existence of one or more non-interacting, i.e. sterile, neutrino species that might be observable since they couple, albeit weakly, to the flavor neutrinos  $|\nu_l\rangle$ . In that case, the neutrino mixing matrix would be  $n \times n$  unitary matrix with  $n > 3$ .

Combined three neutrino analyses determine the squared mass differences and all three mixing angles to within reasonable accuracy. For given  $|\Delta m_{ij}^2|$  a limit on  $m_{\nu_e}^{2(eff)}$  from beta decay defines an upper limit on the maximum value  $m_{max}$  of  $m_{\nu_i}$ :  $m_{max}^2 \leq m_{\nu_e}^{2(eff)} + \sum_{i < j} |\Delta m_{ij}^2|$ . The analysis of the low energy beta decay of tritium, combined with the oscillation results, thus limits *all* active neutrino masses. Traditionally, experimental neutrino mass limits obtained from pion decay  $\pi^+ \rightarrow \mu^+ + \nu_\mu$  or the shape of the spectrum of decay products of the  $\tau$  lepton did not distinguish between flavor and mass eigenstates. These results are reported as limits of the  $\mu$  and  $\tau$  based neutrino

# Lepton Particle Listings

## Neutrino Properties

mass. After the determination of the  $|\Delta m_{ij}^2|$ 's and the mixing angles  $\theta_{ij}$ , the corresponding neutrino mass limits are no longer competitive with those derived from low energy beta decays.

The spread of arrival times of the neutrinos from SN1987A, coupled with the measured neutrino energies, provided a time-of-flight limit on a quantity similar to  $\langle m_\beta \rangle \equiv \sqrt{m_{\nu_e}^{2(eff)}}$ . This statement, clothed in various degrees of sophistication, has been the basis for a very large number of papers. The resulting limits, however, are no longer comparable with the limits from tritium beta decay.

Constraint, or eventually a value, of the sum of the neutrino masses  $m_{tot}$  can be determined from the analysis of the cosmic microwave background anisotropy, combined with the galaxy redshift surveys and other data. These limits are reported in a separate table ( Sum of Neutrino Masses,  $m_{tot}$ ). Obviously,  $m_{tot}$  represents an upper limit for all  $m_i$  values. Note that many reported  $m_{tot}$  limits are considerably more stringent than the listed  $m_{\nu_e}^{eff}$  limits. Discussion concerning the model dependence of the  $m_{tot}$  limit is continuing.

### $\overline{\nu}$ MASS (electron based)

Those limits given below are for the square root of  $m_{\nu_e}^{2(eff)} \equiv \sum_i |U_{ei}|^2 m_{\nu_i}^2$ . Limits that come from the kinematics of  ${}^3\text{H}\beta\text{-}\overline{\nu}$  decay are the square roots of the limits for  $m_{\nu_e}^{2(eff)}$ . Obtained from the measurements reported in the Listings for " $\overline{\nu}$  Mass Squared," below.

VALUE (eV)	CL%	DOCUMENT ID	TECN	COMMENT
< 1.1	90	1 AKER	19 SPEC	${}^3\text{H}\beta$ decay
• • • We do not use the following data for averages, fits, limits, etc. • • •				
< 2.05	95	2 ASEEV	11 SPEC	${}^3\text{H}\beta$ decay
< 5.8	95	3 PAGLIAROLI	10 ASTR	SN1987A
< 2.3	95	4 KRAUS	05 SPEC	${}^3\text{H}\beta$ decay
< 21.7	90	5 ARNABOLDI	03A BOLO	${}^{187}\text{Re}\beta$ decay
< 5.7	95	6 LOREDO	02 ASTR	SN1987A
< 2.5	95	7 LOBASHEV	99 SPEC	${}^3\text{H}\beta$ decay
< 2.8	95	8 WEINHEIMER	99 SPEC	${}^3\text{H}\beta$ decay
< 4.35	95	9 BELESEV	95 SPEC	${}^3\text{H}\beta$ decay
< 12.4	95	10 CHING	95 SPEC	${}^3\text{H}\beta$ decay
< 9.2	95	11 HIDDEMANN	95 SPEC	${}^3\text{H}\beta$ decay
15 $\pm$ 32 -15		HIDDEMANN	95 SPEC	${}^3\text{H}\beta$ decay
< 19.6	95	KERNAN	95 ASTR	SN 1987A
< 7.0	95	12 STOEFL	95 SPEC	${}^3\text{H}\beta$ decay
< 7.2	95	13 WEINHEIMER	93 SPEC	${}^3\text{H}\beta$ decay
< 11.7	95	14 HOLZSCHUH	92B SPEC	${}^3\text{H}\beta$ decay
< 13.1	95	15 KAWAKAMI	91 SPEC	${}^3\text{H}\beta$ decay
< 9.3	95	16 ROBERTSON	91 SPEC	${}^3\text{H}\beta$ decay
< 14	95	AVIGNONE	90 ASTR	SN 1987A
< 16		SPERGEL	88 ASTR	SN 1987A
17 to 40		17 BORIS	87 SPEC	${}^3\text{H}\beta$ decay

<sup>1</sup> AKER 19 report a neutrino mass limit, derived from the first month of data collected by the KATRIN tritium endpoint experiment. The analysis of the electron kinematics shows no evidence for neutrino mass.

<sup>2</sup> ASEEV 11 report the analysis of the entire beta endpoint data, taken with the Troitsk integrating electrostatic spectrometer between 1997 and 2002 (some of the earlier runs were rejected), using a windowless gaseous tritium source. The fitted value of  $m_\nu$ , based on the method of Feldman and Cousins, is obtained from the upper limit of the fit for  $m_\nu^2$ . Previous analysis problems were resolved by careful monitoring of the tritium gas column density. Supersedes LOBASHEV 99 and BELESEV 95.

<sup>3</sup> PAGLIAROLI 10 is critical of the likelihood method used by LOREDO 02.

<sup>4</sup> KRAUS 05 is a continuation of the work reported in WEINHEIMER 99. This result represents the final analysis of data taken from 1997 to 2001. Various sources of systematic uncertainties have been identified and quantified. The background has been reduced compared to the initial running period. A spectral anomaly at the endpoint, reported in LOBASHEV 99, was not observed.

<sup>5</sup> ARNABOLDI 03A *et al.* report kinematical neutrino mass limit using  $\beta$ -decay of  ${}^{187}\text{Re}$ . Bolometric  $\text{AgReO}_4$  micro-calorimeters are used. Mass bound is substantially weaker than those derived from tritium  $\beta$ -decays but has different systematic uncertainties.

<sup>6</sup> LOREDO 02 updates LOREDO 89.

<sup>7</sup> LOBASHEV 99 report a new measurement which continues the work reported in BELESEV 95. This limit depends on phenomenological fit parameters used to derive their best fit to  $m_\nu^2$ , making an unambiguous interpretation difficult. See the footnote under " $\overline{\nu}$  Mass Squared."

<sup>8</sup> WEINHEIMER 99 presents two analyses which exclude the spectral anomaly and result in an acceptable  $m_\nu^2$ . We report the most conservative limit, but the other is nearly the same. See the footnote under " $\overline{\nu}$  Mass Squared."

<sup>9</sup> BELESEV 95 (Moscow) use an integral electrostatic spectrometer with adiabatic magnetic collimation and a gaseous tritium source. A fit to a normal Kurie plot above 18300–18350 eV (to avoid a low-energy anomaly) plus a monochromatic line 7–15 eV below the endpoint yields  $m_\nu^2 = -4.1 \pm 10.9 \text{ eV}^2$ , leading to this Bayesian limit.

<sup>10</sup> CHING 95 quotes results previously given by SUN 93; no experimental details are given. A possible explanation for consistently negative values of  $m_\nu^2$  is given.

<sup>11</sup> HIDDEMANN 95 (Munich) experiment uses atomic tritium embedded in a metal-dioxide lattice. Bayesian limit calculated from the weighted mean  $m_\nu^2 = 221 \pm 4244 \text{ eV}^2$  from the two runs listed below.

<sup>12</sup> STOEFL 95 (LLNL) result is the Bayesian limit obtained from the  $m_\nu^2$  errors given below but with  $m_\nu^2$  set equal to 0. The anomalous endpoint accumulation leads to a value of  $m_\nu^2$  which is negative by more than 5 standard deviations.

<sup>13</sup> WEINHEIMER 93 (Mainz) is a measurement of the endpoint of the tritium  $\beta$  spectrum using an electrostatic spectrometer with a magnetic guiding field. The source is molecular tritium frozen onto an aluminum substrate.

<sup>14</sup> HOLZSCHUH 92B (Zurich) result is obtained from the measurement  $m_\nu^2 = -24 \pm 48 \pm 61$  ( $1\sigma$  errors), in  $\text{eV}^2$ , using the PDG prescription for conversion to a limit in  $m_\nu$ .

<sup>15</sup> KAWAKAMI 91 (Tokyo) experiment uses tritium-labeled arachidic acid. This result is the Bayesian limit obtained from the  $m_\nu^2$  limit with the errors combined in quadrature. This was also done in ROBERTSON 91, although the authors report a different procedure.

<sup>16</sup> ROBERTSON 91 (LANL) experiment uses gaseous molecular tritium. The result is in strong disagreement with the earlier claims by the ITEP group [LUBIMOV 80, BORIS 87 (+ BORIS 88 erratum)] that  $m_\nu$  lies between 17 and 40 eV. However, the probability of a positive  $m^2$  is only 3% if statistical and systematic error are combined in quadrature.

<sup>17</sup> See also comment in BORIS 87B and erratum in BORIS 88.

### $\overline{\nu}$ MASS SQUARED (electron based)

Given troubling systematics which result in improbably negative estimates of  $m_{\nu_e}^{2(eff)} \equiv \sum_i |U_{ei}|^2 m_{\nu_i}^2$ , in many experiments, we use only KRAUS 05, LOBASHEV 99, and AKER 19 for our average.

VALUE (eV <sup>2</sup> )	DOCUMENT ID	TECN	COMMENT
– 0.9 $\pm$ 0.8 + 1.0	<b>OUR AVERAGE</b>		
– 1.0 $\pm$ 0.9 + 1.1	1 AKER	19 SPEC	${}^3\text{H}\beta$ decay
– 0.67 $\pm$ 2.53	2 ASEEV	11 SPEC	${}^3\text{H}\beta$ decay
– 0.6 $\pm$ 2.2 $\pm$ 2.1	3 KRAUS	05 SPEC	${}^3\text{H}\beta$ decay
• • • We do not use the following data for averages, fits, limits, etc. • • •			
– 1.9 $\pm$ 3.4 $\pm$ 2.2	4 LOBASHEV	99 SPEC	${}^3\text{H}\beta$ decay
– 3.7 $\pm$ 5.3 $\pm$ 2.1	5 WEINHEIMER	99 SPEC	${}^3\text{H}\beta$ decay
– 22 $\pm$ 4.8	6 BELESEV	95 SPEC	${}^3\text{H}\beta$ decay
129 $\pm$ 6010	7 HIDDEMANN	95 SPEC	${}^3\text{H}\beta$ decay
313 $\pm$ 5994	7 HIDDEMANN	95 SPEC	${}^3\text{H}\beta$ decay
– 130 $\pm$ 20 $\pm$ 15	8 STOEFL	95 SPEC	${}^3\text{H}\beta$ decay
– 31 $\pm$ 75 $\pm$ 48	9 SUN	93 SPEC	${}^3\text{H}\beta$ decay
– 39 $\pm$ 34 $\pm$ 15	10 WEINHEIMER	93 SPEC	${}^3\text{H}\beta$ decay
– 24 $\pm$ 48 $\pm$ 61	11 HOLZSCHUH	92B SPEC	${}^3\text{H}\beta$ decay
– 65 $\pm$ 85 $\pm$ 65	12 KAWAKAMI	91 SPEC	${}^3\text{H}\beta$ decay
– 147 $\pm$ 68 $\pm$ 41	13 ROBERTSON	91 SPEC	${}^3\text{H}\beta$ decay

<sup>1</sup> AKER 19 use the first month of data collected by the KATRIN experiment to determine  $m_\nu^2$ . The result is consistent with a neutrino mass of zero and is used to place a limit on  $m_\nu$ .

<sup>2</sup> ASEEV 11 report the analysis of the entire beta endpoint data, taken with the Troitsk integrating electrostatic spectrometer between 1997 and 2002, using a windowless gaseous tritium source. The analysis does not use the two additional fit parameters (see LOBASHEV 99) for a step-like structure near the endpoint. Using only the runs where the tritium gas column density was carefully monitored the need for such parameters was eliminated. Supersedes LOBASHEV 99 and BELESEV 95.

<sup>3</sup> KRAUS 05 is a continuation of the work reported in WEINHEIMER 99. This result represents the final analysis of data taken from 1997 to 2001. Problems with significantly negative squared neutrino masses, observed in some earlier experiments, have been resolved in this work.

<sup>4</sup> LOBASHEV 99 report a new measurement which continues the work reported in BELESEV 95. The data were corrected for electron trapping effects in the source, eliminating the dependence of the fitted neutrino mass on the fit interval. The analysis assuming a pure beta spectrum yields significantly negative fitted  $m_\nu^2 \approx -(20-10) \text{ eV}^2$ . This problem is attributed to a discrete spectral anomaly of about  $6 \times 10^{-11}$  intensity with a time-dependent energy of 5–15 eV below the endpoint. The data analysis accounts for this anomaly by introducing two extra phenomenological fit parameters resulting in a best fit of  $m_\nu^2 = -1.9 \pm 3.4 \pm 2.2 \text{ eV}^2$  which is used to derive a neutrino mass limit. However, the introduction of phenomenological fit parameters which are correlated with the derived  $m_\nu^2$  limit makes unambiguous interpretation of this result difficult.

See key on page 999

# Lepton Particle Listings

## Neutrino Properties

<sup>5</sup> WEINHEIMER 99 is a continuation of the work reported in WEINHEIMER 93. Using a lower temperature of the frozen tritium source eliminated the dewetting of the  $T_2$  film, which introduced a dependence of the fitted neutrino mass on the fit interval in the earlier work. An indication for a spectral anomaly reported in LOBASHEV 99 has been seen, but its time dependence does not agree with LOBASHEV 99. Two analyses, which exclude the spectral anomaly either by choice of the analysis interval or by using a particular data set which does not exhibit the anomaly, result in acceptable  $m_\nu^2$  fits and are used to derive the neutrino mass limit published by the authors. We list the most conservative of the two.

<sup>6</sup> BELESEV 95 (Moscow) use an integral electrostatic spectrometer with adiabatic magnetic collimation and a gaseous tritium sources. This value comes from a fit to a normal Kurie plot above 18300–18350 eV (to avoid a low-energy anomaly), including the effects of an apparent peak 7–15 eV below the endpoint.

<sup>7</sup> HIDDENMANN 95 (Munich) experiment uses atomic tritium embedded in a metal-dioxide lattice. They quote measurements from two data sets.

<sup>8</sup> STOEFL 95 (LLNL) uses a gaseous source of molecular tritium. An anomalous pileup of events at the endpoint leads to the negative value for  $m_\nu^2$ . The authors acknowledge that “the negative value for the best fit of  $m_\nu^2$  has no physical meaning” and discuss possible explanations for this effect.

<sup>9</sup> SUN 93 uses a tritiated hydrocarbon source. See also CHING 95.

<sup>10</sup> WEINHEIMER 93 (Mainz) is a measurement of the endpoint of the tritium  $\beta$  spectrum using an electrostatic spectrometer with a magnetic guiding field. The source is molecular tritium frozen onto an aluminum substrate.

<sup>11</sup> HOLZSCHUH 92B (Zurich) source is a monolayer of tritiated hydrocarbon.

<sup>12</sup> KAWAKAMI 91 (Tokyo) experiment uses tritium-labeled arachidic acid.

<sup>13</sup> ROBERTSON 91 (LANL) experiment uses gaseous molecular tritium. The result is in strong disagreement with the earlier claims by the ITEP group [LUBIMOV 80, BORIS 87 (+ BORIS 88 erratum)] that  $m_\nu$  lies between 17 and 40 eV. However, the probability of a positive  $m_\nu^2$  is only 3% if statistical and systematic error are combined in quadrature.

### $\nu$ MASS (electron based)

These are measurement of  $m_\nu$  (in contrast to  $m_{\overline{\nu}}$  given above). The masses can be different for a Dirac neutrino in the absence of CPT invariance. The possible distinction between  $\nu$  and  $\overline{\nu}$  properties is usually ignored elsewhere in these Listings.

VALUE (eV)	CL%	DOCUMENT ID	TECN	COMMENT
<460	68	YASUMI 94	CNTR	$^{163}\text{Ho}$ decay
<225	95	SPRINGER 87	CNTR	$^{163}\text{Ho}$ decay

### $\nu$ MASS (muon based)

Limits given below are for the square root of  $m_{\nu_\mu}^{2(\text{eff})} \equiv \sum_i |U_{\mu i}|^2 m_{\nu_i}^2$ .

In some of the COSM papers listed below, the authors did not distinguish between weak and mass eigenstates.

OUR EVALUATION is based on OUR AVERAGE for the  $\pi^+$  mass and the ASSAMAGAN 96 value for the muon momentum for the  $\pi^+$  decay at rest. The limit is calculated using the unified classical analysis of FELDMAN 98 for a Gaussian distribution near a physical boundary. WARNING: since  $m_{\nu_\mu}^{2(\text{eff})}$  is calculated from the differences of large numbers, it and the corresponding limits are extraordinarily sensitive to small changes in the pion mass, the decay muon momentum, and their errors. For example, the limits obtained using JECKELMANN 94, LENZ 98, and the weighted averages are 0.15, 0.29, and 0.19 MeV, respectively.

VALUE (MeV)	CL%	DOCUMENT ID	TECN	COMMENT
<b>&lt;0.19 (CL = 90%) OUR EVALUATION</b>				
<0.17	90	1 ASSAMAGAN 96	SPEC	$m_\nu^2 = -0.016 \pm 0.023$

• • • We do not use the following data for averages, fits, limits, etc. • • •

<0.15		2 DOLGOV 95	COSM	Nucleosynthesis
<0.48		3 ENQVIST 93	COSM	Nucleosynthesis
<0.3		4 FULLER 91	COSM	Nucleosynthesis
<0.42		4 LAM 91	COSM	Nucleosynthesis
<0.50	90	5 ANDERHUB 82	SPEC	$m_\nu^2 = -0.14 \pm 0.20$
<0.65	90	4 CLARK 74	ASPK	$K_{\mu 3}$ decay

<sup>1</sup> ASSAMAGAN 96 measurement of  $p_\mu$  from  $\pi^+ \rightarrow \mu^+ \nu$  at rest combined with JECKELMANN 94 Solution B pion mass yields  $m_\nu^2 = -0.016 \pm 0.023$  with corresponding Bayesian limit listed above. If Solution A is used,  $m_\nu^2 = -0.143 \pm 0.024$  MeV<sup>2</sup>. Replaces ASSAMAGAN 94.

<sup>2</sup> DOLGOV 95 removes earlier assumptions (DOLGOV 93) about thermal equilibrium below  $T_{\text{QCD}}$  for wrong-helicity Dirac neutrinos (ENQVIST 93, FULLER 91) to set more stringent limits.

<sup>3</sup> ENQVIST 93 bases limit on the fact that thermalized wrong-helicity Dirac neutrinos would speed up expansion of early universe, thus reducing the primordial abundance. FULLER 91 exploits the same mechanism but in the older calculation obtains a larger production rate for these states, and hence a lower limit. Neutrino lifetime assumed to exceed nucleosynthesis time,  $\sim 1$  s.

<sup>4</sup> Assumes neutrino lifetime  $>1$  s. For Dirac neutrinos only. See also ENQVIST 93.

<sup>5</sup> ANDERHUB 82 kinematics is insensitive to the pion mass.

### $\nu$ MASS (tau based)

The limits given below are the square roots of limits for  $m_{\nu_\tau}^{2(\text{eff})} \equiv \sum_i |U_{\tau i}|^2 m_{\nu_i}^2$ .

In some of the ASTR and COSM papers listed below, the authors did not distinguish between weak and mass eigenstates.

VALUE (MeV)	CL%	EVTS	DOCUMENT ID	TECN	COMMENT
<b>&lt; 18.2</b>					
	95		1 BARATE 98F	ALEP	1991–1995 LEP runs
• • • We do not use the following data for averages, fits, limits, etc. • • •					
< 28	95		2 ATHANAS 00	CLEO	$E_{\text{cm}}^{\text{eff}} = 10.6$ GeV
< 27.6	95		3 ACKERSTAFF 98T	OPAL	1990–1995 LEP runs
< 30	95	473	4 AMMAR 98	CLEO	$E_{\text{cm}}^{\text{eff}} = 10.6$ GeV
< 60	95		5 ANASTASSOV 97	CLEO	$E_{\text{cm}}^{\text{eff}} = 10.6$ GeV
< 0.37 or >22			6 FIELDS 97	COSM	Nucleosynthesis
< 68	95		7 SWAIN 97	THEO	$m_\tau, \tau_\tau, \tau$ partial widths
< 29.9	95		8 ALEXANDER 96M	OPAL	1990–1994 LEP runs
<149			9 BOTTINO 96	THEO	$\pi, \mu, \tau$ leptonic decays
<1 or >25			10 HANNSTAD 96C	COSM	Nucleosynthesis
< 71	95		11 SOBIE 96	THEO	$m_\tau, \tau_\tau, B(\tau^- \rightarrow e^- \overline{\nu}_e \nu_\tau)$
< 24	95	25	12 BUSKULIC 95H	ALEP	1991–1993 LEP runs
< 0.19			13 DOLGOV 95	COSM	Nucleosynthesis
< 3			14 SIGL 95	ASTR	SN 1987A
< 0.4 or > 30			15 DODELSON 94	COSM	Nucleosynthesis
< 0.1 or > 50			16 KAWASAKI 94	COSM	Nucleosynthesis
155–225			17 PERES 94	THEO	$\pi, K, \mu, \tau$ weak decays
< 32.6	95	113	18 CINABRO 93	CLEO	$E_{\text{cm}}^{\text{eff}} \approx 10.6$ GeV
< 0.3 or > 35			19 DOLGOV 93	COSM	Nucleosynthesis
< 0.74			20 ENQVIST 93	COSM	Nucleosynthesis
< 31	95	19	21 ALBRECHT 92M	ARG	$E_{\text{cm}}^{\text{eff}} = 9.4\text{--}10.6$ GeV
< 0.3			22 FULLER 91	COSM	Nucleosynthesis
< 0.5 or > 25			23 KOLB 91	COSM	Nucleosynthesis
< 0.42			22 LAM 91	COSM	Nucleosynthesis

<sup>1</sup> BARATE 98F result based on kinematics of 2939  $\tau^- \rightarrow 2\pi^- \pi^+ \nu_\tau$  and 52  $\tau^- \rightarrow 3\pi^- 2\pi^+ (\pi^0) \nu_\tau$  decays. If possible 2.5% excited  $a_1$  decay is included in 3-prong sample analysis, limit increases to 19.2 MeV.

<sup>2</sup> ATHANAS 00 bound comes from analysis of  $\tau^- \rightarrow \pi^- \pi^+ \pi^- \pi^0 \nu_\tau$  decays.

<sup>3</sup> ACKERSTAFF 98T use  $\tau^- \rightarrow 5\pi^\pm \nu_\tau$  decays to obtain a limit of 43.2 MeV (95%CL). They combine this with ALEXANDER 96M value using  $\tau^- \rightarrow 3h^\pm \nu_\tau$  decays to obtain quoted limit.

<sup>4</sup> AMMAR 98 limit comes from analysis of  $\tau^- \rightarrow 3\pi^- 2\pi^+ \nu_\tau$  and  $\tau^- \rightarrow 2\pi^- \pi^+ 2\pi^0 \nu_\tau$  decay modes.

<sup>5</sup> ANASTASSOV 97 derive limit by comparing their  $m_\tau$  measurement (which depends on  $m_{\nu_\tau}$ ) to BAI 96  $m_\tau$  threshold measurement.

<sup>6</sup> FIELDS 97 limit for a Dirac neutrino. For a Majorana neutrino the mass region  $< 0.93$  or  $> 31$  MeV is excluded. These bounds assume  $N_\nu < 4$  from nucleosynthesis; a wider excluded region occurs with a smaller  $N_\nu$  upper limit.

<sup>7</sup> SWAIN 97 derive their limit from the Standard Model relationships between the tau mass, lifetime, branching fractions for  $\tau^- \rightarrow e^- \overline{\nu}_e \nu_\tau, \tau^- \rightarrow \mu^- \overline{\nu}_\mu \nu_\tau, \tau^- \rightarrow \pi^- \nu_\tau$ , and  $\tau^- \rightarrow K^- \nu_\tau$ , and the muon mass and lifetime by assuming lepton universality and using world average values. Limit is reduced to 48 MeV when the CLEO  $\tau$  mass measurement (BALEST 93) is included; see CLEO’s more recent  $m_{\nu_\tau}$  limit (ANASTASSOV 97). Consideration of mixing with a fourth generation heavy neutrino yields  $\sin^2 \theta_L < 0.016$  (95%CL).

<sup>8</sup> ALEXANDER 96M bound comes from analyses of  $\tau^- \rightarrow 3\pi^- 2\pi^+ \nu_\tau$  and  $\tau^- \rightarrow h^- h^- h^+ \nu_\tau$  decays.

<sup>9</sup> BOTTINO 96 assumes three generations of neutrinos with mixing, finds consistency with massless neutrinos with no mixing based on 1995 data for masses, lifetimes, and leptonic partial widths.

<sup>10</sup> HANNSTAD 96C limit is on the mass of a Majorana neutrino. This bound assumes  $N_\nu < 4$  from nucleosynthesis. A wider excluded region occurs with a smaller  $N_\nu$  upper limit. This paper is the corrected version of HANNSTAD 96; see the erratum: HANNSTAD 96B.

<sup>11</sup> SOBIE 96 derive their limit from the Standard Model relationship between the tau mass, lifetime, and leptonic branching fraction, and the muon mass and lifetime, by assuming lepton universality and using world average values.

<sup>12</sup> BUSKULIC 95H bound comes from a two-dimensional fit of the visible energy and invariant mass distribution of  $\tau^- \rightarrow 5\pi (\pi^0) \nu_\tau$  decays. Replaced by BARATE 98F.

<sup>13</sup> DOLGOV 95 removes earlier assumptions (DOLGOV 93) about thermal equilibrium below  $T_{\text{QCD}}$  for wrong-helicity Dirac neutrinos (ENQVIST 93, FULLER 91) to set more stringent limits. DOLGOV 96 argues that a possible window near 20 MeV is excluded.

<sup>14</sup> SIGL 95 exclude massive Dirac or Majorana neutrinos with lifetimes between  $10^{-3}$  and  $10^8$  seconds if the decay products are predominantly  $\gamma$  or  $e^+ e^-$ .

<sup>15</sup> DODELSON 94 calculate constraints on  $\nu_\tau$  mass and lifetime from nucleosynthesis for 4 generic decay modes. Limits depend strongly on decay mode. Quoted limit is valid for



# Lepton Particle Listings

## Neutrino Properties

all decay modes of Majorana neutrinos with lifetime greater than about 300s. For Dirac neutrinos limits change to  $< 0.3$  or  $> 33$ .

<sup>16</sup> KAWASAKI 94 excluded region is for Majorana neutrino with lifetime  $> 1000$  s. Other limits are given as a function of  $\nu_\tau$  lifetime for decays of the type  $\nu_\tau \rightarrow \nu_\mu \phi$  where  $\phi$  is a Nambu-Goldstone boson.

<sup>17</sup> PERES 94 used PDG 92 values for parameters to obtain a value consistent with mixing. Reexamination by BOTTINO 96 which included radiative corrections and 1995 PDG parameters resulted in two allowed regions,  $m_3 < 70$  MeV and  $140$  MeV  $m_3 < 149$  MeV.

<sup>18</sup> CINABRO 93 bound comes from analysis of  $\tau^- \rightarrow 3\pi^- 2\pi^+ \nu_\tau$  and  $\tau^- \rightarrow 2\pi^- \pi^+ 2\pi^0 \nu_\tau$  decay modes.

<sup>19</sup> DOLGOV 93 assumes neutrino lifetime  $> 100$  s. For Majorana neutrinos, the low mass limit is 0.5 MeV. KAWANO 92 points out that these bounds can be overcome for a Dirac neutrino if it possesses a magnetic moment. See also DOLGOV 96.

<sup>20</sup> ENQVIST 93 bases limit on the fact that thermalized wrong-helicity Dirac neutrinos would speed up expansion of early universe, thus reducing the primordial abundance. FULLER 91 exploits the same mechanism but in the older calculation obtains a larger production rate for these states, and hence a lower limit. Neutrino lifetime assumed to exceed nucleosynthesis time,  $\sim 1$  s.

<sup>21</sup> ALBRECHT 92M reports measurement of a slightly lower  $\tau$  mass, which has the effect of reducing the  $\nu_\tau$  mass reported in ALBRECHT 88B. Bound is from analysis of  $\tau^- \rightarrow 3\pi^- 2\pi^+ \nu_\tau$  mode.

<sup>22</sup> Assumes neutrino lifetime  $> 1$  s. For Dirac neutrinos. See also ENQVIST 93.

<sup>23</sup> KOLB 91 exclusion region is for Dirac neutrino with lifetime  $> 1$  s; other limits are given.

Revised September 2019 by K.A. Olive (University of Minnesota).

Neutrinos decouple from thermal equilibrium in the early universe at temperatures  $\mathcal{O}(1)$  MeV. The limits on low mass ( $m_\nu \lesssim 1$  MeV) neutrinos apply to  $m_{\text{tot}}$  given by

$$m_{\text{tot}} = \sum_{\nu} m_{\nu} .$$

Stable neutrinos in this mass range decouple from the thermal bath while still relativistic and make a contribution to the total energy density of the Universe which is given by

$$\rho_{\nu} = m_{\text{tot}} n_{\nu} \simeq m_{\text{tot}} (3/11) (3.045/3)^{3/4} n_{\gamma} ,$$

where the factor  $3/11$  is the ratio of (light) neutrinos to photons and the factor  $(3.045/3)^{3/4}$  corrects for the fact that the effective number of neutrinos in the standard model is 3.045 when taking into account  $e^+e^-$  annihilation during neutrino decoupling. Writing  $\Omega_{\nu} = \rho_{\nu}/\rho_c$ , where  $\rho_c$  is the critical energy density of the Universe, and using  $n_{\gamma} = 410.7 \text{ cm}^{-3}$ , we have

$$\Omega_{\nu} h^2 \simeq m_{\text{tot}} / (93 \text{ eV}) .$$

While an upper limit to the matter density of  $\Omega_m h^2 < 0.12$  would constrain  $m_{\text{tot}} < 11$  eV, much stronger constraints are obtained from a combination of observations of the CMB, the amplitude of density fluctuations on smaller scales from the clustering of galaxies and the Lyman- $\alpha$  forest, baryon acoustic oscillations, and new Hubble parameter data. These combine to give an upper limit of around 0.15 eV, and may, in the near future, be able to provide a lower bound on the sum of the neutrino masses. The current lower bound of  $m_{\text{tot}} > 0.06$  eV implies a lower limit of  $\Omega_{\nu} h^2 > 6 \times 10^{-4}$ . See our review on "Neutrinos in Cosmology" for more details.

### SUM OF THE NEUTRINO MASSES, $m_{\text{tot}}$

This is a sum of the neutrino masses,  $m_{\text{tot}}$ , as defined in the above note, of effectively stable neutrinos, i.e. those with mean lifetimes on cosmological scales. When necessary, we have generalized the results reported so they apply to  $m_{\text{tot}}$ . For other limits, see SZALAY 76, VYSOTSKY 77, BERNSTEIN 81, FREESE 84, SCHRAMM 84, and COWSIK 85. For more information see a note on "Neutrinos in Cosmology" in this Review.

VALUE (eV)	CL%	DOCUMENT ID	TECN	COMMENT
< 0.26	95	1 LOUREIRO	19	COSM
< 0.18	95	2 UPADHYE	19	COSM BOSS and CMB
< 0.152	95	3 CHOUDHURY	18	COSM
0.064 $\pm$ 0.061 -0.005	95	4 SIMPSON	17	COSM
< 0.151	95	5 VAGNOZZI	17	COSM
< 0.14	95	6 YECHE	17	COSM BOSS and XQ-100
< 0.0926	90	7 DIVALENTINO	16	COSM
< 0.18	95	8 HUANG	16	COSM Normal mass hierarchy
< 0.14	95	9 ROSSI	15	COSM
< 0.23	95	10 ADE	14	COSM Planck
0.320 $\pm$ 0.081		11 BATTYE	14	COSM
0.35 $\pm$ 0.10		12 BEUTLER	14	COSM BOSS
0.22 $\pm$ 0.09 -0.10		13 COSTANZI	14	COSM
< 0.22	95	14 GIUSARMA	14	COSM
0.32 $\pm$ 0.11		15 HOU	14	COSM
< 0.26	95	16 LEISTEDT	14	COSM
< 0.18	95	17 RIEMER-SOR...	14	COSM
< 0.24	68	18 MORESCO	12	COSM
< 0.29	95	19 XIA	12	COSM
< 0.81	95	20 SAITO	11	COSM SDSS
< 0.44	95	21 HANNESTAD	10	COSM
< 0.6	95	22 SEKIGUCHI	10	COSM
< 0.28	95	23 THOMAS	10	COSM
< 1.1		24 ICHIKI	09	COSM
< 1.3	95	25 KOMATSU	09	COSM WMAP
< 1.2		26 TEREÑO	09	COSM
< 0.33		27 VIKHLININ	09	COSM
< 0.28		28 BERNARDIS	08	COSM
< 0.17-2.3		29 FOGGLI	07	COSM
< 0.42	95	30 KRISTIANSEN	07	COSM
< 0.63-2.2		31 ZUNCKEL	07	COSM
< 0.24	95	32 CIRELLI	06	COSM
< 0.62	95	33 HANNESTAD	06	COSM
< 1.2		34 SANCHEZ	06	COSM
< 0.17	95	32 SELJAK	06	COSM
< 2.0	95	35 ICHIKAWA	05	COSM
< 0.75		36 BARGER	04	COSM
< 1.0		37 CROTTY	04	COSM
< 0.7		38 SPERGEL	03	COSM WMAP
< 0.9		39 LEWIS	02	COSM
< 4.2		40 WANG	02	COSM CMB
< 2.7		41 FUKUGITA	00	COSM
< 5.5		42 CROFT	99	ASTR Ly $\alpha$ power spec
<180		SZALAY	74	COSM
<132		COWSIK	72	COSM
<280		MARX	72	COSM
<400		GERSHTEIN	66	COSM

<sup>1</sup> LOUREIRO 19 combines data from large scale structure, cosmic microwave background, type Ia supernovae and big bang nucleosynthesis using physically motivated neutrino mass models.

<sup>2</sup> UPADHYE 19 uses the shape of the BOSS redshift-space galaxy power spectrum in combination with the CMB, and supernovae data. Limit weakens to  $< 0.54$  eV if the dark energy equation of state is allowed to vary.

<sup>3</sup> CHOUDHURY 18 combines 2015 Planck CMB temperature data, information from the optical depth to reionization from Planck 2016 intermediate results together with baryon acoustic oscillation data from BOSS, MGS, and 6dFGS as well as supernovae Type Ia data from the Pantheon Sample. The limit is strengthened to 0.118 eV when high- $l$  CMB polarization data is also included.

<sup>4</sup> SIMPSON 17 uses a combination of laboratory and cosmological measurements to determine the light neutrino masses and argue that there is strong evidence for the normal mass ordering.

<sup>5</sup> Combines temperature anisotropies of the CMB from Planck with data on baryon acoustic oscillations and the optical depth to reionization. Limit is strengthened to 0.118 when high multipole polarization data is included. Updates GIUSARMA 16.

<sup>6</sup> Constrains the total mass of neutrinos using the Lyman-alpha forest power spectrum with BOSS (mid-resolution), XQ-100 (high-resolution) and CMB. Without the CMB data, the limit relaxes to 0.8 eV. Supersedes PALANQUE-DELABROUILLE 15A.

<sup>7</sup> Constrains the total mass of neutrinos from Planck CMB data combined with baryon acoustic oscillation and Planck cluster data.

<sup>8</sup> Constrains the total mass of neutrinos from BAO data from SDSS-III/BOSS combined with CMB data from Planck. Limit quoted for normal mass hierarchy. The limit for the inverted mass hierarchy is 0.20 eV and for the degenerate mass hierarchy it is 0.15 eV.

<sup>9</sup> ROSSI 15 sets limits on the sum of neutrino masses using BOSS Lyman alpha forest data combined with Planck CMB data and baryon acoustic oscillations.

- 10 Constrains the total mass of neutrinos from Planck CMB data along with WMAP polarization, high L, and BAO data.
- 11 Finite neutrino mass fit to resolve discrepancy between CMB and lensing measurements.
- 12 Fit to the total mass of neutrinos from BOSS data along with WMAP CMB data and data from other BAO constraints and weak lensing.
- 13 Fit to the total mass of neutrinos from Planck CMB data along with BAO.
- 14 Constrains the total mass of neutrinos from Planck CMB data combined with baryon acoustic oscillation data from BOSS and HST data on the Hubble parameter.
- 15 Fit based on the SPT-SZ survey combined with CMB, BAO, and  $H_0$  data.
- 16 Constrains the total mass of neutrinos (marginalizing over the effective number of neutrino species) from CMB, CMB lensing, BAO, and galaxy clustering data.
- 17 Constrains the total mass of neutrinos from Planck CMB data combined with baryon acoustic oscillation data from BOSS, 6dFGS, SDSS, WiggleZ data on the galaxy power spectrum, and HST data on the Hubble parameter. The limit is increased to 0.25 eV if a lower bound to the sum of neutrino masses of 0.04 eV is assumed.
- 18 Constrains the total mass of neutrinos from observational Hubble parameter data with seven-year WMAP data and the most recent estimate of  $H_0$ .
- 19 Constrains the total mass of neutrinos from the CFHTLS combined with seven-year WMAP data and a prior on the Hubble parameter. Limit is relaxed to 0.41 eV when small scales affected by non-linearities are removed.
- 20 Constrains the total mass of neutrinos from the Sloan Digital Sky Survey and the five-year WMAP data.
- 21 Constrains the total mass of neutrinos from the 7-year WMAP data including SDSS and HST data. Limit relaxes to 1.19 eV when CMB data is used alone. Supersedes HANNESTAD 06.
- 22 Constrains the total mass of neutrinos from a combination of CMB data, a recent measurement of  $H_0$  (SHOES), and baryon acoustic oscillation data from SDSS.
- 23 Constrains the total mass of neutrinos from SDSS MegaZ LRG DR7 galaxy clustering data combined with CMB, HST, supernovae and baryon acoustic oscillation data. Limit relaxes to 0.47 eV when the equation of state parameter,  $w \neq 1$ .
- 24 Constrains the total mass of neutrinos from weak lensing measurements when combined with CMB. Limit improves to 0.54 eV when supernovae and baryon acoustic oscillation observations are included. Assumes  $\Lambda$ CDM model.
- 25 Constrains the total mass of neutrinos from five-year WMAP data. Limit improves to 0.67 eV when supernovae and baryon acoustic oscillation observations are included. Limits quoted assume the  $\Lambda$ CDM model. Supersedes SPERGEL 07.
- 26 Constrains the total mass of neutrinos from weak lensing measurements when combined with CMB. Limit improves to  $0.03 < \Sigma m_\nu < 0.54$  eV when supernovae and baryon acoustic oscillation observations are included. The slight preference for massive neutrinos at the two-sigma level disappears when systematic errors are taken into account. Assumes  $\Lambda$ CDM model.
- 27 Constrains the total mass of neutrinos from recent Chandra X-ray observations of galaxy clusters when combined with CMB, supernovae, and baryon acoustic oscillation measurements. Assumes flat universe and constant dark-energy equation of state,  $w$ .
- 28 Constrains the total mass of neutrinos from recent CMB and SOSS LRG power spectrum data along with bias mass relations from SDSS, DEEP2, and Lyman-Break Galaxies. It assumes  $\Lambda$ CDM model. Limit degrades to 0.59 eV in a more general  $w$ CDM model.
- 29 Constrains the total mass of neutrinos from neutrino oscillation experiments and cosmological data. The most conservative limit uses only WMAP three-year data, while the most stringent limit includes CMB, large-scale structure, supernova, and Lyman-alpha data.
- 30 Constrains the total mass of neutrinos from recent CMB, large scale structure, SNIa, and baryon acoustic oscillation data. The limit relaxes to 1.75 when WMAP data alone is used with no prior. Paper shows results with several combinations of data sets. Supersedes KRISTIANSEN 06.
- 31 Constrains the total mass of neutrinos from the CMB and the large scale structure data. The most conservative limit is obtained when generic initial conditions are allowed.
- 32 Constrains the total mass of neutrinos from recent CMB, large scale structure, Lyman-alpha forest, and SNIa data.
- 33 Constrains the total mass of neutrinos from recent CMB and large scale structure data. See also GOOBAR 06. Superseded by HANNESTAD 10.
- 34 Constrains the total mass of neutrinos from the CMB and the final 2dF Galaxy Redshift Survey.
- 35 Constrains the total mass of neutrinos from the CMB experiments alone, assuming  $\Lambda$ CDM Universe. FUKUGITA 06 show that this result is unchanged by the 3-year WMAP data.
- 36 Constrains the total mass of neutrinos from the power spectrum of fluctuations derived from the Sloan Digital Sky Survey and the 2dF galaxy redshift survey, WMAP and 27 other CMB experiments and measurements by the HST Key project.
- 37 Constrains the total mass of neutrinos from the power spectrum of fluctuations derived from the Sloan Digital Sky Survey, the 2dF galaxy redshift survey, WMAP and ACBAR. The limit is strengthened to 0.6 eV when measurements by the HST Key project and supernovae data are included.
- 38 Constrains the fractional contribution of neutrinos to the total matter density in the Universe from WMAP data combined with other CMB measurements, the 2dFGRS data, and Lyman  $\alpha$  data. The limit does not noticeably change if the Lyman  $\alpha$  data are not used.
- 39 LEVVIS 02 constrains the total mass of neutrinos from the power spectrum of fluctuations derived from the CMB, HST Key project, 2dF galaxy redshift survey, supernovae type Ia, and BBN.
- 40 WANG 02 constrains the total mass of neutrinos from the power spectrum of fluctuations derived from the CMB and other cosmological data sets such as galaxy clustering and the Lyman  $\alpha$  forest.
- 41 FUKUGITA 00 is a limit on neutrino masses from structure formation. The constraint is based on the clustering scale  $\sigma_8$  and the COBE normalization and leads to a conservative limit of 0.9 eV assuming 3 nearly degenerate neutrinos. The quoted limit is on the sum of the light neutrino masses.

42 CROFT 99 result based on the power spectrum of the Ly  $\alpha$  forest. If  $\Omega_{\text{matter}} < 0.5$ , the limit is improved to  $m_\nu < 2.4 (\Omega_{\text{matter}}/0.17-1)$  eV.

**Limits on MASSES of Light Stable Right-Handed  $\nu$  (with necessarily suppressed interaction strengths)**

VALUE (eV)	DOCUMENT ID	TECN	COMMENT
<100-200	1 OLIVE	82 COSM	Dirac $\nu$
<200-2000	1 OLIVE	82 COSM	Majorana $\nu$

• • • We do not use the following data for averages, fits, limits, etc. • • •

<sup>1</sup> Depending on interaction strength  $G_R$  where  $G_R < G_F$ .

**Limits on MASSES of Heavy Stable Right-Handed  $\nu$  (with necessarily suppressed interaction strengths)**

VALUE (GeV)	DOCUMENT ID	TECN	COMMENT
> 10	1 OLIVE	82 COSM	$G_R/G_F < 0.1$
>100	1 OLIVE	82 COSM	$G_R/G_F < 0.01$

• • • We do not use the following data for averages, fits, limits, etc. • • •

<sup>1</sup> These results apply to heavy Majorana neutrinos and are summarized by the equation:  $m_\nu > 1.2$  GeV ( $G_F/G_R$ ). The bound saturates, and if  $G_R$  is too small no mass range is allowed.

**$\nu$  CHARGE**

e = electron charge is the unit of values listed below.

VALUE (e)	CL%	DOCUMENT ID	TECN	COMMENT
<4 x 10 <sup>-35</sup>	95	1 CAPRINI	05 COSM	charge neutral universe

• • • We do not use the following data for averages, fits, limits, etc. • • •

<3 x 10 <sup>-8</sup>	95	2 DELLA-VALLE	16 LASR	magnetic dichroism
<2.1 x 10 <sup>-12</sup>	90	3 CHEN	14A TEXO	nuclear reactor
<1.5 x 10 <sup>-12</sup>	90	4 STUDENIKIN	14	nuclear reactor
<3.7 x 10 <sup>-12</sup>	90	5 GNINENKO	07 RVUE	nuclear reactor
<2 x 10 <sup>-14</sup>		6 RAFFELT	99 ASTR	red giant luminosity
<6 x 10 <sup>-14</sup>		7 RAFFELT	99 ASTR	solar cooling
<4 x 10 <sup>-4</sup>		8 BABU	94 RVUE	BECB beam dump
<3 x 10 <sup>-4</sup>		9 DAVIDSON	91 RVUE	SLAC e <sup>-</sup> beam dump
<2 x 10 <sup>-15</sup>		10 BARBIELLINI	87 ASTR	SN 1987A
<1 x 10 <sup>-13</sup>		11 BERNSTEIN	63 ASTR	solar energy losses

<sup>1</sup> CAPRINI 05 limit derived from the lack of a charge asymmetry in the universe. Limit assumes that charge asymmetries between particles are not anti-correlated.

<sup>2</sup> DELLA-VALLE 16 obtain a limit on the charge of neutrinos valid for masses of less than 10 MeV. For heavier neutrinos the limit increases as a power of mass, reaching 10<sup>-6</sup> e for  $m = 100$  MeV.

<sup>3</sup> CHEN 14A use the Multi-Configuration RPPA method to analyze reactor  $\bar{\nu}_e$  scattering on Ge atoms with 300 eV recoil energy threshold to obtain this limit.

<sup>4</sup> STUDENIKIN 14 uses the limit on  $\mu_\nu$  from BEDA 13 and the 2.8 keV threshold of the electron recoil energy to obtain this limit.

<sup>5</sup> GNINENKO 07 use limit on  $\bar{\nu}_e$  magnetic moment from LI 03b to derive this result. The limit is considerably weaker than the limits on the charge of  $\nu_e$  and  $\bar{\nu}_e$  from various astrophysics considerations.

<sup>6</sup> This RAFFELT 99 limit applies to all neutrino flavors which are light enough (<5 keV) to be emitted from globular-cluster red giants.

<sup>7</sup> This RAFFELT 99 limit is derived from the helioseismological limit on a new energy-loss channel of the Sun, and applies to all neutrino flavors which are light enough (<1 keV) to be emitted from the sun.

<sup>8</sup> BABU 94 use COOPER-SARKAR 92 limit on  $\nu$  magnetic moment to derive quoted result. It applies to  $\nu_\tau$ .

<sup>9</sup> DAVIDSON 91 use data from early SLAC electron beam dump experiment to derive charge limit as a function of neutrino mass. It applies to  $\nu_\tau$ .

<sup>10</sup> Exact BARBIELLINI 87 limit depends on assumptions about the intergalactic or galactic magnetic fields and about the direct distance and time through the field. It applies to  $\nu_e$ .

<sup>11</sup> The limit applies to all flavors.

**$\nu$  (MEAN LIFE) / MASS**

Measures  $[\sum |U_{ej}|^2 \Gamma_j m_j]^{-1}$ , where the sum is over mass eigenstates which cannot be resolved experimentally. Some of the limits constrain the radiative decay and are based on the limit of the corresponding photon flux. Other apply to the decay of a heavier neutrino into the lighter one and a Majoron or other invisible particle. Many of these limits apply to any  $\nu$  within the indicated mass range.

Limits on the radiative decay are either directly based on the limits of the corresponding photon flux, or are derived from the limits on the neutrino magnetic moments. In the later case the transition rate for  $\nu_i \rightarrow \nu_j + \gamma$

is constrained by  $\Gamma_{ij} = \frac{1}{\tau_{ij}} = \frac{(m_i^2 - m_j^2)^3}{m_i^3} \mu_{ij}^2$  where  $\mu_{ij}$  is the neutrino transition moment in the mass eigenstates basis. Typically, the limits on lifetime based on the magnetic moments are many orders of magnitude more restrictive than limits based on the nonobservation of photons.

# Lepton Particle Listings

## Neutrino Properties

VALUE (s/eV)	CL%	DOCUMENT ID	TECN	COMMENT
> 15.4	90	1 KRAKAUER	91 CNTR	$\nu_\mu, \bar{\nu}_\mu$ at LAMPF
> 7 × 10 <sup>9</sup>		2 RAFFELT	85 ASTR	
> 300	90	3 REINES	74 CNTR	$\bar{\nu}_e$
• • • We do not use the following data for averages, fits, limits, etc. • • •				
> 8.08 × 10 <sup>-5</sup>	90	4 AHARMIM	19 SNO	$\nu_2$ invisible nonradiative decay
> 1.92 × 10 <sup>-3</sup>	90	5 AHARMIM	19 FIT	$\nu_2$ invisible nonradiative decay
6–26 × 10 <sup>9</sup>	95	6 ESCUDERO	19 COSM	Invisible decay $m_\nu \geq 0.05$ eV
> 10 <sup>5</sup> – 10 <sup>10</sup>	95	7 CECCHINI	11 ASTR	$\nu_2 \rightarrow \nu_1$ radiative decay
	90	8 MIRIZZI	07 CMB	radiative decay
	90	9 MIRIZZI	07 CIB	radiative decay
	90	10 WONG	07 CNTR	Reactor $\bar{\nu}_e$
> 0.11	90	11 XIN	05 CNTR	Reactor $\nu_e$
	90	12 XIN	05 CNTR	Reactor $\nu_e$
> 0.004	90	13 AHARMIM	04 SNO	quasidegen. $\nu$ masses
> 4.4 × 10 <sup>-5</sup>	90	13 AHARMIM	04 SNO	hierarchical $\nu$ masses
$\gtrsim 100$	95	14 CECCHINI	04 ASTR	Radiative decay for $\nu$ mass $> 0.01$ eV
> 0.067	90	15 EGUCHI	04 KLND	quasidegen. $\nu$ masses
> 1.1 × 10 <sup>-3</sup>	95	15 EGUCHI	04 KLND	hierarchical $\nu$ masses
> 8.7 × 10 <sup>-5</sup>	99	16 BANDYOPA...	03 FIT	nonradiative decay
$\geq 4200$	90	17 DERBIN	02B CNTR	Solar $pp$ and Be $\nu$
> 2.8 × 10 <sup>-5</sup>	99	18 JOSHIPURA	02B FIT	nonradiative decay
		19 DOLGOV	99 COSM	
		20 BILLER	98 ASTR	$m_\nu = 0.05$ –1 eV
> 2.8 × 10 <sup>15</sup>		21,22 BLUDMAN	92 ASTR	$m_\nu < 50$ eV
none 10 <sup>-12</sup> – 5 × 10 <sup>4</sup>		23 DODELSON	92 ASTR	$m_\nu = 1$ –300 keV
< 10 <sup>-12</sup> or > 5 × 10 <sup>4</sup>		23 DODELSON	92 ASTR	$m_\nu = 1$ –300 keV
		24 GRANEK	91 COSM	Decaying $L^0$
> 6.4	90	25 KRAKAUER	91 CNTR	$\nu_e$ at LAMPF
> 1.1 × 10 <sup>15</sup>		26 WALKER	90 ASTR	$m_\nu = 0.03$ – ~2 MeV
> 6.3 × 10 <sup>15</sup>		22,27 CHUPP	89 ASTR	$m_\nu < 20$ eV
> 1.7 × 10 <sup>15</sup>		22 KOLB	89 ASTR	$m_\nu < 20$ eV
		28 RAFFELT	89 RVUE	$\bar{\nu}$ (Dirac, Majorana)
		29 RAFFELT	89B ASTR	
		30 VONFEILIT...	88 ASTR	
> 8.3 × 10 <sup>14</sup>		31 OBERAUER	87 $\bar{\nu}_R$ (Dirac)	
> 22	68	31 OBERAUER	87 $\bar{\nu}$ (Majorana)	
> 38	68	31 OBERAUER	87 $\bar{\nu}_L$ (Dirac)	
> 59	68	31 OBERAUER	87 $\bar{\nu}$ (Dirac)	
> 30	68	KETOV	86 CNTR	$\bar{\nu}$ (Dirac)
> 20	68	KETOV	86 CNTR	$\bar{\nu}$ (Majorana)
		32 BINETRUY	84 COSM	$m_\nu \sim 1$ MeV
> 0.11	90	33 FRANK	81 CNTR	$\nu\bar{\nu}$ LAMPF
> 2 × 10 <sup>21</sup>		34 STECKER	80 ASTR	$m_\nu = 10$ –100 eV
> 1.0 × 10 <sup>-2</sup>	90	33 BLIETSCHAU	78 HLBC	$\nu_\mu$ , CERN GGM
> 1.7 × 10 <sup>-2</sup>	90	33 BLIETSCHAU	78 HLBC	$\bar{\nu}_\mu$ , CERN GGM
< 3 × 10 <sup>-11</sup>		35 FALK	78 ASTR	$m_\nu < 10$ MeV
> 2.2 × 10 <sup>-3</sup>	90	33 BARNES	77 DBC	$\nu$ , ANL 12-ft
		36 COWSIK	77 ASTR	
> 3. × 10 <sup>-3</sup>	90	33 BELLOTTI	76 HLBC	$\nu$ , CERN GGM
> 1.3 × 10 <sup>-2</sup>	90	33 BELLOTTI	76 HLBC	$\bar{\nu}$ , CERN GGM

1 KRAKAUER 91 quotes the limit  $\tau/m_{\nu_1} > (0.75a^2 + 21.65a + 26.3) \text{ s/eV}$ , where  $a$  is a parameter describing the asymmetry in the neutrino decay defined as  $dN_\nu/d\cos\theta = (1/2)(1 + a\cos\theta)$ . The parameter  $a = 0$  for a Majorana neutrino, but can vary from  $-1$  to  $1$  for a Dirac neutrino. The bound given by the authors is the most conservative (which applies for  $a = -1$ ).

2 RAFFELT 85 limit on the radiative decay is from solar  $x$ - and  $\gamma$ -ray fluxes. Limit depends on  $\nu$  flux from  $pp$ , now established from GALLEX and SAGE to be  $> 0.5$  of expectation.

3 REINES 74 looked for  $\nu$  of nonzero mass decaying radiatively to a neutral of lesser mass +  $\gamma$ . Used liquid scintillator detector near fission reactor. Finds lab lifetime  $6 \times 10^7$  s or more. Above value of (mean life)/mass assumes average effective neutrino energy of 0.2 MeV. To obtain the limit  $6 \times 10^7$  s REINES 74 assumed that the full  $\bar{\nu}_e$  reactor flux could be responsible for yielding decays with photon energies in the interval 0.1 MeV – 0.5 MeV. This represents some overestimate so their lower limit is an over-estimate of the lab lifetime (VOGEL 84). If so, OBERAUER 87 may be comparable or better.

4 AHARMIM 19 quotes the limit  $\tau/m_{\nu_2}$  for invisible nonradiative decay of  $\nu_2$ . They obtained this result by analyzing the entire SNO dataset, allowing for the decay of  $\nu_2$  which would cause an energy-dependent distortion of the survival probability of electron-type solar neutrinos.

5 AHARMIM 19 quotes the limit  $\tau/m_{\nu_2}$  for invisible nonradiative decay of  $\nu_2$ . They obtained this result by combining the  $\tau/m_{\nu_2}$  measurements from SNO and other solar neutrino experiments (Super-Kamiokande, KamLAND, and Borexino <sup>8B</sup> results; Borexino and KamLAND <sup>7Be</sup> results; the combined gallium interaction rate from GNO, GALLEX, and SAGE; and the chlorine interaction rate from Homestake). The quoted limit at 99% CL is  $> 1.04 \times 10^{-3}$ .

6 ESCUDERO 19 sets limits on invisible neutrino decays using Planck 2018 data of  $\tau > 1.3$ – $0.3 \times 10^9$  s at 95% C.L. Values in the range  $\tau = 2$ – $16 \times 10^9$  s are preferred at 95% C.L. when Planck polarization data is included. Limits scale as  $(m_\nu/0.05 \text{ eV})^3$ .

7 CECCHINI 11 search for radiative decays of solar neutrinos into visible photons during the 2006 total solar eclipse. The range of (mean life)/mass values corresponds to a range of  $\nu_1$  masses between  $10^{-4}$  and 0.1 eV.

8 MIRIZZI 07 determine a limit on the neutrino radiative decay from analysis of the maximum allowed distortion of the CMB spectrum as measured by the COBE/FIRAS. For the decay  $\nu_2 \rightarrow \nu_1$  the lifetime limit is  $\lesssim 4 \times 10^{20}$  s for  $m_{\min} \lesssim 0.14$  eV. For transition with the  $|\Delta m_{31}|$  mass difference the lifetime limit is  $\sim 2 \times 10^{19}$  s for  $m_{\min} \lesssim 0.14$  eV and  $\sim 5 \times 10^{20}$  s for  $m_{\min} \gtrsim 0.14$  eV.

9 MIRIZZI 07 determine a limit on the neutrino radiative decay from analysis of the cosmic infrared background (CIB) using the Spitzer Observatory data. For transition with the  $|\Delta m_{31}|$  mass difference they obtain the lifetime limit  $\sim 10^{20}$  s for  $m_{\min} \lesssim 0.14$  eV.

10 WONG 07 use their limit on the neutrino magnetic moment together with the assumed experimental value of  $\Delta m_{13}^2 \sim 2 \times 10^{-3} \text{ eV}^2$  to obtain  $\tau_{13}/m_1^3 > 3.2 \times 10^{27} \text{ s/eV}^3$  for the radiative decay in the case of the inverted mass hierarchy. Similarly to RAFFELT 89 this limit can be violated if electric and magnetic moments are equal to each other. Analogous, but numerically somewhat different limits are obtained for  $\tau_{23}$  and  $\tau_{21}$ .

11 XIN 05 search for the  $\gamma$  from radiative decay of  $\nu_e$  produced by the electron capture on <sup>51</sup>Cr. No events were seen and the limit on  $\tau/m_\nu$  was derived. This is a weaker limit on the decay of  $\nu_e$  than KRAKAUER 91.

12 XIN 05 use their limit on the neutrino magnetic moment of  $\nu_e$  together with the assumed experimental value of  $\Delta m_{1,3}^2 \sim 2 \times 10^{-3} \text{ eV}^2$  to obtain  $\tau_{13}/m_1^3 > 1 \times 10^{23} \text{ s/eV}^3$  for the radiative decay in the case of the inverted mass hierarchy. Similarly to RAFFELT 89 this limit can be violated if electric and magnetic moments are equal to each other. Analogous, but numerically somewhat different limits are obtained for  $\tau_{23}$  and  $\tau_{21}$ . Again, this limit is specific for  $\nu_e$ .

13 AHARMIM 04 obtained these results from the solar  $\bar{\nu}_e$  flux limit set by the SNO measurement assuming  $\nu_2$  decay through nonradiative process  $\nu_2 \rightarrow \bar{\nu}_1 X$ , where  $X$  is a Majoron or other invisible particle. Limits are given for the cases of quasidegenerate and hierarchical neutrino masses.

14 CECCHINI 04 obtained this bound through the observations performed on the occasion of the 21 June 2001 total solar eclipse, looking for visible photons from radiative decays of solar neutrinos. Limit is a  $\tau/m_{\nu_2}$  in  $\nu_2 \rightarrow \nu_1 \gamma$ . Limit ranges from  $\sim 100$  to  $10^7 \text{ s/eV}$  for  $0.01 < m_{\nu_1} < 0.1 \text{ eV}$ .

15 EGUCHI 04 obtained these results from the solar  $\bar{\nu}_e$  flux limit set by the KamLAND measurement assuming  $\nu_2$  decay through nonradiative process  $\nu_2 \rightarrow \bar{\nu}_1 X$ , where  $X$  is a Majoron or other invisible particle. Limits are given for the cases of quasidegenerate and hierarchical neutrino masses.

16 The ratio of the lifetime over the mass derived by BANDYOPADHYAY 03 is for  $\nu_2$ . They obtained this result using the following solar-neutrino data: total rates measured in Cl and Ga experiments, the Super-Kamiokande's zenith-angle spectra, and SNO's day and night spectra. They assumed that  $\nu_1$  is the lowest mass, stable or nearly stable neutrino state and  $\nu_2$  decays through nonradiative Majoron emission process,  $\nu_2 \rightarrow \bar{\nu}_1 + J$ , or through nonradiative process with all the final state particles being sterile. The best fit is obtained in the region of the LMA solution.

17 DERBIN 02B (also BACK 03B) obtained this bound for the radiative decay from the results of background measurements with Counting Test Facility (the prototype of the Borexino detector). The laboratory gamma spectrum is given as  $dN_\gamma/d\cos\theta = (1/2)(1 + \alpha\cos\theta)$  with  $\alpha=0$  for a Majorana neutrino, and  $\alpha$  varying to  $-1$  to  $1$  for a Dirac neutrino. The listed bound is for the case of  $\alpha=0$ . The most conservative bound  $1.5 \times 10^{13} \text{ s eV}^{-1}$  is obtained for the case of  $\alpha=-1$ .

18 The ratio of the lifetime over the mass derived by JOSHIPURA 02B is for  $\nu_2$ . They obtained this result from the total rates measured in all solar neutrino experiments. They assumed that  $\nu_1$  is the lowest mass, stable or nearly stable neutrino state and  $\nu_2$  decays through nonradiative process like Majoron emission decay,  $\nu_2 \rightarrow \nu'_1 + J$  where  $\nu'_1$  state is sterile. The exact limit depends on the specific solution of the solar neutrino problem. The quoted limit is for the LMA solution.

19 DOLGOV 99 places limits in the (Majorana)  $\tau$ -associated  $\nu$  mass-lifetime plane based on nucleosynthesis. Results would be considerably modified if neutrino oscillations exist.

20 BILLER 98 use the observed TeV  $\gamma$ -ray spectra to set limits on the mean life of any radiatively decaying neutrino between 0.05 and 1 eV. Curve shows  $\tau_\nu/B_\gamma > 0.15 \times 10^{21} \text{ s}$  at 0.05 eV,  $> 1.2 \times 10^{21} \text{ s}$  at 0.17 eV,  $> 3 \times 10^{21} \text{ s}$  at 1 eV, where  $B_\gamma$  is the branching ratio to photons.

21 BLUDMAN 92 sets additional limits by this method for higher mass ranges. Cosmological limits are also obtained.

22 Limit on the radiative decay based on nonobservation of  $\gamma$ 's in coincidence with  $\nu$ 's from SN 1987A.

23 DODELSON 92 range is for wrong-helicity keV mass Dirac  $\nu$ 's from the core of neutron star in SN 1987A decaying to  $\nu$ 's that would have interacted in KAM2 or LMB detectors.

24 GRANEK 91 considers heavy neutrino decays to  $\gamma\nu_L$  and  $3\nu_L$ , where  $m_{\nu_1} < 100 \text{ keV}$ . Lifetime is calculated as a function of heavy neutrino mass, branching ratio into  $\gamma\nu_L$ , and  $m_{\nu_1}$ .

25 KRAKAUER 91 quotes the limit for  $\nu_e$ ,  $\tau/m_\nu > (0.3a^2 + 9.8a + 15.9) \text{ s/eV}$ , where  $a$  is a parameter describing the asymmetry in the radiative neutrino decay defined as  $dN_\nu/d\cos\theta = (1/2)(1 + a\cos\theta)$   $a = 0$  for a Majorana neutrino, but can vary from  $-1$  to  $1$  for a Dirac neutrino. The bound given by the authors is the most conservative (which applies for  $a = -1$ ).

26 WALKER 90 uses SN 1987A  $\gamma$  flux limits after 289 days.

27 CHUPP 89 should be multiplied by a branching ratio (about 1) and a detection efficiency (about 1/4), and pertains to radiative decay of any neutrino to a lighter or sterile neutrino.

28 RAFFELT 89 uses KYULDJIEV 84 to obtain  $\tau m^3 > 3 \times 10^{18} \text{ s eV}^3$  (based on  $\bar{\nu}_e e^-$  cross sections). The bound for the radiative decay is not valid if electric and magnetic transition moments are equal for Dirac neutrinos.

See key on page 999

# Lepton Particle Listings Neutrino Properties

- <sup>29</sup> RAFFELT 89B analyze stellar evolution and exclude the region  $3 \times 10^{12} < \tau m^3 < 3 \times 10^{21} \text{ s eV}^3$ .
- <sup>30</sup> Model-dependent theoretical analysis of SN1987A neutrinos. Quoted limit is for  $[\sum_j |U_{\ell j}|^2 \Gamma_j m_j]^{-1}$ , where  $\ell = \mu, \tau$ . Limit is  $3.3 \times 10^{14} \text{ s/eV}$  for  $\ell = e$ .
- <sup>31</sup> OBERAUER 87 looks for photons and  $e^+e^-$  pairs from radiative decays of reactor neutrinos.
- <sup>32</sup> BINETRUY 84 finds  $\tau < 10^8 \text{ s}$  for neutrinos in a radiation-dominated universe.
- <sup>33</sup> These experiments look for  $\nu_k \rightarrow \nu_j \gamma$  or  $\bar{\nu}_k \rightarrow \bar{\nu}_j \gamma$ .
- <sup>34</sup> STECKER 80 limit based on UV background; result given is  $\tau > 4 \times 10^{22} \text{ s}$  at  $m_\nu = 20 \text{ eV}$ .
- <sup>35</sup> FALK 78 finds lifetime constraints based on supernova energetics.
- <sup>36</sup> COWSIK 77 considers variety of scenarios. For neutrinos produced in the big bang, present limits on optical photon flux require  $\tau > 10^{23} \text{ s}$  for  $m_\nu \sim 1 \text{ eV}$ . See also COWSIK 79 and GOLDMAN 79.

## μ MAGNETIC MOMENT

The coupling of neutrinos to an electromagnetic field is characterized by a  $3 \times 3$  matrix  $\lambda$  of the magnetic ( $\mu$ ) and electric ( $d$ ) dipole moments ( $\lambda = \mu - id$ ). For Majorana neutrinos the matrix  $\lambda$  is antisymmetric and only transition moments are allowed, while for Dirac neutrinos  $\lambda$  is a general  $3 \times 3$  matrix. In the standard electroweak theory extended to include neutrino masses (see FUJIKAWA 80)  $\mu_\nu = 3eG_F m_\nu / (8\pi^2 \sqrt{2}) = 3.2 \times 10^{-19} (m_\nu / \text{eV}) \mu_B$ , i.e. it is unobservably small given the known small neutrino masses. In more general models there is no longer a proportionality between neutrino mass and its magnetic moment, even though only massive neutrinos have nonvanishing magnetic moments without fine tuning.

Laboratory bounds on  $\lambda$  are obtained via elastic  $\nu$ - $e$  scattering, where the scattered neutrino is not observed. The combinations of matrix elements of  $\lambda$  that are constrained by various experiments depend on the initial neutrino flavor and on its propagation between source and detector (e.g., solar  $\nu_e$  and reactor  $\bar{\nu}_e$  do not constrain the same combinations). The listings below therefore identify the initial neutrino flavor.

Other limits, e.g. from various stellar cooling processes, apply to all neutrino flavors. Analogous flavor independent, but weaker, limits are obtained from the analysis of  $e^+e^- \rightarrow \nu\bar{\nu}\gamma$  collider experiments.

VALUE ( $10^{-10} \mu_B$ )	CL%	DOCUMENT ID	TECN	COMMENT
< 0.28	90	1 AGOSTINI 17A	BORX	Solar $\nu$ spectrum
< 0.29	90	2 BEDA 13	CNTR	Reactor $\bar{\nu}_e$
< 6.8	90	3 AUERBACH 01	LSND	$\nu_e e, \nu_\mu e$ scattering
< 3900	90	4 SCHWIENHO...01	DONU	$\nu_\tau e^- \rightarrow \nu_\tau e^-$
• • • We do not use the following data for averages, fits, limits, etc. • • •				
< 0.022	90	5 ARCEO-DIAZ 15	ASTR	Red giants
< 0.1	95	6 CORSICO 14	ASTR	
< 0.05	95	7 MILLER-BER...14B	ASTR	
< 0.045	95	8 VIAUX 13A	ASTR	Globular cluster M5
< 0.32	90	9 BEDA 10	CNTR	Reactor $\bar{\nu}_e$
< 2.2	90	10 DENIZ 10	TEXO	Reactor $\bar{\nu}_e$
< 0.011-0.027		11 KUZNETSOV 09	ASTR	$\nu_L \rightarrow \nu_R$ in SN1987A
< 0.54	90	12 ARPESELLA 08A	BORX	Solar $\nu$ spectrum
< 0.58	90	13 BEDA 07	CNTR	Reactor $\bar{\nu}_e$
< 0.74	90	14 WONG 07	CNTR	Reactor $\bar{\nu}_e$
< 0.9	90	15 DARAKTCHIEVA 05		Reactor $\bar{\nu}_e$
< 130	90	16 XIN 05	CNTR	Reactor $\nu_e$
< 37	95	17 GRIFOLS 04	FIT	Solar $^8\text{B } \nu$ (SNO NC)
< 3.6	90	18 LIU 04	SKAM	Solar $\nu$ spectrum
< 1.1	90	19 LIU 04	SKAM	Solar $\nu$ spectrum (LMA region)
< 5.5	90	20 BACK 03B	CNTR	Solar $pp$ and Be $\nu$
< 1.0	90	21 DARAKTCH... 03		Reactor $\bar{\nu}_e$
< 1.3	90	22 LI 03B	CNTR	Reactor $\bar{\nu}_e$
< 2	90	23 GRIMUS 02	FIT	solar + reactor (Majorana $\nu$ )
< 80000	90	24 TANIMOTO 00	RVUE	$e^+e^- \rightarrow \nu\bar{\nu}\gamma$
< 0.01-0.04		25 AYALA 99	ASTR	$\nu_L \rightarrow \nu_R$ in SN1987A
< 1.5	90	26 BEACOM 99	SKAM	Solar $\nu$ spectrum
< 0.03		27 RAFFELT 99	ASTR	Red giant luminosity
< 4		28 RAFFELT 99	ASTR	Solar cooling
< 44000	90	29 ABREU 97J	DLPH	$e^+e^- \rightarrow \nu\bar{\nu}\gamma$ at LEP
< 33000	90	29 ACCIARRI 97Q	L3	$e^+e^- \rightarrow \nu\bar{\nu}\gamma$ at LEP
< 0.62		30 ELMFORS 97	COSM	Depolarization in early universe plasma
< 27000	95	31 ESCRIBANO 97	RVUE	$\Gamma(Z \rightarrow \nu\nu)$ at LEP
< 30	90	31 VILAIN 95B	CHM2	$\nu_\mu e \rightarrow \nu_\mu e$
< 55000	90	32 GOULD 94	RVUE	$e^+e^- \rightarrow \nu\bar{\nu}\gamma$ at LEP
< 1.9	95	32 DERBIN 93	CNTR	Reactor $\bar{\nu}_e \rightarrow \bar{\nu}_e$
< 5400	90	33 COOPER... 92	BEBC	$\nu_\tau e^- \rightarrow \nu_\tau e^-$
< 2.4	90	34 VIDYAKIN 92	CNTR	Reactor $\bar{\nu}_e \rightarrow \bar{\nu}_e$
< 56000	90	34 DESHPANDE 91	RVUE	$e^+e^- \rightarrow \nu\bar{\nu}\gamma$
< 100	95	35 DORENBOS... 91	CHRM	$\nu_\mu e \rightarrow \nu_\mu e$
< 8.5	90	AHRENS 90	CNTR	$\nu_\mu e \rightarrow \nu_\mu e$

< 10.8	90	36 KRAKAUER 90	CNTR	LAMPF $\nu e \rightarrow \nu e$
< 7.4	90	36 KRAKAUER 90	CNTR	LAMPF ( $\nu_\mu, \bar{\nu}_\mu$ ) $e$ elast.
< 0.02		37 RAFFELT 90	ASTR	Red giant luminosity
< 0.1		38 RAFFELT 89B	ASTR	Cooling helium stars
		39 FUKUGITA 88	COSM	Primordial magn. fields
< 40000	90	40 GROTH 88	RVUE	$e^+e^- \rightarrow \nu\bar{\nu}\gamma$
$\leq .3$		38 RAFFELT 88B	ASTR	He burning stars
< 0.11		38 FUKUGITA 87	ASTR	Cooling helium stars
< 0.0006		41 NUSSINOV 87	ASTR	Cosmic EM back-grounds
< 0.1-0.2		MORGAN 81	COSM	$^4\text{He}$ abundance
< 0.85		BEG 78	ASTR	Stellar plasmons
< 0.6		42 SUTHERLAND 76	ASTR	Red giants + degenerate dwarfs
< 81		43 KIM 74	RVUE	$\bar{\nu}_\mu e \rightarrow \bar{\nu}_\mu e$
< 1		BERNSTEIN 63	ASTR	Solar cooling
< 14		COWAN 57	CNTR	Reactor $\bar{\nu}$

- <sup>1</sup> AGOSTINI 17A obtained this limit using the shape of the recoil electron energy spectrum from the Borexino Phase-II 1291.5 live days of solar neutrino data and the constraints on the sum of the solar neutrino fluxes from the radiochemical gallium experiments SAGE, Gallex, and GNO. Without radiochemical constraints, the 90% C.L. limit of  $< 4.0 \times 10^{-11} \mu_B$  is obtained.
- <sup>2</sup> BEDA 13 report  $\bar{\nu}_e e^-$  scattering results, using the Kalinin Nuclear Power Plant and a shielded Ge detector. The recoil electron spectrum is analyzed between 2.5 and 55 keV. Supersedes BEDA 07. Supersedes BEDA 10. This is the most stringent limit on the magnetic moment of reactor  $\bar{\nu}_e$ .
- <sup>3</sup> AUERBACH 01 limit is based on the LSND  $\nu_e$  and  $\nu_\mu$  electron scattering measurements. The limit is slightly more stringent than KRAKAUER 90.
- <sup>4</sup> SCHWIENHORST 01 quote an experimental sensitivity of  $4.9 \times 10^{-7}$ .
- <sup>5</sup> ARCEO-DIAZ 15 constrains the neutrino magnetic moment from observation of the tip of the red giant branch in the globular cluster  $\omega$ -Centauri.
- <sup>6</sup> CORSICO 14 constrains the neutrino magnetic moment from observations of white dwarf pulsations.
- <sup>7</sup> MILLER-BERTOLAMI 14B constrains the neutrino magnetic moment from observations of the white dwarf luminosity function of the Galactic disk.
- <sup>8</sup> VIAUX 13A constrains the neutrino magnetic moment from observations of the globular cluster M5.
- <sup>9</sup> BEDA 10 report  $\bar{\nu}_e e^-$  scattering results, using the Kalinin Nuclear Power Plant and a shielded Ge detector. The recoil electron spectrum is analyzed between 2.9 and 45 keV. Supersedes BEDA 07. Superseded by BEDA 13.
- <sup>10</sup> DENIZ 10 observe reactor  $\bar{\nu}_e$  scattering with recoil kinetic energies 3-8 MeV using CsI(Tl) detectors. The observed rate and spectral shape are consistent with the Standard Model prediction, leading to the reported constraint on  $\bar{\nu}_e$  magnetic moment.
- <sup>11</sup> KUZNETSOV 09 obtain a limit on the flavor averaged magnetic moment of Dirac neutrinos from the time averaged neutrino signal of SN1987A. Improves and supersedes the analysis of BARBIERI 88 and AYALA 99.
- <sup>12</sup> ARPESELLA 08A obtained this limit using the shape of the recoil electron energy spectrum from the Borexino 192 live days of solar neutrino data.
- <sup>13</sup> BEDA 07 performed search for electromagnetic  $\bar{\nu}_e$ - $e$  scattering at Kalininskaya nuclear reactor. A Ge detector with active and passive shield was used and the electron recoil spectrum between 3.0 and 61.3 keV analyzed. Superseded by BEDA 10.
- <sup>14</sup> WONG 07 performed search for non-standard  $\bar{\nu}_e$ - $e$  scattering at the Kuo-Sheng nuclear reactor. Ge detector equipped with active anti-Compton shield is used. Most stringent laboratory limit on magnetic moment of reactor  $\bar{\nu}_e$ . Supersedes LI 03B.
- <sup>15</sup> DARAKTCHIEVA 05 present the final analysis of the search for non-standard  $\bar{\nu}_e$ - $e$  scattering component at Bugey nuclear reactor. Full kinematical event reconstruction of both the kinetic energy above 700 keV and scattering angle of the recoil electron, by use of TPC. Most stringent laboratory limit on magnetic moment. Supersedes DARAKTCHIEVA 03.
- <sup>16</sup> XIN 05 evaluated the  $\nu_e$  flux at the Kuo-Sheng nuclear reactor and searched for non-standard  $\nu_e$ - $e$  scattering. Ge detector equipped with active anti-Compton shield was used. This laboratory limit on magnetic moment is considerably less stringent than the limits for reactor  $\bar{\nu}_e$ , but is specific to  $\nu_e$ .
- <sup>17</sup> GRIFOLS 04 obtained this bound using the SNO data of the solar  $^8\text{B}$  neutrino flux measured with deuteron breakup. This bound applies to  $\mu_{\text{eff}} = (\mu_{21}^2 + \mu_{22}^2 + \mu_{23}^2)^{1/2}$ .
- <sup>18</sup> LIU 04 obtained this limit using the shape of the recoil electron energy spectrum from the Super-Kamiokande-I 1496 days of solar neutrino data. Neutrinos are assumed to have only diagonal magnetic moments,  $\mu_{\nu j} = \mu_{j\nu}$ . This limit corresponds to the oscillation parameters in the vacuum oscillation region.
- <sup>19</sup> LIU 04 obtained this limit using the shape of the recoil electron energy spectrum from the Super-Kamiokande-I 1496 live-day solar neutrino data, by limiting the oscillation parameter region in the LMA region allowed by solar neutrino experiments plus KamLAND.  $\mu_{\nu j} = \mu_{j\nu}$  is assumed. In the LMA region, the same limit would be obtained even if neutrinos have off-diagonal magnetic moments.
- <sup>20</sup> BACK 03B obtained this bound from the results of background measurements with Counting Test Facility (the prototype of the Borexino detector). Standard Solar Model flux was assumed. This  $\mu_\nu$  can be different from the reactor  $\mu_\nu$  in certain oscillation scenarios (see BEACOM 99).
- <sup>21</sup> DARAKTCHIEVA 03 searched for non-standard  $\bar{\nu}_e$ - $e$  scattering component at Bugey nuclear reactor. Full kinematical event reconstruction by use of TPC. Superseded by DARAKTCHIEVA 05.
- <sup>22</sup> LI 03B used Ge detector in active shield near nuclear reactor to test for nonstandard  $\bar{\nu}_e$ - $e$  scattering.
- <sup>23</sup> GRIMUS 02 obtain stringent bounds on all Majorana neutrino transition moments from a simultaneous fit of LMA-MSW oscillation parameters and transition moments to global

# Lepton Particle Listings

## Neutrino Properties

solar neutrino data + reactor data. Using only solar neutrino data, a 90% CL bound of  $6.3 \times 10^{-10} \mu_B$  is obtained.

- 24 TANIMOTO 00 combined  $e^+e^- \rightarrow \nu\bar{\nu}\gamma$  data from VENUS, TOPAZ, and AMY.
- 25 AYALA 99 improves the limit of BARBIERI 88.
- 26 BEACOM 99 obtain the limit using the shape, but not the absolute magnitude which is affected by oscillations, of the solar neutrino spectrum obtained by Superkamiokande (825 days). This  $\mu_\nu$  can be different from the reactor  $\mu_\nu$  in certain oscillation scenarios.
- 27 RAFFELT 99 is an update of RAFFELT 90. This limit applies to all neutrino flavors which are light enough ( $< 5$  keV) to be emitted from globular-cluster red giants. This limit pertains equally to electric dipole moments and magnetic transition moments, and it applies to both Dirac and Majorana neutrinos.
- 28 RAFFELT 99 is essentially an update of BERNSTEIN 63, but is derived from the helioseismological limit on a new energy-loss channel of the Sun. This limit applies to all neutrino flavors which are light enough ( $< 1$  keV) to be emitted from the Sun. This limit pertains equally to electric dipole and magnetic transition moments, and it applies to both Dirac and Majorana neutrinos.
- 29 ACCIARRI 97q result applies to both direct and transition magnetic moments and for  $q^2=0$ .
- 30 ELMFORS 97 calculate the rate of depolarization in a plasma for neutrinos with a magnetic moment and use the constraints from a big-bang nucleosynthesis on additional degrees of freedom.
- 31 Applies to absolute value of magnetic moment.
- 32 DERBIN 93 determine the cross section for 0.6–2.0 MeV electron energy as  $(1.28 \pm 0.63) \times \sigma_{\text{weak}}$ . However, the (reactor on - reactor off)/(reactor off) is only  $\sim 1/100$ .
- 33 COOPER-SARKAR 92 assume  $f_D/f_\pi = 2$  and  $D_S, \bar{D}_S$  production cross section =  $2.6 \mu\text{b}$  to calculate  $\nu$  flux.
- 34 VIDYAKIN 92 limit is from a  $e\bar{\nu}$  elastic scattering experiment. No experimental details are given except for the cross section from which this limit is derived. Signal/noise was 1/10. The limit uses  $\sin^2\theta_W = 0.23$  as input.
- 35 DORENBOSCH 91 corrects an incorrect statement in DORENBOSCH 89 that the  $\nu$  magnetic moment is  $< 1 \times 10^{-9}$  at the 95%CL. DORENBOSCH 89 measures both  $\nu_\mu$   $e$  and  $\bar{\nu}$   $e$  elastic scattering and assume  $\mu(\nu) = \mu(\bar{\nu})$ .
- 36 KRAKAUER 90 experiment fully reported in ALLEN 93.
- 37 RAFFELT 90 limit applies for a diagonal magnetic moment of a Dirac neutrino, or for a transition magnetic moment of a Majorana neutrino. In the latter case, the same analysis gives  $< 1.4 \times 10^{-12}$ . Limit at 95%CL obtained from  $\delta M_C$ .
- 38 Significant dependence on details of stellar models.
- 39 FUKUGITA 88 find magnetic dipole moments of any two neutrino species are bounded by  $\mu < 10^{-16} [10^{-9} G/B_0]$  where  $B_0$  is the present-day intergalactic field strength.
- 40 GROTCHE 88 combined data from MAC, ASP, CELLO, and Mark J.
- 41 For  $m_\nu = 8\text{--}200$  eV. NUSSINOV 87 examines transition magnetic moments for  $\nu_\mu \rightarrow \nu_e$  and obtain  $< 3 \times 10^{-15}$  for  $m_\nu > 16$  eV and  $< 6 \times 10^{-14}$  for  $m_\nu > 4$  eV.
- 42 We obtain above limit from SUTHERLAND 76 using their limit  $f < 1/3$ .
- 43 KIM 74 is a theoretical analysis of  $\bar{\nu}_\mu$  reaction data.

### NEUTRINO CHARGE RADIUS SQUARED

We report limits on the so-called neutrino charge radius squared. While the straight-forward definition of a neutrino charge radius has been proven to be gauge-dependent and, hence, unphysical (LEE 77c), there have been recent attempts to define a physically observable neutrino charge radius (BERNABEU 00, BERNABEU 02). The issue is still controversial (FUJIKAWA 03, BERNABEU 03). A more general interpretation of the experimental results is that they are limits on certain nonstandard contributions to neutrino scattering.

VALUE ( $10^{-32} \text{cm}^2$ )	CL%	DOCUMENT ID	TECN	COMMENT
<b>-2.1 to 3.3</b>	90	1 DENIZ 10	TEXO	Reactor $\bar{\nu}_e e$
• • •				We do not use the following data for averages, fits, limits, etc. • • •
-4 to 5.5	90	2 CADEDDU 18		$\nu_\mu$ coherent scat. on Csl
-0.53 to 0.68	90	3 HIRSCH 03		$\nu_\mu e$ scat.
-8.2 to 9.9	90	4 HIRSCH 03		anomalous $e^+e^- \rightarrow \nu\bar{\nu}\gamma$
-2.97 to 4.14	90	5 AUERBACH 01	LSND	$\nu_e e \rightarrow \nu_e e$
-0.6 to 0.6	90	VILAIN 95B	CHM2	$\nu_\mu e$ elastic scat.
0.9 $\pm$ 2.7		ALLEN 93	CNTR	LAMPF $\nu e \rightarrow \nu e$
< 2.3	95	MOURAO 92	ASTR	HOME/KAM2 $\nu$ rates
< 7.3	90	6 VIDYAKIN 92	CNTR	Reactor $\bar{\nu} e \rightarrow \bar{\nu} e$
1.1 $\pm$ 2.3		ALLEN 91	CNTR	Repl. by ALLEN 93
-1.1 $\pm$ 1.0		7 AHRENS 90	CNTR	$\nu_\mu e$ elastic scat.
-0.3 $\pm$ 1.5		7 DORENBOS... 89	CHRM	$\nu_\mu e$ elastic scat.
		8 GRIFOLS 89B	ASTR	SN 1987A

1 DENIZ 10 observe reactor  $\bar{\nu}_e e$  scattering with recoil kinetic energies 3–8 MeV using Csl(Tl) detectors. The observed rate and spectral shape are consistent with the Standard Model prediction, leading to the reported constraint on  $\bar{\nu}_e$  charge radius.

2 CADEDDU 18 use the data of the COHERENT experiment, AKIMOV 18. The limit is  $\langle r_{\nu_\mu}^2 \rangle$  for  $\nu_\mu$  obtained from the time-dependent data. Weaker limits were obtained for charge radii of  $\nu_e$  and for transition charge radii. The published value was divided by 2 to conform to the convention of this table.

- 3 Based on analysis of CCFR 98 results. Limit is on  $\langle r_{\nu_\tau}^2 \rangle + \langle r_{\nu_\mu}^2 \rangle$ . The CHARM II and E734 at BNL results are reanalyzed, and weaker bounds on the charge radius squared than previously published are obtained. The NuTeV result is discussed; when tentatively interpreted as  $\nu_\mu$  charge radius it implies  $\langle r_{\nu_\tau}^2 \rangle + \langle r_{\nu_\mu}^2 \rangle = (4.20 \pm 1.64) \times 10^{-33} \text{cm}^2$ .
- 4 Results of LEP-2 are interpreted as limits on the axial-vector charge radius squared of a Majorana  $\nu_\tau$ . Slightly weaker limits for both vector and axial-vector charge radius squared are obtained for the Dirac case, and somewhat weaker limits are obtained from the analysis of lower energy data (LEP-1.5 and TRISTAN).
- 5 AUERBACH 01 measure  $\nu_e e$  elastic scattering with LSND detector. The cross section agrees with the Standard Model expectation, including the charge and neutral current interference. The 90% CL applies to the range shown.
- 6 VIDYAKIN 92 limit is from a  $e\bar{\nu}$  elastic scattering experiment. No experimental details are given except for the cross section from which this limit is derived. Signal/noise was 1/10. The limit uses  $\sin^2\theta_W = 0.23$  as input.
- 7 Result is obtained from reanalysis given in ALLEN 91, followed by our reduction to obtain  $1\sigma$  errors.
- 8 GRIFOLS 89b sets a limit of  $\langle r^2 \rangle < 0.2 \times 10^{-32} \text{cm}^2$  for right-handed neutrinos.

### REFERENCES FOR Neutrino Properties

AHARMIM 19	PR D99 032013	B. Aharmim <i>et al.</i>	(SNO Collab.)
AKER 19	PRL 123 221802	M. Aker <i>et al.</i>	(KATRIN)
ESCUDERO 19	PR D100 103531	M. Escudero, M. Fairbairn	(LOKCK)
LOUREIRO 19	PRL 123 081301	A. Loureiro <i>et al.</i>	
UPADHYE 19	JCAP 1905 041	A. Upadhye	(WISC)
AKIMOV 18	arXiv:1804.09459	D. Akimov <i>et al.</i>	(COHERENT Collab.)
CADEDDU 18	PR D98 113010	M. Cadeddu <i>et al.</i>	
CHOUDHURY 18	JCAP 1809 017	S.R. Choudhury, S. Choubey	
AGOSTINI 17A	PR D96 091103	M. Agostini <i>et al.</i>	(Borexino Collab.)
SIMPSON 17	JCAP 1706 029	F. Simpson <i>et al.</i>	(BARC)
VAGNOZZI 17	PR D96 123503	S. Vagnozzi <i>et al.</i>	
YECHÉ 17	JCAP 1706 047	C. Yeché <i>et al.</i>	
DELLA-VALLE 16	EPJ C76 24	F. Della Valle <i>et al.</i>	(PVLAS Collab.)
DIVALENTINO 16	PR D93 083527	E. Di Valentinio <i>et al.</i>	
GIUSARMA 16	PR D94 083522	E. Giusarma <i>et al.</i>	
HUANG 16	EPJ C76 489	Q.-G. Huang, K. Wang, S. Wang	
ARCEO-DIAZ 15	ASP 70 1	S. Arceo-Diaz <i>et al.</i>	
PALANQUE... 15A	JCAP 1511 011	N. Palanque-Desabrouille <i>et al.</i>	
ROSSI 15	PR D92 063505	G. Rossi <i>et al.</i>	
ADE 14	AA 571 A16	P.A.R. Ade <i>et al.</i>	(Planck Collab.)
BATTYE 14	PRL 112 051303	R.A. Battye, A. Moss	(MCHS, NOTT)
BEUTLER 14	MNRAS 444 3501	F. Beutler <i>et al.</i>	(BOSS Collab.)
CHEN 14A	PR D90 011301	J.-W. Chen <i>et al.</i>	(TEXONO Collab.)
CORSICO 14	JCAP 1408 054	A.H. Corsico	
COSTANZI 14	JCAP 1410 081	M. Costanzi <i>et al.</i>	(TRST, TRST1)
GIUSARMA 14	PR D90 043507	E. Giusarma <i>et al.</i>	
HOU 14	APJ 782 74	Z. Hou <i>et al.</i>	
LEISTEDT 14	PRL 113 041301	B. Leistedt, H.V. Peiris, L. Verste	
MILLER-BER... 14B	AA 562 A123	M.M. Miller-Berlioni	(MPIG, LAPL)
RIEMER-SOR... 14	PR D89 103505	S. Riemer-Sørensen, D. Parkinson, T.M. Davis	
STUDENIKIN 14	EPL 107 21001	A.I. Studenikin	(GEMMA Collab.)
BEDA 13	PNPL 10 139	A.G. Beda <i>et al.</i>	
VIAUX 13A	PRL 111 231301	N. Viaux <i>et al.</i>	
MORESCO 12	JCAP 1207 053	M. Moresco <i>et al.</i>	
XIA 12	JCAP 1206 010	J.-Q. Xia <i>et al.</i>	
ASEEV 11	PR D84 112003	V.N. Aseev <i>et al.</i>	
CECCHINI 11	ASP 34 486	S. Cecchini <i>et al.</i>	
SAITO 11	PR D83 043529	S. Saito, M. Takada, A. Taruya	
BEDA 10	PNPL 7 406	A.G. Beda <i>et al.</i>	(GEMMA Collab.)
DENIZ 10	PR D81 072001	M. Deniz <i>et al.</i>	(TEXONO Collab.)
NANNESTAD 10	JCAP 1008 001	S. Hannestad <i>et al.</i>	
PAGLIAROLI 10	ASP 33 287	G. Pagliaroli, F. Rossi-Torres, E. Vissani	(INFN+)
SEKIGUCHI 10	JCAP 1003 015	T. Sekiguchi <i>et al.</i>	
THOMAS 10	PRL 105 031301	S.A. Thomas, F.B. Abdalla, O. Lahav	(LOU)
ICHIKI 09	PR D79 023520	K. Ichiki, M. Takada, T. Takahashi	
KOMATSU 09	APJS 180 330	E. Komatsu <i>et al.</i>	
KUZNETSOV 09	IJMP A24 5977	A.V. Kuznetsov, N.V. Mikheyev, A.A. Okrugin	(YARO)
TERENO 09	AA 500 657	I. Tereno <i>et al.</i>	
VIKHLININ 09	APJ 692 1060	A. Vikhlinin <i>et al.</i>	
ARPESELLA 08A	PRL 101 091302	C. Arpessella <i>et al.</i>	(Borexino Collab.)
BERNARDIS 08	PR D78 083535	F. De Bernardis <i>et al.</i>	
BEDA 07	PAN 70 1873	A.G. Beda <i>et al.</i>	
	Translated from YAF 70 1925		
FOGLI 07	PR D75 053001	G.L. Fogli <i>et al.</i>	
GNINENKO 07	PR D75 075014	S.N. Gninenko, N.V. Krasnikov, A. Rubbia	
KRISTIANSEN 07	PR D75 083510	J. Kristiansen, O. Elgaroy, H. Dahle	
MIRIZZI 07	PR D76 053007	A. Mirizzi, D. Montanari, P.D. Serpico	
SPERGEL 07	APJS 170 377	D.N. Spergel <i>et al.</i>	
WONG 07	PR D75 012001	H.T. Wong <i>et al.</i>	(TEXONO Collab.)
ZUNCKEL 07	JCAP 0708 004	C. Zunckel, P. Ferreira	
CIRELLI 06	JCAP 0612 013	M. Cirelli <i>et al.</i>	
FUKUGITA 06	PR D74 027302	M. Fukugita <i>et al.</i>	
GOOBAR 06	JCAP 0606 019	A. Goobar <i>et al.</i>	
HANNENSTAD 06	JCAP 0611 016	S. Hannestad, G. Raffelt	
KRISTIANSEN 06	PR D74 123005	J. Kristiansen, O. Elgaroy, H. Eriksen	
SANCHEZ 06	MNRAS 366 189	A.G. Sanchez <i>et al.</i>	
SELJAK 06	JCAP 0610 014	U. Seljak, A. Slosar, P. McDonald	
CAPRINI 05	JCAP 0502 006	C. Caprini, P.G. Ferreira	(GEVA, OXFTP)
DARAKTCHIEVA 05	PL B615 153	Z. Daraktchieva <i>et al.</i>	(MUNU Collab.)
ICHIKAWA 05	PR D71 043001	K. Ichikawa, M. Fukugita, M. Kawasaki	(ICRR)
KRAUS 05	EPJ C40 447	Ch. Kraus <i>et al.</i>	
XIN 05	PR D72 012006	B. Xin <i>et al.</i>	(TEXONO Collab.)
AHARMIM 04	PR D70 093014	B. Aharmim <i>et al.</i>	(SNO Collab.)
BARGER 04	PL B595 55	V. Barger, D. Marfatia, A. Tregre	
CECCHINI 04	ASP 21 183	S. Cecchini <i>et al.</i>	(BGNA+)
CROTTY 04	PR D69 123007	P. Crotty, J. Lessingourges, S. Pastor	
EGUCHI 04	PRL 92 071301	K. Eguchi <i>et al.</i>	(KamLAND Collab.)
GRIFOLS 04	PL B587 184	J.A. Grifols, E. Masso, S. Mohanty	(BARC, AHMED)
LIU 04	PRL 93 021802	D.W. Liu <i>et al.</i>	(Super-Kamiokande Collab.)
ARNABOLDI 03A	PRL 91 161802	C. Arnaboldi <i>et al.</i>	
BACK 03B	PL B563 35	H.O. Back <i>et al.</i>	(Borexino Collab.)
BANDYOPAD... 03	PL B555 33	A. Bandyopadhyay, S. Choubey, S. Goswami	(SAHA+)
BERNABEU 03	hep-ph/0303202	J. Bernabeu, J. Papavassiliou, J. Vidal	
DARAKTCHIEVA 03	PL B564 190	Z. Daraktchieva <i>et al.</i>	(MUNU Collab.)
FUJIKAWA 03	hep-ph/0303188	K. Fujikawa, R. Shrock	
HIRSCH 03	PR D67 033005	M. Hirsch, E. Nardi, D. Restrepo	
LI 03B	PRL 90 131802	H.B. Li <i>et al.</i>	(TEXONO Collab.)
SPERGEL 03	APJS 148 175	D.N. Spergel <i>et al.</i>	
BERNABEU 02	PRL 89 101802	J. Bernabeu, J. Papavassiliou, J. Vidal	
Also	PRL 89 229902 (errata)	J. Bernabeu, J. Papavassiliou, J. Vidal	
DERBIN 02B	JETPL 76 409	A.V. Derbin, O.Ju. Smirnov	

Translated from ZETFP 76 483.



# Lepton Particle Listings

## Number of Neutrino Types

much more dependent on the Standard Model, the approach described above is favored.

Before SLC and LEP, limits on the number of neutrino generations were placed by experiments at lower-energy  $e^+e^-$  colliders by measuring the cross section of the process  $e^+e^- \rightarrow \nu\bar{\nu}\gamma$ . The ASP, CELLO, MAC, MARK J, and VENUS experiments observed a total of 3.9 events above background [4], leading to a 95% CL limit of  $N_\nu < 4.8$ . This process has a much larger cross section at center-of-mass energies near the  $Z$  mass and has been measured at LEP by the ALEPH, DELPHI, L3, and OPAL experiments [5]. These experiments have observed several thousand such events, and the combined result is  $N_\nu = 3.00 \pm 0.08$ . The same process has also been measured by the LEP experiments at much higher center-of-mass energies, between 130 and 208 GeV, in searches for new physics [6]. Combined with the lower energy data, the result is  $N_\nu = 2.92 \pm 0.05$ .

Experiments at  $p\bar{p}$  colliders also placed limits on  $N_\nu$  by determining the total  $Z$  width from the observed ratio of  $W^\pm \rightarrow \ell^\pm\nu$  to  $Z \rightarrow \ell^+\ell^-$  events [7]. This involved a calculation that assumed Standard Model values for the total  $W$  width and the ratio of  $W$  and  $Z$  leptonic partial widths, and used an estimate of the ratio of  $Z$  to  $W$  production cross sections. Now that the  $Z$  width is very precisely known from the LEP experiments, the approach is now one of those used to determine the  $W$  width.

### References

1. ALEPH, DELPHI, L3, OPAL, and SLD Collaborations, and LEP Electroweak Working Group, and SLD Electroweak Group, and SLD Heavy Flavour Group, Phys. Reports **427**, 257 (2006).
2. P. Janot and S. Jadach, Phys. Lett. **B803**, 135319 (2020).
3. G. Voutsinas *et al.*, Phys. Lett. **B800**, 135068 (2020).
4. VENUS: K. Abe *et al.*, Phys. Lett. **B232**, 431 (1989); ASP: C. Hearty *et al.*, Phys. Rev. **D39**, 3207 (1989); CELLO: H.J. Behrend *et al.*, Phys. Lett. **B215**, 186 (1988); MAC: W.T. Ford *et al.*, Phys. Rev. **D33**, 3472 (1986); MARK J: H. Wu, Ph.D. Thesis, Univ. Hamburg (1986).
5. L3: M. Acciarri *et al.*, Phys. Lett. **B431**, 199 (1998); DELPHI: P. Abreu *et al.*, Z. Phys. **C74**, 577 (1997); OPAL: R. Akers *et al.*, Z. Phys. **C65**, 47 (1995); ALEPH: D. Buskulic *et al.*, Phys. Lett. **B313**, 520 (1993).
6. DELPHI: J. Abdallah *et al.*, Eur. Phys. J. **C38**, 395 (2005); L3: P. Achard *et al.*, Phys. Lett. **B587**, 16 (2004); ALEPH: A. Heister *et al.*, Eur. Phys. J. **C28**, 1 (2003); OPAL: G. Abbiendi *et al.*, Eur. Phys. J. **C18**, 253 (2000).
7. UA1: C. Albajar *et al.*, Phys. Lett. **B198**, 271 (1987); UA2: R. Ansari *et al.*, Phys. Lett. **B186**, 440 (1987).

### Number from $e^+e^-$ Colliders

#### Number of Light $\nu$ Types

VALUE	DOCUMENT ID	TECN
<b>2.9963 ± 0.0074</b>	1 JANOT 20	
2.9918 ± 0.0081	2 VOUTSINAS 20	
2.9840 ± 0.0082	3 LEP-SLC 06 RVUE	
3.00 ± 0.05	4 LEP 92 RVUE	

• • • We do not use the following data for averages, fits, limits, etc. • • •

<sup>1</sup> JANOT 20 applies a correction to LEP-SLC 06 using an updated Bhabha cross section calculation. This result also includes a correction to account for correlated luminosity bias as presented in VOUTSINAS 20.

<sup>2</sup> VOUTSINAS 20 applies a correction to LEP-SLC 06 to account for correlated luminosity bias.

<sup>3</sup> Combined fit from ALEPH, DELPHI, L3 and OPAL Experiments.

<sup>4</sup> Simultaneous fits to all measured cross section data from all four LEP experiments.

#### Number of Light $\nu$ Types from Direct Measurement of Invisible $Z$ Width

In the following, the invisible  $Z$  width is obtained from studies of single-photon events from the reaction  $e^+e^- \rightarrow \nu\bar{\nu}\gamma$ . All are obtained from LEP runs in the  $E_{cm}^{ee}$  range 88–209 GeV.

VALUE	DOCUMENT ID	TECN	COMMENT
<b>2.92 ± 0.05 OUR AVERAGE</b>	Error includes scale factor of 1.2.		
2.84 ± 0.10 ± 0.14	ABDALLAH 05B	DLPH	$\sqrt{s} = 180\text{--}209$ GeV
2.98 ± 0.05 ± 0.04	ACHARD 04E	L3	1990–2000 LEP runs
2.86 ± 0.09	HEISTER 03C	ALEP	$\sqrt{s} = 189\text{--}209$ GeV
2.69 ± 0.13 ± 0.11	ABBIENDI,G 00D	OPAL	1998 LEP run
2.89 ± 0.32 ± 0.19	ABREU 97J	DLPH	1993–1994 LEP runs
3.23 ± 0.16 ± 0.10	AKERS 95C	OPAL	1990–1992 LEP runs
2.68 ± 0.20 ± 0.20	BUSKULIC 93L	ALEP	1990–1991 LEP runs
• • • We do not use the following data for averages, fits, limits, etc. • • •			
2.84 ± 0.15 ± 0.14	ABREU 00Z	DLPH	1997–1998 LEP runs
3.01 ± 0.08	ACCIARRI 99R	L3	1991–1998 LEP runs
3.1 ± 0.6 ± 0.1	ADAM 96C	DLPH	$\sqrt{s} = 130, 136$ GeV

### Limits from Astrophysics and Cosmology

#### Effective Number of Light $\nu$ Types

"Light" means here with a mass  $<$  about 1 MeV. The quoted values correspond to  $N_{\text{eff}}$ , where  $N_{\text{eff}} = 3.045$  in the Standard Model with  $N_\nu = 3$ . See also reviews on "Big-Bang Nucleosynthesis" and "Neutrinos in Cosmology."

VALUE	CL%	DOCUMENT ID	TECN	COMMENT
• • • We do not use the following data for averages, fits, limits, etc. • • •				
2.3–3.2	95	1 VERDE 17	COSM	
2.88 ± 0.20	95	2 ROSSI 15	COSM	
3.3 ± 0.5	95	3 ADE 14	COSM	Planck
3.78 <sup>+0.31</sup> <sub>-0.30</sub>		4 COSTANZI 14	COSM	
3.29 ± 0.31		5 HOU 14	COSM	
$< 3.80$	95	6 LEISTEDT 14	COSM	
$< 4.10$	95	7 MORESCO 12	COSM	
$< 5.79$	95	8 XIA 12	COSM	
$< 4.08$	95	MANGANO 11	COSM	BBN
0.9–8.2		9 ICHIKAWA 07	COSM	
3–7	95	10 CIRELLI 06	COSM	
2.7–4.6	95	11 HANNESTAD 06	COSM	
3.6–7.4	95	10 SELJAK 06	COSM	
$< 4.4$		12 CYBURT 05	COSM	
$< 3.3$		13 BARGER 03C	COSM	
1.4–6.8		14 CROTTY 03	COSM	
1.9–6.6		14 PIERPAOLI 03	COSM	
2–4		LISI 99	COSM	BBN
$< 4.3$		OLIVE 99	COSM	BBN
$< 4.9$		COPI 97		Cosmology
$< 3.6$		HATA 97B		High D/H quasar abs.
$< 4.0$		OLIVE 97		BBN; high $^4\text{He}$ and $^7\text{Li}$
$< 4.7$		CARDALL 96B	COSM	High D/H quasar abs.
$< 3.9$		FIELDS 96	COSM	BBN; high $^4\text{He}$ and $^7\text{Li}$
$< 4.5$		KERNAN 96	COSM	High D/H quasar abs.
$< 3.6$		OLIVE 95		BBN; $\geq 3$ massless $\nu$
$< 3.3$		WALKER 91		Cosmology
$< 3.4$		OLIVE 90		Cosmology
$< 4$		YANG 84		Cosmology
$< 4$		YANG 79		Cosmology
$< 7$		STEIGMAN 77		Cosmology
$< 16$		PEEBLES 71		Cosmology
		15 SHVARTSMAN69		Cosmology
		HOYLE 64		Cosmology

<sup>1</sup> Uses Planck Data combined with an independent standard measure of distance to the sound horizon to set a limit on the total number of neutrinos. Only CMB and early-time information are used.

<sup>2</sup> ROSSI 15 sets limits on the number of neutrino types using BOSS Lyman alpha forest data combined with Planck CMB data and baryon acoustic oscillations.

<sup>3</sup> Fit to the number of neutrino degrees of freedom from Planck CMB data along with WMAP polarization, high L, and BAO data.

<sup>4</sup> Fit to the number of neutrinos degrees of freedom from Planck CMB data along with BAO, shear and cluster data.

<sup>5</sup> Fit based on the SPT-SZ survey combined with CMB, BAO, and  $H_0$  data.

<sup>6</sup> Constrains the number of neutrino degrees of freedom (marginalizing over the total mass) from CMB, CMB lensing, BAO, and galaxy clustering data.

<sup>7</sup> Limit on the number of light neutrino types from observational Hubble parameter data with seven-year WMAP data, SPT, and the most recent estimate of  $H_0$ . Best fit is  $3.45 \pm 0.65$ .

See key on page 999

# Lepton Particle Listings

## Number of Neutrino Types, Double- $\beta$ Decay

- <sup>8</sup> Limit on the number of light neutrino types from the CFHTLS combined with seven-year WMAP data and a prior on the Hubble parameter. Best fit is  $4.17^{+1.62}_{-1.26}$ . Limit is relaxed to  $3.98^{+2.02}_{-1.20}$  when small scales affected by non-linearities are removed.
- <sup>9</sup> Constrains the number of neutrino types from recent CMB and large scale structure data. No priors on other cosmological parameters are used.
- <sup>10</sup> Constrains the number of neutrino types from recent CMB, large scale structure, Lyman-alpha forest, and SN1a data. The slight preference for  $N_\nu > 3$  comes mostly from the Lyman-alpha forest data.
- <sup>11</sup> Constrains the number of neutrino types from recent CMB and large scale structure data. See also HAMANN 07.
- <sup>12</sup> Limit on the number of neutrino types based on <sup>4</sup>He and D/H abundance assuming a baryon density fixed to the WMAP data. Limit relaxes to 4.6 if D/H is not used or to 5.8 if only D/H and the CMB are used. See also CYBURT 01 and CYBURT 03.
- <sup>13</sup> Limit on the number of neutrino types based on combination of WMAP data and big-bang nucleosynthesis. The limit from WMAP data alone is 8.3. See also KNELLER 01.  $N_\nu \geq 3$  is assumed to compute the limit.
- <sup>14</sup> 95% confidence level range on the number of neutrino flavors from WMAP data combined with other CMB measurements, the 2dGRS data, and HST data.
- <sup>15</sup> SHVARTSMAN 69 limit inferred from his equations.

### Number Coupling with Less Than Full Weak Strength

VALUE	DOCUMENT ID	TECN
<20	1 OLIVE	81c COSM
<20	1 STEIGMAN	79 COSM

<sup>1</sup> Limit varies with strength of coupling. See also WALKER 91.

### REFERENCES FOR Limits on Number of Neutrino Types

JANOT	20	PL B803 135319	P. Janot, S. Jadach	(CERN, CRAC)
VOUTSINAS	20	PL B800 135068	G. Voutsinas <i>et al.</i>	(CERN, BOHR)
VERDE	17	JCAP 1704 023	L. Verde <i>et al.</i>	
ROSSI	15	PR D92 063505	G. Rossi <i>et al.</i>	
ADE	14	AA 571 A16	P.A.R. Ade <i>et al.</i>	(Planck Collab.)
COSTANZI	14	JCAP 1410 081	M. Costanzi <i>et al.</i>	(TRST, TRST1)
HOU	14	APJ 782 74	Z. Hou <i>et al.</i>	
LEISTEDT	14	PRL 113 041301	B. Leistedt, H.V. Peiris, L. Verde	
MORESCO	12	JCAP 1207 053	M. Moresco <i>et al.</i>	
XIA	12	JCAP 1206 010	J.-Q. Xia <i>et al.</i>	
MANGANO	11	PL B701 296	P. Mangano, P. Serpico	
HAMANN	07	JCAP 0708 021	J. Hamann <i>et al.</i>	
ICHIKAWA	07	JCAP 0705 007	K. Ichikawa, M. Kawasaki, F. Takahashi	
CIRELLI	06	JCAP 0612 013	M. Cirelli <i>et al.</i>	
HANNESTAD	06	JCAP 0611 016	S. Hannestad, G. Raffelt	
LEP-SLC	06	PRPL 427 257	ALEPH, DELPHI, L3, OPAL, SLD and working groups	
SELJAK	06	JCAP 0610 014	U. Seljak, A. Slosar, P. McDonald	
ABDALLAH	05B	EPJ C38 395	J. Abdallah <i>et al.</i>	(DELPHI Collab.)
CYBURT	05	ASP 23 313	R.H. Cyburt <i>et al.</i>	
ACHARD	04E	PL B587 16	P. Achard <i>et al.</i>	(L3 Collab.)
BARGER	03C	PL B566 8	V. Barger <i>et al.</i>	
CROTTY	03	PR D67 132005	P. Crotty, J. Lesgourgues, S. Pastor	
CYBURT	03	PL B567 227	R.H. Cyburt, B.D. Fields, K.A. Olive	
HEISTER	03C	EPJ C28 1	A. Heister <i>et al.</i>	(ALEPH Collab.)
PIERPAOLI	03	MNRAS 342 L63	E. Pierpaoli	
CYBURT	01	ASP 17 87	R.H. Cyburt, B.D. Fields, K.A. Olive	
KNELLER	01	PR D64 123506	J.P. Kneller <i>et al.</i>	
ABBIENDI.G	00D	EPJ C18 253	G. Abbiendi <i>et al.</i>	(OPAL Collab.)
ABREU	00Z	EPJ C17 53	P. Abreu <i>et al.</i>	(DELPHI Collab.)
ACCIARRI	99R	PL B470 268	M. Acciarri <i>et al.</i>	(L3 Collab.)
LISI	99	PR D59 123520	E. Lisi, S. Sarkar, F.L. Villante	
OLIVE	99	ASP 11 403	K.A. Olive, D. Thomas	
ABREU	97J	ZPHY C74 577	P. Abreu <i>et al.</i>	(DELPHI Collab.)
COP1	97	PR D55 3389	C.J. Copi, D.W. Schramm, M.S. Turner	(CHIC)
HATA	97B	PR D55 540	N. Hata <i>et al.</i>	(OSU, PENN)
OLIVE	97	ASP 7 27	K.A. Olive, D. Thomas	(MINN, FLOR)
ADAM	96C	PL B380 471	W. Adam <i>et al.</i>	(DELPHI Collab.)
CARDALL	96B	APJ 472 435	C.Y. Cardall, G.M. Fuller	(UCSD)
FIELDS	96	New Ast 1 77	B.D. Fields <i>et al.</i>	(NDAM, CERN, MINN+)
KERNAN	96	PR D54 3681	P.S. Kernan, S. Sarkar	(CASE, OXFTP)
AKERS	95C	ZPHY C65 47	R. Akers <i>et al.</i>	(OPAL Collab.)
OLIVE	95	PL B354 357	K.A. Olive, G. Steigman	(MINN, OSU)
BUSKULIC	93L	PL B313 520	D. Buskulic <i>et al.</i>	(ALEPH Collab.)
LEP	92	PL B276 247	LEP Collabs.	(LEP, ALEPH, DELPHI, L3, OPAL)
WALKER	91	APJ 376 51	T.P. Walker <i>et al.</i>	(HSCA, OSU, CHIC+)
OLIVE	90	PL B236 454	K.A. Olive <i>et al.</i>	(MINN, CHIC, OSU+)
YANG	84	APJ 281 493	J. Yang <i>et al.</i>	(CHIC, BART)
OLIVE	81C	NP B180 497	K.A. Olive, D.N. Schramm, G. Steigman	(EFI+)
STEIGMAN	79	PRL 43 239	G. Steigman, K.A. Olive, D.N. Schramm	(BART+)
YANG	79	APJ 227 697	J. Yang <i>et al.</i>	(CHIC, YALE, UVA)
STEIGMAN	77	PL 66B 202	G. Steigman, D.N. Schramm, J.E. Gunn	(YALE, CHIC+)
PEEBLES	71	Physical Cosmology	P.Z. Peebles	(PRIN)
SHVARTSMAN	69	Princeton Univ. Press (1971) JETPL 9 184	V.F. Shvartsman	(MOSU)
HOYLE	64	Translated from ZETFP 9 315. NAT 203 1108	F. Hoyle, R.J. Tayler	(CAMB)

## Double- $\beta$ Decay

OMITTED FROM SUMMARY TABLE

### NEUTRINOLESS DOUBLE- $\beta$ DECAY

Revised August 2019 by A. Piepke (University of Alabama) and P. Vogel (Caltech).

Observation of neutrinoless double-beta ( $0\nu\beta\beta$ ) decay would signal violation of total lepton number conservation. The process can be mediated by an exchange of a light Majorana neutrino, or by an exchange of other particles. However, the existence of  $0\nu\beta\beta$ -decay requires a nonvanishing Majorana neutrino mass, no matter what the actual mechanism is. As long as only a limit on the lifetime is available, limits on the effective Majorana neutrino mass, on the lepton-number violating right-handed current or other possible mechanisms mediating  $0\nu\beta\beta$  decay can be obtained, independently of the actual mechanism, by assuming that one of these “new physics” possibilities dominates. These limits are listed in the Double- $\beta$  Decay Listings of the experimental measurements.

In the following we assume that the exchange of light Majorana neutrinos ( $m_{\nu_i} \leq 10$  MeV) contributes dominantly to the decay rate. Besides a dependence on the phase space ( $G^{0\nu}$ ) and the nuclear matrix element ( $M^{0\nu}$ ), the observable  $0\nu\beta\beta$ -decay rate is proportional then to the square of the effective Majorana mass  $m_{ee}$ ,  $(T_{1/2}^{0\nu})^{-1} = G^{0\nu} \cdot |M^{0\nu}|^2 \cdot m_{ee}^2$ , with  $m_{ee}^2 = |\sum_i U_{ei}^2 m_{\nu_i}|^2$ . The sum contains, in general, complex CP-phases in  $U_{ei}^2$ , i.e., cancellations may occur. For three neutrino flavors there are two physical phases for Majorana neutrinos ( $\eta_1, \eta_2$ ) and one for Dirac neutrinos ( $\delta_{CP}$ ). The relevant Majorana phases affect only processes to which lepton-number changing amplitudes contribute. Given the general  $3 \times 3$  mixing matrix for Majorana neutrinos, one can construct other analogous lepton number violating quantities,  $m_{\ell\ell'} = \sum_i U_{ei} U_{\ell'i} m_{\nu_i}$  ( $\ell$  or  $\ell' \neq e$ ). However, these are currently much less constrained than  $m_{ee}$ .

Nuclear structure calculations are needed to deduce  $m_{ee}$  from the decay rate. While  $G^{0\nu}$  can be calculated accurately, the computation of  $M^{0\nu}$  is subject to uncertainty. Comparing different nuclear model evaluations indicates a factor  $\sim 2$ -3 spread in the calculated nuclear matrix elements. Nuclear structure calculation consistently overestimate Gamow-Teller (axial current) matrix elements. This inability of the nuclear models to reproduce Gamow-Teller decay rates is often parametrized in form of a modified coupling constant  $g_A$ . Many nuclear theorists interpret this shortcoming as evidence that important physics is missing in the modeling of weak nuclear transitions. It is not clear how these observed uncertainties impact  $0\nu\beta\beta$ -matrix elements. Nevertheless, this constitutes an additional element of uncertainty. Recent work, [1] shows how the discrepancy between experimental and theoretical axial current matrix elements might be resolved. However, application of this approach to the  $0\nu\beta\beta$  decay remains to be accomplished. The particle physics quantities to be determined are thus nuclear model-dependent, so the half-life measurements are listed first. Where possible, we reference the nuclear matrix elements used in the subsequent analysis. Since rates for the conventional  $2\nu\beta\beta$  decay serve to constrain the nuclear theory models, results for this process are also given.



# Lepton Particle Listings

## Double- $\beta$ Decay

Oscillation experiments utilizing atmospheric, accelerator, solar, and reactor produced neutrinos and anti-neutrinos show that at least some neutrinos are massive. However, so far the inverted mass ordering (i.e., whether  $\Delta m_{31}^2 < 0$ ) is disfavored only by 2-3  $\sigma$  compared to the normal mass ordering (when  $\Delta m_{31}^2 > 0$ ), while the absolute neutrino mass values or the properties of neutrinos under CPT-conjugation (Dirac or Majorana) remain undetermined. All confirmed oscillation experiments can be consistently described using three interacting neutrino species with two mass splittings and three mixing angles. (For values of the mixing angles and mass square differences see the corresponding tables.)

Based on the 3-neutrino analysis:

$m_{ee}^2 = |\cos^2 \theta_{13} \cos^2 \theta_{12} m_1 + e^{2i(\eta_2 - \eta_1)} \cos^2 \theta_{13} \sin^2 \theta_{12} m_2 + e^{-2i(\eta_1 + \delta_{CP})} \sin^2 \theta_{13} m_3|^2$ , valid for both mass orderings. Given the present knowledge of the neutrino oscillation parameters one can derive a relation between the effective Majorana mass and the mass of the lightest neutrino, as illustrated in Figure 14.11 in the Neutrino Masses, Mixing and Oscillations review. The three mass orderings allowed by the oscillation data: normal ( $m_1 < m_2 \ll m_3$ ), inverted ( $m_3 \ll m_1 < m_2$ ), and degenerate ( $m_1 \approx m_2 \approx m_3$ ), result in different projections. The width of the colored bands reflects the uncertainty introduced by the unknown Majorana and Dirac phases as well as the experimental errors of the oscillation parameters. The latter causes only minor broadening of the bands. Because of the overlap of the different mass scenarios, a measurement of  $m_{ee}$  would not reveal which mass ordering is applicable, provided the value of  $m_{ee}$  is in the overlapping range.

Analogous plots depict the relation of  $m_{ee}$  with the summed neutrino mass  $m_{tot} = m_1 + m_2 + m_3$ , constrained by observational cosmology, and  $m_{ee}$  as a function of the average mass  $m_{\nu_e}^{eff} = [\sum |U_{ei}|^2 m_{\nu_i}^2]^{1/2}$  determined through the analysis of the electron energy distribution in low energy beta decays. (See Fig. 1 of [2].) The oscillation data thus allow to test whether observed values of  $m_{ee}$  and  $m_{tot}$  or  $m_{\nu_e}^{eff}$  are consistent within the 3 neutrino framework. The rather large intrinsic width of the  $\beta\beta$ -decay constraints essentially does not allow to positively identify the mass ordering, and thus the sign of  $\Delta m_{31}^2$ , even in combination with these other observables. Naturally, if a value of  $0 < m_{ee} \leq 0.01$  eV is ever established, then the normal mass ordering becomes the only possible scenario.

It should be noted that systematic uncertainties of the nuclear matrix elements and possible quenching of the axial current matrix elements are sometimes not folded into the mass limits reported by  $\beta\beta$ -decay experiments. Taking this additional uncertainty into account would further widen the projections. The plots are based on a 3-neutrino analysis. If it turns out that additional, i.e. sterile light neutrinos exist, the allowed regions would be modified substantially.

If neutrinoless double-beta decay is observed, it will be possible to fix a range of absolute values of the masses  $m_{\nu_i}$ . Unlike the direct neutrino mass measurements, however, a limit

on  $m_{ee}$  does not allow one to constrain the individual mass values  $m_{\nu_i}$  even when the mass differences  $\Delta m_{ij}^2$  are known.

Neutrino oscillation data imply the existence of a lower limit  $\sim 0.014$  eV for the Majorana neutrino mass for the inverted mass ordering pattern, while  $m_{ee}$  could, by fine tuning, vanish in the case of the normal mass ordering. Several new double-beta searches have been proposed to probe the interesting  $m_{ee}$  mass range, with the prospect of full coverage of the inverted mass ordering region within the next decade.

The  $0\nu\beta\beta$  decay mechanism discussed so far is not the only way in which the decay can occur. Numerous other possible scenarios have been proposed, however, all of them requiring new physics. It will be a challenging task to decide which mechanism was responsible once  $0\nu\beta\beta$  decay is observed. LHC experiments may reveal corresponding signatures for new physics of lepton number violation. If lepton-number violating right-handed weak current interactions exist, its strength can be characterized by the phenomenological coupling constants  $\eta$  and  $\lambda$  ( $\eta$  describes the coupling between the right-handed lepton current and left-handed quark current while  $\lambda$  describes the coupling when both currents are right-handed). The  $0\nu\beta\beta$  decay rate then depends on  $\langle \eta \rangle = \eta \sum_i U_{ei} V_{ei}$  and  $\langle \lambda \rangle = \lambda \sum_i U_{ei} V_{ei}$  that vanish for massless or unmixed neutrinos ( $V_{ij}$  is a matrix analogous to  $U_{ij}$  but describing the mixing with the hypothetical right-handed neutrinos). The observation of the single electron spectra could, in principle, allow to distinguish this mechanism of  $0\nu\beta\beta$  from the light Majorana neutrino exchange driven mode. The limits on  $\langle \eta \rangle$  and  $\langle \lambda \rangle$  are listed in a separate table. The reader is cautioned that a number of earlier experiments did not distinguish between  $\eta$  and  $\lambda$ . In addition, see the section on Majoron searches for additional limits set by these experiments.

### References

1. P. Gysbers *et al.*, Nature Phys. **15**, 5 (2019); [arXiv:1903.00047].
2. M.J. Dolinski, A.W.P. Poon and W. Rodejohann, Ann. Rev. Nucl. Part. Sci. **49**, 219 (2019); [arXiv:1902.04097].

### Half-life $0\nu$ double- $\beta$ decay

In most cases the transitions  $(Z,A) \rightarrow (Z+2,A) + 2e^-$  to the  $0^+$  ground state of the final nucleus are listed. We also list transitions that decrease the nuclear charge ( $2e^+$ ,  $e^+$  CC and double EC) and transitions to an excited state of the final nucleus ( $0^+_i$ ,  $2^+$ , and  $2^+_i$ ). In the following Listings only the best or comparable limits for the half-lives of each transition are reported and only those with about  $T_{1/2} > 10^{23}$  years that are relevant for particle physics.

$T_{1/2}(10^{23} \text{ yr})$	CL% ISOTOPE	TRANSITION METHOD	DOCUMENT ID
• • •	We do not use the following data for averages, fits, limits, etc. • • •		
> 900	90 <sup>76</sup> Ge	GERDA	1 AGOSTINI 19
> 14	90 <sup>130</sup> Te	$g.s \rightarrow 0^+_1$ CUORE-0	2 ALDUINO 19
> 0.95	90 <sup>100</sup> Mo	AMoRE	3 ALENKOV 19
> 270	90 <sup>76</sup> Ge	MAJORANA	4 ALVIS 19
> 350	90 <sup>136</sup> Xe	EXO-200	5 ANTON 19
> 35	90 <sup>82</sup> Se	CUPID-0	6 AZZOLINI 19

> 2.4	90	<sup>136</sup> Xe	PANDAX-II	7	NI	19
> 190	90	<sup>76</sup> Ge	MAJORANA	8	AALSETH	18
> 800	90	<sup>76</sup> Ge	GERDA	9	AGOSTINI	18
> 180	90	<sup>136</sup> Xe	EXO-200	10	ALBERT	18
> 150	90	<sup>130</sup> Te	CUORE	11	ALDUINO	18
> 2.5	90	<sup>82</sup> Se	NEMO-3	12	ARNOLD	18
> 24	90	<sup>82</sup> Se	CUPID-0	13	AZZOLINI	18
> 0.81	90	<sup>82</sup> Se	g.s. → 0 <sub>1</sub> <sup>+</sup>	14	AZZOLINI	18A
> 2.2	90	<sup>116</sup> Cd	AURORA	15	BARABASH	18
> 530	90	<sup>76</sup> Ge	GERDA	16	AGOSTINI	17
> 1.1	90	<sup>134</sup> Xe	EXO-200	17	ALBERT	17C
> 1	90	<sup>116</sup> Cd	NEMO-3	18	ARNOLD	17
> 40	90	<sup>130</sup> Te	CUORE(CINO)	19	ALDUINO	16
> 260	90	<sup>136</sup> Xe	g.s. → 2 <sub>1</sub> <sup>+</sup>	20	ASAKURA	16
> 260	90	<sup>136</sup> Xe	g.s. → 2 <sub>2</sub> <sup>+</sup>	21	ASAKURA	16
> 240	90	<sup>136</sup> Xe	g.s. → 0 <sub>1</sub> <sup>+</sup>	22	ASAKURA	16
>1070	90	<sup>136</sup> Xe	KamLAND-Zen	23	GANDO	16
> 11	90	<sup>100</sup> Mo	NEMO-3	24	ARNOLD	15
> 110	90	<sup>136</sup> Xe	EXO-200	25	ALBERT	14B
> 9.4	90	<sup>130</sup> Te	0 <sup>+</sup> → 0 <sub>1</sub> <sup>+</sup>	26	ANDREOTTI	12
> 3.6	90	<sup>82</sup> Se	NEMO-3	27	BARABASH	11A
> 30	90	<sup>130</sup> Te	CUORICINO	28	ARNABOLDI	08
> 0.58	90	<sup>48</sup> Ca	CaF <sub>2</sub> scint.	29	UMEHARA	08
> 0.89	90	<sup>100</sup> Mo	0 <sup>+</sup> → 0 <sub>1</sub> <sup>+</sup>	30	ARNOLD	07
> 1.6	90	<sup>100</sup> Mo	0 <sup>+</sup> → 2 <sub>1</sub> <sup>+</sup>	31	ARNOLD	07
> 1	90	<sup>82</sup> Se	NEMO-3	32	ARNOLD	05A
> 1.1	90	<sup>128</sup> Te	Cryog. det.	33	ARNABOLDI	03
> 1.7	90	<sup>116</sup> Cd	<sup>116</sup> CdWO <sub>4</sub> scint.	34	DANEVICH	03
> 157	90	<sup>76</sup> Ge	Enriched HPGe	35	AALSETH	02B
> 190	90	<sup>76</sup> Ge	Enriched HPGe	36	KLAPDOR-K...	01

- AGOSTINI 19 use 82.4 kg-yr of data, collected by the GERDA experiment, to search for the 0ν ββ decay of <sup>76</sup>Ge. High resolution Ge-calorimeters, made from isotopically enriched Ge, are used. A median sensitivity of 1.1 × 10<sup>26</sup> yr is reported. Supersedes AGOSTINI 18.
- ALDUINO 19 use the combined data of the CUORICINO and CUORE-0 experiments to place a lower limit on the half life of the 0ν ββ decay of <sup>130</sup>Te to the first excited 0<sup>+</sup> state of <sup>130</sup>Xe. Supersedes ANDREOTTI 12.
- ALENKOV 19 report the 0ν ββ decay half-life limit based on the 52.1 kg-d exposure of <sup>100</sup>Mo, of a cryogenic dual heat and light detector in the Yangyang underground laboratory. The median sensitivity is 1.1 × 10<sup>23</sup> years.
- ALVIS 19 use the MAJORANA Demonstrator with enriched in <sup>76</sup>Ge detectors to set this limit on 0ν ββ half-life of <sup>76</sup>Ge. The exposure is 26.0 kg yr. The sensitivity is 4.8 × 10<sup>25</sup> yr.
- ANTON 19 uses the complete dataset of the EXO-200 detector to search for the 0ν ββ decay. The exposure is 234.1 kg yr. The median sensitivity is 5.0 × 10<sup>25</sup> yr. Supersedes ALBERT 18 and ALBERT 14B.
- AZZOLINI 19 use the CPID-0 scintillating cryogenic bolometer to set this limit on 0ν ββ half-life of <sup>82</sup>Se. The exposure is 5.29 kg yr. The sensitivity is 5 × 10<sup>24</sup> yr.
- NI 19 use the PandaX-II dual phase TPC at CJPL to search for the 0ν ββ decay of <sup>136</sup>Xe. The half-life limit 2.4 × 10<sup>23</sup> yr is obtained from 22.2 kg yr exposure with a sensitivity of 1.9 × 10<sup>23</sup> yr.
- AALSETH 18 uses the MAJORANA Demonstrator to search for the 0ν ββ decay. The exposure is 9.95 kg-year. The median sensitivity is 2.1 × 10<sup>25</sup> yr.
- AGOSTINI 18 uses the GERDA detector to search for the 0ν ββ decay. The exposure is 46.7 kg-year. The median sensitivity is 5.8 × 10<sup>25</sup> yr. Supersedes AGOSTINI 17.
- ALBERT 18 uses the EXO-200 detector to search for the 0ν ββ decay. The exposure is 177.6 kg-year. The median sensitivity is 3.7 × 10<sup>25</sup> years.
- ALDUINO 18 uses the CUORE detector to search for the 0ν ββ decay of <sup>130</sup>Te. The exposure is 86.3 kg-year of natural TeO<sub>2</sub> corresponding to 24.0 kg-year for <sup>130</sup>Te. The median sensitivity is 0.7 × 10<sup>25</sup> yr. The limit is obtained combining the new data from CUORE with those of CUORE0 (9.8 kg-year of <sup>130</sup>Te) and Cuoricino (19.8 kg-year of <sup>130</sup>Te).
- ARNOLD 18 use the NEMO-3 tracking detector to place a limit on the 0ν ββ decay of <sup>82</sup>Se. This is a slightly weaker limit than in BARABASH 11A, using the same detector. Supersedes ARNOLD 05A.
- AZZOLINI 18 uses CUPID-0 detector, a novel scintillating cryogenic calorimeter, operated in the LNGS. This results replaces BARABASH 11A (NEMO-3) as the most stringent limit on the 0ν ββ-decay of <sup>82</sup>Se.
- AZZOLINI 18A data collected by CUPID-0 based on scintillating bolometers is used to derive a new most stringent limit on the 0ν ββ-decay of <sup>82</sup>Se to the 0<sub>1</sub><sup>+</sup> state of <sup>82</sup>Kr.
- BARABASH 18 use 1.162 kg of <sup>116</sup>CdWO<sub>4</sub> scintillating crystals to obtain this limit. Supersedes DANEVICH 03 with analogous source and is more sensitive than ARNOLD 17.
- AGOSTINI 17 result corresponds to data collected with GERDA phase 1 and first release of phase 2 for a total of 343 mol-yr exposure. Supersedes AGOSTINI 13A. The median sensitivity is 4.0 10<sup>25</sup> yr.
- ALBERT 17C uses the EXO-200 detector that contains 19.098 ± 0.014% admixture of <sup>134</sup>Xe to search for the 0ν and 2ν ββ decay modes. The exposure is 29.6 kg-year. The median sensitivity is 1.9 × 10<sup>21</sup> years.
- ARNOLD 17 use the NEMO-3 tracking calorimeter, containing 410 g of enriched <sup>116</sup>Cd exposed for 5.26 yr, to determine the half-life limit. Supersedes BARABASH 11A.

- ALDUINO 16 report result obtained with 9.8 kg y of data collected with the CUORE-0 bolometer, combined with data from the CUORICINO. Supersedes ALFONSO 15.
- ASAKURA 16 use the KamLAND-Zen liquid scintillator calorimeter (<sup>136</sup>Xe 89.5 kg yr) to place a limit on the 0ν ββ-decay into the first excited state of the daughter nuclide.
- ASAKURA 16 use the KamLAND-Zen liquid scintillator calorimeter (<sup>136</sup>Xe 89.5 kg yr) to place a limit on the 0ν ββ-decay into the second excited state of the daughter nuclide.
- ASAKURA 16 use the KamLAND-Zen liquid scintillator calorimeter (<sup>136</sup>Xe 89.5 kg yr) to place a limit on the 0ν ββ-decay into the third excited state of the daughter nuclide.
- GANDO 16 use the KamLAND detector to search for the 0ν decay of <sup>136</sup>Xe. With a significant background reduction, the combination of results of the first (270.7 days) and the second phase (263.8 days) of the experiment leads to about six fold improvement over the previous limit. Supersedes GANDO 13A. The sensitivity is 5.6 10<sup>25</sup> yr.
- ARNOLD 15 use the NEMO-3 tracking calorimeter with 34.3 kg yr exposure to determine the limit of 0ν ββ-half life of <sup>100</sup>Mo. Supersedes ARNOLD 2005A and BARABASH 11A.
- ALBERT 14B use 100 kg yr of exposure of the EXO-200 tracking calorimeter to place a lower limit on the 0ν ββ-half life of <sup>136</sup>Xe. Supersedes AUGER 12.
- ANDREOTTI 12 use high resolution TeO<sub>2</sub> bolometric calorimeter to search for the 0ν ββ decay of <sup>130</sup>Te leading to the excited 0<sub>1</sub><sup>+</sup> state at 1793.5 keV.
- BARABASH 11A use the NEMO-3 detector to measure 2ν ββ rates and place limits on 0ν ββ half lives for various nuclides. Supersedes ARNOLD 05A, ARNOLD 04, ARNOLD 98, and ELLIOTT 92.
- Supersedes ARNABOLDI 04. Bolometric TeO<sub>2</sub> detector array CUORICINO is used for high resolution search for 0ν ββ decay. The half-life limit is derived from 3.09 kg yr <sup>130</sup>Te exposure.
- UMEHARA 08 use CaF<sub>2</sub> scintillation calorimeter to search for double beta decay of <sup>48</sup>Ca. Limit is significantly more stringent than quoted sensitivity: 18 × 10<sup>21</sup> years.
- Limit on 0ν-decay to the first excited 0<sub>1</sub><sup>+</sup>-state of daughter nucleus using NEMO-3 tracking calorimeter. Supersedes DASSIE 95.
- Limit on 0ν-decay to the first excited 2<sup>+</sup>-state of daughter nucleus using NEMO-3 tracking calorimeter.
- NEMO-3 tracking calorimeter is used in ARNOLD 05A to place limit on 0ν ββ half-life of <sup>82</sup>Se. Detector contains 0.93 kg of enriched <sup>82</sup>Se. Supersedes ARNOLD 04.
- Supersedes ALESSANDRELLO 00. Array of TeO<sub>2</sub> crystals in high resolution cryogenic calorimeter. Some enriched in <sup>128</sup>Te. Ground state to ground state decay.
- Limit on 0ν ββ decay of <sup>116</sup>Cd using enriched CdWO<sub>4</sub> scintillators. Supersedes DANEVICH 00.
- AALSETH 02b limit is based on 117 mol-yr of data using enriched Ge detectors. Background reduction by means of pulse shape analysis is applied to part of the data set. Reported limit is slightly less restrictive than that in KLAPDOR-KLEINGROTHAUS 01 However, it excludes part of the allowed half-life range reported in KLAPDOR-KLEINGROTHAUS 01B for the same nuclide. The analysis has been criticized in KLAPDOR-KLEINGROTHAUS 04B. The criticism was addressed and disputed in AALSETH 04.
- KLAPDOR-KLEINGROTHAUS 01 is a continuation of the work published in BAUDIS 99. Isotopically enriched Ge detectors are used in calorimetric measurement. The most stringent bound is derived from the data set in which pulse-shape analysis has been used to reduce background. Exposure time is 35.5 kg y. Supersedes BAUDIS 99 as most stringent result.

Half-life measurements of the two-neutrino double-β decay

The measured half-life values for the transitions (Z,A) → (Z+2,A) + 2e<sup>-</sup> + 2ν̄<sub>e</sub> to the 0<sup>+</sup> ground state of the final nucleus are listed. We also list the transitions to an excited state of the final nucleus (0<sub>i</sub><sup>+</sup>, etc.). We report only the measurements with the smallest (or comparable) uncertainty for each transition.

t <sub>1/2</sub> (10 <sup>21</sup> yr)	ISOTOPE	TRANSITION	METHOD	DOCUMENT ID
• • •	We do not use the following data for averages, fits, limits, etc. • • •			
18 ± 5 ± 1	<sup>124</sup> Xe	2νDEC	XENON1T	1 APRILE 19E
0.00680 ± 0.00001 ± 0.00038	<sup>100</sup> Mo		NEMO-3	2 ARNOLD 19
0.0939 ± 0.0017 ± 0.0058	<sup>82</sup> Se		NEMO-3	3 ARNOLD 18
0.0263 ± 0.0011 ± 0.0012	<sup>116</sup> Cd		AURORA	4 BARABASH 18
> 0.87	<sup>134</sup> Xe		EXO-200	5 ALBERT 17C
0.82 ± 0.02 ± 0.06	<sup>130</sup> Te		CUORE-0	6 ALDUINO 17
0.00690 ± 0.00015 ± 0.00037	<sup>100</sup> Mo		CUPID	7 ARMENGAUD 17
0.0274 ± 0.0004 ± 0.0018	<sup>116</sup> Cd		NEMO-3	8 ARNOLD 17
0.064 ± 0.007 ± 0.012 ± 0.009	<sup>48</sup> Ca		NEMO-3	9 ARNOLD 16
0.00934 ± 0.00022 ± 0.00062	<sup>150</sup> Nd		NEMO-3	10 ARNOLD 16A
1.926 ± 0.094	<sup>76</sup> Ge		GERDA	11 AGOSTINI 15A
0.00693 ± 0.00004	<sup>100</sup> Mo		NEMO-3	12 ARNOLD 15
2.165 ± 0.016 ± 0.059	<sup>136</sup> Xe		EXO-200	13 ALBERT 14
9.2 ± 5.5 ± 1.3	<sup>78</sup> Kr		BAKSAN	14 GAVRILYAK 13
2.38 ± 0.02 ± 0.14	<sup>136</sup> Xe		KamLAND-Zen	15 GANDO 12A
0.7 ± 0.09 ± 0.11	<sup>130</sup> Te		NEMO-3	16 ARNOLD 11
0.0235 ± 0.0014 ± 0.0016	<sup>96</sup> Zr		NEMO-3	17 ARGYRADES 10
0.69 ± 0.10 ± 0.08	<sup>100</sup> Mo	0 <sup>+</sup> → 0 <sub>1</sub> <sup>+</sup>	Ge coinc.	18 BELLI 10
0.57 ± 0.13 ± 0.09	<sup>100</sup> Mo	0 <sup>+</sup> → 0 <sub>1</sub> <sup>+</sup>	NEMO-3	19 ARNOLD 07

## Lepton Particle Listings

Double- $\beta$  Decay

VALUE (eV)	ISOTOPE	METHOD	DOCUMENT ID
0.096 $\pm$ 0.003 $\pm$ 0.010	$^{82}\text{Se}$	NEMO-3	<sup>20</sup> ARNOLD 05A
0.029 $\pm$ 0.004 $\pm$ 0.003	$^{116}\text{Cd}$	$^{116}\text{CdWO}_4$ scint.	<sup>21</sup> DANEVICH 03
< 0.311–0.638	$^{82}\text{Se}$	CUPID-0	<sup>5</sup> AZZOLINI 19
< 1.3–3.5	$^{136}\text{Xe}$	PANDAX-II	<sup>6</sup> NI 19
< 0.24–0.52	$^{76}\text{Ge}$	MAJORANA Dem	<sup>7</sup> AALSETH 18
< 0.12–0.26	$^{76}\text{Ge}$	GERDA	<sup>8</sup> AGOSTINI 18
< 0.15–0.40	$^{136}\text{Xe}$	EXO-200	<sup>9</sup> ALBERT 18
< 0.11–0.52	$^{130}\text{Te}$	CUORE	<sup>10</sup> ALDUINO 18
< 1.2–3.0	$^{82}\text{Se}$	NEMO-3	<sup>11</sup> ARNOLD 18
< 0.376–0.770	$^{82}\text{Se}$	CUPID-0	<sup>12</sup> AZZOLINI 18
< 1.0–1.7	$^{116}\text{Cd}$	AURORA	<sup>13</sup> BARABASH 18
< 0.15–0.33	$^{76}\text{Ge}$	GERDA	<sup>14</sup> AGOSTINI 17
< 1.4–2.5	$^{116}\text{Cd}$	NEMO-3	<sup>15</sup> ARNOLD 17
< 0.27–0.76	$^{130}\text{Te}$	CUORE(CINO)	<sup>16</sup> ALDUINO 16
< 1.6–5.3	$^{150}\text{Nd}$	NEMO-3	<sup>17</sup> ARNOLD 16A
< 0.061–0.165	$^{136}\text{Xe}$	KamLAND-Zen	<sup>18</sup> GANDO 16
< 0.33–0.62	$^{100}\text{Mo}$	NEMO-3	<sup>19</sup> ARNOLD 15
< 0.19–0.45	$^{136}\text{Xe}$	EXO-200	<sup>20</sup> ALBERT 14B
< 0.89–2.43	$^{82}\text{Se}$	NEMO-3	<sup>21</sup> BARABASH 11A
< 7.2–19.5	$^{96}\text{Zr}$	NEMO-3	<sup>22</sup> ARGYRIADES 10
< 3.5–2.2	$^{48}\text{Ca}$	$\text{CaF}_2$ scint.	<sup>23</sup> UMEHARA 08
< 0.2–1.1	$^{130}\text{Te}$	Cryog. det.	<sup>24</sup> ARNABOLDI 05
< 0.37–1.9	$^{130}\text{Te}$	Cryog. det.	<sup>25</sup> ARNABOLDI 04
< 1.5–1.7	$^{116}\text{Cd}$	$^{116}\text{CdWO}_4$ scint.	<sup>26</sup> DANEVICH 03
< 0.350	$^{76}\text{Ge}$	Enriched HPGc	<sup>27</sup> KLAPDOR-K...01
< 8.3	$^{48}\text{Ca}$	$\text{CaF}_2$ scint.	YOU 91
<sup>1</sup> APRILE 19e report first measurement of two-neutrino double electron capture in $^{124}\text{Xe}$ using the XENON1T detector with a 0.73 t-yr exposure. An excess of $126 \pm 29$ events is observed at $64.3 \pm 0.6$ keV decay energy, corresponding to $\sqrt{\Delta\chi^2} = 4.4$ with respect to the background-only hypothesis.			
<sup>2</sup> ARNOLD 19 use the NEMO-3 tracking calorimeter with 34.3 kg y exposure to determine the $2\nu\beta\beta$ half-life of $^{100}\text{Mo}$ . Supersedes ARNOLD 15.			
<sup>3</sup> ARNOLD 18 use the NEMO-3 tracking detector to determine the $2\nu\beta\beta$ half-life of $^{82}\text{Se}$ . 0.93 kg of $^{82}\text{Se}$ was observed for 5.25 y. The half-life value was obtained based on the single-state-dominance (SSD) hypothesis, preferred in this case by about $2\sigma$ . Supersedes ARNOLD 05A.			
<sup>4</sup> BARABASH 18 use 1.162 kg of $^{116}\text{CdWO}_4$ scintillating crystals to obtain this value. Supersedes DANEVICH 03 with an analogous source and agrees with ARNOLD 17 with the NEMO-3 detector.			
<sup>5</sup> ALBERT 17c uses the EXO-200 detector that contains $19.098 \pm 0.014\%$ admixture of $^{134}\text{Xe}$ to search for the $2\nu\beta\beta$ decay mode. The exposure is 29.6 kg-year. The median sensitivity is $1.2 \times 10^{21}$ years.			
<sup>6</sup> ALDUINO 17 use the CUORE-0 detector containing 10.8 kg of $^{130}\text{Te}$ in 52 crystals of $\text{TeO}_2$ . The exposure was 9.3 kg yr of $^{130}\text{Te}$ . This is a more accurate rate determination than in ARNOLD 11 and BARABASH 11A.			
<sup>7</sup> ARMENGAUD 17 use 185.9 $\pm$ 0.1 g crystal of $\text{Li}_2^{100}\text{MoO}_4$ to determine the $^{100}\text{Mo}$ $2\nu\beta\beta$ half-life. The exposure was of 1303 $\pm$ 26 hours only, using novel technique.			
<sup>8</sup> ARNOLD 17 use the NEMO-3 tracking calorimeter, containing 410 grams of enriched $^{116}\text{Cd}$ exposed for 5.26 years, to determine the half-life value.			
<sup>9</sup> ARNOLD 16 use the NEMO-3 detector and a source of 6.99 g of $^{48}\text{Ca}$ . The half-life is based on 36.7 g year exposure. It is consistent, although somewhat longer, than the previous determinations of the half-life. Supersedes BARABASH 11A.			
<sup>10</sup> ARNOLD 16A use the NEMO-3 tracking calorimeter, containing 36.6 g of $^{150}\text{Nd}$ exposed for 1918.5 days, to determine the half-life. Supersedes ARGYRIADES 09.			
<sup>11</sup> AGOSTINI 15A use 17.9 kg yr exposure of the GERDA calorimeter to derive an improved measurement of the $2\nu\beta\beta$ decay half life of $^{76}\text{Ge}$ .			
<sup>12</sup> ARNOLD 15 use the NEMO-3 tracking calorimeter with 34.3 kg yr exposure to determine the $2\nu\beta\beta$ -half life of $^{100}\text{Mo}$ . Supersedes ARNOLD 05A and ARNOLD 04.			
<sup>13</sup> ALBERT 14 use the EXO-200 tracking detector for a re-measurement of the $2\nu\beta\beta$ -half life of $^{136}\text{Xe}$ . A nuclear matrix element of $0.0218 \pm 0.0003 \text{ MeV}^{-1}$ is derived from this data. Supersedes ACKERMAN 11.			
<sup>14</sup> GAVRILYAK 13 use a proportional counter filled with Kr gas to search for the $2\nu 2K$ decay of $^{78}\text{Kr}$ . Data with the enriched and depleted Kr were used to determine signal and background. A $2.5\sigma$ excess of events obtained with the enriched sample is interpreted as an indication for the presence of this decay.			
<sup>15</sup> GANDO 12A use a modification of the existing KamLAND detector. The $\beta\beta$ decay source/detector is 13 tons of enriched $^{136}\text{Xe}$ -loaded scintillator contained in an inner balloon. The $2\nu\beta\beta$ decay rate is derived from the fit to the spectrum between 0.5 and 4.8 MeV. This result is in agreement with ACKERMAN 11.			
<sup>16</sup> ARNOLD 11 use enriched $^{130}\text{Te}$ in the NEMO-3 detector to measure the $2\nu\beta\beta$ decay rate. This result is in agreement with, but more accurate than ARNABOLDI 03.			
<sup>17</sup> ARGYRIADES 10 use $9.4 \pm 0.2$ g of $^{96}\text{Zr}$ in NEMO-3 detector and identify its $2\nu\beta\beta$ decay. The result is in agreement and supersedes ARNOLD 99.			
<sup>18</sup> BELLI 10 use enriched $^{100}\text{Mo}$ with 4 HP Ge detectors to record the 590.8 and 539.5 keV $\gamma$ rays from the decay of the $0_1^+$ state in $^{100}\text{Ru}$ both in singles and coincidences. This result confirms the measurement of KIDD 09 and ARNOLD 07 and supersedes them.			
<sup>19</sup> First exclusive measurement of $2\nu$ -decay to the first excited $0_1^+$ -state of daughter nucleus. ARNOLD 07 use the NEMO-3 tracking calorimeter to detect all particles emitted in decay. Result agrees with the inclusive $(0\nu + 2\nu)$ measurement of DEBRAECKELEER 01.			
<sup>20</sup> ARNOLD 05A use the NEMO-3 tracking detector to determine the $2\nu\beta\beta$ half-life of $^{82}\text{Se}$ with high statistics and low background (389 days of data taking). Supersedes ARNOLD 04.			
<sup>21</sup> Calorimetric measurement of $2\nu\beta\beta$ ground state decay of $^{116}\text{Cd}$ using enriched $\text{CdWO}_4$ scintillators. Agrees with EJIRI 95 and ARNOLD 96. Supersedes DANEVICH 00.			

### $\langle m_{ee} \rangle$ , The Effective Weighted Sum of Majorana Neutrino Masses Contributing to Neutrinoless Double- $\beta$ Decay

$\langle m_{ee} \rangle = |\sum U_{ei}^2 m_{\nu_i}|$ ,  $i = 1, 2, 3$ . It is assumed that  $\nu_i$  are Majorana particles and that the transition is dominated by the known (light) neutrinos. Note that  $U_{ei}^2$  and not  $|U_{ei}|^2$  occur in the sum, and that consequently cancellations are possible. The experiments obtain the limits on  $\langle m_{\nu} \rangle$  from the measured ones on  $T_{1/2}$  using a range of nuclear matrix elements (NME), which is reflected in the spread of  $\langle m_{\nu} \rangle$ . Different experiments may choose different NME. All assume  $g_A = 1.27$ . In the following Listings, only the best or comparable limits for each isotope are reported. When not mentioned explicitly the transition is between ground states, but transitions between excited states are also reported.

VALUE (eV)	ISOTOPE	METHOD	DOCUMENT ID
< 0.07–0.16	$^{76}\text{Ge}$	GERDA	<sup>1</sup> AGOSTINI 19
< 1.2–2.1	$^{100}\text{Mo}$	AMoRE	<sup>2</sup> ALENKOV 19
< 0.200–0.433	$^{76}\text{Ge}$	MAJORANA	<sup>3</sup> ALVIS 19
< 0.093–0.286	$^{136}\text{Xe}$	EXO-200	<sup>4</sup> ANTON 19

• • • We do not use the following data for averages, fits, limits, etc. • • •

- AGOSTINI 19 use 82.4 kg-yr of data collected by the isotopically enriched  $^{76}\text{Ge}$  detectors of the GERDA experiment to derive an upper limit for  $\langle m_{\beta\beta} \rangle$ . The range reflects the variability of the theoretically calculated nuclear matrix elements. Supersedes AGOSTINI 18.
- ALENKOV 19 report the range of the effective masses  $\langle m_{\beta\beta} \rangle$  corresponding to the  $0\nu\beta\beta$  decay half-life limit. It is based on the 52.1 kg-d exposure of  $^{100}\text{Mo}$ , in the Yangyang underground laboratory. The median sensitivity is  $1.1 \times 10^{23}$  years. The range of  $\langle m_{\beta\beta} \rangle$  reflects the uncertainty of nuclear matrix elements.
- ALVIS 19 use the MAJORANA Demonstrator with enriched in  $^{76}\text{Ge}$  detectors to set this limit. The exposure is 26.0 kg yr. The sensitivity is  $4.8 \times 10^{25}$  yr.
- ANTON 19 uses the complete dataset of the EXO-200 experiment to obtain these limits. The spread reflect the uncertainty in the nuclear matrix elements. Supersedes ALBERT 18 and ALBERT 14b.
- AZZOLINI 19 use the CPID-0 scintillating cryogenic bolometer to set this limit. The exposure is 5.29 kg yr. The sensitivity is  $5 \times 10^{24}$  yr.
- NI 19 use the PandaX-II dual phase TPC at CJPL to search for the  $0\nu\beta\beta$  decay of  $^{136}\text{Xe}$  with 22.2 kg yr exposure. The range in the  $m_{\beta\beta}$  limit of 1.3–3.5 eV reflects the range of the calculated nuclear matrix elements. The sensitivity is  $1.9 \times 10^{23}$  yr.
- AALSETH 18 uses the MAJORANA Demonstrator detector to establish this limit.
- AGOSTINI 18 uses the GERDA detector to establish this limit.
- ALBERT 18 uses the EXO-200 experiment to obtain this limit.
- ALDUINO 18 use the combined data of CUORE, CUORE0, and Cuoricino to obtain this limit.
- ARNOLD 18 use the NEMO-3 tracking detector to constrain the  $0\nu\beta\beta$  decay of  $^{82}\text{Se}$ . The limit on  $\langle m_{\beta\beta} \rangle$  is obtained assuming light neutrino exchange; the range reflects different calculations of the nuclear matrix elements. This is a somewhat weaker limit than in BARABASH 11A using the same detector.
- AZZOLINI 18 uses data collected by the CUPID-0 scintillating cryogenic calorimeter, operated in the LNGS, to derive a range of limits on  $\langle m_{\nu} \rangle$ . The reported range reflects the spread of the nuclear matrix element calculations considered in this work. Use  $g_A = 1.269$ .
- BARABASH 18 use 1.162 kg of  $^{116}\text{CdWO}_4$  scintillating crystals to obtain these limits. The spread reflects the estimated uncertainty in the nuclear matrix element. Supersedes DANEVICH 03.
- AGOSTINI 17 is based on 343 mol yr of data from GERDA phase 1 and phase 2 first part and the corresponding limit on  $T_{1/2}$  using the different nuclear matrix elements mentioned by the authors. Supersedes AGOSTINI 13A.
- ARNOLD 17 utilize NEMO-3 data, taken with enriched  $^{116}\text{Cd}$  to limit the effective Majorana neutrino mass. The reported range results from the use of different nuclear matrix elements. Supersedes BARABASH 11A.
- ALDUINO 16 place a limit on the effective Majorana neutrino mass using the combined data of the CUORE-0 and CUORICINO experiments. The range reflects the authors' evaluation of the variability of the nuclear matrix elements. Supersedes ALFONSO 15.
- ARNOLD 16A limit is derived from data taken with the NEMO-3 detector and  $^{150}\text{Nd}$ . A range of nuclear matrix elements that include the effect of nuclear deformation have been used. Supersedes ARGYRIADES 09.
- GANDO 16 result is based on the 2016 KamLAND-Zen half-life limit. The stated range reflects different nuclear matrix elements, an unquenched  $g_A = 1.27$  is used. Supersedes GANDO 13A.
- ARNOLD 15 use the NEMO-3 tracking calorimeter with 34.3 kg yr exposure to determine the neutrino mass limit based on the  $0\nu\beta\beta$ -half life of  $^{100}\text{Mo}$ . The spread range reflects different nuclear matrix elements. Supersedes ARNOLD 14 and BARABASH 11A.
- ALBERT 14b is based on 100 kg yr of exposure of the EXO-200 tracking calorimeter. The mass range reflects the nuclear matrix element calculations. Supersedes AUGER 12.
- BARABASH 11A limit is based on NEMO-3 data for  $^{82}\text{Se}$ . The reported range reflects different nuclear matrix elements. Supersedes ARNOLD 05A and ARNOLD 04.
- ARGYRIADES 10 use  $^{96}\text{Zr}$  and the NEMO-3 tracking detector to obtain the reported mass limit. The range reflects the fluctuation of the nuclear matrix elements considered.

See key on page 999

Lepton Particle Listings
Double-β Decay, Neutrino Mixing

- 23 Limit was obtained using CaF2 scintillation calorimeter to search for double beta decay of 48Ca. Reported range of limits reflects spread of QRPA and SM matrix element calculations used. Supersedes OGAWA 04.
24 Supersedes ARNABOLDI 04. Reported range of limits due to use of different nuclear matrix element calculations.
25 Supersedes ARNABOLDI 03. Reported range of limits due to use of different nuclear matrix element calculations.
26 Limit for <math>\langle m\_{\nu} \rangle</math> is based on the nuclear matrix elements of STAUDT 90 and ARNOLD 96. Supersedes DANEVICH 00.
27 KLAPDOR-KLEINGROTHAUS 01 uses the calculation by STAUDT 90. Using several other models in the literature could worsen the limit up to 1.2eV. This is the most stringent experimental bound on <math>m\_{\nu}</math>. It supersedes BAUDIS 99B.

Limits on Lepton-Number Violating (V+A) Current Admixture

For reasons given in the discussion at the beginning of this section, we list only results from 1989 and later. <math>\langle \lambda \rangle = \lambda \sum U\_{ej} V\_{ej}</math> and <math>\langle \eta \rangle = \eta \sum U\_{ej} V\_{ej}</math>, where the sum is over the number of neutrino generations. This sum vanishes for massless or unmixed neutrinos. In the following Listings, only best or comparable limits or lifetimes for each isotope are reported.

Table with columns: <math>\langle \lambda \rangle (10^{-6})</math>, CL%, <math>\langle \eta \rangle (10^{-8})</math>, CL%, ISOTOPE, METHOD, DOCUMENT ID. Contains data for various isotopes like 82Se, 116Cd, 100Mo, 76Ge, 130Te, 116CdWO4, 100Mo, 76Ge, 136Xe, 128Te.

- 1 ARNOLD 18 use the NEMO03 tracking detector, with 0.93 kg of 82Se mass and 5.25 y exposure to obtain the limits for the hypothetical right-handed currents. Supersedes ARNOLD 05A.
2 BARABASH 18 use 1.162 kg of 116CdWO4 scintillating crystals to obtain this limits for the hypothetical right-handed currents in the 0νββ decay of 116Cd.
3 ARNOLD 14 is based on 34.7 kg yr of exposure of the NEMO-3 tracking calorimeter. The reported range limit on <math>\langle \lambda \rangle</math> and <math>\langle \eta \rangle</math> reflects the nuclear matrix element uncertainty in 100Mo.
4 ARNOLD 07 use NEMO-3 half life limit for 0ν-decay of 100Mo to the first excited 2+ state of daughter nucleus to limit the right-right handed admixture of weak currents <math>\langle \lambda \rangle</math>. This limit is not competitive when compared to the decay to the ground state.
5 Re-analysis of data originally published in KLAPDOR-KLEINGROTHAUS 04A. Modified pulse shape analysis leads the authors to claim 6σ statistical evidence for observation of 0ν-decay. Authors use matrix element of MUTO 89 to determine <math>\langle \lambda \rangle</math> and <math>\langle \eta \rangle</math>. Uncertainty of nuclear matrix element is not reflected in stated errors.
6 ARNOLD 05A derive limit for <math>\langle \lambda \rangle</math> based on 100 Mo data collected with NEMO-3 detector. No limit for <math>\langle \eta \rangle</math> is given. Supersedes ARNOLD 04.
7 ARNOLD 05A derive limit for <math>\langle \lambda \rangle</math> based on 82Se data collected with NEMO-3 detector. No limit for <math>\langle \eta \rangle</math> is given. Supersedes ARNOLD 04.
8 ARNOLD 04 use the matrix elements of SUHONEN 94 to obtain a limit for <math>\langle \lambda \rangle</math>, no limit for <math>\langle \eta \rangle</math> is given. This limit is more stringent than the limit in EJIRI 01 for the same nucleus.
9 ARNOLD 04 use the matrix elements of TOMODA 91 and SUHONEN 91 to obtain a limit for <math>\langle \lambda \rangle</math>, no limit for <math>\langle \eta \rangle</math> is given.
10 Supersedes ALESSANDRELLO 00. Cryogenic calorimeter search. Reported a range reflecting uncertainty in nuclear matrix element calculations.
11 Limits for <math>\langle \lambda \rangle</math> and <math>\langle \eta \rangle</math> are based on nuclear matrix elements of STAUDT 90. Supersedes DANEVICH 00.
12 The range of the reported <math>\langle \lambda \rangle</math> and <math>\langle \eta \rangle</math> values reflects the spread of the nuclear matrix elements. On axis value assuming <math>\langle m\_{\nu} \rangle = 0</math> and <math>\langle \lambda \rangle = \langle \eta \rangle = 0</math>, respectively.
13 GUENTHER 97 limits use the matrix elements of STAUDT 90. Supersedes BALYSH 95 and BALYSH 92.
14 VUILLEUMIER 93 uses the matrix elements of MUTO 89. Based on a half-life limit 2.6 × 1023 y at 90%CL.
15 BERNATOWICZ 92 takes the measured geochemical decay width as a limit on the 0ν width, and uses the SUHONEN 91 coefficients to obtain the least restrictive limit on η. Further details of the experiment are given in BERNATOWICZ 93.

Table with columns: Author, Year, Reference, Collaboration. Lists various authors and their contributions to the field, including collaborations like NEMO-3, CUORE, MAJORANA, GERDA, EXO-200, CUORICINO, DAMA-INR, KamLAND-Zen, CUORICINO, NEMO-3, and others.

Neutrino Mixing

With the possible exceptions of "short-baseline anomalies," such as LSND, all neutrino data can be described within the framework of a 3x3 mixing matrix between the mass eigenstates ν1, ν2, and ν3, leading to the flavor eigenstates νe, νμ, and ντ, as described in the review "Neutrino masses, mixing and oscillations."

The Listings are divided in the following sections:

(A) Neutrino fluxes and event ratios: shows measurements which correspond to various oscillation tests for Accelerator, Reactor, Atmospheric, and Solar neutrino experiments. Typically, ratios involve a measurement in a realm sensitive to oscillations compared to one for which no oscillation effect is expected.

Double-β Decay REFERENCES

Table with columns: Author, Year, Reference, Collaboration. Lists references for Double-β Decay, including AGOSTINI, ALDUINO, ALENKOV, ALVIS, ANTON, APRILE, M. Agostini et al., C. Alduino et al., V. Alenkov et al., S.I. Alvis et al., G. Anton et al., E. Aprile et al., and collaborations like GERDA, CUORE, AMORE, MAJORANA, EXO-200, XENON1T.

Downloaded from https://academic.oup.com/ptep/article/2020/8/083C01/5891211 by guest on 12 November 2020

# Lepton Particle Listings

## Neutrino Mixing

**(B) Neutrino mixing parameters:** shows measurements of  $\sin^2(\theta_{12})$ ,  $\sin^2(\theta_{23})$ ,  $\sin^2(\theta_{13})$ ,  $\Delta m_{21}^2$ ,  $\Delta m_{32}^2$ , and  $\delta_{CP}$  as extracted from the measured data in the quoted publications in the frame of the three-neutrino mixing scheme. The quoted averages are not the result of a global fit, as in the review "Neutrino masses, mixing, and oscillations," and, as a consequence, might slightly differ from them. In some cases, measurements depend on the mass order (normal when  $\Delta m_{32}^2 > 0$  or inverted when  $\Delta m_{32}^2 < 0$ ) or octant of  $\theta_{23}$  (lower when  $\theta_{23} < 45^\circ$  or upper when  $\theta_{23} > 45^\circ$ ).

### (C) Other neutrino mixing results:

The LSND anomaly [AGUILAR 01], reported a signal which is consistent with  $\bar{\nu}_\mu \rightarrow \bar{\nu}_e$  oscillations. In a three neutrino framework, this would be a measurement of  $\theta_{12}$  and  $\Delta m_{21}^2$ . This does not appear to be consistent with the interpretation of other neutrino data. It has been interpreted as evidence for a 4th "sterile" neutrino. The following listings include results which might be relevant towards understanding this observation. They include searches for  $\nu_\mu \rightarrow \nu_e$ ,  $\bar{\nu}_\mu \rightarrow \bar{\nu}_e$ , sterile neutrino oscillations, and others.

### (A) Neutrino fluxes and event ratios

#### Events (observed/expected) from accelerator $\nu_\mu$ experiments.

Some neutrino oscillation experiments compare the flux in two or more detectors. This is usually quoted as the ratio of the event rate in the far detector to the expected rate based on an extrapolation from the near detector in the absence of oscillations.

VALUE	DOCUMENT ID	TECN	COMMENT
• • •	We do not use the following data for averages, fits, limits, etc. • • •		
$1.01 \pm 0.10$	<sup>1</sup> ABE	14B T2K	$\nu_e$ rate in T2K near detect.
$0.71 \pm 0.08$	<sup>2</sup> AHN	06A K2K	K2K to Super-K
$0.64 \pm 0.05$	<sup>3</sup> MICHAEL	06 MINS	All charged current events
$0.71 \pm 0.08$ $-0.09$	<sup>4</sup> ALIU	05 K2K	KEK to Super-K
$0.70 \pm 0.10$ $-0.11$	<sup>5</sup> AHN	03 K2K	KEK to Super-K

<sup>1</sup> The rate of  $\nu_e$  from  $\mu$  decay was measured to be  $0.68 \pm 0.30$  compared to the predicted flux. From  $K$  decay  $1.10 \pm 0.14$  compared to the predicted flux.

<sup>2</sup> Based on the observation of 112 events when  $158.1 \pm 9.2$   
 $-8.6$  were expected without oscillations. Including not only the number of events but also the shape of the energy distribution, the evidence for oscillation is at the level of about  $4.3 \sigma$ . Supersedes ALIU 05.

<sup>3</sup> This ratio is based on the observation of 215 events compared to an expectation of  $336 \pm 14$  without oscillations. See also ADAMSON 08.

<sup>4</sup> This ratio is based on the observation of 107 events at the far detector 250 km away from KEK, and an expectation of  $151 \pm 12$   
 $-10$ .

<sup>5</sup> This ratio is based on the observation of 56 events with an expectation of  $80.1 \pm 6.2$   
 $-5.4$ .

#### Events (observed/expected) from reactor $\bar{\nu}_e$ experiments.

The quoted values are the ratios of the measured reactor  $\bar{\nu}_e$  event rate at the quoted distances, and the rate expected without oscillations. The expected rate is based on the experimental data for the most significant reactor fuels ( $^{235}\text{U}$ ,  $^{239}\text{Pu}$ ,  $^{241}\text{Pu}$ ) and on calculations for  $^{238}\text{U}$ .

A recent re-evaluation of the spectral conversion of electron to  $\bar{\nu}_e$  in MUELLER 11 results in an upward shift of the reactor  $\bar{\nu}_e$  spectrum by 3% and, thus, might require revisions to the ratios listed in this table.

VALUE	DOCUMENT ID	TECN	COMMENT
• • •	We do not use the following data for averages, fits, limits, etc. • • •		
$0.952 \pm 0.027$	<sup>1</sup> ADEY	19 DAYA	DayaBay, Ling Ao/Ao II reactors
$1.08 \pm 0.21 \pm 0.16$	<sup>2</sup> AN	16 DAYA	DayaBay, Ling Ao/Ao II reactors
$0.658 \pm 0.044 \pm 0.047$	<sup>3</sup> DENIZ	10 TEXO	Kuo-Sheng reactor, 28 m
$0.611 \pm 0.085 \pm 0.041$	<sup>4</sup> ARAKI	05 KLND	Japanese react. ~ 180 km
$1.01 \pm 0.024 \pm 0.053$	<sup>5</sup> EGUCHI	03 KLND	Japanese react. ~ 180 km
$1.01 \pm 0.028 \pm 0.027$	<sup>6</sup> BOEHM	01	Palo Verde react. 0.75–0.89 km
$0.987 \pm 0.006 \pm 0.037$	<sup>7</sup> APOLLONIO	99 CHOZ	Chooz reactors 1 km
$0.988 \pm 0.004 \pm 0.05$	<sup>8</sup> GREENWOOD	96	Savannah River, 18.2 m
	ACHKAR	95 CNTR	Bugey reactor, 15 m

$0.994 \pm 0.010 \pm 0.05$	ACHKAR	95 CNTR	Bugey reactor, 40 m
$0.915 \pm 0.132 \pm 0.05$	ACHKAR	95 CNTR	Bugey reactor, 95 m
$0.987 \pm 0.014 \pm 0.027$	<sup>9</sup> DECLAIS	94 CNTR	Bugey reactor, 15 m
$0.985 \pm 0.018 \pm 0.034$	KUVSHINN...	91 CNTR	Rovno reactor
$1.05 \pm 0.02 \pm 0.05$	VUILLEUMIER	82	Gösgen reactor
$0.955 \pm 0.035 \pm 0.110$	<sup>10</sup> KWON	81	$\bar{\nu}_e p \rightarrow e^+ n$
$0.89 \pm 0.15$	<sup>10</sup> BOEHM	80	$\bar{\nu}_e p \rightarrow e^+ n$

<sup>1</sup> ADEY 19 present a re-analysis of 1230 days of Daya Bay near detector data with reduced systematic uncertainties on the neutron detection efficiency. Note that ADEY 19 report the measured to predicted antineutrino ratio using the reactor model of MUELLER 11 (Huber-Mueller model). The ratio using the older ILL-Vogel model is  $1.001 \pm 0.015 \pm 0.027$ .

<sup>2</sup> AN 16 use 217 days of data (338k events) to determine the neutrino flux ratio relative to the prediction of Mueller-Huber and ILL-Vogel models (see AN 16 for details). The reported flux ratios were corrected for  $\theta_{13}$  oscillation effect. The flux measurement is consistent with results from previous short-baseline reactor experiments. The measured inverse beta decay yield is  $(1.55 \pm 0.04) \times 10^{-18} \text{ cm}^2/(\text{GW day})$  or  $\sigma_f = (5.92 \pm 0.14) \times 10^{-43} \text{ cm}^2/\text{fission}$ . About  $4\sigma$  excess of events was observed in the 4–6 MeV prompt energy region.

<sup>3</sup> DENIZ 10 observe reactor  $\bar{\nu}_e e$  scattering with recoil kinetic energies 3–8 MeV using CsI(Tl) detectors. The observed rate is consistent with the Standard Model prediction, leading to a constraint on  $\sin^2 \theta_W = 0.251 \pm 0.031(\text{stat}) \pm 0.024(\text{sys})$ .

<sup>4</sup> Updated result of KamLAND, including the data used in EGUCHI 03. Note that the survival probabilities for different periods are not directly comparable because the effective baseline varies with power output of the reactor sources involved, and there were large variations in the reactor power production in Japan in 2003.

<sup>5</sup> EGUCHI 03 observe reactor neutrino disappearance at ~ 180 km baseline to various Japanese nuclear power reactors.

<sup>6</sup> BOEHM 01 search for neutrino oscillations at 0.75 and 0.89 km distance from the Palo Verde reactors.

<sup>7</sup> APOLLONIO 99, APOLLONIO 98 search for neutrino oscillations at 1.1 km fixed distance from Chooz reactors. They use  $\bar{\nu}_e p \rightarrow e^+ n$  in Gd-loaded scintillator target. APOLLONIO 99 supersedes APOLLONIO 98. See also APOLLONIO 03 for detailed description.

<sup>8</sup> GREENWOOD 96 search for neutrino oscillations at 18 m and 24 m from the reactor at Savannah River.

<sup>9</sup> DECLAIS 94 result based on integral measurement of neutrons only. Result is ratio of measured cross section to that expected in standard V-A theory. Replaced by ACHKAR 95.

<sup>10</sup> KWON 81 represents an analysis of a larger set of data from the same experiment as BOEHM 80.

### Atmospheric neutrinos

Neutrinos and antineutrinos produced in the atmosphere induce  $\mu$ -like and  $e$ -like events in underground detectors. The ratio of the numbers of the two kinds of events is defined as  $\mu/e$ . It has the advantage that systematic effects, such as flux uncertainty, tend to cancel, for both experimental and theoretical values of the ratio. The "ratio of the ratios" of experimental to theoretical  $\mu/e$ ,  $R(\mu/e)$ , or that of experimental to theoretical  $\mu/\text{total}$ ,  $R(\mu/\text{total})$  with  $\text{total} = \mu + e$ , is reported below. If the actual value is not unity, the value obtained in a given experiment may depend on the experimental conditions. In addition, the measured "up-down asymmetry" for  $\mu$  ( $N_{up}(\mu)/N_{down}(\mu)$ ) or  $e$  ( $N_{up}(e)/N_{down}(e)$ ) is reported. The expected "up-down asymmetry" is nearly unity if there is no neutrino oscillation.

#### $R(\mu/e) = (\text{Measured Ratio } \mu/e) / (\text{Expected Ratio } \mu/e)$

VALUE	DOCUMENT ID	TECN	COMMENT
• • •	We do not use the following data for averages, fits, limits, etc. • • •		
$0.658 \pm 0.016 \pm 0.035$	<sup>1</sup> ASHIE	05 SKAM	sub-GeV
$0.702 \pm 0.032 \pm 0.101$ $-0.030$	<sup>2</sup> ASHIE	05 SKAM	multi-GeV
$0.69 \pm 0.10 \pm 0.06$	<sup>3</sup> SANCHEZ	03 SOU2	Calorimeter raw data
$1.00 \pm 0.15 \pm 0.08$	<sup>4</sup> FUKUDA	96B KAMI	Water Cherenkov
$0.60 \pm 0.06 \pm 0.05$ $-0.05$	<sup>5</sup> DAUM	95 FREJ	Calorimeter
$0.57 \pm 0.08 \pm 0.07$ $-0.07$	<sup>6</sup> FUKUDA	94 KAMI	sub-GeV
	<sup>7</sup> FUKUDA	94 KAMI	multi-GeV
	<sup>8</sup> BECKER-SZ...	92B IMB	Water Cherenkov

<sup>1</sup> ASHIE 05 results are based on an exposure of 92 kton yr during the complete Super-Kamiokande I running period. The analyzed data sample consists of fully-contained single-ring  $e$ -like events with  $0.1 \text{ GeV}/c < p_e$  and  $\mu$ -like events  $0.2 \text{ GeV}/c < p_\mu$ , both having a visible energy  $< 1.33 \text{ GeV}$ . These criteria match the definition used by FUKUDA 94.

<sup>2</sup> ASHIE 05 results are based on an exposure of 92 kton yr during the complete Super-Kamiokande I running period. The analyzed data sample consists of fully-contained single-ring events with visible energy  $> 1.33 \text{ GeV}$  and partially-contained events. All partially-contained events are classified as  $\mu$ -like.

<sup>3</sup> SANCHEZ 03 result is based on an exposure of 5.9 kton yr, and updates ALLISON 99 result. The analyzed data sample consists of fully-contained  $e$ -flavor and  $\mu$ -flavor events having lepton momentum  $> 0.3 \text{ GeV}/c$ .

<sup>4</sup> FUKUDA 96B studied neutron background in the atmospheric neutrino sample observed in the Kamiokande detector. No evidence for the background contamination was found.

<sup>5</sup> DAUM 95 results are based on an exposure of 2.0 kton yr which includes the data used by BERGER 90B. This ratio is for the contained and semicontained events. DAUM 95

See key on page 999

# Lepton Particle Listings

## Neutrino Mixing

also report  $R(\mu/e) = 0.99 \pm 0.13 \pm 0.08$  for the total neutrino induced data sample which includes upward going stopping muons and horizontal muons in addition to the contained and semicontained events.

<sup>6</sup>FUKUDA 94 result is based on an exposure of 7.7 kton yr and updates the HIRATA 92 result. The analyzed data sample consists of fully-contained  $e$ -like events with  $0.1 < p_e < 1.33$  GeV/c and fully-contained  $\mu$ -like events with  $0.2 < p_\mu < 1.5$  GeV/c.

<sup>7</sup>FUKUDA 94 analyzed the data sample consisting of fully contained events with visible energy  $> 1.33$  GeV and partially contained  $\mu$ -like events.

<sup>8</sup>BECKER-SZENDY 92B reports the fraction of nonshowering events (mostly muons from atmospheric neutrinos) as  $0.36 \pm 0.02 \pm 0.02$ , as compared with expected fraction  $0.51 \pm 0.01 \pm 0.05$ . After cutting the energy range to the Kamiokande limits, BEIER 92 finds  $R(\mu/e)$  very close to the Kamiokande value.

### $R(\nu_\mu) = (\text{Measured Flux of } \nu_\mu) / (\text{Expected Flux of } \nu_\mu)$

VALUE	DOCUMENT ID	TECN	COMMENT
• • • We do not use the following data for averages, fits, limits, etc. • • •			
$0.84 \pm 0.12$	<sup>1</sup> ADAMSON 06	MINS	MINOS atmospheric
$0.72 \pm 0.026 \pm 0.13$	<sup>2</sup> AMBROSIO 01	MCRO	upward through-going
$0.57 \pm 0.05 \pm 0.15$	<sup>3</sup> AMBROSIO 00	MCRO	upgoing partially contained
$0.71 \pm 0.05 \pm 0.19$	<sup>4</sup> AMBROSIO 00	MCRO	downgoing partially contained + upgoing stopping
$0.74 \pm 0.036 \pm 0.046$	<sup>5</sup> AMBROSIO 98	MCRO	Streamer tubes
	<sup>6</sup> CASPER 91	IMB	Water Cherenkov
	<sup>7</sup> AGLIETTA 89	NUSX	
$0.95 \pm 0.22$	<sup>8</sup> BOLIEV 81	Baksan	
$0.62 \pm 0.17$	CROUCH 78		Case Western /UCI

<sup>1</sup>ADAMSON 06 uses a measurement of 107 total neutrinos compared to an expected rate of  $127 \pm 13$  without oscillations.

<sup>2</sup>AMBROSIO 01 result is based on the upward through-going muon tracks with  $E_\mu > 1$  GeV. The data came from three different detector configurations, but the statistics is largely dominated by the full detector run, from May 1994 to December 2000. The total live time, normalized to the full detector configuration, is 6.17 years. The first error is the statistical error, the second is the systematic error, dominated by the theoretical error in the predicted flux.

<sup>3</sup>AMBROSIO 00 result is based on the upgoing partially contained event sample. It came from 4.1 live years of data taking with the full detector, from April 1994 to February 1999. The average energy of atmospheric muon neutrinos corresponding to this sample is 4 GeV. The first error is statistical, the second is the systematic error, dominated by the 25% theoretical error in the rate (20% in the flux and 15% in the cross section, added in quadrature). Within statistics, the observed deficit is uniform over the zenith angle.

<sup>4</sup>AMBROSIO 00 result is based on the combined samples of downgoing partially contained events and upgoing stopping events. These two subsamples could not be distinguished due to the lack of timing information. The result came from 4.1 live years of data taking with the full detector, from April 1994 to February 1999. The average energy of atmospheric muon neutrinos corresponding to this sample is 4 GeV. The first error is statistical, the second is the systematic error, dominated by the 25% theoretical error in the rate (20% in the flux and 15% in the cross section, added in quadrature). Within statistics, the observed deficit is uniform over the zenith angle.

<sup>5</sup>AMBROSIO 98 result is for all nadir angles and updates AHLEN 95 result. The lower cutoff on the muon energy is 1 GeV. In addition to the statistical and systematic errors, there is a Monte Carlo flux error (theoretical error) of  $\pm 0.13$ . With a neutrino oscillation hypothesis, the fit either to the flux or zenith distribution independently yields  $\sin^2 2\theta = 1.0$  and  $\Delta(m^2) \sim$  a few times  $10^{-3}$  eV<sup>2</sup>. However, the fit to the observed zenith distribution gives a maximum probability for  $\chi^2$  of only 5% for the best oscillation hypothesis.

<sup>6</sup>CASPER 91 correlates showering/nonshowering signature of single-ring events with parent atmospheric-neutrino flavor. They find nonshowering ( $\approx \nu_\mu$  induced) fraction is  $0.41 \pm 0.03 \pm 0.02$ , as compared with expected  $0.51 \pm 0.05$  (syst).

<sup>7</sup>AGLIETTA 89 finds no evidence for any anomaly in the neutrino flux. They define  $\rho = (\text{measured number of } \nu_e\text{'s}) / (\text{measured number of } \nu_\mu\text{'s})$ . They report  $\rho(\text{measured}) = \rho(\text{expected}) = 0.96 \pm \frac{0.32}{-0.28}$ .

<sup>8</sup>From this data BOLIEV 81 obtain the limit  $\Delta(m^2) \leq 6 \times 10^{-3}$  eV<sup>2</sup> for maximal mixing,  $\nu_\mu \leftrightarrow \nu_\mu$  type oscillation.

### $R(\mu/\text{total}) = (\text{Measured Ratio } \mu/\text{total}) / (\text{Expected Ratio } \mu/\text{total})$

VALUE	DOCUMENT ID	TECN	COMMENT
• • • We do not use the following data for averages, fits, limits, etc. • • •			
$1.1 \pm \frac{0.07}{-0.12} \pm 0.11$	<sup>1</sup> CLARK 97	IMB	multi-GeV

<sup>1</sup>CLARK 97 obtained this result by an analysis of fully contained and partially contained events in the IMB water-Cherenkov detector with visible energy  $> 0.95$  GeV.

### $N_{\text{up}}(\mu) / N_{\text{down}}(\mu)$

VALUE	DOCUMENT ID	TECN	COMMENT
• • • We do not use the following data for averages, fits, limits, etc. • • •			
$0.71 \pm 0.06$	<sup>1</sup> ADAMSON 12B	MINS	contained-vertex muons
$0.551 \pm \frac{0.035}{-0.033} \pm 0.004$	<sup>2</sup> ASHIE 05	SKAM	multi-GeV

<sup>1</sup>ADAMSON 12B reports the atmospheric neutrino results obtained with MINOS far detector in 2,553 live days (an exposure of 37.9 kton-yr). This result is obtained with a sample of high resolution contained-vertex muons. The quoted error is statistical only.

<sup>2</sup>ASHIE 05 results are based on an exposure of 92 kton yr during the complete Super-Kamiokande I running period. The analyzed data sample consists of fully-contained single-ring  $\mu$ -like events with visible energy  $> 1.33$  GeV and partially-contained events.

All partially-contained events are classified as  $\mu$ -like. Upward-going events are those with  $-1 < \cos(\text{zenith angle}) < -0.2$  and downward-going events are those with  $0.2 < \cos(\text{zenith angle}) < 1$ . The  $\mu$ -like up-down ratio for the multi-GeV data deviates from 1 (the expectation for no atmospheric  $\nu_\mu$  oscillations) by more than 12 standard deviations.

### $N_{\text{up}}(e) / N_{\text{down}}(e)$

VALUE	DOCUMENT ID	TECN	COMMENT
• • • We do not use the following data for averages, fits, limits, etc. • • •			
$0.961 \pm \frac{0.086}{-0.079} \pm 0.016$	<sup>1</sup> ASHIE 05	SKAM	multi-GeV

<sup>1</sup>ASHIE 05 results are based on an exposure of 92 kton yr during the complete Super-Kamiokande I running period. The analyzed data sample consists of fully-contained single-ring  $e$ -like events with visible energy  $> 1.33$  GeV. Upward-going events are those with  $-1 < \cos(\text{zenith angle}) < -0.2$  and downward-going events are those with  $0.2 < \cos(\text{zenith angle}) < 1$ . The  $e$ -like up-down ratio for the multi-GeV data is consistent with 1 (the expectation for no atmospheric  $\nu_e$  oscillations).

### $R(\text{up/down}; \mu) = (\text{Measured up/down}; \mu) / (\text{Expected up/down}; \mu)$

VALUE	DOCUMENT ID	TECN	COMMENT
• • • We do not use the following data for averages, fits, limits, etc. • • •			
$0.62 \pm 0.05 \pm 0.02$	<sup>1</sup> ADAMSON 12B	MINS	contained-vertex muons
$0.63 \pm \frac{0.19}{-0.14} \pm 0.02$	<sup>2</sup> ADAMSON 06	MINS	atmospheric $\nu$ with far detector

<sup>1</sup>ADAMSON 12B reports the atmospheric neutrino results obtained with MINOS far detector in 2,553 live days (an exposure of 37.9 kton-yr). This result is obtained with a sample of high resolution contained-vertex muons. The expected ratio is calculated with no neutrino oscillation.

<sup>2</sup>ADAMSON 06 result is obtained with the MINOS far detector with an exposure of 4.54 kton yr. The expected ratio is calculated with no neutrino oscillation.

### $N(\mu^+) / N(\mu^-)$

VALUE	DOCUMENT ID	TECN	COMMENT
• • • We do not use the following data for averages, fits, limits, etc. • • •			
$0.46 \pm \frac{0.05}{-0.04}$	<sup>1,2</sup> ADAMSON 12B	MINS	contained-vertex muons
$0.63 \pm \frac{0.09}{-0.08}$	<sup>1,3</sup> ADAMSON 12B	MINS	$\nu$ -induced rock-muons

<sup>1</sup>ADAMSON 12B reports the atmospheric neutrino results obtained with MINOS far detector in 2,553 live days (an exposure of 37.9 kton-yr). The muon charge ratio  $N(\mu^+) / N(\mu^-)$  represents the  $\overline{\nu}_\mu / \nu_\mu$  ratio.

<sup>2</sup>This result is obtained with a charge-separated sample of high resolution contained-vertex muons. The quoted error is statistical only.

<sup>3</sup>This result is obtained with a charge-separated sample of high resolution neutrino-induced rock-muons. The quoted error is statistical only.

### $R(\mu^+ / \mu^-) = (\text{Measured } N(\mu^+) / N(\mu^-)) / (\text{Expected } N(\mu^+) / N(\mu^-))$

VALUE	DOCUMENT ID	TECN	COMMENT
• • • We do not use the following data for averages, fits, limits, etc. • • •			
$0.93 \pm 0.09 \pm 0.09$	<sup>1,2</sup> ADAMSON 12B	MINS	contained-vertex muons
$1.29 \pm \frac{0.19}{-0.17} \pm 0.16$	<sup>1,3</sup> ADAMSON 12B	MINS	$\nu$ -induced rock-muons
$1.03 \pm 0.08 \pm 0.08$	<sup>1,4</sup> ADAMSON 12B	MINS	contained
$1.39 \pm \frac{0.35}{-0.46} \pm 0.08$	<sup>5</sup> ADAMSON 07	MINS	Upward and horizontal $\mu$ with far detector
$0.96 \pm \frac{0.38}{-0.27} \pm 0.15$	<sup>6</sup> ADAMSON 06	MINS	atmospheric $\nu$ with far detector

<sup>1</sup>ADAMSON 12B reports the atmospheric neutrino results obtained with MINOS far detector in 2,553 live days (an exposure of 37.9 kton-yr). The muon charge ratio  $N(\mu^+) / N(\mu^-)$  represents the  $\overline{\nu}_\mu / \nu_\mu$  ratio. As far as the same oscillation parameters are used for  $\nu_s$  and  $\overline{\nu}_s$ , the expected  $\overline{\nu}_\mu / \nu_\mu$  ratio is almost entirely independent of any input oscillations.

<sup>2</sup>This result is obtained with a charge-separated sample of high resolution contained-vertex muons.

<sup>3</sup>This result is obtained with a charge-separated sample of high resolution neutrino-induced rock-muons.

<sup>4</sup>The charge-separated samples of high resolution contained-vertex muons and neutrino-induced rock-muons are combined to obtain this result which is consistent with unity.

<sup>5</sup>ADAMSON 07 result is obtained with the MINOS far detector in 854.24 live days, based on neutrino-induced upward-going and horizontal muons. This result is consistent with CP T conservation.

<sup>6</sup>ADAMSON 06 result is obtained with the MINOS far detector with an exposure of 4.54 kton yr, based on contained events. The expected ratio is calculated by assuming the same oscillation parameters for neutrinos and antineutrinos.

### Solar neutrinos

Solar neutrinos are produced by thermonuclear fusion reactions in the Sun. Radiochemical experiments measure particular combinations of fluxes from various neutrino-producing reactions, whereas water-Cherenkov experiments mainly measure a flux of neutrinos from decay of <sup>8</sup>B. Solar neutrino fluxes are composed of all active neutrino species,  $\nu_e$ ,  $\nu_\mu$ , and  $\nu_\tau$ . In addition, some other mechanisms may cause antineutrino components in solar neutrino fluxes. Each measurement method is sensitive to

# Lepton Particle Listings

## Neutrino Mixing

a particular component or a combination of components of solar neutrino fluxes.

### $\nu_e$ Capture Rates from Radiochemical Experiments

1 SNU (Solar Neutrino Unit) =  $10^{-36}$  captures per atom per second.

VALUE (SNU)	DOCUMENT ID	TECN	COMMENT
73.4 $^{+6.1}_{-6.0}$ $^{+3.7}_{-4.1}$	<sup>1</sup> KAETHER 10	GALX	reanalysis
67.6 $\pm 4.0 \pm 3.2$	<sup>2</sup> KAETHER 10	GNO+GALX	reanalysis combined
65.4 $^{+3.1}_{-3.0}$ $^{+2.6}_{-2.8}$	<sup>3</sup> ABDURASHI... 09	SAGE <sup>71</sup> Ga $\rightarrow$ <sup>71</sup> Ge	
62.9 $^{+5.5}_{-5.3}$ $\pm 2.5$	<sup>4</sup> ALTMANN 05	GNO <sup>71</sup> Ga $\rightarrow$ <sup>71</sup> Ge	
69.3 $\pm 4.1 \pm 3.6$	<sup>5</sup> ALTMANN 05	GNO + GALX	combined
77.5 $\pm 6.2$ $^{+4.3}_{-4.7}$	<sup>6</sup> HAMPEL 99	GALX <sup>71</sup> Ga $\rightarrow$ <sup>71</sup> Ge	
2.56 $\pm 0.16 \pm 0.16$	<sup>7</sup> CLEVELAND 98	HOME <sup>37</sup> Cl $\rightarrow$ <sup>37</sup> Ar	

- • • We do not use the following data for averages, fits, limits, etc. • • •
- <sup>1</sup> KAETHER 10 reports the reanalysis results of a complete GALLEX data (GALLEX I+II+III+IV, reported in HAMPEL 99) based on the event selection with a new pulse shape analysis, which provides a better background reduction than the rise time analysis adopted in HAMPEL 99.
- <sup>2</sup> Combined result of GALLEX I+II+III+IV reanalysis and GNO I+II+III (ALTMANN 05).
- <sup>3</sup> ABDURASHITOV 09 reports a combined analysis of 168 extractions of the SAGE solar neutrino experiment during the period January 1990 through December 2007, and updates the ABDURASHITOV 02 result. The data are consistent with the assumption that the solar neutrino production rate is constant in time. Note that a  $\sim 15\%$  systematic uncertainty in the overall normalization may be added to the ABDURASHITOV 09 result, because calibration experiments for gallium solar neutrino measurements using intense <sup>51</sup>Cr (twice by GALLEX and once by SAGE) and <sup>37</sup>Ar (by SAGE) result in an average ratio of  $0.87 \pm 0.05$  of the observed to calculated rates.
- <sup>4</sup> ALTMANN 05 reports the complete result from the GNO solar neutrino experiment (GNO I+II+III), which is the successor project of GALLEX. Experimental technique of GNO is essentially the same as that of GALLEX. The run data cover the period 20 May 1998 through 9 April 2003.
- <sup>5</sup> Combined result of GALLEX I+II+III+IV (HAMPEL 99) and GNO I+II+III.
- <sup>6</sup> HAMPEL 99 report the combined result for GALLEX I+II+III+IV (65 runs in total), which update the HAMPEL 96 result. The GALLEX IV result (12 runs) is  $118.4 \pm 17.8 \pm 6.6$  SNU. (HAMPEL 99 discuss the consistency of partial results with the mean.) The GALLEX experimental program has been completed with these runs. The total run data cover the period 14 May 1991 through 23 January 1997. A total of 300 <sup>71</sup>Ge events were observed. Note that a  $\sim 15\%$  systematic uncertainty in the overall normalization may be added to the HAMPEL 99 result, because calibration experiments for gallium solar neutrino measurements using intense <sup>51</sup>Cr (twice by GALLEX and once by SAGE) and <sup>37</sup>Ar (by SAGE) result in an average ratio of  $0.87 \pm 0.05$  of the observed to calculated rates.
- <sup>7</sup> CLEVELAND 98 is a detailed report of the <sup>37</sup>Cl experiment at the Homestake Mine. The average solar neutrino-induced <sup>37</sup>Ar production rate from 108 runs between 1970 and 1994 updates the DAVIS 89 result.

### $\phi_{ES} (^8B)$

<sup>8</sup>B solar-neutrino flux measured via  $\nu e$  elastic scattering. This process is sensitive to all active neutrino flavors, but with reduced sensitivity to  $\nu_\mu, \nu_\tau$  due to the cross-section difference,  $\sigma(\nu_{\mu,\tau} e) \sim 0.16\sigma(\nu_e e)$ . If the <sup>8</sup>B solar-neutrino flux involves nonelectron flavor active neutrinos, their contribution to the flux is  $\sim 0.16$  times of  $\nu_e$ .

VALUE ( $10^6 \text{ cm}^{-2}\text{s}^{-1}$ )	DOCUMENT ID	TECN	COMMENT
2.53 $^{+0.31}_{-0.28}$ $^{+0.13}_{-0.10}$	<sup>1</sup> ANDERSON 19	SNO+	Water phase; average flux
2.57 $^{+0.17}_{-0.18}$ $^{+0.07}_{-0.07}$	<sup>2</sup> AGOSTINI 18B	BORX	average flux
2.345 $\pm 0.014 \pm 0.036$	<sup>3</sup> ABE 16C	SKAM SK-I+II+III+IV	average flux
2.308 $\pm 0.020$ $^{+0.039}_{-0.040}$	<sup>4</sup> ABE 16C	SKAM SK-IV	average flux
2.250 $^{+0.030}_{-0.029}$ $\pm 0.038$	<sup>4</sup> ABE 16C	SKAM SK-IV	day flux
2.364 $\pm 0.029 \pm 0.040$	<sup>4</sup> ABE 16C	SKAM SK-IV	night flux
2.404 $\pm 0.039 \pm 0.053$	<sup>5</sup> ABE 16C	SKAM SK-III	average flux
2.41 $\pm 0.05$ $^{+0.16}_{-0.15}$	<sup>6</sup> ABE 11	SKAM SK-II	average flux
2.38 $\pm 0.02 \pm 0.08$	<sup>7</sup> ABE 11	SKAM SK-I	average flux
2.77 $\pm 0.26 \pm 0.32$	<sup>8</sup> ABE 11B	KLND	average flux
2.4 $\pm 0.4 \pm 0.1$	<sup>9</sup> BELLINI 10A	BORX	average flux
1.77 $^{+0.24}_{-0.21}$ $^{+0.09}_{-0.10}$	<sup>10</sup> AHARMIM 08	SNO Phase III	
2.38 $\pm 0.05$ $^{+0.16}_{-0.15}$	<sup>11</sup> CRAVENS 08	SKAM	average flux
2.35 $\pm 0.02 \pm 0.08$	<sup>12</sup> HOSAKA 06	SKAM	average flux
2.35 $\pm 0.22 \pm 0.15$	<sup>13</sup> AHARMIM 05A	SNO Salty D <sub>2</sub> O; <sup>8</sup> B shape not constrained	
2.34 $\pm 0.23$ $^{+0.15}_{-0.14}$	<sup>13</sup> AHARMIM 05A	SNO Salty D <sub>2</sub> O; <sup>8</sup> B shape constrained	
2.39 $^{+0.24}_{-0.23}$ $\pm 0.12$	<sup>14</sup> AHMAD 02	SNO	average flux

• • • We do not use the following data for averages, fits, limits, etc. • • •

2.39 $\pm 0.34$ $^{+0.16}_{-0.14}$	<sup>15</sup> AHMAD 01	SNO	average flux
2.80 $\pm 0.19 \pm 0.33$	<sup>16</sup> FUKUDA 96	KAMI	average flux
2.70 $\pm 0.27$	<sup>16</sup> FUKUDA 96	KAMI	day flux
2.87 $^{+0.27}_{-0.26}$	<sup>16</sup> FUKUDA 96	KAMI	night flux

- <sup>1</sup> ANDERSON 19 reports this result from the  $\nu_e e$  elastic scattering rate using a 69.2 kton-day (or 114.7 days) of exposure from May through December, 2017 during the SNO+ detector's water commissioning phase. The events over the reconstructed electron kinetic energy range of 5–15 MeV were analyzed.
- <sup>2</sup> AGOSTINI 18B obtained this result from the  $\nu_e e$  elastic scattering rate over the period between January 2008 and December 2016.
- <sup>3</sup> ABE 16C reports the combined results of the four phases of the Super-Kamiokande average flux measurements. Here the revised Super-Kamiokande-III result is used.
- <sup>4</sup> ABE 16C reports the Super-Kamiokande-IV results for 1664 live days from September 2008 to February 2014. The analysis threshold is total electron energy of 4.0 MeV.
- <sup>5</sup> ABE 16C revised the Super-Kamiokande-III average flux value reported in ABE 11. Super-Kamiokande-III results are for 548 live days from August 4, 2006 to August 18, 2008. The analysis threshold is 5.0 MeV, but the event sample in the 5.0–6.5 MeV total electron energy range has a total live time of 298 days.
- <sup>6</sup> ABE 11 recalculated the Super-Kamiokande-II results using <sup>8</sup>B spectrum of WINTER 06A.
- <sup>7</sup> ABE 11 recalculated the Super-Kamiokande-I results using <sup>8</sup>B spectrum of WINTER 06A.
- <sup>8</sup> ABE 11B use a 123 kton-day exposure of the KamLAND liquid scintillation detector to measure the <sup>8</sup>B solar neutrino flux. They utilize  $\nu - e$  elastic scattering above a reconstructed-energy threshold of 5.5 MeV, corresponding to 5 MeV electron recoil energy. 299 electron recoil candidate events are reported, of which 157  $\pm 23.6$  are assigned to background.
- <sup>9</sup> BELLINI 10A reports the Borexino result with 3 MeV energy threshold for scattered electrons. The data correspond to 345.3 live days with a target mass of 100 t, between July 15, 2007 and August 23, 2009.
- <sup>10</sup> AHARMIM 08 reports the results from SNO Phase III measurement using an array of <sup>3</sup>He proportional counters to measure the rate of NC interactions in heavy water, over the period between November 27, 2004 and November 28, 2006, corresponding to 385.17 live days. A simultaneous fit was made for the number of NC events detected by the proportional counters and the numbers of NC, CC, and ES events detected by the PMTs, where the spectral distributions of the ES and CC events were not constrained to the <sup>8</sup>B shape.
- <sup>11</sup> CRAVENS 08 reports the Super-Kamiokande-II results for 791 live days from December 2002 to October 2005. The photocathode coverage of the detector is 19% (reduced from 40% of that of Super-Kamiokande-I due to an accident in 2001). The analysis threshold for the average flux is 7 MeV.
- <sup>12</sup> HOSAKA 06 reports the final results for 1496 live days with Super-Kamiokande-I between May 31, 1996 and July 15, 2001, and replace FUKUDA 02 results. The analysis threshold is 5 MeV except for the first 280 live days (6.5 MeV).
- <sup>13</sup> AHARMIM 05A measurements were made with dissolved NaCl (0.195% by weight) in heavy water over the period between July 26, 2001 and August 28, 2003, corresponding to 391.4 live days, and update AHMED 04A. The CC, ES, and NC events were statistically separated. In one method, the <sup>8</sup>B energy spectrum was not constrained. In the other method, the constraint of an undistorted <sup>8</sup>B energy spectrum was added for comparison with AHMAD 02 results.
- <sup>14</sup> AHMAD 02 reports the <sup>8</sup>B solar-neutrino flux measured via  $\nu e$  elastic scattering above the kinetic energy threshold of 5 MeV. The data correspond to 306.4 live days with SNO between November 2, 1999 and May 28, 2001, and updates AHMAD 01 results.
- <sup>15</sup> AHMAD 01 reports the <sup>8</sup>B solar-neutrino flux measured via  $\nu e$  elastic scattering above the kinetic energy threshold of 6.75 MeV. The data correspond to 241 live days with SNO between November 2, 1999 and January 15, 2001.
- <sup>16</sup> FUKUDA 96 results are for a total of 2079 live days with Kamiokande II and III from January 1987 through February 1995, covering the entire solar cycle 22, with threshold  $E_e > 9.3$  MeV (first 449 days),  $> 7.5$  MeV (middle 794 days), and  $> 7.0$  MeV (last 836 days). These results update the HIRATA 90 result for the average <sup>8</sup>B solar-neutrino flux and HIRATA 91 result for the day-night variation in the <sup>8</sup>B solar-neutrino flux. The total data sample was also analyzed for short-term variations: within experimental errors, no strong correlation of the solar-neutrino flux with the sunspot numbers was found.

### $\phi_{CC} (^8B)$

<sup>8</sup>B solar-neutrino flux measured with charged-current reaction which is sensitive exclusively to  $\nu_e$ .

VALUE ( $10^6 \text{ cm}^{-2}\text{s}^{-1}$ )	DOCUMENT ID	TECN	COMMENT
1.67 $^{+0.05}_{-0.04}$ $^{+0.07}_{-0.08}$	<sup>1</sup> AHARMIM 08	SNO	Phase III
1.68 $\pm 0.06$ $^{+0.08}_{-0.09}$	<sup>2</sup> AHARMIM 05A	SNO	Salty D <sub>2</sub> O; <sup>8</sup> B shape not const.
1.72 $\pm 0.05 \pm 0.11$	<sup>2</sup> AHARMIM 05A	SNO	Salty D <sub>2</sub> O; <sup>8</sup> B shape constrained
1.76 $^{+0.06}_{-0.05}$ $\pm 0.09$	<sup>3</sup> AHMAD 02	SNO	average flux
1.75 $\pm 0.07$ $^{+0.12}_{-0.11}$ $\pm 0.05$	<sup>4</sup> AHMAD 01	SNO	average flux

- • • We do not use the following data for averages, fits, limits, etc. • • •
- <sup>1</sup> AHARMIM 08 reports the results from SNO Phase III measurement using an array of <sup>3</sup>He proportional counters to measure the rate of NC interactions in heavy water, over the period between November 27, 2004 and November 28, 2006, corresponding to 385.17 live days. A simultaneous fit was made for the number of NC events detected by the proportional counters and the numbers of NC, CC, and ES events detected by the PMTs, where the spectral distributions of the ES and CC events were not constrained to the <sup>8</sup>B shape.

See key on page 999

# Lepton Particle Listings

## Neutrino Mixing

<sup>2</sup>AHARMIM 05A measurements were made with dissolved NaCl (0.195% by weight) in heavy water over the period between July 26, 2001 and August 28, 2003, corresponding to 391.4 live days, and update AHMED 04A. The CC, ES, and NC events were statistically separated. In one method, the <sup>8</sup>B energy spectrum was not constrained. In the other method, the constraint of an undistorted <sup>8</sup>B energy spectrum was added for comparison with AHMAD 02 results.

<sup>3</sup>AHMAD 02 reports the SNO result of the <sup>8</sup>B solar-neutrino flux measured with charged-current reaction on deuterium,  $\nu_e d \rightarrow ppe^-$ , above the kinetic energy threshold of 5 MeV. The data correspond to 306.4 live days with SNO between November 2, 1999 and May 28, 2001, and updates AHMAD 01 results. The complete description of the SNO Phase I data set is given in AHARMIM 07.

<sup>4</sup>AHMAD 01 reports the first SNO result of the <sup>8</sup>B solar-neutrino flux measured with the charged-current reaction on deuterium,  $\nu_e d \rightarrow ppe^-$ , above the kinetic energy threshold of 6.75 MeV. The data correspond to 241 live days with SNO between November 2, 1999 and January 15, 2001.

### $\phi_{NC}$ (<sup>8</sup>B)

<sup>8</sup>B solar neutrino flux measured with neutral-current reaction, which is equally sensitive to  $\nu_e, \nu_\mu,$  and  $\nu_\tau$ .

VALUE ( $10^6 \text{ cm}^{-2}\text{s}^{-1}$ )	DOCUMENT ID	TECN	COMMENT
• • • We do not use the following data for averages, fits, limits, etc. • • •			
5.25 ± 0.16 <sup>+0.11</sup> / <sub>-0.13</sub>	<sup>1</sup> AHARMIM 13	SNO	All three phases combined
5.140 <sup>+0.160</sup> / <sub>-0.158</sub> <sup>+0.132</sup> / <sub>-0.117</sub>	<sup>2</sup> AHARMIM 10	SNO	Phase I+II, low threshold
5.54 <sup>+0.33</sup> / <sub>-0.31</sub> <sup>+0.36</sup> / <sub>-0.34</sub>	<sup>3</sup> AHARMIM 08	SNO	Phase III, prop. counter + PMT
4.94 ± 0.21 <sup>+0.38</sup> / <sub>-0.34</sub>	<sup>4</sup> AHARMIM 05A	SNO	Salty D <sub>2</sub> O; <sup>8</sup> B shape not const.
4.81 ± 0.19 <sup>+0.28</sup> / <sub>-0.27</sub>	<sup>4</sup> AHARMIM 05A	SNO	Salty D <sub>2</sub> O; <sup>8</sup> B shape constrained
5.09 <sup>+0.44</sup> / <sub>-0.43</sub> <sup>+0.46</sup> / <sub>-0.43</sub>	<sup>5</sup> AHMAD 02	SNO	average flux; <sup>8</sup> B shape const.
6.42 ± 1.57 <sup>+0.55</sup> / <sub>-0.58</sub>	<sup>5</sup> AHMAD 02	SNO	average flux; <sup>8</sup> B shape not const.

<sup>1</sup>AHARMIM 13 obtained this result from a combined analysis of the data from all three phases, SNO-I, II, and III. The measurement of the <sup>8</sup>B flux mostly comes from the NC signal, however, CC contribution is included in the fit.

<sup>2</sup>AHARMIM 10 reports this result from a joint analysis of SNO Phase I+II data with the "effective electron kinetic energy" threshold of 3.5 MeV. This result is obtained with a "binned-histogram unconstrained fit" where binned probability distribution functions of the neutrino signal observables were used without any model constraints on the shape of the neutrino spectrum.

<sup>3</sup>AHARMIM 08 reports the results from SNO Phase III measurement using an array of <sup>3</sup>He proportional counters to measure the rate of NC interactions in heavy water, over the period between November 27, 2004 and November 28, 2006, corresponding to 385.17 live days. A simultaneous fit was made for the number of NC events detected by the proportional counters and the numbers of NC, CC, and ES events detected by the PMTs, where the spectral distributions of the ES and CC events were not constrained to the <sup>8</sup>B shape.

<sup>4</sup>AHARMIM 05A measurements were made with dissolved NaCl (0.195% by weight) in heavy water over the period between July 26, 2001 and August 28, 2003, corresponding to 391.4 live days, and update AHMED 04A. The CC, ES, and NC events were statistically separated. In one method, the <sup>8</sup>B energy spectrum was not constrained. In the other method, the constraint of an undistorted <sup>8</sup>B energy spectrum was added for comparison with AHMAD 02 results.

<sup>5</sup>AHMAD 02 reports the first SNO result of the <sup>8</sup>B solar-neutrino flux measured with the neutral-current reaction on deuterium,  $\nu_e d \rightarrow np\nu_e$ , above the neutral-current reaction threshold of 2.2 MeV. The data correspond to 306.4 live days with SNO between November 2, 1999 and May 28, 2001. The complete description of the SNO Phase I data set is given in AHARMIM 07.

### $\phi_{\nu_\mu + \nu_\tau}$ (<sup>8</sup>B)

Nonelectron-flavor active neutrino component ( $\nu_\mu$  and  $\nu_\tau$ ) in the <sup>8</sup>B solar-neutrino flux.

VALUE ( $10^6 \text{ cm}^{-2}\text{s}^{-1}$ )	DOCUMENT ID	TECN	COMMENT
• • • We do not use the following data for averages, fits, limits, etc. • • •			
3.26 ± 0.25 <sup>+0.40</sup> / <sub>-0.35</sub>	<sup>1</sup> AHARMIM 05A	SNO	From $\phi_{NC}, \phi_{CC},$ and $\phi_{ES}$ ; <sup>8</sup> B shape not const.
3.09 ± 0.22 <sup>+0.30</sup> / <sub>-0.27</sub>	<sup>1</sup> AHARMIM 05A	SNO	From $\phi_{NC}, \phi_{CC},$ and $\phi_{ES}$ ; <sup>8</sup> B shape constrained
3.41 ± 0.45 <sup>+0.48</sup> / <sub>-0.45</sub>	<sup>2</sup> AHMAD 02	SNO	From $\phi_{NC}, \phi_{CC},$ and $\phi_{ES}$
3.69 ± 1.13	<sup>3</sup> AHMAD 01		Derived from SNO+SuperKam, water Cherenkov

<sup>1</sup>AHARMIM 05A measurements were made with dissolved NaCl (0.195% by weight) in heavy water over the period between July 26, 2001 and August 28, 2003, corresponding to 391.4 live days, and update AHMED 04A. The CC, ES, and NC events were statistically separated. In one method, the <sup>8</sup>B energy spectrum was not constrained. In the other method, the constraint of an undistorted <sup>8</sup>B energy spectrum was added for comparison with AHMAD 02 results.

<sup>2</sup>AHMAD 02 deduced the nonelectron-flavor active neutrino component ( $\nu_\mu$  and  $\nu_\tau$ ) in the <sup>8</sup>B solar-neutrino flux, by combining the charged-current result, the  $\nu_e$  elastic-scattering result and the neutral-current result. The complete description of the SNO Phase I data set is given in AHARMIM 07.

<sup>3</sup>AHMAD 01 deduced the nonelectron-flavor active neutrino component ( $\nu_\mu$  and  $\nu_\tau$ ) in the <sup>8</sup>B solar-neutrino flux, by combining the SNO charged-current result (AHMAD 01) and the Super-Kamiokande  $\nu_e$  elastic-scattering result (FUKUDA 01).

### Total Flux of Active pp Solar Neutrinos

Total flux of active neutrinos ( $\nu_e, \nu_\mu, \nu_\tau$ ).

VALUE ( $10^{10} \text{ cm}^{-2}\text{s}^{-1}$ )	DOCUMENT ID	TECN	COMMENT
• • • We do not use the following data for averages, fits, limits, etc. • • •			
6.1 ± 0.5 <sup>+0.3</sup> / <sub>-0.5</sub>	<sup>1</sup> AGOSTINI 18B	BORX	Use $\nu_e e$ scattering rate

<sup>1</sup>AGOSTINI 18B obtained this result from the measured  $\nu_e e$  elastic scattering rate over the period between December 2011 and May 2016, assuming the MSW-LMA oscillation parameters derived by ESTEBAN 17. Assuming a high-metallicity standard solar model, the electron neutrino survival probability for the pp solar neutrino is calculated to be 0.57 ± 0.09.

### Total Flux of Active <sup>7</sup>Be Solar Neutrinos

Total flux of active neutrinos ( $\nu_e, \nu_\mu, \nu_\tau$ ).

VALUE ( $10^9 \text{ cm}^{-2}\text{s}^{-1}$ )	DOCUMENT ID	TECN	COMMENT
• • • We do not use the following data for averages, fits, limits, etc. • • •			
4.99 ± 0.11 <sup>+0.06</sup> / <sub>-0.08</sub>	<sup>1</sup> AGOSTINI 18B	BORX	Use $\nu_e e$ scattering rate

<sup>1</sup>AGOSTINI 18B obtained this result from the measured  $\nu_e e$  elastic scattering rate over the period between December 2011 and May 2016, assuming the MSW-LMA oscillation parameters derived by ESTEBAN 17. Assuming a high-metallicity standard solar model, the electron neutrino survival probability for the <sup>7</sup>Be solar neutrino is calculated to be 0.53 ± 0.05.

### Total Flux of Active pep Solar Neutrinos

Total flux of active neutrinos ( $\nu_e, \nu_\mu, \nu_\tau$ ).

VALUE ( $10^8 \text{ cm}^{-2}\text{s}^{-1}$ )	DOCUMENT ID	TECN	COMMENT
• • • We do not use the following data for averages, fits, limits, etc. • • •			
1.27 ± 0.19 <sup>+0.08</sup> / <sub>-0.12</sub>	<sup>1</sup> AGOSTINI 18B	BORX	Use $\nu_e e$ scattering rate

<sup>1</sup>AGOSTINI 18B obtained this result from the measured  $\nu_e e$  elastic scattering rate over the period between December 2011 and May 2016, assuming the MSW-LMA oscillation parameters derived by ESTEBAN 17 and a high-metallicity standard solar model. The electron neutrino survival probability for the pep solar neutrino is calculated to be 0.43 ± 0.11.

### Total Flux of Active <sup>8</sup>B Solar Neutrinos

Total flux of active neutrinos ( $\nu_e, \nu_\mu,$  and  $\nu_\tau$ ).

VALUE ( $10^6 \text{ cm}^{-2}\text{s}^{-1}$ )	DOCUMENT ID	TECN	COMMENT
• • • We do not use the following data for averages, fits, limits, etc. • • •			
5.95 <sup>+0.75</sup> / <sub>-0.71</sub> <sup>+0.28</sup> / <sub>-0.30</sub>	<sup>1</sup> ANDERSON 19	SNO+	Water phase; $\nu_e e$ scattering rate
5.68 <sup>+0.39</sup> / <sub>-0.41</sub> <sup>+0.03</sup> / <sub>-0.03</sub>	<sup>2</sup> AGOSTINI 18B	BORX	From $\nu_e e$ scattering rate
5.25 ± 0.16 <sup>+0.11</sup> / <sub>-0.13</sub>	<sup>3</sup> AHARMIM 13	SNO	All three phases combined
5.046 <sup>+0.159</sup> / <sub>-0.152</sub> <sup>+0.107</sup> / <sub>-0.123</sub>	<sup>4</sup> AHARMIM 10	SNO	From $\phi_{NC}$ in Phase I+II, low threshold
5.54 <sup>+0.33</sup> / <sub>-0.31</sub> <sup>+0.36</sup> / <sub>-0.34</sub>	<sup>5</sup> AHARMIM 08	SNO	$\phi_{NC}$ in Phase III
4.94 ± 0.21 <sup>+0.38</sup> / <sub>-0.34</sub>	<sup>6</sup> AHARMIM 05A	SNO	From $\phi_{NC}$ ; <sup>8</sup> B shape not const.
4.81 ± 0.19 <sup>+0.28</sup> / <sub>-0.27</sub>	<sup>6</sup> AHARMIM 05A	SNO	From $\phi_{NC}$ ; <sup>8</sup> B shape constrained
5.09 <sup>+0.44</sup> / <sub>-0.43</sub> <sup>+0.46</sup> / <sub>-0.43</sub>	<sup>7</sup> AHMAD 02	SNO	Direct measurement from $\phi_{NC}$
5.44 ± 0.99	<sup>8</sup> AHMAD 01		Derived from SNO+SuperKam, water Cherenkov

<sup>1</sup>ANDERSON 19 reports this result from the measured  $\nu_e e$  elastic scattering rate using a 69.2 kton-day (or 114.7 days) of exposure from May through December, 2017 during the SNO+ detector's water commissioning phase, assuming the neutrino mixing parameters given in PDG 16 and a standard solar model given in BAHCALL 05.

<sup>2</sup>AGOSTINI 18B obtained this result from the measured  $\nu_e e$  elastic scattering rate over the period between January 2008 and December 2016, assuming the MSW-LMA oscillation parameters derived by ESTEBAN 17. Assuming a high-metallicity standard solar model, the electron neutrino survival probability for the <sup>8</sup>B solar neutrino is calculated to be 0.37 ± 0.08.

<sup>3</sup>AHARMIM 13 obtained this result from a combined analysis of the data from all three phases, SNO-I, II, and III. The measurement of the <sup>8</sup>B flux mostly comes from the NC signal, however, CC contribution is included in the fit.

<sup>4</sup>AHARMIM 10 reports this result from a joint analysis of SNO Phase I+II data with the "effective electron kinetic energy" threshold of 3.5 MeV. This result is obtained with the assumption of unitarity, which relates the NC, CC, and ES rates. The data were fit with the free parameters directly describing the total <sup>8</sup>B neutrino flux and the energy-dependent  $\nu_e$  survival probability.

<sup>5</sup>AHARMIM 08 reports the results from SNO Phase III measurement using an array of <sup>3</sup>He proportional counters to measure the rate of NC interactions in heavy water, over the period between November 27, 2004 and November 28, 2006, corresponding to 385.17



# Lepton Particle Listings

## Neutrino Mixing

live days. A simultaneous fit was made for the number of NC events detected by the proportional counters and the numbers of NC, CC, and ES events detected by the PMTs, where the spectral distributions of the ES and CC events were not constrained to the  $^8\text{B}$  shape.

<sup>6</sup> AHARMIM 05A measurements were made with dissolved NaCl (0.195% by weight) in heavy water over the period between July 26, 2001 and August 28, 2003, corresponding to 391.4 live days, and update AHMED 04A. The CC, ES, and NC events were statistically separated. In one method, the  $^8\text{B}$  energy spectrum was not constrained. In the other method, the constraint of an undistorted  $^8\text{B}$  energy spectrum was added for comparison with AHMAD 02 results.

<sup>7</sup> AHMAD 02 determined the total flux of active  $^8\text{B}$  solar neutrinos by directly measuring the neutral-current reaction,  $\nu_e d \rightarrow np\nu_e$ , which is equally sensitive to  $\nu_e$ ,  $\nu_\mu$ , and  $\nu_\tau$ . The complete description of the SNO Phase I data set is given in AHARMIM 07.

<sup>8</sup> AHMAD 01 deduced the total flux of active  $^8\text{B}$  solar neutrinos by combining the SNO charged-current result (AHMAD 01) and the Super-Kamiokande  $\nu e$  elastic-scattering result (FUKUDA 01).

### Total Flux of Active CNO Solar Neutrinos

Total flux of active neutrinos ( $\nu_e, \nu_\mu, \nu_\tau$ ).

VALUE ( $10^8 \text{ cm}^{-2} \text{ s}^{-1}$ )	CL%	DOCUMENT ID	TECN	COMMENT
---	-----	-------------	------	---------

• • • We do not use the following data for averages, fits, limits, etc. • • •

<7.9                    95                    <sup>1</sup> AGOSTINI    18B BORSX    Use  $\nu_e e$  scattering rate

<sup>1</sup> AGOSTINI 18B obtained this result from an upper limit of the  $\nu_e e$  elastic scattering rate for the CNO neutrinos over the period between December 2011 and May 2016, assuming the MSW-LMA oscillation parameters derived by ESTEBAN 17.

### Total Flux of Active hep Solar Neutrinos

Total flux of active neutrinos ( $\nu_e, \nu_\mu, \nu_\tau$ ).

VALUE ( $10^5 \text{ cm}^{-2} \text{ s}^{-1}$ )	CL%	DOCUMENT ID	TECN	COMMENT
---	-----	-------------	------	---------

• • • We do not use the following data for averages, fits, limits, etc. • • •

<2.2                    90                    <sup>1</sup> AGOSTINI    18B BORSX    Use  $\nu_e e$  scattering rate

<sup>1</sup> AGOSTINI 18B obtained this result from an upper limit of the  $\nu_e e$  elastic scattering rate for the hep neutrino using the dataset corresponding to an exposure of 0.8 kt-yr and assuming the MSW-LMA oscillation parameters derived by ESTEBAN 17.

### Day-Night Asymmetry ( $^8\text{B}$ )

$A = (\phi_{\text{night}} - \phi_{\text{day}}) / \phi_{\text{average}}$

VALUE	DOCUMENT ID	TECN	COMMENT
-------	-------------	------	---------

**0.033 ± 0.010 ± 0.005**                    <sup>1</sup> ABE                    16c SKAM    SK combined; Based on  $\phi_{ES}$

• • • We do not use the following data for averages, fits, limits, etc. • • •

0.036 ± 0.016 ± 0.006                    <sup>2</sup> ABE                    16c SKAM    SK-IV; Based on  $\phi_{ES}$

0.032 ± 0.011 ± 0.005                    <sup>3</sup> RENSHAW            14 SKAM    Based on  $\phi_{ES}$

0.063 ± 0.042 ± 0.037                    <sup>4</sup> CRAVENS            08 SKAM    Based on  $\phi_{ES}$

0.021 ± 0.020 ±  $\begin{smallmatrix} 0.012 \\ -0.013 \end{smallmatrix}$                     <sup>5</sup> HOSAKA            06 SKAM    Based on  $\phi_{ES}$

0.017 ± 0.016 ±  $\begin{smallmatrix} 0.012 \\ -0.013 \end{smallmatrix}$                     <sup>6</sup> HOSAKA            06 SKAM    Fitted in the LMA region

-0.056 ± 0.074 ± 0.053                    <sup>7</sup> AHARMIM            05A SNO    From salty SNO  $\phi_{CC}$

-0.037 ± 0.063 ± 0.032                    <sup>7</sup> AHARMIM            05A SNO    From salty SNO  $\phi_{CC}$ ; const. of no  $\phi_{NC}$  asymmetry

0.14 ± 0.063 ±  $\begin{smallmatrix} 0.015 \\ -0.014 \end{smallmatrix}$                     <sup>8</sup> AHMAD            02B SNO    Derived from SNO  $\phi_{CC}$

0.07 ± 0.049 ±  $\begin{smallmatrix} 0.013 \\ -0.012 \end{smallmatrix}$                     <sup>9</sup> AHMAD            02B SNO    Const. of no  $\phi_{NC}$  asymmetry

<sup>1</sup> ABE 16c reports the combined day-night flux asymmetry results of the four phases of the Super-Kamiokande measurements. Amplitude fit method is used. See footnote to RENSHAW 14.

<sup>2</sup> ABE 16c reports the Super-Kamiokande-IV results for 1664 live days from September 2008 to February 2014. The analysis threshold for day-night flux asymmetry is recoil electron energy of 4.49 MeV (total electron energy of 5.0 MeV). Amplitude fit method is used. See footnote to RENSHAW 14.

<sup>3</sup> RENSHAW 14 obtains this result by using the "amplitude fit" introduced in SMY 04. The data from the Super-Kamiokande(SK)-I, -II, -III, and 1306 live days of the SK-IV measurements are used. The analysis threshold is recoil-electron kinetic energy of 4.5 MeV for SK-III, and SK-IV except for 250 live days in SK-III (6.0 MeV). The analysis threshold for SK-I and SK-II is the same as in the previous reports. (Note that in the previous SK solar-neutrino results, the analysis threshold is quoted as recoil-electron total energy.) This day-night asymmetry result is consistent with neutrino oscillations for  $4 \times 10^{-5} \text{ eV}^2 < \Delta m_{21}^2 < 7 \times 10^{-5} \text{ eV}^2$  and large mixing values of  $\theta_{12}$  at the 68% CL.

<sup>4</sup> CRAVENS 08 reports the Super-Kamiokande-II results for 791 live days from December 2002 to October 2005. The photocathode coverage of the detector is 19% (reduced from 40% of that of Super-Kamiokande-I due to an accident in 2001). The analysis threshold for the day and night fluxes is 7.5 MeV except for the first 159 live days (8.0 MeV).

<sup>5</sup> HOSAKA 06 reports the final results for 1496 live days with Super-Kamiokande-I between May 31, 1996 and July 15, 2001, and replace FUKUDA 02 results. The analysis threshold is 5 MeV except for the first 280 live days (6.5 MeV).

<sup>6</sup> This result with reduced statistical uncertainty is obtained by assuming two-neutrino oscillations within the LMA (large mixing angle) region and by fitting the time variation of the solar neutrino flux measured via  $\nu_e e$  elastic scattering to the variations expected from neutrino oscillations. For details, see SMY 04. There is an additional small systematic error of  $\pm 0.0004$  coming from uncertainty of oscillation parameters.

<sup>7</sup> AHARMIM 05A measurements were made with dissolved NaCl (0.195% by weight) in heavy water over the period between July 26, 2001 and August 28, 2003, with 176.5 days of the live time recorded during the day and 214.9 days during the night. This result is obtained with the spectral distribution of the CC events not constrained to the  $^8\text{B}$  shape.

<sup>8</sup> AHMAD 02b results are based on the charged-current interactions recorded between November 2, 1999 and May 28, 2001, with the day and night live times of 128.5 and 177.9 days, respectively. The complete description of the SNO Phase I data set is given in AHARMIM 07.

<sup>9</sup> AHMAD 02b results are derived from the charged-current interactions, neutral-current interactions, and  $\nu e$  elastic scattering, with the total flux of active neutrinos constrained to have no asymmetry. The data were recorded between November 2, 1999 and May 28, 2001, with the day and night live times of 128.5 and 177.9 days, respectively. The complete description of the SNO Phase I data set is given in AHARMIM 07.

### $\phi_{ES}$ ( $^7\text{Be}$ )

$^7\text{Be}$  solar-neutrino flux measured via  $\nu_e e$  elastic scattering. This process is sensitive to all active neutrino flavors, but with reduced sensitivity to  $\nu_\mu, \nu_\tau$  due to the cross-section difference,  $\sigma(\nu_{\mu,\tau} e) \sim 0.2 \sigma(\nu_e e)$ . If the  $^7\text{Be}$  solar-neutrino flux involves nonelectron flavor active neutrinos, their contribution to the flux is  $\sim 0.2$  times that of  $\nu_e$ .

VALUE ( $10^9 \text{ cm}^{-2} \text{ s}^{-1}$ )	DOCUMENT ID	TECN	COMMENT
---	-------------	------	---------

• • • We do not use the following data for averages, fits, limits, etc. • • •

3.26 ± 0.52                    <sup>1</sup> GANDO            15 KLND    average flux

3.10 ± 0.15                    <sup>2</sup> BELLINI            11A BORSX    average flux

<sup>1</sup> GANDO 15 uses 165.4 kton-day exposure of the KamLAND liquid scintillator detector to measure the 862 keV  $^7\text{Be}$  solar neutrino flux via  $\nu - e$  elastic scattering.

<sup>2</sup> BELLINI 11A reports the  $^7\text{Be}$  solar neutrino flux measured via  $\nu - e$  elastic scattering. The data correspond to 740.7 live days between May 16, 2007 and May 8, 2010, and also correspond to 153.6 ton-year fiducial exposure. BELLINI 11A measured the 862 keV  $^7\text{Be}$  solar neutrino flux, which is an 89.6% branch of the  $^7\text{Be}$  solar neutrino flux, to be  $(2.78 \pm 0.13) \times 10^9 \text{ cm}^{-2} \text{ s}^{-1}$ . Supersedes ARPESELLA 08A.

### $\phi_{ES}$ ( $p\bar{p}$ )

$p\bar{p}$  solar-neutrino flux measured via  $\nu_e e$  elastic scattering. This process is sensitive to all active neutrino flavors, but with reduced sensitivity to  $\nu_\mu, \nu_\tau$  due to the cross section difference,  $\sigma(\nu_{\mu,\tau} e) \sim 0.2 \sigma(\nu_e e)$ . If the  $p\bar{p}$  solar-neutrino flux involves non-electron flavor active neutrinos, their contribution to the flux is  $\sim 0.2$  times that of  $\nu_e$ .

VALUE ( $10^8 \text{ cm}^{-2} \text{ s}^{-1}$ )	DOCUMENT ID	TECN	COMMENT
---	-------------	------	---------

• • • We do not use the following data for averages, fits, limits, etc. • • •

1.0 ± 0.2                    <sup>1</sup> BELLINI            12A BORSX    average flux

<sup>1</sup> BELLINI 12A reports 1.44 MeV  $p\bar{p}$  solar-neutrino flux measured via  $\nu_e e$  elastic scattering. The data were collected between January 13, 2008 and May 9, 2010, corresponding to 20,4009 ton-day fiducial exposure. The listed flux value is calculated from the observed rate of  $p\bar{p}$  solar neutrino interactions in Borexino ( $3.1 \pm 0.6 \pm 0.3 \text{ counts}/(\text{day} \cdot 100 \text{ ton})$ ) and the corresponding rate expected for no neutrino flavor oscillations ( $4.47 \pm 0.05 \text{ counts}/(\text{day} \cdot 100 \text{ ton})$ ), using the SSM prediction for the  $p\bar{p}$  solar neutrino flux of  $(1.441 \pm 0.012) \times 10^8 \text{ cm}^{-2} \text{ s}^{-1}$ .

### $\phi_{ES}$ (CNO)

CNO solar-neutrino flux measured via  $\nu_e e$  elastic scattering. This process is sensitive to all active neutrino flavors, but with reduced sensitivity to  $\nu_\mu, \nu_\tau$  due to the cross section difference,  $\sigma(\nu_{\mu,\tau} e) \sim 0.2 \sigma(\nu_e e)$ . If the CNO solar-neutrino flux involves non-electron flavor active neutrinos, their contribution to the flux is  $\sim 0.2$  times that of  $\nu_e$ .

VALUE ( $10^8 \text{ cm}^{-2} \text{ s}^{-1}$ )	CL%	DOCUMENT ID	TECN	COMMENT
---	-----	-------------	------	---------

• • • We do not use the following data for averages, fits, limits, etc. • • •

<7.7                    90                    <sup>1</sup> BELLINI            12A BORSX    MSW-LMA solution assumed

<sup>1</sup> BELLINI 12A reports an upper limit of the CNO solar neutrino flux measured via  $\nu_e e$  elastic scattering. The data were collected between January 13, 2008 and May 9, 2010, corresponding to 20,409 ton-day fiducial exposure.

### $\phi_{ES}(pp)$

$pp$  solar-neutrino flux measured via  $\nu_e e$  elastic scattering. This process is sensitive to all active neutrino flavors, but with reduced sensitivity to  $\nu_\mu, \nu_\tau$  due to the cross section difference,  $\sigma(\nu_{\mu,\tau} e) \sim 0.3 \sigma(\nu_e e)$ . If the  $pp$  solar-neutrino flux involves nonelectron flavor active neutrinos, their contribution to the flux is  $\sim 0.3$  times of  $\nu_e$ .

VALUE ( $10^{10} \text{ cm}^{-2} \text{ s}^{-1}$ )	DOCUMENT ID	TECN	COMMENT
--	-------------	------	---------

• • • We do not use the following data for averages, fits, limits, etc. • • •

4.4 ± 0.5                    <sup>1</sup> BELLINI            14A BORSX    average flux

<sup>1</sup> BELLINI 14A reports  $pp$  solar-neutrino flux measured via  $\nu_e e$  elastic scattering. The data were collected between January 2012 and May 2013, corresponding to 408 days of data. The  $pp$  neutrino interaction rate in Borexino is measured to be  $144 \pm 13 \pm 10 \text{ counts}/(\text{day} \cdot 100 \text{ ton})$  by fitting the measured energy spectrum of events in the 165–590 keV recoil electron kinetic energy window with the expected signal + background spectrum. The listed flux value  $\phi_{ES}(pp)$  is calculated from the observed rate and the number of  $(3.307 \pm 0.003) \times 10^{31}$  electrons for 100 tons of the Borexino scintillator, and the  $\nu_e e$  integrated cross section over the  $pp$  neutrino spectrum,  $\sigma(\nu_e e) = 11.38 \times 10^{-46} \text{ cm}^2$ .

**$\phi_{CC}(pp)$** 

$pp$  solar-neutrino flux measured with charged-current reaction which is sensitive exclusively to  $\nu_e$ .

VALUE ( $10^{10} \text{ cm}^{-2} \text{ s}^{-1}$ )	DOCUMENT ID	TECN	COMMENT
--	-------------	------	---------

• • • We do not use the following data for averages, fits, limits, etc. • • •

3.38 ± 0.47	<sup>1</sup> ABDURASHI...	09	FIT	Fit existing solar- $\nu$ data
-------------	---------------------------	----	-----	--------------------------------

<sup>1</sup> ABDURASHITOV 09 reports the  $pp$  solar-neutrino flux derived from the Ga solar neutrino capture rate by subtracting contributions from  $^8\text{B}$ ,  $^7\text{Be}$ ,  $ppep$  and CNO solar neutrino fluxes determined by other solar neutrino experiments as well as neutrino oscillation parameters determined from available world neutrino oscillation data.

 **$\phi_{ES}(\text{hep})$** 

hep solar-neutrino flux measured via  $\nu e$  elastic scattering. This process is sensitive to all active neutrino flavors, but with reduced sensitivity to  $\nu_\mu, \nu_\tau$  due to the cross-section difference,  $\sigma(\nu_{\mu,\tau} e) \sim 0.16\sigma(\nu_e e)$ . If the hep solar-neutrino flux involves nonelectron flavor active neutrinos, their contribution to the flux is  $\sim 0.16$  times of  $\nu_e$ .

VALUE ( $10^3 \text{ cm}^{-2} \text{ s}^{-1}$ )	CL%	DOCUMENT ID	TECN	COMMENT
---	-----	-------------	------	---------

• • • We do not use the following data for averages, fits, limits, etc. • • •

<73	90	<sup>1</sup> HOSAKA	06	SKAM
-----	----	---------------------	----	------

<sup>1</sup> HOSAKA 06 result is obtained from the recoil electron energy window of 18–21 MeV, and updates FUKUDA 01 result.

 **$\phi_{\bar{\nu}_e}(\text{8B})$** 

Searches are made for electron antineutrino flux from the Sun. Flux limits listed here are derived relative to the BS05(OP) Standard Solar Model  $^8\text{B}$  solar neutrino flux ( $5.69 \times 10^6 \text{ cm}^{-2} \text{ s}^{-1}$ ), with an assumption that solar  $\bar{\nu}_e$ s follow an unoscillated  $^8\text{B}$  neutrino spectrum.

VALUE (%)	CL%	DOCUMENT ID	TECN	COMMENT
-----------	-----	-------------	------	---------

• • • We do not use the following data for averages, fits, limits, etc. • • •

<0.013	90	BELLINI	11	BORX $E_{\bar{\nu}_e} > 1.8 \text{ MeV}$
<1.9	90	<sup>1</sup> BALATA	06	CNTR $1.8 < E_{\bar{\nu}_e} < 20.0 \text{ MeV}$
<0.72	90	AHARMIM	04	SNO $4.0 < E_{\bar{\nu}_e} < 14.8 \text{ MeV}$
<0.022	90	EGUCHI	04	KLND $8.3 < E_{\bar{\nu}_e} < 14.8 \text{ MeV}$
<0.7	90	GANDO	03	SKAM $8.0 < E_{\bar{\nu}_e} < 20.0 \text{ MeV}$
<1.7	90	AGLIETTA	96	LSD $7 < E_{\bar{\nu}_e} < 17 \text{ MeV}$

<sup>1</sup> BALATA 06 obtained this result from the search for  $\bar{\nu}_e$  interactions with Counting Test Facility (the prototype of the Borexino detector).

**(B) Three-neutrino mixing parameters****THREE-NEUTRINO MIXING PARAMETERS**

Updated July 2019 by M. Goodman (ANL).

**Introduction and Notation:** With the exception of possible short-baseline anomalies (such as LSND), current accelerator, reactor, solar and atmospheric neutrino data can be described within the framework of a  $3 \times 3$  mixing matrix between the flavor states  $\nu_e, \nu_\mu$  and  $\nu_\tau$  and mass eigenstates  $\nu_1, \nu_2$  and  $\nu_3$ . (See equation 14.34 of the review “Neutrino Mass, Mixing and Oscillations” by M.C. Gonzalez-Garcia and M. Yokoyama.) Whether or not this is the ultimately correct framework, it is currently widely used to parametrize neutrino mixing data and to plan new experiments.

The mass differences are called  $\Delta m_{21}^2 \equiv m_2^2 - m_1^2$  and  $\Delta m_{32}^2 \equiv m_3^2 - m_2^2$ . Until recently, we assumed

$$\Delta m_{32}^2 \sim \Delta m_{31}^2. \quad (1)$$

But the experimental error is comparable to the difference  $\Delta m_{31}^2 - \Delta m_{32}^2 = \Delta m_{21}^2$ , so we quote them separately when appropriate. The measurements made by  $\nu_\mu$  disappearance at accelerators and by  $\nu_e$  disappearance at reactors are slightly different mixtures of  $\Delta m_{32}^2$  and  $\Delta m_{31}^2$ . The angles are labeled  $\theta_{12}, \theta_{23}$  and  $\theta_{13}$ . The CP violating phase is called  $\delta_{CP}$ .

The familiar two neutrino form for oscillations is

$$P(\nu_a \rightarrow \nu_b; a \neq b) = \sin^2(2\theta) \sin^2(\Delta m^2 L/4E). \quad (2)$$

Despite the fact that the mixing angles have been measured to be much larger than in the quark sector, the two neutrino form is often a very good approximation and is used in many situations.

The angles appear in the equations below in many forms. They often appear as  $\sin^2(2\theta)$ . The listings currently now use  $\sin^2(\theta)$  because this distinguishes the octant, i.e. whether  $\theta_{23}$  is larger or smaller than  $45^\circ$ .

**Accelerator neutrino experiments:** Ignoring  $\Delta m_{21}^2$ , CP violation, and matter effects, the equations for the probability of appearance in an accelerator oscillation experiment are:

$$P(\nu_\mu \rightarrow \nu_\tau) = \sin^2(2\theta_{23}) \cos^4(\theta_{13}) \sin^2(\Delta m_{32}^2 L/4E) \quad (3)$$

$$P(\nu_\mu \rightarrow \nu_e) = \sin^2(2\theta_{13}) \sin^2(\theta_{23}) \sin^2(\Delta m_{32}^2 L/4E) \quad (4)$$

$$P(\nu_e \rightarrow \nu_\mu) = \sin^2(2\theta_{13}) \sin^2(\theta_{23}) \sin^2(\Delta m_{32}^2 L/4E) \quad (5)$$

$$P(\nu_e \rightarrow \nu_\tau) = \sin^2(2\theta_{13}) \cos^2(\theta_{23}) \sin^2(\Delta m_{32}^2 L/4E). \quad (6)$$

Current and future long-baseline accelerator experiments are studying non-zero  $\theta_{13}$  through  $P(\nu_\mu \rightarrow \nu_e)$ . Including the CP terms and low mass scale, the equation for neutrino oscillation in vacuum is:

$$\begin{aligned} P(\nu_\mu \rightarrow \nu_e) &= P1 + P2 + P3 + P4 \\ P1 &= \sin^2(\theta_{23}) \sin^2(2\theta_{13}) \sin^2(\Delta m_{32}^2 L/4E) \\ P2 &= \cos^2(\theta_{23}) \sin^2(2\theta_{13}) \sin^2(\Delta m_{21}^2 L/4E) \\ P3 &= -/+ J \sin(\delta_{CP}) \sin(\Delta m_{32}^2 L/4E) \\ P4 &= J \cos(\delta_{CP}) \cos(\Delta m_{32}^2 L/4E) \end{aligned} \quad (7)$$

where

$$\begin{aligned} J &= \cos(\theta_{13}) \sin(2\theta_{12}) \sin(2\theta_{13}) \sin(2\theta_{23}) \times \\ &\sin(\Delta m_{32}^2 L/4E) \sin(\Delta m_{21}^2 L/4E) \end{aligned} \quad (8)$$

and the sign in P3 is negative for neutrinos and positive for anti-neutrinos respectively. For most new long-baseline accelerator experiments, P2 can safely be neglected. Also, depending on the distance and the mass order, matter effects need to be included.

**Reactor neutrino experiments:** Nuclear reactors are prolific sources of  $\bar{\nu}_e$  with an energy near 4 MeV. The oscillation probability can be expressed

$$\begin{aligned} P(\bar{\nu}_e \rightarrow \bar{\nu}_e) &= 1 - \cos^4(\theta_{13}) \sin^2(2\theta_{12}) \sin^2(\Delta m_{21}^2 L/4E) \\ &- \cos^2(\theta_{12}) \sin^2(2\theta_{13}) \sin^2(\Delta m_{31}^2 L/4E) \\ &- \sin^2(\theta_{12}) \sin^2(2\theta_{13}) \sin^2(\Delta m_{32}^2 L/4E) \end{aligned} \quad (9)$$

not using the approximation in Eq. (1). For short distances ( $L < 5 \text{ km}$ ) we can ignore the second term on the right and can reimpose approximation Eq. (1). This takes the familiar two neutrino form with  $\theta_{13}$  and  $\Delta m_{32}^2$ :

$$P(\bar{\nu}_e \rightarrow \bar{\nu}_e) = 1 - \sin^2(2\theta_{13}) \sin^2(\Delta m_{32}^2 L/4E). \quad (10)$$

## Lepton Particle Listings

## Neutrino Mixing

**Solar and Atmospheric neutrino experiments:** Solar neutrino experiments are sensitive to  $\nu_e$  disappearance and have allowed the measurement of  $\theta_{12}$  and  $\Delta m_{21}^2$ . They are also sensitive to  $\theta_{13}$ . We identify  $\Delta m_{\odot}^2 = \Delta m_{21}^2$  and  $\theta_{\odot} = \theta_{12}$ .

Atmospheric neutrino experiments are primarily sensitive to  $\nu_{\mu}$  disappearance through  $\nu_{\mu} \rightarrow \nu_{\tau}$  oscillations, and have allowed the measurement of  $\theta_{23}$  and  $\Delta m_{32}^2$ . We identify  $\Delta m_A^2 = \Delta m_{32}^2$  and  $\theta_A = \theta_{23}$ . Despite the large  $\nu_e$  component of the atmospheric neutrino flux, it is difficult to measure  $\Delta m_{21}^2$  effects. This is because of a cancellation between  $\nu_{\mu} \rightarrow \nu_e$  and  $\nu_e \rightarrow \nu_{\mu}$  together with the fact that the ratio of  $\nu_{\mu}$  and  $\nu_e$  atmospheric fluxes, which arise from sequential  $\pi$  and  $\mu$  decay, is near 2.

**Oscillation Parameter Listings:** In Section (B) we encode the three mixing angles  $\theta_{12}$ ,  $\theta_{23}$ ,  $\theta_{13}$ ,  $\delta_{CP}$ , and two mass squared differences  $\Delta m_{21}^2$  and  $\Delta m_{32}^2$ . Our knowledge of  $\theta_{12}$  and  $\Delta m_{21}^2$  comes from the KamLAND reactor neutrino experiment together with solar neutrino experiments. Our knowledge of  $\theta_{23}$  and  $\Delta m_{32}^2$  comes from atmospheric, reactor and long-baseline accelerator neutrino experiments. For the earlier experiments, we identified the large mass splitting as  $\Delta m_{32}^2$ . Now that  $\sigma(\Delta m_{32}^2) \approx \Delta m_{21}^2$ , some experiments report separate values for the two mass orders. Results on  $\theta_{13}$  come from reactor antineutrino disappearance experiments. There are also results from long-baseline accelerator experiments looking for  $\nu_e$  appearance. The interpretation of both kinds of results depends on  $\Delta m_{32}^2$ , and the accelerator results also depend on the mass order,  $\theta_{23}$  and the CP violating phase  $\delta_{CP}$ .

Accelerator and atmospheric experiments have some sensitivity to the CP violation phase  $\delta_{CP}$  through Eq. (7). Note that P3 depends on the sign of  $\Delta m_{32}^2$  so the sensitivity depends on the mass order. For non-maximal  $\theta_{23}$  mixing, it also depends on the octant of  $\theta_{23}$ , i.e. whether  $\theta_{23} > \pi/4$  or  $\theta_{23} < \pi/4$ .

 $\sin^2(\theta_{12})$ 

If an experiment reports  $\sin^2(2\theta_{12})$  we convert the value to  $\sin^2(\theta_{12})$ .

VALUE	DOCUMENT ID	TECN	COMMENT
$0.307^{+0.013}_{-0.012}$	1 ABE	16c FIT	KamLAND+global solar; $3\nu$
• • •	We do not use the following data for averages, fits, limits, etc. • • •		
$0.320^{+0.020}_{-0.016}$	DE-SALAS	18 FIT	Global Fit
$0.310 \pm 0.014$	2 ABE	16c FIT	SKAM+SNO; $3\nu$
$0.334^{+0.027}_{-0.023}$	3 ABE	16c FIT	SK-I+II+III+IV; $3\nu$
$0.327^{+0.026}_{-0.031}$	4 ABE	16c FIT	SK-IV; $3\nu$
$0.323 \pm 0.016$	5 FORERO	14 FIT	$3\nu$
$0.304^{+0.013}_{-0.012}$	6 GONZALEZ...	14 FIT	Either mass ordering; global fit
$0.299^{+0.014}_{-0.014}$	7,8 AHARMIM	13 FIT	global solar; $2\nu$
$0.307^{+0.016}_{-0.013}$	8,9 AHARMIM	13 FIT	global solar; $3\nu$
$0.304^{+0.022}_{-0.018}$	8,10 AHARMIM	13 FIT	KamLAND + global solar; $3\nu$
$0.304^{+0.014}_{-0.013}$	11 GANDO	13 FIT	KamLAND + global solar + SBL + accelerator; $3\nu$
$0.304^{+0.014}_{-0.013}$	12 GANDO	13 FIT	KamLAND + global solar; $3\nu$
$0.325^{+0.039}_{-0.039}$	13 GANDO	13 FIT	KamLAND; $3\nu$
$0.30^{+0.02}_{-0.01}$	14 ABE	11 FIT	KamLAND + global solar; $2\nu$
$0.30^{+0.02}_{-0.01}$	15 ABE	11 FIT	global solar; $2\nu$

$0.31^{+0.03}_{-0.02}$	16 ABE	11 FIT	KamLAND + global solar; $3\nu$
$0.31^{+0.03}_{-0.03}$	17 ABE	11 FIT	global solar; $3\nu$
$0.314^{+0.015}_{-0.012}$	18 BELLINI	11A FIT	KamLAND + global solar; $2\nu$
$0.319^{+0.017}_{-0.015}$	19 BELLINI	11A FIT	global solar; $2\nu$
$0.311^{+0.016}_{-0.016}$	20 GANDO	11 FIT	KamLAND + solar; $3\nu$
$0.304^{+0.046}_{-0.042}$	21 GANDO	11 FIT	KamLAND; $3\nu$
$0.314^{+0.018}_{-0.014}$	22,23 AHARMIM	10 FIT	KamLAND + global solar; $2\nu$
$0.314^{+0.017}_{-0.020}$	22,24 AHARMIM	10 FIT	global solar; $2\nu$
$0.319^{+0.019}_{-0.016}$	22,25 AHARMIM	10 FIT	KamLAND + global solar; $3\nu$
$0.319^{+0.023}_{-0.024}$	22,26 AHARMIM	10 FIT	global solar; $3\nu$
$0.36^{+0.05}_{-0.04}$	27 ABE	08A FIT	KamLAND
$0.32 \pm 0.03$	28 ABE	08A FIT	KamLAND + global fit
$0.32 \pm 0.02$	29 AHARMIM	08 FIT	KamLAND + global solar
$0.31^{+0.04}_{-0.04}$	30 HOSAKA	06 FIT	KamLAND + global solar
$0.31^{+0.04}_{-0.03}$	31 HOSAKA	06 FIT	SKAM+SNO+KamLAND
$0.31^{+0.03}_{-0.04}$	32 HOSAKA	06 FIT	SKAM+SNO
$0.31^{+0.02}_{-0.03}$	33 AHARMIM	05A FIT	KamLAND + global solar
0.25-0.39	34 AHARMIM	05A FIT	global solar
0.29 $\pm$ 0.03	35 ARAKI	05 FIT	KamLAND + global solar
$0.29^{+0.03}_{-0.02}$	36 AHMED	04A FIT	KamLAND + global solar
0.23-0.37	37 AHMED	04A FIT	global solar
$0.31^{+0.04}_{-0.04}$	38 SMY	04 FIT	KamLAND + global solar
$0.29^{+0.04}_{-0.04}$	39 SMY	04 FIT	global solar
$0.32^{+0.06}_{-0.05}$	40 SMY	04 FIT	SKAM + SNO
0.19-0.33	41 AHMAD	02B FIT	global solar
0.19-0.39	42 FUKUDA	02 FIT	global solar

<sup>1</sup> ABE 16c obtained this result by a three-neutrino oscillation analysis, with a constraint of  $\sin^2(\theta_{13}) = 0.0219 \pm 0.0014$  coming from reactor neutrino experiments, using all solar data and KamLAND data. *CPT* invariance is assumed.

<sup>2</sup> ABE 16c obtained this result by a three-neutrino oscillation analysis, with a constraint of  $\sin^2(\theta_{13}) = 0.0219 \pm 0.0014$  coming from reactor neutrino experiments, using Super-Kamiokande (I+II+III+IV) and SNO data.

<sup>3</sup> ABE 16c obtained this result by a three-neutrino oscillation analysis, with a constraint of  $\sin^2(\theta_{13}) = 0.0219 \pm 0.0014$  coming from reactor neutrino experiments, by combining the four phases of the Super-Kamiokande solar data.

<sup>4</sup> ABE 16c obtained this result by a three-neutrino oscillation analysis, with a constraint of  $\sin^2(\theta_{13}) = 0.0219 \pm 0.0014$  coming from reactor neutrino experiments, using the Super-Kamiokande-IV data.

<sup>5</sup> FORERO 14 performs a global fit to neutrino oscillations using solar, reactor, long-baseline accelerator, and atmospheric neutrino data.

<sup>6</sup> GONZALEZ-GARCIA 14 result comes from a frequentist global fit. The corresponding Bayesian global fit to the same data results are reported in BERGSTROM 15 as  $0.304^{+0.013}_{-0.012}$  for normal and  $0.305^{+0.012}_{-0.013}$  for inverted mass ordering.

<sup>7</sup> AHARMIM 13 obtained this result by a two-neutrino oscillation analysis using global solar neutrino data.

<sup>8</sup> AHARMIM 13 global solar neutrino data include SNO's all-phases-combined analysis results on the total active  $^8\text{B}$  neutrino flux and energy-dependent  $\nu_e$  survival probability parameters, measurements of Cl (CLEVELAND 98), Ga (ABDURASHITOV 09 which contains combined analysis with GNO (ALTMANN 05 and Ph.D. thesis of F. Kaether)), and  $^7\text{Be}$  (BELLINI 11A) rates, and  $^8\text{B}$  solar-neutrino recoil electron measurements of SK-I (HOSAKA 06) zenith, SK-II (CRAVEN 08) and SK-III (ABE 11) day/night spectra, and Borexino (BELLINI 10A) spectra.

<sup>9</sup> AHARMIM 13 obtained this result by a three-neutrino oscillation analysis with the value of  $\Delta m_{32}^2$  fixed to  $2.45 \times 10^{-3} \text{ eV}^2$ , using global solar neutrino data.

<sup>10</sup> AHARMIM 13 obtained this result by a three-neutrino oscillation analysis with the value of  $\Delta m_{32}^2$  fixed to  $2.45 \times 10^{-3} \text{ eV}^2$ , using global solar neutrino and KamLAND (GANDO 11) data. *CPT* invariance is assumed.

<sup>11</sup> GANDO 13 obtained this result by a three-neutrino oscillation analysis using KamLAND, global solar neutrino, short-baseline (SBL) reactor, and accelerator data, assuming *CPT* invariance. Supersedes GANDO 11.

<sup>12</sup> GANDO 13 obtained this result by a three-neutrino oscillation analysis using KamLAND and global solar neutrino data, assuming *CPT* invariance. Supersedes GANDO 11.

<sup>13</sup> GANDO 13 obtained this result by a three-neutrino oscillation analysis using KamLAND data. Supersedes GANDO 11.

<sup>14</sup> ABE 11 obtained this result by a two-neutrino oscillation analysis using solar neutrino data including Super-Kamiokande, SNO, Borexino (ARPESELLA 08a), Homestake, GALLEX/GNO, SAGE, and KamLAND data. *CPT* invariance is assumed.

<sup>15</sup> ABE 11 obtained this result by a two-neutrino oscillation analysis using solar neutrino data including Super-Kamiokande, SNO, Borexino (ARPESELLA 08a), Homestake, GALLEX/GNO, and SAGE data.

See key on page 999

# Lepton Particle Listings

## Neutrino Mixing

- <sup>16</sup> ABE 11 obtained this result by a three-neutrino oscillation analysis with the value of  $\Delta m_{32}^2$  fixed to  $2.4 \times 10^{-3} \text{ eV}^2$ , using solar neutrino data including Super-Kamiokande, SNO, Borexino (ARPESELLA 08A), Homestake, GALLEX/GNO, SAGE, and KamLAND data. The normal neutrino mass ordering and CPT invariance are assumed.
- <sup>17</sup> ABE 11 obtained this result by a three-neutrino oscillation analysis with the value of  $\Delta m_{32}^2$  fixed to  $2.4 \times 10^{-3} \text{ eV}^2$ , using solar neutrino data including Super-Kamiokande, SNO, Borexino (ARPESELLA 08A), Homestake, and GALLEX/GNO data. The normal neutrino mass ordering is assumed.
- <sup>18</sup> BELLINI 11A obtained this result by a two-neutrino oscillation analysis using KamLAND, Homestake, SAGE, Gallex, GNO, Kamiokande, Super-Kamiokande, SNO, and Borexino (BELLINI 11A) data and the SSM flux prediction in SERENELLI 11 (Astrophysical Journal **743** 24 (2011)) with the exception that the  $^8\text{B}$  flux was left free. CPT invariance is assumed.
- <sup>19</sup> BELLINI 11A obtained this result by a two-neutrino oscillation analysis using Homestake, SAGE, Gallex, GNO, Kamiokande, Super-Kamiokande, SNO, and Borexino (BELLINI 11A) data and the SSM flux prediction in SERENELLI 11 (Astrophysical Journal **743** 24 (2011)) with the exception that the  $^8\text{B}$  flux was left free.
- <sup>20</sup> GAND0 11 obtain this result with three-neutrino fit using the KamLAND + solar data. Superseded by GAND0 13.
- <sup>21</sup> GAND0 11 obtain this result with three-neutrino fit using the KamLAND data only. Superseded by GAND0 13.
- <sup>22</sup> AHARMIM 10 global solar neutrino data include SNO's low-energy-threshold analysis survival probability day/night curves, SNO Phase III integral rates (AHARMIM 08), Cl (CLEVELAND 98), SAGE (ABDURASHITOV 09), Gallex/GNO (HAMPEL 99, ALTMANN 05), Borexino (ARPESELLA 08A), SK-I zenith (HOSAKA 06), and SK-II day/night spectra (CRAVENS 08).
- <sup>23</sup> AHARMIM 10 obtained this result by a two-neutrino oscillation analysis using global solar neutrino data and KamLAND data (ABE 08A). CPT invariance is assumed.
- <sup>24</sup> AHARMIM 10 obtained this result by a two-neutrino oscillation analysis using global solar neutrino data.
- <sup>25</sup> AHARMIM 10 obtained this result by a three-neutrino oscillation analysis with the value of  $\Delta m_{31}^2$  fixed to  $2.3 \times 10^{-3} \text{ eV}^2$ , using global solar neutrino data and KamLAND data (ABE 08A). CPT invariance is assumed.
- <sup>26</sup> AHARMIM 10 obtained this result by a three-neutrino oscillation analysis with the value of  $\Delta m_{31}^2$  fixed to  $2.3 \times 10^{-3} \text{ eV}^2$ , using global solar neutrino data.
- <sup>27</sup> ABE 08A obtained this result by a rate + shape + time combined geoneutrino and reactor two-neutrino fit for  $\Delta m_{21}^2$  and  $\tan^2\theta_{12}$ , using KamLAND data only. Superseded by GAND0 11.
- <sup>28</sup> ABE 08A obtained this result by means of a two-neutrino fit using KamLAND, Homestake, SAGE, GALLEX, GNO, SK (zenith angle and E-spectrum), the SNO  $\chi^2$ -map, and solar flux data. CPT invariance is assumed. Superseded by GAND0 11.
- <sup>29</sup> The result given by AHARMIM 08 is  $\theta = (34.4^{+1.3}_{-1.2})^\circ$ . This result is obtained by a two-neutrino oscillation analysis using solar neutrino data including those of Borexino (ARPESELLA 08A) and Super-Kamiokande-I (HOSAKA 06), and KamLAND data (ABE 08A). CPT invariance is assumed.
- <sup>30</sup> HOSAKA 06 obtained this result by a two-neutrino oscillation analysis using SK  $\nu_e$  data, CC data from other solar neutrino experiments, and KamLAND data (ARAKI 05). CPT invariance is assumed.
- <sup>31</sup> HOSAKA 06 obtained this result by a two-neutrino oscillation analysis using the data from Super-Kamiokande, SNO (AHMAD 02 and AHMAD 02B), and KamLAND (ARAKI 05) experiments. CPT invariance is assumed.
- <sup>32</sup> HOSAKA 06 obtained this result by a two-neutrino oscillation analysis using the Super-Kamiokande and SNO (AHMAD 02 and AHMAD 02B) solar neutrino data.
- <sup>33</sup> The result given by AHARMIM 05A is  $\theta = (33.9 \pm 1.6)^\circ$ . This result is obtained by a two-neutrino oscillation analysis using SNO pure deuterium and salt phase data, SK  $\nu_e$  data, Cl and Ga CC data, and KamLAND data (ARAKI 05). CPT invariance is assumed. AHARMIM 05A also quotes  $\theta = (33.9^{+2.4}_{-2.2})^\circ$  as the error enveloping the 68% CL two-dimensional region. This translates into  $\sin^2 2\theta = 0.86^{+0.05}_{-0.06}$ .
- <sup>34</sup> AHARMIM 05A obtained this result by a two-neutrino oscillation analysis using the data from all solar neutrino experiments. The listed range of the parameter envelops the 95% CL two-dimensional region shown in figure 35a of AHARMIM 05A. AHARMIM 05A also quotes  $\tan^2\theta = 0.45^{+0.09}_{-0.08}$  as the error enveloping the 68% CL two-dimensional region. This translates into  $\sin^2 2\theta = 0.86^{+0.05}_{-0.07}$ .
- <sup>35</sup> ARAKI 05 obtained this result by a two-neutrino oscillation analysis using KamLAND and solar neutrino data. CPT invariance is assumed. The  $1\sigma$  error shown here is translated from the number provided by the KamLAND collaboration,  $\tan^2\theta = 0.40^{+0.07}_{-0.05}$ . The corresponding number quoted in ARAKI 05 is  $\tan^2\theta = 0.40^{+0.10}_{-0.07}$  ( $\sin^2 2\theta = 0.82 \pm 0.07$ ), which envelops the 68% CL two-dimensional region.
- <sup>36</sup> The result given by AHMED 04A is  $\theta = (32.5^{+1.7}_{-1.6})^\circ$ . This result is obtained by a two-neutrino oscillation analysis using solar neutrino and KamLAND data (EGUCHI 03). CPT invariance is assumed. AHMED 04A also quotes  $\theta = (32.5^{+2.4}_{-2.3})^\circ$  as the error enveloping the 68% CL two-dimensional region. This translates into  $\sin^2 2\theta = 0.82 \pm 0.06$ .
- <sup>37</sup> AHMED 04A obtained this result by a two-neutrino oscillation analysis using the data from all solar neutrino experiments. The listed range of the parameter envelops the 95% CL two-dimensional region shown in Fig. 5(a) of AHMED 04A. The best-fit point is  $\Delta(m^2) = 6.5 \times 10^{-5} \text{ eV}^2$ ,  $\tan^2\theta = 0.40$  ( $\sin^2 2\theta = 0.82$ ).
- <sup>38</sup> The result given by SMY 04 is  $\tan^2\theta = 0.44 \pm 0.08$ . This result is obtained by a two-neutrino oscillation analysis using solar neutrino and KamLAND data (IANNI 03). CPT invariance is assumed.
- <sup>39</sup> SMY 04 obtained this result by a two-neutrino oscillation analysis using the data from all solar neutrino experiments. The  $1\sigma$  errors are read from Fig. 6(a) of SMY 04.

<sup>40</sup> SMY 04 obtained this result by a two-neutrino oscillation analysis using the Super-Kamiokande and SNO (AHMAD 02 and AHMAD 02B) solar neutrino data. The  $1\sigma$  errors are read from Fig. 6(a) of SMY 04.

<sup>41</sup> AHMAD 02B obtained this result by a two-neutrino oscillation analysis using the data from all solar neutrino experiments. The listed range of the parameter envelops the 95% CL two-dimensional region shown in Fig. 4(b) of AHMAD 02B. The best fit point is  $\Delta(m^2) = 5.0 \times 10^{-5} \text{ eV}^2$  and  $\tan\theta = 0.34$  ( $\sin^2 2\theta = 0.76$ ).

<sup>42</sup> FUKUDA 02 obtained this result by a two-neutrino oscillation analysis using the data from all solar neutrino experiments. The listed range of the parameter envelops the 95% CL two-dimensional region shown in Fig. 4 of FUKUDA 02. The best fit point is  $\Delta(m^2) = 6.9 \times 10^{-5} \text{ eV}^2$  and  $\tan^2\theta = 0.38$  ( $\sin^2 2\theta = 0.80$ ).

### $\Delta m_{21}^2$

VALUE ( $10^{-5} \text{ eV}^2$ )	DOCUMENT ID	TECN	COMMENT
<b><math>7.53 \pm 0.18</math></b>	<sup>1</sup> GAND0	13 FIT	KamLAND + global solar + SBL + accelerator: $3\nu$
• • • We do not use the following data for averages, fits, limits, etc. • • •			
$7.55^{+0.20}_{-0.16}$	DE-SALAS	18 FIT	Global Fit
$7.49^{+0.19}_{-0.18}$	<sup>2</sup> ABE	16c FIT	KamLAND+global solar; $3\nu$
$4.8^{+1.3}_{-0.6}$	<sup>3</sup> ABE	16c FIT	SKAM+SNO; $3\nu$
$4.8^{+1.5}_{-0.8}$	<sup>4</sup> ABE	16c FIT	SK-I+II+III+IV; $3\nu$
$3.2^{+2.8}_{-0.2}$	<sup>5</sup> ABE	16c FIT	SK-IV; $3\nu$
$7.6^{+0.19}_{-0.18}$	<sup>6</sup> FORERO	14 FIT	$3\nu$
$7.50^{+0.19}_{-0.17}$	<sup>7</sup> GONZALEZ...	14 FIT	Either mass ordering; global fit
$5.13^{+1.29}_{-0.96}$	<sup>8,9</sup> AHARMIM	13 FIT	global solar: $2\nu$
$5.13^{+1.49}_{-0.98}$	<sup>9,10</sup> AHARMIM	13 FIT	global solar: $3\nu$
$7.46^{+0.20}_{-0.19}$	<sup>9,11</sup> AHARMIM	13 FIT	KamLAND + global solar: $3\nu$
$7.53^{+0.19}_{-0.18}$	<sup>12</sup> GAND0	13 FIT	KamLAND + global solar: $3\nu$
$7.54^{+0.19}_{-0.18}$	<sup>13</sup> GAND0	13 FIT	KamLAND: $3\nu$
$7.6 \pm 0.2$	<sup>14</sup> ABE	11 FIT	KamLAND + global solar: $2\nu$
$6.2^{+1.1}_{-1.9}$	<sup>15</sup> ABE	11 FIT	global solar: $2\nu$
$7.7 \pm 0.3$	<sup>16</sup> ABE	11 FIT	KamLAND + global solar: $3\nu$
$6.0^{+2.2}_{-2.5}$	<sup>17</sup> ABE	11 FIT	global solar: $3\nu$
$7.50^{+0.16}_{-0.24}$	<sup>18</sup> BELLINI	11A FIT	KamLAND + global solar: $2\nu$
$5.2^{+1.5}_{-0.9}$	<sup>19</sup> BELLINI	11A FIT	global solar: $2\nu$
$7.50^{+0.19}_{-0.20}$	<sup>20</sup> GAND0	11 FIT	KamLAND + solar: $3\nu$
$7.49 \pm 0.20$	<sup>21</sup> GAND0	11 FIT	KamLAND: $3\nu$
$7.59^{+0.20}_{-0.21}$	<sup>22,23</sup> AHARMIM	10 FIT	KamLAND + global solar: $2\nu$
$5.89^{+2.13}_{-2.16}$	<sup>22,24</sup> AHARMIM	10 FIT	global solar: $2\nu$
$7.59 \pm 0.21$	<sup>22,25</sup> AHARMIM	10 FIT	KamLAND + global solar: $3\nu$
$6.31^{+2.49}_{-2.58}$	<sup>22,26</sup> AHARMIM	10 FIT	global solar: $3\nu$
$7.58^{+0.14}_{-0.13} \pm 0.15$	<sup>27</sup> ABE	08A FIT	KamLAND
$7.59 \pm 0.21$	<sup>28</sup> ABE	08A FIT	KamLAND + global solar
$7.59^{+0.19}_{-0.21}$	<sup>29</sup> AHARMIM	08 FIT	KamLAND + global solar
$8.0 \pm 0.3$	<sup>30</sup> HOSAKA	06 FIT	KamLAND + global solar
$8.0 \pm 0.3$	<sup>31</sup> HOSAKA	06 FIT	SKAM+SNO+KamLAND
$6.3^{+3.7}_{-1.5}$	<sup>32</sup> HOSAKA	06 FIT	SKAM+SNO
5–12	<sup>33</sup> HOSAKA	06 FIT	SKAM day/night in the LMA region
$8.0^{+0.4}_{-0.3}$	<sup>34</sup> AHARMIM	05A FIT	KamLAND + global solar LMA
3.3–14.4	<sup>35</sup> AHARMIM	05A FIT	global solar
$7.9^{+0.4}_{-0.3}$	<sup>36</sup> ARAKI	05 FIT	KamLAND + global solar
$7.1^{+1.0}_{-0.3}$	<sup>37</sup> AHMED	04A FIT	KamLAND + global solar
3.2–13.7	<sup>38</sup> AHMED	04A FIT	global solar
$7.1^{+0.6}_{-0.5}$	<sup>39</sup> SMY	04 FIT	KamLAND + global solar
$6.0^{+1.7}_{-1.6}$	<sup>40</sup> SMY	04 FIT	global solar
$6.0^{+2.5}_{-1.6}$	<sup>41</sup> SMY	04 FIT	SKAM + SNO
2.8–12.0	<sup>42</sup> AHMAD	02B FIT	global solar
3.2–19.1	<sup>43</sup> FUKUDA	02 FIT	global solar

<sup>1</sup> GAND0 13 obtained this result by a three-neutrino oscillation analysis using KamLAND, global solar neutrino, short-baseline (SBL) reactor, and accelerator data, assuming CPT invariance. Supersedes GAND0 11.

<sup>2</sup> ABE 16c obtained this result by a three-neutrino oscillation analysis, with a constraint of  $\sin^2(\theta_{13}) = 0.0219 \pm 0.0014$  coming from reactor neutrino experiments, using all solar data and KamLAND data. CPT invariance is assumed.

## Lepton Particle Listings

## Neutrino Mixing

- <sup>3</sup> ABE 16c obtained this result by a three-neutrino oscillation analysis, with a constraint of  $\sin^2(\theta_{13}) = 0.0219 \pm 0.0014$  coming from reactor neutrino experiments, using Super-Kamiokande (I+II+III+IV) and SNO data.
- <sup>4</sup> ABE 16c obtained this result by a three-neutrino oscillation analysis, with a constraint of  $\sin^2(\theta_{13}) = 0.0219 \pm 0.0014$  coming from reactor neutrino experiments, by combining the four phases of the Super-Kamiokande solar data.
- <sup>5</sup> ABE 16c obtained this result by a three-neutrino oscillation analysis, with a constraint of  $\sin^2(\theta_{13}) = 0.0219 \pm 0.0014$  coming from reactor neutrino experiments, using the Super-Kamiokande-IV data.
- <sup>6</sup> FORERO 14 performs a global fit to  $\Delta m_{21}^2$  using solar, reactor, long-baseline accelerator, and atmospheric neutrino data.
- <sup>7</sup> GONZALEZ-GARCIA 14 result comes from a frequentist global fit. The corresponding Bayesian global fit to the same data results are reported in BERGSTROM 15 as  $(7.50^{+0.19}_{-0.17}) \times 10^{-5} \text{ eV}^2$  for normal and  $(7.50^{+0.18}_{-0.17}) \times 10^{-5} \text{ eV}^2$  for inverted mass ordering.
- <sup>8</sup> AHARMIM 13 obtained this result by a two-neutrino oscillation analysis using global solar neutrino data.
- <sup>9</sup> AHARMIM 13 global solar neutrino data include SNO's all-phases-combined analysis results on the total active  $^8\text{B}$  neutrino flux and energy-dependent  $\nu_e$  survival probability parameters, measurements of Cl (CLEVELAND 98), Ga (ABDURASHITOV 09 which contains combined analysis with GNO (ALTMANN 05 and Ph.D. thesis of F. Kaether)), and  $^7\text{Be}$  (BELLINI 11A) rates, and  $^8\text{B}$  solar-neutrino recoil electron measurements of SK-I (HOSAKA 06) zenith, SK-II (CRAVENS 08), and SK-III (ABE 11) day/night spectra, and Borexino (BELLINI 10A) spectra.
- <sup>10</sup> AHARMIM 13 obtained this result by a three-neutrino oscillation analysis with the value of  $\Delta m_{31}^2$  fixed to  $2.45 \times 10^{-3} \text{ eV}^2$ , using global solar neutrino data.
- <sup>11</sup> AHARMIM 13 obtained this result by a three-neutrino oscillation analysis with the value of  $\Delta m_{31}^2$  fixed to  $2.45 \times 10^{-3} \text{ eV}^2$ , using global solar neutrino and KamLAND data (GANDO 11). *CPT* invariance is assumed.
- <sup>12</sup> GANDO 13 obtained this result by a three-neutrino oscillation analysis using KamLAND and global solar neutrino data, assuming *CPT* invariance. Supersedes GANDO 11.
- <sup>13</sup> GANDO 13 obtained this result by a three-neutrino oscillation analysis using KamLAND data. Supersedes GANDO 11.
- <sup>14</sup> ABE 11 obtained this result by a two-neutrino oscillation analysis using solar neutrino data including Super-Kamiokande, SNO, Borexino (ARPESELLA 08a), Homestake, GALLEX/GNO, SAGE, and KamLAND data. *CPT* invariance is assumed.
- <sup>15</sup> ABE 11 obtained this result by a two-neutrino oscillation analysis using solar neutrino data including Super-Kamiokande, SNO, Borexino (ARPESELLA 08a), Homestake, GALLEX/GNO, and SAGE data.
- <sup>16</sup> ABE 11 obtained this result by a three-neutrino oscillation analysis with the value of  $\Delta m_{32}^2$  fixed to  $2.4 \times 10^{-3} \text{ eV}^2$ , using solar neutrino data including Super-Kamiokande, SNO, Borexino (ARPESELLA 08a), Homestake, GALLEX/GNO, SAGE, and KamLAND data. The normal neutrino mass ordering and *CPT* invariance are assumed.
- <sup>17</sup> ABE 11 obtained this result by a three-neutrino oscillation analysis with the value of  $\Delta m_{32}^2$  fixed to  $2.4 \times 10^{-3} \text{ eV}^2$ , using solar neutrino data including Super-Kamiokande, SNO, Borexino (ARPESELLA 08a), Homestake, and GALLEX/GNO data. The normal neutrino mass ordering is assumed.
- <sup>18</sup> BELLINI 11A obtained this result by a two-neutrino oscillation analysis using KamLAND, Homestake, SAGE, Gallex, GNO, Kamiokande, Super-Kamiokande, SNO, and Borexino (BELLINI 11A) data and the SSM flux prediction in SERENELLI 11 (Astrophysical Journal **743** 24 (2011)) with the exception that the  $^8\text{B}$  flux was left free. *CPT* invariance is assumed.
- <sup>19</sup> BELLINI 11A obtained this result by a two-neutrino oscillation analysis using Homestake, SAGE, Gallex, GNO, Kamiokande, Super-Kamiokande, SNO, and Borexino (BELLINI 11A) data and the SSM flux prediction in SERENELLI 11 (Astrophysical Journal **743** 24 (2011)) with the exception that the  $^8\text{B}$  flux was left free.
- <sup>20</sup> GANDO 11 obtain this result with three-neutrino fit using the KamLAND + solar data. Superseded by GANDO 13.
- <sup>21</sup> GANDO 11 obtain this result with three-neutrino fit using the KamLAND data only. Supersedes ABE 08a.
- <sup>22</sup> AHARMIM 10 global solar neutrino data include SNO's low-energy-threshold analysis survival probability day/night curves, SNO Phase III integral rates (AHARMIM 08), Cl (CLEVELAND 98), SAGE (ABDURASHITOV 09), Gallex/GNO (HAMPEL 99, ALTMANN 05), Borexino (ARPESELLA 08a), SK-I zenith (HOSAKA 06), and SK-II day/night spectra (CRAVENS 08).
- <sup>23</sup> AHARMIM 10 obtained this result by a two-neutrino oscillation analysis using global solar neutrino data and KamLAND data (ABE 08a). *CPT* invariance is assumed.
- <sup>24</sup> AHARMIM 10 obtained this result by a two-neutrino oscillation analysis using global solar neutrino data.
- <sup>25</sup> AHARMIM 10 obtained this result by a three-neutrino oscillation analysis with the value of  $\Delta m_{31}^2$  fixed to  $2.3 \times 10^{-3} \text{ eV}^2$ , using global solar neutrino data and KamLAND data (ABE 08a). *CPT* invariance is assumed.
- <sup>26</sup> AHARMIM 10 obtained this result by a three-neutrino oscillation analysis with the value of  $\Delta m_{31}^2$  fixed to  $2.3 \times 10^{-3} \text{ eV}^2$ , using global solar neutrino data.
- <sup>27</sup> ABE 08a obtained this result by a rate + shape + time combined geoneutrino and reactor two-neutrino fit for  $\Delta m_{21}^2$  and  $\tan^2\theta_{12}$ , using KamLAND data only. Superseded by GANDO 11.
- <sup>28</sup> ABE 08a obtained this result by means of a two-neutrino fit using KamLAND, Homestake, SAGE, GALLEX, GNO, SK (zenith angle and E-spectrum), the SNO  $\chi^2$ -map, and solar flux data. *CPT* invariance is assumed. Superseded by GANDO 11.
- <sup>29</sup> AHARMIM 08 obtained this result by a two-neutrino oscillation analysis using all solar neutrino data including those of Borexino (ARPESELLA 08a) and Super-Kamiokande-I (HOSAKA 06), and KamLAND data (ABE 08a). *CPT* invariance is assumed.
- <sup>30</sup> HOSAKA 06 obtained this result by a two-neutrino oscillation analysis using solar neutrino and KamLAND data (ARAKI 05). *CPT* invariance is assumed.
- <sup>31</sup> HOSAKA 06 obtained this result by a two-neutrino oscillation analysis using the data from Super-Kamiokande, SNO (AHMAD 02 and AHMAD 02b), and KamLAND (ARAKI 05) experiments. *CPT* invariance is assumed.
- <sup>32</sup> HOSAKA 06 obtained this result by a two-neutrino oscillation analysis using the Super-Kamiokande and SNO (AHMAD 02 and AHMAD 02b) solar neutrino data.
- <sup>33</sup> HOSAKA 06 obtained this result from the consistency between the observed and expected day-night flux asymmetry amplitude. The listed 68% CL range is derived from the  $1\sigma$  boundary of the amplitude fit to the data. Oscillation parameters are constrained to be in the LMA region. The mixing angle is fixed at  $\tan^2\theta = 0.44$  because the fit depends only very weakly on it.
- <sup>34</sup> AHARMIM 05a obtained this result by a two-neutrino oscillation analysis using solar neutrino and KamLAND data (ARAKI 05). *CPT* invariance is assumed. AHARMIM 05a also quotes  $\Delta(m^2) = (8.0^{+0.6}_{-0.4}) \times 10^{-5} \text{ eV}^2$  as the error enveloping the 68% CL two-dimensional region.
- <sup>35</sup> AHARMIM 05a obtained this result by a two-neutrino oscillation analysis using the data from all solar neutrino experiments. The listed range of the parameter envelops the 95% CL two-dimensional region shown in figure 35a of AHARMIM 05a. AHARMIM 05a also quotes  $\Delta(m^2) = (6.5^{+4.4}_{-2.3}) \times 10^{-5} \text{ eV}^2$  as the error enveloping the 68% CL two-dimensional region.
- <sup>36</sup> ARAKI 05 obtained this result by a two-neutrino oscillation analysis using KamLAND and solar neutrino data. *CPT* invariance is assumed. The  $1\sigma$  error shown here is provided by the KamLAND collaboration. The error quoted in ARAKI 05,  $\Delta(m^2) = (7.9^{+0.6}_{-0.5}) \times 10^{-5}$ , envelops the 68% CL two-dimensional region.
- <sup>37</sup> AHMED 04a obtained this result by a two-neutrino oscillation analysis using solar neutrino and KamLAND data (EGUCHI 03). *CPT* invariance is assumed. AHMED 04a also quotes  $\Delta(m^2) = (7.1^{+1.2}_{-0.6}) \times 10^{-5} \text{ eV}^2$  as the error enveloping the 68% CL two-dimensional region.
- <sup>38</sup> AHMED 04a obtained this result by a two-neutrino oscillation analysis using the data from all solar neutrino experiments. The listed range of the parameter envelops the 95% CL two-dimensional region shown in Fig. 5(a) of AHMED 04a. The best-fit point is  $\Delta(m^2) = 6.5 \times 10^{-5} \text{ eV}^2$ ,  $\tan^2\theta = 0.40$  ( $\sin^2 2\theta = 0.82$ ).
- <sup>39</sup> SMY 04 obtained this result by a two-neutrino oscillation analysis using solar neutrino and KamLAND data (IANNI 03). *CPT* invariance is assumed.
- <sup>40</sup> SMY 04 obtained this result by a two-neutrino oscillation analysis using the data from all solar neutrino experiments. The  $1\sigma$  errors are read from Fig. 6(a) of SMY 04.
- <sup>41</sup> SMY 04 obtained this result by a two-neutrino oscillation analysis using the Super-Kamiokande and SNO (AHMAD 02 and AHMAD 02b) solar neutrino data. The  $1\sigma$  errors are read from Fig. 6(a) of SMY 04.
- <sup>42</sup> AHMAD 02b obtained this result by a two-neutrino oscillation analysis using the data from all solar neutrino experiments. The listed range of the parameter envelops the 95% CL two-dimensional region shown in Fig. 4(b) of AHMAD 02b. The best fit point is  $\Delta(m^2) = 5.0 \times 10^{-5} \text{ eV}^2$  and  $\tan\theta = 0.34$  ( $\sin^2 2\theta = 0.76$ ).
- <sup>43</sup> FUKUDA 02 obtained this result by a two-neutrino oscillation analysis using the data from all solar neutrino experiments. The listed range of the parameter envelops the 95% CL two-dimensional region shown in Fig. 4 of FUKUDA 02. The best fit point is  $\Delta(m^2) = 6.9 \times 10^{-5} \text{ eV}^2$  and  $\tan^2\theta = 0.38$  ( $\sin^2 2\theta = 0.80$ ).

 $\sin^2(\theta_{23})$ 

The reported limits below correspond to the projection onto the  $\sin^2(\theta_{23})$  axis of the 90% CL contours in the  $\sin^2(\theta_{23}) - \Delta m_{32}^2$  plane presented by the authors. Unless otherwise specified, the limits are 90% CL and the reported uncertainties are 68% CL.

If an experiment reports  $\sin^2(2\theta_{23})$  we convert the value to  $\sin^2(\theta_{23})$ .

VALUE	DOCUMENT ID	TECN	COMMENT
<b>0.547 ± 0.021 OUR FIT</b>	Assuming inverted mass ordering		
<b>0.545 ± 0.021 OUR FIT</b>	Assuming normal mass ordering		
$0.56^{+0.04}_{-0.03}$	1 ACERO	19 NOVA	Normal mass order; octant II for $\theta_{23}$
$0.56^{+0.04}_{-0.03}$	1,2 ACERO	19 NOVA	Inverted mass order; octant II for $\theta_{23}$
$0.51^{+0.07}_{-0.09}$	3 AARTSEN	18a ICCB	Normal mass ordering
$0.588^{+0.031}_{-0.064}$	4 ABE	18b SKAM	Normal mass ordering, $\theta_{13}$ constrained
$0.575^{+0.036}_{-0.073}$	4 ABE	18b SKAM	Inverted mass ordering, $\theta_{13}$ constrained
$0.526^{+0.032}_{-0.036}$	5 ABE	18g T2K	Normal mass ordering, $\theta_{13}$ constrained
$0.530^{+0.030}_{-0.034}$	5 ABE	18g T2K	Inverted mass ordering, $\theta_{13}$ constrained
$0.41^{+0.23}_{-0.06}$	6 ADAMSON	14 MINS	Normal mass ordering
$0.41^{+0.26}_{-0.07}$	6 ADAMSON	14 MINS	Inverted mass ordering
• • • We do not use the following data for averages, fits, limits, etc. • • •			
0.455	7 AARTSEN	20 ICCB	For both mass orderings
$0.58^{+0.04}_{-0.13}$	8 AARTSEN	19c ICCB	
$0.48^{+0.04}_{-0.03}$	1,2 ACERO	19 NOVA	Normal mass order; octant I for $\theta_{23}$
$0.47^{+0.04}_{-0.03}$	1,2 ACERO	19 NOVA	Inverted mass order; octant I for $\theta_{23}$

0.49	$+0.30$ $-0.28$	AGAFONOVA	19	OPER		0.24 to 0.76	<sup>53</sup> HATAKEYAMA98	KAMI	Kamiokande	
0.50	$+0.20$ $-0.19$	<sup>9</sup> ALBERT	19	ANTR	Atmospheric $\nu$ , deep sea telescope	0.20 to 0.80	<sup>54</sup> FUKUDA	94	KAMI	Kamiokande
0.587	$+0.036$ $-0.069$	<sup>10</sup> ABE	18B	SKAM	$3\nu$ osc: normal mass ordering, $\theta_{13}$ free	<sup>1</sup> ACERO 19 is based on a sample size of $12.33 \times 10^{20}$ protons on target. The fit combines both antineutrino and neutrino data to extract the oscillation parameters. The results favor the normal mass ordering by $1.9 \sigma$ and $\theta_{23}$ values in octant II by $1.6 \sigma$ . Supersedes ACERO 18. <sup>2</sup> Errors are from normal mass ordering and $\theta_{13}$ octant II fits. <sup>3</sup> AARTSEN 18A uses three years (April 2012 – May 2015) of neutrino data from full sky with reconstructed energies between 5.6 and 56 GeV, measured with the low-energy subdetector DeepCore of the IceCube neutrino telescope. AARTSEN 18A also reports the best fit result for the inverted mass ordering as $\Delta m_{32}^2 = -2.32 \times 10^{-3} \text{ eV}^2$ and $\sin^2(\theta_{23}) = 0.51$ . Uncertainties for the inverted mass ordering fits were not provided. Supersedes AARTSEN 15A. <sup>4</sup> ABE 18B uses 328 kton-years of Super-Kamiokande I-IV atmospheric neutrino data to obtain this result. The fit is performed over the three parameters, $\Delta m_{21}^2$ , $\sin^2(\theta_{23})$ , and $\delta$ , while the solar parameters and $\sin^2(\theta_{13})$ are fixed to $\Delta m_{21}^2 = (7.53 \pm 0.18) \times 10^{-5} \text{ eV}^2$ , $\sin^2(\theta_{12}) = 0.304 \pm 0.014$ , and $\sin^2(\theta_{13}) = 0.0219 \pm 0.0012$ . <sup>5</sup> ABE 18c data prefers normal mass ordering is with a posterior probability of 87%. Supersedes ABE 17F. <sup>6</sup> ADAMSON 14 uses a complete set of accelerator and atmospheric data. The analysis combines the $\nu_\mu$ disappearance and $\nu_e$ appearance data using three-neutrino oscillation fit. The fit results are obtained for normal and inverted mass ordering assumptions. The best fit is for first $\theta_{23}$ octant and inverted mass ordering. <sup>7</sup> AARTSEN 20 uses the data taken between May 2012 and April 2014 with the low-energy subdetector DeepCore of the IceCube neutrino telescope. The reconstructed energy range is between 4 (5) and 90 (80) GeV for the main (confirmatory) analysis. Though the observed best-fit is in the lower octant for both mass orderings, a substantial range of $\sin^2(\theta_{23}) > 0.5$ is still compatible with the observed data for both mass orderings. <sup>8</sup> AARTSEN 19c uses three years (April 2012 – May 2015) of neutrino data from full sky with reconstructed energies between 5.6 and 56 GeV, measured with the low-energy sub-detector DeepCore of the IceCube neutrino telescope. AARTSEN 19c adopts looser event selection criteria to prioritize the efficiency of selecting neutrino events, different from tighter event selection criteria which closely follow the criteria used by AARTSEN 18A to measure the $\nu_\mu$ disappearance. <sup>9</sup> ALBERT 19 measured the oscillation parameters of atmospheric neutrinos with the ANTARES deep sea neutrino telescope using the data taken from 2007 to 2016 (2830 days of total live time). Supersedes ADRIAN-MARTINEZ 12. <sup>10</sup> ABE 18b uses 328 kton-years of Super-Kamiokande I-IV atmospheric neutrino data to obtain this result. The fit is performed over the four parameters, $\Delta m_{21}^2$ , $\sin^2\theta_{23}$ , $\sin^2\theta_{13}$ , and $\delta$ , while the solar parameters are fixed to $\Delta m_{21}^2 = (7.53 \pm 0.18) \times 10^{-5} \text{ eV}^2$ and $\sin^2\theta_{12} = 0.304 \pm 0.014$ . <sup>11</sup> ACERO 18 performs a joint fit to the data for $\nu_\mu$ disappearance and $\nu_e$ appearance. The overall best fit favors normal mass ordering and $\theta_{23}$ in octant II. No $1\sigma$ confidence intervals are presented for the inverted mass ordering scenarios. Superseded by ACERO 19. <sup>12</sup> Errors are from the projections of the 68% contour on 2D plot of $\Delta m^2$ versus $\sin^2(\theta_{23})$ . ABE 17f supersedes ABE 17A. Superseded by ABE 18g. <sup>13</sup> Superseded by ACERO 18. <sup>14</sup> ABE 16d reports oscillation results using $\bar{\nu}_\mu$ disappearance in an off-axis beam. <sup>15</sup> ADAMSON 16A obtains $\sin^2(\theta_{23})$ in the 68% C.L. range [0.38, 0.65] ([0.37, 0.64]), with two statistically degenerate best-fit values of 0.44 and 0.59 (0.44 and 0.59) for normal (inverted) mass ordering. Superseded by ADAMSON 17A. <sup>16</sup> AARTSEN 15A obtains this result by a three-neutrino oscillation analysis using 10–100 GeV muon neutrino sample from a total of 953 days of measurement with the low-energy subdetector DeepCore of the IceCube neutrino telescope. Superseded by AARTSEN 18A. <sup>17</sup> ABE 14 results are based on $\nu_\mu$ disappearance using three-neutrino oscillation fit. The confidence intervals are derived from one dimensional profiled likelihoods. Superseded by ABE 17A. <sup>18</sup> FORERO 14 performs a global fit to neutrino oscillations using solar, reactor, long-baseline accelerator, and atmospheric neutrino data. <sup>19</sup> GONZALEZ-GARCIA 14 result comes from a frequentist global fit. The corresponding Bayesian global fit to the same data results are reported in BERGSTROM 15 as 68% CL intervals of 0.433–0.496 or 0.530–0.594 for normal and 0.514–0.612 for inverted mass ordering. <sup>20</sup> AARTSEN 13B obtained this result by a two-neutrino oscillation analysis using 20–100 GeV muon neutrino sample from a total of 318.9 days of live-time measurement with the low-energy subdetector DeepCore of the IceCube neutrino telescope. <sup>21</sup> The best fit value is $\sin^2(\theta_{23}) = 0.514 \pm 0.082$ . Superseded by ABE 14. <sup>22</sup> ADAMSON 13B obtained this result from $\nu_\mu$ and $\bar{\nu}_\mu$ disappearance using $\nu_\mu$ (10.71 $\times$ 10 <sup>20</sup> POT) and $\bar{\nu}_\mu$ (3.36 $\times$ 10 <sup>20</sup> POT) beams, and atmospheric (37.88kton-years) data from MINOS. The fit assumed two-flavor neutrino hypothesis and identical $\nu_\mu$ and $\bar{\nu}_\mu$ oscillation parameters. Superseded by ADAMSON 14. <sup>23</sup> ABE 12a obtained this result by a two-neutrino oscillation analysis. The best-fit point is $\sin^2(2\theta_{23}) = 0.98$ . <sup>24</sup> ADAMSON 12 is a two-neutrino oscillation analysis using antineutrinos. The best fit value is $\sin^2(2\theta_{23}) = 0.95^{+0.10}_{-0.11} \pm 0.01$ . <sup>25</sup> ADAMSON 12B obtained this result by a two-neutrino oscillation analysis of the L/E distribution using 37.9 kton-yr atmospheric neutrino data with the MINOS far detector. <sup>26</sup> The best fit point is $\Delta m^2 = 0.0019 \text{ eV}^2$ and $\sin^2 2\theta = 0.99$ . The 90% single-parameter confidence interval at the best fit point is $\sin^2 2\theta > 0.86$ . <sup>27</sup> The data are separated into pure samples of $\nu_S$ and $\bar{\nu}_S$ , and separate oscillation parameters for $\nu_S$ and $\bar{\nu}_S$ are fit to the data. The best fit point is $(\Delta m^2, \sin^2 2\theta) = (0.0022 \text{ eV}^2, 0.99)$ and $(\Delta \bar{m}^2, \sin^2 2\bar{\theta}) = (0.0016 \text{ eV}^2, 1.00)$ . The quoted result is taken from the				
0.551	$+0.044$ $-0.075$	<sup>10</sup> ABE	18B	SKAM	$3\nu$ osc: inverted mass ordering, $\theta_{13}$ free					
0.56	$\pm 0.04$	<sup>11</sup> ACERO	18	NOVA	Normal mass order; octant II for $\theta_{23}$					
0.47	$\pm 0.04$	<sup>11</sup> ACERO	18	NOVA	Normal mass order; octant I for $\theta_{23}$					
0.547	$+0.020$ $-0.030$	DE-SALAS	18	FIT	Normal mass ordering, global fit					
0.551	$+0.018$ $-0.030$	DE-SALAS	18	FIT	Inverted mass order, global fit					
0.532	$+0.061$ $-0.087$	<sup>12</sup> ABE	17A	T2K	Normal mass ordering					
0.534	$+0.061$ $-0.087$	<sup>12</sup> ABE	17A	T2K	Inverted mass ordering					
0.51	$+0.08$ $-0.07$	ABE	17C	T2K	Normal mass ordering with neutrinos					
0.42	$+0.25$ $-0.07$	ABE	17C	T2K	Normal mass ordering with antineutrinos					
0.52	$+0.075$ $-0.09$	ABE	17C	T2K	normal mass ordering with neutrinos and antineutrinos					
0.55	$+0.05$ $-0.09$	<sup>12</sup> ABE	17F	T2K	Normal mass ordering					
0.55	$+0.05$ $-0.08$	<sup>12</sup> ABE	17F	T2K	Inverted mass ordering					
0.404	$+0.022$ $-0.030$	<sup>13</sup> ADAMSON	17A	NOVA	Normal mass ordering; octant I for $\theta_{23}$					
0.624	$+0.022$ $-0.030$	<sup>13</sup> ADAMSON	17A	NOVA	Normal mass ordering; octant II for $\theta_{23}$					
0.398	$+0.030$ $-0.022$	<sup>13</sup> ADAMSON	17A	NOVA	Inverted mass ordering; octant I for $\theta_{23}$					
0.618	$+0.022$ $-0.030$	<sup>13</sup> ADAMSON	17A	NOVA	Inverted mass ordering; octant II for $\theta_{23}$					
0.45	$+0.19$ $-0.07$	<sup>14</sup> ABE	16D	T2K	$3\nu$ osc; normal mass ordering; $\bar{\nu}$ beam					
0.38	to 0.65	<sup>15</sup> ADAMSON	16A	NOVA	normal mass ordering					
0.37	to 0.64	<sup>15</sup> ADAMSON	16A	NOVA	Inverted mass ordering					
0.53	$+0.09$ $-0.12$	<sup>16</sup> AARTSEN	15A	ICCB	Normal mass ordering					
0.51	$+0.09$ $-0.11$	<sup>16</sup> AARTSEN	15A	ICCB	Inverted mass ordering					
0.514	$+0.055$ $-0.056$	<sup>17</sup> ABE	14	T2K	$3\nu$ osc.; normal mass ordering					
0.511	$\pm 0.055$	<sup>17</sup> ABE	14	T2K	$3\nu$ osc.; inverted mass ordering					
0.567	$+0.032$ $-0.126$	<sup>18</sup> FORERO	14	FIT	Normal mass ordering					
0.573	$+0.025$ $-0.043$	<sup>18</sup> FORERO	14	FIT	Inverted mass ordering					
0.452	$+0.052$ $-0.028$	<sup>19</sup> GONZALEZ...	14	FIT	Normal mass ordering; global fit					
0.579	$+0.025$ $-0.037$	<sup>19</sup> GONZALEZ...	14	FIT	Inverted mass ordering; global fit					
0.24	to 0.76	<sup>20</sup> AARTSEN	13B	ICCB	DeepCore, $2\nu$ oscillation					
0.514	$\pm 0.082$	<sup>21</sup> ABE	13G	T2K	$3\nu$ osc.; normal mass ordering					
0.388	$+0.051$ $-0.053$	<sup>22</sup> ADAMSON	13B	MINS	Beam + Atmospheric; identical $\nu$ & $\bar{\nu}$					
0.3	to 0.7	<sup>23</sup> ABE	12A	T2K	Off-axis beam					
0.28	to 0.72	<sup>24</sup> ADAMSON	12	MINS	$\bar{\nu}$ beam					
0.25	to 0.75	<sup>25,26</sup> ADAMSON	12B	MINS	MINOS atmospheric					
0.27	to 0.73	<sup>25,27</sup> ADAMSON	12B	MINS	MINOS pure atmospheric $\nu$					
0.21	to 0.79	<sup>25,27</sup> ADAMSON	12B	MINS	MINOS pure atmospheric $\bar{\nu}$					
0.15	to 0.85	<sup>28</sup> ADRIAN-MAR.	12	ANTR	Atmospheric $\nu$ with deep see telescope					
0.39	to 0.61	<sup>29</sup> ABE	11C	SKAM	Super-Kamiokande					
0.34	to 0.66	ADAMSON	11	MINS	$2\nu$ osc.; maximal mixing					
0.31	$+0.10$ $-0.07$	<sup>30</sup> ADAMSON	11B	MINS	$\bar{\nu}$ beam					
0.41	to 0.59	<sup>31</sup> WENDELL	10	SKAM	$3\nu$ osc. with solar terms; $\theta_{13}=0$					
0.39	to 0.61	<sup>32</sup> WENDELL	10	SKAM	$3\nu$ osc.; normal mass ordering					
0.37	to 0.63	<sup>33</sup> WENDELL	10	SKAM	$3\nu$ osc.; inverted mass ordering					
0.31	to 0.69	ADAMSON	08A	MINS	MINOS					
0.05	to 0.95	<sup>34</sup> ADAMSON	06	MINS	Atmospheric $\nu$ with far detector					
0.18	to 0.82	<sup>35</sup> AHN	06A	K2K	KEK to Super-K					
0.23	to 0.77	<sup>36</sup> MICHAEL	06	MINS	MINOS					
0.18	to 0.82	<sup>37</sup> ALIU	05	K2K	KEK to Super-K					
0.18	to 0.82	<sup>38</sup> ALLISON	05	SOU2						
0.36	to 0.64	<sup>39</sup> ASHIE	05	SKAM	Super-Kamiokande					
0.28	to 0.72	<sup>40</sup> AMBROSIO	04	MCRO	MACRO					
0.34	to 0.66	<sup>41</sup> ASHIE	04	SKAM	L/E distribution					
0.08	to 0.92	<sup>42</sup> AHN	03	K2K	KEK to Super-K					
0.13	to 0.87	<sup>43</sup> AMBROSIO	03	MCRO	MACRO					
0.26	to 0.74	<sup>44</sup> AMBROSIO	03	MCRO	MACRO					
0.15	to 0.85	<sup>45</sup> SANCHEZ	03	SOU2	Soudan-2 Atmospheric					
0.28	to 0.72	<sup>46</sup> AMBROSIO	01	MCRO	Upward $\mu$					
0.29	to 0.71	<sup>47</sup> AMBROSIO	01	MCRO	Upward $\mu$					
0.13	to 0.87	<sup>48</sup> FUKUDA	99C	SKAM	Upward $\mu$					
0.23	to 0.77	<sup>49</sup> FUKUDA	99D	SKAM	Upward $\mu$					
0.08	to 0.92	<sup>50</sup> FUKUDA	99D	SKAM	Stop $\mu$ / through					
0.29	to 0.71	<sup>51</sup> FUKUDA	98C	SKAM	Super-Kamiokande					
0.08	to 0.92	<sup>52</sup> HATAKEYAMA98	KAMI	Kamiokande						

## Lepton Particle Listings

## Neutrino Mixing

- 90% C.L. contour in the  $(\Delta m^2, \sin^2 2\theta)$  plane obtained by minimizing the four parameter log-likelihood function with respect to the other oscillation parameters.
- <sup>28</sup>ADRIAN-MARTINEZ 12 measured the oscillation parameters of atmospheric neutrinos with the ANTARES deep sea neutrino telescope using the data taken from 2007 to 2010 (863 days of total live time). Superseded by ALBERT 19.
- <sup>29</sup>ABE 11c obtained this result by a two-neutrino oscillation analysis using the Super-Kamiokande-I+II+III atmospheric neutrino data. ABE 11c also reported results under a two-neutrino disappearance model with separate mixing parameters between  $\nu$  and  $\bar{\nu}$ , and obtained  $\sin^2 2\theta > 0.93$  for  $\nu$  and  $\sin^2 2\theta > 0.83$  for  $\bar{\nu}$  at 90% C.L.
- <sup>30</sup>ADAMSON 11b obtained this result by a two-neutrino oscillation analysis of antineutrinos in an antineutrino enhanced beam with  $1.71 \times 10^{20}$  protons on target. This result is consistent with the neutrino measurements of ADAMSON 11 at 2% C.L.
- <sup>31</sup>WENDELL 10 obtained this result ( $\sin^2 \theta_{23} = 0.407\text{--}0.583$ ) by a three-neutrino oscillation analysis using the Super-Kamiokande-I+II+III atmospheric neutrino data, assuming  $\theta_{13} = 0$  but including the solar oscillation parameters  $\Delta m_{21}^2$  and  $\sin^2 \theta_{12}$  in the fit.
- <sup>32</sup>WENDELL 10 obtained this result ( $\sin^2 \theta_{23} = 0.43\text{--}0.61$ ) by a three-neutrino oscillation analysis with one mass scale dominance ( $\Delta m_{21}^2 = 0$ ) using the Super-Kamiokande-I+II+III atmospheric neutrino data, and updates the HOSAKA 06a result.
- <sup>33</sup>WENDELL 10 obtained this result ( $\sin^2 \theta_{23} = 0.44\text{--}0.63$ ) by a three-neutrino oscillation analysis with one mass scale dominance ( $\Delta m_{21}^2 = 0$ ) using the Super-Kamiokande-I+II+III atmospheric neutrino data, and updates the HOSAKA 06a result.
- <sup>34</sup>ADAMSON 06 obtained this result by a two-neutrino oscillation analysis of the L/E distribution using 4.54 kton yr atmospheric neutrino data with the MINOS far detector.
- <sup>35</sup>Supersedes ALIU 05.
- <sup>36</sup>MICHAEL 06 best fit is for maximal mixing. See also ADAMSON 08.
- <sup>37</sup>The best fit is for maximal mixing.
- <sup>38</sup>ALLISON 05 result is based upon atmospheric neutrino interactions including upward-stopping muons, with an exposure of 5.9 kton yr. From a two-flavor oscillation analysis the best-fit point is  $\Delta m^2 = 0.0017 \text{ eV}^2$  and  $\sin^2(2\theta) = 0.97$ .
- <sup>39</sup>ASHIE 05 obtained this result by a two-neutrino oscillation analysis using 92 kton yr atmospheric neutrino data from the complete Super-Kamiokande I running period.
- <sup>40</sup>AMBROSIO 04 obtained this result, without using the absolute normalization of the neutrino flux, by combining the angular distribution of upward through-going muon tracks with  $E_\mu > 1 \text{ GeV}$ ,  $N_{low}$  and  $N_{high}$ , and the numbers of InDown + UpStop and InUp events. Here,  $N_{low}$  and  $N_{high}$  are the number of events with reconstructed neutrino energies  $< 30 \text{ GeV}$  and  $> 130 \text{ GeV}$ , respectively. InDown and InUp represent events with downward and upward-going tracks starting inside the detector due to neutrino interactions, while UpStop represents entering upward-going tracks which stop in the detector. The best fit is for maximal mixing.
- <sup>41</sup>ASHIE 04 obtained this result from the  $L(\text{flight length})/E(\text{estimated neutrino energy})$  distribution of  $\nu_\mu$  disappearance probability, using the Super-Kamiokande-I 1489 live-day atmospheric neutrino data.
- <sup>42</sup>There are several islands of allowed region from this K2K analysis, extending to high values of  $\Delta m^2$ . We only include the one that overlaps atmospheric neutrino analyses. The best fit is for maximal mixing.
- <sup>43</sup>AMBROSIO 03 obtained this result on the basis of the ratio  $R = N_{low}/N_{high}$ , where  $N_{low}$  and  $N_{high}$  are the number of upward through-going muon events with reconstructed neutrino energy  $< 30 \text{ GeV}$  and  $> 130 \text{ GeV}$ , respectively. The data came from the full detector run started in 1994. The method of FELDMAN 98 is used to obtain the limits.
- <sup>44</sup>AMBROSIO 03 obtained this result by using the ratio  $R$  and the angular distribution of the upward through-going muons.  $R$  is given in the previous note and the angular distribution is reported in AMBROSIO 01. The method of FELDMAN 98 is used to obtain the limits. The best fit is to maximal mixing.
- <sup>45</sup>SANCHEZ 03 is based on an exposure of 5.9 kton yr. The result is obtained using a likelihood analysis of the neutrino L/E distribution for a selection  $\mu$  flavor sample while the  $e$ -flavor sample provides flux normalization. The method of FELDMAN 98 is used to obtain the allowed region. The best fit is  $\sin^2(2\theta) = 0.97$ .
- <sup>46</sup>AMBROSIO 01 result is based on the angular distribution of upward through-going muon tracks with  $E_\mu > 1 \text{ GeV}$ . The data came from three different detector configurations, but the statistics is largely dominated by the full detector run, from May 1994 to December 2000. The total live time, normalized to the full detector configuration is 6.17 years. The best fit is obtained outside the physical region. The method of FELDMAN 98 is used to obtain the limits. The best fit is for maximal mixing.
- <sup>47</sup>AMBROSIO 01 result is based on the angular distribution and normalization of upward through-going muon tracks with  $E_\mu > 1 \text{ GeV}$ . See the previous footnote.
- <sup>48</sup>FUKUDA 99c obtained this result from a total of 537 live days of upward through-going muon data in Super-Kamiokande between April 1996 to January 1998. With a threshold of  $E_\mu > 1.6 \text{ GeV}$ , the observed flux is  $(1.74 \pm 0.07 \pm 0.02) \times 10^{-13} \text{ cm}^{-2}\text{s}^{-1}\text{sr}^{-1}$ . The best fit is  $\sin^2(2\theta) = 0.95$ .
- <sup>49</sup>FUKUDA 99b obtained this result from a simultaneous fitting to zenith angle distributions of upward-stopping and through-going muons. The flux of upward-stopping muons of minimum energy of 1.6 GeV measured between April 1996 and January 1998 is  $(0.39 \pm 0.04 \pm 0.02) \times 10^{-13} \text{ cm}^{-2}\text{s}^{-1}\text{sr}^{-1}$ . This is compared to the expected flux of  $(0.73 \pm 0.16 (\text{theoretical error})) \times 10^{-13} \text{ cm}^{-2}\text{s}^{-1}\text{sr}^{-1}$ . The best fit is to maximal mixing.
- <sup>50</sup>FUKUDA 99d obtained this result from the zenith dependence of the upward-stopping/through-going flux ratio. The best fit is to maximal mixing.
- <sup>51</sup>FUKUDA 98c obtained this result by an analysis of 33.0 kton yr atmospheric neutrino data. The best fit is for maximal mixing.
- <sup>52</sup>HATAKEYAMA 98 obtained this result from a total of 2456 live days of upward-going muon data in Kamiokande between December 1985 and May 1995. With a threshold of  $E_\mu > 1.6 \text{ GeV}$ , the observed flux of upward through-going muons is  $(1.94 \pm 0.10^{+0.07}_{-0.06}) \times$

$10^{-13} \text{ cm}^{-2}\text{s}^{-1}\text{sr}^{-1}$ . This is compared to the expected flux of  $(2.46 \pm 0.54 (\text{theoretical error})) \times 10^{-13} \text{ cm}^{-2}\text{s}^{-1}\text{sr}^{-1}$ . The best fit is for maximal mixing.

- <sup>53</sup>HATAKEYAMA 98 obtained this result from a combined analysis of Kamiokande contained events (FUKUDA 94) and upward going muon events. The best fit is  $\sin^2(2\theta) = 0.95$ .

- <sup>54</sup>FUKUDA 94 obtained the result by a combined analysis of sub- and multi-GeV atmospheric neutrino events in Kamiokande. The best fit is for maximal mixing.

 $\Delta m_{32}^2$ 

The sign of  $\Delta m_{32}^2$  is not known at this time. If given, values are shown separately for the normal and inverted mass ordering. Unless otherwise specified, the ranges below correspond to the projection onto the  $\Delta m_{32}^2$  axis of the 90% CL contours in the  $\sin^2(2\theta_{23}) - \Delta m_{32}^2$  plane presented by the authors. If uncertainties are reported with the value, they correspond to one standard deviation uncertainty.

VALUE ( $10^{-3} \text{ eV}^2$ )	DOCUMENT ID	TECN	COMMENT
<b><math>-2.546^{+0.034}_{-0.040}</math> OUR FIT</b>			Assuming inverted ordering
<b><math>2.453 \pm 0.034</math> OUR FIT</b>			Assuming normal ordering
$2.48^{+0.11}_{-0.06}$	1 ACERO	19 NOVA	Normal mass ordering, octant II for $\theta_{23}$
$-2.54^{+0.06}_{-0.11}$	1 ACERO	19 NOVA	Inverted mass ordering, octant II for $\theta_{23}$
$2.31^{+0.11}_{-0.13}$	2 AARTSEN	18A ICCB	Normal mass ordering
$2.50^{+0.13}_{-0.20}$	3 ABE	18B SKAM	Normal mass ordering, $\theta_{13}$ constrained
$-2.58^{+0.08}_{-0.37}$	3 ABE	18B SKAM	Inverted mass ordering, $\theta_{13}$ constrained
$2.463^{+0.071}_{-0.070}$	4 ABE	18G T2K	Normal mass ordering, $\theta_{13}$ constrained
$-2.507 \pm 0.070$	4.5 ABE	18G T2K	Inverted mass ordering, $\theta_{13}$ constrained
$2.471^{+0.068}_{-0.070}$	6 ADEY	18A DAYA	Normal mass ordering
$-2.575^{+0.068}_{-0.070}$	6 ADEY	18A DAYA	Inverted mass ordering
$2.63 \pm 0.14$	7 BAK	18 RENO	Normal mass ordering
$-2.73 \pm 0.14$	7 BAK	18 RENO	Inverted mass ordering
$2.37 \pm 0.09$	8 ADAMSON	14 MINS	Accel., atmospheric, normal mass ordering
$-2.41^{+0.09}_{-0.12}$	8 ADAMSON	14 MINS	Accel., atmospheric, inverted mass ordering
• • • We do not use the following data for averages, fits, limits, etc. • • •			
$2.55^{+0.12}_{-0.11}$	9 AARTSEN	19c ICCB	
$< 4.1$ at 90% CL	AGAFONOVA	19 OPER	
$2.0^{+0.4}_{-0.3}$	10 ALBERT	19 ANTR	Atmospheric $\nu$ , deep sea telescope
$2.50^{+0.13}_{-0.31}$	11 ABE	18B SKAM	$3\nu$ osc: normal mass ordering, $\theta_{13}$ free
$-2.28^{+0.33}_{-0.13}$	11 ABE	18B SKAM	$3\nu$ osc: inverted mass ordering, $\theta_{13}$ free
$2.44^{+0.08}_{-0.07}$	12 ACERO	18 NOVA	Normal mass order, octant II for $\theta_{23}$
$2.45^{+0.07}_{-0.08}$	12,13 ACERO	18 NOVA	Normal mass order; octant I for $\theta_{23}$
$2.7^{+0.7}_{-0.6}$	14 AGAFONOVA	18 OPER	OPERA $\nu_\tau$ appearance
$2.42 \pm 0.03$	DE-SALAS	18 FIT	Normal mass ordering, global fit
$-2.50^{+0.03}_{-0.04}$	DE-SALAS	18 FIT	Inverted mass order, global fit
$2.57^{+0.21}_{-0.23}$	15 SEO	18 RENO	Normal mass ordering
$-2.67^{+0.23}_{-0.21}$	15 SEO	18 RENO	Inverted mass ordering
$2.53^{+0.15}_{-0.13}$	ABE	17c T2K	Normal mass ordering with neutrinos
$2.55^{+0.33}_{-0.27}$	ABE	17c T2K	Normal mass ordering with antineutrinos
$2.55^{+0.08}_{-0.08}$	ABE	17c T2K	Normal mass ordering with neutrinos and antineutrinos
$-2.63^{+0.08}_{-0.08}$	ABE	17c T2K	Inverted mass ordering with neutrinos and antineutrinos
$2.54 \pm 0.08$	16 ABE	17F T2K	Normal mass ordering; $\nu+\bar{\nu}$
$-2.51 \pm 0.08$	16 ABE	17F T2K	Inverted mass ordering; $\nu+\bar{\nu}$
$2.67 \pm 0.11$	17 ADAMSON	17A NOVA	$3\nu$ osc; normal mass ordering
$-2.72 \pm 0.11$	17 ADAMSON	17A NOVA	$3\nu$ osc; inverted mass ordering
$2.45 \pm 0.06 \pm 0.06$	18 AN	17A DAYA	Normal mass ordering
$-2.56 \pm 0.06 \pm 0.06$	18 AN	17A DAYA	Inverted mass ordering

See key on page 999

# Lepton Particle Listings

## Neutrino Mixing

2.51 <sup>+0.29</sup> <sub>-0.25</sub>	19	ABE	16D	T2K	3ν osc.; normal mass ordering; $\bar{\nu}$ beam
2.52 <sup>+0.20</sup> <sub>-0.18</sub>	20	ADAMSON	16A	NOVA	3ν osc.; normal mass ordering
-2.56 ± 0.19	20	ADAMSON	16A	NOVA	3ν osc.; inverted mass ordering
2.56 <sup>+0.21</sup> <sub>-0.23</sub>	21	CHOI	16	RENO	3ν osc.; normal mass ordering
2.56 <sup>+0.21</sup> <sub>-0.13</sub>	21	CHOI	16	RENO	3ν osc.; normal mass ordering
-2.69 <sup>+0.23</sup> <sub>-0.21</sub>	21	CHOI	16	RENO	3ν osc.; inverted mass ordering
2.72 <sup>+0.19</sup> <sub>-0.20</sub>	22	AARTSEN	15A	ICCB	Normal mass ordering
-2.73 <sup>+0.21</sup> <sub>-0.18</sub>	22	AARTSEN	15A	ICCB	Inverted mass ordering
2.0-5.0	23	AGAFONOVA	15A	OPER	90% CL, 5 events
2.37 ± 0.11	24	AN	15	DAYA	3ν osc.; normal mass ordering
-2.47 ± 0.11	24	AN	15	DAYA	3ν osc.; inverted mass ordering
2.51 ± 0.10	25	ABE	14	T2K	3ν osc.; normal mass ordering
-2.56 ± 0.10	25	ABE	14	T2K	3ν osc.; inverted mass ordering
2.54 <sup>+0.19</sup> <sub>-0.20</sub>	26	AN	14	DAYA	3ν osc.; normal mass ordering
-2.64 <sup>+0.20</sup> <sub>-0.19</sub>	26	AN	14	DAYA	3ν osc.; inverted mass ordering
2.48 <sup>+0.05</sup> <sub>-0.07</sub>	27	FORERO	14	FIT	3ν; normal mass ordering
-2.38 <sup>+0.06</sup> <sub>-0.05</sub>	27	FORERO	14	FIT	3ν; inverted mass ordering
2.457 ± 0.047	28,29	GONZALEZ...	14	FIT	Normal mass ordering; global fit
-2.449 <sup>+0.047</sup> <sub>-0.048</sub>	28	GONZALEZ...	14	FIT	Inverted mass ordering; global fit
2.3 <sup>+0.6</sup> <sub>-0.5</sub>	30	AARTSEN	13B	ICCB	DeepCore, 2ν oscillation
2.44 <sup>+0.17</sup> <sub>-0.15</sub>	31	ABE	13G	T2K	3ν osc.; normal mass ordering
2.41 <sup>+0.09</sup> <sub>-0.10</sub>	32	ADAMSON	13B	MINS	2ν osc.; beam + atmospheric; identical ν & $\bar{\nu}$ off-axis beam
2.2-3.1	33	ABE	12A	T2K	off-axis beam
2.62 <sup>+0.31</sup> <sub>-0.28</sub> ± 0.09	34	ADAMSON	12	MINS	$\bar{\nu}$ beam
1.35-2.55	35,36	ADAMSON	12B	MINS	MINOS atmospheric
1.4-5.6	35,37	ADAMSON	12B	MINS	MINOS pure atmospheric ν
0.9-2.5	35,37	ADAMSON	12B	MINS	MINOS pure atmospheric $\bar{\nu}$
1.8-5.0	38	ADRIAN-MAR.	12	ANTR	Atmospheric ν with deep sea telescope
1.3-4.0	39	ABE	11C	SKAM	atmospheric $\bar{\nu}$
2.32 <sup>+0.12</sup> <sub>-0.08</sub>		ADAMSON	11	MINS	2ν oscillation; maximal mixing
3.36 <sup>+0.46</sup> <sub>-0.40</sub>	40	ADAMSON	11B	MINS	$\bar{\nu}$ beam
< 3.37	41	ADAMSON	11C	MINS	MINOS
1.9-2.6	42	WENDELL	10	SKAM	3ν osc.; normal mass ordering
-1.7- -2.7	42	WENDELL	10	SKAM	3ν osc.; inverted mass ordering
2.43 ± 0.13		ADAMSON	08A	MINS	MINOS
0.07-5.0	43	ADAMSON	06	MINS	atmospheric ν with far detector
1.9-4.0	44,45	AHN	06A	K2K	KEK to Super-K
2.2-3.8	46	MICHAEL	06	MINS	MINOS
1.9-3.6	47	ALIU	05	K2K	KEK to Super-K
0.3-1.2	44	ALLISON	05	SOU2	
1.5-3.4	48	ASHIE	05	SKAM	atmospheric neutrino
0.6-8.0	49	AMBROSIO	04	MCRO	MACRO
1.9 to 3.0	50	ASHIE	04	SKAM	L/E distribution
1.5-3.9	51	AHN	03	K2K	KEK to Super-K
0.25-9.0	52	AMBROSIO	03	MCRO	MACRO
0.6-7.0	53	AMBROSIO	03	MCRO	MACRO
0.15-15	54	SANCHEZ	03	SOU2	Soudan-2 Atmospheric
0.6-15	55	AMBROSIO	01	MCRO	upward μ
1.0-6.0	56	AMBROSIO	01	MCRO	upward μ
1.0-5.0	57	FUKUDA	99C	SKAM	upward μ
1.5-15.0	58	FUKUDA	99D	SKAM	upward μ
0.7-18	59	FUKUDA	99D	SKAM	stop μ / through
0.5-6.0	60	FUKUDA	98C	SKAM	Super-Kamiokande
0.5-5.0	61	HATAKEYAMA	98	KAMI	Kamiokande
4-23	62	HATAKEYAMA	98	KAMI	Kamiokande
5-25	63	FUKUDA	94	KAMI	Kamiokande

<sup>1</sup> ACERO 19 is based on a sample size of  $12.33 \times 10^{20}$  protons on target. The fit combines both antineutrino and neutrino data to extract the oscillation parameters. The results favor the normal mass ordering by  $1.9 \sigma$  and  $\theta_{23}$  values in octant II by  $1.6 \sigma$ . Supersedes ACERO 18.

<sup>2</sup> AARTSEN 18A uses three years (April 2012 – May 2015) of neutrino data from full sky with reconstructed energies between 5.6 and 56 GeV, measured with the low-energy subdetector DeepCore of the IceCube neutrino telescope. AARTSEN 18A also reports the best fit values for the inverted mass ordering as  $\Delta m_{32}^2 = -2.32 \times 10^{-3} \text{ eV}^2$  and  $\sin^2(\theta_{23}) = 0.51$ . Uncertainties for the inverted mass ordering fits were not provided. Supersedes AARTSEN 15A.

<sup>3</sup> ABE 18B uses 328 kton-years of Super-Kamiokande I-IV atmospheric neutrino data to obtain this result. The fit is performed over the three parameters,  $\Delta m_{32}^2$ ,  $\sin^2(\theta_{23})$ , and  $\delta$ , while the solar parameters and  $\sin^2(\theta_{13})$  are fixed to  $\Delta m_{21}^2 = (7.53 \pm 0.18) \times 10^{-5} \text{ eV}^2$ ,  $\sin^2(\theta_{12}) = 0.304 \pm 0.014$ , and  $\sin^2(\theta_{13}) = 0.0219 \pm 0.0012$ .

<sup>4</sup> ABE 18C data prefers normal ordering with a posterior probability of 87%. Supersedes ABE 17F.

<sup>5</sup> ABE 18C reports  $\Delta m_{13}^2 = (2.432 \pm 0.070) \times 10^{-3} \text{ eV}^2$  for inverted mass ordering. We convert to  $\Delta m_{32}^2$  using PDG 18 value of  $\Delta m_{21}^2 = (7.53 \pm 0.18) \times 10^{-5} \text{ eV}^2$ .

<sup>6</sup> ADEY 18A reports results from analysis of 1958 days of data taking with the Daya-Bay experiment, with  $3.9 \times 10^6$   $\bar{\nu}_e$  candidates. The fit to the data gives  $\Delta m_{ee}^2 = (2.522^{+0.068}_{-0.070}) \times 10^{-3} \text{ eV}^2$ . Solar oscillation parameters are fixed in the analysis using the global averages,  $\sin^2(\theta_{12}) = 0.307^{+0.013}_{-0.012}$ ,  $\Delta m_{21}^2 = (7.53 \pm 0.18) \times 10^{-5} \text{ eV}^2$ , from PDG 18. Supersedes AN 17A.

<sup>7</sup> BAK 18 reports results of the RENO experiment using about 2200 live-days of data taken with detectors placed at 410.6 and 1445.7 m from reactors of the Hanbit Nuclear Power Plant. We convert the results to  $\Delta m_{32}^2$  using the PDG 18 values of  $\sin^2 \theta_{12} = 0.307^{+0.013}_{-0.012}$  and  $\Delta m_{21}^2 = (7.53 \pm 0.18) \times 10^{-5} \text{ eV}^2$ . Supersedes SEO 18.

<sup>8</sup> ADAMSON 14 uses a complete set of accelerator and atmospheric data. The analysis combines the analysis combines the  $\nu_\mu$  disappearance and  $\nu_e$  appearance data using three-neutrino oscillation fit. The fit results are obtained for normal and inverted mass ordering assumptions.

<sup>9</sup> AARTSEN 19C uses three years (April 2012 – May 2015) of neutrino data from full sky with reconstructed energies between 5.6 and 56 GeV, measured with the low-energy sub-detector DeepCore of the IceCube neutrino telescope. AARTSEN 19C adopts looser event selection criteria to prioritize the efficiency of selecting neutrino events, different from tighter event selection criteria which closely follow the criteria used by AARTSEN 18A to measure the  $\nu_\mu$  disappearance.

<sup>10</sup> ALBERT 19 measured the oscillation parameters of atmospheric neutrinos with the ANTARES deep sea neutrino telescope using the data taken from 2007 to 2016 (2830 days of total live time). Supersedes ADRIAN-MARTINEZ 12.

<sup>11</sup> ABE 18B uses 328 kton-years of Super-Kamiokande I-IV atmospheric neutrino data to obtain this result. The fit is performed over the four parameters,  $\Delta m_{32}^2$ ,  $\sin^2 \theta_{23}$ ,  $\sin^2 \theta_{13}$ , and  $\delta$ , while the solar parameters are fixed to  $\Delta m_{21}^2 = (7.53 \pm 0.18) \times 10^{-5} \text{ eV}^2$  and  $\sin^2 \theta_{12} = 0.304 \pm 0.014$ .

<sup>12</sup> ACERO 18 performs a joint fit to the data for  $\nu_\mu$  disappearance and  $\nu_e$  appearance. The overall best fit favors normal mass ordering and  $\theta_{23}$  in octant II. No  $1\sigma$  confidence intervals are presented for the inverted mass ordering scenarios. Superseded by ACERO 19.

<sup>13</sup> The error for octant I is taken from the result for octant II.

<sup>14</sup> AGAFONOVA 18 assumes maximal  $\theta_{23}$  mixing.

<sup>15</sup> SEO 18 reports result of the RENO experiment from a rate and shape analysis of 500 days of data. A simultaneous fit to  $\theta_{13}$  and  $\Delta m_{ee}^2$  yields  $\Delta m_{ee}^2 = (2.62^{+0.21}_{-0.23} \pm 0.12) \times 10^{-3} \text{ eV}^2$ . We convert the results to  $\Delta m_{32}^2$  using the PDG 18 values of  $\sin^2 \theta_{12}$  and  $\Delta m_{21}^2$ . SEO 18 is a detailed description of the results published in CHOI 16, which it supersedes. Superseded by BAK 18.

<sup>16</sup> ABE 17F confidence intervals are obtained using a frequentist analysis including  $\theta_{13}$  constraint from reactor experiments. Bayesian intervals based on Markov Chain Monte Carlo method are also provided by the authors. Superseded by ABE 18G.

<sup>17</sup> Superseded by ACERO 18.

<sup>18</sup> AN 17A report results from combined rate and spectral shape analysis of 1230 days of data taken with the Daya Bay reactor experiment. The data set contains more than  $2.5 \times 10^6$  inverse beta-decay events with neutron capture on Gd. The fit to the data gives  $\Delta_{ee}^2 = (2.50 \pm 0.06 \pm 0.06) \times 10^{-3} \text{ eV}^2$ . Superseded by ADEY 18A.

<sup>19</sup> ABE 16D reports oscillation results using  $\bar{\nu}_\mu$  disappearance in an off-axis beam.

<sup>20</sup> Superseded by ADAMSON 17A.

<sup>21</sup> CHOI 16 reports result of the RENO experiment from a rate and shape analysis of 500 days of data. A simultaneous fit to  $\theta_{13}$  and  $\Delta m_{ee}^2$  yields  $\Delta m_{ee}^2 = (2.62^{+0.21}_{-0.23} \pm 0.12) \times 10^{-3} \text{ eV}^2$ . We convert the results to  $\Delta m_{32}^2$  using PDG 18 values of  $\sin^2(\theta_{12})$  and  $\Delta m_{21}^2$ .

<sup>22</sup> AARTSEN 15A obtains this result by a three-neutrino oscillation analysis using 10–100 GeV muon neutrino sample from a total of 953 days of measurements with the low-energy subdetector DeepCore of the IceCube neutrino telescope. Superseded by AARTSEN 18A.

<sup>23</sup> AGAFONOVA 15A result is based on 5  $\nu_\mu \rightarrow \nu_\tau$  appearance candidates with an expected background of  $0.25 \pm 0.05$  events. The best fit is for  $\Delta m_{32}^2 = 3.3 \times 10^{-3} \text{ eV}^2$ .

<sup>24</sup> AN 15 uses all eight identical detectors, with four placed near the reactor cores and the remaining four at the far hall to determine prompt energy spectra. The results correspond to the exposure of  $6.9 \times 10^5 \text{ GW}_{th}\text{-ton-days}$ . They derive  $\Delta m_{ee}^2 = (2.42 \pm 0.11) \times 10^{-3} \text{ eV}^2$ . Assuming the normal (inverted) ordering, the fitted  $\Delta m_{32}^2 = (2.37 \pm 0.11) \times 10^{-3} ((2.47 \pm 0.11) \times 10^{-3}) \text{ eV}^2$ . Superseded by AN 17A.

<sup>25</sup> ABE 14 results are based on  $\nu_\mu$  disappearance using three-neutrino oscillation fit. The confidence intervals are derived from one dimensional profiled likelihoods. In ABE 14 the inverted mass ordering result is reported as  $\Delta m_{13}^2 = (2.48 \pm 0.10) \times 10^{-3} \text{ eV}^2$  which we converted to  $\Delta m_{32}^2$  by adding PDG 14 value of  $\Delta m_{21}^2 = (7.53 \pm 0.18) \times 10^{-5} \text{ eV}^2$ . Superseded by ABE 17C.

<sup>26</sup> AN 14 uses six identical detectors, with three placed near the reactor cores (flux-weighted baselines of 512 and 561 m) and the remaining three at the far hall (at the flux averaged distance of 1579 m from all six reactor cores) to determine prompt energy spectra and derive  $\Delta m_{ee}^2 = (2.59^{+0.19}_{-0.20}) \times 10^{-3} \text{ eV}^2$ . Assuming the normal (inverted) ordering, the fitted  $\Delta m_{32}^2 = (2.54^{+0.19}_{-0.20}) \times 10^{-3} ((2.64^{+0.19}_{-0.20}) \times 10^{-3}) \text{ eV}^2$ . Superseded by AN 15.

<sup>27</sup> FORERO 14 performs a global fit to  $\Delta m_{31}^2$  using solar, reactor, long-baseline accelerator, and atmospheric neutrino data.

<sup>28</sup> GONZALEZ-GARCIA 14 result comes from a frequentist global fit. The corresponding Bayesian global fit to the same data results are reported in BERGSTROM 15 as  $(2.460 \pm 0.046) \times 10^{-3} \text{ eV}^2$  for normal and  $(2.445^{+0.047}_{-0.045}) \times 10^{-3} \text{ eV}^2$  for inverted mass ordering.

<sup>29</sup> The value for normal mass ordering is actually a measurement of  $\Delta m_{31}^2$  which differs from  $\Delta m_{32}^2$  by a much smaller value of  $\Delta m_{21}^2$ .

<sup>30</sup> AARTSEN 13B obtained this result by a two-neutrino oscillation analysis using 20–100 GeV muon neutrino sample from a total of 318.9 days of live-time measurement with the low-energy subdetector DeepCore of the IceCube neutrino telescope.



# Lepton Particle Listings

## Neutrino Mixing

- <sup>31</sup> Based on the observation of 58  $\nu_\mu$  events with  $205 \pm 17$ (syst) expected in the absence of neutrino oscillations. Superseded by ABE 14.
- <sup>32</sup> ADAMSON 13B obtained this result from  $\nu_\mu$  and  $\bar{\nu}_\mu$  disappearance using  $\nu_\mu$  ( $10.71 \times 10^{20}$  POT) and  $\bar{\nu}_\mu$  ( $3.36 \times 10^{20}$  POT) beams, and atmospheric (37.88 kton-years) data from MINOS. The fit assumed two-flavor neutrino hypothesis and identical  $\nu_\mu$  and  $\bar{\nu}_\mu$  oscillation parameters.
- <sup>33</sup> ABE 12A obtained this result by a two-neutrino oscillation analysis. The best-fit point is  $\Delta m_{32}^2 = 2.65 \times 10^{-3} \text{ eV}^2$ .
- <sup>34</sup> ADAMSON 12 is a two-neutrino oscillation analysis using antineutrinos.
- <sup>35</sup> ADAMSON 12B obtained this result by a two-neutrino oscillation analysis of the L/E distribution using 37.9 kton-yr atmospheric neutrino data with the MINOS far detector.
- <sup>36</sup> The 90% single-parameter confidence interval at the best fit point is  $\Delta m^2 = 0.0019 \pm 0.0004 \text{ eV}^2$ .
- <sup>37</sup> The data are separated into pure samples of  $\nu_s$  and  $\bar{\nu}_s$ , and separate oscillation parameters for  $\nu_s$  and  $\bar{\nu}_s$  are fit to the data. The best fit point is  $(\Delta m^2, \sin^2 2\theta) = (0.0022 \text{ eV}^2, 0.99)$  and  $(\Delta \bar{m}^2, \sin^2 2\bar{\theta}) = (0.0016 \text{ eV}^2, 1.00)$ . The quoted result is taken from the 90% C.L. contour in the  $(\Delta m^2, \sin^2 2\theta)$  plane obtained by minimizing the four parameter log-likelihood function with respect to the other oscillation parameters.
- <sup>38</sup> ADRIAN-MARTINEZ 12 measured the oscillation parameters of atmospheric neutrinos with the ANTARES deep sea neutrino telescope using the data taken from 2007 to 2010 (863 days of total live time). Superseded by ALBERT 19
- <sup>39</sup> ABE 11c obtained this result by a two-neutrino oscillation analysis with separate mixing parameters between neutrinos and antineutrinos, using the Super-Kamiokande-I+II+III atmospheric neutrino data. The corresponding 90% CL neutrino oscillation parameter range obtained from this analysis is  $\Delta m^2 = 1.7\text{--}3.0 \times 10^{-3} \text{ eV}^2$ .
- <sup>40</sup> ADAMSON 11B obtained this result by a two-neutrino oscillation analysis of antineutrinos in an antineutrino enhanced beam with  $1.71 \times 10^{20}$  protons on target. This result is consistent with the neutrino measurements of ADAMSON 11 at 2% C.L.
- <sup>41</sup> ADAMSON 11c obtains this result based on a study of antineutrinos in a neutrino beam and assumes maximal mixing in the two-flavor approximation.
- <sup>42</sup> WENDELL 10 obtained this result by a three-neutrino oscillation analysis with one mass scale dominance ( $\Delta m_{21}^2 = 0$ ) using the Super-Kamiokande-I+II+III atmospheric neutrino data, and updates the HOSAKA 06A result.
- <sup>43</sup> ADAMSON 06 obtained this result by a two-neutrino oscillation analysis of the L/E distribution using 4.54 kton yr atmospheric neutrino data with the MINOS far detector.
- <sup>44</sup> The best fit in the physical region is for  $\Delta m^2 = 2.8 \times 10^{-3} \text{ eV}^2$ .
- <sup>45</sup> Supersedes ALIU 05.
- <sup>46</sup> MICHAEL 06 best fit is  $2.74 \times 10^{-3} \text{ eV}^2$ . See also ADAMSON 08.
- <sup>47</sup> ALLISON 05 result is based on an atmospheric neutrino observation with an exposure of 5.9 kton yr. From a two-flavor oscillation analysis the best-fit point is  $\Delta m^2 = 0.0017 \text{ eV}^2$  and  $\sin^2 2\theta = 0.97$ .
- <sup>48</sup> ASHIE 05 obtained this result by a two-neutrino oscillation analysis using 92 kton yr atmospheric neutrino data from the complete Super-Kamiokande I running period. The best fit is for  $\Delta m^2 = 2.1 \times 10^{-3} \text{ eV}^2$ .
- <sup>49</sup> AMBROSIO 04 obtained this result, without using the absolute normalization of the neutrino flux, by combining the angular distribution of upward through-going muon tracks with  $E_\mu > 1 \text{ GeV}$ ,  $N_{low}$  and  $N_{high}$ , and the numbers of InDown + UpStop and InUp events. Here,  $N_{low}$  and  $N_{high}$  are the number of events with reconstructed neutrino energies  $< 30 \text{ GeV}$  and  $> 130 \text{ GeV}$ , respectively. InDown and InUp represent events with downward and upward-going tracks starting inside the detector due to neutrino interactions, while UpStop represents entering upward-going tracks which stop in the detector. The best fit is for  $\Delta m^2 = 2.3 \times 10^{-3} \text{ eV}^2$ .
- <sup>50</sup> ASHIE 04 obtained this result from the L(flight length)/E(estimated neutrino energy) distribution of  $\nu_\mu$  disappearance probability, using the Super-Kamiokande-I 1489 live-day atmospheric neutrino data. The best fit is for  $\Delta m^2 = 2.4 \times 10^{-3} \text{ eV}^2$ .
- <sup>51</sup> There are several islands of allowed region from this K2K analysis, extending to high values of  $\Delta m^2$ . We only include the one that overlaps atmospheric neutrino analyses. The best fit is for  $\Delta m^2 = 2.8 \times 10^{-3} \text{ eV}^2$ .
- <sup>52</sup> AMBROSIO 03 obtained this result on the basis of the ratio  $R = N_{low}/N_{high}$ , where  $N_{low}$  and  $N_{high}$  are the number of upward through-going muon events with reconstructed neutrino energy  $< 30 \text{ GeV}$  and  $> 130 \text{ GeV}$ , respectively. The data came from the full detector run started in 1994. The method of FELDMAN 98 is used to obtain the limits. The best fit is for  $\Delta m^2 = 2.5 \times 10^{-3} \text{ eV}^2$ .
- <sup>53</sup> AMBROSIO 03 obtained this result by using the ratio R and the angular distribution of the upward through-going muons. R is given in the previous note and the angular distribution is reported in AMBROSIO 01. The method of FELDMAN 98 is used to obtain the limits. The best fit is for  $\Delta m^2 = 2.5 \times 10^{-3} \text{ eV}^2$ .
- <sup>54</sup> SANCHEZ 03 is based on an exposure of 5.9 kton yr. The result is obtained using a likelihood analysis of the neutrino L/E distribution for a selection  $\mu$  flavor sample while the  $e$ -flavor sample provides flux normalization. The method of FELDMAN 98 is used to obtain the allowed region. The best fit is for  $\Delta m^2 = 5.2 \times 10^{-3} \text{ eV}^2$ .
- <sup>55</sup> AMBROSIO 01 result is based on the angular distribution of upward through-going muon tracks with  $E_\mu > 1 \text{ GeV}$ . The data came from three different detector configurations, but the statistics is largely dominated by the full detector run, from May 1994 to December 2000. The total live time, normalized to the full detector configuration is 6.17 years. The best fit is obtained outside the physical region. The method of FELDMAN 98 is used to obtain the limits.
- <sup>56</sup> AMBROSIO 01 result is based on the angular distribution and normalization of upward through-going muon tracks with  $E_\mu > 1 \text{ GeV}$ . See the previous footnote.
- <sup>57</sup> FUKUDA 99c obtained this result from a total of 537 live days of upward through-going muon data in Super-Kamiokande between April 1996 to January 1998. With a threshold of  $E_\mu > 1.6 \text{ GeV}$ , the observed flux is  $(1.74 \pm 0.07 \pm 0.02) \times 10^{-13} \text{ cm}^{-2}\text{s}^{-1}\text{sr}^{-1}$ . The best fit is for  $\Delta m^2 = 5.9 \times 10^{-3} \text{ eV}^2$ .

- <sup>58</sup> FUKUDA 99b obtained this result from a simultaneous fitting to zenith angle distributions of upward-stopping and through-going muons. The flux of upward-stopping muons of minimum energy of 1.6 GeV measured between April 1996 and January 1998 is  $(0.39 \pm 0.04 \pm 0.02) \times 10^{-13} \text{ cm}^{-2}\text{s}^{-1}\text{sr}^{-1}$ . This is compared to the expected flux of  $(0.73 \pm 0.16 \text{ (theoretical error)}) \times 10^{-13} \text{ cm}^{-2}\text{s}^{-1}\text{sr}^{-1}$ . The best fit is for  $\Delta m^2 = 3.9 \times 10^{-3} \text{ eV}^2$ .
- <sup>59</sup> FUKUDA 99d obtained this result from the zenith dependence of the upward-stopping/through-going flux ratio. The best fit is for  $\Delta m^2 = 3.1 \times 10^{-3} \text{ eV}^2$ .
- <sup>60</sup> FUKUDA 98c obtained this result by an analysis of 33.0 kton yr atmospheric neutrino data. The best fit is for  $\Delta m^2 = 2.2 \times 10^{-3} \text{ eV}^2$ .
- <sup>61</sup> HATAKEYAMA 98 obtained this result from a total of 2456 live days of upward-going muon data in Kamiokande between December 1985 and May 1995. With a threshold of  $E_\mu > 1.6 \text{ GeV}$ , the observed flux of upward through-going muons is  $(1.94 \pm 0.10^{+0.07}_{-0.06}) \times 10^{-13} \text{ cm}^{-2}\text{s}^{-1}\text{sr}^{-1}$ . This is compared to the expected flux of  $(2.46 \pm 0.54 \text{ (theoretical error)}) \times 10^{-13} \text{ cm}^{-2}\text{s}^{-1}\text{sr}^{-1}$ . The best fit is for  $\Delta m^2 = 2.2 \times 10^{-3} \text{ eV}^2$ .
- <sup>62</sup> HATAKEYAMA 98 obtained this result from a combined analysis of Kamiokande contained events (FUKUDA 94) and upward going muon events. The best fit is for  $\Delta m^2 = 13 \times 10^{-3} \text{ eV}^2$ .
- <sup>63</sup> FUKUDA 94 obtained the result by a combined analysis of sub- and multi-GeV atmospheric neutrino events in Kamiokande. The best fit is for  $\Delta m^2 = 16 \times 10^{-3} \text{ eV}^2$ .

### $\sin^2(\theta_{13})$

At present time direct measurements of  $\sin^2(\theta_{13})$  are derived from the reactor  $\bar{\nu}_e$  disappearance at distances corresponding to the  $\Delta m_{32}^2$  value, i.e.  $L \sim 1\text{km}$ . Alternatively, limits can also be obtained from the analysis of the solar neutrino data and accelerator-based  $\nu_\mu \rightarrow \nu_e$  experiments.

If an experiment reports  $\sin^2(2\theta_{13})$  we convert the value to  $\sin^2(\theta_{13})$ .

VALUE (units $10^{-2}$ )	CL%	DOCUMENT ID	TECN	COMMENT
<b>2.18 ± 0.07</b>	<b>OUR AVERAGE</b>			
2.188 ± 0.076		<sup>1</sup> ADEY	18A DAYA	DayaBay, LingAo/Ao II reactors
2.29 ± 0.18		<sup>2</sup> BAK	18 RENO	Yonggwang reactors
2.25 ± 0.87		<sup>3</sup> ABE	16B DCHZ	Chooz reactors
1.81 ± 0.29		<sup>4</sup> AN	16A DAYA	DayaBay, Ling Ao/Ao II reactors
• • • We do not use the following data for averages, fits, limits, etc. • • •				
< 3.9	68	AGAFONOVA	19 OPER	
1.8 ± 2.9		<sup>5</sup> ABE	18B SKAM	$3\nu$ osc: normal mass ordering, $\theta_{13}$ free
0.8 ± 1.7		<sup>5</sup> ABE	18B SKAM	$3\nu$ osc: inverted mass ordering, $\theta_{13}$ free
<12	90	<sup>6</sup> AGAFONOVA	18A OPER	OPERA: $\nu_e$ appearance
2.160 <sup>+</sup> 0.083		DE-SALAS	18 FIT	Normal mass ordering, global fit
2.220 <sup>+</sup> 0.074		DE-SALAS	18 FIT	Inverted mass ordering, global fit
2.09 ± 0.23 ± 0.16		<sup>7</sup> SEO	18 RENO	Yonggwang reactors
2.7 ± 0.7		<sup>8</sup> ABE	17F T2K	Normal mass ordering, T2K only
2.149 ± 0.071 ± 0.050		<sup>9</sup> AN	17A DAYA	DayaBay, LingAo/Ao II reactors
2.09 ± 0.23 ± 0.16		<sup>10</sup> CHOI	16 RENO	Yonggwang reactors
2.15 ± 0.13		<sup>11</sup> AN	15 DAYA	DayaBay, Ling Ao/Ao II reactors
2.6 ± 1.2		<sup>12</sup> ABE	14A DCHZ	Chooz reactors
3.0 ± 1.3		<sup>13</sup> ABE	14C T2K	Inverted mass ordering
3.6 ± 1.0		<sup>13</sup> ABE	14C T2K	Normal mass ordering
2.3 ± 0.9		<sup>14</sup> ABE	14H DCHZ	Chooz reactors
2.3 ± 0.2		<sup>15</sup> AN	14 DAYA	DayaBay, Ling Ao/Ao II reactors
2.12 ± 0.47		<sup>16</sup> AN	14B DAYA	DayaBay, Ling Ao/Ao II reactors
2.34 ± 0.20		<sup>17</sup> FORERO	14 FIT	Normal mass ordering
2.40 ± 0.19		<sup>17</sup> FORERO	14 FIT	Inverted mass ordering
2.18 ± 0.10		<sup>18</sup> GONZALEZ...	14 FIT	Normal mass ordering; global fit
2.19 ± 0.11		<sup>18</sup> GONZALEZ...	14 FIT	Inverted mass ordering; global fit
2.5 ± 0.9 ± 0.9		<sup>19</sup> ABE	13C DCHZ	Chooz reactors
2.3 ± 1.3		<sup>20</sup> ABE	13E T2K	Normal mass ordering
2.8 ± 1.6		<sup>20</sup> ABE	13E T2K	Inverted mass ordering
1.6 ± 1.3		<sup>21</sup> ADAMSON	13A MINS	Normal mass ordering
3.0 ± 1.8		<sup>21</sup> ADAMSON	13A MINS	Inverted mass ordering
<13	90	AGAFONOVA	13 OPER	OPERA: $3\nu$
< 3.6	95	22 AHARMIM	13 FIT	global solar: $3\nu$

2.3 ± 0.3 ± 0.1	23	AN	13	DAYA	DayaBay, Ling Ao/Ao II reactors	
2.2 ± 1.1 ± 0.8	24	ABE	12	DCHZ	Chooz reactors	
2.8 ± 0.8 ± 0.7	25	ABE	12B	DCHZ	Chooz reactors	
2.9 ± 0.3 ± 0.5	26	AHN	12	RENO	Yonggwang reactors	
2.4 ± 0.4 ± 0.1	27	AN	12	DAYA	DayaBay, Ling Ao/Ao II reactors	
2.5 + 1.8 - 1.6	28	ABE	11	FIT	KamLAND + global solar	
< 6.1	95	29	ABE	11	FIT	Global solar
1.3 to 5.6	68	30	ABE	11A	T2K Normal mass ordering	
1.5 to 5.6	68	31	ABE	11A	T2K Inverted mass ordering	
0.3 to 2.3	68	32	ADAMSON	11D	MINS Normal mass ordering	
0.8 to 3.9	68	33	ADAMSON	11D	MINS Inverted mass ordering	
8 ± 3		34	FOGLI	11	FIT Global neutrino data	
7.8 ± 6.2		35	GANDO	11	FIT KamLAND + solar: $3\nu$	
12.4 ± 13.3		36	GANDO	11	FIT KamLAND: $3\nu$	
3 + 9 - 7	90	37	ADAMSON	10A	MINS Normal mass ordering	
6 + 14 - 6	90	38	ADAMSON	10A	MINS Inverted mass ordering	
8 + 8 - 7		39,40	AHARMIM	10	FIT KamLAND + global solar: $3\nu$	
< 30	95	39,41	AHARMIM	10	FIT global solar: $3\nu$	
< 15	90	42	WENDELL	10	SKAM $3\nu$ osc.; normal $m$ ordering	
< 33	90	42	WENDELL	10	SKAM $3\nu$ osc.; inverted $m$ ordering	
11 + 11 - 8		43	ADAMSON	09	MINS Normal mass ordering	
18 + 15 - 11		44	ADAMSON	09	MINS Inverted mass ordering	
6 ± 4		45	FOGLI	08	FIT Global neutrino data	
8 ± 7		46	FOGLI	08	FIT Solar + KamLAND data	
5 ± 5		47	FOGLI	08	FIT Atmospheric + LBL + CHOOZ	
< 36	90	48	YAMAMOTO	06	K2K Accelerator experiment	
< 48	90	49	AHN	04	K2K Accelerator experiment	
< 36	90	50	BOEHM	01	Palo Verde react.	
< 45	90	51	BOEHM	00	Palo Verde react.	
< 15	90	52	APOLLONIO	99	CHOZ Reactor Experiment	

1 ADEY 18A reports results from analysis of 1958 days of data taking with the Daya-Bay experiment, with  $3.9 \times 10^6$   $\bar{\nu}_e$  candidates. The fit to the data gives  $\Delta m_{ee}^2 = (2.522 \pm 0.068 \pm 0.070) \times 10^{-3} \text{ eV}^2$ . Solar oscillation parameters are fixed in the analysis using the global averages,  $\sin^2(\theta_{12}) = 0.307^{+0.013}_{-0.012}$ ,  $\Delta m_{21}^2 = (7.53 \pm 0.18) \times 10^{-5} \text{ eV}^2$ , from PDG 18. Supersedes AN 17A.

2 BAK 18 reports results of the RENO experiment using about 2200 live-days of data taken with detectors placed at 410.6 and 1445.7 m from reactors of the Hanbit Nuclear Power Plant. Supersedes SEO 18.

3 ABE 16B uses 455.57 live days of data from a detector 1050 m away from two reactor cores of the Chooz nuclear power station, to determine the mixing parameter  $\sin^2(2\theta_{13})$ . This analysis uses 7.15 reactor-off days for constraining backgrounds. A rate and shape analysis is performed on combined neutron captures on H and Gd. Supersedes ABE 14H and ABE 13C.

4 AN 16A uses data from the eight antineutrino detectors (404 days) and six antineutrino detectors (217 days) runs to determine the mixing parameter  $\sin^2(2\theta_{13})$  using the neutron capture on H only. Supersedes AN 14B.

5 ABE 18B uses 328 kton-years of Super-Kamiokande I-IV atmospheric neutrino data to obtain this result. The fit is performed over the four parameters,  $\Delta m_{21}^2$ ,  $\sin^2\theta_{23}$ ,  $\sin^2\theta_{13}$ , and  $\delta$ , while the solar parameters are fixed to  $\Delta m_{21}^2 = (7.53 \pm 0.18) \times 10^{-5} \text{ eV}^2$  and  $\sin^2\theta_{12} = 0.304 \pm 0.014$ .

6 AGAFONOVA 18A reports  $\sin^2(2\theta_{13}) < 0.43$  at 90% C.L. The result on the sterile neutrino search in the context of 3+1 model is also reported. A 90% C.L. upper limit on  $\sin^2(2\theta_{\mu e}) = 0.021$  for  $\Delta m_{41}^2 \geq 0.1 \text{ eV}^2$  is set.

7 SEO 18 reports results of the RENO experiment using about 500 days of data, performing a rate and shape analysis. Compared to AHN 12, a significant reduction of the systematic uncertainties is reported. A 3% excess of events near 5 MeV of the prompt energy is observed. SEO 18 is a detailed description of the results published in CHOI 16, which it supersedes. Supersedes by BAK 18.

8 Using T2K data only. For inverted mass ordering, all values of  $\theta_{13}$  are ruled out at 68% CL.

9 AN 17A reports results from combined rate and spectral shape analysis of 1230 days of data taken with the Daya Bay reactor experiment. The data set contains more than  $2.5 \times 10^6$  inverse beta-decay events with neutron capture on Gd. A simultaneous fit to  $\theta_{13}$  and  $\Delta m_{ee}^2$  is performed. Supersedes by ADEY 18A.

10 CHOI 16 reports results of the RENO experiment using about 500 days of data, performing a rate and shape analysis. Compared to AHN 12, a significant reduction of the systematic uncertainties is reported. A 3% excess of events near 5 MeV of the prompt energy is observed. Supersedes AHN 12.

11 AN 15 uses all eight identical detectors, with four placed near the reactor cores and the remaining four at the far hall to determine the mixing angle  $\theta_{13}$  using the  $\bar{\nu}_e$  observed interaction rates with neutron capture on Gd and energy spectra. The result corresponds to the exposure of  $6.9 \times 10^5 \text{ GW}_{th}$ -ton-days. Supersedes by AN 17A.

12 ABE 14A uses 467.9 live days of one detector, 1050 m away from two reactor cores of the Chooz nuclear power station, to determine the mixing parameter  $\sin^2(2\theta_{13})$ . The Bugey4 data (DECLAIS 94) is used to constrain the neutrino flux. The data set includes 7.24 reactor-off days. A "rate-modulation" analysis is performed. Supersedes ABE 12B.

13 ABE 14C result is for  $\nu_e$  appearance and assumes  $\Delta m_{32}^2 = 2.4 \times 10^{-3} \text{ eV}^2$ ,  $\sin^2(\theta_{23}) = 0.5$ , and  $\delta = 0$ .

14 ABE 14H uses 467.9 live days of one detector, 1050 m away from two reactor cores of the Chooz nuclear power station, to determine the mixing parameter  $\sin^2(2\theta_{13})$ . The Bugey4 data (DECLAIS 94) is used to constrain the neutrino flux. The data set includes 7.24 reactor-off days. A rate and shape analysis is performed. Superseded by ABE 16B.

15 AN 14 uses six identical detectors, with three placed near the reactor cores (flux-weighted baselines of 512 and 561 m) and the remaining three at the far hall (at the flux averaged distance of 1579 m from all six reactor cores) to determine the mixing angle  $\theta_{13}$  using the  $\bar{\nu}_e$  observed interaction rates with neutron capture on Gd and energy spectra. Supersedes AN 13 and superseded by AN 15.

16 AN 14B uses six identical anti-neutrino detectors with flux-weighted baselines of  $\sim 500 \text{ m}$  and  $\sim 1.6 \text{ km}$  to six power reactors. This rate analysis uses a 217-day data set and neutron capture on protons (not Gd) only.  $\Delta m_{31}^2 = 2.32 \times 10^{-3} \text{ eV}^2$  is assumed. Superseded by AN 16A.

17 FORERO 14 performs a global fit to neutrino oscillations using solar, reactor, long-baseline accelerator, and atmospheric neutrino data.

18 GONZALEZ-GARCIA 14 result comes from a frequentist global fit. The corresponding Bayesian global fit to the same data results are reported in BERGSTROM 15 as  $(2.18^{+0.10}_{-0.11}) \times 10^{-2} \text{ eV}^2$  for normal and  $(2.19^{+0.12}_{-0.10}) \times 10^{-2} \text{ eV}^2$  for inverted mass ordering.

19 ABE 13C uses delayed neutron capture on hydrogen instead of on Gd used previously. The physical volume is thus three times larger. The fit is based on the rate and shape analysis as in ABE 12B. The Bugey4 data (DECLAIS 94) is used to constrain the neutrino flux. Superseded by ABE 16B.

20 ABE 13E assumes maximal  $\theta_{23}$  mixing and CP phase  $\delta = 0$ .

21 ADAMSON 13A results obtained from  $\nu_e$  appearance, assuming  $\delta = 0$ , and  $\sin^2(2\theta_{23}) = 0.957$ .

22 AHARMIM 13 obtained this result by a three-neutrino oscillation analysis with the value of  $\Delta m_{32}^2$  fixed to  $2.45 \times 10^{-3} \text{ eV}^2$ , using global solar neutrino data. AHARMIM 13 global solar neutrino data include SNO's all-phases-combined analysis results on the total active  $^8\text{B}$  neutrino flux and energy-dependent  $\nu_e$  survival probability parameters, measurements of Cl (CLEVELAND 98), Ga (ABDURASHITOV 09 which contains combined analysis with GNO (ALTMANN 05 and Ph.D. thesis of F. Kaether)), and  $^7\text{Be}$  (BELLINI 11A) rates, and  $^8\text{B}$  solar-neutrino recoil electron measurements of SK-I (HOSAKA 06) zenith, SK-II (CRAVENS 08) and SK-II (ABE 11) day/night spectra, and Borexino (BELLINI 10A) spectra. AHARMIM 13 also reported a result combining global solar and KamLAND data, which is  $\sin^2(2\theta_{13}) = (9.1^{+2.9}_{-3.1}) \times 10^{-2}$ .

23 AN 13 uses six identical detectors, with three placed near the reactor cores (flux-weighted baselines of 498 and 555 m) and the remaining three at the far hall (at the flux averaged distance of 1628 m from all six reactor cores) to determine the  $\bar{\nu}_e$  interaction rate ratios. Superseded by AN 14.

24 ABE 12 determines the  $\bar{\nu}_e$  interaction rate in a single detector, located 1050 m from the cores of two reactors. A rate and shape analysis is performed. The rate normalization is fixed by the results of the Bugey4 reactor experiment, thus avoiding any dependence on possible very short baseline oscillations. The value of  $\Delta m_{31}^2 = 2.4 \times 10^{-3} \text{ eV}^2$  is used in the analysis. Superseded by ABE 12B.

25 ABE 12B determines the neutrino mixing angle  $\theta_{13}$  using a single detector, located 1050 m from the cores of two reactors. This result is based on a spectral shape and rate analysis. The Bugey4 data (DECLAIS 94) is used to constrain the neutrino flux. Superseded by ABE 14A.

26 AHN 12 uses two identical detectors, placed at flux weighted distances of 408.56 m and 1433.99 m from six reactor cores, to determine the mixing angle  $\theta_{13}$ . This rate-only analysis excludes the no-oscillation hypothesis at 4.9 standard deviations. The value of  $\Delta m_{31}^2 = (2.32^{+0.12}_{-0.08}) \times 10^{-3} \text{ eV}^2$  was assumed in the analysis. Superseded by CHOI 16.

27 AN 12 uses six identical detectors with three placed near the reactor cores (flux-weighted baselines of 470 m and 576 m) and the remaining three at the far hall (at the flux averaged distance of 1648 m from all six reactor cores) to determine the mixing angle  $\theta_{13}$  using the  $\bar{\nu}_e$  observed interaction rate ratios. This rate-only analysis excludes the no-oscillation hypothesis at 5.2 standard deviations. The value of  $\Delta m_{31}^2 = (2.32^{+0.12}_{-0.08}) \times 10^{-3} \text{ eV}^2$  was assumed in the analysis. Superseded by AN 13.

28 ABE 11 obtained this result by a three-neutrino oscillation analysis with the value of  $\Delta m_{32}^2$  fixed to  $2.4 \times 10^{-3} \text{ eV}^2$ , using solar neutrino data including Super-Kamiokande, SNO, Borexino (ARPESELLA 08A), Homestake, GALLEX/GNO, SAGE, and KamLAND data. This result implies an upper bound of  $\sin^2\theta_{13} < 0.059$  (95% CL) or  $\sin^2 2\theta_{13} < 0.22$  (95% CL). The normal neutrino mass ordering and CPT invariance are assumed.

29 ABE 11 obtained this result by a three-neutrino oscillation analysis with the value of  $\Delta m_{32}^2$  fixed to  $2.4 \times 10^{-3} \text{ eV}^2$ , using solar neutrino data including Super-Kamiokande, SNO, Borexino (ARPESELLA 08A), Homestake, and GALLEX/GNO data. The normal neutrino mass ordering is assumed.

30 The quoted limit is for  $\Delta m_{32}^2 = 2.4 \times 10^{-3} \text{ eV}^2$ ,  $\theta_{23} = \pi/2$ ,  $\delta = 0$ , and the normal mass ordering. For other values of  $\delta$ , the 68% region spans from 0.03 to 0.25, and the 90% region from 0.02 to 0.32.

31 The quoted limit is for  $\Delta m_{32}^2 = 2.4 \times 10^{-3} \text{ eV}^2$ ,  $\theta_{23} = \pi/2$ ,  $\delta = 0$ , and the inverted mass ordering. For other values of  $\delta$ , the 68% region spans from 0.04 to 0.30, and the 90% region from 0.02 to 0.39.

32 The quoted limit is for  $\Delta m_{32}^2 = 2.32 \times 10^{-3} \text{ eV}^2$ ,  $\theta_{23} = \pi/2$ ,  $\delta = 0$ , and the normal mass ordering. For other values of  $\delta$ , the 68% region spans from 0.02 to 0.12, and the 90% region from 0 to 0.16.

33 The quoted limit is for  $\Delta m_{32}^2 = 2.32 \times 10^{-3} \text{ eV}^2$ ,  $\theta_{23} = \pi/2$ ,  $\delta = 0$ , and the inverted mass ordering. For other values of  $\delta$ , the 68% region spans from 0.02 to 0.16, and the 90% region from 0 to 0.21.

34 FOGLI 11 obtained this result from an analysis using the atmospheric, accelerator long baseline, CHOOZ, solar, and KamLAND data. Recently, MUELLER 11 suggested an

# Lepton Particle Listings

## Neutrino Mixing

average increase of about 3.5% in normalization of the reactor  $\bar{\nu}_e$  fluxes, and using these fluxes, the fitted result becomes  $0.10 \pm 0.03$ .

<sup>35</sup> GANDO 11 report  $\sin^2\theta_{13} = 0.020 \pm 0.016$ . This result was obtained with three-neutrino fit using the KamLAND + solar data.

<sup>36</sup> GANDO 11 report  $\sin^2\theta_{13} = 0.032 \pm 0.037$ . This result was obtained with three-neutrino fit using the KamLAND data only.

<sup>37</sup> This result corresponds to the limit of  $<0.12$  at 90% CL for  $\Delta m_{32}^2 = 2.43 \times 10^{-3} \text{ eV}^2$ ,  $\theta_{23} = \pi/2$ , and  $\delta = 0$ . For other values of  $\delta$ , the 90% CL region spans from 0 to 0.16.

<sup>38</sup> This result corresponds to the limit of  $<0.20$  at 90% CL for  $\Delta m_{32}^2 = 2.43 \times 10^{-3} \text{ eV}^2$ ,  $\theta_{23} = \pi/2$ , and  $\delta = 0$ . For other values of  $\delta$ , the 90% CL region spans from 0 to 0.21.

<sup>39</sup> AHARMIM 10 global solar neutrino data include SNO's low-energy-threshold analysis survival probability day/night curves, SNO Phase III integral rates (AHARMIM 08), CL (CLEVELAND 98), SAGE (ABDURASHITOV 09), Gallex/GNO (HAMPEL 99, ALTMANN 05), Borexino (ARPESELLA 08A), SK-I zenith (HOSAKA 06), and SK-II day/night spectra (CRAVENS 08).

<sup>40</sup> AHARMIM 10 obtained this result by a three-neutrino oscillation analysis with the value of  $\Delta m_{31}^2$  fixed to  $2.3 \times 10^{-3} \text{ eV}^2$ , using global solar neutrino data and KamLAND data (ABE 08A). *CPT* invariance is assumed. This result implies an upper bound of  $\sin^2\theta_{13} < 0.057$  (95% CL) or  $\sin^2\theta_{13} < 0.22$  (95% CL).

<sup>41</sup> AHARMIM 10 obtained this result by a three-neutrino oscillation analysis with the value of  $\Delta m_{31}^2$  fixed to  $2.3 \times 10^{-3} \text{ eV}^2$ , using global solar neutrino data.

<sup>42</sup> WENDELL 10 obtained this result by a three-neutrino oscillation analysis with one mass scale dominance ( $\Delta m_{21}^2 = 0$ ) using the Super-Kamiokande-I+II+III atmospheric neutrino data, and updates the HOSAKA 06A result.

<sup>43</sup> The quoted limit is for  $\Delta m_{32}^2 = 2.43 \times 10^{-3} \text{ eV}^2$ ,  $\theta_{23} = \pi/2$ , and  $\delta = 0$ . For other values of  $\delta$ , the 68% CL region spans from 0.02 to 0.26.

<sup>44</sup> The quoted limit is for  $\Delta m_{32}^2 = 2.43 \times 10^{-3} \text{ eV}^2$ ,  $\theta_{23} = \pi/2$ , and  $\delta = 0$ . For other values of  $\delta$ , the 68% CL region spans from 0.04 to 0.34.

<sup>45</sup> FOGLI 08 obtained this result from a global analysis of all neutrino oscillation data, that is, solar + KamLAND + atmospheric + accelerator long baseline + CHOOZ.

<sup>46</sup> FOGLI 08 obtained this result from an analysis using the solar and KamLAND neutrino oscillation data.

<sup>47</sup> FOGLI 08 obtained this result from an analysis using the atmospheric, accelerator long baseline, and CHOOZ neutrino oscillation data.

<sup>48</sup> YAMAMOTO 06 searched for  $\nu_\mu \rightarrow \nu_e$  appearance. Assumes  $2 \sin^2(2\theta_{\mu e}) = \sin^2(2\theta_{13})$ . The quoted limit is for  $\Delta m_{32}^2 = 1.9 \times 10^{-3} \text{ eV}^2$ . That value of  $\Delta m_{32}^2$  is the one- $\sigma$  low value for AHN 06A. For the AHN 06A best fit value of  $2.8 \times 10^{-3} \text{ eV}^2$ , the  $\sin^2(2\theta_{13})$  limit is  $< 0.26$ . Supersedes AHN 04.

<sup>49</sup> AHN 04 searched for  $\nu_\mu \rightarrow \nu_e$  appearance. Assuming  $2 \sin^2(2\theta_{\mu e}) = \sin^2(2\theta_{13})$ , a limit on  $\sin^2(2\theta_{\mu e})$  is converted to a limit on  $\sin^2(2\theta_{13})$ . The quoted limit is for  $\Delta m_{32}^2 = 1.9 \times 10^{-3} \text{ eV}^2$ . That value of  $\Delta m_{32}^2$  is the one- $\sigma$  low value for ALIU 05. For the ALIU 05 best fit value of  $2.8 \times 10^{-3} \text{ eV}^2$ , the  $\sin^2(2\theta_{13})$  limit is  $< 0.30$ .

<sup>50</sup> The quoted limit is for  $\Delta m_{32}^2 = 1.9 \times 10^{-3} \text{ eV}^2$ . That value of  $\Delta m_{32}^2$  is the 1- $\sigma$  low value for ALIU 05. For the ALIU 05 best fit value of  $2.8 \times 10^{-3} \text{ eV}^2$ , the  $\sin^2\theta_{13}$  limit is  $< 0.19$ . In this range, the  $\theta_{13}$  limit is larger for lower values of  $\Delta m_{32}^2$ , and smaller for higher values of  $\Delta m_{32}^2$ .

<sup>51</sup> The quoted limit is for  $\Delta m_{32}^2 = 1.9 \times 10^{-3} \text{ eV}^2$ . That value of  $\Delta m_{32}^2$  is the 1- $\sigma$  low value for ALIU 05. For the ALIU 05 best fit value of  $2.8 \times 10^{-3} \text{ eV}^2$ , the  $\sin^2\theta_{13}$  limit is  $< 0.23$ .

<sup>52</sup> The quoted limit is for  $\Delta m_{32}^2 = 2.43 \times 10^{-3} \text{ eV}^2$ . That value of  $\Delta m_{32}^2$  is the central value for ADAMSON 08. For the ADAMSON 08 1- $\sigma$  low value of  $2.30 \times 10^{-3} \text{ eV}^2$ , the  $\sin^2\theta_{13}$  limit is  $< 0.16$ . See also APOLLONIO 03 for a detailed description of the experiment.

### CP violating phase

#### $\delta$ , CP violating phase

Measurements of  $\delta$  come from atmospheric and accelerator experiments looking at  $\nu_e$  appearance. We encode values between 0 and  $2\pi$ , though it is equivalent to use  $-\pi$  to  $\pi$ .

VALUE ( $\pi$ rad)	CL%	DOCUMENT ID	TECN	COMMENT
<b>1.36<math>\pm</math>0.17 OUR AVERAGE</b>				
0.0 $\pm$ 1.3 -0.4		<sup>1</sup> ACERO	19 NOVA	Normal mass ordering, octant II for $\theta_{23}$
1.33 $\pm$ 0.45 -0.51		<sup>2</sup> ABE	18B SKAM	Normal mass ordering, $\theta_{13}$ constrained
1.40 $\pm$ 0.20		<sup>3</sup> ABE	18G T2K	Normal mass ordering, $\theta_{13}$ constrained
• • • We do not use the following data for averages, fits, limits, etc. • • •				
1.33 $\pm$ 0.46 -0.53		<sup>4</sup> ABE	18B SKAM	$3\nu$ osc: normal mass ordering, $\theta_{13}$ free
1.22 $\pm$ 0.76 -0.67		<sup>4</sup> ABE	18B SKAM	$3\nu$ osc: inverted mass ordering, $\theta_{13}$ free
1.33 $\pm$ 0.48 -0.53		<sup>2</sup> ABE	18B SKAM	$3\nu$ osc: inverted mass ordering, $\theta_{13}$ constrained

1.54 $\pm$ 0.14 -0.12	95	<sup>3</sup> ABE	18G T2K	Inverted mass ordering, $\theta_{13}$ constrained
1.21 $\pm$ 0.91 -0.30		<sup>5</sup> ACERO	18 NOVA	Normal mass ordering, octant II for $\theta_{23}$
1.46 $\pm$ 0.56 -0.42		<sup>5</sup> ACERO	18 NOVA	Normal mass ordering, octant I for $\theta_{23}$
1.32 $\pm$ 0.21 -0.15		DE-SALAS	18 FIT	Normal mass ordering, global fit
1.56 $\pm$ 0.13 -0.15		DE-SALAS	18 FIT	Inverted mass ordering, global fit
1.45 $\pm$ 0.27 -0.26		<sup>6</sup> ABE	17F T2K	Normal mass ordering
1.54 $\pm$ 0.22 -0.23		<sup>6</sup> ABE	17F T2K	Inverted mass ordering
1.50 $\pm$ 0.53 -0.57		<sup>7</sup> ADAMSON	17B NOVA	Inverted mass ordering; $\theta_{23}$ in octant II
0.74 $\pm$ 0.57 -0.93		<sup>7</sup> ADAMSON	17B NOVA	Normal mass ordering; $\theta_{23}$ in octant II
1.48 $\pm$ 0.69 -0.58		<sup>7</sup> ADAMSON	17B NOVA	Normal mass ordering; $\theta_{23}$ in octant I
0.0 to 0.1, 0.5 to 2.0	90	<sup>7,8</sup> ADAMSON	16 NOVA	Inverted mass ordering
0.0 to 2.0 to 0.15, 0.83	90	<sup>8</sup> ADAMSON	16 NOVA	Normal mass ordering
1.09 to 1.92 0.05 to 1.2	90	ABE	15D T2K	Normal mass ordering
1.09 to 1.92 0.05 to 1.2	90	ABE	15D T2K	Inverted mass ordering
1.34 $\pm$ 0.64 -0.38		<sup>9</sup> ADAMSON	14 MINS	Normal mass ordering
1.48 $\pm$ 0.34 -0.32		FORERO	14 FIT	Normal mass ordering
1.48 $\pm$ 0.34 -0.32		FORERO	14 FIT	Inverted mass ordering
1.70 $\pm$ 0.22 -0.39		<sup>10</sup> GONZALEZ...	14 FIT	Normal mass ordering; global fit
1.41 $\pm$ 0.35 -0.34		<sup>10</sup> GONZALEZ...	14 FIT	Inverted mass ordering; global fit
0 to 1.5 or 1.9 to 2	90	<sup>11</sup> ADAMSON	13A MINS	Normal mass ordering

<sup>1</sup> ACERO 19 is based on a sample size of  $1.33 \times 10^{20}$  protons on target with combined antineutrino and neutrino data. Supersedes ACERO 18.

<sup>2</sup> ABE 18B uses 328 kton-years of Super-Kamiokande I-IV atmospheric neutrino data to obtain this result. The fit is performed over the three parameters,  $\Delta m_{32}^2$ ,  $\sin^2\theta_{23}$ , and  $\delta$ , while the solar parameters and  $\sin^2\theta_{13}$  are fixed to  $\Delta m_{21}^2 = (7.53 \pm 0.18) \times 10^{-5} \text{ eV}^2$ ,  $\sin^2\theta_{12} = 0.304 \pm 0.014$ , and  $\sin^2\theta_{13} = 0.0219 \pm 0.0012$ .

<sup>3</sup> ABE 18G confidence intervals are marginalized over both mass orderings. Normal order preferred with a posterior probability of 87%. The 1-sigma result for normal mass ordering used in the average was provided by the experiment via private communications. Supersedes ABE 17F.

<sup>4</sup> ABE 18B uses 328 kton-years of Super-Kamiokande I-IV atmospheric neutrino data to obtain this result. The fit is performed over the four parameters,  $\Delta m_{32}^2$ ,  $\sin^2\theta_{23}$ ,  $\sin^2\theta_{13}$ , and  $\delta$ , while the solar parameters are fixed to  $\Delta m_{21}^2 = (7.53 \pm 0.18) \times 10^{-5} \text{ eV}^2$  and  $\sin^2\theta_{12} = 0.304 \pm 0.014$ .

<sup>5</sup> ACERO 18 performs a joint fit to the data for  $\nu_\mu$  disappearance and  $\nu_e$  appearance. The overall best fit favors normal mass ordering and  $\theta_{23}$  in octant II. No 1- $\sigma$  confidence intervals are presented for the inverted mass ordering scenarios. Superseded by ACERO 19.

<sup>6</sup> ABE 17F confidence intervals are obtained using a frequentist analysis including  $\theta_{13}$  constraint from reactor experiments. Bayesian intervals based on Markov Chain Monte Carlo method are also provided by the authors. Superseded by ABE 18G.

<sup>7</sup> Errors are projections of 68% C.L. curve of  $\delta_{CP}$  vs.  $\sin^2\theta_{23}$ .

<sup>8</sup> ADAMSON 16 result is based on a data sample with  $2.74 \times 10^{20}$  protons on target. The likelihood-based analysis observed 6  $\nu_e$  events with an expected background of  $0.99 \pm 0.11$  events.

<sup>9</sup> ADAMSON 14 result is based on three-flavor formalism and  $\theta_{23} > \pi/4$ . Likelihood as a function of  $\delta$  is also shown for the other three combinations of hierarchy and  $\theta_{23}$  octants; all values of  $\delta$  are allowed at 90% C.L.

<sup>10</sup> GONZALEZ-GARCIA 14 result comes from a frequentist global fit. The corresponding Bayesian global fit to the same data results are reported in BERGSTROM 15 as 68% CL intervals of 1.24–1.94 for normal and 1.15–1.77 for inverted mass ordering.

<sup>11</sup> ADAMSON 13A result is based on  $\nu_e$  appearance in MINOS and the calculated  $\sin^2(2\theta_{23}) = 0.957$ ,  $\theta_{23} > \pi/4$ , and normal mass hierarchy. Likelihood as a function of  $\delta$  is also shown for the other three combinations of hierarchy and  $\theta_{23}$  octants; all values of  $\delta$  are allowed at 90% C.L.

### (C) Other neutrino mixing results

The LSND collaboration reported in AGUILAR 01 a signal which is consistent with  $\bar{\nu}_\mu \rightarrow \bar{\nu}_e$  oscillations. In a three neutrino framework, this would be a measurement of  $\theta_{12}$  and  $\Delta m_{21}^2$ . This does not appear to be consistent with most of the other neutrino data. The following listings include results from  $\nu_\mu \rightarrow \nu_e$ ,  $\bar{\nu}_\mu \rightarrow \bar{\nu}_e$  appearance and  $\nu_\mu$ ,  $\bar{\nu}_\mu$ ,  $\nu_e$ , and  $\bar{\nu}_e$  disappearance experiments, and searches for *CPT* violation.

See key on page 999

# Lepton Particle Listings Neutrino Mixing

## $\Delta(m^2)$ for $\sin^2(2\theta) = 1$ ( $\nu_\mu \rightarrow \nu_e$ )

VALUE (eV <sup>2</sup> )	CL%	DOCUMENT ID	TECN	COMMENT
0.03 to 0.05	90	1 AGUILAR-AR...18c	MBNE	MiniBooNE $\nu_\mu \bar{\nu}_e$ combined
0.015 to 0.050	90	2 AGUILAR-AR...13A	MBNE	MiniBooNE
<0.34	90	3 MAHN 12	MBNE	MiniBooNE/SciBooNE
<0.034	90	AGUILAR-AR...07	MBNE	MiniBooNE
<0.0008	90	AHN 04	K2K	Water Cherenkov
<0.4	90	ASTIER 03	NOMD	CERN SPS
<2.4	90	AVVAKUMOV 02	NTEV	NUTEV FNAL
		4 AGUILAR 01	LSND	$\nu_\mu \rightarrow \nu_e$ osc.prob.
0.03 to 0.3	95	5 ATHANASSO...98	LSND	$\nu_\mu \rightarrow \nu_e$
<2.3	90	6 LOVERRE 96	CHARM/CDHS	
<0.9	90	VILAIN 94c	CHM2	CERN SPS
<0.09	90	ANGELINI 86	HLBC	BEBC CERN PS

- 1 AGUILAR-AREVALO 18c result is based on  $\nu_\mu \rightarrow \nu_e$  appearance of  $460.5 \pm 99.0$  events; The best fit value is  $\Delta m^2 = 0.041$  eV<sup>2</sup>.
- 2 AGUILAR-AREVALO 13A result is based on  $\nu_\mu \rightarrow \nu_e$  appearance of  $162.0 \pm 47.8$  events; marginally compatible with twoneutrino oscillations. The best fit value is  $\Delta m^2 = 3.14$  eV<sup>2</sup>.
- 3 MAHN 12 is a combined spectral fit of MiniBooNE and SciBooNE neutrino data with the range of  $\Delta m^2$  up to  $25$  eV<sup>2</sup>. The best limit is  $0.04$  at  $7$  eV<sup>2</sup>.
- 4 AGUILAR 01 is the final analysis of the LSND full data set. Search is made for the  $\nu_\mu \rightarrow \nu_e$  oscillations using  $\nu_\mu$  from  $\pi^+$  decay in flight by observing beam-on electron events from  $\nu_e C \rightarrow e^- X$ . Present analysis results in  $8.1 \pm 12.2 \pm 1.7$  excess events in the  $60 < E_e < 200$  MeV energy range, corresponding to oscillation probability of  $0.10 \pm 0.16 \pm 0.04\%$ . This is consistent, though less significant, with the previous result of ATHANASSOPOULOS 98, which it supersedes. The present analysis uses selection criteria developed for the decay at rest region, and is less effective in removing the background above 60 MeV than ATHANASSOPOULOS 98.
- 5 ATHANASSOPOULOS 98 is a search for the  $\nu_\mu \rightarrow \nu_e$  oscillations using  $\nu_\mu$  from  $\pi^+$  decay in flight. The 40 observed beam-on electron events are consistent with  $\nu_e C \rightarrow e^- X$ ; the expected background is  $21.9 \pm 2.1$ . Authors interpret this excess as evidence for an oscillation signal corresponding to oscillations with probability  $(0.26 \pm 0.10 \pm 0.05)\%$ . Although the significance is only  $2.3\sigma$ , this measurement is an important and consistent cross check of ATHANASSOPOULOS 96 who reported evidence for  $\bar{\nu}_\mu \rightarrow \bar{\nu}_e$  oscillations from  $\mu^+$  decay at rest. See also ATHANASSOPOULOS 98b.
- 6 LOVERRE 96 uses the charged-current to neutral-current ratio from the combined CHARM (ALLABY 86) and CDHS (ABRAMOWICZ 86) data from 1986.

## $\sin^2(2\theta)$ for "Large" $\Delta(m^2)$ ( $\nu_\mu \rightarrow \nu_e$ )

VALUE (units $10^{-3}$ )	CL%	DOCUMENT ID	TECN	COMMENT
< 5	90	1 AGUILAR-AR...18c	MBNE	MiniBooNE; $\nu_\mu \bar{\nu}_e$
< 7.2	90	AGAFONOVA 13	OPER	$\Delta(m^2) > 0.1$ eV <sup>2</sup>
0.8 to 3	90	2 AGUILAR-AR...13A	MBNE	MiniBooNE
< 11	90	3 ANTONELLO 13	ICAR	$\nu_\mu \rightarrow \nu_e$
< 6.8	90	4 ANTONELLO 13A	ICAR	$\nu_\mu \rightarrow \nu_e$
<100	90	5 MAHN 12	MBNE	MiniBooNE/SciBooNE
< 1.8	90	6 AGUILAR-AR...07	MBNE	MiniBooNE
<110	90	7 AHN 04	K2K	Water Cherenkov
< 1.4	90	ASTIER 03	NOMD	CERN SPS
< 1.6	90	AVVAKUMOV 02	NTEV	NUTEV FNAL
		8 AGUILAR 01	LSND	$\nu_\mu \rightarrow \nu_e$ osc.prob.
0.5 to 30	95	9 ATHANASSO...98	LSND	$\nu_\mu \rightarrow \nu_e$
< 3.0	90	10 LOVERRE 96	CHARM/CDHS	
< 9.4	90	VILAIN 94c	CHM2	CERN SPS
< 5.6	90	11 VILAIN 94c	CHM2	CERN SPS

- 1 AGUILAR-AREVALO 18c result is based on  $\nu_\mu \rightarrow \nu_e$  appearance of  $460.5 \pm 99.0$  events; The best fit value is  $\sin^2(2\theta) = 0.92$ . The quoted limit for the two-neutrino mixing angle  $\theta$  is valid above  $\Delta m^2 = 0.59$  eV<sup>2</sup>.
- 2 AGUILAR-AREVALO 13A result is based on  $\nu_\mu \rightarrow \nu_e$  appearance of  $162.0 \pm 47.8$  events; marginally compatible with two neutrino oscillations. The best fit value is  $\sin^2(2\theta) = 0.002$ .
- 3 ANTONELLO 13 use the ICARUS T600 detector at LNGS and  $\sim 20$  GeV beam of  $\nu_\mu$  from CERN 730 km away to search for an excess of  $\nu_e$  events. Two events are found with  $3.7 \pm 0.6$  expected from conventional sources. This result excludes some parts of the parameter space expected by LSND. Superseded by ANTONELLO 13A.
- 4 Based on four events with a background of  $6.4 \pm 0.9$  from conventional sources with an average energy of 20 GeV and 730 km from the source of  $\nu_\mu$ .
- 5 MAHN 12 is a combined fit of MiniBooNE and SciBooNE neutrino data.
- 6 The limit is  $\sin^2 2\theta < 0.9 \times 10^{-3}$  at  $\Delta m^2 = 2$  eV<sup>2</sup>. That value of  $\Delta m^2$  corresponds to the smallest mixing angle consistent with the reported signal from LSND in AGUILAR 01.
- 7 The limit becomes  $\sin^2 2\theta < 0.15$  at  $\Delta m^2 = 2.8 \times 10^{-3}$  eV<sup>2</sup>, the best-fit value of the  $\nu_\mu$  disappearance analysis in K2K.
- 8 AGUILAR 01 is the final analysis of the LSND full data set of the search for the  $\nu_\mu \rightarrow \nu_e$  oscillations. See footnote in preceding table for further details.
- 9 ATHANASSOPOULOS 98 report ( $0.26 \pm 0.10 \pm 0.05\%$ ) for the oscillation probability; the value of  $\sin^2 2\theta$  for large  $\Delta m^2$  is deduced from this probability. See footnote in

preceding table for further details, and see the paper for a plot showing allowed regions. If effect is due to oscillation, it is most likely to be intermediate  $\sin^2 2\theta$  and  $\Delta m^2$ . See also ATHANASSOPOULOS 98b.

- 10 LOVERRE 96 uses the charged-current to neutral-current ratio from the combined CHARM (ALLABY 86) and CDHS (ABRAMOWICZ 86) data from 1986.
- 11 VILAIN 94c limit derived by combining the  $\nu_\mu$  and  $\bar{\nu}_\mu$  data assuming CP conservation.

## $\Delta(m^2)$ for $\sin^2(2\theta) = 1$ ( $\bar{\nu}_\mu \rightarrow \bar{\nu}_e$ )

VALUE (eV <sup>2</sup> )	CL%	DOCUMENT ID	TECN	COMMENT
0.023 to 0.060	90	1 AGUILAR-AR...13A	MBNE	MiniBooNE
<0.16	90	2 CHENG 12	MBNE	MiniBooNE/SciBooNE
0.03-0.09	90	3 AGUILAR-AR...10	MBNE	$E_\nu > 475$ MeV
0.03-0.07	90	4 AGUILAR-AR...10	MBNE	$E_\nu > 200$ MeV
<0.06	90	AGUILAR-AR...09b	MBNE	MiniBooNE
<0.055	90	5 ARMBRUSTER02	KAR2	Liquid Sci. calor.
<2.6	90	AVVAKUMOV 02	NTEV	NUTEV FNAL
0.03-0.05	90	6 AGUILAR 01	LSND	LAMPF
0.05-0.08	90	7 ATHANASSO...96	LSND	LAMPF
0.048-0.090	80	8 ATHANASSO...95		
<0.07	90	9 HILL 95		
<0.9	90	VILAIN 94c	CHM2	CERN SPS
<0.14	90	10 FREEDMAN 93	CNTR	LAMPF

- 1 Based on  $\bar{\nu}_\mu \rightarrow \bar{\nu}_e$  appearance of  $78.4 \pm 28.5$  events. The best fit values are  $\Delta m^2 = 0.043$  eV<sup>2</sup> and  $\sin^2 2\theta = 0.88$ .
- 2 CHENG 12 is a combined fit of MiniBooNE and SciBooNE antineutrino data.
- 3 This value is for a two neutrino oscillation analysis for excess antineutrino events with  $E_\nu > 475$  MeV. The best fit is at 0.07. The allowed region is consistent with LSND reported by AGUILAR 01. Supersedes AGUILAR-AREVALO 09b.
- 4 This value is for a two neutrino oscillation analysis for excess antineutrino events with  $E_\nu > 200$  MeV with subtraction of the expected 12 events low energy excess seen in the neutrino component of the beam. The best fit value is  $0.007$  for  $\Delta(m^2) = 4.4$  eV<sup>2</sup>.
- 5 ARMBRUSTER 02 is the final analysis of the KARMEN 2 data for 17.7 m distance from the ISIS stopped pion and muon neutrino source. It is a search for  $\bar{\nu}_e$ , detected by the inverse  $\beta$ -decay reaction on protons and <sup>12</sup>C. 15 candidate events are observed, and  $15.8 \pm 0.5$  background events are expected, hence no oscillation signal is detected. The results exclude large regions of the parameter area favored by the LSND experiment.
- 6 AGUILAR 01 is the final analysis of the LSND full data set. It is a search for  $\bar{\nu}_e$  30 m from LAMPF beam stop. Neutrinos originate mainly for  $\pi^+$  decay at rest.  $\bar{\nu}_e$  are detected through  $\bar{\nu}_e p \rightarrow e^+ n$  ( $20 < E_{e^+} < 60$  MeV) in delayed coincidence with  $np \rightarrow d\gamma$ . Authors observe  $87.9 \pm 22.4 \pm 6.0$  total excess events. The observation is attributed to  $\bar{\nu}_\mu \rightarrow \bar{\nu}_e$  oscillations with the oscillation probability of  $0.264 \pm 0.067 \pm 0.045\%$ , consistent with the previously published result. Taking into account all constraints, the most favored allowed region of oscillation parameters is a band of  $\Delta(m^2)$  from  $0.2-2.0$  eV<sup>2</sup>. Supersedes ATHANASSOPOULOS 95, ATHANASSOPOULOS 96, and ATHANASSOPOULOS 98.
- 7 ATHANASSOPOULOS 96 is a search for  $\bar{\nu}_e$  30 m from LAMPF beam stop. Neutrinos originate mainly from  $\pi^+$  decay at rest.  $\bar{\nu}_e$  could come from either  $\bar{\nu}_\mu \rightarrow \bar{\nu}_e$  or  $\nu_e \rightarrow \bar{\nu}_e$ ; our entry assumes the first interpretation. They are detected through  $\bar{\nu}_e p \rightarrow e^+ n$  ( $20 \text{ MeV} < E_{e^+} < 60 \text{ MeV}$ ) in delayed coincidence with  $np \rightarrow d\gamma$ . Authors observe  $51 \pm 20 \pm 8$  total excess events over an estimated background  $12.5 \pm 2.9$ . ATHANASSOPOULOS 96b is a shorter version of this paper.
- 8 ATHANASSOPOULOS 95 error corresponds to the  $1.6\sigma$  band in the plot. The expected background is  $2.7 \pm 0.4$  events. Corresponds to an oscillation probability of  $(0.34 \pm 0.20 \pm 0.07)\%$ . For a different interpretation, see HILL 95. Replaced by ATHANASSOPOULOS 96.
- 9 HILL 95 is a report by one member of the LSND Collaboration, reporting a different conclusion from the analysis of the data of this experiment (see ATHANASSOPOULOS 95). Contrary to the rest of the LSND Collaboration, Hill finds no evidence for the neutrino oscillation  $\bar{\nu}_\mu \rightarrow \bar{\nu}_e$  and obtains only upper limits.
- 10 FREEDMAN 93 is a search at LAMPF for  $\bar{\nu}_e$  generated from any of the three neutrino types  $\nu_\mu, \bar{\nu}_\mu$ , and  $\nu_e$  which come from the beam stop. The  $\bar{\nu}_e$ 's would be detected by the reaction  $\bar{\nu}_e p \rightarrow e^+ n$ . FREEDMAN 93 replaces DURKIN 88.

## $\sin^2(2\theta)$ for "Large" $\Delta(m^2)$ ( $\bar{\nu}_\mu \rightarrow \bar{\nu}_e$ )

VALUE (units $10^{-3}$ )	CL%	DOCUMENT ID	TECN	COMMENT
<640	90	1 ANTONELLO 13A	ICAR	$\bar{\nu}_e$ appearance
<150	90	2 CHENG 12	MBNE	MiniBooNE/SciBooNE
0.4-9.0	90	3 AGUILAR-AR...10	MBNE	$E_\nu > 475$ MeV
0.4-9.0	99	4 AGUILAR-AR...10	MBNE	$E_\nu > 200$ MeV
< 3.3	90	5 AGUILAR-AR...09b	MBNE	MiniBooNE
< 1.7	90	6 ARMBRUSTER02	KAR2	Liquid Sci. calor.
< 1.1	90	AVVAKUMOV 02	NTEV	NUTEV FNAL
5.3±1.3±9.0		7 AGUILAR 01	LSND	LAMPF
6.2±2.4±1.0		8 ATHANASSO...96	LSND	LAMPF
3-12	80	9 ATHANASSO...95		
< 6	90	10 HILL 95		

- 1 ANTONELLO 13A use the ICARUS T600 detector at LNGS and  $\sim 20$  GeV beam of  $\bar{\nu}_\mu$  from CERN 730 km away to search for an excess of  $\bar{\nu}_e$  events. Two events are found with  $3.7 \pm 0.6$  expected from conventional sources. This result excludes some parts of the parameter space expected by LSND. Superseded by ANTONELLO 13A.

Downloaded from https://academic.oup.com/ptep/article/2020/8/083C01/5891211 by guest on 12 November 2020

# Lepton Particle Listings

## Neutrino Mixing

<sup>1</sup> ANTONELLO 13a obtained the limit by assuming  $\bar{\nu}_\mu \rightarrow \bar{\nu}_e$  oscillation from the  $\sim 2\%$  of  $\bar{\nu}_\mu$  events contamination in the CNGS beam.

<sup>2</sup> CHENG 12 is a combined fit of MiniBooNE and SciBooNE antineutrino data.

<sup>3</sup> This value is for a two neutrino oscillation analysis for excess antineutrino events with  $E_\nu > 475$  MeV. At 90% CL there is no solution at high  $\Delta(m^2)$ . The best fit is at maximal mixing. The allowed region is consistent with LSND reported by AGUILAR 01. Supersedes AGUILAR-AREVALO 09b.

<sup>4</sup> This value is for a two neutrino oscillation analysis for excess antineutrino events with  $E_\nu > 200$  MeV with subtraction of the expected 12 events low energy excess seen in the neutrino component of the beam. At 90% CL there is no solution at high  $\Delta(m^2)$ . The best fit value is 0.007 for  $\Delta(m^2) = 4.4 \text{ eV}^2$ .

<sup>5</sup> This result is inconclusive with respect to small amplitude mixing suggested by LSND.

<sup>6</sup> ARMBRUSTER 02 is the final analysis of the KARMEN2 data. See footnote in the preceding table for further details, and the paper for the exclusion plot.

<sup>7</sup> AGUILAR 01 is the final analysis of the LSND full data set. The deduced oscillation probability is  $0.264 \pm 0.067 \pm 0.045\%$ ; the value of  $\sin^2 2\theta$  for large  $\Delta(m^2)$  is twice this probability (although these values are excluded by other constraints). See footnote in preceding table for further details, and the paper for a plot showing allowed regions. Supersedes ATHANASSOPOULOS 95, ATHANASSOPOULOS 96, and ATHANASSOPOULOS 98.

<sup>8</sup> ATHANASSOPOULOS 96 reports  $(0.31 \pm 0.12 \pm 0.05)\%$  for the oscillation probability; the value of  $\sin^2 2\theta$  for large  $\Delta(m^2)$  should be twice this probability. See footnote in preceding table for further details, and see the paper for a plot showing allowed regions.

<sup>9</sup> ATHANASSOPOULOS 95 error corresponds to the  $1.6\sigma$  band in the plot. The expected background is  $2.7 \pm 0.4$  events. Corresponds to an oscillation probability of  $(0.34 \pm 0.20 \pm 0.18 \pm 0.07)\%$ . For a different interpretation, see HILL 95. Replaced by ATHANASSOPOULOS 96.

<sup>10</sup> HILL 95 is a report by one member of the LSND Collaboration, reporting a different conclusion than the analysis of the data of this experiment (see ATHANASSOPOULOS 95). Contrary to the rest of the LSND Collaboration, Hill finds no evidence for the neutrino oscillation  $\bar{\nu}_\mu \rightarrow \bar{\nu}_e$  and obtains only upper limits.

### $\Delta(m^2)$ for $\sin^2(2\theta) = 1$ ( $\nu_\mu(\bar{\nu}_\mu) \rightarrow \nu_e(\bar{\nu}_e)$ )

VALUE (eV <sup>2</sup> )	CL%	DOCUMENT ID	TECN	COMMENT
<0.075	90	BORODOV... 92	CNTR	BNL E776

• • • We do not use the following data for averages, fits, limits, etc. • • •

<1.6	90	<sup>1</sup> ROMOSAN 97	CCFR	FNAL
------	----	-------------------------	------	------

<sup>1</sup> ROMOSAN 97 uses wideband beam with a 0.5 km decay region.

### $\sin^2(2\theta)$ for "Large" $\Delta(m^2)$ ( $\nu_\mu(\bar{\nu}_\mu) \rightarrow \nu_e(\bar{\nu}_e)$ )

VALUE (units $10^{-3}$ )	CL%	DOCUMENT ID	TECN	COMMENT
<1.8	90	<sup>1</sup> ROMOSAN 97	CCFR	FNAL

• • • We do not use the following data for averages, fits, limits, etc. • • •

<3.8	90	<sup>2</sup> MCFARLAND 95	CCFR	FNAL
<3	90	BORODOV... 92	CNTR	BNL E776

<sup>1</sup> ROMOSAN 97 uses wideband beam with a 0.5 km decay region.

<sup>2</sup> MCFARLAND 95 state that "This result is the most stringent to date for  $250 < \Delta(m^2) < 450 \text{ eV}^2$  and also excludes at 90%CL much of the high  $\Delta(m^2)$  region favored by the recent LSND observation." See ATHANASSOPOULOS 95 and ATHANASSOPOULOS 96.

### $\Delta(m^2)$ for $\sin^2(2\theta) = 1$ ( $\bar{\nu}_e \nrightarrow \bar{\nu}_e$ )

VALUE (eV <sup>2</sup> )	CL%	DOCUMENT ID	TECN	COMMENT
<0.01	90	<sup>1</sup> ACHKAR 95	CNTR	Bugey reactor

• • • We do not use the following data for averages, fits, limits, etc. • • •

<sup>1</sup> ACHKAR 95 bound is for  $L=15, 40,$  and  $95 \text{ m}$ .

### $\sin^2(2\theta)$ for "Large" $\Delta(m^2)$ ( $\bar{\nu}_e \nrightarrow \bar{\nu}_e$ )

VALUE	CL%	DOCUMENT ID	TECN	COMMENT
<0.02	90	<sup>1</sup> ACHKAR 95	CNTR	For $\Delta(m^2) = 0.6 \text{ eV}^2$

<sup>1</sup> ACHKAR 95 bound is from data for  $L=15, 40,$  and  $95 \text{ m}$  distance from the Bugey reactor.

## Sterile neutrino limits

### $\Delta(m^2)$ for $\sin^2(2\theta) = 1$ ( $\nu_\mu \rightarrow \nu_s$ )

$\nu_s$  means  $\nu_\tau$  or any sterile (noninteracting)  $\nu$ .

VALUE ( $10^{-5} \text{ eV}^2$ )	CL%	DOCUMENT ID	TECN	COMMENT
<3000 (or <550)	90	<sup>1</sup> OYAMA 89	KAMI	Water Cherenkov
<4.2 (or >54)	90	BIONTA 88	IMB	Flux has $\nu_\mu, \bar{\nu}_\mu, \nu_e,$ and $\bar{\nu}_e$

• • • We do not use the following data for averages, fits, limits, etc. • • •

<sup>1</sup> OYAMA 89 gives a range of limits, depending on assumptions in their analysis. They argue that the region  $\Delta(m^2) = (100-1000) \times 10^{-5} \text{ eV}^2$  is not ruled out by any data for large mixing.

### Search for $\nu_\mu$ or $\nu_e \rightarrow \nu_s$

VALUE	CL%	DOCUMENT ID	TECN	COMMENT
-------	-----	-------------	------	---------

• • • We do not use the following data for averages, fits, limits, etc. • • •

<0.1	99	<sup>1</sup> SEREBROV 19		Neutrino-4
<0.01	90	<sup>2</sup> ALEKSEEV 18		DANSS
<0.06	90	<sup>3</sup> ALMAZAN 18		STEREO
<0.1	95	<sup>4</sup> ASHENFELT... 18		PROSPECT
<0.1	95	<sup>5</sup> SEREBROV 18A		Neutrino-4
<0.4	90	<sup>6</sup> AARTSEN 17B	ICCB	IceCube-DeepCore
<8 $\times 10^{-3}$	95	<sup>7</sup> ABDURASHLI... 17		T $\beta$ decay
<1 $\times 10^{-2}$	90	<sup>8</sup> KO 17		NEOS
<2 $\times 10^{-2}$	90	<sup>9</sup> AARTSEN 16	ICCB	IceCube
<4.5 $\times 10^{-4}$	95	<sup>10</sup> ADAMSON 16B		MINOS, DayaBay
<8.6 $\times 10^{-2}$	95	<sup>11</sup> ADAMSON 16C		MINS
<1.1 $\times 10^{-2}$	95	<sup>12</sup> AN 16B		DAYA
		<sup>13</sup> AMBROSIO 01	MCRO	matter effects
		<sup>14</sup> FUKUDA 00	SKAM	neutral currents + matter effects

<sup>1</sup> SEREBROV 19 searches for  $\bar{\nu}_e \rightarrow \bar{\nu}_s$  oscillations with baseline 6–12 m with SM-3 research reactor that uses highly enriched <sup>235</sup>U fuel. The spectrum is well described by the  $1/L^2$  dependence. However, the shape differs from the theoretical expectations, with the best fit corresponding to  $\Delta m_{41}^2 = 7.34 \pm 0.1 \text{ eV}^2$  and  $\sin^2(2\theta_{14}) = 0.39 \pm 0.12$  at  $3\sigma$  significance.

<sup>2</sup> ALEKSEEV 18 searches for  $\bar{\nu}_e \rightarrow \bar{\nu}_s$  oscillations using the DANSS detector at 10.7, 11.2, and 12.7 m from the 3.1 GW<sub>th</sub> power reactor. The DANSS detector is highly segmented and moveable; the positions are changed usually 3 times a week. The analysis is based on the ratio of the events at top and bottom position; the middle position is used for checks of consistency. The best fit point is at  $\Delta m_{41}^2 = 1.4 \text{ eV}^2$  and  $\sin^2(2\theta_{14}) = 0.05$  with  $\Delta\chi^2 = 13.1$  (statistical errors only) compared to the fit with 3 active neutrinos only. The quoted limit of 0.01 for  $\sin^2(2\theta_{14})$  corresponds to  $\Delta m_{41}^2 \sim 1.0 \text{ eV}^2$ .

<sup>3</sup> ALMAZAN 18 searches for the  $\bar{\nu}_e \rightarrow \bar{\nu}_s$  oscillations with baseline from 9.4 to 11.1 m from the ILL research reactor with highly enriched <sup>235</sup>U fuel. The STEREO detector consists of six separated cells with Gd loaded scintillator, with 15 m water equivalent overburden. The detected rate is  $396.3 \pm 4.7 \bar{\nu}_e/\text{day}$  with signal to background ratio of about 0.9. The reported results corresponds to 66 days of reactor-on. The analysis uses the relative rates normalized to the cell number 1. No indication of the oscillation to the sterile neutrinos is found, the stated limit on  $\sin^2(2\theta_{14})$  correspond to  $\Delta m_{41}^2 \sim 3.5 \text{ eV}^2$  where the exclusion is maximal.

<sup>4</sup> ASHENFELTER 18 searches for the  $\bar{\nu}_e \rightarrow \bar{\nu}_s$  oscillations at baseline from 6.7 to 9.2 m from the 85 MW research reactor with pure <sup>235</sup>U core. The segmented 4 ton <sup>6</sup>Li-doped liquid scintillator is operated with about 1 m water equivalent overburden and recorded 25461  $\pm$  283 IBD events. No indication of oscillations into sterile neutrinos was observed. The stated limit for  $\sin^2(2\theta_{14})$  is for  $\Delta m_{41}^2 \sim 2 \text{ eV}^2$  where the sensitivity is maximal.

<sup>5</sup> SEREBROV 18A searches for the  $\bar{\nu}_e \rightarrow \bar{\nu}_s$  oscillation with baseline 6–12 m from the core of the SM-3 research reactor that uses highly enriched <sup>235</sup>U. They find that oscillations with  $\Delta m_{41}^2 \sim 0.7-0.8 \text{ eV}^2$  and  $\sin^2(2\theta_{14}) \sim 0.10-0.15$  give better fit to the  $L$  and  $E$  dependence than the no oscillation scenario. The significance of this is about 2 $\sigma$ .

<sup>6</sup> AARTSEN 17B uses three years of upward-going atmospheric neutrino data in the energy range of 10–60 GeV to constrain their disappearance into light sterile neutrinos. The reported limit  $\sin^2\theta_{24} < 0.11$  at 90% C.L. is for  $\Delta m_{41}^2 = 1.0 \text{ eV}^2$ . We convert the result to  $\sin^2 2\theta_{24}$  for the listing. AARTSEN 17B also reports  $\cos^2\theta_{24} \cdot \sin^2\theta_{34} < 0.15$  at 90% C.L. for  $\Delta m_{41}^2 = 1.0 \text{ eV}^2$ .

<sup>7</sup> ABDURASHITOV 17 use the Troitsk  $\nu$ -mass experiment to search for sterile neutrinos with mass 0.1 – 2 keV. We convert the reported limit from  $U_{e4}^2 < 0.002$  to  $\sin^2 2\theta_{14} < 0.008$  assume  $U_{e4} \sim \sin\theta_{14}$ . The stated limit corresponds to the smallest  $U_{e4}^2$ . The exclusion curve begins at  $U_{e4}^2$  of 0.02 for  $m_4 = 0.1 \text{ keV}$ .

<sup>8</sup> KO 17 reports on short baseline reactor oscillation search ( $\bar{\nu}_e \rightarrow \bar{\nu}_s$ ), motivated by the so-called "reactor antineutrino anomaly". The experiment is conducted at 23.7 m from the core of unit 5 of the Hanbit Nuclear Power Complex in Korea. The reported limited on  $\sin^2(2\theta_{41})$  for sterile neutrinos was determined using the reactor antineutrino spectrum determined by the Daya Bay experiment for  $\Delta m_{41}^2$  around 0.55 eV<sup>2</sup> where the sensitivity is maximal. A fraction of the parameter space derived from the "reactor antineutrino anomaly" is excluded by this work. Compared to reactor models an event excess is observed at about 5 MeV, in agreement with other experiments.

<sup>9</sup> AARTSEN 16 use one year of upward-going atmospheric muon neutrino data in the energy range of 320 GeV to 20 TeV to constrain their disappearance into light sterile neutrinos. Sterile neutrinos are expected to produce distinctive zenith distribution for these energies for  $0.01 \leq \Delta m^2 \leq 10 \text{ eV}^2$ . The stated limit is for  $\sin^2 2\theta_{24}$  at  $\Delta m^2$  around 0.3 eV<sup>2</sup>.

<sup>10</sup> ADAMSON 16b combine the results of AN 16B, ADAMSON 16C, and Bugey-3 reactor experiments to constrain  $\nu_\mu$  to  $\nu_e$  mixing through oscillations into light sterile neutrinos. The stated limit for  $\sin^2 2\theta_{\mu e}$  is at  $|\Delta m_{41}^2| = 1.2 \text{ eV}^2$ .

<sup>11</sup> ADAMSON 16c use the NuMI beam and exposure of  $10.56 \times 10^{20}$  protons on target to search for the oscillation of  $\nu_\mu$  dominated beam into light sterile neutrinos with detectors at 1.04 and 735 km. The reported limit  $\sin^2(\theta_{24}) < 0.022$  at 95% C.L. is for  $|\Delta m_{41}^2| = 0.5 \text{ eV}^2$ . We convert the result to  $\sin^2(2\theta_{24})$  for the listing.

<sup>12</sup> AN 16B utilize 621 days of data to place limits on the  $\bar{\nu}_e$  disappearance into a light sterile neutrino. The stated limit corresponds to the smallest  $\sin^2(2\theta_{14})$  at  $|\Delta m_{41}^2| \sim 3 \times 10^{-2} \text{ eV}^2$  (obtained from Figure 3 in AN 16B). The exclusion curve begins at  $|\Delta m_{41}^2| \sim 1.5 \times 10^{-4} \text{ eV}^2$  and extends to  $\sim 0.25 \text{ eV}^2$ . The analysis assumes  $\sin^2(2\theta_{12})$

See key on page 999

Lepton Particle Listings  
Neutrino Mixing

= 0.846 ± 0.021, Δm<sub>21</sub><sup>2</sup> = (7.53 ± 0.18) × 10<sup>-5</sup> eV<sup>2</sup>, and |Δm<sub>32</sub><sup>2</sup>| = (2.44 ± 0.06) × 10<sup>-3</sup> eV<sup>2</sup>.

<sup>13</sup>AMBROSIO 01 tested the pure 2-flavor ν<sub>μ</sub> → ν<sub>s</sub> hypothesis using matter effects which change the shape of the zenith-angle distribution of upward through-going muons. With maximum mixing and Δm<sup>2</sup> around 0.0024 eV<sup>2</sup>, the ν<sub>μ</sub> → ν<sub>s</sub> oscillation is disfavored with 99% confidence level with respect to the ν<sub>μ</sub> → ν<sub>τ</sub> hypothesis.

<sup>14</sup>FUKUDA 00 tested the pure 2-flavor ν<sub>μ</sub> → ν<sub>s</sub> hypothesis using three complementary atmospheric-neutrino data samples. With this hypothesis, zenith-angle distributions are expected to show characteristic behavior due to neutral currents and matter effects. In the Δm<sup>2</sup> and sin<sup>2</sup>2θ region preferred by the Super-Kamiokande data, the ν<sub>μ</sub> → ν<sub>s</sub> hypothesis is rejected at the 99% confidence level, while the ν<sub>μ</sub> → ν<sub>τ</sub> hypothesis consistently fits all of the data sample.

CPT tests

Table with 5 columns: (Δm<sub>21</sub><sup>2</sup> - Δm<sub>21</sub><sup>2</sup>), VALUE (10<sup>-4</sup> eV<sup>2</sup>), CL%, DOCUMENT ID, TECN, COMMENT. Row 1: <-1.1, 99.7, 1 DEGOUVEA 05 FIT solar vs. reactor

<sup>1</sup>DEGOUVEA 05 obtained this bound at the 3σ CL from the KamLAND (ARAKI 05) and solar neutrino data.

Table with 5 columns: (Δm<sub>32</sub><sup>2</sup> - Δm<sub>32</sub><sup>2</sup>), VALUE (10<sup>-3</sup> eV<sup>2</sup>), CL%, DOCUMENT ID, TECN, COMMENT. Row 1: -0.12 ± 0.26, 90, 2 ADAMSON 12B MINS MINOS atmospheric

• • • We do not use the following data for averages, fits, limits, etc. • • •

Table with 5 columns: VALUE (10<sup>-3</sup> eV<sup>2</sup>), CL%, DOCUMENT ID, TECN, COMMENT. Row 1: 0.6 ± 2.4 / -0.8, 90, 2 ADAMSON 12B MINS MINOS atmospheric

<sup>1</sup>ADAMSON 13B quotes this difference as a negative of our convention.   
 <sup>2</sup>The quoted result is the single-parameter 90% C.L. interval determined from the 90% C.L. contour in the (Δm<sup>2</sup>, Δm<sup>2</sup>) plane, which is obtained by minimizing the four parameter log-likelihood function with respect to the other oscillation parameters.

REFERENCES FOR Neutrino Mixing

AARTSEN 20 EPJ C80 9 M.G. Aartsen et al. (IceCube Collab.)
AARTSEN 19C PR D99 032007 M.G. Aartsen et al. (IceCube Collab.)
ACERO 19 PRL 123 151803 M.A. Acero et al. (NOvA Collab.)
ADEY 19 PR D100 052004 D. Adey et al. (Daya Bay Collab.)
AGAFONOVA 19 PR D100 051301 N. Agafonova et al. (OPERA Collab.)
ALBERT 19 JHEP 1906 113 A. Albert et al. (ANTARES Collab.)
ANDERSON 19 PR D99 012012 M. Anderson et al. (SNO+ Collab.)
SEREBROV 19 JETPL 109 213 A.P. Serbrov et al. (Neutrino-4 Collab.)
AARTSEN 18A PRL 120 071801 M.G. Aartsen et al. (IceCube Collab.)
ABE 18B PR D97 072001 K. Abe et al. (Super-Kamiokande Collab.)
ABE 18G PRL 121 171802 K. Abe et al. (T2K Collab.)
ACERO 18 PR D98 032012 M.A. Acero et al. (NOvA Collab.)
ADEY 18A PRL 121 241805 D. Adey et al. (Daya Bay Collab.)
AGAFONOVA 18A PRL 120 211801 N. Agafonova et al. (OPERA Collab.)
AGAFONOVA 18A JHEP 1806 151 N. Agafonova et al. (OPERA Collab.)
AGOSTINI 18B NAT 552 505 M. Agostini et al. (Borexino Collab.)
AGUILAR-AR... 18C PRL 121 221801 A.A. Aguilar-Arevalo et al. (MiniBooNE Collab.)
ALEKSEEV 18 PR B787 56 I. Alekseev et al. (DANSS Collab.)
ALMAZAN 18 PRL 121 161801 H. Almazan et al. (STEREO Collab.)
ASHENFELT... 18 PRL 121 251802 J. Ashenfelter et al. (PROSPECT Collab.)
BAK 18 PRL 121 201801 G. Bak et al. (RENO Collab.)
DE-SALAS 18 PR B782 633 P.F. de Salas et al. (PDG Collab.)
PDG 18 PR D98 030001 M. Tanabashi et al. (PDG Collab.)
SEO 18 PR D98 012002 S.H. Seo et al. (RENO Collab.)
SEREBROV 18A PPN 49 701 A.P. Serbrov et al. (Neutrino-4 Collab.)
AARTSEN 17B PR D95 112002 M.G. Aartsen et al. (IceCube Collab.)
ABDURASHI... 17B JETPL 105 753 J.N. Abdurashitov et al. (Troitsk non-mass Collab.)
ABE 17A PRL 118 151801 K. Abe et al. (T2K Collab.)
ABE 17C PR D96 011102 K. Abe et al. (T2K Collab.)
ABE 17F PR D96 092006 K. Abe et al. (T2K Collab.)
Also PR D98 019902 (errat.) K. Abe et al. (T2K Collab.)
ADAMSON 17A PRL 118 151802 P. Adamson et al. (NOvA Collab.)
ADAMSON 17B PRL 118 231801 P. Adamson et al. (NOvA Collab.)
AN 17A PR D95 072006 F.P. An et al. (Daya Bay Collab.)
ESTEBAN 17 JHEP 1701 087 I. Esteban et al. (NEOS Collab.)
KO 17 PRL 118 121802 Y.J. Ko et al. (NEOS Collab.)
AARTSEN 16 PR 117 071801 M.G. Aartsen et al. (IceCube Collab.)
ABE 16B JHEP 1601 163 Y. Abe et al. (Double Chooz Collab.)
ABE 16C PR D94 052010 K. Abe et al. (Super-Kamiokande Collab.)
ABE 16D PRL 116 181801 K. Abe et al. (T2K Collab.)
ADAMSON 16 PR D93 051104 P. Adamson et al. (NOvA Collab.)
ADAMSON 16A PR D93 051104 P. Adamson et al. (NOvA Collab.)
ADAMSON 16B PRL 117 151801 P. Adamson et al. (Daya Bay and MINOS Collab.)
ADAMSON 16C PRL 117 151803 P. Adamson et al. (MINOS Collab.)
AN 16 PR 116 061801 F.P. An et al. (Daya Bay Collab.)
AN 16A PR D93 072011 F.P. An et al. (Daya Bay Collab.)
AN 16B PRL 117 151802 F.P. An et al. (Daya Bay Collab.)
CHOI 16 PR 116 211801 J.H. Choi et al. (RENO Collab.)
PDG 16 CP C40 100001 C. Patrignani et al. (PDG Collab.)
AARTSEN 15A PR D91 072004 M.G. Aartsen et al. (IceCube Collab.)
ABE 15D PR D91 072010 K. Abe et al. (T2K Collab.)
AGAFONOVA 15A PRL 115 121802 N. Agafonova et al. (OPERA Collab.)
AN 15 PRL 115 111802 F.P. An et al. (Daya Bay Collab.)
BERGSTROM 15 JHEP 1509 200 J. Bergstrom et al. (BARC, STON, MADU+ Collab.)
GANDO 15 PR C92 055808 A. Gando et al. (KamLAND Collab.)
ABE 14 PRL 112 181801 K. Abe et al. (T2K Collab.)
Also PR D91 072010 K. Abe et al. (T2K Collab.)
ABE 14A PL B735 51 Y. Abe et al. (Double Chooz Collab.)
ABE 14B PR D89 092003 K. Abe et al. (T2K Collab.)
ABE 14C PRL 112 061802 K. Abe et al. (T2K Collab.)
ABE 14H JHEP 1410 086 Y. Abe et al. (Double Chooz Collab.)
Also JHEP 1502 074 (errat.) Y. Abe et al. (Double Chooz Collab.)
ADAMSON 14 PRL 112 191801 P. Adamson et al. (MINOS Collab.)
AN 14 PRL 112 061801 F.P. An et al. (Daya Bay Collab.)
AN 14B PR D90 071101 F.P. An et al. (Daya Bay Collab.)
BELLINI 14A NAT 512 383 G. Bellini et al. (Borexino Collab.)
FORERO 14 PR D90 093006 D.V. Forero, M. Tortola, J.W.F. Valle

GONZALEZ... 14 JHEP 1411 052
PDG 14 CP C38 070001
RENSHAW 14 PRL 112 091805
AARTSEN 13B PRL 111 081801
ABE 13C PL B723 66
ABE 13E PR D88 032002
ABE 13G PRL 111 211803
ADAMSON 13A PRL 110 171801
ADAMSON 13B PRL 110 251801
AGAFONOVA 13 JHEP 1307 004
AGUILAR-AR... 13A PRL 110 161801
AHARMIM 13 PR C88 02501
AN 13 CP C37 011001
ANTONELLO 13 EPJ C73 2345
ANTONELLO 13A EPJ C73 2599
GANDO 13 PR D88 033001
ABE 12 PRL 108 131801
ABE 12A PR D85 031103
ABE 12B PR D86 052008
ADAMSON 12 PRL 108 191801
ADAMSON 12B PR D86 052007
ADRIAN-MAR... 12 PL B714 224
AHN 12 PRL 108 191802
AN 12 PRL 108 171803
BELLINI 12A PRL 108 051302
CHENG 12 PR D86 052009
MAHN 12 PR D85 032007
ABE 11 PR D83 052010
ABE 11A PRL 107 041801
ABE 11B PR C84 035004
ABE 11C PRL 107 241801
ADAMSON 11 PRL 106 181801
ADAMSON 11B PRL 107 021801
ADAMSON 11C PR D84 071103
ADAMSON 11D PRL 107 181802
BELLINI 11 PL B696 191
BELLINI 11A PRL 107 141302
FOGLI 11 PR D84 053007
GANDO 11 PR D83 052002
MUELLER 11 PR C83 054615
SERENELLI 11 APJ 743 24
ADAMSON 10A PR D82 051102
AGUILAR-AR... 10 PR 105 181801
AHARMIM 10 PR C81 055504
BELLINI 10A PR D82 033006
DENIZ 10 PR D81 072001
KAETHER 10 PL B685 47
WENDELL 10 PR D81 092004
ABDURASHI... 09 PR C80 015807
ADAMSON 09 PRL 103 261802
AGUILAR-AR... 09B PRL 103 111801
ABE 08A PRL 100 221803
Also PRL 101 119904E
ADAMSON 08 PR D77 072002
ADAMSON 08A PRL 101 131802
ADAMSON 08B PRL 101 111301
AHARMIM 08 PR C87 015502
Also PRL 101 091302
ARPESELLA 08A PRL 101 091302
CRAVENS 08 PR D78 032002
FOGLI 08 PRL 101 141801
ADAMSON 07 PR D75 092003
AGUILAR-AR... 07 PRL 98 231801
AHARMIM 07 PR C75 045502
ADAMSON 06 PR D73 072002
AHN 06A PR D74 072003
BALATA 06 EPJ C47 21
HOSAKA 06 PR D73 112001
HOSAKA 06A PR D74 032002
MICHAEL 06 PRL 97 191801
WINTER 06A PR C73 025503
YAMAMOTO 06 PRL 96 181801
AHARMIM 05A PR C72 055502
ALIU 05 PR 94 081802
ALLISON 05 PR D72 052005
ALTMANN 05 PR B616 174
ARAKI 05 PRL 94 081801
ASHIE 05 PR D71 112005
BAHCALL 05 APJ 621 185
DEGOUVEA 05 PR D71 093002
AHARMIM 04 PR D70 093014
AHMED 04A PRL 92 181301
AHN 04 PRL 93 051801
AMBROSIO 04 EPJ C36 323
ASHIE 04 PRL 93 101801
EGUCHI 04 PRL 92 071301
SMY 04 PR D69 011104
AHN 03 PRL 90 041801
AMBROSIO 03 PL B566 35
APOLLONIO 03 EPJ C27 331
ASTIER 03 PL B570 19
EGUCHI 03 PRL 90 021802
GANDO 03 PRL 90 171302
IANNI 03 JP G29 2107
SANCHEZ 03 PR D68 113004
ABDURASHI... 02 JETP 95 181
Translated from ZETF 122 211.
AHMAD 02 PRL 89 011301
AHMAD 02B PRL 89 011302
ARMBRUSTER 02 PR D65 112001
AVAKUMOV 02 PRL 89 011804
FUKUDA 02 PL B539 179
AGUILAR 01 PR D64 112007
AHMAD 01 PRL 87 071301
AMBROSIO 01 PL B517 59
BOEHM 01 PR D64 112001
FUKUDA 01 PRL 86 5651
AMBROSIO 00 PL B478 5
BOEHM 00 PRL 84 3764
FUKUDA 00 PRL 85 3999
ALLISON 99 PL B449 137
APOLLONIO 99 PL B466 415
Also PL B472 434 (errat.)
Y. Fukuda et al.
FUKUDA 99C PRL 82 2644
FUKUDA 99D PL B467 185
HAMPPEL 99 PL B447 127
AMBROSIO 98 PL B434 451
APOLLONIO 98 PL B420 397
ATHANASSO... 98 PRL 81 1774
ATHANASSO... 98B PR C58 2489
CLEVELAND 98 APJ 496 505
FELDMAN 98 PR D57 3873

M.C. Gonzalez-Garcia, M. Maltoni, T. Schwetz (PDG Collab.)
K. Olive et al. (Super-Kamiokande Collab.)
A. Renshaw et al. (IceCube Collab.)
M.G. Aartsen et al. (Double Chooz Collab.)
Y. Abe et al. (T2K Collab.)
K. Abe et al. (T2K Collab.)
K. Abe et al. (MINOS Collab.)
P. Adamson et al. (OPERA Collab.)
N. Agafonova et al. (MiniBooNE Collab.)
A.A. Aguilar-Arevalo et al. (SNO Collab.)
B. Aharmim et al. (Daya Bay Collab.)
F.P. An et al. (ICARUS Collab.)
M. Antonello et al. (ICARUS Collab.)
M. Antonello et al. (KamLAND Collab.)
A. Gando et al. (Double Chooz Collab.)
Y. Abe et al. (T2K Collab.)
K. Abe et al. (Double Chooz Collab.)
Y. Abe et al. (MINOS Collab.)
P. Adamson et al. (MINOS Collab.)
P. Adamson et al. (MINOS Collab.)
S. Adrian-Martinez et al. (ANTARES Collab.)
J.K. Ahn et al. (RENO Collab.)
F.P. An et al. (Daya Bay Collab.)
G. Bellini et al. (Borexino Collab.)
G. Cheng et al. (MiniBooNE/SciBooNE Collab.)
K.B.M. Mahn et al. (MiniBooNE/SciBooNE Collab.)
K. Abe et al. (Super-Kamiokande Collab.)
K. Abe et al. (T2K Collab.)
S. Abe et al. (KamLAND Collab.)
Super-Kamiokande Collab.
K. Abe et al. (MINOS Collab.)
P. Adamson et al. (MINOS Collab.)
P. Adamson et al. (MINOS Collab.)
P. Adamson et al. (MINOS Collab.)
P. Adamson et al. (MINOS Collab.)
G. Bellini et al. (Borexino Collab.)
G. Bellini et al. (Borexino Collab.)
G.L. Fogli et al. (KamLAND Collab.)
Th.A. Mueller et al.
A.M. Serenelli, W.C. Haxton, C. Pena-Garay
P. Adamson et al. (MINOS Collab.)
A.A. Aguilar-Arevalo et al. (MiniBooNE Collab.)
B. Aharmim et al. (SNO Collab.)
G. Bellini et al. (Borexino Collab.)
M. Deniz et al. (TEXONO Collab.)
F. Kaether et al. (Super-Kamiokande Collab.)
R. Wendell et al. (SAGE Collab.)
J.N. Abdurashitov et al. (MINOS Collab.)
P. Adamson et al. (MiniBooNE Collab.)
A.A. Aguilar-Arevalo et al. (KamLAND Collab.)
S. Abe et al. (KamLAND Collab.)
P. Adamson et al. (MINOS Collab.)
P. Adamson et al. (MINOS Collab.)
P. Adamson et al. (MINOS Collab.)
P. Adamson et al. (MINOS Collab.)
P. Adamson et al. (MINOS Collab.)
W.W.M. Allison et al. (SOUDAN-2 Collab.)
M. Altmann et al. (KamLAND Collab.)
T. Araki et al. (KamLAND Collab.)
Y. Ashie et al. (Super-Kamiokande Collab.)
J.N. Bahcall, A.M. Serenelli, S. Basu (IAS+)
A. de Gouvea, C. Pena-Garay
B. Aharmim et al. (SNO Collab.)
S.N. Ahmed et al. (SNO Collab.)
M.H. Ahn et al. (K2K Collab.)
M. Ambrosio et al. (MACRO Collab.)
Y. Ashie et al. (Super-Kamiokande Collab.)
K. Eguchi et al. (KamLAND Collab.)
M.B. Smy et al. (Super-Kamiokande Collab.)
M.H. Ahn et al. (K2K Collab.)
M. Ambrosio et al. (MACRO Collab.)
M. Apollonio et al. (CHOOZ Collab.)
P. Astier et al. (NOMAD Collab.)
K. Eguchi et al. (KamLAND Collab.)
Y. Gando et al. (Super-Kamiokande Collab.)
A. Ianni (INFN Gran Sasso)
M. Sanchez et al. (Soudan 2 Collab.)
J.N. Abdurashitov et al. (SAGE Collab.)
Q.R. Ahmad et al. (SNO Collab.)
Q.R. Ahmad et al. (SNO Collab.)
B. Armbruster et al. (KARMEN 2 Collab.)
S. Avvakumov et al. (NuTeV Collab.)
S. Fukuda et al. (Super-Kamiokande Collab.)
A. Aguilar et al. (LSND Collab.)
Q.R. Ahmad et al. (SNO Collab.)
M. Ambrosio et al. (MACRO Collab.)
F. Boehm et al. (Super-Kamiokande Collab.)
S. Fukuda et al. (MACRO Collab.)
M. Ambrosio et al. (Super-Kamiokande Collab.)
S. Fukuda et al. (Super-Kamiokande Collab.)
W.W.M. Allison et al. (Soudan 2 Collab.)
M. Apollonio et al. (CHOOZ Collab.)
M. Apollonio et al. (CHOOZ Collab.)
Y. Fukuda et al. (Super-Kamiokande Collab.)
Y. Fukuda et al. (Super-Kamiokande Collab.)
W. Hampel et al. (GALLEX Collab.)
M. Ambrosio et al. (MACRO Collab.)
M. Apollonio et al. (CHOOZ Collab.)
C. Athanassopoulos et al. (LSND Collab.)
C. Athanassopoulos et al. (LSND Collab.)
B.T. Cleveland et al. (Homestake Collab.)
G.J. Feldman, R.D. Cousins

Downloaded from https://academic.oup.com/ptep/article/2020/8/1167/5891211 by guest on 12 November 2020

# Lepton Particle Listings

## Neutrino Mixing, Heavy Neutral Leptons, Searches for

FUKUDA	98C	PRL 81 1562	Y. Fukuda <i>et al.</i>	(Super-Kamiokande Collab.)
HATAKEYAMA	98	PRL 81 2016	S. Hatakeyama <i>et al.</i>	(Kamiokande Collab.)
CLARK	97	PRL 79 345	R. Clark <i>et al.</i>	(IMB Collab.)
ROMOSAN	97	PRL 78 2912	A. Romosan <i>et al.</i>	(CCFR Collab.)
AGLIETTA	96	JETPL 63 791	M. Aglietta <i>et al.</i>	(LSND Collab.)
Translated from ZETFP 63 753.				
ATHANASSO...	96	PR C54 2685	C. Athanassopoulos <i>et al.</i>	(LSND Collab.)
ATHANASSO...	96B	PRL 77 3082	C. Athanassopoulos <i>et al.</i>	(LSND Collab.)
FUKUDA	96	PRL 77 1683	Y. Fukuda <i>et al.</i>	(Kamiokande Collab.)
FUKUDA	96B	PL B388 397	Y. Fukuda <i>et al.</i>	(Kamiokande Collab.)
GREENWOOD	96	PR D53 6054	Z.D. Greenwood <i>et al.</i>	(UCI, SVR, S CUC)
HAMPEL	96	PL B388 384	W. Hampel <i>et al.</i>	(GALLEX Collab.)
LOVERRE	96	PL B370 156	P.F. Loverre	
ACHKAR	95	NP B434 503	B. Achkar <i>et al.</i>	(SING, SACLD, CPPM, CDEF+)
AHLEN	95	PL B357 481	S.P. Ahlen <i>et al.</i>	(MACRO Collab.)
ATHANASSO...	95	PRL 75 2650	C. Athanassopoulos <i>et al.</i>	(LSND Collab.)
DAUM	95	ZPHY C66 417	K. Daum <i>et al.</i>	(FREJUS Collab.)
HILL	95	PRL 75 2654	J.E. Hill	(PENN)
MCFARLAND	95	PRL 75 3993	K.S. McFarland <i>et al.</i>	(CCFR Collab.)
DECLAIS	94	PL B338 383	Y. Declais <i>et al.</i>	(Kamiokande Collab.)
FUKUDA	94	PL B335 237	Y. Fukuda <i>et al.</i>	(CHARM II Collab.)
VILAIN	94C	ZPHY C64 539	P. Vilain <i>et al.</i>	(CHARM II Collab.)
FREEDMAN	93	PR D47 811	S.J. Freedman <i>et al.</i>	(LAMPF E645 Collab.)
BECKER-SZ...	92B	PR D46 3720	R.A. Becker-Szendy <i>et al.</i>	(IMB Collab.)
BEIER	92	PL B283 446	E.W. Beier <i>et al.</i>	(KAM2 Collab.)
Also PTRSL A346 63				
BORODOV...	92	PRL 68 274	L. Borodovsky <i>et al.</i>	(COLU, JHU, ILL)
HIRATA	92	PL B280 146	K.S. Hirata <i>et al.</i>	(Kamiokande II Collab.)
CASPER	91	PRL 66 2561	D. Casper <i>et al.</i>	(IMB Collab.)
HIRATA	91	PRL 66 9	K.S. Hirata <i>et al.</i>	(Kamiokande II Collab.)
KUVSHIN...	91	JETPL 54 253	A.A. Kuvshinnikov <i>et al.</i>	(KIAE)
BERGER	90B	PL B245 305	C. Berger <i>et al.</i>	(FREJUS Collab.)
HIRATA	90	PRL 65 1297	K.S. Hirata <i>et al.</i>	(Kamiokande II Collab.)
AGLIETTA	89	EPL 8 611	M. Aglietta <i>et al.</i>	(FREJUS Collab.)
DAVIS	89	ARNPS 39 467	R. Davis, A.K. Mann, L. Wolfenstein	(BNL, PENN+)
OYAMA	89	PR D39 1481	Y. Oyama <i>et al.</i>	(Kamiokande II Collab.)
BIONTA	88	PR D38 768	R.M. Bionta <i>et al.</i>	(IMB Collab.)
DURKIN	88	PRL 61 1811	L.S. Durkin <i>et al.</i>	(OSU, ANL, CIT+)
ABRAMOWICZ	86	PRL 57 298	H. Abramowicz <i>et al.</i>	(CDHS Collab.)
ALLABY	86	PL B177 446	J.V. Allaby <i>et al.</i>	(CHARM Collab.)
ANGELINI	86	PL B179 307	C. Angelini <i>et al.</i>	(PISA, ATHU, PADO+)
VUILLEUMIER	82	PL 114B 298	J.L. Vuilleumier <i>et al.</i>	(CIT, SIN, MUNI)
BOLIEV	81	SJNP 34 787	M.M. Boliev <i>et al.</i>	(INRM)
Translated from YAF 34 1418.				
KWON	81	PR D24 1097	H. Kwon <i>et al.</i>	(CIT, ISNG, MUNI)
BOEHM	80	PL 97B 310	F. Boehm <i>et al.</i>	(ILLG, CIT, ISNG, MUNI)
CROUCH	78	PR D18 2239	M.F. Crouch <i>et al.</i>	(CASE, UCI, WITW)

$<2 \times 10^{-9}$	10,11	BERNARDI	88	CNTR	Near $m_K - m_e$ kin. thres.
$<1 \times 10^{-7}$	90	DORENBOS...	86	CHRM	Near $m_D - m_e$ kin. thres.
$<1 \times 10^{-7}$	90	COOPER...	85	BEBC	Near $m_D - m_e$ kin. thres.

••• We do not use the following data for averages, fits, limits, etc. •••

14	PARK	16	BELL	$m_{\nu_x} \sim 0.2-1.4$ GeV
----	------	----	------	------------------------------

- Limit from prompt lepton number violating trilepton search.
- $K^+ \rightarrow e^+ \nu_x$ , with  $\nu_x$  decay through  $U_{eX}$ . ABE 19B also considers bounds on  $|U_{eX} U_{\ell'X}|$  for combinations of lepton flavors in the  $\nu_x$  decay final state.
- Searches for a Majorana Heavy Neutral Lepton producing a  $\pi^- e^+$  resonance in the same sign dilepton decay  $D \rightarrow K \pi^- e^+ e^+$ .
- Search for  $\pi^+ \rightarrow e^+ \nu_x$ .
- Search for  $K^+ \rightarrow e^+ \nu_x$ .
- Search for prompt  $\nu_x$  decay signatures.
- Search for displaced  $\nu_x$  decay signatures.
- Searches for  $K$  or  $\pi \rightarrow e^+ \nu_x$ ,  $\nu_x \rightarrow e^+ e^- \nu_e$  using a beam dump experiment at the 70 GeV Serpukhov proton synchrotron. BARANOV 93 also considers limits for  $|U_{eX} U_{\mu X}|$  from  $K$  or  $\pi \rightarrow \mu^+ \nu_x$ ,  $\nu_x \rightarrow e^+ e^- \nu_e$ .
- $\pi^+ \rightarrow e^+ \nu_x$ , with  $\nu_x$  decay through  $U_{eX}$ .
- BERNARDI 88 also considers bounds on  $|U_{eX} U_{\mu X}|$ .
- $K^+ \rightarrow e^+ \nu_x$ , with  $\nu_x$  decay through  $U_{eX}$ .
- $D^+ \rightarrow e^+ \nu_x$ , with  $\nu_x \rightarrow e^- \ell^+ \nu_{\ell}$ .
- $D^+ \rightarrow e^+ \nu_x$ , with  $\nu_x \rightarrow e^- \ell^+ \nu_{\ell}$  or  $\nu_x \rightarrow e^- \pi^+$ .
- PARK 16 quotes an approximate limit  $B(B^+ \rightarrow e^+ \nu_x) < 3 \times 10^{-6}$  in the mass range  $m_{\nu_x} \sim 0.2-1.4$  GeV.

### Limits on $|U_{\mu X}|^2$

Quoted limits are either the best limit near the kinematic threshold of the experiment, or a characteristic value in the mass range of the experimental sensitivity

VALUE	CL%	DOCUMENT ID	TECN	COMMENT
$<2 \times 10^{-5}$	95	1 AAD	19F ATLS	$m_{\nu_x} \sim 10-50$ GeV
$<2 \times 10^{-6}$	95	2 AAD	19F ATLS	$m_{\nu_x} \sim 10$ GeV
$<1 \times 10^{-9}$	90	3 ABE	19B T2K	Near $m_K - m_{\mu}$ kin. thres.
$<5 \times 10^{-6}$	90	4,5 AGUILAR-AR...	19B PIEN	$m_{\nu_x} \sim 16-30$ MeV
$<1 \times 10^{-5}$	90	5 AGUILAR-AR...	19B PIEN	Near $m_{\pi} - m_{\mu}$ kin. thres.
$<3 \times 10^{-7}$	90	6 CORTINA-GIL	18 NA62	$m_{\nu_x} \sim 250-350$ MeV
$<3 \times 10^{-6}$	90	6 LAZZERONI	17A NA62	Near $m_K - m_{\mu}$ kin. thres.
$<1 \times 10^{-8}$	90	6 ARTAMONOV	15A B949	$m_{\nu_x} \sim 200-300$ MeV
$<2.0 \times 10^{-8}$	95	7 DAUM	00 KARM	$m_{\nu_x} = 33.905$ MeV
$<8 \times 10^{-8}$	90	8 VAITAITIS	99 CCFR	Near $m_K - m_{\mu}$ kin. thres.
$<6 \times 10^{-8}$	90	9 VAITAITIS	99 CCFR	Near $m_{D_s} - m_{\mu}$ kin. thres.
$<3 \times 10^{-5}$	95	10 ABREU	97I DLPH	$m_{\nu_x} \sim 6-50$ GeV
$<2 \times 10^{-5}$	95	11 ABREU	97I DLPH	Near $m_{\nu_x} \sim 3.5$ GeV
$<3 \times 10^{-5}$	90	12 VILAIN	95C CHM2	Near $m_K - m_{\mu}$ kin. thres.
$<3 \times 10^{-8}$	13,14	BERNARDI	88 CNTR	Near $m_{\mu} + m_{\pi}$ kin. thres.
$<2 \times 10^{-9}$	14,15	BERNARDI	88 CNTR	Near $m_K - m_{\mu}$ kin. thres.
$<1 \times 10^{-7}$	90	16 DORENBOS...	86 CHRM	Near $m_D - m_{\mu}$ kin. thres.
$<1 \times 10^{-7}$	90	17 COOPER...	85 BEBC	Near $m_D - m_{\mu}$ kin. thres.

••• We do not use the following data for averages, fits, limits, etc. •••

18	PARK	16	BELL	$m_{\nu_x} \sim 0.2-1.4$ GeV
----	------	----	------	------------------------------

- Limit from prompt lepton number violating trilepton search.
- Limit from displaced lepton violating or conserving trilepton searches.
- $K^+ \rightarrow \mu^+ \nu_x$ , with  $\nu_x$  decay through  $U_{\mu X}$ . ABE 19B also considers bounds on  $|U_{eX} U_{\ell'X}|$  for combinations of lepton flavors in the  $\nu_x$  decay final state.
- Limit requires muon kinetic energy  $> 1.2$  MeV.
- Search for  $\pi^+ \rightarrow \mu^+ \nu_x$ .
- Search for  $K^+ \rightarrow \mu^+ \nu_x$ .
- DAUM 00 quotes a branching ratio bound  $B(\pi^+ \rightarrow \mu^+ \nu_x) < 6.0 \times 10^{-10}$  at 95% CL.
- $K^+ \rightarrow \mu^+ \nu_x$ , with  $\nu_x \rightarrow \mu X$ .
- $D_s \rightarrow \mu^+ \nu_x$ , with  $\nu_x \rightarrow \mu X$ .
- Search for prompt  $\nu_x$  decay signatures.
- Search for displaced  $\nu_x$  decay signatures.
- Search for Heavy Neutral Leptons produced by neutral current muon neutrino interactions, with  $\nu_x \rightarrow \mu^+ \mu^- \nu_{\mu}$ .
- $K^+ \rightarrow \mu^+ \nu_x$ , with  $\nu_x$  decay through  $U_{\mu X}$  and  $m_{\nu_x} < m_{\mu} + m_{\pi}$ .
- BERNARDI 88 also considers bounds on  $|U_{eX} U_{\mu X}|$ .
- $K^+ \rightarrow \mu^+ \nu_x$ , with  $\nu_x \rightarrow \mu^- \pi^+$ .
- $D^+ \rightarrow \mu^+ \nu_x$ , with  $\nu_x \rightarrow \mu^- \ell^+ \nu_{\ell}$ .

## Heavy Neutral Leptons, Searches for

### OMITTED FROM SUMMARY TABLE

We define searches for Heavy Neutral Leptons (HNLs) as searches for Dirac or Majorana fermions with sterile neutrino quantum numbers, that are heavy enough to not disrupt the simplest Big Bang Nucleosynthesis bounds and/or unstable on cosmological timescales: Typically HNLs have mass  $\sim$  MeV or higher.

Searches for these particles generically set bounds on the mixing between the HNL and the active neutrinos, as parametrized by the extended  $3 \times 4$  PMNS matrix elements  $U_{\ell X}$  (see the "Neutrino mass, mixing and oscillations" review) where  $\ell = e, \mu$  or  $\tau$ , and we denote the HNL as  $\nu_x$ . While many measurements may be interpreted to place bounds on various combinations of these matrix elements, we quote below limits only for those cases in which one matrix element is assumed to be much larger than the other two, i.e.  $|U_{\ell X}| \gg |U_{\ell' X}|$  for  $\ell' \neq \ell$ .

Experimental searches make use of various different strategies, including e.g. resonance searches in missing mass decay distributions or specific final states, searches for lepton number violating decays, and trilepton signatures. The resulting bounds on  $U_{\ell X}$  are typically dependent on the HNL mass. The quoted limits below are either the best limit near an experimental kinematic threshold, or a characteristic value in the mass range of the experimental sensitivity.

### Limits on heavy neutral lepton mixing parameters

#### Limits on $|U_{eX}|^2$

Quoted limits are either the best limit near the kinematic threshold of the experiment, or a characteristic value in the mass range of the experimental sensitivity

VALUE	CL%	DOCUMENT ID	TECN	COMMENT
$<2 \times 10^{-5}$	95	1 AAD	19F ATLS	$m_{\nu_x} \sim 15-40$ GeV
$<1 \times 10^{-9}$	90	2 ABE	19B T2K	Near $m_K - m_e$ kin. thres.
$<1 \times 10^{-4}$	90	3 ABLIKIM	19AL BES3	$m_{\nu_x} \sim 0.3-0.7$ GeV
$<1 \times 10^{-8}$	90	4 AGUILAR-AR...	18A PIEN	$m_{\nu_x} \sim 60-120$ MeV $i_{br}$
$<3 \times 10^{-7}$	90	5 CORTINA-GIL	18 NA62	$m_{\nu_x} \sim 200-400$ MeV
$<3 \times 10^{-5}$	95	6 ABREU	97I DLPH	$m_{\nu_x} \sim 6-50$ GeV
$<2 \times 10^{-5}$	95	7 ABREU	97I DLPH	Near $m_{\nu_x} \sim 3.5$ GeV
$<1 \times 10^{-5}$	90	8 BARANOV	93	Near $m_{\pi} - m_e$ kin. thres.
$<2 \times 10^{-7}$	90	8 BARANOV	93	Near $m_K - m_e$ kin. thres.
$<1 \times 10^{-7}$	9,10	BERNARDI	88 CNTR	Near $m_{\pi} - m_e$ kin. thres.

See key on page 999

# Lepton Particle Listings

## Heavy Neutral Leptons, Searches for

- <sup>17</sup>  $D^+ \rightarrow \mu^+ \nu_X$ , with  $\nu_X \rightarrow \mu^- \ell^+ \nu_\ell$  or  $\nu_X \rightarrow \mu^- \pi^+$ .  
<sup>18</sup> PARK 16 quotes an approximate limit  $B(B^+ \rightarrow \mu^+ \nu_X) < 3 \times 10^{-6}$  in the mass range  $m_{\nu_X} \sim 0.2\text{-}1.4$  GeV.

### Limits on $|U_{\tau X}|^2$

Quoted limits are either the best limit near the kinematic threshold of the experiment, or a characteristic value in the mass range of the experimental sensitivity

VALUE	CL%	DOCUMENT ID	TECN	COMMENT
$< 2 \times 10^{-4}$	90	1 ORLOFF	02	CHRM Near $m_D - m_\tau$ kin. thres.
$< 1 \times 10^{-4}$	90	2 ORLOFF	02	CHRM $m_{\nu_X} \sim 200\text{-}250$ MeV
$< 3 \times 10^{-5}$	95	3 ABREU	97I	DLPH $m_{\nu_X} \sim 6\text{-}50$ GeV
$< 2 \times 10^{-5}$	95	4 ABREU	97I	DLPH Near $m_{\nu_X} \sim 3.5$ GeV

- <sup>1</sup>  $D_S \rightarrow \tau^+ \nu_X$ , with  $\nu_X$  decay via  $U_{\tau X}$ .  
<sup>2</sup>  $D_S \rightarrow \nu_\tau \tau^+$ ,  $\tau^+ \rightarrow \nu_X X$ , with  $\nu_X$  decay via  $U_{\tau X}$ .  
<sup>3</sup> Search for prompt  $\nu_X$  decay signatures.  
<sup>4</sup> Search for displaced  $\nu_X$  decay signatures. Kinematical suppression of  $\nu_X \rightarrow \tau X$  at lower masses leads to rapid loosening of the  $|U_{\tau X}|$  bound compared to that for  $|U_{eX}|$  and  $|U_{\mu X}|$ .

### REFERENCES FOR Heavy Neutral Leptons, Searches for

AAD	19F	JHEP 1910 265	G. Aad <i>et al.</i>	(ATLAS Collab.)
ABE	19B	PR D100 052006	K. Abe <i>et al.</i>	(T2K Collab.)
ABLIKIM	19AL	PR D99 112002	M. Ablikim <i>et al.</i>	(BESIII Collab.)
AGUILAR-AR...	19B	PL B798 134980	A. Aguilar-Arevalo <i>et al.</i>	(PIENU Collab.)
AGUILAR-AR...	18A	PR D97 072012	A. Aguilar-Arevalo <i>et al.</i>	(PIENU Collab.)
CORTINA-GIL	18	PL B778 137	E. Cortina Gil <i>et al.</i>	(NA62 Collab.)
LAZZERONI	17A	PL B772 712	C. Lazzeroni <i>et al.</i>	(NA62 Collab.)
PARK	16	PR D94 012003	C.-S. Park <i>et al.</i>	(BELLE Collab.)
ARTAMONOV	15A	PR D91 052001	A.V. Artamonov <i>et al.</i>	(E949 Collab.)
ORLOFF	02	PL B550 9	J. Orloff <i>et al.</i>	(CHARM Collab.)
DAUM	00	PRL 85 1815	U. Daum <i>et al.</i>	(KARMEN Collab.)
VAITAITIS	99	PRL 83 4943	A. Vaitaitis <i>et al.</i>	(CCFR Collab.)
ABREU	97I	ZPHY C74 67	P. Abreu <i>et al.</i>	(DELPHI Collab.)
Also		ZPHY C75 580 (errat.)	P. Abreu <i>et al.</i>	(DELPHI Collab.)
VILAIN	95C	PL B351 387	P. Vilain <i>et al.</i>	(CHARM II Collab.)
Also		PL B343 453	P. Vilain <i>et al.</i>	(CHARM II Collab.)
BARANOV	93	PL B302 336	S.A. Baranov <i>et al.</i>	(JINR, SERP, BUDA)
BERNARDI	88	PL B203 332	G. Bernardi <i>et al.</i>	(PARIS, CERN, INFN+)
DORENBOS...	86	PL 166B 473	J. Dorenbosch <i>et al.</i>	(CHARM Collab.)
COOPER...	85	PL 160B 207	A.M. Cooper-Sarkar <i>et al.</i>	(CERN, LOIC+)





## QUARKS

<i>u</i> . . . . .	1173
<i>d</i> . . . . .	1173
<i>s</i> . . . . .	1173
<i>c</i> . . . . .	1177
<i>b</i> . . . . .	1179
<i>t</i> . . . . .	1180
<i>b'</i> (Fourth Generation) Quark . . . . .	1197
<i>t'</i> (Fourth Generation) Quark . . . . .	1199
Free Quark Searches . . . . .	1201

## Related Reviews in Volume 1

59. Quark masses (rev.) . . . . .	733
60. Top quark (rev.) . . . . .	741



**QUARKS**

See the related review(s):

Quark Masses

**u**  $I(J^P) = \frac{1}{2}(\frac{1}{2}^+)$

Mass  $m = 2.16^{+0.49}_{-0.26}$  MeV    Charge =  $\frac{2}{3} e$      $I_z = +\frac{1}{2}$

$m_u/m_d = 0.47^{+0.06}_{-0.07}$

**d**  $I(J^P) = \frac{1}{2}(\frac{1}{2}^+)$

Mass  $m = 4.67^{+0.48}_{-0.17}$  MeV    Charge =  $-\frac{1}{3} e$      $I_z = -\frac{1}{2}$

$m_s/m_d = 17-22$

$\bar{m} = (m_u + m_d)/2 = 3.45^{+0.55}_{-0.15}$  MeV

**s**  $I(J^P) = 0(\frac{1}{2}^+)$

Mass  $m = 93^{+11}_{-5}$  MeV    Charge =  $-\frac{1}{3} e$     Strangeness =  $-1$

$(m_s - (m_u + m_d)/2)/(m_d - m_u) = 27.3^{+0.7}_{-1.3}$

**Light Quarks (*u*, *d*, *s*)**

OMITTED FROM SUMMARY TABLE

**u-QUARK MASS**

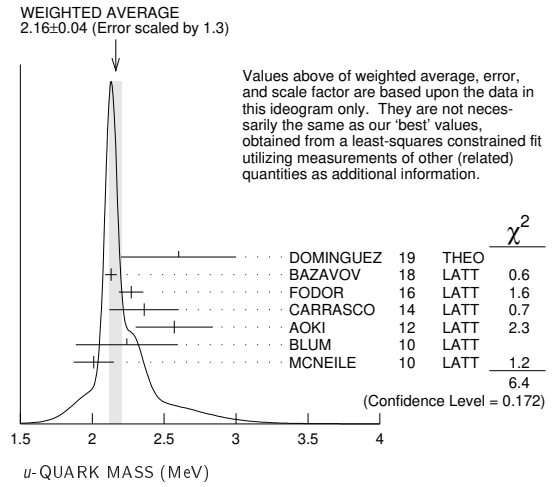
The *u*-, *d*-, and *s*-quark masses are estimates of so-called “current-quark masses,” in a mass-independent subtraction scheme such as  $\overline{MS}$ . The ratios  $m_u/m_d$  and  $m_s/m_d$  are extracted from pion and kaon masses using chiral symmetry. The estimates of *d* and *u* masses are not without controversy and remain under active investigation. Within the literature there are even suggestions that the *u* quark could be essentially massless. The *s*-quark mass is estimated from SU(3) splittings in hadron masses.

We have normalized the  $\overline{MS}$  masses at a renormalization scale of  $\mu = 2$  GeV. Results quoted in the literature at  $\mu = 1$  GeV have been rescaled by dividing by 1.35. The values of “Our Evaluation” were determined in part via Figures 1 and 2.

$\overline{MS}$ MASS (MeV)	DOCUMENT ID	TECN
<b>2.16 <math>^{+0.49}_{-0.26}</math> OUR EVALUATION</b>	See the ideogram below.	
2.6 $\pm 0.4$	1 DOMINGUEZ 19	THEO
2.130 $\pm 0.041$	2 BAZAVOV 18	LATT
2.27 $\pm 0.06 \pm 0.06$	3 FODOR 16	LATT
2.36 $\pm 0.24$	4 CARRASCO 14	LATT
2.57 $\pm 0.26 \pm 0.07$	5 AOKI 12	LATT
2.24 $\pm 0.10 \pm 0.34$	6 BLUM 10	LATT
2.01 $\pm 0.14$	7 MCNEILE 10	LATT
• • • We do not use the following data for averages, fits, limits, etc. • • •		
2.15 $\pm 0.03 \pm 0.10$	8 DURR 11	LATT
1.9 $\pm 0.2$	9 BAZAVOV 10	LATT
2.01 $\pm 0.14$	7 DAVIES 10	LATT
2.9 $\pm 0.2$	10 DOMINGUEZ 09	THEO
2.9 $\pm 0.8$	11 DEANDREA 08	THEO
3.02 $\pm 0.33$	12 BLUM 07	LATT
2.7 $\pm 0.4$	13 JAMIN 06	THEO
1.9 $\pm 0.2$	14 MASON 06	LATT
2.8 $\pm 0.2$	15 NARISON 06	THEO
1.7 $\pm 0.3$	16 AUBIN 04A	LATT

- DOMINGUEZ 19 determine the quark mass from a QCD finite energy sum rule for the divergence of the axial current.
- BAZAVOV 18 determine the quark masses using a lattice computation with staggered fermions and four active quark flavors.
- FODOR 16 is a lattice simulation with  $N_f = 2 + 1$  dynamical flavors and includes partially quenched QED effects.
- CARRASCO 14 is a lattice QCD computation of light quark masses using  $2 + 1 + 1$  dynamical quarks, with  $m_u = m_d \neq m_s \neq m_c$ . The *u* and *d* quark masses are obtained separately by using the *K* meson mass splittings and lattice results for the electromagnetic contributions.
- AOKI 12 is a lattice computation using  $1 + 1 + 1$  dynamical quark flavors.
- BLUM 10 determines light quark masses using a QCD plus QED lattice computation of the electromagnetic mass splittings of the low-lying hadrons. The lattice simulations use  $2+1$  dynamical quark flavors.
- DAVIES 10 and MCNEILE 10 determine  $\bar{m}_c(\mu)/\bar{m}_s(\mu) = 11.85 \pm 0.16$  using a lattice computation with  $N_f = 2 + 1$  dynamical fermions of the pseudoscalar meson masses.

- Mass  $m_u$  is obtained from this using the value of  $m_c$  from ALLISON 08 or MCNEILE 10 and the BAZAVOV 10 values for the light quark mass ratios,  $m_s/\bar{m}$  and  $m_u/m_d$ .
- DURR 11 determine quark mass from a lattice computation of the meson spectrum using  $N_f = 2 + 1$  dynamical flavors. The lattice simulations were done at the physical quark mass, so that extrapolation in the quark mass was not needed. The individual  $m_u$ ,  $m_d$  values are obtained using the lattice determination of the average mass  $m_{ud}$  and of the ratio  $m_s/m_{ud}$  and the value of  $Q = (m_s^2 - m_{ud}^2) / (m_d^2 - m_u^2)$  as determined from  $\eta \rightarrow 3\pi$  decays.
  - BAZAVOV 10 is a lattice computation using  $2+1$  dynamical quark flavors.
  - DOMINGUEZ 09 use QCD finite energy sum rules for the two-point function of the divergence of the axial vector current computed to order  $\alpha_s^4$ .
  - DEANDREA 08 determine  $m_u - m_d$  from  $\eta \rightarrow 3\pi^0$ , and combine with the PDG 06 lattice average value of  $m_u + m_d = 7.6 \pm 1.6$  to determine  $m_u$  and  $m_d$ .
  - BLUM 07 determine quark masses from the pseudoscalar meson masses using a QED plus QCD lattice computation with two dynamical quark flavors.
  - JAMIN 06 determine  $m_u(2 \text{ GeV})$  by combining the value of  $m_s$  obtained from the spectral function for the scalar  $K\pi$  form factor with other determinations of the quark mass ratios.
  - MASON 06 extract light quark masses from a lattice simulation using staggered fermions with an improved action, and three dynamical light quark flavors with degenerate *u* and *d* quarks. Perturbative corrections were included at NNLO order. The quark masses  $m_u$  and  $m_d$  were determined from their  $(m_u + m_d)/2$  measurement and AUBIN 04A  $m_u/m_d$  value.
  - NARISON 06 uses sum rules for  $e^+ e^- \rightarrow$  hadrons to order  $\alpha_s^3$  to determine  $m_s$  combined with other determinations of the quark mass ratios.
  - AUBIN 04A employ a partially quenched lattice calculation of the pseudoscalar meson masses.



**d-QUARK MASS**

See the comment for the *u* quark above.

We have normalized the  $\overline{MS}$  masses at a renormalization scale of  $\mu = 2$  GeV. Results quoted in the literature at  $\mu = 1$  GeV have been rescaled by dividing by 1.35. The values of “Our Evaluation” were determined in part via Figures 1 and 2.

$\overline{MS}$ MASS (MeV)	DOCUMENT ID	TECN
<b>4.67 <math>^{+0.48}_{-0.17}</math> OUR EVALUATION</b>	See the ideogram below.	
5.3 $\pm 0.4$	1 DOMINGUEZ 19	THEO
4.675 $\pm 0.056$	2 BAZAVOV 18	LATT
4.67 $\pm 0.06 \pm 0.06$	3 FODOR 16	LATT
5.03 $\pm 0.26$	4 CARRASCO 14	LATT
3.68 $\pm 0.29 \pm 0.10$	5 AOKI 12	LATT
4.65 $\pm 0.15 \pm 0.32$	6 BLUM 10	LATT
4.77 $\pm 0.15$	7 MCNEILE 10	LATT
• • • We do not use the following data for averages, fits, limits, etc. • • •		
4.79 $\pm 0.07 \pm 0.12$	8 DURR 11	LATT
4.6 $\pm 0.3$	9 BAZAVOV 10	LATT
4.79 $\pm 0.16$	7 DAVIES 10	LATT
5.3 $\pm 0.4$	10 DOMINGUEZ 09	THEO
4.7 $\pm 0.8$	11 DEANDREA 08	THEO
5.49 $\pm 0.39$	12 BLUM 07	LATT
4.8 $\pm 0.5$	13 JAMIN 06	THEO
4.4 $\pm 0.3$	14 MASON 06	LATT
5.1 $\pm 0.4$	15 NARISON 06	THEO
3.9 $\pm 0.5$	16 AUBIN 04A	LATT

# Quark Particle Listings

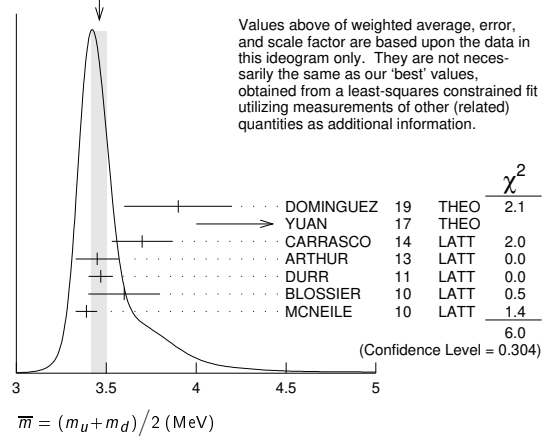
## Light Quarks (*u, d, s*)

- <sup>1</sup> DOMINGUEZ 19 determine the quark mass from a QCD finite energy sum rule for the divergence of the axial current.
- <sup>2</sup> BAZAVOV 18 determine the quark masses using a lattice computation with staggered fermions and four active quark flavors.
- <sup>3</sup> FODOR 16 is a lattice simulation with  $N_f = 2 + 1$  dynamical flavors and includes partially quenched QED effects.
- <sup>4</sup> CARRASCO 14 is a lattice QCD computation of light quark masses using  $2 + 1 + 1$  dynamical quarks, with  $m_u = m_d \neq m_s \neq m_c$ . The  $u$  and  $d$  quark masses are obtained separately by using the  $K$  meson mass splittings and lattice results for the electromagnetic contributions.
- <sup>5</sup> AOKI 12 is a lattice computation using  $1 + 1 + 1$  dynamical quark flavors.
- <sup>6</sup> BLUM 10 determines light quark masses using a QCD plus QED lattice computation of the electromagnetic mass splittings of the low-lying hadrons. The lattice simulations use  $2+1$  dynamical quark flavors.
- <sup>7</sup> DAVIES 10 and MCNEILE 10 determine  $\overline{m}_c(\mu)/\overline{m}_s(\mu) = 11.85 \pm 0.16$  using a lattice computation with  $N_f = 2 + 1$  dynamical fermions of the pseudoscalar meson masses. Mass  $m_d$  is obtained from this using the value of  $m_c$  from ALLISON 08 or MCNEILE 10 and the BAZAVOV 10 values for the light quark mass ratios,  $m_s/\overline{m}$  and  $m_u/m_d$ .
- <sup>8</sup> DURR 11 determine quark mass from a lattice computation of the meson spectrum using  $N_f = 2 + 1$  dynamical flavors. The lattice simulations were done at the physical quark mass, so that extrapolation in the quark mass was not needed. The individual  $m_u, m_d$  values are obtained using the lattice determination of the average mass  $m_{ud}$  and of the ratio  $m_s/m_{ud}$  and the value of  $Q = (m_s^2 - m_{ud}^2) / (m_d^2 - m_u^2)$  as determined from  $\eta \rightarrow 3\pi$  decays.
- <sup>9</sup> BAZAVOV 10 is a lattice computation using  $2+1$  dynamical quark flavors.
- <sup>10</sup> DOMINGUEZ 09 use QCD finite energy sum rules for the two-point function of the divergence of the axial vector current computed to order  $\alpha_s^4$ .
- <sup>11</sup> DEANDREA 08 determine  $m_u - m_d$  from  $\eta \rightarrow 3\pi^0$ , and combine with the PDG 06 lattice average value of  $m_u + m_d = 7.6 \pm 1.6$  to determine  $m_u$  and  $m_d$ .
- <sup>12</sup> BLUM 07 determine quark masses from the pseudoscalar meson masses using a QED plus QCD lattice computation with two dynamical quark flavors.
- <sup>13</sup> JAMIN 06 determine  $m_d(2 \text{ GeV})$  by combining the value of  $m_s$  obtained from the spectral function for the scalar  $K\pi$  form factor with other determinations of the quark mass ratios.
- <sup>14</sup> MASON 06 extract light quark masses from a lattice simulation using staggered fermions with an improved action, and three dynamical light quark flavors with degenerate  $u$  and  $d$  quarks. Perturbative corrections were included at NNLO order. The quark masses  $m_u$  and  $m_d$  were determined from their  $(m_u + m_d)/2$  measurement and AUBIN 04A  $m_u/m_d$  value.
- <sup>15</sup> NARISON 06 uses sum rules for  $e^+ e^- \rightarrow$  hadrons to order  $\alpha_s^3$  to determine  $m_s$  combined with other determinations of the quark mass ratios.
- <sup>16</sup> AUBIN 04A perform three flavor dynamical lattice calculation of pseudoscalar meson masses, with continuum estimate of electromagnetic effects in the kaon masses, and one-loop perturbative renormalization constant.

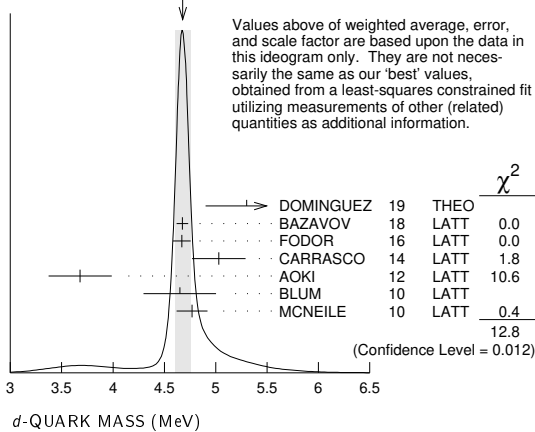
• • • We do not use the following data for averages, fits, limits, etc. • • •

3.59 ± 0.21	<sup>8</sup> AOKI	11A	LATT
3.40 ± 0.07	<sup>7</sup> DAVIES	10	LATT
4.1 ± 0.2	<sup>9</sup> DOMINGUEZ	09	THEO
3.72 ± 0.41	<sup>10</sup> ALLTON	08	LATT
3.85 ± 0.12 ± 0.4	<sup>11</sup> BLOSSIER	08	LATT
≥ 4.85 ± 0.20	<sup>12</sup> DOMINGUEZ..08B	THEO	
3.55 +0.65 -0.28	<sup>13</sup> ISHIKAWA	08	LATT
4.026 ± 0.048	<sup>14</sup> NAKAMURA	08	LATT
4.25 ± 0.35	<sup>15</sup> BLUM	07	LATT
4.08 ± 0.25 ± 0.42	<sup>16</sup> GOCKELER	06	LATT
4.7 ± 0.2 ± 0.3	<sup>17</sup> GOCKELER	06A	LATT
3.2 ± 0.3	<sup>18</sup> MASON	06	LATT
3.95 ± 0.3	<sup>19</sup> NARISON	06	THEO
2.8 ± 0.3	<sup>20</sup> AUBIN	04	LATT
4.29 ± 0.14 ± 0.65	<sup>21</sup> AOKI	03	LATT
3.223 ± 0.3	<sup>22</sup> AOKI	03B	LATT
4.4 ± 0.1 ± 0.4	<sup>23</sup> BECIREVIC	03	LATT
4.1 ± 0.3 ± 1.0	<sup>24</sup> CHIU	03	LATT

WEIGHTED AVERAGE  
3.46±0.04 (Error scaled by 1.1)



WEIGHTED AVERAGE  
4.68±0.08 (Error scaled by 1.8)



$$\overline{m} = (m_u + m_d)/2$$

See the comments for the  $u$  quark above.

We have normalized the  $\overline{m}_S$  masses at a renormalization scale of  $\mu = 2$  GeV. Results quoted in the literature at  $\mu = 1$  GeV have been rescaled by dividing by 1.35. The values of "Our Evaluation" were determined in part via Figures 1 and 2.

$\overline{m}_S$ MASS (MeV)	DOCUMENT ID	TECN
<b>3.45 +0.55 -0.15 OUR EVALUATION</b>	See the ideogram below.	
3.9 ± 0.3	<sup>1</sup> DOMINGUEZ 19	THEO
4.7 +0.8 -0.7	<sup>2</sup> YUAN 17	THEO
3.70 ± 0.17	<sup>3</sup> CARRASCO 14	LATT
3.45 ± 0.12	<sup>4</sup> ARTHUR 13	LATT
3.469 ± 0.047 ± 0.048	<sup>5</sup> DURR 11	LATT
3.6 ± 0.2	<sup>6</sup> BLOSSIER 10	LATT
3.39 ± 0.06	<sup>7</sup> MCNEILE 10	LATT

- <sup>1</sup> DOMINGUEZ 19 determine the quark mass from a QCD finite energy sum rule for the divergence of the axial current.
- <sup>2</sup> YUAN 17 determine  $\overline{m}$  using QCD sum rules in the isospin  $I=0$  scalar channel. At the end of the "Numerical Results" section of YUAN 17 the authors discuss the significance of their larger value of the light quark mass compared to previous determinations.
- <sup>3</sup> CARRASCO 14 is a lattice QCD computation of light quark masses using  $2 + 1 + 1$  dynamical quarks, with  $m_u = m_d \neq m_s \neq m_c$ . The  $u$  and  $d$  quark masses are obtained separately by using the  $K$  meson mass splittings and lattice results for the electromagnetic contributions.
- <sup>4</sup> ARTHUR 13 is a lattice computation using  $2+1$  dynamical domain wall fermions. Masses at  $\mu = 3$  GeV have been converted to  $\mu = 2$  GeV using conversion factors given in their paper.
- <sup>5</sup> DURR 11 determine quark mass from a lattice computation of the meson spectrum using  $N_f = 2 + 1$  dynamical flavors. The lattice simulations were done at the physical quark mass, so that extrapolation in the quark mass was not needed.
- <sup>6</sup> BLOSSIER 10 determines quark masses from a computation of the hadron spectrum using  $N_f=2$  dynamical twisted-mass Wilson fermions.
- <sup>7</sup> DAVIES 10 and MCNEILE 10 determine  $\overline{m}_c(\mu)/\overline{m}_s(\mu) = 11.85 \pm 0.16$  using a lattice computation with  $N_f = 2 + 1$  dynamical fermions of the pseudoscalar meson masses. Mass  $\overline{m}$  is obtained from this using the value of  $m_c$  from ALLISON 08 or MCNEILE 10 and the BAZAVOV 10 values for the light quark mass ratio,  $m_s/\overline{m}$ .
- <sup>8</sup> AOKI 11A determine quark masses from a lattice computation of the hadron spectrum using  $N_f = 2 + 1$  dynamical flavors of domain wall fermions.
- <sup>9</sup> DOMINGUEZ 09 use QCD finite energy sum rules for the two-point function of the divergence of the axial vector current computed to order  $\alpha_s^4$ .
- <sup>10</sup> ALLTON 08 use a lattice computation of the  $\pi, K$ , and  $\Omega$  masses with  $2+1$  dynamical flavors of domain wall quarks, and non-perturbative renormalization.
- <sup>11</sup> BLOSSIER 08 use a lattice computation of pseudoscalar meson masses and decay constants with  $2$  dynamical flavors and non-perturbative renormalization.
- <sup>12</sup> DOMINGUEZ-CLARIMON 08B obtain an inequality from sum rules for the scalar two-point correlator.
- <sup>13</sup> ISHIKAWA 08 use a lattice computation of the light meson spectrum with  $2+1$  dynamical flavors of  $C(a)$  improved Wilson quarks, and one-loop perturbative renormalization.
- <sup>14</sup> NAKAMURA 08 do a lattice computation using quenched domain wall fermions and non-perturbative renormalization.
- <sup>15</sup> BLUM 07 determine quark masses from the pseudoscalar meson masses using a QED plus QCD lattice computation with two dynamical quark flavors.
- <sup>16</sup> GOCKELER 06 use an unquenched lattice computation of the axial Ward Identity with  $N_f = 2$  dynamical light quark flavors, and non-perturbative renormalization, to obtain  $\overline{m}(2 \text{ GeV}) = 4.08 \pm 0.25 \pm 0.19 \pm 0.23$  MeV, where the first error is statistical, the second and third are systematic due to the fit range and force scale uncertainties, respectively. We have combined the systematic errors linearly.
- <sup>17</sup> GOCKELER 06A use an unquenched lattice computation of the pseudoscalar meson masses with  $N_f = 2$  dynamical light quark flavors, and non-perturbative renormalization.

See key on page 999

# Quark Particle Listings

## Light Quarks (*u, d, s*)

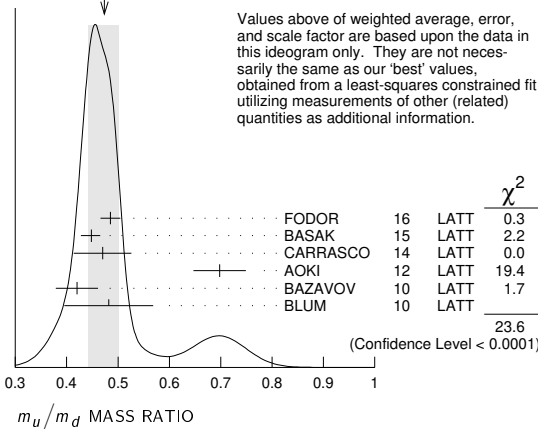
- <sup>18</sup> MASON 06 extract light quark masses from a lattice simulation using staggered fermions with an improved action, and three dynamical light quark flavors with degenerate *u* and *d* quarks. Perturbative corrections were included at NNLO order.
- <sup>19</sup> NARISON 06 uses sum rules for  $e^+e^- \rightarrow$  hadrons to order  $\alpha_s^3$  to determine  $m_s$  combined with other determinations of the quark mass ratios.
- <sup>20</sup> AUBIN 04 perform three flavor dynamical lattice calculation of pseudoscalar meson masses, with one-loop perturbative renormalization constant.
- <sup>21</sup> AOKI 03 uses quenched lattice simulation of the meson and baryon masses with degenerate light quarks. The extrapolations are done using quenched chiral perturbation theory.
- <sup>22</sup> The errors given in AOKI 03b were  $+0.046$   $-0.069$ . We changed them to  $\pm 0.3$  for calculating the overall best values. AOKI 03b uses lattice simulation of the meson and baryon masses with two dynamical light quarks. Simulations are performed using the  $O(a)$  improved Wilson action.
- <sup>23</sup> BECIREVIC 03 perform quenched lattice computation using the vector and axial Ward identities. Uses  $O(a)$  improved Wilson action and nonperturbative renormalization.
- <sup>24</sup> CHIU 03 determines quark masses from the pion and kaon masses using a lattice simulation with a chiral fermion action in quenched approximation.

### $m_u/m_d$ MASS RATIO

VALUE	DOCUMENT ID	TECN	COMMENT
<b>0.47 <math>\pm 0.06</math> <math>\pm 0.07</math> OUR EVALUATION</b>	See the ideogram below.		
0.485 $\pm 0.011 \pm 0.016$	1 FODOR	16 LATT	
0.4482 $\pm 0.0173$ $-0.0206$	2 BASAK	15 LATT	
0.470 $\pm 0.056$	3 CARRASCO	14 LATT	
0.698 $\pm 0.051$	4 AOKI	12 LATT	
0.42 $\pm 0.01 \pm 0.04$	5 BAZAVOV	10 LATT	
0.4818 $\pm 0.0096 \pm 0.0860$	6 BLUM	10 LATT	
••• We do not use the following data for averages, fits, limits, etc. •••			
0.550 $\pm 0.031$	7 BLUM	07 LATT	
0.43 $\pm 0.08$	8 AUBIN	04A LATT	
0.410 $\pm 0.036$	9 NELSON	03 LATT	
0.553 $\pm 0.043$	10 LEUTWYLER	96 THEO	Compilation

- <sup>1</sup> FODOR 16 is a lattice simulation with  $N_f = 2 + 1$  dynamical flavors and includes partially quenched QED effects.
- <sup>2</sup> BASAK 15 is a lattice computation using 2+1 dynamical quark flavors.
- <sup>3</sup> CARRASCO 14 is a lattice QCD computation of light quark masses using 2 + 1 + 1 dynamical quarks, with  $m_u = m_d \neq m_s \neq m_c$ . The *u* and *d* quark masses are obtained separately by using the *K* meson mass splittings and lattice results for the electromagnetic contributions.
- <sup>4</sup> AOKI 12 is a lattice computation using 1 + 1 + 1 dynamical quark flavors.
- <sup>5</sup> BAZAVOV 10 is a lattice computation using 2+1 dynamical quark flavors.
- <sup>6</sup> BLUM 10 is a lattice computation using 2+1 dynamical quark flavors.
- <sup>7</sup> BLUM 07 determine quark masses from the pseudoscalar meson masses using a QED plus QCD lattice computation with two dynamical quark flavors.
- <sup>8</sup> AUBIN 04a perform three flavor dynamical lattice calculation of pseudoscalar meson masses, with continuum estimate of electromagnetic effects in the kaon masses.
- <sup>9</sup> NELSON 03 computes coefficients in the order  $p^4$  chiral Lagrangian using a lattice calculation with three dynamical flavors. The ratio  $m_u/m_d$  is obtained by combining this with the chiral perturbation theory computation of the meson masses to order  $p^4$ .
- <sup>10</sup> LEUTWYLER 96 uses a combined fit to  $\eta \rightarrow 3\pi$  and  $\psi' \rightarrow J/\psi(\pi, \eta)$  decay rates, and the electromagnetic mass differences of the  $\pi$  and *K*.

WEIGHTED AVERAGE  
0.474 $\pm$ 0.029 (Error scaled by 2.4)



### s-QUARK MASS

See the comment for the *u* quark above.

We have normalized the  $\overline{MS}$  masses at a renormalization scale of  $\mu = 2$  GeV. Results quoted in the literature at  $\mu = 1$  GeV have been rescaled by dividing by 1.35.

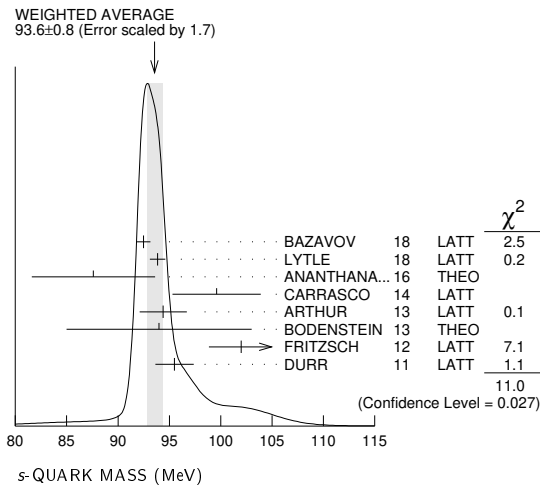
$\overline{MS}$ MASS (MeV)	DOCUMENT ID	TECN
<b>93 <math>\pm 11</math> <math>\pm 5</math> OUR EVALUATION</b>	See the ideogram below.	
92.47 $\pm 0.69$	1 BAZAVOV	18 LATT
93.85 $\pm 0.75$	2 LYTLE	18 LATT
87.6 $\pm 6.0$	3 ANANTHANA	16 THEO
99.6 $\pm 4.3$	4 CARRASCO	14 LATT
94.4 $\pm 2.3$	5 ARTHUR	13 LATT
94 $\pm 9$	6 BODENSTEIN	13 THEO
102 $\pm 3 \pm 1$	7 FRITZSCH	12 LATT
95.5 $\pm 1.1 \pm 1.5$	8 DURR	11 LATT
••• We do not use the following data for averages, fits, limits, etc. •••		
93.6 $\pm 0.8$	9 CHAKRABORTY	15 LATT
96.2 $\pm 2.7$	10 AOKI	11A LATT
95 $\pm 6$	11 BLOSSIER	10 LATT
97.6 $\pm 2.9 \pm 5.5$	12 BLUM	10 LATT
92.4 $\pm 1.5$	13 DAVIES	10 LATT
92.2 $\pm 1.3$	14 MCNEILE	10 LATT
107.3 $\pm 11.7$	15 ALLTON	08 LATT
105 $\pm 3 \pm 9$	16 BLOSSIER	08 LATT
102 $\pm 8$	17 DOMINGUEZ	08A THEO
90.1 $+17.2$ $-6.1$	18 ISHIKAWA	08 LATT
105.6 $\pm 1.2$	19 NAKAMURA	08 LATT
119.5 $\pm 9.3$	20 BLUM	07 LATT
105 $\pm 6 \pm 7$	21 CHETYRKIN	06 THEO
111 $\pm 6 \pm 10$	22 GOCKELER	06 LATT
119 $\pm 5 \pm 8$	23 GOCKELER	06A LATT
92 $\pm 9$	24 JAMIN	06 THEO
87 $\pm 6$	25 MASON	06 LATT
104 $\pm 15$	26 NARISON	06 THEO
$\geq 71 \pm 4, \leq 151 \pm 14$	27 NARISON	06 THEO
96 $+5$ $-16$ $-18$	28 BAIKOV	05 THEO
81 $\pm 22$	29 GAMIZ	05 THEO
125 $\pm 28$	30 GORBUNOV	05 THEO
93 $\pm 32$	31 NARISON	05 THEO
76 $\pm 8$	32 AUBIN	04 LATT
116 $\pm 6 \pm 0.65$	33 AOKI	03 LATT
84.5 $+12$ $-1.7$	34 AOKI	03B LATT
106 $\pm 2 \pm 8$	35 BECIREVIC	03 LATT
92 $\pm 9 \pm 16$	36 CHIU	03 LATT
117 $\pm 17$	37 GAMIZ	03 THEO
103 $\pm 17$	38 GAMIZ	03 THEO

- <sup>1</sup> BAZAVOV 18 determine the quark masses using a lattice computation with staggered fermions and four active quark flavors.
- <sup>2</sup> LYTLE 18 combined with CHAKRABORTY 2015 determine  $\overline{m}_s(3 \text{ GeV}) = 84.78 \pm 0.65$  MeV from a lattice simulation with  $n_f = 2+1+1$  flavors. They also determine the quoted value  $\overline{m}_s(2 \text{ GeV})$  for  $n_f = 4$  dynamical flavors.
- <sup>3</sup> ANANTHANARAYAN 16 determine  $\overline{m}_s(2 \text{ GeV}) = 106.70 \pm 9.36$  MeV and  $74.47 \pm 7.77$  MeV from fits to ALEPH and OPAL  $\tau$  decay data, respectively. We have used the weighted average of the two.
- <sup>4</sup> CARRASCO 14 is a lattice QCD computation of light quark masses using 2 + 1 + 1 dynamical quarks, with  $m_u = m_d \neq m_s \neq m_c$ . The *u* and *d* quark masses are obtained separately by using the *K* meson mass splittings and lattice results for the electromagnetic contributions.
- <sup>5</sup> ARTHUR 13 is a lattice computation using 2+1 dynamical domain wall fermions. Masses at  $\mu = 3$  GeV have been converted to  $\mu = 2$  GeV using conversion factors given in their paper.
- <sup>6</sup> BODENSTEIN 13 determines  $m_s$  from QCD finite energy sum rules, and the perturbative computation of the pseudoscalar correlator to five-loop order.
- <sup>7</sup> FRITZSCH 12 determine  $m_s$  using a lattice computation with  $N_f = 2$  dynamical flavors.
- <sup>8</sup> DURR 11 determine quark mass from a lattice computation of the meson spectrum using  $N_f = 2 + 1$  dynamical flavors. The lattice simulations were done at the physical quark mass, so that extrapolation in the quark mass was not needed.
- <sup>9</sup> CHAKRABORTY 15 is a lattice QCD computation that determines  $m_c$  and  $m_c/m_s$  using pseudoscalar mesons masses tuned on gluon field configurations with 2+1+1 dynamical flavors of HISQ quarks with *u/d* masses down to the physical value.
- <sup>10</sup> AOKI 11A determine quark masses from a lattice computation of the hadron spectrum using  $N_f = 2 + 1$  dynamical flavors of domain wall fermions.
- <sup>11</sup> BLOSSIER 10 determines quark masses from a computation of the hadron spectrum using  $N_f=2$  dynamical twisted-mass Wilson fermions.
- <sup>12</sup> BLUM 10 determines light quark masses using a QCD plus QED lattice computation of the electromagnetic mass splittings of the low-lying hadrons. The lattice simulations use 2+1 dynamical quark flavors.
- <sup>13</sup> DAVIES 10 and MCNEILE 10 determine  $\overline{m}_c(\mu)/\overline{m}_s(\mu) = 11.85 \pm 0.16$  using a lattice computation with  $N_f = 2 + 1$  dynamical fermions of the pseudoscalar meson masses. Mass  $m_s$  is obtained from this using the value of  $m_c$  from ALLISON 08 or MCNEILE 10.
- <sup>14</sup> ALLTON 08 use a lattice computation of the  $\pi$ , *K*, and  $\Omega$  masses with 2+1 dynamical flavors of domain wall quarks, and non-perturbative renormalization.
- <sup>15</sup> BLOSSIER 08 use a lattice computation of pseudoscalar meson masses and decay constants with 2 dynamical flavors and non-perturbative renormalization.
- <sup>16</sup> DOMINGUEZ 08A make determination from QCD finite energy sum rules for the pseudoscalar two-point function computed to order  $a^4$ .
- <sup>17</sup> ISHIKAWA 08 use a lattice computation of the light meson spectrum with 2+1 dynamical flavors of  $O(a)$  improved Wilson quarks, and one-loop perturbative renormalization.
- <sup>18</sup> NAKAMURA 08 do a lattice computation using quenched domain wall fermions and non-perturbative renormalization.

# Quark Particle Listings

## Light Quarks (*u, d, s*)

- <sup>19</sup>BLUM 07 determine quark masses from the pseudoscalar meson masses using a QED plus QCD lattice computation with two dynamical quark flavors.
- <sup>20</sup>CHETYRKIN 06 use QCD sum rules in the pseudoscalar channel to order  $\alpha_s^4$ .
- <sup>21</sup>GOCKELER 06 use an unquenched lattice computation of the axial Ward Identity with  $N_f = 2$  dynamical light quark flavors, and non-perturbative renormalization, to obtain  $\overline{m}_s(2 \text{ GeV}) = 111 \pm 6 \pm 4 \pm 6 \text{ MeV}$ , where the first error is statistical, the second and third are systematic due to the fit range and force scale uncertainties, respectively. We have combined the systematic errors linearly.
- <sup>22</sup>GOCKELER 06A use an unquenched lattice computation of the pseudoscalar meson masses with  $N_f = 2$  dynamical light quark flavors, and non-perturbative renormalization.
- <sup>23</sup>JAMIN 06 determine  $\overline{m}_s(2 \text{ GeV})$  from the spectral function for the scalar  $K\pi$  form factor.
- <sup>24</sup>MASON 06 extract light quark masses from a lattice simulation using staggered fermions with an improved action, and three dynamical light quark flavors with degenerate  $u$  and  $d$  quarks. Perturbative corrections were included at NNLO order.
- <sup>25</sup>NARISON 06 uses sum rules for  $e^+e^- \rightarrow$  hadrons to order  $\alpha_s^3$ .
- <sup>26</sup>NARISON 06 obtains the quoted range from positivity of the spectral functions.
- <sup>27</sup>BAIKOV 05 determines  $\overline{m}_s(M_\tau) = 100^{+5}_{-3} +^{17}_{-19}$  from sum rules using the strange spectral function in  $\tau$  decay. The computations were done to order  $\alpha_s^3$ , with an estimate of the  $\alpha_s^4$  terms. We have converted the result to  $\mu = 2 \text{ GeV}$ .
- <sup>28</sup>GAMIZ 05 determines  $\overline{m}_s(2 \text{ GeV})$  from sum rules using the strange spectral function in  $\tau$  decay. The computations were done to order  $\alpha_s^2$ , with an estimate of the  $\alpha_s^3$  terms.
- <sup>29</sup>GORBUNOV 05 use hadronic tau decays to N3LO, including power corrections.
- <sup>30</sup>NARISON 05 determines  $\overline{m}_s(2 \text{ GeV})$  from sum rules using the strange spectral function in  $\tau$  decay. The computations were done to order  $\alpha_s^3$ .
- <sup>31</sup>AUBIN 04 perform three flavor dynamical lattice calculation of pseudoscalar meson masses, with one-loop perturbative renormalization constant.
- <sup>32</sup>AOKI 03 uses quenched lattice simulation of the meson and baryon masses with degenerate light quarks. The extrapolations are done using quenched chiral perturbation theory. Determines  $m_s = 113.8 \pm 2.3^{+5.8}_{-2.9}$  using  $K$  mass as input and  $m_s = 142.3 \pm 5.8^{+2.2}_{-0}$  using  $\phi$  mass as input. We have performed a weighted average of these values.
- <sup>33</sup>AOKI 03B uses lattice simulation of the meson and baryon masses with two dynamical light quarks. Simulations are performed using the  $\mathcal{O}(a)$  improved Wilson action.
- <sup>34</sup>BEČIREVIĆ 03 perform quenched lattice computation using the vector and axial Ward identities. Uses  $\mathcal{O}(a)$  improved Wilson action and nonperturbative renormalization. They also quote  $\overline{m}/m_s = 24.3 \pm 0.2 \pm 0.6$ .
- <sup>35</sup>CHIU 03 determines quark masses from the pion and kaon masses using a lattice simulation with a chiral fermion action in quenched approximation.
- <sup>36</sup>GAMIZ 03 determines  $m_s$  from SU(3) breaking in the  $\tau$  hadronic width. The value of  $V_{us}$  is chosen to satisfy CKM unitarity.
- <sup>37</sup>GAMIZ 03 determines  $m_s$  from SU(3) breaking in the  $\tau$  hadronic width. The value of  $V_{us}$  is taken from the PDG.



### OTHER LIGHT QUARK MASS RATIOS

#### $m_s/m_d$ MASS RATIO

VALUE	DOCUMENT ID	TECN	COMMENT
<b>17-22 OUR EVALUATION</b>			
20.0	1 GAO 97	THEO	
18.9 ± 0.8	2 LEUTWYLER 96	THEO	Compilation
21	3 DONOGHUE 92	THEO	
18	4 GERARD 90	THEO	
18 to 23	5 LEUTWYLER 90B	THEO	

- <sup>1</sup>GAO 97 uses electromagnetic mass splittings of light mesons.
- <sup>2</sup>LEUTWYLER 96 uses a combined fit to  $\eta \rightarrow 3\pi$  and  $\psi' \rightarrow J/\psi(\pi, \eta)$  decay rates, and the electromagnetic mass differences of the  $\pi$  and  $K$ .
- <sup>3</sup>DONOGHUE 92 result is from a combined analysis of meson masses,  $\eta \rightarrow 3\pi$  using second-order chiral perturbation theory including nonanalytic terms, and  $(\psi(2S) \rightarrow J/\psi(1S)\pi)/(\psi(2S) \rightarrow J/\psi(1S)\eta)$ .
- <sup>4</sup>GERARD 90 uses large  $N$  and  $\eta$ - $\eta'$  mixing.
- <sup>5</sup>LEUTWYLER 90B determines quark mass ratios using second-order chiral perturbation theory for the meson and baryon masses, including nonanalytic corrections. Also uses Weinberg sum rules to determine  $L_7$ .

#### $m_s/\overline{m}$ MASS RATIO

$$\overline{m} \equiv (m_u + m_d)/2$$

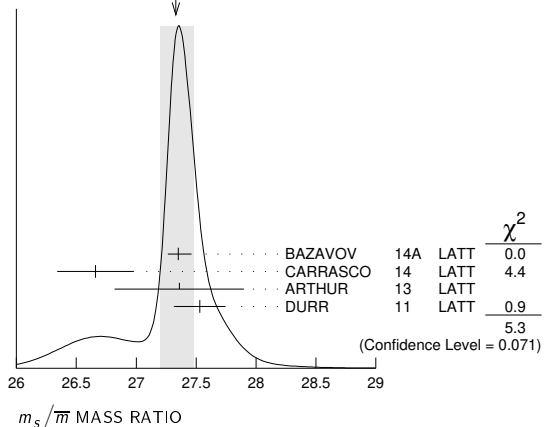
VALUE	DOCUMENT ID	TECN
-------	-------------	------

**27.3 ± 0.7** OUR EVALUATION See the ideogram below.

27.35 ± 0.05 <sup>+0.10</sup> <sub>-0.07</sub>	1 BAZAVOV	14A LATT
26.66 ± 0.32	2 CARRASCO	14 LATT
27.36 ± 0.54	3 ARTHUR	13 LATT
27.53 ± 0.20 ± 0.08	4 DURR	11 LATT
• • • We do not use the following data for averages, fits, limits, etc. • • •		
26.8 ± 1.4	5 AOKI	11A LATT
27.3 ± 0.9	6 BLOSSIER	10 LATT
28.8 ± 1.65	7 ALLTON	08 LATT
27.3 ± 0.3 ± 1.2	8 BLOSSIER	08 LATT
23.5 ± 1.5	9 OLLER	07A THEO
27.4 ± 0.4	10 AUBIN	04 LATT

- <sup>1</sup>BAZAVOV 14A is a lattice computation using 4 dynamical flavors of HISQ fermions.
- <sup>2</sup>CARRASCO 14 is a lattice QCD computation of light quark masses using 2 + 1 + 1 dynamical quarks, with  $m_u = m_d \neq m_s \neq m_c$ . The  $u$  and  $d$  quark masses are obtained separately by using the  $K$  meson mass splittings and lattice results for the electromagnetic contributions.
- <sup>3</sup>ARTHUR 13 is a lattice computation using 2+1 dynamical domain wall fermions.
- <sup>4</sup>DURR 11 determine quark mass from a lattice computation of the meson spectrum using  $N_f = 2 + 1$  dynamical flavors. The lattice simulations were done at the physical quark mass, so that extrapolation in the quark mass was not needed.
- <sup>5</sup>AOKI 11A determine quark masses from a lattice computation of the hadron spectrum using  $N_f = 2 + 1$  dynamical flavors of domain wall fermions.
- <sup>6</sup>BLOSSIER 10 determines quark masses from a computation of the hadron spectrum using  $N_f=2$  dynamical twisted-mass Wilson fermions.
- <sup>7</sup>ALLTON 08 use a lattice computation of the  $\pi$ ,  $K$ , and  $\Omega$  masses with 2+1 dynamical flavors of domain wall quarks, and non-perturbative renormalization.
- <sup>8</sup>BLOSSIER 08 use a lattice computation of pseudoscalar meson masses and decay constants with 2 dynamical flavors and non-perturbative renormalization.
- <sup>9</sup>OLLER 07A use unitarized chiral perturbation theory to order  $p^4$ .
- <sup>10</sup>Three flavor dynamical lattice calculation of pseudoscalar meson masses.

WEIGHTED AVERAGE  
27.33±0.15-0.12 (Error scaled by 1.6)



#### Q MASS RATIO

$$Q \equiv \sqrt{(m^2_s - \overline{m}^2)/(m^2_d - m^2_u)}; \quad \overline{m} \equiv (m_u + m_d)/2$$

VALUE	DOCUMENT ID	TECN
-------	-------------	------

• • • We do not use the following data for averages, fits, limits, etc. • • •

22.1 ± 0.7	1 COLANGELO 18	THEO
22.0 ± 0.7	2 COLANGELO 17	THEO
21.6 ± 1.1	3 GUO 17	THEO
23.4 ± 0.4 ± 0.5	4 FODOR 16	LATT
21.4 ± 0.4	5 GUO 15F	THEO
22.8 ± 0.4	6 MARTEMYA... 05	THEO
22.7 ± 0.8	7 ANISOVICH 96	THEO

- <sup>1</sup>COLANGELO 18 obtain  $Q$  from a dispersive analysis of  $\eta \rightarrow 3\pi$  decay.
- <sup>2</sup>COLANGELO 17 obtain  $Q$  from a dispersive analysis of KLOE collaboration data on  $\eta \rightarrow \pi^+\pi^-\pi^0$  decays and chiral perturbation theory input.
- <sup>3</sup>GUO 17 determine  $Q$  from a dispersive model fit to KLOE and WASA-at-COSY data on  $\eta \rightarrow \pi^+\pi^-\pi^0$  decay and matching to chiral perturbation theory.
- <sup>4</sup>FODOR 16 is a lattice simulation with  $N_f = 2 + 1$  dynamical flavors and includes partially quenched QED effects.
- <sup>5</sup>GUO 15F determine  $Q$  from a Khuri-Treiman analysis of  $\eta \rightarrow 3\pi$  decays.
- <sup>6</sup>MARTEMYANOV 05 determine  $Q$  from  $\eta \rightarrow 3\pi$  decay.
- <sup>7</sup>ANISOVICH 96 find  $Q$  from  $\eta \rightarrow \pi^+\pi^-\pi^0$  decay using dispersion relations and chiral perturbation theory.

LIGHT QUARKS (*u, d, s*) REFERENCES

DOMINGUEZ 19	JHEP 1902 057	C.A. Dominguez, A. Mes, K. Schilcher (CAPE, MAINZ)
BAZAVOV 18	PR D98 054517	A. Bazavov et al. (Fermilab Lattice, MILC, TUMQCD)
COLANGELO 18	EPJ C78 947	G. Colangelo et al.
LYTLE 18	PR D98 014513	A.T. Lytle et al. (HPQCD Collab.)
COLANGELO 17	PRL 118 022001	G. Colangelo et al. (BERN, IND, JLAB)
GUO 17	PL B771 497	P. Guo et al.
YUAN 17	PR D96 014034	J.-M. Yuan et al.
ANANTHANA... 16	PR D94 116014	Z. Ananthanarayan, D. Das (BANG, AHMED)
FODOR 16	PRL 117 082001	F. Fodor et al. (BMW Collab.)
BASAK 15	JPCS 640 012052	S. Basak et al. (MILC Collab.)
CHAKRABOR... 15	PR D91 054508	B. Chakraborty et al. (HPQCD Collab.)
GUO 15	PR D92 054016	P. Guo et al.
BAZAVOV 14A	PR D90 074509	A. Bazavov et al. (Fermi-LAT and MILC Collabs.)
CARRASCO 14	NP B887 19	N. Carrasco et al. (European Twisted Mass Collab.)
ARTHUR 13	PR D87 094514	R. Arthur et al. (RBC and UKQCD Collabs.)
BODENSTEIN 13	JHEP 1307 138	S. Bodenstein, C.A. Dominguez, K. Schilcher (MANZ+)
AOKI 12	PR D86 034507	S. Aoki et al. (PACS-CS Collab.)
FRITZSCH 12	NP B865 397	P. Fritzsche et al. (ALPHA Collab.)
AOKI 11A	PR D83 074508	Y. Aoki et al. (RBC-UKQCD Collab.)
DURR 11	PL B701 265	S. Durr et al. (BMW Collab.)
BAZAVOV 10	RMP 82 1349	A. Bazavov et al. (MILC Collab.)
BLOSSIER 10	PR D82 114513	B. Blossier et al. (ETM Collab.)
BLUM 10	PR D82 094508	T. Blum et al.
DAVIES 10	PRL 104 132003	T.H. Davies et al. (HPQCD Collab.)
MCNEILE 10	PR D82 034512	C. McNeile et al. (HPQCD Collab.)
DOMINGUEZ 09	PR D79 014009	C.A. Dominguez et al.
ALLISON 08	PR D78 054513	L. Allison et al. (HPQCD Collab.)
ALLTON 08	PR D78 114509	C. Allton et al. (RBC and UKQCD Collabs.)
BLOSSIER 08	JHEP 0804 020	B. Blossier et al. (ETM Collab.)
DEANDREA 08	PR D78 034032	A. Deandrea, A. Nehme, P. Talavera
DOMINGUEZ 08A	JHEP 0805 020	C.A. Dominguez et al.
DOMINGUEZ... 08B	PL B660 49	A. Dominguez-Clarimon, E. de Rafael, J. Tarón
ISHIKAWA 08	PR D78 011502	T. Ishikawa et al. (CP-PACS and JLQCD Collabs.)
NAKAMURA 08	PR D78 034502	Y. Nakamura et al. (CP-PACS Collab.)
BLUM 07	PR D76 114508	T. Blum et al.
OLLER 07A	EPJ A34 371	J.A. Oller, L. Roca
CHETYRKIN 06	EPJ C46 721	K.G. Chetyrkin, A. Khodjamirian
GOCKELER 06	PR D73 054508	M. Gockeler et al. (QCDSF and UKQCD Collabs.)
GOCKELER 06A	PL B639 307	M. Gockeler et al. (QCDSF and UKQCD Collabs.)
JAMIN 06	PR D74 074009	M. Jamin, J.A. Oller, A. Pich
MASON 06	PR D73 114501	Q. Mason et al. (HPQCD Collab.)
NARISON 06	PR D74 034013	S. Narison
PDG 06	JG 333 1	W.-M. Yao et al. (PDG Collab.)
BAIKOV 05	PRL 95 012003	P.A. Baikov, K.G. Chetyrkin, J.H. Kuhn
GAMIZ 05	PRL 94 011803	E. Gamiz et al.
GORBUNOV 05	PR D71 013002	D.S. Gorbunov, A.A. Pivovarov
MARTEMYAN... 05	PR D71 017501	B.V. Martemyanov, V.S. Sopot
NARISON 05	PL B626 101	S. Narison
AUBIN 04	PR D70 031504	C. Aubin et al. (HPQCD, MILC, UKQCD Collabs.)
AUBIN 04A	PR D70 114501	C. Aubin et al. (MILC Collab.)
AOKI 03	PR D67 034503	S. Aoki et al. (CP-PACS Collab.)
AOKI 03B	PR D68 054502	S. Aoki et al. (CP-PACS Collab.)
BECIREVIC 03	PL B558 69	D. Becirevic, V. Lubicz, C. Tarantino
CHIU 03	NP B673 217	T.-W. Chiu, T.-H. Hsieh
GAMIZ 03	JHEP 0301 060	E. Gamiz et al.
NELSON 03	PRL 90 021601	D. Nelson, G.T. Fleming, G.W. Kilcup
GAO 97	PR D56 4115	D.N. Gao, B.A. Li, M.-L. Yan
ANISOVICH 96	PL B375 335	A.V. Anisovich, H. Leutwyler
LEUTWYLER 96	PL B378 313	H. Leutwyler
DONOGHUE 92	PRL 69 3444	J.F. Donoghue, B.R. Holstein, D. Wyler (MASA+)
GERARD 90	MPL A5 391	J.M. Gerard (MPIM)
LEUTWYLER 90B	NP B337 108	H. Leutwyler (BERN)

1.26 ± 0.05 ± 0.04	21 ABRAMOWICZ13c COMB
1.282 ± 0.011 ± 0.022	22 DEHNADI 13 THEO
1.286 ± 0.066	23 NARISON 13 THEO
1.36 ± 0.04 ± 0.10	24 ALEKHIN 12 THEO
1.261 ± 0.016	25 NARISON 12A THEO
1.01 ± 0.09 ± 0.03	26 ALEKHIN 11 THEO
1.28 ± 0.04	27 BLOSSIER 10 LATT
1.299 ± 0.026	28 BODENSTEIN 10 THEO
1.273 ± 0.006	29 MCNEILE 10 LATT
1.261 ± 0.018	30 NARISON 10 THEO
1.279 ± 0.013	31 CHETYRKIN 09 THEO
1.268 ± 0.009	32 ALLISON 08 LATT
1.286 ± 0.013	33 KUHN 07 THEO
1.295 ± 0.015	34 BOUGHEZAL 06 THEO
1.24 ± 0.09	35 BUCHMUEL... 06 THEO
1.224 ± 0.017 ± 0.054	36 HOANG 06 THEO
1.33 ± 0.10	37 AUBERT 04x THEO
1.29 ± 0.07	38 HOANG 04 THEO
1.319 ± 0.028	39 DEDIVITIIS 03 LATT
1.19 ± 0.11	40 EIDEMULLER 03 THEO
1.289 ± 0.043	41 ERLER 03 THEO
1.26 ± 0.02	42 ZYABLYUK 03 THEO

- 1 NARISON 20 determines the quark mass using QCD Laplace sum rules from the  $B_c$  mass, combined with previous determinations of the QCD condensates and  $c$  and  $b$  masses.
- 2 ABRAMOWICZ 18 determine  $\overline{m}_c(\overline{m}_c) = 1.290 \pm 0.046 \pm 0.062 \pm 0.003$  from the production of  $c$  quarks in  $e p$  collisions at HERA using combined H1 and ZEUS data. The experimental/fitting errors, and those from modeling and parameterization have been combined in quadrature.
- 3 BAZAVOV 18 determine the quark masses using a lattice computation with staggered fermions and four active quark flavors.
- 4 LYTLE 18 combined with CHAKRABORTY 15 determine  $\overline{m}_c(3 \text{ GeV}) = 0.9874(48) \text{ GeV}$  from a lattice simulation with  $n_f = 2+1+1$  flavors. They also determine the quoted value  $\overline{m}_c(\overline{m}_c)$  for  $n_f = 4$  dynamical flavors.
- 5 PESET 18 determine  $\overline{m}_c(\overline{m}_c)$  and  $\overline{m}_b(\overline{m}_b)$  using an N3LO calculation of the  $\eta_c, \eta_b$  and  $B_c$  masses.
- 6 CHETYRKIN 17 determine  $\overline{m}_c(\mu = 3 \text{ GeV}) = 0.993 \pm 0.008 \text{ GeV}$  and  $\overline{m}_c(\overline{m}_c)$  from a four-loop sum-rule computation of the cross-section for  $e^+e^- \rightarrow$  hadrons in the charm threshold region.
- 7 ERLER 17 determine  $\overline{m}_c(\overline{m}_c) = 1.272 \pm 0.008 \text{ GeV}$  from a three-loop QCD sum-rule computation of the vector current correlator. This result is for fixed  $\alpha_s(M_Z) = 0.1182$ . Including an  $\alpha_s$  uncertainty of  $\pm 0.0016$ , the charm mass error increases from 8 to 9 MeV.
- 8 KIYO 16 determine  $\overline{m}_c(\overline{m}_c)$  from the  $J/\psi(1S)$  mass at order  $\alpha_s^3$  (N3LO).
- 9 DEHNADI 15 determine  $\overline{m}_c(\overline{m}_c)$  using sum rules for  $e^+e^- \rightarrow$  hadrons at order  $\alpha_s^3$  (N3LO), and fitting to both experimental data and lattice results.
- 10 CARRASCO 14 is a lattice QCD computation of light quark masses using  $2+1+1$  dynamical quarks, with  $m_u = m_d \neq m_s \neq m_c$ . The  $u$  and  $d$  quark masses are obtained separately by using the  $K$  meson mass splittings and lattice results for the electromagnetic contributions.
- 11 ALEKHIN 13 determines  $m_c$  from charm production in deep inelastic scattering at HERA using approximate NNLO QCD.
- 12 SAMOYLOV 13 determines  $m_c$  from a study of charm dimuon production in neutrino-iron scattering using the NLO QCD result for the charm quark production cross section.
- 13 BODENSTEIN 11 determine  $\overline{m}_c(3 \text{ GeV}) = 0.987 \pm 0.009 \text{ GeV}$  and  $\overline{m}_c(\overline{m}_c) = 1.278 \pm 0.009 \text{ GeV}$  using QCD sum rules for the charm quark vector current correlator.
- 14 LASCHKA 11 determine the  $c$  mass from the charmonium spectrum. The theoretical computation uses the heavy  $Q\overline{Q}$  potential to order  $1/m_Q$  obtained by matching the short-distance perturbative result onto lattice QCD result at larger scales.
- 15 AUBERT 10A determine the  $b$ - and  $c$ -quark masses from a fit to the inclusive decay spectra in semileptonic  $B$  decays in the kinetic scheme (and convert it to the  $\overline{MS}$  scheme).
- 16 SIGNER 09 determines the  $c$ -quark mass using non-relativistic sum rules to analyze the  $e^+e^- \rightarrow c\overline{c}$  cross-section near threshold. Also determine the PS mass  $m_{PS}(\mu_P = 0.7 \text{ GeV}) = 1.50 \pm 0.04 \text{ GeV}$ .
- 17 NARISON 18A determines simultaneously  $\overline{m}_c(\overline{m}_c)$  and the 4-dimension gluon condensate using QCD exponential sum rules and their ratios evaluated at the optimal scale  $\mu = 2.85 \text{ GeV}$  at N2LO-N3LO of perturbative QCD and including condensates up to dimension 6-8 in the (axial-)vector and (pseudo-)scalar charmonium channels.
- 18 NARISON 18B determines  $\overline{m}_c(\overline{m}_c)$  using QCD vector moment sum rules and their ratios at N2LO-N3LO of perturbative QCD and including condensates up to dimension 8.
- 19 BERTONE 16 determine  $\overline{m}_c(\overline{m}_c)$  from HERA deep inelastic scattering data using the FONLL scheme. Also determine  $\overline{m}_c(\overline{m}_c) = 1.318 \pm 0.054 \pm 0.490 \pm 0.022$  using the fixed flavor number scheme.
- 20 CHAKRABORTY 15 is a lattice QCD computation using  $2+1+1$  dynamical flavors. Moments of pseudoscalar current-current correlators are matched to  $\alpha_s^3$ -accurate QCD perturbation theory with the  $\eta_c$  meson mass tuned to experiment.
- 21 ABRAMOWICZ 13c determines  $m_c$  from charm production in deep inelastic  $e p$  scattering, using the QCD prediction at NLO order. The uncertainties from model and parameterization assumptions, and the value of  $\alpha_s$ , of  $\pm 0.03$ ,  $\pm 0.02$ , and  $\pm 0.02$  respectively, have been combined in quadrature.
- 22 DEHNADI 13 determines  $m_c$  using QCD sum rules for the charmonium spectrum and charm continuum to order  $\alpha_s^3$  (N3LO). The statistical and systematic experimental errors of  $\pm 0.006$  and  $\pm 0.009$  have been combined in quadrature. The theoretical uncertainties  $\pm 0.019$  from truncation of the perturbation series,  $\pm 0.010$  from  $\alpha_s$ , and  $\pm 0.002$  from the gluon condensate have been combined in quadrature.
- 23 NARISON 13 determines  $m_c$  using QCD spectral sum rules to order  $\alpha_s^2$  (NNLO) and including condensates up to dimension 6.
- 24 ALEKHIN 12 determines  $m_c$  from heavy quark production in deep inelastic scattering at HERA using approximate NNLO QCD.
- 25 NARISON 12A determines  $m_c$  using sum rules for the vector current correlator to order  $\alpha_s^3$ , including the effect of gluon condensates up to dimension eight.

**C**

$$J(J^P) = 0(\frac{1}{2}^+)$$

Charge =  $\frac{2}{3} e$  Charm = +1

**c-QUARK MASS**

The  $c$ -quark mass corresponds to the “running” mass  $m_c(\mu = m_c)$  in the  $\overline{MS}$  scheme. We have converted masses in other schemes to the  $\overline{MS}$  scheme using two-loop QCD perturbation theory with  $\alpha_s(\mu = m_c) = 0.38 \pm 0.03$ . The value  $1.27 \pm 0.02 \text{ GeV}$  for the  $\overline{MS}$  mass corresponds to  $1.67 \pm 0.07 \text{ GeV}$  for the pole mass (see the “Note on Quark Masses”).

$\overline{MS}$ MASS (GeV)	DOCUMENT ID	TECN
<b>1.27 ± 0.02</b>	<b>OUR EVALUATION</b>	See the ideogram below.
1.266 ± 0.006	1 NARISON 20	THEO
1.290 +0.077 -0.053	2 ABRAMOWICZ18	HERA
1.273 ± 0.010	3 BAZAVOV 18	LATT
1.2737 ± 0.0077	4 LYTLE 18	LATT
1.223 ± 0.033	5 PESET 18	THEO
1.279 ± 0.008	6 CHETYRKIN 17	THEO
1.272 ± 0.008	7 ERLER 17	THEO
1.246 ± 0.023	8 KIYO 16	THEO
1.288 ± 0.020	9 DEHNADI 15	THEO
1.348 ± 0.046	10 CARRASCO 14	LATT
1.24 ± 0.03 +0.03 -0.07	11 ALEKHIN 13	THEO
1.159 ± 0.075	12 SAMOYLOV 13	NOMD
1.278 ± 0.009	13 BODENSTEIN 11	THEO
1.28 +0.07 -0.06	14 LASCHKA 11	THEO
1.196 ± 0.059 ± 0.050	15 AUBERT 10A	BABR
1.25 ± 0.04	16 SIGNER 09	THEO
• • • We do not use the following data for averages, fits, limits, etc. • • •		
1.263 ± 0.014	17 NARISON 18A	THEO
1.264 ± 0.006	18 NARISON 18B	THEO
1.335 ± 0.043 +0.040 -0.011	19 BERTONE 16	THEO
1.2715 ± 0.0095	20 CHAKRABOR...15	LATT

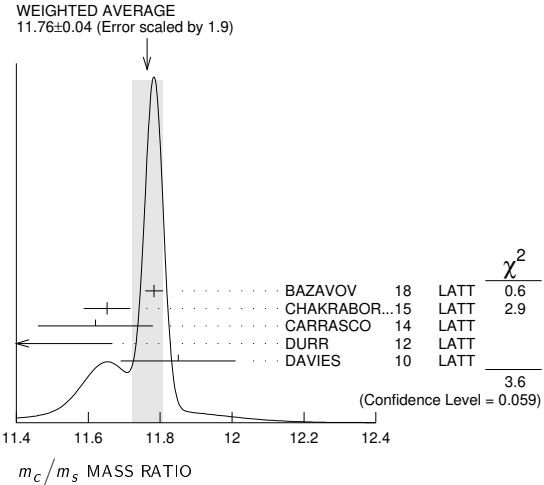


# Quark Particle Listings

## C

- 26 ALEKHIN 11 determines  $m_c$  from heavy quark production in deep inelastic scattering using fixed target and HERA data, and approximate NNLO QCD.
- 27 BLOSSIER 10 determines quark masses from a computation of the hadron spectrum using  $N_f=2$  dynamical twisted-mass Wilson fermions.
- 28 BODENSTEIN 10 determines  $\overline{m}_c(3 \text{ GeV}) = 1.008 \pm 0.026 \text{ GeV}$  using finite energy sum rules for the vector current correlator. The authors have converted this to  $\overline{m}_c(\overline{m}_c)$  using  $\alpha_s(M_Z) = 0.1189 \pm 0.0020$ .
- 29 MCNEILE 10 determines  $m_c$  by comparing the order  $\alpha_s^3$  perturbative results for the pseudo-scalar current to lattice simulations with  $N_f = 2+1$  sea-quarks by the HPQCD collaboration.
- 30 NARISON 10 determines  $m_c$  from ratios of moments of vector current correlators computed to order  $\alpha_s^3$  and including the dimension-six gluon condensate.
- 31 CHETYRKIN 09 determine  $m_c$  and  $m_b$  from the  $e^+e^- \rightarrow Q\overline{Q}$  cross-section and sum rules, using an order  $\alpha_s^3$  computation of the heavy quark vacuum polarization. They also determine  $m_c(3 \text{ GeV}) = 0.986 \pm 0.013 \text{ GeV}$ .
- 32 ALLISON 08 determine  $m_c$  by comparing four-loop perturbative results for the pseudo-scalar current correlator to lattice simulations by the HPQCD collaboration. The result has been updated in MCNEILE 10.
- 33 KUHN 07 determine  $\overline{m}_c(\mu = 3 \text{ GeV}) = 0.986 \pm 0.013 \text{ GeV}$  and  $\overline{m}_c(\overline{m}_c)$  from a four-loop sum-rule computation of the cross-section for  $e^+e^- \rightarrow$  hadrons in the charm threshold region.
- 34 BOUGHEZAL 06 result comes from the first moment of the hadronic production cross-section to order  $\alpha_s^3$ .
- 35 BUCHMUELLER 06 determine  $m_b$  and  $m_c$  by a global fit to inclusive  $B$  decay spectra.
- 36 HOANG 06 determines  $\overline{m}_c(\overline{m}_c)$  from a global fit to inclusive  $B$  decay data. The  $B$  decay distributions were computed to order  $\alpha_s^2\beta_0$ , and the conversion between different  $m_c$  mass schemes to order  $\alpha_s^3$ .
- 37 AUBERT 04x obtain  $m_c$  from a fit to the hadron mass and lepton energy distributions in semileptonic  $B$  decay. The paper quotes values in the kinetic scheme. The  $\overline{M_S}$  value has been provided by the BABAR collaboration.
- 38 HOANG 04 determines  $\overline{m}_c(\overline{m}_c)$  from moments at order  $\alpha_s^2$  of the charm production cross-section in  $e^+e^-$  annihilation.
- 39 DEDIVITIIS 03 use a quenched lattice computation of heavy-heavy and heavy-light meson masses.
- 40 EIDEMULLER 03 determines  $m_b$  and  $m_c$  using QCD sum rules.
- 41 ERLER 03 determines  $m_b$  and  $m_c$  using QCD sum rules. Includes recent BES data.
- 42 ZYABLYUK 03 determines  $m_c$  by using QCD sum rules in the pseudoscalar channel and comparing with the  $\eta_c$  mass.

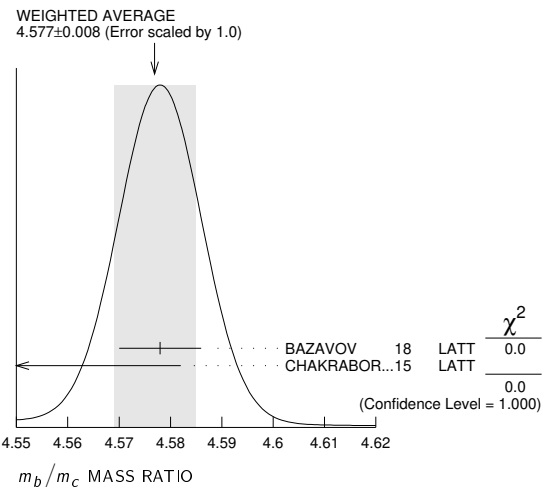
- 5 DAVIES 10 determine  $m_c/m_s$  from meson masses calculated on gluon fields including  $u, d,$  and  $s$  sea quarks with lattice spacing down to 0.045 fm. The Highly Improved Staggered quark formalism is used for the valence quarks.
- 6 BAZAVOV 14A is a lattice computation using 4 dynamical flavors of HISQ fermions.
- 7 BLOSSIER 10 determine  $m_c/m_s$  from a computation of the hadron spectrum using  $N_f = 2$  dynamical twisted-mass Wilson fermions.



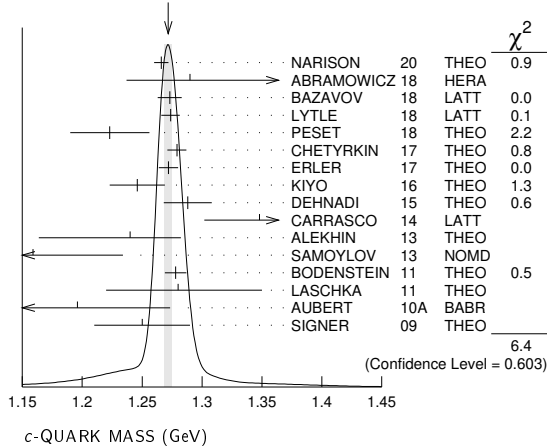
### $m_b/m_c$ MASS RATIO

VALUE	DOCUMENT ID	TECN
<b>4.577 ± 0.008 OUR AVERAGE</b>	See the ideogram below.	
4.578 ± 0.008	1 BAZAVOV 18	LATT
4.528 ± 0.054	2 CHAKRABORTY 15	LATT

- 1 BAZAVOV 18 determine the quark masses using a lattice computation with staggered fermions and four active quark flavors for the  $u, d, s, c$  quarks and five active flavors for the  $b$  quark.
- 2 CHAKRABORTY 15 is a lattice computation using 4 dynamical quark flavors.



### WEIGHTED AVERAGE



### $m_c/m_s$ MASS RATIO

VALUE	DOCUMENT ID	TECN
<b>11.72 ± 0.25 OUR EVALUATION</b>	See the ideogram below.	
11.783 ± 0.025	1 BAZAVOV 18	LATT
11.652 ± 0.065	2 CHAKRABORTY 15	LATT
11.62 ± 0.16	3 CARRASCO 14	LATT
11.27 ± 0.30 ± 0.26	4 DURR 12	LATT
11.85 ± 0.16	5 DAVIES 10	LATT
11.747 ± 0.019 <sup>+</sup> 0.059 -0.043	6 BAZAVOV 14A	LATT
12.0 ± 0.3	7 BLOSSIER 10	LATT

- • • We do not use the following data for averages, fits, limits, etc. • • •
- 1 BAZAVOV 18 determine the quark masses using a lattice computation with staggered fermions and four active quark flavors.
- 2 CHAKRABORTY 15 is a lattice QCD computation on gluon field configurations with 2+1+1 dynamical flavors of HISQ quarks with  $u/d$  masses down to the physical value.  $m_c$  and  $m_s$  are tuned from pseudoscalar meson masses.
- 3 CARRASCO 14 is a lattice QCD computation of light quark masses using 2 + 1 + 1 dynamical quarks, with  $m_u = m_d \neq m_s \neq m_c$ . The  $u$  and  $d$  quark masses are obtained separately by using the  $K$  meson mass splittings and lattice results for the electromagnetic contributions.
- 4 DURR 12 determine  $m_c/m_s$  using a lattice computation with  $N_f = 2$  dynamical fermions. The result is combined with other determinations of  $m_c$  to obtain  $m_s(2 \text{ GeV}) = 97.0 \pm 2.6 \pm 2.5 \text{ MeV}$ .

### $m_b - m_c$ QUARK MASS DIFFERENCE

VALUE (GeV)	DOCUMENT ID	TECN
<b>3.45 ± 0.05 OUR EVALUATION</b>	See the ideogram below.	
3.472 ± 0.032	1 AUBERT 10A	BABR
3.42 ± 0.06	2 ABDALLAH 06B	DLPH
3.44 ± 0.03	3 AUBERT 04x	BABR
3.41 ± 0.01	3 BAUER 04	THEO

- • • We do not use the following data for averages, fits, limits, etc. • • •
- 1 AUBERT 10A determine the  $b$ - and  $c$ -quark masses from a fit to the inclusive decay spectra in semileptonic  $B$  decays in the kinetic scheme.
- 2 ABDALLAH 06B determine  $m_b - m_c$  from moments of the hadron invariant mass and lepton energy spectra in semileptonic inclusive  $B$  decays.
- 3 Determine  $m_b - m_c$  from a global fit to inclusive  $B$  decay spectra.

### c-QUARK REFERENCES

NARISON 20	PL B802 135221	S. Narison	(MONP)
ABRAMOWICZ 18	EPJ C78 473	H. Abramowicz et al.	(HI and ZEUS Collabs.)
BAZAVOV 18	PR D98 054517	A. Bazavov et al.	(Fermilab Lattice, MILC, TUMQCD)
LYTLE 18	PR D98 014513	A.T. Lytle et al.	(HPQCD Collab.)
NARISON 18A	IJMP A33 1850045	S. Narison	(MONP)
NARISON 18B	PL B784 261	S. Narison	(MONP)

PESET	18	JHEP 1809 167	C. Peset, A. Pineda, J. Segovia (BARC, MUNT)
CHETYRKIN	17	PR D96 116007	K.G. Chetyrkin <i>et al.</i>
ERLER	17	EPJ C77 99	J. Erler, P. Masjuan, H. Spiesberger
BERTONE	16	JHEP 1608 050	V. Bertone <i>et al.</i> (xFitter Developers)
KIYO	16	PL B752 122	Y. Kiyo, G. Mishima, Y. Sumino
CHAKRABOR...	15	PR D91 054508	B. Chakraborty <i>et al.</i> (HPQCD Collab.)
DEHNADI	15	JHEP 1508 155	B. Dehnadi, A.H. Hoang, V. Mateu
BAZAVOV	14A	PR D90 074509	A. Bazavov <i>et al.</i> (Fermi-LAT and MILC Collabs.)
CARRASCO	14	NP B887 19	N. Carrasco <i>et al.</i> (European Twisted Mass Collab.)
ABRAMOWICZ	13C	EPJ C73 2311	H. Abramowicz <i>et al.</i> (H1 and Zeuss Collabs.)
ALEKHIN	13	PL B720 172	S. Alekhin <i>et al.</i> (SERP, DESYZ, WUPP+)
DEHNADI	13	JHEP 1309 103	B. Dehnadi <i>et al.</i> (SHRZ, VIEN, MPIM+)
NARISON	13	PL B718 1321	S. Narison (MONP)
SAMOYLOV	13	NP B876 339	O. Samoylov <i>et al.</i> (NOMAD Collab.)
ALEKHIN	12	PL B718 550	S. Alekhin <i>et al.</i> (SERP, WUPP, DESYZ+)
DURR	12	PRL 108 122003	S. Durr, G. Koutsou (WUPP, JULI, CYPR)
NARISON	12A	PL B706 412	S. Narison (MONP)
ALEKHIN	11	PL B699 345	S. Alekhin, S. Moch
BODENSTEIN	11	PR D83 074014	S. Bodenstein <i>et al.</i>
LASCHKA	11	PR D83 094002	A. Laschka, M. Kaiser, W. Weise
AUBERT	10A	PR D81 032003	B. Aubert <i>et al.</i> (BABAR Collab.)
BLOSSIER	10	PR D82 114513	B. Blossier <i>et al.</i> (ETM Collab.)
BODENSTEIN	10	PR D82 114013	S. Bodenstein <i>et al.</i>
DAVIES	10	PRL 104 132003	C.T.H. Davies <i>et al.</i> (HPQCD Collab.)
MCNEILE	10	PR D82 034512	C. McNeile <i>et al.</i> (HPQCD Collab.)
NARISON	10	PL B693 559	S. Narison (MONP)
Also		PL B705 544 (errata.)	S. Narison (MONP)
CHETYRKIN	09	PR D80 074010	K.G. Chetyrkin <i>et al.</i> (KARL, BNL)
SIGNER	09	PL B672 333	A. Signer (DURH)
ALLISON	08	PR D78 054513	I. Allison <i>et al.</i> (HPQCD Collab.)
KUHN	07	NP B779 192	J.H. Kuhn, M. Steinhauser, C. Sturm
ABDALLAH	06B	EPJ C45 35	J. Abdallah <i>et al.</i> (DELPHI Collab.)
BOUGHEZAL	06	PR D74 074006	R. Boughezal, M. Czakon, T. Schutzmeier
BUCHMUEL...	06	PR D73 073008	O.L. Buchmuller, H.U. Flacher (RHBL)
HOANG	06	PL B633 526	A.H. Hoang, A.V. Manohar
AUBERT	04X	PRL 93 011803	B. Aubert <i>et al.</i> (BABAR Collab.)
BAUER	04	PR D70 094017	C. Bauer <i>et al.</i>
HOANG	04	PL B594 127	A.H. Hoang, M. Jamin
DEDIVITIIS	03	NP B675 309	G.M. de Divitiis <i>et al.</i>
EIDEMULLER	03	PR D67 113002	M. Eidemuller
ERLER	03	PL B558 125	J. Erler, M. Luo
ZYABLYUK	03	JHEP 0301 081	K.N. Zybalyuk (ITEP)



$$I(J^P) = 0(\frac{1}{2}^+)$$

$$\text{Charge} = -\frac{1}{3} e \quad \text{Bottom} = -1$$

**b-QUARK MASS**

*b*-quark mass corresponds to the “running mass”  $\overline{m}_b(\mu = \overline{m}_b)$  in the  $\overline{MS}$  scheme. We have converted masses in other schemes to the  $\overline{MS}$  mass using two-loop QCD perturbation theory with  $\alpha_s(\mu = \overline{m}_b) = 0.223 \pm 0.008$ . The value  $4.18^{+0.04}_{-0.03}$  GeV for the  $\overline{MS}$  mass corresponds to  $4.78 \pm 0.06$  GeV for the pole mass, using the two-loop conversion formula. A discussion of masses in different schemes can be found in the “Note on Quark Masses.”

$\overline{MS}$ MASS (GeV)	DOCUMENT ID	TECN.
<b>4.18 <math>\pm</math> 0.03 <math>\overline{MS}</math> OUR EVALUATION</b>	of $\overline{MS}$ Mass. See the ideogram below.	
4.197 $\pm$ 0.008	1 NARISON 20	THEO
4.049 $\pm$ 0.138 $\overline{MS}$	2 ABRAMOWICZ18	HERA
4.195 $\pm$ 0.014	3 BAZAVOV 18	LATT
4.186 $\pm$ 0.037	4 PESET 18	THEO
4.197 $\pm$ 0.022	5 KIYO 16	THEO
4.183 $\pm$ 0.037	6 ALBERTI 15	THEO
4.203 $\pm$ 0.016 $\overline{MS}$	7 BENEKE 15	THEO
4.196 $\pm$ 0.023	8 COLQUHOUN 15	LATT
4.176 $\pm$ 0.023	9 DEHNADI 15	THEO
4.21 $\pm$ 0.11	10 BERNARDONI 14	LATT
4.169 $\pm$ 0.002 $\pm$ 0.008	11 PENIN 14	THEO
4.166 $\pm$ 0.043	12 LEE 13o	LATT
4.247 $\pm$ 0.034	13 LUCHA 13	THEO
4.171 $\pm$ 0.009	14 BODENSTEIN 12	THEO
4.29 $\pm$ 0.14	15 DIMOPOUL... 12	LATT
4.18 $\pm$ 0.05 $\overline{MS}$	16 LASCHKA 11	THEO
4.186 $\pm$ 0.044 $\pm$ 0.015	17 AUBERT 10A	BABR
4.163 $\pm$ 0.016	18 CHETYRKIN 09	THEO
4.243 $\pm$ 0.049	19 SCHWANDA 08	BELL
• • • We do not use the following data for averages, fits, limits, etc. • • •		
4.184 $\pm$ 0.011	20 NARISON 18A	THEO
4.188 $\pm$ 0.008	21 NARISON 18B	THEO
4.07 $\pm$ 0.17	22 ABRAMOWICZ14A	ZEUS
4.201 $\pm$ 0.043	23 AYALA 14A	THEO
4.236 $\pm$ 0.069	24 NARISON 13	THEO
4.213 $\pm$ 0.059	25 NARISON 13A	THEO
4.235 $\pm$ 0.003 $\pm$ 0.055	26 HOANG 12	THEO
4.212 $\pm$ 0.032	27 NARISON 12	THEO
4.177 $\pm$ 0.011	28 NARISON 12	THEO
4.171 $\pm$ 0.014	29 NARISON 12A	THEO
4.164 $\pm$ 0.023	30 MCNEILE 10	LATT
4.173 $\pm$ 0.010	31 NARISON 10	THEO
5.26 $\pm$ 1.2	32 ABDALLAH 08D	DLPH
4.42 $\pm$ 0.06 $\pm$ 0.08	33 GUAZZINI 08	LATT
4.347 $\pm$ 0.048 $\pm$ 0.08	34 DELLA-MOR... 07	LATT
4.164 $\pm$ 0.025	35 KUHN 07	THEO
4.19 $\pm$ 0.40	36 ABDALLAH 06D	DLPH

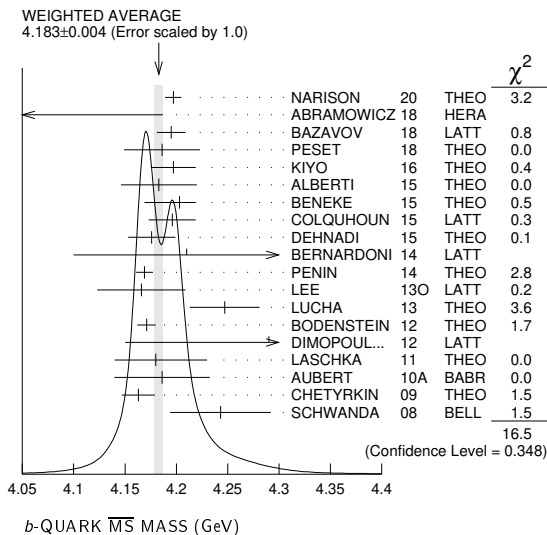
4.205 $\pm$ 0.058	37 BOUGHEZAL 06	THEO
4.20 $\pm$ 0.04	38 BUCHMUEL... 06	THEO
4.19 $\pm$ 0.06	39 PINEDA 06	THEO
4.4 $\pm$ 0.3	40 GRAY 05	LATT
4.22 $\pm$ 0.06	41 AUBERT 04X	THEO
4.17 $\pm$ 0.03	42 BAUER 04	THEO
4.22 $\pm$ 0.11	43 HOANG 04	THEO
4.25 $\pm$ 0.11	44 MCNEILE 04	LATT
4.22 $\pm$ 0.09	45 BAUER 03	THEO
4.19 $\pm$ 0.05	46 BORDES 03	THEO
4.20 $\pm$ 0.09	47 CORCELLA 03	THEO
4.33 $\pm$ 0.10	48 DEDIVITIIS 03	LATT
4.24 $\pm$ 0.10	49 EIDEMULLER 03	THEO
4.207 $\pm$ 0.03	50 ERLER 03	THEO
4.33 $\pm$ 0.06 $\pm$ 0.10	51 MAHMOOD 03	CLEO
4.190 $\pm$ 0.032	52 BRAMBILLA 02	THEO
4.346 $\pm$ 0.070	53 PENIN 02	THEO

- NARISON 20 determines the quark mass using QCD Laplace sum rules from the  $B_c$  mass, combined with previous determinations of the QCD condensates and  $c$  and  $b$  masses.
- ABRAMOWICZ 18 determine  $\overline{m}_b(\overline{m}_b) = 4.049^{+0.104+0.090+0.001}_{-0.109-0.032-0.031}$  from the production of  $b$  quarks in  $e p$  collisions at HERA using combined H1 and ZEUS data. The experimental/fitting errors, and those from modeling and parameterization have been combined in quadrature.
- BAZAVOV 18 determine the  $b$  mass using a lattice computation with staggered fermions and five active quark flavors.
- PESET 18 determine  $\overline{m}_c(\overline{m}_c)$  and  $\overline{m}_b(\overline{m}_b)$  using an N3LO calculation of the  $\eta_c, \eta_b$  and  $B_c$  masses.
- KIYO 16 determine  $\overline{m}_b(\overline{m}_b)$  from the  $\Upsilon(1S)$  mass at order  $\alpha_s^3$  (N3LO).
- ALBERTI 15 determine  $\overline{m}_b(\overline{m}_b)$  from fits to inclusive  $B \rightarrow X_c e \overline{\nu}$  decay. They also find  $m_b^{\text{kin}}(1 \text{ GeV}) = 4.553 \pm 0.020 \text{ GeV}$ .
- BENEKE 15 determine  $\overline{m}_b(\overline{m}_b)$  using sum rules for  $e^+ e^- \rightarrow$  hadrons at order N3LO including finite  $m_c$  effects. They find  $m_b^{\overline{MS}}(2 \text{ GeV}) = 4.532^{+0.013}_{-0.039} \text{ GeV}$ , and  $\overline{m}_b(\overline{m}_b) = 4.193^{+0.022}_{-0.035} \text{ GeV}$ . The value quoted is obtained using the four-loop conversion given in BENEKE 16.
- COLQUHOUN 15 determine  $\overline{m}_b(\overline{m}_b)$  from moments of the vector current correlator computed with a lattice simulation using the NRQCD action.
- DEHNADI 15 determine  $\overline{m}_b(\overline{m}_b)$  using sum rules for  $e^+ e^- \rightarrow$  hadrons at order  $\alpha_s^3$  (N3LO), and fitting to both experimental data and lattice results.
- BERNARDONI 14 determine  $m_b$  from  $N_f = 2$  lattice calculations using heavy quark effective theory non-perturbatively renormalized and matched to QCD at  $1/m$  order.
- PENIN 14 determine  $\overline{m}_b(\overline{m}_b) = 4.169 \pm 0.008 \pm 0.002 \pm 0.002$  using an estimate of the order  $\alpha_s^3$   $b$ -quark vacuum polarization function in the threshold region, including finite  $m_c$  effects. The errors of  $\pm 0.008$  from theoretical uncertainties, and  $\pm 0.002$  from  $\alpha_s$  have been combined in quadrature.
- LEE 13o determines  $m_b$  using lattice calculations of the  $\Upsilon$  and  $B_s$  binding energies in NRQCD, including three light dynamical quark flavors. The quark mass shift in NRQCD is determined to order  $\alpha_s^2$ , with partial  $\alpha_s^3$  contributions.
- LUCHA 13 determines  $m_b$  from QCD sum rules for heavy-light currents using the lattice value for  $f_B$  of  $191.5 \pm 7.3 \text{ GeV}$ .
- BODENSTEIN 12 determine  $m_b$  using sum rules for the vector current correlator and the  $e^+ e^- \rightarrow Q \overline{Q}$  total cross-section.
- DIMOPOULOS 12 determine quark masses from a lattice computation using  $N_f = 2$  dynamical flavors of twisted mass fermions.
- LASCHKA 11 determine the  $b$  mass from the charmonium spectrum. The theoretical computation uses the heavy  $Q \overline{Q}$  potential to order  $1/m_Q$  obtained by matching the short-distance perturbative result onto lattice QCD result at larger scales.
- AUBERT 10A determine the  $b$ - and  $c$ -quark masses from a fit to the inclusive decay spectra in semileptonic  $B$  decays in the kinetic scheme (and convert it to the  $\overline{MS}$  scheme).
- CHETYRKIN 09 determine  $m_c$  and  $m_b$  from the  $e^+ e^- \rightarrow Q \overline{Q}$  cross-section and sum rules, using an order  $\alpha_s^3$  (N3LO) computation of the heavy quark vacuum polarization.
- SCHWANDA 08 measure moments of the inclusive photon spectrum in  $B \rightarrow X_s \gamma$  decay to determine  $m_b^1 S$ . We have converted this to  $\overline{MS}$  scheme.
- NARISON 18A determines  $\overline{m}_b(\overline{m}_b)$  as a function of  $\alpha_s$  using QCD exponential sum rules and their ratios evaluated at the optimal scale  $\mu = 9.5 \text{ GeV}$  at N2LO-N3LO of perturbative QCD and including condensates up to dimension 6–8 in the (axial-)vector and (pseudo-)scalar bottomonium channels.
- NARISON 18B determines  $\overline{m}_b(\overline{m}_b)$  using QCD vector moment sum rules and their ratios at N2LO-N3LO of perturbative QCD and including condensates up to dimension 8.
- ABRAMOWICZ 14A determine  $\overline{m}_b(\overline{m}_b) = 4.07 \pm 0.14^{+0.01+0.05+0.08}_{-0.07-0.00-0.05}$  from the production of  $b$  quarks in  $e p$  collisions at HERA. The errors due to fitting, modeling, PDF parameterization, and theoretical QCD uncertainties due to the values of  $\alpha_s, m_c$ , and the renormalization scale  $\mu$  have been combined in quadrature.
- AYALA 14A determine  $\overline{m}_b(\overline{m}_b)$  from the  $\Upsilon(1S)$  mass computed to N3LO order in perturbation theory using a renormalon subtracted scheme.
- NARISON 13 determines  $m_b$  using QCD spectral sum rules to order  $\alpha_s^2$  (NNLO) and including condensates up to dimension 6.
- NARISON 13A determines  $m_b$  using HQET sum rules to order  $\alpha_s^2$  (NNLO) and the  $B$  meson mass and decay constant.
- HOANG 12 determine  $m_b$  using non-relativistic sum rules for the  $\Upsilon$  system at order  $\alpha_s^2$  (NNLO) with renormalization group improvement.
- NARISON 12 determines  $m_b$  using exponential sum rules for the vector current correlator to order  $\alpha_s^3$ , including the effect of gluon condensates up to dimension eight.
- Determines  $m_b$  to order  $\alpha_s^3$  (N3LO), including the effect of gluon condensates up to dimension eight combining the methods of NARISON 12 and NARISON 12A.
- NARISON 12A determines  $m_b$  using sum rules for the vector current correlator to order  $\alpha_s^3$ , including the effect of gluon condensates up to dimension eight.

# Quark Particle Listings

## b, t

- 30 MCNEILE 10 determines  $m_b$  by comparing order  $\alpha_s^3$  (N3LO) perturbative results for the pseudo-scalar current to lattice simulations with  $N_f = 2+1$  sea-quarks by the HPQCD collaboration.
- 31 NARISON 10 determines  $m_b$  from ratios of moments of vector current correlators computed to order  $\alpha_s^2$  and including the dimension-six gluon condensate. These values are taken from the erratum to that reference.
- 32 ABDALLAH 08d determine  $\overline{m}_b(M_Z) = 3.76 \pm 1.0$  GeV from a leading order study of four-jet rates at LEP.
- 33 GUAZZINI 08 determine  $\overline{m}_b(\overline{m}_b)$  from a quenched lattice simulation of heavy meson masses. The  $\pm 0.08$  is an estimate of the quenching error.
- 34 DELLA-MORTE 07 determine  $\overline{m}_b(\overline{m}_b)$  from a computation of the spin-averaged  $B$  meson mass using quenched lattice HQET at order  $1/m$ . The  $\pm 0.08$  is an estimate of the quenching error.
- 35 KUHN 07 determine  $\overline{m}_b(\mu = 10 \text{ GeV}) = 3.609 \pm 0.025$  GeV and  $\overline{m}_b(\overline{m}_b)$  from a four-loop sum-rule computation of the cross-section for  $e^+e^- \rightarrow$  hadrons in the bottom threshold region.
- 36 ABDALLAH 06d determine  $m_b(M_Z) = 2.85 \pm 0.32$  GeV from  $Z$ -decay three-jet events containing a  $b$ -quark.
- 37 BOUGHEZAL 06  $\overline{MS}$  scheme result comes from the first moment of the hadronic production cross-section to order  $\alpha_s^3$ .
- 38 BUCHMUELLER 06 determine  $m_b$  and  $m_c$  by a global fit to inclusive  $B$  decay spectra.
- 39 PINEDA 06  $\overline{MS}$  scheme result comes from a partial NNLL evaluation (complete at order  $\alpha_s^2$  (NNLO)) of sum rules of the bottom production cross-section in  $e^+e^-$  annihilation.
- 40 GRAY 05 determines  $\overline{m}_b(\overline{m}_b)$  from a lattice computation of the  $\Upsilon$  spectrum. The simulations have  $2+1$  dynamical light flavors. The  $b$  quark is implemented using NRQCD.
- 41 AUBERT 04x obtain  $m_b$  from a fit to the hadron mass and lepton energy distributions in semileptonic  $B$  decay. The paper quotes values in the kinetic scheme. The  $\overline{MS}$  value has been provided by the BABAR collaboration.
- 42 BAUER 04 determine  $m_b$ ,  $m_c$  and  $m_b - m_c$  by a global fit to inclusive  $B$  decay spectra.
- 43 HOANG 04 determines  $\overline{m}_b(\overline{m}_b)$  from moments at order  $\alpha_s^2$  of the bottom production cross-section in  $e^+e^-$  annihilation.
- 44 MCNEILE 04 use lattice QCD with dynamical light quarks and a static heavy quark to compute the masses of heavy-light mesons.
- 45 BAUER 03 determine the  $b$  quark mass by a global fit to  $B$  decay observables. The experimental data includes lepton energy and hadron invariant mass moments in semileptonic  $B \rightarrow X_c \ell \nu_\ell$  decay, and the inclusive photon spectrum in  $B \rightarrow X_s \gamma$  decay. The theoretical expressions used are of order  $1/m^3$ , and  $\alpha_s^2 \beta_0$ .
- 46 BORDES 03 determines  $m_b$  using QCD finite energy sum rules to order  $\alpha_s^2$ .
- 47 CORCELLA 03 determines  $\overline{m}_b$  using sum rules computed to order  $\alpha_s^2$ . Includes charm quark mass effects.
- 48 DEDIVITIIS 03 use a quenched lattice computation of heavy-heavy and heavy-light meson masses.
- 49 EIDEMULLER 03 determines  $\overline{m}_b$  and  $\overline{m}_c$  using QCD sum rules.
- 50 ERLER 03 determines  $\overline{m}_b$  and  $\overline{m}_c$  using QCD sum rules. Includes recent BES data.
- 51 MAHMOOD 03 determines  $m_b^{1S}$  by a fit to the lepton energy moments in  $B \rightarrow X_c \ell \nu_\ell$  decay. The theoretical expressions used are of order  $1/m^3$  and  $\alpha_s^2 \beta_0$ . We have converted their result to the  $\overline{MS}$  scheme.
- 52 BRAMBILLA 02 determine  $\overline{m}_b(\overline{m}_b)$  from a computation of the  $\Upsilon(1S)$  mass to order  $\alpha_s^4$ , including finite  $m_c$  corrections.
- 53 PENIN 02 determines  $\overline{m}_b$  from the spectrum of the  $\Upsilon$  system.



### $m_b/m_s$ MASS RATIO

VALUE	DOCUMENT ID	TECN
<b>53.94 ± 0.12</b>	1 BAZAVOV	18 LATT

1 BAZAVOV 18 determine the quark masses using a lattice computation with staggered fermions and four active quark flavors for the  $u, d, s, c$  quarks and five active flavors for the  $b$  quark.

## b-QUARK REFERENCES

NARISON	20	PL B802 135221	S. Narison	(MONP)
ABRAMOWICZ	18	EPJ C78 473	H. Abramowicz et al.	(HI and ZEUS Collabs.)
BAZAVOV	18	PR D98 054517	A. Bazavov et al.	(Fermilab Lattice, MILC, TUMQCD)
NARISON	18A	IJMP A33 1850045	S. Narison	(MONP)
NARISON	18B	PL B784 261	S. Narison	(MONP)
PESET	18	JHEP 1809 167	C. Peset, A. Pineda, J. Segovia	(BARC, MUNT)
BENEKE	16	PoS RADCOR2015 035	M. Beneke et al.	
KIYO	16	PL B752 122	Y. Kiyo, G. Mishima, Y. Sumino	
ALBERTI	15	PRL 114 061802	A. Alberti et al.	
BENEKE	15	NP B591 42	M. Beneke et al.	
COLQUHOUN	15	PR D91 074514	B. Colquhoun et al.	(HPQCD Collab.)
DEHNADI	15	JHEP 1508 155	B. Dehnadi, A.H. Hoang, V. Mateu	
ABRAMOWICZ	14A	JHEP 1409 127	H. Abramowicz et al.	(ZEUS Collab.)
AYALA	14A	JHEP 1409 045	C. Ayala, G. Cvetič, A. Pineda	
BERNARDONI	14	PL B730 171	F. Bernardoni et al.	(ALPHA Collab.)
PENIN	14	JHEP 1404 120	A.A. Penin, N. Zerb	
LEE	13O	PR D87 074018	A.J. Lee et al.	(HPQCD Collab.)
LUCHA	13	PR D88 056011	W. Lucha, D. Melikhov, S. Simuta	(WIEN, MOSU+)
NARISON	13	PL B718 1321	S. Narison	(MONP)
NARISON	13A	PL B721 269	S. Narison	(MONP)
BODENSTEIN	12	PR D85 034003	S. Bodenstein et al.	(CAPE, VALE, MANZ+)
DIMOPOLU...	12	JHEP 1201 046	P. Dimopoulos et al.	(ETM Collab.)
HOANG	12	JHEP 1210 188	A.H. Hoang, P. Ruiz-Femenia, M. Stahlhofen	(WIEN+)
NARISON	12	PL B707 259	S. Narison	(MONP)
NARISON	12A	PL B706 412	S. Narison	(MONP)
LASCHKA	11	PR D83 094002	A. Laschka, N. Kaiser, W. Weise	
AUBERT	10A	PR D81 032003	B. Aubert et al.	(BABAR Collab.)
MCNEILE	10	PR D82 034512	C. McNeile et al.	(HPQCD Collab.)
NARISON	10	PL B693 559	S. Narison	(MONP)
Also		PL B705 544 (errat.)	S. Narison	(MONP)
CHETYRKIN	09	PR D80 074010	K.G. Chetyrkin et al.	(KARL, BNL)
ABDALLAH	08D	EPJ C55 525	J. Abdallah et al.	(DELPHI Collab.)
GUAZZINI	08	JHEP 0801 076	D. Guazzini, R. Sommer, N. Tantalo	
SCHWANDA	08	PR D78 032016	C. Schwanda et al.	(BELLE Collab.)
DELLA-MOR...	07	JHEP 0701 007	M. Della Morte et al.	
KUHN	07	NP B778 192	J.H. Kuhn, M. Steinhauser, C. Sturm	
ABDALLAH	06D	EPJ C46 569	J. Abdallah et al.	(DELPHI Collab.)
BOUGHEZAL	06	PR D74 074006	R. Boughezal, M. Czakon, T. Schutzmeier	
BUCHMUELL...	06	PR D73 073008	O.L. Buchmuller, H.U. Flacher	(RHBL)
PINEDA	06	PR D73 111501	A. Pineda, A. Signer	
GRAY	05	PR D72 094507	A. Gray et al.	(HPQCD and UKQCD Collab.)
AUBERT	04X	PRL 93 013803	B. Aubert et al.	(BABAR Collab.)
BAUER	04	PR D70 094017	C. Bauer et al.	
HOANG	04	PL B594 127	A.H. Hoang, M. Jamin	
MCNEILE	04	PL B600 77	C. McNeile, C. Michael, G. Thompson	(UKQCD Collab.)
BAUER	03	PR D67 054012	C.W. Bauer et al.	
BORDES	03	PL B562 81	J. Bordes, J. Penarrocha, K. Schilcher	
CORCELLA	03	PL B554 133	G. Corcella, A.H. Hoang	
DEDIVITIIS	03	NP B675 309	G.M. de Divitiis et al.	
EIDEMULLER	03	PR D67 113002	M. Eidemuller	
ERLER	03	PL B558 125	J. Erler, M. Luo	
MAHMOOD	03	PR D67 072001	A.H. Mahmood et al.	(CLEO Collab.)
BRAMBILLA	02	PR D65 034001	N. Brambilla, Y. Sumino, A. Vairo	
PENIN	02	PL B538 335	A. Penin, M. Steinhauser	



$$I(J^P) = 0(\frac{1}{2}^+)$$

$$\text{Charge} = \frac{2}{3} e \quad \text{Top} = +1$$

See the related review(s):

Top Quark

## t-QUARK MASS

We first list the direct measurements of the top quark mass which employ the event kinematics and then list the measurements which extract a top quark mass from the measured  $t\bar{t}$  cross-section using theory calculations. A discussion of the definition of the top quark mass in these measurements can be found in the review "The Top Quark."

For earlier search limits see PDG 96, Physical Review **D54** 1 (1996). We no longer include a compilation of indirect top mass determinations from Standard Model Electroweak fits in the Listings (our last compilation can be found in the Listings of the 2007 partial update). For a discussion of current results see the reviews "The Top Quark" and "Electroweak Model and Constraints on New Physics."

### t-Quark Mass (Direct Measurements)

The following measurements extract a  $t$ -quark mass from the kinematics of  $t\bar{t}$  events. They are sensitive to the top quark mass used in the MC generator that is usually interpreted as the pole mass, but the theoretical uncertainty in this interpretation is hard to quantify. See the review "The Top Quark" and references therein for more information.

OUR AVERAGE of  $172.76 \pm 0.30$  GeV is an average of top mass measurements from LHC and Tevatron Runs. The latest Tevatron average,  $174.30 \pm 0.35 \pm 0.54$  GeV, was provided by the Tevatron Electroweak Working Group (TEVEWWG).

VALUE (GeV)	DOCUMENT ID	TECN	COMMENT
<b>172.76 ± 0.30 OUR AVERAGE</b>			Error includes scale factor of 1.2.
172.69 ± 0.25 ± 0.41	1 AABOUD	19AC ATLAS	7, 8 TeV ATLAS combination
172.26 ± 0.07 ± 0.61	2 SIRUNYAN	19AP CMS	lepton+jets, all-jets channels
172.33 ± 0.14 ± 0.66	3 SIRUNYAN	19AR CMS	dilepton channel ( $e\mu, 2e, 2\mu$ )
			0.72
172.95 ± 0.77 ± 0.97	4 SIRUNYAN	17L CMS	$t$ -channel single top production
			0.93
172.44 ± 0.13 ± 0.47	5 KHACHATRY...	16AK CMS	7, 8 TeV CMS combination
174.30 ± 0.35 ± 0.54	6 TEVEWWG	16 TEVA	Tevatron combination

• • • We do not use the following data for averages, fits, limits, etc. • • •

172.08 ± 0.39 ± 0.82	7	AABOUD	19AC	ATLS	$\ell + \geq 4j$ ( $2b$ )
172.34 ± 0.20 ± 0.70	8	SIRUNYAN	19AP	CMS	$\geq 6$ jets ( $\geq 2b$ )
172.25 ± 0.08 ± 0.62	9	SIRUNYAN	18DE	CMS	$\ell + \geq 4j$ ( $2b$ )
173.72 ± 0.55 ± 1.01	10	AABOUD	17AH	ATLS	$\geq 5$ jets ( $2b$ )
174.95 ± 0.40 ± 0.64	11	ABAZOV	17B	D0	$\ell +$ jets and dilepton channels
170.8 ± 9.0	12	SIRUNYAN	17N	CMS	jet mass in highly-boosted $t\bar{T}$ events
172.22 ± 0.18 ± 0.89 0.93	13	SIRUNYAN	17O	CMS	Dilepton channel
172.99 ± 0.41 ± 0.74	14	AABOUD	16T	ATLS	dilepton channel
172.84 ± 0.34 ± 0.61	15	AABOUD	16T	ATLS	combination of ATLAS
173.32 ± 1.36 ± 0.85	16	ABAZOV	16	D0	$\ell\ell + \cancel{E}_T + \geq 2j$ ( $\geq 2b$ )
173.93 ± 1.61 ± 0.88	17	ABAZOV	16D	D0	$\ell\ell + \cancel{E}_T + \geq 2j$ ( $\geq 2b$ )
172.35 ± 0.16 ± 0.48	18,19	KHACHATRYAN	16AK	CMS	$\ell + \geq 4j$ ( $2b$ )
172.32 ± 0.25 ± 0.59	18,19	KHACHATRYAN	16AK	CMS	$\geq 6$ jets ( $2b$ )
172.82 ± 0.19 ± 1.22	18,20	KHACHATRYAN	16AK	CMS	$(ee/\mu\mu) + \cancel{E}_T + \geq 2b, e\mu + \geq 2b$
173.68 ± 0.20 ± 1.58 0.97	21	KHACHATRYAN	16AL	CMS	semi- + di-leptonic channels
173.5 ± 3.0 ± 0.9	22	KHACHATRYAN	16CB	CMS	$t \rightarrow (W \rightarrow \ell\nu)(b \rightarrow J/\psi X \rightarrow \mu^+\mu^-X)$ small $\cancel{E}_T, \geq 6$ jets ( $2b$ -tag)
175.1 ± 1.4 ± 1.2	23	AAD	15AW	ATLS	$\ell +$ jets and dilepton
172.99 ± 0.48 ± 0.78	24	AAD	15BF	ATLS	$\ell + \cancel{E}_T + \geq 2j$
171.5 ± 1.9 ± 2.5	25	AALTONEN	15D	CDF	small $\cancel{E}_T, 6-8$ jets ( $\geq 1b$ -tag)
175.07 ± 1.19 ± 1.55 1.58	26	AALTONEN	14N	CDF	$\ell + \cancel{E}_T + 4$ jets ( $\geq 1b$ -tag)
174.98 ± 0.58 ± 0.49	27	ABAZOV	14C	D0	$\geq 6$ jets ( $\geq 2b$ -tag)
173.49 ± 0.69 ± 1.21	28	CHATRCHYAN	14AC	CMS	$\cancel{E}_T + \geq 4$ jets ( $\geq 1b$ )
173.93 ± 1.64 ± 0.87	29	AALTONEN	13H	CDF	$\ell + \cancel{E}_T + \geq 2b$ -tag (MT2( $T$ ))
173.9 ± 0.9 ± 1.7 2.1	30	CHATRCHYAN	13S	CMS	$\ell + \cancel{E}_T + \geq 4$ jets ( $\geq 1b$ ), MT
174.5 ± 0.6 ± 2.3	31	AAD	12I	ATLS	$\ell + \cancel{E}_T + \geq 4j$ (0,1,2 <b>b</b> ) template
172.85 ± 0.71 ± 0.85	32	AALTONEN	12AI	CDF	$\tau_h + \cancel{E}_T + 4j$ ( $\geq 1b$ )
172.7 ± 9.3 ± 3.7	33	AALTONEN	12AL	CDF	CDF, D0 combination
173.18 ± 0.56 ± 0.75	34	AALTONEN	12AP	TEVA	6-8 jets with $\geq 1b$
172.5 ± 1.4 ± 1.5	35	AALTONEN	12G	CDF	$\ell + \cancel{E}_T + \geq 2j$ ( $\nu$ WT)
173.7 ± 2.8 ± 1.5	36	ABAZOV	12AB	D0	$\ell\ell + \cancel{E}_T + \geq 2j$ ( $\nu$ WT+MWT)
173.9 ± 1.9 ± 1.6	37	ABAZOV	12AB	D0	$\ell\ell + \cancel{E}_T + \geq 2j$ ( $\geq 1b$ ), AMWT
172.5 ± 0.4 ± 1.5	38	CHATRCHYAN	12BA	CMS	$\ell + \cancel{E}_T + \geq 4j$ ( $\geq 2b$ )
173.49 ± 0.43 ± 0.98	39	CHATRCHYAN	12BP	CMS	$\ell + \cancel{E}_T + 4$ jets ( $\geq 1b$ -tag)
172.4 ± 1.4 ± 1.3	40	AALTONEN	11AC	CDF	Repl. by AALTONEN 13H
172.3 ± 2.4 ± 1.0	41	AALTONEN	11AK	CDF	$\ell +$ jets and dilepton
172.1 ± 1.1 ± 0.9	42	AALTONEN	11E	CDF	$\ell + \cancel{E}_T + 4$ jets ( $\geq 1b$ -tag), $p_T(\ell)$ shape
176.9 ± 8.0 ± 2.7	43	AALTONEN	11T	CDF	$\ell + \cancel{E}_T + 4$ jets ( $\geq 1b$ -tag)
174.94 ± 0.83 ± 1.24	44	ABAZOV	11P	D0	dilepton + $\cancel{E}_T + \geq 2$ jets
174.0 ± 1.8 ± 2.4	45	ABAZOV	11R	D0	dilepton + $\cancel{E}_T$ + jets
175.5 ± 4.6 ± 4.6	46	CHATRCHYAN	11F	CMS	$\ell + \cancel{E}_T + 4$ jets ( $\geq 1b$ -tag), ME method
173.0 ± 0.9 ± 0.9	47	AALTONEN	10AE	CDF	dilepton + $b$ -tag (MT2+NWA)
169.3 ± 2.7 ± 3.2	48	AALTONEN	10C	CDF	$\ell + \cancel{E}_T + 4$ jets ( $b$ -tag)
170.7 ± 6.3 ± 2.6	49	AALTONEN	10D	CDF	$\geq 6$ jets, vtx $b$ -tag
174.8 ± 2.4 ± 1.2 1.0	50	AALTONEN	10E	CDF	$\ell + \cancel{E}_T +$ jets (soft $\mu$ $b$ -tag)
180.5 ± 12.0 ± 3.6	51	AALTONEN	09AK	CDF	$\ell + \cancel{E}_T + 4$ jets ( $b$ -tag)
172.7 ± 1.8 ± 1.2	52	AALTONEN	09J	CDF	6 jets, vtx $b$ -tag
171.1 ± 3.7 ± 2.1	53	AALTONEN	09K	CDF	$\ell +$ jets, $\ell\ell +$ jets
171.9 ± 1.7 ± 1.1	54	AALTONEN	09L	CDF	dilepton
171.2 ± 2.7 ± 2.9	55	AALTONEN	09O	CDF	$\ell\ell + \cancel{E}_T$ ( $\nu\phi$ weighting)
165.5 ± 3.4 ± 3.1 3.3	56	AALTONEN	09X	CDF	dilepton + $b$ -tag ( $\nu$ WT+MWT)
174.7 ± 4.4 ± 2.0	57	ABAZOV	09AH	D0	dilepton, $\sigma_{t\bar{t}}$ constrained
170.7 ± 4.2 ± 3.5 3.9	58,59	AALTONEN	08C	CDF	$\ell + \cancel{E}_T + 4$ jets
171.5 ± 1.8 ± 1.1	60	ABAZOV	08AH	D0	6 jets with $\geq 1b$ vtx
177.1 ± 4.9 ± 4.7	61,62	AALTONEN	07C	CDF	$\geq 4$ jets ( $b$ -tag)
172.3 ± 10.8 ± 9.6	63	AALTONEN	07B	CDF	$\geq 6$ jets, vtx $b$ -tag
174.0 ± 2.2 ± 4.8	64	AALTONEN	07D	CDF	lepton + jets ( $b$ -tag)
170.8 ± 2.2 ± 1.4	65,66	AALTONEN	07I	CDF	lepton + jets
173.7 ± 4.4 ± 2.1 2.0	62,67	ABAZOV	07F	D0	dilepton (MWT)
176.2 ± 9.2 ± 3.9	68	ABAZOV	07W	D0	dilepton ( $\nu$ WT)
179.5 ± 7.4 ± 5.6	68	ABAZOV	07W	D0	dilepton
164.5 ± 3.9 ± 3.9	66,69	ABULENCIA	07D	CDF	lepton + jets
180.7 ± 15.5 ± 13.4	70	ABULENCIA	07J	CDF	lepton + jets ( $b$ -tag)
170.3 ± 4.1 ± 1.2 4.5 - 1.8	66,71	ABAZOV	06U	D0	lepton + jets
173.2 ± 2.6 ± 3.2 2.4	72,73	ABULENCIA	06D	CDF	lepton + jets
173.5 ± 3.7 ± 3.6	59,72	ABULENCIA	06D	CDF	dilepton
165.2 ± 6.1 ± 3.4	66,74	ABULENCIA	06G	CDF	dilepton
170.1 ± 6.0 ± 4.1	59,75	ABULENCIA	06V	CDF	6 or more jets
178.5 ± 13.7 ± 7.7	76,77	ABAZOV	05	D0	lepton + jets
180.1 ± 3.6 ± 3.9	78,79	ABAZOV	04G	D0	lepton + jets
176.1 ± 5.1 ± 5.3	80	AFFOLDER	01	CDF	dilepton, lepton+jets, all-jets
176.1 ± 6.6	81	AFFOLDER	01	CDF	di-lepton, lepton+jets
172.1 ± 5.2 ± 4.9	82	ABBOTT	99G	D0	dilepton, lepton+jets, all-jets
176.0 ± 6.5	83,84	ABE	99B	CDF	dilepton
167.4 ± 10.3 ± 4.8	84,85	ABE	99B	CDF	dilepton

168.4 ± 12.3 ± 3.6	79	ABBOTT	98D	D0	dilepton
173.3 ± 5.6 ± 5.5	79,86	ABBOTT	98F	D0	lepton + jets
175.9 ± 4.8 ± 5.3	85,87	ABE	98E	CDF	lepton + jets
161 ± 17 ± 10	85	ABE	98F	CDF	dilepton
172.1 ± 5.2 ± 4.9	88	BHAT	98B	RVUE	dilepton and lepton+jets
173.8 ± 5.0	89	BHAT	98B	RVUE	dilepton, lepton+jets, all-jets
173.3 ± 5.6 ± 6.2	79	ABACHI	97E	D0	lepton + jets
186 ± 10 ± 5.7	85,90	ABE	97R	CDF	6 or more jets
199 ± 19 ± 21	± 22	ABACHI	95	D0	lepton + jets
176 ± 8 ± 10	± 10	ABE	95F	CDF	lepton + $b$ -jet
174 ± 10 ± 13	± 12	ABE	94E	CDF	lepton + $b$ -jet

- 1 AABOUD 19AC is an ATLAS combination of 7 and 8 TeV top-quark mass determination in the dilepton, lepton + jets, and all jets channels.
- 2 SIRUNYAN 19AP based on 35.9 fb<sup>-1</sup> of  $pp$  data at  $\sqrt{s} = 13$  TeV. A combined measurement using the lepton+jets and all-jets channels through a single likelihood function. See SIRUNYAN 18DE and SIRUNYAN 19AP below.
- 3 SIRUNYAN 19AR based on 35.9 fb<sup>-1</sup> of  $pp$  data at  $\sqrt{s} = 13$  TeV. Obtained from a simultaneous fit of the cross section and the top quark mass in the POWHEG simulation. The cross section is used also to extract the  $\overline{MS}$  mass and the strong coupling constant for different PDF sets.
- 4 SIRUNYAN 17L based on 19.7 fb<sup>-1</sup> of  $pp$  data at  $\sqrt{s} = 8$  TeV.  $m_t$  is reconstructed from a fit to the invariant mass distribution of  $\mu\nu b$ , where  $p_T^{miss}$  and  $W$  mass constraint are used to reconstruct  $\nu$  momentum. The number of events for various contributions, except for the  $t$ -channel single top one, are fixed to the values extracted from simulation.
- 5 KHACHATRYAN 16AK based on 19.7 fb<sup>-1</sup> of  $pp$  data at  $\sqrt{s} = 8$  TeV. Combination of the three top mass measurements in KHACHATRYAN 16AK and with the CMS results at  $\sqrt{s} = 7$  TeV.
- 6 TEVEVWG 16 is the latest Tevatron average (July 2016) provided by the Tevatron Electroweak Working Group. It takes correlated uncertainties into account and has a  $\chi^2$  of 10.8 for 11 degrees of freedom.
- 7 AABOUD 19AC based on 20.2 fb<sup>-1</sup> of  $pp$  collisions at  $\sqrt{s} = 8$  TeV. Uses optimized event selection to suppress less-well-reconstructed events and template fits to determine  $m_t$  together with a global jet energy scale factor and a relative  $b$ -to-light-jet energy scale factor.
- 8 SIRUNYAN 19AP based on 35.9 fb<sup>-1</sup> of  $pp$  data at  $\sqrt{s} = 13$  TeV. A kinematical fit is applied to each event assuming the signal event topology.  $m_t$  is determined simultaneously with a jet energy scale factor (JSF). The second error represents stat.+JSF. Modeling uncertainties are larger than in the measurements at  $\sqrt{s} = 7$  and 8 TeV because of the use of new alternative color reconnection models.
- 9 SIRUNYAN 18DE based on 35.9 fb<sup>-1</sup> of  $pp$  data at  $\sqrt{s} = 13$  TeV.  $m_t$  is determined simultaneously with an overall jet energy scale factor constrained by the mass of the hadronically decayed  $W$ . Compared to the Run 1 analysis a more advanced treatment of modeling uncertainties are employed, in particular concerning color-reconnection models.
- 10 AABOUD 17AH based on 20.2 fb<sup>-1</sup> of  $pp$  data at  $\sqrt{s} = 8$  TeV. Uses template fits to the ratio of the masses of three-jets (from  $t$  candidate) and dijets (from  $W$  candidate), to suppress jet energy scale uncertainty. Large QCD background is modelled using a data-driven method.
- 11 ABZOV 17B is a combination of measurements of the top quark mass by D0 in the lepton+jets and dilepton channels, using all data collected in Run I (1992-1996) at  $\sqrt{s} = 1.8$  TeV and Run II (2001-2011) at  $\sqrt{s} = 1.96$  TeV of the Tevatron, corresponding to integrated luminosities of 0.1 fb<sup>-1</sup> and 9.7 fb<sup>-1</sup>, respectively.
- 12 SIRUNYAN 17N based on 19.7 fb<sup>-1</sup> of  $pp$  data at  $\sqrt{s} = 8$  TeV. The fully hadronic decay of a highly-boosted  $t$  is reconstructed in the  $\ell+$ jets channel and unfolded at the particle level. The sensitivity of the peak position of the  $m_{jet}$  distribution is used to test quality of the modelling by the simulation.
- 13 SIRUNYAN 17O based on 19.7 fb<sup>-1</sup> of  $pp$  data at  $\sqrt{s} = 8$  TeV. Analysis is based on the kinematical observables  $M(b\ell)$ ,  $M_{T2}$  and  $M(b\ell\nu)$ . A fit is performed to determine  $m_t$  and an overall jet energy scale factor simultaneously.
- 14 AABOUD 16T based on 20.2 fb<sup>-1</sup> of  $pp$  data at  $\sqrt{s} = 8$  TeV. The analysis is refined using the  $p_T$  and invariant mass distributions of  $\ell+$  $b$ -jet system. A combination with measurements from  $\sqrt{s} = 7$  TeV data in the dilepton and lepton+jets channels gives  $172.84 \pm 0.34 \pm 0.61$  GeV.
- 15 AABOUD 16T is an ATLAS combination of 8 TeV top-quark mass in the dilepton channel with previous measurements from  $\sqrt{s} = 7$  TeV data in the dilepton and lepton + jets channels.
- 16 ABZOV 16 based on 9.7 fb<sup>-1</sup> of data in  $p\bar{p}$  collisions at  $\sqrt{s} = 1.96$  TeV. Employs improved fit to minimize statistical errors and improved jet energy calibration, using lepton + jets mode, which reduces error of jet energy scale. Based on previous determination in ABZOV 12AB with increased integrated luminosity and improved fit and calibrations.
- 17 ABZOV 16D based on 9.7 fb<sup>-1</sup> of data in  $p\bar{p}$  collisions at  $\sqrt{s} = 1.96$  TeV, using the matrix element technique. Based on previous determination in ABZOV 11R with increased integrated luminosity. There is a strong correlation with the determination in ABZOV 16. (See ABZOV 17B.)
- 18 KHACHATRYAN 16AK based on 19.7 fb<sup>-1</sup> of  $pp$  data at  $\sqrt{s} = 8$  TeV. Combination of the three top mass measurements in KHACHATRYAN 16AK and with the CMS results at  $\sqrt{s} = 7$  TeV gives  $172.44 \pm 0.13 \pm 0.47$  GeV.
- 19 The top mass and jet energy scale factor are determined by a fit.
- 20 Uses the analytical matrix weighting technique method.
- 21 KHACHATRYAN 16AL based on 19.7 fb<sup>-1</sup> in  $pp$  collisions at  $\sqrt{s} = 8$  TeV. Determined from the invariant mass distribution of leptons and reconstructed secondary vertices from  $b$  decays using only charged particles. The uncertainty is dominated by modeling of  $b$  fragmentation and top  $p_T$  distribution.
- 22 KHACHATRYAN 16CB based on 666 candidate reconstructed events corresponding to 19.7 fb<sup>-1</sup> of  $pp$  data at  $\sqrt{s} = 8$  TeV. The measurement exploits correlation of  $m_t$  with  $M(J/\psi b)$  in the same top quark decay, using a high-purity event sample. A study on modeling of  $b$ -quark fragmentation is given in Sec.3.3.
- 23 AAD 15AW based on 4.6 fb<sup>-1</sup> of  $pp$  data at  $\sqrt{s} = 7$  TeV. Uses template fits to the ratio of the masses of three-jets (from  $t$  candidate) and dijets (from  $W$  candidate). Large background from multijet production is modeled with data-driven methods.
- 24 AAD 15BF based on 4.6 fb<sup>-1</sup> in  $pp$  collisions at  $\sqrt{s} = 7$  TeV. Using a three-dimensional template likelihood technique the lepton plus jets ( $\geq 1b$ -tagged) channel gives  $172.33 \pm 0.75 \pm 1.02$  GeV, while exploiting a one dimensional template method using  $m_{\ell b}$  the dilepton channel (1 or 2**b**-tags) gives  $173.79 \pm 0.54 \pm 1.30$  GeV. The results are combined.

## Quark Particle Listings

t

- 25 AALTONEN 15D based on  $9.1 \text{ fb}^{-1}$  of  $p\bar{p}$  data at  $\sqrt{s} = 1.96 \text{ TeV}$ . Uses a template technique to fit a distribution of a variable defined by a linear combination of variables sensitive and insensitive to jet energy scale to optimize reduction of systematic errors.  $b$ -tagged and non- $b$ -tagged events are separately analyzed and combined.
- 26 Based on  $9.3 \text{ fb}^{-1}$  of  $p\bar{p}$  data at  $\sqrt{s} = 1.96 \text{ TeV}$ . Multivariate algorithm is used to discriminate signal from backgrounds, and templates are used to measure  $m_t$ .
- 27 Based on  $9.7 \text{ fb}^{-1}$  of  $p\bar{p}$  data at  $\sqrt{s} = 1.96 \text{ TeV}$ . A matrix element method is used to calculate the probability of an event to be signal or background, and the overall jet energy scale is constrained *in situ* by  $m_W$ . See ABAZOV 15G for further details.
- 28 Based on  $3.54 \text{ fb}^{-1}$  of  $pp$  data at  $\sqrt{s} = 7 \text{ TeV}$ . The mass is reconstructed for each event employing a kinematic fit of the jets to a ttbar hypothesis. The combination with the previous CMS measurements in the dilepton and the lepton+jets channels gives  $173.54 \pm 0.33 \pm 0.96 \text{ GeV}$ .
- 29 Based on  $8.7 \text{ fb}^{-1}$  in  $p\bar{p}$  collisions at  $\sqrt{s} = 1.96 \text{ TeV}$ . Events with an identified charged lepton or small  $E_T$  are rejected from the event sample, so that the measurement is statistically independent from those in the  $\ell + \text{jets}$  and all hadronic channels while being sensitive to those events with a  $\tau$  lepton in the final state.
- 30 Based on  $5.0 \text{ fb}^{-1}$  of  $pp$  data at  $\sqrt{s} = 7 \text{ TeV}$ . CHATRCHYAN 13s studied events with di-lepton +  $E_T + \geq 2$   $b$ -jets, and looked for kinematical endpoints of MT2, MT2 $_T$ , and subsystem variables.
- 31 AAD 12i based on  $1.04 \text{ fb}^{-1}$  of  $pp$  data at  $\sqrt{s} = 7 \text{ TeV}$ . Uses 2d-template analysis (MT) with  $m_t$  and jet energy scale factor (JSF) from  $m_W$  mass fit.
- 32 Based on  $8.7 \text{ fb}^{-1}$  of data in  $p\bar{p}$  collisions at  $1.96 \text{ TeV}$ . The JES is calibrated by using the dijet mass from the  $W$  boson decay.
- 33 Use the ME method based on  $2.2 \text{ fb}^{-1}$  of data in  $p\bar{p}$  collisions at  $1.96 \text{ TeV}$ .
- 34 Combination based on up to  $5.8 \text{ fb}^{-1}$  of data in  $p\bar{p}$  collisions at  $1.96 \text{ TeV}$ .
- 35 Based on  $5.8 \text{ fb}^{-1}$  of data in  $p\bar{p}$  collisions at  $1.96 \text{ TeV}$  the quoted value is  $m_t = 172.5 \pm 1.4(\text{stat}) \pm 1.0(\text{JES}) \pm 1.1(\text{syst}) \text{ GeV}$ . The measurement is performed with a likelihood fit technique which simultaneously determines  $m_t$  and JES (Jet Energy Scale).
- 36 Based on  $4.3 \text{ fb}^{-1}$  of data in  $p$ - $p$ bar collisions at  $1.96 \text{ TeV}$ . The measurement reduces the JES uncertainty by using the single lepton channel study of ABAZOV 11P.
- 37 Combination with the result in  $1 \text{ fb}^{-1}$  of preceding data reported in ABAZOV 09AH as well as the MWT result of ABAZOV 11R with a statistical correlation of 60%.
- 38 Based on  $5.0 \text{ fb}^{-1}$  of  $pp$  data at  $\sqrt{s} = 7 \text{ TeV}$ . Uses an analytical matrix weighting technique (AMWT) and full kinematic analysis (KIN).
- 39 Based on  $5.0 \text{ fb}^{-1}$  of  $pp$  data at  $\sqrt{s} = 7 \text{ TeV}$ . The first error is statistical and JES combined, and the second is systematic. Ideogram method is used to obtain 2D likelihood for the kinematical fit with two parameters  $m_{top}$  and JES.
- 40 Based on  $3.2 \text{ fb}^{-1}$  in  $p\bar{p}$  collisions at  $\sqrt{s} = 1.96 \text{ TeV}$ . The first error is from statistics and JES combined, and the latter is from the other systematic uncertainties. The result is obtained using an unbinned maximum likelihood method where the top quark mass and the JES are measured simultaneously, with  $\Delta_{JES} = 0.3 \pm 0.3(\text{stat})$ .
- 41 Based on  $5.7 \text{ fb}^{-1}$  in  $p\bar{p}$  collisions at  $\sqrt{s} = 1.96 \text{ TeV}$ . Events with an identified charged lepton or small  $E_T$  are rejected from the event sample, so that the measurement is statistically independent from those in the  $\ell + \text{jets}$  and all hadronic channels while being sensitive to those events with a  $\tau$  lepton in the final state. Supersedes AALTONEN 07B.
- 42 AALTONEN 11E based on  $5.6 \text{ fb}^{-1}$  in  $p\bar{p}$  collisions at  $\sqrt{s} = 1.96 \text{ TeV}$ . Employs a multi-dimensional template likelihood technique where the lepton plus jets (one or two  $b$ -tags) channel gives  $172.2 \pm 1.2 \pm 0.9 \text{ GeV}$  while the dilepton channel yields  $170.3 \pm 2.0 \pm 3.1 \text{ GeV}$ . The results are combined. OUR EVALUATION includes the measurement in the dilepton channel only.
- 43 Uses a likelihood fit of the lepton  $p_T$  distribution based on  $2.7 \text{ fb}^{-1}$  in  $p\bar{p}$  collisions at  $\sqrt{s} = 1.96 \text{ TeV}$ .
- 44 Based on  $3.6 \text{ fb}^{-1}$  in  $p\bar{p}$  collisions at  $\sqrt{s} = 1.96 \text{ TeV}$ . ABAZOV 11P reports  $174.94 \pm 0.83 \pm 0.78 \pm 0.96 \text{ GeV}$ , where the first uncertainty is from statistics, the second from JES, and the last from other systematic uncertainties. We combine the JES and systematic uncertainties. A matrix-element method is used where the JES uncertainty is constrained by the  $W$  mass. ABAZOV 11P describes a measurement based on  $2.6 \text{ fb}^{-1}$  that is combined with ABAZOV 08AH, which employs an independent  $1 \text{ fb}^{-1}$  of data.
- 45 Based on a matrix-element method which employs  $5.4 \text{ fb}^{-1}$  in  $p\bar{p}$  collisions at  $\sqrt{s} = 1.96 \text{ TeV}$ . Superseded by ABAZOV 12AB.
- 46 Based on  $36 \text{ pb}^{-1}$  of  $pp$  collisions at  $\sqrt{s} = 7 \text{ TeV}$ . A Kinematic Method using  $b$ -tagging and an analytical Matrix Weighting Technique give consistent results and are combined. Superseded by CHATRCHYAN 12BA.
- 47 Based on  $5.6 \text{ fb}^{-1}$  in  $p\bar{p}$  collisions at  $\sqrt{s} = 1.96 \text{ TeV}$ . The likelihood calculated using a matrix element method gives  $m_t = 173.0 \pm 0.7(\text{stat}) \pm 0.6(\text{JES}) \pm 0.9(\text{syst}) \text{ GeV}$ , for a total uncertainty of  $1.2 \text{ GeV}$ .
- 48 Based on  $3.4 \text{ fb}^{-1}$  of  $p\bar{p}$  collisions at  $\sqrt{s} = 1.96 \text{ TeV}$ . The result is obtained by combining the MT2 variable method and the NWA (Neutrino Weighting Algorithm). The MT2 method alone gives  $m_t = 168.0^{+4.8}_{-4.0}(\text{stat}) \pm 2.9(\text{syst}) \text{ GeV}$  with smaller systematic error due to small JES uncertainty.
- 49 Based on  $1.9 \text{ fb}^{-1}$  in  $p\bar{p}$  collisions at  $\sqrt{s} = 1.96 \text{ TeV}$ . The result is from the measurement using the transverse decay length of  $b$ -hadrons and that using the transverse momentum of the  $W$  decay muons, which are both insensitive to the JES (jet energy scale) uncertainty. OUR EVALUATION uses only the measurement exploiting the decay length significance which yields  $166.9^{+9.5}_{-8.5}(\text{stat}) \pm 2.9(\text{syst}) \text{ GeV}$ . The measurement that uses the lepton transverse momentum is excluded from the average because of a statistical correlation with other samples.
- 50 Based on  $2.9 \text{ fb}^{-1}$  of  $p\bar{p}$  collisions at  $\sqrt{s} = 1.96 \text{ TeV}$ . The first error is from statistics and JES uncertainty, and the latter is from the other systematics. Neural-network-based kinematical selection of 6 highest  $E_T$  jets with a vtx  $b$ -tag is used to distinguish signal from background. Superseded by AALTONEN 12G.
- 51 Based on  $2 \text{ fb}^{-1}$  of data at  $\sqrt{s} = 1.96 \text{ TeV}$ . The top mass is obtained from the measurement of the invariant mass of the lepton ( $e$  or  $\mu$ ) from  $W$  decays and the soft  $\mu$  in  $b$ -jet. The result is insensitive to jet energy scaling.
- 52 Based on  $1.9 \text{ fb}^{-1}$  of data at  $\sqrt{s} = 1.96 \text{ TeV}$ . The first error is from statistics and jet energy scale uncertainty, and the latter is from the other systematics. Matrix element method with effective propagators.
- 53 Based on  $943 \text{ pb}^{-1}$  of data at  $\sqrt{s} = 1.96 \text{ TeV}$ . The first error is from statistical and jet-energy-scale uncertainties, and the latter is from other systematics. AALTONEN 09k selected 6 jet events with one or more vertex  $b$ -tags and used the tree-level matrix element to construct template models of signal and background.
- 54 Based on  $1.9 \text{ fb}^{-1}$  of data at  $\sqrt{s} = 1.96 \text{ TeV}$ . The first error is from statistical and jet-energy-scale (JES) uncertainties, and the second is from other systematics. Events with lepton + jets and those with dilepton + jets were simultaneously fit to constrain  $m_t$  and JES. Lepton + jets data only give  $m_t = 171.8 \pm 2.2 \text{ GeV}$ , and dilepton data only give  $m_t = 171.2^{+5.3}_{-5.1} \text{ GeV}$ .
- 55 Based on  $2 \text{ fb}^{-1}$  of data at  $\sqrt{s} = 1.96 \text{ TeV}$ . Matrix Element method. Optimal selection criteria for candidate events with two high  $p_T$  leptons, high  $E_T$ , and two or more jets with and without  $b$ -tag are obtained by neural network with neuroevolution technique to minimize the statistical error of  $m_t$ .
- 56 Based on  $2.9 \text{ fb}^{-1}$  of data at  $\sqrt{s} = 1.96 \text{ TeV}$ . Mass  $m_t$  is estimated from the likelihood for the eight-fold kinematical solutions in the plane of the azimuthal angles of the two neutrino momenta.
- 57 Based on  $1 \text{ fb}^{-1}$  of data at  $\sqrt{s} = 1.96 \text{ TeV}$ . Events with two identified leptons, and those with one lepton plus one isolated track and a  $b$ -tag were used to constrain  $m_t$ . The result is a combination of the  $\nu$ WT ( $\nu$  Weighting Technique) result of  $176.2 \pm 4.8 \pm 2.1 \text{ GeV}$  and the MWT (Matrix-element Weighting Technique) result of  $173.2 \pm 4.9 \pm 2.0 \text{ GeV}$ .
- 58 Reports measurement of  $170.7^{+4.2}_{-3.9} \pm 2.6 \pm 2.4 \text{ GeV}$  based on  $1.2 \text{ fb}^{-1}$  of data at  $\sqrt{s} = 1.96 \text{ TeV}$ . The last error is due to the theoretical uncertainty on  $\sigma_{t\bar{t}}$ . Without the cross-section constraint a top mass of  $169.7^{+5.2}_{-4.9} \pm 3.1 \text{ GeV}$  is obtained.
- 59 Template method.
- 60 Result is based on  $1 \text{ fb}^{-1}$  of data at  $\sqrt{s} = 1.96 \text{ TeV}$ . The first error is from statistics and jet energy scale uncertainty, and the latter is from the other systematics.
- 61 Based on  $310 \text{ pb}^{-1}$  of data at  $\sqrt{s} = 1.96 \text{ TeV}$ .
- 62 Ideogram method.
- 63 Based on  $311 \text{ pb}^{-1}$  of data at  $\sqrt{s} = 1.96 \text{ TeV}$ . Events with 4 or more jets with  $E_T > 15 \text{ GeV}$ , significant missing  $E_T$ , and secondary vertex  $b$ -tag are used in the fit. About 44% of the signal acceptance is from  $\tau\nu + 4$  jets. Events with identified  $e$  or  $\mu$  are vetoed to provide a statistically independent measurement.
- 64 Based on  $1.02 \text{ fb}^{-1}$  of data at  $\sqrt{s} = 1.96 \text{ TeV}$ . Superseded by AALTONEN 12G.
- 65 Based on  $955 \text{ pb}^{-1}$  of data at  $\sqrt{s} = 1.96 \text{ TeV}$ .  $m_t$  and JES (Jet Energy Scale) are fitted simultaneously, and the first error contains the JES contribution of  $1.5 \text{ GeV}$ .
- 66 Matrix element method.
- 67 Based on  $425 \text{ pb}^{-1}$  of data at  $\sqrt{s} = 1.96 \text{ TeV}$ . The first error is a combination of statistics and JES (Jet Energy Scale) uncertainty, which has been measured simultaneously to give  $JES = 0.989 \pm 0.029(\text{stat})$ .
- 68 Based on  $370 \text{ pb}^{-1}$  of data at  $\sqrt{s} = 1.96 \text{ TeV}$ . Combined result of MWT (Matrix-element Weighting Technique) and  $\nu$ WT ( $\nu$  Weighting Technique) analyses is  $178.1 \pm 6.7 \pm 4.8 \text{ GeV}$ .
- 69 Based on  $1.0 \text{ fb}^{-1}$  of data at  $\sqrt{s} = 1.96 \text{ TeV}$ . ABULENCIA 07D improves the matrix element description by including the effects of initial-state radiation.
- 70 Based on  $695 \text{ pb}^{-1}$  of data at  $\sqrt{s} = 1.96 \text{ TeV}$ . The transverse decay length of the  $b$  hadron is used to determine  $m_t$ , and the result is free from the JES (jet energy scale) uncertainty.
- 71 Based on  $\sim 400 \text{ pb}^{-1}$  of data at  $\sqrt{s} = 1.96 \text{ TeV}$ . The first error includes statistical and systematic jet energy scale uncertainties, the second error is from the other systematics. The result is obtained with the  $b$ -tagging information. The result without  $b$ -tagging is  $169.2^{+5.0+1.5}_{-7.4-1.4} \text{ GeV}$ . Superseded by ABAZOV 08AH.
- 72 Based on  $318 \text{ pb}^{-1}$  of data at  $\sqrt{s} = 1.96 \text{ TeV}$ .
- 73 Dynamical likelihood method.
- 74 Based on  $340 \text{ pb}^{-1}$  of data at  $\sqrt{s} = 1.96 \text{ TeV}$ .
- 75 Based on  $360 \text{ pb}^{-1}$  of data at  $\sqrt{s} = 1.96 \text{ TeV}$ .
- 76 Based on  $110.2 \pm 5.8 \text{ pb}^{-1}$  at  $\sqrt{s} = 1.8 \text{ TeV}$ .
- 77 Based on the all hadronic decays of  $t\bar{t}$  pairs. Single  $b$ -quark tagging via the decay chain  $b \rightarrow c \rightarrow \mu$  was used to select signal enriched multijet events. The result was obtained by the maximum likelihood method after bias correction.
- 78 Obtained by re-analysis of the lepton + jets candidate events that led to ABBOTT 98F. It is based upon the maximum likelihood method which makes use of the leading order matrix elements.
- 79 Based on  $125 \pm 7 \text{ pb}^{-1}$  of data at  $\sqrt{s} = 1.8 \text{ TeV}$ .
- 80 Based on  $\sim 106 \text{ pb}^{-1}$  of data at  $\sqrt{s} = 1.8 \text{ TeV}$ .
- 81 Obtained by combining the measurements in the lepton + jets [AFFOLDER 01], all-jets [ABE 97R, ABE 99B], and dilepton [ABE 99B] decay topologies.
- 82 Obtained by combining the D0 result  $m_t$  (GeV) =  $168.4 \pm 12.3 \pm 3.6$  from 6 di-lepton events (see also ABBOTT 98B) and  $m_t$  (GeV) =  $173.3 \pm 5.6 \pm 5.5$  from lepton+jets events (ABBOTT 98F).
- 83 Obtained by combining the CDF results of  $m_t$  (GeV) =  $167.4 \pm 10.3 \pm 4.8$  from 8 dilepton events,  $m_t$  (GeV) =  $175.9 \pm 4.8 \pm 5.3$  from lepton+jets events (ABE 98E), and  $m_t$  (GeV) =  $186.0 \pm 10.0 \pm 5.7$  from all-jet events (ABE 97R). The systematic errors in the latter two measurements are changed in this paper.
- 84 See AFFOLDER 01 for details of systematic error re-evaluation.
- 85 Based on  $109 \pm 7 \text{ pb}^{-1}$  of data at  $\sqrt{s} = 1.8 \text{ TeV}$ .
- 86 See ABAZOV 04G.
- 87 The updated systematic error is listed. See AFFOLDER 01, appendix C.
- 88 Obtained by combining the D0 results of  $m_t$  (GeV) =  $168.4 \pm 12.3 \pm 3.6$  from 6 dilepton events and  $m_t$  (GeV) =  $173.3 \pm 5.6 \pm 5.5$  from 77 lepton+jets events.
- 89 Obtained by combining the D0 results from dilepton and lepton+jets events, and the CDF results (ABE 99B) from dilepton, lepton+jets events, and all-jet events.
- 90 Based on the first observation of all hadronic decays of  $t\bar{t}$  pairs. Single  $b$ -quark tagging with jet-shape variable constraints was used to select signal enriched multi-jet events. The updated systematic error is listed. See AFFOLDER 01, appendix C.

## t-Quark Mass from Cross-Section Measurements

The top quark  $M\bar{S}$  or pole mass can be extracted from a measurement of  $\sigma(t\bar{t})$  by using theory calculations. We quote below the  $M\bar{S}$  mass. See the review "The Top Quark" and references therein for more information.

VALUE (GeV)	DOCUMENT ID	TECN	COMMENT
<b><math>162.5^{+2.1}_{-1.5}</math> OUR AVERAGE</b>			
$162.9 \pm 0.5 \pm 1.0^{+2.1}_{-1.2}$	1 AAD	19G ATLS	$\ell + E_{T+} \geq 5 j$ ( $2b$ -j)
$160.0^{+4.8}_{-4.3}$	2 ABAZOV	11s D0	$\sigma(t\bar{t})$ + theory
	3 ABAZOV	09AG D0	cross sects, theory + exp
	4 ABAZOV	09R D0	cross sects, theory + exp

• • • We do not use the following data for averages, fits, limits, etc. • • •

<sup>1</sup> AAD 19g based on 20.2 fb<sup>-1</sup> of data in *pp* collisions at  $\sqrt{s} = 8$  TeV. Normalized  $t\bar{t} + 1$ -jet differential cross section as a function of  $t\bar{t}j$  invariant mass is measured in the  $\ell +$  jets mode. The unfolded parton-level distribution is compared with the NLO QCD prediction. The three errors are from statistics, systematics, and theory.

<sup>2</sup> Based on 5.3 fb<sup>-1</sup> in *p* $\bar{p}$  collisions at  $\sqrt{s} = 1.96$  TeV. ABAZOV 11s uses the measured  $t\bar{t}$  production cross section of  $8.13^{+1.02}_{-0.90}$  pb [ABAZOV 11E] in the lepton plus jets channel to obtain the top quark  $\overline{MS}$  mass by using an approximate NNLO computation (MOCH 08, LANGENFELD 09). The corresponding top quark pole mass is  $167.5^{+5.4}_{-4.9}$  GeV. A different theory calculation (AHRENS 10, AHRENS 10A) is also used and yields  $m_t^{\overline{MS}} = 154.5^{+5.0}_{-4.3}$  GeV.

<sup>3</sup> Based on 1 fb<sup>-1</sup> of data at  $\sqrt{s} = 1.96$  TeV. Uses the  $\ell +$  jets,  $\ell\ell$ , and  $\ell\tau +$  jets channels. ABAZOV 09AG extract the pole mass of the top quark using two different calculations that yield  $169.1^{+5.9}_{-5.2}$  GeV (MOCH 08, LANGENFELD 09) and  $168.2^{+5.9}_{-5.4}$  GeV (KIDONAKIS 08).

<sup>4</sup> Based on 1 fb<sup>-1</sup> of data at  $\sqrt{s} = 1.96$  TeV. Uses the  $\ell\ell$  and  $\ell\tau +$  jets channels. ABAZOV 09R extract the pole mass of the top quark using two different calculations that yield  $173.3^{+9.8}_{-8.6}$  GeV (MOCH 08, LANGENFELD 09) and  $171.5^{+9.9}_{-8.8}$  GeV (CACIARI 08).

### t-Quark Pole Mass from Cross-Section Measurements

VALUE (GeV)	DOCUMENT ID	TECN	COMMENT
<b>172.4±0.7 OUR AVERAGE</b>			
171.1±0.4±0.9 <sup>+0.7</sup> <sub>-0.3</sub>	1 AAD	19G ATLS	$\ell + E_T + \geq 5 j$ (2b-j)
173.2±0.9±0.8±1.2	2 AABOUD	17bC ATLS	$e + \mu + \geq 1b$ jets
170.6±2.7	3 SIRUNYAN	17W CMS	$\ell + \geq 1j$
172.8±1.1 <sup>+3.3</sup> <sub>-3.1</sub>	4 ABAZOV	16F D0	$\ell\ell, \ell +$ jets channels
173.8±1.7 <sup>+1.8</sup> <sub>-1.8</sub>	5 KHACHATRYAN...16AW	CMS	$e + \mu + E_T + \geq 0j$
173.7±2.3 <sup>+2.1</sup> <sub>-2.1</sub>	6 AAD	15bWATLS	$\ell + E_T + \geq 5j$ (2b-tag)
172.9±2.5 <sup>+2.6</sup> <sub>-2.6</sub>	7 AAD	14AY ATLS	<i>pp</i> at $\sqrt{s} = 7, 8$ TeV
• • • We do not use the following data for averages, fits, limits, etc. • • •			
176.7±3.0 <sup>+3.0</sup> <sub>-2.8</sub>	8 CHATRCHYAN14	CMS	<i>pp</i> at $\sqrt{s} = 7$ TeV

<sup>1</sup> AAD 19g based on 20.2 fb<sup>-1</sup> of data in *pp* collisions at  $\sqrt{s} = 8$  TeV. Normalized  $t\bar{t} + 1$ -jet differential cross section as a function of  $t\bar{t}j$  invariant mass is measured in the  $\ell +$  jets mode. The unfolded parton-level distribution is compared with the NLO QCD prediction. The three errors are from statistics, systematics, and theory.

<sup>2</sup> AABOUD 17bC based on 20.2 fb<sup>-1</sup> of *pp* data at  $\sqrt{s} = 8$  TeV. The pole mass is extracted from a fit of NLO predictions to eight single lepton and dilepton differential distributions, while simultaneously constraining uncertainties due to PDFs and QCD scales. The three reported uncertainties come from statistics, experimental systematics, and theoretical sources.

<sup>3</sup> SIRUNYAN 17W based on 2.2 fb<sup>-1</sup> of *pp* data at  $\sqrt{s} = 13$  TeV. Events are categorized according to the jet multiplicity and the number of *b*-tagged jets. The pole mass is obtained from the inclusive cross section measurement and the NNLO prediction.

<sup>4</sup> ABAZOV 16F based on 9.7 fb<sup>-1</sup> of data in *p* $\bar{p}$  collisions at  $\sqrt{s} = 1.96$  TeV. The result is obtained from the inclusive cross section measurement and the NNLO+NNLL prediction.

<sup>5</sup> KHACHATRYAN 16AW based on 5.0 fb<sup>-1</sup> of *pp* collisions at 7 TeV and 19.7 fb<sup>-1</sup> at 8 TeV. The 7 TeV data include those used in CHATRCHYAN 14. The result is obtained from the inclusive cross sections.

<sup>6</sup> AAD 15bW based on 4.6 fb<sup>-1</sup> of *pp* data at  $\sqrt{s} = 7$  TeV. Uses normalized differential cross section for  $t\bar{t} + 1$  jet as a function of the inverse of the invariant mass of the  $t\bar{t} + 1$  jet system. The measured cross section is corrected to the parton level. Then a fit to the data using NLO + parton shower prediction is performed.

<sup>7</sup> AAD 14AY used  $\sigma(t\bar{t})$  for  $e\mu$  events. The result is a combination of the measurements  $m_t = 171.4 \pm 2.6$  GeV based on 4.6 fb<sup>-1</sup> of data at 7 TeV and  $m_t = 174.1 \pm 2.6$  GeV based on 20.3 fb<sup>-1</sup> of data at 8 TeV.

<sup>8</sup> CHATRCHYAN 14 used  $\sigma(t\bar{t})$  from *pp* collisions at  $\sqrt{s} = 7$  TeV measured in CHATRCHYAN 12AX to obtain  $m_t(\text{pole}) = 0.1184 \pm 0.0007$ . The errors have been corrected in KHACHATRYAN 14K.

$$m_t - m_{\bar{t}}$$

Test of *CP*T conservation. OUR AVERAGE assumes that the systematic uncertainties are uncorrelated.

VALUE (GeV)	DOCUMENT ID	TECN	COMMENT
<b>-0.16±0.19 OUR AVERAGE</b>			
-0.15±0.19±0.09	1 CHATRCHYAN17	CMS	$\ell + E_T + \geq 4j$ ( $\geq 1b$ j)
0.67±0.61±0.41	2 AAD	14 ATLS	$\ell + E_T + \geq 4j$ ( $\geq 2$ b-tags)
-1.95±1.11±0.59	3 AALTONEN	13E CDF	$\ell + E_T + \geq 4j$ (0,1,2 b-tags)
-0.44±0.46±0.27	4 CHATRCHYAN12Y	CMS	$\ell + E_T + \geq 4j$
0.8±1.8±0.5	5 ABAZOV	11T D0	$\ell + E_T + 4$ jets ( $\geq 1$ b-tag)
• • • We do not use the following data for averages, fits, limits, etc. • • •			
-3.3±1.4±1.0	6 AALTONEN	11K CDF	Repl. by AALTONEN 13E
3.8±3.4±1.2	7 ABAZOV	09AA D0	$\ell + E_T + 4$ jets ( $\geq 1$ b-tag)

<sup>1</sup> CHATRCHYAN 17 based on 19.6 fb<sup>-1</sup> of *pp* data at  $\sqrt{s} = 8$  TeV and an average top mass of  $172.84 \pm 0.10$  (stat) GeV is obtained.

<sup>2</sup> Based on 4.7 fb<sup>-1</sup> of *pp* data at  $\sqrt{s} = 7$  TeV and an average top mass of  $172.5$  GeV/c<sup>2</sup>.

<sup>3</sup> Based on 8.7 fb<sup>-1</sup> of *p* $\bar{p}$  collisions at  $\sqrt{s} = 1.96$  TeV and an average top mass of  $172.5$  GeV/c<sup>2</sup>.

<sup>4</sup> Based on 4.96 fb<sup>-1</sup> of *pp* data at  $\sqrt{s} = 7$  TeV. Based on the fitted  $m_t$  for  $\ell^+$  and  $\ell^-$  events using the Ideogram method.

<sup>5</sup> Based on a matrix-element method which employs 3.6 fb<sup>-1</sup> in *p* $\bar{p}$  collisions at  $\sqrt{s} = 1.96$  TeV.

<sup>6</sup> Based on a template likelihood technique which employs 5.6 fb<sup>-1</sup> in *p* $\bar{p}$  collisions at  $\sqrt{s} = 1.96$  TeV.

<sup>7</sup> Based on 1 fb<sup>-1</sup> of data in *p* $\bar{p}$  collisions at  $\sqrt{s} = 1.96$  TeV.

### t-quark DECAY WIDTH

VALUE (GeV)	CL%	DOCUMENT ID	TECN	COMMENT
<b>1.42±0.19 OUR AVERAGE</b>				Error includes scale factor of 1.4.
1.76±0.33 <sup>+0.79</sup> <sub>-0.68</sub>		1 AABOUD	18AZ ATLS	$\ell + E_T + \geq 4j$ ( $\geq 1$ b)
1.36±0.02 <sup>+0.14</sup> <sub>-0.11</sub>		2 KHACHATRYAN...14E	CMS	$\ell\ell + E_T + 2,4$ jets (0-2b-tag)
2.00±0.47 <sup>+0.47</sup> <sub>-0.43</sub>		3 ABAZOV	12T D0	$\Gamma(t \rightarrow bW)/\Gamma(t \rightarrow bW)$
• • • We do not use the following data for averages, fits, limits, etc. • • •				
< 6.38	95	4 AALTONEN	13Z CDF	$\ell + E_T + \geq 4j$ ( $\geq 0$ b), direct
1.99±0.69 <sup>+0.69</sup> <sub>-0.55</sub>		5 ABAZOV	11B D0	Repl. by ABAZOV 12T
> 1.21	95	5 ABAZOV	11B D0	$\Gamma(t \rightarrow Wb)$
< 7.6	95	6 AALTONEN	10AC CDF	$\ell +$ jets, direct
<13.1	95	7 AALTONEN	09M CDF	$m_t(\text{rec})$ distribution

<sup>1</sup> Based on 20.2 fb<sup>-1</sup> of *pp* data at  $\sqrt{s} = 8$  TeV.  $\Gamma_t$  is measured using a template fit to the reconstructed invariant mass of the *b*-jet of the semileptonically decaying top quark and the corresponding lepton, and the angular distance between  $j_b$  and  $j_l$  in hadronic top decay. Signal templates are generated by reweighting events at parton-level to Breit-Wigner distribution with different  $\Gamma_t$  hypotheses for  $m_t = 172.5$  GeV. The result is consistent with the NNLO SM prediction of 1.322 GeV.

<sup>2</sup> Based on 19.7 fb<sup>-1</sup> of *pp* data at  $\sqrt{s} = 8$  TeV. The result is obtained by combining the measurement of  $R = \Gamma(t \rightarrow Wb)/\Gamma(t \rightarrow Wq (q=b,s,d))$  and a previous CMS measurement of the *t*-channel single top production cross section of CHATRCHYAN 12BQ, by using the theoretical calculation of  $\Gamma(t \rightarrow Wb)$  for  $m_t = 172.5$  GeV.

<sup>3</sup> Based on 5.4 fb<sup>-1</sup> of data in *p* $\bar{p}$  collisions at 1.96 TeV.  $\Gamma(t \rightarrow bW) = 1.87^{+0.44}_{-0.40}$  GeV is obtained from the observed *t*-channel single top quark production cross section, whereas  $B(t \rightarrow bW) = 0.90 \pm 0.04$  is used assuming  $\sum_q B(t \rightarrow qW) = 1$ . The result is valid for  $m_t = 172.5$  GeV. See the paper for the values for  $m_t = 170$  or 175 GeV.

<sup>4</sup> Based on 8.7 fb<sup>-1</sup> of data. The two sided 68% CL interval is  $1.10 \text{ GeV} < \Gamma_t < 4.05$  GeV for  $m_t = 172.5$  GeV.

<sup>5</sup> Based on 2.3 fb<sup>-1</sup> in *p* $\bar{p}$  collisions at  $\sqrt{s} = 1.96$  TeV. ABAZOV 11B extracted  $\Gamma_t$  from the partial width  $\Gamma(t \rightarrow Wb) = 1.92^{+0.58}_{-0.51}$  GeV measured using the *t*-channel single top production cross section, and the branching fraction  $\text{br}(t \rightarrow Wb) = 0.962^{+0.068}_{-0.066}(\text{stat})^{+0.064}_{-0.052}(\text{syst})$ . The  $\Gamma(t \rightarrow Wb)$  measurement gives the 95% CL lowerbound of  $\Gamma(t \rightarrow Wb)$  and hence that of  $\Gamma_t$ .

<sup>6</sup> Results are based on 4.3 fb<sup>-1</sup> of data in *p* $\bar{p}$  collisions at  $\sqrt{s} = 1.96$  TeV. The top quark mass and the hadronically decaying *W* boson mass are reconstructed for each candidate events and compared with templates of different top quark width. The two sided 68% CL interval is  $0.3 \text{ GeV} < \Gamma_t < 4.4 \text{ GeV}$  for  $m_t = 172.5$  GeV.

<sup>7</sup> Based on 955 pb<sup>-1</sup> of *p* $\bar{p}$  collision data at  $\sqrt{s} = 1.96$  TeV. AALTONEN 09M selected  $t\bar{t}$  candidate events for the  $\ell + E_T +$  jets channel with one or two *b*-tags, and examine the decay width dependence of the reconstructed  $m_t$  distribution. The result is for  $m_t = 175$  GeV, whereas the upper limit is lower for smaller  $m_t$ .

### t DECAY MODES

Mode	Fraction ( $\Gamma_i/\Gamma$ )	Confidence level
$\Gamma_1$ $Wq (q = b, s, d)$		
$\Gamma_2$ $Wb$		
$\Gamma_3$ $e\nu_e b$	(11.10±0.30) %	
$\Gamma_4$ $\mu\nu_\mu b$	(11.40±0.20) %	
$\Gamma_5$ $\tau\nu_\tau b$	(11.1 ± 0.9) %	
$\Gamma_6$ $q\bar{q}b$	(66.5 ± 1.4) %	
$\Gamma_7$ $\gamma q (q=u,c)$	[a] < 1.8	$\times 10^{-4}$ 95%
$\Gamma_8$ $H^+b, H^+ \rightarrow \tau\nu_\tau$		

### $\Delta T = 1$ weak neutral current (TI) modes

Mode	TI	[b] <	Confidence level
$\Gamma_9$ $Zq (q=u,c)$	TI	< 5	$\times 10^{-4}$ 95%
$\Gamma_{10}$ $Hu$	TI	< 1.2	$\times 10^{-3}$ 95%
$\Gamma_{11}$ $Hc$	TI	< 1.1	$\times 10^{-3}$ 95%
$\Gamma_{12}$ $\ell^+ \bar{q}q' (q=d,s,b; q'=u,c)$	TI	< 1.6	$\times 10^{-3}$ 95%

[a] This limit is for  $\Gamma(t \rightarrow \gamma q)/\Gamma(t \rightarrow Wb)$ .

[b] This limit is for  $\Gamma(t \rightarrow Zq)/\Gamma(t \rightarrow Wb)$ .

### t BRANCHING RATIOS

$\Gamma(Wb)/\Gamma(Wq (q=b,s,d))$	$\Gamma_2/\Gamma_1$		
<b>0.957±0.034 OUR AVERAGE</b>			
OUR AVERAGE assumes that the systematic uncertainties are uncorrelated.			
VALUE	DOCUMENT ID	TECN	COMMENT
0.87 ± 0.07	1 AALTONEN	14G CDF	$\ell\ell + E_T + \geq 2j$ (0,1,2 b-tag)
1.014 ± 0.003 ± 0.032	2 KHACHATRYAN...14E	CMS	$\ell\ell + E_T + 2,3,4j$ (0-2b-tag)
0.94 ± 0.09	3 AALTONEN	13G CDF	$\ell + E_T + \geq 3$ jets ( $\geq 1$ b-tag)
0.90 ± 0.04	4 ABAZOV	11X D0	

Error includes scale factor of 1.5. See the ideogram below.

<sup>1</sup> AALTONEN 14G CDF  $\ell\ell + E_T + \geq 2j$  (0,1,2 b-tag)

<sup>2</sup> KHACHATRYAN...14E CMS  $\ell\ell + E_T + 2,3,4j$  (0-2b-tag)

<sup>3</sup> AALTONEN 13G CDF  $\ell + E_T + \geq 3$  jets ( $\geq 1$  b-tag)

<sup>4</sup> ABAZOV 11X D0

## Quark Particle Listings

t

• • • We do not use the following data for averages, fits, limits, etc. • • •

0.97 <sup>+0.09</sup> <sub>-0.08</sub>	5	ABAZOV	08M D0	$\ell + n$ jets with 0,1,2 b-tag
1.03 <sup>+0.19</sup> <sub>-0.17</sub>	6	ABAZOV	06k D0	
1.12 <sup>+0.21</sup> <sub>-0.19</sub> <sup>+0.17</sup> <sub>-0.13</sub>	7	ACOSTA	05A CDF	Repl. by AALTONEN 13G
0.94 <sup>+0.26</sup> <sub>-0.21</sub> <sup>+0.17</sup> <sub>-0.12</sub>	8	AFFOLDER	01c CDF	

<sup>1</sup> Based on 8.7 fb<sup>-1</sup> of data. This measurement gives  $|V_{tb}| = 0.93 \pm 0.04$  and  $|V_{tb}| > 0.85$  (95% CL) in the SM.

<sup>2</sup> Based on 19.7 fb<sup>-1</sup> of  $pp$  data at  $\sqrt{s} = 8$  TeV. The result is obtained by counting the number of  $b$  jets per  $t\bar{t}$  signal events in the dilepton channel. The  $t\bar{t}$  production cross section is measured to be  $\sigma(t\bar{t}) = 238 \pm 1 \pm 15$  pb, in good agreement with the SM prediction and the latest CMS measurement of CHATRCHYAN 14F. The measurement gives  $R > 0.995$  (95% CL), or  $|V_{tb}| > 0.975$  (95% CL) in the SM, requiring  $R \leq 1$ .

<sup>3</sup> Based on 8.7 fb<sup>-1</sup> of  $p\bar{p}$  collisions at  $\sqrt{s} = 1.96$  TeV. Measure the fraction of  $t \rightarrow Wb$  decays simultaneously with the  $t\bar{t}$  cross section. The correlation coefficient between those two measurements is  $-0.434$ . Assume unitarity of the  $3 \times 3$  CKM matrix and set  $|V_{tb}| > 0.89$  at 95% CL.

<sup>4</sup> Based on 5.4 fb<sup>-1</sup> of data. The error is statistical and systematic combined. The result is a combination of  $0.95 \pm 0.07$  from  $\ell +$  jets channel and  $0.86 \pm 0.05$  from  $\ell\ell$  channel.  $|V_{tb}| = 0.95 \pm 0.02$  follows from the result by assuming unitarity of the  $3 \times 3$  CKM matrix.

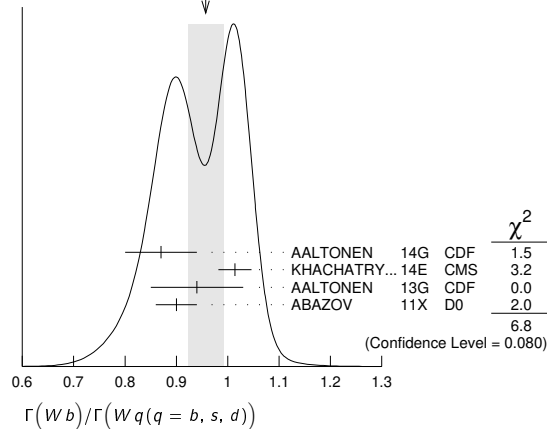
<sup>5</sup> Result is based on 0.9 fb<sup>-1</sup> of data. The 95% CL lower bound  $R > 0.79$  gives  $|V_{tb}| > 0.89$  (95% CL).

<sup>6</sup> ABAZOV 06k result is from the analysis of  $t\bar{t} \rightarrow \ell\nu_\ell + \geq 3$  jets with 230 pb<sup>-1</sup> of data at  $\sqrt{s} = 1.96$  TeV. It gives  $R > 0.61$  and  $|V_{tb}| > 0.78$  at 95% CL. Superseded by ABAZOV 08M.

<sup>7</sup> ACOSTA 05A result is from the analysis of lepton + jets and di-lepton + jets final states of  $t\bar{t}$  candidate events with  $\sim 162$  pb<sup>-1</sup> of data at  $\sqrt{s} = 1.96$  TeV. The first error is statistical and the second systematic. It gives  $R > 0.61$ , or  $|V_{tb}| > 0.78$  at 95% CL.

<sup>8</sup> AFFOLDER 01c measures the top-quark decay width ratio  $R = \Gamma(Wb)/\Gamma(Wq)$ , where  $q$  is a  $d$ ,  $s$ , or  $b$  quark, by using the number of events with multiple btags. The first error is statistical and the second systematic. A numerical integration of the likelihood function gives  $R > 0.61$  (0.56) at 90% (95%) CL. By assuming three generation unitarity,  $|V_{tb}| = 0.97^{+0.16}_{-0.12}$  or  $|V_{tb}| > 0.78$  (0.75) at 90% (95%) CL is obtained. The result is based on 109 pb<sup>-1</sup> of data at  $\sqrt{s} = 1.8$  TeV.

WEIGHTED AVERAGE  
0.957±0.034 (Error scaled by 1.5)



VALUE	DOCUMENT ID	TECN	COMMENT	$\Gamma_3/\Gamma$
<b>0.111 ± 0.003</b>	<sup>1</sup> AAD	15cc ATLS	$\ell +$ jets, $\ell\ell +$ jets, $\ell\tau_h +$ jets	

<sup>1</sup> AAD 15cc based on 4.6 fb<sup>-1</sup> of  $pp$  data at  $\sqrt{s} = 7$  TeV. The original value is given by  $13.3 \pm 0.4 \pm 0.5\%$ , which includes electrons from the decay of  $\tau$  leptons. It is assumed that the top branching ratios to leptons and jets add up to one and that only SM processes contribute to the background. The event selection criteria are optimized for the  $\ell\tau_h +$  jets channel. We have converted the original value to eliminate contributions of electrons from  $\tau$ 's, by using the AAD 15cc measurements of the branching ratios to  $\mu$  and  $\tau$  channels, as well as the PDG values of  $\tau$  branching ratios into  $e$  and  $\mu$  channels.

VALUE	DOCUMENT ID	TECN	COMMENT	$\Gamma_4/\Gamma$
<b>0.114 ± 0.002</b>	<sup>1</sup> AAD	15cc ATLS	$\ell +$ jets, $\ell\ell +$ jets, $\ell\tau_h +$ jets	

<sup>1</sup> AAD 15cc based on 4.6 fb<sup>-1</sup> of  $pp$  data at  $\sqrt{s} = 7$  TeV. The original value is given by  $13.4 \pm 0.3 \pm 0.5\%$ , which includes muons from the decay of  $\tau$  leptons. It is assumed that the top branching ratios to leptons and jets add up to one and that only SM processes contribute to the background. The event selection criteria are optimized for the  $\ell\tau_h +$  jets channel. We have converted the original value to eliminate contributions of muons from  $\tau$ 's, by using the AAD 15cc measurements of the branching ratios to  $\mu$  and  $\tau$  channels, as well as the PDG values of  $\tau$  branching ratios into  $e$  and  $\tau$  channels.

VALUE	DOCUMENT ID	TECN	COMMENT	$\Gamma_5/\Gamma$
<b>0.111 ± 0.009 OUR AVERAGE</b>				
0.112 ± 0.009	<sup>1</sup> AAD	15cc ATLS	$\ell +$ jets, $\ell\ell +$ jets, $\ell\tau_h +$ jets	
0.096 ± 0.028	<sup>2</sup> AALTONEN	14A CDF	$\ell + \tau_h + \geq 2$ jets ( $\geq 1b$ -tag)	

• • • We do not use the following data for averages, fits, limits, etc. • • •

<sup>3</sup> ABULENCIA	06R CDF	$\ell\tau +$ jets
<sup>4</sup> ABE	97V CDF	$\ell\tau +$ jets

<sup>1</sup> AAD 15cc based on 4.6 fb<sup>-1</sup> of  $pp$  data at  $\sqrt{s} = 7$  TeV. The original value is given by  $7.0 \pm 0.3 \pm 0.5\%$ , which includes only the hadronic decay of  $\tau$  leptons. It is assumed that the top branching ratios to leptons and jets add up to one and that only SM processes contribute to the background. The event selection criteria are optimized for the  $\ell\tau_h +$  jets channel. We have converted the original value to include leptonic decays of  $\tau$ 's, by using the AAD 15cc measurements of the branching ratios to  $e$  and  $\mu$  channels, as well as the PDG values of  $\tau$  branching ratios into  $e$  and  $\mu$  channels.

<sup>2</sup> Based on 9 fb<sup>-1</sup> of data. The measurement is in the channel  $t\bar{t} \rightarrow (b\ell\nu)(b\tau\nu)$ , where  $\tau$  decays into hadrons ( $\tau_h$ ), and  $\ell$  ( $e$  or  $\mu$ ) include  $\ell$  from  $\tau$  decays ( $\tau_\ell$ ). The result is consistent with lepton universality.

<sup>3</sup> ABULENCIA 06R looked for  $t\bar{t} \rightarrow (\ell\nu_\ell)(\tau\nu_\tau)b\bar{b}$  events in 194 pb<sup>-1</sup> of  $p\bar{p}$  collisions at  $\sqrt{s} = 1.96$  TeV. 2 events are found where  $1.00 \pm 0.17$  signal and  $1.29 \pm 0.25$  background events are expected, giving a 95% CL upper bound for the partial width ratio  $\Gamma(t \rightarrow \tau\nu q) / \Gamma_{SM}(t \rightarrow \tau\nu q) < 5.2$ .

<sup>4</sup> ABE 97V searched for  $t\bar{t} \rightarrow (\ell\nu_\ell)(\tau\nu_\tau)b\bar{b}$  events in 109 pb<sup>-1</sup> of  $p\bar{p}$  collisions at  $\sqrt{s} = 1.8$  TeV. They observed 4 candidate events where one expects  $\sim 1$  signal and  $\sim 2$  background events. Three of the four observed events have jets identified as  $b$  candidates.

VALUE	DOCUMENT ID	TECN	COMMENT	$\Gamma_6/\Gamma$
<b>0.665 ± 0.004 ± 0.013</b>	<sup>1</sup> AAD	15cc ATLS	$\ell +$ jets, $\ell\ell +$ jets, $\ell\tau_h +$ jets	

<sup>1</sup> AAD 15cc based on 4.6 fb<sup>-1</sup> of  $pp$  data at  $\sqrt{s} = 7$  TeV. Branching ratio of top quark into  $b$  and jets. It is assumed that the top branching ratios to leptons and jets add up to one and that only SM processes contribute to the background. The event selection criteria are optimized for the  $\ell\tau_h +$  jets channel.

VALUE	CL%	DOCUMENT ID	TECN	COMMENT	$\Gamma_7/\Gamma$
<b>&lt; 2.8 × 10<sup>-5</sup></b>	95	<sup>1</sup> AAD	20B ATLS	$B(t \rightarrow \gamma u)$ , left-handed $t u \gamma$ coupling	
<b>&lt; 6.1 × 10<sup>-5</sup></b>	95	<sup>1</sup> AAD	20B ATLS	$B(t \rightarrow \gamma u)$ , right-handed $t u \gamma$ coupling	
<b>&lt; 2.2 × 10<sup>-4</sup></b>	95	<sup>1</sup> AAD	20B ATLS	$B(t \rightarrow \gamma c)$ , left-handed $t c \gamma$ coupling	
<b>&lt; 1.8 × 10<sup>-4</sup></b>	95	<sup>1</sup> AAD	20B ATLS	$B(t \rightarrow \gamma c)$ , right-handed $t c \gamma$ coupling	
< 1.3 × 10 <sup>-4</sup>	95	<sup>2</sup> KHACHATRYAN 16AS	CMS	$B(t \rightarrow \gamma u)$	
< 1.7 × 10 <sup>-3</sup>	95	<sup>2</sup> KHACHATRYAN 16AS	CMS	$B(t \rightarrow \gamma c)$	
< 5.9 × 10 <sup>-3</sup>	95	<sup>3</sup> CHEKANOV 03	ZEUS	$B(t \rightarrow \gamma u)$	

• • • We do not use the following data for averages, fits, limits, etc. • • •

< 0.0064	95	<sup>4</sup> AARON	09A H1	$t \rightarrow \gamma u$
< 0.0465	95	<sup>5</sup> ABDALLAH	04c DLPH	$B(\gamma c$ or $\gamma u)$
< 0.0132	95	<sup>6</sup> AKTAS	04 H1	$B(t \rightarrow \gamma u)$
< 0.041	95	<sup>7</sup> ACHARD	02J L3	$B(t \rightarrow \gamma c$ or $\gamma u)$
< 0.032	95	<sup>8</sup> ABE	98G CDF	$t\bar{t} \rightarrow (Wb)(\gamma c$ or $\gamma u)$

<sup>1</sup> AAD 20B based on 81 fb<sup>-1</sup> of data in  $pp$  collisions at  $\sqrt{s} = 13$  TeV. FCNC through single top production in association with a photon is searched for in the mode  $\ell\gamma + E_T + 1j$  ( $b$ -tag). Anomalous FCNC left-handed and right-handed couplings are searched for, which result in different kinematical properties of top decay such as the lepton distribution. Limits are set on the  $tq\gamma$  couplings in an effective field theory.

<sup>2</sup> KHACHATRYAN 16AS based on 19.8 fb<sup>-1</sup> of data in  $pp$  collisions at  $\sqrt{s} = 8$  TeV. FCNC through single top production in association with a photon is searched for in the mode  $\mu + \gamma + E_T + \geq 1j$  (0,1b). Bounds on the anomalous FCNC couplings are given by  $\kappa_{t u \gamma} < 0.025$  and  $\kappa_{t c \gamma} < 0.091$ .

<sup>3</sup> CHEKANOV 03 looked for single top production via FCNC in the reaction  $e^\pm p \rightarrow e^\pm (t$  or  $\bar{t}) X$  in 130.1 pb<sup>-1</sup> of data at  $\sqrt{s} = 300$ –318 GeV. No evidence for top production and its decay into  $bW$  was found. The result is obtained for  $m_t = 175$  GeV when  $B(\gamma c) = B(\gamma u) = 0$ , where  $q$  is a  $u$  or  $c$  quark. Bounds on the effective  $t-u-\gamma$  and  $t-u-Z$  couplings are found in their Fig. 4. The conversion to the constraint listed is from private communication, E. Gallo, January 2004.

<sup>4</sup> AARON 09A looked for single top production via FCNC in  $e^\pm p$  collisions at HERA with 474 pb<sup>-1</sup>. The upper bound of the cross section gives the bound on the FCNC coupling  $\kappa_{t u \gamma} / \Lambda < 1.03$  TeV<sup>-1</sup>, which corresponds to the result for  $m_t = 175$  GeV.

<sup>5</sup> ABDALLAH 04c looked for single top production via FCNC in the reaction  $e^+ e^- \rightarrow \bar{t} c$  or  $\bar{t} u$  in 541 pb<sup>-1</sup> of data at  $\sqrt{s} = 189$ –208 GeV. No deviation from the SM is found, which leads to the bound on  $B(t \rightarrow \gamma q)$ , where  $q$  is a  $u$  or a  $c$  quark, for  $m_t = 175$  GeV when  $B(\gamma c) = B(\gamma u) = 0$  is assumed. The conversion to the listed bound is from private communication, O. Yushchenko, April 2005. The bounds on the effective  $t-q-\gamma$  and  $t-q-Z$  couplings are given in their Fig. 7 and Table 4, for  $m_t = 170$ –180 GeV, where most conservative bounds are found by choosing the chiral couplings to maximize the negative interference between the virtual  $\gamma$  and  $Z$  exchange amplitudes.

<sup>6</sup> AKTAS 04 looked for single top production via FCNC in  $e^\pm$  collisions at HERA with 118.3 pb<sup>-1</sup>, and found 5 events in the  $e$  or  $\mu$  channels. By assuming that they are due to statistical fluctuation, the upper bound on the  $t u \gamma$  coupling  $\kappa_{t u \gamma} < 0.27$  (95% CL) is obtained. The conversion to the partial width limit, when  $B(\gamma c) = B(\gamma u) = B(\gamma Z) = 0$ , is from private communication, E. Perez, May 2005.

<sup>7</sup> ACHARD 02J looked for single top production via FCNC in the reaction  $e^+ e^- \rightarrow \bar{t} c$  or  $\bar{t} u$  in 634 pb<sup>-1</sup> of data at  $\sqrt{s} = 189$ –209 GeV. No deviation from the SM is found, which leads to a bound on the top-quark decay branching fraction  $B(\gamma q)$ , where  $q$  is a  $u$  or  $c$  quark. The bound assumes  $B(Zq) = 0$  and is for  $m_t = 175$  GeV; bounds for  $m_t = 170$  GeV and 180 GeV and  $B(Zq) \neq 0$  are given in Fig. 5 and Table 7.

<sup>8</sup> ABE 98G looked for  $t\bar{t}$  events where one  $t$  decays into  $q\gamma$  while the other decays into  $bW$ . The quoted bound is for  $\Gamma(\gamma q)/\Gamma(Wb)$ .

$\Gamma(H^+ b, H^+ \rightarrow \tau \nu_\tau)/\Gamma_{\text{total}}$		$\Gamma_8/\Gamma$	
VALUE (%)	CL%	DOCUMENT ID	TECN
<0.25	95	1 AABOUD	18BWATLS

<sup>1</sup>AABOUD 18BW based on  $36.1 \text{ fb}^{-1}$  of  $pp$  data at  $\sqrt{s} = 13 \text{ TeV}$ . In the mass range of  $m_{H^+} = 90\text{--}160 \text{ GeV}$ , assuming the SM cross section for the  $t\bar{t}$  production, the upper limit for the branching fraction  $B(t \rightarrow bH^+) \times B(H^+ \rightarrow \tau \nu_\tau)$  ranges between 0.25% and 0.031%.

$\Gamma(Zq(q=u,c))/\Gamma_{\text{total}}$		$\Gamma_9/\Gamma$	
VALUE (units $10^{-3}$ )	CL%	DOCUMENT ID	TECN

< 0.17	95	1 AABOUD	18AT ATLS	$t \rightarrow Zu$
< 0.24	95	1 AABOUD	18AT ATLS	$t \rightarrow Zc$
< 0.22	95	2 SIRUNYAN	17E CMS	$t \rightarrow Zu$
< 0.49	95	2 SIRUNYAN	17E CMS	$t \rightarrow Zc$
< 0.7	95	3 AAD	16D ATLS	$t \rightarrow Zq (q = u, c)$
< 0.5	95	4 CHATRCHYAN14S	CMS	$t \rightarrow Zq (q = u, c)$
••• We do not use the following data for averages, fits, limits, etc. •••				
< 0.6	95	5 CHATRCHYAN14S	CMS	$t \rightarrow Zq (q = u, c)$
< 2.1	95	6 CHATRCHYAN13F	CMS	$t \rightarrow Zq (q = u, c)$
< 7.3	95	7 AAD	12BT ATLS	$t\bar{t} \rightarrow \ell^+ \ell^- \ell'^{\pm} + E_T + \text{jets}$
< 32	95	8 ABZOV	11M D0	$t \rightarrow Zq (q = u, c)$
< 83	95	9 AALTONEN	09AL CDF	$t \rightarrow Zq (q = c)$
< 37	95	10 AALTONEN	08AD CDF	$t \rightarrow Zq (q = u, c)$
< $1.59 \times 10^2$	95	11 ABDALLAH	04C DLPH	$e^+e^- \rightarrow \bar{t}c \text{ or } \bar{t}u$
< $1.37 \times 10^2$	95	12 ACHARD	02J L3	$e^+e^- \rightarrow \bar{t}c \text{ or } \bar{t}u$
< $1.4 \times 10^2$	95	13 HEISTER	02Q ALEP	$e^+e^- \rightarrow \bar{t}c \text{ or } \bar{t}u$
< $1.37 \times 10^2$	95	14 ABBIENDI	01T OPAL	$e^+e^- \rightarrow \bar{t}c \text{ or } \bar{t}u$
< $1.7 \times 10^2$	95	15 BARATE	00S ALEP	$e^+e^- \rightarrow \bar{t}c \text{ or } \bar{t}u$
< $3.3 \times 10^2$	95	16 ABE	98G CDF	$t\bar{t} \rightarrow (Wb)(Zc \text{ or } Zu)$

<sup>1</sup>Based on  $36.1 \text{ fb}^{-1}$  of  $pp$  data at  $\sqrt{s} = 13 \text{ TeV}$ . The final states  $t\bar{t} \rightarrow \ell^+ \ell^- \ell'^{\pm} \nu$  + jets ( $\ell, \ell' = e, \mu$ ) are investigated and no significant excess over the SM background contributions is observed.

<sup>2</sup>SIRUNYAN 17E based on  $19.7 \text{ fb}^{-1}$  of  $pp$  data at  $\sqrt{s} = 8 \text{ TeV}$ . The final states  $t\bar{t} \rightarrow \ell^+ \ell^- \ell'^{\pm} \nu$  + jets ( $\ell, \ell' = e, \mu$ ) are investigated and the cross section  $\sigma(pp \rightarrow tZq \rightarrow \ell \nu b \ell^+ \ell^- q) = 10^{+8}_{-7} \text{ fb}$  is measured, giving no sign of FCNC decays of the top quark.

<sup>3</sup>AAD 16D based on  $20.3 \text{ fb}^{-1}$  of  $pp$  data at  $\sqrt{s} = 8 \text{ TeV}$ . The FCNC decay is searched for in  $t\bar{t}$  events in the final state  $(bW)(qZ)$  when both  $W$  and  $Z$  decay leptonically, giving 3 charged leptons.

<sup>4</sup>CHATRCHYAN 14S combined search limit from this and CHATRCHYAN 13F data.

<sup>5</sup>Based on  $19.7 \text{ fb}^{-1}$  of  $pp$  data at  $\sqrt{s} = 8 \text{ TeV}$ . The flavor changing decay is searched for in  $t\bar{t}$  events in the final state  $(bW)(qZ)$  when both  $W$  and  $Z$  decay leptonically, giving 3 charged leptons.

<sup>6</sup>Based on  $5.0 \text{ fb}^{-1}$  of  $pp$  data at  $\sqrt{s} = 7 \text{ TeV}$ . Search for FCNC decays of the top quark in  $t\bar{t} \rightarrow \ell^+ \ell^- \ell'^{\pm} \nu$  + jets ( $\ell, \ell' = e, \mu$ ) final states found no excess of signal events.

<sup>7</sup>Based on  $2.1 \text{ fb}^{-1}$  of  $pp$  data at  $\sqrt{s} = 7 \text{ TeV}$ .

<sup>8</sup>Based on  $4.1 \text{ fb}^{-1}$  of data. ABZOV 11M searched for FCNC decays of the top quark in  $t\bar{t} \rightarrow \ell^+ \ell^- \ell'^{\pm} \nu$  + jets ( $\ell, \ell' = e, \mu$ ) final states, and absence of the signal gives the bound.

<sup>9</sup>Based on  $pp$  data of  $1.52 \text{ fb}^{-1}$ . AALTONEN 09AL compared  $t\bar{t} \rightarrow WbWb \rightarrow \ell \nu b j j b$  and  $t\bar{t} \rightarrow ZcWb \rightarrow \ell \ell c j j b$  decay chains, and absence of the latter signal gives the bound. The result is for 100% longitudinally polarized  $Z$  boson and the theoretical  $t\bar{t}$  production cross section. The results for different  $Z$  polarizations and those without the cross section assumption are given in their Table XII.

<sup>10</sup>Result is based on  $1.9 \text{ fb}^{-1}$  of data at  $\sqrt{s} = 1.96 \text{ TeV}$ .  $t\bar{t} \rightarrow WbZq \text{ or } ZqZq$  processes have been looked for in  $Z + \geq 4$  jet events with and without  $b$ -tag. No signal leads to the bound  $B(t \rightarrow Zq) < 0.037 (0.041)$  for  $m_t = 175 (170) \text{ GeV}$ .

<sup>11</sup>ABDALLAH 04C looked for single top production via FCNC in the reaction  $e^+e^- \rightarrow \bar{t}c \text{ or } \bar{t}u$  in  $541 \text{ pb}^{-1}$  of data at  $\sqrt{s} = 189\text{--}208 \text{ GeV}$ . No deviation from the SM is found, which leads to the bound on  $B(t \rightarrow Zq)$ , where  $q$  is a  $u$  or a  $c$  quark, for  $m_t = 175 \text{ GeV}$  when  $B(t \rightarrow \gamma q) = 0$  is assumed. The conversion to the listed bound is from private communication, O. Yushchenko, April 2005. The bounds on the effective  $t$ - $q$ - $\gamma$  and  $t$ - $q$ - $Z$  couplings are given in their Fig. 7 and Table 4, for  $m_t = 170\text{--}180 \text{ GeV}$ , where most conservative bounds are found by choosing the chiral couplings to maximize the negative interference between the virtual  $\gamma$  and  $Z$  exchange amplitudes.

<sup>12</sup>ACHARD 02J looked for single top production via FCNC in the reaction  $e^+e^- \rightarrow \bar{t}c \text{ or } \bar{t}u$  in  $634 \text{ pb}^{-1}$  of data at  $\sqrt{s} = 189\text{--}209 \text{ GeV}$ . No deviation from the SM is found, which leads to a bound on the top-quark decay branching fraction  $B(Zq)$ , where  $q$  is a  $u$  or  $c$  quark. The bound assumes  $B(\gamma q) = 0$  and is for  $m_t = 175 \text{ GeV}$ ; bounds for  $m_t = 170 \text{ GeV}$  and  $180 \text{ GeV}$  and  $B(\gamma q) \neq 0$  are given in Fig. 5 and Table 7. Table 6 gives constraints on  $t$ - $c$ - $e$  four-fermi contact interactions.

<sup>13</sup>HEISTER 02Q looked for single top production via FCNC in the reaction  $e^+e^- \rightarrow \bar{t}c \text{ or } \bar{t}u$  in  $214 \text{ pb}^{-1}$  of data at  $\sqrt{s} = 204\text{--}209 \text{ GeV}$ . No deviation from the SM is found, which leads to a bound on the branching fraction  $B(Zq)$ , where  $q$  is a  $u$  or  $c$  quark. The bound assumes  $B(\gamma q) = 0$  and is for  $m_t = 174 \text{ GeV}$ . Bounds on the effective  $t$ - $(c \text{ or } u)$ - $\gamma$  and  $t$ - $(c \text{ or } u)$ - $Z$  couplings are given in their Fig. 2.

<sup>14</sup>ABBIENDI 01T looked for single top production via FCNC in the reaction  $e^+e^- \rightarrow \bar{t}c \text{ or } \bar{t}u$  in  $600 \text{ pb}^{-1}$  of data at  $\sqrt{s} = 189\text{--}209 \text{ GeV}$ . No deviation from the SM is found, which leads to bounds on the branching fractions  $B(Zq)$  and  $B(\gamma q)$ , where  $q$  is a  $u$  or  $c$  quark. The result is obtained for  $m_t = 174 \text{ GeV}$ . The upper bound becomes 9.7% (20.6%) for  $m_t = 169 (179) \text{ GeV}$ . Bounds on the effective  $t$ - $(c \text{ or } u)$ - $\gamma$  and  $t$ - $(c \text{ or } u)$ - $Z$  couplings are given in their Fig. 4.

<sup>15</sup>BARATE 00S looked for single top production via FCNC in the reaction  $e^+e^- \rightarrow \bar{t}c \text{ or } \bar{t}u$  in  $411 \text{ pb}^{-1}$  of data at c.m. energies between 189 and 202 GeV. No deviation from the SM is found, which leads to a bound on the branching fraction. The bound assumes  $B(\gamma q) = 0$ . Bounds on the effective  $t$ - $(c \text{ or } u)$ - $\gamma$  and  $t$ - $(c \text{ or } u)$ - $Z$  couplings are given in their Fig. 4.

<sup>16</sup>ABE 98G looked for  $t\bar{t}$  events where one  $t$  decays into three jets and the other decays into  $qZ$  with  $Z \rightarrow \ell\ell$ . The quoted bound is for  $\Gamma(Zq)/\Gamma(Wb)$ .

$\Gamma(Hu)/\Gamma_{\text{total}}$		$\Gamma_{10}/\Gamma$	
VALUE (units $10^{-3}$ )	CL%	DOCUMENT ID	TECN

<1.2	95	1 AABOUD	19S ATLS	combination of $t \rightarrow Hu$ ( $H \rightarrow WW, ZZ, \tau\tau, \gamma\gamma, b\bar{b}$ )
••• We do not use the following data for averages, fits, limits, etc. •••				
<5.2	95	2 AABOUD	19S ATLS	$t \rightarrow Hu (H \rightarrow bb)$
<1.7	95	3 AABOUD	19S ATLS	$t \rightarrow Hu (H \rightarrow \tau\tau)$
<1.9	95	4 AABOUD	18X ATLS	$t \rightarrow Hu (H \rightarrow WW, ZZ, \tau\tau)$
<4.7	95	5 SIRUNYAN	18Bc CMS	$t \rightarrow Hu (H \rightarrow bb)$
<2.4	95	6 AABOUD	17AV ATLS	$t \rightarrow Hu (H \rightarrow \gamma\gamma)$
<5.5	95	7 KHACHATRYAN..17I	CMS	$t \rightarrow Hu (H \rightarrow WW, ZZ, \tau\tau, \gamma\gamma, b\bar{b})$
<6.1	95	8 AAD	15CO ATLS	$t \rightarrow Hu (H \rightarrow bb)$
<7.9	95	9 AAD	14AA ATLS	$t \rightarrow Hq (q=u,c; H \rightarrow \gamma\gamma)$

<sup>1</sup>AABOUD 19S based on  $36.1 \text{ fb}^{-1}$  at  $\sqrt{s} = 13 \text{ TeV}$  of  $pp$  data. The searches using  $H \rightarrow bb$  and  $H \rightarrow \tau_h \tau_h$  are combined with searches in diphoton and multilepton final states. The upper limit on the Yukawa coupling  $|Y_{tH}| < 0.066$  (95% CL) is obtained.

<sup>2</sup>AABOUD 19S based on  $36.1 \text{ fb}^{-1}$  at  $\sqrt{s} = 13 \text{ TeV}$  of  $pp$  data. Uses events with one isolated lepton and multiple jets (several of them  $b$ -tagged with high purity). A multivariate analysis is performed to distinguish the signal from backgrounds.

<sup>3</sup>AABOUD 19S based on  $36.1 \text{ fb}^{-1}$  at  $\sqrt{s} = 13 \text{ TeV}$  of  $pp$  data. Uses events with one or two hadronically decaying  $\tau$  and multiple jets. A multivariate analysis is performed to distinguish the signal from backgrounds.

<sup>4</sup>AABOUD 18X based on  $36.1 \text{ fb}^{-1}$  at  $\sqrt{s} = 13 \text{ TeV}$  of  $pp$  data.  $\ell\ell$ (same sign) +  $\geq 4$  jets and  $\ell\ell\ell + \geq 2$  jets mode are targeted and specialized boosted decision trees are used to distinguish signals from backgrounds.

<sup>5</sup>SIRUNYAN 18Bc based on  $35.9 \text{ fb}^{-1}$  at  $\sqrt{s} = 13 \text{ TeV}$  of  $pp$  data. Two channels  $pp \rightarrow tH$  and  $pp \rightarrow t\bar{t}$  in final states with one isolated lepton and  $\geq 3$  jets with  $\geq 2$   $b$  jets are considered assuming a single  $tHc$  FCNC coupling. Reconstructed kinematical variables are fed into a multivariate analysis and no significant deviation is observed from the predicted background.

<sup>6</sup>AABOUD 17AV based on  $36.1 \text{ fb}^{-1}$  at  $\sqrt{s} = 13 \text{ TeV}$  of  $pp$  data. Search for  $t\bar{t}$  events, where the other top quark decays hadronically or semi-leptonically.

<sup>7</sup>KHACHATRYAN 17I based on  $19.7 \text{ fb}^{-1}$  of  $pp$  data at  $\sqrt{s} = 8 \text{ TeV}$ , using the topologies  $t\bar{t} \rightarrow Hq + Wb$ , where  $q = u, c$ .

<sup>8</sup>AAD 15CO based on  $20.3 \text{ fb}^{-1}$  at  $\sqrt{s} = 8 \text{ TeV}$  of  $pp$  data. Searches for  $t\bar{t}$  events, where the other top quark decays semi-leptonically. Exploits high multiplicity of  $b$ -jets and uses a likelihood discriminant. Combining with other ATLAS searches for different Higgs decay modes,  $B(t \rightarrow Hc) < 0.46\%$  and  $B(t \rightarrow Hu) < 0.45\%$  are obtained.

<sup>9</sup>AAD 14AA based on  $4.7 \text{ fb}^{-1}$  at  $\sqrt{s} = 7 \text{ TeV}$  and  $20.3 \text{ fb}^{-1}$  at  $\sqrt{s} = 8 \text{ TeV}$  of  $pp$  data. The upper-bound is for the sum of  $\text{Br}(t \rightarrow Hc)$  and  $\text{Br}(t \rightarrow Hu)$ . Search for  $t\bar{t}$  events, where the other top quark decays hadronically or semi-leptonically. The upper bound constrains the  $H$ - $t$ - $c$  Yukawa couplings  $\sqrt{|Y_{tH}^c}|^2 + |Y_{tH}^u}|^2 < 0.17$  (95% CL).

$\Gamma(Hc)/\Gamma_{\text{total}}$		$\Gamma_{11}/\Gamma$	
VALUE (units $10^{-3}$ )	CL%	DOCUMENT ID	TECN

< 1.1	95	1 AABOUD	19S ATLS	combination of $t \rightarrow Hc$ ( $H \rightarrow WW, ZZ, \tau\tau, \gamma\gamma, b\bar{b}$ )
••• We do not use the following data for averages, fits, limits, etc. •••				
< 4.2	95	2 AABOUD	19S ATLS	$t \rightarrow Hc (H \rightarrow bb)$
< 1.9	95	3 AABOUD	19S ATLS	$t \rightarrow Hc (H \rightarrow \tau\tau)$
< 1.6	95	4 AABOUD	18X ATLS	$t \rightarrow Hc (H \rightarrow WW, ZZ, \tau\tau)$
< 4.7	95	5 SIRUNYAN	18Bc CMS	$t \rightarrow Hc (H \rightarrow bb)$
< 2.2	95	6 AABOUD	17AV ATLS	$t \rightarrow Hc (H \rightarrow \gamma\gamma)$
< 4	95	7 KHACHATRYAN..17I	CMS	$t \rightarrow Hc (H \rightarrow WW, ZZ, \tau\tau, \gamma\gamma, b\bar{b})$
< 5.6	95	8 AAD	15CO ATLS	$t \rightarrow Hc (H \rightarrow bb)$
< 7.9	95	9 AAD	14AA ATLS	$t \rightarrow Hq (q=u,c; H \rightarrow \gamma\gamma)$
< 13	95	10 CHATRCHYAN14R	CMS	$t \rightarrow Hc (H \rightarrow \geq 2 \ell)$
< 5.6	95	11 KHACHATRYAN..14Q	CMS	$t \rightarrow Hc (H \rightarrow \gamma\gamma \text{ or } \text{leptons})$

<sup>1</sup>AABOUD 19S based on  $36.1 \text{ fb}^{-1}$  at  $\sqrt{s} = 13 \text{ TeV}$  of  $pp$  data. The searches using  $H \rightarrow bb$  and  $H \rightarrow \tau_h \tau_h$  are combined with searches in diphoton and multilepton final states. The upper limit on the Yukawa coupling  $|Y_{tH}| < 0.064$  (95% CL) is obtained.

<sup>2</sup>AABOUD 19S based on  $36.1 \text{ fb}^{-1}$  at  $\sqrt{s} = 13 \text{ TeV}$  of  $pp$  data. Uses events with one isolated lepton and multiple jets (several of them  $b$ -tagged with high purity). A multivariate analysis is performed to distinguish the signal from backgrounds.

<sup>3</sup>AABOUD 19S based on  $36.1 \text{ fb}^{-1}$  at  $\sqrt{s} = 13 \text{ TeV}$  of  $pp$  data. Uses events with one or two hadronically decaying  $\tau$  and multiple jets. A multivariate analysis is performed to distinguish the signal from backgrounds.

<sup>4</sup>AABOUD 18X based on  $36.1 \text{ fb}^{-1}$  at  $\sqrt{s} = 13 \text{ TeV}$  of  $pp$  data.  $\ell\ell$ (same sign) +  $\geq 4$  jets and  $\ell\ell\ell + \geq 2$  jets mode are targeted and specialized boosted decision trees are used to distinguish signals from backgrounds.

<sup>5</sup>SIRUNYAN 18Bc based on  $35.9 \text{ fb}^{-1}$  at  $\sqrt{s} = 13 \text{ TeV}$  of  $pp$  data. Two channels  $pp \rightarrow tH$  and  $pp \rightarrow t\bar{t}$  in final states with one isolated lepton and  $\geq 3$  jets with  $\geq 2$   $b$  jets are considered assuming a single  $tHc$  FCNC coupling. Reconstructed kinematical variables are fed into a multivariate analysis and no significant deviation is observed from the predicted background.

<sup>6</sup>AABOUD 17AV based on  $36.1 \text{ fb}^{-1}$  at  $\sqrt{s} = 13 \text{ TeV}$  of  $pp$  data. Search for  $t\bar{t}$  events, where the other top quark decays hadronically or semi-leptonically. The upper bound on the  $H$ - $t$ - $c$  Yukawa couplings is 0.090 (95% CL).

<sup>7</sup>KHACHATRYAN 17I based on  $19.7 \text{ fb}^{-1}$  of  $pp$  data at  $\sqrt{s} = 8 \text{ TeV}$ , using the topologies  $t\bar{t} \rightarrow Hq + Wb$ , where  $q = u, c$ .

<sup>8</sup>AAD 15CO based on  $20.3 \text{ fb}^{-1}$  at  $\sqrt{s} = 8 \text{ TeV}$  of  $pp$  data. Searches for  $t\bar{t}$  events, where the other top quark decays semi-leptonically. Exploits high multiplicity of  $b$ -jets



# Quark Particle Listings

*t*

and uses a likelihood discriminant. Combining with other ATLAS searches for different Higgs decay modes,  $B(t \rightarrow Hc) < 0.46\%$  and  $B(t \rightarrow Hu) < 0.45\%$  are obtained.

<sup>9</sup>AAD 14AA based on  $4.7 \text{ fb}^{-1}$  at  $\sqrt{s} = 7 \text{ TeV}$  and  $20.3 \text{ fb}^{-1}$  at  $\sqrt{s} = 8 \text{ TeV}$  of  $pp$  data. The upper-bound is for the sum of  $B(t \rightarrow Hc)$  and  $B(t \rightarrow Hu)$ . Search for  $t\bar{t}$  events, where the other top quark decays hadronically or semi-leptonically. The upper bound constrains the  $H$ - $t$ - $c$  Yukawa couplings  $\sqrt{|Y_{t_{cL}}^H|^2 + |Y_{t_{cR}}^H|^2} < 0.17$  (95% CL).

<sup>10</sup>Based on  $19.5 \text{ fb}^{-1}$  of  $pp$  data at  $\sqrt{s} = 8 \text{ TeV}$ . Search for final states with 3 or more isolated high  $E_T$  charged leptons ( $\ell = e, \mu$ ) bounds the  $t \rightarrow Hc$  decay in  $t\bar{t}$  events when  $H$  decays contain a pair of leptons. The upper bound constrains the  $H$ - $t$ - $c$  Yukawa couplings  $\sqrt{|Y_{t_{cL}}^H|^2 + |Y_{t_{cR}}^H|^2} < 0.21$  (95% CL).

<sup>11</sup>KHACHATRYAN 14Q based on  $19.5 \text{ fb}^{-1}$  at  $\sqrt{s} = 8 \text{ TeV}$  of  $pp$  data. Search for final states with  $\geq 3$  isolated charged leptons or with a photon pair accompanied by  $\geq 1$  lepton(s).

$\Gamma(\ell^+ \bar{q} q' (q=d,s,b; q'=u,c))/\Gamma_{\text{total}}$		$\Gamma_{12}/\Gamma$	
VALUE	CL%	DOCUMENT ID	TECN COMMENT
$< 1.6 \times 10^{-3}$	95	<sup>1</sup> CHATRCHYAN14O	CMS $\mu + \text{dijets}$
$< 1.7 \times 10^{-3}$	95	<sup>1</sup> CHATRCHYAN14O	CMS $e + \text{dijets}$

<sup>1</sup>Based on  $19.5 \text{ fb}^{-1}$  of  $pp$  data at  $\sqrt{s} = 8 \text{ TeV}$ . Baryon number violating decays of the top quark are searched for in  $t\bar{t}$  production events where one of the pair decays into hadronic three jets.

## $t$ -quark EW Couplings

$W$  helicity fractions in top decays.  $F_0$  is the fraction of longitudinal and  $F_{\pm}$  the fraction of right-handed  $W$  bosons.  $F_{V+A}$  is the fraction of  $V+A$  current in top decays. The effective Lagrangian (cited by ABAZOV 08AI) has terms  $f_1^L$  and  $f_1^R$  for  $V-A$  and  $V+A$  couplings,  $f_2^L$  and  $f_2^R$  for tensor couplings with  $b_R$  and  $b_L$  respectively.

$F_0$			
VALUE	CL%	DOCUMENT ID	TECN COMMENT
<b><math>0.687 \pm 0.018</math></b>	<b>OUR AVERAGE</b>		
$0.70 \pm 0.05$		<sup>1</sup> AABOUD	17BB ATLS $F_0 = 1 - f_1$
$0.681 \pm 0.012 \pm 0.023$		<sup>2</sup> KHACHATRYAN16BU	CMS $F_0 = B(t \rightarrow W_0 b)$
$0.726 \pm 0.066 \pm 0.067$		<sup>3</sup> AALTONEN	13D CDF $F_0 = B(t \rightarrow W_0 b)$
$0.682 \pm 0.030 \pm 0.033$		<sup>4</sup> CHATRCHYAN13BH	CMS $F_0 = B(t \rightarrow W_0 b)$
$0.67 \pm 0.07$		<sup>5</sup> AAD	12BG ATLS $F_0 = B(t \rightarrow W_0 b)$
$0.722 \pm 0.062 \pm 0.052$		<sup>6</sup> AALTONEN	12Z TEVA $F_0 = B(t \rightarrow W_0 b)$
$0.669 \pm 0.078 \pm 0.065$		<sup>7</sup> ABAZOV	11C D0 $F_0 = B(t \rightarrow W_0 b)$
$0.91 \pm 0.37 \pm 0.13$		<sup>8</sup> AFFOLDER	00B CDF $F_0 = B(t \rightarrow W_0 b)$
$0.70 \pm 0.07 \pm 0.04$		<sup>9</sup> AALTONEN	10Q CDF Repl. by AALTONEN 12Z
$0.62 \pm 0.10 \pm 0.05$		<sup>10</sup> AALTONEN	09Q CDF Repl. by AALTONEN 10Q
$0.425 \pm 0.166 \pm 0.102$		<sup>11</sup> ABAZOV	08B D0 Repl. by ABAZOV 11c
$0.85^{+0.15}_{-0.22} \pm 0.06$		<sup>12</sup> ABULENCIA	07I CDF $F_0 = B(t \rightarrow W_0 b)$
$0.74^{+0.22}_{-0.34}$		<sup>13</sup> ABULENCIA	06U CDF $F_0 = B(t \rightarrow W_0 b)$
$0.56 \pm 0.31$		<sup>14</sup> ABAZOV	05G D0 $F_0 = B(t \rightarrow W_0 b)$

<sup>1</sup>AABOUD 17BB based on  $20.2 \text{ fb}^{-1}$  of  $pp$  data at  $\sqrt{s} = 8 \text{ TeV}$ . Triple-differential decay rate of top quark in the  $t$ -channel single-top production is used to simultaneously determine five generalized  $Wtb$  couplings as well as the top polarization. No assumption is made for the other couplings. See this paper for constraints on other couplings not included here. The paper reported  $f_1$ , and we converted it to  $F_0$ .

<sup>2</sup>KHACHATRYAN 16BU based on  $19.8 \text{ fb}^{-1}$  of  $pp$  data at  $\sqrt{s} = 8 \text{ TeV}$  using  $t\bar{t}$  events with  $\ell + E_T + \geq 4$  jets ( $\geq 2 b$ ). The errors of  $F_0$  and  $F_{\pm}$  are correlated with a correlation coefficient  $\rho(F_0, F_{\pm}) = -0.87$ . The result is consistent with the NNLO SM prediction of  $0.687 \pm 0.005$  for  $m_t = 172.8 \pm 1.3 \text{ GeV}$ .

<sup>3</sup>Based on  $8.7 \text{ fb}^{-1}$  of data in  $p\bar{p}$  collisions at  $\sqrt{s} = 1.96 \text{ TeV}$  using  $t\bar{t}$  events with  $\ell + E_T + \geq 4$  jets ( $\geq 1 b$ ), and under the constraint  $F_0 + F_{\pm} + F_{\mp} = 1$ . The statistical errors of  $F_0$  and  $F_{\pm}$  are correlated with correlation coefficient  $\rho(F_0, F_{\pm}) = -0.69$ .

<sup>4</sup>Based on  $5.0 \text{ fb}^{-1}$  of  $pp$  data at  $\sqrt{s} = 7 \text{ TeV}$ . CHATRCHYAN 13BH studied  $tt$  events with large  $E_T$  and  $\ell + \geq 4$  jets using a constrained kinematic fit.

<sup>5</sup>Based on  $1.04 \text{ fb}^{-1}$  of  $pp$  data at  $\sqrt{s} = 7 \text{ TeV}$ . AAD 12BG studied  $tt$  events with large  $E_T$  and either  $\ell + \geq 4j$  or  $\ell\ell + \geq 2j$ . The uncertainties are not independent,  $\rho(F_0, F_{\pm}) = -0.96$ .

<sup>6</sup>Based on  $2.7$  and  $5.1 \text{ fb}^{-1}$  of CDF data in  $\ell +$  jets and dilepton channels, and  $5.4 \text{ fb}^{-1}$  of D0 data in  $\ell +$  jets and dilepton channels.  $F_0 = 0.682 \pm 0.035 \pm 0.046$  if  $F_{\pm} = 0.0017(1)$ , while  $F_{\pm} = -0.015 \pm 0.018 \pm 0.030$  if  $F_0 = 0.688(4)$ , where the assumed fixed values are the SM prediction for  $m_t = 173.3 \pm 1.1 \text{ GeV}$  and  $m_W = 80.399 \pm 0.023 \text{ GeV}$ .

<sup>7</sup>Results are based on  $5.4 \text{ fb}^{-1}$  of data in  $p\bar{p}$  collisions at  $1.96 \text{ TeV}$ , including those of ABAZOV 08B. Under the SM constraint of  $f_0 = 0.698$  (for  $m_t = 173.3 \text{ GeV}$ ,  $m_W = 80.399 \text{ GeV}$ ),  $f_{\pm} = 0.010 \pm 0.022 \pm 0.030$  is obtained.

<sup>8</sup>AFFOLDER 00B studied the angular distribution of leptonic decays of  $W$  bosons in  $t \rightarrow Wb$  events. The ratio  $F_0$  is the fraction of the helicity zero (longitudinal)  $W$  bosons in the decaying top quark rest frame.  $B(t \rightarrow W_{\pm} b)$  is the fraction of positive helicity (right-handed) positive charge  $W$  bosons in the top quark decays. It is obtained by assuming the Standard Model value of  $F_0$ .

<sup>9</sup>Results are based on  $2.7 \text{ fb}^{-1}$  of data in  $p\bar{p}$  collisions at  $\sqrt{s} = 1.96 \text{ TeV}$ .  $F_0$  result is obtained by assuming  $F_{\pm} = 0$ , while  $F_{\pm}$  result is obtained for  $F_0 = 0.70$ , the SM value. Model independent fits for the two fractions give  $F_0 = 0.88 \pm 0.11 \pm 0.06$  and  $F_{\pm} = -0.15 \pm 0.07 \pm 0.06$  with correlation coefficient of  $-0.59$ . The results are for  $m_t = 175 \text{ GeV}$ .

<sup>10</sup>Results are based on  $1.9 \text{ fb}^{-1}$  of data in  $p\bar{p}$  collisions at  $\sqrt{s} = 1.96 \text{ TeV}$ .  $F_0$  result is obtained assuming  $F_{\pm} = 0$ , while  $F_{\pm}$  result is obtained for  $F_0 = 0.70$ , the SM values.

Model independent fits for the two fractions give  $F_0 = 0.66 \pm 0.16 \pm 0.05$  and  $F_{\pm} = -0.03 \pm 0.06 \pm 0.03$ .

<sup>11</sup>Based on  $1 \text{ fb}^{-1}$  at  $\sqrt{s} = 1.96 \text{ TeV}$ .

<sup>12</sup>Based on  $318 \text{ pb}^{-1}$  of data at  $\sqrt{s} = 1.96 \text{ TeV}$ .

<sup>13</sup>Based on  $200 \text{ pb}^{-1}$  of data at  $\sqrt{s} = 1.96 \text{ TeV}$ .  $t \rightarrow Wb \rightarrow \ell\nu b$  ( $\ell = e$  or  $\mu$ ). The errors are stat + syst.

<sup>14</sup>ABAZOV 05G studied the angular distribution of leptonic decays of  $W$  bosons in  $t\bar{t}$  candidate events with lepton + jets final states, and obtained the fraction of longitudinally polarized  $W$  under the constraint of no right-handed current,  $F_{\pm} = 0$ . Based on  $125 \text{ pb}^{-1}$  of data at  $\sqrt{s} = 1.8 \text{ TeV}$ .

## $F_{-}$

VALUE	CL%	DOCUMENT ID	TECN COMMENT
<b><math>0.320 \pm 0.013</math></b>	<b>OUR AVERAGE</b>		
$> 0.264 \pm 0.044$	95	<sup>1</sup> AABOUD	17BB ATLS $F_{-} = f_1(1 - f_1^{\pm})$
$0.323 \pm 0.008 \pm 0.014$		<sup>2</sup> KHACHATRYAN16BU	CMS $F_{-} = B(t \rightarrow W_{-} b)$
$0.310 \pm 0.022 \pm 0.022$		<sup>3</sup> CHATRCHYAN13BH	CMS $F_{-} = B(t \rightarrow W_{-} b)$
$0.32 \pm 0.04$		<sup>4</sup> AAD	12BG ATLS $F_{-} = B(t \rightarrow W_{-} b)$

<sup>1</sup>AABOUD 17BB based on  $20.2 \text{ fb}^{-1}$  of  $pp$  data at  $\sqrt{s} = 8 \text{ TeV}$ . Triple-differential decay rate of top quark in the  $t$ -channel single-top production is used to simultaneously determine five generalized  $Wtb$  couplings as well as the top polarization. No assumption is made for the other couplings. The authors reported  $f_1 = 0.30 \pm 0.05$  and  $f_1^{\pm} < 0.120$  which we converted to  $F_{-} = f_1(1 - f_1^{\pm})$ . See this paper for constraints on other couplings not included here.

<sup>2</sup>KHACHATRYAN 16BU based on  $19.8 \text{ fb}^{-1}$  of  $pp$  data at  $\sqrt{s} = 8 \text{ TeV}$  using  $t\bar{t}$  events with  $\ell + E_T + \geq 4$  jets ( $\geq 2 b$ ). The errors of  $F_0$  and  $F_{\pm}$  are correlated with a correlation coefficient  $\rho(F_0, F_{\pm}) = -0.87$ . The result is consistent with the NNLO SM prediction of  $0.311 \pm 0.005$  for  $m_t = 172.8 \pm 1.3 \text{ GeV}$ .

<sup>3</sup>Based on  $5.0 \text{ fb}^{-1}$  of  $pp$  data at  $\sqrt{s} = 7 \text{ TeV}$ . CHATRCHYAN 13BH studied  $tt$  events with large  $E_T$  and  $\ell + \geq 4$  jets using a constrained kinematic fit.

<sup>4</sup>Based on  $1.04 \text{ fb}^{-1}$  of  $pp$  data at  $\sqrt{s} = 7 \text{ TeV}$ . AAD 12BG studied  $tt$  events with large  $E_T$  and either  $\ell + \geq 4j$  or  $\ell\ell + \geq 2j$ . The uncertainties are not independent,  $\rho(F_0, F_{\pm}) = -0.96$ .

## $F_{+}$

VALUE	CL%	DOCUMENT ID	TECN COMMENT
<b><math>0.002 \pm 0.011</math></b>	<b>OUR AVERAGE</b>		
$< 0.036 \pm 0.006$	95	<sup>1</sup> AABOUD	17BB ATLS $F_{+} = f_1 f_1^{\pm}$
$-0.004 \pm 0.005 \pm 0.014$		<sup>2</sup> KHACHATRYAN16BU	CMS $F_{+} = B(t \rightarrow W_{+} b)$
$-0.045 \pm 0.044 \pm 0.058$		<sup>3</sup> AALTONEN	13D CDF $F_{+} = B(t \rightarrow W_{+} b)$
$0.008 \pm 0.012 \pm 0.014$		<sup>4</sup> CHATRCHYAN13BH	CMS $F_{+} = B(t \rightarrow W_{+} b)$
$0.01 \pm 0.05$		<sup>5</sup> AAD	12BG ATLS $F_{+} = B(t \rightarrow W_{+} b)$
$0.023 \pm 0.041 \pm 0.034$		<sup>6</sup> ABAZOV	11C D0 $F_{+} = B(t \rightarrow W_{+} b)$
$0.11 \pm 0.15$		<sup>7</sup> AFFOLDER	00B CDF $F_{+} = B(t \rightarrow W_{+} b)$
$-0.033 \pm 0.034 \pm 0.031$		<sup>8</sup> AALTONEN	12Z TEVA $F_{+} = B(t \rightarrow W_{+} b)$
$-0.01 \pm 0.02 \pm 0.05$		<sup>9</sup> AALTONEN	10Q CDF Repl. by AALTONEN 13D
$-0.04 \pm 0.04 \pm 0.03$		<sup>10</sup> AALTONEN	09Q CDF Repl. by AALTONEN 10Q
$0.119 \pm 0.090 \pm 0.053$		<sup>11</sup> ABAZOV	08B D0 Repl. by ABAZOV 11c
$0.056 \pm 0.080 \pm 0.057$		<sup>12</sup> ABAZOV	07D D0 $F_{+} = B(t \rightarrow W_{+} b)$
$0.05^{+0.11}_{-0.05} \pm 0.03$		<sup>13</sup> ABULENCIA	07I CDF $F_{+} = B(t \rightarrow W_{+} b)$
$< 0.26$	95	<sup>13</sup> ABULENCIA	07I CDF $F_{+} = B(t \rightarrow W_{+} b)$
$< 0.27$	95	<sup>14</sup> ABULENCIA	06U CDF $F_{+} = B(t \rightarrow W_{+} b)$
$0.00 \pm 0.13 \pm 0.07$		<sup>15</sup> ABAZOV	05L D0 $F_{+} = B(t \rightarrow W_{+} b)$
$< 0.25$	95	<sup>15</sup> ABAZOV	05L D0 $F_{+} = B(t \rightarrow W_{+} b)$
$< 0.24$	95	<sup>16</sup> ACOSTA	05D CDF $F_{+} = B(t \rightarrow W_{+} b)$

<sup>1</sup>AABOUD 17BB based on  $20.2 \text{ fb}^{-1}$  of  $pp$  data at  $\sqrt{s} = 8 \text{ TeV}$ . Triple-differential decay rate of top quark in the  $t$ -channel single-top production is used to simultaneously determine five generalized  $Wtb$  couplings as well as the top polarization. No assumption is made for the other couplings. The authors reported  $f_1 = 0.30 \pm 0.05$  and  $f_1^{\pm} < 0.120$  which we converted to  $F_{+} = f_1 f_1^{\pm}$ . See this paper for constraints on other couplings not included here.

<sup>2</sup>KHACHATRYAN 16BU based on  $19.8 \text{ fb}^{-1}$  of  $pp$  data at  $\sqrt{s} = 8 \text{ TeV}$  using  $t\bar{t}$  events with  $\ell + E_T + \geq 4$  jets ( $\geq 2 b$ ). The result is consistent with the NNLO SM prediction of  $0.0017 \pm 0.0001$  for  $m_t = 172.8 \pm 1.3 \text{ GeV}$ .

<sup>3</sup>Based on  $8.7 \text{ fb}^{-1}$  of data in  $p\bar{p}$  collisions at  $\sqrt{s} = 1.96 \text{ TeV}$  using  $t\bar{t}$  events with  $\ell + E_T + \geq 4$  jets ( $\geq 1 b$ ), and under the constraint  $F_0 + F_{\pm} + F_{\mp} = 1$ . The statistical errors of  $F_0$  and  $F_{\pm}$  are correlated with correlation coefficient  $\rho(F_0, F_{\pm}) = -0.69$ .

<sup>4</sup>Based on  $5.0 \text{ fb}^{-1}$  of  $pp$  data at  $\sqrt{s} = 7 \text{ TeV}$ . CHATRCHYAN 13BH studied  $tt$  events with large  $E_T$  and  $\ell + \geq 4$  jets using a constrained kinematic fit.

<sup>5</sup>Based on  $1.04 \text{ fb}^{-1}$  of  $pp$  data at  $\sqrt{s} = 7 \text{ TeV}$ . AAD 12BG studied  $tt$  events with large  $E_T$  and either  $\ell + \geq 4j$  or  $\ell\ell + \geq 2j$ .

<sup>6</sup>Results are based on  $5.4 \text{ fb}^{-1}$  of data in  $p\bar{p}$  collisions at  $1.96 \text{ TeV}$ , including those of ABAZOV 08B. Under the SM constraint of  $f_0 = 0.698$  (for  $m_t = 173.3 \text{ GeV}$ ,  $m_W = 80.399 \text{ GeV}$ ),  $f_{\pm} = 0.010 \pm 0.022 \pm 0.030$  is obtained.

<sup>7</sup>AFFOLDER 00B studied the angular distribution of leptonic decays of  $W$  bosons in  $t \rightarrow Wb$  events. The ratio  $F_0$  is the fraction of the helicity zero (longitudinal)  $W$  bosons in the decaying top quark rest frame.  $B(t \rightarrow W_{\pm} b)$  is the fraction of positive helicity (right-handed) positive charge  $W$  bosons in the top quark decays. It is obtained by assuming the Standard Model value of  $F_0$ .

<sup>8</sup>Based on  $2.7$  and  $5.1 \text{ fb}^{-1}$  of CDF data in  $\ell +$  jets and dilepton channels, and  $5.4 \text{ fb}^{-1}$  of D0 data in  $\ell +$  jets and dilepton channels.  $F_0 = 0.682 \pm 0.035 \pm 0.046$  if  $F_{\pm} = 0.0017(1)$ , while  $F_{\pm} = -0.015 \pm 0.018 \pm 0.030$  if  $F_0 = 0.688(4)$ , where the assumed

fixed values are the SM prediction for  $m_t = 173.3 \pm 1.1$  GeV and  $m_W = 80.399 \pm 0.023$  GeV.

<sup>9</sup> Results are based on  $2.7 \text{ fb}^{-1}$  of data in  $p\bar{p}$  collisions at  $\sqrt{s} = 1.96$  TeV.  $F_0$  result is obtained by assuming  $F_{\pm} = 0$ , while  $F_{\pm}$  result is obtained for  $F_0 = 0.70$ , the SM value. Model independent fits for the two fractions give  $F_0 = 0.88 \pm 0.11 \pm 0.06$  and  $F_{\pm} = -0.15 \pm 0.07 \pm 0.06$  with correlation coefficient of  $-0.59$ . The results are for  $m_t = 175$  GeV.

<sup>10</sup> Results are based on  $1.9 \text{ fb}^{-1}$  of data in  $p\bar{p}$  collisions at  $\sqrt{s} = 1.96$  TeV.  $F_0$  result is obtained assuming  $F_{\pm} = 0$ , while  $F_{\pm}$  result is obtained for  $F_0 = 0.70$ , the SM values. Model independent fits for the two fractions give  $F_0 = 0.66 \pm 0.16 \pm 0.05$  and  $F_{\pm} = -0.03 \pm 0.06 \pm 0.03$ .

<sup>11</sup> Based on  $1 \text{ fb}^{-1}$  at  $\sqrt{s} = 1.96$  TeV.

<sup>12</sup> Based on  $370 \text{ pb}^{-1}$  of data at  $\sqrt{s} = 1.96$  TeV, using the  $\ell + \text{jets}$  and dilepton decay channels. The result assumes  $F_0 = 0.70$ , and it gives  $F_{\pm} < 0.23$  at 95% CL.

<sup>13</sup> Based on  $318 \text{ pb}^{-1}$  of data at  $\sqrt{s} = 1.96$  TeV.

<sup>14</sup> Based on  $200 \text{ pb}^{-1}$  of data at  $\sqrt{s} = 1.96$  TeV.  $t \rightarrow Wb \rightarrow \ell\nu b$  ( $\ell = e$  or  $\mu$ ). The errors are stat + syst.

<sup>15</sup> ABAZOV 05L studied the angular distribution of leptonic decays of  $W$  bosons in  $t\bar{t}$  events, where one of the  $W$ 's from  $t$  or  $\bar{t}$  decays into  $e$  or  $\mu$  and the other decays hadronically. The fraction of the "+" helicity  $W$  boson is obtained by assuming  $F_0 = 0.7$ , which is the generic prediction for any linear combination of V and A currents. Based on  $230 \pm 15 \text{ pb}^{-1}$  of data at  $\sqrt{s} = 1.96$  TeV.

<sup>16</sup> ACOSTA 05D measures the  $m_{\ell^+b}^2$  distribution in  $t\bar{t}$  production events where one or both  $W$ 's decay leptonically to  $\ell = e$  or  $\mu$ , and finds a bound on the V+A coupling of the  $t b W$  vertex. By assuming the SM value of the longitudinal  $W$  fraction  $F_0 = B(t \rightarrow W_0 b) = 0.70$ , the bound on  $F_{\pm}$  is obtained. If the results are combined with those of AFFOLDER 00B, the bounds become  $F_{V+A} < 0.61$  (95% CL) and  $F_{\pm} < 0.18$  (95% CL), respectively. Based on  $109 \pm 7 \text{ pb}^{-1}$  of data at  $\sqrt{s} = 1.8$  TeV (run I).

### $F_{V+A}$

VALUE	CL%	DOCUMENT ID	TECN	COMMENT
$< 0.29$	95	<sup>1</sup> ABULENCIA 07G CDF		$F_{V+A} = B(t \rightarrow Wb_R)$

• • • We do not use the following data for averages, fits, limits, etc. • • •

$-0.06 \pm 0.22 \pm 0.12$		<sup>1</sup> ABULENCIA 07G CDF		$F_{V+A} = B(t \rightarrow Wb_R)$
$< 0.80$	95	<sup>2</sup> ACOSTA 05D CDF		$F_{V+A} = B(t \rightarrow Wb_R)$

<sup>1</sup> Based on  $700 \text{ pb}^{-1}$  of data at  $\sqrt{s} = 1.96$  TeV.

<sup>2</sup> ACOSTA 05D measures the  $m_{\ell^+b}^2$  distribution in  $t\bar{t}$  production events where one or both  $W$ 's decay leptonically to  $\ell = e$  or  $\mu$ , and finds a bound on the V+A coupling of the  $t b W$  vertex. By assuming the SM value of the longitudinal  $W$  fraction  $F_0 = B(t \rightarrow W_0 b) = 0.70$ , the bound on  $F_{\pm}$  is obtained. If the results are combined with those of AFFOLDER 00B, the bounds become  $F_{V+A} < 0.61$  (95% CL) and  $F_{\pm} < 0.18$  (95% CL), respectively. Based on  $109 \pm 7 \text{ pb}^{-1}$  of data at  $\sqrt{s} = 1.8$  TeV (run I).

### $f_1^R$

VALUE	CL%	DOCUMENT ID	TECN	COMMENT
• • • We do not use the following data for averages, fits, limits, etc. • • •				

$ f_1^R/f_2^R  < 0.37$	95	<sup>1</sup> AABOUD 17BB ATLS		$t$ -channel single top
$ f_1^R  < 0.16$	95	<sup>2</sup> KHACHATRYAN...17G CMS		$t$ -channel single- $t$ prod.
$-0.20 < \text{Re}(V_{tb} f_1^R) < 0.23$	95	<sup>3</sup> AAD 12BG ATLS		Constr. on $Wtb$ vtx
$(V_{tb} f_1^R)^2 < 0.93$	95	<sup>4</sup> ABAZOV 12E D0		Single-top
$ f_1^R ^2 < 0.30$	95	<sup>5</sup> ABAZOV 12I D0		single- $t + W$ helicity
$ f_1^R ^2 < 1.01$	95	<sup>6</sup> ABAZOV 09J D0		$ f_1^L  = 1,  f_2^L  =  f_2^R  = 0$
$ f_1^R ^2 < 2.5$	95	<sup>7</sup> ABAZOV 08AI D0		$ f_1^L ^2 = 1.8^{+1.0}_{-1.3}$

<sup>1</sup> AABOUD 17BB based on  $20.2 \text{ fb}^{-1}$  of  $pp$  data at  $\sqrt{s} = 8$  TeV. Triple-differential decay rate of top quark is used to simultaneously determine five generalized  $Wtb$  couplings as well as the top polarization. No assumption is made for the other couplings. See this paper for constraints on other couplings not included here.

<sup>2</sup> KHACHATRYAN 17G based on  $5.0$  and  $19.7 \text{ fb}^{-1}$  of  $pp$  data at  $\sqrt{s} = 7$  and  $8$  TeV, respectively. A Bayesian neural network technique is used to discriminate between signal and backgrounds. This is a 95% CL exclusion limit obtained by a three-dimensional fit with simultaneous variation of  $(f_1^L, f_1^R, f_2^R)$ .

<sup>3</sup> Based on  $1.04 \text{ fb}^{-1}$  of  $pp$  data at  $\sqrt{s} = 7$  TeV. AAD 12BG studied  $t\bar{t}$  events with large  $E_T$  and either  $\ell + \geq 4j$  or  $\ell\ell + \geq 2j$ .

<sup>4</sup> Based on  $5.4 \text{ fb}^{-1}$  of data. For each value of the form factor quoted the other two are assumed to have their SM value. Their Fig. 4 shows two-dimensional posterior probability density distributions for the anomalous couplings.

<sup>5</sup> Based on  $5.4 \text{ fb}^{-1}$  of data in  $p\bar{p}$  collisions at  $1.96$  TeV. Results are obtained by combining the limits from the  $W$  helicity measurements and those from the single top quark production.

<sup>6</sup> Based on  $1 \text{ fb}^{-1}$  of data at  $p\bar{p}$  collisions  $\sqrt{s} = 1.96$  TeV. Combined result of the  $W$  helicity measurement in  $t\bar{t}$  events (ABAZOV 08B) and the search for anomalous  $t b W$  couplings in the single top production (ABAZOV 08AI). Constraints when  $f_1^L$  and one of the anomalous couplings are simultaneously allowed to vary are given in their Fig. 1 and Table 1.

<sup>7</sup> Result is based on  $0.9 \text{ fb}^{-1}$  of data at  $\sqrt{s} = 1.96$  TeV. Single top quark production events are used to measure the Lorentz structure of the  $t b W$  coupling. The upper bounds on the non-standard couplings are obtained when only one non-standard coupling is allowed to be present together with the SM one,  $f_1^L = V_{tb}^*$ .

### $f_2^L$

VALUE	CL%	DOCUMENT ID	TECN	COMMENT
• • • We do not use the following data for averages, fits, limits, etc. • • •				

$ f_2^L/f_1^L  < 0.29$	95	<sup>1</sup> AABOUD 17BB ATLS		$t$ -channel single top
$ f_2^L  < 0.057$	95	<sup>2</sup> KHACHATRYAN...17G CMS		$t$ -channel single- $t$ prod.
$-0.14 < \text{Re}(f_2^L) < 0.11$	95	<sup>3</sup> AAD 12BG ATLS		Constr. on $Wtb$ vtx

$(V_{tb} f_2^L)^2 < 0.13$	95	<sup>4</sup> ABAZOV 12E D0		Single-top
$ f_2^L ^2 < 0.05$	95	<sup>5</sup> ABAZOV 12I D0		single- $t + W$ helicity
$ f_2^L ^2 < 0.28$	95	<sup>6</sup> ABAZOV 09J D0		$ f_1^L  = 1,  f_1^R  =  f_2^R  = 0$
$ f_2^L ^2 < 0.5$	95	<sup>7</sup> ABAZOV 08AI D0		$ f_1^L ^2 = 1.4^{+0.6}_{-0.5}$

<sup>1</sup> AABOUD 17BB based on  $20.2 \text{ fb}^{-1}$  of  $pp$  data at  $\sqrt{s} = 8$  TeV. Triple-differential decay rate of top quark is used to simultaneously determine five generalized  $Wtb$  couplings as well as the top polarization. No assumption is made for the other couplings. See this paper for constraints on other couplings not included here.

<sup>2</sup> KHACHATRYAN 17G based on  $5.0$  and  $19.7 \text{ fb}^{-1}$  of  $pp$  data at  $\sqrt{s} = 7$  and  $8$  TeV, respectively. A Bayesian neural network technique is used to discriminate between signal and backgrounds. This is a 95% CL exclusion limit obtained by a three-dimensional fit with simultaneous variation of  $(f_1^L, f_2^L, f_2^R)$ .

<sup>3</sup> Based on  $1.04 \text{ fb}^{-1}$  of  $pp$  data at  $\sqrt{s} = 7$  TeV. AAD 12BG studied  $t\bar{t}$  events with large  $E_T$  and either  $\ell + \geq 4j$  or  $\ell\ell + \geq 2j$ .

<sup>4</sup> Based on  $5.4 \text{ fb}^{-1}$  of data. For each value of the form factor quoted the other two are assumed to have their SM value. Their Fig. 4 shows two-dimensional posterior probability density distributions for the anomalous couplings.

<sup>5</sup> Based on  $5.4 \text{ fb}^{-1}$  of data in  $p\bar{p}$  collisions at  $1.96$  TeV. Results are obtained by combining the limits from the  $W$  helicity measurements and those from the single top quark production.

<sup>6</sup> Based on  $1 \text{ fb}^{-1}$  of data at  $p\bar{p}$  collisions  $\sqrt{s} = 1.96$  TeV. Combined result of the  $W$  helicity measurement in  $t\bar{t}$  events (ABAZOV 08B) and the search for anomalous  $t b W$  couplings in the single top production (ABAZOV 08AI). Constraints when  $f_1^L$  and one of the anomalous couplings are simultaneously allowed to vary are given in their Fig. 1 and Table 1.

<sup>7</sup> Result is based on  $0.9 \text{ fb}^{-1}$  of data at  $\sqrt{s} = 1.96$  TeV. Single top quark production events are used to measure the Lorentz structure of the  $t b W$  coupling. The upper bounds on the non-standard couplings are obtained when only one non-standard coupling is allowed to be present together with the SM one,  $f_1^L = V_{tb}^*$ .

### $f_2^R$

VALUE	CL%	DOCUMENT ID	TECN	COMMENT
• • • We do not use the following data for averages, fits, limits, etc. • • •				

$-0.12 < \text{Re}(f_2^R/f_1^L) < 0.17$	95	<sup>1</sup> AABOUD 17BB ATLS		$t$ -channel single top
$-0.07 < \text{Im}(f_2^R/f_1^L) < 0.06$	95	<sup>1</sup> AABOUD 17BB ATLS		$t$ -channel single top
$-0.18 < \text{Im}(f_2^R) < 0.06$	95	<sup>2</sup> AABOUD 17I ATLS		$t$ -channel single top
$-0.049 < f_2^R < 0.048$	95	<sup>3</sup> KHACHATRYAN...17G CMS		$t$ -channel single top
$-0.36 < \text{Re}(f_2^R/f_1^L) < 0.10$	95	<sup>4</sup> AAD 16AK ATLS		Single-top
$-0.17 < \text{Im}(f_2^R/f_1^L) < 0.23$	95	<sup>4</sup> AAD 16AK ATLS		Single-top
$-0.08 < \text{Re}(f_2^R) < 0.04$	95	<sup>5</sup> AAD 12BG ATLS		Constr. on $Wtb$ vtx
$(V_{tb} f_2^R)^2 < 0.06$	95	<sup>6</sup> ABAZOV 12E D0		Single-top
$ f_2^R ^2 < 0.12$	95	<sup>7</sup> ABAZOV 12I D0		single- $t + W$ helicity
$ f_2^R ^2 < 0.23$	95	<sup>8</sup> ABAZOV 09J D0		$ f_1^L  = 1,  f_1^R  =  f_2^L  = 0$
$ f_2^R ^2 < 0.3$	95	<sup>9</sup> ABAZOV 08AI D0		$ f_1^L ^2 = 1.4^{+0.9}_{-0.8}$

<sup>1</sup> AABOUD 17BB based on  $20.2 \text{ fb}^{-1}$  of  $pp$  data at  $\sqrt{s} = 8$  TeV. Triple-differential decay rate of top quark is used to simultaneously determine five generalized  $Wtb$  couplings as well as the top polarization. No assumption is made for the other couplings. See this paper for constraints on other couplings not included here.

<sup>2</sup> AABOUD 17I based on  $20.2 \text{ fb}^{-1}$  of  $pp$  data at  $\sqrt{s} = 8$  TeV. A cut-based analysis is used to discriminate between signal and backgrounds. All anomalous couplings other than  $\text{Im}(f_2^R)$  are assumed to be zero. See this paper for a number of other asymmetries and measurements that are not included here.

<sup>3</sup> KHACHATRYAN 17G based on  $5.0$  and  $19.7 \text{ fb}^{-1}$  of  $pp$  data at  $\sqrt{s} = 7$  and  $8$  TeV, respectively. A Bayesian neural network technique is used to discriminate between signal and backgrounds. This is a 95% CL exclusion limit obtained by a three-dimensional fit with simultaneous variation of  $(f_1^L, f_2^L, f_2^R)$ .

<sup>4</sup> AAD 16AK based on  $4.6 \text{ fb}^{-1}$  of  $pp$  data at  $\sqrt{s} = 7$  TeV. The results are obtained from an analysis of angular distributions of the decay products of single top quarks, assuming  $f_1^R = f_2^R = 0$ . The fraction of decays containing transversely polarized  $W$  is measured to be  $F_{\pm} + F_{\mp} = 0.37 \pm 0.07$ .

<sup>5</sup> Based on  $1.04 \text{ fb}^{-1}$  of  $pp$  data at  $\sqrt{s} = 7$  TeV. AAD 12BG studied  $t\bar{t}$  events with large  $E_T$  and either  $\ell + \geq 4j$  or  $\ell\ell + \geq 2j$ .

<sup>6</sup> Based on  $5.4 \text{ fb}^{-1}$  of data. For each value of the form factor quoted the other two are assumed to have their SM value. Their Fig. 4 shows two-dimensional posterior probability density distributions for the anomalous couplings.

<sup>7</sup> Based on  $5.4 \text{ fb}^{-1}$  of data in  $p\bar{p}$  collisions at  $1.96$  TeV. Results are obtained by combining the limits from the  $W$  helicity measurements and those from the single top quark production.

<sup>8</sup> Based on  $1 \text{ fb}^{-1}$  of data at  $p\bar{p}$  collisions  $\sqrt{s} = 1.96$  TeV. Combined result of the  $W$  helicity measurement in  $t\bar{t}$  events (ABAZOV 08B) and the search for anomalous  $t b W$  couplings in the single top production (ABAZOV 08AI). Constraints when  $f_1^L$  and one of the anomalous couplings are simultaneously allowed to vary are given in their Fig. 1 and Table 1.

<sup>9</sup> Result is based on  $0.9 \text{ fb}^{-1}$  of data at  $\sqrt{s} = 1.96$  TeV. Single top quark production events are used to measure the Lorentz structure of the  $t b W$  coupling. The upper bounds on the non-standard couplings are obtained when only one non-standard coupling is allowed to be present together with the SM one,  $f_1^L = V_{tb}^*$ .

### $|f_{LV} V_{tb}|$

Assumed that the top-quark-related CKM matrix elements obey the relation  $|V_{td}|, |V_{ts}| \ll |V_{tb}|$  and a form factor  $f_{LV}$  is determined for each production mode and centre-of-mass energy.

VALUE	DOCUMENT ID	TECN	COMMENT
<b><math>1.02 \pm 0.04 \pm 0.02</math></b>	<sup>1</sup> AABOUD 19R LHC		ATLAS + CMS at $7, 8$ TeV

<sup>1</sup> The combination of single-top production cross-section measurements in the  $t$ -channel,  $tW$ , and  $s$ -channel production modes from ATLAS and CMS at  $\sqrt{s} = 7$  and  $8$  TeV.

## Quark Particle Listings

t

Chromo-magnetic dipole moment  $\mu_t = g_s \hat{\mu}_t / m_t$ 

VALUE	CL%	DOCUMENT ID	TECN	COMMENT
-------	-----	-------------	------	---------

- • • We do not use the following data for averages, fits, limits, etc. • • •
- $-0.014 < \hat{\mu}_t < 0.004$  95 1 SIRUNYAN 19bx CMS  $\ell\ell + \geq 2j$  ( $\geq 1b$ )
- $-0.053 < \text{Re}(\hat{\mu}_t) < 0.026$  95 2 KHACHATRYAN...16AI CMS  $\ell\ell + \geq 2j$  ( $\geq 1b$ )
- 1 SIRUNYAN 19bx based on 35.9 fb<sup>-1</sup> of  $pp$  data at  $\sqrt{s} = 13$  TeV. A set of parton-level normalized differential cross sections is measured to extract coefficients of the spin-dependent  $t\bar{t}$  production density matrix. The coefficients are compared with the NLO MC simulations and with the NLO QCD calculation including EW corrections.
- 2 KHACHATRYAN 16AI based on 19.5 fb<sup>-1</sup> of  $pp$  data at  $\sqrt{s} = 8$  TeV, using lepton angular distributions as a function of the  $t\bar{t}$ -system kinematical variables.

Chromo-electric dipole moment  $d_t = g_s \hat{d}_t / m_t$ 

VALUE	CL%	DOCUMENT ID	TECN	COMMENT
-------	-----	-------------	------	---------

- • • We do not use the following data for averages, fits, limits, etc. • • •
- $-0.020 < \hat{d}_t < 0.012$  95 1 SIRUNYAN 19bx CMS  $\ell\ell + \geq 2j$  ( $\geq 1b$ )
- $-0.068 < \text{Im}(\hat{d}_t) < 0.067$  95 2 KHACHATRYAN...16AI CMS  $\ell\ell + \geq 2j$  ( $\geq 1b$ )
- 1 SIRUNYAN 19bx based on 35.9 fb<sup>-1</sup> of  $pp$  data at  $\sqrt{s} = 13$  TeV. A set of parton-level normalized differential cross sections is measured to extract coefficients of the spin-dependent  $t\bar{t}$  production density matrix and constrain the anomalous chromomagnetic and chromoelectric dipole moments of the top quark. The coefficients are compared with the NLO MC simulations and with the NLO QCD calculation including EW corrections.
- 2 KHACHATRYAN 16AI based on 19.5 fb<sup>-1</sup> of  $pp$  data at  $\sqrt{s} = 8$  TeV, using lepton angular distributions as a function of the  $t\bar{t}$ -system kinematical variables.

Spin Correlation in  $t\bar{t}$  Production in  $p\bar{p}$  Collisions

C is the correlation strength parameter, f is the ratio of events with correlated t and  $\bar{t}$  spins (SM prediction: f = 1), and  $\kappa$  is the spin correlation coefficient. See "The Top Quark" review for more information.

VALUE	DOCUMENT ID	TECN	COMMENT
-------	-------------	------	---------

- • • We do not use the following data for averages, fits, limits, etc. • • •
- $0.89 \pm 0.22$  1 ABAZOV 16A D0 f ( $\ell\ell + \geq 2$  jets,  $\ell + \geq 4$  jets)
- $0.85 \pm 0.29$  2 ABAZOV 12B D0 f ( $\ell\ell + \geq 2$  jets,  $\ell + \geq 4$  jets)
- $1.15^{+0.42}_{-0.43}$  3 ABAZOV 12B D0 f ( $\ell + \cancel{E}_T + \geq 4$  jets)
- $0.60^{+0.50}_{-0.16}$  4 AALTONEN 11AR CDF  $\kappa$  ( $\ell + \cancel{E}_T + \geq 4$  jets)
- $0.74^{+0.40}_{-0.41}$  5 ABAZOV 11AE D0 f ( $\ell\ell + \cancel{E}_T + \geq 2$  jets)
- $0.10 \pm 0.45$  6 ABAZOV 11AF D0 C ( $\ell\ell + \cancel{E}_T + \geq 2$  jets)
- 1 ABAZOV 16A based on 9.7 fb<sup>-1</sup> of data. A matrix element method is used. It corresponds to evidence of spin correlation at 4.2 $\sigma$  and is in agreement with the NLO SM prediction  $0.80^{+0.01}_{-0.02}$ .
- 2 This is a combination of the lepton + jets analysis presented in ABAZOV 12B and the dilepton measurement of ABAZOV 11AE. It provides a 3.1  $\sigma$  evidence for the  $t\bar{t}$  spin correlation.
- 3 Based on 5.3 fb<sup>-1</sup> of data. The error is statistical and systematic combined. A matrix element method is used.
- 4 Based on 4.3 fb<sup>-1</sup> of data. The measurement is based on the angular study of the top quark decay products in the helicity basis. The theory prediction is  $\kappa \approx 0.40$ .
- 5 Based on 5.4 fb<sup>-1</sup> of data using a matrix element method. The error is statistical and systematic combined. The no-correlation hypothesis is excluded at the 97.7% CL.
- 6 Based on 5.4 fb<sup>-1</sup> of data. The error is statistical and systematic combined. The NLO QCD prediction is C = 0.78  $\pm$  0.03. The neutrino weighting method is used for reconstruction of kinematics.

Spin Correlation in  $t\bar{t}$  Production in  $pp$  Collisions

Spin correlation,  $f_{SM}$ , measures the strength of the correlation between the spins of the pair produced  $t\bar{t}$ .  $f_{SM} = 1$  for the SM, while  $f_{SM} = 0$  for no spin correlation.

VALUE	DOCUMENT ID	TECN	COMMENT
-------	-------------	------	---------

- • • We do not use the following data for averages, fits, limits, etc. • • •
- $0.90 \pm 0.07 \pm 0.09 \pm 0.01$  1 SIRUNYAN 19bx CMS  $C_{kk}$  in  $\ell\ell + \geq 2j$  ( $\geq 1b$ )
- $1.13 \pm 0.32 \pm 0.32^{+0.10}_{-0.13}$  1 SIRUNYAN 19bx CMS  $C_{rr}$  in  $\ell\ell + \geq 2j$  ( $\geq 1b$ )
- $1.01 \pm 0.04 \pm 0.05 \pm 0.01$  1 SIRUNYAN 19bx CMS  $C_{nn}$  in  $\ell\ell + \geq 2j$  ( $\geq 1b$ )
- $0.94 \pm 0.17 \pm 0.26 \pm 0.01$  1 SIRUNYAN 19bx CMS  $C_{rk} + C_{kr}$  in  $\ell\ell + \geq 2j$  ( $\geq 1b$ )
- $0.98 \pm 0.03 \pm 0.04 \pm 0.01$  1 SIRUNYAN 19bx CMS  $(C_{kk} + C_{rr} + C_{nn})/3$  in  $\ell\ell + \geq 2j$  ( $\geq 1b$ )
- $0.74 \pm 0.07 \pm 0.19^{+0.06}_{-0.08}$  1 SIRUNYAN 19bx CMS  $A_{\cos\phi}^{lab}$  in  $\ell\ell + \geq 2j$  ( $\geq 1b$ )
- $1.05 \pm 0.03 \pm 0.08^{+0.09}_{-0.12}$  1 SIRUNYAN 19bx CMS  $A_{|\Delta\phi(\ell\ell)|}$  in  $\ell\ell + \geq 2j$  ( $\geq 1b$ )
- $1.12^{+0.12}_{-0.15}$  2 KHACHATRYAN...16AI CMS  $\ell\ell + \geq 2j$  ( $\geq 1b$ )
- $0.72 \pm 0.08^{+0.15}_{-0.13}$  3 KHACHATRYAN...16X CMS  $\mu + 4, 5j$
- $1.20 \pm 0.05 \pm 0.13$  4 AAD 15J ATLS  $\Delta\phi(\ell\ell)$  in  $\ell\ell + \geq 2j$  ( $\geq 1b$ )
- $1.19 \pm 0.09 \pm 0.18$  5 AAD 14BB ATLS  $\Delta\phi(\ell\ell)$  in  $\ell\ell + \geq 2j$  events
- $1.12 \pm 0.11 \pm 0.22$  5 AAD 14BB ATLS  $\Delta\phi(\ell j)$  in  $\ell + \geq 4j$  events
- $0.87 \pm 0.11 \pm 0.14$  5,6 AAD 14BB ATLS S-ratio in  $\ell\ell + \geq 2j$  events
- $0.75 \pm 0.19 \pm 0.23$  5,7 AAD 14BB ATLS  $\cos\theta(\ell^+) \cos\theta(\ell^-)$  in  $\ell\ell + \geq 2j$  events
- $0.83 \pm 0.14 \pm 0.18$  5,8 AAD 14BB ATLS  $\cos\theta(\ell^+) \cos\theta(\ell^-)$  in  $\ell\ell + \geq 2j$  events
- 1 SIRUNYAN 19bx based on 35.9 fb<sup>-1</sup> of  $pp$  data at  $\sqrt{s} = 13$  TeV. A set of parton-level normalized differential cross sections sensitive to coefficients of the spin-dependent  $t\bar{t}$  production density matrix is measured. The distributions and coefficients are compared with the NLO MC simulations and with the NLO QCD calculation including EW corrections. Three errors are from statistics, experimental systematics, and theory.

- 2 KHACHATRYAN 16AI based on 19.5 fb<sup>-1</sup> of  $pp$  data at  $\sqrt{s} = 8$  TeV, using lepton angular distributions as a function of the  $t\bar{t}$ -system kinematical variables.
- 3 KHACHATRYAN 16x based on 19.7 fb<sup>-1</sup> of  $pp$  data at  $\sqrt{s} = 8$  TeV. Uses a template fit method. Spin correlation strength in the helicity basis is given by  $A_{\text{hel}} = 0.23 \pm 0.03^{+0.05}_{-0.04}$ .
- 4 AAD 15J based on 20.3 fb<sup>-1</sup> of  $pp$  data at  $\sqrt{s} = 8$  TeV. Uses a fit including a linear superposition of  $\Delta\phi$  distribution from the SM NLO simulation with coefficient  $f_{SM}$  and from  $t\bar{t}$  simulation without spin correlation with coefficient  $(1 - f_{SM})$ .
- 5 Based on 4.6 fb<sup>-1</sup> of  $pp$  data at  $\sqrt{s} = 7$  TeV. The results are for  $m_t = 172.5$  GeV.
- 6 The S-ratio is defined as the SM spin correlation in the like-helicity gluon-gluon collisions normalized to the no spin correlation case; see eq. (6) for the LO expression.
- 7 The polar angle correlation along the helicity axis.
- 8 The polar angle correlation along the direction which maximizes the correlation.

t-quark FCNC Couplings  $\kappa_t^{uq}/\Lambda$  and  $\kappa_t^{cq}/\Lambda$ 

VALUE (TeV <sup>-1</sup> )	CL%	DOCUMENT ID	TECN	COMMENT
----------------------------	-----	-------------	------	---------

- • • We do not use the following data for averages, fits, limits, etc. • • •
- $< 0.0041$  95 1 KHACHATRYAN...17G CMS  $|\kappa_t^{tug}|/\Lambda$
- $< 0.018$  95 1 KHACHATRYAN...17G CMS  $|\kappa_t^{tcg}|/\Lambda$
- $< 0.0058$  95 2 AAD 16As ATLS  $\kappa_t^{tug}/\Lambda$
- $< 0.013$  95 2 AAD 16As ATLS  $\kappa_t^{tcg}/\Lambda$
- $< 0.0069$  95 3 AAD 12BP ATLS  $t\bar{t}ug/\Lambda$  ( $t\bar{t}cg = 0$ )
- $< 0.016$  95 3 AAD 12BP ATLS  $t\bar{t}cg/\Lambda$  ( $t\bar{t}ug = 0$ )
- $< 0.013$  95 4 ABAZOV 10K D0  $\kappa_t^{tug}/\Lambda$
- $< 0.057$  95 4 ABAZOV 10K D0  $\kappa_t^{tcg}/\Lambda$
- $< 0.018$  95 5 AALTONEN 09N CDF  $\kappa_t^{tug}/\Lambda$  ( $\kappa_t^{tcg} = 0$ )
- $< 0.069$  95 5 AALTONEN 09N CDF  $\kappa_t^{tcg}/\Lambda$  ( $\kappa_t^{tug} = 0$ )
- $< 0.037$  95 6 ABAZOV 07V D0  $\kappa_t^{tug}/\Lambda$
- $< 0.15$  95 6 ABAZOV 07V D0  $\kappa_t^{cug}/\Lambda$
- 1 KHACHATRYAN 17G based on 5.0 and 19.7 fb<sup>-1</sup> of  $pp$  data at  $\sqrt{s} = 7$  and 8 TeV, respectively.  $t$ -channel single top production is used. The result corresponds to  $B(t \rightarrow ug) < 2.0 \times 10^{-5}$  or  $B(t \rightarrow cg) < 4.1 \times 10^{-4}$ .
- 2 AAD 16As based on 20.3 fb<sup>-1</sup> of  $pp$  data at  $\sqrt{s} = 8$  TeV. The results are obtained from the 95% CL upper limit on the single top-quark production  $\sigma(qg \rightarrow t) \cdot B(t \rightarrow bW) < 3.4$  pb,  $B(t \rightarrow ug) < 4.0 \times 10^{-5}$  and  $B(t \rightarrow cg) < 2.0 \times 10^{-5}$ .
- 3 Based on 2.05 fb<sup>-1</sup> of  $pp$  data at  $\sqrt{s} = 7$  TeV. The results are obtained from the 95% CL upper limit on the single top-quark production  $\sigma(qg \rightarrow t) \cdot B(t \rightarrow bW) < 3.9$  pb, for  $u=q$  or  $q=c$ ,  $B(t \rightarrow ug) < 5.7 \times 10^{-5}$  and  $B(t \rightarrow cg) < 2.7 \times 10^{-4}$ .
- 4 Based on 2.3 fb<sup>-1</sup> of data in  $p\bar{p}$  collisions at  $\sqrt{s} = 1.96$  TeV. Upper limit of single top quark production cross section 0.20 pb and 0.27 pb via FCNC  $t$ - $u$ - $g$  and  $t$ - $c$ - $g$  couplings, respectively, lead to the bounds without assuming the absence of the other coupling.  $B(t \rightarrow u + g) < 2.0 \times 10^{-4}$  and  $B(t \rightarrow c + g) < 3.9 \times 10^{-3}$  follow.
- 5 Based on 2.2 fb<sup>-1</sup> of data in  $p\bar{p}$  collisions at  $\sqrt{s} = 1.96$  TeV. Upper limit of single top quark production cross section  $\sigma(u(c) + g \rightarrow t) < 1.8$  pb (95% CL) via FCNC  $t$ - $u$ - $g$  and  $t$ - $c$ - $g$  couplings lead to the bounds.  $B(t \rightarrow u + g) < 3.9 \times 10^{-4}$  and  $B(t \rightarrow c + g) < 5.7 \times 10^{-3}$  follow.
- 6 Result is based on 230 pb<sup>-1</sup> of data at  $\sqrt{s} = 1.96$  TeV. Absence of single top quark production events via FCNC  $t$ - $u$ - $g$  and  $t$ - $c$ - $g$  couplings lead to the upper bounds on the dimensioned couplings,  $\kappa_t^{tug}/\Lambda$  and  $\kappa_t^{cug}/\Lambda$ , respectively.

t-Quark Yukawa Coupling from  $t\bar{t}$  Kinematic Distributions in  $pp$  Collisions

The ratio of  $t$ -quark Yukawa coupling to its standard model predicted value.

VALUE	DOCUMENT ID	TECN	COMMENT
-------	-------------	------	---------

- • • We do not use the following data for averages, fits, limits, etc. • • •
- $1.07^{+0.34}_{-0.43}$  1 SIRUNYAN 19By CMS  $\ell + \text{jets}$ ,  $t\bar{t}$  threshold
- 1 SIRUNYAN 19By based on 35.8 fb<sup>-1</sup> of data at  $\sqrt{s} = 13$  TeV. Experimental sensitivity is enhanced in the low  $M_{t\bar{t}}$  region. The distributions of  $M_{t\bar{t}}$ ,  $|y_t - y_{\bar{t}}|$ , and the number of reconstructed jets are compared with predictions by different Yukawa couplings which include NNLO QCD and NLO EW corrections.

 $\sigma(Ht\bar{t})/\sigma(Ht\bar{t})_{SM}$ 

VALUE	CL%	DOCUMENT ID	TECN	COMMENT
-------	-----	-------------	------	---------

- • • We do not use the following data for averages, fits, limits, etc. • • •
- $0.72 \pm 0.24 \pm 0.38$  1 SIRUNYAN 19R CMS  $Ht\bar{t}$  ( $H \rightarrow b\bar{b}$ ,  $t\bar{t} \rightarrow \ell + \text{jets}$  or dilepton)
- $0.9 \pm 0.7 \pm 1.3$  2 SIRUNYAN 18BD CMS  $Ht\bar{t}$  ( $H \rightarrow b\bar{b}$ ,  $t\bar{t} \rightarrow \text{all jets}$ )
- $1.26^{+0.31}_{-0.26}$  3 SIRUNYAN 18L CMS combination of CMS
- $< 6.7$  95 4 AAD 15 ATLS  $Ht\bar{t}$ ;  $H \rightarrow \gamma\gamma$
- $2.8 \pm 1.0$  5 KHACHATRYAN...14H CMS  $H \rightarrow b\bar{b}, \tau\bar{\tau}, \gamma\gamma, WW/ZZ$  (leptons)
- 1 SIRUNYAN 19R based on 35.9 fb<sup>-1</sup> of  $pp$  data at 13 TeV. Multivariate techniques are employed to separate the signal from the dominant  $t\bar{t}$ - $jj$  background. The result is for  $m_H = 125$  GeV. The measured ratio corresponds to a signal significance of 1.6 $\sigma$  above the background-only hypothesis.
- 2 SIRUNYAN 18BD based on 35.9 fb<sup>-1</sup> of  $pp$  data at 13 TeV. A combined fit of signal and background templates to data is performed in six event categories separated by jet and  $b$ -jet multiplicities. An upper limit of 3.8 is obtained for the cross section ratio.
- 3 SIRUNYAN 18L based on up to 5.1, 19.7, and 35.9 fb<sup>-1</sup> of  $pp$  data at 7, 8, and 13 TeV, respectively. An excess of events is observed, with a significance of 5.2 standard deviations, over the expectation from the background-only hypothesis. The result is for the Higgs boson mass of 125.09 GeV.
- 4 Based on 4.5 fb<sup>-1</sup> of data at 7 TeV and 20.3 fb<sup>-1</sup> at 8 TeV. The result is for  $m_H = 125.4$  GeV. The measurement constrains the top quark Yukawa coupling strength parameter  $\kappa_t = Y_t/Y_t^{SM}$  to be  $-1.3 < \kappa_t < 8.0$  (95% CL).

<sup>5</sup> Based on  $5.1 \text{ fb}^{-1}$  of  $pp$  data at 7 TeV and  $19.7 \text{ fb}^{-1}$  at 8 TeV. The results are obtained by assuming the SM decay branching fractions for the Higgs boson of mass 125.6 GeV. The signal strength for individual Higgs decay channels are given in Fig. 13, and the preferred region in the  $(\kappa_V, \kappa_f)$  space is given in Fig. 14.

### Single $t$ -Quark Production Cross Section in $p\bar{p}$ Collisions at $\sqrt{s} = 1.8 \text{ TeV}$

Direct probe of the  $t b W$  coupling and possible new physics at  $\sqrt{s} = 1.8 \text{ TeV}$ .

VALUE (pb)	CL%	DOCUMENT ID	TECN	COMMENT
<24	95	<sup>1</sup> ACOSTA	04H	CDF $p\bar{p} \rightarrow tb + X, tqb + X$
<18	95	<sup>2</sup> ACOSTA	02	CDF $p\bar{p} \rightarrow tb + X$
<13	95	<sup>3</sup> ACOSTA	02	CDF $p\bar{p} \rightarrow tqb + X$

<sup>1</sup> ACOSTA 04H bounds single top-quark production from the  $s$ -channel  $W$ -exchange process,  $q'\bar{q} \rightarrow t\bar{b}$ , and the  $t$ -channel  $W$ -exchange process,  $q'g \rightarrow qt\bar{b}$ . Based on  $\sim 106 \text{ pb}^{-1}$  of data.

<sup>2</sup> ACOSTA 02 bounds the cross section for single top-quark production via the  $s$ -channel  $W$ -exchange process,  $q'\bar{q} \rightarrow t\bar{b}$ . Based on  $\sim 106 \text{ pb}^{-1}$  of data.

<sup>3</sup> ACOSTA 02 bounds the cross section for single top-quark production via the  $t$ -channel  $W$ -exchange process,  $q'g \rightarrow qt\bar{b}$ . Based on  $\sim 106 \text{ pb}^{-1}$  of data.

### Single $t$ -Quark Production Cross Section in $p\bar{p}$ Collisions at $\sqrt{s} = 1.96 \text{ TeV}$

Direct probes of the  $t b W$  coupling and possible new physics at  $\sqrt{s} = 1.96 \text{ TeV}$ .

OUR AVERAGE assumes that the systematic uncertainties are uncorrelated.

VALUE (pb)	CL%	DOCUMENT ID	TECN	COMMENT
$3.53^{+1.25}_{-1.16}$		<sup>1</sup> AALTONEN	16	CDF $s- + t$ -channels ( $0\ell + \mathcal{E}_T + 2, 3j$ ( $\geq 1b$ -tag))
$2.25^{+0.29}_{-0.31}$		<sup>2</sup> AALTONEN	15H	TEVA $t$ -channel
$3.30^{+0.52}_{-0.40}$		<sup>2,3</sup> AALTONEN	15H	TEVA $s- + t$ -channels
$1.12^{+0.61}_{-0.57}$		<sup>4</sup> AALTONEN	14K	CDF $s$ -channel ( $0\ell + \mathcal{E}_T + 2, 3j$ ( $\geq 1b$ -tag))
$1.41^{+0.44}_{-0.42}$		<sup>5</sup> AALTONEN	14L	CDF $s$ -channel ( $\ell + \mathcal{E}_T + 2j$ ( $\geq 1b$ -tag))
$1.29^{+0.26}_{-0.24}$		<sup>6</sup> AALTONEN	14M	TEVA $s$ -channel (CDF + D0)
$3.04^{+0.57}_{-0.53}$		<sup>7</sup> AALTONEN	14o	CDF $s + t + Wt$ ( $\ell + \mathcal{E}_T + 2$ or 3 jets ( $\geq 1b$ -tag))
$1.10^{+0.33}_{-0.31}$		<sup>8</sup> ABAZOV	13o	D0 $s$ -channel
$3.07^{+0.54}_{-0.49}$		<sup>8</sup> ABAZOV	13o	D0 $t$ -channel
$4.11^{+0.60}_{-0.55}$		<sup>8</sup> ABAZOV	13o	D0 $s- + t$ -channels
$0.98^{+0.63}_{-0.59}$		<sup>9</sup> ABAZOV	11AA	D0 $s$ -channel
$2.90^{+0.59}_{-0.54}$		<sup>9</sup> ABAZOV	11AA	D0 $t$ -channel
$3.43^{+0.73}_{-0.74}$		<sup>10</sup> ABAZOV	11AD	D0 $s- + t$ -channels
$1.8^{+0.7}_{-0.5}$		<sup>11</sup> AALTONEN	10AB	CDF $s$ -channel
$0.8 \pm 0.4$		<sup>11</sup> AALTONEN	10AB	CDF $t$ -channel
$4.9^{+2.5}_{-2.2}$		<sup>12</sup> AALTONEN	10U	CDF $\mathcal{E}_T + \text{jets decay}$
$3.14^{+0.94}_{-0.80}$		<sup>13</sup> ABAZOV	10	D0 $t$ -channel
$1.05^{+0.81}_{-0.80}$		<sup>13</sup> ABAZOV	10	D0 $s$ -channel
< 7.3	95	<sup>14</sup> ABAZOV	10J	D0 $\tau + \text{jets decay}$
$2.3^{+0.6}_{-0.5}$		<sup>15</sup> AALTONEN	09AT	CDF $s- + t$ -channel
$3.94^{+0.88}_{-0.88}$		<sup>16</sup> ABAZOV	09Z	D0 $s- + t$ -channel
$2.2^{+0.7}_{-0.6}$		<sup>17</sup> AALTONEN	08AH	CDF $s- + t$ -channel
$4.7^{+1.3}_{-1.4}$		<sup>18</sup> ABAZOV	08I	D0 $s- + t$ -channel
$4.9 \pm 1.4$		<sup>19</sup> ABAZOV	07H	D0 $s- + t$ -channel
< 6.4	95	<sup>20</sup> ABAZOV	05P	D0 $p\bar{p} \rightarrow tb + X$
< 5.0	95	<sup>20</sup> ABAZOV	05P	D0 $p\bar{p} \rightarrow tqb + X$
<10.1	95	<sup>21</sup> ACOSTA	05N	CDF $p\bar{p} \rightarrow tqb + X$
<13.6	95	<sup>21</sup> ACOSTA	05N	CDF $p\bar{p} \rightarrow tb + X$
<17.8	95	<sup>21</sup> ACOSTA	05N	CDF $p\bar{p} \rightarrow tb + X, tqb + X$

<sup>1</sup> AALTONEN 16 based on  $9.5 \text{ fb}^{-1}$  of data. This includes, as a part, the result of AALTONEN 14K. Combination of this result with that of AALTONEN 14o gives a  $s + t$  cross section of  $3.02^{+0.49}_{-0.48} \text{ pb}$  and  $|V_{tb}| > 0.84$  (95% CL).

<sup>2</sup> AALTONEN 15H based on  $9.7 \text{ fb}^{-1}$  of data per experiment. The result is for  $m_t = 172.5 \text{ GeV}$ , and is a combination of the CDF measurements (AALTONEN 16) and the D0 measurements (ABAZOV 13o) on the  $t$ -channel single  $t$ -quark production cross section. The result is consistent with the NLO+NNLL SM prediction and gives  $|V_{tb}| = 1.02^{+0.06}_{-0.05}$  and  $|V_{tb}| > 0.92$  (95% CL).

<sup>3</sup> AALTONEN 15H is a combined measurement of  $s$ -channel single top cross section by CDF + D0. AALTONEN 14M is not included.

<sup>4</sup> Based on  $9.45 \text{ fb}^{-1}$  of data, using neural networks to separate signal from backgrounds. The result is for  $m_t = 172.5 \text{ GeV}$ . Combination of this result with the CDF measurement in the 1 lepton channel AALTONEN 14K gives  $1.36^{+0.37}_{-0.32} \text{ pb}$ , consistent with the SM prediction, and is 4.2 sigma away from the background only hypothesis.

<sup>5</sup> Based on  $9.4 \text{ fb}^{-1}$  of data, using neural networks to separate signal from backgrounds. The result is for  $m_t = 172.5 \text{ GeV}$ . The result is 3.8 sigma away from the background only hypothesis.

<sup>6</sup> Based on  $9.7 \text{ fb}^{-1}$  of data per experiment. The result is for  $m_t = 172.5 \text{ GeV}$ , and is a combination of the CDF measurements AALTONEN 14L, AALTONEN 14K and the D0 measurement ABAZOV 13o on the  $s$ -channel single  $t$ -quark production cross section. The result is consistent with the SM prediction of  $1.05 \pm 0.06 \text{ pb}$  and the significance of the observation is of 6.3 standard deviations.

<sup>7</sup> Based on  $7.5 \text{ fb}^{-1}$  of data. Neural network is used to discriminate signals ( $s$ -,  $t$ - and  $Wt$ -channel single top production) from backgrounds. The result is consistent with the SM prediction, and gives  $|V_{tb}| = 0.95 \pm 0.09$  (stat + syst)  $\pm 0.05$  (theory) and  $|V_{tb}| > 0.78$  (95% CL). The result is for  $m_t = 172.5 \text{ GeV}$ .

<sup>8</sup> Based on  $9.7 \text{ fb}^{-1}$  of data. Events with  $\ell + \mathcal{E}_T + 2$  or 3 jets (1 or 2  $b$ -tag) are analysed, assuming  $m_t = 172.5 \text{ GeV}$ . The combined  $s- + t$ -channel cross section gives  $|V_{tb}| f_1^L = 1.12^{+0.09}_{-0.08}$ , or  $|V_{tb}| > 0.92$  at 95% CL for  $f_1^L = 1$  and a flat prior within  $0 \leq |V_{tb}|^2 \leq 1$ .

<sup>9</sup> Based on  $5.4 \text{ fb}^{-1}$  of data. The error is statistical + systematic combined. The results are for  $m_t = 172.5 \text{ GeV}$ . Results for other  $m_t$  values are given in Table 2 of ABAZOV 11AA.

<sup>10</sup> Based on  $5.4 \text{ fb}^{-1}$  of data and for  $m_t = 172.5 \text{ GeV}$ . The error is statistical + systematic combined. Results for other  $m_t$  values are given in Table III of ABAZOV 11AD. The result is obtained by assuming the SM ratio between  $tb$  ( $s$ -channel) and  $tqb$  ( $t$ -channel) productions, and gives  $|V_{tb}| f_1^L = 1.02^{+0.10}_{-0.11}$ , or  $|V_{tb}| > 0.79$  at 95% CL for a flat prior within  $0 < |V_{tb}|^2 < 1$ .

<sup>11</sup> Based on  $3.2 \text{ fb}^{-1}$  of data. For combined  $s- + t$ -channel result see AALTONEN 09AT.

<sup>12</sup> Result is based on  $2.1 \text{ fb}^{-1}$  of data. Events with large missing  $E_T$  and jets with at least one  $b$ -jet without identified electron or muon are selected. Result is obtained when observed  $2.1 \sigma$  excess over the background originates from the signal for  $m_t = 175 \text{ GeV}$ , giving  $|V_{tb}| = 1.24^{+0.34}_{-0.29} \pm 0.07$  (theory).

<sup>13</sup> Result is based on  $2.3 \text{ fb}^{-1}$  of data. Events with isolated  $\ell + \mathcal{E}_T + 2, 3, 4$  jets with one or two  $b$ -tags are selected. The analysis assumes  $m_t = 170 \text{ GeV}$ .

<sup>14</sup> Result is based on  $4.8 \text{ fb}^{-1}$  of data. Events with an isolated reconstructed tau lepton, missing  $E_T + 2, 3$  jets with one or two  $b$ -tags are selected. When combined with ABAZOV 09Z result for  $e + \mu$  channels, the  $s$ - and  $t$ -channels combined cross section is  $3.84^{+0.89}_{-0.83} \text{ pb}$ .

<sup>15</sup> Based on  $3.2 \text{ fb}^{-1}$  of data. Events with isolated  $\ell + \mathcal{E}_T + \text{jets}$  with at least one  $b$ -tag are analyzed and  $s$ - and  $t$ -channel single top events are selected by using the likelihood function, matrix element, neural-network, boosted decision tree, likelihood function optimized for  $s$ -channel process, and neural-network based analysis of events with  $\mathcal{E}_T$  that has sensitivity for  $W \rightarrow \tau\nu$  decays. The result is for  $m_t = 175 \text{ GeV}$ , and the mean value decreases by  $0.02 \text{ pb/GeV}$  for smaller  $m_t$ . The signal has 5.0 sigma significance. The result gives  $|V_{tb}| = 0.91 \pm 0.11$  (stat+syst)  $\pm 0.07$  (theory), or  $|V_{tb}| > 0.71$  at 95% CL.

<sup>16</sup> Based on  $2.3 \text{ fb}^{-1}$  of data. Events with isolated  $\ell + \mathcal{E}_T + \geq 2$  jets with 1 or 2  $b$ -tags are analyzed and  $s$ - and  $t$ -channel single top events are selected by using boosted decision tree, Bayesian neural networks and the matrix element method. The signal has 5.0 sigma significance. The result gives  $|V_{tb}| = 1.07 \pm 0.12$ , or  $|V_{tb}| > 0.78$  at 95% CL. The analysis assumes  $m_t = 170 \text{ GeV}$ .

<sup>17</sup> Result is based on  $2.2 \text{ fb}^{-1}$  of data. Events with isolated  $\ell + \mathcal{E}_T + 2, 3$  jets with at least one  $b$ -tag are selected, and  $s$ - and  $t$ -channel single top events are selected by using likelihood, matrix element, and neural network discriminants. The result can be interpreted as  $|V_{tb}| = 0.88^{+0.13}_{-0.12}$  (stat + syst)  $\pm 0.07$  (theory), and  $|V_{tb}| > 0.66$  (95% CL) under the  $|V_{tb}| < 1$  constraint.

<sup>18</sup> Result is based on  $0.9 \text{ fb}^{-1}$  of data. Events with isolated  $\ell + \mathcal{E}_T + 2, 3, 4$  jets with one or two  $b$ -vertex-tag are selected, and contributions from  $W + \text{jets}$ ,  $t\bar{t}$ ,  $s$ - and  $t$ -channel single top events are identified by using boosted decision trees, Bayesian neural networks, and matrix element analysis. The result can be interpreted as the measurement of the CKM matrix element  $|V_{tb}| = 1.31^{+0.25}_{-0.21}$ , or  $|V_{tb}| > 0.68$  (95% CL) under the  $|V_{tb}| < 1$  constraint.

<sup>19</sup> Result is based on  $0.9 \text{ fb}^{-1}$  of data. This result constrains  $V_{tb}$  to  $0.68 < |V_{tb}| \leq 1$  at 95% CL.

<sup>20</sup> ABAZOV 05P bounds single top-quark production from either the  $s$ -channel  $W$ -exchange process,  $q'\bar{q} \rightarrow t\bar{b}$ , or the  $t$ -channel  $W$ -exchange process,  $q'g \rightarrow qt\bar{b}$ , based on  $\sim 230 \text{ pb}^{-1}$  of data.

<sup>21</sup> ACOSTA 05N bounds single top-quark production from the  $t$ -channel  $W$ -exchange process ( $q'g \rightarrow qt\bar{b}$ ), the  $s$ -channel  $W$ -exchange process ( $q'\bar{q} \rightarrow t\bar{b}$ ), and from the combined cross section of  $t$ - and  $s$ -channel. Based on  $\sim 162 \text{ pb}^{-1}$  of data.

### $t$ -channel Single $t$ Production Cross Section in $pp$ Collisions at $\sqrt{s} = 7 \text{ TeV}$

Direct probe of the  $t b W$  coupling and possible new physics at  $\sqrt{s} = 7 \text{ TeV}$ .

VALUE (pb)	DOCUMENT ID	TECN	COMMENT
$67.5 \pm 5.7$	<sup>1</sup> AABOUD	19R	LHC combination of ATLAS+CMS
$68 \pm 2 \pm 8$	<sup>2</sup> AAD	14BI	ATLS $\ell + \mathcal{E}_T + 2j$ or $3j$
$83 \pm 4^{+20}_{-19}$	<sup>3</sup> AAD	12CH	ATLS $t$ -channel $\ell + \mathcal{E}_T + (2,3)j$ (1b)
$67.2 \pm 6.1$	<sup>4</sup> CHATRCHYAN12BQ	CMS	$t$ -channel $\ell + \mathcal{E}_T + \geq 2j$ (1b)
$83.6 \pm 29.8 \pm 3.3$	<sup>5</sup> CHATRCHYAN11R	CMS	$t$ -channel

<sup>1</sup> AABOUD 19R based on  $1.17$  to  $5.1 \text{ fb}^{-1}$  of data from ATLAS and CMS at 7 TeV.

<sup>2</sup> Based on  $4.9 \text{ fb}^{-1}$  of data, using neural networks for signal and background separation.  $\sigma(tq) = 46 \pm 1 \pm 6 \text{ pb}$  and  $\sigma(\bar{t}q) = 23 \pm 1 \pm 3 \text{ pb}$  are separately measured, as well as their ratio  $R = \sigma(tq)/\sigma(\bar{t}q) = 2.04 \pm 0.13 \pm 0.12$ . The results are for  $m_t = 172.5 \text{ GeV}$ , and those for other  $m_t$  values are given by eq.(4) and Table IV. The measurements give  $|V_{tb}| = 1.02 \pm 0.07$  or  $|V_{tb}| > 0.88$  (95% CL).

<sup>3</sup> Based on  $1.04 \text{ fb}^{-1}$  of data. The result gives  $|V_{tb}| = 1.13^{+0.14}_{-0.13}$  from the ratio  $\sigma(\text{exp})/\sigma(\text{th})$ , where  $\sigma(\text{th})$  is the SM prediction for  $|V_{tb}| = 1$ . The 95% CL lower bound of  $|V_{tb}| > 0.75$  is found if  $|V_{tb}| < 1$  is assumed.  $\sigma(t) = 59^{+18}_{-16} \text{ pb}$  and  $\sigma(\bar{t}) = 33^{+13}_{-12} \text{ pb}$  are found for the separate single  $t$  and  $\bar{t}$  production cross sections, respectively. The results assume  $m_t = 172.5 \text{ GeV}$  for the acceptance.

## Quark Particle Listings

 $t$ 

<sup>4</sup> Based on  $1.17 \text{ fb}^{-1}$  of data for  $\ell = \mu$ ,  $1.56 \text{ fb}^{-1}$  of data for  $\ell = e$  at 7 TeV collected during 2011. The result gives  $|V_{tb}| = 1.020 \pm 0.046(\text{meas}) \pm 0.017(\text{th})$ . The 95% CL lower bound of  $|V_{tb}| > 0.92$  is found if  $|V_{tb}| < 1$  is assumed. The results assume  $m_t = 172.5 \text{ GeV}$  for the acceptance.

<sup>5</sup> Based on  $36 \text{ pb}^{-1}$  of data. The first error is statistical + systematic combined, the second is luminosity. The result gives  $|V_{tb}| = 1.114 \pm 0.22(\text{exp}) \pm 0.02(\text{th})$  from the ratio  $\sigma(\text{exp})/\sigma(\text{th})$ , where  $\sigma(\text{th})$  is the SM prediction for  $|V_{tb}| = 1$ . The 95% CL lower bound of  $|V_{tb}| > 0.62$  (0.68) is found from the 2D (BDT) analysis under the constraint  $0 < |V_{tb}|^2 < 1$ .

**t-channel Single t Production Cross Section in pp Collisions at  $\sqrt{s} = 8 \text{ TeV}$** 

VALUE (pb)	DOCUMENT ID	TECN	COMMENT
• • •			We do not use the following data for averages, fits, limits, etc. • • •
$87.7 \pm 5.8$	<sup>1</sup> AABOUD	19R LHC	combination of ATLAS+CMS
$89.6^{+7.1}_{-6.3}$	<sup>2</sup> AABOUD	17T ATLS	$\ell + \cancel{E}_T + 2j$ (1b j)
$83.6 \pm 2.3 \pm 7.4$	<sup>3</sup> KHACHATRYAN...14F	CMS	$\ell + \cancel{E}_T + \geq 2j$ (1, 2 b, 1 forward j)

<sup>1</sup> AABOUD 19R based on  $12.2$  to  $20.3 \text{ fb}^{-1}$  of data from ATLAS and CMS at 8 TeV.

<sup>2</sup> AABOUD 17T based on  $20.2 \text{ fb}^{-1}$  of data. A maximum-likelihood fit to neural-network discriminant distributions is used to separate signal and background events. Individual cross sections are measured as  $\sigma(tq) = 56.7^{+4.3}_{-3.8} \text{ pb}$  and  $\sigma(\bar{t}q) = 32.9^{+3.0}_{-2.7} \text{ pb}$ , while their ratio is given by  $\sigma(tq)/\sigma(\bar{t}q) = 1.72 \pm 0.09$ . A lower limit  $|V_{tb}| > 0.92$  (95% CL) is obtained. Measured total and differential cross sections are described well by the SM.

<sup>3</sup> Based on  $19.7 \text{ fb}^{-1}$  of data. The  $t$  and  $\bar{t}$  production cross sections are measured separately as  $\sigma_{t\text{-ch.}}(t) = 53.8 \pm 1.5 \pm 4.4 \text{ pb}$  and  $\sigma_{t\text{-ch.}}(\bar{t}) = 27.6 \pm 1.3 \pm 3.7 \text{ pb}$ , respectively, as well as their ratio  $R_{t\text{-ch.}} = \sigma_{t\text{-ch.}}(t)/\sigma_{t\text{-ch.}}(\bar{t}) = 1.95 \pm 0.10 \pm 0.19$ , in agreement with the SM predictions. Combination with a previous CMS result at  $\sqrt{s} = 7 \text{ TeV}$  [CHATRCHYAN 12Bq] gives  $|V_{tb}| = 0.998 \pm 0.038 \pm 0.016$ . Also obtained is the ratio  $R_{8/7} = \sigma_{t\text{-ch.}}(8\text{TeV})/\sigma_{t\text{-ch.}}(7\text{TeV}) = 1.24 \pm 0.08 \pm 0.12$ .

**s-channel Single t Production Cross Section in pp Collisions at  $\sqrt{s} = 8 \text{ TeV}$** 

VALUE (pb)	DOCUMENT ID	TECN	COMMENT
• • •			We do not use the following data for averages, fits, limits, etc. • • •
$4.9 \pm 1.4$	<sup>1</sup> AABOUD	19R LHC	ATLAS + CMS
$4.8 \pm 0.8^{+1.6}_{-1.3}$	<sup>2</sup> AAD	16U ATLS	$\ell + \cancel{E}_T + 2b$
$13.4 \pm 7.3$	<sup>3</sup> KHACHATRYAN...16AZ	CMS	$\ell + \cancel{E}_T + 2b$
$5.0 \pm 4.3$	<sup>4</sup> AAD	15A ATLS	$\ell + \cancel{E}_T + 2b$

<sup>1</sup> AABOUD 19R based on  $12.2$  to  $20.3 \text{ fb}^{-1}$  of data from ATLAS and CMS at 8 TeV.

<sup>2</sup> AAD 16U based on  $20.3 \text{ fb}^{-1}$  of data, using a maximum-likelihood fit of a matrix element method discriminant. The same data set as in AAD 15A is used. The result corresponds to an observed significance of  $3.2\sigma$ .

<sup>3</sup> KHACHATRYAN 16AZ based on  $19.7 \text{ fb}^{-1}$  of data, using a multivariate analysis to separate signal and backgrounds. The same method is applied to  $5.1 \text{ fb}^{-1}$  of data at  $\sqrt{s} = 7 \text{ TeV}$ , giving  $7.1 \pm 8.1 \text{ pb}$ . Combining both measurements, the observed significance is  $2.5\sigma$ . A best fit value of  $2.0 \pm 0.9$  is obtained for the combined ratio of the measured values and SM expectations.

<sup>4</sup> AAD 15A based on  $20.3 \text{ fb}^{-1}$  of data, using a multivariate analysis to separate signal and backgrounds. The 95% CL upper bound of the cross section is  $14.6 \text{ pb}$ . The results are consistent with the SM prediction of  $5.61 \pm 0.22 \text{ pb}$  at approximate NNLO.

**t-channel Single t Production Cross Section in pp Collisions at  $\sqrt{s} = 13 \text{ TeV}$** 

VALUE (pb)	DOCUMENT ID	TECN	COMMENT
• • •			We do not use the following data for averages, fits, limits, etc. • • •
$130 \pm 1 \pm 19$	<sup>1</sup> SIRUNYAN	20D CMS	$\sigma(tq), \ell + \cancel{E}_T + \geq 2j$
$77 \pm 1 \pm 12$	<sup>1</sup> SIRUNYAN	20D CMS	$\sigma(\bar{t}q), \ell + \cancel{E}_T + \geq 2j$
$156 \pm 5 \pm 27 \pm 3$	<sup>2</sup> AABOUD	17H ATLS	$\sigma(tq), \ell + \cancel{E}_T + 2j$ (1b, 1 forward j)
$91 \pm 4 \pm 18 \pm 2$	<sup>2</sup> AABOUD	17H ATLS	$\sigma(\bar{t}q), \ell + \cancel{E}_T + 2j$ (1b, 1 forward j)
$154 \pm 8 \pm 9 \pm 19 \pm 4$	<sup>3</sup> SIRUNYAN	17AA CMS	$\sigma(tq), \mu + \geq 2j$ (1b)
$85 \pm 10 \pm 4 \pm 11 \pm 2$	<sup>3</sup> SIRUNYAN	17AA CMS	$\sigma(\bar{t}q), \mu + \geq 2j$ (1b)

<sup>1</sup> SIRUNYAN 20D based on  $35.9 \text{ fb}^{-1}$  of data. Different categories of jet and b jet multiplicity and multivariate discriminators are used to separate signal and background events. The cross section ratio is measured to be  $\sigma(tq)/\sigma(\bar{t}q) = 1.68 \pm 0.02 \pm 0.05$ . CKM matrix element is obtained as  $|f_{LV} V_{tb}| = 0.98 \pm 0.07(\text{exp}) \pm 0.02(\text{theo})$  where  $f_{LV}$  is an anomalous form factor. All results are in agreement with the SM.

<sup>2</sup> AABOUD 17H based on  $3.2 \text{ fb}^{-1}$  of data. A maximum-likelihood fit to neural-network discriminant distributions is used to separate signal and background events. The third error is for luminosity. The cross section ratio is measured to be  $\sigma(tq)/\sigma(\bar{t}q) = 1.72 \pm 0.09 \pm 0.18$ . A lower limit  $|V_{tb}| > 0.84$  (95% CL) is obtained. All results are in agreement with the SM.

<sup>3</sup> SIRUNYAN 17AA based on  $2.2 \text{ fb}^{-1}$  of data. A multivariate discriminator is used to separate signal and background events. The four errors are from statistics, experimental systematics, theory, and luminosity. The cross section ratio is measured to be  $\sigma(tq)/\sigma(\bar{t}q) = 1.81 \pm 0.18 \pm 0.15$ . CKM matrix element is obtained as  $|V_{tb}| = 1.05 \pm 0.07(\text{exp}) \pm 0.02(\text{theo})$ . All results are in agreement with the SM.

**t $\bar{t}$  Production Cross Section in pp Collisions at  $\sqrt{s} = 13 \text{ TeV}$** 

VALUE (fb)	DOCUMENT ID	TECN	COMMENT
• • •			We do not use the following data for averages, fits, limits, etc. • • •
$670 \pm 90^{+110}_{-100}$	<sup>1</sup> AABOUD	18BK ATLS	$H \rightarrow b\bar{b}, WW^* \tau\tau, \gamma\gamma, ZZ^*$

<sup>1</sup> AABOUD 18BK based on  $79.8 \text{ fb}^{-1}$  of data. The observed significance is  $5.8\sigma$  relative to the background-only hypothesis. The measurement is consistent with the NLO SM prediction of  $507^{+35}_{-50} \text{ fb}$ . See Table 3 and Fig. 5 for measurements of individual modes. Combined with the measurements at 7 and 8 TeV, the observed significance is  $6.3\sigma$ .

**Wt Production Cross Section in pp Collisions at  $\sqrt{s} = 7 \text{ TeV}$** 

VALUE (pb)	DOCUMENT ID	TECN	COMMENT
• • •			We do not use the following data for averages, fits, limits, etc. • • •
$16.3 \pm 4.1$	<sup>1</sup> AABOUD	19R LHC	ATLAS + CMS combined
$16^{+5}_{-4}$	<sup>2</sup> CHATRCHYAN13C	CMS	$t + W$ channel, $2\ell + \cancel{E}_T + 1b$

<sup>1</sup> AABOUD 19R based on  $1.17$  to  $5.1 \text{ fb}^{-1}$  of data from ATLAS and CMS at 7 TeV.  
<sup>2</sup> Based on  $4.9 \text{ fb}^{-1}$  of data. The result gives  $V_{tb} = 1.01^{+0.16}_{-0.13}(\text{exp})^{+0.03}_{-0.04}(\text{th})$ .  $V_{tb} > 0.79$  (95% CL) if  $V_{tb} < 1$  is assumed. The results assume  $m_t = 172.5 \text{ GeV}$  for the acceptance.

**Wt Production Cross Section in pp Collisions at  $\sqrt{s} = 8 \text{ TeV}$** 

VALUE (pb)	DOCUMENT ID	TECN	COMMENT
• • •			We do not use the following data for averages, fits, limits, etc. • • •
$23.1 \pm 3.6$	<sup>1</sup> AABOUD	19R LHC	ATLAS + CMS combined
$23.0 \pm 1.3^{+3.2}_{-3.5} \pm 1.1$	<sup>2</sup> AAD	16B ATLS	$2\ell + \cancel{E}_T + 1b$
$23.4 \pm 5.4$	<sup>3</sup> CHATRCHYAN14AC	CMS	$t + W$ channel, $2\ell + \cancel{E}_T + 1b$

<sup>1</sup> AABOUD 19R based on  $12.2$  to  $20.3 \text{ fb}^{-1}$  of data from ATLAS and CMS at 8 TeV.  
<sup>2</sup> AAD 16B based on  $20.3 \text{ fb}^{-1}$  of data. The result gives  $|V_{tb}| = 1.01 \pm 0.10$  and  $|V_{tb}| > 0.80$  (95% CL) without assuming unitarity of the CKM matrix. The results assume  $m_t = 172.5 \text{ GeV}$  for the acceptance.

<sup>3</sup> Based on  $12.2 \text{ fb}^{-1}$  of data. Events with two oppositely charged leptons, large  $\cancel{E}_T$  and a  $b$ -tagged jet are selected, and a multivariate analysis is used to separate the signal from the backgrounds. The result is consistent with the SM prediction of  $22.2 \pm 0.6(\text{scale}) \pm 1.4(\text{PDF}) \text{ pb}$  at approximate NNLO.

**Wt Production Cross Section in pp Collisions at  $\sqrt{s} = 13 \text{ TeV}$** 

VALUE (pb)	DOCUMENT ID	TECN	COMMENT
• • •			We do not use the following data for averages, fits, limits, etc. • • •
$94 \pm 10^{+28}_{-22} \pm 2$	<sup>1</sup> AABOUD	18H ATLS	$\ell^+ \ell^- + \geq 1j$
$63.1 \pm 1.8 \pm 6.4 \pm 2.1$	<sup>2</sup> SIRUNYAN	18DL CMS	$e^\pm \mu^\mp + \geq 1j(b\text{-tag})$

<sup>1</sup> AABOUD 18H based on  $3.2 \text{ fb}^{-1}$  of data. The last error is from luminosity. A multivariate analysis is used to separate the signal from the backgrounds. The result is consistent with the NLO+NNLL SM prediction of  $71.7 \pm 1.8(\text{scale}) \pm 3.4(\text{PDF}) \text{ pb}$ .

<sup>2</sup> SIRUNYAN 18DL based on  $35.9 \text{ fb}^{-1}$  of data. The last error is from luminosity. A multivariate analysis is used to separate the signal from the backgrounds. The result is consistent with the NLO+NNLL SM prediction of  $71.7 \pm 1.8(\text{scale}) \pm 3.4(\text{PDF}) \text{ pb}$ .

**Zt Production Cross Section in pp Collisions at  $\sqrt{s} = 13 \text{ TeV}$** 

VALUE (fb)	DOCUMENT ID	TECN	COMMENT
• • •			We do not use the following data for averages, fits, limits, etc. • • •
$111 \pm 13^{+11}_{-9}$	<sup>1</sup> SIRUNYAN	19BF CMS	$3\ell + \geq 2j$ ( $\geq 1b_j$ )
$600 \pm 170 \pm 140$	<sup>2</sup> AABOUD	18AE ATLS	$3\ell + 1j + 1b_j$
$123 \pm 33^{+29}_{-31} \pm 23$	<sup>3</sup> SIRUNYAN	18Z CMS	$3\ell + 1j + 1b_j$

<sup>1</sup> SIRUNYAN 19BF based on  $77.4 \text{ fb}^{-1}$  of data. Two BDT's are used in the analysis: one to discriminate prompt leptons from non-prompt ones; and one to discriminate  $tZq$  signal from backgrounds. The result is for the cross section  $\sigma(pp \rightarrow tZq \rightarrow t\bar{t}Zq)$  for dilepton invariant masses above  $30 \text{ GeV}$  and is consistent with the NLO SM prediction of  $94.2 \pm 3.1 \text{ fb}$ .

<sup>2</sup> AABOUD 18AE based on  $36.1 \text{ fb}^{-1}$  of data. A multivariate analysis is used to separate the signal from the backgrounds. The result is consistent with the NLO SM prediction of  $800 \text{ fb}$  with a scale uncertainty of  $+6.1\%$ .

<sup>3</sup> SIRUNYAN 18Z based on  $35.9 \text{ fb}^{-1}$  of data. A multivariate analysis is used to separate the signal from the backgrounds. The result is for the cross section  $\sigma(pp \rightarrow tZq \rightarrow Wb\ell^+ \ell^- q)$  and is consistent with the NLO SM prediction of  $94.2^{+1.9}_{-1.8}(\text{scale}) \pm 2.5(\text{PDF}) \text{ fb}$ . Superseded by SIRUNYAN 19BF.

**Single t-Quark Production Cross Section in ep Collisions**

VALUE (pb)	CL%	DOCUMENT ID	TECN	COMMENT
• • •				We do not use the following data for averages, fits, limits, etc. • • •
$< 0.25$	95	<sup>1</sup> AARON	09A H1	$e^\pm p \rightarrow e^\pm tX$
$< 0.55$	95	<sup>2</sup> AKTAS	04 H1	$e^\pm p \rightarrow e^\pm tX$
$< 0.225$	95	<sup>3</sup> CHEKANOV	03 ZEUS	$e^\pm p \rightarrow e^\pm tX$

<sup>1</sup> AARON 09A looked for single top production via FCNC in  $e^\pm p$  collisions at HERA with  $474 \text{ pb}^{-1}$  of data at  $\sqrt{s} = 301\text{--}319 \text{ GeV}$ . The result supersedes that of AKTAS 04.

<sup>2</sup> AKTAS 04 looked for single top production via FCNC in  $e^\pm$  collisions at HERA with  $118.3 \text{ pb}^{-1}$ , and found 5 events in the  $e$  or  $\mu$  channels while  $1.31 \pm 0.22$  events are expected from the Standard Model background. No excess was found for the hadronic channel. The observed cross section of  $\sigma(ep \rightarrow etX) = 0.29^{+0.15}_{-0.14} \text{ pb}$  at  $\sqrt{s} = 319 \text{ GeV}$  gives the quoted upper bound if the observed events are due to statistical fluctuation.

<sup>3</sup> CHEKANOV 03 looked in  $130.1 \text{ pb}^{-1}$  of data at  $\sqrt{s} = 301$  and  $318 \text{ GeV}$ . The limit is for  $\sqrt{s} = 318 \text{ GeV}$  and assumes  $m_t = 175 \text{ GeV}$ .

**t $\bar{t}$  Production Cross Section in p $\bar{p}$  Collisions at  $\sqrt{s} = 1.8 \text{ TeV}$** 

Only the final combined  $t\bar{t}$  production cross sections obtained from Tevatron Run I by the CDF and D0 experiments are quoted below.

VALUE (pb)	DOCUMENT ID	TECN	COMMENT
• • •			We do not use the following data for averages, fits, limits, etc. • • •
$5.69 \pm 1.21 \pm 1.04$	<sup>1</sup> ABAZOV	03A D0	Combined Run I data
$6.5^{+1.7}_{-1.4}$	<sup>2</sup> AFFOLDER	01A CDF	Combined Run I data

<sup>1</sup> Combined result from  $110 \text{ pb}^{-1}$  of Tevatron Run I data. Assume  $m_t = 172.1 \text{ GeV}$ .

<sup>2</sup> Combined result from  $105 \text{ pb}^{-1}$  of Tevatron Run I data. Assume  $m_t = 175 \text{ GeV}$ .

tT Production Cross Section in pP Collisions at sqrt(s) = 1.96 TeV

Unless otherwise noted the first quoted error is from statistics, the second from systematic uncertainties, and the third from luminosity. If only two errors are quoted the luminosity is included in the systematic uncertainties.

Table with 4 columns: VALUE (pb), DOCUMENT ID, TECN, COMMENT. It lists various production cross sections for tT in pP collisions at sqrt(s) = 1.96 TeV, including entries from AALTONEN, ABAZOV, and ABULENCIA.

1 ABAZOV 16F based on 9.7 fb^-1 of data. The result is for mt = 172.5 GeV, and the mt dependence is shown in Table V and Fig. 9. The result agrees with the NNLO+NNLL SM prediction of 7.35 +/- 0.23 +/- 0.27 pb.
2 Based on 9 fb^-1 of data. The measurement is in the channel tT -> (bLnu)(btau nu), where tau decays into hadrons (tau\_h), and l (e or mu) include l from tau decays (tau\_l). The result is for mt = 173 GeV.
3 Based on 8.8 fb^-1 of data. Combination of CDF and D0 measurements given, respectively, by sigma(tT; CDF) = 7.63 +/- 0.31 +/- 0.36 +/- 0.16 pb, sigma(tT; D0) = 7.56 +/- 0.20 +/- 0.32 +/- 0.46 pb. All the results are for mt = 172.5 GeV. The mt dependence of the mean value is parametrized in eq. (1) and shown in Fig. 2.

production cross section and the b-tagging efficiency and find improvements in both measurements.

9 Based on 2.7 fb^-1. The first error is from statistics and systematics, the second is from luminosity. The result is for mt = 175 GeV. AALTONEN 11W fits simultaneously a jet flavor discriminator between b-, c-, and light-quarks, and find significant reduction in the systematic error.
10 Based on 2.2 fb^-1. The result is for mt = 172.5 GeV. AALTONEN 11Y selects multi-jet events with large ET, and vetoes identified electrons and muons.
11 Based on 5.3 fb^-1. The error is statistical + systematic + luminosity combined. The result is for mt = 172.5 GeV. The results for other mt values are given in Table XII and eq.(10) of ABAZOV 11E.
12 Combination of a dilepton measurement presented in ABAZOV 11Z (based on 5.4 fb^-1), which yields 7.36 +/- 0.90 (stat+syst) pb, and the lepton + jets measurement of ABAZOV 11E. The result is for mt = 172.5 GeV. The results for other mt values is given by eq.(5) of ABAZOV 11A.
13 Based on 2.8 fb^-1. The result is for mt = 175 GeV.
14 Based on 2.9 fb^-1. Result is obtained from the fraction of signal events in the top quark mass measurement in the all hadronic decay channel.
15 Based on 1.7 fb^-1. The result is for mt = 175 GeV. AALTONEN 10V uses soft electrons from b-hadron decays to suppress W+jets background events.
16 Based on 4.6 fb^-1. The result is for mt = 172.5 GeV. The ratio sigma(tT -> l+jets) / sigma(Z/gamma\* -> ll) is measured and then multiplied by the theoretical Z/gamma\* -> ll cross section of sigma(Z/gamma\* -> ll) = 251.3 +/- 5.0 pb, which is free from the luminosity error.
17 Based on 1 fb^-1. The result is for mt = 175 GeV. 7.9 +/- 2.3 pb is found for mt = 170 GeV. ABAZOV 10I uses a likelihood discriminant to separate signal from background, where the background model was created from lower jet-multiplicity data.
18 Based on 1 fb^-1. The result is for mt = 170 GeV. For mt = 175 GeV, the result is 6.3 +/- 1.2 (stat) +/- 0.7 (syst) +/- 0.4 (lumi) pb. Cross section of tT production has been measured in the tT -> tau\_h + jets topology, where tau\_h denotes hadronically decaying tau leptons. The result for the cross section times the branching ratio is sigma(tT -> tau\_h + jets) = 0.60 +/- 0.23 +/- 0.15 +/- 0.04 pb for mt = 170 GeV.
19 Based on 1.1 fb^-1. The result is for B(W -> l nu) = 10.8% and mt = 175 GeV; the mean value is 9.8 for mt = 172.5 GeV and 10.1 for mt = 170 GeV. AALTONEN 09AD used high pT e or mu with an isolated track to select tT decays into dileptons including l = tau. The result is based on the candidate event samples with and without vertex b-tag.
20 Based on 2 fb^-1. The result is for mt = 175 GeV; the mean value is 3% higher for mt = 170 GeV and 4% lower for mt = 180 GeV.
21 Result is based on 1 fb^-1 of data. The result is for mt = 170 GeV, and the mean value decreases with increasing mt; see their Fig. 2. The result is obtained after combining l + jets, ll, and l tau final states, and the ratios of the extracted cross sections are R^ll/llj = 0.86 +/- 0.19 +/- 0.17 and R^l tau/ll-llj = 0.97 +/- 0.32 +/- 0.29, consistent with the SM expectation of R = 1. This leads to the upper bound of B(t -> bH+) as a function of mH+. Results are shown in their Fig. 1 for B(H+ -> tau nu) = 1 and B(H+ -> c s-bar) = 1 cases. Comparison of the mt dependence of the extracted cross section and a partial NNLO prediction gives mt = 169.1 +/- 5.9 +/- 5.2 GeV.
22 Result is based on 1 fb^-1 of data. The result is for mt = 170 GeV, and the mean value changes by -0.07 [mt(GeV)-170] pb near the reference mt value. Comparison of the mt dependence of the extracted cross section and a partial NNLO QCD prediction gives mt = 171.5 +/- 9.9 +/- 8.8 GeV. The l tau channel alone gives 7.6 +/- 4.9 +/- 3.5 +/- 1.4 pb and the ll channel gives 7.5 +/- 1.2 +/- 0.7 +/- 0.7 +/- 1.1 +/- 0.6 +/- 0.5 pb.
23 Result is based on 0.9 fb^-1 of data. The first error is from stat + syst, while the latter error is from luminosity. The result is for mt = 175 GeV, and the mean value changes by -0.09 pb/[mt(GeV)-175].
24 Result is based on 0.9 fb^-1 of data. The cross section is obtained from the l + 3 jet event rates with 1 or 2 b-tag, and also from the kinematical likelihood analysis of the l + 3, 4 jet events. The result is for mt = 172.6 GeV, and its mt dependence shown in Fig. 3 leads to the constraint mt = 170 +/- 7 GeV when compared to the SM prediction.
25 Result is based on 360 pb^-1 of data. Events with high pT oppositely charged dileptons l+ l- (l = e, mu) are used to obtain cross sections for tT, W+ W-, and Z -> tau+ tau- production processes simultaneously. The other cross sections are given in Table IV.
26 Based on 1.02 fb^-1 of data. Result is for mt = 175 GeV. Secondary vertex b-tag and neural network selections are used to achieve a signal-to-background ratio of about 1/2.
27 Based on 425 pb^-1 of data. Result is for mt = 175 GeV. For mt = 170.9 GeV, 7.8 +/- 1.8 (stat + syst) pb is obtained.
28 Based on 405 +/- 25 pb^-1 of data. Result is for mt = 175 GeV. The last error is for luminosity. Secondary vertex b-tag and neural network are used to separate the signal events from the background.
29 Based on 425 pb^-1 of data. Assumes mt = 175 GeV.
30 Based on ~ 425 pb^-1. Assuming mt = 175 GeV. The first error is combined statistical and systematic, the second one is luminosity.
31 Based on ~ 318 pb^-1. Assuming mt = 178 GeV. The cross section changes by +/- 0.08 pb for each +/- GeV change in the assumed mt. Result is for at least one b-tag. For at least two b-tagged jets, tT signal of significance greater than 5 sigma is found, and the cross section is 10.1 +/- 1.6 +/- 2.0 +/- 1.4 +/- 1.3 pb for mt = 178 GeV.
32 Based on ~ 311 pb^-1. Assuming mt = 178 GeV. For mt = 175 GeV, the result is 6.0 +/- 1.2 +/- 0.9 +/- 0.7. This is the first CDF measurement without lepton identification, and hence it has sensitivity to the W -> tau nu mode.
33 ABULENCIA,A 06E measures the tT production cross section in the all hadronic decay mode by selecting events with 6 to 8 jets and at least one b-jet. S/B = 1/5 has been achieved. Based on 311 pb^-1. Assuming mt = 178 GeV.
34 Based on ~ 318 pb^-1. Assuming mt = 178 GeV. Result is for at least one b-tag. For at least two b-tagged jets, the cross section is 11.1 +/- 2.3 +/- 2.5 +/- 1.9 +/- 1.9 pb.
35 ABAZOV 05Q measures the top-quark pair production cross section with ~ 230 pb^-1 of data, based on the analysis of W plus n-jet events where W decays into e or mu plus neutrino, and at least one of the jets is b-jet like. The first error is statistical and systematic, and the second accounts for the luminosity uncertainty. The result assumes

# Quark Particle Listings

*t*

- $m_t = 175$  GeV; the mean value changes by  $(175 - m_t(\text{GeV})) \times 0.06$  pb in the mass range 160 to 190 GeV.
- <sup>36</sup> ABZOV 05R measures the top-quark pair production cross section with 224–243 pb<sup>-1</sup> of data, based on the analysis of events with two charged leptons in the final state. The result assumes  $m_t = 175$  GeV; the mean value changes by  $(175 - m_t(\text{GeV})) \times 0.08$  pb in the mass range 160 to 190 GeV.
- <sup>37</sup> Based on 230 pb<sup>-1</sup>. Assuming  $m_t = 175$  GeV.
- <sup>38</sup> Based on 194 pb<sup>-1</sup>. Assuming  $m_t = 175$  GeV.
- <sup>39</sup> Based on 194 ± 11 pb<sup>-1</sup>. Assuming  $m_t = 175$  GeV.
- <sup>40</sup> Based on 162 ± 10 pb<sup>-1</sup>. Assuming  $m_t = 175$  GeV.
- <sup>41</sup> ACOSTA 05V measures the top-quark pair production cross section with ~ 162 pb<sup>-1</sup> data, based on the analysis of *W* plus *n*-jet events where *W* decays into *e* or  $\mu$  plus neutrino, and at least one of the jets is *b*-jet like. Assumes  $m_t = 175$  GeV.
- <sup>42</sup> ACOSTA 04I measures the top-quark pair production cross section with 197 ± 12 pb<sup>-1</sup> data, based on the analysis of events with two charged leptons in the final state. Assumes  $m_t = 175$  GeV.

## Ratio of the Production Cross Sections of $t\bar{t}\gamma$ to $t\bar{t}$ at $\sqrt{s} = 1.96$ TeV

VALUE	DOCUMENT ID	TECN	COMMENT
0.024 ± 0.009	<sup>1</sup> AALTONEN 11z CDF		$E_T(\gamma) > 10$ GeV, $ \eta(\gamma)  < 1.0$

• • • We do not use the following data for averages, fits, limits, etc. • • •

<sup>1</sup> Based on 6.0 fb<sup>-1</sup> of data. The error is statistical and systematic combined. Events with lepton +  $\cancel{E}_T + \geq 3$  jets ( $\geq 1b$ ) with and without central, high  $E_T$  photon are measured. The result is consistent with the SM prediction of 0.024 ± 0.005. The absolute production cross section is measured to be 0.18 ± 0.08 fb. The statistical significance is 3.0 standard deviations.

## *t* *t* Production Cross Section in *pp* Collisions at $\sqrt{s} = 7$ TeV

VALUE (pb)	CL%	DOCUMENT ID	TECN	COMMENT
< 1.7	95	<sup>1</sup> AAD 12BE ATLS		$\ell^+ \ell^+ + \cancel{E}_T + \geq 2j + HT$

• • • We do not use the following data for averages, fits, limits, etc. • • •

<sup>1</sup> Based on 1.04 fb<sup>-1</sup> of *pp* data at  $\sqrt{s} = 7$  TeV. The upper bounds are the same for LL, LR and RR chiral components of the two top quarks.

## $t\bar{t}$ Production Cross Section in *pp* Collisions at $\sqrt{s} = 5.02$ TeV

Unless otherwise noted the first quoted error is from statistics, the second from systematic uncertainties, and the third from luminosity. If only two errors are quoted the luminosity is included in the systematic uncertainties.

VALUE (pb)	DOCUMENT ID	TECN	COMMENT
69.5 ± 6.1 ± 5.6 ± 1.6	<sup>1</sup> SIRUNYAN 18AQ CMS		$\ell + \text{jets}, \ell\ell + \text{jets}$

• • • We do not use the following data for averages, fits, limits, etc. • • •

<sup>1</sup> SIRUNYAN 18AQ based on 27.4 pb<sup>-1</sup> of data from *pp* collisions at  $\sqrt{s} = 5.02$  TeV. The result is in agreement with the NNLO SM prediction  $68.9_{-2.3}^{+1.9}(\text{scale}) \pm 2.3(\text{PDF})_{-1.0}^{+1.4}(\alpha_s)$  pb.

## $t\bar{t}$ Production Cross Section in *pp* Collisions at $\sqrt{s} = 7$ TeV

Unless otherwise noted the first quoted error is from statistics, the second from systematic uncertainties, and the third from luminosity. If only two errors are quoted the luminosity is included in the systematic uncertainties.

VALUE (pb)	DOCUMENT ID	TECN	COMMENT
161.7 ± 6.0 ± 12.0 ± 3.6	<sup>1</sup> KHACHATRYAN...17B CMS		$\ell + \cancel{E}_T + \geq 4j (\geq 1b)$
173.6 ± 2.1 ± 4.5 ± 3.8	<sup>2</sup> KHACHATRYAN...16AW CMS		$e + \mu + \cancel{E}_T + \geq 0j$
181.2 ± 2.8 ± 10.8 ± 10.6	<sup>3</sup> AAD 15B0 ATLS		$e + \mu + \cancel{E}_T + \geq 0j$
178 ± 3 ± 16 ± 3	<sup>4</sup> AAD 15CC ATLS		$\ell + \text{jets}, \ell\ell + \text{jets}, \ell\tau_h + \text{jets}$
	<sup>5</sup> AAIJ 15R LHCB		$\mu + \geq 1j(\text{b-tag})$ forward region
182.9 ± 3.1 ± 6.4	<sup>6</sup> AAD 14AY ATLS		$e + \mu + 1$ or $2b$ jets
194 ± 18 ± 46	<sup>7</sup> AAD 13X ATLS		$\tau_h + \cancel{E}_T + \geq 5j (\geq 2b)$
139 ± 10 ± 26	<sup>8</sup> CHATRCHYAN13AY CMS		$\geq 6$ jets with $2$ <i>b</i> -tags
158.1 ± 2.1 ± 10.8	<sup>9</sup> CHATRCHYAN13BB CMS		$\ell + \cancel{E}_T + \text{jets} (\geq 1$ <i>b</i> -tag)
152 ± 12 ± 32	<sup>10</sup> CHATRCHYAN13BE CMS		$\tau_h + \cancel{E}_T + \geq 4$ jets ( $\geq 1$ <i>b</i> )
177 ± 20 ± 14 ± 7	<sup>11</sup> AAD 12B ATLS		Repl. by AAD 12BF
176 ± 5 ± 14 ± 11 ± 8	<sup>12</sup> AAD 12BF ATLS		$\ell\ell + \cancel{E}_T + \geq 2j$
187 ± 11 ± 18 ± 17 ± 6	<sup>13</sup> AAD 12B0 ATLS		$\ell + \cancel{E}_T + \geq 3j$ with <i>b</i> -tag
186 ± 13 ± 20 ± 7	<sup>14</sup> AAD 12CG ATLS		$\ell + \tau_h + \cancel{E}_T + \geq 2j (\geq 1b)$
143 ± 14 ± 22 ± 3	<sup>15</sup> CHATRCHYAN12AC CMS		$\ell + \tau_h + \cancel{E}_T + \geq 2j (\geq 1b)$
161.9 ± 2.5 ± 5.1 ± 5.0 ± 3.6	<sup>16</sup> CHATRCHYAN12AX CMS		$\ell\ell + \cancel{E}_T + \geq 2b$
145 ± 31 ± 42 ± 27	<sup>17</sup> AAD 11A ATLS		$\ell + \cancel{E}_T + \geq 4j, \ell\ell + \cancel{E}_T + \geq 2j$
173 ± 39 ± 32 ± 7	<sup>18</sup> CHATRCHYAN11AA CMS		$\ell + \cancel{E}_T + \geq 3$ jets
168 ± 18 ± 14 ± 7	<sup>19</sup> CHATRCHYAN11F CMS		$\ell\ell + \cancel{E}_T + \text{jets}$
154 ± 17 ± 6	<sup>20</sup> CHATRCHYAN11Z CMS		Combination
194 ± 72 ± 24 ± 21	<sup>21</sup> KHACHATRYAN...11A CMS		$\ell\ell + \cancel{E}_T + \geq 2$ jets

• • • We do not use the following data for averages, fits, limits, etc. • • •

<sup>1</sup> KHACHATRYAN 17B based on 5.0 fb<sup>-1</sup> of data, using a binned likelihood fit of templates to the data. Also the ratio  $\sigma(t\bar{t}; 8 \text{ TeV})/\sigma(t\bar{t}; 7 \text{ TeV}) = 1.43 \pm 0.04 \pm 0.07 \pm 0.05$  is reported. The results are in agreement with NNLO SM predictions.

<sup>2</sup> KHACHATRYAN 16AW based on 5.0 fb<sup>-1</sup> of data, using a binned likelihood fit to differential distributions of *b*-tagged and non-*b*-tagged jets. The result is in good agreement with NNLO SM predictions.

<sup>3</sup> Based on 4.6 fb<sup>-1</sup> of data. Uses a template fit to distributions of  $\cancel{E}_T$  and jet multiplicities to measure simultaneously  $t\bar{t}$ , *WW*, and  $Z/\gamma^* \rightarrow \tau\tau$  cross sections, assuming  $m_t = 172.5$  GeV.

- <sup>4</sup> AAD 15CC based on 4.6 fb<sup>-1</sup> of data. The event selection criteria are optimized for the  $\ell\tau_h + \text{jets}$  channel. Using only this channel  $183 \pm 9 \pm 23 \pm 3$  pb is derived for the cross section.
- <sup>5</sup> AAIJ 15R, based on 1.0 fb<sup>-1</sup> of data, reports  $0.239 \pm 0.053 \pm 0.033 \pm 0.024$  pb cross section for the forward fiducial region  $p_T(\mu) > 25$  GeV,  $2.0 < \eta(\mu) < 4.5$ ,  $50 \text{ GeV} < p_T(b) < 100$  GeV,  $2.2 < \eta(b) < 4.2$ ,  $\Delta R(\mu, b) > 0.5$ , and  $p_T(\mu+b) > 20$  GeV. The three errors are from statistics, systematics, and theory. The result agrees with the SM NLO prediction.
- <sup>6</sup> AAD 14AY reports  $182.9 \pm 3.1 \pm 4.2 \pm 3.6 \pm 3.3$  pb value based on 4.6 fb<sup>-1</sup> of data. The four errors are from statistics, systematic, luminosity, and the 0.66% beam energy uncertainty. We have combined the systematic uncertainties in quadrature. The result is for  $m_t = 172.5$  GeV; for other  $m_t$ ,  $\sigma(m_t) = \sigma(172.5 \text{ GeV}) \times [1 - 0.0028 \times (m_t - 172.5 \text{ GeV})]$ . The result is consistent with the SM prediction at NNLO.
- <sup>7</sup> Based on 1.67 fb<sup>-1</sup> of data. The result uses the acceptance for  $m_t = 172.5$  GeV.
- <sup>8</sup> Based on 3.54 fb<sup>-1</sup> of data.
- <sup>9</sup> Based on 2.3 fb<sup>-1</sup> of data.
- <sup>10</sup> Based on 3.9 fb<sup>-1</sup> of data.
- <sup>11</sup> Based on 35 pb<sup>-1</sup> of data for an assumed top quark mass of  $m_t = 172.5$  GeV.
- <sup>12</sup> Based on 0.70 fb<sup>-1</sup> of data. The 3 errors are from statistics, systematics, and luminosity. The result uses the acceptance for  $m_t = 172.5$  GeV.
- <sup>13</sup> Based on 35 pb<sup>-1</sup> of data. The 3 errors are from statistics, systematics, and luminosity. The result uses the acceptance for  $m_t = 172.5$  GeV and  $173 \pm 17_{-16}^{+18} \pm 6$  pb is found without the *b*-tag.
- <sup>14</sup> Based on 2.05 fb<sup>-1</sup> of data. The hadronic  $\tau$  candidates are selected using a BDT technique. The 3 errors are from statistics, systematics, and luminosity. The result uses the acceptance for  $m_t = 172.5$  GeV.
- <sup>15</sup> Based on 2.0 fb<sup>-1</sup> and 2.2 fb<sup>-1</sup> of data for  $\ell = e$  and  $\ell = \mu$ , respectively. The 3 errors are from statistics, systematics, and luminosity. The result uses the acceptance for  $m_t = 172.5$  GeV.
- <sup>16</sup> Based on 2.3 fb<sup>-1</sup> of data. The 3 errors are from statistics, systematics, and luminosity. The result uses the profile likelihood-ratio (PLB) method and an assumed  $m_t$  of 172.5 GeV.
- <sup>17</sup> Based on 2.9 pb<sup>-1</sup> of data. The result for single lepton channels is  $142 \pm 34_{-31}^{+50}$  pb, while for the dilepton channels is  $151 \pm 78_{-62}^{+37} \pm 24$  pb.
- <sup>18</sup> Result is based on 36 pb<sup>-1</sup> of data. The first uncertainty corresponds to the statistical and systematic uncertainties, and the second corresponds to the luminosity.
- <sup>19</sup> Based on 36 pb<sup>-1</sup> of data. The ratio of  $t\bar{t}$  and  $Z/\gamma^*$  cross sections is measured as  $\sigma(pp \rightarrow t\bar{t})/\sigma(pp \rightarrow Z/\gamma^* \rightarrow e^+e^-/\mu^+\mu^-) = 0.175 \pm 0.018(\text{stat}) \pm 0.015(\text{syst})$  for  $60 < m_{\ell\ell} < 120$  GeV, for which they use an NNLO prediction for the denominator cross section of  $972 \pm 42$  pb.
- <sup>20</sup> Result is based on 36 pb<sup>-1</sup> of data. The first error is from statistical and systematic uncertainties, and the second from luminosity. This is a combination of a measurement in the dilepton channel (CHATRCHYAN 11F) and the measurement in the  $\ell + \text{jets}$  channel (CHATRCHYAN 11Z) which yields  $150 \pm 9 \pm 17 \pm 6$  pb.
- <sup>21</sup> Result is based on 3.1 ± 0.3 pb<sup>-1</sup> of data.

## $t\bar{t}$ Production Cross Section in *pp* Collisions at $\sqrt{s} = 8$ TeV

Unless otherwise noted the first quoted error is from statistics, the second from systematic uncertainties, and the third from luminosity. If only two errors are quoted the luminosity is included in the systematic uncertainties.

VALUE (pb)	DOCUMENT ID	TECN	COMMENT
248.3 ± 0.7 ± 13.4 ± 4.7	<sup>1</sup> AABOUD 18BH ATLS		$\ell + \cancel{E}_T + \geq 4j (\geq 1b)$
239 ± 4 ± 28 ± 5	<sup>2</sup> AABOUD 17Z ATLS		$\tau_h + \cancel{E}_T + \geq 2j (\geq 2b)$
228.5 ± 3.8 ± 13.7 ± 6.0	<sup>3</sup> KHACHATRYAN...17B CMS		$\ell + \cancel{E}_T + \geq 4j (\geq 1b)$
242.9 ± 1.7 ± 8.6	<sup>4</sup> AAD 16BK ATLS		$e + \mu + 1$ or $2b$ jets
244.9 ± 1.4 ± 6.3 ± 6.4	<sup>5</sup> KHACHATRYAN...16AW CMS		$e + \mu + \cancel{E}_T + \geq 0j$
275.6 ± 6.1 ± 37.8 ± 7.2	<sup>6</sup> KHACHATRYAN...16BC CMS		$\geq 6j (\geq 2b)$
260 ± 1 ± 24 ± 25	<sup>7</sup> AAD 15BP ATLS		$\ell + \cancel{E}_T + \geq 3j (\geq 1b)$
	<sup>8</sup> AAIJ 15R LHCB		$\mu + \geq 1j(\text{b-tag})$ forward region
242.4 ± 1.7 ± 10.2	<sup>9</sup> AAD 14AY ATLS		$e + \mu + 1$ or $2b$ jets
239 ± 2 ± 11 ± 6	<sup>10</sup> CHATRCHYAN14F CMS		$\ell\ell + \cancel{E}_T + \geq 2j (\geq 1$ <i>b</i> -tag)
257 ± 3 ± 24 ± 7	<sup>11</sup> KHACHATRYAN...14S CMS		$\ell + \tau_h + \cancel{E}_T + \geq 2j (\geq 1b)$

- <sup>1</sup> AABOUD 18BH based on 20.2 fb<sup>-1</sup> of data. The result is for  $m_t = 172.5$  GeV. To reduce effects of uncertainties in the jet energy scale and *b*-tagging efficiency, they are included as nuisance parameters in the fit of discriminant distributions, after separating selected events into three regions. Furthermore the *W*+jets background distribution is modelled using *Z*+jets event data.
- <sup>2</sup> AABOUD 17Z based on 20.2 fb<sup>-1</sup> of data, using the mode  $t\bar{t} \rightarrow \tau\nu q^* \bar{q} b \bar{b}$  with  $\tau$  decaying hadronically. Single prong and 3 prong decays of  $\tau$  are separately analyzed. The result is consistent with the SM. The third quoted uncertainty is due to luminosity.
- <sup>3</sup> KHACHATRYAN 17B based on 19.6 fb<sup>-1</sup> of data, using a binned likelihood fit of templates to the data. Also the ratio  $\sigma(t\bar{t}; 8 \text{ TeV})/\sigma(t\bar{t}; 7 \text{ TeV}) = 1.43 \pm 0.04 \pm 0.07 \pm 0.05$  is reported. The results are in agreement with NNLO SM predictions.
- <sup>4</sup> AAD 16BK is an update of the value from AAD 14AY using the improved luminosity calibration. The value  $242.9 \pm 1.7 \pm 5.5 \pm 5.1 \pm 4.2$  pb is reported, where we have combined the systematic uncertainties in quadrature. Also the ratio  $\sigma(t\bar{t}; 8 \text{ TeV})/\sigma(t\bar{t}; 7 \text{ TeV}) = 1.328 \pm 0.024 \pm 0.015 \pm 0.038 \pm 0.001$  has been updated. The former result is consistent with the SM predictions at NNLO, while the latter result is 2.1  $\sigma$  below the expectation.
- <sup>5</sup> KHACHATRYAN 16AW based on 19.7 fb<sup>-1</sup> of data, using a binned likelihood fit to differential distributions of *b*-tagged and non-*b*-tagged jets. The result is in good agreement with NNLO SM predictions.
- <sup>6</sup> KHACHATRYAN 16BC based on 18.4 fb<sup>-1</sup> of data. The last uncertainty is due to luminosity. Cuts on kinematical fit probability and  $\Delta R(b, b)$  are imposed. The major QCD background is determined from the data. The result is for  $m_t = 172.5$  GeV and in agreement with the SM prediction. The top quark  $p_T$  spectra, also measured, are significantly softer than theoretical predictions.
- <sup>7</sup> AAD 15BP based on 20.3 fb<sup>-1</sup> of data. The result is for  $m_t = 172.5$  GeV and in agreement with the SM prediction  $253_{-15}^{+13}$  pb at NNLO+NNLL. Superseded by AABOUD 18BH.

<sup>8</sup> AAIJ 15R, based on 2.0 fb<sup>-1</sup> of data, reports 0.289 ± 0.043 ± 0.040 ± 0.029 pb cross section for the forward fiducial region  $p_T(\mu) > 25$  GeV,  $2.0 < \eta(\mu) < 4.5$ , 50 GeV <  $p_T(b) < 100$  GeV,  $2.2 < \eta(b) < 4.2$ ,  $\Delta R(\mu, b) > 0.5$ , and  $p_T(\mu+b) > 20$  GeV. The three errors are from statistics, systematics, and theory. The result agrees with the SM NLO prediction.

<sup>9</sup> AAD 14AY reports 242.4 ± 1.7 ± 5.5 ± 7.5 ± 4.2 pb value based on 20.3 fb<sup>-1</sup> of data. The four errors are from statistics, systematic, luminosity, and the 0.66% beam energy uncertainty. We have combined the systematic uncertainties in quadrature. The result is for  $m_t = 172.5$  GeV; for other  $m_t$ ,  $\sigma(m_t) = \sigma(172.5 \text{ GeV}) \times [1 - 0.0028 \times (m_t - 172.5 \text{ GeV})]$ . Also measured is the ratio  $\sigma(t\bar{t}; 8 \text{ TeV})/\sigma(t\bar{t}; 7 \text{ TeV}) = 1.326 \pm 0.024 \pm 0.015 \pm 0.049 \pm 0.001$ . The results are consistent with the SM predictions at NNLO.

<sup>10</sup> Based on 5.3 fb<sup>-1</sup> of data. The result is for  $m_t = 172.5$  GeV, and a parametrization is given in eq.(6.1) for the mean value at other  $m_t$  values. The result is in agreement with the SM prediction 252.9<sup>+6.4</sup><sub>-8.6</sub> pb at NNLO.

<sup>11</sup> Based on 19.6 fb<sup>-1</sup> of data. The measurement is in the channel  $t\bar{t} \rightarrow (b\ell\nu)(b\tau\nu)$ , where  $\tau$  decays into hadrons ( $\tau_h$ ). The result is for  $m_t = 172.5$  GeV. For  $m_t = 173.3$  GeV, the cross section is lower by 3.1 pb.

### t $\bar{t}$ Production Cross Section in pp Collisions at $\sqrt{s} = 13$ TeV

VALUE (pb)	DOCUMENT ID	TECN	COMMENT
803 ± 2 ± 25 ± 20	<sup>1</sup> SIRUNYAN 19AR CMS		dilepton channel ( $e\mu, 2e, 2\mu$ )
	<sup>2</sup> SIRUNYAN 19P CMS		dilepton channel
815 ± 9 ± 38 ± 19	<sup>3</sup> KHACHATRYAN...17N CMS		$e\mu + \geq 2j (\geq 1b j)$
888 ± 2 <sup>+26</sup> <sub>-28</sub> ± 20	<sup>4</sup> SIRUNYAN 17W CMS		$\ell + \geq 1j$
818 ± 8 ± 35	<sup>5</sup> AABOUD 16R ATLS		$e + \mu + 1$ or 2b jets
746 ± 5 ± 8 ± 53 ± 36	<sup>6</sup> KHACHATRYAN...16j CMS		$e + \mu + \geq 2j$

<sup>1</sup> SIRUNYAN 19AR based on 35.9 fb<sup>-1</sup> of data. Obtained from the visible cross section measured using a template fit to multidifferential distributions categorized according to the  $b$ -tagged jet multiplicity. The result is for  $m_t = 172.5$  GeV and in agreement with the SM prediction at NNLO+NNLL.

<sup>2</sup> SIRUNYAN 19P reports differential  $t\bar{t}$  cross sections measured using dilepton events at 13 TeV with 35.9 fb<sup>-1</sup> and compared to NLO predictions.

<sup>3</sup> KHACHATRYAN 17N based on 2.2 fb<sup>-1</sup> of data. The last quoted uncertainty is due to the beam luminosity. This measurement supersedes that of KHACHATRYAN 16j.

<sup>4</sup> SIRUNYAN 17W based on 2.2 fb<sup>-1</sup> of  $pp$  data at  $\sqrt{s} = 13$  TeV. Events are categorized according to the jet multiplicity and the number of  $b$ -tagged jets. A likelihood fit is performed to the event distributions to compare to the NNLO+NNLL prediction.

<sup>5</sup> AABOUD 16R reported value 818 ± 8 ± 27 ± 19 ± 12 pb based on 3.2 fb<sup>-1</sup> of data. The four errors are from statistics, systematic, luminosity, and beam energy. We have combined the systematic uncertainties in quadrature. The result is in agreement with the SM prediction 832<sup>+40</sup><sub>-46</sub> pb at NNLO+NNLL for  $m_t = 172.5$  GeV.

<sup>6</sup> KHACHATRYAN 16j based on 4.3 pb<sup>-1</sup> of data. The last uncertainty is due to luminosity. The result is for  $m_t = 172.5$  GeV and in agreement with the SM prediction 832<sup>+40</sup><sub>-46</sub> pb at NNLO+NNLL.

### t $\bar{t}$ t $\bar{t}$ Production Cross Section in pp Collisions at $\sqrt{s} = 8$ TeV

VALUE (fb)	CL%	DOCUMENT ID	TECN	COMMENT
<23	95	<sup>1</sup> AAD 15AR ATLS		$\ell + \bar{\ell} + \geq 5j (\geq 2b)$
<70	95	<sup>2</sup> AAD 15BY ATLS		$\geq 2\ell + \bar{\ell} + \geq 2j (\geq 1b j)$
<32	95	<sup>3</sup> KHACHATRYAN...14R CMS		$\ell + \bar{\ell} + \geq 6j (\geq 2b)$

<sup>1</sup> AAD 15AR based on 20.3 fb<sup>-1</sup> of data. A fit to  $H_T$  distributions in multi-channels classified by the number of jets and of  $b$ -tagged jets is performed.

<sup>2</sup> AAD 15BY based on 20.3 fb<sup>-1</sup> of data. A same-sign lepton pair is required. An excess over the SM prediction reaches 2.5 $\sigma$  for hypotheses involving heavy resonances decaying into  $t\bar{t}$ .

<sup>3</sup> Based on 19.6 fb<sup>-1</sup> of data, using a multivariate analysis to separate signal from backgrounds. About  $\sigma(t\bar{t}t\bar{t}) = 1$  fb is expected in the SM.

### t $\bar{t}$ t $\bar{t}$ Production Cross Section in pp Collisions at $\sqrt{s} = 13$ TeV

VALUE (fb)	CL%	DOCUMENT ID	TECN	COMMENT
<47	95	<sup>1</sup> AABOUD 19AP ATLS		$\ell + \ell^+ \ell^-$ channels
<49	95	<sup>2</sup> AABOUD 19AP ATLS		combination of ATLAS
13 <sup>+11</sup> <sub>-9</sub>		<sup>3</sup> SIRUNYAN 19CN CMS		combination of CMS
<48	95	<sup>4</sup> SIRUNYAN 19CN CMS		$\ell + \text{jets}, \ell^+ \ell^- + \text{jets}$ channels
<69	95	<sup>5</sup> AABOUD 18CE ATLS		$\geq 2\ell$ (same sign) + $\bar{\ell} + \geq 1b j$
16.9 <sup>+13.8</sup> <sub>-11.4</sub>		<sup>6</sup> SIRUNYAN 18BU CMS		$t\bar{t}t\bar{t} \rightarrow$ (same sign 2 $\ell$ or $\geq 3\ell$ ) + $\geq 4j (\geq 2b)$
<94	95	<sup>7</sup> SIRUNYAN 17AB CMS		$\ell + \text{jets}, \ell^+ \ell^- + \text{jets}$ channels
<42	95	<sup>8</sup> SIRUNYAN 17S CMS		(same sign 2 $\ell$ ) + $\bar{\ell} + \geq 2j$

<sup>1</sup> AABOUD 19AP based on 36.1 fb<sup>-1</sup> of data. The upper limit corresponds to 5.1 times the NLO SM cross section.

<sup>2</sup> AABOUD 19AP limit from data combined with AABOUD 18CE. The upper limit corresponds to 5.3 times the NLO SM cross section. Also a limit on the four-top-quark contact interaction of  $|C_{4t}|/\Lambda^2 < 1.9 \text{ TeV}^{-2}$  (95% CL) is obtained in an EFT model.

<sup>3</sup> SIRUNYAN 19CN based on 35.8 fb<sup>-1</sup> of data, combined with SIRUNYAN 18BU. The results are also interpreted in the effective field theory framework.

<sup>4</sup> SIRUNYAN 19CN based on 35.8 fb<sup>-1</sup> of data. A multivariate analysis using global event and jet properties is performed to discriminate from  $t\bar{t}$  background.

<sup>5</sup> AABOUD 18CE based on 36.1 fb<sup>-1</sup> of proton-proton data taken at  $\sqrt{s} = 13$  TeV. Events including a same-sign lepton pair are used. The result is consistent with the NLO SM cross section of 9.2 fb.

<sup>6</sup> SIRUNYAN 18BU based on 35.9 fb<sup>-1</sup> of proton-proton data taken at  $\sqrt{s} = 13$  TeV. Yields from signal regions and control regions defined based on  $N_{jets}$ ,  $N_b$  and  $N_j$  are combined in a maximum-likelihood fit. The result is in agreement with the NLO SM prediction 9.2<sup>+2.9</sup><sub>-2.4</sub> fb. The measurement constrains the top quark Yukawa coupling strength parameter to be  $|Y_t/Y_t^{SM}| < 2.1$  (95% CL).

<sup>7</sup> SIRUNYAN 17AB based on 2.6 fb<sup>-1</sup> of data. A multivariate analysis is used to discriminate between  $t\bar{t}t\bar{t}$  signal and  $t\bar{t}$  background. A combination with a previous search (CMS, KHACHATRYAN 16BJ) in the same-sign dilepton channel gives an upper limit of 69 fb (95% CL), corresponding to 7.4 (SM prediction).

<sup>8</sup> SIRUNYAN 17S based on 35.9 fb<sup>-1</sup>. The limit is in agreement with the NLO SM prediction 9.2<sup>+2.9</sup><sub>-2.4</sub> fb. Superseded by SIRUNYAN 18BU. The signal events are also used to constrain various new physics models.

### t $\bar{t}$ W Production Cross Section in pp Collisions at $\sqrt{s} = 8$ TeV

VALUE (fb)	DOCUMENT ID	TECN	COMMENT
170 <sup>+90</sup> <sub>-80</sub> ± 70	<sup>1</sup> KHACHATRYAN...14N CMS		$t\bar{t}W \rightarrow$ same sign dilepton + $\bar{\ell} + \text{jets}$

<sup>1</sup> Based on 19.5 fb<sup>-1</sup> of data. The result is consistent with the SM prediction of  $\sigma(t\bar{t}W) = 206<sup>+21</sup><sub>-23</sub> fb.$

### t $\bar{t}$ W Production Cross Section in pp Collisions at $\sqrt{s} = 13$ TeV

VALUE (pb)	DOCUMENT ID	TECN	COMMENT
0.87 ± 0.13 ± 0.14	<sup>1</sup> AABOUD 19AR ATLS		2,3,4 $\ell$ + $\bar{\ell} + \text{jets}$
0.77 ± 0.12 ± 0.13 -0.11 -0.12	<sup>2</sup> SIRUNYAN 18BS CMS		$t\bar{t}W \rightarrow$ same sign dilepton + $\bar{\ell} + \text{jets}$

<sup>1</sup> AABOUD 19AR based on 35.9 fb<sup>-1</sup> of data.  $t\bar{t}W$  and  $t\bar{t}Z$  cross sections are simultaneously measured using a combined fit to the events divided into multiple regions. The result is consistent with the SM prediction at NLO 0.60<sup>+0.08</sup><sub>-0.07</sub> pb. It is also used to constrain the Wilson coefficients for dimension-six operators which modify the  $t\bar{t}Z$  vertex.

<sup>2</sup> Based on 35.9 fb<sup>-1</sup> of proton-proton data taken at  $\sqrt{s} = 13$  TeV. The result is consistent with the SM prediction and is used to constrain the Wilson coefficients for dimension-six operators describing new interactions. The result is consistent with the SM prediction at NLO 0.628 ± 0.082 pb.

### t $\bar{t}$ Z Production Cross Section in pp Collisions at $\sqrt{s} = 8$ TeV

VALUE (fb)	DOCUMENT ID	TECN	COMMENT
200 <sup>+80+40</sup> <sub>-70-30</sub>	<sup>1</sup> KHACHATRYAN...14N CMS		$t\bar{t}Z \rightarrow 3,4 \ell + \bar{\ell} + \text{jets}$

<sup>1</sup> Based on 19.5 fb<sup>-1</sup> of data. The result is consistent with the SM prediction of  $\sigma(t\bar{t}Z) = 197<sup>+22</sup><sub>-25</sub> fb.$

### t $\bar{t}$ Z Production Cross Section in pp Collisions at $\sqrt{s} = 13$ TeV

VALUE (pb)	DOCUMENT ID	TECN	COMMENT
0.95 ± 0.08 ± 0.10	<sup>1</sup> AABOUD 19AR ATLS		2,3,4 $\ell$ + $\bar{\ell} + \text{jets}$
0.99 ± 0.09 ± 0.12 -0.08 -0.10	<sup>2</sup> SIRUNYAN 18BS CMS		$t\bar{t}Z \rightarrow 3,4 \ell + \bar{\ell} + \text{jets}$

<sup>1</sup> AABOUD 19AR based on 35.9 fb<sup>-1</sup> of data.  $t\bar{t}W$  and  $t\bar{t}Z$  cross sections are simultaneously measured using a combined fit to the events divided into multiple regions. The result is consistent with the SM prediction at NLO 0.88<sup>+0.09</sup><sub>-0.11</sub> pb. It is also used to constrain the Wilson coefficients for dimension-six operators which modify the  $t\bar{t}Z$  vertex.

<sup>2</sup> Based on 35.9 fb<sup>-1</sup> of proton-proton data taken at  $\sqrt{s} = 13$  TeV. The result is consistent with the SM prediction and is used to constrain the Wilson coefficients for dimension-six operators describing new interactions. The result is consistent with the SM prediction at NLO 0.839 ± 0.101 pb.

### t $\bar{t}$ γ Production Cross Section in pp Collisions at $\sqrt{s} = 13$ TeV

VALUE (pb)	DOCUMENT ID	TECN	COMMENT
	<sup>1</sup> AABOUD 19AD ATLS		$pp \rightarrow t\bar{t}\gamma$

<sup>1</sup> AABOUD 19AD measured fiducial inclusive and differential cross-sections for  $pp \rightarrow t\bar{t}\gamma$  at 13 TeV with 36.1 fb<sup>-1</sup> of data. The results are in agreement with the theoretical predictions.

### f(Q<sub>0</sub>): t $\bar{t}$ Fraction of Events with a Veto on Additional Central Jet Activity in pp Collisions at $\sqrt{s} = 7$ TeV

VALUE (%)	DOCUMENT ID	TECN	COMMENT
80.0 ± 1.1 ± 1.6	<sup>1</sup> CHATRCHYAN 14AE CMS		$Q_0 = 75 \text{ GeV}$ ( $ \eta  < 2.4$ )
92.0 ± 0.7 ± 0.8	<sup>1</sup> CHATRCHYAN 14AE CMS		$Q_0 = 150 \text{ GeV}$ ( $ \eta  < 2.4$ )
98.0 ± 0.3 ± 0.3	<sup>1</sup> CHATRCHYAN 14AE CMS		$Q_0 = 300 \text{ GeV}$ ( $ \eta  < 2.4$ )
56.4 ± 1.3 ± 2.6 -2.8	<sup>2</sup> AAD 12BL ATLS		$Q_0 = 25 \text{ GeV}$ ( $ \eta  < 2.1$ )
84.7 ± 0.9 ± 1.0	<sup>2</sup> AAD 12BL ATLS		$Q_0 = 75 \text{ GeV}$ ( $ \eta  < 2.1$ )
95.2 <sup>+0.5</sup> <sub>-0.6</sub> ± 0.4	<sup>2</sup> AAD 12BL ATLS		$Q_0 = 150 \text{ GeV}$ ( $ \eta  < 2.1$ )

<sup>1</sup> CHATRCHYAN 15 based on 5.0 fb<sup>-1</sup> of data. The  $t\bar{t}$  events are selected in the dilepton and lepton + jets decay channels. For other values of  $Q_0$  see Table 5.

<sup>2</sup> Based on 2.05 fb<sup>-1</sup> of data. The  $t\bar{t}$  events are selected in the dilepton decay channel with two identified  $b$ -jets.



# Quark Particle Listings

*t*

## Fraction of $t\bar{t}$ + multi-jet Events in $pp$ Collisions at $\sqrt{s} = 7$ TeV

VALUE	DOCUMENT ID	TECN	COMMENT
••• We do not use the following data for averages, fits, limits, etc. •••			
0.332±0.090	<sup>1</sup> AAD	15D ATLS	$\ell + \cancel{E}_T + n_j$ ( $n=3$ to 8)
0.436±0.098	<sup>2</sup> CHATRCHYAN14AE	CMS	$t\bar{t}(\ell\ell) + 0$ jet ( $E_T > 30$ GeV)
0.232±0.125	<sup>2</sup> CHATRCHYAN14AE	CMS	$t\bar{t}(\ell\ell) + 1$ jet ( $E_T > 30$ GeV)
	<sup>2</sup> CHATRCHYAN14AE	CMS	$t\bar{t}(\ell\ell) + \geq 2$ jet ( $E_T > 30$ GeV)

<sup>1</sup> Based on 4.6 fb<sup>-1</sup> of data. Fiducial  $t\bar{t}$  production cross section is presented as a function of the jet multiplicity for up to eight jets with the jet  $p_T$  threshold of 25, 40, 60, and 80 GeV, and as a function of jet  $p_T$  up to the 5th jet. MC models can be discriminated by using data for high jet multiplicity and by  $p_T$  distributions of the leading and 5th jet.

<sup>2</sup> Based on 5.0 fb<sup>-1</sup> of data. Events with two oppositely charged leptons, large  $\cancel{E}_T$  and jets with at least 1  $b$ -tag are used to measure the fraction of  $t\bar{t}$  plus additional jets. The gap fraction ( $n=0$  jet rate) as a function of the jet  $p_T$  and that of  $H_T$ , the scalar sum of the  $p_T$ 's of additional jets, is shown in Fig. 8.

## $t\bar{t}$ Charge Asymmetry ( $A_C$ ) in $pp$ Collisions at $\sqrt{s} = 7$ TeV

$A_C = (N(\Delta|y| > 0) - N(\Delta|y| < 0)) / (N(\Delta|y| > 0) + N(\Delta|y| < 0))$  where  $\Delta|y| = |y_t| - |y_{\bar{t}}|$  is the difference between the absolute values of the top and antitop rapidities and  $N$  is the number of events with  $\Delta|y|$  positive or negative.

VALUE (%)	DOCUMENT ID	TECN	COMMENT
••• We do not use the following data for averages, fits, limits, etc. •••			
0.5±0.7±0.6	<sup>1</sup> AABOUD	18AMLHC	ATLAS+CMS combination (lepton + jets)
2.1±2.5±1.7	<sup>2</sup> AAD	15AJ ATLS	$\ell\ell + \cancel{E}_T + \geq 2j$
0.6±1.0	<sup>3</sup> AAD	14I ATLS	$\ell + \cancel{E}_T + \geq 4j$ ( $\geq 1b$ )
-1.0±1.7±0.8	<sup>4</sup> CHATRCHYAN14D	CMS	$\ell\ell + \cancel{E}_T + \geq 2j$ ( $\geq 1b$ )
-1.9±2.8±2.4	<sup>5</sup> AAD	12BK ATLS	$\ell + \cancel{E}_T + \geq 4j$ ( $\geq 1b$ )
0.4±1.0±1.1	<sup>6</sup> CHATRCHYAN12BB	CMS	$\ell + \cancel{E}_T + \geq 4j$ ( $\geq 1b$ )
-1.3±2.8± <sup>2.9</sup> <sub>-3.1</sub>	<sup>7</sup> CHATRCHYAN12Bs	CMS	$\ell + \cancel{E}_T + \geq 4j$ ( $\geq 1b$ )

<sup>1</sup> ATLAS and CMS combination based on the data of AAD 14I and CHATRCHYAN 12BB. It takes into account the correlations of the measurements and systematic errors. The result is in agreement with the SM prediction (NLO QCD + NLO EW).

<sup>2</sup> AAD 15AJ based on 4.6 fb<sup>-1</sup> of data. After kinematic reconstruction the top quark momenta are corrected for detector resolution and acceptance effects by unfolding, using parton level information of the MC generators. The lepton charge asymmetry is measured as  $A_C^\ell = 0.024 \pm 0.015 \pm 0.009$ . All the measurements are consistent with the SM predictions.

<sup>3</sup> Based on 4.7 fb<sup>-1</sup> of data. The result is consistent with the SM prediction of  $A_C = 0.0123 \pm 0.0005$ . The asymmetry is  $0.011 \pm 0.018$  if restricted to those events where  $\beta_Z(t\bar{t}) > 0.6$ , which is also consistent with the SM prediction of  $0.020^{+0.006}_{-0.007}$ .

<sup>4</sup> Based on 5.0 fb<sup>-1</sup> of data. The lepton charge asymmetry is measured as  $A_C^\ell = 0.009 \pm 0.0010 \pm 0.006$ .  $A_C^\ell$  dependences on  $m_{T\bar{T}}$ ,  $|y(t\bar{t})|$ , and  $p_T(t\bar{t})$  are given in Fig. 5. All measurements are consistent with the SM predictions.

<sup>5</sup> Based on 1.04 fb<sup>-1</sup> of data. The result is consistent with  $A_C = 0.006 \pm 0.002$  (MC at NLO). No significant dependence of  $A_C$  on  $m_{T\bar{T}}$  is observed.

<sup>6</sup> Based on 5.0 fb<sup>-1</sup> of data at 7 TeV.

<sup>7</sup> Based on 1.09 fb<sup>-1</sup> of data. The result is consistent with the SM predictions.

## $t\bar{t}$ Charge Asymmetry ( $A_C$ ) in $pp$ Collisions at $\sqrt{s} = 8$ TeV

VALUE (%)	DOCUMENT ID	TECN	COMMENT
••• We do not use the following data for averages, fits, limits, etc. •••			
0.55±0.23±0.25	<sup>1</sup> AABOUD	18AMLHC	ATLAS+CMS combination (lepton + jets)
2.1 ± 1.6	<sup>2</sup> AAD	16AE ATLS	$\ell\ell + \cancel{E}_T + \geq 2j$
0.9 ± 0.5	<sup>3</sup> AAD	16AZ ATLS	$\ell + \cancel{E}_T + \geq 4j$
4.2 ± 3.2	<sup>4</sup> AAD	16T ATLS	$m_{t\bar{t}} > 0.75$ TeV, $ y_t  -  y_{\bar{t}}  < 2$ , $\ell + \cancel{E}_T + \text{jets}$
1.1 ± 1.1 ± 0.7	<sup>5</sup> KHACHATRYAN...16AD	CMS	$\ell\ell + \cancel{E}_T + \geq 2j$ ( $\geq 1b$ )
0.33±0.26±0.33	<sup>6</sup> KHACHATRYAN...16AH	CMS	$\ell + \cancel{E}_T + \geq 4j$ ( $\geq 1b$ )
0.10±0.68±0.37	<sup>7</sup> KHACHATRYAN...16T	CMS	$\ell + \cancel{E}_T + \geq 4j$ ( $\geq 1b$ )

<sup>1</sup> ATLAS and CMS combination based on the data of AAD 16AZ and KHACHATRYAN 16AH. It takes into account the correlations of the measurements and systematic errors. A combination of the differential measurements of the charge asymmetry is also presented. The results are in agreement with the SM prediction (NNLO QCD + NLO EW).

<sup>2</sup> AAD 16AE is based on 20.3 fb<sup>-1</sup> of data. After kinematic reconstruction, the top quark momenta are corrected for detector resolution and acceptance effects by unfolding, using parton level information of the MC generators. The lepton charge asymmetry is measured as  $A_C^{\ell\ell} = 0.008 \pm 0.006$ . All the measurements are consistent with the SM predictions.

<sup>3</sup> AAD 16AZ based on 20.3 fb<sup>-1</sup> of data. All the differential and inclusive measurements are statistically limited and consistent with the SM predictions.

<sup>4</sup> AAD 16T based on 20.3 fb<sup>-1</sup> of data. Uses reconstruction techniques for the decay topology of highly boosted top quarks. The observed asymmetry is transformed by unfolding to a parton-level result in the shown fiducial region. The result is consistent with the NLO SM prediction.

<sup>5</sup> KHACHATRYAN 16AD based on 19.5 fb<sup>-1</sup> of data. The lepton charge asymmetry is measured as  $A_C^{\ell\ell} = 0.003 \pm 0.006 \pm 0.003$ . All the measurements are consistent with the SM predictions.

<sup>6</sup> KHACHATRYAN 16AH based on 19.6 fb<sup>-1</sup> of data. The same data set as in KHACHATRYAN 16T is used. A template technique is used, which is sensitive to the charge anti-symmetric component of the  $t\bar{t}$  rapidity distributions and statistically advantageous. The result is consistent with the SM predictions.

<sup>7</sup> KHACHATRYAN 16T based on 19.7 fb<sup>-1</sup> of data. The same data set as in KHACHATRYAN 16AH is used. After kinematic reconstruction the top quark momenta are corrected for detector resolution and acceptance effects by unfolding, using parton level information of the MC generators. All the measurements are consistent with the SM predictions.

## $t$ -quark Polarization in $t\bar{t}$ Events in $p\bar{p}$ Collisions at $\sqrt{s} = 1.96$ TeV

VALUE	DOCUMENT ID	TECN	COMMENT
••• We do not use the following data for averages, fits, limits, etc. •••			
0.070±0.055	<sup>1</sup> ABAZOV	17 D0	$\ell + \cancel{E}_T + \geq 3j$ ( $\geq 1b$ )
-0.102±0.061	<sup>2</sup> ABAZOV	17 D0	$\ell + \cancel{E}_T + \geq 3j$ ( $\geq 1b$ )
0.040±0.035	<sup>3</sup> ABAZOV	17 D0	$\ell + \cancel{E}_T + \geq 3j$ ( $\geq 1b$ )
0.113±0.091±0.019	<sup>4</sup> ABAZOV	15K D0	$A_{FB}^\ell$ in $\ell\ell + \cancel{E}_T + \geq 2j$ ( $\geq 1b$ )

<sup>1</sup> ABAZOV 17 based on 9.7 fb<sup>-1</sup> of data. The value is top quark polarization times spin analyzing power in the beam basis. Combination with the result of ABAZOV 15K yields  $0.081 \pm 0.048$ . This result together with the helicity polarization is shown in a 2-dimensional plot in Fig.4. These results are consistent with the SM prediction.

<sup>2</sup> ABAZOV 17 based on 9.7 fb<sup>-1</sup> of data. The value is top quark polarization times spin analyzing power in the helicity basis. The result is consistent with the SM prediction. This result together with the beam polarization is shown in a 2-dimensional plot in Fig.4.

<sup>3</sup> ABAZOV 17 based on 9.7 fb<sup>-1</sup> of data. The value is top quark polarization times spin analyzing power in the transverse basis. The result is consistent with the SM prediction.

<sup>4</sup> ABAZOV 15K based on 9.7 fb<sup>-1</sup> of data. The value is top quark polarization times spin analyzing power in the beam basis. The result is consistent with the SM prediction of  $-0.0019 \pm 0.0005$ .

## $t$ -quark Polarization in $t\bar{t}$ Events in $pp$ Collisions at $\sqrt{s} = 7$ TeV

The double differential distribution in polar angles,  $\theta_1$  ( $\theta_2$ ) of the decay product of the top (anti-top) decay products, is parametrized as  $(1/\sigma)d\sigma/(d\cos\theta_1 d\cos\theta_2) = (1/4) (1 + A_t \cos\theta_1 + A_{\bar{t}} \cos\theta_2 - C \cos\theta_1 \cos\theta_2)$ . The charged lepton is used to tag  $t$  or  $\bar{t}$ . The coefficient  $A_t$  and  $A_{\bar{t}}$  measure the average helicity of  $t$  and  $\bar{t}$ , respectively.  $A_{CP} = A_t = A_{\bar{t}}$  assumes  $CP$  conservation, whereas  $A_{CPV} = A_t = -A_{\bar{t}}$  corresponds to maximal  $CP$  violation.

VALUE	DOCUMENT ID	TECN	COMMENT
••• We do not use the following data for averages, fits, limits, etc. •••			
-0.035±0.014±0.037	<sup>1</sup> AAD	13BE ATLS	$A_{CP}$
0.020±0.016± <sup>0.013</sup> <sub>-0.017</sub>	<sup>1</sup> AAD	13BE ATLS	$A_{CPV}$

<sup>1</sup> Based on 4.7 fb<sup>-1</sup> of data using the final states containing one or two isolated electrons or muons and jets with at least one  $b$ -tag.

## $t$ -quark Polarization in $t\bar{t}$ Events in $pp$ Collisions at $\sqrt{s} = 8$ TeV

$A_t$ ,  $A_{\bar{t}}$ ,  $A_{CP}$ ,  $A_{CPV}$ , and  $A_C$  are defined in header texts in the subsections, just above.

VALUE	DOCUMENT ID	TECN	COMMENT
••• We do not use the following data for averages, fits, limits, etc. •••			
-0.044±0.038±0.027	<sup>1</sup> AABOUD	17G ATLS	$A_t$
-0.064±0.040±0.027	<sup>1</sup> AABOUD	17G ATLS	$A_{\bar{t}}$
0.296±0.093±0.037	<sup>1</sup> AABOUD	17G ATLS	$A_C$
-0.022±0.058	<sup>2</sup> KHACHATRYAN...16AI	CMS	$A_{CP}$
0.000±0.016	<sup>2</sup> KHACHATRYAN...16AI	CMS	$A_{CPV}$

<sup>1</sup> AABOUD 17G based on 20.2 fb<sup>-1</sup> of  $pp$  data, using events with two leptons and two or more jets with at least one  $b$ -tag. Determined from measurements of 15 top quark spin observables. The second error corresponds to a variation of  $m_t$  about 172.5 GeV by 0.7 GeV. The values are consistent with the NLO SM predictions.

<sup>2</sup> KHACHATRYAN 16AI based on 19.5 fb<sup>-1</sup> of  $pp$  data at  $\sqrt{s} = 8$  TeV, using events with two leptons and two or more jets with at least one  $b$ -tag. Determined from the lepton angular distributions as a function of the  $t\bar{t}$ -system kinematical variables.

## $t$ -quark Polarization in Single Top Events in $pp$ Collisions at $\sqrt{s} = 8$ TeV

VALUE	CL%	DOCUMENT ID	TECN	COMMENT
••• We do not use the following data for averages, fits, limits, etc. •••				
>0.72	95	<sup>1</sup> AABOUD	17Bb ATLS	$\alpha_\ell P$ ; t-channel
0.97±0.05±0.11		<sup>2</sup> AABOUD	17I ATLS	$\alpha_\ell P$ ; t-channel
0.25±0.08±0.14		<sup>3</sup> AABOUD	17I ATLS	$(F_+ + F_-)P$ ; t-channel
0.26±0.03±0.10		<sup>4</sup> KHACHATRYAN...16B0	CMS	$(\alpha_\mu P)/2$ ; t-channel

<sup>1</sup> AABOUD 17Bb based on 20.2 fb<sup>-1</sup> of  $pp$  data. Triple-differential decay rate of top quark is used to simultaneously determine five generalized  $Wtb$  couplings as well as the top polarization.  $\alpha_\ell$  denotes the spin analyzing power of charged lepton, and the spin axis of the top polarization  $P$  is taken along the spectator-quark momentum in the top rest frame. The value is compatible with the SM prediction of about 0.9.

<sup>2</sup> AABOUD 17I based on 20.2 fb<sup>-1</sup> of  $pp$  data. A cut-based analysis is used to discriminate between signal and backgrounds.  $\alpha_\ell$  denotes the spin analyzing power of charged lepton, and the spin axis of the top polarization  $P$  is taken along the spectator-quark momentum in the top rest frame. See this paper for a number of other asymmetries and measurements that are not included here.

<sup>3</sup> AABOUD 17I based on 20.2 fb<sup>-1</sup> of  $pp$  data. A cut-based analysis is used to discriminate between signal and backgrounds.  $F_\pm$  denotes  $W$  helicity fraction, and the spin axis of the top polarization  $P$  is taken along the spectator-quark momentum in the top rest frame. See this paper for a number of other asymmetries and measurements that are not included here.

<sup>4</sup> KHACHATRYAN 16B0 based on 19.7 fb<sup>-1</sup> of data. A high-purity sample with a muon is selected by a multivariate analysis. The value is the top spin asymmetry, given by one half of the spin analyzing power  $\alpha_\mu$  ( $=1$  at LO of SM) times the top polarization,  $P$ , where the spin axis is defined as the direction of the untagged jet in the top rest frame. The value is compatible with the SM prediction of 0.44 with a 2.0 $\sigma$  deviation.

## $g\bar{g} \rightarrow t\bar{t}$ Fraction in $p\bar{p}$ Collisions at $\sqrt{s} = 1.96$ TeV

VALUE	CL%	DOCUMENT ID	TECN	COMMENT
••• We do not use the following data for averages, fits, limits, etc. •••				
<0.33	68	<sup>1</sup> AALTONEN	09F CDF	$t\bar{t}$ correlations
0.07±0.14±0.07		<sup>2</sup> AALTONEN	08AG CDF	low $p_T$ number of tracks

<sup>1</sup> Based on 955 pb<sup>-1</sup>. AALTONEN 09F used differences in the  $t\bar{t}$  production angular distribution and polarization correlation to discriminate between  $g\bar{g} \rightarrow t\bar{t}$  and  $q\bar{q} \rightarrow t\bar{t}$  subprocesses. The combination with the result of AALTONEN 08AG yields  $0.07^{+0.15}_{-0.07}$ .





See key on page 999

# Quark Particle Listings

## *t*, *b'* (Fourth Generation) Quark

ABAZOV	06U	PR D74 092005	V.M. Abazov et al.	(DO Collab.)
ABAZOV	06X	PR D74 112004	V.M. Abazov et al.	(DO Collab.)
ABULENCIA	06D	PRL 96 022004	A. Abulencia et al.	(CDF Collab.)
Also		PR D73 032003	A. Abulencia et al.	(CDF Collab.)
Also		PR D73 092002	A. Abulencia et al.	(CDF Collab.)
ABULENCIA	06G	PRL 96 152002	A. Abulencia et al.	(CDF Collab.)
Also		PR D74 032009	A. Abulencia et al.	(CDF Collab.)
ABULENCIA	06R	PL B639 172	A. Abulencia et al.	(CDF Collab.)
ABULENCIA	06U	PR D73 111103	A. Abulencia et al.	(CDF Collab.)
ABULENCIA	06V	PR D73 112006	A. Abulencia et al.	(CDF Collab.)
ABULENCIA	06Z	PRL 97 082004	A. Abulencia et al.	(CDF Collab.)
ABULENCIA, A	06C	PRL 96 202002	A. Abulencia et al.	(CDF Collab.)
ABULENCIA, A	06E	PR D74 072005	A. Abulencia et al.	(CDF Collab.)
ABULENCIA, A	06F	PR D74 072006	A. Abulencia et al.	(CDF Collab.)
ABAZOV	05	PL B606 25	V.M. Abazov et al.	(DO Collab.)
ABAZOV	05G	PL B617 1	V.M. Abazov et al.	(DO Collab.)
ABAZOV	05L	PR D72 011104	V.M. Abazov et al.	(DO Collab.)
ABAZOV	05P	PL B622 265	V.M. Abazov et al.	(DO Collab.)
Also		PL B517 282	V.M. Abazov et al.	(DO Collab.)
Also		PR D53 031101	B. Abbott et al.	(DO Collab.)
Also		PR D75 092007	V.M. Abazov et al.	(DO Collab.)
ABAZOV	05Q	PL B626 35	V.M. Abazov et al.	(DO Collab.)
ABAZOV	05R	PL B626 55	V.M. Abazov et al.	(DO Collab.)
ABAZOV	05X	PL B626 45	V.M. Abazov et al.	(DO Collab.)
ACOSTA	05A	PRL 95 102002	D. Acosta et al.	(CDF Collab.)
ACOSTA	05D	PR D71 031101	D. Acosta et al.	(CDF Collab.)
ACOSTA	05N	PR D71 121005	D. Acosta et al.	(CDF Collab.)
ACOSTA	05S	PR D72 032002	D. Acosta et al.	(CDF Collab.)
ACOSTA	05T	PR D72 052003	D. Acosta et al.	(CDF Collab.)
ACOSTA	05U	PR D71 072005	D. Acosta et al.	(CDF Collab.)
ACOSTA	05V	PR D71 052003	D. Acosta et al.	(CDF Collab.)
ABAZOV	04G	NAT 429 638	V.M. Abazov et al.	(DO Collab.)
ABDALLAH	04C	PL B590 21	J. Abdallah et al.	(DELPHI Collab.)
ACOSTA	04H	PR D69 052003	D. Acosta et al.	(CDF Collab.)
ACOSTA	04I	PRL 93 142001	D. Acosta et al.	(CDF Collab.)
AKTAS	04	EPJ C33 9	A. Aktas et al.	(H1 Collab.)
ABAZOV	03A	PR D67 012004	V.M. Abazov et al.	(DO Collab.)
CHEKANOV	03	PL B559 153	S. Chekanov et al.	(ZEUS Collab.)
ACHARD	02J	PL B549 290	P. Achard et al.	(L3 Collab.)
ACOSTA	02	PR D65 091102	D. Acosta et al.	(CDF Collab.)
HEISTER	02Q	PL B543 173	A. Heister et al.	(ALEPH Collab.)
ABBIEUDI	01T	PL B521 181	G. Abbiendi et al.	(OPAL Collab.)
AFFOLDER	01	PR D63 032003	T. Affolder et al.	(CDF Collab.)
AFFOLDER	01A	PR D64 032002	T. Affolder et al.	(CDF Collab.)
AFFOLDER	01C	PRL 86 3233	T. Affolder et al.	(CDF Collab.)
AFFOLDER	00B	PRL 84 214	T. Affolder et al.	(CDF Collab.)
BARATE	00S	PL B494 33	S. Barate et al.	(ALEPH Collab.)
ABBOTT	99G	PR D60 052001	B. Abbott et al.	(DO Collab.)
ABE	99B	PRL 82 271	F. Abe et al.	(CDF Collab.)
Also		PRL 82 2808 (erratum)	F. Abe et al.	(CDF Collab.)
CHANG	99	PR D59 091503	D. Chang, W. Chang, E. Ma	
ABBOTT	98D	PRL 80 2063	B. Abbott et al.	(DO Collab.)
ABBOTT	98F	PR D58 052001	B. Abbott et al.	(DO Collab.)
ABE	98E	PRL 80 2767	F. Abe et al.	(CDF Collab.)
ABE	98F	PRL 80 2779	F. Abe et al.	(CDF Collab.)
ABE	98G	PRL 80 2525	F. Abe et al.	(CDF Collab.)
BHAT	98B	JUMP A13 5113	P.C. Bhat, H.B. Prosper, S.S. Snyder	
ABACHI	97E	PRL 79 1197	S. Abachi et al.	(DO Collab.)
ABE	97R	PRL 79 1992	F. Abe et al.	(CDF Collab.)
ABE	97V	PRL 79 3585	F. Abe et al.	(CDF Collab.)
PDG	96	PL D54 1	R. M. Barnett et al.	(PDG Collab.)
ABACHI	95	PRL 74 2632	S. Abachi et al.	(DO Collab.)
ABE	95F	PRL 74 2626	F. Abe et al.	(CDF Collab.)
ABE	94E	PR D50 2966	F. Abe et al.	(CDF Collab.)
Also		PRL 73 225	F. Abe et al.	(CDF Collab.)

### *b'* (*4<sup>th</sup>* Generation) Quark, Searches for

#### *b'*(-1/3)-quark/hadron mass limits in *p* $\bar{p}$ and *pp* collisions

VALUE (GeV)	CL%	DOCUMENT ID	TECN	COMMENT
>1130	95	1 SIRUNYAN 19A Q CMS		$B(b' \rightarrow Zb) = 1$
>1230	95	2 SIRUNYAN 19B W CMS		$B(b' \rightarrow Wt) = 1$
>1350	95	3 AABOUD 18A W ATLS		$B(b' \rightarrow Wt) = 1$
>1000	95	4 AABOUD 18C ATLS		$\geq 2\ell + \cancel{E}_T + \geq 1bj$
> 950	95	5 AABOUD 18L ATLS		<i>Wt</i> , <i>Zb</i> , <i>hb</i> modes
>1010	95	6,7 AABOUD 18CP ATLS		2,3 $\ell$ , singlet model
>1140	95	5,8 AABOUD 18CP ATLS		2,3 $\ell$ , doublet model
>1220	95	9,10 AABOUD 18CR ATLS		singlet <i>b'</i> , ATLAS Combination
>1370	95	9,11 AABOUD 18CR ATLS		<i>b'</i> in a weak isospin doublet ( <i>t'</i> , <i>b'</i> ). ATLAS combination.
> 910	95	12 SIRUNYAN 18B M CMS		<i>Wt</i> , <i>Zb</i> , <i>hb</i> modes
> 845	95	13 SIRUNYAN 18Q CMS		$B(b' \rightarrow Wu) = 1$
> 730	95	14 SIRUNYAN 17A U CMS		
> 880	95	15 KHACHATRYAN 16A N CMS		$B(b' \rightarrow Wt) = 1$
> 620	95	16 AAD 15B Y ATLS		<i>Wt</i> , <i>Zb</i> , <i>hb</i> modes
> 730	95	17 AAD 15B Y ATLS		$B(b' \rightarrow Wt) = 1$
> 810	95	18 AAD 15Z ATLS		
> 755	95	19 AAD 14A Z ATLS		$B(b' \rightarrow Wt) = 1$
> 675	95	20 CHATRCHYAN 13I CMS		$B(b' \rightarrow Wt) = 1$
> 190	95	21 ABAZOV 08X D0		$c\tau = 200\text{m}$
> 190	95	22 ACOSTA 03 CDF		quasi-stable <i>b'</i>
<350, 580-635, >700	95	23 AAD 15A R ATLS		$B(b' \rightarrow Hb) = 1$
> 690	95	24 AAD 15C N ATLS		$B(b' \rightarrow Wq) = 1$ ( $q=u$ )
> 480	95	25 AAD 12A T ATLS		$B(b' \rightarrow Wt) = 1$
> 400	95	26 AAD 12A U ATLS		$B(b' \rightarrow Zb) = 1$
> 350	95	27 AAD 12B C ATLS		$B(b' \rightarrow Wq) = 1$ ( $q=u, c$ )
> 450	95	28 AAD 12B E ATLS		$B(b' \rightarrow Wt) = 1$
> 685	95	29 CHATRCHYAN 12B H CMS		$m_{t'} = m_{b'}$

••• We do not use the following data for averages, fits, limits, etc. •••

- > 611 95 30 CHATRCHYAN 12X CMS  $B(b' \rightarrow Wt) = 1$
  - > 372 95 31 AALTONEN 11J CDF  $b' \rightarrow Wt$
  - > 361 95 32 CHATRCHYAN 11L CMS Repl. by CHATRCHYAN 12X
  - > 338 95 33 AALTONEN 10H CDF  $b' \rightarrow Wt$
  - > 380-430 95 34 FLACCO 10 RVUE  $m_{b'} > m_{t'}$
  - > 268 95 35,36 AALTONEN 07C CDF  $B(b' \rightarrow Zb) = 1$
  - > 199 95 37 AFFOLDER 00 CDF NC:  $b' \rightarrow Zb$
  - > 148 95 38 ABE 98N CDF NC:  $b' \rightarrow Zb + \text{vertex}$
  - > 96 95 39 ABACHI 97D D0 NC:  $b' \rightarrow b\gamma$
  - > 128 95 40 ABACHI 95F D0  $\ell\ell + \text{jets}, \ell + \text{jets}$
  - > 75 95 41 MUKHOPAD... 93 RVUE NC:  $b' \rightarrow b\ell\ell$
  - > 85 95 42 ABE 92 CDF CC:  $\ell\ell$
  - > 72 95 43 ABE 90B CDF CC:  $e + \mu$
  - > 54 95 44 AKESSON 90 UA2 CC:  $e + \text{jets} + \cancel{E}_T$
  - > 43 95 45 ALBAJAR 90B UA1 CC:  $\mu + \text{jets}$
  - > 34 95 46 ALBAJAR 88 UA1 CC:  $e \text{ or } \mu + \text{jets}$
- 1 SIRUNYAN 19A Q based on 35.9 fb<sup>-1</sup> of *pp* data at  $\sqrt{s} = 13$  TeV. Pair production of vector-like *b'* is searched for with one *b'* decaying into *Zb* and the other *b'* decaying into *Wt*, *Zb*, *hb*. Events with an opposite-sign lepton pair consistent with coming from *Z* and jets are used. Mass limits are obtained for a variety of branching ratios of *b'*.
  - 2 SIRUNYAN 19B W based on 35.9 fb<sup>-1</sup> of *pp* data at  $\sqrt{s} = 13$  TeV. The limit is for the pair-produced vector-like *b'* using all-hadronic final state. The analysis is made for the *Zb*, *Wt*, *hb* modes and mass limits are obtained for a variety of branching ratios.
  - 3 AABOUD 18A W based on 36.1 fb<sup>-1</sup> of *pp* data at  $\sqrt{s} = 13$  TeV. The limit is for the pair-produced vector-like *b'* using lepton-plus-jets final state. The search is also sensitive to the decays into *Zb* and *Hb* final states.
  - 4 AABOUD 18C E based on 36.1 fb<sup>-1</sup> of proton-proton data taken at  $\sqrt{s} = 13$  TeV. Events including a same-sign lepton pair are used. The limit is for a singlet model, assuming the branching ratios of *b'* into *Zb*, *Wt* and *Hb* as predicted by the model.
  - 5 AABOUD 18C L, AABOUD 18C P based on 36.1 fb<sup>-1</sup> of *pp* data at  $\sqrt{s} = 13$  TeV. The limit is for the pair-produced vector-like *b'* using all-hadronic final state. The analysis is particularly powerful for the *b' \rightarrow hb* mode. Assuming the pure decay only in this mode sets a limit  $m_{b'} > 1010$  GeV.
  - 6 AABOUD 18C P based on 36.1 fb<sup>-1</sup> of *pp* data at  $\sqrt{s} = 13$  TeV. Pair and single production of vector-like *b'* are searched for with at least one *b'* decaying into *Zb*. In the case of  $B(b' \rightarrow Zb) = 1$ , the limit is  $m_{b'} > 1220$  GeV.
  - 7 The limit is for the singlet model, assuming that the branching ratios into *Wt*, *Zb*, *hb* add up to one.
  - 8 The limit is for the doublet model, assuming that the branching ratios into *Wt*, *Zb*, *hb* add up to one.
  - 9 AABOUD 18C R based on 36.1 fb<sup>-1</sup> of *pp* data at  $\sqrt{s} = 13$  TeV. A combination of searches for the pair-produced vector-like *b'* in various decay channels (*b' \rightarrow Wt*, *Zb*, *hb*). Also a model-independent limit is obtained as  $m_{b'} > 1.03$  TeV, assuming that the branching ratios into *Zb*, *Wt*, and *hb* add up to one.
  - 10 The limit is for the singlet *b'*.
  - 11 The limit is for *b'* in a weak isospin doublet (*t'*, *b'*) and  $|V_{t'b}| \ll |V_{tb}|$ . For a *b'* in a doublet with a charge -4/3 vector-like quark, the limit  $m_{b'} > 1.14$  TeV is obtained.
  - 12 SIRUNYAN 18B M based on 35.9 fb<sup>-1</sup> of *pp* data at  $\sqrt{s} = 13$  TeV. The limit is for the pair-produced vector-like *b'*. Three channels (single lepton, same-charge 2 leptons, or at least 3 leptons) are considered for various branching fraction combinations. Assuming  $B(tW) = 1$ , the limit is 1240 GeV and for  $B(bZ) = 1$  it is 960 GeV.
  - 13 SIRUNYAN 18Q based on 19.7 fb<sup>-1</sup> of *pp* data at  $\sqrt{s} = 8$  TeV. The limit is for the pair-produced vector-like *b'* that couple only to light quarks. Upper cross section limits on the single production of a *b'* and constraints for other decay channels (*Zq* and *Hq*) are also given in the paper.
  - 14 SIRUNYAN 17A U based on 2.3-2.6 fb<sup>-1</sup> of *pp* data at  $\sqrt{s} = 13$  TeV. Limit on pair-produced singlet vector-like *b'* using one lepton and several jets. The mass bound is given for a *b'* transforming as a singlet under the electroweak symmetry group, assumed to decay through *W*, *Z* or Higgs boson (which decays to jets) and to a third generation quark.
  - 15 KHACHATRYAN 16A N based on 19.7 fb<sup>-1</sup> of *pp* data at  $\sqrt{s} = 8$  TeV. Limit on pair-produced vector-like *b'* using 1, 2, and >2 leptons as well as fully hadronic final states. Other limits depending on the branching fractions to *tW*, *bZ*, and *bH* are given in Table IX.
  - 16 AAD 15B Y based on 20.3 fb<sup>-1</sup> of *pp* data at  $\sqrt{s} = 8$  TeV. Limit on pair-produced vector-like *b'* assuming the branching fractions to *Wt*, *Zb*, and *hb* modes of the singlet model. Used events containing  $\geq 2\ell + \cancel{E}_T + \geq 2j$  ( $\geq 1b$ ) and including a same-sign lepton pair.
  - 17 AAD 15B Y based on 20.3 fb<sup>-1</sup> of *pp* data at  $\sqrt{s} = 8$  TeV. Limit on pair-produced chiral *b'*-quark. Used events containing  $\geq 2\ell + \cancel{E}_T + \geq 2j$  ( $\geq 1b$ ) and including a same-sign lepton pair.
  - 18 AAD 15Z based on 20.3 fb<sup>-1</sup> of *pp* data at  $\sqrt{s} = 8$  TeV. Used events with  $\ell + \cancel{E}_T + \geq 6j$  ( $\geq 1b$ ) and at least one pair of jets from weak boson decay, primarily designed to select the signature  $b'\bar{b}' \rightarrow WW\tau\tau \rightarrow WWWWb\bar{b}$ . This is a limit on pair-produced vector-like *b'*. The lower mass limit is 640 GeV for a vector-like singlet *b'*.
  - 19 Based on 20.3 fb<sup>-1</sup> of *pp* data at  $\sqrt{s} = 8$  TeV. No significant excess over SM expectation is found in the search for pair production or single production of *b'* in the events with dilepton from a high *p<sub>T</sub>* *Z* and additional jets ( $\geq 1b$ -tag). If instead of  $B(b' \rightarrow Wt) = 1$  an electroweak singlet with  $B(b' \rightarrow Wt) \sim 0.45$  is assumed, the limit reduces to 685 GeV.
  - 20 Based on 5.0 fb<sup>-1</sup> of *pp* data at  $\sqrt{s} = 7$  TeV. CHATRCHYAN 13I looked for events with one isolated electron or muon, large  $\cancel{E}_T$ , and at least four jets with large transverse momenta, where one jet is likely to originate from the decay of a bottom quark.
  - 21 Result is based on 1.1 fb<sup>-1</sup> of data. No signal is found for the search of long-lived particles which decay into final states with two electrons or photons, and upper bound on the cross section times branching fraction is obtained for  $2 < c\tau < 7000$  nm; see Fig. 3. 95% CL excluded region of *b'* lifetime and mass is shown in Fig. 4.

# Quark Particle Listings

## $b'$ (Fourth Generation) Quark

- <sup>22</sup> ACOSTA 03 looked for long-lived fourth generation quarks in the data sample of 90 pb<sup>-1</sup> of  $\sqrt{s}=1.8$  TeV  $p\bar{p}$  collisions by using the muon-like penetration and anomalously high ionization energy loss signature. The corresponding lower mass bound for the charge (2/3)e quark ( $t'$ ) is 220 GeV. The  $t'$  bound is higher than the  $b'$  bound because  $t'$  is more likely to produce charged hadrons than  $b'$ . The 95% CL upper bounds for the production cross sections are given in their Fig. 3.
- <sup>23</sup> AAD 15AR based on 20.3 fb<sup>-1</sup> of  $pp$  data at  $\sqrt{s}=8$  TeV. Used lepton-plus-jets final state. See Fig. 24 for mass limits in the plane of  $B(b' \rightarrow Wt)$  vs.  $B(b' \rightarrow Hb)$  from  $b'\bar{b}' \rightarrow Hb + X$  searches.
- <sup>24</sup> AAD 15CN based on 20.3 fb<sup>-1</sup> of  $pp$  data at  $\sqrt{s}=8$  TeV. Limit on pair-production of chiral  $b'$ -quark. Used events with  $\ell + E_T + \geq 4j$  (non- $b$ -tagged). Limits on a heavy vector-like quark, which decays into  $Wq, Zq, hq$ , are presented in the plane  $B(Q \rightarrow Wq)$  vs.  $B(Q \rightarrow hq)$  in Fig. 12.
- <sup>25</sup> Based on 1.04 fb<sup>-1</sup> of  $pp$  data at  $\sqrt{s}=7$  TeV. No signal is found for the search of heavy quark pair production that decay into  $W$  and a  $t$  quark in the events with a high  $p_T$  isolated lepton, large  $E_T$ , and at least 6 jets in which one, two or more dijets are from  $W$ .
- <sup>26</sup> Based on 2.0 fb<sup>-1</sup> of  $pp$  data at  $\sqrt{s}=7$  TeV. No  $b' \rightarrow Zb$  invariant mass peak is found in the search of heavy quark pair production that decay into  $Z$  and a  $b$  quark in events with  $Z \rightarrow e^+e^-$  and at least one  $b$ -jet. The lower mass limit is 358 GeV for a vector-like singlet  $b'$  mixing solely with the third SM generation.
- <sup>27</sup> Based on 1.04 fb<sup>-1</sup> of  $pp$  data at  $\sqrt{s}=7$  TeV. No signal is found for the search of heavy quark pair production that decay into  $W$  and a quark in the events with dileptons, large  $E_T$ , and  $\geq 2$  jets.
- <sup>28</sup> Based on 1.04 fb<sup>-1</sup> of  $pp$  data at  $\sqrt{s}=7$  TeV. AAD 12BE looked for events with two isolated like-sign leptons and at least 2 jets, large  $E_T$  and  $H_T > 350$  GeV.
- <sup>29</sup> Based on 5 fb<sup>-1</sup> of  $pp$  data at  $\sqrt{s}=7$  TeV. CHATRCHYAN 12BH searched for QCD and EW production of single and pair of degenerate 4th generation quarks that decay to  $bW$  or  $tW$ . Absence of signal in events with one lepton, same-sign dileptons or tripletons gives the bound. With a mass difference of 25 GeV/c<sup>2</sup> between  $m_{t'}$  and  $m_{b'}$ , the corresponding limit shifts by about  $\pm 20$  GeV/c<sup>2</sup>.
- <sup>30</sup> Based on 4.9 fb<sup>-1</sup> of  $pp$  data at  $\sqrt{s}=7$  TeV. CHATRCHYAN 12X looked for events with tripletons or same-sign dileptons and at least one  $b$  jet.
- <sup>31</sup> Based on 4.8 fb<sup>-1</sup> of data in  $p\bar{p}$  collisions at 1.96 TeV. AALTONEN 11J looked for events with  $\ell + E_T + \geq 5j$  ( $\geq 1 b$  or  $c$ ). No signal is observed and the bound  $\sigma(b'\bar{b}') < 30$  fb for  $m_{b'} > 375$  GeV is found for  $B(b' \rightarrow Wt) = 1$ .
- <sup>32</sup> Based on 34 pb<sup>-1</sup> of data in  $pp$  collisions at 7 TeV. CHATRCHYAN 11L looked for multi-jet events with tripletons or same-sign dileptons. No excess above the SM background excludes  $m_{b'}$  between 255 and 361 GeV at 95% CL for  $B(b' \rightarrow Wt) = 1$ .
- <sup>33</sup> Based on 2.7 fb<sup>-1</sup> of data in  $p\bar{p}$  collisions at  $\sqrt{s}=1.96$  TeV. AALTONEN 10H looked for pair production of heavy quarks which decay into  $tW^-$  or  $tW^+$ , in events with same sign dileptons ( $e$  or  $\mu$ ), several jets and large missing  $E_T$ . The result is obtained for  $b'$  which decays into  $tW^-$ . For the charge 5/3 quark ( $T_{5/3}$ ) which decays into  $tW^+$ ,  $m_{T_{5/3}} > 365$  GeV (95% CL) is found when it has the charge  $-1/3$  partner  $B$  of the same mass.
- <sup>34</sup> FLACCO 10 result is obtained from AALTONEN 10H result of  $m_{b'} > 338$  GeV, by relaxing the condition  $B(b' \rightarrow Wt) = 100\%$  when  $m_{b'} > m_{t'}$ .
- <sup>35</sup> Result is based on 1.06 fb<sup>-1</sup> of data. No excess from the SM  $Z$ +jet events is found when  $Z$  decays into  $e$  or  $\mu\mu$ . The  $m_{b'}$  bound is found by comparing the resulting upper bound on  $\sigma(b'\bar{b}') [1 - (1 - B(b' \rightarrow Zb))^2]$  and the LO estimate of the  $b'$  pair production cross section shown in Fig. 38 of the article.
- <sup>36</sup> HUANG 08 reexamined the  $b'$  mass lower bound of 268 GeV obtained in AALTONEN 07c that assumes  $B(b' \rightarrow Zb) = 1$ , which does not hold for  $m_{b'} > 255$  GeV. The lower mass bound is given in the plane of  $\sin^2(\theta_{tb'})$  and  $m_{b'}$ .
- <sup>37</sup> AFFOLDER 00 looked for  $b'$  that decays into  $b+Z$ . The signal searched for is  $bbZZ$  events where one  $Z$  decays into  $e^+e^-$  or  $\mu^+\mu^-$  and the other  $Z$  decays hadronically. The bound assumes  $B(b' \rightarrow Zb) = 100\%$ . Between 100 GeV and 199 GeV, the 95%CL upper bound on  $\sigma(b' \rightarrow \bar{b}') \times B^2(b' \rightarrow Zb)$  is also given (see their Fig. 2).
- <sup>38</sup> ABE 98n looked for  $Z \rightarrow e^+e^-$  decays with displaced vertices. Quoted limit assumes  $B(b' \rightarrow Zb) = 1$  and  $c\tau_{b'} = 1$  cm. The limit is lower than  $m_{Z+m_b}$  ( $\sim 96$  GeV) if  $c\tau > 22$  cm or  $c\tau < 0.009$  cm. See their Fig. 4.
- <sup>39</sup> ABACHI 97D searched for  $b'$  that decays mainly via FCNC. They obtained 95%CL upper bounds on  $B(b'\bar{b}' \rightarrow \gamma + 3 \text{ jets})$  and  $B(b'\bar{b}' \rightarrow 2\gamma + 2 \text{ jets})$ , which can be interpreted as the lower mass bound  $m_{b'} > m_{Z+m_b}$ .
- <sup>40</sup> ABACHI 95F bound on the top-quark also applies to  $b'$  and  $t'$  quarks that decay predominantly into  $W$ . See FROGGATT 97.
- <sup>41</sup> MUKHOPADHYAYA 93 analyze CDF dilepton data of ABE 92g in terms of a new quark decaying via flavor-changing neutral current. The above limit assumes  $B(b' \rightarrow b\ell^+\ell^-) = 1\%$ . For an exotic quark decaying only via virtual  $Z$  [ $B(b\ell^+\ell^-) = 3\%$ ], the limit is 85 GeV.
- <sup>42</sup> ABE 92 dilepton analysis limit of  $>85$  GeV at CL=95% also applies to  $b'$  quarks, as discussed in ABE 90b.
- <sup>43</sup> ABE 90b exclude the region 28–72 GeV.
- <sup>44</sup> AKESSON 90 searched for events having an electron with  $p_T > 12$  GeV, missing momentum  $> 15$  GeV, and a jet with  $E_T > 10$  GeV,  $|\eta| < 2.2$ , and excluded  $m_{b'}$  between 30 and 69 GeV.
- <sup>45</sup> For the reduction of the limit due to non-charged-current decay modes, see Fig. 19 of ALBAJAR 90b.
- <sup>46</sup> ALBAJAR 88 study events at  $E_{cm} = 546$  and 630 GeV with a muon or isolated electron, accompanied by one or more jets and find agreement with Monte Carlo predictions for the production of charm and bottom, without the need for a new quark. The lower mass limit is obtained by using a conservative estimate for the  $b'\bar{b}'$  production cross section and by assuming that it cannot be produced in  $W$  decays. The value quoted here is revised using the full  $O(\alpha_s^3)$  cross section of ALTARELLI 88.

### $b'(-1/3)$ mass limits from single production in $p\bar{p}$ and $pp$ collisions

VALUE (GeV)	CL%	DOCUMENT ID	TECN	COMMENT
>1500	95	<sup>1</sup> AAD	16AH ATLS	$g b \rightarrow b' \rightarrow t W, B(b' \rightarrow t W)=1$
>1390	95	<sup>2</sup> KHACHATRY...16i	CMS	$g b \rightarrow b' \rightarrow t W, B(b' \rightarrow t W)=1$
>1430	95	<sup>3</sup> KHACHATRY...16i	CMS	$g b \rightarrow b' \rightarrow t W, B(b' \rightarrow t W)=1$
>1530	95	<sup>4</sup> KHACHATRY...16i	CMS	$g b \rightarrow b' \rightarrow t W, B(b' \rightarrow t W)=1$
> 693	95	<sup>5</sup> ABAZOV	11F D0	$q u \rightarrow q' b' \rightarrow q'(Wu)$ $\bar{\kappa}_{ub'}=1, B(b' \rightarrow Wu)=1$
> 430	95	<sup>5</sup> ABAZOV	11F D0	$q d \rightarrow q' b' \rightarrow q(Zd)$ $\bar{\kappa}_{db'}=\sqrt{2}, B(b' \rightarrow Zd)=1$

• • • We do not use the following data for averages, fits, limits, etc. • • •

<sup>6</sup> SIRUNYAN 19Ai CMS  $bZ/tW \rightarrow b' \rightarrow tW$

- <sup>1</sup> AAD 16AH based on 20.3 fb<sup>-1</sup> of data in  $pp$  collisions at 8 TeV. No significant excess over SM expectation is found in the search for a vector-like  $b'$  in the single-lepton and dilepton channels ( $\ell$  or  $\ell\ell$ ) + 1,2,3  $j$  ( $\geq 1b$ ). The model assumes that the  $b'$  has the excited quark couplings.
- <sup>2</sup> Based on 19.7 fb<sup>-1</sup> of data in  $pp$  collisions at 8 TeV. Limit on left-handed  $b'$  assuming 100% decay to  $tW$  and using all-hadronic, lepton + jets, and dilepton final states.
- <sup>3</sup> Based on 19.7 fb<sup>-1</sup> of data in  $pp$  collisions at 8 TeV. Limit on right-handed  $b'$  assuming 100% decay to  $tW$  and using all-hadronic, lepton + jets, and dilepton final states.
- <sup>4</sup> Based on 19.7 fb<sup>-1</sup> of data in  $pp$  collisions at 8 TeV. Limit on vector-like  $b'$  assuming 100% decay to  $tW$  and using all-hadronic, lepton+jets, and dilepton final states.
- <sup>5</sup> Based on 5.4 fb<sup>-1</sup> of data in  $p\bar{p}$  collisions at 1.96 TeV. ABAZOV 11F looked for single production of  $b'$  via the  $W$  or  $Z$  coupling to the first generation up or down quarks, respectively. Model independent cross section limits for the single production processes  $p\bar{p} \rightarrow b'q \rightarrow Wuq$ , and  $p\bar{p} \rightarrow b'q \rightarrow Zdq$  are given in Figs. 3 and 4, respectively, and the mass limits are obtained for the model of ATRE 09 with degenerate bi-doublets of vector-like quarks.
- <sup>6</sup> SIRUNYAN 19Ai based on 35.9 fb<sup>-1</sup> of  $pp$  data at  $\sqrt{s}=13$  TeV. Exclusion limits are set on the product of the production cross section and branching fraction for the  $b'(-1/3) + b$  and  $b'(-1/3) + t$  modes as a function of the vector-like quark mass in Figs. 7 and 8 and in Tab. 2 for relative vector-like quark widths between 1 and 30% for left- and right-handed vector-like quark couplings. No significant deviation from the SM prediction is observed.

### MASS LIMITS for $b'$ (4th Generation) Quark or Hadron in $e^+e^-$ Collisions

Search for hadrons containing a fourth-generation  $-1/3$  quark denoted  $b'$ .

The last column specifies the assumption for the decay mode ( $CC$  denotes the conventional charged-current decay) and the event signature which is looked for.

VALUE (GeV)	CL%	DOCUMENT ID	TECN	COMMENT
>46.0	95	<sup>1</sup> DECAMP	90F ALEP	any decay
• • • We do not use the following data for averages, fits, limits, etc. • • •				
none 96–103	95	<sup>2</sup> ABDALLAH	07 DLPH	$b' \rightarrow bZ, cW$
	95	<sup>3</sup> ADRIANI	93G L3	Quarkonium
>44.7	95	ADRIANI	93M L3	$\Gamma(Z)$
>45	95	ABREU	91F DLPH	$\Gamma(Z)$
none 19.4–28.2	95	ABE	90D VNS	Any decay; event shape
>45.0	95	ABREU	90D DLPH	$B(C C) = 1$ ; event shape
>44.5	95	<sup>4</sup> ABREU	90D DLPH	$b' \rightarrow cH^-, H^- \rightarrow \bar{c}s, \tau^- \nu$
>40.5	95	<sup>5</sup> ABREU	90D DLPH	$\Gamma(Z \rightarrow \text{hadrons})$
>28.3	95	ADACHI	90 TOPZ	$B(FCNC)=100\%$ ; isol. $\gamma$ or 4 jets
>41.4	95	<sup>6</sup> AKRAWY	90B OPAL	Any decay; acoplanarity
>45.2	95	<sup>6</sup> AKRAWY	90B OPAL	$B(C C) = 1$ ; acoplanarity
>46	95	<sup>7</sup> AKRAWY	90J OPAL	$b' \rightarrow \gamma + \text{any}$
>27.5	95	<sup>8</sup> ABE	89E VNS	$B(C C) = 1$ ; $\mu, e$
none 11.4–27.3	95	<sup>9</sup> ABE	89G VNS	$B(b' \rightarrow b\gamma) > 10\%$ ; isolated $\gamma$
>44.7	95	<sup>10</sup> ABRAMS	89C MRK2	$B(C C) = 100\%$ ; isol. track
>42.7	95	<sup>10</sup> ABRAMS	89C MRK2	$B(bg) = 100\%$ ; event shape
>42.0	95	<sup>10</sup> ABRAMS	89C MRK2	Any decay; event shape
>28.4	95	<sup>11,12</sup> ADACHI	89C TOPZ	$B(C C) = 1$ ; $\mu$
>28.8	95	<sup>13</sup> ENO	89 AMY	$B(C C) \geq 90\%$ ; $\mu, e$
>27.2	95	<sup>13,14</sup> ENO	89 AMY	any decay; event shape
>29.0	95	<sup>13</sup> ENO	89 AMY	$B(b' \rightarrow bg) \geq 85\%$ ; event shape
>24.4	95	<sup>15</sup> IGARASHI	88 AMY	$\mu, e$
>23.8	95	<sup>16</sup> SAGAWA	88 AMY	event shape
>22.7	95	<sup>17</sup> ADEVA	86 MRKJ	$\mu$
>21	95	<sup>18</sup> ALTHOFF	84C TASS	$R$ , event shape
>19	95	<sup>19</sup> ALTHOFF	84I TASS	Aplanarity

- <sup>1</sup> DECAMP 90F looked for isolated charged particles, for isolated photons, and for four-jet final states. The modes  $b' \rightarrow bg$  for  $B(b' \rightarrow bg) > 65\%$   $b' \rightarrow b\gamma$  for  $B(b' \rightarrow b\gamma) > 5\%$  are excluded. Charged Higgs decay were not discussed.
- <sup>2</sup> ABDALLAH 07 searched for  $b'$  pair production at  $E_{cm}=196\text{--}209$  GeV, with 420 pb<sup>-1</sup>. No signal leads to the 95% CL upper limits on  $B(b' \rightarrow bZ)$  and  $B(b' \rightarrow cW)$  for  $m_{b'} = 96$  to 103 GeV.
- <sup>3</sup> ADRIANI 93g search for vector quarkonium states near  $Z$  and give limit on quarkonium- $Z$  mixing parameter  $\delta m^2 < (10\text{--}30)$  GeV<sup>2</sup> (95%CL) for the mass 88–94.5 GeV. Using



# Quark Particle Listings

## $t'$ (Fourth Generation) Quark

- the events with one lepton, large  $E_T$ , and  $\geq 4$  jets. The lower mass limit 0.87 (1.05) TeV is obtained for the singlet (doublet) model with other possible decay modes.
- SIRUNYAN 17AU based on 2.3–2.6 fb<sup>-1</sup> of  $pp$  data at  $\sqrt{s} = 13$  TeV. Limit on pair-produced singlet vector-like  $t'$  using one lepton and several jets. The mass bound is given for a  $t'$  transforming as a singlet under the electroweak symmetry group, assumed to decay through  $W$ ,  $Z$  or Higgs boson (which decays to jets) and to a third generation quark. For a doublet, the limit is  $>830$  GeV. Other limits are also given in the paper.
  - AAD 15AR based on 20.3 fb<sup>-1</sup> of  $pp$  data at  $\sqrt{s} = 8$  TeV. Used lepton-plus-jets final state. See Fig. 20 for mass limits in the plane of  $B(t' \rightarrow Ht)$  vs.  $B(t' \rightarrow Wb)$  from a combination of  $t't' \rightarrow Wb + X$  and  $t't' \rightarrow Ht + X$  searches. Any branching ratio scenario is excluded for mass below 715 GeV.
  - AAD 15BY based on 20.3 fb<sup>-1</sup> of  $pp$  data at  $\sqrt{s} = 8$  TeV. Limit on pair-produced vector-like  $t'$  assuming the branching fractions to  $W$ ,  $Z$ , and  $h$  modes of the singlet model. Used events containing  $\geq 2\ell + E_T + \geq 2j$  ( $\geq 1b$ ) and including a same-sign lepton pair.
  - KHACHATRYAN 15AI based on 19.7 fb<sup>-1</sup> of  $pp$  data at  $\sqrt{s} = 8$  TeV. The search exploits all-hadronic final states by tagging boosted Higgs boson using jet substructure and  $b$ -tagging.
  - Based on 20.3 fb<sup>-1</sup> of  $pp$  data at  $\sqrt{s} = 8$  TeV. No significant excess over SM expectation is found in the search for pair production or single production of  $t'$  in the events with dilepton from a high  $p_T$   $Z$  and additional jets ( $\geq 1b$ -tag). If instead of  $B(b' \rightarrow Wt)$  is 1 an electroweak singlet with  $B(b' \rightarrow Wt) \sim 0.45$  is assumed, the limit reduces to 685 GeV.
  - Based on 19.5 fb<sup>-1</sup> of  $pp$  data at  $\sqrt{s} = 8$  TeV. The  $t'$  quark is pair produced and is assumed to decay into three different final states of  $bW$ ,  $tZ$ , and  $th$ . The search is carried out using events with at least one isolated lepton.
  - Based on 1.04 fb<sup>-1</sup> of  $pp$  data at  $\sqrt{s} = 7$  TeV. No signal is found for the search of heavy quark pair production that decay into  $W$  and a quark in the events with dileptons, large  $E_T$ , and  $\geq 2$  jets.
  - Based on 1.04 fb<sup>-1</sup> of data in  $pp$  collisions at 7 TeV. AAD 12c looked for  $t't'$  production followed by  $t'$  decaying into a top quark and  $X$ , an invisible particle, in a final state with an isolated high- $p_T$  lepton, four or more jets, and a large missing transverse energy. No excess over the SM  $t\bar{t}$  production gives the upper limit on  $t't'$  production cross section as a function of  $m_{t'}$  and  $m_X$ . The result is obtained for  $B(t' \rightarrow Wt) = 1$ .
  - Based on 5 fb<sup>-1</sup> of  $pp$  data at  $\sqrt{s} = 7$  TeV. CHATRCHYAN 12BH searched for QCD and EW production of single and pair of degenerate 4<sup>th</sup> generation quarks that decay to  $Wb$  or  $Wt$ . Absence of signal in events with one lepton, same-sign dileptons or tripletons gives the bound. With a mass difference of 25 GeV/ $c^2$  between  $m_{t'}$  and  $m_{b'}$ , the corresponding limit shifts by about  $\pm 20$  GeV/ $c^2$ .
  - Based on 5.0 fb<sup>-1</sup> of  $pp$  data at  $\sqrt{s} = 7$  TeV. CHATRCHYAN 12P looked for  $t't'$  production events with two isolated high  $p_T$  leptons, large  $E_T$ , and 2 high  $p_T$  jets with  $b$ -tag. The absence of signal above the SM background gives the limit for  $B(t' \rightarrow Wb) = 1$ .
  - Based on 4.7 fb<sup>-1</sup> of  $pp$  data at  $\sqrt{s} = 7$  TeV. No signal is found for the search of heavy quark pair production that decay into  $W$  and a  $b$  quark in the events with a high  $p_T$  isolated lepton, large  $E_T$ , and at least 3 jets ( $\geq 1b$ -tag). Vector-like quark of charge  $2/3$  with  $400 < m_{t'} < 550$  GeV and  $B(t' \rightarrow Wb) > 0.63$  is excluded at 95% CL.
  - Based on 5.0 fb<sup>-1</sup> of  $pp$  data at  $\sqrt{s} = 7$  TeV. CHATRCHYAN 13I looked for events with one isolated electron or muon, large  $E_T$ , and at least four jets with large transverse momenta, where one jet is likely to originate from the decay of a bottom quark.
  - Based on 1.04 fb<sup>-1</sup> of  $pp$  data at  $\sqrt{s} = 7$  TeV. No signal is found in the search for pair produced heavy quarks that decay into  $W$  boson and a  $b$  quark in the events with a high  $p_T$  isolated lepton, large  $E_T$ , and at least 3 jets ( $\geq 1b$ -tag).
  - Based on 5.0 fb<sup>-1</sup> of  $pp$  data at  $\sqrt{s} = 7$  TeV. CHATRCHYAN 12Bc looked for  $t't'$  production events with a single isolated high  $p_T$  lepton, large  $E_T$ , and at least 4 high  $p_T$  jets with a  $b$ -tag. The absence of signal above the SM background gives the limit for  $B(t' \rightarrow Wb) = 1$ .
  - Based on 5.7 fb<sup>-1</sup> of data in  $p\bar{p}$  collisions at 1.96 TeV. AALTONEN 11AH looked for  $t't'$  production followed by  $t'$  decaying into a top quark and  $X$ , an invisible particle, in the all hadronic decay mode of  $t\bar{t}$ . No excess over the SM  $t\bar{t}$  production gives the upper limit on  $t't'$  production cross section as a function of  $m_{t'}$  and  $m_X$ . The result is obtained for  $B(t' \rightarrow Xt) = 1$ .
  - Based on 5.6 fb<sup>-1</sup> of data in  $p\bar{p}$  collisions at 1.96 TeV. AALTONEN 11AL looked for  $\ell + \geq 4j$  events and set upper limits on  $\sigma(t't')$  as functions of  $m_{t'}$ .
  - Based on 4.8 fb<sup>-1</sup> of data in  $p\bar{p}$  collisions at 1.96 TeV. AALTONEN 11I looked for  $t't'$  production signal when  $t'$  decays into a top quark and  $X$ , an invisible particle, in  $\ell + E_T + jets$  channel. No excess over the SM  $t\bar{t}$  production gives the upper limit on  $t't'$  production cross section as a function of  $m_{t'}$  and  $m_X$ . The result is obtained for  $B(t' \rightarrow Xt) = 1$ .
  - Based on 5.3 fb<sup>-1</sup> of data in  $p\bar{p}$  collisions at 1.96 TeV. ABAZOV 11Q looked for  $\ell + E_T + \geq 4j$  events and set upper limits on  $\sigma(t't')$  as functions of  $m_{t'}$ .
  - Searches for pair production of a new heavy top-like quark  $t'$  decaying to a  $W$  boson and another quark by fitting the observed spectrum of total transverse energy and reconstructed  $t'$  mass in the lepton + jets events.
  - HUANG 08 reexamined the  $t'$  mass lower bound of 256 GeV obtained in AALTONEN 08H that assumes  $B(b' \rightarrow qZ) = 1$  for  $q = u, c$  which does not hold when  $m_{b'} < m_{t'} - m_W$  or the mixing  $\sin^2(\theta_{bt'})$  is so tiny that the decay occurs outside of the vertex detector. Fig. 1 gives that lower bound on  $m_{t'}$  in the plane of  $\sin^2(\theta_{bt'})$  and  $m_{b'}$ .

### $t'(5/3)$ -quark/hadron mass limits in $p\bar{p}$ and $pp$ collisions

VALUE (GeV)	CL%	DOCUMENT ID	TECN	COMMENT
>1330	95	1 SIRUNYAN	19T CMS	$t'_R(5/3) \rightarrow tW^+$
>1300	95	1 SIRUNYAN	19T CMS	$t'_L(5/3) \rightarrow tW^+$
>1350	95	2 AABOUD	18AW ATLS	$t'(5/3) \rightarrow tW^+$

>1190	95	3 AABOUD	18CE ATLS	$\geq 2\ell + E_T + \geq 1bj$
>1020	95	4 SIRUNYAN	17J CMS	$t'_R(5/3) \rightarrow tW^+$
> 990	95	4 SIRUNYAN	17J CMS	$t'_L(5/3) \rightarrow tW^+$
> 750	95	5 AAD	15BY ATLS	$t'(5/3) \rightarrow tW^+$
> 840	95	6 AAD	15Z ATLS	$t'(5/3) \rightarrow tW^+$
> 800	95	7 CHATRCHYAN	14T CMS	$t'(5/3) \rightarrow tW^+$

- SIRUNYAN 19T based on 35.9 fb<sup>-1</sup> of  $pp$  data at  $\sqrt{s} = 13$  TeV. Signals are searched in the final states of  $t't'$  pair production, with same-sign leptons (which come from a  $t'$  decay) or a single lepton (which comes from a  $W$  out of  $4Ws$ ), along with jets, and no excess over the SM expectation is found.
- AABOUD 18AW based on 36.1 fb<sup>-1</sup> of  $pp$  data at  $\sqrt{s} = 13$  TeV. Limit on  $t'(5/3)$  in pair production assuming its coupling to  $Wt$  is equal to one. Lepton-plus-jets final state is used, characterized by  $\ell + E_T + jets$  ( $\geq 1b$ -tagged).
- AABOUD 18CE based on 36.1 fb<sup>-1</sup> of proton-proton data taken at  $\sqrt{s} = 13$  TeV. Events including a same-sign lepton pair are used. The limit is for the pair-produced vector-like  $t'$ . With single  $t'$  production included, assuming  $t'tW$  coupling of one, the limit is  $m_{t'} > 1.6$  TeV.
- SIRUNYAN 17J based on 2.3 fb<sup>-1</sup> of  $pp$  data at  $\sqrt{s} = 13$  TeV. Signals are searched in the final states of  $t't'$  pair production, with same-sign leptons (which come from a  $t'$  decay) or a single lepton (which comes from a  $W$  out of  $4Ws$ ), along with jets, and no excess over the SM expectation is found.
- AAD 15BY based on 20.3 fb<sup>-1</sup> of  $pp$  data at  $\sqrt{s} = 8$  TeV. Limit on  $t'(5/3)$  in pair and single production assuming its coupling to  $Wt$  is equal to one. Used events containing  $\geq 2\ell + E_T + \geq 2j$  ( $\geq 1b$ ) and including a same-sign lepton pair.
- AAD 15Z based on 20.3 fb<sup>-1</sup> of  $pp$  data at  $\sqrt{s} = 8$  TeV. Used events with  $\ell + E_T + \geq 6j$  ( $\geq 1b$ ) and at least one pair of jets from weak boson decay, sensitive to the final state  $b\bar{b}W^+W^-W^+W^-$ .
- CHATRCHYAN 14T based on 19.5 fb<sup>-1</sup> of  $pp$  data at  $\sqrt{s} = 8$  TeV. Non-observation of anomaly in  $H_T$  distribution in the same-sign dilepton events leads to the limit when pair produced  $t'(5/3)$  quark decays exclusively into  $t$  and  $W^+$ , resulting in the final state with  $b\bar{b}W^+W^-W^+W^-$ .

### $t'(2/3)$ mass limits from single production in $p\bar{p}$ and $pp$ collisions

VALUE (GeV)	CL%	DOCUMENT ID	TECN	COMMENT
>950	95	1 AAD	16AV ATLS	$qg \rightarrow q't'b, B(t' \rightarrow Wb)=0.5$
>403	95	2 ABAZOV	11F D0	$qd \rightarrow q't' \rightarrow q'(Wd)$ $\bar{\kappa}_{dt'}=1, B(t' \rightarrow Wd)=1$
>551	95	2 ABAZOV	11F D0	$qu \rightarrow q't' \rightarrow q(Zu)$ $\bar{\kappa}_{ut'}=\sqrt{2}, B(t' \rightarrow Zu)=1$

- AAD 16AV based on 20.3 fb<sup>-1</sup> of  $pp$  data at  $\sqrt{s} = 8$  TeV. No significant excess over SM expectation is found in the search for a fully reconstructed vector-like  $t'$  in the mode  $\ell + E_T + \geq 2j$  ( $\geq 1b$ ). A veto on massive large-radius jets is used to reject the  $t\bar{t}$  background.
- Based on 5.4 fb<sup>-1</sup> of data in  $p\bar{p}$  collisions at 1.96 TeV. ABAZOV 11F looked for single production of  $t'$  via the  $Z$  or  $E$  coupling to the first generation up or down quarks, respectively. Model independent cross section limits for the single production processes  $p\bar{p} \rightarrow t'q \rightarrow (Wd)q$ , and  $p\bar{p} \rightarrow t'q \rightarrow (Zd)q$  are given in Figs. 3 and 4, respectively, and the mass limits are obtained for the model of ATRE 09 with degenerate bi-doublets of vector-like quarks.

### $t'(5/3)$ mass limits from single production in $p\bar{p}$ and $pp$ collisions

VALUE (GeV)	DOCUMENT ID	TECN	COMMENT
•••	1 SIRUNYAN	19AI CMS	$tW \rightarrow t'(5/3) \rightarrow tW$

- SIRUNYAN 19AI based on 35.9 fb<sup>-1</sup> of  $pp$  data at  $\sqrt{s} = 13$  TeV. Exclusion limits are set on the product of the production cross section and branching fraction for the  $b'(-1/3) + t$  and  $t'(5/3) + t$  modes as a function of the vector-like quark mass in Fig. 8 and Tab. 2 for relative vector-like quark widths between 1 and 30% for left- and right-handed vector-like quark couplings. No significant deviation from the SM prediction is observed.

### REFERENCES FOR Searches for (Fourth Generation) $t'$ Quark

SIRUNYAN	19AI	EPJ C79 90	A.M. Sirunyan et al.	(CMS Collab.)
SIRUNYAN	19AQ	EPJ C79 364	A.M. Sirunyan et al.	(CMS Collab.)
SIRUNYAN	19BW	PR D100 072001	A.M. Sirunyan et al.	(CMS Collab.)
SIRUNYAN	19T	JHEP 1903 082	A.M. Sirunyan et al.	(CMS Collab.)
AABOUD	18AW	JHEP 1808 048	M. Aaboud et al.	(ATLAS Collab.)
AABOUD	18CE	JHEP 1812 039	M. Aaboud et al.	(ATLAS Collab.)
AABOUD	18CL	PR D98 092005	M. Aaboud et al.	(ATLAS Collab.)
AABOUD	18CP	PR D98 112010	M. Aaboud et al.	(ATLAS Collab.)
AABOUD	18CR	PRL 121 211801	M. Aaboud et al.	(ATLAS Collab.)
SIRUNYAN	18BM	JHEP 1808 177	A.M. Sirunyan et al.	(CMS Collab.)
SIRUNYAN	18L	PR D97 072008	A.M. Sirunyan et al.	(CMS Collab.)
SIRUNYAN	18W	PL B779 82	A.M. Sirunyan et al.	(CMS Collab.)
AABOUD	17L	JHEP 1708 052	M. Aaboud et al.	(ATLAS Collab.)
SIRUNYAN	17AJ	JHEP 1711 085	A.M. Sirunyan et al.	(CMS Collab.)
SIRUNYAN	17J	JHEP 1708 073	A.M. Sirunyan et al.	(CMS Collab.)
AAD	16AV	EPJ C76 442	G. Aad et al.	(ATLAS Collab.)
AAD	15AR	JHEP 1508 105	G. Aad et al.	(ATLAS Collab.)
AAD	15BY	JHEP 1510 150	G. Aad et al.	(ATLAS Collab.)
AAD	15Z	PR D91 112011	G. Aad et al.	(ATLAS Collab.)
KHACHATRYAN	15AI	JHEP 1506 080	V. Khachatryan et al.	(CMS Collab.)
AAD	14AZ	JHEP 1411 104	G. Aad et al.	(ATLAS Collab.)
CHATRCHYAN	14A	PL B729 149	S. Chatrchyan et al.	(CMS Collab.)
CHATRCHYAN	14T	PRL 112 171801	S. Chatrchyan et al.	(CMS Collab.)
AAD	13F	PL B718 1284	G. Aad et al.	(ATLAS Collab.)
CHATRCHYAN	13I	JHEP 1301 154	S. Chatrchyan et al.	(CMS Collab.)
AAD	12AR	PRL 108 261802	G. Aad et al.	(ATLAS Collab.)
AAD	12C	PR D86 012007	G. Aad et al.	(ATLAS Collab.)
AAD	12B	PRL 108 041805	G. Aad et al.	(ATLAS Collab.)
CHATRCHYAN	12B	PL B718 307	S. Chatrchyan et al.	(CMS Collab.)





# Quark Particle Listings

## Free Quark Searches

<3.E-3	b	±1,2	<2	540	$p\bar{p}$	0	BANNER	83	CNTR
<1.E-4	b	±1,2		106	$^{56}\text{Fe}$	0	LINDGREN	83	CNTR
<3.E-3	b	>  ± 0.1		74	$^{40}\text{Ar}$	0	11 PRICE	83	PLAS
<1.E-2	e	±1,2	<14	29	$e^+e^-$	0	MARINI	82B	CNTR
<8.E-2	e	±1,2	<12	29	$e^+e^-$	0	ROSS	82	CNTR
<3.E-4	e	±2	1.8-2	7	$e^+e^-$	0	WEISS	81	MRK2
<5.E-2	e	+1,2,4,5	2-12	27	$e^+e^-$	0	BARTEL	80	JADE
<2.E-5	g	1,2			$\nu$	0	5,6 BASILE	80	CNTR
<3.E-10	f	±2,4	1-3	200	$p$	0	12 BOZZOLI	79	CNTR
<6.E-11	f	±1	<21	52	$pp$	0	BASILE	78	SPEC
<5.E-3	g				$\nu_\mu$	0	BASILE	78B	CNTR
<2.E-9	f	±1	<26	62	$pp$	0	BASILE	77	SPEC
<7.E-10	f	+1,2	<20	52	$p$	0	13 FABJAN	75	CNTR
		+1,2	>4.5	$\gamma$	0	5,6 GALIK	74	CNTR	
		+1,2	>1.5	12	$e^-$	0	5,6 BELLAMY	68	CNTR
		+1,2	>0.9	$\gamma$	0	6 BATHOW	67	CNTR	
		+1,2	>0.9	6	$\gamma$	0	6 FOSS	67	CNTR

<4.E-10		±1					HANAYAMA	68	CNTR	
<3.E-8		>15					KASHA	68	OSP K	
<2.E-10		+2					KASHA	68B	CNTR	
<2.E-10		+4					KASHA	68c	CNTR	
<2.E-10		+2				6	BARTON	67	CNTR	
<2.E-7		+4				0.008, 0.5 *	BUHLER	67	CNTR	
<5.E-10		1,2				0.008, 0.5 *	BUHLER	67B	CNTR	
<4.E-10		+1,2					GOMEZ	67	CNTR	
<2.E-9		+2					KASHA	67	CNTR	
<2.E-10		+2				220	BARTON	66	CNTR	
<2.E-9		+1,2				0.5 *	BUHLER	66	CNTR	
<3.E-9		+1,2					KASHA	66	CNTR	
<2.E-9		+1,2					LAMB	66	CNTR	
<2.E-8		+1,2				>7	DELISE	65	CNTR	
<5.E-8		+2				>2.5	0.5 *	MASSAM	65	CNTR
<2.E-8		+1					2.5 *	BOWEN	64	CNTR
<2.E-7		+1					0.8	SUNYAR	64	CNTR

<sup>1</sup> HUENTRUP 96 quote 95% CL limits for production of fragments with charge differing by as much as ±1/3 (in units of e) for charge 6 ≤ Z ≤ 10.  
<sup>2</sup> BUSKULIC 93c limits for inclusive quark production are more conservative if the ALEPH hadronic fragmentation function is assumed.  
<sup>3</sup> CECCHINI 93 limit at 90%CL for 23/3 ≤ Z ≤ 40/3, for 16A GeV O, 14.5A Si, and 200A S incident on Cu target. Other limits are 2.3 × 10<sup>-4</sup> for 17/3 ≤ Z ≤ 20/3 and 1.2 × 10<sup>-4</sup> for 20/3 ≤ Z ≤ 23/3.  
<sup>4</sup> GHOSH 92 reports measurement of spallation fragment charge based on ionization in emulsion. Out of 650 measured tracks, 2 were consistent with charge 5e/3, and 4 with 7e/3.  
<sup>5</sup> Hadronic quark.  
<sup>6</sup> Leptonic quark.  
<sup>7</sup> HE 91 limits are for charges of the form N±1/3 from 23/3 to 38/3, and correspond to cross-section limits of 380μb (Pb) and 320μb (Cu).  
<sup>8</sup> The limits apply to projectile fragment charges of 17, 19, 20, 22, 23 in units of e/3.  
<sup>9</sup> The limits apply to projectile fragment charges of 16, 17, 19, 20, 22, 23 in units of e/3.  
<sup>10</sup> Flux limits and mass range depend on charge.  
<sup>11</sup> Bound to nuclei.  
<sup>12</sup> Quark lifetimes > 1 × 10<sup>-8</sup> s.  
<sup>13</sup> One candidate m < 0.17 GeV.

<sup>1</sup> See AGNESE 15 Fig.6 for limits on vertical density as function of charge extending to |q|/e < 1/10.  
<sup>2</sup> AMBROSIO 00c limit is below 11 × 10<sup>-15</sup> for 0.25 < q/e < 0.5, and is changing rapidly near q/e=2/3, where it is 2 × 10<sup>-14</sup>.  
<sup>3</sup> Distribution in celestial sphere was described as anisotropic.  
<sup>4</sup> With telescope axis at zenith angle 40° to the south.  
<sup>5</sup> Leptonic quarks.  
<sup>6</sup> Lifetime > 10<sup>-8</sup> s; charge ±0.70, 0.68, 0.42; and mass >4.4, 4.8, and 20 GeV, respectively.  
<sup>7</sup> Time delayed air shower search.  
<sup>8</sup> Prompt air shower search.  
<sup>9</sup> Also e/4 and e/6 charges.  
<sup>10</sup> No events in subsequent experiments.

## Quark Flux — Cosmic Ray Searches

Shielding values followed with an asterisk indicate altitude in km. Shielding values not followed with an asterisk indicate sea level in kg/cm<sup>2</sup>.

FLUX (cm <sup>-2</sup> sr <sup>-1</sup> s <sup>-1</sup> )	CHG (e/3)	MASS (GeV)	SHIELDING	DOCUMENT ID	TECN
< 1.E-8	±1/6-1/10			1 AGNESE 15	CDMS
< 9.2E-15	±1		3800	2 AMBROSIO 00c	MCRO
<2.1E-15	±1			MORI 91	KAM2
<2.3E-15	±2			MORI 91	KAM2
<2.E-10	±1,2		0.3	WADA 88	CNTR
	±4		0.3	3 WADA 88	CNTR
	±4		0.3	4 WADA 86	CNTR
<1.E-12	±2,3/2		-70.	5 KAWAGOE 84B	PLAS
<9.E-10	±1,2		0.3	WADA 84B	CNTR
<4.E-9	±4		0.3	WADA 84B	CNTR
<2.E-12	±1,2,3		-0.3 *	MASHIMO 83	CNTR
<3.E-10	±1,2		0.3	MARINI 82	CNTR
<2.E-11	±1,2			MASHIMO 82	CNTR
<8.E-10	±1,2		0.3	5 NAPOLITANO 82	CNTR
				6 YOCK 78	CNTR
<1.E-9				7 BRIATORE 76	ELEC
<2.E-11	+1			8 HAZEN 75	CC
<2.E-10	+1,2			KRISOR 75	CNTR
<1.E-7	+1,2			8,9 CLARK 74B	CC
<3.E-10	+1	>20		KIFUNE 74	CNTR
<8.E-11	+1			8 ASHTON 73	CNTR
<2.E-8	+1,2			HICKS 73B	CNTR
<5.E-10	+4		2.8 *	BEAUCHAMP 72	CNTR
<1.E-10	+1,2			8 BOHM 72B	CNTR
<1.E-10	+1,2		2.8 *	COX 72	ELEC
<3.E-10	+2			CROUCH 72	CNTR
<3.E-8			7	7 DARDO 72	CNTR
<4.E-9	+1			8 EVANS 72	CC
<2.E-9		>10		7 TONWAR 72	CNTR
<2.E-10	+1		2.8 *	CHIN 71	CNTR
<3.E-10	+1,2			8 CLARK 71B	CC
<1.E-10	+1,2			8 HAZEN 71	CC
<5.E-10	+1,2		3.5 *	BOSIA 70	CNTR
	+1,2	<6.5		8 CHU 70	HLBC
<2.E-9	+1			FAISSNER 70B	CNTR
<2.E-10	+1,2		0.8 *	KRIDER 70	CNTR
<5.E-11	+2			CAIRNS 69	CC
<8.E-10	+1,2	<10		FUKUSHIMA 69	CNTR
	+2			8,10 MCCUSKER 69	CC
<1.E-10		>5	1.7,3.6	7 BJORNBOE 68	CNTR
<1.E-8	±1,2,4		6.3,2 *	5 BRIATORE 68	CNTR
<3.E-8		>2		FRANZINI 68	CNTR
<9.E-11	±1,2			GARMIRE 68	CNTR

## Quark Density — Matter Searches

QUARKS/ NUCLEON	CHG (e/3)	MASS (GeV)	MATERIAL/METHOD	EVTS	DOCUMENT ID
<1.17E-22			silicone oil drops	0	1 LEE 02
<4.71E-22			silicone oil drops	1	2 HALYO 00
<4.7E-21	±1,2		silicone oil drops	0	MAR 96
<8.E-22	+2		Si/infrared photoionization	0	PERERA 93
<5.E-27	±1,2		sea water/levitation	0	HOMER 92
<4.E-20	±1,2		meteorites/mag. levitation	0	JONES 89
<1.E-19	±1,2		various/spectrometer	0	MLNER 87
<5.E-22	±1,2		W/levitation	0	SMITH 87
<3.E-20	+1,2		org liq/droplet tower	0	VAN POLEN 87
<6.E-20	-1,2		org liq/droplet tower	0	VAN POLEN 87
<3.E-21	±1		Hg drops-untreated	0	SAVAGE 86
<3.E-22	±1,2		levitated niobium	0	SMITH 86
<2.E-26	±1,2		<sup>4</sup> He/levitation	0	SMITH 86B
<2.E-20	>±1	0.2-250	niobium+tungs/ion	0	MLNER 85
<1.E-21	±1		levitated niobium	0	SMITH 85
	+1,2	<100	niobium/mass spec	0	KUTSCHERA 84
<5.E-22			levitated steel	0	MARINELLI 84
<9.E-20	± <13		water/oil drop	0	JOYCE 83
<2.E-21	>  ± 1/2		levitated steel	0	LIEBOWITZ 83
<1.E-19	±1,2		photo ion spec	0	VANDESTEEG 83
<2.E-20			mercury/oil drop	0	3 HODGES 81
1.E-20	+1		levitated niobium	4	4 LARUE 81
1.E-20	-1		levitated niobium	4	4 LARUE 81
<1.E-21			levitated steel	0	MARINELLI 80B
<6.E-16			helium/mass spec	0	BOYD 79
1.E-20	+1		levitated niobium	2	4 LARUE 79
<4.E-28			earth+/ion beam	0	OGOROD... 79
<5.E-15	+1		tungs./mass spec	0	BOYD 78
<5.E-16	+3	<1.7	hydrogen/mass spec	0	BOYD 78B
<1.E-21	±2,4		water/ion beam	0	LUND 78
<6.E-15	>1/2		levitated tungsten	0	PUTT 78
<1.E-22			metals/mass spec	0	SCHIFFER 78
<5.E-15			levitated tungsten ox	0	BLAND 77
<3.E-21			levitated iron	0	GALLINARO 77
2.E-21	-1		levitated niobium	1	4 LARUE 77
4.E-21	+1		levitated niobium	2	4 LARUE 77
<1.E-13	+3	<7.7	hydrogen/mass spec	0	MULLER 77
<5.E-27			water+/ion beam	0	OGOROD... 77
<1.E-21			lunar+/ion spec	0	STEVENS 76
<1.E-15	+1	<60	oxygen+/ion spec	0	ELBERT 70
<5.E-19			levitated graphite	0	MORPURGO 70
<5.E-23			water+/atom beam	0	COOK 69
<1.E-17	±1,2		levitated graphite	0	BRAGINSK 68
<1.E-17			water+/uv spec	0	RANK 68
<3.E-19	±1		levitated iron	0	STOVER 67
<1.E-10			sun/uv spec	0	5 BENNETT 66
<1.E-17	+1,2		meteorites+/ion beam	0	CHUPKA 66
<1.E-16	±1		levitated graphite	0	GALLINARO 66
<1.E-22			argon/electrometer	0	HILLAS 59
	-2		levitated oil	0	MILLIKAN 10

<sup>1</sup> 95% CL limit for fractional charge particles with 0.18e ≤ |Q<sub>residual</sub>| ≤ 0.82e in total of 70.1 mg of silicone oil.





**LIGHT UNFLAVORED MESONS ( $S = C = B = 0$ )**

- $\pi^\pm$  . . . . . 1209
- $\pi^0$  . . . . . 1212
- $\eta$  . . . . . 1214
- $f_0(500)$  aka  $\sigma$ ; was  $f_0(600)$  . . . . . 1219
- $\rho(770)$  . . . . . 1221
- $\omega(782)$  . . . . . 1228
- $\eta'(958)$  . . . . . 1233
- $f_0(980)$  . . . . . 1239
- $a_0(980)$  . . . . . 1242
- $\phi(1020)$  . . . . . 1243
- $h_1(1170)$  . . . . . 1250
- $b_1(1235)$  . . . . . 1251
- $a_1(1260)$  . . . . . 1252
- $f_2(1270)$  . . . . . 1254
- $f_1(1285)$  . . . . . 1257
- $\eta(1295)$  . . . . . 1260
- $\pi(1300)$  . . . . . 1261
- $a_2(1320)$  . . . . . 1262
- $f_0(1370)$  . . . . . 1265
- $\pi_1(1400)$  . . . . . 1268
- $\eta(1405)$  . . . . . 1269
- $h_1(1415)$  was  $h_1(1380)$  . . . . . 1272
- $a_1(1420)$  . . . . . 1272
- $f_1(1420)$  . . . . . 1272
- $\omega(1420)$  . . . . . 1274
- $f_2(1430)$  . . . . . 1275
- $a_0(1450)$  . . . . . 1275
- $\rho(1450)$  . . . . . 1276
- $\eta(1475)$  . . . . . 1281
- $f_0(1500)$  . . . . . 1282
- $f_1(1510)$  . . . . . 1285
- $f_2'(1525)$  . . . . . 1286
- $f_2(1565)$  . . . . . 1289
- $\rho(1570)$  . . . . . 1290
- $h_1(1595)$  . . . . . 1291
- $\pi_1(1600)$  . . . . . 1291
- $a_1(1640)$  . . . . . 1292
- $f_2(1640)$  . . . . . 1293
- $\eta_2(1645)$  . . . . . 1293
- $\omega(1650)$  . . . . . 1293
- $\omega_3(1670)$  . . . . . 1295
- $\pi_2(1670)$  . . . . . 1295
- $\phi(1680)$  . . . . . 1297
- $\rho_3(1690)$  . . . . . 1299
- $\rho(1700)$  . . . . . 1302
- $a_2(1700)$  . . . . . 1307
- $f_0(1710)$  . . . . . 1308
- $\eta(1760)$  . . . . . 1310
- $\pi(1800)$  . . . . . 1311
- $f_2(1810)$  . . . . . 1312
- $X(1835)$  . . . . . 1313
- $\phi_3(1850)$  . . . . . 1314
- $\eta_2(1870)$  . . . . . 1315
- $\pi_2(1880)$  . . . . . 1315
- $\rho(1900)$  . . . . . 1315
- $f_2(1910)$  . . . . . 1316
- $a_0(1950)$  . . . . . 1317
- $f_2(1950)$  . . . . . 1317
- $a_4(1970)$  was  $a_4(2040)$  . . . . . 1318
- $\rho_3(1990)$  . . . . . 1319
- $\pi_2(2005)$  . . . . . 1319
- $f_2(2010)$  . . . . . 1320

• Indicates the particle is in the Meson Summary Table

- $f_0(2020)$  . . . . . 1320
- $f_4(2050)$  . . . . . 1321
- $\pi_2(2100)$  . . . . . 1322
- $f_0(2100)$  . . . . . 1322
- $f_2(2150)$  . . . . . 1323
- $\rho(2150)$  . . . . . 1324
- $\phi(2170)$  . . . . . 1325
- $f_0(2200)$  . . . . . 1326
- $f_J(2220)$  . . . . . 1326
- $\eta(2225)$  . . . . . 1327
- $\rho_3(2250)$  . . . . . 1328
- $f_2(2300)$  . . . . . 1328
- $f_4(2300)$  . . . . . 1329
- $f_0(2330)$  . . . . . 1329
- $f_2(2340)$  . . . . . 1330
- $\rho_5(2350)$  . . . . . 1330
- $f_6(2510)$  . . . . . 1331

**OTHER LIGHT UNFLAVORED ( $S = C = B = 0$ )**

- Further States . . . . . 1332

**STRANGE MESONS ( $S = \pm 1, C = B = 0$ )**

- $K^\pm$  . . . . . 1337
- $K^0$  . . . . . 1353
- $K_S^0$  . . . . . 1354
- $K_L^0$  . . . . . 1358
- $K_0^*(700)$  aka  $\kappa$ ; was  $K_0^*(800)$  . . . . . 1373
- $K^*(892)$  . . . . . 1374
- $K_1(1270)$  . . . . . 1376
- $K_1(1400)$  . . . . . 1378
- $K^*(1410)$  . . . . . 1379
- $K_0^*(1430)$  . . . . . 1379
- $K_2^*(1430)$  . . . . . 1380
- $K(1460)$  . . . . . 1383
- $K_2(1580)$  . . . . . 1383
- $K(1630)$  . . . . . 1383
- $K_1(1650)$  . . . . . 1383
- $K^*(1680)$  . . . . . 1384
- $K_2(1770)$  . . . . . 1384
- $K_3^*(1780)$  . . . . . 1385
- $K_2(1820)$  . . . . . 1386
- $K(1830)$  . . . . . 1387
- $K_0^*(1950)$  . . . . . 1387
- $K_2^*(1980)$  . . . . . 1387
- $K_4^*(2045)$  . . . . . 1388
- $K_2(2250)$  . . . . . 1388
- $K_3(2320)$  . . . . . 1388
- $K_5^*(2380)$  . . . . . 1389
- $K_4(2500)$  . . . . . 1389
- $K(3100)$  . . . . . 1389

**CHARMED MESONS ( $C = \pm 1$ )**

- $D^\pm$  . . . . . 1391
- $D^0$  . . . . . 1406
- $D^*(2007)^0$  . . . . . 1438
- $D^*(2010)^\pm$  . . . . . 1439
- $D_0^*(2300)^0$  was  $D_0^*(2400)^0$  . . . . . 1440
- $D_0^*(2300)^\pm$  was  $D_0^*(2400)^\pm$  . . . . . 1441
- $D_1(2420)^0$  . . . . . 1441
- $D_1(2420)^\pm$  . . . . . 1442
- $D_1(2430)^0$  . . . . . 1443
- $D_2^*(2460)^0$  . . . . . 1443
- $D_2^*(2460)^\pm$  . . . . . 1444

(Continued on the next page)

$D(2550)^0$	1445	• $\chi_{c2}(3930)$ was $\chi_{c2}(2P)$	1761
$D_J^*(2600)$ was $D(2600)$	1445	$X(3940)$	1762
$D^*(2640)^\pm$	1446	• $X(4020)^\pm$	1763
$D(2740)^0$	1446	• $\psi(4040)$	1763
$D_3^*(2750)$	1446	$X(4050)^\pm$	1765
$D(3000)^0$	1447	$X(4055)^\pm$	1766
<b>CHARMED, STRANGE MESONS (<math>C = S = \pm 1</math>)</b>			
• $D_s^\pm$	1448	$X(4100)^\pm$	1766
• $D_s^{*\pm}$	1458	• $\chi_{c1}(4140)$ was $X(4140)$	1767
• $D_{s0}^*(2317)^\pm$	1459	• $\psi(4160)$	1767
• $D_{s1}(2460)^\pm$	1460	$X(4160)$	1770
• $D_{s1}^*(2536)^\pm$	1461	$Z_c(4200)$ was $X(4200)^\pm$	1770
• $D_{s2}^*(2573)$	1463	• $\psi(4230)$ aka $Y(4230)$ ; was $X(4230)$	1770
• $D_{s1}^*(2700)^\pm$	1463	$R_{c0}(4240)$ was $X(4240)^\pm$	1772
$D_{s1}^*(2860)^\pm$	1464	$X(4250)^\pm$	1772
$D_{s3}^*(2860)^\pm$	1464	• $\psi(4260)$ aka $Y(4260)$ ; was $X(4260)$	1772
$D_{sJ}(3040)^\pm$	1464	• $\chi_{c1}(4274)$ was $X(4274)$	1775
<b>BOTTOM MESONS (<math>B = \pm 1</math>)</b>			
• $B^\pm$	1466	$X(4350)$	1775
• $B^0$	1529	• $\psi(4360)$ aka $Y(4360)$ ; was $X(4360)$	1776
• $B^\pm/B^0$ ADMIXTURE	1603	$\psi(4390)$ was $X(4390)$	1777
• $B^\pm/B^0/B_s^0/b$ -baryon ADMIXTURE	1625	• $\psi(4415)$	1777
$V_{cb}$ and $V_{ub}$ CKM Matrix Elements	1633	• $Z_c(4430)$ was $X(4430)^\pm$	1779
• $B^*$	1634	$\chi_{c0}(4500)$ was $X(4500)$	1779
• $B_1(5721)^+$	1635	• $\psi(4660)$ aka $Y(4660)$ ; was $X(4660)$	1780
• $B_1(5721)^0$	1635	$\chi_{c0}(4700)$ was $X(4700)$	1781
$B_J^*(5732)$ aka $B^{**}$	1635	<b><math>b\bar{b}</math> MESONS</b>	
• $B_2^*(5747)^+$	1636	• $\eta_b(1S)$	1783
• $B_2^*(5747)^0$	1636	• $\Upsilon(1S)$	1784
$B_J(5840)^+$	1637	• $\chi_{b0}(1P)$	1790
$B_J(5840)^0$	1637	• $\chi_{b1}(1P)$	1792
• $B_J(5970)^+$	1638	• $h_b(1P)$	1794
• $B_J(5970)^0$	1638	• $\chi_{b2}(1P)$	1794
<b>BOTTOM, STRANGE MESONS (<math>B = \pm 1, S = \mp 1</math>)</b>			
• $B_s^0$	1640	$\eta_b(2S)$	1796
• $B_s^*$	1661	• $\Upsilon(2S)$	1796
$X(5568)^\pm$	1662	• $\Upsilon_2(1D)$ was $\Upsilon(1D)$	1801
• $B_{s1}(5830)^0$	1662	• $\chi_{b0}(2P)$	1802
• $B_{s2}^*(5840)^0$	1663	• $\chi_{b1}(2P)$	1803
$B_{sJ}^*(5850)$	1663	$h_b(2P)$	1806
<b>BOTTOM, CHARMED MESONS (<math>B = C = \pm 1</math>)</b>			
• $B_c^+$	1664	• $\chi_{b2}(2P)$	1806
$B_c(2S)^\pm$	1667	• $\Upsilon(3S)$	1808
<b><math>c\bar{c}</math> MESONS</b>			
• $\eta_c(1S)$	1668	• $\chi_{b1}(3P)$	1812
• $J/\psi(1S)$	1676	• $\chi_{b2}(3P)$	1812
• $\chi_{c0}(1P)$	1699	• $\Upsilon(4S)$ aka $\Upsilon(10580)$	1812
• $\chi_{c1}(1P)$	1709	• $Z_b(10610)$ was $X(10610)$	1814
• $h_c(1P)$	1718	• $Z_b(10650)$ was $X(10650)^\pm$	1816
• $\chi_{c2}(1P)$	1719	$\Upsilon(10753)$	1817
• $\eta_c(2S)$	1730	• $\Upsilon(10860)$	1817
• $\psi(2S)$	1733	• $\Upsilon(11020)$	1820
• $\psi(3770)$	1749	<b>Notes in the Listings</b>	
• $\psi_2(3823)$ was $\psi(3823)$ , $X(3823)$	1756	$\rho(770)$	1221
• $\psi_3(3842)$	1756	$\rho(1450)$ and the $\rho(1700)$ (rev.)	1302
$\chi_{c0}(3860)$	1757	Charged kaon mass	1337
• $\chi_{c1}(3872)$ aka $X(3872)$	1757	Dalitz plot parameters for $K \rightarrow 3\pi$ decays	1345
• $Z_c(3900)$ was $X(3900)$	1759	$K_{\ell 3}^\pm$ and $K_{\ell 3}^0$ form factors	1347
• $X(3915)$ was $\chi_{c0}(3915)$	1761	$CP$ -violation in $K_S \rightarrow 3\pi$	1357
• Indicates the particle is in the Meson Summary Table		Heavy Flavor Averaging Group (rev.)	1465
		Charmonium system	1668
		Branching ratios of $\psi(2S)$ and $\chi_{c0,1,2}$ (rev.)	1698
		Bottomonium system	1782
		Width determination of the $\Upsilon$ states	1782

(Continued on next page.)

## Related Reviews in Volume 1

61. Form factors for rad. pion & kaon decays (rev.) . . . . .	762
62. Scalar mesons below 2 GeV (rev.) . . . . .	764
63. Pseudoscalar and pseudovector mesons . . . . .	771
in the 1400 MeV region (rev.)	
64. Rare kaon decays (rev.) . . . . .	774
65. $CPT$ invariance tests in neutral kaon decay (rev.) . . . . .	779
66. $V_{ud}$ , $V_{us}$ , Cabibbo angle, and CKM unitarity (rev.) . . . . .	781
67. $CP$ -violation in $K_L$ decays . . . . .	784
68. Review of multibody charm analyses (rev.) . . . . .	788
69. $D^0-\bar{D}^0$ mixing (rev.) . . . . .	792
70. $D_s^+$ branching fractions (rev.) . . . . .	801
71. Leptonic decays of charged pseudoscalar mesons (rev.) . . . . .	803
72. Production and decay of $b$ -flavored hadrons (rev.) . . . . .	814
73. Polarization in $B$ decays (rev.) . . . . .	824
74. $B^0-\bar{B}^0$ mixing (rev.) . . . . .	828
75. Semileptonic $B$ decays, $V_{cb}$ and $V_{ub}$ (rev.) . . . . .	835
76. CKM angles from $B$ hadrons, Determination of (new) . . . . .	849
77. Spectroscopy of mesons containing two heavy quarks (rev.) . . . . .	854
78. Non- $q\bar{q}$ mesons (rev.) . . . . .	861



**LIGHT UNFLAVORED MESONS**  
**(S = C = B = 0)**

For  $I = 1$  ( $\pi, \rho, \omega$ ):  $u\bar{d}, (u\bar{u}-d\bar{d})/\sqrt{2}, d\bar{u}$ ;  
for  $I = 0$  ( $\eta, \eta', \phi, f, f'$ ):  $c_1(u\bar{u} + d\bar{d}) + c_2(s\bar{s})$

$\pi^\pm$

$$J^G(J^P) = 1^-(0^-)$$

We have omitted some results that have been superseded by later experiments. The omitted results may be found in our 1988 edition Physics Letters **B204** 1 (1988).

**$\pi^\pm$  MASS**

The most accurate charged pion mass measurements are based upon x-ray wavelength measurements for transitions in  $\pi^-$ -mesonic atoms. The observed line is the blend of three components, corresponding to different K-shell occupancies. JECKELMANN 94 revisits the occupancy question, with the conclusion that two sets of occupancy ratios, resulting in two different pion masses (Solutions A and B), are equally probable. We choose the higher Solution B since only this solution is consistent with a positive mass-squared for the muon neutrino, given the precise muon momentum measurements now available (DAUM 91, ASSAMAGAN 94, and ASSAMAGAN 96) for the decay of pions at rest. Earlier mass determinations with  $\pi^-$ -mesonic atoms may have used incorrect K-shell screening corrections.

Measurements with an error of  $> 0.005$  MeV have been omitted from this Listing.

VALUE (MeV)	DOCUMENT ID	TECN	CHG	COMMENT
<b>139.57039 ± 0.00018 OUR FIT</b>	Error includes scale factor of 1.8.			
<b>139.57039 ± 0.00017 OUR AVERAGE</b>	Error includes scale factor of 1.6. See the ideogram below.			
139.57021 ± 0.00014	<sup>1</sup> DAUM 19	SPEC		$\pi^+ \rightarrow \mu^+ \nu_\mu$
139.57077 ± 0.00018	<sup>2</sup> TRASSINELLI 16	CNTR		X-ray transitions in pionic N2
139.57071 ± 0.00053	<sup>3</sup> LENZ 98	CNTR	-	pionic N2-atoms gas target
139.56995 ± 0.00035	<sup>4</sup> JECKELMANN 94	CNTR	-	$\pi^-$ atom, Soln. B
• • • We do not use the following data for averages, fits, limits, etc. • • •				
139.57022 ± 0.00014	<sup>5</sup> ASSAMAGAN 96	SPEC	+	$\pi^+ \rightarrow \mu^+ \nu_\mu$
139.56782 ± 0.00037	<sup>6</sup> JECKELMANN 94	CNTR	-	$\pi^-$ atom, Soln. A
139.56996 ± 0.00067	<sup>7</sup> DAUM 91	SPEC	+	$\pi^+ \rightarrow \mu^+ \nu$
139.56752 ± 0.00037	<sup>8</sup> JECKELMANN 86b	CNTR	-	Mesonic atoms
139.5704 ± 0.0011	<sup>7</sup> ABELA 84	SPEC	+	See DAUM 91
139.5664 ± 0.0009	<sup>9</sup> LU 80	CNTR	-	Mesonic atoms
139.5686 ± 0.0020	<sup>9,10</sup> CARTER 76	CNTR	-	Mesonic atoms
139.5660 ± 0.0024	<sup>9,10</sup> MARUSHEN... 76	CNTR	-	Mesonic atoms

<sup>1</sup> DAUM 19 value is based on their previous (1991+1996) measurements of the  $\mu^+$  momentum of  $29.79200 \pm 0.00011$  MeV for  $\pi^+$  decay at rest. It also uses  $m_\mu = 105.6583745 \pm 0.0000024$  MeV, and assumes conservatively  $m_{\nu_\mu} = 2.0 \pm 2.0$  MeV. It is the most precise charged pion mass determination.

<sup>2</sup> TRASSINELLI 16 use the muonic oxygen line for online energy calibration of the pionic line.

<sup>3</sup> LENZ 98 result does not suffer K-electron configuration uncertainties as does JECKELMANN 94.

<sup>4</sup> JECKELMANN 94 Solution B (dominant 2-electron K-shell occupancy), chosen for consistency with positive  $m_{\nu_\mu}^2$ .

<sup>5</sup> ASSAMAGAN 96 measures the  $\mu^+$  momentum  $p_\mu$  in  $\pi^+ \rightarrow \mu^+ \nu_\mu$  decay at rest to be  $29.79200 \pm 0.00011$  MeV/c. Combined with the  $\mu^+$  mass and the assumption  $m_{\nu_\mu} = 0$ , this gives the  $\pi^+$  mass above; if  $m_{\nu_\mu} > 0$ ,  $m_{\pi^+}$  given above is a lower limit. Combined instead with  $m_\mu$  and (assuming CPT) the  $\pi^-$  mass of JECKELMANN 94,  $p_\mu$  gives an upper limit on  $m_{\nu_\mu}$  (see the  $\nu_\mu$ ).

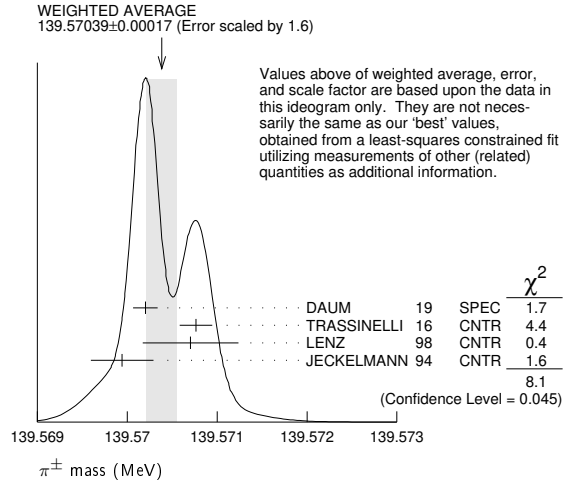
<sup>6</sup> JECKELMANN 94 Solution A (small 2-electron K-shell occupancy) in combination with either the DAUM 91 or ASSAMAGAN 94 pion decay muon momentum measurement yields a significantly negative  $m_{\nu_\mu}^2$ . It is accordingly not used in our fits.

<sup>7</sup> The DAUM 91 value includes the ABELA 84 result. The value is based on a measurement of the  $\mu^+$  momentum for  $\pi^+$  decay at rest,  $p_\mu = 29.79179 \pm 0.00053$  MeV, uses  $m_\mu = 105.658389 \pm 0.000034$  MeV, and assumes that  $m_{\nu_\mu} = 0$ . The last assumption means that in fact the value is a lower limit.

<sup>8</sup> JECKELMANN 86b gives  $m_\pi/m_e = 273.12677(71)$ . We use  $m_e = 0.51099906(15)$  MeV from COHEN 87. The authors note that two solutions for the probability distribution of K-shell occupancy fit equally well, and use other data to choose the lower of the two possible  $\pi^\pm$  masses.

<sup>9</sup> These values are scaled with a new wavelength-energy conversion factor  $V\lambda = 1.23984244(37) \times 10^{-6}$  eV m from COHEN 87. The LU 80 screening correction relies upon a theoretical calculation of inner-shell refilling rates.

<sup>10</sup> This MARUSHENKO 76 value used at the authors' request to use the accepted set of calibration  $\gamma$  energies. Error increased from 0.0017 MeV to include QED calculation error of 0.0017 MeV (12 ppm).



$$m_{\pi^+} - m_{\mu^+}$$

Measurements with an error  $> 0.05$  MeV have been omitted from this Listing.

VALUE (MeV)	EVTS	DOCUMENT ID	TECN	CHG	COMMENT
• • • We do not use the following data for averages, fits, limits, etc. • • •					
33.91157 ± 0.00067		<sup>1</sup> DAUM 91	SPEC	+	$\pi^+ \rightarrow \mu^+ \nu$
33.9111 ± 0.0011		ABELA 84	SPEC		See DAUM 91
33.925 ± 0.025		BOOTH 70	CNTR	+	Magnetic spect.
33.881 ± 0.035	145	HYMAN 67	HEBC	+	$K^-$ He

<sup>1</sup> The DAUM 91 value assumes that  $m_{\nu_\mu} = 0$  and uses our  $m_\mu = 105.658389 \pm 0.000034$  MeV.

$$(m_{\pi^+} - m_{\pi^-}) / m_{\text{average}}$$

A test of CPT invariance.

VALUE (units $10^{-4}$ )	DOCUMENT ID	TECN
<b>2 ± 5</b>	AYRES 71	CNTR

**$\pi^\pm$  MEAN LIFE**

Measurements with an error  $> 0.02 \times 10^{-8}$  s have been omitted.

VALUE ( $10^{-8}$ s)	DOCUMENT ID	TECN	CHG	COMMENT
<b>2.6033 ± 0.0005 OUR AVERAGE</b>	Error includes scale factor of 1.2.			
2.60361 ± 0.00052	<sup>1</sup> KOPTEV 95	SPEC	+	Surface $\mu^+$ 's
2.60231 ± 0.00050 ± 0.00084	NUMAO 95	SPEC	+	Surface $\mu^+$ 's
2.609 ± 0.008	DUNAITSEV 73	CNTR	+	
2.602 ± 0.004	AYRES 71	CNTR	±	
2.604 ± 0.005	NORDBERG 67	CNTR	+	
2.602 ± 0.004	ECKHAUSE 65	CNTR	+	
• • • We do not use the following data for averages, fits, limits, etc. • • •				
2.640 ± 0.008	<sup>2</sup> KINSEY 66	CNTR	+	

<sup>1</sup> KOPTEV 95 combines the statistical and systematic errors; the statistical error dominates.

<sup>2</sup> Systematic errors in the calibration of this experiment are discussed by NORDBERG 67.

$$(\tau_{\pi^+} - \tau_{\pi^-}) / \tau_{\text{average}}$$

A test of CPT invariance.

VALUE (units $10^{-4}$ )	DOCUMENT ID	TECN
<b>5.5 ± 7.1</b>	AYRES 71	CNTR
• • • We do not use the following data for averages, fits, limits, etc. • • •		
-14 ± 29	PETRUKHIN 68	CNTR
40 ± 70	BARDON 66	CNTR
23 ± 40	<sup>1</sup> LOBKOWICZ 66	CNTR

<sup>1</sup> This is the most conservative value given by LOBKOWICZ 66.

**$\pi$  ELECTRIC POLARIZABILITY  $\alpha_\pi$**

See HOLSTEIN 14 for a general review on hadron polarizability.

VALUE ( $10^{-4}$ fm <sup>3</sup> )	EVTS	DOCUMENT ID	TECN	COMMENT
<b>2.0 ± 0.6 ± 0.7</b>	63k	<sup>1</sup> ADOLPH 15A	SPEC	$\pi^- \gamma \rightarrow \pi^- \gamma$ Compton scatt.

<sup>1</sup> Value is derived assuming  $\alpha_\pi = -\beta_\pi$ .



# Meson Particle Listings

$\pi^\pm$

## $\pi^\pm$ DECAY MODES

$\pi^-$  modes are charge conjugates of the modes below.

For decay limits to particles which are not established, see the section on Searches for Axions and Other Very Light Bosons.

Mode	Fraction ( $\Gamma_i/\Gamma$ )	Confidence level
$\Gamma_1$ $\mu^+ \nu_\mu$	[a] (99.98770 ± 0.00004) %	
$\Gamma_2$ $\mu^+ \nu_\mu \gamma$	[b] ( 2.00 ± 0.25 ) × 10 <sup>-4</sup>	
$\Gamma_3$ $e^+ \nu_e$	[a] ( 1.230 ± 0.004 ) × 10 <sup>-4</sup>	
$\Gamma_4$ $e^+ \nu_e \gamma$	[b] ( 7.39 ± 0.05 ) × 10 <sup>-7</sup>	
$\Gamma_5$ $e^+ \nu_e \pi^0$	( 1.036 ± 0.006 ) × 10 <sup>-8</sup>	
$\Gamma_6$ $e^+ \nu_e e^+ e^-$	( 3.2 ± 0.5 ) × 10 <sup>-9</sup>	
$\Gamma_7$ $e^+ \nu_e \nu \bar{\nu}$	< 5 × 10 <sup>-6</sup>	90%

### Lepton Family number (LF) or Lepton number (L) violating modes

$\Gamma_8$ $\mu^+ \bar{\nu}_e$	L	[c] < 1.5	× 10 <sup>-3</sup>	90%
$\Gamma_9$ $\mu^+ \nu_e$	LF	[c] < 8.0	× 10 <sup>-3</sup>	90%
$\Gamma_{10}$ $\mu^- e^+ e^+ \nu$	LF	< 1.6	× 10 <sup>-6</sup>	90%

[a] Measurements of  $\Gamma(e^+ \nu_e)/\Gamma(\mu^+ \nu_\mu)$  always include decays with  $\gamma$ 's, and measurements of  $\Gamma(e^+ \nu_e \gamma)$  and  $\Gamma(\mu^+ \nu_\mu \gamma)$  never include low-energy  $\gamma$ 's. Therefore, since no clean separation is possible, we consider the modes with  $\gamma$ 's to be subreactions of the modes without them, and let  $[\Gamma(e^+ \nu_e) + \Gamma(\mu^+ \nu_\mu)]/\Gamma_{\text{total}} = 100\%$ .

[b] See the Particle Listings below for the energy limits used in this measurement; low-energy  $\gamma$ 's are not included.

[c] Derived from an analysis of neutrino-oscillation experiments.

## $\pi^\pm$ BRANCHING RATIOS

$\Gamma(e^+ \nu_e)/\Gamma_{\text{total}}$   $\Gamma_3/\Gamma$   
 See note [a] in the list of  $\pi^+$  decay modes just above, and see also the next block of data. See also the note on "Decay Constants of Charged Pseudoscalar Mesons" in the  $D_s^+$  Listings.

VALUE (units 10 <sup>-4</sup> )	DOCUMENT ID
<b>1.230 ± 0.004 OUR EVALUATION</b>	

$[\Gamma(e^+ \nu_e) + \Gamma(e^+ \nu_e \gamma)]/[\Gamma(\mu^+ \nu_\mu) + \Gamma(\mu^+ \nu_\mu \gamma)]$   $(\Gamma_3 + \Gamma_4)/(\Gamma_1 + \Gamma_2)$

See note [a] in the list of  $\pi^+$  decay modes above. See NUMAO 92 for a discussion of  $e-\mu$  universality. See also the note on "Decay Constants of Charged Pseudoscalar Mesons" in the  $D_s^+$  Listings.

VALUE (units 10 <sup>-4</sup> )	EVTS	DOCUMENT ID	TECN	CHG	COMMENT
<b>1.2327 ± 0.0023 OUR AVERAGE</b>					
1.2344 ± 0.0023 ± 0.0019	400k	AGUILAR-AR...15	CNTR	+	Stopping $\pi^+$
1.2346 ± 0.0035 ± 0.0036	120k	CZAPEK	93	CALO	Stopping $\pi^+$
1.2265 ± 0.0034 ± 0.0044	190k	BRITTON	92	CNTR	Stopping $\pi^+$
1.218 ± 0.014	32k	BRYMAN	86	CNTR	Stopping $\pi^+$
••• We do not use the following data for averages, fits, limits, etc. •••					
1.273 ± 0.028	11k	<sup>1</sup> DICAPUA	64	CNTR	
1.21 ± 0.07		ANDERSON	60	SPEC	

<sup>1</sup>DICAPUA 64 has been updated using the current mean life.

$\Gamma(\mu^+ \nu_\mu \gamma)/\Gamma_{\text{total}}$   $\Gamma_2/\Gamma$   
 Note that measurements here do not cover the full kinematic range.

VALUE (units 10 <sup>-4</sup> )	EVTS	DOCUMENT ID	TECN	CHG	COMMENT
<b>2.0 ± 0.24 ± 0.08</b>		<sup>1</sup> BRESSI	98	CALO	+

••• We do not use the following data for averages, fits, limits, etc. •••

1.24 ± 0.25	26	CASTAGNOLI	58	EMUL	$KE_\mu < 3.38$ MeV
<sup>1</sup> BRESSI 98 result is given for $E_\gamma > 1$ MeV only. Result agrees with QED expectation, $2.283 \times 10^{-4}$ and does not confirm discrepancy of earlier experiment CASTAGNOLI 58.					

$\Gamma(e^+ \nu_e \gamma)/\Gamma_{\text{total}}$   $\Gamma_4/\Gamma$

The very different values reflect the very different kinematic ranges covered (bigger range, bigger value). And none of them covers the whole kinematic range.

VALUE (units 10 <sup>-8</sup> )	EVTS	DOCUMENT ID	TECN	CHG	COMMENT
<b>73.86 ± 0.54</b>	65k	<sup>1</sup> BYCHKOV	09	PIBE	$e^+ \nu \gamma$ at rest
••• We do not use the following data for averages, fits, limits, etc. •••					
16.1 ± 2.3		<sup>2</sup> BOLOTOV	90b	SPEC	17 GeV $\pi^- \rightarrow e^- \bar{\nu}_e \gamma$
5.6 ± 0.7	226	<sup>3</sup> STETZ	78	SPEC	$P_e > 56$ MeV/c
3.0	143	DEPOMMIER	63b	CNTR	(KE) $e^+ \gamma > 48$ MeV

<sup>1</sup>This BYCHKOV 09 value is for  $E_\gamma > 10$  MeV and  $\Theta_{e^+ \gamma} > 40^\circ$ .

<sup>2</sup>BOLOTOV 90b is for  $E_\gamma > 21$  MeV,  $E_e > 70 - 0.8 E_\gamma$ .

<sup>3</sup>STETZ 78 is for an  $e^- \gamma$  opening angle  $> 132^\circ$ . Obtains 3.7 when using same cutoffs as DEPOMMIER 63b.

## $\Gamma(e^+ \nu_e \pi^0)/\Gamma_{\text{total}}$

$\Gamma_5/\Gamma$

VALUE (units 10 <sup>-8</sup> )	EVTS	DOCUMENT ID	TECN	CHG	COMMENT
<b>1.036 ± 0.006 OUR AVERAGE</b>					
1.036 ± 0.006	64k	<sup>1,2</sup> POCANIC	04	PIBE	+
1.026 ± 0.039	1224	<sup>3</sup> MCFARLANE	85	CNTR	+
1.00 <sup>+0.08</sup> <sub>-0.10</sub>	332	DEPOMMIER	68	CNTR	+
1.07 ± 0.21	38	<sup>4</sup> BACASTOW	65	OSPK	+
1.10 ± 0.26		<sup>4</sup> BERTRAM	65	OSPK	+
1.1 ± 0.2	43	<sup>4</sup> DUNAITSEV	65	CNTR	+
0.97 ± 0.20	36	<sup>4</sup> BARTLETT	64	OSPK	+
••• We do not use the following data for averages, fits, limits, etc. •••					
1.15 ± 0.22	52	<sup>4</sup> DEPOMMIER	63	CNTR	+

See DEPOMMIER 68  
<sup>1</sup>POCANIC 04 normalizes to  $e^+ \nu_e$  decays, using the PDG 2004 value  $B(\pi^+ \rightarrow e^+ \nu_e) = (1.230 \pm 0.004) \times 10^{-4}$ . We add their statistical  $(0.004 \times 10^{-8})$ , systematic  $(0.004 \times 10^{-8})$  and systematic error due to the uncertainty of  $B(\pi^+ \rightarrow e^+ \nu_e)$   $(0.003 \times 10^{-8})$  in quadrature.

<sup>2</sup>This result can be used to calculate  $V_{ud}$  from pion beta decay:  $V_{ud}^{PIBETA} = 0.9728 \pm 0.0030$ .

<sup>3</sup>MCFARLANE 85 combines a measured rate  $(0.394 \pm 0.015)/s$  with 1982 PDG mean life.

<sup>4</sup>DEPOMMIER 68 says the result of DEPOMMIER 63 is at least 10% too large because of a systematic error in the  $\pi^0$  detection efficiency, and that this may be true of all the previous measurements (also V. Soergel, private communication, 1972).

## $\Gamma(e^+ \nu_e e^+ e^-)/\Gamma(\mu^+ \nu_\mu)$

$\Gamma_6/\Gamma_1$

VALUE (units 10 <sup>-9</sup> )	CL%	EVTS	DOCUMENT ID	TECN	COMMENT
<b>3.2 ± 0.5 ± 0.2</b>		98	EGLI	89	SPEC

Uses  $R_{P_{CAC}} = 0.068 \pm 0.004$

••• We do not use the following data for averages, fits, limits, etc. •••

0.46 ± 0.16 ± 0.07	7	<sup>1</sup> BARANOV	92	SPEC	Stopped $\pi^+$
< 4.8	90	KORENCHE...	76b	SPEC	
< 34	90	KORENCHE...	71	OSPK	

<sup>1</sup>This measurement by BARANOV 92 is of the structure-dependent part of the decay. The value depends on values assumed for ratios of form factors.

## $\Gamma(e^+ \nu_e \nu \bar{\nu})/\Gamma_{\text{total}}$

$\Gamma_7/\Gamma$

VALUE (units 10 <sup>-6</sup> )	CL%	DOCUMENT ID	TECN
<b>&lt; 5</b>	90	PICCIOTTO	88

## $\Gamma(\mu^+ \bar{\nu}_e)/\Gamma_{\text{total}}$

$\Gamma_8/\Gamma$

Forbidden by total lepton number conservation. See the note on "Decay Constants of Charged Pseudoscalar Mesons" in the  $D_s^+$  Listings.

VALUE (units 10 <sup>-3</sup> )	CL%	DOCUMENT ID	TECN	COMMENT
<b>&lt; 1.5</b>	90	<sup>1</sup> COOPER	82	HLBC

<sup>1</sup>COOPER 82 limit on  $\bar{\nu}_e$  observation is here interpreted as a limit on lepton number violation.

## $\Gamma(\mu^+ \nu_e)/\Gamma_{\text{total}}$

$\Gamma_9/\Gamma$

Forbidden by lepton family number conservation.

VALUE (units 10 <sup>-3</sup> )	CL%	DOCUMENT ID	TECN	COMMENT
<b>&lt; 8.0</b>	90	<sup>1</sup> COOPER	82	HLBC

<sup>1</sup>COOPER 82 limit on  $\nu_e$  observation is here interpreted as a limit on lepton family number violation.

## $\Gamma(\mu^- e^+ e^+ \nu)/\Gamma_{\text{total}}$

$\Gamma_{10}/\Gamma$

Forbidden by lepton family number conservation.

VALUE (units 10 <sup>-6</sup> )	CL%	DOCUMENT ID	TECN	CHG
<b>&lt; 1.6</b>	90	BARANOV	91b	SPEC
••• We do not use the following data for averages, fits, limits, etc. •••				
< 7.7	90	KORENCHE...	87	SPEC

## $\pi^\pm$ — POLARIZATION OF EMITTED $\mu^\pm$

### $\pi^+ \rightarrow \mu^+ \nu$

Tests the Lorentz structure of leptonic charged weak interactions.

VALUE	CL%	DOCUMENT ID	TECN	CHG	COMMENT
••• We do not use the following data for averages, fits, limits, etc. •••					
< (-0.9959)	90	<sup>1</sup> FETSCHER	84	RVUE	+
-0.99 ± 0.16		<sup>2</sup> ABELA	83	SPEC	- $\mu$ X-rays

<sup>1</sup>FETSCHER 84 uses only the measurement of CARR 83.  
<sup>2</sup>Sign of measurement reversed in ABELA 83 to compare with  $\mu^+$  measurements.

## See the related review(s):

Form Factors for Radiative Pion and Kaon Decays

## $\pi^\pm$ FORM FACTORS

### $F_V$ , VECTOR FORM FACTOR

VALUE	EVTS	DOCUMENT ID	TECN	COMMENT
<b>0.0254 ± 0.0017 OUR AVERAGE</b>				
0.0258 ± 0.0017	65k	<sup>1</sup> BYCHKOV	09	PIBE
0.014 ± 0.009		<sup>2</sup> BOLOTOV	90b	SPEC
$17 \text{ GeV } \pi^- \rightarrow e^- \bar{\nu}_e \gamma$				
0.023 <sup>+0.015</sup> <sub>-0.013</sub>	98	EGLI	89	SPEC

<sup>1</sup>The BYCHKOV 09  $F_A$  and  $F_V$  results are highly (anti-)correlated:  $F_A + 1.0286 F_V = 0.03853 \pm 0.00014$ .

<sup>2</sup>BOLOTOV 90b only determines the absolute value.

F<sub>A</sub>, AXIAL-VECTOR FORM FACTOR

Table with columns: VALUE, EVTS, DOCUMENT ID, TECN, COMMENT. Contains data for various experiments like BYCHKOV, FRLEZ, BOLOTOV, EGLI, BAY, PIILONEN, STETZ.

- 1 These values come from fixing the vector form factor at the CVC prediction, F<sub>V</sub> = 0.0259 ± 0.0005.
2 When F<sub>V</sub> is released, the BYCHKOV 09 F<sub>A</sub> is 0.0117 ± 0.0017, and F<sub>A</sub> and F<sub>V</sub> results are highly (anti-)correlated: F<sub>A</sub> + 1.0286 F<sub>V</sub> = 0.03853 ± 0.00014.
3 The sign of γ = F<sub>A</sub> / F<sub>V</sub> is determined to be positive.
4 Only the absolute value of F<sub>A</sub> is determined.
5 The result of STETZ 78 has a two-fold ambiguity. We take the solution compatible with later determinations.

VECTOR FORM FACTOR SLOPE PARAMETER a

This is a in F<sub>V</sub>(q<sup>2</sup>) = F<sub>V</sub>(0) (1 + a q<sup>2</sup>)

Table with columns: VALUE, EVTS, DOCUMENT ID, TECN, COMMENT. Contains data for BYCHKOV 09.

R, SECOND AXIAL-VECTOR FORM FACTOR

Table with columns: VALUE, EVTS, DOCUMENT ID, TECN, COMMENT. Contains data for EGLI 89.

π± CHARGE RADIUS

The charge radius of the pion √(r<sub>π</sub><sup>2</sup>) is defined in relation to the form factor of the pion electromagnetic vertex, called vector form factor VFF, F<sub>V</sub><sup>V</sup>. The VFF is a function of the squared four-momentum transfer t, or of the squared c.m. energy s, depending on the channel in which the photon exchange takes place. In both cases, it is related to the slope of the VFF at zero, namely

(r<sub>π</sub><sup>2</sup>) = 6 dF<sub>V</sub><sup>V</sup>(q) / dq (q=0) where q = t, s.

The quantity cannot be measured directly. It can be extracted from the cross sections of three processes: pion electroproduction, eN → eNπ, and pion electron scattering eπ → eπ, for the t channel, and positron electron annihilation into two charged pions, e+e- → π+π-, for the s channel. We encode all measurements, but we do not use electroproduction data in averaging because the extraction of the pion radius involves, in this case, theoretical uncertainties that cannot be controlled at the needed level of accuracy. In case of analyses based on the same data set, as ANANTHANARAYAN 17 and COLANGELO 19, which cannot be averaged, we combine the results into a common value, with the uncertainty range chosen to cover both analyses. Note that for consistency the form factor needs to be defined in both channels with the vacuum polarisation removed. For details see COLANGELO 19 or Appendix B of ANANTHANARAYAN 16a.

Table with columns: VALUE (fm), DOCUMENT ID, TECN, COMMENT. Includes 'OUR AVERAGE' and various experimental data points.

- 1 This value combines the measurements of ANANTHANARAYAN 17 and COLANGELO 19 which are based on the same data set. The uncertainty range is chosen to cover both results.
2 COLANGELO 19 fit existing F<sub>V</sub> data, using an extended Omnes dispersive representation. This analysis is based on the same data set of ANANTHANARAYAN 17. Accordingly, they cannot be averaged. We combine the results into a common value, with the uncertainty range chosen to cover the uncertainty ranges of both analyses.
3 ANANTHANARAYAN 17 fit existing F<sub>V</sub> data, using a mixed phase-modulus dispersive representation. This analysis is based on the same data set of COLANGELO 19. Accordingly, they cannot be averaged. We combine the results into a common value, with the uncertainty range chosen to cover the uncertainty ranges of both analyses.
4 According to the authors the uncertainty could be underestimated. The value quoted omits the BaBar data AUBERT 09.
5 The extractions could contain an additional theoretical uncertainty which cannot be sufficiently quantified.

6 BIJNENS 98 fits existing data.

7 The extraction is based on a parametrization that does not have correct analytic properties.

π± REFERENCES

We have omitted some papers that have been superseded by later experiments. The omitted papers may be found in our 1988 edition Physics Letters B204 1 (1988).

COLANGELO 19, DAUM 19, PDG 19, ANANTHANA...17, HANHART 17, ANANTHANA...16A, TRASSINELLI 16, ADOLPH 15A, AGUILAR-AREVALO...15, HOLSTEIN 14, AUBERT 09, BYCHKOV 09, FRLEZ 04, POCANIC 04, ESCHRICH 01, LIESENFELD 99, BIJNENS 98, BRESSI 98, LENZ 98, ASSAMAGAN 96, KOPTEV 95, NUMAO 95, ASSAMAGAN 94, JECKELMANN 94, CZAPEK 93, BARANOV 92, BRITTON 92, Also, NUMAO 92B, DAUM 91, BOLOTOV 90B, EGLI 89, PDG 88, PICCIOTTO 88, COHEN 87, KORENCHENKO...87, AMENDOLIA 86, BAY 86, BRYMAN 86, Also, JECKELMANN 86B, Also, PIILONEN 86, MCFARLANE 85, ABELA 84, Also, AMENDOLIA 84, FETSCHER 84, ABELA 83, CARR 83, COOPER 82, DALLY 82, LLU 80, BEBEK 78, QUENZER 78, STETZ 78, ADYLOV 77, BARDIN 77, DALLY 77, CARTER 76, KORENCHENKO...76B, MARUSHEN...76, Also, DUNAITSSEV 73, AYRES 71, Also, Also, Also, KORENCHENKO...71, BOOTH 70, DEPOMMIER 68, PETRIUKHIN 68, HYMAN 67, NORDBERG 67, BARDON 66, KINSEY 66, LOBKOWICZ 66, BACASTOW 65, BERTRAM 65, DUNAITSSEV 65, ECKHAUSE 65, BARTLETT 64, DICAPUA 64, Also, DEPOMMIER 63, DEPOMMIER 63B, ANDERSON 60, CASTAGNOLI 58, G. Colangelo, M. Hoferichter, P. Stoffer, M. Daum, R. Frosch, P.-R. Kettle, M. Tanabashi et al., B. Ananthanarayan, I. Caprini, D. Das, C. Hanhart et al., B. Ananthanarayan et al., M. Trassinelli et al., C. Adolph et al., A. Aguilar-Arevalo et al., B. Holstein, S. Scherer, B. Aubert et al., M. Bychkov et al., E. Frlze et al., D. Pocanic et al., I. Eschrich et al., A. Liesenfeld et al., J. Bijnens et al., G. Bressi et al., S. Lenz et al., K.A. Assamagan et al., V.P. Koptev et al., Translated from ZETP 61 865, N. Numao et al., K.A. Assamagan et al., B. Jeckelmann, P.F.A. Goudsmit, H.J. Lesi, G. Czapek et al., V.A. Baranov et al., Translated from YAF 55 2940, D.L. Britton et al., D.L. Britton et al., T. Numao, V.A. Baranov et al., Translated from YAF 54 1298, M. Daum et al., V.N. Bolotov et al., S. Egli et al., S. Egli et al., G.P. Yost et al., C.E. Picciotto et al., E.R. Cohen, B.N. Taylor, S.M. Korenchenko et al., Translated from YAF 46 313, S.R. Amendolia et al., A. Bay et al., D.A. Bryman et al., D.A. Bryman et al., B. Jeckelmann et al., B. Jeckelmann et al., L.E. Piilonen et al., W.K. McFarlane et al., R. Abela et al., M. Daum et al., M. Daum et al., S.R. Amendolia et al., W. Fetscher, R. Abela et al., J. Carr et al., A.M. Cooper et al., E.B. Dally et al., C. Lu et al., C.J. Bebek et al., A. Quenzer et al., A.W. Stetz et al., G.T. Adylov et al., G. Bardin et al., E.B. Dally et al., A.L. Carter et al., S.M. Korenchenko et al., Translated from ZETF 71 67, V.I. Marushenko et al., Translated from ZETP 23 80, Private Comm., R.E. Shafer, Private Comm., A. Smirnov, A.F. Dunaitsev et al., Translated from YAF 16 524, D.S. Ayres et al., D.S. Ayres et al., PRL 21 261, D.S. Ayres et al., D.S. Ayres, A.J. Greenberg et al., S.M. Korenchenko et al., Translated from YAF 13 339, P.S.L. Booth et al., P. Depommier et al., P. Petrukhin et al., L.G. Hyman et al., M.E. Nordberg, F. Lobkowicz, R.L. Burman, M. Bardon et al., K.F. Kinsey, F. Lobkowicz, M.E. Nordberg, R.B. Bacastow et al., W.K. Bertram et al., A.F. Dunaitsev et al., Translated from ZETF 47 84, M. Eckhause et al., D. Bartlett et al., M. di Capua et al., L. Pondrom, P. Depommier et al., P. Depommier et al., H.L. Anderson et al., C. Castagnoli, M. Muchnik

Downloaded from https://academic.oup.com/ptep/article/2020/8/083C01/5891211 by guest on 12 November 2020

# Meson Particle Listings

$\pi^0$



$$I^G(J^{PC}) = 1^-(0^{-+})$$

We have omitted some results that have been superseded by later experiments. The omitted results may be found in our 1988 edition Physics Letters **B204** 1 (1988).

### $\pi^0$ MASS

The value is calculated from  $m_{\pi^\pm}$  and  $(m_{\pi^\pm} - m_{\pi^0})$ . See also the notes under the  $\pi^\pm$  Mass Listings.

VALUE (MeV)	DOCUMENT ID
<b>134.9768 ± 0.0005 OUR FIT</b>	Error includes scale factor of 1.1.

### $m_{\pi^\pm} - m_{\pi^0}$

Measurements with an error > 0.01 MeV have been omitted.

VALUE (MeV)	DOCUMENT ID	TECN	COMMENT
<b>4.5936 ± 0.0005 OUR FIT</b>			
<b>4.5936 ± 0.0005 OUR AVERAGE</b>			
4.59364 ± 0.00048	CRAWFORD 91	CNTR	$\pi^- p \rightarrow \pi^0 n, n$ TOF
4.5930 ± 0.0013	CRAWFORD 86	CNTR	$\pi^- p \rightarrow \pi^0 n, n$ TOF
• • •	We do not use the following data for averages, fits, limits, etc. • • •		
4.59366 ± 0.00048	CRAWFORD 88B	CNTR	See CRAWFORD 91
4.6034 ± 0.0052	VASILEVSKY 66	CNTR	
4.6056 ± 0.0055	CZIRR 63	CNTR	

### $\pi^0$ MEAN LIFE

Most experiments measure the  $\pi^0$  width which we convert to a lifetime. ATHERTON 85 is the only direct measurement of the  $\pi^0$  lifetime. Our average based only on indirect measurement yields  $(8.30 \pm 0.19) \times 10^{-17}$  s. The two Primakoff measurements from 1970 have been excluded from our average because they suffered model-related systematics unknown at the time. More information on the  $\pi^0$  lifetime can be found in BERNSTEIN 13.

VALUE ( $10^{-17}$ s)	EVTS	DOCUMENT ID	TECN	COMMENT
<b>8.52 ± 0.18 OUR AVERAGE</b>		Error includes scale factor of 1.2.		
8.32 ± 0.15 ± 0.18		<sup>1</sup> LARIN 11	PRMX	Primakoff effect
8.5 ± 1.1		<sup>2</sup> BYCHKOV 09	PIBE	$\pi^+ \rightarrow e^+ \nu \gamma$ at rest
8.4 ± 0.5 ± 0.5	1182	<sup>3</sup> WILLIAMS 88	CBAL	$e^+ e^- \rightarrow e^+ e^- \pi^0$
8.97 ± 0.22 ± 0.17		ATHERTON 85	CNTR	Direct measurement
8.2 ± 0.4		<sup>4</sup> BROWMAN 74	CNTR	Primakoff effect
• • •	We do not use the following data for averages, fits, limits, etc. • • •			
5.6 ± 0.6		BELLETTINI 70	CNTR	Primakoff effect
9 ± 0.68		KRYSHKIN 70	CNTR	Primakoff effect
7.3 ± 1.1		BELLETTINI 65B	CNTR	Primakoff effect
<sup>1</sup> LARIN 11 reported $\Gamma(\pi^0 \rightarrow \gamma\gamma) = 7.82 \pm 0.14 \pm 0.17$ eV which we converted to mean life $\tau = \hbar/\Gamma(\text{total})$ .				
<sup>2</sup> BYCHKOV 09 obtains this using the conserved-vector-current relation between the vector form factor $F_V$ and the $\pi^0$ lifetime.				
<sup>3</sup> WILLIAMS 88 gives $\Gamma(\gamma\gamma) = 7.7 \pm 0.5 \pm 0.5$ eV. We give here $\tau = \hbar/\Gamma(\text{total})$ .				
<sup>4</sup> BROWMAN 74 gives a $\pi^0$ width $\Gamma = 8.02 \pm 0.42$ eV. The mean life is $\hbar/\Gamma$ .				

### $\pi^0$ DECAY MODES

For decay limits to particles which are not established, see the appropriate Search sections ( $A^0$  (axion) and Other Light Boson ( $X^0$ ) Searches, etc.).

Mode	Fraction ( $\Gamma_i/\Gamma$ )	Scale factor/ Confidence level
$\Gamma_1$ $2\gamma$	$(98.823 \pm 0.034) \%$	S=1.5
$\Gamma_2$ $e^+ e^- \gamma$	$(1.174 \pm 0.035) \%$	S=1.5
$\Gamma_3$ $\gamma$ positronium	$(1.82 \pm 0.29) \times 10^{-9}$	
$\Gamma_4$ $e^+ e^+ e^- e^-$	$(3.34 \pm 0.16) \times 10^{-5}$	
$\Gamma_5$ $e^+ e^-$	$(6.46 \pm 0.33) \times 10^{-8}$	
$\Gamma_6$ $4\gamma$	< 2	CL=90%
$\Gamma_7$ $\nu\bar{\nu}$	[a] < 2.7	$\times 10^{-7}$ CL=90%
$\Gamma_8$ $\nu_e \bar{\nu}_e$	< 1.7	$\times 10^{-6}$ CL=90%
$\Gamma_9$ $\nu_\mu \bar{\nu}_\mu$	< 1.6	$\times 10^{-6}$ CL=90%
$\Gamma_{10}$ $\nu_\tau \bar{\nu}_\tau$	< 2.1	$\times 10^{-6}$ CL=90%
$\Gamma_{11}$ $\gamma \nu \bar{\nu}$	< 1.9	$\times 10^{-7}$ CL=90%

### Charge conjugation (C) or Lepton Family number (LF) violating modes

$\Gamma_{12}$ $3\gamma$	C	< 3.1	$\times 10^{-8}$	CL=90%
$\Gamma_{13}$ $\mu^+ e^-$	LF	< 3.8	$\times 10^{-10}$	CL=90%
$\Gamma_{14}$ $\mu^- e^+$	LF	< 3.4	$\times 10^{-9}$	CL=90%
$\Gamma_{15}$ $\mu^+ e^- + \mu^- e^+$	LF	< 3.6	$\times 10^{-10}$	CL=90%

[a] Astrophysical and cosmological arguments give limits of order  $10^{-13}$ .

### CONSTRAINED FIT INFORMATION

An overall fit to 2 branching ratios uses 6 measurements and one constraint to determine 3 parameters. The overall fit has a  $\chi^2 = 4.6$  for 4 degrees of freedom.

The following *off-diagonal* array elements are the correlation coefficients  $\langle \delta x_i \delta x_j \rangle / (\delta x_i \delta x_j)$ , in percent, from the fit to the branching fractions,  $x_i \equiv \Gamma_i / \Gamma_{\text{total}}$ . The fit constrains the  $x_i$  whose labels appear in this array to sum to one.

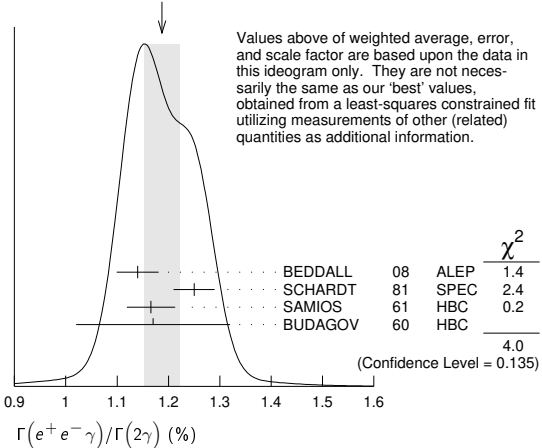
$x_2$	-100	
$x_4$	0	-1
	$x_1$	$x_2$

### $\pi^0$ BRANCHING RATIOS

$\Gamma(e^+ e^- \gamma) / \Gamma(2\gamma)$	VALUE (%)	EVTS	DOCUMENT ID	TECN	COMMENT	$\Gamma_2/\Gamma_1$
<b>1.188 ± 0.035 OUR FIT</b>			Error includes scale factor of 1.5.			
<b>1.188 ± 0.034 OUR AVERAGE</b>			Error includes scale factor of 1.4. See the ideogram below.			
	1.140 ± 0.024 ± 0.033	12.5k	<sup>1</sup> BEDDALL 08	ALEP	$e^+ e^- \rightarrow Z \rightarrow \text{hadrons}$	
	1.25 ± 0.04		SCHARDT 81	SPEC	$\pi^- p \rightarrow n \pi^0$	
	1.166 ± 0.047	3071	<sup>2</sup> SAMIOS 61	HBC	$\pi^- p \rightarrow n \pi^0$	
	1.17 ± 0.15	27	BUDAGOV 60	HBC		
• • •	We do not use the following data for averages, fits, limits, etc. • • •					
	1.1559 ± 0.0047 ± 0.0106	60k	<sup>3</sup> ABOUZAID 19	KTEV	$K_L \rightarrow 3\pi^0$ in flight	
	1.196		JOSEPH 60	THEO	QED calculation	

<sup>1</sup>BEDDALL 08 value is obtained from ALEPH archived data.  
<sup>2</sup>SAMIOS 61 value uses a Panofsky ratio = 1.62.  
<sup>3</sup>ABOUZAID 19 measured a value of  $(0.3920 \pm 0.0016 \pm 0.0036) \%$  from 1999 KTEV data in  $K_L \rightarrow 3\pi^0 \rightarrow 5\gamma e^+ e^-$  decays, normalised to  $K_L \rightarrow 3\pi^0$ , for  $m(ee) > 15$  MeV and then extrapolated it to the full  $m(ee)$  range using the Mikaelian and Smith predictions for the mass spectrum.

WEIGHTED AVERAGE  
1.188 ± 0.034 (Error scaled by 1.4)



### $\Gamma(\gamma$ positronium) $/\Gamma(2\gamma)$

VALUE (units $10^{-9}$ )	EVTS	DOCUMENT ID	TECN	COMMENT
<b>1.84 ± 0.29</b>	277	AFANASYEV 90	CNTR	$pC$ 70 GeV

### $\Gamma(e^+ e^+ e^- e^-) / \Gamma(2\gamma)$

VALUE (units $10^{-5}$ )	EVTS	DOCUMENT ID	TECN	COMMENT
<b>3.38 ± 0.16 OUR FIT</b>				
<b>3.38 ± 0.16 OUR AVERAGE</b>				
3.46 ± 0.19	30.5k	<sup>1</sup> ABOUZAID 08D	KTEV	$K_L^0 \rightarrow \pi^0 \pi^0 \pi_{DD}^0$
3.18 ± 0.30	146	<sup>2</sup> SAMIOS 62B	HBC	

<sup>1</sup>This ABOUZAID 08D value includes all radiative final states. The error includes both statistical and systematic errors. The correlation between the Dalitz-pair planes gives a direct measurement of the  $\pi^0$  parity. The  $\pi^0 2\gamma^*$  form factor is measured and limits are placed on a scalar contribution to the decay.  
<sup>2</sup>SAMIOS 62B value uses a Panofsky ratio = 1.62.

### $\Gamma(e^+ e^-) / \Gamma_{\text{total}}$

Experimental results are listed; branching ratios corrected for radiative effects are given in the footnotes. BERMAN 60 found  $B(\pi^0 \rightarrow e^+ e^-) \geq 4.69 \times 10^{-8}$  via an exact QED calculation.

VALUE (units $10^{-8}$ )	EVTS	DOCUMENT ID	TECN	CHG	COMMENT
<b>6.46 ± 0.33 OUR AVERAGE</b>					
6.44 ± 0.25 ± 0.22	794	<sup>1</sup> ABOUZAID 07	KTEV		$K_L^0 \rightarrow 3\pi^0$ in flight
6.9 ± 2.3 ± 0.6	21	<sup>2</sup> DESHPANDE 93	SPEC		$K^+ \rightarrow \pi^+ \pi^0$
7.6 $\pm$ 2.9 $\pm$ 0.5	8	<sup>3</sup> MCFARLAND 93	SPEC		$K_L^0 \rightarrow 3\pi^0$ in flight

See key on page 999

Meson Particle Listings

$\pi^0$

••• We do not use the following data for averages, fits, limits, etc. •••  
6.09 ± 0.40 ± 0.24 275 4 ALAVI-HARATI 99c SPEC 0 Repl. by ABOUZAID 07

<sup>1</sup> ABOUZAID 07 result is for  $m_{e^+e^-}/m_{\pi^0} > 0.95$ . With radiative corrections the result becomes  $(7.48 \pm 0.29 \pm 0.25) \times 10^{-8}$ .

<sup>2</sup> The DESHPANDE 93 result with bremsstrahlung radiative corrections is  $(8.0 \pm 2.6 \pm 0.6) \times 10^{-8}$ .

<sup>3</sup> The MCFARLAND 93 result is for  $B[\pi^0 \rightarrow e^+e^-, (m_{e^+e^-}/m_{\pi^0})^2 > 0.95]$ . With radiative corrections it becomes  $(8.8_{-3.2}^{+4.5} \pm 0.6) \times 10^{-8}$ .

<sup>4</sup> ALAVI-HARATI 99c quote result for  $B[\pi^0 \rightarrow e^+e^-, (m_{e^+e^-}/m_{\pi^0})^2 > 0.95]$  to minimize radiative contributions from  $\pi^0 \rightarrow e^+e^-\gamma$ . After radiative corrections they obtain  $(7.04 \pm 0.46 \pm 0.28) \times 10^{-8}$ .

$\Gamma(e^+e^-)/\Gamma(2\gamma)$   $\Gamma_5/\Gamma_1$

Table with columns: VALUE (units 10^-7), CL%, EVTS, DOCUMENT ID, TECN, COMMENT. Rows include NIEBUHR 89, ZEPHAT 87, FRANK 83, MISCHKE 82, FISCHER 78B.

$\Gamma(4\gamma)/\Gamma_{total}$   $\Gamma_6/\Gamma$

Table with columns: VALUE (units 10^-8), CL%, EVTS, DOCUMENT ID, TECN, COMMENT. Rows include MCDONOUGH 88, BOLOTOV 86c, AUERBACH 80.

$\Gamma(\nu\bar{\nu})/\Gamma_{total}$   $\Gamma_7/\Gamma$

The astrophysical and cosmological limits are many orders of magnitude lower, but we use the best laboratory limit for the Summary Tables.

Table with columns: VALUE (units 10^-6), CL%, DOCUMENT ID, TECN, COMMENT. Rows include ARTAMONOV 05A, ATIYA 91, LAM 91, NATALE 91, DORENBOS... 88, HERCZEG 81.

<sup>1</sup> This limit applies to all possible  $\nu\nu'$  states as well as to other massless, weakly interacting states.  
<sup>2</sup> LAM 91 considers the production of right-handed neutrinos produced from the cosmic thermal background at the temperature of about the pion mass through the reaction  $\gamma\gamma \rightarrow \pi^0 \rightarrow \nu\bar{\nu}$ .  
<sup>3</sup> NATALE 91 considers the excess energy-loss rate from SN1987A if the process  $\gamma\gamma \rightarrow \pi^0 \rightarrow \nu\bar{\nu}$  occurs, permitted if the neutrinos have a right-handed component. As pointed out in LAM 91 (and confirmed by Natale), there is a factor 4 error in the NATALE 91 published result  $(0.8 \times 10^{-7})$ .

$\Gamma(\nu_e\bar{\nu}_e)/\Gamma_{total}$   $\Gamma_8/\Gamma$

Table with columns: VALUE (units 10^-6), CL%, DOCUMENT ID, TECN, COMMENT. Rows include DORENBOS... 88, HOFFMAN 88.

$\Gamma(\nu_\mu\bar{\nu}_\mu)/\Gamma_{total}$   $\Gamma_9/\Gamma$

Table with columns: VALUE (units 10^-6), CL%, EVTS, DOCUMENT ID, TECN, COMMENT. Rows include AUERBACH 04, HOFFMAN 88, DORENBOS... 88.

$\Gamma(\nu_\tau\bar{\nu}_\tau)/\Gamma_{total}$   $\Gamma_{10}/\Gamma$

Table with columns: VALUE (units 10^-6), CL%, DOCUMENT ID, TECN, COMMENT. Rows include HOFFMAN 88, DORENBOS... 88.

$\Gamma(\gamma\nu\bar{\nu})/\Gamma_{total}$   $\Gamma_{11}/\Gamma$

Table with columns: VALUE, CL%, DOCUMENT ID, TECN, COMMENT. Rows include CORTINA-GIL 19, ATIYA 92.

$\Gamma(3\gamma)/\Gamma_{total}$   $\Gamma_{12}/\Gamma$

Forbidden by C invariance.

Table with columns: VALUE (units 10^-8), CL%, EVTS, DOCUMENT ID, TECN, COMMENT. Rows include MCDONOUGH 88, HIGHLAND 80, AUERBACH 78, DUCLOS 65, KUTIN 65.

$\Gamma(\mu^+e^-)/\Gamma_{total}$   $\Gamma_{13}/\Gamma$

Forbidden by lepton family number conservation.

Table with columns: VALUE (units 10^-3), CL%, EVTS, DOCUMENT ID, TECN, COMMENT. Rows include APPEL 00, LEE 90, CAMPAGNARI 88.

$\Gamma(\mu^-e^+)/\Gamma_{total}$   $\Gamma_{14}/\Gamma$

Forbidden by lepton family number conservation.

Table with columns: VALUE (units 10^-3), CL%, EVTS, DOCUMENT ID, TECN, COMMENT. Rows include APPEL 00B, B865.

$[\Gamma(\mu^+e^-) + \Gamma(\mu^-e^+)]/\Gamma_{total}$   $\Gamma_{15}/\Gamma$

Forbidden by lepton family number conservation.

Table with columns: VALUE (units 10^-3), CL%, DOCUMENT ID, TECN, COMMENT. Rows include ABOUZAID 08c, KROLAK 94, HERCZEG 84, BRYMAN 82.

$\pi^0$  ELECTROMAGNETIC FORM FACTOR

The amplitude for the process  $\pi^0 \rightarrow e^+e^-\gamma$  contains a form factor  $F(x)$  at the  $\pi^0\gamma\gamma$  vertex, where  $x = [m_{e^+e^-}/m_{\pi^0}]^2$ . The parameter  $a$  in the linear expansion  $F(x) = 1 + ax$  is listed below.

All the measurements except that of BEHREND 91 are in the time-like region of momentum transfer.

LINEAR COEFFICIENT OF  $\pi^0$  ELECTROMAGNETIC FORM FACTOR

Table with columns: VALUE (units 10^-2), EVTS, DOCUMENT ID, TECN, COMMENT. Rows include LAZZERONI 17, FARZANPAY 92, MEIJERDREES 92B, BEHREND 91, FONVIEILLE 89, TUPPER 83, FISCHER 78, DEVONS 69, KOBRACK 61, SAMIOS 61.

<sup>1</sup> BEHREND 91 estimates that their systematic error is of the same order of magnitude as their statistical error, and so we have included a systematic error of this magnitude. The value of  $a$  is obtained by extrapolation from the region of large space-like momentum transfer assuming vector dominance.  
<sup>2</sup> TUPPER 83 is a theoretical analysis of FISCHER 78 including 2-photon exchange in the corrections.  
<sup>3</sup> The FISCHER 78 error is statistical only. The result without radiation corrections is  $+0.05 \pm 0.03$ .

$\pi^0$  REFERENCES

We have omitted some papers that have been superseded by later experiments. The omitted papers may be found in our 1988 edition Physics Letters B204 1 (1988).

ABOUZAID 19 PR D100 032003 (KTeV Collab.)  
CORTINA-GIL 19 JHEP 1905 182 (NA62 Collab.)  
LAZZERONI 17 PL B7 69 38 (NA62 Collab.)  
BERNSTEIN 13 RMP 85 49 (AMET, MIT)  
LARIN 11 PRL 106 162303 (PrimEx Collab.)  
BYCHKOV 09 PRL 103 051802 (PSI PIBETA Collab.)  
ABOUZAID 08C PRL 100 131803 (FNAL KTeV Collab.)  
ABOUZAID 08D PRL 100 182001 (FNAL KTeV Collab.)  
BEDDALL 08 EPJ C54 365 (UGAZ)  
ABOUZAID 07 PR D75 012004 (KTeV Collab.)  
ARTAMONOV 05A PR D72 091102 (BNL E949 Collab.)  
AUERBACH 04 PRL 92 091801 (LSND Collab.)  
APPEL 00 PRL 85 2450 (BNL 865 Collab.)  
Also Thesis, Yale Univ. D.R. Bergman  
Also Thesis, Univ. Zurich S. Pistak  
APPEL 00B PRL 85 2877 (BNL 865 Collab.)  
E. Abouzaid et al.  
E. Cortina Gil et al.  
C. Lazzeroni et al.  
A.M. Bernstein, B. R. Holstein  
I. Larin et al.  
M. Bychkov et al.  
E. Abouzaid et al.  
E. Abouzaid et al.  
A. Beddall, A. Beddall  
E. Abouzaid et al.  
A.V. Artamonov et al.  
L.B. Auerbach et al.  
R. Appel et al.  
D.R. Bergman  
S. Pistak  
R. Appel et al.

Downloaded from https://academic.oup.com/ptep/article/2020/8/083C01/5891211 by guest on 12 November 2020

# Meson Particle Listings

## $\pi^0, \eta$

ALAVI-HARATI	99C	PRL 83 922	A. Alavi-Harati et al.	(FNAL KTeV Collab.)
KROLAK	94	PL B320 407	P. Krolak et al.	(EFI, UCLA, COLO, ELMT+)
DESHPANDE	93	PRL 71 27	A. Deshpande et al.	(BNL E851 Collab.)
MCFARLAND	93	PRL 71 31	K.S. McFarland et al.	(EFI, UCLA, COLO+)
ATIYA	92	PRL 69 733	M.S. Atiya et al.	(BNL, LANL, PRIN+)
FARZANPAY	92	PL B278 413	F. Farzanpay et al.	(ORST, TRIU, BRCO+)
MEUERDREES	92B	PR D45 1439	R. Meijer Drees et al.	(PSI SINDRUM-I Collab.)
ATIYA	91	PRL 66 2189	M.S. Atiya et al.	(BNL, LANL, PRIN+)
BEHREND	91	ZPHY C49 401	H.J. Behrend et al.	(CELLO Collab.)
CRAWFORD	91	PR D43 46	J.F. Crawford et al.	(VILL, UVA)
LAM	91	PR D44 3345	W.P. Lam, K.W. Ng	(AST)
NATALE	91	PL B258 227	A.A. Natale	(SPIFT)
AFANASYEV	90	PL B236 116	L.G. Afanasyev et al.	(JINR, MOSU, SERP)
Also		SJNP 51 664	L.G. Afanasyev et al.	(JINR)
LEE	90	PRL 64 165	A.M. Lee et al.	(BNL, FNAL, VILL, WASH+)
FONVIELLE	89	PL B233 65	H. Fonville et al.	(CLER, LYON, SAACL)
NIEBUHR	89	PR D40 2796	C. Niebuhr et al.	(SINDRUM Collab.)
CAMPAGNARI	88	PRL 61 2062	C. Campagnari et al.	(BNL, FNAL, PSI+)
CRAWFORD	88B	PL B213 391	J.F. Crawford et al.	(PSI, UVA)
DORENBOS...	88	ZPHY C40 497	J. Dorenbosch et al.	(CHARM Collab.)
HOFFMAN	88	PL B208 149	C.M. Hoffman	(LANL)
MCDONOUGH	88	PR D38 2121	J.M. McDonough et al.	(TEMP, LANL, CHIC)
PDG	88	PL B204 1	G.P. Yost et al.	(LBL+)
WILLIAMS	88	PR D38 1365	D.A. Williams et al.	(Crystal Ball Collab.)
ZEPHAT	87	JP G13 1375	A.G. Zephath et al.	(OMICRON Collab.)
BOLOTOV	86C	JETPL 43 520	V.N. Bolotov et al.	(INRM)
Translated from ZETFP		43 405		
CRAWFORD	86	PRL 56 1043	J.F. Crawford et al.	(SIN, UVA)
ATHERTON	85	PL 158B 81	H.W. Atherton et al.	(CERN, ISU, LUND+)
HERCZEG	84	PR D29 1954	P. Herczeg, C.M. Hoffman	(LANL)
FRANK	83	PR D28 423	J.S. Frank et al.	(LANL, ARZS)
TUPPER	83	PR D28 2905	G.B. Tupper, T.R. Grose, M.A. Samuel	(OKSU)
BRYMAN	82	PR D26 2538	D.A. Bryman	(TRIU)
MISCHKE	82	PRL 48 1153	R.E. Mischke et al.	(LANL, ARZS)
HERCZEG	81	PL 100B 347	P. Herczeg, C.M. Hoffman	(LANL)
SCHARDT	81	PR D23 639	M.A. Schardt et al.	(ARZS, LANL)
AUERBACH	80	PL 90B 317	L.B. Auerbach et al.	(TEMP, LASL)
HIGHLAND	80	PRL 44 628	V.L. Highland et al.	(TEMP, LASL)
AUERBACH	78	PRL 41 275	L.B. Auerbach et al.	(TEMP, LASL)
FISCHER	78	PL 73B 359	J. Fischer et al.	(GEVA, SAACL)
FISCHER	78B	PL 73B 364	J. Fischer et al.	(GEVA, SAACL)
BROWMAN	74	PRL 33 1400	A. Browman et al.	(CORN, BING)
BELLETTINI	70	NC 66A 243	G. Bellettini et al.	(PISA, BONN)
KRYSHKIN	70	JETP 30 1037	V.I. Kryshkin, A.G. Sterligov, Y.P. Usov	(TMSK)
Translated from ZETFP		57 1917		
DEVONS	69	PR 184 1356	S. Devons et al.	(COLU, ROMA)
VASILEVSKY	66	PL 23 281	I.M. Vasilevsky et al.	(JINR)
BELLETTINI	65B	NC 40A 1139	G. Bellettini et al.	(PISA, FIRZ)
DUCLLOS	65	PL 19 253	J. Duclos et al.	(CERN, HEID)
KUTIN	65	JETPL 2 243	V.M. Kutjin, V.I. Petrukhin, Y.D. Prokoshkin	(JINR)
Translated from ZETFP		2 387		
CZIRR	63	PR 130 341	J.B. Czirr	(LRL)
SAMIOS	62B	PR 126 1844	N.P. Samios et al.	(COLU, BNL)
KOBRAK	61	NC 20 1115	H. Kobrak	(EFI)
SAMIOS	61	PR 121 275	N.P. Samios	(COLU, BNL)
BERMAN	60	NC 38 1192	S. Berman, D. Geffen	
BUDAGOV	60	JETP 11 755	Y.A. Budagov et al.	(JINR)
Translated from ZETFP		38 1047		
JOSEPH	60	NC 16 997	D.W. Joseph	(EFI)

## $\eta$

$$I^G(J^{PC}) = 0^+(0^{-+})$$

We have omitted some results that have been superseded by later experiments. The omitted results may be found in our 1988 edition Physics Letters **B204** (1988).

### $\eta$ MASS

Recent measurements resolve the obvious inconsistency in previous  $\eta$  mass measurements in favor of the higher value first reported by NA48 (LA1 02). We use only precise measurements consistent with this higher mass value for our  $\eta$  mass average.

VALUE (MeV)	EVTS	DOCUMENT ID	TECN	COMMENT
<b>547.862 ± 0.017 OUR AVERAGE</b>				
547.865 ± 0.031 ± 0.062		NIKOLAEV 14	CRYB	$\gamma p \rightarrow p \eta$
547.873 ± 0.005 ± 0.027	1M	GOSLAWSKI 12	SPEC	$d p \rightarrow {}^3\text{He} \eta$
547.874 ± 0.007 ± 0.029		AMBROSINO 07B	KLOE	$e^+ e^- \rightarrow \phi \rightarrow \eta \gamma$
547.785 ± 0.017 ± 0.057	16k	MILLER 07	CLEO	$\psi(2S) \rightarrow J/\psi \eta$
547.843 ± 0.030 ± 0.041	1134	LAI 02	NA48	$\eta \rightarrow 3\pi^0$
• • • We do not use the following data for averages, fits, limits, etc. • • •				
547.311 ± 0.028 ± 0.032		<sup>1</sup> ABDEL-BARY 05	SPEC	$d p \rightarrow {}^3\text{He} \eta$
547.12 ± 0.06 ± 0.25		KRUSCHE 95D	SPEC	$\gamma p \rightarrow \eta p$ , threshold
547.30 ± 0.15		PLOUIN 92	SPEC	$d p \rightarrow {}^3\text{He} \eta$
547.45 ± 0.25		DUANE 74	SPEC	$\pi^- p \rightarrow n$ neutrals
548.2 ± 0.65		FOSTER 65c	HBC	
549.0 ± 0.7	148	FOELSCH 64	HBC	
548.0 ± 1.0	91	ALFF-... 62	HBC	
549.0 ± 1.2	53	BASTIEN 62	HBC	

<sup>1</sup> ABDEL-BARY 05 disagrees significantly with recent measurements of similar or better precision. See comment in the header.

### $\eta$ WIDTH

This is the partial decay rate  $\Gamma(\eta \rightarrow \gamma \gamma)$  divided by the fitted branching fraction for that mode. See the note at the start of the  $\Gamma(2\gamma)$  data block, next below.

VALUE (keV)	DOCUMENT ID
<b>1.31 ± 0.05 OUR FIT</b>	

### $\eta$ DECAY MODES

Mode	Fraction ( $\Gamma_i/\Gamma$ )	Scale factor/ Confidence level
<b>Neutral modes</b>		
$\Gamma_1$ neutral modes	(72.12 ± 0.34) %	S=1.2
$\Gamma_2$ $2\gamma$	(39.41 ± 0.20) %	S=1.1
$\Gamma_3$ $3\pi^0$	(32.68 ± 0.23) %	S=1.1
$\Gamma_4$ $\pi^0 2\gamma$	( 2.56 ± 0.22 ) × 10 <sup>-4</sup>	
$\Gamma_5$ $2\pi^0 2\gamma$	< 1.2 × 10 <sup>-3</sup>	CL=90%
$\Gamma_6$ $4\gamma$	< 2.8 × 10 <sup>-4</sup>	CL=90%
$\Gamma_7$ invisible	< 1.0 × 10 <sup>-4</sup>	CL=90%
<b>Charged modes</b>		
$\Gamma_8$ charged modes	(27.89 ± 0.29) %	S=1.2
$\Gamma_9$ $\pi^+ \pi^- \pi^0$	(22.92 ± 0.28) %	S=1.2
$\Gamma_{10}$ $\pi^+ \pi^- \gamma$	( 4.22 ± 0.08 ) %	S=1.1
$\Gamma_{11}$ $e^+ e^- \gamma$	( 6.9 ± 0.4 ) × 10 <sup>-3</sup>	S=1.3
$\Gamma_{12}$ $\mu^+ \mu^- \gamma$	( 3.1 ± 0.4 ) × 10 <sup>-4</sup>	
$\Gamma_{13}$ $e^+ e^-$	< 7 × 10 <sup>-7</sup>	CL=90%
$\Gamma_{14}$ $\mu^+ \mu^-$	( 5.8 ± 0.8 ) × 10 <sup>-6</sup>	
$\Gamma_{15}$ $2e^+ 2e^-$	( 2.40 ± 0.22 ) × 10 <sup>-5</sup>	
$\Gamma_{16}$ $\pi^+ \pi^- e^+ e^- (\gamma)$	( 2.68 ± 0.11 ) × 10 <sup>-4</sup>	
$\Gamma_{17}$ $e^+ e^- \mu^+ \mu^-$	< 1.6 × 10 <sup>-4</sup>	CL=90%
$\Gamma_{18}$ $2\mu^+ 2\mu^-$	< 3.6 × 10 <sup>-4</sup>	CL=90%
$\Gamma_{19}$ $\mu^+ \mu^- \pi^+ \pi^-$	< 3.6 × 10 <sup>-4</sup>	CL=90%
$\Gamma_{20}$ $\pi^+ e^- \bar{\nu}_e + c.c.$	< 1.7 × 10 <sup>-4</sup>	CL=90%
$\Gamma_{21}$ $\pi^+ \pi^- 2\gamma$	< 2.1 × 10 <sup>-3</sup>	
$\Gamma_{22}$ $\pi^0 \pi^- \pi^0 \gamma$	< 5 × 10 <sup>-4</sup>	CL=90%
$\Gamma_{23}$ $\pi^0 \mu^+ \mu^- \gamma$	< 3 × 10 <sup>-6</sup>	CL=90%

### Charge conjugation (C), Parity (P), Charge conjugation × Parity (CP), or Lepton Family number (LF) violating modes

$\Gamma_{24}$ $\pi^0 \gamma$	C	[a] < 9 × 10 <sup>-5</sup>	CL=90%
$\Gamma_{25}$ $\pi^+ \pi^-$	P, CP	< 1.3 × 10 <sup>-5</sup>	CL=90%
$\Gamma_{26}$ $2\pi^0$	P, CP	< 3.5 × 10 <sup>-4</sup>	CL=90%
$\Gamma_{27}$ $2\pi^0 \gamma$	C	< 5 × 10 <sup>-4</sup>	CL=90%
$\Gamma_{28}$ $3\pi^0 \gamma$	C	< 6 × 10 <sup>-5</sup>	CL=90%
$\Gamma_{29}$ $3\gamma$	C	< 1.6 × 10 <sup>-5</sup>	CL=90%
$\Gamma_{30}$ $4\pi^0$	P, CP	< 6.9 × 10 <sup>-7</sup>	CL=90%
$\Gamma_{31}$ $\pi^0 e^+ e^-$	C	[b] < 8 × 10 <sup>-6</sup>	CL=90%
$\Gamma_{32}$ $\pi^0 \mu^+ \mu^-$	C	[b] < 5 × 10 <sup>-6</sup>	CL=90%
$\Gamma_{33}$ $\mu^+ e^- + \mu^- e^+$	LF	< 6 × 10 <sup>-6</sup>	CL=90%

[a] Forbidden by angular momentum conservation.

[b] C parity forbids this to occur as a single-photon process.

### CONSTRAINED FIT INFORMATION

An overall fit to 2 decay rate and 19 branching ratios uses 50 measurements and one constraint to determine 9 parameters. The overall fit has a  $\chi^2 = 43.8$  for 42 degrees of freedom.

The following *off-diagonal* array elements are the correlation coefficients  $\langle \delta x_i \delta x_j \rangle / (\delta x_i \delta x_j)$ , in percent, from the fit to the branching fractions,  $x_i \equiv \Gamma_i / \Gamma_{\text{total}}$ . The fit constrains the  $x_i$  whose labels appear in this array to sum to one.

$x_3$	24								
$x_4$	4	1							
$x_9$	-73	-80	-4						
$x_{10}$	-56	-60	-3	61					
$x_{11}$	-5	-5	0	-6	-4				
$x_{12}$	-1	0	0	-1	0	0			
$x_{16}$	0	0	0	0	0	0	0		
$\Gamma$	-14	-3	-32	11	8	1	0	0	
	$x_2$	$x_3$	$x_4$	$x_9$	$x_{10}$	$x_{11}$	$x_{12}$	$x_{16}$	

Mode	Rate (keV)	Scale factor
$\Gamma_2$ $2\gamma$	0.515 ± 0.018	
$\Gamma_3$ $3\pi^0$	0.427 ± 0.015	
$\Gamma_4$ $\pi^0 2\gamma$	(3.34 ± 0.28) × 10 <sup>-4</sup>	
$\Gamma_9$ $\pi^+ \pi^- \pi^0$	0.299 ± 0.011	
$\Gamma_{10}$ $\pi^+ \pi^- \gamma$	0.0551 ± 0.0022	
$\Gamma_{11}$ $e^+ e^- \gamma$	0.0090 ± 0.0006	1.2

See key on page 999

## Meson Particle Listings

 $\eta$ 

$\Gamma_{12}$	$\mu^+ \mu^- \gamma$	(4.1 ± 0.5) × 10 <sup>-4</sup>
$\Gamma_{16}$	$\pi^+ \pi^- e^+ e^- (\gamma)$	(3.50 ± 0.19) × 10 <sup>-4</sup>

 $\eta$  DECAY RATES $\Gamma(2\gamma)$  $\Gamma_2$ 

See the table immediately above giving the fitted decay rates. Following the advice of NEFKENS 02, we have removed the Primakoff-effect measurement from the average. See also the "Note on the Decay Width  $\Gamma(\eta \rightarrow \gamma\gamma)$ ," in our 1994 edition, Phys. Rev. D50, 1 August 1994, Part I, p. 1451, for a discussion of the various measurements.

VALUE (keV)	EVTS	DOCUMENT ID	TECN	COMMENT
<b>0.515 ± 0.018 OUR FIT</b>				
<b>0.516 ± 0.018 OUR AVERAGE</b>				
0.520 ± 0.020 ± 0.013		BABUSCI	13A	KLOE $e^+ e^- \rightarrow e^+ e^- \eta$
0.51 ± 0.12 ± 0.05	36	BARU	90	MD1 $e^+ e^- \rightarrow e^+ e^- \eta$
0.490 ± 0.010 ± 0.048	2287	ROE	90	ASP $e^+ e^- \rightarrow e^+ e^- \eta$
0.514 ± 0.017 ± 0.035	1295	WILLIAMS	88	CBAL $e^+ e^- \rightarrow e^+ e^- \eta$
0.53 ± 0.04 ± 0.04		BARTEL	85E	JADE $e^+ e^- \rightarrow e^+ e^- \eta$
• • • We do not use the following data for averages, fits, limits, etc. • • •				
0.476 ± 0.062		<sup>1</sup> RODRIGUES	08	CNTR Reanalysis
0.64 ± 0.14 ± 0.13		AIHARA	86	TPC $e^+ e^- \rightarrow e^+ e^- \eta$
0.56 ± 0.16	56	WEINSTEIN	83	CBAL $e^+ e^- \rightarrow e^+ e^- \eta$
0.324 ± 0.046		BROWMAN	74B	CNTR Primakoff effect
1.00 ± 0.22		<sup>2</sup> BEMPORAD	67	CNTR Primakoff effect

<sup>1</sup>RODRIGUES 08 uses a more sophisticated calculation for the inelastic background due to incoherent photoproduction to reanalyze the  $\eta$  photoproduction data on Be and Cu at 9 GeV from BROWMAN 74B. This brings the value of  $\Gamma(\eta \rightarrow 2\gamma)$  in line with direct measurements of the width. The error here is only statistical.

<sup>2</sup>BEMPORAD 67 gives  $\Gamma(2\gamma) = 1.21 \pm 0.26$  keV assuming  $\Gamma(2\gamma)/\Gamma(\text{total}) = 0.314$ . Bemporad private communication gives  $\Gamma(2\gamma)^2/\Gamma(\text{total}) = 0.380 \pm 0.083$ . We evaluate this using  $\Gamma(2\gamma)/\Gamma(\text{total}) = 0.38 \pm 0.01$ . Not included in average because the uncertainty resulting from the separation of the coulomb and nuclear amplitudes has apparently been underestimated.

 $\Gamma(\pi^0 2\gamma)$  $\Gamma_4$ 

VALUE (eV)	EVTS	DOCUMENT ID	TECN	COMMENT
<b>0.334 ± 0.028 OUR FIT</b>				
<b>0.33 ± 0.03</b>	1200	NEFKENS	14	CRYB $\gamma p \rightarrow \eta p$

 $\eta$  BRANCHING RATIOS

## Neutral modes

 $\Gamma(\text{neutral modes})/\Gamma_{\text{total}}$  $\Gamma_1/\Gamma = (\Gamma_2 + \Gamma_3 + \Gamma_4)/\Gamma$ 

VALUE	EVTS	DOCUMENT ID	TECN	COMMENT
<b>0.7212 ± 0.0034 OUR FIT</b>				Error includes scale factor of 1.2.
<b>0.705 ± 0.008</b>	16k	BASILE	71D	CNTR MM spectrometer
• • • We do not use the following data for averages, fits, limits, etc. • • •				
0.79 ± 0.08		BUNIATOV	67	OSPK

 $\Gamma(2\gamma)/\Gamma_{\text{total}}$  $\Gamma_2/\Gamma$ 

VALUE (units 10 <sup>-2</sup> )	EVTS	DOCUMENT ID	TECN	COMMENT
<b>39.41 ± 0.20 OUR FIT</b>				Error includes scale factor of 1.1.
<b>39.49 ± 0.17 ± 0.30</b>	65k	ABEGG	96	SPEC $pd \rightarrow {}^3\text{He} \eta$
• • • We do not use the following data for averages, fits, limits, etc. • • •				
38.45 ± 0.40 ± 0.36	14k	<sup>1</sup> LOPEZ	07	CLEO $\psi(2S) \rightarrow J/\psi \eta$

<sup>1</sup>Not independent of other results listed for LOPEZ 07. Assuming decays of  $\eta \rightarrow \gamma\gamma$ ,  $3\pi^0$ ,  $\pi^+ \pi^- \pi^0$ ,  $\pi^+ \pi^- \gamma$ , and  $e^+ e^- \gamma$  account for all  $\eta$  decays within a contribution of 0.3% to the systematic error.

 $\Gamma(2\gamma)/\Gamma(\text{neutral modes})$  $\Gamma_2/\Gamma_1 = \Gamma_2/(\Gamma_2 + \Gamma_3 + \Gamma_4)$ 

VALUE	EVTS	DOCUMENT ID	TECN	COMMENT
<b>0.5465 ± 0.0019 OUR FIT</b>				
<b>0.548 ± 0.023 OUR AVERAGE</b>				Error includes scale factor of 1.5.
0.535 ± 0.018		BUTTRAM	70	OSPK
0.59 ± 0.033		BUNIATOV	67	OSPK
• • • We do not use the following data for averages, fits, limits, etc. • • •				
0.52 ± 0.09	88	ABROSIMOV	80	HLBC
0.60 ± 0.14	113	KENDALL	74	OSPK
0.57 ± 0.09		STRUGALSKI	71	HLBC
0.579 ± 0.052		FELDMAN	67	OSPK
0.416 ± 0.044		DIGUGNO	66	CNTR Error doubled
0.44 ± 0.07		GRUNHAUS	66	OSPK
0.39 ± 0.06		<sup>1</sup> JONES	66	CNTR

<sup>1</sup>This result from combining cross sections from two different experiments.

 $\Gamma(3\pi^0)/\Gamma_{\text{total}}$  $\Gamma_3/\Gamma$ 

VALUE (units 10 <sup>-2</sup> )	EVTS	DOCUMENT ID	TECN	COMMENT
<b>32.68 ± 0.23 OUR FIT</b>				Error includes scale factor of 1.1.
• • • We do not use the following data for averages, fits, limits, etc. • • •				
34.03 ± 0.56 ± 0.49	1821	<sup>1</sup> LOPEZ	07	CLEO $\psi(2S) \rightarrow J/\psi \eta$

<sup>1</sup>Not independent of other results listed for LOPEZ 07. Assuming decays of  $\eta \rightarrow \gamma\gamma$ ,  $3\pi^0$ ,  $\pi^+ \pi^- \pi^0$ ,  $\pi^+ \pi^- \gamma$ , and  $e^+ e^- \gamma$  account for all  $\eta$  decays within a contribution of 0.3% to the systematic error.

 $\Gamma(3\pi^0)/\Gamma(\text{neutral modes})$  $\Gamma_3/\Gamma_1 = \Gamma_3/(\Gamma_2 + \Gamma_3 + \Gamma_4)$ 

VALUE	EVTS	DOCUMENT ID	TECN	COMMENT
<b>0.4531 ± 0.0019 OUR FIT</b>				
<b>0.439 ± 0.024</b>				
• • • We do not use the following data for averages, fits, limits, etc. • • •				
0.44 ± 0.08	75	ABROSIMOV	80	HLBC
0.32 ± 0.09		STRUGALSKI	71	HLBC
0.41 ± 0.033		BUNIATOV	67	OSPK Not indep. of $\Gamma(2\gamma)/\Gamma(\text{neutral modes})$
0.177 ± 0.035		FELDMAN	67	OSPK
0.209 ± 0.054		DIGUGNO	66	CNTR Error doubled
0.29 ± 0.10		GRUNHAUS	66	OSPK

 $\Gamma(3\pi^0)/\Gamma(2\gamma)$  $\Gamma_3/\Gamma_2$ 

VALUE	EVTS	DOCUMENT ID	TECN	COMMENT
<b>0.829 ± 0.006 OUR FIT</b>				
<b>0.829 ± 0.007 OUR AVERAGE</b>				
0.884 ± 0.022 ± 0.019	1821	LOPEZ	07	CLEO $\psi(2S) \rightarrow J/\psi \eta$
0.817 ± 0.012 ± 0.032	17.4k	<sup>1</sup> AKHMETSHIN	05	CMD2 $e^+ e^- \rightarrow \phi \rightarrow \eta\gamma$
0.826 ± 0.024		ACHASOV	00D	SND $e^+ e^- \rightarrow \phi \rightarrow \eta\gamma$
0.832 ± 0.005 ± 0.012		KRUSCHE	95D	SPEC $\gamma p \rightarrow \eta p$ , threshold
0.841 ± 0.034		AMSLER	93	CBAR $\bar{p} p \rightarrow \pi^+ \pi^- \eta$ at rest
0.822 ± 0.009		ALDE	84	GAM2
• • • We do not use the following data for averages, fits, limits, etc. • • •				
0.796 ± 0.016 ± 0.016		ACHASOV	00	SND See ACHASOV 00D
0.91 ± 0.14		COX	70B	HBC
0.75 ± 0.09		DEVONS	70	OSPK
0.88 ± 0.16		BALTAY	67D	DBC
1.1 ± 0.2		CENCE	67	OSPK
1.25 ± 0.39		BACCI	63	CNTR Inverse BR reported

<sup>1</sup>Uses result from AKHMETSHIN 01b.

 $\Gamma(\pi^0 2\gamma)/\Gamma_{\text{total}}$  $\Gamma_4/\Gamma$ 

Early results are summarized in the review by LANDSBERG 85.

VALUE (units 10 <sup>-4</sup> )	CL%	EVTS	DOCUMENT ID	TECN	COMMENT
<b>2.56 ± 0.22 OUR FIT</b>					
<b>2.21 ± 0.24 ± 0.47</b>	≈ 500	<sup>1</sup> PRAKHOV	08	CRYB $\pi^- p \rightarrow \eta n$ ≈ threshold	
• • • We do not use the following data for averages, fits, limits, etc. • • •					
3.5 ± 0.7 ± 0.6	1.6k	<sup>2,3</sup> PRAKHOV	05	CRYB See PRAKHOV 08	
<8.4	90	7	ACHASOV	01D	SND $e^+ e^- \rightarrow \phi \rightarrow \eta\gamma$
<30	90	0	DAVYDOV	81	GAM2 $\pi^- p \rightarrow \eta n$

<sup>1</sup>PRAKHOV 08 is a reanalysis of the data of PRAKHOV 05, using for the first time the invariant-mass spectrum of the two photons.

<sup>2</sup>Normalized using  $\Gamma(\eta \rightarrow 2\gamma)/\Gamma = 0.3943 \pm 0.0026$ .

<sup>3</sup>This measurement and the independent analysis of the same data by KNECHT 04 both imply a lower value of  $\Gamma(\pi^0 2\gamma)$  than the one obtained by ALDE 84 from  $\Gamma(\pi^0 2\gamma)/\Gamma(2\gamma)$ .

 $\Gamma(\pi^0 2\gamma)/\Gamma(2\gamma)$  $\Gamma_4/\Gamma_2$ 

VALUE (units 10 <sup>-3</sup> )	EVTS	DOCUMENT ID	TECN	CHG	COMMENT
<b>0.65 ± 0.06 OUR FIT</b>					
<b>1.8 ± 0.4</b>					
• • • We do not use the following data for averages, fits, limits, etc. • • •					
2.5 ± 0.6	70	BINON	82	GAM2	See ALDE 84

 $\Gamma(\pi^0 2\gamma)/\Gamma(3\pi^0)$  $\Gamma_4/\Gamma_3$ 

VALUE (units 10 <sup>-4</sup> )	EVTS	DOCUMENT ID	TECN	COMMENT
<b>7.8 ± 0.7 OUR FIT</b>				
• • • We do not use the following data for averages, fits, limits, etc. • • •				
8.3 ± 2.8 ± 1.4		<sup>1</sup> KNECHT	04	CRYB $\pi^- p \rightarrow \eta n$

<sup>1</sup>Independent analysis of same data as PRAKHOV 05.

 $\Gamma(2\pi^0 2\gamma)/\Gamma_{\text{total}}$  $\Gamma_5/\Gamma$ 

VALUE	CL%	DOCUMENT ID	TECN	COMMENT
<b>&lt;1.2 × 10<sup>-3</sup></b>	90	<sup>1</sup> NEFKENS	05A	CRYB $p(720 \text{ MeV}/c) \pi^- \rightarrow n\eta$
• • • We do not use the following data for averages, fits, limits, etc. • • •				
<4.0 × 10 <sup>-3</sup>	90	BLIK	07	GAM4 $\pi^- p \rightarrow \eta n$

<sup>1</sup>Measurement is done in limited  $\gamma\gamma$  energy range.

 $\Gamma(4\gamma)/\Gamma_{\text{total}}$  $\Gamma_6/\Gamma$ 

VALUE	CL%	DOCUMENT ID	TECN	COMMENT
<b>&lt;2.8 × 10<sup>-4</sup></b>	90	BLIK	07	GAM4 $\pi^- p \rightarrow \eta n$

 $\Gamma(\text{invisible})/\Gamma(2\gamma)$  $\Gamma_7/\Gamma_2$ 

VALUE	CL%	DOCUMENT ID	TECN	COMMENT
<b>&lt;2.6 × 10<sup>-4</sup></b>	90	<sup>1</sup> ABLIKIM	13	BES3 $J/\psi \rightarrow \phi \eta$
• • • We do not use the following data for averages, fits, limits, etc. • • •				
<1.65 × 10 <sup>-3</sup>	90	<sup>2</sup> ABLIKIM	06Q	BES2 $J/\psi \rightarrow \phi \eta$

<sup>1</sup>Based on 225M  $J/\psi$  decays.

<sup>2</sup>Based on 58M  $J/\psi$  decays.

## Meson Particle Listings

 $\eta$ 

## Charged modes

$\Gamma(\pi^+\pi^-\pi^0)/\Gamma_{\text{total}}$	$\Gamma_9/\Gamma$
<b>22.92±0.28 OUR FIT</b>	
Error includes scale factor of 1.2.	

• • • We do not use the following data for averages, fits, limits, etc. • • •

22.60±0.35±0.29 3915 <sup>1</sup> LOPEZ 07 CLEO  $\psi(2S) \rightarrow J/\psi\eta$

<sup>1</sup> Not independent of other results listed for LOPEZ 07. Assuming decays of  $\eta \rightarrow \gamma\gamma$ ,  $3\pi^0$ ,  $\pi^+\pi^-\pi^0$ ,  $\pi^+\pi^-\gamma$ , and  $e^+e^-\gamma$  account for all  $\eta$  decays within a contribution of 0.3% to the systematic error.

$\Gamma(\text{neutral modes})/\Gamma(\pi^+\pi^-\pi^0)$	$\Gamma_1/\Gamma_9 = (\Gamma_2+\Gamma_3+\Gamma_4)/\Gamma_9$
<b>3.15±0.05 OUR FIT</b>	
Error includes scale factor of 1.2.	

• • • We do not use the following data for averages, fits, limits, etc. • • •

2.54±1.89 74 KENDALL 74 OSPK

3.4 ±1.1 29 AGUILAR... 72B HBC

2.83±0.80 70 <sup>1</sup> BLOODWORTH... 72B HBC

3.6 ±0.6 244 FLATTE 67B HBC

2.89±0.56 ALFF... 66 HBC

3.6 ±0.8 50 KRAEMER 64 DBC

3.8 ±1.1 PAULI 64 DBC

<sup>1</sup> Error increased from published value 0.5 by Bloodworth (private communication).

$\Gamma(2\gamma)/\Gamma(\pi^+\pi^-\pi^0)$	$\Gamma_2/\Gamma_9$
<b>1.720±0.028 OUR FIT</b>	
Error includes scale factor of 1.2.	

• • • We do not use the following data for averages, fits, limits, etc. • • •

1.70 ±0.04 OUR AVERAGE

1.704±0.032±0.026 3915 <sup>1</sup> LOPEZ 07 CLEO  $\psi(2S) \rightarrow J/\psi\eta$

1.61 ±0.14 ABLIKIM 06E BES2  $e^+e^- \rightarrow J/\psi \rightarrow \eta\gamma$

1.78 ±0.10 ±0.13 1077 AMSLER 95 CBAR  $\bar{p}p \rightarrow \pi^+\pi^-\eta$  at rest

1.72 ±0.25 401 BAGLIN 69 HLBC

1.61 ±0.39 FOSTER 65 HBC

<sup>1</sup> LOPEZ 07 reports  $\Gamma(\eta \rightarrow \pi^+\pi^-\pi^0) / \Gamma(\eta \rightarrow 2\gamma) = \Gamma_9/\Gamma_2 = 0.587 \pm 0.011 \pm 0.009$ .

$\Gamma(3\pi^0)/\Gamma(\pi^+\pi^-\pi^0)$	$\Gamma_3/\Gamma_9$
<b>1.426±0.026 OUR FIT</b>	
Error includes scale factor of 1.2.	

• • • We do not use the following data for averages, fits, limits, etc. • • •

1.48 ±0.05 OUR AVERAGE

1.46 ±0.03 ±0.09 ACHASOV 06A SND  $e^+e^- \rightarrow \eta\gamma$

1.52 ±0.04 ±0.08 23k <sup>1</sup> AKHMETSHIN 01B CMD2  $e^+e^- \rightarrow \phi \rightarrow \eta\gamma$

1.44 ±0.09 ±0.10 1627 AMSLER 95 CBAR  $\bar{p}p \rightarrow \pi^+\pi^-\eta$  at rest

1.50  $\begin{smallmatrix} +0.15 \\ -0.29 \end{smallmatrix}$  199 BAGLIN 69 HLBC

1.47  $\begin{smallmatrix} +0.20 \\ -0.17 \end{smallmatrix}$  BULLOCK 68 HLBC

• • • We do not use the following data for averages, fits, limits, etc. • • •

1.3 ±0.4 BAGLIN 67B HLBC

0.90 ±0.24 FOSTER 65 HBC

2.0 ±1.0 FOELSCH 64 HBC

0.83 ±0.32 CRAWFORD 63 HBC

<sup>1</sup> AKHMETSHIN 01B uses results from AKHMETSHIN 99F.

$\Gamma(\pi^+\pi^-\pi^0)/[\Gamma(2\gamma) + \Gamma(3\pi^0)]$	$\Gamma_9/(\Gamma_2+\Gamma_3)$
<b>0.318 ±0.005 OUR FIT</b>	
Error includes scale factor of 1.2.	

• • • We do not use the following data for averages, fits, limits, etc. • • •

0.304 ±0.012 ACHASOV 00D SND  $e^+e^- \rightarrow \phi \rightarrow \eta\gamma$

• • • We do not use the following data for averages, fits, limits, etc. • • •

0.3141±0.0081±0.0058 ACHASOV 00B SND See ACHASOV 00D

$\Gamma(\pi^+\pi^-\gamma)/\Gamma_{\text{total}}$	$\Gamma_{10}/\Gamma$
<b>4.22±0.08 OUR FIT</b>	
Error includes scale factor of 1.1.	

• • • We do not use the following data for averages, fits, limits, etc. • • •

3.96±0.14±0.14 859 <sup>1</sup> LOPEZ 07 CLEO  $\psi(2S) \rightarrow J/\psi\eta$

<sup>1</sup> Not independent of other results listed for LOPEZ 07. Assuming decays of  $\eta \rightarrow \gamma\gamma$ ,  $3\pi^0$ ,  $\pi^+\pi^-\pi^0$ ,  $\pi^+\pi^-\gamma$ , and  $e^+e^-\gamma$  account for all  $\eta$  decays within a contribution of 0.3% to the systematic error.

$\Gamma(\pi^+\pi^-\gamma)/\Gamma(\pi^+\pi^-\pi^0)$	$\Gamma_{10}/\Gamma_9$
<b>0.1842±0.0027 OUR FIT</b>	
Error includes scale factor of 1.1.	

• • • We do not use the following data for averages, fits, limits, etc. • • •

0.1856±0.0005±0.0028 200k BABUSCI 13 KLOE  $e^+e^- \rightarrow \phi \rightarrow \eta\gamma$

0.175 ±0.007 ±0.006 859 LOPEZ 07 CLEO  $\psi(2S) \rightarrow J/\psi\eta$

• • • We do not use the following data for averages, fits, limits, etc. • • •

0.209 ±0.004 18k THALER 73 ASPK

0.201 ±0.006 7250 GORMLEY 70 ASPK

0.28 ±0.04 BALTAY 67B DBC

0.25 ±0.035 LITCHEFIELD 67 DBC

0.30 ±0.06 CRAWFORD 66 HBC

0.196 ±0.041 FOSTER 65c HBC

$\Gamma(e^+e^-\gamma)/\Gamma_{\text{total}}$	$\Gamma_{11}/\Gamma$
<b>6.9 ±0.4 OUR FIT</b>	
Error includes scale factor of 1.3.	

• • • We do not use the following data for averages, fits, limits, etc. • • •

6.7 ±0.5 OUR AVERAGE Error includes scale factor of 1.2.

6.6 ±0.4 ±0.4 1345 BERGHAUSER 11 SPEC  $\gamma p \rightarrow p\eta$

7.8 ±0.5 ±0.8 435 ± 31 BERLOWSKI 08 WASA  $pd \rightarrow {}^3\text{He}\eta$

5.15±0.62±0.74 283 ACHASOV 01B SND  $e^+e^- \rightarrow \phi \rightarrow \eta\gamma$

7.10±0.64±0.46 323 AKHMETSHIN 01 CMD2  $e^+e^- \rightarrow \phi \rightarrow \eta\gamma$

• • • We do not use the following data for averages, fits, limits, etc. • • •

9.4 ±0.7 ±0.5 172 <sup>1</sup> LOPEZ 07 CLEO  $\psi(2S) \rightarrow J/\psi\eta$

<sup>1</sup> Not independent of other results listed for LOPEZ 07. Assuming decays of  $\eta \rightarrow \gamma\gamma$ ,  $3\pi^0$ ,  $\pi^+\pi^-\pi^0$ ,  $\pi^+\pi^-\gamma$ , and  $e^+e^-\gamma$  account for all  $\eta$  decays within a contribution of 0.3% to the systematic error.

$\Gamma(e^+e^-\gamma)/\Gamma(\pi^+\pi^-\gamma)$	$\Gamma_{11}/\Gamma_{10}$
<b>0.163±0.011 OUR FIT</b>	
Error includes scale factor of 1.2.	

• • • We do not use the following data for averages, fits, limits, etc. • • •

0.237±0.021±0.015 172 LOPEZ 07 CLEO  $\psi(2S) \rightarrow J/\psi\eta$

$\Gamma(e^+e^-\gamma)/\Gamma(\pi^+\pi^-\pi^0)$	$\Gamma_{11}/\Gamma_9$
<b>3.00±0.19 OUR FIT</b>	
Error includes scale factor of 1.3.	

• • • We do not use the following data for averages, fits, limits, etc. • • •

2.1 ±0.5 80 JANE 75B OSPK See the erratum

$\Gamma(\text{neutral modes})/[\Gamma(\pi^+\pi^-\pi^0) + \Gamma(\pi^+\pi^-\gamma) + \Gamma(e^+e^-\gamma)]$	$\Gamma_1/(\Gamma_9+\Gamma_{10}+\Gamma_{11}) = (\Gamma_2+\Gamma_3+\Gamma_4)/(\Gamma_9+\Gamma_{10}+\Gamma_{11})$
<b>2.59±0.04 OUR FIT</b>	
Error includes scale factor of 1.2.	

• • • We do not use the following data for averages, fits, limits, etc. • • •

2.64±0.23 BALTAY 67B DBC

4.5 ±1.0 280 <sup>1</sup> JAMES 66 HBC

3.20±1.26 53 <sup>1</sup> BASTIEN 62 HBC

2.5 ±1.0 10 <sup>1</sup> PICKUP 62 HBC

<sup>1</sup> These experiments are not used in the averages as they do not separate clearly  $\eta \rightarrow \pi^+\pi^-\pi^0$  and  $\eta \rightarrow \pi^+\pi^-\gamma$  from each other. The reported values thus probably contain some unknown fraction of  $\eta \rightarrow \pi^+\pi^-\gamma$ .

$\Gamma(2\gamma)/[\Gamma(\pi^+\pi^-\pi^0) + \Gamma(\pi^+\pi^-\gamma) + \Gamma(e^+e^-\gamma)]$	$\Gamma_2/(\Gamma_9+\Gamma_{10}+\Gamma_{11})$
<b>1.417±0.023 OUR FIT</b>	
Error includes scale factor of 1.2.	

• • • We do not use the following data for averages, fits, limits, etc. • • •

1.1 ±0.4 OUR AVERAGE

1.51 ±0.93 75 KENDALL 74 OSPK

0.99 ±0.48 CRAWFORD 63 HBC

$\Gamma(\mu^+\mu^-\gamma)/\Gamma_{\text{total}}$	$\Gamma_{12}/\Gamma$
<b>3.1±0.4 OUR FIT</b>	
Error includes scale factor of 1.2.	

• • • We do not use the following data for averages, fits, limits, etc. • • •

3.1±0.4 600 DZHELADIN 80 SPEC  $\pi^-p \rightarrow \eta n$

• • • We do not use the following data for averages, fits, limits, etc. • • •

1.5±0.75 100 BUSHNIN 78 SPEC See DZHELADIN 80

$\Gamma(e^+e^-)/\Gamma_{\text{total}}$	$\Gamma_{13}/\Gamma$
<b>&lt;7 × 10<sup>-7</sup></b>	
Error includes scale factor of 1.2.	

• • • We do not use the following data for averages, fits, limits, etc. • • •

<2.3 × 10<sup>-6</sup> 90 AGAKISHIEV 14  $pp \rightarrow \eta + X$

<5.6 × 10<sup>-6</sup> 90 <sup>1</sup> AGAKISHIEV 12A SPEC  $pp \rightarrow \eta + X$

<2.7 × 10<sup>-5</sup> 90 BERLOWSKI 08 WASA  $pd \rightarrow {}^3\text{He}\eta$

<0.77 × 10<sup>-4</sup> 90 BROWDER 97B CLE2  $e^+e^- \simeq 10.5$  GeV

<2 × 10<sup>-4</sup> 90 WHITE 96 SPEC  $pd \rightarrow \eta^3\text{He}$

<3 × 10<sup>-4</sup> 90 DAVIES 74 RVUE Uses ESTEN 67

<sup>1</sup> AGAKISHIEV 12A uses a data sample of 3.5 GeV proton beam collisions on liquid hydrogen target collected by the HADES detector.

$\Gamma(\mu^+\mu^-)/\Gamma_{\text{total}}$	$\Gamma_{14}/\Gamma$
<b>5.8±0.8 OUR AVERAGE</b>	
Error includes scale factor of 1.2.	

• • • We do not use the following data for averages, fits, limits, etc. • • •

5.7±0.7±0.5 114 ABEGG 94 SPEC  $pd \rightarrow \eta^3\text{He}$

6.5±2.1 27 DZHELADIN 80B SPEC  $\pi^-p \rightarrow \eta n$

• • • We do not use the following data for averages, fits, limits, etc. • • •

5.6 $\begin{smallmatrix} +0.6 \\ -0.7 \end{smallmatrix}$ ±0.5 100 KESSLER 93 SPEC See ABEGG 94

< 20 95 0 WEHMANN 68 OSPK

$\Gamma(\mu^+\mu^-)/\Gamma(2\gamma)$	$\Gamma_{14}/\Gamma_2$
<b>5.9±2.2</b>	
Error includes scale factor of 1.2.	

• • • We do not use the following data for averages, fits, limits, etc. • • •

5.9±2.2 69 HYAMS 69 OSPK

$\Gamma(2e^+2e^-)/\Gamma_{\text{total}}$   $\Gamma_{15}/\Gamma$ 

VALUE (units $10^{-5}$ )	CL%	EVTS	DOCUMENT ID	TECN	COMMENT
$2.4 \pm 0.2 \pm 0.1$		362	<sup>1</sup> AMBROSINO 11B	KLOE	$e^+e^- \rightarrow \phi \rightarrow \eta\gamma$
••• We do not use the following data for averages, fits, limits, etc. •••					
<9.7		90	BERLOWSKI 08	WASA	$pd \rightarrow {}^3\text{He} \eta$
<6.9		90	AKHMETSHIN 01	CMD2	$e^+e^- \rightarrow \phi \rightarrow \eta\gamma$

<sup>1</sup>This measurement is fully inclusive (includes " $2e^+2e^-\gamma$ " channel).

 $\Gamma(\pi^+\pi^-e^+e^-)/\Gamma_{\text{total}}$   $\Gamma_{16}/\Gamma$ 

VALUE (units $10^{-4}$ )	CL%	EVTS	DOCUMENT ID	TECN	COMMENT
$2.68 \pm 0.11$ OUR FIT					
$2.68 \pm 0.09 \pm 0.07$		1555 $\pm$ 52	<sup>1</sup> AMBROSINO 09B	KLOE	$e^+e^- \rightarrow \phi \rightarrow \eta\gamma$
••• We do not use the following data for averages, fits, limits, etc. •••					
$4.3 \pm 2.0 \pm 0.4$		16	BERLOWSKI 08	WASA	$pd \rightarrow {}^3\text{He} \eta$
$4.3 \pm 1.3 \pm 0.4$		16	BARGHOLTZ 07	CNTR	See BERLOWSKI 08
$3.7 \pm 2.5 \pm 0.3$		4	AKHMETSHIN 01	CMD2	$e^+e^- \rightarrow \phi \rightarrow \eta\gamma$

<sup>1</sup>This AMBROSINO 09B value includes radiative events.

 $\Gamma(e^+e^-\mu^+\mu^-)/\Gamma_{\text{total}}$   $\Gamma_{17}/\Gamma$ 

VALUE	CL%	DOCUMENT ID	TECN	COMMENT
$<1.6 \times 10^{-4}$		90	BERLOWSKI 08	WASA $pd \rightarrow {}^3\text{He} \eta$

 $\Gamma(2\mu^+2\mu^-)/\Gamma_{\text{total}}$   $\Gamma_{18}/\Gamma$ 

VALUE	CL%	DOCUMENT ID	TECN	COMMENT
$<3.6 \times 10^{-4}$		90	BERLOWSKI 08	WASA $pd \rightarrow {}^3\text{He} \eta$

 $\Gamma(\mu^+\mu^-\pi^+\pi^-)/\Gamma_{\text{total}}$   $\Gamma_{19}/\Gamma$ 

VALUE	CL%	DOCUMENT ID	TECN	COMMENT
$<3.6 \times 10^{-4}$		90	BERLOWSKI 08	WASA $pd \rightarrow {}^3\text{He} \eta$

 $\Gamma(\pi^+e^-\nu_e + \text{c.c.})/\Gamma(\pi^+\pi^-\pi^0)$   $\Gamma_{20}/\Gamma_9$ 

VALUE	CL%	DOCUMENT ID	TECN	COMMENT
$<7.3 \times 10^{-4}$		90	ABLIKIM 13G	BES3 $J/\psi \rightarrow \phi\eta$

 $\Gamma(\pi^+\pi^-2\gamma)/\Gamma(\pi^+\pi^-\pi^0)$   $\Gamma_{21}/\Gamma_9$ 

VALUE	CL%	DOCUMENT ID	TECN	COMMENT
$<9 \times 10^{-3}$			PRICE 67	HBC
••• We do not use the following data for averages, fits, limits, etc. •••				
$<16 \times 10^{-3}$		95	BALTAY 67B	DBC

 $\Gamma(\pi^+\pi^-\pi^0\gamma)/\Gamma(\pi^+\pi^-\pi^0)$   $\Gamma_{22}/\Gamma_9$ 

VALUE	CL%	EVTS	DOCUMENT ID	TECN	COMMENT
$<0.24 \times 10^{-2}$		90	0	THALER 73	ASPK
••• We do not use the following data for averages, fits, limits, etc. •••					
$<1.7 \times 10^{-2}$		90	ARNOLD 68	HLBC	
$<1.6 \times 10^{-2}$		95	BALTAY 67B	DBC	
$<7.0 \times 10^{-2}$			FLATTE 67	HBC	
$<0.9 \times 10^{-2}$			PRICE 67	HBC	

 $\Gamma(\pi^0\mu^+\mu^-)/\Gamma_{\text{total}}$   $\Gamma_{23}/\Gamma$ 

VALUE	CL%	DOCUMENT ID	TECN	COMMENT
$<3 \times 10^{-6}$		90	DZHELADIN 81	SPEC $\pi^-\rho \rightarrow \eta\eta$

## Forbidden modes

 $\Gamma(\pi^0\gamma)/\Gamma_{\text{total}}$   $\Gamma_{24}/\Gamma$ 

Forbidden by angular momentum conservation.

VALUE	CL%	DOCUMENT ID	TECN	COMMENT
$<9 \times 10^{-5}$		90	NEFKENS 05A	CRYB $p(720 \text{ MeV}/c) \pi^- \rightarrow n\eta$

 $\Gamma(\pi^+\pi^-)/\Gamma_{\text{total}}$   $\Gamma_{25}/\Gamma$ 

Forbidden by  $P$  and  $CP$  invariance.

VALUE	CL%	EVTS	DOCUMENT ID	TECN	COMMENT
$<1.3 \times 10^{-5}$		90	16M	AMBROSINO 05A	KLOE $e^+e^- \rightarrow \phi \rightarrow \eta\gamma$
••• We do not use the following data for averages, fits, limits, etc. •••					
$<5.3 \times 10^{-17}$				<sup>1</sup> ZHEVLAKOV 19	THEO from nEDM limits
$<1.6 \times 10^{-5}$		90	25M	AAIJ 17D	LHCB in $D \rightarrow \pi\pi\pi$ decays
$<3.9 \times 10^{-4}$		90	225M	ABLIKIM 11G	BES3 $e^+e^- \rightarrow J/\psi \rightarrow \eta\gamma$
$<3.3 \times 10^{-4}$		90		AKHMETSHIN 99B	CMD2 $e^+e^- \rightarrow \phi \rightarrow \eta\gamma$
$<9 \times 10^{-4}$		90		AKHMETSHIN 97C	CMD2 See AKHMETSHIN 99B
$<15 \times 10^{-4}$		0		THALER 73	ASPK

<sup>1</sup>ZHEVLAKOV 19 derives the value from the experimental limits of nEDM by a calculation using an effective Lagrangian.

 $\Gamma(2\pi^0)/\Gamma_{\text{total}}$   $\Gamma_{26}/\Gamma$ 

Forbidden by  $P$  and  $CP$  invariance.

VALUE	CL%	EVTS	DOCUMENT ID	TECN	COMMENT
$<3.5 \times 10^{-4}$		90		BLIK 07	GAM4 $\pi^-\rho \rightarrow \eta\eta$

••• We do not use the following data for averages, fits, limits, etc. •••

$<2.7 \times 10^{-17}$				<sup>1</sup> ZHEVLAKOV 19	THEO from nEDM limits
$<6.9 \times 10^{-4}$		90	225M	ABLIKIM 11G	BES3 $e^+e^- \rightarrow J/\psi \rightarrow \eta\gamma$
$<4.3 \times 10^{-4}$		90		AKHMETSHIN 99C	CMD2 $e^+e^- \rightarrow \phi \rightarrow \eta\gamma$
$<6 \times 10^{-4}$		90		<sup>2</sup> ACHASOV 98	SND $e^+e^- \rightarrow \phi \rightarrow \eta\gamma$

<sup>1</sup>ZHEVLAKOV 19 derives the value from the experimental limits of nEDM by a calculation using an effective Lagrangian.

<sup>2</sup>ACHASOV 98 observes one event in a  $\pm 3\sigma$  region around the  $\eta$  mass, while a Monte Carlo calculation gives  $10 \pm 5$  events. The limit here is the Poisson upper limit for one observed event and no background.

 $\Gamma(2\pi^0\gamma)/\Gamma_{\text{total}}$   $\Gamma_{27}/\Gamma$ 

Forbidden by  $C$  invariance.

VALUE	CL%	DOCUMENT ID	TECN	CHG	COMMENT
$<5 \times 10^{-4}$		90	NEFKENS 05	CRYB 0	$p(720 \text{ MeV}/c) \pi^- \rightarrow n\eta$
••• We do not use the following data for averages, fits, limits, etc. •••					
$<17 \times 10^{-4}$		90	BLIK 07	GAM4	$\pi^-\rho \rightarrow \eta\eta$

 $\Gamma(3\pi^0\gamma)/\Gamma_{\text{total}}$   $\Gamma_{28}/\Gamma$ 

Forbidden by  $C$  invariance.

VALUE	CL%	DOCUMENT ID	TECN	CHG	COMMENT
$<6 \times 10^{-5}$		90	NEFKENS 05	CRYB 0	$p(720 \text{ MeV}/c) \pi^- \rightarrow n\eta$
••• We do not use the following data for averages, fits, limits, etc. •••					
$<24 \times 10^{-5}$		90	BLIK 07	GAM4	$\pi^-\rho \rightarrow \eta\eta$

 $\Gamma(3\gamma)/\Gamma_{\text{total}}$   $\Gamma_{29}/\Gamma$ 

Forbidden by  $C$  invariance.

VALUE	CL%	DOCUMENT ID	TECN	CHG	COMMENT
$<6 \times 10^{-5}$		90	NEFKENS 05	CRYB 0	$p(720 \text{ MeV}/c) \pi^- \rightarrow n\eta$
••• We do not use the following data for averages, fits, limits, etc. •••					
$<24 \times 10^{-5}$		90	BLIK 07	GAM4	$\pi^-\rho \rightarrow \eta\eta$

 $\Gamma(3\gamma)/\Gamma_{\text{total}}$   $\Gamma_{29}/\Gamma$ 

Forbidden by  $C$  invariance.

VALUE	CL%	DOCUMENT ID	TECN	CHG	COMMENT
$<16 \times 10^{-5}$		90	BLIK 07	GAM4	$\pi^-\rho \rightarrow \eta\eta$
$<4 \times 10^{-5}$		90	NEFKENS 05A	CRYB	$p(720 \text{ MeV}/c) \pi^- \rightarrow n\eta$

 $\Gamma(3\gamma)/\Gamma(2\gamma)$   $\Gamma_{29}/\Gamma_2$ 

VALUE	CL%	DOCUMENT ID	TECN	CHG	COMMENT
$<1.2 \times 10^{-3}$		95	ALDE 84	GAM2	0

 $\Gamma(3\gamma)/\Gamma(3\pi^0)$   $\Gamma_{29}/\Gamma_3$ 

VALUE	CL%	DOCUMENT ID	TECN	COMMENT
$<4.9 \times 10^{-5}$		90	ALOISIO 04	KLOE $\phi \rightarrow \eta\gamma$

 $\Gamma(4\pi^0)/\Gamma_{\text{total}}$   $\Gamma_{30}/\Gamma$ 

Forbidden by  $P$  and  $CP$  invariance.

VALUE	CL%	DOCUMENT ID	TECN	COMMENT
$<6.9 \times 10^{-7}$		90	PRAKHOV 00	CRYB $\pi^-\rho \rightarrow n\eta$ , 720 MeV/c
••• We do not use the following data for averages, fits, limits, etc. •••				
$<200 \times 10^{-7}$		90	BLIK 07	GAM4 $\pi^-\rho \rightarrow \eta\eta$

 $\Gamma(\pi^0e^+e^-)/\Gamma_{\text{total}}$   $\Gamma_{31}/\Gamma$ 

$C$  parity forbids this to occur as a single-photon process.

VALUE	CL%	DOCUMENT ID	TECN	COMMENT
••• We do not use the following data for averages, fits, limits, etc. •••				
$<7.5 \times 10^{-6}$		90	ADLARSON 18c	WASA $pd \rightarrow \eta^3\text{He}$
$<1.6 \times 10^{-4}$		90	MARTYNOV 76	HLBC
$<8.4 \times 10^{-4}$		90	BAZIN 68	DBC
$<70 \times 10^{-4}$			RITTENBERG 65	HBC

 $\Gamma(\pi^0e^+e^-)/\Gamma(\pi^+\pi^-\pi^0)$   $\Gamma_{31}/\Gamma_9$ 

$C$  parity forbids this to occur as a single-photon process.

VALUE	CL%	DOCUMENT ID	TECN	COMMENT
$<3.28 \times 10^{-5}$		90	ADLARSON 18c	WASA $pd \rightarrow \eta^3\text{He}$
••• We do not use the following data for averages, fits, limits, etc. •••				
$<1.9 \times 10^{-4}$		90	JANE 75	OSPK
$<42 \times 10^{-4}$		90	BAGLIN 67	HLBC
$<16 \times 10^{-4}$		90	BILLING 67	HLBC
$<77 \times 10^{-4}$			FOSTER 65B	HBC
$<110 \times 10^{-4}$			PRICE 65	HBC

 $\Gamma(\pi^0\mu^+\mu^-)/\Gamma_{\text{total}}$   $\Gamma_{32}/\Gamma$ 

$C$  parity forbids this to occur as a single-photon process.

VALUE	CL%	DOCUMENT ID	TECN	COMMENT	
$<5 \times 10^{-6}$		90		DZHELADIN 81	SPEC $\pi^-\rho \rightarrow \eta\eta$
••• We do not use the following data for averages, fits, limits, etc. •••					
$<500 \times 10^{-6}$				WEHMANN 68	OSPK

 $[\Gamma(\mu^+e^-) + \Gamma(\mu^-e^+)]/\Gamma_{\text{total}}$   $\Gamma_{33}/\Gamma$ 

Forbidden by lepton family number conservation.

VALUE	CL%	DOCUMENT ID	TECN	COMMENT
$<6 \times 10^{-6}$		90	WHITE 96	SPEC $pd \rightarrow \eta^3\text{He}$





See key on page 999

Meson Particle Listings
eta, f0(500)

Table of meson particle listings with columns for name, code, and reference. Includes entries like LOPEZ, MILLER, ABLIKIM, etc.

Continuation of meson particle listings with columns for name, code, and reference. Includes entries like FLATTE, LITCHFIELD, RICE, etc.

f0(500)

also known as sigma; was f0(600)
See the related review(s):
Scalar Mesons below 2 GeV

I(G JPC) = 0+(0++)

f0(500) T-MATRIX POLE sqrt(s)

Note that Gamma approx 2 Im(sqrt(s) pole)

Table with columns: VALUE (MeV), DOCUMENT ID, TECN, COMMENT. Contains data for f0(500) T-matrix poles with values like (512 +/- 15) - i(188 +/- 12).

1 S-matrix pole; 8595 events.
2 Applying the chiral unitary approach at NLO to the K eta data of BATLEY 10 and pi N -> pi N data of HYAMS 73, GRAYER 74, and PROTOPESCU 73.

Downloaded from https://academic.oup.com/ptep/article/2020/8/083C01/5891211 by guest on 12 November 2020

## Meson Particle Listings

 $f_0(500)$ 

- <sup>3</sup> Uses the  $K_{e4}$  data of BATLEY 10c and the  $\pi N \rightarrow \pi\pi N$  data of HYAMS 73, GRAYER 74, and PROTOPOESCU 73.
- <sup>4</sup> Analytic continuation using Roy equations.
- <sup>5</sup> Analytic continuation using GKPY equations.
- <sup>6</sup> Using Roy equations.
- <sup>7</sup> Average of three variants of the analytic K-matrix model. Uses the  $K_{e4}$  data of BATLEY 08a and the  $\pi N \rightarrow \pi\pi N$  data of HYAMS 73 and GRAYER 74.
- <sup>8</sup> Average of the analyses of three data sets in the K-matrix model. Uses the data of BATLEY 08a, HYAMS 73, and GRAYER 74, partially of COHEN 80 or ETKIN 82b.
- <sup>9</sup> From the  $K_{e4}$  data of BATLEY 08a and  $\pi N \rightarrow \pi\pi N$  data of HYAMS 73.
- <sup>10</sup> From the  $K_{e4}$  data of BATLEY 08a and  $\pi N \rightarrow \pi\pi N$  data of PROTOPOESCU 73, GRAYER 74, and ESTABROOKS 74.
- <sup>11</sup> From a mean of three different  $f_0(500)$  parameterizations. Uses 40k events.
- <sup>12</sup> From an isobar model using 2.6k events.
- <sup>13</sup> Reanalysis of ABLIKIM 04a, PISLAK 01, and HYAMS 73 data.
- <sup>14</sup> Using the N/D method.
- <sup>15</sup> From the solution of the Roy equation (ROY 71) for the isoscalar S-wave and using a phase-shift analysis of HYAMS 73 and PROTOPOESCU 73 data.
- <sup>16</sup> Reanalysis of the data from PROTOPOESCU 73, ESTABROOKS 74, GRAYER 74, ROSSELET 77, PISLAK 03, and AKHMETSHIN 04.
- <sup>17</sup> From a mean of six different analyses and  $f_0(500)$  parameterizations.
- <sup>18</sup> Using data on  $\psi(2S) \rightarrow J/\psi\pi\pi$  from BAI 00E and on  $\Upsilon(nS) \rightarrow \Upsilon(mS)\pi\pi$  from BUTLER 94b and ALEXANDER 98.
- <sup>19</sup> Reanalysis of data from PROTOPOESCU 73, ESTABROOKS 74, GRAYER 74, and COHEN 80 in the unitarized ChPT model.
- <sup>20</sup> From a combined analysis of HYAMS 73, AUGUSTIN 89, AITALA 01b, and PISLAK 01.
- <sup>21</sup> A similar analysis (KOMADA 01) finds  $(580^{+79}_{-30}) - i(190^{+107}_{-49})$  MeV.
- <sup>22</sup> Coupled channel reanalysis of BATON 70, BENSINGER 71, BAILLON 72, HYAMS 73, HYAMS 75, ROSSELET 77, COHEN 80, and ETKIN 82b using the uniformizing variable.
- <sup>23</sup> Using the inverse amplitude method and data of ESTABROOKS 73, GRAYER 74, and PROTOPOESCU 73.
- <sup>24</sup> Reanalysis of data from HYAMS 73, GRAYER 74, SRINIVASAN 75, and ROSSELET 77 using the interfering amplitude method.
- <sup>25</sup> Average and spread of 4 variants ("up" and "down") of KAMINSKI 97b 3-channel model.
- <sup>26</sup> Uses data from BEIER 72b, OCHS 73, HYAMS 73, GRAYER 74, ROSSELET 77, CASON 83, ASTON 88, and ARMSTRONG 91b. Coupled channel analysis with flavor symmetry and all light two-pseudoscalars systems.
- <sup>27</sup> Demonstrates explicitly that  $f_0(500)$  and  $f_0(1370)$  are two different poles.
- <sup>28</sup> Analysis of data from FALVARD 88.
- <sup>29</sup> Analysis of data from OCHS 73, ESTABROOKS 75, ROSSELET 77, and MUKHIN 80.
- <sup>30</sup> Analysis of data from OCHS 73, GRAYER 74, and ROSSELET 77.
- <sup>31</sup> Coupled-channel analysis using data from PROTOPOESCU 73, HYAMS 73, HYAMS 75, GRAYER 74, ESTABROOKS 74, ESTABROOKS 75, FROGGATT 77, CORDEN 79, BISWAS 81.
- <sup>32</sup> Analysis of data from APEL 72c, GRAYER 74, CASON 76, PAWLICKI 77. Includes spread and errors of 4 solutions.
- <sup>33</sup> Analysis of data from BATON 70, BENSINGER 71, COLTON 71, BAILLON 72, PROTOPOESCU 73, and WALKER 67.

 $f_0(500)$  BREIT-WIGNER MASS OR K-MATRIX POLE PARAMETERS

VALUE (MeV)	DOCUMENT ID	TECN	COMMENT
<b>(400-550) OUR ESTIMATE</b>			
513±32	<sup>34</sup> MURAMATSU 02	CLEO	$e^+e^- \approx 10$ GeV
$478^{+24}_{-23} \pm 17$	AITALA 01b	E791	$D^+ \rightarrow \pi^-\pi^+\pi^+$
$563^{+58}_{-29}$	<sup>35</sup> ISHIDA 01		$\Upsilon(3S) \rightarrow \Upsilon\pi\pi$
555	<sup>36</sup> ASNER 00	CLE2	$\tau^- \rightarrow \pi^-\pi^0\pi^0\nu_\tau$
540±36	ISHIDA 00b		$p\bar{p} \rightarrow \pi^0\pi^0\pi^0$
750±4	ALEKSEEV 99	SPEC	$1.78\pi^-\rho_{\text{polar}} \rightarrow \pi^-\pi^+\pi$
744±5	ALEKSEEV 98	SPEC	$1.78\pi^-\rho_{\text{polar}} \rightarrow \pi^-\pi^+\pi$
759±5	<sup>37</sup> TROYAN 98		$5.2n\rho \rightarrow n\rho\pi^+\pi^-$
780±30	ALDE 97	GAM2	$450pp \rightarrow pp\pi^0\pi^0$
585±20	<sup>38</sup> ISHIDA 97		$\pi\pi \rightarrow \pi\pi$
761±12	<sup>39</sup> SVEC 96	RVUE	$6-17\pi N_{\text{polar}} \rightarrow \pi^+\pi^-\pi$
~ 860	40,41 TORNQVIST 96	RVUE	$\pi\pi \rightarrow \pi\pi, K\bar{K}, K\pi, \eta\pi$
1165±50	42,43 ANISOVICH 95	RVUE	$\pi^-\rho \rightarrow \pi^0\pi^0\pi^0, \pi^0\pi^0\eta, \pi^0\eta\eta$
~ 1000	44 ACHASOV 94	RVUE	$\pi\pi \rightarrow \pi\pi$
414±20	<sup>39</sup> AUGUSTIN 89	DM2	

- <sup>34</sup> Statistical uncertainty only.
- <sup>35</sup> A similar analysis (KOMADA 01) finds  $526^{+48}_{-37}$  MeV.
- <sup>36</sup> From the best fit of the Dalitz plot.
- <sup>37</sup>  $6\sigma$  effect, no PWA.
- <sup>38</sup> Reanalysis of data from HYAMS 73, GRAYER 74, SRINIVASAN 75, and ROSSELET 77 using the interfering amplitude method.
- <sup>39</sup> Breit-Wigner fit to S-wave intensity measured in  $\pi N \rightarrow \pi^-\pi^+\pi$  on polarized targets. The fit does not include  $f_0(980)$ .
- <sup>40</sup> Uses data from ASTON 88, OCHS 73, HYAMS 73, ARMSTRONG 91b, GRAYER 74, CASON 83, ROSSELET 77, and BEIER 72b. Coupled channel analysis with flavor symmetry and all light two-pseudoscalars systems.
- <sup>41</sup> Also observed by ASNER 00 in  $\tau^- \rightarrow \pi^-\pi^0\pi^0\nu_\tau$  decays.
- <sup>42</sup> Uses  $\pi^0\pi^0$  data from ANISOVICH 94, AMSLER 94d, and ALDE 95b,  $\pi^+\pi^-\pi$  data from OCHS 73, GRAYER 74 and ROSSELET 77, and  $\eta\eta$  data from ANISOVICH 94.
- <sup>43</sup> The pole is on Sheet III. Demonstrates explicitly that  $f_0(500)$  and  $f_0(1370)$  are two different poles.

- <sup>44</sup> Analysis of data from OCHS 73, ESTABROOKS 75, ROSSELET 77, and MUKHIN 80.

 $f_0(500)$  BREIT-WIGNER WIDTH

VALUE (MeV)	DOCUMENT ID	TECN	COMMENT
<b>(400-700) OUR ESTIMATE</b>			
• • •	We do not use the following data for averages, fits, limits, etc. • • •		
335±67	<sup>45</sup> MURAMATSU 02	CLEO	$e^+e^- \approx 10$ GeV
$324^{+42}_{-40} \pm 21$	AITALA 01b	E791	$D^+ \rightarrow \pi^-\pi^+\pi^+$
$372^{+229}_{-95}$	<sup>46</sup> ISHIDA 01		$\Upsilon(3S) \rightarrow \Upsilon\pi\pi$
540	<sup>47</sup> ASNER 00	CLE2	$\tau^- \rightarrow \pi^-\pi^0\pi^0\nu_\tau$
372±80	ISHIDA 00b		$p\bar{p} \rightarrow \pi^0\pi^0\pi^0$
119±13	ALEKSEEV 99	SPEC	$1.78\pi^-\rho_{\text{polar}} \rightarrow \pi^-\pi^+\pi$
77±22	ALEKSEEV 98	SPEC	$1.78\pi^-\rho_{\text{polar}} \rightarrow \pi^-\pi^+\pi$
35±12	<sup>48</sup> TROYAN 98		$5.2n\rho \rightarrow n\rho\pi^+\pi^-$
780±60	ALDE 97	GAM2	$450pp \rightarrow pp\pi^0\pi^0$
385±70	<sup>49</sup> ISHIDA 97		$\pi\pi \rightarrow \pi\pi$
290±54	<sup>50</sup> SVEC 96	RVUE	$6-17\pi N_{\text{polar}} \rightarrow \pi^+\pi^-\pi$
~ 880	51,52 TORNQVIST 96	RVUE	$\pi\pi \rightarrow \pi\pi, K\bar{K}, K\pi, \eta\pi$
460±40	53,54 ANISOVICH 95	RVUE	$\pi^-\rho \rightarrow \pi^0\pi^0\pi^0, \pi^0\pi^0\eta, \pi^0\eta\eta$
~ 3200	55 ACHASOV 94	RVUE	$\pi\pi \rightarrow \pi\pi$
494±58	<sup>50</sup> AUGUSTIN 89	DM2	

- <sup>45</sup> Statistical uncertainty only.
- <sup>46</sup> A similar analysis (KOMADA 01) finds  $301^{+145}_{-100}$  MeV.
- <sup>47</sup> From the best fit of the Dalitz plot.
- <sup>48</sup>  $6\sigma$  effect, no PWA.
- <sup>49</sup> Reanalysis of data from HYAMS 73, GRAYER 74, SRINIVASAN 75, and ROSSELET 77 using the interfering amplitude method.
- <sup>50</sup> Breit-Wigner fit to S-wave intensity measured in  $\pi N \rightarrow \pi^-\pi^+\pi$  on polarized targets. The fit does not include  $f_0(980)$ .
- <sup>51</sup> Uses data from ASTON 88, OCHS 73, HYAMS 73, ARMSTRONG 91b, GRAYER 74, CASON 83, ROSSELET 77, and BEIER 72b. Coupled channel analysis with flavor symmetry and all light two-pseudoscalars systems.
- <sup>52</sup> Also observed by ASNER 00 in  $\tau^- \rightarrow \pi^-\pi^0\pi^0\nu_\tau$  decays.
- <sup>53</sup> Uses  $\pi^0\pi^0$  data from ANISOVICH 94, AMSLER 94d, and ALDE 95b,  $\pi^+\pi^-\pi$  data from OCHS 73, GRAYER 74 and ROSSELET 77, and  $\eta\eta$  data from ANISOVICH 94.
- <sup>54</sup> The pole is on Sheet III. Demonstrates explicitly that  $f_0(500)$  and  $f_0(1370)$  are two different poles.
- <sup>55</sup> Analysis of data from OCHS 73, ESTABROOKS 75, ROSSELET 77, and MUKHIN 80.

 $f_0(500)$  DECAY MODES

Mode	Fraction ( $\Gamma_i/\Gamma$ )
$\Gamma_1$ $\pi\pi$	seen
$\Gamma_2$ $\gamma\gamma$	seen

 $f_0(500)$  PARTIAL WIDTHS

$\Gamma(\gamma\gamma)$	VALUE (keV)	DOCUMENT ID	TECN	COMMENT	$\Gamma_2$
• • •	We do not use the following data for averages, fits, limits, etc. • • •				
2.05±0.21	<sup>56</sup> DAI 14A	RVUE	Compilation		
1.7±0.4	<sup>57</sup> HOFERICHTER11	RVUE	Compilation		
3.08±0.82	<sup>58</sup> MENNESSIER 11	RVUE	Compilation		
2.08±0.2 $\pm 0.07$ -0.04	<sup>59</sup> MOUSSALLAM11	RVUE	Compilation		
2.08	<sup>60</sup> MAO 09	RVUE	Compilation		
1.2±0.4	<sup>61</sup> BERNABEU 08	RVUE			
3.9±0.6	<sup>58</sup> MENNESSIER 08	RVUE			
1.8±0.4	<sup>62</sup> OLLER 08	RVUE	Compilation		
1.68±0.15	<sup>62,63</sup> OLLER 08a	RVUE	Compilation		
3.1±0.5	<sup>64,65</sup> PENNINGTON 08	RVUE	Compilation		
2.4±0.4	<sup>65,66</sup> PENNINGTON 08	RVUE	Compilation		
4.1±0.3	<sup>67</sup> PENNINGTON 06	RVUE			
3.8±1.5	<sup>68,69</sup> BOGLIONE 99	RVUE			
5.4±2.3	<sup>68</sup> MORGAN 90	RVUE			
10±6	COURAU 86	DM1			

- <sup>56</sup> Using dispersive analysis with phases from GARCIA-MARTIN 11a and BUETTNER 04 as input.
- <sup>57</sup> Using Roy-Steiner equations with  $\pi\pi$  phase shifts from an update of COLANGELO 01 and from GARCIA-MARTIN 11a.
- <sup>58</sup> Using an analytic K-matrix model.
- <sup>59</sup> Using dispersion integral with phase input from Roy equations and data from MARSISKE 90, BOYER 90, BEHREND 92, UEHARA 08a, and MORI 07.
- <sup>60</sup> Used dispersion theory. The value quoted used the  $f_0(500)$  pole position of  $457 - i276$  MeV.
- <sup>61</sup> Using  $p, n$  polarizabilities from PDG 06 and fitting to  $\pi\pi$  phase motion from GARCIA-MARTIN 07 and  $\sigma$ -poles from GARCIA-MARTIN 07 and CAPRINI 06.
- <sup>62</sup> Using twice-subtracted dispersion integrals.
- <sup>63</sup> Supersedes OLLER 08.
- <sup>64</sup> Solution A (preferred solution based on  $\chi^2$ -analysis).

See key on page 999

Meson Particle Listings

$f_0(500), \rho(770)$

- 65 Dispersion theory based amplitude analysis of BOYER 90, MARSISKE 90, BEHREND 92, and MORI 07.
- 66 Solution B (worse than solution A; still acceptable when systematic uncertainties are included).
- 67 Using unitarity and the  $\sigma$  pole position from CAPRINI 06.
- 68 This width could equally well be assigned to the  $f_0(1370)$ . The authors analyse data from BOYER 90 and MARSISKE 90 and report strong correlation with  $\gamma\gamma$  width of  $f_2(1270)$ .
- 69 Supersedes MORGAN 90.

$f_0(500)$  REFERENCES

ABLIKIM 17	PRL 118 012001	M. Ablikim <i>et al.</i>	(BESIII Collab.)
DAI 14A	PR D90 036004	L.-Y. Dai, M.R. Pennington	(CEBAF)
ALBALADEJO 12	PR D86 034003	M. Albaladejo, J.A. Oller	(MURC)
GARCIA-MAR... 11	PRL 107 072001	R. Garcia-Martin <i>et al.</i>	(MADR, CRAC)
GARCIA-MAR... 11A	PR D83 074004	R. Garcia-Martin <i>et al.</i>	(MADR, CRAC)
HOFERICHTER 11	EPJ C71 1743	M. Hofelicher, D.R. Phillips, C. Schat	(BONN+)
MENNESSIER 11	PL B696 40	G. Mennessier, S. Narison, X.-G. Wang	
MOUSSALLAM 11	EPJ C71 1814	B. Moussallam	
BATLEY 10	PL B686 101	J.R. Batley <i>et al.</i>	(CERN NA48/2 Collab.)
BATLEY 10C	EPJ C70 635	J.R. Batley <i>et al.</i>	(CERN NA48/2 Collab.)
MENNESSIER 10	PL B688 59	G. Mennessier, S. Narison, X.-G. Wang	
MAO 09	PR D79 116008	Y. Mao <i>et al.</i>	
BATLEY 08A	EPJ C54 411	J.R. Batley <i>et al.</i>	(CERN NA48/2 Collab.)
BERNABEU 08	PRL 100 241804	J. Bernabeu, J. Prades	(IFIC, GRAN)
CAPRINI 08	PR D77 114019	I. Caprini	
MENNESSIER 08	PL B665 205	G. Mennessier, S. Narison, W. Ochs	
OLLER 08	PL B659 201	J.A. Oller, L. Roca, C. Schat	(MURC, UBA)
OLLER 08A	EPJ A37 15	J.A. Oller, L. Roca	(MURC)
PENNINGTON 08	EPJ C56 1	M.R. Pennington <i>et al.</i>	
UEHARA 08A	PR D78 052004	S. Uehara <i>et al.</i>	(BELLE Collab.)
ABLIKIM 07A	PL B645 19	M. Ablikim <i>et al.</i>	(BES Collab.)
BONVICINI 07	PR D76 012001	G. Bonvicini <i>et al.</i>	(CLEO Collab.)
BUGG 07A	JP G34 151	D.V. Bugg <i>et al.</i>	
GARCIA-MAR... 07	PR D76 074034	R. Garcia-Martin, J.R. Pelaez, F.J. Yndurain	
MORI 07	PR D75 051101	T. Mori <i>et al.</i>	(BELLE Collab.)
ANISOVICH 06	JMP A21 3615	V.V. Anisovich	
CAPRINI 06	PRL 96 132001	I. Caprini, G. Colangelo, H. Leutwyler	(BCIP+)
PDG 06	JP G33 145	W.-M. Yao <i>et al.</i>	(PDG Collab.)
PENNINGTON 06	PRL 97 011601	M.R. Pennington	
ZHOU 05	JHEP 0502 043	Z.Y. Zhou <i>et al.</i>	
ABLIKIM 04A	PL B598 149	M. Ablikim <i>et al.</i>	(BES Collab.)
AKHMETSHIN 04	PL B578 285	R.R. Akhmetshin <i>et al.</i>	(Novosibirsk CMD-2 Collab.)
BUETTIGER 04	EPJ C33 409	P. Buettiger, S. Descotes-Genon, B. Moussallam	
GALLEGOS 04	PR D69 074033	A. Gallegos <i>et al.</i>	
PELAEZ 04A	MPL A19 2879	J.R. Pelaez	
BUGG 03	PL B572 1	D.V. Bugg	
PISLAK 03	PR D67 072004	S. Pislak <i>et al.</i>	(BNL E865 Collab.)
Also	PR D81 119903E	S. Pislak <i>et al.</i>	(BNL E865 Collab.)
MURAMATSU 02	PRL 89 051802	H. Muramatsu <i>et al.</i>	(CLEO Collab.)
Also	PRL 90 059901 (errata.)	H. Muramatsu <i>et al.</i>	(CLEO Collab.)
AITALA 01B	PRL 86 770	E.M. Aitala <i>et al.</i>	(FNAL E791 Collab.)
BLACK 01	PR D64 014031	D. Black <i>et al.</i>	
COLANGELO 01	NP B603 125	G. Colangelo, J. Gasser, H. Leutwyler	
ISHIDA 01	PL B518 47	M. Ishida <i>et al.</i>	
KOMADA 01	PL B508 31	T. Komada <i>et al.</i>	
PISLAK 01	PRL 87 221801	S. Pislak <i>et al.</i>	(BNL E865 Collab.)
Also	PR D67 072004	S. Pislak <i>et al.</i>	(BNL E865 Collab.)
Also	PRL 105 019901E	S. Pislak <i>et al.</i>	(BNL E865 Collab.)
SUROVITSEV 01	PR D63 054024	S.S. Surovtsev, D. Krupa, M. Nagy	
ASNER 00	PR D61 012002	D.H. Asner <i>et al.</i>	(CLEO Collab.)
BAI 00E	PR D62 032002	J. Bai <i>et al.</i>	(BES Collab.)
ISHIDA 00B	PTP 104 203	M. Ishida <i>et al.</i>	
ALEKSEEV 99	NP B541 3	I.G. Alekseev <i>et al.</i>	
BOGLIONE 99	EPJ C9 11	M. Boglione, M.R. Pennington	
HANNAH 99	PR D60 017502	T. Hannah	
KAMINSKI 99	EPJ C9 141	R. Kaminski, L. Lesniak, B. Loiseau	(CRAC, PARIN)
OLLER 99	PR D60 099906 (erratum)	J.A. Oller <i>et al.</i>	
OLLER 99B	NP A652 407 (erratum)	J.A. Oller, E. Oset	
OLLER 99C	PR D60 074023	J.A. Oller, E. Oset	
ALEKSEEV 98	PAN 61 174	I.G. Alekseev <i>et al.</i>	
ALEXANDER 98	PR D58 052004	J.P. Alexander <i>et al.</i>	(CLEO Collab.)
ANISOVICH 98B	SFU 41 419	V.V. Anisovich <i>et al.</i>	
Translated from UFN	168 481.	V.V. Anisovich <i>et al.</i>	
LOCHER 98	EPJ C4 317	M.P. Locher <i>et al.</i>	(PSI)
TROYAN 98	JINRRC 5-91 33	Yu. Troyan <i>et al.</i>	
ALDE 97	PL B397 350	D.M. Alde <i>et al.</i>	(GAMS Collab.)
DOBADO 97	PR D56 3057	A. Dobado, J.R. Pelaez	
ISHIDA 97	PTP 98 1005	S. Ishida <i>et al.</i>	(TOKY, MIYA, KEK)
KAMINSKI 97B	PL B413 130	R. Kaminski, L. Lesniak, B. Loiseau	(CRAC, IPN)
Also	PTP 95 745	S. Ishida <i>et al.</i>	(TOKY, MIYA, KEK)
SVEC 96	PR D53 2343	M. Svec	(MCGI)
TORNQVIST 96	PRL 76 1575	N.A. Tornqvist, M. Roos	(HEL5)
ALDE 95B	ZPHY C66 375	D.M. Alde <i>et al.</i>	(GAMS Collab.)
ANISOVICH 95	PL B355 363	V.V. Anisovich <i>et al.</i>	(PNPI, SERP)
JANSEN 95	PR D52 2690	G. Jansen <i>et al.</i>	(STON, ADL2, JULI)
ACHASOV 94	PR D49 5779	N.N. Achasov, G.N. Shestakov	(NOVM)
AMSLER 94D	PL B333 277	C. Amisler <i>et al.</i>	(Crystal Barrel Collab.)
ANISOVICH 94	PL B323 233	V.V. Anisovich <i>et al.</i>	(Crystal Barrel Collab.)
BUTLER 94B	PR D49 40	F. Butler <i>et al.</i>	(CLEO Collab.)
KAMINSKI 94	PR D50 3145	R. Kaminski, L. Lesniak, J.P. Maillet	(CRAC+)
ZOU 94B	PR D50 3190	B.S. Zou, D.V. Bugg	(NIIIM, BIEL)
ZOU 93	PR D48 3348	B.S. Zou, D.V. Bugg	(LOQM)
BEHREND 92	ZPHY C56 381	H.J. Behrend	(CELLO Collab.)
ARMSTRONG 91B	ZPHY C52 389	T.A. Armstrong <i>et al.</i>	(ATHU, BARI, BIRM+)
BOYER 90	PR D42 1350	J. Boyer <i>et al.</i>	(Mark II Collab.)
MARSISKE 90	PR D41 3324	H. Marsiske <i>et al.</i>	(Crystal Ball Collab.)
MORGAN 90	ZPHY C48 623	D. Morgan, M.R. Pennington	(RAL, DURH)
AUGUSTIN 89	NP B320 1	J.E. Augustin, G. Cosme	(DM2 Collab.)
ASTON 88	NP B296 493	D. Aston <i>et al.</i>	(SLAC, NAGO, CINC, INUS)
FALVARD 88	PR D38 2706	A. Falvard <i>et al.</i>	(CLER, FRAS, LALO+)
COURAU 86	NP B271 1	A. Courau <i>et al.</i>	(CLER, LALO)
VANBEVEREN 86	ZPHY C30 615	E. van Beveren <i>et al.</i>	(NIIIM, BIEL)
CASON 83	PR D28 1584	N.M. Cason <i>et al.</i>	(NDAM, ANL)
ETKIN 82B	PR D25 1784	A. Etkin <i>et al.</i>	(BNL, CUNY, TUFTS, VAND)
BISWAS 81	PRL 47 1378	N.N. Biswas <i>et al.</i>	(NDAM, ANL)
COHEN 80	PR D22 2595	D. Cohen <i>et al.</i>	(ANL) IJUP
MUKHIN 80	JETPL 32 601	K.N. Mukhin <i>et al.</i>	(KIAE)
Translated from ZETFP	32 616.	M.J. Corden <i>et al.</i>	(BIRM, RHEL, TELA+) JP
CORDEN 79	NP B157 250	P. Estabrooks	(CARL)
ESTABROOKS 79	PR D19 2678	C.D. Froggatt, J.L. Petersen	(GLAS, IORR)
FROGGATT 77	NP B129 89	A.J. Pawlikci <i>et al.</i>	(ANL) IJ
PAWLIKCI 77	PR D15 3196	L. Rossetti <i>et al.</i>	(GEVA, SAEL)
ROSSETT 77	PR D15 574	N.M. Cason <i>et al.</i>	(NDAM, ANL) IJ
CASON 76	PRL 36 1485	P.G. Estabrooks, A.D. Martin	(DURH)
ESTABROOKS 75	NP B95 322	B.D. Hyams <i>et al.</i>	(CERN, MPIM)
HYAMS 75	NP B100 205		

$\rho(770)$

THE  $\rho(770)$

$$I^G(J^{PC}) = 1^+(1^-)$$

Updated September 2019 by S. Eidelman (Novosibirsk) and G. Venanzoni (Pisa).

The determination of the parameters of the  $\rho(770)$  is beset with many difficulties because of its large width. In physical region fits, the line shape does not correspond to a relativistic Breit-Wigner function with a  $P$ -wave width, but requires some additional shape parameter. This dependence on parameterization was demonstrated long ago [1]. Bose-Einstein correlations are another source of shifts in the  $\rho(770)$  line shape, particularly in multiparticle final-state systems [2].

The same model dependence afflicts any other source of resonance parameters, such as the energy dependence of the phase shift  $\delta_1^+$ , or the pole position. It is, therefore, not surprising that a study of  $\rho(770)$  dominance in the decays of the  $\eta$  and  $\eta'$  reveals the need for specific dynamical effects, in addition to the  $\rho(770)$  pole [3,4].

The cleanest determination of the  $\rho(770)$  mass and width comes from  $e^+e^-$  annihilation and  $\tau$ -lepton decays. Analysis of ALEPH [5] showed that the charged  $\rho(770)$  parameters measured from  $\tau$ -lepton decays are consistent with those of the neutral one determined from  $e^+e^-$  data [6]. This conclusion is qualitatively supported by the later studies of CLEO [7] and Belle [8]. However, comparison of the two-pion mass spectrum in  $\tau$  decays from OPAL [9], CLEO [7], and ALEPH [10,11], and the  $e^+e^- \rightarrow \pi^+\pi^-$  cross section from CMD-2 [12,13], showed significant discrepancies between the two shapes which can be as high as 10% above the  $\rho$  meson [14,15]. This discrepancy remains after measurements of the two-pion cross section in  $e^+e^-$  annihilation at KLOE [16,17,18,19], SND [20,21], BaBar [22] and, more recently BESIII [23]. The effect is not accounted for by isospin breaking [24,25,26,27], but the accuracy of its calculation may be overestimated [28,29].

This problem seems to be solved after a recent analysis in [30] which showed that after correcting the  $\tau$  data for the missing  $\rho - \gamma$  mixing contribution, besides the other known isospin symmetry violating corrections, the  $\pi\pi$  I=1 part of the hadronic vacuum polarization contribution to the muon  $g - 2$  is fully compatible between  $\tau$  based and  $e^+e^-$  based evaluations. The global fit of the whole set of the  $\rho$ ,  $\omega$ , and  $\phi$  decays, taking into account mixing effects in the hidden local symmetry model, also showed consistency of the data on  $\tau$  decays to two pions and  $e^+e^-$  annihilation [31,32]. However, because

## Meson Particle Listings

 $\rho(770)$ 

of the progress in  $e^+e^-$  data, the  $\tau$  input is now less precise and less reliable due to additional theoretical uncertainties [33] decreasing importance of  $\tau$  versus  $e^+e^-$  comparison for the determination of  $\rho(770)$  parameters and other applications, like, e.g., calculations of hadronic vacuum polarization.

## References

- J. Pisut and M. Roos, Nucl. Phys. **B6**, 325 (1968).
- G.D. Lafferty, Z. Phys. **C60**, 659 (1993).
- A. Abele *et al.*, Phys. Lett. **B402**, 195 (1997).
- M. Benayoun *et al.*, Eur. Phys. J. **C31**, 525 (2003).
- R. Barate *et al.*, Z. Phys. **C76**, 15 (1997).
- L.M. Barkov *et al.*, Nucl. Phys. **B256**, 365 (1985).
- S. Anderson *et al.*, Phys. Rev. **D61**, 112002 (2000).
- M. Fujikawa *et al.*, Phys. Rev. **D78**, 072006 (2008).
- K. Ackerstaff *et al.*, Eur. Phys. J. **C7**, 571 (1999).
- M. Davier *et al.*, Nucl. Phys. (Proc. Supp.) **B123**, 47 (2003).
- S. Schael *et al.*, Phys. Reports **421**, 191 (2005).
- R.R. Akhmetshin *et al.*, Phys. Lett. **B527**, 161 (2002).
- R.R. Akhmetshin *et al.*, Phys. Lett. **B578**, 285 (2004).
- M. Davier *et al.*, Eur. Phys. J. **C27**, 497 (2003).
- M. Davier *et al.*, Eur. Phys. J. **C31**, 503 (2003).
- A. Aloisio *et al.*, Phys. Lett. **B606**, 12 (2005).
- F. Ambrosino *et al.*, Phys. Lett. **B670**, 285 (2009).
- F. Ambrosino *et al.*, Phys. Lett. **B700**, 102 (2011).
- D. Babusci *et al.*, Phys. Lett. **B720**, 336 (2013).
- M.N. Achasov *et al.*, Sov. Phys. JETP **101**, 1053 (2005).
- M.N. Achasov *et al.*, Sov. Phys. JETP **103**, 380 (2006).
- B. Aubert *et al.*, Phys. Rev. Lett. **103**, 231801 (2009).
- M. Ablikim *et al.*, Phys. Lett. **B753**, 629 (2016).
- R. Alemany *et al.*, Eur. Phys. J. **C2**, 123 (1998).
- H. Czyz and J.J. Kuhn, Eur. Phys. J. **C18**, 497 (2001).
- V. Cirigliano *et al.*, Phys. Lett. **B513**, 361 (2001).
- V. Cirigliano *et al.*, Eur. Phys. J. **C23**, 121 (2002).
- K. Maltman and C.E. Wolfe, Phys. Rev. **D73**, 013004 (2006).
- C.E. Wolfe and K. Maltman, Phys. Rev. **D80**, 114024 (2009).
- F. Jegerlehner and R. Szafron, Eur. Phys. J. **C71**, 1632 (2011).
- M. Benayoun *et al.*, Eur. Phys. J. **C72**, 1848 (2012).
- M. Benayoun *et al.*, Eur. Phys. J. **C73**, 2453 (2013).
- M. Davier *et al.*, Eur. Phys. J. **C77**, 827 (2017).

 $\rho(770)$  MASS

We no longer list  $S$ -wave Breit-Wigner fits, or data with high combinatorial background.

NEUTRAL ONLY,  $e^+e^-$ 

VALUE (MeV)	EVTS	DOCUMENT ID	TECN	COMMENT
<b>775.26 ± 0.25 OUR AVERAGE</b>				
775.02 ± 0.35		<sup>1</sup> LEES	12g	BABR $e^+e^- \rightarrow \pi^+\pi^-\gamma$
775.97 ± 0.46 ± 0.70	900k	<sup>2</sup> AKHMETSHIN 07		$e^+e^- \rightarrow \pi^+\pi^-$
774.6 ± 0.4 ± 0.5	800k	<sup>3,4</sup> ACHASOV	06	SND $e^+e^- \rightarrow \pi^+\pi^-$
775.65 ± 0.64 ± 0.50	114k	<sup>5,6</sup> AKHMETSHIN 04	CMD2	$e^+e^- \rightarrow \pi^+\pi^-$
775.9 ± 0.5 ± 0.5	1.98M	<sup>7</sup> ALOISIO	03	KLOE $1.02 e^+e^- \rightarrow \pi^+\pi^-\pi^0$
775.8 ± 0.9 ± 2.0	500k	<sup>7</sup> ACHASOV	02	SND $1.02 e^+e^- \rightarrow \pi^+\pi^-\pi^0$
775.9 ± 1.1		<sup>8</sup> BARKOV	85	OLYA $e^+e^- \rightarrow \pi^+\pi^-$

••• We do not use the following data for averages, fits, limits, etc. •••

763.49 ± 0.53		<sup>9</sup> BARTOS	17	RVUE $e^+e^- \rightarrow \pi^+\pi^-$
758.23 ± 0.46		<sup>10</sup> BARTOS	17A	RVUE $e^+e^- \rightarrow \pi^+\pi^-$
775.8 ± 0.5 ± 0.3	1.98M	<sup>11</sup> ALOISIO	03	KLOE $1.02 e^+e^- \rightarrow \pi^+\pi^-\pi^0$
775.9 ± 0.6 ± 0.5	1.98M	<sup>12</sup> ALOISIO	03	KLOE $1.02 e^+e^- \rightarrow \pi^+\pi^-\pi^0$
775.0 ± 0.6 ± 1.1	500k	<sup>13</sup> ACHASOV	02	SND $1.02 e^+e^- \rightarrow \pi^+\pi^-\pi^0$
775.1 ± 0.7 ± 5.3		<sup>14</sup> BENAYOUN	98	RVUE $e^+e^- \rightarrow \pi^+\pi^-$ , $\mu^+\mu^-$
770.5 ± 1.9 ± 5.1		<sup>15</sup> GARDNER	98	RVUE $0.28-0.92 e^+e^- \rightarrow \pi^+\pi^-$
764.1 ± 0.7		<sup>16</sup> O'CONNELL	97	RVUE $e^+e^- \rightarrow \pi^+\pi^-$
757.5 ± 1.5		<sup>17</sup> BERNICHA	94	RVUE $e^+e^- \rightarrow \pi^+\pi^-$
768 ± 1		<sup>18</sup> GESHKEN...	89	RVUE $e^+e^- \rightarrow \pi^+\pi^-$

<sup>1</sup> Using the GOUNARIS 68 parametrization with the complex phase of the  $\rho$ - $\omega$  interference and leaving the masses and widths of the  $\rho(1450)$ ,  $\rho(1700)$ , and  $\rho(2150)$  resonances as free parameters of the fit.

<sup>2</sup> A combined fit of AKHMETSHIN 07, AULCHENKO 06, and AULCHENKO 05.

<sup>3</sup> Supersedes ACHASOV 05A.

<sup>4</sup> A fit of the SND data from 400 to 1000 MeV using parameters of the  $\rho(1450)$  and  $\rho(1700)$  from a fit of the data of BARKOV 85, BISELLO 89 and ANDERSON 00A.

<sup>5</sup> Using the GOUNARIS 68 parametrization with the complex phase of the  $\rho$ - $\omega$  interference.

<sup>6</sup> Update of AKHMETSHIN 02.

<sup>7</sup> Assuming  $m_{\rho^+} = m_{\rho^-} = m_{\rho^0}$ ,  $\Gamma_{\rho^+} = \Gamma_{\rho^-}$ .

<sup>8</sup> From the GOUNARIS 68 parametrization of the pion form factor.

<sup>9</sup> Applies the Unitary & Analytic Model of the pion electromagnetic form factor of DUBNICKA 10 to analyze the data of LEES 12g and ABLIKIM 16c.

<sup>10</sup> Applies the Unitary & Analytic Model of the pion electromagnetic form factor of DUBNICKA 10 to analyze the data of ACHASOV 06, AKHMETSHIN 07, AUBERT 09as, and AMBROSINO 11a.

<sup>11</sup> Assuming  $m_{\rho^+} = m_{\rho^-} = m_{\rho^0}$ ,  $\Gamma_{\rho^+} = \Gamma_{\rho^-} = \Gamma_{\rho^0}$ .

<sup>12</sup> Without limitations on masses and widths.

<sup>13</sup> Assuming  $m_{\rho^0} = m_{\rho^\pm}$ ,  $g_{\rho^0\pi\pi} = g_{\rho^\pm\pi\pi}$ .

<sup>14</sup> Using the data of BARKOV 85 in the hidden local symmetry model.

<sup>15</sup> From the fit to  $e^+e^- \rightarrow \pi^+\pi^-$  data from the compilations of HEYN 81 and BARKOV 85, including the GOUNARIS 68 parametrization of the pion form factor.

<sup>16</sup> A fit of BARKOV 85 data assuming the direct  $\omega\pi\pi$  coupling.

<sup>17</sup> Applying the S-matrix formalism to the BARKOV 85 data.

<sup>18</sup> Includes BARKOV 85 data. Model-dependent width definition.

CHARGED ONLY,  $\tau$  DECAYS and  $e^+e^-$ 

VALUE (MeV)	EVTS	DOCUMENT ID	TECN	CHG	COMMENT
<b>775.11 ± 0.34 OUR AVERAGE</b>					
774.6 ± 0.2 ± 0.5	5.4M	<sup>1,2</sup> FUJIKAWA	08	BELL ±	$\tau^- \rightarrow \pi^- \pi^0 \nu_\tau$
775.5 ± 0.7		<sup>2,3</sup> SCHAELE	05c	ALEP	$\tau^- \rightarrow \pi^- \pi^0 \nu_\tau$
775.5 ± 0.5 ± 0.4	1.98M	<sup>4</sup> ALOISIO	03	KLOE	$1.02 e^+e^- \rightarrow \pi^+\pi^-\pi^0$
775.1 ± 1.1 ± 0.5	87k	<sup>5,6</sup> ANDERSON	00A	CLE2	$\tau^- \rightarrow \pi^- \pi^0 \nu_\tau$
761.60 ± 0.95		<sup>7</sup> BARTOS	17A	RVUE	$e^+e^- \rightarrow \pi^-\pi^0 \nu_\tau$
774.8 ± 0.6 ± 0.4	1.98M	<sup>8</sup> ALOISIO	03	KLOE -	$1.02 e^+e^- \rightarrow \pi^+\pi^-\pi^0$
776.3 ± 0.6 ± 0.7	1.98M	<sup>8</sup> ALOISIO	03	KLOE +	$1.02 e^+e^- \rightarrow \pi^+\pi^-\pi^0$
773.9 ± 2.0 ± $\begin{smallmatrix} +0.3 \\ -1.0 \end{smallmatrix}$		<sup>9</sup> SANZ-CILLERO	003	RVUE	$\tau^- \rightarrow \pi^- \pi^0 \nu_\tau$
774.5 ± 0.7 ± 1.5	500k	<sup>4</sup> ACHASOV	02	SND ±	$1.02 e^+e^- \rightarrow \pi^+\pi^-\pi^0$
775.1 ± 0.5		<sup>10</sup> PICH	01	RVUE	$\tau^- \rightarrow \pi^- \pi^0 \nu_\tau$

<sup>1</sup>  $|F_\pi(0)|^2$  fixed to 1.

<sup>2</sup> From the GOUNARIS 68 parametrization of the pion form factor.

<sup>3</sup> The error combines statistical and systematic uncertainties. Supersedes BARATE 97M.

<sup>4</sup> Assuming  $m_{\rho^+} = m_{\rho^-} = m_{\rho^0}$ ,  $\Gamma_{\rho^+} = \Gamma_{\rho^-}$ .

<sup>5</sup>  $\rho(1700)$  mass and width fixed at 1700 MeV and 235 MeV respectively.

<sup>6</sup> From the GOUNARIS 68 parametrization of the pion form factor. The second error is a model error taking into account different parametrizations of the pion form factor.

<sup>7</sup> Applies the Unitary & Analytic Model of the pion electromagnetic form factor of DUBNICKA 10 to analyze the data of FUJIKAWA 08.

<sup>8</sup> Without limitations on masses and widths.

<sup>9</sup> Using the data of BARATE 97M and the effective chiral Lagrangian.

<sup>10</sup> From a fit of the model-independent parameterization of the pion form factor to the data of BARATE 97M.

## MIXED CHARGES, OTHER REACTIONS

VALUE (MeV)	EVTS	DOCUMENT ID	TECN	CHG	COMMENT
<b>763.0 ± 0.3 ± 1.2</b>	600k	<sup>1</sup> ABELE	99e	CBAR	$0 \pm 0.0 \bar{p}p \rightarrow \pi^+\pi^-\pi^0$

<sup>1</sup> Assuming the equality of  $\rho^+$  and  $\rho^-$  masses and widths.

## CHARGED ONLY, HADROPRODUCED

VALUE (MeV)	EVTS	DOCUMENT ID	TECN	CHG	COMMENT
<b>766.5 ± 1.1 OUR AVERAGE</b>					
763.7 ± 3.2		ABELE	97	CBAR	$\bar{p}n \rightarrow \pi^-\pi^0 \pi^0$
768 ± 9		AGUILAR...	91	EHS	400 $pp$
767 ± 3	2935	<sup>1</sup> CAPRARO	87	SPEC -	200 $\pi^- \text{Cu} \rightarrow \pi^-\pi^0 \text{Cu}$
761 ± 5	967	<sup>1</sup> CAPRARO	87	SPEC -	200 $\pi^- \text{Pb} \rightarrow \pi^-\pi^0 \text{Pb}$
771 ± 4		HUSTON	86	SPEC +	202 $\pi^+ \text{A} \rightarrow \pi^+\pi^0 \text{A}$
766 ± 7	6500	<sup>2</sup> BYERLY	73	OSPK -	5 $\pi^- p$

See key on page 999

# Meson Particle Listings

## $\rho(770)$

766.8 ± 1.5	9650	<sup>3</sup> PISUT	68	RVUE	-	1.7-3.2 $\pi^- p$ , $t < 10$
767 ± 6	900	<sup>1</sup> EISNER	67	HBC	-	4.2 $\pi^- p$ , $t < 10$

- <sup>1</sup> Mass errors enlarged by us to  $\Gamma/\sqrt{N}$ ; see the note with the  $K^*(892)$  mass.
- <sup>2</sup> Phase shift analysis. Systematic errors added corresponding to spread of different fits.
- <sup>3</sup> From fit of 3-parameter relativistic P-wave Breit-Wigner to total mass distribution. Includes BATON 68, MILLER 67B, ALFF-STEINBERGER 66, HAGOPIAN 66, HAGOPIAN 66B, JACOBS 66B, JAMES 66, WEST 66, BLIEDEN 65 and CARMONY 64.

### NEUTRAL ONLY, PHOTOPRODUCED

VALUE (MeV)	EVTs	DOCUMENT ID	TECN	COMMENT
<b>769.0 ± 1.0 OUR AVERAGE</b>				
771 ± 2	<sup>+2</sup> <sub>-1</sub> 63.5k	<sup>1</sup> ABRAMOWICZ12	ZEUS	$e p \rightarrow e \pi^+ \pi^- p$
770 ± 2	±1 79k	<sup>2</sup> BREITWEG	98B ZEUS	50-100 $\gamma p$
767.6 ± 2.7		BARTALUCCI	78 CNTR	$\gamma p \rightarrow e^+ e^- p$
775 ± 5		GLADDING	73 CNTR	2.9-4.7 $\gamma p$
767 ± 4	1930	BALLAM	72 HBC	2.8 $\gamma p$
770 ± 4	2430	BALLAM	72 HBC	4.7 $\gamma p$
765 ± 10		ALVENSLEB...	70 CNTR	$\gamma A$ , $t < 0.01$
767.7 ± 1.9	140k	BIGGS	70 CNTR	$< 4.1 \gamma C \rightarrow \pi^+ \pi^- C$
765 ± 5	4000	ASBURY	67B CNTR	$\gamma + Pb$

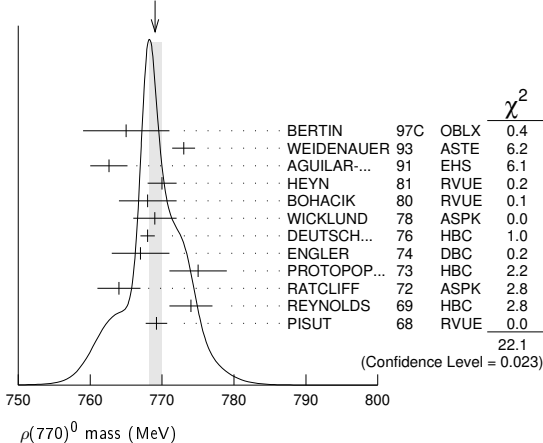
- • • We do not use the following data for averages, fits, limits, etc. • • •
- 771 ± 2     79k     <sup>3</sup>BREITWEG     98B ZEUS     50-100  $\gamma p$
- <sup>1</sup> Using the KUHN 90 parametrization of the pion form factor, neglecting  $\rho-\omega$  interference.
- <sup>2</sup> From the parametrization according to SOEDING 66.
- <sup>3</sup> From the parametrization according to ROSS 66.

### NEUTRAL ONLY, OTHER REACTIONS

VALUE (MeV)	EVTs	DOCUMENT ID	TECN	COMMENT
<b>769.0 ± 0.9 OUR AVERAGE</b>				Error includes scale factor of 1.4. See the ideogram below.
765 ± 6		BERTIN	97C OBLX	0.0 $\bar{p} p \rightarrow \pi^+ \pi^- \pi^0$
773 ± 1.6		WEIDENAUER	93 ASTE	$\bar{p} p \rightarrow \pi^+ \pi^- \omega$
762.6 ± 2.6		AGUILAR...	91 EHS	400 $pp$
770 ± 2		<sup>1</sup> HEYN	81 RVUE	Pion form factor
768 ± 4		<sup>2,3</sup> BOHACIK	80 RVUE	
769 ± 3		<sup>4</sup> WICKLUND	78 ASPK	3,4,6 $\pi^\pm N$
768 ± 1	76k	DEUTSCH...	76 HBC	16 $\pi^+ p$
767 ± 4	4100	ENGLER	74 DBC	6 $\pi^+ n \rightarrow \pi^+ \pi^- p$
775 ± 4	32k	<sup>2</sup> PROTOPOP...	73 HBC	7.1 $\pi^+ p$ , $t < 0.4$
764 ± 3	6.8k	<sup>5</sup> RATCLIFF	72 ASPK	15 $\pi^- p$ , $t < 0.3$
774 ± 3	1.7k	REYNOLDS	69 HBC	2.26 $\pi^- p$
769.2 ± 1.5	13.3k	<sup>6</sup> PISUT	68 RVUE	1.7-3.2 $\pi^- p$ , $t < 10$

- • • We do not use the following data for averages, fits, limits, etc. • • •
- 774.34 ± 0.18 ± 0.35     970k     <sup>7</sup>ABLIKIM     18c BES3      $\eta'(958) \rightarrow \gamma \pi^+ \pi^-$
- 772.93 ± 0.18 ± 0.34     970k     <sup>8</sup>ABLIKIM     18c BES3      $\eta'(958) \rightarrow \gamma \pi^+ \pi^-$
- 773.5 ± 2.5     <sup>9</sup>COLANGELO     01 RVUE      $\pi \pi \rightarrow \pi \pi$
- 762.3 ± 0.5 ± 1.2     600k     <sup>10</sup>ABELE     99E CBAR     0.0  $\bar{p} p \rightarrow \pi^+ \pi^- \pi^0$
- 777 ± 2     4.9k     <sup>11</sup>ADAMS     97 E665     470  $\mu p \rightarrow \mu X B$
- 770 ± 2     <sup>12</sup>BOGOLYUB...     97 MIRA     32  $\bar{p} p \rightarrow \pi^+ \pi^- X$
- 768 ± 8     <sup>12</sup>BOGOLYUB...     97 MIRA     32  $pp \rightarrow \pi^+ \pi^- X$
- 761.1 ± 2.9     <sup>13</sup>DUBNICKA     89 RVUE      $\pi$  form factor
- 777.4 ± 2.0     <sup>13</sup>CHABAUD     83 ASPK     17  $\pi^- p$  polarized
- 769.5 ± 0.7     <sup>2,3</sup>LANG     79 RVUE      $\pi$  form factor
- 770 ± 9     <sup>3</sup>ESTABROOKS     74 RVUE     17  $\pi^- p \rightarrow \pi^+ \pi^- n$
- 773.5 ± 1.7     11.2k     <sup>14</sup>JACOBS     72 HBC     2.8  $\pi^- p$
- 775 ± 3     2.2k     <sup>15</sup>HYAMS     68 OSPK     11.2  $\pi^- p$

WEIGHTED AVERAGE  
769.0 ± 0.9 (Error scaled by 1.4)



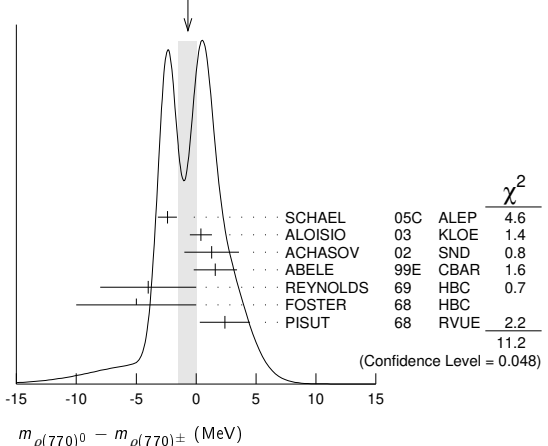
- <sup>6</sup> Includes MALAMUD 69, ARMENISE 68, BACON 67, HUWE 67, MILLER 67B, ALFF-STEINBERGER 66, HAGOPIAN 66, HAGOPIAN 66B, JACOBS 66B, JAMES 66, WEST 66, GOLDBERGER 64, ABOLINS 63.
- <sup>7</sup> From a fit to  $\pi^+ \pi^-$  mass using  $\rho(770)$  (parametrized with the Gounaris-Sakurai approach),  $\omega(782)$ , and box anomaly components.
- <sup>8</sup> From a fit to  $\pi^+ \pi^-$  mass using  $\rho(770)$  (parametrized with the Gounaris-Sakurai approach),  $\omega(782)$ , and  $\rho(1450)$  components.
- <sup>9</sup> Breit-Wigner mass from a phase-shift analysis of HYAMS 73 and PROTOPOESCU 73 data.
- <sup>10</sup> Using relativistic Breit-Wigner and taking into account  $\rho-\omega$  interference.
- <sup>11</sup> Systematic errors not evaluated.
- <sup>12</sup> Systematic effects not studied.
- <sup>13</sup> From fit of 3-parameter relativistic Breit-Wigner to helicity-zero part of P-wave intensity. CHABAUD 83 includes data of GRAYER 74.
- <sup>14</sup> Mass errors enlarged by us to  $\Gamma/\sqrt{N}$ ; see the note with the  $K^*(892)$  mass.
- <sup>15</sup> Of HYAMS 68 six parametrizations, this is theoretically soundest. MR

### $m_{\rho(770)^0} - m_{\rho(770)^\pm}$

VALUE (MeV)	EVTs	DOCUMENT ID	TECN	CHG.	COMMENT
<b>-0.7 ± 0.8 OUR AVERAGE</b>					Error includes scale factor of 1.5. See the ideogram below.
-2.4 ± 0.8		<sup>1</sup> SCHAEEL	05c ALEP		$\tau^- \rightarrow \pi^- \pi^0 \nu_\tau$
0.4 ± 0.7 ± 0.6	1.98M	<sup>2</sup> ALOISIO	03 KLOE		1.02 $e^+ e^- \rightarrow \pi^+ \pi^- \pi^0$
1.3 ± 1.1 ± 2.0	500k	<sup>2</sup> ACHASOV	02 SND		1.02 $e^+ e^- \rightarrow \pi^+ \pi^- \pi^0$
1.6 ± 0.6 ± 1.7	600k	ABELE	99E CBAR	±0	0.0 $\bar{p} p \rightarrow \pi^+ \pi^- \pi^0$
-4 ± 4	3000	<sup>3</sup> REYNOLDS	69 HBC	-0	2.26 $\pi^- p$
-5 ± 5	3600	<sup>3</sup> FOSTER	68 HBC	±0	0.0 $\bar{p} p$
2.4 ± 2.1	22950	<sup>4</sup> PISUT	68 RVUE		$\pi N \rightarrow \rho N$
-3.37 ± 1.06		<sup>5</sup> BARTOS	17A RVUE		$e^+ e^- \rightarrow \pi^+ \pi^-$ , $\tau^- \rightarrow \pi^- \pi^0 \nu_\tau$

- • • We do not use the following data for averages, fits, limits, etc. • • •
- <sup>1</sup> From the combined fit of the  $\tau^-$  data from ANDERSON 00A and SCHAEEL 05c and  $e^+ e^-$  data from the compilation of BARKOV 85, AKHMETSHIN 04, and ALOISIO 05. Supersedes BARATE 97M.
- <sup>2</sup> Assuming  $m_{\rho^+} = m_{\rho^-}$ ,  $\Gamma_{\rho^+} = \Gamma_{\rho^-}$ .
- <sup>3</sup> From quoted masses of charged and neutral modes.
- <sup>4</sup> Includes MALAMUD 69, ARMENISE 68, BATON 68, BACON 67, HUWE 67, MILLER 67B, ALFF-STEINBERGER 66, HAGOPIAN 66, HAGOPIAN 66B, JACOBS 66B, JAMES 66, WEST 66, BLIEDEN 65, CARMONY 64, GOLDBERGER 64, ABOLINS 63.
- <sup>5</sup> Applies the Unitary & Analytic Model of the pion electromagnetic form factor of DUBNICKA 10 to analyze the data of ACHASOV 06, AKHMETSHIN 07, AUBERT 09As, AMBROSINO 11A, and FUJIKAWA 08.

WEIGHTED AVERAGE  
-0.7 ± 0.8 (Error scaled by 1.5)



### $m_{\rho(770)^+} - m_{\rho(770)^-}$

VALUE (MeV)	EVTs	DOCUMENT ID	TECN	COMMENT
<b>1.5 ± 0.8 ± 0.7</b>	1.98M	<sup>1</sup> ALOISIO	03 KLOE	1.02 $e^+ e^- \rightarrow \pi^+ \pi^- \pi^0$

- • • We do not use the following data for averages, fits, limits, etc. • • •
- <sup>1</sup> Without limitations on masses and widths.

### $\rho(770)$ RANGE PARAMETER

The range parameter  $R$  enters an energy-dependent correction to the width, of the form  $(1 + q_r^2 R^2) / (1 + q^2 R^2)$ , where  $q$  is the momentum of one of the pions in the  $\pi\pi$  rest system. At resonance,  $q = q_r$ .

- <sup>1</sup> HEYN 81 includes all spacelike and timelike  $F_\pi$  values until 1978.
- <sup>2</sup> From pole extrapolation.
- <sup>3</sup> From phase shift analysis of GRAYER 74 data.
- <sup>4</sup> Phase shift analysis. Systematic errors added corresponding to spread of different fits.
- <sup>5</sup> Published values contain misprints. Corrected by private communication RATCLIFF 74.

# Meson Particle Listings

## $\rho(770)$

VALUE (GeV <sup>-1</sup> )	DOCUMENT ID	TECN	CHG	COMMENT
<b>5.3<sup>+0.9</sup><sub>-0.7</sub></b>	1 CHABAUD	83	ASPK	0 17 $\pi^- \rho$ polarized

<sup>1</sup>The old PISUT 68 value, properly corrected, was 3.2 ± 0.6.

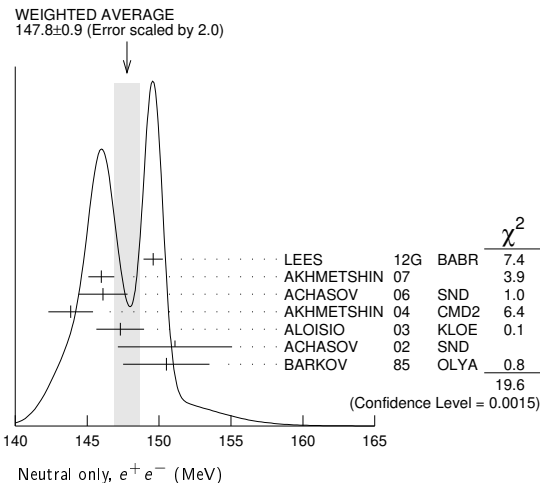
### $\rho(770)$ WIDTH

We no longer list S-wave Breit-Wigner fits, or data with high combinatorial background.

### NEUTRAL ONLY, $e^+e^-$

VALUE (MeV)	EVTS	DOCUMENT ID	TECN	COMMENT
<b>147.8 ± 0.9 OUR AVERAGE</b>				Error includes scale factor of 2.0. See the ideogram below.
149.59 ± 0.67		1 LEES	12G	BABR $e^+e^- \rightarrow \pi^+\pi^-\gamma$
145.98 ± 0.75 ± 0.50	900k	2 AKHMETSHIN	07	$e^+e^- \rightarrow \pi^+\pi^-$
146.1 ± 0.8 ± 1.5	800k	3,4 ACHASOV	06	SND $e^+e^- \rightarrow \pi^+\pi^-$
143.85 ± 1.33 ± 0.80	114k	5,6 AKHMETSHIN	04	CMD2 $e^+e^- \rightarrow \pi^+\pi^-$
147.3 ± 1.5 ± 0.7	1.98M	7 ALOISIO	03	KLOE 1.02 $e^+e^- \rightarrow \pi^+\pi^-$
151.1 ± 2.6 ± 3.0	500k	7 ACHASOV	02	SND 1.02 $e^+e^- \rightarrow \pi^+\pi^-$
150.5 ± 3.0		8 BARKOV	85	OLYA $e^+e^- \rightarrow \pi^+\pi^-$
144.06 ± 0.85		9 BARTOS	17	RVUE $e^+e^- \rightarrow \pi^+\pi^-$
144.56 ± 0.80		10 BARTOS	17A	RVUE $e^+e^- \rightarrow \pi^+\pi^-$
143.9 ± 1.3 ± 1.1	1.98M	11 ALOISIO	03	KLOE 1.02 $e^+e^- \rightarrow \pi^+\pi^-$
147.4 ± 1.5 ± 0.7	1.98M	12 ALOISIO	03	KLOE 1.02 $e^+e^- \rightarrow \pi^+\pi^-$
149.8 ± 2.2 ± 2.0	500k	13 ACHASOV	02	SND 1.02 $e^+e^- \rightarrow \pi^+\pi^-$
147.9 ± 1.5 ± 7.5		14 BENAYOUN	98	RVUE $e^+e^- \rightarrow \pi^+\pi^-$
153.5 ± 1.3 ± 4.6		15 GARDNER	98	RVUE 0.28-0.92 $e^+e^- \rightarrow \mu^+\mu^-$
145.0 ± 1.7		16 O'CONNELL	97	RVUE $e^+e^- \rightarrow \pi^+\pi^-$
142.5 ± 3.5		17 BERNICHA	94	RVUE $e^+e^- \rightarrow \pi^+\pi^-$
138 ± 1		18 GESHKEN...	89	RVUE $e^+e^- \rightarrow \pi^+\pi^-$

- Using the GOUNARIS 68 parametrization with the complex phase of the  $\rho-\omega$  interference and leaving the masses and widths of the  $\rho(1450)$ ,  $\rho(1700)$ , and  $\rho(2150)$  resonances as free parameters of the fit.
- A combined fit of AKHMETSHIN 07, AULCHENKO 06, and AULCHENKO 05.
- Supersedes ACHASOV 05A.
- A fit of the SND data from 400 to 1000 MeV using parameters of the  $\rho(1450)$  and  $\rho(1700)$  from a fit of the data of BARKOV 85, BISELLO 89 and ANDERSON 00A.
- Using the GOUNARIS 68 parametrization with the complex phase of the  $\rho-\omega$  interference.
- From a fit in the energy range 0.61 to 0.96 GeV. Update of AKHMETSHIN 02.
- Assuming  $m_{\rho^+} = m_{\rho^-}$ ,  $\Gamma_{\rho^+} = \Gamma_{\rho^-}$ .
- From the GOUNARIS 68 parametrization of the pion form factor.
- Applies the Unitary & Analytic Model of the pion electromagnetic form factor of DUBNICKA 10 to analyze the data of LEES 12G and ABLIKIM 16C.
- Applies the Unitary & Analytic Model of the pion electromagnetic form factor of DUBNICKA 10 to analyze the data of ACHASOV 06, AKHMETSHIN 07, AUBERT 09as, and AMBROSINO 11A.
- Assuming  $m_{\rho^+} = m_{\rho^-} = m_{\rho^0}$ ,  $\Gamma_{\rho^+} = \Gamma_{\rho^-} = \Gamma_{\rho^0}$ .
- Without limitations on masses and widths.
- Assuming  $m_{\rho^0} = m_{\rho^\pm}$ ,  $g_{\rho^0\pi\pi} = g_{\rho^\pm\pi\pi}$ .
- Using the data of BARKOV 85 in the hidden local symmetry model.
- From the fit to  $e^+e^- \rightarrow \pi^+\pi^-$  data from the compilations of HEYN 81 and BARKOV 85, including the GOUNARIS 68 parametrization of the pion form factor.
- A fit of BARKOV 85 data assuming the direct  $\omega\pi\pi$  coupling.
- Applying the S-matrix formalism to the BARKOV 85 data.
- Includes BARKOV 85 data. Model-dependent width definition.



### CHARGED ONLY, $\tau$ DECAYS and $e^+e^-$

VALUE (MeV)	EVTS	DOCUMENT ID	TECN	CHG	COMMENT
<b>149.1 ± 0.8 OUR FIT</b>					
<b>149.1 ± 0.8 OUR AVERAGE</b>					
148.1 ± 0.4 ± 1.7	5.4M	1,2 FUJIKAWA	08	BELL ±	$\tau^- \rightarrow \pi^- \pi^0 \nu_\tau$
149.0 ± 1.2		2,3 SCHAELE	05c	ALEP	$\tau^- \rightarrow \pi^- \pi^0 \nu_\tau$
149.9 ± 2.3 ± 2.0	500k	4 ACHASOV	02	SND ±	1.02 $e^+e^- \rightarrow \pi^+\pi^-\pi^0$
150.4 ± 1.4 ± 1.4	87k	5,6 ANDERSON	00A	CLE2	$\tau^- \rightarrow \pi^- \pi^0 \nu_\tau$
139.90 ± 0.46		7 BARTOS	17A	RVUE	$\tau^- \rightarrow \pi^- \pi^0 \nu_\tau$
143.7 ± 1.3 ± 1.2	1.98M	4 ALOISIO	03	KLOE ±	1.02 $e^+e^- \rightarrow \pi^+\pi^-\pi^0$
142.9 ± 1.3 ± 1.4	1.98M	8 ALOISIO	03	KLOE -	1.02 $e^+e^- \rightarrow \pi^+\pi^-\pi^0$
144.7 ± 1.4 ± 1.2	1.98M	8 ALOISIO	03	KLOE +	1.02 $e^+e^- \rightarrow \pi^+\pi^-\pi^0$
150.2 ± 2.0 ± 0.7 ± 1.6		9 SANZ-CILLERO	03	RVUE	$\tau^- \rightarrow \pi^- \pi^0 \nu_\tau$
150.9 ± 2.2 ± 2.0	500k	10 ACHASOV	02	SND	1.02 $e^+e^- \rightarrow \pi^+\pi^-\pi^0$

- • • We do not use the following data for averages, fits, limits, etc. • • •
- 1  $|F_\pi(0)|^2$  fixed to 1.
- 2 From the GOUNARIS 68 parametrization of the pion form factor.
- 3 The error combines statistical and systematic uncertainties. Supersedes BARATE 97M.
- 4 Assuming  $m_{\rho^+} = m_{\rho^-}$ ,  $\Gamma_{\rho^+} = \Gamma_{\rho^-}$ .
- 5  $\rho(1700)$  mass and width fixed at 1700 MeV and 235 MeV respectively.
- 6 From the GOUNARIS 68 parametrization of the pion form factor. The second error is a model error taking into account different parametrizations of the pion form factor.
- 7 Applies the Unitary & Analytic Model of the pion electromagnetic form factor of DUBNICKA 10 to analyze the data of FUJIKAWA 08.
- 8 Without limitations on masses and widths.
- 9 Using the data of BARATE 97M and the effective chiral Lagrangian.
- 10 Assuming  $m_{\rho^0} = m_{\rho^\pm}$ ,  $g_{\rho^0\pi\pi} = g_{\rho^\pm\pi\pi}$ .

### MIXED CHARGES, OTHER REACTIONS

VALUE (MeV)	EVTS	DOCUMENT ID	TECN	CHG	COMMENT
<b>149.5 ± 1.3</b>	600k	1 ABELE	99E	CBAR	0 ± 0.0 $\bar{p}p \rightarrow \pi^+\pi^-\pi^0$

<sup>1</sup> Assuming the equality of  $\rho^+$  and  $\rho^-$  masses and widths.

### CHARGED ONLY, HADROPRODUCED

VALUE (MeV)	EVTS	DOCUMENT ID	TECN	CHG	COMMENT
<b>150.2 ± 2.4 OUR FIT</b>					
<b>150.2 ± 2.4 OUR AVERAGE</b>					
152.8 ± 4.3		ABELE	97	CBAR	$\bar{p}n \rightarrow \pi^-\pi^0\pi^0$
155 ± 11	2.9k	1 CAPRARO	87	SPEC -	200 $\pi^-$ Cu $\rightarrow \pi^-\pi^0$ Cu
154 ± 20	967	1 CAPRARO	87	SPEC -	200 $\pi^-$ Pb $\rightarrow \pi^-\pi^0$ Pb
150 ± 5		HUSTON	86	SPEC +	202 $\pi^+$ A $\rightarrow \pi^+\pi^0$ A
146 ± 12	6.5k	2 BYERLY	73	OSPK	5 $\pi^-$ p
148.2 ± 4.1	9.6k	3 PISUT	68	RVUE	1.7-3.2 $\pi^-$ p, $t < 10$
146 ± 13	900	EISNER	67	HBC	4.2 $\pi^-$ p, $t < 10$
137.0 ± 0.4		4 ABLIKIM	17	BES3	$J/\psi \rightarrow \gamma 3\pi$

- • • We do not use the following data for averages, fits, limits, etc. • • •
- 1 Width errors enlarged by us to  $4\Gamma/\sqrt{N}$ ; see the note with the  $K^*(892)$  mass.
- 2 Phase shift analysis. Systematic errors added corresponding to spread of different fits.
- 3 From fit of 3-parameter relativistic P-wave Breit-Wigner to total mass distribution. Includes BATON 68, MILLER 67B, ALFF-STEINBERGER 66, HAGOPIAN 66, HAGOPIAN 66B, JACOBS 66B, JAMES 66, WEST 66, BLIEDEN 65 and CARMONY 64.
- 4 S-matrix pole at a fixed  $\rho$  meson mass of 775.49 MeV.

### NEUTRAL ONLY, PHOTOPRODUCED

VALUE (MeV)	EVTS	DOCUMENT ID	TECN	COMMENT
<b>151.7 ± 2.6 OUR AVERAGE</b>				
155 ± 5 ± 2	63.5k	1 ABRAMOWICZ12	ZEUS	$ep \rightarrow e\pi^+\pi^-\rho$
146 ± 3 ± 13	79k	2 BREITWEG	98B	ZEUS 50-100 $\gamma$ p
150.9 ± 3.0		BARTALUCCI	78	CNTR $\gamma p \rightarrow e^+e^-p$
138 ± 3	79k	3 BREITWEG	98B	ZEUS 50-100 $\gamma$ p
147 ± 11		GLADDING	73	CNTR 2.9-4.7 $\gamma$ p
155 ± 12	2430	BALLAM	72	HBC 4.7 $\gamma$ p
145 ± 13	1930	BALLAM	72	HBC 2.8 $\gamma$ p
140 ± 5		ALVENSLEB...	70	CNTR $\gamma$ A, $t < 0.01$
146.1 ± 2.9	140k	BIGGS	70	CNTR $< 4.1 \gamma$ C $\rightarrow \pi^+\pi^-$ C
160 ± 10		LANZEROTTI	68	CNTR $\gamma$ p
130 ± 5	4000	ASBURY	67B	CNTR $\gamma +$ Pb

- • • We do not use the following data for averages, fits, limits, etc. • • •
- 1 Using the KUHN 90 parametrization of the pion form factor, neglecting  $\rho-\omega$  interference.
- 2 From the parametrization according to SOEDING 66.
- 3 From the parametrization according to ROSS 66.

### NEUTRAL ONLY, OTHER REACTIONS

VALUE (MeV)	EVTS	DOCUMENT ID	TECN	COMMENT
<b>150.9 ± 1.7 OUR AVERAGE</b>				Error includes scale factor of 1.1.
122 ± 20		BERTIN	97c	OBLX 0.0 $\bar{p}p \rightarrow \pi^+\pi^-\pi^0$
145.7 ± 5.3		WEIDENAUER	93	ASTE $\bar{p}p \rightarrow \pi^+\pi^-\omega$
144.9 ± 3.7		DUBNICKA	89	RVUE $\pi$ form factor
148 ± 6		1,2 BOHACIK	80	RVUE
152 ± 9		3 WICKLUND	78	ASPK 3.4, 6 $\pi^\pm$ p N
154 ± 2	76k	DEUTSCH...	76	HBC 16 $\pi^+$ p
157 ± 8	6.8k	4 RATCLIFF	72	ASPK 15 $\pi^-$ p, $t < 0.3$
143 ± 8	1.7k	REYNOLDS	69	HBC 2.26 $\pi^-$ p

••• We do not use the following data for averages, fits, limits, etc. •••

150.85 ± 0.55 ± 0.67	970k	<sup>5</sup> ABLIKIM	18c	BES3	$\eta'(958) \rightarrow \gamma \pi^+ \pi^-$
150.18 ± 0.55 ± 0.65	970k	<sup>6</sup> ABLIKIM	18c	BES3	$\eta(958) \rightarrow \gamma \pi^+ \pi^-$
147.0 ± 2.5	600k	<sup>7</sup> ABELE	99E	CBAR	$0.0 \bar{p} p \rightarrow \pi^+ \pi^- \pi^0$
146 ± 3	4.9k	<sup>8</sup> ADAMS	97	E665	$470 \mu p \rightarrow \mu X B$
160.0 + 4.1 - 4.0		<sup>9</sup> CHABAUD	83	ASPK	$17 \pi^- p$ polarized
155 ± 1		<sup>10</sup> HEYN	81	RVUE	$\pi$ form factor
148.0 ± 1.3		<sup>1,2</sup> LANG	79	RVUE	
146 ± 14	4.1k	ENGLER	74	DBC	$6 \pi^+ n \rightarrow \pi^+ \pi^- p$
143 ± 13		<sup>2</sup> ESTABROOKS	74	RVUE	$17 \pi^- p \rightarrow \pi^+ \pi^- n$
160 ± 10	32k	<sup>1</sup> PROTOPOP...	73	HBC	$7.1 \pi^+ p, t < 0.4$
145 ± 12	2.2k	<sup>3,11</sup> HYAMS	68	OSPK	$11.2 \pi^- p$
163 ± 15	13.3k	<sup>12</sup> PISUT	68	RVUE	$1.7-3.2 \pi^- p, t < 10$

- <sup>1</sup> From pole extrapolation.
- <sup>2</sup> From phase shift analysis of GRAYER 74 data.
- <sup>3</sup> Width errors enlarged by us to  $4\Gamma/\sqrt{N}$ ; see the note with the  $K^*(892)$  mass.
- <sup>4</sup> Published values contain misprints. Corrected by private communication RATCLIFF 74.
- <sup>5</sup> From a fit to  $\pi^+ \pi^-$  mass using  $\rho(770)$  (parametrized with the Gounaris-Sakurai approach),  $\omega(782)$ , and box anomaly components.
- <sup>6</sup> From a fit to  $\pi^+ \pi^-$  mass using  $\rho(770)$  (parametrized with the Gounaris-Sakurai approach),  $\omega(782)$ , and  $\rho(1450)$  components.
- <sup>7</sup> Using relativistic Breit-Wigner and taking into account  $\rho$ - $\omega$  interference.
- <sup>8</sup> Systematic errors not evaluated.
- <sup>9</sup> From fit of 3-parameter relativistic Breit-Wigner to helicity-zero part of  $P$ -wave intensity. CHABAUD 83 includes data of GRAYER 74.
- <sup>10</sup> HEYN 81 includes all spacelike and timelike  $F_\pi$  values until 1978.
- <sup>11</sup> Of HYAMS 68 six parametrizations this is theoretically soundest. MR
- <sup>12</sup> Includes MALAMUD 69, ARMENISE 68, BACON 67, HUWE 67, MILLER 67b, ALFF-STEINBERGER 66, HAGOPIAN 66, HAGOPIAN 66a, JACOBS 66a, JAMES 66, WEST 66, GOLDHABER 64, ABOLINS 63.

$\Gamma(\rho(770)^0) - \Gamma(\rho(770)^\pm)$

VALUE (MeV)	EVTS	DOCUMENT ID	TECN	COMMENT
<b>0.3 ± 1.3 OUR AVERAGE</b>				Error includes scale factor of 1.4.
-0.2 ± 1.0		<sup>1</sup> SCHAEEL	05c	ALEP $\tau^- \rightarrow \pi^- \pi^0 \nu_\tau$
3.6 ± 1.8 ± 1.7 1.98M		<sup>2</sup> ALOISIO	03	KLOE $1.02 e^+ e^- \rightarrow \pi^+ \pi^- \pi^0$

- We do not use the following data for averages, fits, limits, etc. •••
- 4.66 ± 0.85 <sup>3</sup> BARTOS 17A RVUE  $e^+ e^- \rightarrow \pi^+ \pi^-, \tau^- \rightarrow \pi^- \pi^0 \nu_\tau$
- <sup>1</sup> From the combined fit of the  $\tau^-$  data from ANDERSON 00a and SCHAEEL 05c and  $e^+ e^-$  data from the compilation of BARKOV 85, AKHMETSHIN 04, and ALOISIO 05. Supersedes BARATE 97m.
- <sup>2</sup> Assuming  $m_{\rho^+} = m_{\rho^-}, \Gamma_{\rho^+} = \Gamma_{\rho^-}$ .
- <sup>3</sup> Applies the Unitary & Analytic Model of the pion electromagnetic form factor of DUBNICKA 10 to analyze the data of ACHASOV 06, AKHMETSHIN 07, AUBERT 09as, AMBROSINO 11a, and FUJIKAWA 08.

$\Gamma(\rho(770)^+) - \Gamma(\rho(770)^-)$

VALUE	EVTS	DOCUMENT ID	TECN	COMMENT
<b>1.8 ± 2.0 ± 0.5</b>	1.98M	<sup>1</sup> ALOISIO	03	KLOE $1.02 e^+ e^- \rightarrow \pi^+ \pi^- \pi^0$

<sup>1</sup> Without limitations on masses and widths.

$\rho(770)$  DECAY MODES

Mode	Fraction ( $\Gamma_i/\Gamma$ )	Scale factor/ Confidence level
$\Gamma_1 \pi \pi$	~ 100	%

$\rho(770)^\pm$  decays

$\Gamma_2 \pi^\pm \pi^0$	~ 100	%	
$\Gamma_3 \pi^\pm \gamma$	( 4.5 ± 0.5 )	$\times 10^{-4}$	S=2.2
$\Gamma_4 \pi^\pm \eta$	< 6	$\times 10^{-3}$	CL=84%
$\Gamma_5 \pi^\pm \pi^+ \pi^- \pi^0$	< 2.0	$\times 10^{-3}$	CL=84%

$\rho(770)^0$  decays

$\Gamma_6 \pi^+ \pi^-$	~ 100	%	
$\Gamma_7 \pi^+ \pi^- \gamma$	( 9.9 ± 1.6 )	$\times 10^{-3}$	
$\Gamma_8 \pi^0 \gamma$	( 4.7 ± 0.6 )	$\times 10^{-4}$	S=1.4
$\Gamma_9 \eta \gamma$	( 3.00 ± 0.21 )	$\times 10^{-4}$	
$\Gamma_{10} \pi^0 \pi^0 \gamma$	( 4.5 ± 0.8 )	$\times 10^{-5}$	
$\Gamma_{11} \mu^+ \mu^-$	[a]	$\times 10^{-5}$	
$\Gamma_{12} e^+ e^-$	[a]	$\times 10^{-5}$	
$\Gamma_{13} \pi^+ \pi^- \pi^0$	( 1.01 + 0.54 - 0.36 ± 0.34 )	$\times 10^{-4}$	
$\Gamma_{14} \pi^+ \pi^- \pi^+ \pi^-$	( 1.8 ± 0.9 )	$\times 10^{-5}$	
$\Gamma_{15} \pi^+ \pi^- \pi^0 \pi^0$	( 1.6 ± 0.8 )	$\times 10^{-5}$	
$\Gamma_{16} \pi^0 e^+ e^-$	< 1.2	$\times 10^{-5}$	CL=90%
$\Gamma_{17} \eta e^+ e^-$			

[a] The  $\omega\rho$  interference is then due to  $\omega\rho$  mixing only, and is expected to be small. If  $e\mu$  universality holds,  $\Gamma(\rho^0 \rightarrow \mu^+ \mu^-) = \Gamma(\rho^0 \rightarrow e^+ e^-) \times 0.99785$ .

CONSTRAINED FIT INFORMATION

An overall fit to the total width and a partial width uses 10 measurements and one constraint to determine 3 parameters. The overall fit has a  $\chi^2 = 10.7$  for 8 degrees of freedom.

The following *off-diagonal* array elements are the correlation coefficients  $\langle \delta p_i \delta p_j \rangle / (\delta p_i \delta p_j)$ , in percent, from the fit to parameters  $p_i$ , including the branching fractions,  $x_i \equiv \Gamma_i / \Gamma_{\text{total}}$ . The fit constrains the  $x_i$  whose labels appear in this array to sum to one.

$x_3$	-100
$\Gamma$	$\begin{matrix} 15 & -15 \\ x_2 & x_3 \end{matrix}$

Mode	Rate (MeV)	Scale factor
$\Gamma_2 \pi^\pm \pi^0$	150.2 ± 2.4	
$\Gamma_3 \pi^\pm \gamma$	0.068 ± 0.007	2.3

CONSTRAINED FIT INFORMATION

An overall fit to the total width, a partial width, and 7 branching ratios uses 22 measurements and one constraint to determine 9 parameters. The overall fit has a  $\chi^2 = 9.5$  for 14 degrees of freedom.

The following *off-diagonal* array elements are the correlation coefficients  $\langle \delta p_i \delta p_j \rangle / (\delta p_i \delta p_j)$ , in percent, from the fit to parameters  $p_i$ , including the branching fractions,  $x_i \equiv \Gamma_i / \Gamma_{\text{total}}$ . The fit constrains the  $x_i$  whose labels appear in this array to sum to one.

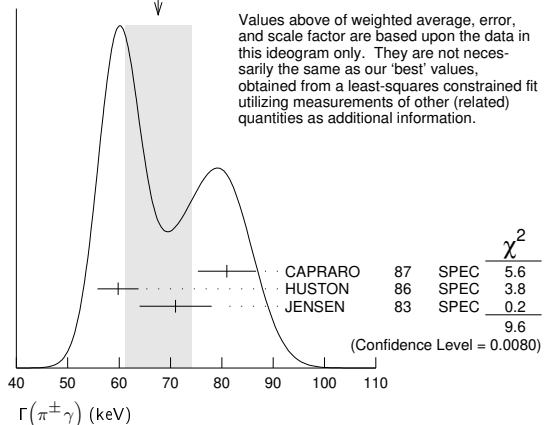
$x_7$	-100						
$x_8$	-4	0					
$x_9$	-1	0	1				
$x_{10}$	-1	0	0	0			
$x_{11}$	2	-3	0	0	0		
$x_{12}$	0	0	-8	-9	0	0	
$x_{14}$	-1	0	0	0	0	0	0
$\Gamma$	0	0	4	5	0	0	-54

Mode	Rate (MeV)	Scale factor
$\Gamma_6 \pi^+ \pi^-$	147.5 ± 0.9	
$\Gamma_7 \pi^+ \pi^- \gamma$	1.48 ± 0.24	
$\Gamma_8 \pi^0 \gamma$	0.070 ± 0.009	1.4
$\Gamma_9 \eta \gamma$	0.0447 ± 0.0032	
$\Gamma_{10} \pi^0 \pi^0 \gamma$	0.0066 ± 0.0012	
$\Gamma_{11} \mu^+ \mu^-$	[a]	0.0068 ± 0.0004
$\Gamma_{12} e^+ e^-$	[a]	0.00704 ± 0.00006
$\Gamma_{14} \pi^+ \pi^- \pi^+ \pi^-$	0.0027 ± 0.0014	

$\rho(770)$  PARTIAL WIDTHS

VALUE (keV)	DOCUMENT ID	TECN	CHG	COMMENT
<b>68 ± 7 OUR FIT</b>				Error includes scale factor of 2.3.
<b>68 ± 7 OUR AVERAGE</b>				Error includes scale factor of 2.2. See the ideogram below.
81 ± 4 ± 4	CAPRARO	87	SPEC	- 200 $\pi^- A \rightarrow \pi^- \pi^0 A$
59.8 ± 4.0	HUSTON	86	SPEC	+ 202 $\pi^+ A \rightarrow \pi^+ \pi^0 A$
71 ± 7	JENSEN	83	SPEC	- 156-260 $\pi^- A \rightarrow \pi^- \pi^0 A$

WEIGHTED AVERAGE  
68 ± 7 (Error scaled by 2.2)





# Meson Particle Listings

## $\rho(770)$

### $\Gamma(\pi^0\gamma)$ G8

VALUE (keV)	EVTS	DOCUMENT ID	TECN	COMMENT
• • • We do not use the following data for averages, fits, limits, etc. • • •				
$77 \pm 17 \pm 11$	36500	<sup>1</sup> ACHASOV 03	SND	$0.60-0.97 e^+e^- \rightarrow \pi^0\gamma$
121 ± 31		DOLINSKY 89	ND	$e^+e^- \rightarrow \pi^0\gamma$

<sup>1</sup> Using  $\Gamma_{\text{total}} = 147.9 \pm 1.3$  MeV and  $B(\rho \rightarrow \pi^0\gamma)$  from ACHASOV 03.

### $\Gamma(\eta\gamma)$ G9

VALUE (keV)	DOCUMENT ID	TECN	COMMENT
• • • We do not use the following data for averages, fits, limits, etc. • • •			
62 ± 17	<sup>1</sup> DOLINSKY 89	ND	$e^+e^- \rightarrow \eta\gamma$

<sup>1</sup> Solution corresponding to constructive  $\omega$ - $\rho$  interference.

### $\Gamma(e^+e^-)$ G12

VALUE (keV)	EVTS	DOCUMENT ID	TECN	COMMENT
<b>7.04 ± 0.06 OUR FIT</b>				
<b>7.04 ± 0.06 OUR AVERAGE</b>				
$7.048 \pm 0.057 \pm 0.050$	900k	<sup>1</sup> AKHMETSHIN 07	SND	$e^+e^- \rightarrow \pi^+\pi^-$
$7.06 \pm 0.11 \pm 0.05$	114k	<sup>2,3</sup> AKHMETSHIN 04	CMD2	$e^+e^- \rightarrow \pi^+\pi^-$
$6.77 \pm 0.10 \pm 0.30$		BARKOV 85	OLYA	$e^+e^- \rightarrow \pi^+\pi^-$
• • • We do not use the following data for averages, fits, limits, etc. • • •				
$7.12 \pm 0.02 \pm 0.11$	800k	<sup>4</sup> ACHASOV 06	SND	$e^+e^- \rightarrow \pi^+\pi^-$
$6.3 \pm 0.1$		<sup>5</sup> BENAYOUN 98	RVUE	$e^+e^- \rightarrow \pi^+\pi^-$ , $\mu^+\mu^-$

<sup>1</sup> A combined fit of AKHMETSHIN 07, AULCHENKO 06, and AULCHENKO 05.  
<sup>2</sup> Using the GOUNARIS 68 parametrization with the complex phase of the  $\rho$ - $\omega$  interference.  
<sup>3</sup> From a fit in the energy range 0.61 to 0.96 GeV. Update of AKHMETSHIN 02.  
<sup>4</sup> Supersedes ACHASOV 05A.  
<sup>5</sup> Using the data of BARKOV 85 in the hidden local symmetry model.

### $\Gamma(\pi^+\pi^-\pi^+\pi^-)$ G14

VALUE (keV)	EVTS	DOCUMENT ID	TECN	COMMENT
• • • We do not use the following data for averages, fits, limits, etc. • • •				
$2.8 \pm 1.4 \pm 0.5$	153	AKHMETSHIN 00	CMD2	$0.6-0.97 e^+e^- \rightarrow \pi^+\pi^-\pi^+\pi^-$

### $\rho(770) \Gamma(e^+e^-)\Gamma(i)/\Gamma^2(\text{total})$

### $\Gamma(e^+e^-)/\Gamma_{\text{total}} \times \Gamma(\pi^+\pi^-)/\Gamma_{\text{total}}$ G12/G × G6/G

VALUE (units $10^{-5}$ )	EVTS	DOCUMENT ID	TECN	COMMENT
<b>4.876 ± 0.023 ± 0.064</b>	800k	<sup>1,2</sup> ACHASOV 06	SND	$e^+e^- \rightarrow \pi^+\pi^-$
• • • We do not use the following data for averages, fits, limits, etc. • • •				
$4.72 \pm 0.02$		<sup>3</sup> BENAYOUN 10	RVUE	$0.4-1.05 e^+e^-$

<sup>1</sup> Supersedes ACHASOV 05A.  
<sup>2</sup> A fit of the SND data from 400 to 1000 MeV using parameters of the  $\rho(1450)$  and  $\rho(1700)$  from a fit of the data of BARKOV 85, BISELLO 89 and ANDERSON 00A.  
<sup>3</sup> A simultaneous fit of  $e^+e^- \rightarrow \pi^+\pi^-$ ,  $\pi^+\pi^-\pi^0$ ,  $\pi^0\gamma$ ,  $\eta\gamma$  data.

### $\Gamma(e^+e^-)/\Gamma_{\text{total}} \times \Gamma(\eta\gamma)/\Gamma_{\text{total}}$ G12/G × G9/G

VALUE (units $10^{-8}$ )	EVTS	DOCUMENT ID	TECN	COMMENT
<b>1.42 ± 0.10 OUR FIT</b>				
<b>1.45 ± 0.12 OUR AVERAGE</b>				
$1.32 \pm 0.14 \pm 0.08$	33k	<sup>1</sup> ACHASOV 07B	SND	$0.6-1.38 e^+e^- \rightarrow \eta\gamma$
$1.50 \pm 0.65 \pm 0.09$	17.4k	<sup>2</sup> AKHMETSHIN 05	CMD2	$0.60-1.38 e^+e^- \rightarrow \eta\gamma$
$1.61 \pm 0.20 \pm 0.11$	23k	<sup>3,4</sup> AKHMETSHIN 01B	CMD2	$e^+e^- \rightarrow \eta\gamma$
$1.85 \pm 0.49$		<sup>5</sup> DOLINSKY 89	ND	$e^+e^- \rightarrow \eta\gamma$
• • • We do not use the following data for averages, fits, limits, etc. • • •				
$1.05 \pm 0.02$		<sup>6</sup> BENAYOUN 10	RVUE	$0.4-1.05 e^+e^-$

<sup>1</sup> From a combined fit of  $\sigma(e^+e^- \rightarrow \eta\gamma)$  with  $\eta \rightarrow 3\pi^0$  and  $\eta \rightarrow \pi^+\pi^-\pi^0$ , and fixing  $B(\eta \rightarrow 3\pi^0) / B(\eta \rightarrow \pi^+\pi^-\pi^0) = 1.44 \pm 0.04$ . Recalculated by us from the cross section at the peak. Supersedes ACHASOV 00D and ACHASOV 06A.  
<sup>2</sup> From the  $\eta \rightarrow 2\gamma$  decay and using  $B(\eta \rightarrow \gamma\gamma) = 39.43 \pm 0.26\%$ .  
<sup>3</sup> From the  $\eta \rightarrow 3\pi^0$  decay and using  $B(\eta \rightarrow 3\pi^0) = (32.24 \pm 0.29) \times 10^{-2}$ .  
<sup>4</sup> The combined fit from 600 to 1380 MeV taking into account  $\rho(770)$ ,  $\omega(782)$ ,  $\phi(1020)$ , and  $\rho(1450)$  (mass and width fixed at 1450 MeV and 310 MeV respectively).  
<sup>5</sup> Recalculated by us from the cross section in the peak.  
<sup>6</sup> A simultaneous fit of  $e^+e^- \rightarrow \pi^+\pi^-$ ,  $\pi^+\pi^-\pi^0$ ,  $\pi^0\gamma$ ,  $\eta\gamma$  data.

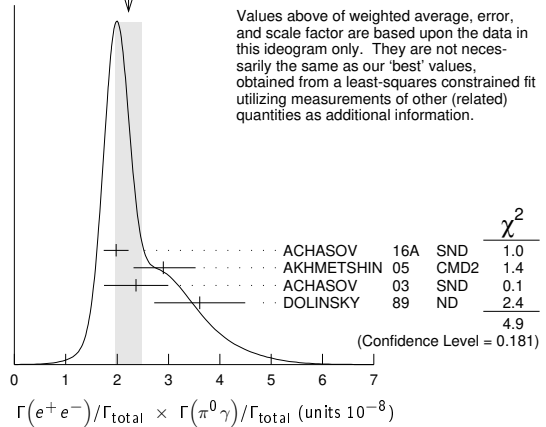
### $\Gamma(e^+e^-)/\Gamma_{\text{total}} \times \Gamma(\pi^0\gamma)/\Gamma_{\text{total}}$ G12/G × G8/G

VALUE (units $10^{-8}$ )	EVTS	DOCUMENT ID	TECN	COMMENT
<b>2.22 ± 0.29 OUR FIT</b>				Error includes scale factor of 1.4.
<b>2.22 ± 0.26 OUR AVERAGE</b>				Error includes scale factor of 1.3. See the ideogram below.
$1.98 \pm 0.22 \pm 0.10$		<sup>1</sup> ACHASOV 16A	SND	$0.60-1.38 e^+e^- \rightarrow \pi^0\gamma$
$2.90 \pm 0.60 \pm 0.18$	18k	AKHMETSHIN 05	CMD2	$0.60-1.38 e^+e^- \rightarrow \pi^0\gamma$
$2.37 \pm 0.53 \pm 0.33$	36k	<sup>2</sup> ACHASOV 03	SND	$0.60-0.97 e^+e^- \rightarrow \pi^0\gamma$
$3.61 \pm 0.74 \pm 0.49$	10k	<sup>3</sup> DOLINSKY 89	ND	$e^+e^- \rightarrow \pi^0\gamma$
• • • We do not use the following data for averages, fits, limits, etc. • • •				
$1.875 \pm 0.026$		<sup>4</sup> BENAYOUN 10	RVUE	$0.4-1.05 e^+e^-$

<sup>1</sup> From the VMD model with the  $\rho(770)$ ,  $\omega(782)$ ,  $\phi(1020)$  resonances, and an additional resonance describing the total contribution of the  $\rho(1450)$  and  $\omega(1420)$  states. Supersedes ACHASOV 03.

<sup>2</sup> Using  $\sigma_{\phi \rightarrow \pi^0\gamma}$  from ACHASOV 00 and  $m_{\rho} = 775.97$  MeV in the model with the energy-independent phase of  $\rho$ - $\omega$  interference equal to  $(-10.2 \pm 7.0)^\circ$ .  
<sup>3</sup> Recalculated by us from the cross section in the peak.  
<sup>4</sup> A simultaneous fit of  $e^+e^- \rightarrow \pi^+\pi^-$ ,  $\pi^+\pi^-\pi^0$ ,  $\pi^0\gamma$ ,  $\eta\gamma$  data.

WEIGHTED AVERAGE  
 $2.22 \pm 0.26$  (Error scaled by 1.3)



### $\Gamma(e^+e^-)/\Gamma_{\text{total}} \times \Gamma(\pi^+\pi^-\pi^0)/\Gamma_{\text{total}}$ G12/G × G13/G

VALUE (units $10^{-9}$ )	EVTS	DOCUMENT ID	TECN	COMMENT
• • • We do not use the following data for averages, fits, limits, etc. • • •				
$0.903 \pm 0.076$		<sup>1</sup> BENAYOUN 10	RVUE	$0.4-1.05 e^+e^-$
$4.58 \pm 2.46 \pm 1.64$	1.2M	<sup>2</sup> ACHASOV 03D	RVUE	$0.44-2.00 e^+e^- \rightarrow \pi^+\pi^-\pi^0$

<sup>1</sup> A simultaneous fit of  $e^+e^- \rightarrow \pi^+\pi^-$ ,  $\pi^+\pi^-\pi^0$ ,  $\pi^0\gamma$ ,  $\eta\gamma$  data.  
<sup>2</sup> Statistical significance is less than 3 $\sigma$ .

### $\rho(770)$ BRANCHING RATIOS

#### $\Gamma(\pi^\pm\eta)/\Gamma(\pi\pi)$ G4/G1

VALUE (units $10^{-4}$ )	CL%	DOCUMENT ID	TECN	CHG	COMMENT
<b>&lt;60</b>	84	FERBEL 66	HBC	±	$\pi^\pm p$ above 2.5

#### $\Gamma(\pi^\pm\pi^+\pi^-\pi^0)/\Gamma(\pi\pi)$ G5/G1

VALUE (units $10^{-4}$ )	CL%	DOCUMENT ID	TECN	CHG	COMMENT
<b>&lt;20</b>	84	FERBEL 66	HBC	±	$\pi^\pm p$ above 2.5
• • • We do not use the following data for averages, fits, limits, etc. • • •					
$35 \pm 40$		JAMES 66	HBC	+	$2.1 \pi^+ p$

#### $\Gamma(\pi^+\pi^-\gamma)/\Gamma_{\text{total}}$ G7/G

VALUE	CL%	DOCUMENT ID	TECN	COMMENT
<b>0.0099 ± 0.0016 OUR FIT</b>				
<b>0.0099 ± 0.0016</b>				
$0.111 \pm 0.0014$		<sup>2</sup> VASSERMAN 88	ND	$e^+e^- \rightarrow \pi^+\pi^-\gamma$
$<0.005$	90	<sup>3</sup> VASSERMAN 88	ND	$e^+e^- \rightarrow \pi^+\pi^-\gamma$

<sup>1</sup> Bremsstrahlung from a decay pion and for photon energy above 50 MeV.  
<sup>2</sup> Superseded by DOLINSKY 91.  
<sup>3</sup> Structure radiation due to quark rearrangement in the decay.

#### $\Gamma(\pi^0\gamma)/\Gamma_{\text{total}}$ G8/G

VALUE (units $10^{-4}$ )	EVTS	DOCUMENT ID	TECN	COMMENT
• • • We do not use the following data for averages, fits, limits, etc. • • •				
$4.20 \pm 0.52$		<sup>1</sup> ACHASOV 16A	SND	$0.60-1.38 e^+e^- \rightarrow \pi^0\gamma$
$6.21 \pm 1.28 \pm 0.39$	18k	<sup>2,3</sup> AKHMETSHIN 05	CMD2	$0.60-1.38 e^+e^- \rightarrow \pi^0\gamma$
$5.22 \pm 1.17 \pm 0.75$	36k	<sup>3,4</sup> ACHASOV 03	SND	$0.60-0.97 e^+e^- \rightarrow \pi^0\gamma$
$6.8 \pm 1.7$		<sup>5</sup> BENAYOUN 96	RVUE	$0.54-1.04 e^+e^- \rightarrow \pi^0\gamma$
$7.9 \pm 2.0$		<sup>3</sup> DOLINSKY 89	ND	$e^+e^- \rightarrow \pi^0\gamma$

<sup>1</sup> Using  $B(\rho \rightarrow e^+e^-)$  from PDG 15. Supersedes ACHASOV 03.  
<sup>2</sup> Using  $B(\rho \rightarrow e^+e^-) = (4.67 \pm 0.09) \times 10^{-5}$ .  
<sup>3</sup> Not independent of the corresponding  $\Gamma(e^+e^-) \times \Gamma(\pi^0\gamma)/\Gamma_{\text{total}}^2$ .  
<sup>4</sup> Using  $B(\rho \rightarrow e^+e^-) = (4.54 \pm 0.10) \times 10^{-5}$ .  
<sup>5</sup> Reanalysis of DRUZHININ 84, DOLINSKY 89, and DOLINSKY 91 taking into account a triangle anomaly contribution.

#### $\Gamma(\eta\gamma)/\Gamma_{\text{total}}$ G9/G

VALUE (units $10^{-4}$ )	EVTS	DOCUMENT ID	TECN	CHG	COMMENT
<b>3.00 ± 0.21 OUR FIT</b>					
<b>2.90 ± 0.32 OUR AVERAGE</b>					
$2.79 \pm 0.34 \pm 0.03$	33k	<sup>1</sup> ACHASOV 07B	SND		$0.6-1.38 e^+e^- \rightarrow \eta\gamma$
$3.6 \pm 0.9$		<sup>2</sup> ANDREWS 77	CNTR	0	$6.7-10 \gamma\text{Cu}$

••• We do not use the following data for averages, fits, limits, etc. •••

3.21 ± 1.39 ± 0.20	17.4k	3,4	AKH METSHIN 05	CMD2	0.60-1.38	$e^+e^- \rightarrow \eta\gamma$
3.39 ± 0.42 ± 0.23		2,5,6	AKH METSHIN 01B	CMD2		$e^+e^- \rightarrow \eta\gamma$
1.9 <sup>+0.6</sup> / <sub>-0.8</sub>		7	BENAYOUN	96 RVUE	0.54-1.04	$e^+e^- \rightarrow \eta\gamma$
4.0 ± 1.1		2,4	DOLINSKY	89 ND		$e^+e^- \rightarrow \eta\gamma$

<sup>1</sup>ACHASOV 07B reports  $[\Gamma(\rho(770) \rightarrow \eta\gamma)/\Gamma_{\text{total}}] \times [B(\rho(770) \rightarrow e^+e^-)] = (1.32 \pm 0.14 \pm 0.08) \times 10^{-8}$  which we divide by our best value  $B(\rho(770) \rightarrow e^+e^-) = (4.72 \pm 0.05) \times 10^{-5}$ . Our first error is their experiment's error and our second error is the systematic error from using our best value. Supersedes ACHASOV 00D and ACHASOV 06A.

<sup>2</sup>Solution corresponding to constructive  $\rho\text{-}\omega$  interference.

<sup>3</sup>Using  $B(\rho \rightarrow e^+e^-) = (4.67 \pm 0.09) \times 10^{-5}$  and  $B(\eta \rightarrow \gamma\gamma) = 39.43 \pm 0.26\%$ .

<sup>4</sup>Not independent of the corresponding  $\Gamma(e^+e^-) \times \Gamma(\eta\gamma)/\Gamma_{\text{total}}^2$ .

<sup>5</sup>The combined fit from 600 to 1380 MeV taking into account  $\rho(770)$ ,  $\omega(782)$ ,  $\phi(1020)$ , and  $\rho(1450)$  (mass and width fixed at 1450 MeV and 310 MeV respectively).

<sup>6</sup>Using  $B(\rho \rightarrow e^+e^-) = (4.75 \pm 0.10) \times 10^{-5}$  from AKHMETSHIN 02 and  $B(\eta \rightarrow 3\pi^0) = (32.24 \pm 0.29) \times 10^{-2}$ .

<sup>7</sup>Reanalysis of DRUZHININ 84, DOLINSKY 89, and DOLINSKY 91 taking into account a triangle anomaly contribution. Constructive  $\rho\text{-}\omega$  interference solution.

$\Gamma(\pi^0\pi^0\gamma)/\Gamma_{\text{total}}$   $\Gamma_{10}/\Gamma$

VALUE (units $10^{-5}$ )	EVTS	DOCUMENT ID	TECN	COMMENT
<b>4.5 ± 0.8 OUR FIT</b>				
<b>4.5 <sup>+0.9</sup>/<sub>-0.8</sub> OUR AVERAGE</b>				

5.2 <sup>+1.5</sup> / <sub>-1.3</sub> ± 0.6	190	<sup>1</sup> AKHMETSHIN 04B	CMD2	0.6-0.97	$e^+e^- \rightarrow \pi^0\pi^0\gamma$
4.1 <sup>+1.0</sup> / <sub>-0.9</sub> ± 0.3	295	<sup>2</sup> ACHASOV	02F SND	0.36-0.97	$e^+e^- \rightarrow \pi^0\pi^0\gamma$
4.8 <sup>+3.4</sup> / <sub>-1.8</sub> ± 0.5	63	<sup>3</sup> ACHASOV	00G SND		$e^+e^- \rightarrow \pi^0\pi^0\gamma$

••• We do not use the following data for averages, fits, limits, etc. •••

<sup>1</sup>This branching ratio includes the conventional VMD mechanism  $\rho \rightarrow \omega\pi^0$ ,  $\omega \rightarrow \pi^0\gamma$ , and the new decay mode  $\rho \rightarrow f_0(500)\gamma$ ,  $f_0(500) \rightarrow \pi^0\pi^0$  with a branching ratio  $(2.0 \pm 1.1 \pm 0.3) \times 10^{-5}$  differing from zero by 2.0 standard deviations.

<sup>2</sup>This branching ratio includes the conventional VMD mechanism  $\rho \rightarrow \omega\pi^0$ ,  $\omega \rightarrow \pi^0\gamma$  and the new decay mode  $\rho \rightarrow f_0(500)\gamma$ ,  $f_0(500) \rightarrow \pi^0\pi^0$  with a branching ratio  $(1.9 \pm 0.9 \pm 0.4) \times 10^{-5}$  differing from zero by 2.4 standard deviations. Supersedes ACHASOV 00G.

<sup>3</sup>Superseded by ACHASOV 02F.

$\Gamma(\mu^+\mu^-)/\Gamma(\pi^+\pi^-)$   $\Gamma_{11}/\Gamma_6$

VALUE (units $10^{-5}$ )	DOCUMENT ID	TECN	COMMENT
<b>4.60 ± 0.28 OUR FIT</b>			
<b>4.6 ± 0.2 ± 0.2</b>			

8.2 <sup>+1.6</sup> / <sub>-3.6</sub>		<sup>1</sup> ROTHWELL	69 CNTR	Photoproduction
5.6 ± 1.5		<sup>2</sup> WEHMANN	69 OSPK	12 $\pi^-$ C, Fe
9.7 <sup>+3.1</sup> / <sub>-3.3</sub>		<sup>3,4</sup> HYAMS	67 OSPK	11 $\pi^-$ Li, H

••• We do not use the following data for averages, fits, limits, etc. •••

<sup>1</sup>Possibly large  $\rho\text{-}\omega$  interference leads us to increase the minus error.

<sup>2</sup>Result contains 11 ± 11% correction using SU(3) for central value. The error on the correction takes account of possible  $\rho\text{-}\omega$  interference and the upper limit agrees with the upper limit of  $\omega \rightarrow \mu^+\mu^-$  from this experiment.

<sup>3</sup>But he even enlarges his error to take residual  $\omega$  contamination into account. Since his value is high, seems the other experiments also can't have too many  $\omega$ 's. But maybe Hyams has additional  $\mu$ 's from  $\rho \rightarrow \pi\pi$ , decaying  $\pi$ 's.

<sup>4</sup>HYAMS 67's mass resolution is 20 MeV. The  $\omega$  region was excluded.

$\Gamma(e^+e^-)/\Gamma(\pi\pi)$   $\Gamma_{12}/\Gamma_1$

VALUE (units $10^{-4}$ )	DOCUMENT ID	TECN	COMMENT
<b>0.40 ± 0.05</b>			

••• We do not use the following data for averages, fits, limits, etc. •••

<sup>1</sup>The  $\rho'$  contribution is not taken into account.

<sup>2</sup>Barkov excludes Auslender and Benaksas for large statistical and systematic errors.

$\Gamma(\pi^+\pi^-\pi^0)/\Gamma_{\text{total}}$   $\Gamma_{13}/\Gamma$

VALUE (units $10^{-4}$ )	CL%	EVTS	DOCUMENT ID	TECN	COMMENT
<b>1.01 <sup>+0.54</sup>/<sub>-0.36</sub> ± 0.34</b>					
<b>&lt;1.2</b>					

••• We do not use the following data for averages, fits, limits, etc. •••

<sup>1</sup>Statistical significance is less than 3 $\sigma$ .

$\Gamma(\pi^+\pi^-\pi^0)/\Gamma(\pi\pi)$   $\Gamma_{13}/\Gamma_1$

VALUE	CL%	DOCUMENT ID	TECN	CHG	COMMENT
<b>~0.01</b>					
<b>&lt;0.01</b>					

••• We do not use the following data for averages, fits, limits, etc. •••

<sup>1</sup>Model dependent, assumes  $l = 1, 2, \text{ or } 3$  for the  $3\pi$  system.

$\Gamma(\pi^+\pi^-\pi^+\pi^-)/\Gamma_{\text{total}}$   $\Gamma_{14}/\Gamma$

VALUE (units $10^{-5}$ )	CL%	EVTS	DOCUMENT ID	TECN	COMMENT
<b>1.8 ± 0.9 OUR FIT</b>					
<b>1.8 ± 0.9 ± 0.3</b>					

••• We do not use the following data for averages, fits, limits, etc. •••

<20	90	KURDADZE	88 OLYA		$e^+e^- \rightarrow \pi^+\pi^-\pi^+\pi^-$
-----	----	----------	---------	--	---

$\Gamma(\pi^+\pi^-\pi^+\pi^-)/\Gamma(\pi\pi)$   $\Gamma_{14}/\Gamma_1$

VALUE (units $10^{-4}$ )	CL%	DOCUMENT ID	TECN	CHG	COMMENT
<b>&lt;15</b>					
<b>&lt;20</b>					
<b>&lt;20</b>					
<b>&lt;80</b>					

$\Gamma(\pi^+\pi^-\pi^0\pi^0)/\Gamma_{\text{total}}$   $\Gamma_{15}/\Gamma$

VALUE (units $10^{-5}$ )	CL%	DOCUMENT ID	TECN	COMMENT
<b>1.60 ± 0.74 ± 0.18</b>				
<4	90	AULCHENKO	87C ND	$e^+e^- \rightarrow \pi^+\pi^-\pi^0\pi^0$
<20	90	KURDADZE	86 OLYA	$e^+e^- \rightarrow \pi^+\pi^-\pi^0\pi^0$

••• We do not use the following data for averages, fits, limits, etc. •••

<sup>1</sup> Assuming no interference between the  $\rho$  and  $\omega$  contributions.

$\Gamma(\pi^0e^+e^-)/\Gamma_{\text{total}}$   $\Gamma_{16}/\Gamma$

VALUE (units $10^{-5}$ )	CL%	DOCUMENT ID	TECN	COMMENT
<b>&lt;1.2</b>				
<4	90	AULCHENKO	87C ND	$e^+e^- \rightarrow \pi^+\pi^-\pi^0\pi^0$
<20	90	KURDADZE	86 OLYA	$e^+e^- \rightarrow \pi^+\pi^-\pi^0\pi^0$

$\Gamma(\eta e^+e^-)/\Gamma_{\text{total}}$   $\Gamma_{17}/\Gamma$

VALUE (units $10^{-5}$ )	DOCUMENT ID	TECN	COMMENT
<b>&lt;0.7</b>			
<0.7		AKHMETSHIN 05A	CMD2 0.72-0.84 $e^+e^-$

**$\rho(770)$  REFERENCES**

ABLIKIM	18C	PRL 120 242003	M. Ablikim et al.	(BESIII Collab.)
ABLIKIM	17	PRL 118 012001	M. Ablikim et al.	(BESIII Collab.)
BARTOS	17	PR D96 113004	E. Bartos et al.	
BARTOS	17A	IJMP A32 1750154	E. Bartos et al.	
ABLIKIM	16C	PL B753 629	M. Ablikim et al.	(BESIII Collab.)
ACHASOV	16A	PR D93 092001	M.N. Achasov et al.	(SND Collab.)
PDG	15	RPP 2015 at pdg.lbl.gov		(PDG Collab.)
ABRAMOWICZ	12	EPJ C72 1869	H. Abramowicz et al.	(ZEUS Collab.)
LEES	12G	PR D86 032013	J.P. Lees et al.	(BABAR Collab.)
AMBROSINO	11A	PL B700 102	F. Ambrosino et al.	(KLOE Collab.)
BENAYOUN	10	EPJ C65 211	M. Benayoun et al.	
DUBNICKA	10	APS 60 1	S. Dubnicka, A.Z. Dubnickova	
ACHASOV	09A	JETP 109 379	M.N. Achasov et al.	(SND Collab.)
AUBERT	09AS	PRL 103 231801	B. Aubert et al.	(BABAR Collab.)
ACHASOV	08	JETP 107 61	M.N. Achasov et al.	(SND Collab.)
FUJIKAWA	08	PR D78 072006	M. Fujikawa et al.	(BELLE Collab.)
ACHASOV	07B	PR D76 077101	M.N. Achasov et al.	(SND Collab.)
AKHMETSHIN	07	PL B648 28	R.R. Akhmetshin et al.	(Novosibirsk CMD-2 Collab.)
ACHASOV	06	JETP 103 380	M.N. Achasov et al.	(Novosibirsk SND Collab.)
ACHASOV	06A	PR D74 014016	M.N. Achasov et al.	(SND Collab.)
AULCHENKO	06	JETPL 84 413	V.M. Aulchenko et al.	(Novosibirsk CMD-2 Collab.)
ACHASOV	05A	JETP 101 1053	M.N. Achasov et al.	(Novosibirsk SND Collab.)
AKHMETSHIN	05	PL B605 26	R.R. Akhmetshin et al.	(Novosibirsk CMD-2 Collab.)
AKHMETSHIN	05A	PL B613 29	R.R. Akhmetshin et al.	(Novosibirsk CMD-2 Collab.)
ALOISIO	05	PL B606 12	A. Aloisio et al.	(KLOE Collab.)
AULCHENKO	05	JETPL 82 743	V.M. Aulchenko et al.	(Novosibirsk CMD-2 Collab.)
SCHAEF	05C	PRPL 421 131	S. Schaefer et al.	(ALEPH Collab.)
AKHMETSHIN	04	PL B578 285	R.R. Akhmetshin et al.	(Novosibirsk CMD-2 Collab.)
AKHMETSHIN	04B	PL B580 119	R.R. Akhmetshin et al.	(Novosibirsk CMD-2 Collab.)
ACHASOV	03	PL B559 171	M.N. Achasov et al.	(Novosibirsk SND Collab.)
ACHASOV	03D	PR D68 052006	M.N. Achasov et al.	(Novosibirsk SND Collab.)
ALOISIO	03	PL B561 55	A. Aloisio et al.	(KLOE Collab.)
SANZ-CILLERO	03	EPJ C27 587	J.J. Sanz-Cillero, A. Pich	
ACHASOV	02	PR D65 032002	M.N. Achasov et al.	(Novosibirsk SND Collab.)
ACHASOV	02F	PL B537 201	M.N. Achasov et al.	(Novosibirsk SND Collab.)
AKHMETSHIN	02	PL B527 161	R.R. Akhmetshin et al.	(Novosibirsk CMD-2 Collab.)
AKHMETSHIN	01B	PL B509 217	R.R. Akhmetshin et al.	(Novosibirsk CMD-2 Collab.)
COLANGELO	01	NP B603 125	G. Colangelo, J. Gasser, H. Leytwyler	
PICH	01	PR D63 093005	A. Pich, J. Portoles	
ACHASOV	00	EPJ C12 25	M.N. Achasov et al.	(Novosibirsk SND Collab.)
ACHASOV	00D	JETPL 72 282	M.N. Achasov et al.	(Novosibirsk SND Collab.)
ACHASOV	00G	JETPL 71 355	M.N. Achasov et al.	(Novosibirsk SND Collab.)
AKHMETSHIN	00	PL B475 190	R.R. Akhmetshin et al.	(Novosibirsk CMD-2 Collab.)
ANDERSON	00A	PR D61 112002	S. Anderson et al.	(CLEO Collab.)
ABELE	99E	PL B469 270	A. Abele et al.	(Crystal Barrel Collab.)
BENAYOUN	98	EPJ C2 269	M. Benayoun et al.	(IPNP, NOVO, ADL+)
BREITWEG	98B	EPJ C2 247	J. Breitweg et al.	(ZEUS Collab.)
GARDNER	98	PR D57 2716	S. Gardner, H.B. O'Connell	
ABELE	97	PL B391 191	A. Abele et al.	(Crystal Barrel Collab.)
ADAMS	97	ZPHY C74 237	M.R. Adams et al.	(E665 Collab.)
BARATE	97M	ZPHY C76 15	R. Barate et al.	(ALEPH Collab.)
BERTIN	97C	PL B408 476	A. Bertin et al.	(OBELIX Collab.)
BOGOLYUB...	97	PAN 60 46	M.Y. Bogolyubsky et al.	(MOSU, SERP)

Translated from YAF 60 53.

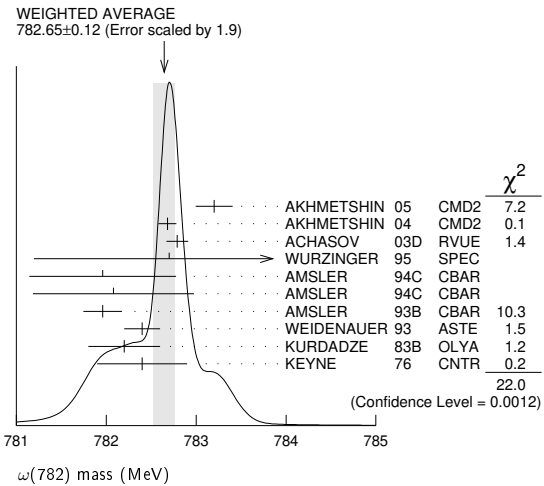
# Meson Particle Listings

## $\rho(770), \omega(782)$

O'CONNELL	97	NP A623 559	H.B. O'Connell et al.	(ADDL)
BENAYOUN	96	ZPHY C72 221	M. Benayoun et al.	(INPN, NOVO)
BERNICHIA	94	PR D50 445	A. Bernichia, G. Lopez Castro, J. Pesticau	(LOUV+)
WEIDENAUER	93	ZPHY C59 387	P. Weidenauer et al.	(ASTERIX Collab.)
AGUILAR...	91	ZPHY C50 405	M. Aguilar-Benitez et al.	(LEBC-EHS Collab.)
DOLINSKY	91	PRPL 202 99	S.I. Dolinsky et al.	(NOVO)
KUHN	90	ZPHY C48 445	J.H. Kuhn et al.	(MPIM)
ANTIPOV	89	ZPHY C42 185	Y.M. Antipov et al.	(SERP, JINR, BGNA+)
BISELLO	89	PR B220 321	D. Bisello et al.	(DM2 Collab.)
DOLINSKY	89	ZPHY C42 511	S.I. Dolinsky et al.	(NOVO)
DUBNICKA	89	JP G15 1349	S.V. Dubnicka et al.	(JINR, SLOV)
GESHKEN	89	ZPHY C45 351	B.V. Geshkenbein	(ITEP)
KURDADZE	88	JETPL 47 512	L.M. Kurdadze et al.	(NOVO)
VASSERMAN	88	SJNP 47 1035	I.B. Vasserman et al.	(NOVO)
VASSERMAN	88B	SJNP 48 480	I.B. Vasserman et al.	(NOVO)
AULCHENKO	87C	IYF 87-90 Preprint	V.M. Aulchenko et al.	(NOVO)
CAPRARO	87	NP B288 659	L. Capraro et al.	(CLER, FRAS, MILA+)
BRAMON	86	PL B173 97	A. Bramon, J. Casulleras	(BARC)
HUSTON	86	PR D33 3199	J. Huston et al.	(ROCH, FNAL, MRN)
KURDADZE	86	JETPL 43 843	L.M. Kurdadze et al.	(NOVO)
BARKOV	85	NP B256 365	L.M. Barkov et al.	(NOVO)
DRUZHININ	84	PL 144B 136	V.P. Druzhinin et al.	(NOVO)
CHABAUD	83	NP B223 1	V. Chabaud et al.	(CERN, CRAC, MPIM)
JENSEN	83	PR D27 26	T. Jensen et al.	(ROCH, FNAL, MINN)
HEYN	81	ZPHY C7 169	M.F. Heyn, C.B. Lang	(GRAZ)
BOHACIK	80	PR D21 1342	J. Bohacik, H. Kuhnelt	(SLOW, WIEN)
LANG	79	PR D19 956	C.B. Lang, A. Mas-Parareda	(GRAZ)
BARTALUCCI	78	NC 44A 567	S. Bartalucci et al.	(DESY, FRAS)
WICKLUND	78	PR D17 1197	A.B. Wicklund et al.	(ARL)
ANDREWS	77	PRL 38 1197	D.E. Andrews et al.	(ROCH)
DEUTSCH...	76	NP B103 426	M. Deuschmann et al.	(AACH3, BERL, BONN+)
ENGLER	74	PR D10 2070	A. Engler et al.	(CMU, CASE)
ESTABROOKS	74	NP B79 301	P.G. Estabrooks, A.D. Martin	(DURH)
GRAYER	74	NP B75 189	G. Grayer et al.	(CERN, MPIM)
RATCLIFF	74	Private Comm.		
BYERLY	73	PR D7 637	W.L. Byerly et al.	(MICH)
GLADDING	73	PR D8 3721	G.E. Gladding et al.	(HARV)
HYAMS	73	NP B64 134	B.D. Hyams et al.	(CERN, MPIM)
PROTOPOP...	73	PR D7 1279	S.D. Protopopescu et al.	(LBL)
BALLAM	72	PR D5 545	J. Ballam et al.	(SLAC, LBL, TUFTS)
BENAKSAS	72	PL 39B 389	J. Benaksas et al.	(ORSAY)
JACOBS	72	PR D6 1291	L.D. Jacobs	(SACL)
RATCLIFF	72	PL 38B 345	B.N. Ratcliff et al.	(SLAC)
ABRAMS	71	PR D4 653	G.S. Abrams et al.	(LBL)
ALVENSLEB...	70	PRL 24 786	H. Alvensleben et al.	(DESY)
BIGGS	70	PRL 24 1197	P.J. Biggs et al.	(DARE)
ERBE	69	PR 188 2060	R. Erbe et al.	(German Bubble Chamber Collab.)
MALAMUD	69	Argonne Conf. 93	E.I. Malamud, P.E. Schlein	(UCLA)
REYNOLDS	69	PR 184 1424	B.G. Reynolds et al.	(FUS)
ROTHWELL	69	PRL 23 1521	P.L. Rothwell et al.	(NEAS)
WEHMANN	69	PR 178 2095	A.A. Wehmann et al.	(HARV, CASE, SLAC+)
ARMENISE	68	NC 54A 999	N. Armenise et al.	(BARI, BGNA, FIRZ+)
BATON	68	PR 176 1574	J.P. Baton, G. Laurens	(SACL)
CHUNG	68	PR 165 1491	S.U. Chung et al.	(LRL)
FOSTER	68	NP B6 107	M. Foster et al.	(CERN, CDEF)
GOUNARIS	68	PRL 21 244	G.J. Gounaris, J.J. Sakurai	(ORSAY, MILA, UCLA)
HUSON	68	PL 28B 208	R. Huson et al.	(CERN, MPIM)
HYAMS	68	NP B7 1	B.D. Hyams et al.	(HARV)
LANZEROTTI	68	PR 166 1365	L.J. Lanzerotti et al.	(CERN)
PISUT	68	NP B6 325	J. Pisut, M. Roos	(DESY, COLU)
ASBURY	67B	PRL 19 865	J.G. Asbury et al.	(BNL)
BACON	67	PR 157 1263	T.C. Bacon et al.	(PURD)
EISNER	67	PL 164 1699	R.L. Eisner et al.	(COLU)
HUWE	67	PL 24B 252	D.O. Huwe et al.	(CERN, MPIM)
HYAMS	67	PL 24B 634	B.D. Hyams et al.	(PURD)
MILLER	67B	PR 153 1423	D.H. Miller et al.	(COLU, RUTG)
ALFF-...	66	PR 145 1072	C. Alff-Steinberger et al.	(ROCH)
FERBEL	66	PL 21 111	T. Ferbel	(PENN, SACL)
HAGOPIAN	66	PR 145 1128	V. Hagopian et al.	(PENN, LRL)
HAGOPIAN	66B	PR 152 1183	V. Hagopian, Y.L. Pan	(LRL)
JACOBS	66B	UCRL 16877	L.D. Jacobs	(YALE, BNL)
JAMES	66	PR 142 896	F.E. James, H.L. Kraybill	
ROSS	66	PR 149 1172	M. Ross, L. Stodolsky	
SOEDING	66	PL B19 702	P. Soeding	
WEST	66	PR 149 1089	E. West et al.	(WISC)
BLIEDEN	65	PL 19 444	H.R. Blieden et al.	(CERN MMS Collab.)
CARMONY	64	PRL 12 254	D.D. Carmony et al.	(UCB)
GOLDBERGER	64	PRL 12 336	G. Goldhaber et al.	(LRL, UCB)
ABOLINS	63	PRL 11 381	M.A. Abolins et al.	(UCSD)

782.7 ± 0.9	535	VANAPEL...	78	HBC	7.2 $\bar{p}p \rightarrow \bar{p}p\omega$
783.5 ± 0.8	2100	GESSAROLI	77	HBC	11 $\pi^- p \rightarrow \omega n$
782.5 ± 0.8	418	AGUILAR...	72B	HBC	3.9, 4.6 $K^- p$
783.4 ± 1.0	248	BIZZARRI	71	HBC	0.0 $\rho\bar{p} \rightarrow K^+ K^- \omega$
781.0 ± 0.6	510	BIZZARRI	71	HBC	0.0 $\rho\bar{p} \rightarrow K_1^+ K_1^- \omega$
783.7 ± 1.0	3583	COYNE	71	HBC	3.7 $\pi^+ p \rightarrow \rho\pi^+ \pi^+ \pi^- \pi^0$
784.1 ± 1.2	750	ABRAMOVI...	70	HBC	3.9 $\pi^- p$
783.2 ± 1.6	9	BIGGS	70B	CNTR	<4.1 $\gamma C \rightarrow \pi^+ \pi^- C$
782.4 ± 0.5	2400	BIZZARRI	69	HBC	0.0 $\bar{p}p$

- Update of AKHMETSIN 00c.
- From the combined fit of ANTONELLI 92, ACHASOV 01e, ACHASOV 02e, and ACHASOV 03d data on the  $\pi^+ \pi^- \pi^0$  and ANTONELLI 92 on the  $\omega \pi^+ \pi^-$  final states. Supersedes ACHASOV 99e and ACHASOV 02e.
- From the  $\eta \rightarrow \gamma\gamma$  decay.
- From the  $\eta \rightarrow 3\pi^0$  decay.
- Observed by threshold-crossing technique. Mass resolution = 4.8 MeV FWHM.
- From the  $\rho-\omega$  interference in the  $\pi^+ \pi^-$  mass spectrum using the Breit-Wigner for the  $\omega$  and leaving its mass and width as free parameters of the fit.
- Systematic uncertainties underestimated.
- From best-resolution sample of COYNE 71.
- From  $\omega-\rho$  interference in the  $\pi^+ \pi^-$  mass spectrum assuming  $\omega$  width 12.6 MeV.



### $\omega(782)$ WIDTH

VALUE (MeV)	EVTS	DOCUMENT ID	TECN	COMMENT
<b>8.49 ± 0.08 OUR AVERAGE</b>				
8.68 ± 0.23 ± 0.10	11200	1 AKHMETSIN 04	CMD2	$e^+e^- \rightarrow \pi^+ \pi^- \pi^0$
8.68 ± 0.04 ± 0.15	1.2M	2 ACHASOV 03D	RVUE	0.44-2.00 $e^+e^- \rightarrow \pi^+ \pi^- \pi^0$
8.2 ± 0.3	19500	WURZINGER 95	SPEC	1.33 $\rho d \rightarrow {}^3\text{He}\omega$
8.4 ± 0.1		3 AULCHENKO 87	ND	$e^+e^- \rightarrow \pi^+ \pi^- \pi^0$
8.30 ± 0.40		BARKOV 87	CMD	$e^+e^- \rightarrow \pi^+ \pi^- \pi^0$
9.8 ± 0.9	1488	KURDADZE 83B	OLYA	$e^+e^- \rightarrow \pi^+ \pi^- \pi^0$
9.0 ± 0.8	433	CORDIER 80	DM1	$e^+e^- \rightarrow \pi^+ \pi^- \pi^0$
9.1 ± 0.8	451	BENAKSAS 72B	OSP K	$e^+e^- \rightarrow \pi^+ \pi^- \pi^0$
8.13 ± 0.45		4 LEES 12G	BABR	$e^+e^- \rightarrow \pi^+ \pi^- \gamma$
12 ± 2	1430	COOPER 78B	HBC	0.7-0.8 $\bar{p}p \rightarrow 5\pi$
9.4 ± 2.5	2100	GESSAROLI 77	HBC	11 $\pi^- p \rightarrow \omega n$
10.22 ± 0.43	20000	5 KEYNE 76	CNTR	$\pi^- p \rightarrow \omega n$
13.3 ± 2	418	AGUILAR...	72B	HBC 3.9, 4.6 $K^- p$
10.5 ± 1.5		BORENSTEIN 72	HBC	2.18 $K^- p$
7.70 ± 0.9 ± 1.15	940	BROWN 72	MMS	2.5 $\pi^- p \rightarrow nMM$
10.3 ± 1.4	510	BIZZARRI 71	HBC	0.0 $\rho\bar{p} \rightarrow K_1^+ K_1^- \omega$
12.8 ± 3.0	248	BIZZARRI 71	HBC	0.0 $\rho\bar{p} \rightarrow K^+ K^- \omega$
9.5 ± 1.0	3583	COYNE 71	HBC	3.7 $\pi^+ p \rightarrow \rho\pi^+ \pi^+ \pi^- \pi^0$

- We do not use the following data for averages, fits, limits, etc. •••
- 1 Update of AKHMETSIN 00c.
- 2 From the combined fit of ANTONELLI 92, ACHASOV 01e, ACHASOV 02e, and ACHASOV 03d data on the  $\pi^+ \pi^- \pi^0$  and ANTONELLI 92 on the  $\omega \pi^+ \pi^-$  final states. Supersedes ACHASOV 99e and ACHASOV 02e.
- 3 Relativistic Breit-Wigner includes radiative corrections.
- 4 From the  $\rho-\omega$  interference in the  $\pi^+ \pi^-$  mass spectrum using the Breit-Wigner for the  $\omega$  and leaving its mass and width as free parameters of the fit.
- 5 Observed by threshold-crossing technique. Mass resolution = 4.8 MeV FWHM.

### $\omega(782)$

$$J^G(J^{PC}) = 0^-(1^{--})$$

### $\omega(782)$ MASS

VALUE (MeV)	EVTS	DOCUMENT ID	TECN	COMMENT
<b>782.65 ± 0.12 OUR AVERAGE</b>				Error includes scale factor of 1.9. See the ideogram below.
783.20 ± 0.13 ± 0.16	18680	AKHMETSIN 05	CMD2	0.60-1.38 $e^+e^- \rightarrow \pi^0 \gamma$
782.68 ± 0.09 ± 0.04	11200	1 AKHMETSIN 04	CMD2	$e^+e^- \rightarrow \pi^+ \pi^- \pi^0$
782.79 ± 0.08 ± 0.09	1.2M	2 ACHASOV 03D	RVUE	0.44-2.00 $e^+e^- \rightarrow \pi^+ \pi^- \pi^0$
782.7 ± 0.1 ± 1.5	19500	WURZINGER 95	SPEC	1.33 $\rho d \rightarrow {}^3\text{He}\omega$
781.96 ± 0.17 ± 0.80	11k	3 AMSLER 94C	CBAR	0.0 $\bar{p}p \rightarrow \omega \eta \pi^0$
782.08 ± 0.36 ± 0.82	3463	4 AMSLER 94C	CBAR	0.0 $\bar{p}p \rightarrow \omega \eta \pi^0$
781.96 ± 0.13 ± 0.17	15k	AMSLER 93B	CBAR	0.0 $\bar{p}p \rightarrow \omega \pi^0 \pi^0$
782.4 ± 0.2	270k	WEIDENAUER 93	ASTE	$\bar{p}p \rightarrow 2\pi^+ 2\pi^- \pi^0$
782.2 ± 0.4	1488	KURDADZE 83B	OLYA	$e^+e^- \rightarrow \pi^+ \pi^- \pi^0$
782.4 ± 0.5	7000	5 KEYNE 76	CNTR	$\pi^- p \rightarrow \omega n$
••• We do not use the following data for averages, fits, limits, etc. •••				
781.91 ± 0.24		6 LEES 12G	BABR	$e^+e^- \rightarrow \pi^+ \pi^- \gamma$
781.78 ± 0.10		7 BARKOV 87	CMD	$e^+e^- \rightarrow \pi^+ \pi^- \pi^0$
783.3 ± 0.4	433	CORDIER 80	DM1	$e^+e^- \rightarrow \pi^+ \pi^- \pi^0$
782.5 ± 0.8	33260	ROOS 80	RVUE	0.0-3.6 $\bar{p}p$
782.6 ± 0.8	3000	BENKHERI 79	OMEG	9-12 $\pi^\pm p$
781.8 ± 0.6	1430	COOPER 78B	HBC	0.7-0.8 $\bar{p}p \rightarrow 5\pi$

$\omega(782)$  DECAY MODES

Mode	Fraction ( $\Gamma_i/\Gamma$ )	Scale factor/ Confidence level
$\Gamma_1$ $\pi^+\pi^-\pi^0$	(89.3 ± 0.6) %	
$\Gamma_2$ $\pi^0\gamma$	( 8.40±0.22) %	S=1.8
$\Gamma_3$ $\pi^+\pi^-$	( 1.53±0.06) %	
$\Gamma_4$ neutrals (excluding $\pi^0\gamma$ )	( 7 <sup>+7</sup> / <sub>-4</sub> ) × 10 <sup>-3</sup>	S=1.1
$\Gamma_5$ $\eta\gamma$	( 4.5 ± 0.4 ) × 10 <sup>-4</sup>	S=1.1
$\Gamma_6$ $\pi^0 e^+ e^-$	( 7.7 ± 0.6 ) × 10 <sup>-4</sup>	
$\Gamma_7$ $\pi^0 \mu^+ \mu^-$	( 1.34±0.18) × 10 <sup>-4</sup>	S=1.5
$\Gamma_8$ $\eta e^+ e^-$		
$\Gamma_9$ $e^+ e^-$	( 7.36±0.15) × 10 <sup>-5</sup>	S=1.5
$\Gamma_{10}$ $\pi^+\pi^-\pi^0\pi^0$	< 2 × 10 <sup>-4</sup>	CL=90%
$\Gamma_{11}$ $\pi^+\pi^-\gamma$	< 3.6 × 10 <sup>-3</sup>	CL=95%
$\Gamma_{12}$ $\pi^+\pi^-\pi^+\pi^--$	< 1 × 10 <sup>-3</sup>	CL=90%
$\Gamma_{13}$ $\pi^0\pi^0\gamma$	( 6.7 ± 1.1 ) × 10 <sup>-5</sup>	
$\Gamma_{14}$ $\eta\pi^0\gamma$	< 3.3 × 10 <sup>-5</sup>	CL=90%
$\Gamma_{15}$ $\mu^+\mu^-$	( 7.4 ± 1.8 ) × 10 <sup>-5</sup>	
$\Gamma_{16}$ $3\gamma$	< 1.9 × 10 <sup>-4</sup>	CL=95%

Charge conjugation (C) violating modes

$\Gamma_{17}$ $\eta\pi^0$	C	< 2.2 × 10 <sup>-4</sup>	CL=90%
$\Gamma_{18}$ $2\pi^0$	C	< 2.2 × 10 <sup>-4</sup>	CL=90%
$\Gamma_{19}$ $3\pi^0$	C	< 2.3 × 10 <sup>-4</sup>	CL=90%
$\Gamma_{20}$ invisible		< 7 × 10 <sup>-5</sup>	CL=90%

CONSTRAINED FIT INFORMATION

An overall fit to 15 branching ratios uses 55 measurements and one constraint to determine 10 parameters. The overall fit has a  $\chi^2 = 57.0$  for 46 degrees of freedom.

The following off-diagonal array elements are the correlation coefficients  $\langle \delta x_i \delta x_j \rangle / (\delta x_i \delta x_j)$ , in percent, from the fit to the branching fractions,  $x_i \equiv \Gamma_i/\Gamma_{total}$ . The fit constrains the  $x_i$  whose labels appear in this array to sum to one.

$x_2$	28								
$x_3$	-9	-3							
$x_4$	-95	-55	0						
$x_5$	7	15	-1	-12					
$x_6$	-1	0	0	0	0				
$x_7$	0	0	0	0	0	0			
$x_9$	-35	-70	3	52	-22	0	0		
$x_{13}$	1	3	0	-2	0	0	0	-2	
$x_{15}$	0	0	0	0	0	0	0	0	0
	$x_1$	$x_2$	$x_3$	$x_4$	$x_5$	$x_6$	$x_7$	$x_9$	$x_{13}$

$\omega(782)$  PARTIAL WIDTHS

$\Gamma(\pi^0\gamma)$	VALUE (keV)	EVTS	DOCUMENT ID	TECN	COMMENT
$\Gamma_2$					
• • • We do not use the following data for averages, fits, limits, etc. • • •					
880±50	7815	1	ACHASOV	13	SND 1.05-2.00 $e^+e^- \rightarrow \pi^0\pi^0\gamma$
788±12±27	36500	2	ACHASOV	03	SND 0.60-0.97 $e^+e^- \rightarrow \pi^0\gamma$
764±51	10625		DOLINSKY	89	ND $e^+e^- \rightarrow \pi^0\gamma$

<sup>1</sup> Systematic uncertainty not estimated.  
<sup>2</sup> Using  $\Gamma_\omega = 8.44 \pm 0.09$  MeV and  $B(\omega \rightarrow \pi^0\gamma)$  from ACHASOV 03.

$\Gamma(\eta\gamma)$	VALUE (keV)	DOCUMENT ID	TECN	COMMENT
$\Gamma_5$				
• • • We do not use the following data for averages, fits, limits, etc. • • •				
6.1±2.5		1	DOLINSKY	89 ND $e^+e^- \rightarrow \eta\gamma$

<sup>1</sup> Using  $\Gamma_\omega = 8.4 \pm 0.1$  MeV and  $B(\omega \rightarrow \eta\gamma)$  from DOLINSKY 89.

$\Gamma(e^+e^-)$	VALUE (keV)	EVTS	DOCUMENT ID	TECN	COMMENT
$\Gamma_9$					
• • • We do not use the following data for averages, fits, limits, etc. • • •					
0.591±0.015	11200	1,2	AKHMETSHIN	04	CMD2 $e^+e^- \rightarrow \pi^+\pi^-\pi^0$
0.653±0.003±0.021	1.2M	3	ACHASOV	03D	RVUE 0.44-2.00 $e^+e^- \rightarrow \pi^+\pi^-\pi^0$
0.600±0.031	10625		DOLINSKY	89	ND $e^+e^- \rightarrow \pi^0\gamma$

<sup>1</sup> Using  $B(\omega \rightarrow \pi^+\pi^-\pi^0) = 0.891 \pm 0.007$  and  $\Gamma_{total} = 8.44 \pm 0.09$  MeV.  
<sup>2</sup> Update of AKHMETSHIN 00c.  
<sup>3</sup> Using ACHASOV 03, ACHASOV 03D and  $B(\omega \rightarrow \pi^+\pi^-) = (1.70 \pm 0.28)\%$ .

$\omega(782) \Gamma(e^+e^-)\Gamma(i)/\Gamma^2(total)$

$\Gamma(e^+e^-)/\Gamma_{total} \times \Gamma(\pi^+\pi^-\pi^0)/\Gamma_{total}$	VALUE (units 10 <sup>-5</sup> )	EVTS	DOCUMENT ID	TECN	COMMENT
$\Gamma_9/\Gamma \times \Gamma_1/\Gamma$					
• • • We do not use the following data for averages, fits, limits, etc. • • •					
6.56±0.12 OUR FIT					Error includes scale factor of 1.6.
6.38±0.10 OUR AVERAGE					Error includes scale factor of 1.1.
6.24±0.11±0.08	11.2k	1	AKHMETSHIN	04	CMD2 $e^+e^- \rightarrow \pi^+\pi^-\pi^0$
6.70±0.06±0.27			AUBERT,B	04N	BABR 10.6 $e^+e^- \rightarrow \pi^+\pi^-\pi^0\gamma$
6.74±0.04±0.24	1.2M	2,3	ACHASOV	03D	RVUE 0.44-2.00 $e^+e^- \rightarrow \pi^+\pi^-\pi^0\gamma$
6.37±0.35			2	DOLINSKY	89 ND $e^+e^- \rightarrow \pi^+\pi^-\pi^0$
6.45±0.24			2	BARKOV	87 CMD $e^+e^- \rightarrow \pi^+\pi^-\pi^0$
5.79±0.42	1488		2	KURDADZE	83B OLYA $e^+e^- \rightarrow \pi^+\pi^-\pi^0$
5.89±0.54	433		2	CORDIER	80 DM1 $e^+e^- \rightarrow \pi^+\pi^-\pi^0$
7.54±0.84	451		2	BENAKSAS	72B OSPK $e^+e^- \rightarrow \pi^+\pi^-\pi^0$
• • • We do not use the following data for averages, fits, limits, etc. • • •					
6.20±0.13			4	BENAYOUN	10 RVUE 0.4-1.05 $e^+e^-$

<sup>1</sup> Update of AKHMETSHIN 00c.  
<sup>2</sup> Recalculated by us from the cross section in the peak.  
<sup>3</sup> From the combined fit of ANTONELLI 92, ACHASOV 01E, ACHASOV 02E, and ACHASOV 03D data on the  $\pi^+\pi^-\pi^0$  and ANTONELLI 92 on the  $\omega\pi^+\pi^-$  final states. Supersedes ACHASOV 99E and ACHASOV 02E.  
<sup>4</sup> A simultaneous fit of  $e^+e^- \rightarrow \pi^+\pi^-, \pi^+\pi^-\pi^0, \pi^0\gamma, \eta\gamma$  data.

$\Gamma(e^+e^-)/\Gamma_{total} \times \Gamma(\pi^0\gamma)/\Gamma_{total}$	VALUE (units 10 <sup>-6</sup> )	EVTS	DOCUMENT ID	TECN	COMMENT
$\Gamma_2/\Gamma \times \Gamma_2/\Gamma$					
• • • We do not use the following data for averages, fits, limits, etc. • • •					
6.18 ± 0.11 OUR FIT					Error includes scale factor of 1.6.
6.37 ± 0.09 OUR AVERAGE					
6.336±0.056±0.089	18k	1	ACHASOV	16A	SND 0.60-1.38 $e^+e^- \rightarrow \pi^0\gamma$
6.47 ± 0.14 ± 0.39	36k	2	AKHMETSHIN	05	CMD2 0.60-1.38 $e^+e^- \rightarrow \pi^0\gamma$
6.50 ± 0.11 ± 0.20	10k	3	ACHASOV	03	SND 0.60-0.97 $e^+e^- \rightarrow \pi^0\gamma$
6.34 ± 0.21 ± 0.21			3	DOLINSKY	89 ND $e^+e^- \rightarrow \pi^0\gamma$
• • • We do not use the following data for averages, fits, limits, etc. • • •					
6.80 ± 0.13			4	BENAYOUN	10 RVUE 0.4-1.05 $e^+e^-$

<sup>1</sup> From the VMD model with the interfering  $\rho(770), \omega(782), \phi(1020)$ , and an additional resonance describing the total contribution of the  $\rho(1450)$  and  $\omega(1420)$  states. Supersedes ACHASOV 03.  
<sup>2</sup> Using  $\sigma_{\phi \rightarrow \pi^0\gamma}$  from ACHASOV 00 and  $m_\omega = 782.57$  MeV in the model with the energy-independent phase of  $\rho$ - $\omega$  interference equal to  $(-10.2 \pm 7.0)^\circ$ .  
<sup>3</sup> Recalculated by us from the cross section in the peak.  
<sup>4</sup> A simultaneous fit of  $e^+e^- \rightarrow \pi^+\pi^-, \pi^+\pi^-\pi^0, \pi^0\gamma, \eta\gamma$  data.

$\Gamma(e^+e^-)/\Gamma_{total} \times \Gamma(\pi^+\pi^-)/\Gamma_{total}$	VALUE (units 10 <sup>-6</sup> )	EVTS	DOCUMENT ID	TECN	COMMENT
$\Gamma_3/\Gamma \times \Gamma_3/\Gamma$					
• • • We do not use the following data for averages, fits, limits, etc. • • •					
1.225 ± 0.058 ± 0.041	800k	1	ACHASOV	06	SND $e^+e^- \rightarrow \pi^+\pi^-$
1.166±0.036			2	BENAYOUN	13 RVUE 0.4-1.05 $e^+e^-$
1.05 ± 0.08			3	DAVIER	13 RVUE $e^+e^- \rightarrow \pi^+\pi^-(\gamma)$
• • • We do not use the following data for averages, fits, limits, etc. • • •					
1.05 ± 0.08			5	BENAYOUN	10 RVUE 0.4-1.05 $e^+e^-$

<sup>1</sup> Supersedes ACHASOV 05A.  
<sup>2</sup> A simultaneous fit to  $e^+e^- \rightarrow \pi^+\pi^-, \pi^+\pi^-\pi^0, \pi^0\gamma, \eta\gamma, K\bar{K}$ , and  $\tau^- \rightarrow \pi^-\pi^0\nu_\tau$  data. Supersedes BENAYOUN 10.  
<sup>3</sup> From  $e^+e^- \rightarrow \pi^+\pi^-(\gamma)$  data of LEES 12G.

$\Gamma(e^+e^-)/\Gamma_{total} \times \Gamma(\eta\gamma)/\Gamma_{total}$	VALUE (units 10 <sup>-8</sup> )	EVTS	DOCUMENT ID	TECN	COMMENT
$\Gamma_5/\Gamma \times \Gamma_5/\Gamma$					
• • • We do not use the following data for averages, fits, limits, etc. • • •					
3.32±0.28 OUR FIT					Error includes scale factor of 1.1.
3.18±0.28 OUR AVERAGE					
3.10±0.31±0.11	33k	1	ACHASOV	07B	SND 0.6-1.38 $e^+e^- \rightarrow \eta\gamma$
3.17±1.85±0.21	17.4k	2	AKHMETSHIN	05	CMD2 0.60-1.38 $e^+e^- \rightarrow \eta\gamma$
3.41±0.52±0.21	23k	3,4	AKHMETSHIN	01B	CMD2 $e^+e^- \rightarrow \eta\gamma$
• • • We do not use the following data for averages, fits, limits, etc. • • •					
4.50±0.10			5	BENAYOUN	10 RVUE 0.4-1.05 $e^+e^-$

<sup>1</sup> From a combined fit of  $\sigma(e^+e^- \rightarrow \eta\gamma)$  with  $\eta \rightarrow 3\pi^0$  and  $\eta \rightarrow \pi^+\pi^-\pi^0$ , and fixing  $B(\eta \rightarrow 3\pi^0) / B(\eta \rightarrow \pi^+\pi^-\pi^0) = 1.44 \pm 0.04$ . Recalculated by us from the cross section at the peak. Supersedes ACHASOV 00D and ACHASOV 06A.  
<sup>2</sup> From the  $\eta \rightarrow 2\gamma$  decay and using  $B(\eta \rightarrow \gamma\gamma) = 39.43 \pm 0.26\%$ .  
<sup>3</sup> From the  $\eta \rightarrow 3\pi^0$  decay and using  $B(\eta \rightarrow 3\pi^0) = (32.24 \pm 0.29) \times 10^{-2}$ .  
<sup>4</sup> The combined fit from 600 to 1380 MeV taking into account  $\rho(770), \omega(782), \phi(1020)$ , and  $\rho(1450)$  (mass and width fixed at 1450 MeV and 310 MeV respectively).  
<sup>5</sup> A simultaneous fit of  $e^+e^- \rightarrow \pi^+\pi^-, \pi^+\pi^-\pi^0, \pi^0\gamma, \eta\gamma$  data.

$\Gamma(e^+e^-)/\Gamma_{total} \times \Gamma(\mu^+\mu^-)/\Gamma_{total}$	VALUE (units 10 <sup>-3</sup> )	EVTS	DOCUMENT ID	TECN	COMMENT
$\Gamma_7/\Gamma \times \Gamma_{15}/\Gamma$					
• • • We do not use the following data for averages, fits, limits, etc. • • •					
4.3±1.8±2.2	4.5M	1	ANASTASI	17	KLOE $e^+e^- \rightarrow \mu^+\mu^- \gamma$

<sup>1</sup> From a fit of the real part of the vacuum polarization by a sum of the leptonic and hadronic contributions, where the hadronic contribution is parametrized as a sum of Breit-Wigner resonances  $\omega(782), \phi(1020)$  and using a GOUNARIS 68 parametrization for the  $\rho(770)$ , and a non-resonant term.

## Meson Particle Listings

 $\omega(782)$  $\omega(782)$  BRANCHING RATIOS

$\Gamma(\pi^+\pi^-\pi^0)/\Gamma_{\text{total}}$   $\Gamma_1/\Gamma$   
 NIECKNIG 12 describes final-state interactions between the three pions in a dispersive framework using data on the  $\pi\pi$   $P$ -wave scattering phase shift.

VALUE	EVTS	DOCUMENT ID	TECN	COMMENT
0.9024 ± 0.0019		1 AMBROSINO 08G	KLOE	1.0-1.03 $e^+e^- \rightarrow \pi^+\pi^-2\pi^0, 2\pi^0\gamma$
0.8965 ± 0.0016 ± 0.0048	1.2M	2,3 ACHASOV 03D	RVUE	0.44-2.00 $e^+e^- \rightarrow \pi^+\pi^-\pi^0$
0.880 ± 0.020 ± 0.032	11200	3,4 AKHMETSHIN 00C	CMD2	$e^+e^- \rightarrow \pi^+\pi^-\pi^0$
0.8942 ± 0.0062		3 DOLINSKY 89	ND	$e^+e^- \rightarrow \pi^+\pi^-\pi^0$

1 Not independent of  $\Gamma(\pi^0\gamma)/\Gamma(\pi^+\pi^-\pi^0)$  from AMBROSINO 08G.  
 2 Using ACHASOV 03, ACHASOV 03D and  $B(\omega \rightarrow \pi^+\pi^-) = (1.70 \pm 0.28)\%$ .  
 3 Not independent of the corresponding  $\Gamma(e^+e^-) \times \Gamma(\pi^+\pi^-\pi^0)/\Gamma_{\text{total}}^2$ .  
 4 Using  $\Gamma(e^+e^-) = 0.60 \pm 0.02$  keV.

$\Gamma(\pi^0\gamma)/\Gamma_{\text{total}}$   $\Gamma_2/\Gamma$

VALUE (units $10^{-2}$ )	EVTS	DOCUMENT ID	TECN	COMMENT
8.88 ± 0.18		1 ACHASOV 16A	SND	0.60-1.38 $e^+e^- \rightarrow \pi^0\gamma$
8.09 ± 0.14		2 AMBROSINO 08G	KLOE	$e^+e^- \rightarrow \pi^+\pi^-2\pi^0, 2\pi^0\gamma$
9.06 ± 0.20 ± 0.57	18k	3,4 AKHMETSHIN 05	CMD2	0.60-1.38 $e^+e^- \rightarrow \pi^0\gamma$
9.34 ± 0.15 ± 0.31	36k	4 ACHASOV 03	SND	0.60-0.97 $e^+e^- \rightarrow \pi^0\gamma$
8.65 ± 0.16 ± 0.42	1.2M	5,6 ACHASOV 03D	RVUE	0.44-2.00 $e^+e^- \rightarrow \pi^+\pi^-\pi^0$
8.39 ± 0.24	9k	7 BENAYOUN 96	RVUE	$e^+e^- \rightarrow \pi^0\gamma$
8.88 ± 0.62	10k	4 DOLINSKY 89	ND	$e^+e^- \rightarrow \pi^0\gamma$

1 Using  $B(\omega \rightarrow e^+e^-)$  from PDG 15. Supersedes ACHASOV 03.  
 2 Not independent of  $\Gamma(\pi^0\gamma)/\Gamma(\pi^+\pi^-\pi^0)$  from AMBROSINO 08G.  
 3 Using  $B(\omega \rightarrow e^+e^-) = (7.14 \pm 0.13) \times 10^{-5}$ .  
 4 Not independent of the corresponding  $\Gamma(e^+e^-) \times \Gamma(\pi^0\gamma)/\Gamma_{\text{total}}^2$ .  
 5 Using ACHASOV 03, ACHASOV 03D and  $B(\omega \rightarrow \pi^+\pi^-) = (1.70 \pm 0.28)\%$ .  
 6 Not independent of the corresponding  $\Gamma(e^+e^-) \times \Gamma(\pi^+\pi^-\pi^0)/\Gamma_{\text{total}}^2$ .  
 7 Reanalysis of DRUZHININ 84, DOLINSKY 89, DOLINSKY 91 taking into account the triangle anomaly contributions.

$\Gamma(\pi^0\gamma)/\Gamma(\pi^+\pi^-\pi^0)$   $\Gamma_2/\Gamma_1$

VALUE (units $10^{-2}$ )	DOCUMENT ID	TECN	COMMENT
<b>9.41 ± 0.23 OUR FIT</b>	Error includes scale factor of 2.0.		
<b>9.05 ± 0.27 OUR AVERAGE</b>	Error includes scale factor of 1.8.		
8.97 ± 0.16	AMBROSINO 08G	KLOE	$e^+e^- \rightarrow \pi^+\pi^-2\pi^0, 2\pi^0\gamma$
9.94 ± 0.36 ± 0.38	1 AULCHENKO 00A	SND	$e^+e^- \rightarrow \pi^+\pi^-2\pi^0, 2\pi^0\gamma$
8.4 ± 1.3	KEYNE 76	CNTR	$\pi^-p \rightarrow \omega n$
10.9 ± 2.5	BENAKSAS 72C	OSPK	$e^+e^- \rightarrow \pi^0\gamma$
8.1 ± 2.0	BALDIN 71	HLBC	2.9 $\pi^+p$
13 ± 4	JACQUET 69B	HLBC	2.05 $\pi^+p \rightarrow \pi^+p\omega$

• • • We do not use the following data for averages, fits, limits, etc. • • •  
 9.7 ± 0.2 ± 0.5 2,3 ACHASOV 03D RVUE 0.44-2.00  $e^+e^- \rightarrow \pi^+\pi^-\pi^0$   
 9.9 ± 0.7 2 DOLINSKY 89 ND  $e^+e^- \rightarrow \pi^0\gamma$

1 From  $\sigma_0^{\omega\pi^0} \rightarrow \pi^0\pi^0\gamma(m_\phi)/\omega\pi^0 \rightarrow \pi^+\pi^-\pi^0\pi^0(m_\phi)$  with a phase-space correction factor of 1/1.023.  
 2 Not independent of the corresponding  $\Gamma(e^+e^-) \times \Gamma(\pi^0\gamma)/\Gamma_{\text{total}}^2$ .  
 3 Using ACHASOV 03. Based on 1.2M events.

$\Gamma(\pi^+\pi^-)/\Gamma_{\text{total}}$   $\Gamma_3/\Gamma$

VALUE (units $10^{-2}$ )	EVTS	DOCUMENT ID	TECN	COMMENT
<b>1.53 ± 0.06 OUR FIT</b>	See also $\Gamma(\pi^+\pi^-)/\Gamma(\pi^+\pi^-\pi^0)$ .			
<b>1.51 ± 0.07 OUR AVERAGE</b>	Error includes scale factor of 1.1.			
1.52 ± 0.08	1 HANHART 18	RVUE	$e^+e^- \rightarrow \pi^+\pi^-$	
1.46 ± 0.12 ± 0.02	900k	2 AKHMETSHIN 07	$e^+e^- \rightarrow \pi^+\pi^-$	
1.30 ± 0.24 ± 0.05	11.2k	3 AKHMETSHIN 04	$e^+e^- \rightarrow \pi^+\pi^-$	
2.30 ± 1.77 ± 0.90 ± 0.18	5.4k	4 ACHASOV 02E	SND 1.1-1.38 $e^+e^- \rightarrow \pi^+\pi^-$	
2.3 ± 0.5	BARKOV 85	OLYA	$e^+e^- \rightarrow \pi^+\pi^-$	
1.6 ± 0.9 ± 0.7	QUENZER 78	DM1	$e^+e^- \rightarrow \pi^+\pi^-$	
3.6 ± 1.9	BENAKSAS 72	OSPK	$e^+e^- \rightarrow \pi^+\pi^-$	

• • • We do not use the following data for averages, fits, limits, etc. • • •  
 1.29 ± 0.22 ± 0.03 970k 5,6 ABLIKIM 18C BES3  $\eta'(958) \rightarrow \gamma\pi^+\pi^-$   
 1.28 ± 0.22 ± 0.03 970k 7,8 ABLIKIM 18C BES3  $\eta'(958) \rightarrow \gamma\pi^+\pi^-$   
 1.75 ± 0.11 4.5M 9 ACHASOV 05A SND  $e^+e^- \rightarrow \pi^+\pi^-$   
 2.01 ± 0.29 10 BENAYOUN 03 RVUE  $e^+e^- \rightarrow \pi^+\pi^-$   
 1.9 ± 0.3 11 GARDNER 99 RVUE  $e^+e^- \rightarrow \pi^+\pi^-$   
 2.3 ± 0.4 12 BENAYOUN 98 RVUE  $e^+e^- \rightarrow \pi^+\pi^-, \mu^+\mu^-$   
 1.0 ± 0.11 13 WICKLUND 78 ASPK 3,4,6  $\pi^\pm N$   
 1.22 ± 0.30 ALVENSLEB... 71C CNTR Photoproduction  
 1.3 ± 1.2 ± 0.9 MOFFEIT 71 HBC 2.8,4,7  $\gamma p$   
 0.80 ± 0.28 ± 0.20 14 BIGGS 70B CNTR 4.2  $\gamma C \rightarrow \pi^+\pi^- C$

1 Dispersive analysis. Value extracted from average of data from AUBERT 09As, AKHMETSHIN 07, ACHASOV 06, AMBROSINO 11A, BABUSCI 13D, ABLIKIM 16b normalised by PDG evaluation for  $\Gamma(\omega \rightarrow e^+e^-)$ .

2 A combined fit of AKHMETSHIN 07, AULCHENKO 06, and AULCHENKO 05.  
 3 Update of AKHMETSHIN 02.

4 From the  $m_{\pi^+\pi^-}$  spectrum taking into account the interference of the  $\rho\pi$  and  $\omega\pi$  amplitudes.  
 5 From a fit to  $\pi^+\pi^-$  mass using  $\rho(770)$  (parametrized with the Gounaris-Sakurai approach),  $\omega(782)$ , and box anomaly components.

6 ABLIKIM 18c reports  $[\Gamma(\omega(782) \rightarrow \pi^+\pi^-)/\Gamma_{\text{total}}] \times [B(\eta'(958) \rightarrow \omega\gamma)] = (3.25 \pm 0.21 \pm 0.52) \times 10^{-4}$  which we divide by our best value  $B(\eta'(958) \rightarrow \omega\gamma) = (2.52 \pm 0.07) \times 10^{-2}$ . Our first error is their experiment's error and our second error is the systematic error from using our best value.

7 From a fit to  $\pi^+\pi^-$  mass using  $\rho(770)$  (parametrized with the Gounaris-Sakurai approach),  $\omega(782)$ , and  $\rho(1450)$  components.

8 ABLIKIM 18c reports  $[\Gamma(\omega(782) \rightarrow \pi^+\pi^-)/\Gamma_{\text{total}}] \times [B(\eta'(958) \rightarrow \omega\gamma)] = (3.22 \pm 0.21 \pm 0.52) \times 10^{-4}$  which we divide by our best value  $B(\eta'(958) \rightarrow \omega\gamma) = (2.52 \pm 0.07) \times 10^{-2}$ . Our first error is their experiment's error and our second error is the systematic error from using our best value.

9 Using  $\Gamma(\omega \rightarrow e^+e^-)$  from the 2004 Edition of this Review (PDG 04).

10 Using the data of AKHMETSHIN 02 in the hidden local symmetry model.

11 Using the data of BARKOV 85.

12 Using the data of BARKOV 85 in the hidden local symmetry model.

13 From a model-dependent analysis assuming complete coherence.

14 Re-evaluated under  $\Gamma(\pi^+\pi^-)/\Gamma(\pi^+\pi^-\pi^0)$  by BEHREND 71 using more accurate  $\omega \rightarrow \rho$  photoproduction cross-section ratio.

$\Gamma(\pi^+\pi^-)/\Gamma(\pi^+\pi^-\pi^0)$   $\Gamma_3/\Gamma_1$

See also  $\Gamma(\pi^+\pi^-)/\Gamma_{\text{total}}$ .

VALUE	DOCUMENT ID	TECN	COMMENT
<b>0.0171 ± 0.0007 OUR FIT</b>			
<b>0.026 ± 0.005 OUR AVERAGE</b>			
0.021 ± 0.028 ± 0.009	1,2 RATCLIFF 72	ASPK	15 $\pi^-p \rightarrow n2\pi$
0.028 ± 0.006	1 BEHREND 71	ASPK	Photoproduction
0.022 ± 0.009 ± 0.01	3 ROOS 70	RVUE	

1 The fitted width of these data is 160 MeV in agreement with present average, thus the  $\omega$  contribution is overestimated. Assuming  $\rho$  width 145 MeV.

2 Significant interference effect observed. NB of  $\omega \rightarrow 3\pi$  comes from an extrapolation.

3 ROOS 70 combines ABRAMOVICH 70 and BIZZARRI 70.

$\Gamma(\pi^+\pi^-)/\Gamma(\pi^0\gamma)$   $\Gamma_3/\Gamma_2$

VALUE	EVTS	DOCUMENT ID	TECN	COMMENT
<b>0.20 ± 0.04</b>	1.98M	1 ALOISIO 03	KLOE	1.02 $e^+e^- \rightarrow \pi^+\pi^-\pi^0$

1 Using the data of ALOISIO 02D.

$\Gamma(\text{neutrals})/\Gamma_{\text{total}}$   $(\Gamma_2+\Gamma_4)/\Gamma$

VALUE	EVTS	DOCUMENT ID	TECN	COMMENT
<b>0.091 ± 0.006 OUR FIT</b>				
<b>0.081 ± 0.011 OUR AVERAGE</b>				
0.075 ± 0.025		BIZZARRI 71	HBC	0.0 $\rho\bar{p}$
0.079 ± 0.019		DEINET 69B	OSPK	1.5 $\pi^-p$
0.084 ± 0.015		BOLLINI 68C	CNTR	2.1 $\pi^-p$

• • • We do not use the following data for averages, fits, limits, etc. • • •  
 0.073 ± 0.018 42 BASILE 72B CNTR 1.67  $\pi^-p$

$\Gamma(\text{neutrals})/\Gamma(\pi^+\pi^-\pi^0)$   $(\Gamma_2+\Gamma_4)/\Gamma_1$

VALUE	EVTS	DOCUMENT ID	TECN	COMMENT
<b>0.102 ± 0.008 OUR FIT</b>				
<b>0.103 ± 0.011 OUR AVERAGE</b>				
0.15 ± 0.04	46	AGUILAR... 72B	HBC	3.9,4.6 $K^-p$
0.10 ± 0.03	19	BARASH 67B	HBC	0.0 $\bar{p}p$
0.134 ± 0.026	850	DIUGNO 66B	CNTR	1.4 $\pi^-p$
0.097 ± 0.016	348	FLATTE 66	HBC	1.4 - 1.7 $K^-p \rightarrow \Lambda MM$
0.06 ± 0.05 ± 0.02		JAMES 66	HBC	2.1 $\pi^+p$
0.08 ± 0.03	35	KRAEMER 64	DBC	1.2 $\pi^+d$
0.11 ± 0.02	20	BUSCHBECK 63	HBC	1.5 $K^-p$

• • • We do not use the following data for averages, fits, limits, etc. • • •

VALUE	CL%	DOCUMENT ID	TECN	COMMENT
0.78 ± 0.07		1 DAKIN 72	OSPK	1.4 $\pi^-p \rightarrow nMM$
> 0.81	90	DEINET 69B	OSPK	

1 Error statistical only. Authors obtain good fit also assuming  $\pi^0\gamma$  as the only neutral decay.

$\Gamma(\text{neutrals})/\Gamma(\text{charged particles})$   $(\Gamma_2+\Gamma_4)/(\Gamma_1+\Gamma_3)$

VALUE	DOCUMENT ID	TECN	COMMENT
<b>0.100 ± 0.008 OUR FIT</b>			
<b>0.124 ± 0.021</b>	FELDMAN 67C	OSPK	1.2 $\pi^-p$

$\Gamma(\eta\gamma)/\Gamma_{total}$			$\Gamma_5/\Gamma$
VALUE (units $10^{-4}$ )	EVTS	DOCUMENT ID	TECN COMMENT
<b>4.5 ± 0.4 OUR FIT</b>			Error includes scale factor of 1.1.
<b>6.3 ± 1.3 OUR AVERAGE</b>			Error includes scale factor of 1.2.
6.6 ± 1.7		<sup>1</sup> ABELE 97E CBAR	0.0 $p\bar{p} \rightarrow 5\gamma$
8.3 ± 2.1		ALDE 93 GAM2	$38\pi^- p \rightarrow \omega n$
3.0 $^{+2.5}_{-1.8}$		<sup>2</sup> ANDREWS 77 CNTR	6.7-10 $\gamma$ Cu

• • • We do not use the following data for averages, fits, limits, etc. • • •

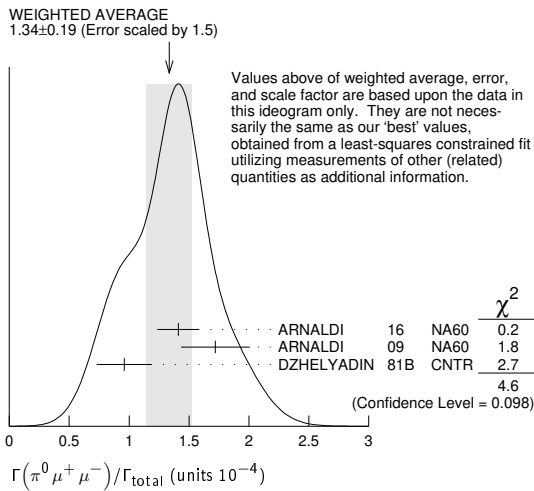
• • • We do not use the following data for averages, fits, limits, etc. • • •

1 No flat  $\eta\eta\gamma$  background assumed.  
 2 Solution corresponding to constructive  $\omega\rho$  interference.  
 3 ACHASOV 07B reports  $[\Gamma(\omega(782) \rightarrow \eta\gamma)/\Gamma_{total}] \times [B(\omega(782) \rightarrow e^+e^-)] = (3.10 \pm 0.31 \pm 0.11) \times 10^{-8}$  which we divide by our best value  $B(\omega(782) \rightarrow e^+e^-) = (7.36 \pm 0.15) \times 10^{-5}$ . Our first error is their experiment's error and our second error is the systematic error from using our best value. Supersedes ACHASOV 00D and ACHASOV 06A.  
 4 Not independent of the corresponding  $\Gamma(e^+e^-) \times \Gamma(\eta\gamma)/\Gamma_{total}^2$ .  
 5 Using  $B(\omega \rightarrow e^+e^-) = (7.14 \pm 0.13) \times 10^{-5}$  and  $B(\eta \rightarrow \gamma\gamma) = 39.43 \pm 0.26\%$ .  
 6 Using  $B(\omega \rightarrow e^+e^-) = (7.07 \pm 0.19) \times 10^{-5}$  and using  $B(\eta \rightarrow 3\pi^0) = (32.24 \pm 0.29) \times 10^{-2}$ . Solution corresponding to constructive  $\omega\rho$  interference. The combined fit from 600 to 1380 MeV taking into account  $\rho(770)$ ,  $\omega(782)$ ,  $\phi(1020)$ , and  $\rho(1450)$  (mass and width fixed at 1450 MeV and 310 MeV respectively). Not independent of the corresponding  $\Gamma(e^+e^-) \times \Gamma(\eta\gamma)/\Gamma_{total}^2$ .  
 7 Depending on the degree of coherence with the flat  $\eta\eta\gamma$  background and using  $B(\omega \rightarrow \pi^0\gamma) = (8.5 \pm 0.5) \times 10^{-2}$ .  
 8 Reanalysis of DRUZHININ 84, DOLINSKY 89, DOLINSKY 91 taking into account the triangle anomaly contributions.

$\Gamma(\eta\gamma)/\Gamma(\pi^0\gamma)$			$\Gamma_5/\Gamma_2$
VALUE	DOCUMENT ID	TECN	COMMENT
• • •			We do not use the following data for averages, fits, limits, etc. • • •
0.0098 ± 0.0024	<sup>1</sup> ALDE 93	GAM2	$38\pi^- p \rightarrow \omega n$
0.0082 ± 0.0033	<sup>2</sup> DOLINSKY 89	ND	$e^+e^- \rightarrow \eta\gamma$
0.010 ± 0.045	APEL 72B	OSPK	$4-8 \pi^- p \rightarrow n3\gamma$

$\Gamma(\pi^0 e^+ e^-)/\Gamma_{total}$			$\Gamma_6/\Gamma$
VALUE (units $10^{-4}$ )	EVTS	DOCUMENT ID	TECN COMMENT
<b>7.7 ± 0.6 OUR FIT</b>			
<b>7.7 ± 0.6 OUR AVERAGE</b>			
7.61 ± 0.53 ± 0.64		ACHASOV 08 SND	0.36-0.97 $e^+e^- \rightarrow \pi^0 e^+ e^-$
8.19 ± 0.71 ± 0.62		AKHMETSHIN 05A CMD2	0.72-0.84 $e^+e^-$
5.9 ± 1.9	43	DOLINSKY 88 ND	$e^+e^- \rightarrow \pi^0 e^+ e^-$

$\Gamma(\pi^0 \mu^+ \mu^-)/\Gamma_{total}$			$\Gamma_7/\Gamma$
VALUE (units $10^{-4}$ )	EVTS	DOCUMENT ID	TECN COMMENT
<b>1.34 ± 0.18 OUR FIT</b>			Error includes scale factor of 1.5.
<b>1.34 ± 0.19 OUR AVERAGE</b>			Error includes scale factor of 1.5. See the ideogram below.
1.41 ± 0.09 ± 0.15		ARNALDI 16 NA60	400 GeV (p-A) collisions
1.72 ± 0.25 ± 0.14	3k	ARNALDI 09 NA60	158A In-In collisions
0.96 ± 0.23		DZHELJADIN 81B CNTR	25-33 $\pi^- p \rightarrow \omega n$



$\Gamma(\eta e^+ e^-)/\Gamma_{total}$			$\Gamma_8/\Gamma$
VALUE (units $10^{-5}$ )	DOCUMENT ID	TECN	COMMENT
• • •			We do not use the following data for averages, fits, limits, etc. • • •
< 1.1	AKHMETSHIN 05A	CMD2	0.72-0.84 $e^+e^-$

$\Gamma(e^+ e^-)/\Gamma_{total}$			$\Gamma_9/\Gamma$
VALUE (units $10^{-4}$ )	EVTS	DOCUMENT ID	TECN COMMENT
<b>0.736 ± 0.015 OUR FIT</b>			Error includes scale factor of 1.5.
• • •			We do not use the following data for averages, fits, limits, etc. • • •
0.700 ± 0.016	11200	<sup>1,2</sup> AKHMETSHIN 04	CMD2 $e^+e^- \rightarrow \pi^+ \pi^- \pi^0$
0.752 ± 0.004 ± 0.024	1.2M	<sup>2,3</sup> ACHASOV 03D	RVUE $0.44-2.00 e^+e^- \rightarrow \pi^+ \pi^- \pi^0$
0.714 ± 0.036		<sup>2</sup> DOLINSKY 89	ND $e^+e^- \rightarrow \pi^+ \pi^- \pi^0$
0.72 ± 0.03		<sup>2</sup> BARKOV 87	CMD $e^+e^- \rightarrow \pi^+ \pi^- \pi^0$
0.64 ± 0.04	1488	<sup>2</sup> KURDADZE 83B	OLYA $e^+e^- \rightarrow \pi^+ \pi^- \pi^0$
0.675 ± 0.069	433	<sup>2</sup> CORDIER 80	DM1 $e^+e^- \rightarrow \pi^+ \pi^- \pi^0$
0.83 ± 0.10	451	<sup>2</sup> BENAKSAS 72B	OSPK $e^+e^- \rightarrow \pi^+ \pi^- \pi^0$
0.77 ± 0.06		<sup>4</sup> AUGUSTIN 69D	OSPK $e^+e^- \rightarrow \pi^+ \pi^- \pi^0$
0.65 ± 0.13	33	<sup>5</sup> ASTVACAT... 68	OSPK Assume SU(3)+mixing

1 Using  $B(\omega \rightarrow \pi^+ \pi^- \pi^0) = 0.891 \pm 0.007$ . Update of AKHMETSHIN 00c.  
 2 Not independent of the corresponding  $\Gamma(e^+e^-) \times \Gamma(\pi^+ \pi^- \pi^0)/\Gamma_{total}^2$ .  
 3 Using ACHASOV 03, ACHASOV 03D and  $B(\omega \rightarrow \pi^+ \pi^-) = (1.70 \pm 0.28)\%$ .  
 4 Rescaled by us to correspond to  $\omega$  width 8.4 MeV. Systematic errors underestimated.  
 5 Not resolved from  $\rho$  decay. Error statistical only.

$\Gamma(\pi^+ \pi^- \pi^0)/\Gamma_{total}$			$\Gamma_{10}/\Gamma$
VALUE (units $10^{-4}$ )	CL%	DOCUMENT ID	TECN COMMENT
< 2	90	ACHASOV 09A	SND $e^+e^- \rightarrow \pi^+ \pi^- \pi^0 \pi^0$
• • •			We do not use the following data for averages, fits, limits, etc. • • •
< 200	90	KURDADZE 86	OLYA $e^+e^- \rightarrow \pi^+ \pi^- \pi^0 \pi^0$

$\Gamma(\pi^+ \pi^- \gamma)/\Gamma_{total}$			$\Gamma_{11}/\Gamma$
VALUE	CL%	DOCUMENT ID	TECN COMMENT
< 0.0036	95	WEIDENAUER 90	ASTE $p\bar{p} \rightarrow \pi^+ \pi^- \pi^+ \pi^- \gamma$
• • •			We do not use the following data for averages, fits, limits, etc. • • •
< 0.004	95	BITYUKOV 88B	SPEC $32 \pi^- p \rightarrow \pi^+ \pi^- \gamma X$

$\Gamma(\pi^+ \pi^- \gamma)/\Gamma(\pi^+ \pi^- \pi^0)$			$\Gamma_{11}/\Gamma_1$
VALUE	CL%	DOCUMENT ID	TECN COMMENT
• • •			We do not use the following data for averages, fits, limits, etc. • • •
< 0.066	90	KALBFLEISCH 75	HBC $2.18 K^- p \rightarrow \Lambda \pi^+ \pi^- \gamma$
< 0.05	90	FLATTE 66	HBC $1.2-1.7 K^- p \rightarrow \Lambda \pi^+ \pi^- \gamma$

$\Gamma(\pi^+ \pi^- \pi^+ \pi^-)/\Gamma_{total}$			$\Gamma_{12}/\Gamma$
VALUE	CL%	DOCUMENT ID	TECN COMMENT
< 1 × 10 <sup>-3</sup>	90	KURDADZE 88	OLYA $e^+e^- \rightarrow \pi^+ \pi^- \pi^+ \pi^-$

$\Gamma(\pi^0 \pi^0 \gamma)/\Gamma_{total}$			$\Gamma_{13}/\Gamma$
VALUE (units $10^{-5}$ )	EVTS	DOCUMENT ID	TECN COMMENT
<b>6.7 ± 1.1 OUR FIT</b>			
<b>6.5 ± 1.2 OUR AVERAGE</b>			
6.4 $^{+2.4}_{-2.0}$ ± 0.8	190	<sup>1</sup> AKHMETSHIN 04B	CMD2 $0.6-0.97 e^+e^- \rightarrow \pi^0 \pi^0 \gamma$
6.6 $^{+1.4}_{-1.3}$ ± 0.6	295	ACHASOV 02F	SND $0.36-0.97 e^+e^- \rightarrow \pi^0 \pi^0 \gamma$
• • •			We do not use the following data for averages, fits, limits, etc. • • •
11.8 $^{+2.1}_{-1.9}$ ± 1.4	190	<sup>2</sup> AKHMETSHIN 04B	CMD2 $0.6-0.97 e^+e^- \rightarrow \pi^0 \pi^0 \gamma$
7.8 ± 2.7 ± 2.0	63	<sup>1,3</sup> ACHASOV 00G	SND $e^+e^- \rightarrow \pi^0 \pi^0 \gamma$
12.7 ± 2.3 ± 2.5	63	<sup>2,3</sup> ACHASOV 00G	SND $e^+e^- \rightarrow \pi^0 \pi^0 \gamma$

1 In the model assuming the  $\rho \rightarrow \pi^0 \pi^0 \gamma$  decay via the  $\omega\pi$  and  $f_0(500)\gamma$  mechanisms.  
 2 In the model assuming the  $\rho \rightarrow \pi^0 \pi^0 \gamma$  decay via the  $\omega\pi$  mechanism only.  
 3 Superseded by ACHASOV 02F.

$\Gamma(\pi^0 \pi^0 \gamma)/\Gamma(\pi^+ \pi^- \pi^0)$			$\Gamma_{13}/\Gamma_1$
VALUE	CL%	DOCUMENT ID	TECN COMMENT
< 0.00045	90	DOLINSKY 89	ND $e^+e^- \rightarrow \pi^0 \pi^0 \gamma$
• • •			We do not use the following data for averages, fits, limits, etc. • • •
< 0.08	95	JACQUET 69B	HLBC $2.05 \pi^+ p \rightarrow \pi^+ \rho\omega$

$\Gamma(\pi^0 \pi^0 \gamma)/\Gamma(\pi^0 \gamma)$			$\Gamma_{13}/\Gamma_2$	
VALUE (units $10^{-4}$ )	CL%	EVTS	DOCUMENT ID	TECN COMMENT
<b>7.9 ± 1.3 OUR FIT</b>				
<b>8.5 ± 2.9</b>				
• • •			We do not use the following data for averages, fits, limits, etc. • • •	
< 50	90		DOLINSKY 89	ND $e^+e^- \rightarrow \pi^0 \pi^0 \gamma$
< 1800	95		KEYNE 76	CNTR $\pi^- p \rightarrow \omega n$
< 1500	90		BENAKSAS 72C	OSPK $e^+e^-$
< 1400			BALDIN 71	HLBC $2.9 \pi^+ p$
< 1000	90		BARMIN 64	HLBC $1.3-2.8 \pi^- p$

## Meson Particle Listings

 $\omega(782)$  $\Gamma(\pi^0\pi^0\gamma)/\Gamma(\text{neutrals})$   $\Gamma_{13}/(\Gamma_2+\Gamma_4)$ 

VALUE	CL%	DOCUMENT ID	TECN	COMMENT
0.22±0.07		<sup>1</sup> DAKIN	72	OSPK 1.4 $\pi^- p \rightarrow nMM$
<0.19	90	DEINET	69B	OSPK

<sup>1</sup> See  $\Gamma(\pi^0\gamma)/\Gamma(\text{neutrals})$ .

 $\Gamma(\eta\pi^0\gamma)/\Gamma_{\text{total}}$   $\Gamma_{14}/\Gamma$ 

VALUE (units $10^{-5}$ )	CL%	DOCUMENT ID	TECN	COMMENT
<3.3	90	AKHMETSHIN 04B	CMD2	0.6-0.97 $e^+e^- \rightarrow \eta\pi^0\gamma$

 $\Gamma(\mu^+\mu^-)/\Gamma_{\text{total}}$   $\Gamma_{15}/\Gamma$ 

VALUE (units $10^{-5}$ )	EVTS	DOCUMENT ID	TECN	COMMENT
<b>7.4±1.8 OUR FIT</b>				
<b>7.4±1.8 OUR AVERAGE</b>				
6.6±1.4±1.7	4.5M	<sup>1</sup> ANASTASI	17	KLOE $e^+e^- \rightarrow \mu^+\mu^-\gamma$
9.0±2.9±1.1	18	HEISTER	02C	ALEP $Z \rightarrow \mu^+\mu^- + X$

<sup>1</sup> Assuming lepton universality in the decay  $\omega \rightarrow \ell^+\ell^-$  and correcting for different phase space between electron and muon final states.

 $\Gamma(\mu^+\mu^-)/\Gamma(\pi^+\pi^-\pi^0)$   $\Gamma_{15}/\Gamma_1$ 

VALUE (units $10^{-3}$ )	CL%	DOCUMENT ID	TECN	COMMENT
<0.2	90	WILSON	69	OSPK 12 $\pi^- C \rightarrow Fe$
<1.7	74	FLATTE	66	HBC 1.2 - 1.7 $K^- p \rightarrow \Lambda\mu^+\mu^-$
<1.2		BARBARO...	65	HBC 2.7 $K^- p$

 $\Gamma(\pi^0\mu^+\mu^-)/\Gamma(\mu^+\mu^-)$   $\Gamma_7/\Gamma_{15}$ 

VALUE	EVTS	DOCUMENT ID	TECN	COMMENT
1.2±0.6	30	<sup>1</sup> DZHELYADIN	79	CNTR 25-33 $\pi^- p$

<sup>1</sup> Superseded by DZHELYADIN 81B result above.

 $\Gamma(3\gamma)/\Gamma_{\text{total}}$   $\Gamma_{16}/\Gamma$ 

VALUE (units $10^{-4}$ )	CL%	DOCUMENT ID	TECN	COMMENT
<1.9	95	<sup>1</sup> ABELE	97E	CBAR 0.0 $\bar{p}p \rightarrow 5\gamma$
<2	90	<sup>1</sup> PROKOSHKIN	95	GAM2 38 $\pi^- p \rightarrow 3\gamma n$

<sup>1</sup> From direct  $3\gamma$  decay search.

 $\Gamma(\eta\pi^0)/\Gamma_{\text{total}}$   $\Gamma_{17}/\Gamma$ 

VALUE	CL%	DOCUMENT ID	TECN	COMMENT
<0.001	90	ALDE	94B	GAM2 38 $\pi^- p \rightarrow \eta\pi^0 n$

 $[\Gamma(\eta\gamma) + \Gamma(\eta\pi^0)]/\Gamma(\pi^+\pi^-\pi^0)$   $(\Gamma_5 + \Gamma_{17})/\Gamma_1$ 

VALUE	CL%	DOCUMENT ID	TECN	COMMENT
<0.016	90	<sup>1</sup> FLATTE	66	HBC 1.2 - 1.7 $K^- p \rightarrow \Lambda\pi^+\pi^- MM$
<0.045	95	JACQUET	69B	HLBC 2.05 $\pi^+ p \rightarrow \pi^+ p \omega$

<sup>1</sup> Restated by us using  $B(\eta \rightarrow \text{charged modes}) = 29.2\%$ .

 $\Gamma(\eta\pi^0)/\Gamma(\pi^0\gamma)$   $\Gamma_{17}/\Gamma_2$ 

VALUE (units $10^{-3}$ )	CL%	DOCUMENT ID	TECN	COMMENT
<2.6	90	<sup>1</sup> STAROSTIN	09	CRYM $\gamma p \rightarrow \eta\pi^0 p$

<sup>1</sup> STAROSTIN 09 reports  $[\Gamma(\omega(782) \rightarrow \eta\pi^0)/\Gamma(\omega(782) \rightarrow \pi^0\gamma)] \times [B(\eta \rightarrow 2\gamma)] < 1.01 \times 10^{-3}$  which we divide by our best value  $B(\eta \rightarrow 2\gamma) = 39.41 \times 10^{-2}$ .

 $\Gamma(2\pi^0)/\Gamma(\pi^0\gamma)$   $\Gamma_{18}/\Gamma_2$ 

VALUE (units $10^{-3}$ )	CL%	DOCUMENT ID	TECN	COMMENT
<2.59	90	STAROSTIN	09	CRYM $\gamma p \rightarrow 2\pi^0 p$

 $\Gamma(3\pi^0)/\Gamma_{\text{total}}$   $\Gamma_{19}/\Gamma$ 

VALUE	CL%	DOCUMENT ID	TECN	COMMENT
<3 × 10 <sup>-4</sup>	90	PROKOSHKIN	95	GAM2 38 $\pi^- p \rightarrow 3\pi^0 n$

 $\Gamma(3\pi^0)/\Gamma(\pi^0\gamma)$   $\Gamma_{19}/\Gamma_2$ 

VALUE (units $10^{-3}$ )	CL%	DOCUMENT ID	TECN	COMMENT
<2.72	90	STAROSTIN	09	CRYM $\gamma p \rightarrow 3\pi^0 p$

 $\Gamma(3\pi^0)/\Gamma(\pi^+\pi^-\pi^0)$   $\Gamma_{19}/\Gamma_1$ 

VALUE	CL%	DOCUMENT ID	TECN	COMMENT
<0.009	90	BARBERIS	01	450 $p p \rightarrow p_f 3\pi^0 p_s$

 $\Gamma(\text{invisible})/\Gamma(\pi^+\pi^-\pi^0)$   $\Gamma_{20}/\Gamma_1$ 

VALUE	CL%	DOCUMENT ID	TECN	COMMENT
<8.1 × 10 <sup>-5</sup>	90	ABLIKIM	18s	BES3 $J/\psi \rightarrow \omega\eta \rightarrow \omega\pi^+\pi^-\pi^0$

PARAMETER  $\Lambda$  IN  $\omega \rightarrow \pi^0\ell^+\ell^-$  DECAY

In the pole approximation the electromagnetic transition form factor for a resonance of mass  $M$  is given by the expression:

$$|F|^2 = (1 - M^2/\Lambda^2)^{-2},$$

where for the parameter  $\Lambda$  vector dominance predicts  $\Lambda = M_p \approx 0.770$  GeV. The ARNALDI 09 measurement is in obvious conflict with this expectation. Note that for  $\eta \rightarrow \gamma\mu^+\mu^-$  decay ARNALDI 09 and DZHELYADIN 80 obtain the value of  $\Lambda$  consistent with vector dominance.

PARAMETER  $\Lambda$  IN  $\omega \rightarrow \pi^0\mu^+\mu^-$  DECAY

VALUE (GeV)	EVTS	DOCUMENT ID	TECN	COMMENT
<b>0.670 ± 0.006 OUR AVERAGE</b>				
0.6707 ± 0.0039 ± 0.0056		<sup>1</sup> ARNALDI	16	NA60 400 GeV ( $p$ -A) collisions
0.668 ± 0.009 ± 0.003	3k	<sup>2</sup> ARNALDI	09	NA60 158A In-In collisions
0.65 ± 0.03		DZHELYADIN	81B	CNTR 25-33 $\pi^- p \rightarrow \omega n$

<sup>1</sup> ARNALDI 16 reports  $\Lambda^{-2}(\omega) = 2.223 \pm 0.026 \pm 0.037$  GeV<sup>-2</sup> which we converted to the quoted  $\Lambda$  value.

<sup>2</sup> ARNALDI 09 reports  $\Lambda^{-2}(\omega) = 2.24 \pm 0.06 \pm 0.02$  GeV<sup>-2</sup> which we converted to the quoted  $\Lambda$  value.

PARAMETER  $\Lambda$  IN  $\omega \rightarrow \pi^0e^+e^-$  DECAY

VALUE (GeV)	EVTS	DOCUMENT ID	TECN	COMMENT
<b>0.709 ± 0.037</b>	1.1k	<sup>1</sup> ADLARSON	17B	A2MM $\gamma p \rightarrow \omega p$
		<sup>1</sup> ADLARSON	17B	reports $\Lambda^{-2}(\omega\pi^0) = 1.99 \pm 0.21$ GeV <sup>-2</sup> that we converted to the quoted $\Lambda$ value.

ENERGY DEPENDENCE OF  $\omega \rightarrow \pi^+\pi^-\pi^0$  DALITZ PLOT

The following experiments fit to one or more of the coefficients  $\alpha, \beta, \gamma$  for  $|matrix\ element|^2 \propto P(1 + 2\alpha Z + 2\beta Z^2 \sin(3\phi) + 2\gamma Z^2 + O(Z^5/2))$  where  $P$  is the  $P$ -wave phase-space factor and  $Z, \phi$  are kinematical variables as defined in ADLARSON 17.

VALUE	EVTS	DOCUMENT ID	TECN	COMMENT
<b>0.133 ± 0.008 OUR AVERAGE</b>				
0.1321 ± 0.0067 ± 0.0046	260k	<sup>1</sup> ABLIKIM	18AD	BES3 $J/\psi \rightarrow \omega\eta$
0.147 ± 0.036	44k	ADLARSON	17	WASA $\alpha$ in $p d \rightarrow {}^3\text{He} \omega, p p \rightarrow p p \omega$

<sup>1</sup> Keeping a term linear in  $Z$  only. A fit with the terms proportional to  $Z$  and  $Z^{3/2}$  gives  $\alpha = 0.133 \pm 0.041$  and  $\beta = 0.037 \pm 0.054$ .

 $\omega(782)$  REFERENCES

ABLIKIM	18AD	PR D98 112007	M. Ablikim et al.	(BESIII Collab.)
ABLIKIM	18C	PRL 120 242003	M. Ablikim et al.	(BESIII Collab.)
ABLIKIM	18S	PR D98 032001	M. Ablikim et al.	(BESIII Collab.)
HANHART	18	EPJ C78 450	C. Hanhart et al.	
ADLARSON	17	PL B770 418	P. Adlarson et al.	(WASA-at-COSY Collab.)
ADLARSON	17B	PR C95 035208	P. Adlarson et al.	(A2 Collab. at MAMI)
ANASTASI	17	PL B767 485	A. Anastasi et al.	(KLOE-2 Collab.)
ABLIKIM	16B	PL B753 103	M. Ablikim et al.	(BESIII Collab.)
ACHASOV	16A	PR D93 092001	M.N. Achasov et al.	(SND Collab.)
ARNALDI	16	PL B757 437	R. Arnaldi et al.	(NA60 Collab.)
PDG	15	RPP 2015 at pub.lnl.gov		(PDG Collab.)
ACHASOV	13	PR D88 054013	M.N. Achasov et al.	(SND Collab.)
BABUSCI	13D	PL B720 336	D. Babusci et al.	(CATA, CALB, BARI)
BENAYOUN	13	EPJ C73 2453	M. Benayoun, P. David, L. DelBuono (PARIN, BERLIN+)	
DAVIER	13	EPJ C73 2597	M. Davier et al.	
LEES	12G	PR D86 032013	J.P. Lees et al.	(BABAR Collab.)
NIECKNIG	12	EPJ C72 2014	F. Niecknig, B. Kubis, S.P. Schneider	(BONN)
AMBROSINO	11A	PL B700 102	F. Ambrosino et al.	(KLOE Collab.)
BENAYOUN	10	EPJ C65 211	M. Benayoun et al.	
ACHASOV	09A	JETP 109 379	M.N. Achasov et al.	(SND Collab.)
ARNALDI	09	PL B677 260	R. Arnaldi et al.	(NA60 Collab.)
AUBERT	09AS	PRL 103 231801	B. Aubert et al.	(BABAR Collab.)
STAROSTIN	09	PR C79 065201	A. Starostin et al.	(Crystal Ball Collab. at MAMI)
ACHASOV	08	JETP 107 61	M.N. Achasov et al.	(SND Collab.)
ACHASOV	08G	PL B669 223	F. Ambrosino et al.	(KLOE Collab.)
ACHASOV	07B	PR D76 077101	M.N. Achasov et al.	(SND Collab.)
AKHMETSHIN	07	PL B648 28	R.R. Akhmetshin et al.	(Novosibirsk CMD-2 Collab.)
ACHASOV	06	JETP 103 380	M.N. Achasov et al.	(Novosibirsk CMD-2 Collab.)
ACHASOV	06A	Translated from ZETF 130 437.		
ACHASOV	06A	PR D74 014016	M.N. Achasov et al.	(SND Collab.)
AULCHENKO	06	JETPL 84 413	V.M. Aulchenko et al.	(Novosibirsk CMD-2 Collab.)
ACHASOV	05A	JETP 101 1053	M.N. Achasov et al.	(Novosibirsk SND Collab.)
ACHMETSHIN	05	PL B605 26	R.R. Akhmetshin et al.	(Novosibirsk CMD-2 Collab.)
AKHMETSHIN	05A	PL B613 29	R.R. Akhmetshin et al.	(Novosibirsk CMD-2 Collab.)
AULCHENKO	05	JETPL 82 743	V.M. Aulchenko et al.	(Novosibirsk CMD-2 Collab.)
		Translated from ZETFP 82 841.		

See key on page 999

Meson Particle Listings

$\omega(782), \eta'(958)$

$\eta'(958)$

$I(G^{JPC}) = 0^+(0^-+)$

$\eta'(958)$  MASS

Table with columns: VALUE (MeV), EVTS, DOCUMENT ID, TECN, COMMENT. Includes summary row: 957.78 ± 0.06 OUR AVERAGE. Lists various experiments like LIBBY, WURZINGER, DUANE, DANBURG, JACOBS, BASILE, BAI, BELADIDZE, ARMSTRONG, AUGUSTIN, GIDAL, BASILE, RITTENBERG.

• • • We do not use the following data for averages, fits, limits, etc. • • •
1 Using all η' decays.
2 Systematic uncertainty not estimated.
3 Using η' decays into neutrals. Not independent of the other listed BASILE 71 η' mass measurement.

$\eta'(958)$  WIDTH

Table with columns: VALUE (MeV), EVTS, DOCUMENT ID, TECN, CHG, COMMENT. Includes summary row: 0.230 ± 0.021 OUR AVERAGE. Lists experiments like CZERWINSKI, WURZINGER, BINNIE, BAI.

• • • We do not use the following data for averages, fits, limits, etc. • • •

$\eta'(958)$  DECAY MODES

Table with columns: Mode, Fraction (Γ<sub>i</sub>/Γ), Confidence level. Lists various decay channels like π<sup>+</sup>π<sup>-</sup>η, ρ<sup>0</sup>γ, π<sup>+</sup>π<sup>-</sup>γ, ωγ, ωe<sup>+</sup>e<sup>-</sup>, γγ, 3π<sup>0</sup>, μ<sup>+</sup>μ<sup>-</sup>γ, π<sup>+</sup>π<sup>-</sup>μ<sup>+</sup>μ<sup>-</sup>, π<sup>+</sup>π<sup>-</sup>π<sup>0</sup>, π<sup>±</sup>ρ<sup>±</sup>, π<sup>0</sup>ρ<sup>0</sup>, 2(π<sup>+</sup>π<sup>-</sup>), π<sup>+</sup>π<sup>-</sup>2π<sup>0</sup>, 2(π<sup>+</sup>π<sup>-</sup>) neutrals, 2(π<sup>+</sup>π<sup>-</sup>)π<sup>0</sup>, 2(π<sup>+</sup>π<sup>-</sup>)2π<sup>0</sup>, 3(π<sup>+</sup>π<sup>-</sup>), K<sup>±</sup>π<sup>∓</sup>, π<sup>+</sup>π<sup>-</sup>e<sup>+</sup>e<sup>-</sup>, π<sup>+</sup>e<sup>-</sup>ν<sub>e</sub>+c.c., γe<sup>+</sup>e<sup>-</sup>, π<sup>0</sup>γγ, π<sup>0</sup>γγ (non resonant), ηγγ, 4π<sup>0</sup>, e<sup>+</sup>e<sup>-</sup>, invisible.

Main reference table listing experiments, values, and comments for η'(958). Includes entries for AKHMETSIN, ACHASOV, ALOISIO, BENAYOUN, HEISTER, BARBERIS, WURZINGER, AMSLER, ALDE, DOLINSKY, KURDADZE, BARKOV, BARKO, DZHELYADIN, CORDIER, ROOS, BENKHEIRI, COOPER, QUENZER, VANAPREL, WICKLUND, ANDREWS, GESSAROLI, KEYNE, GALBFLEISCH, AUILAR..., APEL, BASILE, BENAOKAS, BENAOKAS, BENAOKAS, BORENSTEIN, BROWN, DAKIN, RATCLIFF, ALVENSLEB..., BALDIN, BEHREND, BIZZARRI, COYNE, MOFFETT, ABRAMOV..., BIGGS, BIZZARRI, ROOS, Proc. Daresbury Study Weekend No. 1., AUGUSTIN, BIZZARRI, DEINET, JACQUET, WILSON, ASTVACAT..., BOLLINI, GOUNARIS, BARASH, FELDMAN, DIGIUGNO, FLATTE, JAMES, BARBARO..., BARMIN, KRAEMER, BUSCHBECK.

Downloaded from https://academic.oup.com/ptep/article/2020/8/083C01/5891211 by guest on 12 November 2020



# Meson Particle Listings

## $\eta'(958)$

Charge conjugation (C), Parity (P), Lepton family number (LF) violating modes				
$\Gamma_{31}$	$\pi^+ \pi^-$	$P, CP$	$< 1.8$	$\times 10^{-5}$ 90%
$\Gamma_{32}$	$\pi^0 \pi^0$	$P, CP$	$< 4$	$\times 10^{-4}$ 90%
$\Gamma_{33}$	$\pi^0 e^+ e^-$	C	$[a] < 1.4$	$\times 10^{-3}$ 90%
$\Gamma_{34}$	$\eta e^+ e^-$	C	$[a] < 2.4$	$\times 10^{-3}$ 90%
$\Gamma_{35}$	$3\gamma$	C	$< 1.0$	$\times 10^{-4}$ 90%
$\Gamma_{36}$	$\mu^+ \mu^- \pi^0$	C	$[a] < 6.0$	$\times 10^{-5}$ 90%
$\Gamma_{37}$	$\mu^+ \mu^- \eta$	C	$[a] < 1.5$	$\times 10^{-5}$ 90%
$\Gamma_{38}$	$e \mu$	LF	$< 4.7$	$\times 10^{-4}$ 90%

[a] C parity forbids this to occur as a single-photon process.

### CONSTRAINED FIT INFORMATION

An overall fit to the total width, a partial width, 2 combinations of partial widths obtained from integrated cross section, and 19 branching ratios uses 51 measurements and one constraint to determine 9 parameters. The overall fit has a  $\chi^2 = 69.4$  for 43 degrees of freedom.

The following off-diagonal array elements are the correlation coefficients  $\langle \delta p_i \delta p_j \rangle / (\delta p_i \delta p_j)$ , in percent, from the fit to parameters  $p_i$ , including the branching fractions,  $x_i \equiv \Gamma_i / \Gamma_{\text{total}}$ . The fit constrains the  $x_i$  whose labels appear in this array to sum to one.

$x_2$	-24								
$x_4$	-74	-42							
$x_5$	-7	-6	-2						
$x_7$	-11	-7	9	-1					
$x_8$	-17	-9	19	0	2				
$x_{11}$	-1	-1	-1	0	0	0			
$x_{22}$	-9	-7	-7	-1	-2	-2	0		
$\Gamma$	11	-10	-1	1	-40	0	0	2	
	$x_1$	$x_2$	$x_4$	$x_5$	$x_7$	$x_8$	$x_{11}$	$x_{22}$	

Mode	Rate (MeV)
$\Gamma_1$ $\pi^+ \pi^- \eta$	$0.0799 \pm 0.0029$
$\Gamma_2$ $\rho^0 \gamma$ (including non-resonant $\pi^+ \pi^- \gamma$ )	$0.0554 \pm 0.0019$
$\Gamma_4$ $\pi^0 \pi^0 \eta$	$0.0421 \pm 0.0017$
$\Gamma_5$ $\omega \gamma$	$0.00474 \pm 0.00020$
$\Gamma_7$ $\gamma \gamma$	$0.00434 \pm 0.00013$
$\Gamma_8$ $3\pi^0$	$(4.7 \pm 0.4) \times 10^{-4}$
$\Gamma_{11}$ $\pi^+ \pi^- \pi^0$	$(6.8 \pm 0.4) \times 10^{-4}$
$\Gamma_{22}$ $\pi^+ \pi^- e^+ e^-$	$(4.4 \pm_{-1.8}^{2.3}) \times 10^{-4}$

### $\eta'(958)$ PARTIAL WIDTHS

$\Gamma(\gamma\gamma)$	$\Gamma_7$			
VALUE (keV)	EVTS	DOCUMENT ID	TECN	COMMENT
<b>4.34 ± 0.14 OUR FIT</b>				
<b>4.28 ± 0.19 OUR AVERAGE</b>				
$4.17 \pm 0.10 \pm 0.27$	2000	<sup>1</sup> ACCIARRI	98Q L3	$e^+ e^- \rightarrow e^+ e^- \pi^+ \pi^- \gamma$
$4.53 \pm 0.29 \pm 0.51$	266	KARCH	92 CBAL	$e^+ e^- \rightarrow e^+ e^- \eta \pi^0 \pi^0$
$3.61 \pm 0.13 \pm 0.48$		<sup>2</sup> BEHREND	91 CELL	$e^+ e^- \rightarrow e^+ e^- \eta'(958)$
$4.6 \pm 1.1 \pm 0.6$	23	BARU	90 MD1	$e^+ e^- \rightarrow e^+ e^- \pi^+ \pi^- \gamma$
$4.57 \pm 0.25 \pm 0.44$		BUTLER	90 MRK2	$e^+ e^- \rightarrow e^+ e^- \eta'(958)$
$5.08 \pm 0.24 \pm 0.71$	547	<sup>3</sup> ROE	90 ASP	$e^+ e^- \rightarrow e^+ e^- 2\gamma$
$3.8 \pm 0.7 \pm 0.6$	34	AIHARA	88c TPC	$e^+ e^- \rightarrow e^+ e^- \eta \pi^+ \pi^-$
$4.9 \pm 0.5 \pm 0.5$	136	<sup>4</sup> WILLIAMS	88 CBAL	$e^+ e^- \rightarrow e^+ e^- 2\gamma$
••• We do not use the following data for averages, fits, limits, etc. •••				
$4.7 \pm 0.6 \pm 0.9$	143	<sup>5</sup> GIDAL	87 MRK2	$e^+ e^- \rightarrow e^+ e^- \eta \pi^+ \pi^-$
$4.0 \pm 0.9$		<sup>6</sup> BARTEL	85E JADE	$e^+ e^- \rightarrow e^+ e^- 2\gamma$

<sup>1</sup> No non-resonant  $\pi^+ \pi^-$  contribution found.  
<sup>2</sup> Reevaluated by us using  $B(\eta' \rightarrow \rho(770)\gamma) = (30.2 \pm 1.3)\%$ .  
<sup>3</sup> Reevaluated by us using  $B(\eta' \rightarrow \gamma\gamma) = (2.11 \pm 0.13)\%$ .  
<sup>4</sup> Reevaluated by us using  $B(\eta' \rightarrow \gamma\gamma) = (2.11 \pm 0.13)\%$ .  
<sup>5</sup> Superseded by BUTLER 90.  
<sup>6</sup> Systematic error not evaluated.

$\Gamma(e^+ e^-)$	$\Gamma_{29}$			
VALUE (eV)	CL%	DOCUMENT ID	TECN	COMMENT
<b>&lt; 1.1 × 10<sup>-3</sup></b>	90	<sup>1,2</sup> ACHASOV	15 SND	$0.958 e^+ e^- \rightarrow \pi^+ \pi^- \eta$
••• We do not use the following data for averages, fits, limits, etc. •••				
$< 2.0 \times 10^{-3}$	90	<sup>2</sup> ACHASOV	15 SND	$0.958 e^+ e^- \rightarrow \pi^+ \pi^- \eta$
$< 2.4 \times 10^{-3}$	90	<sup>2</sup> AKHMETSHIN	15 CMD3	$0.958 e^+ e^- \rightarrow \pi^+ \pi^- \eta$

<sup>1</sup> Combining data of ACHASOV 15 and AKHMETSHIN 15.  
<sup>2</sup> Using  $\eta$  and  $\eta'$  branching fractions from PDG 14.

### $\eta'(958) \Gamma(i)\Gamma(\gamma\gamma)/\Gamma(\text{total})$

This combination of a partial width with the partial width into  $\gamma\gamma$  and with the total width is obtained from the integrated cross section into channel(i) in the  $\gamma\gamma$  annihilation.

$\Gamma(\gamma\gamma) \times \Gamma(\rho^0 \gamma$ (including non-resonant $\pi^+ \pi^- \gamma$ )) / $\Gamma_{\text{total}}$	$\Gamma_7 \Gamma_2 / \Gamma$			
VALUE (keV)	EVTS	DOCUMENT ID	TECN	COMMENT
<b>1.28 ± 0.04 OUR FIT</b>				
<b>1.26 ± 0.07 OUR AVERAGE</b>				Error includes scale factor of 1.2.
$1.09 \pm 0.04 \pm 0.13$		BEHREND	91 CELL	$e^+ e^- \rightarrow e^+ e^- \rho(770)^0 \gamma$
$1.35 \pm 0.09 \pm 0.21$		AIHARA	87 TPC	$e^+ e^- \rightarrow e^+ e^- \rho \gamma$
$1.13 \pm 0.04 \pm 0.13$	867	ALBRECHT	87B ARG	$e^+ e^- \rightarrow e^+ e^- \rho \gamma$
$1.53 \pm 0.09 \pm 0.21$		ALTHOFF	84E TASS	$e^+ e^- \rightarrow e^+ e^- \rho \gamma$
$1.14 \pm 0.08 \pm 0.11$	243	BERGER	84B PLUT	$e^+ e^- \rightarrow e^+ e^- \rho \gamma$
$1.73 \pm 0.34 \pm 0.35$	95	JENNI	83 MRK2	$e^+ e^- \rightarrow e^+ e^- \rho \gamma$
$1.49 \pm 0.13 \pm 0.027$	213	BARTEL	82B JADE	$e^+ e^- \rightarrow e^+ e^- \rho \gamma$
••• We do not use the following data for averages, fits, limits, etc. •••				
$1.85 \pm 0.31 \pm 0.24$	43	BEHREND	82c CELL	$e^+ e^- \rightarrow e^+ e^- \rho \gamma$

$\Gamma(\gamma\gamma) \times \Gamma(\pi^0 \pi^0 \eta) / \Gamma_{\text{total}}$	$\Gamma_7 \Gamma_4 / \Gamma$			
VALUE (keV)	EVTS	DOCUMENT ID	TECN	COMMENT
<b>0.97 ± 0.04 OUR FIT</b>				Error includes scale factor of 1.1.
<b>0.92 ± 0.06 ± 0.11</b>		<sup>1</sup> KARCH	92 CBAL	$e^+ e^- \rightarrow e^+ e^- \eta \pi^0 \pi^0$
••• We do not use the following data for averages, fits, limits, etc. •••				
$0.95 \pm 0.05 \pm 0.08$		<sup>2</sup> KARCH	90 CBAL	$e^+ e^- \rightarrow e^+ e^- \eta \pi^0 \pi^0$
$1.00 \pm 0.08 \pm 0.10$		<sup>2,3</sup> ANTREASYSAN	87 CBAL	$e^+ e^- \rightarrow e^+ e^- \eta \pi^0 \pi^0$

<sup>1</sup> Reevaluated by us using  $B(\eta \rightarrow \gamma\gamma) = (39.21 \pm 0.34)\%$ . Supersedes ANTREASYSAN 87 and KARCH 90.  
<sup>2</sup> Superseded by KARCH 92.  
<sup>3</sup> Using  $BR(\eta \rightarrow 2\gamma) = (38.9 \pm 0.5)\%$ .

### $\eta'(958) \Gamma(i)\Gamma(e^+ e^-) / \Gamma(\text{total})$

$\Gamma(\pi^+ \pi^- \eta) \times \Gamma(e^+ e^-) / \Gamma_{\text{total}}$	$\Gamma_1 \Gamma_{29} / \Gamma$			
VALUE (10 <sup>-3</sup> eV)	CL%	DOCUMENT ID	TECN	COMMENT
<b>&lt; 1.0</b>	90	<sup>1</sup> AKHMETSHIN	15 CMD3	$0.958 e^+ e^- \rightarrow \pi^+ \pi^- \eta$
<sup>1</sup> AKHMETSHIN 15 reports $[\Gamma(\eta'(958) \rightarrow \pi^+ \pi^- \eta) \times \Gamma(\eta'(958) \rightarrow e^+ e^-) / \Gamma_{\text{total}}] \times [B(\eta \rightarrow 2\gamma)] < 4.1 \times 10^{-4}$ eV which we divide by our best value $B(\eta \rightarrow 2\gamma) = 39.41 \times 10^{-2}$ .				

### $\eta'(958)$ BRANCHING RATIOS

$\Gamma(\pi^+ \pi^- \eta) / \Gamma_{\text{total}}$	$\Gamma_1 / \Gamma$			
VALUE (units 10 <sup>-2</sup> )	EVTS	DOCUMENT ID	TECN	COMMENT
<b>42.5 ± 0.5 OUR FIT</b>				Error includes scale factor of 1.1.
<b>41.24 ± 0.08 ± 1.24</b>	312k	ABLIKIM	19T BES	$J/\psi \rightarrow \gamma \eta'$
••• We do not use the following data for averages, fits, limits, etc. •••				
$42.4 \pm 1.1 \pm 0.4$	1.2k	<sup>1</sup> PEDLAR	09 CLEO	$J/\psi \rightarrow \gamma \eta'$

<sup>1</sup> Not independent of other  $\eta'$  branching fractions and ratios in PEDLAR 09.

$\Gamma(\pi^+ \pi^- \eta$ (charged decay)) / $\Gamma_{\text{total}}$	$0.2789 \Gamma_1 / \Gamma$			
VALUE	EVTS	DOCUMENT ID	TECN	COMMENT
<b>0.1185 ± 0.0015 OUR FIT</b>				Error includes scale factor of 1.1.
••• We do not use the following data for averages, fits, limits, etc. •••				
$0.123 \pm 0.014$	107	RITTENBERG	69 HBC	$1.7-2.7 K^- p$
$0.10 \pm 0.04$	10	LONDON	66 HBC	$2.24 K^- p \rightarrow \Lambda 2\pi^+ 2\pi^- \pi^0$
$0.07 \pm 0.04$	7	BADIER	65B HBC	$3 K^- p$

$\Gamma(\pi^+ \pi^- \eta$ (neutral decay)) / $\Gamma_{\text{total}}$	$0.7212 \Gamma_1 / \Gamma$			
VALUE	EVTS	DOCUMENT ID	TECN	COMMENT
<b>0.306 ± 0.004 OUR FIT</b>				Error includes scale factor of 1.1.
••• We do not use the following data for averages, fits, limits, etc. •••				
$0.314 \pm 0.026$	281	RITTENBERG	69 HBC	$1.7-2.7 K^- p$

$\Gamma(\rho^0 \gamma$ (including non-resonant $\pi^+ \pi^- \gamma$ )) / $\Gamma_{\text{total}}$	$\Gamma_2 / \Gamma$			
VALUE (units 10 <sup>-2</sup> )	EVTS	DOCUMENT ID	TECN	COMMENT
<b>29.5 ± 0.4 OUR FIT</b>				Error includes scale factor of 1.1.
<b>29.90 ± 0.03 ± 0.55</b>	913k	ABLIKIM	19T BES	$J/\psi \rightarrow \gamma \eta'$
••• We do not use the following data for averages, fits, limits, etc. •••				
$28.7 \pm 0.7 \pm 0.4$	0.2k	<sup>1</sup> PEDLAR	09 CLEO	$J/\psi \rightarrow \gamma \eta'$
$32.9 \pm 3.3$	298	RITTENBERG	69 HBC	$1.7-2.7 K^- p$
$20 \pm 10$	20	LONDON	66 HBC	$2.24 K^- p \rightarrow \Lambda \pi^+ \pi^- \gamma$
$34 \pm 9$	35	BADIER	65B HBC	$3 K^- p$

<sup>1</sup> Not independent of other  $\eta'$  branching fractions and ratios in PEDLAR 09.

$\Gamma(\rho^0 \gamma) / \Gamma_{\text{total}}$	$\Gamma_3 / \Gamma$			
VALUE (%)	EVTS	DOCUMENT ID	TECN	COMMENT
••• We do not use the following data for averages, fits, limits, etc. •••				
$33.34 \pm 0.06 \pm 1.60$	970k	<sup>1</sup> ABLIKIM	18c BES3	$\eta'(958) \rightarrow \gamma \pi^+ \pi^-$
$34.43 \pm 0.52 \pm 1.97$	970k	<sup>2</sup> ABLIKIM	18c BES3	$\eta'(958) \rightarrow \gamma \pi^+ \pi^-$

<sup>1</sup> From a fit to  $\pi^+ \pi^-$  mass using  $\rho(770)$ ,  $\omega(782)$ , and box anomaly components.  
<sup>2</sup> From a fit to  $\pi^+ \pi^-$  mass using  $\rho(770)$ ,  $\omega(782)$ , and  $\rho(1450)$  components.

$\Gamma(\rho^0 \gamma (\text{including non-resonant } \pi^+ \pi^- \gamma)) / \Gamma(\pi^+ \pi^- \eta)$ 

VALUE	DOCUMENT ID	TECN	COMMENT
<b>0.694 ± 0.014 OUR FIT</b>	Error includes scale factor of 1.1.		
<b>0.683 ± 0.020 OUR AVERAGE</b>			
0.677 ± 0.024 ± 0.011	PEDLAR	09 CLE3	$J/\psi \rightarrow \eta' \gamma$
0.69 ± 0.03	ABLIKIM	06E BES2	$J/\psi \rightarrow \eta' \gamma$

 $\Gamma(\rho^0 \gamma (\text{including non-resonant } \pi^+ \pi^- \gamma)) / \Gamma(\pi^+ \pi^- \eta (\text{neutral decay}))$ 

VALUE	EVTs	DOCUMENT ID	TECN	COMMENT
<b>0.972 ± 0.020 OUR FIT</b>	Error includes scale factor of 1.1.			
<b>0.97 ± 0.09 OUR AVERAGE</b>				
0.70 ± 0.22		AMSLER	04B CBAR	$0 \bar{p} p \rightarrow \pi^+ \pi^- \eta$
1.07 ± 0.17		BELADIDZE	92c VES	$36 \pi^- \text{Be} \rightarrow \pi^- \eta' \eta \text{Be}$
0.92 ± 0.14	473	DANBURG	73 HBC	$2.2 K^- p \rightarrow \Lambda X^0$
1.11 ± 0.18	192	JACOBS	73 HBC	$2.9 K^- p \rightarrow \Lambda X^0$

 $\Gamma(\pi^0 \pi^0 \eta) / \Gamma_{\text{total}}$ 

VALUE (units $10^{-2}$ )	EVTs	DOCUMENT ID	TECN	COMMENT
<b>22.4 ± 0.6 OUR FIT</b>	Error includes scale factor of 1.1.			
<b>21.36 ± 0.10 ± 0.92</b>	52k	ABLIKIM	19T BES	$J/\psi \rightarrow \gamma \eta'$
• • • We do not use the following data for averages, fits, limits, etc. • • •				
23.5 ± 1.3 ± 0.4	3.2k	<sup>1</sup> PEDLAR	09 CLEO	$J/\psi \rightarrow \gamma \eta'$

 $\Gamma(\pi^0 \pi^0 \eta (3\pi^0 \text{ decay})) / \Gamma_{\text{total}}$ 

VALUE	EVTs	DOCUMENT ID	TECN	COMMENT
<b>0.0718 ± 0.0018 OUR FIT</b>	Error includes scale factor of 1.1.			
• • • We do not use the following data for averages, fits, limits, etc. • • •				
0.11 ± 0.06	4	BENSINGER	70 DBC	$2.2 \pi^+ d$

 $\Gamma(\pi^0 \pi^0 \eta) / \Gamma(\pi^+ \pi^- \eta)$ 

VALUE	DOCUMENT ID	TECN	COMMENT
<b>0.527 ± 0.019 OUR FIT</b>	Error includes scale factor of 1.1.		
<b>0.555 ± 0.043 ± 0.013</b>	PEDLAR	09 CLE3	$J/\psi \rightarrow \eta' \gamma$

 $\Gamma(\rho^0 \gamma (\text{including non-resonant } \pi^+ \pi^- \gamma)) / \Gamma(\pi \pi \eta)$ 

VALUE	DOCUMENT ID	TECN	COMMENT
<b>0.454 ± 0.009 OUR FIT</b>	Error includes scale factor of 1.1.		
<b>0.43 ± 0.02 ± 0.02</b>	BARBERIS	98c OMEG	$450 p p \rightarrow p_f \eta' p_s$
• • • We do not use the following data for averages, fits, limits, etc. • • •			
0.31 ± 0.15	DAVIS	68 HBC	$5.5 K^- p$

 $\Gamma(\omega \gamma) / \Gamma_{\text{total}}$ 

VALUE (units $10^{-2}$ )	EVTs	DOCUMENT ID	TECN	COMMENT
<b>2.52 ± 0.07 OUR FIT</b>				
<b>2.50 ± 0.07 OUR AVERAGE</b>				
2.489 ± 0.018 ± 0.074	23k	ABLIKIM	19T BES	$J/\psi \rightarrow \gamma \eta'$
2.55 ± 0.03 ± 0.16	33.2k	<sup>1</sup> ABLIKIM	15AD BES3	$J/\psi \rightarrow \eta' \gamma$
• • • We do not use the following data for averages, fits, limits, etc. • • •				
2.34 ± 0.30 ± 0.04	70	<sup>2</sup> PEDLAR	09 CLEO	$J/\psi \rightarrow \gamma \eta'$

 $\Gamma(\omega \gamma) / \Gamma(\pi^+ \pi^- \eta)$ 

VALUE	EVTs	DOCUMENT ID	TECN	COMMENT
<b>0.0593 ± 0.0018 OUR FIT</b>	Error includes scale factor of 1.1.			
<b>0.055 ± 0.007 ± 0.001</b>	PEDLAR	09 CLE3	$J/\psi \rightarrow \eta' \gamma$	
• • • We do not use the following data for averages, fits, limits, etc. • • •				
0.068 ± 0.013	68	ZANFINO	77 ASPK	$8.4 \pi^- p$

 $\Gamma(\omega \gamma) / \Gamma(\pi^0 \pi^0 \eta)$ 

VALUE	DOCUMENT ID	TECN	COMMENT
<b>0.113 ± 0.004 OUR FIT</b>			
<b>0.147 ± 0.016</b>	ALDE	87B GAM2	$38 \pi^- p \rightarrow n 4 \gamma$

 $\Gamma(\omega e^+ e^-) / \Gamma(\omega \gamma)$ 

VALUE (units $10^{-3}$ )	DOCUMENT ID	TECN	COMMENT
• • • We do not use the following data for averages, fits, limits, etc. • • •			
7.71 ± 1.34 ± 0.54	<sup>1</sup> ABLIKIM	15AD BES3	$J/\psi \rightarrow \eta' \gamma$

 $\Gamma(\omega e^+ e^-) / \Gamma_{\text{total}}$ 

VALUE (units $10^{-4}$ )	EVTs	DOCUMENT ID	TECN	COMMENT
<b>1.97 ± 0.34 ± 0.17</b>	66	<sup>1</sup> ABLIKIM	15AD BES3	$J/\psi \rightarrow \eta' \gamma$

 $\Gamma(\rho^0 \gamma (\text{including non-resonant } \pi^+ \pi^- \gamma)) / [\Gamma(\pi^+ \pi^- \eta) + \Gamma(\pi^0 \pi^0 \eta)] + \Gamma(\omega \gamma)$ 

VALUE	DOCUMENT ID	TECN	COMMENT
<b>0.437 ± 0.008 OUR FIT</b>	Error includes scale factor of 1.1.		
• • • We do not use the following data for averages, fits, limits, etc. • • •			
0.25 ± 0.14	DAUBER	64 HBC	$1.95 K^- p$

 $[\Gamma(\pi^0 \pi^0 \eta (\text{charged decay})) + \Gamma(\omega (\text{charged decay}) \gamma)] / \Gamma_{\text{total}} (0.286 \Gamma_4 + 0.89 \Gamma_5) / \Gamma$ 

VALUE	EVTs	DOCUMENT ID	TECN	COMMENT
<b>0.0864 ± 0.0017 OUR FIT</b>	Error includes scale factor of 1.1.			
• • • We do not use the following data for averages, fits, limits, etc. • • •				
0.045 ± 0.029	42	RITTENBERG	69 HBC	$1.7\text{--}2.7 K^- p$

 $\Gamma(\pi^+ \pi^- \text{ neutrals}) / \Gamma_{\text{total}} (0.714 \Gamma_1 + 0.286 \Gamma_4 + 0.89 \Gamma_5) / \Gamma$ 

VALUE	EVTs	DOCUMENT ID	TECN	COMMENT
<b>0.3897 ± 0.0028 OUR FIT</b>	Error includes scale factor of 1.1.			
• • • We do not use the following data for averages, fits, limits, etc. • • •				
0.4 ± 0.1	39	LONDON	66 HBC	$2.24 K^- p \rightarrow \Lambda \pi^+ \pi^- \text{ neutrals}$
0.35 ± 0.06	33	BADIER	65B HBC	$3 K^- p$

 $\Gamma(\gamma \gamma) / \Gamma_{\text{total}}$ 

VALUE (units $10^{-2}$ )	EVTs	DOCUMENT ID	TECN	COMMENT
<b>2.307 ± 0.035 OUR FIT</b>	Error includes scale factor of 1.1.			
<b>2.31 ± 0.06 OUR AVERAGE</b>	Error includes scale factor of 1.8.			
2.331 ± 0.012 ± 0.035	71k	ABLIKIM	19T BES	$J/\psi \rightarrow \gamma \eta'$
1.99 ± 0.31 ± 0.27	114	<sup>1</sup> WICHT	08 BELL	$B^\pm \rightarrow K^\pm \gamma \gamma$
2.00 ± 0.18		<sup>2</sup> STANTON	80 SPEC	$8.45 \pi^- p \rightarrow n \pi^+ \pi^- 2 \gamma$
• • • We do not use the following data for averages, fits, limits, etc. • • •				
2.25 ± 0.16 ± 0.03	0.3k	<sup>3</sup> PEDLAR	09 CLEO	$J/\psi \rightarrow \gamma \eta'$
1.8 ± 0.2	6000	<sup>4</sup> APEL	79 NICE	$15\text{--}40 \pi^- p \rightarrow n 2 \gamma$
2.5 ± 0.7		DUANE	74 MMS	$\pi^- p \rightarrow n \text{MM}$
1.71 ± 0.33	68	DALPIAZ	72 CNTR	$1.6 \pi^- p \rightarrow n X^0$
2.0 ± 0.8 ± 0.6	31	HARVEY	71 OSPK	$3.65 \pi^- p \rightarrow n X^0$

<sup>1</sup> WICHT 08 reports  $[\Gamma(\eta'(958) \rightarrow \gamma \gamma) / \Gamma_{\text{total}}] \times [B(B^+ \rightarrow \eta' K^+)] = (1.40^{+0.16+0.15}_{-0.15-0.12}) \times 10^{-6}$  which we divide by our best value  $B(B^+ \rightarrow \eta' K^+) = (7.04 \pm 0.25) \times 10^{-5}$ . Our first error is their experiment's error and our second error is the systematic error from using our best value.

<sup>2</sup> Includes APEL 79 result.

<sup>3</sup> Not independent of other  $\eta'$  branching fractions and ratios in PEDLAR 09.

<sup>4</sup> Data is included in STANTON 80 evaluation.

 $\Gamma(\gamma \gamma) / \Gamma(\pi^+ \pi^- \eta)$ 

VALUE	DOCUMENT ID	TECN	COMMENT
<b>0.0543 ± 0.0012 OUR FIT</b>	Error includes scale factor of 1.1.		
<b>0.053 ± 0.004 ± 0.001</b>	PEDLAR	09 CLE3	$J/\psi \rightarrow \eta' \gamma$

 $\Gamma(\gamma \gamma) / \Gamma(\rho^0 \gamma (\text{including non-resonant } \pi^+ \pi^- \gamma))$ 

VALUE	DOCUMENT ID	TECN	COMMENT
<b>0.0783 ± 0.0016 OUR FIT</b>	Error includes scale factor of 1.1.		
<b>0.080 ± 0.008</b>	ABLIKIM	06E BES2	$J/\psi \rightarrow \eta' \gamma$

 $\Gamma(\gamma \gamma) / \Gamma(\pi^0 \pi^0 \eta)$ 

VALUE	DOCUMENT ID	TECN	COMMENT
<b>0.1031 ± 0.0028 OUR FIT</b>			
<b>0.105 ± 0.010 OUR AVERAGE</b>	Error includes scale factor of 1.9.		
0.091 ± 0.009	AMSLER	93 CBAR	$0.0 \bar{p} p$
0.112 ± 0.002 ± 0.006	ALDE	87B GAM2	$38 \pi^- p \rightarrow n 2 \gamma$

 $\Gamma(\gamma \gamma) / \Gamma(\pi^0 \pi^0 \eta (\text{neutral decay}))$ 

VALUE	EVTs	DOCUMENT ID	TECN	COMMENT
<b>0.144 ± 0.004 OUR FIT</b>				
• • • We do not use the following data for averages, fits, limits, etc. • • •				
0.188 ± 0.058	16	APEL	72 OSPK	$3.8 \pi^- p \rightarrow n X^0$

 $\Gamma(\text{neutrals}) / \Gamma_{\text{total}} (0.714 \Gamma_4 + 0.09 \Gamma_5 + \Gamma_7) / \Gamma$ 

VALUE	EVTs	DOCUMENT ID	TECN	COMMENT
<b>0.185 ± 0.004 OUR FIT</b>	Error includes scale factor of 1.1.			
• • • We do not use the following data for averages, fits, limits, etc. • • •				
0.185 ± 0.022	535	BASILE	71 CNTR	$1.6 \pi^- p \rightarrow n X^0$
0.189 ± 0.026	123	RITTENBERG	69 HBC	$1.7\text{--}2.7 K^- p$

 $\Gamma(3\pi^0) / \Gamma_{\text{total}}$ 

VALUE (units $10^{-3}$ )	EVTs	DOCUMENT ID	TECN	COMMENT
<b>2.50 ± 0.17 OUR FIT</b>				
<b>3.57 ± 0.26 OUR AVERAGE</b>				
3.522 ± 0.082 ± 0.254	2015	ABLIKIM	17 BES3	$J/\psi \rightarrow \gamma(3\pi^0)$
4.79 ± 0.59 ± 1.14	183	<sup>1</sup> ABLIKIM	15P BES3	$J/\psi \rightarrow K^+ K^- 3 \pi$
• • • We do not use the following data for averages, fits, limits, etc. • • •				
3.56 ± 0.22 ± 0.34	309	<sup>2</sup> ABLIKIM	12E BES3	$J/\psi \rightarrow \gamma(3\pi^0)$

<sup>1</sup> We have added all systematic uncertainties in quadrature to a single value.

<sup>2</sup> Superseded by ABLIKIM 17.

 $\Gamma(3\pi^0) / \Gamma(\pi^0 \pi^0 \eta)$ 

VALUE (units $10^{-4}$ )	EVTs	DOCUMENT ID	TECN	COMMENT
<b>112 ± 8 OUR FIT</b>				
<b>78 ± 10 OUR AVERAGE</b>				
86 ± 19	235	BLIK	08 GAMS	$32 \pi^- p \rightarrow \eta' n$
74 ± 15		ALDE	87B GAM2	$38 \pi^- p \rightarrow n 6 \gamma$
75 ± 18		BINON	84 GAM2	$30\text{--}40 \pi^- p \rightarrow n 6 \gamma$

## Meson Particle Listings

 $\eta'(958)$ 

$\Gamma(\mu^+\mu^-\gamma)/\Gamma(\gamma\gamma)$		$\Gamma_9/\Gamma_7$	
VALUE (units $10^{-3}$ )	EVTS	DOCUMENT ID	TECN COMMENT
<b>4.9±1.2</b>	33	VIKTOROV 80	CNTR 25,33 $\pi^-p \rightarrow 2\mu\gamma$

$\Gamma(\pi^+\pi^-\mu^+\mu^-)/\Gamma_{total}$		$\Gamma_{10}/\Gamma$	
VALUE (units $10^{-4}$ )	CL%	DOCUMENT ID	TECN COMMENT
• • • We do not use the following data for averages, fits, limits, etc. • • •			
<0.29	90	<sup>1</sup> ABLIKIM 130	BES3 $J/\psi \rightarrow \gamma\eta'$
<2.4	90	<sup>2</sup> NAIK 09	CLEO $J/\psi \rightarrow \gamma\eta'$
<sup>1</sup> Using $\Gamma_2/\Gamma = (29.3 \pm 0.6)\%$ from PDG 12.			
<sup>2</sup> Not independent of measured value of $\Gamma_{10}/\Gamma_1$ from NAIK 09.			

$\Gamma(\pi^+\pi^-\mu^+\mu^-)/\Gamma(\pi^+\pi^-\eta)$		$\Gamma_{10}/\Gamma_1$	
VALUE (units $10^{-3}$ )	CL%	DOCUMENT ID	TECN COMMENT
<b>&lt;0.5</b>	90	<sup>1</sup> NAIK 09	CLEO $J/\psi \rightarrow \gamma\eta'$
<sup>1</sup> NAIK 09 reports $[\Gamma(\eta'(958) \rightarrow \pi^+\pi^-\mu^+\mu^-)/\Gamma(\eta'(958) \rightarrow \pi^+\pi^-\eta)] / [B(\eta \rightarrow 2\gamma)] < 1.3 \times 10^{-3}$ which we multiply by our best value $B(\eta \rightarrow 2\gamma) = 39.41 \times 10^{-2}$ .			

$\Gamma(\pi^+\pi^-\mu^+\mu^-)/\Gamma(\rho^0\gamma(\text{including non-resonant } \pi^+\pi^-\gamma))$		$\Gamma_{10}/\Gamma_2$	
VALUE (units $10^{-4}$ )	CL%	DOCUMENT ID	TECN COMMENT
<b>&lt;1.0</b>	90	ABLIKIM 130	BES3 $J/\psi \rightarrow \gamma\eta'$

$\Gamma(\pi^+\pi^-\pi^0)/\Gamma_{total}$		$\Gamma_{11}/\Gamma$	
VALUE (units $10^{-3}$ )	EVTS	DOCUMENT ID	TECN COMMENT
<b>3.61 ± 0.18 OUR FIT</b>			
<b>3.61 ± 0.18 OUR AVERAGE</b>			
3.591 ± 0.054 ± 0.174	6067	ABLIKIM 17	BES3 $J/\psi \rightarrow \gamma(\pi^+\pi^-\pi^0)$
4.28 ± 0.49 ± 1.11	78	<sup>1</sup> ABLIKIM 15P	BES3 $J/\psi \rightarrow K^+K^-3\pi$
3.7 $\begin{smallmatrix} +1.1 \\ -0.9 \end{smallmatrix}$ ± 0.4		<sup>2</sup> NAIK 09	CLEO $J/\psi \rightarrow \gamma\eta'$
• • • We do not use the following data for averages, fits, limits, etc. • • •			
3.83 ± 0.15 ± 0.39	1014	<sup>3</sup> ABLIKIM 12E	BES3 $J/\psi \rightarrow \gamma(\pi^+\pi^-\pi^0)$
<sup>1</sup> We have added all systematic uncertainties in quadrature to a single value.			
<sup>2</sup> Not independent of measured value of $\Gamma_{11}/\Gamma_1$ from NAIK 09.			
<sup>3</sup> Superseded by ABLIKIM 17.			

$\Gamma((\pi^+\pi^-\pi^0) \text{ S-wave})/\Gamma_{total}$		$\Gamma_{12}/\Gamma$	
VALUE (units $10^{-4}$ )	EVTS	DOCUMENT ID	TECN COMMENT
<b>37.63 ± 0.77 ± 5.00</b>	6580	<sup>1</sup> ABLIKIM 17	BES3 $J/\psi \rightarrow \gamma(\pi^+\pi^-\pi^0)$
<sup>1</sup> We have added all systematic uncertainties in quadrature.			

$\Gamma(\pi^+\pi^-\rho^\pm)/\Gamma_{total}$		$\Gamma_{13}/\Gamma$	
VALUE (units $10^{-4}$ )	EVTS	DOCUMENT ID	TECN COMMENT
<b>7.44 ± 0.60 ± 2.23</b>	1231	<sup>1</sup> ABLIKIM 17	BES3 $J/\psi \rightarrow \gamma(\pi^+\pi^-\rho^\pm)$
<sup>1</sup> We have added all systematic uncertainties in quadrature.			

$\Gamma(\pi^+\pi^-\pi^0)/\Gamma(\pi^+\pi^-\eta)$		$\Gamma_{11}/\Gamma_1$	
VALUE (units $10^{-3}$ )	EVTS	DOCUMENT ID	TECN COMMENT
<b>8.5 ± 0.4 OUR FIT</b>			Error includes scale factor of 1.1.
<b>8.28 <math>\begin{smallmatrix} +2.49 \\ -2.12 \end{smallmatrix}</math> ± 0.04</b>	20	<sup>1</sup> NAIK 09	CLEO $J/\psi \rightarrow \gamma\eta'$
<sup>1</sup> NAIK 09 reports $[\Gamma(\eta'(958) \rightarrow \pi^+\pi^-\pi^0)/\Gamma(\eta'(958) \rightarrow \pi^+\pi^-\eta)] / [B(\eta \rightarrow 2\gamma)] = (21 \pm 6 \pm 2) \times 10^{-3}$ which we multiply by our best value $B(\eta \rightarrow 2\gamma) = (39.41 \pm 0.20) \times 10^{-2}$ . Our first error is their experiment's error and our second error is the systematic error from using our best value.			

$\Gamma(\pi^0\rho^0)/\Gamma_{total}$		$\Gamma_{14}/\Gamma$	
VALUE	CL%	DOCUMENT ID	TECN COMMENT
<b>&lt;0.04</b>	90	RITTENBERG 65	HBC 2.7 $K^-p$

$\Gamma(2(\pi^+\pi^-))/\Gamma_{total}$		$\Gamma_{15}/\Gamma$	
VALUE (units $10^{-3}$ )	CL% EVTS	DOCUMENT ID	TECN COMMENT
<b>8.4 ± 0.9 ± 0.1</b>	199	<sup>1</sup> ABLIKIM 14M	BES3 $J/\psi \rightarrow \gamma\eta'$
• • • We do not use the following data for averages, fits, limits, etc. • • •			
< 24	90	<sup>2</sup> NAIK 09	CLEO $J/\psi \rightarrow \gamma\eta'$
<1000	90	RITTENBERG 69	HBC 1.7-2.7 $K^-p$
<sup>1</sup> ABLIKIM 14M reports $[\Gamma(\eta'(958) \rightarrow 2(\pi^+\pi^-))/\Gamma_{total}] \times [B(J/\psi(1S) \rightarrow \gamma\eta'(958))] = (4.40 \pm 0.35 \pm 0.30) \times 10^{-7}$ which we divide by our best value $B(J/\psi(1S) \rightarrow \gamma\eta'(958)) = (5.25 \pm 0.07) \times 10^{-3}$ . Our first error is their experiment's error and our second error is the systematic error from using our best value.			
<sup>2</sup> Not independent of measured value of $\Gamma_{15}/\Gamma_1$ from NAIK 09.			

$\Gamma(2(\pi^+\pi^-))/\Gamma(\pi^+\pi^-\eta)$		$\Gamma_{15}/\Gamma_1$	
VALUE (units $10^{-3}$ )	CL%	DOCUMENT ID	TECN COMMENT
<b>&lt;0.6</b>	90	<sup>1</sup> NAIK 09	CLEO $J/\psi \rightarrow \gamma\eta'$
<sup>1</sup> NAIK 09 reports $[\Gamma(\eta'(958) \rightarrow 2(\pi^+\pi^-))/\Gamma(\eta'(958) \rightarrow \pi^+\pi^-\eta)] / [B(\eta \rightarrow 2\gamma)] < 1.4 \times 10^{-3}$ which we multiply by our best value $B(\eta \rightarrow 2\gamma) = 39.41 \times 10^{-2}$ .			

$\Gamma(\pi^+\pi^-2\pi^0)/\Gamma_{total}$		$\Gamma_{16}/\Gamma$	
VALUE (units $10^{-4}$ )	CL% EVTS	DOCUMENT ID	TECN COMMENT
<b>1.79 ± 0.38 ± 0.02</b>	84	<sup>1</sup> ABLIKIM 14M	BES3 $J/\psi \rightarrow \gamma\eta'$
• • • We do not use the following data for averages, fits, limits, etc. • • •			
<27	90	<sup>2</sup> NAIK 09	CLEO $J/\psi \rightarrow \gamma\eta'$
<sup>1</sup> ABLIKIM 14M reports $[\Gamma(\eta'(958) \rightarrow \pi^+\pi^-2\pi^0)/\Gamma_{total}] \times [B(J/\psi(1S) \rightarrow \gamma\eta'(958))] = (9.38 \pm 1.79 \pm 0.89) \times 10^{-7}$ which we divide by our best value $B(J/\psi(1S) \rightarrow \gamma\eta'(958)) = (5.25 \pm 0.07) \times 10^{-3}$ . Our first error is their experiment's error and our second error is the systematic error from using our best value.			
<sup>2</sup> Not independent of measured value of $\Gamma_{16}/\Gamma_1$ from NAIK 09.			

$\Gamma(\pi^+\pi^-2\pi^0)/\Gamma(\pi^+\pi^-\eta)$		$\Gamma_{16}/\Gamma_1$	
VALUE (units $10^{-3}$ )	CL%	DOCUMENT ID	TECN COMMENT
<b>&lt;6</b>	90	<sup>1</sup> NAIK 09	CLEO $J/\psi \rightarrow \gamma\eta'$
<sup>1</sup> NAIK 09 reports $[\Gamma(\eta'(958) \rightarrow \pi^+\pi^-2\pi^0)/\Gamma(\eta'(958) \rightarrow \pi^+\pi^-\eta)] / [B(\eta \rightarrow 2\gamma)] < 15 \times 10^{-3}$ which we multiply by our best value $B(\eta \rightarrow 2\gamma) = 39.41 \times 10^{-2}$ .			

$\Gamma(2(\pi^+\pi^-) \text{ neutrals})/\Gamma_{total}$		$\Gamma_{17}/\Gamma$	
VALUE	CL%	DOCUMENT ID	TECN COMMENT
<b>&lt;0.01</b>	95	DANBURG 73	HBC 2.2 $K^-p \rightarrow \Lambda\chi^0$
• • • We do not use the following data for averages, fits, limits, etc. • • •			
<0.01	90	RITTENBERG 69	HBC 1.7-2.7 $K^-p$

$\Gamma(2(\pi^+\pi^-)\pi^0)/\Gamma_{total}$		$\Gamma_{18}/\Gamma$	
VALUE	CL%	DOCUMENT ID	TECN COMMENT
• • • We do not use the following data for averages, fits, limits, etc. • • •			
<0.002	90	<sup>1</sup> NAIK 09	CLEO $J/\psi \rightarrow \gamma\eta'$
<0.01	90	RITTENBERG 69	HBC 1.7-2.7 $K^-p$
<sup>1</sup> Not independent of measured value of $\Gamma_{18}/\Gamma_1$ from NAIK 09.			

$\Gamma(2(\pi^+\pi^-)\pi^0)/\Gamma(\pi^+\pi^-\eta)$		$\Gamma_{18}/\Gamma_1$	
VALUE (units $10^{-3}$ )	CL%	DOCUMENT ID	TECN COMMENT
<b>&lt;4</b>	90	<sup>1</sup> NAIK 09	CLEO $J/\psi \rightarrow \gamma\eta'$
<sup>1</sup> NAIK 09 reports $[\Gamma(\eta'(958) \rightarrow 2(\pi^+\pi^-)\pi^0)/\Gamma(\eta'(958) \rightarrow \pi^+\pi^-\eta)] / [B(\eta \rightarrow 2\gamma)] < 11 \times 10^{-3}$ which we multiply by our best value $B(\eta \rightarrow 2\gamma) = 39.41 \times 10^{-2}$ .			

$\Gamma(2(\pi^+\pi^-)2\pi^0)/\Gamma_{total}$		$\Gamma_{19}/\Gamma$	
VALUE	CL%	DOCUMENT ID	TECN COMMENT
<b>&lt;0.01</b>	95	KALBFLEISCH 64B	HBC $K^-p \rightarrow \Lambda 2(\pi^+\pi^-)+MM$
• • • We do not use the following data for averages, fits, limits, etc. • • •			
<0.01	90	LONDON 66	HBC Compilation

$\Gamma(3(\pi^+\pi^-))/\Gamma_{total}$		$\Gamma_{20}/\Gamma$	
VALUE (units $10^{-5}$ )	CL%	DOCUMENT ID	TECN COMMENT
<b>&lt; 3.1</b>	90	<sup>1</sup> ABLIKIM 13U	BES3 $J/\psi \rightarrow \gamma 3(\pi^+\pi^-)$
• • • We do not use the following data for averages, fits, limits, etc. • • •			
< 53	90	<sup>2</sup> NAIK 09	CLEO $J/\psi \rightarrow \gamma\eta'$
<500	95	KALBFLEISCH 64B	HBC $K^-p \rightarrow \Lambda 2(\pi^+\pi^-)$
<sup>1</sup> Using $B(J/\psi \rightarrow \gamma\eta'(958)) = (5.16 \pm 0.15) \times 10^{-3}$ .			
<sup>2</sup> Not independent of measured value of $\Gamma_{20}/\Gamma_1$ from NAIK 09.			

$\Gamma(3(\pi^+\pi^-))/\Gamma(\pi^+\pi^-\eta)$		$\Gamma_{20}/\Gamma_1$	
VALUE (units $10^{-3}$ )	CL%	DOCUMENT ID	TECN COMMENT
<b>&lt;1.2</b>	90	<sup>1</sup> NAIK 09	CLEO $J/\psi \rightarrow \gamma\eta'$
<sup>1</sup> NAIK 09 reports $[\Gamma(\eta'(958) \rightarrow 3(\pi^+\pi^-))/\Gamma(\eta'(958) \rightarrow \pi^+\pi^-\eta)] / [B(\eta \rightarrow 2\gamma)] < 3.0 \times 10^{-3}$ which we multiply by our best value $B(\eta \rightarrow 2\gamma) = 39.41 \times 10^{-2}$ .			

$\Gamma(K^\pm\pi^\mp)/\Gamma(\rho^0\gamma(\text{including non-resonant } \pi^+\pi^-\gamma))$		$\Gamma_{21}/\Gamma_2$	
VALUE	CL%	DOCUMENT ID	TECN COMMENT
<b>&lt;1.3 × 10<sup>-4</sup></b>	90	ABLIKIM 16M	BES3 $e^+e^- \rightarrow J/\psi \rightarrow \text{hadrons}$

$\Gamma(\pi^+\pi^-\pi^0)/\Gamma_{total}$		$\Gamma_{22}/\Gamma$	
VALUE (units $10^{-3}$ )	CL% EVTS	DOCUMENT ID	TECN COMMENT
<b>2.4 <math>\begin{smallmatrix} +1.3 \\ -0.9 \end{smallmatrix}</math> OUR FIT</b>			
• • • We do not use the following data for averages, fits, limits, etc. • • •			
2.11 ± 0.12 ± 0.14	429	<sup>1</sup> ABLIKIM 130	BES3 $J/\psi \rightarrow \gamma\eta'$
2.5 $\begin{smallmatrix} +1.2 \\ -0.9 \end{smallmatrix}$ ± 0.5		<sup>2</sup> NAIK 09	CLEO $J/\psi \rightarrow \gamma\eta'$
<6	90	RITTENBERG 65	HBC 2.7 $K^-p$
<sup>1</sup> Using $\Gamma_2/\Gamma = (29.3 \pm 0.6)\%$ from PDG 12.			
<sup>2</sup> Not independent of measured value of $\Gamma_{22}/\Gamma_1$ from NAIK 09.			

See key on page 999

Meson Particle Listings

$\eta'(958)$

$\Gamma(\pi^+\pi^-e^+e^-)/\Gamma(\pi^+\pi^-\eta)$					$\Gamma_{22}/\Gamma_1$
VALUE (units $10^{-3}$ )	EVTS	DOCUMENT ID	TECN	COMMENT	

5.5  $\pm$   $\frac{3.0}{2.3}$  OUR FIT

5.52  $\pm$   $\frac{3.00}{2.30} \pm 0.03$  8 1 NAIK 09 CLEO  $J/\psi \rightarrow \gamma\eta'$   
 1 NAIK 09 reports  $[\Gamma(\eta'(958) \rightarrow \pi^+\pi^-e^+e^-)/\Gamma(\eta'(958) \rightarrow \pi^+\pi^-\eta)] / [B(\eta \rightarrow 2\gamma)] = (14 \pm 7 \pm 3) \times 10^{-3}$  which we multiply by our best value  $B(\eta \rightarrow 2\gamma) = (39.41 \pm 0.20) \times 10^{-2}$ . Our first error is their experiment's error and our second error is the systematic error from using our best value.

$\Gamma(\pi^+\pi^-e^+e^-)/\Gamma(\rho^0\gamma(\text{including non-resonant } \pi^+\pi^-\gamma))$					$\Gamma_{22}/\Gamma_2$
VALUE (units $10^{-3}$ )	EVTS	DOCUMENT ID	TECN	COMMENT	

7.2  $\pm$   $0.4 \pm 0.5$  429 ABLIKIM 130 BES3  $J/\psi \rightarrow \gamma\eta'$

$\Gamma(\pi^+e^-\nu_e + c.c.)/\Gamma(\pi^+\pi^-\eta)$					$\Gamma_{23}/\Gamma_1$
VALUE (units $10^{-4}$ )	CL%	DOCUMENT ID	TECN	COMMENT	

<5.0 90 ABLIKIM 13G BES3  $J/\psi \rightarrow \phi\eta'$

$\Gamma(\gamma e^+e^-)/\Gamma_{\text{total}}$					$\Gamma_{24}/\Gamma$
VALUE (units $10^{-3}$ )	CL%	DOCUMENT ID	TECN	COMMENT	

<0.9 90 BRIERE 00 CLEO 10.6  $e^+e^-$

$\Gamma(\gamma e^+e^-)/\Gamma(\gamma\gamma)$					$\Gamma_{24}/\Gamma_7$
VALUE (units $10^{-2}$ )	EVTS	DOCUMENT ID	TECN	COMMENT	

2.13  $\pm$   $0.09 \pm 0.07$  864 ABLIKIM 150 BES3  $J/\psi \rightarrow \gamma e^+e^-$

$\Gamma(\pi^0\gamma\gamma)/\Gamma_{\text{total}}$					$\Gamma_{25}/\Gamma$
VALUE (units $10^{-3}$ )	EVTS	DOCUMENT ID	TECN	COMMENT	

3.20  $\pm$   $0.07 \pm 0.23$  3.4k ABLIKIM 17T BES3  $J/\psi \rightarrow \gamma\eta'$

$\Gamma(\pi^0\gamma\gamma(\text{non resonant}))/\Gamma_{\text{total}}$					$\Gamma_{26}/\Gamma$
VALUE (units $10^{-4}$ )	EVTS	DOCUMENT ID	TECN	COMMENT	

6.16  $\pm$   $0.64 \pm 0.67$  655 ABLIKIM 17T BES3  $J/\psi \rightarrow \gamma\eta'$

$\Gamma(\pi^0\gamma\gamma)/\Gamma(\pi^0\pi^0\eta)$					$\Gamma_{25}/\Gamma_4$
VALUE (units $10^{-4}$ )	CL%	DOCUMENT ID	TECN	COMMENT	

<37 90 ALDE 87B GAM2 38  $\pi^-\rho \rightarrow n4\gamma$

$\Gamma(\eta\gamma\gamma)/\Gamma_{\text{total}}$					$\Gamma_{27}/\Gamma$
VALUE	CL%	DOCUMENT ID	TECN	COMMENT	

<1.33  $\times 10^{-4}$  90 ABLIKIM 19AW BES3  $J/\psi \rightarrow \gamma\eta' \rightarrow \gamma\gamma\gamma 2\gamma$

$\Gamma(4\pi^0)/\Gamma_{\text{total}}$					$\Gamma_{28}/\Gamma$
VALUE	CL%	DOCUMENT ID	TECN	COMMENT	

<3.2  $\times 10^{-4}$  90 DONSKOV 14 GAM4 32.5  $\pi^-\rho \rightarrow \eta' n$

$\Gamma(4\pi^0)/\Gamma(\pi^0\pi^0\eta)$					$\Gamma_{28}/\Gamma_4$
VALUE (units $10^{-4}$ )	CL%	DOCUMENT ID	TECN	COMMENT	

<23 90 ALDE 87B GAM2 38  $\pi^-\rho \rightarrow n8\gamma$

$\Gamma(e^+e^-)/\Gamma_{\text{total}}$					$\Gamma_{29}/\Gamma$
VALUE	CL%	DOCUMENT ID	TECN	COMMENT	

< 5.6  $\times 10^{-9}$  90 1 ACHASOV 15 SND 0.958  $e^+e^- \rightarrow \pi\pi\eta$

<12  $\times 10^{-9}$  90 2 AKHMETSHIN 15 CMD3 0.958  $e^+e^- \rightarrow \pi^+\pi^-\eta$

< 2.1  $\times 10^{-7}$  90 VOROBYEV 88 ND  $e^+e^- \rightarrow \pi^+\pi^-\eta$

$\Gamma(\text{invisible})/\Gamma_{\text{total}}$					$\Gamma_{30}/\Gamma$
VALUE (units $10^{-4}$ )	CL%	DOCUMENT ID	TECN	COMMENT	

<9.5 90 1 NAIK 09 CLEO  $J/\psi \rightarrow \gamma\eta'$

1 Not independent of measured value of  $\Gamma_{30}/\Gamma_1$  from NAIK 09.

$\Gamma(\text{invisible})/\Gamma(\gamma\gamma)$					$\Gamma_{30}/\Gamma_7$
VALUE (units $10^{-2}$ )	CL%	DOCUMENT ID	TECN	COMMENT	

<2.4 90 ABLIKIM 13 BES3  $J/\psi \rightarrow \phi\eta'$

<6.69 90 ABLIKIM 06Q BES  $J/\psi \rightarrow \phi\eta'$

$\Gamma(\text{invisible})/\Gamma(\pi^+\pi^-\eta)$					$\Gamma_{30}/\Gamma_1$
VALUE (units $10^{-3}$ )	CL%	DOCUMENT ID	TECN	COMMENT	

<2.1 90 1 NAIK 09 CLEO  $J/\psi \rightarrow \gamma\eta'$

1 NAIK 09 reports  $[\Gamma(\eta'(958) \rightarrow \text{invisible})/\Gamma(\eta'(958) \rightarrow \pi^+\pi^-\eta)] / [B(\eta \rightarrow 2\gamma)] < 5.4 \times 10^{-3}$  which we multiply by our best value  $B(\eta \rightarrow 2\gamma) = 39.41 \times 10^{-2}$ .

$\Gamma(\pi^+\pi^-)/\Gamma_{\text{total}}$					$\Gamma_{31}/\Gamma$
VALUE (units $10^{-4}$ )	CL%	DOCUMENT ID	TECN	COMMENT	

< 0.18 90 1 AAIJ 17D LHCB  $D_{(s)}^+ \rightarrow \pi^+\pi^-\pi^+$

< 0.5 90 2 ABLIKIM 11G BES3  $J/\psi \rightarrow \gamma\pi^+\pi^-$

< 29 90 3 MORI 07A BELL  $\gamma\gamma \rightarrow \pi^+\pi^-$

< 3.3 90 4 MORI 07A BELL  $\gamma\gamma \rightarrow \pi^+\pi^-$

<800 95 DANBURG 73 HBC 2.2  $K^-\rho \rightarrow \Lambda X^0$

<200 90 RITTENBERG 69 HBC 1.7-2.7  $K^-\rho$

1 Using branching fractions of  $D_{(s)}^+$  decays from PDG 15.

2 ABLIKIM 11G reports  $[\Gamma(\eta'(958) \rightarrow \pi^+\pi^-)/\Gamma_{\text{total}}] \times [B(J/\psi(1S) \rightarrow \gamma\eta'(958))] < 2.84 \times 10^{-7}$  which we divide by our best value  $B(J/\psi(1S) \rightarrow \gamma\eta'(958)) = 5.25 \times 10^{-3}$ .

3 Taking into account interference with the  $\gamma\gamma \rightarrow \pi^+\pi^-$  continuum.

4 Without interference with the  $\gamma\gamma \rightarrow \pi^+\pi^-$  continuum.

$\Gamma(\pi^0\pi^0)/\Gamma_{\text{total}}$					$\Gamma_{32}/\Gamma$
VALUE	CL%	DOCUMENT ID	TECN	COMMENT	

<4  $\times 10^{-4}$  90 1 ABLIKIM 11G BES3  $J/\psi \rightarrow \gamma\pi^0\pi^0$

1 ABLIKIM 11G reports  $[\Gamma(\eta'(958) \rightarrow \pi^+\pi^-)/\Gamma_{\text{total}}] \times [B(J/\psi(1S) \rightarrow \gamma\eta'(958))] < 2.84 \times 10^{-7}$  which we divide by our best value  $B(J/\psi(1S) \rightarrow \gamma\eta'(958)) = 5.25 \times 10^{-3}$ .

$\Gamma(\pi^0\pi^0)/\Gamma(\pi^0\pi^0\eta)$					$\Gamma_{32}/\Gamma_4$
VALUE (units $10^{-4}$ )	CL%	DOCUMENT ID	TECN	COMMENT	

<45 90 ALDE 87B GAM2 38  $\pi^-\rho \rightarrow n4\gamma$

$\Gamma(\pi^0e^+e^-)/\Gamma_{\text{total}}$					$\Gamma_{33}/\Gamma$
VALUE (units $10^{-3}$ )	CL%	DOCUMENT ID	TECN	COMMENT	

< 1.4 90 BRIERE 00 CLEO 10.6  $e^+e^-$

<13 90 RITTENBERG 65 HBC 2.7  $K^-\rho$

$\Gamma(\eta e^+e^-)/\Gamma_{\text{total}}$					$\Gamma_{34}/\Gamma$
VALUE (units $10^{-3}$ )	CL%	DOCUMENT ID	TECN	COMMENT	

< 2.4 90 BRIERE 00 CLEO 10.6  $e^+e^-$

<11 90 RITTENBERG 65 HBC 2.7  $K^-\rho$

$\Gamma(3\gamma)/\Gamma(\pi^0\pi^0\eta)$					$\Gamma_{35}/\Gamma_4$
VALUE (units $10^{-4}$ )	CL%	DOCUMENT ID	TECN	COMMENT	

<4.6 90 ALDE 87B GAM2 38  $\pi^-\rho \rightarrow n3\gamma$

$\Gamma(\mu^+\mu^-\pi^0)/\Gamma_{\text{total}}$					$\Gamma_{36}/\Gamma$
VALUE (units $10^{-9}$ )	CL%	DOCUMENT ID	TECN	COMMENT	

<6.0 90 DZHELADIN 81 CNTR 30  $\pi^-\rho \rightarrow \eta' n$

$\Gamma(\mu^+\mu^-\eta)/\Gamma_{\text{total}}$					$\Gamma_{37}/\Gamma$
VALUE (units $10^{-5}$ )	CL%	DOCUMENT ID	TECN	COMMENT	

<1.5 90 DZHELADIN 81 CNTR 30  $\pi^-\rho \rightarrow \eta' n$

$\Gamma(e\mu)/\Gamma_{\text{total}}$					$\Gamma_{38}/\Gamma$
VALUE (units $10^{-4}$ )	CL%	DOCUMENT ID	TECN	COMMENT	

<4.7 90 BRIERE 00 CLEO 10.6  $e^+e^-$

$\eta'(958) \rightarrow \eta\pi\pi$  DECAY PARAMETERS

$|\text{MATRIX ELEMENT}|^2 = |1 + \alpha Y|^2 + CX + DX^2$

X and Y are Dalitz variables;  $\alpha$  is complex and C, and D are real-valued. Parameters C and D are not necessarily equal to c and d, respectively, in the generalized parameterization following this one. May be different for  $\eta'(958) \rightarrow \eta\pi^+\pi^-$  and  $\eta'(958) \rightarrow \eta\pi^0\pi^0$  decays. Because of different initial assumptions and strong correlations of the parameters we do not average the parameters in the section below.

Re( $\alpha$ ) decay parameter

VALUE	EVTS	DOCUMENT ID	TECN	COMMENT
-------	------	-------------	------	---------

-0.034  $\pm$  0.002  $\pm$  0.002 351k ABLIKIM 18 BES3  $\eta' \rightarrow \eta\pi^+\pi^-$

-0.054  $\pm$  0.004  $\pm$  0.001 56k ABLIKIM 18 BES3  $\eta' \rightarrow \eta\pi^0\pi^0$

## Meson Particle Listings

 $\eta'(958)$ 

$-0.033 \pm 0.005 \pm 0.003$	44k	1	ABLIKIM	11	BES3	$J/\psi \rightarrow \gamma \eta \pi^+ \pi^-$
$-0.072 \pm 0.012 \pm 0.006$	7k	2	AMELIN	05A	VES	$28 \pi^- A \rightarrow \eta \pi^+ \pi^- \pi^- A^*$
$-0.021 \pm 0.018 \pm 0.017$	6.7k	3	BRIERE	00	CLEO	$10.6 e^+ e^- \rightarrow \eta \pi^+ \pi^- X$
$-0.058 \pm 0.013 \pm 0.003$	5.4k	4	ALDE	86	GAM2	$38 \pi^- p \rightarrow n \eta \pi^0 \pi^0$
$-0.08 \pm 0.03$		4.5	KALBFLEISCH	74	RVUE	$\eta' \rightarrow \eta \pi^+ \pi^-$

- <sup>1</sup> See ABLIKIM 11 for the full correlation matrix.  
<sup>2</sup> Superseded by DOROFEEV 7, which found this parameterization unacceptable. See below.  
<sup>3</sup> Assuming  $\text{Im}(\alpha) = 0$ ,  $C = 0$ , and  $D = 0$ .  
<sup>4</sup> Assuming  $C = 0$ .  
<sup>5</sup> From the data of DAUBER 64, RITTENBERG 69, AGUILAR-BENITEZ 72B, JACOBS 73, and DANBURG 73.

 **$\text{Im}(\alpha)$  decay parameter**

VALUE	EVTS	DOCUMENT ID	TECN	COMMENT	
$0.000 \pm 0.019 \pm 0.001$	351k	ABLIKIM	18	BES3 $\eta' \rightarrow \eta \pi^+ \pi^-$	
$0.000 \pm 0.038 \pm 0.002$	56k	ABLIKIM	18	BES3 $\eta' \rightarrow \eta \pi^0 \pi^0$	
$0.000 \pm 0.049 \pm 0.001$	44k	1	ABLIKIM	11	BES3 $J/\psi \rightarrow \gamma \eta \pi^+ \pi^-$
$0.0 \pm 0.1 \pm 0.0$	7k	2	AMELIN	05A	VES $28 \pi^- A \rightarrow \eta \pi^+ \pi^- \pi^- A^*$
$-0.00 \pm 0.13 \pm 0.00$	5.4k	3	ALDE	86	GAM2 $38 \pi^- p \rightarrow n \eta \pi^0 \pi^0$
$0.0 \pm 0.3$		3.4	KALBFLEISCH	74	RVUE $\eta' \rightarrow \eta \pi^+ \pi^-$

- <sup>1</sup> See ABLIKIM 11 for the full correlation matrix.  
<sup>2</sup> Superseded by DOROFEEV 07, which found this parameterization unacceptable. See below.  
<sup>3</sup> Assuming  $C = 0$ .  
<sup>4</sup> From the data of DAUBER 64, RITTENBERG 69, AGUILAR-BENITEZ 72B, JACOBS 73, and DANBURG 73.

**C decay parameter**

VALUE	EVTS	DOCUMENT ID	TECN	COMMENT	
$0.0027 \pm 0.0024 \pm 0.0015$	351k	ABLIKIM	18	BES3 $\eta' \rightarrow \eta \pi^+ \pi^-$	
$0.018 \pm 0.009 \pm 0.003$	44k	1	ABLIKIM	11	BES3 $J/\psi \rightarrow \gamma \eta \pi^+ \pi^-$
$0.020 \pm 0.018 \pm 0.004$	7k	2	AMELIN	05A	VES $28 \pi^- A \rightarrow \eta \pi^+ \pi^- \pi^- A^*$

- <sup>1</sup> See ABLIKIM 11 for the full correlation matrix.  
<sup>2</sup> Superseded by DOROFEEV 07, which found this parameterization unacceptable. See below.

**D decay parameter**

VALUE	EVTS	DOCUMENT ID	TECN	COMMENT	
$-0.053 \pm 0.004 \pm 0.004$	351k	ABLIKIM	18	BES3 $\eta' \rightarrow \eta \pi^+ \pi^-$	
$-0.061 \pm 0.009 \pm 0.005$	56k	ABLIKIM	18	BES3 $\eta' \rightarrow \eta \pi^0 \pi^0$	
$-0.059 \pm 0.012 \pm 0.004$	44k	1	ABLIKIM	11	BES3 $J/\psi \rightarrow \gamma \eta \pi^+ \pi^-$
$-0.066 \pm 0.030 \pm 0.015$	7k	2	AMELIN	05A	VES $28 \pi^- A \rightarrow \eta \pi^+ \pi^- \pi^- A^*$
$0.00 \pm 0.03 \pm 0.00$	5.4k	3	ALDE	86	GAM2 $38 \pi^- p \rightarrow n \eta \pi^0 \pi^0$
0		3.4	KALBFLEISCH	74	RVUE $\eta' \rightarrow \eta \pi^+ \pi^-$

- <sup>1</sup> See ABLIKIM 11 for the full correlation matrix.  
<sup>2</sup> Superseded by DOROFEEV 07, which found this parameterization unacceptable. See below.  
<sup>3</sup> Assuming  $C = 0$ .  
<sup>4</sup> From the data of DAUBER 64, RITTENBERG 69, AGUILAR-BENITEZ 72B, JACOBS 73, and DANBURG 73.

 **$\eta'(958) \rightarrow \eta \pi \pi$  DECAY PARAMETERS**

$$|\text{MATRIX ELEMENT}|^2 \propto 1 + a Y + b Y^2 + c X + d X^2$$

$X$  and  $Y$  are Dalitz variables and  $a$ ,  $b$ ,  $c$ , and  $d$  are real-valued parameters. May be different for  $\eta'(958) \rightarrow \eta \pi^+ \pi^-$  and  $\eta'(958) \rightarrow \eta \pi^0 \pi^0$  decays. We do not average measurements in the section below because parameter values from each experiment are strongly correlated.

**a decay parameter**

VALUE	EVTS	DOCUMENT ID	TECN	COMMENT	
$-0.056 \pm 0.004 \pm 0.002$	351k	ABLIKIM	18	BES3 $\eta' \rightarrow \eta \pi^+ \pi^-$	
$-0.087 \pm 0.009 \pm 0.006$	56k	ABLIKIM	18	BES3 $\eta' \rightarrow \eta \pi^0 \pi^0$	
$-0.074 \pm 0.008 \pm 0.006$	124k	ADLARSON	18A	A2MM $\eta' \rightarrow \eta \pi^0 \pi^0$	
$-0.072 \pm 0.007 \pm 0.008$		1	GONZALEZ-S...	18A	RVUE $\eta' \rightarrow \eta \pi^0 \pi^0$
$-0.047 \pm 0.011 \pm 0.003$	44k	2	ABLIKIM	11	BES3 $J/\psi \rightarrow \gamma \eta \pi^+ \pi^-$
$-0.066 \pm 0.016 \pm 0.003$	15k	3	BLIK	09	GAM4 $32.5 \pi^- p \rightarrow \eta' n$
$-0.127 \pm 0.016 \pm 0.008$	20k	4	DOROFEEV	07	VES $27 \pi^- p \rightarrow \eta' n$ , $\pi^- A \rightarrow \eta' \pi^- A^*$

- <sup>1</sup> Theoretical analysis of ADLARSON 18A using resonance chiral perturbation theory to one loop.  
<sup>2</sup> See ABLIKIM 11 for the full correlation matrix.  
<sup>3</sup> From  $\eta' \rightarrow \eta \pi^0 \pi^0$  decay.  
<sup>4</sup> From  $\eta' \rightarrow \eta \pi^+ \pi^-$  decay.

**b decay parameter**

VALUE	EVTS	DOCUMENT ID	TECN	COMMENT	
$-0.049 \pm 0.006 \pm 0.006$	351k	ABLIKIM	18	BES3 $\eta' \rightarrow \eta \pi^+ \pi^-$	
$-0.073 \pm 0.014 \pm 0.005$	56k	ABLIKIM	18	BES3 $\eta' \rightarrow \eta \pi^0 \pi^0$	
$-0.063 \pm 0.014 \pm 0.005$	124k	ADLARSON	18A	A2MM $\eta' \rightarrow \eta \pi^0 \pi^0$	
$-0.052 \pm 0.001 \pm 0.002$		1	GONZALEZ-S...	18A	RVUE $\eta' \rightarrow \eta \pi^0 \pi^0$
$-0.069 \pm 0.019 \pm 0.009$	44k	2	ABLIKIM	11	BES3 $J/\psi \rightarrow \gamma \eta \pi^+ \pi^-$
$-0.063 \pm 0.028 \pm 0.004$	15k	3	BLIK	09	GAM4 $32.5 \pi^- p \rightarrow \eta' n$
$-0.106 \pm 0.028 \pm 0.014$	20k	4	DOROFEEV	07	VES $27 \pi^- p \rightarrow \eta' n$ , $\pi^- A \rightarrow \eta' \pi^- A^*$

- <sup>1</sup> Theoretical analysis of ADLARSON 18A using resonance chiral perturbation theory to one loop.  
<sup>2</sup> See ABLIKIM 11 for the full correlation matrix.  
<sup>3</sup> From  $\eta' \rightarrow \eta \pi^0 \pi^0$  decay.  
<sup>4</sup> From  $\eta' \rightarrow \eta \pi^+ \pi^-$  decay.

**c decay parameter**

VALUE	EVTS	DOCUMENT ID	TECN	COMMENT	
$0.0027 \pm 0.0024 \pm 0.0018$	351k	ABLIKIM	18	BES3 $\eta' \rightarrow \eta \pi^+ \pi^-$	
$0.019 \pm 0.011 \pm 0.003$	44k	1	ABLIKIM	11	BES3 $J/\psi \rightarrow \gamma \eta \pi^+ \pi^-$
$-0.107 \pm 0.096 \pm 0.003$	15k	2	BLIK	09	GAM4 $32.5 \pi^- p \rightarrow \eta' n$
$0.015 \pm 0.011 \pm 0.014$	20k	3	DOROFEEV	07	VES $27 \pi^- p \rightarrow \eta' n$ , $\pi^- A \rightarrow \eta' \pi^- A^*$

- <sup>1</sup> See ABLIKIM 11 for the full correlation matrix.  
<sup>2</sup> From  $\eta' \rightarrow \eta \pi^0 \pi^0$  decay.  
<sup>3</sup> From  $\eta' \rightarrow \eta \pi^+ \pi^-$  decay.

**d decay parameter**

VALUE	EVTS	DOCUMENT ID	TECN	COMMENT	
$-0.063 \pm 0.004 \pm 0.003$	351k	ABLIKIM	18	BES3 $\eta' \rightarrow \eta \pi^+ \pi^-$	
$-0.074 \pm 0.009 \pm 0.004$	56k	ABLIKIM	18	BES3 $\eta' \rightarrow \eta \pi^0 \pi^0$	
$-0.050 \pm 0.009 \pm 0.005$	124k	ADLARSON	18A	A2MM $\eta' \rightarrow \eta \pi^0 \pi^0$	
$-0.051 \pm 0.008 \pm 0.006$		1	GONZALEZ-S...	18A	RVUE $\eta' \rightarrow \eta \pi^0 \pi^0$
$-0.073 \pm 0.012 \pm 0.003$	44k	2	ABLIKIM	11	BES3 $J/\psi \rightarrow \gamma \eta \pi^+ \pi^-$
$0.018 \pm 0.078 \pm 0.006$	15k	3	BLIK	09	GAM4 $32.5 \pi^- p \rightarrow \eta' n$
$-0.082 \pm 0.017 \pm 0.008$	20k	4	DOROFEEV	07	VES $27 \pi^- p \rightarrow \eta' n$ , $\pi^- A \rightarrow \eta' \pi^- A^*$

- <sup>1</sup> Theoretical analysis of ADLARSON 18A using resonance chiral perturbation theory to one loop.  
<sup>2</sup> See ABLIKIM 11 for the full correlation matrix.  
<sup>3</sup> From  $\eta' \rightarrow \eta \pi^0 \pi^0$  decay. If  $c \equiv 0$  from Bose-Einstein symmetry,  $d = -0.067 \pm 0.020 \pm 0.003$ .  
<sup>4</sup> From  $\eta' \rightarrow \eta \pi^+ \pi^-$  decay.

 **$\eta'(958) \beta$  PARAMETER  
|MATRIX ELEMENT|^2 = (1 + 2βZ)**

See the "Note on  $\eta$  Decay Parameters" in our 1994 edition Physical Review D50 1173 (1994), p. 1454.

**β decay parameter**

VALUE	EVTS	DOCUMENT ID	TECN	COMMENT
<b><math>-0.61 \pm 0.08</math> OUR AVERAGE</b>				Error includes scale factor of 1.2.
$-0.640 \pm 0.046 \pm 0.047$	1.8k	ABLIKIM	15G	BES3 $J/\psi \rightarrow \gamma (\pi^0 \pi^0 \pi^0)$
$-0.59 \pm 0.18$	235	BLIK	08	GAMS $32 \pi^- p \rightarrow \eta' n$
$-0.1 \pm 0.3$		ALDE	87B	GAM2 $38 \pi^- p \rightarrow n 3\pi^0$

 **$\eta'(958) C$ -NONCONSERVING DECAY PARAMETER**

See the note on  $\eta$  decay parameters in the Stable Particle Particle Listings for definition of this parameter.

**DECAY ASYMMETRY PARAMETER FOR  $\pi^+ \pi^- \gamma$** 

VALUE	EVTS	DOCUMENT ID	TECN	COMMENT
<b><math>-0.03 \pm 0.04</math> OUR AVERAGE</b>				
$-0.019 \pm 0.056$		AIHARA	87	TPC $2\gamma \rightarrow \pi^+ \pi^- \gamma$
$-0.069 \pm 0.078$	295	GRIGORIAN	75	STRC $2.1 \pi^- p$
$0.00 \pm 0.10$	103	KALBFLEISCH	75	HBC $2.18 K^- p \rightarrow \Lambda \pi^+ \pi^- \gamma$
$0.07 \pm 0.08$	152	RITTENBERG	65	HBC $2.1-2.7 K^- p$

 **$\eta'(958) \rightarrow \gamma \ell^+ \ell^-$  TRANSITION FORM FACTOR SLOPE**

Related to the effective virtual meson mass  $\Lambda$ , via slope  $\approx \Lambda^{-2}$ . See e.g. LANDSBERG 85, eq. (3.8), for a detailed definition.

VALUE (GeV <sup>-2</sup> )	EVTS	DOCUMENT ID	TECN	COMMENT	
<b><math>1.62 \pm 0.17</math> OUR AVERAGE</b>					
$1.60 \pm 0.17 \pm 0.08$	864	1	ABLIKIM	15G	BES3 $J/\psi \rightarrow \gamma e^+ e^-$
$1.7 \pm 0.4$	33	1	VIKTOROV	80	$25,33 \pi^- p \rightarrow 2\mu \gamma$

- <sup>1</sup> In the single-pole Ansatz where slope =  $1/(\Lambda^2 + \gamma^2)$  with  $\Lambda$ ,  $\gamma$  being a Breit-Wigner mass, width for the effective contributing vector meson.



# Meson Particle Listings

## $f_0(980)$

974 ± 4	42 GIDAL	81 MRK2	$J/\psi \rightarrow \pi^+ \pi^- X$
975	43 ACHASOV	80 RVUE	
986 ± 10	42 AGUILAR...	78 HBC	$0.7 \bar{p} p \rightarrow K_S^0 K_S^0$
969 ± 5	42 LEEPER	77 ASPK	$2-2.4 \pi^- p \rightarrow \pi^+ \pi^- n, K^+ K^- n$
987 ± 7	42 BINNIE	73 CNTR	$\pi^- p \rightarrow nMM$
1012 ± 6	44 GRAYER	73 ASPK	$17 \pi^- p \rightarrow \pi^+ \pi^- n$
1007 ± 20	44 HYAMS	73 ASPK	$17 \pi^- p \rightarrow \pi^+ \pi^- n$
997 ± 6	44 PROTOPOP...	73 HBC	$7 \pi^+ p \rightarrow \pi^+ p \pi^+ \pi^-$

- From the  $D^\pm \rightarrow K^\pm K^+ K^-$  Dalitz plot fit with the Triple-M amplitude in the multi-meson model of AOUDE 18.
- Quoted number refers to real part of pole position.
- Analytic continuation using Roy equations. Uses the  $K_{e4}$  data of BATLEY 10c and the  $\pi N \rightarrow \pi \pi N$  data of HYAMS 73, GRAYER 74, and PROTOPODESCU 73.
- Analytic continuation using GKPY equations. Uses the  $K_{e4}$  data of BATLEY 10c and the  $\pi N \rightarrow \pi \pi N$  data of HYAMS 73, GRAYER 74, and PROTOPODESCU 73.
- Pole position. Used Roy equations.
- Average of the analyses of three data sets in the K-matrix model. Uses the data of BATLEY 08a, HYAMS 73, and GRAYER 74, partially of COHEN 80 or ETKIN 82b.
- On sheet II in a 2-pole solution. The other pole is found on sheet III at (850–100i) MeV
- Using a relativistic Breit-Wigner function and taking into account the finite  $D_S$  mass.
- Breit-Wigner mass. Using finite width corrections according to FLATTE 76 and ACHASOV 05, and the ratio  $g_{f_0} K K / g_{f_0} \pi \pi = 0$ .
- In the kaon-loop fit.
- In the no-structure fit.
- Systematic errors not estimated.
- FLATTE 76 parameterization.  $g_{f_0} \pi \pi = 329 \pm 96$  MeV/c<sup>2</sup> assuming  $g_{f_0} K \bar{K} / g_{f_0} \pi \pi = 2$ .
- Breit-Wigner mass. Using finite width corrections according to FLATTE 76 and ACHASOV 05, and the ratio  $g_{f_0} K K / g_{f_0} \pi \pi = 4.21 \pm 0.25 \pm 0.21$  from ABLIKIM 05.
- In the kaon-loop fit following formalism of ACHASOV 89.
- In the no-structure fit assuming a direct coupling of  $\phi$  to  $f_0 \gamma$ .
- FLATTE 76 parameterization. Supersedes GARMASH 05.
- FLATTE 76 parameterization.  $g_{f_0} K \bar{K} / g_{f_0} \pi \pi = 4.21 \pm 0.25 \pm 0.21$ .
- K-matrix pole from combined analysis of  $\pi^- p \rightarrow \pi^0 \pi^0 n, \pi^- p \rightarrow K \bar{K} n, \pi^+ \pi^- \rightarrow \pi^+ \pi^-, \bar{p} p \rightarrow \pi^0 \pi^0 \pi^0, \pi^0 \eta n, \pi^0 \pi^0 \eta, \pi^+ \pi^- \pi^0, K^+ K^- \pi^0, K_S^0 K_S^0 \pi^0, K^+ K_S^0 \pi^-$  at rest,  $\bar{p} n \rightarrow \pi^- \pi^- \pi^+, K_S^0 K^- \pi^0, K_S^0 K_S^0 \pi^-$  at rest.
- From the negative interference with the  $f_0(500)$  meson of AITALA 01b using the ACHASOV 89 parameterization for the  $f_0(980)$ , a Breit-Wigner for the  $f_0(500)$ , and ACHASOV 01f for the  $\rho \pi$  contribution.
- Coupled-channel Breit-Wigner, couplings  $g_{\pi\pi} = 0.09 \pm 0.01 \pm 0.01, g_{K\pi} = 0.02 \pm 0.04 \pm 0.03$ .
- Supersedes ACHASOV 98i. Using the model of ACHASOV 89.
- Supersedes ACHASOV 98i.
- In the "narrow resonance" approximation.
- Assuming  $\Gamma(f_0) = 40$  MeV.
- From a narrow pole fit taking into account  $f_0(980)$  and  $f_0(1200)$  intermediate mechanisms.
- From the combined fit of the photon spectra in the reactions  $e^+ e^- \rightarrow \pi^+ \pi^- \gamma, \pi^0 \pi^0 \gamma$ .
- Supersedes BARBERIS 99 and BARBERIS 99b
- T-matrix pole.
- From invariant mass fit.
- On sheet II in a 2 pole solution. The other pole is found on sheet III at (1039–93i) MeV.
- On sheet II in a 2 pole solution. The other pole is found on sheet III at (963–29i) MeV.
- Reanalysis of data from HYAMS 73, GRAYER 74, SRINIVASAN 75, and ROSSELET 77 using the interfering amplitude method.
- At high  $|t|$ .
- At low  $|t|$ .
- On sheet II in a 4-pole solution, the other poles are found on sheet III at (953–55i) MeV and on sheet IV at (938–35i) MeV.
- Combined fit of ALDE 95b, ANISOVICH 94, AMSLER 94d.
- On sheet II in a 2 pole solution. The other pole is found on sheet III at (996–103i) MeV.
- From sheet II pole position.
- On sheet II in a 2 pole solution. The other pole is found on sheet III at (797–185i) MeV and can be interpreted as a shadow pole.
- On sheet II in a 2 pole solution. The other pole is found on sheet III at (978–28i) MeV.
- From coupled channel analysis.
- Coupled channel analysis with finite width corrections.
- Included in AGUILAR-BENITEZ 78 fit.

### $f_0(980)$ WIDTH

Width determination very model dependent. Peak width in  $\pi \pi$  is about 50 MeV, but decay width can be much larger.

VALUE (MeV)	EVS	DOCUMENT ID	TECN	COMMENT
<b>10 to 100 OUR ESTIMATE</b>				
• • • We do not use the following data for averages, fits, limits, etc. • • •				
15.3 ± 4.7	424	ABLIKIM 15P	BES3	$J/\psi \rightarrow K^+ K^- 3\pi$
9.5 ± 1.1	706	ABLIKIM 12E	BES3	$J/\psi \rightarrow \gamma 3\pi$
42 ± $\frac{+20}{-16}$		1,2 GARCIA-MAR..11	RVUE	Compilation
50 ± $\frac{+20}{-12}$		2,3 GARCIA-MAR..11	RVUE	Compilation
48 ± $\frac{+22}{-6}$		4 MOUSSALLAM11	RVUE	Compilation

36 ± 22	5 MENNESSIER 10	RVUE	Compilation
70 ± $\frac{+20}{-32}$	6 ANISOVICH 09	RVUE	$0.0 \bar{p} p, \pi N$
91 ± $\frac{+30}{-22} \pm 3$	44 7 ECKLUND 09	CLEO	$4.17 e^+ e^- \rightarrow D_S^- D_S^{*+} + c.c.$
66.9 ± $2.2^{+17.6}_{-12.5}$	8 UEHARA 08A	BELL	$10.6 e^+ e^- \rightarrow e^+ e^- \pi^0 \pi^0$
65 ± 13	262 ± 30 9 AUBERT 07AK	BABR	$10.6 e^+ e^- \rightarrow \phi \pi^+ \pi^- \gamma$
81 ± 21	54 ± 9 9 AUBERT 07AK	BABR	$10.6 e^+ e^- \rightarrow \phi \pi^0 \pi^0 \gamma$
51.3 ± $20.8^{+13.2}_{-17.7-3.8}$	10 MORI 07	BELL	$10.6 e^+ e^- \rightarrow e^+ e^- \pi^+ \pi^-$
61 ± $9^{+14}_{-8}$	2584 11 GARMASH 05	BELL	$B^+ \rightarrow K^+ \pi^+ \pi^-$
64 ± 16	12 ANISOVICH 03	RVUE	
121 ± 23	TIKHOIMIROV 03	SPEC	$40.0 \pi^- C \rightarrow K_S^0 K_S^0 K_L^0 X$
~ 70	13 BRAMON 02	RVUE	$1.02 e^+ e^- \rightarrow \pi^0 \pi^0 \gamma$
44 ± 2 ± 2	848 14 AITALA 01A	E791	$D^+ \rightarrow \pi^- \pi^+ \pi^+$
201 ± 28	419 15 ACHASOV 00H	SND	$e^+ e^- \rightarrow \pi^0 \pi^0 \gamma$
122 ± 13	419 16,17 ACHASOV 00H	SND	$e^+ e^- \rightarrow \pi^0 \pi^0 \gamma$
56 ± 20	18 AKHMETSHIN 99C	CMD2	$e^+ e^- \rightarrow \pi^0 \pi^0 \gamma$
65 ± 20	BARBERIS 99	OMEG	$450 pp \rightarrow \rho_S \rho f K^+ K^-$
80 ± 10	BARBERIS 99B	OMEG	$450 pp \rightarrow \rho_S \rho f \pi^+ \pi^-$
80 ± 10	BARBERIS 99C	OMEG	$450 pp \rightarrow \rho_S \rho f \pi^0 \pi^0$
48 ± 12 ± 8	19 BARBERIS 99D	OMEG	$450 pp \rightarrow K^+ K^-, \pi^+ \pi^-$
65 ± 25	BELLAZZINI 99	GAM4	$450 pp \rightarrow \rho p \pi^0 \pi^0$
71 ± 14	20 KAMINSKI 99	RVUE	$\pi \pi \rightarrow \pi \pi, K \bar{K}, \sigma \sigma$
~ 28	20 OLLER 99	RVUE	$\pi \pi \rightarrow \pi \pi, K \bar{K}$
~ 25	20 OLLER 99B	RVUE	$\pi \pi \rightarrow \pi \pi, K \bar{K}$
~ 14	20 OLLER 99C	RVUE	$\pi \pi \rightarrow \pi \pi, K \bar{K}, \eta \eta$
70 ± 20	ALDE 98	GAM4	
86 ± 16	20 ANISOVICH 98B	RVUE	Compilation
54	21 LOCHER 98	RVUE	$\pi \pi \rightarrow \pi \pi, K \bar{K}$
69 ± 15	22 ALDE 97	GAM2	$450 pp \rightarrow \rho p \pi^0 \pi^0$
38 ± 20	23 BERTIN 97C	OBLX	$0.0 \bar{p} p \rightarrow \pi^+ \pi^- \pi^0$
~ 100	24 SHIDA 96	RVUE	$\pi \pi \rightarrow \pi \pi, K \bar{K}$
34	TORNQVIST 96	RVUE	$\pi \pi \rightarrow \pi \pi, K \bar{K}, K \pi, \eta \pi$
48 ± 10	3k 25 ALDE 95B	GAM2	$38 \pi^- p \rightarrow \pi^0 \pi^0 n$
95 ± 20	10k 26 ALDE 95B	GAM2	$38 \pi^- p \rightarrow \pi^0 \pi^0 n$
26 ± 10	AMSLER 95B	CBAR	$0.0 \bar{p} p \rightarrow 3\pi^0$
~ 112	27 AMSLER 95D	CBAR	$0.0 \bar{p} p \rightarrow \pi^0 \pi^0 \pi^0, \pi^0 \eta \eta, \pi^0 \pi^0 \eta$
80 ± 12	28 ANISOVICH 95	RVUE	
30	JANSEN 95	RVUE	$\pi \pi \rightarrow \pi \pi, K \bar{K}$
74	29 BUGG 94	RVUE	$\bar{p} p \rightarrow \eta 2\pi^0$
29 ± 2	30 KAMINSKI 94	RVUE	$\pi \pi \rightarrow \pi \pi, K \bar{K}$
46	31 ZOU 94B	RVUE	
48 ± 12	32 MORGAN 93	RVUE	$\pi \pi(K \bar{K}) \rightarrow \pi \pi(K \bar{K}), J/\psi \rightarrow \phi \pi \pi(K \bar{K}), D_S \rightarrow \pi(\pi \pi)$
37.4 ± 10.6	22 AGUILAR... 91	EHS	400 pp
72 ± 8	33 ARMSTRONG 91	OMEG	300 pp → ppππ, ppK $\bar{K}$
110 ± 30	BREAKSTONE 90	SFM	pp → ppπ $\pi^-$
29 ± 13	22 ABACHI 86B	HRS	$e^+ e^- \rightarrow \pi^+ \pi^- X$
120 ± 281 ± 20	ETKIN 82B	MPS	$23 \pi^- p \rightarrow n 2K_S^0$
28 ± 10	33 GIDAL 81	MRK2	$J/\psi \rightarrow \pi^+ \pi^- X$
70 to 300	34 ACHASOV 80	RVUE	
100 ± 80	35 AGUILAR... 78	HBC	$0.7 \bar{p} p \rightarrow K_S^0 K_S^0$
30 ± 8	33 LEEPER 77	ASPK	$2-2.4 \pi^- p \rightarrow \pi^+ \pi^- n, K^+ K^- n$
48 ± 14	33 BINNIE 73	CNTR	$\pi^- p \rightarrow nMM$
32 ± 10	36 GRAYER 73	ASPK	$17 \pi^- p \rightarrow \pi^+ \pi^- n$
30 ± 10	36 HYAMS 73	ASPK	$17 \pi^- p \rightarrow \pi^+ \pi^- n$
54 ± 16	36 PROTOPOP... 73	HBC	$7 \pi^+ p \rightarrow \pi^+ p \pi^+ \pi^-$

- Analytic continuation using Roy equations. Uses the  $K_{e4}$  data of BATLEY 10c and the  $\pi N \rightarrow \pi \pi N$  data of HYAMS 73, GRAYER 74, and PROTOPODESCU 73.
- Quoted number refers to twice imaginary part of pole position.
- Analytic continuation using GKPY equations. Uses the  $K_{e4}$  data of BATLEY 10c and the  $\pi N \rightarrow \pi \pi N$  data of HYAMS 73, GRAYER 74, and PROTOPODESCU 73.
- Pole position. Used Roy equations.
- Average of the analyses of three data sets in the K-matrix model. Uses the data of BATLEY 08a, HYAMS 73, and GRAYER 74, partially of COHEN 80 or ETKIN 82b.
- On sheet II in a 2-pole solution. The other pole is found on sheet III at (850–100i) MeV
- Using a relativistic Breit-Wigner function and taking into account the finite  $D_S$  mass.
- Breit-Wigner  $\pi \pi$  width. Using finite width corrections according to FLATTE 76 and ACHASOV 05, and the ratio  $g_{f_0} K K / g_{f_0} \pi \pi = 0$ .
- Systematic errors not estimated.





# Meson Particle Listings

## $f_0(980)$ , $a_0(980)$

MARSISKE	90	PR D41 3324	H. Marsiske et al.	(Crystal Ball Collab.)
MORGAN	90	ZPHY C48 623	D. Morgan, M.R. Pennington	(RAL, DURH)
OEST	90	ZPHY C47 343	T. Oest et al.	(JADE Collab.)
ACHASOV	89	NP B315 465	N.N. Achasov, V.N. Ivanchenko	
AUGUSTIN	89	NP B320 1	J.E. Augustin, G. Cosme	(DM2 Collab.)
VOROBYEV	88	SJNP 48 273	P.V. Vorobiev et al.	(NOVO)
ABACHI	86B	PRL 57 1990	S. Abachi et al.	(PURD, ANL, IND, MICH+)
ETKIN	82B	PR D25 1786	A. Etkin et al.	(BNL, CUNY, TUFTS, VAND)
GIDAL	81	PL 107B 153	G. Gidal et al.	(SLAC, LBL)
ACHASOV	80	SJNP 32 566	N.N. Achasov, S.A. Devyanin, G.N. Shestakov	(NOVM)
COHEN	80	PR D22 2595	D. Cohen et al.	(ANL) IJP
LOVERRE	80	ZPHY C6 187	P.F. Loverre et al.	(CERN, CDEF, MADR+)
AGUILAR...	78	NP B140 73	M. Aguilar-Benitez et al.	(MADR, BOMB+)
CASON	78	PRL 41 271	N.M. Cason et al.	(NDAM, ANL)
LEEPER	77	PR D16 2054	R.J. Leeper et al.	(ISU)
ROSSELET	77	PR D15 574	L. Rosselet et al.	(GEVA, SAUCL)
FLATTE	76	PL 63B 224	S.M. Flatte	(CERN)
WETZEL	76	NP B115 208	V. Wetzel et al.	(ETH, CERN, LOIC)
SRINIVASAN	75	PR D12 681	V. Srinivasan et al.	(NDAM, ANL)
GRAYER	74	NP B75 189	G. Grayer et al.	(CERN, MPIM)
BINNIE	73	PRL 31 1534	D.M. Binnie et al.	(CERN, SHMP)
GRAYER	73	Tallahassee	G. Grayer et al.	(CERN, MPIM)
HYAMS	73	NP B64 134	B.D. Hyams et al.	(CERN, MPIM)
PROTOPOP...	73	PR D7 1279	S.D. Protopopescu et al.	(LBL)

### $a_0(980)$

$$J^G(J^{PC}) = 1^-(0^{++})$$

See the review on "Scalar Mesons below 2 GeV."

### $a_0(980)$ MASS

VALUE (MeV)	DOCUMENT ID
<b>980 ± 20 OUR ESTIMATE</b>	Mass determination very model dependent

### $\eta\pi$ FINAL STATE ONLY

VALUE (MeV)	EVTS	DOCUMENT ID	TECN	CHG	COMMENT
• • • We do not use the following data for averages, fits, limits, etc. • • •					
982.5 ± 1.6 ± 1.1	16.9k	<sup>1</sup> AMBROSINO	09F	KLOE	1.02 e <sup>+</sup> e <sup>-</sup> → ηπ <sup>0</sup> γ
986 ± 4		ANISOVICH	09	RVUE	0.0 $\bar{p}p$ , πN
982.3 ± 0.6 ± 3.1 - 0.7 - 4.7		<sup>2</sup> UEHARA	09A	BELL	γγ → π <sup>0</sup> η
987.4 ± 1.0 ± 3.0		<sup>3,4</sup> BUGG	08A	RVUE 0	$\bar{p}p$ → π <sup>0</sup> π <sup>0</sup> η
989.1 ± 1.0 ± 3.0		<sup>4,5</sup> BUGG	08A	RVUE 0	$\bar{p}p$ → π <sup>0</sup> π <sup>0</sup> η
985 ± 4 ± 6	318	ACHARD	02B	L3	183-209 e <sup>+</sup> e <sup>-</sup> → e <sup>+</sup> e <sup>-</sup> ηπ <sup>+</sup> π <sup>-</sup>
995 ± 5.2 - 10	36	<sup>6</sup> ACHASOV	00F	SND	e <sup>+</sup> e <sup>-</sup> → ηπ <sup>0</sup> γ
994 ± 3.3 + 8	36	<sup>7</sup> ACHASOV	00F	SND	e <sup>+</sup> e <sup>-</sup> → ηπ <sup>0</sup> γ
975 ± 7		BARBERIS	00H		450 pp → p <sub>f</sub> ηπ <sup>0</sup> p <sub>s</sub>
988 ± 8		BARBERIS	00H		450 pp → Δ <sub>f</sub> <sup>++</sup> ηπ <sup>-</sup> p <sub>s</sub>
~ 1055		<sup>8</sup> OLLER	99	RVUE	ηπ, K $\bar{K}$
~ 1009.2		<sup>8</sup> OLLER	99B	RVUE	ππ → ππ, K $\bar{K}$
993.1 ± 2.1		<sup>9</sup> TEIGE	99	B852	18.3 π <sup>-</sup> p → ηπ <sup>+</sup> π <sup>-</sup> n
988 ± 6		<sup>8</sup> ANISOVICH	98B	RVUE	Compilation
987		TORNQVIST	96	RVUE	ππ → ππ, K $\bar{K}$ , Kπ, ηπ
991		JANSSEN	95	RVUE	ηπ → ηπ, K $\bar{K}$ , Kπ, ηπ
984.45 ± 1.23 ± 0.34		AMSLER	94C	CBAR	0.0 $\bar{p}p$ → ωηπ <sup>0</sup>
982 ± 2		<sup>10</sup> AMSLER	92	CBAR	0.0 $\bar{p}p$ → ηηπ <sup>0</sup>
984 ± 4	1040	<sup>10</sup> ARMSTRONG	91B	OMEG ±	300 pp → ppηπ <sup>+</sup> π <sup>-</sup>
976 ± 6		ATKINSON	84E	OMEG ±	25-55 γp → ηπn
986 ± 3	500	<sup>11</sup> EVANGELIS...	81	OMEG ±	12 π <sup>-</sup> p → ηπ <sup>+</sup> π <sup>-</sup> π <sup>-</sup> p
990 ± 7	145	<sup>11</sup> GURTU	79	HBC ±	4.2 K <sup>-</sup> p → Λη2π
980 ± 11	47	CONFORTO	78	OSPK -	4.5 π <sup>-</sup> p → ρX <sup>-</sup>
978 ± 16	50	CORDEN	78	OMEG ±	12-15 π <sup>-</sup> p → nη2π
977 ± 7		GRASSLER	77	HBC -	16 π <sup>+</sup> p → ρη3π
989 ± 4	70	WELLS	75	HBC -	3.1-6 K <sup>-</sup> p → Λη2π
972 ± 10	150	DEFOIX	72	HBC ±	0.7 $\bar{p}p$ → 7π
970 ± 15	20	BARNES	69C	HBC -	4-5 K <sup>-</sup> p → Λη2π
980 ± 10		CAMPBELL	69	DBC ±	2.7 π <sup>+</sup> d
980 ± 10	15	MILLER	69B	HBC -	4.5 K <sup>-</sup> N → ηπΛ
980 ± 10	30	AMMAR	68	HBC ±	5.5 K <sup>-</sup> p → Λη2π

<sup>1</sup> Using the model of ACHASOV 89 and ACHASOV 03b.  
<sup>2</sup> From a fit with the S-wave amplitude including two interfering Breit-Wigners plus a background term.  
<sup>3</sup> Parameterizes couplings to  $\bar{K}K$ , πη, and πη'.  
<sup>4</sup> Using AMSLER 94d and ABELE 98.  
<sup>5</sup> From the T-matrix pole on sheet II.  
<sup>6</sup> Using the model of ACHASOV 89. Supersedes ACHASOV 98b.  
<sup>7</sup> Using the model of JAFFE 77. Supersedes ACHASOV 98b.  
<sup>8</sup> T-matrix pole.  
<sup>9</sup> Breit-Wigner fit, average between  $a_0^±$  and  $a_0^0$ . The fit favors a slightly heavier  $a_0^±$ .  
<sup>10</sup> From a single Breit-Wigner fit.  
<sup>11</sup> From  $f_1(1285)$  decay.

### $K\bar{K}$ ONLY

VALUE (MeV)	EVTS	DOCUMENT ID	TECN	COMMENT
• • • We do not use the following data for averages, fits, limits, etc. • • •				
947.7 ± 5.5 - 5.0 ± 6.6		<sup>1</sup> AAIJ	19H	LHCB pp → D <sup>±</sup> X
925 ± 5 ± 8	190k	<sup>2</sup> AAIJ	16N	LHCB D <sup>0</sup> → K <sub>S</sub> <sup>0</sup> K <sup>±</sup> π <sup>∓</sup>
~ 1053		<sup>3</sup> OLLER	99C	RVUE ππ → ππ, K $\bar{K}$
982 ± 3		<sup>4</sup> ABELE	98	CBAR 0.0 $\bar{p}p$ → K <sub>L</sub> <sup>0</sup> K <sup>±</sup> π <sup>∓</sup>
975 ± 15		BERTIN	98B	OBLX 0.0 $\bar{p}p$ → K <sub>L</sub> <sup>0</sup> K <sup>±</sup> π <sup>∓</sup>
976 ± 6	316	DEBILLY	80	HBC 1.2-2 $\bar{p}p$ → f <sub>1</sub> (1285)ω
1016 ± 10	100	<sup>5</sup> ASTIER	67	HBC 0.0 $\bar{p}p$
1003.3 ± 7.0	143	<sup>6</sup> ROSENFELD	65	RVUE
<sup>1</sup> From the D <sup>±</sup> → K <sup>±</sup> K <sup>+</sup> K <sup>-</sup> Dalitz plot fit with the Triple-M amplitude in the multi-meson model of AOUE 18. <sup>2</sup> Using a two-channel resonance parametrization with couplings fixed to ABELE 98. <sup>3</sup> T-matrix pole. <sup>4</sup> T-matrix pole on sheet II, the pole on sheet III is at 1006-i49 MeV. <sup>5</sup> ASTIER 67 includes data of BARLOW 67, CONFORTO 67, ARMENTEROS 65. <sup>6</sup> Plus systematic errors.				

### $a_0(980)$ WIDTH

VALUE (MeV)	EVTS	DOCUMENT ID	TECN	CHG	COMMENT
• • • We do not use the following data for averages, fits, limits, etc. • • •					
75.6 ± 1.6 ± 17.4 - 10.0		<sup>1</sup> UEHARA	09A	BELL	γγ → π <sup>0</sup> η
80.2 ± 3.8 ± 5.4		<sup>2</sup> BUGG	08A	RVUE 0	$\bar{p}p$ → π <sup>0</sup> π <sup>0</sup> η
50 ± 13 ± 4	318	ACHARD	02B	L3	183-209 e <sup>+</sup> e <sup>-</sup> → e <sup>+</sup> e <sup>-</sup> ηπ <sup>+</sup> π <sup>-</sup>
72 ± 16		BARBERIS	00H		450 pp → p <sub>f</sub> ηπ <sup>0</sup> p <sub>s</sub>
61 ± 19		BARBERIS	00H		450 pp → Δ <sub>f</sub> <sup>++</sup> ηπ <sup>-</sup> p <sub>s</sub>
~ 42		<sup>3</sup> OLLER	99	RVUE	ηπ, K $\bar{K}$
~ 112		<sup>3</sup> OLLER	99B	RVUE	ππ → ηπ, K $\bar{K}$
71 ± 7		TEIGE	99	B852	18.3 π <sup>-</sup> p → ηπ <sup>+</sup> π <sup>-</sup> n
92 ± 20		<sup>3</sup> ANISOVICH	98B	RVUE	Compilation
65 ± 10		<sup>4</sup> BERTIN	98B	OBLX ±	0.0 $\bar{p}p$ → K <sup>±</sup> K <sub>S</sub> <sup>∓</sup> π <sup>∓</sup>
~ 100		TORNQVIST	96	RVUE	ππ → ππ, K $\bar{K}$ , Kπ, ηπ
202		JANSSEN	95	RVUE	ηπ → ηπ, K $\bar{K}$ , Kπ, ηπ
54.12 ± 0.34 ± 0.12		AMSLER	94C	CBAR	0.0 $\bar{p}p$ → ωηπ <sup>0</sup>
54 ± 10		<sup>5</sup> AMSLER	92	CBAR	0.0 $\bar{p}p$ → ηηπ <sup>0</sup>
95 ± 14	1040	<sup>5</sup> ARMSTRONG	91B	OMEG ±	300 pp → ppηπ <sup>+</sup> π <sup>-</sup>
62 ± 15	500	<sup>6</sup> EVANGELIS...	81	OMEG ±	12 π <sup>-</sup> p → ηπ <sup>+</sup> π <sup>-</sup> π <sup>-</sup> p
60 ± 20	145	<sup>6</sup> GURTU	79	HBC ±	4.2 K <sup>-</sup> p → Λη2π
60 ± 50 + 30	47	CONFORTO	78	OSPK -	4.5 π <sup>-</sup> p → ρX <sup>-</sup>
86.0 ± 60.0 - 50.0	50	CORDEN	78	OMEG ±	12-15 π <sup>-</sup> p → nη2π
44 ± 22		GRASSLER	77	HBC -	16 π <sup>+</sup> p → ρη3π
80 to 300		<sup>7</sup> FLATTE	76	RVUE -	4.2 K <sup>-</sup> p → Λη2π
16.0 ± 25.0 + 16.0	70	WELLS	75	HBC -	3.1-6 K <sup>-</sup> p → Λη2π
30 ± 5	150	DEFOIX	72	HBC ±	0.7 $\bar{p}p$ → 7π
40 ± 15		CAMPBELL	69	DBC ±	2.7 π <sup>+</sup> d
60 ± 30	15	MILLER	69B	HBC -	4.5 K <sup>-</sup> N → ηπΛ
80 ± 30	30	AMMAR	68	HBC ±	5.5 K <sup>-</sup> p → Λη2π

<sup>1</sup> From a fit with the S-wave amplitude including two interfering Breit-Wigners plus a background term.  
<sup>2</sup> From the T-matrix pole on sheet II, using AMSLER 94d and ABELE 98.  
<sup>3</sup> T-matrix pole.  
<sup>4</sup> The ηπ width.  
<sup>5</sup> From a single Breit-Wigner fit.  
<sup>6</sup> From  $f_1(1285)$  decay.  
<sup>7</sup> Using a two-channel resonance parametrization of GAY 76b data.

### $K\bar{K}$ ONLY

VALUE (MeV)	EVTS	DOCUMENT ID	TECN	CHG	COMMENT
• • • We do not use the following data for averages, fits, limits, etc. • • •					
<b>92 ± 8</b>		<sup>1</sup> ABELE	98	CBAR	0.0 $\bar{p}p$ → K <sub>L</sub> <sup>0</sup> K <sup>±</sup> π <sup>∓</sup>
~ 24		<sup>2</sup> OLLER	99C	RVUE	ππ → ππ, K $\bar{K}$
~ 25	100	<sup>3</sup> ASTIER	67	HBC ±	
57 ± 13	143	<sup>4</sup> ROSENFELD	65	RVUE ±	
<sup>1</sup> T-matrix pole on sheet II, the pole on sheet III is at 1006-i49 MeV. <sup>2</sup> T-matrix pole. <sup>3</sup> ASTIER 67 includes data of BARLOW 67, CONFORTO 67, ARMENTEROS 65. <sup>4</sup> Plus systematic errors.					

a<sub>0</sub>(980), ϕ(1020)

a<sub>0</sub>(980) DECAY MODES

Table with 3 columns: Mode, Fraction (Γ<sub>i</sub>/Γ), and Γ<sub>1</sub>Γ<sub>4</sub>/Γ. Rows include ηπ, K $\bar{K}$ , ρπ, γγ, and e<sup>+</sup>e<sup>-</sup>.

a<sub>0</sub>(980) PARTIAL WIDTHS

Table with 3 columns: Γ(γγ), VALUE (keV), DOCUMENT ID, TECN, COMMENT. Includes a note about data usage and a reference to AMSLER 98 RVUE.

a<sub>0</sub>(980) Γ(η)Γ(γγ)/Γ(total)

Table with 5 columns: Γ(ηπ) × Γ(γγ)/Γ<sub>total</sub>, VALUE (keV), DOCUMENT ID, TECN, COMMENT. Includes 'OUR AVERAGE' and a note about the fit.

Table with 5 columns: Γ(ηπ) × Γ(e<sup>+</sup>e<sup>-</sup>)/Γ<sub>total</sub>, VALUE (eV), CL%, DOCUMENT ID, TECN, COMMENT. Includes 'OUR AVERAGE' and a note about the fit.

a<sub>0</sub>(980) BRANCHING RATIOS

Table with 5 columns: Γ(K $\bar{K}$ )/Γ(ηπ), VALUE, DOCUMENT ID, TECN, CHG, COMMENT. Includes 'OUR AVERAGE' and various branching ratio data points.

Table with 5 columns: Γ(ρπ)/Γ(ηπ), VALUE, CL%, DOCUMENT ID, TECN, CHG, COMMENT. Includes a note about data usage.

Table with 5 columns: VALUE, CL%, DOCUMENT ID, TECN, CHG, COMMENT. Includes a note about data usage and a reference to AMSLER 94D.

a<sub>0</sub>(980) REFERENCES

List of references for a<sub>0</sub>(980) decay modes and branching ratios, including authors like AAIJ, AOUDE, and AMSLER.

List of references for a<sub>0</sub>(980) partial widths and branching ratios, including authors like BUGG, AMSLER, and ARMSTRONG.

ϕ(1020)

I<sup>G(J<sup>PC</sup>)</sup> = 0<sup>-</sup>(1<sup>-</sup>-)

ϕ(1020) MASS

Table with 5 columns: VALUE (MeV), EVTS, DOCUMENT ID, TECN, COMMENT. Includes 'OUR AVERAGE' and various mass measurements from experiments like KOZYREV and LEES.

# Meson Particle Listings

## $\phi(1020)$

1019.4 ± 0.7		BINNIE	73B	CNTR	$\pi^- p \rightarrow \phi n$
1019.6 ± 0.5	120	<sup>13</sup> AGUILAR-...	72B	HBC	$3.9, 4.6 K^- p \rightarrow \Lambda K^+ K^-$
1019.9 ± 0.5	100	<sup>13</sup> AGUILAR-...	72B	HBC	$3.9, 4.6 K^- p \rightarrow K^- p K^+ K^-$
1020.4 ± 0.5	131	COLLEY	72	HBC	$10 K^+ p \rightarrow K^+ p \phi$
1019.9 ± 0.3	410	STOTTLE...	71	HBC	$2.9 K^- p \rightarrow \Sigma / \Lambda K \bar{K}$

- <sup>1</sup> Average of KOZYREV 16 and KOZYREV 18 values taking into account the correlated uncertainties. Supersedes individual KOZYREV 16 and KOZYREV 18 results.
- <sup>2</sup> Using a vector meson dominance model with contribution from  $\phi(1020)$  and higher mass excitations of  $\rho(770)$ ,  $\omega(782)$ , and  $\phi(1020)$ .
- <sup>3</sup> Using a phenomenological model based on KUHN 90 with a sum of Breit-Wigner resonances for  $\rho(770)$ ,  $\omega(782)$ ,  $\phi(1020)$  and their higher mass excitations.
- <sup>4</sup> Update of AKHMETSHIN 99b
- <sup>5</sup> From the combined fit assuming that the total  $\phi(1020)$  production cross section is saturated by those of  $K^+ K^-$ ,  $K_S K_L$ ,  $\pi^+ \pi^- \pi^0$ , and  $\eta \gamma$  decays modes and using ACHASOV 00b for the  $\eta \gamma$  decay mode.
- <sup>6</sup> Using a total width of  $4.43 \pm 0.05$  MeV. Systematic uncertainty included.
- <sup>7</sup> Using a total width of  $4.43 \pm 0.05$  MeV.
- <sup>8</sup> PELLINEN 82 review includes AKERLOF 77, DAUM 81, BALDI 77, AYRES 74, DE-GROOT 74.
- <sup>9</sup> From the  $D^\pm \rightarrow K^\pm K^+ K^-$  Dalitz plot fit with the Triple-M amplitude in the multi-meson model of AOUDE 18.
- <sup>10</sup> Strongly correlated with AKHMETSHIN 04.
- <sup>11</sup> Systematic errors not evaluated.
- <sup>12</sup> Weighted and scaled average of 12 measurements of DIJKSTRA 86.
- <sup>13</sup> Mass errors enlarged by us to  $\Gamma/\sqrt{N}$ ; see the note with the  $K^*(892)$  mass.

### $\phi(1020)$ WIDTH

VALUE (MeV)	EVTS	DOCUMENT ID	TECN	COMMENT
<b>4.249 ± 0.013 OUR AVERAGE</b>		Error includes scale factor of 1.1.		
4.245 ± 0.013	2.3M	<sup>1</sup> KOZYREV	18	CMD3 $e^+ e^- \rightarrow K^+ K^-$ , $K_S^0 K_L^0$
4.205 ± 0.103 ± 0.067	28k	<sup>2</sup> LEES	14H	BABR $e^+ e^- \rightarrow K_S^0 K_L^0 \gamma$
4.29 ± 0.04 ± 0.07		<sup>3</sup> LEES	13Q	BABR $e^+ e^- \rightarrow K^+ K^- \gamma$
4.30 ± 0.06 ± 0.17	105k	AKHMETSHIN 06	CMD2	$0.98-1.06 e^+ e^- \rightarrow \pi^+ \pi^- \pi^0$
4.280 ± 0.033 ± 0.025	272k	<sup>4</sup> AKHMETSHIN 04	CMD2	$e^+ e^- \rightarrow K_S^0 K_L^0$
4.21 ± 0.04	1900k	<sup>5</sup> ACHASOV	01E	SND $e^+ e^- \rightarrow K^+ K^-$ , $K_S K_L$ , $\pi^+ \pi^- \pi^0$
4.44 ± 0.09	55 600	AKHMETSHIN 95	CMD2	$e^+ e^- \rightarrow$ hadrons
4.5 ± 0.7	1500	ARENTON	82	AEMS 11.8 polar. $pp \rightarrow K K$
4.2 ± 0.6	766	<sup>6</sup> IVANOV	81	OLYA 1-1.4 $e^+ e^- \rightarrow K^+ K^-$
4.3 ± 0.6		<sup>6</sup> CORDIER	80	DMI $e^+ e^- \rightarrow \pi^+ \pi^- \pi^0$
4.36 ± 0.29	3681	<sup>6</sup> BUKIN	78C	OLYA $e^+ e^- \rightarrow$ hadrons
4.4 ± 0.6	984	<sup>6</sup> BESCH	74	CNTR $2 \gamma p \rightarrow p K^+ K^-$
4.67 ± 0.72	681	<sup>6</sup> BALAKIN	71	OSPK $e^+ e^- \rightarrow$ hadrons
4.09 ± 0.29		BIZOT	70	OSPK $e^+ e^- \rightarrow$ hadrons
● ● ● We do not use the following data for averages, fits, limits, etc. ● ● ●				
4.249 ± 0.015	1.7M	KOZYREV	18	CMD3 $e^+ e^- \rightarrow K^+ K^-$
4.240 ± 0.017	610k	KOZYREV	16	CMD3 $e^+ e^- \rightarrow K_S^0 K_L^0$
4.37 ± 0.02		LEES	13F	BABR $D^+ \rightarrow K^+ K^- \pi^+$
4.24 ± 0.02 ± 0.03	542k	<sup>7</sup> AKHMETSHIN 08	CMD2	$1.02 e^+ e^- \rightarrow K^+ K^-$
4.28 ± 0.13	12540	<sup>8</sup> AUBERT, B	05J	BABR $D^0 \rightarrow \bar{K}^0 K^+ K^-$
4.45 ± 0.06	271k	DIJKSTRA	86	SPEC 100 $\pi^-$ Be
3.6 ± 0.8	337	<sup>6</sup> COOPER	78B	HBC $0.7-0.8 \bar{p} p \rightarrow K_S^0 K_L^0 \pi^+ \pi^-$
4.5 ± 0.50	1300	<sup>6,8</sup> AKERLOF	77	SPEC 400 pA $\rightarrow K^+ K^- X$
4.5 ± 0.8	500	<sup>6,8</sup> AYRES	74	ASPK $3-6 \pi^- p \rightarrow K^+ K^- n$ , $K^- p \rightarrow K^+ K^- \Lambda / \Sigma^0$
3.81 ± 0.37		COSME	74B	OSPK $e^+ e^- \rightarrow K_L^0 K_S^0$
3.8 ± 0.7	454	<sup>6</sup> BORENSTEIN	72	HBC 2.18 $K^- p \rightarrow K \bar{K} n$

- <sup>1</sup> Average of KOZYREV 16 and KOZYREV 18 values taking into account the correlated uncertainties. Supersedes individual KOZYREV 16 and KOZYREV 18 results.
- <sup>2</sup> Using a vector meson dominance model with contribution from  $\phi(1020)$  and higher mass excitations of  $\rho(770)$ ,  $\omega(782)$ , and  $\phi(1020)$ .
- <sup>3</sup> Using a phenomenological model based on KUHN 90 with a sum of Breit-Wigner resonances for  $\rho(770)$ ,  $\omega(782)$ ,  $\phi(1020)$  and their higher mass excitations.
- <sup>4</sup> Update of AKHMETSHIN 99b
- <sup>5</sup> From the combined fit assuming that the total  $\phi(1020)$  production cross section is saturated by those of  $K^+ K^-$ ,  $K_S K_L$ ,  $\pi^+ \pi^- \pi^0$ , and  $\eta \gamma$  decays modes and using ACHASOV 00b for the  $\eta \gamma$  decay mode.
- <sup>6</sup> Width errors enlarged by us to  $4\Gamma/\sqrt{N}$ ; see the note with the  $K^*(892)$  mass.
- <sup>7</sup> Strongly correlated with AKHMETSHIN 04.
- <sup>8</sup> Systematic errors not evaluated.

### $\phi(1020)$ DECAY MODES

Mode	Fraction ( $\Gamma_i/\Gamma$ )	Scale factor/Confidence level
$\Gamma_1 K^+ K^-$	(49.2 ± 0.5 ) %	S=1.3
$\Gamma_2 K_L^0 K_S^0$	(34.0 ± 0.4 ) %	S=1.3

$\Gamma_3 \rho \pi^+ + \pi^+ \pi^- \pi^0$	(15.24 ± 0.33 ) %	S=1.2
$\Gamma_4 \rho \pi$		
$\Gamma_5 \pi^+ \pi^- \pi^0$		
$\Gamma_6 \eta \gamma$	( 1.303 ± 0.025 ) %	S=1.2
$\Gamma_7 \pi^0 \gamma$	( 1.30 ± 0.05 ) × 10 <sup>-3</sup>	
$\Gamma_8 \ell^+ \ell^-$	—	
$\Gamma_9 e^+ e^-$	( 2.973 ± 0.034 ) × 10 <sup>-4</sup>	S=1.3
$\Gamma_{10} \mu^+ \mu^-$	( 2.86 ± 0.19 ) × 10 <sup>-4</sup>	
$\Gamma_{11} \eta e^+ e^-$	( 1.08 ± 0.04 ) × 10 <sup>-4</sup>	
$\Gamma_{12} \pi^+ \pi^-$	( 7.3 ± 1.3 ) × 10 <sup>-5</sup>	
$\Gamma_{13} \omega \pi^0$	( 4.7 ± 0.5 ) × 10 <sup>-5</sup>	
$\Gamma_{14} \omega \gamma$	< 5 %	CL=84%
$\Gamma_{15} \rho \gamma$	< 1.2 × 10 <sup>-5</sup>	CL=90%
$\Gamma_{16} \pi^+ \pi^- \gamma$	( 4.1 ± 1.3 ) × 10 <sup>-5</sup>	
$\Gamma_{17} f_0(980) \gamma$	( 3.22 ± 0.19 ) × 10 <sup>-4</sup>	S=1.1
$\Gamma_{18} \pi^0 \pi^0 \gamma$	( 1.12 ± 0.06 ) × 10 <sup>-4</sup>	
$\Gamma_{19} \pi^+ \pi^- \pi^+ \pi^-$	( 3.9 <sup>+2.8</sup> <sub>-2.2</sub> ) × 10 <sup>-6</sup>	
$\Gamma_{20} \pi^+ \pi^+ \pi^- \pi^- \pi^0$	< 4.6 × 10 <sup>-6</sup>	CL=90%
$\Gamma_{21} \pi^0 e^+ e^-$	( 1.33 <sup>+0.07</sup> <sub>-0.10</sub> ) × 10 <sup>-5</sup>	
$\Gamma_{22} \pi^0 \eta \gamma$	( 7.27 ± 0.30 ) × 10 <sup>-5</sup>	S=1.5
$\Gamma_{23} a_0(980) \gamma$	( 7.6 ± 0.6 ) × 10 <sup>-5</sup>	
$\Gamma_{24} K^0 \bar{K}^0 \gamma$	< 1.9 × 10 <sup>-8</sup>	CL=90%
$\Gamma_{25} \eta'(958) \gamma$	( 6.22 ± 0.21 ) × 10 <sup>-5</sup>	
$\Gamma_{26} \eta \pi^0 \pi^0 \gamma$	< 2 × 10 <sup>-5</sup>	CL=90%
$\Gamma_{27} \mu^+ \mu^- \gamma$	( 1.4 ± 0.5 ) × 10 <sup>-5</sup>	
$\Gamma_{28} \rho \gamma \gamma$	< 1.2 × 10 <sup>-4</sup>	CL=90%
$\Gamma_{29} \eta \pi^+ \pi^-$	< 1.8 × 10 <sup>-5</sup>	CL=90%
$\Gamma_{30} \eta \mu^+ \mu^-$	< 9.4 × 10 <sup>-6</sup>	CL=90%
$\Gamma_{31} \eta U \rightarrow \eta e^+ e^-$	< 1 × 10 <sup>-6</sup>	CL=90%
$\Gamma_{32}$ invisible	< 1.7 × 10 <sup>-4</sup>	CL=90%

### Lepton Family number (LF) violating modes

$\Gamma_{33} e^\pm \mu^\mp$	LF < 2	× 10 <sup>-6</sup>	CL=90%
-----------------------------	--------	--------------------	--------

### CONSTRAINED FIT INFORMATION

An overall fit to 30 branching ratios uses 82 measurements and one constraint to determine 14 parameters. The overall fit has a  $\chi^2 = 63.7$  for 69 degrees of freedom.

The following *off-diagonal* array elements are the correlation coefficients  $\langle \delta x_i \delta x_j \rangle / (\delta x_i \delta x_j)$ , in percent, from the fit to the branching fractions,  $x_i \equiv \Gamma_i / \Gamma_{\text{total}}$ . The fit constrains the  $x_i$  whose labels appear in this array to sum to one.

$x_2$	-78																			
$x_3$	-59	-4																		
$x_6$	-23	19	6																	
$x_7$	-15	14	4	10																
$x_9$	54	-52	-17	-38	-27															
$x_{10}$	-7	7	2	5	3	-13														
$x_{12}$	-3	3	1	2	2	-6	1													
$x_{13}$	-5	4	1	3	2	-8	1	1												
$x_{17}$	0	0	0	0	0	0	0	0	0											
$x_{18}$	-11	10	3	19	5	-20	2	1	2	0										
$x_{19}$	-1	1	0	1	0	-2	0	0	0	0										
$x_{23}$	0	0	0	0	0	0	0	0	0	0										
$x_{25}$	-8	6	2	33	3	-12	2	1	1	0										
	$x_1$	$x_2$	$x_3$	$x_6$	$x_7$	$x_9$	$x_{10}$	$x_{12}$	$x_{13}$	$x_{17}$										
$x_{19}$	0																			
$x_{23}$	0	0																		
$x_{25}$	6	0	0																	
	$x_{18}$	$x_{19}$	$x_{23}$																	

### $\phi(1020)$ PARTIAL WIDTHS

$\Gamma(\eta \gamma)$	VALUE (keV)	DOCUMENT ID	TECN	COMMENT	$\Gamma_6$
-----------------------	-------------	-------------	------	---------	------------

- ● ● We do not use the following data for averages, fits, limits, etc. ● ● ●
- 58.9 ± 0.5 ± 2.4 ACHASOV 00 SND  $e^+ e^- \rightarrow \eta \gamma$

$\Gamma(\pi^0\gamma)$   $\Gamma_7$

VALUE (keV)	DOCUMENT ID	TECN	COMMENT
5.40 ± 0.16 <sup>+0.43</sup> <sub>-0.40</sub>	ACHASOV 00	SND	$e^+e^- \rightarrow \pi^0\gamma$

• • • We do not use the following data for averages, fits, limits, etc. • • •

$\Gamma(e^+e^-)$   $\Gamma_8$

VALUE (keV)	DOCUMENT ID	TECN	COMMENT
1.320 ± 0.017 ± 0.015	1 AMBROSINO 05	KLOE	1.02 $e^+e^- \rightarrow \mu^+\mu^-$

1 Weighted average of  $\Gamma_{ee}$  and  $\sqrt{\Gamma_{ee}\Gamma_{\mu\mu}}$  from AMBROSINO 05 assuming lepton universality.

$\Gamma(e^+e^-)$   $\Gamma_9$

VALUE (keV)	DOCUMENT ID	TECN	COMMENT
<b>1.27 ± 0.04 OUR EVALUATION</b>			
<b>1.251 ± 0.021 OUR AVERAGE</b>			Error includes scale factor of 1.1.
1.235 ± 0.006 ± 0.022	1 AKHMETSHIN 11	CMD2	1.02 $e^+e^- \rightarrow \phi$
1.32 ± 0.05 ± 0.03	2 AMBROSINO 05	KLOE	1.02 $e^+e^- \rightarrow e^+\mu^-$
1.28 ± 0.05	AKHMETSHIN 95	CMD2	1.02 $e^+e^- \rightarrow \phi$

1 Combined analysis of the CMD-2 data on  $\phi \rightarrow K^+K^-, K_S^0 K_L^0, \pi^+\pi^-\pi^0, \eta\gamma$  assuming that the sum of their branching fractions is 0.99741 ± 0.00007.  
2 From forward-backward asymmetry and using  $\Gamma_{total} = 4.26 \pm 0.05$  MeV from the 2004 edition of this Review.

$(\Gamma(e^+e^-) \times \Gamma(\mu^+\mu^-))^{1/2}$   $(\Gamma_9\Gamma_{10})^{1/2}$

VALUE (keV)	DOCUMENT ID	TECN	COMMENT
<b>1.320 ± 0.018 ± 0.017</b>	AMBROSINO 05	KLOE	1.02 $e^+e^- \rightarrow \mu^+\mu^-$

$\phi(1020) \Gamma(i)\Gamma(e^+e^-)/\Gamma(total)$

$\Gamma(K^+K^-) \times \Gamma(e^+e^-)/\Gamma total$   $\Gamma_1\Gamma_9/\Gamma$

VALUE (keV)	EVTS	DOCUMENT ID	TECN	COMMENT
<b>0.6340 ± 0.0070 ± 0.0039</b>		1 LEES 13Q	BABR	$e^+e^- \rightarrow K^+K^-\gamma$
0.669 ± 0.001 ± 0.023	1.7M	KOZYREV 18	CMD3	$e^+e^- \rightarrow K^+K^-$

• • • We do not use the following data for averages, fits, limits, etc. • • •

1 Using a phenomenological model based on KUHN 90 with a sum of Breit-Wigner resonances for  $\rho(770), \omega(782), \phi(1020)$  and their higher mass excitations. The first error combines statistical and systematic uncertainties. The second one is due to the parametrization of the charged kaon form factor and mass calibration.

$\Gamma(K_S^0 K_L^0) \times \Gamma(e^+e^-)/\Gamma total$   $\Gamma_2\Gamma_9/\Gamma$

VALUE (keV)	EVTS	DOCUMENT ID	TECN	COMMENT
<b>0.4200 ± 0.0033 ± 0.0123</b>	28k	1 LEES 14H	BABR	$e^+e^- \rightarrow K_S^0 K_L^0 \gamma$

1 Using a vector meson dominance model with contribution from  $\phi(1020)$  and higher mass excitations of  $\rho(770), \omega(782)$ , and  $\phi(1020)$ .

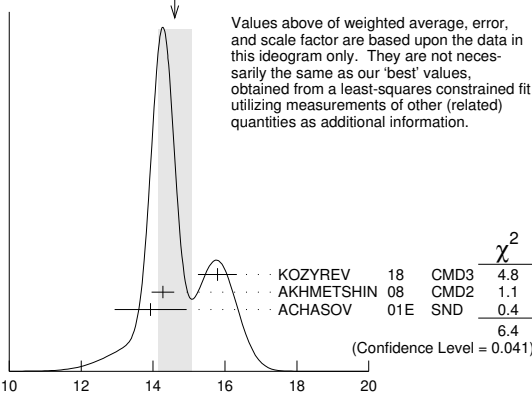
$\phi(1020) \Gamma(i)\Gamma(e^+e^-)/\Gamma^2(total)$

$\Gamma(K^+K^-)/\Gamma total \times \Gamma(e^+e^-)/\Gamma total$   $\Gamma_1/\Gamma \times \Gamma_9/\Gamma$

VALUE (units 10 <sup>-9</sup> )	EVTS	DOCUMENT ID	TECN	COMMENT
<b>14.63 ± 0.29 OUR FIT</b>				Error includes scale factor of 1.5.
<b>14.6 ± 0.5 OUR AVERAGE</b>				Error includes scale factor of 1.8. See the ideogram below.
15.789 ± 0.541	1.7M	KOZYREV 18	CMD3	$e^+e^- \rightarrow K^+K^-$
14.27 ± 0.05 ± 0.31	542k	AKHMETSHIN 08	CMD2	1.02 $e^+e^- \rightarrow K^+K^-$
13.93 ± 0.14 ± 0.99	1000k	1 ACHASOV 01E	SND	$e^+e^- \rightarrow K^+K^-, K_S K_L, \pi^+\pi^-\pi^0$

1 From the combined fit assuming that the total  $\phi(1020)$  production cross section is saturated by those of  $K^+K^-, K_S K_L, \pi^+\pi^-\pi^0$ , and  $\eta\gamma$  decays modes and using ACHASOV 00b for the  $\eta\gamma$  decay mode.

WEIGHTED AVERAGE  
14.6 ± 0.5 (Error scaled by 1.8)



$\Gamma(K_L^0 K_S^0)/\Gamma total \times \Gamma(e^+e^-)/\Gamma total$   $\Gamma_2/\Gamma \times \Gamma_9/\Gamma$

VALUE (units 10 <sup>-9</sup> )	EVTS	DOCUMENT ID	TECN	COMMENT
<b>10.10 ± 0.12 OUR FIT</b>				Error includes scale factor of 1.1.
<b>10.07 ± 0.13 OUR AVERAGE</b>				
10.078 ± 0.223	610k	1 KOZYREV 16	CMD3	$e^+e^- \rightarrow K_S^0 K_L^0$
10.01 ± 0.04 ± 0.17	272k	2 AKHMETSHIN 04	CMD2	$e^+e^- \rightarrow K_L^0 K_S^0$
10.27 ± 0.07 ± 0.34	500k	3 ACHASOV 01E	SND	$e^+e^- \rightarrow K^+K^-, K_S K_L, \pi^+\pi^-\pi^0$

1 KOZYREV 16 also reports  $\Gamma(e^+e^-) B(\phi \rightarrow K_S^0 K_L^0) = (0.428 \pm 0.001 \pm 0.009)$  keV.  
2 Update of AKHMETSHIN 99d  
3 From the combined fit assuming that the total  $\phi(1020)$  production cross section is saturated by those of  $K^+K^-, K_S K_L, \pi^+\pi^-\pi^0$ , and  $\eta\gamma$  decays modes and using ACHASOV 00b for the  $\eta\gamma$  decay mode.

$[\Gamma(\rho\pi) + \Gamma(\pi^+\pi^-\pi^0)]/\Gamma total \times \Gamma(e^+e^-)/\Gamma total$   $\Gamma_3/\Gamma \times \Gamma_9/\Gamma$

VALUE (units 10 <sup>-5</sup> )	EVTS	DOCUMENT ID	TECN	COMMENT
<b>4.53 ± 0.10 OUR FIT</b>				Error includes scale factor of 1.1.
<b>4.46 ± 0.12 OUR AVERAGE</b>				
4.51 ± 0.16 ± 0.11	105k	AKHMETSHIN 06	CMD2	0.98-1.06 $e^+e^- \rightarrow \pi^+\pi^-\pi^0$
4.30 ± 0.08 ± 0.21		AUBERT,B 04N	BABR	10.6 $e^+e^- \rightarrow \pi^+\pi^-\pi^0\gamma$
4.665 ± 0.042 ± 0.261	400k	1 ACHASOV 01E	SND	$e^+e^- \rightarrow K^+K^-, K_S K_L, \pi^+\pi^-\pi^0$
4.35 ± 0.27 ± 0.08	11169	2 AKHMETSHIN 98	CMD2	$e^+e^- \rightarrow \pi^+\pi^-\pi^0$
4.38 ± 0.12		BENAYOUN 10	RVUE	0.4-1.05 $e^+e^-$

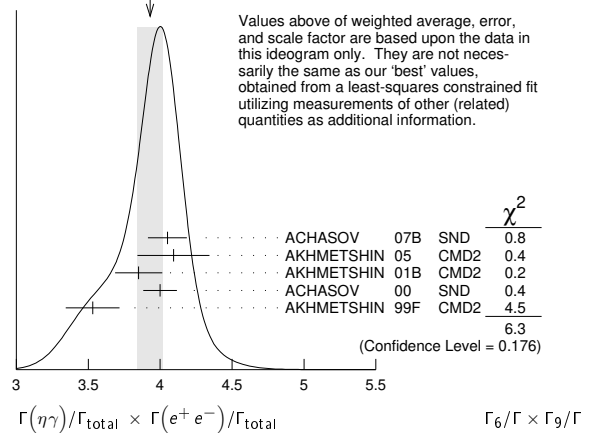
• • • We do not use the following data for averages, fits, limits, etc. • • •  
1 From the combined fit assuming that the total  $\phi(1020)$  production cross section is saturated by those of  $K^+K^-, K_S K_L, \pi^+\pi^-\pi^0$ , and  $\eta\gamma$  decays modes and using ACHASOV 00b for the  $\eta\gamma$  decay mode.  
2 Recalculated by us from the cross section in the peak.

$\Gamma(\eta\gamma)/\Gamma total \times \Gamma(e^+e^-)/\Gamma total$   $\Gamma_6/\Gamma \times \Gamma_9/\Gamma$

VALUE (units 10 <sup>-6</sup> )	EVTS	DOCUMENT ID	TECN	COMMENT
<b>3.87 ± 0.07 OUR FIT</b>				Error includes scale factor of 1.2.
<b>3.93 ± 0.09 OUR AVERAGE</b>				Error includes scale factor of 1.3. See the ideogram below.
4.050 ± 0.067 ± 0.118	33k	1 ACHASOV 07B	SND	0.6-1.38 $e^+e^- \rightarrow \eta\gamma$
4.093 ± 0.040 ± 0.247	17.4k	2 AKHMETSHIN 05	CMD2	0.60-1.38 $e^+e^- \rightarrow \eta\gamma$
3.850 ± 0.041 ± 0.159	23k	3,4 AKHMETSHIN 01B	CMD2	$e^+e^- \rightarrow \eta\gamma$
4.00 ± 0.04 ± 0.11		5 ACHASOV 00	SND	$e^+e^- \rightarrow \eta\gamma$
3.53 ± 0.08 ± 0.17	2200	6,7 AKHMETSHIN 99F	CMD2	$e^+e^- \rightarrow \eta\gamma$
4.19 ± 0.06		8 BENAYOUN 10	RVUE	0.4-1.05 $e^+e^-$

1 From a combined fit of  $\sigma(e^+e^- \rightarrow \eta\gamma)$  with  $\eta \rightarrow 3\pi^0$  and  $\eta \rightarrow \pi^+\pi^-\pi^0$ , and fixing  $B(\eta \rightarrow 3\pi^0) / B(\eta \rightarrow \pi^+\pi^-\pi^0) = 1.44 \pm 0.04$ . Recalculated by us from the cross section at the peak. Supersedes ACHASOV 00d and ACHASOV 06a.  
2 From the  $\eta \rightarrow 2\gamma$  decay and using  $B(\eta \rightarrow \gamma\gamma) = 39.43 \pm 0.26\%$ .  
3 From the  $\eta \rightarrow 3\pi^0$  decay and using  $B(\eta \rightarrow 3\pi^0) = (32.24 \pm 0.29) \times 10^{-2}$ .  
4 The combined fit from 600 to 1380 MeV taking into account  $\rho(770), \omega(782), \phi(1020)$ , and  $\rho(1450)$  (mass and width fixed at 1450 MeV and 310 MeV respectively).  
5 From the  $\eta \rightarrow 2\gamma$  decay and using  $B(\eta \rightarrow 2\gamma) = (39.21 \pm 0.34) \times 10^{-2}$ .  
6 Recalculated by the authors from the cross section in the peak.  
7 From the  $\eta \rightarrow \pi^+\pi^-\pi^0$  decay and using  $B(\eta \rightarrow \pi^+\pi^-\pi^0) = (23.1 \pm 0.5) \times 10^{-2}$ .  
8 A simultaneous fit of  $e^+e^- \rightarrow \pi^+\pi^-, \pi^+\pi^-\pi^0, \pi^0\gamma, \eta\gamma$  data.

WEIGHTED AVERAGE  
3.93 ± 0.09 (Error scaled by 1.3)



# Meson Particle Listings

## $\phi(1020)$

$$\Gamma(\pi^0\gamma)/\Gamma_{\text{total}} \times \Gamma(e^+e^-)/\Gamma_{\text{total}} \quad \Gamma_7/\Gamma \times \Gamma_9/\Gamma$$

VALUE (units $10^{-7}$ )	EVTS	DOCUMENT ID	TECN	COMMENT
<b>3.88 ± 0.14 OUR FIT</b>				
<b>3.87 ± 0.15 OUR AVERAGE</b>				
4.04 ± 0.09 ± 0.19		<sup>1</sup> ACHASOV 16A	SND	0.60-1.38 $e^+e^- \rightarrow \pi^0\gamma$
3.75 ± 0.11 ± 0.29	18k	AKHMETSHIN 05	CMD2	0.60-1.38 $e^+e^- \rightarrow \pi^0\gamma$
3.67 ± 0.10 ± 0.27 -0.25		<sup>2</sup> ACHASOV 00	SND	$e^+e^- \rightarrow \pi^0\gamma$
4.29 ± 0.11		<sup>3</sup> BENAYOUN 10	RVUE	0.4-1.05 $e^+e^-$

• • • We do not use the following data for averages, fits, limits, etc. • • •

<sup>1</sup> From the VMD model with the interfering  $\rho(770)$ ,  $\omega(782)$ ,  $\phi(1020)$  resonances, and an additional resonance describing the total contribution of the  $\rho(1450)$  and  $\omega(1420)$  states. Supersedes ACHASOV 00.

<sup>2</sup> From the  $\pi^0 \rightarrow 2\gamma$  decay and using  $B(\pi^0 \rightarrow 2\gamma) = (98.798 \pm 0.032) \times 10^{-2}$ .

<sup>3</sup> A simultaneous fit of  $e^+e^- \rightarrow \pi^+\pi^-, \pi^+\pi^-\pi^0, \pi^0\gamma, \eta\gamma$  data.

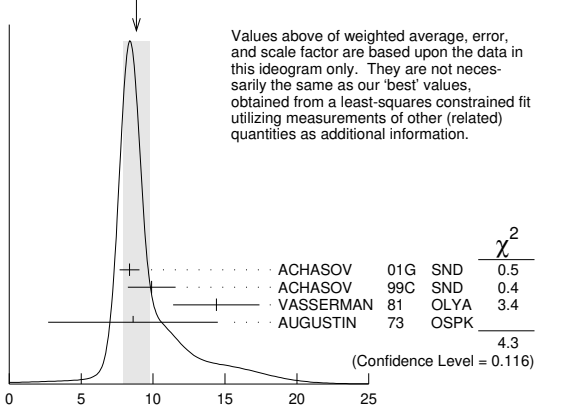
$$\Gamma(\mu^+\mu^-)/\Gamma_{\text{total}} \times \Gamma(e^+e^-)/\Gamma_{\text{total}} \quad \Gamma_{10}/\Gamma \times \Gamma_9/\Gamma$$

VALUE (units $10^{-8}$ )	DOCUMENT ID	TECN	COMMENT
<b>8.5 ± 0.5 OUR FIT</b>			
<b>8.8 ± 0.9 OUR AVERAGE</b>			Error includes scale factor of 1.5. See the ideogram below.
8.36 ± 0.59 ± 0.37	ACHASOV 01G	SND	$e^+e^- \rightarrow \mu^+\mu^-$
9.9 ± 1.4 ± 0.9	<sup>1</sup> ACHASOV 99C	SND	$e^+e^- \rightarrow \mu^+\mu^-$
14.4 ± 3.0	<sup>2</sup> VASSERMAN 81	OLYA	$e^+e^- \rightarrow \mu^+\mu^-$
8.6 ± 5.9	<sup>2</sup> AUGUSTIN 73	OSPK	$e^+e^- \rightarrow \mu^+\mu^-$

<sup>1</sup> Recalculated by the authors from the cross section in the peak.

<sup>2</sup> Recalculated by us from the cross section in the peak.

WEIGHTED AVERAGE  
8.8 ± 0.9 (Error scaled by 1.5)



Values above of weighted average, error, and scale factor are based upon the data in this ideogram only. They are not necessarily the same as our 'best' values, obtained from a least-squares constrained fit utilizing measurements of other (related) quantities as additional information.

$$\Gamma(\mu^+\mu^-)/\Gamma_{\text{total}} \times \Gamma(e^+e^-)/\Gamma_{\text{total}} \quad \Gamma_{10}/\Gamma \times \Gamma_9/\Gamma$$

$$\Gamma(\pi^+\pi^-)/\Gamma_{\text{total}} \times \Gamma(e^+e^-)/\Gamma_{\text{total}} \quad \Gamma_{12}/\Gamma \times \Gamma_9/\Gamma$$

VALUE (units $10^{-8}$ )	DOCUMENT ID	TECN	COMMENT
<b>2.2 ± 0.4 OUR FIT</b>			
<b>2.2 ± 0.4 OUR AVERAGE</b>			
2.1 ± 0.3 ± 0.3	<sup>1</sup> ACHASOV 00C	SND	$e^+e^- \rightarrow \pi^+\pi^-$
1.95 ± 1.15 -0.87	<sup>2</sup> GOLUBEV 86	ND	$e^+e^- \rightarrow \pi^+\pi^-$
6.01 ± 3.19 -2.51	<sup>2</sup> VASSERMAN 81	OLYA	$e^+e^- \rightarrow \pi^+\pi^-$
3.31 ± 0.99	<sup>3</sup> BENAYOUN 13	RVUE	0.4-1.05 $e^+e^-$

• • • We do not use the following data for averages, fits, limits, etc. • • •

<sup>1</sup> Recalculated by the authors from the cross section in the peak.

<sup>2</sup> Recalculated by us from the cross section in the peak.

<sup>3</sup> A simultaneous fit to  $e^+e^- \rightarrow \pi^+\pi^-, \pi^+\pi^-\pi^0, \pi^0\gamma, \eta\gamma, K\bar{K}$ , and  $\tau^- \rightarrow \pi^-\pi^0\nu_\tau$  data.

$$\Gamma(\omega\pi^0)/\Gamma_{\text{total}} \times \Gamma(e^+e^-)/\Gamma_{\text{total}} \quad \Gamma_{13}/\Gamma \times \Gamma_9/\Gamma$$

VALUE (units $10^{-8}$ )	DOCUMENT ID	TECN	COMMENT
<b>1.40 ± 0.15 OUR FIT</b>			
<b>1.37 ± 0.17 ± 0.01</b>	<sup>1,2</sup> AMBROSINO 08G	KLOE	$e^+e^- \rightarrow \pi^+\pi^-\pi^0, 2\pi^0\gamma$

<sup>1</sup> Recalculated by the authors from the cross section at the peak.

<sup>2</sup> AMBROSINO 08G reports  $[\Gamma(\phi(1020) \rightarrow \omega\pi^0)/\Gamma_{\text{total}} \times \Gamma(\phi(1020) \rightarrow e^+e^-)/\Gamma_{\text{total}}] \times [B(\omega(782) \rightarrow \pi^+\pi^-\pi^0)] = (1.22 \pm 0.13 \pm 0.08) \times 10^{-8}$  which we divide by our best value  $B(\omega(782) \rightarrow \pi^+\pi^-\pi^0) = (89.3 \pm 0.6) \times 10^{-2}$ . Our first error is their experiment's error and our second error is the systematic error from using our best value.

$$\Gamma(\pi^0\pi^0\gamma)/\Gamma_{\text{total}} \times \Gamma(e^+e^-)/\Gamma_{\text{total}} \quad \Gamma_{18}/\Gamma \times \Gamma_9/\Gamma$$

VALUE (units $10^{-8}$ )	DOCUMENT ID	TECN	COMMENT
<b>3.34 ± 0.17 OUR FIT</b>			
<b>3.33 ± 0.04 ± 0.19 -0.20</b>	<sup>1</sup> AMBROSINO 07	KLOE	$e^+e^- \rightarrow \pi^0\pi^0\gamma$

<sup>1</sup> Calculated by the authors from the cross section at the peak.

$$\Gamma(\pi^+\pi^-\pi^+\pi^-)/\Gamma_{\text{total}} \times \Gamma(e^+e^-)/\Gamma_{\text{total}} \quad \Gamma_{19}/\Gamma \times \Gamma_9/\Gamma$$

VALUE (units $10^{-9}$ )	EVTS	DOCUMENT ID	TECN	COMMENT
<b>1.2 ± 0.8 -0.7 OUR FIT</b>				
<b>1.17 ± 0.52 ± 0.64</b>	3285	<sup>1</sup> AKHMETSHIN 00E	CMD2	$e^+e^- \rightarrow \pi^+\pi^-\pi^+\pi^-$

<sup>1</sup> Recalculated by the authors from the cross section in the peak.

### $\phi(1020)$ BRANCHING RATIOS

$$\Gamma(K^+K^-)/\Gamma_{\text{total}} \quad \Gamma_1/\Gamma$$

VALUE	EVTS	DOCUMENT ID	TECN	COMMENT
<b>0.492 ± 0.005 OUR FIT</b>				Error includes scale factor of 1.3.
<b>0.493 ± 0.010 OUR AVERAGE</b>				
0.492 ± 0.012	2913	AKHMETSHIN 95	CMD2	$e^+e^- \rightarrow K^+K^-$
0.44 ± 0.05	321	KALBFLEISCH 76	HBC	2.18 $K^-p \rightarrow \Lambda K^+K^-$
0.49 ± 0.06	270	DEGROOT 74	HBC	4.2 $K^-p \rightarrow \Lambda\phi$
0.540 ± 0.034	565	BALAKIN 71	OSPK	$e^+e^- \rightarrow K^+K^-$
0.48 ± 0.04	252	LINDSEY 66	HBC	2.1-2.7 $K^-p \rightarrow \Lambda K^+K^-$

• • • We do not use the following data for averages, fits, limits, etc. • • •

0.493 ± 0.003 ± 0.007 <sup>1</sup>AKHMETSHIN 11 CMD2 1.02  $e^+e^- \rightarrow K^+K^-$

0.476 ± 0.017 100k <sup>2</sup>ACHASOV 01E SND  $e^+e^- \rightarrow K^+K^-, K_S^0 K_L^0, \pi^+\pi^-\pi^0$

<sup>1</sup> Combined analysis of the CMD-2 data on  $\phi \rightarrow K^+K^-, K_L^0 K_S^0, \pi^+\pi^-\pi^0, \eta\gamma$  assuming that the sum of their branching fractions is  $0.99741 \pm 0.00007$ .

<sup>2</sup> Using  $B(\phi \rightarrow e^+e^-) = (2.93 \pm 0.14) \times 10^{-4}$ .

$$\Gamma(K_L^0 K_S^0)/\Gamma_{\text{total}} \quad \Gamma_2/\Gamma$$

VALUE	EVTS	DOCUMENT ID	TECN	COMMENT
<b>0.340 ± 0.004 OUR FIT</b>				Error includes scale factor of 1.3.
<b>0.331 ± 0.009 OUR AVERAGE</b>				
0.335 ± 0.010	40644	AKHMETSHIN 95	CMD2	$e^+e^- \rightarrow K_L^0 K_S^0$
0.326 ± 0.035		DOLINSKY 91	ND	$e^+e^- \rightarrow K_L^0 K_S^0$
0.310 ± 0.024		DRUZHININ 84	ND	$e^+e^- \rightarrow K_L^0 K_S^0$
0.336 ± 0.002 ± 0.006		<sup>1</sup> AKHMETSHIN 11	CMD2	1.02 $e^+e^- \rightarrow K_S^0 K_L^0$
0.351 ± 0.013	500k	<sup>2</sup> ACHASOV 01E	SND	$e^+e^- \rightarrow K^+K^-, K_S^0 K_L^0, \pi^+\pi^-\pi^0$
0.27 ± 0.03	133	KALBFLEISCH 76	HBC	2.18 $K^-p \rightarrow \Lambda K_L^0 K_S^0$
0.257 ± 0.030	95	<sup>3</sup> BALAKIN 71	OSPK	$e^+e^- \rightarrow K_L^0 K_S^0$
0.40 ± 0.04	167	LINDSEY 66	HBC	2.1-2.7 $K^-p \rightarrow \Lambda K_L^0 K_S^0$

• • • We do not use the following data for averages, fits, limits, etc. • • •

0.351 ± 0.013 500k <sup>1</sup>AKHMETSHIN 11 CMD2 1.02  $e^+e^- \rightarrow K_S^0 K_L^0$

0.351 ± 0.013 500k <sup>2</sup>ACHASOV 01E SND  $e^+e^- \rightarrow K^+K^-, K_S^0 K_L^0, \pi^+\pi^-\pi^0$

0.27 ± 0.03 133 KALBFLEISCH 76 HBC 2.18  $K^-p \rightarrow \Lambda K_L^0 K_S^0$

0.257 ± 0.030 95 <sup>3</sup>BALAKIN 71 OSPK  $e^+e^- \rightarrow K_L^0 K_S^0$

0.40 ± 0.04 167 LINDSEY 66 HBC 2.1-2.7  $K^-p \rightarrow \Lambda K_L^0 K_S^0$

<sup>1</sup> Combined analysis of the CMD-2 data on  $\phi \rightarrow K^+K^-, K_L^0 K_S^0, \pi^+\pi^-\pi^0, \eta\gamma$  assuming that the sum of their branching fractions is  $0.99741 \pm 0.00007$ .

<sup>2</sup> Using  $B(\phi \rightarrow e^+e^-) = (2.93 \pm 0.14) \times 10^{-4}$ .

<sup>3</sup> Balakin error increased by Paul.

$$\Gamma(K_L^0 K_S^0)/\Gamma(K^+K^-) \quad \Gamma_2/\Gamma_1$$

VALUE	EVTS	DOCUMENT ID	TECN	COMMENT
<b>0.690 ± 0.015 OUR FIT</b>				Error includes scale factor of 1.3.
<b>0.740 ± 0.031 OUR AVERAGE</b>				
0.70 ± 0.06	2732	BUKIN 78c	OLYA	$e^+e^- \rightarrow K_L^0 K_S^0$
0.82 ± 0.08		LOSTY 78	HBC	4.2 $K^-p \rightarrow \phi$ hyperon
0.71 ± 0.05		LAVEN 77	HBC	10 $K^-p \rightarrow K^+K^- \Lambda$
0.71 ± 0.08		LYONS 77	HBC	3-4 $K^-p \rightarrow \Lambda\phi$
0.89 ± 0.10	144	AGUILAR-...	72B	HBC 3.9,4.6 $K^-p$
0.638 ± 0.022	2.3M	<sup>1</sup> KOZYREV 18	CMD3	$e^+e^- \rightarrow K_L^0 K_S^0, K^+K^-$
0.68 ± 0.03		<sup>2</sup> AKHMETSHIN 95	CMD2	$e^+e^- \rightarrow K_L^0 K_S^0, K^+K^-$

<sup>1</sup> The prediction taking into account phase-space difference, radiative corrections, isospin breaking, and the Sommerfeld-Gamow-Sakharov factor gives 0.630.

<sup>2</sup> Theoretical analysis of BRAMON 00 taking into account phase-space difference, electromagnetic radiative corrections, as well as isospin breaking, predicts 0.62. FLOREZ-BAEZ 08 predicts 0.63 considering also structure-dependent radiative corrections. FISCHBACH 02 calculates additional corrections caused by the close threshold and predicts 0.68. See also BENAYOUN 01 and DUBYNSKIY 07. BENAYOUN 12 obtains  $0.71 \pm 0.01$  in the HLS model.

$$\Gamma(K_L^0 K_S^0)/\Gamma(K\bar{K}) \quad \Gamma_2/(\Gamma_1 + \Gamma_2)$$

VALUE	EVTS	DOCUMENT ID	TECN	COMMENT
<b>0.408 ± 0.005 OUR FIT</b>				Error includes scale factor of 1.3.
<b>0.45 ± 0.04 OUR AVERAGE</b>				
0.44 ± 0.07		<sup>1</sup> LONDON 66	HBC	2.24 $K^-p \rightarrow \Lambda K\bar{K}$
0.48 ± 0.07	52	BADIER 65B	HBC	3 $K^-p$
0.40 ± 0.10	34	SCHLEIN 63	HBC	1.95 $K^-p \rightarrow \Lambda K\bar{K}$

<sup>1</sup> This is probably not affected by their controversial background subtraction; the value is from their numbers of  $K_1 K_2$  vs  $K^+K^-$  events.

$$[\Gamma(\rho\pi) + \Gamma(\pi^+\pi^-\pi^0)]/\Gamma_{\text{total}} \quad \Gamma_3/\Gamma$$

VALUE	EVTS	DOCUMENT ID	TECN	COMMENT
<b>0.1524 ± 0.0033 OUR FIT</b>				Error includes scale factor of 1.2.
<b>0.151 ± 0.009 OUR AVERAGE</b>				Error includes scale factor of 1.7.
0.161 ± 0.008	11761	AKHMETSHIN 95	CMD2	$e^+e^- \rightarrow \pi^+\pi^-\pi^0$
0.143 ± 0.007		DOLINSKY 91	ND	$e^+e^- \rightarrow \pi^+\pi^-\pi^0$

# Meson Particle Listings

## $\phi(1020)$

• • • We do not use the following data for averages, fits, limits, etc. • • •

0.155 ± 0.002 ± 0.005	1	AKHMETSHIN 11	CMD2	1.02	$e^+e^- \rightarrow \pi^+\pi^-\pi^0$
0.159 ± 0.008	400k	2	ACHASOV	01E	$SND \ e^+e^- \rightarrow K^+K^-, K_S^0 K_L^0, \pi^+\pi^-\pi^0$
0.145 ± 0.009 ± 0.003	11169	3	AKHMETSHIN 98	CMD2	$e^+e^- \rightarrow \pi^+\pi^-\pi^0$
0.139 ± 0.007		4	PARROUR	76B	OSPK $e^+e^-$

- 1 Combined analysis of the CMD-2 data on  $\phi \rightarrow K^+K^-, K_S^0 K_L^0, \pi^+\pi^-\pi^0, \eta\gamma$  assuming that the sum of their branching fractions is  $0.99741 \pm 0.00007$ .
- 2 Using  $B(\phi \rightarrow e^+e^-) = (2.93 \pm 0.14) \times 10^{-4}$ .
- 3 Using  $B(\phi \rightarrow e^+e^-) = (2.99 \pm 0.08) \times 10^{-4}$ .
- 4 Using  $\Gamma(\phi) = 4.1$  MeV. If interference between the  $\rho\pi$  and  $3\pi$  modes is neglected, the fraction of the  $\rho\pi$  is more than 80% at the 90% confidence level.

$\frac{\Gamma(\rho\pi) + \Gamma(\pi^+\pi^-\pi^0)}{\Gamma(K^+K^-)}$   $\Gamma_3/\Gamma_1$

VALUE	EVTS	DOCUMENT ID	TECN	COMMENT
<b>0.310 ± 0.009 OUR FIT</b>				Error includes scale factor of 1.2.
<b>0.28 ± 0.09</b>	34	AGUILAR-...	72B	HBC 3.9,4.6 $K^-\rho$

$\frac{\Gamma(\rho\pi) + \Gamma(\pi^+\pi^-\pi^0)}{\Gamma(K\bar{K})}$   $\Gamma_3/(\Gamma_1+\Gamma_2)$

VALUE	DOCUMENT ID	TECN	COMMENT
<b>0.183 ± 0.005 OUR FIT</b>			Error includes scale factor of 1.2.
<b>0.24 ± 0.04 OUR AVERAGE</b>			
0.237 ± 0.039	CERRADA	77B	HBC 4.2 $K^-\rho \rightarrow \Lambda 3\pi$
0.30 ± 0.15	LONDON	66	HBC 2.24 $K^-\rho \rightarrow \Lambda\pi^+\pi^-\pi^0$

$\frac{\Gamma(\rho\pi) + \Gamma(\pi^+\pi^-\pi^0)}{\Gamma(K_S^0 K_L^0)}$   $\Gamma_3/\Gamma_2$

VALUE	EVTS	DOCUMENT ID	TECN	COMMENT
<b>0.448 ± 0.011 OUR FIT</b>				Error includes scale factor of 1.1.
<b>0.51 ± 0.05 OUR AVERAGE</b>				
0.56 ± 0.07	3681	BUKIN	78c	OLYA $e^+e^- \rightarrow K_L^0 K_S^0, \pi^+\pi^-\pi^0$
0.47 ± 0.06	516	COSME	74	OSPK $e^+e^- \rightarrow \pi^+\pi^-\pi^0$

$\Gamma(\pi^+\pi^-\pi^0)/\Gamma_{total}$   $\Gamma_5/\Gamma$

VALUE	CL%	EVTS	DOCUMENT ID	TECN	COMMENT
• • • We do not use the following data for averages, fits, limits, etc. • • •					
≈ 0.0087	1.98M	1,2	ALOISIO	03	KLOE 1.02 $e^+e^- \rightarrow \pi^+\pi^-\pi^0$
< 0.0006	90	3	ACHASOV	02	SND 1.02 $e^+e^- \rightarrow \pi^+\pi^-\pi^0$
< 0.23	90	3	CORDIER	80	DM1 $e^+e^- \rightarrow \pi^+\pi^-\pi^0$
< 0.20	90	3	PARROUR	76B	OSPK $e^+e^- \rightarrow \pi^+\pi^-\pi^0$

- 1 From a fit without limitations on charged and neutral  $\rho$  masses and widths.
- 2 Adding the direct and  $\omega\pi$  contributions and considering the interference between the  $\rho\pi$  and  $\pi^+\pi^-\pi^0$ .
- 3 Neglecting the interference between the  $\rho\pi$  and  $\pi^+\pi^-\pi^0$ .

$\Gamma(\eta\gamma)/\Gamma_{total}$   $\Gamma_6/\Gamma$

VALUE (units $10^{-2}$ )	EVTS	DOCUMENT ID	TECN	COMMENT	
<b>1.303 ± 0.025 OUR FIT</b>				Error includes scale factor of 1.2.	
<b>1.26 ± 0.04 OUR AVERAGE</b>					
1.246 ± 0.025 ± 0.057	10k	1	ACHASOV	98F	SND $e^+e^- \rightarrow 7\gamma$
1.18 ± 0.11	279	2	AKHMETSHIN 95	CMD2	$e^+e^- \rightarrow \pi^+\pi^-\pi^0 3\gamma$
1.30 ± 0.06		3	DRUZHININ	84	ND $e^+e^- \rightarrow 3\gamma$
1.4 ± 0.2		4	DRUZHININ	84	ND $e^+e^- \rightarrow 6\gamma$
0.88 ± 0.20	290		KURDADZE	83c	OLYA $e^+e^- \rightarrow 3\gamma$
1.35 ± 0.29			ANDREWS	77	CNTR 6.7-10 $\gamma Cu$
1.5 ± 0.4	54	3	COSME	76	OSPK $e^+e^-$

- • • We do not use the following data for averages, fits, limits, etc. • • •
- |                       |       |      |                |      |  |
|-----------------------|-------|------|----------------|------|--|
| 1.38 ± 0.02 ± 0.02    |       | 5    | AKHMETSHIN 11  | CMD2 | 1.02 $e^+e^- \rightarrow \eta\gamma$           |
| 1.36 ± 0.05 ± 0.02    | 33k   | 6    | ACHASOV        | 07B  | SND 0.6-1.38 $e^+e^- \rightarrow \eta\gamma$   |
| 1.373 ± 0.014 ± 0.085 | 17.4k | 7,8  | AKHMETSHIN 05  | CMD2 | 0.60-1.38 $e^+e^- \rightarrow \eta\gamma$      |
| 1.287 ± 0.013 ± 0.063 |       | 9,10 | AKHMETSHIN 01B | CMD2 | $e^+e^- \rightarrow \eta\gamma$                |
| 1.338 ± 0.012 ± 0.052 |       | 11   | ACHASOV        | 00   | SND $e^+e^- \rightarrow \eta\gamma$            |
| 1.18 ± 0.03 ± 0.06    | 2200  | 12   | AKHMETSHIN 99F | CMD2 | $e^+e^- \rightarrow \eta\gamma$                |
| 1.21 ± 0.07           |       | 13   | BENAYOUN       | 96   | RVUE 0.54-1.04 $e^+e^- \rightarrow \eta\gamma$ |
- 1 Using  $B(\phi \rightarrow e^+e^-) = (2.99 \pm 0.08) \times 10^{-4}$  and  $B(\eta \rightarrow 3\pi^0) = (32.2 \pm 0.4) \times 10^{-2}$ .
  - 2 From  $\pi^+\pi^-\pi^0$  decay mode of  $\eta$ .
  - 3 From  $2\gamma$  decay mode of  $\eta$ .
  - 4 From  $3\pi^0$  decay mode of  $\eta$ .
  - 5 Combined analysis of the CMD-2 data on  $\phi \rightarrow K^+K^-, K_S^0 K_L^0, \pi^+\pi^-\pi^0, \eta\gamma$  assuming that the sum of their branching fractions is  $0.99741 \pm 0.00007$ .
  - 6 ACHASOV 07B reports  $[\Gamma(\phi(1020) \rightarrow \eta\gamma)/\Gamma_{total}] \times [B(\phi(1020) \rightarrow e^+e^-)] = (4.050 \pm 0.067 \pm 0.118) \times 10^{-6}$  which we divide by our best value  $B(\phi(1020) \rightarrow e^+e^-) = (2.973 \pm 0.034) \times 10^{-4}$ . Our first error is their experiment's error and our second error is the systematic error from using our best value. Supersedes ACHASOV 00b and ACHASOV 06a.
  - 7 Using  $B(\phi \rightarrow e^+e^-) = (2.98 \pm 0.04) \times 10^{-4}$  and  $B(\eta \rightarrow \gamma\gamma) = 39.43 \pm 0.26\%$ .
  - 8 Not independent of the corresponding  $\Gamma(e^+e^-) \times \Gamma(\eta\gamma)/\Gamma_{total}^2$ .
  - 9 Using  $B(\phi \rightarrow e^+e^-) = (2.99 \pm 0.08) \times 10^{-4}$  and  $B(\eta \rightarrow 3\pi^0) = (32.24 \pm 0.29) \times 10^{-2}$ .
  - 10 The combined fit from 600 to 1380 MeV taking into account  $\rho(770), \omega(782), \phi(1020)$ , and  $\rho(1450)$  (mass and width fixed at 1450 MeV and 310 MeV respectively).
  - 11 From the  $\eta \rightarrow 2\gamma$  decay and using  $B(\phi \rightarrow e^+e^-) = (2.99 \pm 0.08) \times 10^{-4}$ .
  - 12 From  $\pi^+\pi^-\pi^0$  decay mode of  $\eta$  and using  $B(\phi \rightarrow e^+e^-) = (2.99 \pm 0.08) \times 10^{-4}$ .
  - 13 Reanalysis of DRUZHININ 84, DOLINSKY 89, and DOLINSKY 91 taking into account a triangle anomaly contribution.

$\Gamma(\pi^0\gamma)/\Gamma_{total}$   $\Gamma_7/\Gamma$

VALUE (units $10^{-3}$ )	EVTS	DOCUMENT ID	TECN	COMMENT
<b>1.30 ± 0.05 OUR FIT</b>				
<b>1.31 ± 0.13 OUR AVERAGE</b>				
1.30 ± 0.13		DRUZHININ	84	ND $e^+e^- \rightarrow 3\gamma$
1.4 ± 0.5	32	COSME	76	OSPK $e^+e^-$

- • • We do not use the following data for averages, fits, limits, etc. • • •
- |                       |     |     |               |      |   |
|-----------------------|-----|-----|---------------|------|---|
| 1.367 ± 0.072         |     | 1   | ACHASOV       | 16A  | SND 0.60-1.38 $e^+e^- \rightarrow \pi^0\gamma$  |
| 1.258 ± 0.037 ± 0.077 | 18k | 2,3 | AKHMETSHIN 05 | CMD2 | 0.60-1.38 $e^+e^- \rightarrow \pi^0\gamma$      |
| 1.226 ± 0.036 ± 0.096 |     | 4   | ACHASOV       | 00   | SND $e^+e^- \rightarrow \pi^0\gamma$            |
| 1.26 ± 0.17           |     | 5   | BENAYOUN      | 96   | RVUE 0.54-1.04 $e^+e^- \rightarrow \pi^0\gamma$ |
- 1 Using  $B(\phi \rightarrow e^+e^-)$  from PDG 15. Supersedes ACHASOV 00.
  - 2 Using  $B(\phi \rightarrow e^+e^-) = (2.98 \pm 0.04) \times 10^{-4}$ .
  - 3 Not independent of the corresponding  $\Gamma(e^+e^-) \times \Gamma(\pi^0\gamma)/\Gamma_{total}^2$ .
  - 4 From the  $\pi^0 \rightarrow 2\gamma$  decay and using  $B(\phi \rightarrow e^+e^-) = (2.99 \pm 0.08) \times 10^{-4}$ .
  - 5 Reanalysis of DRUZHININ 84, DOLINSKY 89, and DOLINSKY 91 taking into account a triangle anomaly contribution.

$\Gamma(\eta\gamma)/\Gamma(\pi^0\gamma)$   $\Gamma_6/\Gamma_7$

VALUE	DOCUMENT ID	TECN	COMMENT
• • • We do not use the following data for averages, fits, limits, etc. • • •			
10.9 ± 0.3 ± 0.7	ACHASOV	00	SND $e^+e^- \rightarrow \eta\gamma, \pi^0\gamma$

$\Gamma(e^+e^-)/\Gamma_{total}$   $\Gamma_9/\Gamma$

VALUE (units $10^{-4}$ )	EVTS	DOCUMENT ID	TECN	COMMENT	
<b>2.973 ± 0.034 OUR FIT</b>				Error includes scale factor of 1.3.	
<b>2.98 ± 0.07 OUR AVERAGE</b>				Error includes scale factor of 1.1.	
2.93 ± 0.14	1900k	1	ACHASOV	01E	SND $e^+e^- \rightarrow K^+K^-, K_S^0 K_L^0, \pi^+\pi^-\pi^0$
2.88 ± 0.09	55600		AKHMETSHIN 95	CMD2	$e^+e^- \rightarrow$ hadrons
3.00 ± 0.21	3681		BUKIN	78c	OLYA $e^+e^- \rightarrow$ hadrons
3.10 ± 0.14		2	PARROUR	76	OSPK $e^+e^-$
3.3 ± 0.3			COSME	74	OSPK $e^+e^- \rightarrow$ hadrons
2.81 ± 0.25	681		BALAKIN	71	OSPK $e^+e^- \rightarrow$ hadrons
3.50 ± 0.27			CHATELUS	71	OSPK $e^+e^-$

- 1 From the combined fit assuming that the total  $\phi(1020)$  production cross section is saturated by those of  $K^+K^-, K_S^0 K_L^0, \pi^+\pi^-\pi^0$ , and  $\eta\gamma$  decays modes and using ACHASOV 00b for the  $\eta\gamma$  decay mode.
- 2 Using total width 4.2 MeV. They detect  $3\pi$  mode and observe significant interference with  $\omega$  tail. This is accounted for in the result quoted above.

$\Gamma(\mu^+\mu^-)/\Gamma_{total}$   $\Gamma_{10}/\Gamma$

VALUE (units $10^{-4}$ )	DOCUMENT ID	TECN	COMMENT	
<b>2.86 ± 0.19 OUR FIT</b>				
<b>2.5 ± 0.4 OUR AVERAGE</b>				
2.69 ± 0.46	1	HAYES	71	CNTR 8.3,9.8 $\gamma C \rightarrow \mu^+\mu^- X$
2.17 ± 0.60	1	EARLES	70	CNTR 6.0 $\gamma C \rightarrow \mu^+\mu^- X$

• • • We do not use the following data for averages, fits, limits, etc. • • •

2.87 ± 0.20 ± 0.14		2	ACHASOV	01g	SND $e^+e^- \rightarrow \mu^+\mu^-$
3.30 ± 0.45 ± 0.32		3	ACHASOV	99c	SND $e^+e^- \rightarrow \mu^+\mu^-$
4.83 ± 1.02		4	VASSERMAN	81	OLYA $e^+e^- \rightarrow \mu^+\mu^-$
2.87 ± 1.98		4	AUGUSTIN	73	OSPK $e^+e^- \rightarrow \mu^+\mu^-$

- 1 Neglecting interference between resonance and continuum.
- 2 Using  $B(\phi \rightarrow e^+e^-) = (2.91 \pm 0.07) \times 10^{-4}$ .
- 3 Using  $B(\phi \rightarrow e^+e^-) = (2.99 \pm 0.08) \times 10^{-4}$ .
- 4 Recalculated by us using  $B(\phi \rightarrow e^+e^-) = (2.99 \pm 0.08) \times 10^{-4}$ .

$\Gamma(\eta e^+e^-)/\Gamma_{total}$   $\Gamma_{11}/\Gamma$

VALUE (units $10^{-4}$ )	EVTS	DOCUMENT ID	TECN	COMMENT	
<b>1.08 ± 0.007 OUR FIT</b>					
<b>1.075 ± 0.004 OUR AVERAGE</b>					
1.075 ± 0.007 ± 0.038	30k	1	BABUSCI	15	KLOE 1.02 $e^+e^- \rightarrow \eta e^+e^-$
1.19 ± 0.19 ± 0.12	213	2	ACHASOV	01B	SND $e^+e^- \rightarrow \eta e^+e^-$
1.14 ± 0.10 ± 0.06	355	3	AKHMETSHIN 01	CMD2	$e^+e^- \rightarrow \eta e^+e^-$

- • • We do not use the following data for averages, fits, limits, etc. • • •
- |                    |     |   |               |      |                                     |
|--------------------|-----|---|---------------|------|-------------------------------------|
| 1.13 ± 0.14 ± 0.07 | 183 | 4 | AKHMETSHIN 01 | CMD2 | $e^+e^- \rightarrow \eta e^+e^-$    |
| 1.21 ± 0.14 ± 0.09 | 130 | 5 | AKHMETSHIN 01 | CMD2 | $e^+e^- \rightarrow \eta e^+e^-$    |
| 1.04 ± 0.20 ± 0.08 | 42  | 6 | AKHMETSHIN 01 | CMD2 | $e^+e^- \rightarrow \eta e^+e^-$    |
| 1.3 ± 0.8          | 7   |   | GOLUBEV       | 85   | ND $e^+e^- \rightarrow \eta e^+e^-$ |
- 1 Using  $B(\eta \rightarrow 3\pi^0) = (32.57 \pm 0.23)\%$  from PDG 12.
  - 2 Using  $B(\eta \rightarrow \gamma\gamma) = (39.25 \pm 0.32)\%$ ,  $B(\phi \rightarrow \eta\gamma) = (1.26 \pm 0.06)\%$ , and  $B(\phi \rightarrow e^+e^-) = (3.00 \pm 0.06) \times 10^{-4}$ .
  - 3 The average of the branching ratios separately obtained from the  $\eta \rightarrow \gamma\gamma, 3\pi^0, \pi^+\pi^-\pi^0$  decays.
  - 4 From  $\eta \rightarrow \gamma\gamma$  decays and using  $B(\eta \rightarrow \gamma\gamma) = (39.33 \pm 0.25) \times 10^{-2}$ ,  $B(\eta \rightarrow \pi^+\pi^-\pi^0) = (4.75 \pm 11) \times 10^{-2}$ , and  $B(\phi \rightarrow \eta\gamma) = (1.297 \pm 0.033) \times 10^{-2}$ .
  - 5 From  $\eta \rightarrow 3\pi^0$  decays and using  $B(\pi^0 \rightarrow \gamma\gamma) = (98.798 \pm 0.033) \times 10^{-2}$ ,  $B(\eta \rightarrow 3\pi^0) = (32.24 \pm 0.29) \times 10^{-2}$ ,  $B(\eta \rightarrow \pi^+\pi^-\pi^0) = (4.75 \pm 0.11) \times 10^{-2}$ , and  $B(\phi \rightarrow \eta\gamma) = (1.297 \pm 0.033) \times 10^{-2}$ .
  - 6 From  $\eta \rightarrow \pi^+\pi^-\pi^0$  decays and using  $B(\pi^0 \rightarrow \gamma\gamma) = (98.798 \pm 0.033) \times 10^{-2}$ ,  $B(\pi^0 \rightarrow e^+e^-) = (1.198 \pm 0.032) \times 10^{-2}$ ,  $B(\eta \rightarrow \pi^+\pi^-\pi^0) = (23.0 \pm 0.4) \times 10^{-2}$ ,  $B(\phi \rightarrow \pi^+\pi^-\pi^0) = (15.5 \pm 0.6) \times 10^{-2}$ , and  $B(\phi \rightarrow \eta\gamma) = (1.297 \pm 0.033) \times 10^{-2}$ .

## Meson Particle Listings

 $\phi(1020)$  $\Gamma(\pi^+\pi^-)/\Gamma_{\text{total}}$ 

VALUE (units $10^{-4}$ )	CL%	DOCUMENT ID	TECN	COMMENT
$0.71 \pm 0.11 \pm 0.09$		<sup>1</sup> ACHASOV	00c	SND $e^+e^- \rightarrow \pi^+\pi^-$
$0.65_{-0.29}^{+0.38}$		<sup>1</sup> GOLUBEV	86	ND $e^+e^- \rightarrow \pi^+\pi^-$
$2.01_{-0.84}^{+1.07}$		<sup>1</sup> VASSERMAN	81	OLYA $e^+e^- \rightarrow \pi^+\pi^-$
<6.6	95	BUKIN	78B	OLYA $e^+e^- \rightarrow \pi^+\pi^-$
<2.7	95	ALVENSLEB...	72	CNTR $6.7\gamma C \rightarrow C\pi^+\pi^-$

<sup>1</sup> Using  $B(\phi \rightarrow e^+e^-) = (2.99 \pm 0.08) \times 10^{-4}$ .

 $\Gamma(\omega\pi^0)/\Gamma_{\text{total}}$ 

VALUE (units $10^{-5}$ )	DOCUMENT ID	TECN	COMMENT
<b>4.7 ± 0.5 OUR FIT</b>			
$5.2_{-1.1}^{+1.3}$	<sup>1,2</sup> AULCHENKO	00A	SND $e^+e^- \rightarrow \pi^+\pi^-\pi^0\pi^0$
$4.4 \pm 0.6$	<sup>3</sup> AMBROSINO	08G	KLOE $e^+e^- \rightarrow \pi^+\pi^-\pi^0, 2\pi^0\gamma$
~5.4	<sup>4</sup> ACHASOV	00E	SND $e^+e^- \rightarrow \pi^0\pi^0\gamma$
$5.5_{-1.4}^{+1.6} \pm 0.3$	<sup>2,5</sup> AULCHENKO	00A	SND $e^+e^- \rightarrow \pi^+\pi^-\pi^0\pi^0$
$4.8_{-1.7}^{+1.9} \pm 0.8$	<sup>4</sup> ACHASOV	99	SND $e^+e^- \rightarrow \pi^+\pi^-\pi^0\pi^0$

<sup>1</sup> Using the 1996 and 1998 data.  
<sup>2</sup> (2.3 ± 0.3)% correction for other decay modes of the  $\omega(782)$  applied.  
<sup>3</sup> Not independent of the corresponding  $\Gamma(\omega\pi^0) \times \Gamma(e^+e^-) / \Gamma^2(\text{total})$ .  
<sup>4</sup> Using the 1996 data.  
<sup>5</sup> Using the 1998 data.

 $\Gamma(\omega\gamma)/\Gamma_{\text{total}}$ 

VALUE	CL%	DOCUMENT ID	TECN	COMMENT
<b>&lt;0.05</b>	84	LINDSEY	66	HBC 2.1-2.7 $K^-\rho \rightarrow \Lambda\pi^+\pi^-\text{neutrals}$

 $\Gamma(\rho\gamma)/\Gamma_{\text{total}}$ 

VALUE (units $10^{-4}$ )	CL%	DOCUMENT ID	TECN	COMMENT
<b>&lt; 0.12</b>	90	<sup>1</sup> AKHMETSHIN	99B	CMD2 $e^+e^- \rightarrow \pi^+\pi^-\gamma$
	90	AKHMETSHIN	97c	CMD2 $e^+e^- \rightarrow \pi^+\pi^-\gamma$
<200	84	LINDSEY	66	HBC 2.1-2.7 $K^-\rho \rightarrow \Lambda\pi^+\pi^-\text{neutrals}$

<sup>1</sup> Supersedes AKHMETSHIN 97c.

 $\Gamma(\pi^+\pi^-\gamma)/\Gamma_{\text{total}}$ 

VALUE (units $10^{-4}$ )	CL%	EVTS	DOCUMENT ID	TECN	COMMENT
<b>0.41 ± 0.12 ± 0.04</b>		30175	<sup>1</sup> AKHMETSHIN	99B	CMD2 $e^+e^- \rightarrow \pi^+\pi^-\gamma$
	90	90	<sup>2</sup> AKHMETSHIN	97c	CMD2 $e^+e^- \rightarrow \pi^+\pi^-\gamma$
<600	90	90	KALBFLEISCH	75	HBC 2.18 $K^-\rho \rightarrow \Lambda\pi^+\pi^-\gamma$
<70	90	90	COSME	74	OSPK $e^+e^- \rightarrow \pi^+\pi^-\gamma$
<400	90	90	LINDSEY	65	HBC 2.1-2.7 $K^-\rho \rightarrow \Lambda\pi^+\pi^-\text{neutrals}$

<sup>1</sup> For  $E_\gamma > 20$  MeV and assuming that  $B(\phi(1020) \rightarrow f_0(980)\gamma)$  is negligible. Supersedes AKHMETSHIN 97c.  
<sup>2</sup> For  $E_\gamma > 20$  MeV and assuming that  $B(\phi(1020) \rightarrow f_0(980)\gamma)$  is negligible.

 $\Gamma(f_0(980)\gamma)/\Gamma_{\text{total}}$ 

VALUE (units $10^{-4}$ )	CL%	EVTS	DOCUMENT ID	TECN	COMMENT
<b>3.22 ± 0.19 OUR FIT</b>					Error includes scale factor of 1.1.
<b>3.21 ± 0.19 OUR AVERAGE</b>					
$3.21_{-0.09}^{+0.03} \pm 0.18$			<sup>1</sup> AMBROSINO	07	KLOE $e^+e^- \rightarrow \pi^0\pi^0\gamma$
$2.90 \pm 0.21 \pm 1.54$			<sup>2</sup> AKHMETSHIN	99c	CMD2 $e^+e^- \rightarrow \pi^+\pi^-\gamma, \pi^0\pi^0\gamma$
$4.47 \pm 0.21$		2438	<sup>3</sup> ALOISIO	02D	KLOE $e^+e^- \rightarrow \pi^0\pi^0\gamma$
$3.5 \pm 0.3_{-0.5}^{+1.3}$		419	<sup>4,5</sup> ACHASOV	00H	SND $e^+e^- \rightarrow \pi^0\pi^0\gamma$
$1.93 \pm 0.46 \pm 0.50$		27188	<sup>6</sup> AKHMETSHIN	99B	CMD2 $e^+e^- \rightarrow \pi^+\pi^-\gamma$
$3.05 \pm 0.25 \pm 0.72$		268	<sup>7</sup> AKHMETSHIN	99c	CMD2 $e^+e^- \rightarrow \pi^0\pi^0\gamma$
$1.5 \pm 0.5$		268	<sup>8</sup> AKHMETSHIN	99c	CMD2 $e^+e^- \rightarrow \pi^0\pi^0\gamma$
$3.42 \pm 0.30 \pm 0.36$		164	<sup>4</sup> ACHASOV	98I	SND $e^+e^- \rightarrow 5\gamma$
<1	90	90	<sup>9</sup> AKHMETSHIN	97c	CMD2 $e^+e^- \rightarrow \pi^+\pi^-\gamma$
<7	90	90	<sup>10</sup> AKHMETSHIN	97c	CMD2 $e^+e^- \rightarrow \pi^+\pi^-\gamma$
<20	90	90	DRUZHNININ	87	ND $e^+e^- \rightarrow \pi^0\pi^0\gamma$

<sup>1</sup> Obtained by the authors taking into account the  $\pi^+\pi^-$  decay mode. Includes a component due to  $\pi\pi$  production via the  $f_0(500)$  meson. Supersedes ALOISIO 02D.  
<sup>2</sup> From the combined fit of the photon spectra in the reactions  $e^+e^- \rightarrow \pi^+\pi^-\gamma, \pi^0\pi^0\gamma$ .  
<sup>3</sup> From the negative interference with the  $f_0(500)$  meson of AITALA 01B using the ACHASOV 89 parameterization for the  $f_0(980)$ , a Breit-Wigner for the  $f_0(500)$ , and ACHASOV 01F for the  $\rho\pi$  contribution. Superseded by AMBROSINO 07.  
<sup>4</sup> Assuming that the  $\pi^0\pi^0\gamma$  final state is completely determined by the  $f_0\gamma$  mechanism, neglecting the decay  $B(\phi \rightarrow K\bar{K}\gamma)$  and using  $B(f_0 \rightarrow \pi^+\pi^-) = 2B(f_0 \rightarrow \pi^0\pi^0)$ .

<sup>5</sup> Using the value  $B(\phi \rightarrow \eta\gamma) = (1.338 \pm 0.053) \times 10^{-2}$ .

<sup>6</sup> For  $E_\gamma > 20$  MeV. Supersedes AKHMETSHIN 97c.

<sup>7</sup> Neglecting other intermediate mechanisms ( $\rho\pi, \sigma\gamma$ ).

<sup>8</sup> A narrow pole fit taking into account  $f_0(980)$  and  $f_0(1200)$  intermediate mechanisms.

<sup>9</sup> For destructive interference with the Bremsstrahlung process

<sup>10</sup> For constructive interference with the Bremsstrahlung process

 $\Gamma(f_0(980)\gamma)/\Gamma(\eta\gamma)$ 

VALUE (units $10^{-2}$ )	EVTS	DOCUMENT ID	TECN	COMMENT
<b>2.47 ± 0.15 OUR FIT</b>				Error includes scale factor of 1.1.
<b>2.6 ± 0.2 ± 0.8</b>	419	<sup>1</sup> ACHASOV	00H	SND $e^+e^- \rightarrow \pi^0\pi^0\gamma$

<sup>1</sup> Assuming that the  $\pi^0\pi^0\gamma$  final state is completely determined by the  $f_0\gamma$  mechanism, neglecting the decay  $B(\phi \rightarrow K\bar{K}\gamma)$  and using  $B(f_0 \rightarrow \pi^+\pi^-) = 2B(f_0 \rightarrow \pi^0\pi^0)$ .

 $\Gamma(\pi^0\pi^0\gamma)/\Gamma_{\text{total}}$ 

VALUE (units $10^{-4}$ )	CL%	EVTS	DOCUMENT ID	TECN	COMMENT
<b>1.07 ± 0.06 OUR AVERAGE</b>					
$1.07_{-0.06}^{+0.01} + 0.06$			<sup>1</sup> AMBROSINO	07	KLOE $e^+e^- \rightarrow \pi^0\pi^0\gamma$
$1.08 \pm 0.17 \pm 0.09$		268	AKHMETSHIN	99c	CMD2 $e^+e^- \rightarrow \pi^0\pi^0\gamma$
$1.09 \pm 0.03 \pm 0.05$		2438	ALOISIO	02D	KLOE $e^+e^- \rightarrow \pi^0\pi^0\gamma$
$1.158 \pm 0.093 \pm 0.052$		419	<sup>2,3</sup> ACHASOV	00H	SND $e^+e^- \rightarrow \pi^0\pi^0\gamma$
<10	90	90	DRUZHNININ	87	ND $e^+e^- \rightarrow 5\gamma$

<sup>1</sup> Supersedes ALOISIO 02D.  
<sup>2</sup> Using the value  $B(\phi \rightarrow \eta\gamma) = (1.338 \pm 0.053) \times 10^{-2}$ .  
<sup>3</sup> Supersedes ACHASOV 98I. Excluding  $\omega\pi^0$ .

 $\Gamma(\pi^0\pi^0\gamma)/\Gamma(\eta\gamma)$ 

VALUE (units $10^{-2}$ )	EVTS	DOCUMENT ID	TECN	COMMENT
<b>0.86 ± 0.04 OUR FIT</b>				
<b>0.865 ± 0.070 ± 0.017</b>	419	<sup>1</sup> ACHASOV	00H	SND $e^+e^- \rightarrow \pi^0\pi^0\gamma$
$0.90 \pm 0.08 \pm 0.07$	164	ACHASOV	98I	SND $e^+e^- \rightarrow 5\gamma$

<sup>1</sup> Supersedes ACHASOV 98I. Excluding  $\omega\pi^0$ .

 $\Gamma(\pi^+\pi^-\pi^+\pi^-)/\Gamma_{\text{total}}$ 

VALUE (units $10^{-6}$ )	CL%	EVTS	DOCUMENT ID	TECN	COMMENT
<b>6.5 ± 2.7 ± 1.6</b>		6.8k	<sup>1</sup> AKHMETSHIN	17	CMD3 $e^+e^- \rightarrow \pi^+\pi^-\pi^+\pi^-$
$3.93 \pm 1.74 \pm 2.14$		3.3k	AKHMETSHIN	00E	CMD2 $e^+e^- \rightarrow \pi^+\pi^-\pi^+\pi^-$
<870	90	90	CORDIER	79	WIRE $e^+e^- \rightarrow \pi^+\pi^-\pi^+\pi^-$

<sup>1</sup> Using the cross section at the  $\phi$  meson peak  $\sigma(\phi) = 4172 \pm 42$  nb, the nonresonant cross section  $\sigma(0) = 1.263 \pm 0.027$  nb and  $\text{Re}(Z) = 0.146 \pm 0.030, \text{Im}(Z) = -0.002 \pm 0.024$  for the complex amplitude of the  $\phi \rightarrow \pi^+\pi^-\pi^+\pi^-$  transition.

 $\Gamma(\pi^+\pi^+\pi^-\pi^-)/\Gamma_{\text{total}}$ 

VALUE (units $10^{-6}$ )	CL%	DOCUMENT ID	TECN	COMMENT
<b>&lt; 4.6</b>	90	AKHMETSHIN	00E	CMD2 $e^+e^- \rightarrow \pi^+\pi^-\pi^+\pi^-$
<150	95	BARKOV	88	CMD $e^+e^- \rightarrow \pi^+\pi^-\pi^+\pi^-$

 $\Gamma(\pi^0 e^+ e^-)/\Gamma_{\text{total}}$ 

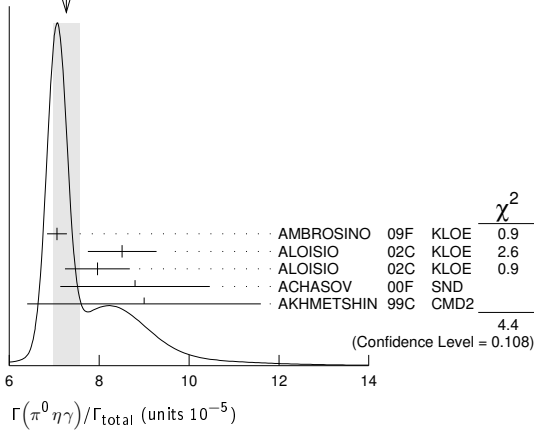
VALUE (units $10^{-5}$ )	CL%	EVTS	DOCUMENT ID	TECN	COMMENT
<b>1.33 ± 0.07 OUR AVERAGE</b>					
$1.35 \pm 0.05_{-0.10}^{+0.05}$		9.5k	<sup>1</sup> ANASTASI	16B	KLOE $e^+e^- \rightarrow \pi^0 e^+ e^-$
$1.01 \pm 0.28 \pm 0.29$		52	<sup>2</sup> ACHASOV	02D	SND $e^+e^- \rightarrow \pi^0 e^+ e^-$
$1.22 \pm 0.34 \pm 0.21$		46	<sup>3</sup> AKHMETSHIN	01c	CMD2 $e^+e^- \rightarrow \pi^0 e^+ e^-$
<12	90	90	DOLINSKY	88	ND $e^+e^- \rightarrow \pi^0 e^+ e^-$

<sup>1</sup> Using  $B(\pi^0 \rightarrow \gamma\gamma)$  from the 2014 Edition of this Review (PDG 14).  
<sup>2</sup> Using various branching ratios from the 2000 Edition of this Review (PDG 00).  
<sup>3</sup> Using  $B(\pi^0 \rightarrow \gamma\gamma) = 0.98798 \pm 0.00032, B(\phi \rightarrow \eta\gamma) = (1.297 \pm 0.033) \times 10^{-2}$ , and  $B(\eta \rightarrow \pi^+\pi^-\gamma) = (4.75 \pm 0.11) \times 10^{-2}$ .

 $\Gamma(\pi^0\eta\gamma)/\Gamma_{\text{total}}$ 

VALUE (units $10^{-5}$ )	CL%	EVTS	DOCUMENT ID	TECN	COMMENT
<b>7.27 ± 0.30 OUR AVERAGE</b>					Error includes scale factor of 1.5. See the ideogram below.
$7.06 \pm 0.22$		16.9k	<sup>1</sup> AMBROSINO	09F	KLOE $1.02 e^+e^- \rightarrow \eta\pi^0\gamma$
$8.51 \pm 0.51 \pm 0.57$		607	<sup>2</sup> ALOISIO	02c	KLOE $e^+e^- \rightarrow \eta\pi^0\gamma$
$7.96 \pm 0.60 \pm 0.40$		197	<sup>3</sup> ALOISIO	02c	KLOE $e^+e^- \rightarrow \eta\pi^0\gamma$
$8.8 \pm 1.4 \pm 0.9$		36	<sup>4</sup> ACHASOV	00F	SND $e^+e^- \rightarrow \eta\pi^0\gamma$
$9.0 \pm 2.4 \pm 1.0$		80	AKHMETSHIN	99c	CMD2 $e^+e^- \rightarrow \eta\pi^0\gamma$
$7.01 \pm 0.10 \pm 0.20$		13.3k	<sup>2,5</sup> AMBROSINO	09F	KLOE $1.02 e^+e^- \rightarrow \eta\pi^0\gamma$
$7.12 \pm 0.13 \pm 0.22$		3.6k	<sup>3,6</sup> AMBROSINO	09F	KLOE $1.02 e^+e^- \rightarrow \eta\pi^0\gamma$
$8.3 \pm 2.3 \pm 1.2$		20	ACHASOV	98B	SND $e^+e^- \rightarrow 5\gamma$
<250	90	90	DOLINSKY	91	ND $e^+e^- \rightarrow \pi^0\eta\gamma$

WEIGHTED AVERAGE  
7.27±0.30 (Error scaled by 1.5)



- 1 Combined results of  $\eta \rightarrow \gamma\gamma$  and  $\eta \rightarrow \pi^+\pi^-\pi^0$  decay modes measurements.
- 2 From the decay mode  $\eta \rightarrow \gamma\gamma$ .
- 3 From the decay mode  $\eta \rightarrow \pi^+\pi^-\pi^0$ .
- 4 Supersedes ACHASOV 98B.
- 5 Using  $B(\phi \rightarrow \eta\gamma) = (1.304 \pm 0.025)\%$ ,  $B(\eta \rightarrow 3\pi^0) = (32.56 \pm 0.23)\%$ , and  $B(\eta \rightarrow \gamma\gamma) = (39.31 \pm 0.20)\%$ .
- 6 Using  $B(\phi \rightarrow \eta\gamma) = (1.304 \pm 0.025)\%$ ,  $B(\eta \rightarrow 3\pi^0) = (32.56 \pm 0.23)\%$ , and  $B(\eta \rightarrow \pi^+\pi^-\pi^0) = (22.73 \pm 0.28)\%$ .

$\Gamma(a_0(980)\gamma)/\Gamma_{total}$   $\Gamma_{23}/\Gamma$

VALUE (units $10^{-5}$ )	CL%	EVTS	DOCUMENT ID	TECN	COMMENT
<b>7.6±0.6 OUR FIT</b>					
<b>7.6±0.6 OUR AVERAGE</b>					
7.4±0.7			1 ALOISIO 02C	KLOE	$e^+e^- \rightarrow \eta\pi^0\gamma$
8.8±1.7	36		2 ACHASOV 00F	SND	$e^+e^- \rightarrow \eta\pi^0\gamma$
• • • We do not use the following data for averages, fits, limits, etc. • • •					
11 ± 2			3 GOKALP 02	RVUE	$e^+e^- \rightarrow \eta\pi^0\gamma$
<50	90		DOLINSKY 91	ND	$e^+e^- \rightarrow \pi^0\eta\gamma$
1 Using $M_{a_0(980)}=984.8$ MeV and assuming $a_0(980)\gamma$ dominance.					
2 Assuming $a_0(980)\gamma$ dominance in the $\eta\pi^0\gamma$ final state.					
3 Using data of ACHASOV 00F.					

$\Gamma(f_0(980)\gamma)/\Gamma(a_0(980)\gamma)$   $\Gamma_{17}/\Gamma_{23}$

VALUE	DOCUMENT ID	TECN	COMMENT
<b>6.1±0.6</b>	1 ALOISIO 02C	KLOE	$e^+e^- \rightarrow \eta\pi^0\gamma$
1 Using results of ALOISIO 02D and assuming that $f_0(980)$ decays into $\pi\pi$ only and $a_0(980)$ into $\eta\pi$ only.			

$\Gamma(K^0\bar{K}^0\gamma)/\Gamma_{total}$   $\Gamma_{24}/\Gamma$

VALUE	CL%	DOCUMENT ID	TECN	COMMENT
<b>&lt;1.9 × 10<sup>-8</sup></b>	90	AMBROSINO 09c	KLOE	$e^+e^- \rightarrow K_S^0 K_S^0 \gamma$

$\Gamma(\eta'(958)\gamma)/\Gamma_{total}$   $\Gamma_{25}/\Gamma$

VALUE (units $10^{-5}$ )	CL%	EVTS	DOCUMENT ID	TECN	COMMENT
<b>6.22±0.21 OUR FIT</b>					
<b>6.22±0.30 OUR AVERAGE</b>					
6.22±0.27±0.12		3407	1 AMBROSINO 07A	KLOE	$1.02 e^+e^- \rightarrow \pi^+\pi^-\pi^0\gamma$
6.7 ± <sub>-2.4</sub> ±0.8		12	2 AULCHENKO 03B	SND	$e^+e^- \rightarrow \eta'\gamma$
• • • We do not use the following data for averages, fits, limits, etc. • • •					
6.7 ± <sub>-4.2</sub> ±1.5		7	AULCHENKO 03B	SND	$e^+e^- \rightarrow \gamma\gamma$
6.10±0.61±0.43		120	3 ALOISIO 02E	KLOE	$1.02 e^+e^- \rightarrow \pi^+\pi^-\pi^0\gamma$
8.2 ± <sub>-1.9</sub> ±1.1		21	4 AKHMETSHIN 00B	CMD2	$e^+e^- \rightarrow \pi^+\pi^-\pi^0\gamma$
4.9 ± <sub>-1.8</sub> ±0.6		9	5 AKHMETSHIN 00F	CMD2	$e^+e^- \rightarrow \pi^+\pi^-\pi^+\pi^-\pi^0\gamma$
6.4 ±1.6		30	6 AKHMETSHIN 00F	CMD2	$e^+e^- \rightarrow \eta'(958)\gamma$
6.7 ± <sub>-2.9</sub> ±1.0		5	7 AULCHENKO 99	SND	$e^+e^- \rightarrow \pi^+\pi^-\pi^0\gamma$
<11	90		AULCHENKO 98	SND	$e^+e^- \rightarrow \gamma\gamma$
12 ± <sub>-5</sub> ±2		6	4 AKHMETSHIN 97B	CMD2	$e^+e^- \rightarrow \pi^+\pi^-\pi^0\gamma$
<41	90		DRUZHININ 87	ND	$e^+e^- \rightarrow \gamma\eta\pi^+\pi^-$

- 1 AMBROSINO 07A reports  $[\Gamma(\phi(1020) \rightarrow \eta'(958)\gamma)/\Gamma_{total}] / [B(\phi(1020) \rightarrow \eta\gamma)] = (4.77 \pm 0.09 \pm 0.19) \times 10^{-3}$  which we multiply by our best value  $B(\phi(1020) \rightarrow \eta\gamma) = (1.303 \pm 0.025) \times 10^{-2}$ . Our first error is their experiment's error and our second error is the systematic error from using our best value.
- 2 Averaging AULCHENKO 03B with AULCHENKO 99.
- 3 Using  $B(\phi \rightarrow \eta\gamma) = (1.297 \pm 0.033)\%$ .

- 4 Using the value  $B(\phi \rightarrow \eta\gamma) = (1.26 \pm 0.06) \times 10^{-2}$ .
- 5 Using  $B(\phi \rightarrow K_L^0 K_S^0) = (33.8 \pm 0.6)\%$ .
- 6 Averaging AKHMETSHIN 00B with AKHMETSHIN 00F.
- 7 Using the value  $B(\eta' \rightarrow \eta\pi^+\pi^-) = (43.7 \pm 1.5) \times 10^{-2}$  and  $B(\eta \rightarrow \gamma\gamma) = (39.25 \pm 0.31) \times 10^{-2}$ .

$\Gamma(\eta'(958)\gamma)/\Gamma(K_L^0 K_S^0)$   $\Gamma_{25}/\Gamma_2$

VALUE (units $10^{-4}$ )	CL%	EVTS	DOCUMENT ID	TECN	COMMENT
<b>1.83±0.06 OUR FIT</b>					
1.46 ± <sub>-0.54</sub> ±0.18		9	1 AKHMETSHIN 00F	CMD2	$e^+e^- \rightarrow \pi^+\pi^-\pi^+\pi^- \geq 2\gamma$

- 1 Using various branching ratios of  $K_S^0, K_L^0, \eta, \eta'$  from the 2000 edition (The European Physical Journal **C15** 1 (2000)) of this Review.

$\Gamma(\eta'(958)\gamma)/\Gamma(\eta\gamma)$   $\Gamma_{25}/\Gamma_6$

VALUE (units $10^{-3}$ )	CL%	EVTS	DOCUMENT ID	TECN	COMMENT
<b>4.77±0.15 OUR FIT</b>					
<b>4.78±0.20 OUR AVERAGE</b>					
4.77±0.09±0.19		3407	AMBROSINO 07A	KLOE	$1.02 e^+e^- \rightarrow \pi^+\pi^-\pi^0\gamma$
4.70±0.47±0.31		120	1 ALOISIO 02E	KLOE	$1.02 e^+e^- \rightarrow \pi^+\pi^-\pi^0\gamma$
6.5 ± <sub>-1.5</sub> ±0.8		21	AKHMETSHIN 00B	CMD2	$e^+e^- \rightarrow \pi^+\pi^-\pi^0\gamma$
• • • We do not use the following data for averages, fits, limits, etc. • • •					
9.5 ± <sub>-4.0</sub> ±1.4		6	2 AKHMETSHIN 97B	CMD2	$e^+e^- \rightarrow \pi^+\pi^-\pi^0\gamma$

- 1 From the decay mode  $\eta' \rightarrow \eta\pi^+\pi^-, \eta \rightarrow \gamma\gamma$ .
- 2 Superseded by AKHMETSHIN 00B.

$\Gamma(\eta\pi^0\pi^0\gamma)/\Gamma_{total}$   $\Gamma_{26}/\Gamma$

VALUE (units $10^{-5}$ )	CL%	DOCUMENT ID	TECN	COMMENT
<b>&lt;2</b>	90	AULCHENKO 98	SND	$e^+e^- \rightarrow \gamma\gamma$

$\Gamma(\mu^+\mu^-\gamma)/\Gamma_{total}$   $\Gamma_{27}/\Gamma$

VALUE (units $10^{-5}$ )	CL%	EVTS	DOCUMENT ID	TECN	COMMENT
<b>1.43±0.45±0.14</b>		27188	1 AKHMETSHIN 99B	CMD2	$e^+e^- \rightarrow \mu^+\mu^-\gamma$
• • • We do not use the following data for averages, fits, limits, etc. • • •					
2.3 ±1.0		824 ± 33	2 AKHMETSHIN 97C	CMD2	$e^+e^- \rightarrow \mu^+\mu^-\gamma$
1 For $E_\gamma > 20$ MeV. Supersedes AKHMETSHIN 97C.					
2 For $E_\gamma > 20$ MeV.					

$\Gamma(\rho\gamma\gamma)/\Gamma_{total}$   $\Gamma_{28}/\Gamma$

VALUE (units $10^{-4}$ )	CL%	DOCUMENT ID	TECN	COMMENT
<b>&lt;1.2</b>	90	AULCHENKO 08	CMD2	$\phi \rightarrow \pi^+\pi^-\gamma\gamma$
• • • We do not use the following data for averages, fits, limits, etc. • • •				
<5	90	AKHMETSHIN 98	CMD2	$e^+e^- \rightarrow \pi^+\pi^-\gamma\gamma$

$\Gamma(\eta\pi^+\pi^-)/\Gamma_{total}$   $\Gamma_{29}/\Gamma$

VALUE (units $10^{-5}$ )	CL%	DOCUMENT ID	TECN	COMMENT
<b>&lt; 1.8</b>	90	AKHMETSHIN 00E	CMD2	$e^+e^- \rightarrow \pi^+\pi^-\pi^+\pi^-\pi^0$
• • • We do not use the following data for averages, fits, limits, etc. • • •				
< 6.1	90	AULCHENKO 08	CMD2	$\phi \rightarrow \eta\pi^+\pi^-$
<30	90	AKHMETSHIN 98	CMD2	$e^+e^- \rightarrow \pi^+\pi^-\gamma\gamma$

$\Gamma(\eta\mu^+\mu^-)/\Gamma_{total}$   $\Gamma_{30}/\Gamma$

VALUE (units $10^{-6}$ )	CL%	DOCUMENT ID	TECN	COMMENT
<b>&lt;9.4</b>	90	AKHMETSHIN 01	CMD2	$e^+e^- \rightarrow \eta e^+e^-$

$\Gamma(\eta U \rightarrow \eta e^+e^-)/\Gamma_{total}$   $\Gamma_{31}/\Gamma$

VALUE	CL%	DOCUMENT ID	TECN	COMMENT
<b>&lt;1 × 10<sup>-6</sup></b>	90	1 BABUSCI 13B	KLOE	$1.02 e^+e^- \rightarrow \eta e^+e^-$
1 For a narrow vector $U$ with mass between 5 and 470 MeV, from the combined analysis of $\eta \rightarrow \pi^+\pi^-\pi^0$ and $\eta \rightarrow \pi^0\pi^0\pi^0$ from ARCHILLI 12. Measured 90% CL limits as a function of $m_U$ range from $2.2 \times 10^{-8}$ to $10^{-6}$ .				

$\Gamma(\text{invisible})/\Gamma(K^+K^-)$   $\Gamma_{32}/\Gamma_1$

VALUE	CL%	DOCUMENT ID	TECN	COMMENT
<b>&lt;3.4 × 10<sup>-4</sup></b>	90	ABLIKIM 18s	BES3	$J/\psi \rightarrow \phi\eta \rightarrow \phi\pi^+\pi^-\pi^0$

Lepton Family number (LF) violating modes

$\Gamma(e^\pm\mu^\mp)/\Gamma_{total}$   $\Gamma_{33}/\Gamma$

VALUE	CL%	DOCUMENT ID	TECN	COMMENT
<b>&lt;2 × 10<sup>-6</sup></b>	90	ACHASOV 10A	SND	$e^+e^- \rightarrow e^\pm\mu^\mp$

$\pi^+\pi^-\pi^0 / \rho\pi$  AMPLITUDE RATIO  $a_1$  IN DECAY OF  $\phi \rightarrow \pi^+\pi^-\pi^0$

NIECKNIG 12 describes final-state interactions between the three pions in a dispersive framework using data on the  $\pi\pi$  P-wave scattering phase shift.





See key on page 999

# Meson Particle Listings

## $h_1(1170), b_1(1235)$

••• We do not use the following data for averages, fits, limits, etc. •••  
 1168 ± 4 ANDO 92 SPEC  $8 \pi^- p \rightarrow \pi^+ \pi^- \pi^0 n$   
 1190 ± 60 <sup>2</sup>DANKOWY... 81 SPEC 0  $8 \pi p \rightarrow 3\pi n$   
<sup>1</sup>Average and spread of values using 2 variants of the model of BOWLER 75.  
<sup>2</sup>Uses the model of BOWLER 75.

### $h_1(1170)$ WIDTH

VALUE (MeV)	DOCUMENT ID	TECN	CHG	COMMENT
<b>375 ± 6 ± 34</b>	<sup>3</sup> ANDO 92	SPEC		$8 \pi^- p \rightarrow \pi^+ \pi^- \pi^0 n$

••• We do not use the following data for averages, fits, limits, etc. •••  
 345 ± 6 ANDO 92 SPEC  $8 \pi^- p \rightarrow \pi^+ \pi^- \pi^0 n$   
 320 ± 50 <sup>4</sup>DANKOWY... 81 SPEC 0  $8 \pi p \rightarrow 3\pi n$   
<sup>3</sup>Average and spread of values using 2 variants of the model of BOWLER 75.  
<sup>4</sup>Uses the model of BOWLER 75.

### $h_1(1170)$ DECAY MODES

Mode	Fraction ( $\Gamma_i/\Gamma$ )
$\Gamma_1 \rho\pi$	seen

### $h_1(1170)$ BRANCHING RATIOS

$\Gamma(\rho\pi)/\Gamma_{total}$	DOCUMENT ID	TECN	COMMENT	$\Gamma_i/\Gamma$
••• We do not use the following data for averages, fits, limits, etc. •••				
seen	ANDO 92	SPEC	$8 \pi^- p \rightarrow \pi^+ \pi^- \pi^0 n$	
seen	ATKINSON 84	OMEG	$20-70 \gamma p \rightarrow \pi^+ \pi^- \pi^0 p$	
seen	DANKOWY... 81	SPEC	$8 \pi p \rightarrow 3\pi n$	

### $h_1(1170)$ REFERENCES

ANDO 92	PL B291 496	A. Ando et al.	(KEK, KYOT, NIRS, SAGA+)
ATKINSON 84	NP B231 15	M. Atkinson et al.	(BOONN, CERN, GLAS+)
DANKOWY... 81	PRL 46 580	J.A. Dankowych et al.	(TNT, BNL, CARL+)
BOWLER 75	NP B97 227	M.G. Bowler et al.	(OXFPP, DARE)

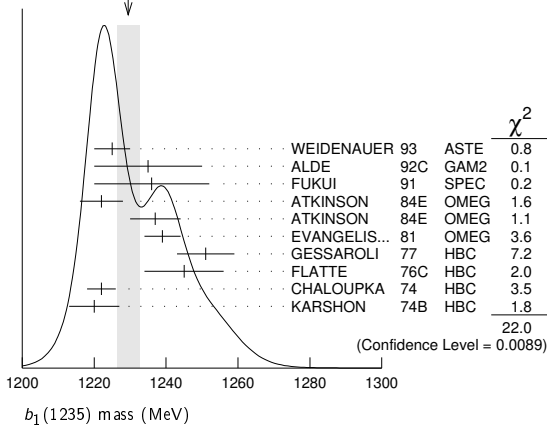
## $b_1(1235)$

$$I^G(J^{PC}) = 1^+(1^{+-})$$

### $b_1(1235)$ MASS

VALUE (MeV)	EVTs	DOCUMENT ID	TECN	CHG	COMMENT
<b>1229.5 ± 3.2 OUR AVERAGE</b>					Error includes scale factor of 1.6. See the ideogram below.
1225 ± 5		WEIDENAUER 93	ASTE		$\bar{p}p \rightarrow 2\pi^+ 2\pi^- \pi^0$
1235 ± 15		ALDE 92c	GAM2		$38,100 \pi^- p \rightarrow \omega \pi^0 n$
1236 ± 16		FUKUI 91	SPEC		$8.95 \pi^- p \rightarrow \omega \pi^0 n$
1222 ± 6		ATKINSON 84E	OMEG ±		$25-55 \gamma p \rightarrow \omega \pi X$
1237 ± 7		ATKINSON 84E	OMEG 0		$25-55 \gamma p \rightarrow \omega \pi X$
1239 ± 5		EVANGELIS... 81	OMEG -		$12 \pi^- p \rightarrow \omega \pi p$
1251 ± 8	450	GESSAROLI 77	HBC -		$11 \pi^- p \rightarrow \pi^- \omega p$
1245 ± 11	890	FLATTE 76c	HBC -		$4.2 K^- p \rightarrow \pi^- \omega \Sigma^+$
1222 ± 4	1400	CHALOUKKA 74	HBC -		$3.9 \pi^- p$
1220 ± 7	600	KARSHON 74B	HBC +		$4.9 \pi^+ p$
••• We do not use the following data for averages, fits, limits, etc. •••					
1190 ± 10		AUGUSTIN 89	DM2 ±		$e^+ e^- \rightarrow 5\pi$
1213 ± 5		ATKINSON 84c	OMEG 0		$20-70 \gamma p$
1271 ± 11		COLLICK 84	SPEC +		$200 \pi^+ Z \rightarrow Z \pi \omega$

WEIGHTED AVERAGE  
1229.5 ± 3.2 (Error scaled by 1.6)



### $b_1(1235)$ WIDTH

VALUE (MeV)	EVTs	DOCUMENT ID	TECN	CHG	COMMENT
<b>142 ± 9 OUR AVERAGE</b>					Error includes scale factor of 1.2.
113 ± 12		WEIDENAUER 93	ASTE		$\bar{p}p \rightarrow 2\pi^+ 2\pi^- \pi^0$
160 ± 30		ALDE 92c	GAM2		$38,100 \pi^- p \rightarrow \omega \pi^0 n$
151 ± 31		FUKUI 91	SPEC		$8.95 \pi^- p \rightarrow \omega \pi^0 n$
170 ± 15		EVANGELIS... 81	OMEG -		$12 \pi^- p \rightarrow \omega \pi p$
170 ± 50	225	BALTAY 78B	HBC +		$15 \pi^+ p \rightarrow p 4\pi$
155 ± 32	450	GESSAROLI 77	HBC -		$11 \pi^- p \rightarrow \pi^- \omega p$
182 ± 45	890	FLATTE 76c	HBC -		$4.2 K^- p \rightarrow \pi^- \omega \Sigma^+$
135 ± 20	1400	CHALOUKKA 74	HBC -		$3.9 \pi^- p$
156 ± 22	600	KARSHON 74B	HBC +		$4.9 \pi^+ p$
••• We do not use the following data for averages, fits, limits, etc. •••					
210 ± 19		AUGUSTIN 89	DM2 ±		$e^+ e^- \rightarrow 5\pi$
231 ± 14		ATKINSON 84c	OMEG 0		$20-70 \gamma p$
232 ± 29		COLLICK 84	SPEC +		$200 \pi^+ Z \rightarrow Z \pi \omega$

### $b_1(1235)$ DECAY MODES

Mode	Fraction ( $\Gamma_i/\Gamma$ )	Confidence level
$\Gamma_1 \omega\pi$	seen	
$\Gamma_2 \pi^\pm \gamma$	( $D/S$ amplitude ratio = $0.277 \pm 0.027$ )	
$\Gamma_3 \eta\rho$	seen	
$\Gamma_4 \pi^+ \pi^+ \pi^- \pi^0$	< 50 %	84%
$\Gamma_5 K^*(892)^\pm K^\mp$	seen	
$\Gamma_6 (K\bar{K})^\pm \pi^0$	< 8 %	90%
$\Gamma_7 K_S^0 K_S^0 \pi^\pm$	< 6 %	90%
$\Gamma_8 K_S^0 K_S^0 \pi^\pm$	< 2 %	90%
$\Gamma_9 \phi\pi$	< 1.5 %	84%

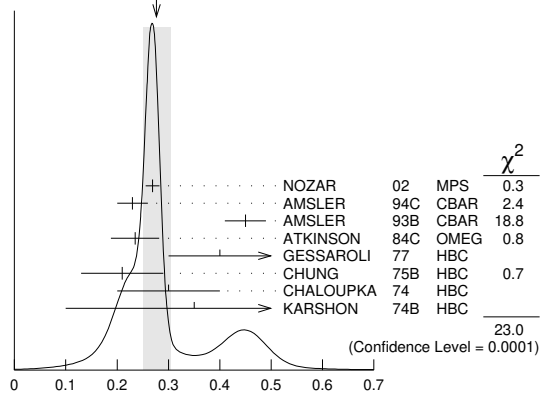
### $b_1(1235)$ PARTIAL WIDTHS

$\Gamma(\pi^\pm \gamma)$	DOCUMENT ID	TECN	CHG	COMMENT	$\Gamma_2$
<b>230 ± 60</b>	COLLICK 84	SPEC	+	$200 \pi^+ Z \rightarrow Z \pi \omega$	

### $b_1(1235)$ D-wave/S-wave AMPLITUDE RATIO IN DECAY OF $b_1(1235) \rightarrow \omega\pi$

VALUE	EVTs	DOCUMENT ID	TECN	CHG	COMMENT
<b>0.277 ± 0.027 OUR AVERAGE</b>					Error includes scale factor of 2.4. See the ideogram below.
0.269 ± 0.009 ± 0.010		NOZAR 02	MPS -		$18 \pi^- p \rightarrow \omega \pi^- p$
0.23 ± 0.03		AMSLER 94c	CBAR		$0.0 \bar{p}p \rightarrow \omega \eta \pi^0$
0.45 ± 0.04		AMSLER 93B	CBAR		$0.0 \bar{p}p \rightarrow \omega \pi^0 \pi^0$
0.235 ± 0.047		ATKINSON 84c	OMEG		$20-70 \gamma p$
0.4 + 0.1 - 0.1		GESSAROLI 77	HBC -		$11 \pi^- p \rightarrow \pi^- \omega p$
0.21 ± 0.08		CHUNG 75B	HBC +		$7.1 \pi^+ p$
0.3 ± 0.1		CHALOUKKA 74	HBC -		$3.9-7.5 \pi^- p$
0.35 ± 0.25	600	KARSHON 74B	HBC +		$4.9 \pi^+ p$

WEIGHTED AVERAGE  
0.277 ± 0.027 (Error scaled by 2.4)



$b_1(1235)$  D-wave/S-wave amplitude ratio in decay of  $b_1(1235) \rightarrow \omega\pi$

### $b_1(1235)$ D-wave/S-wave AMPLITUDE PHASE DIFFERENCE IN DECAY OF $b_1(1235) \rightarrow \omega\pi$

VALUE (°)	DOCUMENT ID	TECN	CHG	COMMENT
<b>10.5 ± 2.4 ± 3.9</b>	NOZAR 02	MPS	-	$18 \pi^- p \rightarrow \omega \pi^- p$

# Meson Particle Listings

## $b_1(1235), a_1(1260)$

### $b_1(1235)$ BRANCHING RATIOS

$\Gamma(\eta\rho)/\Gamma(\omega\pi)$		$\Gamma_3/\Gamma_1$	
VALUE	DOCUMENT ID	TECN	COMMENT
<0.10	ATKINSON	84D	OMEG 20-70 $\gamma p$
$\Gamma(\pi^+\pi^-\pi^0)/\Gamma(\omega\pi)$		$\Gamma_4/\Gamma_1$	
VALUE	DOCUMENT ID	TECN	CHG
<0.5	ABOLINS	63	HBC + 3.5 $\pi^+ p$
$\Gamma(K^*(892)^\pm K^\mp)/\Gamma_{total}$		$\Gamma_5/\Gamma$	
VALUE	DOCUMENT ID	TECN	COMMENT
seen	1 ABLIKIM	10E	BES2 $J/\psi \rightarrow K^\pm K_S^0 \pi^+ \pi^0$
1 From a fit including ten additional resonances and energy-independent Breit-Wigner width.			
$\Gamma((K\bar{K})^\pm \pi^0)/\Gamma(\omega\pi)$		$\Gamma_6/\Gamma_1$	
VALUE	DOCUMENT ID	TECN	CHG
<0.08	BALTAY	67	HBC $\pm$ 0.0 $\bar{p} p$
$\Gamma(K_S^0 K_L^0 \pi^\pm)/\Gamma(\omega\pi)$		$\Gamma_7/\Gamma_1$	
VALUE	DOCUMENT ID	TECN	CHG
<0.06	BALTAY	67	HBC $\pm$ 0.0 $\bar{p} p$
$\Gamma(K_S^0 K_S^0 \pi^\pm)/\Gamma(\omega\pi)$		$\Gamma_8/\Gamma_1$	
VALUE	DOCUMENT ID	TECN	CHG
<0.02	BALTAY	67	HBC $\pm$ 0.0 $\bar{p} p$
$\Gamma(\phi\pi)/\Gamma(\omega\pi)$		$\Gamma_9/\Gamma_1$	
VALUE	DOCUMENT ID	TECN	CHG
<0.004	VIKTOROV	96	SPEC 0 32.5 $\pi^- p \rightarrow K^+ K^- \pi^0 n$
••• We do not use the following data for averages, fits, limits, etc. •••			
<0.04	BIZZARRI	69	HBC $\pm$ 0.0 $\bar{p} p$
<0.015	DAHL	67	HBC 1.6-4.2 $\pi^- p$

### $b_1(1235)$ REFERENCES

ABLIKIM	10E	PL B693 88	M. Ablikim et al.	(BES II Collab.)
NOZAR	02	PL B541 35	M. Nozar et al.	
VIKTOROV	96	PAN 59 1184	V.A. Viktorov et al.	(SERP)
Translated from YAF 59 1239.				
AMSLER	94C	PL B327 425	C. Amstler et al.	(Crystal Barrel Collab.)
AMSLER	93B	PL B311 362	C. Amstler et al.	(Crystal Barrel Collab.)
WEIDENAUER	93	ZPHY C59 387	C. Weidenauer et al.	(ASTERIX Collab.)
ALDE	92C	ZPHY C54 553	D.M. Alde et al.	(BELG, SERP, KEK, LANL+)
FUKUI	91	PL B257 241	S. Fukui et al.	(SUGI, NAGO, KEK, KYOT+)
AUGUSTIN	89	NP B320 1	J.E. Augustin, G. Cosme	(DM2 Collab.)
ATKINSON	84C	NP B243 1	M. Atkinson et al.	(BONN, CERN, GLAS+ JP)
ATKINSON	84D	NP B242 269	M. Atkinson et al.	(BONN, CERN, GLAS+)
ATKINSON	84E	PL 138B 459	M. Atkinson et al.	(BONN, CERN, GLAS+)
COLLICK	84	PRL 53 2374	B. Collick et al.	(MINN, ROCH, FNAL)
EVANGELISTA...	81	NP B178 197	C. Evangelista et al.	(BARI, BONN, CERN+)
BALTAY	78B	PR D17 62	C. Baltay et al.	(COLU, BING)
GESSAROLI	77	NP B126 382	R. Gessaroli et al.	(BGN, FIRZ, GENO+ JP)
FLATTE	76C	PL 64B 225	S.M. Flatte et al.	(CERN, AMST, NIJH+ JP)
CHUNG	75B	PR D11 2426	S.U. Chung et al.	(BNL, LBL, UCSC) JP
CHALOUPIKA	74	PL 51B 407	V. Chaloupka et al.	(CERN) JP
KARSHON	74B	PR D10 3608	U. Karshon et al.	(REHO) JP
BIZZARRI	69	NP B14 169	R. Bizzarri et al.	(CERN, CDEF)
BALTAY	67	PRL 18 93	C. Baltay et al.	(COLU)
DAHL	67	PR 163 1377	O.L. Dahl et al.	(LRL)
ABOLINS	63	PRL 11 381	M.A. Abolins et al.	(UCSD)

## $a_1(1260)$

$$I^G(JPC) = 1^-(1^{++})$$

See also our review under the  $a_1(1260)$  in PDG 06, Journal of Physics **G33** 1 (2006).

### $a_1(1260)$ MASS

VALUE (MeV)	EVTS	DOCUMENT ID	TECN	COMMENT
<b>1230 <math>\pm</math> 40</b>	<b>OUR ESTIMATE</b>			
<b>1299 <math>\pm</math> 12</b>	<b>46M</b>	1 AGHASYAN	18B	COMP 190 $\pi^- p \rightarrow \pi^- \pi^+ \pi^- p$
••• We do not use the following data for averages, fits, limits, etc. •••				
1195.05 $\pm$ 1.05 $\pm$ 6.33	894k	AAIJ	18A1	LHCB $D^0 \rightarrow K^\mp \pi^\pm \pi^\pm \pi^\mp$
1209 $\pm$ 4 $\pm$ 12		2 MIKHASENKO	18	RVUE $\tau^- \rightarrow \pi^- \pi^+ \pi^- \nu_\tau$
1225 $\pm$ 9 $\pm$ 20	7k	3 DARGENT	17	RVUE $D^0 \rightarrow \pi^- \pi^+ \pi^- \pi^+$
1255 $\pm$ 6 $\pm$ 7	420k	4 ALEKSEEV	10	COMP 190 $\pi^- P_b \rightarrow \pi^- \pi^- \pi^+ P_b'$
1243 $\pm$ 12 $\pm$ 20		5 AUBERT	07AU	BABR 10.6 $e^+ e^- \rightarrow \rho^0 \pi^\pm \pi^\mp \gamma$
1230-1270	6360	6 LINK	07A	FOCS $D^0 \rightarrow \pi^- \pi^+ \pi^- \pi^+$
1203 $\pm$ 3		7 GOMEZ-DUM...	04	RVUE $\tau^+ \rightarrow \pi^+ \pi^+ \pi^- \nu_\tau$
1330 $\pm$ 24	90k	8 SALVINI	04	OBLX $\bar{p} p \rightarrow 2\pi^+ 2\pi^-$
1331 $\pm$ 10 $\pm$ 3	37k	8 ASNER	00	CLE2 10.6 $e^+ e^- \rightarrow \tau^+ \tau^-$
1255 $\pm$ 7 $\pm$ 6	5904	9 ABREU	98G	DLPH $e^+ e^-$
1207 $\pm$ 5 $\pm$ 8	5904	10 ABREU	98G	DLPH $e^+ e^-$
1196 $\pm$ 4 $\pm$ 5	5904	11,12 ABREU	98G	DLPH $e^+ e^-$

1240 $\pm$ 10		BARBERIS	98B	450 $\rho p \rightarrow p_f \pi^+ \pi^- \pi^0 p_S$
1262 $\pm$ 9 $\pm$ 7	9,13	ACKERSTAFF	97R	OPAL $E_{cm}^{ee} = 88-94, \tau \rightarrow 3\pi\nu$
1210 $\pm$ 7 $\pm$ 2	10,13	ACKERSTAFF	97R	OPAL $E_{cm}^{ee} = 88-94, \tau \rightarrow 3\pi\nu$
1211 $\pm$ 7 $\pm$ 50		10 ALBRECHT	93C	ARG $\tau^+ \rightarrow \pi^+ \pi^+ \pi^- \nu$
1121 $\pm$ 8		14 ANDO	92	SPEC $8 \pi^- p \rightarrow \pi^+ \pi^- \pi^0 n$
1242 $\pm$ 37		15 IVANOV	91	RVUE $\tau \rightarrow \pi^+ \pi^+ \pi^- \nu$
1260 $\pm$ 14		16 IVANOV	91	RVUE $\tau \rightarrow \pi^+ \pi^+ \pi^- \nu$
1250 $\pm$ 9		17 IVANOV	91	RVUE $\tau \rightarrow \pi^+ \pi^+ \pi^- \nu$
1208 $\pm$ 15		ARMSTRONG	90	OMEG 300.0 $\rho p \rightarrow p p \pi^+ \pi^- \pi^0$
1220 $\pm$ 15		18 ISGUR	89	RVUE $\tau^+ \rightarrow \pi^+ \pi^+ \pi^- \nu$
1260 $\pm$ 25		19 BOWLER	88	RVUE $\tau^+ \rightarrow \pi^+ \pi^+ \pi^- \nu$
1166 $\pm$ 18 $\pm$ 11		BAND	87	MAC $\tau^+ \rightarrow \pi^+ \pi^+ \pi^- \nu$
1164 $\pm$ 41 $\pm$ 23		BAND	87	MAC $\tau^+ \rightarrow \pi^+ \pi^0 \pi^0 \nu$
1250 $\pm$ 40		18 TORNVIST	87	RVUE
1046 $\pm$ 11		ALBRECHT	86B	ARG $\tau^+ \rightarrow \pi^+ \pi^+ \pi^- \nu$
1056 $\pm$ 20 $\pm$ 15		RUCKSTUHL	86	DLCO $\tau^+ \rightarrow \pi^+ \pi^+ \pi^- \nu$
1194 $\pm$ 14 $\pm$ 10		SCHMIDKE	86	MRK2 $\tau^+ \rightarrow \pi^+ \pi^+ \pi^- \nu$
1255 $\pm$ 23		BELLINI	85	SPEC 40 $\pi^- A \rightarrow \pi^- \pi^+ \pi^- A$
1240 $\pm$ 80		20 DANKOWY...	81	SPEC 8.45 $\pi^- p \rightarrow n 3\pi$
1280 $\pm$ 30		20 DAUM	81B	CNTR 63,94 $\pi^- p \rightarrow p 3\pi$
1041 $\pm$ 13		21 GAVILLET	77	HBC 4.2 $K^- p \rightarrow \Sigma 3\pi$

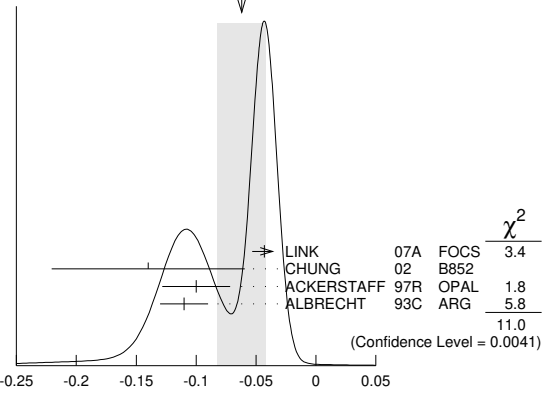
- Statistical error negligible.
- From the pole position. Using an amplitude analysis based on approximate three-body unitarity of  $\tau$  data from SCHAEEL 05c.
- Reanalysis of CLEO data using Breit-Wigner parameterization.
- Superseded by AGHASYAN 2018B.
- The  $\rho^\pm \pi^\mp$  state can be also due to the  $\pi(1300)$ .
- Using the Breit-Wigner parameterization; strong correlation between mass and width.
- Using the data of BARATE 98R.
- From a fit to the  $3\pi$  mass spectrum including the  $K\bar{K}^*(892)$  threshold.
- Uses the model of KUHN 90.
- Uses the model of ISGUR 89.
- Includes the effect of a possible  $a_1'$  state.
- Uses the model of FEINDT 90.
- Supersedes AKERS 95P.
- Average and spread of values using 2 variants of the model of BOWLER 75.
- Reanalysis of RUCKSTUHL 86.
- Reanalysis of SCHMIDKE 86.
- Reanalysis of ALBRECHT 86B.
- From a combined reanalysis of ALBRECHT 86B, SCHMIDKE 86, and RUCKSTUHL 86.
- From a combined reanalysis of ALBRECHT 86B and DAUM 81B.
- Uses the model of BOWLER 75.
- Produced in  $K^-$  backward scattering.

### $a_1(1260)$ WIDTH

VALUE (MeV)	EVTS	DOCUMENT ID	TECN	COMMENT
<b>250 to 600</b>	<b>OUR ESTIMATE</b>			
<b>420 <math>\pm</math> 35</b>	<b>OUR AVERAGE</b>			
430 $\pm$ 80	46M	1 AGHASYAN	18B	COMP 190 $\pi^- p \rightarrow \pi^- \pi^+ \pi^- p$
430 $\pm$ 24 $\pm$ 31		DARGENT	17	RVUE $D^0 \rightarrow \pi^- \pi^+ \pi^- \pi^+$
422.01 $\pm$ 2.10 $\pm$ 12.72	894k	AAIJ	18A1	LHCB $D^0 \rightarrow K^\mp \pi^\pm \pi^\pm \pi^\mp$
576 $\pm$ 11 $\pm$ 89		2 MIKHASENKO	18	RVUE $\tau^- \rightarrow \pi^- \pi^+ \pi^- \nu_\tau$
367 $\pm$ 9 $\pm$ 28	420k	3 ALEKSEEV	10	COMP 190 $\pi^- P_b \rightarrow \pi^- \pi^- \pi^+ P_b'$
410 $\pm$ 31 $\pm$ 30		4 AUBERT	07AU	BABR 10.6 $e^+ e^- \rightarrow \rho^0 \pi^\pm \pi^\mp \gamma$
520-680	6360	5 LINK	07A	FOCS $D^0 \rightarrow \pi^- \pi^+ \pi^- \pi^+$
480 $\pm$ 20		6 GOMEZ-DUM...	04	RVUE $\tau^+ \rightarrow \pi^+ \pi^+ \pi^- \nu_\tau$
580 $\pm$ 41	90k	SALVINI	04	OBLX $\bar{p} p \rightarrow 2\pi^+ 2\pi^-$
460 $\pm$ 85	205	7 DRUTSKOY	02	BELL $B \rightarrow D^*(*) K^- K^+ 0$
814 $\pm$ 36 $\pm$ 13	37k	8 ASNER	00	CLE2 10.6 $e^+ e^- \rightarrow \tau^+ \tau^-$
450 $\pm$ 50	22k	9 AKHMETSHIN	99E	CMD2 1.05-1.38 $e^+ e^- \rightarrow \pi^+ \pi^- \pi^0 \pi^0$
570 $\pm$ 10		10 BONDAR	99	RVUE $e^+ e^- \rightarrow 4\pi, \tau \rightarrow 3\pi\nu_\tau$
587 $\pm$ 27 $\pm$ 21	5904	11 ABREU	98G	DLPH $e^+ e^-$
478 $\pm$ 3 $\pm$ 15	5904	12 ABREU	98G	DLPH $e^+ e^-$
425 $\pm$ 14 $\pm$ 8	5904	13,14 ABREU	98G	DLPH $e^+ e^-$
400 $\pm$ 35		BARBERIS	98B	450 $\rho p \rightarrow p_f \pi^+ \pi^- \pi^0 p_S$
621 $\pm$ 32 $\pm$ 58		11,15 ACKERSTAFF	97R	OPAL $E_{cm}^{ee} = 88-94, \tau \rightarrow 3\pi\nu$
457 $\pm$ 15 $\pm$ 17		12,15 ACKERSTAFF	97R	OPAL $E_{cm}^{ee} = 88-94, \tau \rightarrow 3\pi\nu$
446 $\pm$ 21 $\pm$ 140		12 ALBRECHT	93C	ARG $\tau^+ \rightarrow \pi^+ \pi^+ \pi^- \nu$

239	$\pm 11$	ANDO	92	SPEC	$8 \pi^- \rho \rightarrow \pi^+ \pi^- \pi^0 n$
266	$\pm 13 \pm 4$	<sup>16</sup> ANDO	92	SPEC	$8 \pi^- \rho \rightarrow \pi^+ \pi^- \pi^0 n$
465	$+228$ $-143$	17 IVANOV	91	RVUE	$\tau \rightarrow \pi^+ \pi^+ \pi^- \nu$
298	$+40$ $-34$	18 IVANOV	91	RVUE	$\tau \rightarrow \pi^+ \pi^+ \pi^- \nu$
488	$\pm 32$	19 IVANOV	91	RVUE	$\tau \rightarrow \pi^+ \pi^+ \pi^- \nu$
430	$\pm 50$	ARMSTRONG	90	OMEG	$300.0 \rho \rho \rightarrow \rho \rho \pi^+ \pi^- \pi^0$
420	$\pm 40$	20 ISGUR	89	RVUE	$\tau^+ \rightarrow \pi^+ \pi^+ \pi^- \nu$
396	$\pm 43$	21 BOWLER	88	RVUE	
405	$\pm 75 \pm 25$	BAND	87	MAC	$\tau^+ \rightarrow \pi^+ \pi^+ \pi^- \nu$
419	$\pm 108 \pm 57$	BAND	87	MAC	$\tau^+ \rightarrow \pi^+ \pi^0 \pi^0 \nu$
521	$\pm 27$	ALBRECHT	86B	ARG	$\tau^+ \rightarrow \pi^+ \pi^+ \pi^- \nu$
476	$+132$ $-120$	RUCKSTUHL	86	DLCO	$\tau^+ \rightarrow \pi^+ \pi^+ \pi^- \nu$
462	$\pm 56 \pm 30$	SCHMIDKE	86	MRK2	$\tau^+ \rightarrow \pi^+ \pi^+ \pi^- \nu$
292	$\pm 40$	BELLINI	85	SPEC	$40 \pi^- A \rightarrow \pi^- \pi^+ \pi^- A$
380	$\pm 100$	22 DANKOWY...	81	SPEC	$8.45 \pi^- \rho \rightarrow n 3\pi$
300	$\pm 50$	22 DAUM	81B	CNTR	$63.94 \pi^- \rho \rightarrow \rho 3\pi$
230	$\pm 50$	23 GAVILLET	77	HBC	$4.2 K^- \rho \rightarrow \Sigma 3\pi$

WEIGHTED AVERAGE  
-0.062±0.020 (Error scaled by 2.3)



D-wave/S-wave AMPLITUDE RATIO IN DECAY OF  $a_1(1260) \rightarrow \rho \pi$

- <sup>1</sup> Deck-type background not subtracted.
- <sup>2</sup> Uses the model of ISGUR 89.
- <sup>3</sup> Supersedes AKERS 95P.

- <sup>1</sup> Statistical error negligible.
- <sup>2</sup> From the pole position. Using an amplitude analysis based on approximate three-body unitary of  $\tau$  data from SCHAEEL 05c.
- <sup>3</sup> Superseded by AGHASYAN 2018B.
- <sup>4</sup> The  $\rho^\pm \pi^\mp$  state can be also due to the  $\pi(1300)$ .
- <sup>5</sup> Using the Breit-Wigner parameterization; strong correlation between mass and width.
- <sup>6</sup> Using the data of BARATE 98R.
- <sup>7</sup> From a fit of the  $K^- K^*0$  distribution assuming  $m_{a_1} = 1230$  MeV and purely resonant production of the  $K^- K^*0$  system.
- <sup>8</sup> From a fit to the  $3\pi$  mass spectrum including the  $K \bar{K}^*(892)$  threshold.
- <sup>9</sup> Using the  $a_1(1260)$  mass of 1230 MeV.
- <sup>10</sup> From AKHMETSHIN 99E and ASNER 00 data using the  $a_1(1260)$  mass of 1230 MeV.
- <sup>11</sup> Uses the model of KUHN 90.
- <sup>12</sup> Uses the model of ISGUR 89.
- <sup>13</sup> Includes the effect of a possible  $a_1'$  state.
- <sup>14</sup> Uses the model of FEINDT 90.
- <sup>15</sup> Supersedes AKERS 95P.
- <sup>16</sup> Average and spread of values using 2 variants of the model of BOWLER 75.
- <sup>17</sup> Reanalysis of RUCKSTUHL 86.
- <sup>18</sup> Reanalysis of SCHMIDKE 86.
- <sup>19</sup> Reanalysis of ALBRECHT 86B.
- <sup>20</sup> From a combined reanalysis of ALBRECHT 86B, SCHMIDKE 86, and RUCKSTUHL 86.
- <sup>21</sup> From a combined reanalysis of ALBRECHT 86B and DAUM 81B.
- <sup>22</sup> Uses the model of BOWLER 75.
- <sup>23</sup> Produced in  $K^-$  backward scattering.

$a_1(1260)$  DECAY MODES

Mode	Fraction ( $\Gamma_i/\Gamma$ )
$\Gamma_1$ $3\pi$	seen
$\Gamma_2$ $(\rho\pi)S$ -wave, $\rho \rightarrow \pi\pi$	seen
$\Gamma_3$ $(\rho\pi)D$ -wave, $\rho \rightarrow \pi\pi$	seen
$\Gamma_4$ $(\rho(1450)\pi)S$ -wave, $\rho \rightarrow \pi\pi$	seen
$\Gamma_5$ $(\rho(1450)\pi)D$ -wave, $\rho \rightarrow \pi\pi$	seen
$\Gamma_6$ $f_0(500)\pi, f_0 \rightarrow \pi\pi$	seen
$\Gamma_7$ $f_0(980)\pi, f_0 \rightarrow \pi\pi$	not seen
$\Gamma_8$ $f_0(1370)\pi, f_0 \rightarrow \pi\pi$	seen
$\Gamma_9$ $f_2(1270)\pi, f_2 \rightarrow \pi\pi$	seen
$\Gamma_{10}$ $\pi^+ \pi^- \pi^0$	seen
$\Gamma_{11}$ $\pi^0 \pi^0 \pi^0$	not seen
$\Gamma_{12}$ $K K \pi$	seen
$\Gamma_{13}$ $K^*(892) K$	seen
$\Gamma_{14}$ $\pi \gamma$	seen

$a_1(1260)$  PARTIAL WIDTHS

$\Gamma(\pi\gamma)$	VALUE (keV)	DOCUMENT ID	TECN	COMMENT	$\Gamma_{14}$
	$640 \pm 246$	ZIELINSKI	84c	SPEC	200 $\pi^+ Z \rightarrow Z 3\pi$

D-wave/S-wave AMPLITUDE RATIO IN DECAY OF  $a_1(1260) \rightarrow \rho \pi$

VALUE	DOCUMENT ID	TECN	COMMENT
<b>-0.062±0.020 OUR AVERAGE</b>	Error includes scale factor of 2.3. See the ideogram below.		
-0.043±0.009±0.005	LINK	07A	FOCS $D^0 \rightarrow \pi^- \pi^+ \pi^- \pi^+$
-0.14±0.04±0.07	<sup>1</sup> CHUNG	02	B852 $18.3 \pi^- \rho \rightarrow \pi^+ \pi^- \pi^- \nu$
-0.10±0.02±0.02	<sup>2,3</sup> ACKERSTAFF	97R	OPAL $E_{cm}^{ee} = 88-94, \tau \rightarrow 3\pi \nu$
-0.11±0.02	<sup>2</sup> ALBRECHT	93C	ARG $\tau^+ \rightarrow \pi^+ \pi^+ \pi^- \nu$

$a_1(1260)$  BRANCHING RATIOS

$\Gamma((\rho\pi)S$ -wave, $\rho \rightarrow \pi\pi)/\Gamma_{total}$	VALUE (units $10^{-2}$ )	EVTS	DOCUMENT ID	TECN	COMMENT	$\Gamma_2/\Gamma$
••• We do not use the following data for averages, fits, limits, etc. •••						
	60.19	37k	<sup>1</sup> ASNER	00	CLE2 $10.6 e^+ e^- \rightarrow \tau^+ \tau^-$ $\tau^- \rightarrow \pi^- \pi^0 \pi^0 \nu_\tau$	

$\Gamma((\rho\pi)D$ -wave, $\rho \rightarrow \pi\pi)/\Gamma_{total}$	VALUE (units $10^{-2}$ )	EVTS	DOCUMENT ID	TECN	COMMENT	$\Gamma_3/\Gamma$
••• We do not use the following data for averages, fits, limits, etc. •••						
	$1.30 \pm 0.60 \pm 0.22$	37k	<sup>1</sup> ASNER	00	CLE2 $10.6 e^+ e^- \rightarrow \tau^+ \tau^-$ $\tau^- \rightarrow \pi^- \pi^0 \pi^0 \nu_\tau$	

$\Gamma((\rho(1450)\pi)S$ -wave, $\rho \rightarrow \pi\pi)/\Gamma_{total}$	VALUE (units $10^{-2}$ )	EVTS	DOCUMENT ID	TECN	COMMENT	$\Gamma_4/\Gamma$
••• We do not use the following data for averages, fits, limits, etc. •••						
	$0.56 \pm 0.84 \pm 0.32$	37k	<sup>1,2</sup> ASNER	00	CLE2 $10.6 e^+ e^- \rightarrow \tau^+ \tau^-$ $\tau^- \rightarrow \pi^- \pi^0 \pi^0 \nu_\tau$	

$\Gamma((\rho(1450)\pi)D$ -wave, $\rho \rightarrow \pi\pi)/\Gamma_{total}$	VALUE (units $10^{-2}$ )	EVTS	DOCUMENT ID	TECN	COMMENT	$\Gamma_5/\Gamma$
••• We do not use the following data for averages, fits, limits, etc. •••						
	$2.04 \pm 1.20 \pm 0.28$	37k	<sup>1,2</sup> ASNER	00	CLE2 $10.6 e^+ e^- \rightarrow \tau^+ \tau^-$ $\tau^- \rightarrow \pi^- \pi^0 \pi^0 \nu_\tau$	

$\Gamma(f_0(500)\pi, f_0 \rightarrow \pi\pi)/\Gamma_{total}$	VALUE (units $10^{-2}$ )	EVTS	DOCUMENT ID	TECN	COMMENT	$\Gamma_6/\Gamma$
••• We do not use the following data for averages, fits, limits, etc. •••						
	seen		CHUNG	02	B852 $18.3 \pi^- \rho \rightarrow \pi^+ \pi^- \pi^- \nu$	
	$18.76 \pm 4.29 \pm 1.48$	37k	<sup>1,3</sup> ASNER	00	CLE2 $10.6 e^+ e^- \rightarrow \tau^+ \tau^-$ $\tau^- \rightarrow \pi^- \pi^0 \pi^0 \nu_\tau$	

$\Gamma(f_0(500)\pi, f_0 \rightarrow \pi\pi)/\Gamma((\rho\pi)S$ -wave, $\rho \rightarrow \pi\pi)$	VALUE	EVTS	DOCUMENT ID	TECN	COMMENT	$\Gamma_6/\Gamma_2$
••• We do not use the following data for averages, fits, limits, etc. •••						
	$0.06 \pm 0.05$	90k	SALVINI	04	OBLX $\bar{p} p \rightarrow 2\pi^+ 2\pi^-$	
	$\sim 0.3$	28k	AKHMETSHIN 99E	CMD2	$1.05-1.38 e^+ e^- \rightarrow \pi^+ \pi^- \pi^+ \pi^-$	
	$0.003 \pm 0.003$		<sup>4</sup> LONGACRE	82	RVUE	

$\Gamma(f_0(980)\pi, f_0 \rightarrow \pi\pi)/\Gamma_{total}$	VALUE (units $10^{-2}$ )	EVTS	DOCUMENT ID	TECN	COMMENT	$\Gamma_7/\Gamma$
••• We do not use the following data for averages, fits, limits, etc. •••						
	not seen	37k	ASNER	00	CLE2 $10.6 e^+ e^- \rightarrow \tau^+ \tau^-$ $\tau^- \rightarrow \pi^- \pi^0 \pi^0 \nu_\tau$	

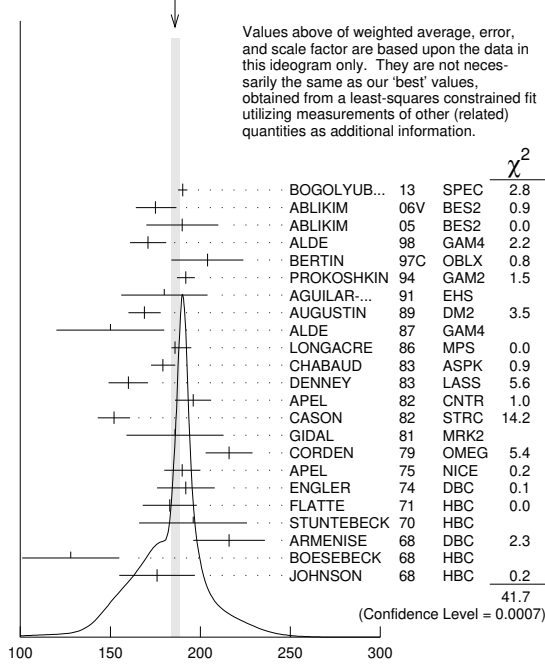
$\Gamma(f_0(1370)\pi, f_0 \rightarrow \pi\pi)/\Gamma_{total}$	VALUE (units $10^{-2}$ )	EVTS	DOCUMENT ID	TECN	COMMENT	$\Gamma_8/\Gamma$
••• We do not use the following data for averages, fits, limits, etc. •••						
	$7.40 \pm 2.71 \pm 1.26$	37k	<sup>1,5</sup> ASNER	00	CLE2 $10.6 e^+ e^- \rightarrow \tau^+ \tau^-$ $\tau^- \rightarrow \pi^- \pi^0 \pi^0 \nu_\tau$	



196 ±10	3k	APEL	82	CNTR	25	$\pi^- p \rightarrow n2\pi^0$
152 ± 9		7 CASON	82	STRC	8	$\pi^+ p \rightarrow \Delta^{++}\pi^0\pi^0$
186 ±27	11600	GIDAL	81	MRK2		$J/\psi$ decay
216 ±13		8 CORDEN	79	OMEG	12-15	$\pi^- p \rightarrow n2\pi$
190 ±10	10k	APEL	75	NICE	40	$\pi^- p \rightarrow n2\pi^0$
192 ±16	4600	ENGLER	74	DBC	6	$\pi^+ n \rightarrow \pi^+\pi^-p$
183 ±15	5300	FLATTE	71	HBC	7	$\pi^+ p \rightarrow \Delta^{++}f_2$
196 ±30		4 STUNTEBECK	70	HBC	8	$\pi^- p, 5.4 \pi^+ d$
216 ±20	1960	4 ARMENISE	68	DBC	5.1	$\pi^+ n \rightarrow p\pi^+MM^-$
128 ±27		4 BOESEBECK	68	HBC	8	$\pi^+ p$
176 ±21		4,9 JOHNSON	68	HBC	3.7-4.2	$\pi^- p$
194 ±36		10 ANISOVICH	09	RVUE	0.0	$\bar{p}p, \pi N$
195 ±15	870	11 SCHEGELSKY	06A	RVUE	$\gamma\gamma \rightarrow K_S^0 K_S^0$	
121 ±26		TIKHOMIROV	03	SPEC	40.0	$\pi^- C \rightarrow K_S^0 K_S^0 K_L^0 X$
187 ±20		12 ALDE	97	GAM2	45.0	$pp \rightarrow p p \pi^0 \pi^0$
184 ±10		12 GRYGOREV	96	SPEC	40	$\pi^- N \rightarrow K_S^0 K_S^0 X$
200 ±10		AKER	91	CBAR	0.0	$\bar{p}p \rightarrow 3\pi^0$
240 ±40	3k	BINON	83	GAM2	38	$\pi^- p \rightarrow n2\eta$
187 ±30	650	4 ANTIPOV	77	CIBS	25	$\pi^- p \rightarrow p3\pi$
225 ±38	16000	DEUTSCH...	76	HBC	16	$\pi^+ p$
166 ±28	600	4 TAKAHASHI	72	HBC	8	$\pi^- p \rightarrow n2\pi$
173 ±53		4 ARMENISE	70	HBC	9	$\pi^+ n \rightarrow p\pi^+\pi^-$

- 1 Averaged over six nuclear targets, no statistically significant dependence on target nucleus observed.
- 2 Breit-Wigner width
- 3 T-matrix pole.
- 4 Width errors enlarged by us to  $4\Gamma/\sqrt{N}$ ; see the note with the  $K^*(892)$  mass.
- 5 From a partial-wave analysis of data using a K-matrix formalism with 5 poles.
- 6 From an energy-independent partial-wave analysis.
- 7 From an amplitude analysis of the reaction  $\pi^+\pi^- \rightarrow 2\pi^0$ .
- 8 From an amplitude analysis of  $\pi^+\pi^- \rightarrow \pi^+\pi^-$  scattering data.
- 9 JOHNSON 68 includes BONDAR 63, LEE 64, DERADO 65, EISNER 67.
- 10 4-poles, 5-channel K matrix fit.
- 11 From analysis of L3 data at 91 and 183-209 GeV.
- 12 Systematic uncertainties not estimated.

WEIGHTED AVERAGE  
185.9±2.8-2.1 (Error scaled by 1.6)



Values above of weighted average, error, and scale factor are based upon the data in this ideogram only. They are not necessarily the same as our 'best' values, obtained from a least-squares constrained fit utilizing measurements of other (related) quantities as additional information.

$\Gamma_5$	$\eta\eta$	$(4.0 \pm 0.8) \times 10^{-3}$	S=2.1
$\Gamma_6$	$4\pi^0$	$(3.0 \pm 1.0) \times 10^{-3}$	
$\Gamma_7$	$\gamma\gamma$	$(1.42 \pm 0.24) \times 10^{-5}$	S=1.4
$\Gamma_8$	$\eta\pi\pi$	$< 8 \times 10^{-3}$	CL=95%
$\Gamma_9$	$K^0 K^- \pi^+ + c.c.$	$< 3.4 \times 10^{-3}$	CL=95%
$\Gamma_{10}$	$e^+ e^-$	$< 6 \times 10^{-10}$	CL=90%

CONSTRAINED FIT INFORMATION

An overall fit to the total width, 4 partial widths, a combination of partial widths obtained from integrated cross sections, and 6 branching ratios uses 45 measurements and one constraint to determine 8 parameters. The overall fit has a  $\chi^2 = 83.0$  for 38 degrees of freedom.

The following off-diagonal array elements are the correlation coefficients  $\langle \delta p_i \delta p_j \rangle / (\delta p_i \delta p_j)$ , in percent, from the fit to parameters  $p_i$ , including the branching fractions,  $x_i \equiv \Gamma_i / \Gamma_{total}$ . The fit constrains the  $x_i$  whose labels appear in this array to sum to one.

$x_2$	-90						
$x_3$	10	-39					
$x_4$	10	-38	1				
$x_5$	1	-6	0	0			
$x_6$	0	-7	0	0	0		
$x_7$	3	1	-15	0	0	0	
$\Gamma$	-71	65	-10	-7	-1	0	-6
	$x_1$	$x_2$	$x_3$	$x_4$	$x_5$	$x_6$	$x_7$

Mode	Rate (MeV)	Scale factor	
$\Gamma_1$	$\pi\pi$	157.2 $\pm$ 4.0 / -1.1	
$\Gamma_2$	$\pi^+\pi^-2\pi^0$	14.4 $\pm$ 2.1 / -6.0	1.2
$\Gamma_3$	$K\bar{K}$	8.5 $\pm$ 0.8	2.8
$\Gamma_4$	$2\pi^+2\pi^-$	5.2 $\pm$ 0.7	1.2
$\Gamma_5$	$\eta\eta$	0.75 $\pm$ 0.14	2.1
$\Gamma_6$	$4\pi^0$	0.56 $\pm$ 0.19	
$\Gamma_7$	$\gamma\gamma$	0.0026 $\pm$ 0.0005	1.4

$f_2(1270)$  PARTIAL WIDTHS

$\Gamma(\pi\pi)$	VALUE (MeV)	EVTS	DOCUMENT ID	TECN	COMMENT	$\Gamma_1$
<b>157.2 ± 4.0 OUR FIT</b>						
<b>157.0 ± 6.0</b>			1 LONGACRE 86	MPS	22 $\pi^- p \rightarrow n2K_S^0$	
152 ± 8		870	2 SCHEGELSKY 06A	RVUE	$\gamma\gamma \rightarrow K_S^0 K_S^0$	
<b><math>\Gamma(K\bar{K})</math></b>						$\Gamma_3$
<b>8.5 ± 0.8 OUR FIT</b>					Error includes scale factor of 2.8.	
<b>9.0 ± 0.7</b>			1 LONGACRE 86	MPS	22 $\pi^- p \rightarrow n2K_S^0$	
7.5 ± 2.0		870	2 SCHEGELSKY 06A	RVUE	$\gamma\gamma \rightarrow K_S^0 K_S^0$	
<b><math>\Gamma(\eta\eta)</math></b>						$\Gamma_5$
<b>0.75 ± 0.14 OUR FIT</b>					Error includes scale factor of 2.1.	
<b>1.0 ± 0.1</b>			1 LONGACRE 86	MPS	22 $\pi^- p \rightarrow n2K_S^0$	
1.8 ± 0.4		870	2 SCHEGELSKY 06A	RVUE	$\gamma\gamma \rightarrow K_S^0 K_S^0$	
<b><math>\Gamma(\gamma\gamma)</math></b>						$\Gamma_7$

The value of this width depends on the theoretical model used. Unitary approaches with scalars typically (with exception of PENNINGTON 08) give values clustering around 2.6 keV; without an S-wave contribution, values are systematically higher (typically around 3 keV).

VALUE (keV)	EVTS	DOCUMENT ID	TECN	COMMENT
<b>2.6 ± 0.5 OUR FIT</b>				Error includes scale factor of 1.4.
<b>2.93 ± 0.40</b>		3 DAI 14A	RVUE	Compilation
3.14 ± 0.20		4,5 PENNINGTON 08	RVUE	Compilation
3.82 ± 0.30		5,6 PENNINGTON 08	RVUE	Compilation
2.55 ± 0.15	870	2 SCHEGELSKY 06A	RVUE	$\gamma\gamma \rightarrow K_S^0 K_S^0$
2.84 ± 0.35		BOGLIONE 99	RVUE	$\gamma\gamma \rightarrow \pi^+\pi^-, \pi^0\pi^0$
2.93 ± 0.23 ± 0.32		7 YABUKI 95	VNS	
2.58 ± 0.13 $\pm$ 0.36 / -0.27		8 BEHREND 92	CELL	$e^+e^- \rightarrow e^+e^-\pi^+\pi^-$

$f_2(1270)$  DECAY MODES

Mode	Fraction ( $\Gamma_i/\Gamma$ )	Scale factor/Confidence level
$\Gamma_1$	$\pi\pi$	(84.2 $\pm$ 2.9 / -0.9) % S=1.1
$\Gamma_2$	$\pi^+\pi^-2\pi^0$	(7.7 $\pm$ 1.1 / -3.2) % S=1.2
$\Gamma_3$	$K\bar{K}$	(4.6 $\pm$ 0.5 / -0.4) % S=2.7
$\Gamma_4$	$2\pi^+2\pi^-$	(2.8 $\pm$ 0.4) % S=1.2

## Meson Particle Listings

 $f_2(1270)$ 

3.10 ± 0.35 ± 0.35		9	BLINOV	92	MD1	$e^+e^- \rightarrow e^+e^-\pi^+\pi^-$
2.27 ± 0.47 ± 0.11			ADACHI	90D	TOPZ	$e^+e^- \rightarrow e^+e^-\pi^+\pi^-$
3.15 ± 0.04 ± 0.39			BOYER	90	MRK2	$e^+e^- \rightarrow e^+e^-\pi^+\pi^-$
3.19 ± 0.16 ± 0.29			MARSISKE	90	CBAL	$e^+e^- \rightarrow e^+e^-\pi^0\pi^0$
2.35 ± 0.65			MORGAN	90	RVUE	$\gamma\gamma \rightarrow \pi^+\pi^-, \pi^0\pi^0$
3.19 ± 0.09 ± 0.22	2177		OEST	90	JADE	$e^+e^- \rightarrow e^+e^-\pi^0\pi^0$
3.2 ± 0.1 ± 0.4			AIHARA	86B	TPC	$e^+e^- \rightarrow e^+e^-\pi^+\pi^-$
2.5 ± 0.1 ± 0.5			BEHREND	84B	CELL	$e^+e^- \rightarrow e^+e^-\pi^+\pi^-$
2.85 ± 0.25 ± 0.5			BERGER	84	PLUT	$e^+e^- \rightarrow e^+e^-2\pi^+$
2.70 ± 0.05 ± 0.20			COURAU	84	DLCO	$e^+e^- \rightarrow e^+e^-\pi^+\pi^-$
2.5 ± 0.13 ± 0.38			SMITH	84C	MRK2	$e^+e^- \rightarrow e^+e^-\pi^+\pi^-$
2.7 ± 0.2 ± 0.6			EDWARDS	82F	CBAL	$e^+e^- \rightarrow e^+e^-2\pi^0$
2.9 ± 0.6 ± 0.6			EDWARDS	82F	CBAL	$e^+e^- \rightarrow e^+e^-2\pi^0$
3.2 ± 0.2 ± 0.6			BRANDELIK	81B	TASS	$e^+e^- \rightarrow e^+e^-\pi^+\pi^-$
3.6 ± 0.3 ± 0.5			ROUSSARIE	81	MRK2	$e^+e^- \rightarrow e^+e^-\pi^+\pi^-$
2.3 ± 0.8			BERGER	80B	PLUT	$e^+e^-$

$\Gamma(e^+e^-)$					$\Gamma_{10}$
VALUE (eV)	CL%	DOCUMENT ID	TECN	COMMENT	
<0.11	90	ACHASOV	00K	SND $e^+e^- \rightarrow \pi^0\pi^0$	
• • • We do not use the following data for averages, fits, limits, etc. • • •					
<1.7	90	VOROBYEV	88	ND $e^+e^- \rightarrow \pi^0\pi^0$	

- From a partial-wave analysis of data using a K-matrix formalism with 5 poles.
- From analysis of L3 data at 91 and 183–209 GeV and using SU(3) relations.
- Based on a K-matrix analysis of BELLE data from MORI 07, UEHARA 08a, UEHARA 09 and UEHARA 13. The width is derived for the pole on the third sheet which is closest to the physical axis. Supersedes PENNINGTON 08.
- Solution A (preferred solution based on  $\chi^2$ -analysis).
- Dispersion theory based amplitude analysis of BOYER 90, MARSISKE 90, BEHREND 92, and MORI 07.
- Solution B (worse than solution A; still acceptable when systematic uncertainties are included).
- With a narrow scalar state around 1220 MeV.
- Using a unitarized model with a 300–500 keV wide scalar at 1100 MeV.
- Using the unitarized model of LYTH 85.
- Error includes spread of different solutions. Data of MARK2 and CRYSTAL BALL used in the analysis. Authors report strong correlations with  $\gamma\gamma$  width of  $f_0(1370)$ :  $\Gamma(f_2) + 1/4 \Gamma(f_0) = 3.6 \pm 0.3$  KeV.
- Radiative corrections modify the partial widths; for instance the COURAU 84 value becomes  $2.66 \pm 0.21$  in the calculation of LANDRO 86.
- Using the MENNESSIER 83 model.
- Superseded by BOYER 90.
- If helicity = 2 assumption is not made.
- Using mass, width and  $B(f_2(1270) \rightarrow 2\pi)$  from PDG 78.

 $f_2(1270) \Gamma(i)\Gamma(\gamma\gamma)/\Gamma(\text{total})$ 

$\Gamma(K\bar{K}) \times \Gamma(\gamma\gamma)/\Gamma_{\text{total}}$					$\Gamma_3\Gamma_7/\Gamma$
VALUE (keV)	DOCUMENT ID	TECN	COMMENT		
<b>0.121 ± 0.020 OUR FIT</b>	Error includes scale factor of 1.3.				
<b>0.091 ± 0.007 ± 0.027</b>	1	ALBRECHT	90G	ARG $e^+e^- \rightarrow e^+e^-K^+K^-$	
• • • We do not use the following data for averages, fits, limits, etc. • • •					
0.104 ± 0.007 ± 0.072	2	ALBRECHT	90G	ARG $e^+e^- \rightarrow e^+e^-K^+K^-$	
1 Using an incoherent background.					
2 Using a coherent background.					

$\Gamma(\eta) \times \Gamma(\gamma\gamma)/\Gamma_{\text{total}}$					$\Gamma_5\Gamma_7/\Gamma$
VALUE (eV)	DOCUMENT ID	TECN	COMMENT		
<b>11.5 ± 1.8 + 4.5</b> <b>-2.0 - 3.7</b>	1	UEHARA	10A	BELL $10.6 e^+e^- \rightarrow e^+e^-\eta\eta$	
1 Including interference with the $f_2'(1525)$ (parameters fixed to the values from the 2008 edition of this review, PDG 08) and $f_0(Y)$ .					

Helicity-0/Helicity-2 RATIO IN  $\gamma\gamma \rightarrow f_2(1270) \rightarrow \pi\pi$ 

VALUE (units $10^{-2}$ )	DOCUMENT ID	TECN	COMMENT		
<b>3.7 ± 0.3 + 15.9</b> <b>-2.9</b>	UEHARA	08A	BELL $10.6 e^+e^- \rightarrow e^+e^-\pi^0\pi^0$		
• • • We do not use the following data for averages, fits, limits, etc. • • •					
9.5 ± 1.8	1	DAI	14A	RVUE	Compilation
13	2,3	PENNINGTON	08	RVUE	Compilation
26	3,4	PENNINGTON	08	RVUE	Compilation

- Based on a K-matrix analysis of BELLE data from MORI 07, UEHARA 08a, UEHARA 09 and UEHARA 13. The width is derived for the pole on the third sheet which is closest to the physical axis.
- Solution A (preferred solution based on  $\chi^2$ -analysis).
- Dispersion theory based amplitude analysis of BOYER 90, MARSISKE 90, BEHREND 92, and MORI 07.
- Solution B (worse than solution A; still acceptable when systematic uncertainties are included).

 $f_2(1270)$  BRANCHING RATIOS

$\Gamma(\pi\pi)/\Gamma_{\text{total}}$					$\Gamma_1/\Gamma$	
VALUE	EVTS	DOCUMENT ID	TECN	COMMENT		
<b>0.842 ± 0.029</b>	OUR FIT Error includes scale factor of 1.1.					
<b>0.837 ± 0.020</b>	OUR AVERAGE					
0.849 ± 0.025		CHABAUD	83	ASPK	$17 \pi^-p$ polarized	
0.85 ± 0.05	250	BEAUPRE	71	HBC	$8 \pi^+p \rightarrow \Delta^{++}f_2$	
0.8 ± 0.04	600	OH	70	HBC	$1.26 \pi^-p \rightarrow \pi^+\pi^-n$	

$\Gamma(\pi^+\pi^-2\pi^0)/\Gamma(\pi\pi)$					$\Gamma_2/\Gamma_1$	
VALUE	EVTS	DOCUMENT ID	TECN	COMMENT		
Should be twice $\Gamma(2\pi^+2\pi^-)/\Gamma(\pi\pi)$ if decay is $\rho\rho$ . (See ASCOLI 68D.)						
<b>0.091 ± 0.014</b>	OUR FIT Error includes scale factor of 1.2.					
<b>0.15 ± 0.06</b>	600	EISENBERG	74	HBC	$4.9 \pi^+p \rightarrow \Delta^{++}f_2$	
• • • We do not use the following data for averages, fits, limits, etc. • • •						
0.07		EMMS	75D	DBC	$4 \pi^+n \rightarrow pf_2$	

$\Gamma(K\bar{K})/\Gamma(\pi\pi)$					$\Gamma_3/\Gamma_1$	
VALUE	EVTS	DOCUMENT ID	TECN	COMMENT		
We average only experiments which either take into account $f_2(1270)$ - $a_2(1320)$ interference explicitly or demonstrate that $a_2(1320)$ production is negligible.						
<b>0.054 ± 0.005</b>	OUR FIT Error includes scale factor of 2.7.					
<b>0.041 ± 0.004</b>	OUR AVERAGE					
0.045 ± 0.01		1	BARGIOTTI	03	OBLX $\bar{p}p$	
0.037 ± 0.008			ETKIN	82B	MPS $23 \pi^-p \rightarrow n2K_S^0$	
0.045 ± 0.009			CHABAUD	81	ASPK $17 \pi^-p$ polarized	
0.039 ± 0.008			LOVERRE	80	HBC $4 \pi^-p \rightarrow K\bar{K}N$	
• • • We do not use the following data for averages, fits, limits, etc. • • •						
0.052 ± 0.025			ABLIKIM	04E	BES2 $J/\psi \rightarrow \omega K^+K^-$	
0.036 ± 0.005			2	COSTA	80	OMEG $1-2.2 \pi^-p \rightarrow K^+K^-n$
0.030 ± 0.005			3	MARTIN	79	RVUE
0.027 ± 0.009			4	POLYCHRO...	79	STRC $7 \pi^-p \rightarrow n2K_S^0$
0.025 ± 0.015			EMMS	75D	DBC	$4 \pi^+n \rightarrow pf_2$
0.031 ± 0.012	20	ADERHOLZ	69	HBC	$8 \pi^+p \rightarrow K^+K^-\pi^+p$	

$\Gamma(2\pi^+2\pi^-)/\Gamma(\pi\pi)$					$\Gamma_4/\Gamma_1$	
VALUE	EVTS	DOCUMENT ID	TECN	COMMENT		
<b>0.033 ± 0.005</b>	OUR FIT Error includes scale factor of 1.2.					
<b>0.033 ± 0.004</b>	OUR AVERAGE Error includes scale factor of 1.1.					
0.024 ± 0.006	160	EMMS	75D	DBC	$4 \pi^+n \rightarrow pf_2$	
0.051 ± 0.025	70	EISENBERG	74	HBC	$4.9 \pi^+p \rightarrow \Delta^{++}f_2$	
0.043 ± 0.007	285	LOUIE	74	HBC	$3.9 \pi^-p \rightarrow pf_2$	
0.037 ± 0.007	154	ANDERSON	73	DBC	$6 \pi^+n \rightarrow pf_2$	
0.047 ± 0.013		OH	70	HBC	$1.26 \pi^-p \rightarrow \pi^+\pi^-n$	

$\Gamma(\eta\eta)/\Gamma_{\text{total}}$					$\Gamma_5/\Gamma$	
VALUE (units $10^{-3}$ )	DOCUMENT ID	TECN	COMMENT			
<b>4.0 ± 0.8</b>	OUR FIT Error includes scale factor of 2.1.					
<b>2.9 ± 0.5</b>	OUR AVERAGE					
2.7 ± 0.7		BINON	05	GAMS	$33 \pi^-p \rightarrow \eta\eta n$	
2.8 ± 0.7		ALDE	86D	GAM4	$100 \pi^-p \rightarrow 2\eta n$	
5.2 ± 1.7		BINON	83	GAM2	$38 \pi^-p \rightarrow 2\eta n$	

$\Gamma(\eta\eta)/\Gamma(\pi\pi)$					$\Gamma_5/\Gamma_1$	
VALUE	CL%	DOCUMENT ID	TECN	COMMENT		
<b>0.003 ± 0.001</b>		BARBERIS	00E	450 $p\rho \rightarrow p_f\eta\eta p_S$		
• • • We do not use the following data for averages, fits, limits, etc. • • •						
<0.05	95	EDWARDS	82F	CBAL $e^+e^- \rightarrow e^+e^-2\eta$		
<0.016	95	EMMS	75D	DBC $4 \pi^+n \rightarrow pf_2$		
<0.09	95	EISENBERG	74	HBC	$4.9 \pi^+p \rightarrow \Delta^{++}f_2$	

$\Gamma(4\pi^0)/\Gamma_{\text{total}}$					$\Gamma_6/\Gamma$	
VALUE	EVTS	DOCUMENT ID	TECN	COMMENT		
<b>0.0030 ± 0.0010</b>	OUR FIT					
<b>0.003 ± 0.001</b>	400 ± 50	ALDE	87	GAM4	$100 \pi^-p \rightarrow 4\pi^0 n$	

$\Gamma(\gamma\gamma)/\Gamma_{\text{total}}$					$\Gamma_7/\Gamma$
VALUE (units $10^{-5}$ )	DOCUMENT ID	TECN	COMMENT		
• • • We do not use the following data for averages, fits, limits, etc. • • •					
1.57 ± 0.01 + 1.39		UEHARA	08A	BELL $10.6 e^+e^- \rightarrow e^+e^-\pi^0\pi^0$	
-0.14					

$\Gamma(\eta\pi\pi)/\Gamma(\pi\pi)$					$\Gamma_8/\Gamma_1$
VALUE	CL%	DOCUMENT ID	TECN	COMMENT	
<0.010	95	EMMS	75D	DBC	$4 \pi^+n \rightarrow pf_2$

See key on page 999

Meson Particle Listings
f2(1270), f1(1285)

Gamma(K0 K- pi+ + c.c.) / Gamma(pi pi)
Gamma(e+ e-) / Gamma(total)
VALUE CL% DOCUMENT ID TECN COMMENT

JOHNSON 68 PR 176 1651 P.B. Johnson et al. (NDAM, PURD, SLAC)
EISNER 67 PR 164 1699 R.L. Eisner et al. (PURD)
DERADO 65 PRL 14 872 L. Derado et al. (NDAM)
LEE 64 PRL 12 342 Y.Y. Lee et al. (MICH)
BONDAR 63 PL 5 153 L. Bondar et al. (AACH, BIRM, BONN, DESY+)

f1(1285)

I^G(J^PC) = 0+(1++)

f1(1285) MASS

VALUE (MeV) EVTS DOCUMENT ID TECN COMMENT
1281.9 +/- 0.5 OUR AVERAGE
1281.0 +/- 0.8 DICKSON 16 CLAS 2.55 gamma p -> eta pi+ pi- p
1287.4 +/- 3.0 87 ABLIKIM 15P BES3 J/psi -> K+ K- 3pi
1281.16 +/- 0.39 +/- 0.45 1 LEES 12X BABR tau- -> pi- f1(1285) nu\_tau
1285.1 +/- 1.0 +/- 1.6 +/- 0.3 2 ABLIKIM 11J BES3 J/psi -> omega(pi+ pi-)
1281 +/- 2 +/- 1 AUBERT 07AU BABR 10.6 e+ e- -> f1(1285) pi+ pi- gamma
1276.1 +/- 8.1 +/- 8.0 203 BAI 04J BES2 J/psi -> gamma gamma pi+ pi-
1274 +/- 6 237 ABDALLAH 03H DLPH 91.2 K\_S^0 e+ e- -> K\_S^0 K\_S^0 pi+ pi+ + X
1280 +/- 4 ACCIARRI 01G L3
1288 +/- 4 +/- 5 20k ADAMS 01B B852 18 GeV pi- p -> K+ K- pi0 n
1284 +/- 6 1400 ALDE 97B GAM4 100 pi- p -> eta pi0 pi0 n
1281 +/- 1 BARBERIS 97B OMEG 450 pp -> pp2(pi+ pi-)
1281 +/- 1 BARBERIS 97C OMEG 450 pp -> ppK\_S^0 K\_S^0 pi+ pi-
1280 +/- 2 3 ANTINORI 95 OMEG 300,450 pp -> pp2(pi+ pi-)
1282.2 +/- 1.5 LEE 94 MPS2 18 pi- p -> K+ K0 2pi- p
1279 +/- 5 FUKUI 91C SPEC 8.95 pi- p -> eta pi+ pi- n
1278 +/- 2 140 ARMSTRONG 89 OMEG 300 pp -> K K pi pi
1278 +/- 2 ARMSTRONG 89G OMEG 85 pi+ p -> 4pi pi pi, pp -> 4pi pi pi
1280.1 +/- 2.1 60 RATH 89 MPS 21.4 pi- p -> K\_S^0 K\_S^0 pi0 n
1285 +/- 1 4750 4 BIRMAN 88 MPS 8 pi- p -> K+ K0 pi- n
1280 +/- 1 504 BITYUKOV 88 SPEC 32.5 pi- p -> K+ K- pi0 n
1280 +/- 4 ANDO 86 SPEC 8 pi- p -> eta pi+ pi- n
1277 +/- 2 420 REEVES 86 SPEC 6.6 p p -> K K pi X
1285 +/- 2 CHUNG 85 SPEC 8 pi- p -> N K K pi
1279 +/- 2 604 ARMSTRONG 84 OMEG 85 pi+ p -> K K pi pi pi, pp -> K K pi pi pi
1286 +/- 1 CHAUVAT 84 SPEC ISR 31.5 pp
1278 +/- 4 EVANGELIS... 81 OMEG 12 pi- p -> eta pi+ pi- pi- p
1283 +/- 3 103 DIONISI 80 HBC 4 pi- p -> K K pi n
1282 +/- 2 320 NACASCH 78 HBC 0.7, 0.76 p p -> K K 3pi
1279 +/- 5 210 GRASSLER 77 HBC 16 pi+ p
1286 +/- 3 180 DUBOC 72 HBC 1.2 p p -> 2K4pi
1283 +/- 5 DAHL 67 HBC 1.6-4.2 pi- p
1289.3 +/- 2.8 234 ABLIKIM 19BA BES3 e+ e- -> psi(2S)
1284.2 +/- 2.2 5 AAIJ 14V LHCB B0(s) -> J/psi 2(pi+ pi-)
1281.9 +/- 5 SOSA 99 SPEC pp -> Pslow (K\_S^0 K+ pi-) Pfast
1282.8 +/- 0.6 5 SOSA 99 SPEC pp -> Pslow (K\_S^0 K- pi+) Pfast
1270 +/- 10 AMELIN 95 YES 37 pi- N -> pi- pi+ pi- gamma N
1280 +/- 2 ABATZIS 94 OMEG 450 pp -> pp2(pi+ pi-)
1282 +/- 4 ARMSTRONG 93C E760 p p -> pi0 eta -> 6gamma
1270 +/- 6 +/- 10 ARMSTRONG 92C OMEG 300 pp -> pp pi+ pi- gamma
1281 +/- 1 ARMSTRONG 89E OMEG 300 pp -> pp2(pi+ pi-)
1279 +/- 6 +/- 10 16 BECKER 87 MRK3 e+ e- -> phi K K pi
1286 +/- 9 GIDAL 87 MRK2 e+ e- -> e+ e- eta pi+ pi-
1287 +/- 5 353 BITYUKOV 84B SPEC 32 pi- p -> K+ K- pi0 n
~1279 6 TORNQVIST 82B RVUE
1275 +/- 6 31 BROMBERG 80 SPEC 100 pi- p -> K K pi X
1288 +/- 9 200 GURTU 79 HBC 4.2 K- p -> n eta 2pi
~1275.0 46 7 STANTON 79 CNTR 8.5 pi- p -> n2 gamma 2pi
1271 +/- 10 34 CORDEN 78 OMEG 12-15 pi- p -> K+ K- pi n
1295 +/- 12 85 CORDEN 78 OMEG 12-15 pi- p -> n5pi
1292 +/- 10 150 DEFOIX 72 HBC 0.7 p p -> 7pi
1280 +/- 3 500 8 THUN 72 MMS 13.4 pi- p
1303 +/- 8 BARDADIN... 71 HBC 8 pi+ p -> p6pi
1283 +/- 6 BOESEBECK 71 HBC 16.0 pi -> p5pi
1270 +/- 10 CAMPBELL 69 DBC 2.7 pi+ d
1285 +/- 7 LORSTAD 69 HBC 0.7 p p, 4.5-body
1290 +/- 7 D'ANDLAU 68 HBC 1.2 p p, 5-6 body

f2(1270) REFERENCES

DOBBS 15 PR D91 052006 S. Dobbs et al. (NWES)
DAI 14A PR D90 036004 L.-Y. Dai, M.R. Pennington (CEBAF)
BOGOLYUB... 13 PAN 76 1324 M.Yu. Bogolyubsky et al. (HYPERON-M Collab.)
UEHARA 13 PTEP 2013 123C01 S. Uehara et al. (BELLE Collab.)
UEHARA 10A PR D92 114031 S. Uehara et al. (BELLE Collab.)
ANISOVICH 09 UMP A24 2481 V.V. Anisovich, A.V. Sarantsev
UEHARA 09 PR D79 052009 S. Uehara et al. (BELLE Collab.)
PDG 08 PL B667 1 C. Amsler et al. (PDG Collab.)
PENNINGTON 08 EPJ C56 1 M.R. Pennington et al.
UEHARA 08A PR D78 052004 S. Uehara et al. (BELLE Collab.)
MORI 07 PR D75 051101 T. Mori et al. (BELLE Collab.)
SABLIKIM 06V PL B642 441 M. Ablikim et al. (BES Collab.)
SCHEGELSKY 06A EPJ A27 207 V.A. Schegelsky et al.
ABLIKIM 05 PL B607 243 M. Ablikim et al. (BES Collab.)
BINON 05 PAN 68 960 F. Binon et al.
Translated from YAF 68 998.
ABLIKIM 04E PL B603 138 M. Ablikim et al. (BES Collab.)
BARGIOTTI 03 EPJ C26 371 M. Bargiotti et al. (OBELIX Collab.)
TIKHOMIROV 03 PAN 66 828 G.D. Tikhomirov et al.
Translated from YAF 66 860.
ACHASOV 00K PL B492 8 M.N. Achasov et al. (Novosibirsk SND Collab.)
BARBERIS 00E PL B479 59 D.M. Barberis et al. (WA 102 Collab.)
BOGLIONE 99 EPJ C9 11 M. Boglione, M.R. Pennington
ALDE 98 EPJ A3 361 D. Alde et al. (GAM4 Collab.)
Also PAN 62 405 D. Alde et al. (GAMS Collab.)
ALDE 97 PL B397 350 D.M. Alde et al. (GAMS Collab.)
BERTIN 97C PL B408 476 A. Bertin et al. (OBELIX Collab.)
GRYGOREV 96 PAN 59 2105 V.K. Grigoriev, O.N. Baloshin, B.P. Barkov (ITEP)
Translated from YAF 59 2187.
YABUKI 95 JPS J 64 435 F. Yabuki et al. (VENUS Collab.)
PROKOSHIN 94 PD 39 420 Y.D. Prokoshin, A.A. Kondashov (SERP)
Translated from DANS 336 613.
BEHREND 92 ZPHY C56 381 H.J. Behrend et al. (CELLO Collab.)
BLINOV 92 ZPHY C53 33 A.E. Blinov et al. (NOVO)
AGUILAR... 91 ZPHY C50 405 M. Aguilar-Benitez et al. (LEBC-EHS Collab.)
AKER 91 PL B260 249 E. Aker et al. (Crystal Barrel Collab.)
ADACHI 90D PL B234 185 I. Adachi et al. (TOPAZ Collab.)
ALBRECHT 90G ZPHY C48 183 H. Albrecht et al. (ARGUS Collab.)
BOYER 90 PR D42 1350 J. Boyer et al. (Mark II Collab.)
BREAKSTONE 90 ZPHY C48 569 A.M. Breakstone et al. (ISU, BGNA, CERN+)
MARSIKSE 90 PR D41 3324 H. Marsiske et al. (Crystal Ball Collab.)
MORGAN 90 ZPHY C48 623 D. Morgan, M.R. Pennington (RAL, DURH)
OEST 90 ZPHY C47 343 T. Oest et al. (JADE Collab.)
AUGUSTIN 89 NP B320 1 J.E. Augustin, G. Cosme (DM2 Collab.)
VOROBYEV 88 SJNP 48 273 P.V. Vorobyev et al. (NOVO)
Translated from YAF 48 436.
ALDE 87 PL B198 286 D.M. Alde et al. (LANL, BRUX, SERP, LAPP)
AUGUSTIN 87 ZPHY C36 369 J.E. Augustin et al. (LALO, CLER, FRAS+)
ABACHI 86B PRL 57 1990 J.F. Abachi et al. (PURD, ANL, IND, MICH+)
AIHARA 86B PRL 57 404 H. Aihara et al. (TPC-2 gamma Collab.)
ALDE 86D NP B269 485 D.M. Alde et al. (BELG, LAPP, SERP, CERN+)
LANDRO 86 PL B172 445 M. Landro, K.J. Mork, H.A. Olsen (UTRO)
LONGACRE 86 PL B177 223 R.S. Longacre et al. (BNL, BRAN, CERN+)
LYTH 85 JP G11 459 D.L. Lyth
BEHREND 84B ZPHY C23 223 H.J. Behrend et al. (CELLO Collab.)
BERGER 84 ZPHY C26 199 C. Berger et al. (PLUTO Collab.)
COURAU 84 PL 147B 227 A. Courau et al. (CIT, SLAC)
SMITH 84C PR D30 851 J.R. Smith et al. (SLAC, LBL, HARV)
BINON 83 NC 78A 313 F.G. Binon et al. (BELG, LAPP, SERP+)
Also SJNP 38 561 F.G. Binon et al. (BELG, LAPP, SERP+)
Translated from YAF 38 934.
CHABAUD 83 NP B223 1 V. Chabaud et al. (CERN, CRAC, MPIM)
DENNEY 83 PR D28 2726 D.L. Denney et al. (IOWA, MICH)
MENNESSIER 83 ZPHY C16 241 G. Mennessier (MONP)
APEL 82 NP B201 197 W.D. Apel et al. (KARLK, KARLE, PISA, SERP+)
CASON 82 PRL 48 1316 N.M. Cason et al. (NDAM, ANL)
EDWARDS 82F PL 110B 82 C. Edwards et al. (CIT, HARV, PRIN+)
ETKIN 82B PR D25 1786 A. Etkin et al. (BNL, CUNY, TUFTS, VAND)
BRANDELK 81B ZPHY C10 117 R. Brandelik et al. (TASSO Collab.)
CHABAUD 81 APP B12 575 V. Chabaud et al. (CERN, CRAC, MPIM)
GIDAL 81 PL 107B 153 G. Gidal et al. (SLAC, LBL)
ROUSSARIE 81 PL 105B 304 A. Roussarie et al. (SLAC, LBL)
BERGER 80B PL 94B 254 C. Berger et al. (PLUTO Collab.)
COSTA 80 NP B175 402 G. Costa et al. (BARI, BONN, CERN, GLAS+)
LOVERRE 80 ZPHY C6 187 P.F. Loverre et al. (CERN, CDF, MADR+)
CORDEN 79 NP B157 250 M.J. Corden et al. (BIRM, RHEL, TELA+)
MARTIN 79 NP B158 520 A.D. Martin, E.N. Ozmutlu (DURH)
POLYCHRO... 79 PR D19 1317 V.A. Polychronakos et al. (NDAM, ANL)
PDG 78 PL 75B 1 C. Brifman et al.
ANTIPOV 77 NP B119 45 Y.M. Antipov et al. (SERP, GEVA)
PAWLICKI 77 PR D15 3196 A.J. Pawlicki et al. (ANL)
DEUTSCH... 76 NP B103 426 M. Deuschmann et al. (AACH3, BERL, BONN+)
APEL 75 PL 57B 398 W.D. Apel et al. (KARLK, KARLE, PISA, SERP+)
EMMS 75D NP B96 155 M.J. Emms et al. (BIRM, DURH, RHEL)
EISENBERG 74 PL 52B 239 Y. Eisenberg et al. (REHO)
ENGLER 74 PR D10 2070 A. Engler et al. (CMU, CASE)
LOUIE 74 PL 48B 385 J. Louie et al. (SACL, CERN)
ANDERSON 73 PRL 31 562 J.C. Anderson et al. (CMU, CASE)
TAKAHASHI 72 PR D6 1266 K. Takahashi et al. (TOHOK, PENN, NDAM+)
BEAUPRE 71 NP B28 77 J.V. Beaupre et al. (AACH, BERL, CERN)
FLATTE 71 PL 34B 551 S.M. Flatte et al. (LBL)
ARMENISE 70 LNC 4 199 N. Armenise et al. (BARI, BGNA, FIRZ)
OH 70 PR D1 2494 B.Y. Oh et al. (WISC, TNTO) JP
STUNTEBECK 70 PL 32B 391 P.H. Stuntebeck et al. (NDAM)
ADERHOLZ 69 NP B11 259 M. Aderholz et al. (AACH3, BERL, CERN+)
ARMENISE 68 NC 54A 999 N. Armenise et al. (BARI, BGNA, FIRZ+)
ASCOLI 68D PRL 21 1712 G. Ascoli et al. (ILL)
BOESEBECK 68 NP B4 501 K. Boesebeck et al. (AACH, BERL, CERN)

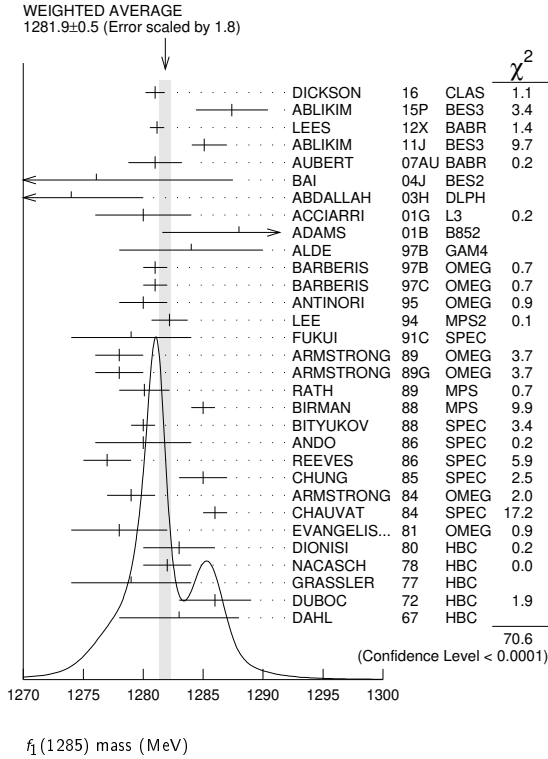
1 Using the 2pi+2pi- and pi+pi- eta modes of f1(1285) decay.



# Meson Particle Listings

## $f_1(1285)$

- <sup>2</sup>The selected process is  $J/\psi \rightarrow \omega a_0(980)\pi$ .
- <sup>3</sup>Supersedes ABATZIS 94, ARMSTRONG 89E.
- <sup>4</sup>From partial wave analysis of  $K^+ \bar{K}^0 \pi^-$  system.
- <sup>5</sup>No systematic error given.
- <sup>6</sup>From a unitarized quark-model calculation.
- <sup>7</sup>From phase shift analysis of  $\eta\pi^+\pi^-$  system.
- <sup>8</sup>Seen in the missing mass spectrum.



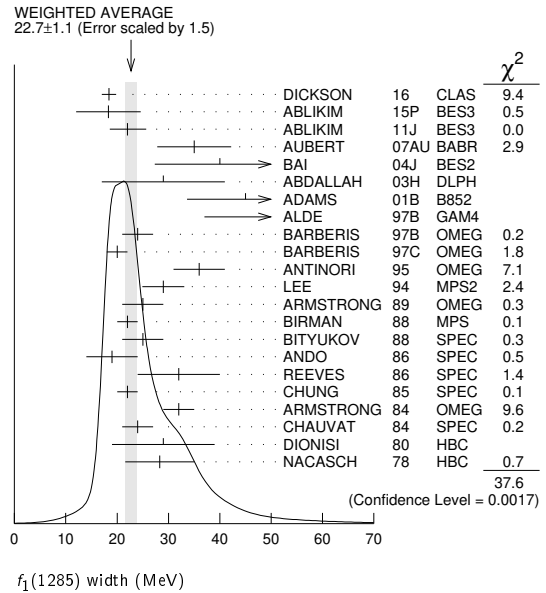
### $f_1(1285)$ WIDTH

Only experiments giving width error less than 20 MeV are kept for averaging.

VALUE (MeV)	EVTS	DOCUMENT ID	TECN	COMMENT
<b>22.7 ± 1.1 OUR AVERAGE</b>		Error includes scale factor of 1.5. See the ideogram below.		
18.4 ± 1.4		DICKSON 16	CLAS	2.55 $\gamma p \rightarrow \eta\pi^+\pi^-p$
18.3 ± 6.3	87	ABLIKIM 15P	BES3	$J/\psi \rightarrow K^+K^-3\pi$
22.0 ± 3.1 ± <sup>2.0</sup> / <sub>1.5</sub>		<sup>1</sup> ABLIKIM 11J	BES3	$J/\psi \rightarrow \omega(\eta\pi^+\pi^-)$
35 ± 6 ± 4		AUBERT 07AU	BABR	10.6 $e^+e^- \rightarrow f_1(1285)\pi^+\pi^-\gamma$
40.0 ± 8.6 ± 9.3	203	BAI 04J	BES2	$J/\psi \rightarrow \gamma\gamma\pi^+\pi^-$
29 ± 12	237	ABDALLAH 03H	DLPH	91.2 $e^+e^- \rightarrow K_S^0 K^\pm \pi^\mp + X$
45 ± 9 ± 7	20k	ADAMS 01B	B852	18 GeV $\pi^-p \rightarrow K^+K^-\pi^0n$
55 ± 18	1400	ALDE 97B	GAM4	100 $\pi^-p \rightarrow \eta\pi^0\pi^0n$
24 ± 3		BARBERIS 97B	OMEG	450 $pp \rightarrow pp2(\pi^+\pi^-)$
20 ± 2		BARBERIS 97C	OMEG	450 $pp \rightarrow ppK_S^0 K^\pm \pi^\mp$
36 ± 5		<sup>2</sup> ANTINORI 95	OMEG	300,450 $pp \rightarrow pp2(\pi^+\pi^-)$
29.0 ± 4.1		LEE 94	MPS2	18 $\pi^-p \rightarrow K^+ \bar{K}^0 2\pi^-p$
25 ± 4	140	ARMSTRONG 89	OMEG	300 $pp \rightarrow K \bar{K} \pi pp$
22 ± 2	4750	<sup>3</sup> BIRMAN 88	MPS	8 $\pi^-p \rightarrow K^+ \bar{K}^0 \pi^-n$
25 ± 4	504	BITYUKOV 88	SPEC	32.5 $\pi^-p \rightarrow K^+K^-\pi^0n$
19 ± 5		ANDO 86	SPEC	8 $\pi^-p \rightarrow \eta\pi^+\pi^-n$
32 ± 8	420	REEVES 86	SPEC	6.6 $p\bar{p} \rightarrow K K \pi X$
22 ± 2		CHUNG 85	SPEC	8 $\pi^-p \rightarrow N K \bar{K} \pi$
32 ± 3	604	ARMSTRONG 84	OMEG	85 $\pi^+p \rightarrow K \bar{K} \pi \pi p$ , $pp \rightarrow K \bar{K} \pi pp$
24 ± 3		CHAUVAT 84	SPEC	ISR 31.5 $pp$
29 ± 10	103	DIONISI 80	HBC	4 $\pi^-p \rightarrow K \bar{K} \pi n$
28.3 ± 6.7	320	NACASCH 78	HBC	0.7,0.76 $p\bar{p} \rightarrow K \bar{K} 3\pi$
• • • We do not use the following data for averages, fits, limits, etc. • • •				
17.1 ± 3.4	234	ABLIKIM 19BA	BES3	$e^+e^- \rightarrow \psi(2S)$
32.4 ± 5.8		<sup>4</sup> AAIJ 14Y	LHCB	$\bar{B}^0(s) \rightarrow J/\psi 2(\pi^+\pi^-)$
18.2 ± 1.2		<sup>4</sup> SOSA 99	SPEC	$pp \rightarrow p_{slow} (K_S^0 K^+\pi^-)_{P_{fast}}$

19.4 ± 1.5		<sup>4</sup> SOSA 99	SPEC	$pp \rightarrow p_{slow} (K_S^0 K^+\pi^-)_{P_{fast}}$
40 ± 5		ABATZIS 94	OMEG	450 $pp \rightarrow pp2(\pi^+\pi^-)$
31 ± 5		ARMSTRONG 89E	OMEG	300 $pp \rightarrow pp2(\pi^+\pi^-)$
41 ± 12		ARMSTRONG 89G	OMEG	85 $\pi^+p \rightarrow 4\pi\pi p$ , $pp \rightarrow 4\pi pp$
17.9 ± 10.9	60	RATH 89	MPS	21.4 $\pi^-p \rightarrow K_S^0 K_S^0 \pi^0 n$
14 + <sup>20</sup> / <sub>-14</sub> ± 10	16	BECKER 87	MRK3	$e^+e^- \rightarrow \phi K \bar{K} \pi$
26 ± 12		EVANGELIS... 81	OMEG	12 $\pi^-p \rightarrow \eta\pi^+\pi^-\pi^-p$
25 ± 15	200	GURTU 79	HBC	4.2 $K^-p \rightarrow \eta\eta 2\pi$
~ 10		<sup>5</sup> STANTON 79	CNTR	8.5 $\pi^-p \rightarrow n2\gamma 2\pi$
24 ± 18	210	GRASSLER 77	HBC	16 $\pi^+p$
28 ± 5	150	<sup>6</sup> DEFOIX 72	HBC	0.7 $p\bar{p} \rightarrow 7\pi$
46 ± 9	180	DUBOC 72	HBC	1.2 $p\bar{p} \rightarrow 2K 4\pi$
37 ± 5	500	<sup>7</sup> THUN 72	MMS	13.4 $\pi^-p$
10 ± 10		BOESEBECK 71	HBC	16.0 $\pi p \rightarrow p5\pi$
30 ± 15		CAMPBELL 69	DBC	2.7 $\pi^+d$
60 ± 15		<sup>6</sup> LORSTAD 69	HBC	0.7 $p\bar{p}$ , 4,5-body
35 ± 10		<sup>6</sup> DAHL 67	HBC	1.6-4.2 $\pi^-p$

- <sup>1</sup>The selected process is  $J/\psi \rightarrow \omega a_0(980)\pi$ .
- <sup>2</sup>Supersedes ABATZIS 94, ARMSTRONG 89E.
- <sup>3</sup>From partial wave analysis of  $K^+ \bar{K}^0 \pi^-$  system.
- <sup>4</sup>No systematic error given.
- <sup>5</sup>From phase shift analysis of  $\eta\pi^+\pi^-$  system.
- <sup>6</sup>Resolution is not unfolded.
- <sup>7</sup>Seen in the missing mass spectrum.



### $f_1(1285)$ DECAY MODES

Mode	Fraction ( $\Gamma_i/\Gamma$ )	Scale factor/ Confidence level
$\Gamma_1$ $4\pi$	(32.7 ± 1.9) %	S=1.2
$\Gamma_2$ $\pi^0\pi^0\pi^+\pi^-$	(21.8 ± 1.3) %	S=1.2
$\Gamma_3$ $2\pi^+2\pi^-$	(10.9 ± 0.6) %	S=1.2
$\Gamma_4$ $\rho^0\pi^+\pi^-$	(10.9 ± 0.6) %	S=1.2
$\Gamma_5$ $\rho^0\rho^0$	seen	
$\Gamma_6$ $4\pi^0$	< 7 × 10 <sup>-4</sup>	CL=90%
$\Gamma_7$ $\eta\pi^+\pi^-$	(35 ± 15) %	
$\Gamma_8$ $\eta\pi\pi$	(52.2 ± 2.0) %	S=1.2
$\Gamma_9$ $a_0(980)\pi$ [ignoring $a_0(980) \rightarrow K \bar{K}$ ]	(38 ± 4) %	
$\Gamma_{10}$ $\eta\pi\pi$ [excluding $a_0(980)\pi$ ]	(14 ± 4) %	
$\Gamma_{11}$ $K \bar{K} \pi$	(9.0 ± 0.4) %	S=1.1
$\Gamma_{12}$ $K \bar{K}^*(892)$	not seen	
$\Gamma_{13}$ $\pi^+\pi^-\pi^0$	(3.0 ± 0.9) × 10 <sup>-3</sup>	
$\Gamma_{14}$ $\rho^\pm\pi^\mp$	< 3.1 × 10 <sup>-3</sup>	CL=95%
$\Gamma_{15}$ $\gamma\rho^0$	(6.1 ± 1.0) %	S=1.7
$\Gamma_{16}$ $\phi\gamma$	(7.4 ± 2.6) × 10 <sup>-4</sup>	
$\Gamma_{17}$ $e^+e^-$	< 9.4 × 10 <sup>-9</sup>	CL=90%
$\Gamma_{18}$ $\gamma\gamma^*$		
$\Gamma_{19}$ $\gamma\gamma$		

See key on page 999

Meson Particle Listings

$f_1(1285)$

CONSTRAINED FIT INFORMATION

An overall fit to 6 branching ratios uses 18 measurements and one constraint to determine 5 parameters. The overall fit has a  $\chi^2 = 24.0$  for 14 degrees of freedom.

The following *off-diagonal* array elements are the correlation coefficients  $\langle \delta x_i \delta x_j \rangle / (\delta x_i \delta x_j)$ , in percent, from the fit to the branching fractions,  $x_i \equiv \Gamma_i / \Gamma_{\text{total}}$ . The fit constrains the  $x_i$  whose labels appear in this array to sum to one.

$x_9$	-30			
$x_{10}$	-12	-88		
$x_{11}$	22	-10	-4	
$x_{15}$	-25	-7	-3	-27
	$x_1$	$x_9$	$x_{10}$	$x_{11}$

$f_1(1285) \Gamma(i) \Gamma(\gamma\gamma) / \Gamma(\text{total})$

$\Gamma(\eta\pi\pi) \times \Gamma(\gamma\gamma) / \Gamma_{\text{total}}$		$\Gamma_8 \Gamma_{19} / \Gamma = (\Gamma_9 + \Gamma_{10}) \Gamma_{19} / \Gamma$			
VALUE (keV)	CL%	DOCUMENT ID	TECN	COMMENT	
<0.62	95	GIDAL	87	MRK2	$e^+e^- \rightarrow e^+e^-\eta\pi^+\pi^-$

$\Gamma(\eta\pi\pi) \times \Gamma(\gamma\gamma^*) / \Gamma_{\text{total}}$		$\Gamma_8 \Gamma_{18} / \Gamma = (\Gamma_9 + \Gamma_{10}) \Gamma_{18} / \Gamma$			
VALUE (keV)	EVTS	DOCUMENT ID	TECN	COMMENT	
<b>1.4 ± 0.4 OUR AVERAGE</b>		Error includes scale factor of 1.4.			
1.18 ± 0.25 ± 0.20	26	1,2 AIHARA	88B	TPC	$e^+e^- \rightarrow e^+e^-\eta\pi^+\pi^-$
2.30 ± 0.61 ± 0.42		1,3 GIDAL	87	MRK2	$e^+e^- \rightarrow e^+e^-\eta\pi^+\pi^-$
••• We do not use the following data for averages, fits, limits, etc. •••					
1.8 ± 0.3 ± 0.3	420	4 ACHARD	02B	L3	183-209 $e^+e^- \rightarrow e^+e^-\eta\pi^+\pi^-$

- <sup>1</sup> Assuming a  $\rho$ -pole form factor.
- <sup>2</sup> Published value multiplied by  $\eta\pi\pi$  branching ratio 0.49.
- <sup>3</sup> Published value divided by 2 and multiplied by the  $\eta\pi\pi$  branching ratio 0.49.
- <sup>4</sup> Published value multiplied by the  $\eta\pi\pi$  branching ratio 0.52.

$f_1(1285)$  BRANCHING RATIOS

$\Gamma(K\bar{K}\pi) / \Gamma(4\pi)$		$\Gamma_{11} / \Gamma_1$			
VALUE	DOCUMENT ID	TECN	COMMENT		
<b>0.274 ± 0.017 OUR FIT</b>	Error includes scale factor of 1.4.				
<b>0.271 ± 0.016 OUR AVERAGE</b>	Error includes scale factor of 1.2.				
0.265 ± 0.014	1 BARBERIS	97c	OMEG	450 $pp \rightarrow p\rho K_S^0 K^\pm \pi^\mp$	
0.28 ± 0.05	2 ARMSTRONG	89E	OMEG	300 $pp \rightarrow p\rho f_1(1285)$	
0.37 ± 0.03 ± 0.05	3 ARMSTRONG	89c	OMEG	85 $\pi p \rightarrow 4\pi X$	

- <sup>1</sup> Using  $2(\pi^+\pi^-)$  data from BARBERIS 97b.
- <sup>2</sup> Assuming  $\rho\pi\pi$  and  $a_0(980)\pi$  intermediate states.
- <sup>3</sup>  $4\pi$  consistent with being entirely  $\rho\pi\pi$ .

$\Gamma(\pi^0\pi^0\pi^+\pi^-) / \Gamma_{\text{total}}$		$\Gamma_2 / \Gamma = \frac{2}{3} \Gamma_1 / \Gamma$			
VALUE	DOCUMENT ID	TECN	COMMENT		
<b>0.218 ± 0.013 OUR FIT</b>	Error includes scale factor of 1.2.				

$\Gamma(2\pi^+2\pi^-) / \Gamma_{\text{total}}$		$\Gamma_3 / \Gamma = \frac{1}{3} \Gamma_1 / \Gamma$			
VALUE	DOCUMENT ID	TECN	COMMENT		
<b>0.109 ± 0.006 OUR FIT</b>	Error includes scale factor of 1.2.				

$\Gamma(\rho^0\pi^+\pi^-) / \Gamma_{\text{total}}$		$\Gamma_4 / \Gamma = \frac{1}{3} \Gamma_1 / \Gamma$			
VALUE	DOCUMENT ID	TECN	COMMENT		
<b>0.109 ± 0.006 OUR FIT</b>	Error includes scale factor of 1.2.				

$\Gamma(\rho^0\pi^+\pi^-) / \Gamma(2\pi^+2\pi^-)$		$\Gamma_4 / \Gamma_3$			
VALUE	DOCUMENT ID	TECN	COMMENT		
1.0 ± 0.4	GRASSLER	77	HBC	16 GeV	$\pi^\pm p$

$\Gamma(\rho^0\rho^0) / \Gamma_{\text{total}}$		$\Gamma_5 / \Gamma$			
VALUE	DOCUMENT ID	TECN	COMMENT		
seen	BARBERIS	00c	450 $pp \rightarrow p_f 4\pi p_S$		

$\Gamma(4\pi^0) / \Gamma_{\text{total}}$		$\Gamma_6 / \Gamma$			
VALUE (units $10^{-4}$ )	CL%	DOCUMENT ID	TECN	COMMENT	
<7	90	ALDE	87	GAM4	100 $\pi^- p \rightarrow 4\pi^0 n$

$\Gamma(\pi^+\pi^-\pi^0) / \Gamma(\eta\pi^+\pi^-)$		$\Gamma_{13} / \Gamma_7$			
VALUE (%)	EVTS	DOCUMENT ID	TECN	COMMENT	
<b>0.86 ± 0.16 ± 0.20</b>	2.3k	1 DOROFEEV	11	VES	$\pi^- N \rightarrow \pi^- f_1(1285) N$

- <sup>1</sup> Value obtained selecting the region corresponding to  $f_0(980)$  in the  $\pi^+\pi^-$  mass spectrum.

$\Gamma(\eta\pi\pi) / \Gamma_{\text{total}}$		$\Gamma_8 / \Gamma = (\Gamma_9 + \Gamma_{10}) / \Gamma$			
VALUE	DOCUMENT ID	TECN	COMMENT		
<b>0.522 ± 0.020 OUR FIT</b>	Error includes scale factor of 1.2.				

$\Gamma(4\pi) / \Gamma(\eta\pi\pi)$

VALUE	DOCUMENT ID	TECN	COMMENT
<b>0.63 ± 0.06 OUR FIT</b>	Error includes scale factor of 1.3.		
<b>0.41 ± 0.14 OUR AVERAGE</b>			
0.37 ± 0.11 ± 0.11	BOLTON	92	MRK3 $J/\psi \rightarrow \gamma f_1(1285)$
0.64 ± 0.40	GURTU	79	HBC 4.2 $K^- p$
••• We do not use the following data for averages, fits, limits, etc. •••			
0.93 ± 0.30	1 GRASSLER	77	HBC 16 $\pi^\mp p$
<sup>1</sup> Assuming $\rho\pi\pi$ and $a_0(980)\pi$ intermediate states.			

$\Gamma(2\pi^+2\pi^-) / \Gamma(\eta\pi\pi)$

VALUE	DOCUMENT ID	TECN	COMMENT
<b>0.28 ± 0.02 ± 0.02</b>	1 LEES	12x	BABR $\tau^- \rightarrow \pi^- f_1(1285) \nu_\tau$
<sup>1</sup> Assuming $B(f_1(1285) \rightarrow \pi\pi\eta) = 3/2 B(f_1(1285) \rightarrow \pi^+\pi^-\eta)$ .			

$\Gamma(a_0(980)\pi \text{ [ignoring } a_0(980) \rightarrow K\bar{K}]) / \Gamma(\eta\pi\pi)$

VALUE	CL%	DOCUMENT ID	TECN	COMMENT
<b>0.72 ± 0.08 OUR FIT</b>				
<b>0.72 ± 0.07 OUR AVERAGE</b>				
0.74 ± 0.02 ± 0.09		DICKSON	16	CLAS $\gamma p \rightarrow f_1(1285) p$
0.72 ± 0.15		GURTU	79	HBC 4.2 $K^- p$
0.6 $\begin{smallmatrix} +0.3 \\ -0.2 \end{smallmatrix}$		CORDEN	78	OMEG 12-15 $\pi^- p$
••• We do not use the following data for averages, fits, limits, etc. •••				
>0.69	95	ACHARD	02B	L3 183-209 $e^+e^- \rightarrow e^+e^-\eta\pi^+\pi^-$
0.28 ± 0.07		ALDE	97B	GAM4 100 $\pi^- p \rightarrow \eta\pi^0\pi^0 n$
1.0 ± 0.3		GRASSLER	77	HBC 16 $\pi^\mp p$

$\Gamma(K\bar{K}\pi) / \Gamma(\eta\pi\pi)$

VALUE	DOCUMENT ID	TECN	COMMENT
<b>0.172 ± 0.012 OUR FIT</b>	Error includes scale factor of 1.1.		
<b>0.176 ± 0.012 OUR AVERAGE</b>			
0.216 ± 0.010 ± 0.031	DICKSON	16	CLAS $\gamma p \rightarrow f_1(1285) p$
0.166 ± 0.01 ± 0.008	BARBERIS	98c	OMEG 450 $pp \rightarrow p_f f_1(1285) p_S$
0.42 ± 0.15	GURTU	79	HBC 4.2 $K^- p$
0.5 ± 0.2	1 CORDEN	78	OMEG 12-15 $\pi^- p$
0.20 ± 0.08	2 DEFOIX	72	HBC 0.7 $\bar{p} p \rightarrow 7\pi$
0.16 ± 0.08	CAMPBELL	69	DBC 2.7 $\pi^+ d$

- <sup>1</sup> CORDEN 78 assumes low-mass  $\eta\pi\pi$  region is dominantly  $1^{++}$ . See BARBERIS 98c and MANAK 00a for discussion.
- <sup>2</sup>  $K\bar{K}$  system characterized by the  $l = 1$  threshold enhancement. (See under  $a_0(980)$ ).

$\Gamma(K\bar{K}^*(892)) / \Gamma_{\text{total}}$

VALUE	DOCUMENT ID	TECN	COMMENT
not seen	NACASCH	78	HBC 0.7, 0.76 $\bar{p} p \rightarrow K\bar{K} 3\pi$
••• We do not use the following data for averages, fits, limits, etc. •••			
seen	1 ACHARD	07	L3 183-209 $e^+e^- \rightarrow e^+e^- K_S^0 K^\pm \pi^\mp$
<sup>1</sup> A clear signal of 19.8 ± 4.4 events observed at high $Q^2$ .			

$\Gamma(\pi^+\pi^-\pi^0) / \Gamma_{\text{total}}$

VALUE (%)	EVTS	DOCUMENT ID	TECN	COMMENT
<b>0.30 ± 0.055 ± 0.074</b>	2.3k	1 DOROFEEV	11	VES $\pi^- N \rightarrow \pi^- f_1(1285) N$
<sup>1</sup> Value obtained selecting the region corresponding to $f_0(980)$ in the $\pi^+\pi^-$ mass spectrum. The systematic error includes the uncertainty on the partial width $f_1 \rightarrow \eta\pi\pi$ obtained from PDG 10 data.				

$\Gamma(\rho^\pm\pi^\mp) / \Gamma_{\text{total}}$

VALUE (%)	CL%	DOCUMENT ID	TECN	COMMENT
<0.31	95	DOROFEEV	11	VES $\pi^- N \rightarrow \pi^- f_1(1285) N$

$\Gamma(\gamma\rho^0) / \Gamma_{\text{total}}$

VALUE (units $10^{-2}$ )	CL%	DOCUMENT ID	TECN	COMMENT
<b>6.1 ± 1.0 OUR FIT</b>	Error includes scale factor of 1.7.			
••• We do not use the following data for averages, fits, limits, etc. •••				
2.8 ± 0.7 ± 0.6		1 AMELIN	95	VES 37 $\pi^- N \rightarrow \pi^- \pi^+ \pi^- \gamma N$
<5	95	BITYUKOV	91B	SPEC 32 $\pi^- p \rightarrow \pi^+ \pi^- \gamma n$
<sup>1</sup> Not an independent measurement.				

$\Gamma(\gamma\rho^0) / \Gamma(2\pi^+2\pi^-)$

VALUE	DOCUMENT ID	TECN	COMMENT
<b>0.55 ± 0.10 OUR FIT</b>	Error includes scale factor of 1.5.		
<b>0.45 ± 0.18</b>	1 COFFMAN	90	MRK3 $J/\psi \rightarrow \gamma\gamma\pi^+\pi^-$
<sup>1</sup> Using $B(J/\psi \rightarrow \gamma f_1(1285) \rightarrow \gamma\gamma\rho^0) = 0.25 \times 10^{-4}$ and $B(J/\psi \rightarrow \gamma f_1(1285) \rightarrow \gamma 2\pi^+ 2\pi^-) = 0.55 \times 10^{-4}$ given by MIR 88.			

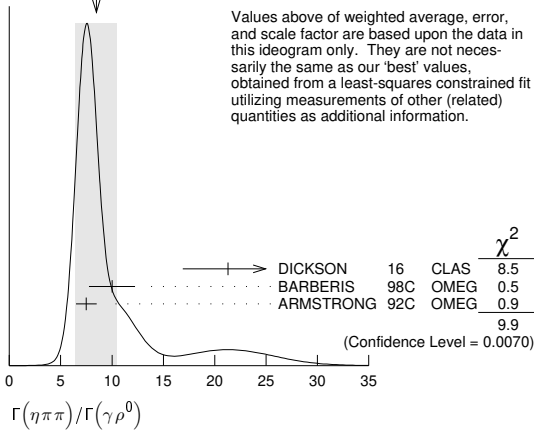
$\Gamma(\eta\pi\pi) / \Gamma(\gamma\rho^0)$

VALUE	DOCUMENT ID	TECN	COMMENT
<b>8.6 ± 1.6 OUR FIT</b>	Error includes scale factor of 1.9.		
<b>8.5 ± 2.0 OUR AVERAGE</b>	Error includes scale factor of 2.2. See the ideogram below.		
21.3 ± 4.4	DICKSON	16	CLAS $\gamma p \rightarrow f_1(1285) p$
10.0 ± 1.0 ± 2.0	BARBERIS	98c	OMEG 450 $pp \rightarrow p_f f_1(1285) p_S$
7.5 ± 1.0	1 ARMSTRONG	92c	OMEG 300 $pp \rightarrow pp\pi^+\pi^-\gamma, pp\eta\pi^+\pi^-$
<sup>1</sup> Published value multiplied by 1.5.			

# Meson Particle Listings

## $f_1(1285), \eta(1295)$

WEIGHTED AVERAGE  
8.5±2.0 (Error scaled by 2.2)



Values above of weighted average, error, and scale factor are based upon the data in this ideogram only. They are not necessarily the same as our 'best' values, obtained from a least-squares constrained fit utilizing measurements of other (related) quantities as additional information.

### $\Gamma(\gamma\rho^0)/\Gamma(K\bar{K}\pi)$ Γ<sub>15</sub>/Γ<sub>11</sub>

VALUE	CL%	DOCUMENT ID	TECN	COMMENT
••• We do not use the following data for averages, fits, limits, etc. •••				
>0.035	90	<sup>1</sup> COFFMAN 90	MRK3	$J/\psi \rightarrow \gamma\gamma\pi^+\pi^-$
<sup>1</sup> Using $B(J/\psi \rightarrow \gamma f_1(1285) \rightarrow \gamma\gamma\rho^0) = 0.25 \times 10^{-4}$ and $B(J/\psi \rightarrow \gamma f_1(1285) \rightarrow \gamma K\bar{K}\pi) < 0.72 \times 10^{-3}$ .				

### $\Gamma(\phi\gamma)/\Gamma(K\bar{K}\pi)$ Γ<sub>16</sub>/Γ<sub>11</sub>

VALUE (units 10 <sup>-2</sup> )	CL%	EVTS	DOCUMENT ID	TECN	COMMENT
<b>0.82 ± 0.21 ± 0.20</b>		19	BITYUKOV 88	SPEC	$32.5 \pi^- \rho \rightarrow K^+ K^- \pi^0 n$
••• We do not use the following data for averages, fits, limits, etc. •••					
<0.50	95		BARBERIS 98C	OMEG	$450 p\rho \rightarrow p f_1(1285) \rho_S$
<0.93	95		AMELIN 95	VES	$37 \pi^- N \rightarrow \pi^- \pi^+ \pi^- \gamma N$

### $\Gamma(e^+e^-)/\Gamma_{total}$ Γ<sub>17</sub>/Γ

VALUE	CL%	DOCUMENT ID	TECN	COMMENT
<b>&lt;9.4 × 10<sup>-9</sup></b>	90	<sup>1</sup> ACHASOV 20	SND	$e^+e^- \rightarrow \eta\pi^0\pi^0$
<sup>1</sup> ACHASOV 20 reports two candidate events corresponding to a significance of 2.5 σ and the branching fraction of $(5.1^{+3.7}_{-2.7}) \times 10^{-9}$ .				

### f<sub>1</sub>(1285) REFERENCES

ACHASOV 20	PL B800 135074	M.N. Achasov et al.	(SND Collab.)
ABLIKIM 19BA	PR D100 092003	M. Ablikim et al.	(BESIII Collab.)
DICKSON 16	PR C93 065202	R. Dickson et al.	(JLab CLAS Collab.)
ABLIKIM 15P	PR D92 012007	M. Ablikim et al.	(BESIII Collab.)
AAJ 14Y	PRL 112 091802	R. Aaij et al.	(LHCb Collab.)
LEES 12X	PR D86 092010	J.P. Lees et al.	(BABAR Collab.)
ABLIKIM 11J	PRL 107 182001	M. Ablikim et al.	(BESIII Collab.)
DOROFEEV 11	EPJ A47 48	V. Dorofeev et al.	(SERP, MIPT)
PDG 10	JP G37 075021	K. Nakamura et al.	(PDG Collab.)
ACHARD 07	JHEP 0703 018	P. Achard et al.	(L3 Collab.)
AUBERT 07AU	PR D76 092005	B. Aubert et al.	(BABAR Collab.)
BAI 04J	PL B594 47	J.Z. Bai et al.	(BES Collab.)
ABDALLAH 03H	PL B569 129	J. Abdallah et al.	(DELPHI Collab.)
ACHARD 02B	PL B526 269	P. Achard et al.	(L3 Collab.)
ACCIARRI 01G	PL B501 1	M. Acciarri et al.	(L3 Collab.)
ADAMS 01B	PL B516 264	G.S. Adams et al.	(BNL E852 Collab.)
BARBERIS 00C	PL B471 440	D. Barberis et al.	(WA 102 Collab.)
MANAK 00A	PR D62 012003	J.J. Manak et al.	(BNL E852 Collab.)
SOSA 99	PRL 83 913	M. Sosa et al.	
BARBERIS 98C	PL B440 225	D. Barberis et al.	(WA 102 Collab.)
ALDE 97B	PAN 60 386	D. Alde et al.	(GAMS Collab.)
Translated from YAF 60 458.			
BARBERIS 97B	PL B413 217	D. Barberis et al.	(WA 102 Collab.)
BARBERIS 97C	PL B413 225	D. Barberis et al.	(WA 102 Collab.)
AMELIN 95	ZPHY C66 71	D.V. Amelin et al.	(VES Collab.)
ANTINORI 95	PL B353 589	F. Antinori et al.	(ATHU, BARI, BIRM+)
ABATZIS 94	PL B324 509	S. Abatzis et al.	(ATHU, BARI, BIRM+)
LEE 94	PL B323 227	M. Lee et al.	(BNL, IND, KYUIN, MASD+)
ARMSTRONG 93C	PL B307 394	T.A. Armstrong et al.	(FNAL, FERR, GENO+)
ARMSTRONG 92C	ZPHY C54 371	T.A. Armstrong et al.	(ATHU, BARI, BIRM+)
BOLTON 92	PL B278 495	T. Bolton et al.	(Mark III Collab.)
BITYUKOV 91B	SJNP 54 318	S.I. Bityukov et al.	(SERP)
Translated from YAF 54 529.			
FUKUI 91C	PL B267 293	S. Fukui et al.	(SUGI, NAGO, KEK, KYOT+)
COFFMAN 90	PR D41 1410	D.M. Coffman et al.	(Mark III Collab.)
ARMSTRONG 89	PL B221 216	T.A. Armstrong et al.	(CERN, CDEF, BIRM+)
ARMSTRONG 89E	PL B228 536	T.A. Armstrong, M. Benayoun	(ATHU, BARI, BIRM+)
ARMSTRONG 89G	ZPHY C43 55	T.A. Armstrong et al.	(CERN, BIRM, BARI+)
RATH 89	PR D40 693	M.G. Rath et al.	(NDAM, BRAN, BNL, CUNY+)
AIHARA 88B	PL B209 107	H. Aihara et al.	(TPC-2γ Collab.)
BIRMAN 88	PRL 61 1557	A. Birman et al.	(BNL, FSU, IND, MASD)JP
BITYUKOV 88	PL B203 327	S.I. Bityukov et al.	(SERP)
MIR 88	Photon-Photon 88, 126	R. Mir	(Mark III Collab.)
Conference			
ALDE 87	PL B198 286	D.M. Alde et al.	(LANL, BRUX, SERP, LAPP)
BECKER 87	PRL 59 186	J.J. Becker et al.	(Mark III Collab.)
GIDAL 87	PRL 59 2012	G. Gidal et al.	(LBL, SLAC, HARV)
ANDO 86	PRL 57 1296	A. Ando et al.	(KEK, KYOT, NIRS, SAGA+)JP

REEVES 86	PR D34 1960	D.F. Reeves et al.	(FLOR, BNL, IND+)JP
CHUNG 85	PRL 55 779	S.U. Chung et al.	(BNL, FLOR, IND+)JP
ARMSTRONG 84	PL 146B 273	T.A. Armstrong et al.	(ATHU, BARI, BIRM+)JP
BITYUKOV 84B	PL 144B 133	S.I. Bityukov et al.	(SERP)
CHAUVAT 84	PL 148B 382	P. Chauvat et al.	(CERN, CLER, UCLA+)
TORNQVIST 82B	NP B203 268	N.A. Tornqvist	(HELS)
EVANGELIS... 81	NP B178 197	C. Evangelista et al.	(BARI, BONN, CERN+)
BROMBERG 80	PR D22 1513	C.M. Bromberg et al.	(CIT, FNAL, ILLC+)
DIONISI 80	NP B169 1	C. Dionisi et al.	(CERN, MADR, CDEF+)
GURTU 79	NP B151 181	A. Gurto et al.	(CERN, ZEEM, NIJM, OXF)
STANTON 79	PRL 42 346	N.R. Stanton et al.	(OSU, CARL, MCGI+)
CORDEN 78	NP B144 253	M.J. Corden et al.	(BIRM, RHEL, TELA+)
NACASCH 78	NP B135 203	R. Nacasch et al.	(PARIS, MADR, CERN)
GRASSLER 77	NP B121 189	H. Grassler et al.	(AACH3, BERL, BONN+)
DEFOIX 72	NP B44 125	C. Defoix et al.	(CDEF, CERN)
DUBOC 72	NP B46 429	J. Duboc et al.	(PARIS, LIVP)
THUN 72	PRL 28 1733	R. Thun et al.	(STON, NEAS)
BARDADIN... 71	PR D4 2711	M. Bardadin-Otwinowska et al.	(WARSA)
BOESEBECK 71	PL 34B 659	K. Boesebeck	(AACH, BERL, BONN, CERN, CRAC+)
CAMPBELL 69	PRL 22 1204	J.H. Campbell et al.	(RURD)
LORSTAD 69	NP B14 63	B. Lorstad et al.	(CDEF, CERN)JP
D'ANDLAU 68	NP B5 693	C. d'Andlau et al.	(CDEF, CERN, IRAD+)JP
DAHL 67	PR 163 1377	O.I. Dahl et al.	(LRL)JP

## $\eta(1295)$

$$J^{PC} = 0^+(0^-)$$

See the review on "Pseudoscalar and pseudovector mesons in the 1400 MeV region."

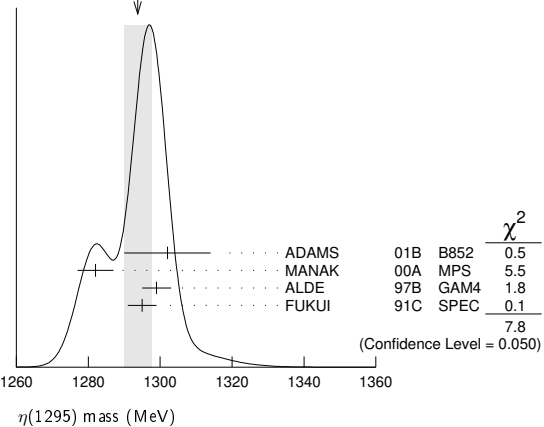
### η(1295) MASS

VALUE (MeV)	EVTS	DOCUMENT ID	TECN	COMMENT
<b>1294 ± 4 OUR AVERAGE</b>	Error	includes scale factor of 1.6. See the ideogram below.		
1302 ± 9 ± 8	20k	ADAMS	01B B852	18 GeV $\pi^- \rho \rightarrow K^+ K^- \pi^0 n$
1282 ± 5	9082	MANAK	00A MPS	18 $\pi^- \rho \rightarrow \eta\pi^+\pi^- n$
1299 ± 4	2100	ALDE	97B GAM4	100 $\pi^- \rho \rightarrow \eta\pi^0\pi^0 n$
1295 ± 4		FUKUI	91C SPEC	8.95 $\pi^- \rho \rightarrow \eta\pi^+\pi^- n$

••• We do not use the following data for averages, fits, limits, etc. •••

1264 ± 8		<sup>1</sup> AUGUSTIN 90	DM2	$J/\psi \rightarrow \gamma\eta\pi^+\pi^-$
~ 1275		STANTON 79	CNTR	$8.4 \pi^- \rho \rightarrow n\eta 2\pi$

WEIGHTED AVERAGE  
1294±4 (Error scaled by 1.6)



<sup>1</sup> PWA analysis of AUGUSTIN 92 assigns 0<sup>-+</sup> quantum numbers to this state rather than 1<sup>++</sup> as before.

### η(1295) WIDTH

VALUE (MeV)	EVTS	DOCUMENT ID	TECN	COMMENT
<b>55 ± 5 OUR AVERAGE</b>				
57 ± 23 ± 21	20k	ADAMS	01B B852	18 GeV $\pi^- \rho \rightarrow K^+ K^- \pi^0 n$
66 ± 13	9082	MANAK	00A MPS	18 $\pi^- \rho \rightarrow \eta\pi^+\pi^- n$
53 ± 6		FUKUI	91C SPEC	8.95 $\pi^- \rho \rightarrow \eta\pi^+\pi^- n$

••• We do not use the following data for averages, fits, limits, etc. •••

<40	2100	ALDE	97B GAM4	100 $\pi^- \rho \rightarrow \eta\pi^0\pi^0 n$
44 ± 20		<sup>2</sup> AUGUSTIN 90	DM2	$J/\psi \rightarrow \gamma\eta\pi^+\pi^-$
~ 70		STANTON 79	CNTR	$8.4 \pi^- \rho \rightarrow n\eta 2\pi$

<sup>2</sup> PWA analysis of AUGUSTIN 92 assigns 0<sup>-+</sup> quantum numbers to this state rather than 1<sup>++</sup> as before.

$\eta(1295), \pi(1300)$

$\eta(1295)$  DECAY MODES

Mode	Fraction ( $\Gamma_i/\Gamma$ )
$\Gamma_1$ $\eta \pi^+ \pi^-$	seen
$\Gamma_2$ $a_0(980) \pi$	seen
$\Gamma_3$ $\gamma \gamma$	
$\Gamma_4$ $\eta \pi^0 \pi^0$	seen
$\Gamma_5$ $\eta(\pi\pi)$ -s-wave	seen
$\Gamma_6$ $\sigma \eta$	
$\Gamma_7$ $K \bar{K} \pi$	

$\eta(1295) \Gamma(i)\Gamma(\gamma\gamma)/\Gamma(\text{total})$

$\Gamma(\eta \pi^+ \pi^-) \times \Gamma(\gamma\gamma)/\Gamma_{\text{total}}$	$\Gamma_1 \Gamma_3/\Gamma$			
VALUE (keV)	CL%	DOCUMENT ID	TECN	COMMENT
<0.066	95	ACCIARRI 01G	L3	183–202 $e^+ e^- \rightarrow e^+ e^- \eta \pi^+ \pi^-$

••• We do not use the following data for averages, fits, limits, etc. •••

<0.6	90	AIHARA 88c	TPC	449±39±47 $e^+ e^- \rightarrow e^+ e^- \eta \pi^+ \pi^-$
<0.3		ANTREASYAN 87	CBAL	$e^+ e^- \rightarrow e^+ e^- \eta \pi \pi$

$\Gamma(K \bar{K} \pi) \times \Gamma(\gamma\gamma)/\Gamma_{\text{total}}$	$\Gamma_7 \Gamma_3/\Gamma$			
VALUE (keV)	CL%	DOCUMENT ID	TECN	COMMENT
<0.014	90	3,4 AHOHE 05	CLE2	10.6 $e^+ e^- \rightarrow e^+ e^- K_S^0 K^\pm \pi^\mp$

<sup>3</sup> Using  $\eta(1295)$  mass and width 1294 MeV and 55 MeV, respectively.  
<sup>4</sup> Assuming three-body phase-space decay to  $K_S^0 K^\pm \pi^\mp$ .

$\eta(1295)$  BRANCHING RATIOS

$\Gamma(a_0(980) \pi)/\Gamma_{\text{total}}$	$\Gamma_2/\Gamma$		
VALUE	DOCUMENT ID	TECN	COMMENT
not seen	BERTIN 97	OBLX	0.0 $\bar{p} p \rightarrow K^\pm(K^0) \pi^\mp \pi^+ \pi^-$
seen	BIRMAN 88	MPS	8 $\pi^- p \rightarrow K^+ \bar{K}^0 \pi^- n$
large	ANDO 86	SPEC	8 $\pi^- p \rightarrow \eta \pi^+ \pi^- n$
large	STANTON 79	CNTR	8.4 $\pi^- p \rightarrow n \eta 2\pi$

$\Gamma(a_0(980) \pi)/\Gamma(\eta \pi^0 \pi^0)$	$\Gamma_2/\Gamma_4$		
VALUE	DOCUMENT ID	TECN	COMMENT
0.65±0.10	5 ALDE 97B	GAM4	100 $\pi^- p \rightarrow \eta \pi^0 \pi^0 n$

<sup>5</sup> Assuming that  $a_0(980)$  decays only to  $\eta \pi$ .

$\Gamma(\eta(\pi\pi)$ -s-wave)/ $\Gamma(\eta \pi^0 \pi^0)$	$\Gamma_5/\Gamma_4$		
VALUE	DOCUMENT ID	TECN	COMMENT
0.35±0.10	ALDE 97B	GAM4	100 $\pi^- p \rightarrow \eta \pi^0 \pi^0 n$

$\Gamma(a_0(980) \pi)/\Gamma(\sigma \eta)$	$\Gamma_2/\Gamma_6$			
VALUE	EVTs	DOCUMENT ID	TECN	COMMENT
0.48±0.22	9082	MANAK 00A	MPS	18 $\pi^- p \rightarrow \eta \pi^+ \pi^- n$

$\eta(1295)$  REFERENCES

AHOHE 05	PR D71 072001	R. Ahohe et al.	(CLEO Collab.)
ACCIARRI 01G	PL B501 1	M. Acciari et al.	(L3 Collab.)
ADAMS 01B	PL B516 264	G.S. Adams et al.	(BNL E852 Collab.)
MANAK 00A	PR D62 012003	J.J. Manak et al.	(BNL E852 Collab.)
ALDE 97B	PAN 60 386	D. Alde et al.	(GAMS Collab.)
Translated from YAF 60 458.			
BERTIN 97	PL B400 226	A. Bertin et al.	(OBELIX Collab.)
AUGUSTIN 92	PR D46 1951	J.E. Augustin, G. Cosme	(DM2 Collab.)
FUKUI 91C	PL B267 293	S. Fukui et al.	(SUGI, NAGO, KEK, KYOT+)
AUGUSTIN 90	PR D42 10	J.E. Augustin et al.	(DM2 Collab.)
AIHARA 88C	PR D38 1	H. Aihara et al.	(TPC-2 $\gamma$ Collab.)
BIRMAN 88	PRL 61 1557	A. Birman et al.	(BNL, FSU, IND, MASD)JP
ANTREASYAN 87	PR D36 2633	D. Antreasyan et al.	(Crystal Ball Collab.)
ANDO 86	PRL 57 1296	A. Ando et al.	(KEK, KYOT, NIRS, SAGA+)JP
STANTON 79	PRL 42 346	N.R. Stanton et al.	(OSU, CARL, MCGI+)JP

$\pi(1300)$

$$I^G(J^{PC}) = 1^-(0^{-+})$$

$\pi(1300)$  MASS

VALUE (MeV)	EVTs	DOCUMENT ID	TECN	COMMENT
-------------	------	-------------	------	---------

1300±100 OUR ESTIMATE

••• We do not use the following data for averages, fits, limits, etc. •••

1128±26±70		DARGENT 17	RVUE	$D^0 \rightarrow \pi^- \pi^+ \pi^- \pi^+$
1345±8±10	18k	<sup>1</sup> SCHEGELSKY 06	RVUE	$\gamma \gamma \rightarrow \pi^+ \pi^- \pi^0$
1200±40	90k	SALVINI 04	OBLX	$\bar{p} p \rightarrow 2\pi^+ 2\pi^-$
1343±15±24		CHUNG 02	B852	18.3 $\pi^- p \rightarrow \pi^+ \pi^- \pi^- p$

1375±40	ABELE 01	CBAR	0.0 $\bar{p} d \rightarrow \pi^- 4\pi^0 p$
1275±15	BERTIN 97D	OBLX	0.05 $\bar{p} p \rightarrow 2\pi^+ 2\pi^-$
~1114	ABELE 96	CBAR	0.0 $\bar{p} p \rightarrow 5\pi^0$
1190±30	ZIELINSKI 84	SPEC	200 $\pi^+ Z \rightarrow Z 3\pi$
1240±30	BELLINI 82	SPEC	40 $\pi^- A \rightarrow A 3\pi$
1273±50	<sup>2</sup> AARON 81	RVUE	
1342±20	BONESINI 81	OMEG	12 $\pi^- p \rightarrow p 3\pi$
~1400	DAUM 81B	SPEC	63,94 $\pi^- p$

<sup>1</sup> From analysis of L3 data at 183–209 GeV.

<sup>2</sup> Uses multichannel Aitchison-Bowler model (BOWLER 75). Uses data from DAUM 80 and DANKOWYCH 81.

$\pi(1300)$  WIDTH

VALUE (MeV)	EVTs	DOCUMENT ID	TECN	COMMENT
-------------	------	-------------	------	---------

200 to 600 OUR ESTIMATE

••• We do not use the following data for averages, fits, limits, etc. •••

314±39±66		DARGENT 17	RVUE	$D^0 \rightarrow \pi^- \pi^+ \pi^- \pi^+$
260±20±30	18k	<sup>3</sup> SCHEGELSKY 06	RVUE	$\gamma \gamma \rightarrow \pi^+ \pi^- \pi^0$
470±120	90k	SALVINI 04	OBLX	$\bar{p} p \rightarrow 2\pi^+ 2\pi^-$
449±39±47		CHUNG 02	B852	18.3 $\pi^- p \rightarrow \pi^+ \pi^- \pi^- p$
268±50		ABELE 01	CBAR	0.0 $\bar{p} d \rightarrow \pi^- 4\pi^0 p$
218±100		BERTIN 97D	OBLX	0.05 $\bar{p} p \rightarrow 2\pi^+ 2\pi^-$
~340		ABELE 96	CBAR	0.0 $\bar{p} p \rightarrow 5\pi^0$
440±80		ZIELINSKI 84	SPEC	200 $\pi^+ Z \rightarrow Z 3\pi$
360±120		BELLINI 82	SPEC	40 $\pi^- A \rightarrow A 3\pi$
580±100		<sup>4</sup> AARON 81	RVUE	
220±70		BONESINI 81	OMEG	12 $\pi^- p \rightarrow p 3\pi$
~600		DAUM 81B	SPEC	63,94 $\pi^- p$

<sup>3</sup> From analysis of L3 data at 183–209 GeV.

<sup>4</sup> Uses multichannel Aitchison-Bowler model (BOWLER 75). Uses data from DAUM 80 and DANKOWYCH 81.

$\pi(1300)$  DECAY MODES

Mode	Fraction ( $\Gamma_i/\Gamma$ )
$\Gamma_1$ $\rho \pi$	seen
$\Gamma_2$ $\pi(\pi\pi)$ -s-wave	seen
$\Gamma_3$ $\gamma \gamma$	

$\pi(1300) \Gamma(i)\Gamma(\gamma\gamma)/\Gamma(\text{total})$

$\Gamma(\rho \pi) \times \Gamma(\gamma\gamma)/\Gamma_{\text{total}}$	$\Gamma_1 \Gamma_3/\Gamma$			
VALUE (keV)	CL%	DOCUMENT ID	TECN	COMMENT
<0.085	90	ACCIARRI 97T	L3	$e^+ e^- \rightarrow e^+ e^- \pi^+ \pi^- \pi^0$
<0.8	95	<sup>5</sup> SCHEGELSKY 06	RVUE	$\gamma \gamma \rightarrow \pi^+ \pi^- \pi^0$
<0.54	90	ALBRECHT 97B	ARG	$e^+ e^- \rightarrow e^+ e^- \pi^+ \pi^- \pi^0$

<sup>5</sup> From analysis of L3 data at 183–209 GeV.

$\pi(1300)$  BRANCHING RATIOS

$\Gamma(\pi(\pi\pi)$ -s-wave)/ $\Gamma(\rho \pi)$	$\Gamma_2/\Gamma_1$				
VALUE	CL%	EVTs	DOCUMENT ID	TECN	COMMENT
2.2±0.4		90k	SALVINI 04	OBLX	$\bar{p} p \rightarrow 2\pi^+ 2\pi^-$
seen			CHUNG 02	B852	18.3 $\pi^- p \rightarrow \pi^+ 2\pi^- p$
<0.15	90		ABELE 01	CBAR	0.0 $\bar{p} d \rightarrow \pi^- 4\pi^0 p$
2.12			<sup>6</sup> AARON 81	RVUE	

<sup>6</sup> Uses multichannel Aitchison-Bowler model (BOWLER 75). Uses data from DAUM 80 and DANKOWYCH 81.

$\pi(1300)$  REFERENCES

DARGENT 17	JHEP 1705 143	P. d'Argent et al.	(HEID, BRIS)
SCHEGELSKY 06	EPJ A27 199	V.A. Schegelsky et al.	
SALVINI 04	EPJ C35 21	P. Salvini et al.	(OBELIX Collab.)
CHUNG 02	PR D65 072001	S.U. Chung et al.	(BNL E852 Collab.)
ABELE 01	EPJ C19 667	A. Abele et al.	(Crystal Barrel Collab.)
ACCIARRI 97T	PL B413 147	M. Acciari et al.	(L3 Collab.)
ALBRECHT 97B	ZPHY C74 469	H. Albrecht et al.	(ARGUS Collab.)
BERTIN 97D	PL B414 220	A. Bertin et al.	(OBELIX Collab.)
ABELE 96	PL B380 453	A. Abele et al.	(Crystal Barrel Collab.)
ZIELINSKI 84	PR D30 1855	M. Zielinski et al.	(ROCH, MINN, FNAL)
BELLINI 82	PRL 48 1697	G. Bellini et al.	(MILA, BGNA, JINR)
AARON 81	PR D24 1207	R.A. Aaron, R.S. Longacre	(NEAS, BNL)
BONESINI 81	PL 103B 75	M. Bonesini et al.	(MILA, LIVP, DARE+)
DANKOWYCH... 81	PRL 46 580	J.A. Dankowych et al.	(TNT0, BNL, CARE+)
DAUM 81B	NP B182 269	C. Daum et al.	(AMST, CERN, CRAC, MPIM+)
DAUM 80	PL 89B 281	C. Daum et al.	(AMST, CERN, CRAC, MPIM+)
BOWLER 75	NP B97 227	M.G. Bowler et al.	(OXFT, DARE)

# Meson Particle Listings

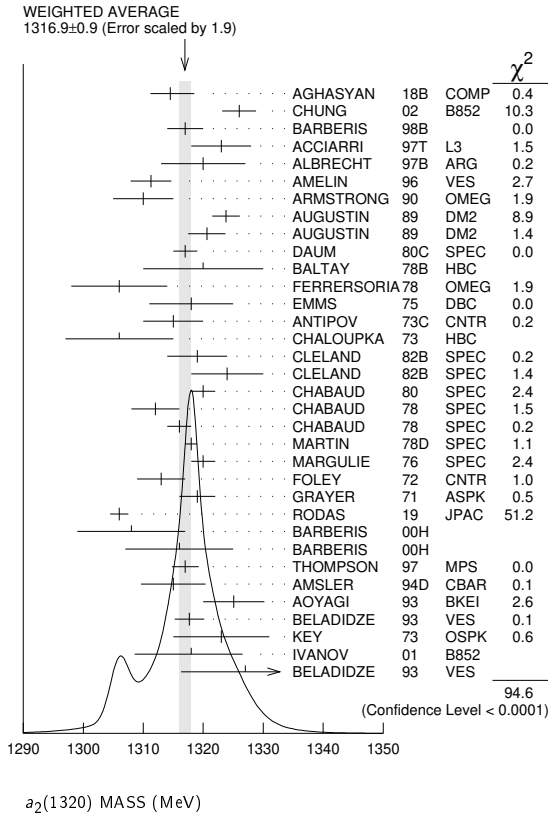
## $a_2(1320)$

**$a_2(1320)$**

$$J^G(J^{PC}) = 1^-(2^{++})$$

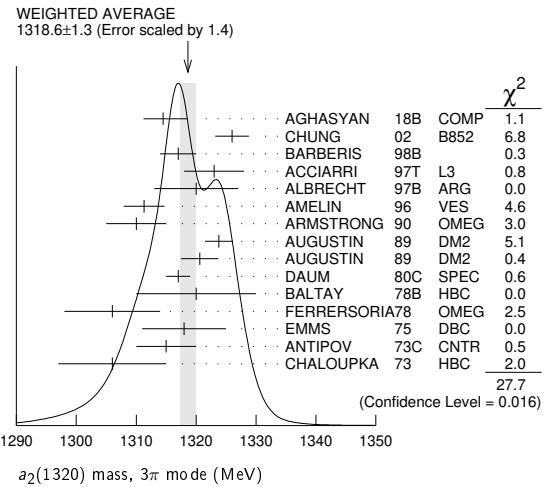
### $a_2(1320)$ MASS

VALUE (MeV) DOCUMENT ID  
**1316.9 ± 0.9 OUR AVERAGE** Includes data from the 4 datablocks that follow this one. Error includes scale factor of 1.9. See the ideogram below.



1309 ± 5	5k	BINNIE	71	MMS	-	$\pi^- p$ near $a_2$ thresh-old
1299 ± 6	28k	BOWEN	71	MMS	-	$5 \pi^- p$
1300 ± 6	24k	BOWEN	71	MMS	+	$5 \pi^+ p$
1309 ± 4	17k	BOWEN	71	MMS	-	$7 \pi^- p$
1306 ± 4	941	ALSTON...	70	HBC	+	$7.0 \pi^+ p \rightarrow 3 \pi p$

- 1 Statistical error negligible.
- 2 From a fit to  $J^P = 2^+ \rho \pi$  partial wave.
- 3 Superseded by AGHASYAN 2018B.
- 4 From analysis of L3 data at 183-209 GeV.



### $K\bar{K}$ MODE

VALUE (MeV) EVTS DOCUMENT ID TECN CHG COMMENT  
 The data in this block is included in the average printed for a previous datablock.

**1318.1 ± 0.7 OUR AVERAGE**

1319 ± 5	4700	<sup>1,2</sup> CLELAND	82B	SPEC	+	$50 \pi^+ p \rightarrow K_S^0 K^+ p$
1324 ± 6	5200	<sup>1,2</sup> CLELAND	82B	SPEC	-	$50 \pi^- p \rightarrow K_S^0 K^- p$
1320 ± 2	4000	CHABAUD	80	SPEC	-	$17 \pi^- A \rightarrow K_S^0 K^- A$
1312 ± 4	11000	CHABAUD	78	SPEC	-	$9.8 \pi^- p \rightarrow K^- K_S^0 p$
1316 ± 2	4730	CHABAUD	78	SPEC	-	$18.8 \pi^- p \rightarrow K^- K_S^0 p$
1318 ± 1		<sup>1,3</sup> MARTIN	78D	SPEC	-	$10 \pi^- p \rightarrow K_S^0 K^- p$
1320 ± 2	2724	MARGULIE	76	SPEC	-	$23 \pi^- p \rightarrow K^- K_S^0 p$
1313 ± 4	730	FOLEY	72	CNTR	-	$20.3 \pi^- p \rightarrow K^- K_S^0 p$
1319 ± 3	1500	<sup>3</sup> GRAYER	71	ASPK	-	$17.2 \pi^- p \rightarrow K^- K_S^0 p$

• • • We do not use the following data for averages, fits, limits, etc. • • •

1304 ± 10	870	<sup>4</sup> SCHEGELSKY	06A	RVUE	0	$\gamma \gamma \rightarrow K_S^0 K_S^0$
1330 ± 11	1000	<sup>1,2</sup> CLELAND	82B	SPEC	+	$30 \pi^+ p \rightarrow K_S^0 K^+ p$
1324 ± 5	350	HYAMS	78	ASPK	+	$12.7 \pi^+ p \rightarrow K^+ K_S^0 p$

- 1 From a fit to  $J^P = 2^+$  partial wave.
- 2 Number of events evaluated by us.
- 3 Systematic error in mass scale subtracted.
- 4 From analysis of L3 data at 91 and 183-209 GeV.

### $\eta \pi$ MODE

VALUE (MeV) EVTS DOCUMENT ID TECN CHG COMMENT  
 The data in this block is included in the average printed for a previous datablock.

**1312.2 ± 2.8 OUR AVERAGE** Error includes scale factor of 2.6. See the ideogram below.

1306.0 ± 0.8 ± 1.3		<sup>1</sup> RODAS	19	JPAC		$191 \pi^- p \rightarrow \eta^{(\prime)} \pi^- p$
1308 ± 9		BARBERIS	00H			$450 \rho p \rightarrow \rho f \eta \pi^0 p_S$
1316 ± 9		BARBERIS	00H			$450 \rho p \rightarrow \Delta_f^+ \eta \pi^- p_S$
1317 ± 1 ± 2		THOMPSON	97	MPS		$18 \pi^- p \rightarrow \eta \pi^- p$
1315 ± 5 ± 2		<sup>2</sup> AMSLER	94D	CBAR		$0.0 \bar{p} p \rightarrow \pi^0 \pi^0 \eta$
1325.1 ± 5.1		AOYAGI	93	BKEI		$\pi^- p \rightarrow \eta \pi^- p$
1317.7 ± 1.4 ± 2.0		BELADIDZE	93	VES		$37 \pi^- N \rightarrow \eta \pi^- N$
1323 ± 8	1000	<sup>3</sup> KEY	73	OSPK	-	$6 \pi^- p \rightarrow \rho \pi^- \eta$

• • • We do not use the following data for averages, fits, limits, etc. • • •

1307 ± 1 ± 6		<sup>4</sup> JACKURA	18	JPAC		$\pi^- p \rightarrow \eta \pi^- p$
1315 ± 12		<sup>5</sup> ADOLPH	15	COMP		$191 \pi^- p \rightarrow \eta^{(\prime)} \pi^- p$
1309 ± 4		ANISOVICH	09	RVUE		$\bar{p} p, \pi N$
1324 ± 5		ARMSTRONG	93C	E760	0	$\bar{p} p \rightarrow \pi^0 \eta \eta \rightarrow 6 \gamma$
1336.2 ± 1.7	2561	DELFOSE	81	SPEC	+	$\pi^\pm p \rightarrow \rho \pi^\pm \eta$
1330.7 ± 2.4	1653	DELFOSE	81	SPEC	-	$\pi^\pm p \rightarrow \rho \pi^\pm \eta$
1324 ± 8	6200	<sup>3,6</sup> CONFORTO	73	OSPK	-	$6 \pi^- p \rightarrow \rho \pi^- \eta$

- 1 The coupled-channel analysis of both the  $\eta \pi$  and  $\eta' \pi$  systems using ADOLPH 15data. The mass is extracted from the T-matrix pole.
- 2 The systematic error of 2 MeV corresponds to the spread of solutions.
- 3 Error includes 5 MeV systematic mass-scale error.

### 3π MODE

VALUE (MeV) EVTS DOCUMENT ID TECN CHG COMMENT  
 The data in this block is included in the average printed for a previous datablock.

**1318.6 ± 1.3 OUR AVERAGE** Error includes scale factor of 1.4. See the ideogram below.

1314.5 ± $\begin{smallmatrix} 4.0 \\ 3.3 \end{smallmatrix}$	46M	<sup>1</sup> AGHASYAN	18B	COMP		$190 \pi^- p \rightarrow \pi^- \pi^+ \pi^- p$
1326 ± 2 ± 2		CHUNG	02	B852		$18.3 \pi^- p \rightarrow \pi^+ \pi^- \pi^- p$
1317 ± 3		BARBERIS	98B			$450 \rho p \rightarrow \rho f \pi^+ \pi^- \pi^0 p_S$
1323 ± 4 ± 3		ACCIARRI	97T	L3		$e^+ e^- \rightarrow e^+ \pi^+ \pi^- \pi^0$
1320 ± 7		ALBRECHT	97B	ARG		$e^+ e^- \rightarrow e^+ \pi^+ \pi^- \pi^0$
1311.3 ± 1.6 ± 3.0	72.4k	AMELIN	96	VES		$36 \pi^- p \rightarrow \pi^+ \pi^- \pi^0 n$
1310 ± 5		ARMSTRONG	90	OMEG	0	$300.0 \rho p \rightarrow \rho \rho \pi^+ \pi^- \pi^0$
1323.8 ± 2.3	4022	AUGUSTIN	89	DM2	±	$J/\psi \rightarrow \rho^\pm a_2^\mp$
1320.6 ± 3.1	3562	AUGUSTIN	89	DM2	0	$J/\psi \rightarrow \rho^0 a_2^0$
1317 ± 2	25k	<sup>2</sup> DAUM	80C	SPEC	-	$63,94 \pi^- p \rightarrow 3 \pi p$
1320 ± 10	1097	<sup>2</sup> BALTAY	78B	HBC	+0	$15 \pi^+ p \rightarrow \rho 4 \pi$
1306 ± 8		FERRERSORIA	78	OMEG	-	$9 \pi^- p \rightarrow \rho 3 \pi$
1318 ± 7	1.6k	<sup>2</sup> EMMS	75	DBC	0	$4 \pi^+ n \rightarrow \rho(3 \pi)^0$
1315 ± 5		<sup>2</sup> ANTIPOV	73C	CNTR	-	$25,40 \pi^- p \rightarrow \rho \eta \pi^-$
1306 ± 9	1580	CHALOUKPA	73	HBC	-	$3.9 \pi^- p$

• • • We do not use the following data for averages, fits, limits, etc. • • •

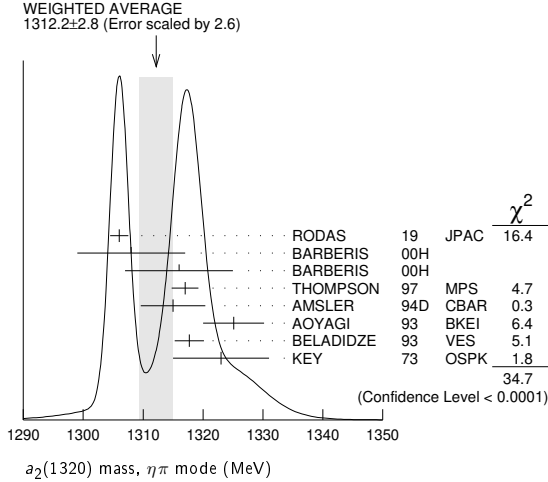
1321 ± 1 ± $\begin{smallmatrix} 0 \\ -7 \end{smallmatrix}$	420k	<sup>3</sup> ALEKSEEV	10	COMP		$190 \pi^- p \rightarrow \pi^- \pi^+ \pi^+ p b'$
1300 ± 2 ± 4	18k	<sup>4</sup> SCHEGELSKY	06	RVUE	0	$\gamma \gamma \rightarrow \pi^+ \pi^- \pi^0$
1305 ± 14		CONDO	93	SHF		$\gamma p \rightarrow n \pi^+ \pi^+ \pi^-$
1310 ± 2		<sup>2</sup> EVANGELIS...	81	OMEG	-	$12 \pi^- p \rightarrow 3 \pi p$
1343 ± 11	490	BALTAY	78B	HBC	0	$15 \pi^+ p \rightarrow \Delta 3 \pi$

See key on page 999

Meson Particle Listings

$a_2(1320)$

- <sup>4</sup> Superseded by RODAS 19.
- <sup>5</sup> ADOLPH 15 value is derived from a Breit-Wigner fit with mass-dependent width taking the  $\eta\pi$  and  $\rho\pi$  channels into account.
- <sup>6</sup> Missing mass with enriched MMS =  $\eta\pi^-$ ,  $\eta = 2\gamma$ .



$\eta/\pi$  MODE

VALUE (MeV)	DOCUMENT ID	TECN	COMMENT
-------------	-------------	------	---------

The data in this block is included in the average printed for a previous datablock.

**1322 ± 7 OUR AVERAGE**

1318 ± 8 <sup>+3</sup> <sub>-5</sub>	IVANOV	01	B852	18 $\pi^- p \rightarrow \eta' \pi^- p$
1327.0 ± 10.7	BELADIDZE	93	VES	37 $\pi^- N \rightarrow \eta' \pi^- N$

$a_2(1320)$  WIDTH

**3 $\pi$  MODE**

VALUE (MeV)	EVTS	DOCUMENT ID	TECN	CHG	COMMENT
-------------	------	-------------	------	-----	---------

**105.0<sup>+</sup> ± 1.7 OUR AVERAGE**

106.6 <sup>+</sup> ± 3.4 <sub>-7.0</sub>	46M	<sup>1</sup> AGHASYAN	18B	COMP	190 $\pi^- p \rightarrow \pi^- \pi^+ \pi^- p$
108 ± 3 ± 15		CHUNG	02	B852	18.3 $\pi^- p \rightarrow \pi^+ \pi^- \pi^- p$
120 ± 10		BARBERIS	98B		450 $\rho p \rightarrow \rho_f \pi^+ \pi^- \pi^0 \rho_S$
105 ± 10 ± 11		ACCIARRI	97T	L3	$e^+ e^- \rightarrow \pi^+ \pi^- \pi^0$
120 ± 10		ALBRECHT	97B	ARG	$e^+ e^- \rightarrow \pi^+ \pi^- \pi^0$
103.0 ± 6.0 ± 3.3	72.4k	AMELIN	96	VES	36 $\pi^- p \rightarrow \pi^+ \pi^- \pi^0 n$
120 ± 10		ARMSTRONG	90	OMEG 0	300.0 $\rho p \rightarrow \rho p \pi^+ \pi^- \pi^0$
107.0 ± 9.7	4022	AUGUSTIN	89	DM2 ±	$J/\psi \rightarrow \rho^\pm a_2^\mp$
118.5 ± 12.5	3562	AUGUSTIN	89	DM2 0	$J/\psi \rightarrow \rho^0 a_2^0$
97 ± 5		<sup>2</sup> EVANGELIS...	81	OMEG -	12 $\pi^- p \rightarrow 3\pi p$
96 ± 9	25k	<sup>2</sup> DAUM	80C	SPEC -	63,94 $\pi^- p \rightarrow 3\pi p$
110 ± 15	1097	<sup>2</sup> BALTAY	78B	HBC +0	15 $\pi^+ p \rightarrow p 4\pi$
112 ± 18	1.6k	<sup>2</sup> EMMS	75	DBC 0	4 $\pi^+ n \rightarrow \rho(3\pi)^0$
122 ± 14	1.2k	<sup>2,3</sup> WAGNER	75	HBC 0	7 $\pi^+ p \rightarrow \Delta^{++}(3\pi)^0$
115 ± 15		<sup>2</sup> ANTIPOV	73C	CNTR -	25,40 $\pi^- p \rightarrow \rho \eta \pi^-$
99 ± 15	1580	CHALOUPKA	73	HBC -	3.9 $\pi^- p$
105 ± 5	28k	BOWEN	71	MMS -	5 $\pi^- p$
99 ± 5	24k	BOWEN	71	MMS +	5 $\pi^+ p$
103 ± 5	17k	BOWEN	71	MMS -	7 $\pi^- p$

- • • We do not use the following data for averages, fits, limits, etc. • • •
  - 110 ± 2 <sup>+2</sup><sub>-15</sub> 420k <sup>4</sup> ALEKSEEV 10 COMP 190  $\pi^- p \rightarrow \pi^- \pi^- \pi^+ p b'$
  - 117 ± 6 ± 20 18k <sup>5</sup> SCHEGELSKY 06 RVUE 0  $\gamma\gamma \rightarrow \pi^+ \pi^- \pi^0$
  - 120 ± 40 CONDO 93 SHF  $\gamma p \rightarrow n \pi^+ \pi^+ \pi^-$
  - 115 ± 14 490 BALTAY 78B HBC 0 15  $\pi^+ p \rightarrow \Delta 3\pi$
  - 72 ± 16 5k BINNIE 71 MMS -  $\pi^- p$  near  $a_2$  threshold
  - 79 ± 12 941 ALSTON... 70 HBC + 7.0  $\pi^+ p \rightarrow 3\pi p$
- <sup>1</sup> Statistical error negligible.  
<sup>2</sup> From a fit to  $J^P = 2^+ \rho\pi$  partial wave.  
<sup>3</sup> Width errors enlarged by us to  $4\Gamma/\sqrt{N}$ ; see the note with the  $K^*(892)$  mass.  
<sup>4</sup> Superseded by AGHASYAN 2018B.  
<sup>5</sup> From analysis of L3 data at 183–209 GeV.

**$K\bar{K}$  AND  $\eta\pi$  MODES**

VALUE (MeV)	DOCUMENT ID
-------------	-------------

**107 ± 5 OUR ESTIMATE**

**112.5 ± 1.2 OUR AVERAGE** Includes data from the 2 datablocks that follow this one.

**$K\bar{K}$  MODE**

VALUE (MeV)	EVTS	DOCUMENT ID	TECN	CHG	COMMENT
-------------	------	-------------	------	-----	---------

The data in this block is included in the average printed for a previous datablock.

**109.8 ± 2.4 OUR AVERAGE**

112 ± 20	4700	<sup>1,2</sup> CLELAND	82B	SPEC +	50 $\pi^+ p \rightarrow K_S^0 K^+ p$
120 ± 25	5200	<sup>1,2</sup> CLELAND	82B	SPEC -	50 $\pi^- p \rightarrow K_S^0 K^- p$
106 ± 4	4000	CHABAUD	80	SPEC -	17 $\pi^- A \rightarrow K_S^0 K^- A$
126 ± 11	11000	CHABAUD	78	SPEC -	9.8 $\pi^- p \rightarrow K^- K_S^0 p$
101 ± 8	4730	CHABAUD	78	SPEC -	18.8 $\pi^- p \rightarrow K^- K_S^0 p$
113 ± 4		<sup>1,3</sup> MARTIN	78D	SPEC -	10 $\pi^- p \rightarrow K_S^0 K^- p$
105 ± 8	2724	<sup>3</sup> MARGULIE	76	SPEC -	23 $\pi^- p \rightarrow K^- K_S^0 p$
113 ± 19	730	FOLEY	72	CNTR -	20.3 $\pi^- p \rightarrow K^- K_S^0 p$
123 ± 13	1500	<sup>3</sup> GRAYER	71	ASPK -	17.2 $\pi^- p \rightarrow K^- K_S^0 p$
• • •		We do not use the following data for averages, fits, limits, etc. • • •			
120 ± 15	870	<sup>4</sup> SCHEGELSKY	06A	RVUE 0	$\gamma\gamma \rightarrow K_S^0 K_S^0$
121 ± 51	1000	<sup>1,2</sup> CLELAND	82B	SPEC +	30 $\pi^+ p \rightarrow K_S^0 K^+ p$
110 ± 18	350	HYAMS	78	ASPK +	12.7 $\pi^+ p \rightarrow K^+ K_S^0 p$

- <sup>1</sup> From a fit to  $J^P = 2^+$  partial wave.
- <sup>2</sup> Number of events evaluated by us.
- <sup>3</sup> Width errors enlarged by us to  $4\Gamma/\sqrt{N}$ ; see the note with the  $K^*(892)$  mass.
- <sup>4</sup> From analysis of L3 data at 91 and 183–209 GeV.

**$\eta\pi$  MODE**

VALUE (MeV)	EVTS	DOCUMENT ID	TECN	CHG	COMMENT
-------------	------	-------------	------	-----	---------

The data in this block is included in the average printed for a previous datablock.

**113.4 ± 1.3 OUR AVERAGE**

114.4 ± 1.6 ± 0.0		<sup>1</sup> RODAS	19	JPAC	191 $\pi^- p \rightarrow \eta^{(\prime)} \pi^- p$
115 ± 20		BARBERIS	00H		450 $\rho p \rightarrow \rho_f \eta \pi^0 \rho_S$
112 ± 14		BARBERIS	00H		450 $\rho p \rightarrow \Delta_f^{++} \eta \pi^- \rho_S$
112 ± 3 ± 2		<sup>2</sup> AMSLER	94D	CBAR	0.0 $\bar{p} p \rightarrow \pi^0 \pi^0 \eta$
103 ± 6 ± 3		BELADIDZE	93	VES	37 $\pi^- N \rightarrow \eta \pi^- N$
112.2 ± 5.7	2561	DELFOSSÉ	81	SPEC +	$\pi^\pm p \rightarrow \rho \pi^\pm \eta$
116.6 ± 7.7	1653	DELFOSSÉ	81	SPEC -	$\pi^\pm p \rightarrow \rho \pi^\pm \eta$
108 ± 9	1000	KEY	73	OSPK -	6 $\pi^- p \rightarrow \rho \pi^- \eta$
• • •		We do not use the following data for averages, fits, limits, etc. • • •			
112 ± 1 ± 8		<sup>3</sup> JACKURA	18	JPAC	$\pi^- p \rightarrow \eta \pi^- p$
119 ± 14		<sup>4</sup> ADOLPH	15	COMP	191 $\pi^- p \rightarrow \eta^{(\prime)} \pi^- p$
110 ± 4		ANISOVICH	09	RVUE	$\bar{p} p, \pi N$
127 ± 2 ± 2		<sup>5</sup> THOMPSON	97	MPS	18 $\pi^- p \rightarrow \eta \pi^- p$
118 ± 10		ARMSTRONG	93C	E760 0	$\bar{p} p \rightarrow \pi^0 \eta \eta \rightarrow 6\gamma$
104 ± 9	6200	<sup>6</sup> CONFORTO	73	OSPK -	6 $\pi^- p \rightarrow \rho \text{MM}^-$

- <sup>1</sup> The coupled-channel analysis of both the  $\eta\pi$  and  $\eta'\pi$  systems using ADOLPH 15 data. The width is extracted from the T-matrix pole.
- <sup>2</sup> The systematic error of 2 MeV corresponds to the spread of solutions.
- <sup>3</sup> Superseded by RODAS 19.
- <sup>4</sup> ADOLPH 15 value is derived from a Breit-Wigner fit with mass-dependent width taking the  $\eta\pi$  and  $\rho\pi$  channels into account.
- <sup>5</sup> Resolution is not unfolded.
- <sup>6</sup> Missing mass with enriched MMS =  $\eta\pi^-$ ,  $\eta = 2\gamma$ .

**$\eta/\pi$  MODE**

VALUE (MeV)	DOCUMENT ID	TECN	COMMENT
-------------	-------------	------	---------

**119 ± 25 OUR AVERAGE**

140 ± 35 ± 20	IVANOV	01	B852	18 $\pi^- p \rightarrow \eta' \pi^- p$
106 ± 32	BELADIDZE	93	VES	37 $\pi^- N \rightarrow \eta' \pi^- N$

$a_2(1320)$  DECAY MODES

Mode	Fraction ( $\Gamma_i/\Gamma$ )	Scale factor/Confidence level
$\Gamma_1$ 3 $\pi$	(70.1 ± 2.7) %	S=1.2
$\Gamma_2$ $\rho(770)\pi$		
$\Gamma_3$ $f_2(1270)\pi$		
$\Gamma_4$ $\rho(1450)\pi$		
$\Gamma_5$ $\eta\pi$	(14.5 ± 1.2) %	
$\Gamma_6$ $\omega\pi\pi$	(10.6 ± 3.2) %	S=1.3
$\Gamma_7$ $K\bar{K}$	(4.9 ± 0.8) %	
$\Gamma_8$ $\eta'(958)\pi$	(5.5 ± 0.9) × 10 <sup>-3</sup>	
$\Gamma_9$ $\pi^\pm\gamma$	(2.91 ± 0.27) × 10 <sup>-3</sup>	
$\Gamma_{10}$ $\gamma\gamma$	(9.4 ± 0.7) × 10 <sup>-6</sup>	
$\Gamma_{11}$ $e^+e^-$	< 5 × 10 <sup>-9</sup>	CL=90%

# Meson Particle Listings

## $a_2(1320)$

### CONSTRAINED FIT INFORMATION

An overall fit to 5 branching ratios uses 18 measurements and one constraint to determine 4 parameters. The overall fit has a  $\chi^2 = 9.3$  for 15 degrees of freedom.

The following *off-diagonal* array elements are the correlation coefficients  $\langle \delta x_i \delta x_j \rangle / (\delta x_i \delta x_j)$ , in percent, from the fit to the branching fractions,  $x_i \equiv \Gamma_i / \Gamma_{\text{total}}$ . The fit constrains the  $x_i$  whose labels appear in this array to sum to one.

$x_5$	10		
$x_6$	-89	-46	
$x_7$	-1	-2	-24
	$x_1$	$x_5$	$x_6$

### $a_2(1320)$ PARTIAL WIDTHS

$\Gamma(\eta\pi)$	$\Gamma_5$				
VALUE (MeV)	EVTS	DOCUMENT ID	TECN	CHG	COMMENT
••• We do not use the following data for averages, fits, limits, etc. •••					
18.5 ± 3.0	870	<sup>1</sup> SCHEGELSKY 06A	RVUE	0	$\gamma\gamma \rightarrow K_S^0 K_S^0$
<sup>1</sup> From analysis of L3 data at 91 and 183–209 GeV, using $\Gamma(a_2(1320) \rightarrow \gamma\gamma) = 0.91$ keV and SU(3) relations.					

$\Gamma(K\bar{K})$	$\Gamma_7$				
VALUE (MeV)	EVTS	DOCUMENT ID	TECN	CHG	COMMENT
••• We do not use the following data for averages, fits, limits, etc. •••					
7.0 ± 2.0	870	<sup>1</sup> SCHEGELSKY 06A	RVUE	0	$\gamma\gamma \rightarrow K^0 K_S^0$
-1.5					
<sup>1</sup> From analysis of L3 data at 91 and 183–209 GeV, using $\Gamma(a_2(1320) \rightarrow \gamma\gamma) = 0.91$ keV and SU(3) relations.					

$\Gamma(\pi^\pm\gamma)$	$\Gamma_9$				
VALUE (keV)	EVTS	DOCUMENT ID	TECN	CHG	COMMENT
<b>311 ± 25 OUR AVERAGE</b>					
358 ± 6 ± 42		<sup>1</sup> ADOLPH 14	COMP	-	190 $\pi^- \text{Pb} \rightarrow \pi^+ \pi^- \pi^- \text{Pb}'$
284 ± 25 ± 25	7.1k	MOLCHANOV 01	SELX		600 $\pi^- \text{A} \rightarrow \pi^+ \pi^- \pi^- \text{A}$
295 ± 60		CIHANGIR 82	SPEC	+	200 $\pi^+ \text{A}$
••• We do not use the following data for averages, fits, limits, etc. •••					
461 ± 110		<sup>2</sup> MAY 77	SPEC	±	9.7 $\gamma \text{A}$
<sup>1</sup> Primakoff reaction using $a_2(1320) \rightarrow 3\pi$ branching ratio of 70.1%.					
<sup>2</sup> Assuming one-pion exchange.					

$\Gamma(\gamma\gamma)$	$\Gamma_{10}$				
VALUE (keV)	EVTS	DOCUMENT ID	TECN	CHG	COMMENT
<b>1.00 ± 0.06 OUR AVERAGE</b>					
0.98 ± 0.05 ± 0.09		ACCIARRI 97T	L3		$e^+e^- \rightarrow e^+e^- \pi^+ \pi^- \pi^0$
0.96 ± 0.03 ± 0.13		ALBRECHT 97b	ARG		$e^+e^- \rightarrow e^+e^- \pi^+ \pi^- \pi^0$
1.26 ± 0.26 ± 0.18	36	BARU 90	MD1		$e^+e^- \rightarrow e^+e^- \pi^+ \pi^- \pi^0$
1.00 ± 0.07 ± 0.15	415	BEHREND 90c	CELL	0	$e^+e^- \rightarrow e^+e^- \pi^+ \pi^- \pi^0$
1.03 ± 0.13 ± 0.21		BUTLER 90	MRK2		$e^+e^- \rightarrow e^+e^- \pi^+ \pi^- \pi^0$
1.01 ± 0.14 ± 0.22	85	OEST 90	JADE		$e^+e^- \rightarrow e^+e^- \pi^0 \eta$
0.90 ± 0.27 ± 0.15	56	<sup>1</sup> ALTHOFF 86	TASS	0	$e^+e^- \rightarrow e^+e^- 3\pi$
1.14 ± 0.20 ± 0.26		<sup>2</sup> ANTREASYSAN 86	CBAL	0	$e^+e^- \rightarrow e^+e^- \pi^0 \eta$
1.06 ± 0.18 ± 0.19		BERGER 84c	PLUT	0	$e^+e^- \rightarrow e^+e^- 3\pi$
••• We do not use the following data for averages, fits, limits, etc. •••					
0.81 ± 0.19 ± 0.42	35	<sup>1</sup> BEHREND 82c	CELL	0	$e^+e^- \rightarrow e^+e^- 3\pi$
0.77 ± 0.18 ± 0.27	22	<sup>2</sup> EDWARDS 82f	CBAL	0	$e^+e^- \rightarrow e^+e^- \pi^0 \eta$
<sup>1</sup> From $\rho\pi$ decay mode.					
<sup>2</sup> From $\eta\pi^0$ decay mode.					

$\Gamma(e^+e^-)$	$\Gamma_{11}$			
VALUE (eV)	CL%	DOCUMENT ID	TECN	COMMENT
<b>&lt; 0.56</b>	90	ACHASOV 00k	SND	$e^+e^- \rightarrow \pi^0 \pi^0$
••• We do not use the following data for averages, fits, limits, etc. •••				
< 25	90	VOROBYEV 88	ND	$e^+e^- \rightarrow \pi^0 \eta$

### $a_2(1320)$ $\Gamma(i)\Gamma(\gamma\gamma)/\Gamma(\text{total})$

$\Gamma(3\pi) \times \Gamma(\gamma\gamma)/\Gamma_{\text{total}}$	$\Gamma_1\Gamma_{10}/\Gamma$			
VALUE (keV)	EVTS	DOCUMENT ID	TECN	COMMENT
••• We do not use the following data for averages, fits, limits, etc. •••				
0.65 ± 0.02 ± 0.02	18k	<sup>1</sup> SCHEGELSKY 06	RVUE	$\gamma\gamma \rightarrow \pi^+ \pi^- \pi^0$
<sup>1</sup> From analysis of L3 data at 183–209 GeV.				

$\Gamma(\eta\pi) \times \Gamma(\gamma\gamma)/\Gamma_{\text{total}}$	$\Gamma_5\Gamma_{10}/\Gamma$		
VALUE (keV)	DOCUMENT ID	TECN	COMMENT
••• We do not use the following data for averages, fits, limits, etc. •••			
0.145 ± 0.097	<sup>1</sup> UEHARA 09A	BELL	$e^+e^- \rightarrow e^+e^- \eta \pi^0$
-0.034			
<sup>1</sup> From the $D_2$ -wave. The fraction of the $D_0$ -wave is $3.4^{+2.3}_{-1.1}\%$ .			

$\Gamma(K\bar{K}) \times \Gamma(\gamma\gamma)/\Gamma_{\text{total}}$	$\Gamma_7\Gamma_{10}/\Gamma$		
VALUE (keV)	DOCUMENT ID	TECN	COMMENT
<b>0.126 ± 0.007 ± 0.028</b>	<sup>1</sup> ALBRECHT 90G	ARG	$e^+e^- \rightarrow e^+e^- K^+ K^-$
••• We do not use the following data for averages, fits, limits, etc. •••			
0.081 ± 0.006 ± 0.027	<sup>2</sup> ALBRECHT 90G	ARG	$e^+e^- \rightarrow e^+e^- K^+ K^-$
<sup>1</sup> Using an incoherent background.			
<sup>2</sup> Using a coherent background.			

### $a_2(1320)$ BRANCHING RATIOS

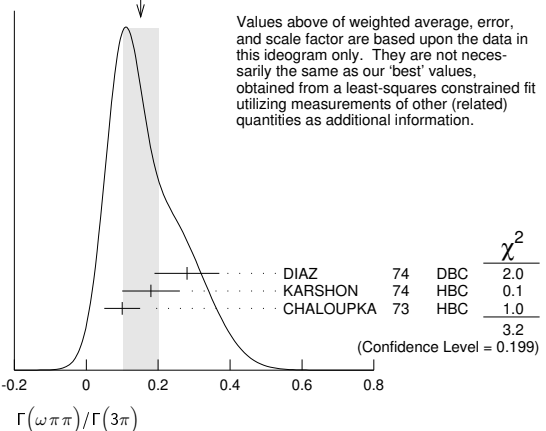
$[\Gamma(\rho(1270)\pi) + \Gamma(\rho(1450)\pi)] / \Gamma(\rho(770)\pi)$	$(\Gamma_3 + \Gamma_4) / \Gamma_2$				
VALUE	CL%	DOCUMENT ID	TECN	CHG	COMMENT
<b>&lt; 0.12</b>	90	ABRAMOVI... 70b	HBC	-	3.93 $\pi^- p$

$\Gamma(\rho(770)\pi) / \Gamma(\rho(1270)\pi)$	$\Gamma_2 / \Gamma_3$			
VALUE	EVTS	DOCUMENT ID	TECN	COMMENT
<b>16.5 ± 1.2</b>	46M	<sup>1</sup> AGHASYAN 18b	COMP	190 $\pi^- p \rightarrow \pi^- \pi^+ \pi^- p$
-2.4				
<sup>1</sup> Statistical error negligible.				

$\Gamma(\eta\pi) / \Gamma(3\pi)$	$\Gamma_5 / \Gamma_1$				
VALUE	EVTS	DOCUMENT ID	TECN	CHG	COMMENT
<b>0.207 ± 0.018 OUR FIT</b>					
<b>0.213 ± 0.020 OUR AVERAGE</b>					
0.18 ± 0.05		FORINO 76	HBC		11 $\pi^- p$
0.22 ± 0.05	52	ANTIPOV 73	CNTR	-	40 $\pi^- p$
0.211 ± 0.044	149	CHALOUKPA 73	HBC	-	3.9 $\pi^- p$
0.246 ± 0.042	167	ALSTON-... 71	HBC	+	7.0 $\pi^+ p$
0.25 ± 0.09	15	BOECKMANN 70	HBC	+	5.0 $\pi^+ p$
0.23 ± 0.08	22	ASCOLI 68	HBC	-	5 $\pi^- p$
0.12 ± 0.08		CHUNG 68	HBC	-	3.2 $\pi^- p$
0.22 ± 0.09		CONTE 67	HBC	-	11.0 $\pi^- p$

$\Gamma(\omega\pi\pi) / \Gamma(3\pi)$	$\Gamma_6 / \Gamma_1$				
VALUE	EVTS	DOCUMENT ID	TECN	CHG	COMMENT
<b>0.15 ± 0.05 OUR FIT</b>					Error includes scale factor of 1.3.
<b>0.15 ± 0.05 OUR AVERAGE</b>					Error includes scale factor of 1.3. See the ideogram below.
0.28 ± 0.09	60	DIAZ 74	DBC	0	6 $\pi^+ n$
0.18 ± 0.08		<sup>1</sup> KARSHON 74	HBC		Avg. of above two
0.10 ± 0.05	279	<sup>2</sup> CHALOUKPA 73	HBC	-	3.9 $\pi^- p$
••• We do not use the following data for averages, fits, limits, etc. •••					
0.29 ± 0.08	140	<sup>1</sup> KARSHON 74	HBC	+	4.9 $\pi^+ p$
0.10 ± 0.04	60	<sup>1</sup> KARSHON 74	HBC	+	4.9 $\pi^+ p$
0.19 ± 0.08		DEFOIX 73	HBC	0	0.7 $\bar{p} p$
<sup>1</sup> KARSHON 74 suggest an additional $l = 0$ state strongly coupled to $\omega\pi\pi$ which could explain discrepancies in branching ratios and masses. We use a central value and a systematic spread.					
<sup>2</sup> Decays to $b_1(1040)\pi$ , $b_1 \rightarrow \omega\pi$ . Error increased to account for possible systematic errors of complicated analysis.					

WEIGHTED AVERAGE  
0.15 ± 0.05 (Error scaled by 1.3)



See key on page 999

Meson Particle Listings
a2(1320), f0(1370)

Gamma(KK-bar)/Gamma(3pi) G7/G1

Table with columns: VALUE, EVTS, DOCUMENT ID, TECN, CHG, COMMENT. Includes data for 0.070 +/- 0.012 OUR FIT and 0.078 +/- 0.017. References include BERTIN, CHALOUPIKA, ALSTON-..., ABRAMOVI..., CHUNG.

Gamma(KK-bar)/Gamma(eta pi) G7/G5

Table with columns: VALUE, DOCUMENT ID, TECN, COMMENT. Includes data for 0.08 +/- 0.02. Reference: BERTIN.

Gamma(eta pi) / [Gamma(3pi) + Gamma(eta pi) + Gamma(KK-bar)] G5 / (G1 + G5 + G7)

Table with columns: VALUE, EVTS, DOCUMENT ID, TECN, CHG, COMMENT. Includes data for 0.162 +/- 0.012 OUR FIT and 0.140 +/- 0.028 OUR AVERAGE. Reference: ESPIGAT.

Gamma(KK-bar) / [Gamma(3pi) + Gamma(eta pi) + Gamma(KK-bar)] G7 / (G1 + G5 + G7)

Table with columns: VALUE, EVTS, DOCUMENT ID, TECN, CHG, COMMENT. Includes data for 0.054 +/- 0.009 OUR FIT and 0.048 +/- 0.012 OUR AVERAGE. References include TOET, DAMERI, BARNHAM, ESPIGAT.

Gamma(eta(958) pi) / Gamma total G8/G

Table with columns: VALUE, CL%, DOCUMENT ID, TECN, CHG, COMMENT. Includes data for <0.006 and <0.02. Reference: BARNHAM.

Gamma(eta(958) pi) / Gamma(3pi) G8/G1

Table with columns: VALUE, CL%, DOCUMENT ID, TECN, CHG, COMMENT. Includes data for <0.011 and <0.04. Reference: EISENSTEIN.

Gamma(eta(958) pi) / Gamma(eta pi) G8/G5

Table with columns: VALUE, DOCUMENT ID, TECN, COMMENT. Includes data for 0.038 +/- 0.005 OUR AVERAGE. Reference: ADOLPH.

Gamma(pi+ pi-) / Gamma total G9/G

Table with columns: VALUE, DOCUMENT ID, TECN, COMMENT. Includes data for 0.005 +/- 0.005. Reference: EISENBERG.

Gamma(e+ e-) / Gamma total G11/G

Table with columns: VALUE (units 10^-9), CL%, DOCUMENT ID, TECN, COMMENT. Includes data for <6. Reference: ACHASOV.

a2(1320) REFERENCES

List of references for a2(1320) and f0(1370) decays, including authors like Rodas, Aghasyan, Jackura, Adolph, etc., and their respective publications.

f0(1370)

I(G JP C) = 0+ (0 + +)

See the review on "Scalar Mesons below 2 GeV" and a note on "Non-q q-bar Candidates" in PDG 06, Journal of Physics G33 1 (2006).

f0(1370) T-MATRIX POLE POSITION

Note that Gamma approx 2 Im(sqrt(s) pole).

Table with columns: VALUE (MeV), DOCUMENT ID, TECN, COMMENT. Includes data for (1290 +/- 50) - i(170 +/- 20) and other pole positions.

Downloaded from https://academic.oup.com/ptep/article/2020/8/083C01/5891211 by guest on 12 November 2020



# Meson Particle Listings

## $f_0(1370)$

(1548 ± 40) - i(560 ± 40)	BERTIN	97c	OBLX	0.0 $\bar{p}p \rightarrow \pi^+ \pi^- \pi^0$
(1380 ± 40) - i(180 ± 25)	ABELE	96b	CBAR	0.0 $\bar{p}p \rightarrow \pi^0 K_L^0 K_L^0$
(1300 ± 15) - i(115 ± 8)	BUGG	96	RVUE	
(1330 ± 50) - i(150 ± 40)	<sup>5</sup> AMSLER	95b	CBAR	$\bar{p}p \rightarrow 3\pi^0$
(1360 ± 35) - i(150-300)	<sup>5</sup> AMSLER	95c	CBAR	$\bar{p}p \rightarrow \pi^0 \eta \eta$
(1390 ± 30) - i(190 ± 40)	<sup>6</sup> AMSLER	95d	CBAR	$\bar{p}p \rightarrow 3\pi^0, \pi^0 \eta \eta,$ $\pi^0 \pi^0 \eta$
1346 - i249	<sup>7,8</sup> JANSSEN	95	RVUE	$\pi \pi \rightarrow \pi \pi, K \bar{K}$
1214 - i168	<sup>8,9</sup> TORNQVIST	95	RVUE	$\pi \pi \rightarrow \pi \pi, K \bar{K}, K \pi,$ $\eta \pi$
1364 - i139	AMSLER	94d	CBAR	$\bar{p}p \rightarrow \pi^0 \pi^0 \eta$
(1365 <sup>+20</sup> <sub>-55</sub> ) - i(134 ± 35)	ANISOVICH	94	CBAR	$\bar{p}p \rightarrow 3\pi^0, \pi^0 \eta \eta$
(1340 ± 40) - i(127 <sup>+30</sup> <sub>-20</sub> )	<sup>10</sup> BUGG	94	RVUE	$\bar{p}p \rightarrow 3\pi^0, \eta \eta \pi^0,$ $\eta \pi^0 \pi^0$
(1430 ± 5) - i(73 ± 13)	<sup>11</sup> KAMINSKI	94	RVUE	$\pi \pi \rightarrow \pi \pi, K \bar{K}$
1420 - i220	<sup>12</sup> AU	87	RVUE	$\pi \pi \rightarrow \pi \pi, K \bar{K}$

- Another pole is found at  $(1510 \pm 130) - i(800 \pm 100)_{-150}$  MeV.
- Coupled channel analysis of  $\pi^+ \pi^- \pi^0, K^+ K^- \pi^0,$  and  $K^\pm K_S^0 \pi^\mp$ .
- Average between  $\pi^+ \pi^- 2\pi^0$  and  $2(\pi^+ \pi^-)$ .
- T-matrix pole on sheet ---.
- Supersedes ANISOVICH 94.
- Coupled-channel analysis of  $\bar{p}p \rightarrow 3\pi^0, \pi^0 \eta \eta,$  and  $\pi^0 \pi^0 \eta$  on sheet IV. Demonstrates explicitly that  $f_0(500)$  and  $f_0(1370)$  are two different poles.
- Analysis of data from FALVARD 88.
- The pole is on Sheet III. Demonstrates explicitly that  $f_0(500)$  and  $f_0(1370)$  are two different poles.
- Uses data from BEIER 72b, OCHS 73, HYAMS 73, GRAYER 74, ROSSELET 77, CASON 83, ASTON 88, and ARMSTRONG 91b. Coupled channel analysis with flavor symmetry and all light two-pseudoscalars systems.
- Reanalysis of ANISOVICH 94 data.
- T-matrix pole on sheet III.
- Analysis of data from OCHS 73, GRAYER 74, BECKER 79, and CASON 83.

### $f_0(1370)$ BREIT-WIGNER MASS OR K-MATRIX POLE PARAMETER

VALUE (MeV)	DOCUMENT ID
<b>1200 to 1500 OUR ESTIMATE</b>	
<b><math>\pi\pi</math> MODE</b>	
VALUE (MeV)	EVTS DOCUMENT ID TECN COMMENT
••• We do not use the following data for averages, fits, limits, etc. •••	
1400 ± 40	<sup>1</sup> AUBERT 09L BABR $B^\pm \rightarrow \pi^\pm \pi^\pm \pi^\mp$
1470 <sup>+6</sup> <sub>-7</sub> <sup>+72</sup> <sub>-255</sub>	<sup>2</sup> UEHARA 08A BELL $10.6 e^+ e^- \rightarrow e^+ e^- \pi^0 \pi^0$
1259 ± 55	2.6k BONVICINI 07 CLEO $D^+ \rightarrow \pi^- \pi^+ \pi^+$
1309 ± 1 ± 15	<sup>3</sup> BUGG 07A RVUE $0.0 p\bar{p} \rightarrow 3\pi^0$
1449 ± 13	4.3k <sup>4</sup> GARMASH 06 BELL $B^+ \rightarrow K^+ \pi^+ \pi^-$
1350 ± 50	ABLIKIM 05 BES2 $J/\psi \rightarrow \phi \pi^+ \pi^-$
1265 ± 30 <sup>+20</sup> <sub>-35</sub>	ABLIKIM 05Q BES2 $\psi(2S) \rightarrow \gamma \pi^+ \pi^- K^+ K^-$
1434 ± 18 ± 9	848 AITALA 01A E791 $D_s^+ \rightarrow \pi^- \pi^+ \pi^+$
1308 ± 10	BARBERIS 99B OMEG $450 pp \rightarrow p_S p_f \pi^+ \pi^-$
1315 ± 50	BELLAZZINI 99 GAM4 $450 pp \rightarrow p p \pi^0 \pi^0$
1315 ± 30	ALDE 98 GAM4 $100 \pi^- p \rightarrow \pi^0 \pi^0 n$
1280 ± 55	BERTIN 98 OBLX $0.05-0.405 \bar{p}p \rightarrow \pi^+ \pi^+ \pi^-$
1186	<sup>5,6</sup> TORNQVIST 95 RVUE $\pi \pi \rightarrow \pi \pi, K \bar{K}, K \pi, \eta \pi$
1472 ± 12	ARMSTRONG 91 OMEG $300 pp \rightarrow p p \pi \pi, p p K \bar{K}$
1275 ± 20	BREAKSTONE 90 SFM $62 pp \rightarrow p p \pi^+ \pi^-$
1420 ± 20	AKESSON 86 SPEC $63 pp \rightarrow p p \pi^+ \pi^-$
1256	FROGGATT 77 RVUE $\pi^+ \pi^-$ channel

- Breit-Wigner mass.
- Breit-Wigner mass. May also be the  $f_0(1500)$ .
- Reanalysis of ABELE 96c data.
- Also observed by GARMASH 07 in  $B^0 \rightarrow K_S^0 \pi^+ \pi^-$  decays. Supersedes GARMASH 05.
- Uses data from BEIER 72b, OCHS 73, HYAMS 73, GRAYER 74, ROSSELET 77, CASON 83, ASTON 88, and ARMSTRONG 91b. Coupled channel analysis with flavor symmetry and all light two-pseudoscalars systems.
- Also observed by ASNER 00 in  $\tau^- \rightarrow \pi^- \pi^0 \pi^0 \nu_\tau$  decays

### $K\bar{K}$ MODE

VALUE (MeV)	EVTS DOCUMENT ID TECN COMMENT
••• We do not use the following data for averages, fits, limits, etc. •••	
1422 ± 15 ± 28	<sup>1</sup> AAIJ 19H LHCB $pp \rightarrow D^\pm X$
1360 ± 31 ± 28	4.30 <sup>2,3</sup> DOBBS 15 $J/\psi \rightarrow \gamma K^+ K^-$
1350 ± 48 ± 15	1.68 <sup>2,3</sup> DOBBS 15 $\psi(2S) \rightarrow \gamma K^+ K^-$
1440 ± 6	VLADIMIRSK...06 SPEC $40 \pi^- p \rightarrow K_S^0 K_S^0 n$
1391 ± 10	TIKHOMIROV 03 SPEC $40.0 \pi^- C \rightarrow K_S^0 K_S^0 K_L^0 X$
1440 ± 50	BOLONKIN 88 SPEC $40 \pi^- p \rightarrow K_S^0 K_S^0 n$
1463 ± 9	ETKIN 82B MPS $23 \pi^- p \rightarrow n 2K_S^0$
1425 ± 15	WICKLUND 80 SPEC $6 \pi N \rightarrow K^+ K^- N$
~ 1300	POLYCHRO... 79 STRC $7 \pi^- p \rightarrow n 2K_S^0$

- From the  $D^\pm \rightarrow K^\pm K^+ K^-$  Dalitz plot fit with the isobar model A.
- Using CLEO-c data but not authorized by the CLEO Collaboration.
- From a fit to a Breit-Wigner line shape with fixed  $\Gamma = 346$  MeV.

### $4\pi$ MODE $2(\pi\pi)_S + \rho\rho$

VALUE (MeV)	EVTS DOCUMENT ID TECN COMMENT
••• We do not use the following data for averages, fits, limits, etc. •••	
1395 ± 40	ABELE 01 CBAR $0.0 \bar{p}d \rightarrow \pi^- 4\pi^0 p$
1374 ± 38	AMSLER 94 CBAR $0.0 \bar{p}p \rightarrow \pi^+ \pi^- 3\pi^0$
1345 ± 12	ADAMO 93 OBLX $\bar{p}p \rightarrow 3\pi^+ 2\pi^-$
1386 ± 30	GASPERO 93 DBC $0.0 \bar{p}n \rightarrow 2\pi^+ 3\pi^-$
~ 1410	5751 <sup>1</sup> BETTINI 66 DBC $0.0 \bar{p}n \rightarrow 2\pi^+ 3\pi^-$
<sup>1</sup> $\rho\rho$ dominant.	

### $\eta\eta$ MODE

VALUE (MeV)	DOCUMENT ID TECN COMMENT
••• We do not use the following data for averages, fits, limits, etc. •••	
1262 <sup>+51</sup> <sub>-78</sub> <sup>+82</sup> <sub>-103</sub>	<sup>1</sup> UEHARA 10A BELL $10.6 e^+ e^- \rightarrow e^+ e^- \eta \eta$
1430	AMSLER 92 CBAR $0.0 \bar{p}p \rightarrow \pi^0 \eta \eta$
1220 ± 40	ALDE 86D GAM4 $100 \pi^- p \rightarrow n 2\eta$
<sup>1</sup> Breit-Wigner mass. May also be the $f_0(1500)$ .	

### COUPLED CHANNEL MODE

VALUE (MeV)	DOCUMENT ID TECN COMMENT
••• We do not use the following data for averages, fits, limits, etc. •••	
1330.2 <sup>+5.9</sup> <sub>-6.5</sub> ± 5.1	<sup>1</sup> AAIJ 19H LHCB $pp \rightarrow D^\pm X$
1306 ± 20	<sup>2</sup> ANISOVICH 03 RVUE
<sup>1</sup> From the $D^\pm \rightarrow K^\pm K^+ K^-$ Dalitz plot fit with the Triple-M amplitude in the multi-meson model of AOUDE 18.	
<sup>2</sup> K-matrix pole from combined analysis of $\pi^- p \rightarrow \pi^0 \pi^0 n, \pi^- p \rightarrow K \bar{K} n,$ $\pi^+ \pi^- \rightarrow \pi^+ \pi^-, \bar{p}p \rightarrow \pi^0 \pi^0 \pi^0, \pi^0 \eta \eta, \pi^0 \pi^0 \eta, \pi^+ \pi^- \pi^0, K^+ K^- \pi^0, K_S^0 K_S^0 \pi^0,$ $K^+ K_S^0 \pi^-$ at rest, $\bar{p}n \rightarrow \pi^- \pi^- \pi^+, K_S^0 K^- \pi^0, K_S^0 K_S^0 \pi^-$ at rest.	

### $f_0(1370)$ BREIT-WIGNER WIDTH

VALUE (MeV)	DOCUMENT ID
<b>200 to 500 OUR ESTIMATE</b>	
<b><math>\pi\pi</math> MODE</b>	
VALUE (MeV)	EVTS DOCUMENT ID TECN COMMENT
••• We do not use the following data for averages, fits, limits, etc. •••	
300 ± 80	<sup>1</sup> AUBERT 09L BABR $B^\pm \rightarrow \pi^\pm \pi^\pm \pi^\mp$
90 <sup>+2</sup> <sub>-1</sub> <sup>+50</sup> <sub>-22</sub>	<sup>2</sup> UEHARA 08A BELL $10.6 e^+ e^- \rightarrow e^+ e^- \pi^0 \pi^0$
298 ± 21	2.6k BONVICINI 07 CLEO $D^+ \rightarrow \pi^- \pi^+ \pi^+$
126 ± 25	4286 <sup>3</sup> GARMASH 06 BELL $B^+ \rightarrow K^+ \pi^+ \pi^-$
265 ± 40	ABLIKIM 05 BES2 $J/\psi \rightarrow \phi \pi^+ \pi^-$
350 ± 100 <sup>+105</sup> <sub>-60</sub>	ABLIKIM 05Q BES2 $\psi(2S) \rightarrow \gamma \pi^+ \pi^- K^+ K^-$
173 ± 32 ± 6	848 AITALA 01A E791 $D_s^+ \rightarrow \pi^- \pi^+ \pi^+$
222 ± 20	BARBERIS 99B OMEG $450 pp \rightarrow p_S p_f \pi^+ \pi^-$
255 ± 60	BELLAZZINI 99 GAM4 $450 pp \rightarrow p p \pi^0 \pi^0$
190 ± 50	ALDE 98 GAM4 $100 \pi^- p \rightarrow \pi^0 \pi^0 n$
323 ± 13	BERTIN 98 OBLX $0.05-0.405 \bar{p}p \rightarrow \pi^+ \pi^+ \pi^-$
350	<sup>4,5</sup> TORNQVIST 95 RVUE $\pi \pi \rightarrow \pi \pi, K \bar{K}, K \pi, \eta \pi$
195 ± 33	ARMSTRONG 91 OMEG $300 pp \rightarrow p p \pi \pi, p p K \bar{K}$
285 ± 60	BREAKSTONE 90 SFM $62 pp \rightarrow p p \pi^+ \pi^-$
460 ± 50	AKESSON 86 SPEC $63 pp \rightarrow p p \pi^+ \pi^-$
~ 400	<sup>6</sup> FROGGATT 77 RVUE $\pi^+ \pi^-$ channel

- The systematic errors are not reported.
- Breit-Wigner width. May also be the  $f_0(1500)$ .
- Also observed by GARMASH 07 in  $B^0 \rightarrow K_S^0 \pi^+ \pi^-$  decays. Supersedes GARMASH 05.
- Uses data from BEIER 72b, OCHS 73, HYAMS 73, GRAYER 74, ROSSELET 77, CASON 83, ASTON 88, and ARMSTRONG 91b. Coupled channel analysis with flavor symmetry and all light two-pseudoscalars systems.
- Also observed by ASNER 00 in  $\tau^- \rightarrow \pi^- \pi^0 \pi^0 \nu_\tau$  decays
- Width defined as distance between 45 and 135° phase shift.

### $K\bar{K}$ MODE

VALUE (MeV)	DOCUMENT ID TECN COMMENT
••• We do not use the following data for averages, fits, limits, etc. •••	
324 ± 38 ± 42	<sup>1</sup> AAIJ 19H LHCB $pp \rightarrow D^\pm X$
121 ± 15	VLADIMIRSK...06 SPEC $40 \pi^- p \rightarrow K_S^0 K_S^0 n$
55 ± 26	TIKHOMIROV 03 SPEC $40.0 \pi^- C \rightarrow K_S^0 K_S^0 K_L^0 X$
250 ± 80	BOLONKIN 88 SPEC $40 \pi^- p \rightarrow K_S^0 K_S^0 n$
118 <sup>+138</sup> <sub>-16</sub>	ETKIN 82B MPS $23 \pi^- p \rightarrow n 2K_S^0$
160 ± 30	WICKLUND 80 SPEC $6 \pi N \rightarrow K^+ K^- N$
~ 150	POLYCHRO... 79 STRC $7 \pi^- p \rightarrow n 2K_S^0$
<sup>1</sup> From the $D^\pm \rightarrow K^\pm K^+ K^-$ Dalitz plot fit with the isobar model A.	

### $4\pi$ MODE $2(\pi\pi)_S + \rho\rho$

VALUE (MeV)	EVTS DOCUMENT ID TECN COMMENT
••• We do not use the following data for averages, fits, limits, etc. •••	
275 ± 55	ABELE 01 CBAR $0.0 \bar{p}d \rightarrow \pi^- 4\pi^0 p$

375 ± 61	AMSLER	94	CBAR	0.0 $\bar{p}p \rightarrow \pi^+\pi^-3\pi^0$	
398 ± 26	ADAMO	93	OBLX	$\bar{p}p \rightarrow 3\pi^+2\pi^-$	
310 ± 50	GASPERO	93	DBC	0.0 $\bar{p}n \rightarrow 2\pi^+3\pi^-$	
~ 90	5751	<sup>1</sup> BETTINI	66	DBC	0.0 $\bar{p}n \rightarrow 2\pi^+3\pi^-$

<sup>1</sup>  $\rho\rho$  dominant.

**$\eta\eta$  MODE**

VALUE (MeV)	DOCUMENT ID	TECN	COMMENT
484 +246 +246 / -170 -263	<sup>1</sup> UEHARA	10A	BELL 10.6 $e^+e^- \rightarrow e^+e^-\eta\eta$
250	AMSLER	92	CBAR 0.0 $\bar{p}p \rightarrow \pi^0\eta\eta$
320 ± 40	ALDE	86D	GAM4 100 $\pi^-\rho \rightarrow n2\eta$

<sup>1</sup> Breit-Wigner width. May also be the  $f_0(1500)$ .

**COUPLED CHANNEL MODE**

VALUE (MeV)	DOCUMENT ID	TECN	COMMENT
147 +30 / -50	<sup>1</sup> ANISOVICH	03	RVUE

<sup>1</sup> K-matrix pole from combined analysis of  $\pi^-\rho \rightarrow \pi^0\pi^0n$ ,  $\pi^-\rho \rightarrow K\bar{K}n$ ,  $\pi^+\pi^- \rightarrow \pi^+\pi^-\pi^0$ ,  $\bar{p}p \rightarrow \pi^0\pi^0\pi^0$ ,  $\pi^0\eta\eta$ ,  $\pi^0\pi^0\eta$ ,  $\pi^+\pi^-\pi^0$ ,  $K^+K^-\pi^0$ ,  $K_S^0K_S^0\pi^0$ ,  $K^+K_S^0\pi^-$  at rest,  $\bar{p}n \rightarrow \pi^-\pi^-\pi^+$ ,  $K_S^0K^-\pi^0$ ,  $K_S^0K_S^0\pi^-$  at rest.

**$f_0(1370)$  DECAY MODES**

Mode	Fraction ( $\Gamma_i/\Gamma$ )
$\Gamma_1$ $\pi\pi$	seen
$\Gamma_2$ $4\pi$	seen
$\Gamma_3$ $4\pi^0$	seen
$\Gamma_4$ $2\pi^+2\pi^-$	seen
$\Gamma_5$ $\pi^+\pi^-2\pi^0$	seen
$\Gamma_6$ $\rho\rho$	seen
$\Gamma_7$ $2(\pi\pi)S$ -wave	seen
$\Gamma_8$ $\pi(1300)\pi$	seen
$\Gamma_9$ $a_1(1260)\pi$	seen
$\Gamma_{10}$ $\eta\eta$	seen
$\Gamma_{11}$ $K\bar{K}$	seen
$\Gamma_{12}$ $K\bar{K}n\pi$	not seen
$\Gamma_{13}$ $6\pi$	not seen
$\Gamma_{14}$ $\omega\omega$	not seen
$\Gamma_{15}$ $\gamma\gamma$	seen
$\Gamma_{16}$ $e^+e^-$	not seen

**$f_0(1370)$  PARTIAL WIDTHS**

$\Gamma(\gamma\gamma)$	$\Gamma_{15}$
See $\gamma\gamma$ widths under $f_0(500)$ and MORGAN 90.	

$\Gamma(e^+e^-)$	$\Gamma_{16}$			
VALUE (eV)	CL%	DOCUMENT ID	TECN	COMMENT
<20	90	VOROBYEV	88	ND $e^+e^- \rightarrow \pi^0\pi^0$

**$f_0(1370)$   $\Gamma(i)\Gamma(\gamma\gamma)/\Gamma(\text{total})$**

$\Gamma(\eta\eta) \times \Gamma(\gamma\gamma)/\Gamma_{\text{total}}$	$\Gamma_{10}\Gamma_{15}/\Gamma$		
VALUE (eV)	DOCUMENT ID	TECN	COMMENT
121 +133 +169 / -53 -106	<sup>1</sup> UEHARA	10A	BELL 10.6 $e^+e^- \rightarrow e^+e^-\eta\eta$

<sup>1</sup> Including interference with the  $f_2'(1525)$  (parameters fixed to the values from the 2008 edition of this review, PDG 08) and  $f_2(1270)$ . May also be the  $f_0(1500)$ .

**$f_0(1370)$  BRANCHING RATIOS**

$\Gamma(\pi\pi)/\Gamma_{\text{total}}$	$\Gamma_1/\Gamma$			
VALUE	CL%	DOCUMENT ID	TECN	COMMENT
<0.10	95	OCHS	13	RVUE
0.26 ± 0.09		BUGG	96	RVUE
<0.15		<sup>1</sup> AMSLER	94	CBAR $\bar{p}p \rightarrow \pi^+\pi^-3\pi^0$
<0.06		GASPERO	93	DBC 0.0 $\bar{p}n \rightarrow \text{hadrons}$

<sup>1</sup> Using AMSLER 95B ( $3\pi^0$ ).

$\Gamma(4\pi)/\Gamma_{\text{total}}$	$\Gamma_2/\Gamma = (\Gamma_3+\Gamma_4+\Gamma_5)/\Gamma$		
VALUE	DOCUMENT ID	TECN	COMMENT
>0.72	GASPERO	93	DBC 0.0 $\bar{p}n \rightarrow \text{hadrons}$

$\Gamma(4\pi^0)/\Gamma(4\pi)$	$\Gamma_3/\Gamma_2$		
VALUE	DOCUMENT ID	TECN	COMMENT
0.068 ± 0.005	<sup>1</sup> ABELE	96	CBAR 0.0 $\bar{p}p \rightarrow 5\pi^0$
	<sup>1</sup> GASPERO	93	DBC 0.0 $\bar{p}n \rightarrow \text{hadrons}$

<sup>1</sup> Model-dependent evaluation.

$\Gamma(2\pi^+2\pi^-)/\Gamma(4\pi)$	$\Gamma_4/\Gamma_2 = \Gamma_4/(\Gamma_3+\Gamma_4+\Gamma_5)$		
VALUE	DOCUMENT ID	TECN	COMMENT
0.420 ± 0.014	<sup>1</sup> GASPERO	93	DBC 0.0 $\bar{p}n \rightarrow 2\pi^+3\pi^-$

<sup>1</sup> Model-dependent evaluation.

$\Gamma(\pi^+\pi^-2\pi^0)/\Gamma(4\pi)$	$\Gamma_5/\Gamma_2 = \Gamma_5/(\Gamma_3+\Gamma_4+\Gamma_5)$		
VALUE	DOCUMENT ID	TECN	COMMENT
0.512 ± 0.019	<sup>1</sup> GASPERO	93	DBC 0.0 $\bar{p}n \rightarrow \text{hadrons}$

<sup>1</sup> Model-dependent evaluation.

$\Gamma(\rho\rho)/\Gamma(4\pi)$	$\Gamma_6/\Gamma_2$		
VALUE	DOCUMENT ID	TECN	COMMENT
0.26 ± 0.07	ABELE	01B	CBAR 0.0 $\bar{p}d \rightarrow 5\pi\rho$

$\Gamma(2(\pi\pi)S\text{-wave})/\Gamma(\pi\pi)$	$\Gamma_7/\Gamma_1$		
VALUE	DOCUMENT ID	TECN	COMMENT
5.6 ± 2.6	<sup>1</sup> ABELE	01	CBAR 0.0 $\bar{p}d \rightarrow \pi^-4\pi^0\rho$

<sup>1</sup> From the combined data of ABELE 96 and ABELE 96C.

$\Gamma(2(\pi\pi)S\text{-wave})/\Gamma(4\pi)$	$\Gamma_7/\Gamma_2$		
VALUE	DOCUMENT ID	TECN	COMMENT
0.51 ± 0.09	ABELE	01B	CBAR 0.0 $\bar{p}d \rightarrow 5\pi\rho$

$\Gamma(\rho\rho)/\Gamma(2(\pi\pi)S\text{-wave})$	$\Gamma_6/\Gamma_7$		
VALUE	DOCUMENT ID	TECN	COMMENT
large	BARBERIS	00c	450 $\rho\rho \rightarrow p_f 4\pi\rho_S$
1.6 ± 0.2	AMSLER	94	CBAR $\bar{p}p \rightarrow \pi^+\pi^-3\pi^0$
~ 0.65	GASPERO	93	DBC 0.0 $\bar{p}n \rightarrow \text{hadrons}$

$\Gamma(\pi(1300)\pi)/\Gamma(4\pi)$	$\Gamma_8/\Gamma_2$		
VALUE	DOCUMENT ID	TECN	COMMENT
0.17 ± 0.06	ABELE	01B	CBAR 0.0 $\bar{p}d \rightarrow 5\pi\rho$

$\Gamma(a_1(1260)\pi)/\Gamma(4\pi)$	$\Gamma_9/\Gamma_2$		
VALUE	DOCUMENT ID	TECN	COMMENT
0.06 ± 0.02	ABELE	01B	CBAR 0.0 $\bar{p}d \rightarrow 5\pi\rho$

$\Gamma(\eta\eta)/\Gamma(4\pi)$	$\Gamma_{10}/\Gamma_2 = \Gamma_{10}/(\Gamma_3+\Gamma_4+\Gamma_5)$		
VALUE	DOCUMENT ID	TECN	COMMENT
(28 ± 11) × 10 <sup>-3</sup>	<sup>1</sup> ANISOVICH	02D	SPEC Combined fit
(4.7 ± 2.0) × 10 <sup>-3</sup>	BARBERIS	00e	450 $\rho\rho \rightarrow p_f\eta\eta\rho_S$

<sup>1</sup> From a combined K-matrix analysis of Crystal Barrel (0.  $\rho\bar{p} \rightarrow \pi^0\pi^0\pi^0$ ,  $\pi^0\eta\eta$ ,  $\pi^0\pi^0\eta$ ), GAMS ( $\pi\rho \rightarrow \pi^0\pi^0n$ ,  $\eta\eta n$ ,  $\eta\eta'n$ ), and BNL ( $\pi\rho \rightarrow K\bar{K}n$ ) data.

$\Gamma(K\bar{K})/\Gamma_{\text{total}}$	$\Gamma_{11}/\Gamma$		
VALUE	DOCUMENT ID	TECN	COMMENT
0.35 ± 0.13	BUGG	96	RVUE

$\Gamma(K\bar{K})/\Gamma(\pi\pi)$	$\Gamma_{11}/\Gamma_1$		
VALUE	DOCUMENT ID	TECN	COMMENT
0.08 ± 0.08	ABLIKIM	05	BES2 $J/\psi \rightarrow \phi\pi^+\pi^-, \phi K^+K^-$
0.91 ± 0.20	<sup>1</sup> BARGIOTTI	03	OBLX $\bar{p}p$
0.12 ± 0.06	<sup>2</sup> ANISOVICH	02D	SPEC Combined fit
0.46 ± 0.15 ± 0.11	BARBERIS	99D	OMEG 450 $\rho\rho \rightarrow K^+K^-, \pi^+\pi^-$

<sup>1</sup> Coupled channel analysis of  $\pi^+\pi^-\pi^0$ ,  $K^+K^-\pi^0$ , and  $K_S^0K_S^0\pi^\mp$ .  
<sup>2</sup> From a combined K-matrix analysis of Crystal Barrel (0.  $\rho\bar{p} \rightarrow \pi^0\pi^0\pi^0$ ,  $\pi^0\eta\eta$ ,  $\pi^0\pi^0\eta$ ), GAMS ( $\pi\rho \rightarrow \pi^0\pi^0n$ ,  $\eta\eta n$ ,  $\eta\eta'n$ ), and BNL ( $\pi\rho \rightarrow K\bar{K}n$ ) data.

$\Gamma(K\bar{K}n\pi)/\Gamma_{\text{total}}$	$\Gamma_{12}/\Gamma$		
VALUE	DOCUMENT ID	TECN	COMMENT
<0.03	GASPERO	93	DBC 0.0 $\bar{p}n \rightarrow \text{hadrons}$

# Meson Particle Listings

## $f_0(1370), \pi_1(1400)$

$\Gamma(6\pi)/\Gamma_{total}$	DOCUMENT ID	TECN	COMMENT	$\Gamma_{13}/\Gamma$
VALUE				
••• We do not use the following data for averages, fits, limits, etc. •••				
<0.22	GASPERO 93	DBC	0.0 $\bar{p}n \rightarrow$ hadrons	

$\Gamma(\omega\omega)/\Gamma_{total}$	DOCUMENT ID	TECN	COMMENT	$\Gamma_{14}/\Gamma$
VALUE				
••• We do not use the following data for averages, fits, limits, etc. •••				
<0.13	GASPERO 93	DBC	0.0 $\bar{p}n \rightarrow$ hadrons	

### $f_0(1370)$ REFERENCES

AAJ 19H	JHEP 1904 063	R. Aaij et al.	(LHCb Collab.)
AOUDE 18	PR D98 056021	R.T. Aoude et al.	
DOBBS 15	PR D91 052006	S. Dobbs et al.	(NWES)
OCHS 13	JP G40 043001	W. Ochs	
UEHARA 10A	PR D82 114031	S. Uehara et al.	(BELLE Collab.)
ANISOVICH 09	JMP A24 2481	V.V. Anisovich, A.V. Sarantsev	
AUBERT 09L	PR D79 072006	B. Aubert et al.	(BABAR Collab.)
PDG 08	PL B667 1	C. Amisler et al.	(PDG Collab.)
UEHARA 08A	PR D78 052004	S. Uehara et al.	(BELLE Collab.)
BONVICINI 07	PR D76 012001	G. Bonvicini et al.	(CLEO Collab.)
BUGG 07A	JP G34 151	D.V. Bugg et al.	
GARMASH 07	PR D75 012006	A. Garmash et al.	(BELLE Collab.)
GARMASH 06	PRL 96 251803	A. Garmash et al.	(BELLE Collab.)
PDG 06	JP G33 1	W.-M. Yao et al.	(PDG Collab.)
VLADIMIRSK... 06	PAN 69 493	V.V. Vladimirov et al.	(ITEP, Moscow)
Translated from YAF 69 515.			
ABLIKIM 05	PL B607 243	M. Ablikim et al.	(BES Collab.)
ABLIKIM 05Q	PR D72 092002	M. Ablikim et al.	(BES Collab.)
GARMASH 05	PR D71 092003	A. Garmash et al.	(BELLE Collab.)
ANISOVICH 03	EPJ A16 229	V.V. Anisovich et al.	
BARGIOTTI 03	EPJ C26 371	M. Bargiotti et al.	(OBELIX Collab.)
TIKHOMIROV 03	PAN 66 828	G.D. Tikhomirov et al.	
Translated from YAF 66 860.			
ANISOVICH 02D	PAN 65 1545	V.V. Anisovich et al.	
Translated from YAF 65 1553.			
ABELE 01	EPJ C19 667	A. Abele et al.	(Crystal Barrel Collab.)
ABELE 01B	EPJ C21 261	A. Abele et al.	(Crystal Barrel Collab.)
AITALA 01A	PRL 86 765	E.M. Aitala et al.	(FNAL E791 Collab.)
ASNER 00	PR D61 012002	D.M. Asner et al.	(CLEO Collab.)
BARBERIS 00C	PL B471 440	D. Barberis et al.	(WA 102 Collab.)
BARBERIS 00E	PL B479 59	D. Barberis et al.	(WA 102 Collab.)
BARBERIS 99B	PL B453 316	D. Barberis et al.	(Omega Expt.)
BARBERIS 99D	PL B462 462	D. Barberis et al.	(Omega Expt.)
BELLAZZINI 99	PL B467 296	R. Bellazzini et al.	
KAMINSKI 99	EPJ C9 141	R. Kaminski, L. Lesniak, B. Loiseau	(CRAC, PARIN)
ALDE 98	EPJ A3 361	D. Alde et al.	(GAM4 Collab.)
Also PAN 62 405			
Translated from YAF 62 446.			
ANISOVICH 98B	SPU 41 419	V.V. Anisovich et al.	
Translated from UFN 168 481.			
BERTIN 98	PR D57 55	A. Bertin et al.	(OBELIX Collab.)
BARBERIS 97B	PL B413 217	D. Barberis et al.	(WA 102 Collab.)
BERTIN 97C	PL B408 476	A. Bertin et al.	(OBELIX Collab.)
ABELE 96	PL B380 453	A. Abele et al.	(Crystal Barrel Collab.)
ABELE 96B	PL B385 425	A. Abele et al.	(Crystal Barrel Collab.)
ABELE 96C	NP A609 562	A. Abele et al.	(Crystal Barrel Collab.)
BUGG 96	NP B471 59	D.V. Bugg, A.V. Sarantsev, B.S. Zou	(LOQM, PNPI)
AMSLER 95B	PL B342 433	C. Amisler et al.	(Crystal Barrel Collab.)
AMSLER 95C	PL B353 571	C. Amisler et al.	(Crystal Barrel Collab.)
AMSLER 95D	PL B355 425	C. Amisler et al.	(Crystal Barrel Collab.)
JANSSEN 95	PR D92 2690	G. Janssen et al.	(STON, ADLD, JULI)
TORNVIST 95	ZPHY C68 647	N.A. Tornqvist	(HELS)
AMSLER 94	PL B322 431	C. Amisler et al.	(Crystal Barrel Collab.)
AMSLER 94D	PL B333 277	C. Amisler et al.	(Crystal Barrel Collab.)
ANISOVICH 94	PL B323 233	V.V. Anisovich et al.	(Crystal Barrel Collab.)
BUGG 94	PR D50 4412	D.V. Bugg et al.	(LOQM)
KAMINSKI 94	PR D50 3145	R. Kaminski, L. Lesniak, J.P. Maillet	(CRAC+)
ADAMO 93	NP A558 13C	A. Adamo et al.	(OBELIX Collab.)
GASPERO 93	NP A562 407	M. Gaspero	(ROMAI) JPC
AMSLER 92	PL B291 347	C. Amisler et al.	(Crystal Barrel Collab.)
ARMSTRONG 91	ZPHY C51 351	T.A. Armstrong et al.	(ATHU, BARI, BIRM+)
ARMSTRONG 91B	ZPHY C52 389	T.A. Armstrong et al.	(ATHU, BARI, BIRM+)
BREAKSTONE 90	ZPHY C48 569	A.M. Breakstone et al.	(ISU, BGN, CERN+)
MORGAN 90	ZPHY C48 623	D. Morgan, M.R. Pennington	(RAL, DURH)
ASTON 88	NP B296 493	D. Aston et al.	(SLAC, NAGO, CINC, INUS)
BOLONKIN 88	NP B309 426	B.V. Bolonkin et al.	(ITEP, SERP)
FALVARD 88	PR D38 2706	A. Falvard et al.	(CLER, FRAS, LALO+)
VOROBYEV 88	SJNP 48 273	P.V. Vorobiev et al.	(NOVO)
Translated from YAF 48 436.			
AU 87	PR D35 1633	K.L. Au, D. Morgan, M.R. Pennington	(DURH, RAL)
AKESSON 86	NP B264 154	T. Akesson et al.	(Axial Field Spec. Collab.)
ALDE 86D	NP B269 485	D.M. Alde et al.	(BELG, LAPP, SERP, CERN+)
CASON 83	PR D28 1586	N.M. Cason et al.	(NDAM, ANL)
ETKIN 82B	PR D25 1786	A. Etkin et al.	(BNL, CUNY, TUFTS, VAND)
WICKLUND 80	PRL 45 1469	A.B. Wicklund et al.	(ANL)
BECKER 79	NP B151 46	H. Becker et al.	(MPIM, CERN, ZEEM, CRAC)
POLYCHRO... 79	PR D19 1317	V.A. Polychronakos et al.	(NDAM, ANL)
FROGGATT 77	NP B129 89	C.D. Froggatt, J.L. Petersen	(GLAS, NORD)
ROSSELET 77	PR D15 574	L. Rosselet et al.	(GEVA, SACL)
GRAYER 74	NP B75 189	G. Grayer et al.	(CERN, MPIM)
HYAMS 73	NP B64 134	B.D. Hyams et al.	(CERN, MPIM)
OCHS 73	Thesis	W. Ochs	(MPIM, MUNI)
BEIER 72B	PRL 29 511	E.W. Beier et al.	(PENN)
BETTINI 66	NC 42A 695	A. Bettini et al.	(PADO, PISA)

### $\pi_1(1400)$

$$J^G(J^{PC}) = 1^-(1^-+)$$

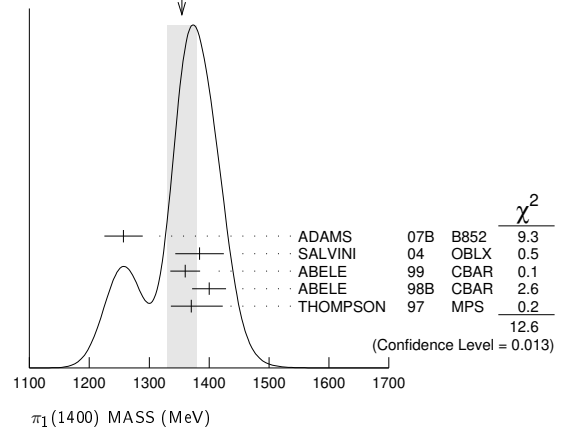
See the review on "Non- $q\bar{q}$  Mesons" and a note in PDG 06, Journal of Physics **G33** 1 (2006).

### $\pi_1(1400)$ MASS

VALUE (MeV)	EVTS	DOCUMENT ID	TECN	CHG	COMMENT
<b>1354 ± 25</b>	<b>OUR AVERAGE</b>	Error includes scale factor of 1.8. See the ideogram below.			
1257 ± 20 ± 25	23.5k	ADAMS	07b	B852	18 $\pi^- p \rightarrow \eta\pi^0 n$

1384 ± 20 ± 35	90k	SALVINI	04	OBLX	$\bar{p}p \rightarrow 2\pi^+ 2\pi^-$
1360 ± 25		ABELE	99	CBAR	0.0 $\bar{p}p \rightarrow \pi^0 \pi^0 \eta$
1400 ± 20 ± 20		ABELE	98b	CBAR	0.0 $\bar{p}n \rightarrow \pi^- \pi^0 \eta$
1370 ± 16	$^{+50}_{-30}$	<sup>1</sup> THOMPSON	97	MPS	18 $\pi^- p \rightarrow \eta\pi^- p$
••• We do not use the following data for averages, fits, limits, etc. •••					
1323.1 ± 4.6		<sup>2</sup> AOYAGI	93	BKEI	$\pi^- p \rightarrow \eta\pi^- p$
1406 ± 20		<sup>3</sup> ALDE	88b	GAM4 0	100 $\pi^- p \rightarrow \eta\pi^0 n$
<sup>1</sup> Natural parity exchange, questioned by DZIERBA 03.					
<sup>2</sup> Unnatural parity exchange.					
<sup>3</sup> Seen in the $P_0$ -wave intensity of the $\eta\pi^0$ system, unnatural parity exchange.					

WEIGHTED AVERAGE  
1354±25 (Error scaled by 1.8)



### $\pi_1(1400)$ WIDTH

VALUE (MeV)	EVTS	DOCUMENT ID	TECN	CHG	COMMENT
<b>330 ± 35</b>	<b>OUR AVERAGE</b>				
354 ± 64 ± 58	23.5k	ADAMS	07b	B852	18 $\pi^- p \rightarrow \eta\pi^0 n$
378 ± 50 ± 50	90k	SALVINI	04	OBLX	$\bar{p}p \rightarrow 2\pi^+ 2\pi^-$
220 ± 90		ABELE	99	CBAR	0.0 $\bar{p}p \rightarrow \pi^0 \pi^0 \eta$
310 ± 50	$^{+50}_{-30}$	ABELE	98b	CBAR	0.0 $\bar{p}n \rightarrow \pi^- \pi^0 \eta$
385 ± 40	$^{+65}_{-105}$	<sup>4</sup> THOMPSON	97	MPS	18 $\pi^- p \rightarrow \eta\pi^- p$
••• We do not use the following data for averages, fits, limits, etc. •••					
143.2 ± 12.5		<sup>5</sup> AOYAGI	93	BKEI	$\pi^- p \rightarrow \eta\pi^- p$
180 ± 20		<sup>6</sup> ALDE	88b	GAM4 0	100 $\pi^- p \rightarrow \eta\pi^0 n$
<sup>4</sup> Resolution is not unfolded, natural parity exchange, questioned by DZIERBA 03.					
<sup>5</sup> Unnatural parity exchange.					
<sup>6</sup> Seen in the $P_0$ -wave intensity of the $\eta\pi^0$ system, unnatural parity exchange.					

### $\pi_1(1400)$ DECAY MODES

Mode	Fraction ( $\Gamma_i/\Gamma$ )
$\Gamma_1 \eta\pi^0$	seen
$\Gamma_2 \eta\pi^-$	seen
$\Gamma_3 \eta'\pi$	
$\Gamma_4 \rho(770)\pi$	not seen

### $\pi_1(1400)$ BRANCHING RATIOS

$\Gamma(\eta\pi^0)/\Gamma_{total}$	DOCUMENT ID	TECN	CHG	COMMENT	$\Gamma_1/\Gamma$
VALUE					
••• We do not use the following data for averages, fits, limits, etc. •••					
not seen	PROKOSHKIN 95b	GAM4		100 $\pi^- p \rightarrow \eta\pi^0 n$	
not seen	<sup>7</sup> BUGG	94	RVUE	$\bar{p}p \rightarrow \eta 2\pi^0$	
not seen	<sup>8</sup> APEL	81	NICE 0	40 $\pi^- p \rightarrow \eta\pi^0 n$	
<sup>7</sup> Using Crystal Barrel data.					
<sup>8</sup> A general fit allowing S, D, and P waves (including m=0) is not done because of limited statistics.					

$\Gamma(\eta\pi^-)/\Gamma_{total}$	DOCUMENT ID	TECN	COMMENT	$\Gamma_2/\Gamma$
VALUE				
••• We do not use the following data for averages, fits, limits, etc. •••				
possibly seen	BELADIDZE 93	VES	37 $\pi^- N \rightarrow \eta\pi^- N$	

See key on page 999

Meson Particle Listings

$\pi_1(1400), \eta(1405)$

$\Gamma(\eta'/\pi)/\Gamma(\eta\pi^0)$

VALUE	CL%	DOCUMENT ID	TECN	COMMENT
<0.80	95	BOUTEMEUR 90	GAM4	100 $\pi^- p \rightarrow 4\gamma n$

$\Gamma(\rho(770)\pi)/\Gamma_{total}$

VALUE	DOCUMENT ID	TECN	COMMENT
not seen	AGHASYAN 18B	COMP	190 $\pi^- p \rightarrow \pi^- \pi^+ \pi^- p$

$\pi_1(1400)$  REFERENCES

AGHASYAN 18B	PR D98 092003	M. Aghasyan et al.	(COMPASS Collab.)
ADAMS 07B	PL B657 27	G.S. Adams et al.	(BNL E852 Collab.)
PDG 06	JP G33 1	W.-M. Yao et al.	(PDG Collab.)
SALVINI 04	EPJ C35 21	P. Salvini et al.	(OBELIX Collab.)
DZIERBA 03	PR D67 094015	A.R. Dzierba et al.	
ABELE 99	PL B446 349	A. Abele et al.	(Crystal Barrel Collab.)
ABELE 98B	PL B423 175	A. Abele et al.	(Crystal Barrel Collab.)
THOMPSON 97	PRL 79 1630	D.R. Thompson et al.	(BNL E852 Collab.)
PROKOSHKIN 95B	PAN 58 606	Y.D. Prokoshkin, S.A. Sadovsky	(SERP)
BUGG 94	PR D50 4412	D.V. Bugg et al.	(LOQM)
AOYAGI 93	PL B314 246	H. Aoyagi et al.	(BKEI Collab.)
BEHADIDZE 93	PL B313 276	G.M. Behadidze et al.	(VES Collab.)
BOUTEMEUR 90	Hadron 89 Conf. p 119	M. BoutemEUR, M. Poulet	(SERP, BELG, LANL)
ALDE 88B	PL B205 397	D.M. Alde et al.	(SERP, BELG, LANL, LAPP)
APEL 81	NP B193 269	W.D. Apel et al.	(SERP, CERN)

$\eta(1405)$

$I^G(JPC) = 0^+(0^-+)$

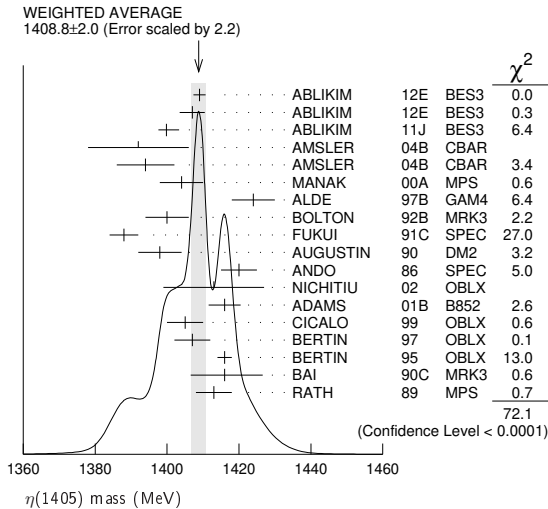
See also the  $\eta(1475)$ .

See the related review(s):

Pseudoscalar and Pseudovector Mesons in the 1400 MeV Region

$\eta(1405)$  MASS

**1408.8 ± 2.0 OUR AVERAGE** Includes data from the 2 datablocks that follow this one. Error includes scale factor of 2.2. See the ideogram below.



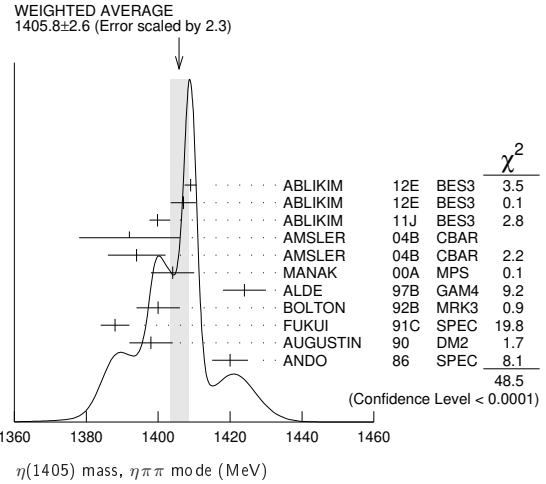
$\eta\pi\pi$  MODE

**1405.8 ± 2.6 OUR AVERAGE** Error includes scale factor of 2.3. See the ideogram below.

1409.0 ± 1.7	743	ABLIKIM 12E	BES3	$J/\psi \rightarrow \gamma(\pi^+ \pi^- \pi^0)$
1407.0 ± 3.5	198	ABLIKIM 12E	BES3	$J/\psi \rightarrow \gamma(\pi^0 \pi^0 \pi^0)$
1399.8 ± 2.2 <sup>+2.8</sup> <sub>-0.1</sub>		1 ABLIKIM 11J	BES3	$J/\psi \rightarrow \omega(\eta\pi^+\pi^-)$
1392 ± 14	900 ± 375	AMSLER 04B	CBAR	$0 \bar{p}p \rightarrow \pi^+ \pi^- \pi^+ \pi^- \eta$
1394 ± 8	6.6 ± 2.0k	AMSLER 04B	CBAR	$0 \bar{p}p \rightarrow \pi^+ \pi^- \pi^0 \pi^0 \eta$
1404 ± 6	9082	MANAK 00A	MPS	$18 \pi^- p \rightarrow \eta\pi^+\pi^- n$
1424 ± 6	2200	ALDE 97B	GAM4	$100 \pi^- p \rightarrow \eta\pi^0 \pi^0 n$
1400 ± 6		2 BOLTON 92B	MRK3	$J/\psi \rightarrow \gamma\eta\pi^+\pi^-$
1388 ± 4		FUKUI 91C	SPEC	$8.95 \pi^- p \rightarrow \eta\pi^+\pi^- n$
1398 ± 6	261	3 AUGUSTIN 90	DM2	$J/\psi \rightarrow \gamma\eta\pi^+\pi^-$
1420 ± 5		ANDO 86	SPEC	$8 \pi^- p \rightarrow \eta\pi^+\pi^- n$
1404.0 ± 11.0	195	ABLIKIM 19B	BES3	$e^+ e^- \rightarrow \psi(2S)$
1385 ± 7		BAI 99	BES	$J/\psi \rightarrow \gamma\eta\pi^+\pi^-$
1409 ± 3		4 AMSLER 95F	CBAR	$0 \bar{p}p \rightarrow \pi^+ \pi^- \pi^0 \pi^0 \eta$

1 The selected process is  $J/\psi \rightarrow \omega a_0(980)\pi$ .

2 From fit to the  $a_0(980)\pi^0$  partial wave.  
 3 Best fit with a single Breit Wigner.  
 4 Superseded by AMSLER 04B.



$K\bar{K}\pi$  MODE ( $a_0(980)\pi$  or direct  $K\bar{K}\pi$ )

**1413.9 ± 1.7 OUR AVERAGE** Error includes scale factor of 1.1.

1413 ± 14	3651	1 NICHITIU 02	OBLX	$0 \bar{p}p \rightarrow K^+ K^- \pi^+ \pi^- \pi^0$
1416 ± 4 ± 2	20k	ADAMS 01B	B852	$18 \text{ GeV } \pi^- p \rightarrow K^+ K^- \pi^0 n$
1405 ± 5		2 CICALO 99	OBLX	$0 \bar{p}p \rightarrow K^\pm K_S^0 \pi^\mp \pi^+ \pi^-$
1407 ± 5		2 BERTIN 97	OBLX	$0 \bar{p}p \rightarrow K^\pm(K^0) \pi^\mp \pi^+ \pi^-$
1416 ± 2		2 BERTIN 95	OBLX	$0 \bar{p}p \rightarrow K\bar{K}\pi\pi$
1416 ± 8 ± 7	700	3 BAI 90C	MRK3	$J/\psi \rightarrow \gamma K_S^0 K^\pm \pi^\mp$
1413 ± 5		3 RATH 89	MPS	$21.4 \pi^- p \rightarrow n K_S^0 K^\pm \pi^0$
1459 ± 5		4 AUGUSTIN 92	DM2	$J/\psi \rightarrow \gamma K\bar{K}\pi$

1 Decaying dominantly directly to  $K^+ K^- \pi^0$ .  
 2 Decaying into  $(K\bar{K})_S \pi$ ,  $(K\pi)_S \bar{K}$ , and  $a_0(980)\pi$ .  
 3 From fit to the  $a_0(980)\pi^0$  partial wave. Cannot rule out a  $a_0(980)\pi^{1^+}$  partial wave.  
 4 Excluded from averaging because averaging would be meaningless.

$\pi\pi\gamma$  MODE

**1403 ± 17 OUR AVERAGE** Error includes scale factor of 1.8.

1390 ± 12	235 ± 91	AMSLER 04B	CBAR	$0 \bar{p}p \rightarrow \pi^+ \pi^- \pi^+ \pi^- \eta$
1424 ± 10 ± 11	547	BAI 04J	BES2	$J/\psi \rightarrow \gamma\gamma\pi^+\pi^-$
1401 ± 18		1,2 AUGUSTIN 90	DM2	$J/\psi \rightarrow \pi^+ \pi^- \gamma\gamma$
1432 ± 8		2 COFFMAN 90	MRK3	$J/\psi \rightarrow \pi^+ \pi^- 2\gamma$

1 Best fit with a single Breit Wigner.  
 2 This peak in the  $\gamma\rho$  channel may not be related to the  $\eta(1405)$ .

4 $\pi$  MODE

1420 ± 20		BUGG 95	MRK3	$J/\psi \rightarrow \gamma\pi^+ \pi^- \pi^+ \pi^-$
1489 ± 12	3270	1 BISELLO 89B	DM2	$J/\psi \rightarrow 4\pi\gamma$

$K\bar{K}\pi$  MODE (unresolved)

1452.7 ± 3.3	191	1,2 ABLIKIM 13M	BES3	$\psi(2S) \rightarrow \omega K\bar{K}\pi$
1437.6 ± 3.2	249 ± 35	1,2 ABLIKIM 08E	BES2	$J/\psi \rightarrow \omega K_S^0 K^+ \pi^- + c.c.$
1445.9 ± 5.7	62 ± 18	1,2 ABLIKIM 08E	BES2	$J/\psi \rightarrow \omega K^+ K^- \pi^0$
1442 ± 10	410	1 BAI 98C	BES	$J/\psi \rightarrow \gamma K^+ K^- \pi^0$
1445 ± 8	693	1 AUGUSTIN 90	DM2	$J/\psi \rightarrow \gamma K_S^0 K^\pm \pi^\mp$
1433 ± 8	296	1 AUGUSTIN 90	DM2	$J/\psi \rightarrow \gamma K^+ K^- \pi^-$
1413 ± 8	500	1 DUCH 89	ASTE	$\bar{p}p \rightarrow \pi^+ \pi^- K^\pm \pi^\mp K^0$
1453 ± 7	170	1 RATH 89	MPS	$21.4 \pi^- p \rightarrow K_S^0 K^0 \pi^0 n$
1419 ± 1	8800	1 BIRMAN 88	MPS	$8 \pi^- p \rightarrow K^+ \bar{K}^0 \pi^- n$
1424 ± 3	620	1 REEVES 86	SPEC	$6.6 \bar{p}p \rightarrow K\bar{K}\pi X$
1421 ± 2		1 CHUNG 85	SPEC	$8 \pi^- p \rightarrow K\bar{K}\pi n$
1440 ± 20	174	1 EDWARDS 82E	CBAL	$J/\psi \rightarrow \gamma K^+ K^- \pi^0$

# Meson Particle Listings

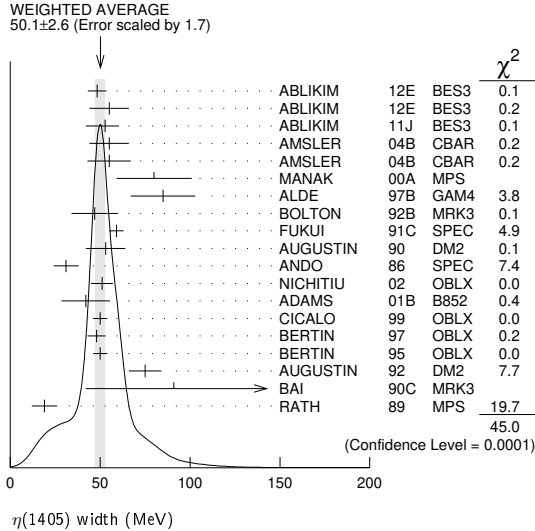
## $\eta(1405)$

1440	$+10$ $-15$	1	SCHARRE	80	MRK2	$J/\psi \rightarrow \gamma K_S^0 K^\pm \pi^\mp$	
1425	$\pm 7$	800	1,3	BAILLON	67	HBC	$0 \bar{p} p \rightarrow K \bar{K} \pi \pi \pi$

<sup>1</sup> These experiments identify only one pseudoscalar in the 1400–1500 range. Data could also refer to  $\eta(1475)$ .  
<sup>2</sup> Systematic uncertainty not evaluated.  
<sup>3</sup> From best fit of  $0^-+$  partial wave, 50%  $K^*(892)K$ , 50%  $a_0(980)\pi$ .

### $\eta(1405)$ WIDTH

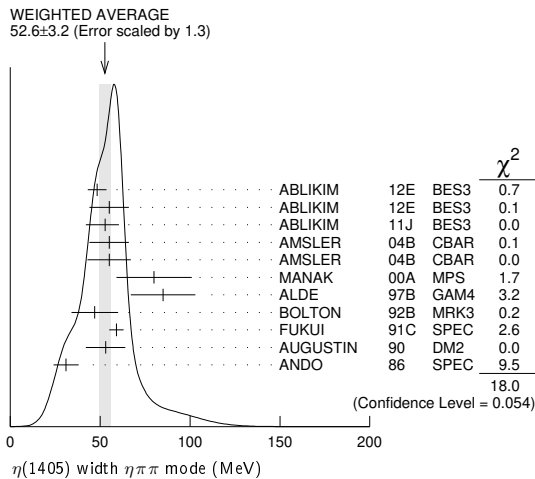
**50.1 ± 2.6 OUR AVERAGE** Includes data from the 2 datablocks that follow this one. Error includes scale factor of 1.7. See the ideogram below.



### $\eta\pi\pi$ MODE

**52.6 ± 3.2 OUR AVERAGE** Error includes scale factor of 1.3. See the ideogram below.

VALUE (MeV)	EVTS	DOCUMENT ID	TECN	COMMENT
48.3 ± 5.2	743	ABLIKIM 12E BES3		$J/\psi \rightarrow \gamma(\pi^+ \pi^- \pi^0)$
55.0 ± 11.0	198	ABLIKIM 12E BES3		$J/\psi \rightarrow \gamma(\pi^0 \pi^0 \pi^0)$
52.8 ± 7.6 <sup>+0.1</sup> <sub>-7.6</sub>		1 ABLIKIM 11J BES3		$J/\psi \rightarrow \omega(\eta\pi^+ \pi^-)$
55 ± 11	900	AMSLER 04B CBAR		$0 \bar{p} p \rightarrow \pi^+ \pi^- \pi^+ \pi^- \eta$
55 ± 12	6.6k	AMSLER 04B CBAR		$0 \bar{p} p \rightarrow \pi^+ \pi^- \pi^0 \pi^0 \gamma$
80 ± 21	9.0k	MANAK 00A MPS		$18 \pi^- p \rightarrow \eta\pi^+ \pi^- n$
85 ± 18	2.2k	ALDE 97B GAM4		$100 \pi^- p \rightarrow \eta\pi^0 \pi^0 n$
47 ± 13		2 BOLTON 92B MRK3		$J/\psi \rightarrow \gamma\eta\pi^+ \pi^-$
59 ± 4		FUKUI 91C SPEC		$8.95 \pi^- p \rightarrow \eta\pi^+ \pi^- n$
53 ± 11		3 AUGUSTIN 90 DM2		$J/\psi \rightarrow \gamma\eta\pi^+ \pi^-$
31 ± 7		ANDO 86 SPEC		$8 \pi^- p \rightarrow \eta\pi^+ \pi^- n$
• • • We do not use the following data for averages, fits, limits, etc. • • •				
79.0 ± 16.0	195	ABLIKIM 19BA BES3		$e^+ e^- \rightarrow \psi(2S)$
86 ± 10		4 AMSLER 95F CBAR		$0 \bar{p} p \rightarrow \pi^+ \pi^- \pi^0 \pi^0 \eta$



<sup>1</sup> The selected process is  $J/\psi \rightarrow \omega a_0(980)\pi$ .  
<sup>2</sup> From fit to the  $a_0(980)\pi 0^-+$  partial wave.

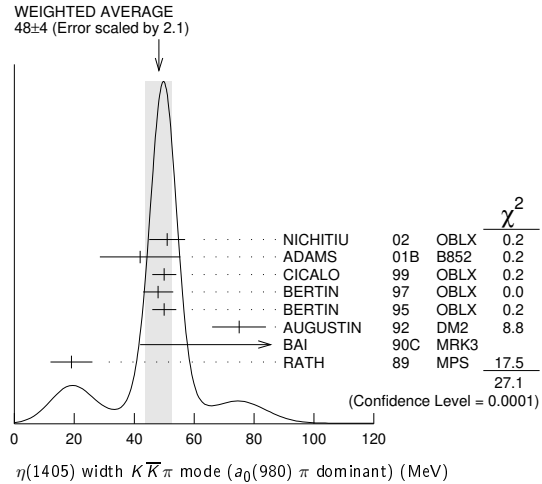
<sup>3</sup> From  $\eta\pi^+ \pi^-$  mass distribution - mainly  $a_0(980)\pi$  - no spin-parity determination available.  
<sup>4</sup> Superseded by AMSLER 04B.

### $K\bar{K}\pi$ MODE ( $a_0(980)\pi$ or direct $K\bar{K}\pi$ )

The data in this block is included in the average printed for a previous datablock.

VALUE (MeV)	EVTS	DOCUMENT ID	TECN	COMMENT
<b>48 ± 4 OUR AVERAGE</b>				Error includes scale factor of 2.1. See the ideogram below.
51 ± 6	3651	1 NICHITIU 02 OBLX		$0 \bar{p} p \rightarrow K^+ K^- \pi^+ \pi^- \pi^0$
42 ± 10 ± 9	20k	ADAMS 01B B852		$18 \text{ GeV } \pi^- p \rightarrow K^+ K^- \pi^0 n$
50 ± 4		CICALO 99 OBLX		$0 \bar{p} p \rightarrow K^\pm K_S^0 \pi^\mp \pi^+ \pi^-$
48 ± 5		2 BERTIN 97 OBLX		$0.0 \bar{p} p \rightarrow K^\pm (K^0) \pi^\mp \pi^+ \pi^-$
50 ± 4		2 BERTIN 95 OBLX		$0 \bar{p} p \rightarrow K \bar{K} \pi \pi \pi$
75 ± 9		AUGUSTIN 92 DM2		$J/\psi \rightarrow \gamma K \bar{K} \pi$
91 <sup>+67</sup> <sub>-31</sub> ± 15 <sup>+38</sup>		3 BAI 90C MRK3		$J/\psi \rightarrow \gamma K_S^0 K^\pm \pi^\mp$
19 ± 7		3 RATH 89 MPS		$21.4 \pi^- p \rightarrow n K_S^0 K_S^0 \pi^0$

<sup>1</sup> Decaying dominantly directly to  $K^+ K^- \pi^0$ .  
<sup>2</sup> Decaying into  $(K \bar{K})_S \pi$ ,  $(K \pi)_S \bar{K}$ , and  $a_0(980)\pi$ .  
<sup>3</sup> From fit to the  $a_0(980)\pi 0^-+$  partial wave, but  $a_0(980)\pi 1^++$  cannot be excluded.



### $\pi\pi\gamma$ MODE

**89 ± 17 OUR AVERAGE** Error includes scale factor of 1.7.

VALUE (MeV)	EVTS	DOCUMENT ID	TECN	COMMENT
64 ± 18	235 ± 91	AMSLER 04B CBAR		$0 \bar{p} p \rightarrow \pi^+ \pi^- \pi^+ \pi^- \gamma$
101.0 ± 8.8 ± 8.8	547	BAI 04J BES2		$J/\psi \rightarrow \gamma\gamma\pi^+ \pi^-$
• • • We do not use the following data for averages, fits, limits, etc. • • •				
174 ± 44		AUGUSTIN 90 DM2		$J/\psi \rightarrow \pi^+ \pi^- \gamma\gamma$
90 ± 26		1 COFFMAN 90 MRK3		$J/\psi \rightarrow \pi^+ \pi^- 2\gamma$

<sup>1</sup> This peak in the  $\gamma\rho$  channel may not be related to the  $\eta(1405)$ .

### 4 $\pi$ MODE

**144 ± 13 OUR AVERAGE** Error includes scale factor of 1.7.

VALUE (MeV)	EVTS	DOCUMENT ID	TECN	COMMENT
160 ± 30		BUGG 95 MRK3		$J/\psi \rightarrow \gamma\pi^+ \pi^- \pi^+ \pi^-$
144 ± 13	3270	1 BISELLO 89B DM2		$J/\psi \rightarrow 4\pi\gamma$

<sup>1</sup> Estimated by us from various fits.

### $K\bar{K}\pi$ MODE (unresolved)

**105 ± 10 OUR AVERAGE** Error includes scale factor of 1.7.

VALUE (MeV)	EVTS	DOCUMENT ID	TECN	COMMENT
45.9 ± 8.2	191	1,2 ABLIKIM 13M BES3		$\psi(2S) \rightarrow \omega K K \pi$
48.9 ± 9.0	249 ± 35	1,2 ABLIKIM 08E BES2		$J/\psi \rightarrow \omega K_S^0 K^+ \pi^- + c.c.$
34.2 ± 18.5	62 ± 18	1,2 ABLIKIM 08E BES2		$J/\psi \rightarrow \omega K^+ K^- \pi^0$
93 ± 14	296	1 AUGUSTIN 90 DM2		$J/\psi \rightarrow \gamma K^+ K^- \pi^0$
105 ± 10	693	1 AUGUSTIN 90 DM2		$J/\psi \rightarrow \gamma K_S^0 K^\pm \pi^\mp$
62 ± 16	500	1 DUCH 89 ASTE		$\bar{p} p \rightarrow K \bar{K} \pi \pi \pi$
100 ± 11	170	1 RATH 89 MPS		$21.4 \pi^- p \rightarrow K_S^0 K_S^0 \pi^0 n$
66 ± 2	8800	1 BIRMAN 88 MPS		$8 \pi^- p \rightarrow K^+ \bar{K}^0 \pi^- n$
60 ± 10	620	1 REEVES 86 SPEC		$6.6 \rho \bar{p} \rightarrow K K \pi X$
60 ± 10		1 CHUNG 85 SPEC		$8 \pi^- p \rightarrow K \bar{K} \pi n$
55 <sup>+20</sup> <sub>-30</sub> ± 10	174	1 EDWARDS 82E CBAL		$J/\psi \rightarrow \gamma K^+ K^- \pi^0$
50 ± 20		1 SCHARRE 80 MRK2		$J/\psi \rightarrow \gamma K_S^0 K^\pm \pi^\mp$
80 ± 10	800	1,3 BAILLON 67 HBC		$0 \bar{p} p \rightarrow K \bar{K} \pi \pi \pi$

<sup>1</sup> These experiments identify only one pseudoscalar in the 1400–1500 range. Data could also refer to  $\eta(1475)$ .  
<sup>2</sup> Systematic uncertainty not evaluated.  
<sup>3</sup> From best fit to  $0^-+$  partial wave, 50%  $K^*(892)K$ , 50%  $a_0(980)\pi$ .

$\eta(1405)$  DECAY MODES

Table with 3 columns: Mode, Fraction ( $\Gamma_i/\Gamma$ ), Confidence level. Rows include  $K\bar{K}\pi$ ,  $\eta\pi\pi$ ,  $a_0(980)\pi$ ,  $\eta(\pi\pi)$  s-wave,  $f_0(980)\pi^0 \rightarrow \pi^+\pi^-\pi^0$ ,  $f_0(980)\eta$ ,  $4\pi$ ,  $\rho\rho$ ,  $\gamma\gamma$ ,  $\rho^0\gamma$ ,  $\phi\gamma$ ,  $K^*(892)K$ .

$\eta(1405)$   $\Gamma(\eta)\Gamma(\gamma\gamma)/\Gamma(\text{total})$

Table with 5 columns: VALUE (keV), CL%, DOCUMENT ID, TECN, COMMENT. Row for  $\Gamma(K\bar{K}\pi) \times \Gamma(\gamma\gamma)/\Gamma_{\text{total}}$  with value <0.035 and document ID 1,2 AHOHE.

• • • We do not use the following data for averages, fits, limits, etc. • • •
Using  $\eta(1405)$  mass and width 1410 MeV and 51 MeV, respectively.
Assuming three-body phase-space decay to  $K_S^0 K^\pm \pi^\mp$ .

Table with 5 columns: VALUE (keV), CL%, DOCUMENT ID, TECN, COMMENT. Row for  $\Gamma(\eta\pi\pi) \times \Gamma(\gamma\gamma)/\Gamma_{\text{total}}$  with value <0.095 and document ID ACCIARRI.

Table with 5 columns: VALUE (keV), CL%, DOCUMENT ID, TECN, COMMENT. Row for  $\Gamma(\rho^0\gamma) \times \Gamma(\gamma\gamma)/\Gamma_{\text{total}}$  with value <1.5 and document ID ALTHOFF.

$\eta(1405)$  BRANCHING RATIOS

Table with 5 columns: VALUE, CL%, DOCUMENT ID, TECN, COMMENT. Row for  $\Gamma(\eta\pi\pi)/\Gamma(K\bar{K}\pi)$  with value 1.09 ± 0.48 and document ID AMSLER.

• • • We do not use the following data for averages, fits, limits, etc. • • •
Using the data of BAILLON 67 on  $\bar{p}p \rightarrow K\bar{K}\pi$ .

Table with 5 columns: VALUE, DOCUMENT ID, TECN, COMMENT. Row for  $\Gamma(\rho^0\gamma)/\Gamma(\eta\pi\pi)$  with value 0.111 ± 0.064 and document ID AMSLER.

Table with 5 columns: VALUE, EVTS, DOCUMENT ID, TECN, COMMENT. Row for  $\Gamma(a_0(980)\pi)/\Gamma(K\bar{K}\pi)$  with value ~0.15 and document ID BERTIN.

• • • We do not use the following data for averages, fits, limits, etc. • • •
Assuming that the  $a_0(980)$  decays only into  $K\bar{K}$ .

Table with 5 columns: VALUE, EVTS, DOCUMENT ID, TECN, COMMENT. Row for  $\Gamma(a_0(980)\pi)/\Gamma(\eta\pi\pi)$  with value 0.29 ± 0.10 and document ID ABELE.

• • • We do not use the following data for averages, fits, limits, etc. • • •
Assuming that the  $a_0(980)$  decays only into  $\eta\pi$ .

Table with 5 columns: VALUE, EVTS, DOCUMENT ID, TECN, COMMENT. Row for  $\Gamma(a_0(980)\pi)/\Gamma(\eta(\pi\pi)\text{s-wave})$  with value 0.91 ± 0.12 and document ID ANISOVICH.

• • • We do not use the following data for averages, fits, limits, etc. • • •
Statistical error only.
Assuming that the  $a_0(980)$  decays only into  $\eta\pi$ .

Table with 5 columns: VALUE, DOCUMENT ID, TECN, COMMENT. Row for  $\Gamma(\rho^0\gamma)/\Gamma(K\bar{K}\pi)$  with value 0.0152 ± 0.0038 and document ID COFFMAN.

Using  $B(J/\psi \rightarrow \gamma\eta(1405) \rightarrow \gamma K\bar{K}\pi) = 4.2 \times 10^{-3}$  and  $B(J/\psi \rightarrow \gamma\eta(1405) \rightarrow \gamma\gamma\rho^0) = 6.4 \times 10^{-5}$ .

Table with 5 columns: VALUE, CL%, DOCUMENT ID, TECN, COMMENT. Row for  $\Gamma(\gamma\gamma)/\Gamma(K\bar{K}\pi)$  with value <1.78 × 10<sup>-3</sup> and document ID ABLIKIM.

Using results from BAI 00d.

Table with 5 columns: VALUE, EVTS, DOCUMENT ID, TECN, COMMENT. Row for  $\Gamma(\eta(\pi\pi)\text{s-wave})/\Gamma(\eta\pi\pi)$  with value 0.81 ± 0.04 and document ID ALDE.

• • • We do not use the following data for averages, fits, limits, etc. • • •

Table with 5 columns: VALUE, DOCUMENT ID, TECN, COMMENT. Row for  $\Gamma(f_0(980)\eta)/\Gamma(\eta\pi\pi)$  with value 0.32 ± 0.07 and document ID ANISOVICH.

Using preliminary Crystal Barrel data.

Table with 5 columns: VALUE, DOCUMENT ID, TECN, COMMENT. Row for  $\Gamma(f_0(980)\pi^0 \rightarrow \pi^+\pi^-\pi^0)/\Gamma_{\text{total}}$  with value not seen and document ID ABLIKIM.

ABLIKIM 17A reports  $B(\psi(2S) \rightarrow \gamma\eta(1405) \rightarrow \gamma f_0(980)\pi^0 \rightarrow \gamma\pi^+\pi^-\pi^0) < 5.0 \times 10^{-7}$ .

Table with 5 columns: VALUE, CL%, DOCUMENT ID, TECN, COMMENT. Row for  $\Gamma(\rho\rho)/\Gamma_{\text{total}}$  with value <0.58 and document ID AMSLER.

Assuming that the  $\eta(1405)$  decays are saturated by the  $\pi\eta\eta$ ,  $K\bar{K}\pi$  and  $\rho\rho$  modes.
Using the data of BAILLON 67 on  $\bar{p}p \rightarrow K\bar{K}\pi$ .

Table with 5 columns: VALUE, DOCUMENT ID, TECN, COMMENT. Row for  $\Gamma(K^*(892)K)/\Gamma(a_0(980)\pi)$  with value 0.084 ± 0.024 and document ID ADAMS.

• • • We do not use the following data for averages, fits, limits, etc. • • •

Statistical error only.

Table with 5 columns: VALUE, CL%, DOCUMENT ID, TECN, COMMENT. Row for  $\Gamma(\phi\gamma)/\Gamma(\rho^0\gamma)$  with value 0.09 ± 0.03 and document ID ABLIKIM.

• • • We do not use the following data for averages, fits, limits, etc. • • •
Constructive interference between  $X(1835)$  and  $\eta(1405)/\eta(1475)$  decays to  $\gamma\phi$  is assumed. Also see  $\eta(1475)$ . ABLIKIM 18i reports the inverse as  $11.10 \pm 3.5$ .
Destructive interference between  $X(1835)$  and  $\eta(1405)/\eta(1475)$  decays to  $\gamma\phi$  is assumed. Also see  $\eta(1475)$ . ABLIKIM 18i reports the inverse as  $7.53 \pm 2.49$ .
Calculated by us from  $B(J/\psi \rightarrow \eta(1405)\gamma \rightarrow \phi\gamma\gamma) < 0.82 \times 10^{-4}$  and  $B(J/\psi \rightarrow \eta(1405)\gamma \rightarrow \rho^0\gamma\gamma) = (1.07 \pm 0.17 \pm 0.11) \times 10^{-4}$ .

$\eta(1405)$  REFERENCES

ABLIKIM 19BA PR D100 092003 M. Ablikim et al. (BESIII Collab.)
ABLIKIM 18i PR D37 051101 M. Ablikim et al. (BESIII Collab.)
ABLIKIM 18O PR D37 072014 M. Ablikim et al. (BESIII Collab.)
ABLIKIM 17AJ PR D36 122008 M. Ablikim et al. (BESIII Collab.)
ABLIKIM 13M PR D87 092006 M. Ablikim et al. (BESIII Collab.)
ABLIKIM 11E PRL 108 182001 M. Ablikim et al. (BESIII Collab.)
ABLIKIM 12J PRL 107 182001 M. Ablikim et al. (BESIII Collab.)
ABLIKIM 08E PR D77 032005 M. Ablikim et al. (BES Collab.)
ABLIKIM 05 PR D71 072001 R. Ahohe et al. (CLEO Collab.)
AMSLER 04B EPJ C33 23 C. Amisler et al. (Crystal Barrel Collab.)
BAI 04J PL B594 47 J.Z. Bai et al. (BES Collab.)
NICHITIU 02 PL B545 261 F. Nichitiu et al. (OBELIX Collab.)
ACCIARRI 01G PL B501 1 M. Acciarrri et al. (L3 Collab.)
ADAMS 01B PL B516 264 G.S. Adams et al. (BNL E852 Collab.)
ANISOVICH 01 NP A490 567 A.V. Anisovich et al.
ANISOVICH 00 PL B472 168 A.V. Anisovich et al.
BAI 00D PL B476 25 J.Z. Bai et al. (BES Collab.)
MANAK 00A PR D62 012003 J.J. Manak et al. (BNL E852 Collab.)
BAI 99 PL B446 356 J.Z. Bai et al. (BES Collab.)
CICALO 99 PL B462 453 C. Cicalo et al. (OBELIX Collab.)
ABELE 98E NP B514 45 A. Abele et al. (Crystal Barrel Collab.)
BAI 98C PL B440 217 J.Z. Bai et al. (BES Collab.)
ALDE 97B PAN 60 386 D. Alde et al. (GAMS Collab.)
BERTIN 97 PL B400 226 Bertin et al. (YAF 60 458)
AMSLER 95F PL B358 389 C. Amisler et al. (Crystal Barrel Collab.)
BERTIN 95 PL B361 187 A. Bertin et al. (OBELIX Collab.)
BUGG 95 PL B353 378 D.V. Bugg et al. (LOQM, PNPI, WASH)
AUGUSTIN 92 PR D46 1951 J.E. Augustin, G. Cosme (DM2 Collab.)
BOLTON 92B PRL 69 1328 T. Bolton et al. (Mark III Collab.)
FUKUI 91C PL B267 293 S. Fukui et al. (SUGI, NAGO, KEK, KYOT+)
AUGUSTIN 90 PR D42 10 J.E. Augustin et al. (DM2 Collab.)
BAI 90C PRL 65 2507 Z. Bai et al. (Mark III Collab.)
COFFMAN 90 PR D41 1410 D.M. Coffman et al. (Mark III Collab.)
BISELLO 89B PR D39 701 G. Bisello et al. (DM2 Collab.)
DUCH 89 ZPHY C45 223 K.D. Duch et al. (ASTERIX Collab.)
RATH 89 PR D40 693 M.G. Rath et al. (NDAM, BRAN, BNL, CUNY+)
BIRMAN 88 PRL 61 1557 A. Birman et al. (BNL, FSU, IND, MASD)JP
ANDO 86 PRL 57 1296 A. Ando et al. (KEK, KYOT, NIRS, SAGA+)JP
REEVES 86 PR D34 1960 D.F. Reeves et al. (FLOR, BNL, IND+)JP
CHUNG 85 PRL 55 779 S.U. Chung et al. (BNL, FLOR, IND+)JP
ALTHOFF 84E PL 147B 487 M. Althoff et al. (TASSO Collab.)
EDWARDS 83B PRL 51 859 C. Edwards et al. (CIT, HARV, PRIN+)
EDWARDS 82E PR 49 253 C. Edwards et al. (CIT, HARV, PRIN+)
Also PR 50 219 C. Edwards et al. (CIT, HARV, PRIN+)
SCHARRE 80 PL 97B 329 D.L. Scharre et al. (SLAC, LBL)
FOSTER 68B NP B8 174 M. Foster et al. (CERN, CDEF)
BAILLON 67 NC 50A 393 P.H. Baillon et al. (CERN, CDEF, IRAD)

# Meson Particle Listings

## $h_1(1415)$ , $a_1(1420)$ , $f_1(1420)$

### $h_1(1415)$

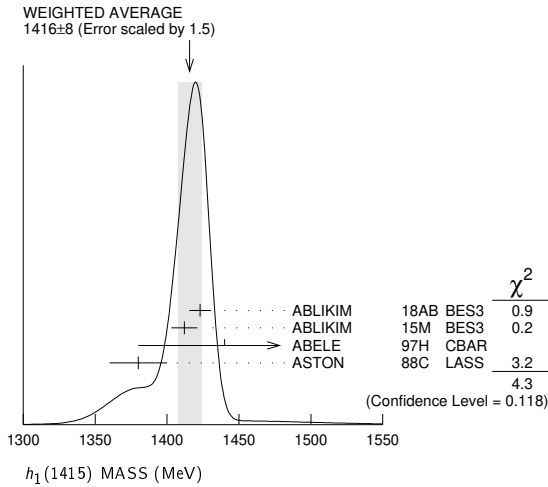
$$J^{PC} = 0^-(1^+ -)$$

was  $h_1(1380)$

#### $h_1(1415)$ MASS

VALUE (MeV)	EVTS	DOCUMENT ID	TECN	COMMENT
<b>1416 ± 8</b>	<b>OUR AVERAGE</b>	Error includes scale factor of 1.5. See the ideogram below.		
1423 ± 2.1 ± 7.3	2.2k	<sup>1</sup> ABLIKIM	18AB BES3	$J/\psi \rightarrow \eta' h_1 \rightarrow \eta' K^* \bar{K}$
1412 ± 4 ± 8		<sup>1</sup> ABLIKIM	15M BES3	$\psi(2S) \rightarrow \gamma \chi_{c1,2} \rightarrow \gamma \phi(h_1 \rightarrow K^* \bar{K})$
1440 ± 60		ABELE	97H CBAR	$\bar{p} p \rightarrow K_L^0 K_S^0 \pi^0 \pi^0$
1380 ± 20		ASTON	88C LASS	11 $K^- p \rightarrow K_S^0 K^\pm \pi^\mp \Lambda$

<sup>1</sup> Final states  $K^+ K^- \pi^0$  and  $K_S^0 K^\pm \pi^\mp$ .



#### $h_1(1415)$ WIDTH

VALUE (MeV)	EVTS	DOCUMENT ID	TECN	COMMENT
<b>90 ± 15</b>	<b>OUR AVERAGE</b>	Error includes scale factor of 1.1.		
90.3 ± 9.8 ± 17.5	2.2k	<sup>1</sup> ABLIKIM	18AB BES3	$J/\psi \rightarrow \eta' h_1 \rightarrow \eta' K^* \bar{K}$
84 ± 12 ± 40		<sup>1</sup> ABLIKIM	15M BES3	$\psi(2S) \rightarrow \gamma \chi_{c1,2} \rightarrow \gamma \phi(h_1 \rightarrow K^* \bar{K})$
170 ± 80		ABELE	97H CBAR	$\bar{p} p \rightarrow K_L^0 K_S^0 \pi^0 \pi^0$
80 ± 30		ASTON	88C LASS	11 $K^- p \rightarrow K_S^0 K^\pm \pi^\mp \Lambda$

<sup>1</sup> Final states  $K^+ K^- \pi^0$  and  $K_S^0 K^\pm \pi^\mp$ .

#### $h_1(1415)$ DECAY MODES

Mode	Fraction ( $\Gamma_i/\Gamma$ )
$\Gamma_1$ $K \bar{K}^*(892) + c.c.$	seen

#### $h_1(1415)$ REFERENCES

ABLIKIM	18AB PR D98 072005	M. Ablikim <i>et al.</i>	(BESIII Collab.)
ABLIKIM	15M PR D91 112008	M. Ablikim <i>et al.</i>	(BESIII Collab.)
ABELE	97H PL B415 280	A. Abele <i>et al.</i>	(Crystal Barrel Collab.)
ASTON	88C PL B201 573	D. Aston <i>et al.</i>	(SLAC, NAGO, CIN, INUS)

### $a_1(1420)$

$$J^{PC} = 1^-(1^+ +)$$

OMITTED FROM SUMMARY TABLE

#### $a_1(1420)$ MASS

VALUE (MeV)	EVTS	DOCUMENT ID	TECN	COMMENT
<b>1411 ± 4</b>	<b>OUR AVERAGE</b>	Error includes scale factor of 1.1.		
1414 ± 15	46M	<sup>1</sup> AGHASYAN	18B COMP	190 $\pi^- p \rightarrow \pi^- \pi^+ \pi^- p$
1412 ± 4 ± 8		<sup>2,3</sup> ADOLPH	15c COMP	190 $\pi^- p \rightarrow \pi^- \pi^+ \pi^- p$

• • • We do not use the following data for averages, fits, limits, etc. • • •

<sup>1</sup> Statistical error negligible.  
<sup>2</sup> Using the isobar model and partial-wave analysis with 88 waves.  
<sup>3</sup> Superseded by AGHASYAN 2018B.

#### $a_1(1420)$ WIDTH

VALUE (MeV)	EVTS	DOCUMENT ID	TECN	COMMENT
<b>161<sup>+11</sup><sub>-14</sub></b>	46M	<sup>1</sup> AGHASYAN	18B COMP	190 $\pi^- p \rightarrow \pi^- \pi^+ \pi^- p$
153 <sup>+8</sup> <sub>-23</sub>		<sup>2,3</sup> ADOLPH	15c COMP	190 $\pi^- p \rightarrow \pi^- \pi^+ \pi^- p$

• • • We do not use the following data for averages, fits, limits, etc. • • •

<sup>1</sup> Statistical error negligible.  
<sup>2</sup> Using the isobar model and partial-wave analysis with 88 waves.  
<sup>3</sup> Superseded by AGHASYAN 2018B.

#### $a_1(1420)$ DECAY MODES

Mode	Fraction ( $\Gamma_i/\Gamma$ )
$\Gamma_1$ $f_0(980) \pi$	seen

#### $a_1(1420)$ BRANCHING RATIOS

$\Gamma(f_0(980) \pi) / \Gamma_{total}$	Fraction ( $\Gamma_i/\Gamma$ )
<b>seen</b>	<b>seen</b>

<sup>1</sup> Using the isobar model and partial-wave analysis with 88 waves.

#### $a_1(1420)$ REFERENCES

AGHASYAN	18B PR D98 092003	M. Aghasyan <i>et al.</i>	(COMPASS Collab.)
ADOLPH	15C PRL 115 082001	C. Adolph <i>et al.</i>	(COMPASS Collab.)

### $f_1(1420)$

$$J^{PC} = 0^+(1^+ +)$$

See the review on "Pseudoscalar and Pseudovector Mesons in the 1400 MeV Region."

#### $f_1(1420)$ MASS

VALUE (MeV)	EVTS	DOCUMENT ID	TECN	COMMENT
<b>1426.3 ± 0.9</b>	<b>OUR AVERAGE</b>	Error includes scale factor of 1.1.		
1434 ± 5 ± 5	133	<sup>1</sup> AACHARD	07 L3	183-209 $e^+ e^- \rightarrow e^+ e^- K_S^0 K^\pm \pi^\mp$
1426 ± 6	711	ABDALLAH	03H DLPH	91.2 $e^+ e^- \rightarrow K_S^0 K^\pm \pi^\mp + X$
1420 ± 14	3651	NICHITIU	02 OBLX	0 $\bar{p} p \rightarrow K^+ K^- \pi^+ \pi^- \pi^0$
1428 ± 4 ± 2	20k	ADAMS	01B B852	18 GeV $\pi^- p \rightarrow K^+ K^- \pi^0 n$
1426 ± 1		BARBERIS	97c OMEG	450 $pp \rightarrow pp K_S^0 K^\pm \pi^\mp$
1425 ± 8		BERTIN	97 OBLX	0.0 $\bar{p} p \rightarrow K^\pm (K^0) \pi^\mp \pi^+ \pi^-$
1430 ± 4		<sup>2</sup> ARMSTRONG	92E OMEG	85,300 $\pi^+ p, pp \rightarrow \pi^+ p, pp (K \bar{K} \pi)$
1462 ± 20		<sup>3</sup> AUGUSTIN	92 DM2	$J/\psi \rightarrow \gamma K \bar{K} \pi$
1443 ± 7 ± 3	1100	BAI	90C MRK3	$J/\psi \rightarrow \gamma K_S^0 K^\pm \pi^\mp$
1425 ± 10	17	BEHREND	89 CELL	$\gamma \gamma \rightarrow K_S^0 K^\pm \pi^\mp$
1442 ± 5 ± 10	111	BECKER	87 MRK3	$e^+ e^-, \omega K \bar{K} \pi$
1423 ± 4		GIDAL	87B MRK2	$e^+ e^- \rightarrow e^+ e^- K \bar{K} \pi$
1417 ± 13	13	AIHARA	86c TPC	$e^+ e^- \rightarrow e^+ e^- K \bar{K} \pi$
1422 ± 3		CHAUVAT	84 SPEC	ISR 31.5 $pp$
1440 ± 10		<sup>4</sup> BROMBERG	80 SPEC	100 $\pi^- p \rightarrow K \bar{K} \pi X$
1426 ± 6	221	DIONISI	80 HBC	4 $\pi^- p \rightarrow K \bar{K} \pi n$
1420 ± 20		DAHL	87 HBC	1.6-4.2 $\pi^- p$
1430.8 ± 0.9		<sup>5</sup> SOSA	99 SPEC	$pp \rightarrow p_{slow} (K_S^0 K^+ \pi^-) p_{fast}$
1433.4 ± 0.8		<sup>5</sup> SOSA	99 SPEC	$pp \rightarrow p_{slow} (K_S^0 K^- \pi^+) p_{fast}$
1435 ± 9		PROKOSHKIN	97B GAM4	100 $\pi^- p \rightarrow \eta \pi^0 \pi^0 n$
1429 ± 3	389	ARMSTRONG	89 OMEG	300 $pp \rightarrow K \bar{K} \pi pp$
1425 ± 2	1520	ARMSTRONG	84 OMEG	85 $\pi^+ p, pp \rightarrow (\pi^+, p) (K \bar{K} \pi) p$
~ 1420		BITYUKOV	84 SPEC	32 $K^- p \rightarrow K^+ K^- \pi^0 \gamma$

• • • We do not use the following data for averages, fits, limits, etc. • • •

<sup>1</sup> From a fit with a width fixed at 55 MeV.  
<sup>2</sup> This result supersedes ARMSTRONG 84, ARMSTRONG 89.  
<sup>3</sup> From fit to the  $K^*(892) K 1^+ +$  partial wave.  
<sup>4</sup> Mass error increased to account for  $a_0(980)$  mass cut uncertainties.  
<sup>5</sup> No systematic error given.

f<sub>1</sub>(1420) WIDTH

Table with columns: VALUE (MeV), EVTS, DOCUMENT ID, TECN, COMMENT. Includes data for various decay channels like K\_S^0 K^+ pi^-, K\_S^0 K^+ pi^+ pi^-, etc.

6 This result supersedes ARMSTRONG 84, ARMSTRONG 89.
7 From fit to the K\*(892) K 1++ partial wave.
8 No systematic error given.

f<sub>1</sub>(1420) DECAY MODES

Table with columns: Mode, Fraction (Gamma\_j / Gamma). Lists decay modes like K K pi, K K\*(892) + c.c., eta pi pi, etc.

f<sub>1</sub>(1420) Gamma(i) Gamma(gamma gamma) / Gamma(total)

Table with columns: VALUE (keV), CL%, EVTS, DOCUMENT ID, TECN, COMMENT. Shows branching ratios for various decay channels.

9 From a fit with a width fixed at 55 MeV.
10 The form factor parameter from the fit is 926 +/- 78 MeV.
11 Assume a rho-pole form factor.
12 A phi-pole form factor gives considerably smaller widths.
13 Published value divided by 2.

f<sub>1</sub>(1420) BRANCHING RATIOS

Table with columns: VALUE, DOCUMENT ID, TECN, COMMENT, Gamma\_2 / Gamma\_1. Shows branching ratios for K K\*(892) + c.c. / Gamma(K K pi).

Gamma(K K pi) / Gamma(K K pi)

Table with columns: VALUE, CL%, DOCUMENT ID, TECN, COMMENT. Shows ratios for various decay channels.

Gamma(eta pi pi) / Gamma(K K pi)

Table with columns: VALUE, CL%, DOCUMENT ID, TECN, COMMENT. Shows ratios for eta pi pi decays.

Gamma(a\_0(980) pi) / Gamma(eta pi pi)

Table with columns: VALUE, CL%, DOCUMENT ID, TECN, COMMENT. Shows ratios for a\_0(980) pi decays.

Gamma(4 pi) / Gamma(K K\*(892) + c.c.)

Table with columns: VALUE, CL%, DOCUMENT ID, TECN, COMMENT. Shows ratios for 4 pi decays.

Gamma(K K pi) / [Gamma(K K\*(892) + c.c.) + Gamma(a\_0(980) pi)]

Table with columns: VALUE, DOCUMENT ID, TECN, COMMENT. Shows ratios for K K pi decays.

Gamma(a\_0(980) pi) / Gamma(K K\*(892) + c.c.)

Table with columns: VALUE, CL%, DOCUMENT ID, TECN, COMMENT. Shows ratios for a\_0(980) pi decays.

Gamma(4 pi) / Gamma(K K pi)

Table with columns: VALUE, CL%, DOCUMENT ID, TECN, COMMENT. Shows ratios for 4 pi decays.

Gamma(rho^0 gamma) / Gamma(total)

Table with columns: VALUE, CL%, DOCUMENT ID, TECN, COMMENT. Shows ratios for rho^0 gamma decays.

Gamma(rho^0 gamma) / Gamma(K K pi)

Table with columns: VALUE, CL%, DOCUMENT ID, TECN, COMMENT. Shows ratios for rho^0 gamma decays.

Gamma(phi gamma) / Gamma(K K pi)

Table with columns: VALUE, DOCUMENT ID, TECN, COMMENT. Shows ratios for phi gamma decays.

f<sub>1</sub>(1420) REFERENCES

List of references for f1(1420) measurements, including authors like Achard et al., Abdallah et al., etc.

Downloaded from https://academic.oup.com/ptep/article/2020/8/083C01/5891211 by guest on 12 November 2020



## Meson Particle Listings

 $f_1(1420), \omega(1420)$ 

CHAUVAT	84	PL 148B 382	P. Chauvat <i>et al.</i>	(CERN, CLER, UCLA+)
JENNI	83	PR D27 1031	P. Jenni <i>et al.</i>	(SLAC, LBL)
BROMBERG	80	PR D22 1513	C.M. Bromberg <i>et al.</i>	(CIT, FNAL, ILLC+)
DIONISI	80	NP B169 1	C. Dionisi <i>et al.</i>	(CERN, MADR, CDEF+) <sup>1</sup>
CORDEN	78	NP B144 253	M.J. Corden <i>et al.</i>	(BIRM, RHEL, TELA+)
DEFOIX	72	NP B44 125	C. Defoix <i>et al.</i>	(CDEF, CERN)
DAHL	67	PR 163 1377	O.I. Dahl <i>et al.</i>	(LRL) <sup>1</sup>
Also		PRL 14 1074	D.H. Miller <i>et al.</i>	(LRL, UCB)

 $\omega(1420)$ 

$$I^G(J^{PC}) = 0^-(1^{--})$$

See also the  $\omega(1650)$  particle listing. $\omega(1420)$  MASS

VALUE (MeV)	EVTs	DOCUMENT ID	TECN	COMMENT
<b>1410 ± 60 OUR ESTIMATE</b>				
• • • We do not use the following data for averages, fits, limits, etc. • • •				
1418 ± 30 ± 10	824	<sup>1</sup> AKHMETSHIN 17A	CMD3	1.4–2.0 $e^+e^- \rightarrow \omega\eta$
1470 ± 50	13.1k	<sup>2</sup> AULCHENKO 15A	SND	1.05–1.80 $e^+e^- \rightarrow \pi^+\pi^-\pi^0$
1382 ± 23 ± 70		AUBERT	07AU BABR	10.6 $e^+e^- \rightarrow \omega\pi^+\pi^-\gamma$
1350 ± 20 ± 20		AUBERT,B	04N BABR	10.6 $e^+e^- \rightarrow \pi^+\pi^-\pi^0\gamma$
1400 ± 50 ± 130	1.2M	<sup>3</sup> ACHASOV	03D RVUE	0.44–2.00 $e^+e^- \rightarrow \pi^+\pi^-\pi^0\gamma$
1450 ± 10		<sup>4</sup> HENNER	02 RVUE	1.2–2.0 $e^+e^- \rightarrow \rho\pi, \omega\pi\pi$
1373 ± 70	177	<sup>5</sup> AKHMETSHIN 00D	CMD2	1.2–1.38 $e^+e^- \rightarrow \omega\pi^+\pi^-$
1370 ± 25	5095	ANISOVICH	00H SPEC	0.0 $p\bar{p} \rightarrow \omega\pi^0\pi^0\pi^0$
1400 <sup>+100</sup> <sub>-200</sub>		<sup>6</sup> ACHASOV	98H RVUE	$e^+e^- \rightarrow \pi^+\pi^-\pi^0$
~1400		<sup>7</sup> ACHASOV	98H RVUE	$e^+e^- \rightarrow \omega\pi^+\pi^-$
~1460		<sup>8</sup> ACHASOV	98H RVUE	$e^+e^- \rightarrow K^+K^-$
1440 ± 70		<sup>9</sup> CLEGG	94 RVUE	
1419 ± 31	315	<sup>10</sup> ANTONELLI	92 DM2	1.34–2.4 $e^+e^- \rightarrow \rho\pi$

- From a fit of the interfering  $\omega(1420)$  and  $\omega(1650)$  with a relative phase of  $\pi$  and other parameters floating.
- From a fit with contributions from  $\omega(782)$ ,  $\phi(1020)$ ,  $\omega(1420)$ , and  $\omega(1650)$ .
- From the combined fit of ANTONELLI 92, ACHASOV 01E, ACHASOV 02E, and ACHASOV 03D data on the  $\pi^+\pi^-\pi^0$  and ANTONELLI 92 on the  $\omega\pi^+\pi^-$  final states. Supersedes ACHASOV 99E and ACHASOV 02E.
- Using results of CORDIER 81 and preliminary data of DOLINSKY 91 and ANTONELLI 92.
- Using the data of AKHMETSHIN 00D and ANTONELLI 92. The  $\rho\pi$  dominance for the energy dependence of the  $\omega(1420)$  and  $\omega(1650)$  width assumed.
- Using data from BARKOV 87, DOLINSKY 91, and ANTONELLI 92.
- Using the data from ANTONELLI 92.
- Using the data from IVANOV 81 and BISELLO 88b.
- From a fit to two Breit-Wigner functions and using the data of DOLINSKY 91 and ANTONELLI 92.
- From a fit to two Breit-Wigner functions interfering between them and with the  $\omega, \phi$  tails with fixed (+, -, +) phases.

 $\omega(1420)$  WIDTH

VALUE (MeV)	EVTs	DOCUMENT ID	TECN	COMMENT
<b>290 ± 190 OUR ESTIMATE</b>				
• • • We do not use the following data for averages, fits, limits, etc. • • •				
104 ± 35 ± 10	824	<sup>1</sup> AKHMETSHIN 17A	CMD3	1.4–2.0 $e^+e^- \rightarrow \omega\eta$
880 ± 170	13.1k	<sup>2</sup> AULCHENKO 15A	SND	1.05–1.80 $e^+e^- \rightarrow \pi^+\pi^-\pi^0$
480 ± 180		<sup>3</sup> ACHASOV	10D SND	1.075–2.0 $e^+e^- \rightarrow \pi^0\gamma$
130 ± 50 ± 100		AUBERT	07AU BABR	10.6 $e^+e^- \rightarrow \omega\pi^+\pi^-\gamma$
450 ± 70 ± 70		AUBERT,B	04N BABR	10.6 $e^+e^- \rightarrow \pi^+\pi^-\pi^0\gamma$
870 <sup>+500</sup> <sub>-300</sub> ± 450	1.2M	<sup>4</sup> ACHASOV	03D RVUE	0.44–2.00 $e^+e^- \rightarrow \pi^+\pi^-\pi^0\gamma$
199 ± 15		<sup>5</sup> HENNER	02 RVUE	1.2–2.0 $e^+e^- \rightarrow \rho\pi, \omega\pi\pi$
188 ± 45	177	<sup>6</sup> AKHMETSHIN 00D	CMD2	1.2–1.38 $e^+e^- \rightarrow \omega\pi^+\pi^-$
360 <sup>+100</sup> <sub>-60</sub>	5095	ANISOVICH	00H SPEC	0.0 $p\bar{p} \rightarrow \omega\pi^0\pi^0\pi^0$
240 ± 70		<sup>7</sup> CLEGG	94 RVUE	
174 ± 59	315	<sup>8</sup> ANTONELLI	92 DM2	1.34–2.4 $e^+e^- \rightarrow \rho\pi$

- From a fit of the interfering  $\omega(1420)$  and  $\omega(1650)$  with a relative phase of  $\pi$  and other parameters floating.
- From a fit with contributions from  $\omega(782)$ ,  $\phi(1020)$ ,  $\omega(1420)$ , and  $\omega(1650)$ .
- From a fit of a VMD model with two effective resonances with masses of 1450 MeV and 1700 MeV to describe the excited vector states  $\omega(1420)$ ,  $\rho(1450)$ ,  $\omega(1650)$ , and  $\rho(1700)$ . Systematic errors not evaluated.
- From the combined fit of ANTONELLI 92, ACHASOV 01E, ACHASOV 02E, and ACHASOV 03D data on the  $\pi^+\pi^-\pi^0$  and ANTONELLI 92 on the  $\omega\pi^+\pi^-$  final states. Supersedes ACHASOV 99E and ACHASOV 02E.
- Using results of CORDIER 81 and preliminary data of DOLINSKY 91 and ANTONELLI 92.
- Using the data of AKHMETSHIN 00D and ANTONELLI 92. The  $\rho\pi$  dominance for the energy dependence of the  $\omega(1420)$  and  $\omega(1650)$  width assumed.
- From a fit to two Breit-Wigner functions and using the data of DOLINSKY 91 and ANTONELLI 92.
- From a fit to two Breit-Wigner functions interfering between them and with the  $\omega, \phi$  tails with fixed (+, -, +) phases.

 $\omega(1420)$  DECAY MODES

Mode	Fraction ( $\Gamma_i/\Gamma$ )
$\Gamma_1$ $\rho\pi$	seen
$\Gamma_2$ $\omega\pi\pi$	seen
$\Gamma_3$ $\omega\eta$	
$\Gamma_4$ $b_1(1235)\pi$	seen
$\Gamma_5$ $e^+e^-$	seen
$\Gamma_6$ $\pi^0\gamma$	

 $\omega(1420)$   $\Gamma(i)\Gamma(e^+e^-)/\Gamma^2(\text{total})$ 

$\Gamma(\rho\pi)/\Gamma_{\text{total}} \times \Gamma(e^+e^-)/\Gamma_{\text{total}}$	$\Gamma_1/\Gamma \times \Gamma_5/\Gamma$			
VALUE (units $10^{-6}$ )	EVTs	DOCUMENT ID	TECN	COMMENT
• • • We do not use the following data for averages, fits, limits, etc. • • •				
0.73 ± 0.08	13.1k	<sup>1</sup> AULCHENKO 15A	SND	1.05–1.80 $e^+e^- \rightarrow \pi^+\pi^-\pi^0$
0.82 ± 0.05 ± 0.06		AUBERT,B	04N BABR	10.6 $e^+e^- \rightarrow \pi^+\pi^-\pi^0\gamma$
0.65 ± 0.13 ± 0.21	1.2M	<sup>2,3</sup> ACHASOV	03D RVUE	0.44–2.00 $e^+e^- \rightarrow \pi^+\pi^-\pi^0\gamma$
0.625 ± 0.160		<sup>4,5</sup> CLEGG	94 RVUE	
0.466 ± 0.178		<sup>6,7</sup> ANTONELLI	92 DM2	1.34–2.4 $e^+e^- \rightarrow \rho\pi$

- From a fit with contributions from  $\omega(782)$ ,  $\phi(1020)$ ,  $\omega(1420)$ , and  $\omega(1650)$ .
- Calculated by us from the cross section at the peak.
- From the combined fit of ANTONELLI 92, ACHASOV 01E, ACHASOV 02E, and ACHASOV 03D data on the  $\pi^+\pi^-\pi^0$  and ANTONELLI 92 on the  $\omega\pi^+\pi^-$  final states. Supersedes ACHASOV 99E and ACHASOV 02E.
- From a fit to two Breit-Wigner functions and using the data of DOLINSKY 91 and ANTONELLI 92.
- From the partial and leptonic width given by the authors.
- From a fit to two Breit-Wigner functions interfering between them and with the  $\omega, \phi$  tails with fixed (+, -, +) phases.
- From the product of the leptonic width and partial branching ratio given by the authors.

 $\Gamma(\omega\pi\pi)/\Gamma_{\text{total}} \times \Gamma(e^+e^-)/\Gamma_{\text{total}}$   $\Gamma_2/\Gamma \times \Gamma_5/\Gamma$ 

VALUE (units $10^{-8}$ )	DOCUMENT ID	TECN	COMMENT
• • • We do not use the following data for averages, fits, limits, etc. • • •			
19.7 ± 5.7	AUBERT	07AU BABR	10.6 $e^+e^- \rightarrow \omega\pi^+\pi^-\gamma$
1.9 ± 1.9	<sup>1</sup> AKHMETSHIN 00D	CMD2	1.2–2.4 $e^+e^- \rightarrow \omega\pi^+\pi^-$

- Using the data of AKHMETSHIN 00D and ANTONELLI 92. The  $\rho\pi$  dominance for the energy dependence of the  $\omega(1420)$  and  $\omega(1650)$  width assumed.

 $\Gamma(\omega\eta)/\Gamma_{\text{total}} \times \Gamma(e^+e^-)/\Gamma_{\text{total}}$   $\Gamma_3/\Gamma \times \Gamma_5/\Gamma$ 

VALUE (units $10^{-8}$ )	EVTs	DOCUMENT ID	TECN	COMMENT
• • • We do not use the following data for averages, fits, limits, etc. • • •				
2.1 <sup>+1.0</sup> <sub>-0.8</sub>		ACHASOV	19 SND	$e^+e^- \rightarrow \pi^+\pi^-\pi^0\eta$
5.0 ± 2.6 ± 0.3	824	<sup>1</sup> AKHMETSHIN 17A	CMD3	1.4–2.0 $e^+e^- \rightarrow \omega\eta$
1.6 <sup>+0.9</sup> <sub>-0.7</sub>	898	<sup>2</sup> ACHASOV	16B SND	1.34–2.00 $e^+e^- \rightarrow \omega\eta$

- From a fit of the interfering  $\omega(1420)$  and  $\omega(1650)$  with a relative phase of  $\pi$  and other parameters floating. From an alternative fit  $\Gamma(\omega(1420) \rightarrow \omega\eta)/\Gamma_{\text{total}} \times \Gamma(\omega(1420) \rightarrow e^+e^-) = 5.3 \pm 1.6$  eV.
- From a fit with contributions from  $\omega(1420)$ ,  $\omega(1650)$ , and  $\phi(1680)$ . The mass and the width of  $\omega(1420)$  are fixed to the 2014 edition (PDG 14) of this review.

 $\Gamma(\pi^0\gamma)/\Gamma_{\text{total}} \times \Gamma(e^+e^-)/\Gamma_{\text{total}}$   $\Gamma_6/\Gamma \times \Gamma_5/\Gamma$ 

VALUE (units $10^{-8}$ )	DOCUMENT ID	TECN	COMMENT
• • • We do not use the following data for averages, fits, limits, etc. • • •			
0.23 ± 0.14	<sup>1</sup> ACHASOV	10D SND	1.075–2.0 $e^+e^- \rightarrow \pi^0\gamma$
2.03 <sup>+0.70</sup> <sub>-0.75</sub>	<sup>2</sup> AKHMETSHIN 05	CMD2	0.60–1.38 $e^+e^- \rightarrow \pi^0\gamma$

- From a fit of a VMD model with two effective resonances with masses of 1450 MeV and 1700 MeV to describe the excited vector states  $\omega(1420)$ ,  $\rho(1450)$ ,  $\omega(1650)$ , and  $\rho(1700)$ . Systematic errors not evaluated.
- Using 1420 MeV and 220 MeV for the  $\omega(1420)$  mass and width.

 $\omega(1420)$  BRANCHING RATIOS

$\Gamma(\omega\pi\pi)/\Gamma_{\text{total}}$	$\Gamma_2/\Gamma$		
VALUE	DOCUMENT ID	TECN	COMMENT

- • • We do not use the following data for averages, fits, limits, etc. • • •
- 0.301 ± 0.029
- <sup>1</sup> HENNER 02 RVUE 1.2–2.0  $e^+e^- \rightarrow \rho\pi, \omega\pi\pi$  possibly seen
- AKHMETSHIN 00D CMD2  $e^+e^- \rightarrow \omega\pi^+\pi^-$

$\Gamma(\omega\pi\pi)/\Gamma(b_1(1235)\pi)$	$\Gamma_2/\Gamma_4$			
VALUE	EVTs	DOCUMENT ID	TECN	COMMENT

- • • We do not use the following data for averages, fits, limits, etc. • • •
- 0.60 ± 0.16
- 5095
- ANISOVICH 00H SPEC 0.0  $p\bar{p} \rightarrow \omega\pi^0\pi^0\pi^0$

See key on page 999

# Meson Particle Listings

## $\omega(1420)$ , $f_2(1430)$ , $a_0(1450)$

$\Gamma(\rho\pi)/\Gamma_{total}$				$\Gamma_1/\Gamma$
VALUE	DOCUMENT ID	TECN	COMMENT	
••• We do not use the following data for averages, fits, limits, etc. •••				
0.699 ± 0.029	<sup>1</sup> HENNER	02	RVUE 1.2–2.0 $e^+e^- \rightarrow \rho\pi, \omega\pi\pi$	

$\Gamma(e^+e^-)/\Gamma_{total}$				$\Gamma_5/\Gamma$
VALUE (units $10^{-7}$ )	EVTS	DOCUMENT ID	TECN	COMMENT
••• We do not use the following data for averages, fits, limits, etc. •••				
~ 6.6	1.2M	<sup>2,3</sup> ACHASOV	03d	RVUE 0.44–2.00 $e^+e^- \rightarrow \pi^+\pi^-\pi^0$
23 ± 1		<sup>1</sup> HENNER	02	RVUE 1.2–2.0 $e^+e^- \rightarrow \rho\pi, \omega\pi\pi$
<sup>1</sup> Assuming that the $\omega(1420)$ decays into $\rho\pi$ and $\omega\pi\pi$ only.				
<sup>2</sup> Calculated by us from the cross section at the peak.				
<sup>3</sup> Assuming that the $\omega(1420)$ decays into $\rho\pi$ only.				

### $\omega(1420)$ REFERENCES

ACHASOV	19	PR D99 112004	M.N. Achasov et al.	(SND Collab.)
AKHMETSHIN	17A	PL B773 150	R.R. Akhmetshin et al.	(CMD-3 Collab.)
ACHASOV	16B	PR D94 092002	M.N. Achasov et al.	(SND Collab.)
AULCHENKO	15A	JETP 121 27	V.M. Aulchenko et al.	(SND Collab.)
Translated from ZETF 148 34.				
PDG	14	CP C38 070001	K. Olive et al.	(PDG Collab.)
ACHASOV	10D	PR D98 112001	M.N. Achasov et al.	(SND Collab.)
AUBERT	07AU	PR D76 092005	B. Aubert et al.	(BABAR Collab.)
AKHMETSHIN	05	PL B605 26	R.R. Akhmetshin et al.	(Novosibirsk CMD-2 Collab.)
AUBERT	04N	PR D70 072004	B. Aubert et al.	(BABAR Collab.)
ACHASOV	03D	PR D68 052006	M.N. Achasov et al.	(Novosibirsk SND Collab.)
ACHASOV	02E	PR D66 032001	M.N. Achasov et al.	(Novosibirsk SND Collab.)
HENNER	02	EPL C26 3	V.K. Henner et al.	
ACHASOV	01E	PR D63 072002	M.N. Achasov et al.	(Novosibirsk SND Collab.)
AKHMETSHIN	00D	PL B489 125	R.R. Akhmetshin et al.	(Novosibirsk CMD-2 Collab.)
ANISOVICH	00H	PL B485 341	A.V. Anisovich et al.	(Novosibirsk SND Collab.)
ACHASOV	99E	PL B462 365	M.N. Achasov et al.	(Novosibirsk SND Collab.)
ACHASOV	98H	PR D57 4334	N.N. Achasov, A.A. Kozhevnikov	
CLEGG	94	ZPHY C62 455	A.B. Clegg, A. Donnachie	(LANC, MCHS)
ANTONELLI	92	ZPHY C56 15	A. Antonelli et al.	(DM2 Collab.)
DOLINSKY	91	PRPL 202 99	S.I. Dolinsky et al.	(NOVO)
BISELLO	88B	ZPHY C39 13	D. Bisello et al.	(PADO, CLER, FRAS+)
BARKOV	87	JETPL 46 164	L.M. Barkov et al.	(NOVO)
Translated from ZETFP 46 132.				
CORDIER	81	PL 106B 155	A. Cordier et al.	(ORSAY)
IVANOV	81	PL 107B 297	P.M. Ivanov et al.	(NOVO)

### $f_2(1430)$ $I^G(J^{PC}) = 0^+(2^{++})$

OMITTED FROM SUMMARY TABLE  
 This entry lists nearby peaks observed in the  $D$  wave of the  $K\bar{K}$  and  $\pi^+\pi^-$  systems. Needs confirmation.

### $f_2(1430)$ MASS

VALUE (MeV)	DOCUMENT ID	TECN	COMMENT
<b>~ 1430 OUR ESTIMATE</b>			
••• We do not use the following data for averages, fits, limits, etc. •••			
1453 ± 4	<sup>1</sup> VLADIMIRSK..01	SPEC	40 $\pi^-p \rightarrow K_S^0 K_S^0 n$
1421 ± 5	AUGUSTIN	87	DM2 $J/\psi \rightarrow \gamma\pi^+\pi^-$
1480 ± 5.0	AKESSON	86	SPEC $pp \rightarrow pp\pi^+\pi^-$
1436 $^{+26}_{-16}$	DAUM	84	CNTR 17–18 $\pi^-p \rightarrow K^+K^-n$
1412 ± 3	DAUM	84	CNTR 63 $\pi^-p \rightarrow K_S^0 K_S^0 n, K^+K^-n$
1439 $^{+5}_{-6}$	<sup>2</sup> BEUSCH	67	OSPK 5,7,12 $\pi^-p \rightarrow K_S^0 K_S^0 n$
<sup>1</sup> $J^{PC} = 0^{++}$ or $2^{++}$ .			
<sup>2</sup> Not seen by WETZEL 76.			

### $f_2(1430)$ WIDTH

VALUE (MeV)	DOCUMENT ID	TECN	COMMENT
••• We do not use the following data for averages, fits, limits, etc. •••			
13 ± 5	<sup>3</sup> VLADIMIRSK..01	SPEC	40 $\pi^-p \rightarrow K_S^0 K_S^0 n$
30 ± 9	AUGUSTIN	87	DM2 $J/\psi \rightarrow \gamma\pi^+\pi^-$
150 ± 5.0	AKESSON	86	SPEC $pp \rightarrow pp\pi^+\pi^-$
81 $^{+56}_{-29}$	DAUM	84	CNTR 17–18 $\pi^-p \rightarrow K^+K^-n$
14 ± 6	DAUM	84	CNTR 63 $\pi^-p \rightarrow K_S^0 K_S^0 n, K^+K^-n$
43 $^{+17}_{-18}$	<sup>4</sup> BEUSCH	67	OSPK 5,7,12 $\pi^-p \rightarrow K_S^0 K_S^0 n$
<sup>3</sup> $J^{PC} = 0^{++}$ or $2^{++}$ .			
<sup>4</sup> Not seen by WETZEL 76.			

### $f_2(1430)$ DECAY MODES

Mode	
$\Gamma_1$	$K\bar{K}$
$\Gamma_2$	$\pi\pi$

### $f_2(1430)$ REFERENCES

VLADIMIRSK..01	PAN 64 1895	V.V. Vladimirov et al.
AUGUSTIN	87	Translated from YAF 64 1979.
AKESSON	86	ZPHY C36 369
DAUM	84	NP B264 154
WETZEL	76	ZPHY C23 339
BEUSCH	67	NP B115 208
		PL 25B 357
		J.E. Augustin et al. (LALO, CLER, FRAS+)
		T. Akesson et al. (Axial Field Spec. Collab.)
		C. Daum et al. (AMST, CERN, CRAC, MPIM+)
		W. Wetzel et al. (ETH, CERN, LOIC)
		W. Beusch et al. (ETH, CERN)

### $a_0(1450)$

$$I^G(J^{PC}) = 1^-(0^{++})$$

See the review on "Scalar Mesons below 2 GeV."

### $a_0(1450)$ MASS

VALUE (MeV)	EVTS	DOCUMENT ID	TECN	COMMENT
<b>1474 ± 19 OUR AVERAGE</b>				
1480 ± 30		ABELE	98	CBAR 0.0 $\bar{p}p \rightarrow K^0 K^\pm \pi^\mp$
1470 ± 25		<sup>1</sup> AMSLER	95D	CBAR 0.0 $\bar{p}p \rightarrow \pi^0 \pi^0 \pi^0, \pi^0 \eta, \pi^0 \pi^0 \eta$
••• We do not use the following data for averages, fits, limits, etc. •••				
1458 ± 14 ± 15	190k	<sup>2</sup> AAIJ	16N	LHCB $D^0 \rightarrow K_S^0 K^\pm \pi^\mp$
1515 ± 30		<sup>3</sup> ANISOVICH	09	RVUE 0.0 $\bar{p}p, \pi N$
1316.8 $^{+0.7}_{-1.0} + 24.7_{-4.6}$		<sup>4</sup> UEHARA	09A	BELL $\gamma\gamma \rightarrow \pi^0 \eta$
1432 ± 13 ± 25		<sup>5</sup> BUGG	08A	RVUE $\bar{p}p$
1477 ± 10	80k	<sup>6</sup> UMAN	06	E835 5.2 $\bar{p}p \rightarrow \eta\eta\pi^0$
1441 $^{+40}_{-15}$	35280	<sup>3</sup> BAKER	03	SPEC $\bar{p}p \rightarrow \omega\pi^+\pi^-\pi^0$
1303 ± 16		<sup>7</sup> BARGIOTTI	03	OBLX $\bar{p}p$
1296 ± 10		<sup>8</sup> AMSLER	02	CBAR 0.9 $\bar{p}p \rightarrow \pi^0 \pi^0 \eta$
1565 ± 30		<sup>9</sup> ANISOVICH	98B	RVUE Compilation
1290 ± 10		<sup>9</sup> BERTIN	98B	OBLX 0.0 $\bar{p}p \rightarrow K^\pm K_S \pi^\mp$
1450 ± 40		AMSLER	94D	CBAR 0.0 $\bar{p}p \rightarrow \pi^0 \pi^0 \eta$
1410 ± 25		ETKIN	82C	MPS 23 $\pi^-p \rightarrow n2K_S^0$
~ 1300		MARTIN	78	SPEC 10 $K^\pm p \rightarrow K_S^0 \pi p$
1255 ± 5		<sup>10</sup> CASON	76	
<sup>1</sup> Coupled-channel analysis of AMSLER 95B, AMSLER 95c, and AMSLER 94D.				
<sup>2</sup> Using a model with Gaussian constraints to the PDG averaged values.				
<sup>3</sup> From the pole position.				
<sup>4</sup> May be a different state.				
<sup>5</sup> Using data from AMSLER 94D, ABELE 98, and BAKER 03. Supersedes BUGG 94.				
<sup>6</sup> Statistical error only.				
<sup>7</sup> Coupled channel analysis of $\pi^+\pi^-\pi^0, K^+K^-\pi^0$ , and $K^\pm K_S^0 \pi^\mp$ .				
<sup>8</sup> T-matrix pole.				
<sup>9</sup> Not confirmed by BUGG 08A.				
<sup>10</sup> Isospin 0 not excluded.				

### $a_0(1450)$ WIDTH

VALUE (MeV)	EVTS	DOCUMENT ID	TECN	COMMENT
<b>265 ± 13 OUR AVERAGE</b>				
265 ± 15		ABELE	98	CBAR 0.0 $\bar{p}p \rightarrow K^0 K^\pm \pi^\mp$
265 ± 30		<sup>1</sup> AMSLER	95D	CBAR 0.0 $\bar{p}p \rightarrow \pi^0 \pi^0 \pi^0, \pi^0 \eta, \pi^0 \pi^0 \eta$
••• We do not use the following data for averages, fits, limits, etc. •••				
282 ± 12 ± 13	190k	<sup>2</sup> AAIJ	16N	LHCB $D^0 \rightarrow K_S^0 K^\pm \pi^\mp$
230 ± 36		<sup>3</sup> ANISOVICH	09	RVUE 0.0 $\bar{p}p, \pi N$
65.0 $^{+2.1}_{-5.4} + 99.1_{-32.6}$		<sup>4</sup> UEHARA	09A	BELL $\gamma\gamma \rightarrow \pi^0 \eta$
196 ± 10 ± 10		<sup>5</sup> BUGG	08A	RVUE $\bar{p}p$
267 ± 11	80k	<sup>6</sup> UMAN	06	E835 5.2 $\bar{p}p \rightarrow \eta\eta\pi^0$
110 ± 14	35280	<sup>3</sup> BAKER	03	SPEC $\bar{p}p \rightarrow \omega\pi^+\pi^-\pi^0$
92 ± 16		<sup>7</sup> BARGIOTTI	03	OBLX $\bar{p}p$
81 ± 21		<sup>8</sup> AMSLER	02	CBAR 0.9 $\bar{p}p \rightarrow \pi^0 \pi^0 \eta$
292 ± 40		<sup>9</sup> ANISOVICH	98B	RVUE Compilation
80 ± 5		<sup>9</sup> BERTIN	98B	OBLX 0.0 $\bar{p}p \rightarrow K^\pm K_S \pi^\mp$
270 ± 40		AMSLER	94D	CBAR 0.0 $\bar{p}p \rightarrow \pi^0 \pi^0 \eta$
230 ± 30		ETKIN	82C	MPS 23 $\pi^-p \rightarrow n2K_S^0$
~ 250		MARTIN	78	SPEC 10 $K^\pm p \rightarrow K_S^0 \pi p$
79 ± 10		<sup>10</sup> CASON	76	
<sup>1</sup> Coupled-channel analysis of AMSLER 95B, AMSLER 95c, and AMSLER 94D.				
<sup>2</sup> Using a model with Gaussian constraints to the PDG averaged values.				
<sup>3</sup> From the pole position.				
<sup>4</sup> May be a different state.				
<sup>5</sup> Using data from AMSLER 94D, ABELE 98, and BAKER 03. Supersedes BUGG 94.				
<sup>6</sup> Statistical error only.				
<sup>7</sup> Coupled channel analysis of $\pi^+\pi^-\pi^0, K^+K^-\pi^0$ , and $K^\pm K_S^0 \pi^\mp$ .				
<sup>8</sup> T-matrix pole.				
<sup>9</sup> Not confirmed by BUGG 08A.				
<sup>10</sup> Isospin 0 not excluded.				

## Meson Particle Listings

 $a_0(1450)$ ,  $\rho(1450)$  $a_0(1450)$  DECAY MODES

Mode	Fraction ( $\Gamma_i/\Gamma$ )
$\Gamma_1$ $\pi\eta$	$0.093 \pm 0.020$
$\Gamma_2$ $\pi\eta'(958)$	$0.033 \pm 0.017$
$\Gamma_3$ $K\bar{K}$	$0.082 \pm 0.028$
$\Gamma_4$ $\omega\pi\pi$	<b>DEFINED AS 1</b>
$\Gamma_5$ $a_0(980)\pi\pi$	seen
$\Gamma_6$ $\gamma\gamma$	seen

 $a_0(1450)$   $\Gamma(i)\Gamma(\gamma\gamma)/\Gamma(\text{total})$ 

$\Gamma(\pi\eta) \times \Gamma(\gamma\gamma)/\Gamma_{\text{total}}$	DOCUMENT ID	TECN	COMMENT	$\Gamma_1\Gamma_6/\Gamma$
VALUE (eV)				
$432 \pm 6 \pm_{256}^{+1073}$	<sup>1</sup> UEHARA	09A	BELL	$\gamma\gamma \rightarrow \pi^0\eta$
<sup>1</sup> May be a different state.				

 $a_0(1450)$  BRANCHING RATIOS

$\Gamma(\pi\eta'(958))/\Gamma(\pi\eta)$	DOCUMENT ID	TECN	COMMENT	$\Gamma_2/\Gamma_1$
VALUE				
$0.35 \pm 0.16$	<sup>1</sup> ABELE	98	CBAR	$0.0 \bar{p}p \rightarrow K_L^0 K^\pm \pi^\mp$
<b>•••</b> We do not use the following data for averages, fits, limits, etc. <b>•••</b>				
$0.43 \pm 0.19$	ABELE	97c	CBAR	$0.0 \bar{p}p \rightarrow \pi^0\pi^0\eta'$
<sup>1</sup> Using $\pi^0\eta$ from AMSLER 94d.				

$\Gamma(K\bar{K})/\Gamma(\pi\eta)$	DOCUMENT ID	TECN	COMMENT	$\Gamma_3/\Gamma_1$
VALUE				
$0.88 \pm 0.23$	<sup>1</sup> ABELE	98	CBAR	$0.0 \bar{p}p \rightarrow K_L^0 K^\pm \pi^\mp$
<sup>1</sup> Using $\pi^0\eta$ from AMSLER 94d.				

$\Gamma(\omega\pi\pi)/\Gamma(\pi\eta)$	DOCUMENT ID	TECN	COMMENT	$\Gamma_4/\Gamma_1$
VALUE				
$10.7 \pm 2.3$	<sup>1</sup> BAKER	03	SPEC	$\bar{p}p \rightarrow \omega\pi^+\pi^-\pi^0$
<sup>1</sup> Using results on $\bar{p}p \rightarrow a_0(1450)^0\pi^0$ , $a_0(1450) \rightarrow \eta\pi^0$ from ABELE 96c and assuming the $\omega\rho$ mechanism for the $\omega\pi\pi$ state.				

$\Gamma(a_0(980)\pi\pi)/\Gamma_{\text{total}}$	DOCUMENT ID	TECN	COMMENT	$\Gamma_5/\Gamma$
VALUE				
seen	BUGG	08A	RVUE	$\bar{p}p$

$\Gamma(a_0(980)\pi\pi)/\Gamma(\pi\eta)$	DOCUMENT ID	TECN	CHG	COMMENT	$\Gamma_5/\Gamma_1$
VALUE					
$\leq 4.3$	ANISOVICH	01	RVUE	0	$\bar{p}p \rightarrow \eta 2\pi^+ 2\pi^-$
<b>•••</b> We do not use the following data for averages, fits, limits, etc. <b>•••</b>					

$\Gamma(\gamma\gamma)/\Gamma_{\text{total}}$	DOCUMENT ID	TECN	COMMENT	$\Gamma_6/\Gamma$
VALUE				
seen	<sup>1</sup> UEHARA	09A	BELL	$\gamma\gamma \rightarrow \pi^0\eta$
<sup>1</sup> May be a different state.				

 $a_0(1450)$  REFERENCES

AJJ	16N	PR D93 052018	R. Ajai et al.	(LHCb Collab.)
ANISOVICH	09	JMP A24 2481	V.V. Anisovich, A.V. Sarantsev	
UEHARA	09A	PR D80 032001	S. Uehara et al.	(BELLE Collab.)
BUGG	08A	PR D78 074023	D.V. Bugg	(LOQM)
UMAN	06	PR D73 052009	I. Uman et al.	(FNAL E835)
BAKER	03	PL B563 140	C.A. Baker et al.	
BARGIOTTI	03	EPJ C26 371	M. Bargiotti et al.	(OBELIX Collab.)
AMSLER	02	EPJ C23 29	C. Amisler et al.	
ANISOVICH	01	NP A690 567	A.V. Anisovich et al.	
ABELE	98	PR D57 3860	A. Abele et al.	(Crystal Barrel Collab.)
ANISOVICH	98B	SPU 411 419	V.V. Anisovich et al.	
		Translated from UFN 168 481.		
BERTIN	98B	PL B434 180	A. Bertin et al.	(OBELIX Collab.)
ABELE	97C	PL B404 179	A. Abele et al.	(Crystal Barrel Collab.)
ABELE	96C	NP A609 562	A. Abele et al.	(Crystal Barrel Collab.)
AMSLER	95B	PL B342 433	C. Amisler et al.	(Crystal Barrel Collab.)
AMSLER	95C	PL B353 571	C. Amisler et al.	(Crystal Barrel Collab.)
AMSLER	95D	PL B355 425	C. Amisler et al.	(Crystal Barrel Collab.)
AMSLER	94D	PL B333 277	C. Amisler et al.	(Crystal Barrel Collab.)
BUGG	94	PR D50 4412	D.V. Bugg et al.	(LOQM)
ETKIN	82C	NP D25 2446	A. Etkin et al.	(BNL, CUNY, TUFTS, VAND)
MARTIN	78	NP B134 392	A.D. Martin et al.	(DURH, GEVA)
CASON	76	PRL 36 1465	N.M. Cason et al.	(NDAM, ANL)

 $\rho(1450)$ 

$$I^G(J^{PC}) = 1^+(1^-)$$

THE  $\rho(1450)$  AND THE  $\rho(1700)$ 

Updated September 2019 by S. Eidelman (Novosibirsk), C. Hanhart (Juelich) and G. Venanzoni (Pisa).

In our 1988 edition, we replaced the  $\rho(1600)$  entry with two new ones, the  $\rho(1450)$  and the  $\rho(1700)$ , because there was emerging evidence that the 1600-MeV region actually contains two  $\rho$ -like resonances. Erkal [1] had pointed out this possibility with a theoretical analysis on the consistency of  $2\pi$  and  $4\pi$  electromagnetic form factors and the  $\pi\pi$  scattering length. Donnachie [2], with a full analysis of data on the  $2\pi$  and  $4\pi$  final states in  $e^+e^-$  annihilation and photoproduction reactions, had also argued that in order to obtain a consistent picture, two resonances were necessary. The existence of  $\rho(1450)$  was supported by the analysis of  $\eta\rho^0$  mass spectra obtained in photoproduction and  $e^+e^-$  annihilation [3], as well as that of  $e^+e^- \rightarrow \omega\pi$  [4].

The analysis of [2] was further extended by [5,6] to include new data on  $4\pi$ -systems produced in  $e^+e^-$  annihilation, and in  $\tau$ -decays ( $\tau$  decays to  $4\pi$ , and  $e^+e^-$  annihilation to  $4\pi$  can be related by the Conserved Vector Current assumption). These systems were successfully analyzed using interfering contributions from two  $\rho$ -like states, and from the tail of the  $\rho(770)$  decaying into two-body states. While specific conclusions on  $\rho(1450) \rightarrow 4\pi$  were obtained, little could be said about the  $\rho(1700)$ .

Independent evidence for two  $1^-$  states is provided by [7] in  $4\pi$  electroproduction at  $\langle Q^2 \rangle = 1$  (GeV/c)<sup>2</sup>, and by [8] in a high-statistics sample of the  $\eta\pi\pi$  system in  $\pi^-p$  charge exchange.

This scenario with two overlapping resonances is supported by other data. Bisello [9] measured the pion form factor in the interval 1.35–2.4 GeV, and observed a deep minimum around 1.6 GeV. The best fit was obtained with the hypothesis of  $\rho$ -like resonances at 1420 and 1770 MeV, with widths of about 250 MeV. Antonelli [10] found that the  $e^+e^- \rightarrow \eta\pi^+\pi^-$  cross section is better fitted with two fully interfering Breit-Wigners, with parameters in fair agreement with those of [2] and [9]. These results can be considered as a confirmation of the  $\rho(1450)$ .

Decisive evidence for the  $\pi\pi$  decay mode of both  $\rho(1450)$  and  $\rho(1700)$  comes from  $\bar{p}p$  annihilation at rest [11]. It has been shown that these resonances also possess a  $K\bar{K}$  decay mode [12–14]. High-statistics studies of the decays  $\tau \rightarrow \pi\pi\nu_\tau$  [15,16], and  $\tau \rightarrow 4\pi\nu_\tau$  [17] also require the  $\rho(1450)$ , but are not sensitive to the  $\rho(1700)$ , because it is too close to the  $\tau$  mass. A recent very-high-statistics study of the  $\tau \rightarrow \pi\pi\nu_\tau$  decay performed at Belle [18] reports the first observation of both  $\rho(1450)$  and  $\rho(1700)$  in  $\tau$  decays. A clear picture of the two  $\pi^+\pi^-$  resonances interfering with the  $\rho(770)$  in  $e^+e^-$  annihilation was also reported by BaBar using the ISR method [19].

The structure of these  $\rho$  states is not yet completely clear. Barnes [20] and Close [21] claim that  $\rho(1450)$  has a mass

consistent with radial  $2S$ , but its decays show characteristics of hybrids, and suggest that this state may be a  $2S$ -hybrid mixture. Donnachie [22] argues that hybrid states could have a  $4\pi$  decay mode dominated by the  $a_1\pi$ . Such behavior has been observed by [23] in  $e^+e^- \rightarrow 4\pi$  in the energy range 1.05–1.38 GeV, and by [17] in  $\tau \rightarrow 4\pi$  decays. CLEO [24] and Belle [25] observe the  $\rho(1450) \rightarrow \omega\pi$  decay mode in  $B$ -meson decays, however, do not find  $\rho(1700) \rightarrow \omega\pi^0$ . A similar conclusion is made by [26,27], who studied the process  $e^+e^- \rightarrow \omega\pi^0$  and do not observe a statistically significant signal of the  $\rho(1700)$ . Various decay modes of the  $\rho(1450)$  and  $\rho(1700)$  are observed in  $\bar{p}n$  and  $\bar{p}p$  annihilation [28,29], but no definite conclusions can be drawn. More data should be collected to clarify the nature of the  $\rho$  states, particularly in the energy range above 1.6 GeV.

We now list under a separate entry the  $\rho(1570)$ , the  $\phi\pi$  state with  $J^{PC} = 1^{--}$  earlier observed by [30] (referred to as  $C(1480)$ ) and recently confirmed by [31]. While [32] shows that it may be a threshold effect, [5] and [33] suggest two independent vector states with this decay mode. The  $C(1480)$  has not been seen in the  $\bar{p}p$  [34] and  $e^+e^-$  [35,36] experiments. However, the sensitivity of the two latter is an order of magnitude lower than that of [31]. Note that [31] can not exclude that their observation is due to an OZI-suppressed decay mode of the  $\rho(1700)$ .

Several observations on the  $\omega\pi$  system in the 1200-MeV region [37–43] may be interpreted in terms of either  $J^P = 1^-$   $\rho(770) \rightarrow \omega\pi$  production [44], or  $J^P = 1^+$   $b_1(1235)$  production [42,43]. We argue that no special entry for a  $\rho(1250)$  is needed. The LASS amplitude analysis [45] showing evidence for  $\rho(1270)$  is preliminary and needs confirmation. For completeness, the relevant observations are listed under the  $\rho(1450)$ .

Recently [46] reported a very broad  $1^{--}$  resonance-like  $K^+K^-$  state in  $J/\psi \rightarrow K^+K^-\pi^0$  decays. Its pole position corresponds to mass of 1576 MeV and width of 818 MeV. [47–49] suggest its exotic structure (molecular or multi-quark), while [50] and [51] explain it by the interference between the  $\rho(1450)$  and  $\rho(1700)$ . The latter statement is qualitatively supported by BaBar [52] and SND [53]. We quote [46] as  $X(1575)$  in the section “Further States.”

Evidence for  $\rho$ -like mesons decaying into  $6\pi$  states was first noted by [54] in the analysis of  $6\pi$  mass spectra from  $e^+e^-$  annihilation [55,56] and diffractive photoproduction [57]. Clegg [54] argued that two states at about 2.1 and 1.8 GeV exist: while the former is a candidate for the  $\rho(2150)$ , the latter could be a manifestation of the  $\rho(1700)$  distorted by threshold effects. BaBar reported observations of the new decay modes of the  $\rho(2150)$  in the channels  $\eta'(958)\pi^+\pi^-$  and  $f_1(1285)\pi^+\pi^-$  [58]. The relativistic quark model [59] predicts the  $2^3D_1$  state with  $J^{PC} = 1^{--}$  at 2.15 GeV which can be identified with the  $\rho(2150)$ .

We no longer list under a separate particle  $\rho(1900)$  various observations of irregular behavior of the cross sections near the  $N\bar{N}$  threshold. Dips of various width around 1.9

GeV were reported by the E687 Collaboration (a narrow one in the  $3\pi^+3\pi^-$  diffractive photoproduction [60,61]), by the FENICE experiment (a narrow structure in the  $R$  value [62]), by BaBar in ISR (a narrow structure in  $e^+e^- \rightarrow \phi\pi$  final state [63], but much broader in  $e^+e^- \rightarrow 3\pi^+3\pi^-$  and  $e^+e^- \rightarrow 2(\pi^+\pi^-\pi^0)$  [64]), by CMD-3 (also a rather broad dip in  $e^+e^- \rightarrow 3\pi^+3\pi^-$  [65]). A dedicated scan of the  $N\bar{N}$ -threshold region by CMD-3 confirms this effect in the  $e^+e^- \rightarrow 3\pi^+3\pi^-$  and  $e^+e^- \rightarrow K^+K^-\pi^+\pi^-$  final states, but does not see it in the cross section of  $e^+e^- \rightarrow 2\pi^+2\pi^-$  [66]. Most probably, these structures emerge as a threshold effect due to the opening of the  $N\bar{N}$  channel [67,68,69].

## References

1. C. Erkal, Z. Phys. **C31**, 615 (1986).
2. A. Donnachie and H. Mirzaie, Z. Phys. **C33**, 407 (1987).
3. A. Donnachie and A.B. Clegg, Z. Phys. **C34**, 257 (1987).
4. A. Donnachie and A.B. Clegg, Z. Phys. **C51**, 689 (1991).
5. A.B. Clegg and A. Donnachie, Z. Phys. **C40**, 313 (1988).
6. A.B. Clegg and A. Donnachie, Z. Phys. **C62**, 455 (1994).
7. T.J. Killian *et al.*, Phys. Rev. **D21**, 3005 (1980).
8. S. Fukui *et al.*, Phys. Lett. **B202**, 441 (1988).
9. D. Bisello *et al.*, Phys. Lett. **B220**, 321 (1989).
10. A. Antonelli *et al.*, Phys. Lett. **B212**, 133 (1988).
11. A. Abele *et al.*, Phys. Lett. **B391**, 191 (1997).
12. A. Abele *et al.*, Phys. Rev. **D57**, 3860 (1998).
13. A. Bertin *et al.*, Phys. Lett. **B434**, 180 (1998).
14. A. Abele *et al.*, Phys. Lett. **B468**, 178 (1999).
15. R. Barate *et al.*, Z. Phys. **C76**, 15 (1997).
16. S. Anderson, Phys. Rev. **D61**, 112002 (2000).
17. K.W. Edwards *et al.*, Phys. Rev. **D61**, 072003 (2000).
18. M. Fujikawa *et al.*, Phys. Rev. **D78**, 072006 (2008).
19. J.P. Lees *et al.*, Phys. Rev. **D86**, 032013 (2012).
20. T. Barnes *et al.*, Phys. Rev. **D55**, 4157 (1997).
21. F.E. Close *et al.*, Phys. Rev. **D56**, 1584 (1997).
22. A. Donnachie and Yu.S. Kalashnikova, Phys. Rev. **D60**, 114011 (1999).
23. R.R. Akhmetshin *et al.*, Phys. Lett. **B466**, 392 (1999).
24. J.P. Alexander *et al.*, Phys. Rev. **D64**, 092001 (2001).
25. D. Matvienko *et al.*, Phys. Rev. **D92**, 012013 (2015).
26. R.R. Akhmetshin *et al.*, Phys. Lett. **B562**, 173 (2003).
27. M.N. Achasov *et al.*, Phys. Rev. **D94**, 112001 (2016).
28. A. Abele *et al.*, Eur. Phys. J. **C21**, 261 (2001).
29. M. Bargiotti *et al.*, Phys. Lett. **B561**, 233 (2003).
30. S.I. Bityukov *et al.*, Phys. Lett. **B188**, 383 (1987).
31. B. Aubert *et al.*, Phys. Rev. **D77**, 092002 (2008).
32. N.N. Achasov and G.N. Shestakov, Phys. Atom. Nucl. **59**, 1262 (1996).
33. L.G. Landsberg, Sov. J. Nucl. Phys. **55**, 1051 (1992).
34. A. Abele *et al.*, Phys. Lett. **B415**, 280 (1997).
35. V.M. Aulchenko *et al.*, Sov. Phys. JETP Lett. **45**, 145 (1987).
36. D. Bisello *et al.*, Z. Phys. **C52**, 227 (1991).
37. P. Frenkiel *et al.*, Nucl. Phys. **B47**, 61 (1972).
38. G. Cosme *et al.*, Phys. Lett. **B63**, 352 (1976).

## Meson Particle Listings

 $\rho(1450)$ 

39. D.P. Barber *et al.*, Z. Phys. **C4**, 169 (1980).  
 40. D. Aston, Phys. Lett. **B92**, 211 (1980).  
 41. M. Atkinson *et al.*, Nucl. Phys. **B243**, 1 (1984).  
 42. J.E. Brau *et al.*, Phys. Rev. **D37**, 2379 (1988).  
 43. C. Amsler *et al.*, Phys. Lett. **B311**, 362 (1993).  
 44. J. Layssac and F.M. Renard, Nuovo Cimento **6A**, 134 (1971).  
 45. D. Aston *et al.*, Nucl. Phys. (Proc. Supp.) **B21**, 105 (1991).  
 46. M. Ablikim *et al.*, Phys. Rev. Lett. **97**, 142002 (2006).  
 47. G.-J. Ding and M.-L. Yan, Phys. Lett. **B643**, 33 (2006).  
 48. F.K. Guo *et al.*, Nucl. Phys. **A773**, 78 (2006).  
 49. A. Zhang *et al.*, Phys. Rev. **D76**, 036004 (2007).  
 50. B.A. Li, Phys. Rev. **D76**, 094016 (2007).  
 51. X. Liu *et al.*, Phys. Rev. **D75**, 074017 (2007).  
 52. J.P. Lees *et al.*, Phys. Rev. **D88**, 032013 (2013).  
 53. M.N. Achasov *et al.*, Phys. Rev. **D94**, 112006 (2016).  
 54. A.B. Clegg and A. Donnachie, Z. Phys. **C45**, 677 (1990).  
 55. D. Bisello *et al.*, Phys. Lett. **107B**, 145 (1981).  
 56. A. Castro *et al.*, LAL-88-58(1988).  
 57. M. Atkinson *et al.*, Z. Phys. **C29**, 333 (1985).  
 58. B. Aubert *et al.*, Phys. Rev. **D76**, 092005 (2007).  
 59. S. Godfrey and N. Isgur, Phys. Rev. **D32**, 189 (1985).  
 60. P.L. Frabetti *et al.*, Phys. Lett. **B514**, 240 (2001).  
 61. P.L. Frabetti *et al.*, Phys. Lett. **B578**, 290 (2004).  
 62. A. Antonelli *et al.*, Phys. Lett. **B365**, 427 (1996).  
 63. B. Aubert *et al.*, Phys. Rev. **D77**, 092002 (2008).  
 64. B. Aubert *et al.*, Phys. Rev. **D73**, 052003 (2006).  
 65. R.R. Akhmetshin *et al.*, Phys. Lett. **B723**, 83 (2013).  
 66. R.R. Akhmetshin *et al.*, Phys. Lett. **B794**, 64 (2019).  
 67. A. Obrazovsky and S. Serednyakov, Sov. Phys. JETP Lett. **99**, 315 (2014).  
 68. J. Heidenauer *et al.*, Phys. Rev. **D92**, 054032 (2015).  
 69. A.I. Milstein and S.G. Salmikov, Nucl. Phys. **A977**, 60 (2018).

 $\rho(1450)$  MASS $\rho(1450)$  MASS

VALUE (MeV) DOCUMENT ID  
**1465 ± 25 OUR ESTIMATE** This is only an educated guess; the error given is larger than the error on the average of the published values.

 $\eta\rho^0$  MODE

VALUE (MeV)	EVTS	DOCUMENT ID	TECN	COMMENT
1500 ± 10	7.4k	<sup>1</sup> ACHASOV 18	SND	1.22–2.00 $e^+e^- \rightarrow \eta\pi^+\pi^-$
1497 ± 14		<sup>2</sup> AKHMETSHIN 01B	CMD2	$e^+e^- \rightarrow \eta\gamma$
1421 ± 15		<sup>3</sup> AKHMETSHIN 00D	CMD2	$e^+e^- \rightarrow \eta\pi^+\pi^-$
1470 ± 20		ANTONELLI 88	DM2	$e^+e^- \rightarrow \eta\pi^+\pi^-$
1446 ± 10		FUKUI 88	SPEC	8.95 $\pi^-p \rightarrow \eta\pi^+\pi^-n$

<sup>1</sup> From the combined fit of AULCHENKO 15 and ACHASOV 18 in the model with the interfering  $\rho(1450)$ ,  $\rho(1700)$  and  $\rho(2150)$  with the parameters of the  $\rho(1450)$  and  $\rho(1700)$  floating and the mass and width of the  $\rho(2150)$  fixed at 2155 MeV and 320 MeV, respectively. The phases of the resonances are  $\pi$ , 0 and  $\pi$ , respectively.

<sup>2</sup> Using the data of AKHMETSHIN 01B on  $e^+e^- \rightarrow \eta\gamma$ , AKHMETSHIN 00D and ANTONELLI 88 on  $e^+e^- \rightarrow \eta\pi^+\pi^-$ .

<sup>3</sup> Using the data of ANTONELLI 88, DOLINSKY 91, and AKHMETSHIN 00D. The energy-independent width of the  $\rho(1450)$  and  $\rho(1700)$  mesons assumed.

 $\omega\pi$  MODE

VALUE (MeV)	EVTS	DOCUMENT ID	TECN	COMMENT
1510 ± 7	10.2k	<sup>1</sup> ACHASOV 16D	SND	1.05–2.00 $e^+e^- \rightarrow \pi^0\pi^0\gamma$
1544 ± 22 ± 11/46	821	<sup>2</sup> MATVIENKO 15	BELL	$\bar{B}^0 \rightarrow D^{*+}\omega\pi^-$

1491 ± 19	7815	<sup>3</sup> ACHASOV 13	SND	1.05–2.00 $e^+e^- \rightarrow \pi^0\pi^0\gamma$
1582 ± 17 ± 25	2382	<sup>4</sup> AKHMETSHIN 03B	CMD2	$e^+e^- \rightarrow \pi^0\pi^0\gamma$
1349 ± 25 ± 10/5	341	<sup>5</sup> ALEXANDER 01B	CLE2	$B \rightarrow D^{(*)}\omega\pi^-$
1523 ± 10		<sup>6</sup> EDWARDS 00A	CLE2	$\tau^- \rightarrow \omega\pi^- \nu_\tau$
1463 ± 25		<sup>7</sup> CLEGG 94	RVUE	
1250		<sup>8</sup> ASTON 80C	OMEG	20–70 $\gamma p \rightarrow \omega\pi^0 p$
1290 ± 40		<sup>8</sup> BARBER 80C	SPEC	3–5 $\gamma p \rightarrow \omega\pi^0 p$

<sup>1</sup> From a phenomenological model based on vector meson dominance with interfering  $\rho(770)$ ,  $\rho(1450)$ , and  $\rho(1700)$ . The  $\rho(1700)$  mass and width are fixed at 1720 MeV and 250 MeV, respectively. Systematic uncertainties not estimated. Supersedes ACHASOV 13.

<sup>2</sup> Using Breit-Wigner parameterization of the  $\rho(1450)$  and assuming equal probabilities of the  $\rho(1450) \rightarrow \pi\pi$  and  $\rho(1450) \rightarrow \omega\pi$  decays.

<sup>3</sup> From a phenomenological model based on vector meson dominance with the interfering  $\rho(1450)$  and  $\rho(1700)$  and their widths fixed at 400 and 250 MeV, respectively. Systematic uncertainty not estimated.

<sup>4</sup> Using the data of AKHMETSHIN 03B and BISELLO 91B assuming the  $\omega\pi^0$  and  $\pi^+\pi^-$  mass dependence of the total width.  $\rho(1700)$  mass and width fixed at 1700 MeV and 240 MeV, respectively.

<sup>5</sup> Using Breit-Wigner parameterization of the  $\rho(1450)$  and assuming the  $\omega\pi^-$  mass dependence for the total width.

<sup>6</sup> Mass-independent width parameterization.  $\rho(1700)$  mass and width fixed at 1700 MeV and 235 MeV respectively.

<sup>7</sup> Using data from BISELLO 91B, DOLINSKY 86 and ALBRECHT 87L.

<sup>8</sup> Not separated from  $b_1(1235)$ , not pure  $J^P = 1^-$  effect.

4 $\pi$  MODE

VALUE (MeV)	DOCUMENT ID	TECN	COMMENT
1435 ± 40	ABELE 01B	CBAR	0.0 $\bar{p}n \rightarrow 2\pi^-2\pi^0\pi^+$
1350 ± 50	ACHASOV 97	RVUE	$e^+e^- \rightarrow 2(\pi^+\pi^-)$
1449 ± 4	<sup>1</sup> ARMSTRONG 89E	OMEG	300 $pp \rightarrow pp2(\pi^+\pi^-)$

<sup>1</sup> Not clear whether this observation has  $l=1$  or 0.

 $\pi\pi$  MODE

VALUE (MeV)	EVTS	DOCUMENT ID	TECN	COMMENT
1326.35 ± 3.46		<sup>1</sup> BARTOS 17	RVUE	$e^+e^- \rightarrow \pi^+\pi^-$
1342.31 ± 46.62		<sup>2</sup> BARTOS 17A	RVUE	$e^+e^- \rightarrow \pi^+\pi^-$
1373.83 ± 11.37		<sup>3</sup> BARTOS 17A	RVUE	$\tau^- \rightarrow \pi^- \pi^0 \nu_\tau$
1429 ± 41	20K	<sup>4</sup> LEES 17C	BABR	$J/\psi \rightarrow \pi^+\pi^-\pi^0$
1350 ± 20	+20/-30 63.5k	<sup>5</sup> ABRAMOWICZ12	ZEUS	$ep \rightarrow e\pi^+\pi^-p$
1493 ± 15		<sup>6</sup> LEES 12G	BABR	$e^+e^- \rightarrow \pi^+\pi^-\gamma$
1446 ± 7	± 28 5.4 M	<sup>7,8</sup> FUJIKAWA 08	BELL	$\tau^- \rightarrow \pi^- \pi^0 \nu_\tau$
1328 ± 15		<sup>9</sup> SCHAEEL 05C	ALEP	$\tau^- \rightarrow \pi^- \pi^0 \nu_\tau$
1406 ± 15	87k	<sup>7,10</sup> ANDERSON 00A	CLE2	$\tau^- \rightarrow \pi^- \pi^0 \nu_\tau$
~ 1368		<sup>11</sup> ABELE 99C	CBAR	0.0 $\bar{p}d \rightarrow \pi^+\pi^-\pi^-p$
1348 ± 33		BERTIN 98	OBLX	0.05–0.405 $\bar{p}p \rightarrow \pi^+\pi^-$
1411 ± 14		<sup>12</sup> ABELE 97	CBAR	$\bar{p}n \rightarrow \pi^-\pi^0\pi^0$
1370 ± 90/-70		ACHASOV 97	RVUE	$e^+e^- \rightarrow \pi^+\pi^-$
1359 ± 40		<sup>10</sup> BERTIN 97C	OBLX	0.0 $\bar{p}p \rightarrow \pi^+\pi^-\pi^0$
1282 ± 37		BERTIN 97D	OBLX	0.05 $\bar{p}p \rightarrow 2\pi^+2\pi^-$
1424 ± 25		BISELLO 89	DM2	$e^+e^- \rightarrow \pi^+\pi^-$
1265.5 ± 75.3		DUBNICKA 89	RVUE	$e^+e^- \rightarrow \pi^+\pi^-$
1292 ± 17		<sup>13</sup> KURDADZE 83	OLYA	0.64–1.4 $e^+e^- \rightarrow \pi^+\pi^-$

<sup>1</sup> Applies the Unitary & Analytic Model of the pion electromagnetic form factor of DUBNICKA 10 to analyze the data of LEES 12G and ABLIKIM 16c.

<sup>2</sup> Applies the Unitary & Analytic Model of the pion electromagnetic form factor of DUBNICKA 10 to analyze the data of ACHASOV 06, AKHMETSHIN 07, AUBERT 09As, and AMBROSINO 11A.

<sup>3</sup> Applies the Unitary & Analytic Model of the pion electromagnetic form factor of DUBNICKA 10 to analyze the data of FUJIKAWA 08.

<sup>4</sup> From a Dalitz plot analysis in an isobar model with  $\rho(1450)$  and  $\rho(1700)$  masses and widths floating.

<sup>5</sup> Using the KUHN 90 parametrization of the pion form factor, neglecting  $\rho-\omega$  interference.

<sup>6</sup> Using the GOUNARIS 68 parametrization of the pion form factor leaving the masses and widths of the  $\rho(1450)$ ,  $\rho(1700)$ , and  $\rho(2150)$  resonances as free parameters of the fit.

<sup>7</sup> From the GOUNARIS 68 parametrization of the pion form factor.

<sup>8</sup>  $|F_\pi(0)|^2$  fixed to 1.

<sup>9</sup> From the combined fit of the  $\tau^-$  data from ANDERSON 00A and SCHAEEL 05C and  $e^+e^-$  data from the compilation of BARKOV 85, AKHMETSHIN 04, and AL OISI 05.  $\rho(1700)$  mass and width fixed at 1713 MeV and 235 MeV, respectively. Supersedes BARATE 97m.

<sup>10</sup>  $\rho(1700)$  mass and width fixed at 1700 MeV and 235 MeV, respectively.

<sup>11</sup>  $\rho(1700)$  mass and width fixed at 1780 MeV and 275 MeV respectively.

<sup>12</sup> T-matrix pole.

<sup>13</sup> Using for  $\rho(1700)$  mass and width 1600 ± 20 and 300 ± 10 MeV respectively.

 $K\bar{K}$  MODE

VALUE (MeV)	EVTS	DOCUMENT ID	TECN	CHG	COMMENT
1208 ± 8 ± 9	190k	<sup>1</sup> AAIJ 16N	LHCB		$D^0 \rightarrow K_S^0 K^{\pm}\pi^{\mp}$
1422.8 ± 6.5	27k	<sup>2</sup> ABELE 99D	CBAR	±	0.0 $\bar{p}p \rightarrow K^+ K^- \pi^0$

<sup>1</sup> Using the GOUNARIS 68 parameterization with fixed width.

<sup>2</sup> K-matrix pole. Isospin not determined, could be  $\omega(1420)$ .

$\rho(1450)$

$K\bar{K}^*(892) + c.c. \text{ MODE}$

VALUE (MeV)	DOCUMENT ID	TECN	COMMENT
1505 ± 19 ± 7	AUBERT	08s	BABR 10.6 $e^+e^- \rightarrow K\bar{K}^*(892)\gamma$

$m_{\rho(1450)^0} - m_{\rho(1450)^\pm}$

VALUE (MeV)	DOCUMENT ID	TECN	COMMENT
-31.53 ± 47.99	1 BARTOS	17A	RVUE $e^+e^- \rightarrow \pi^+\pi^-$ , $\tau^- \rightarrow \pi^-\pi^0\nu_\tau$

<sup>1</sup> Applies the Unitary & Analytic Model of the pion electromagnetic form factor of DUB-NICKA 10 to analyze the data of ACHASOV 06, AKHMETSHIN 07, AUBERT 09As, AMBROSINO 11A, and FUJIKAWA 08.

$\rho(1450) \text{ WIDTH}$

$\rho(1450) \text{ WIDTH}$

VALUE (MeV)	DOCUMENT ID	TECN	COMMENT
400 ± 60 OUR ESTIMATE			This is only an educated guess; the error given is larger than the error on the average of the published values.

<sup>1</sup> From a fit of a VMD model with two effective resonances with masses of 1450 MeV and 1700 MeV to describe the excited vector states  $\omega(1420)$ ,  $\rho(1450)$ ,  $\omega(1650)$ , and  $\rho(1700)$ . Systematic errors not evaluated.

$\eta\rho^0 \text{ MODE}$

VALUE (MeV)	EVTS	DOCUMENT ID	TECN	COMMENT
280 ± 20	7.4k	1 ACHASOV	18	SND 1.22-2.00 $e^+e^- \rightarrow \eta\pi^+\pi^-$
226 ± 44		2 AKHMETSHIN 01B	CMD2	$e^+e^- \rightarrow \eta\gamma$
211 ± 31		3 AKHMETSHIN 00D	CMD2	$e^+e^- \rightarrow \eta\pi^+\pi^-$
230 ± 30		ANTONELLI 88	DM2	$e^+e^- \rightarrow \eta\pi^+\pi^-$
60 ± 15		FUKUI 88	SPEC	8.95 $\pi^-p \rightarrow \eta\pi^+\pi^-n$

<sup>1</sup> From the combined fit of AULCHENKO 15 and ACHASOV 18 in the model with the interfering  $\rho(1450)$ ,  $\rho(1700)$  and  $\rho(2150)$  with the parameters of the  $\rho(1450)$  and  $\rho(1700)$  floating and the mass and width of the  $\rho(2150)$  fixed at 2155 MeV and 320 MeV, respectively. The phases of the resonances are  $\pi$ , 0 and  $\pi$ , respectively.  
<sup>2</sup> Using the data of AKHMETSHIN 01B on  $e^+e^- \rightarrow \eta\gamma$ , AKHMETSHIN 00D and ANTONELLI 88 on  $e^+e^- \rightarrow \eta\pi^+\pi^-$ .  
<sup>3</sup> Using the data of ANTONELLI 88, DOLINSKY 91, and AKHMETSHIN 00D. The energy-independent width of the  $\rho(1450)$  and  $\rho(1700)$  mesons assumed.

$\omega\pi \text{ MODE}$

VALUE (MeV)	EVTS	DOCUMENT ID	TECN	COMMENT
440 ± 40	10.2k	1 ACHASOV	16D	SND 1.05-2.00 $e^+e^- \rightarrow \pi^0\pi^0\gamma$
303 + 31 + 69 / - 52 - 7	821	2 MATVIENKO	15	BELL $\bar{B}^0 \rightarrow D^{*+}\omega\pi^-$
429 ± 42 ± 10	2382	3 AKHMETSHIN 03B	CMD2	$e^+e^- \rightarrow \pi^0\pi^0\gamma$
547 ± 86 + 46 / - 45	341	4 ALEXANDER	01B	CLE2 $B \rightarrow D^{(*)}\omega\pi^-$
400 ± 35		5 EDWARDS	00A	CLE2 $\tau^- \rightarrow \omega\pi^-\nu_\tau$
311 ± 62		6 CLEGG	94	RVUE
300		7 ASTON	80C	OMEG 20-70 $\gamma p \rightarrow \omega\pi^0 p$
320 ± 100		7 BARBER	80C	SPEC 3-5 $\gamma p \rightarrow \omega\pi^0 p$

<sup>1</sup> From a phenomenological model based on vector meson dominance with interfering  $\rho(770)$ ,  $\rho(1450)$ , and  $\rho(1700)$ . The  $\rho(1700)$  mass and width are fixed at 1720 MeV and 250 MeV, respectively. Systematic uncertainties not estimated. Supersedes ACHASOV 13.  
<sup>2</sup> Using Breit-Wigner parameterization of the  $\rho(1450)$  and assuming equal probabilities of the  $\rho(1450) \rightarrow \pi\pi$  and  $\rho(1450) \rightarrow \omega\pi$  decays.  
<sup>3</sup> Using the data of AKHMETSHIN 03B and BISELLO 91B assuming the  $\omega\pi^0$  and  $\pi^+\pi^-$  mass dependence of the total width.  $\rho(1700)$  mass and width fixed at 1700 MeV and 240 MeV, respectively.  
<sup>4</sup> Using Breit-Wigner parameterization of the  $\rho(1450)$  and assuming the  $\omega\pi^-$  mass dependence for the total width.  
<sup>5</sup> Mass-independent width parameterization.  $\rho(1700)$  mass and width fixed at 1700 MeV and 235 MeV respectively.  
<sup>6</sup> Using data from BISELLO 91B, DOLINSKY 86 and ALBRECHT 87L.  
<sup>7</sup> Not separated from  $b_1(1235)$ , not pure  $J^P = 1^-$  effect.

$4\pi \text{ MODE}$

VALUE (MeV)	DOCUMENT ID	TECN	COMMENT
325 ± 100	ABELE	01B	CBAR 0.0 $\bar{p}n \rightarrow 2\pi^-2\pi^0\pi^+$

$\pi\pi \text{ MODE}$

VALUE (MeV)	EVTS	DOCUMENT ID	TECN	COMMENT
324.13 ± 12.01		1 BARTOS	17	RVUE $e^+e^- \rightarrow \pi^+\pi^-$
492.17 ± 138.38		2 BARTOS	17A	RVUE $e^+e^- \rightarrow \pi^+\pi^-$
340.87 ± 23.84		3 BARTOS	17A	RVUE $\tau^- \rightarrow \pi^-\pi^0\nu_\tau$
576 ± 29	20K	4 LEES	17c	BABR $J/\psi \rightarrow \pi^+\pi^-\pi^0$

460 ± 30	+40 / -45	63.5k	5	ABRAMOWICZ12	ZEUS	$ep \rightarrow e\pi^+\pi^-p$
427 ± 31			6	LEES	12G	BABR $e^+e^- \rightarrow \pi^+\pi^-\gamma$
434 ± 16	± 60	5.4M	7,8	FUJIKAWA	08	BELL $\tau^- \rightarrow \pi^-\pi^0\nu_\tau$
468 ± 41			9	SCHAEEL	05c	ALEP $\tau^- \rightarrow \pi^-\pi^0\nu_\tau$
455 ± 41		87k	7,10	ANDERSON	00A	CLE2 $\tau^- \rightarrow \pi^-\pi^0\nu_\tau$
~ 374			11	ABELE	99c	CBAR 0.0 $\bar{p}d \rightarrow \pi^+\pi^-\pi^-p$
275 ± 10				BERTIN	98	OBLX 0.05-0.405 $\bar{p}p \rightarrow \pi^+\pi^-\pi^0$
343 ± 20			12	ABELE	97	CBAR $\bar{p}n \rightarrow \pi^-\pi^0$
310 ± 40			10	BERTIN	97c	OBLX 0.0 $\bar{p}p \rightarrow \pi^+\pi^-\pi^0$
236 ± 36				BERTIN	97D	OBLX 0.05 $\bar{p}p \rightarrow 2\pi^+2\pi^-$
269 ± 31				BISELLO	89	DM2 $e^+e^- \rightarrow \pi^+\pi^-$
391 ± 70				DUBNICKA	89	RVUE $e^+e^- \rightarrow \pi^+\pi^-$
218 ± 46			13	KURDADZE	83	OLYA 0.64-1.4 $e^+e^- \rightarrow \pi^+\pi^-$

<sup>1</sup> Applies the Unitary & Analytic Model of the pion electromagnetic form factor of DUB-NICKA 10 to analyze the data of LEES 12G and ABLIKIM 16c.  
<sup>2</sup> Applies the Unitary & Analytic Model of the pion electromagnetic form factor of DUB-NICKA 10 to analyze the data of ACHASOV 06, AKHMETSHIN 07, AUBERT 09As, and AMBROSINO 11A.  
<sup>3</sup> Applies the Unitary & Analytic Model of the pion electromagnetic form factor of DUB-NICKA 10 to analyze the data of FUJIKAWA 08.  
<sup>4</sup> From a Dalitz plot analysis in an isobar model with  $\rho(1450)$  and  $\rho(1700)$  masses and widths floating.  
<sup>5</sup> Using the KUHN 90 parametrization of the pion form factor, neglecting  $\rho-\omega$  interference.  
<sup>6</sup> Using the GOUNARIS 68 parametrization of the pion form factor leaving the masses and widths of the  $\rho(1450)$ ,  $\rho(1700)$ , and  $\rho(2150)$  resonances as free parameters of the fit.  
<sup>7</sup> From the GOUNARIS 68 parametrization of the pion form factor.  
<sup>8</sup>  $|F_\pi(0)|^2$  fixed to 1.  
<sup>9</sup> From the combined fit of the  $\tau^-$  data from ANDERSON 00A and SCHAEEL 05c and  $e^+e^-$  data from the compilation of BARKOV 85, AKHMETSHIN 04, and AL OISI O5.  $\rho(1700)$  mass and width fixed at 1713 MeV and 235 MeV, respectively. Supersedes BARATE 97m.  
<sup>10</sup>  $\rho(1700)$  mass and width fixed at 1700 MeV and 235 MeV, respectively.  
<sup>11</sup>  $\rho(1700)$  mass and width fixed at 1780 MeV and 275 MeV respectively.  
<sup>12</sup> T-matrix pole.  
<sup>13</sup> Using for  $\rho(1700)$  mass and width 1600 ± 20 and 300 ± 10 MeV respectively.

$K\bar{K} \text{ MODE}$

VALUE (MeV)	EVTS	DOCUMENT ID	TECN	CHG	COMMENT
410 ± 19 ± 35	190k	1 AAIJ	16N	LHCB	$D^0 \rightarrow K_S^0 K^\pm \pi^\mp$
146.5 ± 10.5	27k	2 ABELE	99D	CBAR ±	0.0 $\bar{p}p \rightarrow K^+ K^- \pi^0$

<sup>1</sup> Using the GOUNARIS 68 parametrization with fixed mass.  
<sup>2</sup> K-matrix pole. Isospin not determined, could be  $\omega(1420)$ .

$K\bar{K}^*(892) + c.c. \text{ MODE}$

VALUE (MeV)	DOCUMENT ID	TECN	COMMENT
418 ± 25 ± 4	AUBERT	08s	BABR 10.6 $e^+e^- \rightarrow K\bar{K}^*(892)\gamma$

$\Gamma_{\rho(1450)^0} - \Gamma_{\rho(1450)^\pm}$

VALUE (MeV)	DOCUMENT ID	TECN	COMMENT
151.30 ± 140.42	1 BARTOS	17A	RVUE $e^+e^- \rightarrow \pi^+\pi^-$ , $\tau^- \rightarrow \pi^-\pi^0\nu_\tau$

<sup>1</sup> Applies the Unitary & Analytic Model of the pion electromagnetic form factor of DUB-NICKA 10 to analyze the data of ACHASOV 06, AKHMETSHIN 07, AUBERT 09As, AMBROSINO 11A, and FUJIKAWA 08.

$\rho(1450) \text{ DECAY MODES}$

Mode	Fraction ( $\Gamma_i/\Gamma$ )
$\Gamma_1$ $\pi\pi$	seen
$\Gamma_2$ $\pi^+\pi^-$	seen
$\Gamma_3$ $4\pi$	seen
$\Gamma_4$ $\omega\pi$	
$\Gamma_5$ $a_1(1260)\pi$	
$\Gamma_6$ $h_1(1170)\pi$	
$\Gamma_7$ $\pi(1300)\pi$	
$\Gamma_8$ $\rho\rho$	
$\Gamma_9$ $\rho(\pi\pi)S\text{-wave}$	
$\Gamma_{10}$ $e^+e^-$	seen
$\Gamma_{11}$ $\eta\rho$	seen
$\Gamma_{12}$ $a_2(1320)\pi$	not seen
$\Gamma_{13}$ $K\bar{K}$	seen
$\Gamma_{14}$ $K^+K^-$	seen
$\Gamma_{15}$ $K\bar{K}^*(892) + c.c.$	possibly seen
$\Gamma_{16}$ $\pi^0\gamma$	
$\Gamma_{17}$ $\eta\gamma$	seen
$\Gamma_{18}$ $f_0(500)\gamma$	not seen
$\Gamma_{19}$ $f_0(980)\gamma$	not seen
$\Gamma_{20}$ $f_0(1370)\gamma$	not seen
$\Gamma_{21}$ $f_2(1270)\gamma$	not seen

## Meson Particle Listings

 $\rho(1450)$ 

$\rho(1450) \Gamma(i) \Gamma(e^+ e^-) / \Gamma(\text{total})$				
$\Gamma(\pi\pi) \times \Gamma(e^+ e^-) / \Gamma(\text{total})$	$\Gamma_{11} \Gamma_{10} / \Gamma$			
VALUE (keV)	DOCUMENT ID	TECN	COMMENT	
0.12	<sup>1</sup> DIEKMAN 88	RVUE	$e^+ e^- \rightarrow \pi^+ \pi^-$	
$0.027^{+0.015}_{-0.010}$	<sup>2</sup> KURDADZE 83	OLYA	$0.64-1.4 e^+ e^- \rightarrow \pi^+ \pi^-$	
<sup>1</sup> Using total width = 235 MeV.				
<sup>2</sup> Using for $\rho(1700)$ mass and width $1600 \pm 20$ and $300 \pm 10$ MeV respectively.				

$\Gamma(\eta\rho) \times \Gamma(e^+ e^-) / \Gamma(\text{total})$				
VALUE (eV)	DOCUMENT ID	TECN	COMMENT	$\Gamma_{11} \Gamma_{10} / \Gamma$
$210 \pm 24 \pm 10$	<sup>1</sup> LEES 18	BABR	$e^+ e^- \rightarrow \eta \pi^+ \pi^-$	
$74 \pm 20$	<sup>2</sup> AKHMETSHIN 00D	CMD2	$e^+ e^- \rightarrow \eta \pi^+ \pi^-$	
$91 \pm 19$	ANTONELLI 88	DM2	$e^+ e^- \rightarrow \eta \pi^+ \pi^-$	
<sup>1</sup> Includes non-resonant contribution. The selected fit model includes three $\rho$ excited states. Model uncertainty is 20%.				
<sup>2</sup> Using the data of ANTONELLI 88, DOLINSKY 91, and AKHMETSHIN 00D. The energy-independent width of the $\rho(1450)$ and $\rho(1700)$ mesons assumed.				

$\Gamma(\eta\gamma) \times \Gamma(e^+ e^-) / \Gamma(\text{total})$				
VALUE (eV)	DOCUMENT ID	TECN	COMMENT	$\Gamma_{17} \Gamma_{10} / \Gamma$
$<16.4$	<sup>1</sup> AKHMETSHIN 05	CMD2	$0.60-1.38 e^+ e^- \rightarrow \eta\gamma$	
$2.2 \pm 0.5 \pm 0.3$	<sup>2</sup> AKHMETSHIN 01B	CMD2	$e^+ e^- \rightarrow \eta\gamma$	
<sup>1</sup> From $2\gamma$ decay mode of $\eta$ using 1465 MeV and 310 MeV for the $\rho(1450)$ mass and width. Recalculated by us.				
<sup>2</sup> Using the data of AKHMETSHIN 01B on $e^+ e^- \rightarrow \eta\gamma$ , AKHMETSHIN 00D and ANTONELLI 88 on $e^+ e^- \rightarrow \eta \pi^+ \pi^-$ . Recalculated by us using width of 226 MeV.				

$\Gamma(K\bar{K}^*(892) + \text{c.c.}) \times \Gamma(e^+ e^-) / \Gamma(\text{total})$				
VALUE (eV)	DOCUMENT ID	TECN	COMMENT	$\Gamma_{15} \Gamma_{10} / \Gamma$
$127 \pm 15 \pm 6$	AUBERT 08s	BABR	$10.6 e^+ e^- \rightarrow K\bar{K}^*(892)\gamma$	

$\rho(1450) \Gamma(i) / \Gamma(\text{total}) \times \Gamma(e^+ e^-) / \Gamma(\text{total})$				
$\Gamma(\omega\pi) / \Gamma(\text{total}) \times \Gamma(e^+ e^-) / \Gamma(\text{total})$	$\Gamma_4 / \Gamma \times \Gamma_{10} / \Gamma$			
VALUE (units $10^{-6}$ )	EVTS	DOCUMENT ID	TECN	COMMENT
$2.1 \pm 0.4$	10.2k	<sup>1</sup> ACHASOV 16D	SND	$1.05-2.00 e^+ e^- \rightarrow \pi^0 \pi^0 \gamma$
$5.3 \pm 0.4$	7815	<sup>2</sup> ACHASOV 13	SND	$1.05-2.00 e^+ e^- \rightarrow \pi^0 \pi^0 \gamma$
<sup>1</sup> From a phenomenological model based on vector meson dominance with interfering $\rho(770)$ , $\rho(1450)$ , and $\rho(1700)$ . The $\rho(1700)$ mass and width are fixed at 1720 MeV and 250 MeV, respectively. Systematic uncertainties not estimated. Supersedes ACHASOV 13.				
<sup>2</sup> From a phenomenological model based on vector meson dominance with the interfering $\rho(1450)$ and $\rho(1700)$ and their widths fixed at 400 and 250 MeV, respectively. Systematic uncertainty not estimated.				

$\Gamma(\eta\rho) / \Gamma(\text{total}) \times \Gamma(e^+ e^-) / \Gamma(\text{total})$				
VALUE (units $10^{-7}$ )	EVTS	DOCUMENT ID	TECN	COMMENT
$7.3 \pm 0.3$	7.4k	<sup>1</sup> ACHASOV 18	SND	$1.22-2.00 e^+ e^- \rightarrow \eta \pi^+ \pi^-$
$4.3^{+1.1}_{-0.9} \pm 0.2$	4.9k	<sup>2</sup> AULCHENKO 15	SND	$1.22-2.00 e^+ e^- \rightarrow \eta \pi^+ \pi^-$
<sup>1</sup> From the combined fit of AULCHENKO 15 and ACHASOV 18 in the model with the interfering $\rho(1450)$ , $\rho(1700)$ and $\rho(2150)$ with the parameters of the $\rho(1450)$ and $\rho(1700)$ floating and the mass and width of the $\rho(2150)$ fixed at 2155 MeV and 320 MeV, respectively. The phases of the resonances are $\pi$ , 0 and $\pi$ , respectively.				
<sup>2</sup> From a fit to the $e^+ e^- \rightarrow \eta \pi^+ \pi^-$ cross section with vector meson dominance model including $\rho(770)$ , $\rho(1450)$ , and $\rho(1700)$ decaying exclusively via $\eta\rho(770)$ . Masses and widths of vector states are fixed to PDG 14. Coupling constants are assumed to be real.				

$\Gamma(\rho(500)\gamma) / \Gamma(\text{total}) \times \Gamma(e^+ e^-) / \Gamma(\text{total})$				
VALUE (units $10^{-9}$ )	CL%	DOCUMENT ID	TECN	COMMENT
$<4.0$	90	ACHASOV 11	SND	$e^+ e^- \rightarrow \pi^0 \pi^0 \gamma$

$\Gamma(\pi^0\gamma) / \Gamma(\text{total}) \times \Gamma(e^+ e^-) / \Gamma(\text{total})$				
VALUE (units $10^{-9}$ )	DOCUMENT ID	TECN	COMMENT	$\Gamma_{16} / \Gamma \times \Gamma_{10} / \Gamma$
$2.3 \pm 1.4$	<sup>1</sup> ACHASOV 10D	SND	$1.075-2.0 e^+ e^- \rightarrow \pi^0 \gamma$	
<sup>1</sup> From a fit of a VMD model with two effective resonances with masses of 1450 MeV and 1700 MeV to describe the excited vector states $\omega(1420)$ , $\rho(1450)$ , $\omega(1650)$ , and $\rho(1700)$ . Systematic errors not evaluated.				

$\Gamma(\rho(980)\gamma) / \Gamma(\text{total}) \times \Gamma(e^+ e^-) / \Gamma(\text{total})$				
VALUE (units $10^{-9}$ )	CL%	DOCUMENT ID	TECN	COMMENT
$<2.6$	90	ACHASOV 11	SND	$e^+ e^- \rightarrow \pi^0 \pi^0 \gamma$

$\Gamma(\rho(1370)\gamma) / \Gamma(\text{total}) \times \Gamma(e^+ e^-) / \Gamma(\text{total})$				
VALUE (units $10^{-9}$ )	CL%	DOCUMENT ID	TECN	COMMENT
$<3.5$	90	ACHASOV 11	SND	$e^+ e^- \rightarrow \pi^0 \pi^0 \gamma$

$\Gamma(\rho(1270)\gamma) / \Gamma(\text{total}) \times \Gamma(e^+ e^-) / \Gamma(\text{total})$				
VALUE (units $10^{-9}$ )	CL%	DOCUMENT ID	TECN	COMMENT
$<0.8$	90	<sup>1</sup> ACHASOV 11	SND	$e^+ e^- \rightarrow \pi^0 \pi^0 \gamma$
<sup>1</sup> Using Breit-Wigner parametrization of the $\rho(1450)$ with mass and width of 1465 MeV and 400 MeV, respectively.				

 $\rho(1450)$  BRANCHING RATIOS

$\Gamma(\pi\pi) / \Gamma(4\pi)$				$\Gamma_1 / \Gamma_3$
VALUE	DOCUMENT ID	TECN	COMMENT	
$0.37 \pm 0.10$	<sup>1,2</sup> ABELE 01B	CBAR	$0.0 \bar{p}n \rightarrow 5\pi$	
<sup>1</sup> $\omega\pi$ not included.				
<sup>2</sup> Using ABELE 97.				

$\Gamma(K^+ K^-) / \Gamma(\pi^+ \pi^-)$				$\Gamma_{14} / \Gamma_2$
VALUE (%)	EVTS	DOCUMENT ID	TECN	COMMENT
$30.7 \pm 8.4 \pm 8.2$	20K	<sup>1</sup> LEES 17C	BABR	$J/\psi \rightarrow h^+ h^- \pi^0$
<sup>1</sup> From Dalitz plot analyses in isobar models.				

$\Gamma(\omega\pi) / \Gamma(\text{total})$				$\Gamma_4 / \Gamma$
VALUE	EVTS	DOCUMENT ID	TECN	COMMENT
seen	821	<sup>1</sup> MATVIENKO 15	BELL	$\bar{B}^0 \rightarrow D^{*+} \omega \pi^-$
seen	1.6k	ACHASOV 12	SND	$e^+ e^- \rightarrow \pi^0 \pi^0 \gamma$
$\sim 0.21$		CLEGG 94	RVUE	
<sup>1</sup> Using Breit-Wigner parameterization of the $\rho(1450)$ and assuming equal probabilities of the $\rho(1450) \rightarrow \pi\pi$ and $\rho(1450) \rightarrow \omega\pi$ decays.				

$\Gamma(\pi\pi) / \Gamma(\omega\pi)$			$\Gamma_1 / \Gamma_4$
VALUE	DOCUMENT ID	TECN	COMMENT
$\sim 0.32$	CLEGG 94	RVUE	

$\Gamma(\omega\pi) / \Gamma(4\pi)$				$\Gamma_4 / \Gamma_3$
VALUE	DOCUMENT ID	TECN	COMMENT	
$<0.14$	CLEGG 88	RVUE		

$\Gamma(a_1(1260)\pi) / \Gamma(4\pi)$				$\Gamma_5 / \Gamma_3$
VALUE	DOCUMENT ID	TECN	COMMENT	
$0.27 \pm 0.08$	<sup>1</sup> ABELE 01B	CBAR	$0.0 \bar{p}n \rightarrow 5\pi$	
<sup>1</sup> $\omega\pi$ not included.				

$\Gamma(h_1(1170)\pi) / \Gamma(4\pi)$				$\Gamma_6 / \Gamma_3$
VALUE	DOCUMENT ID	TECN	COMMENT	
$0.08 \pm 0.04$	<sup>1</sup> ABELE 01B	CBAR	$0.0 \bar{p}n \rightarrow 5\pi$	
<sup>1</sup> $\omega\pi$ not included.				

$\Gamma(\pi(1300)\pi) / \Gamma(4\pi)$				$\Gamma_7 / \Gamma_3$
VALUE	DOCUMENT ID	TECN	COMMENT	
$0.37 \pm 0.13$	<sup>1</sup> ABELE 01B	CBAR	$0.0 \bar{p}n \rightarrow 5\pi$	
<sup>1</sup> $\omega\pi$ not included.				

$\Gamma(\rho\rho) / \Gamma(4\pi)$				$\Gamma_8 / \Gamma_3$
VALUE	DOCUMENT ID	TECN	COMMENT	
$0.11 \pm 0.05$	<sup>1</sup> ABELE 01B	CBAR	$0.0 \bar{p}n \rightarrow 5\pi$	
<sup>1</sup> $\omega\pi$ not included.				

$\Gamma(\rho(\pi\pi) s\text{-wave}) / \Gamma(4\pi)$				$\Gamma_9 / \Gamma_3$
VALUE	DOCUMENT ID	TECN	COMMENT	
$0.17 \pm 0.09$	<sup>1</sup> ABELE 01B	CBAR	$0.0 \bar{p}n \rightarrow 5\pi$	
<sup>1</sup> $\omega\pi$ not included.				

$\Gamma(\eta\rho) / \Gamma(\text{total})$				$\Gamma_{11} / \Gamma$
VALUE	EVTS	DOCUMENT ID	TECN	COMMENT
seen	35	<sup>1</sup> ACHASOV 14	SND	$1.15-2.00 e^+ e^- \rightarrow \eta\gamma$
$<0.04$		DONNACHIE 87B	RVUE	
<sup>1</sup> From a phenomenological model based on vector meson dominance with $\rho(1450)$ and $\phi(1680)$ masses and widths from the PDG 12.				

See key on page 999

# Meson Particle Listings

## $\rho(1450)$ , $\eta(1475)$

### $\Gamma(\eta\rho)/\Gamma(\omega\rho)$ $\Gamma_{11}/\Gamma_4$

VALUE	DOCUMENT ID	TECN	COMMENT
0.081 ± 0.020	<sup>1,2</sup> AULCHENKO 15	SND	1.22–2.00 $e^+e^- \rightarrow \eta\pi^+\pi^-$
<0.24	<sup>3</sup> DONNACHIE 91	RVUE	
>2	FUKUI 91	SPEC	8.95 $\pi^-p \rightarrow \omega\pi^0n$

<sup>1</sup> From a fit to the  $e^+e^- \rightarrow \eta\pi^+\pi^-$  cross section with vector meson dominance model including  $\rho(770)$ ,  $\rho(1450)$ , and  $\rho(1700)$  decaying exclusively via  $\eta\rho(770)$ . Masses and widths of vector states are fixed to PDG 14. Coupling constants are assumed to be real.  
<sup>2</sup> Reports the inverse of the quoted value as  $12.3 \pm 3.1$ .  
<sup>3</sup> Using data from BISELLO 91b, DOLINSKY 86 and ALBRECHT 87L.

### $\Gamma(\pi\pi)/\Gamma(\eta\rho)$ $\Gamma_1/\Gamma_{11}$

VALUE	DOCUMENT ID	TECN	COMMENT
1.3 ± 0.4	<sup>1</sup> AULCHENKO 15	SND	1.22–2.00 $e^+e^- \rightarrow \eta\pi^+\pi^-$

<sup>1</sup> From a fit to the  $e^+e^- \rightarrow \eta\pi^+\pi^-$  cross section with vector meson dominance model including  $\rho(770)$ ,  $\rho(1450)$ , and  $\rho(1700)$  decaying exclusively via  $\eta\rho(770)$ . Masses and widths of vector states are fixed to PDG 14. Coupling constants are assumed to be real.

### $\Gamma(a_2(1320)\pi)/\Gamma_{total}$ $\Gamma_{12}/\Gamma$

VALUE	DOCUMENT ID	TECN	COMMENT
not seen	AMELIN 00	VES	37 $\pi^-p \rightarrow \eta\pi^+\pi^-n$

### $\Gamma(K\bar{K})/\Gamma(\omega\rho)$ $\Gamma_{13}/\Gamma_4$

VALUE	DOCUMENT ID	TECN	COMMENT
<0.08	<sup>1</sup> DONNACHIE 91	RVUE	

<sup>1</sup> Using data from BISELLO 91b, DOLINSKY 86 and ALBRECHT 87L.

### $\Gamma(K\bar{K}^*(892) + c.c.)/\Gamma_{total}$ $\Gamma_{15}/\Gamma$

VALUE	DOCUMENT ID	TECN	COMMENT
possibly seen	COAN 04	CLEO	$\tau^- \rightarrow K^-\pi^-K^+\nu_\tau$

### $\Gamma(\eta\gamma)/\Gamma_{total}$ $\Gamma_{17}/\Gamma$

VALUE	EVTS	DOCUMENT ID	TECN	COMMENT
seen	35	<sup>1</sup> ACHASOV 14	SND	1.15–2.00 $e^+e^- \rightarrow \eta\gamma$

<sup>1</sup> From a phenomenological model based on vector meson dominance with  $\rho(1450)$  and  $\phi(1680)$  masses and widths from the PDG 12.

### $\rho(1450)$ REFERENCES

ACHASOV	18	PR D97 012008	M.N. Achasov et al.	(SND Collab.)
LEES	18	PR D97 052007	J.P. Lees et al.	(BABAR Collab.)
BARTOS	17	PR D96 113004	E. Bartos et al.	
BARTOS	17A	JUMP A32 1750154	E. Bartos et al.	
LEES	17C	PR D95 072007	J.P. Lees et al.	(BABAR Collab.)
AALI	16N	PR D93 052018	R. Aaij et al.	(LHCb Collab.)
ABLIKIM	16C	PL B753 629	M. Ablikim et al.	(BESIII Collab.)
ACHASOV	16D	PR D94 112001	M.N. Achasov et al.	(SND Collab.)
AULCHENKO	15	PR D91 052013	V.M. Aulchenko et al.	(SND Collab.)
MATVIENKO	15	PR D92 012013	D. Matvienko et al.	(BELLE Collab.)
ACHASOV	14	PR D90 032002	M.N. Achasov et al.	(SND Collab.)
PDG	14	CP C38 070001	K. Olive et al.	(PDG Collab.)
ACHASOV	13	PR D88 054013	M.N. Achasov et al.	(SND Collab.)
ABRAMOWICZ	12	EPJ C72 1849	H. Abramowicz et al.	(ZEUS Collab.)
ACHASOV	12	JETPL 94 734	M.N. Achasov et al.	
LEES	12G	PR D86 032013	J.P. Lees et al.	(BABAR Collab.)
PDG	12	PR D86 010001	J. Beringer et al.	(PDG Collab.)
ACHASOV	11	JETP 113 75	M.N. Achasov et al.	(SND Collab.)
ACHASOV	11	Translated from ZETFP 140 87.		
AMBROSINO	11A	PL B700 102	F. Ambrosino et al.	(KLOE Collab.)
ACHASOV	10D	PR D98 112001	M.N. Achasov et al.	(SND Collab.)
DUBNICKA	10	APS 60 1	S. Dubnicka, A.Z. Dubnickova	
AUBERT	09AS	PRL 103 231801	B. Aubert et al.	(BABAR Collab.)
AUBERT	08S	PR D77 092002	B. Aubert et al.	(BABAR Collab.)
FUJIKAWA	08	PR D78 072006	M. Fujikawa et al.	(BELLE Collab.)
AKHMETSHIN	07	PL B648 28	R.R. Akhmetshin et al.	(Novosibirsk CMD-2 Collab.)
ACHASOV	06	JETP 103 380	M.N. Achasov et al.	(Novosibirsk SND Collab.)
ACHASOV	06	Translated from ZETFP 130 437.		
AKHMETSHIN	05	PL B605 26	R.R. Akhmetshin et al.	(Novosibirsk CMD-2 Collab.)
ALOISIO	05	PL B606 12	A. Aloisio et al.	(CLEO Collab.)
SCHAEL	05C	PRPL 421 191	S. Schael et al.	(ALEPH Collab.)
AKHMETSHIN	04	PL B578 285	R.R. Akhmetshin et al.	(Novosibirsk CMD-2 Collab.)
COAN	04	PRL 92 232001	T.E. Coan et al.	(CLEO Collab.)
AKHMETSHIN	03B	PL B562 173	R.R. Akhmetshin et al.	(Novosibirsk CMD-2 Collab.)
ABELE	01B	EPJ C21 261	A. Abele et al.	(Crystal Barrel Collab.)
AKHMETSHIN	01B	PL B509 217	R.R. Akhmetshin et al.	(Novosibirsk CMD-2 Collab.)
ALEXANDER	01B	PR D64 092001	J.P. Alexander et al.	(CLEO Collab.)
AKHMETSHIN	00D	PL B489 125	R.R. Akhmetshin et al.	(Novosibirsk CMD-2 Collab.)
AMELIN	00	NP A668 83	D. Amelin et al.	(VES Collab.)
ANDERSON	00A	PR D61 112002	S. Anderson et al.	(CLEO Collab.)
EDWARDS	00A	PR D61 072003	K.W. Edwards et al.	(CLEO Collab.)
ABELE	99C	PL B450 275	A. Abele et al.	(Crystal Barrel Collab.)
ABELE	99D	PL B468 178	A. Abele et al.	(Crystal Barrel Collab.)
BERTIN	98	PR D57 55	A. Bertin et al.	(OBELIX Collab.)
ABELE	97	PL B391 191	A. Abele et al.	(Crystal Barrel Collab.)
ACHASOV	97	PR D55 2663	M.N. Achasov et al.	(NOVM)
BARATE	97M	ZPHY C76 15	R. Barate et al.	(ALEPH Collab.)
BERTIN	97C	PL B408 476	A. Bertin et al.	(OBELIX Collab.)
BERTIN	97D	PL B414 220	A. Bertin et al.	(OBELIX Collab.)
CLEGG	94	ZPHY C62 455	A.B. Clegg, A. Donnachie	(LANC, MCHS)
BISELLO	91B	NPBPS 821 111	D. Bisello	(DM2 Collab.)

DOLINSKY	91	PRPL 202 99	S.I. Dolinsky et al.	(NOVO)
DONNACHIE	91	ZPHY C51 689	A. Donnachie, A.B. Clegg	(MCHS, LANC)
FUKUI	91	PL B257 241	S. Fukui et al.	(SUGI, NAGO, KEK, KYOT+)
KUHN	90	ZPHY C48 445	J.H. Kuhn et al.	(M2M)
ARMSTRONG	89E	PL B228 536	T.A. Armstrong, M. Benayoun	(ATHU, BARI, BIRM+)
BISELLO	89	PL B220 321	D. Bisello et al.	(DM2 Collab.)
DUBNICKA	89	JP G15 1349	S. Dubnicka et al.	(JINR, SLOV)
ANTONELLI	88	PL B212 133	A. Antonelli et al.	(DM2 Collab.)
CLEGG	88	ZPHY C40 313	A.B. Clegg, A. Donnachie	(MCHS, LANC)
DIKMAN	88	PRPL 159 99	B. Diekmann	(BOHN)
FUKUI	88	PL B202 441	S. Fukui et al.	(SUGI, NAGO, KEK, KYOT+)
ALBRECHT	87L	PL B185 223	H. Albrecht et al.	(ARGUS Collab.)
DONNACHIE	87B	ZPHY C34 257	A. Donnachie, A.B. Clegg	(MCHS, LANC)
DOLINSKY	86	PL B174 453	S.I. Dolinsky et al.	(NOVO)
BARKOV	85	NP B256 365	L.M. Barkov et al.	(NOVO)
KURDADZE	83	JETPL 37 733	L.M. Kurdadze et al.	(NOVO)
ASTON	80C	PL 92B 211	D. Aston	(BOHN, CERN, EPOL, GLAS, LANC+)
BARBER	80C	ZPHY C4 169	D.P. Barber et al.	(DARE, LANC, SHEP)
GOUNARIS	68	PRL 21 244	G.J. Gounaris, J.J. Sakurai	

## $\eta(1475)$

$$J^{PC} = 0^+(0^-+)$$

See the  $\eta(1405)$  and the related review on "Pseudoscalar and Pseudovector Mesons in the 1400 MeV Region."

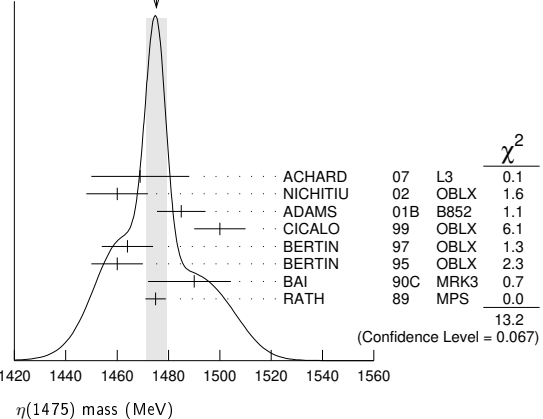
### $\eta(1475)$ MASS

VALUE (MeV)	EVTS	DOCUMENT ID	TECN	COMMENT
<b>1475 ± 4 OUR AVERAGE</b>				Error includes scale factor of 1.4. See the ideogram below.
1469 ± 14 ± 13	74	ACHARD 07	L3	183–209 $e^+e^- \rightarrow e^+e^-K_S^0K_{\pm}^0\pi^{\mp}$
1460 ± 12	3651	NICHITIU 02	OBLX	0 $\bar{p}p \rightarrow K^+K^-\pi^+\pi^-\pi^0$
1485 ± 8 ± 5	20k	ADAMS 01B	B852	18 GeV $\pi^-p \rightarrow K^+K^-\pi^0n$
1500 ± 10		CICALO 99	OBLX	0 $\bar{p}p \rightarrow K^{\pm}K_S^0\pi^{\mp}\pi^{\pm}\pi^{\mp}$
1464 ± 10		BERTIN 97	OBLX	0 $\bar{p}p \rightarrow K^{\pm}(K^0)\pi^{\mp}\pi^{\pm}\pi^{\mp}$
1460 ± 10		BERTIN 95	OBLX	0 $\bar{p}p \rightarrow K\bar{K}\pi\pi\pi$
1490 <sup>+14</sup> <sub>-8</sub> <sup>+3</sup> <sub>-16</sub>	1100	BAI 90C	MRK3	$J/\psi \rightarrow \gamma K_S^0 K_{\pm}^0 \pi^{\mp}$
1475 ± 4		RATH 89	MPS	21.4 $\pi^-p \rightarrow nK_S^0 K_S^0 \pi^0$
1477 ± 7 ± 13		<sup>1</sup> ABLIKIM 18i	BES3	$J/\psi \rightarrow \gamma\gamma\phi(1020)$
1565 ± 8 <sup>+0</sup> <sub>-63</sub>		<sup>2</sup> ABLIKIM 15T	BES3	$J/\psi \rightarrow \gamma K_S^0 K_S^0 \eta$
1421 ± 14		AUGUSTIN 92	DM2	$J/\psi \rightarrow \gamma K\bar{K}\pi$

<sup>1</sup> From a fit to  $\gamma\phi$  invariant mass. Angular analysis consistent with  $J^{PC} = 0^-+$ . Other  $J^{PC}$  not excluded.  
<sup>2</sup> Could also be the  $\eta(1405)$ .

### WEIGHTED AVERAGE

1475±4 (Error scaled by 1.4)



### $\eta(1475)$ WIDTH

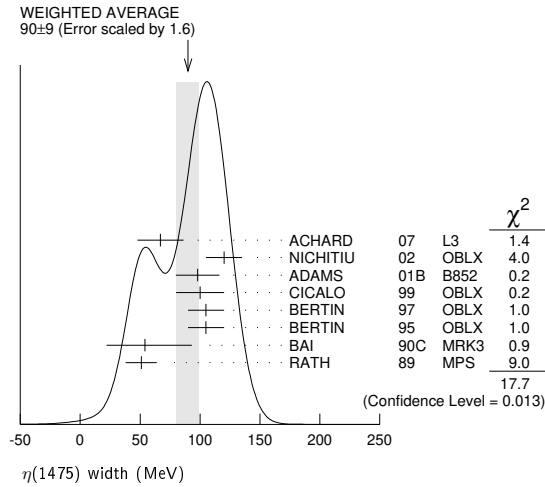
VALUE (MeV)	EVTS	DOCUMENT ID	TECN	COMMENT
<b>90 ± 9 OUR AVERAGE</b>				Error includes scale factor of 1.6. See the ideogram below.
67 ± 18 ± 7	74	ACHARD 07	L3	183–209 $e^+e^- \rightarrow e^+e^-K_S^0K_{\pm}^0\pi^{\mp}$
120 ± 15	3651	NICHITIU 02	OBLX	0 $\bar{p}p \rightarrow K^+K^-\pi^+\pi^-\pi^0$
98 ± 18 ± 3	20k	ADAMS 01B	B852	18 GeV $\pi^-p \rightarrow K^+K^-\pi^0n$
100 ± 20		CICALO 99	OBLX	0 $\bar{p}p \rightarrow K^{\pm}K_S^0\pi^{\mp}\pi^{\pm}\pi^{\mp}$
105 ± 15		BERTIN 97	OBLX	0.0 $\bar{p}p \rightarrow K^{\pm}(K^0)\pi^{\mp}\pi^{\pm}\pi^{\mp}$
105 ± 15		BERTIN 95	OBLX	0 $\bar{p}p \rightarrow K\bar{K}\pi\pi\pi$
54 <sup>+37</sup> <sub>-21</sub> <sup>+13</sup> <sub>-24</sub>		BAI 90C	MRK3	$J/\psi \rightarrow \gamma K_S^0 K_{\pm}^0 \pi^{\mp}$
51 ± 13		RATH 89	MPS	21.4 $\pi^-p \rightarrow nK_S^0 K_S^0 \pi^0$



# Meson Particle Listings

## $\eta(1475)$ , $f_0(1500)$

- • • We do not use the following data for averages, fits, limits, etc. • • •
  - 118 ± 22 ± 17 <sup>1</sup> ABLIKIM 18i BES3  $J/\psi \rightarrow \gamma\gamma\phi(1020)$
  - 45 <sup>+14</sup> <sub>-13</sub> - 28 <sup>2</sup> ABLIKIM 15T BES3  $J/\psi \rightarrow \gamma K_S^0 K_S^0 \eta$
  - 63 ± 18 AUGUSTIN 92 DM2  $J/\psi \rightarrow \gamma K \bar{K} \pi$
- <sup>1</sup> From a fit to  $\gamma\phi$  invariant mass. Angular analysis consistent with  $J^{PC} = 0^{-+}$ . Other  $J^{PC}$  not excluded.  
<sup>2</sup> Could also be the  $\eta(1405)$ .



### $\eta(1475)$ DECAY MODES

Mode	Fraction ( $\Gamma_i/\Gamma$ )
$\Gamma_1$ $K \bar{K} \pi$	seen
$\Gamma_2$ $K \bar{K}^*(892) + c.c.$	seen
$\Gamma_3$ $a_0(980)\pi$	seen
$\Gamma_4$ $\gamma\gamma$	seen
$\Gamma_5$ $K_S^0 K_S^0 \eta$	possibly seen
$\Gamma_6$ $\gamma\phi(1020)$	possibly seen

### $\eta(1475)$ $\Gamma(i)\Gamma(\gamma\gamma)/\Gamma(\text{total})$

VALUE (keV)	CL%	EVTS	DOCUMENT ID	TECN	COMMENT	$\Gamma_1\Gamma_4/\Gamma$
0.23 ± 0.05 ± 0.05		74	<sup>1</sup> ACHARD 07 L3		183-209 $e^+e^- \rightarrow e^+e^- K_S^0 K_S^0 K^\pm \pi^\mp$	

- • • We do not use the following data for averages, fits, limits, etc. • • •
  - < 0.089 90 <sup>2,3</sup> AHOHE 05 CLE2 10.6  $e^+e^- \rightarrow e^+e^- K_S^0 K_S^0 K^\pm \pi^\mp$
- <sup>1</sup> Supersedes ACCIARRI 01G. Using  $B(K_S^0 \rightarrow \pi^+ \pi^-) = 0.6895$ .  
<sup>2</sup> Using  $\eta(1475)$  mass of 1481 MeV and width of 48 MeV. The upper limit increases to 0.140 keV if the world average value, 87 MeV, of the width is used.  
<sup>3</sup> Assuming three-body phase-space decay to  $K_S^0 K^\pm \pi^\mp$ .

### $\eta(1475)$ BRANCHING RATIOS

VALUE	DOCUMENT ID	TECN	COMMENT	$\Gamma_2/\Gamma_1$
-------	-------------	------	---------	---------------------

- • • We do not use the following data for averages, fits, limits, etc. • • •
  - 0.50 ± 0.10 <sup>1</sup> BAILLON 67 HBC 0.0  $\bar{p}p \rightarrow K \bar{K} \pi \pi$
- <sup>1</sup> Data could also refer to  $\eta(1405)$ .

VALUE	CL%	DOCUMENT ID	TECN	COMMENT	$\Gamma_2/(\Gamma_2+\Gamma_3)$
-------	-----	-------------	------	---------	--------------------------------

- • • We do not use the following data for averages, fits, limits, etc. • • •
- < 0.25 90 EDWARDS 82E CBAL  $J/\psi \rightarrow K^+ K^- \pi^0 \gamma$

VALUE	CL%	DOCUMENT ID	TECN	COMMENT	$\Gamma_4/\Gamma_1$
-------	-----	-------------	------	---------	---------------------

- • • We do not use the following data for averages, fits, limits, etc. • • •
  - < 1.27 × 10<sup>-3</sup> 90 <sup>1</sup> ABLIKIM 18i BES3  $\psi(2S) \rightarrow \pi^+ \pi^- \gamma \gamma \gamma$
- <sup>1</sup> Using results from BAI 00D.

VALUE	DOCUMENT ID	TECN	COMMENT	$\Gamma_6/\Gamma$
-------	-------------	------	---------	-------------------

- possibly seen <sup>1</sup> ABLIKIM 18i BES3  $J/\psi \rightarrow \gamma\gamma\phi(1020)$
- <sup>1</sup> Seen as a peak in  $\gamma\phi$  invariant mass. Angular analysis consistent with  $J^{PC} = 0^{-+}$ . Other  $J^{PC}$  not excluded. Also see  $\eta(1405)$ .

### $\eta(1475)$ REFERENCES

ABLIKIM 18i PR D97 051101	M. Ablikim et al.	(BESIII Collab.)
ABLIKIM 18o PR D97 072014	M. Ablikim et al.	(BESIII Collab.)
ABLIKIM 15T PRL 115 091803	M. Ablikim et al.	(BESIII Collab.)
ACHARD 07 JHEP 0703 018	P. Achard et al.	(L3 Collab.)
AHOHE 05 PR D71 072001	R. Ahohe et al.	(CLEO Collab.)
NICHITIU 02 PL B545 261	F. Nitchitui et al.	(OBELIX Collab.)
ACCIARRI 01G PL B501 1	M. Acciarri et al.	(L3 Collab.)
ADAMS 01B PL B516 264	G.S. Adams et al.	(BNL E852 Collab.)
BAI 00D PL B476 25	J.Z. Bai et al.	(BES Collab.)
CICALO 99 PL B462 453	C. Cicalo et al.	(OBELIX Collab.)
BERTIN 97 PL B400 226	A. Bertin et al.	(OBELIX Collab.)
BERTIN 95 PL B361 187	A. Bertin et al.	(OBELIX Collab.)
AUGUSTIN 92 PR D46 1951	J.E. Augustin, G. Cosme	(DM2 Collab.)
BAI 90C PRL 65 2507	Z. Bai et al.	(Mark III Collab.)
RATH 89 PR D40 693	M.G. Rath et al.	(NDAM, BRAN, BNL, CUNY+)
EDWARDS 82E PRL 49 259	C. Edwards et al.	(CIT, HARV, PRIN+)
BAILLON 67 NC 50A 393	P.H. Baillon et al.	(CERN, CDEF, IRAD)

### $f_0(1500)$

$$J^G(J^{PC}) = 0^+(0^{++})$$

See the reviews on "Scalar Mesons below 2 GeV" and on "Non- $q\bar{q}$  Mesons".

### $f_0(1500)$ MASS

VALUE (MeV)	EVTS	DOCUMENT ID	TECN	COMMENT
<b>1506 ± 6</b>	<b>OUR AVERAGE</b>			Error includes scale factor of 1.4. See the ideogram below.
1515 ± 12		<sup>1</sup> BARBERIS 00A		450 $pp \rightarrow p_f \eta \eta p_S$
1511 ± 9		<sup>1,2</sup> BARBERIS 00C		450 $pp \rightarrow p_f 4\pi p_S$
1510 ± 8		<sup>1</sup> BARBERIS 00E		450 $pp \rightarrow p_f \eta \eta p_S$
1522 ± 25		<sup>1</sup> BERTIN 98	OBLX	0.05-0.405 $\bar{p}p \rightarrow \pi^+ \pi^+ \pi^-$
1449 ± 20		<sup>1</sup> BERTIN 97C	OBLX	0.0 $\bar{p}p \rightarrow \pi^+ \pi^- \pi^0$
1500 ± 10		<sup>3</sup> AMSLER 95D	CBAR	0.0 $\bar{p}p \rightarrow \pi^0 \pi^0 \pi^0, \pi^0 \eta \eta, \pi^0 \pi^0 \eta$

- • • We do not use the following data for averages, fits, limits, etc. • • •
- 1465 ± 18 <sup>4</sup> ROPERTZ 18 RVUE  $\bar{B}_S^0 \rightarrow J/\psi(\pi^+ \pi^- / K^+ K^-)$
- 1447 ± 16 ± 13 163 <sup>5,6</sup> DOBBS 15  $J/\psi \rightarrow \gamma \pi^+ \pi^-$
- 1442 ± 9 ± 4 261 <sup>5,6</sup> DOBBS 15  $\psi(2S) \rightarrow \gamma \pi^+ \pi^-$
- 1460.9 ± 2.9 <sup>7</sup> AAIJ 14BR LHCB  $\bar{B}_S^0 \rightarrow J/\psi \pi^+ \pi^-$
- 1468 <sup>+14</sup> <sub>-15</sub> ± <sup>23</sup> <sub>-74</sub> 5.5k <sup>8</sup> ABLIKIM 13N BES3  $e^+e^- \rightarrow J/\psi \rightarrow \gamma \eta \eta$
- 1486 ± 10 <sup>1</sup> ANISOVICH 09 RVUE 0.0  $\bar{p}p, \pi N$
- 1470 ± 60 568 <sup>9</sup> KLEMP T 08 E791  $D_S^+ \rightarrow \pi^- \pi^+ \pi^+$
- 1470 <sup>+6</sup> <sub>-7</sub> ± <sup>72</sup> <sub>-255</sub> <sup>10</sup> UEHARA 08A BELL 10.6  $e^+e^- \rightarrow e^+e^- \pi^0 \pi^0$
- 1466 ± 6 ± 20 <sup>11</sup> ABLIKIM 06V BES2  $e^+e^- \rightarrow J/\psi \rightarrow \gamma \pi^+ \pi^-$
- 1495 ± 4 AMSLER 06 CBAR 0.9  $\bar{p}p \rightarrow K^+ K^- \pi^0$
- 1539 ± 20 9.9k AUBERT 06O BABR  $B^+ \rightarrow K^+ K^+ K^-$
- 1473 ± 5 80k <sup>11,12</sup> UMAN 06 E835 5.2  $\bar{p}p \rightarrow \eta \eta \pi^0$
- 1478 ± 6 VLADIMIRSK...06 SPEC 40  $\pi^- p \rightarrow K_S^0 K_S^0 n$
- 1493 ± 7 <sup>11</sup> BINON 05 GAMS 33  $\pi^- p \rightarrow \eta \eta n$
- 1524 ± 14 1400 <sup>13</sup> GARMASH 05 BELL  $B^+ \rightarrow K^+ K^+ K^-$
- 1489 ± 8 <sup>14</sup> ANISOVICH 03 RVUE
- 1490 ± 30 <sup>11</sup> ABELE 01 CBAR 0.0  $\bar{p}d \rightarrow \pi^- 4\pi^0 p$
- 1497 ± 10 <sup>11</sup> BARBERIS 99 OMEG 450  $pp \rightarrow p_S p_f K^+ K^-$
- 1502 ± 10 <sup>11</sup> BARBERIS 99B OMEG 450  $pp \rightarrow p_S p_f \pi^+ \pi^-$
- 1502 ± 12 ± 10 <sup>15</sup> BARBERIS 99D OMEG 450  $pp \rightarrow K^+ K^-$
- 1530 ± 45 <sup>11</sup> BELLAZZINI 99 GAM4 450  $pp \rightarrow pp \pi^0 \pi^0$
- 1505 ± 18 <sup>11</sup> FRENCH 99 300  $pp \rightarrow p_f(K^+ K^-) p_S$
- 1447 ± 27 <sup>16</sup> KAMINSKI 99 RVUE  $\pi\pi \rightarrow \pi\pi, K \bar{K}, \sigma\sigma$
- 1580 ± 80 <sup>11</sup> ALDE 98 GAM4 100  $\pi^- p \rightarrow \pi^0 \pi^0 n$
- 1499 ± 8 <sup>1</sup> ANISOVICH 98B RVUE Compilation
- ~ 1520 REYES 98 SPEC 800  $pp \rightarrow p_S p_f K_S^0 K_S^0$
- 1510 ± 20 <sup>1</sup> BARBERIS 97B OMEG 450  $pp \rightarrow pp 2(\pi^+ \pi^-)$
- ~ 1475 FRABETTI 97D E687  $D_S^\pm \rightarrow \pi^\mp \pi^\pm \pi^\pm$
- ~ 1505 ABELE 96 CBAR 0.0  $\bar{p}p \rightarrow 5\pi^0$
- 1515 ± 20 ABELE 96B CBAR 0.0  $\bar{p}p \rightarrow \pi^0 K_L^0 K_L^0$
- 1500 ± 8 <sup>1</sup> ABELE 96C RVUE Compilation
- 1460 ± 20 120 <sup>11</sup> AMELIN 96B RVES 37  $\pi^- A \rightarrow \eta \eta \pi^- A$
- 1500 ± 8 BUGG 96 RVUE
- 1500 ± 15 <sup>17</sup> AMSLER 95B CBAR 0.0  $\bar{p}p \rightarrow 3\pi^0$
- 1505 ± 15 <sup>18</sup> AMSLER 95C CBAR 0.0  $\bar{p}p \rightarrow \eta \eta \pi^0$
- 1445 ± 5 <sup>19</sup> ANTINORI 95 OMEG 300,450  $pp \rightarrow pp 2(\pi^+ \pi^-)$
- 1497 ± 30 <sup>11</sup> ANTINORI 95 OMEG 300,450  $pp \rightarrow pp \pi^+ \pi^-$
- ~ 1505 BUGG 95 MRK3  $J/\psi \rightarrow \gamma \pi^+ \pi^- \pi^+ \pi^-$
- 1446 ± 5 <sup>11</sup> ABATZIS 94 OMEG 450  $pp \rightarrow pp 2(\pi^+ \pi^-)$
- 1545 ± 25 <sup>11</sup> AMSLER 94E CBAR 0.0  $\bar{p}p \rightarrow \pi^0 \eta \eta'$
- 1520 ± 25 <sup>1,20</sup> ANISOVICH 94 CBAR 0.0  $\bar{p}p \rightarrow 3\pi^0, \pi^0 \eta \eta$
- 1505 ± 20 <sup>1,21</sup> BUGG 94 RVUE  $\bar{p}p \rightarrow 3\pi^0, \eta \eta \pi^0, \eta \pi^0 \pi^0$

See key on page 999

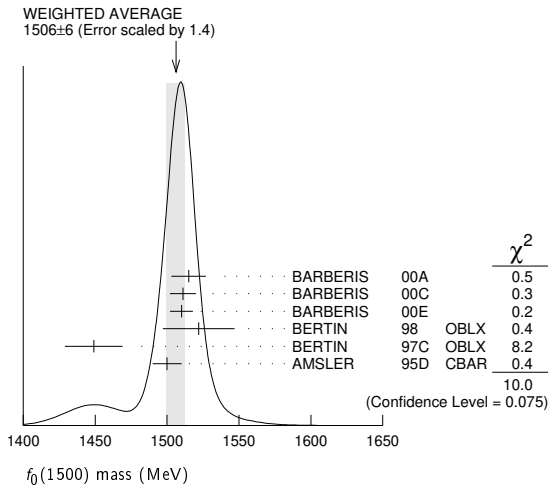
Meson Particle Listings

$f_0(1500)$

1560 ± 25	11 AMSLER	92 CBAR	0.0 $\bar{p}p \rightarrow \pi^0 \eta \eta$
1550 ± 45 ± 30	11 BELADIDZE	92c VES	36 $\pi^- \text{Be} \rightarrow \pi^- \eta' \eta \text{Be}$
1449 ± 4	11 ARMSTRONG	89E OMEG	300 $pp \rightarrow pp 2(\pi^+ \pi^-)$
1610 ± 20	11 ALDE	88 GAM4	300 $\pi^- N \rightarrow \pi^- N 2\eta$
~ 1525	ASTON	88D LASS	11 $K^- p \rightarrow K_S^0 K_S^0 \Lambda$
1570 ± 20	600 11 ALDE	87 GAM4	100 $\pi^- p \rightarrow 4\pi^0 n$
1575 ± 45	22 ALDE	86D GAM4	100 $\pi^- p \rightarrow 2\eta n$
1568 ± 33	11 BINON	84c GAM2	38 $\pi^- p \rightarrow \eta \eta' n$
1592 ± 25	11 BINON	83 GAM2	38 $\pi^- p \rightarrow 2\eta n$
1525 ± 5	11 GRAY	83 DBC	0.0 $\bar{p}N \rightarrow 3\pi$

108 ± 9	80k 8,9 UMAN	06 E835	5.2 $\bar{p}p \rightarrow \eta \eta \pi^0$
119 ± 10	VLADIMIRSK...06	SPEC	40 $\pi^- p \rightarrow K_S^0 K_S^0 n$
90 ± 15	8 BINON	05 GAMS	33 $\pi^- p \rightarrow \eta \eta n$
136 ± 23	10 GARMASH	05 BELL	$B^+ \rightarrow K^+ K^+ K^-$
102 ± 10	11 ANISOVICH	03 RVUE	
140 ± 40	8 ABELE	01 CBAR	0.0 $\bar{p}d \rightarrow \pi^- 4\pi^0 p$
104 ± 25	8 BARBERIS	99 OMEG	450 $pp \rightarrow p_S p_f K^+ K^-$
131 ± 15	8 BARBERIS	99B OMEG	450 $pp \rightarrow p_S p_f \pi^+ \pi^-$
98 ± 18 ± 16	12 BARBERIS	99D OMEG	450 $pp \rightarrow K^+ K^-, \pi^+ \pi^-$
160 ± 50	8 BELLAZZINI	99 GAM4	450 $pp \rightarrow pp \pi^0 \pi^0$
100 ± 33	8 FRENCH	99	300 $pp \rightarrow p_f(K^+ K^-) p_S$
108 ± 46	13 KAMINSKI	99 RVUE	$\pi \pi \rightarrow \pi \pi, K \bar{K}, \sigma \sigma$
280 ± 100	8 ALDE	98 GAM4	100 $\pi^- p \rightarrow \pi^0 \pi^0 n$
130 ± 20	1 ANISOVICH	98B RVUE	Compilation
120 ± 35	1 BARBERIS	97B OMEG	450 $pp \rightarrow pp 2(\pi^+ \pi^-)$
~ 100	FRABETTI	97D E687	$D_S^\pm \rightarrow \pi^\mp \pi^\pm \pi^\pm$
~ 169	8 ABELE	96 CBAR	0.0 $\bar{p}p \rightarrow 5\pi^0$
105 ± 15	8 ABELE	96B CBAR	0.0 $\bar{p}p \rightarrow \pi^0 K_L^0 K_L^0$
100 ± 30	120 8 AMELIN	96B VES	37 $\pi^- A \rightarrow \eta \eta \pi^- A$
132 ± 15	BUGG	96 RVUE	
120 ± 25	14 AMSLER	95B CBAR	0.0 $\bar{p}p \rightarrow 3\pi^0$
120 ± 30	15 AMSLER	95C CBAR	0.0 $\bar{p}p \rightarrow \eta \eta \pi^0$
65 ± 10	16 AN TINORI	95 OMEG	300,450 $pp \rightarrow pp 2(\pi^+ \pi^-)$
199 ± 30	8 AN TINORI	95 OMEG	300,450 $pp \rightarrow pp \pi^+ \pi^-$
56 ± 12	8 ABATZIS	94 OMEG	450 $pp \rightarrow pp 2(\pi^+ \pi^-)$
100 ± 40	8 AMSLER	94E CBAR	0.0 $\bar{p}p \rightarrow \pi^0 \eta \eta'$
148 ± 20	1,17 ANISOVICH	94 CBAR	0.0 $\bar{p}p \rightarrow 3\pi^0, \pi^0 \eta \eta$
150 ± 20	1,18 BUGG	94 RVUE	$\bar{p}p \rightarrow 3\pi^0, \eta \eta \pi^0, \eta \pi^0 \pi^0$
245 ± 50	8 AMSLER	92 CBAR	0.0 $\bar{p}p \rightarrow \pi^0 \eta \eta$
153 ± 67 ± 50	8 BELADIDZE	92c VES	36 $\pi^- \text{Be} \rightarrow \pi^- \eta' \eta \text{Be}$
78 ± 18	8 ARMSTRONG	89E OMEG	300 $pp \rightarrow pp 2(\pi^+ \pi^-)$
170 ± 40	8 ALDE	88 GAM4	300 $\pi^- N \rightarrow \pi^- N 2\eta$
150 ± 20	600 8 ALDE	87 GAM4	100 $\pi^- p \rightarrow 4\pi^0 n$
265 ± 65	19 ALDE	86D GAM4	100 $\pi^- p \rightarrow 2\eta n$
260 ± 60	8 BINON	84c GAM2	38 $\pi^- p \rightarrow \eta \eta' n$
210 ± 40	8 BINON	83 GAM2	38 $\pi^- p \rightarrow 2\eta n$
101 ± 13	8 GRAY	83 DBC	0.0 $\bar{p}N \rightarrow 3\pi$

- 1 T-matrix pole.
- 2 Average between  $\pi^+ \pi^- 2\pi^0$  and  $2(\pi^+ \pi^-)$ .
- 3 T-matrix pole. Coupled-channel analysis of AMSLER 95B, AMSLER 95c, and AMSLER 94d.
- 4 T-matrix pole of 3 channel unitary model fit to data from AAIJ 14BR and AAIJ 17V extracted using Pade approximants.
- 5 Using CLEO-c data but not authored by the CLEO Collaboration.
- 6 From a fit to a Breit-Wigner line shape with fixed  $\Gamma = 109$  MeV.
- 7 Solution 1, statistical error only.
- 8 From partial wave analysis including all possible combinations of  $0^{++}, 2^{++}$ , and  $4^{++}$  resonances.
- 9 Reanalysis of AITALA 01A data. This state could also be  $f_0(1370)$ .
- 10 Breit-Wigner mass. May also be the  $f_0(1370)$ .
- 11 Breit-Wigner mass.
- 12 Statistical error only.
- 13 Breit-Wigner, solution 1, PWA ambiguous.
- 14 K-matrix pole from combined analysis of  $\pi^- p \rightarrow \pi^0 \pi^0 n, \pi^- p \rightarrow K \bar{K} n, \pi^+ \pi^- \rightarrow \pi^+ \pi^-, \bar{p}p \rightarrow \pi^0 \pi^0 \pi^0, \pi^0 \eta \eta, \pi^0 \pi^0 \eta, \pi^+ \pi^- \pi^0, K^+ K^- \pi^0, K_S^0 K_S^0 \pi^0, K^+ K_S^0 \pi^-$  at rest,  $\bar{p}n \rightarrow \pi^- \pi^- \pi^+, K_S^0 K^- \pi^0, K_S^0 K_S^0 \pi^-$  at rest.
- 15 Supersedes BARBERIS 99 and BARBERIS 99b.
- 16 T-matrix pole on sheet  $--+$ .
- 17 T-matrix pole, supersedes ANISOVICH 94.
- 18 T-matrix pole, supersedes ANISOVICH 94 and AMSLER 92.
- 19 Supersedes ABATZIS 94, ARMSTRONG 89E. Breit-Wigner mass.
- 20 From a simultaneous analysis of the annihilations  $\bar{p}p \rightarrow 3\pi^0, \pi^0 \eta \eta$ .
- 21 Reanalysis of ANISOVICH 94 data.
- 22 From central value and spread of two solutions. Breit-Wigner mass.



$f_0(1500)$  WIDTH

VALUE (MeV)	EVTS	DOCUMENT ID	TECN	COMMENT
<b>112 ± 9 OUR AVERAGE</b>				
110 ± 24		1 BARBERIS 00A		450 $pp \rightarrow p_f \eta \eta p_S$
102 ± 18		1,2 BARBERIS 00C		450 $pp \rightarrow p_f 4\pi p_S$
110 ± 16		1 BARBERIS 00E		450 $pp \rightarrow p_f \eta \eta p_S$
108 ± 33		1 BERTIN 98 OBLX		0.05-0.405 $\bar{p}p \rightarrow \pi^+ \pi^+ \pi^-$
114 ± 30		1 BERTIN 97C OBLX		0.0 $\bar{p}p \rightarrow \pi^+ \pi^- \pi^0$
154 ± 30		3 AMSLER 95D CBAR		0.0 $\bar{p}p \rightarrow \pi^0 \pi^0 \pi^0, \pi^0 \eta \eta, \pi^0 \pi^0 \eta$
• • • We do not use the following data for averages, fits, limits, etc. • • •				
100 ± 18		4 ROPERTZ 18 RVUE		$\bar{B}_S^0 \rightarrow J/\psi(\pi^+ \pi^- / K^+ K^-)$
124 ± 7		5 AAIJ 14BR LHCB		$\bar{B}_S^0 \rightarrow J/\psi \pi^+ \pi^-$
136 ± 41 ± 28 26 ± 100	5.5k	6 ABLIKIM 13N BES3		$e^+ e^- \rightarrow J/\psi \rightarrow \gamma \eta \eta$
114 ± 10		1 ANISOVICH 09 RVUE		0.0 $\bar{p}p, \pi N$
90 ± 2 ± 50 1 ± 22		7 UEHARA 08A BELL		10.6 $e^+ e^- \rightarrow e^+ e^- \pi^0 \pi^0$
108 ± 14 ± 25 11 ± 25		8 ABLIKIM 06V BES2		$e^+ e^- \rightarrow J/\psi \rightarrow \gamma \pi^+ \pi^-$
121 ± 8		AMSLER 06 CBAR		0.9 $\bar{p}p \rightarrow K^+ K^- \pi^0$
257 ± 33	9.9k	AUBERT 06o BABR		$B^+ \rightarrow K^+ K^+ K^-$

$f_0(1500)$  DECAY MODES

Mode	Fraction ( $\Gamma_i/\Gamma$ )	Scale factor
$\Gamma_1$ $\pi \pi$	(34.5 ± 2.2) %	1.2
$\Gamma_2$ $\pi^+ \pi^-$	seen	
$\Gamma_3$ $2\pi^0$	seen	
$\Gamma_4$ $4\pi$	(48.9 ± 3.3) %	1.2
$\Gamma_5$ $4\pi^0$	seen	
$\Gamma_6$ $2\pi^+ 2\pi^-$	seen	
$\Gamma_7$ $2(\pi\pi)S$ -wave	seen	
$\Gamma_8$ $\rho\rho$	seen	
$\Gamma_9$ $\pi(1300)\pi$	seen	
$\Gamma_{10}$ $a_1(1260)\pi$	seen	
$\Gamma_{11}$ $\eta\eta$	( 6.0 ± 0.9) %	1.1
$\Gamma_{12}$ $\eta\eta'(958)$	( 2.2 ± 0.8) %	1.4
$\Gamma_{13}$ $K\bar{K}$	( 8.5 ± 1.0) %	1.1
$\Gamma_{14}$ $\gamma\gamma$	not seen	

Downloaded from https://academic.oup.com/ptep/article/2020/8/083C01/5891211 by guest on 12 November 2020

## Meson Particle Listings

 $f_0(1500)$ 

## CONSTRAINED FIT INFORMATION

An overall fit to 6 branching ratios uses 10 measurements and one constraint to determine 5 parameters. The overall fit has a  $\chi^2 = 5.6$  for 6 degrees of freedom.

The following *off-diagonal* array elements are the correlation coefficients  $\langle \delta x_i \delta x_j \rangle / (\delta x_i \delta x_j)$ , in percent, from the fit to the branching fractions,  $x_i \equiv \Gamma_i / \Gamma_{\text{total}}$ . The fit constrains the  $x_i$  whose labels appear in this array to sum to one.

$x_4$	-88				
$x_{11}$	27	-56			
$x_{12}$	3	-32	26		
$x_{13}$	43	-64	20	2	
	$x_1$	$x_4$	$x_{11}$	$x_{12}$	

 $f_0(1500) \Gamma(i) \Gamma(\gamma\gamma) / \Gamma(\text{total})$ 

$\Gamma(\pi\pi) \times \Gamma(\gamma\gamma) / \Gamma_{\text{total}}$	CL%	DOCUMENT ID	TECN	COMMENT	$\Gamma_{14} / \Gamma$
••• We do not use the following data for averages, fits, limits, etc. •••					
$33^{+12}_{-6} + 1809_{-21}$		<sup>1</sup> UEHARA	08A BELL	$10.6 e^+ e^- \rightarrow e^+ e^- \pi^0 \pi^0$	
not seen		ACCIARRI	01H L3	$\gamma\gamma \rightarrow K_S^0 K_S^0, E_{\text{cm}}^{\text{res}} = 91, 183-209 \text{ GeV}$	
<460	95	BARATE	00E ALEP	$\gamma\gamma \rightarrow \pi^+ \pi^-$	
<sup>1</sup> May also be the $f_0(1370)$ . Multiplied by us by 3 to obtain the $\pi\pi$ value.					

 $f_0(1500)$  BRANCHING RATIOS

$\Gamma(\pi\pi) / \Gamma_{\text{total}}$	$\Gamma_1 / \Gamma$
••• We do not use the following data for averages, fits, limits, etc. •••	
$0.454 \pm 0.104$	BUGG 96 RVUE

$\Gamma(\pi^+ \pi^-) / \Gamma_{\text{total}}$	$\Gamma_2 / \Gamma$
••• We do not use the following data for averages, fits, limits, etc. •••	
seen	BERTIN 98 OBLX 0.05-0.405 $\bar{p}p \rightarrow \pi^+ \pi^+ \pi^-$
possibly seen	FRABETTI 97D E687 $D_S^\pm \rightarrow \pi^\mp \pi^\pm \pi^\pm$

$\Gamma(4\pi) / \Gamma(\pi\pi)$	$\Gamma_4 / \Gamma_1$
••• We do not use the following data for averages, fits, limits, etc. •••	
$1.42 \pm 0.18$ OUR FIT	Error includes scale factor of 1.2.
$1.42 \pm 0.18$ OUR AVERAGE	Error includes scale factor of 1.2.
$1.37 \pm 0.16$	BARBERIS 00D 450 $pp \rightarrow p_f 4\pi p_S$
$2.1 \pm 0.6$	<sup>1</sup> AMSLER 98 RVUE
••• We do not use the following data for averages, fits, limits, etc. •••	
$2.1 \pm 0.2$	<sup>2</sup> ANISOVICH 02D SPEC Combined fit
$3.4 \pm 0.8$	<sup>1</sup> ABELE 96 CBAR $0.0 \bar{p}d \rightarrow 5\pi^0$
<sup>1</sup> Excluding $\rho\rho$ contribution to $4\pi$ .	
<sup>2</sup> From a combined K-matrix analysis of Crystal Barrel ( $0. \bar{p}p \rightarrow \pi^0 \pi^0 \pi^0, \pi^0 \eta \eta, \pi^0 \pi^0 \eta$ ), GAMS ( $\pi\rho \rightarrow \pi^0 \pi^0 n, \eta \eta n, \eta \eta' n$ ), and BNL ( $\pi\rho \rightarrow K\bar{K}n$ ) data.	

$\Gamma(2(\pi\pi)_{s\text{-wave}}) / \Gamma(\pi\pi)$	$\Gamma_7 / \Gamma_1$
••• We do not use the following data for averages, fits, limits, etc. •••	
$0.42 \pm 0.26$	<sup>1</sup> ABELE 01 CBAR $0.0 \bar{p}d \rightarrow \pi^- 4\pi^0 p$
<sup>1</sup> From the combined data of ABELE 96 and ABELE 96c.	

$\Gamma(2(\pi\pi)_{s\text{-wave}}) / \Gamma(4\pi)$	$\Gamma_7 / \Gamma_4$
••• We do not use the following data for averages, fits, limits, etc. •••	
$0.26 \pm 0.07$	ABELE 01B CBAR $0.0 \bar{p}d \rightarrow 5\pi p$

$\Gamma(\rho\rho) / \Gamma(4\pi)$	$\Gamma_8 / \Gamma_4$
••• We do not use the following data for averages, fits, limits, etc. •••	
$0.13 \pm 0.08$	ABELE 01B CBAR $0.0 \bar{p}d \rightarrow 5\pi p$

$\Gamma(\rho\rho) / \Gamma(2(\pi\pi)_{s\text{-wave}})$	$\Gamma_8 / \Gamma_7$
••• We do not use the following data for averages, fits, limits, etc. •••	
$2.87 \pm 0.34$ OUR AVERAGE	Error includes scale factor of 1.1.
$3.3 \pm 0.5$	BARBERIS 00C 450 $pp \rightarrow p_f \pi^+ \pi^- 2\pi^0 p_S$
$2.6 \pm 0.4$	BARBERIS 00C 450 $pp \rightarrow p_f 2(\pi^+ \pi^-) p_S$

$\Gamma(\pi(1300)\pi) / \Gamma(4\pi)$	$\Gamma_9 / \Gamma_4$
••• We do not use the following data for averages, fits, limits, etc. •••	
$0.50 \pm 0.25$	ABELE 01B CBAR $0.0 \bar{p}d \rightarrow 5\pi p$

$\Gamma(a_1(1260)\pi) / \Gamma(4\pi)$	$\Gamma_{10} / \Gamma_4$
••• We do not use the following data for averages, fits, limits, etc. •••	
$0.12 \pm 0.05$	ABELE 01B CBAR $0.0 \bar{p}d \rightarrow 5\pi p$

$\Gamma(\eta\eta) / \Gamma_{\text{total}}$	$\Gamma_{11} / \Gamma$
••• We do not use the following data for averages, fits, limits, etc. •••	
large	ALDE 88 GAM4 $300 \pi^- N \rightarrow \eta \eta \pi^- N$
large	BINON 83 GAM2 $38 \pi^- p \rightarrow 2\eta n$

$\Gamma(\eta\eta) / \Gamma(\pi\pi)$	$\Gamma_{11} / \Gamma_1$
••• We do not use the following data for averages, fits, limits, etc. •••	
$0.173 \pm 0.024$ OUR FIT	Error includes scale factor of 1.1.
$0.175 \pm 0.027$ OUR AVERAGE	
$0.18 \pm 0.03$	BARBERIS 00E 450 $pp \rightarrow p_f \eta \eta p_S$
$0.157 \pm 0.060$	<sup>1</sup> AMSLER 95D CBAR $0.0 \bar{p}p \rightarrow \pi^0 \pi^0 \pi^0, \pi^0 \eta \eta, \pi^0 \pi^0 \eta$
••• We do not use the following data for averages, fits, limits, etc. •••	
$0.080 \pm 0.033$	AMSLER 02 CBAR $0.9 \bar{p}p \rightarrow \pi^0 \eta \eta, \pi^0 \pi^0 \pi^0$
$0.11 \pm 0.03$	<sup>2</sup> ANISOVICH 02D SPEC Combined fit
$0.078 \pm 0.013$	<sup>3</sup> ABELE 96C RVUE Compilation
$0.230 \pm 0.097$	<sup>4</sup> AMSLER 95C CBAR $0.0 \bar{p}p \rightarrow \eta \eta \pi^0$
<sup>1</sup> Coupled-channel analysis of AMSLER 95B, AMSLER 95c, and AMSLER 94D.	
<sup>2</sup> From a combined K-matrix analysis of Crystal Barrel ( $0. \bar{p}p \rightarrow \pi^0 \pi^0 \pi^0, \pi^0 \eta \eta, \pi^0 \pi^0 \eta$ ), GAMS ( $\pi\rho \rightarrow \pi^0 \pi^0 n, \eta \eta n, \eta \eta' n$ ), and BNL ( $\pi\rho \rightarrow K\bar{K}n$ ) data.	
<sup>3</sup> $2\pi$ width determined to be $60 \pm 12 \text{ MeV}$ .	
<sup>4</sup> Using AMSLER 95B ( $3\pi^0$ ).	

$\Gamma(4\pi^0) / \Gamma(\eta\eta)$	$\Gamma_5 / \Gamma_{11}$
••• We do not use the following data for averages, fits, limits, etc. •••	
$0.8 \pm 0.3$	ALDE 87 GAM4 $100 \pi^- p \rightarrow 4\pi^0 n$

$\Gamma(\eta\eta(958)) / \Gamma(\pi\pi)$	$\Gamma_{12} / \Gamma_1$
••• We do not use the following data for averages, fits, limits, etc. •••	
$0.064 \pm 0.022$ OUR FIT	Error includes scale factor of 1.4.
$0.095 \pm 0.026$	BARBERIS 00A 450 $pp \rightarrow p_f \eta \eta p_S$
••• We do not use the following data for averages, fits, limits, etc. •••	
$0.005 \pm 0.003$	<sup>1</sup> ANISOVICH 02D SPEC Combined fit
<sup>1</sup> From a combined K-matrix analysis of Crystal Barrel ( $0. \bar{p}p \rightarrow \pi^0 \pi^0 \pi^0, \pi^0 \eta \eta, \pi^0 \pi^0 \eta$ ), GAMS ( $\pi\rho \rightarrow \pi^0 \pi^0 n, \eta \eta n, \eta \eta' n$ ), and BNL ( $\pi\rho \rightarrow K\bar{K}n$ ) data.	

$\Gamma(\eta\eta'(958)) / \Gamma(\eta\eta)$	$\Gamma_{12} / \Gamma_{11}$
••• We do not use the following data for averages, fits, limits, etc. •••	
$0.37 \pm 0.13$ OUR FIT	Error includes scale factor of 1.5.
$0.29 \pm 0.10$	<sup>1</sup> AMSLER 95C CBAR $0.0 \bar{p}p \rightarrow \eta \eta \pi^0$
••• We do not use the following data for averages, fits, limits, etc. •••	
$0.05 \pm 0.03$	<sup>2</sup> ANISOVICH 02D SPEC Combined fit
$0.84 \pm 0.23$	ABELE 96C RVUE Compilation
$2.7 \pm 0.8$	BINON 84C GAM2 $38 \pi^- p \rightarrow \eta \eta' n$
<sup>1</sup> Using AMSLER 94E ( $\eta \eta' \pi^0$ ).	
<sup>2</sup> From a combined K-matrix analysis of Crystal Barrel ( $0. \bar{p}p \rightarrow \pi^0 \pi^0 \pi^0, \pi^0 \eta \eta, \pi^0 \pi^0 \eta$ ), GAMS ( $\pi\rho \rightarrow \pi^0 \pi^0 n, \eta \eta n, \eta \eta' n$ ), and BNL ( $\pi\rho \rightarrow K\bar{K}n$ ) data.	

$\Gamma(K\bar{K}) / \Gamma_{\text{total}}$	$\Gamma_{13} / \Gamma$
••• We do not use the following data for averages, fits, limits, etc. •••	
$0.044 \pm 0.021$	BUGG 96 RVUE

$\Gamma(K\bar{K}) / \Gamma(\pi\pi)$	$\Gamma_{13} / \Gamma_1$
••• We do not use the following data for averages, fits, limits, etc. •••	
$0.246 \pm 0.025$ OUR FIT	
$0.236 \pm 0.026$ OUR AVERAGE	
$0.25 \pm 0.03$	<sup>1</sup> BARGIOTTI 03 OBLX $\bar{p}p$
$0.19 \pm 0.07$	<sup>2</sup> ABELE 98 CBAR $0.0 \bar{p}p \rightarrow K_L^0 K^\pm \pi^\mp$
$0.20 \pm 0.08$	<sup>3</sup> ABELE 96B CBAR $0.0 \bar{p}p \rightarrow \pi^0 K_L^0 K_L^0$
••• We do not use the following data for averages, fits, limits, etc. •••	
$0.16 \pm 0.05$	<sup>4</sup> ANISOVICH 02D SPEC Combined fit
$0.33 \pm 0.03 \pm 0.07$	BARBERIS 99D OMEG $450 pp \rightarrow K^+ K^-, \pi^+ \pi^-$
<sup>1</sup> Coupled channel analysis of $\pi^+ \pi^- \pi^0, K^+ K^- \pi^0$ , and $K^\pm K_S^0 \pi^\mp$ .	
<sup>2</sup> Using $\pi^0 \pi^0$ from AMSLER 95B.	
<sup>3</sup> Using AMSLER 95B ( $3\pi^0$ ), AMSLER 94C ( $2\pi^0 \eta$ ) and SU(3).	
<sup>4</sup> From a combined K-matrix analysis of Crystal Barrel ( $0. \bar{p}p \rightarrow \pi^0 \pi^0 \pi^0, \pi^0 \eta \eta, \pi^0 \pi^0 \eta$ ), GAMS ( $\pi\rho \rightarrow \pi^0 \pi^0 n, \eta \eta n, \eta \eta' n$ ), and BNL ( $\pi\rho \rightarrow K\bar{K}n$ ) data.	

$\Gamma(K\bar{K}) / \Gamma(\eta\eta)$	$\Gamma_{13} / \Gamma_{11}$
••• We do not use the following data for averages, fits, limits, etc. •••	
$1.43 \pm 0.24$ OUR FIT	Error includes scale factor of 1.1.
$1.85 \pm 0.41$	BARBERIS 00E 450 $pp \rightarrow p_f \eta \eta p_S$
••• We do not use the following data for averages, fits, limits, etc. •••	
$1.5 \pm 0.6$	<sup>1</sup> ANISOVICH 02D SPEC Combined fit
<0.4	<sup>2</sup> PROKOSHIN 91 GAM4 $300 \pi^- p \rightarrow \pi^- \rho \eta \eta$

See key on page 999

# Meson Particle Listings

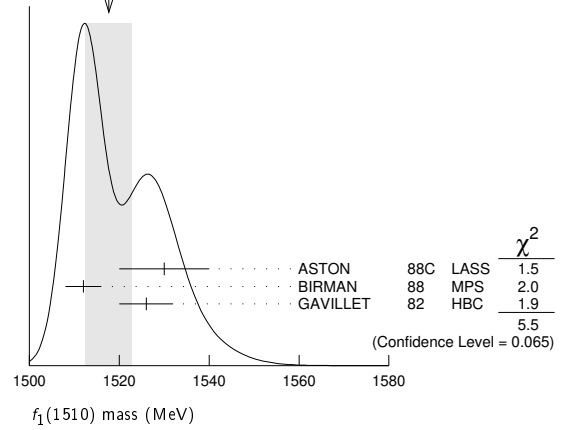
## $f_0(1500)$ , $f_1(1510)$

<0.6 <sup>3</sup> BINON 83 GAM2 38  $\pi^- p \rightarrow 2\eta n$   
<sup>1</sup> From a combined K-matrix analysis of Crystal Barrel ( $0. p\bar{p} \rightarrow \pi^0 \pi^0 \pi^0, \pi^0 \eta \eta, \pi^0 \pi^0 \eta$ ), GAMS ( $\pi p \rightarrow \pi^0 \pi^0 n, \eta \eta n, \eta \eta' n$ ), and BNL ( $\pi p \rightarrow K \bar{K} n$ ) data.  
<sup>2</sup> Combining results of GAM4 with those of WA76 on  $K \bar{K}$  central production.  
<sup>3</sup> Using ETKIN 82b and COHEN 80.

### $f_0(1500)$ REFERENCES

ROPERTZ 18	EPJ C78 1000	S. Ropertz, C. Hanhart, B. Kubis	(BONN, JULI)
AAJ 17V	JHEP 1708 037	R. Aaij <i>et al.</i>	(LHCb Collab.)
DOBBS 15	PR D91 052006	S. Dobbs <i>et al.</i>	(NWES)
AAJ 14BR	PR D89 092006	R. Aaij <i>et al.</i>	(LHCb Collab.)
ABLIKIM 13N	PR D87 092009	Ablikim M. <i>et al.</i>	(BESIII Collab.)
ANISOVICH 09	IJMP A24 2481	V.V. Anisovich, A.V. Sarantsev	(BONN+)
KLEMPF 08	EPJ C35 39	E. Klempf, M. Matveev, A.V. Sarantsev	(BELLE Collab.)
UEHARA 08A	PR D78 092004	S. Uehara <i>et al.</i>	(BES Collab.)
ABLIKIM 06V	PL B642 441	M. Ablikim <i>et al.</i>	(CBAR Collab.)
AMSLER 06P	PL B639 165	C. Amstler <i>et al.</i>	(BABAR Collab.)
AUBERT 06O	PR D74 032003	B. Aubert <i>et al.</i>	(FNAL E835)
UMAN 06	PR D73 052009	I. Uman <i>et al.</i>	(ITEP, Moscow)
VLADIMIRSK... 06	PAN 69 493	V.V. Vladimirovsky <i>et al.</i>	(ITEP, Moscow)
Translated from YAF 69 515.			
BINON 05	PAN 68 960	F. Binon <i>et al.</i>	(Crystal Barrel Collab.)
Translated from YAF 68 938.			
GARMASH 05	PR D71 092003	A. Garmash <i>et al.</i>	(BELLE Collab.)
ANISOVICH 03	EPJ A16 229	V.V. Anisovich <i>et al.</i>	(OBELIX Collab.)
BARGIOTTI 03	EPJ C26 371	M. Bargiotti <i>et al.</i>	(OBELIX Collab.)
AMSLER 02	EPJ C23 29	C. Amstler <i>et al.</i>	(OBELIX Collab.)
ANISOVICH 02D	PAN 65 1545	V.V. Anisovich <i>et al.</i>	(OBELIX Collab.)
Translated from YAF 65 1583.			
ABELE 01	EPJ C19 667	A. Abele <i>et al.</i>	(Crystal Barrel Collab.)
ABELE 01B	EPJ C21 261	A. Abele <i>et al.</i>	(Crystal Barrel Collab.)
ACCIARRI 01H	PL B501 173	M. Acciari <i>et al.</i>	(L3 Collab.)
AITALA 01A	PRL 86 765	E.M. Aitala <i>et al.</i>	(FNAL E791 Collab.)
BARATE 00E	PL B472 189	R. Barate <i>et al.</i>	(ALEPH Collab.)
BARBERIS 00A	PL B471 429	D. Barberis <i>et al.</i>	(WA 102 Collab.)
BARBERIS 00C	PL B471 440	D. Barberis <i>et al.</i>	(WA 102 Collab.)
BARBERIS 00D	PL B474 423	D. Barberis <i>et al.</i>	(WA 102 Collab.)
BARBERIS 00E	PL B479 59	D. Barberis <i>et al.</i>	(WA 102 Collab.)
BARBERIS 99	PL B453 305	D. Barberis <i>et al.</i>	(Omega Expt.)
BARBERIS 99B	PL B453 316	D. Barberis <i>et al.</i>	(Omega Expt.)
BARBERIS 99D	PL B462 462	D. Barberis <i>et al.</i>	(Omega Expt.)
BELLAZZINI 99	PL B467 296	R. Bellazzini <i>et al.</i>	(Omega Expt.)
FRENCH 99	PL B460 213	B. French <i>et al.</i>	(WA76 Collab.)
KAMINSKI 99	EPJ C9 141	R. Kaminski, L. Lesniak, B. Loiseau	(CRAC, PARIN)
ABELE 98	PR D57 3860	A. Abele <i>et al.</i>	(Crystal Barrel Collab.)
ALDE 98	EPJ A3 361	D. Alde <i>et al.</i>	(GAM4 Collab.)
Also	PAN 62 405	D. Alde <i>et al.</i>	(GAMS Collab.)
Translated from YAF 62 446.			
AMSLER 98	RMP 70 1293	C. Amstler	(GAMS Collab.)
ANISOVICH 98B	SPU 41 419	V.V. Anisovich <i>et al.</i>	(GAMS Collab.)
Translated from UFN 168 481.			
BERTIN 98	PR D57 55	A. Bertin <i>et al.</i>	(OBELIX Collab.)
REYES 98	PRL 81 4079	M.A. Reyes <i>et al.</i>	(OBELIX Collab.)
BARBERIS 97B	PL B413 217	D. Barberis <i>et al.</i>	(WA 102 Collab.)
BERTIN 97C	PL B408 476	A. Bertin <i>et al.</i>	(OBELIX Collab.)
FRABETTI 97D	PL B407 79	P.L. Frabetti <i>et al.</i>	(FNAL E687 Collab.)
ABELE 96	PL B380 453	A. Abele <i>et al.</i>	(Crystal Barrel Collab.)
ABELE 96B	PL B385 425	A. Abele <i>et al.</i>	(Crystal Barrel Collab.)
ABELE 96C	NP A609 562	A. Abele <i>et al.</i>	(Crystal Barrel Collab.)
AMELIN 96B	PAN 59 976	D.V. Amelin <i>et al.</i>	(SERP, TBIL)
Translated from YAF 59 1021.			
BUGG 96	NP B471 59	D.V. Bugg, A.V. Sarantsev, B.S. Zou	(LOQM, PNPI)
AMSLER 95B	PL B342 433	C. Amstler <i>et al.</i>	(Crystal Barrel Collab.)
AMSLER 95C	PL B353 571	C. Amstler <i>et al.</i>	(Crystal Barrel Collab.)
AMSLER 95D	PL B355 425	C. Amstler <i>et al.</i>	(Crystal Barrel Collab.)
ANTINORI 95	PL B353 589	F. Antinori <i>et al.</i>	(ATHU, BARI, BIRM+)
BUGG 95	PL B353 378	D.V. Bugg <i>et al.</i>	(LOQM, PNPI, WASH)
ABATZIS 94	PL B324 509	S. Abatzis <i>et al.</i>	(ATHU, BARI, BIRM+)
AMSLER 94C	PL B327 425	C. Amstler <i>et al.</i>	(Crystal Barrel Collab.)
AMSLER 94D	PL B333 277	C. Amstler <i>et al.</i>	(Crystal Barrel Collab.)
AMSLER 94E	PL B340 259	C. Amstler <i>et al.</i>	(Crystal Barrel Collab.)
ANISOVICH 94	PL B323 233	V.V. Anisovich <i>et al.</i>	(Crystal Barrel Collab.)
BUGG 94	PR D50 4412	D.V. Bugg <i>et al.</i>	(LOQM)
AMSLER 92	PL B291 347	C. Amstler <i>et al.</i>	(Crystal Barrel Collab.)
BELADIDZE 92C	SJNP 55 1535	G.M. Beladidze, S.I. Bityukov, G.V. Borisov	(SERP+)
Translated from YAF 55 2748.			
PROKOSHKIN 91	SPD 36 155	Y.D. Prokoshkin	(GAM2 and GAM4 Collab.)
Translated from DANS 316 900.			
ARMSTRONG 89E	PL B228 536	T.A. Armstrong, M. Benayoun	(ATHU, BARI, BIRM+)
ALDE 88	PL B201 160	D.M. Alde <i>et al.</i>	(SERP, BELG, LANL, LAPP+)
ASTON 88D	NP B301 525	D. Aston <i>et al.</i>	(SLAC, NAGO, CIN, INUS)
ALDE 87	PL B198 286	D.M. Alde <i>et al.</i>	(LANL, BRUX, SERP, LAPP)
ALDE 86D	NP B269 485	D.M. Alde <i>et al.</i>	(BELG, LAPP, SERP, CERN+)
BINON 84C	NC 80A 363	F.G. Binon <i>et al.</i>	(BELG, LAPP, SERP+)
BINON 83	NC 78A 313	F.G. Binon <i>et al.</i>	(BELG, LAPP, SERP+)
Also	SJNP 38 561	F.G. Binon <i>et al.</i>	(BELG, LAPP, SERP+)
Translated from YAF 38 934.			
GRAY 83	PR D27 307	L. Gray <i>et al.</i>	(SYRA)
ETKIN 82B	PR D25 1786	A. Etkin <i>et al.</i>	(BNL, CUNY, TUFTS, VAND)
COHEN 80	PR D22 2595	D. Cohen <i>et al.</i>	(ANL)

WEIGHTED AVERAGE  
1518±5 (Error scaled by 1.7)

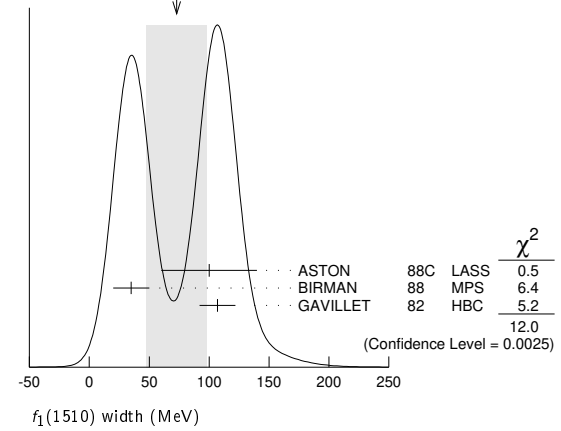


### $f_1(1510)$ WIDTH

VALUE (MeV)	EVTS	DOCUMENT ID	TECN	COMMENT
<b>73±25 OUR AVERAGE</b>	Error	includes scale factor of 2.5. See the ideogram below.		
100±40	600	ASTON	88C LASS	11 $K^- p \rightarrow K_S^0 K^\pm \pi^\mp \Lambda$
35±15	271	BIRMAN	88 MPS	8 $\pi^- p \rightarrow K^+ \bar{K}^0 \pi^- n$
107±15	271	GAVILLET	82 HBC	4.2 $K^- p \rightarrow \Lambda K K \pi$

<sup>3</sup> From partial wave analysis of  $K^+ \bar{K}^0 \pi^-$  state.

WEIGHTED AVERAGE  
73±25 (Error scaled by 2.5)



### $f_1(1510)$ DECAY MODES

Mode	Fraction ( $\Gamma_i/\Gamma$ )
$\Gamma_1$ $K \bar{K}^*(892) + c.c.$	seen
$\Gamma_2$ $\pi^+ \pi^- \eta'$	seen

### $f_1(1510)$ BRANCHING RATIOS

$\Gamma(\pi^+ \pi^- \eta')/\Gamma_{total}$	$\Gamma_2/\Gamma$
seen	230
	ABL IKIM 11C BES3 $J/\psi \rightarrow \gamma \pi^+ \pi^- \eta'$

### $f_1(1510)$ REFERENCES

ABLIKIM 11C	PRL 106 072002	M. Ablikim <i>et al.</i>	(BESIII Collab.)
BAUER 93B	PR D48 3976	D.A. Bauer <i>et al.</i>	(SLAC)
AIHARA 88C	PR D38 1	H. Aihara <i>et al.</i>	(TPC-2 $\gamma$ Collab.)
ASTON 88C	PL B201 573	D. Aston <i>et al.</i>	(SLAC, NAGO, CIN, INUS) JIP
BIRMAN 88P	PRL 61 1557	A. Birman <i>et al.</i>	(BNL, FSU, IND, MASD) JIP
GAVILLET 82	ZPHY C16 119	P. Gavillet <i>et al.</i>	(CERN, CDEF, PADO+)

### $f_1(1510)$

$$J^G(J^{PC}) = 0^+(1^{++})$$

OMITTED FROM SUMMARY TABLE  
See the minireview under  $\eta(1405)$ .

### $f_1(1510)$ MASS

VALUE (MeV)	EVTS	DOCUMENT ID	TECN	COMMENT
<b>1518±5 OUR AVERAGE</b>	Error	includes scale factor of 1.7. See the ideogram below.		
1530±10		ASTON	88C LASS	11 $K^- p \rightarrow K_S^0 K^\pm \pi^\mp \Lambda$
1512±4	600	BIRMAN	88 MPS	8 $\pi^- p \rightarrow K^+ \bar{K}^0 \pi^- n$
1526±6	271	GAVILLET	82 HBC	4.2 $K^- p \rightarrow \Lambda K K \pi$
••• We do not use the following data for averages, fits, limits, etc. •••				
~1525		BAUER	93B	$\gamma \gamma^* \rightarrow \pi^+ \pi^- \pi^0 \pi^0$

<sup>1</sup> From partial wave analysis of  $K^+ \bar{K}^0 \pi^-$  state.

<sup>2</sup> Not seen by AIHARA 88C in the  $K_S^0 K^\pm \pi^\mp$  final state.

# Meson Particle Listings

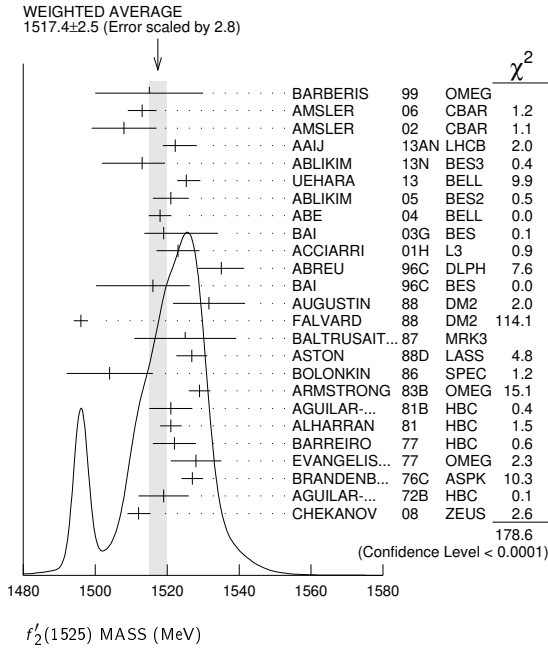
## $f_2'(1525)$

$f_2'(1525)$

$$J^G(J^{PC}) = 0^+(2^{++})$$

### $f_2'(1525)$ MASS

**1517.4 ± 2.5 OUR AVERAGE** Includes data from the 6 datablocks that follow this one. Error includes scale factor of 2.8. See the ideogram below.



### PRODUCED BY PION BEAM

The data in this block is included in the average printed for a previous datablock.

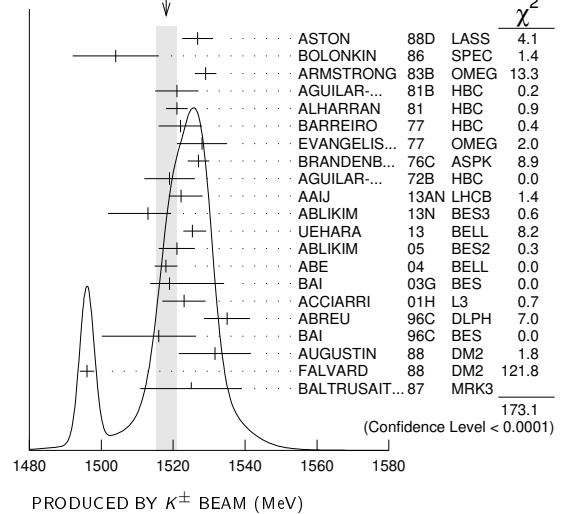
- • • We do not use the following data for averages, fits, limits, etc. • • •
- 1521 ± 13 TIKHOMIROV 03 SPEC 40.0  $\pi^- C \rightarrow K_S^0 K_S^0 K_L^0 X$
- 1547<sup>+10</sup>/<sub>-2</sub> 1 LONGACRE 86 MPS 22  $\pi^- p \rightarrow K_S^0 K_S^0 n$
- 1496<sup>+9</sup>/<sub>-8</sub> 2 CHABAUD 81 ASPK 6  $\pi^- p \rightarrow K^+ K^- n$
- 1497<sup>+8</sup>/<sub>-9</sub> CHABAUD 81 ASPK 18.4  $\pi^- p \rightarrow K^+ K^- n$
- 1492 ± 29 GORLICH 80 ASPK 17  $\pi^- p$  polarized  $\rightarrow K^+ K^- n$
- 1502 ± 25 3 CORDEN 79 OMEG 12-15  $\pi^- p \rightarrow \pi^+ \pi^- n$
- 1480 14 CRENNELL 66 HBC 6.0  $\pi^- p \rightarrow K_S^0 K_S^0 n$

### PRODUCED BY $K^\pm$ BEAM

The data in this block is included in the average printed for a previous datablock.

- 1518.1 ± 2.8 OUR AVERAGE** Includes data from the datablock that follows this one. Error includes scale factor of 3.0. See the ideogram below.
- |              |              |     |      |          |   |
|--------------|--------------|-----|------|----------|---|
| 1526.8 ± 4.3 | ASTON        | 88D | LASS | 11       | $K^- p \rightarrow K_S^0 K_S^0 \Lambda$         |
| 1504 ± 12    | BOLONKIN     | 86  | SPEC | 40       | $K^- p \rightarrow K_S^0 K_S^0 \Upsilon$        |
| 1529 ± 3     | ARMSTRONG    | 83B | OMEG | 18.5     | $K^- p \rightarrow K^- K^+ \Lambda$             |
| 1521 ± 6     | AGUILAR...   | 81B | HBC  | 4.2      | $K^- p \rightarrow \Lambda K^+ K^-$             |
| 1521 ± 3     | ALHARRAN     | 81  | HBC  | 8.25     | $K^- p \rightarrow \Lambda K \bar{K}$           |
| 1522 ± 6     | BARREIRO     | 77  | HBC  | 4.15     | $K^- p \rightarrow \Lambda K_S^0 K_S^0$         |
| 1528 ± 7     | EVANGELIS... | 77  | OMEG | 10       | $K^- p \rightarrow K^+ K^- (\Lambda, \Sigma)$   |
| 1527 ± 3     | BRANDENB...  | 76C | ASPK | 13       | $K^- p \rightarrow K^+ K^- (\Lambda, \Sigma)$   |
| 1519 ± 7     | AGUILAR...   | 72B | HBC  | 3.9, 4.6 | $K^- p \rightarrow K \bar{K} (\Lambda, \Sigma)$ |
- • • We do not use the following data for averages, fits, limits, etc. • • •
  - 1514 ± 8 61 BINON 07 GAMS 32.5  $K^- p \rightarrow \eta \eta (\Lambda / \Sigma^0)$
  - 1513 ± 10 4 BARKOV 99 SPEC 40  $K^- p \rightarrow K_S^0 K_S^0 \Upsilon$

WEIGHTED AVERAGE  
1518.1 ± 2.8 (Error scaled by 3.0)

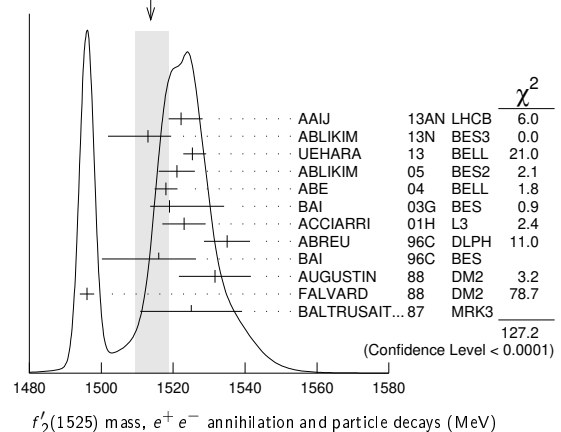


### PRODUCED IN $e^+ e^-$ ANNIHILATION AND PARTICLE DECAYS

The data in this block is included in the average printed for a previous datablock.

- 1514 ± 5 / 4 OUR AVERAGE** Error includes scale factor of 3.8. See the ideogram below.
- |  |               |            |  |
|--|---------------|------------|--|
| 1522.2 ± 2.8 <sup>+5.3</sup> / <sub>-2.0</sub> | AAIJ          | 13AN LHCB  | $\bar{B}_S^0 \rightarrow J/\psi K^+ K^-$                           |
| 1513 ± 5 <sup>+4</sup> / <sub>-10</sub>        | 5.5k          | 5 ABLIKIM  | 13N BES3 $e^+ e^- \rightarrow J/\psi \rightarrow \gamma \eta \eta$ |
| 1525.3 ± 1.2 <sup>+3.7</sup> / <sub>-1.4</sub> | UEHARA        | 13 BELL    | $\gamma \gamma \rightarrow K_S^0 K_S^0$                            |
| 1521 ± 5                                       | ABLIKIM       | 05 BES2    | $J/\psi \rightarrow \phi K^+ K^-$                                  |
| 1518 ± 1 ± 3                                   | ABE           | 04 BELL    | 10.6 $e^+ e^- \rightarrow e^+ e^- K^+ K^-$                         |
| 1519 ± 2 ± 15 <sup>+15</sup> / <sub>-5</sub>   | BAI           | 03G BES    | $J/\psi \rightarrow \gamma K \bar{K}$                              |
| 1523 ± 6                                       | 331           | 6 ACCIARRI | 01H L3 91, 183-209 $e^+ e^- \rightarrow e^+ e^- K_S^0 K_S^0$       |
| 1535 ± 5 ± 4                                   | ABREU         | 96C DLPH   | $Z^0 \rightarrow K^+ K^- + X$                                      |
| 1516 ± 5 ± 15 <sup>+9</sup> / <sub>-15</sub>   | BAI           | 96C BES    | $J/\psi \rightarrow \gamma K^+ K^-$                                |
| 1531.6 ± 10.0                                  | AUGUSTIN      | 88 DM2     | $J/\psi \rightarrow \gamma K^+ K^-$                                |
| 1496 ± 2                                       | 7 FALVARD     | 88 DM2     | $J/\psi \rightarrow \phi K^+ K^-$                                  |
| 1525 ± 10 ± 10                                 | BALTRUSAIT... | 87 MRK3    | $J/\psi \rightarrow \gamma K^+ K^-$                                |
- • • We do not use the following data for averages, fits, limits, etc. • • •
  - 1532 ± 3 ± 6 644 8,9 DOBBS 15  $J/\psi \rightarrow \gamma K^+ K^-$
  - 1557 ± 9 ± 3 113 8,9 DOBBS 15  $\psi(2S) \rightarrow \gamma K^+ K^-$
  - 1526 ± 7 29 10 LEES 14H BABR  $e^+ e^- \rightarrow K_S^0 K_S^0 K^+ K^- \gamma$
  - 1523 ± 5 870 11 SCHEGELSKY 06A RVUE  $\gamma \gamma \rightarrow K_S^0 K_S^0$
  - 1515 ± 5 12 FALVARD 88 DM2  $J/\psi \rightarrow \phi K^+ K^-$

WEIGHTED AVERAGE  
1514 ± 5.4 (Error scaled by 3.8)



**PRODUCED IN  $\bar{p}p$  ANNIHILATION**

VALUE (MeV)	DOCUMENT ID	TECN	COMMENT
-------------	-------------	------	---------

The data in this block is included in the average printed for a previous datablock.

**1512 ± 4 OUR AVERAGE**

1513 ± 4	AMSLER 06	CBAR	0.9 $\bar{p}p \rightarrow K^+ K^- \pi^0$
1508 ± 9	13 AMSLER 02	CBAR	0.9 $\bar{p}p \rightarrow \pi^0 \eta \eta, \pi^0 \pi^0 \pi^0$
• • •	We do not use the following data for averages, fits, limits, etc. • • •		
1530 ± 12	14 ANISOVICH 09	RVUE	0.0 $\bar{p}p, \pi N$

**CENTRAL PRODUCTION**

VALUE (MeV)	DOCUMENT ID	TECN	COMMENT
-------------	-------------	------	---------

The data in this block is included in the average printed for a previous datablock.

**1515 ± 15**

BARBERIS 99	OMEG	450 $pp \rightarrow p_S p_f K^+ K^-$
-------------	------	--------------------------------------

**PRODUCED IN  $e p$  COLLISIONS**

VALUE (MeV)	EVTS	DOCUMENT ID	TECN	COMMENT
-------------	------	-------------	------	---------

The data in this block is included in the average printed for a previous datablock.

**1512 ± 3<sup>+1.4</sup><sub>-0.5</sub>**

15	CHEKANOV 08	ZEUS	$e p \rightarrow K_S^0 K_S^0 X$
----	-------------	------	---------------------------------

• • • We do not use the following data for averages, fits, limits, etc. • • •

1537 <sup>+9</sup> <sub>-8</sub>	84	16 CHEKANOV 04	ZEUS $e p \rightarrow K_S^0 K_S^0 X$
----------------------------------	----	----------------	--------------------------------------

- From a partial-wave analysis of data using a K-matrix formalism with 5 poles.
- CHABAUD 81 is a reanalysis of PAWLICKI 77 data.
- From an amplitude analysis where the  $f_2'(1525)$  width and elasticity are in complete disagreement with the values obtained from  $K\bar{K}$  channel, making the solution dubious.
- Systematic errors not estimated.
- From partial wave analysis including all possible combinations of  $0^{++}, 2^{++}$ , and  $4^{++}$  resonances.
- Supersedes ACCIARRI 95j.
- From an analysis including interference with  $f_0(1710)$ .
- Using CLEO-c data but not authored by the CLEO Collaboration.
- From a fit to a Breit-Wigner line shape with fixed  $\Gamma = 73$  MeV.
- From a fit to a Breit-Wigner line shape plus a second-order polynomial function. Systematic errors not evaluated.
- From analysis of L3 data at 91 and 183–209 GeV.
- From an analysis ignoring interference with  $f_0(1710)$ .
- T-matrix pole.
- 4-poles, 5-channel K matrix fit.
- In the SU(3) based model with a specific interference pattern of the  $f_2(1270), a_2^0(1320)$ , and  $f_2'(1525)$  mesons incoherently added to the  $f_0(1710)$  and non-resonant background.
- Systematic errors not estimated.

**$f_2'(1525)$  WIDTH**

VALUE (MeV)	DOCUMENT ID	COMMENT
<b>86 ± 5 OUR FIT</b>		Error includes scale factor of 2.2.
<b>86.9 ± 2.3<sub>-2.1</sub></b>	PDG 18	Average of width measurements

**PRODUCED BY PION BEAM**

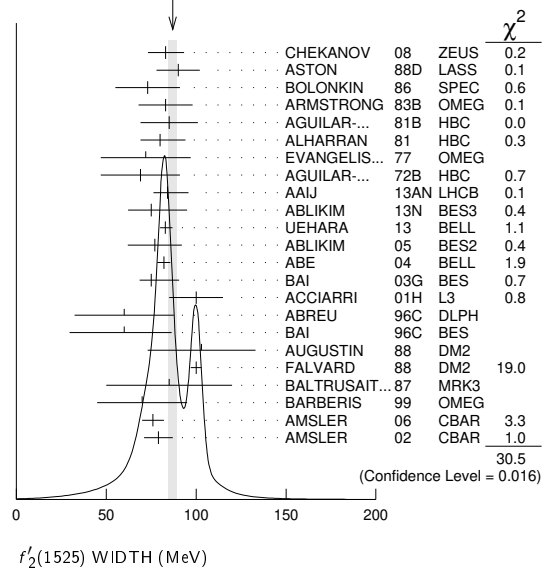
VALUE (MeV)	DOCUMENT ID	TECN	COMMENT
-------------	-------------	------	---------

**86.9 ± 2.3<sub>-2.1</sub> OUR AVERAGE** Includes data from the 5 datablocks that follow this one. Error includes scale factor of 1.4. See the ideogram below.

• • • We do not use the following data for averages, fits, limits, etc. • • •

102 ± 4.2	TIKHOMIROV 03	SPEC	40.0 $\pi^- C \rightarrow K_S^0 K_S^0 K_L^0 X$
108 ± 5 <sub>-2</sub>	17 LONGACRE 86	MPS	22 $\pi^- p \rightarrow K_S^0 K_S^0 n$
69 ± 22 <sub>-16</sub>	18 CHABAUD 81	ASPK	6 $\pi^- p \rightarrow K^+ K^- n$
137 ± 23 <sub>-21</sub>	CHABAUD 81	ASPK	18.4 $\pi^- p \rightarrow K^+ K^- n$
150 ± 83 <sub>-50</sub>	GORLICH 80	ASPK	17 $\pi^- p$ polarized $\rightarrow K^+ K^- n$
165 ± 4.2	19 CORDEN 79	OMEG	12–15 $\pi^- p \rightarrow \pi^+ \pi^- n$
92 ± 39 <sub>-22</sub>	20 POLYCHRO... 79	STRC	7 $\pi^- p \rightarrow n K_S^0 K_S^0$

WEIGHTED AVERAGE  
86.9±2.3-2.1 (Error scaled by 1.4)



**PRODUCED BY  $K^\pm$  BEAM**

VALUE (MeV)	EVTS	DOCUMENT ID	TECN	COMMENT
-------------	------	-------------	------	---------

The data in this block is included in the average printed for a previous datablock.

**82 ± 6 OUR AVERAGE**

90 ± 12	ASTON 88D	LASS	11 $K^- p \rightarrow K_S^0 K_S^0 \Lambda$
73 ± 18	BOLONKIN 86	SPEC	40 $K^- p \rightarrow K_S^0 K_S^0 Y$
83 ± 15	ARMSTRONG 83B	OMEG	18.5 $K^- p \rightarrow K^- K^+ \Lambda$
85 ± 16	650 AGUILAR... 81B	HBC	4.2 $K^- p \rightarrow \Lambda K^+ K^-$
80 ± 14 <sub>-11</sub>	572 ALHARRAN 81	HBC	8.25 $K^- p \rightarrow \Lambda K\bar{K}$
72 ± 25	166 EVANGELIS... 77	OMEG	10 $K^- p \rightarrow K^+ K^- (\Lambda, \Sigma)$
69 ± 22	100 AGUILAR... 72B	HBC	3.9, 4.6 $K^- p \rightarrow K\bar{K} (\Lambda, \Sigma)$
• • •	We do not use the following data for averages, fits, limits, etc. • • •		
92 ± 25 <sub>-16</sub>	61 BINON 07	GAMS	32.5 $K^- p \rightarrow \eta \eta (\Lambda / \Sigma^0)$
75 ± 20	21 BARKOV 99	SPEC	40 $K^- p \rightarrow K_S^0 K_S^0 y$
62 ± 19 <sub>-14</sub>	123 BARREIRO 77	HBC	4.15 $K^- p \rightarrow \Lambda K_S^0 K_S^0$
61 ± 8	120 BRANDENB... 76C	ASPK	13 $K^- p \rightarrow K^+ K^- (\Lambda, \Sigma)$

**PRODUCED IN  $e^+ e^-$  ANNIHILATION AND PARTICLE DECAYS**

VALUE (MeV)	EVTS	DOCUMENT ID	TECN	COMMENT
-------------	------	-------------	------	---------

The data in this block is included in the average printed for a previous datablock.

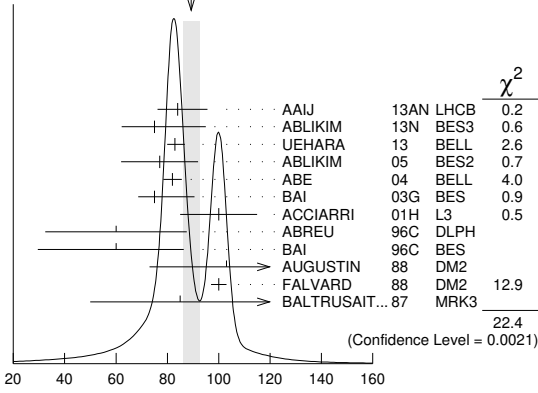
**89.2 ± 3.4<sub>-3.0</sub> OUR AVERAGE** Error includes scale factor of 1.8. See the ideogram below.

84 ± 6 <sub>-5</sub>	AAIJ 13AN	LHCB	$\bar{B}_S^0 \rightarrow J/\psi K^+ K^-$
75 ± 12 <sub>-10</sub> ± 16 <sub>-8</sub>	5.5k 22	ABLIKIM 13N	BES3 $e^+ e^- \rightarrow J/\psi \rightarrow \gamma \eta \eta$
82.9 ± 2.1 <sub>-2.2</sub> ± 3.3 <sub>-2.0</sub>	UEHARA 13	BELL	$\gamma \gamma \rightarrow K_S^0 K_S^0$
77 ± 15	ABLIKIM 05	BES2	$J/\psi \rightarrow \phi K^+ K^-$
82 ± 2 ± 3	ABE 04	BELL	10.6 $e^+ e^- \rightarrow e^+ e^- K^+ K^-$
75 ± 4 ± 15 <sub>-5</sub>	BAI 03G	BES	$J/\psi \rightarrow \gamma K\bar{K}$
100 ± 15	331 23	ACCIARRI 01H	L3 91, 183–209 $e^+ e^- \rightarrow e^+ e^- K_S^0 K_S^0$
60 ± 20 ± 19	ABREU 96C	DLPH	$Z^0 \rightarrow K^+ K^- + X$
60 ± 23 ± 13 <sub>-20</sub>	BAI 96C	BES	$J/\psi \rightarrow \gamma K^+ K^-$
103 ± 30	AUGUSTIN 88	DM2	$J/\psi \rightarrow \gamma K^+ K^-$
100 ± 3	24 FALVARD 88	DM2	$J/\psi \rightarrow \phi K^+ K^-$
85 ± 35	BALTRUSAIT... 87	MRK3	$J/\psi \rightarrow \gamma K^+ K^-$
• • •	We do not use the following data for averages, fits, limits, etc. • • •		
37 ± 12	29	25 LEES 14H	BABR $e^+ e^- \rightarrow K_S^0 K_S^0 K^+ K^- \gamma$
104 ± 10	870	26 SCHEGELSKY 06A	RVUE $\gamma \gamma \rightarrow K_S^0 K_S^0$
62 ± 10	27 FALVARD 88	DM2	$J/\psi \rightarrow \phi K^+ K^-$

# Meson Particle Listings

## $f'_2(1525)$

WEIGHTED AVERAGE  
89.2±3.4-3.0 (Error scaled by 1.8)



$f'_2(1525)$  width,  $e^+e^-$  annihilation and particle decays (MeV)

### PRODUCED IN $\bar{p}p$ ANNIHILATION

VALUE (MeV)	DOCUMENT ID	TECN	COMMENT
<b>77 ± 5 OUR AVERAGE</b>			
76 ± 6	AMSLER 06 CBAR	0.9 $\bar{p}p \rightarrow K^+ K^- \pi^0$	
79 ± 8	28 AMSLER 02 CBAR	0.9 $\bar{p}p \rightarrow \pi^0 \eta \eta, \pi^0 \pi^0 \pi^0$	
128 ± 20	29 ANISOVICH 09 RVUE	0.0 $\bar{p}p, \pi N$	

• • • We do not use the following data for averages, fits, limits, etc. • • •

### CENTRAL PRODUCTION

VALUE (MeV)	DOCUMENT ID	TECN	COMMENT
<b>70 ± 25</b>	BARBERIS 99 OMEG	450 $pp \rightarrow p_S p_f K^+ K^-$	

### PRODUCED IN $e p$ COLLISIONS

VALUE (MeV)	EVTS	DOCUMENT ID	TECN	COMMENT
-------------	------	-------------	------	---------

The data in this block is included in the average printed for a previous datablock.

<b>83 ± 9<sup>+5</sup><sub>-4</sub></b>	30 CHEKANOV 08 ZEUS	$e p \rightarrow K_S^0 K_S^0 X$	
---	---------------------	---------------------------------	--

- • • We do not use the following data for averages, fits, limits, etc. • • •
- 50 ± 34<sub>-22</sub> 84 31 CHEKANOV 04 ZEUS  $e p \rightarrow K_S^0 K_S^0 X$
- 17 From a partial-wave analysis of data using a K-matrix formalism with 5 poles.
- 18 CHABAUD 81 is a reanalysis of PAWLICKI 77 data.
- 19 From an amplitude analysis where the  $f'_2(1525)$  width and elasticity are in complete disagreement with the values obtained from  $K\bar{K}$  channel, making the solution dubious.
- 20 From a fit to the  $D$  with  $f_2(1270)$ - $f'_2(1525)$  interference. Mass fixed at 1516 MeV.
- 21 Systematic errors not estimated.
- 22 From partial wave analysis including all possible combinations of  $0^{++}$ ,  $2^{++}$ , and  $4^{++}$  resonances.
- 23 Supersedes ACCIARRI 95J.
- 24 From an analysis including interference with  $f_0(1710)$ .
- 25 From a fit to a Breit-Wigner line shape plus a second-order polynomial function. Systematic errors not evaluated.
- 26 From analysis of L3 data at 91 and 183–209 GeV.
- 27 From an analysis ignoring interference with  $f_0(1710)$ .
- 28 T-matrix pole.
- 29 4-poles, 5-channel K matrix fit.
- 30 In the SU(3) based model with a specific interference pattern of the  $f_2(1270)$ ,  $a_2^0(1320)$ , and  $f'_2(1525)$  mesons incoherently added to the  $f_0(1710)$  and non-resonant background.
- 31 Systematic errors not estimated.

### $f'_2(1525)$ DECAY MODES

Mode	Fraction ( $\Gamma_i/\Gamma$ )	Scale factor
$\Gamma_1$ $K\bar{K}$	(87.6±2.2) %	1.1
$\Gamma_2$ $\eta\eta$	(11.6±2.2) %	1.1
$\Gamma_3$ $\pi\pi$	( 8.3±1.6) × 10 <sup>-3</sup>	
$\Gamma_4$ $K\bar{K}^*(892) + c.c.$		
$\Gamma_5$ $\pi K\bar{K}$		
$\Gamma_6$ $\pi\pi\eta$		
$\Gamma_7$ $\pi^+\pi^+\pi^-\pi^-$		
$\Gamma_8$ $\gamma\gamma$	( 9.5±1.1) × 10 <sup>-7</sup>	1.1

### CONSTRAINED FIT INFORMATION

An overall fit to the total width, 2 partial widths, a combination of partial widths obtained from integrated cross sections, and 3 branching ratios uses 17 measurements and one constraint to determine 5 parameters. The overall fit has a  $\chi^2 = 18.2$  for 13 degrees of freedom.

The following *off-diagonal* array elements are the correlation coefficients  $\langle \delta p_i \delta p_j \rangle / (\delta p_i \delta p_j)$ , in percent, from the fit to parameters  $p_i$ , including the branching fractions,  $x_i \equiv \Gamma_i/\Gamma_{\text{total}}$ . The fit constrains the  $x_i$  whose labels appear in this array to sum to one.

$x_2$	-100			
$x_3$	-6	-1		
$x_8$	-19	19	1	
$\Gamma$	-4	4	0	-44
	$x_1$	$x_2$	$x_3$	$x_8$

Mode	Rate (MeV)	Scale factor
$\Gamma_1$ $K\bar{K}$	75 ± 4	1.8
$\Gamma_2$ $\eta\eta$	9.9 ± 1.9	1.1
$\Gamma_3$ $\pi\pi$	0.71 ± 0.14	1.1
$\Gamma_8$ $\gamma\gamma$	( 8.2 ± 0.9) × 10 <sup>-5</sup>	

### $f'_2(1525)$ PARTIAL WIDTHS

$\Gamma(K\bar{K})$	VALUE (MeV)	DOCUMENT ID	TECN	COMMENT	$\Gamma_1$
<b>75 ± 4 OUR FIT</b>				Error includes scale factor of 1.8.	
<b>63<sup>+6</sup><sub>-5</sub></b>	32 LONGACRE 86 MPS	22 $\pi^- p \rightarrow K_S^0 K_S^0 \eta$			

$\Gamma(\eta\eta)$	VALUE (MeV)	EVTS	DOCUMENT ID	TECN	COMMENT	$\Gamma_2$
<b>9.9 ± 1.9 OUR FIT</b>					Error includes scale factor of 1.1.	
5.0 ± 0.8	870 33 SCHEGELSKY 06A RVUE	$\gamma\gamma \rightarrow K_S^0 K_S^0$				
24 <sup>+3</sup> <sub>-1</sub>	32 LONGACRE 86 MPS	22 $\pi^- p \rightarrow K_S^0 K_S^0 \eta$				

$\Gamma(\pi\pi)$	VALUE (MeV)	EVTS	DOCUMENT ID	TECN	COMMENT	$\Gamma_3$
<b>0.71 ± 0.14 OUR FIT</b>					Error includes scale factor of 1.1.	
<b>1.4<sup>+1.0</sup><sub>-0.5</sub></b>	32 LONGACRE 86 MPS	22 $\pi^- p \rightarrow K_S^0 K_S^0 \eta$				
0.2 <sup>+1.0</sup> <sub>-0.2</sub>	870 33 SCHEGELSKY 06A RVUE	$\gamma\gamma \rightarrow K_S^0 K_S^0$				

$\Gamma(\gamma\gamma)$	VALUE (keV)	EVTS	DOCUMENT ID	TECN	COMMENT	$\Gamma_8$
<b>0.082 ± 0.009 OUR FIT</b>						
0.13 ± 0.03	870 33 SCHEGELSKY 06A RVUE	$\gamma\gamma \rightarrow K_S^0 K_S^0$				
32		From a partial-wave analysis of data using a K-matrix formalism with 5 poles.				
33		From analysis of L3 data at 91 and 183–209 GeV, using $\Gamma(f'_2(1525) \rightarrow K\bar{K}) = 68$ MeV and SU(3) relations.				

### $f'_2(1525)$ $\Gamma(i)\Gamma(\gamma\gamma)/\Gamma(\text{total})$

$\Gamma(K\bar{K}) \times \Gamma(\gamma\gamma)/\Gamma_{\text{total}}$	VALUE (keV)	EVTS	DOCUMENT ID	TECN	COMMENT	$\Gamma_1\Gamma_8/\Gamma$
<b>0.072 ± 0.007 OUR FIT</b>						
<b>0.072 ± 0.007 OUR AVERAGE</b>						
0.048 <sup>+0.067</sup> <sub>-0.008</sub> <sup>+0.108</sup> <sub>-0.012</sub>	UEHARA 13 BELL	$\gamma\gamma \rightarrow K_S^0 K_S^0$				
0.0564 ± 0.0048 ± 0.0116	ABE 04 BELL	10.6 $e^+e^- \rightarrow e^+e^- K^+ K^-$				
0.076 ± 0.006 ± 0.011 331	34 ACCIARRI 01H L3	$e^+e^- \rightarrow e^+e^- K_S^0 K_S^0$				
0.067 ± 0.008 ± 0.015	35 ALBRECHT 90G ARG	$e^+e^- \rightarrow e^+e^- K^+ K^-$				
0.11 <sup>+0.03</sup> <sub>-0.02</sub> ± 0.02	BEHREND 89C CELL	$e^+e^- \rightarrow e^+e^- K_S^0 K_S^0$				
0.10 <sup>+0.04</sup> <sub>-0.03</sub> <sup>+0.03</sup> <sub>-0.02</sub>	BERGER 88 PLUT	$e^+e^- \rightarrow e^+e^- K_S^0 K_S^0$				
0.12 ± 0.07 ± 0.04	35 AIHARA 86B TPC	$e^+e^- \rightarrow e^+e^- K^+ K^-$				
0.11 ± 0.02 ± 0.04	35 ALTHOFF 83 TASS	$e^+e^- \rightarrow e^+e^- K\bar{K}$				
0.0314 ± 0.0050 ± 0.0077	36 ALBRECHT 90G ARG	$e^+e^- \rightarrow e^+e^- K^+ K^-$				
34		Supersedes ACCIARRI 95J. From analysis of L3 data at 91 and 183–209 GeV,				
35		Using an incoherent background.				
36		Using a coherent background.				

See key on page 999

Meson Particle Listings

f'\_2(1525), f\_2(1565)

f'\_2(1525) BRANCHING RATIOS

Table with columns: Γ(ηη)/Γtotal, DOCUMENT ID, TECN, COMMENT, Γ2/Γ. Includes data for UEHARA 10A BELL and PROKOSHKIN 91 GAM4.

37 Combining results of GAM4 with those of WA76 on K-K central production and results of CBAL, MRK3 and DM2 on J/ψ → γηη.

Γ(ηη)/Γ(KK̄)

Table with columns: VALUE, CL%, EVTS, DOCUMENT ID, TECN, COMMENT, Γ2/Γ1. Includes data for BINON 61 38 and PROKOSHKIN 91 GAM4.

• • • We do not use the following data for averages, fits, limits, etc. • • •

38 Using the compilation of the cross sections for f'\_2(1525) production in K-p collisions from ASTON 88D.

39 Combining results of GAM4 with those of WA76 on K-K central production and results of CBAL, MRK3 and DM2 on J/ψ → γηη.

Γ(ππ)/Γtotal

Table with columns: VALUE, CL%, DOCUMENT ID, TECN, COMMENT, Γ3/Γ. Includes data for COSTA 80 OMEG and GORLICH 80 ASPK.

• • • We do not use the following data for averages, fits, limits, etc. • • •

40 Assuming that the f'\_2(1525) is produced by an one-pion exchange production mechanism.

41 MARTIN 79 uses the PAWLICKI 77 data with different input value of the f'\_2(1525) → K-K branching ratio.

Γ(ππ)/Γ(KK̄)

Table with columns: VALUE, DOCUMENT ID, TECN, COMMENT, Γ3/Γ1. Includes data for AUGUSTIN 87 DM2.

[Γ(KK\*(892)+c.c.)+Γ(πKK̄)]/Γ(KK̄)

Table with columns: VALUE, CL%, DOCUMENT ID, TECN, COMMENT, (Γ4+Γ5)/Γ1. Includes data for AGUILAR... 95 and AMMAR 67.

Γ(ππη)/Γ(KK̄)

Table with columns: VALUE, CL%, DOCUMENT ID, TECN, COMMENT, Γ6/Γ1. Includes data for AGUILAR... 95 and AMMAR 67.

Γ(π+π+π-π-)/Γ(KK̄)

Table with columns: VALUE, CL%, DOCUMENT ID, TECN, COMMENT, Γ7/Γ1. Includes data for AGUILAR... 95.

f'\_2(1525) REFERENCES

List of references for f'\_2(1525) including PDG, DOBBS, LEES, AALI, ABLIKIM, UEHARA, ANISOVICH, CHEKANOV, BINON, AMSLER, SCHEGELSKY, ABLIKIM, ABE, CHEKANOV, BAI, TIKHOMIROV.

Table listing various meson decays and production channels with columns for author, document ID, and comment.

f\_2(1565)

I^G(JPC) = 0+(2++)

OMITTED FROM SUMMARY TABLE. Seen mostly in antineutron-nucleon annihilation. Needs confirmation in other channels.

f\_2(1565) MASS

Table with columns: VALUE (MeV), DOCUMENT ID, TECN, COMMENT. Includes data for AMSLER 02 CBAR, BERTIN 98 OBLX, and ANISOVICH 09 RVUE.

- 1 T-matrix pole.
2 On sheet II in a two-pole solution.
3 Supersedes the ωω state of BELADIDZE 92B earlier assigned to the f\_2(1640).
4 Breit-Wigner width.
5 T-matrix pole, large coupling to ρρ and ωω, could be f\_2(1640).
6 Coupled-channel analysis of AMSLER 95B, AMSLER 95C, and AMSLER 94D.
7 From a simultaneous analysis of the annihilations p-bar p → 3π^0, π^0 ηη including AKER 91 data.
8 J^P not determined, could be partly f\_0(1500).
9 J^P not determined.
10 Superseded by AMSLER 95B.

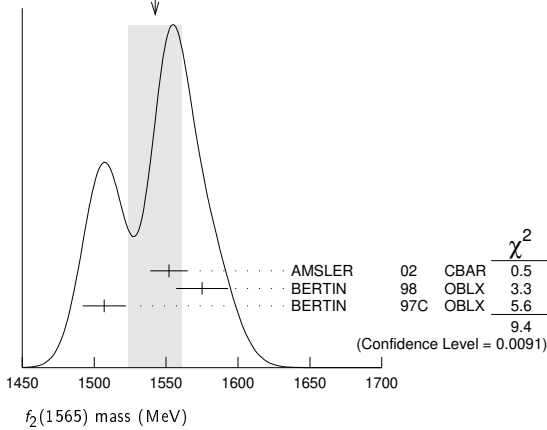
Downloaded from https://academic.oup.com/ptep/article/2020/8/083C01/5891211 by guest on 12 November 2020



# Meson Particle Listings

## $f_2(1565), \rho(1570)$

WEIGHTED AVERAGE  
1542±19 (Error scaled by 2.2)



### $f_2(1565)$ WIDTH

VALUE (MeV)	DOCUMENT ID	TECN	COMMENT
<b>122± 13 OUR AVERAGE</b>			
113± 23	11 AMSLER	02 CBAR	$0.9 \bar{p}p \rightarrow \pi^0 \eta \eta, \pi^0 \pi^0 \pi^0$
119± 24	11 BERTIN	98 OBLX	$0.05-0.405 \bar{p}p \rightarrow \pi^+ \pi^+ \pi^-$
130± 20	11 BERTIN	97c OBLX	$0.0 \bar{p}p \rightarrow \pi^+ \pi^- \pi^0$
• • • We do not use the following data for averages, fits, limits, etc. • • •			
280± 40	12 ANISOVICH	09 RVUE	$0.0 \bar{p}p, \pi N$
140± 11	13,14 AMELIN	06 VES	$36 \pi^- p \rightarrow \omega \omega n$
130± 20±40	14 AMELIN	00 VES	$37 \pi^- p \rightarrow \eta \pi^+ \pi^- n$
180± 60	15 ABELE	96c RVUE	Compilation
~ 142	16 AMSLER	95D CBAR	$0.0 \bar{p}p \rightarrow \pi^0 \pi^0 \pi^0, \pi^0 \eta \eta, \pi^0 \pi^0 \eta$
263±101	BALOSHIN	95 SPEC	$40 \pi^- C \rightarrow K_S^0 K_S^0 X$
166± 80 20	17 ANISOVICH	94 CBAR	$0.0 \bar{p}p \rightarrow 3\pi^0, \eta \eta \pi^0$
130± 10	18 ADAMO	93 OBLX	$\bar{p}p \rightarrow \pi^+ \pi^+ \pi^-$
148± 27	19 ARMSTRONG	93c E760	$\bar{p}p \rightarrow \pi^0 \eta \eta \rightarrow 6\gamma$
103± 15	19 ARMSTRONG	93d E760	$\bar{p}p \rightarrow 3\pi^0 \rightarrow 6\gamma$
111± 10	19 ARMSTRONG	93d E760	$\bar{p}p \rightarrow \eta \pi^0 \pi^0 \rightarrow 6\gamma$
~ 206	20 WEIDENAUER	93 ASTE	$0.0 \bar{p}N \rightarrow 3\pi^- 2\pi^+$
132± 37	19 ADAMO	92 OBLX	$\bar{p}p \rightarrow \pi^+ \pi^+ \pi^-$
120± 10	21 AKER	91 CBAR	$0.0 \bar{p}p \rightarrow 3\pi^0$
170± 40	MAY	90 ASTE	$0.0 \bar{p}p \rightarrow \pi^+ \pi^- \pi^0$
116± 9	BRIDGES	86c DBC	$0.0 \bar{p}N \rightarrow 3\pi^- 2\pi^+$

- 11 T-matrix pole.
- 12 On sheet II in a two-pole solution.
- 13 Supersedes the  $\omega\omega$  state of BELADIDZE 92b earlier assigned to the  $f_2(1640)$ .
- 14 Breit-Wigner width.
- 15 T-matrix pole, large coupling to  $\rho\rho$  and  $\omega\omega$ , could be  $f_2(1640)$ .
- 16 Coupled-channel analysis of AMSLER 95b, AMSLER 95c, and AMSLER 94d.
- 17 From a simultaneous analysis of the annihilations  $\bar{p}p \rightarrow 3\pi^0, \pi^0 \eta \eta$  including AKER 91 data.
- 18 Supersedes ADAMO 92.
- 19  $J^P$  not determined, could be partly  $f_0(1500)$ .
- 20  $J^P$  not determined.
- 21 Superseded by AMSLER 95b.

### $f_2(1565)$ DECAY MODES

Mode	Fraction ( $\Gamma_i/\Gamma$ )
$\Gamma_1$ $\pi \pi$	seen
$\Gamma_2$ $\pi^+ \pi^-$	seen
$\Gamma_3$ $\pi^0 \pi^0$	seen
$\Gamma_4$ $\rho^0 \rho^0$	seen
$\Gamma_5$ $2\pi^+ 2\pi^-$	seen
$\Gamma_6$ $\eta \eta$	seen
$\Gamma_7$ $\omega \omega$	seen
$\Gamma_8$ $K \bar{K}$	seen
$\Gamma_9$ $\gamma \gamma$	seen

### $f_2(1565)$ PARTIAL WIDTHS

$\Gamma(\eta\eta)$	VALUE (MeV)	EVTS	DOCUMENT ID	TECN	COMMENT
• • • We do not use the following data for averages, fits, limits, etc. • • •					
	1.2±0.3	870	22 SCHEGELSKY 06A	RVUE	$\gamma\gamma \rightarrow K_S^0 K_S^0$

### $\Gamma(K\bar{K})$

VALUE (MeV)	EVTS	DOCUMENT ID	TECN	COMMENT
• • • We do not use the following data for averages, fits, limits, etc. • • •				
2.0±1.0	870	22 SCHEGELSKY 06A	RVUE	$\gamma\gamma \rightarrow K_S^0 K_S^0$

### $\Gamma(\gamma\gamma)$

VALUE (keV)	EVTS	DOCUMENT ID	TECN	COMMENT
• • • We do not use the following data for averages, fits, limits, etc. • • •				
0.70±0.14	870	22 SCHEGELSKY 06A	RVUE	$\gamma\gamma \rightarrow K_S^0 K_S^0$
22 From analysis of L3 data at 91 and 183–209 GeV, using $f_2(1565)$ mass of 1570 MeV, width of 160 MeV, $\Gamma(\pi\pi) = 25$ MeV, and SU(3) relations.				

### $f_2(1565)$ BRANCHING RATIOS

$\Gamma(\pi\pi)/\Gamma_{total}$	VALUE	DOCUMENT ID	TECN	COMMENT
• • • We do not use the following data for averages, fits, limits, etc. • • •				
seen		BAKER	99B SPEC	$0 \bar{p}p \rightarrow \omega \omega \pi^0$

$\Gamma(\pi^+ \pi^-)/\Gamma_{total}$	VALUE	DOCUMENT ID	TECN	COMMENT
• • • We do not use the following data for averages, fits, limits, etc. • • •				
seen		BERTIN	98 OBLX	$0.05-0.405 \bar{p}p \rightarrow \pi^+ \pi^+ \pi^-$
not seen		23 ANISOVICH	94B RVUE	$\bar{p}p \rightarrow \pi^+ \pi^- \pi^0$
seen		MAY	89 ASTE	$\bar{p}p \rightarrow \pi^+ \pi^- \pi^0$
23 ANISOVICH 94b is from a reanalysis of MAY 90.				

$\Gamma(\pi^0 \pi^0)/\Gamma_{total}$	VALUE	DOCUMENT ID	TECN	COMMENT
• • • We do not use the following data for averages, fits, limits, etc. • • •				
seen		AMSLER	95B CBAR	$0.0 \bar{p}p \rightarrow 3\pi^0$

$\Gamma(\pi^+ \pi^-)/\Gamma(\rho^0 \rho^0)$	VALUE	DOCUMENT ID	TECN	COMMENT
• • • We do not use the following data for averages, fits, limits, etc. • • •				
0.042±0.013		BRIDGES	86B DBC	$\bar{p}N \rightarrow 3\pi^- 2\pi^+$

$\Gamma(\eta\eta)/\Gamma(\pi^0 \pi^0)$	VALUE	DOCUMENT ID	TECN	COMMENT
• • • We do not use the following data for averages, fits, limits, etc. • • •				
0.024±0.005±0.012		24 ARMSTRONG	93c E760	$\bar{p}p \rightarrow \pi^0 \eta \eta \rightarrow 6\gamma$
24 $J^P$ not determined, could be partly $f_0(1500)$ .				

$\Gamma(\omega\omega)/\Gamma_{total}$	VALUE	DOCUMENT ID	TECN	COMMENT
• • • We do not use the following data for averages, fits, limits, etc. • • •				
seen		BAKER	99B SPEC	$0 \bar{p}p \rightarrow \omega \omega \pi^0$

### $f_2(1565)$ REFERENCES

ANISOVICH 09	IJMP A24 2481	V.V. Anisovich, A.V. Sarantsev
AMELIN 06	PAN 69 690	D.V. Amelin et al.
	Translated from YAF 69 715.	(VES Collab.)
SCHEGELSKY 06A	EPJ A27 207	V.A. Schegelsky et al.
AMSLER 02	EPJ C23 29	C. Amisler et al.
AMELIN 00	NP A668 83	D. Amelin et al.
BAKER 99B	PL B467 147	C.A. Baker et al.
BERTIN 98	PR D57 55	A. Bertin et al.
BERTIN 97C	PL B408 476	A. Bertin et al.
ABELE 96C	NP A609 562	A. Abele et al.
AMSLER 95B	PL B342 433	C. Amisler et al.
AMSLER 95C	PL B353 571	C. Amisler et al.
AMSLER 95D	PL B355 425	C. Amisler et al.
BALOSHIN 95	PAN 58 46	O.M. Baloshin et al.
	Translated from YAF 58 50.	(ITEP)
AMSLER 94D	PL B333 277	C. Amisler et al.
ANISOVICH 94	PL B323 233	V.V. Anisovich et al.
ANISOVICH 94B	PR D50 1972	V.V. Anisovich et al.
ADAMO 93C	NP A558 13C	A. Adamo et al.
ARMSTRONG 93C	PL B307 394	T.A. Armstrong et al.
ARMSTRONG 93D	PL B307 399	T.A. Armstrong et al.
WEIDENAUER 93	ZPHY C59 387	P. Weidenauer et al.
ADAMO 92	PL B287 368	A. Adamo et al.
BELADIDZE 92B	ZPHY C54 367	G.M. Beladidze et al.
AKER 91	PL B260 249	E. Aker et al.
MAY 90	ZPHY C46 203	B. May et al.
MAY 89	PL B225 450	B. May et al.
BRIDGES 86B	PRL 56 215	D.L. Bridges et al.
BRIDGES 86C	PRL 57 1534	D.L. Bridges et al.

## $\rho(1570)$

$$I^G(J^{PC}) = 1^+(1^{-})$$

OMITTED FROM SUMMARY TABLE

May be an OZI-violating decay mode of  $\rho(1700)$ . See our mini-review under the  $\rho(1700)$ .

See key on page 999

# Meson Particle Listings

## $\rho(1570)$ , $h_1(1595)$ , $\pi_1(1600)$

### $\rho(1570)$ MASS

VALUE (MeV)	EVTS	DOCUMENT ID	TECN	COMMENT
<b>1570 ± 36 ± 62</b>	54	<sup>1</sup> AUBERT 08s	BABR	10.6 $e^+e^- \rightarrow \phi\pi^0\gamma$
1480 ± 40		<sup>2</sup> BITYUKOV 87	SPEC	32.5 $\pi^-p \rightarrow \phi\pi^0n$

• • • We do not use the following data for averages, fits, limits, etc. • • •

<sup>1</sup> From the fit with two resonances.  
<sup>2</sup> Systematic errors not estimated.

### $\rho(1570)$ WIDTH

VALUE (MeV)	EVTS	DOCUMENT ID	TECN	COMMENT
<b>144 ± 75 ± 43</b>	54	<sup>3</sup> AUBERT 08s	BABR	10.6 $e^+e^- \rightarrow \phi\pi^0\gamma$
130 ± 60		<sup>4</sup> BITYUKOV 87	SPEC	32.5 $\pi^-p \rightarrow \phi\pi^0n$

• • • We do not use the following data for averages, fits, limits, etc. • • •

<sup>3</sup> From the fit with two resonances.  
<sup>4</sup> Systematic errors not estimated.

### $\rho(1570)$ DECAY MODES

Mode	Fraction ( $\Gamma_i/\Gamma$ )
$\Gamma_1$ $e^+e^-$	
$\Gamma_2$ $\phi\pi$	not seen
$\Gamma_3$ $\omega\pi$	

### $\rho(1570)$ $\Gamma(i)\Gamma(e^+e^-)/\Gamma(\text{total})$

$\Gamma(\phi\pi) \times \Gamma(e^+e^-)/\Gamma_{\text{total}}$	CL%	EVTS	DOCUMENT ID	TECN	COMMENT	$\Gamma_2/\Gamma_1$
<b>3.5 ± 0.9 ± 0.3</b>		54	<sup>5</sup> AUBERT 08s	BABR	10.6 $e^+e^- \rightarrow \phi\pi^0\gamma$	
<70	90		<sup>6</sup> AULCHENKO 87b	ND	$e^+e^- \rightarrow K_S^0 K_L^0 \pi^0$	

• • • We do not use the following data for averages, fits, limits, etc. • • •

<sup>5</sup> From the fit with two resonances.  
<sup>6</sup> Using mass and width of BITYUKOV 87.

### $\rho(1570)$ BRANCHING RATIOS

$\Gamma(\phi\pi)/\Gamma_{\text{total}}$	DOCUMENT ID	TECN	COMMENT	$\Gamma_2/\Gamma$
not seen	ABELE 97H	CBAR	$\bar{p}p \rightarrow K_L^0 K_S^0 \pi^0$	
<0.01	<sup>7</sup> DONNACHIE 91	RVUE		

• • • We do not use the following data for averages, fits, limits, etc. • • •

<sup>7</sup> Using data from BISELLO 91b, DOLINSKY 86, and ALBRECHT 87L.

$\Gamma(\phi\pi)/\Gamma(\omega\pi)$	CL%	DOCUMENT ID	TECN	COMMENT	$\Gamma_2/\Gamma_3$
>0.5	95	BITYUKOV 87	SPEC	32.5 $\pi^-p \rightarrow \phi\pi^0n$	

• • • We do not use the following data for averages, fits, limits, etc. • • •

### $\rho(1570)$ REFERENCES

AUBERT 08s	PR D77 092002	B. Aubert et al.	(BABAR Collab.)
ABELE 97H	PL B415 280	A. Abele et al.	(Crystal Barrel Collab.)
BISELLO 91b	NPBPS B21 111	D. Bisello	(DM2 Collab.)
DONNACHIE 91	ZPHY C51 689	A. Donnachie, A.B. Clegg	(MCHS, LANC)
ALBRECHT 87L	PL B185 223	H. Albrecht et al.	(ARGUS Collab.)
AULCHENKO 87b	JETPL 45 145	V.M. Aulchenko et al.	(NOVO)
BITYUKOV 87	Translated from ZETFP 45 118		
DOLINSKY 86	PL B188 383	S.I. Bityukov et al.	(SERP)
	PL B174 453	S.I. Dolinsky et al.	(NOVO)

## $h_1(1595)$

$$I^G(J^{PC}) = 0^-(1^{+-})$$

OMITTED FROM SUMMARY TABLE

Seen in a partial-wave analysis of the  $\omega\eta$  system produced in the reaction  $\pi^-p \rightarrow \omega\eta n$  at 18 GeV/c.

### $h_1(1595)$ MASS

VALUE (MeV)	DOCUMENT ID	TECN	COMMENT
<b>1594 ± 15 ± 10 ± 60</b>	EUGENIO 01	SPEC	18 $\pi^-p \rightarrow \omega\eta n$

### $h_1(1595)$ WIDTH

VALUE (MeV)	DOCUMENT ID	TECN	COMMENT
<b>384 ± 60 ± 70 ± 100</b>	EUGENIO 01	SPEC	18 $\pi^-p \rightarrow \omega\eta n$

### $h_1(1595)$ DECAY MODES

Mode	Fraction ( $\Gamma_i/\Gamma$ )
$\Gamma_1$ $\omega\eta$	seen

### $h_1(1595)$ REFERENCES

EUGENIO 01	PL B497 190	P. Eugenio et al.
------------	-------------	-------------------

## $\pi_1(1600)$

$$I^G(J^{PC}) = 1^-(1^{-+})$$

See the review on "Non- $q\bar{q}$  Mesons" and a note in PDG 06, Journal of Physics **G33** 1 (2006).

### $\pi_1(1600)$ MASS

VALUE (MeV)	EVTS	DOCUMENT ID	TECN	COMMENT
<b>1660 ± 15 ± 11 OUR AVERAGE</b>				Error includes scale factor of 1.2.
1564 ± 24 ± 86		<sup>1</sup> RODAS 19	JPAC	191 $\pi^-p \rightarrow \eta^{(\prime)}\pi^-p$
1600 ± 110 ± 60	46M	<sup>2</sup> AGHASYAN 18B	COMP	190 $\pi^-p \rightarrow \pi^-\pi^+\pi^-p$
1664 ± 8 ± 10	145k	<sup>3</sup> LU 05	B852	18 $\pi^-p \rightarrow \omega\pi^-\pi^0p$
1709 ± 24 ± 41	69k	<sup>4</sup> KUHN 04	B852	18 $\pi^-p \rightarrow \eta\pi^+\pi^-\pi^-p$
1597 ± 10 ± 45 ± 10		<sup>4</sup> IVANOV 01	B852	18 $\pi^-p \rightarrow \eta'\pi^-p$
1660 ± 10 ± 64	420k	<sup>5</sup> ALEKSEEV 10	COMP	190 $\pi^-Pb \rightarrow \pi^-\pi^-\pi^+Pb'$
1593 ± 8 ± 29 ± 47		<sup>4,6</sup> ADAMS 98B	B852	18.3 $\pi^-p \rightarrow \pi^+\pi^-\pi^-p$

• • • We do not use the following data for averages, fits, limits, etc. • • •

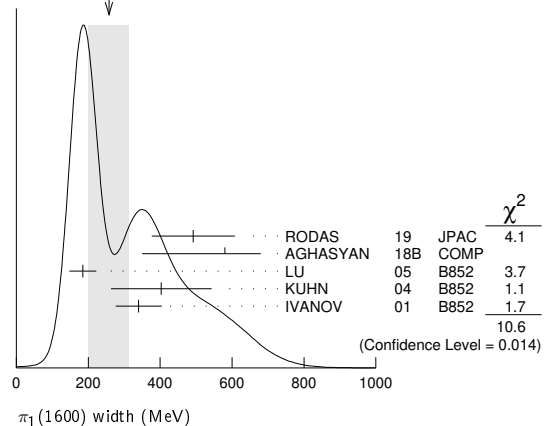
- The coupled-channel analysis of both the  $\eta\pi$  and  $\eta'\pi$  systems using ADOLPH 15data. The mass is extracted from the T-matrix pole.
- Statistical error negligible.
- May be a different state: natural and unnatural parity exchanges.
- Natural parity exchange.
- Superseded by AGHASYAN 2018B.
- Superseded by DZIERBA 06 excluding this state in a more refined PWA analysis, with 2.6 M events of  $\pi^-p \rightarrow \pi^-\pi^-\pi^+p$  and 3 M events of  $\pi^-p \rightarrow \pi^-\pi^0\pi^0p$  of E852 data.

### $\pi_1(1600)$ WIDTH

VALUE (MeV)	EVTS	DOCUMENT ID	TECN	COMMENT
<b>257 ± 60 OUR AVERAGE</b>				Error includes scale factor of 1.9. See the ideogram below.
492 ± 54 ± 102		<sup>1</sup> RODAS 19	JPAC	191 $\pi^-p \rightarrow \eta^{(\prime)}\pi^-p$
580 ± 100 ± 230	46M	<sup>2</sup> AGHASYAN 18B	COMP	190 $\pi^-p \rightarrow \pi^-\pi^+\pi^-p$
185 ± 25 ± 28	145k	<sup>3</sup> LU 05	B852	18 $\pi^-p \rightarrow \omega\pi^-\pi^0p$
403 ± 80 ± 115	69k	<sup>4</sup> KUHN 04	B852	18 $\pi^-p \rightarrow \eta\pi^+\pi^-\pi^-p$
340 ± 40 ± 50		<sup>4</sup> IVANOV 01	B852	18 $\pi^-p \rightarrow \eta'\pi^-p$
269 ± 21 ± 42 ± 64	420k	<sup>5</sup> ALEKSEEV 10	COMP	190 $\pi^-Pb \rightarrow \pi^-\pi^-\pi^+Pb'$
168 ± 20 ± 150 ± 12		<sup>4,6</sup> ADAMS 98B	B852	18.3 $\pi^-p \rightarrow \pi^+\pi^-\pi^-p$

• • • We do not use the following data for averages, fits, limits, etc. • • •

WEIGHTED AVERAGE  
257±60 (Error scaled by 1.9)



- The coupled-channel analysis of both the  $\eta\pi$  and  $\eta'\pi$  systems using ADOLPH 15data. The width is extracted from the T-matrix pole.
- Statistical error negligible.
- May be a different state: natural and unnatural parity exchanges.

# Meson Particle Listings

## $\pi_1(1600)$ , $a_1(1640)$

<sup>4</sup> Natural parity exchange.  
<sup>5</sup> Superseded by AGHASYAN 2018B.  
<sup>6</sup> Superseded by DZIERBA 06 excluding this state in a more refined PWA analysis, with 2.6 M events of  $\pi^- p \rightarrow \pi^- \pi^- \pi^+ p$  and 3 M events of  $\pi^- p \rightarrow \pi^- \pi^0 \pi^0 p$  of E852 data.

### $\pi_1(1600)$ DECAY MODES

Mode	Fraction ( $\Gamma_i/\Gamma$ )
$\Gamma_1$ $\pi \pi \pi$	seen
$\Gamma_2$ $\rho^0 \pi^-$	seen
$\Gamma_3$ $f_2(1270) \pi^-$	not seen
$\Gamma_4$ $b_1(1235) \pi$	seen
$\Gamma_5$ $\eta'(958) \pi^-$	seen
$\Gamma_6$ $f_1(1285) \pi$	seen

### $\pi_1(1600)$ BRANCHING RATIOS

$\Gamma(\rho^0 \pi^-)/\Gamma_{total}$	VALUE	DOCUMENT ID	TECN	COMMENT	$\Gamma_2/\Gamma$
seen		ALEKSEEV	10	COMP	190 $\pi^- p b \rightarrow \pi^- \pi^- \pi^+ p b'$
not seen		NOZAR	09	CLAS	$\gamma p \rightarrow 2\pi^+ \pi^- n$
not seen		<sup>1</sup> DZIERBA	06	B852	18 $\pi^- p$

<sup>1</sup> From the PWA analysis of 2.6 M  $\pi^- p \rightarrow \pi^- \pi^- \pi^+ p$  and 3 M events of  $\pi^- p \rightarrow \pi^- \pi^0 \pi^0 p$  of E852 data. Supersedes ADAMS 98B.

$\Gamma(f_2(1270) \pi^-)/\Gamma_{total}$	VALUE	DOCUMENT ID	TECN	COMMENT	$\Gamma_3/\Gamma$
not seen		<sup>1</sup> DZIERBA	06	B852	18 $\pi^- p$

<sup>1</sup> From the PWA analysis of 2.6 M  $\pi^- p \rightarrow \pi^- \pi^- \pi^+ p$  and 3 M events of  $\pi^- p \rightarrow \pi^- \pi^0 \pi^0 p$  of E852 data. Supersedes CHUNG 02.

$\Gamma(b_1(1235) \pi)/\Gamma_{total}$	VALUE	EVTS	DOCUMENT ID	TECN	COMMENT	$\Gamma_4/\Gamma$
seen		35280	<sup>1</sup> BAKER	03	SPEC	$\bar{p} p \rightarrow \omega \pi^+ \pi^- \pi^0$
seen		145k	LU	05	B852	18 $\pi^- p \rightarrow \omega \pi^- \pi^0 p$

<sup>1</sup>  $B((b_1 \pi)_{D-wave})/B((b_1 \pi)_{S-wave}) = 0.3 \pm 0.1$ .

$\Gamma(\eta'(958) \pi^-)/\Gamma_{total}$	VALUE	DOCUMENT ID	TECN	COMMENT	$\Gamma_5/\Gamma$
seen		IVANOV	01	B852	18 $\pi^- p \rightarrow \eta' \pi^- p$

$\Gamma(f_1(1285) \pi)/\Gamma(\eta'(958) \pi^-)$	VALUE	EVTS	DOCUMENT ID	TECN	COMMENT	$\Gamma_6/\Gamma_5$
<b>3.80 ± 0.78</b>		69k	<sup>1</sup> KUHN	04	B852	18 $\pi^- p \rightarrow \eta \pi^+ \pi^- \pi^- p$

<sup>1</sup> Using  $\eta'(958)$   $\pi$  data from IVANOV 01.

### $\pi_1(1600)$ REFERENCES

RODAS	19	PRL 122 042002	A. Rodas et al.	(JPAC Collab.)
AGHASYAN	18B	PR D98 092003	M. Aghasyan et al.	(COMPASS Collab.)
ADOLPH	15	PL B740 303	M. Adolph et al.	(COMPASS Collab.)
ALEKSEEV	10	PRL 104 241803	M. G. Alekseev et al.	(COMPASS Collab.)
NOZAR	09	PRL 102 102002	M. Nozar et al.	(JLab CLAS Collab.)
DZIERBA	06	PR D73 072001	A.R. Dzierba et al.	(BNL E852 Collab.)
PDG	06	JP G33 1	W.-M. Yao et al.	(PDG Collab.)
LU	05	PRL 94 032002	M. Lu et al.	(BNL E852 Collab.)
KUHN	04	PL B595 109	J. Kuhn et al.	(BNL E852 Collab.)
BAKER	03	PL B563 140	C.A. Baker et al.	(BNL E852 Collab.)
CHUNG	02	PR D65 072001	S.U. Chung et al.	(BNL E852 Collab.)
IVANOV	01	PRL 86 3977	E.I. Ivanov et al.	(BNL E852 Collab.)
ADAMS	98B	PRL 81 5760	G.S. Adams et al.	(BNL E852 Collab.)

**$a_1(1640)$**   $I^G(J^{PC}) = 1^-(1^{++})$

Possibly seen in the study of the hadronic structure in decay  $\tau \rightarrow 3\pi \nu_\tau$  (ABREU 98G and ASNER 00).

### $a_1(1640)$ MASS

VALUE (MeV)	EVTS	DOCUMENT ID	TECN	COMMENT
<b>1655 ± 16 OUR AVERAGE</b>				Error includes scale factor of 1.2.
1700 ± 35	46M	<sup>1</sup> AGHASYAN	18B	COMP
1691 ± 18 ± 30		DARGENT	17	RVUE
1630 ± 20	35k	<sup>2</sup> BAKER	03	SPEC
1714 ± 9 ± 36		CHUNG	02	B852
1640 ± 12 ± 30		BAKER	99	SPEC

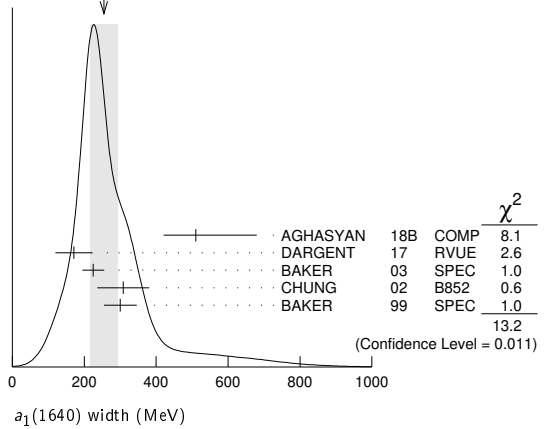
• • • We do not use the following data for averages, fits, limits, etc. • • •  
 1760 ± 90 BELLINI 85 SPEC 40  $\pi^- A \rightarrow \pi^- \pi^+ \pi^- A$   
<sup>1</sup> Statistical error negligible.  
<sup>2</sup> Using the  $a_1(1260)$  mass and width results of BOWLER 88.

### $a_1(1640)$ WIDTH

VALUE (MeV)	EVTS	DOCUMENT ID	TECN	COMMENT
<b>254 ± 40 OUR AVERAGE</b>				Error includes scale factor of 1.8. See the ideogram below.
510 <sup>+170</sup> <sub>-90</sub>	46M	<sup>1</sup> AGHASYAN	18B	COMP
171 ± 33 ± 40		DARGENT	17	RVUE
225 ± 30	35k	<sup>2</sup> BAKER	03	SPEC
308 ± 37 ± 62		CHUNG	02	B852
300 ± 22 ± 40		BAKER	99	SPEC
300 ± 100		BELLINI	85	SPEC

<sup>1</sup> Statistical error negligible.  
<sup>2</sup> Using the  $a_1(1260)$  mass and width results of BOWLER 88.

WEIGHTED AVERAGE  
 254±40 (Error scaled by 1.8)



### $a_1(1640)$ DECAY MODES

Mode	Fraction ( $\Gamma_i/\Gamma$ )
$\Gamma_1$ $\pi \pi \pi$	seen
$\Gamma_2$ $f_2(1270) \pi$	seen
$\Gamma_3$ $\sigma \pi$	seen
$\Gamma_4$ $\rho \pi S$ -wave	seen
$\Gamma_5$ $\rho \pi D$ -wave	seen
$\Gamma_6$ $\omega \pi \pi$	seen
$\Gamma_7$ $f_1(1285) \pi$	seen
$\Gamma_8$ $a_1(1260) \eta$	not seen

### $a_1(1640)$ BRANCHING RATIOS

$\Gamma(f_2(1270) \pi)/\Gamma(\sigma \pi)$	VALUE	DOCUMENT ID	TECN	COMMENT	$\Gamma_2/\Gamma_3$
<b>0.24 ± 0.07</b>		BAKER	99	SPEC	1.94 $\bar{p} p \rightarrow 4\pi^0$

$\Gamma(\rho \pi D\text{-wave})/\Gamma_{total}$	VALUE	DOCUMENT ID	TECN	COMMENT	$\Gamma_5/\Gamma$
seen		CHUNG	02	B852	18.3 $\pi^- p \rightarrow \pi^+ \pi^- \pi^- p$
seen		AMELIN	95B	VES	36 $\pi^- A \rightarrow \pi^+ \pi^- \pi^- A$

$\Gamma(\omega \pi \pi)/\Gamma_{total}$	VALUE	EVTS	DOCUMENT ID	TECN	COMMENT	$\Gamma_6/\Gamma$
seen		35280	<sup>1</sup> BAKER	03	SPEC	$\bar{p} p \rightarrow \omega \pi^+ \pi^- \pi^0$

<sup>1</sup> Assuming the  $\omega \rho$  mechanism for the  $\omega \pi \pi$  state.

$\Gamma(f_1(1285) \pi)/\Gamma_{total}$	VALUE	DOCUMENT ID	TECN	COMMENT	$\Gamma_7/\Gamma$
not seen		KUHN	04	B852	18 $\pi^- p \rightarrow \eta \pi^+ \pi^- \pi^- p$
seen		LEE	94	MPS2	18 $\pi^- p \rightarrow K^+ \bar{K}^0 \pi^- \pi^- p$

See key on page 999

# Meson Particle Listings

## $a_1(1640), f_2(1640), \eta_2(1645), \omega(1650)$

$\Gamma(a_1(1260)\eta)/\Gamma_{total}$	DOCUMENT ID	TECN	COMMENT	$\Gamma_8/\Gamma$
not seen	KUHN	04	B852	$18 \pi^- p \rightarrow \eta \pi^+ \pi^- \pi^- p$

### $a_1(1640)$ REFERENCES

Author	Year	Pub	Doc ID	TECN	Comment
AGHASYAN	18B	PR D98 092003	M. Aghasyan et al.	(COMPASS Collab.)	
DARGENT	17	JHEP 1705 143	P. d'Argent et al.	(HEID, BRIS)	
KUHN	04	PL B595 109	J. Kuhn et al.	(BNL E852 Collab.)	
BAKER	03	PL B563 140	C.A. Baker et al.		
CHUNG	02	PR D65 072001	S.U. Chung et al.	(BNL E852 Collab.)	
ASNER	00	PR D61 012002	D.M. Asner et al.	(CLEO Collab.)	
BAKER	99	PL B449 114	C.A. Baker et al.		
ABREU	98G	PL B426 411	P. Abreu et al.	(DELPHI Collab.)	
AMELIN	95B	PL B356 595	D.V. Amelin et al.	(SERP, TBIL)	
LEE	94	PL B323 227	J.H. Lee et al.	(BNL, IND, KYUN, MASD+)	
BOWLER	88	PL B209 99	M.G. Bowler	(SERP, TBIL)	
BELLINI	85	SJNP 41 781	D. Bellini et al.	(OXF)	
Translated from YAF 41 1223.					

$f_2(1640)$	$I^G(J^{PC}) = 0^+(2^{++})$
OMITTED FROM SUMMARY TABLE	

### $f_2(1640)$ MASS

VALUE (MeV)	DOCUMENT ID	TECN	COMMENT
<b>1639 ± 6 OUR AVERAGE</b>	Error includes scale factor of 1.2.		
1620 ± 16	BUGG	95	MRK3 $J/\psi \rightarrow \gamma \pi^+ \pi^- \pi^+ \pi^-$
1647 ± 7	ADAMO	92	OBLX $\bar{p} p \rightarrow 3\pi^+ 2\pi^-$
1635 ± 7	ALDE	90	GAM2 $38 \pi^- p \rightarrow \omega \omega n$
• • • We do not use the following data for averages, fits, limits, etc. • • •			
1640 ± 5	AMSLER	06	CBAR $0.9 \bar{p} p \rightarrow K^+ K^- \pi^0$
1659 ± 6	VLADIMIRSK..06	SPEC	$40 \pi^- p \rightarrow K_S^0 K_S^0 n$
1643 ± 7	<sup>1</sup> ALDE	89B	GAM2 $38 \pi^- p \rightarrow \omega \omega n$
<sup>1</sup> Superseded by ALDE 90.			

### $f_2(1640)$ WIDTH

VALUE (MeV)	CL%	DOCUMENT ID	TECN	COMMENT
<b>99<sup>+60</sup><sub>-40</sub> OUR AVERAGE</b>	Error includes scale factor of 2.9.			
140 <sup>+60</sup> <sub>-20</sub>		BUGG	95	MRK3 $J/\psi \rightarrow \gamma \pi^+ \pi^- \pi^+ \pi^-$
58 ± 20		ADAMO	92	OBLX $\bar{p} p \rightarrow 3\pi^+ 2\pi^-$
• • • We do not use the following data for averages, fits, limits, etc. • • •				
44 ± 9		AMSLER	06	CBAR $0.9 \bar{p} p \rightarrow K^+ K^- \pi^0$
152 ± 18		VLADIMIRSK..06	SPEC	$40 \pi^- p \rightarrow K_S^0 K_S^0 n$
< 70	90	ALDE	90	GAM2 $38 \pi^- p \rightarrow \omega \omega n$

### $f_2(1640)$ DECAY MODES

Mode	Fraction ( $\Gamma_i/\Gamma$ )
$\Gamma_1$ $\omega \omega$	seen
$\Gamma_2$ $4\pi$	seen
$\Gamma_3$ $K\bar{K}$	seen

### $f_2(1640)$ BRANCHING RATIOS

$\Gamma(K\bar{K})/\Gamma_{total}$	DOCUMENT ID	TECN	COMMENT	$\Gamma_3/\Gamma$
seen	AMSLER	06	CBAR $0.9 \bar{p} p \rightarrow K^+ K^- \pi^0$	

### $f_2(1640)$ REFERENCES

Author	Year	Pub	Doc ID	TECN	Comment
AMSLER	06	PL B639 165	C. Amstler et al.	(CBAR Collab.)	
VLADIMIRSK..06	06	PAN 69 433	V.V. Vladimirov et al.	(ITEP, Moscow)	
Translated from YAF 69 515.					
BUGG	95	PL B353 378	D.V. Bugg et al.	(LOQM, PNPI, WASH)JP	
ADAMO	92	PL B287 368	A. Adamo et al.	(OBELIX Collab.)	
ALDE	90	PL B241 600	D.M. Alde et al.	(SERP, BELG, LANL, LAPP+)	
ALDE	89B	PL B216 451	D.M. Alde et al.	(SERP, BELG, LANL, LAPP+)IGJPC	

$\eta_2(1645)$	$I^G(J^{PC}) = 0^+(2^{-+})$
----------------	-----------------------------

### $\eta_2(1645)$ MASS

VALUE (MeV)	DOCUMENT ID	TECN	CHG	COMMENT
<b>1617 ± 5 OUR AVERAGE</b>				
1613 ± 8	BARBERIS	00B		$450 pp \rightarrow p_f \eta \pi^+ \pi^- p_S$
1617 ± 8	BARBERIS	00C		$450 pp \rightarrow p_f 4\pi p_S$
1620 ± 20	BARBERIS	97B	OMEG	$450 pp \rightarrow pp 2(\pi^+ \pi^-)$
1645 ± 14 ± 15	ADOMEIT	96	CBAR 0	$1.94 \bar{p} p \rightarrow \eta 3\pi^0$

• • • We do not use the following data for averages, fits, limits, etc. • • •  
 1645 ± 6 ± 20 ANISOVICH 00E SPEC 0.9-1.94  $\bar{p} p \rightarrow \eta 3\pi^0$

### $\eta_2(1645)$ WIDTH

VALUE (MeV)	DOCUMENT ID	TECN	CHG	COMMENT
<b>181 ± 11 OUR AVERAGE</b>				
185 ± 17	BARBERIS	00B		$450 pp \rightarrow p_f \eta \pi^+ \pi^- p_S$
177 ± 18	BARBERIS	00C		$450 pp \rightarrow p_f 4\pi p_S$
180 ± 25	BARBERIS	97B	OMEG	$450 pp \rightarrow pp 2(\pi^+ \pi^-)$
180 <sup>+40</sup> <sub>-21</sub> ± 25	ADOMEIT	96	CBAR 0	$1.94 \bar{p} p \rightarrow \eta 3\pi^0$
• • • We do not use the following data for averages, fits, limits, etc. • • •				
200 ± 25	ANISOVICH	00E	SPEC	$0.9-1.94 \bar{p} p \rightarrow \eta 3\pi^0$

### $\eta_2(1645)$ DECAY MODES

Mode	Fraction ( $\Gamma_i/\Gamma$ )
$\Gamma_1$ $a_2(1320)\pi$	seen
$\Gamma_2$ $K\bar{K}\pi$	seen
$\Gamma_3$ $K^*\bar{K}$	seen
$\Gamma_4$ $\eta \pi^+ \pi^-$	seen
$\Gamma_5$ $a_0(980)\pi$	seen
$\Gamma_6$ $f_2(1270)\eta$	not seen

### $\eta_2(1645)$ BRANCHING RATIOS

$\Gamma(K\bar{K}\pi)/\Gamma(a_2(1320)\pi)$	DOCUMENT ID	TECN	COMMENT	$\Gamma_2/\Gamma_1$
<b>0.07 ± 0.03</b>	<sup>1</sup> BARBERIS	97C	OMEG $450 pp \rightarrow pp K\bar{K}\pi$	
<sup>1</sup> Using $2(\pi^+ \pi^-)$ data from BARBERIS 97B.				

$\Gamma(a_2(1320)\pi)/\Gamma(a_0(980)\pi)$	DOCUMENT ID	TECN	COMMENT	$\Gamma_1/\Gamma_5$
<b>13.1 ± 2.3 OUR AVERAGE</b>				
13.5 ± 4.6	<sup>2</sup> ANISOVICH	11	SPEC	$0.9-1.94 p\bar{p}$
13.0 ± 2.7	BARBERIS	00B		$450 pp \rightarrow p_f \eta \pi^+ \pi^- p_S$
<sup>2</sup> Reanalysis of ADOMEIT 96 and ANISOVICH 00E.				

$\Gamma(f_2(1270)\eta)/\Gamma_{total}$	DOCUMENT ID	COMMENT	$\Gamma_6/\Gamma$
not seen	BARBERIS	00B $450 pp \rightarrow p_f \eta \pi^+ \pi^- p_S$	

### $\eta_2(1645)$ REFERENCES

Author	Year	Pub	Doc ID	TECN	Comment
ANISOVICH	11	EPL C71 1511	A.V. Anisovich et al.	(LOQM, RAL, PNPI)	
ANISOVICH	00E	PL B477 19	A.V. Anisovich et al.		
BARBERIS	00B	PL B471 435	D. Barberis et al.	(WA 102 Collab.)	
BARBERIS	00C	PL B471 440	D. Barberis et al.	(WA 102 Collab.)	
BARBERIS	97B	PL B413 217	D. Barberis et al.	(WA 102 Collab.)	
BARBERIS	97C	PL B413 225	D. Barberis et al.	(WA 102 Collab.)	
ADOMEIT	96	ZPHY C71 227	J. Adomeit et al.	(Crystal Barrel Collab.)	

$\omega(1650)$	$I^G(J^{PC}) = 0^-(1^{-+})$
----------------	-----------------------------

See also the  $\omega(1420)$  particle listing.

### $\omega(1650)$ MASS

VALUE (MeV)	EVTS	DOCUMENT ID	TECN	COMMENT
<b>1670 ± 30 OUR ESTIMATE</b>				
1651 ± 3 <sup>+16</sup> <sub>-6</sub>	183k	<sup>1</sup> ABLIKIM	19AQ BES	$J/\psi \rightarrow K^+ K^- \pi^0$
1673 ± 6 <sup>+7</sup> <sub>-7</sub>		ACHASOV	19	SND $e^+ e^- \rightarrow \pi^+ \pi^- \pi^0 \eta$
1671 ± 6 ± 10	824	<sup>2</sup> AKHMETSHIN	17A CMD3	$1.4-2.0 e^+ e^- \rightarrow \omega \eta$
1660 ± 10	898	<sup>3</sup> ACHASOV	16B SND	$1.34-2.00 e^+ e^- \rightarrow \omega \eta$
1680 ± 10	13.1k	<sup>4</sup> AULCHENKO	15A SND	$1.05-1.80 e^+ e^- \rightarrow \pi^+ \pi^- \pi^0$
1667 ± 13 ± 6		AUBERT	07AU BABR	$10.6 e^+ e^- \rightarrow \omega \pi^+ \pi^- \gamma$
1645 ± 8	13	AUBERT	06D BABR	$10.6 e^+ e^- \rightarrow \omega \eta \gamma$
1660 ± 10 ± 2		AUBERT,B	04N BABR	$10.6 e^+ e^- \rightarrow \pi^+ \pi^- \pi^0 \gamma$
1770 ± 50 ± 60	1.2M	<sup>5</sup> ACHASOV	03D RVUE	$0.44-2.00 e^+ e^- \rightarrow \pi^+ \pi^- \pi^0$
1619 ± 5		<sup>6</sup> HENNER	02	RVUE $1.2-2.0 e^+ e^- \rightarrow \rho \pi,$ $\omega \pi \pi$
1700 ± 20		EUGENIO	01	SPEC $18 \pi^- p \rightarrow \omega \eta n$
1705 ± 26	612	<sup>7</sup> AKHMETSHIN	00D CMD2	$e^+ e^- \rightarrow \omega \pi^+ \pi^-$
1820 <sup>+190</sup> <sub>-150</sub>		<sup>8</sup> ACHASOV	98H RVUE	$e^+ e^- \rightarrow \pi^+ \pi^- \pi^0$
1840 <sup>+100</sup> <sub>-70</sub>		<sup>9</sup> ACHASOV	98H RVUE	$e^+ e^- \rightarrow \omega \pi^+ \pi^-$

# Meson Particle Listings

## $\omega(1650)$

$1780^{+170}_{-300}$	10	ACHASOV	98H	RVUE	$e^+e^- \rightarrow K^+K^-$
$\sim 2100$	11	ACHASOV	98H	RVUE	$e^+e^- \rightarrow K_S^0 K^\pm \pi^\mp$
$1606 \pm 9$	12	CLEGG	94	RVUE	
$1662 \pm 13$	750	13 ANTONELLI	92	DM2	$1.34-2.4e^+e^- \rightarrow \rho\pi,$
$1670 \pm 20$		ATKINSON	83B	OMEG	$20-70 \gamma\rho \rightarrow 3\pi X$
$1657 \pm 13$		CORDIER	81	DM1	$e^+e^- \rightarrow \omega 2\pi$
$1679 \pm 34$	21	ESPOSITO	80	FRAM	$e^+e^- \rightarrow 3\pi$
$1652 \pm 17$		COSME	79	OSPK	$e^+e^- \rightarrow 3\pi$

- 1 Could also be  $\rho(1700)$ . Branching ratio  $J/\psi \rightarrow X \pi^0 \rightarrow K^+K^-\pi^0 = (5.3 \pm 0.3^{+0.6}_{-0.5}) \times 10^{-5}$ .
- 2 From a fit of the interfering  $\omega(1420)$  and  $\omega(1650)$  with a relative phase of  $\pi$  and other parameters floating.
- 3 From a fit with contributions from  $\omega(1420)$ ,  $\omega(1650)$ , and  $\phi(1680)$ .
- 4 From a fit with contributions from  $\omega(782)$ ,  $\phi(1020)$ ,  $\omega(1420)$ , and  $\omega(1650)$ .
- 5 From the combined fit of ANTONELLI 92, ACHASOV 01E, ACHASOV 02E, and ACHASOV 03D data on the  $\pi^+\pi^-\pi^0$  and ANTONELLI 92 on the  $\omega\pi^+\pi^-$  final states. Supersedes ACHASOV 99E and ACHASOV 02E.
- 6 Using results of CORDIER 81 and preliminary data of DOLINSKY 91 and ANTONELLI 92.
- 7 Using the data of AKHMETSHIN 00D and ANTONELLI 92. The  $\rho\pi$  dominance for the energy dependence of the  $\omega(1420)$  and  $\omega(1650)$  width assumed.
- 8 Using data from BARKOV 87, DOLINSKY 91, and ANTONELLI 92.
- 9 Using the data from ANTONELLI 92.
- 10 Using the data from IVANOV 81 and BISELLO 88B.
- 11 Using the data from BISELLO 91c.
- 12 From a fit to two Breit-Wigner functions and using the data of DOLINSKY 91 and ANTONELLI 92.
- 13 From the combined fit of the  $\rho\pi$  and  $\omega\pi\pi$  final states.

### $\omega(1650)$ WIDTH

VALUE (MeV)	EVTS	DOCUMENT ID	TECN	COMMENT
<b>315 ± 35 OUR ESTIMATE</b>				
• • • We do not use the following data for averages, fits, limits, etc. • • •				
$194 \pm 8^{+15}_{-7}$	183k	1 ABLIKIM	19AQ	BES $J/\psi \rightarrow K^+K^-\pi^0$
$95 \pm 11$		ACHASOV	19	SND $e^+e^- \rightarrow \pi^+\pi^-\pi^0\eta$
$113 \pm 9 \pm 10$	824	2 AKHMETSHIN	17A	CMD3 $1.4-2.0 e^+e^- \rightarrow \omega\eta$
$110 \pm 20$	898	3 ACHASOV	16B	SND $1.34-2.00 e^+e^- \rightarrow \omega\eta$
$310 \pm 30$	13.1k	4 AULCHENKO	15A	SND $1.05-1.80 e^+e^- \rightarrow \omega\eta$
$222 \pm 25 \pm 20$		AUBERT	07AU	BABR $10.6 e^+e^- \rightarrow \omega\pi^+\pi^-\gamma$
$114 \pm 14$	13	AUBERT	06D	BABR $10.6 e^+e^- \rightarrow \omega\eta\eta$
$230 \pm 30 \pm 20$		AUBERT,B	04N	BABR $10.6 e^+e^- \rightarrow \pi^+\pi^-\pi^0\gamma$
$490^{+200}_{-150} \pm 130$	1.2M	5 ACHASOV	03D	RVUE $0.44-2.00 e^+e^- \rightarrow \pi^+\pi^-\pi^0$
$250 \pm 14$		6 HENNER	02	RVUE $1.2-2.0 e^+e^- \rightarrow \rho\pi, \omega\pi\pi$
$250 \pm 50$		EUGENIO	01	SPEC $18 \pi^-\rho \rightarrow \omega\eta\eta$
$370 \pm 25$	612	7 AKHMETSHIN	00D	CMD2 $e^+e^- \rightarrow \omega\pi^+\pi^-$
$113 \pm 20$		8 CLEGG	94	RVUE
$280 \pm 24$	750	9 ANTONELLI	92	DM2 $1.34-2.4e^+e^- \rightarrow \rho\pi, \omega\pi\pi$
$160 \pm 20$		ATKINSON	83B	OMEG $20-70 \gamma\rho \rightarrow 3\pi X$
$136 \pm 46$		CORDIER	81	DM1 $e^+e^- \rightarrow \omega 2\pi$
$99 \pm 49$	21	ESPOSITO	80	FRAM $e^+e^- \rightarrow 3\pi$
$42 \pm 17$		COSME	79	OSPK $e^+e^- \rightarrow 3\pi$

- 1 Could also be  $\rho(1700)$ . Branching ratio  $J/\psi \rightarrow X \pi^0 \rightarrow K^+K^-\pi^0 = (5.3 \pm 0.3^{+0.6}_{-0.5}) \times 10^{-5}$ .
- 2 From a fit of the interfering  $\omega(1420)$  and  $\omega(1650)$  with a relative phase of  $\pi$  and other parameters floating.
- 3 From a fit with contributions from  $\omega(1420)$ ,  $\omega(1650)$ , and  $\phi(1680)$ .
- 4 From a fit with contributions from  $\omega(782)$ ,  $\phi(1020)$ ,  $\omega(1420)$ , and  $\omega(1650)$ .
- 5 From the combined fit of ANTONELLI 92, ACHASOV 01E, ACHASOV 02E, and ACHASOV 03D data on the  $\pi^+\pi^-\pi^0$  and ANTONELLI 92 on the  $\omega\pi^+\pi^-$  final states. Supersedes ACHASOV 99E and ACHASOV 02E.
- 6 Using results of CORDIER 81 and preliminary data of DOLINSKY 91 and ANTONELLI 92.
- 7 Using the data of AKHMETSHIN 00D and ANTONELLI 92. The  $\rho\pi$  dominance for the energy dependence of the  $\omega(1420)$  and  $\omega(1650)$  width assumed.
- 8 From a fit to two Breit-Wigner functions and using the data of DOLINSKY 91 and ANTONELLI 92.
- 9 From the combined fit of the  $\rho\pi$  and  $\omega\pi\pi$  final states.

### $\omega(1650)$ DECAY MODES

Mode	Fraction ( $\Gamma_i/\Gamma$ )
$\Gamma_1$ $\rho\pi$	seen
$\Gamma_2$ $\omega\pi\pi$	seen
$\Gamma_3$ $\omega\eta$	seen
$\Gamma_4$ $e^+e^-$	seen
$\Gamma_5$ $\pi^0\gamma$	not seen

### $\omega(1650) \Gamma(\rho\pi)/\Gamma^2(\text{total})$

VALUE (units $10^{-6}$ )	EVTS	DOCUMENT ID	TECN	COMMENT
• • • We do not use the following data for averages, fits, limits, etc. • • •				
$1.56 \pm 0.23$	13.1k	1 AULCHENKO	15A	SND $1.05-1.80 e^+e^- \rightarrow \pi^+\pi^-\pi^0$
$1.3 \pm 0.1 \pm 0.1$		AUBERT,B	04N	BABR $10.6 e^+e^- \rightarrow \pi^+\pi^-\pi^0\gamma$
$1.2^{+0.4}_{-0.1} \pm 0.8$	1.2M	2,3 ACHASOV	03D	RVUE $0.44-2.00 e^+e^- \rightarrow \pi^+\pi^-\pi^0$
$0.921 \pm 0.230$		4,5 CLEGG	94	RVUE
$0.479 \pm 0.050$	750	6,7 ANTONELLI	92	DM2 $1.34-2.4e^+e^- \rightarrow \rho\pi,$

- 1 From a fit with contributions from  $\omega(782)$ ,  $\phi(1020)$ ,  $\omega(1420)$ , and  $\omega(1650)$ .
- 2 Calculated by us from the cross section at the peak.
- 3 From the combined fit of ANTONELLI 92, ACHASOV 01E, ACHASOV 02E, and ACHASOV 03D data on the  $\pi^+\pi^-\pi^0$  and ANTONELLI 92 on the  $\omega\pi^+\pi^-$  final states. Supersedes ACHASOV 99E and ACHASOV 02E.
- 4 From a fit to two Breit-Wigner functions and using the data of DOLINSKY 91 and ANTONELLI 92.
- 5 From the partial and leptonic width given by the authors.
- 6 From the combined fit of the  $\rho\pi$  and  $\omega\pi\pi$  final states.
- 7 From the product of the leptonic width and partial branching ratio given by the authors.

### $\Gamma(\omega\pi\pi)/\Gamma_{\text{total}} \times \Gamma(e^+e^-)/\Gamma_{\text{total}}$

VALUE (units $10^{-7}$ )	EVTS	DOCUMENT ID	TECN	COMMENT
• • • We do not use the following data for averages, fits, limits, etc. • • •				
$7.0 \pm 0.5$		AUBERT	07AU	BABR $10.6 e^+e^- \rightarrow \omega\pi^+\pi^-\gamma$
$4.1 \pm 0.9 \pm 1.3$	1.2M	1,2 ACHASOV	03D	RVUE $0.44-2.00 e^+e^- \rightarrow \pi^+\pi^-\pi^0$
$5.40 \pm 0.95$		3 AKHMETSHIN	00D	CMD2 $1.2-1.38 e^+e^- \rightarrow \omega\pi^+\pi^-$
$3.18 \pm 0.80$		4,5 CLEGG	94	RVUE
$6.07 \pm 0.61$	750	6,7 ANTONELLI	92	DM2 $1.34-2.4 e^+e^- \rightarrow \rho\pi, \omega\pi\pi$

- 1 Calculated by us from the cross section at the peak.
- 2 From the combined fit of ANTONELLI 92, ACHASOV 01E, ACHASOV 02E, and ACHASOV 03D data on the  $\pi^+\pi^-\pi^0$  and ANTONELLI 92 on the  $\omega\pi^+\pi^-$  final states. Supersedes ACHASOV 99E and ACHASOV 02E.
- 3 Using the data of AKHMETSHIN 00D and ANTONELLI 92. The  $\rho\pi$  dominance for the energy dependence of the  $\omega(1420)$  and  $\omega(1650)$  width assumed.
- 4 From a fit to two Breit-Wigner functions and using the data of DOLINSKY 91 and ANTONELLI 92.
- 5 From the partial and leptonic width given by the authors.
- 6 From the combined fit of the  $\rho\pi$  and  $\omega\pi\pi$  final states.
- 7 From the product of the leptonic width and partial branching ratio given by the authors.

### $\Gamma(\omega\eta)/\Gamma_{\text{total}} \times \Gamma(e^+e^-)/\Gamma_{\text{total}}$

VALUE (units $10^{-7}$ )	EVTS	DOCUMENT ID	TECN	COMMENT
• • • We do not use the following data for averages, fits, limits, etc. • • •				
$5.62^{+0.45}_{-0.42}$		ACHASOV	19	SND $e^+e^- \rightarrow \pi^+\pi^-\pi^0\eta$
$4.5 \pm 0.3 \pm 0.3$	824	1 AKHMETSHIN	17A	CMD3 $1.4-2.0 e^+e^- \rightarrow \omega\eta$
$4.4 \pm 0.5$	898	2 ACHASOV	16B	SND $1.34-2.00 e^+e^- \rightarrow \omega\eta$
$5.7 \pm 0.6$	13	AUBERT	06D	BABR $10.6 e^+e^- \rightarrow \omega\eta\eta$
$< 60$ at 90% CL		3 AKHMETSHIN	03B	CMD2 $e^+e^- \rightarrow \eta\pi^0\gamma$

- 1 From a fit of the interfering  $\omega(1420)$  and  $\omega(1650)$  with a relative phase of  $\pi$  and other parameters floating. From an alternative fit  $\Gamma(\omega(1650) \rightarrow \omega\eta)/\Gamma_{\text{total}} \times \Gamma(\omega(1650) \rightarrow e^+e^-) = 51 \pm 3$  eV.
- 2 From a fit with contributions from  $\omega(1420)$ ,  $\omega(1650)$ , and  $\phi(1680)$ .
- 3  $\omega(1650)$  mass and width fixed at 1700 MeV and 250 MeV, respectively.

### $\omega(1650)$ BRANCHING RATIOS

$\Gamma(\rho\pi)/\Gamma_{\text{total}}$	VALUE	EVTS	DOCUMENT ID	TECN	COMMENT
• • • We do not use the following data for averages, fits, limits, etc. • • •					
$\sim 0.65$	1.2M	1	ACHASOV	03D	RVUE $0.44-2.00 e^+e^- \rightarrow \pi^+\pi^-\pi^0$
$0.380 \pm 0.014$		2	HENNER	02	RVUE $1.2-2.0 e^+e^- \rightarrow \rho\pi, \omega\pi\pi$
1 From the combined fit of ANTONELLI 92, ACHASOV 01E, ACHASOV 02E, and ACHASOV 03D data on the $\pi^+\pi^-\pi^0$ and ANTONELLI 92 on the $\omega\pi^+\pi^-$ final states. Supersedes ACHASOV 99E and ACHASOV 02E.					
2 Assuming that the $\omega(1650)$ decays into $\rho\pi$ and $\omega\pi\pi$ only.					

### $\Gamma(\omega\pi\pi)/\Gamma_{\text{total}}$

VALUE	EVTS	DOCUMENT ID	TECN	COMMENT	
• • • We do not use the following data for averages, fits, limits, etc. • • •					
$\sim 0.35$	1.2M	1	ACHASOV	03D	RVUE $0.44-2.00 e^+e^- \rightarrow \pi^+\pi^-\pi^0$
$0.620 \pm 0.014$		2	HENNER	02	RVUE $1.2-2.0 e^+e^- \rightarrow \rho\pi, \omega\pi\pi$
1 From the combined fit of ANTONELLI 92, ACHASOV 01E, ACHASOV 02E, and ACHASOV 03D data on the $\pi^+\pi^-\pi^0$ and ANTONELLI 92 on the $\omega\pi^+\pi^-$ final states. Supersedes ACHASOV 99E and ACHASOV 02E.					
2 Assuming that the $\omega(1650)$ decays into $\rho\pi$ and $\omega\pi\pi$ only.					

See key on page 999

# Meson Particle Listings

## $\omega(1650), \omega_3(1670), \pi_2(1670)$

$\Gamma(e^+e^-)/\Gamma_{total}$

VALUE (units $10^{-7}$ )	EVTS	DOCUMENT ID	TECN	COMMENT
$\sim 18$	1.2M	<sup>1,2</sup> ACHASOV	03D	RVUE $0.44-2.00 e^+e^- \rightarrow \pi^+\pi^-\pi^0$
$32 \pm 1$		<sup>2</sup> HENNER	02	RVUE $1.2-2.0 e^+e^- \rightarrow \rho\pi, \omega\pi\pi$

<sup>1</sup> Calculated by us from the cross section at the peak.  
<sup>2</sup> Assuming that the  $\omega(1650)$  decays into  $\rho\pi$  and  $\omega\pi\pi$  only.

$\Gamma(\pi^0\gamma)/\Gamma_{total}$

VALUE	DOCUMENT ID	TECN	COMMENT
not seen	<sup>1</sup> ACHASOV	10D	SND $1.075-2.0 e^+e^- \rightarrow \pi^0\gamma$

<sup>1</sup> From a fit of a VMD model with two effective resonances with masses of 1450 MeV and 1700 MeV to describe the excited vector states  $\omega(1420), \rho(1450), \omega(1650)$ , and  $\rho(1700)$ . The width of the highest mass effective resonance is fixed at 315 MeV.

**$\omega(1650)$  REFERENCES**

ABBREVIATION	YEAR	PAPER	AUTHORS	COLLABORATION
ABLIKIM	19A	Q	D100 032004	M. Ablikim et al. (BESIII Collab.)
ACHASOV	19	PR	D99 112004	M.N. Achasov et al. (SND Collab.)
AKHMETSHIN	17A	PL	B773 150	R.R. Akhmetshin et al. (CMD-3 Collab.)
ACHASOV	16B	PR	D94 092002	M.N. Achasov et al. (SND Collab.)
AULCHENKO	15A	JETP	121 27	V.M. Aulchenko et al. (SND Collab.)
ACHASOV	10D	PR	D98 112001	M.N. Achasov et al. (SND Collab.)
AUBERT	07AU	PR	D76 092005	B. Aubert et al. (BABAR Collab.)
AUBERT	06D	PR	D73 052003	B. Aubert et al. (BABAR Collab.)
AUBERT	04N	PR	D70 072004	B. Aubert et al. (BABAR Collab.)
ACHASOV	03D	PR	D68 052006	M.N. Achasov et al. (Novosibirsk SND Collab.)
AKHMETSHIN	03B	PL	B562 173	R.R. Akhmetshin et al. (Novosibirsk CMD-2 Collab.)
ACHASOV	02E	PR	D66 032001	M.N. Achasov et al. (Novosibirsk SND Collab.)
HENNER	02	EPJ	C26 3	V.K. Henner et al.
ACHASOV	01E	PR	D63 072002	M.N. Achasov et al. (Novosibirsk SND Collab.)
EUGENIO	01	PL	B497 190	P. Eugenio et al.
AKHMETSHIN	00D	PL	B489 125	R.R. Akhmetshin et al. (Novosibirsk CMD-2 Collab.)
ACHASOV	99E	PL	B462 365	M.N. Achasov et al. (Novosibirsk SND Collab.)
ACHASOV	98H	PR	D57 4334	M.N. Achasov et al. (Novosibirsk SND Collab.)
CLEGG	94	ZPHY	C62 455	A.B. Clegg, A. Donnachie (LANC, MCHS)
ANTONELLI	92	ZPHY	C56 15	A. Antonelli et al. (DM2 Collab.)
BISELLO	91C	ZPHY	C52 227	D. Bisello et al. (DM2 Collab.)
DOLINSKY	91	PR	L202 99	S.I. Dolinsky et al. (NOVO)
BISELLO	88B	ZPHY	C39 13	D. Bisello et al. (PADO, CLER, FRAS+)
BARKOV	87	JETPL	46 164	L.M. Barkov et al. (NOVO)
ATKINSON	83B	PL	127B 132	M. Atkinson et al. (BONN, CERN, GLAS+)
CORDIER	81	PL	106B 155	A. Cordier et al. (ORSAY)
IVANOV	81	PL	107B 297	P.M. Ivanov et al. (NOVO)
ESPOSITO	80	LNC	28 195	B. Esposito et al. (FRAS, NAPL, PADO+)
COSME	79	NP	B152 215	G. Cosme et al. (IPN)

**$\omega_3(1670)$**

$I^G(J^{PC}) = 0^-(3^{--})$

**$\omega_3(1670)$  MASS**

VALUE (MeV)	EVTS	DOCUMENT ID	TECN	COMMENT
<b>1667 ± 4</b>	<b>OUR AVERAGE</b>			
1665.3 ± 5.2 ± 4.5	23400	AMELIN	96	VES $36 \pi^-p \rightarrow \pi^+\pi^-\pi^0 n$
1685 ± 20	60	BAUBILLIER	79	HBC $8.2 K^-p$ backward
1673 ± 12	430	<sup>1,2</sup> BALTAY	78E	HBC $15 \pi^+p \rightarrow \Delta 3\pi$
1650 ± 12		CORDEN	78B	OMEG $8-12 \pi^-p \rightarrow N3\pi$
1669 ± 11	600	<sup>2</sup> WAGNER	75	HBC $7 \pi^+p \rightarrow \Delta^{++} 3\pi$
1678 ± 14	500	DIAZ	74	DBC $6 \pi^+n \rightarrow p 3\pi^0$
1660 ± 13	200	DIAZ	74	DBC $6 \pi^+n \rightarrow p \omega \pi^0 \pi^0$
1679 ± 17	200	MATTHEWS	71D	DBC $7.0 \pi^+n \rightarrow p 3\pi^0$
1670 ± 20		KENYON	69	DBC $8 \pi^+n \rightarrow p 3\pi^0$
$\sim 1700$	110	<sup>1</sup> CERRADA	77B	HBC $4.2 K^-p \rightarrow \Lambda 3\pi$
1695 ± 20		BARNES	69B	HBC $4.6 K^-p \rightarrow \omega 2\pi X$
1636 ± 20		ARMENISE	68B	DBC $5.1 \pi^+n \rightarrow p 3\pi^0$

<sup>1</sup> Phase rotation seen for  $J^P = 3^- \rho\pi$  wave.  
<sup>2</sup> From a fit to  $I(J^P) = 0(3^-) \rho\pi$  partial wave.

**$\omega_3(1670)$  WIDTH**

VALUE (MeV)	EVTS	DOCUMENT ID	TECN	COMMENT
<b>168 ± 10</b>	<b>OUR AVERAGE</b>			
149 ± 19 ± 7	23400	AMELIN	96	VES $36 \pi^-p \rightarrow \pi^+\pi^-\pi^0 n$
160 ± 80	60	<sup>3</sup> BAUBILLIER	79	HBC $8.2 K^-p$ backward
173 ± 16	430	<sup>4,5</sup> BALTAY	78E	HBC $15 \pi^+p \rightarrow \Delta 3\pi$
253 ± 39		CORDEN	78B	OMEG $8-12 \pi^-p \rightarrow N3\pi$
173 ± 28	600	<sup>3,5</sup> WAGNER	75	HBC $7 \pi^+p \rightarrow \Delta^{++} 3\pi$
167 ± 40	500	DIAZ	74	DBC $6 \pi^+n \rightarrow p 3\pi^0$
122 ± 39	200	DIAZ	74	DBC $6 \pi^+n \rightarrow p \omega \pi^0 \pi^0$
155 ± 40	200	<sup>3</sup> MATTHEWS	71D	DBC $7.0 \pi^+n \rightarrow p 3\pi^0$
90 ± 20		BARNES	69B	HBC $4.6 K^-p \rightarrow \omega 2\pi$
100 ± 40		KENYON	69	DBC $8 \pi^+n \rightarrow p 3\pi^0$
112 ± 60		ARMENISE	68B	DBC $5.1 \pi^+n \rightarrow p 3\pi^0$

<sup>3</sup> Width errors enlarged by us to  $4\Gamma/\sqrt{N}$ ; see the note with the  $K^*(892)$  mass.  
<sup>4</sup> Phase rotation seen for  $J^P = 3^- \rho\pi$  wave.  
<sup>5</sup> From a fit to  $I(J^P) = 0(3^-) \rho\pi$  partial wave.

**$\omega_3(1670)$  DECAY MODES**

Mode	Fraction ( $\Gamma_i/\Gamma$ )
$\Gamma_1 \rho\pi$	seen
$\Gamma_2 \omega\pi\pi$	seen
$\Gamma_3 b_1(1235)\pi$	possibly seen

**$\omega_3(1670)$  BRANCHING RATIOS**

$\Gamma(\omega\pi\pi)/\Gamma(\rho\pi)$

VALUE	EVTS	DOCUMENT ID	TECN	COMMENT
$0.71 \pm 0.27$	100	DIAZ	74	DBC $6 \pi^+n \rightarrow p 5\pi^0$

$\Gamma(b_1(1235)\pi)/\Gamma(\rho\pi)$

VALUE	DOCUMENT ID	TECN	COMMENT
possibly seen	DIAZ	74	DBC $6 \pi^+n \rightarrow p 5\pi^0$

$\Gamma(b_1(1235)\pi)/\Gamma(\omega\pi\pi)$

VALUE	CL%	DOCUMENT ID	TECN	COMMENT
$>0.75$	68	BAUBILLIER	79	HBC $8.2 K^-p$ backward

• • • We do not use the following data for averages, fits, limits, etc. • • •

**$\omega_3(1670)$  REFERENCES**

ABBREVIATION	YEAR	PAPER	AUTHORS	COLLABORATION
AMELIN	96	ZPHY	C70 71	D.V. Amelin et al. (SERP, TBIL)
BAUBILLIER	79	PL	B9B 131	M. Baubillier et al. (BIRM, CERN, GLAS+)
BALTAY	78E	PR	L40 87	C. Baltay, C.V. Cautis, M. Kaelker (COLU)JP
CORDEN	78B	NP	B138 235	M.J. Corden et al. (BIRM, RHEL, TELA+)
CERRADA	77B	NP	B126 241	M. Cerrada et al. (AMST, CERN, NUMJ+JP)
WAGNER	75	PL	S8B 201	F. Wagner, M. Tabak, D.M. Chew (LBL)JP
DIAZ	74	PR	L32 260	J. Diaz et al. (CASE, CMU)
MATTHEWS	71D	PR	D3 2561	J.A.J. Matthews et al. (TNTO, WISC)
BARNES	69B	PR	L23 142	V.E. Barnes et al. (BNL)
KENYON	69	PR	L23 146	I.R. Kenyon et al. (BNL, UCND, ORNL)
ARMENISE	68B	PL	B26B 336	N. Armenise et al. (BARI, BGNA, FIRZ+)

**$\pi_2(1670)$**

$I^G(J^{PC}) = 1^-(2^{-+})$

**$\pi_2(1670)$  MASS**

VALUE (MeV)	EVTS	DOCUMENT ID	TECN	CHG	COMMENT
<b>1670.6 ± 1.9</b>	<b>OUR AVERAGE</b>				
1642 ± $\frac{+12}{-1}$	46M	<sup>1</sup> AGHASYAN	18B	COMP	$190 \pi^-p \rightarrow \pi^-\pi^+\pi^-p$
1749 ± 10 ± 100	145k	LU	05	B852	$18 \pi^-p \rightarrow \omega\pi^-\pi^0 p$
1676 ± 3 ± 8		<sup>2</sup> CHUNG	02	B852	$18.3 \pi^-p \rightarrow \pi^+\pi^-\pi^-p$
1685 ± 10 ± 30		BARBERIS	01		$450 pp \rightarrow pf 3\pi^0 p_S$
1687 ± 9 ± 15		AMELIN	99	VES	$37 \pi^-A \rightarrow \omega\pi^-\pi^0 A^*$
1669 ± 4		BARBERIS	98B		$450 pp \rightarrow pf \rho\pi p_S$
1670 ± 4		BARBERIS	98B		$450 pp \rightarrow pf f_2(1270) \pi p_S$
1690 ± 14		<sup>3</sup> BERDNIKOV	94	VES	$37 \pi^-A \rightarrow K^+ K^- \pi^- A$
1710 ± 20	700	ANTIPOV	87	SIGM	$50 \pi^-Cu \rightarrow \mu^+ \mu^- \pi^- Cu$
1676 ± 6		<sup>3</sup> EVANGELIS...	81	OMEG	$12 \pi^-p \rightarrow 3\pi p$
1657 ± 14		<sup>3,4</sup> DAUM	80D	SPEC	$63-94 \pi p \rightarrow 3\pi X$
1662 ± 10	2000	<sup>3</sup> BALTAY	77	HBC	$15 \pi^+p \rightarrow p 3\pi$

• • • We do not use the following data for averages, fits, limits, etc. • • •

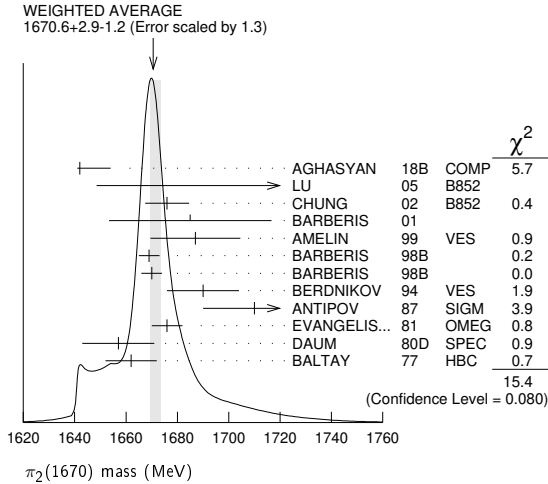
1658 ± 3 ± $\frac{+24}{-8}$	420k	<sup>5</sup> ALEKSEEV	10	COMP	$190 \pi^-p \rightarrow \pi^-\pi^-\pi^+\pi^+ p'$
1730 ± 20		<sup>6</sup> AMELIN	95B	VES	$36 \pi^-A \rightarrow \pi^+\pi^-\pi^- A$
1742 ± 31 ± 49		ANTREASYAN	90	CBAL	$e^+e^- \rightarrow e^+e^-\pi^0\pi^0\pi^0$
1624 ± 21		<sup>2</sup> BELLINI	85	SPEC	$40 \pi^-A \rightarrow \pi^-\pi^+\pi^- A$
1622 ± 35		<sup>7</sup> BELLINI	85	SPEC	$40 \pi^-A \rightarrow \pi^-\pi^+\pi^- A$
1693 ± 28		<sup>8</sup> BELLINI	85	SPEC	$40 \pi^-A \rightarrow \pi^-\pi^+\pi^- A$
1710 ± 20		<sup>9</sup> DAUM	81B	SPEC	$63,94 \pi^-p$
1660 ± 10		<sup>3</sup> ASCOLI	73	HBC	$5-25 \pi^-p \rightarrow p 2\pi$

<sup>1</sup> Statistical error negligible.  
<sup>2</sup> From  $f_2(1270)\pi$  decay.  
<sup>3</sup> From a fit to  $J^P = 2^- S$ -wave  $f_2(1270)\pi$  partial wave.  
<sup>4</sup> Clear phase rotation seen in  $2^- S, 2^- P, 2^- D$  waves. We quote central value and spread of single-resonance fits to three channels.  
<sup>5</sup> Superseded by AGHASYAN 2018B.  
<sup>6</sup>  $J^PC$  ambiguous.

# Meson Particle Listings

## $\pi_2(1670)$

<sup>7</sup> From  $\rho\pi$  decay.  
<sup>8</sup> From  $\sigma\pi$  decay.  
<sup>9</sup> From a two-resonance fit to four  $2^-0^+$  waves. This should not be averaged with all the single resonance fits.



### $\pi_2(1670)$ WIDTH

VALUE (MeV)	EVTS	DOCUMENT ID	TECN	CHG	COMMENT
<b>258<sup>+</sup><sub>-9</sub></b>	<b>OUR AVERAGE</b>	Error includes scale factor of 1.2.			
311 <sup>+</sup> <sub>-23</sub>	46M	<sup>10</sup> AGHASYAN	18B	COMP	190 $\pi^- p \rightarrow \pi^- \pi^+ \pi^- p$
408 <sup>+</sup> <sub>60 ± 250</sub>	145k	LU	05	B852	18 $\pi^- p \rightarrow \omega \pi^- \pi^0 p$
254 <sup>+</sup> <sub>3 ± 31</sub>		<sup>11</sup> CHUNG	02	B852	18.3 $\pi^- p \rightarrow \pi^+ \pi^- \pi^- p$
265 <sup>+</sup> <sub>30 ± 40</sub>		BARBERIS	01		450 $\rho p \rightarrow \rho_f 3\pi^0 p_s$
168 <sup>+</sup> <sub>43 ± 53</sub>		AMELIN	99	VES	37 $\pi^- A \rightarrow \omega \pi^- \pi^0 A^*$
268 <sup>+</sup> <sub>15</sub>		BARBERIS	98B		450 $\rho p \rightarrow \rho_f \rho \pi p_s$
256 <sup>+</sup> <sub>15</sub>		BARBERIS	98B		450 $\rho p \rightarrow \rho_f f_2(1270) \pi p_s$
190 <sup>+</sup> <sub>50</sub>		<sup>12</sup> BERDNIKOV	94	VES	37 $\pi^- A \rightarrow K^+ K^- \pi^- A$
170 <sup>+</sup> <sub>80</sub>	700	ANTIPOV	87	SIGM	50 $\pi^- Cu \rightarrow \mu^+ \mu^- \pi^- Cu$
260 <sup>+</sup> <sub>20</sub>		<sup>12</sup> EVANGELIS...	81	OMEG	12 $\pi^- p \rightarrow 3\pi p$
219 <sup>+</sup> <sub>20</sub>		<sup>12,13</sup> DAUM	80D	SPEC	63-94 $\pi p \rightarrow 3\pi X$
285 <sup>+</sup> <sub>60</sub>	2000	<sup>12</sup> BALTAY	77	HBC	15 $\pi^+ p \rightarrow \rho 3\pi$
••• We do not use the following data for averages, fits, limits, etc. •••					
271 <sup>+</sup> <sub>9<sup>+</sup><sub>24</sub></sub>	420k	<sup>14</sup> ALEKSEEV	10	COMP	190 $\pi^- Pb \rightarrow \pi^- \pi^- \pi^+ Pb'$
310 <sup>+</sup> <sub>20</sub>		<sup>15</sup> AMELIN	95B	VES	36 $\pi^- A \rightarrow \pi^+ \pi^- \pi^- A$
236 <sup>+</sup> <sub>49 ± 36</sub>		ANTREASYAN	90	CBAL	$e^+ e^- \rightarrow \pi^0 \pi^0 \pi^0$
304 <sup>+</sup> <sub>22</sub>		<sup>11</sup> BELLINI	85	SPEC	40 $\pi^- A \rightarrow \pi^- \pi^+ \pi^- A$
404 <sup>+</sup> <sub>±108</sub>		<sup>16</sup> BELLINI	85	SPEC	40 $\pi^- A \rightarrow \pi^- \pi^+ \pi^- A$
330 <sup>+</sup> <sub>90</sub>		<sup>17</sup> BELLINI	85	SPEC	40 $\pi^- A \rightarrow \pi^- \pi^+ \pi^- A$
312 <sup>+</sup> <sub>50</sub>		<sup>18</sup> DAUM	81B	SPEC	63,94 $\pi^- p$
270 <sup>+</sup> <sub>60</sub>		<sup>12</sup> ASCOLI	73	HBC	5-25 $\pi^- p \rightarrow \rho \pi_2$

<sup>10</sup> Statistical error negligible.  
<sup>11</sup> From  $f_2(1270)\pi$  decay.  
<sup>12</sup> From a fit to  $J^P = 2^- 2^- f_2(1270)\pi$  partial wave.  
<sup>13</sup> Clear phase rotation seen in  $2^-S, 2^-P, 2^-D$  waves. We quote central value and spread of single-resonance fits to three channels.  
<sup>14</sup> Superseded by AGHASYAN 2018B.  
<sup>15</sup>  $J^{PC}$  ambiguous.  
<sup>16</sup> From  $\rho\pi$  decay.  
<sup>17</sup> From  $\sigma\pi$  decay.  
<sup>18</sup> From a two-resonance fit to four  $2^-0^+$  waves. This should not be averaged with all the single resonance fits.

### $\pi_2(1670)$ DECAY MODES

Mode	Fraction ( $\Gamma_i/\Gamma$ )	Confidence level
$\Gamma_1$ $3\pi$	(95.8 ± 1.4) %	
$\Gamma_2$ $\pi^+ \pi^- \pi^0$		
$\Gamma_3$ $\pi^0 \pi^0 \pi^0$		
$\Gamma_4$ $f_2(1270)\pi$	(56.3 ± 3.2) %	
$\Gamma_5$ $\rho\pi$	(31 ± 4) %	

$\Gamma_6$ $\sigma\pi$	(10 ± 4) %	
$\Gamma_7$ $\pi(\pi\pi)_S$ -wave	(8.7 ± 3.4) %	
$\Gamma_8$ $\pi^+ \pi^+ \pi^-$	(53 ± 4) %	
$\Gamma_9$ $K\bar{K}^*(892) + c.c.$	(4.2 ± 1.4) %	
$\Gamma_{10}$ $\omega\rho$	(2.7 ± 1.1) %	
$\Gamma_{11}$ $\pi^\pm \gamma$	(7.0 ± 1.2) × 10 <sup>-4</sup>	
$\Gamma_{12}$ $\gamma\gamma$	< 2.8 × 10 <sup>-7</sup>	90%
$\Gamma_{13}$ $\eta\pi$	< 5 %	
$\Gamma_{14}$ $\pi^\pm 2\pi^+ 2\pi^-$	< 5 %	
$\Gamma_{15}$ $\rho(1450)\pi$	< 3.6 × 10 <sup>-3</sup>	97.7%
$\Gamma_{16}$ $b_1(1235)\pi$	< 1.9 × 10 <sup>-3</sup>	97.7%
$\Gamma_{17}$ $\eta 3\pi$		
$\Gamma_{18}$ $f_1(1285)\pi$	possibly seen	
$\Gamma_{19}$ $a_2(1320)\pi$	not seen	

### CONSTRAINED FIT INFORMATION

An overall fit to 4 branching ratios uses 6 measurements and one constraint to determine 4 parameters. The overall fit has a  $\chi^2 = 1.9$  for 3 degrees of freedom.

The following off-diagonal array elements are the correlation coefficients  $\langle \delta x_i \delta x_j \rangle / (\delta x_i \delta x_j)$ , in percent, from the fit to the branching fractions,  $x_i \equiv \Gamma_i/\Gamma_{total}$ . The fit constrains the  $x_i$  whose labels appear in this array to sum to one.

$x_5$	-53		
$x_7$	-29	-59	
$x_9$	-8	-21	-9
	$x_4$	$x_5$	$x_7$

### $\pi_2(1670)$ PARTIAL WIDTHS

$\Gamma(\pi^\pm \gamma)$	VALUE (keV)	DOCUMENT ID	TECN	CHG	COMMENT	$\Gamma_{11}$	
<b>181 ± 11 ± 27</b>		<sup>19</sup> ADOLPH	14	COMP	190 $\pi^- Pb \rightarrow \pi^+ \pi^- \pi^- Pb'$		
<sup>19</sup> Primakoff reaction. Assumes incoherent $f_2(1270)\pi$ contribution to $3\pi$ final state and uses $B(\pi_2(1670) \rightarrow f_2\pi) = 56\%$ .							
$\Gamma(\gamma\gamma)$	VALUE (keV)	CL%	DOCUMENT ID	TECN	CHG	COMMENT	$\Gamma_{12}$
<b>&lt;0.072</b>		90	<sup>20</sup> ACCIARRI	97T	L3	$e^+ e^- \rightarrow e^+ e^- \pi^+ \pi^- \pi^0$	
••• We do not use the following data for averages, fits, limits, etc. •••							
	<0.19	90	<sup>20</sup> ALBRECHT	97B	ARG	$e^+ e^- \rightarrow e^+ e^- \pi^+ \pi^- \pi^0$	
	1.41 ± 0.23 ± 0.28		ANTREASYAN	90	CBAL	0 $e^+ e^- \rightarrow e^+ e^- \pi^0 \pi^0 \pi^0$	
	0.8 ± 0.3 ± 0.12		<sup>21</sup> BEHREND	90c	CELL	0 $e^+ e^- \rightarrow e^+ e^- \pi^+ \pi^- \pi^0$	
	1.3 ± 0.3 ± 0.2		<sup>22</sup> BEHREND	90c	CELL	0 $e^+ e^- \rightarrow e^+ e^- \pi^+ \pi^- \pi^0$	
<sup>20</sup> Decaying into $f_2(1270)\pi$ and $\rho\pi$ .							
<sup>21</sup> Constructive interference between $f_2(1270)\pi, \rho\pi$ and background.							
<sup>22</sup> Incoherent Ansatz.							

### $\pi_2(1670)$ $\Gamma(i)\Gamma(\gamma\gamma)/\Gamma(total)$

$\Gamma(\pi^+ \pi^- \pi^0) \times \Gamma(\gamma\gamma)/\Gamma_{total}$	VALUE (keV)	CL%	DOCUMENT ID	TECN	COMMENT	$\Gamma_2 \Gamma_{12}/\Gamma$
<b>&lt;0.1</b>		95	<sup>23</sup> SCHEGELSKY	06	RVUE $\gamma\gamma \rightarrow \pi^+ \pi^- \pi^0$	
<sup>23</sup> From analysis of L3 data at 183-209 GeV.						

### $\pi_2(1670)$ BRANCHING RATIOS

$\Gamma(3\pi)/\Gamma_{total}$	VALUE	DOCUMENT ID	TECN	COMMENT	$\Gamma_1/\Gamma = (\Gamma_4 + \Gamma_5 + \Gamma_7)/\Gamma$
<b>0.958 ± 0.014 OUR FIT</b>					
$\Gamma(\pi^0 \pi^0 \pi^0)/\Gamma(\pi^+ \pi^- \pi^0)$	VALUE	DOCUMENT ID	COMMENT	$\Gamma_3/\Gamma_2$	
<b>0.29 ± 0.03 ± 0.05</b>		BARBERIS 01	450 $\rho p \rightarrow \rho_f 3\pi^0 p_s$		
$\Gamma(\rho\pi)/0.565\Gamma(f_2(1270)\pi)$	VALUE	DOCUMENT ID	TECN	COMMENT	$\Gamma_5/0.565\Gamma_4$
<b>0.97 ± 0.09 OUR AVERAGE</b>		Error includes scale factor of 1.9.			
0.76 ± 0.07 ± 0.10		CHUNG 02	B852	18.3 $\pi^- p \rightarrow \pi^+ \pi^- \pi^- p$	
1.01 ± 0.05		BARBERIS 98B		450 $\rho p \rightarrow \rho_f \pi^+ \pi^- \pi^0 p_s$	
$\Gamma(\sigma\pi)/\Gamma(f_2(1270)\pi)$	VALUE	DOCUMENT ID	TECN	COMMENT	$\Gamma_6/\Gamma_4$
<b>0.17 ± 0.02 ± 0.07</b>		CHUNG 02	B852	18.3 $\pi^- p \rightarrow \pi^+ \pi^- \pi^- p$	

See key on page 999

Meson Particle Listings

$\pi_2(1670)$ ,  $\phi(1680)$

••• We do not use the following data for averages, fits, limits, etc. •••  
 0.24±0.10 24,25 BAKER 99 SPEC 1.94  $\bar{p}p \rightarrow 4\pi^0$

$\frac{1}{2}\Gamma(\rho\pi)/\Gamma(\pi^\pm\pi^+\pi^-)$   $\frac{1}{2}\Gamma_5/\Gamma_8 = \frac{1}{2}\Gamma_5/(0.565\Gamma_4 + \frac{1}{2}\Gamma_5 + 0.624\Gamma_7)$

VALUE	DOCUMENT ID	TECN	CHG	COMMENT
<b>0.29±0.04 OUR FIT</b>				
<b>0.29±0.05</b>	26 DAUM	81B	SPEC	63,94 $\pi^-p$
<0.3	BARTSCH	68	HBC	+ 8 $\pi^+p \rightarrow 3\pi p$

$0.565\Gamma(f_2(1270)\pi)/\Gamma(\pi^\pm\pi^+\pi^-)$   
 $0.565\Gamma_4/\Gamma_8 = 0.565\Gamma_4/(0.565\Gamma_4 + \frac{1}{2}\Gamma_5 + 0.624\Gamma_7)$   
 (With  $f_2(1270) \rightarrow \pi^+\pi^-$ )

VALUE	DOCUMENT ID	TECN	CHG	COMMENT
<b>0.604±0.035 OUR FIT</b>				
<b>0.60 ±0.05 OUR AVERAGE</b>	Error includes scale factor of 1.3.			
0.61 ±0.04	26 DAUM	81B	SPEC	63,94 $\pi^-p$
0.76 $\pm_{-0.34}^{+0.24}$	ARMENISE	69	DBC	+ 5.1 $\pi^+d \rightarrow d3\pi$
0.35 ±0.20	BALTAY	68	HBC	+ 7-8.5 $\pi^+p$
••• We do not use the following data for averages, fits, limits, etc. •••				
0.59	BARTSCH	68	HBC	+ 8 $\pi^+p \rightarrow 3\pi p$

$0.624\Gamma(\pi(\pi\pi)_{s\text{-wave}})/\Gamma(\pi^\pm\pi^+\pi^-)$   
 $0.624\Gamma_7/\Gamma_8 = 0.624\Gamma_7/(0.565\Gamma_4 + \frac{1}{2}\Gamma_5 + 0.624\Gamma_7)$   
 (With  $(\pi\pi)_{s\text{-wave}} \rightarrow \pi^+\pi^-$ )

VALUE	DOCUMENT ID	TECN	CHG	COMMENT
<b>0.10±0.04 OUR FIT</b>				
<b>0.10±0.05</b>	26 DAUM	81B	SPEC	63,94 $\pi^-p$

$\Gamma(K\bar{K}^*(892) + c.c.)/\Gamma(f_2(1270)\pi)$   $\Gamma_9/\Gamma_4$

VALUE	DOCUMENT ID	TECN	CHG	COMMENT
<b>0.075±0.025 OUR FIT</b>				
<b>0.075±0.025</b>	27 ARMSTRONG	82B	OMEG	- 16 $\pi^-p \rightarrow K^+K^-\pi^-p$

$\Gamma(\omega\rho)/\Gamma_{\text{total}}$   $\Gamma_{10}/\Gamma$

VALUE	DOCUMENT ID	TECN	CHG	COMMENT
<b>0.027±0.004±0.010</b>	28 AMELIN	99	VES	37 $\pi^-A \rightarrow \omega\pi^-\pi^0A^*$

$\Gamma(\eta\pi)/\Gamma(\pi^\pm\pi^+\pi^-)$   $\Gamma_{13}/\Gamma_8 = \Gamma_{13}/(0.565\Gamma_4 + \frac{1}{2}\Gamma_5 + 0.624\Gamma_7)$   
 (All  $\eta$  decays.)

VALUE	DOCUMENT ID	TECN	CHG	COMMENT
<0.09	BALTAY	68	HBC	+ 7-8.5 $\pi^+p$
••• We do not use the following data for averages, fits, limits, etc. •••				
<0.10	CRENNELL	70	HBC	- 6 $\pi^-p \rightarrow f_2\pi^-N$

$\Gamma(\pi^\pm 2\pi^+ 2\pi^-)/\Gamma(\pi^\pm\pi^+\pi^-)$   $\Gamma_{14}/\Gamma_8 = \Gamma_{14}/(0.565\Gamma_4 + \frac{1}{2}\Gamma_5 + 0.624\Gamma_7)$

VALUE	DOCUMENT ID	TECN	CHG	COMMENT
<0.10	CRENNELL	70	HBC	- 6 $\pi^-p \rightarrow f_2\pi^-N$
••• We do not use the following data for averages, fits, limits, etc. •••				
<0.1	BALTAY	68	HBC	+ 7,8.5 $\pi^+p$

$\Gamma(\rho(1450)\pi)/\Gamma_{\text{total}}$   $\Gamma_{15}/\Gamma$

VALUE	CL%	DOCUMENT ID	TECN	COMMENT
<0.0036	97.7	AMELIN	99	VES 37 $\pi^-A \rightarrow \omega\pi^-\pi^0A^*$

$\Gamma(b_1(1235)\pi)/\Gamma_{\text{total}}$   $\Gamma_{16}/\Gamma$

VALUE	CL%	DOCUMENT ID	TECN	COMMENT
<0.0019	97.7	AMELIN	99	VES 37 $\pi^-A \rightarrow \omega\pi^-\pi^0A^*$

$\Gamma(f_1(1285)\pi)/\Gamma_{\text{total}}$   $\Gamma_{18}/\Gamma$

VALUE	EVTS	DOCUMENT ID	TECN	COMMENT
possibly seen	69k	KUHN	04	B852 18 $\pi^-p \rightarrow \eta\pi^+\pi^-\pi^-p$

$\Gamma(a_2(1320)\pi)/\Gamma_{\text{total}}$   $\Gamma_{19}/\Gamma$

VALUE	EVTS	DOCUMENT ID	TECN	COMMENT
not seen	69k	KUHN	04	B852 18 $\pi^-p \rightarrow \eta\pi^+\pi^-\pi^-p$

**D-wave/S-wave RATIO FOR  $\pi_2(1670) \rightarrow f_2(1270)\pi$**

VALUE	DOCUMENT ID	TECN	COMMENT
<b>-0.18±0.06</b>	24 BAKER	99	SPEC 1.94 $\bar{p}p \rightarrow 4\pi^0$
••• We do not use the following data for averages, fits, limits, etc. •••			
0.22±0.10	26 DAUM	81B	SPEC 63,94 $\pi^-p$

**F-wave/P-wave RATIO FOR  $\pi_2(1670) \rightarrow \rho\pi$**

VALUE	DOCUMENT ID	TECN	COMMENT
<b>-0.72±0.07±0.14</b>	CHUNG	02	B852 18.3 $\pi^-p \rightarrow \pi^+\pi^-\pi^-p$

<sup>24</sup> Using preliminary CBAR data.  
<sup>25</sup> With the  $\sigma\pi$  in  $L=2$  and the  $f_2(1270)\pi$  in  $L=0$ .  
<sup>26</sup> From a two-resonance fit to four  $2^-0^+$  waves.  
<sup>27</sup> From a partial-wave analysis of  $K^+K^-\pi^-$  system.  
<sup>28</sup> Normalized to the  $B(\pi_2(1670) \rightarrow f_2\pi)$ .

**$\pi_2(1670)$  REFERENCES**

AGHASYAN 18B	PR D98 092003	M. Aghasyan et al.	(COMPASS Collab.)
ADOLPH 14	EPJ A50 79	C. Adolph et al.	(COMPASS Collab.)
ALEKSEEV 10	PRL 104 241803	M.G. Alekseev et al.	(COMPASS Collab.)
SCHEGELSKY 06	EPJ A27 199	V.A. Schegelsky et al.	
LU 05	PRL 94 032002	M. Lu et al.	(BNL E852 Collab.)
KUHN 04	PL B595 109	J. Kuhn et al.	(BNL E852 Collab.)
CHUNG 02	PR D65 072001	S.U. Chung et al.	(BNL E852 Collab.)
BARBERIS 01	PL B507 14	D. Barberis et al.	
AMELIN 99	PAN 62 445	D.V. Amelin et al.	(VES Collab.)
	Translated from YAF 62 487.		
BAKER 99	PL B449 114	C.A. Baker et al.	
BARBERIS 98B	PL B422 399	D. Barberis et al.	(WA 102 Collab.)
ACCIARRI 97T	PL B413 147	M. Acciarri et al.	(L3 Collab.)
ALBRECHT 97B	ZPHY C74 469	H. Albrecht et al.	(ARGUS Collab.)
AMELIN 95B	PL B356 595	D.V. Amelin et al.	(SERP, TBIL)
BERDNIKOV 94	PL B337 219	E.B. Berdnikov et al.	(SERP, TBIL)
ANTREASYAN 90	ZPHY C48 561	D. Antreasyan et al.	(Crystal Ball Collab.)
BEHREND 90C	ZPHY C46 583	H.J. Behrend et al.	(CELLO Collab.)
ANTIPOV 87	EPL 4 403	Y.M. Antipov et al.	(SERP, JINR, INRM+)
BELLINI 85	SJNP 41 781	D. Bellini et al.	
	Translated from YAF 41 1223.		
ARMSTRONG 82B	NP B202 1	T.A. Armstrong, B. Baccari	(AACH3, BARI, BONN+)
DAUM 81B	NP B182 269	C. Daum et al.	(AMST, CERN, CRAC, MPIM+)
EVANGELISTA 81	NP B178 197	C. Evangelista et al.	(BARI, BONN, CERN+)
	Also NP B186 594		
DAUM 80D	PL 898 285	C. Daum et al.	(AMST, CERN, CRAC, MPIM+)JP
BALTAY 77	PRL 39 591	C. Baltay, C.V. Curtis, M. Katelkar	(COLU)JP
ASCOLI 73	PR D7 669	G. Ascoli et al.	(ILL, TNTO, GENO, HAMB, MILA+JP)
CRENNELL 70	PRL 24 781	D.J. Crennell et al.	(BNL)
ARMENISE 69	LNC 2 501	N. Armenise et al.	(BARI, BGNA, FIRZ)
BALTAY 68	PRL 20 887	C. Baltay et al.	(COLU, ROCH, RUTG, YALE)I
BARTSCH 68	NP B7 345	J. Bartsch et al.	(AACH, BERL, CERN)JP

**$\phi(1680)$**   $I^G(J^{PC}) = 0^-(1^{--})$

**$\phi(1680)$  MASS**

**$e^+e^-$  PRODUCTION**

VALUE (MeV)	EVTS	DOCUMENT ID	TECN	COMMENT
<b>1680±20 OUR ESTIMATE</b>				
••• We do not use the following data for averages, fits, limits, etc. •••				
1641 $\pm_{-18}^{+24}$		ACHASOV	19	SND $e^+e^- \rightarrow \pi^+\pi^-\pi^0\eta$
1667±5±11	3k	1 IVANOV	19A	CMD3 1.59-2.007 $e^+e^- \rightarrow K^+K^-\eta$
1700±23	2k	2 ACHASOV	18A	SND 1.3-2.0 $e^+e^- \rightarrow K_S^0 K_L^0 \pi^0$
1674±12±6	6.2k	3 LEES	14H	BABR $e^+e^- \rightarrow K_S^0 K_L^0 \gamma$
1733±10±10		4 LEES	12F	BABR 10.6 $e^+e^- \rightarrow \phi\pi^+\pi^-\gamma$
1689±7±10	4.8k	5 SHEN	09	BELL 10.6 $e^+e^- \rightarrow K^+K^-\pi^+\pi^-\gamma$
1709±20±43		6 AUBERT	08s	BABR 10.6 $e^+e^- \rightarrow$ hadrons
1623±20	948	7 AKHMETSHIN	03	CMD2 1.05-1.38 $e^+e^- \rightarrow K_L^0 K_S^0$
~1500		8 ACHASOV	98H	RVUE $e^+e^- \rightarrow \pi^+\pi^-\pi^0, \omega\pi^+\pi^-, K^+K^-$
~1900		9 ACHASOV	98H	RVUE $e^+e^- \rightarrow K_S^0 K^\pm\pi^\mp$
1700±20		10 CLEGG	94	RVUE $e^+e^- \rightarrow K^+K^-, K_S^0 K\pi$
1657±27	367	BISELLO	91c	DM2 $e^+e^- \rightarrow K_S^0 K^\pm\pi^\mp$
1655±17		11 BISELLO	88B	DM2 $e^+e^- \rightarrow K^+K^-$
1680±10		12 BUON	82	DM1 $e^+e^- \rightarrow$ hadrons
1677±12		13 MANE	82	DM1 $e^+e^- \rightarrow K_S^0 K\pi$

<sup>1</sup> From a fit with coherent interference of the  $\phi(1680)$  with a non-resonant contribution.  
<sup>2</sup> Assuming the  $K\bar{K}^*(892) + c.c.$  dynamics. Systematic uncertainties not estimated.  
<sup>3</sup> Using a vector meson dominance model with contribution from  $\phi(1020)$ ,  $\phi(1680)$ , and higher mass excitations of  $\rho(770)$  and  $\omega(782)$ .  
<sup>4</sup> Using events with  $\pi\pi$  invariant mass less than 0.85 GeV.  
<sup>5</sup> From a fit with two incoherent Breit-Wigners.  
<sup>6</sup> From the simultaneous fit to the  $K\bar{K}^*(892) + c.c.$  and  $\phi\eta$  data from AUBERT 08s using the results of AUBERT 07AK.  
<sup>7</sup> From the combined fit of AKHMETSHIN 03 and MANE 81 also including  $\rho, \omega$ , and  $\phi$ . Neither isospin nor flavor structure known.  
<sup>8</sup> Using data from IVANOV 81, BARKOV 87, BISELLO 88b, DOLINSKY 91, and ANTONELLI 92.  
<sup>9</sup> Using the data from BISELLO 91c.  
<sup>10</sup> Using BISELLO 88b and MANE 82 data.  
<sup>11</sup> From global fit including  $\rho, \omega, \phi$  and  $\rho(1700)$  assume mass 1570 MeV and width 510 MeV for  $\rho$  radial excitation.  
<sup>12</sup> From global fit of  $\rho, \omega, \phi$  and their radial excitations to channels  $\omega\pi^+\pi^-, K^+K^-, K_S^0 K_L^0, K_S^0 K^\pm\pi^\mp$ . Assume mass 1570 MeV and width 510 MeV for  $\rho$  radial excitations, mass 1570 and width 500 MeV for  $\omega$  radial excitation.  
<sup>13</sup> Fit to one channel only, neglecting interference with  $\omega, \rho(1700)$ .



# Meson Particle Listings

## $\phi(1680)$

### PHOTOPRODUCTION

VALUE (MeV)	DOCUMENT ID	TECN	COMMENT
••• We do not use the following data for averages, fits, limits, etc. •••			
1753 ± 3	<sup>1</sup> LINK 02k	FOCS	20-160 $\gamma p \rightarrow K^+ K^- p$
1726 ± 22	<sup>1</sup> BUSENITZ 89	TPS	$\gamma p \rightarrow K^+ K^- X$
1760 ± 20	<sup>1</sup> ATKINSON 85c	OMEG	20-70 $\gamma p \rightarrow K^+ K^- X$
1690 ± 10	<sup>1</sup> ASTON 81f	OMEG	25-70 $\gamma p \rightarrow K^+ K^- X$

<sup>1</sup> We list here a state decaying into  $K^+ K^-$  possibly different from  $\phi(1680)$ .

### $p\bar{p}$ ANNIHILATION

VALUE (MeV)	DOCUMENT ID	TECN	COMMENT
••• We do not use the following data for averages, fits, limits, etc. •••			
1700 ± 8	<sup>1</sup> AMSLER 06	CBAR	0.9 $\bar{p} p \rightarrow K^+ K^- \pi^0$

<sup>1</sup> Could also be  $\rho(1700)$ .

### $\phi(1680)$ WIDTH

#### $e^+e^-$ PRODUCTION

VALUE (MeV)	EVTS	DOCUMENT ID	TECN	COMMENT
<b>150 ± 50 OUR ESTIMATE</b> This is only an educated guess; the error given is larger than the error on the average of the published values.				
••• We do not use the following data for averages, fits, limits, etc. •••				
103 ± <sup>26</sup> / <sub>24</sub>		ACHASOV 19	SND	$e^+e^- \rightarrow \pi^+ \pi^- \pi^0 \eta$
176 ± 23 ± 38	3k	<sup>1</sup> IVANOV 19a	CMD3	1.59-2.007 $e^+e^- \rightarrow K^+ K^- \eta$
300 ± 50	2k	<sup>2</sup> ACHASOV 18a	SND	1.3-2.0 $e^+e^- \rightarrow K_S^0 K_L^0 \pi^0$
165 ± 38 ± 70	6.2k	<sup>3</sup> LEES 14h	BABR	$e^+e^- \rightarrow K_S^0 K_L^0 \gamma$
300 ± 15 ± 37		<sup>4</sup> LEES 12f	BABR	10.6 $e^+e^- \rightarrow \phi \pi^+ \pi^- \gamma$
211 ± 14 ± 19	4.8k	<sup>5</sup> SHEN 09	BELL	10.6 $e^+e^- \rightarrow K^+ K^- \pi^+ \pi^- \gamma$
322 ± 77 ± 160		<sup>6</sup> AUBERT 08s	BABR	10.6 $e^+e^- \rightarrow$ hadrons
139 ± 60	948	<sup>7</sup> AKHMETSHIN 03	CMD2	1.05-1.38 $e^+e^- \rightarrow K_L^0 K_S^0$
300 ± 60		<sup>8</sup> CLEGG 94	RVUE	$e^+e^- \rightarrow K^+ K^-, K_S^0 K \pi$
146 ± 55	367	<sup>9</sup> BISELLO 91c	DM2	$e^+e^- \rightarrow K_S^0 K^\pm \pi^\mp$
207 ± 45		<sup>9</sup> BISELLO 88b	DM2	$e^+e^- \rightarrow K^+ K^-$
185 ± 22		<sup>10</sup> BUON 82	DM1	$e^+e^- \rightarrow$ hadrons
102 ± 36		<sup>11</sup> MANE 82	DM1	$e^+e^- \rightarrow K_S^0 K \pi$

<sup>1</sup> From a fit with coherent interference of the  $\phi(1680)$  with a non-resonant contribution.  
<sup>2</sup> Assuming the  $K \bar{K}^*(892) + c.c.$  dynamics. Systematic uncertainties not estimated.  
<sup>3</sup> Using a vector meson dominance model with contribution from  $\phi(1020)$ ,  $\phi(1680)$ , and higher mass excitations of  $\rho(770)$  and  $\omega(782)$ .  
<sup>4</sup> Using events with  $\pi\pi$  invariant mass less than 0.85 GeV.  
<sup>5</sup> From a fit with two incoherent Breit-Wigners.  
<sup>6</sup> From the simultaneous fit to the  $K \bar{K}^*(892) + c.c.$  and  $\phi\eta$  data from AUBERT 08s using the results of AUBERT 07AK.  
<sup>7</sup> From the combined fit of AKHMETSHIN 03 and MANE 81 also including  $\rho, \omega$ , and  $\phi$ . Neither isospin nor flavor structure known.  
<sup>8</sup> Using BISELLO 88b and MANE 82 data.  
<sup>9</sup> From global fit including  $\rho, \omega, \phi$  and  $\rho(1700)$   
<sup>10</sup> From global fit of  $\rho, \omega, \phi$  and their radial excitations to channels  $\omega\pi^+\pi^-, K^+K^-, K_S^0 K_L^0, K_S^0 K^\pm \pi^\mp$ . Assume mass 1570 MeV and width 510 MeV for  $\rho$  radial excitations, mass 1570 and width 500 MeV for  $\omega$  radial excitation.  
<sup>11</sup> Fit to one channel only, neglecting interference with  $\omega, \rho(1700)$ .

### PHOTOPRODUCTION

VALUE (MeV)	DOCUMENT ID	TECN	COMMENT
••• We do not use the following data for averages, fits, limits, etc. •••			
122 ± 63	<sup>1</sup> LINK 02k	FOCS	20-160 $\gamma p \rightarrow K^+ K^- p$
121 ± 47	<sup>1</sup> BUSENITZ 89	TPS	$\gamma p \rightarrow K^+ K^- X$
80 ± 40	<sup>1</sup> ATKINSON 85c	OMEG	20-70 $\gamma p \rightarrow K^+ K^- X$
100 ± 40	<sup>1</sup> ASTON 81f	OMEG	25-70 $\gamma p \rightarrow K^+ K^- X$

<sup>1</sup> We list here a state decaying into  $K^+ K^-$  possibly different from  $\phi(1680)$ .

### $p\bar{p}$ ANNIHILATION

VALUE (MeV)	DOCUMENT ID	TECN	COMMENT
••• We do not use the following data for averages, fits, limits, etc. •••			
143 ± 24	<sup>1</sup> AMSLER 06	CBAR	0.9 $\bar{p} p \rightarrow K^+ K^- \pi^0$

<sup>1</sup> Could also be  $\rho(1700)$ .

### $\phi(1680)$ DECAY MODES

Mode	Fraction ( $\Gamma_i/\Gamma$ )
$\Gamma_1$ $K \bar{K}^*(892) + c.c.$	seen
$\Gamma_2$ $K_S^0 K \pi$	seen
$\Gamma_3$ $K \bar{K}$	seen
$\Gamma_4$ $K_L^0 K_S^0$	
$\Gamma_5$ $e^+ e^-$	seen
$\Gamma_6$ $\omega \pi \pi$	not seen
$\Gamma_7$ $\phi \pi \pi$	
$\Gamma_8$ $K^+ K^- \pi^+ \pi^-$	seen
$\Gamma_9$ $\eta \phi$	seen
$\Gamma_{10}$ $K^+ K^- \eta$	
$\Gamma_{11}$ $\eta \gamma$	seen
$\Gamma_{12}$ $K^+ K^- \pi^0$	

### $\phi(1680) \Gamma(i)\Gamma(e^+e^-)/\Gamma(\text{total})$

This combination of a partial width with the partial width into  $e^+e^-$  and with the total width is obtained from the integrated cross section into channel (i) in  $e^+e^-$  annihilation. We list only data that have not been used to determine the partial width  $\Gamma(i)$  or the branching ratio  $\Gamma(i)/\text{total}$ .

#### $\Gamma(K_L^0 K_S^0) \times \Gamma(e^+e^-)/\Gamma_{\text{total}}$ $\Gamma_4 \Gamma_5/\Gamma$

VALUE (eV)	EVTS	DOCUMENT ID	TECN	COMMENT
••• We do not use the following data for averages, fits, limits, etc. •••				
14.3 ± 2.4 ± 6.2	6.2k	<sup>1</sup> LEES 14h	BABR	$e^+e^- \rightarrow K_S^0 K_L^0 \gamma$

<sup>1</sup> Using a vector meson dominance model with contribution from  $\phi(1020)$ ,  $\phi(1680)$ , and higher mass excitations of  $\rho(770)$  and  $\omega(782)$ .

#### $\Gamma(\phi \pi \pi) \times \Gamma(e^+e^-)/\Gamma_{\text{total}}$ $\Gamma_7 \Gamma_5/\Gamma$

VALUE ( $10^{-2}$ keV)	DOCUMENT ID	TECN	COMMENT
••• We do not use the following data for averages, fits, limits, etc. •••			
4.2 ± 0.2 ± 0.3	LEES 12f	BABR	10.6 $e^+e^- \rightarrow \phi \pi^+ \pi^- \gamma$

#### $\Gamma(\eta \phi) \times \Gamma(e^+e^-)/\Gamma_{\text{total}}$ $\Gamma_9 \Gamma_5/\Gamma$

VALUE (eV)	EVTS	DOCUMENT ID	TECN	COMMENT
••• We do not use the following data for averages, fits, limits, etc. •••				
94 ± 13 ± 15	3k	<sup>1</sup> IVANOV 19a	CMD3	1.59-2.007 $e^+e^- \rightarrow K^+ K^- \eta$

<sup>1</sup> From a fit with coherent interference of the  $\phi(1680)$  with a non-resonant contribution.

### $\phi(1680) \Gamma(i)\Gamma(e^+e^-)/\Gamma^2(\text{total})$

This combination of a branching ratio into channel (i) and branching ratio into  $e^+e^-$  is directly measured and obtained from the cross section at the peak. We list only data that have not been used to determine the branching ratio into (i) or  $e^+e^-$ .

#### $\Gamma(K_L^0 K_S^0)/\Gamma_{\text{total}} \times \Gamma(e^+e^-)/\Gamma_{\text{total}}$ $\Gamma_4/\Gamma \times \Gamma_5/\Gamma$

VALUE (units $10^{-6}$ )	EVTS	DOCUMENT ID	TECN	COMMENT
••• We do not use the following data for averages, fits, limits, etc. •••				
0.131 ± 0.059	948	<sup>1</sup> AKHMETSHIN 03	CMD2	1.05-1.38 $e^+e^- \rightarrow K_L^0 K_S^0$

<sup>1</sup> From the combined fit of AKHMETSHIN 03 and MANE 81 also including  $\rho, \omega$ , and  $\phi$ . Neither isospin nor flavor structure known. Recalculated by us.

#### $\Gamma(K \bar{K}^*(892) + c.c.)/\Gamma_{\text{total}} \times \Gamma(e^+e^-)/\Gamma_{\text{total}}$ $\Gamma_1/\Gamma \times \Gamma_5/\Gamma$

VALUE (units $10^{-6}$ )	EVTS	DOCUMENT ID	TECN	COMMENT
••• We do not use the following data for averages, fits, limits, etc. •••				
1.15 ± 0.16 ± 0.01		<sup>1</sup> AUBERT 08s	BABR	10.6 $e^+e^- \rightarrow K \bar{K}^*(892) \gamma + c.c.$
3.29 ± 1.57	367	<sup>2</sup> BISELLO 91c	DM2	1.35-2.40 $e^+e^- \rightarrow K_S^0 K^\pm \pi^\mp$

<sup>1</sup> From the simultaneous fit to the  $K \bar{K}^*(892) + c.c.$  and  $\phi\eta$  data from AUBERT 08s using the results of AUBERT 07AK.  
<sup>2</sup> Recalculated by us with the published value of  $B(K \bar{K}^*(892) + c.c.) \times \Gamma(e^+e^-)$ .

#### $\Gamma(\phi \pi \pi)/\Gamma_{\text{total}} \times \Gamma(e^+e^-)/\Gamma_{\text{total}}$ $\Gamma_7/\Gamma \times \Gamma_5/\Gamma$

VALUE (units $10^{-7}$ )	EVTS	DOCUMENT ID	TECN	COMMENT
••• We do not use the following data for averages, fits, limits, etc. •••				
1.86 ± 0.14 ± 0.21	4.8k	<sup>1</sup> SHEN 09	BELL	10.6 $e^+e^- \rightarrow K^+ K^- \pi^+ \pi^- \gamma$

<sup>1</sup> Multiplied by 3/2 to take into account the  $\phi\pi^0\pi^0$  mode. Using  $B(\phi \rightarrow K^+ K^-) = (49.2 \pm 0.6)\%$ .

#### $\Gamma(\eta \phi)/\Gamma_{\text{total}} \times \Gamma(e^+e^-)/\Gamma_{\text{total}}$ $\Gamma_9/\Gamma \times \Gamma_5/\Gamma$

VALUE (units $10^{-7}$ )	EVTS	DOCUMENT ID	TECN	COMMENT
••• We do not use the following data for averages, fits, limits, etc. •••				
5.64 ± <sup>1.74</sup> / <sub>1.80</sub>		ACHASOV 19	SND	$e^+e^- \rightarrow \pi^+ \pi^- \pi^0 \eta$
5.3 ± 0.6 ± 0.9	3k	<sup>1</sup> IVANOV 19a	CMD3	1.59-2.007 $e^+e^- \rightarrow K^+ K^- \eta$
4.3 ± 1.0 ± 0.9		<sup>2</sup> AUBERT 08s	BABR	10.6 $e^+e^- \rightarrow \phi \eta \gamma$

<sup>1</sup> From a fit with coherent interference of the  $\phi(1680)$  with a non-resonant contribution.  
<sup>2</sup> From the simultaneous fit to the  $K \bar{K}^*(892) + c.c.$  and  $\phi\eta$  data from AUBERT 08s using the results of AUBERT 07AK.

### $\phi(1680)$ BRANCHING RATIOS

#### $\Gamma(K \bar{K}^*(892) + c.c.)/\Gamma(K_S^0 K \pi)$ $\Gamma_1/\Gamma_2$

VALUE	DOCUMENT ID	TECN	COMMENT
dominant	MANE 82	DM1	$e^+e^- \rightarrow K_S^0 K^\pm \pi^\mp$

#### $\Gamma(K \bar{K})/\Gamma(K \bar{K}^*(892) + c.c.)$ $\Gamma_3/\Gamma_1$

VALUE	DOCUMENT ID	TECN	COMMENT
••• We do not use the following data for averages, fits, limits, etc. •••			
0.07 ± 0.01	BUON 82	DM1	$e^+e^-$

$\Gamma(\omega\pi\pi)/\Gamma(K\bar{K}^*(892) + c.c.)$				$\Gamma_6/\Gamma_1$
VALUE	DOCUMENT ID	TECN	COMMENT	
<0.10	BUON	82	DM1	$e^+e^-$

$\Gamma(\eta\phi)/\Gamma_{total}$				$\Gamma_9/\Gamma$	
VALUE	EVTS	DOCUMENT ID	TECN	COMMENT	
seen	35	<sup>1</sup> ACHASOV	14	SND	$1.15-2.00 e^+e^- \rightarrow \eta\gamma$

<sup>1</sup> From a phenomenological model based on vector meson dominance with  $\rho(1450)$  and  $\phi(1680)$  masses and widths from the PDG 12.

$\Gamma(\eta\phi)/\Gamma(K\bar{K}^*(892) + c.c.)$				$\Gamma_9/\Gamma_1$
VALUE	DOCUMENT ID	TECN	COMMENT	
•••	We do not use the following data for averages, fits, limits, etc. •••			
$\approx 0.37$	<sup>1</sup> AUBERT	08s	BABR	$10.6 e^+e^- \rightarrow \text{hadrons}$

$\Gamma(\eta\gamma)/\Gamma_{total}$				$\Gamma_{11}/\Gamma$	
VALUE	EVTS	DOCUMENT ID	TECN	COMMENT	
seen	35	<sup>1</sup> ACHASOV	14	SND	$1.15-2.00 e^+e^- \rightarrow \eta\gamma$

<sup>1</sup> From a phenomenological model based on vector meson dominance with  $\rho(1450)$  and  $\phi(1680)$  masses and widths from the PDG 12.

$\phi(1680)$  REFERENCES

ACHASOV	19	PR D99 112004	M.N. Achasov et al.	(SND Collab.)
IVANOV	19A	PL B798 134946	V.L. Ivanov et al.	(CMD-3 Collab.)
ACHASOV	18A	PR D97 032011	M.N. Achasov et al.	(SND Collab.)
ACHASOV	14	PR D90 032002	M.N. Achasov et al.	(SND Collab.)
LEES	14H	PR D89 092002	J.P. Lees et al.	(BABAR Collab.)
LEES	12F	PR D86 012008	J.P. Lees et al.	(BABAR Collab.)
PDG	12	PR D86 010001	J. Beringer et al.	(PDG Collab.)
SHEN	09	PR D80 031101	C.P. Shen et al.	(BELLE Collab.)
AUBERT	08S	PR D77 092002	M. Aubert et al.	(BABAR Collab.)
AUBERT	07AK	PR D76 012008	M. Aubert et al.	(BABAR Collab.)
AMSLER	06	PL B639 165	C. Amisler et al.	(CBAR Collab.)
AKHMETSHIN	03	PL B551 27	R.R. Akhmetshin et al.	(Novosibirsk CMD-2 Collab.)
Also		PAN 65 1222	E.V. Anashkin, V.M. Aulchenko, R.R. Akhmetshin	
LINK	02K	PL B545 50	J.M. Link et al.	(FNAL FOCUS Collab.)
ACHASOV	98H	PR D57 4334	M.N. Achasov, A.A. Kozhevnikov	
CLEGG	94	ZPHY C62 455	A.B. Clegg, A. Donnachie	(LANC, MCHS)
ANTONELLI	92	ZPHY C56 15	A. Antonelli et al.	(DM2 Collab.)
BISELLO	91C	ZPHY C52 227	D. Bisello et al.	(DM2 Collab.)
DOLINSKY	91	PRPL 202 99	S.I. Dolinsky et al.	(NOVO)
BUSENITZ	89	PR D40 1	J.K. Busenitz et al.	(ILL, FNAL)
BISELLO	88B	ZPHY C39 13	D. Bisello et al.	(PADO, CLER, FRAS+)
BARKOV	87	JETPL 46 164	L.M. Barkov et al.	(NOVO)
ATKINSON	85C	ZPHY C27 233	M. Atkinson et al.	(BONN, CERN, GLAS+)
BUON	82	PL 118B 221	J. Buon et al.	(LALO, MONP)
MANE	82	PL 112B 178	F. Mane et al.	(LALO)
ASTON	81F	PL 104B 231	D. Aston	(BONN, CERN, EPOL, GLAS, LANC+)
IVANOV	81	PL 107B 297	P.M. Ivanov et al.	(NOVO)
MANE	81	PL 99B 261	F. Mane et al.	(ORSAY)

$\rho_3(1690)$

 $I^G(J^{PC}) = 1^+(3^{--})$ 

$\rho_3(1690)$  MASS

VALUE (MeV)	DOCUMENT ID
<b>1688.8 ± 2.1 OUR AVERAGE</b>	Includes data from the 5 datablocks that follow this one.

<b>2π MODE</b>				
VALUE (MeV)	EVTS	DOCUMENT ID	TECN	CHG COMMENT
The data in this block is included in the average printed for a previous datablock.				

<b>1686 ± 4 OUR AVERAGE</b>					
1677 ± 14		EVANGELIS...	81	OMEG -	$12 \pi^- \rho \rightarrow 2\pi\rho$
1679 ± 11	476	BALTAY	78B	HBC 0	$15 \pi^+ \rho \rightarrow \pi^+ \pi^- n$
1678 ± 12	175	<sup>1</sup> ANTIPOV	77	CIBS 0	$25 \pi^- \rho \rightarrow \rho 3\pi$
1690 ± 7	600	<sup>1</sup> ENGLER	74	DBC 0	$6 \pi^+ n \rightarrow \pi^+ \pi^- p$
1693 ± 8		<sup>2</sup> GRAY	74	ASPK 0	$17 \pi^- \rho \rightarrow \pi^+ \pi^- n$
1678 ± 12		MATTHEWS	71c	DBC 0	$7 \pi^+ n$
•••	We do not use the following data for averages, fits, limits, etc. •••				
1734 ± 10		<sup>3</sup> CORDEN	79	OMEG	$12-15 \pi^- \rho \rightarrow n2\pi$
1692 ± 12		<sup>2,4</sup> ESTABROOKS	75	RVUE	$17 \pi^- \rho \rightarrow \pi^+ \pi^- n$
1737 ± 23		ARMENISE	70	DBC 0	$9 \pi^+ n$
1650 ± 35	122	BARTSCH	70B	HBC +	$8 \pi^+ \rho \rightarrow N2\pi$
1687 ± 21		STUNTEBECK	70	HDBC 0	$8 \pi^- \rho, 5.4 \pi^+ d$
1683 ± 13		ARMENISE	68	DBC 0	$5.1 \pi^+ d$
1670 ± 30		GOLDBERG	65	HBC 0	$6 \pi^+ d, 8 \pi^- p$

<sup>1</sup> Mass errors enlarged by us to  $\Gamma/\sqrt{N}$ ; see the note with the  $K^*(892)$  mass.  
<sup>2</sup> Uses same data as HYAMS 75.  
<sup>3</sup> From a phase shift solution containing a  $f'_2(1525)$  width two times larger than the  $K\bar{K}$  result.  
<sup>4</sup> From phase-shift analysis. Error takes account of spread of different phase-shift solutions.

<b><math>K\bar{K}</math> AND <math>K\bar{K}\pi</math> MODES</b>					
VALUE (MeV)	EVTS	DOCUMENT ID	TECN	CHG	COMMENT
The data in this block is included in the average printed for a previous datablock.					

<b>1696 ± 4 OUR AVERAGE</b>					
1699 ± 5		ALPER	80	CNTR 0	$62 \pi^- \rho \rightarrow K^+ K^- n$
1698 ± 12	6k	<sup>5,6</sup> MARTIN	78D	SPEC	$10 \pi \rho \rightarrow K_S^0 K^- \rho$
1692 ± 6		BLUM	75	ASPK 0	$18.4 \pi^- \rho \rightarrow nK^+ K^-$
1690 ± 16		ADERHOLZ	69	HBC +	$8 \pi^+ \rho \rightarrow K\bar{K}\pi$
•••	We do not use the following data for averages, fits, limits, etc. •••				
1694 ± 8		<sup>7</sup> COSTA	80	OMEG	$10 \pi^- \rho \rightarrow K^+ K^- n$
<sup>5</sup>	From a fit to $J^P = 3^-$ partial wave.				
<sup>6</sup>	Systematic error on mass scale subtracted.				
<sup>7</sup>	They cannot distinguish between $\rho_3(1690)$ and $\omega_3(1670)$ .				

<b>(4π)<sup>±</sup> MODE</b>					
VALUE (MeV)	EVTS	DOCUMENT ID	TECN	CHG	COMMENT
The data in this block is included in the average printed for a previous datablock.					

<b>1686 ± 5 OUR AVERAGE</b>					
1694 ± 6		<sup>8</sup> EVANGELIS...	81	OMEG -	$12 \pi^- \rho \rightarrow p4\pi$
1665 ± 15	177	BALTAY	78B	HBC +	$15 \pi^+ \rho \rightarrow p4\pi$
1670 ± 10		THOMPSON	74	HBC +	$13 \pi^+ \rho$
1687 ± 20		CASON	73	HBC -	$8,18.5 \pi^- \rho$
1685 ± 14		<sup>9</sup> CASON	73	HBC -	$8,18.5 \pi^- \rho$
1680 ± 40	144	BARTSCH	70B	HBC +	$8 \pi^+ \rho \rightarrow N4\pi$
1689 ± 20	102	<sup>9</sup> BARTSCH	70B	HBC +	$8 \pi^+ \rho \rightarrow N2\rho$
1705 ± 21		CASO	70	HBC -	$11.2 \pi^- \rho \rightarrow n\rho 2\pi$
•••	We do not use the following data for averages, fits, limits, etc. •••				
1718 ± 10		<sup>10</sup> EVANGELIS...	81	OMEG -	$12 \pi^- \rho \rightarrow p4\pi$
1673 ± 9		<sup>11</sup> EVANGELIS...	81	OMEG -	$12 \pi^- \rho \rightarrow p4\pi$
1733 ± 9	66	<sup>9</sup> KLIGER	74	HBC -	$4.5 \pi^- \rho \rightarrow p4\pi$
1630 ± 15		HOLMES	72	HBC +	$10-12 K^+ \rho$
1720 ± 15		BALTAY	68	HBC +	$7, 8.5 \pi^+ \rho$

<sup>8</sup> From  $\rho^- \rho^0$  mode, not independent of the other two EVANGELISTA 81 entries.  
<sup>9</sup> From  $\rho^\pm \rho^0$  mode.  
<sup>10</sup> From  $a_2(1320)^- \pi^0$  mode, not independent of the other two EVANGELISTA 81 entries.  
<sup>11</sup> From  $a_2(1320)^0 \pi^-$  mode, not independent of the other two EVANGELISTA 81 entries.

<b><math>\omega\pi</math> MODE</b>				
VALUE (MeV)	DOCUMENT ID	TECN	CHG	COMMENT
The data in this block is included in the average printed for a previous datablock.				

<b>1681 ± 7 OUR AVERAGE</b>					
1670 ± 25		<sup>12</sup> ALDE	95	GAM2	$38 \pi^- \rho \rightarrow \omega\pi^0 n$
1690 ± 15		EVANGELIS...	81	OMEG -	$12 \pi^- \rho \rightarrow \omega\pi\rho$
1666 ± 14		GESSAROLI	77	HBC	$11 \pi^- \rho \rightarrow \omega\pi\rho$
1686 ± 9		THOMPSON	74	HBC +	$13 \pi^+ \rho$
•••	We do not use the following data for averages, fits, limits, etc. •••				
1654 ± 24		BARNHAM	70	HBC +	$10 K^+ \rho \rightarrow \omega\pi X$
<sup>12</sup>	Supersedes ALDE 92c.				

<b><math>\eta\pi^+ \pi^-</math> MODE</b>				
(For difficulties with MMS experiments, see the $a_2(1320)$ mini-review in the 1973 edition.)				
VALUE (MeV)	DOCUMENT ID	TECN	CHG	COMMENT
The data in this block is included in the average printed for a previous datablock.				

<b>1682 ± 12 OUR AVERAGE</b>					
1685 ± 10 ± 20		AMELIN	00	VES	$37 \pi^- \rho \rightarrow \eta\pi^+ \pi^- n$
1680 ± 15		FUKUI	88	SPEC 0	$8.95 \pi^- \rho \rightarrow \eta\pi^+ \pi^- n$
•••	We do not use the following data for averages, fits, limits, etc. •••				
1700 ± 47		<sup>13</sup> ANDERSON	69	MMS -	$16 \pi^- \rho$ backward
1632 ± 15		<sup>13,14</sup> FOCACCI	66	MMS -	$7-12 \pi^- \rho \rightarrow pMM$
1700 ± 15		<sup>13,14</sup> FOCACCI	66	MMS -	$7-12 \pi^- \rho \rightarrow pMM$
1748 ± 15		<sup>13,14</sup> FOCACCI	66	MMS -	$7-12 \pi^- \rho \rightarrow pMM$
<sup>13</sup>	Seen in 2.5-3 GeV/c $\bar{p}p$ . $2\pi^+ 2\pi^-$ , with 0, 1, 2 $\pi^+ \pi^-$ pairs in $\rho$ band not seen by OREN 74 (2.3 GeV/c $\bar{p}p$ ) with more statistics. (Jan. 1976)				
<sup>14</sup>	Not seen by BOWEN 72.				

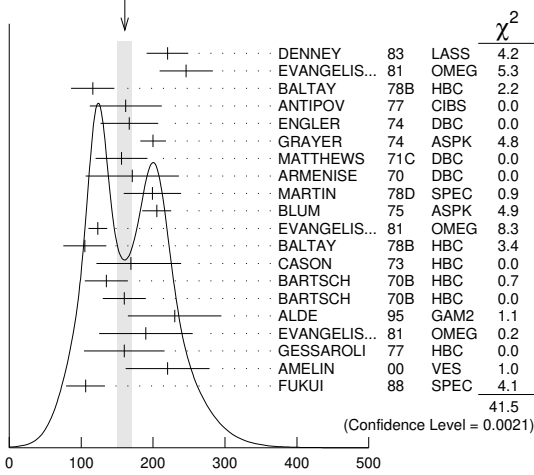
$\rho_3(1690)$  WIDTH

<b>2π, <math>K\bar{K}</math>, AND <math>K\bar{K}\pi</math> MODES</b>				
VALUE (MeV)	DOCUMENT ID			
<b>161 ± 10 OUR AVERAGE</b>	Includes data from the 5 datablocks that follow this one. Error includes scale factor of 1.5. See the ideogram below.			

# Meson Particle Listings

## $\rho_3(1690)$

WEIGHTED AVERAGE  
161±10 (Error scaled by 1.5)



$\rho_3(1690)$  width,  $2\pi$ ,  $K\bar{K}$ , and  $K\bar{K}\pi$  modes (MeV)

### $2\pi$ MODE

VALUE (MeV)	EVTs	DOCUMENT ID	TECN	CHG	COMMENT
-------------	------	-------------	------	-----	---------

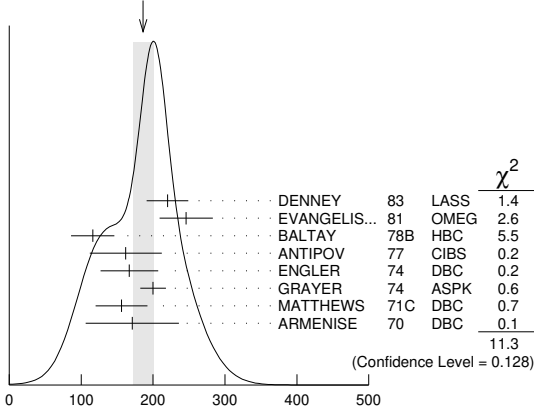
The data in this block is included in the average printed for a previous datablock.

**186±14 OUR AVERAGE** Error includes scale factor of 1.3. See the ideogram below.

220±29		DENNEY	83	LASS	10 $\pi^+ N$
246±37		EVANGELIS...	81	OMEG	12 $\pi^- p \rightarrow 2\pi p$
116±30	476	BALTAY	78B	HBC	15 $\pi^+ p \rightarrow \pi^+ \pi^- n$
162±5.0	175	15 ANTIPOV	77	CIBS	0 25 $\pi^- p \rightarrow p3\pi$
167±4.0	600	ENGLER	74	DBC	0 6 $\pi^+ n \rightarrow \pi^+ \pi^- p$
200±18		16 GRAYER	74	ASPK	0 17 $\pi^- p \rightarrow \pi^+ \pi^- n$
156±36		MATTHEWS	71C	DBC	0 7 $\pi^+ n$
171±65		ARMENISE	70	DBC	0 9 $\pi^+ d$
••• We do not use the following data for averages, fits, limits, etc. •••					
322±35		17 CORDEN	79	OMEG	12-15 $\pi^- p \rightarrow n2\pi$
240±30		16,18 ESTABROOKS	75	RVUE	17 $\pi^- p \rightarrow \pi^+ \pi^- n$
180±30	122	BARTSCH	70B	HBC	+ 8 $\pi^+ p \rightarrow N2\pi$
267±72		STUNTEBECK	70	HDHC	0 8 $\pi^- p, 5.4 \pi^+ d$
188±49		ARMENISE	68	DBC	0 5.1 $\pi^+ d$
180±40		GOLDBERG	65	HBC	0 6 $\pi^+ d, 8 \pi^- p$

15 Width errors enlarged by us to  $4\Gamma/\sqrt{N}$ ; see the note with the  $K^*(892)$  mass.  
 16 Uses same data as HYAMS 75 and BECKER 79.  
 17 From a phase shift solution containing a  $f'_2(1525)$  width two times larger than the  $K\bar{K}$  result.  
 18 From phase-shift analysis. Error takes account of spread of different phase-shift solutions.

WEIGHTED AVERAGE  
186±14 (Error scaled by 1.3)



$\rho_3(1690)$  width,  $2\pi$  mode (MeV)

### $K\bar{K}$ AND $K\bar{K}\pi$ MODES

VALUE (MeV)	EVTs	DOCUMENT ID	TECN	CHG	COMMENT
-------------	------	-------------	------	-----	---------

The data in this block is included in the average printed for a previous datablock.

**204±18 OUR AVERAGE**

199±40	6000	19 MARTIN	78D	SPEC	10 $\pi p \rightarrow K_S^0 K^- p$
205±20		BLUM	75	ASPK	0 18.4 $\pi^- p \rightarrow nK^+ K^-$

••• We do not use the following data for averages, fits, limits, etc. •••

219±4		ALPER	80	CNTR	0 62 $\pi^- p \rightarrow K^+ K^- n$
186±11		20 COSTA	80	OMEG	10 $\pi^- p \rightarrow K^+ K^- n$
112±60		ADERHOLZ	69	HBC	+ 8 $\pi^+ p \rightarrow K\bar{K}\pi$

19 From a fit to  $J^P = 3^-$  partial wave.  
 20 They cannot distinguish between  $\rho_3(1690)$  and  $\omega_3(1670)$ .

### ( $4\pi$ ) $^\pm$ MODE

VALUE (MeV)	EVTs	DOCUMENT ID	TECN	CHG	COMMENT
-------------	------	-------------	------	-----	---------

The data in this block is included in the average printed for a previous datablock.

**129±10 OUR AVERAGE**

123±13		21 EVANGELIS...	81	OMEG	- 12 $\pi^- p \rightarrow p4\pi$
105±30	177	BALTAY	78B	HBC	+ 15 $\pi^+ p \rightarrow p4\pi$
169±70		CASON	73	HBC	- 8,18.5 $\pi^- p$
135±30	144	BARTSCH	70B	HBC	+ 8 $\pi^+ p \rightarrow N4\pi$
160±30	102	BARTSCH	70B	HBC	+ 8 $\pi^+ p \rightarrow N2\rho$

••• We do not use the following data for averages, fits, limits, etc. •••

230±28		22 EVANGELIS...	81	OMEG	- 12 $\pi^- p \rightarrow p4\pi$
184±33		23 EVANGELIS...	81	OMEG	- 12 $\pi^- p \rightarrow p4\pi$
150	66	24 KLIGER	74	HBC	- 4.5 $\pi^- p \rightarrow p4\pi$
106±25		THOMPSON	74	HBC	+ 13 $\pi^+ p$
125±83		24 CASON	73	HBC	- 8,18.5 $\pi^- p$
130±30		HOLMES	72	HBC	+ 10-12 $K^+ p$
180±30	90	24 BARTSCH	70B	HBC	+ 8 $\pi^+ p \rightarrow Na_2\pi$
100±35		BALTAY	68	HBC	+ 7, 8.5 $\pi^+ p$

21 From  $\rho^- \rho^0$  mode, not independent of the other two EVANGELISTA 81 entries.  
 22 From  $a_2(1320) \pi^0$  mode, not independent of the other two EVANGELISTA 81 entries.  
 23 From  $a_2(1320) \pi^-$  mode, not independent of the other two EVANGELISTA 81 entries.  
 24 From  $\rho^\pm \rho^0$  mode.

### $\omega\pi$ MODE

VALUE (MeV)	DOCUMENT ID	TECN	CHG	COMMENT
-------------	-------------	------	-----	---------

The data in this block is included in the average printed for a previous datablock.

**190±40 OUR AVERAGE**

230±65	25	ALDE	95	GAM2	38 $\pi^- p \rightarrow \omega\pi^0 n$
190±65		EVANGELIS...	81	OMEG	- 12 $\pi^- p \rightarrow \omega\pi p$
160±56		GESSAROLI	77	HBC	11 $\pi^- p \rightarrow \omega\pi p$

••• We do not use the following data for averages, fits, limits, etc. •••

89±25		THOMPSON	74	HBC	+ 13 $\pi^+ p$
130±73		BARNHAM	70	HBC	+ 10 $K^+ p \rightarrow \omega\pi X$

25 Supersedes ALDE 92c.

### $\eta\pi^+\pi^-$ MODE

(For difficulties with MMS experiments, see the  $a_2(1320)$  mini-review in the 1973 edition.)

VALUE (MeV)	DOCUMENT ID	TECN	CHG	COMMENT
-------------	-------------	------	-----	---------

The data in this block is included in the average printed for a previous datablock.

**126±40 OUR AVERAGE** Error includes scale factor of 1.8.

220±30±50		AMELIN	00	VES	37 $\pi^- p \rightarrow \eta\pi^+\pi^- n$
106±27		FUKUI	88	SPEC	0 8.95 $\pi^- p \rightarrow \eta\pi^+\pi^- n$

••• We do not use the following data for averages, fits, limits, etc. •••

195		26 ANDERSON	69	MMS	- 16 $\pi^- p$ backward
< 21	26,27	FOCACCI	66	MMS	- 7-12 $\pi^- p \rightarrow pMM$
< 30	26,27	FOCACCI	66	MMS	- 7-12 $\pi^- p \rightarrow pMM$
< 38	26,27	FOCACCI	66	MMS	- 7-12 $\pi^- p \rightarrow pMM$

26 Seen in 2.5-3 GeV/c  $\bar{p}p$ .  $2\pi^+2\pi^-$ , with 0, 1, 2  $\pi^+\pi^-$  pairs in  $\rho^0$  band not seen by OREN 74 (2.3 GeV/c  $\bar{p}p$ ) with more statistics. (Jan. 1979)  
 27 Not seen by BOWEN 72.

### $\rho_3(1690)$ DECAY MODES

Mode	Fraction ( $\Gamma_i/\Gamma$ )	Scale factor
$\Gamma_1$ $4\pi$	(71.1 ± 1.9) %	
$\Gamma_2$ $\pi^\pm \pi^+ \pi^- \pi^0$	(67 ± 22) %	
$\Gamma_3$ $\omega\pi$	(16 ± 6) %	
$\Gamma_4$ $\pi\pi$	(23.6 ± 1.3) %	
$\Gamma_5$ $K\bar{K}\pi$	( 3.8 ± 1.2) %	
$\Gamma_6$ $K\bar{K}$	( 1.58 ± 0.26) %	1.2
$\Gamma_7$ $\eta\pi^+\pi^-$	seen	
$\Gamma_8$ $\rho(770)\eta$	seen	
$\Gamma_9$ $\pi\pi\rho$	seen	
$\Gamma_{10}$ $a_2(1320)\pi$	seen	
$\Gamma_{11}$ $\rho\rho$	seen	
$\Gamma_{12}$ $\phi\pi$		
$\Gamma_{13}$ $\eta\pi$		
$\Gamma_{14}$ $\pi^\pm 2\pi^+ 2\pi^- \pi^0$		

**CONSTRAINED FIT INFORMATION**

An overall fit to 5 branching ratios uses 10 measurements and one constraint to determine 4 parameters. The overall fit has a  $\chi^2 = 14.7$  for 7 degrees of freedom.

The following *off-diagonal* array elements are the correlation coefficients  $\langle \delta x_i \delta x_j \rangle / (\delta x_i \delta x_j)$ , in percent, from the fit to the branching fractions,  $x_i \equiv \Gamma_i / \Gamma_{\text{total}}$ . The fit constrains the  $x_i$  whose labels appear in this array to sum to one.

$x_4$	-77		
$x_5$	-74	17	
$x_6$	-15	2	0
	$x_1$	$x_4$	$x_5$

**$\rho_3(1690)$  BRANCHING RATIOS**

$\Gamma(\pi\pi)/\Gamma_{\text{total}}$	DOCUMENT ID	TECN	CHG	COMMENT	$\Gamma_4/\Gamma$
<b>0.236 ± 0.013 OUR FIT</b>					
<b>0.243 ± 0.013 OUR AVERAGE</b>					

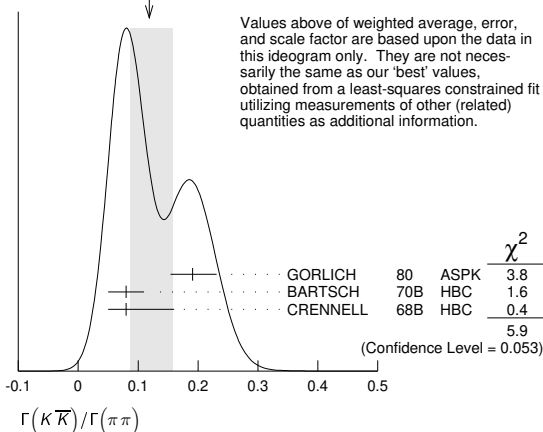
0.259 <sup>+0.018</sup> <sub>-0.019</sub>	BECKER	79	ASPK	0	17 $\pi^- \rho$ polarized
0.23 ± 0.02	CORDEN	79	OMEG		12-15 $\pi^- \rho \rightarrow n2\pi$
0.22 ± 0.04	<sup>28</sup> MATTHEWS	71c	HDBC	0	7 $\pi^+ n \rightarrow \pi^- \rho$
• • • We do not use the following data for averages, fits, limits, etc. • • •					
0.245 ± 0.006	<sup>29</sup> ESTABROOKS	75	RVUE		17 $\pi^- \rho \rightarrow \pi^+ \pi^- n$
<sup>28</sup> One-pion-exchange model used in this estimation.					
<sup>29</sup> From phase-shift analysis of HYAMS 75 data.					

$\Gamma(\pi\pi)/\Gamma(\pi^+\pi^+\pi^-\pi^0)$	DOCUMENT ID	TECN	CHG	COMMENT	$\Gamma_4/\Gamma_2$
<b>0.35 ± 0.11</b>	CASON	73	HBC	-	8,18.5 $\pi^- \rho$
• • • We do not use the following data for averages, fits, limits, etc. • • •					
<0.2	HOLMES	72	HBC	+	10-12 $K^+ \rho$
<0.12	BALLAM	71b	HBC	-	16 $\pi^- \rho$

$\Gamma(\pi\pi)/\Gamma(4\pi)$	DOCUMENT ID	TECN	CHG	COMMENT	$\Gamma_4/\Gamma_1$
<b>0.332 ± 0.026 OUR FIT</b>	Error includes scale factor of 1.1.				
<b>0.30 ± 0.10</b>	BALTAY	78b	HBC	0	15 $\pi^+ \rho \rightarrow p4\pi$

$\Gamma(K\bar{K})/\Gamma(\pi\pi)$	DOCUMENT ID	TECN	CHG	COMMENT	$\Gamma_6/\Gamma_4$
<b>0.067 ± 0.011 OUR FIT</b>	Error includes scale factor of 1.2.				
<b>0.118 ± 0.040</b>	Error includes scale factor of 1.7. See the ideogram below.				
<b>0.118 ± 0.040</b>	OUR AVERAGE				
0.191 <sup>+0.040</sup> <sub>-0.037</sub>	GORLICH	80	ASPK	0	17,18 $\pi^- \rho$ polarized
0.08 ± 0.03	BARTSCH	70b	HBC	+	8 $\pi^+ \rho$
0.08 ± 0.08	CRENNELL	68b	HBC		6.0 $\pi^- \rho$

WEIGHTED AVERAGE  
0.118 ± 0.040 - 0.032 (Error scaled by 1.7)



$\Gamma(K\bar{K}\pi)/\Gamma(\pi\pi)$	DOCUMENT ID	TECN	CHG	COMMENT	$\Gamma_5/\Gamma_4$
<b>0.16 ± 0.05 OUR FIT</b>					
<b>0.16 ± 0.05</b>	<sup>30</sup> BARTSCH	70b	HBC	+	8 $\pi^+ \rho$

<sup>30</sup> Increased by us to correspond to  $B(\rho_3(1690) \rightarrow \pi\pi) = 0.24$ .

$[\Gamma(\pi\pi\rho) + \Gamma(a_2(1320)\pi) + \Gamma(\rho\rho)]/\Gamma(\pi^+\pi^+\pi^-\pi^0)$	DOCUMENT ID	TECN	CHG	COMMENT	$(\Gamma_9 + \Gamma_{10} + \Gamma_{11})/\Gamma_2$
<b>0.94 ± 0.09 OUR AVERAGE</b>					
0.96 ± 0.21	BALTAY	78b	HBC	+	15 $\pi^+ \rho \rightarrow p4\pi$
0.88 ± 0.15	BALLAM	71b	HBC	-	16 $\pi^- \rho$
1 ± 0.15	BARTSCH	70b	HBC	+	8 $\pi^+ \rho$
consistent with 1					
	CASO	68	HBC	-	11 $\pi^- \rho$

$\Gamma(\rho\rho)/\Gamma(\pi^+\pi^+\pi^-\pi^0)$	DOCUMENT ID	TECN	CHG	COMMENT	$\Gamma_{11}/\Gamma_2$
<b>0.12 ± 0.11</b>	BALTAY	78b	HBC	+	15 $\pi^+ \rho \rightarrow p4\pi$
0.56	KLIGER	74	HBC	-	4.5 $\pi^- \rho \rightarrow p4\pi$
0.13 ± 0.09	<sup>31</sup> THOMPSON	74	HBC	+	13 $\pi^+ \rho$
0.7 ± 0.15	BARTSCH	70b	HBC	+	8 $\pi^+ \rho$
<sup>31</sup> $\rho\rho$ and $a_2(1320)\pi$ modes are indistinguishable.					

$\Gamma(\rho\rho)/[\Gamma(\pi\pi\rho) + \Gamma(a_2(1320)\pi) + \Gamma(\rho\rho)]$	DOCUMENT ID	TECN	CHG	COMMENT	$\Gamma_{11}/(\Gamma_9 + \Gamma_{10} + \Gamma_{11})$
<b>0.48 ± 0.16</b>	CASO	68	HBC	-	11 $\pi^- \rho$

$\Gamma(a_2(1320)\pi)/\Gamma(\pi^+\pi^+\pi^-\pi^0)$	DOCUMENT ID	TECN	CHG	COMMENT	$\Gamma_{10}/\Gamma_2$
<b>0.66 ± 0.08</b>	BALTAY	78b	HBC	+	15 $\pi^+ \rho \rightarrow p4\pi$
0.36 ± 0.14	<sup>32</sup> THOMPSON	74	HBC	+	13 $\pi^+ \rho$
not seen	CASON	73	HBC	-	8,18.5 $\pi^- \rho$
0.6 ± 0.15	BARTSCH	70b	HBC	+	8 $\pi^+ \rho$
0.6	BALTAY	68	HBC	+	7,8.5 $\pi^+ \rho$
<sup>32</sup> $\rho\rho$ and $a_2(1320)\pi$ modes are indistinguishable.					

$\Gamma(\omega\pi)/\Gamma(\pi^+\pi^+\pi^-\pi^0)$	DOCUMENT ID	TECN	CHG	COMMENT	$\Gamma_3/\Gamma_2$	
<b>0.23 ± 0.05 OUR AVERAGE</b>	Error includes scale factor of 1.2.					
0.33 ± 0.07	THOMPSON	74	HBC	+	13 $\pi^+ \rho$	
0.12 ± 0.07	BALLAM	71b	HBC	-	16 $\pi^- \rho$	
0.25 ± 0.10	BALTAY	68	HBC	+	7,8.5 $\pi^+ \rho$	
0.25 ± 0.10	JOHNSTON	68	HBC	-	7.0 $\pi^- \rho$	
• • • We do not use the following data for averages, fits, limits, etc. • • •						
<0.11	95	BALTAY	78b	HBC	+	15 $\pi^+ \rho \rightarrow p4\pi$
<0.09	KLIGER	74	HBC	-	4.5 $\pi^- \rho \rightarrow p4\pi$	

$\Gamma(\phi\pi)/\Gamma(\pi^+\pi^+\pi^-\pi^0)$	DOCUMENT ID	TECN	CHG	COMMENT	$\Gamma_{12}/\Gamma_2$
<b>0.11 ± 0.04</b>	Error includes scale factor of 1.7. See the ideogram below.				
<b>0.11 ± 0.04</b>	OUR AVERAGE				
<0.11	BALTAY	68	HBC	+	7,8.5 $\pi^+ \rho$

$\Gamma(\pi^+2\pi^+2\pi^-\pi^0)/\Gamma(\pi^+\pi^+\pi^-\pi^0)$	DOCUMENT ID	TECN	CHG	COMMENT	$\Gamma_{14}/\Gamma_2$
<b>0.11 ± 0.04</b>	Error includes scale factor of 1.7. See the ideogram below.				
<b>0.11 ± 0.04</b>	OUR AVERAGE				
<0.15	BALTAY	68	HBC	+	7,8.5 $\pi^+ \rho$

$\Gamma(\eta\pi)/\Gamma(\pi^+\pi^+\pi^-\pi^0)$	DOCUMENT ID	TECN	CHG	COMMENT	$\Gamma_{13}/\Gamma_2$
<b>0.11 ± 0.04</b>	Error includes scale factor of 1.7. See the ideogram below.				
<b>0.11 ± 0.04</b>	OUR AVERAGE				
<0.02	THOMPSON	74	HBC	+	13 $\pi^+ \rho$

$\Gamma(K\bar{K})/\Gamma_{\text{total}}$	DOCUMENT ID	TECN	CHG	COMMENT	$\Gamma_6/\Gamma$
<b>0.0158 ± 0.0026 OUR FIT</b>	Error includes scale factor of 1.2.				
<b>0.0130 ± 0.0024 OUR AVERAGE</b>					
0.013 ± 0.003	COSTA	80	OMEG	0	10 $\pi^- \rho \rightarrow K^+ K^- n$
0.013 ± 0.004	<sup>33</sup> MARTIN	78b	SPEC	-	10 $\pi \rho \rightarrow K_S^0 K^- \rho$
<sup>33</sup> From $(\Gamma_4 \Gamma_6)^{1/2} = 0.056 \pm 0.034$ assuming $B(\rho_3(1690) \rightarrow \pi\pi) = 0.24$ .					

$\Gamma(\omega\pi)/[\Gamma(\omega\pi) + \Gamma(\rho\rho)]$	DOCUMENT ID	TECN	CHG	COMMENT	$\Gamma_3/(\Gamma_3 + \Gamma_{11})$
<b>0.22 ± 0.08</b>	CASON	73	HBC	-	8,18.5 $\pi^- \rho$

$\Gamma(\eta\pi^+\pi^-)/\Gamma_{\text{total}}$	DOCUMENT ID	TECN	COMMENT	$\Gamma_7/\Gamma$
<b>0.22 ± 0.08</b>	FUKUI	88	SPEC	8.95 $\pi^- \rho \rightarrow \eta\pi^+\pi^- n$

$\Gamma(a_2(1320)\pi)/\Gamma(\rho(770)\eta)$	DOCUMENT ID	TECN	COMMENT	$\Gamma_{10}/\Gamma_8$
<b>5.5 ± 2.0</b>	AMELIN	00	VES	37 $\pi^- \rho \rightarrow \eta\pi^+\pi^- n$

## Meson Particle Listings

 $\rho_3(1690)$ ,  $\rho(1700)$  $\rho_3(1690)$  REFERENCES

AMELIN	00	NP A668 83	D. Amelin et al.	(VES Collab.)
ALDE	95	ZPHY C66 379	D.M. Alde et al.	(GAMS Collab.) JP
ALDE	92C	ZPHY C54 553	D.M. Alde et al.	(BELG, SERP, KEK, LANL+)
FUKUI	88	PL B202 441	S. Fukui et al.	(SUGI, NAGO, KEK, KYOT+)
DENNEY	83	PR D28 2726	D.L. Denney et al.	(IOWA, MICH)
EVANGELIS...	81	NP B178 197	C. Evangelista et al.	(BARI, BONN, CERN+)
ALPER	80	PL 94B 422	B. Alper et al.	(AMST, CERN, CRAC, MPIM+)
COSTA	80	NP B175 402	G. Costa et al.	(BARI, BONN, CERN, GLAS+)
GÖRGLICH	80	NP B174 16	L. Gorlich et al.	(CRAC, MPIM, CERN+)
BECKER	79	NP B151 46	H. Becker et al.	(MPIM, CERN, ZEEM, CRAC)
CORDEN	79	NP B157 250	M.J. Corden et al.	(BIRM, RHEL, TEHA+)
BALTAY	78B	PR D17 62	C. Baltay et al.	(COLU, BING)
MARTIN	78B	NP B140 158	A.D. Martin et al.	(DURH, GEVA)
MARTIN	78D	PL 74B 417	A.D. Martin et al.	(DURH, GEVA)
ANTIPOV	77	NP B119 45	Y.M. Antipov et al.	(SERP, GEVA)
GESSAROLI	77	NP B126 382	R. Gessaroli et al.	(BGNA, FIRZ, GENO+)
BLUM	75	PL 57B 403	W. Blum et al.	(CERN, MPIM) JP
ESTABROOKS	75	NP B95 322	P.G. Estabrooks, A.D. Martin	(DURH)
HYAMS	75	NP B100 205	B.D. Hyams et al.	(CERN, MPIM)
ENGLER	74	PR D10 2070	A. Engler et al.	(CMU, CASE)
GRAVER	74	NP B75 189	G. Grayer et al.	(CERN, MPIM)
KLIGER	74	SJNP 19 428	G.K. Kliger et al.	(ITEP)
		Translated from YAF 19 839.		
OREN	74	NP B71 189	Y. Oren et al.	(ANL, OXF)
THOMPSON	74	NP B69 220	G. Thompson et al.	(PURD)
CASON	73	PR D7 1971	N.M. Cason et al.	(NDAM)
BOWEN	72	PRL 29 890	D.R. Bowen et al.	(NEAS, STON)
HOLMES	72	PR D6 3336	R. Holmes et al.	(ROCH)
BALLAM	71B	NP D3 2606	J. Ballam et al.	(SLAC)
MATTHEWS	71C	NP B33 1	J.A.J. Matthews et al.	(TNTO, WISC) JP
ARMENISE	70	LNC 4 199	N. Armenise et al.	(BARI, BGNA, FIRZ)
BARNHAM	70	PRL 24 1083	K.W.J. Barnham et al.	(BIRM)
BARTSCH	70B	NP B22 109	J. Bartsch et al.	(AACH, BERL, CERN)
CASO	70	LNC 3 707	C. Caso et al.	(GENO, HAMB, MILA, SACL)
STUNTEBECK	70	PL 32B 391	P.H. Stuntebeck et al.	(NDAM)
ADERHOLZ	69	NP B11 259	M. Aderholz et al.	(AACH3, BERL, CERN+)
ANDERSON	69	PRL 22 1390	E.W. Anderson et al.	(BNL, CMU)
ARMENISE	68	NC 54A 999	N. Armenise et al.	(BARI, BGNA, FIRZ+)
BALTAY	68	PRL 20 887	C. Baltay et al.	(COLU, ROCH, RUTG, YALE)
CASO	68	NC 54A 983	C. Caso et al.	(GENO, HAMB, MILA, SACL)
CRENNELL	68B	PL 28B 136	D.J. Crennell et al.	(BNL)
JOHNSTON	68	PRL 20 1414	T.F. Johnston et al.	(TNTO, WISC) JP
FOCACCI	66	PRL 17 890	M.N. Focacci et al.	(CERN)
GOLDBERG	65	PL 17 354	M. Goldberg et al.	(CERN, EPOL, ORSAY+)

 $\rho(1700)$ 

$$J^G(J^{PC}) = 1^+(1^{--})$$

THE  $\rho(1450)$  AND THE  $\rho(1700)$ 

Updated September 2019 by S. Eidelman (Novosibirsk), C. Hanhart (Juelich) and G. Venanzoni (Pisa).

In our 1988 edition, we replaced the  $\rho(1600)$  entry with two new ones, the  $\rho(1450)$  and the  $\rho(1700)$ , because there was emerging evidence that the 1600-MeV region actually contains two  $\rho$ -like resonances. Erkal [1] had pointed out this possibility with a theoretical analysis on the consistency of  $2\pi$  and  $4\pi$  electromagnetic form factors and the  $\pi\pi$  scattering length. Donnachie [2], with a full analysis of data on the  $2\pi$  and  $4\pi$  final states in  $e^+e^-$  annihilation and photoproduction reactions, had also argued that in order to obtain a consistent picture, two resonances were necessary. The existence of  $\rho(1450)$  was supported by the analysis of  $\eta\rho^0$  mass spectra obtained in photoproduction and  $e^+e^-$  annihilation [3], as well as that of  $e^+e^- \rightarrow \omega\pi$  [4].

The analysis of [2] was further extended by [5,6] to include new data on  $4\pi$ -systems produced in  $e^+e^-$  annihilation, and in  $\tau$ -decays ( $\tau$  decays to  $4\pi$ , and  $e^+e^-$  annihilation to  $4\pi$  can be related by the Conserved Vector Current assumption). These systems were successfully analyzed using interfering contributions from two  $\rho$ -like states, and from the tail of the  $\rho(770)$  decaying into two-body states. While specific conclusions on  $\rho(1450) \rightarrow 4\pi$  were obtained, little could be said about the  $\rho(1700)$ .

Independent evidence for two  $1^-$  states is provided by [7] in  $4\pi$  electroproduction at  $\langle Q^2 \rangle = 1$  (GeV/c)<sup>2</sup>, and by [8] in a high-statistics sample of the  $\eta\pi\pi$  system in  $\pi^-p$  charge exchange.

This scenario with two overlapping resonances is supported by other data. Bisello [9] measured the pion form factor in the interval 1.35–2.4 GeV, and observed a deep minimum around 1.6 GeV. The best fit was obtained with the hypothesis of  $\rho$ -like resonances at 1420 and 1770 MeV, with widths of about 250 MeV. Antonelli [10] found that the  $e^+e^- \rightarrow \eta\pi^+\pi^-$  cross section is better fitted with two fully interfering Breit-Wigners, with parameters in fair agreement with those of [2] and [9]. These results can be considered as a confirmation of the  $\rho(1450)$ .

Decisive evidence for the  $\pi\pi$  decay mode of both  $\rho(1450)$  and  $\rho(1700)$  comes from  $\bar{p}p$  annihilation at rest [11]. It has been shown that these resonances also possess a  $K\bar{K}$  decay mode [12–14]. High-statistics studies of the decays  $\tau \rightarrow \pi\pi\nu_\tau$  [15,16], and  $\tau \rightarrow 4\pi\nu_\tau$  [17] also require the  $\rho(1450)$ , but are not sensitive to the  $\rho(1700)$ , because it is too close to the  $\tau$  mass. A recent very-high-statistics study of the  $\tau \rightarrow \pi\pi\nu_\tau$  decay performed at Belle [18] reports the first observation of both  $\rho(1450)$  and  $\rho(1700)$  in  $\tau$  decays. A clear picture of the two  $\pi^+\pi^-$  resonances interfering with the  $\rho(770)$  in  $e^+e^-$  annihilation was also reported by BaBar using the ISR method [19].

The structure of these  $\rho$  states is not yet completely clear. Barnes [20] and Close [21] claim that  $\rho(1450)$  has a mass consistent with radial  $2S$ , but its decays show characteristics of hybrids, and suggest that this state may be a  $2S$ -hybrid mixture. Donnachie [22] argues that hybrid states could have a  $4\pi$  decay mode dominated by the  $a_1\pi$ . Such behavior has been observed by [23] in  $e^+e^- \rightarrow 4\pi$  in the energy range 1.05–1.38 GeV, and by [17] in  $\tau \rightarrow 4\pi$  decays. CLEO [24] and Belle [25] observe the  $\rho(1450) \rightarrow \omega\pi$  decay mode in  $B$ -meson decays, however, do not find  $\rho(1700) \rightarrow \omega\pi^0$ . A similar conclusion is made by [26,27], who studied the process  $e^+e^- \rightarrow \omega\pi^0$  and do not observe a statistically significant signal of the  $\rho(1700)$ . Various decay modes of the  $\rho(1450)$  and  $\rho(1700)$  are observed in  $\bar{p}n$  and  $\bar{p}p$  annihilation [28,29], but no definite conclusions can be drawn. More data should be collected to clarify the nature of the  $\rho$  states, particularly in the energy range above 1.6 GeV.

We now list under a separate entry the  $\rho(1570)$ , the  $\phi\pi$  state with  $J^{PC} = 1^{--}$  earlier observed by [30] (referred to as  $C(1480)$ ) and recently confirmed by [31]. While [32] shows that it may be a threshold effect, [5] and [33] suggest two independent vector states with this decay mode. The  $C(1480)$  has not been seen in the  $\bar{p}p$  [34] and  $e^+e^-$  [35,36] experiments. However, the sensitivity of the two latter is an order of magnitude lower than that of [31]. Note that [31] can not exclude that their observation is due to an OZI-suppressed decay mode of the  $\rho(1700)$ .

Several observations on the  $\omega\pi$  system in the 1200-MeV region [37–43] may be interpreted in terms of either  $J^P = 1^- \rho(770) \rightarrow \omega\pi$  production [44], or  $J^P = 1^+ b_1(1235)$  production [42,43]. We argue that no special entry for a  $\rho(1250)$  is needed. The LASS amplitude analysis [45] showing evidence for  $\rho(1270)$  is preliminary and needs confirmation.

For completeness, the relevant observations are listed under the  $\rho(1450)$ .

Recently [46] reported a very broad  $1^{--}$  resonance-like  $K^+K^-$  state in  $J/\psi \rightarrow K^+K^-\pi^0$  decays. Its pole position corresponds to mass of 1576 MeV and width of 818 MeV. [47–49] suggest its exotic structure (molecular or multiquark), while [50] and [51] explain it by the interference between the  $\rho(1450)$  and  $\rho(1700)$ . The latter statement is qualitatively supported by BaBar [52] and SND [53]. We quote [46] as  $X(1575)$  in the section “Further States.”

Evidence for  $\rho$ -like mesons decaying into  $6\pi$  states was first noted by [54] in the analysis of  $6\pi$  mass spectra from  $e^+e^-$  annihilation [55,56] and diffractive photoproduction [57]. Clegg [54] argued that two states at about 2.1 and 1.8 GeV exist: while the former is a candidate for the  $\rho(2150)$ , the latter could be a manifestation of the  $\rho(1700)$  distorted by threshold effects. BaBar reported observations of the new decay modes of the  $\rho(2150)$  in the channels  $\eta'(958)\pi^+\pi^-$  and  $f_1(1285)\pi^+\pi^-$  [58]. The relativistic quark model [59] predicts the  $2^3D_1$  state with  $J^{PC} = 1^{--}$  at 2.15 GeV which can be identified with the  $\rho(2150)$ .

We no longer list under a separate particle  $\rho(1900)$  various observations of irregular behavior of the cross sections near the  $N\bar{N}$  threshold. Dips of various width around 1.9 GeV were reported by the E687 Collaboration (a narrow one in the  $3\pi^+3\pi^-$  diffractive photoproduction [60,61]), by the FENICE experiment (a narrow structure in the  $R$  value [62]), by BaBar in ISR (a narrow structure in  $e^+e^- \rightarrow \phi\pi$  final state [63], but much broader in  $e^+e^- \rightarrow 3\pi^+3\pi^-$  and  $e^+e^- \rightarrow 2(\pi^+\pi^-\pi^0)$  [64]), by CMD-3 (also a rather broad dip in  $e^+e^- \rightarrow 3\pi^+3\pi^-$  [65]). A dedicated scan of the  $N\bar{N}$ -threshold region by CMD-3 confirms this effect in the  $e^+e^- \rightarrow 3\pi^+3\pi^-$  and  $e^+e^- \rightarrow K^+K^-\pi^+\pi^-$  final states, but does not see it in the cross section of  $e^+e^- \rightarrow 2\pi^+2\pi^-$  [66]. Most probably, these structures emerge as a threshold effect due to the opening of the  $N\bar{N}$  channel [67,68,69].

## References

1. C. Erkal, Z. Phys. **C31**, 615 (1986).
2. A. Donnachie and H. Mirzaie, Z. Phys. **C33**, 407 (1987).
3. A. Donnachie and A.B. Clegg, Z. Phys. **C34**, 257 (1987).
4. A. Donnachie and A.B. Clegg, Z. Phys. **C51**, 689 (1991).
5. A.B. Clegg and A. Donnachie, Z. Phys. **C40**, 313 (1988).
6. A.B. Clegg and A. Donnachie, Z. Phys. **C62**, 455 (1994).
7. T.J. Killian *et al.*, Phys. Rev. **D21**, 3005 (1980).
8. S. Fukui *et al.*, Phys. Lett. **B202**, 441 (1988).
9. D. Bisello *et al.*, Phys. Lett. **B220**, 321 (1989).
10. A. Antonelli *et al.*, Phys. Lett. **B212**, 133 (1988).
11. A. Abele *et al.*, Phys. Lett. **B391**, 191 (1997).
12. A. Abele *et al.*, Phys. Rev. **D57**, 3860 (1998).
13. A. Bertin *et al.*, Phys. Lett. **B434**, 180 (1998).
14. A. Abele *et al.*, Phys. Lett. **B468**, 178 (1999).
15. R. Barate *et al.*, Z. Phys. **C76**, 15 (1997).
16. S. Anderson, Phys. Rev. **D61**, 112002 (2000).
17. K.W. Edwards *et al.*, Phys. Rev. **D61**, 072003 (2000).
18. M. Fujikawa *et al.*, Phys. Rev. **D78**, 072006 (2008).
19. J.P. Lees *et al.*, Phys. Rev. **D86**, 032013 (2012).
20. T. Barnes *et al.*, Phys. Rev. **D55**, 4157 (1997).
21. F.E. Close *et al.*, Phys. Rev. **D56**, 1584 (1997).
22. A. Donnachie and Yu.S. Kalashnikova, Phys. Rev. **D60**, 114011 (1999).
23. R.R. Akhmetshin *et al.*, Phys. Lett. **B466**, 392 (1999).
24. J.P. Alexander *et al.*, Phys. Rev. **D64**, 092001 (2001).
25. D. Matvienko *et al.*, Phys. Rev. **D92**, 012013 (2015).
26. R.R. Akhmetshin *et al.*, Phys. Lett. **B562**, 173 (2003).
27. M.N. Achasov *et al.*, Phys. Rev. **D94**, 112001 (2016).
28. A. Abele *et al.*, Eur. Phys. J. **C21**, 261 (2001).
29. M. Bargiotti *et al.*, Phys. Lett. **B561**, 233 (2003).
30. S.I. Bityukov *et al.*, Phys. Lett. **B188**, 383 (1987).
31. B. Aubert *et al.*, Phys. Rev. **D77**, 092002 (2008).
32. N.N. Achasov and G.N. Shestakov, Phys. Atom. Nucl. **59**, 1262 (1996).
33. L.G. Landsberg, Sov. J. Nucl. Phys. **55**, 1051 (1992).
34. A. Abele *et al.*, Phys. Lett. **B415**, 280 (1997).
35. V.M. Aulchenko *et al.*, Sov. Phys. JETP Lett. **45**, 145 (1987).
36. D. Bisello *et al.*, Z. Phys. **C52**, 227 (1991).
37. P. Frenkiel *et al.*, Nucl. Phys. **B47**, 61 (1972).
38. G. Cosme *et al.*, Phys. Lett. **B63**, 352 (1976).
39. D.P. Barber *et al.*, Z. Phys. **C4**, 169 (1980).
40. D. Aston, Phys. Lett. **B92**, 211 (1980).
41. M. Atkinson *et al.*, Nucl. Phys. **B243**, 1 (1984).
42. J.E. Brau *et al.*, Phys. Rev. **D37**, 2379 (1988).
43. C. Amsler *et al.*, Phys. Lett. **B311**, 362 (1993).
44. J. Layssac and F.M. Renard, Nuovo Cimento **6A**, 134 (1971).
45. D. Aston *et al.*, Nucl. Phys. (Proc. Supp.) **B21**, 105 (1991).
46. M. Ablikim *et al.*, Phys. Rev. Lett. **97**, 142002 (2006).
47. G.-J. Ding and M.-L. Yan, Phys. Lett. **B643**, 33 (2006).
48. F.K. Guo *et al.*, Nucl. Phys. **A773**, 78 (2006).
49. A. Zhang *et al.*, Phys. Rev. **D76**, 036004 (2007).
50. B.A. Li, Phys. Rev. **D76**, 094016 (2007).
51. X. Liu *et al.*, Phys. Rev. **D75**, 074017 (2007).
52. J.P. Lees *et al.*, Phys. Rev. **D88**, 032013 (2013).
53. M.N. Achasov *et al.*, Phys. Rev. **D94**, 112006 (2016).
54. A.B. Clegg and A. Donnachie, Z. Phys. **C45**, 677 (1990).
55. D. Bisello *et al.*, Phys. Lett. **107B**, 145 (1981).
56. A. Castro *et al.*, LAL-88-58(1988).
57. M. Atkinson *et al.*, Z. Phys. **C29**, 333 (1985).
58. B. Aubert *et al.*, Phys. Rev. **D76**, 092005 (2007).
59. S. Godfrey and N. Isgur, Phys. Rev. **D32**, 189 (1985).
60. P.L. Frabetti *et al.*, Phys. Lett. **B514**, 240 (2001).
61. P.L. Frabetti *et al.*, Phys. Lett. **B578**, 290 (2004).
62. A. Antonelli *et al.*, Phys. Lett. **B365**, 427 (1996).
63. B. Aubert *et al.*, Phys. Rev. **D77**, 092002 (2008).
64. B. Aubert *et al.*, Phys. Rev. **D73**, 052003 (2006).
65. R.R. Akhmetshin *et al.*, Phys. Lett. **B723**, 83 (2013).
66. R.R. Akhmetshin *et al.*, Phys. Lett. **B794**, 64 (2019).

## Meson Particle Listings

 $\rho(1700)$ 

67. A. Obrazovsky and S. Serednyakov, Sov. Phys. JETP Lett. **99**, 315 (2014).
68. J. Heidenauer *et al.*, Phys. Rev. **D92**, 054032 (2015).
69. A.I. Milstein and S.G. Salmikov, Nucl. Phys. **A977**, 60 (2018).

 $\rho(1700)$  MASS $\eta\rho^0$  AND  $\pi^+\pi^-$  MODES

VALUE (MeV)	DOCUMENT ID
<b>1720±20 OUR ESTIMATE</b>	

 $\eta\rho^0$  MODE

VALUE (MeV)	EVTS	DOCUMENT ID	TECN	COMMENT
The data in this block is included in the average printed for a previous datablock.				

• • • We do not use the following data for averages, fits, limits, etc. • • •

1840±10	7.4k	<sup>1</sup> ACHASOV	18	SND	1.22–2.00 $e^+e^- \rightarrow \eta\pi^+\pi^-$
1740±20		ANTONELLI	88	DM2	$e^+e^- \rightarrow \eta\pi^+\pi^-$
1701±15		<sup>2</sup> FUKUI	88	SPEC	8.95 $\pi^-p \rightarrow \eta\pi^+\pi^-n$

<sup>1</sup> From the combined fit of AULCHENKO 15 and ACHASOV 18 in the model with the interfering  $\rho(1450)$ ,  $\rho(1700)$  and  $\rho(2150)$  with the parameters of the  $\rho(1450)$  and  $\rho(1700)$  floating and the mass and width of the  $\rho(2150)$  fixed at 2155 MeV and 320 MeV, respectively. The phases of the resonances are  $\pi$ , 0 and  $\pi$ , respectively.

<sup>2</sup> Assuming  $\rho^+ f_0(1370)$  decay mode interferes with  $a_1(1260)^+\pi$  background. From a two Breit-Wigner fit.

 $\pi\pi$  MODE

VALUE (MeV)	EVTS	DOCUMENT ID	TECN	COMMENT
The data in this block is included in the average printed for a previous datablock.				

• • • We do not use the following data for averages, fits, limits, etc. • • •

1770.54 ± 5.49		<sup>1</sup> BARTOS	17	RVUE	$e^+e^- \rightarrow \pi^+\pi^-$	
1718.50 ± 65.44		<sup>2</sup> BARTOS	17A	RVUE	$e^+e^- \rightarrow \pi^+\pi^-$	
1766.80 ± 52.36		<sup>3</sup> BARTOS	17A	RVUE	$\tau^- \rightarrow \pi^-\pi^0\nu_\tau$	
1644 ± 36	20K	<sup>4</sup> LEES	17c	BABR	$J/\psi \rightarrow \pi^+\pi^-\pi^0$	
1780 ± 20	+15 -20	63.5k	<sup>5</sup> ABRAMOWICZ12	ZEUS	$e p \rightarrow e\pi^+\pi^-p$	
1861 ± 17		<sup>6</sup> LEES	12G	BABR	$e^+e^- \rightarrow \pi^+\pi^-\gamma$	
1728 ± 17	± 89	5.4M	<sup>7,8</sup> FUJIKAWA	08	BELL	$\tau^- \rightarrow \pi^-\pi^0\nu_\tau$
1780 ± 37 -29		<sup>9</sup> ABELE	97	CBAR	$\bar{p}n \rightarrow \pi^-\pi^0\pi^0$	
1719 ± 15		<sup>9</sup> BERTIN	97c	OBLX	$0.0 \bar{p}p \rightarrow \pi^+\pi^-\pi^0$	
1730 ± 30		CLEGG	94	RVUE	$e^+e^- \rightarrow \pi^+\pi^-$	
1768 ± 21		BISELLO	89	DM2	$e^+e^- \rightarrow \pi^+\pi^-$	
1745.7 ± 91.9		DUBNICKA	89	RVUE	$e^+e^- \rightarrow \pi^+\pi^-$	
1546 ± 26		GESHKEN...	89	RVUE		
1650		<sup>10</sup> ERKAL	85	RVUE	20–70 $\gamma p \rightarrow \gamma\pi$	
1550 ± 70		ABE	84B	HYBR	20 $\gamma p \rightarrow \pi^+\pi^-p$	
1590 ± 20		<sup>11</sup> ASTON	80	OMEG	20–70 $\gamma p \rightarrow p2\pi$	
1600 ± 10		<sup>12</sup> ATIYA	79B	SPEC	50 $\gamma C \rightarrow C2\pi$	
1598 ± 24 -22		BECKER	79	ASPK	17 $\pi^-p$ polarized	
1659 ± 25		<sup>10</sup> LANG	79	RVUE		
1575		<sup>10</sup> MARTIN	78c	RVUE	17 $\pi^-p \rightarrow \pi^+\pi^-n$	
1610 ± 30		<sup>10</sup> FROGGATT	77	RVUE	17 $\pi^-p \rightarrow \pi^+\pi^-n$	
1590 ± 20		<sup>13</sup> HYAMS	73	ASPK	17 $\pi^-p \rightarrow \pi^+\pi^-n$	

<sup>1</sup> Applies the Unitary & Analytic Model of the pion electromagnetic form factor of DUBNICKA 10 to analyze the data of LEES 12G and ABLIKIM 16c.

<sup>2</sup> Applies the Unitary & Analytic Model of the pion electromagnetic form factor of DUBNICKA 10 to analyze the data of ACHASOV 06, AKHMETSHIN 07, AUBERT 09as, and AMBROSINO 11A.

<sup>3</sup> Applies the Unitary & Analytic Model of the pion electromagnetic form factor of DUBNICKA 10 to analyze the data of FUJIKAWA 08.

<sup>4</sup> From a Dalitz plot analysis in an isobar model with  $\rho(1450)$  and  $\rho(1700)$  masses and widths floating.

<sup>5</sup> Using the KUHN 90 parametrization of the pion form factor, neglecting  $\rho-\omega$  interference.

<sup>6</sup> Using the GOUNARIS 68 parametrization of the pion form factor leaving the masses and widths of the  $\rho(1450)$ ,  $\rho(1700)$ , and  $\rho(2150)$  resonances as free parameters of the fit.

<sup>7</sup>  $|F_\pi(0)|^2$  fixed to 1.

<sup>8</sup> From the GOUNARIS 68 parametrization of the pion form factor.

<sup>9</sup> T-matrix pole.

<sup>10</sup> From phase shift analysis of HYAMS 73 data.

<sup>11</sup> Simple relativistic Breit-Wigner fit with constant width.

<sup>12</sup> An additional 40 MeV uncertainty in both the mass and width is present due to the choice of the background shape.

<sup>13</sup> Included in BECKER 79 analysis.

 $\pi\omega$  MODE

VALUE (MeV)	EVTS	DOCUMENT ID	TECN	COMMENT
• • • We do not use the following data for averages, fits, limits, etc. • • •				

1708±41	7815	<sup>1</sup> ACHASOV	13	SND	1.05–2.00 $e^+e^- \rightarrow \pi^0\pi^0\gamma$
1550 to 1620		<sup>2</sup> ACHASOV	00i	SND	$e^+e^- \rightarrow \pi^0\pi^0\gamma$

1580 to 1710		<sup>3</sup> ACHASOV	00i	SND	$e^+e^- \rightarrow \pi^0\pi^0\gamma$
1710±90		ACHASOV	97	RVUE	$e^+e^- \rightarrow \omega\pi^0$

<sup>1</sup> From a phenomenological model based on vector meson dominance with the interfering  $\rho(1450)$  and  $\rho(1700)$  and their widths fixed at 400 and 250 MeV, respectively. Systematic uncertainty not estimated.

<sup>2</sup> Taking into account both  $\rho(1450)$  and  $\rho(1700)$  contributions. Using the data of ACHASOV 00i on  $e^+e^- \rightarrow \omega\pi^0$  and of EDWARDS 00A on  $\tau^- \rightarrow \omega\pi^-\nu_\tau$ .  $\rho(1450)$  mass and width fixed at 1400 MeV and 500 MeV respectively.

<sup>3</sup> Taking into account the  $\rho(1700)$  contribution only. Using the data of ACHASOV 00i on  $e^+e^- \rightarrow \omega\pi^0$  and of EDWARDS 00A on  $\tau^- \rightarrow \omega\pi^-\nu_\tau$ .

 $K\bar{K}$  MODE

VALUE (MeV)	EVTS	DOCUMENT ID	TECN	CHG	COMMENT
• • • We do not use the following data for averages, fits, limits, etc. • • •					

1541 ± 12 ± 33	190k	<sup>1</sup> AAIJ	16N	LHCB	$D^0 \rightarrow K_S^0 K^\pm \pi^\mp$
1740.8 ± 22.2	27k	<sup>2</sup> ABELE	99D	CBAR	$\pm 0.0 \bar{p}p \rightarrow K^+K^-\pi^0$
1582 ± 36	1600	CLELAND	82B	SPEC	$\pm 5.0 \pi p \rightarrow K_S^0 K^\pm p$

<sup>1</sup> Using the GOUNARIS 68 parameterization with a fixed width. Value is average using different  $K\pi$  S-wave parameterizations in fit.

<sup>2</sup> K-matrix pole. Isospin not determined, could be  $\omega(1650)$  or  $\phi(1680)$ .

 $2(\pi^+\pi^-)$  MODE

VALUE (MeV)	EVTS	DOCUMENT ID	TECN	COMMENT
• • • We do not use the following data for averages, fits, limits, etc. • • •				

1851 ± 27 -24		ACHASOV	97	RVUE	$e^+e^- \rightarrow 2(\pi^+\pi^-)$
1570 ± 20		<sup>1</sup> CORDIER	82	DM1	$e^+e^- \rightarrow 2(\pi^+\pi^-)$
1520 ± 30		<sup>2</sup> ASTON	81E	OMEG	20–70 $\gamma p \rightarrow p4\pi$
1654 ± 25		<sup>3</sup> DIBIANCA	81	DBC	$\pi^+d \rightarrow p\rho 2(\pi^+\pi^-)$
1666 ± 39		<sup>1</sup> BACCI	80	FRAG	$e^+e^- \rightarrow 2(\pi^+\pi^-)$
1780	34	KILLIAN	80	SPEC	11 $e^-p \rightarrow 2(\pi^+\pi^-)$
1500		<sup>4</sup> ATIYA	79B	SPEC	50 $\gamma C \rightarrow C4\pi^\pm$
1570 ± 60	65	<sup>5</sup> ALEXANDER	75	HBC	7.5 $\gamma p \rightarrow p4\pi$
1550 ± 60		<sup>2</sup> CONVERSI	74	OSPK	$e^+e^- \rightarrow 2(\pi^+\pi^-)$
1550 ± 50	160	SCHACHT	74	STRC	5.5–9 $\gamma p \rightarrow p4\pi$
1450 ± 100	340	SCHACHT	74	STRC	9–18 $\gamma p \rightarrow p4\pi$
1430 ± 50	400	BINGHAM	72B	HBC	9.3 $\gamma p \rightarrow p4\pi$

<sup>1</sup> Simple relativistic Breit-Wigner fit with model dependent width.

<sup>2</sup> Simple relativistic Breit-Wigner fit with constant width.

<sup>3</sup> One peak fit result.

<sup>4</sup> Parameters roughly estimated, not from a fit.

<sup>5</sup> Skew mass distribution compensated by Ross-Stodolsky factor.

 $\pi^+\pi^-\pi^0\pi^0$  MODE

VALUE (MeV)	DOCUMENT ID	TECN	COMMENT
• • • We do not use the following data for averages, fits, limits, etc. • • •			

1660 ± 30	AT KINSON	85B	OMEG 20–70 $\gamma p$
-----------	-----------	-----	-----------------------

 $3(\pi^+\pi^-)$  AND  $2(\pi^+\pi^-\pi^0)$  MODES

VALUE (MeV)	DOCUMENT ID	TECN	COMMENT
• • • We do not use the following data for averages, fits, limits, etc. • • •			

1730 ± 34	<sup>1</sup> FRABETTI	04	E687 $\gamma p \rightarrow 3\pi^+3\pi^-p$
1783 ± 15	CLEGG	90	RVUE $e^+e^- \rightarrow 3(\pi^+\pi^-)2(\pi^+\pi^-\pi^0)$

<sup>1</sup> From a fit with two resonances with the JACOB 72 continuum.

 $m_{\rho(1700)^0} - m_{\rho(1700)^\pm}$ 

VALUE (MeV)	DOCUMENT ID	TECN	COMMENT
• • • We do not use the following data for averages, fits, limits, etc. • • •			

-48.30 ± 83.81	<sup>1</sup> BARTOS	17A	RVUE $e^+e^- \rightarrow \pi^+\pi^-, \tau^- \rightarrow \pi^-\pi^0\nu_\tau$
----------------	---------------------	-----	---

<sup>1</sup> Applies the Unitary & Analytic Model of the pion electromagnetic form factor of DUBNICKA 10 to analyze the data of ACHASOV 06, AKHMETSHIN 07, AUBERT 09as, AMBROSINO 11A, and FUJIKAWA 08.

 $\rho(1700)$  WIDTH $\eta\rho^0$  AND  $\pi^+\pi^-$  MODES

VALUE (MeV)	DOCUMENT ID
<b>250±100 OUR ESTIMATE</b>	

 $\eta\rho^0$  MODE

VALUE (MeV)	EVTS	DOCUMENT ID	TECN	COMMENT
The data in this block is included in the average printed for a previous datablock.				

• • • We do not use the following data for averages, fits, limits, etc. • • •

132±40	7.4k	<sup>1</sup> ACHASOV	18	SND	1.22–2.00 $e^+e^- \rightarrow \eta\pi^+\pi^-$
150±30		ANTONELLI	88	DM2	$e^+e^- \rightarrow \eta\pi^+\pi^-$
282±44		<sup>2</sup> FUKUI	88	SPEC	8.95 $\pi^-p \rightarrow \eta\pi^+\pi^-n$

<sup>1</sup> From the combined fit of AULCHENKO 15 and ACHASOV 18 in the model with the interfering  $\rho(1450)$ ,  $\rho(1700)$  and  $\rho(2150)$  with the parameters of the  $\rho(1450)$  and  $\rho(1700)$  floating and the mass and width of the  $\rho(2150)$  fixed at 2155 MeV and 320 MeV, respectively. The phases of the resonances are  $\pi$ , 0 and  $\pi$ , respectively.

<sup>2</sup> Assuming  $\rho^+ f_0(1370)$  decay mode interferes with  $a_1(1260)^+\pi$  background. From a two Breit-Wigner fit.

**$\pi\pi$  MODE**

VALUE (MeV)	EVTS	DOCUMENT ID	TECN	COMMENT
-------------	------	-------------	------	---------

The data in this block is included in the average printed for a previous datablock.

• • • We do not use the following data for averages, fits, limits, etc. • • •				
268.98 ± 11.40		<sup>1</sup> BARTOS 17	RVUE	$e^+e^- \rightarrow \pi^+\pi^-$
489.58 ± 16.95		<sup>2</sup> BARTOS 17A	RVUE	$e^+e^- \rightarrow \pi^+\pi^-$
414.71 ± 119.48		<sup>3</sup> BARTOS 17A	RVUE	$\tau^- \rightarrow \pi^-\pi^0\nu_\tau$
109 ± 19	20K	<sup>4</sup> LEES 17C	BABR	$J/\psi \rightarrow \pi^+\pi^-\pi^0$
310 ± 30	$^{+25}_{-35}$ 63.5k	<sup>5</sup> ABRAMOWICZ12	ZEUS	$e\rho \rightarrow e\pi^+\pi^-p$
316 ± 26		<sup>6</sup> LEES 12G	BABR	$e^+e^- \rightarrow \pi^+\pi^-\gamma$
164 ± 21	$^{+89}_{-26}$ 5.4M	<sup>7,8</sup> FUJIKAWA 08	BELL	$\tau^- \rightarrow \pi^-\pi^0\nu_\tau$
275 ± 45		<sup>9</sup> ABELE 97	CBAR	$\bar{p}n \rightarrow \pi^-\pi^0\pi^0$
310 ± 40		<sup>9</sup> BERTIN 97C	OBLX	$0.0\bar{p}p \rightarrow \pi^+\pi^-\pi^0$
400 ± 100		<sup>9</sup> CLEGG 94	RVUE	$e^+e^- \rightarrow \pi^+\pi^-$
224 ± 22		<sup>9</sup> BISELLO 89	DM2	$e^+e^- \rightarrow \pi^+\pi^-$
242.5 ± 163.0		<sup>9</sup> DUBNICKA 89	RVUE	$e^+e^- \rightarrow \pi^+\pi^-$
620 ± 60		<sup>9</sup> GESHKEN... 89	RVUE	$e^+e^- \rightarrow \pi^+\pi^-$
<315		<sup>10</sup> ERKAL 85	RVUE	20-70 $\gamma\rho \rightarrow \gamma\pi$
280 ± 30		<sup>10</sup> ABE 84B	HYBR	20 $\gamma\rho \rightarrow \pi^+\pi^-p$
230 ± 80		<sup>11</sup> ASTON 80	OMEG	20-70 $\gamma\rho \rightarrow p2\pi$
283 ± 14		<sup>12</sup> ATIYA 79B	SPEC	50 $\gamma C \rightarrow C2\pi$
175 ± 98		<sup>12</sup> BECKER 79	ASPK	17 $\pi^-p$ polarized
232 ± 34		<sup>10</sup> LANG 79	RVUE	
340		<sup>10</sup> MARTIN 78C	RVUE	17 $\pi^-p \rightarrow \pi^+\pi^-n$
300 ± 100		<sup>10</sup> FROGGATT 77	RVUE	17 $\pi^-p \rightarrow \pi^+\pi^-n$
180 ± 50		<sup>13</sup> HYAMS 73	ASPK	17 $\pi^-p \rightarrow \pi^+\pi^-n$

- Applies the Unitary & Analytic Model of the pion electromagnetic form factor of DUBNICKA 10 to analyze the data of LEES 12G and ABLIKIM 16c.
- Applies the Unitary & Analytic Model of the pion electromagnetic form factor of DUBNICKA 10 to analyze the data of ACHASOV 06, AKHMETSIN 07, AUBERT 09as, and AMBROSINO 11a.
- Applies the Unitary & Analytic Model of the pion electromagnetic form factor of DUBNICKA 10 to analyze the data of FUJIKAWA 08.
- From a Dalitz plot analysis in an isobar model with  $\rho(1450)$  and  $\rho(1700)$  masses and widths floating.
- Using the KUHN 90 parametrization of the pion form factor, neglecting  $\rho-\omega$  interference.
- Using the GOUNARIS 68 parametrization of the pion form factor leaving the masses and widths of the  $\rho(1450)$ ,  $\rho(1700)$ , and  $\rho(2150)$  resonances as free parameters of the fit.
- $|F_\pi(0)|^2$  fixed to 1.
- From the GOUNARIS 68 parametrization of the pion form factor.
- T-matrix pole.
- From phase shift analysis of HYAMS 73 data.
- Simple relativistic Breit-Wigner fit with constant width.
- An additional 40 MeV uncertainty in both the mass and width is present due to the choice of the background shape.
- Included in BECKER 79 analysis.

**$K\bar{K}$  MODE**

VALUE (MeV)	EVTS	DOCUMENT ID	TECN	CHG	COMMENT
-------------	------	-------------	------	-----	---------

• • • We do not use the following data for averages, fits, limits, etc. • • •					
187.2 ± 26.7	27k	<sup>1</sup> ABELE 99D	CBAR	±	0.0 $\bar{p}p \rightarrow K^+K^-\pi^0$
265 ± 120	1600	CLELAND 82B	SPEC	±	5.0 $\pi p \rightarrow K_S^0 K^\pm p$

<sup>1</sup> K-matrix pole. Isospin not determined, could be  $\omega(1650)$  or  $\phi(1680)$ .

**$2(\pi^+\pi^-)$  MODE**

VALUE (MeV)	EVTS	DOCUMENT ID	TECN	COMMENT
-------------	------	-------------	------	---------

• • • We do not use the following data for averages, fits, limits, etc. • • •				
510 ± 40		<sup>1</sup> CORDIER 82	DM1	$e^+e^- \rightarrow 2(\pi^+\pi^-)$
400 ± 50		<sup>2</sup> ASTON 81E	OMEG	20-70 $\gamma\rho \rightarrow p4\pi$
400 ± 146		<sup>3</sup> DIBIANCA 81	DBC	$\pi^+d \rightarrow pp2(\pi^+\pi^-)$
700 ± 160		<sup>1</sup> BACCI 80	FRAG	$e^+e^- \rightarrow 2(\pi^+\pi^-)$
100	34	KILLIAN 80	SPEC	11 $e^-p \rightarrow 2(\pi^+\pi^-)$
600		<sup>4</sup> ATIYA 79B	SPEC	50 $\gamma C \rightarrow C4\pi^\pm$
340 ± 160	65	<sup>5</sup> ALEXANDER 75	HBC	7.5 $\gamma\rho \rightarrow p4\pi$
360 ± 100		<sup>2</sup> CONVERSI 74	OSPK	$e^+e^- \rightarrow 2(\pi^+\pi^-)$
400 ± 120	160	<sup>6</sup> SCHACHT 74	STRC	5.5-9 $\gamma\rho \rightarrow p4\pi$
850 ± 200	340	<sup>6</sup> SCHACHT 74	STRC	9-18 $\gamma\rho \rightarrow p4\pi$
650 ± 100	400	BINGHAM 72B	HBC	9.3 $\gamma\rho \rightarrow p4\pi$

- Simple relativistic Breit-Wigner fit with model-dependent width.
- Simple relativistic Breit-Wigner fit with constant width.
- One peak fit result.
- Parameters roughly estimated, not from a fit.
- Skew mass distribution compensated by Ross-Stodolsky factor.
- Width errors enlarged by us to  $4\Gamma/\sqrt{N}$ ; see the note with the  $K^*(892)$  mass.

**$\pi^+\pi^-\pi^0\pi^0$  MODE**

VALUE (MeV)	DOCUMENT ID	TECN	COMMENT
-------------	-------------	------	---------

• • • We do not use the following data for averages, fits, limits, etc. • • •			
300 ± 50	ATKINSON 85B	OMEG	20-70 $\gamma\rho$

**$\omega\pi^0$  MODE**

VALUE (MeV)	DOCUMENT ID	TECN	COMMENT
-------------	-------------	------	---------

• • • We do not use the following data for averages, fits, limits, etc. • • •			
350 to 580	<sup>1</sup> ACHASOV 00i	SND	$e^+e^- \rightarrow \pi^0\pi^0\gamma$
490 to 1040	<sup>2</sup> ACHASOV 00i	SND	$e^+e^- \rightarrow \pi^0\pi^0\gamma$

- Taking into account both  $\rho(1450)$  and  $\rho(1700)$  contributions. Using the data of ACHASOV 00i on  $e^+e^- \rightarrow \omega\pi^0$  and of EDWARDS 00a on  $\tau^- \rightarrow \omega\pi^-\nu_\tau$ .  $\rho(1450)$  mass and width fixed at 1400 MeV and 500 MeV respectively.
- Taking into account the  $\rho(1700)$  contribution only. Using the data of ACHASOV 00i on  $e^+e^- \rightarrow \omega\pi^0$  and of EDWARDS 00a on  $\tau^- \rightarrow \omega\pi^-\nu_\tau$ .

**$3(\pi^+\pi^-)$  AND  $2(\pi^+\pi^-\pi^0)$  MODES**

VALUE (MeV)	DOCUMENT ID	TECN	COMMENT
-------------	-------------	------	---------

• • • We do not use the following data for averages, fits, limits, etc. • • •			
315 ± 100	<sup>1</sup> FRABETTI 04	E687	$\gamma\rho \rightarrow 3\pi^+3\pi^-p$
285 ± 20	CLEGG 90	RVUE	$e^+e^- \rightarrow 3(\pi^+\pi^-)2(\pi^+\pi^-\pi^0)$

<sup>1</sup> From a fit with two resonances with the JACOB 72 continuum.

**$\Gamma_{\rho(1700)^0} - \Gamma_{\rho(1700)^\pm}$**

VALUE (MeV)	DOCUMENT ID	TECN	COMMENT
-------------	-------------	------	---------

• • • We do not use the following data for averages, fits, limits, etc. • • •			
74.87 ± 120.67	<sup>1</sup> BARTOS 17A	RVUE	$e^+e^- \rightarrow \pi^+\pi^-\tau^+ \rightarrow \pi^-\pi^0\nu_\tau$

- Applies the Unitary & Analytic Model of the pion electromagnetic form factor of DUBNICKA 10 to analyze the data of ACHASOV 06, AKHMETSIN 07, AUBERT 09as, AMBROSINO 11a, and FUJIKAWA 08.

**$\rho(1700)$  DECAY MODES**

Mode	Fraction ( $\Gamma_i/\Gamma$ )
$\Gamma_1$ $4\pi$	
$\Gamma_2$ $2(\pi^+\pi^-)$	seen
$\Gamma_3$ $\rho\pi\pi$	seen
$\Gamma_4$ $\rho^0\pi^+\pi^-$	seen
$\Gamma_5$ $\rho^0\pi^0\pi^0$	
$\Gamma_6$ $\rho^\pm\pi^\mp\pi^0$	seen
$\Gamma_7$ $a_1(1260)\pi$	seen
$\Gamma_8$ $h_1(1170)\pi$	seen
$\Gamma_9$ $\pi(1300)\pi$	seen
$\Gamma_{10}$ $\rho\rho$	seen
$\Gamma_{11}$ $\pi^+\pi^-$	seen
$\Gamma_{12}$ $\pi\pi$	seen
$\Gamma_{13}$ $K\bar{K}^*(892) + c.c.$	seen
$\Gamma_{14}$ $\eta\rho$	seen
$\Gamma_{15}$ $a_2(1320)\pi$	not seen
$\Gamma_{16}$ $K\bar{K}$	seen
$\Gamma_{17}$ $e^+e^-$	seen
$\Gamma_{18}$ $\pi^0\omega$	seen
$\Gamma_{19}$ $\pi^0\gamma$	not seen

**$\rho(1700) \Gamma(i)\Gamma(e^+e^-)/\Gamma(\text{total})$**

This combination of a partial width with the partial width into  $e^+e^-$  and with the total width is obtained from the cross-section into channel in  $e^+e^-$  annihilation.

**$\Gamma(2(\pi^+\pi^-)) \times \Gamma(e^+e^-)/\Gamma_{\text{total}}$   $\Gamma_2\Gamma_{17}/\Gamma$**

VALUE (keV)	DOCUMENT ID	TECN	COMMENT
-------------	-------------	------	---------

• • • We do not use the following data for averages, fits, limits, etc. • • •			
2.6 ± 0.2	DEL COURT 81B	DM1	$e^+e^- \rightarrow 2(\pi^+\pi^-)$
2.83 ± 0.42	BACCI 80	FRAG	$e^+e^- \rightarrow 2(\pi^+\pi^-)$

**$\Gamma(\pi^+\pi^-) \times \Gamma(e^+e^-)/\Gamma_{\text{total}}$   $\Gamma_{11}\Gamma_{17}/\Gamma$**

VALUE (keV)	DOCUMENT ID	TECN	COMMENT
-------------	-------------	------	---------

• • • We do not use the following data for averages, fits, limits, etc. • • •			
0.13	<sup>1</sup> DIEKMAN 88	RVUE	$e^+e^- \rightarrow \pi^+\pi^-$
0.029 $^{+0.016}_{-0.012}$	KURDADZE 83	OLYA	0.64-1.4 $e^+e^- \rightarrow \pi^+\pi^-$

<sup>1</sup> Using total width = 220 MeV.

**$\Gamma(K\bar{K}^*(892) + c.c.) \times \Gamma(e^+e^-)/\Gamma_{\text{total}}$   $\Gamma_{13}\Gamma_{17}/\Gamma$**

VALUE (keV)	DOCUMENT ID	TECN	COMMENT
-------------	-------------	------	---------

• • • We do not use the following data for averages, fits, limits, etc. • • •			
0.305 ± 0.071	<sup>1</sup> BIZOT 80	DM1	$e^+e^-$

<sup>1</sup> Model dependent.



## Meson Particle Listings

 $\rho(1700)$ 

$\Gamma(\eta\rho) \times \Gamma(e^+e^-)/\Gamma_{\text{total}}$   $\Gamma_{14}\Gamma_{17}/\Gamma$   
 VALUE (keV) DOCUMENT ID TECN COMMENT

••• We do not use the following data for averages, fits, limits, etc. •••  
 $84 \pm 26 \pm 4$  <sup>1</sup> LEES 18 BABR  $e^+e^- \rightarrow \eta\pi^+\pi^-$   
 $7 \pm 3$  ANTONELLI 88 DM2  $e^+e^- \rightarrow \eta\pi^+\pi^-$   
<sup>1</sup> Includes non-resonant contribution. The selected fit model includes three  $\rho$  excited states. Model uncertainty is 80%.

$\Gamma(K\bar{K}) \times \Gamma(e^+e^-)/\Gamma_{\text{total}}$   $\Gamma_{16}\Gamma_{17}/\Gamma$   
 VALUE (keV) DOCUMENT ID TECN COMMENT

••• We do not use the following data for averages, fits, limits, etc. •••  
 $0.035 \pm 0.029$  <sup>1</sup> BIZOT 80 DM1  $e^+e^-$   
<sup>1</sup> Model dependent.

$\Gamma(\rho\pi\pi) \times \Gamma(e^+e^-)/\Gamma_{\text{total}}$   $\Gamma_3\Gamma_{17}/\Gamma$   
 VALUE (keV) DOCUMENT ID TECN COMMENT

••• We do not use the following data for averages, fits, limits, etc. •••  
 $3.510 \pm 0.090$  <sup>1</sup> BIZOT 80 DM1  $e^+e^-$   
<sup>1</sup> Model dependent.

 $\rho(1700) \Gamma(i)/\Gamma(\text{total}) \times \Gamma(e^+e^-)/\Gamma(\text{total})$ 

$\Gamma(\pi^0\omega)/\Gamma_{\text{total}} \times \Gamma(e^+e^-)/\Gamma_{\text{total}}$   $\Gamma_{18}/\Gamma \times \Gamma_{17}/\Gamma$   
 VALUE (units  $10^{-8}$ ) EVTS DOCUMENT ID TECN COMMENT

••• We do not use the following data for averages, fits, limits, etc. •••  
 $0.09 \pm 0.05$  10.2k <sup>1</sup> ACHASOV 16D SND 1.05–2.00  $e^+e^- \rightarrow \pi^0\pi^0\gamma$   
 $1.7 \pm 0.4$  7815 <sup>2</sup> ACHASOV 13 SND 1.05–2.00  $e^+e^- \rightarrow \pi^0\pi^0\gamma$   
<sup>1</sup> From a phenomenological model based on vector meson dominance with interfering  $\rho(700)$ ,  $\rho(1450)$ , and  $\rho(1700)$ . The  $\rho(1700)$  mass and width are fixed at 1720 MeV and 250 MeV, respectively. Systematic uncertainty not estimated. Supersedes ACHASOV 13.  
<sup>2</sup> From a phenomenological model based on vector meson dominance with the interfering  $\rho(1450)$  and  $\rho(1700)$  and their widths fixed at 400 and 250 MeV, respectively. Systematic uncertainty not estimated.

$\Gamma(\eta\rho)/\Gamma_{\text{total}} \times \Gamma(e^+e^-)/\Gamma_{\text{total}}$   $\Gamma_{14}/\Gamma \times \Gamma_{17}/\Gamma$   
 VALUE (units  $10^{-8}$ ) EVTS DOCUMENT ID TECN COMMENT

••• We do not use the following data for averages, fits, limits, etc. •••  
 $8.3^{+3.8}_{-3.1}$  7.4k <sup>1</sup> ACHASOV 18 SND 1.22–2.00  $e^+e^- \rightarrow \eta\pi^+\pi^-$   
<sup>1</sup> From the combined fit of AULCHENKO 15 and ACHASOV 18 in the model with the interfering  $\rho(1450)$ ,  $\rho(1700)$  and  $\rho(2150)$  with the parameters of the  $\rho(1450)$  and  $\rho(1700)$  floating and the mass and width of the  $\rho(2150)$  fixed at 2155 MeV and 320 MeV, respectively. The phases of the resonances are  $\pi$ , 0 and  $\pi$ , respectively.

 $\rho(1700)$  BRANCHING RATIOS

$\Gamma(\rho\pi\pi)/\Gamma(4\pi)$   $\Gamma_3/\Gamma_1$   
 VALUE DOCUMENT ID TECN COMMENT

••• We do not use the following data for averages, fits, limits, etc. •••  
 $0.28 \pm 0.06$  <sup>1</sup> ABELE 01B CBAR  $0.0 \bar{p}n \rightarrow 5\pi$   
<sup>1</sup>  $\omega\pi$  not included.

$\Gamma(\rho^0\pi^+\pi^-)/\Gamma(2(\pi^+\pi^-))$   $\Gamma_4/\Gamma_2$   
 VALUE EVTS DOCUMENT ID TECN COMMENT

••• We do not use the following data for averages, fits, limits, etc. •••  
 $\sim 1.0$  DELCOURT 81B DM1  $e^+e^- \rightarrow 2(\pi^+\pi^-)$   
 $0.7 \pm 0.1$  500 SCHACHT 74 STRC  $5.5\text{--}18 \gamma\rho \rightarrow p4\pi$   
 $0.80$  <sup>1</sup> BINGHAM 72B HBC  $9.3 \gamma\rho \rightarrow p4\pi$   
<sup>1</sup> The  $\pi\pi$  system is in S-wave.

$\Gamma(\rho^0\pi^0\pi^0)/\Gamma(\rho^\pm\pi^\mp\pi^0)$   $\Gamma_5/\Gamma_6$   
 VALUE DOCUMENT ID TECN CHG COMMENT

••• We do not use the following data for averages, fits, limits, etc. •••  
 $<0.10$  ATKINSON 85B OMEG  $20\text{--}70 \gamma\rho$   
 $<0.15$  ATKINSON 82 OMEG 0  $20\text{--}70 \gamma\rho \rightarrow p4\pi$

$\Gamma(a_1(1260)\pi)/\Gamma(4\pi)$   $\Gamma_7/\Gamma_1$   
 VALUE DOCUMENT ID TECN COMMENT

••• We do not use the following data for averages, fits, limits, etc. •••  
 $0.16 \pm 0.05$  <sup>1</sup> ABELE 01B CBAR  $0.0 \bar{p}n \rightarrow 5\pi$   
<sup>1</sup>  $\omega\pi$  not included.

$\Gamma(h_1(1170)\pi)/\Gamma(4\pi)$   $\Gamma_8/\Gamma_1$   
 VALUE DOCUMENT ID TECN COMMENT

••• We do not use the following data for averages, fits, limits, etc. •••  
 $0.17 \pm 0.06$  <sup>1</sup> ABELE 01B CBAR  $0.0 \bar{p}n \rightarrow 5\pi$   
<sup>1</sup>  $\omega\pi$  not included.

$\Gamma(\pi(1300)\pi)/\Gamma(4\pi)$   $\Gamma_9/\Gamma_1$   
 VALUE DOCUMENT ID TECN COMMENT

••• We do not use the following data for averages, fits, limits, etc. •••  
 $0.30 \pm 0.10$  <sup>1</sup> ABELE 01B CBAR  $0.0 \bar{p}n \rightarrow 5\pi$   
<sup>1</sup>  $\omega\pi$  not included.

$\Gamma(\rho\rho)/\Gamma(4\pi)$   $\Gamma_{10}/\Gamma_1$   
 VALUE DOCUMENT ID TECN COMMENT

••• We do not use the following data for averages, fits, limits, etc. •••  
 $0.09 \pm 0.03$  <sup>1</sup> ABELE 01B CBAR  $0.0 \bar{p}n \rightarrow 5\pi$   
<sup>1</sup>  $\omega\pi$  not included.

$\Gamma(\pi^+\pi^-)/\Gamma_{\text{total}}$   $\Gamma_{11}/\Gamma$   
 VALUE DOCUMENT ID TECN COMMENT

••• We do not use the following data for averages, fits, limits, etc. •••  
 $0.287^{+0.043}_{-0.042}$  BECKER 79 ASPK  $17 \pi^- p$  polarized  
 $0.15$  to  $0.30$  <sup>1</sup> MARTIN 78C RVUE  $17 \pi^- p \rightarrow \pi^+\pi^-n$   
 $<0.20$  <sup>2</sup> COSTA... 77B RVUE  $e^+e^- \rightarrow 2\pi, 4\pi$   
 $0.30 \pm 0.05$  <sup>1</sup> FROGGATT 77 RVUE  $17 \pi^- p \rightarrow \pi^+\pi^-n$   
 $<0.15$  <sup>3</sup> EISENBERG 73 HBC  $5 \pi^+ p \rightarrow \Delta^{++}2\pi$   
 $0.25 \pm 0.05$  <sup>4</sup> HYAMS 73 ASPK  $17 \pi^- p \rightarrow \pi^+\pi^-n$   
<sup>1</sup> From phase shift analysis of HYAMS 73 data.  
<sup>2</sup> Estimate using unitarity, time reversal invariance, Breit-Wigner.  
<sup>3</sup> Estimated using one-pion-exchange model.  
<sup>4</sup> Included in BECKER 79 analysis.

$\Gamma(\pi^+\pi^-)/\Gamma(2(\pi^+\pi^-))$   $\Gamma_{11}/\Gamma_2$   
 VALUE DOCUMENT ID TECN COMMENT

••• We do not use the following data for averages, fits, limits, etc. •••  
 $0.13 \pm 0.05$  ASTON 80 OMEG  $20\text{--}70 \gamma\rho \rightarrow p2\pi$   
 $<0.14$  <sup>1</sup> DAVIER 73 STRC  $6\text{--}18 \gamma\rho \rightarrow p4\pi$   
 $<0.2$  <sup>2</sup> BINGHAM 72B HBC  $9.3 \gamma\rho \rightarrow p2\pi$   
<sup>1</sup> Upper limit is estimate.  
<sup>2</sup>  $2\sigma$  upper limit.

$\Gamma(\pi\pi)/\Gamma(4\pi)$   $\Gamma_{12}/\Gamma_1$   
 VALUE DOCUMENT ID TECN COMMENT

••• We do not use the following data for averages, fits, limits, etc. •••  
 $0.16 \pm 0.04$  <sup>1,2</sup> ABELE 01B CBAR  $0.0 \bar{p}n \rightarrow 5\pi$   
<sup>1</sup> Using ABELE 97.  
<sup>2</sup>  $\omega\pi$  not included.

$\Gamma(K\bar{K}^*(892) + \text{c.c.})/\Gamma_{\text{total}}$   $\Gamma_{13}/\Gamma$   
 VALUE DOCUMENT ID TECN COMMENT

••• We do not use the following data for averages, fits, limits, etc. •••  
 possibly seen COAN 04 CLEO  $\tau^- \rightarrow K^-\pi^-K^+\nu_\tau$

$\Gamma(K\bar{K}^*(892) + \text{c.c.})/\Gamma(2(\pi^+\pi^-))$   $\Gamma_{13}/\Gamma_2$   
 VALUE DOCUMENT ID TECN COMMENT

••• We do not use the following data for averages, fits, limits, etc. •••  
 $0.15 \pm 0.03$  <sup>1</sup> DELCOURT 81B DM1  $e^+e^- \rightarrow \bar{K}K\pi$   
<sup>1</sup> Assuming  $\rho(1700)$  and  $\omega$  radial excitations to be degenerate in mass.

$\Gamma(\eta\rho)/\Gamma_{\text{total}}$   $\Gamma_{14}/\Gamma$   
 VALUE CL% DOCUMENT ID TECN COMMENT

••• We do not use the following data for averages, fits, limits, etc. •••  
 possibly seen AKHMETSHIN 00D CMD2  $e^+e^- \rightarrow \eta\pi^+\pi^-$   
 $<0.04$  DONNACHIE 87B RVUE  
 $<0.02$  58 ATKINSON 86B OMEG  $20\text{--}70 \gamma\rho$

$\Gamma(\eta\rho)/\Gamma(2(\pi^+\pi^-))$   $\Gamma_{14}/\Gamma_2$   
 VALUE DOCUMENT ID TECN COMMENT

••• We do not use the following data for averages, fits, limits, etc. •••  
 $0.123 \pm 0.027$  DELCOURT 82 DM1  $e^+e^- \rightarrow \pi^+\pi^-MM$   
 $\sim 0.1$  ASTON 80 OMEG  $20\text{--}70 \gamma\rho$

$\Gamma(\pi^+\pi^- \text{ neutrals})/\Gamma(2(\pi^+\pi^-))$   $(\Gamma_5 + \Gamma_6 + 0.714\Gamma_{14})/\Gamma_2$   
 VALUE DOCUMENT ID TECN COMMENT

••• We do not use the following data for averages, fits, limits, etc. •••  
 $2.6 \pm 0.4$  <sup>1</sup> BALLAM 74 HBC  $9.3 \gamma\rho$   
<sup>1</sup> Upper limit. Background not subtracted.

$\Gamma(a_2(1320)\pi)/\Gamma_{\text{total}}$   $\Gamma_{15}/\Gamma$   
 VALUE DOCUMENT ID TECN COMMENT

••• We do not use the following data for averages, fits, limits, etc. •••  
 not seen AMELIN 00 VES  $37 \pi^- p \rightarrow \eta\pi^+\pi^-n$

See key on page 999

Meson Particle Listings

$\rho(1700), a_2(1700)$

$\Gamma(K\bar{K})/\Gamma(2\pi^+\pi^-)$   $\Gamma_{16}/\Gamma_2$

Table with columns: VALUE, CL%, DOCUMENT ID, TECN, CHG, COMMENT. Includes data for DELCOURT 81B DM1 and BINGHAM 72B HBC 0.

$\Gamma(K\bar{K})/\Gamma(K\bar{K}^*(892)+c.c.)$   $\Gamma_{16}/\Gamma_{13}$

Table with columns: VALUE, DOCUMENT ID, TECN, COMMENT. Includes data for BUON 82 DM1.

$\Gamma(\pi^0\omega)/\Gamma_{total}$   $\Gamma_{18}/\Gamma$

Table with columns: VALUE, EVTS, DOCUMENT ID, TECN, COMMENT. Includes data for MATVIENKO 15 BELL and ACHASOV 12 SND.

$\Gamma(\pi^0\gamma)/\Gamma_{total}$   $\Gamma_{19}/\Gamma$

Table with columns: VALUE, DOCUMENT ID, TECN, COMMENT. Includes data for ACHASOV 10D SND. Includes a note about VMD model.

$\rho(1700)$  REFERENCES

Large reference table listing authors, document IDs, and collaborations for the rho(1700) meson.

$a_2(1700)$

$J^{PC} = 1^-(2^+)$

$a_2(1700)$  MASS

Table with columns: VALUE (MeV), EVTS, DOCUMENT ID, TECN, COMMENT. Includes 'OUR AVERAGE' and data from RODAS, AMSLER, AGHASYAN, etc.

- 1 The coupled-channel analysis of both the  $\eta\pi$  and  $\eta'\pi$  systems using ADOLPH 15data.
2 T-matrix pole.
3 Statistical error negligible.
4 Breit-Wigner mass.
5 Superseded by RODAS 19.
6 From analysis of L3 data at 183-209 GeV.
7 Statistical error only.
8 Spin 2 dominant, isospin not determined, could also be  $I=1$ .
9 Possibly two  $J^P = 2^+$  resonances with isospins 0 and 1.

$a_2(1700)$  WIDTH

Table with columns: VALUE (MeV), EVTS, DOCUMENT ID, TECN, COMMENT. Includes 'OUR AVERAGE' and data from RODAS, AMSLER, AGHASYAN, etc.

- 1 The coupled-channel analysis of both the  $\eta\pi$  and  $\eta'\pi$  systems using ADOLPH 15data. The width is extracted from the T-matrix pole.
2 T-matrix pole.
3 Statistical error negligible.
4 Breit-Wigner width.
5 Superseded by RODAS 19.
6 From analysis of L3 data at 183-209 GeV.
7 Statistical error only.
8 Spin 2 dominant, isospin not determined, could also be  $I=1$ .

$a_2(1700)$  DECAY MODES

Table with columns: Mode, Fraction ( $\Gamma_i/\Gamma$ ). Lists decay modes like  $\eta\pi$ ,  $\gamma\gamma$ ,  $\rho\pi$ ,  $f_2(1270)\pi$ ,  $K\bar{K}$ ,  $\omega\pi^-\pi^0$ ,  $\omega\rho$ .

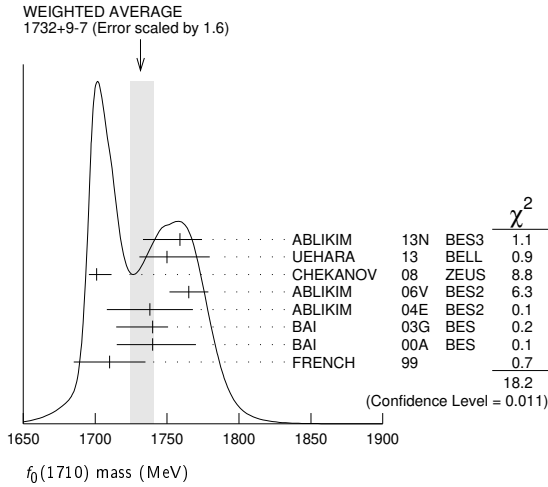
$a_2(1700)$  PARTIAL WIDTHS

Table with columns: VALUE (MeV), EVTS, DOCUMENT ID, TECN, COMMENT. Includes data for SCHEGELSKY 06A RVUE.

Downloaded from https://academic.oup.com/ptep/article/2020/8/083C01/5891211 by guest on 12 November 2020



<sup>29</sup> Superseded by LONGACRE 86.



$f_0(1710)$  WIDTH

OUR EVALUATION below is based on T-matrix poles from BARBERIS 00E and BARBERIS 99B.

VALUE (MeV)	EVTs	DOCUMENT ID	TECN	COMMENT
<b>123 ± 18</b>	<b>OUR EVALUATION</b>			
<b>147 ± 12</b>	<b>OUR AVERAGE</b>	Error includes scale factor of 1.2.		
172 ± 10	5.5k	1 ABLIKIM	13N BES3	$e^+e^- \rightarrow J/\psi \rightarrow \gamma\eta\eta$
139 ± 11		2 UEHARA	13 BELL	$\gamma\gamma \rightarrow K_S^0 K_S^0$
100 ± 24	4k	3 CHEKANOV	08 ZEUS	$ep \rightarrow K_S^0 K_S^0 X$
145 ± 8	±69	4 ABLIKIM	06V BES2	$e^+e^- \rightarrow J/\psi \rightarrow \gamma\pi^+\pi^-$
125 ± 20		ABLIKIM	04E BES2	$J/\psi \rightarrow \omega K^+K^-$
166 ± 5	+15	BAI	03G BES	$J/\psi \rightarrow \gamma K\bar{K}$
120 ± 50	-40	BAI	00A BES	$J/\psi \rightarrow \gamma(\pi^+\pi^-\pi^+\pi^-)$
105 ± 34		5 FRENCH	99	$300 pp \rightarrow p_f(K^+K^-)p_s$
••• We do not use the following data for averages, fits, limits, etc. •••				
148 ± 40		AMSLER	06 CBAR	$1.64 \bar{p}p \rightarrow K^+K^-\pi^0$
188 ± 13	80k	4,6 UMAN	06 E835	$5.2 \bar{p}p \rightarrow \eta\eta\pi^0$
250 ± 30		VLADIMIRSK..06	SPEC	$40 \pi^-\pi^0 \rightarrow K_S^0 K_S^0 n$
270 ± 60		7 ABLIKIM	05 BES2	$J/\psi \rightarrow \phi\pi^+\pi^-$
125 ± 25	+10	4 ABLIKIM	05Q BES2	$\psi(2S) \rightarrow \gamma\pi^+\pi^-K^+K^-$
260 ± 50		4 BINON	05 GAMS	$33 \pi^-\pi^0 \rightarrow \eta\eta n$
144 ± 30		8,9 ANISOVICH	03 RVUE	
320 ± 50		9,10 ANISOVICH	03 RVUE	
102 ± 26		TIKHOMIROV	03 SPEC	$40.0 \pi^-\pi^0 \rightarrow K_S^0 K_S^0 K_S^0 X$
267 ± 44	3651	11 NICHITIU	02 OBLX	$0 \bar{p}p \rightarrow K^+K^-\pi^+\pi^-\pi^0$
120 ± 26		12 BARBERIS	00E	$450 pp \rightarrow p_f\eta\eta p_s$
220 ± 40		13,14 ANISOVICH	99B SPEC	$0.6-1.2 p\bar{p} \rightarrow \eta\eta\pi^0$
100 ± 25		BARBERIS	99 OMEG	$450 pp \rightarrow p_s p_f K^+K^-$
160 ± 30		BARBERIS	99B OMEG	$450 pp \rightarrow p_s p_f \pi^+\pi^-$
126 ± 16	±18	12,15 BARBERIS	99D OMEG	$450 pp \rightarrow K^+K^-, \pi^+\pi^-$
250 ± 140		16 ANISOVICH	98B RVUE	Compilation
30 ± 7	57	17 BARKOV	98	$\pi^-\pi^0 \rightarrow K_S^0 K_S^0 n$
103 ± 18	+30	18 BAI	96C BES	$J/\psi \rightarrow \gamma K^+K^-$
85 ± 24	+22	BAI	96C BES	$J/\psi \rightarrow \gamma K^+K^-$
56 ± 19		BALOSHIN	95 SPEC	$40 \pi^-\pi^0 \rightarrow K_S^0 K_S^0 X$
160 ± 40		19 BUGG	95 MRK3	$J/\psi \rightarrow \gamma\pi^+\pi^-\pi^+\pi^-$
160 ± 60		BUGG	95 MRK3	$J/\psi \rightarrow \gamma\pi^+\pi^-\pi^+\pi^-$
264 ± 25		20 ARMSTRONG	93c E760	$\bar{p}p \rightarrow \pi^0\eta\eta \rightarrow 6\gamma$
200 to 300		BREAKSTONE	93 SFM	$pp \rightarrow pp\pi^+\pi^-\pi^+\pi^-$
< 80 90% CL		21 ALDE	92D GAM2	$38 \pi^-\pi^0 \rightarrow \eta\eta N^*$
181 ± 30		22 ARMSTRONG	89D OMEG	$300 pp \rightarrow ppK^+K^-$
104 ± 30		22 ARMSTRONG	89D OMEG	$300 pp \rightarrow ppK_S^0 K_S^0$
166.4 ± 33.2		20 AUGUSTIN	88 DM2	$J/\psi \rightarrow \gamma K^+K^-, K_S^0 K_S^0$
30 ± 20		18 BOLONKIN	88 SPEC	$40 \pi^-\pi^0 \rightarrow K_S^0 K_S^0 n$
350 ± 150		BOLONKIN	88 SPEC	$40 \pi^-\pi^0 \rightarrow K_S^0 K_S^0 n$
148 ± 17		23 FALVARD	88 DM2	$J/\psi \rightarrow \phi K^+K^-, K_S^0 K_S^0$

184 ± 6	24 FALVARD	88 DM2	$J/\psi \rightarrow \phi K^+K^-, K_S^0 K_S^0$
136 ± 28	20 AUGUSTIN	87 DM2	$J/\psi \rightarrow \gamma\pi^+\pi^-$
130 ± 20	18 BALTRUSAIT..87	MRK3	$J/\psi \rightarrow \gamma K^+K^-$
122 ± 74	25 LONGACRE	86 RVUE	$22 \pi^-\pi^0 \rightarrow n2K_S^0$
15			
57 ± 38	26 WILLIAMS	84 MP5F	$200 \pi^-\pi^0 \rightarrow 2K_S^0 X$
160 ± 80	BLOOM	83 CBAL	$J/\psi \rightarrow \gamma 2\eta$
200 ± 100	BURKE	82 MRK2	$J/\psi \rightarrow \gamma 2\rho$
220 ± 100	27,28 EDWARDS	82D CBAL	$J/\psi \rightarrow \gamma 2\eta$
70			
200 ± 156	29 ETKIN	82B MPS	$23 \pi^-\pi^0 \rightarrow n2K_S^0$
9			

- From partial wave analysis including all possible combinations of  $0^{++}$ ,  $2^{++}$ , and  $4^{++}$  resonances.
- Spin 0 favored over spin 2.
- In the SU(3) based model with a specific interference pattern of the  $f_2(1270)$ ,  $\rho_2^0(1320)$ , and  $f_2'(1525)$  mesons incoherently added to the  $f_0(1710)$  and non-resonant background.
- Breit-Wigner width.
- $J^P = 0^+$ , superseded by ARMSTRONG 89D.
- Systematic errors not estimated.
- This state may be different from  $f_0(1710)$ , see CLOSE 05.
- (Solution I)
- K-matrix pole, assuming  $J^P = 0^+$ , from combined analysis of  $\pi^-\pi^0 \rightarrow \pi^0\pi^0 n$ ,  $\pi^-\pi^0 \rightarrow K\bar{K}n$ ,  $\pi^+\pi^-\pi^0 \rightarrow \pi^+\pi^-\pi^0$ ,  $\bar{p}p \rightarrow \pi^0\pi^0\pi^0$ ,  $\pi^0\eta\eta$ ,  $\pi^0\pi^0\eta$ ,  $\pi^+\pi^-\pi^0$ ,  $K^+K^-\pi^0$ ,  $K_S^0 K_S^0 \pi^0$ ,  $K^+K_S^0 \pi^-$  at rest,  $\bar{p}n \rightarrow \pi^-\pi^-\pi^+$ ,  $K_S^0 K^-\pi^0$ ,  $K_S^0 K_S^0 \pi^-$  at rest.
- (Solution I)
- Decaying to  $f_0(1370)\pi\pi$ .
- T-matrix pole.
- $J^P = 0^+$ .
- Not seen by AMSLER 02.
- Supersedes BARBERIS 99 and BARBERIS 99B.
- T-matrix pole, assuming  $J^P = 0^+$
- No  $J^{PC}$  determination.
- $J^P = 2^+$ .
- From a fit to the  $0^+$  partial wave.
- No  $J^{PC}$  determination.
- ALDE 92D combines all the GAMS-2000 data.
- $J^P = 2^+$ , ( $0^+$  excluded).
- From an analysis ignoring interference with  $f_2'(1525)$ .
- From an analysis including interference with  $f_2'(1525)$ .
- Uses MRK3 data. From a partial-wave analysis of data using a K-matrix formalism with 5 poles, but assuming spin 2. Fit with constrained inelasticity.
- No  $J^{PC}$  determination.
- $J^P = 2^+$  preferred.
- From fit neglecting nearby  $f_2'(1525)$ . Replaced by BLOOM 83.
- From an amplitude analysis of the  $K_S^0 K_S^0$  system, superseded by LONGACRE 86.

$f_0(1710)$  DECAY MODES

Mode	Fraction ( $\Gamma_i/\Gamma$ )
$\Gamma_1$ $K\bar{K}$	seen
$\Gamma_2$ $\eta\eta$	seen
$\Gamma_3$ $\pi\pi$	seen
$\Gamma_4$ $\gamma\gamma$	seen
$\Gamma_5$ $\omega\omega$	seen

$f_0(1710)$   $\Gamma(i)\Gamma(\gamma\gamma)/\Gamma(\text{total})$

VALUE (eV)	CL%	DOCUMENT ID	TECN	COMMENT	$\Gamma_1\Gamma_4/\Gamma$
<b>12 ± 3 + 227</b>		UEHARA	13 BELL	$\gamma\gamma \rightarrow K_S^0 K_S^0$	
<b>-2 - 8</b>					

VALUE (eV)	CL%	DOCUMENT ID	TECN	COMMENT
<480	95	ALBRECHT	90G ARG	$\gamma\gamma \rightarrow K^+K^-$
<110	95	1 BEHREND	89C CELL	$\gamma\gamma \rightarrow K_S^0 K_S^0$
<280	95	1 ALTHOFF	85B TASS	$\gamma\gamma \rightarrow K\bar{K}\pi$

1 Assuming helicity 2.

VALUE (keV)	CL%	DOCUMENT ID	TECN	COMMENT	$\Gamma_3\Gamma_4/\Gamma$
<b>&lt;0.82</b>	95	1 BARATE	00E ALEP	$\gamma\gamma \rightarrow \pi^+\pi^-$	

1 Assuming spin 0.

$f_0(1710)$  BRANCHING RATIOS

VALUE	EVTs	DOCUMENT ID	TECN	COMMENT	$\Gamma_1/\Gamma$
seen	1004	1 DOBBS	15	$J/\psi \rightarrow \gamma K^+K^-$	
seen	349	1 DOBBS	15	$\psi(2S) \rightarrow \gamma K^+K^-$	
0.36 ± 0.12		ALBALADEJO	80	RVUE	
0.38 ± 0.09		2 LONGACRE	86 MPS	$22 \pi^-\pi^0 \rightarrow n2K_S^0$	
0.38 ± 0.19					

- Using CLEO-c data but not authored by the CLEO Collaboration.
- From a partial-wave analysis of data using a K-matrix formalism with 5 poles, but assuming spin 2. Fit with constrained inelasticity.

# Meson Particle Listings

## $f_0(1710), \eta(1760)$

### $\Gamma(\eta\eta)/\Gamma_{total}$ $\Gamma_2/\Gamma$

VALUE	DOCUMENT ID	TECN
0.22 ± 0.12	ALBALADEJO 08	RVUE
0.18 <sup>+0.03</sup> <sub>-0.13</sub>	<sup>1</sup> LONGACRE 86	RVUE

<sup>1</sup> From a partial-wave analysis of data using a K-matrix formalism with 5 poles, but assuming spin 2. Fit with constrained inelasticity.

### $\Gamma(\pi\pi)/\Gamma_{total}$ $\Gamma_3/\Gamma$

VALUE	EVTs	DOCUMENT ID	TECN	COMMENT
seen	381	<sup>1</sup> DOBBS 15		$J/\psi \rightarrow \gamma\pi^+\pi^-$
seen	237	<sup>1</sup> DOBBS 15		$\psi(2S) \rightarrow \gamma\pi^+\pi^-$
not seen		AMSLER 02	CBAR	$0.9\bar{p}p \rightarrow \pi^0\eta\eta, \pi^0\pi^0\pi^0$
0.039 <sup>+0.002</sup> <sub>-0.024</sub>		<sup>2</sup> LONGACRE 86	RVUE	

<sup>1</sup> Using CLEO-c data but not authored by the CLEO Collaboration.  
<sup>2</sup> From a partial-wave analysis of data using a K-matrix formalism with 5 poles, but assuming spin 2. Fit with constrained inelasticity.

### $\Gamma(\pi\pi)/\Gamma(K\bar{K})$ $\Gamma_3/\Gamma_1$

VALUE	CL%	DOCUMENT ID	TECN	COMMENT
<b>0.23 ± 0.05</b>	<b>OUR AVERAGE</b>	Error includes scale factor of 1.2.		
0.64 ± 0.27	± 0.18	LEES 18A	BABR	$\Upsilon(1S) \rightarrow \gamma\pi^+\pi^-, \gamma K^+K^-$
0.41 <sup>+0.11</sup> <sub>-0.17</sub>		ABLIKIM 06V	BES2	$e^+e^- \rightarrow J/\psi \rightarrow \gamma\pi^+\pi^-$
0.2 ± 0.024 ± 0.036		BARBERIS 99D	OMEG 450	$pp \rightarrow K^+K^-, \pi^+\pi^-$
0.39 ± 0.14		ARMSTRONG 91	OMEG 300	$pp \rightarrow \rho\rho\pi\pi, \rho\rho K\bar{K}$
0.32 ± 0.14		ALBALADEJO 08	RVUE	
< 0.11	95	<sup>1</sup> ABLIKIM 04E	BES2	$J/\psi \rightarrow \omega K^+K^-$
5.8 <sup>+9.1</sup> <sub>-5.5</sub>		<sup>2</sup> ANISOVICH 02D	SPEC	Combined fit

<sup>1</sup> Using data from ABLIKIM 04a.  
<sup>2</sup> From a combined K-matrix analysis of Crystal Barrel ( $0. p\bar{p} \rightarrow \pi^0\pi^0\pi^0, \pi^0\eta\eta, \pi^0\pi^0\eta$ ), GAMS ( $\pi\rho \rightarrow \pi^0\pi^0n, \eta\eta n, \eta\eta'n$ ), and BNL ( $\pi\rho \rightarrow K\bar{K}n$ ) data.

### $\Gamma(\eta\eta)/\Gamma(K\bar{K})$ $\Gamma_2/\Gamma_1$

VALUE	CL%	DOCUMENT ID	TECN	COMMENT
<b>0.48 ± 0.15</b>		BARBERIS 00E		450 $pp \rightarrow \rho f \eta \eta \rho_S$
0.46 <sup>+0.70</sup> <sub>-0.38</sub>		<sup>1</sup> ANISOVICH 02D	SPEC	Combined fit
< 0.02	90	<sup>2</sup> PROKOSHKIN 91	GA24	300 $\pi^-p \rightarrow \pi^- \rho \eta \eta$

<sup>1</sup> From a combined K-matrix analysis of Crystal Barrel ( $0. p\bar{p} \rightarrow \pi^0\pi^0\pi^0, \pi^0\eta\eta, \pi^0\pi^0\eta$ ), GAMS ( $\pi\rho \rightarrow \pi^0\pi^0n, \eta\eta n, \eta\eta'n$ ), and BNL ( $\pi\rho \rightarrow K\bar{K}n$ ) data.  
<sup>2</sup> Combining results of GAM4 with those of ARMSTRONG 89D.

### $\Gamma(\omega\omega)/\Gamma_{total}$ $\Gamma_5/\Gamma$

VALUE	EVTs	DOCUMENT ID	TECN	COMMENT
seen	180	ABLIKIM 06H	BES	$J/\psi \rightarrow \gamma\omega\omega$

### $f_0(1710)$ REFERENCES

LEES 18A	PR D97 112006	J.P. Lees et al.	(BABAR Collab.)
DOBBS 15	PR D91 052006	S. Dobbs et al.	(NWES)
ABLIKIM 13N	PR D87 092009	Ablikim M. et al.	(BESIII Collab.)
UEHARA 13	PTEP 2013 123C01	S. Uehara et al.	(BELLE Collab.)
ALBALADEJO 08	PRL 101 252002	M. Albaladejo, J.A. Oller	
CHEKANOV 08	PRL 101 112003	S. Chekanov et al.	(ZEUS Collab.)
ABLIKIM 06H	PR D73 112007	M. Ablikim et al.	(BES Collab.)
ABLIKIM 06V	PL B642 441	M. Ablikim et al.	(BES Collab.)
AMSLER 06	PL B639 165	C. Amisler et al.	(CBAR Collab.)
UMAN 06	PR D73 052009	I. Uman et al.	(FNAL E835)
VLADIMIRSK... 06	PAN 69 493	V.V. Vladimirov et al.	(ITEP, Moscow)
ABLIKIM 05	PL B607 243	M. Ablikim et al.	(BES Collab.)
ABLIKIM 05Q	PR D72 092002	M. Ablikim et al.	(BES Collab.)
BINON 05	PAN 68 960	F. Binon et al.	
CLOSE 05	PR D71 094022	F.E. Close, Q. Zhao	
ABLIKIM 04A	PL B598 149	M. Ablikim et al.	(BES Collab.)
ABLIKIM 04E	PL B603 138	M. Ablikim et al.	(BES Collab.)
ANISOVICH 03	EPJ A16 229	V.V. Anisovich et al.	
BAI 03G	PR D68 052003	J.Z. Bai et al.	(BES Collab.)
TIKHOMIROV 03	PAN 66 828	G.D. Tikhomirov et al.	
AMSLER 02	EPJ C23 29	C. Amisler et al.	
ANISOVICH 02D	PAN 65 1545	V.V. Anisovich et al.	
NICHITIU 02	PL B545 261	F. Nichitiu et al.	(OBELIX Collab.)
BAI 00A	PL B472 207	J.Z. Bai et al.	(BES Collab.)
BARATE 00E	PL B472 189	R. Barate et al.	(ALEPH Collab.)
BARBERIS 00E	PL B479 59	D. Barberis et al.	(WA 102 Collab.)
ANISOVICH 99B	PL B449 154	A.V. Anisovich et al.	
BARBERIS 99	PL B453 305	D. Barberis et al.	(Omega Expt.)
BARBERIS 99B	PL B453 316	D. Barberis et al.	(Omega Expt.)
BARBERIS 99D	PL B462 462	D. Barberis et al.	(Omega Expt.)
FRENCH 99	PL B460 213	B. French et al.	(WA76 Collab.)
ANISOVICH 98B	SFU 41 419	V.V. Anisovich et al.	
BAI 98H	PRL 81 1179	J.Z. Bai et al.	(BES Collab.)
BARKOV 98	JETPL 68 764	B.P. Barkov et al.	
ABREU 96C	PL B379 309	P. Abreu et al.	(DELPHI Collab.)
BAI 96C	PRL 77 3959	J.Z. Bai et al.	(BES Collab.)
BALOSHIN 95	PAN 58 46	O.N. Baloshin et al.	(ITEP)
	Translated from YAF 58 50.		

BUGG 95	PL B353 378	D.V. Bugg et al.	(LOQM, PNPI, WASH)
ARMSTRONG 93C	PL B307 394	T.A. Armstrong et al.	(FNAL, FERR, GENO+)
BREAKSTONE 93	ZPHY C58 251	A.M. Breakstone et al.	(IOWA, CERN, DORT+)
ALDE 92D	PL B284 457	D.M. Alde et al.	(GAM2 Collab.)
	Also SJNP 54 451	D.M. Alde et al.	(GAM2 Collab.)
	Translated from YAF 54 745.		
ARMSTRONG 91	ZPHY C51 351	T.A. Armstrong et al.	(ATHU, BARI, BIRM+)
PROKOSHKIN 91	SPD 36 155	Y.D. Prokoshkin	(GAM2 and GAM4 Collab.)
	Translated from DANS 316 900.		
ALBRECHT 90G	ZPHY C48 183	H. Albrecht et al.	(ARGUS Collab.)
ARMSTRONG 89D	PL B227 186	T.A. Armstrong, M. Benayoun	(ATHU, BARI, BIRM+)
BEHREND 89C	ZPHY C43 91	H.J. Behrend et al.	(CELLO Collab.)
AUGUSTIN 88	PRL 60 2238	J.E. Augustin et al.	(DM2 Collab.)
BOLONKIN 88	NP B309 426	B.V. Bolonkin et al.	(ITEP, SERP)
FALVARD 88	PR D38 2706	A. Falvard et al.	(CLER, FRAS, LALO+)
AUGUSTIN 87	ZPHY C36 369	J.E. Augustin et al.	(LALO, CLER, FRAS+)
BALTRUSAITIS... 87	PR D35 2077	R.M. Baltrusaitis et al.	(Mark III Collab.)
ALDE 86C	PL B182 105	D.M. Alde et al.	(SERP, BELG, LAM, LAPP)
LONGACRE 86	PL B177 223	R.S. Longacre et al.	(BNL, BRAN, CUNY+)
ALTHOFF 85B	ZPHY C29 189	M. Althoff et al.	(TASSO Collab.)
WILLIAMS 84	PR D30 877	E.G.H. Williams et al.	(VAND, NDAM, TUFTS+)
BLOOM 83	ARNS 33 143	E.D. Bloom, C. Peck	(SLAC, CIT)
BURKE 82	PRL 49 632	D.L. Burke et al.	(LBL, SLAC)
EDWARDS 82D	PRL 48 458	C. Edwards et al.	(CIT, HARV, PRIN+)
ETKIN 82B	PR D25 1786	A. Etkin et al.	(BNL, CUNY, TUFTS, VAND)
ETKIN 82C	PR D25 2446	A. Etkin et al.	(BNL, CUNY, TUFTS, VAND)

### $\eta(1760)$ $I^G(J^{PC}) = 0^+(0^-+)$

OMITTED FROM SUMMARY TABLE  
 Seen by DM2 in the  $\rho\rho$  system (BISELLO 89B). Structure in this region has been reported before in the same system (BALTRUSAITIS 86B) and in the  $\omega\omega$  system (BALTRUSAITIS 85C, BISELLO 87).

### $\eta(1760)$ MASS

VALUE (MeV)	EVTs	DOCUMENT ID	TECN	COMMENT
<b>1751 ± 15</b>	<b>OUR AVERAGE</b>			
1768 <sup>+24</sup> <sub>-25</sub> ± 10	465	<sup>1</sup> ZHANG 12A	BELL	$e^+e^- \rightarrow e^+e^-\eta'\pi^+\pi^-$
1744 ± 10 ± 15	1045	<sup>2</sup> ABLIKIM 06H	BES	$J/\psi \rightarrow \gamma\omega\omega$
1703 <sup>+12</sup> <sub>-11</sub> ± 2		<sup>3</sup> ZHANG 12A	BELL	$e^+e^- \rightarrow e^+e^-\eta'\pi^+\pi^-$
1760 ± 11	320	<sup>4</sup> BISELLO 89B	DM2	$J/\psi \rightarrow 4\pi\gamma$

<sup>1</sup> From a single-resonance fit.  
<sup>2</sup> From a partial wave analysis including  $\eta(1760), f_0(1710), f_2(1640),$  and  $f_2(1910)$ .  
<sup>3</sup> From a two-resonance fit.  
<sup>4</sup> Estimated by us from various fits. Systematic uncertainties not estimated.

### $\eta(1760)$ WIDTH

VALUE (MeV)	EVTs	DOCUMENT ID	TECN	COMMENT
<b>240 ± 30</b>	<b>OUR AVERAGE</b>			
224 <sup>+62</sup> <sub>-56</sub> ± 25	465	<sup>5</sup> ZHANG 12A	BELL	$e^+e^- \rightarrow e^+e^-\eta'\pi^+\pi^-$
244 <sup>+24</sup> <sub>-21</sub> ± 25	1045	<sup>6</sup> ABLIKIM 06H	BES	$J/\psi \rightarrow \gamma\omega\omega$
42 <sup>+36</sup> <sub>-22</sub> ± 15		<sup>7</sup> ZHANG 12A	BELL	$e^+e^- \rightarrow e^+e^-\eta'\pi^+\pi^-$
60 ± 16	320	<sup>8</sup> BISELLO 89B	DM2	$J/\psi \rightarrow 4\pi\gamma$

<sup>5</sup> From a single-resonance fit.  
<sup>6</sup> From a partial wave analysis including  $\eta(1760), f_0(1710), f_2(1640),$  and  $f_2(1910)$ .  
<sup>7</sup> From a two-resonance fit.  
<sup>8</sup> Estimated by us from various fits. Systematic uncertainties not estimated.

### $\eta(1760)$ DECAY MODES

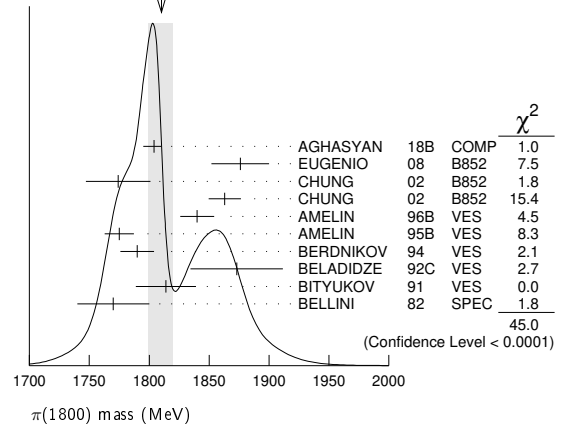
Mode	Fraction ( $\Gamma_i/\Gamma$ )
$\Gamma_1$	$4\pi$
$\Gamma_2$	$2\pi^+2\pi^-$
$\Gamma_3$	$\pi^+\pi^--2\pi^0$
$\Gamma_4$	$\rho^0\rho^0$
$\Gamma_5$	$\rho^+\rho^-$
$\Gamma_6$	$\omega\omega$
$\Gamma_7$	$\eta'\pi^+\pi^-$
$\Gamma_8$	$\gamma\gamma$

### $\eta(1760)$ $\Gamma(i)\Gamma(\gamma)/\Gamma_{total}$

VALUE (eV)	EVTs	DOCUMENT ID	TECN	COMMENT
<b>28.2<sup>+7.9</sup><sub>-7.5</sub> ± 3.7</b>	465	<sup>9</sup> ZHANG 12A	BELL	$e^+e^- \rightarrow e^+e^-\eta'\pi^+\pi^-$

- • • We do not use the following data for averages, fits, limits, etc. • • •
  - 3.0<sup>+2.0</sup><sub>-1.2</sub> ± 0.8    52    10 ZHANG    12A BELL     $e^+e^- \rightarrow e^+e^- \eta' \pi^+ \pi^-$
  - 18    <sup>+13</sup><sub>-10</sub> ± 5    315    11 ZHANG    12A BELL     $e^+e^- \rightarrow e^+e^- \eta' \pi^+ \pi^-$
- <sup>9</sup> From a single-resonance fit.  
<sup>10</sup> From a two-resonance fit. For constructive interference with the X(1835).  
<sup>11</sup> From a two-resonance fit. For destructive interference with the X(1835).

WEIGHTED AVERAGE  
1810+9-11 (Error scaled by 2.2)



**$\eta(1760)$  BRANCHING RATIOS**

$\Gamma(2\pi^+ 2\pi^-)/\Gamma_{total}$		$\Gamma_2/\Gamma$	
VALUE	DOCUMENT ID	TECN	COMMENT
seen	BISELLO	89B DM2	$J/\psi \rightarrow \gamma 2\pi^+ 2\pi^-$

$\Gamma(\pi^+ \pi^- 2\pi^0)/\Gamma_{total}$		$\Gamma_3/\Gamma$	
VALUE	DOCUMENT ID	TECN	COMMENT
seen	BISELLO	89B DM2	$J/\psi \rightarrow \gamma \pi^+ \pi^- 2\pi^0$

$\Gamma(\rho^0 \rho^0)/\Gamma_{total}$		$\Gamma_4/\Gamma$	
VALUE	DOCUMENT ID	TECN	COMMENT
seen	BISELLO	89B DM2	$J/\psi \rightarrow \gamma \rho^0 \rho^0$
seen	BALTRUSAIT...86	MRK3	$J/\psi \rightarrow \gamma \rho^0 \rho^0$

$\Gamma(\rho^+ \rho^-)/\Gamma_{total}$		$\Gamma_5/\Gamma$	
VALUE	DOCUMENT ID	TECN	COMMENT
seen	BISELLO	89B DM2	$J/\psi \rightarrow \gamma \rho^+ \rho^-$
seen	BALTRUSAIT...86	MRK3	$J/\psi \rightarrow \gamma \rho^+ \rho^-$

$\Gamma(\omega\omega)/\Gamma_{total}$		$\Gamma_6/\Gamma$	
VALUE	DOCUMENT ID	TECN	COMMENT
seen	BISELLO	87 DM2	$J/\psi \rightarrow \gamma \omega\omega$
seen	BALTRUSAIT...85C	MRK3	$J/\psi \rightarrow \gamma \omega\omega$

$\Gamma(\gamma\gamma)/\Gamma(\omega\omega)$		$\Gamma_8/\Gamma_6$		
VALUE	CL%	DOCUMENT ID	TECN	COMMENT
<b><math>&lt;2.48 \times 10^{-3}</math></b>	90	12 ABLIKIM	180 BES3	$\psi(2S) \rightarrow \pi^+ \pi^- \gamma \gamma \gamma$

<sup>12</sup> Using results from ABLIKIM 06H.

**$\pi(1800)$  WIDTH**

VALUE (MeV)	EVTS	DOCUMENT ID	TECN	CHG	COMMENT
<b>215<sup>+8</sup><sub>-11</sub></b>	46M	<sup>8</sup> AGHASYAN	18B COMP		190 $\pi^- p \rightarrow \pi^- \pi^+ \pi^- p$
221 ± 26 ± 38	4k	<sup>9</sup> EUGENIO	08 B852	-	18 $\pi^- p \rightarrow \eta \eta \pi^- p$
223 ± 48 ± 50		<sup>10</sup> CHUNG	02 B852		18.3 $\pi^- p \rightarrow \pi^+ \pi^- \pi^- p$
191 ± 21 ± 20		<sup>11</sup> CHUNG	02 B852		18.3 $\pi^- p \rightarrow \pi^+ \pi^- \pi^- p$
210 ± 30 ± 30	1.2k	AMELIN	96B VES	-	37 $\pi^- A \rightarrow \eta \eta \pi^- A$
190 ± 15 ± 15		<sup>12</sup> AMELIN	95B VES	-	36 $\pi^- A \rightarrow \pi^+ \pi^- \pi^- A$
210 ± 70		<sup>13</sup> BERDNIKOV	94 VES	-	37 $\pi^- A \rightarrow K^+ K^- \pi^- A$
225 ± 35 ± 20		BELADIDZE	92C VES	-	36 $\pi^- Be \rightarrow \pi^- \eta' \eta Be$
205 ± 18 ± 32	426	BITYUKOV	91 VES	-	36 $\pi^- C \rightarrow \pi^- \eta \eta C$
310 ± 50	1.1k	BELLINI	82 SPEC	-	40 $\pi^- A \rightarrow 3\pi A$

- • • We do not use the following data for averages, fits, limits, etc. • • •
  - 208 ± 22 ± 37    420k    <sup>14</sup> ALEKSEEV    10 COMP    190  $\pi^- Pb \rightarrow \pi^- \pi^- \pi^+ Pb$
  - 259 ± 19 ± 6    AMELIN    99 VES    37  $\pi^- A \rightarrow \omega \pi^- \pi^0 A^*$
- <sup>8</sup> Statistical error negligible.  
<sup>9</sup> From a single-pole fit.  
<sup>10</sup> In the  $f_0(980)\pi$  wave.  
<sup>11</sup> In the  $f_0(500)\pi$  wave.  
<sup>12</sup> From a fit to  $J^{PC} = 0^- + f_0(980)\pi, f_0(1370)\pi$  waves.  
<sup>13</sup> From a fit to  $J^{PC} = 0^- + K_0^*(1430)K^-$  and  $f_0(980)\pi^-$  waves.  
<sup>14</sup> Superseded by AGHASYAN 2018B.

**$\eta(1760)$  REFERENCES**

ABLIKIM 180 PR D97 072014	M. Ablikim et al.	(BESIII Collab.)
ZHANG 12A PR D86 052002	C.C. Zhang et al.	(BELLE Collab.)
ABLIKIM 06H PR D73 112007	M. Ablikim et al.	(BES Collab.)
BISELLO 89B PR D39 701	G. Busetto et al.	(DM2 Collab.)
BISELLO 87 PL B192 239	D. Bisello et al.	(PADO, CLER, FRAS+)
BALTRUSAIT...86 PR D33 629	R.M. Baltrusaitis et al.	(Mark III Collab.)
BALTRUSAIT...86B PR D33 1222	R.M. Baltrusaitis et al.	(Mark III Collab.)
BALTRUSAIT...85C PRL 55 1723	R.M. Baltrusaitis et al.	(CIT, UCSC+)

**$\pi(1800)$**

$I^G(J^{PC}) = 1^-(0^-+)$

See the review on "Non- $q\bar{q}$  Mesons."

**$\pi(1800)$  MASS**

VALUE (MeV)	EVTS	DOCUMENT ID	TECN	CHG	COMMENT
<b>1810<sup>+9</sup><sub>-11</sub></b>		<b>OUR AVERAGE</b>			Error includes scale factor of 2.2. See the ideogram below.
1804 ± <sup>6</sup> <sub>9</sub>	46M	<sup>1</sup> AGHASYAN	18B COMP		190 $\pi^- p \rightarrow \pi^- \pi^+ \pi^- p$
1876 ± 18 ± 16	4k	<sup>2</sup> EUGENIO	08 B852	-	18 $\pi^- p \rightarrow \eta \eta \pi^- p$
1774 ± 18 ± 20		<sup>3</sup> CHUNG	02 B852		18.3 $\pi^- p \rightarrow \pi^+ \pi^- \pi^- p$
1863 ± 9 ± 10		<sup>4</sup> CHUNG	02 B852		18.3 $\pi^- p \rightarrow \pi^+ \pi^- \pi^- p$
1840 ± 10 ± 10	1.2k	AMELIN	96B VES	-	37 $\pi^- A \rightarrow \eta \eta \pi^- A$
1775 ± 7 ± 10		<sup>5</sup> AMELIN	95B VES	-	36 $\pi^- A \rightarrow \pi^+ \pi^- \pi^- A$
1790 ± 14		<sup>6</sup> BERDNIKOV	94 VES	-	37 $\pi^- A \rightarrow K^+ K^- \pi^- A$
1873 ± 33 ± 20		BELADIDZE	92C VES	-	36 $\pi^- Be \rightarrow \pi^- \eta' \eta Be$
1814 ± 10 ± 23	426	BITYUKOV	91 VES	-	36 $\pi^- C \rightarrow \pi^- \eta \eta C$
1770 ± 30	1.1k	BELLINI	82 SPEC	-	40 $\pi^- A \rightarrow 3\pi A$

- • • We do not use the following data for averages, fits, limits, etc. • • •
  - 1785 ± 9 ± <sup>12</sup><sub>6</sub>    420k    <sup>7</sup> ALEKSEEV    10 COMP    190  $\pi^- Pb \rightarrow \pi^- \pi^- \pi^+ Pb'$
  - 1737 ± 5 ± 15    AMELIN    99 VES    37  $\pi^- A \rightarrow \omega \pi^- \pi^0 A^*$
- <sup>1</sup> Statistical error negligible.  
<sup>2</sup> From a single-pole fit.  
<sup>3</sup> In the  $f_0(980)\pi$  wave.  
<sup>4</sup> In the  $f_0(500)\pi$  wave.  
<sup>5</sup> From a fit to  $J^{PC} = 0^- + f_0(980)\pi, f_0(1370)\pi$  waves.  
<sup>6</sup> From a fit to  $J^{PC} = 0^- + K_0^*(1430)K^-$  and  $f_0(980)\pi^-$  waves.  
<sup>7</sup> Superseded by AGHASYAN 2018B.

**$\pi(1800)$  DECAY MODES**

Mode	Fraction ( $\Gamma_i/\Gamma$ )
$\Gamma_1$ $\pi^+ \pi^- \pi^-$	seen
$\Gamma_2$ $f_0(500)\pi^-$	seen
$\Gamma_3$ $f_0(980)\pi^-$	seen
$\Gamma_4$ $f_0(1370)\pi^-$	seen
$\Gamma_5$ $f_0(1500)\pi^-$	not seen
$\Gamma_6$ $\rho\pi^-$	not seen
$\Gamma_7$ $\eta\eta\pi^-$	seen
$\Gamma_8$ $a_0(980)\eta$	seen
$\Gamma_9$ $a_2(1320)\eta$	not seen
$\Gamma_{10}$ $f_2'(1270)\pi$	not seen
$\Gamma_{11}$ $f_0(1370)\pi^-$	not seen
$\Gamma_{12}$ $f_0(1500)\pi^-$	seen
$\Gamma_{13}$ $\eta\eta'(958)\pi^-$	seen
$\Gamma_{14}$ $K_0^*(1430)K^-$	seen
$\Gamma_{15}$ $K^*(892)K^-$	not seen

**$\pi(1800)$  BRANCHING RATIOS**

$\Gamma(f_0(980)\pi^-)/\Gamma(f_0(500)\pi^-)$		$\Gamma_3/\Gamma_2$	
VALUE	DOCUMENT ID	TECN	COMMENT
<b>0.44 ± 0.08 ± 0.38</b>	<sup>15</sup> CHUNG	02 B852	18.3 $\pi^- p \rightarrow \pi^+ \pi^- \pi^- p$

# Meson Particle Listings

## $\pi(1800)$ , $f_2(1810)$

### $\Gamma(f_0(980)\pi^-)/\Gamma(f_0(1370)\pi^-)$ $\Gamma_3/\Gamma_4$

VALUE	DOCUMENT ID	TECN	CHG	COMMENT
$1.7 \pm 1.3$	16 AMELIN	95B	VES	- $36 \pi^- A \rightarrow \pi^+ \pi^- \pi^- A$

### $\Gamma(f_0(1370)\pi^-)/\Gamma_{total}$ $\Gamma_4/\Gamma$

VALUE	DOCUMENT ID	TECN	CHG	COMMENT
seen	BELLINI	82	SPEC	- $40 \pi^- A \rightarrow 3\pi A$

### $\Gamma(f_0(1500)\pi^-)/\Gamma_{total}$ $\Gamma_5/\Gamma$

VALUE	DOCUMENT ID	TECN	COMMENT
not seen	CHUNG	02	B852 $18.3 \pi^- p \rightarrow \pi^+ \pi^- \pi^- p$

### $\Gamma(\rho\pi^-)/\Gamma_{total}$ $\Gamma_6/\Gamma$

VALUE	DOCUMENT ID	TECN	CHG	COMMENT
not seen	BELLINI	82	SPEC	- $40 \pi^- A \rightarrow 3\pi A$

### $\Gamma(\rho\pi^-)/\Gamma(f_0(980)\pi^-)$ $\Gamma_6/\Gamma_3$

VALUE	CL%	DOCUMENT ID	TECN	CHG	COMMENT
$<0.25$		CHUNG	02	B852	$18.3 \pi^- p \rightarrow \pi^+ \pi^- \pi^- p$
$<0.14$	90	AMELIN	95B	VES	- $36 \pi^- A \rightarrow \pi^+ \pi^- \pi^- A$

### $\Gamma(\eta\eta\pi^-)/\Gamma(\pi^+ \pi^- \pi^-)$ $\Gamma_7/\Gamma_1$

VALUE	EVTs	DOCUMENT ID	TECN	CHG	COMMENT
$0.5 \pm 0.1$	1200	16 AMELIN	96B	VES	- $37 \pi^- A \rightarrow \eta\eta\pi^- A$

### $\Gamma(a_2(1320)\eta)/\Gamma_{total}$ $\Gamma_9/\Gamma$

VALUE	DOCUMENT ID	TECN	COMMENT
not seen	EUGENIO	08	B852 $18 \pi^- p \rightarrow \eta\eta\pi^- p$

### $\Gamma(f_2(1270)\pi)/\Gamma_{total}$ $\Gamma_{10}/\Gamma$

VALUE	DOCUMENT ID	TECN	COMMENT
not seen	EUGENIO	08	B852 $18 \pi^- p \rightarrow \eta\eta\pi^- p$

### $\Gamma(f_0(1370)\pi^-)/\Gamma_{total}$ $\Gamma_{11}/\Gamma$

VALUE	DOCUMENT ID	TECN	COMMENT
not seen	EUGENIO	08	B852 $18 \pi^- p \rightarrow \eta\eta\pi^- p$

### $\Gamma(f_0(1500)\pi^-)/\Gamma(a_0(980)\eta)$ $\Gamma_{12}/\Gamma_8$

VALUE	EVTs	DOCUMENT ID	TECN	CHG	COMMENT
$0.48 \pm 0.17$	4k	16,17 EUGENIO	08	B852	- $18 \pi^- p \rightarrow \eta\eta\pi^- p$
$0.030 \pm 0.014$		16 ANISOVICH	01B	SPEC	0 $0.6-1.94 p\bar{p} \rightarrow \eta\eta\pi^0 \pi^0$
$-0.011$					
$0.08 \pm 0.03$	1200	16,18 AMELIN	96B	VES	- $37 \pi^- A \rightarrow \eta\eta\pi^- A$

### $\Gamma(\eta\eta'(958)\pi^-)/\Gamma(\eta\eta\pi^-)$ $\Gamma_{13}/\Gamma_7$

VALUE	EVTs	DOCUMENT ID	TECN	CHG	COMMENT
$0.29 \pm 0.07$		16 BELADIDZE	92C	VES	- $36 \pi^- Be \rightarrow \pi^- \eta' \eta Be$
$0.3 \pm 0.1$	426 ± 57	16 BITYUKOV	91	VES	- $36 \pi^- C \rightarrow \pi^- \eta\eta C$

### $\Gamma(K_0^*(1430)K^-)/\Gamma_{total}$ $\Gamma_{14}/\Gamma$

VALUE	DOCUMENT ID	TECN	CHG	COMMENT
seen	BERDNIKOV	94	VES	- $37 \pi^- A \rightarrow K^+ K^- \pi^- A$

### $\Gamma(K^*(892)K^-)/\Gamma_{total}$ $\Gamma_{15}/\Gamma$

VALUE	DOCUMENT ID	TECN	CHG	COMMENT
not seen	BERDNIKOV	94	VES	- $37 \pi^- A \rightarrow K^+ K^- \pi^- A$

15 Assuming that  $f_0(980)$  decays only to  $\pi\pi$ .  
 16 Systematic errors not estimated.  
 17 From a single-pole fit.  
 18 Assuming that  $f_0(1500)$  decays only to  $\eta\eta$  and  $a_0(980)$  decays only to  $\eta\pi$ .

### $\pi(1800)$ REFERENCES

AGHASYAN	18B	PR D98 092003	M. Aghasyan et al.	(COMPASS Collab.)
ALEKSEEV	10	PRL 104 241803	M.G. Alekseev et al.	(COMPASS Collab.)
EUGENIO	08	PL B660 466	P. Eugenio et al.	(BNL E852 Collab.)
CHUNG	02	PR D65 072001	S.U. Chung et al.	(BNL E852 Collab.)
ANISOVICH	01B	PL B500 222	A.V. Anisovich et al.	(BNL E852 Collab.)
AMELIN	99	PAN 62 445	D.V. Amelin et al.	(VES Collab.)
		Translated from YAF 62 487.		
AMELIN	96B	PAN 59 976	D.V. Amelin et al.	(SERP, TBIL)IGJPC
		Translated from YAF 59 1021.		
AMELIN	95B	PL B356 595	D.V. Amelin et al.	(SERP, TBIL)
BERDNIKOV	94	PL B337 219	E.B. Berdnikov et al.	(SERP, TBIL)
BELADIDZE	92C	SJMP 55 1535	G.M. Beladidze, S.I. Bityukov, G.V. Borisov	(SERP+)
		Translated from YAF 55 2748.		
BITYUKOV	91	PL B268 137	S.I. Bityukov et al.	(SERP, TBIL)
BELLINI	82	PRL 48 1697	G. Bellini et al.	(MILA, BGNA, JINR)

## $f_2(1810)$

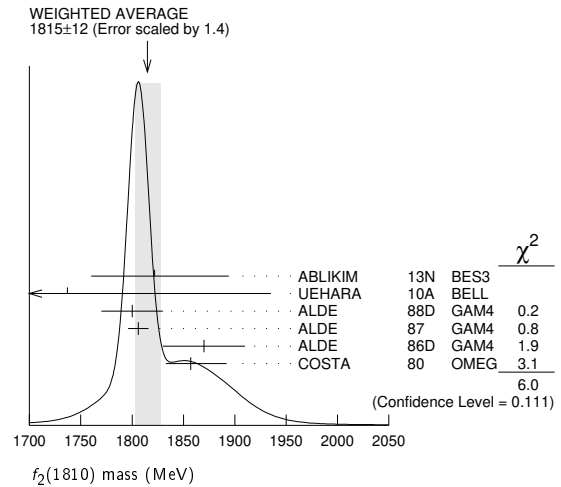
$$I^G(J^{PC}) = 0^+(2^{++})$$

OMITTED FROM SUMMARY TABLE  
Needs confirmation.

### $f_2(1810)$ MASS

VALUE (MeV)	EVTs	DOCUMENT ID	TECN	COMMENT
<b><math>1815 \pm 12</math> OUR AVERAGE</b>				Error includes scale factor of 1.4. See the ideogram below.
$1822^{+29}_{-24} +^{66}_{-57}$	5.5k	1 ABLIKIM	13N	BES3 $e^+ e^- \rightarrow J/\psi \rightarrow \gamma\eta\eta$
$1737 \pm 9^{+198}_{-65}$		2 UEHARA	10A	BELL $10.6 e^+ e^- \rightarrow e^+ e^- \eta\eta$
$1800 \pm 30$	40	ALDE	88D	GAM4 $300 \pi^- p \rightarrow \pi^- p 4\pi^0$
$1806 \pm 10$	1600	ALDE	87	GAM4 $100 \pi^- p \rightarrow 4\pi^0 n$
$1870 \pm 40$		3 ALDE	86D	GAM4 $100 \pi^- p \rightarrow \eta\eta n$
$1857^{+35}_{-24}$		4 COSTA	80	OMEG $10 \pi^- p \rightarrow K^+ K^- n$
$1858^{+18}_{-71}$		5 LONGACRE	86	RVUE Compilation
$1799 \pm 15$		6 CASON	82	STRC $8 \pi^+ p \rightarrow \Delta^{++} \pi^0 \pi^0$

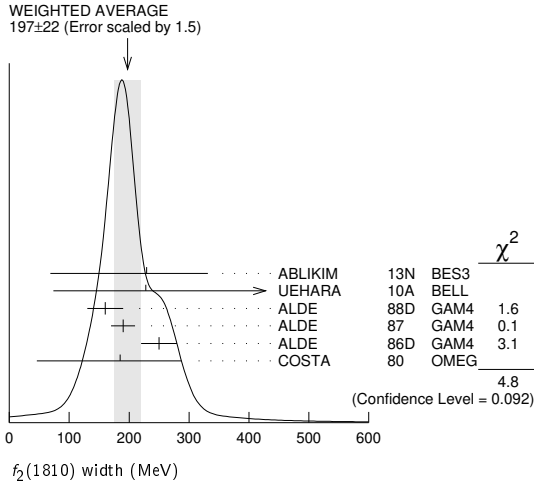
1 From partial wave analysis including all possible combinations of  $0^{++}$ ,  $2^{++}$ , and  $4^{++}$  resonances.  
 2 Breit-Wigner mass. Could also be the  $f_2(1910)$ .  
 3 Seen in only one solution.  
 4 Error increased by spread of two solutions. Included in LONGACRE 86 global analysis.  
 5 From a partial-wave analysis of data using a K-matrix formalism with 5 poles. Includes compilation of several other experiments.  
 6 From an amplitude analysis of the reaction  $\pi^+ \pi^- \rightarrow 2\pi^0$ . The resonance in the  $2\pi^0$  final state is not confirmed by PROKOSHKIN 97.



### $f_2(1810)$ WIDTH

VALUE (MeV)	EVTs	DOCUMENT ID	TECN	COMMENT
<b><math>197 \pm 22</math> OUR AVERAGE</b>				Error includes scale factor of 1.5. See the ideogram below.
$229^{+52}_{-42} +^{88}_{-155}$	5.5k	7 ABLIKIM	13N	BES3 $e^+ e^- \rightarrow J/\psi \rightarrow \gamma\eta\eta$
$228^{+21}_{-20} +^{234}_{-153}$		8 UEHARA	10A	BELL $10.6 e^+ e^- \rightarrow e^+ e^- \eta\eta$
$160 \pm 30$	40	ALDE	88D	GAM4 $300 \pi^- p \rightarrow \pi^- p 4\pi^0$
$190 \pm 20$	1600	ALDE	87	GAM4 $100 \pi^- p \rightarrow 4\pi^0 n$
$250 \pm 30$		9 ALDE	86D	GAM4 $100 \pi^- p \rightarrow \eta\eta n$
$185^{+102}_{-139}$		10 COSTA	80	OMEG $10 \pi^- p \rightarrow K^+ K^- n$

11 LONGACRE 86 RVUE Compilation  
 12 CASON 82 STRC  $8 \pi^+ p \rightarrow \Delta^{++} \pi^0 \pi^0$   
 7 From partial wave analysis including all possible combinations of  $0^{++}$ ,  $2^{++}$ , and  $4^{++}$  resonances.  
 8 Breit-Wigner width. Could also be the  $f_2(1910)$ .  
 9 Seen in only one solution.  
 10 Error increased by spread of two solutions. Included in LONGACRE 86 global analysis.  
 11 From a partial-wave analysis of data using a K-matrix formalism with 5 poles. Includes compilation of several other experiments.  
 12 From an amplitude analysis of the reaction  $\pi^+ \pi^- \rightarrow 2\pi^0$ . The resonance in the  $2\pi^0$  final state is not confirmed by PROKOSHKIN 97.



$f_2(1810)$  REFERENCES

ABLIKIM	13N	PR D87 092009	Ablikim <i>et al.</i>	(BESIII Collab.)
UEHARA	10A	PR D82 114031	S. Uehara <i>et al.</i>	(BELLE Collab.)
PDG	08	PL B667 1	C. Amsler <i>et al.</i>	(PDG Collab.)
AMSLER	02	EPJ C23 29	C. Amsler <i>et al.</i>	
PROKOSHKIN	97	PD 42 117	Y.D. Prokoshkin <i>et al.</i>	(SERP)
		Translated from DANS 353 323.		
ALDE	88D	SJNP 47 810	D.M. Alde <i>et al.</i>	(SERP, BELG, LANL, LAPP+)
		Translated from YAF 47 1273.		
ALDE	87	PL B198 286	D.M. Alde <i>et al.</i>	(LANL, BRUX, SERP, LAPP)
ALDE	86D	NP B269 485	D.M. Alde <i>et al.</i>	(BELG, LAPP, SERP, CERN+)
LONGACRE	86	PL B177 223	R.S. Longacre <i>et al.</i>	(BNL, BRAN, CUNY+)
CASON	82	PRL 48 1316	N.M. Cason <i>et al.</i>	(NDAM, ANL)
COSTA	80	NP B175 402	G. Costa <i>et al.</i>	(BARI, BONN, CERN, GLAS+)

$X(1835)$

$$J^G(J^{PC}) = ?(0^{-+})$$

OMITTED FROM SUMMARY TABLE

Could be a superposition of two states, one with small width appearing as threshold enhancement in  $p\bar{p}$ , the other one with a larger width. For the former ABLIKIM 12D determine  $J^{PC} = 0^{-+}$ .

$X(1835)$  MASS

VALUE (MeV)	EVTS	DOCUMENT ID	TECN	COMMENT		
<b>1826.5 ± 13.0</b>	<b>3.4</b>	<b>OUR AVERAGE</b>				
1825.3 ± 2.4	17.3	1	ABLIKIM	16J BES3 $J/\psi \rightarrow \gamma\pi^+\pi^-\eta'$		
1844 ± 9	16	25	ABLIKIM	15T BES3 $J/\psi \rightarrow \gamma K_S^0 K_S^0 \eta$		
1839 ± 26	± 26	2	ABLIKIM	18I BES3 $J/\psi \rightarrow \gamma\gamma\phi(1020)$		
1909.5 ± 15.9	9.4	27.5	3	ABLIKIM	16J BES3 $J/\psi \rightarrow \gamma\pi^+\pi^-\eta'$	
1842.2 ± 4.2	7.1	2.6	0.6k	ABLIKIM	13U BES3 $J/\psi \rightarrow \gamma 3(\pi^+\pi^-)$	
1832 ± 19	± 26	4	ABLIKIM	12D BES3 $J/\psi \rightarrow \gamma p\bar{p}$		
1836.5 ± 3.0	5.6	2.1	4265	5	ABLIKIM	11C BES3 $J/\psi \rightarrow \gamma\pi^+\pi^-\eta'$
1877.3 ± 6.3	3.4	7.4	6	ABLIKIM	11J BES3 $J/\psi \rightarrow \omega(\eta\pi^+\pi^-)$	
1837 ± 10	9	7	231	7,8	ALEXANDER	10 CLEO $J/\psi \rightarrow \gamma p\bar{p}$
1833.7 ± 6.1	± 2.7	264	8,9	ABLIKIM	05R BES2 $J/\psi \rightarrow \gamma\pi^+\pi^-\eta'$	
1831 ± 7	8,9	ABLIKIM	05R	BES2	$J/\psi \rightarrow \gamma p\bar{p}$	
1859 ± 3	5	25	8	BAI	03F BES2 $J/\psi \rightarrow \gamma p\bar{p}$	

- From a fit of the measured  $\pi^+\pi^-\eta'$  lineshape that accounts for the abrupt distortion observed at the  $p\bar{p}$  threshold through interference with a second previously unseen narrow resonance near 1870 MeV. The fit uses Breit-Wigner functions for the signal shapes and includes known backgrounds and contributors.
- From a fit to  $\gamma\phi$  invariant mass. Angular analysis consistent with  $J^{PC} = 0^{-+}$ . Other  $J^{PC}$  not excluded.
- Pole mass from a fit of the measured  $\pi^+\pi^-\eta'$  lineshape to a Flatte formula that accounts for the abrupt distortion observed at the  $p\bar{p}$  threshold; the fit also includes known backgrounds and contributors, as well as an *ad hoc* Breit-Wigner function ( $M \approx 1919$  MeV;  $\Gamma \approx 51$  MeV) that is required for a good fit.
- From the fit including final state interaction effects in isospin 0 S-wave according to SIBIRTSSEV 05A. Supersedes ABLIKIM 10G.
- From a fit of the  $\pi^+\pi^-\eta'$  mass distribution to a combination of  $\gamma f_1(1510)$ ,  $\gamma X(1835)$ , and two unconfirmed states  $\gamma X(2120)$ , and  $\gamma X(2370)$ , for  $M(p\bar{p}) < 2.8$  GeV, and accounting for backgrounds from non- $\eta'$  events and  $J/\psi \rightarrow \pi^0\pi^+\pi^-\eta'$ .
- The selected process is  $J/\psi \rightarrow \omega a_0(980)\pi$ . This state may be due also to  $\eta_2(1870)$  or to a combination of  $X(1835)$  and  $\eta_2(1870)$ .
- From a fit of the  $p\bar{p}$  mass distribution to a combination of  $\gamma X(1835)$ ,  $\gamma R$  with  $M(R) = 2100$  MeV and  $\Gamma(R) = 160$  MeV, and  $\gamma p\bar{p}$  phase space, for  $M(p\bar{p}) < 2.85$  GeV.
- Evidence for a threshold enhancement in the  $p\bar{p}$  mass spectrum was also reported by ABE 02k, AUBERT, B 05L, and WANG 05A in  $B^+ \rightarrow p\bar{p}K^+$ , WANG 05A in  $B^0 \rightarrow p\bar{p}K_S^0$ , ABE 02w in  $\bar{B}^0 \rightarrow p\bar{p}D^0$ , DEL-AMO-SANCHEZ 12 in  $B \rightarrow D(D^*)p\bar{p}(\pi)$ , and WEI 08 in  $B^+ \rightarrow p\bar{p}\pi^+$  decays. Not seen by ATHAR 06 in  $\Upsilon(1S) \rightarrow p\bar{p}\gamma$ .
- From the fit including final state interaction effects in isospin 0 S-wave according to SIBIRTSSEV 05A. Systematic errors not estimated.

$X(1835)$  WIDTH

VALUE (MeV)	CL%	EVTS	DOCUMENT ID	TECN	COMMENT	
<b>242 ± 14</b>	<b>-15</b>	<b>OUR AVERAGE</b>				
245.2 ± 13.1	4.6	9.6	1	ABLIKIM	16J BES3 $J/\psi \rightarrow \gamma\pi^+\pi^-\eta'$	
192 ± 20	± 62	-17 -43	2	ABLIKIM	15T BES3 $J/\psi \rightarrow \gamma K_S^0 K_S^0 \eta$	
175 ± 5.7	± 25	273.5 ± 21.4	6.1	3	ABLIKIM	16J BES3 $J/\psi \rightarrow \gamma\pi^+\pi^-\eta'$
83 ± 14	± 11	64.0	0.6k	ABLIKIM	13U BES3 $J/\psi \rightarrow \gamma 3(\pi^+\pi^-)$	
< 76	90	4	ABLIKIM	12D BES3 $J/\psi \rightarrow \gamma p\bar{p}$		

$f_2(1810)$  DECAY MODES

Mode	Fraction ( $\Gamma_i/\Gamma$ )
$\Gamma_1$ $\pi\pi$	
$\Gamma_2$ $\eta\eta$	seen
$\Gamma_3$ $4\pi^0$	seen
$\Gamma_4$ $K^+K^-$	
$\Gamma_5$ $\gamma\gamma$	seen

$f_2(1810)$   $\Gamma(\eta)/\Gamma(\text{total})$

VALUE (eV)	DOCUMENT ID	TECN	COMMENT
<b>5.2 ± 0.9 + 37.3</b>	13	UEHARA	10A BELL 10.6 $e^+e^- \rightarrow e^+e^-\eta\eta$
<b>-0.8 - 4.5</b>			

<sup>13</sup>Including interference with the  $f_2'(1525)$  (parameters fixed to the values from the 2008 edition of this review, PDG 08) and  $f_2(1270)$ . May also be the  $f_0(1500)$ .

$f_2(1810)$  BRANCHING RATIOS

$\Gamma(\pi\pi)/\Gamma_{\text{total}}$	DOCUMENT ID	TECN	COMMENT
• • • We do not use the following data for averages, fits, limits, etc. • • •			
not seen	AMSLER	02	CBAR 0.9 $p\bar{p} \rightarrow \pi^0\eta\eta, \pi^0\pi^0\pi^0$
not seen	PROKOSHKIN	97	GAM2 38 $\pi^-p \rightarrow \pi^0\pi^0n$
0.21 ± 0.02	14	LONGACRE	86 RVUE Compilation
-0.03			
0.44 ± 0.03	15	CASON	82 STRC 8 $\pi^+p \rightarrow \Delta^+\pi^0$

<sup>14</sup>From a partial-wave analysis of data using a K-matrix formalism with 5 poles. Includes compilation of several other experiments.

<sup>15</sup>Included in LONGACRE 86 global analysis.

$\Gamma(\eta\eta)/\Gamma_{\text{total}}$	DOCUMENT ID	TECN	COMMENT
seen	ABLIKIM	13N	BES3 PWA of $J/\psi \rightarrow \gamma\eta\eta$
• • • We do not use the following data for averages, fits, limits, etc. • • •			
0.008 ± 0.028	16	LONGACRE	86 RVUE Compilation
-0.003			

<sup>16</sup>From a partial-wave analysis of data using a K-matrix formalism with 5 poles. Includes compilation of several other experiments.

$\Gamma(\pi\pi)/\Gamma(4\pi^0)$	DOCUMENT ID	TECN	COMMENT
• • • We do not use the following data for averages, fits, limits, etc. • • •			
< 0.75	ALDE	87	GAM4 100 $\pi^-p \rightarrow 4\pi^0n$

$\Gamma(4\pi^0)/\Gamma(\eta\eta)$	DOCUMENT ID	TECN	COMMENT
• • • We do not use the following data for averages, fits, limits, etc. • • •			
0.8 ± 0.3	ALDE	87	GAM4 100 $\pi^-p \rightarrow 4\pi^0n$

$\Gamma(K^+K^-)/\Gamma_{\text{total}}$	DOCUMENT ID	TECN	COMMENT
• • • We do not use the following data for averages, fits, limits, etc. • • •			
0.003 ± 0.019	17	LONGACRE	86 RVUE Compilation
-0.002			
seen	COSTA	80	OMEG 10 $\pi^-p \rightarrow K^+K^-n$

<sup>17</sup>From a partial-wave analysis of data using a K-matrix formalism with 5 poles. Includes compilation of several other experiments.



# Meson Particle Listings

## X(1835), $\phi_3(1850)$

190 ± 9 <sup>+38</sup> / <sub>-36</sub>	4265	<sup>5</sup> ABLIKIM	11c	BES3	$J/\psi \rightarrow \gamma\pi^+\pi^-\eta'$
57 ± 12 <sup>+19</sup> / <sub>-4</sub>		<sup>6</sup> ABLIKIM	11j	BES3	$J/\psi \rightarrow \omega(\eta\pi^+\pi^-)$
0 <sup>+44</sup> / <sub>-0</sub>	231	<sup>7,8</sup> ALEXANDER	10	CLEO	$J/\psi \rightarrow \gamma\rho\bar{p}$
67.7±20.3± 7.7	264	<sup>9</sup> ABLIKIM	05R	BES2	$J/\psi \rightarrow \gamma\pi^+\pi^-\eta'$
< 153	90	<sup>8,9</sup> ABLIKIM	05R	BES2	$J/\psi \rightarrow \gamma\rho\bar{p}$
< 30		<sup>8</sup> BAI	03F	BES2	$J/\psi \rightarrow \gamma\rho\bar{p}$

- From a fit of the measured  $\pi^+\pi^-\eta'$  lineshape that accounts for the abrupt distortion observed at the  $p\bar{p}$  threshold through interference with a second previously unseen narrow resonance near 1870 MeV. The fit uses Breit-Wigner functions for the signal shapes and includes known backgrounds and contributors.
- From a fit to  $\gamma\phi$  invariant mass. Angular analysis consistent with  $J^{PC} = 0^{-+}$ . Other  $J^{PC}$  not excluded.
- Pole width from a fit of the measured  $\pi^+\pi^-\eta'$  lineshape to a Flatte formula that accounts for the abrupt distortion observed at the  $p\bar{p}$  threshold; the fit also includes known backgrounds and contributors, as well as an *ad hoc* Breit-Wigner function ( $M \approx 1919$  MeV;  $\Gamma \approx 51$  MeV) that is required for a good fit.
- From the fit including final state interaction effects in isospin 0 S-wave according to SIBIRTSSEV 05A. Supersedes ABLIKIM 10G.
- From a fit of the  $\pi^+\pi^-\eta'$  mass distribution to a combination of  $\gamma f_1(1510)$ ,  $\gamma X(1835)$ , and two unconfirmed states  $\gamma X(2120)$ , and  $\gamma X(2370)$ , for  $M(p\bar{p}) < 2.8$  GeV, and accounting for backgrounds from non- $\eta'$  events and  $J/\psi \rightarrow \pi^0\pi^+\pi^-\eta'$ .
- The selected process is  $J/\psi \rightarrow \omega\pi_0(980)\pi$ . This state may be due also to  $\eta_2(1870)$  or to a combination of  $X(1835)$  and  $\eta_2(1870)$ .
- From a fit of the  $p\bar{p}$  mass distribution to a combination of  $\gamma X(1835)$ ,  $\gamma R$  with  $M(R) = 2100$  MeV and  $\Gamma(R) = 160$  MeV, and  $\gamma p\bar{p}$  phase space, for  $M(p\bar{p}) < 2.85$  GeV.
- Evidence for a threshold enhancement in the  $p\bar{p}$  mass spectrum was also reported by ABE 02K, AUBERT,B 05L, and WANG 05A in  $B^+ \rightarrow p\bar{p}K^+$ , WANG 05A in  $B^0 \rightarrow p\bar{p}K_S^0$ , ABE 02W in  $\bar{B}^0 \rightarrow p\bar{p}D^0$ , DEL-AMO-SANCHEZ 12 in  $B \rightarrow D(D^*)p\bar{p}(\pi)$ , and WEI 08 in  $B^+ \rightarrow p\bar{p}\pi^+$  decays. Not seen by ATHAR 06 in  $\Upsilon(1S) \rightarrow p\bar{p}\gamma$ .
- From the fit including final state interaction effects in isospin 0 S-wave according to SIBIRTSSEV 05A. Systematic errors not estimated.

### X(1835) DECAY MODES

Mode	Fraction ( $\Gamma_i/\Gamma$ )
$\Gamma_1$ $p\bar{p}$	seen
$\Gamma_2$ $\eta'\pi^+\pi^-$	seen
$\Gamma_3$ $\gamma\gamma$	
$\Gamma_4$ $K_S^0 K_S^0 \eta$	seen
$\Gamma_5$ $\gamma\phi(1020)$	possibly seen
$\Gamma_6$ $3(\pi^+\pi^-)$	seen

### X(1835) $\Gamma(i)\Gamma(\gamma\gamma)/\Gamma(\text{total})$

$\Gamma(\eta'\pi^+\pi^-) \times \Gamma(\gamma\gamma)/\Gamma_{\text{total}}$	$\Gamma_2/\Gamma_3/\Gamma$
VALUE (eV)	CL% DOCUMENT ID TECN COMMENT
••• We do not use the following data for averages, fits, limits, etc. •••	
<35.6	90 <sup>1</sup> ZHANG 12A BELL $e^+e^- \rightarrow e^+e^-\eta'\pi^+\pi^-$
<83	90 <sup>2</sup> ZHANG 12A BELL $e^+e^- \rightarrow e^+e^-\eta'\pi^+\pi^-$

- From a two-resonance fit and constructive interference of the  $\eta(1760)$  and  $X(1835)$ , a significance of 2.8  $\sigma$ .
- From a two-resonance fit and destructive interference of the  $\eta(1760)$  and  $X(1835)$ , a significance of 2.8  $\sigma$ .

### X(1835) BRANCHING RATIOS

$\Gamma(p\bar{p})/\Gamma(\eta'\pi^+\pi^-)$	$\Gamma_1/\Gamma_2$
VALUE	DOCUMENT ID TECN COMMENT
••• We do not use the following data for averages, fits, limits, etc. •••	
0.333	ABLIKIM 05R BES2 $J/\psi \rightarrow \gamma\pi^+\pi^-\eta'$

$\Gamma(\eta'\pi^+\pi^-)/\Gamma(K_S^0 K_S^0 \eta)$	$\Gamma_2/\Gamma_4$
VALUE	DOCUMENT ID TECN COMMENT
••• We do not use the following data for averages, fits, limits, etc. •••	
6.7±1.8	<sup>1</sup> ABLIKIM 15T BES3 $J/\psi \rightarrow \gamma K_S^0 K_S^0 \eta$

- Using results from ABLIKIM 05R.

$\Gamma(\eta'\pi^+\pi^-)/\Gamma_{\text{total}}$	$\Gamma_2/\Gamma$
VALUE	DOCUMENT ID TECN COMMENT
seen	<sup>1</sup> ABLIKIM 16j BES3 $J/\psi \rightarrow \gamma\pi^+\pi^-\eta'$

- ABLIKIM 16j quotes  $B(J/\psi \rightarrow \gamma X(1835)) \times B(X(1835) \rightarrow \pi^+\pi^-\eta') = (3.93 \pm 0.38^{+0.31}_{-0.84}) \times 10^{-4}$  from a fit of the measured  $\pi^+\pi^-\eta'$  lineshape that accounts for the abrupt distortion observed at the  $p\bar{p}$  threshold with a Flatte formula in addition to known backgrounds and contributors, as well as an *ad hoc* Breit-Wigner ( $M \approx 1919$  MeV;  $\Gamma \approx 51$  MeV) that is required for a good fit. Another explanation for the distortion provided by ABLIKIM 16j is that a second resonance near 1870 MeV interferes with the  $X(1835)$ ; fits to this possibility yield product branching fraction values compatible with that shown within the respective systematic uncertainties.

$\Gamma(\gamma\phi(1020))/\Gamma_{\text{total}}$	$\Gamma_5/\Gamma$
VALUE	DOCUMENT ID TECN COMMENT
possibly seen	<sup>1</sup> ABLIKIM 18i BES3 $J/\psi \rightarrow \gamma\gamma\phi(1020)$

- Seen as a peak in  $\gamma\phi$  invariant mass. Angular analysis consistent with  $J^{PC} = 0^{-+}$ . Other  $J^{PC}$  not excluded.

$\Gamma(\gamma\gamma)/\Gamma(\eta'\pi^+\pi^-)$	$\Gamma_3/\Gamma_2$
VALUE	CL% DOCUMENT ID TECN COMMENT
<9.80 × 10 <sup>-3</sup>	90 <sup>1</sup> ABLIKIM 18o BES3 $\psi(2S) \rightarrow \pi^+\pi^-\gamma\gamma$

- Using results from ABLIKIM 16j.

$\Gamma(3(\pi^+\pi^-))/\Gamma_{\text{total}}$	$\Gamma_6/\Gamma$
VALUE	EVTS DOCUMENT ID TECN COMMENT
seen	0.6k ABLIKIM 13u BES3 $J/\psi \rightarrow \gamma 3(\pi^+\pi^-)$

### X(1835) REFERENCES

ABLIKIM 18i	PR D97 051101	M. Ablikim <i>et al.</i>	(BESIII Collab.)
ABLIKIM 18o	PR D97 072014	M. Ablikim <i>et al.</i>	(BESIII Collab.)
ABLIKIM 16j	PRL 117 042002	M. Ablikim <i>et al.</i>	(BESIII Collab.)
ABLIKIM 15T	PRL 115 091803	M. Ablikim <i>et al.</i>	(BESIII Collab.)
ABLIKIM 13u	PR D88 091502	M. Ablikim <i>et al.</i>	(BESIII Collab.)
ABLIKIM 12D	PRL 108 112003	M. Ablikim <i>et al.</i>	(BESIII Collab.) JPC
DEL-AMO-SA...	PR D85 092017	P. del Amo Sanchez <i>et al.</i>	(BABAR Collab.)
ZHANG 12A	PR D86 052002	C.C. Zhang <i>et al.</i>	(BELLE Collab.)
ABLIKIM 11C	PRL 106 072002	M. Ablikim <i>et al.</i>	(BESIII Collab.)
ABLIKIM 11J	PRL 107 182001	M. Ablikim <i>et al.</i>	(BESIII Collab.)
ABLIKIM 10G	CP C34 421	M. Ablikim <i>et al.</i>	(BESIII Collab.)
ALEXANDER 10	PR D82 092002	J.P. Alexander <i>et al.</i>	(CLEO Collab.)
WEI 08	PL B659 80	J.-T. Wei <i>et al.</i>	(BELLE Collab.)
ATHAR 06	PR D73 032001	S.B. Athar <i>et al.</i>	(CLEO Collab.)
ABLIKIM 05R	PRL 95 292001	M. Ablikim <i>et al.</i>	(BES Collab.)
AUBERT,B 05L	PR D72 051101	B. Aubert <i>et al.</i>	(BABAR Collab.)
SIBIRTSSEV 05A	PR D71 054010	A. Sibirtsev, J. Haidenbauer	
WANG 05A	PL B617 141	M.-Z. Wang <i>et al.</i>	(BELLE Collab.)
BAI 03F	PRL 91 022001	J.Z. Bai <i>et al.</i>	(BES II Collab.)
ABE 02K	PRL 88 181803	K. Abe <i>et al.</i>	(BELLE Collab.)
ABE 02W	PRL 89 151802	K. Abe <i>et al.</i>	(BELLE Collab.)

## $\phi_3(1850)$

$$I^G(J^{PC}) = 0^-(3^{-})$$

### $\phi_3(1850)$ MASS

VALUE (MeV)	EVTS	DOCUMENT ID	TECN	COMMENT
<b>1854 ± 7</b>	<b>OUR AVERAGE</b>			
1855 ± 10		ASTON	88E LASS	11 $K^-p \rightarrow K^-K^+\Lambda$ , $K_S^0 K^\pm \pi^\mp \Lambda$
1870 <sup>+30</sup> / <sub>-20</sub>	430	ARMSTRONG 82	OMEG	18.5 $K^-p \rightarrow K^-K^+\Lambda$
1850 ± 10	123	ALHARRAN 81B	HBC	8.25 $K^-p \rightarrow K\bar{K}\Lambda$

### $\phi_3(1850)$ WIDTH

VALUE (MeV)	EVTS	DOCUMENT ID	TECN	COMMENT
<b>87 <sup>+28</sup>/<sub>-23</sub></b>	<b>OUR AVERAGE</b>			Error includes scale factor of 1.2.
64 ± 31		ASTON	88E LASS	11 $K^-p \rightarrow K^-K^+\Lambda$ , $K_S^0 K^\pm \pi^\mp \Lambda$
160 <sup>+90</sup> / <sub>-50</sub>	430	ARMSTRONG 82	OMEG	18.5 $K^-p \rightarrow K^-K^+\Lambda$
80 <sup>+40</sup> / <sub>-30</sub>	123	ALHARRAN 81B	HBC	8.25 $K^-p \rightarrow K\bar{K}\Lambda$

### $\phi_3(1850)$ DECAY MODES

Mode	Fraction ( $\Gamma_i/\Gamma$ )
$\Gamma_1$ $K\bar{K}$	seen
$\Gamma_2$ $K\bar{K}^*(892) + \text{c.c.}$	seen

### $\phi_3(1850)$ BRANCHING RATIOS

$\Gamma(K\bar{K}^*(892) + \text{c.c.})/\Gamma(K\bar{K})$	$\Gamma_2/\Gamma_1$
VALUE	DOCUMENT ID TECN COMMENT
<b>0.55 <sup>+0.85</sup>/<sub>-0.45</sub></b>	ASTON 88E LASS 11 $K^-p \rightarrow K^-K^+\Lambda$ , $K_S^0 K^\pm \pi^\mp \Lambda$

- We do not use the following data for averages, fits, limits, etc. •••

0.8 ± 0.4	ALHARRAN 81B HBC 8.25 $K^-p \rightarrow K\bar{K}\pi\Lambda$
-----------	---

### $\phi_3(1850)$ REFERENCES

ASTON 88E	PL B208 324	D. Aston <i>et al.</i>	(SLAC, NAGO, CINC, INUS)IGJPC
ARMSTRONG 82	PL 110B 77	T.A. Armstrong <i>et al.</i>	(BARI, BIRM, CERN+)JP
ALHARRAN 81B	PL 101B 357	S. Al-Harran <i>et al.</i>	(BIRM, CERN, GLAS+)

See key on page 999

# Meson Particle Listings

## $\eta_2(1870), \pi_2(1880), \rho(1900)$

### $\eta_2(1870)$ $I^G(J^{PC}) = 0^+(2^-)$

**$\eta_2(1870)$  MASS**

VALUE (MeV)	EVTS	DOCUMENT ID	TECN	COMMENT
<b>1842 ± 8</b>	<b>8</b>	<b>OUR AVERAGE</b>		
1835 ± 12		BARBERIS	00B	450 $pp \rightarrow \rho_f \eta \pi^+ \pi^- \rho_S$
1844 ± 13		BARBERIS	00C	450 $pp \rightarrow \rho_f 4 \pi \rho_S$
1840 ± 25		BARBERIS	97B	OMEG 450 $pp \rightarrow \rho p 2(\pi^+ \pi^-)$
1875 ± 20 ± 35		ADOMEIT	96	CBAR 1.94 $\bar{p}p \rightarrow \eta 3\pi^0$
1881 ± 32 ± 40	26	KARCH	92	CBAL $e^+ e^- \rightarrow e^+ e^- \eta \pi^0 \pi^0$
• • • We do not use the following data for averages, fits, limits, etc. • • •				
1860 ± 5 ± 15		ANISOVICH	00E	SPEC 0.9-1.94 $\bar{p}p \rightarrow \eta 3\pi^0$
1840 ± 15		BAI	99	BES $J/\psi \rightarrow \gamma \eta \pi^+ \pi^-$

**$\eta_2(1870)$  WIDTH**

VALUE (MeV)	EVTS	DOCUMENT ID	TECN	COMMENT
<b>225 ± 14</b>	<b>14</b>	<b>OUR AVERAGE</b>		
235 ± 22		BARBERIS	00B	450 $pp \rightarrow \rho_f \eta \pi^+ \pi^- \rho_S$
228 ± 23		BARBERIS	00C	450 $pp \rightarrow \rho_f 4 \pi \rho_S$
200 ± 40		BARBERIS	97B	OMEG 450 $pp \rightarrow \rho p 2(\pi^+ \pi^-)$
200 ± 25 ± 45		ADOMEIT	96	CBAR 1.94 $\bar{p}p \rightarrow \eta 3\pi^0$
221 ± 92 ± 44	26	KARCH	92	CBAL $e^+ e^- \rightarrow e^+ e^- \eta \pi^0 \pi^0$
• • • We do not use the following data for averages, fits, limits, etc. • • •				
250 ± 25 ± 50	-35	ANISOVICH	00E	SPEC 0.9-1.94 $\bar{p}p \rightarrow \eta 3\pi^0$
170 ± 40		BAI	99	BES $J/\psi \rightarrow \gamma \eta \pi^+ \pi^-$

**$\eta_2(1870)$  DECAY MODES**

Mode	Fraction ( $\Gamma_i/\Gamma$ )
$\Gamma_1$ $\eta \pi \pi$	
$\Gamma_2$ $a_2(1320) \pi$	
$\Gamma_3$ $f_2(1270) \eta$	
$\Gamma_4$ $a_0(980) \pi$	
$\Gamma_5$ $\gamma \gamma$	seen

**$\eta_2(1870)$  BRANCHING RATIOS**

$\Gamma(a_2(1320)\pi)/\Gamma(f_2(1270)\eta)$   $\Gamma_2/\Gamma_3$

VALUE	DOCUMENT ID	TECN	COMMENT
<b>1.7 ± 0.4</b>	<b>14</b>	<b>OUR AVERAGE</b>	
1.60 ± 0.40	1	ANISOVICH	11 SPEC 0.9-1.94 $p\bar{p}$
20.4 ± 6.6		BARBERIS	00B 450 $pp \rightarrow \rho_f \eta \pi^+ \pi^- \rho_S$
4.1 ± 2.3		ADOMEIT	96 CBAR 1.94 $\bar{p}p \rightarrow \eta 3\pi^0$
1 Reanalysis of ADOMEIT 96 and ANISOVICH 00E.			

$\Gamma(a_2(1320)\pi)/\Gamma(a_0(980)\pi)$   $\Gamma_2/\Gamma_4$

VALUE	DOCUMENT ID	COMMENT
<b>32.6 ± 12.6</b>	<b>1</b>	<b>OUR AVERAGE</b>
	BARBERIS	00B 450 $pp \rightarrow \rho_f \eta \pi^+ \pi^- \rho_S$

$\Gamma(a_0(980)\pi)/\Gamma(f_2(1270)\eta)$   $\Gamma_4/\Gamma_3$

VALUE	DOCUMENT ID	TECN	COMMENT
<b>0.48 ± 0.45</b>	<b>1</b>	<b>OUR AVERAGE</b>	
	ANISOVICH	11 SPEC	0.9-1.94 $p\bar{p}$
1 Reanalysis of ADOMEIT 96 and ANISOVICH 00E.			

$\Gamma(\gamma\gamma)/\Gamma_{total}$   $\Gamma_5/\Gamma$

VALUE	DOCUMENT ID	TECN	COMMENT
seen	KARCH	92 CBAL	$e^+ e^- \rightarrow e^+ e^- \eta \pi^0 \pi^0$

**$\eta_2(1870)$  REFERENCES**

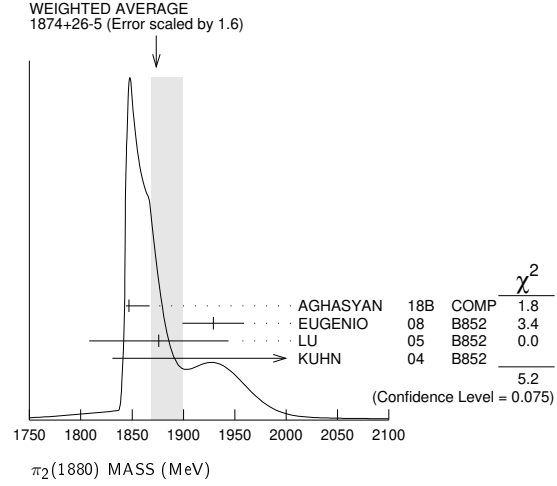
ANISOVICH	11	EPJ C71 1511	A.V. Anisovich et al.	(LOQM, RAL, PNPI)
ANISOVICH	00E	PL B477 19	A.V. Anisovich et al.	
BARBERIS	00B	PL B471 435	D. Barberis et al.	(WA 102 Collab.)
BARBERIS	00C	PL B471 440	D. Barberis et al.	(WA 102 Collab.)
BAI	99	PL B446 356	J.Z. Bai et al.	(BES Collab.)
BARBERIS	97B	PL B413 217	D. Barberis et al.	(WA 102 Collab.)
ADOMEIT	96	ZPHY C71 227	J. Adomeit et al.	(Crystal Barrel Collab.)
KARCH	92	ZPHY C54 33	K. Karch et al.	(Crystal Ball Collab.)

### $\pi_2(1880)$ $I^G(J^{PC}) = 1^-(2^-)$

**$\pi_2(1880)$  MASS**

VALUE (MeV)	EVTS	DOCUMENT ID	TECN	CHG	COMMENT
<b>1874 ± 26</b>	<b>5</b>	<b>OUR AVERAGE</b>			
1847 ± 20	46M	1	AGHASYAN	18B	COMP 190 $\pi^- p \rightarrow \pi^- \pi^+ \pi^- p$
1929 ± 24 ± 18	4k	EUGENIO	08	B852	- 18 $\pi^- p \rightarrow \eta \eta \pi^- p$
1876 ± 11 ± 67	145k	LU	05	B852	- 18 $\pi^- p \rightarrow \omega \pi^- \pi^0 p$
2003 ± 88 ± 148	69k	KUHN	04	B852	- 18 $\pi^- p \rightarrow \eta \pi^+ \pi^- \pi^- p$

• • • We do not use the following data for averages, fits, limits, etc. • • •  
 1880 ± 20 ANISOVICH 01B SPEC 0 0.6-1.94  $\bar{p}p \rightarrow \eta \eta \pi^0 \pi^0$   
 1 Statistical error negligible.



**$\pi_2(1880)$  WIDTH**

VALUE (MeV)	EVTS	DOCUMENT ID	TECN	CHG	COMMENT
<b>237 ± 33</b>	<b>30</b>	<b>OUR AVERAGE</b>			
246 ± 28	46M	2	AGHASYAN	18B	COMP Error includes scale factor of 1.2.
323 ± 87 ± 43	4k	EUGENIO	08	B852	- 18 $\pi^- p \rightarrow \eta \eta \pi^- p$
146 ± 17 ± 62	145k	LU	05	B852	- 18 $\pi^- p \rightarrow \omega \pi^- \pi^0 p$
306 ± 132 ± 121	69k	KUHN	04	B852	- 18 $\pi^- p \rightarrow \eta \pi^+ \pi^- \pi^- p$
• • • We do not use the following data for averages, fits, limits, etc. • • •					
255 ± 45		ANISOVICH	01B	SPEC	0 0.6-1.94 $\bar{p}p \rightarrow \eta \eta \pi^0 \pi^0$
2 Statistical error negligible.					

**$\pi_2(1880)$  DECAY MODES**

Mode
$\Gamma_1$ $\eta \eta \pi^-$
$\Gamma_2$ $a_0(980) \eta$
$\Gamma_3$ $a_2(1320) \eta$
$\Gamma_4$ $f_0(1500) \pi$
$\Gamma_5$ $f_1(1285) \pi$
$\Gamma_6$ $\omega \pi^- \pi^0$

$\Gamma(a_2(1320)\eta)/\Gamma(f_1(1285)\pi)$   $\Gamma_3/\Gamma_5$

VALUE	EVTS	DOCUMENT ID	TECN	CHG	COMMENT
<b>22.7 ± 7.3</b>	<b>69k</b>	<b>1</b>	<b>OUR AVERAGE</b>		
		KUHN	04	B852	- 18 $\pi^- p \rightarrow \eta \pi^+ \pi^- \pi^- p$

$\Gamma(f_0(1500)\pi)/\Gamma(a_0(980)\eta)$   $\Gamma_4/\Gamma_2$

VALUE	DOCUMENT ID	TECN	CHG	COMMENT
<b>0.28 ± 0.20</b>	<b>3</b>	<b>OUR AVERAGE</b>		
-0.15		ANISOVICH	01B	SPEC 0 0.6-1.94 $\bar{p}p \rightarrow \eta \eta \pi^0 \pi^0$
3 Systematic errors not estimated.				

**$\pi_2(1880)$  REFERENCES**

AGHASYAN	18B	PR D98 092003	M. Aghasyan et al.	(COMPASS Collab.)
EUGENIO	08	PL B660 466	P. Eugenio et al.	(BNL E852 Collab.)
LU	05	PRL 94 032002	M. Lu et al.	(BNL E852 Collab.)
KUHN	04	PL B595 109	J. Kuhn et al.	(BNL E852 Collab.)
ANISOVICH	01B	PL B500 222	A.V. Anisovich et al.	

### $\rho(1900)$ $I^G(J^{PC}) = 1^+(1^-)$

OMITTED FROM SUMMARY TABLE  
 See our mini-review under the  $\rho(1700)$ .

# Meson Particle Listings

## $\rho(1900)$ , $f_2(1910)$

### $\rho(1900)$ MASS

VALUE (MeV)	EVTs	DOCUMENT ID	TECN	COMMENT
• • • We do not use the following data for averages, fits, limits, etc. • • •				
1909 ± 17 ± 25	54	<sup>1</sup> AUBERT	08s BABR	10.6 e <sup>+</sup> e <sup>-</sup> → φπ <sup>0</sup> γ
1880 ± 30		AUBERT	06D BABR	10.6 e <sup>+</sup> e <sup>-</sup> → 3π <sup>+</sup> 3π <sup>-</sup> γ
1860 ± 20		AUBERT	06D BABR	10.6 e <sup>+</sup> e <sup>-</sup> → 2(π <sup>+</sup> π <sup>-</sup> π <sup>0</sup> )γ
1910 ± 10	2,3	FRABETTI	04 E687	γp → 3π <sup>+</sup> 3π <sup>-</sup> p
1870 ± 10		ANTONELLI	96 SPEC	e <sup>+</sup> e <sup>-</sup> → hadrons

<sup>1</sup> From the fit with two resonances.  
<sup>2</sup> From a fit with two resonances with the JACOB 72 continuum.  
<sup>3</sup> Supersedes FRABETTI 01.

### $\rho(1900)$ WIDTH

VALUE (MeV)	EVTs	DOCUMENT ID	TECN	COMMENT
• • • We do not use the following data for averages, fits, limits, etc. • • •				
48 ± 17 ± 2	54	<sup>4</sup> AUBERT	08s BABR	10.6 e <sup>+</sup> e <sup>-</sup> → φπ <sup>0</sup> γ
130 ± 30		AUBERT	06D BABR	10.6 e <sup>+</sup> e <sup>-</sup> → 3π <sup>+</sup> 3π <sup>-</sup> γ
160 ± 20		AUBERT	06D BABR	10.6 e <sup>+</sup> e <sup>-</sup> → 2(π <sup>+</sup> π <sup>-</sup> π <sup>0</sup> )γ
37 ± 13	5,6	FRABETTI	04 E687	γp → 3π <sup>+</sup> 3π <sup>-</sup> p
10 ± 5		ANTONELLI	96 SPEC	e <sup>+</sup> e <sup>-</sup> → hadrons

<sup>4</sup> From the fit with two resonances.  
<sup>5</sup> From a fit with two resonances with the JACOB 72 continuum.  
<sup>6</sup> Supersedes FRABETTI 01.

### $\rho(1900)$ $\Gamma(\pi)\Gamma(e^+e^-)/\Gamma^2(\text{total})$

VALUE (units 10 <sup>-8</sup> )	EVTs	DOCUMENT ID	TECN	COMMENT
• • • We do not use the following data for averages, fits, limits, etc. • • •				
4.2 ± 1.2 ± 0.8	54	<sup>7</sup> AUBERT	08s BABR	10.6 e <sup>+</sup> e <sup>-</sup> → φπ <sup>0</sup> γ

<sup>7</sup> From the fit with two resonances.

### $\rho(1900)$ DECAY MODES

Mode	Fraction ( $\Gamma_i/\Gamma$ )
$\Gamma_1$ 6π	seen
$\Gamma_2$ 3π <sup>+</sup> 3π <sup>-</sup>	seen
$\Gamma_3$ 2π <sup>+</sup> 2π <sup>-</sup> 2π <sup>0</sup>	
$\Gamma_4$ φπ	
$\Gamma_5$ hadrons	seen
$\Gamma_6$ e <sup>+</sup> e <sup>-</sup>	seen
$\Gamma_7$ $\bar{N}N$	not seen

### $\rho(1900)$ BRANCHING RATIOS

$\Gamma(6\pi)/\Gamma_{\text{total}}$	VALUE	EVTs	DOCUMENT ID	TECN	COMMENT
seen		8k	AKHMETSHIN 13	CMD3	e <sup>+</sup> e <sup>-</sup> → 3π <sup>+</sup> 3π <sup>-</sup>
not seen			AGNELLO 02	OBLX	$\bar{n}p \rightarrow 3\pi^+2\pi^- \pi^0$
seen			FRABETTI 01	E687	γp → 3π <sup>+</sup> 3π <sup>-</sup> p
seen			ANTONELLI 96	SPEC	e <sup>+</sup> e <sup>-</sup> → hadrons

### $\rho(1900)$ REFERENCES

AKHMETSHIN 13	PL B723 82	R.R. Akhmetshin et al.	(CMD-3 Collab.)
AUBERT 08s	PR D77 092002	B. Aubert et al.	(BABAR Collab.)
AUBERT 06D	PR D73 052003	B. Aubert et al.	(BABAR Collab.)
FRABETTI 04	PL B578 290	P.L. Frabetti et al.	(FNAL E687 Collab.)
AGNELLO 02	PL B527 39	M. Agnello et al.	(OBELIX Collab.)
FRABETTI 01	PL B514 240	P.L. Frabetti et al.	(FNAL E687 Collab.)
ANTONELLI 96	PL B365 427	A. Antonelli et al.	(FENICE Collab.)
JACOB 72	PR D5 1847	M. Jacob, R. Slansky	

## $f_2(1910)$

$$J^{PC} = 0^+(2^{++})$$

OMITTED FROM SUMMARY TABLE

We list here three different peaks with close masses and widths seen in the mass distributions of ωω, ηη', and K<sup>+</sup>K<sup>-</sup> final states. ALDE 91B argues that they are of different nature.

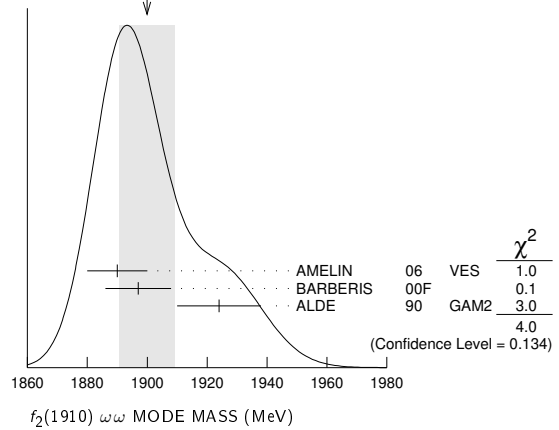
### $f_2(1910)$ MASS

#### $f_2(1910)$ ωω MODE

VALUE (MeV)	DOCUMENT ID	TECN	COMMENT
<b>1900 ± 9 OUR AVERAGE</b> Error includes scale factor of 1.4. See the ideogram below.			
1890 ± 10	<sup>1</sup> AMELIN	06 VES	36 π <sup>-</sup> p → ωωn
1897 ± 11	BARBERIS	00F	450 pp → p <sub>f</sub> ωωp <sub>s</sub>
1924 ± 14	ALDE	90 GAM2	38 π <sup>-</sup> p → ωωn

<sup>1</sup> Supersedes BELADIDZE 92b.

WEIGHTED AVERAGE  
1900 ± 9 (Error scaled by 1.4)



#### $f_2(1910)$ ηη' MODE

VALUE (MeV)	DOCUMENT ID	TECN	COMMENT
<b>1934 ± 16</b>			
	<sup>1</sup> BARBERIS	00A	450 pp → p <sub>f</sub> ηη'p <sub>s</sub>
• • • We do not use the following data for averages, fits, limits, etc. • • •			
1934 ± 20	<sup>2</sup> ANISOVICH	00J	SPEC
1911 ± 10	ALDE	91B	GAM2 38 π <sup>-</sup> p → ηη'n

<sup>1</sup> Also compatible with J<sup>PC</sup>=1<sup>-</sup>+.  
<sup>2</sup> Combined fit with ηη, ππ, and ηππ.

#### $f_2(1910)$ K<sup>+</sup>K<sup>-</sup> MODE

VALUE (MeV)	DOCUMENT ID	TECN	COMMENT
• • • We do not use the following data for averages, fits, limits, etc. • • •			
1941 ± 18	<sup>1</sup> AMSLER	06	CBAR 1.64 $\bar{p}p \rightarrow K^+K^-\pi^0$

<sup>1</sup> Tentative, could be f<sub>2</sub>(1950).

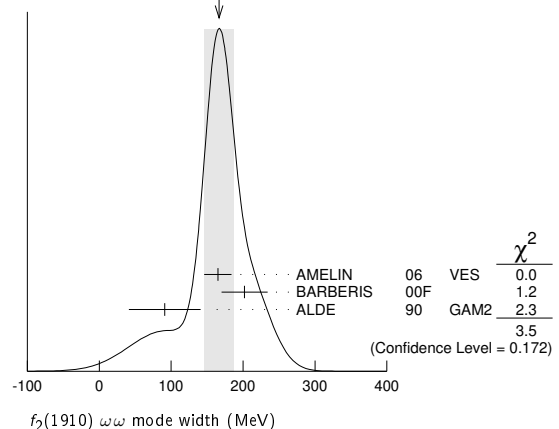
### $f_2(1910)$ WIDTH

#### $f_2(1910)$ ωω MODE

VALUE (MeV)	DOCUMENT ID	TECN	COMMENT
<b>167 ± 21 OUR AVERAGE</b> Error includes scale factor of 1.3. See the ideogram below.			
165 ± 19	<sup>1</sup> AMELIN	06 VES	36 π <sup>-</sup> p → ωωn
202 ± 32	BARBERIS	00F	450 pp → p <sub>f</sub> ωωp <sub>s</sub>
91 ± 50	ALDE	90	GAM2 38 π <sup>-</sup> p → ωωn

<sup>1</sup> Supersedes BELADIDZE 92b.

WEIGHTED AVERAGE  
167 ± 21 (Error scaled by 1.3)



#### $f_2(1910)$ ηη' MODE

VALUE (MeV)	DOCUMENT ID	TECN	COMMENT
<b>141 ± 41</b>			
	<sup>1</sup> BARBERIS	00A	450 pp → p <sub>f</sub> ηη'p <sub>s</sub>
• • • We do not use the following data for averages, fits, limits, etc. • • •			
271 ± 25	<sup>2</sup> ANISOVICH	00J	SPEC
90 ± 35	ALDE	91B	GAM2 38 π <sup>-</sup> p → ηη'n

<sup>1</sup> Also compatible with J<sup>PC</sup>=1<sup>-</sup>+.  
<sup>2</sup> Combined fit with ηη, ππ, and ηππ.

See key on page 999

# Meson Particle Listings

## $f_2(1910)$ , $a_0(1950)$ , $f_2(1950)$

### $f_2(1910) K^+ K^-$ MODE

VALUE (MeV)	DOCUMENT ID	TECN	COMMENT
120 ± 40	AMSLER 06	CBAR	1.64 $\bar{p}p \rightarrow K^+ K^- \pi^0$

### $f_2(1910)$ DECAY MODES

Mode	Fraction ( $\Gamma_i/\Gamma$ )
$\Gamma_1 \pi^0 \pi^0$	
$\Gamma_2 K^+ K^-$	seen
$\Gamma_3 K_S^0 K_S^0$	
$\Gamma_4 \eta \eta$	seen
$\Gamma_5 \omega \omega$	seen
$\Gamma_6 \eta \eta'$	seen
$\Gamma_7 \eta' \eta'$	
$\Gamma_8 \rho \rho$	seen
$\Gamma_9 a_2(1320) \pi$	seen
$\Gamma_{10} f_2(1270) \eta$	seen

### $f_2(1910)$ BRANCHING RATIOS

$\Gamma(K^+ K^-)/\Gamma_{total}$	DOCUMENT ID	TECN	COMMENT	$\Gamma_2/\Gamma$
seen	<sup>1</sup> AMSLER 06	CBAR	1.64 $\bar{p}p \rightarrow K^+ K^- \pi^0$	

<sup>1</sup> Tentative, could be  $f_2(1950)$ .

$\Gamma(\pi^0 \pi^0)/\Gamma(\eta \eta')$	DOCUMENT ID	TECN	COMMENT	$\Gamma_1/\Gamma_6$
<0.1	ALDE 89	GAM2	$38 \pi^- p \rightarrow \eta \eta' n$	

$\Gamma(K_S^0 K_S^0)/\Gamma(\eta \eta')$	DOCUMENT ID	TECN	COMMENT	$\Gamma_3/\Gamma_6$
<0.066	90	BALOSHIN 86	SPEC $40 \pi p \rightarrow K_S^0 K_S^0 n$	

$\Gamma(\eta \eta)/\Gamma(\eta \eta')$	DOCUMENT ID	TECN	COMMENT	$\Gamma_4/\Gamma_6$
<0.05	90	ALDE 91B	GAM2 $38 \pi^- p \rightarrow \eta \eta' n$	

$\Gamma(\omega \omega)/\Gamma(\eta \eta')$	DOCUMENT ID	COMMENT	$\Gamma_5/\Gamma_6$
2.6 ± 0.6	BARBERIS 00F	450 $p p \rightarrow p_f \omega p_S$	

$\Gamma(\eta' \eta')/\Gamma_{total}$	DOCUMENT ID	TECN	COMMENT	$\Gamma_7/\Gamma$
probably not seen possibly seen	BARBERIS 00A BELADIDZE 92D	00A VES	450 $p p \rightarrow p_f \eta' \eta' p_S$ 37 $\pi^- p \rightarrow \eta' \eta' n$	

$\Gamma(\rho \rho)/\Gamma(\omega \omega)$	DOCUMENT ID	COMMENT	$\Gamma_8/\Gamma_5$
2.6 ± 0.4	BARBERIS 00F	450 $p p \rightarrow p_f \omega p_S$	

$\Gamma(f_2(1270) \eta)/\Gamma(a_2(1320) \pi)$	DOCUMENT ID	TECN	COMMENT	$\Gamma_{10}/\Gamma_9$
0.09 ± 0.05	<sup>1</sup> ANISOVICH 11	SPEC	0.9-1.94 $p \bar{p}$	

<sup>1</sup> Reanalysis of ADOMEIT 96 and ANISOVICH 00E.

### $f_2(1910)$ REFERENCES

ANISOVICH 11	EPJ C71 1511	A.V. Anisovich et al.	(LOQM, RAL, PNPI)
AMELIN 06	PAN 69 690	D.V. Amelin et al.	(VES Collab.)
AMSLER 06	PL B639 165	C. Amstler et al.	(CBAR Collab.)
ANISOVICH 00E	PL B477 19	A.V. Anisovich et al.	
ANISOVICH 00J	PL B491 47	A.V. Anisovich et al.	(RAL, LOQM, PNPI+)
BARBERIS 00A	PL B471 429	D. Barberis et al.	(WA 102 Collab.)
BARBERIS 00F	PL B484 198	D. Barberis et al.	(WA 102 Collab.)
ADOMEIT 96	ZPHY C71 227	J. Adomeit et al.	(Crystal Barrel Collab.)
BELADIDZE 92B	ZPHY C54 367	G.M. Beladidze et al.	(VES Collab.)
BELADIDZE 92D	ZPHY C57 13	G.M. Beladidze et al.	(VES Collab.)
ALDE 91B	SJNP 54 455	D.M. Alde et al.	(SERP, BELG, LANL, LAPP+)
Also	Translated from YAF 54 751.		
ALDE 90	PL B276 375	D.M. Alde et al.	(BELG, SERP, KEK, LANL+)
ALDE 89	PL B241 600	D.M. Alde et al.	(SERP, BELG, LANL, LAPP+)
Also	PL B216 447	D.M. Alde et al.	(SERP, BELG, LANL, LAPP)
Also	SJNP 48 1035	D.M. Alde et al.	(BELG, SERP, LANL, LAPP)
Also	Translated from YAF 48 1724.		
BALOSHIN 86	SJNP 43 959	O.N. Baloshin et al.	(ITEP)
Also	Translated from YAF 43 1487.		

### $a_0(1950)$

$$I^G(J^{PC}) = 1^-(0^{++})$$

OMITTED FROM SUMMARY TABLE

Needs confirmation. Seen in  $\gamma \gamma \rightarrow \eta_c(1S) \rightarrow K \bar{K} \pi$  by LEES 16A with significance 2.5  $\sigma$  in  $K_S^0 K^\pm \pi^\mp$  and 4.2  $\sigma$  in  $K^+ K^- \pi^0$ .

### $a_0(1950)$ MASS

VALUE (MeV)	EVTs	DOCUMENT ID	TECN	COMMENT
1931 ± 14 ± 22	12k	<sup>1,2</sup> LEES	16A	BABR $\gamma \gamma \rightarrow \eta_c(1S) \rightarrow K \bar{K} \pi$
1949 ± 32 ± 76	8k	<sup>1</sup> LEES	16A	BABR $\gamma \gamma \rightarrow \eta_c(1S) \rightarrow K_S^0 K^\pm \pi^\mp$
1927 ± 15 ± 23	4k	<sup>1</sup> LEES	16A	BABR $\gamma \gamma \rightarrow \eta_c(1S) \rightarrow K^+ K^- \pi^0$

<sup>1</sup> From a model-independent partial wave analysis fit to a relativistic Breit-Wigner function with a floating width.  
<sup>2</sup> Weighted average of the  $K_S^0 K^\pm$  and  $K^+ K^-$  decay modes.

### $a_0(1950)$ WIDTH

VALUE (MeV)	EVTs	DOCUMENT ID	TECN	COMMENT
271 ± 22 ± 29	12k	<sup>1,2</sup> LEES	16A	BABR $\gamma \gamma \rightarrow \eta_c(1S) \rightarrow K \bar{K} \pi$
265 ± 36 ± 110	8k	<sup>1</sup> LEES	16A	BABR $\gamma \gamma \rightarrow \eta_c(1S) \rightarrow K_S^0 K^\pm \pi^\mp$
274 ± 28 ± 30	4k	<sup>1</sup> LEES	16A	BABR $\gamma \gamma \rightarrow \eta_c(1S) \rightarrow K^+ K^- \pi^0$

<sup>1</sup> From a model-independent partial wave analysis fit to a relativistic Breit-Wigner function with a floating mass.  
<sup>2</sup> Weighted average of the  $K_S^0 K^\pm$  and  $K^+ K^-$  decay modes.

### $a_0(1950)$ DECAY MODES

Mode	Fraction ( $\Gamma_i/\Gamma$ )
$\Gamma_1 K \bar{K}$	seen

### $a_0(1950)$ BRANCHING RATIOS

$\Gamma(K \bar{K})/\Gamma_{total}$	DOCUMENT ID	TECN	COMMENT	$\Gamma_1/\Gamma$
seen	12k	<sup>1</sup> LEES	16A	BABR $\gamma \gamma \rightarrow \eta_c(1S) \rightarrow K \bar{K} \pi$

<sup>1</sup> From a model-independent partial wave analysis.

### $a_0(1950)$ REFERENCES

LEES 16A PR D93 012005 J.P. Lees et al. (BABAR Collab.)

### $f_2(1950)$

$$I^G(J^{PC}) = 0^+(2^{++})$$

### $f_2(1950)$ MASS

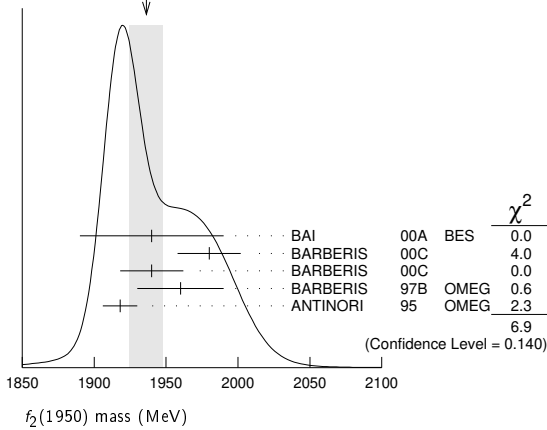
VALUE (MeV)	DOCUMENT ID	TECN	COMMENT
1936 ± 12 OUR AVERAGE			Error includes scale factor of 1.3. See the ideogram below.
1940 ± 50	BAI 00A	BES	$J/\psi \rightarrow \gamma(\pi^+ \pi^- \pi^+ \pi^-)$
1980 ± 22	<sup>1</sup> BARBERIS 00C		450 $p p \rightarrow p p 4 \pi$
1940 ± 22	<sup>2</sup> BARBERIS 00C		450 $p p \rightarrow p p 2 \pi 2 \pi^0$
1960 ± 30	BARBERIS 97B	OMEG	450 $p p \rightarrow p p 2(\pi^+ \pi^-)$
1918 ± 12	ANTINORI 95	OMEG	300,450 $p p \rightarrow p p 2(\pi^+ \pi^-)$
2038 <sup>+13+12</sup> <sub>-11-73</sub>	<sup>3</sup> UEHARA 09	BELL	10.6 $e^+ e^- \rightarrow e^+ e^- \pi^0 \pi^0$
1930 ± 25	<sup>4</sup> BINON 05	GAMS	33 $\pi^- p \rightarrow \eta \eta n$
1980 ± 2 ± 14	ABE 04	BELL	10.6 $e^+ e^- \rightarrow e^+ e^- K^+ K^-$
1867 ± 46	<sup>5</sup> AMSLER 02	CBAR	0.9 $\bar{p}p \rightarrow \pi^0 \eta \eta, \pi^0 \pi^0 \pi^0$
2010 ± 25	ANISOVICH 00J	SPEC	
1980 ± 50	ANISOVICH 99B	SPEC	1.35-1.94 $p \bar{p} \rightarrow \eta \eta \pi^0$
~ 1990	<sup>6</sup> OAKDEN 94	RVUE	0.36-1.55 $p \bar{p} \rightarrow \pi \pi$
1950 ± 15	<sup>7</sup> ASTON 91	LASS	11 $K^- p \rightarrow \Lambda K \bar{K} \pi \pi$

<sup>1</sup> Decaying into  $\pi^+ \pi^- 2 \pi^0$ .  
<sup>2</sup> Decaying into  $2(\pi^+ \pi^-)$ .  
<sup>3</sup> Taking into account  $f_4(2050)$ .  
<sup>4</sup> First solution, PWA is ambiguous.  
<sup>5</sup> T-matrix pole.  
<sup>6</sup> From solution B of amplitude analysis of data on  $p \bar{p} \rightarrow \pi \pi$ . See however KLOET 96 who fit  $\pi^+ \pi^-$  only and find waves only up to  $J = 3$  to be important but not significantly resonant.  
<sup>7</sup> Cannot determine spin to be 2.

# Meson Particle Listings

## $f_2(1950)$ , $a_4(1970)$

WEIGHTED AVERAGE  
1936±12 (Error scaled by 1.3)



### $f_2(1950)$ WIDTH

VALUE (MeV)	DOCUMENT ID	TECN	COMMENT
<b>464±24 OUR AVERAGE</b>			
380 <sup>+120</sup> <sub>-90</sub>	BAI	00A	BES $J/\psi \rightarrow \gamma(\pi^+\pi^-\pi^+\pi^-)$
520±50	<sup>8</sup> BARBERIS	00c	450 $pp \rightarrow pp4\pi$
485±55	<sup>9</sup> BARBERIS	00c	450 $pp \rightarrow pp4\pi$
460±40	BARBERIS	97B	OMEG 450 $pp \rightarrow pp2(\pi^+\pi^-)$
390±60	ANTINORI	95	OMEG 300,450 $pp \rightarrow pp2(\pi^+\pi^-)$
441 <sup>+27+28</sup> <sub>-25-192</sub>	<sup>10</sup> UEHARA	09	BELL 10.6 $e^+e^- \rightarrow e^+e^-\pi^0\pi^0$
450±50	<sup>11</sup> BINON	05	GAMS 33 $\pi^-p \rightarrow \eta\eta n$
297±12±6	ABE	04	BELL 10.6 $e^+e^- \rightarrow e^+e^-K^+K^-$
385±58	<sup>12</sup> AMSLER	02	CBAR 0.9 $\bar{p}p \rightarrow \pi^0\eta\eta, \pi^0\pi^0\pi^0$
495±35	ANISOVICH	00j	SPEC
500±100	ANISOVICH	99B	SPEC 1.35-1.94 $\bar{p}p \rightarrow \eta\eta\pi^0$
~100	<sup>13</sup> OAKDEN	94	RVUE 0.36-1.55 $\bar{p}p \rightarrow \pi\pi$
25±50	<sup>14</sup> ASTON	91	LASS 11 $K^-p \rightarrow \Lambda K\bar{K}\pi\pi$

- • • We do not use the following data for averages, fits, limits, etc. • • •
- <sup>8</sup> Decaying into  $\pi^+\pi^-\pi^0$ .
- <sup>9</sup> Decaying into  $2(\pi^+\pi^-)$ .
- <sup>10</sup> Taking into account  $f_4(2050)$ .
- <sup>11</sup> First solution, PWA is ambiguous.
- <sup>12</sup> T-matrix pole.
- <sup>13</sup> From solution B of amplitude analysis of data on  $\bar{p}p \rightarrow \pi\pi$ . See however KLOET 96 who fit  $\pi^+\pi^-$  only and find waves only up to  $J=3$  to be important but not significantly resonant.
- <sup>14</sup> Cannot determine spin to be 2.

### $f_2(1950)$ DECAY MODES

Mode	Fraction ( $\Gamma_i/\Gamma$ )
$\Gamma_1$ $K^*(892)\bar{K}^*(892)$	seen
$\Gamma_2$ $\pi\pi$	
$\Gamma_3$ $\pi^+\pi^-$	seen
$\Gamma_4$ $\pi^0\pi^0$	seen
$\Gamma_5$ $4\pi$	seen
$\Gamma_6$ $\pi^+\pi^-\pi^+\pi^-$	
$\Gamma_7$ $a_2(1320)\pi$	
$\Gamma_8$ $f_2(1270)\pi\pi$	
$\Gamma_9$ $\eta\eta$	seen
$\Gamma_{10}$ $K\bar{K}$	seen
$\Gamma_{11}$ $\gamma\gamma$	seen
$\Gamma_{12}$ $\rho\bar{\rho}$	seen

### $f_2(1950)$ $\Gamma(i)\Gamma(\gamma\gamma)/\Gamma(\text{total})$

VALUE (eV)	DOCUMENT ID	TECN	COMMENT	$\Gamma_{10}\Gamma_{11}/\Gamma$
<b>122±4±26</b>	<sup>15</sup> ABE	04	BELL 10.6 $e^+e^- \rightarrow e^+e^-K^+K^-$	

<sup>15</sup> Assuming spin 2.

### $\Gamma(\pi\pi) \times \Gamma(\gamma\gamma)/\Gamma_{\text{total}}$ $\Gamma_2\Gamma_{11}/\Gamma$

VALUE	DOCUMENT ID	TECN	COMMENT
<b>162<sup>+69+1137</sup><sub>-42-204</sub></b>	<sup>16</sup> UEHARA	09	BELL 10.6 $e^+e^- \rightarrow e^+e^-\pi^0\pi^0$

<sup>16</sup> Taking into account  $f_4(2050)$ .

### $f_2(1950)$ BRANCHING RATIOS

$\Gamma(K^*(892)\bar{K}^*(892))/\Gamma_{\text{total}}$	$\Gamma_1/\Gamma$
seen	ASTON 91 LASS 0 11 $K^-p \rightarrow \Lambda K\bar{K}\pi\pi$

### $\Gamma(a_2(1320)\pi)/\Gamma_{\text{total}}$ $\Gamma_7/\Gamma$

VALUE	DOCUMENT ID	TECN	COMMENT
not seen	BARBERIS	00B	450 $pp \rightarrow p_f\eta\pi^+\pi^-\rho_S$
not seen	BARBERIS	00c	450 $pp \rightarrow p_f4\pi\rho_S$
possibly seen	BARBERIS	97B	OMEG 450 $pp \rightarrow pp2(\pi^+\pi^-)$

### $\Gamma(\eta\eta)/\Gamma(4\pi)$ $\Gamma_9/\Gamma_5$

VALUE	CL%	DOCUMENT ID	COMMENT
<b>&lt;5.0 × 10<sup>-3</sup></b>	90	BARBERIS	00E 450 $pp \rightarrow p_f\eta\eta\rho_S$

### $\Gamma(\eta\eta)/\Gamma(\pi^+\pi^-)$ $\Gamma_9/\Gamma_3$

VALUE	DOCUMENT ID	TECN	COMMENT
<b>0.14±0.05</b>	AMSLER	02	CBAR 0.9 $\bar{p}p \rightarrow \pi^0\eta\eta, \pi^0\pi^0\pi^0$

### $\Gamma(\rho\bar{\rho})/\Gamma_{\text{total}}$ $\Gamma_{12}/\Gamma$

VALUE	EVTs	DOCUMENT ID	TECN	COMMENT
seen	111	ALEXANDER	10	CLEO $\psi(2S) \rightarrow \gamma\rho\bar{\rho}$

### $f_2(1950)$ REFERENCES

ALEXANDER	10	PR D82 092002	J.P. Alexander et al.	(CLEO Collab.)
UEHARA	09	PR D79 052009	S. Uehara et al.	(BELLE Collab.)
BINON	05	PAN 68 960	F. Binon et al.	
		Translated from YAF 68 998.		
ABE	04	EPJ C32 323	K. Abe et al.	(BELLE Collab.)
AMSLER	02	EPJ C23 29	C. Amisler et al.	
ANISOVICH	00j	PL B491 47	A.V. Anisovich et al.	(RAL, LOQM, FNPI+)
BAI	00A	PL B472 207	J.Z. Bai et al.	(BES Collab.)
BARBERIS	00B	PL B471 435	D. Barberis et al.	(WA 102 Collab.)
BARBERIS	00c	PL B471 440	D. Barberis et al.	(WA 102 Collab.)
BARBERIS	00E	PL B479 59	D. Barberis et al.	(WA 102 Collab.)
ANISOVICH	99B	PL B449 154	A.V. Anisovich et al.	
BARBERIS	97B	PL B413 217	D. Barberis et al.	(WA 102 Collab.)
KLOET	96	PR D53 6120	W.M. Kloet, F. Myhrer	(RUTG, NORD)
ANTINORI	95	PL B353 589	F. Antinori et al.	(ATHU, BARI, BIRN+JP)
OAKDEN	94	NP A574 731	M.N. Oakden, M.R. Pennington	(DURH)
ASTON	91	NPBS B21 5	D. Aston et al.	(LASS Collab.)

## $a_4(1970)$

$$I^G(J^{PC}) = 1^-(4^{++})$$

was  $a_4(2040)$

### $a_4(1970)$ MASS

VALUE (MeV)	EVTs	DOCUMENT ID	TECN	CHG	COMMENT
<b>1967±16 OUR AVERAGE</b>		Error includes scale factor of 2.1. See the ideogram below.			
1935 <sup>+11</sup> <sub>-13</sub>	46M	<sup>1</sup> AGHASYAN	18B	COMP	190 $\pi^-p \rightarrow \pi^-\pi^+\pi^-p$
1900 <sup>+80</sup> <sub>-20</sub>		ADOLPH	15	COMP	191 $\pi^-p \rightarrow \eta^{(\prime)}\pi^-p$
1985±10±13	145k	LU	05	B852	18 $\pi^-p \rightarrow \omega\pi^-\pi^0p$
1996±25±43		CHUNG	02	B852	18.3 $\pi^-p \rightarrow 3\pi p$
2000±40 <sup>+60</sup> <sub>-20</sub>		IVANOV	01	B852	18 $\pi^-p \rightarrow \eta'\pi^-p$
2010±20		<sup>2</sup> DONSKOV	96	GAM2 0	38 $\pi^-p \rightarrow \eta\pi^0 n$
2040±30		<sup>3</sup> CLELAND	82B	SPEC ±	50 $\pi p \rightarrow K_S^0 K^\pm p$
1885±13 <sup>+50</sup> <sub>-2</sub>	420k	<sup>4</sup> ALEKSEEV	10	COMP	190 $\pi^-p \rightarrow \pi^-\pi^-\pi^+\rho b'$
2004±6	80k	<sup>5</sup> UMAN	06	E835	5.2 $\bar{p}p \rightarrow \eta\eta\pi^0$
2005 <sup>+25</sup> <sub>-45</sub>		<sup>6</sup> ANISOVICH	01F	SPEC	2.0 $\bar{p}p \rightarrow 3\pi^0, \pi^0\eta, \pi^0\eta'$
1944±8±50		<sup>7</sup> AMELIN	99	VES	37 $\pi^-A \rightarrow \omega\pi^-\pi^0 A^*$
1903±10		<sup>8</sup> BALDI	78	SPEC	10 $\pi^-p \rightarrow \rho K_S^0 K^-$
2030±50		<sup>9</sup> CORDEN	78c	OMEG 0	15 $\pi^-p \rightarrow 3\pi n$

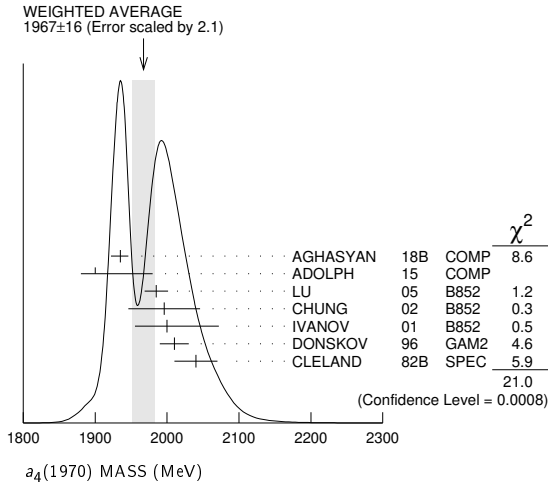
- • • We do not use the following data for averages, fits, limits, etc. • • •
- <sup>1</sup> Statistical error negligible.
- <sup>2</sup> From a simultaneous fit to the  $G_+$  and  $G_0$  wave intensities.
- <sup>3</sup> From an amplitude analysis.
- <sup>4</sup> Superseded by AGHASYAN 2018B.
- <sup>5</sup> Statistical error only.
- <sup>6</sup> From the combined analysis of ANISOVICH 99c, ANISOVICH 99e, and ANISOVICH 01F.

See key on page 999

# Meson Particle Listings

## $a_4(1970), \rho_3(1990), \pi_2(2005)$

<sup>7</sup> May be a different state.  
<sup>8</sup> From a fit to the  $Y_8^0$  moment. Limited by phase space.  
<sup>9</sup>  $J^P = 4^+$  is favored, though  $J^P = 2^+$  cannot be excluded.



### $a_4(1970)$ WIDTH

VALUE (MeV)	EVTS	DOCUMENT ID	TECN	CHG	COMMENT
<b><math>324 \pm \frac{15}{18}</math> OUR AVERAGE</b>					
$333 \pm \frac{16}{21}$	46M	<sup>1</sup> AGHASYAN	18B	COMP	$190 \pi^- p \rightarrow \pi^- \pi^+ \pi^- p$
$300 \pm \frac{80}{100}$		ADOLPH	15	COMP	$191 \pi^- p \rightarrow \eta^{(\prime)} \pi^- p$
$231 \pm \frac{30 \pm 46}{81 \pm 85}$	145k	LU	05	B852	$18 \pi^- p \rightarrow \omega \pi^- \pi^0 p$
$298 \pm \frac{81 \pm 85}{50}$		CHUNG	02	B852	$18.3 \pi^- p \rightarrow 3\pi p$
$350 \pm \frac{100 \pm 70}{50}$		IVANOV	01	B852	$18 \pi^- p \rightarrow \eta' \pi^- p$
$370 \pm 80$		<sup>2</sup> DONSKOV	96	GAM2 0	$38 \pi^- p \rightarrow \eta \pi^0 n$
$380 \pm 150$		<sup>3</sup> CLELAND	82B	SPEC $\pm$	$50 \pi^- p \rightarrow K_S^0 K^\pm p$
• • • We do not use the following data for averages, fits, limits, etc. • • •					
$294 \pm \frac{25 \pm 46}{19}$	420k	<sup>4</sup> ALEKSEEV	10	COMP	$190 \pi^- p \rightarrow \pi^- \pi^- \pi^+ P b'$
$401 \pm 16$	80k	<sup>5</sup> UMAN	06	E835	$5.2 \bar{p} p \rightarrow \eta \eta \pi^0$
$180 \pm 30$		<sup>6</sup> ANISOVICH	01F	SPEC	$2.0 \bar{p} p \rightarrow 3\pi^0, \pi^0 \eta, \pi^0 \eta'$
$324 \pm 26 \pm 75$		<sup>7</sup> AMELIN	99	VES	$37 \pi^- A \rightarrow \omega \pi^- \pi^0 A^*$
$166 \pm 43$		<sup>8</sup> BALDI	78	SPEC $-$	$10 \pi^- p \rightarrow \rho K_S^0 K^-$
$510 \pm 200$		<sup>9</sup> CORDEN	78C	OMEG 0	$15 \pi^- p \rightarrow 3\pi n$

<sup>1</sup> Statistical error negligible.  
<sup>2</sup> From a simultaneous fit to the  $G_+$  and  $G_0$  wave intensities.  
<sup>3</sup> From an amplitude analysis.  
<sup>4</sup> Superseded by AGHASYAN 2018B.  
<sup>5</sup> Statistical error only.  
<sup>6</sup> From the combined analysis of ANISOVICH 99C, ANISOVICH 99E, and ANISOVICH 01F.  
<sup>7</sup> May be a different state.  
<sup>8</sup> From a fit to the  $Y_8^0$  moment. Limited by phase space.  
<sup>9</sup>  $J^P = 4^+$  is favored, though  $J^P = 2^+$  cannot be excluded.

### $a_4(1970)$ DECAY MODES

Mode	Fraction ( $\Gamma_i/\Gamma$ )
$\Gamma_1$ $K\bar{K}$	seen
$\Gamma_2$ $\pi^+ \pi^- \pi^0$	seen
$\Gamma_3$ $\rho\pi$	seen
$\Gamma_4$ $f_2(1270)\pi$	seen
$\Gamma_5$ $\omega \pi^- \pi^0$	seen
$\Gamma_6$ $\omega\rho$	seen
$\Gamma_7$ $\eta\pi$	seen
$\Gamma_8$ $\eta'(958)\pi$	seen

### $a_4(1970)$ BRANCHING RATIOS

$\Gamma(K\bar{K})/\Gamma_{total}$					$\Gamma_1/\Gamma$
VALUE	DOCUMENT ID	TECN	CHG	COMMENT	
seen	BALDI	78	SPEC $\pm$	$10 \pi^- p \rightarrow K_S^0 K^- p$	
$\Gamma(\pi^+ \pi^- \pi^0)/\Gamma_{total}$					$\Gamma_2/\Gamma$
VALUE	DOCUMENT ID	TECN	CHG	COMMENT	
seen	CORDEN	78C	OMEG 0	$15 \pi^- p \rightarrow 3\pi n$	

### $\Gamma(\rho\pi)/\Gamma(f_2(1270)\pi)$

VALUE	EVTS	DOCUMENT ID	TECN	COMMENT	$\Gamma_3/\Gamma_4$
<b><math>1.7 \pm \frac{0.9}{0.8}</math> OUR AVERAGE</b>				Error includes scale factor of 3.7.	
$2.9 \pm \frac{0.6}{0.4}$	46M	<sup>1</sup> AGHASYAN	18B	COMP	$190 \pi^- p \rightarrow \pi^- \pi^+ \pi^- p$
$1.1 \pm 0.2 \pm 0.2$		CHUNG	02	B852	$18.3 \pi^- p \rightarrow 3\pi p$
<sup>1</sup> Statistical error negligible.					

### $\Gamma(\eta\pi)/\Gamma_{total}$

VALUE	DOCUMENT ID	TECN	CHG	COMMENT	$\Gamma_7/\Gamma$
seen	DONSKOV	96	GAM2 0	$38 \pi^- p \rightarrow \eta \pi^0 n$	

### $\Gamma(\eta'(958)\pi)/\Gamma(\eta\pi)$

VALUE	DOCUMENT ID	TECN	COMMENT	$\Gamma_8/\Gamma_7$	
<b><math>0.23 \pm 0.07</math></b>	ADOLPH	15	COMP	$191 \pi^- p \rightarrow \eta^{(\prime)} \pi^- p$	

### $\Gamma(\omega\rho)/\Gamma_{total}$

VALUE	EVTS	DOCUMENT ID	TECN	COMMENT	$\Gamma_6/\Gamma$
seen	145k	LU	05	B852	$18 \pi^- p \rightarrow \omega \pi^- \pi^0 p$

### $a_4(1970)$ REFERENCES

AGHASYAN	18B	PR D98 092003	M. Aghasyan et al.	(COMPASS Collab.)
ADOLPH	15	PL B740 303	M. Adolph et al.	(COMPASS Collab.)
ALEKSEEV	10	PRL 104 241803	M.G. Aleksev et al.	(COMPASS Collab.)
UMAN	06	PR D73 052009	I. Uman et al.	(FNAL E835)
LU	05	PRL 94 032002	M. Lu et al.	(BNL E852 Collab.)
CHUNG	02	PR D65 072001	S.U. Chung et al.	(BNL E852 Collab.)
ANISOVICH	01F	PL B517 261	A.V. Anisovich et al.	
IVANOV	01	PRL 86 3977	E.I. Ivanov et al.	(BNL E852 Collab.)
AMELIN	99	PAN 62 445	D.V. Amelin et al.	(VES Collab.)
Translated from YAF 62 487.				
ANISOVICH	99C	PL B452 173	A.V. Anisovich et al.	
ANISOVICH	99E	PL B452 187	A.V. Anisovich et al.	
DONSKOV	96	PAN 59 982	S.V. Donskov et al.	(GAMS Collab.) IJGPC
Translated from YAF 59 1027.				
CLELAND	82B	NP B208 228	W.E. Cleland et al.	(DURH, GEVA, LAUS+)
BALDI	78	PL 74B 413	R. Baldi et al.	(GEVA) JP
CORDEN	78C	NP B136 77	M.J. Corden et al.	(BIRM, RHEL, TELA+JP)

### $\rho_3(1990)$

$$I^G(J^{PC}) = 1^+(3^{--})$$

OMITTED FROM SUMMARY TABLE

### $\rho_3(1990)$ MASS

VALUE (MeV)	DOCUMENT ID	TECN	COMMENT
• • • We do not use the following data for averages, fits, limits, etc. • • •			
$1982 \pm 14$	<sup>1</sup> ANISOVICH	02	SPEC $0.6-1.9 \rho \bar{p} \rightarrow \omega \pi^0, \omega \eta \pi^0, \pi^+ \pi^-$
$\sim 2007$	HASAN	94	RVUE $\bar{p} p \rightarrow \pi \pi$
<sup>1</sup> From the combined analysis of ANISOVICH 00J, ANISOVICH 01D, ANISOVICH 01E, and ANISOVICH 02.			

### $\rho_3(1990)$ WIDTH

VALUE (MeV)	DOCUMENT ID	TECN	COMMENT
• • • We do not use the following data for averages, fits, limits, etc. • • •			
$188 \pm 24$	<sup>2</sup> ANISOVICH	02	SPEC $0.6-1.9 \rho \bar{p} \rightarrow \omega \pi^0, \omega \eta \pi^0, \pi^+ \pi^-$
$\sim 287$	HASAN	94	RVUE $\bar{p} p \rightarrow \pi \pi$
<sup>2</sup> From the combined analysis of ANISOVICH 00J, ANISOVICH 01D, ANISOVICH 01E, and ANISOVICH 02.			

### $\rho_3(1990)$ REFERENCES

ANISOVICH	02	PL B542 8	A.V. Anisovich et al.
ANISOVICH	01D	PL B508 6	A.V. Anisovich et al.
ANISOVICH	01E	PL B513 281	A.V. Anisovich et al.
ANISOVICH	00J	PL B491 47	A.V. Anisovich et al.
HASAN	94	PL B334 215	A. Hasan, D.V. Bugg

### $\pi_2(2005)$

$$I^G(J^{PC}) = 1^-(2^{-+})$$

OMITTED FROM SUMMARY TABLE

### $\pi_2(2005)$ MASS

VALUE (MeV)	EVTS	DOCUMENT ID	TECN	COMMENT	
<b><math>1963 \pm \frac{17}{27}</math> OUR AVERAGE</b>					
$1962 \pm \frac{17}{29}$	46M	<sup>1</sup> AGHASYAN	18B	COMP	$190 \pi^- p \rightarrow \pi^- \pi^+ \pi^- p$
$1974 \pm 14 \pm 83$	145k	LU	05	B852	$18 \pi^- p \rightarrow \omega \pi^- \pi^0 p$
$2005 \pm 15$		ANISOVICH	01F	SPEC	$2.0 \bar{p} p \rightarrow 3\pi^0, \pi^0 \eta, \pi^0 \eta'$
<sup>1</sup> Statistical uncertainty negligible.					

# Meson Particle Listings

$\pi_2(2005)$ ,  $f_2(2010)$ ,  $f_0(2020)$

## $\pi_2(2005)$ WIDTH

VALUE (MeV)	EVTs	DOCUMENT ID	TECN	COMMENT
<b><math>370^{+16}_{-120}</math></b>	<b>46M</b>	<sup>1</sup> AGHASYAN	18B COMP	$190 \pi^- p \rightarrow \pi^- \pi^+ \pi^- p$
<b><math>341 \pm 61 \pm 139</math></b>	<b>145k</b>	LU	05 B852	$18 \pi^- p \rightarrow \omega \pi^- \pi^0 p$
• • • We do not use the following data for averages, fits, limits, etc. • • •				
<b><math>200 \pm 40</math></b>		ANISOVICH	01F SPEC	$2.0 \bar{p} p \rightarrow 3\pi^0, \pi^0 \eta, \pi^0 \eta'$
<sup>1</sup> Statistical uncertainty negligible.				

## $\pi_2(2005)$ DECAY MODES

Mode	Fraction ( $\Gamma_i/\Gamma$ )
$\Gamma_1 \pi^- \pi^+ \pi^-$	seen
$\Gamma_2 \omega \pi^0 \pi^-$	seen

## $\pi_2(2005)$ BRANCHING RATIOS

$\Gamma(\pi^- \pi^+ \pi^-)/\Gamma_{total}$	$\Gamma_1/\Gamma$		
VALUE	DOCUMENT ID	TECN	COMMENT
seen	AGHASYAN	18B COMP	$190 \pi^- p \rightarrow \pi^- \pi^+ \pi^- p$
$\Gamma(\omega \pi^0 \pi^-)/\Gamma_{total}$	$\Gamma_2/\Gamma$		
VALUE	DOCUMENT ID	TECN	COMMENT
seen	LU	05 B852	$18 \pi^- p \rightarrow \omega \pi^- \pi^0 p$

## $\pi_2(2005)$ REFERENCES

AGHASYAN	18B	PR D98 092003	M. Aghasyan et al.	(COMPASS Collab.)
LU	05	PRL 94 032002	M. Lu et al.	(BNL E852 Collab.)
ANISOVICH	01F	PL B517 261	A.V. Anisovich et al.	

## $f_2(2010)$

$$J^G(J^{PC}) = 0^+(2^{++})$$

## $f_2(2010)$ MASS

VALUE (MeV)	DOCUMENT ID	TECN	COMMENT
<b><math>2011^{+62}_{-76}</math></b>	<sup>1</sup> ETKIN	88 MPS	$22 \pi^- p \rightarrow \phi \phi n$
• • • We do not use the following data for averages, fits, limits, etc. • • •			
$2005 \pm 12$	VLADIMIRSK...06	SPEC	$40 \pi^- p \rightarrow K_S^0 K_S^0 n$
$1980 \pm 20$	<sup>2</sup> BOLONKIN	88 SPEC	$40 \pi^- p \rightarrow K_S^0 K_S^0 n$
$2050^{+90}_{-50}$	ETKIN	85 MPS	$22 \pi^- p \rightarrow 2\phi n$
$2120^{+20}_{-120}$	LINDENBAUM	84 RVUE	
$2160 \pm 50$	ETKIN	82 MPS	$22 \pi^- p \rightarrow 2\phi n$

<sup>1</sup>Includes data of ETKIN 85. The percentage of the resonance going into  $\phi \phi 2^{++} S_2$ ,  $D_2$ , and  $D_0$  is  $98^{+1}_{-3}$ ,  $0^{+1}_{-0}$ , and  $2^{+2}_{-1}$ , respectively.  
<sup>2</sup>Statistically very weak, only 1.4 s.d.

## $f_2(2010)$ WIDTH

VALUE (MeV)	DOCUMENT ID	TECN	COMMENT
<b><math>202^{+67}_{-62}</math></b>	<sup>3</sup> ETKIN	88 MPS	$22 \pi^- p \rightarrow \phi \phi n$
• • • We do not use the following data for averages, fits, limits, etc. • • •			
$209 \pm 32$	VLADIMIRSK...06	SPEC	$40 \pi^- p \rightarrow K_S^0 K_S^0 n$
$145 \pm 50$	<sup>4</sup> BOLONKIN	88 SPEC	$40 \pi^- p \rightarrow K_S^0 K_S^0 n$
$200^{+160}_{-50}$	ETKIN	85 MPS	$22 \pi^- p \rightarrow 2\phi n$
$300^{+150}_{-50}$	LINDENBAUM	84 RVUE	
$310 \pm 70$	ETKIN	82 MPS	$22 \pi^- p \rightarrow 2\phi n$

<sup>3</sup>Includes data of ETKIN 85.  
<sup>4</sup>Statistically very weak, only 1.4 s.d.

## $f_2(2010)$ DECAY MODES

Mode	Fraction ( $\Gamma_i/\Gamma$ )
$\Gamma_1 \phi \phi$	seen
$\Gamma_2 K \bar{K}$	seen

## $f_2(2010)$ BRANCHING RATIOS

$\Gamma(K \bar{K})/\Gamma_{total}$	$\Gamma_2/\Gamma$		
VALUE	DOCUMENT ID	TECN	COMMENT
seen	VLADIMIRSK...06	SPEC	$40 \pi^- p \rightarrow K_S^0 K_S^0 n$

## $f_2(2010)$ REFERENCES

VLADIMIRSK...06	PAN 69 493	V.V. Vladimirov et al.	(ITEP, Moscow)
	Translated from YAF 69 515.		
BOLONKIN	88 NP B309 426	B.V. Bolonkin et al.	(ITEP, SERP)
ETKIN	88 PL B201 568	A. Etkin et al.	(BNL, CUNY)
ETKIN	85 PL 165B 217	A. Etkin et al.	(BNL, CUNY)
LINDENBAUM	84 CNPP 13 285	S.J. Lindenbaum	(CUNY)
ETKIN	82 PRL 49 1620	A. Etkin et al.	(BNL, CUNY)
Also	Brighton Conf. 351	S.J. Lindenbaum	(BNL, CUNY)

## $f_0(2020)$

$$J^G(J^{PC}) = 0^+(0^{++})$$

OMITTED FROM SUMMARY TABLE  
 Needs confirmation.

## $f_0(2020)$ MASS

VALUE (MeV)	EVTs	DOCUMENT ID	TECN	COMMENT
<b><math>1992 \pm 16</math></b>		<sup>1,2</sup> BARBERIS	00C	$450 pp \rightarrow p_f 4\pi p_s$
• • • We do not use the following data for averages, fits, limits, etc. • • •				
$1910 \pm 50$		<sup>3</sup> ROPERTZ	18 RVUE	$\bar{B}_S^0 \rightarrow J/\psi(\pi^+ \pi^- / K^+ K^-)$
$2037 \pm 8$	80k	<sup>4</sup> UMAN	06 E835	$5.2 \bar{p} p \rightarrow \eta \eta \pi^0$
$2040 \pm 38$		ANISOVICH	00J SPEC	
$2010 \pm 60$		ALDE	98 GAM4	$100 \pi^- p \rightarrow \pi^0 \pi^0 n$
$2020 \pm 35$		BARBERIS	97B OMEG	$450 pp \rightarrow p p 2(\pi^+ \pi^-)$

<sup>1</sup>Average between  $\pi^+ \pi^- 2\pi^0$  and  $2(\pi^+ \pi^-)$ .  
<sup>2</sup>T-matrix pole.  
<sup>3</sup>T-matrix pole of 3 channel unitary model fit to data from AAIJ 14Br and AAIJ 17v extracted using Pade approximants.  
<sup>4</sup>Statistical error only.

## $f_0(2020)$ WIDTH

VALUE (MeV)	EVTs	DOCUMENT ID	TECN	COMMENT
<b><math>442 \pm 60</math></b>		<sup>1,2</sup> BARBERIS	00C	$450 pp \rightarrow p_f 4\pi p_s$
• • • We do not use the following data for averages, fits, limits, etc. • • •				
$400 \pm 80$		<sup>3</sup> ROPERTZ	18 RVUE	$\bar{B}_S^0 \rightarrow J/\psi(\pi^+ \pi^- / K^+ K^-)$
$296 \pm 17$	80k	<sup>4</sup> UMAN	06 E835	$5.2 \bar{p} p \rightarrow \eta \eta \pi^0$
$405 \pm 40$		ANISOVICH	00J SPEC	
$240 \pm 100$		ALDE	98 GAM4	$100 \pi^- p \rightarrow \pi^0 \pi^0 n$
$410 \pm 50$		BARBERIS	97B OMEG	$450 pp \rightarrow p p 2(\pi^+ \pi^-)$

<sup>1</sup>Average between  $\pi^+ \pi^- 2\pi^0$  and  $2(\pi^+ \pi^-)$ .  
<sup>2</sup>T-matrix pole.  
<sup>3</sup>T-matrix pole of 3 channel unitary model fit to data from AAIJ 14Br and AAIJ 17v extracted using Pade approximants.  
<sup>4</sup>Statistical error only.

## $f_0(2020)$ DECAY MODES

Mode	Fraction ( $\Gamma_i/\Gamma$ )
$\Gamma_1 \rho \pi \pi$	seen
$\Gamma_2 \pi^0 \pi^0$	seen
$\Gamma_3 \rho \rho$	seen
$\Gamma_4 \omega \omega$	seen
$\Gamma_5 \eta \eta$	seen

## $f_0(2020)$ BRANCHING RATIOS

$\Gamma(\rho \rho)/\Gamma(\omega \omega)$	$\Gamma_3/\Gamma_4$		
VALUE	DOCUMENT ID	TECN	COMMENT
$\sim 3$	BARBERIS	00F	$450 pp \rightarrow p_f \omega \omega p_s$
$\Gamma(\eta \eta)/\Gamma_{total}$	$\Gamma_5/\Gamma$		
VALUE	DOCUMENT ID	TECN	COMMENT
seen	UMAN	06 E835	$5.2 \bar{p} p \rightarrow \eta \eta \pi^0$

## $f_0(2020)$ REFERENCES

ROPERTZ	18	EPJ C78 1000	S. Ropertz, C. Hanhart, B. Kubis	(BONN, JULI)
AAIJ	17V	JHEP 1708 037	R. Aaij et al.	(LHCb Collab.)
AAIJ	14BR	PR D89 092006	R. Aaij et al.	(LHCb Collab.)
UMAN	06	PR D73 052009	L. Uman et al.	(FNAL E835)
ANISOVICH	00J	PL B491 47	A.V. Anisovich et al.	(RAL, LOQM, PNPI+)
BARBERIS	00C	PL B471 440	D. Barberis et al.	(WA 102 Collab.)
BARBERIS	00F	PL B484 198	D. Barberis et al.	(WA 102 Collab.)
ALDE	98	EPJ A3 361	D. Alde et al.	(GAM4 Collab.)
Also	PAN	62 405	D. Alde et al.	(GAMS Collab.)
BARBERIS	97B	PL B413 217	D. Barberis et al.	(WA 102 Collab.)
		Translated from YAF 62 446.		

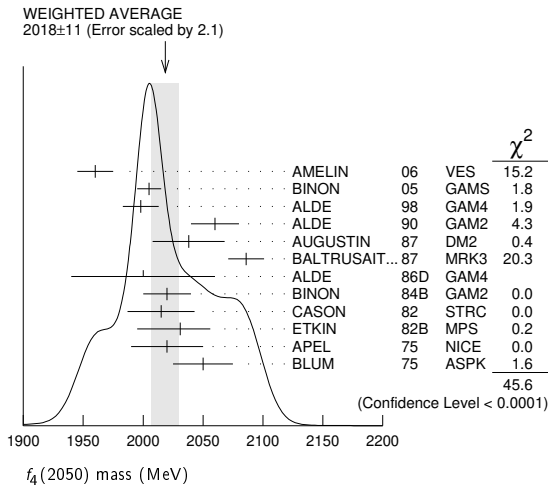
$f_4(2050)$

$I^G(J^{PC}) = 0^+(4^{++})$

$f_4(2050)$  MASS

VALUE (MeV)	EVTs	DOCUMENT ID	TECN	COMMENT
<b>2018±11 OUR AVERAGE</b>		Error includes scale factor of 2.1. See the ideogram below.		
1960±15		AMELIN 06	VES	$36 \pi^- p \rightarrow \omega \omega n$
2005±10	1	BINON 05	GAMS	$33 \pi^- p \rightarrow \eta \eta n$
1998±15		ALDE 98	GAM4	$100 \pi^- p \rightarrow \pi^0 \pi^0 n$
2060±20		ALDE 90	GAM2	$38 \pi^- p \rightarrow \omega \omega n$
2038±30		AUGUSTIN 87	DM2	$J/\psi \rightarrow \gamma \pi^+ \pi^-$
2086±15		BALTRUSAIT...87	MRK3	$J/\psi \rightarrow \gamma \pi^+ \pi^-$
2000±60		ALDE 86D	GAM4	$100 \pi^- p \rightarrow n2\eta$
2020±20	40k	BINON 84B	GAM2	$38 \pi^- p \rightarrow n2\pi^0$
2015±28		CASON 82	STRC	$8 \pi^+ p \rightarrow \Delta^{++} \pi^0 \pi^0$
2031 <sup>+25</sup> <sub>-36</sub>		ETKIN 82B	MPS	$23 \pi^- p \rightarrow n2K^0_S$
2020±30	700	APEL 75	NICE	$40 \pi^- p \rightarrow n2\pi^0$
2050±25		BLUM 75	ASPK	$18.4 \pi^- p \rightarrow nK^+ K^-$
1966±25		4 ANISOVICH 09	RVUE	$0.0 \bar{p} p, \pi N$
1885 <sup>+14+218</sup> <sub>-13-25</sub>		5 UEHARA 09	BELL	$10.6 e^+ e^- \rightarrow e^+ e^- \pi^0 \pi^0$
2018± 6		ANISOVICH 00j	SPEC	$2.0 \bar{p} p \rightarrow \eta \pi^0 \pi^0, \pi^0 \pi^0,$ $\eta \eta, \eta \eta', \pi \pi$
~ 2000		6 MARTIN 98	RVUE	$N\bar{N} \rightarrow \pi \pi$
~ 2010		7 MARTIN 97	RVUE	$N\bar{N} \rightarrow \pi \pi$
~ 2040		8 OAKDEN 94	RVUE	$0.36-1.55 \bar{p} p \rightarrow \pi \pi$
~ 1990		9 OAKDEN 94	RVUE	$0.36-1.55 \bar{p} p \rightarrow \pi \pi$
1978± 5		10 ALPER 80	CNTR	$62 \pi^- p \rightarrow K^+ K^- n$
2040±10		10 ROZANSKA 80	SPRK	$18 \pi^- p \rightarrow p\bar{p} n$
1935±13		10 CORDEN 79	OMEG	$12-15 \pi^- p \rightarrow n2\pi$
1988± 7		10 EVANGELIS... 79B	OMEG	$10 \pi^- p \rightarrow K^+ K^- n$
1922±14		11 ANTIPOV 77	CIBS	$25 \pi^- p \rightarrow p3\pi$

- 1 From the first PWA solution.
- 2 From a partial-wave analysis of the data.
- 3 From an amplitude analysis of the reaction  $\pi^+ \pi^- \rightarrow 2\pi^0$ .
- 4 K matrix pole.
- 5 Taking into account the  $f_2(1950)$ . Helicity-2 production favored.
- 6 Energy-dependent analysis.
- 7 Single energy analysis.
- 8 From solution A of amplitude analysis of data on  $\bar{p} p \rightarrow \pi \pi$ . See however KLOET 96 who fit  $\pi^+ \pi^-$  only and find waves only up to  $J = 3$  to be important but not significantly resonant.
- 9 From solution B of amplitude analysis of data on  $\bar{p} p \rightarrow \pi \pi$ . See however KLOET 96 who fit  $\pi^+ \pi^-$  only and find waves only up to  $J = 3$  to be important but not significantly resonant.
- 10  $I(J^{PC}) = 0(4^+)$  from amplitude analysis assuming one-pion exchange.
- 11 Width errors enlarged by us to  $4\Gamma/\sqrt{N}$ ; see the note with the  $K^*(892)$  mass.

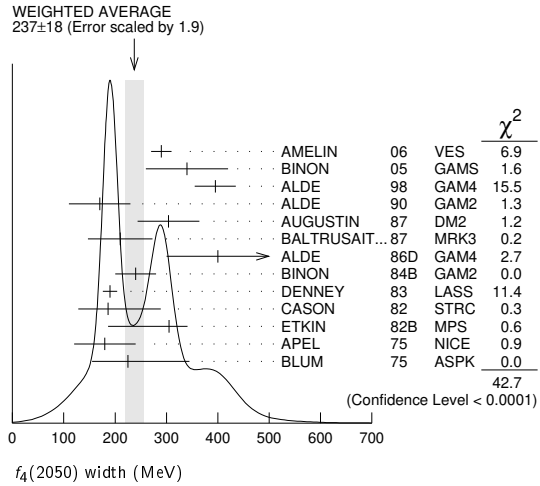


$f_4(2050)$  WIDTH

VALUE (MeV)	EVTs	DOCUMENT ID	TECN	COMMENT
<b>237± 18 OUR AVERAGE</b>		Error includes scale factor of 1.9. See the ideogram below.		
290± 20		AMELIN 06	VES	$36 \pi^- p \rightarrow \omega \omega n$
340± 80	12	BINON 05	GAMS	$33 \pi^- p \rightarrow \eta \eta n$
395± 40		ALDE 98	GAM4	$100 \pi^- p \rightarrow \pi^0 \pi^0 n$
170± 60		ALDE 90	GAM2	$38 \pi^- p \rightarrow \omega \omega n$
304± 60		AUGUSTIN 87	DM2	$J/\psi \rightarrow \gamma \pi^+ \pi^-$
210± 63		BALTRUSAIT...87	MRK3	$J/\psi \rightarrow \gamma \pi^+ \pi^-$

400±100		ALDE 86D	GAM4	$100 \pi^- p \rightarrow n2\eta$
240± 40	40k	13 BINON 05	GAM2	$38 \pi^- p \rightarrow n2\pi^0$
190± 14		DENNEY 83	LASS	$10 \pi^+ n/\pi^+ p$
186 <sup>+103</sup> <sub>-58</sub>		14 CASON 82	STRC	$8 \pi^+ p \rightarrow \Delta^{++} \pi^0 \pi^0$
305 <sup>+36</sup> <sub>-119</sub>		ETKIN 82B	MPS	$23 \pi^- p \rightarrow n2K^0_S$
180± 60	700	APEL 75	NICE	$40 \pi^- p \rightarrow n2\pi^0$
225 <sup>+120</sup> <sub>-70</sub>		BLUM 75	ASPK	$18.4 \pi^- p \rightarrow nK^+ K^-$

- • • We do not use the following data for averages, fits, limits, etc. • • •
- 260± 40
- 453± 20<sup>+31</sup><sub>-129</sub>
- 182± 7
- ~ 170
- ~ 200
- ~ 60
- ~ 80
- 243± 16
- 140± 15
- 263± 57
- 100± 28
- 107± 56
- 12 From the first PWA solution.
- 13 From a partial-wave analysis of the data.
- 14 From an amplitude analysis of the reaction  $\pi^+ \pi^- \rightarrow 2\pi^0$ .
- 15 K matrix pole.
- 16 Taking into account the  $f_2(1950)$ . Helicity-2 production favored.
- 17 Energy-dependent analysis.
- 18 Single energy analysis.
- 19 From solution A of amplitude analysis of data on  $\bar{p} p \rightarrow \pi \pi$ . See however KLOET 96 who fit  $\pi^+ \pi^-$  only and find waves only up to  $J = 3$  to be important but not significantly resonant.
- 20 From solution B of amplitude analysis of data on  $\bar{p} p \rightarrow \pi \pi$ . See however KLOET 96 who fit  $\pi^+ \pi^-$  only and find waves only up to  $J = 3$  to be important but not significantly resonant.
- 21  $I(J^{PC}) = 0(4^+)$  from amplitude analysis assuming one-pion exchange.
- 22 Width errors enlarged by us to  $4\Gamma/\sqrt{N}$ ; see the note with the  $K^*(892)$  mass.



$f_4(2050)$  DECAY MODES

Mode	Fraction ( $\Gamma_i/\Gamma$ )
$\Gamma_1$ $\omega \omega$	seen
$\Gamma_2$ $\pi \pi$	(17.0±1.5) %
$\Gamma_3$ $K \bar{K}$	( 6.8 <sup>+3.4</sup> <sub>-1.8</sub> ) × 10 <sup>-3</sup>
$\Gamma_4$ $\eta \eta$	( 2.1±0.8) × 10 <sup>-3</sup>
$\Gamma_5$ $4\pi^0$	< 1.2 %
$\Gamma_6$ $\gamma \gamma$	
$\Gamma_7$ $a_2(1320) \pi$	seen

$f_4(2050)$   $\Gamma(i)\Gamma(\gamma\gamma)/\Gamma(\text{total})$

$\Gamma(K\bar{K}) \times \Gamma(\gamma\gamma)/\Gamma_{\text{total}}$	CL%	DOCUMENT ID	TECN	COMMENT	$\Gamma_3\Gamma_6/\Gamma$
<0.29	95	ALTHOFF 85B	TASS	$\gamma \gamma \rightarrow K\bar{K} \pi$	

- • • We do not use the following data for averages, fits, limits, etc. • • •



# Meson Particle Listings

## $f_4(2050)$ , $\pi_2(2100)$ , $f_0(2100)$

$\Gamma(\pi\pi) \times \Gamma(\gamma\gamma)/\Gamma_{total}$			$\Gamma_2\Gamma_6/\Gamma$		
VALUE (eV)	CL%	EVTS	DOCUMENT ID	TECN	COMMENT
• • • We do not use the following data for averages, fits, limits, etc. • • •					
$23.1^{+3.6+70.5}_{-3.3-15.6}$			23 UEHARA	09 BELL	$10.6 e^+ e^- \rightarrow e^+ e^- \pi^0 \pi^0$
<1100	95	13 ± 4	OEST	90 JADE	$e^+ e^- \rightarrow e^+ e^- \pi^0 \pi^0$

<sup>23</sup> Taking into account the  $f_2(1950)$ . Helicity-2 production favored.

### $f_4(2050)$ BRANCHING RATIOS

$\Gamma(\omega\omega)/\Gamma_{total}$			$\Gamma_1/\Gamma$		
VALUE	DOCUMENT ID	TECN	COMMENT		
seen	AMELIN	06 VES	36 $\pi^- p \rightarrow \omega\omega n$		
• • • We do not use the following data for averages, fits, limits, etc. • • •					
not seen	BARBERIS	00F	450 $pp \rightarrow p_f \omega\omega p_s$		

$\Gamma(\omega\omega)/\Gamma(\pi\pi)$			$\Gamma_1/\Gamma_2$		
VALUE	DOCUMENT ID	TECN	COMMENT		
<b>1.5 ± 0.3</b>	ALDE	90 GAM2	38 $\pi^- p \rightarrow \omega\omega n$		

$\Gamma(\pi\pi)/\Gamma_{total}$			$\Gamma_2/\Gamma$		
VALUE	DOCUMENT ID	TECN	COMMENT		
<b>0.170 ± 0.015 OUR AVERAGE</b>					
0.18 ± 0.03	24 BINON	83C GAM2	38 $\pi^- p \rightarrow n4\gamma$		
0.16 ± 0.03	24 CASON	82 STRC	8 $\pi^+ p \rightarrow \Delta^{++} \pi^0 \pi^0$		
0.17 ± 0.02	24 CORDEN	79 OMEG	12-15 $\pi^- p \rightarrow n2\pi$		

<sup>24</sup> Assuming one pion exchange.

$\Gamma(K\bar{K})/\Gamma(\pi\pi)$			$\Gamma_3/\Gamma_2$		
VALUE	DOCUMENT ID	TECN	COMMENT		
<b>0.04 ± 0.02</b> <b>-0.01</b>	ETKIN	82B MPS	23 $\pi^- p \rightarrow n2K_S^0$		

$\Gamma(\eta\eta)/\Gamma_{total}$			$\Gamma_4/\Gamma$		
VALUE (units 10 <sup>-3</sup> )	DOCUMENT ID	TECN	COMMENT		
<b>2.1 ± 0.8</b>	ALDE	86D GAM4	100 $\pi^- p \rightarrow n4\gamma$		

$\Gamma(4\pi^0)/\Gamma_{total}$			$\Gamma_5/\Gamma$		
VALUE	DOCUMENT ID	TECN	COMMENT		
<0.012	ALDE	87 GAM4	100 $\pi^- p \rightarrow 4\pi^0 n$		

$\Gamma(a_2(1320)\pi)/\Gamma_{total}$			$\Gamma_7/\Gamma$		
VALUE	DOCUMENT ID	TECN	COMMENT		
seen	AMELIN	00 VES	37 $\pi^- p \rightarrow \eta\pi^+ \pi^- n$		

### $f_4(2050)$ REFERENCES

ANISOVICH	09	IJMP A24 2481	V.V. Anisovich, A.V. Sarantsev		
UEHARA	09	PR D79 052009	S. Uehara et al.	(BELLE Collab.)	
AMELIN	06	PAN 69 690	D.V. Amelin et al.	(VES Collab.)	
		Translated from YAF 69 715.			
BINON	05	PAN 68 960	F. Binon et al.		
		Translated from YAF 68 998.			
AMELIN	00	NP A668 83	D. Amelin et al.	(VES Collab.)	
ANISOVICH	00J	PL B491 47	A.V. Anisovich et al.	(RAL, LOQM, PNPI+)	
BARBERIS	00F	PL B484 198	D. Barberis et al.	(WA 102 Collab.)	
ALDE	98	EPJ A3 361	D. Alde et al.	(GAM4 Collab.)	
		Also PAN 62 405	D. Alde et al.	(GAMS Collab.)	
		Translated from YAF 62 446.			
MARTIN	98	PR C57 3492	B.R. Martin et al.		
MARTIN	97	PR C56 1114	B.R. Martin, G.C. Oades	(LOUC, AARH)	
KLOET	96	PR D53 6120	W.M. Kloet, F. Myhrer	(RUTG, NORD)	
OAKDEN	94	NP A574 731	M.N. Oakden, M.R. Pennington	(DURH)	
ALDE	90	PL B241 600	D.M. Alde et al.	(SERP, BELG, LANL, LAPP+)	
OEST	90	ZPHY C47 343	T. Oest et al.	(JADE Collab.)	
ALDE	87	PL B198 286	D.M. Alde et al.	(LANL, BRUX, SERP, LAPP)	
AUGUSTIN	87	ZPHY C36 369	J.E. Augustin et al.	(LALO, CLER, FRAS+)	
BALTRUSAITIS	87	PR D35 2077	R.M. Baltrusaitis et al.	(Mark III Collab.)	
ALDE	86D	NP B269 485	D.M. Alde et al.	(MPIM, CERN)	
ALTHOFF	85B	ZPHY C29 189	M. Althoff et al.	(TASSO Collab.)	
BINON	84B	LNC 39 41	F.G. Binon et al.	(SERP, BELG, LAPP)	
BINON	83C	SJNP 38 723	F.G. Binon et al.	(SERP, BRUX+)	
		Translated from YAF 38 1199.			
DENNEY	83	PR D28 2726	D.L. Denney et al.	(IOWA, MICH)	
CASON	82	PRL 48 1316	N.M. Cason et al.	(NDAM, ANL)	
ETKIN	82B	PR D25 1786	A. Etkin et al.	(BNL, CUNY, TUFTS, VAND)	
ALPER	80	PL 94B 422	B. Alper et al.	(AMST, CERN, CRAC, MPIM+)	
ROZANSKA	80	NP B162 505	M. Rozanska et al.	(MPIM, CERN)	
CORDEN	79	NP B157 250	M.J. Corden et al.	(BIRM, RHEL, TEHA+)	JIP
EVANGELIS...	79B	NP B154 381	C. Evangelista et al.	(BARI, BONN, CERN+)	
ANTIPOV	77	NP B119 45	Y.M. Antipov et al.	(SERP, GEVA)	
APEL	75	PL 57B 398	W.D. Apel et al.	(KARLK, KARLE, PISA, SERP+)	JIP
BLUM	75	PL 57B 403	W. Blum et al.	(CERN, MPIM)	JIP

## $\pi_2(2100)$

$$I^G(J^{PC}) = 1^-(2^-+)$$

OMITTED FROM SUMMARY TABLE  
Needs confirmation.

### $\pi_2(2100)$ MASS

VALUE (MeV)	DOCUMENT ID	TECN	COMMENT
<b>2090 ± 29 OUR AVERAGE</b>			
2090 ± 30	<sup>1</sup> AMELIN	95B VES	36 $\pi^- A \rightarrow \pi^+ \pi^- \pi^- A$
2100 ± 150	<sup>2</sup> DAUM	81B CNTR	63,94 $\pi^- p \rightarrow 3\pi X$

<sup>1</sup> From a fit to  $J^{PC} = 2^- + f_2(1270)\pi, (\pi\pi)_S\pi$  waves.  
<sup>2</sup> From a two-resonance fit to four  $2^-0^+$  waves.

### $\pi_2(2100)$ WIDTH

VALUE (MeV)	DOCUMENT ID	TECN	COMMENT
<b>625 ± 50 OUR AVERAGE</b> Error includes scale factor of 1.2.			
520 ± 100	<sup>3</sup> AMELIN	95B VES	36 $\pi^- A \rightarrow \pi^+ \pi^- \pi^- A$
651 ± 50	<sup>4</sup> DAUM	81B CNTR	63,94 $\pi^- p \rightarrow 3\pi X$

<sup>3</sup> From a fit to  $J^{PC} = 2^- + f_2(1270)\pi, (\pi\pi)_S\pi$  waves.  
<sup>4</sup> From a two-resonance fit to four  $2^-0^+$  waves.

### $\pi_2(2100)$ DECAY MODES

Mode	Fraction ( $\Gamma_i/\Gamma$ )
$\Gamma_1$ 3 $\pi$	seen
$\Gamma_2$ $\rho\pi$	seen
$\Gamma_3$ $f_2(1270)\pi$	seen
$\Gamma_4$ $(\pi\pi)_S\pi$	seen

### $\pi_2(2100)$ BRANCHING RATIOS

$\Gamma(\rho\pi)/\Gamma(3\pi)$			$\Gamma_2/\Gamma_1$		
VALUE	DOCUMENT ID	TECN	COMMENT		
<b>0.19 ± 0.05</b>	<sup>5</sup> DAUM	81B CNTR	63,94 $\pi^- p$		

$\Gamma(f_2(1270)\pi)/\Gamma(3\pi)$			$\Gamma_3/\Gamma_1$		
VALUE	DOCUMENT ID	TECN	COMMENT		
<b>0.36 ± 0.09</b>	<sup>5</sup> DAUM	81B CNTR	63,94 $\pi^- p$		

$\Gamma((\pi\pi)_S\pi)/\Gamma(3\pi)$			$\Gamma_4/\Gamma_1$		
VALUE	DOCUMENT ID	TECN	COMMENT		
<b>0.45 ± 0.07</b>	<sup>5</sup> DAUM	81B CNTR	63,94 $\pi^- p$		

D-wave/S-wave RATIO FOR $\pi_2(2100) \rightarrow f_2(1270)\pi$			
VALUE	DOCUMENT ID	TECN	COMMENT
<b>0.39 ± 0.23</b>	<sup>5</sup> DAUM	81B CNTR	63,94 $\pi^- p$

<sup>5</sup> From a two-resonance fit to four  $2^-0^+$  waves.

### $\pi_2(2100)$ REFERENCES

AMELIN	95B	PL B356 595	D.V. Amelin et al.	(SERP, TBLI)
DAUM	81B	NP B182 269	C. Daum et al.	(AMST, CERN, CRAC, MPIM+)

## $f_0(2100)$

$$I^G(J^{PC}) = 0^+(0^{++})$$

OMITTED FROM SUMMARY TABLE  
Needs confirmation.

### $f_0(2100)$ MASS

VALUE (MeV)	EVTS	DOCUMENT ID	TECN	COMMENT
<b>2086 ± 20 OUR AVERAGE</b>				
$2081^{+13+24}_{-36}$	5.5k	<sup>1</sup> ABLIKIM	13N BES3	$e^+ e^- \rightarrow J/\psi \rightarrow \gamma\eta\eta$
2090 ± 30		BAI	00A BES	$J/\psi \rightarrow \gamma(\pi^+ \pi^- \pi^+ \pi^-)$

• • • We do not use the following data for averages, fits, limits, etc. • • •

2090 ± 10 ± 6	529	<sup>2,3</sup> DOBBS	15	$J/\psi \rightarrow \gamma\pi^+ \pi^-$
2099 ± 17 ± 8	283	<sup>2,3</sup> DOBBS	15	$\psi(2S) \rightarrow \gamma\pi^+ \pi^-$
2105 ± 8	80k	<sup>4</sup> UMAN	06 E835	5.2 $\bar{p}p \rightarrow \eta\eta\pi^0$
2102 ± 13		<sup>5</sup> ANISOVICH	00J SPEC	2.0 $\bar{p}p \rightarrow \eta\pi^0 \pi^0, \pi^0 \pi^0, \eta\eta, \eta\eta', \pi^+ \pi^-$
2105 ± 10		ANISOVICH	99K SPEC	0.6-1.94 $\bar{p}p \rightarrow \eta\eta, \eta\eta'$
~2104		BUGG	95	$J/\psi \rightarrow \gamma\pi^+ \pi^- \pi^+ \pi^-$
~2122		HASAN	94 RVUE	$\bar{p}p \rightarrow \pi\pi$

<sup>1</sup> From partial wave analysis including all possible combinations of  $0^{++}, 2^{++},$  and  $4^{++}$  resonances.  
<sup>2</sup> Using CLEO-c data but not authored by the CLEO Collaboration.  
<sup>3</sup> From a fit to a Breit-Wigner line shape with fixed  $\Gamma = 209$  MeV.  
<sup>4</sup> Statistical error only.  
<sup>5</sup> Includes the data of ANISOVICH 00B indicating to exotic decay pattern.

See key on page 999

# Meson Particle Listings

## $f_0(2100)$ , $f_2(2150)$

### $f_0(2100)$ WIDTH

VALUE (MeV)	EVTS	DOCUMENT ID	TECN	COMMENT
<b>284<sup>+60</sup><sub>-32</sub> OUR AVERAGE</b>				
273 <sup>+27</sup> <sub>-24</sub> <sup>+70</sup> <sub>-23</sub>	5.5k	<sup>6</sup> ABLIKIM	13N BES3	$e^+e^- \rightarrow J/\psi \rightarrow \gamma\eta\eta$
330±100		BAI	00A BES	$J/\psi \rightarrow \gamma(\pi^+\pi^-\pi^+\pi^-)$
• • • We do not use the following data for averages, fits, limits, etc. • • •				
236±14	80k	<sup>7</sup> UMAN	06 E835	$5.2 \bar{p}p \rightarrow \eta\eta\pi^0$
211±29		<sup>8</sup> ANISOVICH	00J SPEC	$2.0 \bar{p}p \rightarrow \eta\pi^0\pi^0, \pi^0\pi^0, \eta\eta, \eta\eta', \pi^+\pi^-$
200±25		ANISOVICH	99K SPEC	$0.6-1.94 \bar{p}p \rightarrow \eta\eta, \eta\eta'$
~203		BUGG	95	$J/\psi \rightarrow \gamma\pi^+\pi^-\pi^+\pi^-$
~273		HASAN	94 RVUE	$\bar{p}p \rightarrow \pi\pi$

<sup>6</sup> From partial wave analysis including all possible combinations of  $0^{++}$ ,  $2^{++}$ , and  $4^{++}$  resonances.  
<sup>7</sup> Statistical error only.  
<sup>8</sup> Includes the data of ANISOVICH 00B indicating to exotic decay pattern.

### $f_0(2100)$ REFERENCES

DOBBS	15	PR D91 052006	S. Dobbs <i>et al.</i>	(NWES)
ABLIKIM	13N	PR D87 092009	Ablikim M. <i>et al.</i>	(BESIII Collab.)
UMAN	06	PR D73 052009	I. Uman <i>et al.</i>	(FNAL E835)
ANISOVICH	00B	NP A662 319	A.V. Anisovich <i>et al.</i>	
ANISOVICH	00J	PL B491 47	A.V. Anisovich <i>et al.</i>	(RAL, LOQM, PNPI+)
BAI	00A	PL B472 207	J.Z. Bai <i>et al.</i>	(BES Collab.)
ANISOVICH	99K	PL B468 309	A.V. Anisovich <i>et al.</i>	
BUGG	95	PL B353 378	D.V. Bugg <i>et al.</i>	(LOQM, PNPI, WASH)
HASAN	94	PL B334 215	A. Hasan, D.V. Bugg	(LOQM)

## $f_2(2150)$

$$I^G(J^{PC}) = 0^+(2^{++})$$

OMITTED FROM SUMMARY TABLE  
 This entry was previously called  $T_0$ .

### $f_2(2150)$ MASS

#### $f_2(2150)$ MASS, COMBINED MODES (MeV)

VALUE (MeV)	EVTS	DOCUMENT ID	TECN	COMMENT
<b>152±30 OUR AVERAGE</b>				Includes data from the datablock that follows this one.
• • • We do not use the following data for averages, fits, limits, etc. • • •				
2170±6	80k	<sup>1</sup> UMAN	06 E835	$5.2 \bar{p}p \rightarrow \eta\eta\pi^0$

<sup>1</sup> Statistical error only.

#### $\eta\eta$ MODE

VALUE (MeV)	DOCUMENT ID	TECN	COMMENT
The data in this block is included in the average printed for a previous datablock.			

#### 2157±12 OUR AVERAGE

2151±16	BARBERIS	00E	450 $pp \rightarrow p_f\eta\eta p_S$	
2175±20	PROKOSHKIN	95D GAM4	$300 \pi^- N \rightarrow \pi^- N 2\eta,$ $450 pp \rightarrow pp 2\eta$	
2130±35	SINGOVSKI	94 GAM4	$450 pp \rightarrow pp 2\eta$	
• • • We do not use the following data for averages, fits, limits, etc. • • •				
2140±30	<sup>2</sup> ABELE	99B CBAR	$1.94 \bar{p}p \rightarrow \pi^0\eta\eta$	
2104±20	<sup>3</sup> ARMSTRONG	93C E760	$\bar{p}p \rightarrow \pi^0\eta\eta \rightarrow 6\gamma$	

<sup>2</sup> Spin not determined.  
<sup>3</sup> No  $J^{PC}$  determination.

#### $\eta\pi\pi$ MODE

VALUE (MeV)	DOCUMENT ID	TECN	CHG	COMMENT
• • • We do not use the following data for averages, fits, limits, etc. • • •				
2135±20±45	<sup>4</sup> ADOMEIT	96 CBAR	0	$1.94 \bar{p}p \rightarrow \eta 3\pi^0$

<sup>4</sup> ANISOVICH 00E recommends to withdraw ADOMEIT 96 that assumed a single  $J^P = 2^+$  resonance.

#### $\bar{p}p \rightarrow \pi\pi$

VALUE (MeV)	DOCUMENT ID	TECN	COMMENT
• • • We do not use the following data for averages, fits, limits, etc. • • •			
~2090	<sup>5</sup> OAKDEN	94 RVUE	$0.36-1.55 \bar{p}p \rightarrow \pi\pi$
~2120	<sup>6</sup> OAKDEN	94 RVUE	$0.36-1.55 \bar{p}p \rightarrow \pi\pi$
~2170	<sup>7</sup> MARTIN	80B RVUE	
~2150	<sup>7</sup> MARTIN	80C RVUE	
~2150	<sup>8</sup> DULUDE	78B OSPK	$1-2 \bar{p}p \rightarrow \pi^0\pi^0$

<sup>5</sup> OAKDEN 94 makes an amplitude analysis of LEAR data on  $\bar{p}p \rightarrow \pi\pi$  using a method based on Barrelet zeros. This is solution A. The amplitude analysis of HASAN 94 includes earlier data as well, and assume that the data can be parametrized in terms of towers of nearly degenerate resonances on the leading Regge trajectory. See also KLOET 96 and MARTIN 97 who make related analyses.

<sup>6</sup> From solution B of amplitude analysis of data on  $\bar{p}p \rightarrow \pi\pi$ .

<sup>7</sup>  $I(J^P) = 0(2^+)$  from simultaneous analysis of  $p\bar{p} \rightarrow \pi^-\pi^+$  and  $\pi^0\pi^0$ .  
<sup>8</sup>  $I^G(J^P) = 0^+(2^+)$  from partial-wave amplitude analysis.

### S-CHANNEL $\bar{p}p, \bar{N}N$ or $\bar{K}K$

VALUE (MeV)	DOCUMENT ID	TECN	CHG	COMMENT
• • • We do not use the following data for averages, fits, limits, etc. • • •				
2139 <sup>+8</sup> <sub>-9</sub>	<sup>9</sup> EVANGELIS...	97 SPEC		$0.6-2.4 \bar{p}p \rightarrow K_S^0 K_S^0$
~2190	<sup>9</sup> CUTTS	78B CNTR		$0.97-3 \bar{p}p \rightarrow \bar{N}N$
2155±15	<sup>9,10</sup> COUPLAND	77 CNTR	0	$0.7-2.4 \bar{p}p \rightarrow \bar{p}p$
2193±2	<sup>9,11</sup> ALSPECTOR	73 CNTR		$\bar{p}p$ S channel

<sup>9</sup> Isospins 0 and 1 not separated.  
<sup>10</sup> From a fit to the total elastic cross section.  
<sup>11</sup> Referred to as  $T$  or  $T$  region by ALSPECTOR 73.

### $K\bar{K}$ MODE

VALUE (MeV)	DOCUMENT ID	TECN	COMMENT
• • • We do not use the following data for averages, fits, limits, etc. • • •			
2200±13	VLADIMIRSK..	06 SPEC	$40 \pi^- p \rightarrow K_S^0 K_S^0 n$
2150±20	ABLIKIM	04E BES2	$J/\psi \rightarrow \omega K^+ K^-$
2130±35	BARBERIS	99 OMEG	$450 pp \rightarrow p_S p_f K^+ K^-$

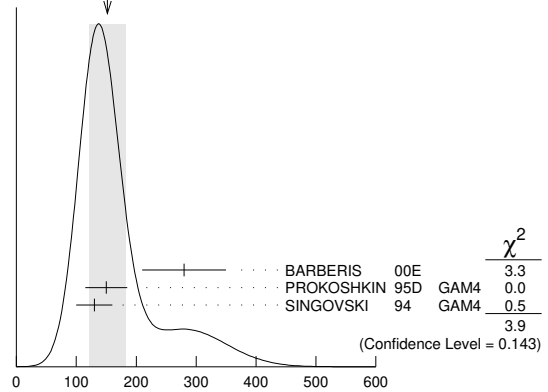
### $f_2(2150)$ WIDTH

#### $f_2(2150)$ WIDTH, COMBINED MODES (MeV)

VALUE (MeV)	EVTS	DOCUMENT ID	TECN	COMMENT
<b>152±30 OUR AVERAGE</b>				Includes data from the datablock that follows this one. Error includes scale factor of 1.4. See the ideogram below.
• • • We do not use the following data for averages, fits, limits, etc. • • •				
182±11	80k	<sup>12</sup> UMAN	06 E835	$5.2 \bar{p}p \rightarrow \eta\eta\pi^0$

<sup>12</sup> Statistical error only.

WEIGHTED AVERAGE  
 152±30 (Error scaled by 1.4)



$f_2(2150)$  width, combined modes (MeV)

#### $\eta\eta$ MODE

VALUE (MeV)	DOCUMENT ID	TECN	COMMENT
The data in this block is included in the average printed for a previous datablock.			

#### 152±30 OUR AVERAGE

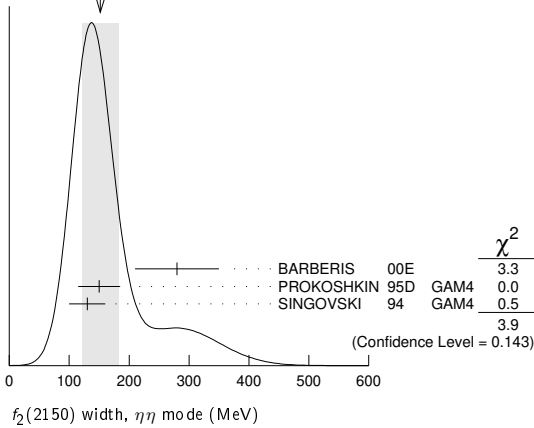
280±70	BARBERIS	00E	450 $pp \rightarrow p_f\eta\eta p_S$	
150±35	PROKOSHKIN	95D GAM4	$300 \pi^- N \rightarrow \pi^- N 2\eta,$ $450 pp \rightarrow pp 2\eta$	
130±30	SINGOVSKI	94 GAM4	$450 pp \rightarrow pp 2\eta$	
• • • We do not use the following data for averages, fits, limits, etc. • • •				
310±50	<sup>13</sup> ABELE	99B CBAR	$1.94 \bar{p}p \rightarrow \pi^0\eta\eta$	
203±10	<sup>14</sup> ARMSTRONG	93C E760	$\bar{p}p \rightarrow \pi^0\eta\eta \rightarrow 6\gamma$	

<sup>13</sup> Spin not determined.  
<sup>14</sup> No  $J^{PC}$  determination.

# Meson Particle Listings

## $f_2(2150), \rho(2150)$

WEIGHTED AVERAGE  
152±30 (Error scaled by 1.4)



### $\eta\pi\pi$ MODE

VALUE (MeV)	DOCUMENT ID	TECN	CHG	COMMENT
250±25±45	15 ADOMEIT 96	CBAR	0	1.94 $\bar{p}p \rightarrow \eta 3\pi^0$

• • • We do not use the following data for averages, fits, limits, etc. • • •

15 ANISOVICH 00E recommends to withdraw ADOMEIT 96 that assumed a single  $J^P = 2^+$  resonance.

### $\bar{p}p \rightarrow \pi\pi$

VALUE (MeV)	DOCUMENT ID	TECN	COMMENT
<b>250 OUR ESTIMATE</b>			
~ 70	16 OAKDEN 94	RVUE	0.36-1.55 $\bar{p}p \rightarrow \pi\pi$
~ 250	17 MARTIN 80B	RVUE	
~ 250	17 MARTIN 80C	RVUE	
~ 250	18 DULUDE 78B	OSPK	1-2 $\bar{p}p \rightarrow \pi^0\pi^0$

• • • We do not use the following data for averages, fits, limits, etc. • • •

16 See however KLOET 96 who fit  $\pi^+\pi^-$  only and find waves only up to  $J = 3$  to be important but not significantly resonant.

17  $I(J^P) = 0(2^+)$  from simultaneous analysis of  $p\bar{p} \rightarrow \pi^-\pi^+$  and  $\pi^0\pi^0$ .

18  $I(J^P) = 0^+(2^+)$  from partial-wave amplitude analysis.

### S-CHANNEL $\bar{p}p, \bar{N}N$ or $\bar{K}K$

VALUE (MeV)	DOCUMENT ID	TECN	CHG	COMMENT
56 <sup>+31</sup> <sub>-16</sub>	19 EVANGELIS... 97	SPEC		0.6-2.4 $\bar{p}p \rightarrow K_S^0 K_S^0$
135±75	20,21 COUPLAND 77	CNTR	0	0.7-2.4 $\bar{p}p \rightarrow \bar{p}p$
98±8	21 ALSPECTOR 73	CNTR		$\bar{p}p$ S channel

• • • We do not use the following data for averages, fits, limits, etc. • • •

19 Isospin 0 and 2 not separated.

20 From a fit to the total elastic cross section.

21 Isospins 0 and 1 not separated.

### $K\bar{K}$ MODE

VALUE (MeV)	DOCUMENT ID	TECN	COMMENT
91±62	VLADIMIRSK...06	SPEC	40 $\pi^-\rho \rightarrow K_S^0 K_S^0 n$
150±30	ABLIKIM 04E	BES2	$J/\psi \rightarrow \omega K^+ K^-$
270±50	BARBERIS 99	OMEG	450 $pp \rightarrow p_S p_f K^+ K^-$

### $f_2(2150)$ DECAY MODES

Mode	Fraction ( $\Gamma_i/\Gamma$ )
$\Gamma_1$ $\pi\pi$	
$\Gamma_2$ $\eta\eta$	seen
$\Gamma_3$ $K\bar{K}$	seen
$\Gamma_4$ $f_2(1270)\eta$	seen
$\Gamma_5$ $a_2(1320)\pi$	seen
$\Gamma_6$ $\rho\bar{\rho}$	seen

### $f_2(2150)$ BRANCHING RATIOS

$\Gamma(K\bar{K})/\Gamma(\eta\eta)$	CL%	DOCUMENT ID	TECN	COMMENT	$\Gamma_3/\Gamma_2$
1.28±0.23		BARBERIS 00E		450 $pp \rightarrow p_f \eta \eta p_S$	
<0.1	95	22 PROKOSHKIN 95D	GAM4	300 $\pi^- N \rightarrow \pi^- N 2\eta$ , 450 $pp \rightarrow p p 2\eta$	

• • • We do not use the following data for averages, fits, limits, etc. • • •

22 Using data from ARMSTRONG 89D.

### $\Gamma(\pi\pi)/\Gamma(\eta\eta)$

VALUE	CL%	DOCUMENT ID	TECN	COMMENT	$\Gamma_1/\Gamma_2$
<0.33	95	23 PROKOSHKIN 95D	GAM4	300 $\pi^- N \rightarrow \pi^- N 2\eta$ , 450 $pp \rightarrow p p 2\eta$	

• • • We do not use the following data for averages, fits, limits, etc. • • •

23 Derived from a  $\pi^0\pi^0/\eta\eta$  limit.

### $\Gamma(f_2(1270)\eta)/\Gamma(a_2(1320)\pi)$

VALUE	DOCUMENT ID	TECN	COMMENT	$\Gamma_4/\Gamma_5$
0.79±0.11	24 ADOMEIT 96	CBAR	1.94 $\bar{p}p \rightarrow \eta 3\pi^0$	

24 Using  $B(a_2(1320) \rightarrow \eta\pi) = 0.145$

### $\Gamma(\rho\bar{\rho})/\Gamma_{total}$

VALUE	EVTS	DOCUMENT ID	TECN	COMMENT	$\Gamma_6/\Gamma$
seen	73	ALEXANDER 10	CLEO	$\psi(2S) \rightarrow \gamma\rho\bar{\rho}$	

### $f_2(2150)$ REFERENCES

ALEXANDER 10	PR D82 092002	J.P. Alexander et al.	(CLEO Collab.)
UMAN 06	PR D73 052009	I. Uman et al.	(FNAL E835)
VLADIMIRSK...06	PAN 69 493	V.V. Vladimirov et al.	(ITEP, Moscow)
ABLIKIM 04E	PL B603 138	M. Ablikim et al.	(BES Collab.)
ANISOVICH 00E	PL B477 19	A.V. Anisovich et al.	(WA 102 Collab.)
BARBERIS 00E	PL B479 59	D. Barberis et al.	(Crystal Barrel Collab.)
ABELE 99B	EPJ C8 67	A. Abele et al.	(Omega Expt.)
BARBERIS 99B	PL B453 305	D. Barberis et al.	(LEAR Collab.)
EVANGELIS... 97	PR D56 3803	C. Evangelista et al.	(LOUC, AARH)
MARTIN 97	PR C56 1114	B.R. Martin, G.C. Oades	(Crystal Barrel Collab.)
ADOMEIT 96	ZPHY C71 227	J. Adomeit et al.	(RUTG, NORD)
KLOET 96	PR D53 6120	W.M. Kloet, F. Myhrer	(SERP)IGJPC
PROKOSHKIN 95D	PD 40 495	Y.D. Prokoshkin	
HASAN 94	PL B334 215	A. Hasan, D.V. Bugg	(LOQM)
OAKDEN 94	NP A574 731	M.N. Oakden, M.R. Pennington	(DURH)
SINGOVSKI 94	NC A107 1911	A.V. Singovsky	(SERP)
ARMSTRONG 89D	PL B307 394	T.A. Armstrong et al.	(FNAL, FERR, GENO+)
ARMSTRONG 89D	PL B227 186	T.A. Armstrong, M. Benayoun	(ATHU, BARI, BIRM+)
MARTIN 80B	NP B176 355	B.R. Martin, D. Morgan	(LOUC, RHEL)JP
MARTIN 80C	NP B169 216	A.D. Martin, M.R. Pennington	(DURH)JP
CUTTS 78B	PR D17 16	D. Cutts et al.	(STON, WISC)
DULUDE 78B	PL 79B 335	R.S. Dulude et al.	(BROW, MIT, BARI)JP
COUPLAND 77	PL 71B 460	M. Coupland et al.	(LOQM, RHEL)
ALSPECTOR 73	PRL 30 511	J. Alspector et al.	(RUTG, UPNJ)

### $\rho(2150)$

$$I^G(J^PC) = 1^+(1^-)$$

OMITTED FROM SUMMARY TABLE

This entry was previously called  $T_1(2190)$ . See our mini-review under the  $\rho(1700)$ .

### $\rho(2150)$ MASS

#### $e^+e^-$ PRODUCED

VALUE (MeV)	DOCUMENT ID	TECN	COMMENT
2201 ± 19	1 LEES 20	BABR	$e^+e^- \rightarrow K^+ K^- \gamma$
2227 ± 9 ± 9	2 LEES 20	RVUE	$e^+e^- \rightarrow K^+ K^-$
2039 ± 8 <sup>+36</sup> <sub>-18</sub>	3 ABLIKIM 19Aq	BES3	$J/\psi \rightarrow K^+ K^- \pi^0$
2239.2± 7.1±11.3	4 ABLIKIM 19L	BES3	$e^+e^- \rightarrow K^+ K^-$
2254 ± 22	5 LEES 12G	BABR	$e^+e^- \rightarrow \pi^+ \pi^- \gamma$
2150 ± 40 ± 50	AUBERT 07Au	BABR	10.6 $e^+e^- \rightarrow f_1(1285)\pi^+\pi^-\gamma$
1990 ± 80	AUBERT 07Au	BABR	10.6 $e^+e^- \rightarrow \eta^+\pi^+\pi^-\gamma$
2153 ± 37	BIAGINI 91	RVUE	$e^+e^- \rightarrow \pi^+\pi^-, K^+ K^-$
2110 ± 50	6 CLEGG 90	RVUE	$e^+e^- \rightarrow 3(\pi^+\pi^-), 2(\pi^+\pi^-\pi^0)$

- From the fit to the BABAR data of LEES 13Q assuming a coherent sum of a single Breit-Wigner resonance and a nonresonant contribution. The resonance significance is 3.5  $\sigma$ .
- From the fit to the BABAR data of LEES 13Q and BESIII data of ABLIKIM 19L assuming a coherent sum of a single Breit-Wigner resonance and a nonresonant contribution.
- Could also be another state. Seen in  $J/\psi$  decay with branching ratio  $J/\psi \rightarrow X\pi^0 \rightarrow K^+ K^- \pi^0 = (6.7 \pm 1.1 \pm 2.2 \pm 1.8) \times 10^{-6}$ .
- The observed structure can be due to both the  $\phi(2170)$  and  $\rho(2150)$ .
- Using the GOUNARIS 68 parametrization of the pion form factor leaving the masses and widths of the  $\rho(1450)$ ,  $\rho(1700)$ , and  $\rho(2150)$  resonances as free parameters of the fit.
- Includes ATKINSON 85.

#### $\bar{p}p \rightarrow \pi\pi$

VALUE (MeV)	DOCUMENT ID	TECN	COMMENT
~ 2191	HASAN 94	RVUE	$\bar{p}p \rightarrow \pi\pi$
~ 2070	1 OAKDEN 94	RVUE	0.36-1.55 $\bar{p}p \rightarrow \pi\pi$
~ 2170	2 MARTIN 80B	RVUE	
~ 2100	2 MARTIN 80C	RVUE	

- • • We do not use the following data for averages, fits, limits, etc. • • •
- 1 See however KLOET 96 who fit  $\pi^+\pi^-$  only and find waves only up to  $J = 3$  to be important but not significantly resonant.
- 2  $I(J^P) = 1(1^-)$  from simultaneous analysis of  $p\bar{p} \rightarrow \pi^-\pi^+$  and  $\pi^0\pi^0$ .

See key on page 999

Meson Particle Listings

$\rho(2150), \phi(2170)$

S-CHANNEL  $\bar{N}N$

VALUE (MeV)	DOCUMENT ID	TECN	COMMENT
••• We do not use the following data for averages, fits, limits, etc. •••			
2110±35	<sup>1</sup> ANISOVICH 02	SPEC	0.6-1.9 $p\bar{p} \rightarrow \omega\pi^0, \omega\eta\pi^0, \pi^+\pi^-$
~2190	<sup>2</sup> CUTTS 78B	CNTR	0.97-3 $\bar{p}p \rightarrow \bar{N}N$
2155±15	<sup>2,3</sup> COUPLAND 77	CNTR	0.7-2.4 $\bar{p}p \rightarrow \bar{p}p$
2193±2	<sup>2,4</sup> ALSPECTOR 73	CNTR	$\bar{p}p$ S channel
2190±10	<sup>5</sup> ABRAMS 70	CNTR	S channel $\bar{p}N$

<sup>1</sup> From the combined analysis of ANISOVICH 00J, ANISOVICH 01D, ANISOVICH 01E, and ANISOVICH 02.  
<sup>2</sup> Isospins 0 and 1 not separated.  
<sup>3</sup> From a fit to the total elastic cross section.  
<sup>4</sup> Referred to as T or T' region by ALSPECTOR 73.  
<sup>5</sup> Seen as bump in l = 1 state. See also COOPER 68. PEASLEE 75 confirm  $\bar{p}p$  results of ABRAMS 70, no narrow structure.

$\pi^-p \rightarrow \omega\pi^0n$

VALUE (MeV)	DOCUMENT ID	TECN	COMMENT
••• We do not use the following data for averages, fits, limits, etc. •••			
2140±30	ALDE 95	GAM2	38 $\pi^-p \rightarrow \omega\pi^0n$
2170±30	ALDE 92c	GAM4	100 $\pi^-p \rightarrow \omega\pi^0n$

$\rho(2150)$  WIDTH

$e^+e^-$  PRODUCED

VALUE (MeV)	DOCUMENT ID	TECN	COMMENT
••• We do not use the following data for averages, fits, limits, etc. •••			
70 ± 38	<sup>1</sup> LEES 20	BABR	$e^+e^- \rightarrow K^+K^-\gamma$
127 ± 14 ± 4	<sup>2</sup> LEES 20	RVUE	$e^+e^- \rightarrow K^+K^-$
196 ± 23 <sup>+25</sup> / <sub>-27</sub>	<sup>3</sup> ABLIKIM 19AQ	BES	$J/\psi \rightarrow K^+K^-\pi^0$
139.8 ± 12.3 ± 20.6	<sup>4</sup> ABLIKIM 19L	BES3	$e^+e^- \rightarrow K^+K^-$
109 ± 76	<sup>5</sup> LEES 12G	BABR	$e^+e^- \rightarrow \pi^+\pi^-\gamma$
350 ± 40 ± 50	AUBERT 07AU	BABR	10.6 $e^+e^- \rightarrow f_1(1285)\pi^+\pi^-\gamma$
310 ± 140	AUBERT 07AU	BABR	10.6 $e^+e^- \rightarrow \eta'\pi^+\pi^-\gamma$
389 ± 79	BIAGINI 91	RVUE	$e^+e^- \rightarrow \pi^+\pi^-, K^+K^-$
410 ± 100	<sup>6</sup> CLEGG 90	RVUE	$e^+e^- \rightarrow 3(\pi^+\pi^-), 2(\pi^+\pi^-\pi^0)$

<sup>1</sup> From the fit to the BABAR data of LEES 13Q assuming a coherent sum of a single Breit-Wigner resonance and a nonresonant contribution. The resonance significance is 3.5  $\sigma$ .  
<sup>2</sup> From the fit to the BABAR data of LEES 13Q and BESIII data of ABLIKIM 19L assuming a coherent sum of a single Breit-Wigner resonance and a nonresonant contribution.  
<sup>3</sup> Could also be another state. Seen in  $J/\psi$  decay with branching ratio  $J/\psi \rightarrow X\pi^0 \rightarrow K^+K^-\pi^0 = (6.7 \pm 1.1 \pm 2.2 \pm 1.8) \times 10^{-6}$ .  
<sup>4</sup> The observed structure can be due to both the  $\phi(2170)$  and  $\rho(2150)$ .  
<sup>5</sup> Using the GOUNARIS 68 parametrization of the pion form factor leaving the masses and widths of the  $\rho(1450)$ ,  $\rho(1700)$ , and  $\rho(2150)$  resonances as free parameters of the fit.  
<sup>6</sup> Includes ATKINSON 85.

$\bar{p}p \rightarrow \pi\pi$

VALUE (MeV)	DOCUMENT ID	TECN	COMMENT
••• We do not use the following data for averages, fits, limits, etc. •••			
~296	HASAN 94	RVUE	$\bar{p}p \rightarrow \pi\pi$
~40	<sup>1</sup> OAKDEN 94	RVUE	0.36-1.55 $\bar{p}p \rightarrow \pi\pi$
~250	<sup>2</sup> MARTIN 80B	RVUE	
~200	<sup>2</sup> MARTIN 80C	RVUE	

<sup>1</sup> See however KLOET 96 who fit  $\pi^+\pi^-$  only and find waves only up to J = 3 to be important but not significantly resonant.  
<sup>2</sup>  $I(J^P) = 1(1^-)$  from simultaneous analysis of  $p\bar{p} \rightarrow \pi^-\pi^+$  and  $\pi^0\pi^0$ .

S-CHANNEL  $\bar{N}N$

VALUE (MeV)	DOCUMENT ID	TECN	COMMENT
••• We do not use the following data for averages, fits, limits, etc. •••			
230±50	<sup>1</sup> ANISOVICH 02	SPEC	0.6-1.9 $p\bar{p} \rightarrow \omega\pi^0, \omega\eta\pi^0, \pi^+\pi^-$
135±75	<sup>2,3</sup> COUPLAND 77	CNTR	0.7-2.4 $\bar{p}p \rightarrow \bar{p}p$
98±8	<sup>3</sup> ALSPECTOR 73	CNTR	$\bar{p}p$ S channel
~85	<sup>4</sup> ABRAMS 70	CNTR	S channel $\bar{p}N$

<sup>1</sup> From the combined analysis of ANISOVICH 00J, ANISOVICH 01D, ANISOVICH 01E, and ANISOVICH 02.  
<sup>2</sup> From a fit to the total elastic cross section.  
<sup>3</sup> Isospins 0 and 1 not separated.  
<sup>4</sup> Seen as bump in l = 1 state. See also COOPER 68. PEASLEE 75 confirm  $\bar{p}p$  results of ABRAMS 70, no narrow structure.

$\pi^-p \rightarrow \omega\pi^0n$

VALUE (MeV)	DOCUMENT ID	TECN	COMMENT
••• We do not use the following data for averages, fits, limits, etc. •••			
320±70	ALDE 95	GAM2	38 $\pi^-p \rightarrow \omega\pi^0n$
~300	ALDE 92c	GAM4	100 $\pi^-p \rightarrow \omega\pi^0n$

$\rho(2150)$  DECAY MODES

Mode	Fraction ( $\Gamma_i/\Gamma$ )
$\Gamma_1$ $e^+e^-$	
$\Gamma_2$ $\pi^+\pi^-$	seen
$\Gamma_3$ $K^+K^-$	seen
$\Gamma_4$ $3(\pi^+\pi^-)$	seen
$\Gamma_5$ $2(\pi^+\pi^-\pi^0)$	seen
$\Gamma_6$ $\eta'\pi^+\pi^-$	seen
$\Gamma_7$ $f_1(1285)\pi^+\pi^-$	seen
$\Gamma_8$ $\omega\pi^0$	seen
$\Gamma_9$ $\omega\pi^0\eta$	seen
$\Gamma_{10}$ $\rho\bar{\rho}$	

$\rho(2150) \Gamma(i)\Gamma(e^+e^-)/\Gamma^2(\text{total})$

$\Gamma(f_1(1285)\pi^+\pi^-)/\Gamma_{\text{total}} \times \Gamma(e^+e^-)/\Gamma_{\text{total}}$	$\Gamma_7/\Gamma \times \Gamma_1/\Gamma$		
VALUE (units $10^{-7}$ )	DOCUMENT ID	TECN	COMMENT
<b>3.1 ± 0.6 ± 0.5</b>	<sup>1</sup> AUBERT 07AU	BABR	10.6 $e^+e^- \rightarrow f_1(1285)\pi^+\pi^-\gamma$

<sup>1</sup> Calculated by us from the reported value of cross section at the peak.

$\Gamma(\eta'\pi^+\pi^-)/\Gamma_{\text{total}} \times \Gamma(e^+e^-)/\Gamma_{\text{total}}$	$\Gamma_6/\Gamma \times \Gamma_1/\Gamma$		
VALUE (units $10^{-8}$ )	DOCUMENT ID	TECN	COMMENT
<b>4.9 ± 1.9</b>	<sup>1</sup> AUBERT 07AU	BABR	10.6 $e^+e^- \rightarrow \eta'\pi^+\pi^-\gamma$

<sup>1</sup> Calculated by us from the reported value of cross section at the peak.

$\rho(2150)$  REFERENCES

LEES 20	PR D101 012011	J.P. Lees et al.	(BESIII Collab.)
ABLIKIM 19AQ	PR D100 032004	M. Ablikim et al.	(BESIII Collab.)
ABLIKIM 19L	PR D99 032001	M. Ablikim et al.	(BESIII Collab.)
LEES 13Q	PR D88 032013	J.P. Lees et al.	(BABAR Collab.)
LEES 12G	PR D86 032013	J.P. Lees et al.	(BABAR Collab.)
AUBERT 07AU	PR D76 092005	B. Aubert et al.	(BABAR Collab.)
ANISOVICH 02	PL B542 8	A.V. Anisovich et al.	
ANISOVICH 01D	PL B508 6	A.V. Anisovich et al.	
ANISOVICH 01E	PL B513 281	A.V. Anisovich et al.	
ANISOVICH 00J	PL B491 47	A.V. Anisovich et al.	(RAL, LOQM, PNPI+)
KLOET 96	PR D53 6120	W.M. Kloet, F. Myhrer	(RUTG, NORD)
ALDE 95	ZPHY C66 379	D.M. Alde et al.	(GAMS Collab.) JP
HASAN 94	PL B334 215	A. Hasan, D.V. Bugg	(LOQM)
OAKDEN 94	NP A574 731	M.N. Oakden, M.R. Pennington	(DURH)
ALDE 92C	ZPHY C54 553	D.M. Alde et al.	(BELG, SERP, KEK, LANL+)
BIAGINI 91	NC 104A 363	M.E. Biagini et al.	(FRAS, PRAG)
CLEGG 90	ZPHY C45 677	A.B. Clegg, A. Donnachie	(LANC, NCHS)
ATKINSON 85	ZPHY C29 333	M. Atkinson et al.	(BONN, CERN, GLAS+)
MARTIN 80B	NP B176 355	B.R. Martin, D. Morgan	(LOUC, RHEL) JP
MARTIN 80C	NP B169 216	A.D. Martin, M.R. Pennington	(DURH) JP
CUTTS 78B	PR D17 16	D. Cutts et al.	(STON, WISC)
COUPLAND 77	PL 71B 460	M. Coupland et al.	(LOQM, RHEL)
PEASLEE 75	PL 57B 189	D.C. Peaslee et al.	(CANB, BARI, BROW+)
ALSPECTOR 73	PRL 30 511	J. Alspector et al.	(RUTG, UPNJ)
ABRAMS 70	PR D1 1917	R.J. Abrams et al.	(BNL)
COOPER 68	PRL 20 1059	W.A. Cooper et al.	(ANL)
GOUNARIS 68	PRL 21 244	G.J. Gounaris, J.J. Sakurai	

$\phi(2170)$

$I(G^{JPC}) = 0^-(1^-)$

$\phi(2170)$  MASS

VALUE (MeV)	EVTS	DOCUMENT ID	TECN	COMMENT
<b>2160 ± 80</b>	<b>OUR EVALUATION</b>			
••• We do not use the following data for averages, fits, limits, etc. •••				
2135 ± 8 ± 9	95	ABLIKIM 19I	BES3	$e^+e^- \rightarrow \eta\phi f_0(980)$
2239.2 ± 7.1 ± 11.3		<sup>1</sup> ABLIKIM 19L	BES3	$e^+e^- \rightarrow K^+K^-$
2200 ± 6 ± 5	471	ABLIKIM 15H	BES3	$J/\psi \rightarrow \eta\phi\pi^+\pi^-$
2180 ± 8 ± 8		<sup>2,3</sup> LEES 12F	BABR	10.6 $e^+e^- \rightarrow \phi\pi^+\pi^-\gamma$
2079 ± 13 <sup>+79</sup> / <sub>-28</sub>	4.8k	<sup>4</sup> SHEN 09	BELL	10.6 $e^+e^- \rightarrow K^+K^-\pi^+\pi^-\gamma$
2186 ± 10 ± 6	52	ABLIKIM 08F	BES	$J/\psi \rightarrow \eta\phi f_0(980)$
2125 ± 22 ± 10	483	AUBERT 08s	BABR	10.6 $e^+e^- \rightarrow \phi\eta\gamma$
2192 ± 14	116	<sup>5</sup> AUBERT 07AK	BABR	10.6 $e^+e^- \rightarrow K^+K^-\pi^+\pi^-\gamma$
2169 ± 20	149	<sup>5</sup> AUBERT 07AK	BABR	10.6 $e^+e^- \rightarrow K^+K^-\pi^0\pi^0\gamma$
2175 ± 10 ± 15	201	<sup>3,6</sup> AUBERT, BE	06D	10.6 $e^+e^- \rightarrow K^+K^-\pi\pi\gamma$

<sup>1</sup> The observed structure can be due to both the  $\phi(2170)$  and  $\rho(2150)$ .  
<sup>2</sup> Fit includes interference with the  $\phi(1680)$ .  
<sup>3</sup> From the  $\phi f_0(980)$  component.  
<sup>4</sup> From a fit with two incoherent Breit-Wigners.  
<sup>5</sup> From the  $K^+K^-f_0(980)$  component.  
<sup>6</sup> Superseded by LEES 12F.

# Meson Particle Listings

## $\phi(2170)$ , $f_0(2200)$ , $f_j(2220)$

### $\phi(2170)$ WIDTH

VALUE (MeV)	EVTS	DOCUMENT ID	TECN	COMMENT
<b>125 ± 65 OUR EVALUATION</b>				
• • • We do not use the following data for averages, fits, limits, etc. • • •				
104 ± 24 ± 12	95	ABLIKIM 19I	BES3	$e^+e^- \rightarrow \eta\phi f_0(980)$
139.8 ± 12.3 ± 20.6		<sup>1</sup> ABLIKIM 19L	BES3	$e^+e^- \rightarrow K^+K^-$
104 ± 15 ± 15	471	ABLIKIM 15H	BES3	$J/\psi \rightarrow \eta\phi\pi^+\pi^-$
77 ± 15 ± 10		<sup>2,3</sup> LEES 12F	BABR	$10.6 e^+e^- \rightarrow \phi\pi^+\pi^-\gamma$
192 ± 23 ± <sup>25</sup> / <sub>-61</sub>	4.8k	<sup>4</sup> SHEN 09	BELL	$10.6 e^+e^- \rightarrow K^+K^-\pi^+\pi^-\gamma$
65 ± 23 ± 17	52	ABLIKIM 08F	BES	$J/\psi \rightarrow \eta\phi f_0(980)$
61 ± 5.0 ± 13	483	AUBERT 08S	BABR	$10.6 e^+e^- \rightarrow \phi\eta\gamma$
71 ± 21	116	<sup>5</sup> AUBERT 07AK	BABR	$10.6 e^+e^- \rightarrow K^+K^-\pi^+\pi^-\gamma$
102 ± 27	149	<sup>5</sup> AUBERT 07AK	BABR	$10.6 e^+e^- \rightarrow K^+K^-\pi^0\pi^0\gamma$
58 ± 16 ± 20	201	<sup>3,6</sup> AUBERT, BE 06D	BABR	$10.6 e^+e^- \rightarrow K^+K^-\pi\pi\gamma$

<sup>1</sup>The observed structure can be due to both the  $\phi(2170)$  and  $\rho(2150)$ .

<sup>2</sup>Fit includes interference with the  $\phi(1680)$ .

<sup>3</sup>From the  $\phi f_0(980)$  component.

<sup>4</sup>From a fit with two incoherent Breit-Wigners.

<sup>5</sup>From the  $K^+K^-f_0(980)$  component.

<sup>6</sup>Superseded by LEES 12F.

### $\phi(2170)$ DECAY MODES

Mode	Fraction ( $\Gamma_i/\Gamma$ )
$\Gamma_1 e^+e^-$	seen
$\Gamma_2 \phi\eta$	
$\Gamma_3 \phi\pi\pi$	
$\Gamma_4 \phi f_0(980)$	seen
$\Gamma_5 K^+K^-\pi^+\pi^-$	
$\Gamma_6 K^+K^-f_0(980) \rightarrow K^+K^-\pi^+\pi^-$	seen
$\Gamma_7 K^+K^-\pi^0\pi^0$	
$\Gamma_8 K^+K^-f_0(980) \rightarrow K^+K^-\pi^0\pi^0$	seen
$\Gamma_9 K^{*0}K^\pm\pi^\mp$	not seen
$\Gamma_{10} K^*(892)^0\bar{K}^*(892)^0$	not seen

### $\phi(2170)$ $\Gamma(i)\Gamma(e^+e^-)/\Gamma(\text{total})$

$\Gamma(\phi\eta) \times \Gamma(e^+e^-)/\Gamma_{\text{total}}$	$\Gamma_2\Gamma_1/\Gamma$			
VALUE (eV)	EVTS	DOCUMENT ID	TECN	COMMENT
• • • We do not use the following data for averages, fits, limits, etc. • • •				
1.7 ± 0.7 ± 1.3	483	AUBERT 08S	BABR	$10.6 e^+e^- \rightarrow \phi\eta\gamma$

$\Gamma(\phi f_0(980)) \times \Gamma(e^+e^-)/\Gamma_{\text{total}}$	$\Gamma_4\Gamma_1/\Gamma$			
VALUE (eV)	EVTS	DOCUMENT ID	TECN	COMMENT
<b>2.3 ± 0.3 ± 0.3</b>		<sup>1,2</sup> LEES 12F	BABR	$10.6 e^+e^- \rightarrow \phi\pi^+\pi^-\gamma$
• • • We do not use the following data for averages, fits, limits, etc. • • •				
2.5 ± 0.8 ± 0.4	201	<sup>2,3</sup> AUBERT, BE 06D	BABR	$10.6 e^+e^- \rightarrow K^+K^-\pi\pi\gamma$

<sup>1</sup>From a fit with constructive interference with the  $\phi(1680)$ . In a fit with destructive interference, the value is larger by a factor of 1.2.

<sup>2</sup>From the  $\phi f_0(980)$  component.

<sup>3</sup>Superseded by LEES 12F.

### $\phi(2170)$ $\Gamma(i)\Gamma(e^+e^-)/\Gamma^2(\text{total})$

$\Gamma(\phi\pi\pi)/\Gamma_{\text{total}} \times \Gamma(e^+e^-)/\Gamma_{\text{total}}$	$\Gamma_3/\Gamma \times \Gamma_1/\Gamma$			
VALUE (units $10^{-7}$ )	EVTS	DOCUMENT ID	TECN	COMMENT
• • • We do not use the following data for averages, fits, limits, etc. • • •				
1.65 ± 0.15 ± 0.18	4.8k	<sup>1</sup> SHEN 09	BELL	$10.6 e^+e^- \rightarrow K^+K^-\pi^+\pi^-\gamma$
<sup>1</sup> Multiplied by 3/2 to take into account the $\phi\pi^0\pi^0$ mode. Using $B(\phi \rightarrow K^+K^-) = (49.2 \pm 0.6)\%$ .				

### $\phi(2170)$ BRANCHING RATIOS

$\Gamma(K^+K^-f_0(980) \rightarrow K^+K^-\pi^+\pi^-)/\Gamma_{\text{total}}$	$\Gamma_6/\Gamma$		
VALUE	DOCUMENT ID	TECN	COMMENT
seen	AUBERT 07AK	BABR	$10.6 e^+e^- \rightarrow K^+K^-\pi^+\pi^-\gamma$
$\Gamma(K^+K^-f_0(980) \rightarrow K^+K^-\pi^0\pi^0)/\Gamma_{\text{total}}$	$\Gamma_8/\Gamma$		
VALUE	DOCUMENT ID	TECN	COMMENT
seen	AUBERT 07AK	BABR	$10.6 e^+e^- \rightarrow K^+K^-\pi^0\pi^0\gamma$
$\Gamma(K^{*0}K^\pm\pi^\mp)/\Gamma_{\text{total}}$	$\Gamma_9/\Gamma$		
VALUE	DOCUMENT ID	TECN	COMMENT
not seen	AUBERT 07AK	BABR	$10.6 \text{ GeV } e^+e^-$

### $\Gamma(K^*(892)^0\bar{K}^*(892)^0)/\Gamma_{\text{total}}$

VALUE	DOCUMENT ID	TECN	COMMENT	$\Gamma_{10}/\Gamma$	
not seen	ABLIKIM	10c	BES2	$J/\psi \rightarrow \eta K^+\pi^- K^-\pi^+$	

### $\phi(2170)$ REFERENCES

ABLIKIM 19I	PR D99 012014	M. Ablikim et al.	(BESIII Collab.)
ABLIKIM 19L	PR D99 032001	M. Ablikim et al.	(BESIII Collab.)
ABLIKIM 15H	PR D91 052017	M. Ablikim et al.	(BESIII Collab.)
LEES 12F	PR D86 012008	J.P. Lees et al.	(BABAR Collab.)
ABLIKIM 10C	PL B685 27	M. Ablikim et al.	(BES II Collab.)
SHEN 09	PR D80 031101	C.P. Shen et al.	(BELLE Collab.)
ABLIKIM 08F	PRL 100 102003	M. Ablikim et al.	(BES Collab.)
AUBERT 08S	PR D77 092002	B. Aubert et al.	(BABAR Collab.)
AUBERT 07AK	PR D76 012008	B. Aubert et al.	(BABAR Collab.)
AUBERT, BE 06D	PR D74 091103	B. Aubert et al.	(BABAR Collab.)

## $f_0(2200)$

$$I^G(J^{PC}) = 0^+(0^{++})$$

OMITTED FROM SUMMARY TABLE

Seen in  $K_S^0 K_S^0$  (AUGUSTIN 88),  $K^+K^-$  (ABLIKIM 05Q) and  $\eta\eta$  (BINON 05) system. Not seen in  $\mathcal{T}(1S)$  radiative decays (BARU 89).

### $f_0(2200)$ MASS

VALUE (MeV)	EVTS	DOCUMENT ID	TECN	COMMENT
<b>2187 ± 14 OUR AVERAGE</b>				
2170 ± 20 ± <sup>10</sup> / <sub>-15</sub>		ABLIKIM	05Q	BES2 $\psi(2S) \rightarrow \gamma\pi^+\pi^-K^+K^-$
2197 ± 17		<sup>1</sup> AUGUSTIN 88	DM2	$J/\psi \rightarrow \gamma K_S^0 K_S^0$
• • • We do not use the following data for averages, fits, limits, etc. • • •				
2206 ± 12 ± 8	381	<sup>2,3</sup> DOBBS 15		$J/\psi \rightarrow \gamma K^+K^-$
2188 ± 17 ± 16	203	<sup>2,3</sup> DOBBS 15		$\psi(2S) \rightarrow \gamma K^+K^-$
2210 ± 5.0		<sup>4</sup> BINON 05	GAMS	$33 \pi^-\rho \rightarrow \eta\eta\eta$
~ 2122		HASAN 94	RVUE	$\bar{p}p \rightarrow \pi\pi$
~ 2321		HASAN 94	RVUE	$\bar{p}p \rightarrow \pi\pi$

<sup>1</sup>Cannot determine spin to be 0.

<sup>2</sup>Using CLEO-c data but not authored by the CLEO Collaboration.

<sup>3</sup>From a fit to a Breit-Wigner line shape with fixed  $\Gamma = 238$  MeV.

<sup>4</sup>First solution, PWA is ambiguous.

### $f_0(2200)$ WIDTH

VALUE (MeV)	DOCUMENT ID	TECN	COMMENT
<b>207 ± 40 OUR AVERAGE</b>			
220 ± 60 ± <sup>40</sup> / <sub>-45</sub>	ABLIKIM	05Q	BES2 $\psi(2S) \rightarrow \gamma\pi^+\pi^-K^+K^-$
201 ± 5.1	<sup>5</sup> AUGUSTIN 88	DM2	$J/\psi \rightarrow \gamma K_S^0 K_S^0$
• • • We do not use the following data for averages, fits, limits, etc. • • •			
380 ± 90	<sup>6</sup> BINON 05	GAMS	$33 \pi^-\rho \rightarrow \eta\eta\eta$
~ 273	HASAN 94	RVUE	$\bar{p}p \rightarrow \pi\pi$
~ 223	HASAN 94	RVUE	$\bar{p}p \rightarrow \pi\pi$
<sup>5</sup> Cannot determine spin to be 0.			
<sup>6</sup> First solution, PWA is ambiguous.			

### $f_0(2200)$ REFERENCES

DOBBS 15	PR D91 052006	S. Dobbs et al.	(NWES)
ABLIKIM 05Q	PR D72 092002	M. Ablikim et al.	(BES Collab.)
BINON 05	PAN 68 960	F. Binon et al.	
	Translated from YAF 68 998.		
HASAN 94	PL B334 215	A. Hasan, D.V. Bugg	(LOQM)
BARU 89	ZPHY C42 505	S.E. Baru et al.	(NOVO)
AUGUSTIN 88	PRL 60 2238	J.E. Augustin et al.	(DM2 Collab.)

## $f_j(2220)$

$$I^G(J^{PC}) = 0^+(2^{++} \text{ or } 4^{++})$$

OMITTED FROM SUMMARY TABLE

Needs confirmation. See our mini-review in the 2004 edition of this Review, PDG 04.

### $f_j(2220)$ MASS

VALUE (MeV)	EVTS	DOCUMENT ID	TECN	COMMENT
<b>2231.1 ± 3.5 OUR AVERAGE</b>				
2235 ± 4 ± 6	74	BAI 96B	BES	$e^+e^- \rightarrow J/\psi \rightarrow \gamma\pi^+\pi^-$
2230 ± <sup>6</sup> / <sub>-7</sub> ± 16	46	BAI 96B	BES	$e^+e^- \rightarrow J/\psi \rightarrow \gamma K^+K^-$
2232 ± <sup>8</sup> / <sub>-7</sub> ± 15	23	BAI 96B	BES	$e^+e^- \rightarrow J/\psi \rightarrow \gamma K_S^0 K_S^0$
2235 ± 4 ± 5	32	BAI 96B	BES	$e^+e^- \rightarrow J/\psi \rightarrow \gamma\rho\bar{\rho}$
2209 ± 17 ± 15 ± 10		ASTON 88F	LASS	$11 K^-\rho \rightarrow K^+K^-\Lambda$
2230 ± 20		BOLONKIN 88	SPEC	$40 \pi^-\rho \rightarrow K_S^0 K_S^0 n$
2220 ± 10	41	<sup>1</sup> ALDE 86B	GA24	$38-100 \pi\rho \rightarrow n\eta\eta'$
2230 ± 6 ± 14	93	BALTRUSAIT...86D	MRK3	$e^+e^- \rightarrow \gamma K^+K^-$
2232 ± 7 ± 7	23	BALTRUSAIT...86D	MRK3	$e^+e^- \rightarrow \gamma K_S^0 K_S^0$

• • • We do not use the following data for averages, fits, limits, etc. • • •  
 2223.9 ± 2.5 <sup>2</sup>VLADIMIRSK...08 SPEC 40  $\pi^- p \rightarrow K_S^0 K_S^0 n + m\pi^0$   
 2246 ± 36 BAI 98H BES  $J/\psi \rightarrow \gamma \pi^0 \pi^0$   
<sup>1</sup>ALDE 86B uses data from both the GAMS-2000 and GAMS-4000 detectors.  
<sup>2</sup> $J^{PC} = 2^+ +$ . Systematic uncertainties not evaluated

**$f_j(2220)$  WIDTH**

VALUE (MeV)	CL%	EVTS	DOCUMENT ID	TECN	COMMENT
<b>23<sup>+</sup><sub>5</sub> <sup>9</sup></b>					<b>OUR AVERAGE</b>
19 <sup>+</sup> <sub>11</sub> ± 12	74		BAI	96B BES	$e^+ e^- \rightarrow J/\psi \rightarrow \gamma \pi^+ \pi^-$
20 <sup>+</sup> <sub>15</sub> ± 17	46		BAI	96B BES	$e^+ e^- \rightarrow J/\psi \rightarrow \gamma K^+ K^-$
20 <sup>+</sup> <sub>16</sub> ± 14	23		BAI	96B BES	$e^+ e^- \rightarrow J/\psi \rightarrow \gamma K_S^0 K_S^0$
15 <sup>+</sup> <sub>9</sub> ± 9	32		BAI	96B BES	$e^+ e^- \rightarrow J/\psi \rightarrow \gamma \rho \bar{\rho}$
60 <sup>+</sup> <sub>57</sub>			ASTON	88F LASS	11 $K^- p \rightarrow K^+ K^- \Lambda$
80 ± 30			BOLONKIN	88 SPEC	40 $\pi^- p \rightarrow K_S^0 K_S^0 n$
26 <sup>+</sup> <sub>16</sub> ± 17	93		BALTRUSAIT...86D	MRK3	$e^+ e^- \rightarrow \gamma K^+ K^-$
18 <sup>+</sup> <sub>15</sub> ± 10	23		BALTRUSAIT...86D	MRK3	$e^+ e^- \rightarrow \gamma K_S^0 K_S^0$
• • • We do not use the following data for averages, fits, limits, etc. • • •					
8.6 ± 2.5			<sup>1</sup> VLADIMIRSK...08	SPEC	40 $\pi^- p \rightarrow K_S^0 K_S^0 n + m\pi^0$
<80	90		ALDE	87C GAM2	38 $\pi^- p \rightarrow \eta' \eta n$
<sup>1</sup> $J^{PC} = 2^+ +$ . Systematic uncertainties not evaluated					

**$f_j(2220)$  DECAY MODES**

Mode	Fraction ( $\Gamma_i/\Gamma$ )
$\Gamma_1$ $\pi \pi$	not seen
$\Gamma_2$ $\pi^+ \pi^-$	not seen
$\Gamma_3$ $K \bar{K}$	not seen
$\Gamma_4$ $\rho \bar{\rho}$	not seen
$\Gamma_5$ $\gamma \gamma$	not seen
$\Gamma_6$ $\eta \eta' (958)$	seen
$\Gamma_7$ $\phi \phi$	not seen
$\Gamma_8$ $\eta \eta$	not seen

**$f_j(2220)$   $\Gamma(i)\Gamma(\gamma\gamma)/\Gamma(\text{total})$**

VALUE (eV)	CL%	DOCUMENT ID	TECN	COMMENT	$\Gamma_3 \Gamma_5 / \Gamma$
< 1.4	95	<sup>1</sup> ACCIARRI 01H L3		$\gamma \gamma \rightarrow K_S^0 K_S^0, E_{\text{cm}}^{\text{ee}} = 91, 183-209 \text{ GeV}$	
• • • We do not use the following data for averages, fits, limits, etc. • • •					
< 5.6		<sup>1</sup> GODANG 97 CLE2		$\gamma \gamma \rightarrow K_S^0 K_S^0$	
< 86	95	<sup>1</sup> ALBRECHT 90G ARG		$\gamma \gamma \rightarrow K^+ K^-$	
<1000	95	<sup>2</sup> ALTHOFF 85B TASS		$\gamma \gamma, K \bar{K} \pi$	

VALUE (eV)	CL%	DOCUMENT ID	TECN	COMMENT	$\Gamma_1 \Gamma_5 / \Gamma$
<2.5	95	ALAM 98C CLE2		$\gamma \gamma \rightarrow \pi^+ \pi^-$	
<sup>1</sup> Assuming $J^P = 2^+$ . <sup>2</sup> True for $J^P = 0^+$ and $J^P = 2^+$ .					

**$f_j(2220)$   $\Gamma(i)\Gamma(\rho\bar{\rho})/\Gamma^2(\text{total})$**

VALUE (units 10 <sup>-5</sup> )	CL%	DOCUMENT ID	TECN	COMMENT	$\Gamma_4/\Gamma \times \Gamma_1/\Gamma$
<18	95	<sup>1</sup> AMSLER 01 CBAR		1.4-1.5 $\rho \bar{\rho} \rightarrow \pi^0 \pi^0$	
• • • We do not use the following data for averages, fits, limits, etc. • • •					
<(11-42)	99	<sup>2</sup> HASAN 96 SPEC		1.35-1.55 $\rho \bar{\rho} \rightarrow \pi^+ \pi^-$	

VALUE (units 10 <sup>-5</sup> )	CL%	DOCUMENT ID	TECN	COMMENT	$\Gamma_4/\Gamma \times \Gamma_7/\Gamma$
<6	95	<sup>3</sup> EVANGELIS... 98	SPEC	1.1-2.0 $\rho \bar{\rho} \rightarrow \phi \phi$	

VALUE (units 10 <sup>-5</sup> )	CL%	DOCUMENT ID	TECN	COMMENT	$\Gamma_4/\Gamma \times \Gamma_8/\Gamma$
<4	95	<sup>1</sup> AMSLER 01 CBAR		1.4-1.5 $\rho \bar{\rho} \rightarrow \eta \eta$	

<sup>1</sup> For  $J^P = 2^+$  in the mass range 2222-2240 MeV and the total width between 10 and 20 MeV.  
<sup>2</sup> For  $J^P = 2^+$  and  $J^P = 4^+$  in the mass range 2220-2245 MeV and the total width of 15 MeV.  
<sup>3</sup> For  $J^P = 2^+$ , the mass of 2235 MeV and the total width of 15 MeV.

**$f_j(2220)$  BRANCHING RATIOS**

$\Gamma(\pi\pi)/\Gamma_{\text{total}}$	$\Gamma_1/\Gamma$
VALUE	DOCUMENT ID COMMENT
not seen	<sup>1</sup> DOBBS 15 $J/\psi \rightarrow \gamma \pi \pi$
not seen	<sup>1</sup> DOBBS 15 $\psi(2S) \rightarrow \gamma \pi \pi$
<sup>1</sup> Using CLEO-c data but not authored by the CLEO Collaboration.	

$\Gamma(K\bar{K})/\Gamma_{\text{total}}$	$\Gamma_3/\Gamma$
VALUE	DOCUMENT ID COMMENT
not seen	<sup>1</sup> DOBBS 15 $J/\psi \rightarrow \gamma K \bar{K}$
not seen	<sup>1</sup> DOBBS 15 $\psi(2S) \rightarrow \gamma K \bar{K}$
<sup>1</sup> Using CLEO-c data but not authored by the CLEO Collaboration.	

$\Gamma(\pi\pi)/\Gamma(K\bar{K})$	$\Gamma_1/\Gamma_3$
VALUE	DOCUMENT ID TECN COMMENT
<b>1.0 ± 0.5</b>	BAI 96B BES $e^+ e^- \rightarrow J/\psi \rightarrow \gamma \pi, K \bar{K}$

$\Gamma(\rho\bar{\rho})/\Gamma_{\text{total}}$	$\Gamma_4/\Gamma$
VALUE (units 10 <sup>-4</sup> )	DOCUMENT ID TECN COMMENT
• • • We do not use the following data for averages, fits, limits, etc. • • •	
not seen	<sup>1</sup> AUBERT 07AV BABR $B \rightarrow \rho \bar{\rho} K^*$
not seen	WANG 05A BELL $B^+ \rightarrow \bar{p} p K^+$
<3.0	95 <sup>2</sup> EVANGELIS... 97 SPEC 1.96-2.40 $\bar{p} p \rightarrow K_S^0 K_S^0$
<1.1	99.7 <sup>3</sup> BARNES 93 SPEC 1.3-1.57 $\bar{p} p \rightarrow K_S^0 K_S^0$
<2.6	99.7 <sup>3</sup> BARDIN 87 CNTR 1.3-1.5 $\bar{p} p \rightarrow K^+ K^-$
<3.6	99.7 <sup>3</sup> SCULLI 87 CNTR 1.29-1.55 $\bar{p} p \rightarrow K^+ K^-$
<sup>1</sup> Assuming $\Gamma < 30 \text{ MeV}$ . <sup>2</sup> Assuming $\Gamma \sim 20 \text{ MeV}$ , $J^P = 2^+$ and $B(f_j(2220) \rightarrow K \bar{K}) = 100\%$ . <sup>3</sup> Assuming $\Gamma = 30-35 \text{ MeV}$ , $J^P = 2^+$ and $B(f_j(2220) \rightarrow K \bar{K}) = 100\%$ .	

$\Gamma(\rho\bar{\rho})/\Gamma(K\bar{K})$	$\Gamma_4/\Gamma_3$
VALUE	DOCUMENT ID TECN COMMENT
<b>0.17 ± 0.09</b>	BAI 96B BES $e^+ e^- \rightarrow J/\psi \rightarrow \gamma \rho \bar{\rho}, K \bar{K}$

**$f_j(2220)$  REFERENCES**

DOBBS 15 PR D91 052006 S. Dobbs et al. (NWES)  
 VLADIMIRSK... 08 PAN 71 2129 V.V. Vladimirov et al. (ITEP)  
 Translated from YAF 71 2166.  
 AUBERT 07AV PR D76 092004 B. Aubert et al. (BABAR Collab.)  
 WANG 05A PL B617 141 M.-Z. Wang et al. (BELLE Collab.)  
 PDG 04 PL B592 1 S. Eidelman et al. (PDG Collab.)  
 ACCIARRI 01H PL B501 173 M. Acciari et al. (L3 Collab.)  
 AMSLER 01 PL B520 175 C. Amisler et al. (Crystal Barrel Collab.)  
 ALAM 98C PRL 81 3328 M.S. Alam et al. (CLEO Collab.)  
 BAI 98H PRL 81 1179 J.Z. Bai et al. (BES Collab.)  
 EVANGELIS... 98 PR D57 6370 C. Evangelista et al. (JETSET Collab.)  
 EVANGELIS... 97 PR D56 3803 C. Evangelista et al. (LEAR Collab.)  
 GODANG 97 PRL 79 3829 R. Godang et al. (CLEO Collab.)  
 BAI 96B PRL 76 3502 J.Z. Bai et al. (BES Collab.)  
 HASAN 96 PL B388 376 A. Hasan, D.V. Bugg (BRUN, LOQM)  
 BARNES 93 PL B309 469 P.D. Barnes et al. (PS185 Collab.)  
 ALBRECHT 90G ZPHY C48 183 H. Albrecht et al. (ARGUS Collab.)  
 ASTON 88F PL B215 199 D. Aston et al. (SLAC, NAGO, CIN, INUS, JP)  
 BOLONKIN 88 NP B309 426 B.V. Bolonkin et al. (ITEP, SERP)  
 ALDE 87C SJNP 45 255 D. Alde et al.  
 Translated from YAF 45 405.  
 BARDIN 87 PL B195 292 G. Bardini et al. (SACL, FERR, CERN, PADO+)  
 SCULLI 87 PRL 58 1715 J. Sculli et al. (NYU, BNL)  
 ALDE 86B PL B177 120 D.M. Alde et al. (SERP, BELG, LANL, LAPP)  
 BALTRUSAIT... 86D PRL 56 107 R.M. Baltrusaitis (CIT, UCSC, ILL, SLAC+)  
 ALTHOFF 85B ZPHY C29 189 M. Althoff et al. (TASSO Collab.)

**OTHER RELATED PAPERS**

DEL-AMO-SA... 100	PRL 105 172001	P. del Amo Sanchez et al. (BABAR Collab.)
-------------------	----------------	---

$\eta(2225)$

$I^G(J^{PC}) = 0^+(0^-+)$

OMITTED FROM SUMMARY TABLE  
 Seen in  $J/\psi \rightarrow \gamma \phi \phi$ . Possibly seen in  $B \rightarrow \phi \phi K$  by LEES 11A.

**$\eta(2225)$  MASS**

VALUE (MeV)	EVTS	DOCUMENT ID	TECN	COMMENT
<b>2221<sup>+</sup><sub>10</sub> <sup>13</sup></b>				<b>OUR AVERAGE</b>
2216 <sup>+</sup> <sub>5</sub> ± 11		<sup>1</sup> ABLIKIM 16N BES3		$J/\psi \rightarrow \gamma K^+ K^- K^+ K^-$
2240 <sup>+</sup> <sub>20</sub> ± 30	196 ± 19	ABLIKIM 08I BES		$J/\psi \rightarrow \gamma K^+ K^- K_S^0 K_L^0$
2230 ± 25 ± 15		BAI 90B MRK3		$J/\psi \rightarrow \gamma K^+ K^- K^+ K^-$
2214 ± 20 ± 13		BAI 90B MRK3		$J/\psi \rightarrow \gamma K^+ K^- K_S^0 K_L^0$
• • • We do not use the following data for averages, fits, limits, etc. • • •				
~ 2220		BISELLO 86B DM2		$J/\psi \rightarrow \gamma K^+ K^- K^+ K^-$

<sup>1</sup> From a partial wave analysis of  $J/\psi \rightarrow \gamma \phi \phi$  that also finds significant signals for for  $\eta(2100)$ ,  $0^- +$  phase space,  $f_0(2100)$ ,  $f_2(2010)$ ,  $f_2(2300)$ ,  $f_2(2340)$ , and a previously unseen  $0^- +$  state  $X(2500)$  ( $M = 2470^{+15+101}_{-19-23} \text{ MeV}$ ,  $\Gamma = 230^{+64+56}_{-35-33} \text{ MeV}$ ).

## Meson Particle Listings

 $\eta(2225)$ ,  $\rho_3(2250)$ ,  $f_2(2300)$  $\eta(2225)$  WIDTH

VALUE (MeV)	EVTS	DOCUMENT ID	TECN	CHG	COMMENT
<b>185 ± 40</b>	<b>20</b>	<b>OUR AVERAGE</b>			
185 ± 12+43 14-17		<sup>1</sup> ABLIKIM	16N	BES3	$J/\psi \rightarrow \gamma K^+ K^- K^+ K^-$
190 ± 30+60 40	196 ± 19	ABLIKIM	08I	BES	$J/\psi \rightarrow \gamma K^+ K^- K_S^0 K_L^0$
150 ± 300 60 ± 60		BAI	90B	MRK3	$J/\psi \rightarrow \gamma K^+ K^- K^+ K^-$
••• We do not use the following data for averages, fits, limits, etc. •••					
~ 80		BISELLO	86B	DM2	$J/\psi \rightarrow \gamma K^+ K^- K^+ K^-$

<sup>1</sup> From a partial wave analysis of  $J/\psi \rightarrow \gamma \phi \phi$  that also finds significant signals for  $\eta(2100)$ ,  $0^{-+}$  phase space,  $f_0(2100)$ ,  $f_2(2010)$ ,  $f_2(2300)$ ,  $f_2(2340)$ , and a previously unseen  $0^{-+}$  state  $X(2500)$  ( $M = 2470^{+15+101}_{-19-23}$  MeV,  $\Gamma = 230^{+64+56}_{-35-33}$  MeV).

 $\eta(2225)$  REFERENCES

ABLIKIM	16N	PR D93 112011	M. Ablikim	(BESIII Collab.)
LEES	11A	PR D84 012001	J.P. Lees et al.	(BABAR Collab.)
ABLIKIM	08I	PL B662 330	M. Ablikim et al.	(BES Collab.)
BAI	90B	PRL 65 1309	Z. Bai et al.	(Mark III Collab.)
BISELLO	86B	PL B179 294	D. Bisello et al.	(DM2 Collab.)

 $\rho_3(2250)$ 

$$I^G(J^{PC}) = 1^+(3^{--})$$

OMITTED FROM SUMMARY TABLE

Contains results mostly from formation experiments. For further production experiments see the Further States entry. See also  $\rho(2150)$ ,  $f_2(2150)$ ,  $f_4(2300)$ ,  $\rho_5(2350)$ .

 $\rho_3(2250)$  MASS $\bar{p}p \rightarrow \pi\pi$  or  $K\bar{K}$ 

VALUE (MeV)	DOCUMENT ID	TECN	CHG	COMMENT
••• We do not use the following data for averages, fits, limits, etc. •••				
~ 2232	HASAN	94	RVUE	$\bar{p}p \rightarrow \pi\pi$
~ 2090	<sup>1</sup> OAKDEN	94	RVUE	0.36-1.55 $\bar{p}p \rightarrow \pi\pi$
~ 2250	<sup>2</sup> MARTIN	80B	RVUE	
~ 2300	<sup>2</sup> MARTIN	80C	RVUE	
~ 2140	<sup>3</sup> CARTER	78B	CNTR 0	0.7-2.4 $\bar{p}p \rightarrow K^- K^+$
~ 2150	<sup>4</sup> CARTER	77	CNTR 0	0.7-2.4 $\bar{p}p \rightarrow \pi\pi$

<sup>1</sup> See however KLOET 96 who fit  $\pi^+\pi^-$  only and find waves only up to  $J = 3$  to be important but not significantly resonant.

<sup>2</sup>  $I(J^P) = 1(3^-)$  from simultaneous analysis of  $p\bar{p} \rightarrow \pi^-\pi^+$  and  $\pi^0\pi^0$ .

<sup>3</sup>  $I = 0, 1$ .  $J^P = 3^-$  from Barrelet-zero analysis.

<sup>4</sup>  $I(J^P) = 1(3^-)$  from amplitude analysis.

S-CHANNEL  $\bar{N}N$ 

VALUE (MeV)	DOCUMENT ID	TECN	CHG	COMMENT
••• We do not use the following data for averages, fits, limits, etc. •••				
2260 ± 20	<sup>5</sup> ANISOVICH	02	SPEC	0.6-1.9 $p\bar{p} \rightarrow \omega\pi^0$ , $\omega\eta\pi^0$ , $\pi^+\pi^-$
~ 2190	<sup>6</sup> CUTTS	78B	CNTR	0.97-3 $\bar{p}p \rightarrow \bar{N}N$
2155 ± 15	<sup>6,7</sup> COUPLAND	77	CNTR 0	0.7-2.4 $\bar{p}p \rightarrow \bar{p}p$
2193 ± 2	<sup>6,8</sup> ALSPECTOR	73	CNTR	$\bar{p}p$ S channel
2190 ± 10	<sup>9</sup> ABRAMS	70	CNTR	S channel $\bar{p}N$

<sup>5</sup> From the combined analysis of ANISOVICH 00J, ANISOVICH 01D, ANISOVICH 01E, and ANISOVICH 02.

<sup>6</sup> Isospins 0 and 1 not separated.

<sup>7</sup> From a fit to the total elastic cross section.

<sup>8</sup> Referred to as  $T$  or  $T'$  region by ALSPECTOR 73.

<sup>9</sup> Seen as bump in  $I = 1$  state. See also COOPER 68. PEASLEE 75 confirm  $\bar{p}p$  results of ABRAMS 70, no narrow structure.

 $\pi^-p \rightarrow \eta\pi\pi$ 

VALUE (MeV)	DOCUMENT ID	TECN	CHG	COMMENT
••• We do not use the following data for averages, fits, limits, etc. •••				
2290 ± 20 ± 30	AMELIN	00	VES	37 $\pi^-p \rightarrow \eta\pi^+\pi^-n$

 $\rho_3(2250)$  WIDTH $\bar{p}p \rightarrow \pi\pi$  or  $K\bar{K}$ 

VALUE (MeV)	DOCUMENT ID	TECN	CHG	COMMENT
••• We do not use the following data for averages, fits, limits, etc. •••				
~ 220	HASAN	94	RVUE	$\bar{p}p \rightarrow \pi\pi$
~ 60	<sup>10</sup> OAKDEN	94	RVUE	0.36-1.55 $\bar{p}p \rightarrow \pi\pi$
~ 250	<sup>11</sup> MARTIN	80B	RVUE	
~ 200	<sup>11</sup> MARTIN	80C	RVUE	
~ 150	<sup>12</sup> CARTER	78B	CNTR 0	0.7-2.4 $\bar{p}p \rightarrow K^- K^+$
~ 200	<sup>13</sup> CARTER	77	CNTR 0	0.7-2.4 $\bar{p}p \rightarrow \pi\pi$

<sup>10</sup> See however KLOET 96 who fit  $\pi^+\pi^-$  only and find waves only up to  $J = 3$  to be important but not significantly resonant.

<sup>11</sup>  $I(J^P) = 1(3^-)$  from simultaneous analysis of  $p\bar{p} \rightarrow \pi^-\pi^+$  and  $\pi^0\pi^0$ .

<sup>12</sup>  $I = 0, 1$ .  $J^P = 3^-$  from Barrelet-zero analysis.

<sup>13</sup>  $I(J^P) = 1(3^-)$  from amplitude analysis.

S-CHANNEL  $\bar{N}N$ 

VALUE (MeV)	DOCUMENT ID	TECN	CHG	COMMENT
••• We do not use the following data for averages, fits, limits, etc. •••				
160 ± 25	<sup>14</sup> ANISOVICH	02	SPEC	0.6-1.9 $p\bar{p} \rightarrow \omega\pi^0$ , $\omega\eta\pi^0$ , $\pi^+\pi^-$
135 ± 75	<sup>15,16</sup> COUPLAND	77	CNTR 0	0.7-2.4 $\bar{p}p \rightarrow \bar{p}p$
98 ± 8	<sup>16</sup> ALSPECTOR	73	CNTR	$\bar{p}p$ S channel
~ 85	<sup>17</sup> ABRAMS	70	CNTR	S channel $\bar{p}N$

<sup>14</sup> From the combined analysis of ANISOVICH 00J, ANISOVICH 01D, ANISOVICH 01E, and ANISOVICH 02.

<sup>15</sup> From a fit to the total elastic cross section.

<sup>16</sup> Isospins 0 and 1 not separated.

<sup>17</sup> Seen as bump in  $I = 1$  state. See also COOPER 68. PEASLEE 75 confirm  $\bar{p}p$  results of ABRAMS 70, no narrow structure.

 $\pi^-p \rightarrow \eta\pi\pi$ 

VALUE (MeV)	DOCUMENT ID	TECN	CHG	COMMENT
••• We do not use the following data for averages, fits, limits, etc. •••				
230 ± 50 ± 80	AMELIN	00	VES	37 $\pi^-p \rightarrow \eta\pi^+\pi^-n$

 $\rho_3(2250)$  REFERENCES

ANISOVICH	02	PL B542 8	A.V. Anisovich et al.	
ANISOVICH	01D	PL B508 6	A.V. Anisovich et al.	
ANISOVICH	01E	PL B513 281	A.V. Anisovich et al.	
AMELIN	00	NP A668 83	D. Amelin et al.	(VES Collab.)
ANISOVICH	00J	PL B491 47	A.V. Anisovich et al.	(RAL, LOQM, FNPI+)
KLOET	96	PR D53 6120	W.M. Kloet, F. Myhrer	(RUTG, IORD)
HASAN	94	PL B334 215	A. Hasan, D.V. Bugg	(LOQM)
OAKDEN	94	NP A574 731	M.N. Oakden, M.R. Pennington	(DURH)
MARTIN	80B	NP B176 355	B.R. Martin, D. Morgan	(LOUC, RHEL)JP
MARTIN	80C	NP B169 216	A.D. Martin, M.R. Pennington	(DURH)JP
CARTER	78B	NP B141 467	A.A. Carter	(LOQM)
CUTTS	78B	PR D17 16	D. Cutts et al.	(STON, WISC)
CARTER	77	PL 67B 117	A.A. Carter et al.	(LOQM, RHEL)JP
COUPLAND	77	PL 71B 460	M. Coupland et al.	(LOQM, RHEL)
PEASLEE	75	PL 57B 189	D.C. Peaslee et al.	(CANB, BARI, BROW+)
ALSPECTOR	73	PRL 30 511	J. Alspector et al.	(RUTG, UPNJ)
ABRAMS	70	PR D1 1917	R.J. Abrams et al.	(BNL)
COOPER	68	PRL 20 1059	W.A. Cooper et al.	(ANL)

 $f_2(2300)$ 

$$I^G(J^{PC}) = 0^+(2^{++})$$

 $f_2(2300)$  MASS

VALUE (MeV)	DOCUMENT ID	TECN	CHG	COMMENT
<b>2297 ± 28</b>	<sup>1</sup> ETKIN	88	MPS	22 $\pi^-p \rightarrow \phi\phi n$
••• We do not use the following data for averages, fits, limits, etc. •••				
2243 ± 7+3 6-29	<sup>2</sup> UEHARA	13	BELL	$\gamma\gamma \rightarrow K_S^0 K_S^0$
2270 ± 12	VLADIMIRSK..06	SPEC	40	$\pi^-p \rightarrow K_S^0 K_S^0 n$
2327 ± 9 ± 6	ABE	04	BELL	10.6 $e^+e^- \rightarrow e^+e^- K^+ K^-$
2231 ± 10	BOOTH	86	OMEG	85 $\pi^-Be \rightarrow 2\phi Be$
2220 ± 90 20	LINDENBAUM	84	RVUE	
2320 ± 40	ETKIN	82	MPS	22 $\pi^-p \rightarrow 2\phi n$

<sup>1</sup> Includes data of ETKIN 85. The percentage of the resonance going into  $\phi\phi 2^{++} S_2$ ,  $D_2$ , and  $D_0$  is  $6^{+15}_{-5}$ ,  $25^{+18}_{-14}$ , and  $69^{+16}_{-27}$ , respectively.

<sup>2</sup> Spin 2 preferred, tentatively assigned to  $f_2(2300)$ .

 $f_2(2300)$  WIDTH

VALUE (MeV)	DOCUMENT ID	TECN	CHG	COMMENT
<b>149 ± 41</b>	<sup>3</sup> ETKIN	88	MPS	22 $\pi^-p \rightarrow \phi\phi n$
••• We do not use the following data for averages, fits, limits, etc. •••				
145 ± 12+27 -34	<sup>4</sup> UEHARA	13	BELL	$\gamma\gamma \rightarrow K_S^0 K_S^0$
90 ± 29	VLADIMIRSK..06	SPEC	40	$\pi^-p \rightarrow K_S^0 K_S^0 n$
275 ± 36 ± 20	ABE	04	BELL	10.6 $e^+e^- \rightarrow e^+e^- K^+ K^-$
133 ± 50	BOOTH	86	OMEG	85 $\pi^-Be \rightarrow 2\phi Be$
200 ± 50	LINDENBAUM	84	RVUE	
220 ± 70	ETKIN	82	MPS	22 $\pi^-p \rightarrow 2\phi n$

<sup>3</sup> Includes data of ETKIN 85.

<sup>4</sup> Spin 2 preferred, tentatively assigned to  $f_2(2300)$ .

 $f_2(2300)$  DECAY MODES

Mode	Fraction ( $\Gamma_i/\Gamma$ )
$\Gamma_1$ $\phi\phi$	seen
$\Gamma_2$ $K\bar{K}$	seen
$\Gamma_3$ $\gamma\gamma$	seen

See key on page 999

# Meson Particle Listings

## $f_2(2300)$ , $f_4(2300)$ , $f_0(2330)$

### $f_2(2300) \Gamma(i)\Gamma(\gamma\gamma)/\Gamma(\text{total})$

$\Gamma(K\bar{K}) \times \Gamma(\gamma\gamma)/\Gamma_{\text{total}}$	DOCUMENT ID	TECN	COMMENT	$\Gamma_2\Gamma_3/\Gamma$
$3.2^{+0.5+1.3}_{-0.4-2.2}$	UEHARA	13	BELL $\gamma\gamma \rightarrow K_S^0 K_S^0$	
$44 \pm 6 \pm 12$	<sup>5</sup> ABE	04	BELL $10.6 e^+ e^- \rightarrow e^+ e^- K^+ K^-$	

<sup>5</sup> Assuming spin 2.

### $f_2(2300)$ REFERENCES

UEHARA 13	PTEP 2013 123C01	S. Uehara et al.	(BELLE Collab.)
VLADIMIRSK... 06	PAN 69 493	V.V. Vladimirov et al.	(ITEP, Moscow)
ABE 04	EPJ C32 323	K. Abe et al.	(BELLE Collab.)
ETKIN 88	PL B201 568	A. Etkin et al.	(BNL, CUNY)
BOOTH 86	NP B273 677	P.S.L. Booth et al.	(LIVP, GLAS, CERN)
ETKIN 85	PL 165B 217	A. Etkin et al.	(BNL, CUNY)
LINDENBAUM 84	CNPP 13 285	S.J. Lindenbaum	(CUNY)
ETKIN 82	PRL 49 1620	A. Etkin et al.	(BNL, CUNY)

### $f_4(2300)$

$$I^G(J^{PC}) = 0^+(4^{++})$$

OMITTED FROM SUMMARY TABLE

This entry was previously called  $U_0(2350)$ . Contains results mostly from formation experiments. For further production experiments see the Further States entry. See also  $\rho(2150)$ ,  $f_2(2150)$ ,  $\rho_3(2250)$ ,  $\rho_5(2350)$ .

### $f_4(2300)$ MASS

### $\bar{p}p \rightarrow \pi\pi \text{ or } \bar{K}K$

VALUE (MeV)	DOCUMENT ID	TECN	COMMENT
$\sim 2314$	HASAN 94	RVUE	$\bar{p}p \rightarrow \pi\pi$
$\sim 2300$	<sup>1</sup> MARTIN 80B	RVUE	
$\sim 2300$	<sup>1</sup> MARTIN 80C	RVUE	
$\sim 2340$	<sup>2</sup> CARTER 78B	CNTR	$0.7-2.4 \bar{p}p \rightarrow K^- K^+$
$\sim 2330$	DULUDE 78B	OSPK	$1-2 \bar{p}p \rightarrow \pi^0 \pi^0$
$\sim 2310$	<sup>3</sup> CARTER 77	CNTR	$0.7-2.4 \bar{p}p \rightarrow \pi\pi$

<sup>1</sup>  $I(J^P) = 0(4^+)$  from simultaneous analysis of  $p\bar{p} \rightarrow \pi^- \pi^+$  and  $\pi^0 \pi^0$ .  
<sup>2</sup>  $I(J^P) = 0(4^+)$  from Barrelet-zero analysis.  
<sup>3</sup>  $I(J^P) = 0(4^+)$  from amplitude analysis.

### S-CHANNEL $\bar{p}p \text{ or } \bar{N}N$

VALUE (MeV)	DOCUMENT ID	TECN	COMMENT
$2283 \pm 17$	<sup>4</sup> ANISOVICH 00J	SPEC	
$\sim 2380$	<sup>5</sup> CUTTS 78B	CNTR	$0.97-3 \bar{p}p \rightarrow \bar{N}N$
$2345 \pm 15$	<sup>5,6</sup> COUPLAND 77	CNTR	$0.7-2.4 \bar{p}p \rightarrow \bar{p}p$
$2359 \pm 2$	<sup>5,7</sup> ALSPECTOR 73	CNTR	$\bar{p}p$ S channel
$2375 \pm 10$	ABRAMS 70	CNTR	S channel $\bar{N}N$

<sup>4</sup> From the combined analysis of ANISOVICH 99c and ANISOVICH 99f on  $\bar{p}p \rightarrow \eta\pi^0 \pi^0$ ,  $\pi^0 \pi^0$ ,  $\eta\eta$ ,  $\eta\eta'$ ,  $\pi^+ \pi^-$ .  
<sup>5</sup> Isospins 0 and 1 not separated.  
<sup>6</sup> From a fit to the total elastic cross section.  
<sup>7</sup> Referred to as  $U$  or  $U$  region by ALSPECTOR 73.

### $\pi^- p \rightarrow \eta\pi\pi n$

VALUE (MeV)	DOCUMENT ID	TECN	COMMENT
$2330 \pm 20 \pm 40$	AMELIN 00	VES	$37 \pi^- p \rightarrow \eta\pi^+ \pi^- n$

### $pp$ CENTRAL PRODUCTION

VALUE (MeV)	DOCUMENT ID	COMMENT
<b><math>2320 \pm 60</math> OUR ESTIMATE</b>		
$2332 \pm 15$	BARBERIS 00F	$450 pp \rightarrow p_f \omega p_S$

### $f_4(2300)$ WIDTH

### $\bar{p}p \rightarrow \pi\pi \text{ or } \bar{K}K$

VALUE (MeV)	DOCUMENT ID	TECN	COMMENT
$\sim 278$	HASAN 94	RVUE	$\bar{p}p \rightarrow \pi\pi$
$\sim 200$	<sup>8</sup> MARTIN 80C	RVUE	
$\sim 150$	<sup>9</sup> CARTER 78B	CNTR	$0.7-2.4 \bar{p}p \rightarrow K^- K^+$
$\sim 210$	<sup>10</sup> CARTER 77	CNTR	$0.7-2.4 \bar{p}p \rightarrow \pi\pi$

<sup>8</sup>  $I(J^P) = 0(4^+)$  from simultaneous analysis of  $p\bar{p} \rightarrow \pi^- \pi^+$  and  $\pi^0 \pi^0$ .  
<sup>9</sup>  $I(J^P) = 0(4^+)$  from Barrelet-zero analysis.  
<sup>10</sup>  $I(J^P) = 0(4^+)$  from amplitude analysis.

### S-CHANNEL $\bar{p}p \text{ or } \bar{N}N$

VALUE (MeV)	DOCUMENT ID	TECN	COMMENT
$310 \pm 25$	<sup>11</sup> ANISOVICH 00J	SPEC	
$135^{+150}_{-65}$	<sup>12,13</sup> COUPLAND 77	CNTR	$0.7-2.4 \bar{p}p \rightarrow \bar{p}p$
$165^{+18}_{-8}$	<sup>13</sup> ALSPECTOR 73	CNTR	$\bar{p}p$ S channel
$\sim 190$	ABRAMS 70	CNTR	S channel $\bar{N}N$

<sup>11</sup> From the combined analysis of ANISOVICH 99c and ANISOVICH 99f on  $\bar{p}p \rightarrow \eta\pi^0 \pi^0$ ,  $\pi^0 \pi^0$ ,  $\eta\eta$ ,  $\eta\eta'$ ,  $\pi^+ \pi^-$ .  
<sup>12</sup> From a fit to the total elastic cross section.  
<sup>13</sup> Isospins 0 and 1 not separated.

### $\pi^- p \rightarrow \eta\pi\pi n$

VALUE (MeV)	DOCUMENT ID	TECN	COMMENT
$235 \pm 50 \pm 40$	AMELIN 00	VES	$37 \pi^- p \rightarrow \eta\pi^+ \pi^- n$

### $pp$ CENTRAL PRODUCTION

VALUE (MeV)	DOCUMENT ID	COMMENT
<b><math>250 \pm 80</math> OUR ESTIMATE</b>		
$260 \pm 57$	BARBERIS 00F	$450 pp \rightarrow p_f \omega p_S$

### $f_4(2300)$ DECAY MODES

Mode	Fraction ( $\Gamma_i/\Gamma$ )
$\Gamma_1$ $\rho\rho$	seen
$\Gamma_2$ $\omega\omega$	seen
$\Gamma_3$ $\eta\pi\pi$	seen
$\Gamma_4$ $\pi\pi$	seen
$\Gamma_5$ $K\bar{K}$	seen
$\Gamma_6$ $N\bar{N}$	seen

### $f_4(2300)$ BRANCHING RATIOS

$\Gamma(\rho\rho)/\Gamma(\omega\omega)$	DOCUMENT ID	COMMENT	$\Gamma_1/\Gamma_2$
$2.8 \pm 0.5$	BARBERIS 00F	$450 pp \rightarrow p_f \omega p_S$	

### $f_4(2300)$ REFERENCES

AMELIN 00	NP A668 83	D. Amelin et al.	(VES Collab.)
ANISOVICH 00J	PL B491 47	A.V. Anisovich et al.	(RAL, LOQM, PNPI+)
BARBERIS 00F	PL B484 198	D. Barberis et al.	(WA 102 Collab.)
ANISOVICH 99C	PL B452 173	A.V. Anisovich et al.	
ANISOVICH 99F	NP A551 253	A.V. Anisovich et al.	(LOQM)
HASAN 94	PL B334 215	A. Hasan, D.V. Bugg	(LOUQ, RHEL) JP
MARTIN 80B	NP B176 355	B.R. Martin, D. Morgan	(DURH) JP
MARTIN 80C	NP B169 216	A.D. Martin, M.R. Pennington	(DURH) JP
CARTER 78B	NP B141 467	A.A. Carter	(LOQM)
CUTTS 78B	PR D17 16	D. Cutts et al.	(STON, WISC)
DULUDE 78B	PL 79B 335	R.S. Dulude et al.	(BROW, MIT, BARI) JP
CARTER 77	PL 67B 117	A.A. Carter et al.	(LOQM, RHEL) JP
COUPLAND 77	PL 71B 460	M. Coupland et al.	(LOQM, RHEL)
ALSPECTOR 73	PRL 30 511	J. Alspector et al.	(RUTG, UPNJ)
ABRAMS 70	PR D1 1917	R.J. Abrams et al.	(BNL)

### $f_0(2330)$

$$I^G(J^{PC}) = 0^+(0^{++})$$

OMITTED FROM SUMMARY TABLE

### $f_0(2330)$ MASS

VALUE (MeV)	DOCUMENT ID	TECN	COMMENT
$2314 \pm 25$	<sup>1</sup> BUGG 04A	RVUE	
$2337 \pm 14$	ANISOVICH 00J	SPEC	$2.0 \bar{p}p \rightarrow \pi\pi, \eta\eta$
$\sim 2321$	HASAN 94	RVUE	$\bar{p}p \rightarrow \pi\pi$

<sup>1</sup> Partial wave analysis of the data on  $p\bar{p} \rightarrow \bar{\Lambda}\Lambda$  from BARNES 00.

### $f_0(2330)$ WIDTH

VALUE (MeV)	DOCUMENT ID	TECN	COMMENT
$144 \pm 20$	<sup>2</sup> BUGG 04A	RVUE	
$217 \pm 33$	ANISOVICH 00J	SPEC	$2.0 \bar{p}p \rightarrow \pi\pi, \eta\eta$
$\sim 223$	HASAN 94	RVUE	$\bar{p}p \rightarrow \pi\pi$

<sup>2</sup> Partial wave analysis of the data on  $p\bar{p} \rightarrow \bar{\Lambda}\Lambda$  from BARNES 00.

### $f_0(2330)$ REFERENCES

BUGG 04A	EPJ C36 161	D.V. Bugg	(LOQM)
ANISOVICH 00J	PL B491 47	A.V. Anisovich et al.	(RAL, LOQM, PNPI+)
BARNES 00	PR C62 055203	P.D. Barnes et al.	
HASAN 94	PL B334 215	A. Hasan, D.V. Bugg	(LOQM)



# Meson Particle Listings

## $f_2(2340)$ , $\rho_5(2350)$

### $f_2(2340)$

$$I^G(J^{PC}) = 0^+(2^{++})$$

#### $f_2(2340)$ MASS

VALUE (MeV)	EVTS	DOCUMENT ID	TECN	COMMENT
<b>2345 ± 50 OUR AVERAGE</b>				
2362 ± 31 +140 -30 -63	5.5k	1 ABLIKIM	13N BES3	$e^+e^- \rightarrow J/\psi \rightarrow \gamma\eta\eta$
2339 ± 55		2 ETKIN	88 MPS	$22 \pi^- p \rightarrow \phi\phi n$
2350 ± 7	80k	3 UMAN	06 E835	$5.2 \bar{p}p \rightarrow \eta\eta\pi^0$
2392 ± 10		BOOTH	86 OMEG	$85 \pi^- Be \rightarrow 2\phi Be$
2360 ± 20		LINDENBAUM	84 RVUE	

• • • We do not use the following data for averages, fits, limits, etc. • • •  
 1 From partial wave analysis including all possible combinations of  $0^{++}$ ,  $2^{++}$ , and  $4^{++}$  resonances.  
 2 Includes data of ETKIN 85. The percentage of the resonance going into  $\phi\phi 2^{++} S_2$ ,  $D_2$ , and  $D_0$  is  $37 \pm 19$ ,  $4 \pm 12$ , and  $59 \pm 21$ , respectively.  
 3 Statistical error only.

#### $f_2(2340)$ WIDTH

VALUE (MeV)	EVTS	DOCUMENT ID	TECN	COMMENT
<b>322 ± 70 OUR AVERAGE</b>				
334 ± 62 +165 -54 -100	5.5k	4 ABLIKIM	13N BES3	$e^+e^- \rightarrow J/\psi \rightarrow \gamma\eta\eta$
319 ± 81 -69		5 ETKIN	88 MPS	$22 \pi^- p \rightarrow \phi\phi n$
218 ± 16	80k	6 UMAN	06 E835	$5.2 \bar{p}p \rightarrow \eta\eta\pi^0$
198 ± 50		BOOTH	86 OMEG	$85 \pi^- Be \rightarrow 2\phi Be$
150 ± 150 -50		LINDENBAUM	84 RVUE	

• • • We do not use the following data for averages, fits, limits, etc. • • •  
 4 From partial wave analysis including all possible combinations of  $0^{++}$ ,  $2^{++}$ , and  $4^{++}$  resonances.  
 5 Includes data of ETKIN 85.  
 6 Statistical error only.

#### $f_2(2340)$ DECAY MODES

Mode	Fraction ( $\Gamma_i/\Gamma$ )
$\Gamma_1$ $\phi\phi$	seen
$\Gamma_2$ $\eta\eta$	seen

#### $f_2(2340)$ BRANCHING RATIOS

$\Gamma(\eta\eta)/\Gamma_{total}$	DOCUMENT ID	TECN	COMMENT	$\Gamma_2/\Gamma$
seen	UMAN	06 E835	$5.2 \bar{p}p \rightarrow \eta\eta\pi^0$	

#### $f_2(2340)$ REFERENCES

ABLIKIM	13N	PR D87 092009	Ablikim M. et al.	(BESIII Collab.)
UMAN	06	PR D73 052009	I. Uman et al.	(FNAL E835)
ETKIN	88	PL B201 568	A. Etkin et al.	(BNL, CUNY)
BOOTH	86	NP B273 677	P.S.L. Booth et al.	(LIVP, GLAS, CERN)
ETKIN	85	PL 165B 217	A. Etkin et al.	(BNL, CUNY)
LINDENBAUM	84	CNPP 13 285	S.J. Lindenbaum	(CUNY)

### $\rho_5(2350)$

$$I^G(J^{PC}) = 1^+(5^{--})$$

OMITTED FROM SUMMARY TABLE

This entry was previously called  $U_1(2400)$ . See also  $\rho(2150)$ ,  $f_2(2150)$ ,  $\rho_3(2250)$ ,  $f_4(2300)$ .

#### $\rho_5(2350)$ MASS

VALUE (MeV)	DOCUMENT ID	TECN	CHG	COMMENT
<b><math>\pi^- p \rightarrow \omega\pi^0 n</math></b>				
2330 ± 35	ALDE	95	GAM2	$38 \pi^- p \rightarrow \omega\pi^0 n$
<b><math>\bar{p}p \rightarrow \pi\pi</math> or <math>\bar{K}K</math></b>				
~ 2303	HASAN	94	RVUE	$\bar{p}p \rightarrow \pi\pi$
~ 2300	1 MARTIN	80B	RVUE	
~ 2250	1 MARTIN	80C	RVUE	
~ 2500	2 CARTER	78B	CNTR 0	$0.7-2.4 \bar{p}p \rightarrow K^- K^+$
~ 2480	3 CARTER	77	CNTR 0	$0.7-2.4 \bar{p}p \rightarrow \pi\pi$

#### S-CHANNEL $\bar{N}N$

VALUE (MeV)	DOCUMENT ID	TECN	CHG	COMMENT
• • • We do not use the following data for averages, fits, limits, etc. • • •				
2300 ± 45	4 ANISOVICH	02	SPEC	$0.6-1.9 p\bar{p} \rightarrow \omega\pi^0$ , $\omega\eta\pi^0, \pi^+\pi^-$
2295 ± 30	ANISOVICH	00J	SPEC	
~ 2380	5 CUTTS	78B	CNTR	$0.97-3 \bar{p}p \rightarrow \bar{N}N$
2345 ± 15	5,6 COUPLAND	77	CNTR 0	$0.7-2.4 \bar{p}p \rightarrow \bar{p}p$
2359 ± 2	5,7 ALSPECTOR	73	CNTR	$\bar{p}p$ S channel
2350 ± 10	8 ABRAMS	70	CNTR	S channel $\bar{N}N$
2360 ± 25	9 OH	70B	HDBC -0	$\bar{p}(p n), K^* K 2\pi$

#### $\pi^- p \rightarrow K^+ K^- n$

VALUE (MeV)	DOCUMENT ID	TECN	CHG	COMMENT
• • • We do not use the following data for averages, fits, limits, etc. • • •				
2307 ± 6	ALPER	80	CNTR 0	$62 \pi^- p \rightarrow K^+ K^- n$
1 ( $J^P$ ) = 1(5 <sup>-</sup> )				from simultaneous analysis of $p\bar{p} \rightarrow \pi^- \pi^+$ and $\pi^0 \pi^0$ .
2 ( $J^P$ ) = 0(1); $J^P$ = 5 <sup>-</sup>				from Barrelet-zero analysis.
3 ( $J^P$ ) = 1(5 <sup>-</sup> )				from amplitude analysis.
4				From the combined analysis of ANISOVICH 00J, ANISOVICH 01D, ANISOVICH 01E, and ANISOVICH 02.
5				Isospins 0 and 1 not separated.
6				From a fit to the total elastic cross section.
7				Referred to as U or U region by ALSPECTOR 73.
8				For $l = 1 \bar{N}N$ .
9				No evidence for this bump seen in the $\bar{p}p$ data of CHAPMAN 71B. Narrow state not confirmed by OH 73 with more data.

#### $\rho_5(2350)$ WIDTH

VALUE (MeV)	DOCUMENT ID	TECN	COMMENT
<b><math>\pi^- p \rightarrow \omega\pi^0 n</math></b>			
400 ± 100	ALDE	95	GAM2 $38 \pi^- p \rightarrow \omega\pi^0 n$

#### $\bar{p}p \rightarrow \pi\pi$ or $\bar{K}K$

VALUE (MeV)	DOCUMENT ID	TECN	CHG	COMMENT
• • • We do not use the following data for averages, fits, limits, etc. • • •				
~ 169	HASAN	94	RVUE	$\bar{p}p \rightarrow \pi\pi$
~ 250	10 MARTIN	80B	RVUE	
~ 300	10 MARTIN	80C	RVUE	
~ 150	11 CARTER	78B	CNTR 0	$0.7-2.4 \bar{p}p \rightarrow K^- K^+$
~ 210	12 CARTER	77	CNTR 0	$0.7-2.4 \bar{p}p \rightarrow \pi\pi$

#### S-CHANNEL $\bar{N}N$

VALUE (MeV)	DOCUMENT ID	TECN	CHG	COMMENT
• • • We do not use the following data for averages, fits, limits, etc. • • •				
260 ± 75	13 ANISOVICH	02	SPEC	$0.6-1.9 p\bar{p} \rightarrow \omega\pi^0$ , $\omega\eta\pi^0, \pi^+\pi^-$
235 ± 65 -40	ANISOVICH	00J	SPEC	
135 ± 150 -65	14,15 COUPLAND	77	CNTR 0	$0.7-2.4 \bar{p}p \rightarrow \bar{p}p$
165 ± 18 -8	15 ALSPECTOR	73	CNTR	$\bar{p}p$ S channel
< 60	16 OH	70B	HDBC -0	$\bar{p}(p n), K^* K 2\pi$
~ 140	ABRAMS	67C	CNTR	S channel $\bar{p}N$

#### $\pi^- p \rightarrow K^+ K^- n$

VALUE (MeV)	DOCUMENT ID	TECN	CHG	COMMENT
• • • We do not use the following data for averages, fits, limits, etc. • • •				
245 ± 20	ALPER	80	CNTR 0	$62 \pi^- p \rightarrow K^+ K^- n$
10 ( $J^P$ ) = 1(5 <sup>-</sup> )				from simultaneous analysis of $p\bar{p} \rightarrow \pi^- \pi^+$ and $\pi^0 \pi^0$ .
11 ( $J^P$ ) = 0(1); $J^P$ = 5 <sup>-</sup>				from Barrelet-zero analysis.
12 ( $J^P$ ) = 1(5 <sup>-</sup> )				from amplitude analysis.
13				From the combined analysis of ANISOVICH 00J, ANISOVICH 01D, ANISOVICH 01E, and ANISOVICH 02.
14				From a fit to the total elastic cross section.
15				Isospins 0 and 1 not separated.
16				No evidence for this bump seen in the $\bar{p}p$ data of CHAPMAN 71B. Narrow state not confirmed by OH 73 with more data.

#### $\rho_5(2350)$ REFERENCES

ANISOVICH	02	PL B542 8	A.V. Anisovich et al.	
ANISOVICH	01D	PL B508 6	A.V. Anisovich et al.	
ANISOVICH	01E	PL B513 281	A.V. Anisovich et al.	
ANISOVICH	00J	PL B491 47	A.V. Anisovich et al.	(RAL, LOQM, PNPI+)
ALDE	95	ZPHY C66 379	D.H. Alde et al.	(GAMS Collab) JP
HASAN	94	PL B334 215	A. Hasan et al.	(LOQM)
ALPER	80	PL 94B 422	B. Alper et al.	(AMST, CERN, CRAC, MPIM+)
MARTIN	80B	NP B176 355	B.R. Martin, D. Morgan	(LOUC, RHEL) JP
MARTIN	80C	NP B169 216	A.D. Martin, M.R. Pennington	(BURH) JP
CARTER	78B	NP B141 467	A.A. Carter	(LOQM)
CUTTS	78B	PR D17 16	D. Cutts et al.	(STON, WISC)
CARTER	77	PL 67B 117	A.A. Carter et al.	(LOQM, RHEL) JP
COUPLAND	77	PL 71B 460	M. Coupland et al.	(LOQM, RHEL)
ALSPECTOR	73	PRL 30 511	J. Alspector et al.	(RUTG, UPNJ)
OH	73	NP B51 57	B.Y. Oh et al.	(MSU)
CHAPMAN	71B	PR D1 1275	J.W. Chapman et al.	(MICH)
ABRAMS	70	PR D1 1917	R.J. Abrams et al.	(BNL)
OH	70B	PRL 24 1257	B.Y. Oh et al.	(MSU)
ABRAMS	67C	PRL 18 1209	R.J. Abrams et al.	(BNL)

See key on page 999

Meson Particle Listings

$f_6(2510)$

$f_6(2510)$

$$I^G(J^{PC}) = 0^+(6^{++})$$

OMITTED FROM SUMMARY TABLE  
Needs confirmation.

$f_6(2510)$  MASS

VALUE (MeV)	DOCUMENT ID	TECN	COMMENT
<b>2465 ± 50 OUR AVERAGE</b>	Error includes scale factor of 2.1.		
2420 ± 30	ALDE 98	GAM4	100 $\pi^- p \rightarrow \pi^0 \pi^0 n$
2510 ± 30	BINON 84B	GAM2	38 $\pi^- p \rightarrow n 2\pi^0$
• • • We do not use the following data for averages, fits, limits, etc. • • •			
2485 ± 40	<sup>1</sup> ANISOVICH 00J	SPEC	1.92–2.41 $p\bar{p}$
<sup>1</sup> From the combined analysis of ANISOVICH 99c, ANISOVICH 99f, ANISOVICH 99j, ANISOVICH 99k, and ANISOVICH 00b.			

$f_6(2510)$  WIDTH

VALUE (MeV)	DOCUMENT ID	TECN	COMMENT
<b>255 ± 40 OUR AVERAGE</b>			
270 ± 60	ALDE 98	GAM4	100 $\pi^- p \rightarrow \pi^0 \pi^0 n$
240 ± 60	BINON 84B	GAM2	38 $\pi^- p \rightarrow n 2\pi^0$
• • • We do not use the following data for averages, fits, limits, etc. • • •			
410 ± 90	<sup>2</sup> ANISOVICH 00J	SPEC	1.92–2.41 $p\bar{p}$
<sup>2</sup> From the combined analysis of ANISOVICH 99c, ANISOVICH 99f, ANISOVICH 99j, ANISOVICH 99k, and ANISOVICH 00b.			

$f_6(2510)$  DECAY MODES

Mode	Fraction ( $\Gamma_i/\Gamma$ )
$\Gamma_1 \pi\pi$	(6.0 ± 1.0) %

$f_6(2510)$  BRANCHING RATIOS

$\Gamma(\pi\pi)/\Gamma_{total}$	DOCUMENT ID	TECN	COMMENT	$\Gamma_1/\Gamma$
<b>0.06 ± 0.01</b>	<sup>3</sup> BINON 83C	GAM2	38 $\pi^- p \rightarrow n 4\gamma$	
<sup>3</sup> Assuming one pion exchange and using data of BOLOTOV 74.				

$f_6(2510)$  REFERENCES

ANISOVICH 00B	NP A662 319	A.V. Anisovich <i>et al.</i>	
ANISOVICH 00J	PL B491 47	A.V. Anisovich <i>et al.</i>	(RAL, LOQM, PNPI+)
ANISOVICH 99C	PL B452 173	A.V. Anisovich <i>et al.</i>	
ANISOVICH 99F	NP A651 253	A.V. Anisovich <i>et al.</i>	
ANISOVICH 99J	PL B471 271	A.V. Anisovich <i>et al.</i>	
ANISOVICH 99K	PL B468 309	A.V. Anisovich <i>et al.</i>	
ALDE 98	EPJ A3 361	D. Alde <i>et al.</i>	(GAM4 Collab.)
Also	PAN 62 405	D. Alde <i>et al.</i>	(GAMS Collab.)
	Translated from YAF 62 446.		
BINON 84B	LNC 39 41	F.G. Binon <i>et al.</i>	(SERP, BELG, LAPP)JP
BINON 83C	SJNP 38 723	F.G. Binon <i>et al.</i>	(SERP, BRUX+)
	Translated from YAF 38 1199.		
BOLOTOV 74	PL 52B 489	V.N. Bolotov <i>et al.</i>	(SERP)

# Meson Particle Listings

## Further States

### OTHER LIGHT MESONS

#### Further States

OMITTED FROM SUMMARY TABLE

This section contains states observed by a single group or states poorly established that thus need confirmation.

QUANTUM NUMBERS, MASSES, WIDTHS, AND BRANCHING RATIOS

**X(360)**  $I^G(J^{PC}) = ??(??^+)$

MASS (MeV)	WIDTH (MeV)	EVTs	DOCUMENT ID	TECN	COMMENT
360 ± 7 ± 9	64 ± 18	2.3k	<sup>1</sup> ABRAAMYAN 09	CNTR	2.75 dC → γγX

<sup>1</sup> Not seen in pC → γγX at 5.5 GeV/c.

**X(1070)**  $I^G(J^{PC}) = ?(0^{++})$

MASS (MeV)	WIDTH (MeV)	DOCUMENT ID	COMMENT
1072 ± 1	3.5 ± 0.5	<sup>2</sup> VLADIMIRSK...08	40 π <sup>-</sup> p → K <sub>S</sub> <sup>0</sup> K <sub>S</sub> <sup>0</sup> n + mπ <sup>0</sup>

<sup>2</sup> Supersedes GRIGOR'EV 05.

**X(1110)**  $I^G(J^{PC}) = 0^+(\text{even}^{++})$

MASS (MeV)	WIDTH (MeV)	DOCUMENT ID	TECN	COMMENT
1107 ± 4	111 ± 8 ± 15	DAFTARI 87	DBC	0. $\bar{p}n \rightarrow \rho^-\pi^+\pi^-$

**η<sub>2</sub>(1200-1600)**  $I^G(J^{PC}) = 0^+(0^{++})$

MASS (MeV)	WIDTH (MeV)	DOCUMENT ID	TECN	COMMENT
1323 ± 8	237 ± 20	VLADIMIRSK...06	SPEC	40 π <sup>-</sup> p → K <sub>S</sub> <sup>0</sup> K <sub>S</sub> <sup>0</sup> n
1480 <sup>+100</sup> <sub>-150</sub>	1030 <sup>+80</sup> <sub>-170</sub>	<sup>3</sup> ANISOVICH 03	SPEC	
1530 <sup>+90</sup> <sub>-250</sub>	560 ± 40	<sup>4</sup> ANISOVICH 03	SPEC	

<sup>3</sup> K-matrix pole from combined analysis of π<sup>-</sup>p → π<sup>0</sup>π<sup>0</sup>n, π<sup>-</sup>p → K $\bar{K}$ n, π<sup>+</sup>π<sup>-</sup> → π<sup>+</sup>π<sup>-</sup>,  $\bar{p}p \rightarrow \pi^0\pi^0\pi^0, \pi^0\eta\eta, \pi^0\pi^0\eta, \pi^+\pi^-\pi^0, K^+K^-\pi^0, K_S^0K_S^0\pi^0, K^+K_S^0\pi^-$  at rest,  $\bar{p}n \rightarrow \pi^-\pi^+\pi^+, K_S^0K^-\pi^0, K_S^0K_S^0\pi^-$  at rest.

<sup>4</sup> K-matrix pole from combined analysis of π<sup>-</sup>p → π<sup>0</sup>π<sup>0</sup>n, π<sup>-</sup>p → K $\bar{K}$ n,  $\bar{p}p \rightarrow \pi^0\pi^0\pi^0, \pi^0\eta\eta, \pi^0\pi^0\eta$  at rest.

**X(1420)**  $I^G(J^{PC}) = 2^+(0^{++})$

MASS (MeV)	WIDTH (MeV)	DOCUMENT ID	TECN	COMMENT
1420 ± 20	160 ± 10	FILIPPI 00	OBLX	0 $\bar{p}p \rightarrow \pi^+\pi^+\pi^-$

**X(1545)**  $I^G(J^{PC}) = ?(??^{++})$

MASS (MeV)	WIDTH (MeV)	DOCUMENT ID	COMMENT
1545 ± 3	6.0 ± 2.5	<sup>5</sup> VLADIMIRSK...08	40 π <sup>-</sup> p → K <sub>S</sub> <sup>0</sup> K <sub>S</sub> <sup>0</sup> n + mπ <sup>0</sup>

<sup>5</sup> Supersedes VLADIMIRSKII 00.

**X(1575)**  $I^G(J^{PC}) = ?(1^{--})$

MASS (MeV)	WIDTH (MeV)	DOCUMENT ID	TECN	COMMENT
1576 <sup>+49+98</sup> <sub>-55-91</sub>	818 <sup>+22+64</sup> <sub>-23-133</sub>	<sup>6</sup> ABLIKIM 06s	BES	J/ψ → K <sup>+</sup> K <sup>-</sup> π <sup>0</sup>

<sup>6</sup> A broad peak observed at K<sup>+</sup>K<sup>-</sup> invariant mass. Mass and width above are its pole position. The observed branching ratio is B(J/ψ → Xπ<sup>0</sup>) B(X → K<sup>+</sup>K<sup>-</sup>) = (8.5 ± 0.6<sup>+2.7</sup><sub>-3.6</sub>) × 10<sup>-4</sup>.

**X(1600)**  $I^G(J^{PC}) = 2^+(2^{++})$

MASS (MeV)	WIDTH (MeV)	DOCUMENT ID	TECN	COMMENT
1600 ± 100	400 ± 200	<sup>7</sup> ALBRECHT 91F	ARG	10.2 e <sup>+</sup> e <sup>-</sup> → e <sup>+</sup> e <sup>-</sup> 2(π <sup>+</sup> π <sup>-</sup> )

<sup>7</sup> Our estimate.

**X(1650)**  $I^G(J^{PC}) = 0^-(??^-)$

MASS (MeV)	WIDTH (MeV)	EVTs	DOCUMENT ID	TECN	COMMENT
1652 ± 7	<50	100	PROKOSHKIN 96	GAM2	32,38 πp → ωηn

**X(1730)**  $I^G(J^{PC}) = ?(??^+)$

MASS (MeV)	WIDTH (MeV)	EVTs	DOCUMENT ID	TECN	COMMENT
1731.0 ± 1.2 ± 2.0	3.2 ± 0.8 ± 1.3	58	VLADIMIRSK...07	SPEC	40 π <sup>-</sup> p → K <sub>S</sub> <sup>0</sup> K <sub>S</sub> <sup>0</sup> X

**X(1750)**  $I^G(J^{PC}) = ?(1^{--})$

MASS (MeV)	WIDTH (MeV)	DOCUMENT ID	TECN	COMMENT
1753.5 ± 1.5 ± 2.3	122.2 ± 6.2 ± 8.0	LINK 02k	FOCS	20-160 γp → K <sup>+</sup> K <sup>-</sup> π <sup>0</sup>

**B(X(1750) → K\*(892)<sup>0</sup> K<sup>0</sup> → K<sup>±</sup>π<sup>∓</sup>K<sub>S</sub><sup>0</sup>)/B(X(1750) → K<sup>+</sup>K<sup>-</sup>)**

VALUE	CL%	DOCUMENT ID	TECN
<0.065	90	LINK	02k FOCS

**B(X(1750) → K\*(892)<sup>±</sup> K<sup>∓</sup> → K<sub>S</sub><sup>0</sup>π<sup>±</sup>K<sup>∓</sup>)/B(X(1750) → K<sup>+</sup>K<sup>-</sup>)**

VALUE	CL%	DOCUMENT ID	TECN
<0.183	90	LINK	02k FOCS

**η<sub>2</sub>(1750)**  $I^G(J^{PC}) = 0^+(2^{++})$

MASS (MeV)	WIDTH (MeV)	EVTs	DOCUMENT ID	TECN	COMMENT
1755 ± 10	67 ± 12	870	<sup>8</sup> SCHEGELSKY 06A	RVUE	γγ → K <sub>S</sub> <sup>0</sup> K <sub>S</sub> <sup>0</sup>

**Γ(K $\bar{K}$ )**

VALUE (MeV)	EVTs	DOCUMENT ID	TECN	COMMENT
17 ± 5	870	<sup>9</sup> SCHEGELSKY 06A	RVUE	γγ → K <sub>S</sub> <sup>0</sup> K <sub>S</sub> <sup>0</sup>

**Γ(γγ)**

VALUE (MeV)	EVTs	DOCUMENT ID	TECN	COMMENT
0.13 ± 0.04	870	<sup>9</sup> SCHEGELSKY 06A	RVUE	γγ → K <sub>S</sub> <sup>0</sup> K <sub>S</sub> <sup>0</sup>

**Γ(ππ)**

VALUE (MeV)	EVTs	DOCUMENT ID	TECN	COMMENT
1.3 ± 1.0	870	<sup>9</sup> SCHEGELSKY 06A	RVUE	γγ → K <sub>S</sub> <sup>0</sup> K <sub>S</sub> <sup>0</sup>

**Γ(ηη)**

VALUE (MeV)	EVTs	DOCUMENT ID	TECN	COMMENT
2.0 ± 0.5	870	<sup>9</sup> SCHEGELSKY 06A	RVUE	γγ → K <sub>S</sub> <sup>0</sup> K <sub>S</sub> <sup>0</sup>

<sup>8</sup> From analysis of L3 data at 91 and 183-209 GeV.  
<sup>9</sup> From analysis of L3 data at 91 and 183-209 GeV and using SU(3) relations.

**X(1775)**  $I^G(J^{PC}) = 1^-(?^{-+})$

MASS (MeV)	WIDTH (MeV)	DOCUMENT ID	TECN	COMMENT
1763 ± 20	192 ± 60	CONDO 91	SHF	γp → (pπ <sup>+</sup> )(π <sup>+</sup> π <sup>-</sup> π <sup>-</sup> )
1787 ± 18	118 ± 60	CONDO 91	SHF	γp → nπ <sup>+</sup> π <sup>+</sup> π <sup>-</sup>

**η<sub>2</sub>(1800)**  $I^G(J^{PC}) = 0^+(0^{++})$

MASS (MeV)	WIDTH (MeV)	DOCUMENT ID	TECN	COMMENT
1795 ± 7 <sup>+23</sup> <sub>-20</sub>	95 ± 10 <sup>+78</sup> <sub>-82</sub>	ABLIKIM 13J	BES3	J/ψ → γωφ
1812 <sup>+19</sup> <sub>-26</sub> ± 18	105 ± 20 ± 28	<sup>10</sup> ABLIKIM 06J	BES2	J/ψ → γωφ

<sup>10</sup> Not seen by LIU 09 in B<sup>±</sup> → K<sup>±</sup>ωφ.

**X(1850 - 3100)**  $I^G(J^{PC}) = ?(1^{--})$

Γ(e <sup>+</sup> e <sup>-</sup> )/B(X → hadrons) (eV)	CL%	DOCUMENT ID	TECN	COMMENT
<120	90	<sup>11</sup> ANASHIN 11	KEDR	e <sup>+</sup> e <sup>-</sup> → hadrons

<sup>11</sup> This limit is center-of-mass energy dependent. We quote the most stringent one.

**X(1855)**  $I^G(J^{PC}) = ?(??^?)$

MASS (MeV)	WIDTH (MeV)	DOCUMENT ID	TECN	COMMENT
1856.6 ± 5	20 ± 5	BRIDGES 86D	SPEC	0. $\bar{p}d \rightarrow \pi\pi N$

**X(1870)**  $I^G(J^{PC}) = ?(2^{??})$

MASS (MeV)	WIDTH (MeV)	DOCUMENT ID	TECN	COMMENT
1870 ± 40	250 ± 30	ALDE 86D	GAM4	100 π <sup>-</sup> p → 2ηX

**a<sub>3</sub>(1875)**  $I^G(J^{PC}) = 1^-(3^{++})$

MASS (MeV)	WIDTH (MeV)	DOCUMENT ID	TECN	COMMENT
1874 ± 43 ± 96	385 ± 121 ± 114	CHUNG 02	B852	18.3 π <sup>-</sup> p → π <sup>+</sup> π <sup>-</sup> π <sup>-</sup> p

**B(a<sub>3</sub>(1875) → f<sub>2</sub>(1270)π)/B(a<sub>3</sub>(1875) → ρπ)**

VALUE	DOCUMENT ID	TECN	COMMENT
0.8 ± 0.2	<sup>12</sup> CHUNG 02	B852	18.3 π <sup>-</sup> p → π <sup>+</sup> π <sup>-</sup> π <sup>-</sup> p

<sup>12</sup> Using the observable fractions of 50.0% ρπ, 56.5% f<sub>2</sub>π, and 11.8% ρ<sub>3</sub>π.

**B(a<sub>3</sub>(1875) → ρ<sub>3</sub>(1690)π)/B(a<sub>3</sub>(1875) → ρπ)**

VALUE	DOCUMENT ID	TECN	COMMENT
0.9 ± 0.3	<sup>13</sup> CHUNG 02	B852	18.3 π <sup>-</sup> p → π <sup>+</sup> π <sup>-</sup> π <sup>-</sup> p

<sup>13</sup> Using the observable fractions of 50.0% ρπ, 56.5% f<sub>2</sub>π, and 11.8% ρ<sub>3</sub>π.

**a<sub>1</sub>(1930)**  $I^G(J^{PC}) = 1^-(1^{++})$

MASS (MeV)	WIDTH (MeV)	DOCUMENT ID	TECN	COMMENT
1930 <sup>+30</sup> <sub>-70</sub>	155 ± 45	ANISOVICH 01F	SPEC	2.0 $\bar{p}p \rightarrow 3\pi^0, \pi^0\eta, \pi^0\eta'$

See key on page 999

# Meson Particle Listings

## Further States

**X(1935)**  $I^G(J^{PC}) = 1^+(1^{-?})$

MASS (MeV)	WIDTH (MeV)	DOCUMENT ID	TECN	COMMENT
1935 ± 20	215 ± 30	EVANGELIS... 79	OMEG	10,16 $\pi^- p \rightarrow \bar{p} p n$

**$\rho_2(1940)$**   $I^G(J^{PC}) = 1^+(2^{- -})$

MASS (MeV)	WIDTH (MeV)	DOCUMENT ID	TECN	COMMENT
1940 ± 40	155 ± 40	14 ANISOVICH	02	SPEC 0.6-1.9 $p\bar{p} \rightarrow \omega\pi^0, \omega\eta\pi^0, \pi^+\pi^-$

<sup>14</sup>From the combined analysis of ANISOVICH 00J, ANISOVICH 01D, ANISOVICH 01E, and ANISOVICH 02.

**$\omega_3(1945)$**   $I^G(J^{PC}) = 0^-(3^{- -})$

MASS (MeV)	WIDTH (MeV)	DOCUMENT ID	TECN	COMMENT
1945 ± 20	115 ± 22	15 ANISOVICH	02B	SPEC 0.6-1.9 $p\bar{p} \rightarrow \omega\eta, \omega\pi^0\pi^0$

<sup>15</sup>From the combined analysis of ANISOVICH 00D, ANISOVICH 01C, and ANISOVICH 02B.

**$a_2(1950)$**   $I^G(J^{PC}) = 1^-(2^{+ +})$

MASS (MeV)	WIDTH (MeV)	DOCUMENT ID	TECN	COMMENT
1950 <sup>+30</sup> <sub>-70</sub>	180 <sup>+30</sup> <sub>-70</sub>	16 ANISOVICH	01F	SPEC 1.96-2.41 $\bar{p}p$

<sup>16</sup>From the combined analysis of ANISOVICH 99C, ANISOVICH 99E, and ANISOVICH 01F.

**$\omega(1960)$**   $I^G(J^{PC}) = 0^-(1^{- -})$

MASS (MeV)	WIDTH (MeV)	DOCUMENT ID	TECN	COMMENT
1960 ± 25	195 ± 60	17 ANISOVICH	02B	SPEC 0.6-1.9 $p\bar{p} \rightarrow \omega\eta, \omega\pi^0\pi^0$

<sup>17</sup>From the combined analysis of ANISOVICH 00D, ANISOVICH 01C, and ANISOVICH 02B.

**$b_1(1960)$**   $I^G(J^{PC}) = 1^+(1^{+ -})$

MASS (MeV)	WIDTH (MeV)	DOCUMENT ID	TECN	COMMENT
1960 ± 35	230 ± 50	18 ANISOVICH	02	SPEC 0.6-1.9 $p\bar{p} \rightarrow \omega\pi^0, \omega\eta\pi^0, \pi^+\pi^-$

<sup>18</sup>From the combined analysis of ANISOVICH 00J, ANISOVICH 01D, ANISOVICH 01E, and ANISOVICH 02.

**$h_1(1965)$**   $I^G(J^{PC}) = 0^-(1^{+ -})$

MASS (MeV)	WIDTH (MeV)	DOCUMENT ID	TECN	COMMENT
1965 ± 45	345 ± 75	19 ANISOVICH	02B	SPEC 0.6-1.9 $p\bar{p} \rightarrow \omega\eta, \omega\pi^0\pi^0$

<sup>19</sup>From the combined analysis of ANISOVICH 00D, ANISOVICH 01C, and ANISOVICH 02B.

**$f_1(1970)$**   $I^G(J^{PC}) = 0^+(1^{+ +})$

MASS (MeV)	WIDTH (MeV)	DOCUMENT ID	TECN	COMMENT
1971 ± 15	240 ± 45	ANISOVICH	00J	SPEC

**X(1970)**  $I^G(J^{PC}) = ?^?(?^{??})$

MASS (MeV)	WIDTH (MeV)	DOCUMENT ID	TECN	COMMENT
1970 ± 10	40 ± 20	CHLIAPNIK... 80	HBC	32 $K^+ p \rightarrow 2K_S^0 2\pi X$

**X(1975)**  $I^G(J^{PC}) = ?^?(?^{??})$

MASS (MeV)	WIDTH (MeV)	EVTS	DOCUMENT ID	TECN	COMMENT
1973 ± 15	80	30	CASO	70	HBC 11.2 $\pi^- p \rightarrow \rho 2\pi$

**$\omega_2(1975)$**   $I^G(J^{PC}) = 0^-(2^{- -})$

MASS (MeV)	WIDTH (MeV)	DOCUMENT ID	TECN	COMMENT
1975 ± 20	175 ± 25	20 ANISOVICH	02B	SPEC 0.6-1.9 $p\bar{p} \rightarrow \omega\eta, \omega\pi^0\pi^0$

<sup>20</sup>From the combined analysis of ANISOVICH 00D, ANISOVICH 01C, and ANISOVICH 02B.

**$a_2(1990)$**   $I^G(J^{PC}) = 1^-(2^{+ +})$

MASS (MeV)	WIDTH (MeV)	EVTS	DOCUMENT ID	TECN	COMMENT
2050 ± 10 ± 40	190 ± 22 ± 100	18k	21 SCHEGELSKY	06	RVUE $\gamma\gamma \rightarrow \pi^+\pi^-\pi^0$
2003 ± 10 ± 19	249 ± 23 ± 32		LU	05	B852 18 $\pi^- p \rightarrow \omega\pi^-\pi^0\pi^0$

<sup>21</sup>From analysis of L3 data at 183-209 GeV.

**$\Gamma(\gamma\gamma) \Gamma(\pi^+\pi^-\pi^0) / \Gamma(\text{total})$**

VALUE (keV)	EVTS	DOCUMENT ID	TECN	COMMENT
0.11 ± 0.04 ± 0.05	18k	22 SCHEGELSKY	06	RVUE $\gamma\gamma \rightarrow \pi^+\pi^-\pi^0$

<sup>22</sup>From analysis of L3 data at 183-209 GeV.

**$\rho(2000)$**   $I^G(J^{PC}) = 1^+(1^{- -})$

MASS (MeV)	WIDTH (MeV)	DOCUMENT ID	TECN	COMMENT
2000 ± 30	260 ± 45	23 BUGG	04C	RVUE Compilation
~ 1988	~ 244	HASAN	94	RVUE $\bar{p}p \rightarrow \pi\pi$

<sup>23</sup>From the combined analysis of ANISOVICH 00J, ANISOVICH 01D, ANISOVICH 01E, and ANISOVICH 02.

**$f_2(2000)$**   $I^G(J^{PC}) = 0^+(2^{+ +})$

MASS (MeV)	WIDTH (MeV)	DOCUMENT ID	TECN	COMMENT
2001 ± 10	312 ± 32	ANISOVICH	00J	SPEC
~ 1996	~ 134	HASAN	94	RVUE $\bar{p}p \rightarrow \pi\pi$

**X(2000)**  $I^G(J^{PC}) = 1^-(?^{?+})$

MASS (MeV)	WIDTH (MeV)	DOCUMENT ID	TECN	CHG	COMMENT
1964 ± 35	225 ± 50	24 ARMSTRONG	93D	E760	$\bar{p}p \rightarrow 3\pi^0 \rightarrow 6\gamma$
~ 2100	~ 500	24 ANTIPOV	77	CIBS	- 25 $\pi^- p \rightarrow \rho\pi^- \rho_3$
2214 ± 15	355 ± 21	25 BALTAY	77	HBC	0 15 $\pi^- p \rightarrow \Delta^{++} 3\pi$
2080 ± 40	340 ± 80	KALELKAR	75	HBC	+ 15 $\pi^+ p \rightarrow \rho\pi^+ \rho_3$

<sup>24</sup>Cannot determine spin to be 3.

<sup>25</sup>BALTAY 77 favors  $J^P = ,3^+$ .

**X(2000)**  $I^G(J^{PC}) = ?^?(4^{+ +})$

MASS (MeV)	WIDTH (MeV)	DOCUMENT ID	TECN	COMMENT
1998 ± 3 ± 5	< 15	VLADIMIRSK...03	SPEC	$\pi^- p \rightarrow K_S^0 K_S^0 M M$

**$\eta(2010)$**   $I^G(J^{PC}) = 0^+(0^{- +})$

MASS (MeV)	WIDTH (MeV)	DOCUMENT ID	TECN	COMMENT
2010 <sup>+35</sup> <sub>-60</sub>	270 ± 60	ANISOVICH	00J	SPEC

**$\pi_1(2015)$**   $I^G(J^{PC}) = 1^-(1^{- +})$

MASS (MeV)	WIDTH (MeV)	EVTS	DOCUMENT ID	TECN	COMMENT
2014 ± 20 ± 16	230 ± 32 ± 73	145k	LU	05	B852 18 $\pi^- p \rightarrow \omega\pi^-\pi^0 p$
2001 ± 30 ± 92	333 ± 52 ± 49	69k	KUHN	04	B852 18 $\pi^- p \rightarrow \eta\pi^+\pi^-\pi^- p$

**$a_0(2020)$**   $I^G(J^{PC}) = 1^-(0^{+ +})$

MASS (MeV)	WIDTH (MeV)	DOCUMENT ID	TECN	COMMENT
2025 ± 30	330 ± 75	ANISOVICH	99C	SPEC

**X(2020)**  $I^G(J^{PC}) = ?^?(?^{??})$

MASS (MeV)	WIDTH (MeV)	DOCUMENT ID	TECN	COMMENT
2015 ± 3	10 ± 4	FERRER	99	RVUE $\pi p \rightarrow p\rho\bar{p}\pi(\pi)$

**$h_3(2025)$**   $I^G(J^{PC}) = 0^-(3^{+ -})$

MASS (MeV)	WIDTH (MeV)	DOCUMENT ID	TECN	COMMENT
2025 ± 20	145 ± 30	26 ANISOVICH	02B	SPEC 0.6-1.9 $p\bar{p} \rightarrow \omega\eta, \omega\pi^0\pi^0$

<sup>26</sup>From the combined analysis of ANISOVICH 00D, ANISOVICH 01C, and ANISOVICH 02B.

**$b_3(2030)$**   $I^G(J^{PC}) = 1^+(3^{+ -})$

MASS (MeV)	WIDTH (MeV)	DOCUMENT ID	TECN	COMMENT
2032 ± 12	117 ± 11	27 ANISOVICH	02	SPEC 0.6-1.9 $p\bar{p} \rightarrow \omega\pi^0, \omega\eta\pi^0, \pi^+\pi^-$

<sup>27</sup>From the combined analysis of ANISOVICH 00J, ANISOVICH 01D, ANISOVICH 01E, and ANISOVICH 02.

**$a_2(2030)$**   $I^G(J^{PC}) = 1^-(2^{+ +})$

MASS (MeV)	WIDTH (MeV)	DOCUMENT ID	TECN	COMMENT
2030 ± 20	205 ± 30	28 ANISOVICH	01F	SPEC 1.96-2.41 $\bar{p}p$

<sup>28</sup>From the combined analysis of ANISOVICH 99C, ANISOVICH 99E, and ANISOVICH 01F.

**$a_3(2030)$**   $I^G(J^{PC}) = 1^-(3^{+ +})$

MASS (MeV)	WIDTH (MeV)	DOCUMENT ID	TECN	COMMENT
2031 ± 12	150 ± 18	29 ANISOVICH	01F	SPEC 1.96-2.41 $\bar{p}p$

<sup>29</sup>From the combined analysis of ANISOVICH 99C, ANISOVICH 99E, and ANISOVICH 01F.

**$\eta_2(2030)$**   $I^G(J^{PC}) = 0^+(2^{- +})$

MASS (MeV)	WIDTH (MeV)	DOCUMENT ID	TECN	COMMENT
2030 ± 5 ± 15	205 ± 10 ± 15	ANISOVICH	00E	SPEC

# Meson Particle Listings

## Further States

<b>B(a<sub>2</sub>π)<sub>L=0</sub>/B(a<sub>2</sub>π)<sub>L=2</sub></b>				
VALUE	DOCUMENT ID	TECN	COMMENT	
0.05±0.03	30 ANISOVICH	11	SPEC	0.9–1.94 $\rho\bar{p}$

<sup>30</sup> Reanalysis of ADOMEIT 96 and ANISOVICH 00E.

<b>B(a<sub>0</sub>π)/B(a<sub>2</sub>π)<sub>L=2</sub></b>				
VALUE	DOCUMENT ID	TECN	COMMENT	
0.10±0.08	31 ANISOVICH	11	SPEC	0.9–1.94 $\rho\bar{p}$

<sup>31</sup> Reanalysis of ADOMEIT 96 and ANISOVICH 00E.

<b>B(f<sub>2</sub>η)/B(a<sub>2</sub>π)<sub>L=2</sub></b>				
VALUE	DOCUMENT ID	TECN	COMMENT	
0.13±0.06	32 ANISOVICH	11	SPEC	0.9–1.94 $\rho\bar{p}$

<sup>32</sup> Reanalysis of ADOMEIT 96 and ANISOVICH 00E.

<b>f<sub>3</sub>(2050) I<sup>G</sup>(J<sup>PC</sup>) = 0<sup>+</sup>(3<sup>++</sup>)</b>				
MASS (MeV)	WIDTH (MeV)	DOCUMENT ID	TECN	COMMENT
2048±8	213±34	ANISOVICH	00J	SPEC 2.0 $\rho\bar{p} \rightarrow \eta\pi^0\pi^0$

<b>f<sub>0</sub>(2060) I<sup>G</sup>(J<sup>PC</sup>) = 0<sup>+</sup>(0<sup>++</sup>)</b>				
MASS (MeV)	WIDTH (MeV)	DOCUMENT ID	TECN	COMMENT
~ 2050	~ 120	33 OAKDEN	94	RVUE 0.36–1.55 $\bar{p}p \rightarrow \pi\pi$
~ 2060	~ 50	33 OAKDEN	94	RVUE 0.36–1.55 $\bar{p}p \rightarrow \pi\pi$

<sup>33</sup> See SEMENOV 99 and KLOET 96.

<b>π(2070) I<sup>G</sup>(J<sup>PC</sup>) = 1<sup>-</sup>(0<sup>-+</sup>)</b>				
MASS (MeV)	WIDTH (MeV)	DOCUMENT ID	TECN	COMMENT
2070±35	310 <sup>+100</sup> <sub>-50</sub>	ANISOVICH	01F	SPEC 2.0 $\bar{p}p \rightarrow 3\pi^0, \pi^0\eta, \pi^0\eta'$

<b>X(2075) I<sup>G</sup>(J<sup>PC</sup>) = ?<sup>?</sup>(???)</b>				
MASS (MeV)	WIDTH (MeV)	DOCUMENT ID	TECN	COMMENT
2075±12±5	90±35±9	34 ABLIKIM	04J	BES2 J/ψ → K <sup>-</sup> ρ <sup>+</sup> $\bar{\Lambda}$

<sup>34</sup> From a fit in the region  $M_{\rho\bar{\Lambda}} - M_{\rho} - M_{\Lambda} < 150$  MeV. S-wave in the  $\rho\bar{\Lambda}$  system preferred. A similar near-threshold enhancement in the  $\rho\bar{\Lambda}$  system is observed in  $B^+ \rightarrow \rho\bar{\Lambda}\bar{D}^0$  by CHEN 11F.

<b>X(2080) I<sup>G</sup>(J<sup>PC</sup>) = ?<sup>?</sup>(???)</b>				
MASS (MeV)	WIDTH (MeV)	DOCUMENT ID	TECN	COMMENT
2080±10	110±20	KREYMER	80	STRC 13 $\pi^- d \rightarrow \rho\bar{p}n(n_S)$

<b>X(2080) I<sup>G</sup>(J<sup>PC</sup>) = ?<sup>?</sup>(3<sup>-2</sup>)</b>				
MASS (MeV)	WIDTH (MeV)	DOCUMENT ID	TECN	COMMENT
2080±10	190±15	ROZANSKA	80	SPRK 18 $\pi^- p \rightarrow \rho\bar{p}n$

<b>a<sub>1</sub>(2095) I<sup>G</sup>(J<sup>PC</sup>) = 1<sup>-</sup>(1<sup>++</sup>)</b>					
MASS (MeV)	WIDTH (MeV)	EVS	DOCUMENT ID	TECN	COMMENT
2096±17±121	451±41±81	69k	KUHN	04	B852 18 $\pi^- p \rightarrow \eta\pi^+\pi^-\pi^-p$

<b>B(a<sub>1</sub>(2095) → f<sub>1</sub>(1285)π) / B(a<sub>1</sub>(2095) → a<sub>1</sub>(1260))</b>				
VALUE	EVS	DOCUMENT ID	TECN	COMMENT
3.18±0.64	69k	KUHN	04	B852 18 $\pi^- p \rightarrow \eta\pi^+\pi^-\pi^-p$

<b>η(2100) I<sup>G</sup>(J<sup>PC</sup>) = 0<sup>+</sup>(0<sup>-+</sup>)</b>					
MASS (MeV)	WIDTH (MeV)	EVS	DOCUMENT ID	TECN	COMMENT
2050 <sup>+30+75</sup> <sub>-24-26</sub>	250 <sup>+36+181</sup> <sub>-30-164</sub>	35	ABLIKIM	16N	BES3 J/ψ → γK <sup>+</sup>
2103±50	187±75	586	36 BISELLO	89B	DM2 J/ψ → 4πγ

<sup>35</sup> From a partial wave analysis of  $J/\psi \rightarrow \gamma\phi\phi$ , for which the primary signal is  $\eta(2225) \rightarrow \phi\phi$ , and that also finds significant signals for for 0<sup>-+</sup> phase space, f<sub>0</sub>(2100), f<sub>2</sub>(2010), f<sub>2</sub>(2300), f<sub>2</sub>(2340), and a previously unseen 0<sup>-+</sup> state X(2500) (M = 2470<sup>+15+101</sup><sub>-19-23</sub> MeV, Γ = 230<sup>+64+56</sup><sub>-35-33</sub> MeV).

<sup>36</sup> ASTON 81B sees no peak, has 850 events in Ajinenko+Barth bins. ARESTOV 80 sees no peak.

<b>X(2100) I<sup>G</sup>(J<sup>PC</sup>) = ?<sup>?</sup>(0<sup>??</sup>)</b>				
MASS (MeV)	WIDTH (MeV)	DOCUMENT ID	TECN	COMMENT
2100±40	250±40	ALDE	86D	GAMA 100 $\pi^- p \rightarrow 2\eta X$

<b>X(2110) I<sup>G</sup>(J<sup>PC</sup>) = 1<sup>+</sup>(3<sup>-2</sup>)</b>				
MASS (MeV)	WIDTH (MeV)	DOCUMENT ID	TECN	COMMENT
2110±10	330±20	EVANGELIS...	79	OMEG 10,16 $\pi^- p \rightarrow \bar{p}pn$

<b>f<sub>2</sub>(2140) I<sup>G</sup>(J<sup>PC</sup>) = 0<sup>+</sup>(2<sup>++</sup>)</b>					
MASS (MeV)	WIDTH (MeV)	EVS	DOCUMENT ID	TECN	COMMENT
2141±12	49±28	389	GREEN	86	MPSF 400 $pA \rightarrow 4KX$

<b>X(2150) I<sup>G</sup>(J<sup>PC</sup>) = ?<sup>?</sup>(2<sup>++</sup>)</b>					
MASS (MeV)	WIDTH (MeV)	DOCUMENT ID	TECN	COMMENT	
2150±10	260±10	ROZANSKA	80	SPRK	18 $\pi^- p \rightarrow \rho\bar{p}n$

<b>a<sub>2</sub>(2175) I<sup>G</sup>(J<sup>PC</sup>) = 1<sup>-</sup>(2<sup>++</sup>)</b>					
MASS (MeV)	WIDTH (MeV)	DOCUMENT ID	TECN	COMMENT	
2175±40	310 <sup>+90</sup> <sub>-45</sub>	ANISOVICH	01F	SPEC	2.0 $\bar{p}p \rightarrow 3\pi^0, \pi^0\eta, \pi^0\eta'$

<b>η(2190) I<sup>G</sup>(J<sup>PC</sup>) = 0<sup>+</sup>(0<sup>-+</sup>)</b>					
MASS (MeV)	WIDTH (MeV)	DOCUMENT ID	TECN	COMMENT	
2190±50	850±100	BUGG	99	BES	

<b>ω<sub>2</sub>(2195) I<sup>G</sup>(J<sup>PC</sup>) = 0<sup>-</sup>(2<sup>--</sup>)</b>					
MASS (MeV)	WIDTH (MeV)	DOCUMENT ID	TECN	COMMENT	
2195±30	225±40	37 ANISOVICH	02B	SPEC	0.6–1.9 $\rho\bar{p} \rightarrow \omega\eta, \omega\pi^0\pi^0$

<sup>37</sup> From the combined analysis of A NISOVICH 00D, ANISOVICH 01C, and ANISOVICH 02B.

<b>ω(2205) I<sup>G</sup>(J<sup>PC</sup>) = 0<sup>-</sup>(1<sup>--</sup>)</b>					
MASS (MeV)	WIDTH (MeV)	DOCUMENT ID	TECN	COMMENT	
2205±30	350±90	38 ANISOVICH	02B	SPEC	0.6–1.9 $\rho\bar{p} \rightarrow \omega\eta, \omega\pi^0\pi^0$

<sup>38</sup> From the combined analysis of A NISOVICH 00D, ANISOVICH 01C, and ANISOVICH 02B.

<b>X(2210) I<sup>G</sup>(J<sup>PC</sup>) = ?<sup>?</sup>(???)</b>					
MASS (MeV)	WIDTH (MeV)	DOCUMENT ID	TECN	COMMENT	
2210 <sup>+79</sup> <sub>-21</sub>	203 <sup>+437</sup> <sub>-87</sub>	EVANGELIS...	79B	OMEG	10 $\pi^- p \rightarrow K^+ K^- n$

<b>X(2210) I<sup>G</sup>(J<sup>PC</sup>) = ?<sup>?</sup>(???)</b>					
MASS (MeV)	WIDTH (MeV)	DOCUMENT ID	TECN	COMMENT	
2207±22	130	CASO	70	HBC	11.2 $\pi^- p$

<b>h<sub>1</sub>(2215) I<sup>G</sup>(J<sup>PC</sup>) = 0<sup>-</sup>(1<sup>+-</sup>)</b>					
MASS (MeV)	WIDTH (MeV)	DOCUMENT ID	TECN	COMMENT	
2215±40	325±55	39 ANISOVICH	02B	SPEC	0.6–1.9 $\rho\bar{p} \rightarrow \omega\eta, \omega\pi^0\pi^0$

<sup>39</sup> From the combined analysis of A NISOVICH 00D, ANISOVICH 01C, and ANISOVICH 02B.

<b>ρ<sub>2</sub>(2225) I<sup>G</sup>(J<sup>PC</sup>) = 1<sup>+</sup>(2<sup>--</sup>)</b>					
MASS (MeV)	WIDTH (MeV)	DOCUMENT ID	TECN	COMMENT	
2225±35	335 <sup>+100</sup> <sub>-50</sub>	40 ANISOVICH	02	SPEC	0.6–1.9 $\rho\bar{p} \rightarrow \omega\pi^0, \omega\eta\pi^0, \pi^+\pi^-$

<sup>40</sup> From the combined analysis of ANISOVICH 00J, ANISOVICH 01D, ANISOVICH 01E, and ANISOVICH 02.

<b>ρ<sub>4</sub>(2230) I<sup>G</sup>(J<sup>PC</sup>) = 1<sup>+</sup>(4<sup>--</sup>)</b>					
MASS (MeV)	WIDTH (MeV)	DOCUMENT ID	TECN	COMMENT	
2230±25	210±30	41 ANISOVICH	02	SPEC	0.6–1.9 $\rho\bar{p} \rightarrow \omega\pi^0, \omega\eta\pi^0, \pi^+\pi^-$

<sup>41</sup> From the combined analysis of ANISOVICH 00J, ANISOVICH 01D, ANISOVICH 01E, and ANISOVICH 02.

<b>b<sub>1</sub>(2240) I<sup>G</sup>(J<sup>PC</sup>) = 1<sup>+</sup>(1<sup>+-</sup>)</b>					
MASS (MeV)	WIDTH (MeV)	DOCUMENT ID	TECN	COMMENT	
2240±35	320±85	42 ANISOVICH	02	SPEC	0.6–1.9 $\rho\bar{p} \rightarrow \omega\pi^0, \omega\eta\pi^0, \pi^+\pi^-$

<sup>42</sup> From the combined analysis of ANISOVICH 00J, ANISOVICH 01D, ANISOVICH 01E, and ANISOVICH 02.

<b>f<sub>2</sub>(2240) I<sup>G</sup>(J<sup>PC</sup>) = 0<sup>+</sup>(2<sup>++</sup>)</b>					
MASS (MeV)	WIDTH (MeV)	DOCUMENT ID	TECN	COMMENT	
2240±15	241±30	43 ANISOVICH	00J	SPEC	1.92–2.41 $\rho\bar{p}$

••• We do not use the following data for averages, fits, limits, etc. •••

~ 2226 ~ 226 HASAN 94 RVUE  $\rho\bar{p} \rightarrow \pi\pi$

<sup>43</sup> From the combined analysis of ANISOVICH 99C, ANISOVICH 99F, ANISOVICH 99J, ANISOVICH 99K, and ANISOVICH 00B. See also ANISOVICH 12.

<b><math>b_3(2245)</math></b> $I^G(J^{PC}) = 1^+(3^+ -)$				
MASS (MeV)	WIDTH (MeV)	DOCUMENT ID	TECN	COMMENT
2245 ± 50	320 ± 70	44 BUGG	04c	RVUE

<sup>44</sup> From the combined analysis of ANISOVICH 00j, ANISOVICH 01d, ANISOVICH 01e, and ANISOVICH 02.

<b><math>\eta_2(2250)</math></b> $I^G(J^{PC}) = 0^+(2^- +)$				
MASS (MeV)	WIDTH (MeV)	DOCUMENT ID	TECN	COMMENT
2248 ± 20	280 ± 20	ANISOVICH	00i	SPEC
2267 ± 14	290 ± 50	ANISOVICH	00j	SPEC

<b><math>\pi_4(2250)</math></b> $I^G(J^{PC}) = 1^-(4^- +)$				
MASS (MeV)	WIDTH (MeV)	DOCUMENT ID	TECN	COMMENT
2250 ± 15	215 ± 25	ANISOVICH	01f	SPEC 2.0 $\bar{p}p \rightarrow 3\pi^0, \pi^0\eta, \pi^0\eta'$

<b><math>\omega_4(2250)</math></b> $I^G(J^{PC}) = 0^-(4^- -)$				
MASS (MeV)	WIDTH (MeV)	DOCUMENT ID	TECN	COMMENT
2250 ± 30	150 ± 50	45 ANISOVICH	02b	SPEC 0.6–1.9 $p\bar{p} \rightarrow \omega\eta, \omega\pi^0\pi^0$

<sup>45</sup> From the combined analysis of ANISOVICH 00d, ANISOVICH 01c, and ANISOVICH 02b.

<b><math>\omega_5(2250)</math></b> $I^G(J^{PC}) = 0^-(5^- -)$				
MASS (MeV)	WIDTH (MeV)	DOCUMENT ID	TECN	COMMENT
2250 ± 70	320 ± 95	46 BUGG	04	RVUE

<sup>46</sup> From the combined analysis of ANISOVICH 00d, ANISOVICH 01c, and ANISOVICH 02b.

<b><math>\omega_3(2255)</math></b> $I^G(J^{PC}) = 0^-(3^- -)$				
MASS (MeV)	WIDTH (MeV)	DOCUMENT ID	TECN	COMMENT
2255 ± 15	175 ± 30	47 ANISOVICH	02b	SPEC 0.6–1.9 $p\bar{p} \rightarrow \omega\eta, \omega\pi^0\pi^0$

<sup>47</sup> From the combined analysis of ANISOVICH 00d, ANISOVICH 01c, and ANISOVICH 02b.

<b><math>a_4(2255)</math></b> $I^G(J^{PC}) = 1^-(4^+ +)$				
MASS (MeV)	WIDTH (MeV)	DOCUMENT ID	TECN	COMMENT
2237 ± 5	291 ± 12	UMAN	06	E835 5.2 $\bar{p}p \rightarrow \eta\eta\pi^0$
2255 ± 40	330 <sup>+110</sup> <sub>-50</sub>	48 ANISOVICH	01f	SPEC 1.96–2.41 $\bar{p}p$

<sup>48</sup> From the combined analysis of ANISOVICH 99c, ANISOVICH 99e, and ANISOVICH 01f.

<b><math>a_2(2255)</math></b> $I^G(J^{PC}) = 1^-(2^+ +)$				
MASS (MeV)	WIDTH (MeV)	DOCUMENT ID	TECN	COMMENT
2255 ± 20	230 ± 15	49 ANISOVICH	01g	SPEC 1.96–2.41 $\bar{p}p$

<sup>49</sup> From the combined analysis of ANISOVICH 99c, ANISOVICH 99e, ANISOVICH 01f, and ANISOVICH 01g.

<b><math>X(2260)</math></b> $I^G(J^{PC}) = 0^+(4^+?)$				
MASS (MeV)	WIDTH (MeV)	DOCUMENT ID	TECN	COMMENT
2260 ± 20	400 ± 100	EVANGELIS...	79	OMEG 10.16 $\pi^- p \rightarrow \bar{p}pn$

<b><math>\rho(2270)</math></b> $I^G(J^{PC}) = 1^+(1^- -)$				
MASS (MeV)	WIDTH (MeV)	DOCUMENT ID	TECN	COMMENT
2265 ± 40	325 ± 80	50 ANISOVICH	02	SPEC 0.6–1.9 $p\bar{p} \rightarrow \omega\pi^0, \omega\eta\pi^0, \pi^+\pi^-$
2280 ± 50	440 ± 110	ATKINSON	85	OMEG 20–70 $\gamma p \rightarrow p\omega\pi^+\pi^-\pi^0$

<sup>50</sup> From the combined analysis of ANISOVICH 00j, ANISOVICH 01d, ANISOVICH 01e, and ANISOVICH 02.

<b><math>a_1(2270)</math></b> $I^G(J^{PC}) = 1^-(1^+ +)$				
MASS (MeV)	WIDTH (MeV)	DOCUMENT ID	TECN	COMMENT
2270 ± 55	305 <sup>+70</sup> <sub>-40</sub>	ANISOVICH	01f	SPEC 2.0 $\bar{p}p \rightarrow 3\pi^0, \pi^0\eta, \pi^0\eta'$

<b><math>h_3(2275)</math></b> $I^G(J^{PC}) = 0^-(3^+ -)$				
MASS (MeV)	WIDTH (MeV)	DOCUMENT ID	TECN	COMMENT
2275 ± 25	190 ± 45	51 ANISOVICH	02b	SPEC 0.6–1.9 $p\bar{p} \rightarrow \omega\eta, \omega\pi^0\pi^0$

<sup>51</sup> From the combined analysis of ANISOVICH 00d, ANISOVICH 01c, and ANISOVICH 02b.

<b><math>a_3(2275)</math></b> $I^G(J^{PC}) = 1^-(3^+ +)$				
MASS (MeV)	WIDTH (MeV)	DOCUMENT ID	TECN	COMMENT
2275 ± 35	350 <sup>+100</sup> <sub>-50</sub>	52 ANISOVICH	01g	SPEC 1.96–2.41 $\bar{p}p$

<sup>52</sup> From the combined analysis of ANISOVICH 99c, ANISOVICH 99e, ANISOVICH 01f, and ANISOVICH 01g.

<b><math>\pi_2(2285)</math></b> $I^G(J^{PC}) = 1^-(2^- +)$				
MASS (MeV)	WIDTH (MeV)	DOCUMENT ID	TECN	COMMENT
2285 ± 20 ± 25	250 ± 20 ± 25	53 ANISOVICH	11	SPEC 0.9–1.94 $p\bar{p}$

<sup>53</sup> Reanalysis of ADOMEIT 96 and ANISOVICH 00e.

<b><math>\omega_3(2285)</math></b> $I^G(J^{PC}) = 0^-(3^- -)$				
MASS (MeV)	WIDTH (MeV)	DOCUMENT ID	TECN	COMMENT
2278 ± 28	224 ± 50	54 BUGG	04a	RVUE
2285 ± 60	230 ± 40	55 ANISOVICH	02b	SPEC 0.6–1.9 $p\bar{p} \rightarrow \omega\eta, \omega\pi^0\pi^0$

<sup>54</sup> Partial wave analysis of the data on  $p\bar{p} \rightarrow \bar{\Lambda}\Lambda$  from BARNES 00.

<sup>55</sup> From the combined analysis of ANISOVICH 00d, ANISOVICH 01c, and ANISOVICH 02b.

<b><math>\omega(2290)</math></b> $I^G(J^{PC}) = 0^-(1^- -)$				
MASS (MeV)	WIDTH (MeV)	DOCUMENT ID	TECN	COMMENT
2290 ± 20	275 ± 35	56 BUGG	04a	RVUE

<sup>56</sup> Partial wave analysis of the data on  $p\bar{p} \rightarrow \bar{\Lambda}\Lambda$  from BARNES 00.

<b><math>f_2(2295)</math></b> $I^G(J^{PC}) = 0^+(2^+ +)$				
MASS (MeV)	WIDTH (MeV)	DOCUMENT ID	TECN	COMMENT
2293 ± 13	216 ± 37	57 ANISOVICH	00j	SPEC 1.92–2.41 $p\bar{p}$

<sup>57</sup> From the combined analysis of ANISOVICH 99c, ANISOVICH 99f, ANISOVICH 99j, ANISOVICH 99k, and ANISOVICH 00b. See also ANISOVICH 12.

<b><math>f_3(2300)</math></b> $I^G(J^{PC}) = 0^+(3^+ +)$				
MASS (MeV)	WIDTH (MeV)	DOCUMENT ID	TECN	COMMENT
2334 ± 25	200 ± 20	58 BUGG	04a	RVUE

<sup>58</sup> Partial wave analysis of the data on  $p\bar{p} \rightarrow \bar{\Lambda}\Lambda$  from BARNES 00.

<b><math>f_1(2310)</math></b> $I^G(J^{PC}) = 0^+(1^+ +)$				
MASS (MeV)	WIDTH (MeV)	DOCUMENT ID	TECN	COMMENT
2310 ± 60	255 ± 70	ANISOVICH	00j	SPEC

<b><math>\eta(2320)</math></b> $I^G(J^{PC}) = 0^+(0^- +)$				
MASS (MeV)	WIDTH (MeV)	DOCUMENT ID	TECN	COMMENT
2320 ± 15	230 ± 35	59 ANISOVICH	00m	SPEC

<sup>59</sup> From the combined analysis of  $\bar{p}p \rightarrow \eta\eta\eta$  from ANISOVICH 00m and  $\bar{p}p \rightarrow \eta\pi^0\pi^0$  from ANISOVICH 00j.

<b><math>\eta_4(2330)</math></b> $I^G(J^{PC}) = 0^+(4^- +)$				
MASS (MeV)	WIDTH (MeV)	DOCUMENT ID	TECN	COMMENT
2328 ± 38	240 ± 90	ANISOVICH	00j	SPEC 2.0 $p\bar{p} \rightarrow \eta\pi^0\pi^0$

<b><math>\omega(2330)</math></b> $I^G(J^{PC}) = 0^-(1^- -)$				
MASS (MeV)	WIDTH (MeV)	DOCUMENT ID	TECN	COMMENT
2330 ± 30	435 ± 75	ATKINSON	88	OMEG 25–50 $\gamma p \rightarrow \rho^\pm \rho^0 \pi^\mp$

<b><math>X(2340)</math></b> $I^G(J^{PC}) = ?(???)$					
MASS (MeV)	WIDTH (MeV)	EVTS	DOCUMENT ID	TECN	COMMENT
2340 ± 20	180 ± 60	126	60 BALTAY	75	HBC 15 $\pi^+ p \rightarrow p\pi\pi$

<sup>60</sup> Dominant decay into  $\rho^0\rho^0\pi^+$ . BALTAY 78 finds confirmation in  $2\pi^+\pi^-2\pi^0$  events which contain  $\rho^+\rho^0\pi^0$  and  $2\rho^+\pi^-$ .

<b><math>\pi(2360)</math></b> $I^G(J^{PC}) = 1^-(0^- +)$				
MASS (MeV)	WIDTH (MeV)	DOCUMENT ID	TECN	COMMENT
2360 ± 25	300 <sup>+100</sup> <sub>-50</sub>	ANISOVICH	01f	SPEC 2.0 $\bar{p}p \rightarrow 3\pi^0, \pi^0\eta, \pi^0\eta'$

<b><math>X(2360)</math></b> $I^G(J^{PC}) = ?(4^+?)$				
MASS (MeV)	WIDTH (MeV)	DOCUMENT ID	TECN	COMMENT
2360 ± 10	430 ± 30	ROZANSKA	80	SPRK 18 $\pi^- p \rightarrow p\bar{p}n$

<b><math>X(2440)</math></b> $I^G(J^{PC}) = ?(5^-?)$				
MASS (MeV)	WIDTH (MeV)	DOCUMENT ID	TECN	COMMENT
2440 ± 10	310 ± 20	ROZANSKA	80	SPRK 18 $\pi^- p \rightarrow p\bar{p}n$

<b><math>a_6(2450)</math></b> $I^G(J^{PC}) = 1^-(6^+ +)$				
MASS (MeV)	WIDTH (MeV)	DOCUMENT ID	TECN	COMMENT
2450 ± 130	400 ± 250	CLELAND	82b	SPEC 50 $\pi p \rightarrow K_S^0 K^\pm p$

<b><math>X(2540)</math></b> $I^G(J^{PC}) = 0^+(0^+ +)$				
MASS (MeV)	WIDTH (MeV)	DOCUMENT ID	TECN	COMMENT
2539 ± 14 <sup>+38</sup> <sub>-14</sub>	274 <sup>+77+126</sup> <sub>-61-163</sub>	UEHARA	13	BELL $\gamma\gamma \rightarrow K_S^0 K_S^0$

# Meson Particle Listings

## Further States

$\Gamma(\gamma\gamma) \times B(K\bar{K})$				
VALUE (eV)	DOCUMENT ID	TECN	COMMENT	
$40^{+9+17}_{-7-40}$	UEHARA	13	BELL	$\gamma\gamma \rightarrow K_S^0 K_S^0$

$X(2632) \quad I^G(J^{PC}) = ?^?(?^{??})$				
MASS (MeV)	WIDTH (MeV)	DOCUMENT ID	TECN	COMMENT
$2635.2 \pm 3.3$		61 EVDOKIMOV 04	SELX	$X(2632) \rightarrow D_s^+ \eta$
$2631.6 \pm 2.1$	$< 17$	62 EVDOKIMOV 04	SELX	$X(2632) \rightarrow D_s^0 K^+$
61 From a mass difference to $D_s^+$ of $666.9 \pm 3.3$ MeV.				
62 From a mass difference to $D_s^0$ of $767.0 \pm 2.0$ MeV.				

$B(X(2632) \rightarrow D^0 K^+)/B(X(2632) \rightarrow D_s^+ \eta)$				
VALUE	DOCUMENT ID	TECN	COMMENT	
$0.14 \pm 0.06$	63 EVDOKIMOV 04	SELX		
63 Possible interpretation of this decay pattern is discussed by YASUI 07.				

$X(2680) \quad I^G(J^{PC}) = ?^?(?^{??})$				
MASS (MeV)	WIDTH (MeV)	DOCUMENT ID	TECN	COMMENT
$2676 \pm 27$	150	CASO 70	HBC	$11.2 \pi^- p \rightarrow \rho^- \pi^+ \pi^- p$

$X(2710) \quad I^G(J^{PC}) = ?^?(6^{+?})$				
MASS (MeV)	WIDTH (MeV)	DOCUMENT ID	TECN	COMMENT
$2710 \pm 20$	$170 \pm 40$	ROZANSKA 80	SPRK	$18 \pi^- p \rightarrow p \bar{p} n$

$X(2750) \quad I^G(J^{PC}) = ?^?(7^{-?})$				
MASS (MeV)	WIDTH (MeV)	DOCUMENT ID	TECN	COMMENT
$2747 \pm 32$	$195 \pm 75$	DENNEY 83	LASS	$10 \pi^+ p \rightarrow K^+ K^- \pi^+ p$

$f_6(3100) \quad I^G(J^{PC}) = 0^+(6^{++})$				
MASS (MeV)	WIDTH (MeV)	DOCUMENT ID	TECN	COMMENT
$3100 \pm 100$	$700 \pm 130$	BINON 05	GAMS	$33 \pi^- p \rightarrow \eta \eta n$

$X(3250) \quad I^G(J^{PC}) = ?^?(?^{??})$ 3-Body Decays				
MASS (MeV)	WIDTH (MeV)	DOCUMENT ID	TECN	COMMENT
$3250 \pm 8 \pm 20$	$45 \pm 18$	ALEEV 93	BIS2	$X(3250) \rightarrow \Lambda \bar{p} K^+$
$3265 \pm 7 \pm 20$	$40 \pm 18$	ALEEV 93	BIS2	$X(3250) \rightarrow \bar{\Lambda} p K^-$

$X(3250) \quad I^G(J^{PC}) = ?^?(?^{??})$ 4-Body Decays				
MASS (MeV)	WIDTH (MeV)	DOCUMENT ID	TECN	COMMENT
$3245 \pm 8 \pm 20$	$25 \pm 11$	ALEEV 93	BIS2	$X(3250) \rightarrow \Lambda \bar{p} K^+ \pi^\pm$
$3250 \pm 9 \pm 20$	$50 \pm 20$	ALEEV 93	BIS2	$X(3250) \rightarrow \bar{\Lambda} p K^- \pi^\mp$
$3270 \pm 8 \pm 20$	$25 \pm 11$	ALEEV 93	BIS2	$X(3250) \rightarrow K_S^0 p \bar{p} K^\pm$

$X(3350) \quad I^G(J^{PC}) = ?^?(?^{??})$				
MASS (MeV)	WIDTH (MeV)	EVTS	DOCUMENT ID	TECN COMMENT
$3350^{+10}_{-20} \pm 20$	$70^{+40}_{-30} \pm 40$	$50 \pm 10$	64 GABYSHEV 06A	BELL $B^- \rightarrow \Lambda_c^+ \bar{p} \pi^-$
64 A similar enhancement in the $\Lambda_c^+ \bar{p}$ final state is also reported by BABAR collaboration in AUBERT 10H.				

### REFERENCES for Further States

ABLIKIM 16N	PR D93 112011	M. Ablikim		(BESIII Collab.)
ABLIKIM 13J	PR D87 032008	M. Ablikim et al.		(BESIII Collab.)
UEHARA 13	PTEP 2013 123C01	S. Uehara et al.		(BELLE Collab.)
ANISOVICH 12	PR D85 014001	A.V. Anisovich et al.		
ANASHIN 11	PL B703 543	V.V. Anashin et al.		(KEDR Collab.)

ANISOVICH 11	EPJ C71 1511	A.V. Anisovich et al.		(LOQM, RAL, PNPI)
CHEN 11F	PR D84 071501	P. Chen et al.		(BELLE Collab.)
AUBERT 10H	PR D82 031102	B. Aubert et al.		(BABAR Collab.)
ABRAAMYAN 09	PR C80 034001	Kh.U. Abraamyan et al.		
LIU 09	PR D79 071102	C. Liu et al.		(BELLE Collab.)
VLADIMIRSK... 08	PAN 71 2129	V.V. Vladimirov et al.		(ITEP)
VLADIMIRSK... 07	PAN 70 1706	V.V. Vladimirov et al.		
YASUI 07	PR D76 034009	S. Yasui, M. Oka		
ABLIKIM 06J	PRL 96 162002	M. Ablikim et al.		(BES Collab.)
ABLIKIM 06S	PRL 97 142002	M. Ablikim et al.		(BES Collab.)
GABYSHEV 06A	PRL 97 242001	N. Gabyshev et al.		(BELLE Collab.)
SCHEGELSKY 06A	EPJ A27 199	V.A. Schegelsky et al.		
SCHEGELSKY 06A	EPJ A27 207	V.A. Schegelsky et al.		
UMAN 06	PR D73 052009	I. Uman et al.		(FNAL E835)
VLADIMIRSK... 06	PAN 69 493	V.V. Vladimirov et al.		(ITEP, Moscow)
BINON 05	PAN 68 960	F. Binon et al.		
GRIGOR'EV 05	PAN 68 1271	V.K. Grigor'ev et al.		(ITEP)
LU 05	PRL 94 032002	M. Lu et al.		(BNL E852 Collab.)
ABLIKIM 04J	PRL 93 112002	M. Ablikim et al.		(BES Collab.)
BUGG 04	PL B595 556 (err.)	D.V. Bugg		
BUGG 04A	EPJ C36 161	D.V. Bugg		
BUGG 04C	PRPL 397 257	D.V. Bugg		
EVDOKIMOV 04	PRL 93 242001	A.V. Evdokimov et al.		(SELEX Collab.)
KUHN 04	PL B595 109	J. Kuhn et al.		(BNL E852 Collab.)
ANISOVICH 03	EPJ A16 229	V.V. Anisovich et al.		
VLADIMIRSK... 03	PAN 66 700	V.V. Vladimirov et al.		
ANISOVICH 02	PL B542 8	A.V. Anisovich et al.		
ANISOVICH 02B	PL B542 19	A.V. Anisovich et al.		
CHUNG 02	PR D65 072001	S.U. Chung et al.		(BNL E852 Collab.)
LINK 02K	PL B545 50	J.M. Link et al.		(FNAL FOCUS Collab.)
ANISOVICH 01C	PL B507 23	A.V. Anisovich et al.		
ANISOVICH 01D	PL B508 6	A.V. Anisovich et al.		
ANISOVICH 01E	PL B513 281	A.V. Anisovich et al.		
ANISOVICH 01F	PL B517 261	A.V. Anisovich et al.		
ANISOVICH 01G	PL B517 273	A.V. Anisovich et al.		
ANISOVICH 00B	NP A662 319	A.V. Anisovich et al.		
ANISOVICH 00D	PL B476 15	A.V. Anisovich et al.		
ANISOVICH 00E	PL B477 19	A.V. Anisovich et al.		
ANISOVICH 00J	PL B491 40	A.V. Anisovich et al.		
ANISOVICH 00I	PL B491 47	A.V. Anisovich et al.		(RAL, LOQM, PNPI+)
ANISOVICH 00M	PL B496 145	A.V. Anisovich et al.		
BARNES 00	PR C62 055203	P.D. Barnes et al.		
FILIPPI 00	PL B495 284	A. Filippi et al.		(OBELIX Experiment)
VLADIMIRSK... 00	JETPL 72 486	V.V. Vladimirov et al.		
ANISOVICH 99C	PL B452 173	A.V. Anisovich et al.		
ANISOVICH 99E	PL B452 187	A.V. Anisovich et al.		
ANISOVICH 99F	NP A651 253	A.V. Anisovich et al.		
ANISOVICH 99J	PL B471 271	A.V. Anisovich et al.		
ANISOVICH 99K	PL B468 309	A.V. Anisovich et al.		
BUGG 99	PL B458 511	D.V. Bugg et al.		
FERRER 99	EPJ C10 249	A. Ferrer et al.		
SEMENOV 99	SFU 42 847	S.V. Semenov		
ADOMEIT 96	Translated from UFN 42 937	J. Adomeit et al.		(Crystal Barrel Collab.)
KLOET 96	ZPHY C71 227	W.M. Kloet, F. Myhrer		(RUTG, NORD)
PROKOSHKIN 96	PD 41 247	Y.D. Prokoshkin, V.D. Samoilenko		(SERP)
HASAN 94	PL B334 215	A. Hasan, D.V. Bugg		(LOQM)
OAKDEN 94	NP A574 731	M.N. Oakden, M.R. Pennington		(DURH)
ALEEV 93	PAN 56 1358	A.N. Aleev et al.		(BIS-2 Collab.)
ARMSTRONG 93D	Translated from YAF 56 100	T.A. Armstrong et al.		(FNAL, FERR, GENO+)
ALBRECHT 91F	ZPHY C50 1	H. Albrecht et al.		(ARGUS Collab.)
CONDO 91	PR D43 2787	G.T. Condo et al.		(SLAC Hybrid Collab.)
BISELLO 89B	PR D39 701	G. Busetto et al.		(DM2 Collab.)
ATKINSON 88	ZPHY C38 635	M. Atkinson et al.		(BONN, CERN, GLAS+)
DAFTARI 87	PRL 58 859	I.K. Daftari et al.		(SYRA)
ALDE 86D	NP B269 485	D.M. Alde et al.		(BELG, LAPP, SERP, CERN+)
BRIDGES 86D	PL B180 313	D.L. Bridges et al.		(SYRA, BNL, CASE+)
GREEN 86	PRL 56 1639	D.R. Green et al.		(FNAL, ARIZ, FSU+)
ATKINSON 85	ZPHY C29 333	M. Atkinson et al.		(BONN, CERN, GLAS+)
DENNEY 83	PR D28 2726	D.L. Denney et al.		(IOWA, MICH)
CLELAND 82B	NP B208 228	W.E. Cleland et al.		(DURH, GEVA, LAUS+)
ASTON 81B	NP B189 205	D. Aston et al.		(BONN, CERN, EPOL, GLAS+)
ARESTOV 80	IHEP 80-165	Y.I. Arestov et al.		(SERP)
CHLIAPNIK... 80	ZPHY C3 285	P.V. Chliapnikov et al.		(SERP, BRUX, MONS)
KREYMER 80	PR D22 36	A.E. Kreymer et al.		(IND, PURD, SLAC+)
ROZANSKA 80	NP B162 505	M. Rozanska et al.		(MPIM, CERN)
EVANGELIS... 79	NP B153 253	C. Evangelista et al.		(BARI, BONN, CERN+)
EVANGELIS... 79B	NP B154 381	C. Evangelista et al.		(BARI, BONN, CERN+)
BALTAY 78	PR D17 52	C. Baltay et al.		(COLU, BING)
ANTIPOV 77	NP B119 45	Y.M. Antipov et al.		(SERP, GEVA)
BALTAY 77	PRL 39 591	C. Baltay, C.V. Cautis, M. Kaelkar		(COLU)
BALTAY 75	PRL 35 891	C. Baltay et al.		(COLU, BING)
KALELKAR 75	Thesis Nevis 207	M.S. Kaelkar		(COLU)
CASO 70	LNC 3 707	C. Caso et al.		(GENO, HAMB, MILA, SACL)

**STRANGE MESONS**  
**( $S = \pm 1, C = B = 0$ )**  
 $K^+ = u\bar{s}, K^0 = d\bar{s}, \bar{K}^0 = \bar{d}s, K^- = \bar{u}s,$  similarly for  $K^{*s}$

$K^\pm$

$$I(J^P) = \frac{1}{2}(0^-)$$

**CHARGED KAON MASS**

Revised 1994 by T.G. Trippe (LBNL).

The average of the six charged kaon mass measurements which we use in the Particle Listings is

$$m_{K^\pm} = 493.677 \pm 0.013 \text{ MeV } (S = 2.4), \quad (1)$$

where the error has been increased by the scale factor  $S$ . The large scale factor indicates a serious disagreement between different input data. The average before scaling the error is

$$m_{K^\pm} = 493.677 \pm 0.005 \text{ MeV }, \quad \chi^2 = 22.9 \text{ for } 5 \text{ D.F.}, \text{ Prob.} = 0.04\%, \quad (2)$$

where the high  $\chi^2$  and correspondingly low  $\chi^2$  probability further quantify the disagreement.

The main disagreement is between the two most recent and precise results,

$$m_{K^\pm} = 493.696 \pm 0.007 \text{ MeV} \quad \text{DENISOV 91}$$

$$m_{K^\pm} = 493.636 \pm 0.011 \text{ MeV } (S = 1.5) \quad \text{GALL 88}$$

---


$$\text{Average} = 493.679 \pm 0.006 \text{ MeV}$$

$$\chi^2 = 21.2 \text{ for } 1 \text{ D.F.}, \text{ Prob.} = 0.0004\%, \quad (3)$$

both of which are measurements of x-ray energies from kaonic atoms. Comparing the average in Eq. (3) with the overall average in Eq. (2), it is clear that DENISOV 91 and GALL 88 dominate the overall average, and that their disagreement is responsible for most of the high  $\chi^2$ .

The GALL 88 measurement was made using four different kaonic atom transitions,  $K^- \text{Pb } (9 \rightarrow 8)$ ,  $K^- \text{Pb } (11 \rightarrow 10)$ ,  $K^- \text{W } (9 \rightarrow 8)$ , and  $K^- \text{W } (11 \rightarrow 10)$ . The  $m_{K^\pm}$  values they obtain from each of these transitions is shown in the Particle Listings and in Fig. 1. Their  $K^- \text{Pb } (9 \rightarrow 8)$   $m_{K^\pm}$  is below and somewhat inconsistent with their other three transitions. The average of their four measurements is

$$m_{K^\pm} = 493.636 \pm 0.007,$$

$$\chi^2 = 7.0 \text{ for } 3 \text{ D.F.}, \text{ Prob.} = 7.2\%. \quad (4)$$

This is a low but acceptable  $\chi^2$  probability so, to be conservative, GALL 88 scaled up the error on their average by  $S=1.5$  to obtain their published error  $\pm 0.011$  shown in Eq. (3) above and used in the Particle Listings average.

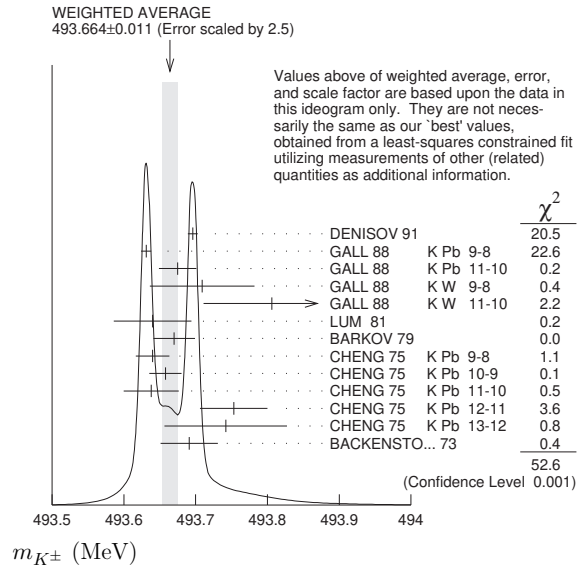


**Figure 1:** Ideogram of  $m_{K^\pm}$  mass measurements. GALL 88 and CHENG 75 measurements are shown separately for each transition they measured.

The ideogram in Fig. 1 shows that the DENISOV 91 measurement and the GALL 88  $K^- \text{Pb } (9 \rightarrow 8)$  measurement yield two well-separated peaks. One might suspect the GALL 88  $K^- \text{Pb } (9 \rightarrow 8)$  measurement since it is responsible both for the internal inconsistency in the GALL 88 measurements and the disagreement with DENISOV 91.

To see if the disagreement could result from a systematic problem with the  $K^- \text{Pb } (9 \rightarrow 8)$  transition, we have separated the CHENG 75 data, which also used  $K^- \text{Pb}$ , into its separate transitions. Figure 1 shows that the CHENG 75 and GALL 88  $K^- \text{Pb } (9 \rightarrow 8)$  values are consistent, suggesting the possibility of a common effect such as contaminant nuclear  $\gamma$  rays near the  $K^- \text{Pb } (9 \rightarrow 8)$  transition energy, although the CHENG 75 errors are too large to make a strong conclusion. The average of all 13 measurements has a  $\chi^2$  of 52.6 as shown in Fig. 1 and the first line of Table 1, yielding an unacceptable  $\chi^2$  probability of 0.00005%. The second line of Table 1 excludes both the GALL 88 and CHENG 75 measurements of the  $K^- \text{Pb } (9 \rightarrow 8)$  transition and yields a  $\chi^2$  probability of 43%. The third [fourth] line of Table 1 excludes only the GALL 88  $K^- \text{Pb } (9 \rightarrow 8)$  [DENISOV 91] measurement and yields a  $\chi^2$  probability of 20% [8.6%]. Table 1 shows that removing both measurements of the  $K^- \text{Pb } (9 \rightarrow 8)$  transition produces the most consistent set of data, but that excluding only the GALL 88  $K^- \text{Pb } (9 \rightarrow 8)$  transition or DENISOV 91 also produces acceptable probabilities.



## Meson Particle Listings

 $K^\pm$ **Table 1:**  $m_{K^\pm}$  averages for some combinations of Fig. 1 data.

$m_{K^\pm}$ (MeV)	$\chi^2$	D.F.	Prob. (%)	Measurements used
$493.664 \pm 0.004$	52.6	12	0.00005	all 13 measurements
$493.690 \pm 0.006$	10.1	10	43	no $K^-$ Pb(9→8)
$493.687 \pm 0.006$	14.6	11	20	no GALL 88 $K^-$ Pb(9→8)
$493.642 \pm 0.006$	17.8	11	8.6	no DENISOV 91

Yu.M. Ivanov, representing DENISOV 91, has estimated corrections needed for the older experiments because of improved  $^{192}\text{Ir}$  and  $^{198}\text{Au}$  calibration  $\gamma$ -ray energies. He estimates that CHENG 75 and BACKENSTOSS 73  $m_{K^\pm}$  values could be raised by about 15 keV and 22 keV, respectively. With these estimated corrections, Table 1 becomes Table 2. The last line of Table 2 shows that if such corrections are assumed, then GALL 88  $K^-$  Pb (9 → 8) is inconsistent with the rest of the data even when DENISOV 91 is excluded. Yu.M. Ivanov warns that these are rough estimates. Accordingly, we do not use Table 2 to reject the GALL 88  $K^-$  Pb (9 → 8) transition, but we note that a future reanalysis of the CHENG 75 data could be useful because it might provide supporting evidence for such a rejection.

**Table 2:**  $m_{K^\pm}$  averages for some combinations of Fig. 1 data after raising CHENG 75 and BACKENSTOSS 73 values by 0.015 and 0.022 MeV respectively.

$m_{K^\pm}$ (MeV)	$\chi^2$	D.F.	Prob. (%)	Measurements used
$493.666 \pm 0.004$	53.9	12	0.00003	all 13 measurements
$493.693 \pm 0.006$	9.0	10	53	no $K^-$ Pb(9→8)
$493.690 \pm 0.006$	11.5	11	40	no GALL 88 $K^-$ Pb(9→8)
$493.645 \pm 0.006$	23.0	11	1.8	no DENISOV 91

The GALL 88 measurement uses a Ge semiconductor spectrometer which has a resolution of about 1 keV, so they run the risk of some contaminant nuclear  $\gamma$  rays. Studies of  $\gamma$  rays following stopped  $\pi^-$  and  $\Sigma^-$  absorption in nuclei (unpublished) do not show any evidence for contaminants according to GALL 88 spokesperson, B.L. Roberts. The DENISOV 91 measurement uses a crystal diffraction spectrometer with a resolution of 6.3 eV for radiation at 22.1 keV to measure the 4f-3d transition in  $K^-$   $^{12}\text{C}$ . The high resolution and the light nucleus reduce the probability for overlap by contaminant  $\gamma$  rays, compared with the measurement of GALL 88. The DENISOV 91 measurement is supported by their high-precision measurement of the 4d-2p transition energy in  $\pi^-$   $^{12}\text{C}$ , which is good agreement with the calculated energy.

While we suspect that the GALL 88  $K^-$  Pb (9 → 8) measurements could be the problem, we are unable to find clear grounds for rejecting it. Therefore, we retain their measurement in the average and accept the large scale factor until further information can be obtained from new measurements and/or from reanalysis of GALL 88 and CHENG 75 data.

We thank B.L. Roberts (Boston Univ.) and Yu.M. Ivanov (Petersburg Nuclear Physics Inst.) for their extensive help in understanding this problem.

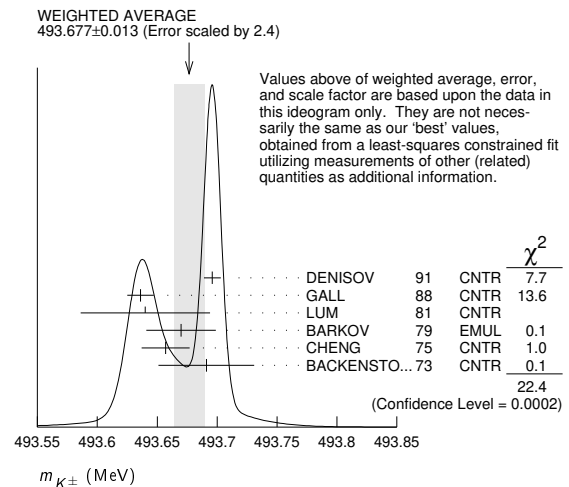
 **$K^\pm$  MASS**

VALUE (MeV)	DOCUMENT ID	TECN	CHG	COMMENT
<b><math>493.677 \pm 0.016</math> OUR FIT</b>	Error includes scale factor of 2.8.			
<b><math>493.677 \pm 0.013</math> OUR AVERAGE</b>	Error includes scale factor of 2.4. See the ideogram below.			
$493.696 \pm 0.007$	<sup>1</sup> DENISOV	91	CNTR	— Kaonic atoms
$493.636 \pm 0.011$	<sup>2</sup> GALL	88	CNTR	— Kaonic atoms
$493.640 \pm 0.054$	LUM	81	CNTR	— Kaonic atoms
$493.670 \pm 0.029$	BARKOV	79	EMUL	± $e^+ e^- \rightarrow K^+ K^-$
$493.657 \pm 0.020$	<sup>2</sup> CHENG	75	CNTR	— Kaonic atoms
$493.691 \pm 0.040$	BACKENSTO...73	CNTR	—	Kaonic atoms
• • • We do not use the following data for averages, fits, limits, etc. • • •				
$493.631 \pm 0.007$	GALL	88	CNTR	— $K^-$ Pb (9 → 8)
$493.675 \pm 0.026$	GALL	88	CNTR	— $K^-$ Pb (11 → 10)
$493.709 \pm 0.073$	GALL	88	CNTR	— $K^-$ W (9 → 8)
$493.806 \pm 0.095$	GALL	88	CNTR	— $K^-$ W (11 → 10)
$493.640 \pm 0.022 \pm 0.008$	<sup>3</sup> CHENG	75	CNTR	— $K^-$ Pb (9 → 8)
$493.658 \pm 0.019 \pm 0.012$	<sup>3</sup> CHENG	75	CNTR	— $K^-$ Pb (10 → 9)
$493.638 \pm 0.035 \pm 0.016$	<sup>3</sup> CHENG	75	CNTR	— $K^-$ Pb (11 → 10)
$493.753 \pm 0.042 \pm 0.021$	<sup>3</sup> CHENG	75	CNTR	— $K^-$ Pb (12 → 11)
$493.742 \pm 0.081 \pm 0.027$	<sup>3</sup> CHENG	75	CNTR	— $K^-$ Pb (13 → 12)

<sup>1</sup> Error increased from 0.0059 based on the error analysis in IVANOV 92.

<sup>2</sup> This value is the authors' combination of all of the separate transitions listed for this paper.

<sup>3</sup> The CHENG 75 values for separate transitions were calculated from their Table 7 transition energies. The first error includes a 20% systematic error in the noncircular contaminant shift. The second error is due to a  $\pm 5$  eV uncertainty in the theoretical transition energies.

 **$m_{K^+} - m_{K^-}$** 

Test of CPT.

VALUE (MeV)	EVTS	DOCUMENT ID	TECN	CHG
<b><math>-0.032 \pm 0.090</math></b>	1.5M	<sup>1</sup> FORD	72	ASPK ±

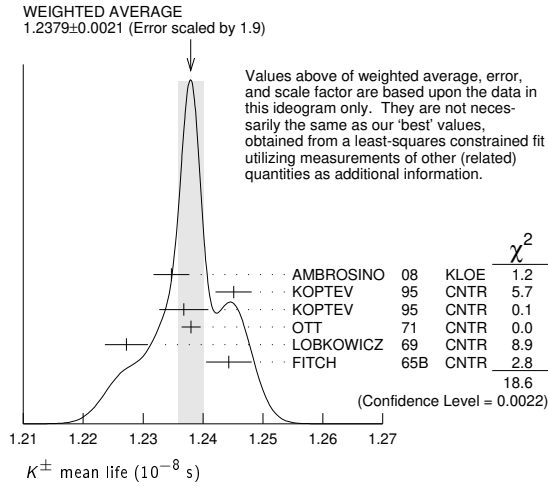
<sup>1</sup> FORD 72 uses  $m_{\pi^+} - m_{\pi^-} = +28 \pm 70$  keV.

 **$K^\pm$  MEAN LIFE**

VALUE ( $10^{-8}$ s)	EVTS	DOCUMENT ID	TECN	CHG	COMMENT
<b><math>1.2380 \pm 0.0020</math> OUR FIT</b>	Error includes scale factor of 1.8.				
<b><math>1.2379 \pm 0.0021</math> OUR AVERAGE</b>	Error includes scale factor of 1.9. See the ideogram below.				
$1.2347 \pm 0.0030$	15M	<sup>1</sup> AMBROSINO	08	KLOE ±	$\phi \rightarrow K^+ K^-$
$1.2451 \pm 0.0030$	250k	KOPTEV	95	CNTR	$K$ at rest, U target
$1.2368 \pm 0.0041$	150k	KOPTEV	95	CNTR	$K$ at rest, Cu target
$1.2380 \pm 0.0016$	3M	OTT	71	CNTR	+ $K$ at rest
$1.2272 \pm 0.0036$		LOBKOWICZ	69	CNTR	+ $K$ in flight
$1.2443 \pm 0.0038$		FITCH	65B	CNTR	+ $K$ at rest
• • • We do not use the following data for averages, fits, limits, etc. • • •					
$1.2415 \pm 0.0024$	400k	<sup>2</sup> KOPTEV	95	CNTR	$K$ at rest
$1.221 \pm 0.011$		FORD	67	CNTR	±
$1.231 \pm 0.011$		BOYARSKI	62	CNTR	+

<sup>1</sup> Result obtained by averaging the decay length and decay time analyses taking correlations into account.

<sup>2</sup> KOPTEV 95 report this weighted average of their U-target and Cu-target results, where they have weighted by  $1/\sigma$  rather than  $1/\sigma^2$ .



$$\frac{(\tau_{K^+} - \tau_{K^-})}{\tau_{\text{average}}}$$

This quantity is a measure of CPT invariance in weak interactions.

VALUE (%)	DOCUMENT ID	TECN
<b>0.10 ± 0.09 OUR AVERAGE</b>	Error includes scale factor of 1.2.	
-0.4 ± 0.4	AMBROSINO 08	KLOE
0.090 ± 0.078	LOBKOWICZ 69	CNTR
0.47 ± 0.30	FORD 67	CNTR

See the related review(s):  
Rare Kaon Decays

**$K^\pm$  DECAY MODES**

$K^-$  modes are charge conjugates of the modes below.

Mode	Fraction ( $\Gamma_i/\Gamma$ )	Scale factor/ Confidence level
<b>Leptonic and semileptonic modes</b>		
$\Gamma_1$ $e^+ \nu_e$	( 1.582 ± 0.007 ) × 10 <sup>-5</sup>	
$\Gamma_2$ $\mu^+ \nu_\mu$	( 63.56 ± 0.11 ) %	S=1.2
$\Gamma_3$ $\pi^0 e^+ \nu_e$	( 5.07 ± 0.04 ) %	S=2.1
Called $K_{e3}^+$ .		
$\Gamma_4$ $\pi^0 \mu^+ \nu_\mu$	( 3.352 ± 0.033 ) %	S=1.9
Called $K_{\mu3}^+$ .		
$\Gamma_5$ $\pi^0 \pi^0 e^+ \nu_e$	( 2.55 ± 0.04 ) × 10 <sup>-5</sup>	S=1.1
$\Gamma_6$ $\pi^+ \pi^- e^+ \nu_e$	( 4.247 ± 0.024 ) × 10 <sup>-5</sup>	
$\Gamma_7$ $\pi^+ \pi^- \mu^+ \nu_\mu$	( 1.4 ± 0.9 ) × 10 <sup>-5</sup>	
$\Gamma_8$ $\pi^0 \pi^0 \pi^0 e^+ \nu_e$	< 3.5 × 10 <sup>-6</sup>	CL=90%
<b>Hadronic modes</b>		
$\Gamma_9$ $\pi^+ \pi^0$	( 20.67 ± 0.08 ) %	S=1.2
$\Gamma_{10}$ $\pi^+ \pi^0 \pi^0$	( 1.760 ± 0.023 ) %	S=1.1
$\Gamma_{11}$ $\pi^+ \pi^+ \pi^-$	( 5.583 ± 0.024 ) %	
<b>Leptonic and semileptonic modes with photons</b>		
$\Gamma_{12}$ $\mu^+ \nu_\mu \gamma$	[a,b] ( 6.2 ± 0.8 ) × 10 <sup>-3</sup>	
$\Gamma_{13}$ $\mu^+ \nu_\mu \gamma$ (SD <sup>+</sup> )	[c,d] ( 1.33 ± 0.22 ) × 10 <sup>-5</sup>	
$\Gamma_{14}$ $\mu^+ \nu_\mu \gamma$ (SD <sup>+</sup> INT)	[c,d] < 2.7 × 10 <sup>-5</sup>	CL=90%
$\Gamma_{15}$ $\mu^+ \nu_\mu \gamma$ (SD <sup>-</sup> + SD <sup>-</sup> INT)	[c,d] < 2.6 × 10 <sup>-4</sup>	CL=90%
$\Gamma_{16}$ $e^+ \nu_e \gamma$	( 9.4 ± 0.4 ) × 10 <sup>-6</sup>	
$\Gamma_{17}$ $\pi^0 e^+ \nu_e \gamma$	[a,b] ( 2.56 ± 0.16 ) × 10 <sup>-4</sup>	
$\Gamma_{18}$ $\pi^0 e^+ \nu_e \gamma$ (SD)	[c,d] < 5.3 × 10 <sup>-5</sup>	CL=90%
$\Gamma_{19}$ $\pi^0 \mu^+ \nu_\mu \gamma$	[a,b] ( 1.25 ± 0.25 ) × 10 <sup>-5</sup>	
$\Gamma_{20}$ $\pi^0 \pi^0 e^+ \nu_e \gamma$	< 5 × 10 <sup>-6</sup>	CL=90%
<b>Hadronic modes with photons or <math>\ell\bar{\ell}</math> pairs</b>		
$\Gamma_{21}$ $\pi^+ \pi^0 \gamma$ (INT)	( -4.2 ± 0.9 ) × 10 <sup>-6</sup>	
$\Gamma_{22}$ $\pi^+ \pi^0 \gamma$ (DE)	[a,e] ( 6.0 ± 0.4 ) × 10 <sup>-6</sup>	
$\Gamma_{23}$ $\pi^+ \pi^0 e^+ e^-$	( 4.24 ± 0.14 ) × 10 <sup>-6</sup>	
$\Gamma_{24}$ $\pi^+ \pi^0 \pi^0 \gamma$	[a,b] ( 7.6 ± 6.0 / -3.0 ) × 10 <sup>-6</sup>	
$\Gamma_{25}$ $\pi^+ \pi^+ \pi^- \gamma$	[a,b] ( 7.1 ± 0.5 ) × 10 <sup>-6</sup>	

$\Gamma_{26}$ $\pi^+ \gamma \gamma$	[a] ( 1.01 ± 0.06 ) × 10 <sup>-6</sup>	
$\Gamma_{27}$ $\pi^+ 3\gamma$	[a] < 1.0 × 10 <sup>-4</sup>	CL=90%
$\Gamma_{28}$ $\pi^+ e^+ e^- \gamma$	( 1.19 ± 0.13 ) × 10 <sup>-8</sup>	

**Leptonic modes with  $\ell\bar{\ell}$  pairs**

$\Gamma_{29}$ $e^+ \nu_e \nu \bar{\nu}$	< 6 × 10 <sup>-5</sup>	CL=90%
$\Gamma_{30}$ $\mu^+ \nu_\mu \nu \bar{\nu}$	< 2.4 × 10 <sup>-6</sup>	CL=90%
$\Gamma_{31}$ $e^+ \nu_e e^+ e^-$	( 2.48 ± 0.20 ) × 10 <sup>-8</sup>	
$\Gamma_{32}$ $\mu^+ \nu_\mu e^+ e^-$	( 7.06 ± 0.31 ) × 10 <sup>-8</sup>	
$\Gamma_{33}$ $e^+ \nu_e \mu^+ \mu^-$	( 1.7 ± 0.5 ) × 10 <sup>-8</sup>	
$\Gamma_{34}$ $\mu^+ \nu_\mu \mu^+ \mu^-$	< 4.1 × 10 <sup>-7</sup>	CL=90%

**Lepton family number (LF), Lepton number (L),  $\Delta S = \Delta Q$  (SQ) violating modes, or  $\Delta S = 1$  weak neutral current (S1) modes**

$\Gamma_{35}$ $\pi^+ \pi^+ e^- \bar{\nu}_e$	SQ	< 1.3 × 10 <sup>-8</sup>	CL=90%
$\Gamma_{36}$ $\pi^+ \pi^+ \mu^- \bar{\nu}_\mu$	SQ	< 3.0 × 10 <sup>-6</sup>	CL=95%
$\Gamma_{37}$ $\pi^+ e^+ e^-$	S1	( 3.00 ± 0.09 ) × 10 <sup>-7</sup>	
$\Gamma_{38}$ $\pi^+ \mu^+ \mu^-$	S1	( 9.4 ± 0.6 ) × 10 <sup>-8</sup>	S=2.6
$\Gamma_{39}$ $\pi^+ \nu \bar{\nu}$	S1	( 1.7 ± 1.1 ) × 10 <sup>-10</sup>	
$\Gamma_{40}$ $\pi^+ \pi^0 \nu \bar{\nu}$	S1	< 4.3 × 10 <sup>-5</sup>	CL=90%
$\Gamma_{41}$ $\mu^- \nu e^+ e^+$	LF	< 2.1 × 10 <sup>-8</sup>	CL=90%
$\Gamma_{42}$ $\mu^+ \nu_e$	LF	[f] < 4 × 10 <sup>-3</sup>	CL=90%
$\Gamma_{43}$ $\pi^+ \mu^+ e^-$	LF	< 1.3 × 10 <sup>-11</sup>	CL=90%
$\Gamma_{44}$ $\pi^+ \mu^- e^+$	LF	< 5.2 × 10 <sup>-10</sup>	CL=90%
$\Gamma_{45}$ $\pi^- \mu^+ e^+$	L	< 5.0 × 10 <sup>-10</sup>	CL=90%
$\Gamma_{46}$ $\pi^- e^+ e^+$	L	< 2.2 × 10 <sup>-10</sup>	CL=90%
$\Gamma_{47}$ $\pi^- \mu^+ \mu^+$	L	< 4.2 × 10 <sup>-11</sup>	CL=90%
$\Gamma_{48}$ $\mu^+ \bar{\nu}_e$	L	[f] < 3.3 × 10 <sup>-3</sup>	CL=90%
$\Gamma_{49}$ $\pi^0 e^+ \bar{\nu}_e$	L	< 3 × 10 <sup>-3</sup>	CL=90%
$\Gamma_{50}$ $\pi^+ \gamma$	[g] < 2.3 × 10 <sup>-9</sup>	CL=90%	

- [a] See the Particle Listings below for the energy limits used in this measurement.
- [b] Most of this radiative mode, the low-momentum  $\gamma$  part, is also included in the parent mode listed without  $\gamma$ 's.
- [c] Structure-dependent part.
- [d] See the review on "Form Factors for Radiative Pion and Kaon Decays" for definitions and details.
- [e] Direct-emission branching fraction.
- [f] Derived from an analysis of neutrino-oscillation experiments.
- [g] Violates angular-momentum conservation.

**CONSTRAINED FIT INFORMATION**

An overall fit to the mean life, a decay rate, and 15 branching ratios uses 35 measurements and one constraint to determine 8 parameters. The overall fit has a  $\chi^2 = 53.4$  for 28 degrees of freedom.

The following *off-diagonal* array elements are the correlation coefficients  $\langle \delta p_i \delta p_j \rangle / (\delta p_i \delta p_j)$ , in percent, from the fit to parameters  $p_i$ , including the branching fractions,  $x_i \equiv \Gamma_i / \Gamma_{\text{total}}$ . The fit constrains the  $x_i$  whose labels appear in this array to sum to one.

$x_3$	-66					
$x_4$	-64	90				
$x_5$	-12	-5	-5			
$x_9$	-67	0	-1	-6		
$x_{10}$	-13	-6	-5	91	-6	
$x_{11}$	-14	-6	-6	2	-7	2
$\Gamma$	3	1	1	0	2	0 -24
	$x_2$	$x_3$	$x_4$	$x_5$	$x_9$	$x_{10}$ $x_{11}$

Mode	Rate (10 <sup>8</sup> s <sup>-1</sup> )	Scale factor
$\Gamma_2$ $\mu^+ \nu_\mu$	0.5134 ± 0.0012	1.5
$\Gamma_3$ $\pi^0 e^+ \nu_e$	0.0410 ± 0.0004	2.1
Called $K_{e3}^+$ .		
$\Gamma_4$ $\pi^0 \mu^+ \nu_\mu$	0.02707 ± 0.00027	1.9
Called $K_{\mu3}^+$ .		
$\Gamma_5$ $\pi^0 \pi^0 e^+ \nu_e$	(2.059 ± 0.029 ) × 10 <sup>-5</sup>	1.1
$\Gamma_9$ $\pi^+ \pi^0$	0.1670 ± 0.0007	1.3
$\Gamma_{10}$ $\pi^+ \pi^0 \pi^0$	0.01421 ± 0.00018	1.1
$\Gamma_{11}$ $\pi^+ \pi^+ \pi^-$	0.04510 ± 0.00019	

## Meson Particle Listings

 $K^\pm$  $K^\pm$  DECAY RATES

$\Gamma(\mu^+ \nu_\mu)$		$\Gamma_2$	
VALUE ( $10^6 \text{ s}^{-1}$ )	DOCUMENT ID	TECN	CHG
<b>51.34 ± 0.12 OUR FIT</b>	Error includes scale factor of 1.5.		
• • • We do not use the following data for averages, fits, limits, etc. • • •			
51.2 ± 0.8	FORD	67	CNTR ±
$\Gamma(\pi^+ \pi^+ \pi^-)$		$\Gamma_{11}$	
VALUE ( $10^6 \text{ s}^{-1}$ )	EVTS	DOCUMENT ID	TECN CHG
<b>4.510 ± 0.019 OUR FIT</b>	Error includes scale factor of 1.5.		
<b>4.511 ± 0.024</b>	1 FORD 70 ASPK		
• • • We do not use the following data for averages, fits, limits, etc. • • •			
4.529 ± 0.032	3.2M	1 FORD	70 ASPK
4.496 ± 0.030		1 FORD	67 CNTR ±
1 First FORD 70 value is second FORD 70 combined with FORD 67.			

 $K^+$  BRANCHING RATIOS

## Leptonic and semileptonic modes

$\Gamma(e^+ \nu_e)/\Gamma(\mu^+ \nu_\mu)$		$\Gamma_1/\Gamma_2$	
See the note on "Decay Constants of Charged Pseudoscalar Mesons" in the $D_S^+$ Listings.			
VALUE (units $10^{-5}$ )	EVTS	DOCUMENT ID	TECN CHG
<b>2.488 ± 0.009 OUR AVERAGE</b>	Error includes scale factor of 1.5.		
2.488 ± 0.007 ± 0.007	150k	1 LAZZERONI	13 NA62 ±
2.493 ± 0.025 ± 0.019	13.8k	2 AMBROSINO	09E KLOE ±
• • • We do not use the following data for averages, fits, limits, etc. • • •			
2.487 ± 0.011 ± 0.007	60k	3 LAZZERONI	11 NA62 +
2.51 ± 0.15	404	HEINTZE	76 SPEC +
2.37 ± 0.17	534	HEARD	75B SPEC +
2.42 ± 0.42	112	CLARK	72 OSPK +
1 LAZZERONI 13 uses full data sample collected from 2007 to 2008. This ratio is defined to be fully inclusive, including internal-bremsstrahlung.			
2 The ratio is defined to include internal-bremsstrahlung, ignoring direct-emission contributions. AMBROSINO 09E determined the ratio from the measurement of $\Gamma(K \rightarrow e \nu(\gamma), E_\gamma < 10 \text{ MeV}) / \Gamma(K \rightarrow \mu \nu(\gamma))$ . 89.8% of $K \rightarrow e \nu(\gamma)$ events had $E_\gamma < 10 \text{ MeV}$ .			
3 This ratio is defined to be fully inclusive, including internal-bremsstrahlung.			

$\Gamma(\mu^+ \nu_\mu)/\Gamma_{\text{total}}$		$\Gamma_2/\Gamma$	
See the note on "Decay Constants of Charged Pseudoscalar Mesons" in the $D_S^+$ Listings.			
VALUE (units $10^{-2}$ )	EVTS	DOCUMENT ID	TECN CHG COMMENT
<b>63.56 ± 0.11 OUR FIT</b>	Error includes scale factor of 1.2.		
<b>63.60 ± 0.16 OUR AVERAGE</b>	Error includes scale factor of 1.2.		
63.66 ± 0.09 ± 0.15	865k	1 AMBROSINO	06A KLOE +
63.24 ± 0.44	62k	CHIANG	72 OSPK + 1.84 GeV/c $K^+$
1 Fully inclusive. Used tagged kaons from $\phi$ decays.			

$\Gamma(\pi^0 e^+ \nu_e)/\Gamma_{\text{total}}$		$\Gamma_3/\Gamma$	
VALUE (units $10^{-2}$ )	EVTS	DOCUMENT ID	TECN CHG COMMENT
<b>5.07 ± 0.04 OUR FIT</b>	Error includes scale factor of 2.1.		
<b>4.94 ± 0.05 OUR AVERAGE</b>	Error includes scale factor of 2.1.		
4.965 ± 0.038 ± 0.037		1 AMBROSINO	08A KLOE ±
4.86 ± 0.10	3516	CHIANG	72 OSPK + 1.84 GeV/c $K^+$
• • • We do not use the following data for averages, fits, limits, etc. • • •			
4.7 ± 0.3	429	SHAKLEE	64 HLBC +
5.0 ± 0.5		ROE	61 HLBC +
1 Depends on $K^+$ lifetime $\tau$ . AMBROSINO 08A uses PDG 06 value of $\tau = (1.2385 \pm 0.0024) \times 10^{-8}$ sec. The correlation between $K_{e3}^+$ and $K_{\mu 3}^+$ branching fraction measurements is 62.7%.			

$\Gamma(\pi^0 e^+ \nu_e)/\Gamma(\mu^+ \nu_\mu)$		$\Gamma_3/\Gamma_2$	
VALUE	EVTS	DOCUMENT ID	TECN CHG
<b>0.0798 ± 0.0008 OUR FIT</b>	Error includes scale factor of 1.9.		
• • • We do not use the following data for averages, fits, limits, etc. • • •			
0.069 ± 0.006	350	ZELLER	69 ASPK +
0.0775 ± 0.0033	960	BOTTERILL	68C ASPK +
0.069 ± 0.006	561	GARLAND	68 OSPK +
0.0791 ± 0.0054	295	1 AUERBACH	67 OSPK +
1 AUERBACH 67 changed from 0.0797 ± 0.0054. See comment with ratio $\Gamma(\pi^0 \mu^+ \nu_\mu)/\Gamma(\mu^+ \nu_\mu)$ . The value 0.0785 ± 0.0025 given in AUERBACH 67 is an average of AUERBACH 67 $\Gamma(\pi^0 e^+ \nu_e)/\Gamma(\mu^+ \nu_\mu)$ and CESTER 66 $\Gamma(\pi^0 e^+ \nu_e)/[\Gamma(\mu^+ \nu_\mu) + \Gamma(\pi^+ \pi^0)]$ .			

$\Gamma(\pi^0 e^+ \nu_e)/[\Gamma(\mu^+ \nu_\mu) + \Gamma(\pi^+ \pi^0)]$		$\Gamma_3/(\Gamma_2 + \Gamma_0)$	
VALUE (units $10^{-2}$ )	EVTS	DOCUMENT ID	TECN CHG
<b>6.02 ± 0.06 OUR FIT</b>	Error includes scale factor of 2.1.		
<b>6.02 ± 0.15 OUR AVERAGE</b>	Error includes scale factor of 2.1.		
6.16 ± 0.22	5110	ESCHSTRUTH	68 OSPK +
5.89 ± 0.21	1679	CESTER	66 OSPK +

• • • We do not use the following data for averages, fits, limits, etc. • • •  
 5.92 ± 0.65 <sup>1</sup>WEISSENBERG... 76 SPEC +  
<sup>1</sup> Value calculated from WEISSENBERG 76 ( $\pi^0 e \nu$ ), ( $\mu \nu$ ), and ( $\pi \pi^0$ ) values to eliminate dependence on our 1974 ( $\pi 2\pi^0$ ) and ( $\pi \pi^+ \pi^-$ ) fractions.

$\Gamma(\pi^0 e^+ \nu_e)/[\Gamma(\pi^0 \mu^+ \nu_\mu) + \Gamma(\pi^+ \pi^0) + \Gamma(\pi^+ \pi^0 \pi^0)]$		$\Gamma_3/(\Gamma_4 + \Gamma_9 + \Gamma_{10})$	
VALUE	EVTS	DOCUMENT ID	TECN CHG
<b>0.1967 ± 0.0016 OUR FIT</b>	Error includes scale factor of 2.5.		
<b>0.1962 ± 0.0008 ± 0.0035</b>	71k	SHER	03 B865 +

$\Gamma(\pi^0 e^+ \nu_e)/\Gamma(\pi^+ \pi^0)$		$\Gamma_3/\Gamma_9$	
VALUE	EVTS	DOCUMENT ID	TECN CHG COMMENT
<b>0.2454 ± 0.0023 OUR FIT</b>	Error includes scale factor of 2.6.		
<b>0.2467 ± 0.0011 OUR AVERAGE</b>	Error includes scale factor of 1.1.		
0.2423 ± 0.0015 ± 0.0037	31k	UVAROV	14 ISTR - ISTR +
0.2470 ± 0.0009 ± 0.0004	87k	BATLEY	07A NA48 ±
• • • We do not use the following data for averages, fits, limits, etc. • • •			
0.221 ± 0.012	786	1 LUCAS	73B HBC - Dalitz pairs only
1 LUCAS 73B gives $N(K_{e3}) = 786 \pm 3.1\%$ , $N(2\pi) = 3564 \pm 3.1\%$ . We use these values to obtain quoted result.			

$\Gamma(\pi^0 e^+ \nu_e)/\Gamma(\pi^+ \pi^+ \pi^-)$		$\Gamma_3/\Gamma_{11}$	
VALUE	EVTS	DOCUMENT ID	TECN CHG
<b>0.908 ± 0.009 OUR FIT</b>	Error includes scale factor of 1.6.		
• • • We do not use the following data for averages, fits, limits, etc. • • •			
0.867 ± 0.027	2768	BARMIN	87 XEBC +
0.856 ± 0.040	2827	BRAUN	75 HLBC +
0.850 ± 0.019	4385	1 HAIDT	71 HLBC +
0.846 ± 0.021	4385	1 EICHTEN	68 HLBC +
0.94 ± 0.09	854	BELLOTTI	67B HLBC
0.90 ± 0.06	230	BORREANI	64 HBC +
1 HAIDT 71 is a reanalysis of EICHTEN 68. Not included in average because of large discrepancy in $\Gamma(\pi^0 \mu^+ \nu)/\Gamma(\pi^0 e^+ \nu)$ with more precise results.			

$\Gamma(\pi^0 \mu^+ \nu_\mu)/\Gamma_{\text{total}}$		$\Gamma_4/\Gamma$	
VALUE (units $10^{-2}$ )	EVTS	DOCUMENT ID	TECN CHG COMMENT
<b>3.352 ± 0.033 OUR FIT</b>	Error includes scale factor of 1.9.		
<b>3.24 ± 0.04 OUR AVERAGE</b>	Error includes scale factor of 1.9.		
3.233 ± 0.029 ± 0.026		1 AMBROSINO	08A KLOE ±
3.33 ± 0.16	2345	CHIANG	72 OSPK + 1.84 GeV/c $K^+$
• • • We do not use the following data for averages, fits, limits, etc. • • •			
2.8 ± 0.4		2 TAYLOR	59 EMUL +
1 Depends on $K^+$ lifetime $\tau$ . AMBROSINO 08A uses PDG 06 value of $\tau = (1.2385 \pm 0.0024) \times 10^{-8}$ sec. The correlation between $K_{e3}^+$ and $K_{\mu 3}^+$ branching fraction measurements is 62.7%.			
2 Earlier experiments not averaged.			

$\Gamma(\pi^0 \mu^+ \nu_\mu)/\Gamma(\mu^+ \nu_\mu)$		$\Gamma_4/\Gamma_2$	
VALUE	EVTS	DOCUMENT ID	TECN CHG
<b>0.0527 ± 0.0006 OUR FIT</b>	Error includes scale factor of 1.8.		
• • • We do not use the following data for averages, fits, limits, etc. • • •			
0.054 ± 0.009	240	ZELLER	69 ASPK +
0.0480 ± 0.0037	424	1 GARLAND	68 OSPK +
0.0486 ± 0.0040	307	2 AUERBACH	67 OSPK +
1 GARLAND 68 changed from 0.055 ± 0.004 in agreement with $\mu$ -spectrum calculation of GAILLARD 70 appendix B. L.G.Pondrom, (private communication 73).			
2 AUERBACH 67 changed from 0.0602 ± 0.0046 by erratum which brings the $\mu$ -spectrum calculation into agreement with GAILLARD 70 appendix B.			

$\Gamma(\pi^0 \mu^+ \nu_\mu)/\Gamma(\pi^0 e^+ \nu_e)$		$\Gamma_4/\Gamma_3$	
VALUE	EVTS	DOCUMENT ID	TECN CHG COMMENT
<b>0.6608 ± 0.0029 OUR FIT</b>	Error includes scale factor of 1.1.		
<b>0.6618 ± 0.0027 OUR AVERAGE</b>	Error includes scale factor of 1.1.		
0.663 ± 0.003 ± 0.001	77k	BATLEY	07A NA48 ±
0.671 ± 0.007 ± 0.008	24k	HORIE	01 SPEC
0.670 ± 0.014		1 HEINTZE	77 SPEC +
0.667 ± 0.017	5601	BOTTERILL	68B ASPK +
• • • We use the following data for averages but not for fits. • • •			
0.6511 ± 0.0064		2 AMBROSINO	08A KLOE ±
• • • We do not use the following data for averages, fits, limits, etc. • • •			
0.608 ± 0.014	1585	3 BRAUN	75 HLBC +
0.705 ± 0.063	554	4 LUCAS	73B HBC - Dalitz pairs only
0.698 ± 0.025	3480	5 CHIANG	72 OSPK + 1.84 GeV/c $K^+$
0.596 ± 0.025		6 HAIDT	71 HLBC +
0.604 ± 0.022	1398	6 EICHTEN	68 HLBC
0.703 ± 0.056	1509	CALLAHAN	66B HLBC
1 HEINTZE 77 value from fit to $\lambda_0$ . Assumes $\mu$ -e universality.			
2 Not used in the fit. This result enters the fit via correlation of $K_{e3}^+$ and $K_{\mu 3}^+$ branching fraction measurements of AMBROSINO 08A.			
3 BRAUN 75 value is from form factor fit. Assumes $\mu$ -e universality.			
4 LUCAS 73B gives $N(K_{\mu 3}) = 554 \pm 7.6\%$ , $N(K_{e3}) = 786 \pm 3.1\%$ . We divide.			
5 CHIANG 72 $\Gamma(\pi^0 \mu^+ \nu_\mu)/\Gamma(\pi^0 e^+ \nu_e)$ is statistically independent of CHIANG 72 $\Gamma(\pi^0 \mu^+ \nu_\mu)/\Gamma_{\text{total}}$ and $\Gamma(\pi^0 e^+ \nu_e)/\Gamma_{\text{total}}$ .			
6 HAIDT 71 is a reanalysis of EICHTEN 68. Not included in average because of large discrepancy with more precise results.			

$[\Gamma(\pi^0 \mu^+ \nu_\mu) + \Gamma(\pi^+ \pi^0)]/\Gamma_{\text{total}}$  ( $\Gamma_4 + \Gamma_9$ )/ $\Gamma$   
 We combine these two modes for experiments measuring them in xenon bubble chamber because of difficulties of separating them there.

VALUE (units $10^{-2}$ )	EVTS	DOCUMENT ID	TECN	CHG
<b>24.02 ± 0.08 OUR FIT</b>				Error includes scale factor of 1.2.
• • • We do not use the following data for averages, fits, limits, etc. • • •				
25.4 ± 0.9	886	SHAKLEE	64	HLBC +
23.4 ± 1.1		ROE	61	HLBC +

$\Gamma(\pi^0 \mu^+ \nu_\mu)/\Gamma(\pi^+ \pi^0)$   $\Gamma_4/\Gamma_9$   
 VALUE (units  $10^{-2}$ ) EVTS DOCUMENT ID TECN CHG  
**0.1637 ± 0.0006 ± 0.0003** 77k BATLEY 07A NA48 ±

$\Gamma(\pi^0 \mu^+ \nu_\mu)/\Gamma(\pi^+ \pi^+ \pi^-)$   $\Gamma_4/\Gamma_{11}$   
 VALUE (units  $10^{-3}$ ) EVTS DOCUMENT ID TECN CHG COMMENT  
**0.600 ± 0.007 OUR FIT** Error includes scale factor of 1.6.  
 • • • We do not use the following data for averages, fits, limits, etc. • • •  
 0.503 ± 0.019 1505 1 HAIDT 71 HLBC +  
 0.510 ± 0.017 1505 1 EICHTEN 68 HLBC +  
 0.63 ± 0.07 2845 2 BISI 65B BC + HBC+HLBC

<sup>1</sup> HAIDT 71 is a reanalysis of EICHTEN 68. Not included in average because of large discrepancy in  $\Gamma(\pi^0 \mu^+ \nu)/\Gamma(\pi^0 e^+ \nu)$  with more precise results.  
<sup>2</sup> Error enlarged for background problems. See GAILLARD 70.

$\Gamma(\pi^0 \pi^0 e^+ \nu_e)/\Gamma_{\text{total}}$   $\Gamma_5/\Gamma$   
 VALUE (units  $10^{-5}$ ) EVTS DOCUMENT ID TECN CHG  
**2.55 ± 0.04 OUR FIT** Error includes scale factor of 1.1.  
**2.54 ± 0.89** 10 BARMIN 88B HLBC +

$\Gamma(\pi^0 \pi^0 e^+ \nu_e)/\Gamma(\pi^+ \pi^0 \pi^0)$   $\Gamma_5/\Gamma_{10}$   
 VALUE (units  $10^{-3}$ ) EVTS DOCUMENT ID TECN CHG  
**1.449 ± 0.008 OUR FIT**  
**1.449 ± 0.006 ± 0.006** 65.2k 1 BATLEY 14A NA48 ±

<sup>1</sup> Data collected in 2003-2004. This leads to the scalar form factor  $(1 + \delta_{EM}) f_5 = 6.079 \pm 0.012 \pm 0.027 \pm 0.046$  where the last error is due to the normalizing decay mode uncertainty.

$\Gamma(\pi^0 \pi^0 e^+ \nu_e)/\Gamma(\pi^0 e^+ \nu_e)$   $\Gamma_5/\Gamma_3$   
 VALUE (units  $10^{-4}$ ) EVTS DOCUMENT ID TECN CHG  
**5.03 ± 0.09 OUR FIT** Error includes scale factor of 1.2.  
**4.1 ± 1.0 OUR AVERAGE**  
 -0.7  
 4.2 ± 1.0 25 BOLOTOV 86B CALO -  
 -0.9  
 3.8 ± 5.0 2 LJUNG 73 HLBC +  
 -1.2

$\Gamma(\pi^+ \pi^- e^+ \nu_e)/\Gamma(\pi^+ \pi^+ \pi^-)$   $\Gamma_6/\Gamma_{11}$   
 VALUE (units  $10^{-4}$ ) EVTS DOCUMENT ID TECN CHG  
**7.606 ± 0.029 OUR AVERAGE**  
 7.615 ± 0.008 ± 0.028 1.1M 1 BATLEY 12 NA48 ±  
 7.35 ± 0.01 ± 0.19 388k 2 PISLAK 01 B865  
 7.21 ± 0.32 30k ROSSELET 77 SPEC +  
 • • • We do not use the following data for averages, fits, limits, etc. • • •  
 7.36 ± 0.68 500 BOURQUIN 71 ASPK  
 7.0 ± 0.9 106 SCHWEINB... 71 HLBC +  
 5.83 ± 0.63 269 ELY 69 HLBC +

<sup>1</sup> BATLEY 12 uses data collected in 2003-2004. The result is inclusive of  $K^\pm \rightarrow \pi^+ \pi^- e^\pm \nu_\gamma$  decays. Using PDG 12 value for  $\Gamma(\pi^+ \pi^- \pi^+ \pi^-)/\Gamma = (5.59 \pm 0.04) \times 10^{-2}$ . BATLEY 12 obtains  $B(\pi^+ \pi^- e \nu) = (4.257 \pm 0.004 \pm 0.035) \times 10^{-5}$  where the syst. error is dominated by the error on the normalization mode.  
<sup>2</sup> PISLAK 01 reports  $\Gamma(\pi^+ \pi^- e^+ \nu_e)/\Gamma_{\text{total}} = (4.109 \pm 0.008 \pm 0.110) \times 10^{-5}$  using the PDG 00 value  $\Gamma(\pi^+ \pi^+ \pi^-)/\Gamma_{\text{total}} = (5.59 \pm 0.05) \times 10^{-2}$ . We divide by the PDG value and unfold its error from the systematic error. PISLAK 03 and PISLAK 10A give additional details on the branching ratio measurement and give improved errors on the S-wave  $\pi\pi$  scattering length:  $a_0^0 = 0.235 \pm 0.013$  and  $a_0^2 = -0.0410 \pm 0.0027$ .

$\Gamma(\pi^+ \pi^- \mu^+ \nu_\mu)/\Gamma_{\text{total}}$   $\Gamma_7/\Gamma$   
 VALUE (units  $10^{-5}$ ) EVTS DOCUMENT ID TECN CHG  
 • • • We do not use the following data for averages, fits, limits, etc. • • •  
 0.77 ± 0.54 1 CLINE 65 FBC +  
 -0.50

$\Gamma(\pi^+ \pi^- \mu^+ \nu_\mu)/\Gamma(\pi^+ \pi^+ \pi^-)$   $\Gamma_7/\Gamma_{11}$   
 VALUE (units  $10^{-4}$ ) EVTS DOCUMENT ID TECN CHG  
**2.57 ± 1.55** 7 BISI 67 DBC +  
 • • • We do not use the following data for averages, fits, limits, etc. • • •  
 ~ 2.5 1 GREINER 64 EMUL +

$\Gamma(\pi^0 \pi^0 \pi^0 e^+ \nu_e)/\Gamma_{\text{total}}$   $\Gamma_8/\Gamma$   
 VALUE (units  $10^{-6}$ ) CL% EVTS DOCUMENT ID TECN CHG  
**<3.5** 90 0 BOLOTOV 88 SPEC -  
 • • • We do not use the following data for averages, fits, limits, etc. • • •  
 <9 90 0 BARMIN 92 XEBC +

Hadronic modes

$\Gamma(\pi^+ \pi^0)/\Gamma_{\text{total}}$   $\Gamma_9/\Gamma$   
 VALUE (units  $10^{-2}$ ) EVTS DOCUMENT ID TECN CHG COMMENT  
**20.67 ± 0.08 OUR FIT** Error includes scale factor of 1.2.  
**20.70 ± 0.16 OUR AVERAGE** Error includes scale factor of 1.8.

20.65 ± 0.05 ± 0.08	1.4M	1 AMBROSINO 08E	KLOE +	$\phi \rightarrow K^+ K^-$
21.18 ± 0.28	16k	CHIANG 72	OSPK +	1.84 GeV/c $K^+$
• • • We do not use the following data for averages, fits, limits, etc. • • •				
21.0 ± 0.6		CALLAHAN 65	HLBC	See $\Gamma_9/\Gamma_{11}$

<sup>1</sup> Fully inclusive of final-state radiation. The branching ratio is evaluated using  $K^+$  lifetime,  $\tau = 12.385$  ns.

$\Gamma(\pi^+ \pi^0)/\Gamma(\pi^+ \pi^+ \pi^-)$   $\Gamma_9/\Gamma_{11}$   
 VALUE (units  $10^{-2}$ ) EVTS DOCUMENT ID TECN CHG  
**3.702 ± 0.022 OUR FIT** Error includes scale factor of 1.1.  
 • • • We do not use the following data for averages, fits, limits, etc. • • •  
 3.96 ± 0.15 1045 CALLAHAN 66 FBC +

$\Gamma(\pi^+ \pi^0)/\Gamma(\mu^+ \nu_\mu)$   $\Gamma_9/\Gamma_2$   
 VALUE (units  $10^{-2}$ ) EVTS DOCUMENT ID TECN CHG COMMENT  
**0.3252 ± 0.0016 OUR FIT** Error includes scale factor of 1.2.  
**0.3325 ± 0.0032 OUR AVERAGE**  
 0.3329 ± 0.0047 ± 0.0010 45k USHER 92 SPEC +  $p\bar{p}$  at rest  
 0.3355 ± 0.0057 1 WEISSENBE... 76 SPEC +  
 0.3277 ± 0.0065 4517 2 AUERBACH 67 OSPK +  
 • • • We do not use the following data for averages, fits, limits, etc. • • •  
 0.328 ± 0.005 25k 1 WEISSENBE... 74 STRC +  
 0.305 ± 0.018 1600 ZELLER 69 ASPK +

<sup>1</sup> WEISSENBERG 76 revises WEISSENBERG 74.  
<sup>2</sup> AUERBACH 67 changed from 0.3253 ± 0.0065. See comment with ratio  $\Gamma(\pi^0 \mu^+ \nu_\mu)/\Gamma(\mu^+ \nu_\mu)$ .

$\Gamma(\pi^+ \pi^0 \pi^0)/\Gamma_{\text{total}}$   $\Gamma_{10}/\Gamma$   
 VALUE (units  $10^{-2}$ ) EVTS DOCUMENT ID TECN CHG COMMENT  
**1.760 ± 0.023 OUR FIT** Error includes scale factor of 1.1.  
**1.775 ± 0.028 OUR AVERAGE** Error includes scale factor of 1.2.  
 1.763 ± 0.013 ± 0.022 ALOISIO 04A KLOE ±  
 1.84 ± 0.06 1307 CHIANG 72 OSPK + 1.84 GeV/c  $K^+$   
 • • • We do not use the following data for averages, fits, limits, etc. • • •  
 1.53 ± 0.11 198 1 PANDOULAS 70 EMUL +  
 1.8 ± 0.2 108 SHAKLEE 64 HLBC +  
 1.7 ± 0.2 ROE 61 HLBC +  
 1.5 ± 0.2 2 TAYLOR 59 EMUL +

<sup>1</sup> Includes events of TAYLOR 59.  
<sup>2</sup> Earlier experiments not averaged.

$\Gamma(\pi^+ \pi^0 \pi^0)/\Gamma(\pi^+ \pi^0)$   $\Gamma_{10}/\Gamma_9$   
 VALUE (units  $10^{-2}$ ) EVTS DOCUMENT ID TECN CHG COMMENT  
**0.0851 ± 0.0012 OUR FIT** Error includes scale factor of 1.1.  
 • • • We do not use the following data for averages, fits, limits, etc. • • •  
 0.081 ± 0.005 574 1 LUCAS 73B HBC - Dalitz pairs only  
<sup>1</sup> LUCAS 73B gives  $N(\pi^2 \pi^0) = 574 \pm 5.9\%$ ,  $N(2\pi) = 3564 \pm 3.1\%$ . We quote  $0.5N(\pi^2 \pi^0)/N(2\pi)$  where 0.5 is because only Dalitz pair  $\pi^0$ s were used.

$\Gamma(\pi^+ \pi^0 \pi^0)/\Gamma(\pi^+ \pi^+ \pi^-)$   $\Gamma_{10}/\Gamma_{11}$   
 VALUE (units  $10^{-2}$ ) EVTS DOCUMENT ID TECN CHG COMMENT  
**0.315 ± 0.004 OUR FIT** Error includes scale factor of 1.1.  
**0.303 ± 0.009** 2027 BISI 65 BC + HBC+HLBC  
 • • • We do not use the following data for averages, fits, limits, etc. • • •  
 0.393 ± 0.099 17 YOUNG 65 EMUL +

$\Gamma(\pi^+ \pi^+ \pi^-)/\Gamma_{\text{total}}$   $\Gamma_{11}/\Gamma$   
 VALUE (units  $10^{-2}$ ) EVTS DOCUMENT ID TECN CHG COMMENT  
**5.583 ± 0.024 OUR FIT**  
**5.565 ± 0.031 ± 0.025** 68K 1 BABUSCI 14B KLOE +  
 • • • We do not use the following data for averages, fits, limits, etc. • • •  
 5.56 ± 0.20 2330 2 CHIANG 72 OSPK + 1.84 GeV/c  $K^+$   
 5.34 ± 0.21 693 3 PANDOULAS 70 EMUL +  
 5.71 ± 0.15 DEMARCO 65 HBC  
 6.0 ± 0.4 YOUNG 65 EMUL +  
 5.54 ± 0.12 2332 CALLAHAN 64 HLBC +  
 5.1 ± 0.2 540 SHAKLEE 64 HLBC +  
 5.7 ± 0.3 ROE 61 HLBC +

<sup>1</sup> Inclusive of final-state radiation. Result obtained from averaging two branching ratios: one from a sample with  $K^- \rightarrow \mu \nu(\gamma)$  tagging and another with  $K^- \rightarrow \pi^- \pi^0(\gamma)$  tagging.  
<sup>2</sup> Value is not independent of CHIANG 72  $\Gamma(\mu^+ \nu_\mu)/\Gamma_{\text{total}}$ ,  $\Gamma(\pi^+ \pi^0)/\Gamma_{\text{total}}$ ,  $\Gamma(\pi^+ \pi^0 \pi^0)/\Gamma_{\text{total}}$ ,  $\Gamma(\pi^0 \mu^+ \nu_\mu)/\Gamma_{\text{total}}$ , and  $\Gamma(\pi^0 e^+ \nu_e)/\Gamma_{\text{total}}$ .  
<sup>3</sup> Includes events of TAYLOR 59.

# Meson Particle Listings

$K^\pm$

## Leptonic and semileptonic modes with photons

$\Gamma(\mu^+ \nu_\mu \gamma) / \Gamma_{\text{total}}$	$\Gamma_{12} / \Gamma$				
VALUE (units $10^{-3}$ )	EVTS	DOCUMENT ID	TECN	CHG	COMMENT
<b><math>6.2 \pm 0.8</math> OUR AVERAGE</b>					
$6.6 \pm 1.5$		1,2 DEMIDOV	90	XEBC	$P(\mu) < 231.5$ MeV/c
$6.0 \pm 0.9$		BARMIN	88	HLBC +	$P(\mu) < 231.5$ MeV/c

$3.5 \pm 0.8$		2,3 DEMIDOV	90	XEBC	$E(\gamma) > 20$ MeV
$3.2 \pm 0.5$	57	4 BARMIN	88	HLBC +	$E(\gamma) > 20$ MeV
$5.4 \pm 0.3$		5 AKIBA	85	SPEC	$P(\mu) < 231.5$ MeV/c

1  $P(\mu)$  cut given in DEMIDOV 90 paper, 235.1 MeV/c, is a misprint according to authors (private communication).  
 2 DEMIDOV 90 quotes only inner bremsstrahlung (IB) part.  
 3 Not independent of above DEMIDOV 90 value. Cuts differ.  
 4 Not independent of above BARMIN 88 value. Cuts differ.  
 5 Assumes  $\mu$ -e universality and uses constraints from  $K \rightarrow e \nu \gamma$ .

$\Gamma(\mu^+ \nu_\mu \gamma (SD^+)) / \Gamma_{\text{total}}$	$\Gamma_{13} / \Gamma$				
VALUE (units $10^{-5}$ )	CL% EVTS	DOCUMENT ID	TECN	CHG	COMMENT
<b><math>1.33 \pm 0.12 \pm 0.18</math></b>	2588	1 ADLER	00B	B787	

Structure-dependent part with  $+\gamma$  helicity ( $SD^+$  term). See the "Note on  $\pi^\pm \rightarrow \ell^\pm \nu \gamma$  and  $K^\pm \rightarrow \ell^\pm \nu \gamma$  Form Factors" in the  $\pi^\pm$  section of the Particle Data Listings above.  
 • • • We do not use the following data for averages, fits, limits, etc. • • •  
 $< 3.0$  90 AKIBA 85 SPEC  
 1 ADLER 00B obtains the branching ratio by extrapolating the measurement in the kinematic region  $E_\mu > 137$  MeV,  $E_\gamma > 90$  MeV to the full  $SD^+$  phase-space. Also reports  $|F_V + F_A| = 0.165 \pm 0.007 \pm 0.011$  and  $-0.04 < F_V - F_A < 0.24$  at 90% CL.

$\Gamma(\mu^+ \nu_\mu \gamma (SD^+ INT)) / \Gamma_{\text{total}}$	$\Gamma_{14} / \Gamma$				
VALUE (units $10^{-5}$ )	CL% EVTS	DOCUMENT ID	TECN	CHG	COMMENT
<b><math>&lt; 2.7</math></b>	90	AKIBA	85	SPEC	

Interference term between internal Bremsstrahlung and  $SD^+$  term. See the "Note on  $\pi^\pm \rightarrow \ell^\pm \nu \gamma$  and  $K^\pm \rightarrow \ell^\pm \nu \gamma$  Form Factors" in the  $\pi^\pm$  section of the Particle Data Listings above.

$\Gamma(\mu^+ \nu_\mu \gamma (SD^- + SD^- INT)) / \Gamma_{\text{total}}$	$\Gamma_{15} / \Gamma$				
VALUE (units $10^{-4}$ )	CL% EVTS	DOCUMENT ID	TECN	CHG	COMMENT
<b><math>&lt; 2.6</math></b>	90	1 AKIBA	85	SPEC	

Sum of structure-dependent part with  $-\gamma$  helicity ( $SD^-$  term) and interference term between internal Bremsstrahlung and  $SD^-$  term. See the "Note on  $\pi^\pm \rightarrow \ell^\pm \nu \gamma$  and  $K^\pm \rightarrow \ell^\pm \nu \gamma$  Form Factors" in the  $\pi^\pm$  section of the Particle Data Listings above.  
 1 Assumes  $\mu$ -e universality and uses constraints from  $K \rightarrow e \nu \gamma$ .

$\Gamma(e^+ \nu_e \gamma) / \Gamma(\mu^+ \nu_\mu)$	$\Gamma_{16} / \Gamma_2$				
VALUE (units $10^{-5}$ )	EVTS	DOCUMENT ID	TECN	CHG	COMMENT
<b><math>1.483 \pm 0.066 \pm 0.013</math></b>	1.4K	1 AMBROSINO	09E	KLOE	$\pm E_\gamma$ in 10–250 MeV, $p_e > 200$ MeV/c

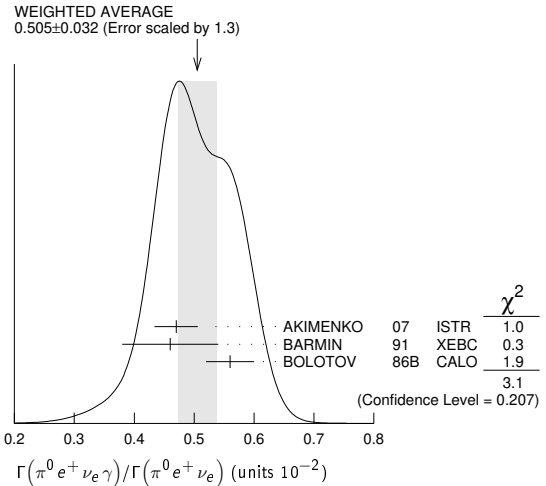
1 AMBROSINO 09E measured the differential width  $dR_\gamma/dE_\gamma = (1/\Gamma(K \rightarrow \mu \nu)) (d\Gamma(K \rightarrow e \nu \gamma)/dE_\gamma)$ . Result obtained by integrating the differential width over  $E_\gamma$  from 10 to 250 MeV.

$\Gamma(\pi^0 e^+ \nu_e \gamma) / \Gamma(\pi^0 e^+ \nu_e)$	$\Gamma_{17} / \Gamma_3$				
VALUE (units $10^{-2}$ )	EVTS	DOCUMENT ID	TECN	CHG	COMMENT
<b><math>0.505 \pm 0.032</math> OUR AVERAGE</b>					Error includes scale factor of 1.3. See the ideogram below.
$0.47 \pm 0.02 \pm 0.03$	4476	1 AKIMENKO	07	ISTR	$E_\gamma > 10$ MeV, $0.6 < \cos(\theta_{e\gamma}) < 0.9$
$0.46 \pm 0.08$	82	2 BARMIN	91	XEBC	$E_\gamma > 10$ MeV, $0.6 < \cos(\theta_{e\gamma}) < 0.9$
$0.56 \pm 0.04$	192	3 BOLOTOV	86B	CALO	$E_\gamma > 10$ MeV

• • • We do not use the following data for averages, fits, limits, etc. • • •  
 $1.81 \pm 0.03 \pm 0.07$  4476 1 AKIMENKO 07 ISTR  $E_\gamma > 10$  MeV,  $\theta_{e\gamma} > 10^\circ$   
 $0.63 \pm 0.02 \pm 0.03$  4476 1 AKIMENKO 07 ISTR  $E_\gamma > 30$  MeV,  $\theta_{e\gamma} > 20^\circ$   
 $1.51 \pm 0.25$  82 2 BARMIN 91 XEBC  $E_\gamma > 10$  MeV,  $\cos(\theta_{e\gamma}) < 0.98$   
 $0.48 \pm 0.20$  16 4 LJUNG 73 HLBC  $E_\gamma > 30$  MeV  
 $0.22 \pm 0.15$  4 LJUNG 73 HLBC  $E_\gamma > 30$  MeV  
 $-0.10$   
 $0.76 \pm 0.28$  13 5 ROMANO 71 HLBC  $E_\gamma > 10$  MeV  
 $0.53 \pm 0.22$  5 ROMANO 71 HLBC  $E_\gamma > 30$  MeV  
 $1.2 \pm 0.8$  BELLOTTI 67 HLBC  $E_\gamma > 30$  MeV

1 AKIMENKO 07 provides values for three kinematic regions. For averaging, we use value with  $E_\gamma > 10$  MeV and  $0.6 < \cos(\theta_{e\gamma}) < 0.9$ .  
 2 BARMIN 91 quotes branching ratio  $\Gamma(K \rightarrow e \pi^0 \nu \gamma) / \Gamma_{\text{all}}$ . The measured normalization is  $[\Gamma(K \rightarrow e \pi^0 \nu) + \Gamma(K \rightarrow \pi^+ \pi^+ \pi^-)]$ . For comparison with other experiments we used  $\Gamma(K \rightarrow e \pi^0 \nu) / \Gamma_{\text{all}} = 0.0482$  to calculate the values quoted here.  
 3  $\cos(\theta_{e\gamma})$  between 0.6 and 0.9.  
 4 First LJUNG 73 value is for  $\cos(\theta_{e\gamma}) < 0.9$ , second value is for  $\cos(\theta_{e\gamma})$  between 0.6 and 0.9 for comparison with ROMANO 71.

5 Both ROMANO 71 values are for  $\cos(\theta_{e\gamma})$  between 0.6 and 0.9. Second value is for comparison with second LJUNG 73 value. We use lowest  $E_\gamma$  cut for Summary Table value. See ROMANO 71 for  $E_\gamma$  dependence.



$\Gamma(\pi^0 e^+ \nu_e \gamma (SD)) / \Gamma_{\text{total}}$	$\Gamma_{18} / \Gamma$				
VALUE (units $10^{-5}$ )	CL% EVTS	DOCUMENT ID	TECN	CHG	COMMENT
<b><math>&lt; 5.3</math></b>	90	BOLOTOV	86B	CALO	

$\Gamma(\pi^0 \mu^+ \nu_\mu \gamma) / \Gamma_{\text{total}}$	$\Gamma_{19} / \Gamma$				
VALUE (units $10^{-5}$ )	CL% EVTS	DOCUMENT ID	TECN	CHG	COMMENT
<b><math>1.25 \pm 0.25</math> OUR AVERAGE</b>					
$1.10 \pm 0.32 \pm 0.05$		1 ADLER	10	B787	$30 < E_\gamma < 60$ MeV
$1.46 \pm 0.22 \pm 0.32$	153	2 TCHIKILEV	07	ISTR	$30 < E_\gamma < 60$ MeV

• • • We do not use the following data for averages, fits, limits, etc. • • •  
 $2.4 \pm 0.5 \pm 0.6$  125 SHIMIZU 06 K470  $E_\gamma > 30$  MeV;  $\theta_{\mu\gamma} > 20^\circ$   
 $< 6.1$  90 0 LJUNG 73 HLBC  $E(\gamma) > 30$  MeV

1 Value obtained from  $B(K^+ \rightarrow \pi^0 \mu^+ \nu_\mu \gamma) = (2.51 \pm 0.74 \pm 0.12) \times 10^{-5}$  obtained in the kinematic region  $E_\gamma > 20$  MeV, and then theoretical  $K_{\mu 3\gamma}$  spectrum has been used. Also  $B(K^+ \rightarrow \pi^0 \mu^+ \nu_\mu \gamma) = (1.58 \pm 0.46 \pm 0.08) \times 10^{-5}$ , for  $E_\gamma > 30$  MeV and  $\theta_{\mu\gamma} > 20^\circ$ , was determined.  
 2 Obtained from measuring  $B(K_{\mu 3\gamma}) / B(K_{\mu 3})$  and using PDG 02 value  $B(K_{\mu 3}) = 3.27\%$ .  $B(K_{\mu 3\gamma}) = (8.82 \pm 0.94 \pm 0.86) \times 10^{-5}$  is obtained for  $5 \text{ MeV} < E_\gamma < 30 \text{ MeV}$ .

$\Gamma(\pi^0 \pi^0 e^+ \nu_e \gamma) / \Gamma_{\text{total}}$	$\Gamma_{20} / \Gamma$				
VALUE (units $10^{-6}$ )	CL% EVTS	DOCUMENT ID	TECN	CHG	COMMENT
<b><math>&lt; 5</math></b>	90	0	BARMIN	92	XEBC $E_\gamma > 10$ MeV

## Hadronic modes with photons

$\Gamma(\pi^+ \pi^0 \gamma (INT)) / \Gamma_{\text{total}}$	$\Gamma_{21} / \Gamma$				
VALUE (units $10^{-6}$ )	EVTS	DOCUMENT ID	TECN	CHG	COMMENT
<b><math>-4.24 \pm 0.63 \pm 0.70</math></b>	600k	1 BATLEY	10A	NA48	$\pm T_{\pi^+}$ 0–80 MeV

The  $K^+ \rightarrow \pi^+ \pi^0 \gamma$  differential decay rate can be described in terms of  $T_{\pi^+}$ , the charged pion kinetic energy, and  $W^2 = (P_K \cdot P_\gamma) (P_{\pi^+} \cdot P_\gamma) / (m_K m_{\pi^+})^2$ ; then we can write  $d^2\Gamma(K^+ \rightarrow \pi^+ \pi^0 \gamma) / (dT_{\pi^+} dW^2) = d^2\Gamma(K^+ \rightarrow \pi^+ \pi^0 \gamma)_{IB} / (dT_{\pi^+} dW^2) [1 + 2 \cos(\phi + \delta_1^+ - \delta_0^0) m_\pi^2 m_K^2 W^2 X_E + m_\pi^4 m_K^4 (X_E^2 + X_M^2) W^4]$ . The IB differential and total branching ratios are expressed in terms of the non-radiative experimental width  $\Gamma(K^+ \rightarrow \pi^+ \pi^0)$  by Low's theorem. Using PDG 10  $B(K^+ \rightarrow \pi^+ \pi^0) = 0.2066 \pm 0.0008$ , one obtains respectively  $B(K^+ \rightarrow \pi^+ \pi^0 \gamma)_{IB} (55 < T_{\pi^+} < 90 \text{ MeV}) = 2.55 \times 10^{-4}$  and  $B(K^+ \rightarrow \pi^+ \pi^0 \gamma)_{IB} (0 < T_{\pi^+} < 80 \text{ MeV}) = 1.80 \times 10^{-4}$ . Fitting respectively the piece proportional to  $W^2$  and the piece proportional to  $W^4$ , the interference contribution (INT), proportional to  $X_E$ , and the direct contribution (DE) proportional to  $X_E^2 + X_M^2$  are extracted.

$\Gamma(\pi^+ \pi^0 \gamma (DE)) / \Gamma_{\text{total}}$	$\Gamma_{22} / \Gamma$				
VALUE (units $10^{-6}$ )	EVTS	DOCUMENT ID	TECN	CHG	COMMENT
<b><math>5.99 \pm 0.27 \pm 0.25</math></b>	600k	1 BATLEY	10A	NA48	$\pm T_{\pi^+}$ 0–80 MeV

1 The cut on the photon energy implies  $W^2 > 0.2$ . BATLEY 10A obtains the INT and DE fractional branchings with respect to IB from a simultaneous kinematical fit of INT and DE and then we use the PDG 10 value for  $B(K^+ \rightarrow \pi^+ \pi^0) = 0.2066 \pm 0.0008$  to determine the IB. The INT and DE correlation coefficients  $-0.83$ . Assuming a constant electric amplitude,  $X_E$ , this INT value implies  $X_E = -24 \pm 6 \text{ GeV}^{-4}$ .

$\Gamma(\pi^+ \pi^0 \gamma (INT)) / \Gamma_{\text{total}}$	$\Gamma_{22} / \Gamma$				
VALUE (units $10^{-6}$ )	EVTS	DOCUMENT ID	TECN	CHG	COMMENT
<b><math>5.99 \pm 0.27 \pm 0.25</math></b>	600k	1 BATLEY	10A	NA48	$\pm T_{\pi^+}$ 0–80 MeV

Direct emission (DE) part of  $\Gamma(\pi^+ \pi^0 \gamma) / \Gamma_{\text{total}}$ , assuming that interference (INT) component is zero.

••• We do not use the following data for averages, fits, limits, etc. •••

3.8 ± 0.8 ± 0.7	10k	ALIEV	06	K470	+	$T_{\pi^+}$	55–90 MeV
3.7 ± 3.9 ± 1.0	930	UVAROV	06	ISTR	–	$T_{\pi^-}$	55–90 MeV
3.2 ± 1.3 ± 1.0	4k	ALIEV	03	K470	+	$T_{\pi^+}$	55–90 MeV
6.1 ± 2.5 ± 1.9	4k	ALIEV	03	K470	+	$T_{\pi^+}$	full range
4.7 ± 0.8 ± 0.3	20k	<sup>2</sup> ADLER	00c	B787	+	$T_{\pi^+}$	55–90 MeV
20.5 ± 4.6	+3.9	BOLOTOV	87	WIRE	–	$T_{\pi^-}$	55–90 MeV
–2.3	–2.3						
15.6 ± 3.5 ± 5.0		ABRAMS	72	ASPK	±	$T_{\pi^\pm}$	55–90 MeV

<sup>1</sup> The cut on the photon energy implies  $W^2 > 0.2$ . BATLEY 10a obtains the INT and DE fractional branchings with respect to IB from a simultaneous kinematical fit of INT and DE and then we use the PDG 10 value for  $B(K^+ \rightarrow \pi^+ \pi^0) = 20.66 \pm 0.08$  to determine the IB. The INT and DE correlation coefficients  $-0.93$ . Assuming constant electric and magnetic amplitudes,  $X_E$  and  $X_M$ , these INT and DE values imply  $X_E = -24 \pm 6 \text{ GeV}^{-4}$  and  $X_M = -254 \pm 9 \text{ GeV}^{-4}$ .

<sup>2</sup> ADLER 00c measures the INT component to be  $(-0.4 \pm 1.6)\%$  of the inner bremsstrahlung (IB) component.

$\Gamma(\pi^+ \pi^0 \pi^0 \gamma) / \Gamma(\pi^+ \pi^0 \pi^0)$   $\Gamma_{24} / \Gamma_{10}$

VALUE (units $10^{-4}$ )	DOCUMENT ID	TECN	CHG	COMMENT	
<b>4.3 ± 3.2</b>	BOLOTOV	85	SPEC	–	$E(\gamma) > 10 \text{ MeV}$

$\Gamma(\pi^+ \pi^+ \pi^- \gamma) / \Gamma_{\text{total}}$   $\Gamma_{25} / \Gamma$

VALUE (units $10^{-4}$ )	EVTS	DOCUMENT ID	TECN	CHG	COMMENT	
<b>0.071 ± 0.005 OUR AVERAGE</b>						
0.071 ± 0.005	450	SHAPKIN	19	OKA	+	$E(\gamma) > 30 \text{ MeV}$
1.10 ± 0.48	7	BARMIN	89	XEBC		$E(\gamma) > 5 \text{ MeV}$
1.0 ± 0.4		STAMER	65	EMUL	+	$E(\gamma) > 11 \text{ MeV}$

$\Gamma(\pi^+ \pi^0 e^+ e^-) / \Gamma_{\text{total}}$   $\Gamma_{23} / \Gamma$

VALUE (units $10^{-6}$ )	EVTS	DOCUMENT ID	TECN
<b>4.24 ± 0.14</b>	4.9K	<sup>1</sup> BATLEY	19 NA48

<sup>1</sup> BATLEY 19 result is obtained from an exposure of  $1.7 \times 10^{11}$  charged kaon decays recorded in 2003–2004. The study of the kinematic space shows evidence for a structure dependent contribution consistent with predictions from chiral perturbation theory.

$\Gamma(\pi^+ \gamma \gamma) / \Gamma_{\text{total}}$   $\Gamma_{26} / \Gamma$

VALUE (units $10^{-7}$ )	CL%	EVTS	DOCUMENT ID	TECN	CHG	COMMENT
<b>10.1 ± 0.6 OUR AVERAGE</b>						
10.03 ± 0.51 ± 0.24	215	<sup>1</sup> LAZZERONI	14 NA62	±		
11 ± 3 ± 1	31	<sup>2</sup> KITCHING	97 B787	+		
9.10 ± 0.72 ± 0.22	149	<sup>3</sup> BATLEY	14 NA48	±		
< 0.083	90	<sup>4</sup> ARTAMONOV	05 B949	+	$P_{\pi^-} > 213 \text{ MeV}/c$	
< 10	90	0 ATIYA	90b B787	+	$T_{\pi^-} 117\text{--}127 \text{ MeV}$	
< 84	90	0 ASANO	82 CNTR	+	$T_{\pi^-} 117\text{--}127 \text{ MeV}$	
< 420 ± 520	0	0 ABRAMS	77 SPEC	+	$T_{\pi^-} < 92 \text{ MeV}$	
< 350	90	0 LJUNG	73 HLBC	+	6–102, 114–127 MeV	
< 500	90	0 KLEMS	71 OSPK	+	$T_{\pi^-} < 117 \text{ MeV}$	
< 100 ± 600		0 CHEN	68 OSPK	+	$T_{\pi^-} 60\text{--}90 \text{ MeV}$	

<sup>1</sup> LAZZERONI 14 combines NA62 and NA48/2 results. The result for the full kinematic range is extrapolated from the model-independent branching fraction  $(9.65 \pm 0.61 \pm 0.14) \times 10^{-7}$  for  $(m_{\gamma\gamma}/m_K)^2 > 0.2$ . The measured ChPT parameter  $\tilde{c} = 1.86 \pm 0.25$ .

<sup>2</sup> KITCHING 97 is extrapolated from their model-independent branching fraction  $(6.0 \pm 1.5 \pm 0.7) \times 10^{-7}$  for  $100 \text{ MeV}/c < P_{\pi^+} < 180 \text{ MeV}/c$  using Chiral Perturbation Theory.

<sup>3</sup> BATLEY 14 uses data collected in 2003 and 2004. Branching ratio is obtained by determining the parameter  $\tilde{c} = 1.41 \pm 0.38 \pm 0.11$  and integrating the  $O(p^6)$  chiral spectrum. A model independent value for the branching ratio is also obtained  $(8.77 \pm 0.87 \pm 0.17) \times 10^{-7}$  for kinematic range  $(m_{\gamma\gamma}/m_K)^2 > 0.2$ .

<sup>4</sup> ARTAMONOV 05 limit assumes ChPT with  $\tilde{c} = 1.8$  with unitarity corrections. With  $\tilde{c} = 1.6$  and no unitarity corrections they obtain  $< 2.3 \times 10^{-8}$  at 90% CL. This partial branching ratio is predicted to be  $6.10 \times 10^{-9}$  and  $0.49 \times 10^{-9}$  for the cases with and without unitarity correction.

$\Gamma(\pi^+ 3\gamma) / \Gamma_{\text{total}}$   $\Gamma_{27} / \Gamma$

Values given here assume a phase space pion energy spectrum.

VALUE (units $10^{-4}$ )	CL%	DOCUMENT ID	TECN	CHG	COMMENT	
<b>&lt; 1.0</b>	90	ASANO	82	CNTR	+	$T(\pi) 117\text{--}127 \text{ MeV}$

••• We do not use the following data for averages, fits, limits, etc. •••

< 3.0	90	KLEMS	71	OSPK	+	$T(\pi) > 117 \text{ MeV}$
-------	----	-------	----	------	---	----------------------------

$\Gamma(\pi^+ e^+ e^- \gamma) / \Gamma_{\text{total}}$   $\Gamma_{28} / \Gamma$

VALUE (units $10^{-8}$ )	EVTS	DOCUMENT ID	TECN	COMMENT
<b>1.19 ± 0.12 ± 0.04</b>	113	<sup>1</sup> BATLEY	08 NA48	$m_{ee\gamma} > 260 \text{ MeV}$

<sup>1</sup> BATLEY 08 also reports the Chiral Perturbation Theory parameter  $\tilde{c} = 0.9 \pm 0.45$  obtained using the shape of the  $e^+ e^- \gamma$  invariant mass spectrum. By extrapolating the theoretical amplitude to  $m_{ee\gamma} < 260 \text{ MeV}$ , it obtains the inclusive  $B(K^+ \rightarrow \pi^+ e^+ e^- \gamma) = (1.29 \pm 0.13 \pm 0.03) \times 10^{-8}$ , where the first error is the combined statistical and systematic errors and the second error is from the uncertainty in  $\tilde{c}$ .

Leptonic modes with  $\ell\bar{\ell}$  pairs

$\Gamma(e^+ \nu_e \nu \bar{\nu}) / \Gamma(e^+ \nu_e)$   $\Gamma_{29} / \Gamma_1$

VALUE	CL%	EVTS	DOCUMENT ID	TECN	CHG	
<b>&lt; 3.8</b>	90	0	HEINTZE	79	SPEC	+

$\Gamma(\mu^+ \nu_\mu \nu \bar{\nu}) / \Gamma_{\text{total}}$   $\Gamma_{30} / \Gamma$

VALUE	CL%	DOCUMENT ID	TECN	CHG
<b>&lt; 2.4 × 10<sup>-6</sup></b>	90	<sup>1</sup> ARTA MONOV	16 B949	+
< 6.0 × 10 <sup>-6</sup>	90	<sup>2</sup> PANG	73 CNTR	+

••• We do not use the following data for averages, fits, limits, etc. •••

<sup>1</sup> ARTAMONOV 16 assumes Standard model  $\mu$  spectrum. The search is performed in the muon momentum region between 130 and 175 MeV/c.

<sup>2</sup> PANG 73 assumes  $\mu$  spectrum from  $\nu\text{-}\nu$  interaction of BARDIN 70.

$\Gamma(e^+ \nu_e e^+ e^-) / \Gamma_{\text{total}}$   $\Gamma_{31} / \Gamma$

VALUE (units $10^{-8}$ )	EVTS	DOCUMENT ID	TECN	CHG	COMMENT	
<b>2.48 ± 0.14 ± 0.14</b>	410	POBLAGUEV	02 B865	+	$m_{ee} > 150 \text{ MeV}$	
20 ± 20	4	DIAMANT...	76	SPEC	+	$m_{e^+e^-} > 140 \text{ MeV}$

••• We do not use the following data for averages, fits, limits, etc. •••

$\Gamma(\mu^+ \nu_\mu e^+ e^-) / \Gamma_{\text{total}}$   $\Gamma_{32} / \Gamma$

VALUE (units $10^{-8}$ )	EVTS	DOCUMENT ID	TECN	CHG	COMMENT	
<b>7.06 ± 0.16 ± 0.26</b>	2.7k	POBLAGUEV	02 B865	+	$m_{ee} > 145 \text{ MeV}$	
100 ± 30	14	DIAMANT...	76	SPEC	+	$m_{e^+e^-} > 140 \text{ MeV}$

••• We do not use the following data for averages, fits, limits, etc. •••

$\Gamma(e^+ \nu_e \mu^+ \mu^-) / \Gamma_{\text{total}}$   $\Gamma_{33} / \Gamma$

VALUE (units $10^{-8}$ )	CL%	DOCUMENT ID	TECN
<b>1.72 ± 0.45</b>		MA	06 B865
< 50	90	ADLER	98 B787

••• We do not use the following data for averages, fits, limits, etc. •••

$\Gamma(\mu^+ \nu_\mu \mu^+ \mu^-) / \Gamma_{\text{total}}$   $\Gamma_{34} / \Gamma$

VALUE (units $10^{-7}$ )	CL%	DOCUMENT ID	TECN	CHG	
<b>&lt; 4.1</b>	90	ATIYA	89	B787	+

Lepton Family number (LF), Lepton number (L),  $\Delta S = \Delta Q$  (SQ) violating modes, or  $\Delta S = 1$  weak neutral current (S1) modes

$\Gamma(\pi^+ \pi^+ e^- \bar{\nu}_e) / \Gamma_{\text{total}}$   $\Gamma_{35} / \Gamma$

Test of  $\Delta S = \Delta Q$  rule.

VALUE (units $10^{-7}$ )	CL%	EVTS	DOCUMENT ID	TECN	CHG	
< 9.0	95	0	SCHWEINB...	71	HLBC	+
< 6.9	95	0	ELY	69	HLBC	+
< 20.	95	0	BIRGE	65	FBC	+

••• We do not use the following data for averages, fits, limits, etc. •••

$\Gamma(\pi^+ \pi^+ e^- \bar{\nu}_e) / \Gamma(\pi^+ \pi^- e^+ \nu_e)$   $\Gamma_{35} / \Gamma_6$

Test of  $\Delta S = \Delta Q$  rule.

VALUE (units $10^{-4}$ )	CL%	EVTS	DOCUMENT ID	TECN	
<b>&lt; 3</b>	90	3	<sup>1</sup> BLOCH	76	SPEC
< 130.	95	0	BOURQUIN	71	ASPK

••• We do not use the following data for averages, fits, limits, etc. •••

<sup>1</sup> BLOCH 76 quotes  $3.6 \times 10^{-4}$  at CL = 95%, we convert.

$\Gamma(\pi^+ \pi^+ \mu^- \bar{\nu}_\mu) / \Gamma_{\text{total}}$   $\Gamma_{36} / \Gamma$

Test of  $\Delta S = \Delta Q$  rule.

VALUE (units $10^{-6}$ )	CL%	EVTS	DOCUMENT ID	TECN	CHG	
<b>&lt; 3.0</b>	95	0	BIRGE	65	FBC	+

$\Gamma(\pi^+ e^+ e^-) / \Gamma_{\text{total}}$   $\Gamma_{37} / \Gamma$

Test for  $\Delta S = 1$  weak neutral current. Allowed by combined first-order weak and electromagnetic interactions.

VALUE (units $10^{-7}$ )	EVTS	DOCUMENT ID	TECN	CHG	
<b>3.00 ± 0.09 OUR AVERAGE</b>					
3.11 ± 0.04 ± 0.12	7253	<sup>1</sup> BATLEY	09 NA48	±	
2.94 ± 0.05 ± 0.14	10300	<sup>2</sup> APPEL	99	SPEC	+
2.75 ± 0.23 ± 0.13	500	<sup>3</sup> ALLIEGRO	92	SPEC	+
2.7 ± 0.5	41	<sup>4</sup> BLOCH	75	SPEC	+

<sup>1</sup> Value extrapolated from a measurement in the region  $z = (m_{ee}/m_K)^2 > 0.08$ . BATLEY 09 also evaluated the shape of the form factor using four different theoretical models.

<sup>2</sup> APPEL 99 establishes vector nature of this decay and determines form factor  $f(z) = f_0(1 + \delta Z)$ ,  $Z = M_{ee}^2/m_K^2$ ,  $\delta = 2.14 \pm 0.13 \pm 0.15$ .

<sup>3</sup> ALLIEGRO 92 assumes a vector interaction with a form factor given by  $\lambda = 0.105 \pm 0.035 \pm 0.015$  and a correlation coefficient of  $-0.82$ .

<sup>4</sup> BLOCH 75 assumes a vector interaction.

# Meson Particle Listings

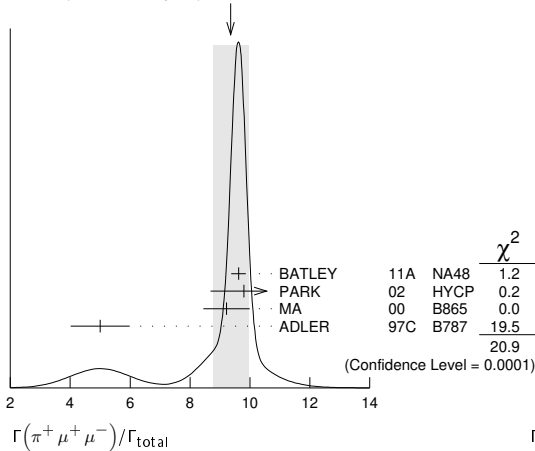
$K^\pm$

$\Gamma(\pi^+ \mu^+ \mu^-)/\Gamma_{total}$   $\Gamma_{38}/\Gamma$   
 Test for  $\Delta S = 1$  weak neutral current. Allowed by higher-order electroweak interactions.

VALUE (units $10^{-8}$ )	CL%	EVTS	DOCUMENT ID	TECN	CHG	COMMENT
<b>9.4 ± 0.6</b>	<b>OUR AVERAGE</b>					Error includes scale factor of 2.6. See the ideogram below.
9.62 ± 0.21 ± 0.13		3120	<sup>1</sup> BATLEY	11A	NA48	± 2003-04 data
9.8 ± 1.0 ± 0.5		110	<sup>2</sup> PARK	02	HYCP	±
9.22 ± 0.60 ± 0.49		402	<sup>3</sup> MA	00	B865	+
5.0 ± 0.4 ± 0.9		207	<sup>4</sup> ADLER	97c	B787	+

- • • We do not use the following data for averages, fits, limits, etc. • • •
  - 9.7 ± 1.2 ± 0.4      65      PARK      02      HYCP      +
  - 10.0 ± 1.9 ± 0.7      35      PARK      02      HYCP      -
  - <23                      90                      ATIYA                      89                      B787                      +
- <sup>1</sup> BATLEY 11A also studies the form factor  $f(z)$  dependence of the decay, described via single photon exchange: i) assuming a linear form factor,  $f(z) = f_0 (1 + \delta z)$ ,  $z = (M_{\mu\mu}/m_K)^2$ , finding  $f_0 = 0.470 \pm 0.040$  and  $\delta = 3.11 \pm 0.57$  and ii) assuming a linear form factor including  $\pi$ - $\pi$  rescattering,  $W_{\pi\pi}$ , as in DAMBROSIO 98A, finding  $f(z) = G_F m_K^2 (a_+ + b_+ z) + W_{\pi\pi}(z)$ ,  $a_+ = -0.575 \pm 0.039$ ,  $b_+ = -0.813 \pm 0.145$ .
- <sup>2</sup> PARK 02 “±” result comes from combining  $K^+ \rightarrow \pi^+ \mu^+ \mu^-$  and  $K^- \rightarrow \pi^- \mu^+ \mu^-$ , assuming CP is conserved.
- <sup>3</sup> MA 00 establishes vector nature of this decay and determines form factor  $f(z) = f_0 (1 + \delta z)$ ,  $z = (M_{\mu\mu}/m_K)^2$ ,  $\delta = 2.45_{-0.95}^{+1.30}$ .
- <sup>4</sup> ADLER 97c gives systematic error  $0.7 \times 10^{-8}$  and theoretical uncertainty  $0.6 \times 10^{-8}$ , which we combine in quadrature to obtain our second error.

WEIGHTED AVERAGE  
9.4±0.6 (Error scaled by 2.6)



$\Gamma(\pi^+ \nu \mu)/\Gamma_{total}$   $\Gamma_{39}/\Gamma$   
 Test for  $\Delta S = 1$  weak neutral current. Allowed by higher-order electroweak interactions. Branching ratio values are extrapolated from the momentum or energy regions shown in the comments assuming Standard Model phase space except for those labeled “Scalar” or “Tensor” to indicate the assumed non-Standard-Model interaction.

VALUE (units $10^{-9}$ )	CL%	EVTS	DOCUMENT ID	TECN	CHG	COMMENT
<b>0.173 ± 0.115</b>		7	<sup>1</sup> ARTAMONOV 08	B949	+	$140 < P_\pi < 199$ MeV, $211 < P_\pi < 229$ MeV
< 1.1	90	1	<sup>2</sup> CORTINA-GIL 19B	NA62	+	decay-in-flight
0.789 ± 0.926		3	<sup>3</sup> ARTAMONOV 08	B949	+	$140 < P_\pi < 199$ MeV
< 2.2	90	1	<sup>4</sup> ADLER	04	B787	+ $211 < P_\pi < 229$ MeV
< 2.7	90		ADLER	04	B787	+ Scalar
< 1.8	90		ADLER	04	B787	+ Tensor
0.147 ± 0.130		3	<sup>5</sup> ANISIMOVSK...04	B949	+	$211 < P_\pi < 229$ MeV
0.157 ± 0.175		2	ADLER	02	B787	+ $P_\pi > 211$ MeV/c
< 4.2	90	1	ADLER	02c	B787	+ $140 < P_\pi < 195$ MeV
< 4.7	90		ADLER	02c	B787	+ Scalar
< 2.5	90		ADLER	02c	B787	+ Tensor
0.15 ± 0.34		1	ADLER	00	B787	In ADLER 02
0.42 ± 0.97		1	ADLER	97	B787	
< 2.4	90		ADLER	96	B787	
< 7.5	90		ATIYA	93	B787	+ $T(\pi)$ 115-127 MeV
< 5.2	90		ATIYA	93	B787	+
< 17	90	0	ATIYA	93B	B787	+ $T(\pi)$ 60-100 MeV
< 34	90		ATIYA	90	B787	+
<140	90		ASANO	81B	CNTR	+ $T(\pi)$ 116-127 MeV

- • • We do not use the following data for averages, fits, limits, etc. • • •
- <sup>1</sup> Value obtained combining ANISIMOVSKY 04, ADLER 04, and the present ARTAMONOV 08 results.
- <sup>2</sup> Based on a sample of  $1.21 \times 10^{11}$   $K^+$  decays collected in 2016. One signal candidate is observed while the expected background is 0.152 events. The single-event-sensitivity is estimated to be  $3.15 \times 10^{-10}$ .

- <sup>3</sup> Observed 3 events with an estimated background of  $0.93 \pm 0.17_{-0.24}^{+0.32}$ . Signal-to-background ratio for each of these 3 events is 0.20, 0.42, and 0.47.
- <sup>4</sup> Value obtained combining the previous result ADLER 02c with 1 event and the present result with 0 events to obtain an expected background  $1.22 \pm 0.24$  events and 1 event observed.
- <sup>5</sup> Value obtained combining the previous E787 result ADLER 02 with 2 events and the present E949 with 1 event. The additional event has a signal-to-background ratio 0.9. Superseded by ARTAMONOV 08.
- <sup>6</sup> Superseded by ADLER 04.
- <sup>7</sup> Combining ATIYA 93 and ATIYA 93B results. Superseded by ADLER 96.

$\Gamma(\pi^+ \pi^0 \nu \mu)/\Gamma_{total}$   $\Gamma_{40}/\Gamma$   
 Test for  $\Delta S = 1$  weak neutral current. Allowed by higher-order electroweak interactions.

VALUE (units $10^{-5}$ )	CL%	DOCUMENT ID	TECN
<b>&lt;4.3</b>	90	<sup>1</sup> ADLER	01 SPEC

$\Gamma(\mu^- \nu e^+ e^+)/\Gamma(\pi^+ \pi^- e^+ \nu_e)$   $\Gamma_{41}/\Gamma_6$   
 Test of lepton family number conservation.

VALUE (units $10^{-3}$ )	CL%	EVTS	DOCUMENT ID	TECN	CHG
<b>&lt;0.5</b>	90	0	<sup>1</sup> DIAMANT-...	76	SPEC +

- <sup>1</sup> DIAMANT-BERGER 76 quotes this result times our 1975  $\pi^+ \pi^- e \nu$  BR ratio.

$\Gamma(\mu^- \nu_e)/\Gamma_{total}$   $\Gamma_{42}/\Gamma$   
 Forbidden by lepton family number conservation.

VALUE	CL%	EVTS	DOCUMENT ID	TECN	COMMENT
<b>&lt;0.004</b>	90	0	<sup>1</sup> LYONS	81	HLBC 200 GeV $K^+$ narrow band $\nu$ beam

- • • We do not use the following data for averages, fits, limits, etc. • • •
- <0.012      90                      <sup>1</sup> COOPER                      82                      HLBC                      Wideband  $\nu$  beam
- <sup>1</sup> COOPER 82 and LYONS 81 limits on  $\nu_e$  observation are here interpreted as limits on lepton family number violation in the absence of mixing.

$\Gamma(\pi^+ \mu^+ e^-)/\Gamma_{total}$   $\Gamma_{43}/\Gamma$   
 Test of lepton family number conservation.

VALUE (units $10^{-10}$ )	CL%	DOCUMENT ID	TECN	CHG
<b>&lt;0.13</b>	90	<sup>1</sup> SHER	05	RVUE +
<0.21	90	SHER	05	B865 +
<0.39	90	APPEL	00	B865 +
<2.1	90	LEE	90	SPEC +

- • • We do not use the following data for averages, fits, limits, etc. • • •
- <sup>1</sup> This result combines SHER 05 1998 data, APPEL 00 1996 data, and data from BERGMAN 97 and PISLAK 97 theses, all from BNL-E865, with LEE 90 BNL-E777 data.

$\Gamma(\pi^+ \mu^- e^+)/\Gamma_{total}$   $\Gamma_{44}/\Gamma$   
 Test of lepton family number conservation.

VALUE (units $10^{-10}$ )	CL%	EVTS	DOCUMENT ID	TECN	CHG
<b>&lt; 5.2</b>	90	0	APPEL	00B	B865 +

- • • We do not use the following data for averages, fits, limits, etc. • • •
- <70                      90                      0                      <sup>1</sup> DIAMANT-...                      76                      SPEC +

$\Gamma(\pi^- \mu^+ e^+)/\Gamma_{total}$   $\Gamma_{45}/\Gamma$   
 Test of total lepton number conservation.

VALUE (units $10^{-10}$ )	CL%	EVTS	DOCUMENT ID	TECN	CHG
<b>&lt; 5.0</b>	90	0	APPEL	00B	B865 +

- • • We do not use the following data for averages, fits, limits, etc. • • •
- <70                      90                      0                      <sup>1</sup> DIAMANT-...                      76                      SPEC +

$\Gamma(\pi^- e^+ e^+)/\Gamma_{total}$   $\Gamma_{46}/\Gamma$   
 Test of total lepton number conservation.

VALUE	CL%	DOCUMENT ID	TECN	CHG	COMMENT
<b>&lt;2.2 × 10<sup>-10</sup></b>	90	<sup>1</sup> CORTINA-GIL 19A	NA 62	+	decay-in-flight
<6.4 × 10 <sup>-10</sup>	90	APPEL	00B	B865	+
<9.2 × 10 <sup>-9</sup>	90	DIAMANT-...	76	SPEC	+
<1.5 × 10 <sup>-5</sup>		CHANG	68	HBC	-

- <sup>1</sup> CORTINA-GIL 19A results are obtained with 2017 data.

$\Gamma(\pi^- \mu^+ \mu^+)/\Gamma_{total}$   $\Gamma_{47}/\Gamma$   
 Forbidden by total lepton number conservation.

VALUE	CL%	DOCUMENT ID	TECN	CHG	COMMENT
<b>&lt;4.2 × 10<sup>-11</sup></b>	90	<sup>1</sup> CORTINA-GIL 19A	NA 62	+	decay-in-flight
<8.6 × 10 <sup>-11</sup>	90	<sup>2</sup> BATLEY	17	NA 48	±
<1.1 × 10 <sup>-9</sup>	90	BATLEY	11A	NA 48	±
<3.0 × 10 <sup>-9</sup>	90	APPEL	00B	B865	+
<1.5 × 10 <sup>-4</sup>	90	<sup>3</sup> LITTEMBERG	92	HBC	

- <sup>1</sup> CORTINA-GIL 19A results are obtained with 2017 data.
- <sup>2</sup> BATLEY 17 result is based on data taken in 2003 to 2004. Limits for two-body resonance  $X$  in  $K^\pm \rightarrow \pi \mu \mu$  decays are also reported.
- <sup>3</sup> LITTEMBERG 92 is from retroactive data analysis of CHANG 68 bubble chamber data.

$\Gamma(\mu^+ \bar{\nu}_e) / \Gamma_{\text{total}}$   $\Gamma_{48} / \Gamma$   
 Forbidden by total lepton number conservation.

VALUE (units $10^{-3}$ )	CL%	DOCUMENT ID	TECN	COMMENT
<3.3	90	<sup>1</sup> COOPER 82	HLBC	Wideband $\nu$ beam

<sup>1</sup> COOPER 82 limit on  $\bar{\nu}_e$  observation is here interpreted as a limit on lepton number violation in the absence of mixing.

$\Gamma(\pi^0 e^+ \bar{\nu}_e) / \Gamma_{\text{total}}$   $\Gamma_{49} / \Gamma$   
 Forbidden by total lepton number conservation.

VALUE	CL%	DOCUMENT ID	TECN	COMMENT
<0.003	90	<sup>1</sup> COOPER 82	HLBC	Wideband $\nu$ beam

<sup>1</sup> COOPER 82 limit on  $\bar{\nu}_e$  observation is here interpreted as a limit on lepton number violation in the absence of mixing.

$\Gamma(\pi^+ \gamma) / \Gamma_{\text{total}}$   $\Gamma_{50} / \Gamma$   
 Violates angular momentum conservation and gauge invariance. Current interest in this decay is as a search for non-commutative space-time effects as discussed in ARTAMONOV 05 and for exotic physics such as a vacuum expectation value of a new vector field, non-local Superstring effects, or departures from Lorentz invariance, as discussed in ADLER 02b.

VALUE (units $10^{-3}$ )	CL%	DOCUMENT ID	TECN	CHG
< 2.3	90	ARTAMONOV 05	B949	+
• • • We do not use the following data for averages, fits, limits, etc. • • •				
< 360	90	ADLER 02b	B787	+
<1400	90	ASANO 82	CNTR	+
<4000	90	<sup>1</sup> KLEMS 71	OSPK	+

<sup>1</sup> Test of model of Selleri, Nuovo Cimento **60A** 291 (1969).

**CPT VIOLATION TESTS IN  $K^\pm$  DECAYS**

$$\Delta = (\Gamma(K^+) - \Gamma(K^-)) / (\Gamma(K^+) + \Gamma(K^-))$$

$\Delta(K^\pm \rightarrow \mu^\pm \nu_\mu)$  RATE DIFFERENCE/SUM

VALUE (%)	DOCUMENT ID	TECN
-0.27 ± 0.21	FORD 67	CNTR

$\Delta(K^\pm \rightarrow \pi^\pm \pi^0)$  RATE DIFFERENCE/SUM

VALUE (%)	DOCUMENT ID	TECN
0.4 ± 0.6	HERZO 69	OSPK

**CP VIOLATION TESTS IN  $K^\pm$  DECAYS**

$$\Delta = (\Gamma(K^+) - \Gamma(K^-)) / (\Gamma(K^+) + \Gamma(K^-))$$

$\Delta(K^\pm \rightarrow \pi^\pm e^+ e^-)$  RATE DIFFERENCE/SUM

VALUE (units $10^{-2}$ )	DOCUMENT ID	TECN
-2.2 ± 1.5 ± 0.6	<sup>1</sup> BATLEY 09	NA48

<sup>1</sup> This implies an upper limit of  $2.1 \times 10^{-2}$  at 90% CL.

$\Delta(K^\pm \rightarrow \pi^\pm \mu^+ \mu^-)$  RATE DIFFERENCE/SUM

VALUE	DOCUMENT ID	TECN
0.010 ± 0.023 OUR AVERAGE		
0.011 ± 0.023	<sup>1</sup> BATLEY 11a	NA48
-0.02 ± 0.11 ± 0.04	PARK 02	HYCP

<sup>1</sup> This corresponds to the asymmetry upper limit of  $< 2.9 \times 10^{-2}$  at 90% CL.

$\Delta(K^\pm \rightarrow \pi^\pm \pi^0 \gamma)$  RATE DIFFERENCE/SUM

VALUE (units $10^{-3}$ )	EVTS	DOCUMENT ID	TECN	CHG	COMMENT
0.0 ± 1.2 OUR AVERAGE					
0.0 ± 1.0 ± 0.6	1M	<sup>1</sup> BATLEY 10a	NA48		
4 ± 29	2461	SMITH 76	WIRE	±	$E_\pi$ 55-90 MeV
5 ± 20	4000	ABRAMS 73b	ASPK	±	$E_\pi$ 51-100 MeV

<sup>1</sup> This value implies the upper bound for this asymmetry  $1.5 \times 10^{-3}$  at 90% CL.

$\Delta(K^\pm \rightarrow \pi^\pm \pi^+ \pi^-)$  RATE DIFFERENCE/SUM

VALUE (%)	EVTS	DOCUMENT ID	TECN	CHG
0.04 ± 0.06		<sup>1</sup> FORD 70	ASPK	
• • • We do not use the following data for averages, fits, limits, etc. • • •				
-0.01 ± 0.08		<sup>2</sup> SMITH 73	ASPK	±
0.05 ± 0.07	3.2M	<sup>1</sup> FORD 70	ASPK	
-0.25 ± 0.45		FLETCHER 67	OSPK	
-0.02 ± 0.11		<sup>1</sup> FORD 67	CNTR	

<sup>1</sup> First FORD 70 value is second FORD 70 combined with FORD 67.  
<sup>2</sup> SMITH 73 value of  $K^\pm \rightarrow \pi^\pm \pi^+ \pi^-$  rate difference is derived from SMITH 73 value of  $K^\pm \rightarrow \pi^\pm 2\pi^0$  rate difference.

$\Delta(K^\pm \rightarrow \pi^\pm \pi^0 \pi^0)$  RATE DIFFERENCE/SUM

VALUE (%)	EVTS	DOCUMENT ID	TECN	CHG
-0.02 ± 0.28 OUR AVERAGE				
0.04 ± 0.29		SMITH 73	ASPK	±
-0.6 ± 0.9	1802	HERZO 69	OSPK	

**T VIOLATION TESTS IN  $K^+$  AND  $K^-$  DECAYS**

$P_T$  in  $K^+ \rightarrow \pi^0 \mu^+ \nu_\mu$

T-violating muon polarization. Sensitive to new sources of CP violation beyond the Standard Model.

VALUE (units $10^{-3}$ )	EVTS	DOCUMENT ID	TECN	CHG
-1.7 ± 2.3 ± 1.1		<sup>1</sup> ABE 04f	K246	+
• • • We do not use the following data for averages, fits, limits, etc. • • •				
-4.2 ± 4.9 ± 0.9	3.9M	ABE 99s	K246	+

<sup>1</sup> Includes three sets of data: 96-97 (ABE 99s), 98, and 99-00 totaling about three times the ABE 99s data sample. Corresponds to  $P_T < 5.0 \times 10^{-3}$  at 90% CL.

$P_T$  in  $K^+ \rightarrow \mu^+ \nu_\mu \gamma$

T-violating muon polarization. Sensitive to new sources of CP violation beyond the Standard Model.

VALUE (units $10^{-2}$ )	EVTS	DOCUMENT ID	TECN	CHG
-0.64 ± 1.85 ± 0.10	114k	<sup>1</sup> ANISIMOVSK...03	K246	+

<sup>1</sup> Muons stopped and polarization measured from decay to positrons.

$\text{Im}(\xi)$  in  $K^+ \rightarrow \pi^0 \mu^+ \nu_\mu$  DECAY (from transverse  $\mu$  pol.)

Test of T reversal invariance.

VALUE	EVTS	DOCUMENT ID	TECN	CHG	COMMENT
-0.006 ± 0.008 OUR AVERAGE					
-0.0053 ± 0.0071 ± 0.0036		<sup>1</sup> ABE 04f	K246	+	
-0.016 ± 0.025	20M	CAMPBELL 81	CNTR	+	Pol.
• • • We do not use the following data for averages, fits, limits, etc. • • •					
-0.013 ± 0.016 ± 0.003	3.9M	ABE 99s	CNTR	+	$\rho_T K^+$ at rest

<sup>1</sup> Includes three sets of data: 96-97 (ABE 99s), 98, and 99-00 totaling about three times the ABE 99s data sample. Corresponds to  $\text{Im}(\xi) < 0.016$  at 90% CL.

**DALITZ PLOT PARAMETERS FOR  $K \rightarrow 3\pi$  DECAYS**

Revised 1999 by T.G. Trippe (LBNL).

The Dalitz plot distribution for  $K^\pm \rightarrow \pi^\pm \pi^\pm \pi^\mp$ ,  $K^\pm \rightarrow \pi^0 \pi^0 \pi^\pm$ , and  $K_L^0 \rightarrow \pi^+ \pi^- \pi^0$  can be parameterized by a series expansion such as that introduced by Weinberg [1]. We use the form

$$\begin{aligned} |M|^2 \propto & 1 + g \frac{(s_3 - s_0)}{m_{\pi^+}^2} + h \left[ \frac{s_3 - s_0}{m_{\pi^+}^2} \right]^2 \\ & + j \frac{(s_2 - s_1)}{m_{\pi^+}^2} + k \left[ \frac{s_2 - s_1}{m_{\pi^+}^2} \right]^2 \\ & + f \frac{(s_2 - s_1)(s_3 - s_0)}{m_{\pi^+}^2 m_{\pi^+}^2} + \dots, \end{aligned} \quad (1)$$

where  $m_{\pi^+}^2$  has been introduced to make the coefficients  $g$ ,  $h$ ,  $j$ , and  $k$  dimensionless, and

$$\begin{aligned} s_i &= (P_K - P_i)^2 = (m_K - m_i)^2 - 2m_K T_i, \quad i = 1, 2, 3, \\ s_0 &= \frac{1}{3} \sum_i s_i = \frac{1}{3} (m_K^2 + m_1^2 + m_2^2 + m_3^2). \end{aligned}$$

Here the  $P_i$  are four-vectors,  $m_i$  and  $T_i$  are the mass and kinetic energy of the  $i^{\text{th}}$  pion, and the index 3 is used for the odd pion.

The coefficient  $g$  is a measure of the slope in the variable  $s_3$  (or  $T_3$ ) of the Dalitz plot, while  $h$  and  $k$  measure the quadratic dependence on  $s_3$  and  $(s_2 - s_1)$ , respectively. The coefficient  $j$  is related to the asymmetry of the plot and must be zero if CP invariance holds. Note also that if CP is good,  $g$ ,  $h$ , and  $k$  must be the same for  $K^+ \rightarrow \pi^+ \pi^+ \pi^-$  as for  $K^- \rightarrow \pi^- \pi^- \pi^+$ .

Since different experiments use different forms for  $|M|^2$ , in order to compare the experiments we have converted to  $g$ ,  $h$ ,  $j$ , and  $k$  whatever coefficients have been measured. Where such conversions have been done, the measured coefficient  $a_y$ ,  $a_t$ ,  $a_u$ , or  $a_v$  is given in the comment at the right. For definitions of



# Meson Particle Listings

## $K^\pm$

these coefficients, details of this conversion, and discussion of the data, see the April 1982 version of this note [2].

### References

- S. Weinberg, Phys. Rev. Lett. **4**, 87 (1960).
- Particle Data Group, Phys. Lett. **111B**, 69 (1982).

### ENERGY DEPENDENCE OF $K^\pm$ DALITZ PLOT

$$|\text{matrix element}|^2 = 1 + gu + hu^2 + kv^2$$

where  $u = (s_3 - s_0) / m_\pi^2$  and  $v = (s_2 - s_1) / m_\pi^2$

### LINEAR COEFFICIENT $g$ FOR $K^\pm \rightarrow \pi^\pm \pi^+ \pi^-$

Some experiments use Dalitz variables  $x$  and  $y$ . In the comments we give  $a_y =$  coefficient of  $y$  term. See note above on "Dalitz Plot Parameters for  $K \rightarrow 3\pi$  Decays." For discussion of the conversion of  $a_y$  to  $g$ , see the earlier version of the same note in the Review published in Physics Letters **111B** 70 (1982).

VALUE	EVTS	DOCUMENT ID	TECN	CHG	COMMENT
<b>-0.21134 ± 0.00017</b>	471M	<sup>1</sup> BATLEY	07B	NA48	±
•••	We do not use the following data for averages, fits, limits, etc. •••				
-0.2221 ± 0.0065	225k	DEVAUX	77	SPEC	+ $a_y = .2814 \pm .0082$
-0.199 ± 0.008	81k	<sup>2</sup> LUCAS	73	HBC	- $a_y = 0.252 \pm 0.011$
-0.2157 ± 0.0028	750k	FORD	72	ASPK	+ $a_y = .2734 \pm .0035$
-0.2186 ± 0.0028	750k	FORD	72	ASPK	- $a_y = .2770 \pm .0035$
-0.200 ± 0.009	39819	<sup>3</sup> HOFFMASTER	72	HLBC	+
-0.196 ± 0.012	17898	<sup>4</sup> GRAUMAN	70	HLBC	+ $a_y = 0.228 \pm 0.030$
-0.193 ± 0.010	50919	MAST	69	HBC	- $a_y = 0.244 \pm 0.013$
-0.218 ± 0.016	9994	<sup>5</sup> BUTLER	68	HBC	+ $a_y = 0.277 \pm 0.020$
-0.190 ± 0.023	5778	<sup>5,6</sup> MOSCOSO	68	HBC	- $a_y = 0.242 \pm 0.029$
-0.22 ± 0.024	5428	<sup>5,6</sup> ZINCHENKO	67	HBC	+ $a_y = 0.28 \pm 0.03$
-0.220 ± 0.035	1347	<sup>7</sup> FERRO-LUZZI	61	HBC	- $a_y = 0.28 \pm 0.045$

- Final state strong interaction and radiative corrections not included in the fit.
- Quadratic dependence is required by  $K_L^0$  experiments.
- HOFFMASTER 72 includes GRAUMAN 70 data.
- Emulsion data added — all events included by HOFFMASTER 72.
- Experiments with large errors not included in average.
- Also includes DBC events.
- No radiative corrections included.

### QUADRATIC COEFFICIENT $h$ FOR $K^\pm \rightarrow \pi^\pm \pi^+ \pi^-$

VALUE (units $10^{-2}$ )	EVTS	DOCUMENT ID	TECN	CHG	
<b>1.848 ± 0.040</b>	471M	<sup>1</sup> BATLEY	07B	NA48	±
•••	We do not use the following data for averages, fits, limits, etc. •••				
-0.06 ± 1.43	225k	DEVAUX	77	SPEC	+
1.87 ± 0.62	750k	FORD	72	ASPK	+
1.25 ± 0.62	750k	FORD	72	ASPK	-
-0.9 ± 1.4	39819	HOFFMASTER	72	HLBC	+
-0.1 ± 1.2	50919	MAST	69	HBC	-

- Final state strong interaction and radiative corrections not included in the fit.

### QUADRATIC COEFFICIENT $k$ FOR $K^\pm \rightarrow \pi^\pm \pi^+ \pi^-$

VALUE (units $10^{-3}$ )	EVTS	DOCUMENT ID	TECN	CHG	
<b>-4.63 ± 0.14</b>	471M	<sup>1</sup> BATLEY	07B	NA48	±
•••	We do not use the following data for averages, fits, limits, etc. •••				
-20.5 ± 3.9	225k	DEVAUX	77	SPEC	+
-7.5 ± 1.9	750k	FORD	72	ASPK	+
-8.3 ± 1.9	750k	FORD	72	ASPK	-
-10.5 ± 4.5	39819	HOFFMASTER	72	HLBC	+
-14 ± 12	50919	MAST	69	HBC	-

- Final state strong interaction and radiative corrections not included in the fit.

### $(g_+ - g_-) / (g_+ + g_-)$ FOR $K^\pm \rightarrow \pi^\pm \pi^+ \pi^-$

This is a CP violating asymmetry between linear coefficients  $g_+$  for  $K^+ \rightarrow \pi^+ \pi^+ \pi^-$  decay and  $g_-$  for  $K^- \rightarrow \pi^- \pi^+ \pi^-$  decay.

VALUE (units $10^{-4}$ )	EVTS	DOCUMENT ID	TECN
<b>-1.5 ± 1.5 ± 1.6</b>	3.1G	<sup>1</sup> BATLEY	07E NA48
•••	We do not use the following data for averages, fits, limits, etc. •••		
1.7 ± 2.1 ± 2.0	1.7G	<sup>2</sup> BATLEY	06 NA48
-70.0 ± 53	3.2M	FORD	70 ASPK

- BATLEY 07E includes data from BATLEY 06. Uses quadratic parametrization and value  $g_+ + g_- = 2g$  from BATLEY 07B. This measurement neglects any possible charge asymmetries in higher order slope parameters  $h$  or  $k$ .
- This measurement neglects any possible charge asymmetries in higher order slope parameters  $h$  or  $k$ .

### LINEAR COEFFICIENT $g$ FOR $K^\pm \rightarrow \pi^\pm \pi^0 \pi^0$

Unless otherwise stated, all experiments include terms quadratic in  $(s_3 - s_0) / m_\pi^2$ . See note above on "Dalitz Plot Parameters for  $K \rightarrow 3\pi$  Decays."

See BATUSOV 98 for a discussion of the discrepancy between their result and others, especially BOLOTOV 86. At this time we have no way to resolve the discrepancy so we depend on the large scale factor as a warning.

VALUE	EVTS	DOCUMENT ID	TECN	CHG	COMMENT
<b>0.626 ± 0.007 OUR AVERAGE</b>					
0.6259 ± 0.0043 ± 0.0093	493k	AKOPDZHAN..05B	TNF	±	
0.627 ± 0.004 ± 0.010	252k	<sup>1,2</sup> AJINENKO	03B	ISTR	-
•••	We do not use the following data for averages, fits, limits, etc. •••				
0.736 ± 0.014 ± 0.012	33k	BATUSOV	98	SPEC	+
0.582 ± 0.021	43k	BOLOTOV	86	CALO	-
0.670 ± 0.054	3263	BRAUN	76B	HLBC	+
0.630 ± 0.038	5635	SHEAFF	75	HLBC	+
0.510 ± 0.060	27k	SMITH	75	WIRE	+
0.67 ± 0.06	1365	AUBERT	72	HLBC	+
0.544 ± 0.048	4048	DAVISON	69	HLBC	+ Also emulsion

- Measured using in-flight decays of the 25 GeV negative secondary beam.
- They form new world averages  $g_- = (0.617 \pm 0.018)$  and  $g_+ = (0.684 \pm 0.033)$  which give  $\Delta g_{\pi^0} = 0.051 \pm 0.028$ .

### QUADRATIC COEFFICIENT $h$ FOR $K^\pm \rightarrow \pi^\pm \pi^0 \pi^0$

VALUE	EVTS	DOCUMENT ID	TECN	CHG	COMMENT
<b>0.052 ± 0.008 OUR AVERAGE</b>					
0.0551 ± 0.0044 ± 0.0086	493k	AKOPDZHAN..05B	TNF	±	
0.046 ± 0.004 ± 0.012	252k	<sup>1</sup> AJINENKO	03B	ISTR	-
•••	We do not use the following data for averages, fits, limits, etc. •••				
0.128 ± 0.015 ± 0.024	33k	BATUSOV	98	SPEC	+
0.037 ± 0.024	43k	BOLOTOV	86	CALO	-
0.152 ± 0.082	3263	BRAUN	76B	HLBC	+
0.041 ± 0.030	5635	SHEAFF	75	HLBC	+
0.009 ± 0.040	27k	SMITH	75	WIRE	+
-0.01 ± 0.08	1365	AUBERT	72	HLBC	+
0.026 ± 0.050	4048	DAVISON	69	HLBC	+ Also emulsion

- Measured using in-flight decays of the 25 GeV negative secondary beam.

### QUADRATIC COEFFICIENT $k$ FOR $K^\pm \rightarrow \pi^\pm \pi^0 \pi^0$

VALUE	EVTS	DOCUMENT ID	TECN	CHG	
<b>0.0054 ± 0.0035 OUR AVERAGE</b>					
0.0082 ± 0.0011 ± 0.0014	493k	AKOPDZHAN..05B	TNF	±	
0.001 ± 0.001 ± 0.002	252k	<sup>1</sup> AJINENKO	03B	ISTR	-
•••	We do not use the following data for averages, fits, limits, etc. •••				
0.0197 ± 0.0045 ± 0.0029	33k	BATUSOV	98	SPEC	+

- Measured using in-flight decays of the 25 GeV negative secondary beam.

### $(g_+ - g_-) / (g_+ + g_-)$ FOR $K^\pm \rightarrow \pi^\pm \pi^0 \pi^0$

A nonzero value for this quantity indicates CP violation.

VALUE (units $10^{-4}$ )	EVTS	DOCUMENT ID	TECN
<b>1.8 ± 1.8 OUR AVERAGE</b>			
1.8 ± 1.7 ± 0.6	91.3M	<sup>1</sup> BATLEY	07E NA48
2 ± 18 ± 5	619k	<sup>2</sup> AKOPDZHA..05	TNF
•••	We do not use the following data for averages, fits, limits, etc. •••		
1.8 ± 2.2 ± 1.3	47M	<sup>3</sup> BATLEY	06A NA48

- BATLEY 07E includes data from BATLEY 06A. Uses quadratic parametrization and PDG 06 value  $g = 0.626 \pm 0.007$  to obtain  $g_+ - g_- = (2.2 \pm 2.1 \pm 0.7) \times 10^{-4}$ . Neglects any possible charge asymmetries in higher order slope parameters  $h$  or  $k$ .
- Asymmetry obtained assuming that  $g_+ + g_- = 2 \times 0.652$  (PDG 02) and that asymmetries in  $h$  and  $k$  are zero.
- Linear and quadratic slopes from PDG 04 are used. Any possible charge asymmetries in higher order slope parameters  $h$  or  $k$  are neglected.

### ALTERNATIVE PARAMETRIZATIONS OF $K^\pm \rightarrow \pi^\pm \pi^0 \pi^0$ DALITZ PLOT

The following functional form for the matrix element suggested by  $\pi\pi$  rescattering in  $K^+ \rightarrow \pi^+ \pi^+ \pi^0 \rightarrow \pi^+ \pi^0 \pi^0$  is used for this fit (CABIBBO 04A, CABIBBO 05): Matrix element =  $M_0 + M_1$  where  $M_0 = 1 + (1/2)g_0 u + (1/2)h' u^2 + (1/2)k_0 v^2$  with  $u = (s_3 - s_0) / (m_{\pi^+})^2$ ,  $v = (s_2 - s_1) / (m_{\pi^+})^2$  and where  $M_1$  takes into account the non-analytic piece due to  $\pi\pi$  rescattering amplitudes  $a_0$  and  $a_2$ ; The parameters  $g_0$  and  $h'$  are related to the parameters  $g$  and  $h$  of the matrix element squared given in the previous section by the approximations  $g_0 \sim g^{PDG}$  and  $h' \sim h^{PDG} - (g/2)^2$  and  $k_0 \sim k^{PDG}$ .

In addition, we also consider the effective field theory framework of COLANGELO 06A and BISSEGGER 09 to extract  $g_{BB}$  and  $h'_{BB}$ .

### LINEAR COEFFICIENT $g_0$ FOR $K^\pm \rightarrow \pi^\pm \pi^0 \pi^0$

VALUE	EVTS	DOCUMENT ID	TECN	CHG	
<b>0.6525 ± 0.0009 ± 0.0033</b>	60M	<sup>1</sup> BATLEY	09A	NA48	±
•••	We do not use the following data for averages, fits, limits, etc. •••				
0.645 ± 0.004 ± 0.009	23M	<sup>2</sup> BATLEY	06B	NA48	±

- This fit is obtained with the CABIBBO 05 matrix element in the  $2\pi^0$  invariant mass squared range  $0.074094 < m_{2\pi^0}^2 < 0.104244 \text{ GeV}^2$ . Electromagnetic corrections and CHPT constraints for  $\pi\pi$  phase shifts ( $a_0$  and  $a_2$ ) have been used. Also measured  $(a_0 - a_2) m_{\pi^+} = 0.2646 \pm 0.0021 \pm 0.0023$ , where  $k_0$  was kept fixed in the fit at  $-0.0099$ .
- Superseded by BATLEY 09A. This fit is obtained with the CABIBBO 05 matrix element in the  $2\pi^0$  invariant mass squared range  $0.074 \text{ GeV}^2 < m_{2\pi^0}^2 < 0.097 \text{ GeV}^2$ , assuming  $k = 0$  (no term proportional to  $(s_2 - s_1)^2$ ) and excluding the kinematic region around the cusp ( $m_{2\pi^0}^2 = (2m_{\pi^+})^2 \pm 0.000525 \text{ GeV}^2$ ). Also  $\pi\pi$  phase shifts  $a_0$  and  $a_2$  are measured:  $(a_0 - a_2) m_{\pi^+} = 0.268 \pm 0.010 \pm 0.004 \pm 0.013$  (external) and  $a_2 m_{\pi^+} = -0.041 \pm 0.022 \pm 0.014$ .

**QUADRATIC COEFFICIENT  $h'$  FOR  $K^\pm \rightarrow \pi^\pm \pi^0 \pi^0$** 

VALUE	EVTS	DOCUMENT ID	TECN	CHG
$-0.0433 \pm 0.0008 \pm 0.0026$	60M	<sup>1</sup> BATLEY	09A NA48	$\pm$

••• We do not use the following data for averages, fits, limits, etc. •••

$-0.047 \pm 0.012 \pm 0.011$	23M	<sup>2</sup> BATLEY	06B NA48	$\pm$
------------------------------	-----	---------------------	----------	-------

<sup>1</sup>This fit is obtained with the CABIBBO 05 matrix element in the  $2\pi^0$  invariant mass squared range  $0.074094 < m_{2\pi^0}^2 < 0.104244$  GeV<sup>2</sup>. Electromagnetic corrections and CHPT constraints for  $\pi\pi$  phase shifts ( $a_0$  and  $a_2$ ) have been used. Also measured  $(a_0 - a_2) m_{\pi^+} = 0.2646 \pm 0.0021 \pm 0.0023$ , where  $k_0$  was kept fixed in the fit at  $-0.0099$ .

<sup>2</sup>Superseded by BATLEY 09A. This fit is obtained with the CABIBBO 05 matrix element in the  $2\pi^0$  invariant mass squared range  $0.074$  GeV<sup>2</sup>  $< m_{2\pi^0}^2 < 0.097$  GeV<sup>2</sup>, assuming  $k = 0$  (no term proportional to  $(s_2 - s_1)^2$ ) and excluding the kinematic region around the cusp ( $m_{2\pi^0}^2 = (2m_{\pi^+})^2 \pm 0.000525$  GeV<sup>2</sup>). Also  $\pi\pi$  phase shifts  $a_0$  and  $a_2$  are measured:  $(a_0 - a_2) m_{\pi^+} = 0.268 \pm 0.010 \pm 0.004 \pm 0.013$ (external) and  $a_2 m_{\pi^+} = -0.041 \pm 0.022 \pm 0.014$ .

**QUADRATIC COEFFICIENT  $k_0$  FOR  $K^\pm \rightarrow \pi^\pm \pi^0 \pi^0$** 

VALUE	EVTS	DOCUMENT ID	TECN	CHG
$0.0095 \pm 0.00017 \pm 0.00048$	60M	<sup>1</sup> BATLEY	09A NA48	$\pm$

<sup>1</sup>Assumed  $a_2 m_{\pi^+} = -0.0044$  in the fit.

**LINEAR COEFFICIENT  $g_{BB}$  FOR  $K^\pm \rightarrow \pi^\pm \pi^0 \pi^0$** 

VALUE	EVTS	DOCUMENT ID	TECN	CHG
$0.6219 \pm 0.0009 \pm 0.0033$	60M	<sup>1</sup> BATLEY	09A NA48	$\pm$

<sup>1</sup>This fit is obtained using parametrizations of COLANGELO 06A and BISSEGGER 09 in the  $2\pi^0$  invariant mass squared range  $0.074094 < m_{2\pi^0}^2 < 0.104244$  GeV<sup>2</sup>. Electromagnetic corrections and CHPT constraints for  $\pi\pi$  phase shifts ( $a_0$  and  $a_2$ ) have been used. Also measured  $(a_0 - a_2) m_{\pi^+} = 0.2633 \pm 0.0024 \pm 0.0024$ , where  $k_0$  was kept fixed in the fit at 0.0085.

**QUADRATIC COEFFICIENT  $h'_{BB}$  FOR  $K^\pm \rightarrow \pi^\pm \pi^0 \pi^0$** 

VALUE	EVTS	DOCUMENT ID	TECN	CHG
$-0.0520 \pm 0.0009 \pm 0.0026$	60M	<sup>1</sup> BATLEY	09A NA48	$\pm$

<sup>1</sup>This fit is obtained using parametrizations of COLANGELO 06A and BISSEGGER 09 in the  $2\pi^0$  invariant mass squared range  $0.074094 < m_{2\pi^0}^2 < 0.104244$  GeV<sup>2</sup>. Electromagnetic corrections and CHPT constraints for  $\pi\pi$  phase shifts ( $a_0$  and  $a_2$ ) have been used. Also measured  $(a_0 - a_2) m_{\pi^+} = 0.2633 \pm 0.0024 \pm 0.0024$ , where  $k_0$  was kept fixed in the fit at 0.0085.

 **$K_{e3}^\pm$  AND  $K_{e3}^0$  FORM FACTORS**

Updated September 2013 by T.G. Trippe (LBNL) and C.-J. Lin (LBNL).

Assuming that only the vector current contributes to  $K \rightarrow \pi \ell \nu$  decays, we write the matrix element as

$$M \propto f_+(t) [(P_K + P_\pi)_\mu \bar{\ell} \gamma_\mu (1 + \gamma_5) \nu] + f_-(t) [m_\ell \bar{\ell} (1 + \gamma_5) \nu], \quad (1)$$

where  $P_K$  and  $P_\pi$  are the four-momenta of the  $K$  and  $\pi$  mesons,  $m_\ell$  is the lepton mass, and  $f_+$  and  $f_-$  are dimensionless form factors which can depend only on  $t = (P_K - P_\pi)^2$ , the square of the four-momentum transfer to the leptons. If time-reversal invariance holds,  $f_+$  and  $f_-$  are relatively real.  $K_{\mu 3}$  experiments, discussed immediately below, measure  $f_+$  and  $f_-$ , while  $K_{e3}$  experiments, discussed further below, are sensitive only to  $f_+$  because the small electron mass makes the  $f_-$  term negligible.

**$K_{\mu 3}$  Experiments.** Analyses of  $K_{\mu 3}$  data frequently assume a linear dependence of  $f_+$  and  $f_-$  on  $t$ , i.e.,

$$f_\pm(t) = f_\pm(0) [1 + \lambda_\pm(t/m_{\pi^+}^2)]. \quad (2)$$

Most  $K_{\mu 3}$  data are adequately described by Eq. (2) for  $f_+$  and a constant  $f_-$  (i.e.,  $\lambda_- = 0$ ).

**Two commonly used equivalent parametrizations:**

(1)  $\lambda_+, \xi(0)$  parametrization. Older analyses of  $K_{\mu 3}$  data often introduce the ratio of the two form factors

$$\xi(t) = f_-(t)/f_+(t). \quad (3)$$

The  $K_{\mu 3}$  decay distribution is then described by the two parameters  $\lambda_+$  and  $\xi(0)$  (assuming time reversal invariance and  $\lambda_- = 0$ ).

(2)  $\lambda_+, \lambda_0$  parametrization. More recent  $K_{\mu 3}$  analyses have parametrized in terms of the form factors  $f_+$  and  $f_0$ , which are associated with vector and scalar exchange, respectively, to the lepton pair.  $f_0$  is related to  $f_+$  and  $f_-$  by

$$f_0(t) = f_+(t) + [t/(m_K^2 - m_\pi^2)] f_-(t). \quad (4)$$

Here  $f_0(0)$  must equal  $f_+(0)$  unless  $f_-(t)$  diverges at  $t = 0$ . The earlier assumption that  $f_+$  is linear in  $t$  and  $f_-$  is constant leads to  $f_0$  linear in  $t$ :

$$f_0(t) = f_0(0) [1 + \lambda_0(t/m_{\pi^+}^2)]. \quad (5)$$

With the assumption that  $f_0(0) = f_+(0)$ , the two parametrizations,  $(\lambda_+, \xi(0))$  and  $(\lambda_+, \lambda_0)$  are equivalent as long as correlation information is retained.  $(\lambda_+, \lambda_0)$  correlations tend to be less strong than  $(\lambda_+, \xi(0))$  correlations.

Since the 2006 edition of the *Review* [4], we no longer quote results in the  $(\lambda_+, \xi(0))$  parametrization. We have removed many older low statistics results from the Listings. See the 2004 version of this note [5] for these older results, and the 1982 version [6] for additional discussion of the  $K_{\mu 3}^0$  parameters, correlations, and conversion between parametrizations.

**Quadratic Parametrization.** More recent high-statistics experiments have included a quadratic term in the expansion of  $f_+(t)$ ,

$$f_+(t) = f_+(0) \left[ 1 + \lambda'_+(t/m_{\pi^+}^2) + \frac{\lambda''_+}{2}(t/m_{\pi^+}^2)^2 \right]. \quad (6)$$

If there is a non-vanishing quadratic term, then  $\lambda_+$  of Eq. (2) represents the average slope, which is then different from  $\lambda'_+$ . Our convention is to include the factor  $\frac{1}{2}$  in the quadratic term, and to use  $m_{\pi^+}$  even for  $K_{e3}^+$  and  $K_{\mu 3}^+$  decays. We have converted other's parametrizations to match our conventions, as noted in the beginning of the " $K_{e3}^\pm$  and  $K_{e3}^0$  Form Factors" sections of the Listings.

**Pole Parametrization.** The pole model describes the  $t$ -dependence of  $f_+(t)$  and  $f_0(t)$  in terms of the exchange of the lightest vector and scalar  $K^*$  mesons with masses  $M_v$  and  $M_s$ , respectively:

$$f_+(t) = f_+(0) \left[ \frac{M_v^2}{M_v^2 - t} \right], \quad f_0(t) = f_0(0) \left[ \frac{M_s^2}{M_s^2 - t} \right]. \quad (7)$$

**Dispersive Parametrization.** This approach [7,8] uses dispersive techniques and the known low-energy  $K\pi$  phases to parametrize the vector and scalar form factors:

$$f_+(t) = f_+(0) \exp \left[ \frac{t}{m_\pi^2} (\Lambda_+ + H(t)) \right]; \quad (8)$$

$$f_0(t) = f_+(0) \exp \left[ \frac{t}{(m_K^2 - m_\pi^2)} (\ln[C] - G(t)) \right], \quad (9)$$

where  $\Lambda_+$  is the slope of the vector form factor, and  $\ln[C] = \ln[f_0(m_K^2 - m_\pi^2)]$  is the logarithm of the scalar form factor at

## Meson Particle Listings

 $K^\pm$ 

the Callan-Treiman point. The functions  $H(t)$  and  $G(t)$  are dispersive integrals.

**$K_{e3}$  Experiments.** Analysis of  $K_{e3}$  data is simpler than that of  $K_{\mu 3}$  because the second term of the matrix element assuming a pure vector current [Eq. (1) above] can be neglected. Here  $f_+$  can be assumed to be linear in  $t$ , in which case the linear coefficient  $\lambda_+$  of Eq. (2) is determined, or quadratic, in which case the linear coefficient  $\lambda'_+$  and quadratic coefficient  $\lambda''_+$  of Eq. (6) are determined.

If we remove the assumption of a pure vector current, then the matrix element for the decay, in addition to the terms in Eq. (1), would contain

$$+2m_K f_S \bar{\ell}(1 + \gamma_5)\nu + (2f_T/m_K)(P_K)_\lambda(P_\pi)_\mu \bar{\ell}\sigma_{\lambda\mu}(1 + \gamma_5)\nu, \quad (10)$$

where  $f_S$  is the scalar form factor, and  $f_T$  is the tensor form factor. In the case of the  $K_{e3}$  decays where the  $f_-$  term can be neglected, experiments have yielded limits on  $|f_S/f_+|$  and  $|f_T/f_+|$ .

**Fits for  $K_{e3}$  Form Factors.** For  $K_{e3}$  data, we determine best values for the three parametrizations: linear ( $\lambda_+$ ), quadratic ( $\lambda'_+$ ,  $\lambda''_+$ ) and pole ( $M_v$ ). For  $K_{\mu 3}$  data, we determine best values for the three parametrizations: linear ( $\lambda_+$ ,  $\lambda_0$ ), quadratic ( $\lambda'_+$ ,  $\lambda''_+$ ,  $\lambda_0$ ) and pole ( $M_v$ ,  $M_s$ ). We then assume  $\mu - e$  universality so that we can combine  $K_{e3}$  and  $K_{\mu 3}$  data, and again determine best values for the three parametrizations: linear ( $\lambda_+$ ,  $\lambda_0$ ), quadratic ( $\lambda'_+$ ,  $\lambda''_+$ ,  $\lambda_0$ ), and pole ( $M_v$ ,  $M_s$ ). When there is more than one parameter, fits are done including input correlations. Simple averages suffice in the two  $K_{e3}$  cases where there is only one parameter: linear ( $\lambda_+$ ) and pole ( $M_v$ ).

Both KTeV and KLOE see an improvement in the quality of their fits relative to linear fits when a quadratic term is introduced, as well as when the pole parametrization is used. The quadratic parametrization has the disadvantage that the quadratic parameter  $\lambda''_+$  is highly correlated with the linear parameter  $\lambda'_+$ , in the neighborhood of 95%, and that neither parameter is very well determined. The pole fit has the same number of parameters as the linear fit, but yields slightly better fit probabilities, so that it would be advisable for all experiments to include the pole parametrization as one of their choices [9].

The “Kaon Particle Listings” show the results with and without assuming  $\mu - e$  universality. The “Meson Summary Tables” show all of the results assuming  $\mu - e$  universality, but most results not assuming  $\mu - e$  universality are given only in the Listings.

## References

1. L.M. Chounet, J.M. Gaillard, and M.K. Gaillard, Phys. Reports **4C**, 199 (1972).
2. H.W. Fearing, E. Fischbach, and J. Smith, Phys. Rev. **D2**, 542 (1970).
3. N. Cabibbo and A. Maksymowicz, Phys. Lett. **9**, 352 (1964).
4. W.-M. Yao *et al.*, Particle Data Group, J. Phys. **G33**, 1 (2006).

5. S. Eidelman *et al.*, Particle Data Group, Phys. Lett. **B592**, 1 (2004).
6. M. Roos *et al.*, Particle Data Group, Phys. Lett. **111B**, 73 (1982).
7. V. Bernard *et al.*, Phys. Lett. **B638**, 48 (2006).
8. A. Lai *et al.*, Phys. Lett. **B647**, 341 (2007), and references therein.
9. We thank P. Franzini (Rome U. and Frascati) for useful discussions on this point.

 $K_{e3}^\pm$  FORM FACTORS

In the form factor comments, the following symbols are used.

$f_+$  and  $f_-$  are form factors for the vector matrix element.

$f_S$  and  $f_T$  refer to the scalar and tensor term.

$f_0 = f_+ + f_- t/(m_{K^+}^2 - m_{\pi^0}^2)$ .

$t =$  momentum transfer to the  $\pi$ .

$\lambda_+$  and  $\lambda_0$  are the linear expansion coefficients of  $f_+$  and  $f_0$ :

$f_+(t) = f_+(0) (1 + \lambda_+ t/m_{\pi^+}^2)$

For quadratic expansion

$f_+(t) = f_+(0) (1 + \lambda'_+ t/m_{\pi^+}^2 + \frac{\lambda''_+}{2} t^2/m_{\pi^+}^4)$

as used by KTeV. If there is a non-vanishing quadratic term, then  $\lambda_+$  represents an average slope, which is then different from  $\lambda'_+$ .

NA48/2 and OKA quadratic expansion coefficients are converted with  $\lambda'_+{}^{PDG} = \lambda'_+{}^{NA48/2}$  and  $\lambda''_+{}^{PDG} = 2 \lambda''_+{}^{NA48/2}$

$\lambda'_+{}^{PDG} = (\frac{m_{\pi^+}}{m_{\pi^0}})^2 \lambda'_+{}^{OKA}$  and

$\lambda''_+{}^{PDG} = 2 (\frac{m_{\pi^+}}{m_{\pi^0}})^4 \lambda''_+{}^{OKA}$

OKA linear expansion coefficients are converted with  $\lambda_+{}^{PDG} = (\frac{m_{\pi^+}}{m_{\pi^0}})^2 \lambda_+{}^{OKA}$  and  $\lambda_0{}^{PDG} = (\frac{m_{\pi^+}}{m_{\pi^0}})^2 \lambda_0{}^{OKA}$

The pole parametrization is

$f_+(t) = f_+(0) (\frac{M_V^2}{M_V^2 - t})$

$f_0(t) = f_0(0) (\frac{M_S^2}{M_S^2 - t})$

where  $M_V$  and  $M_S$  are the vector and scalar pole masses.

The following abbreviations are used:

DP = Dalitz plot analysis.

PI =  $\pi$  spectrum analysis.

MU =  $\mu$  spectrum analysis.

POL =  $\mu$  polarization analysis.

BR =  $K_{\mu 3}^\pm/K_{e3}^\pm$  branching ratio analysis.

E = positron or electron spectrum analysis.

RC = radiative corrections.

For previous  $\lambda'_+$  and  $\lambda''_+$  parametrizations used by NA48 (e.g. LAI 07A) and ISTRA (e.g. YUSHCHENKO 04B) see PDG 18.

 $\lambda_+$  (LINEAR ENERGY DEPENDENCE OF  $f_+$  IN  $K_{e3}^\pm$  DECAY)

These results are for a linear expansion only. See the next section for fits including a quadratic term. For radiative correction of the  $K_{e3}^\pm$  Dalitz plot, see GINSBERG 67, BECHERRAWY 70, CIRIGLIANO 02, CIRIGLIANO 04, and ANDRE 07. Results labeled OUR FIT are discussed in the review “ $K_{e3}^\pm$  and  $K_{\mu 3}^0$  Form Factors” above. For earlier, lower statistics results, see the 2004 edition of this review, Physics Letters **B592** 1 (2004).

VALUE (units $10^{-2}$ )	EVTS	DOCUMENT ID	TECN	CHG	COMMENT
<b>2.959 ± 0.025 OUR FIT</b>	Assuming $\mu - e$ universality				
<b>2.956 ± 0.025 OUR AVERAGE</b>					
2.95 ± 0.022 ± 0.018	5.25M	YUSHCHENKO 18	OKA	+	
3.044 ± 0.083 ± 0.074	1.1M	AKOPDZANOV 09	TNF	±	
2.966 ± 0.050 ± 0.034	919k	<sup>1</sup> YUSHCHENKO 04B	ISTR	-	DP
2.78 ± 0.26 ± 0.30	41k	SHIMIZU	00	SPEC	+
2.84 ± 0.27 ± 0.20	32k	<sup>2</sup> AKIMENKO 91	SPEC		PI, no RC
2.9 ± 0.4	62k	<sup>3</sup> BOLOTOV 88	SPEC		PI, no RC
3.06 ± 0.09 ± 0.06	550k	<sup>1,4</sup> AJINENKO 03c	ISTR	-	DP
2.93 ± 0.15 ± 0.2	130k	<sup>4</sup> AJINENKO 02	SPEC		DP

••• We do not use the following data for averages, fits, limits, etc. •••

<sup>1</sup> Rescaled to agree with our conventions as noted above.

<sup>2</sup> AKIMENKO 91 state that radiative corrections would raise  $\lambda_+$  by 0.0013.

<sup>3</sup> BOLOTOV 88 state radiative corrections of GINSBERG 67 would raise  $\lambda_+$  by 0.002.

<sup>4</sup> Superseded by YUSHCHENKO 04B.

$\lambda_+$  (LINEAR ENERGY DEPENDENCE OF  $f_+$  IN  $K_{e3}^\pm$  DECAY)

Results labeled OUR FIT are discussed in the review " $K_{e3}^\pm$  and  $K_{\mu 3}^0$  Form Factors" above. For earlier, lower statistics results, see the 2004 edition of this review, Physics Letters **B592** 1 (2004).

VALUE (units $10^{-2}$ )	EVTS	DOCUMENT ID	TECN	CHG	COMMENT
<b>2.959 ± 0.025 OUR FIT</b>					Assuming $\mu-e$ universality
<b>3.09 ± 0.25 OUR FIT</b>					Error includes scale factor of 1.5. Not assuming $\mu-e$ universality
2.96 ± 0.14 ± 0.10	540k	<sup>1</sup> YUSHCHENKO04	ISTR	-	DP
• • •					We do not use the following data for averages, fits, limits, etc. • • •
3.21 ± 0.45	112k	<sup>2</sup> AJINENKO	03	ISTR	- DP

<sup>1</sup> Rescaled to agree with our conventions as noted above.  
<sup>2</sup> Superseded by YUSHCHENKO 04.

$\lambda_0$  (LINEAR ENERGY DEPENDENCE OF  $f_0$  IN  $K_{e3}^\pm$  DECAY)

Results labeled OUR FIT are discussed in the review " $K_{e3}^\pm$  and  $K_{\mu 3}^0$  Form Factors" above. For earlier, lower statistics results, see the 2004 edition of this review, Physics Letters **B592** 1 (2004).

VALUE (units $10^{-2}$ )	$d\lambda_0/d\lambda_+$	EVTS	DOCUMENT ID	TECN	CHG	COMMENT
<b>1.76 ± 0.25 OUR FIT</b>						Error includes scale factor of 2.7. Assuming $\mu-e$ universality
<b>1.73 ± 0.27 OUR FIT</b>						Error includes scale factor of 2.6. Not assuming $\mu-e$ universality
1.420 ± 0.114 ± 0.107		2.3M	<sup>1</sup> BATLEY	18	NA48	±
1.96 ± 0.12 ± 0.06	-0.348	540k	<sup>2</sup> YUSHCHENKO04	ISTR	-	DP
• • •						We do not use the following data for averages, fits, limits, etc. • • •
2.09 ± 0.45	-0.46	112k	<sup>3</sup> AJINENKO	03	ISTR	- DP
1.9 ± 0.64		24k	<sup>4</sup> HORIE	01	SPEC	+ BR
1.9 ± 1.0	+0.03	55k	<sup>5</sup> HEINTZE	77	SPEC	+ BR

<sup>1</sup> Data collected in 2004 by NA48/2. Obtained from a fit with a quadratic vector form factor. Correlation coefficient with linear slope is 0.511, with quadratic slope is -0.513.  $\chi^2/NDF = 409.9/381$ . BATLEY 18 also performed a combined  $K_{e3}^\pm$  and  $K_{\mu 3}^\pm$  fit assuming  $\mu-e$  universality and obtained  $(14.47 \pm 0.63 \pm 1.17) \times 10^{-3}$ .  
<sup>2</sup> Rescaled to agree with our conventions as noted above.  
<sup>3</sup> Superseded by YUSHCHENKO 04.  
<sup>4</sup> HORIE 01 assumes  $\mu-e$  universality in  $K_{e3}^\pm$  decay and uses SHIMIZU 00 value  $\lambda = 0.0278 \pm 0.0040$  from  $K_{e3}^\pm$  decay.  
<sup>5</sup> HEINTZE 77 uses  $\lambda_+ = 0.029 \pm 0.003$ .  $d\lambda_0/d\lambda_+$  estimated by us.

$\lambda_+^*$  (LINEAR  $K_{e3}^\pm$  FORM FACTOR FROM QUADRATIC FIT)

VALUE (units $10^{-2}$ )	EVTS	DOCUMENT ID	TECN	CHG	COMMENT
<b>2.59 ± 0.04 OUR AVERAGE</b>					
2.426 ± 0.078 ± 0.130	4.4M	<sup>1</sup> BATLEY	18	NA48	±
2.611 ± 0.035 ± 0.028	5.25M	YUSHCHENKO18	OKA	+	
2.485 ± 0.163 ± 0.034	919k	<sup>2,3</sup> YUSHCHENKO04B	ISTR	-	DP
• • •					We do not use the following data for averages, fits, limits, etc. • • •
3.07 ± 0.21	550k	<sup>2,4</sup> AJINENKO	03c	ISTR	- DP

<sup>1</sup> Data collected in 2004 by NA48/2. Correlation coefficient with quadratic slope is -0.929.  $\chi^2/NDF = 569.1/687$ . BATLEY 18 also performed a combined  $K_{e3}^\pm$  and  $K_{\mu 3}^\pm$  fit assuming  $\mu-e$  universality and obtained  $(24.24 \pm 0.75 \pm 1.3) \times 10^{-3}$ .  
<sup>2</sup> Rescaled to agree with our conventions as noted above.  
<sup>3</sup> YUSHCHENKO 04B  $\lambda_+^*$  and  $\lambda_+^{**}$  are strongly correlated with coefficient  $\rho(\lambda_+^*, \lambda_+^{**}) = -0.95$ .  
<sup>4</sup> Superseded by YUSHCHENKO 04B.

$\lambda_+^{**}$  (QUADRATIC  $K_{e3}^\pm$  FORM FACTOR)

VALUE (units $10^{-2}$ )	EVTS	DOCUMENT ID	TECN	CHG	COMMENT
<b>0.186 ± 0.021 OUR AVERAGE</b>					
0.164 ± 0.030 ± 0.039	4.4M	<sup>1</sup> BATLEY	18	NA48	±
0.191 ± 0.019 ± 0.014	5.25M	YUSHCHENKO18	OKA	+	
0.192 ± 0.062 ± 0.071	919k	<sup>2,3</sup> YUSHCHENKO04B	ISTR	-	DP
• • •					We do not use the following data for averages, fits, limits, etc. • • •
-0.5 ± 0.7 ± 1.5	550k	<sup>2,4</sup> AJINENKO	03c	ISTR	- DP

<sup>1</sup> Data collected in 2004 by NA48/2. Correlation coefficient with quadratic slope is -0.929.  $\chi^2/NDF = 569.1/687$ . BATLEY 18 also performed a combined  $K_{e3}^\pm$  and  $K_{\mu 3}^\pm$  fit assuming  $\mu-e$  universality and obtained  $(1.67 \pm 0.29 \pm 0.41) \times 10^{-3}$ .  
<sup>2</sup> Rescaled to agree with our conventions as noted above.  
<sup>3</sup> YUSHCHENKO 04B  $\lambda_+^*$  and  $\lambda_+^{**}$  are strongly correlated with coefficient  $\rho(\lambda_+^*, \lambda_+^{**}) = -0.95$ .  
<sup>4</sup> Superseded by YUSHCHENKO 04B.

$\lambda_+^{\dagger}$  (LINEAR  $K_{\mu 3}^\pm$  FORM FACTOR FROM QUADRATIC FIT)

VALUE (units $10^{-3}$ )	EVTS	DOCUMENT ID	TECN	CHG	COMMENT
<b>24.27 ± 2.88 ± 2.89</b>	2.3M	<sup>1</sup> BATLEY	18	NA48	±

<sup>1</sup> Data collected in 2004 by NA48/2. Correlation coefficient with quadratic slope is -0.974, with scalar slope is 0.511.  $\chi^2/NDF = 409.9/381$ . BATLEY 18 also performed a combined  $K_{e3}^\pm$  and  $K_{\mu 3}^\pm$  fit assuming  $\mu-e$  universality and obtained  $(24.24 \pm 0.75 \pm 1.3) \times 10^{-3}$ .

$\lambda_+^{\dagger\dagger}$  (QUADRATIC  $K_{\mu 3}^\pm$  FORM FACTOR)

VALUE (units $10^{-3}$ )	EVTS	DOCUMENT ID	TECN	CHG	
<b>1.83 ± 1.05 ± 1.09</b>	2.3M	<sup>1</sup> BATLEY	18	NA48	±

<sup>1</sup> Data collected in 2004 by NA48/2. Correlation coefficient with linear slope is -0.974, with scalar slope is 0.513.  $\chi^2/NDF = 409.9/381$ . BATLEY 18 also performed a combined  $K_{e3}^\pm$  and  $K_{\mu 3}^\pm$  fit assuming  $\mu-e$  universality and obtained  $(1.67 \pm 0.29 \pm 0.41) \times 10^{-3}$ .

$M_V$  (VECTOR POLE MASS FOR  $K_{e3}^\pm$  DECAY)

See the review on  $K_{13}^\pm$  and  $K_{13}^0$  Form Factors for details.

VALUE (MeV)	EVTS	DOCUMENT ID	TECN	CHG	
<b>890.3 ± 2.8 OUR AVERAGE</b>					
885.2 ± 3.3 ± 7.2	4.4M	<sup>1</sup> BATLEY	18	NA48	±
891 ± 3	5.25M	<sup>2</sup> YUSHCHENKO18	OKA	+	

<sup>1</sup> Data collected in 2004 by NA48/2.  $\chi^2/NDF = 568.9/688$ . BATLEY 18 also performed a combined  $K_{e3}^\pm$  and  $K_{\mu 3}^\pm$  fit assuming  $\mu-e$  universality and obtained  $884.4 \pm 3.1 \pm 6.7$  MeV.  
<sup>2</sup> Assumed no scalar or tensor contributions to the form factor.

$M_V$  (VECTOR POLE MASS FOR  $K_{\mu 3}^\pm$  DECAY)

VALUE (MeV)	EVTS	DOCUMENT ID	TECN	CHG	
<b>878.4 ± 8.8 ± 8.3</b>	2.3M	<sup>1</sup> BATLEY	18	NA48	±

<sup>1</sup> Data collected in 2004 by NA48/2.  $\chi^2/NDF = 409.9/382$ . BATLEY 18 also performed a combined  $K_{e3}^\pm$  and  $K_{\mu 3}^\pm$  fit assuming  $\mu-e$  universality and obtained  $884.4 \pm 3.1 \pm 6.7$  MeV.

$M_S$  (SCALAR POLE MASS FOR  $K_{\mu 3}^\pm$  DECAY)

VALUE (MeV)	EVTS	DOCUMENT ID	TECN	CHG	
<b>1214.8 ± 23.5 ± 49.2</b>	2.3M	<sup>1</sup> BATLEY	18	NA48	±

<sup>1</sup> Data collected in 2004 by NA48/2.  $\chi^2/NDF = 409.9/382$ . BATLEY 18 also performed a combined  $K_{e3}^\pm$  and  $K_{\mu 3}^\pm$  fit assuming  $\mu-e$  universality and obtained  $1208.3 \pm 21.2 \pm 47.5$  MeV.

$A_+$  (DISPERSIVE VECTOR FORM FACTOR IN  $K_{e3}^\pm$  DECAY)

See the review on  $K_{13}^\pm$  and  $K_{13}^0$  Form Factors for details.

VALUE (units $10^{-2}$ )	EVTS	DOCUMENT ID	TECN	CHG	
<b>2.460 ± 0.017 OUR AVERAGE</b>					
2.494 ± 0.021 ± 0.064	4.4M	<sup>1</sup> BATLEY	18	NA48	±
2.458 ± 0.018	5.25M	<sup>2</sup> YUSHCHENKO18	OKA	+	

<sup>1</sup> Data collected in 2004 by NA48/2.  $\chi^2/NDF = 569.0/688$ . BATLEY 18 also performed a combined  $K_{e3}^\pm$  and  $K_{\mu 3}^\pm$  fit assuming  $\mu-e$  universality and obtained  $(24.99 \pm 0.20 \pm 0.62) \times 10^{-3}$ .  
<sup>2</sup> Assumed no scalar or tensor contributions to the form factor.

$A_+$  (DISPERSIVE VECTOR FORM FACTOR IN  $K_{\mu 3}^\pm$  DECAY)

VALUE (units $10^{-3}$ )	EVTS	DOCUMENT ID	TECN	CHG	
<b>25.36 ± 0.58 ± 0.72</b>	2.3M	<sup>1</sup> BATLEY	18	NA48	±

<sup>1</sup> Data collected in 2004 by NA48/2.  $\chi^2/NDF = 410.3/382$ . BATLEY 18 also performed a combined  $K_{e3}^\pm$  and  $K_{\mu 3}^\pm$  fit assuming  $\mu-e$  universality and obtained  $(24.99 \pm 0.20 \pm 0.62) \times 10^{-3}$ .

$\ln(C)$  (DISPERSIVE SCALAR FORM FACTOR IN  $K_{\mu 3}^\pm$  decays)

VALUE (units $10^{-3}$ )	EVTS	DOCUMENT ID	TECN	CHG	
<b>182.17 ± 6.31 ± 14.45</b>	2.3M	<sup>1</sup> BATLEY	18	NA48	±

<sup>1</sup> Data collected in 2004 by NA48/2. Combined fit with dispersive vector form factor  $A_+ = 25.36 \pm 0.58 \pm 0.72$ . Correlation coefficient is 0.104.  $\chi^2/NDF = 410.3/382$ . BATLEY 18 also performed a combined  $K_{e3}^\pm$  and  $K_{\mu 3}^\pm$  fit assuming  $\mu-e$  universality and obtained  $(183.65 \pm 5.92 \pm 14.25) \times 10^{-3}$ .

$|f_S/f_+|$  FOR  $K_{e3}^\pm$  DECAY

Ratio of scalar to  $f_+$  couplings.

VALUE (units $10^{-2}$ )	CL%	EVTS	DOCUMENT ID	TECN	CHG	COMMENT
<b>-0.08 ± 0.34 ± 0.40 OUR AVERAGE</b>						

0.01 ± 0.38 ± 0.46		5.25M	YUSHCHENKO18	OKA	+	$\lambda_+^{\dagger\dagger}, \lambda_+^{\dagger}, f_S$ fit
-0.37 ± 0.66 ± 0.41		919k	YUSHCHENKO04B	ISTR	-	$\lambda_+^{\dagger\dagger}, \lambda_+^{\dagger}, f_S$ fit
0.2 ± 2.6 ± 1.4		41k	SHIMIZU	00	SPEC	$\lambda_+, f_S, f_T$ fit
• • •						We do not use the following data for averages, fits, limits, etc. • • •
0.2 ± 2.0 ± 2.2 ± 0.3		550k	<sup>1</sup> AJINENKO	03c	ISTR	$\lambda_+, f_S, f_T$ fit
-1.9 ± 2.5 ± 1.6		130k	<sup>1</sup> AJINENKO	02	SPEC	$\lambda_+, f_S$ fit
7.0 ± 1.6 ± 1.6		32k	AKIMENKO	91	SPEC	$\lambda_+, f_S, f_T, \phi$ fit
0 ± 10		2827	<sup>2</sup> BRAUN	75	HLBC	+
< 13		4017	CHIANG	72	OSPK	+
14 ± 3 ± 4		2707	<sup>2</sup> STEINER	71	HLBC	$\lambda_+, f_S, f_T, \phi$ fit
< 23		90	BOTTERILL	68c	ASPK	

## Meson Particle Listings

 $K^\pm$ 

< 18	90	BELLOTTI	67B	HLBC
< 30	95	KALMUS	67	HLBC +

- <sup>1</sup> Superseded by YUSHCHENKO 04b.  
<sup>2</sup> Statistical errors only.

 $|f_T/f_+|$  FOR  $K_{e3}^\pm$  DECAYRatio of tensor to  $f_+$  couplings.

VALUE (units $10^{-2}$ )	EVTS	DOCUMENT ID	TECN	CHG	COMMENT
<b><math>-1.2 \pm 1.3</math></b>					<b>OUR AVERAGE</b>
$-1.24 \pm 1.6$	5.25M	YUSHCHENKO18	OKA	+	$\lambda'_+, \lambda''_+, f_T$ fit
$-1.2 \pm 2.1 \pm 1.1$	919k	YUSHCHENKO04B	ISTR	-	$\lambda'_+, \lambda''_+, f_T$ fit
$1 \pm 14 \pm 9$	41k	SHIMIZU	00	SPEC	$\lambda_+, f_S, f_T$ fit
••• We do not use the following data for averages, fits, limits, etc. •••					
$2.1 \pm 6.4$	550k	1 AJJENKO	03c	ISTR	$\lambda_+, f_S, f_T$ fit
$-4.5 \pm 6.0$	130k	1 AJJENKO	02	SPEC	$\lambda_+, f_T$ fit
$53 \pm 9$	32k	AKIMENKO	91	SPEC	$\lambda_+, f_S, f_T, \phi$ fit

- <sup>1</sup> Superseded by YUSHCHENKO 04b.

 $f_S/f_+$  FOR  $K_{\mu 3}^\pm$  DECAYRatio of scalar to  $f_+$  couplings.

VALUE (units $10^{-2}$ )	EVTS	DOCUMENT ID	TECN	CHG	COMMENT
<b><math>0.17 \pm 0.14 \pm 0.54</math></b>	540k	1 YUSHCHENKO04	ISTR	-	DP
••• We do not use the following data for averages, fits, limits, etc. •••					
$0.4 \pm 0.5 \pm 0.5$	112k	2 AJJENKO	03	ISTR	DP

- <sup>1</sup> The second error is the theoretical error from the uncertainty in the chiral perturbation theory prediction for  $\lambda_0$ ,  $\pm 0.0053$ , combined in quadrature with the systematic error  $\pm 0.0009$ .  
<sup>2</sup> The second error is the theoretical error from the uncertainty in the chiral perturbation theory prediction for  $\lambda_0$ . Superseded by YUSHCHENKO 04.

 $f_T/f_+$  FOR  $K_{\mu 3}^\pm$  DECAYRatio of tensor to  $f_+$  couplings.

VALUE (units $10^{-2}$ )	EVTS	DOCUMENT ID	TECN	CHG	COMMENT
<b><math>-0.07 \pm 0.71 \pm 0.20</math></b>	540k	YUSHCHENKO04	ISTR	-	DP
••• We do not use the following data for averages, fits, limits, etc. •••					
$-2.1 \pm 2.8 \pm 1.4$	112k	1 AJJENKO	03	ISTR	DP
$2 \pm 12$	1585	BRAUN	75	HLBC	

- <sup>1</sup> The second error is the theoretical error from the uncertainty in the chiral perturbation theory prediction for  $\lambda_0$ . Superseded by YUSHCHENKO 04.

 $K_{24}^\pm$  FORM FACTORS

Based on the parametrizations of AMOROS 99, the  $K_{24}^\pm$  form factors can be expressed as

$$F_S = f_S + f'_S q^2 + f''_S q^4 + f'_e S_e / 4m_\pi^2$$

$$F_P = f_P$$

$$G_P = g_P + g'_P q^2$$

$$H_P = h_P$$

where  $q^2 = (S_\pi / 4m_\pi^2) - 1$ ,  $S_\pi$  is the invariant mass squared of the dipion, and  $S_e$  is the invariant mass squared of the dilepton.

 $f_S$  FOR  $K^\pm \rightarrow \pi^+ \pi^- e^\pm \nu$  DECAY

VALUE	EVTS	DOCUMENT ID	TECN	CHG
<b><math>5.712 \pm 0.032</math></b>				
$5.705 \pm 0.003 \pm 0.035$	1.1M	1 BATLEY	12	NA48 ±
$5.75 \pm 0.02 \pm 0.08$	400k	2 PISLAK	03	B865 +

- <sup>1</sup> BATLEY 12 uses data collected in 2003–2004. The result is obtained from a measurement of  $\Gamma(\pi^+ \pi^- e \nu) / \Gamma(\pi^+ \pi^- \pi^+) / \Gamma(\pi^+ \pi^- \pi^+) / \Gamma = (5.59 \pm 0.04) \times 10^{-2}$ .  
<sup>2</sup> Radiative corrections included. Using Roy equations and not including isospin breaking, PISLAK 03 obtains the following  $\pi\pi$  scattering lengths  $a_0^0 = 0.228 \pm 0.012 \pm 0.004 \pm 0.012$  (theor.) and  $a_0^2 = -0.0365 \pm 0.0023 \pm 0.0008 \pm 0.0031 \pm 0.0026$  (theor.).

 $f'_S/f_S$  FOR  $K^\pm \rightarrow \pi^+ \pi^- e^\pm \nu$  DECAY

VALUE (units $10^{-2}$ )	EVTS	DOCUMENT ID	TECN	CHG
<b><math>15.2 \pm 0.7 \pm 0.5</math></b>	1.13M	1 BATLEY	10c	NA48 ±
••• We do not use the following data for averages, fits, limits, etc. •••				
$17.2 \pm 0.9 \pm 0.6$	670k	2 BATLEY	08A	NA48 ±

- <sup>1</sup> Radiative corrections included. Using Roy equations and including isospin breaking, BATLEY 10c obtains the following scattering lengths  $a_0^0 = 0.2220 \pm 0.0128 \pm 0.0050 \pm 0.0037$  (theor.),  $a_0^2 = -0.0432 \pm 0.0086 \pm 0.0034 \pm 0.0028$  (theor.). The correlation with  $f''_S/f_S = -0.954$  and with  $f'_e/f_S = 0.080$ . Supersedes BATLEY 08A.  
<sup>2</sup> Radiative corrections included. Using Roy equations and not including isospin breaking, BATLEY 08A obtains the following  $\pi\pi$  scattering length  $a_0^0 = 0.233 \pm 0.016 \pm 0.007$   $a_0^2 = -0.0471 \pm 0.011 \pm 0.004$ .

 $f''_S/f_S$  FOR  $K^\pm \rightarrow \pi^+ \pi^- e^\pm \nu$  DECAY

VALUE (units $10^{-2}$ )	EVTS	DOCUMENT ID	TECN	CHG
<b><math>-7.3 \pm 0.7 \pm 0.6</math></b>	1.13M	1 BATLEY	10c	NA48 ±
••• We do not use the following data for averages, fits, limits, etc. •••				
$-9.0 \pm 0.9 \pm 0.7$	670k	2 BATLEY	08A	NA48 ±

- <sup>1</sup> Radiative corrections included. Using Roy equations and including isospin breaking, BATLEY 10c obtains the following scattering lengths  $a_0^0 = 0.2220 \pm 0.0128 \pm 0.0050 \pm 0.0037$  (theor.),  $a_0^2 = -0.0432 \pm 0.0086 \pm 0.0034 \pm 0.0028$  (theor.). The correlation with  $f'_S/f_S = -0.954$  and with  $f'_e/f_S = 0.019$ . Supersedes BATLEY 08A.

- <sup>2</sup> Radiative corrections included. Using Roy equations and not including isospin breaking, BATLEY 08A obtains the following  $\pi\pi$  scattering length  $a_0^0 = 0.233 \pm 0.016 \pm 0.007$   $a_0^2 = -0.0471 \pm 0.011 \pm 0.004$ .

 $f'_e/f_S$  FOR  $K^\pm \rightarrow \pi^+ \pi^- e^\pm \nu$  DECAY

VALUE (units $10^{-2}$ )	EVTS	DOCUMENT ID	TECN	CHG
<b><math>6.8 \pm 0.6 \pm 0.7</math></b>	1.13M	1 BATLEY	10c	NA48 ±
••• We do not use the following data for averages, fits, limits, etc. •••				
$8.1 \pm 0.8 \pm 0.9$	670k	2 BATLEY	08A	NA48 ±

- <sup>1</sup> Radiative corrections included. Using Roy equations and including isospin breaking, BATLEY 10c obtains the following scattering lengths  $a_0^0 = 0.2220 \pm 0.0128 \pm 0.0050 \pm 0.0037$  (theor.),  $a_0^2 = -0.0432 \pm 0.0086 \pm 0.0034 \pm 0.0028$  (theor.). The correlation with  $f'_S/f_S = 0.080$  and with  $f''_S/f_S = 0.019$ . Supersedes BATLEY 08A.

- <sup>2</sup> Radiative corrections included. Using Roy equations and not including isospin breaking, BATLEY 08A obtains the following  $\pi\pi$  scattering length  $a_0^0 = 0.233 \pm 0.016 \pm 0.007$   $a_0^2 = -0.0471 \pm 0.011 \pm 0.004$ .

 $f_P/f_S$  FOR  $K^\pm \rightarrow \pi^+ \pi^- e^\pm \nu$  DECAY

VALUE (units $10^{-2}$ )	EVTS	DOCUMENT ID	TECN	CHG
<b><math>-4.8 \pm 0.3 \pm 0.4</math></b>	1.13M	1 BATLEY	10c	NA48 ±
••• We do not use the following data for averages, fits, limits, etc. •••				
$-4.8 \pm 0.4 \pm 0.4$	670k	2 BATLEY	08A	NA48 ±

- <sup>1</sup> Radiative corrections included. Using Roy equations and including isospin breaking, BATLEY 10c obtains the following scattering lengths  $a_0^0 = 0.2220 \pm 0.0128 \pm 0.0050 \pm 0.0037$  (theor.),  $a_0^2 = -0.0432 \pm 0.0086 \pm 0.0034 \pm 0.0028$  (theor.). Supersedes BATLEY 08A.

- <sup>2</sup> Radiative corrections included. Using Roy equations and not including isospin breaking, BATLEY 08A obtains the following  $\pi\pi$  scattering length  $a_0^0 = 0.233 \pm 0.016 \pm 0.007$   $a_0^2 = -0.0471 \pm 0.011 \pm 0.004$ .

 $g_P/f_S$  FOR  $K^\pm \rightarrow \pi^+ \pi^- e^\pm \nu$  DECAY

VALUE (units $10^{-2}$ )	EVTS	DOCUMENT ID	TECN	CHG
<b><math>86.8 \pm 1.0 \pm 1.0</math></b>	1.13M	1 BATLEY	10c	NA48 ±
••• We do not use the following data for averages, fits, limits, etc. •••				
$87.3 \pm 1.3 \pm 1.2$	670k	2 BATLEY	08A	NA48 ±
$80.9 \pm 0.9 \pm 1.2$	400k	3 PISLAK	03	B865 ±

- <sup>1</sup> Radiative corrections included. Using Roy equations and including isospin breaking, BATLEY 10c obtains the following scattering lengths  $a_0^0 = 0.2220 \pm 0.0128 \pm 0.0050 \pm 0.0037$  (theor.),  $a_0^2 = -0.0432 \pm 0.0086 \pm 0.0034 \pm 0.0028$  (theor.). Supersedes BATLEY 08A. The correlation with  $g'_P/f_S = -0.914$ . Supersedes BATLEY 08A.

- <sup>2</sup> Radiative corrections included. Using Roy equations and not including isospin breaking, BATLEY 08A obtains the following  $\pi\pi$  scattering length  $a_0^0 = 0.233 \pm 0.016 \pm 0.007$   $a_0^2 = -0.0471 \pm 0.011 \pm 0.004$ .

- <sup>3</sup> Radiative corrections included. Using Roy equations PISLAK 03 obtains the following scattering lengths  $a_0^0 = 0.203 \pm 0.033 \pm 0.004$ ,  $a_0^2 = -0.055 \pm 0.023 \pm 0.003$ .

 $g'_P/f_S$  FOR  $K^\pm \rightarrow \pi^+ \pi^- e^\pm \nu$  DECAY

VALUE (units $10^{-2}$ )	EVTS	DOCUMENT ID	TECN	CHG
<b><math>8.9 \pm 1.7 \pm 1.3</math></b>	1.13M	1 BATLEY	10c	NA48 ±
••• We do not use the following data for averages, fits, limits, etc. •••				
$8.1 \pm 2.2 \pm 1.5$	670k	2 BATLEY	08A	NA48 ±
$12.0 \pm 1.9 \pm 0.7$	400k	3 PISLAK	03	B865 ±

- <sup>1</sup> Radiative corrections included. Using Roy equations and including isospin breaking, BATLEY 10c obtains the following scattering lengths  $a_0^0 = 0.2220 \pm 0.0128 \pm 0.0050 \pm 0.0037$  (theor.),  $a_0^2 = -0.0432 \pm 0.0086 \pm 0.0034 \pm 0.0028$  (theor.). The correlation with  $g_P/f_S = -0.914$ . Supersedes BATLEY 08A.

- <sup>2</sup> Radiative corrections included. Using Roy equations and not including isospin breaking, BATLEY 08A obtains the following  $\pi\pi$  scattering length  $a_0^0 = 0.233 \pm 0.016 \pm 0.007$   $a_0^2 = -0.0471 \pm 0.011 \pm 0.004$ .

- <sup>3</sup> Radiative corrections included. Using Roy equations PISLAK 03 obtains the following scattering lengths  $a_0^0 = 0.203 \pm 0.033 \pm 0.004$ ,  $a_0^2 = -0.055 \pm 0.023 \pm 0.003$ .

 $h_P/f_S$  FOR  $K^\pm \rightarrow \pi^+ \pi^- e^\pm \nu$  DECAY

VALUE (units $10^{-2}$ )	EVTS	DOCUMENT ID	TECN	CHG
<b><math>-39.8 \pm 1.5 \pm 0.8</math></b>	1.13M	1 BATLEY	10c	NA48 ±

••• We do not use the following data for averages, fits, limits, etc. •••

-41.1 ± 1.9 ± 0.8	670k	<sup>2</sup> BATLEY	08A	NA48	±
-51.3 ± 3.3 ± 3.5	400k	<sup>3</sup> PISLAK	03	B865	±

<sup>1</sup> Radiative corrections included. Using Roy equations and including isospin breaking, BATLEY 10c obtains the following scattering lengths  $a_0^0 = 0.2220 \pm 0.0128 \pm 0.0050 \pm 0.0037$  (theor.),  $a_0^2 = -0.0432 \pm 0.0086 \pm 0.0034 \pm 0.0028$  (theor.). Supersedes BATLEY 08A.

<sup>2</sup> Radiative corrections included. Using Roy equations and not including isospin breaking, BATLEY 08A obtains the following  $\pi\pi$  scattering length  $a_0^0 = 0.233 \pm 0.016 \pm 0.007$ ,  $a_0^2 = -0.0471 \pm 0.011 \pm 0.004$ .

<sup>3</sup> Radiative corrections included. Using Roy equations PISLAK 03 obtains the following scattering lengths  $a_0^0 = 0.203 \pm 0.033 \pm 0.004$ ,  $a_0^2 = -0.055 \pm 0.023 \pm 0.003$ .

**DECAY FORM FACTOR FOR  $K^\pm \rightarrow \pi^0 \pi^\pm e^\pm \nu$**   
 Given in BOLOTOV 86b, BARMIN 88b, and SHIMIZU 04.

**$K^\pm \rightarrow \ell^\pm \nu \gamma$  FORM FACTORS**

For definitions of the axial-vector  $F_A$  and vector  $F_V$  form factor, see the "Note on  $\pi^\pm \rightarrow \ell^\pm \nu \gamma$  and  $K^\pm \rightarrow \ell^\pm \nu \gamma$  Form Factors" in the  $\pi^\pm$  section. In the kaon literature, often different definitions  $a_K = F_A/m_K$  and  $v_K = F_V/m_K$  are used.

**$F_A + F_V$ , SUM OF AXIAL-VECTOR AND VECTOR FORM FACTOR FOR  $K \rightarrow e \nu e \gamma$**

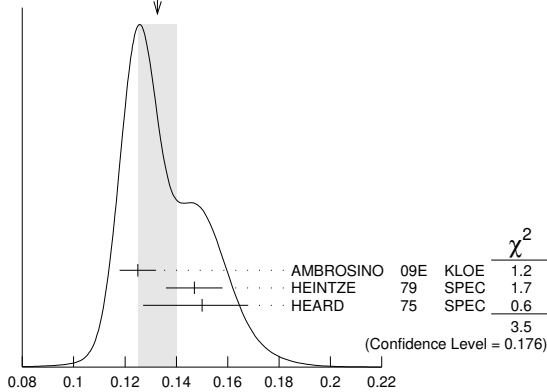
VALUE	EVTS	DOCUMENT ID	TECN	COMMENT
<b>0.133 ± 0.008 OUR AVERAGE</b>		Error includes scale factor of 1.3.		See the ideogram below.
0.125 ± 0.007 ± 0.001	1.4K	<sup>1</sup> AMBROSINO 09E	KLOE	$E_\gamma$ in 10–250 MeV, $p_e > 200$ MeV/c
0.147 ± 0.011	51	<sup>2</sup> HEINTZE 79	SPEC	
0.150 ± 0.018 –0.023	56	<sup>3</sup> HEARD 75	SPEC	

<sup>1</sup> AMBROSINO 09E measures the absolute value  $|F_A + F_V|$  which is parametrized as  $|F_A + F_V| = F_V (1 + \lambda(1-x)) + F_A$ ,  $x = 2E_\gamma/m_K$ . ( $F_A + F_V$ ) and  $\lambda$  are fit parameters. The fitted value of  $\lambda = 0.38 \pm 0.20 \pm 0.02$  with a correlation of –0.93 between ( $F_A + F_V$ ) and  $\lambda$ .

<sup>2</sup> HEINTZE 79 quotes absolute value of  $|F_A + F_V| \sin\theta_c$ . We use  $\sin\theta_c = V_{us} = 0.2205$ .

<sup>3</sup> HEARD 75 quotes absolute value of  $|F_A + F_V| \sin\theta_c$ . We use  $\sin\theta_c = V_{us} = 0.2205$ .

WEIGHTED AVERAGE  
 0.133 ± 0.008 (Error scaled by 1.3)



**$F_A + F_V$ , SUM OF AXIAL-VECTOR AND VECTOR FORM FACTOR FOR  $K \rightarrow e \nu e \gamma$**

**$F_A + F_V$ , SUM OF AXIAL-VECTOR AND VECTOR FORM FACTOR FOR  $K \rightarrow \mu \nu \mu \gamma$**

VALUE	CL%	EVTS	DOCUMENT ID	TECN	CHG
<b>0.165 ± 0.007 ± 0.011</b>		2588	<sup>1</sup> ADLER	00B	B787 +
–1.2 to 1.1	90		DEMIDOV	90	XEBC
< 0.23	90		<sup>1</sup> AKIBA	85	SPEC

••• We do not use the following data for averages, fits, limits, etc. •••

<sup>1</sup> Quotes absolute value. Sign not determined.

**$F_A - F_V$ , DIFFERENCE OF AXIAL-VECTOR AND VECTOR FORM FACTOR FOR  $K \rightarrow e \nu e \gamma$**

VALUE	CL%	DOCUMENT ID	TECN
<b>&lt; 0.49</b>		<sup>1</sup> HEINTZE 79	SPEC

<sup>1</sup> HEINTZE 79 quotes  $|F_A - F_V| < \sqrt{11} |F_A + F_V|$ .

**$F_A - F_V$ , DIFFERENCE OF AXIAL-VECTOR AND VECTOR FORM FACTOR FOR  $K \rightarrow \mu \nu \mu \gamma$**

VALUE	CL%	EVTS	DOCUMENT ID	TECN	CHG
<b>–0.153 ± 0.033 OUR AVERAGE</b>			Error includes scale factor of 1.1.		
–0.134 ± 0.021 ± 0.027	95K		KRAVTSOV 19	OKA	+
–0.21 ± 0.06	22K		DUK 11	ISTR	–

••• We do not use the following data for averages, fits, limits, etc. •••

–0.24 to 0.04	90	2588	ADLER	00B	B787 +
–2.2 to 0.6	90		DEMIDOV	90	XEBC
–2.5 to 0.3	90		AKIBA	85	SPEC

**$K^\pm$  CHARGE RADIUS**

VALUE (fm)	DOCUMENT ID	COMMENT
<b>0.560 ± 0.031 OUR AVERAGE</b>		
0.580 ± 0.040	AMENDOLIA 86B	$Ke \rightarrow Ke$
0.530 ± 0.050	DALLY 80	$Ke \rightarrow Ke$
0.620 ± 0.037	BLATNIK 79	VMD + dispersion relations

••• We do not use the following data for averages, fits, limits, etc. •••

**$K^+$  LONGITUDINAL POLARIZATION OF EMITTED  $\mu^+$**

VALUE	CL%	DOCUMENT ID	TECN	CHG	COMMENT
<b>&lt; –0.990</b>	90	<sup>1</sup> AOKI 94	SPEC	+	
< –0.990	90	IMAZATO 92	SPEC	+	Repl. by AOKI 94
–0.970 ± 0.047		<sup>2</sup> YAMANAKA 86	SPEC	+	
–1.0 ± 0.1		<sup>2</sup> CUTTS 69	SPRK	+	
–0.96 ± 0.12		<sup>2</sup> COOMBES 57	CNTR	+	

<sup>1</sup> AOKI 94 measures  $\xi P_\mu = -0.9996 \pm 0.0030 \pm 0.0048$ . The above limit is obtained by summing the statistical and systematic errors in quadrature, normalizing to the physically significant region ( $|\xi P_\mu| < 1$ ) and assuming that  $\xi=1$ , its maximum value.

<sup>2</sup> Assumes  $\xi=1$ .

**FORWARD-BACKWARD ASYMMETRY IN  $K^\pm$  DECAYS**

$$A_{FB}(K^\pm_{\pi\mu\mu}) = \frac{\Gamma(\cos\theta_{K\mu}) > 0 - \Gamma(\cos\theta_{K\mu}) < 0}{\Gamma(\cos\theta_{K\mu}) > 0 + \Gamma(\cos\theta_{K\mu}) < 0}$$

VALUE	CL%	DOCUMENT ID	TECN
<b>&lt; 2.3 × 10<sup>–2</sup></b>	90	<sup>1</sup> BATLEY 11A	NA48

<sup>1</sup> BATLEY 11A gives a corresponding value of the asymmetry  $A_{FB} = (-2.4 \pm 1.8) \times 10^{-2}$ .

**$K^\pm$  REFERENCES**

BATLEY 19	PL B788 552	J.R. Batley et al.	(NA48/2 Collab.)
CORTINA-GIL 19A	PL B797 134794	E. Cortina Gil et al.	(NA62 Collab.)
CORTINA-GIL 19B	PL B791 156	E. Cortina Gil et al.	(NA62 Collab.)
KRAVTSOV 19	EPJ C79 635	V.I. Kravtsov et al.	(OKA Collab.)
SHAPKIN 19	EPJ C79 296	M.M. Shapkin et al.	(OKA Collab.)
BATLEY 18	JHEP 1810 150	J.R. Batley et al.	(NA48/2 Collab.)
PDG 18	PR D98 030001	M. Tanabashi et al.	(PDG Collab.)
YUSHCHENKO 18	JETPL 107 139	G.P. Yushchenko et al.	(OKA Collab.)
BATLEY 17	PL B769 67	J.R. Batley et al.	(NA48/2 Collab.)
ARTAMONOV 16	PR D94 032012	A.V. Artamonov et al.	(BNL E949 Collab.)
BABUSCI 14B	PL B738 128	D. Babusci et al.	(KLOE and KLOE-2 Collab.)
BATLEY 14	PL B730 141	J.R. Batley et al.	(CERN NA48/2 Collab.)
BATLEY 14A	JHEP 1408 159	J.R. Batley et al.	(CERN NA48/2 Collab.)
LAZZERONI 14	PL B732 65	C. Lazzeroni et al.	(CERN NA62 Collab.)
UVAROV 14	PAN 77 725	V.A. Uvarov et al.	(ISTRA+ Collab.)
LAZZERONI 13	PL B719 326	C. Lazzeroni et al.	(CERN NA62 Collab.)
BATLEY 12	PL B715 105	J.R. Batley et al.	(CERN NA48/2 Collab.)
PDG 12	PR D86 010001	J. Beringer et al.	(PDG Collab.)
BATLEY 11A	PL B697 107	J.R. Batley et al.	(CERN NA48/2 Collab.)
DUK 11	PL B695 59	V.A. Duk et al.	(ISTRA+ Collab.)
LAZZERONI 11	PL B698 105	C. Lazzeroni et al.	(CERN NA62 Collab.)
ADLER 10	PR D81 092001	S. Adler et al.	(BNL E787 Collab.)
BATLEY 10A	EPJ C68 75	J.R. Batley et al.	(CERN NA48/2 Collab.)
BATLEY 10C	EPJ C70 635	J.R. Batley et al.	(CERN NA48/2 Collab.)
PDG 10	JP G37 075021	K. Nakamura et al.	(PDG Collab.)
PISLAK 10A	PRL 105 019901E	S. Pislak et al.	(BNL E865 Collab.)
AKOPDZHANOV 09	PAN 71 2074	G.A. Akopdzhanov et al.	(IHEP Collab.)
AMBROSINO 09E	EPJ C64 627	F. Ambrosino et al.	(KLOE Collab.)
Also	EPJ C65 703 (err.)	F. Ambrosino et al.	(KLOE Collab.)
BATLEY 09	PL B677 246	J.R. Batley et al.	(CERN NA48/2 Collab.)
BATLEY 09A	EPJ C64 589	J.R. Batley et al.	(CERN NA48/2 Collab.)
BISSEGER 09	NP B806 178	M. Bissegger et al.	(KLOE Collab.)
AMBROSINO 08A	JHEP 0801 073	F. Ambrosino et al.	(KLOE Collab.)
AMBROSINO 08B	JHEP 0802 098	F. Ambrosino et al.	(KLOE Collab.)
AMBROSINO 08E	PL B666 305	F. Ambrosino et al.	(KLOE Collab.)
ARTAMONOV 08	PRL 101 191802	A.V. Artamonov et al.	(BNL E949 Collab.)
Also	PR D79 092004	A.V. Artamonov et al.	(BNL E949 Collab.)
BATLEY 08	PL B659 493	J.R. Batley et al.	(CERN NA48/2 Collab.)
BATLEY 08A	EPJ C54 411	J.R. Batley et al.	(CERN NA48/2 Collab.)
AKIMENKO 07	PAN 70 702	S.A. Akimenko et al.	(ISTRA+ Collab.)
ANDRE 07	ANP 322 2518	T. Andre	(EFI Collab.)
BATLEY 07A	EPJ C50 329	J.R. Batley et al.	(CERN NA48/2 Collab.)
Also	EPJ C52 1021 (err.)	J.R. Batley et al.	(CERN NA48/2 Collab.)
BATLEY 07B	PL B649 349	J.R. Batley et al.	(CERN NA48/2 Collab.)
BATLEY 07E	EPJ C52 875	J.R. Batley et al.	(CERN NA48/2 Collab.)
LAI 07A	PL B647 341	A. Lai et al.	(CERN NA48 Collab.)
TCHIKILEV 07	PAN 70 29	O.G. Tchikilev et al.	(ISTRA+ Collab.)
ALIEV 06	EPJ C46 61	M.A. Aliev et al.	(KEK E470 Collab.)
AMBROSINO 06A	PL B632 76	F. Ambrosino et al.	(KLOE Collab.)
BATLEY 06	PL B634 474	J.R. Batley et al.	(CERN NA48/2 Collab.)
BATLEY 06A	PL B638 22	J.R. Batley et al.	(CERN NA48/2 Collab.)
Also	PL B640 297 (err.)	J.R. Batley et al.	(CERN NA48/2 Collab.)
BATLEY 06B	PL B633 173	J.R. Batley et al.	(CERN NA48/2 Collab.)
COLANGELO 06A	PL B638 187	G. Colangelo et al.	(CERN NA48/2 Collab.)
MA 06	PR D73 037101	H. Ma et al.	(BNL E865 Collab.)
PDG 06	JP G33 1	W.-M. Yao et al.	(PDG Collab.)
SHIMIZU 06	PL B633 190	S. Shimizu et al.	(KEK E470 Collab.)
UVAROV 06	PAN 69 26	V.A. Uvarov et al.	(ISTRA+ Collab.)
AKOPDZHAN...05	EPJ C40 343	G.A. Akopdzhanov et al.	(IHEP Collab.)
Also	PAN 68 948	G.A. Akopdzhanov et al.	(IHEP Collab.)
AKOPDZHAN...05B	JETPL 82 675	G.A. Akopdzhanov et al.	(IHEP Collab.)
Translated from YAF 68 966.			
Translated from ZETFP 82 771.			



See key on page 999

Meson Particle Listings

$K^\pm, K^0$

Also	PL 11 360	N. Cabibbo, A. Maksymowicz	(CERN)
Also	PL 14 72	N. Cabibbo, A. Maksymowicz	(CERN)
BIRGE	63 PRL 11 35	R.W. Birge <i>et al.</i>	(LRL, WISC, BARI)
BLOCK	62B CERN Conf. 371	M.M. Block, L. Lendinara, L. Monari	(NWES, BGNA)
BRENE	61 NP 22 553	N. Brene, L. Egardt, B. Qvist	(NORD)



$$I(J^P) = \frac{1}{2}(0^-)$$

**K<sup>0</sup> MASS**

VALUE (MeV)	EVTS	DOCUMENT ID	TECN	COMMENT
<b>497.611 ± 0.013 OUR FIT</b>	Error includes scale factor of 1.2.			
<b>497.611 ± 0.013 OUR AVERAGE</b>	Error includes scale factor of 1.2.			
497.607 ± 0.007 ± 0.015	261k	<sup>1</sup> TOMARADZE 14		$\psi(2S) \rightarrow K_S^0 X$
497.583 ± 0.005 ± 0.020	35k	AMBROSINO 07B	KLOE	$e^+e^- \rightarrow K_L^0 K_S^0$
497.625 ± 0.001 ± 0.031	655k	LAI 02	NA48	$K^0$ beam
497.661 ± 0.033	3713	BARKOV 87B	CMD	$e^+e^- \rightarrow K_L^0 K_S^0$
497.742 ± 0.085	780	BARKOV 85B	CMD	$e^+e^- \rightarrow K_L^0 K_S^0$
• • • We do not use the following data for averages, fits, limits, etc. • • •				
497.44 ± 0.50		FITCH 67	OSP K	
498.9 ± 0.5	4500	BALTAY 66	HBC	$K^0$ from $\bar{p}p$
497.44 ± 0.33	2223	KIM 65B	HBC	$K^0$ from $\bar{p}p$
498.1 ± 0.4		CHRISTENS... 64	OSP K	

<sup>1</sup> Obtained by analyzing CLEO-c data but not authored by the CLEO Collaboration.

**m<sub>K<sup>0</sup></sub> - m<sub>K<sup>±</sup></sub>**

VALUE (MeV)	EVTS	DOCUMENT ID	TECN	CHG	COMMENT
<b>3.934 ± 0.020 OUR FIT</b>	Error includes scale factor of 1.6.				
• • • We do not use the following data for averages, fits, limits, etc. • • •					
3.95 ± 0.21	417	HILL 68B	DBC	+	$K^+d \rightarrow K^0 pp$
3.90 ± 0.25	9	BURNSTEIN 65	HBC	-	
3.71 ± 0.35	7	KIM 65B	HBC	-	$K^-p \rightarrow n\bar{K}^0$
5.4 ± 1.1		CRAWFORD 59	HBC	+	
3.9 ± 0.6		ROSENFELD 59	HBC	-	

**K<sup>0</sup> MEAN SQUARE CHARGE RADIUS**

VALUE (fm <sup>2</sup> )	EVTS	DOCUMENT ID	TECN	COMMENT
<b>-0.077 ± 0.010 OUR AVERAGE</b>				
-0.077 ± 0.007 ± 0.011	5037	ABOUZAID 06	KTEV	$K_L^0 \rightarrow \pi^+\pi^- e^+e^-$
-0.090 ± 0.021		LAI 03C	NA48	$K_L^0 \rightarrow \pi^+\pi^- e^+e^-$
-0.054 ± 0.026		MOLZON 78		$K_S$ regen. by electrons
• • • We do not use the following data for averages, fits, limits, etc. • • •				
-0.087 ± 0.046		BLATNIK 79		VMD + dispersion relations
-0.050 ± 0.130		FOETHK 69B		$K_S$ regen. by electrons

**T-VIOLATION PARAMETER IN K<sup>0</sup>-K<sup>0</sup> MIXING**

The asymmetry  $A_T = \frac{\Gamma(\bar{K}^0 \rightarrow K^0) - \Gamma(K^0 \rightarrow \bar{K}^0)}{\Gamma(\bar{K}^0 \rightarrow K^0) + \Gamma(K^0 \rightarrow \bar{K}^0)}$  must vanish if  $T$  invariance holds.

**ASYMMETRY A<sub>T</sub> IN K<sup>0</sup>-K<sup>0</sup> MIXING**

VALUE (units 10 <sup>-3</sup> )	EVTS	DOCUMENT ID	TECN
<b>6.6 ± 1.3 ± 1.0</b>	640k	<sup>1</sup> ANGELOPOULOS... 98E	CPLR

<sup>1</sup> ANGELOPOULOS 98E measures the asymmetry  $A_T = [\Gamma(\bar{K}^0_{t=0} \rightarrow e^+\pi^-\nu_{t=\tau}) - \Gamma(K^0_{t=0} \rightarrow e^-\pi^+\bar{\nu}_{t=\tau})] / [\Gamma(\bar{K}^0_{t=0} \rightarrow e^+\pi^-\nu_{t=\tau}) + \Gamma(K^0_{t=0} \rightarrow e^-\pi^+\bar{\nu}_{t=\tau})]$  as a function of the neutral-kaon eigentime  $\tau$ . The initial strangeness of the neutral kaon is tagged by the charge of the accompanying charged kaon in the reactions  $p\bar{p} \rightarrow K^-\pi^+K^0$  and  $p\bar{p} \rightarrow K^+\pi^-K^0$ . The strangeness at the time of the decay is tagged by the lepton charge. The reported result is the average value of  $A_T$  over the interval  $1\tau_S < \tau < 20\tau_S$ . From this value of  $A_T$  ANGELOPOULOS 01B, assuming  $CP$   $T$  invariance in the  $e\pi\nu$  decay amplitude, determine the  $T$ -violating as  $\Delta S = \Delta S$  conserving parameter (for its definition, see Review below)  $4\text{Re}(\epsilon) = (6.2 \pm 1.4 \pm 1.0) \times 10^{-3}$ .

**See the related review(s):**

[CPT Invariance Tests in Neutral Kaon Decay](#)

**CP-VIOLATION PARAMETERS**

**Re(ε)**

VALUE (units 10 <sup>-3</sup> )	DOCUMENT ID	TECN
<b>1.596 ± 0.013</b>	<sup>1</sup> AMBROSINO 06H	KLOE
• • • We do not use the following data for averages, fits, limits, etc. • • •		
1.664 ± 0.010	<sup>2</sup> LAI 05A	NA48

<sup>1</sup> AMBROSINO 06H uses Bell-Steinberger relations with the following measurements:  $B(K_L^0 \rightarrow \pi^+\pi^-)$  in AMBROSINO 06F,  $B(K_S^0 \rightarrow \pi^0\pi^0\pi^0)$  in AMBROSINO 05B, the  $K_S^0$ -semileptonic charge asymmetry in AMBROSINO 06E, and  $K^0$ -semileptonic results in ANGELOPOULOS 98F.

<sup>2</sup> LAI 05A values are obtained through unitarity (Bell-Steinberger relations), improving determination of  $\eta_{000}$  and combining other data from PDG 04 and APOSTOLAKIS 99B.

**CPT-VIOLATION PARAMETERS**

In  $K^0$ - $\bar{K}^0$  mixing, if  $CP$ -violating interactions include a  $T$  conserving part then

$$|K_S\rangle = [|K_1\rangle + (\epsilon + \delta)|K_2\rangle] / \sqrt{|1 + |\epsilon + \delta|^2|}$$

$$|K_L\rangle = [|K_2\rangle + (\epsilon - \delta)|K_1\rangle] / \sqrt{|1 + |\epsilon - \delta|^2|}$$

where

$$|K_1\rangle = [ |K^0\rangle + |\bar{K}^0\rangle ] / \sqrt{2}$$

$$|K_2\rangle = [ |K^0\rangle - |\bar{K}^0\rangle ] / \sqrt{2}$$

and

$$|\bar{K}^0\rangle = CP|K^0\rangle.$$

The parameter  $\delta$  specifies the  $CP$ -violating part.

Estimates of  $\delta$  are given below assuming the validity of the  $\Delta S = \Delta Q$  rule. See also THOMSON 95 for a test of  $CP$ -symmetry conservation in  $K^0$  decays using the Bell-Steinberger relation.

**REAL PART OF δ**

A nonzero value violates  $CP$   $T$  invariance.

VALUE (units 10 <sup>-4</sup> )	EVTS	DOCUMENT ID	TECN	COMMENT
<b>2.51 ± 2.25</b>		<sup>1</sup> ABOUZAID 11	KTEV	
• • • We do not use the following data for averages, fits, limits, etc. • • •				
2.3 ± 2.7		<sup>2</sup> AMBROSINO 06H	KLOE	
2.4 ± 2.8		<sup>3</sup> APOSTOLA... 99B	RVUE	
2.9 ± 2.6 ± 0.6	1.3M	<sup>4</sup> ANGELOPOULOS... 98F	CPLR	
180 ± 200	6481	<sup>5</sup> DEMIDOV 95		$K_{\ell 3}$ reanalysis

- <sup>1</sup> ABOUZAID 11 uses Bell-Steinberger relations.
- <sup>2</sup> AMBROSINO 06H uses Bell-Steinberger relations with the following measurements:  $B(K^0 \rightarrow \pi^+\pi^-)$  in AMBROSINO 06F,  $B(K^0 \rightarrow \pi^0\pi^0\pi^0)$  in AMBROSINO 05B, the  $K_S^0$ -semileptonic charge asymmetry in AMBROSINO 06E, and  $K^0$ -semileptonic results in ANGELOPOULOS 98F.
- <sup>3</sup> APOSTOLAKIS 99B assumes only unitarity and combines CPLEAR and other results.
- <sup>4</sup> ANGELOPOULOS 98F use  $\Delta S = \Delta Q$ . If  $\Delta S = \Delta Q$  is not assumed, they find  $\text{Re}\delta = (3.0 \pm 3.3 \pm 0.6) \times 10^{-4}$ .
- <sup>5</sup> DEMIDOV 95 reanalyzes data from HART 73 and NIEBERGALL 74.

**IMAGINARY PART OF δ**

A nonzero value violates  $CP$   $T$  invariance.

VALUE (units 10 <sup>-5</sup> )	EVTS	DOCUMENT ID	TECN	COMMENT
<b>-1.5 ± 1.6</b>		<sup>1</sup> ABOUZAID 11	KTEV	
• • • We do not use the following data for averages, fits, limits, etc. • • •				
0.4 ± 2.1		<sup>2</sup> AMBROSINO 06H	KLOE	
-0.2 ± 2.0		<sup>3</sup> LAI 05A	NA48	
2.4 ± 5.0		<sup>4</sup> APOSTOLA... 99B	RVUE	
-90 ± 290 ± 100	1.3M	<sup>5</sup> ANGELOPOULOS... 98F	CPLR	
2100 ± 3700	6481	<sup>6</sup> DEMIDOV 95		$K_{\ell 3}$ reanalysis

- <sup>1</sup> ABOUZAID 11 uses Bell-Steinberger relations.
- <sup>2</sup> AMBROSINO 06H uses Bell-Steinberger relations with the following measurements:  $B(K_L^0 \rightarrow \pi^+\pi^-)$  in AMBROSINO 06F,  $B(K_S^0 \rightarrow \pi^0\pi^0\pi^0)$  in AMBROSINO 05B, the  $K^0$ -semileptonic charge asymmetry in AMBROSINO 06E, and  $K^0$ -semileptonic results in ANGELOPOULOS 98F.
- <sup>3</sup> LAI 05A values are obtained through unitarity (Bell-Steinberger relations), improving determination of  $\eta_{000}$  and combining other data from PDG 04 and APOSTOLAKIS 99B.
- <sup>4</sup> APOSTOLAKIS 99B assumes only unitarity and combines CPLEAR and other results.
- <sup>5</sup> If  $\Delta S = \Delta Q$  is not assumed, ANGELOPOULOS 98F finds  $\text{Im}\delta = (-15 \pm 23 \pm 3) \times 10^{-3}$ .
- <sup>6</sup> DEMIDOV 95 reanalyzes data from HART 73 and NIEBERGALL 74.

**Re(y)**

A non-zero value would violate  $CP$   $T$  invariance in  $\Delta S = \Delta Q$  amplitude.  $\text{Re}(y)$  is the following combination of  $K_{e3}$  decay amplitudes:

$$\text{Re}(y) = \text{Re} \left( \frac{A(\bar{K}^0 \rightarrow e^-\pi^+\bar{\nu}_e) - A(K^0 \rightarrow e^+\pi^-\nu_e)}{A(\bar{K}^0 \rightarrow e^-\pi^+\bar{\nu}_e) + A(K^0 \rightarrow e^+\pi^-\nu_e)} \right)$$

VALUE (units 10 <sup>-3</sup> )	EVTS	DOCUMENT ID	TECN
<b>0.4 ± 2.5</b>	13k	<sup>1</sup> AMBROSINO 06E	KLOE
• • • We do not use the following data for averages, fits, limits, etc. • • •			
0.3 ± 3.1		<sup>2</sup> APOSTOLA... 99B	CPLR

- <sup>1</sup> They use the PDG 04 for the  $K_L^0$  semileptonic charge asymmetry and PDG 04 ( $CP$  review,  $CP$  NOT ASSUMED) for  $\text{Re}(\epsilon)$ .
- <sup>2</sup> Constrained by Bell-Steinberger (or unitarity) relation.

**Re(x<sub>-</sub>)**

A non-zero value would violate  $CP$   $T$  invariance in decay amplitudes with  $\Delta S \neq \Delta Q$ .  $x_-$ , used here to define  $\text{Re}(x_-)$ , and  $x_+$ , used below in the  $\Delta S = \Delta Q$  section are the following combinations of  $K_{e3}$  decay amplitudes:

$$x_- = \frac{1}{2} \left( \frac{A(\bar{K}^0 \rightarrow \pi^-\pi^+\nu_e) + A(K^0 \rightarrow \pi^+\pi^-\bar{\nu}_e)}{A(K^0 \rightarrow \pi^-\pi^+\nu_e)} \right)$$

VALUE (units 10 <sup>-3</sup> )	EVTS	DOCUMENT ID	TECN	COMMENT
<b>-2.9 ± 2.0</b>		<sup>1</sup> AMBROSINO 06H	KLOE	



# Meson Particle Listings

## $K^0, K_S^0$

••• We do not use the following data for averages, fits, limits, etc. •••

- 0.8 ± 2.5      13k      <sup>2</sup> AMBROSINO 06E KLOE
- 0.5 ± 3.0      <sup>3</sup> APOSTOLA... 99B CPLR Strangeness tagged
- 2 ± 13 ± 3      650k      ANGELOPO... 98F CPLR Strangeness tagged

- 1 AMBROSINO 06H uses Bell-Steinberger relations with the following measurements:  $B(K_L^0 \rightarrow \pi^+ \pi^-)$  in AMBROSINO 06F,  $B(K_S^0 \rightarrow \pi^0 \pi^0 \pi^0)$  in AMBROSINO 05B, the  $K_S^0$ -semileptonic charge asymmetry in AMBROSINO 06E, and  $K^0$ -semileptonic results in ANGELOPOULOS 98F.
- 2 Uses PDG 04 for the  $K_L^0$  semileptonic charge asymmetry and  $\text{Re}(\delta)$  from CPLEAR, ANGELOPOULOS 98F.
- 3 Constrained by Bell-Steinberger (or unitarity) relation.

$$|m_{K^0} - m_{\bar{K}^0}| / m_{\text{average}}$$

A test of *CPT* invariance. "Our Evaluation" is described in the "Tests of Conservation Laws" section. It assumes *CPT* invariance in the decay and neglects some contributions from decay channels other than  $\pi\pi$ .

VALUE	CL%	DOCUMENT ID	TECN
<b>&lt;6 × 10<sup>-19</sup></b>	90	PDG	12

••• We do not use the following data for averages, fits, limits, etc. •••

- (-3 ± 4) × 10<sup>-18</sup>      <sup>1</sup> ANGELOPO... 99B RVUE
- <sup>1</sup> ANGELOPOULOS 99B assumes only unitarity and combines CPLEAR and other results.

$$(\Gamma_{K^0} - \Gamma_{\bar{K}^0}) / m_{\text{average}}$$

A test of *CPT* invariance.

VALUE	DOCUMENT ID	TECN
<b>(7.8 ± 8.4) × 10<sup>-18</sup></b>	<sup>1</sup> ANGELOPO... 99B RVUE	

- <sup>1</sup> ANGELOPOULOS 99B assumes only unitarity and combines CPLEAR with other results. Correlated with  $(m_{K^0} - m_{\bar{K}^0}) / m_{\text{average}}$  with a correlation coefficient of -0.95.

### TESTS OF $\Delta S = \Delta Q$ RULE

#### $\text{Re}(x_+)$

A non-zero value would violate the  $\Delta S = \Delta Q$  rule in *CPT* conserving transitions.  $x_+$  is defined above in the  $\text{Re}(x_-)$  section.

VALUE (units 10 <sup>-3</sup> )	EVTS	DOCUMENT ID	TECN
<b>-0.9 ± 3.0 OUR AVERAGE</b>			
-2 ± 10		<sup>1</sup> BATLEY 07D NA48	
-0.5 ± 3.6	13k	<sup>2</sup> AMBROSINO 06E KLOE	
-1.8 ± 6.1		<sup>3</sup> ANGELOPO... 98D CPLR	

- <sup>1</sup> Result obtained from the measurement  $\Gamma(K_S^0 \rightarrow \pi e \nu) / \Gamma(K_L^0 \rightarrow \pi e \nu) = 0.993 \pm 0.34$ , neglecting possible *CPT* non-invariance and using PDG 06 values of  $B(K_L^0 \rightarrow \pi e \nu) = 0.4053 \pm 0.0015$ ,  $\tau_L = (5.114 \pm 0.021) \times 10^{-8}$  s and  $\tau_S = (0.8958 \pm 0.0005) \times 10^{-10}$  s.
- <sup>2</sup>  $\text{Re}(x_+)$  can be shown to be equal to the following combination of rates:
- $$\text{Re}(x_+) = \frac{1}{2} \frac{\Gamma(K_S^0 \rightarrow \pi e \nu) - \Gamma(K_L^0 \rightarrow \pi e \nu)}{\Gamma(K_S^0 \rightarrow \pi e \nu) + \Gamma(K_L^0 \rightarrow \pi e \nu)}$$
- which is valid up to first order in terms violating *CPT* and/or the  $\Delta S = \Delta Q$  rule.
- <sup>3</sup> Obtained neglecting *CPT* violating amplitudes.

### $K^0$ REFERENCES

TOMARADZE 14 PR D89 031501	A. Tomaradze <i>et al.</i>	(NWES, WAYN)
PDG 12 PR D86 010001	J. Berlinger <i>et al.</i>	(PDG Collab.)
ABOUZAID 11 PR D83 092001	E. Abouzaid <i>et al.</i>	(FNAL KTeV Collab.)
AMBROSINO 07B JHEP 0712 073	F. Ambrosino <i>et al.</i>	(KLOE Collab.)
BATLEY 07D PL B653 145	J.R. Batley <i>et al.</i>	(CERN NA48 Collab.)
ABOUZAID 06 PRL 96 101801	E. Abouzaid <i>et al.</i>	(KTeV Collab.)
AMBROSINO 06E PL B636 173	F. Ambrosino <i>et al.</i>	(KLOE Collab.)
AMBROSINO 06F PL B638 140	F. Ambrosino <i>et al.</i>	(KLOE Collab.)
AMBROSINO 06H JHEP 0612 011	F. Ambrosino <i>et al.</i>	(KLOE Collab.)
PDG 06 JP G33 1	W.-M. Yao <i>et al.</i>	(PDG Collab.)
AMBROSINO 05B PL B619 61	F. Ambrosino <i>et al.</i>	(KLOE Collab.)
LAI 05A PL B610 165	A. Lai <i>et al.</i>	(CERN NA48 Collab.)
PDG 04 PL B592 1	S. Eidelman <i>et al.</i>	(PDG Collab.)
LAI 03C EPJ C30 33	A. Lai <i>et al.</i>	(CERN NA48 Collab.)
LAI 02 PL B533 196	A. Lai <i>et al.</i>	(CERN NA48 Collab.)
ANGELOPO... 01B EPJ C22 55	A. Angelopoulos <i>et al.</i>	(CLEAR Collab.)
ANGELOPO... 99B PL B471 332	A. Angelopoulos <i>et al.</i>	(CLEAR Collab.)
APOSTOLA... 99B PL B456 297	A. Apostolakis <i>et al.</i>	(CLEAR Collab.)
ANGELOPO... 98D PL B444 38	A. Angelopoulos <i>et al.</i>	(CLEAR Collab.)
Also EPJ C22 55	A. Angelopoulos <i>et al.</i>	(CLEAR Collab.)
ANGELOPO... 98E PL B444 43	A. Angelopoulos <i>et al.</i>	(CLEAR Collab.)
ANGELOPO... 98F PL B444 52	A. Angelopoulos <i>et al.</i>	(CLEAR Collab.)
Also EPJ C22 55	A. Angelopoulos <i>et al.</i>	(CLEAR Collab.)
DEMIDOV 95 PAN 58 968	V. Demidov, K. Gusev, E. Shabalina	(ITEP)
From YAF 58 1041		
THOMSON 95 PR D51 1412	G.B. Thomson, Y. Zou	(RUTG)
BARKOV 87B SJNP 46 630	L.M. Barkov <i>et al.</i>	(NOVO)
Translated from YAF 46 1088,		
BARKOV 85B JETPL 42 138	L.M. Barkov <i>et al.</i>	(NOVO)
Translated from ZETFP 42 113,		
BLATNIK 79 LNC 24 39	S. Blatnik, J. Stahov, C.B. Lang	(TUZL, GRAZ)
MOLZON 78 PRL 41 1213	W.R. Molzon <i>et al.</i>	(EFI+)
NIEBERGALL 74 PL 49B 103	F. Niebergall <i>et al.</i>	(CERN, ORSAY, VIEN)
HART 73 NP B66 317	J.C. Hart <i>et al.</i>	(CAVE, RHUL)
FOETH 69B PL 30B 276	H. Foeth <i>et al.</i>	(AACH, CERN, TORI)
HILL 68B PR 168 1534	D.G. Hill <i>et al.</i>	(BNL, CMU)
FITCH 67 PR 164 1711	V.L. Fitch <i>et al.</i>	(PRIN)
BALTAY 66 PR 142 932	C. Baltay <i>et al.</i>	(YALE, BNL)
BURNSTEIN 65 PR 138 B895	R.A. Burnstein, H.A. Rubin	(UMD)
KIM 65B PR 140 B1334	J.K. Kim, L. Kirsch, D. Miller	(COLU)
CHRISTENS... 64 PRL 13 138	J.H. Christenson <i>et al.</i>	(PRIN)
CRAWFORD 59 PRL 2 112	F.S. Crawford <i>et al.</i>	(LRL)
ROSENFELD 59 PRL 2 110	A.H. Rosenfeld, F.T. Solmitz, R.D. Tripp	(LRL)



$$I(J^P) = \frac{1}{2}(0^-)$$

### $K_S^0$ MEAN LIFE

For earlier measurements, beginning with BOLDT 58B, see our 1986 edition, Physics Letters **170B** 130 (1986).

OUR FIT is described in the note on "*CP* violation in  $K_L$  decays" in the  $K_L^0$  Particle Listings. The result labeled "OUR FIT Assuming *CP T*" ["OUR FIT Not assuming *CP T*"] includes all measurements except those with the comment "Not assuming *CP T*" ["Assuming *CP T*"]. Measurements with neither comment do not assume *CPT* and enter both fits.

VALUE (10 <sup>-10</sup> s)	EVTS	DOCUMENT ID	TECN	COMMENT
<b>0.8954 ± 0.0004 OUR FIT</b>				Error includes scale factor of 1.1. Assuming <i>CPT</i>
<b>0.89564 ± 0.00033 OUR FIT</b>				Not assuming <i>CP T</i>
0.89589 ± 0.00070		<sup>1,2</sup> ABOUZAID 11	KTEV	Not assuming <i>CP T</i>
0.89623 ± 0.00047		<sup>1,3</sup> ABOUZAID 11	KTEV	Assuming <i>CP T</i>
0.89562 ± 0.00029 ± 0.00043	20M	<sup>4</sup> AMBROSINO 11	KLOE	Not assuming <i>CP T</i>
0.89598 ± 0.00048 ± 0.00051	16M	LAI	02c NA48	
0.8971 ± 0.0021		BERTANZA 97	NA31	
0.8941 ± 0.0014 ± 0.0009		SCHWINGEN... 95	E773	Assuming <i>CP T</i>
0.8929 ± 0.0016		GIBBONS 93	E731	Assuming <i>CP T</i>
••• We do not use the following data for averages, fits, limits, etc. •••				
0.8965 ± 0.0007		<sup>5</sup> ALAVI-HARATI 03	KTEV	Assuming <i>CP T</i>
0.8958 ± 0.0013		<sup>6</sup> ALAVI-HARATI 03	KTEV	Not assuming <i>CP T</i>
0.8920 ± 0.0044	214k	GROSSMAN 87	SPEC	
0.905 ± 0.007		<sup>7</sup> ARONSON 82B	SPEC	
0.881 ± 0.009	26k	ARONSON 76	SPEC	
0.8926 ± 0.0032 ± 0.0002		<sup>8</sup> CARITHERS 75	SPEC	
0.8937 ± 0.0048	6M	GEWENGER 74B	ASP K	
0.8958 ± 0.0045	50k	<sup>9</sup> SKJEGGEST... 72	HBC	
0.856 ± 0.008	19994	<sup>10</sup> DONALD 68B	HBC	
0.872 ± 0.009	20000	<sup>9,10</sup> HILL 68	DBC	

- <sup>1</sup> The two ABOUZAID 11 values use the same full KTeV dataset from 1996, 1997, and 1999. The first enters the "assuming *CPT*" fit and the second enters the "not assuming *CP T*" fit.
- <sup>2</sup> ABOUZAID 11 fit has  $\Delta m$ ,  $\tau_S$ ,  $\phi_e$ ,  $\text{Re}(\epsilon'/\epsilon)$ , and  $\text{Im}(\epsilon'/\epsilon)$  as free parameters. See  $\text{Im}(\epsilon'/\epsilon)$  in the " $K_L^0$  *CP* violation" section for correlation information.
- <sup>3</sup> ABOUZAID 11 fit has  $\Delta m$  and  $\tau_S$  free but constrains  $\phi_e$  to the Superweak value, i.e. assumes *CP T*. This  $\tau_S$  value is correlated with their  $\Delta m = m_{K_L^0} - m_{K_S^0}$  measurement in the  $K_L^0$  listings. The correlation coefficient  $\rho(\tau_S, \Delta m) = -0.670$ .
- <sup>4</sup> Fit to the proper time distribution.
- <sup>5</sup> This ALAVI-HARATI 03 fit has  $\Delta m$  and  $\tau_S$  free but constrains  $\phi_{+-}$  to the Superweak value, i.e. assumes *CPT*. This  $\tau_S$  value is correlated with their  $\Delta m = m_{K_L^0} - m_{K_S^0}$  measurement in the  $K_L^0$  listings. The correlation coefficient  $\rho(\tau_S, \Delta m) = -0.396$ . Superseded by ABOUZAID 11.
- <sup>6</sup> This ALAVI-HARATI 03 fit has  $\Delta m$ ,  $\phi_{+-}$ , and  $\tau_{K_S}$  free. See  $\phi_{+-}$  in the " $K_L$  *CP* violation" section for correlation information. Superseded by ABOUZAID 11.
- <sup>7</sup> ARONSON 82 find that  $K_S^0$  mean life may depend on the kaon energy.
- <sup>8</sup> CARITHERS 75 measures the  $\Delta m$  dependence of the total decay rate (inverse mean life) to be  $\Gamma(K_S^0) = [(1.122 \pm 0.004) + 0.16(\Delta m - 0.5348)/\Delta m] 10^{10} / \text{s}$ , or, in terms of mean life, CARITHERS 75 measures  $\tau_S = (0.8913 \pm 0.0032) - 0.238 [\Delta m - 0.5348] (10^{-10} \text{ s})$ . We have adjusted the measurement to use our best values of  $(\Delta m = 0.5293 \pm 0.0009) (10^{10} \text{ h s}^{-1})$ . Our first error is their experiment's error and our second error is the systematic error from using our best values.
- <sup>9</sup> HILL 68 has been changed by the authors from the published value  $(0.865 \pm 0.009)$  because of a correction in the shift due to  $\eta_{+-}$ . SKJEGGESTAD 72 and HILL 68 give detailed discussions of systematics encountered in this type of experiment.
- <sup>10</sup> Pre-1971 experiments are excluded from the average because of disagreement with later more precise experiments.

### $K_S^0$ DECAY MODES

Mode	Fraction ( $\Gamma_i/\Gamma$ )	Scale factor/ Confidence level
<b>Hadronic modes</b>		
$\Gamma_1$ $\pi^0 \pi^0$	(30.69 ± 0.05) %	
$\Gamma_2$ $\pi^+ \pi^-$	(69.20 ± 0.05) %	
$\Gamma_3$ $\pi^+ \pi^- \pi^0$	( 3.5 ± 1.1 - 0.9 ) × 10 <sup>-7</sup>	
<b>Modes with photons or <math>\ell\bar{\ell}</math> pairs</b>		
$\Gamma_4$ $\pi^+ \pi^- \gamma$	[a,b] ( 1.79 ± 0.05 ) × 10 <sup>-3</sup>	
$\Gamma_5$ $\pi^+ \pi^- e^+ e^-$	( 4.79 ± 0.15 ) × 10 <sup>-5</sup>	
$\Gamma_6$ $\pi^0 \gamma \gamma$	[a] ( 4.9 ± 1.8 ) × 10 <sup>-8</sup>	
$\Gamma_7$ $\gamma \gamma$	( 2.63 ± 0.17 ) × 10 <sup>-6</sup>	S=3.0
<b>Semileptonic modes</b>		
$\Gamma_8$ $\pi^\pm e^\mp \nu_e$	[c] ( 7.04 ± 0.08 ) × 10 <sup>-4</sup>	
$\Gamma_9$ $\pi^\pm \mu^\mp \nu_\mu$	[c,d] ( 4.69 ± 0.05 ) × 10 <sup>-4</sup>	

**CP violating (CP) and  $\Delta S = 1$  weak neutral current (S1) modes**

$\Gamma_{10}$	$3\pi^0$	CP	< 2.6	$\times 10^{-8}$	CL=90%
$\Gamma_{11}$	$\mu^+\mu^-$	S1	< 8	$\times 10^{-10}$	CL=90%
$\Gamma_{12}$	$e^+e^-$	S1	< 9	$\times 10^{-9}$	CL=90%
$\Gamma_{13}$	$\pi^0 e^+ e^-$	S1	[a]	$(3.0 \pm_{-1.2}^{+1.5}) \times 10^{-9}$	
$\Gamma_{14}$	$\pi^0 \mu^+ \mu^-$	S1		$(2.9 \pm_{-1.2}^{+1.5}) \times 10^{-9}$	

[a] See the Particle Listings below for the energy limits used in this measurement.

[b] Most of this radiative mode, the low-momentum  $\gamma$  part, is also included in the parent mode listed without  $\gamma$ 's.

[c] The value is for the sum of the charge states or particle/antiparticle states indicated.

[d] Not a measurement. Calculated as  $0.666 \cdot B(\pi^\pm e^\mp \nu_e)$ .

**CONSTRAINED FIT INFORMATION**

An overall fit to 4 branching ratios uses 5 measurements and one constraint to determine 4 parameters. The overall fit has a  $\chi^2 = 0.1$  for 2 degrees of freedom.

The following *off-diagonal* array elements are the correlation coefficients  $\langle \delta x_i \delta x_j \rangle / (\delta x_i \delta x_j)$ , in percent, from the fit to the branching fractions,  $x_i \equiv \Gamma_i / \Gamma_{\text{total}}$ . The fit constrains the  $x_i$  whose labels appear in this array to sum to one.

$x_2$	-100		
$x_8$	-6	3	
$x_9$	-6	3	100
	$x_1$	$x_2$	$x_8$

**$K_S^0$  DECAY RATES**

$\Gamma(\pi^\pm e^\mp \nu_e)$	$\Gamma_8$			
VALUE ( $10^6 \text{ s}^{-1}$ )	EVTS	DOCUMENT ID	TECN	COMMENT

8.1 $\pm$ 1.6	75	1 AKHMETSHIN 99	CMD2	Tagged $K_S^0$ using $\phi \rightarrow K_L^0 K_S^0$
7.50 $\pm$ 0.08		2 PDG	98	
seen		BURGUN 72	HBC	$K^+ p \rightarrow K^0 p \pi^+$
9.3 $\pm$ 2.5		AUBERT 65	HLBC	$\Delta S = \Delta Q$ , CP cons. not assumed

1 AKHMETSHIN 99 is from a measured branching ratio  $B(K_S^0 \rightarrow \pi e \nu_e) = (7.2 \pm 1.4) \times 10^{-4}$  and  $\tau_{K_S^0} = (0.8934 \pm 0.0008) \times 10^{-10}$  s. Not independent of measured branching ratio.

2 PDG 98 from  $K_L^0$  measurements, assuming that  $\Delta S = \Delta Q$  in  $K^0$  decay so that  $\Gamma(K_S^0 \rightarrow \pi^\pm e^\mp \nu_e) = \Gamma(K_L^0 \rightarrow \pi^\pm e^\mp \nu_e)$ .

$\Gamma(\pi^\pm \mu^\mp \nu_\mu)$	$\Gamma_9$		
VALUE ( $10^6 \text{ s}^{-1}$ )	DOCUMENT ID	TECN	COMMENT

5.25 $\pm$ 0.07	1 PDG	98	
-----------------	-------	----	--

1 PDG 98 from  $K_L^0$  measurements, assuming that  $\Delta S = \Delta Q$  in  $K^0$  decay so that  $\Gamma(K_S^0 \rightarrow \pi^\pm \mu^\mp \nu_\mu) = \Gamma(K_L^0 \rightarrow \pi^\pm \mu^\mp \nu_\mu)$ .

**$K_S^0$  BRANCHING RATIOS**

**Hadronic modes**

$\Gamma(\pi^0 \pi^0) / \Gamma_{\text{total}}$	$\Gamma_1 / \Gamma$			
VALUE	EVTS	DOCUMENT ID	TECN	COMMENT

0.3069 $\pm$ 0.0005	<b>OUR FIT</b>			
0.335 $\pm$ 0.014	1066	BROWN 63	HLBC	
0.288 $\pm$ 0.021	198	CHRETIEN 63	HLBC	
0.30 $\pm$ 0.035		BROWN 61	HLBC	

$\Gamma(\pi^+ \pi^-) / \Gamma_{\text{total}}$	$\Gamma_2 / \Gamma$			
VALUE	EVTS	DOCUMENT ID	TECN	COMMENT

0.670 $\pm$ 0.010	3447	DOYLE 69	HBC	$\pi^- p \rightarrow \Lambda K^0$
-------------------	------	----------	-----	-----------------------------------

$\Gamma(\pi^+ \pi^-) / \Gamma(\pi^0 \pi^0)$	$\Gamma_2 / \Gamma_1$			
VALUE	EVTS	DOCUMENT ID	TECN	COMMENT

2.255 $\pm$ 0.005	<b>OUR FIT</b>			
2.2549 $\pm$ 0.0054		1 AMBROSINO 06c	KLOE	

• • • We do not use the following data for averages, fits, limits, etc. • • •

2.2555 $\pm$ 0.0012 $\pm$ 0.0054	2 AMBROSINO 06c	KLOE
2.236 $\pm$ 0.003 $\pm$ 0.015	2 ALOISIO 02b	KLOE
2.11 $\pm$ 0.09	1315	EVERHART 76
2.169 $\pm$ 0.094	16k	COWELL 74
2.16 $\pm$ 0.08	4799	HILL 73
2.22 $\pm$ 0.10	3068	3 ALITTI 72
2.22 $\pm$ 0.08	6380	MORSE 72b
2.10 $\pm$ 0.11	701	4 NAGY 72
2.22 $\pm$ 0.095	6150	5 BALTAY 71
2.282 $\pm$ 0.043	7944	6 MOFFETT 70
2.12 $\pm$ 0.17	267	4 BOZOKI 69
2.285 $\pm$ 0.055	3016	6 GOBBI 69
2.10 $\pm$ 0.06	3700	MORFIN 69

1 This result combines AMBROSINO 06c KLOE 2001-02 data with ALOISIO 02b KLOE 2000 data.  $K_S^0 \rightarrow \pi^+ \pi^-$  fully inclusive.

2 Includes radiative decays  $\pi^+ \pi^- \gamma$ .

3 The directly measured quantity is  $K_S^0 \rightarrow \pi^+ \pi^- / \text{all } K^0 = 0.345 \pm 0.005$ .

4 NAGY 72 is a final result which includes BOZOKI 69.

5 The directly measured quantity is  $K_S^0 \rightarrow \pi^+ \pi^- / \text{all } \pi^0 = 0.345 \pm 0.005$ .

6 MOFFETT 70 is a final result which includes GOBBI 69.

$\Gamma(\pi^+ \pi^- \pi^0) / \Gamma_{\text{total}}$	$\Gamma_3 / \Gamma$			
VALUE (units $10^{-7}$ )	EVTS	DOCUMENT ID	TECN	COMMENT

3.5 $\pm$ 1.1	<b>OUR AVERAGE</b>			
4.7 $\pm$ 1.7	1	BATLEY 05	NA48	
2.5 $\pm$ 1.3	500k	2 ADLER 97b	CPLR	
4.8 $\pm$ 2.2		3 ZOU 96	E621	

• • • We do not use the following data for averages, fits, limits, etc. • • •

4.1 $\pm$ 2.5		4 ADLER 96e	CPLR	Sup. by ADLER 97b
3.9 $\pm$ 5.4		5 THOMSON 94	E621	Sup. by ZOU 96

1 BATLEY 05 is obtained by measuring the interference parameters in  $K_S, K_L \rightarrow \pi^+ \pi^- \pi^0$ .  $\text{Re}(\lambda) = 0.038 \pm 0.008 \pm 0.006$  and  $\text{Im}(\lambda) = -0.013 \pm 0.005 \pm 0.004$ ; the correlation coeff. between  $\text{Re}(\lambda)$  and  $\text{Im}(\lambda)$  is 0.66 (statistical only).

2 ADLER 97b find the CP-conserving parameters  $\text{Re}(\lambda) = (28 \pm 7 \pm 3) \times 10^{-3}$ ,  $\text{Im}(\lambda) = (-10 \pm 8 \pm 2) \times 10^{-3}$ . They estimate  $B(K_S^0 \rightarrow \pi^+ \pi^- \pi^0)$  from  $\text{Re}(\lambda)$  and the  $K_L^0$  decay parameters. See also ANGELOPOULOS 98c.

3 ZOU 96 is from the the measured quantities  $|\rho_{+-0}| = 0.039 \pm_{-0.006}^{+0.009} \pm 0.005$  and  $\phi_\rho = (-9 \pm 18)^\circ$ .

4 ADLER 96e is from the measured quantities  $\text{Re}(\lambda) = 0.036 \pm 0.010 \pm_{-0.005}^{+0.002}$  and  $\text{Im}(\lambda)$  consistent with zero. Note that the quantity  $\lambda$  is the same as  $\rho_{+-0}$  used in other footnotes.

5 THOMSON 94 calculates this branching ratio from their measurements  $|\rho_{+-0}| = 0.035 \pm_{-0.011}^{+0.019} \pm 0.004$  and  $\phi_\rho = (-59 \pm 48)^\circ$  where  $|\rho_{+-0}| e^{i\phi_\rho} = A(K_S^0 \rightarrow \pi^+ \pi^- \pi^0, I = 2) / A(K_L^0 \rightarrow \pi^+ \pi^- \pi^0)$ .

**Modes with photons or  $\ell\bar{\ell}$  pairs**

$\Gamma(\pi^+ \pi^- \gamma) / \Gamma(\pi^+ \pi^-)$	$\Gamma_4 / \Gamma_2$			
VALUE (units $10^{-3}$ )	EVTS	DOCUMENT ID	TECN	COMMENT

2.59 $\pm$ 0.08	<b>OUR AVERAGE</b>			
2.56 $\pm$ 0.09	1286	RAMBERG 93	E731	$p_\gamma > 50$ MeV/c
2.68 $\pm$ 0.15		1 TAUREG 76	SPEC	$p_\gamma > 50$ MeV/c
7.10 $\pm$ 0.22	3723	RAMBERG 93	E731	$p_\gamma > 20$ MeV/c
3.0 $\pm$ 0.6	29	2 BOBISUT 74	HLBC	$p_\gamma > 40$ MeV/c
2.8 $\pm$ 0.6		3 BURGUN 73	HBC	$p_\gamma > 50$ MeV/c

1 TAUREG 76 find direct emission contribution  $< 0.06$ , CL = 90%.

2 BOBISUT 74 not included in average because  $p_\gamma$  cut differs. Estimates direct emission contribution to be 0.5 or less, CL = 95%.

3 BURGUN 73 estimates that direct emission contribution is  $0.3 \pm 0.6$ .

$\Gamma(\pi^+ \pi^- e^+ e^-) / \Gamma_{\text{total}}$	$\Gamma_5 / \Gamma$			
VALUE (units $10^{-5}$ )	EVTS	DOCUMENT ID	TECN	COMMENT

4.79 $\pm$ 0.15	<b>OUR AVERAGE</b>			
4.83 $\pm$ 0.11 $\pm$ 0.14	23k	1 BATLEY 11	NA48	2002 data
4.69 $\pm$ 0.30	676	2 LAI 03c	NA48	1998+1999 data
4.71 $\pm$ 0.23 $\pm$ 0.22	620	2,3 LAI 03c	NA48	1999 data
4.5 $\pm$ 0.7 $\pm$ 0.4	56	LAI 00b	NA48	1998 data

1 BATLEY 11 reports  $[\Gamma(K_S^0 \rightarrow \pi^+ \pi^- e^+ e^-) / \Gamma_{\text{total}}] / [B(K_L^0 \rightarrow \pi^+ \pi^- \pi^0) / B(\pi^0 \rightarrow e^+ e^- \gamma)] = (3.28 \pm 0.06 \pm 0.04) \times 10^{-2}$  which we multiply by our best values  $B(K_L^0 \rightarrow \pi^+ \pi^- \pi^0) = (12.54 \pm 0.05) \times 10^{-2}$ ,  $B(\pi^0 \rightarrow e^+ e^- \gamma) = (1.174 \pm 0.035) \times 10^{-2}$ . Our first error is their experiment's error and our second error is the systematic error from using our best values. Also a limit on the absolute value of the interference between bremsstrahlung and E1 transition is given :  $< 4 \times 10^{-7}$  at 90% CL.

2 Uses normalization  $\text{BR}(K_L \rightarrow \pi^+ \pi^- \pi^0) * \text{BR}(\pi^0 \rightarrow e^+ e^-) = (1.505 \pm 0.047) \times 10^{-3}$  from our 2000 Edition.

3 Second error is  $0.16(\text{sys}) \pm 0.15(\text{norm})$  combined in quadrature.



**CP VIOLATION IN  $K_S \rightarrow 3\pi$**

Written 1996 by T. Nakada (Paul Scherrer Institute) and L. Wolfenstein (Carnegie-Mellon University).

The possible final states for the decay  $K^0 \rightarrow \pi^+\pi^-\pi^0$  have isospin  $I = 0, 1, 2$ , and  $3$ . The  $I = 0$  and  $I = 2$  states have  $CP = +1$  and  $K_S$  can decay into them without violating  $CP$  symmetry, but they are expected to be strongly suppressed by centrifugal barrier effects. The  $I = 1$  and  $I = 3$  states, which have no centrifugal barrier, have  $CP = -1$  so that the  $K_S$  decay to these requires  $CP$  violation.

In order to see  $CP$  violation in  $K_S \rightarrow \pi^+\pi^-\pi^0$ , it is necessary to observe the interference between  $K_S$  and  $K_L$  decay, which determines the amplitude ratio

$$\eta_{+-0} = \frac{A(K_S \rightarrow \pi^+\pi^-\pi^0)}{A(K_L \rightarrow \pi^+\pi^-\pi^0)} \quad (1)$$

If  $\eta_{+-0}$  is obtained from an integration over the whole Dalitz plot, there is no contribution from the  $I = 0$  and  $I = 2$  final states and a nonzero value of  $\eta_{+-0}$  is entirely due to  $CP$  violation.

Only  $I = 1$  and  $I = 3$  states, which are  $CP = -1$ , are allowed for  $K^0 \rightarrow \pi^0\pi^0\pi^0$  decays and the decay of  $K_S$  into  $3\pi^0$  is an unambiguous sign of  $CP$  violation. Similarly to  $\eta_{+-0}$ ,  $\eta_{000}$  is defined as

$$\eta_{000} = \frac{A(K_S \rightarrow \pi^0\pi^0\pi^0)}{A(K_L \rightarrow \pi^0\pi^0\pi^0)} \quad (2)$$

If one assumes that  $CPT$  invariance holds and that there are no transitions to  $I = 3$  (or to nonsymmetric  $I = 1$  states), it can be shown that

$$\eta_{+-0} = \eta_{000} = \epsilon + i \frac{\text{Im } a_1}{\text{Re } a_1} \quad (3)$$

With the Wu-Yang phase convention,  $a_1$  is the weak decay amplitude for  $K^0$  into  $I = 1$  final states;  $\epsilon$  is determined from  $CP$  violation in  $K_L \rightarrow 2\pi$  decays. The real parts of  $\eta_{+-0}$  and  $\eta_{000}$  are equal to  $\text{Re}(\epsilon)$ . Since currently-known upper limits on  $|\eta_{+-0}|$  and  $|\eta_{000}|$  are much larger than  $|\epsilon|$ , they can be interpreted as upper limits on  $\text{Im}(\eta_{+-0})$  and  $\text{Im}(\eta_{000})$  and so as limits on the  $CP$ -violating phase of the decay amplitude  $a_1$ .

**CP-VIOLATION PARAMETERS IN  $K_S^0$  DECAY**

$$A_S = [\Gamma(K_S^0 \rightarrow \pi^- e^+ \nu_e) - \Gamma(K_S^0 \rightarrow \pi^+ e^- \bar{\nu}_e)] / \text{SUM}$$

Such asymmetry violates  $CP$ . If  $CPT$  is assumed then  $A_S = 2 \text{Re}(\epsilon)$ .

VALUE (units $10^{-3}$ )	EVTS	DOCUMENT ID	TECN
<b>-3.8 ± 5.0 ± 2.6</b>	83K	<sup>1</sup> ANASTASI 18A	KLOE
••• We do not use the following data for averages, fits, limits, etc. •••			
1.5 ± 9.6 ± 2.9	13k	AMBROSINO 06E	KLOE

<sup>1</sup> ANASTASI 18A result is a combination of the new measurement and AMBROSINO 06E. The new ANASTASI 18A measurement using data collected from 2004–2005, which corresponds to an integrated luminosity of  $1.63 \text{ fb}^{-1}$  is  $A_S = (-4.9 \pm 5.7 \pm 2.6) \times 10^{-3}$ .

**PARAMETERS FOR  $K_S^0 \rightarrow 3\pi$  DECAY**

$$\text{Im}(\eta_{+-0})^2 = \Gamma(K_S^0 \rightarrow \pi^+\pi^-\pi^0, CP\text{-violating}) / \Gamma(K_L^0 \rightarrow \pi^+\pi^-\pi^0)$$

$CPT$  assumed valid (i.e.  $\text{Re}(\eta_{+-0}) \simeq 0$ ).

VALUE	CL%	EVTS	DOCUMENT ID	TECN
••• We do not use the following data for averages, fits, limits, etc. •••				
<0.23	90	601	<sup>1</sup> BARMIN 85	HLBC
<0.12	90	384	METCALF 72	ASPK

<sup>1</sup> BARMIN 85 find  $\text{Re}(\eta_{+-0}) = (0.05 \pm 0.17)$  and  $\text{Im}(\eta_{+-0}) = (0.15 \pm 0.33)$ . Includes events of BALDO-CEOLIN 75.

$$\text{Im}(\eta_{+-0}) = \text{Im}(A(K_S^0 \rightarrow \pi^+\pi^-\pi^0, CP\text{-violating}) / A(K_L^0 \rightarrow \pi^+\pi^-\pi^0))$$

VALUE	CL%	EVTS	DOCUMENT ID	TECN	COMMENT
<b>-0.002 ± 0.009 ± 0.002 - 0.001</b>		500k	<sup>1</sup> ADLER	97B	CPLR
••• We do not use the following data for averages, fits, limits, etc. •••					
-0.002 ± 0.018 ± 0.003		137k	<sup>2</sup> ADLER	96D	CPLR Sup. by ADLER 97B
-0.015 ± 0.017 ± 0.025		272k	<sup>3</sup> ZOU	94	SPEC
<sup>1</sup> ADLER 97B also find $\text{Re}(\eta_{+-0}) = -0.002 \pm 0.007 \pm 0.004 - 0.001$ . See also ANGELOPOULOS 98C.					
<sup>2</sup> The ADLER 96D fit also yields $\text{Re}(\eta_{+-0}) = 0.006 \pm 0.013 \pm 0.001$ with a correlation +0.66 between real and imaginary parts. Their results correspond to $ \eta_{+-0}  < 0.037$ with 90% CL.					
<sup>3</sup> ZOU 94 use theoretical constraint $\text{Re}(\eta_{+-0}) = \text{Re}(\epsilon) = 0.0016$ . Without this constraint they find $\text{Im}(\eta_{+-0}) = 0.019 \pm 0.061$ and $\text{Re}(\eta_{+-0}) = 0.019 \pm 0.027$ .					

$$\text{Im}(\eta_{000})^2 = \Gamma(K_S^0 \rightarrow 3\pi^0) / \Gamma(K_L^0 \rightarrow 3\pi^0)$$

$CPT$  assumed valid (i.e.  $\text{Re}(\eta_{000}) \simeq 0$ ). This limit determines branching ratio  $\Gamma(3\pi^0)/\Gamma_{\text{total}}$  above.

VALUE	CL%	EVTS	DOCUMENT ID	TECN	COMMENT
••• We do not use the following data for averages, fits, limits, etc. •••					
<0.1	90	632	<sup>1</sup> BARMIN 83	HLBC	
<0.28	90		<sup>2</sup> GJESDAL 74B	SPEC	Indirect meas.
<sup>1</sup> BARMIN 83 find $\text{Re}(\eta_{000}) = (-0.08 \pm 0.18)$ and $\text{Im}(\eta_{000}) = (-0.05 \pm 0.27)$ . Assuming $CPT$ invariance they obtain the limit quoted above.					
<sup>2</sup> GJESDAL 74B uses $K_{2\pi}, K_{\mu 3}$ , and $K_{e3}$ decay results, unitarity, and $CPT$ . Calculates $ \langle \eta_{000} \rangle  = 0.26 \pm 0.20$ . We convert to upper limit.					

$$\text{Im}(\eta_{000}) = \text{Im}(A(K_S^0 \rightarrow \pi^0\pi^0\pi^0) / A(K_L^0 \rightarrow \pi^0\pi^0\pi^0))$$

$K_S^0 \rightarrow \pi^0\pi^0\pi^0$  violates  $CP$  conservation, in contrast to  $K_S^0 \rightarrow \pi^+\pi^-\pi^0$  which has a  $CP$ -conserving part.

VALUE	CL%	EVTS	DOCUMENT ID	TECN	COMMENT
<b>-0.001 ± 0.016 OUR AVERAGE</b>					
0.000 ± 0.009 ± 0.013		4.9M	<sup>1</sup> LAI 05A	NA48	Assumes $CPT$
-0.05 ± 0.12 ± 0.05		17300	<sup>2</sup> ANGELOPOULOS 98B	CPLR	Assumes $CPT$
<sup>1</sup> LAI 05A assumes $\text{Re}(\eta_{000}) = \text{Re}(\epsilon) = 1.66 \times 10^{-3}$ . The equivalent limit is $ \eta_{000} _{CPT} < 0.025$ at 90% CL. Without assuming $CPT$ invariance, they obtain $\text{Re}(\eta_{000}) = -0.002 \pm 0.011 \pm 0.015$ and $\text{Im}(\eta_{000}) = -0.003 \pm 0.013 \pm 0.017$ with a statistical correlation coefficient of 0.77 and an overall correlation coefficient of 0.57 between imaginary and real part. The equivalent limit is $ \eta_{000}  < 0.045$ at 90% CL.					
<sup>2</sup> ANGELOPOULOS 98B assumes $\text{Re}(\eta_{000}) = \text{Re}(\epsilon) = 1.635 \times 10^{-3}$ . Without assuming $CPT$ invariance, they obtain $\text{Re}(\eta_{000}) = 0.18 \pm 0.14 \pm 0.06$ and $\text{Im}(\eta_{000}) = 0.15 \pm 0.20 \pm 0.03$ .					

$$|\eta_{000}| = |A(K_S^0 \rightarrow 3\pi^0) / A(K_L^0 \rightarrow 3\pi^0)|$$

A non-zero value violates  $CP$  invariance.

VALUE	CL%	EVTS	DOCUMENT ID	TECN	COMMENT
<b>&lt;0.0088</b>		90 590M	BABUSCI	13C	KLOE
••• We do not use the following data for averages, fits, limits, etc. •••					
<0.018	90	37.8M	AMBROSINO 05B	KLOE	
<0.045	90	4.9M	LAI 05A	NA48	

**DECAY-PLANE ASYMMETRY IN  $\pi^+\pi^-e^+e^-$  DECAYS**

This is the  $CP$ -violating asymmetry

$$A = \frac{N_{\sin\phi\cos\phi>0.0} - N_{\sin\phi\cos\phi<0.0}}{N_{\sin\phi\cos\phi>0.0} + N_{\sin\phi\cos\phi<0.0}}$$

where  $\phi$  is the angle between the  $e^+e^-$  and  $\pi^+\pi^-$  planes in the  $K_S^0$  rest frame.

$$CP \text{ asymmetry } A \text{ in } K_S^0 \rightarrow \pi^+\pi^-e^+e^-$$

VALUE (%)	DOCUMENT ID	TECN	COMMENT
<b>-0.4 ± 0.8 OUR AVERAGE</b>			
-0.4 ± 0.8	<sup>1</sup> BATLEY 11	NA48	2002 data
-1.1 ± 4.1	LAI 03C	NA48	1998+1999 data
••• We do not use the following data for averages, fits, limits, etc. •••			
0.5 ± 4.0 ± 1.6	LAI 03C	NA48	1999 data
<sup>1</sup> The result is used to set the limit $A < 1.5\%$ at 90% C.L.			

**$K_S^0$  REFERENCES**

ANASTASI 18A	JHEP 1809 021	A. Anastasi et al.	(KLOE-2 Collab.)
AJAI 17BQ	EPJ C77 678	R. Ajai et al.	(LHCb Collab.)
PDG 16	CP C40 100001	C. Patrignani et al.	(PDG Collab.)
AJAI 13G	JHEP 1301 090	R. Ajai et al.	(LHCb Collab.)
BABUSCI 13C	PL B723 54	D. Babusci et al.	(KLOE-2 Collab.)
ABOUZAID 11	PR D83 092001	E. Abouzaid et al.	(FNAL KTeV Collab.)
AMBROSINO 11	EPJ C71 1604	F. Ambrosino et al.	(KLOE Collab.)
BATLEY 11	PL B694 301	J.R. Batley et al.	(CERN NA48/1 Collab.)
AMBROSINO 09A	PL B672 203	F. Ambrosino et al.	(KLOE Collab.)
AMBROSINO 08C	JHEP 0805 051	F. Ambrosino et al.	(KLOE Collab.)
ANDRE 07	ANP 322 2518	T. Andre	(EFT)
BATLEY 07D	PL B653 145	J.R. Batley et al.	(CERN NA48 Collab.)
AMBROSINO 06C	EPJ C48 767	F. Ambrosino et al.	(KLOE Collab.)
AMBROSINO 06E	PL B636 173	F. Ambrosino et al.	(KLOE Collab.)
PDG 06	JP G33 1	W.-M. Yao et al.	(PDG Collab.)
AMBROSINO 05B	PL B619 61	F. Ambrosino et al.	(KLOE Collab.)
BATLEY 05	PL B630 31	J.R. Batley et al.	(NA48 Collab.)
LAI 05A	PL B610 165	A. Lai et al.	(CERN NA48 Collab.)
ALEXOPOU... 04A	PR D70 092007	T. Alexopoulos et al.	(FNAL KTeV Collab.)
BATLEY 04A	PL B599 197	J.R. Batley et al.	(NA48 Collab.)
LAI 04	PL B578 276	A. Lai et al.	(CERN NA48 Collab.)



See key on page 999

Meson Particle Listings

$K_L^0$

$\Gamma_2$	$\pi^\pm \mu^\mp \nu_\mu$ Called $K_{\mu 3}^0$ .	[a]	$(27.04 \pm 0.07) \%$	S=1.1
------------	---	-----	-----------------------	-------

$\Gamma_3$	$(\pi \mu \text{atom}) \nu$		$(1.05 \pm 0.11) \times 10^{-7}$	
$\Gamma_4$	$\pi^0 \pi^\pm e^\mp \nu$	[a]	$(5.20 \pm 0.11) \times 10^{-5}$	
$\Gamma_5$	$\pi^\pm e^\mp \nu e^+ e^-$	[a]	$(1.26 \pm 0.04) \times 10^{-5}$	

**Hadronic modes, including Charge conjugation  $\times$  Parity Violating (CPV) modes**

$\Gamma_6$	$3\pi^0$		$(19.52 \pm 0.12) \%$	S=1.6
$\Gamma_7$	$\pi^+ \pi^- \pi^0$		$(12.54 \pm 0.05) \%$	
$\Gamma_8$	$\pi^+ \pi^-$	CPV [b]	$(1.967 \pm 0.010) \times 10^{-3}$	S=1.5
$\Gamma_9$	$\pi^0 \pi^0$	CPV	$(8.64 \pm 0.06) \times 10^{-4}$	S=1.8

**Semileptonic modes with photons**

$\Gamma_{10}$	$\pi^\pm e^\mp \nu_e \gamma$	[a,c,d]	$(3.79 \pm 0.06) \times 10^{-3}$	
$\Gamma_{11}$	$\pi^\pm \mu^\mp \nu_\mu \gamma$		$(5.65 \pm 0.23) \times 10^{-4}$	

**Hadronic modes with photons or  $\ell\bar{\ell}$  pairs**

$\Gamma_{12}$	$\pi^0 \pi^0 \gamma$		$< 2.43 \times 10^{-7}$	CL=90%
$\Gamma_{13}$	$\pi^+ \pi^- \gamma$	[c,d]	$(4.15 \pm 0.15) \times 10^{-5}$	S=2.8
$\Gamma_{14}$	$\pi^+ \pi^- \gamma$ (DE)		$(2.84 \pm 0.11) \times 10^{-5}$	S=2.0
$\Gamma_{15}$	$\pi^0 2\gamma$	[c]	$(1.273 \pm 0.033) \times 10^{-6}$	
$\Gamma_{16}$	$\pi^0 \gamma e^+ e^-$		$(1.62 \pm 0.17) \times 10^{-8}$	

**Other modes with photons or  $\ell\bar{\ell}$  pairs**

$\Gamma_{17}$	$2\gamma$		$(5.47 \pm 0.04) \times 10^{-4}$	S=1.1
$\Gamma_{18}$	$3\gamma$		$< 7.4 \times 10^{-8}$	CL=90%
$\Gamma_{19}$	$e^+ e^- \gamma$		$(9.4 \pm 0.4) \times 10^{-6}$	S=2.0
$\Gamma_{20}$	$\mu^+ \mu^- \gamma$		$(3.59 \pm 0.11) \times 10^{-7}$	S=1.3
$\Gamma_{21}$	$e^+ e^- \gamma \gamma$	[c]	$(5.95 \pm 0.33) \times 10^{-7}$	
$\Gamma_{22}$	$\mu^+ \mu^- \gamma \gamma$	[c]	$(1.0 \pm_{-0.6}^{+0.8}) \times 10^{-8}$	

**Charge conjugation  $\times$  Parity (CP) or Lepton Family number (LF) violating modes, or  $\Delta S = 1$  weak neutral current (SI) modes**

$\Gamma_{23}$	$\mu^+ \mu^-$	SI	$(6.84 \pm 0.11) \times 10^{-9}$	
$\Gamma_{24}$	$e^+ e^-$	SI	$(9 \pm_{-4}^{+6}) \times 10^{-12}$	
$\Gamma_{25}$	$\pi^+ \pi^- e^+ e^-$	SI [c]	$(3.11 \pm 0.19) \times 10^{-7}$	
$\Gamma_{26}$	$\pi^0 \pi^0 e^+ e^-$	SI	$< 6.6 \times 10^{-9}$	CL=90%
$\Gamma_{27}$	$\pi^0 \pi^0 \mu^+ \mu^-$	SI	$< 9.2 \times 10^{-11}$	CL=90%
$\Gamma_{28}$	$\mu^+ \mu^- e^+ e^-$	SI	$(2.69 \pm 0.27) \times 10^{-9}$	
$\Gamma_{29}$	$e^+ e^- e^+ e^-$	SI	$(3.56 \pm 0.21) \times 10^{-8}$	
$\Gamma_{30}$	$\pi^0 \mu^+ \mu^-$	CP,SI [e]	$< 3.8 \times 10^{-10}$	CL=90%
$\Gamma_{31}$	$\pi^0 e^+ e^-$	CP,SI [e]	$< 2.8 \times 10^{-10}$	CL=90%
$\Gamma_{32}$	$\pi^0 \nu \bar{\nu}$	CP,SI [f]	$< 3.0 \times 10^{-9}$	CL=90%
$\Gamma_{33}$	$\pi^0 \pi^0 \nu \bar{\nu}$	SI	$< 8.1 \times 10^{-7}$	CL=90%
$\Gamma_{34}$	$e^\pm \mu^\mp$	LF [a]	$< 4.7 \times 10^{-12}$	CL=90%
$\Gamma_{35}$	$e^\pm e^\pm \mu^\mp \mu^\mp$	LF [a]	$< 4.12 \times 10^{-11}$	CL=90%
$\Gamma_{36}$	$\pi^0 \mu^\pm e^\mp$	LF [a]	$< 7.6 \times 10^{-11}$	CL=90%
$\Gamma_{37}$	$\pi^0 \pi^0 \mu^\pm e^\mp$	LF	$< 1.7 \times 10^{-10}$	CL=90%

- [a] The value is for the sum of the charge states or particle/antiparticle states indicated.
- [b] This mode includes gammas from inner bremsstrahlung but not the direct emission mode  $K_L^0 \rightarrow \pi^+ \pi^- \gamma$  (DE).
- [c] See the Particle Listings below for the energy limits used in this measurement.
- [d] Most of this radiative mode, the low-momentum  $\gamma$  part, is also included in the parent mode listed without  $\gamma$ 's.
- [e] Allowed by higher-order electroweak interactions.
- [f] Violates CP in leading order. Test of direct CP violation since the indirect CP-violating and CP-conserving contributions are expected to be suppressed.

**CONSTRAINED FIT INFORMATION**

An overall fit to the mean life and 15 branching ratios uses 27 measurements and one constraint to determine 11 parameters. The overall fit has a  $\chi^2 = 37.4$  for 17 degrees of freedom.

The following *off-diagonal* array elements are the correlation coefficients  $\langle \delta p_i \delta p_j \rangle / (\delta p_i \delta p_j)$ , in percent, from the fit to parameters  $p_i$ , including the branching fractions,  $x_i \equiv \Gamma_i / \Gamma_{\text{total}}$ . The fit constrains the  $x_i$  whose labels appear in this array to sum to one.

$x_2$	-21									
$x_6$	-77	-29								
$x_7$	-15	-20	-18							
$x_8$	53	-11	-47	4						
$x_9$	30	-23	-11	-12	64					
$x_{13}$	6	-1	-6	0	12	8				
$x_{14}$	6	-1	-6	0	11	7	93			
$x_{17}$	-46	-22	64	-14	-21	8	-3	-3		
$x_{19}$	-5	-2	7	-1	-3	-1	0	0	4	
$\Gamma$	-27	-9	24	15	-13	-6	-2	-2	15	2

Mode	Rate ( $10^8 \text{ s}^{-1}$ )	Scale factor
$\Gamma_1$ $\pi^\pm e^\mp \nu_e$ Called $K_{e3}^0$ .	[a] 0.07927 $\pm$ 0.00034	1.1
$\Gamma_2$ $\pi^\pm \mu^\mp \nu_\mu$ Called $K_{\mu 3}^0$ .	[a] 0.05286 $\pm$ 0.00025	1.1
$\Gamma_6$ $3\pi^0$	0.03815 $\pm$ 0.00030	1.5
$\Gamma_7$ $\pi^+ \pi^- \pi^0$	0.02451 $\pm$ 0.00015	
$\Gamma_8$ $\pi^+ \pi^-$	[b] (3.844 $\pm$ 0.023) $\times 10^{-4}$	1.2
$\Gamma_9$ $\pi^0 \pi^0$	(1.690 $\pm$ 0.013) $\times 10^{-4}$	1.4
$\Gamma_{13}$ $\pi^+ \pi^- \gamma$	[c,d] (8.11 $\pm$ 0.29) $\times 10^{-6}$	2.7
$\Gamma_{14}$ $\pi^+ \pi^- \gamma$ (DE)	(5.55 $\pm$ 0.21) $\times 10^{-6}$	2.0
$\Gamma_{17}$ $2\gamma$	(1.069 $\pm$ 0.010) $\times 10^{-4}$	1.2
$\Gamma_{19}$ $e^+ e^- \gamma$	(1.84 $\pm$ 0.08) $\times 10^{-6}$	1.9

**$K_L^0$  DECAY RATES**

**$\Gamma(\pi^+ \pi^- \pi^0)$   $\Gamma_7$**

VALUE ( $10^6 \text{ s}^{-1}$ )	EVTS	DOCUMENT ID	TECN	COMMENT
<b>2.451 <math>\pm</math> 0.015 OUR FIT</b>				
• • • We do not use the following data for averages, fits, limits, etc. • • •				
2.32 $\pm_{-0.15}^{+0.13}$	192	BALDO...	75	HLBC Assumes CP
2.35 $\pm$ 0.20	180	<sup>1</sup> JAMES	72	HBC Assumes CP
2.71 $\pm$ 0.28	99	CHO	71	DBC Assumes CP
2.5 $\pm$ 0.3	98	<sup>1</sup> JAMES	71	HBC Assumes CP
2.12 $\pm$ 0.33	50	MEISNER	71	HBC Assumes CP
2.20 $\pm$ 0.35	53	WEBBER	70	HBC Assumes CP
2.62 $\pm_{-0.27}^{+0.28}$	136	BEHR	66	HLBC Assumes CP
3.26 $\pm$ 0.77	18	ANDERSON	65	HBC
1.4 $\pm$ 0.4	14	FRANZINI	65	HBC
<sup>1</sup> JAMES 72 is a final measurement and includes JAMES 71.				

**$\Gamma(\pi^\pm e^\mp \nu_e)$   $\Gamma_1$**

VALUE ( $10^6 \text{ s}^{-1}$ )	EVTS	DOCUMENT ID	TECN	COMMENT
<b>7.927 <math>\pm</math> 0.034 OUR FIT</b>				Error includes scale factor of 1.1.
• • • We do not use the following data for averages, fits, limits, etc. • • •				
7.81 $\pm$ 0.56	620	CHAN	71	HBC
7.52 $\pm_{-0.72}^{+0.85}$		AUBERT	65	HLBC $\Delta S = \Delta Q$ , CP assumed

**$\Gamma(\pi^\pm e^\mp \nu_e) + \Gamma(\pi^\pm \mu^\mp \nu_\mu)$   $(\Gamma_1 + \Gamma_2)$**

VALUE ( $10^6 \text{ s}^{-1}$ )	EVTS	DOCUMENT ID	TECN	COMMENT
<b>13.21 <math>\pm</math> 0.05 OUR FIT</b>				
• • • We do not use the following data for averages, fits, limits, etc. • • •				
12.4 $\pm$ 0.7	410	<sup>1</sup> BURGUN	72	HBC $K^+ p \rightarrow K^0 p \pi^+$
8.47 $\pm$ 1.69	126	<sup>1</sup> MANN	72	HBC $K^- p \rightarrow n \bar{K}^0$
13.1 $\pm$ 1.3	252	<sup>1</sup> WEBBER	71	HBC $K^- p \rightarrow n \bar{K}^0$
11.6 $\pm$ 0.9	393	<sup>1,2</sup> CHO	70	DBC $K^+ n \rightarrow K^0 p$
10.3 $\pm$ 0.8	335	<sup>2</sup> HILL	67	DBC $K^+ n \rightarrow K^0 p$
9.85 $\pm_{-1.05}^{+1.15}$	109	<sup>1</sup> FRANZINI	65	HBC
<sup>1</sup> Assumes $\Delta S = \Delta Q$ rule.				
<sup>2</sup> CHO 70 includes events of HILL 67.				

**$K_L^0$  BRANCHING RATIOS**

**Semileptonic modes**

**$\Gamma(\pi^\pm e^\mp \nu_e) / \Gamma_{\text{total}}$   $\Gamma_1 / \Gamma$**

VALUE	EVTS	DOCUMENT ID	TECN
<b>0.4055 <math>\pm</math> 0.0011 OUR FIT</b>			Error includes scale factor of 1.7.
<b>0.4047 <math>\pm</math> 0.0028 OUR AVERAGE</b>			Error includes scale factor of 3.1.
0.4007 $\pm$ 0.0005 $\pm$ 0.0015	13M	<sup>1</sup> AMBROSINO	06 KLOE
0.4067 $\pm$ 0.0011		<sup>2</sup> ALEXOPOU...	04 KTEV

<sup>1</sup> There are correlations between these five KLOE measurements:  $B(K_L \rightarrow \pi e \nu)$ ,  $B(K_L \rightarrow \pi \mu \nu)$ ,  $B(K_L \rightarrow 3\pi^0)$ ,  $B(K_L \rightarrow \pi^+ \pi^- \pi^0)$ , and  $\tau_{K_L}$  measured in AMBROSINO 06. See the footnote for the  $\tau_{K_L}$  measurement for the correlation matrix.

## Meson Particle Listings

 $K_L^0$ 

<sup>2</sup>ALEXOPOULOS 04 constrains  $\sum_i B_i = 0.9993$  for the six major  $K_L$  branching fractions. The correlations among these branching fractions are taken into account in our fit. The correlation matrix is

	$K_{e3}$	$K_{\mu 3}$	$3\pi^0$	$\pi^+\pi^-\pi^0$	$\pi^+\pi^-$	$\pi^0\pi^0$
$K_{e3}$	1					
$K_{\mu 3}$	0.15	1				
$3\pi^0$	-0.77	-0.62	1			
$\pi^+\pi^-\pi^0$	0.18	0.08	-0.54	1		
$\pi^+\pi^-$	0.28	0.22	-0.48	0.49	1	
$\pi^0\pi^0$	-0.72	-0.54	0.89	-0.46	-0.39	1

$\Gamma(\pi^\pm \mu^\mp \nu_\mu)/\Gamma_{\text{total}}$	$\Gamma_2/\Gamma$
<b>0.2704 ± 0.0007 OUR FIT</b>	Error includes scale factor of 1.1.
<b>0.2700 ± 0.0008 OUR AVERAGE</b>	
0.2698 ± 0.0005 ± 0.0015	13M <sup>1</sup> AMBROSINO 06 KLOE
0.2701 ± 0.0009	<sup>2</sup> ALEXOPOU... 04 KTEV

<sup>1</sup>There are correlations between these five KLOE measurements:  $B(K_L \rightarrow \pi e \nu)$ ,  $B(K_L \rightarrow \pi \mu \nu)$ ,  $B(K_L \rightarrow 3\pi^0)$ ,  $B(K_L \rightarrow \pi^+\pi^-\pi^0)$ , and  $\tau_{K_L}$  measured in AMBROSINO 06. See the footnote for the  $\tau_{K_L}$  measurement for the correlation matrix.

<sup>2</sup>For correlations with other ALEXOPOULOS 04 measurements, see the footnote with their  $B(K_L \rightarrow \pi e \nu)$  measurement.

$[\Gamma(\pi^\pm e^\mp \nu_e) + \Gamma(\pi^\pm \mu^\mp \nu_\mu)]/\Gamma_{\text{total}}$	$(\Gamma_1 + \Gamma_2)/\Gamma$
<b>0.6760 ± 0.0012 OUR FIT</b>	Error includes scale factor of 1.6.

$\Gamma(\pi^\pm \mu^\mp \nu_\mu)/\Gamma(\pi^\pm e^\mp \nu_e)$	$\Gamma_2/\Gamma_1$
<b>0.6669 ± 0.0027 OUR FIT</b>	Error includes scale factor of 1.2.
<b>0.666 ± 0.004 OUR AVERAGE</b>	Error includes scale factor of 1.6.
••• We use the following data for averages but not for fits. •••	
0.6740 ± 0.0059	13M <sup>1</sup> AMBROSINO 06 KLOE Not in fit
0.6640 ± 0.0014 ± 0.0022	394K <sup>2</sup> ALEXOPOU... 04 KTEV Not in fit
••• We do not use the following data for averages, fits, limits, etc. •••	
0.702 ± 0.011	33k CHO 80 HBC
0.662 ± 0.037	10k WILLIAMS 74 ASPK
0.741 ± 0.044	6700 BRANDENB... 73 HBC
0.662 ± 0.030	1309 EVANS 73 HLBC
0.68 ± 0.08	3548 BASILE 70 OSPK
0.71 ± 0.05	770 BUDAGOV 68 HLBC

<sup>1</sup>AMBROSINO 06 enters the fit via their separate measurements of these two modes.

<sup>2</sup>ALEXOPOULOS 04 enters the fit via their separate measurements of these two modes.

$\Gamma(\pi^\pm \mu^\mp \nu_\mu)/\Gamma(\pi^\pm e^\mp \nu_e)$	$\Gamma_3/\Gamma_2$
<b>3.90 ± 0.39</b>	155 <sup>1</sup> ARONSON 86 SPEC
••• We do not use the following data for averages, fits, limits, etc. •••	
seen	18 COOMBES 76 WIRE
	<sup>1</sup> ARONSON 86 quote theoretical value of $(4.31 \pm 0.08) \times 10^{-7}$ .

<sup>1</sup>AMBROSINO 06 enters the fit via their separate measurements of these two modes.

<sup>2</sup>ALEXOPOULOS 04 enters the fit via their separate measurements of these two modes.

$\Gamma(\pi^0 \pi^\pm e^\mp \nu)/\Gamma_{\text{total}}$	$\Gamma_4/\Gamma$
<b>5.20 ± 0.11 OUR AVERAGE</b>	
5.21 ± 0.07 ± 0.09	5402 BATLEY 04 NA48
5.16 ± 0.20 ± 0.22	729 MAKOFF 93 E731
••• We do not use the following data for averages, fits, limits, etc. •••	
6.2 ± 2.0	16 CARROLL 80c SPEC
< 220	90 <sup>1</sup> DONALDSON 74 SPEC
	<sup>1</sup> DONALDSON 74 uses $K_L^0 \rightarrow \pi^+\pi^-\pi^0$ /(all $K_L^0$ decays) = 0.126.

<sup>1</sup>DONALDSON 74 uses  $K_L^0 \rightarrow \pi^+\pi^-\pi^0$ /(all  $K_L^0$  decays) = 0.126.

$\Gamma(\pi^\pm e^\mp \nu e^+ e^-)/\Gamma(\pi^+\pi^-\pi^0)$	$\Gamma_5/\Gamma_7$
<b>10.02 ± 0.17 ± 0.29</b>	19k <sup>1</sup> ABOUZAI 07c KTEV $M_{ee} > 5 \text{ MeV}$ , $E_{ee}^* > 30 \text{ MeV}$
<b>1E*</b>	is the energy of the $e^+e^-$ pair in the kaon rest frame. ABOUZAI 07c reports $[\Gamma(K_L^0 \rightarrow \pi^\pm e^\mp \nu e^+ e^-)/\Gamma(K_L^0 \rightarrow \pi^+\pi^-\pi^0)] / [B(\pi^0 \rightarrow e^+e^-\gamma)] = (8.54 \pm 0.07 \pm 0.13) \times 10^{-3}$ which we multiply by our best value $B(\pi^0 \rightarrow e^+e^-\gamma) = (1.174 \pm 0.035) \times 10^{-2}$ . Our first error is their experiment's error and our second error is the systematic error from using our best value.

## Hadronic modes,

including Charge conjugation×Parity Violating (CPV) modes

$\Gamma(3\pi^0)/\Gamma_{\text{total}}$	$\Gamma_6/\Gamma$
<b>0.1952 ± 0.0012 OUR FIT</b>	Error includes scale factor of 1.6.
<b>0.1969 ± 0.0026 OUR AVERAGE</b>	Error includes scale factor of 2.0.
••• We use the following data for averages but not for fits. •••	
0.1997 ± 0.0003 ± 0.0019	13M <sup>1</sup> AMBROSINO 06 KLOE Not fitted
0.1945 ± 0.0018	<sup>1</sup> ALEXOPOU... 04 KTEV Not fitted

<sup>1</sup>We exclude these  $B(K_L \rightarrow 3\pi^0)$  measurements from our fit because the authors have constrained  $K_L$  branching fractions to sum to one. It enters our fit via the other measurements from the experiment and their correlations, along with our constraint that the fitted branching fractions sum to one.

$\Gamma(3\pi^0)/\Gamma(\pi^\pm e^\mp \nu_e)$	$\Gamma_6/\Gamma_1$
--	---------------------

**0.481 ± 0.004 OUR FIT** Error includes scale factor of 1.8.

••• We use the following data for averages but not for fits. •••

**0.4782 ± 0.0014 ± 0.0053** 209K <sup>1</sup>ALEXOPOU... 04 KTEV Not in fit

••• We do not use the following data for averages, fits, limits, etc. •••

0.545 ± 0.004 ± 0.009 38k KREUTZ 95 NA31

<sup>1</sup>This measurement enters the fit via their separate measurements of these two modes.

$\Gamma(3\pi^0)/[\Gamma(\pi^\pm e^\mp \nu_e) + \Gamma(\pi^\pm \mu^\mp \nu_\mu) + \Gamma(\pi^+\pi^-\pi^0)]$	$\Gamma_6/(\Gamma_1 + \Gamma_2 + \Gamma_7)$
--	---

**0.2436 ± 0.0018 OUR FIT** Error includes scale factor of 1.6.

••• We do not use the following data for averages, fits, limits, etc. •••

0.251 ± 0.014 549 BUDAGOV 68 HLBC ORSAY measur.

0.277 ± 0.021 444 BUDAGOV 68 HLBC Ecole polytec.meas

0.31 ± 0.07 29 KULYUKINA 68 CC

0.24 ± 0.08 24 ANIKINA 64 CC

$\Gamma(3\pi^0)/\Gamma(\pi^+\pi^-\pi^0)$	$\Gamma_6/\Gamma_7$
--	---------------------

**1.557 ± 0.012 OUR FIT** Error includes scale factor of 1.3.

••• We use the following data for averages but not for fits. •••

**1.582 ± 0.027** 13M <sup>1</sup>AMBROSINO 06 KLOE Not in fit

••• We do not use the following data for averages, fits, limits, etc. •••

1.611 ± 0.014 ± 0.034 28k KREUTZ 95 NA31

1.65 ± 0.07 883 BARMIN 72B HLBC Error statistical only

1.80 ± 0.13 1010 BUDAGOV 68 HLBC

2.0 ± 0.6 188 ALEKSANYAN 64B FBC

<sup>1</sup>AMBROSINO 06 enters the fit via their separate measurements of these two modes.

$\Gamma(\pi^+\pi^-\pi^0)/\Gamma_{\text{total}}$	$\Gamma_7/\Gamma$
---	-------------------

**0.1254 ± 0.0005 OUR FIT**

**0.1255 ± 0.0006 OUR AVERAGE**

0.1263 ± 0.0004 ± 0.0011 13M <sup>1</sup>AMBROSINO 06 KLOE

0.1252 ± 0.0007 <sup>2</sup>ALEXOPOU... 04 KTEV

<sup>1</sup>There are correlations between these five KLOE measurements:  $B(K_L \rightarrow \pi e \nu)$ ,  $B(K_L \rightarrow \pi \mu \nu)$ ,  $B(K_L \rightarrow 3\pi^0)$ ,  $B(K_L \rightarrow \pi^+\pi^-\pi^0)$ , and  $\tau_{K_L}$  measured in AMBROSINO 06. See the footnote for the  $\tau_{K_L}$  measurement for the correlation matrix.

<sup>2</sup>For correlations with other ALEXOPOULOS 04 measurements, see the footnote with their  $B(K_L \rightarrow \pi e \nu)$  measurement.

$\Gamma(\pi^+\pi^-\pi^0)/\Gamma(\pi^\pm e^\mp \nu_e)$	$\Gamma_7/\Gamma_1$
---	---------------------

**0.3092 ± 0.0016 OUR FIT** Error includes scale factor of 1.1.

••• We use the following data for averages but not for fits. •••

**0.3078 ± 0.0005 ± 0.0017** 799K <sup>1</sup>ALEXOPOU... 04 KTEV Not in fit

••• We do not use the following data for averages, fits, limits, etc. •••

0.336 ± 0.003 ± 0.007 28k KREUTZ 95 NA31

<sup>1</sup>This measurement enters the fit via their separate measurements for the two modes.

$\Gamma(\pi^+\pi^-\pi^0)/[\Gamma(\pi^\pm e^\mp \nu_e) + \Gamma(\pi^\pm \mu^\mp \nu_\mu) + \Gamma(\pi^+\pi^-\pi^0)]$	$\Gamma_7/(\Gamma_1 + \Gamma_2 + \Gamma_7)$
---	---

**0.1565 ± 0.0006 OUR FIT** Error includes scale factor of 1.1.

••• We do not use the following data for averages, fits, limits, etc. •••

0.163 ± 0.003 6499 CHO 77 HBC

0.1605 ± 0.0038 1590 ALEXANDER 73B HBC

0.146 ± 0.004 3200 BRANDENB... 73 HBC

0.159 ± 0.010 558 EVANS 73 HLBC

0.167 ± 0.016 1402 KULYUKINA 68 CC

0.161 ± 0.005 HOPKINS 67 HBC

0.162 ± 0.015 126 HAWKINS 66 HBC

0.159 ± 0.015 326 ASTBURY 65B CC

0.178 ± 0.017 566 GUIDONI 65 HBC

0.144 ± 0.004 1729 HOPKINS 65 HBC See HOPKINS 67

$\Gamma(\pi^+\pi^-)/\Gamma_{\text{total}}$	$\Gamma_8/\Gamma$
--	-------------------

Violates CP conservation.

**1.967 ± 0.010 OUR FIT** Error includes scale factor of 1.5.

**1.975 ± 0.012** <sup>1</sup>ALEXOPOU... 04 KTEV

<sup>1</sup>For correlations with other ALEXOPOULOS 04 measurements, see the footnote with their  $B(K_L \rightarrow \pi e \nu)$  measurement.

$\Gamma(\pi^+\pi^-)/\Gamma(\pi^\pm e^\mp \nu_e)$	$\Gamma_8/\Gamma_1$
--	---------------------

**4.849 ± 0.020 OUR FIT** Error includes scale factor of 1.1.

**4.840 ± 0.020 OUR AVERAGE**

4.826 ± 0.022 ± 0.016 47k <sup>1</sup>LAI 07 NA48

••• We use the following data for averages but not for fits. •••

4.856 ± 0.017 ± 0.023 84k <sup>2</sup>ALEXOPOU... 04 KTEV Not in fit

<sup>1</sup>The LAI 07 central value of  $4.835 \times 10^{-3}$  has been reduced by 0.19% to  $4.826 \times 10^{-3}$  to subtract the contribution from the direct emission mode  $K_L^0 \rightarrow \pi^+\pi^-\gamma$ (DE).

<sup>2</sup>This measurement enters the fit via their separate measurements for the two modes.

$[\Gamma(\pi^+\pi^-) + \Gamma(\pi^+\pi^-\gamma(\text{DE}))]/\Gamma(\pi^\pm\mu^\mp\nu_\mu)$   $(\Gamma_8+\Gamma_{14})/\Gamma_2$

VALUE (units $10^{-3}$ )	EVTS	DOCUMENT ID	TECN
<b>7.38 ± 0.04 OUR FIT</b>			Error includes scale factor of 1.4.
<b>7.275 ± 0.042 ± 0.054</b>	45k	<sup>1</sup> AMBROSINO 06F KLOE	

<sup>1</sup>Fully inclusive. Taking  $B(K_L^0 \rightarrow \pi\mu\nu)$  from KLOE, AMBROSINO 06,  $B(K_L^0 \rightarrow \pi^+\pi^-\pi^+\pi^-\gamma(\text{DE})) = (1.963 \pm 0.012 \pm 0.017) \times 10^{-3}$  is obtained.

$\Gamma(\pi^+\pi^-)/[\Gamma(\pi^\pm e^\mp\nu_e) + \Gamma(\pi^\pm\mu^\mp\nu_\mu)]$   $\Gamma_8/(\Gamma_1+\Gamma_2)$

Violates CP conservation.

VALUE (units $10^{-3}$ )	EVTS	DOCUMENT ID	TECN	COMMENT
<b>2.909 ± 0.013 OUR FIT</b>				Error includes scale factor of 1.3.

- • • We do not use the following data for averages, fits, limits, etc. • • •
- 3.13 ± 0.14 1687 COUPAL 85 SPEC  $\eta_{+-} = 2.28 \pm 0.06$
- 3.04 ± 0.14 2703 DEVOE 77 SPEC  $\eta_{+-} = 2.25 \pm 0.05$
- 2.51 ± 0.23 309 <sup>1</sup>DEBOUARD 67 OSPK  $\eta_{+-} = 2.00 \pm 0.09$
- 2.35 ± 0.19 525 <sup>1</sup>FITCH 67 OSPK  $\eta_{+-} = 1.94 \pm 0.08$

<sup>1</sup>Old experiments excluded from fit. See subsection on  $\eta_{+-}$  in section on "PARAMETERS FOR  $K_L^0 \rightarrow 2\pi$  DECAY" below for average  $\eta_{+-}$  of these experiments and for note on discrepancy.

$\Gamma(\pi^\pm e^\mp\nu_e)/\Gamma(2 \text{ tracks})$   $\Gamma_1/(\Gamma_1+\Gamma_2+0.03508\Gamma_6+\Gamma_7+\Gamma_8)$

$\Gamma(2 \text{ tracks}) = \Gamma(\pi^\pm e^\mp\nu_e) + \Gamma(\pi^\pm\mu^\mp\nu_\mu) + 0.03508 \Gamma(3\pi^0) + \Gamma(\pi^+\pi^-\pi^0) + \Gamma(\pi^+\pi^-)$  where 0.03508 is the fraction of  $3\pi^0$  events with one Dalitz decay ( $\pi^0 \rightarrow \gamma e^+e^-$ ).

VALUE	EVTS	DOCUMENT ID	TECN
<b>0.5006 ± 0.0009 OUR FIT</b>			Error includes scale factor of 1.3.
<b>0.4978 ± 0.0035</b>	6.8M	LAI 04B NA48	

$\Gamma(\pi^+\pi^-)/[\Gamma(\pi^\pm e^\mp\nu_e) + \Gamma(\pi^\pm\mu^\mp\nu_\mu) + \Gamma(\pi^+\pi^-\pi^0)]$   $\Gamma_8/(\Gamma_1+\Gamma_2+\Gamma_7)$

Violates CP conservation.

VALUE (units $10^{-3}$ )	EVTS	DOCUMENT ID	TECN	COMMENT
<b>2.454 ± 0.011 OUR FIT</b>				Error includes scale factor of 1.3.

- • • We do not use the following data for averages, fits, limits, etc. • • •
  - 2.60 ± 0.07 4200 <sup>1</sup>MESSNER 73 ASPK  $\eta_{+-} = 2.23 \pm 0.05$
- <sup>1</sup>From same data as  $\Gamma(\pi^+\pi^-)/\Gamma(\pi^+\pi^-\pi^0)$  MESSNER 73, but with different normalization.

$\Gamma(\pi^+\pi^-)/\Gamma(\pi^+\pi^-\pi^0)$   $\Gamma_8/\Gamma_7$

Violates CP conservation.

VALUE (units $10^{-2}$ )	EVTS	DOCUMENT ID	TECN	COMMENT
<b>1.568 ± 0.010 OUR FIT</b>				Error includes scale factor of 1.3.

- • • We do not use the following data for averages, fits, limits, etc. • • •
- 1.64 ± 0.04 4200 MESSNER 73 ASPK  $\eta_{+-} = 2.23$

$\Gamma(\pi^0\pi^0)/\Gamma_{\text{total}}$   $\Gamma_9/\Gamma$

Violates CP conservation.

VALUE (units $10^{-3}$ )	DOCUMENT ID	TECN
<b>0.864 ± 0.006 OUR FIT</b>		
<b>0.865 ± 0.012</b>	<sup>1</sup> ALEXOPOU... 04 KTEV	

<sup>1</sup>For correlations with other ALEXOPOULOS 04 measurements, see the footnote with their  $B(K_L \rightarrow \pi e \nu)$  measurement.

$\Gamma(\pi^0\pi^0)/\Gamma(\pi^+\pi^-)$   $\Gamma_9/\Gamma_8$

Violates CP conservation.

VALUE	DOCUMENT ID	TECN	COMMENT
<b>0.4395 ± 0.0023 OUR FIT</b>			Error includes scale factor of 2.0.
<b>0.4390 ± 0.0012</b>	ETAFIT 16		

$\Gamma(\pi^0\pi^0)/\Gamma(3\pi^0)$   $\Gamma_9/\Gamma_6$

Violates CP conservation.

VALUE (units $10^{-2}$ )	EVTS	DOCUMENT ID	TECN	COMMENT
<b>0.443 ± 0.004 OUR FIT</b>				Error includes scale factor of 2.1.

- • • We use the following data for averages but not for fits. • • •
  - 0.4446 ± 0.0016 ± 0.0019** 100K <sup>1</sup>ALEXOPOU... 04 KTEV Not in fit
  - • • We do not use the following data for averages, fits, limits, etc. • • •
  - 0.37 ± 0.08 29 BARMIN 70 HLBC  $\eta_{00} = 2.02 \pm 0.23$
  - 0.32 ± 0.15 30 BUDAGOV 70 HLBC  $\eta_{00} = 1.9 \pm 0.5$
  - 0.46 ± 0.11 57 BANNER 69 OSPK  $\eta_{00} = 2.2 \pm 0.3$
- <sup>1</sup>This measurement enters the fit via their separate measurements for the two modes.

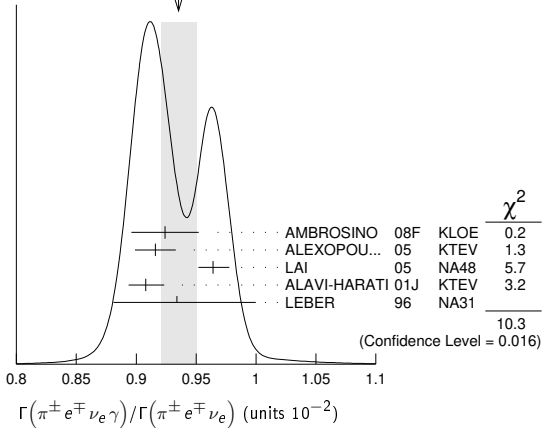
———— Semileptonic modes with photons ————

$\Gamma(\pi^\pm e^\mp\nu_e)/\Gamma(\pi^\pm e^\mp\nu_e)$   $\Gamma_{10}/\Gamma_1$

VALUE (units $10^{-2}$ )	EVTS	DOCUMENT ID	TECN	COMMENT
<b>0.935 ± 0.015 OUR AVERAGE</b>				Error includes scale factor of 1.9. See the ideogram below.
0.924 ± 0.023 ± 0.016	9k	<sup>1</sup> AMBROSINO 08F KLOE		$E_\gamma^* > 30 \text{ MeV}, \theta_{e\gamma}^* > 20^\circ$
0.916 ± 0.017	4309	<sup>2</sup> ALEXOPOU... 05 KTEV		$E_\gamma^* > 30 \text{ MeV}, \theta_{e\gamma}^* > 20^\circ$
0.964 ± 0.008 ± $^{+0.011}_{-0.009}$	19K	LAI 05 NA48		$E_\gamma^* > 30 \text{ MeV}, \theta_{e\gamma}^* > 20^\circ$
0.908 ± 0.008 ± $^{+0.013}_{-0.012}$	15k	ALAVI-HARATI01J KTEV		$E_\gamma^* \geq 30 \text{ MeV}, \theta_{e\gamma}^* \geq 20^\circ$
0.934 ± 0.036 ± $^{+0.055}_{-0.039}$	1384	LEBER 96 NA31		$E_\gamma^* \geq 30 \text{ MeV}, \theta_{e\gamma}^* \geq 20^\circ$

<sup>1</sup>Direct emission contribution measured  $\langle X \rangle = -2.3 \pm 1.3 \pm 1.4$ .  
<sup>2</sup>Also measured cut  $E_\gamma^* > 10 \text{ MeV}, \theta_{e\gamma}^* > 0^\circ$  14221 evts:  $\Gamma(\pi^\pm e^\mp\nu_e\gamma) / \Gamma(\pi^\pm e^\mp\nu_e) = (4.942 \pm 0.062)\%$ .

WEIGHTED AVERAGE  
0.935±0.015 (Error scaled by 1.9)



$\Gamma(\pi^\pm\mu^\mp\nu_\mu\gamma)/\Gamma(\pi^\pm\mu^\mp\nu_\mu)$   $\Gamma_{11}/\Gamma_2$

VALUE (units $10^{-3}$ )	EVTS	DOCUMENT ID	TECN	COMMENT
<b>2.09 ± 0.08 OUR AVERAGE</b>				
2.09 ± 0.09		<sup>1</sup> ALEXOPOU... 05	KTEV	$E_\gamma^* > 30 \text{ MeV}$
2.08 ± 0.17 ± $^{+0.16}_{-0.21}$	252	BENDER 98	NA48	$E_\gamma^* \geq 30 \text{ MeV}$

<sup>1</sup>Also measured cut  $E_\gamma^* > 10 \text{ MeV}$ , 1385 evts:  $\Gamma(\pi^\pm\mu^\mp\nu_\mu\gamma) / \Gamma(\pi^\pm\mu^\mp\nu_\mu) = (0.530 \pm 0.014 \pm 0.012)\%$ .

———— Hadronic modes with photons or  $e\bar{e}$  pairs ————

$\Gamma(\pi^0\pi^0\gamma)/\Gamma_{\text{total}}$   $\Gamma_{12}/\Gamma$

VALUE (units $10^{-6}$ )	CL%	DOCUMENT ID	TECN	COMMENT
<b>&lt; 0.243</b>	90	ABOUZAID 08B	KTEV	$K_L^0 \rightarrow \pi^0\pi_D^0\gamma, \pi_D^0 \rightarrow e\bar{e}\gamma$
• • • We do not use the following data for averages, fits, limits, etc. • • •				
< 5.6	90	BARR 94	NA31	
< 230	90	ROBERTS 94	E799	

$\Gamma(\pi^+\pi^-\gamma)/\Gamma(\pi^+\pi^-\pi^0)$   $\Gamma_{13}/\Gamma_7$

For earlier limits see our 1992 edition Physical Review **D45** S1 (1992).

VALUE (units $10^{-4}$ )	EVTS	DOCUMENT ID	TECN	COMMENT
• • • We do not use the following data for averages, fits, limits, etc. • • •				
1.23 ± 0.13	516	<sup>1,2</sup> CARROLL 80B	SPEC	$E_\gamma^* > 20 \text{ MeV}$
2.33 ± 0.23	546	<sup>1,3</sup> CARROLL 80B	SPEC	
3.56 ± 0.26	1062	<sup>1,4</sup> CARROLL 80B	SPEC	$E_\gamma^* > 20 \text{ MeV}$

<sup>1</sup>CARROLL 80B quotes  $B(\pi^+\pi^-\gamma)$  using normalization  $B(\pi^+\pi^-\pi^0) = 0.1239$ . We divide by this value to obtain their measured  $\Gamma(\pi^+\pi^-\gamma) / \Gamma(\pi^+\pi^-\pi^0)$ .

- <sup>2</sup>Internal Bremsstrahlung component only.
- <sup>3</sup>Direct  $\gamma$  emission component only.
- <sup>4</sup>Both IB and DE components.

$\Gamma(\pi^+\pi^-\gamma)/\Gamma(\pi^+\pi^-)$   $\Gamma_{13}/\Gamma_8$

VALUE (units $10^{-2}$ )	EVTS	DOCUMENT ID	TECN	COMMENT
<b>2.11 ± 0.08 OUR FIT</b>				Error includes scale factor of 2.9.
<b>2.11 ± 0.08 OUR AVERAGE</b>				Error includes scale factor of 2.9.
2.08 ± 0.02 ± 0.02	8669	<sup>1</sup> ALAVI-HARATI01B	KTEV	$E_\gamma^* > 20 \text{ MeV}$
2.30 ± 0.07	3136	RAMBERG 93	E731	$E_\gamma^* > 20 \text{ MeV}$

<sup>1</sup>ALAVI-HARATI 01B includes both Direct Emission (DE) and Inner Bremsstrahlung (IB) processes.

$\Gamma(\pi^+\pi^-\gamma(\text{DE}))/\Gamma(\pi^+\pi^-)$   $\Gamma_{14}/\Gamma_{13}$

These values assume that  $\Gamma(K_L^0 \rightarrow \pi^+\pi^-\gamma) = \Gamma(K_L^0 \rightarrow \pi^+\pi^-\gamma(\text{DE})) + \Gamma(K_L^0 \rightarrow \pi^+\pi^-\gamma(\text{IB}))$ , the sum of widths for the direct emission (DE) and inner bremsstrahlung (IB) processes, with no IB-DE interference. DE assumes a form factor as described in RAMBERG 93.

VALUE	EVTS	DOCUMENT ID	TECN	COMMENT
<b>0.684 ± 0.009 OUR FIT</b>				
<b>0.684 ± 0.009 OUR AVERAGE</b>				
0.689 ± 0.021	111k	ABOUZAID 06A	KTEV	$E_\gamma^* > 20 \text{ MeV}$
0.683 ± 0.011	8669	ALAVI-HARATI01B	KTEV	$E_\gamma^* > 20 \text{ MeV}$
0.685 ± 0.041	3136	RAMBERG 93	E731	$E_\gamma^* > 20 \text{ MeV}$



# Meson Particle Listings

$K_L^0$

## $\Gamma(\pi^0 2\gamma)/\Gamma_{\text{total}}$ $\Gamma_{15}/\Gamma$

VALUE (units $10^{-6}$ )	CL%	EVTS	DOCUMENT ID	TECN	COMMENT
<b>1.273 ± 0.033 OUR AVERAGE</b>					
1.28 ± 0.06 ± 0.01		1.4k	<sup>1</sup> ABOUZAIID 08	KTEV	
1.27 ± 0.04 ± 0.01		2.5k	<sup>2</sup> LAI 02b	NA48	
• • • We do not use the following data for averages, fits, limits, etc. • • •					
1.68 ± 0.07 ± 0.08		884	<sup>3</sup> ALAVI-HARATI 99b	KTEV	
1.7 ± 0.2 ± 0.2		63	<sup>4</sup> BARR 92	NA31	$m_{\gamma\gamma} > 280$ MeV
1.86 ± 0.60 ± 0.60		60	PAPADIMITR...91	E731	$m_{\gamma\gamma} < 264$ MeV
<5.1		90	PAPADIMITR...91	E731	$m_{\gamma\gamma} < 264$ MeV
2.1 ± 0.6		14	<sup>5</sup> BARR 90c	NA31	$m_{\gamma\gamma} > 280$ MeV

<sup>1</sup> ABOUZAIID 08 reports  $(1.29 \pm 0.03 \pm 0.05) \times 10^{-6}$  from a measurement of  $[\Gamma(K_L^0 \rightarrow \pi^0 2\gamma)/\Gamma_{\text{total}}] / [B(K_L^0 \rightarrow \pi^0 \pi^0)]$  assuming  $B(K_L^0 \rightarrow \pi^0 \pi^0) = (8.69 \pm 0.04) \times 10^{-4}$ , which we rescale to our best value  $B(K_L^0 \rightarrow \pi^0 \pi^0) = (8.64 \pm 0.06) \times 10^{-4}$ . Our first error is their experiment's error and our second error is the systematic error from using our best value.

<sup>2</sup> LAI 02b reports  $[\Gamma(K_L^0 \rightarrow \pi^0 2\gamma)/\Gamma_{\text{total}}] / [B(K_L^0 \rightarrow \pi^0 \pi^0)] = (1.467 \pm 0.032 \pm 0.032) \times 10^{-3}$  which we multiply by our best value  $B(K_L^0 \rightarrow \pi^0 \pi^0) = (8.64 \pm 0.06) \times 10^{-4}$ . Our first error is their experiment's error and our second error is the systematic error from using our best value. They also find that  $B(\pi^0 2\gamma, m_{\gamma\gamma} < 110$  MeV)  $< 0.6 \times 10^{-8}$  (90% CL).

<sup>3</sup> ALAVI-HARATI 99b finds that  $\Gamma(\pi^0 2\gamma, m_{\gamma\gamma} < 240$  MeV) /  $\Gamma(\pi^0 2\gamma) = (17.3 \pm 1.3 \pm 1.5)\%$ . Superseded by ABOUZAIID 08.

<sup>4</sup> BARR 92 find that  $\Gamma(\pi^0 2\gamma, m_{\gamma\gamma} < 240$  MeV) /  $\Gamma(\pi^0 2\gamma) < 0.09$  (90% CL).

<sup>5</sup> BARR 90c superseded by BARR 92.

## $\Gamma(\pi^0 \gamma e^+ e^-)/\Gamma_{\text{total}}$ $\Gamma_{16}/\Gamma$

VALUE (units $10^{-8}$ )	CL%	EVTS	DOCUMENT ID	TECN	COMMENT
<b>1.62 ± 0.14 ± 0.09</b>					
2.34 ± 0.35 ± 0.13		44	ALAVI-HARATI 01E	KTEV	
<71		90	MURAKAMI 99	SPEC	

<sup>1</sup> ABOUZAIID 07D includes 1997 (ALAVI-HARATI 01E) and 1999 data. It measures the ratio of  $B(K_L^0 \rightarrow \pi^0 \gamma e^+ e^-) / B(K_L^0 \rightarrow \pi^0 \pi^0)$ , where  $\pi_D^0$  is the Dalitz decaying  $\pi^0$ , and uses PDG 06 values  $B(K_L^0 \rightarrow \pi^0 \pi^0) = (8.69 \pm 0.04) \times 10^{-4}$ , and  $B(\pi_D^0 \rightarrow e^+ e^- \gamma) = (1.198 \pm 0.032) \times 10^{-2}$ . Supersedes ALAVI-HARATI 01E result.

### Other modes with photons or $\ell\bar{\ell}$ pairs

## $\Gamma(2\gamma)/\Gamma_{\text{total}}$ $\Gamma_{17}/\Gamma$

VALUE (units $10^{-4}$ )	EVTS	DOCUMENT ID	TECN	COMMENT
<b>5.87 ± 0.04 OUR FIT</b> Error includes scale factor of 1.1.				
• • • We do not use the following data for averages, fits, limits, etc. • • •				
4.54 ± 0.84		<sup>1</sup> BANNER 72b	OSPK	
4.5 ± 1.0		ENSTROM 71	OSPK	$K_L^0$ 1.5–9 GeV/c
5.0 ± 1.0		<sup>2</sup> REPELLIN 71	OSPK	
5.5 ± 1.1		90 KUNZ 68	OSPK	Norm.to 3 $\pi$ (C+N)

<sup>1</sup> This value uses  $(\eta_{00}/\eta_{+-})^2 = 1.05 \pm 0.14$ . In general,  $\Gamma(2\gamma)/\Gamma_{\text{total}} = [(4.32 \pm 0.55) \times 10^{-4}] [(\eta_{00}/\eta_{+-})^2]$ .

<sup>2</sup> Assumes regeneration amplitude in copper at 2 GeV is 22 mb. To evaluate for a given regeneration amplitude and error, multiply by (regeneration amplitude/22mb)<sup>2</sup>.

## $\Gamma(2\gamma)/\Gamma(3\pi^0)$ $\Gamma_{17}/\Gamma_6$

VALUE (units $10^{-3}$ )	EVTS	DOCUMENT ID	TECN	COMMENT
<b>2.802 ± 0.017 OUR FIT</b>				
<b>2.802 ± 0.018 OUR AVERAGE</b>				
2.79 ± 0.02 ± 0.02	27k	ADINOLFI 03	KLOE	
2.81 ± 0.01 ± 0.02		LAI 03	NA48	
• • • We do not use the following data for averages, fits, limits, etc. • • •				
2.13 ± 0.43	28	BARMIN 71	HLBC	
2.24 ± 0.28	115	BANNER 69	OSPK	
2.5 ± 0.7	16	ARNOLD 68b	HLBC	Vacuum decay

## $\Gamma(2\gamma)/\Gamma(\pi^0 \pi^0)$ $\Gamma_{17}/\Gamma_9$

VALUE	EVTS	DOCUMENT ID	TECN	COMMENT
<b>0.633 ± 0.006 OUR FIT</b> Error includes scale factor of 1.4.				
<b>0.632 ± 0.004 ± 0.008</b>				
	110k	BURKHARDT 87	NA31	

## $\Gamma(3\gamma)/\Gamma_{\text{total}}$ $\Gamma_{18}/\Gamma$

VALUE	CL%	DOCUMENT ID	TECN	COMMENT
<b>&lt;7.4 × 10<sup>-8</sup></b>				
	90	<sup>1</sup> TUNG 11	11 K391	
• • • We do not use the following data for averages, fits, limits, etc. • • •				
<2.4 × 10 <sup>-7</sup>		<sup>2</sup> BARR 95c	NA31	

<sup>1</sup> TUNG 11 reports the result assuming parity violating interaction and using 2005 data (Run-II and III). Assuming parity conserving or phase space interaction, the 90% upper limits obtained are  $7.5 \times 10^{-8}$  and  $8.6 \times 10^{-8}$ , respectively.

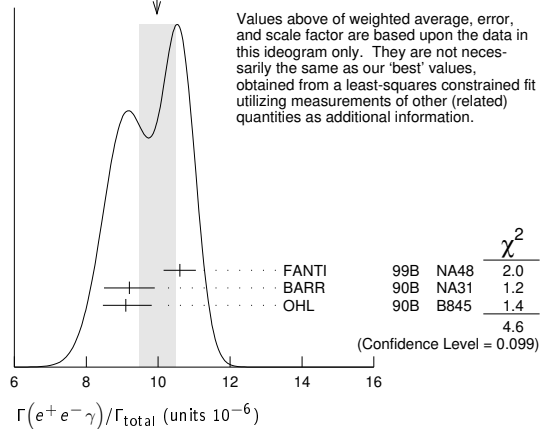
<sup>2</sup> Assumes a phase-space decay distribution.

## $\Gamma(e^+ e^- \gamma)/\Gamma_{\text{total}}$ $\Gamma_{19}/\Gamma$

VALUE (units $10^{-6}$ )	EVTS	DOCUMENT ID	TECN	COMMENT
<b>9.4 ± 0.4 OUR FIT</b> Error includes scale factor of 2.0.				
<b>10.0 ± 0.5 OUR AVERAGE</b> Error includes scale factor of 1.5. See the ideogram below.				
10.6 ± 0.2 ± 0.4	6864	<sup>1</sup> FANTI 99b	NA48	
9.2 ± 0.5 ± 0.5	1053	BARR 90b	NA31	
9.1 ± 0.4 <sup>+0.6</sup> <sub>-0.5</sub>	919	OHL 90b	B845	

<sup>1</sup> For FANTI 99b, the ± 0.4 systematic error includes for uncertainties in the calculation, primarily uncertainties in the  $\pi^0 \rightarrow e^+ e^- \gamma$  and  $K_L^0 \rightarrow \pi^0 \pi^0$  branching ratios, evaluated using our 1999 Web edition values.

WEIGHTED AVERAGE  
10.0 ± 0.5 (Error scaled by 1.5)



## $\Gamma(e^+ e^- \gamma)/\Gamma(3\pi^0)$ $\Gamma_{19}/\Gamma_6$

VALUE (units $10^{-5}$ )	EVTS	DOCUMENT ID	TECN	COMMENT
<b>4.82 ± 0.21 OUR FIT</b> Error includes scale factor of 2.0.				
<b>4.63 ± 0.04 ± 0.13</b>				
	83k	<sup>1</sup> ABOUZAIID 07b	KTEV	

<sup>1</sup> ABOUZAIID 07b reports  $[\Gamma(K_L^0 \rightarrow e^+ e^- \gamma)/\Gamma(K_L^0 \rightarrow 3\pi^0)] / [3\Gamma(\pi^0 \rightarrow 2\gamma)/\Gamma_{\text{total}} \times \Gamma(\pi^0 \rightarrow e^+ e^- \gamma)/\Gamma_{\text{total}}] = (1.3302 \pm 0.0046 \pm 0.0103) \times 10^{-3}$  which we multiply by our best value  $3\Gamma(\pi^0 \rightarrow 2\gamma)/\Gamma_{\text{total}} \times \Gamma(\pi^0 \rightarrow e^+ e^- \gamma)/\Gamma_{\text{total}} = 0.0348 \pm 0.0010$ . Our first error is their experiment's error and our second error is the systematic error from using our best value.

## $\Gamma(\mu^+ \mu^- \gamma)/\Gamma_{\text{total}}$ $\Gamma_{20}/\Gamma$

VALUE (units $10^{-7}$ )	EVTS	DOCUMENT ID	TECN	COMMENT
<b>3.59 ± 0.11 OUR AVERAGE</b> Error includes scale factor of 1.3.				
3.62 ± 0.04 ± 0.08	9100	ALAVI-HARATI 01G	KTEV	
3.4 ± 0.6 ± 0.4	45	FANTI 97	NA48	
3.23 ± 0.23 ± 0.19	197	SPENCER 95	E799	

## $\Gamma(e^+ e^- \gamma)/\Gamma_{\text{total}}$ $\Gamma_{21}/\Gamma$

VALUE (units $10^{-7}$ )	EVTS	DOCUMENT ID	TECN	COMMENT
<b>5.95 ± 0.33 OUR AVERAGE</b>				
5.84 ± 0.15 ± 0.32	1543	ALAVI-HARATI 01F	KTEV	$E_{\gamma}^* > 5$ MeV
8.0 ± 1.5 <sup>+1.4</sup> <sub>-1.2</sub>	40	SETZU 98	NA31	$E_{\gamma}^* > 5$ MeV
6.5 ± 1.2 ± 0.6	58	NAKAYA 94	E799	$E_{\gamma}^* > 5$ MeV
6.6 ± 3.2		MORSE 92	B845	$E_{\gamma}^* > 5$ MeV

## $\Gamma(\mu^+ \mu^- \gamma\gamma)/\Gamma_{\text{total}}$ $\Gamma_{22}/\Gamma$

VALUE (units $10^{-9}$ )	EVTS	DOCUMENT ID	TECN	COMMENT
<b>10.4<sup>+7.5</sup><sub>-5.9</sub> ± 0.7</b>				
	4	ALAVI-HARATI 00E	KTEV	$m_{\gamma\gamma} \geq 1$ MeV/c <sup>2</sup>

### Charge conjugation × Parity (CP) or Lepton Family number (LF) violating modes, or $\Delta S = 1$ weak neutral current (S1) modes

## $\Gamma(\mu^+ \mu^-)/\Gamma(\pi^+ \pi^-)$ $\Gamma_{23}/\Gamma_8$

Test for  $\Delta S = 1$  weak neutral current. Allowed by higher-order electroweak interaction.

VALUE (units $10^{-6}$ )	EVTS	DOCUMENT ID	TECN	COMMENT
<b>3.48 ± 0.05 OUR AVERAGE</b>				
3.474 ± 0.057	6210	AMBROSE 00	B871	
3.87 ± 0.30	179	<sup>1</sup> AKAGI 95	SPEC	
3.38 ± 0.17	707	HEINSON 95	B791	
• • • We do not use the following data for averages, fits, limits, etc. • • •				
3.9 ± 0.3 ± 0.1	178	<sup>2</sup> AKAGI 91b	SPEC	In AKAGI 95
3.45 ± 0.18 ± 0.13	368	<sup>3</sup> HEINSON 91	SPEC	In HEINSON 95
4.1 ± 0.5	54	INAGAKI 89	SPEC	In AKAGI 91b
2.8 ± 0.3 ± 0.2	87	MATHIAZHA...89b	SPEC	In HEINSON 91

<sup>1</sup> AKAGI 95 gives this number multiplied by the PDG 1992 average for  $\Gamma(K_L^0 \rightarrow \pi^+ \pi^-)/\Gamma_{\text{total}}$ .

$K_L^0$

<sup>2</sup>AKAGI 91B give this number multiplied by the 1990 PDG average for  $\Gamma(K_L^0 \rightarrow \pi^+ \pi^-)/\Gamma(\text{total})$ .  
<sup>3</sup>HEINSON 91 give  $\Gamma(K_L^0 \rightarrow \mu\mu)/\Gamma(\text{total})$ . We divide out the  $\Gamma(K_L^0 \rightarrow \pi^+ \pi^-)/\Gamma(\text{total})$  PDG average which they used.

$\Gamma(e^+ e^-)/\Gamma_{\text{total}}$   
Test for  $\Delta S = 1$  weak neutral current. Allowed by higher-order electroweak interaction.

VALUE (units $10^{-10}$ )	CL%	EVTS	DOCUMENT ID	TECN
<b>0.087 ± 0.057</b> <b>-0.041</b>		4	AMBROSE 98	B871
<1.6	90	1	AKAGI 95	SPEC
<0.41	90	0	<sup>1</sup> ARISAKA 93B	B791

<sup>1</sup>ARISAKA 93B includes all events with <6 MeV radiated energy.

$\Gamma(\pi^+ \pi^- e^+ e^-)/\Gamma_{\text{total}}$   
Test for  $\Delta S = 1$  weak neutral current. Allowed by higher-order electroweak interaction.

VALUE (units $10^{-7}$ )	CL%	EVTS	DOCUMENT ID	TECN	COMMENT
<b>3.11 ± 0.19 OUR AVERAGE</b>					
3.08 ± 0.09 ± 0.18	1125		<sup>1</sup> LAI 03c	03c	NA48
3.2 ± 0.6 ± 0.4	37		ADAMS 98		KTEV
4.4 ± 1.3 ± 0.5	13		TAKEUCHI 98		SPEC
<4.6	90		NOMURA 97		SPEC $m_{ee} > 4 \text{ MeV}$

<sup>1</sup>LAI 03c second error is 0.15(syst)±0.10(norm) combined in quadrature. The normalization uses  $\text{BR}(K_L^0 \rightarrow \pi^+ \pi^- \pi^0) * \text{BR}(\pi^0 \rightarrow e^+ e^-) = (1.505 \pm 0.047) \times 10^{-3}$  from our 2000 Edition.

$\Gamma(\pi^0 \pi^0 e^+ e^-)/\Gamma_{\text{total}}$   
Test for  $\Delta S = 1$  weak neutral current. Allowed by higher-order electroweak interaction.

VALUE (units $10^{-9}$ )	CL%	EVTS	DOCUMENT ID	TECN
<b>&lt;6.6</b>	90	1	ALAVI-HARATI 02c	E799

$\Gamma(\pi^0 \pi^0 \mu^+ \mu^-)/\Gamma_{\text{total}}$   
Test for  $\Delta S = 1$  weak neutral current. Allowed by higher-order electroweak interaction.

VALUE	CL%	DOCUMENT ID	TECN
<b>&lt;9.2 × 10<sup>-11</sup></b>	90	<sup>1</sup> ABOUZAIID 11A	E799

<sup>1</sup>ABOUZAIID 11A also reports  $\text{B}(K_L^0 \rightarrow \pi^0 \pi^0 X^0 \rightarrow \pi^0 \pi^0 \mu^+ \mu^-) < 1.0 \times 10^{-10}$  at 90% C.L., where the  $X^0$  is a possible new neutral boson that was reported by PARK 05 with a mass of  $214.3 \pm 0.5 \text{ MeV}/c^2$ .

$\Gamma(\mu^+ \mu^- e^+ e^-)/\Gamma_{\text{total}}$   
Test for  $\Delta S = 1$  weak neutral current. Allowed by higher-order electroweak interaction.

VALUE (units $10^{-9}$ )	CL%	EVTS	DOCUMENT ID	TECN	COMMENT
<b>2.69 ± 0.27 OUR AVERAGE</b>					
2.69 ± 0.24 ± 0.12	131		<sup>1</sup> ALAVI-HARATI 03B		KTEV
2.9 ± 0.7	1		GU 96		E799
<2.4					
2.62 ± 0.40 ± 0.17	43		ALAVI-HARATI 01H		KTEV Sup. by ALAVI-HARATI 03B
<4900	90		BALATS 83		SPEC

<sup>1</sup>ALAVI-HARATI 03B also measures the linear slope  $\alpha = -1.59 \pm 0.37$ .

$\Gamma(e^+ e^- e^+ e^-)/\Gamma_{\text{total}}$   
Test for  $\Delta S = 1$  weak neutral current. Allowed by higher-order electroweak interaction.

VALUE (units $10^{-8}$ )	EVTS	DOCUMENT ID	TECN	COMMENT
<b>3.56 ± 0.21 OUR AVERAGE</b>				
3.30 ± 0.24 ± 0.25	200	<sup>1</sup> LAI	05B	NA48
3.72 ± 0.18 ± 0.23	441	ALAVI-HARATI 01D		KTEV
3.96 ± 0.78 ± 0.32	27	GU	94	E799
3.07 ± 1.25 ± 0.26	6	VAGINS 93		B845
<6 ± 2 ± 1	18	<sup>2</sup> AKAGI 95		SPEC $m_{ee} > 470 \text{ MeV}$
7 ± 3 ± 2	6	<sup>2</sup> AKAGI 95		SPEC $m_{ee} > 470 \text{ MeV}$
10.4 ± 3.7 ± 1.1	8	<sup>3</sup> BARR 95		NA31
6 ± 2 ± 1	18	AKAGI 93		CNTR Sup. by AKAGI 95
4 ± 3	2	BARR 91		NA31 Sup. by BARR 95

<sup>1</sup>LAI 05B uses 1998 and 1999 data. Data are normalized to the observed events of  $K_L^0 \rightarrow \pi^+ \pi^- \pi^0$  ( $\pi^0$  into Dalitz pair) and PDG 04 values are used for  $\text{B}(K_L^0 \rightarrow \pi^+ \pi^- \pi^0)$  and  $\text{B}(\pi^0 \rightarrow e^+ e^- \gamma)$ . The systematic error includes a normalization error of ±0.10.  
<sup>2</sup>Values are for the total branching fraction, acceptance-corrected for the  $m_{ee}$  cuts shown.  
<sup>3</sup>Distribution of angles between two  $e^+ e^-$  pair planes favors  $CP = -1$  for  $K_L^0$ .

$\Gamma(\pi^0 \mu^+ \mu^-)/\Gamma_{\text{total}}$   
Violates CP in leading order. Test for  $\Delta S = 1$  weak neutral current. Allowed by higher-order electroweak interaction.

VALUE (units $10^{-9}$ )	CL%	EVTS	DOCUMENT ID	TECN
<b>&lt;0.38</b>	90		ALAVI-HARATI 00D	KTEV
<5.1	90	0	HARRIS 93	E799

$\Gamma(\pi^0 e^+ e^-)/\Gamma_{\text{total}}$   
Violates CP in leading order. Direct and indirect CP-violating contributions are expected to be comparable and to dominate the CP-conserving part. LAI 02B result suggests that CP-violation effects dominate. Test for  $\Delta S = 1$  weak neutral current. Allowed by higher-order electroweak interaction.

VALUE (units $10^{-10}$ )	CL%	EVTS	DOCUMENT ID	TECN	COMMENT
<b>&lt; 2.8</b>	90		<sup>1</sup> ALAVI-HARATI 04A		KTEV combined result
< 3.5	90		ALAVI-HARATI 04A		KTEV
0.0047 <sup>+0.0022</sup> -0.0018			<sup>2</sup> LAI	02B	NA48 CP-conserving part
< 5.1	90	2	ALAVI-HARATI 01		KTEV
0.01 to 0.02			ALAVI-HARATI 99B		KTEV CP-conserving part
< 43	90	0	HARRIS 93B		E799
< 75	90	0	BARKER 90		E731
< 55	90	0	OHL 90		B845
< 400	90		BARR 88		NA31
<3200	90		JASTRZEM... 88		SPEC

<sup>1</sup> Combined result of ALAVI-HARATI 04A 1999-2000 data set and ALAVI-HARATI 01 1997 data set.  
<sup>2</sup> LAI 02B uses the absence of a signal in  $K_L^0 \rightarrow \pi^0 \gamma \gamma$  with  $m(\gamma\gamma) < m(\pi^0)$  and their  $a_V$  value to predict this value.

$\Gamma(\pi^0 \nu \bar{\nu})/\Gamma_{\text{total}}$   
Violates CP in leading order. Test of direct CP violation since the indirect CP-violating and CP-conserving contributions are expected to be suppressed. Test of  $\Delta S = 1$  weak neutral current.

VALUE (units $10^{-8}$ )	CL%	DOCUMENT ID	TECN
<b>&lt; 0.30</b>	90	<sup>1</sup> AHN 19	KOTO
< 5.1	90	<sup>2</sup> AHN 17	KOTO
< 2.6	90	<sup>3</sup> AHN 10	K391
< 6.7	90	<sup>4</sup> AHN 08	K391
< 21	90	<sup>5</sup> AHN 06	K391
< 59	90	ALAVI-HARATI 00	KTEV

<sup>1</sup> AHN 19 result is based on data collected in 2015, which corresponds to  $2.2 \times 10^{19}$  protons on target. A single event sensitivity of  $(1.30 \pm 0.01 \pm 0.14) \times 10^{-9}$  was achieved with no candidate events observed. An upper limit of  $< 2.4 \times 10^{-9}$  at the 90% C.L. for the  $K_L \rightarrow \pi^0 X^0$  decay was also set, where  $X^0$  is an invisible particle with a mass of 135  $\text{MeV}/c^2$ .  
<sup>2</sup> AHN 17 result is based on the first 100 hours of physics running in 2013. One candidate event was observed with an expected background of  $0.34 \pm 0.16$  events. An upper limit of  $< 3.7 \times 10^{-8}$  at the 90% C.L. for the  $K_L \rightarrow \pi^0 X^0$  decay was also set, where  $X^0$  is an invisible particle with a mass of 135  $\text{MeV}/c^2$ .  
<sup>3</sup> Obtained combining Run-2 (AHN 08) and Run-3 data.  
<sup>4</sup> Value obtained using data from February to April 2005.  
<sup>5</sup> Value obtained analyzing 10% of data of RUN 1 (performed in 2004).

$\Gamma(\pi^0 \pi^0 \nu \bar{\nu})/\Gamma_{\text{total}}$   
Violates CP in leading order. Test of direct CP violation since the indirect CP-violating and CP-conserving contributions are expected to be suppressed. Test of  $\Delta S = 1$  weak neutral current.

VALUE	CL%	DOCUMENT ID	TECN
<b>&lt;8.1 × 10<sup>-7</sup></b>	90	<sup>1</sup> OGATA 11	K391
<4.7 × 10 <sup>-5</sup>	90	<sup>2</sup> NIX 07	K391

<sup>1</sup> Using 2005 Run-I data. OGATA 11 also sets a limit on the  $K_L^0 \rightarrow \pi^0 \pi^0 X \rightarrow$  invisible particles process: the limit on the branching fraction varied from  $7.0 \times 10^{-7}$  to  $4.0 \times 10^{-5}$  for the mass of X ranging from 50 to 200  $\text{MeV}/c^2$ .  
<sup>2</sup> Observed 1 event with expected background of  $0.43 \pm 0.35$  events. NIX 07 also measured  $\text{B}(K_L^0 \rightarrow \pi^0 \pi^0 P) < 1.2 \times 10^{-6}$  at 90% CL, where P is the pseudoscalar particle and  $m_P < 100 \text{ MeV}$ .

$\Gamma(e^\pm \mu^\mp)/\Gamma_{\text{total}}$   
Test of lepton family number conservation.

VALUE (units $10^{-11}$ )	CL%	EVTS	DOCUMENT ID	TECN
<b>&lt;0.47</b>	90		AMBROSE 98B	B871
<9.4	90	0	AKAGI 95	SPEC
<3.9	90	0	ARISA KA 93	B791
<3.3	90	0	<sup>1</sup> ARISA KA 93	B791

<sup>1</sup> This is the combined result of ARISA KA 93 and MATHIAZHAGAN 89.

$\Gamma(e^\pm e^\pm \mu^\mp \mu^\mp)/\Gamma_{\text{total}}$   
Test of lepton family number conservation.

VALUE (units $10^{-11}$ )	CL%	EVTS	DOCUMENT ID	TECN	COMMENT
<b>&lt; 4.12</b>	90	0	ALAVI-HARATI 03B		KTEV
< 12.3	90	0	<sup>1</sup> ALAVI-HARATI 01H		KTEV Sup. by ALAVI-HARATI 03B
< 610	90	0	<sup>1</sup> GU 96		E799

<sup>1</sup> Assuming uniform phase space distribution.

$\Gamma(\pi^0 \mu^\pm e^\mp)/\Gamma_{\text{total}}$   
Test of lepton family number conservation.

VALUE (units $10^{-10}$ )	CL%	DOCUMENT ID	TECN
<b>&lt; 0.76</b>	90	ABOUZAIID 08c	KTEV
< 62	90	ARISA KA 98	E799

Downloaded from https://academic.oup.com/ptep/article/2020/8/083C01/5891211 by guest on 12 November 2020

# Meson Particle Listings

$K_L^0$

$\Gamma(\pi^0 \pi^0 \mu^\pm e^\mp) / \Gamma_{\text{total}}$			
Test of lepton family number conservation.			
VALUE (units $10^{-10}$ )	CL%	DOCUMENT ID	TECN
<1.7	90	ABOUZAID	08c KTEV

See the related review(s):  
 $V_{ud}, V_{us}$  the Cabibbo Angle, and CKM Unitarity

## ENERGY DEPENDENCE OF $K_L^0$ DALITZ PLOT

For discussion, see note on Dalitz plot parameters in the  $K^\pm$  section of the Particle Listings above. For definitions of  $a_v, a_t, a_{ll}$ , and  $a_y$ , see the earlier version of the same note in the 1982 edition of this Review published in Physics Letters **111B** 70 (1982).

$$|\text{matrix element}|^2 = 1 + gu + hu^2 + jv + kv^2 + fuv$$

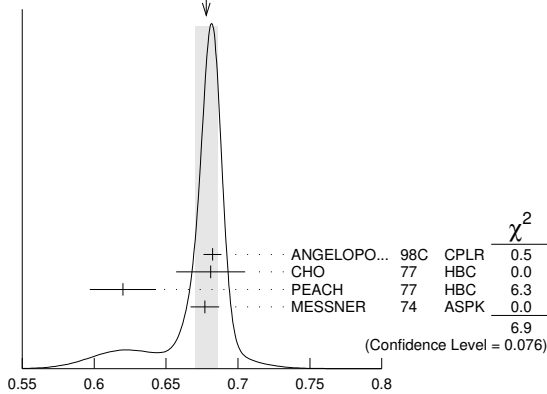
where  $u = (s_3 - s_0) / m_\pi^2$  and  $v = (s_2 - s_1) / m_\pi^2$

## LINEAR COEFFICIENT $g$ FOR $K_L^0 \rightarrow \pi^+ \pi^- \pi^0$

VALUE	EVTS	DOCUMENT ID	TECN	COMMENT
<b>0.678 ± 0.008 OUR AVERAGE</b>				Error includes scale factor of 1.5. See the ideogram below.
0.6823 ± 0.0044 ± 0.0044	500k	ANGELOPO...	98c CPLR	
0.681 ± 0.024	6499	CHO	77 HBC	
0.620 ± 0.023	4709	PEACH	77 HBC	
0.677 ± 0.010	509k	MESSNER	74 ASPK	$a_y = -0.917 \pm 0.013$
• • • We do not use the following data for averages, fits, limits, etc. • • •				
0.69 ± 0.07	192	<sup>1</sup> BALDO...	75 HLBC	
0.590 ± 0.022	56k	<sup>1</sup> BUCHANAN	75 SPEC	$a_{ll} = -0.277 \pm 0.010$
0.619 ± 0.027	20k	<sup>1,2</sup> BISI	74 ASPK	$a_t = -0.282 \pm 0.011$
0.612 ± 0.032		<sup>1</sup> ALEXANDER	73B HBC	
0.73 ± 0.04	3200	<sup>1</sup> BRANDENB...	73 HBC	
0.608 ± 0.043	1486	<sup>1</sup> KRENZ	72 HLBC	$a_t = -0.277 \pm 0.018$
0.650 ± 0.012	29k	<sup>1</sup> ALBROW	70 ASPK	$a_y = -0.858 \pm 0.015$
0.593 ± 0.022	36k	<sup>1,3</sup> BUCHANAN	70 SPEC	$a_{ll} = -0.278 \pm 0.010$
0.664 ± 0.056	4400	<sup>1</sup> SMITH	70 OSPK	$a_t = -0.306 \pm 0.024$
0.400 ± 0.045	2446	<sup>1</sup> BASILE	68B OSPK	$a_t = -0.188 \pm 0.020$
0.649 ± 0.044	1350	<sup>1</sup> HOPKINS	67 HBC	$a_t = -0.294 \pm 0.018$
0.428 ± 0.055	1198	<sup>1</sup> NEFKENS	67 OSPK	$a_{ll} = -0.204 \pm 0.025$

- Quadratic dependence required by some experiments. (See sections on "QUADRATIC COEFFICIENT  $h$ " and "QUADRATIC COEFFICIENT  $k$ " below.) Correlations prevent us from averaging results of fits not including  $g, h,$  and  $k$  terms.
- BISI 74 value comes from quadratic fit with quad. term consistent with zero.  $g$  error is thus larger than if linear fit were used.
- BUCHANAN 70 result revised by BUCHANAN 75 to include radiative correlations and to use more reliable  $K_L^0$  momentum spectrum of second experiment (had same beam).

WEIGHTED AVERAGE  
 0.678±0.008 (Error scaled by 1.5)



Linear coeff.  $g$  for  $K_L^0 \rightarrow \pi^+ \pi^- \pi^0$  matrix element squared

## QUADRATIC COEFFICIENT $h$ FOR $K_L^0 \rightarrow \pi^+ \pi^- \pi^0$

See notes in section "LINEAR COEFFICIENT  $g$  FOR  $K_L^0 \rightarrow \pi^+ \pi^- \pi^0$  |MATRIX ELEMENT<sup>2</sup>" above.

VALUE	EVTS	DOCUMENT ID	TECN
<b>0.076 ± 0.006 OUR AVERAGE</b>			
0.061 ± 0.004 ± 0.015	500k	ANGELOPO...	98c CPLR
0.095 ± 0.032	6499	CHO	77 HBC
0.048 ± 0.036	4709	PEACH	77 HBC
0.079 ± 0.007	509k	MESSNER	74 ASPK
• • • We do not use the following data for averages, fits, limits, etc. • • •			
-0.011 ± 0.018	29k	<sup>1</sup> ALBROW	70 ASPK
0.043 ± 0.052	4400	<sup>1</sup> SMITH	70 OSPK

- Quadratic coefficients  $h$  and  $k$  required by some experiments. (See section on "QUADRATIC COEFFICIENT  $k$ " below.) Correlations prevent us from averaging results of fits not including  $g, h,$  and  $k$  terms.

## QUADRATIC COEFFICIENT $k$ FOR $K_L^0 \rightarrow \pi^+ \pi^- \pi^0$

VALUE	EVTS	DOCUMENT ID	TECN
<b>0.0099 ± 0.0015 OUR AVERAGE</b>			
0.0104 ± 0.0017 ± 0.0024	500k	ANGELOPO...	98c CPLR
0.024 ± 0.010	6499	CHO	77 HBC
-0.008 ± 0.012	4709	PEACH	77 HBC
0.0097 ± 0.0018	509k	MESSNER	74 ASPK

## LINEAR COEFFICIENT $j$ FOR $K_L^0 \rightarrow \pi^+ \pi^- \pi^0$ (CP-VIOLATING TERM)

Listed in CP-violation section below.

## QUADRATIC COEFFICIENT $f$ FOR $K_L^0 \rightarrow \pi^+ \pi^- \pi^0$ (CP-VIOLATING TERM)

Listed in CP-violation section below.

## QUADRATIC COEFFICIENT $h$ FOR $K_L^0 \rightarrow \pi^0 \pi^0 \pi^0$

We do not average measurements that do not account for the effect of final state rescattering.

VALUE (units $10^{-3}$ )	EVTS	DOCUMENT ID	TECN
<b>+0.59 ± 0.20 ± 1.16</b>	68M	<sup>1</sup> ABOUZAID	08A KTEV
• • • We do not use the following data for averages, fits, limits, etc. • • •			
-6.1 ± 0.9 ± 0.5	14.7M	<sup>2</sup> LAI	01B NA48
-3.3 ± 1.1 ± 0.7	5M	<sup>2,3</sup> SOMALWAR	92 E731

- Result obtained using C13pl model of CABIBBO 05 to include  $\pi\pi$  rescattering effects. The systematic error includes an external error of  $1.06 \times 10^{-3}$  from the parametrization input of  $(a_0 - a_2) m_{\pi^+} = 0.268 \pm 0.017$  from BATLEY 06B.
- LAI 01B and SOMALWAR 92 results do not include  $\pi\pi$  final state rescattering effects.
- SOMALWAR 92 chose  $m_{\pi^+}$  as normalization to make it compatible with the Particle Data Group  $K_L^0 \rightarrow \pi^+ \pi^- \pi^0$  definitions.

## $K_L^0$ FORM FACTORS

For discussion, see note on form factors in the  $K^\pm$  section of the Particle Listings above.

In the form factor comments, the following symbols are used.

$f_+$  and  $f_-$  are form factors for the vector matrix element.

$f_S$  and  $f_T$  refer to the scalar and tensor term.

$$f_0(t) = f_+(t) + f_-(t) t / (m_{K^0}^2 - m_{\pi^+}^2).$$

$t$  = momentum transfer to the  $\pi$ .

$\lambda_+$  and  $\lambda_0$  are the linear expansion coefficients of  $f_+$  and  $f_0$ :

$$f_+(t) = f_+(0) (1 + \lambda_+ t / m_{\pi^+}^2)$$

For quadratic expansion

$$f_+(t) = f_+(0) (1 + \lambda'_+ t / m_{\pi^+}^2 + \frac{\lambda''_+}{2} t^2 / m_{\pi^+}^4)$$

as used by KTeV. If there is a non-vanishing quadratic term, then  $\lambda_+$  represents an average slope, which is then different from  $\lambda'_+$ .

NA48 ( $K_{e3}$ ) and ISTRA quadratic expansion coefficients are converted with

$$\lambda'_+ PDG = \lambda_+ NA48 \text{ and } \lambda''_+ PDG = 2 \lambda'_+ NA48$$

$$\lambda'_+ PDG = (\frac{m_{\pi^+}}{m_{\pi^0}})^2 \lambda_+ ISTRA \text{ and}$$

$$\lambda''_+ PDG = 2 (\frac{m_{\pi^+}}{m_{\pi^0}})^4 \lambda'_+ ISTRA$$

ISTRA linear expansion coefficients are converted with

$$\lambda_+ PDG = (\frac{m_{\pi^+}}{m_{\pi^0}})^2 \lambda_+ ISTRA \text{ and } \lambda_0 PDG = (\frac{m_{\pi^+}}{m_{\pi^0}})^2 \lambda_0 ISTRA$$

The pole parametrization is

$$f_+(t) = f_+(0) (\frac{M_V^2}{M_V^2 - t})$$

$$f_0(t) = f_0(0) (\frac{M_S^2}{M_S^2 - t})$$

where  $M_V$  and  $M_S$  are the vector and scalar pole masses.

The dispersive parametrization is

$$f_+(t) = f_+(0) \exp[\frac{t}{m_{\pi^+}^2} (\Lambda_+ + H(t))];$$

$$f_0(t) = f_0(0) \exp[\frac{t}{m_{\pi^+}^2 - m_{\pi^0}^2} (\ln[C] - G(t))],$$

where  $\Lambda_+$  is the slope parameter and  $\ln[C] = \ln[f_0(m_K^2 - m_\pi^2)]$

is the logarithm of the scalar form factor at the Callan-Treiman point.

$H(t)$  and  $G(t)$  are dispersive integrals.

The following abbreviations are used:

DP = Dalitz plot analysis.

PI =  $\pi$  spectrum analysis.

MU =  $\mu$  spectrum analysis.

POL =  $\mu$  polarization analysis.

BR =  $K_{\mu 3}^0 / K_{e 3}^0$  branching ratio analysis.

E = positron or electron spectrum analysis.

RC = radiative corrections.

$\lambda_+$  (LINEAR ENERGY DEPENDENCE OF  $f_+$  IN  $K_{e3}^0$  DECAY)

For radiative correction of  $K_{e3}^0$  DP, see GINSBERG 67, BECHERRAWY 70, CIRIGLIANO 02, CIRIGLIANO 04, and ANDRE 07. Results labeled OUR FIT are discussed in the review “ $K_{e3}^\pm$  and  $K_{e3}^0$  Form Factors” in the  $K^\pm$  Listings. For earlier, lower statistics results, see the 2004 edition of this review, Physics Letters **B592** 1 (2004).

VALUE (units $10^{-2}$ )	EVTS	DOCUMENT ID	TECN	COMMENT
<b>2.82 ± 0.04 OUR FIT</b>				Error includes scale factor of 1.1. Assuming $\mu$ -e universality
<b>2.85 ± 0.04 OUR AVERAGE</b>				
2.86 ± 0.05 ± 0.04	2M	AMBROSINO 06D	KLOE	
2.832 ± 0.037 ± 0.043	1.9M	ALEXOPOU... 04A	KTEV	PI, no $\mu = e$
2.88 ± 0.04 ± 0.11	5.6M	<sup>1</sup> LAI 04c	NA48	DP
• • • We do not use the following data for averages, fits, limits, etc. • • •				
2.84 ± 0.07 ± 0.13	5.6M	<sup>2</sup> LAI 04c	NA48	DP
2.45 ± 0.12 ± 0.22	366k	APOSTOLA... 00	CPLR	DP
3.06 ± 0.34	74k	BIRULEV 81	SPEC	DP
3.12 ± 0.25	500k	GJESDAL 76	SPEC	DP
2.70 ± 0.28	25k	BLUMENTHAL 75	SPEC	DP

<sup>1</sup> Results from linear fit and assuming only vector and axial couplings.  
<sup>2</sup> Results from linear fit with  $|f_S/f_+|$  and  $|f_T/f_+|$  free.

$\lambda_+$  (LINEAR ENERGY DEPENDENCE OF  $f_+$  IN  $K_{\mu 3}^0$  DECAY)

Results labeled OUR FIT are discussed in the review “ $K_{e3}^\pm$  and  $K_{e3}^0$  Form Factors” in the  $K^\pm$  Listings. For earlier, lower statistics results, see the 2004 edition of this review, Physics Letters **B592** 1 (2004).

VALUE (units $10^{-2}$ )	EVTS	DOCUMENT ID	TECN	COMMENT
<b>2.82 ± 0.04 OUR FIT</b>				Error includes scale factor of 1.1. Assuming $\mu$ -e universality
<b>2.71 ± 0.10 OUR FIT</b>				Error includes scale factor of 1.4. Not assuming $\mu$ -e universality
2.67 ± 0.06 ± 0.08	2.3M	<sup>1</sup> LAI 07A	NA48	DP
2.745 ± 0.088 ± 0.063	1.5M	ALEXOPOU... 04A	KTEV	DP, no $\mu = e$
2.813 ± 0.051	3.4M	ALEXOPOU... 04A	KTEV	PI, DP, $\mu = e$
3.0 ± 0.3	1.6M	DONALDSON 74B	SPEC	DP
• • • We do not use the following data for averages, fits, limits, etc. • • •				
4.27 ± 0.44	150k	BIRULEV 81	SPEC	DP

<sup>1</sup> LAI 07A gives a correlation  $-0.40$  between their  $\lambda_0$  and  $\lambda_+$  measurements.

$\lambda_0$  (LINEAR ENERGY DEPENDENCE OF  $f_0$  IN  $K_{\mu 3}^0$  DECAY)

Wherever possible, we have converted the above values of  $\xi(0)$  into values of  $\lambda_0$  using the associated  $\lambda_+^H$  and  $d\xi(0)/d\lambda_+$ . Results labeled OUR FIT are discussed in the review “ $K_{e3}^\pm$  and  $K_{e3}^0$  Form Factors” in the  $K^\pm$  Listings. For earlier, lower statistics results, see the 2004 edition of this review, Physics Letters **B592** 1 (2004).

VALUE (units $10^{-2}$ )	$d\lambda_0/d\lambda_+$	EVTS	DOCUMENT ID	TECN	COMMENT
<b>1.38 ± 0.18 OUR FIT</b>					Error includes scale factor of 2.2. Assuming $\mu$ -e universality
<b>1.42 ± 0.23 OUR FIT</b>					Error includes scale factor of 2.8. Not assuming $\mu$ -e universality
1.17 ± 0.07 ± 0.10		2.3M	<sup>1</sup> LAI 07A	NA48	DP
1.657 ± 0.125	-0.44	1.5M	<sup>2</sup> ALEXOPOU... 04A	KTEV	DP, no $\mu = e$
1.635 ± 0.121	-0.85	3.4M	<sup>3</sup> ALEXOPOU... 04A	KTEV	PI, DP, $\mu = e$
+1.9 ± 0.4	-0.47	1.6M	<sup>4</sup> DONALDSON 74B	SPEC	DP
• • • We do not use the following data for averages, fits, limits, etc. • • •					
3.41 ± 0.67	unknown	150k	<sup>5</sup> BIRULEV 81	SPEC	DP

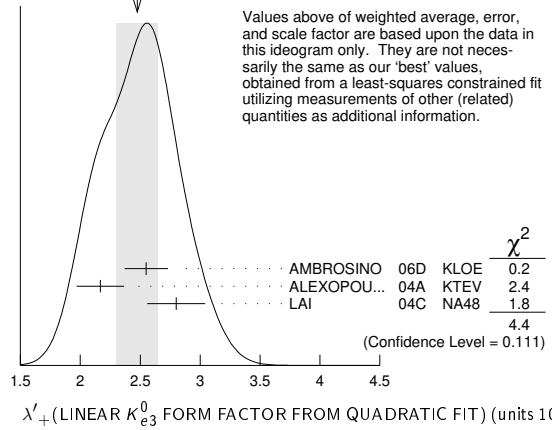
<sup>1</sup> LAI 07A gives a correlation  $-0.40$  between their  $\lambda_0$  and  $\lambda_+$  measurements.  
<sup>2</sup> ALEXOPOULOS 04A gives a correlation  $-0.38$  between their  $\lambda_0$  and  $\lambda_+$  measurements.  
<sup>3</sup> ALEXOPOULOS 04A gives a correlation  $-0.36$  between their  $\lambda_0$  and  $\lambda_+$  measurements.  
<sup>4</sup> DONALDSON 74B  $d\lambda_0/d\lambda_+$  obtained from figure 18.  
<sup>5</sup> BIRULEV 81 gives  $d\lambda_0/d\lambda_+ = -1.5$ , giving an unreasonably narrow error ellipse which dominates all other results. We use  $d\lambda_0/d\lambda_+ = 0$ .

$\lambda'_+$  (LINEAR  $K_{e3}^0$  FORM FACTOR FROM QUADRATIC FIT)

VALUE (units $10^{-2}$ )	EVTS	DOCUMENT ID	TECN	COMMENT
<b>2.40 ± 0.12 OUR FIT</b>				Error includes scale factor of 1.2. Assuming $\mu$ -e universality
<b>2.49 ± 0.13 OUR FIT</b>				Error includes scale factor of 1.1. Not assuming $\mu$ -e universality
<b>2.48 ± 0.17 OUR AVERAGE</b>				Error includes scale factor of 1.5. See the ideogram below.
2.55 ± 0.15 ± 0.10	2M	<sup>1</sup> AMBROSINO 06D	KLOE	
2.167 ± 0.137 ± 0.143	1.9M	<sup>2</sup> ALEXOPOU... 04A	KTEV	PI, no $\mu = e$
2.80 ± 0.19 ± 0.15	5.6M	<sup>3</sup> LAI 04c	NA48	DP

<sup>1</sup> We use AMBROSINO 06D result in the fit not assuming  $\mu$ -e universality. This result enters the fit assuming  $\mu$ -e universality via AMBROSINO 07C measurement of  $\lambda'_+$  in  $K_{\mu 3}$  decays. AMBROSINO 06D gives a correlation  $-0.95$  between their  $\lambda'_+$  and  $\lambda''_+$ .  
<sup>2</sup> ALEXOPOULOS 04A gives a correlation  $-0.97$  between their  $\lambda'_+$  and  $\lambda''_+$ .  
<sup>3</sup> For LAI 04c we calculate a correlation  $-0.88$  between their  $\lambda'_+$  and  $\lambda''_+$ .

WEIGHTED AVERAGE  
2.48±0.17 (Error scaled by 1.5)



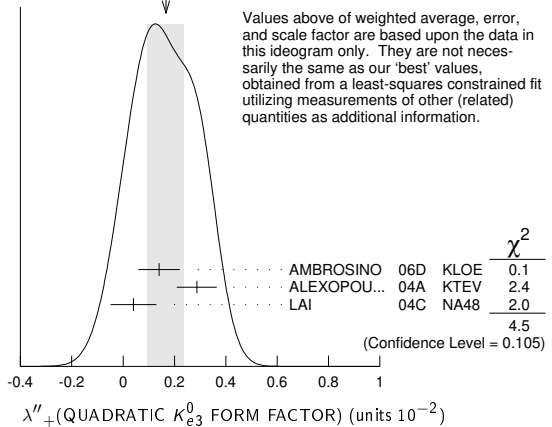
Values above of weighted average, error, and scale factor are based upon the data in this ideogram only. They are not necessarily the same as our 'best' values, obtained from a least-squares constrained fit utilizing measurements of other (related) quantities as additional information.

$\lambda''_+$  (QUADRATIC  $K_{e3}^0$  FORM FACTOR)

VALUE (units $10^{-2}$ )	EVTS	DOCUMENT ID	TECN	COMMENT
<b>0.20 ± 0.05 OUR FIT</b>				Error includes scale factor of 1.2. Assuming $\mu$ -e universality
<b>0.16 ± 0.05 OUR FIT</b>				Error includes scale factor of 1.1. Not assuming $\mu$ -e universality
<b>0.17 ± 0.07 OUR AVERAGE</b>				Error includes scale factor of 1.5. See the ideogram below.
0.14 ± 0.07 ± 0.04	2M	<sup>1</sup> AMBROSINO 06D	KLOE	
0.287 ± 0.057 ± 0.053	1.9M	<sup>2</sup> ALEXOPOU... 04A	KTEV	PI, no $\mu = e$
0.04 ± 0.08 ± 0.04	5.6M	<sup>3,4</sup> LAI 04c	NA48	DP

<sup>1</sup> We use AMBROSINO 06D result in the fit not assuming  $\mu$ -e universality. This result enters the fit assuming  $\mu$ -e universality via AMBROSINO 07C measurement of  $\lambda''_+$  in  $K_{\mu 3}$  decays. AMBROSINO 06D gives a correlation  $-0.95$  between their  $\lambda'_+$  and  $\lambda''_+$ .  
<sup>2</sup> ALEXOPOULOS 04A gives a correlation  $-0.97$  between their  $\lambda'_+$  and  $\lambda''_+$ .  
<sup>3</sup> Values doubled to agree with PDG conventions described above.  
<sup>4</sup> LAI 04c gives a correlation  $-0.88$  between their  $\lambda'_+$  and  $\lambda''_+$ .

WEIGHTED AVERAGE  
0.17±0.07 (Error scaled by 1.5)



Values above of weighted average, error, and scale factor are based upon the data in this ideogram only. They are not necessarily the same as our 'best' values, obtained from a least-squares constrained fit utilizing measurements of other (related) quantities as additional information.

$\lambda'_+$  (LINEAR  $K_{\mu 3}^0$  FORM FACTOR FROM QUADRATIC FIT)

VALUE (units $10^{-2}$ )	EVTS	DOCUMENT ID	TECN	COMMENT
<b>2.40 ± 0.12 OUR FIT</b>				Error includes scale factor of 1.2. Assuming $\mu$ -e universality
<b>1.89 ± 0.24 OUR FIT</b>				Not assuming $\mu$ -e universality
2.23 ± 0.98 ± 0.37	1.8M	<sup>1</sup> AMBROSINO 07C	KLOE	no $\mu = e$
2.56 ± 0.15 ± 0.09	3.8M	<sup>1</sup> AMBROSINO 07C	KLOE	$\mu = e$
2.05 ± 0.22 ± 0.24	2.3M	<sup>1</sup> LAI 07A	NA48	DP
1.703 ± 0.319 ± 0.177	1.5M	<sup>1</sup> ALEXOPOU... 04A	KTEV	DP, no $\mu = e$
2.064 ± 0.175	3.4M	<sup>1</sup> ALEXOPOU... 04A	KTEV	PI, DP, $\mu = e$

<sup>1</sup> See section  $\lambda_0$  below for correlations.

$\lambda''_+$  (QUADRATIC  $K_{\mu 3}^0$  FORM FACTOR)

VALUE (units $10^{-2}$ )	EVTS	DOCUMENT ID	TECN	COMMENT
<b>0.20 ± 0.05 OUR FIT</b>				Error includes scale factor of 1.2. Assuming $\mu$ -e universality
<b>0.37 ± 0.12 OUR FIT</b>				Error includes scale factor of 1.3. Not assuming $\mu$ -e universality
0.48 ± 0.49 ± 0.16	1.8M	<sup>1</sup> AMBROSINO 07C	KLOE	no $\mu = e$
0.15 ± 0.07 ± 0.04	3.8M	<sup>1</sup> AMBROSINO 07C	KLOE	$\mu = e$
0.26 ± 0.09 ± 0.10	2.3M	<sup>1</sup> LAI 07A	NA48	DP
0.443 ± 0.131 ± 0.072	1.5M	<sup>1</sup> ALEXOPOU... 04A	KTEV	DP, no $\mu = e$
0.320 ± 0.069	3.4M	<sup>1</sup> ALEXOPOU... 04A	KTEV	PI, DP, $\mu = e$

<sup>1</sup> See section  $\lambda_0$  below for correlations.

# Meson Particle Listings

$K_L^0$

## $\lambda_0$ (LINEAR $f_0$ $K_{\mu 3}^0$ FORM FACTOR FROM QUADRATIC FIT)

VALUE (units $10^{-2}$ )	EVTS	DOCUMENT ID	TECN	COMMENT
<b>1.16 ± 0.09 OUR FIT</b>				Error includes scale factor of 1.2. Assuming $\mu$ -e universality
<b>1.07 ± 0.14 OUR FIT</b>				Error includes scale factor of 1.3. Not assuming $\mu$ -e universality
0.91 ± 0.59 ± 0.26	1.8M	<sup>1</sup> AMBROSINO 07c	KLOE	no $\mu = e$
1.54 ± 0.18 ± 0.13	3.8M	<sup>2</sup> AMBROSINO 07c	KLOE	$\mu = e$
0.95 ± 0.11 ± 0.08	2.3M	<sup>3</sup> LAI 07A	NA48	DP
1.281 ± 0.136 ± 0.122	1.5M	<sup>4</sup> ALEXOPOU... 04A	KTEV	DP, no $\mu = e$
1.372 ± 0.131	3.4M	<sup>5</sup> ALEXOPOU... 04A	KTEV	PI, DP, $\mu = e$

<sup>1</sup> AMBROSINO 07c, not assuming  $\mu$ -e universality, gives a correlation matrix

$\chi''_+$	$\chi''_+$
$\chi''_+$	-0.97
$\lambda_0$	0.81
	-0.91

<sup>2</sup> AMBROSINO 07c, assuming  $\mu$ -e universality, gives a correlation matrix

$\chi''_+$	$\chi''_+$
$\chi''_+$	-0.95
$\lambda_0$	0.29
	-0.38

<sup>3</sup> LAI 07A gives a correlation matrix

$\chi''_+$	$\chi''_+$
$\chi''_+$	-0.96
$\lambda_0$	0.63
	-0.73

<sup>4</sup> ALEXOPOULOS 04A, not assuming  $\mu$ -e universality, gives a correlation matrix

$\chi''_+$	$\chi''_+$	$\lambda_0$
$\chi''_+$	1	
$\chi''_+$	-0.96	1
$\lambda_0$	0.65	-0.75
		1

<sup>5</sup> ALEXOPOULOS 04A, assuming  $\mu$ -e universality, gives a correlation matrix

$\chi''_+$	$\chi''_+$	$\lambda_0$
$\chi''_+$	1	
$\chi''_+$	-0.97	1
$\lambda_0$	0.34	-0.44
		1

## $M_V^e$ (POLE MASS FOR $K_{e 3}^0$ DECAY)

VALUE (MeV)	EVTS	DOCUMENT ID	TECN	COMMENT
<b>878 ± 6 OUR FIT</b>				Error includes scale factor of 1.1. Assuming $\mu$ -e universality
<b>875 ± 5 OUR AVERAGE</b>				
870 ± 6 ± 7	2M	AMBROSINO 06D	KLOE	
881.03 ± 5.12 ± 4.94	1.9M	ALEXOPOU... 04A	KTEV	PI, no $\mu = e$
859 ± 18	5.6M	LAI 04C	NA48	

## $M_V^\mu$ (POLE MASS FOR $K_{\mu 3}^0$ DECAY)

VALUE (MeV)	EVTS	DOCUMENT ID	TECN	COMMENT
<b>878 ± 6 OUR FIT</b>				Error includes scale factor of 1.1. Assuming $\mu$ -e universality
<b>900 ± 21 OUR FIT</b>				Error includes scale factor of 1.7. Not assuming $\mu$ -e universality
905 ± 9 ± 17	2.3M	<sup>1</sup> LAI 07A	NA48	DP
889.19 ± 12.81 ± 9.92	1.5M	<sup>1</sup> ALEXOPOU... 04A	KTEV	DP, no $\mu = e$
882.32 ± 6.54	3.4M	<sup>1</sup> ALEXOPOU... 04A	KTEV	PI, DP, $\mu = e$

<sup>1</sup> See section  $M_S^\mu$  below for correlations.

## $M_S^\mu$ (POLE MASS FOR $K_{\mu 3}^0$ DECAY)

VALUE (MeV)	EVTS	DOCUMENT ID	TECN	COMMENT
<b>1252 ± 90 OUR FIT</b>				Error includes scale factor of 2.6. Assuming $\mu$ -e universality
<b>1222 ± 80 OUR FIT</b>				Error includes scale factor of 2.3. Not assuming $\mu$ -e universality
1400 ± 46 ± 53	2.3M	<sup>1</sup> LAI 07A	NA48	DP
1167.14 ± 28.30 ± 31.04	1.5M	<sup>2</sup> ALEXOPOU... 04A	KTEV	PI, no $\mu = e$
1173.80 ± 39.47	3.4M	<sup>3</sup> ALEXOPOU... 04A	KTEV	PI, DP, $\mu = e$

<sup>1</sup> LAI 07A gives a correlation  $-0.47$  between their  $M_S^\mu$  and  $M_V^\mu$  measurements, not assuming  $\mu$ -e universality.

<sup>2</sup> ALEXOPOULOS 04A gives a correlation  $-0.46$  between their  $M_S^\mu$  and  $M_V^\mu$  measurements, not assuming  $\mu$ -e universality.

<sup>3</sup> ALEXOPOULOS 04A gives a correlation  $-0.40$  between their  $M_S^\mu$  and  $M_V^\mu$  measurements, assuming  $\mu$ -e universality.

## $\Lambda_+$ (DISPERSIVE VECTOR FORM FACTOR FOR $K_{\mu 3}^0$ DECAY)

See the review on " $K_{e 3}^0$  and  $K_{\mu 3}^0$  Form Factors" for details of the dispersive parametrization.

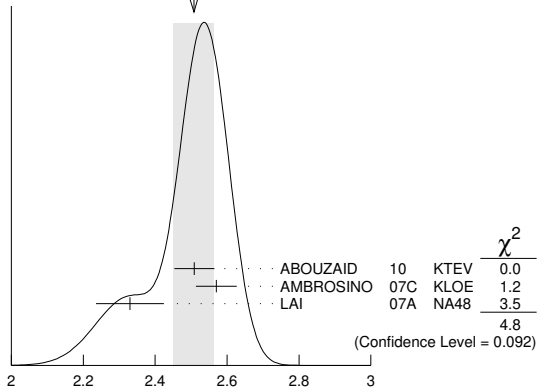
VALUE (units $10^{-2}$ )	EVTS	DOCUMENT ID	TECN	COMMENT
<b>2.51 ± 0.06 OUR AVERAGE</b>				Error includes scale factor of 1.5. See the ideogram below.
2.509 ± 0.035 ± 0.043	3.4M	<sup>1</sup> ABOUZAID 10	KTEV	$\mu = e$
2.57 ± 0.04 ± 0.04	3.8M	<sup>2</sup> AMBROSINO 07c	KLOE	$\mu = e$
2.33 ± 0.05 ± 0.08	2.3M	<sup>3</sup> LAI 07A	NA48	DP

<sup>1</sup> Obtained from a sample of 1.9 M  $K_{e 3}$  and 1.5 M  $K_{\mu 3}$ . The correlation between  $\Lambda_+$  and  $\ln(C)$  is  $-0.269$ .

<sup>2</sup> AMBROSINO 07c results include 2M  $K_{e 3}$  events from AMBROSINO 06D. The correlation between  $\Lambda_+$  and  $\ln(C)$  is  $-0.26$ .

<sup>3</sup> LAI 07A gives a correlation  $-0.44$  between their  $\Lambda_+$  and  $\ln(C)$  measurements.

WEIGHTED AVERAGE  
2.51±0.06 (Error scaled by 1.5)



$\Lambda_+$  (DISPERSIVE VECTOR FORM FACTOR FOR  $K_{\mu 3}^0$  DECAY) (units  $10^{-2}$ )

## $\ln(C)$ (DISPERSIVE SCALAR FORM FACTOR FOR $K_{\mu 3}^0$ DECAY)

See the review on " $K_{e 3}^0$  and  $K_{\mu 3}^0$  Form Factors" for details of the dispersive parametrization.

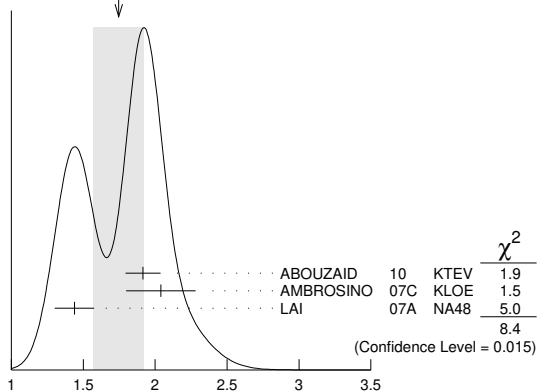
VALUE (units $10^{-1}$ )	EVTS	DOCUMENT ID	TECN	COMMENT
<b>1.75 ± 0.18 OUR AVERAGE</b>				Error includes scale factor of 2.0. See the ideogram below.
1.915 ± 0.078 ± 0.094	3.4M	<sup>1</sup> ABOUZAID 10	KTEV	$\mu = e$
2.04 ± 0.19 ± 0.15	3.8M	<sup>2</sup> AMBROSINO 07c	KLOE	$\mu = e$
1.438 ± 0.080 ± 0.112	2.3M	<sup>3</sup> LAI 07A	NA48	DP

<sup>1</sup> Obtained from a sample of 1.9 M  $K_{e 3}$  and 1.5 M  $K_{\mu 3}$ . The correlation between  $\Lambda_+$  and  $\ln(C)$  is  $-0.269$ .

<sup>2</sup> AMBROSINO 07c results include 2M  $K_{e 3}$  events from AMBROSINO 06D. We convert  $(\Lambda_+, \Lambda_0)$  to  $(\Lambda_+, \ln(C))$  parametrization using  $\ln(C) = (\Lambda_0 \cdot 11.713 + 0.0398) \pm 0.0041$ , where the error is due to theory parametrization of the form factor. The correlation between  $\Lambda_+$  and  $\ln(C)$  is  $-0.26$ .

<sup>3</sup> LAI 07A gives a correlation  $-0.44$  between their  $\Lambda_+$  and  $\ln(C)$  measurements.

WEIGHTED AVERAGE  
1.75±0.18 (Error scaled by 2.0)



$\ln(C)$  (DISPERSIVE SCALAR FORM FACTOR FOR  $K_{\mu 3}^0$  DECAY) (units  $10^{-1}$ )

## $a_1(t_0, Q^2)$ FORM FACTOR PARAMETER

See HILL 06 for a definition of this parameter.

VALUE	EVTS	DOCUMENT ID	TECN
<b>1.023 ± 0.028 ± 0.029</b>	2M	<sup>1</sup> ABOUZAID 06c	KTEV

<sup>1</sup>  $Q^2 = 2 \text{ GeV}^2$ ,  $t_0 = 0.49 (m_K - m_\pi)^2$ . Correlation between  $a_1$  and  $a_2$ :  $\rho_{12} = -0.064$ .

## $a_2(t_0, Q^2)$ FORM FACTOR PARAMETER

See HILL 06 for a definition of this parameter.

VALUE	EVTS	DOCUMENT ID	TECN
<b>0.75 ± 1.58 ± 1.47</b>	2M	<sup>1</sup> ABOUZAID 06c	KTEV

<sup>1</sup>  $Q^2 = 2 \text{ GeV}^2$ ,  $t_0 = 0.49 (m_K - m_\pi)^2$ . Correlation between  $a_1$  and  $a_2$ :  $\rho_{12} = -0.064$ .

**$|f_S/f_+|$  FOR  $K_{e3}^0$  DECAY**

Ratio of scalar to  $f_+$  couplings.

VALUE (units $10^{-2}$ )	CL%	EVTS	DOCUMENT ID	TECN	COMMENT
$1.5^{+0.7}_{-1.0} \pm 1.2$		5.6M	<sup>1</sup> LAI	04C	NA48
• • • We do not use the following data for averages, fits, limits, etc. • • •					
<9.5	95	18k	HILL	78	STRC
<7.	68	48k	BIRULEV	76	SPEC See also BIRULEV 81
<4.	68	25k	BLUMENTHAL75	SPEC	

<sup>1</sup> Results from linear fit with  $|f_S/f_+|$  and  $|f_T/f_+|$  free.

**$|f_T/f_+|$  FOR  $K_{e3}^0$  DECAY**

Ratio of tensor to  $f_+$  couplings.

VALUE (units $10^{-2}$ )	CL%	EVTS	DOCUMENT ID	TECN	COMMENT
$5^{+3}_{-4} \pm 3$		5.6M	<sup>1</sup> LAI	04C	NA48
• • • We do not use the following data for averages, fits, limits, etc. • • •					
<40.	95	18k	HILL	78	STRC
<34.	68	48k	BIRULEV	76	SPEC See also BIRULEV 81
<23.	68	25k	BLUMENTHAL75	SPEC	

<sup>1</sup> Results from linear fit with  $|f_S/f_+|$  and  $|f_T/f_+|$  free.

**$|f_T/f_+|$  FOR  $K_{\mu 3}^0$  DECAY**

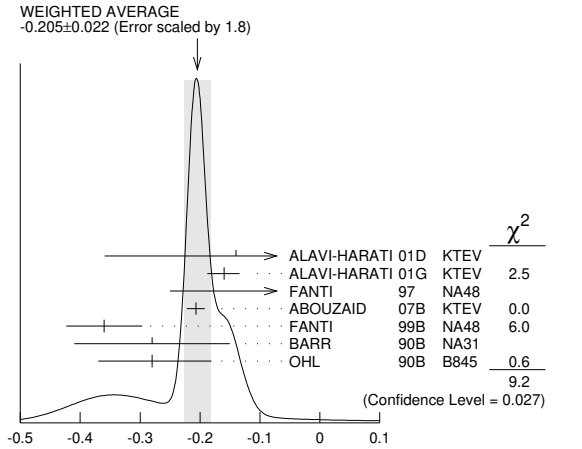
Ratio of tensor to  $f_+$  couplings.

VALUE (units $10^{-2}$ )	DOCUMENT ID	TECN
$12. \pm 12.$	BIRULEV 81	SPEC

**$\alpha_{K^*}$  DECAY FORM FACTOR FOR  $K_L \rightarrow \ell^+ \ell^- \gamma, K_L^0 \rightarrow \ell^+ \ell^- \ell^+ \ell^-$**

Average of all  $\alpha_{K^*}$  measurements (from each of three datablocks following this one) assuming lepton universality.

VALUE	DOCUMENT ID
$-0.205 \pm 0.022$ OUR AVERAGE	Includes data from the 3 datablocks that follow this one. Error includes scale factor of 1.8. See the ideogram below.



$\alpha_{K^*}$  DECAY FORM FACTOR FOR  $K_L \rightarrow \ell^+ \ell^- \gamma, K_L^0 \rightarrow \ell^+ \ell^- \ell^+ \ell^-$

**$\alpha_{K^*}$  DECAY FORM FACTOR FOR  $K_L \rightarrow e^+ e^- \gamma$**

$\alpha_{K^*}$  is the constant in the model of BERGSTROM 83 which measures the relative strength of the vector-vector transition  $K_L \rightarrow K^* \gamma$  with  $K^* \rightarrow \rho, \omega, \phi \rightarrow \gamma^*$  and the pseudoscalar-pseudoscalar transition  $K_L \rightarrow \pi, \eta, \eta' \rightarrow \gamma \gamma^*$ .

VALUE	EVTS	DOCUMENT ID	TECN
$-0.217 \pm 0.034$ OUR AVERAGE		Error includes scale factor of 2.4.	
$-0.207 \pm 0.012 \pm 0.009$	83k	<sup>1</sup> ABOUZAID 07B	KTEV
$-0.36 \pm 0.06 \pm 0.02$	6864	FANTI 99B	NA48
$-0.28 \pm 0.13$		BARR 90B	NA31
$-0.280^{+0.099}_{-0.090}$		OHL 90B	B845

<sup>1</sup> ABOUZAID 07B measures  $C \cdot \alpha_{K^*} = -0.517 \pm 0.030 \pm 0.022$ . We assume  $C = 2.5$ , as in all other measurements.

**$\alpha_{K^*}$  DECAY FORM FACTOR FOR  $K_L \rightarrow \mu^+ \mu^- \gamma$**

$\alpha_{K^*}$  is the constant in the model of BERGSTROM 83 described in the previous section.

VALUE	EVTS	DOCUMENT ID	TECN
$-0.158 \pm 0.027$ OUR AVERAGE			
$-0.160^{+0.026}_{-0.028}$	9100	ALAVI-HARATI01G	KTEV
$-0.04^{+0.24}_{-0.21}$		FANTI 97	NA48

**$\alpha_{K^*}^{\text{eff}}$  DECAY FORM FACTOR FOR  $K_L \rightarrow e^+ e^- e^+ e^-$**

$\alpha_{K^*}^{\text{eff}}$  is the parameter describing the relative strength of an intermediate pseudoscalar decay amplitude and a vector meson decay amplitude in the model of BERGSTROM 83. It takes into account both the radiative effects and the form factor. Since there are two  $e^+ e^-$  pairs here compared with one in  $e^+ e^- \gamma$  decays, a factorized expression is used for the  $e^+ e^- e^+ e^-$  decay form factor.

VALUE	EVTS	DOCUMENT ID	TECN
$-0.14 \pm 0.16 \pm 0.15$	441	ALAVI-HARATI01D	KTEV

**$\alpha_{DIP}$  DECAY FORM FACTOR FOR  $K_L^0 \rightarrow \ell^+ \ell^- \gamma, K_L^0 \rightarrow \ell^+ \ell^- \ell^+ \ell^-$**

Average of all  $\alpha_{DIP}$  measurements (from each of three datablocks following this one) assuming lepton universality.

VALUE	DOCUMENT ID
$-1.69 \pm 0.08$ OUR AVERAGE	Includes data from the 3 datablocks that follow this one. Error includes scale factor of 1.7.

**$\alpha_{DIP}$  DECAY FORM FACTOR FOR  $K_L^0 \rightarrow e^+ e^- \gamma$**

$\alpha_{DIP}$  parameter in  $K_L^0 \rightarrow \gamma^* \gamma^*$  form factor by DAMBROSIO 98, motivated by vector meson dominance and a proper short distance behavior.

VALUE	EVTS	DOCUMENT ID	TECN
$-1.729 \pm 0.043 \pm 0.028$	83k	ABOUZAID 07B	KTEV

**$\alpha_{DIP}$  DECAY FORM FACTOR FOR  $K_L^0 \rightarrow \mu^+ \mu^- \gamma$**

$\alpha_{DIP}$  is a constant in the model of DAMBROSIO 98 described in the previous section.

VALUE	EVTS	DOCUMENT ID	TECN
$-1.54 \pm 0.10$	9100	ALAVI-HARATI01G	KTEV

**$\alpha_{DIP}$  DECAY FORM FACTOR FOR  $K_L^0 \rightarrow e^+ e^- \mu^+ \mu^-$**

$\alpha_{DIP}$  is a constant in the model of DAMBROSIO 98 described in the previous section.

VALUE	EVTS	DOCUMENT ID	TECN
$-1.59 \pm 0.37$	131	ALAVI-HARATI03B	KTEV

**$a_1/a_2$  FORM FACTOR FOR M1 DIRECT EMISSION AMPLITUDE**

Form factor =  $\tilde{g}_{M1} [1 + \frac{a_1/a_2}{(M_p^2 - M_K^2) + 2M_K E_\gamma}]$  as described in ALAVI-HARATI 00b.

VALUE (GeV <sup>2</sup> )	EVTS	DOCUMENT ID	TECN	COMMENT
$-0.737 \pm 0.014$ OUR AVERAGE				
$-0.744 \pm 0.027 \pm 0.032$	5241	<sup>1</sup> ABOUZAID 06	KTEV	$\pi^+ \pi^- e^+ e^-$
$-0.738 \pm 0.007 \pm 0.018$	111k	<sup>2</sup> ABOUZAID 06A	KTEV	$\pi^+ \pi^+ \gamma$
$-0.81^{+0.07}_{-0.13} \pm 0.02$		<sup>3</sup> LAI 03c	NA48	$\pi^+ \pi^- e^+ e^-$
$-0.737 \pm 0.026 \pm 0.022$		<sup>4</sup> ALAVI-HARATI01B		$\pi^+ \pi^- \gamma$
$-0.720 \pm 0.028 \pm 0.009$	1766	<sup>5</sup> ALAVI-HARATI00B	KTEV	$\pi^+ \pi^- e^+ e^-$

<sup>1</sup> ABOUZAID 06 also measured  $|\tilde{g}_{M1}| = 1.11 \pm 0.14$ .  
<sup>2</sup> ABOUZAID 06A also measured  $|\tilde{g}_{M1}| = 1.198 \pm 0.035 \pm 0.086$ .  
<sup>3</sup> LAI 03c also measured  $\tilde{g}_{M1} = 0.99^{+0.28}_{-0.27} \pm 0.07$ .  
<sup>4</sup> ALAVI-HARATI 01B fit gives  $\chi^2/\text{DOF} = 38.8/27$ . Linear and quadratic fits give  $\chi^2/\text{DOF} = 43.2/27$  and  $37.6/26$  respectively.  
<sup>5</sup> ALAVI-HARATI 00B also measured  $|\tilde{g}_{M1}| = 1.35^{+0.20}_{-0.17} \pm 0.04$ .

**$\overline{f}_S$  DECAY FORM FACTOR FOR  $K_L^0 \rightarrow \pi^\pm \pi^0 e^\mp \nu_e$**

VALUE	DOCUMENT ID	TECN
$0.049 \pm 0.011$ OUR AVERAGE	Error includes scale factor of 1.7.	
$0.052 \pm 0.006 \pm 0.002$	BATLEY 04	NA48
$0.010 \pm 0.016 \pm 0.017$	MAKOFF 93	E731

**$\overline{f}_P$  DECAY FORM FACTOR FOR  $K_L^0 \rightarrow \pi^\pm \pi^0 e^\mp \nu_e$**

VALUE	DOCUMENT ID	TECN
$-0.052 \pm 0.012$ OUR AVERAGE		
$-0.051 \pm 0.011 \pm 0.005$	BATLEY 04	NA48
$-0.079 \pm 0.049 \pm 0.022$	MAKOFF 93	E731

**$\lambda_\gamma$  DECAY FORM FACTOR FOR  $K_L^0 \rightarrow \pi^\pm \pi^0 e^\mp \nu_e$**

VALUE	DOCUMENT ID	TECN
$0.085 \pm 0.020$ OUR AVERAGE		
$0.087 \pm 0.019 \pm 0.006$	BATLEY 04	NA48
$0.014 \pm 0.087 \pm 0.070$	MAKOFF 93	E731

**$\overline{h}$  DECAY FORM FACTOR FOR  $K_L^0 \rightarrow \pi^\pm \pi^0 e^\mp \nu_e$**

VALUE	DOCUMENT ID	TECN
$-0.30 \pm 0.13$ OUR AVERAGE		
$-0.32 \pm 0.12 \pm 0.07$	BATLEY 04	NA48
$-0.07 \pm 0.31 \pm 0.31$	MAKOFF 93	E731

**$L_3$  CHIRAL PERT. THEO. PARAM. FOR  $K_L^0 \rightarrow \pi^\pm \pi^0 e^\mp \nu_e$**

VALUE (units $10^{-3}$ )	DOCUMENT ID	TECN
$-3.96 \pm 0.28$ OUR AVERAGE	Error includes scale factor of 1.6.	
$-4.1 \pm 0.2$	BATLEY 04	NA48
$-3.4 \pm 0.4$	<sup>1</sup> MAKOFF 93	E731

<sup>1</sup> MAKOFF 93 sign has been changed to negative to agree with the sign convention used in BATLEY 04.

# Meson Particle Listings

## K<sub>L</sub><sup>0</sup>

### a<sub>V</sub>, VECTOR MESON EXCHANGE CONTRIBUTION

VALUE	EVTS	DOCUMENT ID	TECN	COMMENT
<b>-0.43 ± 0.06 OUR AVERAGE</b> Error includes scale factor of 1.5.				
-0.31 ± 0.05 ± 0.07	1.4k	<sup>1</sup> ABOUZAID 08	KTEV	
-0.46 ± 0.03 ± 0.04		LAI 02B	NA48	K <sub>L</sub> <sup>0</sup> → π <sup>0</sup> 2γ
-0.67 ± 0.21 ± 0.12		ALAVI-HARATI 01E	KTEV	K <sub>L</sub> <sup>0</sup> → π <sup>0</sup> e <sup>+</sup> e <sup>-</sup> γ
• • • We do not use the following data for averages, fits, limits, etc. • • •				
-0.72 ± 0.05 ± 0.06		<sup>2</sup> ALAVI-HARATI 199B	KTEV	K <sub>L</sub> <sup>0</sup> → π <sup>0</sup> 2γ
<sup>1</sup> Using KTeV dataset collected in 1996, 1997, and 1999.				
<sup>2</sup> Superseded by ABOUZAID 08.				

See the related review(s):  
[CP Violation in K<sub>L</sub><sup>0</sup> Decays](#)

### CP-VIOLATION PARAMETERS IN K<sub>L</sub><sup>0</sup> DECAYS

#### CHARGE ASYMMETRY IN K<sub>S</sub><sup>0</sup> DECAYS

Such asymmetry violates CP. It is related to Re(ε).

#### A<sub>L</sub>(μ) = weighted average of A<sub>L</sub>(μ) and A<sub>L</sub>(e)

In previous editions and in the literature the symbol used for this asymmetry was δ<sub>L</sub> or δ. We use A<sub>L</sub> for consistency with B<sup>0</sup> asymmetry notation and with recent K<sub>S</sub><sup>0</sup> notation.

VALUE (%)	EVTS	DOCUMENT ID	TECN	COMMENT
<b>0.332 ± 0.006 OUR AVERAGE</b> Includes data from the 2 datablocks that follow this one.				
0.333 ± 0.050	33M	WILLIAMS 73	ASPK	K <sub>μ3</sub> + K <sub>e3</sub>

#### A<sub>L</sub>(μ) = [Γ(π<sup>-</sup> μ<sup>+</sup> ν<sub>μ</sub>) - Γ(π<sup>+</sup> μ<sup>-</sup> ν̄<sub>μ</sub>)]/SUM

Only the combined value below is put into the Meson Summary Table.

VALUE (%)	EVTS	DOCUMENT ID	TECN
The data in this block is included in the average printed for a previous datablock.			

#### 0.304 ± 0.025 OUR AVERAGE

0.313 ± 0.029	15M	GEWENIGER 74	ASPK
0.278 ± 0.051	7.7M	PICCIONI 72	ASPK
• • • We do not use the following data for averages, fits, limits, etc. • • •			
0.60 ± 0.14	4.1M	MCCARTHY 73	CNTR
0.57 ± 0.17	1M	<sup>1</sup> PACIOTTI 69	OSPK
0.403 ± 0.134	1M	<sup>1</sup> DORFAN 67	OSPK

<sup>1</sup> PACIOTTI 69 is a reanalysis of DORFAN 67 and is corrected for μ<sup>+</sup> μ<sup>-</sup> range difference in MCCARTHY 72.

#### A<sub>L</sub>(e) = [Γ(π<sup>-</sup> e<sup>+</sup> ν<sub>e</sub>) - Γ(π<sup>+</sup> e<sup>-</sup> ν̄<sub>e</sub>)]/SUM

Only the combined value below is put into the Meson Summary Table.

VALUE (%)	EVTS	DOCUMENT ID	TECN
The data in this block is included in the average printed for a previous datablock.			

#### 0.334 ± 0.007 OUR AVERAGE

0.3322 ± 0.0058 ± 0.0047	298M	ALAVI-HARATI 02	
0.341 ± 0.018	34M	GEWENIGER 74	ASPK
0.318 ± 0.038	40M	FITCH 73	ASPK
0.346 ± 0.033	10M	MARX 70	CNTR
• • • We do not use the following data for averages, fits, limits, etc. • • •			
0.36 ± 0.18	600k	ASHFORD 72	ASPK
0.246 ± 0.059	10M	<sup>1</sup> SAAL 69	CNTR
0.224 ± 0.036	10M	<sup>1</sup> BENNETT 67	CNTR

<sup>1</sup> SAAL 69 is a reanalysis of BENNETT 67.

#### PARAMETERS FOR K<sub>L</sub><sup>0</sup> → 2π DECAY

$$\eta_{+-} = A(K_L^0 \rightarrow \pi^+ \pi^-) / A(K_S^0 \rightarrow \pi^+ \pi^-)$$

$$\eta_{00} = A(K_L^0 \rightarrow \pi^0 \pi^0) / A(K_S^0 \rightarrow \pi^0 \pi^0)$$

The fitted values of |η<sub>+-</sub>| and |η<sub>00</sub>| given below are the results of a fit to |η<sub>+-</sub>|, |η<sub>00</sub>|, |η<sub>00</sub>/η<sub>+-</sub>|, and Re(ε'/ε). Independent information on |η<sub>+-</sub>| and |η<sub>00</sub>| can be obtained from the fitted values of the K<sub>L</sub><sup>0</sup> → ππ and K<sub>S</sub><sup>0</sup> → ππ branching ratios and the K<sub>L</sub><sup>0</sup> and K<sub>S</sub><sup>0</sup> lifetimes. This information is included as data in the |η<sub>+-</sub>| and |η<sub>00</sub>| sections with a Document ID "BRFIT." See the note "CP violation in K<sub>L</sub> decays" above for details.

#### |η<sub>00</sub>| = |A(K<sub>L</sub><sup>0</sup> → 2π<sup>0</sup>) / A(K<sub>S</sub><sup>0</sup> → 2π<sup>0</sup>)|

VALUE (units 10 <sup>-3</sup> )	DOCUMENT ID	TECN	COMMENT
<b>2.220 ± 0.011 OUR FIT</b> Error includes scale factor of 1.8.			
<b>2.243 ± 0.014</b>	BRFIT 16		
• • • We do not use the following data for averages, fits, limits, etc. • • •			
2.47 ± 0.31 ± 0.24	ANGELOPO... 98	CPLR	
2.49 ± 0.40	<sup>1</sup> ADLER 96B	CPLR	Sup. by ANGELOPOULOS 98
2.33 ± 0.18	CHRISTENS... 79	ASPK	
2.71 ± 0.37	<sup>2</sup> WOLFF 71	OSPK	Cu reg., 4γ's
2.95 ± 0.63	<sup>2</sup> CHOLLET 70	OSPK	Cu reg., 4γ's
<sup>1</sup> Error is statistical only.			

<sup>2</sup> CHOLLET 70 gives |η<sub>00</sub>| = (1.23 ± 0.24) × (regeneration amplitude, 2 GeV/c Cu)/10000mb. WOLFF 71 gives |η<sub>00</sub>| = (1.13 ± 0.12) × (regeneration amplitude, 2 GeV/c Cu)/10000mb. We compute both |η<sub>00</sub>| values for (regeneration amplitude, 2 GeV/c Cu) = 24 ± 2mb. This regeneration amplitude results from averaging over FAISSNER 69, extrapolated using optical-model calculations of Bohm et al., Physics Letters **27B** 594 (1968) and the data of BALATS 71. (From H. Faissner, private communication).

#### |η<sub>+-</sub>| = |A(K<sub>L</sub><sup>0</sup> → π<sup>+</sup> π<sup>-</sup>) / A(K<sub>S</sub><sup>0</sup> → π<sup>+</sup> π<sup>-</sup>)|

VALUE (units 10 <sup>-3</sup> )	EVTS	DOCUMENT ID	TECN	COMMENT
<b>2.232 ± 0.011 OUR FIT</b> Error includes scale factor of 1.8.				
<b>2.226 ± 0.007</b>	BRFIT 16			
• • • We do not use the following data for averages, fits, limits, etc. • • •				
2.223 ± 0.012		<sup>1</sup> LAI 07	NA48	
2.219 ± 0.013		<sup>2</sup> AMBROSINO 06F	KLOE	
2.228 ± 0.010		<sup>3</sup> ALEXOPOU... 04	KTEV	
2.286 ± 0.023 ± 0.026	70M	<sup>4</sup> APOSTOLA... 99C	CPLR	K <sub>L</sub> <sup>0</sup> -K <sub>S</sub> <sup>0</sup> asymmetry
2.310 ± 0.043 ± 0.031		<sup>5</sup> ADLER 95B	CPLR	K <sub>L</sub> <sup>0</sup> -K <sub>S</sub> <sup>0</sup> asymmetry
2.32 ± 0.14 ± 0.03	10 <sup>5</sup>	ADLER 92B	CPLR	K <sub>L</sub> <sup>0</sup> -K <sub>S</sub> <sup>0</sup> asymmetry
2.30 ± 0.035		GEWENIGER 74B	ASPK	

<sup>1</sup> Value obtained from the NA48 measurements of Γ(K<sub>L</sub><sup>0</sup> → π<sup>+</sup> π<sup>-</sup>)/Γ(K<sub>L</sub><sup>0</sup> → π ν e) and τ<sub>K<sub>S</sub><sup>0</sup></sub> and KLOE measurements of B(K<sub>S</sub><sup>0</sup> → π<sup>+</sup> π<sup>-</sup>) and τ<sub>K<sub>L</sub><sup>0</sup></sub>. Γ(K<sub>L</sub><sup>0</sup> → π<sup>+</sup> π<sup>-</sup>) is defined to include the inner bremsstrahlung component Γ(K<sub>L</sub><sup>0</sup> → π<sup>+</sup> π<sup>-</sup> γ (IB)) but exclude the direct emission component B(K<sub>S</sub><sup>0</sup> → π<sup>+</sup> π<sup>-</sup> (DE)). Their |η<sub>+-</sub>| value is not directly used in our fit, but enters the fit via their branching ratio and lifetime measurements.

<sup>2</sup> AMBROSINO 06F uses KLOE branching ratios and τ<sub>L</sub> together with τ<sub>S</sub> from PDG 04. Their |η<sub>+-</sub>| value is not directly used in our fit, but enters the fit via their branching ratio and lifetime measurements.

<sup>3</sup> ALEXOPOULOS 04 |η<sub>+-</sub>| uses their K<sub>L</sub><sup>0</sup> → ππ branching fractions, τ<sub>S</sub> = (0.8963 ± 0.0005) × 10<sup>-10</sup> s from the average of KTeV and NA48 τ<sub>S</sub> measurements, and assumes that Γ(K<sub>S</sub><sup>0</sup> → π ℓ ν ℓ) = Γ(K<sub>L</sub><sup>0</sup> → π ℓ ν ℓ) giving B(K<sub>S</sub><sup>0</sup> → π ℓ ν ℓ) = 0.118%. Their η<sub>+-</sub> is not directly used in our fit, but enters our fit via their branching ratio measurements.

<sup>4</sup> APOSTOLAKIS 99C report (2.264 ± 0.023 ± 0.026 + 9.1[τ<sub>S</sub> - 0.8934]) × 10<sup>-3</sup>. We evaluate for our 2006 best value τ<sub>S</sub> = (0.8958 ± 0.0005) × 10<sup>-10</sup> s.

<sup>5</sup> ADLER 95B report (2.312 ± 0.043 ± 0.030 - 1[Δm - 0.5274] + 9.1[τ<sub>S</sub> - 0.8926]) × 10<sup>-3</sup>. We evaluate for our 1996 best values Δm = (0.5304 ± 0.0014) × 10<sup>-10</sup> ħs<sup>-1</sup> and τ<sub>S</sub> = (0.8927 ± 0.0009) × 10<sup>-10</sup> s. Superseded by APOSTOLAKIS 99C.

#### |ε| = (2|η<sub>+-</sub>| + |η<sub>00</sub>|)/3

This expression is a very good approximation, good to about one part in 10<sup>-4</sup> because of the small measured value of φ<sub>00</sub> - φ<sub>+-</sub> and small theoretical ambiguities.

VALUE (units 10 <sup>-3</sup> )	DOCUMENT ID
<b>2.228 ± 0.011 OUR FIT</b> Error includes scale factor of 1.8.	

#### |η<sub>00</sub>/η<sub>+-</sub>|

VALUE	EVTS	DOCUMENT ID	TECN
<b>0.9950 ± 0.0007 OUR FIT</b> Error includes scale factor of 1.6.			
<b>0.9930 ± 0.0020 OUR AVERAGE</b>			
0.9931 ± 0.0020		<sup>1,2</sup> BARR 93D	NA31
0.9904 ± 0.0084 ± 0.0036		<sup>3</sup> WOODS 88	E731
• • • We do not use the following data for averages, fits, limits, etc. • • •			
0.9939 ± 0.0013 ± 0.0015	1M	<sup>1</sup> BARR 93D	NA31
0.9899 ± 0.0020 ± 0.0025		<sup>1</sup> BURKHARDT 88	NA31

<sup>1</sup> This is the square root of the ratio R given by BURKHARDT 88 and BARR 93D.  
<sup>2</sup> This is the combined results from BARR 93D and BURKHARDT 88, taking into account a common systematic uncertainty of 0.0014.  
<sup>3</sup> We calculate |η<sub>00</sub>/η<sub>+-</sub>| = 1 - 3(ε'/ε) from WOODS 88 (ε'/ε) value.

#### Re(ε'/ε) = (1 - |η<sub>00</sub>/η<sub>+-</sub>|)/3

We have neglected terms of order ω · Re(ε'/ε), where ω = Re(A<sub>2</sub>)/Re(A<sub>0</sub>) ≈ 1/22. If included, this correction would lower Re(ε'/ε) by about 0.04 × 10<sup>-3</sup>. See SOZZI 04.

VALUE (units 10 <sup>-3</sup> )	DOCUMENT ID	TECN	COMMENT
<b>1.66 ± 0.23 OUR FIT</b> Error includes scale factor of 1.6.			
<b>1.68 ± 0.20 OUR AVERAGE</b> Error includes scale factor of 1.4. See the ideogram below.			
1.92 ± 0.21		<sup>1</sup> ABOUZAID 11	KTEV Assuming CPT
1.47 ± 0.22		BATLEY 02	NA48
0.74 ± 0.52 ± 0.29		GIBBONS 93B	E731
• • • We use the following data for averages but not for fits. • • •			
2.3 ± 0.65		<sup>2,3</sup> BARR 93D	NA31
• • • We do not use the following data for averages, fits, limits, etc. • • •			
2.110 ± 0.343		<sup>1,4</sup> ABOUZAID 11	KTEV Not assuming CPT
2.07 ± 0.28		ALAVI-HARATI 03	KTEV In ABOUZAID 11
1.53 ± 0.26		LAI 01C	NA48 Incl. in BATLEY 02
2.80 ± 0.30 ± 0.28		ALAVI-HARATI 99D	KTEV In ALAVI-HARATI 03
1.85 ± 0.45 ± 0.58		FANTI 99C	NA48 In LAI 01C
2.0 ± 0.7		<sup>5</sup> BARR 93D	NA31
-0.4 ± 1.4 ± 0.6		PATTERSON 90	E731 in GIBBONS 93B
3.3 ± 1.1		<sup>5</sup> BURKHARDT 88	NA31
3.2 ± 2.8 ± 1.2		<sup>2</sup> WOODS 88	E731

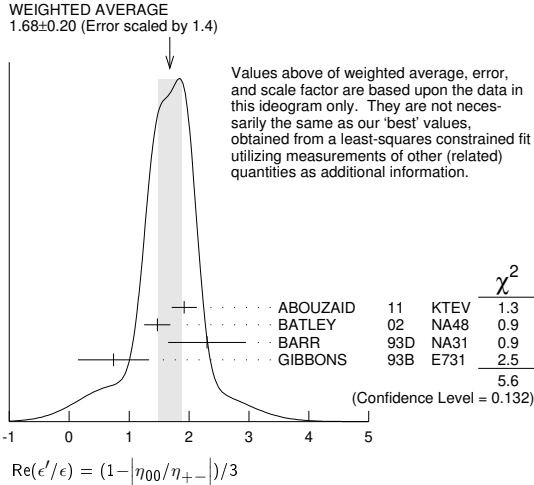
<sup>1</sup> The two ABOUZAID 11 values use the same data. The fits are performed with and without CPT invariance requirement.

See key on page 999

# Meson Particle Listings

$K_L^0$

- <sup>2</sup> These values are derived from  $|\eta_{00}/\eta_{+-}|$  measurements. They enter the average in this section but enter the fit via the  $|\eta_{00}/\eta_{+-}|$  only.
- <sup>3</sup> This is the combined results from BARR 93D and BURKHARDT 88, taking into account their common systematic uncertainty.
- <sup>4</sup> We use ABOUZAID 11  $\text{Re}(\epsilon'/\epsilon)$  value with *CPT* assumption in our fits for  $|\eta_{+-}|$ ,  $|\eta_{00}|$ , and  $\text{Re}(\epsilon'/\epsilon)$ .
- <sup>5</sup> These values are derived from  $|\eta_{00}/\eta_{+-}|$  measurements.



## $\phi_{+-}$ , PHASE OF $\eta_{+-}$

The dependence of the phase on  $\Delta m$  and  $\tau_S$  is given for each experiment in the comments below, where  $\Delta m$  is the  $K_L^0 - K_S^0$  mass difference in units  $10^{10} \text{h s}^{-1}$  and  $\tau_S$  is the  $K_S$  mean life in units  $10^{-10} \text{s}$ . We also give the regeneration phase  $\phi_f$  in the comments below.

OUR FIT is described in the note on “*CP* violation in  $K_L$  decays” in the  $K_L^0$  Particle Listings. Most experiments in this section are included in both the “Not Assuming *CPT*” and “Assuming *CPT*” fits. In the latter fit, they have little direct influence on  $\phi_{+-}$  because their errors are large compared to that assuming *CPT*, but they influence  $\Delta m$  and  $\tau_S$  through their dependencies on these parameters, which are given in the footnotes.

VALUE (°)	EVTs	DOCUMENT ID	TECN	COMMENT
<b>43.51 ± 0.05 OUR FIT</b>				Error includes scale factor of 1.2. Assuming <i>CPT</i>
<b>43.4 ± 0.5 OUR FIT</b>				Error includes scale factor of 1.2. Not assuming <i>CPT</i>
42.9 ± 0.6 ± 0.3	70M	<sup>1</sup> APOSTOLA... 99c	CPLR	$K^0 - \bar{K}^0$ asymmetry
42.9 ± 0.8 ± 0.2		<sup>2,3</sup> SCHWINGENHEUER...95	E773	$\text{CH}_{11}$ regenerator
41.4 ± 0.9 ± 0.2		<sup>3,4</sup> GIBBONS 93	E731	$\text{B}_4\text{C}$ regenerator
44.5 ± 1.6 ± 0.6		<sup>5</sup> CAROSI 90	NA31	Vacuum regen.
43.3 ± 1.0 ± 0.5		<sup>6</sup> GEWENIGER 74B	ASPK	Vacuum regen.
••• We do not use the following data for averages, fits, limits, etc. •••				
43.76 ± 0.64		<sup>7</sup> ABOUZAID 11	KTEV	Not assuming <i>CPT</i>
44.12 ± 0.72 ± 1.20		<sup>8</sup> ALAVI-HARATI03	KTEV	Not assuming <i>CPT</i>
42.5 ± 0.4 ± 0.3		<sup>9,10</sup> ADLER 96C	RVUE	
43.4 ± 1.1 ± 0.3		<sup>11</sup> ADLER 95B	CPLR	$K^0 - \bar{K}^0$ asymmetry
42.3 ± 4.4 ± 1.4	100k	<sup>12</sup> ADLER 92B	CPLR	$K^0 - \bar{K}^0$ asymmetry
47.7 ± 2.0 ± 0.9		<sup>3,13</sup> KARLSSON 90	E731	
44.3 ± 2.8 ± 0.2		<sup>14</sup> CARITHERS 75	SPEC	C regenerator

- <sup>1</sup> APOSTOLAKIS 99c measures  $\phi_{+-} = (43.19 \pm 0.53 \pm 0.28) + 300 [\Delta m - 0.5301] (\circ)$ . We have adjusted the measurement to use our best values of  $(\Delta m = 0.5293 \pm 0.0009) (10^{10} \text{h s}^{-1})$ . Our first error is their experiment's error and our second error is the systematic error from using our best values.
- <sup>2</sup> SCHWINGENHEUER 95 measures  $\phi_{+-} = (43.53 \pm 0.76) + 173 [\Delta m - 0.5282] - 275 [\tau_S - 0.8926] (\circ)$ . We have adjusted the measurement to use our best values of  $(\Delta m = 0.5293 \pm 0.0009) (10^{10} \text{h s}^{-1})$ ,  $(\tau_S = 0.8954 \pm 0.0004) (10^{-10} \text{s})$ . Our first error is their experiment's error and our second error is the systematic error from using our best values.
- <sup>3</sup> These experiments measure  $\phi_{+-} - \phi_f$  and calculate the regeneration phase from the power law momentum dependence of the regeneration amplitude using analyticity and dispersion relations. SCHWINGENHEUER 95 [GIBBONS 93] includes a systematic error of  $0.35^\circ [0.5^\circ]$  for uncertainties in their modeling of the regeneration amplitude.
- <sup>4</sup> GIBBONS 93 measures  $\phi_{+-} = (42.21 \pm 0.9) + 189 [\Delta m - 0.5257] - 460 [\tau_S - 0.8922] (\circ)$ . We have adjusted the measurement to use our best values of  $(\Delta m = 0.5293 \pm 0.0009) (10^{10} \text{h s}^{-1})$ ,  $(\tau_S = 0.8954 \pm 0.0004) (10^{-10} \text{s})$ . Our first error is their experiment's error and our second error is the systematic error from using our best values. This is actually reported in SCHWINGENHEUER 95, footnote 8. GIBBONS 93 reports  $\phi_{+-} (42.2 \pm 1.4)^\circ$ . They measure  $\phi_{+-} - \phi_f$  and calculate the regeneration phase  $\phi_f$  from the power law momentum dependence of the regeneration amplitude using analyticity. An error of  $0.6^\circ$  is included for possible uncertainties in the regeneration phase.
- <sup>5</sup> CAROSI 90 measures  $\phi_{+-} = (46.9 \pm 1.4 \pm 0.7) + 579 [\Delta m - 0.5351] + 303 [\tau_S - 0.8922] (\circ)$ . We have adjusted the measurement to use our best values of  $(\Delta m = 0.5293 \pm 0.0009) (10^{10} \text{h s}^{-1})$ ,  $(\tau_S = 0.8954 \pm 0.0004) (10^{-10} \text{s})$ . Our first error is their experiment's error and our second error is the systematic error from using our best values.

- <sup>6</sup> GEWENIGER 74B measures  $\phi_{+-} = (49.4 \pm 1.0) + 565 [\Delta m - 0.540] (\circ)$ . We have adjusted the measurement to use our best values of  $(\Delta m = 0.5293 \pm 0.0009) (10^{10} \text{h s}^{-1})$ . Our first error is their experiment's error and our second error is the systematic error from using our best values.
- <sup>7</sup> Not independent of other phase parameters reported in ABOUZAID 11.
- <sup>8</sup> ALAVI-HARATI 03  $\phi_{+-}$  is correlated with their  $\Delta m = m_{K_L^0} - m_{K_S^0}$  and  $\tau_{K_S}$  measurements in the  $K_L^0$  and  $K_S^0$  sections respectively. The correlation coefficients are  $\rho(\phi_{+-}, \Delta m) = +0.955$ ,  $\rho(\phi_{+-}, \tau_S) = -0.871$ , and  $\rho(\tau_S, \Delta m) = -0.840$ . *CPT* is not assumed. Uses scintillator Pb regenerator. Superseded by ABOUZAID 11.
- <sup>9</sup> ADLER 96C measures  $\phi_{+-} = (43.82 \pm 0.41) + 339 [\Delta m - 0.5307] - 252 [\tau_S - 0.8922] (\circ)$ . We have adjusted the measurement to use our best values of  $(\Delta m = 0.5293 \pm 0.0009) (10^{10} \text{h s}^{-1})$ ,  $(\tau_S = 0.8954 \pm 0.0004) (10^{-10} \text{s})$ . Our first error is their experiment's error and our second error is the systematic error from using our best values.
- <sup>10</sup> ADLER 96C is the result of a fit which includes nearly the same data as entered into the “OUR FIT” value in the 1996 edition of this Review (Physical Review **D54** 1 (1996)).
- <sup>11</sup> ADLER 95B measures  $\phi_{+-} = (42.7 \pm 0.9 \pm 0.6) + 316 [\Delta m - 0.5274] + 30 [\tau_S - 0.8926] (\circ)$ . We have adjusted the measurement to use our best values of  $(\Delta m = 0.5293 \pm 0.0009) (10^{10} \text{h s}^{-1})$ ,  $(\tau_S = 0.8954 \pm 0.0004) (10^{-10} \text{s})$ . Our first error is their experiment's error and our second error is the systematic error from using our best values.
- <sup>12</sup> ADLER 92B quote separately two systematic errors:  $\pm 0.4$  from their experiment and  $\pm 1.0$  degrees due to the uncertainty in the value of  $\Delta m$ .
- <sup>13</sup> KARLSSON 90 systematic error does not include regeneration phase uncertainty.
- <sup>14</sup> CARITHERS 75 measures  $\phi_{+-} = (45.5 \pm 2.8) + 224 [\Delta m - 0.5348] (\circ)$ . We have adjusted the measurement to use our best values of  $(\Delta m = 0.5293 \pm 0.0009) (10^{10} \text{h s}^{-1})$ . Our first error is their experiment's error and our second error is the systematic error from using our best values.  $\phi_f = -40.9 \pm 2.6^\circ$ .

## $\phi_{00}$ , PHASE OF $\eta_{00}$

See comment in  $\phi_{+-}$  header above for treatment of  $\Delta m$  and  $\tau_S$  dependence, as well as for the inclusion of data in both the “Assuming *CPT*” and “Not Assuming *CPT*” fits.

OUR FIT is described in the note on “*CP* violation in  $K_L$  decays” in the  $K_L^0$  Particle Listings.

VALUE (°)	DOCUMENT ID	TECN	COMMENT
<b>43.52 ± 0.05 OUR FIT</b>			Error includes scale factor of 1.3. Assuming <i>CPT</i>
<b>43.7 ± 0.6 OUR FIT</b>			Error includes scale factor of 1.2. Not assuming <i>CPT</i>
44.5 ± 2.3 ± 0.5	<sup>1</sup> CAROSI 90	NA31	
••• We do not use the following data for averages, fits, limits, etc. •••			
44.06 ± 0.68	<sup>2</sup> ABOUZAID 11	KTEV	Not assuming <i>CPT</i>
41.7 ± 5.9 ± 0.2	<sup>3</sup> ANGELOPOU... 98	CPLR	
50.8 ± 7.1 ± 1.7	<sup>4</sup> ADLER 96B	CPLR	Sup. by ANGELOPOULOS 98
47.4 ± 1.4 ± 0.9	<sup>5</sup> KARLSSON 90	E731	
<sup>1</sup> CAROSI 90 measures $\phi_{00} = (47.1 \pm 2.1 \pm 1.0) + 579 [\Delta m - 0.5351] + 252 [\tau_S - 0.8922] (\circ)$ . We have adjusted the measurement to use our best values of $(\Delta m = 0.5293 \pm 0.0009) (10^{10} \text{h s}^{-1})$ , $(\tau_S = 0.8954 \pm 0.0004) (10^{-10} \text{s})$ . Our first error is their experiment's error and our second error is the systematic error from using our best values.			
<sup>2</sup> Not independent of other phase parameters reported in ABOUZAID 11.			
<sup>3</sup> ANGELOPOULOS 98 measures $\phi_{00} = (42.0 \pm 5.6 \pm 1.9) + 240 [\Delta m - 0.5307] (\circ)$ . We have adjusted the measurement to use our best values of $(\Delta m = 0.5293 \pm 0.0009) (10^{10} \text{h s}^{-1})$ . Our first error is their experiment's error and our second error is the systematic error from using our best values. The $\tau_S$ dependence is negligible.			
<sup>4</sup> ADLER 96B identified initial neutral kaon individually as being a $K^0$ or a $\bar{K}^0$ . The systematic uncertainty is $\pm 1.5^\circ$ combined in quadrature with $\pm 0.8^\circ$ due to $\Delta m$ .			
<sup>5</sup> KARLSSON 90 systematic error does not include regeneration phase uncertainty.			

## $\phi_\epsilon = (2\phi_{+-} + \phi_{00})/3$

This expression is a very good approximation, good to about  $10^{-3}$  degrees because of the small measured values of  $\phi_{00} - \phi_{+-}$  and  $\text{Re}(\epsilon'/\epsilon)$ , and small theoretical ambiguities.

VALUE (°)	DOCUMENT ID	TECN	COMMENT
<b>43.52 ± 0.05 OUR FIT</b>			Error includes scale factor of 1.2. Assuming <i>CPT</i>
<b>43.5 ± 0.5 OUR FIT</b>			Error includes scale factor of 1.3. Not assuming <i>CPT</i>
43.5164 ± 0.0002 ± 0.0518	<sup>1</sup> SUPERWEAK 16		Assuming <i>CPT</i>
43.86 ± 0.63	<sup>2</sup> ABOUZAID 11	KTEV	Not assuming <i>CPT</i>
<sup>1</sup> SUPERWEAK 16 is a fake measurement used to impose the <i>CPT</i> or Superweak constraint $\phi_{+-} = \phi_{\text{SW}} = \tan^{-1}[2 \frac{\Delta m}{\hbar} (\frac{\tau_S \tau_L}{\tau_S - \tau_L})]$ . This “measurement” is linearized using values near the PDG 04 edition values of $\Delta m$ , $\tau_S$ and $\tau_L$ , and then adjusted to our current values as described in the following “measurement”. SUPERWEAK 16 measures $\phi_\epsilon = (43.50258 \pm 0.00021) + 54.1 [\Delta m - 0.5289] + 32.0 [\tau_S - 0.89564] (\circ)$ . We have adjusted the measurement to use our best values of $(\Delta m = 0.5293 \pm 0.0009) (10^{10} \text{h s}^{-1})$ , $(\tau_S = 0.8954 \pm 0.0004) (10^{-10} \text{s})$ . Our first error is their experiment's error and our second error is the systematic error from using our best values.			
<sup>2</sup> ABOUZAID 11 uses the full KTeV dataset collected in 1996, 1997, and 1999. See $\text{Im}(\epsilon'/\epsilon)$ section for correlation information.			

## $\text{Im}(\epsilon'/\epsilon) = -(\phi_{00} - \phi_{+-})/3$

For small  $|\epsilon'/\epsilon|$ ,  $\text{Im}(\epsilon'/\epsilon)$  is related to the phases of  $\eta_{00}$  and  $\eta_{+-}$  by the above expression.

VALUE (°)	DOCUMENT ID	TECN	COMMENT
<b>-0.002 ± 0.005 OUR FIT</b>			Error includes scale factor of 1.7. Assuming <i>CPT</i>
<b>-0.11 ± 0.11 OUR FIT</b>			Not assuming <i>CPT</i>
<b>-0.0985 ± 0.1157</b>	<sup>1</sup> ABOUZAID 11	KTEV	Not assuming <i>CPT</i>
<sup>1</sup> ABOUZAID 11 uses the full KTeV dataset collected in 1996, 1997, and 1999. The fit has $\Delta m$ , $\tau_S$ , $\phi_\epsilon$ , $\text{Re}(\epsilon'/\epsilon)$ , and $\text{Im}(\epsilon'/\epsilon)$ as free parameters. The reported value of $\text{Im}(\epsilon'/\epsilon) = (-17.20 \pm 20.20) \times 10^{-4}$ rad. The correlation coefficients are $\rho(\phi_\epsilon, \Delta m) = 0.828$ , $\rho(\phi_\epsilon, \tau_S) = -0.765$ , $\rho(\Delta m, \tau_S) = -0.858$ , $\rho(\text{Im}(\epsilon'/\epsilon), \phi_\epsilon) = -0.041$ , $\rho(\text{Im}(\epsilon'/\epsilon), \Delta m) = 0.026$ , $\rho(\text{Im}(\epsilon'/\epsilon), \tau_S) = -0.010$ .			



# Meson Particle Listings

$K_L^0$

## DECAY-PLANE ASYMMETRY IN $\pi^+\pi^-\pi^+\pi^0$ DECAYS

This is the  $CP$ -violating asymmetry

$$A = \frac{N_{\sin\phi\cos\phi>0.0} - N_{\sin\phi\cos\phi<0.0}}{N_{\sin\phi\cos\phi>0.0} + N_{\sin\phi\cos\phi<0.0}}$$

where  $\phi$  is the angle between the  $e^+e^-$  and  $\pi^+\pi^-$  planes in the  $K_L^0$  rest frame.

## CP ASYMMETRY $A$ in $K_L^0 \rightarrow \pi^+\pi^-\pi^+\pi^0$

VALUE (%)	DOCUMENT ID	TECN
<b>13.7 ± 1.5 OUR AVERAGE</b>		
13.6 ± 1.4 ± 1.5	ABOUZAID 06	KTEV
14.2 ± 3.0 ± 1.9	LAI 03C	NA48
13.6 ± 2.5 ± 1.2	ALAVI-HARATI00B	KTEV

## PARAMETERS FOR $e^+e^-\pi^+\pi^0$ DECAYS

These are the  $CP$ -violating parameters in the  $\phi$  distribution, where  $\phi$  is the angle between the planes of the two  $e^+e^-$  pairs in the kaon rest frame:

$$d\Gamma/d\phi \propto 1 + \beta_{CP} \cos(2\phi) + \gamma_{CP} \sin(2\phi)$$

where  $\beta_{CP} = -0.20$  and  $\gamma_{CP} = 0$  values correspond to no  $CP$  violation.

## $\beta_{CP}$ from $K_L^0 \rightarrow e^+e^-\pi^+\pi^0$

VALUE	EVTS	DOCUMENT ID	TECN	COMMENT
<b>-0.19 ± 0.07 OUR AVERAGE</b>				
-0.13 ± 0.10 ± 0.03	200	1 LAI	05B	NA48
-0.23 ± 0.09 ± 0.02	441	ALAVI-HARATI01D	KTEV	$M_{ee} > 8 \text{ MeV}/c^2$

1 LAI 05B obtains  $\beta_{CP} = -0.13 \pm 0.10$  (stat) if  $\gamma_{CP} = 0$  is assumed.

## $\gamma_{CP}$ from $K_L^0 \rightarrow e^+e^-\pi^+\pi^0$

VALUE	EVTS	DOCUMENT ID	TECN	COMMENT
<b>0.01 ± 0.11 OUR AVERAGE</b>				Error includes scale factor of 1.6.
+0.13 ± 0.10 ± 0.03	200	LAI	05B	NA48
-0.09 ± 0.09 ± 0.02	441	ALAVI-HARATI01D	KTEV	$M_{ee} > 8 \text{ MeV}/c^2$

## CHARGE ASYMMETRY IN $\pi^+\pi^-\pi^0$ DECAYS

These are  $CP$ -violating charge-asymmetry parameters, defined at beginning of section "LINEAR COEFFICIENT  $g$  FOR  $K_L^0 \rightarrow \pi^+\pi^-\pi^0$ " above. See also note on Dalitz plot parameters in  $K^\pm$  section and note on " $CP$  violation in  $K_L$  decays" above.

## LINEAR COEFFICIENT $j$ FOR $K_L^0 \rightarrow \pi^+\pi^-\pi^0$

VALUE	EVTS	DOCUMENT ID	TECN
<b>0.0012 ± 0.0008 OUR AVERAGE</b>			
0.0010 ± 0.0024 ± 0.0030	500k	ANGELOPO...	98C CPLR
-0.001 ± 0.011	6499	CHO	77
0.001 ± 0.003	4709	PEACH	77
0.0013 ± 0.0009	3M	SCRIBANO	70
0.0 ± 0.017	4400	SMITH	70 OSPK
0.001 ± 0.004	238k	BLANPIED	68

## QUADRATIC COEFFICIENT $f$ FOR $K_L^0 \rightarrow \pi^+\pi^-\pi^0$

VALUE	EVTS	DOCUMENT ID	TECN
<b>0.0045 ± 0.0024 ± 0.0059</b>	500k	ANGELOPO...	98C CPLR

## PARAMETERS for $K_L^0 \rightarrow \pi^+\pi^-\gamma$ DECAY

$$|\eta_{+-\gamma}| = |A(K_L^0 \rightarrow \pi^+\pi^-\gamma, CP \text{ violating})/A(K_S^0 \rightarrow \pi^+\pi^-\gamma)|$$

VALUE (units $10^{-3}$ )	EVTS	DOCUMENT ID	TECN
<b>2.35 ± 0.07 OUR AVERAGE</b>			
2.359 ± 0.062 ± 0.040	9045	MATTHEWS 95	E773
2.15 ± 0.26 ± 0.20	3671	RAMBERG 93B	E731

## $\phi_{+-\gamma}$ = phase of $\eta_{+-\gamma}$

VALUE (°)	EVTS	DOCUMENT ID	TECN
<b>44 ± 4 OUR AVERAGE</b>			
43.8 ± 3.5 ± 1.9	9045	MATTHEWS 95	E773
72 ± 23 ± 17	3671	RAMBERG 93B	E731

## $|\epsilon'_{+-\gamma}|/\epsilon$ for $K_L^0 \rightarrow \pi^+\pi^-\gamma$

VALUE	CL%	EVTS	DOCUMENT ID	TECN
<b>&lt;0.3</b>	90	3671	1 RAMBERG 93B	E731

1 RAMBERG 93B limit on  $|\epsilon'_{+-\gamma}|/\epsilon$  assumes than any difference between  $\eta_{+-}$  and  $\eta_{+-\gamma}$  is due to direct  $CP$  violation.

## $|g_{E1}|$ for $K_L^0 \rightarrow \pi^+\pi^-\gamma$

This parameter is the amplitude of the direct emission of a  $CP$  violating E1 electric dipole photon.

VALUE	CL%	EVTS	DOCUMENT ID	TECN	COMMENT
<b>&lt;0.21</b>	90	111k	ABOUZAID 06A	KTEV	$E_{\gamma}^* > 20 \text{ MeV}$

## T VIOLATION TESTS IN $K_L^0$ DECAYS

### Im( $\xi$ ) in $K_{\mu 3}^0$ DECAY (from transverse $\mu$ pol.)

VALUE	EVTS	DOCUMENT ID	TECN	COMMENT
<b>-0.007 ± 0.026 OUR AVERAGE</b>				
0.009 ± 0.030	12M	MORSE	80	CNTR Polarization
0.35 ± 0.30	207k	1 CLARK	77	SPEC POL, $t=0$
-0.085 ± 0.064	2.2M	2 SANDWEISS	73	CNTR POL, $t=0$
-0.02 ± 0.08		LONGO	69	CNTR POL, $t=3.3$
-0.2 ± 0.6		ABRAMS	68B	OSPK Polarization
0.012 ± 0.026		SCHMIDT	79	CNTR Repl. by MORSE 80

• • • We do not use the following data for averages, fits, limits, etc. • • •

1 CLARK 77 value has additional  $\xi(0)$  dependence  $+0.21\text{Re}[\xi(0)]$ .  
 2 SANDWEISS 73 value corrected from value quoted in their paper due to new value of  $\text{Re}(\xi)$ . See footnote 4 of SCHMIDT 79.

## CPT-INVARIANCE TESTS IN $K_L^0$ DECAYS

### PHASE DIFFERENCE $\phi_{00} - \phi_{+-}$

Test of  $CPT$ .

OUR FIT is described in the note on " $CP$  violation in  $K_L$  decays" in the  $K_L^0$  Particle Listings.

VALUE (°)	DOCUMENT ID	TECN	COMMENT
<b>0.006 ± 0.014 OUR FIT</b>			Error includes scale factor of 1.7. Assuming $CPT$
<b>0.34 ± 0.32 OUR FIT</b>			Not assuming $CPT$
0.006 ± 0.008	1 SUPERWEAK 16		Assuming $CPT$
-0.30 ± 0.88	2 SCHWINGEN...95		Combined E731, E773
0.30 ± 0.35	3 ABOUZAID 11	KTEV	Not assuming $CPT$
0.39 ± 0.22 ± 0.45	4 ALAVI-HARATI03	KTEV	
0.62 ± 0.71 ± 0.75	SCHWINGEN...95		E773
-1.6 ± 1.2	5 GIBBONS 93	E731	
0.2 ± 2.6 ± 1.2	6 CAROSI 90	NA31	
-0.3 ± 2.4 ± 1.2	KARLSSON 90	E731	

- 1 SUPERWEAK 16 is a fake experiment to constrain  $\phi_{00} - \phi_{+-}$  to a small value as described in the note "CP violation in  $K_L$  decays."
- 2 This SCHWINGENHEUER 95 values is the combined result of SCHWINGENHEUER 95 and GIBBONS 93, accounting for correlated systematic errors.
- 3 Not independent of other phase parameters reported in ABOUZAID 11.
- 4 ALAVI-HARATI 03 fit  $\text{Re}(\epsilon'/\epsilon)$ ,  $\text{Im}(\epsilon'/\epsilon)$ ,  $\Delta m$ ,  $\tau_S$ , and  $\phi_{+-}$  simultaneously, not assuming  $CPT$ . Phase difference is obtained from  $\phi_{00} - \phi_{+-} \approx -3\text{Im}(\epsilon'/\epsilon)$  for small  $|\epsilon'/\epsilon|$ . Superseded by ABOUZAID 11.
- 5 GIBBONS 93 give detailed dependence of systematic error on lifetime (see the section on the  $K_S^0$  mean life) and mass difference (see the section on  $m_{K_L^0} - m_{K_S^0}$ ).
- 6 CAROSI 90 is excluded from the fit because it it is not independent of  $\phi_{+-}$  and  $\phi_{00}$  values.

### PHASE DIFFERENCE $\phi_{+-} - \phi_{SW}$

Test of  $CPT$ . The Superweak phase  $\phi_{SW} \equiv \tan^{-1}(2\Delta m/\Delta\Gamma)$  where  $\Delta m = m_{K_L^0} - m_{K_S^0}$  and  $\Delta\Gamma = \hbar(\tau_L - \tau_S)/(\tau_L\tau_S)$ .

VALUE (°)	DOCUMENT ID	TECN
<b>0.61 ± 0.62 ± 1.01</b>	1 ALAVI-HARATI03	KTEV

1 ALAVI-HARATI 03 fit is the same as their  $\phi_{+-}$ ,  $\tau_{K_S}$ ,  $\Delta m$  fit, except that the parameter  $\phi_{+-} - \phi_{SW}$  is used in place of  $\phi$ .

### $\text{Re}(\frac{2}{3}\eta_{+-} + \frac{1}{3}\eta_{00}) - \frac{A_L}{2}$

VALUE (units $10^{-6}$ )	DOCUMENT ID	TECN	COMMENT
<b>-3 ± 35</b>	1 ALAVI-HARATI02	E799	Uses $A_L$ from $K_{e3}$ decays

1 ALAVI-HARATI 02 uses PDG 00 values of  $\eta_{+-}$  and  $\eta_{00}$ .

## $\Delta S = \Delta Q$ IN $K^0$ DECAYS

The relative amount of  $\Delta S \neq \Delta Q$  component present is measured by the parameter  $x$ , defined as

$$x = A(\bar{K}^0 \rightarrow \pi^-\ell^+\nu)/A(K^0 \rightarrow \pi^-\ell^+\nu)$$

We list  $\text{Re}\{x\}$  and  $\text{Im}\{x\}$  for  $K_{e3}$  and  $K_{\mu 3}$  combined.

$$x = A(\bar{K}^0 \rightarrow \pi^-\ell^+\nu)/A(K^0 \rightarrow \pi^-\ell^+\nu) = A(\Delta S = -\Delta Q)/A(\Delta S = \Delta Q)$$

## REAL PART OF $x$

VALUE	EVTS	DOCUMENT ID	TECN	COMMENT
<b>-0.0018 ± 0.0041 ± 0.0045</b>		ANGELOPO... 98D	CPLR	$K_{e3}$ from $K^0$

• • • We do not use the following data for averages, fits, limits, etc. • • •

Table with columns for value, error, and reference numbers. Entries include SMITH 75B WIRE, NIEBERGALL 74 ASPK, FACKLER 73 OSPK, HART 73 OSPK, MALLARY 73 OSPK, BURGUN 72 HBC, GRAHAM 72 OSPK, MANN 72 HBC, MANTSCH 72 OSPK, WEBBER 71 HBC, CHO 70 DBC, BENNETT 69 CNTR, JAMES 68 HBC, FELDMAN 67B OSPK, HILL 67 DBC, AUBERT 65 HLBC, BALDO... 65 HLBC, FRANZINI 65 HBC.

1 BURGUN 72 is a final result which includes BURGUN 71.
2 First GRAHAM 72 value is second GRAHAM 72 value combined with MANTSCH 72.
3 CHO 70 is analysis of unambiguous events in new data and HILL 67.
4 BENNETT 69 is a reanalysis of BENNETT 68.
5 BALDO-CEOLIN 65 gives x and theta converted by us to Re(x) and Im(x).
6 FRANZINI 65 gives x and theta for Re(x) and Im(x). See SCHMIDT 67.

IMAGINARY PART OF x

Assumes  $m_{K_L^0} - m_{K_S^0}$  positive. See Listings above.

Table with columns: VALUE, EVTS, DOCUMENT ID, TECN, COMMENT. Entry: 0.0012 ± 0.0019 ± 0.0009 640k ANGELOPO... 01B CPLR K23 from K0

• • • We do not use the following data for averages, fits, limits, etc. • • •

Table with columns for value, error, and reference numbers. Entries include ANGELOPO... 98E CPLR, SMITH 75B WIRE, NIEBERGALL 74 ASPK, FACKLER 73 OSPK, HART 73 OSPK, MALLARY 73 OSPK, BURGUN 72 HBC, GRAHAM 72 OSPK, MANN 72 HBC, MANTSCH 72 OSPK, BURGUN 71 HBC, WEBBER 71 HBC, CHO 70 DBC, LITTENBERG 69 OSPK, JAMES 68 HBC, FELDMAN 67B OSPK, HILL 67 DBC, AUBERT 65 HLBC, BALDO... 65 HLBC, FRANZINI 65 HBC.

1 Superseded by ANGELOPOULOS 01B.
2 BURGUN 72 is a final result which includes BURGUN 71.
3 First GRAHAM 72 value is second GRAHAM 72 value combined with MANTSCH 72.
4 Footnote 10 of HILL 67 should read +0.58, not -0.58 (private communication) CHO 70 is analysis of unambiguous events in new data and HILL 67.
5 BALDO-CEOLIN 65 gives x and theta converted by us to Re(x) and Im(x).
6 FRANZINI 65 gives x and theta for Re(x) and Im(x). See SCHMIDT 67.

$K_L^0$  REFERENCES

Table with columns: Author, Year, Document ID, Journal, Collaboration. Entries: AHN 19 PRL 122 021802 J.K. Ahn et al. (KOTO Collab.), AHN 17 PTEP 2017 021C01 J.K. Ahn et al. (KOTO Collab.), BRFIT 16 RPP 2016 edition C.-J. Lin (PDG Collab.)

Large table of references for K\_L^0 mesons. Columns include Author, Year, Document ID, Journal, Collaboration. Entries include ETAFIT 16 RPP 2016 edition, SUPERWEAK 16 RPP 2016 edition, ABOUZAIID 11 PR D83 092001, ABOUZAIID 11A PRL 107 201803, OGATA 11 PR D84 052009, TUNG 11 PR D83 031101, ABOUZAIID 10 PR D81 052001, AHN 10 PR D81 072004, ABOUZAIID 08 PR D77 112004, ABOUZAIID 08A PR D78 032009, ABOUZAIID 08B PR D78 032014, ABOUZAIID 08C PRL 100 131803, AHN 08 PRL 100 201802, AMBROSINO 08F EPJ C55 539, ABOUZAIID 07B PRL 99 051804, ABOUZAIID 07C PRL 99 081803, ABOUZAIID 07D PR D76 052001, AMBROSINO 07C JHEP 0712 105, ANDRE 07 ANP 322 2518, LAI 07 PL B645 261, LAI 07A PR B647 341, NIX 07 PR D76 011101, ABOUZAIID 06 PR 96 101801, ABOUZAIID 06A PR D74 032004, ABOUZAIID 06C PR D74 097101, AHN 06 PR D74 051105, AHN 06 PR D74 079901 (err.), AMBROSINO 06 PL B632 43, AMBROSINO 06F PL B636 166, AMBROSINO 06D PL B638 140, BATLEY 06B PL B633 173, HILL 06 PR D78 096006, PDG 06 JP G33 1, ALEXOPOU... 05 PR D71 012001, AMBROSINO 05C PL B626 15, CABIBBO 05 JHEP 0503 021, LAI 05 PL B605 247, LAI 05B PL B615 31, PARK 05 PRL 94 021801, ALAVI-HARATI 04A PRL 93 021805, ALEXOPOU... 04 PR D70 092006, ALEXOPOU... 04 PR D70 092007, BATLEY 04 PL B595 75, CIRIGLIANO 04 EPJ C35 53, LAI 04B PL B602 41, LAI 04C PL B604 1, PDG 04 PL B592 1, SOZZI 04 EPJ C36 37, ADINOLFI 03 PL B566 61, ALAVI-HARATI 03 PR D67 012005, ALAVI-HARATI 03B PRL 90 141801, LAI 03 PR B551 7, LAI 03C EPJ C30 33, ALAVI-HARATI 02 PR 88 181601, ALAVI-HARATI 02C PRL 89 211801, BATLEY 02 PL B544 97, CIRIGLIANO 02 EPJ C23 121, LAI 02B PL B536 229, ALAVI-HARATI 01 PRL 86 397, ALAVI-HARATI 01B PRL 86 761, ALAVI-HARATI 01D PRL 86 5425, ALAVI-HARATI 01E PRL 87 021801, ALAVI-HARATI 01F PRL D62 112001, ALAVI-HARATI 01G PRL 87 071801, ALAVI-HARATI 01H PRL 87 111802, ALAVI-HARATI 01J PR D64 112004, ANGELOPO... 01 PL B503 49, ANGELOPO... 01B EPJ C22 55, LAI 01B PL B515 261, LAI 01C EPJ C22 231, ALAVI-HARATI 00 PR D61 072006, ALAVI-HARATI 00B PRL 84 408, ALAVI-HARATI 00D PRL 84 5279, ALAVI-HARATI 00E PR D62 112001, AMBROSIO 00 PR 84 1339, APOSTOLA... 00 PL B473 186, PDG 00 EPJ C15 1, ALAVI-HARATI 99B PRL 83 917, ALAVI-HARATI 99D PRL 83 22, APOSTOLA... 99C PL B458 545, FANTI 99B PL B458 553, FANTI 99C PL B465 335, MURAKAMI 99 PL B463 333, ADAMS 98 PRL 80 4123, AMBROSE 98 PRL 81 4309, AMBROSE 98B PRL 81 5734, ANGELOPO... 98 PL B420 191, ANGELOPO... 98C EPJ C5 389, ANGELOPO... 98D PL B444 38, ANGELOPO... 98E PL B444 43, ARISAKA 98 PL B432 230, BENDER 98 PL B418 411, DAMBROSIO 98 PL B423 385, SETZU 98 PL B420 205, TAKEUCHI 98 PR B443 409, FANTI 97 ZPHY C76 653, NOMURA 97 PL B408 445, ADLER 96B ZPHY C70 211, ADLER 96C PL B369 367, GU 96 PRL 76 4312, LEBER 96 PL B369 69, PDG 96 PR D54 1, ADLER 95 PL B363 237, ADLER 95B PL B363 243, AKAGI 95 PR D51 2061, AMBROSE 95 ZPHY C65 361, BARR 95C PL B358 399, HEINSON 95 PR D51 985, KREUTZ 95 ZPHY C65 67, MATTHEWS 95 PRL 75 2803, SCHWINGEN... 95 PRL 74 4376, SPENCER 95 PRL 74 3323, BARR 94 PL B328 528, GU 94 PRL 72 3000, NAKAYA 94 PRL 73 2169, ROBERTS 94 PR D50 1874, AKAGI 93 PR D47 2644, ARISAKA 93 PRL 70 1049, C.-J. Lin (PDG Collab.), C.-J. Lin (PDG Collab.), E. Abouzaid et al. (FNAL KTeV Collab.), E. Abouzaid et al. (KTeV Collab.), R. Ogata et al. (KEK E391a Collab.), Y.C. Tung et al. (KEK E391a Collab.), E. Abouzaid et al. (FNAL KTeV Collab.), J.K. Ahn et al. (KEK E391a Collab.), E. Abouzaid et al. (FNAL KTeV Collab.), E. Abouzaid et al. (FNAL KTeV Collab.), E. Abouzaid et al. (FNAL KTeV Collab.), E. Abouzaid et al. (FNAL KTeV Collab.), F. Ambrosino et al. (KLOE Collab.), E. Abouzaid et al. (FNAL KTeV Collab.), E. Abouzaid et al. (FNAL KTeV Collab.), E. Abouzaid et al. (FNAL KTeV Collab.), F. Ambrosino et al. (KLOE Collab.), T. Andre (EFT), A. Lai et al. (CERN NA48 Collab.), A. Lai et al. (CERN NA48 Collab.), J. Nix et al. (KEK E391a Collab.), E. Abouzaid et al. (KTeV Collab.), E. Abouzaid et al. (KTeV Collab.), E. Abouzaid et al. (KTeV Collab.), E. Abouzaid et al. (KTeV Collab.), J.K. Ahn et al. (KEK E391a Collab.), J.K. Ahn et al. (KEK E391a Collab.), F. Ambrosino et al. (KLOE Collab.), F. Ambrosino et al. (KLOE Collab.), F. Ambrosino et al. (KLOE Collab.), J.R. Batley et al. (CERN NA48/2 Collab.), R.J. Hill (FNAL), W.-M. Yao et al. (PDG Collab.), T. Alexopoulos et al. (FNAL KTeV Collab.), F. Ambrosino et al. (KLOE Collab.), N. Cabibbo, G. Isidori (CERN, ROMA1, FRAS), A. Lai et al. (CERN NA48 Collab.), A. Lai et al. (CERN NA48 Collab.), H.K. Park et al. (FNAL HyperCP Collab.), A. Alavi-Harati et al. (FNAL KTeV/E799 Collab.), T. Alexopoulos et al. (FNAL KTeV Collab.), J.R. Batley et al. (CERN NA48 Collab.), V. Cirigliano, H. Neufeld, H. Pichl (CIT, VALE+), A. Lai et al. (CERN NA48 Collab.), A. Lai et al. (CERN NA48 Collab.), S. Eidelman et al. (PDG Collab.), M. Sozzi (PISA), M. Adinolfi et al. (KLOE Collab.), A. Alavi-Harati et al. (FNAL KTeV Collab.), A. Alavi-Harati et al. (FNAL KTeV Collab.), A. Alavi-Harati et al. (FNAL KTeV Collab.), A. Lai et al. (CERN NA48 Collab.), A. Lai et al. (CERN NA48 Collab.), A. Alavi-Harati et al. (FNAL KTeV Collab.), A. Alavi-Harati et al. (FNAL KTeV Collab.), A. Alavi-Harati et al. (FNAL KTeV Collab.), A. Alavi-Harati et al. (FNAL KTeV Collab.), J.R. Batley et al. (CERN NA48 Collab.), V. Cirigliano et al. (VIEN, VALE, MARS), A. Lai et al. (CERN NA48 Collab.), A. Alavi-Harati et al. (FNAL KTeV Collab.), A. Alavi-Harati et al. (FNAL KTeV Collab.), A. Alavi-Harati et al. (FNAL KTeV Collab.), A. Alavi-Harati et al. (FNAL KTeV Collab.), A. Alavi-Harati et al. (FNAL KTeV Collab.), D. Ambrose et al. (BNL E871 Collab.), A. Apostolakis et al. (CLEAR Collab.), D.E. Groom et al. (PDG Collab.), A. Alavi-Harati et al. (FNAL KTeV Collab.), A. Alavi-Harati et al. (FNAL KTeV Collab.), J. Adams et al. (FNAL KTeV Collab.), D. Ambrose et al. (BNL E871 Collab.), D. Ambrose et al. (BNL E871 Collab.), A. Angelopoulos et al. (CLEAR Collab.), A. Angelopoulos et al. (CLEAR Collab.), A. Lai et al. (CERN NA48 Collab.), A. Lai et al. (CERN NA48 Collab.), A. Alavi-Harati et al. (FNAL KTeV Collab.), A. Alavi-Harati et al. (FNAL KTeV Collab.), V. Fanti et al. (CERN NA48 Collab.), V. Fanti et al. (CERN NA48 Collab.), K. Murakami et al. (KEK E162 Collab.), D. Ambrose et al. (FNAL KTeV Collab.), D. Ambrose et al. (BNL E871 Collab.), D. Ambrose et al. (BNL E871 Collab.), A. Angelopoulos et al. (CLEAR Collab.), A. Angelopoulos et al. (CLEAR Collab.), A. Angelopoulos et al. (CLEAR Collab.), A. Angelopoulos et al. (CLEAR Collab.), K. Arisaka et al. (FNAL E799 Collab.), M. Bender et al. (CERN NA48 Collab.), G. D'Ambrosio, G. Isidori, J. Portoles, M.G. Setzu et al. (KYOT, KEK, HIRO), Y. Takeuchi et al. (CERN NA48 Collab.), V. Fanti et al. (KYOT, KEK, HIRO), T. Nomura et al. (CLEAR Collab.), R. Adler et al. (CLEAR Collab.), R. Adler et al. (CLEAR Collab.), P. Gu et al. (RUTG, UCLA, EFI, COLO+), F. Leber et al. (MANZ, CERN, EDIN, ORSAY+), R. M. Barnett et al. (PDG Collab.), R. Adler et al. (CLEAR Collab.), R. Adler et al. (CLEAR Collab.), T. Akagi et al. (TOHOK, TOKY, KYOT, KEK), G.D. Barr et al. (CERN, EDIN, MANZ, LALO+), G.D. Barr et al. (CERN, EDIN, MANZ, LALO+), A.P. Heinson et al. (BNL E791 Collab.), A. Kreutz et al. (SIEG, EDIN, MANZ, ORSAY+), J.N. Matthews et al. (RUTG, EFI, ELMT+), B. Schwingerheuer et al. (EFI, CHIC+), M.B. Spencer et al. (UCLA, EFI, COLO+), G.D. Barr et al. (CERN, EDIN, MANZ, LALO+), P. Gu et al. (RUTG, UCLA, EFI, COLO+), T. Nakaya et al. (OSAK, UCLA, EFI, COLO+), D. Roberts et al. (UCLA, EFI, COLO+), T. Akagi et al. (TOHOK, TOKY, KYOT, KEK), K. Arisaka et al. (BNL E791 Collab.)

Downloaded from https://academic.oup.com/ptep/article/2020/8/083C01/5891211 by guest on 12 November 2020



FIRESTONE 66B PRL 17 116 A. Firestone *et al.* (YALE, BNL)  
 BEHR 65 Argonne Conf. 59 L. Behr *et al.* (EPOL, MILA, PADO)  
 MESTVIRISH... 65 JINR P 2449 A.N. Mestvirishvili *et al.* (JINR)  
 TRILLING 65B UCRL 16473 G.N. Trilling (LRL)  
 Updated from 1965 Argonne Conference, page 115.  
 JOVANOVI... 63 BNL Conf. 42 J.V. Jovanovich *et al.* (BNL, UMD)

$K_0^*(700)$

$I(J^P) = \frac{1}{2}(0^+)$

also known as  $\kappa$ ; was  $K_0^*(800)$

Needs confirmation. See the mini-review on scalar mesons under  $f_0(500)$  (see the index for the page number).

$K_0^*(700)$  T-Matrix Pole  $\sqrt{s}$

VALUE (MeV)	DOCUMENT ID	TECN	COMMENT
<b>(630-730) - i (260-340) OUR EVALUATION</b>			
• • • We do not use the following data for averages, fits, limits, etc. • • •			
$(670 \pm 18) - i (295 \pm 28)$	1 PELAEZ 17	RVUE	
$(764 \pm 63^{+71}_{-54}) - i (306 \pm 149^{+143}_{-85})$	2 ABLIKIM 11B	BES2	1.3k $J/\psi \rightarrow K_S^0 K_S^0 \pi^+ \pi^-$
$(665 \pm 9) - i (268^{+21}_{-6})$	3 GUO 11B	RVUE	
$(849 \pm 77^{+18}_{-14}) - i (256 \pm 40^{+46}_{-22})$	2 ABLIKIM 10E	BES2	1.4k $J/\psi \rightarrow K^\pm K_S^0 \pi^\mp \pi^0$
$(663 \pm 8 \pm 34) - i (329 \pm 5 \pm 22)$	4 BUGG 10	RVUE	S-matrix pole
$(706.0 \pm 1.8 \pm 22.8) - i (319.4 \pm 2.2 \pm 20.2)$	5 BONVICINI 08A	CLEO	141k $D^+ \rightarrow K^- \pi^+ \pi^+$
$(841 \pm 30^{+81}_{-73}) - i (309 \pm 45^{+48}_{-72})$	2 ABLIKIM 06C	BES2	25k $J/\psi \rightarrow \bar{K}^*(892)^0 K^+ \pi^-$
$(750^{+30}_{-55}) - i (342 \pm 60)$	6 BUGG 06	RVUE	
$(658 \pm 13) - i (279 \pm 12)$	7 DESCOTES-G... 06	RVUE	$\pi K \rightarrow \pi K$
$(757 \pm 33) - i (279 \pm 41)$	8 GUO 06	RVUE	
$(694 \pm 53) - i (303 \pm 30)$	9 ZHOU 06	RVUE	$K\rho \rightarrow K^- \pi^+ n$
$(754 \pm 22) - i (230 \pm 27)$	10 PELAEZ 04A	RVUE	$K\rho \rightarrow K\rho$
$(594 \pm 79) - i (362 \pm 166)$	9 ZHENG 04	RVUE	$K^- \rho \rightarrow K^- \pi^+ n$
$(722 \pm 60) - i (386 \pm 50)$	9 BUGG 03	RVUE	11 $K^- \rho \rightarrow K^- \pi^+ n$
$(875 \pm 75) - i (335 \pm 110)$	11 ISHIDA 97B	RVUE	11 $K^- \rho \rightarrow K^- \pi^+ n$
727 - i 263	12 VANBEVEREN 86	RVUE	

- 1 Extracted from Forward Dispersion Relations using sequences of Pade approximants .
- 2 Extracted from Breit-Wigner parameters.
- 3 Fit to scattering phase shifts using UChPT amplitudes with explicit resonances.
- 4 Supersedes BUGG 06. Combined analysis of ASTON 88, ABLIKIM 06c, AITALA 06, and LINK 09 using an s-dependent width with couplings to  $K\pi$  and  $K\eta'$ , and the Adler zero near thresholds.
- 5 From a complex pole included in the fit. Using parameters from the model that fits data best.
- 6 Reanalysis of ASTON 88, AITALA 02, and ABLIKIM 06c using for the  $\kappa$  an s-dependent width with an Adler zero near threshold.
- 7 Using Roy-Steiner equations (ROY 71) consistent with unitarity, analyticity and crossing symmetry constraints.
- 8 From UChPT fitted to MERCER 71, BINGHAM 72 and ESTABROOKS 78. Amplitude shown to be consistent with data of ABLIKIM 06c.
- 9 Reanalysis of ASTON 88 data.
- 10 Reanalysis of data from LINGLIN 73, ESTABROOKS 78, and ASTON 88 using the Inverse Amplitude Method.
- 11 Reanalysis of ASTON 88 using interfering Breit-Wigner amplitudes. Extracted from Breit-Wigner parameters.
- 12 Unitarized Quark Model.

$K_0^*(700)$  Breit-Wigner Mass

VALUE (MeV)	EVTS	DOCUMENT ID	TECN	COMMENT
<b>824 ± 30 OUR AVERAGE</b>				
$826 \pm 49^{+49}_{-34}$	1.3k	1 ABLIKIM 11B	BES2	$J/\psi \rightarrow K_S^0 K_S^0 \pi^+ \pi^-$
$810 \pm 68^{+15}_{-24}$	1.4k	2 ABLIKIM 10E	BES2	$J/\psi \rightarrow K^\pm K_S^0 \pi^\mp \pi^0$
$878 \pm 23^{+64}_{-55}$	25k	3 ABLIKIM 06C	BES2	$J/\psi \rightarrow \bar{K}^*(892)^0 K^+ \pi^-$
$797 \pm 19 \pm 43$	15k	4,5 AITALA 02	E791	$D^+ \rightarrow K^- \pi^+ \pi^+$
• • • We do not use the following data for averages, fits, limits, etc. • • •				
$888.0 \pm 1.9$	141k	6 BONVICINI 08A	CLEO	$D^+ \rightarrow K^- \pi^+ \pi^+$
$856 \pm 17 \pm 13$	54k	7 LINK 07B	FOCS	$D^+ \rightarrow K^- \pi^+ \pi^+$
$855 \pm 15$	0.6k	8 CAWLFIELD 06A	CLEO	$D^0 \rightarrow K^+ K^- \pi^0$
$905^{+65}_{-30}$		9 ISHIDA 97B	RVUE	11 $K^- \rho \rightarrow K^- \pi^+ n$

- 1 The Breit-Wigner parameters from a fit with seven intermediate resonances. The S-matrix pole position is  $(764 \pm 63^{+71}_{-54}) - i (306 \pm 149^{+143}_{-85})$  MeV.
- 2 From a fit including ten additional resonances and energy-independent Breit-Wigner width.
- 3 A fit in the  $K_0^*(700) + K^*(892) + K^*(1410)$  model with mass and width of the  $K_0^*(700)$  from ABLIKIM 06c well describes the left slope of the  $K_S^0 \pi^-$  invariant mass spectrum in  $\tau^- \rightarrow K_S^0 \pi^- \nu_\tau$  decay studied by EPIFANOV 07. Averaged value from different parameterizations.

- 4 Not seen by KOPP 01 using 7070 events of  $D^0 \rightarrow K^- \pi^+ \pi^0$ . LINK 02e and LINK 05i show clear evidence for a constant non-resonant scalar amplitude rather than  $K_0^*(700)$  in their high statistics analysis of  $D^+ \rightarrow K^- \pi^+ \mu^+ \nu_\mu$ .
- 5 AUBERT 07r does not find evidence for the charged  $K_0^*(700)$  using 11k events of  $D^0 \rightarrow K^- K^+ \pi^0$ .
- 6 Using parameters from the model that fits data best.
- 7 A Breit-Wigner mass and width.
- 8 Breit-Wigner parameters. A significant S-wave can be also modeled as a non-resonant contribution.
- 9 Reanalysis of ASTON 88 using interfering Breit-Wigner amplitudes.

$K_0^*(700)$  Breit-Wigner Width

VALUE (MeV)	EVTS	DOCUMENT ID	TECN	COMMENT
<b>478 ± 50 OUR AVERAGE</b>				
$449 \pm 156^{+144}_{-81}$	1.3k	1 ABLIKIM 11B	BES2	$J/\psi \rightarrow K_S^0 K_S^0 \pi^+ \pi^-$
$536 \pm 87^{+106}_{-47}$	1.4k	2 ABLIKIM 10E	BES2	$J/\psi \rightarrow K^\pm K_S^0 \pi^\mp \pi^0$
$499 \pm 52^{+55}_{-87}$	25k	3 ABLIKIM 06C	BES2	$J/\psi \rightarrow \bar{K}^*(892)^0 K^+ \pi^-$
$410 \pm 43 \pm 87$	15k	4,5 AITALA 02	E791	$D^+ \rightarrow K^- \pi^+ \pi^+$
• • • We do not use the following data for averages, fits, limits, etc. • • •				
$550.4 \pm 11.8$	141k	6 BONVICINI 08A	CLEO	$D^+ \rightarrow K^- \pi^+ \pi^+$
$464 \pm 28 \pm 22$	54k	7 LINK 07B	FOCS	$D^+ \rightarrow K^- \pi^+ \pi^+$
$251 \pm 48$	0.6k	8 CAWLFIELD 06A	CLEO	$D^0 \rightarrow K^+ K^- \pi^0$
$545^{+235}_{-110}$		9 ISHIDA 97B	RVUE	11 $K^- \rho \rightarrow K^- \pi^+ n$

- 1 The Breit-Wigner parameters from a fit with seven intermediate resonances. The S-matrix pole position is  $(764 \pm 63^{+71}_{-54}) - i (306 \pm 149^{+143}_{-85})$  MeV.
- 2 From a fit including ten additional resonances and energy-independent Breit-Wigner width.
- 3 A fit in the  $K_0^*(700) + K^*(892) + K^*(1410)$  model with mass and width of the  $K_0^*(700)$  from ABLIKIM 06c well describes the left slope of the  $K_S^0 \pi^-$  invariant mass spectrum in  $\tau^- \rightarrow K_S^0 \pi^- \nu_\tau$  decay studied by EPIFANOV 07. Averaged value from different parameterizations.
- 4 Not seen by KOPP 01 using 7070 events of  $D^0 \rightarrow K^- \pi^+ \pi^0$ . LINK 02e and LINK 05i show clear evidence for a constant non-resonant scalar amplitude rather than  $K_0^*(700)$  in their high statistics analysis of  $D^+ \rightarrow K^- \pi^+ \mu^+ \nu_\mu$ .
- 5 AUBERT 07r does not find evidence for the charged  $K_0^*(700)$  using 11k events of  $D^0 \rightarrow K^- K^+ \pi^0$ .
- 6 Using parameters from the model that fits data best.
- 7 A Breit-Wigner mass and width.
- 8 Statistical error only. A fit to the Dalitz plot including the  $K_0^*(700)^\pm, K^*(892)^\pm$ , and  $\phi$  resonances modeled as Breit-Wigners. A significant S-wave can be also modeled as a non-resonant contribution.
- 9 Reanalysis of ASTON 88 using interfering Breit-Wigner amplitudes.

$K_0^*(700)$  DECAY MODES

Mode	Fraction ( $\Gamma_i/\Gamma$ )
$\Gamma_1$ $K\pi$	100 %

$K_0^*(700)$  REFERENCES

PELAEZ 17	EPJ C77 91	J.R. Pelaez, A.Rodas, J.Ruiz de Elvira
ABLIKIM 11B	PL B698 183	M. Ablikim <i>et al.</i> (BES II Collab.)
GUO 11B	PR D84 034005	Z.-H. Guo, J.A. Oller
ABLIKIM 10E	PL B693 88	M. Ablikim <i>et al.</i> (BES II Collab.)
BUGG 10	PR D81 014002	D.V. Bugg (LOQM)
LINK 09	PL B681 14	J.M. Link <i>et al.</i> (FNAL FOCUS Collab.)
BONVICINI 08A	PR D78 052001	G. Bonvicini <i>et al.</i> (CLEO Collab.)
AUBERT 07T	PR D76 011102	B. Aubert <i>et al.</i> (BABAR Collab.)
EPIFANOV 07	PL B654 65	D. Epifanov <i>et al.</i> (BELLE Collab.)
LINK 07B	PL B653 1	J.M. Link <i>et al.</i> (FNAL FOCUS Collab.)
ABLIKIM 06C	PL B633 681	M. Ablikim <i>et al.</i> (BES Collab.)
AITALA 06	PR D73 032004	E.M. Aitala <i>et al.</i> (FNAL E791 Collab.)
Also	PR D74 059901 (errat.)	E.M. Aitala <i>et al.</i> (FNAL E791 Collab.)
BUGG 06	PL B632 471	D.V. Bugg (LOQM)
CAWLFIELD 06A	PR D74 031108	C. Cawfield <i>et al.</i> (CLEO Collab.)
DESCOTES-G... 06	EPJ C48 553	S. Descotes-Genon, B. Moussallam
GUO 06	NP A773 78	F.K. Guo <i>et al.</i>
ZHOU 06	NP A775 212	Z.Y. Zhou, H.Q. Zheng
LINK 05I	PL B621 72	J.M. Link <i>et al.</i> (FNAL FOCUS Collab.)
PELAEZ 04A	MPL A19 2879	J.R. Pelaez
ZHENG 04	NP A733 235	H.Q. Zheng <i>et al.</i>
BUGG 03	PL B572 1	D.V. Bugg
AITALA 02	PRL 89 121801	E.M. Aitala <i>et al.</i> (FNAL E791 Collab.)
LINK 02E	PL B535 43	J.M. Link <i>et al.</i> (FNAL FOCUS Collab.)
KOPP 01	PR D63 092001	S. Kopp <i>et al.</i> (CLEO Collab.)
ISHIDA 97B	PTP 98 621	S. Ishida <i>et al.</i>
ASTON 88	NP B296 493	D. Aston <i>et al.</i> (SLAC, NAGO, CIN, INUS)
VANBEVEREN 86	ZPHY C30 615	E. van Beveren <i>et al.</i> (NUM, BIEL)
ESTABROOKS 78	NP B133 490	P.G. Estabrooks <i>et al.</i> (MCGI, CARL, DURH+)
LINGLIN 73	NP B55 408	D. Linglin (CERN)
BINGHAM 72	NP B41 1	H.H. Bingham <i>et al.</i> (International $K^+$ Collab.)
MERCER 71	NP B32 381	R. Mercer <i>et al.</i> (JHU)
ROY 71	PL 36B 353	S.M. Roy

# Meson Particle Listings

## $K^*(892)$

$K^*(892)$

$$I(J^P) = \frac{1}{2}(1^-)$$

### $K^*(892)$ MASS

#### CHARGED ONLY, HADROPRODUCED

VALUE (MeV)	EVTS	DOCUMENT ID	TECN	CHG	COMMENT
<b>891.66 ± 0.26</b>	<b>OUR AVERAGE</b>				
892.6 ± 0.5	5840	BAUBILLIER 84B	HBC	-	8.25 $K^- p \rightarrow \bar{K}^0 \pi^- p$
888 ± 3		NAPIER 84	SPEC	+	200 $\pi^- p \rightarrow 2K_S^0 X$
891 ± 1		NAPIER 84	SPEC	-	200 $\pi^- p \rightarrow 2K_S^0 X$
891.7 ± 2.1	3700	BARTH 83	HBC	+	70 $K^+ p \rightarrow K_S^0 \pi^+ X$
891 ± 1	4100	TOAFF 81	HBC	-	6.5 $K^- p \rightarrow \bar{K}^0 \pi^- p$
892.8 ± 1.6		AJINENKO 80	HBC	+	32 $K^+ p \rightarrow K_S^0 \pi^+ X$
890.7 ± 0.9	1800	AGUILAR... 78B	HBC	±	0.76 $\bar{p} p \rightarrow K^\mp K_S^0 \pi^\pm$
886.6 ± 2.4	1225	BALAND 78	HBC	±	12 $\bar{p} p \rightarrow (K\pi)^\pm X$
891.7 ± 0.6	6706	COOPER 78	HBC	±	0.76 $\bar{p} p \rightarrow (K\pi)^\pm X$
891.9 ± 0.7	9000	1 PALER 75	HBC	-	14.3 $K^- p \rightarrow (K\pi)^- X$
892.2 ± 1.5	4404	AGUILAR... 71B	HBC	-	3.9,4.6 $K^- p \rightarrow (K\pi)^- p$
891 ± 2	1000	CRENNELL 69D	DBC	-	3.9 $K^- N \rightarrow K^0 \pi^- X$
890 ± 3.0	720	BARLOW 67	HBC	±	1.2 $\bar{p} p \rightarrow (K^0 \pi)^\pm K^\mp$
889 ± 3.0	600	BARLOW 67	HBC	±	1.2 $\bar{p} p \rightarrow (K^0 \pi)^\pm K\pi$
891 ± 2.3	620	2 DEBAERE 67B	HBC	±	3.5 $K^+ p \rightarrow K^0 \pi^+ p$
891.0 ± 1.2	1700	3 WOJCICKI 64	HBC	-	1.7 $K^- p \rightarrow \bar{K}^0 \pi^- p$

- • • We do not use the following data for averages, fits, limits, etc. • • •
- 893.6 ± 0.1  $^{+0.2}_{-0.3}$  183k ABLIKIM 19AQ BES ±  $J/\psi \rightarrow K^+ K^- \pi^0$
- 895.6 ± 0.8 4K 4 LEES 17C BABR  $J/\psi \rightarrow K_S^0 K^\pm \pi^\mp$
- 893.2 ± 0.1 ± 1.0 190k 5 AAIJ 16N LHCB  $D^0 \rightarrow K_S^0 K^\pm \pi^\mp$
- 893.5 ± 1.1 27k 6 ABELE 99D CBAR ± 0.0  $\bar{p} p \rightarrow K^+ K^- \pi^0$
- 890.4 ± 0.2 ± 0.5 80k 7 BIRD 89 LASS - 11  $K^- p \rightarrow \bar{K}^0 \pi^- p$
- 890.0 ± 2.3 800 2,3 CLELAND 82 SPEC + 30  $K^+ p \rightarrow K_S^0 \pi^+ p$
- 896.0 ± 1.1 3200 2,3 CLELAND 82 SPEC + 50  $K^+ p \rightarrow K_S^0 \pi^+ p$
- 893 ± 1 3600 2,3 CLELAND 82 SPEC - 50  $K^+ p \rightarrow K_S^0 \pi^- p$
- 896.0 ± 1.9 380 DELFOSSE 81 SPEC + 50  $K^\pm p \rightarrow K^\pm \pi^0 p$
- 886.0 ± 2.3 187 DELFOSSE 81 SPEC - 50  $K^\pm p \rightarrow K^\pm \pi^0 p$
- 894.2 ± 2.0 765 2 CLARK 73 HBC - 3.13  $K^- p \rightarrow \bar{K}^0 \pi^- p$
- 894.3 ± 1.5 1150 2,3 CLARK 73 HBC - 3.3  $K^- p \rightarrow \bar{K}^0 \pi^- p$
- 892.0 ± 2.6 341 2 SCHWEING...68 HBC - 5.5  $K^- p \rightarrow \bar{K}^0 \pi^- p$

#### CHARGED ONLY, PRODUCED IN $\tau$ LEPTON DECAYS

VALUE (MeV)	EVTS	DOCUMENT ID	TECN	COMMENT
<b>895.47 ± 0.20 ± 0.74</b>	<b>53k</b>	1 EPIFANOV 07	BELL	$\tau^- \rightarrow K_S^0 \pi^- \nu_\tau$
892.0 ± 0.5		2 BOITO 10	RVUE	$\tau^- \rightarrow K_S^0 \pi^- \nu_\tau$
892.0 ± 0.9		3,4 BOITO 09	RVUE	$\tau^- \rightarrow K_S^0 \pi^- \nu_\tau$
895.3 ± 0.2		4,5 JAMIN 08	RVUE	$\tau^- \rightarrow K_S^0 \pi^- \nu_\tau$
896.4 ± 0.9	12k	6 BONVICINI 02	CLEO	$\tau^- \rightarrow K^- \pi^0 \nu_\tau$
895 ± 2		7 BARATE 99R	ALEP	$\tau^- \rightarrow K^- \pi^0 \nu_\tau$

- 1 From a fit in the  $K_S^0(700) + K^*(892) + K^*(1410)$  model.
- 2 From the pole position of the  $K\pi$  vector form factor using EPIFANOV 07 and constraints from  $K_{f3}$  decays in ANTONELLI 10.
- 3 From the pole position of the  $K\pi$  vector form factor in the complex  $s$ -plane and using EPIFANOV 07 data.
- 4 Systematic uncertainties not estimated.
- 5 Reanalysis of EPIFANOV 07 using resonance chiral theory.
- 6 Calculated by us from the shift by  $4.7 \pm 0.9$  MeV (statistical uncertainty only) reported in BONVICINI 02 with respect to the world average value from PDG 00.
- 7 With mass and width of the  $K^*(1410)$  fixed at 1412 MeV and 227 MeV, respectively.

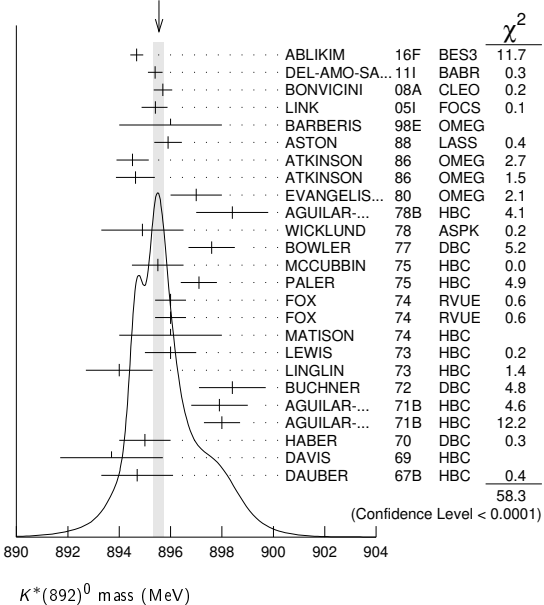
#### NEUTRAL ONLY

VALUE (MeV)	EVTS	DOCUMENT ID	TECN	COMMENT
<b>895.55 ± 0.20</b>	<b>OUR AVERAGE</b>			
894.68 ± 0.25 ± 0.05		1 ABLIKIM 16F	BES3	$D^+ \rightarrow K^- \pi^+ e^+ \nu_e$
895.4 ± 0.2 ± 0.2	243k	2 DEL-AMO-SA...11I	BABR	$D^+ \rightarrow K^- \pi^+ e^+ \nu_e$
895.7 ± 0.2 ± 0.3	141k	3 BONVICINI 08A	CLEO	$D^+ \rightarrow K^- \pi^+ \pi^+$
895.41 ± 0.32 $^{+0.35}_{-0.43}$	18k	4 LINK 05I	FOCS	$D^+ \rightarrow K^- \pi^+ \mu^+ \nu_\mu$
896 ± 2		BARBERIS 98E	OMEG	450 $pp \rightarrow p_f p_S K^* \bar{K}^*$
895.9 ± 0.5 ± 0.2		ASTON 88	LASS	11 $K^- p \rightarrow K^- \pi^+ n$
894.52 ± 0.63	25k	5 ATKINSON 86	OMEG	20-70 $\gamma p$
894.63 ± 0.76	20k	5 ATKINSON 86	OMEG	20-70 $\gamma p$
897 ± 1	28k	EVANGELIS... 80	OMEG	10 $\pi^- p \rightarrow K^+ \pi^- (\Lambda, \Sigma)$
898.4 ± 1.4	1180	AGUILAR... 78B	HBC	0.76 $\bar{p} p \rightarrow K^\mp K_S^0 \pi^\pm$

894.9 ± 1.6		WICKLUND 78	ASPK	3,4,6 $K^\pm N \rightarrow (K\pi)^0 N$
897.6 ± 0.9		BOWLER 77	DBC	5.4 $K^+ d \rightarrow K^+ \pi^- p p$
895.5 ± 1.0	3600	MCCUBBIN 75	HBC	3.6 $K^- p \rightarrow K^- \pi^+ n$
897.1 ± 0.7	22k	5 PALER 75	HBC	14.3 $K^- p \rightarrow (K\pi)^0 X$
896.0 ± 0.6	10k	FOX 74	RVUE	2 $K^- p \rightarrow K^- \pi^+ n$
896.0 ± 0.6		FOX 74	RVUE	2 $K^+ n \rightarrow K^+ \pi^- p$
896 ± 2		6 MATISON 74	HBC	12 $K^+ p \rightarrow K^+ \pi^- \Delta$
896 ± 1	3186	LEWIS 73	HBC	2.1-2.7 $K^+ p \rightarrow K\pi\pi p$
894.0 ± 1.3		6 LINGLIN 73	HBC	2-13 $K^+ p \rightarrow K^+ \pi^- \pi^+ p$
898.4 ± 1.3	1700	7 BUCHNER 72	DBC	4.6 $K^+ n \rightarrow K^+ \pi^- p$
897.9 ± 1.1	2934	7 AGUILAR... 71B	HBC	3.9,4.6 $K^- p \rightarrow K^- \pi^+ n$
898.0 ± 0.7	5362	7 AGUILAR... 71B	HBC	3.9,4.6 $K^- p \rightarrow K^- \pi^+ \pi^- p$
895 ± 1	4300	8 HABER 70	DBC	3 $K^- N \rightarrow K^- \pi^+ X$
893.7 ± 2.0	10k	DAVIS 69	HBC	12 $K^+ p \rightarrow K^+ \pi^- \pi^+ p$
894.7 ± 1.4	1040	7 DAUBER 67B	HBC	2.0 $K^- p \rightarrow K^- \pi^+ \pi^- p$
• • • We do not use the following data for averages, fits, limits, etc. • • •				
898.1 ± 1.0	4K	9 LEES 17C	BABR	$J/\psi \rightarrow K_S^0 K^\pm \pi^\mp$
895.53 ± 0.17		LEES 13F	BABR	$D^+ \rightarrow K^+ K^- \pi^+$
894.9 ± 0.5 ± 0.7	14.4k	10 MITCHELL 09A	CLEO	$D_S^+ \rightarrow K^+ K^- \pi^+$
896.2 ± 0.3	20k	11 AUBERT 07AK	BABR	10.6 $e^+ e^- \rightarrow K^{*0} K^\pm \pi^\mp \gamma$
900.7 ± 1.1	5900	BARTH 83	HBC	70 $K^+ p \rightarrow K^+ \pi^- X$

- 1 Taking also into account the  $K_S^0(1430)^0$  and  $K_2^*(1430)^0$ .
- 2 Taking into account the  $K^*(892)^0$ ,  $S$ -wave and  $P$ -wave ( $K^*(1410)^0$ ).
- 3 From the isobar model with a complex pole for the  $\kappa$ .
- 4 Fit to  $K\pi$  mass spectrum includes a non-resonant scalar component.
- 5 Inclusive reaction. Complicated background and phase-space effects.
- 6 From pole extrapolation.
- 7 Mass errors enlarged by us to  $\Gamma/\sqrt{N}$ . See note.
- 8 Number of events in peak reevaluated by us.
- 9 From a Dalitz plot analysis in an isobar model with charged and neutral  $K^*(892)$  masses and widths floating.
- 10 This value comes from a fit with  $\chi^2$  of 178/117.
- 11 Systematic uncertainties not estimated.

WEIGHTED AVERAGE  
895.55 ± 0.20 (Error scaled by 1.7)



### $K^*(892)$ MASSES AND MASS DIFFERENCES

Unrealistically small errors have been reported by some experiments. We use simple “realistic” tests for the minimum errors on the determination of a mass and width from a sample of  $N$  events:

$$\delta_{\min}(m) = \frac{\Gamma}{\sqrt{N}}, \quad \delta_{\min}(\Gamma) = 4 \frac{\Gamma}{\sqrt{N}}. \quad (1)$$

We consistently increase unrealistic errors before averaging. For a detailed discussion, see the 1971 edition of this Note.

K\*(892)

m\_{K\*(892)^0} - m\_{K\*(892)^±}

Table with columns: VALUE (MeV), EVTS, DOCUMENT ID, TECN, CHG, COMMENT. Includes data for AGUILAR... and BARASH.

1 Number of events in peak reevaluated by us.

K\*(892) RANGE PARAMETER

All from partial wave amplitude analyses.

Table with columns: VALUE (GeV^-1), EVTS, DOCUMENT ID, TECN, CHG, COMMENT. Includes data for DEL-AMO-SA... and LINK.

• • • We do not use the following data for averages, fits, limits, etc. • • •

1 Taking into account the K\*(892)^0, S-wave and P-wave (K\*(1410)^0).
2 Fit to K pi mass spectrum includes a non-resonant scalar component.

K\*(892) WIDTH

CHARGED ONLY, HADROPRODUCED

Table with columns: VALUE (MeV), EVTS, DOCUMENT ID, TECN, CHG, COMMENT. Includes data for BAUBILLIER, NAPIER, TOAFF, AJINENKO, AGUILAR..., COOPER, PALER, CLARK, CLARK, AGUILAR..., WOJCICKI.

• • • We do not use the following data for averages, fits, limits, etc. • • •

Table with columns: VALUE (MeV), EVTS, DOCUMENT ID, TECN, CHG, COMMENT. Includes data for ABLIKIM, LEES, AAIJ, ABELE, BIRD, BARTH, CLELAND, CLELAND, CLELAND, DELFOSSE, DELFOSSE.

1 Width errors enlarged by us to 4 x Gamma/sqrt(N); see note.
2 Inclusive reaction. Complicated background and phase-space effects.
3 Number of events in peak reevaluated by us.
4 From a Dalitz plot analysis in an isobar model with charged and neutral K\*(892) masses and widths floating.
5 Average of fit results with different parametrizations for the K pi S-wave.
6 K-matrix pole.
7 From a partial wave amplitude analysis.

CHARGED ONLY, PRODUCED IN tau LEPTON DECAYS

Table with columns: VALUE (MeV), EVTS, DOCUMENT ID, TECN, COMMENT. Includes data for EPIFANOV, BOITO, BOITO, JAMIN, BARATE.

1 From a fit in the K0(700) + K\*(892) + K\*(1410) model.
2 From the pole position of the K pi vector form factor using EPIFANOV 07 and constraints from K13 decays in ANTONELLI 10.
3 From the pole position of the K pi vector form factor in the complex s-plane and using EPIFANOV 07 data.
4 Systematic uncertainties not estimated.
5 Reanalysis of EPIFANOV 07 using resonance chiral theory.
6 With mass and width of the K\*(1410) fixed at 1412 MeV and 227 MeV, respectively.

NEUTRAL ONLY

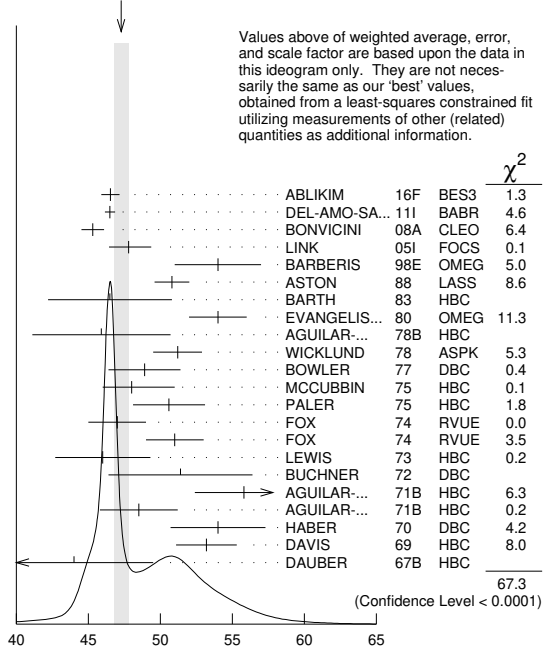
Table with columns: VALUE (MeV), EVTS, DOCUMENT ID, TECN, COMMENT. Includes data for ABLIKIM, DEL-AMO-SA..., BONVICINI, LINK, BARBERIS, ASTON, BARTH, EVANGELIS..., AGUILAR..., WICKLUND, BOWLER, MCCUBBIN, PALER, FOX, LEWIS, BUCHNER, AGUILAR..., HABER, DAVIS, DAUBER.

• • • We do not use the following data for averages, fits, limits, etc. • • •

Table with columns: VALUE (MeV), EVTS, DOCUMENT ID, TECN, COMMENT. Includes data for LEES, LEES, MITCHELL, AUBERT.

1 Taking also into account the K0\*(1430)^0 and K2\*(1430)^0.
2 Taking into account the K\*(892)^0, S-wave and P-wave (K\*(1410)^0).
3 From the isobar model with a complex pole for the xi.
4 Fit to K pi mass spectrum includes a non-resonant scalar component.
5 Inclusive reaction. Complicated background and phase-space effects.
6 Width errors enlarged by us to 4 x Gamma/sqrt(N); see note.
7 Number of events in peak reevaluated by us.
8 From a Dalitz plot analysis in an isobar model with charged and neutral K\*(892) masses and widths floating.
9 This value comes from a fit with chi^2 of 178/117.
10 Systematic uncertainties not estimated.

WEIGHTED AVERAGE 47.3±0.5 (Error scaled by 2.0)



NEUTRAL ONLY (MeV)

# Meson Particle Listings

## $K^*(892), K_1(1270)$

### $K^*(892)$ DECAY MODES

Mode	Fraction ( $\Gamma_i/\Gamma$ )	Confidence level
$\Gamma_1$ $K\pi$	$\sim 100$	%
$\Gamma_2$ $(K\pi)^\pm$	$(99.901 \pm 0.009)$	%
$\Gamma_3$ $(K\pi)^0$	$(99.754 \pm 0.021)$	%
$\Gamma_4$ $K^0\gamma$	$(2.46 \pm 0.21) \times 10^{-3}$	
$\Gamma_5$ $K^\pm\gamma$	$(9.9 \pm 0.9) \times 10^{-4}$	
$\Gamma_6$ $K\pi\pi$	$< 7$	$\times 10^{-4}$

### CONSTRAINED FIT INFORMATION

An overall fit to the total width and a partial width uses 13 measurements and one constraint to determine 3 parameters. The overall fit has a  $\chi^2 = 7.8$  for 11 degrees of freedom.

The following *off-diagonal* array elements are the correlation coefficients  $\langle \delta p_i \delta p_j \rangle / (\delta p_i \delta p_j)$ , in percent, from the fit to parameters  $p_i$ , including the branching fractions,  $x_i \equiv \Gamma_i/\Gamma_{\text{total}}$ . The fit constrains the  $x_i$  whose labels appear in this array to sum to one.

$x_5$	-100	
$\Gamma$	19	-19
		$x_2$ $x_5$

Mode	Rate (MeV)
$\Gamma_2$ $(K\pi)^\pm$	$50.7 \pm 0.9$
$\Gamma_5$ $K^\pm\gamma$	$0.050 \pm 0.005$

### CONSTRAINED FIT INFORMATION

An overall fit to the total width and a partial width uses 23 measurements and one constraint to determine 3 parameters. The overall fit has a  $\chi^2 = 68.4$  for 21 degrees of freedom.

The following *off-diagonal* array elements are the correlation coefficients  $\langle \delta p_i \delta p_j \rangle / (\delta p_i \delta p_j)$ , in percent, from the fit to parameters  $p_i$ , including the branching fractions,  $x_i \equiv \Gamma_i/\Gamma_{\text{total}}$ . The fit constrains the  $x_i$  whose labels appear in this array to sum to one.

$x_4$	-100	
$\Gamma$	12	-12
		$x_3$ $x_4$

Mode	Rate (MeV)	Scale factor
$\Gamma_3$ $(K\pi)^0$	$47.2 \pm 0.5$	1.9
$\Gamma_4$ $K^0\gamma$	$0.117 \pm 0.010$	

### $K^*(892)$ PARTIAL WIDTHS

$\Gamma(K^0\gamma)$	VALUE (keV)	EVTS	DOCUMENT ID	TECN	CHG	COMMENT	$\Gamma_4$
$116 \pm 10$ OUR FIT							
$116.5 \pm 9.9$	584		CARLSMITH 86	SPEC	0	$K_L^0 A \rightarrow K_S^0 \pi^0 A$	

$\Gamma(K^\pm\gamma)$	VALUE (keV)	DOCUMENT ID	TECN	CHG	COMMENT	$\Gamma_5$
$50 \pm 5$ OUR FIT						
$50 \pm 5$ OUR AVERAGE						
$48 \pm 11$		BERG 83	SPEC	-	$156 K^- A \rightarrow \bar{K}^0 \pi A$	
$51 \pm 5$		CHANDLEE 83	SPEC	+	$200 K^+ A \rightarrow K \pi A$	

### $K^*(892)$ BRANCHING RATIOS

$\Gamma(K^0\gamma)/\Gamma_{\text{total}}$	VALUE (units $10^{-3}$ )	DOCUMENT ID	TECN	CHG	COMMENT	$\Gamma_4/\Gamma$
$2.46 \pm 0.21$ OUR FIT						
$1.5 \pm 0.7$		CARITHERS 75B	CNTR	0	8-16 $\bar{K}^0 A$	

$\Gamma(K^\pm\gamma)/\Gamma_{\text{total}}$	VALUE (units $10^{-3}$ )	CL%	DOCUMENT ID	TECN	CHG	COMMENT	$\Gamma_5/\Gamma$
$0.99 \pm 0.09$ OUR FIT							
$< 1.6$	95		BEMPORAD 73	CNTR	+	10-16 $K^+ A$	

### $\Gamma(K\pi\pi)/\Gamma((K\pi)^\pm)$

VALUE	CL%	DOCUMENT ID	TECN	CHG	COMMENT	$\Gamma_6/\Gamma_2$
$< 7 \times 10^{-4}$	95	JONGEJANS 78	HBC		$4 K^- p \rightarrow p \bar{K}^0 2\pi$	
$< 20 \times 10^{-4}$		WOJCICKI 64	HBC	-	$1.7 K^- p \rightarrow \bar{K}^0 \pi^- p$	

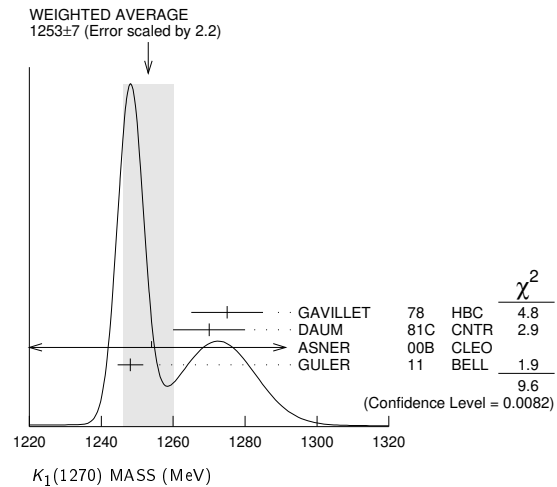
### $K^*(892)$ REFERENCES

ABLIKIM 19AQ	PR D100 032004	M. Ablikim <i>et al.</i>	(BESIII Collab.)
LEES 17C	PR D95 072007	J.P. Lees <i>et al.</i>	(BABAR Collab.)
AAJ 16N	PR D93 052018	R. Aaij <i>et al.</i>	(LHCb Collab.)
ABLIKIM 16F	PR D94 032001	M. Ablikim <i>et al.</i>	(BESIII Collab.)
LEES 13F	PR D87 052010	J.P. Lees <i>et al.</i>	(BABAR Collab.)
DEL-AMO-SA... 11I	PR D83 072001	P. del Amo Sanchez <i>et al.</i>	(BABAR Collab.)
ANTONELLI 10	EPJ C69 399	M. Antonelli <i>et al.</i>	(FlaviaNet Working Group)
BOITO 10	JHEP 1009 031	D.R. Boito, R. Escribano, M. Jamin	(BARC)
BOITO 09	EPJ C59 821	D.R. Boito, R. Escribano, M. Jamin	
MITCHELL 09A	PR D79 072008	R.E. Mitchell <i>et al.</i>	(CLEO Collab.)
BONVICINI 08A	PR D78 052001	G. Bonvicini <i>et al.</i>	(CLEO Collab.)
JAMIN 08	PL B664 78	M. Jamin, A. Pich, J. Portoles	
AUBERT 07AK	PR D76 012008	B. Aubert <i>et al.</i>	(BABAR Collab.)
EPIFANOV 07	PL B654 65	D. Epifanov <i>et al.</i>	(BELLE Collab.)
LINK 05I	PL B621 72	J.M. Link <i>et al.</i>	(FNAL FOCUS Collab.)
BONVICINI 02	PRL 88 111803	G. Bonvicini <i>et al.</i>	(CLEO Collab.)
PDG 00	EPJ C15 1	D.E. Groom <i>et al.</i>	(PDG Collab.)
ABELE 99D	PL B468 178	A. Abele <i>et al.</i>	(Crystal Barrel Collab.)
BARATE 99R	EPJ C11 599	R. Barate <i>et al.</i>	(ALEPH Collab.)
BARBERIS 98E	PL B436 204	D. Barberis <i>et al.</i>	(Omega Expt.)
BIRD 89	SLAC-332	P.F. Bird	(SLAC)
ASTON 88	NP B296 493	D. Aston <i>et al.</i>	(SLAC, NAGO, CIN, INUS)
ATKINSON 86	ZPHY C30 621	M. Atkinson <i>et al.</i>	(BONN, CERN, GLAS+)
CARLSMITH 86	PRL 56 18	D. Carlsmith <i>et al.</i>	(EPI, SACL)
BAUBILLIER 84B	ZPHY C26 37	M. Baubillier <i>et al.</i>	(BIRM, CERN, GLAS+)
NAPIER 84	PL B49B 514	A. Napier <i>et al.</i>	(TUFTS, ARIZ, FNAL, FLO+)
BARTH 83	NP B223 296	M. Barth <i>et al.</i>	(BRUX, CERN, GENO, MONS+)
BERG 83	Thesis UMI 83-21652	D.M. Berg	(ROCH)
CHANDLEE 83	PRL 51 168	C. Chandlee <i>et al.</i>	(ROCH, FNAL, MINN)
CLELAND 82	NP B208 189	W.E. Cleland <i>et al.</i>	(DURH, GEVA, LAUS+)
DELFOSE 81	NP B183 349	A. Delfosse <i>et al.</i>	(GEVA, LAUS)
TOAFF 81	PR D23 1500	S. Toaff <i>et al.</i>	(ANL, KANS)
AJINENKO 80	ZPHY C5 177	I.V. Ajinenko <i>et al.</i>	(SERP, BRUX, MONS+)
EVANGELIS... 80	NP B165 383	C. Evangelista <i>et al.</i>	(BARI, BONN, CERN+)
AGUILAR... 78B	NP B141 101	M. Aguilar-Benitez <i>et al.</i>	(MADR, TATA+)
BALAND 78	NP B140 220	J.F. Baland <i>et al.</i>	(MONS, BELG, CERN+)
COOPER 78	NP B136 365	A.M. Cooper <i>et al.</i>	(TATA, CERN, CDEF+)
JONGEJANS 78	NP B139 383	B. Jongejans <i>et al.</i>	(ZEEM, CERN, NIJN+)
WICKLUND 78	PR D17 1197	A.B. Wicklund <i>et al.</i>	(ANL)
BOWLER 77	NP B126 31	M.G. Bowler <i>et al.</i>	(OXF)
CARITHERS 75B	PRL 35 349	W.C.J. Carithers <i>et al.</i>	(ROCH, MCGI)
MCCUBBIN 75	NP B86 13	N.A. McCubbin, L. Lyons	(OXF)
PALER 75	NP B96 1	K. Paler <i>et al.</i>	(RHEL, SACL, EPOL)
FOX 74	NP B80 403	G.C. Fox, M.L. Griss	(CIT)
MATISON 74	PR D9 1872	M.J. Matison <i>et al.</i>	(LBL)
BEMPORAD 73	NP B51 1	C. Bemporad <i>et al.</i>	(CERN, ETH, LOIC)
CLARK 73	NP B54 432	A.G. Clark, L. Lyons, D. Radojicic	(OXF)
LEWIS 73	NP B40 288	PH. Lewis <i>et al.</i>	(LOWC, LOIC, CDEF)
LINGLIN 73	NP B55 488	D. Linglin	(CERN)
BUCHNER 72	NP B45 333	K. Buchner <i>et al.</i>	(MPIM, CERN, BRUX)
AGUILAR... 71B	PR D4 2583	M. Aguilar-Benitez, R.L. Eisner, J.B. Kinson	(BNL)
HABER 70	NP B17 289	B. Haber <i>et al.</i>	(REHO, SACL, BGNA, EPOL)
CRENNELL 69D	PRL 22 487	D.J. Crennell <i>et al.</i>	(BNL)
DAVIS 69	PRL 23 1071	P.J. Davis <i>et al.</i>	(LRL)
SCHWEING... 68	PR 166 1317	F. Schweingruber <i>et al.</i>	(ANL, NWES)
BARASH 67B	PR 156 1399	N. Barash <i>et al.</i>	(COLU)
BARLOW 67	NC 50A 701	J. Barlow <i>et al.</i>	(CERN, CDEF, IRAD, LIVA)
DAUBER 67B	NP 153 1403	P.M. Dauber <i>et al.</i>	(UCLA)
DEBAERE 67B	NC 51A 401	W. de Baere <i>et al.</i>	(BRUX, CERN)
WOJCICKI 64	PR 135 B484	S.G. Wojcicki	(LRL)

$$K_1(1270) \quad J(P) = \frac{1}{2}(1^+)$$

### $K_1(1270)$ MASS

VALUE (MeV) DOCUMENT ID  
**1253 ± 7 OUR AVERAGE** Includes data from the 4 datablocks that follow this one. Error includes scale factor of 2.2. See the ideogram below.



See key on page 999

# Meson Particle Listings

## $K_1(1270)$

### PRODUCED BY $K^-$ , BACKWARD SCATTERING, HYPERON EXCHANGE

VALUE (MeV)	EVTS	DOCUMENT ID	TECN	CHG	COMMENT
The data in this block is included in the average printed for a previous datablock.					

1275 ± 10    700    GAVILLET    78    HBC    +    4.2  $K^- p \rightarrow \Xi^-(K\pi\pi)^+$

### PRODUCED BY K BEAMS

VALUE (MeV)	EVTS	DOCUMENT ID	TECN	CHG	COMMENT
The data in this block is included in the average printed for a previous datablock.					

1270 ± 10    1 DAUM    81c    CNTR    -    63  $K^- p \rightarrow K^- 2\pi$

••• We do not use the following data for averages, fits, limits, etc. •••

~ 1276	2	TORNQVIST	82B	RVUE	
~ 1300		VERGEEST	79	HBC	- 4.2 $K^- p \rightarrow (\bar{K}\pi\pi)^- p$
1289 ± 25	3	CARNEGIE	77	ASPK	± 13 $K^\pm p \rightarrow (K\pi\pi)^\pm p$
~ 1300		BRANDENB...	76	ASPK	± 13 $K^\pm p \rightarrow (K\pi\pi)^\pm p$
~ 1270		OTTER	76	HBC	- 10,14,16 $K^- p \rightarrow (\bar{K}\pi\pi)^- p$
1260		DAVIS	72	HBC	+ 12 $K^+ p$
1234 ± 12		FIRESTONE	72B	DBC	+ 12 $K^+ d$

<sup>1</sup> Well described in the chiral unitary approach of GENG 07 with two poles at 1195 and 1284 MeV and widths of 246 and 146 MeV, respectively.

<sup>2</sup> From a unitarized quark-model calculation.

<sup>3</sup> From a model-dependent fit with Gaussian background to BRANDENBURG 76 data.

### PRODUCED BY BEAMS OTHER THAN K MESONS

VALUE (MeV)	EVTS	DOCUMENT ID	TECN	CHG	COMMENT
The data in this block is included in the average printed for a previous datablock.					

1248.1 ± 3.3 ± 1.4    GULER    11    BELL     $B^+ \rightarrow J/\psi K^+ \pi^+ \pi^-$

••• We do not use the following data for averages, fits, limits, etc. •••

1289.81 ± 0.56 ± 1.66	894k	AAIJ	18A1	LHCB	$D^0 \rightarrow K^+ \pi^\pm \pi^\pm \pi^\mp$
1279 ± 10	25k	1	ABLIIKIM	06c	BES2 $J/\psi \rightarrow \bar{K}^*(892)^0 K^+ \pi^-$
1294 ± 10	310	RODEBACK	81	HBC	$4 \pi^- p \rightarrow \Lambda K 2\pi$
1300	40	CRENNELL	72	HBC	$4.5 \pi^- p \rightarrow \Lambda K 2\pi$
1242 + 9 / - 10	2	ASTIER	69	HBC	$\bar{p} p$
1300	45	CRENNELL	67	HBC	$6 \pi^- p \rightarrow \Lambda K 2\pi$

<sup>1</sup> Systematic errors not estimated.

<sup>2</sup> This was called the C meson.

### PRODUCED IN $\tau$ LEPTON DECAYS

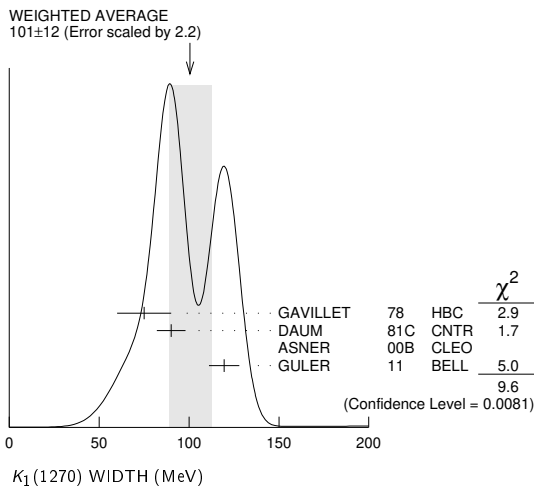
VALUE (MeV)	EVTS	DOCUMENT ID	TECN	CHG	COMMENT
The data in this block is included in the average printed for a previous datablock.					

1254 ± 33 ± 34    7k    ASNER    00B    CLEO    ±     $\tau^- \rightarrow K^- \pi^+ \pi^- \nu_\tau$

### $K_1(1270)$ WIDTH

90 ± 20 OUR ESTIMATE    This is only an educated guess; the error given is larger than the error on the average of the published values.

101 ± 12 OUR AVERAGE    Includes data from the 4 datablocks that follow this one. Error includes scale factor of 2.2. See the ideogram below.



### PRODUCED BY $K^-$ , BACKWARD SCATTERING, HYPERON EXCHANGE

VALUE (MeV)	EVTS	DOCUMENT ID	TECN	CHG	COMMENT
The data in this block is included in the average printed for a previous datablock.					

75 ± 15    700    GAVILLET    78    HBC    +    4.2  $K^- p \rightarrow \Xi^- K\pi\pi$

### PRODUCED BY K BEAMS

VALUE (MeV)	EVTS	DOCUMENT ID	TECN	CHG	COMMENT
The data in this block is included in the average printed for a previous datablock.					

90 ± 8    1 DAUM    81c    CNTR    -    63  $K^- p \rightarrow K^- 2\pi$

••• We do not use the following data for averages, fits, limits, etc. •••

~ 150		VERGEEST	79	HBC	- 4.2 $K^- p \rightarrow (\bar{K}\pi\pi)^- p$
150 ± 71	2	CARNEGIE	77	ASPK	± 13 $K^\pm p \rightarrow (K\pi\pi)^\pm p$
~ 200		BRANDENB...	76	ASPK	± 13 $K^\pm p \rightarrow (K\pi\pi)^\pm p$
120		DAVIS	72	HBC	+ 12 $K^+ p$
188 ± 21		FIRESTONE	72B	DBC	+ 12 $K^+ d$

<sup>1</sup> Well described in the chiral unitary approach of GENG 07 with two poles at 1195 and 1284 MeV and widths of 246 and 146 MeV, respectively.

<sup>2</sup> From a model-dependent fit with Gaussian background to BRANDENBURG 76 data.

### PRODUCED BY BEAMS OTHER THAN K MESONS

VALUE (MeV)	EVTS	DOCUMENT ID	TECN	CHG	COMMENT
The data in this block is included in the average printed for a previous datablock.					

119.5 ± 5.2 ± 6.7    GULER    11    BELL     $B^+ \rightarrow J/\psi K^+ \pi^+ \pi^-$

••• We do not use the following data for averages, fits, limits, etc. •••

116.11 ± 1.65 ± 2.96	894k	AAIJ	18A1	LHCB	$D^0 \rightarrow K^+ \pi^\pm \pi^\pm \pi^\mp$
131 ± 21	25k	1	ABLIIKIM	06c	BES2 $J/\psi \rightarrow \bar{K}^*(892)^0 K^+ \pi^-$
66 ± 15	310	RODEBACK	81	HBC	$4 \pi^- p \rightarrow \Lambda K 2\pi$
60	40	CRENNELL	72	HBC	$4.5 \pi^- p \rightarrow \Lambda K 2\pi$
127 + 7 / - 25	2	ASTIER	69	HBC	$\bar{p} p$
60	45	CRENNELL	67	HBC	$6 \pi^- p \rightarrow \Lambda K 2\pi$

<sup>1</sup> Systematic errors not estimated.

### PRODUCED IN $\tau$ LEPTON DECAYS

VALUE (MeV)	EVTS	DOCUMENT ID	TECN	CHG	COMMENT
The data in this block is included in the average printed for a previous datablock.					

260 + 90 / - 70 ± 80    7k    ASNER    00B    CLEO    ±     $\tau^- \rightarrow K^- \pi^+ \pi^- \nu_\tau$

### $K_1(1270)$ DECAY MODES

Mode	Fraction ( $\Gamma_j/\Gamma$ )
$\Gamma_1$ $K \rho$	(42 ± 6) %
$\Gamma_2$ $K_0^*(1430) \pi$	(28 ± 4) %
$\Gamma_3$ $K^*(892) \pi$	(16 ± 5) %
$\Gamma_4$ $K \omega$	(11.0 ± 2.0) %
$\Gamma_5$ $K f_0(1370)$	( 3.0 ± 2.0) %
$\Gamma_6$ $\gamma K^0$	seen

### $K_1(1270)$ PARTIAL WIDTHS

#### $\Gamma(K\rho)$ $\Gamma_1$

VALUE (MeV)	DOCUMENT ID	TECN	CHG	COMMENT
••• We do not use the following data for averages, fits, limits, etc. •••				

57 ± 5	MAZZUCATO	79	HBC	+ 4.2 $K^- p \rightarrow \Xi^- (K\pi\pi)^+$
75 ± 6	CARNEGIE	77B	ASPK	± 13 $K^\pm p \rightarrow (K\pi\pi)^\pm p$

#### $\Gamma(K_0^*(1430)\pi)$ $\Gamma_2$

VALUE (MeV)	DOCUMENT ID	TECN	CHG	COMMENT
••• We do not use the following data for averages, fits, limits, etc. •••				

26 ± 6	CARNEGIE	77B	ASPK	± 13 $K^\pm p \rightarrow (K\pi\pi)^\pm p$
--------	----------	-----	------	--

#### $\Gamma(K^*(892)\pi)$ $\Gamma_3$

VALUE (MeV)	DOCUMENT ID	TECN	CHG	COMMENT
••• We do not use the following data for averages, fits, limits, etc. •••				

14 ± 11	MAZZUCATO	79	HBC	+ 4.2 $K^- p \rightarrow \Xi^- (K\pi\pi)^+$
2 ± 2	CARNEGIE	77B	ASPK	± 13 $K^\pm p \rightarrow (K\pi\pi)^\pm p$

#### $\Gamma(K\omega)$ $\Gamma_4$

VALUE (MeV)	DOCUMENT ID	TECN	CHG	COMMENT
••• We do not use the following data for averages, fits, limits, etc. •••				

4 ± 4	MAZZUCATO	79	HBC	+ 4.2 $K^- p \rightarrow \Xi^- (K\pi\pi)^+$
24 ± 3	CARNEGIE	77B	ASPK	± 13 $K^\pm p \rightarrow (K\pi\pi)^\pm p$

#### $\Gamma(K f_0(1370))$ $\Gamma_5$

VALUE (MeV)	DOCUMENT ID	TECN	CHG	COMMENT
••• We do not use the following data for averages, fits, limits, etc. •••				

22 ± 5	CARNEGIE	77B	ASPK	± 13 $K^\pm p \rightarrow (K\pi\pi)^\pm p$
--------	----------	-----	------	--

#### $\Gamma(\gamma K^0)$ $\Gamma_6$

VALUE (keV)	DOCUMENT ID	TECN	COMMENT
73.2 ± 6.1 ± 28.3	ALAVI-HARATI02B	KTEV	$K + A \rightarrow K^* + A$



# Meson Particle Listings

## $K_1(1270), K_1(1400)$

### $K_1(1270)$ BRANCHING RATIOS

$\Gamma(K\rho)/\Gamma_{total}$   $\Gamma_1/\Gamma$

VALUE	DOCUMENT ID	TECN	COMMENT
<b>0.42 ± 0.06</b>	<sup>1</sup> DAUM	81c CNTR	63 $K^-p \rightarrow K^-2\pi p$
••• We do not use the following data for averages, fits, limits, etc. •••			
0.584 ± 0.043	<sup>2</sup> GULER	11 BELL	$B^+ \rightarrow J/\psi K^+ \pi^+ \pi^-$
dominant	RODEBACK	81 HBC	$4 \pi^- p \rightarrow \Lambda K 2\pi$

$\Gamma(K_0^*(1430)\pi)/\Gamma_{total}$   $\Gamma_2/\Gamma$

VALUE	DOCUMENT ID	TECN	COMMENT
<b>0.28 ± 0.04</b>	<sup>1</sup> DAUM	81c CNTR	63 $K^-p \rightarrow K^-2\pi p$
••• We do not use the following data for averages, fits, limits, etc. •••			
0.0201 ± 0.0064	<sup>2</sup> GULER	11 BELL	$B^+ \rightarrow J/\psi K^+ \pi^+ \pi^-$

$\Gamma(K^*(892)\pi)/\Gamma_{total}$   $\Gamma_3/\Gamma$

VALUE	DOCUMENT ID	TECN	COMMENT
<b>0.16 ± 0.05</b>	<sup>1</sup> DAUM	81c CNTR	63 $K^-p \rightarrow K^-2\pi p$
••• We do not use the following data for averages, fits, limits, etc. •••			
0.171 ± 0.023	<sup>2</sup> GULER	11 BELL	$B^+ \rightarrow J/\psi K^+ \pi^+ \pi^-$

$\Gamma(K\omega)/\Gamma_{total}$   $\Gamma_4/\Gamma$

VALUE	DOCUMENT ID	TECN	COMMENT
<b>0.11 ± 0.02</b>	<sup>1</sup> DAUM	81c CNTR	63 $K^-p \rightarrow K^-2\pi p$
••• We do not use the following data for averages, fits, limits, etc. •••			
0.225 ± 0.052	<sup>2</sup> GULER	11 BELL	$B^+ \rightarrow J/\psi K^+ \pi^+ \pi^-$

$\Gamma(K\omega)/\Gamma(K\rho)$   $\Gamma_4/\Gamma_1$

VALUE	CL%	DOCUMENT ID	TECN	COMMENT
<0.30	95	RODEBACK	81 HBC	$4 \pi^- p \rightarrow \Lambda K 2\pi$
••• We do not use the following data for averages, fits, limits, etc. •••				

$\Gamma(K f_0(1370))/\Gamma_{total}$   $\Gamma_5/\Gamma$

VALUE	DOCUMENT ID	TECN	COMMENT
<b>0.03 ± 0.02</b>	<sup>1</sup> DAUM	81c CNTR	63 $K^-p \rightarrow K^-2\pi p$

### D-wave/S-wave RATIO FOR $K_1(1270) \rightarrow K^*(892)\pi$

VALUE	DOCUMENT ID	TECN	COMMENT
<b>1.0 ± 0.7</b>	<sup>1</sup> DAUM	81c CNTR	63 $K^-p \rightarrow K^-2\pi p$

<sup>1</sup> Average from low and high  $t$  data.  
<sup>2</sup> Assuming that decays are saturated by the  $K\rho, K_0^*(1430)\pi, K^*(892)\pi, K\omega$  decay modes and neglecting interference between them. The values  $B(\omega \rightarrow \pi^+\pi^-) = (1.53^{+0.11}_{-0.13})\%$  and  $B(K_0^*(1430) \rightarrow K\pi) = (93 \pm 10)\%$  are used. Systematic uncertainties not estimated.

### $K_1(1270)$ REFERENCES

AAIJ	18AI	EPJ C78 443	R. Aaij <i>et al.</i>	(LHCb Collab.)
GULER	11	PR D83 032005	H. Guler <i>et al.</i>	(BELLE Collab.)
GENG	07	PR D75 014017	L.S. Geng <i>et al.</i>	(BES Collab.)
ABLIKIM	06C	PL B633 681	M. Ablikim <i>et al.</i>	(FNAL KTeV Collab.)
ALAVI-HARATI	02B	PRL 89 072001	A. Alavi-Harati <i>et al.</i>	(CLEO Collab.)
ASNER	00B	PR D62 072006	D.M. Asner <i>et al.</i>	(HELS)
TORNQVIST	82B	NP B203 268	N.A. Tornqvist	(AMST, CERN, CRAC, MPIM+)
DAUM	81C	NP B187 1	C. Daum <i>et al.</i>	(CERN, CDEF, MADR+)
RODEBACK	81	ZPHY C9 9	S. Rodeback <i>et al.</i>	(CERN, ZEEM, NIJM+)
MAZZUCATO	79	NP B156 532	M. Mazzucato <i>et al.</i>	(NIJM, AMST, CERN+)
VERGEEST	79	NP B158 265	J.S.M. Vergeest <i>et al.</i>	(AMST, CERN, NIJM+)
GAVILLET	78	PL 76B 517	P. Gavillet <i>et al.</i>	(SLAC)
CARNEGIE	77	NP B127 509	R.K. Carnegie <i>et al.</i>	(SLAC)
CARNEGIE	77B	PL 68B 287	R.K. Carnegie <i>et al.</i>	(SLAC)
BRANDENB...	76	PRL 36 703	G.W. Brandenburg <i>et al.</i>	(AACH3, BERL, CERN, LOIC+)
OTTER	76	NP B106 77	G. Otter <i>et al.</i>	(BNL)
CRENNELL	72	PR D6 1220	D.J. Crennell <i>et al.</i>	(LBL)
DAVIS	72	PR D5 2688	P.J. Davis <i>et al.</i>	(LBL)
FIRESTONE	72B	PR D5 505	A. Firestone <i>et al.</i>	(CDEF, CERN, IPNP, LIVP)
ASTIER	69	NP B10 65	A. Astier <i>et al.</i>	(BNL)1
CRENNELL	67	PRL 19 44	D.J. Crennell <i>et al.</i>	(BNL)1

## $K_1(1400)$

$$J(P) = \frac{1}{2}(1^+)$$

### $K_1(1400)$ MASS

VALUE (MeV)	EVTs	DOCUMENT ID	TECN	CHG	COMMENT
<b>1403 ± 7 OUR AVERAGE</b>					
1463 ± 64 ± 68	7k	ASNER	00B CLEO	±	$\tau^- \rightarrow K^- \pi^+ \pi^- \nu_\tau$
1373 ± 14 ± 18		<sup>1</sup> ASTON	87 LASS	0	$11 K^- p \rightarrow \bar{K}^0 \pi^+ \pi^- n$
1392 ± 18		BAUBILLIER	82B HBC	0	$8.25 K^- p \rightarrow K_S^0 \pi^+ \pi^- n$
1410 ± 25		DAUM	81C CNTR	-	$63 K^- p \rightarrow K^- 2\pi p$
1415 ± 15		ETKIN	80 MPS	0	$6 K^- p \rightarrow \bar{K}^0 \pi^+ \pi^- n$
1404 ± 10		<sup>2</sup> CARNEGIE	77 ASPK	±	$13 K^\pm p \rightarrow (K\pi\pi)^\pm p$

••• We do not use the following data for averages, fits, limits, etc. •••

1418 ± 8	25k	<sup>3</sup> ABLIKIM	06c BES2	$J/\psi \rightarrow \bar{K}^*(892)^0 K^+ \pi^-$
~1350		<sup>4</sup> TORNQVIST	82B RVUE	
~1400		VERGEEST	79 HBC	$4.2 K^- p \rightarrow (\bar{K}\pi\pi)^- p$
~1400		BRANDENB...	76 ASPK	$13 K^\pm p \rightarrow (K\pi\pi)^\pm p$
1420		DAVIS	72 HBC	$12 K^+ p$
1368 ± 18		FIRESTONE	72B DBC	$12 K^+ d$

<sup>1</sup> From partial-wave analysis of  $K^0 \pi^+ \pi^-$  system.  
<sup>2</sup> From a model-dependent fit with Gaussian background to BRANDENBURG 76 data.  
<sup>3</sup> Systematic errors not estimated.  
<sup>4</sup> From a unitarized quark-model calculation.

### $K_1(1400)$ WIDTH

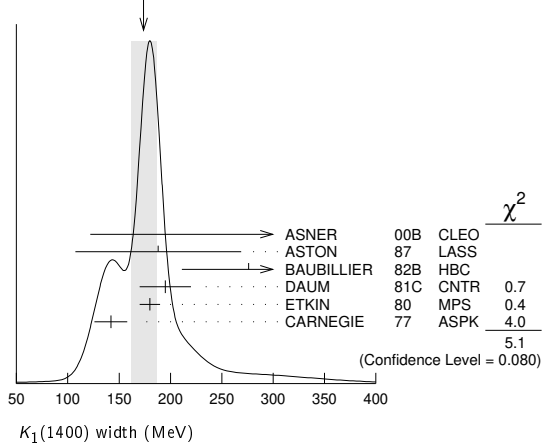
**174 ± 13 OUR AVERAGE** Error includes scale factor of 1.6. See the ideogram below.

VALUE (MeV)	EVTs	DOCUMENT ID	TECN	CHG	COMMENT
$300^{+370}_{-110} \pm 140$	7k	ASNER	00B CLEO	±	$\tau^- \rightarrow K^- \pi^+ \pi^- \nu_\tau$
$188 \pm 54 \pm 60$		<sup>5</sup> ASTON	87 LASS	0	$11 K^- p \rightarrow \bar{K}^0 \pi^+ \pi^- n$
$276 \pm 65$		BAUBILLIER	82B HBC	0	$8.25 K^- p \rightarrow K_S^0 \pi^+ \pi^- n$
195 ± 25		DAUM	81C CNTR	-	$63 K^- p \rightarrow K^- 2\pi p$
180 ± 10		ETKIN	80 MPS	0	$6 K^- p \rightarrow \bar{K}^0 \pi^+ \pi^- n$
142 ± 16		<sup>6</sup> CARNEGIE	77 ASPK	±	$13 K^\pm p \rightarrow (K\pi\pi)^\pm p$
152 ± 16	25k	<sup>7</sup> ABLIKIM	06c BES2		$J/\psi \rightarrow \bar{K}^*(892)^0 K^+ \pi^-$

~200		VERGEEST	79 HBC	-	$4.2 K^- p \rightarrow (\bar{K}\pi\pi)^- p$
~160		BRANDENB...	76 ASPK	±	$13 K^\pm p \rightarrow (K\pi\pi)^\pm p$
80		DAVIS	72 HBC	+	$12 K^+ p$
241 ± 30		FIRESTONE	72B DBC	+	$12 K^+ d$

<sup>5</sup> From partial-wave analysis of  $K^0 \pi^+ \pi^-$  system.  
<sup>6</sup> From a model-dependent fit with Gaussian background to BRANDENBURG 76 data.  
<sup>7</sup> Systematic errors not estimated.

WEIGHTED AVERAGE  
 174 ± 13 (Error scaled by 1.6)



### $K_1(1400)$ DECAY MODES

Mode	Fraction ( $\Gamma_i/\Gamma$ )
$\Gamma_1 K^*(892)\pi$	(94 ± 6) %
$\Gamma_2 K\rho$	( 3.0 ± 3.0) %
$\Gamma_3 K f_0(1370)$	( 2.0 ± 2.0) %
$\Gamma_4 K\omega$	( 1.0 ± 1.0) %
$\Gamma_5 K_0^*(1430)\pi$	not seen
$\Gamma_6 \gamma K^0$	seen

### $K_1(1400)$ PARTIAL WIDTHS

$\Gamma(K^*(892)\pi)$	$\Gamma_1$			
VALUE (MeV)	DOCUMENT ID	TECN	CHG	COMMENT
<b>117 ± 10</b>	CARNEGIE	77 ASPK	±	$13 K^\pm p \rightarrow (K\pi\pi)^\pm p$

$\Gamma(K\rho)$	$\Gamma_2$			
VALUE (MeV)	DOCUMENT ID	TECN	CHG	COMMENT
<b>2 ± 1</b>	CARNEGIE	77 ASPK	±	$13 K^\pm p \rightarrow (K\pi\pi)^\pm p$

Meson Particle Listings
K1(1400), K\*(1410), K0\*(1430)

Gamma(K omega) table with columns: VALUE (MeV), DOCUMENT ID, TECN, CHG, COMMENT. Entry: 23 +/- 12, CARNEGIE 77 ASPK +/- 13 K+/- p -> (K pi pi) +/- p

Gamma(gamma K0) table with columns: VALUE (keV), DOCUMENT ID, TECN, COMMENT. Entry: 280.8 +/- 23.2 +/- 40.4, ALAVI-HARATI02B KTEV K + A -> K\* + A

K1(1400) BRANCHING RATIOS

Gamma(K\*(892) pi)/Gamma total table with columns: VALUE, DOCUMENT ID, TECN, COMMENT. Entry: 0.94 +/- 0.06, 8 DAUM 81c CNTR 63 K- p -> K- 2 pi p

Gamma(K rho)/Gamma total table with columns: VALUE, DOCUMENT ID, TECN, COMMENT. Entry: 0.03 +/- 0.03, 8 DAUM 81c CNTR 63 K- p -> K- 2 pi p

Gamma(K f0(1370))/Gamma total table with columns: VALUE, DOCUMENT ID, TECN, COMMENT. Entry: 0.02 +/- 0.02, 8 DAUM 81c CNTR 63 K- p -> K- 2 pi p

Gamma(K omega)/Gamma total table with columns: VALUE, DOCUMENT ID, TECN, COMMENT. Entry: 0.01 +/- 0.01, 8 DAUM 81c CNTR 63 K- p -> K- 2 pi p

Gamma(K0\*(1430) pi)/Gamma total table with columns: VALUE, DOCUMENT ID, TECN, COMMENT. Entry: not seen, 8 DAUM 81c CNTR 63 K- p -> K- 2 pi p

D-wave/S-wave RATIO FOR K1(1400) -> K\*(892) pi table with columns: VALUE, DOCUMENT ID, TECN, COMMENT. Entry: 0.04 +/- 0.01, 8 DAUM 81c CNTR 63 K- p -> K- 2 pi p

K1(1400) REFERENCES

References table for K1(1400) listing authors, document IDs, and collaborations like BES, FNAL, CLEO, SLAC, etc.

K\*(1410) J(JP) = 1/2(1-)

K\*(1410) MASS

Mass table for K\*(1410) with columns: VALUE (MeV), EVTS, DOCUMENT ID, TECN, CHG, COMMENT. Entry: 1414 +/- 15 OUR AVERAGE

Table with experimental data points for K\*(1410) mass, including values like 1380 +/- 21 +/- 19 and 1420 +/- 7 +/- 10.

Footnotes explaining parametrization methods and data sources for the K\*(1410) mass table.

K\*(1410) WIDTH

Width table for K\*(1410) with columns: VALUE (MeV), EVTS, DOCUMENT ID, TECN, CHG, COMMENT. Entry: 232 +/- 21 OUR AVERAGE

... We do not use the following data for averages, fits, limits, etc. ...

Table listing excluded data points for various decays like D0 -> (K0S pi pi) K +/- and tau- -> K0S pi- nu tau.

Footnotes explaining why certain data points are excluded, such as parametrization choices and systematic uncertainties.

K\*(1410) DECAY MODES

Decay modes table for K\*(1410) showing Mode, Fraction (Gamma\_i/Gamma), and Confidence level.

K\*(1410) PARTIAL WIDTHS

Gamma(gamma K0) table with columns: VALUE (keV), CL%, DOCUMENT ID, TECN, COMMENT. Entry: <52.9, 90 ALAVI-HARATI02B KTEV K + A -> K\* + A

K\*(1410) BRANCHING RATIOS

Gamma(K rho)/Gamma(K\*(892) pi) table with columns: VALUE, CL%, DOCUMENT ID, TECN, CHG, COMMENT. Entry: <0.17, 95 ASTON 84 LASS 0 11 K- p -> K0 2 pi n

Gamma(K pi)/Gamma(K\*(892) pi) table with columns: VALUE, CL%, DOCUMENT ID, TECN, CHG, COMMENT. Entry: <0.16, 95 ASTON 84 LASS 0 11 K- p -> K0 2 pi n

Gamma(K pi)/Gamma total table with columns: VALUE, DOCUMENT ID, TECN, CHG, COMMENT. Entry: 0.066 +/- 0.010 +/- 0.008, ASTON 88 LASS 0 11 K- p -> K- pi+ n

K\*(1410) REFERENCES

References table for K\*(1410) listing authors, document IDs, and collaborations like LHCb, Belle, FNAL, CLEO, etc.

K0\*(1430) J(JP) = 1/2(0+)

See our minireview in the 1994 edition and in this edition under the f0(500).

K0\*(1430) MASS

Mass table for K0\*(1430) with columns: VALUE (MeV), EVTS, DOCUMENT ID, TECN, COMMENT. Entry: 1425 +/- 50 OUR ESTIMATE

Table with experimental data points for K0\*(1430) mass, including values like 1438 +/- 8 +/- 4 and 1427 +/- 4 +/- 13.

Footnotes explaining parametrization methods and data sources for the K0\*(1430) mass table.

# Meson Particle Listings

## $K_0^*(1430)$ , $K_2^*(1430)$

1415 ±25 ~ 1450	<sup>9</sup> ANISOVICH 97c	RVUE	11	$K^- p \rightarrow K^- \pi^+ n$
1412 ± 6	<sup>14</sup> TORNQVIST 96	RVUE	$\pi\pi \rightarrow \pi\pi, K\bar{K}, K\pi$	
~ 1430	<sup>15</sup> ASTON 88	LASS	11	$K^- p \rightarrow K^- \pi^+ n$
~ 1425	BAUBILLIER 84B	HBC	8.25	$K^- p \rightarrow \bar{K}^0 \pi^- p$
~ 1450.0	<sup>16</sup> ESTABROOKS 78	ASPK	13	$K^\pm p \rightarrow K^\pm \pi^\pm (n, \Delta)$
	MARTIN 78	SPEC	10	$K^\pm p \rightarrow K_S^0 \pi p$

- Using both  $\eta \rightarrow \gamma\gamma$  and  $\eta \rightarrow \pi^+\pi^-\pi^0$ . From a likelihood scan in the presence of several interfering scalar-meson resonances with fixed width  $\Gamma(K_0^*(1430)) = 210$  MeV.
- S-matrix pole. Supersedes BUGG 06. Combined analysis of ASTON 88, ABLIKIM 06c, AITALA 06, and LINK 09 using an s-dependent width with couplings to  $K\pi$  and  $K\eta'$ , and the Adler zero near thresholds.
- From the isobar model with a complex pole for the  $\kappa$ .
- From a non-parametric analysis.
- A Breit-Wigner mass and width.
- S-matrix pole. Reanalysis of ASTON 88, AITALA 02, and ABLIKIM 06c including the  $\kappa$  with an s-dependent width and an Adler zero near threshold.
- S-matrix pole. Using ASTON 88 and assuming  $K_0^*(700)$ ,  $K_0^*(1950)$ .
- Using ASTON 88 and assuming  $K_0^*(700)$ .
- T-matrix pole. Reanalysis of ASTON 88 data.
- Breit-Wigner fit. Using ASTON 88.
- Assuming a low-mass scalar  $K\pi$  resonance,  $\kappa(700)$ .
- T-matrix pole. Using data from ESTABROOKS 78 and ASTON 88.
- $J^P$  not determined, could be  $K_2^*(1430)$ .
- T-matrix pole.
- Uses a model for the background, without this background they get a mass 1340 MeV, where the phase shift passes 90°.
- Mass defined by pole position. From elastic  $K\pi$  partial-wave analysis.

### $K_0^*(1430)$ WIDTH

VALUE (MeV)	EVTs	DOCUMENT ID	TECN	COMMENT
<b>270 ±80</b>	<b>OUR ESTIMATE</b>			
• • •	We do not use the following data for averages, fits, limits, etc. • • •			
210 ±20 ±12	5.4k	<sup>1</sup> LEES	14E	BABR $\eta_C(1S) \rightarrow K^+ K^- \eta/\pi^0$
270 ±10 ±40		<sup>2</sup> BUGG	10	RVUE S-matrix pole
174.2 ± 1.9 ± 3.2	141k	<sup>3</sup> BONVICINI	08A	CLEO $D^+ \rightarrow K^- \pi^+ \pi^+$
~ 500		<sup>4</sup> LINK	07	FOCS $D^+ \rightarrow K^- K^+ \pi^+$
177.0 ± 8.0 ± 3.4	54k	<sup>5</sup> LINK	07B	FOCS $D^+ \rightarrow K^- \pi^+ \pi^+$
350 ±40		<sup>6</sup> BUGG	06	RVUE
288 ±22		<sup>7</sup> ZHOU	06	RVUE $Kp \rightarrow K^- \pi^+ n$
270 ±45 <sup>+30</sup> / <sub>-35</sub>		ABLIKIM	05Q	BES2 $\psi(2S) \rightarrow \gamma\pi^+\pi^- K^+ K^-$
217 ±31		<sup>8</sup> ZHENG	04	RVUE $K^- p \rightarrow K^- \pi^+ n$
~ 316		<sup>9</sup> BUGG	03	RVUE $11 K^- p \rightarrow K^- \pi^+ n$
~ 350		<sup>10</sup> LI	03	RVUE $11 K^- p \rightarrow K^- \pi^+ n$
175 ±17	15k	<sup>11</sup> AITALA	02	E791 $D^+ \rightarrow K^- \pi^+ \pi^+$
~ 300		<sup>12</sup> JAMIN	00	RVUE $Kp \rightarrow Kp$
196 ±45		<sup>13</sup> BARBERIS	98E	OMEG 450 $pp \rightarrow p_f p_s K^+ K^- \pi^+ \pi^-$
330 ±50		<sup>9</sup> ANISOVICH 97c	RVUE	11 $K^- p \rightarrow K^- \pi^+ n$
~ 320		<sup>14</sup> TORNQVIST 96	RVUE	$\pi\pi \rightarrow \pi\pi, K\bar{K}, K\pi$
294 ±23		ASTON 88	LASS	11 $K^- p \rightarrow K^- \pi^+ n$
~ 200		BAUBILLIER 84B	HBC	8.25 $K^- p \rightarrow \bar{K}^0 \pi^- p$
200 to 300		<sup>15</sup> ESTABROOKS 78	ASPK	13 $K^\pm p \rightarrow K^\pm \pi^\pm (n, \Delta)$

- Using both  $\eta \rightarrow \gamma\gamma$  and  $\eta \rightarrow \pi^+\pi^-\pi^0$ . From a likelihood scan in the presence of several interfering scalar-meson resonances with fixed mass  $M(K_0^*(1430)) = 1435$  MeV.
- S-matrix pole. Supersedes BUGG 06. Combined analysis of ASTON 88, ABLIKIM 06c, AITALA 06, and LINK 09 using an s-dependent width with couplings to  $K\pi$  and  $K\eta'$ , and the Adler zero near thresholds.
- From the isobar model with a complex pole for the  $\kappa$ .
- From a non-parametric analysis.
- A Breit-Wigner mass and width.
- S-matrix pole. Reanalysis of ASTON 88, AITALA 02, and ABLIKIM 06c including the  $\kappa$  with an s-dependent width and an Adler zero near threshold.
- S-matrix pole. Using ASTON 88 and assuming  $K_0^*(700)$ ,  $K_0^*(1950)$ .
- Using ASTON 88 and assuming  $K_0^*(700)$ .
- T-matrix pole. Reanalysis of ASTON 88 data.
- Breit-Wigner fit. Using ASTON 88.
- Assuming a low-mass scalar  $K\pi$  resonance,  $\kappa(700)$ .
- T-matrix pole. Using data from ESTABROOKS 78 and ASTON 88.
- $J^P$  not determined, could be  $K_2^*(1430)$ .
- T-matrix pole.
- From elastic  $K\pi$  partial-wave analysis.

### $K_0^*(1430)$ DECAY MODES

Mode	Fraction ( $\Gamma_i/\Gamma$ )
$\Gamma_1$ $K\pi$	(93 ±10 ) %
$\Gamma_2$ $K\eta$	( 8.6 ± 2.7 / 3.4 ) %
$\Gamma_3$ $K\eta'(958)$	seen

### $K_0^*(1430)$ BRANCHING RATIOS

$\Gamma(K\pi)/\Gamma_{total}$	DOCUMENT ID	TECN	CHG	COMMENT	$\Gamma_1/\Gamma$
0.93 ± 0.04 ± 0.09	ASTON	88	LASS	0	11 $K^- p \rightarrow K^- \pi^+ n$

$\Gamma(K\eta)/\Gamma(K\pi)$	DOCUMENT ID	TECN	COMMENT	$\Gamma_2/\Gamma_1$
9.2 ± 2.5 <sup>+1.0</sup> / <sub>-2.5</sub>	1 LEES	14E	BABR $\eta_C(1S) \rightarrow K^+ K^- \eta/\pi^0$	

<sup>1</sup> Using both  $\eta \rightarrow \gamma\gamma$  and  $\eta \rightarrow \pi^+\pi^-\pi^0$ . From a Dalitz analysis in the presence of several interfering scalar-meson resonances.

$\Gamma(K\eta'(958))/\Gamma_{total}$	DOCUMENT ID	TECN	COMMENT	$\Gamma_3/\Gamma$
seen	ABLIKIM	14J	BES3	$\psi(2S) \rightarrow \gamma K^+ K^- \eta'(958)$

### $K_0^*(1430)$ REFERENCES

ABLIKIM 14J	PR D89 074030	M. Ablikim <i>et al.</i>	(BESIII Collab.)
LEES 14E	PR D89 112004	J.P. Lees <i>et al.</i>	(BABAR Collab.)
BUGG 10	PR D81 014002	D.V. Bugg	(LOQM)
LINK 09	PL B681 14	J.M. Link <i>et al.</i>	(FNAL FOCUS Collab.)
BONVICINI 08A	PR D78 052001	G. Bonvicini <i>et al.</i>	(CLEO Collab.)
LINK 07	PL B648 156	J.M. Link <i>et al.</i>	(FNAL FOCUS Collab.)
LINK 07B	PL B653 1	J.M. Link <i>et al.</i>	(FNAL FOCUS Collab.)
ABLIKIM 06C	PL B633 681	M. Ablikim <i>et al.</i>	(BES Collab.)
AITALA 06	PR D73 032004	E.M. Aitala <i>et al.</i>	(FNAL E791 Collab.)
Also	PR D74 059901 (errat.)	E.M. Aitala <i>et al.</i>	(FNAL E791 Collab.)
BUGG 06	PL B632 471	D.V. Bugg	(LOQM)
ZHOU 06	NP A775 212	Z.Y. Zhou, H.Q. Zheng	
ABLIKIM 05Q	PR D72 092002	M. Ablikim <i>et al.</i>	(BES Collab.)
ZHENG 04	NP A733 235	H.Q. Zheng <i>et al.</i>	
BUGG 03	PL B572 1	D.V. Bugg	
LI 03	PR D67 034025	L. Li, B. Zou, G. Li	
AITALA 02	PRL 89 121801	E.M. Aitala <i>et al.</i>	(FNAL E791 Collab.)
JAMIN 00	NP B587 331	M. Jamin <i>et al.</i>	
BARBERIS 98E	PL B436 204	D. Barberis <i>et al.</i>	(Omega Expt.)
ANISOVICH 97C	PL B413 137	A.V. Anisovich, A.V. Sarantsev	
TORNQVIST 96	PRL 76 1575	N.A. Tornqvist, M. Roos	(HELS)
ASTON 88	NP B296 493	D. Aston <i>et al.</i>	(SLAC, NAGO, CIN, INUS)
BAUBILLIER 84B	ZPHY C26 37	M. Baubillier <i>et al.</i>	(BIRM, CERN, GLAS+)
ESTABROOKS 78	NP B133 490	P.G. Estabrooks <i>et al.</i>	(MCGI, CARL, DURH+)
MARTIN 78	NP B134 392	A.D. Martin <i>et al.</i>	(DURH, GEVA)

### $K_2^*(1430)$

$$J(J^P) = \frac{1}{2}(2^+)$$

We consider that phase-shift analyses provide more reliable determinations of the mass and width.

### $K_2^*(1430)$ MASS

#### CHARGED ONLY, WITH FINAL STATE $K\pi$

VALUE (MeV)	EVTs	DOCUMENT ID	TECN	CHG	COMMENT
<b>1427.3 ± 1.5</b>	<b>OUR AVERAGE</b>	Error includes scale factor of 1.3. See the ideogram below.			
1432.7 ± 0.7 <sup>+2.2</sup> / <sub>-2.3</sub>	183k	ABLIKIM	19AQ	BES	$J/\psi \rightarrow K^+ K^- \pi^0$
1420 ± 4	1587	BAUBILLIER	84B	HBC	8.25 $K^- p \rightarrow \bar{K}^0 \pi^- p$
1436 ± 5.5	400	<sup>1,2</sup> CLELAND	82	SPEC	+ 30 $K^+ p \rightarrow K_S^0 \pi^+ p$
1430 ± 3.2	1500	<sup>1,2</sup> CLELAND	82	SPEC	+ 50 $K^+ p \rightarrow K_S^0 \pi^+ p$
1430 ± 3.2	1200	<sup>1,2</sup> CLELAND	82	SPEC	- 50 $K^+ p \rightarrow K_S^0 \pi^- p$
1423 ± 5	935	TOAFF	81	HBC	- 6.5 $K^- p \rightarrow \bar{K}^0 \pi^- p$
1428.0 ± 4.6		<sup>3</sup> MARTIN	78	SPEC	+ 10 $K^\pm p \rightarrow K_S^0 \pi p$
1423.8 ± 4.6		<sup>3</sup> MARTIN	78	SPEC	- 10 $K^\pm p \rightarrow K_S^0 \pi p$
1420.0 ± 3.1	1400	AGUILAR...	71B	HBC	- 3.9, 4.6 $K^- p$
1425 ± 8.0	225	<sup>1,2</sup> BARNHAM	71c	HBC	+ $K^+ p \rightarrow K^0 \pi^+ p$
1416 ± 10	220	CRENNELL	69D	DBC	- 3.9 $K^- N \rightarrow \bar{K}^0 \pi^- N$
1414 ± 13.0	60	<sup>1</sup> LIND	69	HBC	+ 9 $K^+ p \rightarrow K^0 \pi^+ p$
1427 ± 12	63	<sup>1</sup> SCHWEING...	68	HBC	+ 5.5 $K^- p \rightarrow \bar{K} \pi N$
1423 ± 11.0	39	<sup>1</sup> BASSANO	67	HBC	- 4.6-5.0 $K^- p \rightarrow \bar{K}^0 \pi^- p$

• • • We do not use the following data for averages, fits, limits, etc. • • •

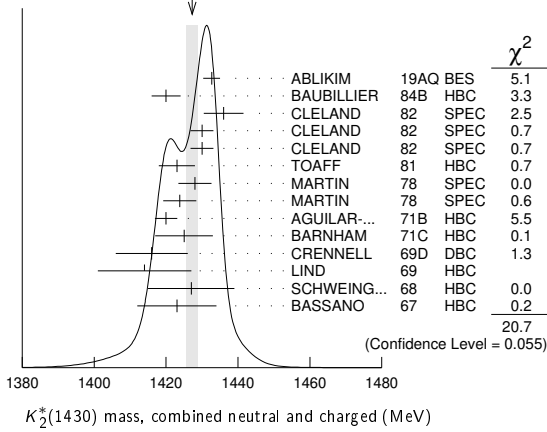
1423.4 ± 2 ± 3	24809 ± 820	<sup>4</sup> BIRD	89	LASS	- 11 $K^- p \rightarrow \bar{K}^0 \pi^- p$
----------------	-------------	-------------------	----	------	--

See key on page 999

# Meson Particle Listings

## $K_2^*(1430)$

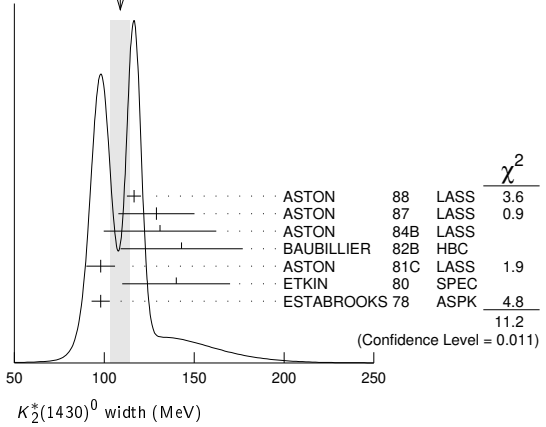
WEIGHTED AVERAGE  
1427.3±1.5 (Error scaled by 1.3)



••• We do not use the following data for averages, fits, limits, etc. •••

113.7 ± 9.2	1786 ± 127	<sup>12</sup> AUBERT	07AK BABR	10.6 $e^+e^- \rightarrow K^{*0}K^\pm\pi^\mp\gamma$
125 ± 29	300	<sup>8</sup> HENDRICK	76 DBC	8.25 $K^+N \rightarrow K^+\pi N$
116 ± 18	800	MCCUBBIN	75 HBC	3.6 $K^-p \rightarrow K^-\pi^+n$
61 ± 14		<sup>13</sup> LINGLIN	73 HBC	2-13 $K^+p \rightarrow K^+\pi^-X$
116.6 <sup>+10.3</sup> <sub>-15.5</sub>	1800	AGUILAR...	71B HBC	3.9,4.6 $K^-p$
144 ± 24.0	600	<sup>8</sup> CORDS	71 DBC	9 $K^+n \rightarrow K^+\pi^-p$
101 ± 10	2200	DAVIS	69 HBC	12 $K^+p \rightarrow K^+\pi^-\pi^+p$

WEIGHTED AVERAGE  
109±5 (Error scaled by 1.9)



### NEUTRAL ONLY

VALUE (MeV)	EVTS	DOCUMENT ID	TECN	COMMENT
<b>1432.4 ± 1.3 OUR AVERAGE</b>				
1431.2 ± 1.8 ± 0.7	5	ASTON 88	LASS	11 $K^-p \rightarrow K^-\pi^+n$
1434 ± 4 ± 6	5	ASTON 87	LASS	11 $K^-p \rightarrow \bar{K}^0\pi^+\pi^-n$
1433 ± 6 ± 10	5	ASTON 84B	LASS	11 $K^-p \rightarrow \bar{K}^02\pi n$
1471 ± 12	5	BAUBILLIER 82B	HBC	8.25 $K^-p \rightarrow NK_S^0\pi\pi$
1428 ± 3	5	ASTON 81C	LASS	11 $K^-p \rightarrow K^-\pi^+n$
1434 ± 2	5	ESTABROOKS 78	ASPK	13 $K^\pm p \rightarrow \rho K\pi$
1440 ± 10	5	BOWLER 77	DBC	5.5 $K^+d \rightarrow K\pi pp$

••• We do not use the following data for averages, fits, limits, etc. •••

1428.5 ± 3.9	1786 ± 127	<sup>6</sup> AUBERT	07AK BABR	10.6 $e^+e^- \rightarrow K^{*0}K^\pm\pi^\mp\gamma$
1420 ± 7	300	HENDRICK	76 DBC	8.25 $K^+N \rightarrow K^+\pi N$
1421.6 ± 4.2	800	MCCUBBIN	75 HBC	3.6 $K^-p \rightarrow K^-\pi^+n$
1420.1 ± 4.3		<sup>7</sup> LINGLIN	73 HBC	2-13 $K^+p \rightarrow K^+\pi^-X$
1419.1 ± 3.7	1800	AGUILAR...	71B HBC	3.9,4.6 $K^-p$
1416 ± 6	600	CORDS	71 DBC	9 $K^+n \rightarrow K^+\pi^-p$
1421.1 ± 2.6	2200	DAVIS	69 HBC	12 $K^+p \rightarrow K^+\pi^-X$

- Errors enlarged by us to  $\Gamma/\sqrt{N}$ ; see the note with the  $K^*(892)$  mass.
- Number of events in peak re-evaluated by us.
- Systematic error added by us.
- From a partial wave amplitude analysis.
- From phase shift or partial-wave analysis.
- Systematic errors not estimated.
- From pole extrapolation, using world  $K^+p$  data summary tape.

### $K_2^*(1430)$ WIDTH

#### CHARGED ONLY, WITH FINAL STATE $K\pi$

VALUE (MeV)	EVTS	DOCUMENT ID	TECN	CHG	COMMENT
<b>100.0 ± 2.1 OUR FIT</b>					
<b>100.0 ± 2.2 OUR AVERAGE</b>					Error includes scale factor of 1.1.
102.5 ± 1.6 <sup>+3.1</sup> <sub>-2.8</sub>	183k	ABLIKIM	19AQ BES	±	$J/\psi \rightarrow K^+K^-\pi^0$
109 ± 22	400	<sup>8,9</sup> CLELAND	82 SPEC	+	30 $K^+p \rightarrow K_S^0\pi^+p$
114 ± 12.8	1500	<sup>8,9</sup> CLELAND	82 SPEC	+	50 $K^+p \rightarrow K_S^0\pi^+p$
113 ± 12.8	1200	<sup>8,9</sup> CLELAND	82 SPEC	-	50 $K^+p \rightarrow K_S^0\pi^-p$
85 ± 16	935	TOAFF	81 HBC	-	6.5 $K^-p \rightarrow \bar{K}^0\pi^-p$
96.5 ± 3.8		MARTIN	78 SPEC	+	10 $K^\pm p \rightarrow K_S^0\pi p$
97.7 ± 4.0		MARTIN	78 SPEC	-	10 $K^\pm p \rightarrow K_S^0\pi p$
94.7 <sup>+15.1</sup> <sub>-12.5</sub>	1400	AGUILAR...	71B HBC	-	3.9,4.6 $K^-p$
98 ± 4 ± 4	25k	<sup>10</sup> BIRD	89 LASS	-	11 $K^-p \rightarrow \bar{K}^0\pi^-p$

### NEUTRAL ONLY

VALUE (MeV)	EVTS	DOCUMENT ID	TECN	COMMENT
<b>109 ± 5 OUR AVERAGE</b>				Error includes scale factor of 1.9. See the ideogram below.
116.5 ± 3.6 ± 1.7	11	ASTON 88	LASS	11 $K^-p \rightarrow K^-\pi^+n$
129 ± 15 ± 15	11	ASTON 87	LASS	11 $K^-p \rightarrow \bar{K}^0\pi^+\pi^-n$
131 ± 24 ± 20	11	ASTON 84B	LASS	11 $K^-p \rightarrow \bar{K}^02\pi n$
143 ± 34	11	BAUBILLIER 82B	HBC	8.25 $K^-p \rightarrow NK_S^0\pi\pi$
98 ± 8	11	ASTON 81C	LASS	11 $K^-p \rightarrow K^-\pi^+n$
140 ± 30	11	ETKIN 80	SPEC	6 $K^-p \rightarrow \bar{K}^0\pi^+\pi^-n$
98 ± 5	11	ESTABROOKS 78	ASPK	13 $K^\pm p \rightarrow \rho K\pi$

<sup>8</sup> Errors enlarged by us to  $4\Gamma/\sqrt{N}$ ; see the note with the  $K^*(892)$  mass.

<sup>9</sup> Number of events in peak re-evaluated by us.

<sup>10</sup> From a partial wave amplitude analysis.

<sup>11</sup> From phase shift or partial-wave analysis.

<sup>12</sup> Systematic errors not estimated.

<sup>13</sup> From pole extrapolation, using world  $K^+p$  data summary tape.

### $K_2^*(1430)$ DECAY MODES

Mode	Fraction ( $\Gamma_i/\Gamma$ )	Scale factor/ Confidence level
$\Gamma_1$ $K\pi$	(49.9 ± 1.2) %	
$\Gamma_2$ $K^*(892)\pi$	(24.7 ± 1.5) %	
$\Gamma_3$ $K^*(892)\pi\pi$	(13.4 ± 2.2) %	
$\Gamma_4$ $K\rho$	( 8.7 ± 0.8) %	S=1.2
$\Gamma_5$ $K\omega$	( 2.9 ± 0.8) %	
$\Gamma_6$ $K^+\gamma$	( 2.4 ± 0.5) × 10 <sup>-3</sup>	S=1.1
$\Gamma_7$ $K\eta$	( 1.5 <sup>+3.4</sup> <sub>-1.0</sub> ) × 10 <sup>-3</sup>	S=1.3
$\Gamma_8$ $K\omega\pi$	< 7.2 × 10 <sup>-4</sup>	CL=95%
$\Gamma_9$ $K^0\gamma$	< 9 × 10 <sup>-4</sup>	CL=90%

### CONSTRAINED FIT INFORMATION

An overall fit to the total width, a partial width, and 10 branching ratios uses 32 measurements and one constraint to determine 8 parameters. The overall fit has a  $\chi^2 = 21.1$  for 25 degrees of freedom.

The following *off-diagonal* array elements are the correlation coefficients  $\langle \delta p_i \delta p_j \rangle / (\delta p_i \delta p_j)$ , in percent, from the fit to parameters  $p_i$ , including the branching fractions,  $x_i \equiv \Gamma_i/\Gamma_{\text{total}}$ . The fit constrains the  $x_i$  whose labels appear in this array to sum to one.

$x_2$	-9						
$x_3$	-40	-73					
$x_4$	-8	36	-52				
$x_5$	-11	-3	-26	-7			
$x_6$	-1	-1	-1	-1	0		
$x_7$	-4	-7	-5	-5	-2	0	
$\Gamma$	0	0	0	0	0	-10	0
	$x_1$	$x_2$	$x_3$	$x_4$	$x_5$	$x_6$	$x_7$

# Meson Particle Listings

## $K_2^*(1430)$

Mode	Rate (MeV)	Scale factor
$\Gamma_1$ $K\pi$	$49.9 \pm 1.6$	
$\Gamma_2$ $K^*(892)\pi$	$24.7 \pm 1.6$	
$\Gamma_3$ $K^*(892)\pi\pi$	$13.5 \pm 2.3$	
$\Gamma_4$ $K\rho$	$8.7 \pm 0.8$	1.2
$\Gamma_5$ $K\omega$	$2.9 \pm 0.8$	
$\Gamma_6$ $K^+\gamma$	$0.24 \pm 0.05$	1.1
$\Gamma_7$ $K\eta$	$0.15^{+0.34}_{-0.10}$	1.3

### $K_2^*(1430)$ PARTIAL WIDTHS

$\Gamma(K^+\gamma)$						$\Gamma_6$
VALUE (keV)	DOCUMENT ID	TECN	CHG	COMMENT		
<b><math>241 \pm 50</math> OUR FIT</b>	Error includes scale factor of 1.1.					
<b><math>240 \pm 45</math></b>	CIHANGIR	82	SPEC	+	$200 K^+ Z \rightarrow Z K^+ \pi^0, Z K_S^0 \pi^+$	

$\Gamma(K^0\gamma)$						$\Gamma_9$
VALUE (keV)	CL%	DOCUMENT ID	TECN	CHG	COMMENT	
<b><math>&lt; 5.4</math></b>	90	ALAVI-HARATI02B	KTEV		$K^+ A \rightarrow K^* + A$	
••• We do not use the following data for averages, fits, limits, etc. •••						
<b><math>&lt; 84</math></b>	90	CARLSMITH	87	SPEC	0	$60\text{--}200 K_L^0 A \rightarrow K_S^0 \pi^0 A$

### $K_2^*(1430)$ BRANCHING RATIOS

$\Gamma(K\pi)/\Gamma_{\text{total}}$						$\Gamma_1/\Gamma$
VALUE	DOCUMENT ID	TECN	CHG	COMMENT		
<b><math>0.499 \pm 0.012</math> OUR FIT</b>						
<b><math>0.488 \pm 0.014</math> OUR AVERAGE</b>						
$0.485 \pm 0.006 \pm 0.020$	<sup>14</sup> ASTON	88	LASS	0	$11 K^- p \rightarrow K^- \pi^+ n$	
$0.49 \pm 0.02$	<sup>14</sup> ESTABROOKS	78	ASPK	$\pm$	$13 K^\pm p \rightarrow p K \pi$	

$\Gamma(K^*(892)\pi)/\Gamma(K\pi)$						$\Gamma_2/\Gamma_1$
VALUE	DOCUMENT ID	TECN	CHG	COMMENT		
<b><math>0.496 \pm 0.034</math> OUR FIT</b>						
<b><math>0.47 \pm 0.04</math> OUR AVERAGE</b>						
$0.44 \pm 0.09$	ASTON	84B	LASS	0	$11 K^- p \rightarrow \bar{K}^0 2\pi n$	
$0.62 \pm 0.19$	LAUSCHER	75	HBC	0	$10,16 K^- p \rightarrow K^- \pi^+ n$	
$0.54 \pm 0.16$	DEHM	74	DBC	0	$4.6 K^+ N$	
$0.47 \pm 0.08$	AGUILAR...	71B	HBC		$3,9,4,6 K^- p$	
$0.47 \pm 0.10$	BASSANO	67	HBC	-0	$4,6,5,0 K^- p$	
$0.45 \pm 0.13$	BADIER	65c	HBC	-	$3 K^- p$	

$\Gamma(K\omega)/\Gamma(K\pi)$						$\Gamma_5/\Gamma_1$
VALUE	DOCUMENT ID	TECN	CHG	COMMENT		
<b><math>0.059 \pm 0.017</math> OUR FIT</b>						
<b><math>0.070 \pm 0.035</math> OUR AVERAGE</b>						
$0.05 \pm 0.04$	AGUILAR...	71B	HBC		$3,9,4,6 K^- p$	
$0.13 \pm 0.07$	BASSOMPIE...	69	HBC	0	$5 K^+ p$	

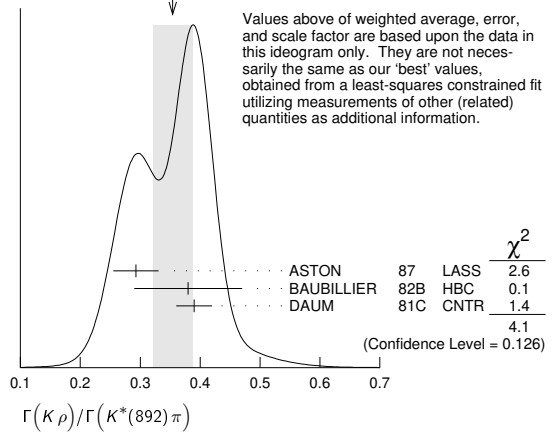
  

$\Gamma(K\rho)/\Gamma(K\pi)$						$\Gamma_4/\Gamma_1$
VALUE	DOCUMENT ID	TECN	CHG	COMMENT		
<b><math>0.174 \pm 0.017</math> OUR FIT</b>	Error includes scale factor of 1.2.					
<b><math>0.150^{+0.029}_{-0.017}</math> OUR AVERAGE</b>						
$0.18 \pm 0.05$	ASTON	84B	LASS	0	$11 K^- p \rightarrow \bar{K}^0 2\pi n$	
$0.02^{+0.10}_{-0.02}$	DEHM	74	DBC	0	$4.6 K^+ N$	
$0.16 \pm 0.05$	AGUILAR...	71B	HBC		$3,9,4,6 K^- p$	
$0.14 \pm 0.10$	BASSANO	67	HBC	-0	$4,6,5,0 K^- p$	
$0.14 \pm 0.07$	BADIER	65c	HBC	-	$3 K^- p$	

$\Gamma(K\rho)/\Gamma(K^*(892)\pi)$						$\Gamma_4/\Gamma_2$
VALUE	DOCUMENT ID	TECN	CHG	COMMENT		
<b><math>0.350 \pm 0.031</math> OUR FIT</b>	Error includes scale factor of 1.4.					
<b><math>0.354 \pm 0.033</math> OUR AVERAGE</b>	Error includes scale factor of 1.4. See the ideogram below.					
$0.293 \pm 0.032 \pm 0.020$	ASTON	87	LASS	0	$11 K^- p \rightarrow \bar{K}^0 \pi^+ \pi^- n$	
$0.38 \pm 0.09$	BAUBILLIER	82B	HBC	0	$8.25 K^- p \rightarrow N K_S^0 \pi \pi$	
$0.39 \pm 0.03$	DAUM	81c	CNTR		$63 K^- p \rightarrow K^- 2\pi p$	

WEIGHTED AVERAGE  
0.354±0.033 (Error scaled by 1.4)



$\Gamma(K\omega)/\Gamma(K^*(892)\pi)$						$\Gamma_5/\Gamma_2$
VALUE	DOCUMENT ID	TECN	CHG	COMMENT		
<b><math>0.118 \pm 0.034</math> OUR FIT</b>						
<b><math>0.10 \pm 0.04</math></b>	FIELD	67	HBC	-	$3.8 K^- p$	

$\Gamma(K\eta)/\Gamma(K^*(892)\pi)$						$\Gamma_7/\Gamma_2$
VALUE	DOCUMENT ID	TECN	CHG	COMMENT		
<b><math>0.006^{+0.014}_{-0.004}</math> OUR FIT</b>	Error includes scale factor of 1.2.					
<b><math>0.07 \pm 0.04</math></b>	FIELD	67	HBC	-	$3.8 K^- p$	

$\Gamma(K\eta)/\Gamma(K\pi)$						$\Gamma_7/\Gamma_1$
VALUE	CL%	DOCUMENT ID	TECN	CHG	COMMENT	
<b><math>0.0030^{+0.0070}_{-0.0020}</math> OUR FIT</b>	Error includes scale factor of 1.3.					
<b><math>0 \pm 0.0056</math></b>		<sup>15</sup> ASTON	88B	LASS	-	$11 K^- p \rightarrow K^- \eta p$
••• We do not use the following data for averages, fits, limits, etc. •••						
$< 0.04$	95	AGUILAR...	71B	HBC		$3,9,4,6 K^- p$
$< 0.065$		<sup>16</sup> BASSOMPIE...	69	HBC		$5.0 K^+ p$
$< 0.02$		BISHOP	69	HBC		$3.5 K^+ p$

$\Gamma(K^*(892)\pi\pi)/\Gamma_{\text{total}}$						$\Gamma_3/\Gamma$
VALUE	DOCUMENT ID	TECN	CHG	COMMENT		
<b><math>0.134 \pm 0.022</math> OUR FIT</b>						
<b><math>0.12 \pm 0.04</math></b>	<sup>17</sup> GOLDBERG	76	HBC	-	$3 K^- p \rightarrow p \bar{K}^0 \pi \pi$	

$\Gamma(K^*(892)\pi\pi)/\Gamma(K\pi)$						$\Gamma_3/\Gamma_1$
VALUE	DOCUMENT ID	TECN	CHG	COMMENT		
<b><math>0.27 \pm 0.05</math> OUR FIT</b>						
<b><math>0.21 \pm 0.08</math></b>	<sup>16,17</sup> JONGEJANS	78	HBC	-	$4 K^- p \rightarrow p \bar{K}^0 \pi \pi$	

$\Gamma(K\omega\pi)/\Gamma_{\text{total}}$						$\Gamma_8/\Gamma$
VALUE (units $10^{-3}$ )	CL%	EVTS	DOCUMENT ID	TECN	COMMENT	
<b><math>&lt; 0.72</math></b>	95	0	JONGEJANS	78	HBC	$4 K^- p \rightarrow p \bar{K}^0 4\pi$

<sup>14</sup> From phase shift analysis.  
<sup>15</sup> ASTON 88B quote  $< 0.0092$  at CL=95%. We convert this to a central value and 1 sigma error in order to be able to use it in our constrained fit.  
<sup>16</sup> Restated by us.  
<sup>17</sup> Assuming  $\pi\pi$  system has isospin 1, which is supported by the data.

### $K_2^*(1430)$ REFERENCES

ABLIKIM	19AQ	PR D100 032004	M. Ablikim et al.	(BESIII Collab.)
AUBERT	07AK	PR D76 012008	B. Aubert et al.	(BABAR Collab.)
ALAVI-HARATI	02B	PRL 89 072001	A. Alavi-Harati et al.	(FNAL KTeV Collab.)
BIRD	89	SLAC-332	P.F. Bird	(SLAC)
ASTON	88	NP B296 493	D. Aston et al.	(SLAC, NAGO, CINC, INUS)
ASTON	88B	PL B201 169	D. Aston et al.	(SLAC, NAGO, CINC, INUS)
ASTON	87	NP B292 693	D. Aston et al.	(SLAC, NAGO, CINC, INUS)
CARLSMITH	87	PR D36 3502	D. Carlsmith et al.	(EFT, SAFL)
ASTON	84B	NP B247 261	D. Aston et al.	(SLAC, CARL, OTTA)
BAUBILLIER	84B	ZPHY C26 37	M. Baubillier et al.	(BIRM, CERN, GLAS+)
BAUBILLIER	82B	NP B202 21	M. Baubillier et al.	(BIRM, CERN, GLAS+)
CIHANGIR	82	PL 117B 123	S. Chhangir et al.	(FNAL, MINN, ROCH)
CLELAND	82	NP B208 189	W.E. Cleland et al.	(DURH, GEVA, LAUS+)
ASTON	81C	PL 106B 235	D. Aston et al.	(SLAC, CARL, OTTA) JP
DAUM	81C	NP B187 1	C. Daum et al.	(AMST, CERN, CRAC, MPIM+)
TOAFF	81	PR D23 1500	S. Toaff et al.	(ANL, KANS)
ETKIN	80	PR D22 42	A. Etkin et al.	(BNL, CUNY) JP
ESTABROOKS	78	NP B133 490	P.G. Estabrooks et al.	(MCGI, CARL, DURH+)
Also		PR D17 658	P.G. Estabrooks et al.	(MCGI, CARL, DURH+)
JONGEJANS	78	NP B139 383	R. Jongejans et al.	(ZEEM, CERN, NUM+)
MARTIN	78	NP B134 392	A.D. Martin et al.	(DURH, GEVA)
BOWLER	77	NP B126 31	M.G. Bowler et al.	(OXF)
GOLDBERG	76	LCN 17 253	J. Goldberg	(HAIF)

See key on page 999

Meson Particle Listings

$K_2^*(1430)$ ,  $K(1460)$ ,  $K_2(1580)$ ,  $K(1630)$ ,  $K_1(1650)$

HENDRICK	76	NP B112 189	K. Hendrickx et al.	(MONS, SACL, PARIS+)
LAUSCHER	75	NP B86 189	P. Lauscher et al.	(ABCLV Collab.) JP
MCCUBBIN	75	NP B86 13	N.A. McCubbin, L. Lyons	(OXF)
DEHM	74	NP B75 47	G. Dehm et al.	(MPIM, BRUX, MONS, CERN)
LINGLIN	73	NP B55 408	D. Linglin	(CERN)
AGUILAR...	71B	PR D4 2583	M. Aguilar-Benitez, R.L. Eisner, J.B. Kinson	(BNL)
BARNHAM	71C	NP B28 171	K.W.J. Barnham et al.	(BIRM, GLAS)
CORDS	71	PR D4 1974	D. Cords et al.	(PURD, UCD, IUPU)
BASSOMPIE...	69	NP B13 189	G. Bassompierre et al.	(CERN, BRUX) JP
BISHOP	69	NP B9 403	J.M. Bishop et al.	(WISC)
CRENNELL	69D	PRL 22 487	D.J. Crennell et al.	(BNL)
DAVIS	69	PRL 23 1071	P.J. Davis et al.	(LRL)
LIND	69	NP B14 1	V.G. Lind et al.	(LRL) JP
SCHWEING...	68	PR 166 1317	F. Schweingruber et al.	(ANL, NWES)
Also		Thesis	F.L. Schweingruber	(NWES, NWES)
BASSANO	67	PRL 19 968	D. Bassano et al.	(BNL, SYRA)
FIELD	67	PL 24B 638	J.H. Field et al.	(UCSD)
BADIER	65C	PL 19 612	J. Badier et al.	(EPOL, SACL, AMST)

**$K(1460)$**

$I(J^P) = \frac{1}{2}(0^-)$

OMITTED FROM SUMMARY TABLE  
Observed in  $K\pi\pi$  partial-wave analysis.

**$K(1460)$  MASS**

VALUE (MeV)	EVTS	DOCUMENT ID	TECN	CHG	COMMENT
1482.40 ± 3.58 ± 15.22	894k	AAIJ	18A1	LHCB	$D^0 \rightarrow K\bar{\pi} 2\pi^\pm \pi^\mp$
~ 1460	63	DAUM	81c	CNTR	$K^- p \rightarrow K^- 2\pi p$
~ 1400	13	<sup>1</sup> BRANDENB...	76B	ASPK	$K^\pm p \rightarrow K^\pm 2\pi p$

<sup>1</sup> Coupled mainly to  $K f_0(1370)$ . Decay into  $K^*(892)\pi$  seen.

**$K(1460)$  WIDTH**

VALUE (MeV)	EVTS	DOCUMENT ID	TECN	CHG	COMMENT
335.60 ± 6.20 ± 8.65	894k	AAIJ	18A1	LHCB	$D^0 \rightarrow K\bar{\pi} 2\pi^\pm \pi^\mp$
~ 260	63	DAUM	81c	CNTR	$K^- p \rightarrow K^- 2\pi p$
~ 250	15	<sup>1</sup> BRANDENB...	76B	ASPK	$K^\pm p \rightarrow K^\pm 2\pi p$

<sup>1</sup> Coupled mainly to  $K f_0(1370)$ . Decay into  $K^*(892)\pi$  seen.

**$K(1460)$  DECAY MODES**

Mode	Fraction ( $\Gamma_i/\Gamma$ )
$\Gamma_1$ $K^*(892)\pi$	seen
$\Gamma_2$ $K\rho$	seen
$\Gamma_3$ $K_0^0(1430)\pi$	seen

**$K(1460)$  PARTIAL WIDTHS**

$\Gamma(K^*(892)\pi)$	$\Gamma_1$		
VALUE (MeV)	DOCUMENT ID	TECN	COMMENT
~ 109	DAUM	81c	CNTR 63 $K^- p \rightarrow K^- 2\pi p$

$\Gamma(K\rho)$	$\Gamma_2$		
VALUE (MeV)	DOCUMENT ID	TECN	COMMENT
~ 34	DAUM	81c	CNTR 63 $K^- p \rightarrow K^- 2\pi p$

$\Gamma(K_0^0(1430)\pi)$	$\Gamma_3$		
VALUE (MeV)	DOCUMENT ID	TECN	COMMENT
~ 117	DAUM	81c	CNTR 63 $K^- p \rightarrow K^- 2\pi p$

**$K(1460)$  REFERENCES**

AAIJ	18A1	EPJ C78 443	R. Aaij et al.	(LHCb Collab.)
DAUM	81C	NP B187 1	C. Daum et al.	(AMST, CERN, CRAC, MPIM+)
BRANDENB...	76B	PRL 36 1239	G.W. Brandenburg et al.	(SLAC) JP

**$K_2(1580)$**

$I(J^P) = \frac{1}{2}(2^-)$

OMITTED FROM SUMMARY TABLE  
Seen in partial-wave analysis of the  $K^- \pi^+ \pi^-$  system. Needs confirmation.

**$K_2(1580)$  MASS**

VALUE (MeV)	DOCUMENT ID	CHG	COMMENT
~ 1580	OTTER	79	- 10,14,16 $K^- p$

**$K_2(1580)$  WIDTH**

VALUE (MeV)	DOCUMENT ID	CHG	COMMENT
~ 110	OTTER	79	- 10,14,16 $K^- p$

• • • We do not use the following data for averages, fits, limits, etc. • • •

**$K_2(1580)$  DECAY MODES**

Mode	Fraction ( $\Gamma_i/\Gamma$ )
$\Gamma_1$ $K^*(892)\pi$	seen
$\Gamma_2$ $K_2^*(1430)\pi$	possibly seen

**$K_2(1580)$  BRANCHING RATIOS**

$\Gamma(K^*(892)\pi)/\Gamma_{total}$	$\Gamma_1/\Gamma$			
VALUE	DOCUMENT ID	TECN	CHG	COMMENT
seen	OTTER	79	HBC	- 10,14,16 $K^- p$

• • • We do not use the following data for averages, fits, limits, etc. • • •

possibly seen
 GULER | 11 | BELL | $B^+ \rightarrow J/\psi K^+ \pi^+ \pi^-$ |

$\Gamma(K_2^*(1430)\pi)/\Gamma_{total}$	$\Gamma_2/\Gamma$			
VALUE	DOCUMENT ID	TECN	CHG	COMMENT
possibly seen	OTTER	79	HBC	- 10,14,16 $K^- p$

**$K_2(1580)$  REFERENCES**

GULER	11	PR D83 032005	H. Guler et al.	(BELLE Collab.)
OTTER	79	NP B147 1	G. Otter et al.	(AACH3, BERL, CERN, LOIC+) JP

**$K(1630)$**

$I(J^P) = \frac{1}{2}(?^-)$

OMITTED FROM SUMMARY TABLE  
Seen as a narrow peak, compatible with the experimental resolution, in the invariant mass of the  $K_S^0 \pi^+ \pi^-$  system produced in  $\pi^- p$  interactions at high momentum transfers.

**$K(1630)$  MASS**

VALUE (MeV)	EVTS	DOCUMENT ID	TECN	COMMENT
1629 ± 7	~ 75	KARNAUKHOV98	BC	16.0 $\pi^- p \rightarrow (K_S^0 \pi^+ \pi^-) X^+ \pi^- X^0$

**$K(1630)$  WIDTH**

VALUE (MeV)	EVTS	DOCUMENT ID	TECN	COMMENT
16 ± 19 16	~ 75	<sup>1</sup> KARNAUKHOV98	BC	16.0 $\pi^- p \rightarrow (K_S^0 \pi^+ \pi^-) X^+ \pi^- X^0$

<sup>1</sup> Compatible with an experimental resolution of 14 ± 1 MeV.

**$K(1630)$  DECAY MODES**

Mode	Fraction ( $\Gamma_i/\Gamma$ )
$\Gamma_1$ $K_S^0 \pi^+ \pi^-$	

**$K(1630)$  REFERENCES**

KARNAUKHOV 98	PAN 61 203	V.M. Karnaukhov, C. Coca, V.I. Moroz
	Translated from YAF 61 252.	

**$K_1(1650)$**

$I(J^P) = \frac{1}{2}(1^+)$

OMITTED FROM SUMMARY TABLE  
This entry contains various peaks in strange meson systems ( $K^+ \phi$ ,  $K\pi\pi$ ) reported in partial-wave analysis in the 1600–1900 mass region.

**$K_1(1650)$  MASS**

VALUE (MeV)	EVTS	DOCUMENT ID	TECN	CHG	COMMENT
1672 ± 50	OUR AVERAGE	Error includes scale factor of 1.1.			
1793 ± 59 ± 153 101	4289	<sup>1</sup> AAIJ	17c	LHCB	$B^+ \rightarrow J/\psi \phi K^+$
1650 ± 50		FRAME	86	OMEG +	13 $K^+ p \rightarrow \phi K^+ p$

• • • We do not use the following data for averages, fits, limits, etc. • • •

~ 1840
 ARMSTRONG | 83 | OMEG - | 18.5  $K^- p \rightarrow 3K p$ |

<sup>1</sup> From an amplitude analysis of the decay  $B^+ \rightarrow J/\psi \phi K^+$  with a significance of 7.6  $\sigma$ .

# Meson Particle Listings

## $K_1(1650)$ , $K^*(1680)$ , $K_2(1770)$

### $K_1(1650)$ WIDTH

VALUE (MeV)	EVTS	DOCUMENT ID	TECN	CHG	COMMENT
<b>158 ± 50 OUR AVERAGE</b>					
365 ± 157 <sup>+138</sup> <sub>-215</sub>	4289	<sup>2</sup> AAIJ	17c	LHCB	$B^+ \rightarrow J/\psi \phi K^+$
150 ± 50		FRAME	86	OMEG +	13 $K^+ p \rightarrow \phi K^+ p$
• • • We do not use the following data for averages, fits, limits, etc. • • •					
~ 250		DAUM	81c	CNTR -	63 $K^- p \rightarrow K^- 2\pi p$
<sup>2</sup> From an amplitude analysis of the decay $B^+ \rightarrow J/\psi \phi K^+$ with a significance of 7.6 $\sigma$ .					

### $K_1(1650)$ DECAY MODES

Mode	Fraction ( $\Gamma_i/\Gamma$ )
$\Gamma_1$ $K \pi \pi$	
$\Gamma_2$ $K \phi$	

### $K_1(1650)$ REFERENCES

AAIJ	17C	PRL 118 022003	R. Aaij et al.	(LHCb Collab.)
Also	PR D95 012002	R. Aaij et al.	(LHCb Collab.)	
FRAME	86	NP B276 667	D. Frame et al.	(GLAS)
ARMSTRONG	83	NP B221 1	T.A. Armstrong et al.	(BARI, BIRM, CERN+)
DAUM	81C	NP B187 1	C. Daum et al.	(AMST, CERN, CRAC, MPIM+)

## $K^*(1680)$

$$I(J^P) = \frac{1}{2}(1^-)$$

### $K^*(1680)$ MASS

VALUE (MeV)	EVTS	DOCUMENT ID	TECN	CHG	COMMENT
<b>1718 ± 18 OUR AVERAGE</b>					
1722 ± 20 <sup>+33</sup> <sub>-109</sub>	4289	<sup>1</sup> AAIJ	17c	LHCB	$B^+ \rightarrow J/\psi \phi K^+$
1677 ± 10 ± 32		ASTON	88	LASS 0	11 $K^- p \rightarrow K^- \pi^+ n$
					$K^- p \rightarrow \bar{K}^0 \pi^+ n$
1735 ± 10 ± 20		ASTON	87	LASS 0	11 $K^- p \rightarrow \bar{K}^0 \pi^+ \pi^- n$
• • • We do not use the following data for averages, fits, limits, etc. • • •					
1678 ± 64		BIRD	89	LASS -	11 $K^- p \rightarrow \bar{K}^0 \pi^- p$
1800 ± 70		ETKIN	80	MPS 0	6 $K^- p \rightarrow \bar{K}^0 \pi^+ \pi^- n$
~ 1650		ESTABROOKS	78	ASPK 0	13 $K^\pm p \rightarrow K^\pm \pi^\pm n$
<sup>1</sup> From an amplitude analysis of the decay $B^+ \rightarrow J/\psi \phi K^+$ with a significance of 8.5 $\sigma$ .					

### $K^*(1680)$ WIDTH

VALUE (MeV)	EVTS	DOCUMENT ID	TECN	CHG	COMMENT
<b>322 ± 110 OUR AVERAGE</b>					Error includes scale factor of 4.2.
354 ± 75 <sup>+140</sup> <sub>-181</sub>	4289	<sup>2</sup> AAIJ	17c	LHCB	$B^+ \rightarrow J/\psi \phi K^+$
205 ± 16 ± 34		ASTON	88	LASS 0	11 $K^- p \rightarrow K^- \pi^+ n$
					$K^- p \rightarrow \bar{K}^0 \pi^+ \pi^- n$
423 ± 18 ± 30		ASTON	87	LASS 0	11 $K^- p \rightarrow \bar{K}^0 \pi^+ \pi^- n$
• • • We do not use the following data for averages, fits, limits, etc. • • •					
454 ± 270		BIRD	89	LASS -	11 $K^- p \rightarrow \bar{K}^0 \pi^- p$
170 ± 30		ETKIN	80	MPS 0	6 $K^- p \rightarrow \bar{K}^0 \pi^+ \pi^- n$
250 to 300		ESTABROOKS	78	ASPK 0	13 $K^\pm p \rightarrow K^\pm \pi^\pm n$
<sup>2</sup> From an amplitude analysis of the decay $B^+ \rightarrow J/\psi \phi K^+$ with a significance of 8.5 $\sigma$ .					

### $K^*(1680)$ DECAY MODES

Mode	Fraction ( $\Gamma_i/\Gamma$ )
$\Gamma_1$ $K \pi$	(38.7 ± 2.5) %
$\Gamma_2$ $K \rho$	(31.4 <sup>+5.0</sup> <sub>-2.1</sub> ) %
$\Gamma_3$ $K^*(892)\pi$	(29.9 <sup>+2.2</sup> <sub>-5.0</sub> ) %
$\Gamma_4$ $K \phi$	seen

### CONSTRAINED FIT INFORMATION

An overall fit to 4 branching ratios uses 4 measurements and one constraint to determine 3 parameters. The overall fit has a  $\chi^2 = 2.9$  for 2 degrees of freedom.

The following *off-diagonal* array elements are the correlation coefficients  $\langle \delta x_i \delta x_j \rangle / (\delta x_i \delta x_j)$ , in percent, from the fit to the branching fractions,  $x_i \equiv \Gamma_i/\Gamma_{\text{total}}$ . The fit constrains the  $x_i$  whose labels appear in this array to sum to one.

$$\begin{matrix} x_2 & | & -36 \\ x_3 & | & -39 & -72 \\ & x_1 & x_2 \end{matrix}$$

### $K^*(1680)$ BRANCHING RATIOS

$\Gamma(K\pi)/\Gamma_{\text{total}}$	DOCUMENT ID	TECN	CHG	COMMENT	$\Gamma_1/\Gamma$
<b>0.387 ± 0.026 OUR FIT</b>					
<b>0.388 ± 0.014 ± 0.022</b>	ASTON	88	LASS 0	11 $K^- p \rightarrow K^- \pi^+ n$	
$\Gamma(K\pi)/\Gamma(K^*(892)\pi)$	DOCUMENT ID	TECN	CHG	COMMENT	$\Gamma_1/\Gamma_3$
<b>1.30<sup>+0.23</sup><sub>-0.14</sub> OUR FIT</b>					
<b>2.8 ± 1.1</b>	ASTON	84	LASS 0	11 $K^- p \rightarrow \bar{K}^0 2\pi n$	
$\Gamma(K\rho)/\Gamma(K\pi)$	DOCUMENT ID	TECN	CHG	COMMENT	$\Gamma_2/\Gamma_1$
<b>0.81<sup>+0.14</sup><sub>-0.09</sub> OUR FIT</b>					
<b>1.2 ± 0.4</b>	ASTON	84	LASS 0	11 $K^- p \rightarrow \bar{K}^0 2\pi n$	
$\Gamma(K\rho)/\Gamma(K^*(892)\pi)$	DOCUMENT ID	TECN	CHG	COMMENT	$\Gamma_2/\Gamma_3$
<b>1.05<sup>+0.27</sup><sub>-0.11</sub> OUR FIT</b>					
<b>0.97 ± 0.09<sup>+0.30</sup><sub>-0.10</sub></b>	ASTON	87	LASS 0	11 $K^- p \rightarrow \bar{K}^0 \pi^+ \pi^- n$	
$\Gamma(K\phi)/\Gamma_{\text{total}}$	EVTS	DOCUMENT ID	TECN	COMMENT	$\Gamma_4/\Gamma$
seen	4289	<sup>3</sup> AAIJ	17c	LHCB $B^+ \rightarrow J/\psi \phi K^+$	
<sup>3</sup> From an amplitude analysis of the decay $B^+ \rightarrow J/\psi \phi K^+$ with a significance of 8.5 $\sigma$ .					

### $K^*(1680)$ REFERENCES

AAIJ	17C	PRL 118 022003	R. Aaij et al.	(LHCb Collab.)
Also	PR D95 012002	R. Aaij et al. <td>(LHCb Collab.)</td> <td></td>	(LHCb Collab.)	
BIRD	89	SLAC-332	P.F. Bird	(SLAC)
ASTON	88	NP B296 493	D. Aston et al.	(SLAC, NAGO, CIN, INUS)
ASTON	87	NP B292 693	D. Aston et al.	(SLAC, NAGO, CIN, INUS)
ASTON	84	PL 149B 258	D. Aston et al.	(SLAC, CARL, OTTA) JP
ETKIN	80	PR D22 42	A. Etkin et al.	(BNL, CUNY) JP
ESTABROOKS	78	NP B133 490	P.G. Estabrooks et al.	(MCGI, CARL, DURH+) JP

## $K_2(1770)$

$$I(J^P) = \frac{1}{2}(2^-)$$

See our mini-review in the 2004 edition of this Review, PDG 04.

### $K_2(1770)$ MASS

VALUE (MeV)	EVTS	DOCUMENT ID	TECN	CHG	COMMENT
<b>1773 ± 8 OUR AVERAGE</b>					
1777 ± 35 <sup>+122</sup> <sub>-77</sub>	4289	<sup>1</sup> AAIJ	17c	LHCB	$B^+ \rightarrow J/\psi \phi K^+$
1773 ± 8		<sup>2</sup> ASTON	93	LASS	11 $K^- p \rightarrow K^- \omega p$
• • • We do not use the following data for averages, fits, limits, etc. • • •					
1743 ± 15		TIKHOMIROV	03	SPEC	40.0 $\pi^- C \rightarrow K_S^0 K_S^0 K_L^0 X$
1810 ± 20		FRAME	86	OMEG +	13 $K^+ p \rightarrow \phi K^+ p$
~ 1730		ARMSTRONG	83	OMEG -	18.5 $K^- p \rightarrow 3K p$
~ 1780		<sup>3</sup> DAUM	81c	CNTR -	63 $K^- p \rightarrow K^- 2\pi p$
1710 ± 15	60	CHUNG	74	HBC -	7.3 $K^- p \rightarrow K^- \omega p$
1767 ± 6		BLIEDEN	72	MMS -	11-16 $K^- p$
1730 ± 20	306	<sup>4</sup> FIRESTONE	72B	DBC +	12 $K^+ d$
1765 ± 40		<sup>5</sup> COLLEY	71	HBC +	10 $K^+ p \rightarrow K_2 \pi N$
1740		DENEGRI	71	DBC -	12.6 $K^- d \rightarrow \bar{K} 2\pi d$
1745 ± 20		AGUILAR...	70C	HBC -	4.6 $K^- p$
1780 ± 15		BARTSCH	70c	HBC -	10.1 $K^- p$
1760 ± 15		LUDLAM	70	HBC -	12.6 $K^- p$

- <sup>1</sup> From an amplitude analysis of the decay  $B^+ \rightarrow J/\psi \phi K^+$  with a significance of 5.0  $\sigma$ .
- <sup>2</sup> From a partial wave analysis of the  $K^- \omega$  system.
- <sup>3</sup> From a partial wave analysis of the  $K^- 2\pi$  system.
- <sup>4</sup> Produced in conjunction with excited deuteron.
- <sup>5</sup> Systematic errors added correspond to spread of different fits.

### $K_2(1770)$ WIDTH

VALUE (MeV)	EVTS	DOCUMENT ID	TECN	CHG	COMMENT
<b>186 ± 14 OUR AVERAGE</b>					
217 ± 116 <sup>+221</sup> <sub>-154</sub>	4289	<sup>6</sup> AAIJ	17c	LHCB	$B^+ \rightarrow J/\psi \phi K^+$
186 ± 14		<sup>7</sup> ASTON	93	LASS	11 $K^- p \rightarrow K^- \omega p$

See key on page 999

Meson Particle Listings

$K_2(1770)$ ,  $K_3^*(1780)$

••• We do not use the following data for averages, fits, limits, etc. •••

$147 \pm 70$	TIKHOMIROV 03	SPEC	$40.0 \frac{\pi^- C \rightarrow K_S^0 K_S^0 K_L^0 X}{K_S^0 K_S^0 K_L^0 X}$
$140 \pm 40$	FRAME 86	OMEG +	$13 K^+ p \rightarrow \phi K^+ p$
$\sim 220$	ARMSTRONG 83	OMEG -	$18.5 K^- p \rightarrow 3K p$
$\sim 210$	8 DAUM 81c	CNTR -	$63 K^- p \rightarrow K^- 2\pi p$
$110 \pm 50$	60 CHUNG 74	HBC -	$7.3 K^- p \rightarrow K^- \omega p$
$100 \pm 26$	BLIEDEN 72	MMS -	$11-16 K^- p$
$210 \pm 30$	306 9 FIRESTONE 72B	DBC +	$12 K^+ d$
$90 \pm 70$	10 COLLEY 71	HBC +	$10 K^+ p \rightarrow K 2\pi N$
130	DENEGRI 71	DBC -	$12.6 K^- d \rightarrow \bar{K} 2\pi d$
$100 \pm 50$	AGUILAR... 70c	HBC -	$4.6 K^- p$
$138 \pm 40$	BARTSCH 70c	HBC -	$10.1 K^- p$
$50 \pm \frac{40}{20}$	LUDLAM 70	HBC -	$12.6 K^- p$

6 From an amplitude analysis of the decay  $B^+ \rightarrow J/\psi \phi K^+$  with a significance of 5.0  $\sigma$ .  
 7 From a partial wave analysis of the  $K^- \omega$  system.  
 8 From a partial wave analysis of the  $K^- 2\pi$  system.  
 9 Produced in conjunction with excited deuteron.  
 10 Systematic errors added correspond to spread of different fits.

$K_2(1770)$  DECAY MODES

Mode	Fraction ( $\Gamma_i/\Gamma$ )
$\Gamma_1$ $K \pi \pi$	
$\Gamma_2$ $K_2^*(1430) \pi$	seen
$\Gamma_3$ $K^*(892) \pi$	seen
$\Gamma_4$ $K f_2(1270)$	seen
$\Gamma_5$ $K f_0(980)$	
$\Gamma_6$ $K \phi$	seen
$\Gamma_7$ $K \omega$	seen

$K_2(1770)$  BRANCHING RATIOS

$\Gamma(K_2^*(1430)\pi)/\Gamma(K\pi\pi)$   $\Gamma_2/\Gamma_1$   
 ( $K_2^*(1430) \rightarrow K\pi$ )

VALUE	DOCUMENT ID	TECN	CHG	COMMENT
$\sim 0.03$	DAUM 81c	CNTR		$63 K^- p \rightarrow K^- 2\pi p$
$\sim 1.0$	11 FIRESTONE 72B	DBC +		$12 K^+ d$
$< 1.0$	COLLEY 71	HBC		$10 K^+ p$
$0.2 \pm 0.2$	AGUILAR... 70c	HBC -		$4.6 K^- p$
$< 1.0$	BARTSCH 70c	HBC -		$10.1 K^- p$
1.0	BARBARO... 69	HBC +		$12.0 K^+ p$

11 Produced in conjunction with excited deuteron.

$\Gamma(K^*(892)\pi)/\Gamma(K\pi\pi)$   $\Gamma_3/\Gamma_1$

VALUE	DOCUMENT ID	TECN	COMMENT
$\sim 0.23$	DAUM 81c	CNTR	$63 K^- p \rightarrow K^- 2\pi p$

$\Gamma(K f_2(1270))/\Gamma(K\pi\pi)$   $\Gamma_4/\Gamma_1$   
 ( $f_2(1270) \rightarrow \pi\pi$ )

VALUE	DOCUMENT ID	TECN	COMMENT
$\sim 0.74$	DAUM 81c	CNTR	$63 K^- p \rightarrow K^- 2\pi p$

$\Gamma(K f_0(980))/\Gamma_{total}$   $\Gamma_5/\Gamma$

VALUE	DOCUMENT ID	TECN	COMMENT
possibly seen	TIKHOMIROV 03	SPEC	$40.0 \frac{\pi^- C \rightarrow K_S^0 K_S^0 K_L^0 X}{K_S^0 K_S^0 K_L^0 X}$

$\Gamma(K\phi)/\Gamma_{total}$   $\Gamma_6/\Gamma$

VALUE	EVTS	DOCUMENT ID	TECN	CHG	COMMENT
seen	4289	12 AAJ 17c	LHCB		$B^+ \rightarrow J/\psi \phi K^+$
seen		ARMSTRONG 83	OMEG -		$18.5 K^- p \rightarrow K^- \phi N$

12 From an amplitude analysis of the decay  $B^+ \rightarrow J/\psi \phi K^+$  with a significance of 5.0  $\sigma$ .

$\Gamma(K\omega)/\Gamma_{total}$   $\Gamma_7/\Gamma$

VALUE	DOCUMENT ID	TECN	CHG	COMMENT
seen	OTTER 81	HBC	$\pm$	$8.25, 10, 16 K^\pm p$
seen	CHUNG 74	HBC	-	$7.3 K^- p \rightarrow K^- \omega p$

$K_2(1770)$  REFERENCES

AAJ 17c	PRL 118 022003	R. Aajj et al.	(LHCB Collab.)
Also	PR D95 012002	R. Aajj et al.	(LHCB Collab.)
PDG 04	PL B592 1	S. Eidelman et al.	(PDG Collab.)
TIKHOMIROV 03	PAN 66 828	G.D. Tikhomirov et al.	
ASTON 93	Translated from YAF 66 860. PL B308 186	D. Aston et al.	(SLAC, NAGO, CINC, INUS)

FRAME 86	NP B276 667	D. Frame et al.	(GLAS)
ARMSTRONG 83	NP B221 1	T.A. Armstrong et al.	(BARI, BIRM, CERN+)
DAUM 81c	NP B187 1	C. Daum et al.	(AMST, CERN, CRAC, MPIM+)
OTTER 81	NP B181 1	G. Otter	(AACH3, BERL, LOIC, VIEN, BIRM+)
CHUNG 74	PL 51B 413	S.U. Chung et al.	(BNL)
BLIEDEN 72	PL 39B 668	H.R. Blieden et al.	(STON, NEAS)
FIRESTONE 72B	PR D5 505	A. Firestone et al.	(LBL)
COLLEY 71	NP B26 71	D.C. Colley et al.	(BIRM, GLAS)
DENEGRI 71	NP B28 13	D. Denegri et al.	(JHU) JP
AGUILAR... 70c	PRL 25 54	M. Aguilar-Benitez et al.	(BNL)
BARTSCH 70c	PL 33B 186	J. Bartsch et al.	(AACH, BERL, CERN+)
LUDLAM 70	PR D2 1234	T. Ludlam, J. Sandweiss, A.J. Slaughter	(YALE)
BARBARO... 69	PRL 22 1207	A. Barbaro-Galtieri et al.	(LRL)

$K_3^*(1780)$

$I(J^P) = \frac{1}{2}(3^-)$

$K_3^*(1780)$  MASS

VALUE (MeV)	EVTS	DOCUMENT ID	TECN	CHG	COMMENT
<b>1776 ± 7 OUR AVERAGE</b>		Error includes scale factor of 1.1.			
$1781 \pm 8 \pm 4$		1 ASTON 88	LASS	0	$11 K^- p \rightarrow K^- \pi^+ n$
$1740 \pm 14 \pm 15$		1 ASTON 87	LASS	0	$11 K^- p \rightarrow \bar{K}^0 \pi^+ \pi^- n$
$1779 \pm 11$		2 BALDI 76	SPEC +		$10 K^+ p \rightarrow K^0 \pi^+ p$
$1776 \pm 26$		3 BRANDENB... 76D	ASPK	0	$13 K^\pm p \rightarrow K^\pm \pi^\mp N$

••• We do not use the following data for averages, fits, limits, etc. •••

$1720 \pm 10 \pm 15$	6111	4 BIRD 89	LASS	-	$11 K^- p \rightarrow \bar{K}^0 \pi^- p$
$1749 \pm 10$		ASTON 88B	LASS	-	$11 K^- p \rightarrow K^- \eta p$
$1780 \pm 9$	300	BAUBILLIER 84B	HBC	-	$8.25 K^- p \rightarrow \bar{K}^0 \pi^- p$
$1790 \pm 15$		BAUBILLIER 82B	HBC	0	$8.25 K^- p \rightarrow K_S^0 2\pi N$
$1784 \pm 9$	2060	CLELAND 82	SPEC	$\pm$	$50 K^+ p \rightarrow K_S^0 \pi^\pm p$
$1786 \pm 15$		5 ASTON 81D	LASS	0	$11 K^- p \rightarrow K^- \pi^+ n$
$1762 \pm 9$	190	TOAFF 81	HBC	-	$6.5 K^- p \rightarrow \bar{K}^0 \pi^- p$
$1850 \pm 50$		ETKIN 80	MPS	0	$6 K^- p \rightarrow \bar{K}^0 \pi^+ \pi^-$
$1812 \pm 28$		BEUSCH 78	OMEG		$10 K^- p \rightarrow \bar{K}^0 \pi^+ \pi^-$
$1786 \pm 8$		CHUNG 78	MPS	0	$6 K^- p \rightarrow \bar{K}^0 \pi^+ \pi^- n$

1 From energy-independent partial-wave analysis.  
 2 From a fit to  $Y_6^2$  moment.  $J^P = 3^-$  found.  
 3 Confirmed by phase shift analysis of ESTABROOKS 78, yields  $J^P = 3^-$ .  
 4 From a partial wave amplitude analysis.  
 5 From a fit to the  $Y_6^0$  moment.

$K_3^*(1780)$  WIDTH

VALUE (MeV)	EVTS	DOCUMENT ID	TECN	CHG	COMMENT
<b>159 ± 21 OUR AVERAGE</b>		Error includes scale factor of 1.3. See the ideogram below.			
$203 \pm 30 \pm 8$		6 ASTON 88	LASS	0	$11 K^- p \rightarrow K^- \pi^+ n$
$171 \pm 42 \pm 20$		6 ASTON 87	LASS	0	$11 K^- p \rightarrow \bar{K}^0 \pi^+ \pi^- n$
$135 \pm 22$		7 BALDI 76	SPEC +		$10 K^+ p \rightarrow K^0 \pi^+ p$
$187 \pm 31 \pm 20$	6111	8 BIRD 89	LASS	-	$11 K^- p \rightarrow \bar{K}^0 \pi^- p$
$193 \pm \frac{51}{37}$		ASTON 88B	LASS	-	$11 K^- p \rightarrow K^- \eta p$
$99 \pm 30$	300	BAUBILLIER 84B	HBC	-	$8.25 K^- p \rightarrow \bar{K}^0 \pi^- p$
$\sim 130$		BAUBILLIER 82B	HBC	0	$8.25 K^- p \rightarrow K_S^0 2\pi N$
$191 \pm 24$	2060	CLELAND 82	SPEC	$\pm$	$50 K^+ p \rightarrow K_S^0 \pi^\pm p$
$225 \pm 60$		9 ASTON 81D	LASS	0	$11 K^- p \rightarrow K^- \pi^+ n$
$\sim 80$	190	TOAFF 81	HBC	-	$6.5 K^- p \rightarrow \bar{K}^0 \pi^- p$
$240 \pm 50$		ETKIN 80	MPS	0	$6 K^- p \rightarrow \bar{K}^0 \pi^+ \pi^-$
$181 \pm 44$		10 BEUSCH 78	OMEG		$10 K^- p \rightarrow \bar{K}^0 \pi^+ \pi^-$
$96 \pm 31$		CHUNG 78	MPS	0	$6 K^- p \rightarrow \bar{K}^0 \pi^+ \pi^- n$
$270 \pm 70$		11 BRANDENB... 76D	ASPK	0	$13 K^\pm p \rightarrow K^\pm \pi^\mp N$

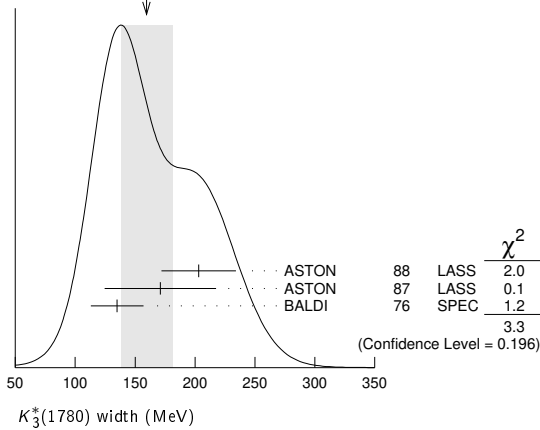
6 From energy-independent partial-wave analysis.  
 7 From a fit to  $Y_6^2$  moment.  $J^P = 3^-$  found.  
 8 From a partial wave amplitude analysis.  
 9 From a fit to  $Y_6^0$  moment.  
 10 Errors enlarged by us to  $4\Gamma/\sqrt{N}$ ; see the note with the  $K^*(892)$  mass.  
 11 ESTABROOKS 78 find that BRANDENBURG 76D data are consistent with 175 MeV width. Not averaged.



# Meson Particle Listings

## $K_3^*(1780)$ , $K_2(1820)$

WEIGHTED AVERAGE  
159±21 (Error scaled by 1.3)



### $K_3^*(1780)$ DECAY MODES

Mode	Fraction ( $\Gamma_i/\Gamma$ )	Confidence level
$\Gamma_1$ $K\rho$	(31 ± 9) %	95%
$\Gamma_2$ $K^*(892)\pi$	(20 ± 5) %	
$\Gamma_3$ $K\pi$	(18.8 ± 1.0) %	
$\Gamma_4$ $K\eta$	(30 ± 13) %	
$\Gamma_5$ $K_2^*(1430)\pi$	< 16 %	

### CONSTRAINED FIT INFORMATION

An overall fit to 3 branching ratios uses 4 measurements and one constraint to determine 4 parameters. The overall fit has a  $\chi^2 = 0.0$  for 1 degrees of freedom.

The following *off-diagonal* array elements are the correlation coefficients  $\langle \delta x_i \delta x_j \rangle / (\delta x_i \delta x_j)$ , in percent, from the fit to the branching fractions,  $x_i \equiv \Gamma_i / \Gamma_{\text{total}}$ . The fit constrains the  $x_i$  whose labels appear in this array to sum to one.

$x_2$	85		
$x_3$	18	21	
$x_4$	-98	-94	-27
	$x_1$	$x_2$	$x_3$

### $K_3^*(1780)$ BRANCHING RATIOS

Mode	Value	Document ID	TECN	CHG	COMMENT	$\Gamma_i/\Gamma_2$
$\Gamma(K\rho)/\Gamma(K^*(892)\pi)$	<b>1.52 ± 0.23 OUR FIT</b>					
	1.52 ± 0.21 ± 0.10	ASTON	87	LASS	0	11 $K^-p \rightarrow \bar{K}^0 \pi^+ \pi^- n$
$\Gamma(K^*(892)\pi)/\Gamma(K\pi)$	<b>1.09 ± 0.26 OUR FIT</b>					
	1.09 ± 0.26	ASTON	84B	LASS	0	11 $K^-p \rightarrow \bar{K}^0 2\pi n$
$\Gamma(K\pi)/\Gamma_{\text{total}}$	<b>0.188 ± 0.010 OUR FIT</b>					
	0.188 ± 0.010 OUR AVERAGE					
	0.187 ± 0.008 ± 0.008	ASTON	88	LASS	0	11 $K^-p \rightarrow K^- \pi^+ n$
	0.19 ± 0.02	ESTABROOKS	78	ASPK	0	13 $K^\pm p \rightarrow K\pi n$
$\Gamma(K\eta)/\Gamma(K\pi)$	<b>1.6 ± 0.7 OUR FIT</b>					
	0.41 ± 0.050	<sup>12</sup> BIRD	89	LASS	-	11 $K^-p \rightarrow \bar{K}^0 \pi^- p$
	0.50 ± 0.18	ASTON	88B	LASS	-	11 $K^-p \rightarrow K^- \eta p$
	<sup>12</sup> This result supersedes ASTON 88B.					
$\Gamma(K_2^*(1430)\pi)/\Gamma(K^*(892)\pi)$	<b>&lt; 0.78</b>					
	95	ASTON	87	LASS	0	11 $K^-p \rightarrow \bar{K}^0 \pi^+ \pi^- n$

### $K_3^*(1780)$ REFERENCES

BIRD	89	SLAC-332	P.F. Bird	(SLAC)
ASTON	88	NP B296 493	D. Aston <i>et al.</i>	(SLAC, NAGO, CINC, INUS)
ASTON	88B	PL B201 169	D. Aston <i>et al.</i>	(SLAC, NAGO, CINC, INUS) JP
ASTON	87	NP B292 693	D. Aston <i>et al.</i>	(SLAC, NAGO, CINC, INUS)
ASTON	84B	NP B247 261	D. Aston <i>et al.</i>	(SLAC, CARL, OTTA)
BAUBILLIER	84B	ZPHY C26 37	M. Baubillier <i>et al.</i>	(BIRM, CERN, GLAS+)
BAUBILLIER	82B	NP B202 21	M. Baubillier <i>et al.</i>	(BIRM, CERN, GLAS+)
CLELAND	82	NP B208 189	W.E. Cleland <i>et al.</i>	(DURH, GEVA, LAUS+)
ASTON	81D	PL 99B 502	D. Aston <i>et al.</i>	(SLAC, CARL, OTTA) JP
TOAFF	81	PR D23 1500	S. Toaff <i>et al.</i>	(ANL, KANS)
ETKIN	80	PR D22 42	A. Etkin <i>et al.</i>	(BNL, CUNY) JP
BEUSCH	78	PL 74B 282	W. Beusch <i>et al.</i>	(CERN, AACH3, ETH) JP
CHUNG	78	PRL 40 355	S.U. Chung <i>et al.</i>	(BNL, BRAN, CUNY+) JP
ESTABROOKS	78	NP B133 490	P.G. Estabrooks <i>et al.</i>	(MCGI, CARL, DURH+) JP
	Also	PR D17 658	P.G. Estabrooks <i>et al.</i>	(MCGI, CARL, DURH+)
BALDI	76	PL 63B 344	R. Baldi <i>et al.</i>	(GEVA) JP
BRANDENB...	76D	PL 60B 478	G.W. Brandenburg <i>et al.</i>	(SLAC) JP

### $K_2(1820)$

$$I(J^P) = \frac{1}{2}(2^-)$$

See our mini-review in the 2004 edition of this Review (PDG 04) under  $K_2(1770)$ .

### $K_2(1820)$ MASS

VALUE (MeV)	EVTS	DOCUMENT ID	TECN	COMMENT
<b>1819 ± 12 OUR AVERAGE</b>				
1853 ± 27 <sup>+18</sup> <sub>-35</sub>	4289	<sup>1</sup> AAIJ	17c	LHCB $B^+ \rightarrow J/\psi \phi K^+$
1816 ± 13		<sup>2</sup> ASTON	93	LASS $11K^-p \rightarrow K^- \omega p$
• • • We do not use the following data for averages, fits, limits, etc. • • •				
~ 1840		<sup>3</sup> DAUM	81c	CNTR $63K^-p \rightarrow K^- 2\pi p$
		<sup>1</sup>		From an amplitude analysis of the decay $B^+ \rightarrow J/\psi \phi K^+$ with a significance of 3.0 $\sigma$ .
		<sup>2</sup>		From a partial wave analysis of the $K^- \omega$ system.
		<sup>3</sup>		From a partial wave analysis of the $K^- 2\pi$ system.

### $K_2(1820)$ WIDTH

VALUE (MeV)	EVTS	DOCUMENT ID	TECN	COMMENT
<b>264 ± 34 OUR AVERAGE</b>				
167 ± 58 <sup>+82</sup> <sub>-72</sub>	4289	<sup>4</sup> AAIJ	17c	LHCB $B^+ \rightarrow J/\psi \phi K^+$
276 ± 35		<sup>5</sup> ASTON	93	LASS $11K^-p \rightarrow K^- \omega p$
• • • We do not use the following data for averages, fits, limits, etc. • • •				
~ 230		<sup>6</sup> DAUM	81c	CNTR $63K^-p \rightarrow K^- 2\pi p$
		<sup>4</sup>		From an amplitude analysis of the decay $B^+ \rightarrow J/\psi \phi K^+$ with a significance of 3.0 $\sigma$ .
		<sup>5</sup>		From a partial wave analysis of the $K^- \omega$ system.
		<sup>6</sup>		From a partial wave analysis of the $K^- 2\pi$ system.

### $K_2(1820)$ DECAY MODES

Mode	Fraction ( $\Gamma_i/\Gamma$ )
$\Gamma_1$ $K\pi\pi$	seen
$\Gamma_2$ $K_2^*(1430)\pi$	seen
$\Gamma_3$ $K^*(892)\pi$	seen
$\Gamma_4$ $Kf_2(1270)$	seen
$\Gamma_5$ $K\omega$	seen
$\Gamma_6$ $K\phi$	seen

### $K_2(1820)$ BRANCHING RATIOS

Mode	Value	Document ID	TECN	COMMENT	$\Gamma_2/\Gamma_1$
$\Gamma(K_2^*(1430)\pi)/\Gamma(K\pi\pi)$	<b>~ 0.77</b>				
	~ 0.77	DAUM	81c	CNTR $63K^-p \rightarrow \bar{K}2\pi p$	
$\Gamma(K^*(892)\pi)/\Gamma(K\pi\pi)$	<b>~ 0.05</b>				
	~ 0.05	DAUM	81c	CNTR $63K^-p \rightarrow \bar{K}2\pi p$	
$\Gamma(Kf_2(1270))/\Gamma(K\pi\pi)$	<b>~ 0.18</b>				
	~ 0.18	DAUM	81c	CNTR $63K^-p \rightarrow \bar{K}2\pi p$	
$\Gamma(K\phi)/\Gamma_{\text{total}}$	<b>seen</b>				
	4289	<sup>7</sup> AAIJ	17c	LHCB $B^+ \rightarrow J/\psi \phi K^+$	
		<sup>7</sup>		From an amplitude analysis of the decay $B^+ \rightarrow J/\psi \phi K^+$ with a significance of 3.0 $\sigma$ .	

See key on page 999

Meson Particle Listings

$K_2(1820)$ ,  $K(1830)$ ,  $K_0^*(1950)$ ,  $K_2^*(1980)$

$K_2(1820)$  REFERENCES

AAJ	17C	PRL 118 022003	R. Aaij et al.	(LHCb Collab.)
Also		PR D95 012002	R. Aaij et al.	(LHCb Collab.)
PDG	04	PL B592 1	S. Edelman et al.	(PDG Collab.)
ASTON	93	PL B308 186	D. Aston et al.	(SLAC, NAGO, CIN, INUS)
DAUM	81C	NP B187 1	C. Daum et al.	(AMST, CERN, CRAC, MPIM+)

$K(1830)$

$$I(J^P) = \frac{1}{2}(0^-)$$

OMITTED FROM SUMMARY TABLE

Seen in partial-wave analysis of  $K\phi$  system. Needs confirmation.

$K(1830)$  MASS

VALUE (MeV)	EVTS	DOCUMENT ID	TECN	CHG	COMMENT
$1874 \pm 43 \pm_{-115}^{59}$	4289	<sup>1</sup> AAIJ	17c	LHCB	$B^+ \rightarrow J/\psi\phi K^+$

••• We do not use the following data for averages, fits, limits, etc. •••

~ 1830 ARMSTRONG 83 OMEG -  $18.5 K^-p \rightarrow 3Kp$

<sup>1</sup>From an amplitude analysis of the decay  $B^+ \rightarrow J/\psi\phi K^+$  with a significance of 3.5  $\sigma$ .

$K(1830)$  WIDTH

VALUE (MeV)	EVTS	DOCUMENT ID	TECN	CHG	COMMENT
$168 \pm 90 \pm_{-104}^{280}$	4289	<sup>2</sup> AAIJ	17c	LHCB	$B^+ \rightarrow J/\psi\phi K^+$

••• We do not use the following data for averages, fits, limits, etc. •••

~ 250 ARMSTRONG 83 OMEG -  $18.5 K^-p \rightarrow 3Kp$

<sup>2</sup>From an amplitude analysis of the decay  $B^+ \rightarrow J/\psi\phi K^+$  with a significance of 3.5  $\sigma$ .

$K(1830)$  DECAY MODES

Mode

$\Gamma_1$	$K\phi$
------------	---------

$K(1830)$  REFERENCES

AAJ	17C	PRL 118 022003	R. Aaij et al.	(LHCb Collab.)
Also		PR D95 012002	R. Aaij et al.	(LHCb Collab.)
ARMSTRONG	83	NP B221 1	T.A. Armstrong et al.	(BARI, BIRM, CERN+) <sup>JP</sup>

$K_0^*(1950)$

$$I(J^P) = \frac{1}{2}(0^+)$$

OMITTED FROM SUMMARY TABLE

Seen in partial-wave analysis of the  $K^- \pi^+$  system. Needs confirmation.

$K_0^*(1950)$  MASS

VALUE (MeV)	DOCUMENT ID	TECN	CHG	COMMENT
$1945 \pm 10 \pm 20$	<sup>1</sup> ASTON 88 LASS 0	11	$K^-p \rightarrow K^- \pi^+ n$	

••• We do not use the following data for averages, fits, limits, etc. •••

1917  $\pm$  12 <sup>2</sup>ZHOU 06 RVUE  $Kp \rightarrow K^- \pi^+ n$

1820  $\pm$  40 <sup>3</sup>ANISOVICH 97c RVUE  $11 K^-p \rightarrow K^- \pi^+ n$

<sup>1</sup>We take the central value of the two solutions and the larger error given.

<sup>2</sup>S-matrix pole. Using ASTON 88 and assuming  $K_0^*(700)$ ,  $K_0^*(1430)$ .

<sup>3</sup>T-matrix pole. Reanalysis of ASTON 88 data.

$K_0^*(1950)$  WIDTH

VALUE (MeV)	DOCUMENT ID	TECN	CHG	COMMENT
$201 \pm 34 \pm 79$	<sup>4</sup> ASTON 88 LASS 0	11	$K^-p \rightarrow K^- \pi^+ n$	

••• We do not use the following data for averages, fits, limits, etc. •••

145  $\pm$  38 <sup>5</sup>ZHOU 06 RVUE  $Kp \rightarrow K^- \pi^+ n$

250  $\pm$  100 <sup>6</sup>ANISOVICH 97c RVUE  $11 K^-p \rightarrow K^- \pi^+ n$

<sup>4</sup>We take the central value of the two solutions and the larger error given.

<sup>5</sup>S-matrix pole. Using ASTON 88 and assuming  $K_0^*(700)$ ,  $K_0^*(1430)$ .

<sup>6</sup>T-matrix pole. Reanalysis of ASTON 88 data.

$K_0^*(1950)$  DECAY MODES

Mode Fraction ( $\Gamma_i/\Gamma$ )

$\Gamma_1$	$K^- \pi^+$	(52 $\pm$ 14) %
------------	-------------	-----------------

$K_0^*(1950)$  BRANCHING RATIOS

$$\frac{\Gamma(K^- \pi^+)}{\Gamma_{\text{total}}} \quad \Gamma_1/\Gamma$$

VALUE	DOCUMENT ID	TECN	CHG	COMMENT
$0.52 \pm 0.08 \pm 0.12$	<sup>7</sup> ASTON 88 LASS 0	11	$K^-p \rightarrow K^- \pi^+ n$	

••• We do not use the following data for averages, fits, limits, etc. •••

~ 0.60 <sup>8</sup>ZHOU 06 RVUE  $Kp \rightarrow K^- \pi^+ n$

<sup>7</sup>We take the central value of the two solutions and the larger error given.

<sup>8</sup>S-matrix pole. Using ASTON 88 and assuming  $K_0^*(700)$ ,  $K_0^*(1430)$ .

$K_0^*(1950)$  REFERENCES

ZHOU	06	NP A775 212	Z.Y. Zhou, H.Q. Zheng	
ANISOVICH	97C	PL B413 137	A.V. Anisovich, A.V. Sarantsev	
ASTON	88	NP B296 493	D. Aston et al.	(SLAC, NAGO, CIN, INUS)

$K_2^*(1980)$

$$I(J^P) = \frac{1}{2}(2^+)$$

OMITTED FROM SUMMARY TABLE

Needs confirmation.

$K_2^*(1980)$  MASS

VALUE (MeV)	EVTS	DOCUMENT ID	TECN	CHG	COMMENT
$1943 \pm 50$ OUR AVERAGE					Error includes scale factor of 2.2.

1868  $\pm$  8  $\pm_{-57}^{40}$  183k ABLIKIM 19AQBES  $\pm$   $J/\psi \rightarrow K^+ K^- \pi^0$

2073  $\pm$  94  $\pm_{-240}^{245}$  4289 <sup>1</sup>AAIJ 17c LHCB  $B^+ \rightarrow J/\psi\phi K^+$

1973  $\pm$  8  $\pm$  25 ASTON 87 LASS 0  $11 K^-p \rightarrow \overline{K}^0 \pi^+ \pi^- n$

••• We do not use the following data for averages, fits, limits, etc. •••

2020  $\pm$  20 TIKHOMIROV 03 SPEC  $40.0 \pi^- C \rightarrow K_S^0 K_S^0 K_L^0 X$

1978  $\pm$  40 241 BIRD 89 LASS -  $11 K^-p \rightarrow \overline{K}^0 \pi^- p$

<sup>1</sup>From an amplitude analysis of the decay  $B^+ \rightarrow J/\psi\phi K^+$  with a significance of 5.4  $\sigma$ .

$K_2^*(1980)$  WIDTH

VALUE (MeV)	EVTS	DOCUMENT ID	TECN	CHG	COMMENT
$307 \pm_{-51}^{50}$ OUR AVERAGE					Error includes scale factor of 1.2.

272  $\pm$  24  $\pm_{-15}^{50}$  183k ABLIKIM 19AQBES  $\pm$   $J/\psi \rightarrow K^+ K^- \pi^0$

678  $\pm$  311  $\pm_{-559}^{1153}$  4289 <sup>2</sup>AAIJ 17c LHCB  $B^+ \rightarrow J/\psi\phi K^+$

373  $\pm$  33  $\pm$  60 ASTON 87 LASS 0  $11 K^-p \rightarrow \overline{K}^0 \pi^+ \pi^- n$

••• We do not use the following data for averages, fits, limits, etc. •••

180  $\pm$  70 TIKHOMIROV 03 SPEC  $40.0 \pi^- C \rightarrow K_S^0 K_S^0 K_L^0 X$

398  $\pm$  47 241 BIRD 89 LASS -  $11 K^-p \rightarrow \overline{K}^0 \pi^- p$

<sup>2</sup>From an amplitude analysis of the decay  $B^+ \rightarrow J/\psi\phi K^+$  with a significance of 5.4  $\sigma$ .

$K_2^*(1980)$  DECAY MODES

Mode	Fraction ( $\Gamma_i/\Gamma$ )
$\Gamma_1$ $K^*(892)\pi$	possibly seen
$\Gamma_2$ $K\rho$	possibly seen
$\Gamma_3$ $K f_2(1270)$	possibly seen
$\Gamma_4$ $K\phi$	seen

$K_2^*(1980)$  BRANCHING RATIOS

$$\frac{\Gamma(K^*(892)\pi)}{\Gamma_{\text{total}}} \quad \Gamma_1/\Gamma$$

VALUE	DOCUMENT ID	TECN	COMMENT
possibly seen	GULER 11 BELL		$B^+ \rightarrow J/\psi K^+ \pi^+ \pi^-$

$$\frac{\Gamma(K\rho)}{\Gamma_{\text{total}}} \quad \Gamma_2/\Gamma$$

VALUE	DOCUMENT ID	TECN	COMMENT
possibly seen	GULER 11 BELL		$B^+ \rightarrow J/\psi K^+ \pi^+ \pi^-$

$$\frac{\Gamma(K\rho)}{\Gamma(K^*(892)\pi)} \quad \Gamma_2/\Gamma_1$$

VALUE	DOCUMENT ID	TECN	CHG	COMMENT
$1.49 \pm 0.24 \pm 0.09$	ASTON 87 LASS 0	11	$K^-p \rightarrow \overline{K}^0 \pi^+ \pi^- n$	

$$\frac{\Gamma(K f_2(1270))}{\Gamma_{\text{total}}} \quad \Gamma_3/\Gamma$$

VALUE	DOCUMENT ID	TECN	COMMENT
possibly seen	TIKHOMIROV 03 SPEC		$40.0 \pi^- C \rightarrow K_S^0 K_S^0 K_L^0 X$

$$\frac{\Gamma(K\phi)}{\Gamma_{\text{total}}} \quad \Gamma_4/\Gamma$$

VALUE	EVTS	DOCUMENT ID	TECN	COMMENT
seen	4289	<sup>3</sup> AAIJ	17c	LHCB $B^+ \rightarrow J/\psi\phi K^+$

<sup>3</sup>From an amplitude analysis of the decay  $B^+ \rightarrow J/\psi\phi K^+$  with a significance of 5.4  $\sigma$ .

## Meson Particle Listings

 $K_2^*(1980)$ ,  $K_4^*(2045)$ ,  $K_2(2250)$ ,  $K_3(2320)$  $K_4^*(1980)$  REFERENCES

ABLIKIM	19AQ	PR D100 032004	M. Ablikim <i>et al.</i>	(BESIII Collab.)
AAU	17C	PRL 118 022003	R. Aaij <i>et al.</i>	(LHCb Collab.)
Albo		PR D95 012002	R. Aaij <i>et al.</i>	(LHCb Collab.)
GULER	11	PR D83 032005	H. Guler <i>et al.</i>	(BELLE Collab.)
TIKHOMIROV	03	PAN 66 828	G.D. Tikhomirov <i>et al.</i>	(BELLE Collab.)
		Translated from YAF 66 860.		
BIRD	89	SLAC-332	P.F. Bird	(SLAC)
ASTON	87	NP B292 693	D. Aston <i>et al.</i>	(SLAC, NAGO, CINC, INUS)

 $K_4^*(2045)$ 

$$I(J^P) = \frac{1}{2}(4^+)$$

 $K_4^*(2045)$  MASS

VALUE (MeV)	EVTS	DOCUMENT ID	TECN	CHG	COMMENT
<b>2048<sup>+8</sup><sub>-9</sub></b>	<b>OUR AVERAGE</b>	Error includes scale factor of 1.1.			
2090 ± 9 <sup>+11</sup> <sub>-29</sub>	183k	ABLIKIM	19AQ	BES	± $J/\psi \rightarrow K^+ K^- \pi^0$
2062 ± 14 ± 13		<sup>1</sup> ASTON	86	LASS	0 $11 K^- p \rightarrow K^- \pi^+ n$
2039 ± 10	400	<sup>2,3</sup> CLELAND	82	SPEC	± $50 K^+ p \rightarrow K_S^0 \pi^\pm p$
2070 <sup>+100</sup> <sub>-40</sub>		<sup>4</sup> ASTON	81c	LASS	0 $11 K^- p \rightarrow K^- \pi^+ n$
• • • We do not use the following data for averages, fits, limits, etc. • • •					
2079 ± 7	431	TORRES	86	MPSF	400 pA → 4KX
2088 ± 20	650	BAUBILLIER	82	HBC	- 8.25 $K^- p \rightarrow K_S^0 \pi^- p$
2115 ± 46	488	CARMONY	77	HBC	0 $9 K^+ d \rightarrow K^+ \pi^+ X$
<sup>1</sup> From a fit to all moments.					
<sup>2</sup> From a fit to 8 moments.					
<sup>3</sup> Number of events evaluated by us.					
<sup>4</sup> From energy-independent partial-wave analysis.					

 $K_4^*(2045)$  WIDTH

VALUE (MeV)	EVTS	DOCUMENT ID	TECN	CHG	COMMENT
<b>199<sup>+27</sup><sub>-19</sub></b>	<b>OUR AVERAGE</b>				
201 ± 19 <sup>+57</sup> <sub>-17</sub>	183k	ABLIKIM	19AQ	BES	± $J/\psi \rightarrow K^+ K^- \pi^0$
221 ± 48 ± 27		<sup>5</sup> ASTON	86	LASS	0 $11 K^- p \rightarrow K^- \pi^+ n$
189 ± 35	400	<sup>6,7</sup> CLELAND	82	SPEC	± $50 K^+ p \rightarrow K_S^0 \pi^\pm p$
• • • We do not use the following data for averages, fits, limits, etc. • • •					
61 ± 58	431	TORRES	86	MPSF	400 pA → 4KX
170 <sup>+100</sup> <sub>-50</sub>	650	BAUBILLIER	82	HBC	- 8.25 $K^- p \rightarrow K_S^0 \pi^- p$
240 <sup>+500</sup> <sub>-100</sub>		<sup>8</sup> ASTON	81c	LASS	0 $11 K^- p \rightarrow K^- \pi^+ n$
300 ± 200		CARMONY	77	HBC	0 $9 K^+ d \rightarrow K^+ \pi^+ X$
<sup>5</sup> From a fit to all moments.					
<sup>6</sup> From a fit to 8 moments.					
<sup>7</sup> Number of events evaluated by us.					
<sup>8</sup> From energy-independent partial-wave analysis.					

 $K_4^*(2045)$  DECAY MODES

Mode	Fraction ( $\Gamma_i/\Gamma$ )
$\Gamma_1$ $K\pi$	(9.9 ± 1.2) %
$\Gamma_2$ $K^*(892)\pi\pi$	(9 ± 5) %
$\Gamma_3$ $K^*(892)\pi\pi\pi$	(7 ± 5) %
$\Gamma_4$ $\rho K\pi$	(5.7 ± 3.2) %
$\Gamma_5$ $\omega K\pi$	(5.0 ± 3.0) %
$\Gamma_6$ $\phi K\pi$	(2.8 ± 1.4) %
$\Gamma_7$ $\phi K^*(892)$	(1.4 ± 0.7) %

 $K_4^*(2045)$  BRANCHING RATIOS

$\Gamma(K\pi)/\Gamma_{\text{total}}$	$\Gamma_1/\Gamma$			
<b>0.099 ± 0.012</b>				
VALUE	DOCUMENT ID	TECN	CHG	COMMENT
	ASTON	88	LASS	0 $11 K^- p \rightarrow K^- \pi^+ n$
$\Gamma(K^*(892)\pi\pi)/\Gamma(K\pi)$	$\Gamma_2/\Gamma_1$			
<b>0.89 ± 0.53</b>				
VALUE	DOCUMENT ID	TECN	CHG	COMMENT
	BAUBILLIER	82	HBC	- 8.25 $K^- p \rightarrow \rho K_S^0 3\pi$
$\Gamma(K^*(892)\pi\pi\pi)/\Gamma(K\pi)$	$\Gamma_3/\Gamma_1$			
<b>0.75 ± 0.49</b>				
VALUE	DOCUMENT ID	TECN	CHG	COMMENT
	BAUBILLIER	82	HBC	- 8.25 $K^- p \rightarrow \rho K_S^0 3\pi$
$\Gamma(\rho K\pi)/\Gamma(K\pi)$	$\Gamma_4/\Gamma_1$			
<b>0.58 ± 0.32</b>				
VALUE	DOCUMENT ID	TECN	CHG	COMMENT
	BAUBILLIER	82	HBC	- 8.25 $K^- p \rightarrow \rho K_S^0 3\pi$

 $\Gamma(\omega K\pi)/\Gamma(K\pi)$ 

VALUE	DOCUMENT ID	TECN	CHG	COMMENT	$\Gamma_5/\Gamma_1$
<b>0.50 ± 0.30</b>	BAUBILLIER	82	HBC	- 8.25 $K^- p \rightarrow \rho K_S^0 3\pi$	

 $\Gamma(\phi K\pi)/\Gamma_{\text{total}}$ 

VALUE	DOCUMENT ID	TECN	COMMENT	$\Gamma_6/\Gamma$
<b>0.028 ± 0.014</b>	<sup>9</sup> TORRES	86	MPSF 400 pA → 4KX	

 $\Gamma(\phi K^*(892))/\Gamma_{\text{total}}$ 

VALUE	DOCUMENT ID	TECN	COMMENT	$\Gamma_7/\Gamma$
<b>0.014 ± 0.007</b>	<sup>9</sup> TORRES	86	MPSF 400 pA → 4KX	

<sup>9</sup> Error determination is model dependent. $K_2^*(2045)$  REFERENCES

ABLIKIM	19AQ	PR D100 032004	M. Ablikim <i>et al.</i>	(BESIII Collab.)
ASTON	88	NP B296 493	D. Aston <i>et al.</i>	(SLAC, NAGO, CINC, INUS)
ASTON	86	PL B180 308	D. Aston <i>et al.</i>	(SLAC, NAGO, CINC, INUS)
TORRES	86	PR D34 707	S. Torres <i>et al.</i>	(VPI, ARIZ, FNAL, FSU+)
BAUBILLIER	82	PL 118B 447	M. Baubillier <i>et al.</i>	(BIRM, CERN, GLAS+)
CLELAND	82	NP B208 189	W.E. Cleland <i>et al.</i>	(DURH, GEVA, LAUS+)
ASTON	81c	PL 106B 235	D. Aston <i>et al.</i>	(SLAC, CARL, OTTA)JP
CARMONY	77	PR D16 1251	D.D. Carmony <i>et al.</i>	(PURD, UCD, IUPUI)

 $K_2(2250)$ 

$$I(J^P) = \frac{1}{2}(2^-)$$

## OMITTED FROM SUMMARY TABLE

This entry contains various peaks in strange meson systems reported in the 2150–2260 MeV region, as well as enhancements seen in the antihyperon-nucleon system, either in the mass spectra or in the  $J^P = 2^-$  wave.

 $K_2(2250)$  MASS

VALUE (MeV)	EVTS	DOCUMENT ID	TECN	CHG	COMMENT
<b>2247 ± 17</b>	<b>OUR AVERAGE</b>				
2200 ± 40		<sup>1</sup> ARMSTRONG	83c	OMEG	- 18 $K^- p \rightarrow \Lambda \bar{p} X$
2235 ± 50		<sup>1</sup> BAUBILLIER	81	HBC	- 8 $K^- p \rightarrow \Lambda \bar{p} X$
2260 ± 20		<sup>1</sup> CLELAND	81	SPEC	± 50 $K^+ p \rightarrow \Lambda \bar{p} X$
• • • We do not use the following data for averages, fits, limits, etc. • • •					
2280 ± 20		TIKHOMIROV	03	SPEC	$40.0 \frac{\pi^- C}{K_S^0 K_S^0 K_L^0} X$
2147 ± 4	37	CHLIAPNIK...	79	HBC	+ 32 $K^+ p \rightarrow \bar{\Lambda} p X$
2240 ± 20	20	LISSAUER	70	HBC	9 $K^+ p$
<sup>1</sup> $J^P = 2^-$ from moments analysis.					

 $K_2(2250)$  WIDTH

VALUE (MeV)	EVTS	DOCUMENT ID	TECN	CHG	COMMENT
<b>180 ± 30</b>	<b>OUR AVERAGE</b>	Error includes scale factor of 1.4.			
150 ± 30		<sup>2</sup> ARMSTRONG	83c	OMEG	- 18 $K^- p \rightarrow \Lambda \bar{p} X$
210 ± 30		<sup>2</sup> CLELAND	81	SPEC	± 50 $K^+ p \rightarrow \Lambda \bar{p} X$
• • • We do not use the following data for averages, fits, limits, etc. • • •					
180 ± 60		TIKHOMIROV	03	SPEC	$40.0 \frac{\pi^- C}{K_S^0 K_S^0 K_L^0} X$
~ 200		<sup>2</sup> BAUBILLIER	81	HBC	- 8 $K^- p \rightarrow \Lambda \bar{p} X$
~ 40	37	CHLIAPNIK...	79	HBC	+ 32 $K^+ p \rightarrow \bar{\Lambda} p X$
80 ± 20	20	LISSAUER	70	HBC	9 $K^+ p$
<sup>2</sup> $J^P = 2^-$ from moments analysis.					

 $K_2(2250)$  DECAY MODES

Mode	Fraction ( $\Gamma_i/\Gamma$ )
$\Gamma_1$ $K\pi\pi$	
$\Gamma_2$ $K f_2(1270)$	
$\Gamma_3$ $K^*(892) f_0(980)$	
$\Gamma_4$ $\rho \bar{\Lambda}$	

 $K_2(2250)$  REFERENCES

TIKHOMIROV	03	PAN 66 828	G.D. Tikhomirov <i>et al.</i>	(BESIII Collab.)
ARMSTRONG	83c	NP B227 365 <td>T.A. Armstrong <i>et al.</i></td> <td>(BIRM, CERN, GLAS+)</td>	T.A. Armstrong <i>et al.</i>	(BIRM, CERN, GLAS+)
BAUBILLIER	81	NP B183 1 <td>M. Baubillier <i>et al.</i></td> <td>(BIRM, CERN, GLAS+)</td>	M. Baubillier <i>et al.</i>	(BIRM, CERN, GLAS+)
CLELAND	81	NP B184 1 <td>W.E. Cleland <i>et al.</i></td> <td>(PITT, GEVA, LAUS+)</td>	W.E. Cleland <i>et al.</i>	(PITT, GEVA, LAUS+)
CHLIAPNIK...	79	NP B158 253 <td>P.V. Chliapnikov <i>et al.</i></td> <td>(CERN, BELG, MONS)</td>	P.V. Chliapnikov <i>et al.</i>	(CERN, BELG, MONS)
LISSAUER	70	NP B18 491 <td>D. Lissauer <i>et al.</i></td> <td>(LBL)</td>	D. Lissauer <i>et al.</i>	(LBL)

 $K_3(2320)$ 

$$I(J^P) = \frac{1}{2}(3^+)$$

## OMITTED FROM SUMMARY TABLE

Seen in the  $J^P = 3^+$  wave of the antihyperon-nucleon system. Needs confirmation.

See key on page 999

Meson Particle Listings

$K_3(2320)$ ,  $K_5^*(2380)$ ,  $K_4(2500)$ ,  $K(3100)$

**$K_3(2320)$  MASS**

VALUE (MeV)	DOCUMENT ID	TECN	CHG	COMMENT
<b>2324 ± 24 OUR AVERAGE</b>				
2330 ± 40	<sup>1</sup> ARMSTRONG 83c	OMEG	-	18 $K^- p \rightarrow \Lambda \bar{p} X$
2320 ± 30	<sup>1</sup> CLELAND 81	SPEC	±	50 $K^+ p \rightarrow \Lambda \bar{p} X$
<sup>1</sup> $J^P = 3^+$ from moments analysis.				

**$K_3(2320)$  WIDTH**

VALUE (MeV)	DOCUMENT ID	TECN	CHG	COMMENT
<b>150 ± 30</b>				
	<sup>2</sup> ARMSTRONG 83c	OMEG	-	18 $K^- p \rightarrow \Lambda \bar{p} X$
• • •	We do not use the following data for averages, fits, limits, etc. • • •			
~ 250	<sup>2</sup> CLELAND 81	SPEC	±	50 $K^+ p \rightarrow \Lambda \bar{p} X$
<sup>2</sup> $J^P = 3^+$ from moments analysis.				

**$K_3(2320)$  DECAY MODES**

Mode	Fraction ( $\Gamma_i/\Gamma$ )
$\Gamma_1$ $\rho \bar{\Lambda}$	(6.1 ± 1.2) %

**$K_3(2320)$  REFERENCES**

ARMSTRONG 83c	NP B227 365	T.A. Armstrong et al.	(BARI, BIRM, CERN+)
CLELAND 81	NP B184 1	W.E. Cleland et al.	(PITT, GEVA, LAUS+)

**$K_5^*(2380)$**

$I(J^P) = \frac{1}{2}(5^-)$

OMITTED FROM SUMMARY TABLE  
Needs confirmation.

**$K_5^*(2380)$  MASS**

VALUE (MeV)	DOCUMENT ID	TECN	CHG	COMMENT
<b>2382 ± 14 ± 19</b>				
	<sup>1</sup> ASTON 86	LASS	0	11 $K^- p \rightarrow K^- \pi^+ n$
<sup>1</sup> From a fit to all the moments.				

**$K_5^*(2380)$  WIDTH**

VALUE (MeV)	DOCUMENT ID	TECN	CHG	COMMENT
<b>178 ± 37 ± 32</b>				
	<sup>2</sup> ASTON 86	LASS	0	11 $K^- p \rightarrow K^- \pi^+ n$
<sup>2</sup> From a fit to all the moments.				

**$K_5^*(2380)$  DECAY MODES**

Mode	Fraction ( $\Gamma_i/\Gamma$ )
$\Gamma_1$ $K \pi$	(6.1 ± 1.2) %

**$K_5^*(2380)$  BRANCHING RATIOS**

$\Gamma(K \pi)/\Gamma_{total}$	DOCUMENT ID	TECN	CHG	COMMENT	$\Gamma_1/\Gamma$
<b>0.061 ± 0.012</b>	ASTON 88	LASS	0	11 $K^- p \rightarrow K^- \pi^+ n$	

**$K_5^*(2380)$  REFERENCES**

ASTON 88	NP B296 493	D. Aston et al.	(SLAC, NAGO, CINC, INUS)
ASTON 86	PL B180 308	D. Aston et al.	(SLAC, NAGO, CINC, INUS)

**$K_4(2500)$**

$I(J^P) = \frac{1}{2}(4^-)$

OMITTED FROM SUMMARY TABLE  
Needs confirmation.

**$K_4(2500)$  MASS**

VALUE (MeV)	DOCUMENT ID	TECN	CHG	COMMENT
<b>2490 ± 20</b>				
	<sup>1</sup> CLELAND 81	SPEC	±	50 $K^+ p \rightarrow \Lambda \bar{p}$
<sup>1</sup> $J^P = 4^-$ from moments analysis.				

**$K_4(2500)$  WIDTH**

VALUE (MeV)	DOCUMENT ID	TECN	CHG	COMMENT
• • • We do not use the following data for averages, fits, limits, etc. • • •				
~ 250	<sup>2</sup> CLELAND 81	SPEC	±	50 $K^+ p \rightarrow \Lambda \bar{p}$
<sup>2</sup> $J^P = 4^-$ from moments analysis.				

**$K_4(2500)$  DECAY MODES**

Mode	Fraction ( $\Gamma_i/\Gamma$ )
$\Gamma_1$ $\rho \bar{\Lambda}$	

**$K_4(2500)$  REFERENCES**

CLELAND 81	NP B184 1	W.E. Cleland et al.	(PITT, GEVA, LAUS+)
------------	-----------	---------------------	---------------------

**$K(3100)$**

$I^G(J^{PC}) = ?^?(?^{??})$

OMITTED FROM SUMMARY TABLE

Narrow peak observed in several ( $\Lambda \bar{p}$  + pions) and ( $\bar{\Lambda} p$  + pions) states in  $\Sigma^-$  Be reactions by BOURQUIN 86 and in  $n p$  and  $n A$  reactions by ALEEV 93. Not seen by BOEHNLEIN 91. If due to strong decays, this state has exotic quantum numbers ( $B=0, Q=+1, S=-1$  for  $\Lambda \bar{p} \pi^+ \pi^+$  and  $I \geq 3/2$  for  $\Lambda \bar{p} \pi^-$ ). Needs confirmation.

**$K(3100)$  MASS**

VALUE (MeV)	DOCUMENT ID
<b>≈ 3100 OUR ESTIMATE</b>	

**3-BODY DECAYS**

VALUE (MeV)	DOCUMENT ID	TECN	COMMENT
<b>3054 ± 11 OUR AVERAGE</b>			
3060 ± 7 ± 20	<sup>1</sup> ALEEV 93	BIS2	$K(3100) \rightarrow \Lambda \bar{p} \pi^+$
3056 ± 7 ± 20	<sup>1</sup> ALEEV 93	BIS2	$K(3100) \rightarrow \bar{\Lambda} p \pi^-$
3055 ± 8 ± 20	<sup>1</sup> ALEEV 93	BIS2	$K(3100) \rightarrow \Lambda \bar{p} \pi^-$
3045 ± 8 ± 20	<sup>1</sup> ALEEV 93	BIS2	$K(3100) \rightarrow \bar{\Lambda} p \pi^+$

**4-BODY DECAYS**

VALUE (MeV)	DOCUMENT ID	TECN	COMMENT
<b>3059 ± 11 OUR AVERAGE</b>			
3067 ± 6 ± 20	<sup>1</sup> ALEEV 93	BIS2	$K(3100) \rightarrow \Lambda \bar{p} \pi^+ \pi^+$
3060 ± 8 ± 20	<sup>1</sup> ALEEV 93	BIS2	$K(3100) \rightarrow \Lambda \bar{p} \pi^+ \pi^-$
3055 ± 7 ± 20	<sup>1</sup> ALEEV 93	BIS2	$K(3100) \rightarrow \bar{\Lambda} p \pi^- \pi^-$
3052 ± 8 ± 20	<sup>1</sup> ALEEV 93	BIS2	$K(3100) \rightarrow \bar{\Lambda} p \pi^- \pi^+$
• • • We do not use the following data for averages, fits, limits, etc. • • •			
3105 ± 30	BOURQUIN 86	SPEC	$K(3100) \rightarrow \Lambda \bar{p} \pi^+ \pi^+$
3115 ± 30	BOURQUIN 86	SPEC	$K(3100) \rightarrow \Lambda \bar{p} \pi^+ \pi^-$

**5-BODY DECAYS**

VALUE (MeV)	DOCUMENT ID	TECN	COMMENT
• • • We do not use the following data for averages, fits, limits, etc. • • •			
3095 ± 30	BOURQUIN 86	SPEC	$K(3100) \rightarrow \Lambda \bar{p} \pi^+ \pi^+ \pi^-$
<sup>1</sup> Supersedes ALEEV 90.			

**$K(3100)$  WIDTH**

**3-BODY DECAYS**

VALUE (MeV)	DOCUMENT ID	TECN	COMMENT
• • • We do not use the following data for averages, fits, limits, etc. • • •			
42 ± 16	<sup>2</sup> ALEEV 93	BIS2	$K(3100) \rightarrow \Lambda \bar{p} \pi^+$
36 ± 15	<sup>2</sup> ALEEV 93	BIS2	$K(3100) \rightarrow \bar{\Lambda} p \pi^-$
50 ± 18	<sup>2</sup> ALEEV 93	BIS2	$K(3100) \rightarrow \Lambda \bar{p} \pi^-$
30 ± 15	<sup>2</sup> ALEEV 93	BIS2	$K(3100) \rightarrow \bar{\Lambda} p \pi^+$

**4-BODY DECAYS**

VALUE (MeV)	CL%	DOCUMENT ID	TECN	COMMENT
• • • We do not use the following data for averages, fits, limits, etc. • • •				
22 ± 8		<sup>2</sup> ALEEV 93	BIS2	$K(3100) \rightarrow \Lambda \bar{p} \pi^+ \pi^+$
28 ± 12		<sup>2</sup> ALEEV 93	BIS2	$K(3100) \rightarrow \Lambda \bar{p} \pi^+ \pi^-$
32 ± 15		<sup>2</sup> ALEEV 93	BIS2	$K(3100) \rightarrow \bar{\Lambda} p \pi^- \pi^-$
30 ± 15		<sup>2</sup> ALEEV 93	BIS2	$K(3100) \rightarrow \bar{\Lambda} p \pi^- \pi^+$
<30	90	BOURQUIN 86	SPEC	$K(3100) \rightarrow \Lambda \bar{p} \pi^+ \pi^+$
<80	90	BOURQUIN 86	SPEC	$K(3100) \rightarrow \Lambda \bar{p} \pi^+ \pi^-$

**5-BODY DECAYS**

VALUE (MeV)	CL%	DOCUMENT ID	TECN	COMMENT
• • • We do not use the following data for averages, fits, limits, etc. • • •				
<30	90	BOURQUIN 86	SPEC	$K(3100) \rightarrow \Lambda \bar{p} \pi^+ \pi^+ \pi^-$
<sup>2</sup> Supersedes ALEEV 90.				

**$K(3100)$  DECAY MODES**

Mode	Fraction ( $\Gamma_i/\Gamma$ )
$\Gamma_1$ $K(3100)^0 \rightarrow \Lambda \bar{p} \pi^+$	
$\Gamma_2$ $K(3100)^{--} \rightarrow \bar{\Lambda} p \pi^-$	
$\Gamma_3$ $K(3100)^- \rightarrow \Lambda \bar{p} \pi^+ \pi^-$	

## Meson Particle Listings

 $K(3100)$ 

$\Gamma_4$	$K(3100)^+ \rightarrow \Lambda \bar{p} \pi^+ \pi^+$
$\Gamma_5$	$K(3100)^0 \rightarrow \Lambda \bar{p} \pi^+ \pi^+ \pi^-$
$\Gamma_6$	$K(3100)^0 \rightarrow \Sigma(1385)^+ \bar{p}$

 **$K(3100)$  REFERENCES**

ALEEV	93	PAN 56 1358	A.N. Aleev <i>et al.</i>	(BIS-2 Collab.)
		Translated from YAF 56 100.		
BOEHNLEIN	91	NPBPS B21 174	A. Boehnlein <i>et al.</i>	(FLOR, BNL, IND+)
ALEEV	90	ZPHY C47 533	A.N. Aleev <i>et al.</i>	(BIS-2 Collab.)
BOURQUIN	86	PL B172 113	M.H. Bourquin <i>et al.</i>	(GEVA, RAL, HEIDP+)

$\Gamma(\Sigma(1385)^+ \bar{p}) / \Gamma(\Lambda \bar{p} \pi^+)$					$\Gamma_6 / \Gamma_1$
VALUE	CL%	DOCUMENT ID	TECN	COMMENT	
<0.04	90	ALEEV	93	BIS2	$K(3100)^0 \rightarrow \Sigma(1385)^+ \bar{p}$

# CHARMED MESONS

## ( $C = \pm 1$ )

$D^+ = c\bar{d}, D^0 = c\bar{u}, \bar{D}^0 = \bar{c}u, D^- = \bar{c}d,$  similarly for  $D^{*s}$

$D^\pm$

$$J(P) = \frac{1}{2}(0^-)$$

### $D^\pm$ MASS

The fit includes  $D^\pm, D^0, D_S^\pm, D^{*0}, D^{*+}, D_S^{*0}, D_1(2420)^0, D_2^*(2460)^0,$  and  $D_{S1}(2536)^\pm$  mass and mass difference measurements.

VALUE (MeV)	EVTS	DOCUMENT ID	TECN	COMMENT
<b>1869.65 ± 0.05 OUR FIT</b>				
<b>1869.5 ± 0.4 OUR AVERAGE</b>				
1869.53 ± 0.49 ± 0.20	110 ± 15	ANASHIN	10A	KEDR $e^+e^-$ at $\psi(3770)$
1870.0 ± 0.5 ± 1.0	317	BARLAG	90c	ACCM $\pi^-$ Cu 230 GeV
1869.4 ± 0.6		1 TRILLING	81	RVUE $e^+e^-$ 3.77 GeV
• • • We do not use the following data for averages, fits, limits, etc. • • •				
1875 ± 10	9	ADAMOVICH	87	EMUL Photoproduction
1860 ± 16	6	ADAMOVICH	84	EMUL Photoproduction
1863 ± 4		DERRICK	84	HRS $e^+e^-$ 29 GeV
1868.4 ± 0.5		1 SCHINDLER	81	MRK2 $e^+e^-$ 3.77 GeV
1874 ± 5		GOLDHABER	77	MRK1 $D^0, D^+$ recoil spectra
1868.3 ± 0.9		1 PERUZZI	77	LGW $e^+e^-$ 3.77 GeV
1874 ± 11		PICCOLO	77	MRK1 $e^+e^-$ 4.03, 4.41 GeV
1876 ± 15	50	PERUZZI	76	MRK1 $K^\mp \pi^\pm \pi^\pm$

<sup>1</sup>PERUZZI 77 and SCHINDLER 81 errors do not include the 0.13% uncertainty in the absolute SPEAR energy calibration. TRILLING 81 uses the high precision  $J/\psi(1S)$  and  $\psi(2S)$  measurements of ZHOLENTZ 80 to determine this uncertainty and combines the PERUZZI 77 and SCHINDLER 81 results to obtain the value quoted.

### $D^\pm$ MEAN LIFE

Measurements with an error  $> 100 \times 10^{-15}$  s have been omitted from the Listings.

VALUE ( $10^{-15}$ s)	EVTS	DOCUMENT ID	TECN	COMMENT
<b>1040 ± 7 OUR AVERAGE</b>				
1039.4 ± 4.3 ± 7.0	110k	LINK	02F	FOCS $\gamma$ nucleus, $\approx 180$ GeV
1033.6 ± 22.1 ± 9.9 ± 12.7	3.7k	BONVICINI	99	CLEO $e^+e^- \approx \Upsilon(4S)$
1048 ± 15 ± 11	9k	FRABETTI	94D	E687 $D^+ \rightarrow K^- \pi^+ \pi^+$
• • • We do not use the following data for averages, fits, limits, etc. • • •				
1075 ± 40 ± 18	2.4k	FRABETTI	91	E687 $\gamma$ Be, $D^+ \rightarrow K^- \pi^+ \pi^+$
1030 ± 80 ± 60	200	ALVAREZ	90	NA14 $\gamma, D^+ \rightarrow K^- \pi^+ \pi^+$
1050 ± 77 ± 72	317	1 BARLAG	90c	ACCM $\pi^-$ Cu 230 GeV
1050 ± 80 ± 70	363	ALBRECHT	88i	ARG $e^+e^-$ 10 GeV
1090 ± 30 ± 25	2.9k	RAAB	88	E691 Photoproduction

<sup>1</sup>BARLAG 90c estimates the systematic error to be negligible.

### $D^+$ DECAY MODES

Most decay modes (other than the semileptonic modes) that involve a neutral  $K$  meson are now given as  $K_S^0$  modes, not as  $\bar{K}^0$  modes. Nearly always it is a  $K_S^0$  that is measured, and interference between Cabibbo-allowed and doubly Cabibbo-suppressed modes can invalidate the assumption that  $2\Gamma(K_S^0) = \Gamma(\bar{K}^0)$ .

Mode	Fraction ( $\Gamma_i/\Gamma$ )	Scale factor/ Confidence level
------	--------------------------------	-----------------------------------

#### Inclusive modes

$\Gamma_1$	$e^+$ semileptonic	(16.07 ± 0.30) %	
$\Gamma_2$	$\mu^+$ anything	(17.6 ± 3.2) %	
$\Gamma_3$	$K^-$ anything	(25.7 ± 1.4) %	
$\Gamma_4$	$\bar{K}^0$ anything + $K^0$ anything	(61 ± 5) %	
$\Gamma_5$	$K^+$ anything	(5.9 ± 0.8) %	
$\Gamma_6$	$K^*(892)^-$ anything	(6 ± 5) %	
$\Gamma_7$	$\bar{K}^*(892)^0$ anything	(23 ± 5) %	
$\Gamma_8$	$K^*(892)^0$ anything	< 6.6 %	CL=90%
$\Gamma_9$	$\eta$ anything	(6.3 ± 0.7) %	
$\Gamma_{10}$	$\eta'$ anything	(1.04 ± 0.18) %	
$\Gamma_{11}$	$\phi$ anything	(1.12 ± 0.04) %	

### Leptonic and semileptonic modes

$\Gamma_{12}$	$e^+ \nu_e$	< 8.8	$\times 10^{-6}$	CL=90%
$\Gamma_{13}$	$\gamma e^+ \nu_e$	< 3.0	$\times 10^{-5}$	CL=90%
$\Gamma_{14}$	$\mu^+ \nu_\mu$	(3.74 ± 0.17)	$\times 10^{-4}$	
$\Gamma_{15}$	$\tau^+ \nu_\tau$	(1.20 ± 0.27)	$\times 10^{-3}$	
$\Gamma_{16}$	$\bar{K}^0 e^+ \nu_e$	(8.73 ± 0.10) %		
$\Gamma_{17}$	$\bar{K}^0 \mu^+ \nu_\mu$	(8.76 ± 0.19) %		
$\Gamma_{18}$	$K^- \pi^+ e^+ \nu_e$	(4.02 ± 0.18) %		S=3.2
$\Gamma_{19}$	$\bar{K}^*(892)^0 e^+ \nu_e, \bar{K}^*(892)^0 \rightarrow K^- \pi^+$	(3.77 ± 0.17) %		
$\Gamma_{20}$	$(K^- \pi^+)_{[0.8-1.0]\text{GeV}} e^+ \nu_e$	(3.39 ± 0.09) %		
$\Gamma_{21}$	$(K^- \pi^+)_{S\text{-wave}} e^+ \nu_e$	(2.28 ± 0.11)	$\times 10^{-3}$	
$\Gamma_{22}$	$\bar{K}^*(1410)^0 e^+ \nu_e, \bar{K}^*(1410)^0 \rightarrow K^- \pi^+$	< 6	$\times 10^{-3}$	CL=90%
$\Gamma_{23}$	$\bar{K}_2^*(1430)^0 e^+ \nu_e, \bar{K}_2^*(1430)^0 \rightarrow K^- \pi^+$	< 5	$\times 10^{-4}$	CL=90%
$\Gamma_{24}$	$K^- \pi^+ e^+ \nu_e$ nonresonant	< 7	$\times 10^{-3}$	CL=90%
$\Gamma_{25}$	$\bar{K}^*(892)^0 e^+ \nu_e$	(5.40 ± 0.10) %		S=1.1
$\Gamma_{26}$	$K^- \pi^+ \mu^+ \nu_\mu$	(3.65 ± 0.34) %		
$\Gamma_{27}$	$\bar{K}^*(892)^0 \mu^+ \nu_\mu, \bar{K}^*(892)^0 \rightarrow K^- \pi^+$	(3.52 ± 0.10) %		
$\Gamma_{28}$	$K^- \pi^+ \mu^+ \nu_\mu$ nonresonant	(1.9 ± 0.5)	$\times 10^{-3}$	
$\Gamma_{29}$	$\bar{K}^*(892)^0 \mu^+ \nu_\mu$	(5.27 ± 0.15) %		
$\Gamma_{30}$	$K^- \pi^+ \pi^0 \mu^+ \nu_\mu$	< 1.5	$\times 10^{-3}$	CL=90%
$\Gamma_{31}$	$\bar{K}_1(1270)^0 e^+ \nu_e, \bar{K}_1^0 \rightarrow K^- \pi^+ \pi^0$	(1.06 ± 0.15)	$\times 10^{-3}$	
$\Gamma_{32}$	$\bar{K}_0^*(1430)^0 \mu^+ \nu_\mu$	< 2.3	$\times 10^{-4}$	CL=90%
$\Gamma_{33}$	$\bar{K}^*(1680)^0 \mu^+ \nu_\mu$	< 1.5	$\times 10^{-3}$	CL=90%
$\Gamma_{34}$	$\pi^0 e^+ \nu_e$	(3.72 ± 0.17)	$\times 10^{-3}$	S=2.0
$\Gamma_{35}$	$\pi^0 \mu^+ \nu_\mu$	(3.50 ± 0.15)	$\times 10^{-3}$	
$\Gamma_{36}$	$\eta e^+ \nu_e$	(1.11 ± 0.07)	$\times 10^{-3}$	
$\Gamma_{37}$	$\pi^- \pi^+ e^+ \nu_e$	(2.45 ± 0.10)	$\times 10^{-3}$	
$\Gamma_{38}$	$f_0(500)^0 e^+ \nu_e, f_0(500)^0 \rightarrow \pi^+ \pi^-$	(6.3 ± 0.5)	$\times 10^{-4}$	
$\Gamma_{39}$	$\rho^0 e^+ \nu_e$	(2.18 ± 0.17 ± 0.25)	$\times 10^{-3}$	
$\Gamma_{40}$	$\rho^0 \mu^+ \nu_\mu$	(2.4 ± 0.4)	$\times 10^{-3}$	
$\Gamma_{41}$	$\omega e^+ \nu_e$	(1.69 ± 0.11)	$\times 10^{-3}$	
$\Gamma_{42}$	$\eta'(958) e^+ \nu_e$	(2.0 ± 0.4)	$\times 10^{-4}$	
$\Gamma_{43}$	$a(980)^0 e^+ \nu_e, a(980)^0 \rightarrow \eta \pi^0$	(1.7 ± 0.8 ± 0.7)	$\times 10^{-4}$	
$\Gamma_{44}$	$\phi e^+ \nu_e$	< 1.3	$\times 10^{-5}$	CL=90%
$\Gamma_{45}$	$D^0 e^+ \nu_e$	< 1.0	$\times 10^{-4}$	CL=90%

### Hadronic modes with a $\bar{K}$ or $\bar{K}K\bar{K}$

$\Gamma_{46}$	$K_S^0 \pi^+$	(1.562 ± 0.031) %		S=1.7
$\Gamma_{47}$	$K_L^0 \pi^+$	(1.46 ± 0.05) %		
$\Gamma_{48}$	$K^- 2\pi^+$	[a] (9.38 ± 0.16) %		S=1.6
$\Gamma_{49}$	$(K^- \pi^+)_{S\text{-wave}} \pi^+$	(7.52 ± 0.17) %		
$\Gamma_{50}$	$\bar{K}_0^*(700)^0 \pi^+, \bar{K}_0^*(700)^0 \rightarrow K^- \pi^+$			
$\Gamma_{51}$	$\bar{K}_0^*(1430)^0 \pi^+, \bar{K}_0^*(1430)^0 \rightarrow K^- \pi^+$	[b] (1.25 ± 0.06) %		
$\Gamma_{52}$	$\bar{K}^*(892)^0 \pi^+, \bar{K}^*(892)^0 \rightarrow K^- \pi^+$	(1.04 ± 0.12) %		
$\Gamma_{53}$	$\bar{K}^*(1410)^0 \pi^+, \bar{K}^{*0} \rightarrow$	not seen		
$\Gamma_{54}$	$\bar{K}_2^*(1430)^0 \pi^+, \bar{K}_2^*(1430)^0 \rightarrow K^- \pi^+$	[b] (2.3 ± 0.7)	$\times 10^{-4}$	
$\Gamma_{55}$	$\bar{K}^*(1680)^0 \pi^+, \bar{K}^*(1680)^0 \rightarrow K^- \pi^+$	[b] (2.2 ± 1.1)	$\times 10^{-4}$	
$\Gamma_{56}$	$K^- (2\pi^+)_{I=2}$	(1.45 ± 0.26) %		
$\Gamma_{57}$	$K^- 2\pi^+$ nonresonant			
$\Gamma_{58}$	$K_S^0 \pi^+ \pi^0$	[a] (7.36 ± 0.21) %		
$\Gamma_{59}$	$K_S^0 \rho^+$	(6.14 ± 0.60 ± 1.4)		
$\Gamma_{60}$	$K_S^0 \rho(1450)^+, \rho^+ \rightarrow \pi^+ \pi^0$	(1.5 ± 1.2)	$\times 10^{-3}$	
$\Gamma_{61}$	$\bar{K}^*(892)^0 \pi^+, \bar{K}^*(892)^0 \rightarrow K_S^0 \pi^0$	(2.64 ± 0.32)	$\times 10^{-3}$	
$\Gamma_{62}$	$\bar{K}_0^*(1430)^0 \pi^+, \bar{K}_0^*(1430)^0 \rightarrow K_S^0 \pi^0$	(2.7 ± 0.9)	$\times 10^{-3}$	
$\Gamma_{63}$	$\bar{K}_0^*(1680)^0 \pi^+, \bar{K}_0^*(1680)^0 \rightarrow K_S^0 \pi^0$	(10 ± 7 ± 10)	$\times 10^{-4}$	
$\Gamma_{64}$	$\bar{K}^0 \pi^+, \bar{K}^0 \rightarrow K_S^0 \pi^0$	(6 ± 5 ± 4)	$\times 10^{-3}$	

## Meson Particle Listings

 $D^\pm$ 

$\Gamma_{65}$	$K_S^0 \pi^+ \pi^0$ nonresonant	$(3 \pm 4) \times 10^{-3}$	$\Gamma_{117}$	$K^+ K_S^0 \pi^+ \pi^-$	$(1.74 \pm 0.18) \times 10^{-3}$
$\Gamma_{66}$	$K_S^0 \pi^+ \pi^0$ nonresonant and $\bar{K}^0 \pi^+$	$(1.37 \pm_{-0.40}^{+0.21}) \%$	$\Gamma_{118}$	$K_S^0 K^- 2\pi^+$	$(2.38 \pm 0.17) \times 10^{-3}$
$\Gamma_{67}$	$(K_S^0 \pi^0)_{S\text{-wave}} \pi^+$	$(1.27 \pm_{-0.33}^{+0.27}) \%$	$\Gamma_{119}$	$K^+ K^- 2\pi^+ \pi^-$	$(2.3 \pm 1.2) \times 10^{-4}$
$\Gamma_{68}$	$K_S^0 \pi^+ \eta'(958)$	$(1.90 \pm 0.21) \times 10^{-3}$	A few poorly measured branching fractions:		
$\Gamma_{69}$	$K^- 2\pi^+ \pi^0$	[c] $(6.25 \pm 0.18) \%$	$\Gamma_{120}$	$\phi \pi^+ \pi^0$	$(2.3 \pm 1.0) \%$
$\Gamma_{70}$	$K_S^0 2\pi^+ \pi^-$	[c] $(3.10 \pm 0.09) \%$	$\Gamma_{121}$	$\phi \rho^+$	$< 1.5 \%$ CL=90%
$\Gamma_{71}$	$K^- 3\pi^+ \pi^-$	[a] $(5.7 \pm 0.5) \times 10^{-3}$	$\Gamma_{122}$	$K^+ K^- \pi^+ \pi^0$ non- $\phi$	$(1.5 \pm_{-0.6}^{+0.7}) \%$
$\Gamma_{72}$	$\bar{K}^*(892)^0 2\pi^+ \pi^-$ , $\bar{K}^*(892)^0 \rightarrow K^- \pi^+$	$(1.2 \pm 0.4) \times 10^{-3}$	$\Gamma_{123}$	$K^*(892)^+ K_S^0$	$(1.7 \pm 0.8) \%$
$\Gamma_{73}$	$\bar{K}^*(892)^0 \rho^0 \pi^+$ , $\bar{K}^*(892)^0 \rightarrow K^- \pi^+$	$(2.3 \pm 0.4) \times 10^{-3}$	<b>Doubly Cabibbo-suppressed modes</b>		
$\Gamma_{74}$	$\bar{K}^*(892)^0 a_1(1260)^+$	[d] $(9.3 \pm 1.9) \times 10^{-3}$	$\Gamma_{124}$	$K^+ \pi^0$	$(2.08 \pm 0.21) \times 10^{-4}$ S=1.4
$\Gamma_{75}$	$\bar{K}^*(892)^0 2\pi^+ \pi^-$ no- $\rho$ , $\bar{K}^*(892)^0 \rightarrow K^- \pi^+$		$\Gamma_{125}$	$K^+ \eta$	$(1.25 \pm 0.16) \times 10^{-4}$ S=1.1
$\Gamma_{76}$	$K^- \rho^0 2\pi^+$	$(1.72 \pm 0.28) \times 10^{-3}$	$\Gamma_{126}$	$K^+ \eta'(958)$	$(1.85 \pm 0.20) \times 10^{-4}$
$\Gamma_{77}$	$K^- 3\pi^+ \pi^-$ nonresonant	$(4.0 \pm 2.9) \times 10^{-4}$	$\Gamma_{127}$	$K^+ \pi^+ \pi^-$	$(4.91 \pm 0.09) \times 10^{-4}$
$\Gamma_{78}$	$K^+ 2K_S^0$	$(2.54 \pm 0.13) \times 10^{-3}$	$\Gamma_{128}$	$K^+ \rho^0$	$(1.9 \pm 0.5) \times 10^{-4}$
$\Gamma_{79}$	$K^+ K^- K_S^0 \pi^+$	$(2.4 \pm 0.5) \times 10^{-4}$	$\Gamma_{129}$	$K^*(892)^0 \pi^+$ , $K^*(892)^0 \rightarrow K^+ \pi^-$	$(2.3 \pm 0.4) \times 10^{-4}$
<b>Pionic modes</b>			$\Gamma_{130}$	$K^+ f_0(980)$ , $f_0(980) \rightarrow \pi^+ \pi^-$	$(4.4 \pm 2.6) \times 10^{-5}$
$\Gamma_{80}$	$\pi^+ \pi^0$	$(1.247 \pm 0.033) \times 10^{-3}$	$\Gamma_{131}$	$K_2^*(1430)^0 \pi^+$ , $K_2^*(1430)^0 \rightarrow K^+ \pi^-$	$(3.9 \pm 2.7) \times 10^{-5}$
$\Gamma_{81}$	$2\pi^+ \pi^-$	$(3.27 \pm 0.18) \times 10^{-3}$	$\Gamma_{132}$	$K^+ \pi^+ \pi^-$ nonresonant	not seen
$\Gamma_{82}$	$\rho^0 \pi^+$	$(8.3 \pm 1.5) \times 10^{-4}$	$\Gamma_{133}$	$2K^+ K^-$	$(6.14 \pm 0.11) \times 10^{-5}$
$\Gamma_{83}$	$\pi^+(\pi^+ \pi^-)_{S\text{-wave}}$	$(1.83 \pm 0.16) \times 10^{-3}$	$\Gamma_{134}$	$\phi(1020)^0 K^+$	$< 2.1 \times 10^{-5}$ CL=90%
$\Gamma_{84}$	$\sigma \pi^+$ , $\sigma \rightarrow \pi^+ \pi^-$	$(1.38 \pm 0.12) \times 10^{-3}$	$\Gamma_{135}$	$K^+ \phi(1020)$ , $\phi \rightarrow K^+ K^-$	$(4.4 \pm 0.6) \times 10^{-6}$
$\Gamma_{85}$	$f_0(980) \pi^+$ , $f_0(980) \rightarrow \pi^+ \pi^-$	$(1.56 \pm 0.33) \times 10^{-4}$	$\Gamma_{136}$	$K^+(K^+ K^-)_{S\text{-wave}}$	$(5.77 \pm 0.12) \times 10^{-5}$
$\Gamma_{86}$	$f_0(1370) \pi^+$ , $f_0(1370) \rightarrow \pi^+ \pi^-$	$(8 \pm 4) \times 10^{-5}$	<b><math>\Delta C = 1</math> weak neutral current (CI) modes, or Lepton Family number (LF) or Lepton number (L) violating modes</b>		
$\Gamma_{87}$	$f_2(1270) \pi^+$ , $f_2(1270) \rightarrow \pi^+ \pi^-$	$(5.0 \pm 0.9) \times 10^{-4}$	$\Gamma_{137}$	$\pi^+ e^+ e^-$	CI $< 1.1 \times 10^{-6}$ CL=90%
$\Gamma_{88}$	$\rho(1450)^0 \pi^+$ , $\rho(1450)^0 \rightarrow \pi^+ \pi^-$	$< 8 \times 10^{-5}$ CL=95%	$\Gamma_{138}$	$\pi^+ \pi^0 e^+ e^-$	$< 1.4 \times 10^{-5}$ CL=90%
$\Gamma_{89}$	$f_0(1500) \pi^+$ , $f_0(1500) \rightarrow \pi^+ \pi^-$	$(1.1 \pm 0.4) \times 10^{-4}$	$\Gamma_{139}$	$\pi^+ \phi$ , $\phi \rightarrow e^+ e^-$	[e] $(1.7 \pm_{-0.9}^{+1.4}) \times 10^{-6}$
$\Gamma_{90}$	$f_0(1710) \pi^+$ , $f_0(1710) \rightarrow \pi^+ \pi^-$	$< 5 \times 10^{-5}$ CL=95%	$\Gamma_{140}$	$\pi^+ \mu^+ \mu^-$	CI $< 7.3 \times 10^{-8}$ CL=90%
$\Gamma_{91}$	$f_0(1790) \pi^+$ , $f_0(1790) \rightarrow \pi^+ \pi^-$	$< 7 \times 10^{-5}$ CL=95%	$\Gamma_{141}$	$\pi^+ \phi$ , $\phi \rightarrow \mu^+ \mu^-$	[e] $(1.8 \pm 0.8) \times 10^{-6}$ CL=90%
$\Gamma_{92}$	$(\pi^+ \pi^+)_{S\text{-wave}} \pi^-$	$< 1.2 \times 10^{-4}$ CL=95%	$\Gamma_{142}$	$\rho^+ \mu^+ \mu^-$	CI $< 5.6 \times 10^{-4}$ CL=90%
$\Gamma_{93}$	$2\pi^+ \pi^-$ nonresonant	$< 1.1 \times 10^{-4}$ CL=95%	$\Gamma_{143}$	$K^+ e^+ e^-$	[f] $< 1.0 \times 10^{-6}$ CL=90%
$\Gamma_{94}$	$\pi^+ 2\pi^0$	$(4.7 \pm 0.4) \times 10^{-3}$	$\Gamma_{144}$	$K^+ \pi^0 e^+ e^-$	$< 1.5 \times 10^{-5}$ CL=90%
$\Gamma_{95}$	$2\pi^+ \pi^- \pi^0$	$(1.16 \pm 0.08) \%$	$\Gamma_{145}$	$K_S^0 \pi^+ e^+ e^-$	$< 2.6 \times 10^{-5}$ CL=90%
$\Gamma_{96}$	$3\pi^+ 2\pi^-$	$(1.66 \pm 0.16) \times 10^{-3}$	$\Gamma_{146}$	$K_S^0 K^+ e^+ e^-$	$< 1.1 \times 10^{-5}$ CL=90%
$\Gamma_{97}$	$\eta \pi^+$	$(3.77 \pm 0.09) \times 10^{-3}$	$\Gamma_{147}$	$K^+ \mu^+ \mu^-$	[f] $< 4.3 \times 10^{-6}$ CL=90%
$\Gamma_{98}$	$\eta \pi^+ \pi^0$	$(1.38 \pm 0.35) \times 10^{-3}$	$\Gamma_{148}$	$\pi^+ e^+ \mu^-$	LF $< 2.9 \times 10^{-6}$ CL=90%
$\Gamma_{99}$	$\omega \pi^+$	$(2.8 \pm 0.6) \times 10^{-4}$	$\Gamma_{149}$	$\pi^+ e^- \mu^+$	LF $< 3.6 \times 10^{-6}$ CL=90%
$\Gamma_{100}$	$\eta'(958) \pi^+$	$(4.97 \pm 0.19) \times 10^{-3}$	$\Gamma_{150}$	$K^+ e^+ \mu^-$	LF $< 1.2 \times 10^{-6}$ CL=90%
$\Gamma_{101}$	$\eta'(958) \pi^+ \pi^0$	$(1.6 \pm 0.5) \times 10^{-3}$	$\Gamma_{151}$	$K^+ e^- \mu^+$	LF $< 2.8 \times 10^{-6}$ CL=90%
<b>Hadronic modes with a <math>K\bar{K}</math> pair</b>			$\Gamma_{152}$	$\pi^- 2e^+$	L $< 1.1 \times 10^{-6}$ CL=90%
$\Gamma_{102}$	$K^+ K_S^0$	$(3.04 \pm 0.09) \times 10^{-3}$	$\Gamma_{153}$	$\pi^- 2\mu^+$	L $< 2.2 \times 10^{-8}$ CL=90%
$\Gamma_{103}$	$K_S^0 K^+$		$\Gamma_{154}$	$\pi^- e^+ \mu^+$	L $< 2.0 \times 10^{-6}$ CL=90%
$\Gamma_{104}$	$K_S^0 K^+$	$(3.21 \pm 0.16) \times 10^{-3}$	$\Gamma_{155}$	$\rho^- 2\mu^+$	L $< 5.6 \times 10^{-4}$ CL=90%
$\Gamma_{105}$	$K_S^0 K^+ \pi^0$	$(5.07 \pm 0.30) \times 10^{-3}$	$\Gamma_{156}$	$K^- 2e^+$	L $< 9 \times 10^{-7}$ CL=90%
$\Gamma_{106}$	$K_S^0 K^+ \pi^0$	$(5.24 \pm 0.31) \times 10^{-3}$	$\Gamma_{157}$	$K_S^0 \pi^- 2e^+$	$< 3.3 \times 10^{-6}$ CL=90%
$\Gamma_{107}$	$K^+ K^- \pi^+$	[a] $(9.68 \pm 0.18) \times 10^{-3}$	$\Gamma_{158}$	$K^- \pi^0 2e^+$	$< 8.5 \times 10^{-6}$ CL=90%
$\Gamma_{108}$	$\phi \pi^+$	$(5.70 \pm 0.14) \times 10^{-3}$	$\Gamma_{159}$	$K^- 2\mu^+$	L $< 1.0 \times 10^{-5}$ CL=90%
$\Gamma_{109}$	$\phi \pi^+$ , $\phi \rightarrow K^+ K^-$	$(2.69 \pm_{-0.08}^{+0.07}) \times 10^{-3}$	$\Gamma_{160}$	$K^- e^+ \mu^+$	L $< 1.9 \times 10^{-6}$ CL=90%
$\Gamma_{110}$	$K^+ \bar{K}^*(892)^0$ , $\bar{K}^*(892)^0 \rightarrow K^- \pi^+$	$(2.49 \pm_{-0.13}^{+0.08}) \times 10^{-3}$	$\Gamma_{161}$	$K^*(892)^- 2\mu^+$	L $< 8.5 \times 10^{-4}$ CL=90%
$\Gamma_{111}$	$K^+ \bar{K}_0^*(1430)^0$ , $\bar{K}_0^*(1430)^0 \rightarrow K^- \pi^+$	$(1.82 \pm 0.35) \times 10^{-3}$	$\Gamma_{162}$	Unaccounted decay modes	$(63.3 \pm 0.4) \%$ S=1.3
$\Gamma_{112}$	$K^+ \bar{K}_2^*(1430)^0$ , $\bar{K}_2^* \rightarrow K^- \pi^+$	$(1.6 \pm_{-0.8}^{+1.2}) \times 10^{-4}$	[a] The branching fraction for this mode may differ from the sum of the submodes that contribute to it, due to interference effects. See the relevant papers.		
$\Gamma_{113}$	$K^+ \bar{K}_0^*(700)$ , $\bar{K}_0^* \rightarrow K^- \pi^+$	$(6.8 \pm_{-2.1}^{+3.5}) \times 10^{-4}$	[b] These subfractions of the $K^- 2\pi^+$ mode are uncertain: see the Particle Listings.		
$\Gamma_{114}$	$a_0(1450)^0 \pi^+$ , $a_0^0 \rightarrow K^+ K^-$	$(4.5 \pm_{-1.8}^{+7.0}) \times 10^{-4}$	[c] Submodes of the $D^+ \rightarrow K^- 2\pi^+ \pi^0$ and $K_S^0 2\pi^+ \pi^-$ were studied by ANJOS 92C and COFFMAN 92B, but with at most 142 events for the first mode and 229 for the second – not enough for precise results. With nothing new for 18 years, we refer to our 2008 edition, Physics Letters <b>B667</b> 1 (2008), for those results.		
$\Gamma_{115}$	$\phi(1680) \pi^+$ , $\phi \rightarrow K^+ K^-$	$(4.9 \pm_{-1.9}^{+4.0}) \times 10^{-5}$	[d] The unseen decay modes of the resonances are included.		
$\Gamma_{116}$	$K_S^0 K_S^0 \pi^+$	$(2.70 \pm 0.13) \times 10^{-3}$	[e] This is <i>not</i> a test for the $\Delta C=1$ weak neutral current, but leads to the $\pi^+ \ell^+ \ell^-$ final state.		
			[f] This mode is not a useful test for a $\Delta C=1$ weak neutral current because both quarks must change flavor in this decay.		

CONSTRAINED FIT INFORMATION

An overall fit to 31 branching ratios uses 41 measurements and one constraint to determine 17 parameters. The overall fit has a  $\chi^2 = 62.8$  for 25 degrees of freedom.

The following off-diagonal array elements are the correlation coefficients  $\langle \delta x_i \delta x_j \rangle / (\delta x_i \delta x_j)$ , in percent, from the fit to the branching fractions,  $x_i \equiv \Gamma_i / \Gamma_{total}$ . The fit constrains the  $x_i$  whose labels appear in this array to sum to one.

Correlation matrix table with parameters x18 through x162 and their correlations.

D+ BRANCHING RATIOS

Some now-obsolete measurements have been omitted from these Listings.

c-quark decays

Γ(c → e+ anything) / Γ(c → anything)

For the Summary Table, we only use the average of e+ and μ+ measurements from Z0 → cτ decays; see the second data block below.

Table with columns VALUE, EVTS, DOCUMENT ID, TECN, COMMENT for c → e+ anything.

1 ABBIENDI 99k uses the excess of right-sign over wrong-sign leptons opposite reconstructed D\*(2010)+ → D0 π+ decays in Z0 → cτ.

Γ(c → μ+ anything) / Γ(c → anything)

For the Summary Table, we only use the average of e+ and μ+ measurements from Z0 → cτ decays; see the next data block.

Table with columns VALUE, EVTS, DOCUMENT ID, TECN, COMMENT for c → μ+ anything.

••• We do not use the following data for averages, fits, limits, etc. •••

1 ABBIENDI 99k uses the excess of right-sign over wrong-sign leptons opposite reconstructed D\*(2010)+ → D0 π+ decays in Z0 → cτ.
2 ALBRECHT 92f uses the excess of right-sign over wrong-sign leptons in a sample of events tagged by fully reconstructed D\*(2010)+ → D0 π+ decays.

Γ(c → ℓ+ anything) / Γ(c → anything)

This is an average (not a sum) of e+ and μ+ measurements.

Table with columns VALUE, EVTS, DOCUMENT ID, TECN, COMMENT for c → ℓ+ anything.

1 ABREU 00o uses leptons opposite fully reconstructed D\*(2010)+, D+, or D0 mesons.
2 ABBIENDI 99k uses the excess of right-sign over wrong-sign leptons opposite reconstructed D\*(2010)+ → D0 π+ decays in Z0 → cτ.

Γ(c → D\*(2010)+ anything) / Γ(c → anything)

Table with columns VALUE, EVTS, DOCUMENT ID, TECN, COMMENT for c → D\*(2010)+ anything.

1 ABREU 00o uses slow pions opposite fully reconstructed D\*(2010)+, D+, or D0 mesons as a signal of D\*(2010)- production.

Inclusive modes

Γ(e+ semileptonic) / Γtotal

The sum of our K0 e+ νe, K\*(892)0 e+ νe, π0 e+ νe, η e+ νe, ρ0 e+ νe, and ω e+ νe branching fractions is 15.3 ± 0.3%.

Table with columns VALUE (%), EVTS, DOCUMENT ID, TECN, COMMENT for e+ semileptonic.

1 ASNER 10 CLEO e+ e- at 3774 MeV
15.2 ± 0.9 ± 0.8 521 ± 32 ABLIKIM 07G BES2 e+ e- ≈ ψ(3770)
••• We do not use the following data for averages, fits, limits, etc. •••
16.13 ± 0.20 ± 0.33 8798 ± 105 2 ADAM 06A CLEO See ASNER 10
17.0 ± 1.9 ± 0.7 158 BALTRUSAIT...85B MRK3 e+ e- 3.77 GeV

1 Using the D+ and D0 lifetimes, ASNER 10 finds that the ratio of the D+ and D0 semileptonic widths is 0.985 ± 0.015 ± 0.024.
2 Using the D+ and D0 lifetimes, ADAM 06A finds that the ratio of the D+ and D0 inclusive e+ widths is 0.985 ± 0.028 ± 0.015, consistent with the isospin-invariance prediction of 1.

Γ(μ+ anything) / Γtotal

Table with columns VALUE (%), EVTS, DOCUMENT ID, TECN, COMMENT for μ+ anything.

1 ABLIKIM 08L finds the ratio of D+ → μ+ X and D0 → μ+ X branching fractions to be 2.59 ± 0.70 ± 0.25, in accord with the ratio of D+ and D0 lifetimes, 2.54 ± 0.02.

Γ(K- anything) / Γtotal

Table with columns VALUE (%), EVTS, DOCUMENT ID, TECN, COMMENT for K- anything.

24.7 ± 1.3 ± 1.2 631 ± 33 ABLIKIM 07G BES2 e+ e- ≈ ψ(3770)
27.8 ± 3.6 3.1 BARLAG 92c ACCM π- Cu 230 GeV
27.1 ± 2.3 ± 2.4 COFFMAN 91 MRK3 e+ e- 3.77 GeV

Γ(K0 anything) + Γ(K0 anything) / Γtotal

Table with columns VALUE (%), EVTS, DOCUMENT ID, TECN, COMMENT for K0 anything.

61 ± 5 OUR AVERAGE
60.5 ± 5.5 ± 3.3 244 ± 22 ABLIKIM 06u BES2 e+ e- at 3773 MeV
61.2 ± 6.5 ± 4.3 COFFMAN 91 MRK3 e+ e- 3.77 GeV

Γ(K+ anything) / Γtotal

Table with columns VALUE (%), EVTS, DOCUMENT ID, TECN, COMMENT for K+ anything.

5.9 ± 0.8 OUR AVERAGE
6.1 ± 0.9 ± 0.4 189 ± 27 ABLIKIM 07G BES2 e+ e- ≈ ψ(3770)
5.5 ± 1.3 ± 0.9 COFFMAN 91 MRK3 e+ e- 3.77 GeV

Γ(K\*(892)- anything) / Γtotal

Table with columns VALUE (%), EVTS, DOCUMENT ID, TECN, COMMENT for K\*(892)- anything.

5.7 ± 5.2 ± 0.7 7.2 ± 6.5 ABLIKIM 06u BES2 e+ e- at 3773 MeV

Γ(K\*(892)0 anything) / Γtotal

Table with columns VALUE (%), EVTS, DOCUMENT ID, TECN, COMMENT for K\*(892)0 anything.

23.2 ± 4.5 ± 3.0 189 ± 36 ABLIKIM 05P BES e+ e- ≈ 3773 MeV

Γ(K\*(892)0 anything) / Γtotal

Table with columns VALUE (%), CL%, DOCUMENT ID, TECN, COMMENT for K\*(892)0 anything.

<6.6 90 ABLIKIM 05P BES e+ e- ≈ 3773 MeV

Γ(η anything) / Γtotal

This ratio includes η particles from η' decays.

Table with columns VALUE (%), EVTS, DOCUMENT ID, TECN, COMMENT for η anything.

6.3 ± 0.5 ± 0.5 1972 ± 142 HUANG 06B CLEO e+ e- at ψ(3770)

Γ(η' anything) / Γtotal

Table with columns VALUE (%), EVTS, DOCUMENT ID, TECN, COMMENT for η' anything.

1.04 ± 0.16 ± 0.09 82 ± 13 HUANG 06B CLEO e+ e- at ψ(3770)







# Meson Particle Listings

## $D^\pm$

$$\Gamma(D^0 e^+ \nu_e) / \Gamma_{total} \quad \Gamma_{45} / \Gamma_{48}$$

VALUE	CL%	DOCUMENT ID	TECN	COMMENT
$< 1.0 \times 10^{-4}$	90	ABLIKIM	17AD BES3	$e^+ e^-$ at 3.773 GeV

### Hadronic modes with a $\bar{K}$ or $\bar{K}K\bar{K}$

$$\Gamma(K_S^0 \pi^+) / \Gamma_{total} \quad \Gamma_{46} / \Gamma_{48}$$

VALUE (units $10^{-2}$ )	EVTs	DOCUMENT ID	TECN	COMMENT
<b>1.562 ± 0.031 OUR FIT</b>				Error includes scale factor of 1.7.
<b>1.591 ± 0.006 ± 0.030</b>	94k	ABLIKIM	18W BES3	$e^+ e^-$ , 3773 MeV
• • • We do not use the following data for averages, fits, limits, etc. • • •				
1.526 ± 0.022 ± 0.038		1 DOBBS	07 CLEO	See MENDEZ 10
1.55 ± 0.05 ± 0.06	2.2k	1 HE	05 CLEO	See DOBBS 07
1.6 ± 0.3 ± 0.1	161	ADLER	88c MRK3	$e^+ e^-$ 3.77 GeV
1 DOBBS 07 and HE 05 use single- and double-tagged events in an overall fit. DOBBS 07 supersedes HE 05.				

$$\Gamma(K_S^0 \pi^+) / \Gamma(K^- 2\pi^+) \quad \Gamma_{46} / \Gamma_{48}$$

VALUE	EVTs	DOCUMENT ID	TECN	COMMENT
<b>0.167 ± 0.004 OUR FIT</b>				Error includes scale factor of 2.4.
<b>0.162 ± 0.009 OUR AVERAGE</b>				Error includes scale factor of 4.5.
0.171 ± 0.002 ± 0.002		BONVICINI	14 CLEO	All CLEO-c runs
0.1530 ± 0.0023 ± 0.0016	10.6k	LINK	02B FOCS	$\gamma$ nucleus, $E_\gamma \approx 180$ GeV
• • • We do not use the following data for averages, fits, limits, etc. • • •				
0.1682 ± 0.0012 ± 0.0037	30k	MENDEZ	10 CLEO	See BONVICINI 14
0.174 ± 0.012 ± 0.011	473	1 BISHAI	97 CLEO	$e^+ e^- \approx \Upsilon(4S)$
0.137 ± 0.015 ± 0.016	264	ANJOS	90c E691	Photoproduction
1 See BISHAI 97 for an isospin analysis of $D^+ \rightarrow \bar{K} \pi$ amplitudes.				

$$\Gamma(K_S^0 \pi^+) / \Gamma_{total} \quad \Gamma_{47} / \Gamma_{48}$$

VALUE (units $10^{-2}$ )	EVTs	DOCUMENT ID	TECN	COMMENT
<b>1.460 ± 0.040 ± 0.035</b>	2023 ± 54	1 HE	08 CLEO	$e^+ e^-$ at $\psi(3770)$
1 The difference of CLEO $D^+ \rightarrow K_S^0 \pi^+$ and $K_L^0 \pi^+$ branching fractions over the sum (DOBBS 07 and HE 08) is $+0.022 \pm 0.016 \pm 0.018$ .				

$$\Gamma(K^- 2\pi^+) / \Gamma_{total} \quad \Gamma_{48} / \Gamma_{48}$$

VALUE (units $10^{-2}$ )	EVTs	DOCUMENT ID	TECN	COMMENT
<b>9.38 ± 0.16 OUR FIT</b>				Error includes scale factor of 1.6.
<b>9.224 ± 0.059 ± 0.157</b>		BONVICINI	14 CLEO	All CLEO-c runs
• • • We do not use the following data for averages, fits, limits, etc. • • •				
9.14 ± 0.10 ± 0.17		1 DOBBS	07 CLEO	See BONVICINI 14
9.5 ± 0.2 ± 0.3	15.1k	1 HE	05 CLEO	See DOBBS 07
9.3 ± 0.6 ± 0.8	1502	2 BALEST	94 CLEO	$e^+ e^- \approx \Upsilon(4S)$
6.4 $^{+1.5}_{-1.4}$		3 BARLAG	92c ACCM	$\pi^-$ Cu 230 GeV
9.1 ± 1.3 ± 0.4	1164	ADLER	88c MRK3	$e^+ e^-$ 3.77 GeV
9.1 ± 1.9	239	4 SCHINDLER	81 MRK2	$e^+ e^-$ 3.771 GeV
1 DOBBS 07 and HE 05 use single- and double-tagged events in an overall fit. DOBBS 07 supersedes HE 05.				
2 BALEST 94 measures the ratio of $D^+ \rightarrow K^- \pi^+ \pi^+$ and $D^0 \rightarrow K^- \pi^+$ branching fractions to be $2.35 \pm 0.16 \pm 0.16$ and uses their absolute measurement of the $D^0 \rightarrow K^- \pi^+$ fraction (AKERIB 93).				
3 BARLAG 92c computes the branching fraction by topological normalization.				
4 SCHINDLER 81 (MARK-2) measures $\sigma(e^+ e^- \rightarrow \psi(3770)) \times$ branching fraction to be $0.38 \pm 0.05$ nb. We use the MARK-3 (ADLER 88c) value of $\sigma = 4.2 \pm 0.6 \pm 0.3$ nb.				

### See the related review(s): Review of Multibody Charm Analyses

$$\Gamma((K^- \pi^+)_{S\text{-wave}} \pi^+) / \Gamma(K^- 2\pi^+) \quad \Gamma_{49} / \Gamma_{48}$$

This is the “fit fraction” from the Dalitz-plot analysis. The  $K^- \pi^+ S$ -wave includes a broad scalar  $\kappa$  ( $\bar{K}_0^*(700)$ ), the  $\bar{K}_0^*(1430)^0$ , and non-resonant background.

VALUE	DOCUMENT ID	TECN	COMMENT
<b>0.801 ± 0.012 OUR AVERAGE</b>			
0.8024 ± 0.0138 ± 0.0043	1 LINK	09 FOCS	MIPWA fit, 53k evts
0.838 ± 0.038	2 BONVICINI	08A CLEO	QMIPWA fit, 141k evts
0.786 ± 0.014 ± 0.018	AITALA	06 E791	Dalitz fit, 15.1k events
• • • We do not use the following data for averages, fits, limits, etc. • • •			
0.8323 ± 0.0150 ± 0.0008	3 LINK	07B FOCS	See LINK 09

1 This LINK 09 model-independent partial-wave analysis of the  $K^- \pi^+ S$ -wave slices the  $K^- \pi^+$  mass range into 39 bins.

2 The BONVICINI 08A QMIPWA (quasi-model-independent partial-wave analysis) of the  $K^- \pi^+ S$ -wave amplitude slices the  $K^- \pi^+$  mass range into 26 bins but keeps the Breit-Wigner  $\bar{K}_0^*(1430)^0$ .

3 This LINK 07B fit uses a K matrix. The  $K^- \pi^+ S$ -wave fit fraction given above breaks down into  $(207.3 \pm 25.5 \pm 12.4)\%$  isospin-1/2 and  $(40.5 \pm 9.6 \pm 3.2)\%$  isospin-3/2 — with large interference between the two. The isospin-1/2 component includes the  $\kappa$  (or  $\bar{K}_0^*(700)^0$ ) and  $\bar{K}_0^*(1430)^0$ .

$$\Gamma(\bar{K}_0^*(700)^0 \pi^+, \bar{K}_0^*(700) \rightarrow K^- \pi^+) / \Gamma(K^- 2\pi^+) \quad \Gamma_{50} / \Gamma_{48}$$

This is the “fit fraction” from the Dalitz-plot analysis.

VALUE	DOCUMENT ID	TECN	COMMENT
• • • We do not use the following data for averages, fits, limits, etc. • • •			
0.478 ± 0.121 ± 0.053	AITALA	02 E791	See AITALA 06

$$\Gamma(\bar{K}_0^*(1430)^0 \pi^+, \bar{K}_0^*(1430)^0 \rightarrow K^- \pi^+) / \Gamma(K^- 2\pi^+) \quad \Gamma_{51} / \Gamma_{48}$$

This is the “fit fraction” from the Dalitz-plot analysis.

VALUE	DOCUMENT ID	TECN	COMMENT
<b>0.1330 ± 0.0062</b>	BONVICINI	08A CLEO	QMIPWA fit, 141k evts
• • • We do not use the following data for averages, fits, limits, etc. • • •			
0.125 ± 0.014 ± 0.005	AITALA	02 E791	See AITALA 06
0.284 ± 0.022 ± 0.059	FRABETTI	94G E687	Dalitz fit, 8800 evts
0.248 ± 0.019 ± 0.017	ANJOS	93 E691	$\gamma$ Be 90–260 GeV

$$\Gamma(\bar{K}^*(892)^0 \pi^+, \bar{K}^*(892)^0 \rightarrow K^- \pi^+) / \Gamma(K^- 2\pi^+) \quad \Gamma_{52} / \Gamma_{48}$$

This is the “fit fraction” from the Dalitz-plot analysis.

VALUE	DOCUMENT ID	TECN	COMMENT
<b>0.111 ± 0.012 OUR AVERAGE</b>			Error includes scale factor of 3.7.
0.1236 ± 0.0034 ± 0.0034	LINK	09 FOCS	MIPWA fit, 53k evts
0.0988 ± 0.0046	BONVICINI	08A CLEO	QMIPWA fit, 141k evts
0.119 ± 0.002 ± 0.020	AITALA	06 E791	Dalitz fit, 15.1k events
• • • We do not use the following data for averages, fits, limits, etc. • • •			
0.1361 ± 0.0041 ± 0.0030	1 LINK	07B FOCS	See LINK 09
0.123 ± 0.010 ± 0.009	AITALA	02 E791	See AITALA 06
0.137 ± 0.006 ± 0.009	FRABETTI	94G E687	Dalitz fit, 8800 evts
0.170 ± 0.009 ± 0.034	ANJOS	93 E691	$\gamma$ Be 90–260 GeV
0.14 ± 0.04 ± 0.04	ALVAREZ	91B NA14	Photoproduction
0.13 ± 0.01 ± 0.07	ADLER	87 MRK3	$e^+ e^-$ 3.77 GeV
1 The statistical error on this LINK 07B value is corrected in LINK 09.			

$$\Gamma(\bar{K}^*(1410)^0 \pi^+, \bar{K}^{*0} \rightarrow K^- \pi^+) / \Gamma(K^- 2\pi^+) \quad \Gamma_{53} / \Gamma_{48}$$

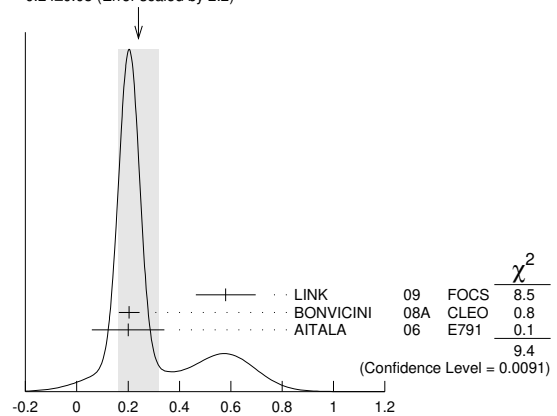
VALUE (units $10^{-3}$ )	DOCUMENT ID	TECN	COMMENT
<b>not seen</b>	LINK	09 FOCS	MIPWA fit, 53k evts
<b>not seen</b>	BONVICINI	08A CLEO	QMIPWA fit, 141k evts
• • • We do not use the following data for averages, fits, limits, etc. • • •			
4.8 ± 2.1 ± 1.7	LINK	07B FOCS	See LINK 09

$$\Gamma(\bar{K}_2^*(1430)^0 \pi^+, \bar{K}_2^*(1430)^0 \rightarrow K^- \pi^+) / \Gamma(K^- 2\pi^+) \quad \Gamma_{54} / \Gamma_{48}$$

This is the “fit fraction” from the Dalitz-plot analysis.

VALUE (units $10^{-2}$ )	DOCUMENT ID	TECN	COMMENT
<b>0.24 ± 0.08 OUR AVERAGE</b>			Error includes scale factor of 2.2. See the ideogram below.
0.58 ± 0.10 ± 0.06	LINK	09 FOCS	MIPWA fit, 53k evts
0.204 ± 0.040	BONVICINI	08A CLEO	QMIPWA fit, 141k evts
0.2 ± 0.1 ± 0.1	AITALA	06 E791	Dalitz fit, 15.1k events
• • • We do not use the following data for averages, fits, limits, etc. • • •			
0.39 ± 0.09 ± 0.05	LINK	07B FOCS	See LINK 09
0.5 ± 0.1 ± 0.2	AITALA	02 E791	See AITALA 06

WEIGHTED AVERAGE  
0.24±0.08 (Error scaled by 2.2)



$$\Gamma(\bar{K}_2^*(1430)^0 \pi^+, \bar{K}_2^*(1430)^0 \rightarrow K^- \pi^+) / \Gamma(K^- 2\pi^+) \quad \Gamma_{54} / \Gamma_{48}$$

(units  $10^{-2}$ )

$$\Gamma(\bar{K}^*(1680)^0 \pi^+, \bar{K}^*(1680)^0 \rightarrow K^- \pi^+) / \Gamma(K^- 2\pi^+) \quad \Gamma_{55} / \Gamma_{48}$$

This is the “fit fraction” from the Dalitz-plot analysis.

VALUE (units $10^{-2}$ )	DOCUMENT ID	TECN	COMMENT
<b>0.23 ± 0.12 OUR AVERAGE</b>			
1.75 ± 0.62 ± 0.54	LINK	09 FOCS	MIPWA fit, 53k evts
0.196 ± 0.118	BONVICINI	08A CLEO	QMIPWA fit, 141k evts
1.2 ± 0.6 ± 1.2	AITALA	06 E791	Dalitz fit, 15.1k events
• • • We do not use the following data for averages, fits, limits, etc. • • •			
1.90 ± 0.63 ± 0.43	LINK	07B FOCS	See LINK 09
2.5 ± 0.7 ± 0.3	AITALA	02 E791	See AITALA 06
4.7 ± 0.6 ± 0.7	FRABETTI	94G E687	Dalitz fit, 8800 evts
3.0 ± 0.4 ± 1.3	ANJOS	93 E691	$\gamma$ Be 90–260 GeV

$$\Gamma(K^- (2\pi^+)_{I=2}) / \Gamma(K^- 2\pi^+) \quad \Gamma_{56} / \Gamma_{48}$$

VALUE	DOCUMENT ID	TECN	COMMENT
<b>0.155 ± 0.028</b>	BONVICINI	08A CLEO	QMIPWA fit, 141k evts



# Meson Particle Listings

## $D^\pm$

• • • We do not use the following data for averages, fits, limits, etc. • • •  
 <0.026      90      FRABETTI    97c    E687     $\gamma$ Be,  $\bar{E}_\gamma \approx 200$  GeV

$\Gamma(K^+ 2K_S^0)/\Gamma_{total}$   $\Gamma_{78}/\Gamma$

VALUE (units $10^{-4}$ )	EVTS	DOCUMENT ID	TECN	COMMENT
<b>25.4 ± 0.5 ± 1.2</b>	3551	ABLIKIM	17A	BES3 $e^+ e^- \rightarrow \psi(3770)$

$\Gamma(K^+ 2K_S^0)/\Gamma(K^- 2\pi^+)$   $\Gamma_{78}/\Gamma_{48}$

VALUE	EVTS	DOCUMENT ID	TECN	COMMENT
0.035 ± 0.010 ± 0.005	39 ± 9	ALBRECHT	94i	ARG $e^+ e^- \approx 10$ GeV
0.085 ± 0.018	70 ± 12	AMMAR	91	CLEO $e^+ e^- \approx 10.5$ GeV

• • • We do not use the following data for averages, fits, limits, etc. • • •

$\Gamma(\phi(1020)^0 K^+)/\Gamma_{total}$   $\Gamma_{134}/\Gamma$

VALUE	CL%	DOCUMENT ID	TECN	COMMENT
<b>&lt;2.1 × 10<sup>-5</sup></b>	90	ABLIKIM	19B1	BES3 $e^+ e^-$ at 3773 MeV

$\Gamma(K^+ K^- K_S^0 \pi^+)/\Gamma(K_S^0 2\pi^+ \pi^-)$   $\Gamma_{79}/\Gamma_{70}$

VALUE (units $10^{-3}$ )	EVTS	DOCUMENT ID	TECN	COMMENT
<b>7.7 ± 1.5 ± 0.9</b>	35 ± 7	LINK	01c	FOCS $\gamma$ nucleus, $\bar{E}_\gamma \approx 180$ GeV

### Pionic modes

$\Gamma(\pi^+ \pi^0)/\Gamma_{total}$   $\Gamma_{80}/\Gamma$

VALUE (units $10^{-3}$ )	EVTS	DOCUMENT ID	TECN	COMMENT
<b>1.247 ± 0.033 OUR FIT</b>				
<b>1.259 ± 0.033 ± 0.023</b>	10k	ABLIKIM	18w	BES3 $e^+ e^-$ , 3773 MeV

$\Gamma(\pi^+ \pi^0)/\Gamma(K^- 2\pi^+)$   $\Gamma_{80}/\Gamma_{48}$

VALUE (units $10^{-2}$ )	EVTS	DOCUMENT ID	TECN	COMMENT
<b>1.33 ± 0.04 OUR FIT</b>				Error includes scale factor of 1.1.
<b>1.31 ± 0.06 OUR AVERAGE</b>				
1.29 ± 0.04 ± 0.05	2649 ± 76	MENDEZ	10	CLEO $e^+ e^-$ at 3774 MeV
1.33 ± 0.11 ± 0.09	1229 ± 99	AUBERT,B	06f	BABR $e^+ e^- \approx \Upsilon(4S)$
1.44 ± 0.19 ± 0.10	171 ± 22	ARMS	04	CLEO $e^+ e^- \approx 10$ GeV

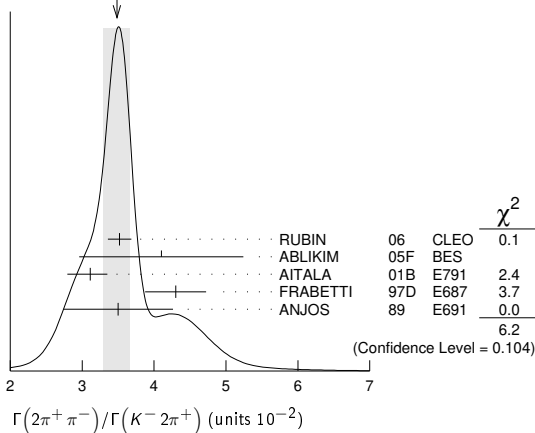
• • • We do not use the following data for averages, fits, limits, etc. • • •

1.33 ± 0.07 ± 0.06	914 ± 46	RUBIN	06	CLEO See MENDEZ 10
--------------------	----------	-------	----	--------------------

$\Gamma(2\pi^+ \pi^-)/\Gamma(K^- 2\pi^+)$   $\Gamma_{81}/\Gamma_{48}$

VALUE (units $10^{-2}$ )	EVTS	DOCUMENT ID	TECN	COMMENT
<b>3.48 ± 0.19 OUR AVERAGE</b>				Error includes scale factor of 1.4. See the ideogram below.
3.52 ± 0.11 ± 0.12	3303 ± 95	RUBIN	06	CLEO $e^+ e^-$ at $\psi(3770)$
4.1 ± 1.1 ± 0.3	85 ± 22	ABLIKIM	05f	BES $e^+ e^- \approx \psi(3770)$
3.11 ± 0.18 <sup>+0.16</sup> <sub>-0.26</sub>	1172	AITALA	01B	E791 $\pi^-$ nucleus, 500 GeV
4.3 ± 0.3 ± 0.3	236	FRABETTI	97D	E687 $\gamma$ Be $\approx 200$ GeV
3.5 ± 0.7 ± 0.3	83	ANJOS	89	E691 Photoproduction

WEIGHTED AVERAGE  
3.48 ± 0.19 (Error scaled by 1.4)

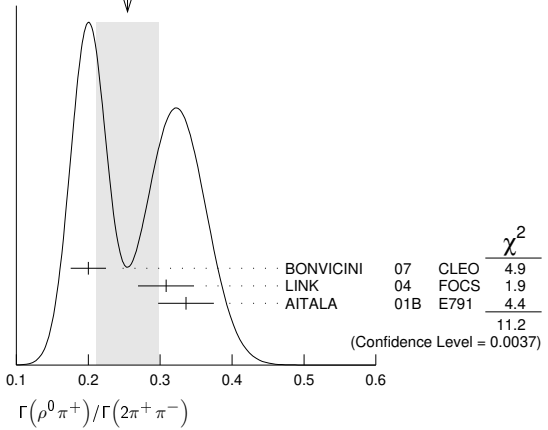


$\Gamma(\rho^0 \pi^+)/\Gamma(2\pi^+ \pi^-)$   $\Gamma_{82}/\Gamma_{81}$

This is the "fit fraction" from the Dalitz-plot analysis.

VALUE	DOCUMENT ID	TECN	COMMENT
<b>0.25 ± 0.04 OUR AVERAGE</b>			Error includes scale factor of 2.4. See the ideogram below.
0.200 ± 0.023 ± 0.009	BONVICINI	07	CLEO Dalitz fit, $\approx 2240$ evts
0.3082 ± 0.0314 ± 0.0230	LINK	04	FOCS Dalitz fit, 1527 ± 51 evts
0.336 ± 0.032 ± 0.022	AITALA	01B	E791 Dalitz fit, 1172 evts

WEIGHTED AVERAGE  
0.25 ± 0.04 (Error scaled by 2.4)



$\Gamma(\pi^+ (\pi^+ \pi^-)_{S\text{-wave}})/\Gamma(2\pi^+ \pi^-)$   $\Gamma_{83}/\Gamma_{81}$

This is the "fit fraction" from the Dalitz-plot analysis. See also the next three data blocks.

VALUE	DOCUMENT ID	TECN	COMMENT	
<b>0.5600 ± 0.0324 ± 0.0214</b>	1	LINK	04	FOCS Dalitz fit, 1527 ± 51 evts

<sup>1</sup>LINK 04 borrows a K-matrix parametrization from ANISOVICH 03 of the full  $\pi-\pi$  S-wave isoscalar scattering amplitude to describe the  $\pi^+ \pi^-$  S-wave component of the  $\pi^+ \pi^+ \pi^-$  state. The fit fraction given above is a sum over five  $f_0$  mesons, the  $f_0(980)$ ,  $f_0(1300)$ ,  $f_0(1200-1600)$ ,  $f_0(1500)$ , and  $f_0(1750)$ . See LINK 04 for details and discussion.

$\Gamma(\sigma \pi^+, \sigma \rightarrow \pi^+ \pi^-)/\Gamma(2\pi^+ \pi^-)$   $\Gamma_{84}/\Gamma_{81}$

This is the "fit fraction" from the Dalitz-plot analysis.

VALUE	DOCUMENT ID	TECN	COMMENT
<b>0.422 ± 0.027 OUR AVERAGE</b>			
0.418 ± 0.014 ± 0.025	BONVICINI	07	CLEO Dalitz fit, $\approx 2240$ evts
0.463 ± 0.090 ± 0.021	AITALA	01B	E791 Dalitz fit, 1172 evts

$\Gamma(f_0(980) \pi^+, f_0(980) \rightarrow \pi^+ \pi^-)/\Gamma(2\pi^+ \pi^-)$   $\Gamma_{85}/\Gamma_{81}$

This is the "fit fraction" from the Dalitz-plot analysis.

VALUE	DOCUMENT ID	TECN	COMMENT
<b>0.048 ± 0.010 OUR AVERAGE</b>			Error includes scale factor of 1.3.
0.041 ± 0.009 ± 0.003	BONVICINI	07	CLEO Dalitz fit, $\approx 2240$ evts
0.062 ± 0.013 ± 0.004	AITALA	01B	E791 Dalitz fit, 1172 evts

$\Gamma(f_0(1370) \pi^+, f_0(1370) \rightarrow \pi^+ \pi^-)/\Gamma(2\pi^+ \pi^-)$   $\Gamma_{86}/\Gamma_{81}$

This is the "fit fraction" from the Dalitz-plot analysis.

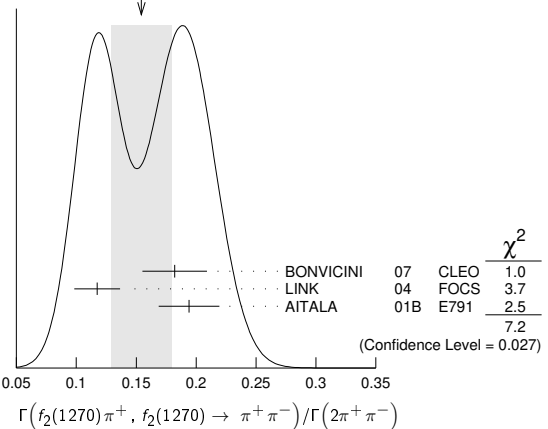
VALUE	DOCUMENT ID	TECN	COMMENT
<b>0.024 ± 0.013 OUR AVERAGE</b>			
0.026 ± 0.018 ± 0.006	BONVICINI	07	CLEO Dalitz fit, $\approx 2240$ evts
0.023 ± 0.015 ± 0.008	AITALA	01B	E791 Dalitz fit, 1172 evts

$\Gamma(f_2(1270) \pi^+, f_2(1270) \rightarrow \pi^+ \pi^-)/\Gamma(2\pi^+ \pi^-)$   $\Gamma_{87}/\Gamma_{81}$

This is the "fit fraction" from the Dalitz-plot analysis.

VALUE	DOCUMENT ID	TECN	COMMENT
<b>0.154 ± 0.025 OUR AVERAGE</b>			Error includes scale factor of 1.9. See the ideogram below.
0.182 ± 0.026 ± 0.007	BONVICINI	07	CLEO Dalitz fit, $\approx 2240$ evts
0.1174 ± 0.0190 ± 0.0029	LINK	04	FOCS Dalitz fit, 1527 ± 51 evts
0.194 ± 0.025 ± 0.004	AITALA	01B	E791 Dalitz fit, 1172 evts

WEIGHTED AVERAGE  
0.154 ± 0.025 (Error scaled by 1.9)



Γ(ρ(1450)<sup>0</sup>π<sup>+</sup>, ρ(1450)<sup>0</sup> → π<sup>+</sup>π<sup>-</sup>)/Γ(2π<sup>+</sup>π<sup>-</sup>) Γ<sub>88</sub>/Γ<sub>81</sub>  
This is the "fit fraction" from the Dalitz-plot analysis.

Table with columns: VALUE, CL%, DOCUMENT ID, TECN, COMMENT. Data rows include BONVICINI 07 CLEO Dalitz fit, ≈ 2240 evts and AITALA 01B E791 Dalitz fit, 1172 evts.

Γ(f<sub>0</sub>(1500)π<sup>+</sup>, f<sub>0</sub>(1500) → π<sup>+</sup>π<sup>-</sup>)/Γ(2π<sup>+</sup>π<sup>-</sup>) Γ<sub>89</sub>/Γ<sub>81</sub>  
This is the "fit fraction" from the Dalitz-plot analysis.

Table with columns: VALUE, DOCUMENT ID, TECN, COMMENT. Data row: BONVICINI 07 CLEO Dalitz fit, ≈ 2240 evts.

Γ(f<sub>0</sub>(1710)π<sup>+</sup>, f<sub>0</sub>(1710) → π<sup>+</sup>π<sup>-</sup>)/Γ(2π<sup>+</sup>π<sup>-</sup>) Γ<sub>90</sub>/Γ<sub>81</sub>  
This is the "fit fraction" from the Dalitz-plot analysis.

Table with columns: VALUE, CL%, DOCUMENT ID, TECN, COMMENT. Data row: BONVICINI 07 CLEO Dalitz fit, ≈ 2240 evts.

Γ(f<sub>0</sub>(1790)π<sup>+</sup>, f<sub>0</sub>(1790) → π<sup>+</sup>π<sup>-</sup>)/Γ(2π<sup>+</sup>π<sup>-</sup>) Γ<sub>91</sub>/Γ<sub>81</sub>  
This is the "fit fraction" from the Dalitz-plot analysis.

Table with columns: VALUE, CL%, DOCUMENT ID, TECN, COMMENT. Data row: BONVICINI 07 CLEO Dalitz fit, ≈ 2240 evts.

Γ((π<sup>+</sup>π<sup>+</sup>)<sub>S-wave</sub>π<sup>-</sup>)/Γ(2π<sup>+</sup>π<sup>-</sup>) Γ<sub>92</sub>/Γ<sub>81</sub>  
This is the "fit fraction" from the Dalitz-plot analysis.

Table with columns: VALUE, CL%, DOCUMENT ID, TECN, COMMENT. Data row: BONVICINI 07 CLEO Dalitz fit, ≈ 2240 evts.

Γ(2π<sup>+</sup>π<sup>-</sup> nonresonant)/Γ(2π<sup>+</sup>π<sup>-</sup>) Γ<sub>93</sub>/Γ<sub>81</sub>  
This is the "fit fraction" from the Dalitz-plot analysis.

Table with columns: VALUE, CL%, DOCUMENT ID, TECN, COMMENT. Data row: AITALA 01B E791 Dalitz fit, 1172 evts.

Γ(π<sup>+</sup>2π<sup>0</sup>)/Γ(K<sup>-</sup>2π<sup>+</sup>) Γ<sub>94</sub>/Γ<sub>48</sub>

Table with columns: VALUE (units 10<sup>-2</sup>), EVTS, DOCUMENT ID, TECN, COMMENT. Data row: RUBIN 06 CLEO e<sup>+</sup>e<sup>-</sup> at ψ(3770).

Γ(2π<sup>+</sup>π<sup>-</sup>π<sup>0</sup>)/Γ(K<sup>-</sup>2π<sup>+</sup>) Γ<sub>95</sub>/Γ<sub>48</sub>

Table with columns: VALUE (units 10<sup>-2</sup>), EVTS, DOCUMENT ID, TECN, COMMENT. Data row: RUBIN 06 CLEO e<sup>+</sup>e<sup>-</sup> at ψ(3770).

Γ(3π<sup>+</sup>2π<sup>-</sup>)/Γ(K<sup>-</sup>2π<sup>+</sup>) Γ<sub>96</sub>/Γ<sub>48</sub>

Table with columns: VALUE (units 10<sup>-2</sup>), EVTS, DOCUMENT ID, TECN, COMMENT. Data row: RUBIN 06 CLEO e<sup>+</sup>e<sup>-</sup> at ψ(3770).

Γ(3π<sup>+</sup>2π<sup>-</sup>)/Γ(K<sup>-</sup>3π<sup>+</sup>π<sup>-</sup>) Γ<sub>96</sub>/Γ<sub>71</sub>

Table with columns: VALUE, EVTS, DOCUMENT ID, TECN, COMMENT. Data row: LINK 03D FOCUS γ A, E<sub>γ</sub> ≈ 180 GeV.

Γ(ηπ<sup>+</sup>)/Γ<sub>total</sub> Γ<sub>97</sub>/Γ

Unseen decay modes of the η are included.

Table with columns: VALUE (units 10<sup>-4</sup>), EVTS, DOCUMENT ID, TECN, COMMENT. Data rows include ABLIKIM 18w BES3 e<sup>+</sup>e<sup>-</sup>, 3773 MeV and ARTUSO 08 CLEO See MENDEZ 10.

Γ(ηπ<sup>+</sup>)/Γ(K<sup>-</sup>2π<sup>+</sup>) Γ<sub>97</sub>/Γ<sub>48</sub>

Unseen decay modes of the η are included.

Table with columns: VALUE (units 10<sup>-2</sup>), EVTS, DOCUMENT ID, TECN, COMMENT. Data row: MENDEZ 10 CLEO e<sup>+</sup>e<sup>-</sup> at 3774 MeV.

Γ(ηπ<sup>+</sup>π<sup>0</sup>)/Γ<sub>total</sub> Γ<sub>98</sub>/Γ

Unseen decay modes of the η are included.

4.02±0.11 OUR FIT Error includes scale factor of 1.1.

Table with columns: VALUE (units 10<sup>-4</sup>), CL%, EVTS, DOCUMENT ID, TECN, COMMENT. Data row: RUBIN 06 CLEO e<sup>+</sup>e<sup>-</sup> at ψ(3770).

Γ(ωπ<sup>+</sup>)/Γ<sub>total</sub> Γ<sub>99</sub>/Γ

Unseen decay modes of the ω are included.

Γ(η'(958)π<sup>+</sup>)/Γ<sub>total</sub> Γ<sub>100</sub>/Γ

Unseen decay modes of the η'(958) are included.

Table with columns: VALUE (units 10<sup>-4</sup>), EVTS, DOCUMENT ID, TECN, COMMENT. Data rows include ABLIKIM 18w BES3 e<sup>+</sup>e<sup>-</sup>, 3773 MeV and ARTUSO 08 CLEO See MENDEZ 10.

Γ(η'(958)π<sup>+</sup>)/Γ(K<sup>-</sup>2π<sup>+</sup>) Γ<sub>100</sub>/Γ<sub>48</sub>

Unseen decay modes of the η'(958) are included.

5.30±0.21 OUR FIT Error includes scale factor of 2.8.

5.12±0.17±0.25 1037 ± 35 MENDEZ 10 CLEO e<sup>+</sup>e<sup>-</sup> at 3774 MeV

Γ(η'(958)π<sup>+</sup>π<sup>0</sup>)/Γ<sub>total</sub> Γ<sub>101</sub>/Γ

Unseen decay modes of the η'(958) are included.

15.7±4.3±2.5 33 ± 9 ARTUSO 08 CLEO e<sup>+</sup>e<sup>-</sup> at ψ(3770)

Hadronic modes with a K $\bar{K}$  pair

Γ(K<sup>+</sup>K<sub>S</sub><sup>0</sup>)/Γ<sub>total</sub> Γ<sub>102</sub>/Γ

3.04 ± 0.09 OUR FIT Error includes scale factor of 2.2.

Table with columns: VALUE (units 10<sup>-3</sup>), EVTS, DOCUMENT ID, TECN, COMMENT. Data rows include ABLIKIM 18w BES3 e<sup>+</sup>e<sup>-</sup>, 3773 MeV and BONVICINI 08 CLEO See MENDEZ 10.

Γ(K<sup>+</sup>K<sub>S</sub><sup>0</sup>)/Γ(K<sub>S</sub><sup>0</sup>π<sup>+</sup>) Γ<sub>102</sub>/Γ<sub>46</sub>

0.194 ± 0.006 OUR FIT Error includes scale factor of 2.8.

Table with columns: VALUE, EVTS, DOCUMENT ID, TECN, COMMENT. Data rows include WONG 09 BELL e<sup>+</sup>e<sup>-</sup> at 7(45) and SCHINDLER 81 MRK2 e<sup>+</sup>e<sup>-</sup> 3.771 GeV.

Γ(K<sup>+</sup>K<sub>S</sub><sup>0</sup>)/Γ(K<sup>-</sup>2π<sup>+</sup>) Γ<sub>102</sub>/Γ<sub>48</sub>

3.24±0.09 OUR FIT Error includes scale factor of 2.3.

Table with columns: VALUE (units 10<sup>-2</sup>), EVTS, DOCUMENT ID, TECN, COMMENT. Data rows include MENDEZ 10 CLEO e<sup>+</sup>e<sup>-</sup> at 3774 MeV and LINK 02B FOCUS γ nucleus, E<sub>γ</sub> ≈ 180 GeV.

Γ(K<sub>L</sub><sup>0</sup>K<sup>+</sup>)/Γ<sub>total</sub> Γ<sub>104</sub>/Γ

3.21±0.11±0.11 650 ABLIKIM 19M BES3 e<sup>+</sup>e<sup>-</sup> at 3773 MeV

Γ(K<sub>S</sub><sup>0</sup>K<sup>+</sup>π<sup>0</sup>)/Γ<sub>total</sub> Γ<sub>105</sub>/Γ

5.07±0.19±0.23 470 ABLIKIM 19M BES3 e<sup>+</sup>e<sup>-</sup> at 3773 MeV

Γ(K<sub>L</sub><sup>0</sup>K<sup>+</sup>π<sup>0</sup>)/Γ<sub>total</sub> Γ<sub>106</sub>/Γ

5.24±0.22±0.22 410 ABLIKIM 19M BES3 e<sup>+</sup>e<sup>-</sup> at 3773 MeV

Γ(K<sup>+</sup>K<sup>-</sup>π<sup>+</sup>)/Γ<sub>total</sub> Γ<sub>107</sub>/Γ

0.935±0.017±0.024 Error includes scale factor of 1.4. See the ideogram below.

Table with columns: VALUE (units 10<sup>-2</sup>), EVTS, DOCUMENT ID, TECN, COMMENT. Data rows include DOBBS 07 CLEO See BONVICINI 14 and ABLIKIM 19G LHCb pp at 8 TeV.

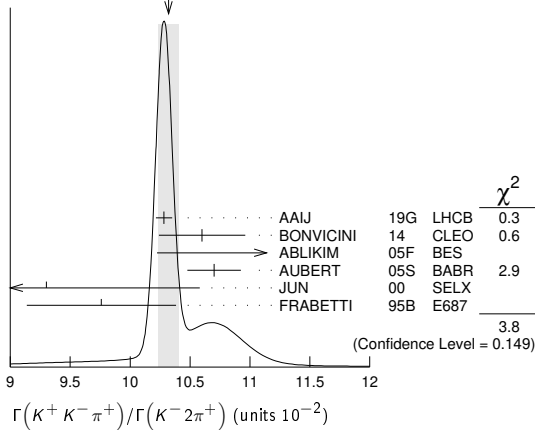
10.32 ± 0.09 OUR AVERAGE Error includes scale factor of 1.4. See the ideogram below.

Table with columns: VALUE (units 10<sup>-2</sup>), EVTS, DOCUMENT ID, TECN, COMMENT. Data rows include ABLIKIM 16D BES3 e<sup>+</sup>e<sup>-</sup> at 3773 MeV and FRABETTI 95B E687 γ Be, E<sub>γ</sub> ≈ 200 GeV.

# Meson Particle Listings

$D^{\pm}$

WEIGHTED AVERAGE  
10.32±0.09 (Error scaled by 1.4)



$\Gamma(\phi\pi^+)/\Gamma_{total}$   $\Gamma_{108}/\Gamma$

VALUE (units $10^{-3}$ )	EVTS	DOCUMENT ID	TECN	COMMENT
<b>5.70±0.05±0.13</b>	18k	ABLIKIM	19B1 BES3	$e^+e^-$ at 3773 MeV

$\Gamma(\phi\pi^+, \phi \rightarrow K^+K^-)/\Gamma(K^+K^-\pi^+)$   $\Gamma_{109}/\Gamma_{107}$

This is the "fit fraction" from the Dalitz-plot analysis.

VALUE (%)	DOCUMENT ID	TECN	COMMENT
<b>27.8±0.4±0.2</b> -0.5	RUBIN	08 CLEO	Dalitz fit, 19,458±163 evts
29.2±3.1±3.0	FRABETTI	95B E687	Dalitz fit, 915 evts

••• We do not use the following data for averages, fits, limits, etc. •••

$\Gamma(K^+\bar{K}^*(892)^0, \bar{K}^*(892)^0 \rightarrow K^-\pi^+)/\Gamma(K^+K^-\pi^+)$   $\Gamma_{110}/\Gamma_{107}$

This is the "fit fraction" from the Dalitz-plot analysis.

VALUE (%)	DOCUMENT ID	TECN	COMMENT
<b>25.7±0.5±0.4</b> -1.2	RUBIN	08 CLEO	Dalitz fit, 19,458±163 evts
30.1±2.0±2.5	FRABETTI	95B E687	Dalitz fit, 915 evts

••• We do not use the following data for averages, fits, limits, etc. •••

$\Gamma(K^+\bar{K}_0^*(1430)^0, \bar{K}_0^*(1430)^0 \rightarrow K^-\pi^+)/\Gamma(K^+K^-\pi^+)$   $\Gamma_{111}/\Gamma_{107}$

This is the "fit fraction" from the Dalitz-plot analysis.

VALUE (%)	DOCUMENT ID	TECN	COMMENT
<b>18.8±1.2±3.3</b> -3.4	RUBIN	08 CLEO	Dalitz fit, 19,458±163 evts
37.0±3.5±1.8	FRABETTI	95B E687	Dalitz fit, 915 evts

••• We do not use the following data for averages, fits, limits, etc. •••

$\Gamma(K^+\bar{K}_2^*(1430)^0, \bar{K}_2^*(1430)^0 \rightarrow K^-\pi^+)/\Gamma(K^+K^-\pi^+)$   $\Gamma_{112}/\Gamma_{107}$

This is the "fit fraction" from the Dalitz-plot analysis.

VALUE (%)	DOCUMENT ID	TECN	COMMENT
<b>1.7±0.4±0.7</b> -0.2	RUBIN	08 CLEO	Dalitz fit, 19,458±163 evts

$\Gamma(K^+\bar{K}_0^*(700), \bar{K}_0^*(700) \rightarrow K^-\pi^+)/\Gamma(K^+K^-\pi^+)$   $\Gamma_{113}/\Gamma_{107}$

This is the "fit fraction" from the Dalitz-plot analysis.

VALUE (%)	DOCUMENT ID	TECN	COMMENT
<b>7.0±0.8±3.5</b> -2.0	RUBIN	08 CLEO	Dalitz fit, 19,458±163 evts

$\Gamma(a_0(1450)^0\pi^+, a_0^0 \rightarrow K^+K^-)/\Gamma(K^+K^-\pi^+)$   $\Gamma_{114}/\Gamma_{107}$

This is the "fit fraction" from the Dalitz-plot analysis.

VALUE (%)	DOCUMENT ID	TECN	COMMENT
<b>4.6±0.6±7.2</b> -1.8	RUBIN	08 CLEO	Dalitz fit, 19,458±163 evts

$\Gamma(\phi(1680)\pi^+, \phi \rightarrow K^+K^-)/\Gamma(K^+K^-\pi^+)$   $\Gamma_{115}/\Gamma_{107}$

This is the "fit fraction" from the Dalitz-plot analysis.

VALUE (%)	DOCUMENT ID	TECN	COMMENT
<b>0.51±0.11±0.37</b> -0.16	RUBIN	08 CLEO	Dalitz fit, 19,458±163 evts

$\Gamma(K_S^0 K_S^0 \pi^+)/\Gamma_{total}$   $\Gamma_{116}/\Gamma$

VALUE (units $10^{-4}$ )	EVTS	DOCUMENT ID	TECN	COMMENT
<b>27.0±0.5±1.2</b>	4897	ABLIKIM	17A BES3	$e^+e^- \rightarrow \psi(3770)$

$\Gamma(K^+ K_S^0 \pi^+ \pi^-)/\Gamma(K_S^0 2\pi^+ \pi^-)$   $\Gamma_{117}/\Gamma_{70}$

VALUE (units $10^{-2}$ )	EVTS	DOCUMENT ID	TECN	COMMENT
<b>5.62±0.39±0.40</b>	469 ± 32	LINK	01c FOCS	$\gamma$ nucleus, $\bar{E}_\gamma \approx 180$ GeV

$\Gamma(K_S^0 K^- 2\pi^+)/\Gamma(K_S^0 2\pi^+ \pi^-)$   $\Gamma_{118}/\Gamma_{70}$

VALUE (units $10^{-2}$ )	EVTS	DOCUMENT ID	TECN	COMMENT
<b>7.68±0.41±0.32</b>	670 ± 35	LINK	01c FOCS	$\gamma$ nucleus, $\bar{E}_\gamma \approx 180$ GeV

$\Gamma(K^+ K^- 2\pi^+ \pi^-)/\Gamma(K^- 3\pi^+ \pi^-)$   $\Gamma_{119}/\Gamma_{71}$

VALUE	EVTS	DOCUMENT ID	TECN	COMMENT
<b>0.040±0.009±0.019</b>	38	LINK	03D FOCS	$\gamma$ A, $\bar{E}_\gamma \approx 180$ GeV

$\Gamma(\phi\pi^+\pi^0)/\Gamma_{total}$   $\Gamma_{120}/\Gamma$

Unseen decay modes of the  $\phi$  are included.

VALUE	DOCUMENT ID	TECN	COMMENT
<b>0.023±0.010</b>	<sup>1</sup> BARLAG	92c ACCM	$\pi^-$ Cu 230 GeV

<sup>1</sup>BARLAG 92c computes the branching fraction using topological normalization.

$\Gamma(\phi\rho^+)/\Gamma(K^- 2\pi^+)$   $\Gamma_{121}/\Gamma_{48}$

Unseen decay modes of the  $\phi$  are included.

VALUE	CL%	DOCUMENT ID	TECN	COMMENT
<b>&lt;0.16</b>	90	DAOUDI	92 CLEO	$e^+e^- \approx 10.5$ GeV

$\Gamma(K^+ K^- \pi^+ \pi^0 \text{ non-}\phi)/\Gamma_{total}$   $\Gamma_{122}/\Gamma$

VALUE	DOCUMENT ID	TECN	COMMENT
<b>0.015±0.007</b> -0.006	<sup>1</sup> BARLAG	92c ACCM	$\pi^-$ Cu 230 GeV

<sup>1</sup>BARLAG 92c computes the branching fraction using topological normalization.

$\Gamma(K^+ K^- \pi^+ \pi^0 \text{ non-}\phi)/\Gamma(K^- 2\pi^+)$   $\Gamma_{122}/\Gamma_{48}$

VALUE	CL%	DOCUMENT ID	TECN	COMMENT
<b>&lt;0.25</b>	90	ANJOS	89E E691	Photoproduction

••• We do not use the following data for averages, fits, limits, etc. •••

$\Gamma(K^*(892)^+ K_S^0)/\Gamma(K_S^0 \pi^+)$   $\Gamma_{123}/\Gamma_{46}$

Unseen decay modes of the  $K^*(892)^+$  are included.

VALUE	EVTS	DOCUMENT ID	TECN	COMMENT
<b>1.1±0.3±0.4</b>	67	FRABETTI	95 E687	$\gamma$ Be $\bar{E}_\gamma \approx 200$ GeV

**Doubly Cabibbo-suppressed modes**

$\Gamma(K^+\pi^0)/\Gamma_{total}$   $\Gamma_{124}/\Gamma$

VALUE (units $10^{-4}$ )	EVTS	DOCUMENT ID	TECN	COMMENT
<b>2.08±0.21 OUR FIT</b>				Error includes scale factor of 1.4.
<b>2.35±0.20 OUR AVERAGE</b>				
2.32±0.21±0.06	1.8k	ABLIKIM	18w BES3	$e^+e^-$ , 3773 MeV
2.52±0.47±0.26	189 ± 37	AUBERT,B	06F BABR	$e^+e^- \approx \gamma(4S)$
2.28±0.36±0.17	148 ± 23	DYTMAN	06 CLEO	See MENDEZ 10

••• We do not use the following data for averages, fits, limits, etc. •••

$\Gamma(K^+\pi^0)/\Gamma(K^- 2\pi^+)$   $\Gamma_{124}/\Gamma_{48}$

VALUE (units $10^{-3}$ )	EVTS	DOCUMENT ID	TECN	COMMENT
<b>2.21±0.23 OUR FIT</b>				Error includes scale factor of 1.5.
<b>1.9 ±0.2 ±0.1</b>	343 ± 37	MENDEZ	10 CLEO	$e^+e^-$ at 3774 MeV

$\Gamma(K^+\eta)/\Gamma_{total}$   $\Gamma_{125}/\Gamma$

VALUE (units $10^{-3}$ )	EVTS	DOCUMENT ID	TECN	COMMENT
<b>0.125±0.016 OUR FIT</b>				Error includes scale factor of 1.1.
<b>0.151±0.025±0.014</b>	439	ABLIKIM	18w BES3	$e^+e^-$ , 3773 MeV

$\Gamma(K^+\eta)/\Gamma(\eta\pi^+)$   $\Gamma_{125}/\Gamma_{97}$

VALUE (%)	EVTS	DOCUMENT ID	TECN	COMMENT
<b>3.3 ±0.4 OUR FIT</b>				Error includes scale factor of 1.1.
<b>3.06±0.43±0.14</b>	166 ± 23	WON	11 BELL	$e^+e^- \approx \gamma(4S)$

$\Gamma(K^+\eta'(958))/\Gamma_{total}$   $\Gamma_{126}/\Gamma$

VALUE (units $10^{-3}$ )	EVTS	DOCUMENT ID	TECN	COMMENT
<b>0.185±0.020 OUR FIT</b>				
<b>0.164±0.051±0.024</b>	87	ABLIKIM	18w BES3	$e^+e^-$ , 3773 MeV

$\Gamma(K^+\eta'(958))/\Gamma(\eta'(958)\pi^+)$   $\Gamma_{126}/\Gamma_{100}$

VALUE (%)	EVTS	DOCUMENT ID	TECN	COMMENT
<b>3.7 ±0.4 OUR FIT</b>				
<b>3.77±0.39±0.10</b>	180 ± 19	WON	11 BELL	$e^+e^- \approx \gamma(4S)$

$\Gamma(K^+\pi^+\pi^-)/\Gamma(K^- 2\pi^+)$   $\Gamma_{127}/\Gamma_{48}$

VALUE (units $10^{-3}$ )	EVTS	DOCUMENT ID	TECN	COMMENT
<b>5.238±0.025 OUR AVERAGE</b>				
5.231±0.009±0.023	795k	AAIJ	19G LHCb	$p\bar{p}$ at 8 TeV
5.69±0.18±0.14	2638 ± 84	KO	09 BELL	$e^+e^-$ at $\gamma(4S)$
6.5 ±0.8 ±0.4	189 ± 24	LINK	04F FOCS	$\gamma$ A, $\bar{E}_\gamma \approx 180$ GeV
7.7 ±1.7 ±0.8	59 ± 13	AITALA	97c E791	$\pi^-$ A, 500 GeV
7.2 ±2.3 ±1.7	21	FRABETTI	95E E687	$\gamma$ Be, $\bar{E}_\gamma \approx 220$ GeV

$\Gamma(K^+\rho^0)/\Gamma(K^+\pi^+\pi^-)$   $\Gamma_{128}/\Gamma_{127}$

This is the "fit fraction" from the Dalitz-plot analysis.

VALUE	DOCUMENT ID	TECN	COMMENT
<b>0.39 ±0.09 OUR AVERAGE</b>			
0.3943±0.0787±0.0815	LINK	04F FOCS	Dalitz fit, 189 evts
0.37 ±0.14 ±0.07	AITALA	97c E791	Dalitz fit, 59 evts

$\Gamma(K^*(892)^0 \pi^+, K^*(892)^0 \rightarrow K^+ \pi^-) / \Gamma(K^+ \pi^+ \pi^-)$   $\Gamma_{129} / \Gamma_{127}$

This is the "fit fraction" from the Dalitz-plot analysis.
VALUE DOCUMENT ID TECN COMMENT
0.47 ± 0.08 OUR AVERAGE
0.5220 ± 0.0684 ± 0.0638 LINK 04F FOCS Dalitz fit, 189 evts
0.35 ± 0.14 ± 0.01 AITALA 97c E791 Dalitz fit, 59 evts

$\Gamma(K^+ f_0(980), f_0(980) \rightarrow \pi^+ \pi^-) / \Gamma(K^+ \pi^+ \pi^-)$   $\Gamma_{130} / \Gamma_{127}$

This is the "fit fraction" from the Dalitz-plot analysis.
VALUE DOCUMENT ID TECN COMMENT
0.0892 ± 0.0333 ± 0.0412 LINK 04F FOCS Dalitz fit, 189 evts

$\Gamma(K_2^*(1430)^0 \pi^+, K_2^*(1430)^0 \rightarrow K^+ \pi^-) / \Gamma(K^+ \pi^+ \pi^-)$   $\Gamma_{131} / \Gamma_{127}$

This is the "fit fraction" from the Dalitz-plot analysis.
VALUE DOCUMENT ID TECN COMMENT
0.0803 ± 0.0372 ± 0.0391 LINK 04F FOCS Dalitz fit, 189 evts

$\Gamma(K^+ \pi^+ \pi^- \text{ nonresonant}) / \Gamma(K^+ \pi^+ \pi^-)$   $\Gamma_{132} / \Gamma_{127}$

This is the "fit fraction" from the Dalitz-plot analysis.
VALUE DOCUMENT ID TECN COMMENT
0.36 ± 0.14 ± 0.07 1 AITALA 97c E791 Dalitz fit, 59 evts
1 LINK 04F, with three times as many events, finds no need for a nonresonant amplitude.

$\Gamma(2K^+ K^-) / \Gamma(K^- 2\pi^+)$   $\Gamma_{133} / \Gamma_{48}$

VALUE (units 10<sup>-4</sup>) EVTS DOCUMENT ID TECN COMMENT
6.54 ± 0.05 OUR AVERAGE
6.541 ± 0.025 ± 0.042 134k AAJ 19G LHCB pp at 8 TeV
9.49 ± 2.17 ± 0.22 65 1 LINK 02i FOCS γ nucleus, ≈ 180 GeV
1 LINK 02i finds little evidence for φ K<sup>+</sup> or f<sub>0</sub>(980) K<sup>+</sup> submodes.

$\Gamma(K^+ \phi(1020), \phi \rightarrow K^+ K^-) / \Gamma(2K^+ K^-)$   $\Gamma_{135} / \Gamma_{133}$

VALUE (%) DOCUMENT ID TECN COMMENT
7.1 ± 0.9 1 AAJ 19H LHCB pp at 8TeV
1 Fit fraction from a Dalitz plot analysis of D<sup>+</sup> → K<sup>+</sup> K<sup>+</sup> K<sup>-</sup> decays. The last uncertainty is due to the amplitude model.

$\Gamma(K^+ (K^+ K^-)_{s\text{-wave}}) / \Gamma(2K^+ K^-)$   $\Gamma_{136} / \Gamma_{133}$

VALUE DOCUMENT ID TECN COMMENT
0.94 ± 0.01 1 AAJ 19H LHCB pp at 8TeV
1 Fit fraction from a Dalitz plot analysis of D<sup>+</sup> → K<sup>+</sup> K<sup>+</sup> K<sup>-</sup> decays. The last uncertainty is due to the amplitude model.

Rare or forbidden modes

$\Gamma(\pi^+ e^+ e^-) / \Gamma_{\text{total}}$   $\Gamma_{137} / \Gamma$

A test for the ΔC = 1 weak neutral current. Allowed by higher-order electroweak interactions.
VALUE CL% DOCUMENT ID TECN COMMENT
<1.1 × 10<sup>-6</sup> 90 LEES 11G BABR e<sup>+</sup>e<sup>-</sup> ≈ 7(4S)
... We do not use the following data for averages, fits, limits, etc.
<5.9 × 10<sup>-6</sup> 90 1 RUBIN 10 CLEO e<sup>+</sup>e<sup>-</sup> at ψ(3770)
<7.4 × 10<sup>-6</sup> 90 HE 05A CLEO See RUBIN 10
<5.2 × 10<sup>-5</sup> 90 AITALA 99G E791 π<sup>-</sup> N 500 GeV
<1.1 × 10<sup>-4</sup> 90 FRABETTI 97B E687 γ Be, E<sub>γ</sub> ≈ 220 GeV
<6.6 × 10<sup>-5</sup> 90 AITALA 96 E791 π<sup>-</sup> N 500 GeV
<2.5 × 10<sup>-3</sup> 90 WEIR 90B MRK2 e<sup>+</sup>e<sup>-</sup> 29 GeV
<2.6 × 10<sup>-3</sup> 90 HAAS 88 CLEO e<sup>+</sup>e<sup>-</sup> 10 GeV
1 This RUBIN 10 limit is for the e<sup>+</sup>e<sup>-</sup> mass in the continuum away from the φ(1020). See the next data block.

$\Gamma(\pi^+ \pi^0 e^+ e^-) / \Gamma_{\text{total}}$   $\Gamma_{138} / \Gamma$

VALUE CL% DOCUMENT ID TECN COMMENT
<1.4 × 10<sup>-5</sup> 90 ABLIKIM 18P BES3 e<sup>+</sup>e<sup>-</sup>, 3773 MeV

$\Gamma(\pi^+ \phi, \phi \rightarrow e^+ e^-) / \Gamma_{\text{total}}$   $\Gamma_{139} / \Gamma$

This is not a test for the ΔC = 1 weak neutral current, but leads to the π<sup>+</sup>e<sup>+</sup>e<sup>-</sup> final state.
VALUE EVTS DOCUMENT ID TECN COMMENT
(1.7 ± 1.4 ± 0.1) × 10<sup>-6</sup> 4 1 RUBIN 10 CLEO e<sup>+</sup>e<sup>-</sup> at ψ(3770)
... We do not use the following data for averages, fits, limits, etc.
(2.7 ± 3.6 ± 0.2) × 10<sup>-6</sup> 2 HE 05A CLEO See RUBIN 10
1 This RUBIN 10 result is consistent with the known D<sup>+</sup> → φπ<sup>+</sup> and φ → e<sup>+</sup>e<sup>-</sup> fractions.

$\Gamma(\pi^+ \mu^+ \mu^-) / \Gamma_{\text{total}}$   $\Gamma_{140} / \Gamma$

A test for the ΔC = 1 weak neutral current. Allowed by higher-order electroweak interactions.
VALUE CL% DOCUMENT ID TECN COMMENT
<7.3 × 10<sup>-8</sup> 90 AAJ 13Af LHCB pp at 7 TeV

... We do not use the following data for averages, fits, limits, etc. ...

<6.5 × 10<sup>-6</sup> 90 LEES 11G BABR e<sup>+</sup>e<sup>-</sup> ≈ 7(4S)
<3.9 × 10<sup>-6</sup> 90 1 ABAZOV 08D D0 p p-bar, E<sub>cm</sub> = 1.96 TeV
<8.8 × 10<sup>-6</sup> 90 LINK 03F FOCS γ A, E<sub>γ</sub> ≈ 180 GeV
<1.5 × 10<sup>-5</sup> 90 AITALA 99G E791 π<sup>-</sup> N 500 GeV
<8.9 × 10<sup>-5</sup> 90 FRABETTI 97B E687 γ Be, E<sub>γ</sub> ≈ 220 GeV
<1.8 × 10<sup>-5</sup> 90 AITALA 96 E791 π<sup>-</sup> N 500 GeV
<2.2 × 10<sup>-4</sup> 90 KODAMA 95 E653 π<sup>-</sup> emulsion 600 GeV
<5.9 × 10<sup>-3</sup> 90 WEIR 90B MRK2 e<sup>+</sup>e<sup>-</sup> 29 GeV
<2.9 × 10<sup>-3</sup> 90 HAAS 88 CLEO e<sup>+</sup>e<sup>-</sup> 10 GeV

1 This ABAZOV 08D limit is for the μ<sup>+</sup>μ<sup>-</sup> mass in the continuum away from the φ(1020). See the next data block.

$\Gamma(\pi^+ \phi, \phi \rightarrow \mu^+ \mu^-) / \Gamma_{\text{total}}$   $\Gamma_{141} / \Gamma$

This is not a test for the ΔC = 1 weak neutral current, but leads to the π<sup>+</sup>μ<sup>+</sup>μ<sup>-</sup> final state.
VALUE DOCUMENT ID TECN COMMENT
(1.8 ± 0.5 ± 0.6) × 10<sup>-6</sup> 1 ABAZOV 08D D0 p p-bar, E<sub>cm</sub> = 1.96 TeV
1 This ABAZOV 08D value is consistent with the known D<sup>+</sup> → φπ<sup>+</sup> and φ → μ<sup>+</sup>μ<sup>-</sup> fractions.

$\Gamma(\rho^+ \mu^+ \mu^-) / \Gamma_{\text{total}}$   $\Gamma_{142} / \Gamma$

A test for the ΔC = 1 weak neutral current. Allowed by higher-order electroweak interactions.
VALUE CL% DOCUMENT ID TECN COMMENT
<5.6 × 10<sup>-4</sup> 90 KODAMA 95 E653 π<sup>-</sup> emulsion 600 GeV

$\Gamma(K^+ e^+ e^-) / \Gamma_{\text{total}}$   $\Gamma_{143} / \Gamma$

Both quarks would have to change flavor for this decay to occur.
VALUE CL% DOCUMENT ID TECN COMMENT
<1.0 × 10<sup>-6</sup> 90 LEES 11G BABR e<sup>+</sup>e<sup>-</sup> ≈ 7(4S)
... We do not use the following data for averages, fits, limits, etc.
<3.0 × 10<sup>-6</sup> 90 RUBIN 10 CLEO e<sup>+</sup>e<sup>-</sup> at ψ(3770)
<6.2 × 10<sup>-6</sup> 90 HE 05A CLEO See RUBIN 10
<2.0 × 10<sup>-4</sup> 90 AITALA 99G E791 π<sup>-</sup> N 500 GeV
<2.0 × 10<sup>-4</sup> 90 FRABETTI 97B E687 γ Be, E<sub>γ</sub> ≈ 220 GeV
<4.8 × 10<sup>-3</sup> 90 WEIR 90B MRK2 e<sup>+</sup>e<sup>-</sup> 29 GeV

$\Gamma(K^+ \pi^0 e^+ e^-) / \Gamma_{\text{total}}$   $\Gamma_{144} / \Gamma$

VALUE CL% DOCUMENT ID TECN COMMENT
<1.5 × 10<sup>-5</sup> 90 ABLIKIM 18P BES3 e<sup>+</sup>e<sup>-</sup>, 3773 MeV

$\Gamma(K_2^0 \pi^+ e^+ e^-) / \Gamma_{\text{total}}$   $\Gamma_{145} / \Gamma$

VALUE CL% DOCUMENT ID TECN COMMENT
<2.6 × 10<sup>-5</sup> 90 ABLIKIM 18P BES3 e<sup>+</sup>e<sup>-</sup>, 3773 MeV

$\Gamma(K_2^0 K^+ e^+ e^-) / \Gamma_{\text{total}}$   $\Gamma_{146} / \Gamma$

VALUE CL% DOCUMENT ID TECN COMMENT
<1.1 × 10<sup>-5</sup> 90 ABLIKIM 18P BES3 e<sup>+</sup>e<sup>-</sup>, 3773 MeV

$\Gamma(K^+ \mu^+ \mu^-) / \Gamma_{\text{total}}$   $\Gamma_{147} / \Gamma$

Both quarks would have to change flavor for this decay to occur.
VALUE CL% DOCUMENT ID TECN COMMENT
<4.3 × 10<sup>-6</sup> 90 LEES 11G BABR e<sup>+</sup>e<sup>-</sup> ≈ 7(4S)
... We do not use the following data for averages, fits, limits, etc.
<9.2 × 10<sup>-6</sup> 90 LINK 03F FOCS γ A, E<sub>γ</sub> ≈ 180 GeV
<4.4 × 10<sup>-5</sup> 90 AITALA 99G E791 π<sup>-</sup> N 500 GeV
<9.7 × 10<sup>-5</sup> 90 FRABETTI 97B E687 γ Be, E<sub>γ</sub> ≈ 220 GeV
<3.2 × 10<sup>-4</sup> 90 KODAMA 95 E653 π<sup>-</sup> emulsion 600 GeV
<9.2 × 10<sup>-3</sup> 90 WEIR 90B MRK2 e<sup>+</sup>e<sup>-</sup> 29 GeV

$\Gamma(\pi^+ e^+ \mu^-) / \Gamma_{\text{total}}$   $\Gamma_{148} / \Gamma$

A test of lepton-family-number conservation.
VALUE CL% DOCUMENT ID TECN COMMENT
<2.9 × 10<sup>-6</sup> 90 LEES 11G BABR e<sup>+</sup>e<sup>-</sup> ≈ 7(4S)
... We do not use the following data for averages, fits, limits, etc.
<1.1 × 10<sup>-4</sup> 90 FRABETTI 97B E687 γ Be, E<sub>γ</sub> ≈ 220 GeV
<3.3 × 10<sup>-3</sup> 90 WEIR 90B MRK2 e<sup>+</sup>e<sup>-</sup> 29 GeV

$\Gamma(\pi^+ e^- \mu^+) / \Gamma_{\text{total}}$   $\Gamma_{149} / \Gamma$

A test of lepton-family-number conservation.
VALUE CL% DOCUMENT ID TECN COMMENT
<3.6 × 10<sup>-6</sup> 90 LEES 11G BABR e<sup>+</sup>e<sup>-</sup> ≈ 7(4S)
... We do not use the following data for averages, fits, limits, etc.
<1.3 × 10<sup>-4</sup> 90 FRABETTI 97B E687 γ Be, E<sub>γ</sub> ≈ 220 GeV
<3.3 × 10<sup>-3</sup> 90 WEIR 90B MRK2 e<sup>+</sup>e<sup>-</sup> 29 GeV

$\Gamma(K^+ e^+ \mu^-) / \Gamma_{\text{total}}$   $\Gamma_{150} / \Gamma$

A test of lepton-family-number conservation.
VALUE CL% DOCUMENT ID TECN COMMENT
<1.2 × 10<sup>-6</sup> 90 LEES 11G BABR e<sup>+</sup>e<sup>-</sup> ≈ 7(4S)
... We do not use the following data for averages, fits, limits, etc.
<1.3 × 10<sup>-4</sup> 90 FRABETTI 97B E687 γ Be, E<sub>γ</sub> ≈ 220 GeV
<3.4 × 10<sup>-3</sup> 90 WEIR 90B MRK2 e<sup>+</sup>e<sup>-</sup> 29 GeV





See key on page 999

# Meson Particle Listings

## $D^\pm$

### $A_{CP}(\bar{K}^0/K^0 K^\pm)$ in $D^+ \rightarrow \bar{K}^0 K^+, D^- \rightarrow K^0 K^-$

VALUE (%)	EVTS	DOCUMENT ID	TECN	COMMENT
<b>0.11 ± 0.17 OUR AVERAGE</b>				
0.03 ± 0.17 ± 0.14	1.0M	1 AAIJ	14BD LHCb	$pp$ at 7, 8 TeV
0.08 ± 0.28 ± 0.14	277k	KO	13 BELL	$e^+e^-$ at $\Upsilon(4S)$
0.46 ± 0.36 ± 0.25	159k	LEES	13E BABR	$e^+e^-$ at $\Upsilon(4S)$

<sup>1</sup> AAIJ 14BD reports its result as  $A_{CP}(D^\pm \rightarrow K_S^0 \pi^\pm)$  with  $CP$ -violation effects in the  $K^0 - \bar{K}^0$  system subtracted. It also measures  $A_{CP}(D^\pm \rightarrow \bar{K}^0/K^0 K^\pm) + A_{CP}(D_S^\pm \rightarrow \bar{K}^0/K^0 \pi^\pm) = (0.41 \pm 0.49 \pm 0.26)\%$ .

### $A_{CP}(K_S^0 K^\pm)$ in $D^\pm \rightarrow K_S^0 K^\pm$

VALUE (%)	EVTS	DOCUMENT ID	TECN	COMMENT
<b>-0.01 ± 0.07 OUR AVERAGE</b>				
-0.004 ± 0.061 ± 0.045	6M	AAIJ	19T LHCb	$pp$ at 7, 8, 13 TeV
-1.8 ± 2.7 ± 1.6	780	ABLIKIM	19M BES3	$e^+e^-$ at 3773 MeV
-0.25 ± 0.28 ± 0.14	277k	KO	13 BELL	$e^+e^-$ at $\Upsilon(nS)$
0.13 ± 0.36 ± 0.25	159k	LEES	13E BABR	$e^+e^-$ at $\Upsilon(4S)$
-0.2 ± 1.5 ± 0.9	5.2k	MENDEZ	10 CLEO	$e^+e^-$ at 3774 MeV
7.1 ± 6.1 ± 1.2	949	1 LINK	02B FOCS	$\gamma$ nucleus, $\bar{E}_\gamma \approx 180$ GeV

• • • We do not use the following data for averages, fits, limits, etc. • • •

-0.16 ± 0.58 ± 0.25  
6.9 ± 6.0 ± 1.5 949 2 LINK 02B FOCS  $\gamma$  nucleus,  $\bar{E}_\gamma \approx 180$  GeV

<sup>1</sup> LINK 02B measures  $N(D^+ \rightarrow K_S^0 K^+)/N(D^+ \rightarrow K_S^0 \pi^+)$ , the ratio of numbers of events observed, and similarly for the  $D^-$ .

<sup>2</sup> LINK 02B measures  $N(D^+ \rightarrow K_S^0 K^+)/N(D^+ \rightarrow K^- \pi^+ \pi^+)$ , the ratio of numbers of events observed, and similarly for the  $D^-$ .

### $A_{CP}(K_S^0 K^\pm \pi^0)$ in $D^\pm \rightarrow K_S^0 K^\pm \pi^0$

VALUE (units $10^{-2}$ )	EVTS	DOCUMENT ID	TECN	COMMENT
<b>1.4 ± 3.7 ± 2.4</b>	470	ABLIKIM	19M BES3	$e^+e^-$ at 3773 MeV

### $A_{CP}(K_L^0 K^\pm \pi^0)$ in $D^\pm \rightarrow K_L^0 K^\pm \pi^0$

VALUE (units $10^{-2}$ )	EVTS	DOCUMENT ID	TECN	COMMENT
<b>-0.6 ± 4.1 ± 1.7</b>	410	ABLIKIM	19M BES3	$e^+e^-$ at 3773 MeV

### $A_{CP}(K^+ K^- \pi^\pm)$ in $D^\pm \rightarrow K^+ K^- \pi^\pm$

See also AAIJ 11G for a search for  $CP$  asymmetry in the  $D^\pm \rightarrow K^+ K^- \pi^\pm$  Dalitz plots using 370k decays and four different binning schemes. No evidence for  $CP$  asymmetry was found.

VALUE (%)	EVTS	DOCUMENT ID	TECN	COMMENT
<b>0.37 ± 0.29 OUR AVERAGE</b>				
0.37 ± 0.30 ± 0.15	224k	1 LEES	13F BABR	$e^+e^-$ at $\Upsilon(4S)$
-0.03 ± 0.84 ± 0.29		RUBIN	08 CLEO	$e^+e^-$ at 3774 MeV
1.4 ± 1.0 ± 0.8	43k	2 AUBERT	05s BABR	$e^+e^-$ at $\Upsilon(4S)$
0.6 ± 1.1 ± 0.5	14k	3 LINK	00B FOCS	
-1.4 ± 2.9		3 AITALA	97B E791	-0.062 $<A_{CP} <$ +0.034 (90% CL)
-3.1 ± 6.8		3 FRABETTI	94I E687	-0.14 $<A_{CP} <$ +0.081 (90% CL)

• • • We do not use the following data for averages, fits, limits, etc. • • •

-0.1 ± 0.9 ± 0.4  
-0.1 ± 1.5 ± 0.8 4 BONVICINI 14 CLEO See RUBIN 08  
DOBBS 07 CLEO See BONVICINI 14 and RUBIN 08

<sup>1</sup> This is the integrated  $CP$  asymmetry. LEES 13F also searches for  $CP$  asymmetries in four regions of the Dalitz plots (two of which are listed below); in comparisons of binned  $D^+$  and  $D^-$  Dalitz plots; in parametrized fits to those plots, including 2-body submodes; and in comparisons of Legendre-polynomial distributions for the  $K^+ K^-$  and  $K^- \pi^+$  systems.

<sup>2</sup> AUBERT 05s measures  $N(D^+ \rightarrow K^+ K^- \pi^+)/N(D_S^+ \rightarrow K^+ K^- \pi^+)$ , the ratio of the numbers of events observed, and similarly for the  $D^-$ .

<sup>3</sup> FRABETTI 94I, AITALA 98C, and LINK 00B measure  $N(D^+ \rightarrow K^- K^+ \pi^+)/N(D^+ \rightarrow K^- \pi^+ \pi^+)$ , the ratio of numbers of events observed, and similarly for the  $D^-$ .

<sup>4</sup> RUBIN 08 performs a dedicated analysis of this decay mode on the same dataset, with slightly better precision. We therefore take it that BONVICINI 14 does not supersede RUBIN 08's  $A_{CP}$  result.

### $A_{CP}(K^\pm K^*0)$ in $D^+ \rightarrow K^+ \bar{K}^{*0}, D^- \rightarrow K^- K^{*0}$

VALUE (%)	EVTS	DOCUMENT ID	TECN	COMMENT
<b>-0.3 ± 0.4 OUR AVERAGE</b>				
-0.3 ± 0.4 ± 0.2	73k	1 LEES	13F BABR	$e^+e^-$ at $\Upsilon(4S)$
-0.4 ± 2.0 ± 0.6		RUBIN	08 CLEO	Fit-fraction asymmetry
+0.9 ± 1.7 ± 0.7	11k	2 AUBERT	05s BABR	$e^+e^-$ at $\Upsilon(4S)$
-1.0 ± 5.0		3 AITALA	97B E791	-0.092 $<A_{CP} <$ +0.072 (90% CL)
-12 ± 13		3 FRABETTI	94I E687	-0.33 $<A_{CP} <$ +0.094 (90% CL)

<sup>1</sup> This LEES 13F result is for the  $K^\mp \pi^\pm$  mass-squared between 0.4 and 1.0  $\text{GeV}^2$ , and does not actually separate out the  $K^*$ .

<sup>2</sup> AUBERT 05s measures  $N(D^+ \rightarrow K^+ \bar{K}^{*0})/N(D_S^+ \rightarrow K^+ K^- \pi^+)$ , the ratio of the numbers of events observed, and similarly for the  $D^-$ .

<sup>3</sup> FRABETTI 94I and AITALA 97B measure  $N(D^+ \rightarrow K^+ \bar{K}^*(892)^0)/N(D^+ \rightarrow K^- \pi^+ \pi^+)$ , the ratio of numbers of events observed, and similarly for the  $D^-$ .

### $A_{CP}(\phi \pi^\pm)$ in $D^\pm \rightarrow \phi \pi^\pm$

VALUE (%)	EVTS	DOCUMENT ID	TECN	COMMENT
<b>0.01 ± 0.09 OUR AVERAGE</b>				Error includes scale factor of 1.8.
0.003 ± 0.040 ± 0.029	55M	AAIJ	19T LHCb	$pp$ at 7, 8, 13 TeV
-0.3 ± 0.3 ± 0.5	97k	1 LEES	13F BABR	$e^+e^-$ at $\Upsilon(4S)$
+0.51 ± 0.28 ± 0.05	237k	STARIC	12 BELL	Mainly at $\Upsilon(4S)$
-1.8 ± 1.6 ± 0.2 ± 0.4		RUBIN	08 CLEO	Fit-fraction asymmetry
+0.2 ± 1.5 ± 0.6	10k	2 AUBERT	05s BABR	$e^+e^-$ at $\Upsilon(4S)$
-2.8 ± 3.6		3 AITALA	97B E791	-0.087 $<A_{CP} <$ +0.031 (90% CL)
+6.6 ± 8.6		3 FRABETTI	94I E687	-0.075 $<A_{CP} <$ +0.21 (90% CL)

• • • We do not use the following data for averages, fits, limits, etc. • • •

-0.04 ± 0.14 ± 0.14 1.58M 4 AAIJ 13W LHCb  $pp$  at 7 TeV

<sup>1</sup> This LEES 13F result is for the  $K^+ K^-$  mass-squared less than 1.3  $\text{GeV}^2$  and the  $K^\mp \pi^\pm$  mass-squared above 1.0  $\text{GeV}^2$ , and does not actually separate out the  $\phi$ .

<sup>2</sup> AUBERT 05s measures  $N(D^+ \rightarrow \phi \pi^+)/N(D_S^+ \rightarrow K^+ K^- \pi^+)$ , the ratio of the numbers of events observed, and similarly for the  $D^-$ .

<sup>3</sup> FRABETTI 94I and AITALA 97B measure  $N(D^+ \rightarrow \phi \pi^+)/N(D^+ \rightarrow K^- \pi^+ \pi^+)$ , the ratio of numbers of events observed, and similarly for the  $D^-$ .

<sup>4</sup> See AAIJ 19T.

### $A_{CP}(K^\pm K_S^0(1430)^0)$ in $D^+ \rightarrow K^+ \bar{K}_S^0(1430)^0, D^- \rightarrow K^- K_S^0(1430)^0$

VALUE (%)	DOCUMENT ID	TECN	COMMENT
<b>+8 ± 6 ± 4</b>	RUBIN 08	CLEO	Fit-fraction asymmetry

### $A_{CP}(K^\pm K_2^*(1430)^0)$ in $D^+ \rightarrow K^+ \bar{K}_2^*(1430)^0, D^- \rightarrow K^- K_2^*(1430)^0$

VALUE (%)	DOCUMENT ID	TECN	COMMENT
<b>+43 ± 19 ± 5</b>	RUBIN 08	CLEO	Fit-fraction asymmetry

### $A_{CP}(K^\pm K_0^*(700))$ in $D^+ \rightarrow K^+ \bar{K}_0^*(700), D^- \rightarrow K^- K_0^*(700)$

VALUE (%)	DOCUMENT ID	TECN	COMMENT
<b>-12 ± 11 ± 14</b>	RUBIN 08	CLEO	Fit-fraction asymmetry

### $A_{CP}(a_0(1450)^0 \pi^\pm)$ in $D^\pm \rightarrow a_0(1450)^0 \pi^\pm$

VALUE (%)	DOCUMENT ID	TECN	COMMENT
<b>-19 ± 12 ± 11</b>	RUBIN 08	CLEO	Fit-fraction asymmetry

### $A_{CP}(\phi(1680) \pi^\pm)$ in $D^\pm \rightarrow \phi(1680) \pi^\pm$

VALUE (%)	DOCUMENT ID	TECN	COMMENT
<b>-9 ± 22 ± 14</b>	RUBIN 08	CLEO	Fit-fraction asymmetry

### $A_{CP}(\pi^+ \pi^- \pi^\pm)$ in $D^\pm \rightarrow \pi^+ \pi^- \pi^\pm$

See also AAIJ 14C for a search for  $CP$  violation in  $D^\pm \rightarrow \pi^+ \pi^- \pi^\pm$  Dalitz plots using model-independent binned and unbinned methods. No evidence was found.

VALUE (%)	DOCUMENT ID	TECN	COMMENT
<b>-1.7 ± 4.2</b>	1 AITALA 97B E791	-0.086 $<A_{CP} <$ +0.052 (90% CL)	

<sup>1</sup> AITALA 97B measure  $N(D^+ \rightarrow \pi^+ \pi^- \pi^+)/N(D^+ \rightarrow K^- \pi^+ \pi^+)$ , the ratio of numbers of events observed, and similarly for the  $D^-$ .

### $A_{CP}(K_S^0 K^\pm \pi^+ \pi^-)$ in $D^\pm \rightarrow K_S^0 K^\pm \pi^+ \pi^-$

VALUE (%)	EVTS	DOCUMENT ID	TECN	COMMENT
<b>-4.2 ± 6.4 ± 2.2</b>	523 ± 32	LINK	05E FOCS	$\gamma$ A, $\bar{E}_\gamma \approx 180$ GeV

### $A_{CP}(K^\pm \pi^0)$ in $D^\pm \rightarrow K^\pm \pi^0$

VALUE (%)	EVTS	DOCUMENT ID	TECN	COMMENT
<b>-3.5 ± 10.7 ± 0.9</b>	343 ± 37	MENDEZ	10 CLEO	$e^+e^-$ at 3774 MeV

## $D^\pm \chi^2$ TESTS OF $CP$ -VIOLATION ( $CPV$ )

We list model-independent searches for local  $CP$  violation in phase-space distributions of multi-body decays.

Most of these searches divide phase space (Dalitz plot for 3-body decays, five-dimensional equivalent for 4-body decays) into bins, and perform a  $\chi^2$  test comparing normalised yields  $N_i, \bar{N}_i$  in  $CP$ -conjugate bin pairs  $i$ :  $\chi^2 = \sum_i (N_i - \alpha \bar{N}_i) / \sigma(N_i - \alpha \bar{N}_i)$ . The factor  $\alpha = (\sum_i N_i) / (\sum_i \bar{N}_i)$  removes the dependence on phase-space-integrated rate asymmetries. The result is used to obtain the probability (p-value) to obtain the measured  $\chi^2$  or larger under the assumption of  $CP$  conservation [AUBERT 08AO, BEDIAGA 09]. Alternative methods obtain p-values from other test variables based on unbinned analyses [WILLIAMS 11, AAIJ 14C]. Results can be combined using Fisher's method [MOSTELLER 48].

### Local $CPV$ in $D^\pm \rightarrow \pi^+ \pi^- \pi^\pm$

p-value (%)	EVTS	DOCUMENT ID	TECN	COMMENT
<b>78.1</b>	3.1M	1 AAIJ	14C LHCb	$\chi^2$

<sup>1</sup> AAIJ 14C uses binned and unbinned methods, and finds slightly better sensitivity with the former. We took the first value in the table of results for the binned method.

# Meson Particle Listings

$D^\pm$

## Local CPV in $D^\pm \rightarrow K^+ K^- \pi^\pm$

p-value (%)	EVTS	DOCUMENT ID	TECN	COMMENT
<b>31 OUR EVALUATION</b>				
72	224k	LEES	13F BABR	$\chi^2$
12.7	370k	1 AAIJ	11G LHCB	$\chi^2$

<sup>1</sup> AAIJ 11G publishes results for several binning schemes. We picked the first value in their table of results.

## CP VIOLATING ASYMMETRIES OF P-ODD (T-ODD) MOMENTS

### $A_{Tviol}(K_S^0 K^\pm \pi^\pm \pi^\mp)$ in $D^\pm \rightarrow K_S^0 K^\pm \pi^\pm \pi^\mp$

$C_T \equiv \bar{p}_{K^+} \cdot (\bar{p}_{\pi^+} \times \bar{p}_{\pi^-})$  is a parity-odd correlation of the  $K^+$ ,  $\pi^+$ , and  $\pi^-$  momenta for the  $D^+$ .  $\bar{C}_T \equiv \bar{p}_{K^-} \cdot (\bar{p}_{\pi^-} \times \bar{p}_{\pi^+})$  is the corresponding quantity for the  $D^-$ . Then  $A_T \equiv [\Gamma(C_T > 0) - \Gamma(C_T < 0)] / [\Gamma(C_T > 0) + \Gamma(C_T < 0)]$ , and  $\bar{A}_T \equiv [\Gamma(-\bar{C}_T > 0) - \Gamma(-\bar{C}_T < 0)] / [\Gamma(-\bar{C}_T > 0) + \Gamma(-\bar{C}_T < 0)]$ , and  $A_{Tviol} \equiv \frac{1}{2}(A_T - \bar{A}_T)$ .  $C_T$  and  $\bar{C}_T$  are commonly referred to as T-odd moments, because they are odd under T reversal. However, the T-conjugate process  $K_S^0 K^\pm \pi^\pm \pi^\mp \rightarrow D^\pm$  is not accessible, while the P-conjugate process is.

VALUE (units $10^{-3}$ )	EVTS	DOCUMENT ID	TECN	COMMENT
<b><math>-12.0 \pm 10.0 \pm 4.6</math></b>	<b>21.2 ± 0.4k</b>	<b>LEES</b>	<b>11E BABR</b>	<b><math>e^+e^- \approx \Upsilon(4S)</math></b>
•••	We do not use the following data for averages, fits, limits, etc.	•••	•••	•••
23 ± 6.2 ± 2.2	523 ± 32	LINK	05E FOCS	$\gamma A, \bar{E}\gamma \approx 180$ GeV

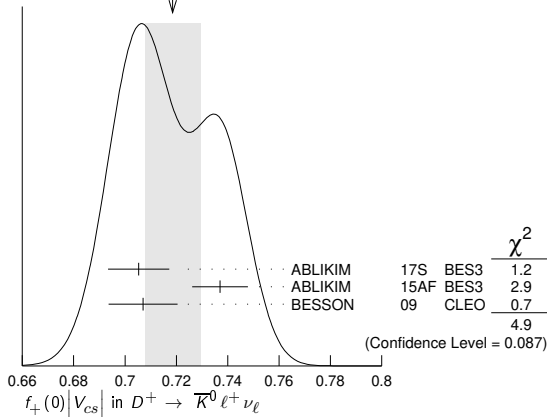
## SEMILEPTONIC FORM FACTORS

### $f_+(0)|V_{cs}|$ in $D^+ \rightarrow \bar{K}^0 \ell^+ \nu_\ell$

VALUE	EVTS	DOCUMENT ID	TECN	COMMENT
<b><math>0.719 \pm 0.011</math></b>	<b>OUR AVERAGE</b>	Error includes scale factor of 1.6. See the ideogram below.		
0.7053 ± 0.0040 ± 0.0112	ABLIKIM	17s BES3	$K_S^0 e^+ \nu_e$	2-parameter fit
0.737 ± 0.006 ± 0.009	<sup>1</sup> ABLIKIM	15AF BES3	$K_L e^+ \nu_e$	3-parameter fit
0.707 ± 0.010 ± 0.009	<sup>2</sup> BESSON	09 CLEO	$K_S e^+ \nu_e$	3-parameter fit

<sup>1</sup> ABLIKIM 15AF finds  $0.728 \pm 0.006 \pm 0.011$  for a 2-parameter fit.  
<sup>2</sup> BESSON 09 finds  $0.716 \pm 0.007 \pm 0.009$  for a 2-parameter fit.

WEIGHTED AVERAGE  
 $0.719 \pm 0.011$  (Error scaled by 1.6)



### $r_1 \equiv a_1/a_0$ in $D^+ \rightarrow \bar{K}^0 \ell^+ \nu_\ell$

VALUE	EVTS	DOCUMENT ID	TECN	COMMENT
<b><math>-2.13 \pm 0.14</math></b>	<b>OUR AVERAGE</b>	Error includes scale factor of 1.5.		
-2.18 ± 0.14 ± 0.05	ABLIKIM	17s BES3	$K_S^0 e^+ \nu_e$	2-parameter fit
-2.23 ± 0.42 ± 0.53	40k	<sup>1</sup> ABLIKIM	15AF BES3	$K_L e^+ \nu_e$ 3-parameter fit
-1.66 ± 0.44 ± 0.10		<sup>2</sup> BESSON	09 CLEO	$K_S e^+ \nu_e$ 3-parameter fit

<sup>1</sup> ABLIKIM 15AF finds  $r_1 = -1.91 \pm 0.33 \pm 0.28$  for a 2-parameter fit.  
<sup>2</sup> BESSON 09 finds  $r_1 = -2.10 \pm 0.25 \pm 0.08$  for 2-parameter fit.

### $r_2 \equiv a_2/a_0$ in $D^+ \rightarrow \bar{K}^0 \ell^+ \nu_\ell$

VALUE	EVTS	DOCUMENT ID	TECN	COMMENT
<b><math>-3 \pm 12</math></b>	<b>OUR AVERAGE</b>	Error includes scale factor of 1.5.		
+11 ± 9 ± 9	40k	ABLIKIM	15AF BES3	$K_L e^+ \nu_e$ 3-parameter fit
-14 ± 11 ± 1		BESSON	09 CLEO	$K_S e^+ \nu_e$ 3-parameter fit

### $f_+(0)|V_{cd}|$ in $D^+ \rightarrow \pi^0 \ell^+ \nu_\ell$

VALUE	EVTS	DOCUMENT ID	TECN	COMMENT
<b><math>0.1407 \pm 0.0025</math></b>	<b>OUR AVERAGE</b>	Error includes scale factor of 1.5.		
0.1400 ± 0.0026 ± 0.0007	ABLIKIM	17s BES3	$\pi^0 e^+ \nu_e$	2-parameter fit
0.146 ± 0.007 ± 0.002	BESSON	09 CLEO	$\pi^0 e^+ \nu_e$	3-parameter fit

### $r_1 \equiv a_1/a_0$ in $D^+ \rightarrow \pi^0 \ell^+ \nu_\ell$

VALUE	EVTS	DOCUMENT ID	TECN	COMMENT
<b><math>-2.00 \pm 0.13</math></b>	<b>OUR AVERAGE</b>	Error includes scale factor of 1.5.		
-2.01 ± 0.13 ± 0.02	ABLIKIM	17s BES3	$\pi^0 e^+ \nu_e$	2-parameter fit
-1.37 ± 0.88 ± 0.24	BESSON	09 CLEO	$\pi^0 e^+ \nu_e$	3-parameter fit

### $r_2 \equiv a_2/a_0$ in $D^+ \rightarrow \pi^0 \ell^+ \nu_\ell$

VALUE	EVTS	DOCUMENT ID	TECN	COMMENT
<b><math>-4 \pm 5 \pm 1</math></b>	<b>OUR AVERAGE</b>	Error includes scale factor of 1.9.		
		BESSON	09 CLEO	$\pi^0 e^+ \nu_e$ 3-parameter fit

### $f_+(0)|V_{cd}|$ in $D^+ \rightarrow \eta e^+ \nu_e$

VALUE (units $10^{-2}$ )	EVTS	DOCUMENT ID	TECN	COMMENT
<b><math>8.3 \pm 0.5</math></b>	<b>OUR AVERAGE</b>	Error includes scale factor of 1.9.		
7.86 ± 0.64 ± 0.21	373	ABLIKIM	18R BES3	z expansion
8.6 ± 0.6 ± 0.1		YELTON	11 CLEO	z expansion

### $r_1 \equiv a_1/a_0$ in $D^+ \rightarrow \eta e^+ \nu_e$

VALUE	EVTS	DOCUMENT ID	TECN	COMMENT
<b><math>-5.3 \pm 2.7</math></b>	<b>OUR AVERAGE</b>	Error includes scale factor of 1.9.		
-7.33 ± 1.69 ± 0.40	373	ABLIKIM	18R BES3	z expansion
-1.83 ± 2.23 ± 0.28		YELTON	11 CLEO	z expansion

### $r_V \equiv V(0)/A_1(0)$ in $D^+ \rightarrow \omega e^+ \nu_e$

VALUE	EVTS	DOCUMENT ID	TECN	COMMENT
<b><math>1.24 \pm 0.09 \pm 0.06</math></b>	<b>OUR AVERAGE</b>	Error includes scale factor of 1.2.		
1.695 ± 0.083 ± 0.051	2.5k	<sup>1</sup> ABLIKIM	19c BES3	$e^+e^-$ at 3773 MeV
1.48 ± 0.15 ± 0.05		<sup>1,2</sup> DOBBS	13 CLEO	$e^+e^-$ at $\psi(3770)$

### $r_2 \equiv A_2(0)/A_1(0)$ in $D^+ \rightarrow \omega e^+ \nu_e$

VALUE	EVTS	DOCUMENT ID	TECN	COMMENT
<b><math>1.06 \pm 0.15 \pm 0.05</math></b>	<b>OUR AVERAGE</b>	Error includes scale factor of 1.2.		
0.845 ± 0.056 ± 0.039	2.5k	<sup>1</sup> ABLIKIM	19c BES3	$e^+e^-$ at 3773 MeV
0.83 ± 0.11 ± 0.04		<sup>1,2</sup> DOBBS	13 CLEO	$e^+e^-$ at $\psi(3770)$

### $r_V \equiv V(0)/A_1(0)$ in $D^+, D^0 \rightarrow \rho e^+ \nu_e$

VALUE	EVTS	DOCUMENT ID	TECN	COMMENT
<b><math>1.64 \pm 0.10</math></b>	<b>OUR AVERAGE</b>	Error includes scale factor of 1.2.		
1.695 ± 0.083 ± 0.051	2.5k	<sup>1</sup> ABLIKIM	19c BES3	$e^+e^-$ at 3773 MeV
1.48 ± 0.15 ± 0.05		<sup>1,2</sup> DOBBS	13 CLEO	$e^+e^-$ at $\psi(3770)$

<sup>1</sup> Uses both  $D^+$  and  $D^0$  events.  
<sup>2</sup> Using PDG 10 values of  $V_{cd}$  and lifetimes, DOBBS 13 gets  $A_1(0) = 0.56 \pm 0.01 \pm 0.02$ ,  $A_2(0) = 0.47 \pm 0.06 \pm 0.04$ , and  $V(0) = 0.84 \pm 0.09 \pm 0.05$ .

### $r_2 \equiv A_2(0)/A_1(0)$ in $D^+, D^0 \rightarrow \rho e^+ \nu_e$

VALUE	EVTS	DOCUMENT ID	TECN	COMMENT
<b><math>0.84 \pm 0.06</math></b>	<b>OUR AVERAGE</b>	Error includes scale factor of 1.2.		
0.845 ± 0.056 ± 0.039	2.5k	<sup>1</sup> ABLIKIM	19c BES3	$e^+e^-$ at 3773 MeV
0.83 ± 0.11 ± 0.04		<sup>1,2</sup> DOBBS	13 CLEO	$e^+e^-$ at $\psi(3770)$

<sup>1</sup> Uses both  $D^+$  and  $D^0$  events.  
<sup>2</sup> Using PDG 10 values of  $V_{cd}$  and lifetimes, DOBBS 13 gets  $A_1(0) = 0.56 \pm 0.01 \pm 0.02$ ,  $A_2(0) = 0.47 \pm 0.06 \pm 0.04$ , and  $V(0) = 0.84 \pm 0.09 \pm 0.05$ .

### $r_V \equiv V(0)/A_1(0)$ in $D^+ \rightarrow \bar{K}^*(892)^0 \ell^+ \nu_\ell$

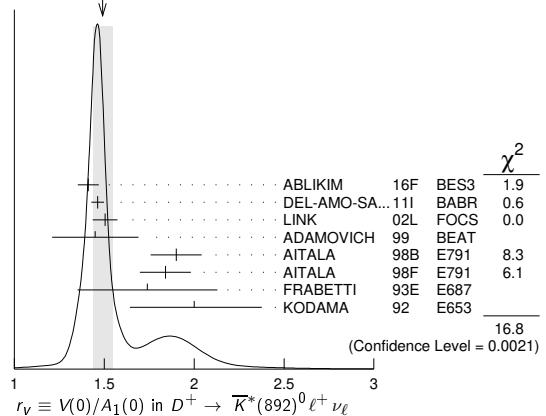
See also BRIERE 10 for  $\bar{K}^* \ell^+ \nu_\ell$  helicity-basis form-factor measurements.

VALUE	EVTS	DOCUMENT ID	TECN	COMMENT
<b><math>1.49 \pm 0.05</math></b>	<b>OUR AVERAGE</b>	Error includes scale factor of 2.1. See the ideogram below.		
1.411 ± 0.058 ± 0.007	16.2k	ABLIKIM	16F BES3	$\bar{K}^*(892)^0 e^+ \nu_e$
1.463 ± 0.017 ± 0.031		<sup>1</sup> DEL-AMO-SA...	11I BABR	
1.504 ± 0.057 ± 0.039	15k	<sup>2</sup> LINK	02L FOCS	$\bar{K}^*(892)^0 \mu^+ \nu_\mu$
1.45 ± 0.23 ± 0.07	763	ADAMOVICH	99 BEAT	$\bar{K}^*(892)^0 \mu^+ \nu_\mu$
1.90 ± 0.11 ± 0.09	3000	<sup>3</sup> AITALA	98B E791	$\bar{K}^*(892)^0 e^+ \nu_e$
1.84 ± 0.11 ± 0.09	3034	AITALA	98F E791	$\bar{K}^*(892)^0 \mu^+ \nu_\mu$
1.74 ± 0.27 ± 0.28	874	FRABETTI	93E E687	$\bar{K}^*(892)^0 \mu^+ \nu_\mu$
2.00 ± 0.34 ± 0.16	305	KODAMA	92 E653	$\bar{K}^*(892)^0 \mu^+ \nu_\mu$

••• We do not use the following data for averages, fits, limits, etc. •••

VALUE	EVTS	DOCUMENT ID	TECN	COMMENT
2.0 ± 0.6 ± 0.3	183	ANJOS	90E E691	$\bar{K}^*(892)^0 e^+ \nu_e$

WEIGHTED AVERAGE  
 $1.49 \pm 0.05$  (Error scaled by 2.1)



<sup>1</sup> DEL-AMO-SANCHEZ 11I finds the pole mass  $m_A = (2.63 \pm 0.10 \pm 0.13)$  GeV ( $m_V$  is fixed at 2 GeV).  
<sup>2</sup> LINK 02L includes the effects of interference with an S-wave background. This much improves the goodness of fit, but does not much shift the values of the form factors.

See key on page 999

Meson Particle Listings D±

3 This is slightly different from the AITALA 98B value: see ref. [5] in AITALA 98F.

r2 ≡ A2(0)/A1(0) in D+ → K\*(892)0 e+ νe

See also BRIERE 10 for K\* e+ νe helicity-basis form-factor measurements.

Table with columns: VALUE, EVTS, DOCUMENT ID, TECN, COMMENT. Contains data for various experiments like ABLIKIM, DEL-AMO-SA, ADAMOVICH, AITALA, FRABETTI, KODAMA, ANJOS.

••• We do not use the following data for averages, fits, limits, etc. •••

1 DEL-AMO-SANCHEZ 11i finds the pole mass mA = (2.63 ± 0.10 ± 0.13) GeV (mV is fixed at 2 GeV).

2 LINK 02L includes the effects of interference with an S-wave background. This much improves the goodness of fit, but does not much shift the values of the form factors.

r3 ≡ A3(0)/A1(0) in D+ → K\*(892)0 e+ νe

See also BRIERE 10 for K\* e+ νe helicity-basis form-factor measurements.

Table with columns: VALUE, EVTS, DOCUMENT ID, TECN, COMMENT. Contains data for AITALA 98F E791.

ΓL/ΓT in D+ → K\*(892)0 e+ νe

See also BRIERE 10 for K\* e+ νe helicity-basis form-factor measurements.

Table with columns: VALUE, EVTS, DOCUMENT ID, TECN, COMMENT. Contains data for ADAMOVICH, FRABETTI, KODAMA, ANJOS.

••• We do not use the following data for averages, fits, limits, etc. •••

Γ+/Γ- in D+ → K\*(892)0 e+ νe

See also BRIERE 10 for K\* e+ νe helicity-basis form-factor measurements.

Table with columns: VALUE, EVTS, DOCUMENT ID, TECN, COMMENT. Contains data for ADAMOVICH, KODAMA, ANJOS.

Amplitude analyses

D → Kπππ partial wave analyses

Amplitude analyses of D+ decays to a variety of 4-body kaon or pion final states, fitting simultaneously different partial wave components.

Table with columns: VALUE, DOCUMENT ID, TECN, COMMENT. Contains data for ABLIKIM 19A Z BES3 D+ → K S0 π+ π+ π-.

D± REFERENCES

Large table listing references for D± mesons, including authors, document IDs, and techniques.

Large table listing references for D± mesons, including authors, document IDs, and techniques.

Downloaded from https://academic.oup.com/ptep/article/2020/8/083C01/5891211 by guest on 12 November 2020



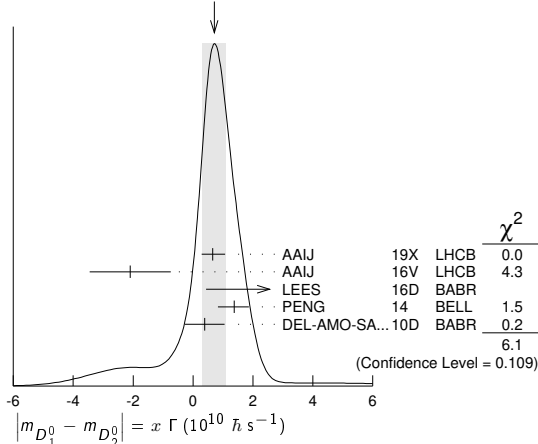
See key on page 999

# Meson Particle Listings

## $D^0$

- <sup>7</sup>Based on  $9.6 \text{ fb}^{-1}$  of data collected at the Tevatron. Assumes no  $CP$  violation. Reported  $x'^2 = (0.08 \pm 0.18) \times 10^{-3}$  and  $y' = (4.3 \pm 4.3) \times 10^{-3}$ , where  $x' = x \cos(\delta) + y \sin(\delta)$ ,  $y' = y \cos(\delta) - x \sin(\delta)$  and  $\delta$  is the strong phase between the  $D^0 \rightarrow K^+ \pi^-$  and  $\bar{D}^0 \rightarrow K^+ \pi^-$ .
- <sup>8</sup>DEL-AMO-SANCHEZ 10D uses  $540,800 \pm 800 K_S^0 \pi^+ \pi^-$  and  $79,900 \pm 300 K_S^0 K^+ K^-$  events in a time-dependent amplitude analysis of the  $D^0$  and  $\bar{D}^0$  Dalitz plots. No evidence was found for  $CP$  violation, and the values here assume no such violation.
- <sup>9</sup>The result was established with  $D^0$  from prompt and secondary  $D^*$ . Based on  $3 \text{ fb}^{-1}$  of data collected at  $\sqrt{s} = 7, 8 \text{ TeV}$ . Assumes no  $CP$  violation. Reported  $x'^2 = (3.6 \pm 4.3) \times 10^{-5}$  and  $y' = (5.23 \pm 0.84) \times 10^{-3}$ , where  $x' = x \cos(\delta) + y \sin(\delta)$ ,  $y' = y \cos(\delta) - x \sin(\delta)$  and  $\delta$  is the strong phase between the  $D^0 \rightarrow K^+ \pi^-$  and  $\bar{D}^0 \rightarrow K^+ \pi^-$ .
- <sup>10</sup>Based on  $3 \text{ fb}^{-1}$  of data collected at  $\sqrt{s} = 7, 8 \text{ TeV}$ . Assumes no  $CP$  violation. Reported  $x'^2 = (5.5 \pm 4.9) \times 10^{-4}$  and  $y' = (4.8 \pm 1.0) \times 10^{-3}$ , where  $x' = x \cos(\delta) + y \sin(\delta)$ ,  $y' = y \cos(\delta) - x \sin(\delta)$  and  $\delta$  is the strong phase between the  $D^0 \rightarrow K^+ \pi^-$  and  $\bar{D}^0 \rightarrow K^+ \pi^-$ .
- <sup>11</sup>Based on  $1 \text{ fb}^{-1}$  of data collected at  $\sqrt{s} = 7 \text{ TeV}$  in 2011. Assumes no  $CP$  violation. Reported  $x'^2 = (-0.9 \pm 1.3) \times 10^{-4}$  and  $y' = (7.2 \pm 2.4) \times 10^{-3}$ , where  $x' = x \cos(\delta) + y \sin(\delta)$ ,  $y' = y \cos(\delta) - x \sin(\delta)$  and  $\delta$  is the strong phase between the  $D^0 \rightarrow K^+ \pi^-$  and  $\bar{D}^0 \rightarrow K^+ \pi^-$ .
- <sup>12</sup>The AUBERT 09AN values are inferred from the branching ratio  $\Gamma(D^0 \rightarrow K^+ \pi^- \pi^0) / \Gamma(D^0 \rightarrow K^+ \pi^- \pi^0)$  given near the end of this Listings. Mixing is distinguished from DCS decays using decay-time information. Interference between mixing and DCS is allowed. The phase between  $D^0 \rightarrow K^+ \pi^- \pi^0$  and  $\bar{D}^0 \rightarrow K^+ \pi^- \pi^0$  is assumed to be small. The width difference here is  $y''$ , which is not the same as  $y_{CP}$  in the note on  $D^0$ - $\bar{D}^0$  mixing.
- <sup>13</sup>LOWREY 09 uses quantum correlations in  $e^+ e^- \rightarrow D^0 \bar{D}^0$  at the  $\psi(3770)$ . See below for coherence factors and average relative strong phases for both  $D^0 \rightarrow K^+ \pi^- \pi^0$  and  $D^0 \rightarrow K^+ \pi^- 2\pi^+$ . A fit that includes external measurements of charm mixing parameters gets  $\Delta m = (2.34 \pm 0.61) \times 10^{10} \text{ h s}^{-1}$ .
- <sup>14</sup>The ASNER 05 and ZHANG 07b values are from the time-dependent Dalitz plot analysis of  $D^0 \rightarrow K_S^0 \pi^+ \pi^-$ . Decay-time information and interference on the Dalitz plot are used to distinguish doubly Cabibbo-suppressed decays from mixing and to measure the relative phase between  $D^0 \rightarrow K^{*+} \pi^-$  and  $\bar{D}^0 \rightarrow K^{*+} \pi^-$ . This value allows  $CP$  violation and is sensitive to the sign of  $\Delta m$ .
- <sup>15</sup>The AUBERT 03Z, LI 05A, and ZHANG 06 limits are inferred from the  $D^0$ - $\bar{D}^0$  mixing ratio  $\Gamma(K^+ \pi^-) / \Gamma(K^+ \pi^-)$  (via  $\bar{D}^0$ ) /  $\Gamma(K^+ \pi^-)$  given near the end of this  $D^0$  Listings. Decay-time information is used to distinguish DCS decays from  $D^0$ - $\bar{D}^0$  mixing. The limit allows interference between the DCS and mixing ratios, and also allows  $CP$  violation. The limit allows interference between the DCS and mixing ratios, and also allows  $CP$  violation. AUBERT 03Z assumes the strong phase between  $D^0 \rightarrow K^+ \pi^-$  and  $\bar{D}^0 \rightarrow K^+ \pi^-$  amplitudes is small; if an arbitrary phase is allowed, the limit degrades by 20%. The LI 05A and ZHANG 06 limits are valid for an arbitrary strong phase.
- <sup>16</sup>This LINK 05H limit is inferred from the  $D^0$ - $\bar{D}^0$  mixing ratio  $\Gamma(K^+ \pi^-)$  (via  $\bar{D}^0$ ) /  $\Gamma(K^+ \pi^-)$  given near the end of this  $D^0$  Listings. Decay-time information is used to distinguish DCS decays from  $D^0$ - $\bar{D}^0$  mixing. The limit allows interference between the DCS and mixing ratios, and also allows  $CP$  violation. The strong phase between  $D^0 \rightarrow K^+ \pi^-$  and  $\bar{D}^0 \rightarrow K^+ \pi^-$  is assumed to be small. If an arbitrary relative strong phase is allowed, the limit degrades by 25%.
- <sup>17</sup>This GODANG 00 limit is inferred from the  $D^0$ - $\bar{D}^0$  mixing ratio  $\Gamma(K^+ \pi^-)$  (via  $\bar{D}^0$ ) /  $\Gamma(K^+ \pi^-)$  given near the end of this  $D^0$  Listings. Decay-time information is used to distinguish DCS decays from  $D^0$ - $\bar{D}^0$  mixing. The limit allows interference between the DCS and mixing ratios, and also allows  $CP$  violation. The strong phase between  $D^0 \rightarrow K^+ \pi^-$  and  $\bar{D}^0 \rightarrow K^+ \pi^-$  is assumed to be small. If an arbitrary relative strong phase is allowed, the limit degrades by a factor of two.
- <sup>18</sup>AITALA 98 allows interference between the doubly Cabibbo-suppressed and mixing amplitudes, and also allows  $CP$  violation in this term, but assumes that  $A_D = A_R = 0$ . See the note on " $D^0$ - $\bar{D}^0$  Mixing," above.
- <sup>19</sup>This limit is inferred from  $R_M$  for  $f = K^+ \pi^-$  and  $f = K^+ \pi^- \pi^+ \pi^-$ . See the note on " $D^0$ - $\bar{D}^0$  Mixing," above. Decay-time information is used to distinguish doubly Cabibbo-suppressed decays from  $D^0$ - $\bar{D}^0$  mixing.
- <sup>20</sup>This limit is inferred from  $R_M$  for  $f = K^+ \ell^- \bar{\nu}_\ell$ . See the note on " $D^0$ - $\bar{D}^0$  Mixing," above.
- <sup>21</sup>ANJOS 88c assumes that  $y = 0$ . See the note on " $D^0$ - $\bar{D}^0$  Mixing," above. Without this assumption, the limit degrades by about a factor of two.

WEIGHTED AVERAGE  
 $0.7 \pm 0.4$  (Error scaled by 1.4)



$$(\Gamma_{D_1^0} - \Gamma_{D_2^0}) / \Gamma = 2y$$

The  $D_1^0$  and  $D_2^0$  are the mass eigenstates of the  $D^0$  meson, as described in the note on " $D^0$ - $\bar{D}^0$  Mixing," above.

Due to the strong phase difference between  $D^0 \rightarrow K^+ \pi^-$  and  $\bar{D}^0 \rightarrow K^+ \pi^-$ , we exclude from the average those measurements of  $y'$  that are inferred from the  $D^0$ - $\bar{D}^0$  mixing ratio  $\Gamma(K^+ \pi^- \text{ via } \bar{D}^0) / \Gamma(K^+ \pi^-)$  given near the end of this  $D^0$  Listings.

Some early results have been omitted. See our 2006 Review (Journal of Physics **G33** 1 (2006)).

"OUR EVALUATION" comes from CPV allowing averages provided by the Heavy Flavor Averaging Group, see the note on " $D^0$ - $\bar{D}^0$  Mixing."

VALUE (units $10^{-2}$ )	EVTS	DOCUMENT ID	TECN	COMMENT
<b><math>1.29 \pm 0.14</math></b>				<b>OUR EVALUATION</b>
<b><math>1.10 \pm 0.19</math></b>				<b>OUR AVERAGE</b> Error includes scale factor of 1.2.
$1.14 \pm 0.26 \pm 0.18$		1 AAIJ	19 LHCB	$pp$ at 7, 8 TeV
$1.48 \pm 0.74$	2.3M	2 AAIJ	19X LHCB	$D^0 \rightarrow K_S^0 \pi^+ \pi^-$
		3 AAIJ	18K LHCB	$pp$ at 7, 8, 13 TeV
$0.06 \pm 0.92 \pm 0.26$		4 AAIJ	16V LHCB	$pp$ at 7 TeV
$0.4 \pm 1.8 \pm 1.0$		5 LEES	16D BABR	$e^+ e^- \rightarrow 10.6 \text{ GeV}$
$2.22 \pm 0.44 \pm 0.18$		6 STARIC	16 BELL	$e^+ e^- \rightarrow \Upsilon(1S)$
$-4.0 \pm 2.6 \pm 1.4$		7 ABLIKIM	15D BES3	$e^+ e^-$ at $\psi(3770)$
		8 KO	14 BELL	$e^+ e^- \rightarrow \Upsilon(1S)$
$0.60 \pm 0.30 \pm 0.10$		9 PENG	14 BELL	$e^+ e^- \rightarrow \Upsilon(1S)$
		10 AALTONEN	13AE CDF	$p\bar{p}$ at 1.96 TeV
$1.44 \pm 0.36 \pm 0.24$		11 LEES	13 BABR	$e^+ e^- \rightarrow \Upsilon(4S)$
$0.55 \pm 0.63 \pm 0.41$		12 AAIJ	12K LHCB	$pp$ at 7 TeV
$1.14 \pm 0.40 \pm 0.30$		13 DEL-AMO-SA...	10D BABR	$e^+ e^- \rightarrow 10.6 \text{ GeV}$
$0.22 \pm 1.22 \pm 1.04$		14 ZUPANC	09 BELL	$e^+ e^- \approx \Upsilon(4S)$
$-1.0 \pm 2.0 \pm 1.4$	18k	15 ABE	02i BELL	$e^+ e^- \approx \Upsilon(4S)$
$-2.4 \pm 5.0 \pm 2.8$	3393	16 CSORNA	02 CLE2	$e^+ e^- \approx \Upsilon(4S)$
$6.84 \pm 2.78 \pm 1.48$	10k	15 LINK	00 FOCS	$\gamma$ nucleus
$\pm 1.6 \pm 5.8 \pm 2.1$		15 AITALA	E791	$K^+ \pi^+, K^+ K^-$
••• We do not use the following data for averages, fits, limits, etc. •••				
		17 AAIJ	17A0 LHCB	Repl. by AAIJ 18k
		18 AAIJ	13CE LHCB	Repl. by AAIJ 17A0
		19 AAIJ	13N LHCB	Repl. by AAIJ 13CE
		20 AUBERT	09A1 BABR	See LEES 13
		21 AUBERT	09AN BABR	$e^+ e^-$ at 10.58 GeV
		22 LOWREY	09 CLEO	$e^+ e^-$ at $\psi(3770)$
		23 AALTONEN	08E CDF	$p\bar{p}$ , $\sqrt{s} = 1.96 \text{ TeV}$
		24 AUBERT	08U BABR	See AUBERT 09A1
		23 AUBERT	07W BABR	$e^+ e^- \approx 10.6 \text{ GeV}$
		25 STARIC	07 BELL	Repl. by STARIC 16
		26 ZHANG	07B BELL	Repl. by PENG 14
		23,27 ZHANG	06 BELL	$e^+ e^-$
		26 ASNER	05 CLEO	$e^+ e^- \approx 10 \text{ GeV}$
		23,27 LI	05A BELL	See ZHANG 06
		23,27 LINK	05H FOCS	$\gamma$ nucleus
		28 AUBERT	03P BABR	See AUBERT 08U
		23,27 AUBERT	03Z BABR	$e^+ e^- \rightarrow 10.6 \text{ GeV}$
		23 GODANG	00 CLE2	$e^+ e^-$

- <sup>1</sup>Based on  $3 \text{ fb}^{-1}$  of data collected at  $\sqrt{s} = 7, 8 \text{ TeV}$ . Measures the lifetime difference between  $D^0 \rightarrow K^- K^+$  and  $D^0 \rightarrow \pi^- \pi^+$  ( $CP$  even) decays and  $D^0 \rightarrow K^- \pi^+$  ( $CP$  mixed) decays, or  $y_{CP} = (\Gamma_{CP+} - \Gamma_{CP-}) / (\Gamma_{CP+} + \Gamma_{CP-})$ . The  $D^0$  mesons are required to originate from semimuonic decays of  $B$  mesons. We list  $2y_{CP} = \Delta \Gamma / \Gamma$ .
- <sup>2</sup>AAIJ 19X  $D^0$  come from  $D^{*+}$  and  $\bar{B}^0 \rightarrow D^0 \mu^- X$  decays (and c.c.) in  $pp$  collisions at 7 and 8 TeV. Measurement allows for  $CP$  violation (none seen).
- <sup>3</sup>The result was established with  $D^0$  from prompt and secondary  $D^*$ . Based on  $5 \text{ fb}^{-1}$  of data collected at  $\sqrt{s} = 7, 8, 13 \text{ TeV}$ . Assumes no  $CP$  violation. Reported  $x'^2 = (3.9 \pm 2.7) \times 10^{-5}$  and  $y' = (5.28 \pm 0.52) \times 10^{-3}$ , where  $x' = x \cos(\delta) + y \sin(\delta)$ ,  $y' = y \cos(\delta) - x \sin(\delta)$  and  $\delta$  is the strong phase between the  $D^0 \rightarrow K^+ \pi^-$  and  $\bar{D}^0 \rightarrow K^+ \pi^-$ .
- <sup>4</sup>Model-independent measurement of the charm mixing parameters in the decay  $D^0 \rightarrow K_S^0 \pi^+ \pi^-$  using  $1.0 \text{ fb}^{-1}$  of LHCb data at  $\sqrt{s} = 7 \text{ TeV}$ .
- <sup>5</sup>Time-dependent amplitude analysis of  $D^0 \rightarrow \pi^+ \pi^- \pi^0$ .
- <sup>6</sup>An improved measurement of  $\bar{D}^0 - D^0$  mixing and a search for  $CP$  violation in  $D^0$  decays to  $CP$ -even final states  $K^+ K^-$  and  $\pi^+ \pi^-$  using the final Belle data sample of  $976 \text{ fb}^{-1}$ .
- <sup>7</sup>ABLIKIM 15D uses quantum correlations in  $e^+ e^- \rightarrow D^0 \bar{D}^0$  at the  $\psi(3770)$ .
- <sup>8</sup>Based on  $976 \text{ fb}^{-1}$  of data collected at  $Y(1S)$  resonances. Assumes no  $CP$  violation. Reported  $x'^2 = (0.09 \pm 0.22) \times 10^{-3}$  and  $y' = (4.6 \pm 3.4) \times 10^{-3}$ , where  $x' = x \cos(\delta) + y \sin(\delta)$ ,  $y' = y \cos(\delta) - x \sin(\delta)$  and  $\delta$  is the strong phase between  $D^0 \rightarrow K^+ \pi^-$  and  $\bar{D}^0 \rightarrow K^+ \pi^-$ .

# Meson Particle Listings

## $D^0$

- <sup>9</sup>The time-dependent Dalitz-plot analysis of  $D^0 \rightarrow K_S^0 \pi^+ \pi^-$  is employed. Decay-time information and interference on the Dalitz plot are used to distinguish doubly Cabibbo-suppressed decays from mixing and to measure the relative phase between  $D^0 \rightarrow K^{*+} \pi^-$  and  $\bar{D}^0 \rightarrow K^{*+} \pi^-$ . This value allows  $CP$  violation and is sensitive to the sign of  $\Delta m$ .
- <sup>10</sup>Based on  $9.6 \text{ fb}^{-1}$  of data collected at the Tevatron. Assumes no  $CP$  violation. Reported  $x'^2 = (0.08 \pm 0.18) \times 10^{-3}$  and  $y' = (4.3 \pm 4.3) \times 10^{-3}$ , where  $x' = x \cos(\delta) + y \sin(\delta)$ ,  $y' = y \cos(\delta) - x \sin(\delta)$  and  $\delta$  is the strong phase between the  $D^0 \rightarrow K^+ \pi^-$  and  $\bar{D}^0 \rightarrow K^+ \pi^-$ .
- <sup>11</sup>Obtained  $y_{CP} = (0.72 \pm 0.18 \pm 0.12)\%$  based on three effective  $D^0$  lifetimes measured in  $K^+ \pi^-$ ,  $K^- K^+$ , and  $\pi^- \pi^+$ . We list  $2y_{CP} = \Delta\Gamma/\Gamma$ .
- <sup>12</sup>Compared the lifetimes of  $D^0$  decay to the  $CP$  eigenstate  $K^+ K^-$  with  $D^0$  decay to  $\pi^+ \pi^-$ . The values here assume no  $CP$  violation.
- <sup>13</sup>DEL-AMO-SANCHEZ 10b uses  $540,800 \pm 800 K_S^0 \pi^+ \pi^-$  and  $79,900 \pm 300 K_S^0 K^+ K^-$  events in a time-dependent amplitude analyses of the  $D^0$  and  $\bar{D}^0$  Dalitz plots. No evidence was found for  $CP$  violation, and the values here assume no such violation.
- <sup>14</sup>ZUPANC 09 uses a method based on measuring the mean decay time of  $D^0 \rightarrow K_S^0 K^+ K^-$  events for different  $K^+ K^-$  mass intervals.
- <sup>15</sup>LINK 00, AITALA 99E, and ABE 02i measure the lifetime difference between  $D^0 \rightarrow K^- K^+$  ( $CP$  even) decays and  $D^0 \rightarrow K^- \pi^+$  ( $CP$  mixed) decays, or  $y_{CP} = [\Gamma(CP+) - \Gamma(CP-)] / [\Gamma(CP+) + \Gamma(CP-)]$ . We list  $2y_{CP} = \Delta\Gamma/\Gamma$ .
- <sup>16</sup>CSORNA 02 measures the lifetime difference between  $D^0 \rightarrow K^- K^+$  and  $\pi^- \pi^+$  ( $CP$  even) decays and  $D^0 \rightarrow K^- \pi^+$  ( $CP$  mixed) decays, or  $y_{CP} = [\Gamma(CP+) - \Gamma(CP-)] / [\Gamma(CP+) + \Gamma(CP-)]$ . We list  $2y_{CP} = \Delta\Gamma/\Gamma$ .
- <sup>17</sup>The result was established with  $D^0$  from prompt and secondary  $D^*$ . Based on  $3 \text{ fb}^{-1}$  of data collected at  $\sqrt{s} = 7, 8 \text{ TeV}$ . Assumes no  $CP$  violation. Reported  $x'^2 = (3.6 \pm 4.3) \times 10^{-5}$  and  $y' = (5.23 \pm 0.84) \times 10^{-3}$ , where  $x' = x \cos(\delta) + y \sin(\delta)$ ,  $y' = y \cos(\delta) - x \sin(\delta)$  and  $\delta$  is the strong phase between the  $D^0 \rightarrow K^+ \pi^-$  and  $\bar{D}^0 \rightarrow K^+ \pi^-$ .
- <sup>18</sup>Based on  $3 \text{ fb}^{-1}$  of data collected at  $\sqrt{s} = 7, 8 \text{ TeV}$ . Assumes no  $CP$  violation. Reported  $x'^2 = (5.5 \pm 4.9) \times 10^{-4}$  and  $y' = (4.8 \pm 1.0) \times 10^{-3}$ , where  $x' = x \cos(\delta) + y \sin(\delta)$ ,  $y' = y \cos(\delta) - x \sin(\delta)$  and  $\delta$  is the strong phase between the  $D^0 \rightarrow K^+ \pi^-$  and  $\bar{D}^0 \rightarrow K^+ \pi^-$ .
- <sup>19</sup>Based on  $1 \text{ fb}^{-1}$  of data collected at  $\sqrt{s} = 7 \text{ TeV}$  in 2011. Assumes no  $CP$  violation. Reported  $x'^2 = (-0.9 \pm 1.3) \times 10^{-4}$  and  $y' = (7.2 \pm 2.4) \times 10^{-3}$ , where  $x' = x \cos(\delta) + y \sin(\delta)$ ,  $y' = y \cos(\delta) - x \sin(\delta)$  and  $\delta$  is the strong phase between the  $D^0 \rightarrow K^+ \pi^-$  and  $\bar{D}^0 \rightarrow K^+ \pi^-$ .
- <sup>20</sup>This combines the  $y_{CP} = (\tau_{K\pi} / \tau_{KK}) - 1$  using untagged  $K^- \pi^+$  and  $K^- K^+$  events of AUBERT 09A1 with the disjoint  $y_{CP}$  using tagged  $K^- \pi^+$ ,  $K^- K^+$ , and  $\pi^- \pi^+$  events of AUBERT 08U.
- <sup>21</sup>The AUBERT 09AN values are inferred from the branching ratio  $\Gamma(D^0 \rightarrow K^+ \pi^- \pi^0)$  via  $\bar{D}^0 / \Gamma(D^0 \rightarrow K^- \pi^+ \pi^0)$  given near the end of this Listings. Mixing is distinguished from DCS decays using decay-time information. Interference between mixing and DCS is allowed. The phase between  $D^0 \rightarrow K^+ \pi^- \pi^0$  and  $\bar{D}^0 \rightarrow K^+ \pi^- \pi^0$  is assumed to be small. The width difference here is  $y''$ , which is not the same as  $y_{CP}$  in the note on  $D^0$ - $\bar{D}^0$  mixing.
- <sup>22</sup>LOWREY 09 uses quantum correlations in  $e^+ e^- \rightarrow D^0 \bar{D}^0$  at the  $\psi(3770)$ . See below for coherence factors and average relative strong phases for both  $D^0 \rightarrow K^- \pi^+ \pi^0$  and  $D^0 \rightarrow K^- \pi^- 2\pi^+$ . A fit that includes external measurements of charm mixing parameters gets  $2y = (1.62 \pm 0.32) \times 10^{-2}$ .
- <sup>23</sup>The GODANG 00, AUBERT 03Z, LINK 05H, LI 05A, ZHANG 06, AUBERT 07w, and AALTONEN 08E limits are inferred from the  $D^0$ - $\bar{D}^0$  mixing ratio  $\Gamma(K^+ \pi^-) / \Gamma(K^- \pi^+)$  given near the end of this  $D^0$  Listings. Decay-time information is used to distinguish DCS decays from  $D^0$ - $\bar{D}^0$  mixing. The limits allow interference between the DCS and mixing ratios, and all except AUBERT 07w and AALTONEN 08E also allow  $CP$  violation. The phase between  $D^0 \rightarrow K^+ \pi^-$  and  $\bar{D}^0 \rightarrow K^+ \pi^-$  is assumed to be small. This is a measurement of  $y'$  and is not the same as the  $y_{CP}$  of our note above on " $D^0$ - $\bar{D}^0$  Mixing."
- <sup>24</sup>This value combines the results of AUBERT 08U and AUBERT 03P.
- <sup>25</sup>STARIC 07 compares the lifetimes of  $D^0$  decay to the  $CP$  eigenstates  $K^+ K^-$  and  $\pi^+ \pi^-$  with  $D^0$  decay to  $K^- \pi^+$ .
- <sup>26</sup>The ASNER 05 and ZHANG 07B values are from the time-dependent Dalitz-plot analysis of  $D^0 \rightarrow K_S^0 \pi^+ \pi^-$ . Decay-time information and interference on the Dalitz plot are used to distinguish doubly Cabibbo-suppressed decays from mixing and to measure the relative phase between  $D^0 \rightarrow K^{*+} \pi^-$  and  $\bar{D}^0 \rightarrow K^{*+} \pi^-$ . This limit allows  $CP$  violation.
- <sup>27</sup>The ranges of AUBERT 03Z, LINK 05H, LI 05A, and ZHANG 06 measurements are for 95% confidence level.
- <sup>28</sup>AUBERT 03P measures  $Y \equiv 2\tau^0 / (\tau^+ + \tau^-) - 1$ , where  $\tau^0$  is the  $D^0 \rightarrow K^- \pi^+$  (and  $\bar{D}^0 \rightarrow K^+ \pi^-$ ) lifetime, and  $\tau^+$  and  $\tau^-$  are the  $D^0$  and  $\bar{D}^0$  lifetimes to  $CP$ -even states (here  $K^- K^+$  and  $\pi^- \pi^+$ ). In the limit of  $CP$  conservation,  $Y = Y \equiv \Delta\Gamma / 2\Gamma$  (we list  $2y = \Delta\Gamma/\Gamma$ ). AUBERT 03P also uses  $\tau^+ - \tau^-$  to get  $\Delta Y = -0.008 \pm 0.006 \pm 0.002$ .

### $|q/p|$

The mass eigenstates  $D_1^0$  and  $D_2^0$  are related to the  $C = \pm 1$  states by  $|D_{1,2}^0\rangle = p|D^0\rangle + q|\bar{D}^0\rangle$ . See the note on " $D^0$ - $\bar{D}^0$  Mixing" above.

"OUR EVALUATION" comes from CPV allowing averages provided by the Heavy Flavor Averaging Group. This would include as-yet-unpublished results, see the note on " $D^0$ - $\bar{D}^0$  Mixing."

VALUE	EVTS	DOCUMENT ID	TECN	COMMENT
<b><math>0.92^{+0.12}_{-0.09}</math> OUR EVALUATION</b>		HFAG fit; see the note on " $D^0$ - $\bar{D}^0$ Mixing."		
<b><math>0.97^{+0.14}_{-0.12}</math> OUR AVERAGE</b>				
$1.05^{+0.22}_{-0.17}$	2.3M	1 AAIJ	19X LHCb	$D^0 \rightarrow K_S^0 \pi^+ \pi^-$

$0.90^{+0.16+0.08}_{-0.15-0.06}$	2 AAIJ	18k LHCb	$pp$ at 7, 8, 13 TeV
	3 PENG	14 BELL	$e^+ e^- \rightarrow \Upsilon(nS)$
	4 AAIJ	13CE LHCb	Repl. by AAIJ 18K
$0.86^{+0.30+0.10}_{-0.29-0.08}$	5 ZHANG	07B BELL	Repl. by PENG 14

• • • We do not use the following data for averages, fits, limits, etc. • • •

- <sup>1</sup>AAIJ 19X  $D^0$  come from  $D^{*+}$  and  $\bar{B} \rightarrow D^0 \mu^- X$  decays (and c.c.) in  $pp$  collisions at 7 and 8 TeV.
- <sup>2</sup>Based on  $5 \text{ fb}^{-1}$  of data collected at  $\sqrt{s} = 7, 8, 13 \text{ TeV}$ . Allowing for  $CP$  violation, the direct  $CP$  violation in mixing is reported  $1.00 < |q/p| < 1.35$  at the 68.3% CL for the  $D^0 \rightarrow K^+ \pi^-$  and  $\bar{D}^0 \rightarrow K^+ \pi^-$ .
- <sup>3</sup>The time-dependent Dalitz-plot analysis of  $D^0 \rightarrow K_S^0 \pi^+ \pi^-$  is employed. Decay-time information and interference on the Dalitz plot are used to distinguish doubly Cabibbo-suppressed decays from mixing and to measure the relative phase between  $D^0 \rightarrow K^{*+} \pi^-$  and  $\bar{D}^0 \rightarrow K^{*+} \pi^-$ . This value allows  $CP$  violation and is sensitive to the sign of  $\Delta m$ .
- <sup>4</sup>Based on  $3 \text{ fb}^{-1}$  of data collected at  $\sqrt{s} = 7, 8 \text{ TeV}$ . Allowing for  $CP$  violation, the direct  $CP$  violation in mixing is reported  $0.75 < |q/p| < 1.24$  at the 68.3% CL for the  $D^0 \rightarrow K^+ \pi^-$  and  $\bar{D}^0 \rightarrow K^+ \pi^-$ .
- <sup>5</sup>The phase of  $p/q$  is  $(-14^{+16}_{-18} \pm 5)^\circ$ . The ZHANG 07B value is from the time-dependent Dalitz-plot analysis of  $D^0 \rightarrow K_S^0 \pi^+ \pi^-$ . Decay-time information and interference on the Dalitz plot are used to distinguish doubly Cabibbo-suppressed decays from mixing and to measure the relative phase between  $D^0 \rightarrow K^{*+} \pi^-$  and  $\bar{D}^0 \rightarrow K^{*+} \pi^-$ . This value allows  $CP$  violation.

### $A_\Gamma$

$A_\Gamma$  is the decay-rate asymmetry for  $CP$ -even final states  $A_\Gamma = (\bar{\tau}_+ - \tau_+) / (\bar{\tau}_+ + \tau_+)$ . See the note on " $D^0$ - $\bar{D}^0$  Mixing" above.

VALUE (units $10^{-3}$ )	EVTS	DOCUMENT ID	TECN	COMMENT
<b><math>-0.125 \pm 0.526</math> OUR EVALUATION</b>				
<b><math>-0.31 \pm 0.23</math> OUR AVERAGE</b>				Error includes scale factor of 1.1.
$-0.44 \pm 0.23 \pm 0.06$	21M	1 AAIJ	20 LHCb	$D^0 \rightarrow K^+ K^-$
$0.25 \pm 0.43 \pm 0.07$	7M	2 AAIJ	20 LHCb	$D^0 \rightarrow \pi^+ \pi^-$
$-0.3 \pm 0.2 \pm 0.7$		3 STARIC	16 BELL	$e^+ e^- \rightarrow \Upsilon(nS)$
$-1.2 \pm 1.2$	1.8M	4 AALTONEN	14Q CDF	$p\bar{p}$ , $\sqrt{s} = 1.96 \text{ TeV}$
$0.9 \pm 2.6 \pm 0.6$	0.7M	LEES	13 BABR	$e^+ e^- \rightarrow \Upsilon(4S)$
$-5.9 \pm 5.9 \pm 2.1$		5 AAIJ	12k LHCb	$pp$ at 7 TeV, 2010 data.
				• • • We do not use the following data for averages, fits, limits, etc. • • •
$-0.30 \pm 0.32 \pm 0.10$	9.6M	5 AAIJ	17AK LHCb	Repl. by AAIJ 20
$0.46 \pm 0.58 \pm 0.12$	3.0M	6 AAIJ	17AK LHCb	Repl. by AAIJ 20
$-1.34 \pm 0.77^{+0.26}_{-0.34}$	2.3M	7 AAIJ	15AA LHCb	Repl. by AAIJ 20
$-0.92 \pm 1.45^{+0.25}_{-0.33}$	0.8M	8 AAIJ	15AA LHCb	Repl. by AAIJ 20
$-0.35 \pm 0.62 \pm 0.12$		5 AAIJ	14AL LHCb	Repl. by AAIJ 17AK
$0.33 \pm 1.06 \pm 0.14$		6 AAIJ	14AL LHCb	Repl. by AAIJ 17AK
$2.6 \pm 3.6 \pm 0.8$		AUBERT	08U BABR	See LEES 13
$0.1 \pm 3.0 \pm 2.5$		STARIC	07 BELL	Repl. by STARIC 16
$8 \pm 6 \pm 2$		AUBERT	03P BABR	$e^+ e^- \approx \Upsilon(4S)$

- <sup>1</sup>Measured using  $D^0 \rightarrow K^+ K^-$  decays, combines measurements with  $D^0$  either from partially reconstructed semileptonic  $B$  hadron decays or from  $D^{*+} \rightarrow D^0 \pi^+$ .
- <sup>2</sup>Measured using  $D^0 \rightarrow \pi^+ \pi^-$  decays, combines measurements with  $D^0$  either from partially reconstructed semileptonic  $B$  hadron decays or from  $D^{*+} \rightarrow D^0 \pi^+$ .
- <sup>3</sup>An improved measurement of  $\bar{D}^0 - D^0$  mixing and a search for  $CP$  violation in  $D^0$  decays to  $CP$ -even final states  $K^+ K^-$  and  $\pi^+ \pi^-$  using the final Belle data sample of  $976 \text{ fb}^{-1}$ .
- <sup>4</sup>Combined result from  $D^0 \rightarrow K^+ K^-$  and  $D^0 \rightarrow \pi^+ \pi^-$ , with  $D^0$  from  $D^{*+} \rightarrow D^0 \pi^+$  (and cc).
- <sup>5</sup>Measured using  $D^{*+} \rightarrow D^0 \pi^+$ ,  $D^0 \rightarrow K^+ K^-$  decays (and cc).
- <sup>6</sup>Measured using  $D^{*+} \rightarrow D^0 \pi^+$ ,  $D^0 \rightarrow \pi^+ \pi^-$  decays (and cc).
- <sup>7</sup>Measured using  $D^0 \rightarrow K^+ K^-$  decays, with  $D^0$  from partially reconstructed semileptonic  $B$  hadron decays.
- <sup>8</sup>Measured using  $D^0 \rightarrow \pi^+ \pi^-$  decays, with  $D^0$  from partially reconstructed semileptonic  $B$  hadron decays.

### $\phi_{K_S^0 \pi^+ \pi^-}$

Parametrizes  $CP$  violation in the interference between  $D^0$  mixing and decay. The mass eigenstates  $D_1^0$  and  $D_2^0$  are related to the  $C = \pm 1$  states by  $|D_{1,2}^0\rangle = p|D^0\rangle + q|\bar{D}^0\rangle$ . In the absence of  $CP$  violation in the decay, and using the usual phase convention where  $CP$  conservation implies  $q/p$  is real,  $\phi_{K_S^0 \pi^+ \pi^-}$  is identical to the decay-mode-independent parameter  $\phi = \arg(q/p)$ .

VALUE	EVTS	DOCUMENT ID	TECN	COMMENT
<b><math>-0.09 \pm 0.10_{-0.13}</math> OUR AVERAGE</b>				
$-0.09 \pm 0.11_{-0.16}$	2.3M	1 AAIJ	19X LHCb	$D^0 \rightarrow K_S^0 \pi^+ \pi^-$
$-0.10 \pm 0.19 \pm 0.05 \pm 0.05_{-0.07}$	1.2M	2 PENG	14 BELL	$e^+ e^-$ at $\Upsilon(4S, 5S)$

- <sup>1</sup>AAIJ 19X  $D^0$  come from  $D^{*+}$  and  $\bar{B} \rightarrow D^0 \mu^- X$  decays (and c.c.) in  $pp$  collisions at 7 and 8 TeV.
- <sup>2</sup>The last uncertainty is due to the amplitude model.

**cos  $\delta$**

$\delta$  is the  $D^0 \rightarrow K^+\pi^-$  relative strong phase.

VALUE	DOCUMENT ID	TECN	COMMENT
<b>0.97 ± 0.11 OUR AVERAGE</b>			
1.02 ± 0.11 ± 0.06	<sup>1</sup> ABLIKIM	14c	BES3 $e^+e^- \rightarrow D^0\bar{D}^0$ , 3.77 GeV
0.81 <sup>+0.22+0.07</sup> <sub>-0.18-0.05</sub>	<sup>2</sup> ASNER	12	CLEO $e^+e^- \rightarrow D^0\bar{D}^0$ , 3.77 GeV
1.03 <sup>+0.31</sup> <sub>-0.17</sub> ± 0.06	<sup>3</sup> ASNER	08	CLEO Repl. by ASNER 12

- • • We do not use the following data for averages, fits, limits, etc. • • •
- <sup>1</sup> Uses quantum correlations in  $e^+e^- \rightarrow D^0\bar{D}^0$  at the  $\psi(3770)$  to measure the asymmetry of the branching fraction of  $D^0 \rightarrow K^-\pi^+$  in  $CP$ -odd and  $CP$ -even eigenstates to be  $(12.7 \pm 1.3 \pm 0.7)\%$ . A fit that includes external measurements of charm mixing parameters finds the value quoted above.
- <sup>2</sup> Uses quantum correlations in  $e^+e^- \rightarrow D^0\bar{D}^0$  at the  $\psi(3770)$ , where decay rates of  $CP$ -tagged  $K\pi$  final states depend on the strong phases between the decays of  $D^0 \rightarrow K^+\pi^-$  and  $\bar{D}^0 \rightarrow K^+\pi^-$ . The measurements obtained  $\sin(\delta) = -0.01 \pm 0.41 \pm 0.04$  and  $|\delta| = (10^{+28+13}_{-53-00})^\circ$  as well. A fit that includes external measurements of charm mixing parameters finds  $\cos(\delta) = 1.15^{+0.19+0.00}_{-0.17-0.08}$ ,  $\sin(\delta) = 0.56^{+0.32+0.21}_{-0.31-0.20}$ , and  $|\delta| = (18^{+11}_{-17})^\circ$ .
- <sup>3</sup> ASNER 08 uses quantum correlations in  $e^+e^- \rightarrow D^0\bar{D}^0$  at the  $\psi(3770)$ , where decay rates of  $CP$ -tagged  $K\pi$  final states depend on  $\cos \delta$  because of interfering amplitudes. The above measurement implies  $|\delta| < 75^\circ$  with a confidence level of 95%. A fit that includes external measurements of charm mixing parameters finds  $\cos \delta = 1.10 \pm 0.35 \pm 0.07$ . See also the note on " $D^0-\bar{D}^0$  Mixing" p. 783 in our 2008 Review (PDG 08).

**$D^0 \rightarrow K^-\pi^+\pi^0$  COHERENCE FACTOR  $R_{K\pi\pi^0}$**

See the note on ' $D^0-\bar{D}^0$  Mixing' for the definition.  $R_{K\pi\pi^0}$  can have any value between 0 and 1. A value near 1 indicates the decay is dominated by a few intermediate states with limited interference.

VALUE	DOCUMENT ID	TECN	COMMENT
<b>0.82 ± 0.06</b>	1,2,3 EVANS	16	$e^+e^- \rightarrow D^0\bar{D}^0$ at $\psi(3770)$
0.82 ± 0.07	1,3 LIBBY	14	Repl. by EVANS 16
0.78 <sup>+0.11</sup> <sub>-0.25</sub>	<sup>4</sup> LOWREY	09	CLEO Repl. by LIBBY 14

- • • We do not use the following data for averages, fits, limits, etc. • • •
- <sup>1</sup> Uses quantum correlations in  $e^+e^- \rightarrow D^0\bar{D}^0$  at the  $\psi(3770)$ , where the decay rates of  $CP$ -tagged  $K^-\pi^+\pi^0$  final states depend on  $R_{K\pi\pi^0}$  and  $\delta K\pi\pi^0$ .
- <sup>2</sup> A combined fit with a recent LHCb  $D^0\bar{D}^0$  mixing results in AAIJ 16f is also reported to be  $0.81 \pm 0.06$ .
- <sup>3</sup> Obtained by analyzing CLEO-c data but not authored by the CLEO Collaboration.
- <sup>4</sup> LOWREY 09 uses quantum correlations in  $e^+e^- \rightarrow D^0\bar{D}^0$  at the  $\psi(3770)$ , where the decay rates of  $CP$ -tagged  $K^-\pi^+\pi^0$  final states depend on  $R_{K\pi\pi^0}$  and  $\delta K\pi\pi^0$ . A fit that includes external measurements of charm mixing parameters gets  $R_{K\pi\pi^0} = 0.84 \pm 0.07$ .

**$D^0 \rightarrow K^-\pi^+\pi^0$  AVERAGE RELATIVE STRONG PHASE  $\delta K\pi\pi^0$**

The quoted value of  $\delta$  is based on the same sign  $CP$  phase of  $D^0$  and  $\bar{D}^0$  convention.

VALUE ( $^\circ$ )	DOCUMENT ID	TECN	COMMENT
<b>199<sup>+13</sup><sub>-14</sub></b>	1,2,3 EVANS	16	$e^+e^- \rightarrow D^0\bar{D}^0$ at $\psi(3770)$
164 <sup>+20</sup> <sub>-14</sub>	1,3 LIBBY	14	Repl. by EVANS 16
239 <sup>+32</sup> <sub>-28</sub>	<sup>4</sup> LOWREY	09	CLEO Repl. by LIBBY 14

- • • We do not use the following data for averages, fits, limits, etc. • • •
- <sup>1</sup> Uses quantum correlations in  $e^+e^- \rightarrow D^0\bar{D}^0$  at the  $\psi(3770)$ , where the decay rates of  $CP$ -tagged  $K^-\pi^+\pi^0$  final states depend on  $R_{K\pi\pi^0}$  and  $\delta K\pi\pi^0$ .
- <sup>2</sup> A combined fit with a recent LHCb  $D^0\bar{D}^0$  mixing results in AAIJ 16f is also reported to be  $198^{+14}_{-15}$  degree.
- <sup>3</sup> Obtained by analyzing CLEO-c data but not authored by the CLEO Collaboration.
- <sup>4</sup> LOWREY 09 uses quantum correlations in  $e^+e^- \rightarrow D^0\bar{D}^0$  at the  $\psi(3770)$ , where the decay rates of  $CP$ -tagged  $K^-\pi^+\pi^0$  final states depend on  $R_{K\pi\pi^0}$  and  $\delta K\pi\pi^0$ . A fit that includes external measurements of charm mixing parameters gets  $\delta K\pi\pi^0 = (227^{+14}_{-17})^\circ$ .

**$D^0 \rightarrow K^-\pi^-2\pi^+$  COHERENCE FACTOR  $R_{K3\pi}$**

See the note on ' $D^0-\bar{D}^0$  Mixing' for the definition.  $R_{K3\pi}$  can have any value between 0 and 1. A value near 1 indicates the decay is dominated by a few intermediate states with limited interference.

VALUE	EVTS	DOCUMENT ID	TECN	COMMENT
<b>0.53<sup>+0.18</sup><sub>-0.21</sub></b>	1,2,3	EVANS	16	$e^+e^- \rightarrow D^0\bar{D}^0$ at $\psi(3770)$ , $pp$ at 7,8 TeV
0.458 ± 0.010 ± 0.023	0.9M,3k	<sup>4</sup> AAIJ	18A1	LHCb amplitude models
0.32 <sup>+0.20</sup> <sub>-0.28</sub>	1,3	LIBBY	14	Repl. by EVANS 16
0.36 <sup>+0.24</sup> <sub>-0.30</sub>	5	LOWREY	09	CLEO Repl. by LIBBY 14

- • • We do not use the following data for averages, fits, limits, etc. • • •
- <sup>1</sup> Uses quantum correlations in  $e^+e^- \rightarrow D^0\bar{D}^0$  at the  $\psi(3770)$ , where the decay rates of  $CP$ -tagged  $K^-\pi^-2\pi^+$  final states depend on  $R_{K3\pi}$  and  $\delta K3\pi$ .
- <sup>2</sup> A combined fit with a recent LHCb  $D^0\bar{D}^0$  mixing results in AAIJ 16f is also reported, to be  $0.43^{+0.17}_{-0.13}$ .

- <sup>3</sup> Obtained by analyzing CLEO-c data but not authored by the CLEO Collaboration.
- <sup>4</sup> Calculated from amplitude models to  $D^0 \rightarrow K^-\pi^-2\pi^+$  and  $D^0 \rightarrow K^+\pi^+2\pi^-$  and cc. Reports  $0.458 \pm 0.010 \pm 0.012 \pm 0.020$  value where the 3rd uncertainty is the model uncertainty. We combined both systematic uncertainties in quadrature. Because of the importance of model independence in the practical use of the coherence factor, we do not include model-derived results in the average.
- <sup>5</sup> LOWREY 09 uses quantum correlations in  $e^+e^- \rightarrow D^0\bar{D}^0$  at the  $\psi(3770)$ , where the decay rates of  $CP$ -tagged  $K^-\pi^-2\pi^+$  final states depend on  $R_{K3\pi}$  and  $\delta K3\pi$ . A fit that includes external measurements of charm mixing parameters gets  $R_{K3\pi} = 0.33^{+0.26}_{-0.23}$ .

**$D^0 \rightarrow K^-\pi^-2\pi^+$  AVERAGE RELATIVE STRONG PHASE  $\delta K3\pi$**

The quoted value of  $\delta$  is based on the same sign  $CP$  phase of  $D^0$  and  $\bar{D}^0$  convention.

VALUE ( $^\circ$ )	DOCUMENT ID	TECN	COMMENT
<b>125<sup>+22</sup><sub>-14</sub></b>	1,2,3	EVANS	16 $e^+e^- \rightarrow D^0\bar{D}^0$ at $\psi(3770)$
255 <sup>+21</sup> <sub>-78</sub>	1,3	LIBBY	14 Repl. by EVANS 16
118 <sup>+62</sup> <sub>-53</sub>	4	LOWREY	09 CLEO Repl. by LIBBY 14

- • • We do not use the following data for averages, fits, limits, etc. • • •
- <sup>1</sup> Uses quantum correlations in  $e^+e^- \rightarrow D^0\bar{D}^0$  at the  $\psi(3770)$ , where the decay rates of  $CP$ -tagged  $K^-\pi^-2\pi^+$  final states depend on  $R_{K3\pi}$  and  $\delta K3\pi$ .
- <sup>2</sup> A combined fit with a recent LHCb  $D^0\bar{D}^0$  mixing results in AAIJ 16f is also reported to be  $(128^{+28}_{-17})^\circ$ .
- <sup>3</sup> Obtained by analyzing CLEO-c data but not authored by the CLEO Collaboration.
- <sup>4</sup> LOWREY 09 uses quantum correlations in  $e^+e^- \rightarrow D^0\bar{D}^0$  at the  $\psi(3770)$ , where the decay rates of  $CP$ -tagged  $K^-\pi^-2\pi^+$  final states depend on  $R_{K3\pi}$  and  $\delta K3\pi$ . A fit that includes external measurements of charm mixing parameters gets  $\delta K3\pi = (114^{+26}_{-23})^\circ$ .

**$D^0 \rightarrow K^-\pi^-2\pi^+$ ,  $R_{K3\pi}$  ( $y \cos\delta K3\pi - x \sin\delta K3\pi$ )**

VALUE ( $10^{-3} \text{TeV}^{-1}$ )	EVTS	DOCUMENT ID	TECN	COMMENT
<b>-3.0 ± 0.7</b>	42.5k	<sup>1</sup> AAIJ	16f	LHCb $pp$ at 7, 8 TeV

- <sup>1</sup> From a time-dependent analysis of  $D$  mixing in  $D^0 \rightarrow K^+\pi^-\pi^+$ . This result uses external constraints on  $R_M = 1/2(x^2 + y^2)$ . Without such constraints, AAIJ 16f measure  $(0.3 \pm 1.8) \times 10^{-3}$ , with a large correlation coefficient to  $R_M$ .

**$D^0 \rightarrow K_S^0 K^+\pi^-$  COHERENCE FACTOR  $R_{K_S^0 K\pi}$**

VALUE	DOCUMENT ID	TECN	COMMENT
<b>0.70 ± 0.08</b>	<sup>1</sup> INSLER	12	CLEO $e^+e^- \rightarrow D^0\bar{D}^0$ at 3.77 GeV

- <sup>1</sup> Uses quantum correlations in  $e^+e^- \rightarrow D^0\bar{D}^0$  at the  $\psi(3770)$ , where the signal side  $D$  decays to  $K_S^0 K\pi$  and the tag-side  $D$  decays to  $K\pi$ ,  $K\pi\pi\pi$ ,  $K\pi\pi^0$ , and 10 additional  $CP$ -even,  $CP$ -odd, and mixed  $CP$  modes involving  $K_S^0$  or  $K_L^0$ .

**$D^0 \rightarrow K_S^0 K^+\pi^-$  AVERAGE RELATIVE STRONG PHASE  $\delta K_S^0 K\pi$**

The quoted value of  $\delta$  is based on the same sign  $CP$  phase of  $D^0$  and  $\bar{D}^0$  convention.

VALUE ( $^\circ$ )	DOCUMENT ID	TECN	COMMENT
<b>0.1 ± 15.7</b>	<sup>1</sup> INSLER	12	CLEO $e^+e^- \rightarrow D^0\bar{D}^0$ at 3.77 GeV

- <sup>1</sup> Uses quantum correlations in  $e^+e^- \rightarrow D^0\bar{D}^0$  at the  $\psi(3770)$ , where the signal side  $D$  decays to  $K_S^0 K\pi$  and the tag-side  $D$  decays to  $K\pi$ ,  $K\pi\pi\pi$ ,  $K\pi\pi^0$ , and 10 additional  $CP$ -even,  $CP$ -odd, and mixed  $CP$  modes involving  $K_S^0$  or  $K_L^0$ .

**$D^0 \rightarrow K^* K$  COHERENCE FACTOR  $R_{K^* K}$**

VALUE	DOCUMENT ID	TECN	COMMENT
<b>0.94 ± 0.12</b>	<sup>1</sup> INSLER	12	CLEO $e^+e^- \rightarrow D^0\bar{D}^0$ at 3.77 GeV

- <sup>1</sup> Uses quantum correlations in  $e^+e^- \rightarrow D^0\bar{D}^0$  at the  $\psi(3770)$ , where the signal side  $D$  decays to  $K_S^0 K\pi$  and the tag-side  $D$  decays to  $K\pi$ ,  $K\pi\pi\pi$ ,  $K\pi\pi^0$ , and 10 additional  $CP$ -even,  $CP$ -odd, and mixed  $CP$  modes involving  $K_S^0$  or  $K_L^0$ .

**$D^0 \rightarrow K^* K$  AVERAGE RELATIVE STRONG PHASE  $\delta K^* K$**

The quoted value of  $\delta$  is based on the same sign  $CP$  phase of  $D^0$  and  $\bar{D}^0$  convention.

VALUE ( $^\circ$ )	DOCUMENT ID	TECN	COMMENT
<b>-16.6 ± 18.4</b>	<sup>1</sup> INSLER	12	CLEO $e^+e^- \rightarrow D^0\bar{D}^0$ at 3.77 GeV

- <sup>1</sup> Uses quantum correlations in  $e^+e^- \rightarrow D^0\bar{D}^0$  at the  $\psi(3770)$ , where the signal side  $D$  decays to  $K_S^0 K\pi$  and the tag-side  $D$  decays to  $K\pi$ ,  $K\pi\pi\pi$ ,  $K\pi\pi^0$ , and 10 additional  $CP$ -even,  $CP$ -odd, and mixed  $CP$  modes involving  $K_S^0$  or  $K_L^0$ .

**$D^0$  DECAY MODES**

Most decay modes (other than the semileptonic modes) that involve a neutral  $K$  meson are now given as  $K_S^0$  modes, not as  $\bar{K}^0$  modes. Nearly always it is a  $K_S^0$  that is measured, and interference between Cabibbo-allowed and doubly Cabibbo-suppressed modes can invalidate the assumption that  $2\Gamma(K_S^0) = \Gamma(\bar{K}^0)$ .



Mode	Fraction ( $\Gamma_i/\Gamma$ )	Scale factor/ Confidence level			
<b>Topological modes</b>					
$\Gamma_1$	0-prongs	[a] (15 ± 6) %			
$\Gamma_2$	2-prongs	(71 ± 6) %			
$\Gamma_3$	4-prongs	[b] (14.6 ± 0.5) %			
$\Gamma_4$	6-prongs	[c] (6.5 ± 1.3) × 10 <sup>-4</sup>			
<b>Inclusive modes</b>					
$\Gamma_5$	$e^+$ anything	[d] (6.49 ± 0.11) %			
$\Gamma_6$	$\mu^+$ anything	(6.8 ± 0.6) %			
$\Gamma_7$	$K^-$ anything	(54.7 ± 2.8) %	S=1.3		
$\Gamma_8$	$\bar{K}^0$ anything + $K^0$ anything	(47 ± 4) %			
$\Gamma_9$	$K^+$ anything	(3.4 ± 0.4) %			
$\Gamma_{10}$	$K^*(892)^-$ anything	(15 ± 9) %			
$\Gamma_{11}$	$\bar{K}^*(892)^0$ anything	(9 ± 4) %			
$\Gamma_{12}$	$K^*(892)^+$ anything	< 3.6 %	CL=90%		
$\Gamma_{13}$	$K^*(892)^0$ anything	(2.8 ± 1.3) %			
$\Gamma_{14}$	$\eta$ anything	(9.5 ± 0.9) %			
$\Gamma_{15}$	$\eta'$ anything	(2.48 ± 0.27) %			
$\Gamma_{16}$	$\phi$ anything	(1.08 ± 0.04) %			
$\Gamma_{17}$	invisibles	< 9.4 × 10 <sup>-5</sup>	CL=90%		
<b>Semileptonic modes</b>					
$\Gamma_{18}$	$K^- \ell^+ \nu_\ell$				
$\Gamma_{19}$	$K^- e^+ \nu_e$	(3.542 ± 0.035) %	S=1.3		
$\Gamma_{20}$	$K^- \mu^+ \nu_\mu$	(3.41 ± 0.04) %			
$\Gamma_{21}$	$K^*(892)^- e^+ \nu_e$	(2.15 ± 0.16) %			
$\Gamma_{22}$	$K^*(892)^- \mu^+ \nu_\mu$	(1.89 ± 0.24) %			
$\Gamma_{23}$	$K^- \pi^0 e^+ \nu_e$	(1.6 ± 1.3) %			
$\Gamma_{24}$	$\bar{K}^0 \pi^- e^+ \nu_e$	(1.44 ± 0.04) %			
$\Gamma_{25}$	$(\bar{K}^0 \pi^-)_{S-wave} e^+ \nu_e$	(7.9 ± 1.7) × 10 <sup>-4</sup>			
$\Gamma_{26}$	$K^- \pi^+ \pi^- e^+ \nu_e$	(2.8 ± 1.4) × 10 <sup>-4</sup>			
$\Gamma_{27}$	$K_1(1270)^- e^+ \nu_e$	(7.6 ± 4.0) × 10 <sup>-4</sup>			
$\Gamma_{28}$	$K^- \pi^+ \pi^- \mu^+ \nu_\mu$	< 1.3 × 10 <sup>-3</sup>	CL=90%		
$\Gamma_{29}$	$(\bar{K}^*(892) \pi^-) \mu^+ \nu_\mu$	< 1.5 × 10 <sup>-3</sup>	CL=90%		
$\Gamma_{30}$	$\pi^- e^+ \nu_e$	(2.91 ± 0.04) × 10 <sup>-3</sup>			
$\Gamma_{31}$	$\pi^- \mu^+ \nu_\mu$	(2.67 ± 0.12) × 10 <sup>-3</sup>	S=1.3		
$\Gamma_{32}$	$\pi^- \pi^0 e^+ \nu_e$	(1.45 ± 0.07) × 10 <sup>-3</sup>			
$\Gamma_{33}$	$\rho^- e^+ \nu_e$	(1.50 ± 0.12) × 10 <sup>-3</sup>	S=1.9		
$\Gamma_{34}$	$a(980)^- e^+ \nu_e, a^- \rightarrow \eta \pi^-$	(1.33 ± 0.34) × 10 <sup>-4</sup>			
<b>Hadronic modes with one <math>\bar{K}</math></b>					
$\Gamma_{35}$	$K^- \pi^+$	(3.950 ± 0.031) %	S=1.2		
$\Gamma_{36}$	$K_S^0 \pi^0$	(1.240 ± 0.022) %			
$\Gamma_{37}$	$K_L^0 \pi^0$	(10.0 ± 0.7) × 10 <sup>-3</sup>			
$\Gamma_{38}$	$K_S^0 \pi^+ \pi^-$	[e] (2.80 ± 0.18) %	S=1.1		
$\Gamma_{39}$	$K_S^0 \rho^0$	(6.3 ± 0.6) × 10 <sup>-3</sup>			
$\Gamma_{40}$	$K_S^0 \omega, \omega \rightarrow \pi^+ \pi^-$	(2.0 ± 0.6) × 10 <sup>-4</sup>			
$\Gamma_{41}$	$K_S^0 (\pi^+ \pi^-)_{S-wave}$	(3.3 ± 0.8) × 10 <sup>-3</sup>			
$\Gamma_{42}$	$K_S^0 f_0(980), f_0 \rightarrow \pi^+ \pi^-$	(1.20 ± 0.40) × 10 <sup>-3</sup>			
$\Gamma_{43}$	$K_S^0 f_0(1370), f_0 \rightarrow \pi^+ \pi^-$	(2.8 ± 0.9) × 10 <sup>-3</sup>			
$\Gamma_{44}$	$K_S^0 f_2(1270), f_2 \rightarrow \pi^+ \pi^-$	(9 ± 10) × 10 <sup>-5</sup>			
$\Gamma_{45}$	$K^*(892)^- \pi^+, K^{*-} \rightarrow K_S^0 \pi^-$	(1.64 ± 0.14) %			
$\Gamma_{46}$	$K_0^*(1430)^- \pi^+, K_0^{*-} \rightarrow K_S^0 \pi^-$	(2.67 ± 0.40) × 10 <sup>-3</sup>			
$\Gamma_{47}$	$K_2^*(1430)^- \pi^+, K_2^{*-} \rightarrow K_S^0 \pi^-$	(3.4 ± 1.9) × 10 <sup>-4</sup>			
$\Gamma_{48}$	$K^*(1680)^- \pi^+, K^{*-} \rightarrow K_S^0 \pi^-$	(4.4 ± 3.5) × 10 <sup>-4</sup>			
$\Gamma_{49}$	$K^*(892)^+ \pi^-, K^{*+} \rightarrow K_S^0 \pi^+$	[f] (1.13 ± 0.60) × 10 <sup>-4</sup>			
$\Gamma_{50}$	$K_0^*(1430)^+ \pi^-, K_0^{*+} \rightarrow K_S^0 \pi^+$	[f] < 1.4 × 10 <sup>-5</sup>	CL=95%		
$\Gamma_{51}$	$K_2^*(1430)^+ \pi^-, K_2^{*+} \rightarrow K_S^0 \pi^+$	[f] < 3.4 × 10 <sup>-5</sup>	CL=95%		
$\Gamma_{52}$	$K_S^0 \pi^+ \pi^-$ nonresonant	(2.5 ± 6.0) × 10 <sup>-4</sup>			
$\Gamma_{53}$	$K^- \pi^+ \pi^0$	[e] (14.4 ± 0.5) %	S=2.0		
$\Gamma_{54}$	$K^- \rho^+$	(11.3 ± 0.7) %			
$\Gamma_{55}$	$K^- \rho(1700)^+, \rho^+ \rightarrow \pi^+ \pi^0$	(8.2 ± 1.8) × 10 <sup>-3</sup>			
$\Gamma_{56}$	$K^*(892)^- \pi^+, K^*(892)^- \rightarrow K^- \pi^0$	(2.31 ± 0.20) %			
$\Gamma_{57}$	$\bar{K}^*(892)^0 \pi^0, \bar{K}^*(892)^0 \rightarrow K^- \pi^+$	(1.95 ± 0.24) %			
$\Gamma_{58}$	$K_0^*(1430)^- \pi^+, K_0^{*-} \rightarrow K^- \pi^0$	(4.8 ± 2.2) × 10 <sup>-3</sup>			
$\Gamma_{59}$	$\bar{K}_0^*(1430)^0 \pi^0, \bar{K}_0^{*0} \rightarrow K^- \pi^+$	(5.9 ± 5.0) × 10 <sup>-3</sup>			
$\Gamma_{60}$	$K^*(1680)^- \pi^+, K^{*-} \rightarrow K^- \pi^0$	(1.9 ± 0.7) × 10 <sup>-3</sup>			
$\Gamma_{61}$	$K^- \pi^+ \pi^0$ nonresonant	(1.15 ± 0.60) %			
$\Gamma_{62}$	$K_S^0 2\pi^0$	(9.1 ± 1.1) × 10 <sup>-3</sup>	S=2.2		
$\Gamma_{63}$	$K_S^0 (2\pi^0)_{S-wave}$	(2.6 ± 0.7) × 10 <sup>-3</sup>			
$\Gamma_{64}$	$\bar{K}^*(892)^0 \pi^0, \bar{K}^{*0} \rightarrow K_S^0 \pi^0$	(8.1 ± 0.7) × 10 <sup>-3</sup>			
$\Gamma_{65}$	$\bar{K}_0^*(1430)^0 \pi^0, \bar{K}_0^{*0} \rightarrow K_S^0 \pi^0$	(4 ± 23) × 10 <sup>-5</sup>			
$\Gamma_{66}$	$\bar{K}^*(1680)^0 \pi^0, \bar{K}^{*0} \rightarrow K_S^0 \pi^0$	(1.0 ± 0.4) × 10 <sup>-3</sup>			
$\Gamma_{67}$	$K_S^0 f_2(1270), f_2 \rightarrow 2\pi^0$	(2.3 ± 1.1) × 10 <sup>-4</sup>			
$\Gamma_{68}$	$2K_S^0, \text{one } K_S^0 \rightarrow 2\pi^0$	(3.2 ± 1.1) × 10 <sup>-4</sup>			
$\Gamma_{69}$	$K_S^0 2\pi^0$ nonresonant				
$\Gamma_{70}$	$K^- 2\pi^+ \pi^-$	[e] (8.23 ± 0.14) %	S=1.1		
$\Gamma_{71}$	$K^- \pi^+ \rho^0$ total	(6.87 ± 0.31) %			
$\Gamma_{72}$	$K^- \pi^+ \rho^0 3\text{-body}$	(6.1 ± 1.6) × 10 <sup>-3</sup>			
$\Gamma_{73}$	$\bar{K}^*(892)^0 \rho^0, \bar{K}^{*0} \rightarrow K^- \pi^+$	(1.01 ± 0.05) %			
$\Gamma_{74}$	$\bar{K}^*(892)^0 \rho^0$ transverse,	(1.2 ± 0.4) %			
$\Gamma_{75}$	$K^- a_1(1260)^+, a_1^+ \rightarrow \rho^0 \pi^+$	(4.33 ± 0.32) %			
$\Gamma_{76}$	$K_1(1270)^- \pi^+, K_1^- \rightarrow K^- \pi^+ \pi^-$ total,	(3.9 ± 0.4) × 10 <sup>-3</sup>			
$\Gamma_{77}$	$\bar{K}^*(892)^0 \pi^+ \pi^-$ total,				
$\Gamma_{78}$	$\bar{K}^*(892)^0 \rightarrow K^- \pi^+$				
$\Gamma_{79}$	$K_1(1270)^- \pi^+, K_1^- \rightarrow \bar{K}^*(892)^0 \pi^-, \bar{K}^{*0} \rightarrow K^- \pi^+$	(6.6 ± 2.3) × 10 <sup>-4</sup>			
$\Gamma_{80}$	$K^- 2\pi^+ \pi^-$ nonresonant	(1.81 ± 0.07) %			
$\Gamma_{81}$	$K_S^0 \pi^+ \pi^- \pi^0$	[g] (5.2 ± 0.6) %			
$\Gamma_{82}$	$K_S^0 \eta, \eta \rightarrow \pi^+ \pi^- \pi^0$	(1.17 ± 0.03) × 10 <sup>-3</sup>			
$\Gamma_{83}$	$K_S^0 \omega, \omega \rightarrow \pi^+ \pi^- \pi^0$	(9.9 ± 0.6) × 10 <sup>-3</sup>			
$\Gamma_{84}$	$K^- \pi^+ 2\pi^0$	(8.86 ± 0.23) %			
$\Gamma_{85}$	$K^- 2\pi^+ \pi^- \pi^0$	(4.3 ± 0.4) %			
$\Gamma_{86}$	$\bar{K}^*(892)^0 \pi^+ \pi^- \pi^0, \bar{K}^{*0} \rightarrow K^- \pi^+$	(1.3 ± 0.6) %			
$\Gamma_{87}$	$K^- \pi^+ \omega, \omega \rightarrow \pi^+ \pi^- \pi^0$	(2.8 ± 0.5) %			
$\Gamma_{88}$	$\bar{K}^*(892)^0 \omega, \bar{K}^{*0} \rightarrow K^- \pi^+, \omega \rightarrow \pi^+ \pi^- \pi^0$	(6.5 ± 3.0) × 10 <sup>-3</sup>			
$\Gamma_{89}$	$K_S^0 \eta \pi^0$	(5.7 ± 1.1) × 10 <sup>-3</sup>			
$\Gamma_{90}$	$K_S^0 a_0(980), a_0 \rightarrow \eta \pi^0$	(6.8 ± 2.1) × 10 <sup>-3</sup>			
$\Gamma_{91}$	$\bar{K}^*(892)^0 \eta, \bar{K}^{*0} \rightarrow K_S^0 \pi^0$	(1.7 ± 0.5) × 10 <sup>-3</sup>			
$\Gamma_{92}$	$K_S^0 2\pi^+ 2\pi^-$	(2.66 ± 0.30) × 10 <sup>-3</sup>			
$\Gamma_{93}$	$K_S^0 \rho^0 \pi^+ \pi^-, \text{no } K^*(892)^-$	(1.1 ± 0.7) × 10 <sup>-3</sup>			
$\Gamma_{94}$	$K^*(892)^- 2\pi^+ \pi^-, K^*(892)^- \rightarrow K_S^0 \pi^-, \text{no } \rho^0$	(5 ± 7) × 10 <sup>-4</sup>			
$\Gamma_{95}$	$K^*(892)^- \rho^0 \pi^+, K^*(892)^- \rightarrow K_S^0 \pi^-$	(1.6 ± 0.6) × 10 <sup>-3</sup>			
$\Gamma_{96}$	$K_S^0 2\pi^+ 2\pi^-$ nonresonant	< 1.2 × 10 <sup>-3</sup>	CL=90%		
$\Gamma_{97}$	$\bar{K}^0 \pi^+ \pi^- 2\pi^0 (\pi^0)$				
$\Gamma_{98}$	$K^- 3\pi^+ 2\pi^-$	(2.2 ± 0.6) × 10 <sup>-4</sup>			
Fractions of some of the following modes with resonances have already appeared above as submodes of particular charged-particle modes. These nine modes below are all corrected for unseen decays of the resonances.					
$\Gamma_{99}$	$K_S^0 \eta$	(5.09 ± 0.13) × 10 <sup>-3</sup>			
$\Gamma_{100}$	$K_S^0 \omega$	(1.11 ± 0.06) %			
$\Gamma_{101}$	$K_S^0 \eta'(958)$	(9.49 ± 0.32) × 10 <sup>-3</sup>			
$\Gamma_{102}$	$\bar{K}^*(892)^0 \pi^+ \pi^- \pi^0$	(1.9 ± 0.9) %			
$\Gamma_{103}$	$\bar{K}^*(892)^0 \eta$				

Γ <sub>104</sub>	$K^- \pi^+ \omega$	( 3.1 ± 0.6 ) %		Γ <sub>163</sub>	Resonant $(\pi^+ \pi^-) \pi^+ \pi^-$	( 1.51 ± 0.12 ) × 10 <sup>-3</sup>	
Γ <sub>105</sub>	$\bar{K}^*(892)^0 \omega$	( 1.1 ± 0.5 ) %			3-body total		
Γ <sub>106</sub>	$K^- \pi^+ \eta'(958)$	( 6.43 ± 0.34 ) × 10 <sup>-3</sup>		Γ <sub>164</sub>	$\sigma \pi^+ \pi^-$	( 6.2 ± 0.9 ) × 10 <sup>-4</sup>	
Γ <sub>107</sub>	$K_S^0 \eta'(958) \pi^0$	( 2.52 ± 0.27 ) × 10 <sup>-3</sup>		Γ <sub>165</sub>	$\sigma \rho(770)^0$	( 5.0 ± 2.5 ) × 10 <sup>-4</sup>	
Γ <sub>108</sub>	$K^*(892)^0 \eta'(958)$	< 1.0 × 10 <sup>-3</sup>	CL=90%	Γ <sub>166</sub>	$f_0(980) \pi^+ \pi^-$ , $f_0 \rightarrow \pi^+ \pi^-$	( 1.8 ± 0.5 ) × 10 <sup>-4</sup>	
<b>Hadronic modes with three K's</b>							
Γ <sub>109</sub>	$K_S^0 K^+ K^-$	( 4.42 ± 0.32 ) × 10 <sup>-3</sup>		Γ <sub>167</sub>	$f_2(1270) \pi^+ \pi^-$ , $f_2 \rightarrow \pi^+ \pi^-$	( 3.7 ± 0.6 ) × 10 <sup>-4</sup>	
Γ <sub>110</sub>	$K_S^0 a_0(980)^0$ , $a_0^0 \rightarrow K^+ K^-$	( 2.9 ± 0.4 ) × 10 <sup>-3</sup>		Γ <sub>168</sub>	$2f_2(1270)$ , $f_2 \rightarrow \pi^+ \pi^-$	( 1.6 ± 1.8 ) × 10 <sup>-4</sup>	
Γ <sub>111</sub>	$K^- a_0(980)^+$ , $a_0^+ \rightarrow K^+ K_S^0$	( 5.9 ± 1.8 ) × 10 <sup>-4</sup>		Γ <sub>169</sub>	$f_0(1370) \sigma$ , $f_0 \rightarrow \pi^+ \pi^-$	( 1.6 ± 0.5 ) × 10 <sup>-3</sup>	
Γ <sub>112</sub>	$K^+ a_0(980)^-$ , $a_0^- \rightarrow K^- K_S^0$	< 1.1 × 10 <sup>-4</sup>	CL=95%	Γ <sub>170</sub>	$\pi^+ \pi^- 2\pi^0$	( 1.02 ± 0.09 ) %	
Γ <sub>113</sub>	$K_S^0 f_0(980)$ , $f_0 \rightarrow K^+ K^-$	< 9 × 10 <sup>-5</sup>	CL=95%	Γ <sub>171</sub>	$\eta \pi^0$	[h] ( 6.3 ± 0.6 ) × 10 <sup>-4</sup>	S=1.1
Γ <sub>114</sub>	$K_S^0 \phi$ , $\phi \rightarrow K^+ K^-$	( 2.03 ± 0.15 ) × 10 <sup>-3</sup>		Γ <sub>172</sub>	$\omega \pi^0$	[h] ( 1.17 ± 0.35 ) × 10 <sup>-4</sup>	
Γ <sub>115</sub>	$K_S^0 f_0(1370)$ , $f_0 \rightarrow K^+ K^-$	( 1.7 ± 1.1 ) × 10 <sup>-4</sup>		Γ <sub>173</sub>	$\omega \eta$	( 1.98 ± 0.18 ) × 10 <sup>-3</sup>	S=1.1
Γ <sub>116</sub>	$3K_S^0$	( 7.5 ± 0.7 ) × 10 <sup>-4</sup>	S=1.4	Γ <sub>174</sub>	$2\pi^+ 2\pi^- \pi^0$	( 4.2 ± 0.5 ) × 10 <sup>-3</sup>	
Γ <sub>117</sub>	$K^+ 2K^- \pi^+$	( 2.25 ± 0.32 ) × 10 <sup>-4</sup>		Γ <sub>175</sub>	$\eta \pi^+ \pi^-$	[h] ( 1.09 ± 0.16 ) × 10 <sup>-3</sup>	
Γ <sub>118</sub>	$K^+ K^- \bar{K}^*(892)^0$ , $\bar{K}^{*0} \rightarrow K^- \pi^+$	( 4.5 ± 1.8 ) × 10 <sup>-5</sup>		Γ <sub>176</sub>	$\omega \pi^+ \pi^-$	[h] ( 1.6 ± 0.5 ) × 10 <sup>-3</sup>	
Γ <sub>119</sub>	$K^- \pi^+ \phi$ , $\phi \rightarrow K^+ K^-$	( 4.1 ± 1.7 ) × 10 <sup>-5</sup>		Γ <sub>177</sub>	$\eta 2\pi^0$	( 3.8 ± 1.3 ) × 10 <sup>-4</sup>	
Γ <sub>120</sub>	$\phi \bar{K}^*(892)^0$ , $\phi \rightarrow K^+ K^-$ , $\bar{K}^{*0} \rightarrow K^- \pi^+$	( 1.08 ± 0.21 ) × 10 <sup>-4</sup>		Γ <sub>178</sub>	$3\pi^+ 3\pi^-$	( 4.3 ± 1.2 ) × 10 <sup>-4</sup>	
Γ <sub>121</sub>	$K^+ 2K^- \pi^+$ nonresonant	( 3.4 ± 1.5 ) × 10 <sup>-5</sup>		Γ <sub>179</sub>	$\eta'(958) \pi^0$	( 9.2 ± 1.0 ) × 10 <sup>-4</sup>	
Γ <sub>122</sub>	$2K_S^0 K^\pm \pi^\mp$	( 5.9 ± 1.3 ) × 10 <sup>-4</sup>		Γ <sub>180</sub>	$\eta'(958) \pi^+ \pi^-$	( 4.5 ± 1.7 ) × 10 <sup>-4</sup>	
<b>Pionic modes</b>							
Γ <sub>123</sub>	$\pi^+ \pi^-$	( 1.455 ± 0.024 ) × 10 <sup>-3</sup>	S=1.3	Γ <sub>181</sub>	$2\eta$	( 2.11 ± 0.19 ) × 10 <sup>-3</sup>	S=2.2
Γ <sub>124</sub>	$2\pi^0$	( 8.26 ± 0.25 ) × 10 <sup>-4</sup>		Γ <sub>182</sub>	$2\eta \pi^0$	( 7.3 ± 2.2 ) × 10 <sup>-4</sup>	
Γ <sub>125</sub>	$\pi^+ \pi^- \pi^0$	( 1.49 ± 0.06 ) %	S=2.1	Γ <sub>183</sub>	$3\eta$	< 1.3 × 10 <sup>-4</sup>	CL=90%
Γ <sub>126</sub>	$\rho^+ \pi^-$	( 1.01 ± 0.04 ) %		Γ <sub>184</sub>	$\eta \eta'(958)$	( 1.01 ± 0.19 ) × 10 <sup>-3</sup>	
Γ <sub>127</sub>	$\rho^0 \pi^0$	( 3.86 ± 0.23 ) × 10 <sup>-3</sup>		<b>Hadronic modes with a <math>K\bar{K}</math> pair</b>			
Γ <sub>128</sub>	$\rho^- \pi^+$	( 5.15 ± 0.25 ) × 10 <sup>-3</sup>		Γ <sub>185</sub>	$K^+ K^-$	( 4.08 ± 0.06 ) × 10 <sup>-3</sup>	S=1.6
Γ <sub>129</sub>	$\rho(1450)^+ \pi^-$ , $\rho^+ \rightarrow \pi^+ \pi^0$	( 1.6 ± 2.1 ) × 10 <sup>-5</sup>		Γ <sub>186</sub>	$2K_S^0$	( 1.41 ± 0.05 ) × 10 <sup>-4</sup>	S=1.1
Γ <sub>130</sub>	$\rho(1450)^0 \pi^0$ , $\rho^0 \rightarrow \pi^+ \pi^-$	( 4.5 ± 2.0 ) × 10 <sup>-5</sup>		Γ <sub>187</sub>	$K_S^0 K^- \pi^+$	( 3.3 ± 0.5 ) × 10 <sup>-3</sup>	S=1.1
Γ <sub>131</sub>	$\rho(1450)^- \pi^+$ , $\rho^- \rightarrow \pi^- \pi^0$	( 2.7 ± 0.4 ) × 10 <sup>-4</sup>		Γ <sub>188</sub>	$\bar{K}^*(892)^0 K_S^0$ , $\bar{K}^{*0} \rightarrow K^- \pi^+$	( 8.2 ± 1.6 ) × 10 <sup>-5</sup>	
Γ <sub>132</sub>	$\rho(1700)^+ \pi^-$ , $\rho^+ \rightarrow \pi^+ \pi^0$	( 6.1 ± 1.5 ) × 10 <sup>-4</sup>		Γ <sub>189</sub>	$K^*(892)^+ K^-$ , $K^{*+} \rightarrow K_S^0 \pi^+$	( 1.89 ± 0.30 ) × 10 <sup>-3</sup>	
Γ <sub>133</sub>	$\rho(1700)^0 \pi^0$ , $\rho^0 \rightarrow \pi^+ \pi^-$	( 7.4 ± 1.8 ) × 10 <sup>-4</sup>		Γ <sub>190</sub>	$\bar{K}^*(1410)^0 K_S^0$ , $\bar{K}^{*0} \rightarrow K^- \pi^+$	( 1.3 ± 1.9 ) × 10 <sup>-4</sup>	
Γ <sub>134</sub>	$\rho(1700)^- \pi^+$ , $\rho^- \rightarrow \pi^- \pi^0$	( 4.8 ± 1.1 ) × 10 <sup>-4</sup>		Γ <sub>191</sub>	$K^*(1410)^+ K^-$ , $K^{*+} \rightarrow K_S^0 \pi^+$	( 3.2 ± 1.9 ) × 10 <sup>-4</sup>	
Γ <sub>135</sub>	$f_0(980) \pi^0$ , $f_0 \rightarrow \pi^+ \pi^-$	( 3.7 ± 0.9 ) × 10 <sup>-5</sup>		Γ <sub>192</sub>	$(K^- \pi^+)_{S\text{-wave}} K_S^0$	( 6.0 ± 2.9 ) × 10 <sup>-4</sup>	
Γ <sub>136</sub>	$f_0(500) \pi^0$ , $f_0 \rightarrow \pi^+ \pi^-$	( 1.22 ± 0.22 ) × 10 <sup>-4</sup>		Γ <sub>193</sub>	$(K_S^0 \pi^+)_{S\text{-wave}} K^-$	( 3.9 ± 1.0 ) × 10 <sup>-4</sup>	
Γ <sub>137</sub>	$f_0(1370) \pi^0$ , $f_0 \rightarrow \pi^+ \pi^-$	( 5.5 ± 2.1 ) × 10 <sup>-5</sup>		Γ <sub>194</sub>	$a_0(980)^- \pi^+$ , $a_0^- \rightarrow K_S^0 K^-$	( 1.3 ± 1.4 ) × 10 <sup>-4</sup>	
Γ <sub>138</sub>	$f_0(1500) \pi^0$ , $f_0 \rightarrow \pi^+ \pi^-$	( 5.8 ± 1.6 ) × 10 <sup>-5</sup>		Γ <sub>195</sub>	$a_0(1450)^- \pi^+$ , $a_0^- \rightarrow K_S^0 K^-$	( 2.5 ± 2.0 ) × 10 <sup>-5</sup>	
Γ <sub>139</sub>	$f_0(1710) \pi^0$ , $f_0 \rightarrow \pi^+ \pi^-$	( 4.6 ± 1.6 ) × 10 <sup>-5</sup>		Γ <sub>196</sub>	$a_2(1320)^- \pi^+$ , $a_2^- \rightarrow K_S^0 K^-$	( 5 ± 5 ) × 10 <sup>-6</sup>	
Γ <sub>140</sub>	$f_2(1270) \pi^0$ , $f_2 \rightarrow \pi^+ \pi^-$	( 1.97 ± 0.21 ) × 10 <sup>-4</sup>		Γ <sub>197</sub>	$\rho(1450)^- \pi^+$ , $\rho^- \rightarrow K_S^0 K^-$	( 4.6 ± 2.5 ) × 10 <sup>-5</sup>	
Γ <sub>141</sub>	$\pi^+ \pi^- \pi^0$ nonresonant	( 1.3 ± 0.4 ) × 10 <sup>-4</sup>		Γ <sub>198</sub>	$K_S^0 K^+ \pi^-$	( 2.17 ± 0.34 ) × 10 <sup>-3</sup>	S=1.1
Γ <sub>142</sub>	$3\pi^0$	( 2.0 ± 0.5 ) × 10 <sup>-4</sup>		Γ <sub>199</sub>	$K^*(892)^0 K_S^0$ , $K^{*0} \rightarrow K^+ \pi^-$	( 1.12 ± 0.21 ) × 10 <sup>-4</sup>	
Γ <sub>143</sub>	$2\pi^+ 2\pi^-$	( 7.56 ± 0.20 ) × 10 <sup>-3</sup>		Γ <sub>200</sub>	$K^*(892)^- K^+$ , $K^{*-} \rightarrow K_S^0 \pi^-$	( 6.2 ± 1.0 ) × 10 <sup>-4</sup>	
Γ <sub>144</sub>	$a_1(1260)^+ \pi^-$ , $a_1^+ \rightarrow 2\pi^+ \pi^-$ total	( 4.54 ± 0.31 ) × 10 <sup>-3</sup>		Γ <sub>201</sub>	$K^*(1410)^0 K_S^0$ , $K^{*0} \rightarrow K^+ \pi^-$	( 5 ± 8 ) × 10 <sup>-5</sup>	
Γ <sub>145</sub>	$a_1(1260)^+ \pi^-$ , $a_1^+ \rightarrow \rho^0 \pi^+ S\text{-wave}$	( 3.14 ± 0.21 ) × 10 <sup>-3</sup>		Γ <sub>202</sub>	$K^*(1410)^- K^+$ , $K^{*-} \rightarrow K_S^0 \pi^-$	( 2.6 ± 2.0 ) × 10 <sup>-4</sup>	
Γ <sub>146</sub>	$a_1(1260)^+ \pi^-$ , $a_1^+ \rightarrow \rho^0 \pi^+ D\text{-wave}$	( 1.9 ± 0.5 ) × 10 <sup>-4</sup>		Γ <sub>203</sub>	$(K^+ \pi^-)_{S\text{-wave}} K_S^0$	( 3.7 ± 1.9 ) × 10 <sup>-4</sup>	
Γ <sub>147</sub>	$a_1(1260)^+ \pi^-$ , $a_1^+ \rightarrow \sigma \pi^+$	( 6.4 ± 0.7 ) × 10 <sup>-4</sup>		Γ <sub>204</sub>	$(K_S^0 \pi^-)_{S\text{-wave}} K^+$	( 1.4 ± 0.6 ) × 10 <sup>-4</sup>	
Γ <sub>148</sub>	$a_1(1260)^- \pi^+$ , $a_1^- \rightarrow \rho^0 \pi^- S\text{-wave}$	( 2.3 ± 0.9 ) × 10 <sup>-4</sup>		Γ <sub>205</sub>	$a_0(980)^+ \pi^-$ , $a_0^+ \rightarrow K_S^0 K^+$	( 6 ± 4 ) × 10 <sup>-4</sup>	
Γ <sub>149</sub>	$a_1(1260)^- \pi^+$ , $a_1^- \rightarrow \sigma \pi^-$	( 6.1 ± 3.4 ) × 10 <sup>-5</sup>		Γ <sub>206</sub>	$a_0(1450)^+ \pi^-$ , $a_0^+ \rightarrow K_S^0 K^+$	( 3.2 ± 2.5 ) × 10 <sup>-5</sup>	
Γ <sub>150</sub>	$\pi(1300)^+ \pi^-$ , $\pi(1300)^+ \rightarrow \sigma \pi^+$	( 5.1 ± 2.7 ) × 10 <sup>-4</sup>		Γ <sub>207</sub>	$\rho(1700)^+ \pi^-$ , $\rho^+ \rightarrow K_S^0 K^+$	( 1.1 ± 0.6 ) × 10 <sup>-5</sup>	
Γ <sub>151</sub>	$\pi(1300)^- \pi^+$ , $\pi(1300)^- \rightarrow \sigma \pi^-$	( 2.3 ± 2.2 ) × 10 <sup>-4</sup>		Γ <sub>208</sub>	$K^+ K^- \pi^0$	( 3.42 ± 0.14 ) × 10 <sup>-3</sup>	
Γ <sub>152</sub>	$a_1(1640)^+ \pi^-$ , $a_1^+ \rightarrow \rho^0 \pi^+ D\text{-wave}$	( 3.2 ± 1.6 ) × 10 <sup>-4</sup>		Γ <sub>209</sub>	$K^*(892)^+ K^-$ , $K^*(892)^+ \rightarrow K^+ \pi^0$	( 1.52 ± 0.07 ) × 10 <sup>-3</sup>	
Γ <sub>153</sub>	$a_1(1640)^+ \pi^-$ , $a_1^+ \rightarrow \sigma \pi^+$	( 1.8 ± 1.4 ) × 10 <sup>-4</sup>		Γ <sub>210</sub>	$K^*(892)^- K^+$ , $K^*(892)^- \rightarrow K^- \pi^0$	( 5.4 ± 0.4 ) × 10 <sup>-4</sup>	
Γ <sub>154</sub>	$\pi_2(1670)^+ \pi^-$ , $\pi_2^+ \rightarrow f_2(1270)^0 \pi^+$ , $f_2^0 \rightarrow \pi^+ \pi^-$	( 2.0 ± 0.9 ) × 10 <sup>-4</sup>		Γ <sub>211</sub>	$(K^+ \pi^0)_{S\text{-wave}} K^-$	( 2.43 ± 0.18 ) × 10 <sup>-3</sup>	
Γ <sub>155</sub>	$\pi_2(1670)^+ \pi^-$ , $\pi_2^+ \rightarrow \sigma \pi^+$	( 2.6 ± 1.0 ) × 10 <sup>-4</sup>		Γ <sub>212</sub>	$(K^- \pi^0)_{S\text{-wave}} K^+$	( 1.3 ± 0.5 ) × 10 <sup>-4</sup>	
Γ <sub>156</sub>	$2\rho^0$ total	( 1.85 ± 0.13 ) × 10 <sup>-3</sup>		Γ <sub>213</sub>	$f_0(980) \pi^0$ , $f_0 \rightarrow K^+ K^-$	( 3.6 ± 0.6 ) × 10 <sup>-4</sup>	
Γ <sub>157</sub>	$2\rho^0$ , parallel helicities	( 8.3 ± 3.2 ) × 10 <sup>-5</sup>		Γ <sub>214</sub>	$\phi \pi^0$ , $\phi \rightarrow K^+ K^-$	( 6.6 ± 0.4 ) × 10 <sup>-4</sup>	
Γ <sub>158</sub>	$2\rho^0$ , perpendicular helicities	( 4.8 ± 0.6 ) × 10 <sup>-4</sup>		Γ <sub>215</sub>	$K^+ K^- \pi^0$ nonresonant		
Γ <sub>159</sub>	$2\rho^0$ , longitudinal helicities	( 1.27 ± 0.10 ) × 10 <sup>-3</sup>		Γ <sub>216</sub>	$2K_S^0 \pi^0$	< 5.9 × 10 <sup>-4</sup>	
Γ <sub>160</sub>	$2\rho(770)^0$ , S-wave	( 1.8 ± 1.3 ) × 10 <sup>-4</sup>		Γ <sub>217</sub>	$K^+ K^- \pi^+ \pi^-$	( 2.47 ± 0.11 ) × 10 <sup>-3</sup>	
Γ <sub>161</sub>	$2\rho(770)^0$ , P-wave	( 5.3 ± 1.3 ) × 10 <sup>-4</sup>		Γ <sub>218</sub>	$\phi(\pi^+ \pi^-)_{S\text{-wave}}$ , $\phi \rightarrow K^+ K^-$	( 10 ± 5 ) × 10 <sup>-5</sup>	
Γ <sub>162</sub>	$2\rho(770)^0$ , D-wave	( 6.2 ± 3.0 ) × 10 <sup>-4</sup>					

## Meson Particle Listings

 $D^0$ 

$\Gamma_{219}$	$(\phi\rho^0)_{S\text{-wave}}, \phi \rightarrow K^+ K^-$	$(6.9 \pm 0.6) \times 10^{-4}$			
$\Gamma_{220}$	$(\phi\rho^0)_{P\text{-wave}}, \phi \rightarrow K^+ K^-$	$(4.0 \pm 1.9) \times 10^{-5}$			
$\Gamma_{221}$	$(\phi\rho^0)_{D\text{-wave}}, \phi \rightarrow K^+ K^-$	$(4.2 \pm 1.4) \times 10^{-5}$			
$\Gamma_{222}$	$K^*(892)^0 \bar{K}^*(892)^0, K^{*0} \rightarrow K^\pm \pi^\mp$				
$\Gamma_{223}$	$K^+ K^- \rho^0$ 3-body				
$\Gamma_{224}$	$f_0(980) \pi^+ \pi^-, f_0 \rightarrow K^+ K^-$				
$\Gamma_{225}$	$(K^*(892)^0 \bar{K}^*(892)^0)_{S\text{-wave}}, K^{*0} \rightarrow K^\pm \pi^\mp$	$(2.24 \pm 0.13) \times 10^{-4}$			
$\Gamma_{226}$	$(K^*(892)^0 \bar{K}^*(892)^0)_{P\text{-wave}}, K^* \rightarrow K^\pm \pi^\mp$	$(1.20 \pm 0.08) \times 10^{-4}$			
$\Gamma_{227}$	$(K^*(892)^0 \bar{K}^*(892)^0)_{D\text{-wave}}, K^* \rightarrow K^\pm \pi^\mp$	$(4.7 \pm 0.4) \times 10^{-5}$			
$\Gamma_{228}$	$K^*(892)^0 K^\mp \pi^\pm$ 3-body, $K^{*0} \rightarrow K^\pm \pi^\mp$				
$\Gamma_{229}$	$K^*(892)^0 (K^- \pi^+)_{S\text{-wave}}$ 3-body, $K^{*0} \rightarrow K^+ \pi^-$	$(1.4 \pm 0.6) \times 10^{-4}$			
$\Gamma_{230}$	$(K^- \pi^+)_{P\text{-wave}}, (K^+ \pi^-)_{S\text{-wave}}$				
$\Gamma_{231}$	$K_1(1270)^\pm K^\mp, K_1^\pm \rightarrow K^\pm \pi^\pm \pi^\mp$				
$\Gamma_{232}$	$K_1(1270)^+ K^-, K_1^+ \rightarrow K^{*0} \pi^+$	$(1.4 \pm 0.9) \times 10^{-4}$			
$\Gamma_{233}$	$K_1(1270)^+ K^-, K_1^+ \rightarrow K^*(1430)^0 \pi^+, K^{*0} \rightarrow K^+ \pi^-$	$(1.5 \pm 0.5) \times 10^{-4}$			
$\Gamma_{234}$	$K_1(1270)^+ K^-, K_1^+ \rightarrow \rho^0 K^+$	$(2.2 \pm 0.6) \times 10^{-4}$			
$\Gamma_{235}$	$K_1(1270)^+ K^-, K_1^+ \rightarrow \omega(782) K^+, \omega \rightarrow \pi^+ \pi^-$	$(1.5 \pm 1.2) \times 10^{-5}$			
$\Gamma_{236}$	$K_1(1270)^- K^+, K_1^- \rightarrow \bar{K}^{*0} \pi^-$				
$\Gamma_{237}$	$K_1(1270)^- K^+, K_1^- \rightarrow \rho^0 K^-$	$(1.3 \pm 0.4) \times 10^{-4}$			
$\Gamma_{238}$	$K_1(1400)^\pm K^\mp, K_1^\pm \rightarrow K^\pm \pi^+ \pi^-$				
$\Gamma_{239}$	$K_1(1400)^+ K^-, K_1^+ \rightarrow K^*(892)^0 \pi^+, K^{*0} \rightarrow K^+ \pi^-$	$(4.6 \pm 0.4) \times 10^{-4}$			
$\Gamma_{240}$	$K^*(1410)^+ K^-, K^{*+} \rightarrow K^{*0} \pi^+$				
$\Gamma_{241}$	$K^*(1410)^- K^+, K^{*-} \rightarrow \bar{K}^{*0} \pi^-$	$(7.0 \pm 1.1) \times 10^{-5}$			
$\Gamma_{242}$	$K_1(1680)^+ K^-, K_1^+ \rightarrow K^{*0} \pi^+, K^{*0} \rightarrow K^+ \pi^-$	$(8.9 \pm 3.2) \times 10^{-5}$			
$\Gamma_{243}$	$K^+ K^- \pi^+ \pi^-$ non-resonant	$(2.7 \pm 0.6) \times 10^{-4}$			
$\Gamma_{244}$	$2K_S^0 \pi^+ \pi^-$	$(1.22 \pm 0.23) \times 10^{-3}$			
$\Gamma_{245}$	$K_S^0 K^- 2\pi^+ \pi^-$	$< 1.4 \times 10^{-4}$	CL=90%		
$\Gamma_{246}$	$K^+ K^- \pi^+ \pi^- \pi^0$	$(3.1 \pm 2.0) \times 10^{-3}$			
Other $K\bar{K}X$ modes. They include all decay modes of the $\phi, \eta,$ and $\omega$ .					
$\Gamma_{247}$	$\phi \pi^0$	$(1.17 \pm 0.04) \times 10^{-3}$			
$\Gamma_{248}$	$\phi \eta$	$(1.8 \pm 0.5) \times 10^{-4}$			
$\Gamma_{249}$	$\phi \omega$	$< 2.1 \times 10^{-3}$	CL=90%		
<b>Radiative modes</b>					
$\Gamma_{250}$	$\rho^0 \gamma$	$(1.82 \pm 0.32) \times 10^{-5}$			
$\Gamma_{251}$	$\omega \gamma$	$< 2.4 \times 10^{-4}$	CL=90%		
$\Gamma_{252}$	$\phi \gamma$	$(2.81 \pm 0.19) \times 10^{-5}$			
$\Gamma_{253}$	$\bar{K}^*(892)^0 \gamma$	$(4.2 \pm 0.7) \times 10^{-4}$			
<b>Doubly Cabibbo suppressed (DC) modes or <math>\Delta C = 2</math> forbidden via mixing (C2M) modes</b>					
$\Gamma_{254}$	$K^+ \ell^- \bar{\nu}_\ell$ via $\bar{D}^0$	$< 2.2 \times 10^{-5}$	CL=90%		
$\Gamma_{255}$	$K^+ \text{ or } K^*(892)^+ e^- \bar{\nu}_e$ via $\bar{D}^0$	$< 6 \times 10^{-5}$	CL=90%		
$\Gamma_{256}$	$K^+ \pi^-$	$(1.50 \pm 0.07) \times 10^{-4}$		S=3.0	
$\Gamma_{257}$	$K^+ \pi^-$ via DCS	$(1.364 \pm 0.026) \times 10^{-4}$			
$\Gamma_{258}$	$K^+ \pi^-$ via $\bar{D}^0$	$< 1.6 \times 10^{-5}$	CL=95%		
$\Gamma_{259}$	$K_S^0 \pi^+ \pi^-$ in $D^0 \rightarrow \bar{D}^0$	$< 1.8 \times 10^{-4}$	CL=95%		
$\Gamma_{260}$	$K^*(892)^+ \pi^-, K^{*+} \rightarrow K_S^0 \pi^+$	$(1.13 \pm_{0.34}^{0.60}) \times 10^{-4}$			
$\Gamma_{261}$	$K_0^*(1430)^+ \pi^-, K_0^{*+} \rightarrow K_S^0 \pi^+$	$< 1.4 \times 10^{-5}$			
$\Gamma_{262}$	$K_2^*(1430)^+ \pi^-, K_2^{*+} \rightarrow K_S^0 \pi^+$	$< 3.4 \times 10^{-5}$			
$\Gamma_{263}$	$K^+ \pi^- \pi^0$	DC	$(3.06 \pm 0.15) \times 10^{-4}$		
$\Gamma_{264}$	$K^+ \pi^- \pi^0$ via $\bar{D}^0$		$(7.6 \pm_{0.6}^{0.5}) \times 10^{-4}$		
$\Gamma_{265}$	$K^+ \pi^+ 2\pi^-$ via DCS		$(2.49 \pm 0.07) \times 10^{-4}$		
$\Gamma_{266}$	$K^+ \pi^+ 2\pi^-$	DC	$(2.65 \pm 0.06) \times 10^{-4}$		
$\Gamma_{267}$	$K^+ \pi^+ 2\pi^-$ via $\bar{D}^0$		$(7.9 \pm 3.0) \times 10^{-6}$		
$\Gamma_{268}$	$K^+ \pi^-$ or $K^+ \pi^+ 2\pi^-$ via $\bar{D}^0$				
$\Gamma_{269}$	$\mu^-$ anything via $\bar{D}^0$	$< 4$	$\times 10^{-4}$	CL=90%	
<b><math>\Delta C = 1</math> weak neutral current (CI) modes, Lepton Family number (LF) violating modes, Lepton (L) or Baryon (B) number violating modes</b>					
$\Gamma_{270}$	$\gamma \gamma$	CI	$< 8.5 \times 10^{-7}$	CL=90%	
$\Gamma_{271}$	$e^+ e^-$	CI	$< 7.9 \times 10^{-8}$	CL=90%	
$\Gamma_{272}$	$\mu^+ \mu^-$	CI	$< 6.2 \times 10^{-9}$	CL=90%	
$\Gamma_{273}$	$\pi^0 e^+ e^-$	CI	$< 4 \times 10^{-6}$	CL=90%	
$\Gamma_{274}$	$\pi^0 \mu^+ \mu^-$	CI	$< 1.8 \times 10^{-4}$	CL=90%	
$\Gamma_{275}$	$\eta e^+ e^-$	CI	$< 3 \times 10^{-6}$	CL=90%	
$\Gamma_{276}$	$\eta \mu^+ \mu^-$	CI	$< 5.3 \times 10^{-4}$	CL=90%	
$\Gamma_{277}$	$\pi^+ \pi^- e^+ e^-$	CI	$< 7 \times 10^{-6}$	CL=90%	
$\Gamma_{278}$	$\rho^0 e^+ e^-$	CI	$< 1.0 \times 10^{-4}$	CL=90%	
$\Gamma_{279}$	$\pi^+ \pi^- \mu^+ \mu^-$	CI	$(9.6 \pm 1.2) \times 10^{-7}$		
$\Gamma_{280}$	$\pi^+ \pi^- \mu^+ \mu^-$ (non-res)		$< 5.5 \times 10^{-7}$	CL=90%	
$\Gamma_{281}$	$\rho^0 \mu^+ \mu^-$	CI	$< 2.2 \times 10^{-5}$	CL=90%	
$\Gamma_{282}$	$\omega e^+ e^-$	CI	$< 6 \times 10^{-6}$	CL=90%	
$\Gamma_{283}$	$\omega \mu^+ \mu^-$	CI	$< 8.3 \times 10^{-4}$	CL=90%	
$\Gamma_{284}$	$K^- K^+ e^+ e^-$	CI	$< 1.1 \times 10^{-5}$	CL=90%	
$\Gamma_{285}$	$\phi e^+ e^-$	CI	$< 5.2 \times 10^{-5}$	CL=90%	
$\Gamma_{286}$	$K^- K^+ \mu^+ \mu^-$	CI	$(1.54 \pm 0.32) \times 10^{-7}$		
$\Gamma_{287}$	$K^- K^+ \mu^+ \mu^-$ (non-res)		$< 3.3 \times 10^{-5}$	CL=90%	
$\Gamma_{288}$	$\phi \mu^+ \mu^-$	CI	$< 3.1 \times 10^{-5}$	CL=90%	
$\Gamma_{289}$	$\bar{K}^0 e^+ e^-$	[j]	$< 2.4 \times 10^{-5}$	CL=90%	
$\Gamma_{290}$	$\bar{K}^0 \mu^+ \mu^-$	[j]	$< 2.6 \times 10^{-4}$	CL=90%	
$\Gamma_{291}$	$K^- \pi^+ e^+ e^-$				
$\Gamma_{292}$	$K^- \pi^+ e^+ e^-, 675 < m_{ee} < 875 \text{ MeV}$		$(4.0 \pm 0.5) \times 10^{-6}$		
$\Gamma_{293}$	$K^- \pi^+ e^+ e^-, 1.005 < m_{ee} < 1.035 \text{ GeV}$		$< 5 \times 10^{-7}$	CL=90%	
$\Gamma_{294}$	$\bar{K}^*(892)^0 e^+ e^-$	[j]	$< 4.7 \times 10^{-5}$	CL=90%	
$\Gamma_{295}$	$K^- \pi^+ \mu^+ \mu^-$	CI	$< 3.59 \times 10^{-4}$	CL=90%	
$\Gamma_{296}$	$K^- \pi^+ \mu^+ \mu^-, 675 < m_{\mu\mu} < 875 \text{ MeV}$		$(4.2 \pm 0.4) \times 10^{-6}$		
$\Gamma_{297}$	$\bar{K}^*(892)^0 \mu^+ \mu^-$	[j]	$< 2.4 \times 10^{-5}$	CL=90%	
$\Gamma_{298}$	$\pi^+ \pi^- \pi^0 \mu^+ \mu^-$	CI	$< 8.1 \times 10^{-4}$	CL=90%	
$\Gamma_{299}$	$\mu^\pm e^\mp$	LF	[j] $< 1.3 \times 10^{-8}$	CL=90%	
$\Gamma_{300}$	$\pi^0 e^\pm \mu^\mp$	LF	[j] $< 8.6 \times 10^{-5}$	CL=90%	
$\Gamma_{301}$	$\eta e^\pm \mu^\mp$	LF	[j] $< 1.0 \times 10^{-4}$	CL=90%	
$\Gamma_{302}$	$\pi^+ \pi^- e^\pm \mu^\mp$	LF	[j] $< 1.5 \times 10^{-5}$	CL=90%	
$\Gamma_{303}$	$\rho^0 e^\pm \mu^\mp$	LF	[j] $< 4.9 \times 10^{-5}$	CL=90%	
$\Gamma_{304}$	$\omega e^\pm \mu^\mp$	LF	[j] $< 1.2 \times 10^{-4}$	CL=90%	
$\Gamma_{305}$	$K^- K^+ e^\pm \mu^\mp$	LF	[j] $< 1.8 \times 10^{-4}$	CL=90%	
$\Gamma_{306}$	$\phi e^\pm \mu^\mp$	LF	[j] $< 3.4 \times 10^{-5}$	CL=90%	
$\Gamma_{307}$	$\bar{K}^0 e^\pm \mu^\mp$	LF	[j] $< 1.0 \times 10^{-4}$	CL=90%	
$\Gamma_{308}$	$K^- \pi^+ e^\pm \mu^\mp$	LF	[j] $< 5.53 \times 10^{-4}$	CL=90%	
$\Gamma_{309}$	$\bar{K}^*(892)^0 e^\pm \mu^\mp$	LF	[j] $< 8.3 \times 10^{-5}$	CL=90%	
$\Gamma_{310}$	$2\pi^- 2e^+ + \text{c.c.}$	L	$< 1.12 \times 10^{-4}$	CL=90%	
$\Gamma_{311}$	$2\pi^- 2\mu^+ + \text{c.c.}$	L	$< 2.9 \times 10^{-5}$	CL=90%	
$\Gamma_{312}$	$K^- \pi^- 2e^+ + \text{c.c.}$				
$\Gamma_{313}$	$K^- \pi^- 2e^+$		$< 2.8 \times 10^{-6}$	CL=90%	
$\Gamma_{314}$	$K^- \pi^- 2\mu^+ + \text{c.c.}$	L	$< 3.9 \times 10^{-4}$	CL=90%	
$\Gamma_{315}$	$2K^- 2e^+ + \text{c.c.}$	L	$< 1.52 \times 10^{-4}$	CL=90%	
$\Gamma_{316}$	$2K^- 2\mu^+ + \text{c.c.}$	L	$< 9.4 \times 10^{-5}$	CL=90%	
$\Gamma_{317}$	$\pi^- \pi^- e^+ \mu^+ + \text{c.c.}$	L	$< 7.9 \times 10^{-5}$	CL=90%	
$\Gamma_{318}$	$K^- \pi^- e^+ \mu^+ + \text{c.c.}$	L	$< 2.18 \times 10^{-4}$	CL=90%	
$\Gamma_{319}$	$2K^- e^+ \mu^+ + \text{c.c.}$	L	$< 5.7 \times 10^{-5}$	CL=90%	
$\Gamma_{320}$	$p e^-$	L,B	[k] $< 1.0 \times 10^{-5}$	CL=90%	
$\Gamma_{321}$	$\bar{p} e^+$	L,B	[l] $< 1.1 \times 10^{-5}$	CL=90%	
$\Gamma_{322}$	Unaccounted decay modes		$(36.9 \pm 1.2) \%$	S=1.1	

[a] This value is obtained by subtracting the branching fractions for 2-, 4- and 6-prongs from unity.

[b] This is the sum of our  $K^- 2\pi^+ \pi^-$ ,  $K^- 2\pi^+ \pi^- \pi^0$ ,  $\bar{K}^0 2\pi^+ 2\pi^-$ ,  $K^+ 2K^- \pi^+$ ,  $2\pi^+ 2\pi^-$ ,  $2\pi^+ 2\pi^- \pi^0$ ,  $K^+ K^- \pi^+ \pi^-$ , and  $K^+ K^- \pi^+ \pi^- \pi^0$ , branching fractions.



## Meson Particle Listings

 $D^0$  $\Gamma(4\text{-prongs})/\Gamma_{\text{total}}$ 

This is the sum of our  $K^-2\pi^+\pi^-$ ,  $K^-2\pi^+\pi^-\pi^0$ ,  $\bar{K}^02\pi^+2\pi^-$ ,  $K^+2K^-\pi^+$ ,  $2\pi^+2\pi^-$ ,  $2\pi^+2\pi^-\pi^0$ ,  $K^+K^-\pi^+\pi^-$ , and  $K^+K^-\pi^+\pi^-\pi^0$  branching fractions.

VALUE	DOCUMENT ID	TECN	COMMENT
<b>0.146±0.005 OUR FIT</b>			
<b>0.146±0.005</b>	PDG	19	

 $\Gamma(6\text{-prongs})/\Gamma_{\text{total}}$ 

This is the sum of our  $K^-3\pi^+2\pi^-$  and  $3\pi^+3\pi^-$  branching fractions.

VALUE (units $10^{-4}$ )	DOCUMENT ID	TECN	COMMENT
<b>6.5±1.3 OUR FIT</b>			
<b>6.5±1.3</b>	PDG	19	

## Inclusive modes

 $\Gamma(e^+\text{ anything})/\Gamma_{\text{total}}$ 

The branching fractions for the  $K^-e^+\nu_e$ ,  $K^*(892)^-e^+\nu_e$ ,  $\pi^-e^+\nu_e$ , and  $\rho^-e^+\nu_e$  modes add up to  $6.17 \pm 0.17\%$ .

VALUE (%)	EVTS	DOCUMENT ID	TECN	COMMENT
<b>6.49±0.11 OUR AVERAGE</b>				
6.46±0.09±0.11	6584 ± 96	<sup>1</sup> ASNER	10 CLEO	$e^+e^-$ at 3774 MeV
6.3 ± 0.7 ± 0.4	290 ± 32	ABLIKIM	07G BES2	$e^+e^- \approx \psi(3770)$
6.46±0.17±0.13	2246 ± 57	ADAM	06A CLEO	See ASNER 10
6.9 ± 0.3 ± 0.5	1670	ALBRECHT	96C ARG	$e^+e^- \approx 10$ GeV
6.64±0.18±0.29	4609	KUBOTA	96B CLE2	$e^+e^- \approx \Upsilon(4S)$

<sup>1</sup> Using the  $D^+$  and  $D^0$  lifetimes, ASNER 10 finds that the ratio of the  $D^+$  and  $D^0$  semileptonic widths is  $0.985 \pm 0.015 \pm 0.024$ .

 $\Gamma(\mu^+\text{ anything})/\Gamma_{\text{total}}$ 

VALUE (%)	EVTS	DOCUMENT ID	TECN	COMMENT
<b>6.8±0.6 OUR FIT</b>				
<b>6.4±0.8 OUR AVERAGE</b>				
6.8±1.5±0.8	79 ± 10	<sup>1</sup> ABLIKIM	08L BES2	$e^+e^- \approx \psi(3772)$
6.5±1.2±0.3	36	KAYIS-TOPAK.05	CHRS	$\nu_\mu$ emulsion
6.0±0.7±1.2	310	ALBRECHT	96C ARG	$e^+e^- \approx 10$ GeV

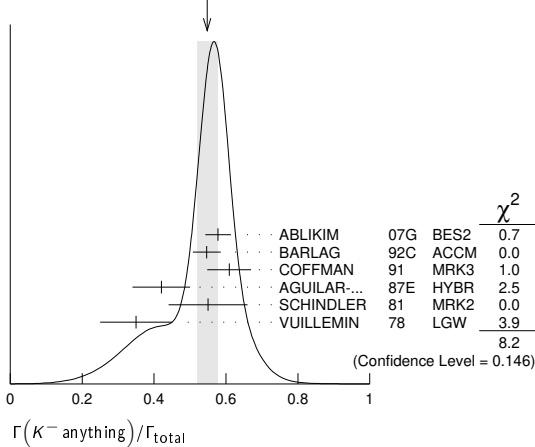
<sup>1</sup> ABLIKIM 08L finds the ratio of  $D^+ \rightarrow \mu^+X$  and  $D^0 \rightarrow \mu^+X$  branching fractions to be  $2.59 \pm 0.70 \pm 0.25$ , in accord with the ratio of  $D^+$  and  $D^0$  lifetimes,  $2.54 \pm 0.02$ .

 $\Gamma(K^-\text{ anything})/\Gamma_{\text{total}}$ 

VALUE	EVTS	DOCUMENT ID	TECN	COMMENT
<b>0.547±0.028 OUR AVERAGE</b>				Error includes scale factor of 1.3. See the ideogram below.
0.578±0.016±0.032	2098 ± 59	ABLIKIM	07G BES2	$e^+e^- \approx \psi(3770)$
0.546 <sup>+0.039</sup> <sub>-0.038</sub>		<sup>1</sup> BARLAG	92c ACCM	$\pi^-$ Cu 230 GeV
0.609±0.032±0.052		COFFMAN	91 MRK3	$e^+e^-$ 3.77 GeV
0.42 ± 0.08		AGUILAR...	87E HYBR	$\pi p, pp$ 360, 400 GeV
0.55 ± 0.11	121	SCHINDLER	81 MRK2	$e^+e^-$ 3.771 GeV
0.35 ± 0.10	19	VUILLEMIN	78 LGW	$e^+e^-$ 3.772 GeV

<sup>1</sup> BARLAG 92c computes the branching fraction using topological normalization.

WEIGHTED AVERAGE  
0.547±0.028 (Error scaled by 1.3)

 $[\Gamma(K^0\text{ anything}) + \Gamma(K^-\text{ anything})]/\Gamma_{\text{total}}$ 

VALUE	EVTS	DOCUMENT ID	TECN	COMMENT
<b>0.47 ± 0.04 OUR AVERAGE</b>				
0.476±0.048±0.030	250 ± 25	ABLIKIM	06u BES2	$e^+e^-$ at 3773 MeV
0.455±0.050±0.032		COFFMAN	91 MRK3	$e^+e^-$ 3.77 GeV

 $\Gamma(K^+\text{ anything})/\Gamma_{\text{total}}$ 

VALUE	EVTS	DOCUMENT ID	TECN	COMMENT
<b>0.034±0.004 OUR AVERAGE</b>				
0.035±0.007±0.003	119 ± 23	ABLIKIM	07G BES2	$e^+e^- \approx \psi(3770)$
0.034 <sup>+0.007</sup> <sub>-0.005</sub>		<sup>1</sup> BARLAG	92c ACCM	$\pi^-$ Cu 230 GeV
0.028±0.009±0.004		COFFMAN	91 MRK3	$e^+e^-$ 3.77 GeV
0.03 <sup>+0.05</sup> <sub>-0.02</sub>		AGUILAR...	87E HYBR	$\pi p, pp$ 360, 400 GeV
0.08 ± 0.03	25	SCHINDLER	81 MRK2	$e^+e^-$ 3.771 GeV

<sup>1</sup> BARLAG 92c computes the branching fraction using topological normalization.

 $\Gamma(K^*(892)^-\text{ anything})/\Gamma_{\text{total}}$ 

VALUE	EVTS	DOCUMENT ID	TECN	COMMENT
<b>0.153±0.083±0.019</b>	28 ± 15	ABLIKIM	06u BES2	$e^+e^-$ at 3773 MeV

 $\Gamma(K^*(892)^0\text{ anything})/\Gamma_{\text{total}}$ 

VALUE	EVTS	DOCUMENT ID	TECN	COMMENT
<b>0.087±0.040±0.012</b>	96 ± 44	ABLIKIM	05P BES	$e^+e^- \approx 3773$ MeV

 $\Gamma(K^*(892)^+\text{ anything})/\Gamma_{\text{total}}$ 

VALUE	CL%	DOCUMENT ID	TECN	COMMENT
<b>&lt;0.036</b>	90	ABLIKIM	06u BES2	$e^+e^-$ at 3773 MeV

 $\Gamma(K^*(892)^0\text{ anything})/\Gamma_{\text{total}}$ 

VALUE	EVTS	DOCUMENT ID	TECN	COMMENT
<b>0.028±0.012±0.004</b>	31 ± 12	ABLIKIM	05P BES	$e^+e^- \approx 3773$ MeV

 $\Gamma(\eta\text{ anything})/\Gamma_{\text{total}}$ 

VALUE (%)	EVTS	DOCUMENT ID	TECN	COMMENT
<b>9.5±0.4±0.8</b>	4463 ± 197	HUANG	06B CLEO	$e^+e^-$ at $\psi(3770)$

 $\Gamma(\eta'\text{ anything})/\Gamma_{\text{total}}$ 

VALUE (%)	EVTS	DOCUMENT ID	TECN	COMMENT
<b>2.48±0.17±0.21</b>	299 ± 21	HUANG	06B CLEO	$e^+e^-$ at $\psi(3770)$

 $\Gamma(\phi\text{ anything})/\Gamma_{\text{total}}$ 

VALUE (%)	EVTS	DOCUMENT ID	TECN	COMMENT
<b>1.08 ± 0.04 OUR AVERAGE</b>				
1.091±0.027±0.035	4.1k	ABLIKIM	19AYBES3	$e^+e^-$ at 3773 MeV
1.05 ± 0.08 ± 0.07	368 ± 24	HUANG	06B CLEO	$e^+e^-$ at $\psi(3770)$
••• We do not use the following data for averages, fits, limits, etc. •••				
1.71 <sup>+0.76</sup> <sub>-0.71</sub> ± 0.17	9	BAI	00c BES	$e^+e^- \rightarrow D\bar{D}^*, D^*\bar{D}^*$

 $\Gamma(\text{invisibles})/\Gamma_{\text{total}}$ 

VALUE	CL%	DOCUMENT ID	TECN	COMMENT
<b>&lt;9.4 × 10<sup>-5</sup></b>	90	LAI	17 BELL	$e^+e^-$ at $\Upsilon(nS)$ , n=4,5

## Semileptonic modes

 $\Gamma(K^-e^+\nu_e)/\Gamma_{\text{total}}$ 

VALUE (%)	EVTS	DOCUMENT ID	TECN	COMMENT
<b>3.542±0.035 OUR FIT</b>				Error includes scale factor of 1.3.
<b>3.503±0.029 OUR AVERAGE</b>				
3.505±0.014±0.033	71k	<sup>1</sup> ABLIKIM	15x BES3	2.92 fb <sup>-1</sup> , 3.773 GeV
3.50 ± 0.03 ± 0.04	14.1k	<sup>1</sup> BESSON	09 CLEO	$e^+e^-$ at $\psi(3770)$
3.45 ± 0.10 ± 0.19	1.3k	<sup>2</sup> WIDHALM	06 BELL	$e^+e^- \approx \Upsilon(4S)$
3.82 ± 0.40 ± 0.27	104	ABLIKIM	04c BES	$e^+e^-$ , 3.773 GeV
3.4 ± 0.5 ± 0.4	55	ADLER	89 MRK3	$e^+e^-$ 3.77 GeV
••• We do not use the following data for averages, fits, limits, etc. •••				
3.56 ± 0.03 ± 0.09		<sup>3</sup> DOBBS	08 CLEO	See BESSON 09
3.44 ± 0.10 ± 0.10	1.3k	COAN	05 CLEO	See DOBBS 08

<sup>1</sup> See the form-factor parameters near the end of this  $D^0$  Listing.

<sup>2</sup> The  $\pi^-e^+\nu_e$  and  $K^-e^+\nu_e$  results of WIDHALM 06 give  $|\frac{V_{cd}}{V_{cs}} \cdot \frac{f_+^{\pi^0}(0)}{f_+^{K^0}(0)}|^2 = 0.042 \pm 0.003 \pm 0.003$ .

<sup>3</sup> DOBBS 08 establishes  $|\frac{V_{cd}}{V_{cs}} \cdot \frac{f_+^{\pi^0}(0)}{f_+^{K^0}(0)}| = 0.188 \pm 0.008 \pm 0.002$  from the  $D^+$  and  $D^0$  decays to  $\bar{K}e^+\nu_e$  and  $\pi e^+\nu_e$ .

 $\Gamma(K^-e^+\nu_e)/\Gamma(K^-\pi^+)$ 

VALUE	EVTS	DOCUMENT ID	TECN	COMMENT
<b>0.897±0.011 OUR FIT</b>				Error includes scale factor of 1.4.
<b>0.930±0.013 OUR AVERAGE</b>				
0.927±0.007±0.012	76k ± 323	<sup>1</sup> AUBERT	07Bg BABR	$e^+e^- \approx \Upsilon(4S)$
0.978±0.027±0.044	2510	<sup>2</sup> BEAN	93c CLE2	$e^+e^- \approx \Upsilon(4S)$
0.90 ± 0.06 ± 0.06	584	<sup>3</sup> CRAWFORD	91B CLEO	$e^+e^- \approx 10.5$ GeV
0.91 ± 0.07 ± 0.11	250	<sup>4</sup> ANJOS	89F E691	Photoproduction

<sup>1</sup> The event samples in this AUBERT 07Bg result include radiative photons. The  $D^0 \rightarrow K^-e^+\nu_e$  form factor at  $q^2 = 0$  is  $f_+(0) = 0.727 \pm 0.007 \pm 0.005 \pm 0.007$ .





• • • We do not use the following data for averages, fits, limits, etc. • • •
0.042±0.005±0.011... ASNER 04A CLEO See MURAMATSU 02
0.068±0.016±0.018... FRABETTI 94G E687 Dalitz fit, 597 evts
0.046±0.018±0.006... ALBRECHT 93D ARG Dalitz fit, 440 evts

$\Gamma(K_S^0 f_0(1370), f_0 \to \pi^+ \pi^-)/\Gamma(K_S^0 \pi^+ \pi^-)$   $\Gamma_{43}/\Gamma_{38}$ 
This is the "fit fraction" from the Dalitz-plot analysis.

0.099±0.011±0.028... MURAMATSU 02 CLE2 Dalitz fit, 5299 evts
• • • We do not use the following data for averages, fits, limits, etc. • • •

0.098±0.014±0.026... ASNER 04A CLEO See MURAMATSU 02
0.077±0.022±0.031... FRABETTI 94G E687 Dalitz fit, 597 evts
0.082±0.028±0.013... ALBRECHT 93D ARG Dalitz fit, 440 evts

$\Gamma(K_S^0 f_2(1270), f_2 \to \pi^+ \pi^-)/\Gamma(K_S^0 \pi^+ \pi^-)$   $\Gamma_{44}/\Gamma_{38}$ 
This is the "fit fraction" from the Dalitz-plot analysis.

0.0032±0.0035 OUR AVERAGE
0.006 ± 0.007
0.0027±0.0015±0.0037... MURAMATSU 02 CLE2 Dalitz fit, 5299 evts

• • • We do not use the following data for averages, fits, limits, etc. • • •
0.0036±0.0022±0.0032... ASNER 04A CLEO See MURAMATSU 02

0.037 ± 0.014 ± 0.017... FRABETTI 94G E687 Dalitz fit, 597 evts
0.050 ± 0.021 ± 0.008... ALBRECHT 93D ARG Dalitz fit, 440 evts
1 The error on this AUBERT 08AL value includes both statistical and systematic uncertainties; the latter dominates.

$\Gamma(K^*(892)^- \pi^+, K^{*-} \to K_S^0 \pi^-)/\Gamma(K_S^0 \pi^+ \pi^-)$   $\Gamma_{45}/\Gamma_{38}$ 
This is the "fit fraction" from the Dalitz-plot analysis.

0.588±0.034 OUR AVERAGE Error includes scale factor of 2.0.
0.557±0.028
1 AUBERT 08AL BABR Dalitz fit, ≈ 487 k evts

0.657±0.013±0.018... MURAMATSU 02 CLE2 Dalitz fit, 5299 evts
• • • We do not use the following data for averages, fits, limits, etc. • • •

0.663±0.013±0.024... ASNER 04A CLEO See MURAMATSU 02
0.625±0.036±0.026... FRABETTI 94G E687 Dalitz fit, 597 evts
0.718±0.042±0.030... ALBRECHT 93D ARG Dalitz fit, 440 evts

0.480±0.097... ANJOS 93 E691 γBe 90–260 GeV
0.56 ± 0.04 ± 0.05... ADLER 87 MRK3 e+ e- 3.77 GeV
1 The error on this AUBERT 08AL value includes both statistical and systematic uncertainties; the latter dominates.

$\Gamma(K_S^0(1430)^- \pi^+, K_0^{*-} \to K_S^0 \pi^-)/\Gamma(K_S^0 \pi^+ \pi^-)$   $\Gamma_{46}/\Gamma_{38}$ 
This is the "fit fraction" from the Dalitz-plot analysis.

0.095±0.014 OUR AVERAGE
0.102±0.015
1 AUBERT 08AL BABR Dalitz fit, ≈ 487 k evts

0.073±0.007±0.031... MURAMATSU 02 CLE2 Dalitz fit, 5299 evts
• • • We do not use the following data for averages, fits, limits, etc. • • •

0.072±0.007±0.014... ASNER 04A CLEO See MURAMATSU 02
0.109±0.027±0.029... FRABETTI 94G E687 Dalitz fit, 597 evts
0.129±0.034±0.021... ALBRECHT 93D ARG Dalitz fit, 440 evts

1 The error on this AUBERT 08AL value includes both statistical and systematic uncertainties; the latter dominates.
1 The error on this AUBERT 08AL value includes both statistical and systematic uncertainties; the latter dominates.

$\Gamma(K_S^0(1430)^- \pi^+, K_2^{*-} \to K_S^0 \pi^-)/\Gamma(K_S^0 \pi^+ \pi^-)$   $\Gamma_{47}/\Gamma_{38}$ 
This is the "fit fraction" from the Dalitz-plot analysis.

0.0120±0.0070 OUR AVERAGE
0.022 ± 0.016
1 AUBERT 08AL BABR Dalitz fit, ≈ 487 k evts

0.011 ± 0.002 ± 0.007... MURAMATSU 02 CLE2 Dalitz fit, 5299 evts
• • • We do not use the following data for averages, fits, limits, etc. • • •

0.011 ± 0.002 ± 0.005... ASNER 04A CLEO See MURAMATSU 02
1 The error on this AUBERT 08AL value includes both statistical and systematic uncertainties; the latter dominates.

$\Gamma(K^*(1680)^- \pi^+, K^{*-} \to K_S^0 \pi^-)/\Gamma(K_S^0 \pi^+ \pi^-)$   $\Gamma_{48}/\Gamma_{38}$ 
This is the "fit fraction" from the Dalitz-plot analysis.

0.016±0.013 OUR AVERAGE
0.007±0.019
1 AUBERT 08AL BABR Dalitz fit, ≈ 487 k evts

0.022±0.004±0.018... MURAMATSU 02 CLE2 Dalitz fit, 5299 evts
• • • We do not use the following data for averages, fits, limits, etc. • • •

0.023±0.005±0.007... ASNER 04A CLEO See MURAMATSU 02
1 The error on this AUBERT 08AL value includes both statistical and systematic uncertainties; the latter dominates.

$\Gamma(K^*(892)^+ \pi^-, K^{*+} \to K_S^0 \pi^+)/\Gamma(K_S^0 \pi^+ \pi^-)$   $\Gamma_{49}/\Gamma_{38}$

This is the "fit fraction" from the Dalitz-plot analysis. This is a doubly Cabibbo-suppressed mode.
VALUE (units 10^-3) DOCUMENT ID TECN COMMENT

4.0±2.0 OUR AVERAGE

4.6±2.3 1 AUBERT 08AL BABR Dalitz fit, ≈ 487 k evts
3.4±1.3±4.1... MURAMATSU 02 CLE2 Dalitz fit, 5299 evts

• • • We do not use the following data for averages, fits, limits, etc. • • •
3.4±1.3±3.6... ASNER 04A CLEO See MURAMATSU 02

1 The error on this AUBERT 08AL value includes both statistical and systematic uncertainties; the latter dominates.

$\Gamma(K_0^*(1430)^+ \pi^-, K_0^{*+} \to K_S^0 \pi^+)/\Gamma(K_S^0 \pi^+ \pi^-)$   $\Gamma_{50}/\Gamma_{38}$

This is the "fit fraction" from the Dalitz-plot analysis. This is a doubly Cabibbo-suppressed mode.
VALUE CL% DOCUMENT ID TECN COMMENT

<5 × 10^-4 95 AUBERT 08AL BABR Dalitz fit, ≈ 487 k evts

$\Gamma(K_2^*(1430)^+ \pi^-, K_2^{*+} \to K_S^0 \pi^+)/\Gamma(K_S^0 \pi^+ \pi^-)$   $\Gamma_{51}/\Gamma_{38}$

This is the "fit fraction" from the Dalitz-plot analysis. This is a doubly Cabibbo-suppressed mode.
VALUE CL% DOCUMENT ID TECN COMMENT

<1.2 × 10^-3 95 AUBERT 08AL BABR Dalitz fit, ≈ 487 k evts

$\Gamma(K_S^0 \pi^+ \pi^- \text{ nonresonant})/\Gamma(K_S^0 \pi^+ \pi^-)$   $\Gamma_{52}/\Gamma_{38}$

This is the "fit fraction" from the Dalitz-plot analysis. Neither FRABETTI 94G nor ALBRECHT 93D (quoted in many of the earlier submodes of K\_S^0 π+ π-) sees evidence for a nonresonant component.

0.009±0.004±0.020 OUR AVERAGE Error includes scale factor of 2.0.
0.007±0.007±0.021... ASNER 04A CLEO See MURAMATSU 02

0.263±0.024±0.041... ANJOS 93 E691 γBe 90–260 GeV
0.26 ± 0.08 ± 0.05... FRABETTI 92B E687 γ Be, Eγ = 221 GeV

0.33 ± 0.05 ± 0.10... ADLER 87 MRK3 e+ e- 3.77 GeV
• • • We do not use the following data for averages, fits, limits, etc. • • •

$\Gamma(K^- \pi^+ \pi^0)/\Gamma_{\text{total}}$   $\Gamma_{53}/\Gamma$

VALUE (%) EVTS DOCUMENT ID TECN COMMENT
14.57±0.12±0.38 1 DOBBS 07 CLEO See BONVICINI 14
14.9 ± 0.3 ± 0.5 19k ± 150 1 HE 05 CLEO See DOBBS 07

13.3 ± 1.2 ± 1.3 931 ADLER 88C MRK3 e+ e- 3.77 GeV
11.7 ± 4.3 37 2 SCHINDLER 81 MRK2 e+ e- 3.771 GeV
1 DOBBS 07 and HE 05 use single- and double-tagged events in an overall fit. DOBBS 07 supersedes HE 05.

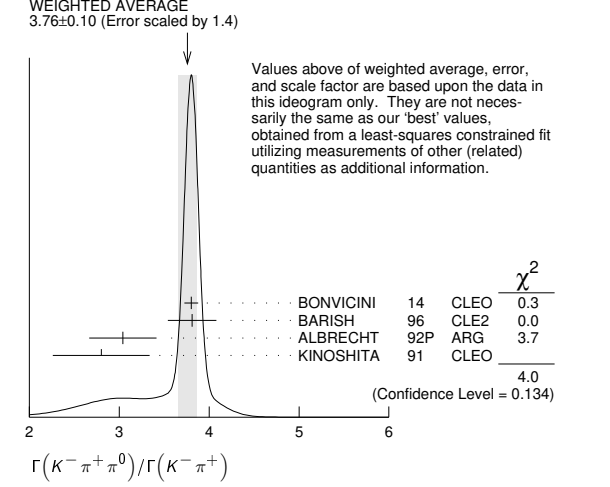
2 SCHINDLER 81 (MARK-2) measures σ(e+ e- → ψ(3770)) × branching fraction to be 0.68 ± 0.23 nb. We use the MARK-3 (ADLER 88c) value of σ = 5.8 ± 0.5 ± 0.6 nb.

$\Gamma(K^- \pi^+ \pi^0)/\Gamma(K^- \pi^+)$   $\Gamma_{53}/\Gamma_{35}$

3.65 ± 0.13 OUR FIT Error includes scale factor of 2.1.
3.76 ± 0.10 OUR AVERAGE Error includes scale factor of 1.4. See the ideogram below.

3.802±0.022±0.073 BONVICINI 14 CLEO All CLEO-c runs
3.81 ± 0.07 ± 0.26 10k BARISH 96 CLE2 e+ e- ≈ 7(4S)
3.04 ± 0.16 ± 0.34 931 1 ALBRECHT 92P ARG e+ e- ≈ 10 GeV
2.8 ± 0.14 ± 0.52 1050 KINOSHITA 91 CLEO e+ e- ~ 10.7 GeV

1 This value is calculated from numbers in Table 1 of ALBRECHT 92P.







Γ(K<sup>-</sup>a<sub>1</sub>(1260)<sup>+</sup>, a<sub>1</sub><sup>+</sup> → ρ<sup>0</sup>π<sup>+</sup>)/Γ(K<sup>-</sup>2π<sup>+</sup>π<sup>-</sup>) Γ<sub>75</sub>/Γ<sub>70</sub>

Table with columns: VALUE (units 10<sup>-2</sup>), EVTS, DOCUMENT ID, TECN, COMMENT. Includes OUR AVERAGE and data from ABLIKIM, BES3, ANJOS, E691, COFFMAN, MRK3.

Γ(K<sub>1</sub>(1270)<sup>-</sup>π<sup>+</sup>, K<sub>1</sub><sup>-</sup> → K<sup>-</sup>π<sup>+</sup>π<sup>-</sup>-total)/Γ(K<sup>-</sup>2π<sup>+</sup>π<sup>-</sup>) Γ<sub>76</sub>/Γ<sub>70</sub>

Table with columns: VALUE (units 10<sup>-2</sup>), EVTS, DOCUMENT ID, TECN, COMMENT. Includes OUR AVERAGE and data from AAIJ, LHCb, COFFMAN, MRK3.

The 3rd error is due to the uncertainty in the amplitude model composition.

Γ(K<sub>1</sub>(1270)<sup>-</sup>π<sup>+</sup>, K<sub>1</sub><sup>-</sup> → K<sup>-</sup>\*(892)<sup>0</sup>π<sup>-</sup>, K<sup>-</sup>\* → K<sup>-</sup>π<sup>+</sup>)/Γ(K<sup>-</sup>2π<sup>+</sup>π<sup>-</sup>) Γ<sub>79</sub>/Γ<sub>70</sub>

Table with columns: VALUE (units 10<sup>-2</sup>), EVTS, DOCUMENT ID, TECN, COMMENT. Includes OUR AVERAGE and data from ABLIKIM, BES3.

Γ(K<sup>-</sup>2π<sup>+</sup>π<sup>-</sup> nonresonant)/Γ(K<sup>-</sup>2π<sup>+</sup>π<sup>-</sup>) Γ<sub>80</sub>/Γ<sub>70</sub>

Table with columns: VALUE (units 10<sup>-2</sup>), EVTS, DOCUMENT ID, TECN, COMMENT. Includes OUR AVERAGE and data from AAIJ, LHCb, ABLIKIM, BES3, ANJOS, E691, COFFMAN, MRK3.

The 3rd error is due to the uncertainty in the amplitude model composition. In addition to the 14 ABLIKIM 17o branching ratios we have listed, the paper gives 15 more ratios for mostly non-resonant modes. Four of the 15 have less than 2-standard-deviation significance. Here are some of the omitted modes, with S, P, V, A, and T for scalar, pseudo-scalar, vector, axial-vector, and tensor spin sub-structures: π<sup>+</sup>(K<sup>-</sup>ρ<sup>0</sup>)<sub>P</sub>, π<sup>+</sup>(K<sup>-</sup>ρ<sup>0</sup>)<sub>V</sub>, π<sup>+</sup>(K<sup>-</sup>\*<sup>0</sup>π<sup>-</sup>)<sub>P</sub>, π<sup>+</sup>(K<sup>-</sup>\*<sup>0</sup>π<sup>-</sup>)<sub>V</sub>, π<sup>+</sup>(π<sup>-</sup>(K<sup>-</sup>π<sup>+</sup>)<sub>S-wave</sub>)<sub>A</sub>, π<sup>+</sup>(K<sup>-</sup>π<sup>+</sup>)<sub>V</sub>, π<sup>+</sup>(π<sup>+</sup>π<sup>-</sup>)<sub>S</sub>, π<sup>+</sup>(K<sup>-</sup>π<sup>+</sup>)<sub>T</sub>, π<sup>+</sup>(π<sup>+</sup>π<sup>-</sup>)<sub>S</sub>...

Γ(K<sub>S</sub><sup>0</sup>π<sup>+</sup>π<sup>-</sup>π<sup>0</sup>)/Γ<sub>total</sub> Γ<sub>81</sub>/Γ

Table with columns: VALUE (%), EVTS, DOCUMENT ID, TECN, COMMENT. Includes OUR FIT and OUR AVERAGE, and data from COFFMAN, MRK3, BARLAG.

BARLAG 92c computes the branching fraction using topological normalization.

Γ(K<sub>S</sub><sup>0</sup>π<sup>+</sup>π<sup>-</sup>π<sup>0</sup>)/Γ(K<sub>S</sub><sup>0</sup>π<sup>+</sup>π<sup>-</sup>) Γ<sub>81</sub>/Γ<sub>38</sub>

Branching fractions for submodes of this mode with narrow resonances (the η, ω, η') are fairly well determined (see below). COFFMAN 92B gives fractions of K\* and ρ submodes, but with only 140 ± 28 events above background could not determine them with much accuracy. We omit those measurements here; they are in our 2008 Review (Physics Letters B667 1 (2008)).

Table with columns: VALUE (%), EVTS, DOCUMENT ID, TECN, COMMENT. Includes OUR FIT and OUR AVERAGE, and data from ALBRECHT, ANJOS, KINOSHITA.

This value is calculated from numbers in Table 1 of ALBRECHT 92P.

Γ(K<sup>-</sup>π<sup>+</sup>2π<sup>0</sup>)/Γ<sub>total</sub> Γ<sub>84</sub>/Γ

Table with columns: VALUE (%), EVTS, DOCUMENT ID, TECN, COMMENT. Includes OUR FIT and OUR AVERAGE, and data from ABLIKIM, BARLAG, ADLER, AGUILAR...

AGUILAR-BENITEZ 87F and BARLAG 92c compute the branching fraction using topological normalization. They do not distinguish the presence of a third π<sup>0</sup>, and thus are not included in the average.

ADLER 88c uses an absolute normalization method finding this decay channel opposite a detected D<sup>0</sup> → K<sup>+</sup>π<sup>-</sup> in pure D D<sup>-</sup> events.

Γ(K<sup>-</sup>2π<sup>+</sup>π<sup>-</sup>π<sup>0</sup>)/Γ(K<sup>-</sup>π<sup>+</sup>) Γ<sub>85</sub>/Γ<sub>35</sub>

Table with columns: VALUE (%), EVTS, DOCUMENT ID, TECN, COMMENT. Includes OUR FIT and OUR AVERAGE, and data from ALBRECHT.

This value is calculated from numbers in Table 1 of ALBRECHT 92P.

Γ(K<sup>-</sup>2π<sup>+</sup>π<sup>-</sup>π<sup>0</sup>)/Γ(K<sup>-</sup>2π<sup>+</sup>π<sup>-</sup>) Γ<sub>85</sub>/Γ<sub>70</sub>

Table with columns: VALUE (%), EVTS, DOCUMENT ID, TECN, COMMENT. Includes OUR FIT and OUR AVERAGE, and data from KINOSHITA, ANJOS.

Γ(K<sub>S</sub><sup>0</sup>ηπ<sup>0</sup>)/Γ(K<sub>S</sub><sup>0</sup>π<sup>0</sup>) Γ<sub>89</sub>/Γ<sub>36</sub>

Table with columns: VALUE (%), EVTS, DOCUMENT ID, TECN, COMMENT. Includes OUR FIT and data from RUBIN.

The η here is detected in its γγ mode, but other η modes are included in the value given.

Γ(K<sub>S</sub><sup>0</sup>a<sub>0</sub>(980), a<sub>0</sub> → ηπ<sup>0</sup>)/Γ(K<sub>S</sub><sup>0</sup>ηπ<sup>0</sup>) Γ<sub>90</sub>/Γ<sub>89</sub>

Table with columns: VALUE (%), EVTS, DOCUMENT ID, TECN, COMMENT. Includes OUR FIT and data from RUBIN.

This is the "fit fraction" from the Dalitz-plot analysis, with interference.

In addition to K<sub>S</sub><sup>0</sup>a<sub>0</sub>(980) and K<sup>\*</sup>(892)<sup>0</sup>η modes, RUBIN 04 finds a fit fraction of 0.246 ± 0.092 ± 0.091 for other, undetermined modes.

Γ(K<sup>\*</sup>(892)<sup>0</sup>η, K<sup>\*</sup>\* → K<sub>S</sub><sup>0</sup>π<sup>0</sup>)/Γ(K<sub>S</sub><sup>0</sup>ηπ<sup>0</sup>) Γ<sub>91</sub>/Γ<sub>89</sub>

Table with columns: VALUE (%), EVTS, DOCUMENT ID, TECN, COMMENT. Includes OUR FIT and data from RUBIN.

This is the "fit fraction" from the Dalitz-plot analysis, with interference.

See the note on RUBIN 04 in the preceding data block.

Γ(K<sub>S</sub><sup>0</sup>2π<sup>+</sup>2π<sup>-</sup>)/Γ(K<sub>S</sub><sup>0</sup>π<sup>+</sup>π<sup>-</sup>) Γ<sub>92</sub>/Γ<sub>38</sub>

Table with columns: VALUE (%), EVTS, DOCUMENT ID, TECN, COMMENT. Includes OUR FIT and data from LINK, FOCUS, ALBRECHT, ANMAR, ANJOS.

This value is calculated from numbers in Table 1 of ALBRECHT 92P.

Γ(K<sub>S</sub><sup>0</sup>ρ<sup>0</sup>π<sup>+</sup>π<sup>-</sup>, no K\*(892)<sup>-</sup>)/Γ(K<sub>S</sub><sup>0</sup>2π<sup>+</sup>2π<sup>-</sup>) Γ<sub>93</sub>/Γ<sub>92</sub>

Table with columns: VALUE (%), EVTS, DOCUMENT ID, TECN, COMMENT. Includes data from LINK, FOCUS.

Γ(K\*(892)<sup>-</sup>2π<sup>+</sup>π<sup>-</sup>, K\*(892)<sup>-</sup> → K<sub>S</sub><sup>0</sup>π<sup>-</sup>, no ρ<sup>0</sup>)/Γ(K<sub>S</sub><sup>0</sup>2π<sup>+</sup>2π<sup>-</sup>) Γ<sub>94</sub>/Γ<sub>92</sub>

Table with columns: VALUE (%), EVTS, DOCUMENT ID, TECN, COMMENT. Includes data from LINK, FOCUS.

Γ(K\*(892)<sup>-</sup>ρ<sup>0</sup>π<sup>+</sup>, K\*(892)<sup>-</sup> → K<sub>S</sub><sup>0</sup>π<sup>-</sup>)/Γ(K<sub>S</sub><sup>0</sup>2π<sup>+</sup>2π<sup>-</sup>) Γ<sub>95</sub>/Γ<sub>92</sub>

Table with columns: VALUE (%), EVTS, DOCUMENT ID, TECN, COMMENT. Includes data from LINK, FOCUS.

Γ(K<sub>S</sub><sup>0</sup>2π<sup>+</sup>2π<sup>-</sup> nonresonant)/Γ(K<sub>S</sub><sup>0</sup>2π<sup>+</sup>2π<sup>-</sup>) Γ<sub>96</sub>/Γ<sub>92</sub>

Table with columns: VALUE (%), CL%, DOCUMENT ID, TECN, COMMENT. Includes data from LINK, FOCUS.

Γ(K<sup>-</sup>3π<sup>+</sup>2π<sup>-</sup>)/Γ(K<sup>-</sup>2π<sup>+</sup>π<sup>-</sup>) Γ<sub>98</sub>/Γ<sub>70</sub>

Table with columns: VALUE (units 10<sup>-3</sup>), EVTS, DOCUMENT ID, TECN, COMMENT. Includes data from LINK, FOCUS.

Γ(K<sub>S</sub><sup>0</sup>η)/Γ<sub>total</sub> Γ<sub>99</sub>/Γ

Unseen decay modes of the η are included.

Table with columns: VALUE (units 10<sup>-3</sup>), EVTS, DOCUMENT ID, TECN, COMMENT. Includes OUR FIT and data from ABLIKIM, ASNER.

We do not use the following data for averages, fits, limits, etc. ....

Γ(K<sub>S</sub><sup>0</sup>η)/[Γ(K<sup>-</sup>π<sup>+</sup>) + Γ(K<sup>+</sup>π<sup>-</sup>)] Γ<sub>99</sub>/Γ<sub>35</sub>+Γ<sub>256</sub>

Unseen decay modes of the η are included.

Table with columns: VALUE (units 10<sup>-2</sup>), EVTS, DOCUMENT ID, TECN, COMMENT. Includes OUR FIT and data from MENDEZ.

Γ(K<sub>S</sub><sup>0</sup>η)/Γ(K<sub>S</sub><sup>0</sup>π<sup>0</sup>) Γ<sub>99</sub>/Γ<sub>36</sub>

Table with columns: VALUE (%), EVTS, DOCUMENT ID, TECN, COMMENT. Includes data from PROCARIO.

We do not use the following data for averages, fits, limits, etc. ....

Γ(K<sub>S</sub><sup>0</sup>η)/Γ(K<sub>S</sub><sup>0</sup>π<sup>+</sup>π<sup>-</sup>) Γ<sub>99</sub>/Γ<sub>38</sub>

Unseen decay modes of the η are included.

Table with columns: VALUE (%), EVTS, DOCUMENT ID, TECN, COMMENT. Includes data from PROCARIO.

We do not use the following data for averages, fits, limits, etc. ....

Γ(K<sub>S</sub><sup>0</sup>ω)/Γ<sub>total</sub> Γ<sub>100</sub>/Γ

Unseen decay modes of the ω are included.

Table with columns: VALUE (%), DOCUMENT ID, TECN, COMMENT. Includes OUR FIT and data from ASNER.

Γ(K<sub>S</sub><sup>0</sup>ω)/Γ(K<sup>-</sup>π<sup>+</sup>) Γ<sub>100</sub>/Γ<sub>35</sub>

Unseen decay modes of the ω are included.

Table with columns: VALUE (%), DOCUMENT ID, TECN, COMMENT. Includes data from ALBRECHT.

We do not use the following data for averages, fits, limits, etc. ....

## Meson Particle Listings

 $D^0$  $\Gamma(K_S^0 \omega)/\Gamma(K_S^0 \pi^+ \pi^-)$   $\Gamma_{100}/\Gamma_{38}$ 

Unseen decay modes of the  $\omega$  are included.  
 VALUE EVTS DOCUMENT ID TECN COMMENT  
**0.396 ± 0.032 OUR FIT** Error includes scale factor of 1.1.

**0.33 ± 0.09 OUR AVERAGE** Error includes scale factor of 1.1.  
 0.29 ± 0.08 ± 0.05 16 <sup>1</sup> ALBRECHT 92P ARG  $e^+ e^- \approx 10$  GeV  
 0.54 ± 0.14 ± 0.16 40 KINOSHITA 91 CLEO  $e^+ e^- \approx 10.7$  GeV

<sup>1</sup> This value is calculated from numbers in Table 1 of ALBRECHT 92P.

 $\Gamma(K_S^0 \omega)/\Gamma(K_S^0 \pi^+ \pi^- \pi^0)$   $\Gamma_{100}/\Gamma_{81}$ 

Unseen decay modes of the  $\omega$  are included.  
 VALUE DOCUMENT ID TECN COMMENT  
**0.215 ± 0.026 OUR FIT**  
**0.220 ± 0.048 ± 0.0116** COFFMAN 92B MRK3 1281 ± 45  $K^- 2\pi^+ \pi^-$  evts

 $\Gamma(K_S^0 \eta(958))/\Gamma_{total}$   $\Gamma_{101}/\Gamma$ 

VALUE (units  $10^{-3}$ ) EVTS DOCUMENT ID TECN COMMENT  
**9.49 ± 0.32 OUR FIT**  
**9.49 ± 0.20 ± 0.36** 3k ABLIKIM 18W BES3  $e^+ e^-$ , 3773 MeV

 $\Gamma(K_S^0 \eta(958))/[\Gamma(K^- \pi^+) + \Gamma(K^+ \pi^-)]$   $\Gamma_{101}/(\Gamma_{35} + \Gamma_{256})$ 

Unseen decay modes of the  $\eta(958)$  are included.  
 VALUE (units  $10^{-2}$ ) EVTS DOCUMENT ID TECN COMMENT  
**23.9 ± 0.8 OUR FIT**  
**24.3 ± 0.8 ± 1.1** 1321 ± 42 MENDEZ 10 CLEO  $e^+ e^-$  at 3774 MeV

 $\Gamma(K_S^0 \eta(958))/\Gamma(K_S^0 \pi^+ \pi^-)$   $\Gamma_{101}/\Gamma_{38}$ 

Unseen decay modes of the  $\eta(958)$  are included.  
 VALUE EVTS DOCUMENT ID TECN COMMENT  
**0.339 ± 0.023 OUR FIT**  
**0.32 ± 0.04 OUR AVERAGE**  
 0.31 ± 0.02 ± 0.04 594 PROCARIO 93B CLE2  $\eta' \rightarrow \eta \pi^+ \pi^-, \rho^0 \gamma$   
 0.37 ± 0.13 ± 0.06 18 <sup>1</sup> ALBRECHT 92P ARG  $e^+ e^- \approx 10$  GeV

<sup>1</sup> This value is calculated from numbers in Table 1 of ALBRECHT 92P.

 $\Gamma(\bar{K}^*(892)^0 \pi^+ \pi^- \pi^0)/\Gamma(K^- 2\pi^+ \pi^- \pi^0)$   $\Gamma_{102}/\Gamma_{85}$ 

Unseen decay modes of the  $\bar{K}^*(892)^0$  are included.  
 VALUE DOCUMENT ID TECN COMMENT  
**0.45 ± 0.15 ± 0.15** ANJOS 90D E691 Photoproduction

 $\Gamma(\bar{K}^*(892)^0 \eta)/\Gamma(K^- \pi^+)$   $\Gamma_{103}/\Gamma_{35}$ 

Unseen decay modes of the  $\bar{K}^*(892)^0$  and  $\eta$  are included.  
 VALUE EVTS DOCUMENT ID TECN COMMENT  
 • • • We do not use the following data for averages, fits, limits, etc. • • •  
 0.58 ± 0.19  $^{+0.24}_{-0.28}$  46 KINOSHITA 91 CLEO  $e^+ e^- \approx 10.7$  GeV

 $\Gamma(\bar{K}^*(892)^0 \eta)/\Gamma(K^- \pi^+ \pi^0)$   $\Gamma_{103}/\Gamma_{53}$ 

Unseen decay modes of the  $\bar{K}^*(892)^0$  and  $\eta$  are included.  
 VALUE EVTS DOCUMENT ID TECN COMMENT  
 • • • We do not use the following data for averages, fits, limits, etc. • • •  
 0.13 ± 0.02 ± 0.03 214 PROCARIO 93B CLE2  $\bar{K}^{*0} \eta \rightarrow K^- \pi^+ / \gamma \gamma$

 $\Gamma(K^- \pi^+ \omega)/\Gamma(K^- \pi^+)$   $\Gamma_{104}/\Gamma_{35}$ 

Unseen decay modes of the  $\omega$  are included.  
 VALUE EVTS DOCUMENT ID TECN COMMENT  
**0.78 ± 0.12 ± 0.10** 99 <sup>1</sup> ALBRECHT 92P ARG  $e^+ e^- \approx 10$  GeV

<sup>1</sup> This value is calculated from numbers in Table 1 of ALBRECHT 92P.

 $\Gamma(\bar{K}^*(892)^0 \omega)/\Gamma(K^- \pi^+)$   $\Gamma_{105}/\Gamma_{35}$ 

Unseen decay modes of the  $\bar{K}^*(892)^0$  and  $\omega$  are included.  
 VALUE EVTS DOCUMENT ID TECN COMMENT  
**0.28 ± 0.11 ± 0.04** 17 <sup>1</sup> ALBRECHT 92P ARG  $e^+ e^- \approx 10$  GeV

<sup>1</sup> This value is calculated from numbers in Table 1 of ALBRECHT 92P.

 $\Gamma(K^- \pi^+ \eta(958))/\Gamma_{total}$   $\Gamma_{106}/\Gamma$ 

VALUE (units  $10^{-3}$ ) EVTS DOCUMENT ID TECN COMMENT  
**6.43 ± 0.15 ± 0.31** 2.5k ABLIKIM 18Ac BES3  $e^+ e^-$ , 3773 MeV

 $\Gamma(K^- \pi^+ \eta(958))/\Gamma(K^- 2\pi^+ \pi^-)$   $\Gamma_{106}/\Gamma_{70}$ 

Unseen decay modes of the  $\eta(958)$  are included.  
 VALUE EVTS DOCUMENT ID TECN COMMENT  
**0.093 ± 0.014 ± 0.019** 286 PROCARIO 93B CLE2  $\eta' \rightarrow \eta \pi^+ \pi^-, \rho^0 \gamma$

 $\Gamma(K_S^0 \eta(958) \pi^0)/\Gamma_{total}$   $\Gamma_{107}/\Gamma$ 

VALUE (units  $10^{-3}$ ) EVTS DOCUMENT ID TECN COMMENT  
**2.52 ± 0.22 ± 0.15** 289 ABLIKIM 18Ac BES3  $e^+ e^-$ , 3773 MeV

 $\Gamma(\bar{K}^*(892)^0 \eta(958))/\Gamma(K^- \pi^+ \eta(958))$   $\Gamma_{108}/\Gamma_{106}$ 

Unseen decay modes of the  $\bar{K}^*(892)^0$  are included.  
 VALUE CL% DOCUMENT ID TECN  
**<0.15** 90 PROCARIO 93B CLE2

Hadronic modes with three  $K$ 's $\Gamma(K_S^0 K^+ K^-)/\Gamma(K_S^0 \pi^+ \pi^-)$   $\Gamma_{109}/\Gamma_{38}$ 

VALUE EVTS DOCUMENT ID TECN COMMENT  
**0.158 ± 0.001 ± 0.005** 14k ± 116 AUBERT,B 05J BABR  $e^+ e^- \approx \Upsilon(4S)$   
 • • • We do not use the following data for averages, fits, limits, etc. • • •  
 0.20 ± 0.05 ± 0.04 47 FRABETTI 92B E687  $\gamma$  Be,  $\bar{E}_\gamma = 221$  GeV  
 0.170 ± 0.022 136 AMMAR 91 CLEO  $e^+ e^- \approx 10.5$  GeV  
 0.24 ± 0.08 BEBEK 86 CLEO  $e^+ e^-$  near  $\Upsilon(4S)$   
 0.185 ± 0.055 52 ALBRECHT 85B ARG  $e^+ e^- 10$  GeV

 $\Gamma(K_S^0 a_0(980)^0, a_0^0 \rightarrow K^+ K^-)/\Gamma(K_S^0 K^+ K^-)$   $\Gamma_{110}/\Gamma_{109}$ 

This is the "fit fraction" from the Dalitz-plot analysis, with interference.  
 VALUE DOCUMENT ID TECN COMMENT  
**0.664 ± 0.016 ± 0.070** AUBERT,B 05J BABR Dalitz fit, 12540 ± 112 evts

 $\Gamma(K^- a_0(980)^+, a_0^+ \rightarrow K^+ K_S^0)/\Gamma(K_S^0 K^+ K^-)$   $\Gamma_{111}/\Gamma_{109}$ 

This is the "fit fraction" from the Dalitz-plot analysis, with interference.  
 VALUE DOCUMENT ID TECN COMMENT  
**0.134 ± 0.011 ± 0.037** AUBERT,B 05J BABR Dalitz fit, 12540 ± 112 evts

 $\Gamma(K^+ a_0(980)^-, a_0^- \rightarrow K^- K_S^0)/\Gamma(K_S^0 K^+ K^-)$   $\Gamma_{112}/\Gamma_{109}$ 

This is a doubly Cabibbo-suppressed mode.  
 VALUE CL% DOCUMENT ID TECN COMMENT  
**<0.025** 95 AUBERT,B 05J BABR Dalitz fit, 12540 ± 112 evts

 $\Gamma(K_S^0 f_0(980), f_0 \rightarrow K^+ K^-)/\Gamma(K_S^0 K^+ K^-)$   $\Gamma_{113}/\Gamma_{109}$ 

VALUE CL% DOCUMENT ID TECN COMMENT  
**<0.021** 95 AUBERT,B 05J BABR Dalitz fit, 12540 ± 112 evts

 $\Gamma(K_S^0 \phi, \phi \rightarrow K^+ K^-)/\Gamma(K_S^0 K^+ K^-)$   $\Gamma_{114}/\Gamma_{109}$ 

This is the "fit fraction" from the Dalitz-plot analysis, with interference.  
 VALUE DOCUMENT ID TECN COMMENT  
**0.459 ± 0.007 ± 0.007** AUBERT,B 05J BABR Dalitz fit, 12540 ± 112 evts

 $\Gamma(K_S^0 f_0(1370), f_0 \rightarrow K^+ K^-)/\Gamma(K_S^0 K^+ K^-)$   $\Gamma_{115}/\Gamma_{109}$ 

This is the "fit fraction" from the Dalitz-plot analysis, with interference.  
 VALUE DOCUMENT ID TECN COMMENT  
**0.038 ± 0.007 ± 0.023** <sup>1</sup> AUBERT,B 05J BABR Dalitz fit, 12540 ± 112 evts  
<sup>1</sup> AUBERT,B 05J calls the mode  $K_S^0 f_0(1400)$ , but insofar as it is seen here at all, it is certainly the same as  $f_0(1370)$ .

 $\Gamma(3K_S^0)/\Gamma_{total}$   $\Gamma_{116}/\Gamma$ 

VALUE (units  $10^{-4}$ ) EVTS DOCUMENT ID TECN COMMENT  
**7.5 ± 0.7 OUR FIT** Error includes scale factor of 1.4.  
**7.21 ± 0.33 ± 0.44** 597 ABLIKIM 17A BES3  $e^+ e^- \rightarrow \psi(3770)$

 $\Gamma(3K_S^0)/\Gamma(K_S^0 \pi^+ \pi^-)$   $\Gamma_{116}/\Gamma_{38}$ 

VALUE (units  $10^{-2}$ ) EVTS DOCUMENT ID TECN COMMENT  
**2.70 ± 0.26 OUR FIT** Error includes scale factor of 1.2.  
**3.2 ± 0.4 OUR AVERAGE**  
 3.58 ± 0.54 ± 0.52 170 ± 26 LINK 05A FOCS  $\gamma$  Be,  $\bar{E}_\gamma \approx 180$  GeV  
 2.78 ± 0.38 ± 0.48 61 ASNER 96B CLE2  $e^+ e^- \approx \Upsilon(4S)$   
 7.0 ± 2.4 ± 1.2 10 ± 3 FRABETTI 94J E687  $\gamma$  Be,  $\bar{E}_\gamma = 220$  GeV  
 3.2 ± 1.0 22 AMMAR 91 CLEO  $e^+ e^- \approx 10.5$  GeV  
 3.4 ± 1.4 ± 1.0 5 ALBRECHT 90c ARG  $e^+ e^- \approx 10$  GeV

 $\Gamma(K^+ 2K^- \pi^+)/\Gamma(K^- 2\pi^+ \pi^-)$   $\Gamma_{117}/\Gamma_{70}$ 

VALUE EVTS DOCUMENT ID TECN COMMENT  
**0.0027 ± 0.0004 OUR AVERAGE** Error includes scale factor of 1.1.  
 0.00257 ± 0.00034 ± 0.00024 143 LINK 03G FOCS  $\gamma$  A,  $\bar{E}_\gamma \approx 180$  GeV  
 0.0054 ± 0.0016 ± 0.0008 18 AITALA 01b E791  $\pi^-$  A, 500 GeV  
 0.0028 ± 0.0007 ± 0.0001 20 FRABETTI 95c E687  $\gamma$  Be,  $\bar{E}_\gamma \approx 200$  GeV

 $\Gamma(K^+ K^- \bar{K}^*(892)^0, \bar{K}^{*0} \rightarrow K^- \pi^+)/\Gamma(K^+ 2K^- \pi^+)$   $\Gamma_{118}/\Gamma_{117}$ 

VALUE DOCUMENT ID TECN COMMENT  
**0.20 ± 0.07 ± 0.02** LINK 03G FOCS  $\gamma$  A,  $\bar{E}_\gamma \approx 180$  GeV

 $\Gamma(K^- \pi^+ \phi, \phi \rightarrow K^+ K^-)/\Gamma(K^+ 2K^- \pi^+)$   $\Gamma_{119}/\Gamma_{117}$ 

VALUE DOCUMENT ID TECN COMMENT  
**0.18 ± 0.06 ± 0.04** LINK 03G FOCS  $\gamma$  A,  $\bar{E}_\gamma \approx 180$  GeV

 $\Gamma(\phi \bar{K}^*(892)^0, \phi \rightarrow K^+ K^-, \bar{K}^{*0} \rightarrow K^- \pi^+)/\Gamma(K^+ 2K^- \pi^+)$   $\Gamma_{120}/\Gamma_{117}$ 

VALUE DOCUMENT ID TECN COMMENT  
**0.48 ± 0.06 ± 0.01** LINK 03G FOCS  $\gamma$  A,  $\bar{E}_\gamma \approx 180$  GeV

 $\Gamma(K^+ 2K^- \pi^+ \text{nonresonant})/\Gamma(K^+ 2K^- \pi^+)$   $\Gamma_{121}/\Gamma_{117}$ 

VALUE DOCUMENT ID TECN COMMENT  
**0.15 ± 0.06 ± 0.02** LINK 03G FOCS  $\gamma$  A,  $\bar{E}_\gamma \approx 180$  GeV





• • • We do not use the following data for averages, fits, limits, etc. • • •

6.5 ± 0.9 ± 0.4	75	ABLIKIM	16D	BES3	See ABLIKIM 18L
6.4 ± 1.0 ± 0.4	156 ± 24	ARTUSO	08	CLEO	See MENDEZ 10

**Γ(ηπ<sup>0</sup>)/Γ(K<sup>-</sup>π<sup>+</sup>)** Γ<sub>171</sub>/Γ<sub>35</sub>  
 Unseen decay modes of the η are included.

VALUE (units 10 <sup>-2</sup> )	EVTS	DOCUMENT ID	TECN	COMMENT
1.47 ± 0.34 ± 0.11	62 ± 14	RUBIN	06	CLEO See ARTUSO 08

• • • We do not use the following data for averages, fits, limits, etc. • • •

**Γ(ηπ<sup>0</sup>)/[Γ(K<sup>-</sup>π<sup>+</sup>) + Γ(K<sup>+</sup>π<sup>-</sup>)]** Γ<sub>171</sub>/(Γ<sub>35</sub>+Γ<sub>256</sub>)  
 Unseen decay modes of the η are included.

VALUE (units 10 <sup>-2</sup> )	EVTS	DOCUMENT ID	TECN	COMMENT
<b>1.60 ± 0.14 OUR FIT</b>				Error includes scale factor of 1.1.
1.74 ± 0.15 ± 0.11	481 ± 40	MENDEZ	10	CLEO e <sup>+</sup> e <sup>-</sup> at 3774 MeV

**Γ(ωπ<sup>0</sup>)/Γ<sub>total</sub>** Γ<sub>172</sub>/Γ  
 Unseen decay modes of the ω are included.

VALUE (units 10 <sup>-4</sup> )	EVTS	DOCUMENT ID	TECN	COMMENT
1.17 ± 0.34 ± 0.07	45	ABLIKIM	16D	BES3 e <sup>+</sup> e <sup>-</sup> , 3773 MeV

**Γ(2π<sup>+</sup>2π<sup>-</sup>π<sup>0</sup>)/Γ(K<sup>-</sup>π<sup>+</sup>)** Γ<sub>174</sub>/Γ<sub>35</sub>

VALUE (units 10 <sup>-2</sup> )	EVTS	DOCUMENT ID	TECN	COMMENT
10.7 ± 1.2 ± 0.5	1614 ± 171	RUBIN	06	CLEO e <sup>+</sup> e <sup>-</sup> at ψ(3770)

**Γ(ηπ<sup>+</sup>π<sup>-</sup>)/Γ<sub>total</sub>** Γ<sub>175</sub>/Γ  
 Unseen decay modes of the η are included.

VALUE (units 10 <sup>-4</sup> )	EVTS	DOCUMENT ID	TECN	COMMENT
10.9 ± 1.3 ± 0.9	257	ARTUSO	08	CLEO e <sup>+</sup> e <sup>-</sup> at ψ(3770)

**Γ(η2π<sup>0</sup>)/Γ<sub>total</sub>** Γ<sub>177</sub>/Γ

VALUE (units 10 <sup>-4</sup> )	EVTS	DOCUMENT ID	TECN	COMMENT
3.8 ± 1.1 ± 0.7	42	1 ABLIKIM	18x	BES3 e <sup>+</sup> e <sup>-</sup> , 3773 MeV

<sup>1</sup> Significance of signal reported by ABLIKIM 18x is 3.8σ.

**Γ(ωη)/Γ<sub>total</sub>** Γ<sub>173</sub>/Γ

VALUE (units 10 <sup>-3</sup> )	EVTS	DOCUMENT ID	TECN	COMMENT
<b>1.98 ± 0.18 OUR AVERAGE</b>				Error includes scale factor of 1.1.
2.15 ± 0.17 ± 0.15	2.2k	ABLIKIM	18L	BES3 e <sup>+</sup> e <sup>-</sup> , 3773 MeV
1.78 ± 0.19 ± 0.15	600	1 SMITH	18	e <sup>+</sup> e <sup>-</sup> , 3773 MeV

<sup>1</sup> Obtained by analyzing CLEO-c data but not authored by the CLEO Collaboration.

**Γ(ωπ<sup>+</sup>π<sup>-</sup>)/Γ(K<sup>-</sup>π<sup>+</sup>)** Γ<sub>176</sub>/Γ<sub>35</sub>  
 Unseen decay modes of the ω are included.

VALUE (units 10 <sup>-2</sup> )	EVTS	DOCUMENT ID	TECN	COMMENT
4.1 ± 1.2 ± 0.4	472 ± 132	RUBIN	06	CLEO e <sup>+</sup> e <sup>-</sup> at ψ(3770)

**Γ(3π<sup>+</sup>3π<sup>-</sup>)/Γ(K<sup>-</sup>2π<sup>+</sup>π<sup>-</sup>)** Γ<sub>178</sub>/Γ<sub>70</sub>

VALUE (units 10 <sup>-3</sup> )	EVTS	DOCUMENT ID	TECN	COMMENT
5.23 ± 0.59 ± 1.35	149 ± 17	LINK	04B	FOCS γA, E <sub>γ</sub> ≈ 180 GeV

**Γ(3π<sup>+</sup>3π<sup>-</sup>)/Γ(K<sup>-</sup>3π<sup>+</sup>2π<sup>-</sup>)** Γ<sub>178</sub>/Γ<sub>98</sub>

VALUE	DOCUMENT ID	TECN	COMMENT
1.93 ± 0.47 ± 0.48	1 LINK	04B	FOCS γA, E <sub>γ</sub> ≈ 180 GeV

<sup>1</sup> This LINK 04B result is not independent of other results in these Listings.

**Γ(η'(958)π<sup>0</sup>)/Γ<sub>total</sub>** Γ<sub>179</sub>/Γ  
 Unseen decay modes of the η'(958) are included.

VALUE (units 10 <sup>-4</sup> )	EVTS	DOCUMENT ID	TECN	COMMENT
<b>9.2 ± 1.0 OUR FIT</b>				
9.3 ± 1.1 ± 0.9	469 ± 56	ABLIKIM	18L	BES3 e <sup>+</sup> e <sup>-</sup> , 3773 MeV

• • • We do not use the following data for averages, fits, limits, etc. • • •

8.1 ± 1.5 ± 0.6	50 ± 9	ARTUSO	08	CLEO See MENDEZ 10
-----------------	--------	--------	----	--------------------

**Γ(η'(958)π<sup>0</sup>)/[Γ(K<sup>-</sup>π<sup>+</sup>) + Γ(K<sup>+</sup>π<sup>-</sup>)]** Γ<sub>179</sub>/(Γ<sub>35</sub>+Γ<sub>256</sub>)  
 Unseen decay modes of the η'(958) are included.

VALUE (units 10 <sup>-2</sup> )	EVTS	DOCUMENT ID	TECN	COMMENT
<b>2.32 ± 0.25 OUR FIT</b>				
2.3 ± 0.3 ± 0.2	159 ± 19	MENDEZ	10	CLEO e <sup>+</sup> e <sup>-</sup> at 3774 MeV

**Γ(η'(958)π<sup>+</sup>π<sup>-</sup>)/Γ<sub>total</sub>** Γ<sub>180</sub>/Γ  
 Unseen decay modes of the η'(958) are included.

VALUE (units 10 <sup>-4</sup> )	EVTS	DOCUMENT ID	TECN	COMMENT
4.5 ± 1.6 ± 0.5	21 ± 8	ARTUSO	08	CLEO e <sup>+</sup> e <sup>-</sup> at ψ(3770)

**Γ(2η)/Γ<sub>total</sub>** Γ<sub>181</sub>/Γ  
 Unseen decay modes of the η are included.

VALUE (units 10 <sup>-4</sup> )	EVTS	DOCUMENT ID	TECN	COMMENT
<b>21.1 ± 1.9 OUR FIT</b>				Error includes scale factor of 2.2.
22.0 ± 0.7 ± 0.6	3.4k	ABLIKIM	18L	BES3 e <sup>+</sup> e <sup>-</sup> , 3773 MeV

• • • We do not use the following data for averages, fits, limits, etc. • • •

16.7 ± 1.4 ± 1.3	255 ± 22	ARTUSO	08	CLEO See MENDEZ 10
------------------	----------	--------	----	--------------------

**Γ(2η)/[Γ(K<sup>-</sup>π<sup>+</sup>) + Γ(K<sup>+</sup>π<sup>-</sup>)]** Γ<sub>181</sub>/(Γ<sub>35</sub>+Γ<sub>256</sub>)  
 Unseen decay modes of the η are included.

VALUE (units 10 <sup>-2</sup> )	EVTS	DOCUMENT ID	TECN	COMMENT
<b>5.3 ± 0.5 OUR FIT</b>				Error includes scale factor of 2.2.
4.3 ± 0.3 ± 0.4	430 ± 29	MENDEZ	10	CLEO e <sup>+</sup> e <sup>-</sup> at 3774 MeV

**Γ(2ηπ<sup>0</sup>)/Γ<sub>total</sub>** Γ<sub>182</sub>/Γ

VALUE (units 10 <sup>-4</sup> )	EVTS	DOCUMENT ID	TECN	COMMENT
<b>7.3 ± 1.6 ± 1.5</b>	27	1 ABLIKIM	18x	BES3 e <sup>+</sup> e <sup>-</sup> , 3773 MeV

<sup>1</sup> Significance of signal reported by ABLIKIM 18x is 5.5σ.

**Γ(3η)/Γ<sub>total</sub>** Γ<sub>183</sub>/Γ

VALUE	CL%	DOCUMENT ID	TECN	COMMENT
<1.3 × 10 <sup>-4</sup>	90	ABLIKIM	18x	BES3 e <sup>+</sup> e <sup>-</sup> , 3773 MeV

**Γ(ηη'(958))/Γ<sub>total</sub>** Γ<sub>184</sub>/Γ  
 Unseen decay modes of the η and η'(958) are included.

VALUE (units 10 <sup>-4</sup> )	EVTS	DOCUMENT ID	TECN	COMMENT
<b>10.1 ± 1.9 OUR FIT</b>				
9.4 ± 2.5 ± 1.1	158 ± 41	ABLIKIM	18L	BES3 e <sup>+</sup> e <sup>-</sup> , 3773 MeV

• • • We do not use the following data for averages, fits, limits, etc. • • •

12.6 ± 2.5 ± 1.1	46 ± 9	ARTUSO	08	CLEO See MENDEZ 10
------------------	--------	--------	----	--------------------

**Γ(ηη'(958))/[Γ(K<sup>-</sup>π<sup>+</sup>) + Γ(K<sup>+</sup>π<sup>-</sup>)]** Γ<sub>184</sub>/(Γ<sub>35</sub>+Γ<sub>256</sub>)  
 Unseen decay modes of the η and η'(958) are included.

VALUE (units 10 <sup>-2</sup> )	EVTS	DOCUMENT ID	TECN	COMMENT
<b>2.5 ± 0.5 OUR FIT</b>				
2.7 ± 0.6 ± 0.3	66 ± 15	MENDEZ	10	CLEO e <sup>+</sup> e <sup>-</sup> at 3774 MeV

**Hadronic modes with a K<sup>+</sup>K<sup>-</sup> pair**

**Γ(K<sup>+</sup>K<sup>-</sup>)/Γ<sub>total</sub>** Γ<sub>185</sub>/Γ

VALUE (units 10 <sup>-3</sup> )	EVTS	DOCUMENT ID	TECN	COMMENT
<b>4.08 ± 0.06 OUR FIT</b>				Error includes scale factor of 1.6.
4.233 ± 0.021 ± 0.064	56k	ABLIKIM	18w	BES3 e <sup>+</sup> e <sup>-</sup> , 3773 MeV

• • • We do not use the following data for averages, fits, limits, etc. • • •

4.08 ± 0.08 ± 0.09	4.7k	BONVICINI	08	CLEO See MENDEZ 10
--------------------	------	-----------	----	--------------------

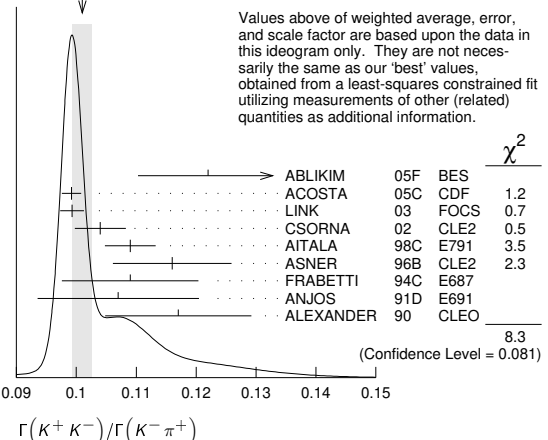
**Γ(K<sup>+</sup>K<sup>-</sup>)/Γ(K<sup>-</sup>π<sup>+</sup>)** Γ<sub>185</sub>/Γ<sub>35</sub>

VALUE	EVTS	DOCUMENT ID	TECN	COMMENT
<b>0.1033 ± 0.0013 OUR FIT</b>				Error includes scale factor of 1.6.
0.1010 ± 0.0016 OUR AVERAGE				Error includes scale factor of 1.4. See the ideogram below.
0.122 ± 0.011 ± 0.004	242 ± 20	ABLIKIM	05F	BES e <sup>+</sup> e <sup>-</sup> ≈ ψ(3770)
0.0992 ± 0.0011 ± 0.0012	16k ± 200	ACOSTA	05c	CDF p $\bar{p}$ , √s=1.96 TeV
0.0993 ± 0.0014 ± 0.0014	11k	LINK	03	FOCS γ nucleus, E <sub>γ</sub> ≈ 180 GeV
0.1040 ± 0.0033 ± 0.0027	1900	CSORNA	02	CLE2 e <sup>+</sup> e <sup>-</sup> ≈ γ(4S)
0.109 ± 0.003 ± 0.003	3317	AITALA	98c	E791 π <sup>-</sup> nucleus, 500 GeV
0.116 ± 0.007 ± 0.007	1102	ASNER	96B	CLE2 e <sup>+</sup> e <sup>-</sup> ≈ γ(4S)
0.109 ± 0.007 ± 0.009	581	FRABETTI	94c	E687 γBe E <sub>γ</sub> = 220 GeV
0.107 ± 0.010 ± 0.009	193	ANJOS	91D	E691 Photoproduction
0.117 ± 0.010 ± 0.007	249	ALEXANDER	90	CLEO e <sup>+</sup> e <sup>-</sup> 10.5–11 GeV

• • • We do not use the following data for averages, fits, limits, etc. • • •

0.107 ± 0.029 ± 0.015	103	ADAMOVICH	92	OMEG π <sup>-</sup> 340 GeV
0.138 ± 0.027 ± 0.010	155	FRABETTI	92	E687 γBe
0.16 ± 0.05	34	ALVAREZ	91B	NA14 Photoproduction
0.10 ± 0.02 ± 0.01	131	ALBRECHT	90c	ARG e <sup>+</sup> e <sup>-</sup> ≈ 10 GeV
0.122 ± 0.018 ± 0.012	118	BALTRUSAITIS	85E	MRK3 e <sup>+</sup> e <sup>-</sup> 3.77 GeV
0.113 ± 0.030		ABRAMS	79D	MRK2 e <sup>+</sup> e <sup>-</sup> 3.77 GeV

WEIGHTED AVERAGE  
0.1010 ± 0.0016 (Error scaled by 1.4)





$\Gamma(K^*(892)^0 K_S^0, K^{*0} \rightarrow K^+ \pi^-) / \Gamma(K^*(892)^0 K_S^0, \bar{K}^{*0} \rightarrow K^- \pi^+)$   
Γ<sub>199</sub>/Γ<sub>188</sub>

VALUE	CL%	DOCUMENT ID	TECN	COMMENT
<b>0.356 ± 0.034 ± 0.007</b>		<sup>1</sup> INSLER 12	CLEO	$e^+ e^- \rightarrow D^0 \bar{D}^0$ , 3.77 GeV
• • • We do not use the following data for averages, fits, limits, etc. • • •				
<0.010	90	AMMAR 91	CLEO	$e^+ e^- \approx 10.5$ GeV
<sup>1</sup> Uses quantum correlations in $e^+ e^- \rightarrow D^0 \bar{D}^0$ at the $\psi(3770)$ , where the signal side $D$ decays to $K_S^0 K \pi$ and the tag-side $D$ decays to $K \pi, K \pi \pi, K \pi \pi^0$ , and 10 additional CP-even, CP-odd, and mixed CP modes involving $K_S^0$ or $K_L^0$ .				

$\Gamma(K^*(892)^0 K_S^0, K^{*0} \rightarrow K^+ \pi^-) / \Gamma(K_S^0 K^+ \pi^-)$   
Fit fraction from Dalitz plot analyses.  
Γ<sub>199</sub>/Γ<sub>198</sub>

VALUE (units 10 <sup>-2</sup> )	EVTS	DOCUMENT ID	TECN	COMMENT
<b>5.17 ± 0.21 ± 0.47</b>	76k	<sup>1</sup> AAIJ 16N	LHCB	Dalitz plot fit
<sup>1</sup> AAIJ 16N gives results for two S-wave parameterisations. We take the values from the model with LASS parametrization, and the difference as a systematic uncertainty.				

$\Gamma(K^*(892)^- K^+, K^{*-} \rightarrow K_S^0 \pi^-) / \Gamma(K_S^0 K^+ \pi^-)$   
Fit fraction from Dalitz plot analyses.  
Γ<sub>200</sub>/Γ<sub>198</sub>

VALUE (units 10 <sup>-2</sup> )	EVTS	DOCUMENT ID	TECN	COMMENT
<b>28.8 ± 0.4 ± 1.5</b>	76k	<sup>1</sup> AAIJ 16N	LHCB	Dalitz plot fit
<sup>1</sup> AAIJ 16N gives results for two S-wave parameterisations. We take the values from the model with LASS parametrization, and the difference as a systematic uncertainty.				

$\Gamma(K^*(1410)^0 K_S^0, K^{*0} \rightarrow K^+ \pi^+) / \Gamma(K_S^0 K^+ \pi^-)$   
Fit fraction from Dalitz plot analyses.  
Γ<sub>201</sub>/Γ<sub>198</sub>

VALUE (units 10 <sup>-2</sup> )	EVTS	DOCUMENT ID	TECN	COMMENT
<b>2.2 ± 0.6 ± 3.7</b>	76k	<sup>1</sup> AAIJ 16N	LHCB	Dalitz plot fit
<sup>1</sup> AAIJ 16N gives results for two S-wave parameterisations. We take the values from the model with LASS parametrization, and the difference as a systematic uncertainty (which in this case dominates).				

$\Gamma(K^*(1410)^- K^+, K^{*-} \rightarrow K_S^0 \pi^-) / \Gamma(K_S^0 K^+ \pi^-)$   
Fit fraction from Dalitz plot analyses.  
Γ<sub>202</sub>/Γ<sub>198</sub>

VALUE (units 10 <sup>-2</sup> )	EVTS	DOCUMENT ID	TECN	COMMENT
<b>11.9 ± 1.5 ± 9.1</b>	76k	<sup>1</sup> AAIJ 16N	LHCB	Dalitz plot fit
<sup>1</sup> AAIJ 16N gives results for two S-wave parameterisations. We take the values from the model with LASS parametrization, and the difference as a systematic uncertainty (which in this case dominates).				

$\Gamma((K^+ \pi^-)_{S\text{-wave}} K_S^0) / \Gamma(K_S^0 K^+ \pi^-)$   
Fit fraction from Dalitz plot analyses.  
Γ<sub>203</sub>/Γ<sub>198</sub>

VALUE (units 10 <sup>-2</sup> )	EVTS	DOCUMENT ID	TECN	COMMENT
<b>17 ± 2 ± 8</b>	76k	<sup>1</sup> AAIJ 16N	LHCB	Dalitz plot fit
<sup>1</sup> AAIJ 16N gives results for two S-wave parameterisations. We take the values from the model with LASS parametrization, and the difference as a systematic uncertainty.				

$\Gamma((K_S^0 \pi^-)_{S\text{-wave}} K^+) / \Gamma(K_S^0 K^+ \pi^-)$   
Fit fraction from Dalitz plot analyses.  
Γ<sub>204</sub>/Γ<sub>198</sub>

VALUE (units 10 <sup>-2</sup> )	EVTS	DOCUMENT ID	TECN	COMMENT
<b>6.3 ± 0.9 ± 2.3</b>	76k	<sup>1</sup> AAIJ 16N	LHCB	Dalitz plot fit
<sup>1</sup> AAIJ 16N gives results for two S-wave parameterisations. We take the values from the model with LASS parametrization, and the difference as a systematic uncertainty.				

$\Gamma(a_0(980)^+ \pi^-, a_0^+ \rightarrow K_S^0 K^+) / \Gamma(K_S^0 K^+ \pi^-)$   
Fit fraction from Dalitz plot analyses.  
Γ<sub>205</sub>/Γ<sub>198</sub>

VALUE (units 10 <sup>-2</sup> )	EVTS	DOCUMENT ID	TECN	COMMENT
<b>26 ± 2 ± 18</b>	76k	<sup>1</sup> AAIJ 16N	LHCB	Dalitz plot fit
<sup>1</sup> AAIJ 16N gives results for two S-wave parameterisations. We take the values from the model with LASS parametrization, and the difference as a systematic uncertainty (which in this case dominates).				

$\Gamma(a_0(1450)^+ \pi^-, a_0^+ \rightarrow K_S^0 K^+) / \Gamma(K_S^0 K^+ \pi^-)$   
Fit fraction from Dalitz plot analyses.  
Γ<sub>206</sub>/Γ<sub>198</sub>

VALUE (units 10 <sup>-2</sup> )	EVTS	DOCUMENT ID	TECN	COMMENT
<b>1.5 ± 0.3 ± 1.1</b>	76k	<sup>1</sup> AAIJ 16N	LHCB	Dalitz plot fit
<sup>1</sup> AAIJ 16N gives results for two S-wave parameterisations. We take the values from the model with LASS parametrization, and the difference as a systematic uncertainty (which in this case dominates).				

$\Gamma(\rho(1700)^+ \pi^-, \rho^+ \rightarrow K_S^0 K^+) / \Gamma(K_S^0 K^+ \pi^-)$   
Fit fraction from Dalitz plot analyses.  
Γ<sub>207</sub>/Γ<sub>198</sub>

VALUE (units 10 <sup>-2</sup> )	EVTS	DOCUMENT ID	TECN	COMMENT
<b>0.53 ± 0.11 ± 0.23</b>	76k	<sup>1</sup> AAIJ 16N	LHCB	Dalitz plot fit
<sup>1</sup> AAIJ 16N gives results for two S-wave parameterisations. We take the values from the model with LASS parametrization, and the difference as a systematic uncertainty.				

$\Gamma(K^+ K^- \pi^0) / \Gamma(K^- \pi^+ \pi^0)$   
Γ<sub>208</sub>/Γ<sub>53</sub>

VALUE (units 10 <sup>-2</sup> )	EVTS	DOCUMENT ID	TECN	COMMENT
<b>2.37 ± 0.03 ± 0.04</b>	11k ± 122	AUBERT, B	06x BABR	$e^+ e^- \approx \Upsilon(4S)$
• • • We do not use the following data for averages, fits, limits, etc. • • •				
0.95 ± 0.26	151	ASNER 96b	CLE2	$e^+ e^- \approx \Upsilon(4S)$

$\Gamma(K^*(892)^+ K^-, K^*(892)^+ \rightarrow K^+ \pi^0) / \Gamma(K^+ K^- \pi^0)$   
This is the "fit fraction" from the Dalitz-plot analysis with interference.  
Γ<sub>209</sub>/Γ<sub>208</sub>

VALUE (units 10 <sup>-2</sup> )	DOCUMENT ID	TECN	COMMENT
<b>44.4 ± 0.8 ± 0.6</b>	AUBERT 07T	BABR	Dalitz fit II, 11k evts
• • • We do not use the following data for averages, fits, limits, etc. • • •			
46.1 ± 3.1	<sup>1</sup> CAWLFIELD 06A	CLEO	Dalitz fit, 627 ± 30 evts
<sup>1</sup> The error on this CAWLFIELD 06A result is statistical only.			

$\Gamma(K^*(892)^- K^+, K^*(892)^- \rightarrow K^- \pi^0) / \Gamma(K^+ K^- \pi^0)$   
This is the "fit fraction" from the Dalitz-plot analysis with interference.  
Γ<sub>210</sub>/Γ<sub>208</sub>

VALUE (units 10 <sup>-2</sup> )	DOCUMENT ID	TECN	COMMENT
<b>15.9 ± 0.7 ± 0.6</b>	AUBERT 07T	BABR	Dalitz fit II, 11k evts
• • • We do not use the following data for averages, fits, limits, etc. • • •			
12.3 ± 2.2	<sup>1</sup> CAWLFIELD 06A	CLEO	Dalitz fit, 627 ± 30 evts
<sup>1</sup> The error on this CAWLFIELD 06A result is statistical only.			

$\Gamma((K^+ \pi^0)_{S\text{-wave}} K^-) / \Gamma(K^+ K^- \pi^0)$   
This is the "fit fraction" from the Dalitz-plot analysis with interference.  
Γ<sub>211</sub>/Γ<sub>208</sub>

VALUE (units 10 <sup>-2</sup> )	DOCUMENT ID	TECN	COMMENT
<b>71.1 ± 3.7 ± 1.9</b>	<sup>1</sup> AUBERT 07T	BABR	Dalitz fit II, 11k evts
<sup>1</sup> The only major difference between fits I and II in the AUBERT 07T analysis is in this mode, where the fit-I fraction is (16.3 ± 3.4 ± 2.1)%.			

$\Gamma((K^- \pi^0)_{S\text{-wave}} K^+) / \Gamma(K^+ K^- \pi^0)$   
This is the "fit fraction" from the Dalitz-plot analysis with interference.  
Γ<sub>212</sub>/Γ<sub>208</sub>

VALUE (units 10 <sup>-2</sup> )	DOCUMENT ID	TECN	COMMENT
<b>3.9 ± 0.9 ± 1.0</b>	AUBERT 07T	BABR	Dalitz fit II, 11k evts

$\Gamma(f_0(980) \pi^0, f_0 \rightarrow K^+ K^-) / \Gamma(K^+ K^- \pi^0)$   
This is the "fit fraction" from the Dalitz-plot analysis with interference.  
Γ<sub>213</sub>/Γ<sub>208</sub>

VALUE (units 10 <sup>-2</sup> )	DOCUMENT ID	TECN	COMMENT
<b>10.5 ± 1.1 ± 1.2</b>	<sup>1</sup> AUBERT 07T	BABR	Dalitz fit II, 11k evts
<sup>1</sup> When AUBERT 07T replace the $f_0(980) \pi^0$ mode with $a_0(980) \pi^0$ , the fit fraction is a negligibly different (11.0 ± 1.5 ± 1.2)%.			

$\Gamma(\phi \pi^0, \phi \rightarrow K^+ K^-) / \Gamma(K^+ K^- \pi^0)$   
This is the "fit fraction" from the Dalitz-plot analysis with interference.  
Γ<sub>214</sub>/Γ<sub>208</sub>

VALUE (units 10 <sup>-2</sup> )	DOCUMENT ID	TECN	COMMENT
<b>19.4 ± 0.6 ± 0.5</b>	AUBERT 07T	BABR	Dalitz fit II, 11k evts
• • • We do not use the following data for averages, fits, limits, etc. • • •			
14.9 ± 1.6	<sup>1</sup> CAWLFIELD 06A	CLEO	Dalitz fit, 627 ± 30 evts
<sup>1</sup> The error on this CAWLFIELD 06A result is statistical only.			

$\Gamma(K^+ K^- \pi^0 \text{ nonresonant}) / \Gamma(K^+ K^- \pi^0)$   
This is the "fit fraction" from the Dalitz-plot analysis with interference.  
Γ<sub>215</sub>/Γ<sub>208</sub>

VALUE	DOCUMENT ID	TECN	COMMENT
0.360 ± 0.037	<sup>1</sup> CAWLFIELD 06A	CLEO	Dalitz fit, 627 ± 30 evts
<sup>1</sup> The error is statistical only. CAWLFIELD 06A also fits the Dalitz plot replacing this flat nonresonant background with broad S-wave $\kappa^\pm \rightarrow K^\pm \pi^0$ resonances. There is no significant improvement in the fit, and $K^{*\pm} K^\mp$ and $\phi \pi^0$ results are not much changed.			

$\Gamma(2K_S^0 \pi^0) / \Gamma_{\text{total}}$   
Γ<sub>216</sub>/Γ

VALUE	DOCUMENT ID	TECN	COMMENT
<b>&lt;0.00059</b>	ASNER 96b	CLE2	$e^+ e^- \approx \Upsilon(4S)$

$\Gamma(K^+ K^- \pi^+ \pi^-) / \Gamma(K^- 2\pi^+ \pi^-)$   
Γ<sub>217</sub>/Γ<sub>70</sub>

VALUE (units 10 <sup>-2</sup> )	EVTS	DOCUMENT ID	TECN	COMMENT
<b>3.00 ± 0.13 OUR AVERAGE</b>				
2.95 ± 0.11 ± 0.08	2669 ± 101	<sup>1</sup> LINK	05G FOCUS	$\gamma \text{Be}, \bar{E}_\gamma \approx 180$ GeV
3.13 ± 0.37 ± 0.36	136 ± 15	AITALA	98D E791	$\pi^-$ nucleus, 500 GeV
3.5 ± 0.4 ± 0.2	244 ± 26	FRABETTI	95C E687	$\gamma \text{Be}, \bar{E}_\gamma \approx 200$ GeV
• • • We do not use the following data for averages, fits, limits, etc. • • •				
4.4 ± 1.8 ± 0.5	19 ± 8	ABLIKIM	05F BES	$e^+ e^- \approx \psi(3770)$
4.1 ± 0.7 ± 0.5	114 ± 20	ALBRECHT	94I ARG	$e^+ e^- \approx 10$ GeV
3.14 ± 1.0	89 ± 29	AMMAR	91 CLEO	$e^+ e^- \approx 10.5$ GeV
2.8 <sup>+0.8</sup> <sub>-0.7</sub>		ANJOS	91 E691	$\gamma \text{Be}$ 80-240 GeV
<sup>1</sup> LINK 05G uses a smaller, cleaner subset of 1279 ± 48 events for the amplitude analysis that gives the results in the next data blocks.				

$\Gamma(\phi(\pi^+ \pi^-)_{S\text{-wave}}, \phi \rightarrow K^+ K^-) / \Gamma(K^+ K^- \pi^+ \pi^-)$   
This is the fraction from a coherent amplitude analysis.  
Γ<sub>218</sub>/Γ<sub>217</sub>

VALUE (units 10 <sup>-2</sup> )	EVTS	DOCUMENT ID	TECN	COMMENT
<b>4.0 ± 0.6 ± 2.1</b>	3k	<sup>1</sup> DARGENT 17		4-body fit, $K K \pi \pi$ events
• • • We do not use the following data for averages, fits, limits, etc. • • •				
10.3 ± 1.0 ± 0.8	3k	<sup>2</sup> ARTUSO 12	CLEO	4-body fit, $K K \pi \pi$ events
1 ± 1	1.3k	LINK	05G FOCUS	4-body fit, $K K \pi \pi$ events
<sup>1</sup> Obtained by analyzing CLEO data but not authored by the CLEO Collaboration. <sup>2</sup> See DARGENT 17				



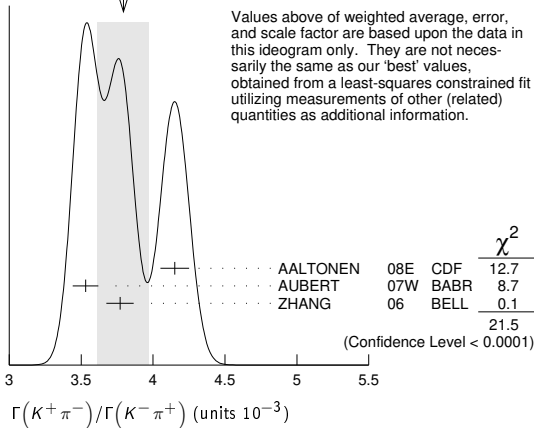




# Meson Particle Listings

$D^0$

WEIGHTED AVERAGE  
3.79±0.18 (Error scaled by 3.3)



Values above of weighted average, error, and scale factor are based upon the data in this ideogram only. They are not necessarily the same as our 'best' values, obtained from a least-squares constrained fit utilizing measurements of other (related) quantities as additional information.

## $\Gamma(K^+\pi^- \text{ via DCS})/\Gamma(K^-\pi^+)$

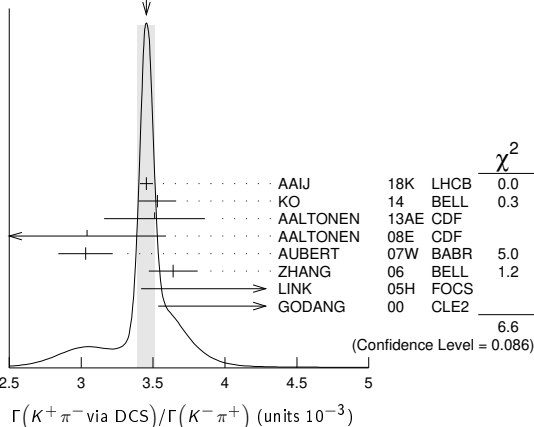
$\Gamma_{257}/\Gamma_{35}$

This is  $R_D$ , the doubly Cabibbo-suppressed ratio when mixing is allowed.

VALUE (units $10^{-3}$ )	EVTS	DOCUMENT ID	TECN	COMMENT
<b>3.45 ± 0.06 OUR AVERAGE</b>				Error includes scale factor of 1.5. See the ideogram below.
3.454 ± 0.040 ± 0.020	722k	1 AAIJ	18K LHCB	$pp$ at 7, 8, 13 TeV
3.53 ± 0.13		2 KO	14 BELL	$e^+e^- \rightarrow \Upsilon(nS)$
3.51 ± 0.35		3 AALTONEN	13AE CDF	$p\bar{p}$ at 1.96 TeV
3.04 ± 0.55	13k	AALTONEN	08E CDF	$p\bar{p}$ , $\sqrt{s} = 1.96$ TeV
3.03 ± 0.16 ± 0.10	4.0k	4 AUBERT	07W BABR	$e^+e^- \approx 10.6$ GeV
3.64 ± 0.17	4.0k	5 ZHANG	06 BELL	$e^+e^-$
5.17 $^{+1.47}_{-1.58}$ ± 0.76	234	6 LINK	05H FOCS	$\gamma$ nucleus
4.8 ± 1.2 ± 0.4	45	7 GODANG	00 CLE2	$e^+e^-$

- • • We do not use the following data for averages, fits, limits, etc. • • •
- 1 This AAIJ 18K value is for direct and indirect  $CP$  violation allowed. The value is the same if either one or the other is not allowed, but in each case the error then is  $(0.028 \pm 0.014) \times 10^{-3}$ .
- 2 Based on  $976 \text{ fb}^{-1}$  of data collected at  $\Upsilon(nS)$  resonances. Assumes no  $CP$  violation.
- 3 Based on  $9.6 \text{ fb}^{-1}$  of data collected at the Tevatron. Assumes no  $CP$  violation.
- 4 Result is the same whether or not  $CP$  violation is allowed.
- 5 This ZHANG 06 assumes no  $CP$  violation.
- 6 This LINK 05H result allows  $CP$  violation. Allowing mixing but not  $CP$  violation,  $R_D = (3.81^{+1.67}_{-1.63} \pm 0.92) \times 10^{-3}$ .
- 7 This GODANG 00 result allows  $CP$  violation.
- 8 The result was established with  $D^0$  from prompt and secondary  $D^*$  assuming no  $CPV$  or no direct  $CPV$ .
- 9 Based on  $3 \text{ fb}^{-1}$  of data collected at  $\sqrt{s} = 7, 8$  TeV. Assumes no  $CP$  violation.
- 10 Based on  $1 \text{ fb}^{-1}$  of data collected at  $\sqrt{s} = 7$  TeV in 2011. Assumes no  $CP$  violation.

WEIGHTED AVERAGE  
3.45±0.06 (Error scaled by 1.5)



## $\Gamma(K^+\pi^- \text{ via } \bar{D}^0)/\Gamma(K^-\pi^+)$

$\Gamma_{258}/\Gamma_{35}$

This is  $R_M$  in the note on " $D^0-\bar{D}^0$  Mixing" near the start of the  $D^0$  Listings. The experiments here (1) use the charge of the pion in  $D^*(2010)^\pm \rightarrow (D^0 \text{ or } \bar{D}^0) \pi^\pm$  decay to tell whether a  $D^0$  or a  $\bar{D}^0$  was born; and (2) use the decay-time distribution to disentangle doubly Cabibbo-suppressed decay and mixing. For the limits on  $|m_1 - m_2|$  and  $(\Gamma_1 - \Gamma_2)/\Gamma$  that come from the best mixing limit, see near the beginning of these  $D^0$  Listings.

VALUE	CL%	DOCUMENT ID	TECN	COMMENT
<b>&lt;0.00040</b>	95	1 ZHANG	06 BELL	$e^+e^-$
• • • We do not use the following data for averages, fits, limits, etc. • • •				
<0.00046	95	2 LI	05A BELL	See ZHANG 06
<0.0063	95	3 LINK	05H FOCS	$\gamma$ nucleus
<0.0013	95	4 AUBERT	03Z BABR	$e^+e^-$ , 10.6 GeV
<0.00041	95	5 GODANG	00 CLE2	$e^+e^-$
<0.0092	95	6 BARATE	98W ALEP	$e^+e^-$ at $Z^0$
<0.005	90	7 ANJOS	88c E691	Photoproduction

- 1 This ZHANG 06 result allows  $CP$  violation, but the result does not change if  $CP$  violation is not allowed.
- 2 This LI 05A result allows  $CP$  violation. The limit becomes  $< 0.00042$  (95% CL) if  $CP$  violation is not allowed.
- 3 LINK 05H obtains the same result whether or not  $CP$  violation is allowed.
- 4 This AUBERT 03Z result allows  $CP$  violation and assumes that the strong phase between  $D^0 \rightarrow K^+\pi^-$  and  $\bar{D}^0 \rightarrow K^+\pi^-$  is small, and limits only  $D^0 \rightarrow \bar{D}^0$  transitions via off-shell intermediate states. The limit on transitions via on-shell intermediate states is 0.0016.
- 5 This GODANG 00 result allows  $CP$  violation and assumes that the strong phase between  $D^0 \rightarrow K^+\pi^-$  and  $\bar{D}^0 \rightarrow K^+\pi^-$  is small, and limits only  $D^0 \rightarrow \bar{D}^0$  transitions via off-shell intermediate states. The limit on transitions via on-shell intermediate states is 0.0017.
- 6 This BARATE 98W result assumes no interference between the DCS and mixing amplitudes ( $\gamma = 0$  in the note on " $D^0-\bar{D}^0$  Mixing" near the start of the  $D^0$  Listings). When interference is allowed, the limit degrades to 0.036 (95%CL).
- 7 This ANJOS 88c result assumes no interference between the DCS and mixing amplitudes ( $\gamma = 0$  in the note on " $D^0-\bar{D}^0$  Mixing" near the start of the  $D^0$  Listings). When interference is allowed, the limit degrades to 0.019.

## $\Gamma(K_S^0 \pi^+ \pi^- \text{ in } D^0 \rightarrow \bar{D}^0)/\Gamma(K_S^0 \pi^+ \pi^-)$

$\Gamma_{259}/\Gamma_{38}$

This is  $R_M$  in the note on " $D^0-\bar{D}^0$  Mixing" near the start of the  $D^0$  Listings. The experiments here (1) use the charge of the pion in  $D^*(2010)^\pm \rightarrow (D^0 \text{ or } \bar{D}^0) \pi^\pm$  decay to tell whether a  $D^0$  or a  $\bar{D}^0$  was born; and (2) use the decay-time distribution to disentangle doubly Cabibbo-suppressed decay and mixing. For the limits on  $|m_1 - m_2|$  and  $(\Gamma_1 - \Gamma_2)/\Gamma$  that come from the best mixing limit, see near the beginning of these  $D^0$  Listings.

VALUE	CL%	DOCUMENT ID	TECN	COMMENT
<b>&lt;0.0063</b>	95	1 ASNER	05 CLEO	$e^+e^- \approx 10$ GeV

- 1 This ASNER 05 limit allows  $CP$  violation. If  $CP$  violation is not allowed, the limit is 0.0042 at 95% CL.

## $\Gamma(K^+\pi^-\pi^0)/\Gamma(K^-\pi^+\pi^0)$

$\Gamma_{263}/\Gamma_{53}$

The experiments here use the charge of the pion in  $D^*(2010)^\pm \rightarrow (D^0 \text{ or } \bar{D}^0) \pi^\pm$  decay to tell whether a  $D^0$  or a  $\bar{D}^0$  was born. The  $D^0 \rightarrow K^+\pi^-\pi^0$  decay can occur directly by doubly Cabibbo-suppressed (DCS) decay, or indirectly by  $D^0 \rightarrow \bar{D}^0$  mixing followed by  $\bar{D}^0 \rightarrow K^+\pi^-\pi^0$  decay.

VALUE (units $10^{-3}$ )	EVTS	DOCUMENT ID	TECN	COMMENT
<b>2.12 ± 0.07 OUR AVERAGE</b>				
2.01 ± 0.11		1 EVANS	16 CLEO	$e^+e^- \rightarrow D^0\bar{D}^0$ at $\psi(3770)$
2.14 ± 0.08 ± 0.08	763	2 AUBERT,B	06N BABR	$e^+e^- \approx \Upsilon(4S)$
2.29 ± 0.15 $^{+0.13}_{-0.09}$	1.9k	TIAN	05 BELL	$e^+e^- \approx \Upsilon(4S)$
4.3 $^{+1.1}_{-1.0}$ ± 0.7	38	BRANDENB...	01 CLE2	$e^+e^- \approx \Upsilon(4S)$

- 1 A combined fit with a recent LHCb  $D^0\bar{D}^0$  mixing results in AAIJ 16F is also reported to be  $(2.00 \pm 0.11) \times 10^{-3}$ .
- 2 This AUBERT,B 06N result assumes no mixing.

## $\Gamma(K^+\pi^-\pi^0 \text{ via } \bar{D}^0)/\Gamma(K^-\pi^+\pi^0)$

$\Gamma_{264}/\Gamma_{53}$

This is  $R_M$  in the note on " $D^0-\bar{D}^0$  Mixing" near the start of the  $D^0$  Listings. The experiments here (1) use the charge of the pion in  $D^*(2010)^\pm \rightarrow (D^0 \text{ or } \bar{D}^0) \pi^\pm$  decay to tell whether a  $D^0$  or a  $\bar{D}^0$  was born; and (2) use the decay-time distribution to disentangle doubly Cabibbo-suppressed decay and mixing. For the limits on  $|m_1 - m_2|$  and  $(\Gamma_1 - \Gamma_2)/\Gamma$  that come from the best mixing limit, see near the beginning of these  $D^0$  Listings.

VALUE (units $10^{-3}$ )	CL%	DOCUMENT ID	TECN	COMMENT
<b>5.25 <math>^{+0.25}_{-0.31}</math> ± 0.12</b>		AUBERT	09AN BABR	$e^+e^-$ at 10.58 GeV

- • • We do not use the following data for averages, fits, limits, etc. • • •
- <0.54
- 95
- 1 AUBERT,B
- 06N BABR
- $e^+e^- \approx \Upsilon(4S)$
- 1 This AUBERT,B 06N limit assumes no  $CP$  violation. The measured value corresponding to the limit is  $(2.3^{+1.8}_{-1.4} \pm 0.4) \times 10^{-4}$ . If  $CP$  violation is allowed, this becomes  $(1.0^{+2.2}_{-0.7} \pm 0.3) \times 10^{-4}$ .

Γ(K<sup>+</sup>π<sup>+</sup>2π<sup>-</sup> via DCS)/Γ(K<sup>-</sup>2π<sup>+</sup>π<sup>-</sup>) Γ<sub>265</sub>/Γ<sub>70</sub>

Table with columns: VALUE (units 10<sup>-3</sup>), EVTS, DOCUMENT ID, TECN, COMMENT. Includes 'OUR AVERAGE' and data from AAIJ and EVANS.

1 This result uses external input on the mixing parameters x, y. Without this input, the result is (3.215 ± 0.136) × 10<sup>-3</sup>.
2 A combined fit with a recent LHCb D<sup>0</sup>D<sup>0</sup> mixing results in AAIJ 16F is also reported to be (3.01 ± 0.07) × 10<sup>-3</sup>.

Γ(K<sup>+</sup>π<sup>+</sup>2π<sup>-</sup>)/Γ(K<sup>-</sup>2π<sup>+</sup>π<sup>-</sup>) Γ<sub>266</sub>/Γ<sub>70</sub>

The experiments here use the charge of the pion in D\*(2010)<sup>±</sup> → (D<sup>0</sup> or D<sup>0</sup>)π<sup>±</sup> decay to tell whether a D<sup>0</sup> or a D<sup>0</sup> was born. The D<sup>0</sup> → K<sup>+</sup>π<sup>-</sup>π<sup>+</sup>π<sup>-</sup> decay can occur directly by doubly Cabibbo-suppressed (DCS) decay, or indirectly by D<sup>0</sup> → D<sup>0</sup> mixing followed by D<sup>0</sup> → K<sup>+</sup>π<sup>-</sup>π<sup>+</sup>π<sup>-</sup> decay. Some of the experiments can use the decay-time information to disentangle the two mechanisms. Here, we list the experimental branching ratio, which if there is no mixing is the DCS ratio; in the next data block we give the limits on the mixing ratio.

Some early limits have been omitted from this Listing; see our 1998 edition (EPJ C3 1).

Table with columns: VALUE (units 10<sup>-3</sup>), CL%, EVTS, DOCUMENT ID, TECN, COMMENT. Includes 'OUR AVERAGE' and data from AAIJ, WHITE, DYTMAN.

Table with columns: VALUE (units 10<sup>-3</sup>), CL%, EVTS, DOCUMENT ID, TECN, COMMENT. Includes data from AAIJ, WHITE, DYTMAN, AITALA, TIAN, AMMAR, ANJOS.

• • • We do not use the following data for averages, fits, limits, etc. • • •
3.20 ± 0.18 +0.18 -0.13 1.7k 2 TIAN 05 BELL See WHITE 13
<18 90 2 AMMAR 91 CLEO e<sup>+</sup>e<sup>-</sup> ≈ 10.5 GeV
<18 90 4 ANJOS 88c E691 Photoproduction

1 AAIJ 16F result comes from time-dependent analysis that uses external input on the mixing parameters x, y. Without this input, the result is (3.29 ± 0.08) × 10<sup>-3</sup>.
2 AMMAR 91 cannot and DYTMAN 01, TIAN 05 do not distinguish between doubly Cabibbo-suppressed decay and D<sup>0</sup>-D<sup>0</sup> mixing.
3 This AITALA 98 result assumes no D<sup>0</sup>-D<sup>0</sup> mixing (R<sub>M</sub> in the note on "D<sup>0</sup>-D<sup>0</sup> Mixing"). It becomes -0.0020 ± 0.0117 ± 0.0106 ± 0.0035 when mixing is allowed and decay-time information is used to distinguish doubly Cabibbo-suppressed decays from mixing.
4 ANJOS 88c uses decay-time information to distinguish doubly Cabibbo-suppressed (DCS) decays from D<sup>0</sup>-D<sup>0</sup> mixing. However, the result assumes no interference between the DCS and mixing amplitudes (y' = 0 in the note on "D<sup>0</sup>-D<sup>0</sup> Mixing" near the start of the D<sup>0</sup> Listings). When interference is allowed, the limit degrades to 0.033.

Γ(K<sup>+</sup>π<sup>+</sup>2π<sup>-</sup> via D<sup>0</sup>)/Γ(K<sup>-</sup>2π<sup>+</sup>π<sup>-</sup>) Γ<sub>267</sub>/Γ<sub>70</sub>

This is a D<sup>0</sup>-D<sup>0</sup> mixing limit. The experiments here (1) use the charge of the pion in D\*(2010)<sup>±</sup> → (D<sup>0</sup> or D<sup>0</sup>)π<sup>±</sup> decay to tell whether a D<sup>0</sup> or a D<sup>0</sup> was born; and (2) use the decay-time distribution to disentangle doubly Cabibbo-suppressed decay and mixing. For the limits on |m<sub>D<sub>1</sub><sup>0</sup> - m<sub>D<sub>2</sub><sup>0</sup></sub>| and (Γ<sub>D<sub>1</sub><sup>0</sup></sub> - Γ<sub>D<sub>2</sub><sup>0</sup></sub>)/Γ<sub>D<sub>0</sub></sub> that come from the best mixing limit, see near the beginning of these D<sup>0</sup> Listings.</sub>

Table with columns: VALUE (units 10<sup>-5</sup>), CL%, DOCUMENT ID, TECN, COMMENT. Includes 'OUR AVERAGE' and data from AAIJ.

• • • We do not use the following data for averages, fits, limits, etc. • • •
<500 90 2 ANJOS 88c E691 Photoproduction

1 AAIJ 16F result comes from an unconstrained decay-time dependent fit to the wrong-sign to right-sign decay rates ratio as (x<sup>2</sup> + y<sup>2</sup>)/2.
2 ANJOS 88c uses decay-time information to distinguish doubly Cabibbo-suppressed (DCS) decays from D<sup>0</sup>-D<sup>0</sup> mixing. However, the result assumes no interference between the DCS and mixing amplitudes (y' = 0 in the note on "D<sup>0</sup>-D<sup>0</sup> Mixing" near the start of the D<sup>0</sup> Listings). When interference is allowed, the limit degrades to 0.007.

Γ(K<sup>+</sup>π<sup>-</sup> or K<sup>+</sup>π<sup>+</sup>2π<sup>-</sup> via D<sup>0</sup>)/Γ(K<sup>-</sup>π<sup>+</sup> or K<sup>-</sup>2π<sup>+</sup>π<sup>-</sup>) Γ<sub>268</sub>/Γ<sub>0</sub>

This is a D<sup>0</sup>-D<sup>0</sup> mixing limit. For the limits on |m<sub>D<sub>1</sub><sup>0</sup> - m<sub>D<sub>2</sub><sup>0</sup></sub>| and (Γ<sub>D<sub>0</sub></sub> - Γ<sub>D<sub>2</sub><sup>0</sup></sub>)/Γ<sub>D<sub>0</sub></sub> that come from the best mixing limit, see near the beginning of these D<sup>0</sup> Listings.</sub>

Table with columns: VALUE, CL%, DOCUMENT ID, TECN, COMMENT. Includes data from AITALA and ANJOS.

• • • We do not use the following data for averages, fits, limits, etc. • • •
<0.0085 90 1 AITALA 98 E791 π<sup>-</sup> nucleus, 500 GeV
<0.0037 90 2 ANJOS 88c E691 Photoproduction

1 AITALA 98 uses decay-time information to distinguish doubly Cabibbo-suppressed decays from D<sup>0</sup>-D<sup>0</sup> mixing. The fit allows interference between the two amplitudes, and also allows CP violation in this term. The central value obtained is 0.0039 ± 0.0036 ± 0.0016 -0.0032 ± 0.0016. When interference is disallowed, the result becomes 0.0021 ± 0.0009 ± 0.0002.
2 This combines results of ANJOS 88c on K<sup>+</sup>π<sup>-</sup> and K<sup>+</sup>π<sup>-</sup>π<sup>+</sup>π<sup>-</sup> (via D<sup>0</sup>) reported in the data block above (see footnotes there). It assumes no interference.

Γ(μ<sup>-</sup> anything via D<sup>0</sup>)/Γ(μ<sup>+</sup> anything) Γ<sub>269</sub>/Γ<sub>6</sub>

This is a D<sup>0</sup>-D<sup>0</sup> mixing limit. See the somewhat better limits above.

Table with columns: VALUE, CL%, DOCUMENT ID, TECN, COMMENT. Includes 'OUR AVERAGE' and data from LOUIS.

• • • We do not use the following data for averages, fits, limits, etc. • • •
<0.012 90 BENVENUTI 85 CNTR μ<sub>C</sub>, 200 GeV
<0.044 90 BODEK 82 SPEC π<sup>-</sup>, pFe → D<sup>0</sup>

Rare or forbidden modes

Γ(γγ)/Γ<sub>total</sub> Γ<sub>270</sub>/Γ

D<sup>0</sup> → γγ is a flavor-changing neutral-current decay, forbidden in the Standard Model at the tree level.

Table with columns: VALUE, CL%, DOCUMENT ID, TECN, COMMENT. Includes data from NISAR, ABLIKIM, LEES, COAN.

Γ(e<sup>+</sup>e<sup>-</sup>)/Γ<sub>total</sub> Γ<sub>271</sub>/Γ

A test for the ΔC = 1 weak neutral current. Allowed by first-order weak interaction combined with electromagnetic interaction.

Table with columns: VALUE, CL%, DOCUMENT ID, TECN, COMMENT. Includes data from PETRIC, BELL, LEES, AUBERT.B, PRIPSTEIN, AITALA, FREYBERGER, ADLER, ALBRECHT, HAAS.

Γ(μ<sup>+</sup>μ<sup>-</sup>)/Γ<sub>total</sub> Γ<sub>272</sub>/Γ

A test for the ΔC = 1 weak neutral current. Allowed by first-order weak interaction combined with electromagnetic interaction.

Table with columns: VALUE, CL%, DOCUMENT ID, TECN, COMMENT. Includes data from AAIJ, LEES, AALTONEN, PETRIC, ABT, AUBERT.B, ACOSTA, PRIPSTEIN, AITALA, ADAMOVIICH, ALEXOPOU..., FREYBERGER, ADAMOVIICH, KODAMA, MISHRA, ALBRECHT, LOUIS, AUBERT.

1 LEES 12q gives a 2-sided range.
2 Here MISHRA 94 uses "the statistical approach advocated by the PDG." For an alternate approach, giving a limit of 9 × 10<sup>-6</sup> at 90% confidence level, see the paper.

Γ(π<sup>0</sup>e<sup>+</sup>e<sup>-</sup>)/Γ<sub>total</sub> Γ<sub>273</sub>/Γ

A test for the ΔC = 1 weak neutral current. Allowed by higher-order electroweak interactions.

Table with columns: VALUE, CL%, DOCUMENT ID, TECN, COMMENT. Includes data from ABLIKIM, FREYBERGER.

Γ(π<sup>0</sup>μ<sup>+</sup>μ<sup>-</sup>)/Γ<sub>total</sub> Γ<sub>274</sub>/Γ

A test for the ΔC=1 weak neutral current. Allowed by higher-order electroweak interactions.

Table with columns: VALUE, CL%, DOCUMENT ID, TECN, COMMENT. Includes data from KODAMA, FREYBERGER.

Γ(ηe<sup>+</sup>e<sup>-</sup>)/Γ<sub>total</sub> Γ<sub>275</sub>/Γ

A test for the ΔC = 1 weak neutral current. Allowed by higher-order electroweak interactions.

Table with columns: VALUE, CL%, DOCUMENT ID, TECN, COMMENT. Includes data from ABLIKIM, FREYBERGER.

Γ(ημ<sup>+</sup>μ<sup>-</sup>)/Γ<sub>total</sub> Γ<sub>276</sub>/Γ

A test for the ΔC = 1 weak neutral current. Allowed by higher-order electroweak interactions.

Table with columns: VALUE, CL%, DOCUMENT ID, TECN, COMMENT. Includes data from FREYBERGER.

## Meson Particle Listings

 $D^0$ 

$\Gamma(\pi^+\pi^-\pi^+\pi^-)/\Gamma_{\text{total}}$   $\Gamma_{277}/\Gamma$   
A test for the  $\Delta C = 1$  weak neutral current. Allowed by higher-order electroweak interactions.

VALUE	CL%	DOCUMENT ID	TECN	COMMENT
$<7 \times 10^{-6}$	90	ABLIKIM 18P	BES3	$e^+e^-$ , 3773 MeV
•••		We do not use the following data for averages, fits, limits, etc. •••		
$<3.73 \times 10^{-4}$	90	AITALA 01c	E791	$\pi^-$ nucleus, 500 GeV

$\Gamma(\rho^0 e^+ e^-)/\Gamma_{\text{total}}$   $\Gamma_{278}/\Gamma$   
A test for the  $\Delta C = 1$  weak neutral current. Allowed by higher-order electroweak interactions.

VALUE	CL%	DOCUMENT ID	TECN	COMMENT
$<1.0 \times 10^{-4}$	90	<sup>1</sup> FREYBERGER 96	CLE2	$e^+e^- \approx \Upsilon(4S)$
•••		We do not use the following data for averages, fits, limits, etc. •••		
$<1.24 \times 10^{-4}$	90	AITALA 01c	E791	$\pi^-$ nucleus, 500 GeV
$<4.5 \times 10^{-4}$	90	HAAS 88	CLEO	$e^+e^-$ 10 GeV

<sup>1</sup>This FREYBERGER 96 limit is obtained using a phase-space model. The limit changes to  $<1.8 \times 10^{-4}$  using a photon pole amplitude model.

$\Gamma(\pi^+\pi^-\mu^+\mu^-)/\Gamma_{\text{total}}$   $\Gamma_{279}/\Gamma$   
A test for the  $\Delta C = 1$  weak neutral current. Allowed by higher-order electroweak interactions.

VALUE (units $10^{-7}$ )	EVTS	DOCUMENT ID	TECN	COMMENT
$9.64 \pm 0.48 \pm 1.10$	561	<sup>1</sup> AAIJ	17Bg LHCb	$pp$ at 8 TeV

<sup>1</sup>The second AAJ17Bg error is the systematic  $0.51 \times 10^{-7}$  and normalization  $0.97 \times 10^{-7}$  mode errors added in quadrature.

$\Gamma(\pi^+\pi^-\mu^+\mu^- \text{ (non-res)})/\Gamma_{\text{total}}$   $\Gamma_{280}/\Gamma$

VALUE	CL%	DOCUMENT ID	TECN	COMMENT
$<5.5 \times 10^{-7}$	90	<sup>1</sup> AAIJ	14B LHCb	$pp$ at 7 TeV
•••		We do not use the following data for averages, fits, limits, etc. •••		
$<3.0 \times 10^{-5}$	90	AITALA 01c	E791	$\pi^-$ nucleus, 500 GeV

<sup>1</sup>AAIJ 14B measures this branching-fraction limit relative to the  $\pi^+\pi^-\phi$ ,  $\phi \rightarrow \mu^+\mu^-$  fraction. The above limit excludes the resonant  $\phi$ ,  $\omega$ , and  $\rho$  regions, and then fills those gaps with a phase-space model.

$\Gamma(\rho^0 \mu^+ \mu^-)/\Gamma_{\text{total}}$   $\Gamma_{281}/\Gamma$   
A test for the  $\Delta C = 1$  weak neutral current. Allowed by higher-order electroweak interactions.

VALUE	CL%	DOCUMENT ID	TECN	COMMENT
$<2.2 \times 10^{-5}$	90	AITALA 01c	E791	$\pi^-$ nucleus, 500 GeV
•••		We do not use the following data for averages, fits, limits, etc. •••		
$<4.9 \times 10^{-4}$	90	<sup>1</sup> FREYBERGER 96	CLE2	$e^+e^- \approx \Upsilon(4S)$
$<2.3 \times 10^{-4}$	90	KODAMA 95	E653	$\pi^-$ emulsion 600 GeV
$<8.1 \times 10^{-4}$	90	HAAS 88	CLEO	$e^+e^-$ 10 GeV

<sup>1</sup>This FREYBERGER 96 limit is obtained using a phase-space model. The limit changes to  $<4.5 \times 10^{-4}$  using a photon pole amplitude model.

$\Gamma(\omega e^+ e^-)/\Gamma_{\text{total}}$   $\Gamma_{282}/\Gamma$   
A test for the  $\Delta C = 1$  weak neutral current. Allowed by higher-order electroweak interactions.

VALUE	CL%	DOCUMENT ID	TECN	COMMENT
$<6 \times 10^{-6}$	90	ABLIKIM 18P	BES3	$e^+e^-$ , 3773 MeV
•••		We do not use the following data for averages, fits, limits, etc. •••		
$<1.8 \times 10^{-4}$	90	<sup>1</sup> FREYBERGER 96	CLE2	$e^+e^- \approx \Upsilon(4S)$

<sup>1</sup>This FREYBERGER 96 limit is obtained using a phase-space model. The limit changes to  $<2.7 \times 10^{-4}$  using a photon pole amplitude model.

$\Gamma(\omega \mu^+ \mu^-)/\Gamma_{\text{total}}$   $\Gamma_{283}/\Gamma$   
A test for the  $\Delta C = 1$  weak neutral current. Allowed by higher-order electroweak interactions.

VALUE	CL%	DOCUMENT ID	TECN	COMMENT
$<8.3 \times 10^{-4}$	90	<sup>1</sup> FREYBERGER 96	CLE2	$e^+e^- \approx \Upsilon(4S)$

<sup>1</sup>This FREYBERGER 96 limit is obtained using a phase-space model. The limit changes to  $<6.5 \times 10^{-4}$  using a photon pole amplitude model.

$\Gamma(K^-K^+e^+e^-)/\Gamma_{\text{total}}$   $\Gamma_{284}/\Gamma$   
A test for the  $\Delta C = 1$  weak neutral current. Allowed by higher-order electroweak interactions.

VALUE	CL%	DOCUMENT ID	TECN	COMMENT
$<1.1 \times 10^{-5}$	90	ABLIKIM 18P	BES3	$e^+e^-$ , 3773 MeV
•••		We do not use the following data for averages, fits, limits, etc. •••		
$<3.15 \times 10^{-4}$	90	AITALA 01c	E791	$\pi^-$ nucleus, 500 GeV

$\Gamma(K^- \pi^+ e^+ e^-, 675 < m_{ee} < 875 \text{ MeV})/\Gamma_{\text{total}}$   $\Gamma_{292}/\Gamma$

VALUE (units $10^{-6}$ )	EVTS	DOCUMENT ID	TECN	COMMENT
$4.0 \pm 0.5 \pm 0.2 \pm 0.1$	68	<sup>1,2</sup> LEES	19A BABR	$e^+e^-$ near $\Upsilon(4S)$

<sup>1</sup>Observation with 9.7  $\sigma$  significance. The last uncertainty is due to the uncertainty on the branching fraction of the normalization mode,  $D^0 \rightarrow K^- \pi^+ \pi^+ \pi^-$ . The second uncertainty is other systematic and is dominated by the model parameterization.

<sup>2</sup>LEES 19A also sets an upper limit for non-resonant regions, where long-distance effects are expected to be small:  $<3.1 \times 10^{-6}$  at 90% CL.

$\Gamma(K^- \pi^+ e^+ e^-, 1.005 < m_{ee} < 1.035 \text{ GeV})/\Gamma_{\text{total}}$   $\Gamma_{293}/\Gamma$

VALUE	CL%	DOCUMENT ID	TECN	COMMENT
$<5 \times 10^{-7}$	90	<sup>1</sup> LEES	19A BABR	$e^+e^-$ near $\Upsilon(4S)$

<sup>1</sup>LEES 19A also sets an upper limit for non-resonant regions, where long-distance effects are expected to be small:  $<3.1 \times 10^{-6}$  at 90% CL.

$\Gamma(\phi e^+ e^-)/\Gamma_{\text{total}}$   $\Gamma_{285}/\Gamma$

A test for the  $\Delta C = 1$  weak neutral current. Allowed by higher-order electroweak interactions.

VALUE	CL%	DOCUMENT ID	TECN	COMMENT
$<5.2 \times 10^{-5}$	90	<sup>1</sup> FREYBERGER 96	CLE2	$e^+e^- \approx \Upsilon(4S)$
•••		We do not use the following data for averages, fits, limits, etc. •••		
$<5.9 \times 10^{-5}$	90	AITALA 01c	E791	$\pi^-$ nucleus, 500 GeV

<sup>1</sup>This FREYBERGER 96 limit is obtained using a phase-space model. The limit changes to  $<7.6 \times 10^{-5}$  using a photon pole amplitude model.

$\Gamma(K^- K^+ \mu^+ \mu^-)/\Gamma_{\text{total}}$   $\Gamma_{286}/\Gamma$

A test for the  $\Delta C = 1$  weak neutral current. Allowed by higher-order electroweak interactions.

VALUE (units $10^{-7}$ )	EVTS	DOCUMENT ID	TECN	COMMENT
$1.54 \pm 0.27 \pm 0.18$	34	<sup>1</sup> AAIJ	17Bg LHCb	$pp$ at 8 TeV

<sup>1</sup>The second AAJ17Bg error is the systematic  $0.09 \times 10^{-7}$  and normalization  $0.16 \times 10^{-7}$  mode errors added in quadrature.

$\Gamma(K^- K^+ \mu^+ \mu^- \text{ (non-res)})/\Gamma_{\text{total}}$   $\Gamma_{287}/\Gamma$

VALUE	CL%	DOCUMENT ID	TECN	COMMENT
$<3.3 \times 10^{-5}$	90	AITALA 01c	E791	$\pi^-$ nucleus, 500 GeV

$\Gamma(\phi \mu^+ \mu^-)/\Gamma_{\text{total}}$   $\Gamma_{288}/\Gamma$

A test for the  $\Delta C = 1$  weak neutral current. Allowed by higher-order electroweak interactions.

VALUE	CL%	DOCUMENT ID	TECN	COMMENT
$<3.1 \times 10^{-5}$	90	AITALA 01c	E791	$\pi^-$ nucleus, 500 GeV
•••		We do not use the following data for averages, fits, limits, etc. •••		
$<4.1 \times 10^{-4}$	90	<sup>1</sup> FREYBERGER 96	CLE2	$e^+e^- \approx \Upsilon(4S)$

<sup>1</sup>This FREYBERGER 96 limit is obtained using a phase-space model. The limit changes to  $<2.4 \times 10^{-4}$  using a photon pole amplitude model.

$\Gamma(\bar{K}^0 e^+ e^-)/\Gamma_{\text{total}}$   $\Gamma_{289}/\Gamma$

Not a useful test for  $\Delta C = 1$  weak neutral current because both quarks must change flavor.

VALUE	CL%	DOCUMENT ID	TECN	COMMENT
$<2.4 \times 10^{-5}$	90	<sup>1</sup> ABLIKIM 18P	BES3	$e^+e^-$ , 3773 MeV
•••		We do not use the following data for averages, fits, limits, etc. •••		
$<1.1 \times 10^{-4}$	90	FREYBERGER 96	CLE2	$e^+e^- \approx \Upsilon(4S)$
$<1.7 \times 10^{-3}$	90	ADLER 89c	MRK3	$e^+e^-$ 3.77 GeV

<sup>1</sup>ABLIKIM 18P report a 90% C.L. limit on  $D^0 \rightarrow \bar{K}_S^0 e^+ e^-$  of  $1.2 \times 10^{-5}$  which is here interpreted in terms of  $D^0 \rightarrow \bar{K}^0 e^+ e^-$ .

$\Gamma(\bar{K}^0 \mu^+ \mu^-)/\Gamma_{\text{total}}$   $\Gamma_{290}/\Gamma$

Not a useful test for  $\Delta C = 1$  weak neutral current because both quarks must change flavor.

VALUE	CL%	DOCUMENT ID	TECN	COMMENT
$<2.6 \times 10^{-4}$	90	KODAMA 95	E653	$\pi^-$ emulsion 600 GeV
•••		We do not use the following data for averages, fits, limits, etc. •••		
$<6.7 \times 10^{-4}$	90	FREYBERGER 96	CLE2	$e^+e^- \approx \Upsilon(4S)$

$\Gamma(K^- \pi^+ e^+ e^-)/\Gamma_{\text{total}}$   $\Gamma_{291}/\Gamma$

A test for the  $\Delta C = 1$  weak neutral current. Allowed by higher-order electroweak interactions.

VALUE	CL%	DOCUMENT ID	TECN	COMMENT
•••		We do not use the following data for averages, fits, limits, etc. •••		
$<4.1 \times 10^{-5}$	90	ABLIKIM 18P	BES3	see LEES 19A
$<3.85 \times 10^{-4}$	90	AITALA 01c	E791	$\pi^-$ nucleus, 500 GeV

$\Gamma(\bar{K}^*(892)^0 e^+ e^-)/\Gamma_{\text{total}}$   $\Gamma_{294}/\Gamma$

Not a useful test for  $\Delta C = 1$  weak neutral current because both quarks must change flavor.

VALUE	CL%	DOCUMENT ID	TECN	COMMENT
$<4.7 \times 10^{-5}$	90	AITALA 01c	E791	$\pi^-$ nucleus, 500 GeV
•••		We do not use the following data for averages, fits, limits, etc. •••		
$<1.4 \times 10^{-4}$	90	<sup>1</sup> FREYBERGER 96	CLE2	$e^+e^- \approx \Upsilon(4S)$

<sup>1</sup>This FREYBERGER 96 limit is obtained using a phase-space model. The limit changes to  $<2.0 \times 10^{-4}$  using a photon pole amplitude model.

$\Gamma(K^- \pi^+ \mu^+ \mu^-)/\Gamma_{\text{total}}$   $\Gamma_{295}/\Gamma$

A test for the  $\Delta C = 1$  weak neutral current. Allowed by higher-order electroweak interactions.

VALUE	CL%	DOCUMENT ID	TECN	COMMENT
$<3.59 \times 10^{-4}$	90	AITALA 01c	E791	$\pi^-$ nucleus, 500 GeV

$\Gamma(K^- \pi^+ \mu^+ \mu^-, 675 < m_{\mu\mu} < 875 \text{ MeV})/\Gamma_{\text{total}}$   $\Gamma_{296}/\Gamma$

VALUE (units $10^{-6}$ )	EVTS	DOCUMENT ID	TECN	COMMENT
$4.17 \pm 0.12 \pm 0.40$	2.4k	<sup>1</sup> AAIJ	16i	LHCB $pp$ at 8 TeV

<sup>1</sup> AAIJ 16i uses  $B(D^0 \rightarrow K^- \pi^+ \pi^+ \pi^-) = (8.287 \pm 0.043 \pm 0.200) \times 10^{-2}$  value for the normalization mode.

$\Gamma(\bar{K}^*(892)^0 \mu^+ \mu^-)/\Gamma_{\text{total}}$   $\Gamma_{297}/\Gamma$

Not a useful test for  $\Delta C=1$  weak neutral current because both quarks must change flavor.

VALUE	CL%	DOCUMENT ID	TECN	COMMENT
$< 2.4 \times 10^{-5}$	90	AITALA	01c	E791 $\pi^-$ nucleus, 500 GeV

• • • We do not use the following data for averages, fits, limits, etc. • • •

VALUE	CL%	DOCUMENT ID	TECN	COMMENT
$< 1.18 \times 10^{-3}$	90	<sup>1</sup> FREYBERGER 96	CLE2	$e^+ e^- \approx \gamma(4S)$

<sup>1</sup> This FREYBERGER 96 limit is obtained using a phase-space model. The limit changes to  $< 1.0 \times 10^{-3}$  using a photon pole amplitude model.

$\Gamma(\pi^+ \pi^- \pi^0 \mu^+ \mu^-)/\Gamma_{\text{total}}$   $\Gamma_{298}/\Gamma$

A test for the  $\Delta C=1$  weak neutral current. Allowed by higher-order electroweak interactions.

VALUE	CL%	DOCUMENT ID	TECN	COMMENT
$< 8.1 \times 10^{-4}$	90	KODAMA	95	E653 $\pi^-$ emulsion 600 GeV

$\Gamma(\mu^\pm e^\mp)/\Gamma_{\text{total}}$   $\Gamma_{299}/\Gamma$

A test of lepton family number conservation.

VALUE	CL%	DOCUMENT ID	TECN	COMMENT
$< 1.3 \times 10^{-8}$	90	AAIJ	16h	LHCB $pp$ at 7, 8 GeV

• • • We do not use the following data for averages, fits, limits, etc. • • •

$< 3.3 \times 10^{-7}$	90	LEES	12q	BABR $e^+ e^- \approx 10.58 \text{ GeV}$
$< 2.6 \times 10^{-7}$	90	PETRIC	10	BELL $e^+ e^- \approx \gamma(4S)$
$< 8.1 \times 10^{-7}$	90	AUBERT,B	04y	BABR $e^+ e^- \approx \gamma(4S)$
$< 1.72 \times 10^{-5}$	90	PRIPSTEIN	00	E789 $p$ nucleus, 800 GeV
$< 8.1 \times 10^{-6}$	90	AITALA	99g	E791 $\pi^- N$ 500 GeV
$< 1.9 \times 10^{-5}$	90	<sup>1</sup> FREYBERGER 96	CLE2	$e^+ e^- \approx \gamma(4S)$
$< 1.0 \times 10^{-4}$	90	ALBRECHT	88g	ARG $e^+ e^-$ 10 GeV
$< 2.7 \times 10^{-4}$	90	HAAS	88	CLEO $e^+ e^-$ 10 GeV
$< 1.2 \times 10^{-4}$	90	BECKER	87c	MRK3 $e^+ e^-$ 3.77 GeV
$< 9 \times 10^{-4}$	90	PALKA	87	SILI 200 GeV $\pi p$
$< 21 \times 10^{-4}$	90	<sup>2</sup> RILES	87	MRK2 $e^+ e^-$ 29 GeV

<sup>1</sup> This is the corrected result given in the erratum to FREYBERGER 96.  
<sup>2</sup> RILES 87 assumes  $B(D \rightarrow K \pi) = 3.0\%$  and has production model dependency.

$\Gamma(\pi^0 e^\pm \mu^\mp)/\Gamma_{\text{total}}$   $\Gamma_{300}/\Gamma$

A test of lepton family number conservation. The value is for the sum of the two charge states.

VALUE	CL%	DOCUMENT ID	TECN	COMMENT
$< 8.6 \times 10^{-5}$	90	FREYBERGER 96	CLE2	$e^+ e^- \approx \gamma(4S)$

$\Gamma(\eta e^\pm \mu^\mp)/\Gamma_{\text{total}}$   $\Gamma_{301}/\Gamma$

A test of lepton family number conservation. The value is for the sum of the two charge states.

VALUE	CL%	DOCUMENT ID	TECN	COMMENT
$< 1.0 \times 10^{-4}$	90	FREYBERGER 96	CLE2	$e^+ e^- \approx \gamma(4S)$

$\Gamma(\pi^+ \pi^- e^\pm \mu^\mp)/\Gamma_{\text{total}}$   $\Gamma_{302}/\Gamma$

A test of lepton family-number conservation. The value is for the sum of the two charge states.

VALUE	CL%	DOCUMENT ID	TECN	COMMENT
$< 1.5 \times 10^{-5}$	90	AITALA	01c	E791 $\pi^-$ nucleus, 500 GeV

$\Gamma(\rho^0 e^\pm \mu^\mp)/\Gamma_{\text{total}}$   $\Gamma_{303}/\Gamma$

A test of lepton family number conservation. The value is for the sum of the two charge states.

VALUE	CL%	DOCUMENT ID	TECN	COMMENT
$< 4.9 \times 10^{-5}$	90	<sup>1</sup> FREYBERGER 96	CLE2	$e^+ e^- \approx \gamma(4S)$

• • • We do not use the following data for averages, fits, limits, etc. • • •

$< 6.6 \times 10^{-5}$	90	AITALA	01c	E791 $\pi^-$ nucleus, 500 GeV
------------------------	----	--------	-----	-------------------------------

<sup>1</sup> This FREYBERGER 96 limit is obtained using a phase-space model. The limit changes to  $< 5.0 \times 10^{-5}$  using a photon pole amplitude model.

$\Gamma(\omega e^\pm \mu^\mp)/\Gamma_{\text{total}}$   $\Gamma_{304}/\Gamma$

A test of lepton family number conservation. The value is for the sum of the two charge states.

VALUE	CL%	DOCUMENT ID	TECN	COMMENT
$< 1.2 \times 10^{-4}$	90	<sup>1</sup> FREYBERGER 96	CLE2	$e^+ e^- \approx \gamma(4S)$

<sup>1</sup> This FREYBERGER 96 limit is obtained using a phase-space model. The same limit is obtained using a photon pole amplitude model.

$\Gamma(K^- K^+ e^\pm \mu^\mp)/\Gamma_{\text{total}}$   $\Gamma_{305}/\Gamma$

A test of lepton family-number conservation. The value is for the sum of the two charge states.

VALUE	CL%	DOCUMENT ID	TECN	COMMENT
$< 1.8 \times 10^{-4}$	90	AITALA	01c	E791 $\pi^-$ nucleus, 500 GeV

$\Gamma(\phi e^\pm \mu^\mp)/\Gamma_{\text{total}}$   $\Gamma_{306}/\Gamma$

A test of lepton family number conservation. The value is for the sum of the two charge states.

VALUE	CL%	DOCUMENT ID	TECN	COMMENT
$< 3.4 \times 10^{-5}$	90	<sup>1</sup> FREYBERGER 96	CLE2	$e^+ e^- \approx \gamma(4S)$

• • • We do not use the following data for averages, fits, limits, etc. • • •

$< 4.7 \times 10^{-5}$	90	AITALA	01c	E791 $\pi^-$ nucleus, 500 GeV
------------------------	----	--------	-----	-------------------------------

<sup>1</sup> This FREYBERGER 96 limit is obtained using a phase-space model. The limit changes to  $< 3.3 \times 10^{-5}$  using a photon pole amplitude model.

$\Gamma(\bar{K}^0 e^\pm \mu^\mp)/\Gamma_{\text{total}}$   $\Gamma_{307}/\Gamma$

A test of lepton family number conservation. The value is for the sum of the two charge states.

VALUE	CL%	DOCUMENT ID	TECN	COMMENT
$< 1.0 \times 10^{-4}$	90	FREYBERGER 96	CLE2	$e^+ e^- \approx \gamma(4S)$

$\Gamma(K^- \pi^+ e^\pm \mu^\mp)/\Gamma_{\text{total}}$   $\Gamma_{308}/\Gamma$

A test of lepton family-number conservation. The value is for the sum of the two charge states.

VALUE	CL%	DOCUMENT ID	TECN	COMMENT
$< 5.53 \times 10^{-4}$	90	AITALA	01c	E791 $\pi^-$ nucleus, 500 GeV

$\Gamma(\bar{K}^*(892)^0 e^\pm \mu^\mp)/\Gamma_{\text{total}}$   $\Gamma_{309}/\Gamma$

A test of lepton family number conservation. The value is for the sum of the two charge states.

VALUE	CL%	DOCUMENT ID	TECN	COMMENT
$< 8.3 \times 10^{-5}$	90	AITALA	01c	E791 $\pi^-$ nucleus, 500 GeV

• • • We do not use the following data for averages, fits, limits, etc. • • •

$< 1.0 \times 10^{-4}$	90	<sup>1</sup> FREYBERGER 96	CLE2	$e^+ e^- \approx \gamma(4S)$
------------------------	----	----------------------------	------	------------------------------

<sup>1</sup> This FREYBERGER 96 limit is obtained using a phase-space model. The same limit is obtained using a photon pole amplitude model.

$\Gamma(2\pi^- 2e^+ + c.c.)/\Gamma_{\text{total}}$   $\Gamma_{310}/\Gamma$

A test of lepton-number conservation. The value is for the sum of the two charge states.

VALUE	CL%	DOCUMENT ID	TECN	COMMENT
$< 1.12 \times 10^{-4}$	90	AITALA	01c	E791 $\pi^-$ nucleus, 500 GeV

$\Gamma(2\pi^- 2\mu^+ + c.c.)/\Gamma_{\text{total}}$   $\Gamma_{311}/\Gamma$

A test of lepton-number conservation. The value is for the sum of the two charge states.

VALUE	CL%	DOCUMENT ID	TECN	COMMENT
$< 2.9 \times 10^{-5}$	90	AITALA	01c	E791 $\pi^-$ nucleus, 500 GeV

$\Gamma(K^- \pi^- 2e^+ + c.c.)/\Gamma_{\text{total}}$   $\Gamma_{312}/\Gamma$

A test of lepton-number conservation. The value is for the sum of the two charge states.

VALUE	CL%	DOCUMENT ID	TECN	COMMENT
$< 2.06 \times 10^{-4}$	90	<sup>1</sup> AITALA	01c	E791 $\pi^-$ nucleus, 500 GeV

<sup>1</sup> ABLIKIM 19AL find  $\Gamma(D^0 \rightarrow K^- \pi^- 2e^+)/\Gamma(\text{total}) < 2.8 \times 10^{-6}$  at 90% CL (note their limit does not include decay to c.c. final state).

$\Gamma(K^- \pi^- 2e^+)/\Gamma_{\text{total}}$   $\Gamma_{313}/\Gamma$

VALUE	CL%	DOCUMENT ID	TECN	COMMENT
$< 2.8 \times 10^{-6}$	90	ABLIKIM	19AL	BES3 $e^+ e^-$ at 3773 MeV

$\Gamma(K^- \pi^- 2\mu^+ + c.c.)/\Gamma_{\text{total}}$   $\Gamma_{314}/\Gamma$

A test of lepton-number conservation. The value is for the sum of the two charge states.

VALUE	CL%	DOCUMENT ID	TECN	COMMENT
$< 3.9 \times 10^{-4}$	90	AITALA	01c	E791 $\pi^-$ nucleus, 500 GeV

$\Gamma(2K^- 2e^+ + c.c.)/\Gamma_{\text{total}}$   $\Gamma_{315}/\Gamma$

A test of lepton-number conservation. The value is for the sum of the two charge states.

VALUE	CL%	DOCUMENT ID	TECN	COMMENT
$< 1.52 \times 10^{-4}$	90	AITALA	01c	E791 $\pi^-$ nucleus, 500 GeV

$\Gamma(2K^- 2\mu^+ + c.c.)/\Gamma_{\text{total}}$   $\Gamma_{316}/\Gamma$

A test of lepton-number conservation. The value is for the sum of the two charge states.

VALUE	CL%	DOCUMENT ID	TECN	COMMENT
$< 9.4 \times 10^{-5}$	90	AITALA	01c	E791 $\pi^-$ nucleus, 500 GeV

$\Gamma(\pi^- \pi^- e^+ \mu^+ + c.c.)/\Gamma_{\text{total}}$   $\Gamma_{317}/\Gamma$

A test of lepton-number conservation. The value is for the sum of the two charge states.

VALUE	CL%	DOCUMENT ID	TECN	COMMENT
$< 7.9 \times 10^{-5}$	90	AITALA	01c	E791 $\pi^-$ nucleus, 500 GeV

$\Gamma(K^- \pi^- e^+ \mu^+ + c.c.)/\Gamma_{\text{total}}$   $\Gamma_{318}/\Gamma$

A test of lepton-number conservation. The value is for the sum of the two charge states.

VALUE	CL%	DOCUMENT ID	TECN	COMMENT
$< 2.18 \times 10^{-4}$	90	AITALA	01c	E791 $\pi^-$ nucleus, 500 GeV









See key on page 999

Meson Particle Listings D<sup>0</sup>

A<sub>CP</sub>(K<sub>1</sub><sup>\*(1270)</sup>- K<sup>+</sup> → K<sup>+</sup>K<sup>-</sup>π<sup>+</sup>π<sup>-</sup>) in D<sup>0</sup> → K<sub>1</sub><sup>\*(1270)</sup>- K<sup>+</sup>, D<sup>0</sup> → c.c.

Table with 5 columns: VALUE (%), EVTS, DOCUMENT ID, TECN, COMMENT. Includes 'OUR AVERAGE' and data from AAIJ and DARGENT.

A<sub>CP</sub>(K<sub>1</sub><sup>\*(1270)</sup>+ K<sup>-</sup> → ρ<sup>0</sup>K<sup>+</sup>K<sup>-</sup>) in D<sup>0</sup> → K<sub>1</sub><sup>\*(1270)</sup>+ K<sup>-</sup>, D<sup>0</sup> → c.c.

Table with 5 columns: VALUE (%), EVTS, DOCUMENT ID, TECN, COMMENT. Includes data from ARTUSO.

A<sub>CP</sub>(K<sub>1</sub><sup>\*(1270)</sup>- K<sup>+</sup> → ρ<sup>0</sup>K<sup>-</sup>K<sup>+</sup>) in D<sup>0</sup> → K<sub>1</sub><sup>\*(1270)</sup>- K<sup>+</sup>, D<sup>0</sup> → c.c.

Table with 5 columns: VALUE (%), EVTS, DOCUMENT ID, TECN, COMMENT. Includes data from ARTUSO.

A<sub>CP</sub>(K<sub>1</sub>(1400)+ K<sup>-</sup> → K<sup>+</sup>K<sup>-</sup>π<sup>+</sup>π<sup>-</sup>) in D<sup>0</sup> → K<sub>1</sub>(1400)+ K<sup>-</sup>, D<sup>0</sup> → c.c.

Table with 5 columns: VALUE (%), EVTS, DOCUMENT ID, TECN, COMMENT. Includes 'OUR AVERAGE' and data from AAIJ and DARGENT.

A<sub>CP</sub>(K<sup>\*</sup>(1410)+ K<sup>-</sup> → K<sup>\*0</sup>π<sup>+</sup>K<sup>-</sup>) in D<sup>0</sup> → K<sup>\*</sup>(1410)+ K<sup>-</sup>, D<sup>0</sup> → c.c.

Table with 5 columns: VALUE (%), EVTS, DOCUMENT ID, TECN, COMMENT. Includes data from ARTUSO.

A<sub>CP</sub>(K<sup>\*</sup>(1410)- K<sup>+</sup> → K<sup>\*0</sup>π<sup>-</sup>K<sup>+</sup>) in D<sup>0</sup> → K<sup>\*</sup>(1410)- K<sup>+</sup>, D<sup>0</sup> → c.c.

Table with 5 columns: VALUE (%), EVTS, DOCUMENT ID, TECN, COMMENT. Includes data from ARTUSO.

A<sub>CP</sub>(K<sup>\*</sup>(1680)+ K<sup>-</sup> → K<sup>+</sup>K<sup>-</sup>π<sup>+</sup>π<sup>-</sup>) in D<sup>0</sup> → K<sup>\*</sup>(1680)+ K<sup>-</sup>, D<sup>0</sup> → c.c.

Table with 5 columns: VALUE (%), EVTS, DOCUMENT ID, TECN, COMMENT. Includes 'OUR AVERAGE' and data from DARGENT.

A<sub>CP</sub>(K<sup>\*0</sup>K<sup>\*0</sup>) in D<sup>0</sup>, D<sup>0</sup> → K<sup>\*0</sup>K<sup>\*0</sup>

Table with 5 columns: VALUE (%), EVTS, DOCUMENT ID, COMMENT. Includes data from DARGENT.

A<sub>CP</sub>(K<sup>\*0</sup>K<sup>\*0</sup> S-wave) in D<sup>0</sup>, D<sup>0</sup> → K<sup>\*0</sup>K<sup>\*0</sup> S-wave

Table with 5 columns: VALUE (%), EVTS, DOCUMENT ID, TECN, COMMENT. Includes 'OUR AVERAGE' and data from AAIJ and ARTUSO.

A<sub>CP</sub>(φρ<sup>0</sup>) in D<sup>0</sup>, D<sup>0</sup> → φρ<sup>0</sup>

Table with 5 columns: VALUE (%), EVTS, DOCUMENT ID, COMMENT. Includes data from DARGENT.

A<sub>CP</sub>(φρ<sup>0</sup> S-wave) in D<sup>0</sup>, D<sup>0</sup> → φρ<sup>0</sup> S-wave

Table with 5 columns: VALUE (%), DOCUMENT ID, TECN, COMMENT. Includes data from ARTUSO.

A<sub>CP</sub>(φρ<sup>0</sup> D-wave) in D<sup>0</sup>, D<sup>0</sup> → φρ<sup>0</sup> D-wave

Table with 5 columns: VALUE (%), DOCUMENT ID, TECN, COMMENT. Includes data from ARTUSO.

A<sub>CP</sub>(φ(π<sup>+</sup>π<sup>-</sup>)s-wave) in D<sup>0</sup>, D<sup>0</sup> → φ(π<sup>+</sup>π<sup>-</sup>)s-wave

Table with 5 columns: VALUE (%), EVTS, DOCUMENT ID, TECN, COMMENT. Includes 'OUR AVERAGE' and data from AAIJ, DARGENT, and ARTUSO.

A<sub>CP</sub>(K<sup>\*</sup>(892)<sup>0</sup>(K<sup>-</sup>π<sup>+</sup>)s-wave) in D<sup>0</sup>, D<sup>0</sup> → K<sup>\*</sup>(892)<sup>0</sup>(K<sup>-</sup>π<sup>+</sup>)s-wave

Table with 5 columns: VALUE (%), EVTS, DOCUMENT ID, COMMENT. Includes data from DARGENT.

A<sub>CP</sub>(K<sup>+</sup>K<sup>-</sup>π<sup>+</sup>π<sup>-</sup> non-resonant) in D<sup>0</sup>, D<sup>0</sup> → K<sup>+</sup>K<sup>-</sup>π<sup>+</sup>π<sup>-</sup> non-resonant

Table with 3 columns: VALUE (%), DOCUMENT ID, COMMENT. Includes data from DARGENT.

A<sub>CP</sub>((K<sup>-</sup>π<sup>+</sup>)P-wave (K<sup>+</sup>π<sup>-</sup>)S-wave) in D<sup>0</sup> → (K<sup>-</sup>π<sup>+</sup>)P-wave (K<sup>+</sup>π<sup>-</sup>)S-wave, D<sup>0</sup> → c.c.

Table with 4 columns: VALUE (%), DOCUMENT ID, TECN, COMMENT. Includes data from ARTUSO.

A<sub>CP</sub>(K<sup>+</sup>K<sup>-</sup>μ<sup>+</sup>μ<sup>-</sup>) in D<sup>0</sup>, D<sup>0</sup> → K<sup>+</sup>K<sup>-</sup>μ<sup>+</sup>μ<sup>-</sup>

Table with 5 columns: VALUE (%), EVTS, DOCUMENT ID, TECN, COMMENT. Includes data from AAIJ.

A<sub>CP</sub>(π<sup>+</sup>π<sup>-</sup>μ<sup>+</sup>μ<sup>-</sup>) in D<sup>0</sup>, D<sup>0</sup> → π<sup>+</sup>π<sup>-</sup>μ<sup>+</sup>μ<sup>-</sup>

Table with 5 columns: VALUE (%), EVTS, DOCUMENT ID, TECN, COMMENT. Includes data from AAIJ.

D<sup>0</sup> CP-EVEN FRACTIONS

The CP-even fraction F<sub>+</sub>, defined for self-conjugate final states, like the coherence factor is useful for measuring the unitary triangle angle γ in B → DK decays.

CP-even fraction in D<sup>0</sup> → π<sup>+</sup>π<sup>-</sup>π<sup>0</sup> decays

Table with 3 columns: VALUE (%), DOCUMENT ID, COMMENT. Includes data from MALDE and NAYAK.

CP-even fraction in D<sup>0</sup> → K<sup>+</sup>K<sup>-</sup>π<sup>0</sup> decays

Table with 3 columns: VALUE (%), DOCUMENT ID, COMMENT. Includes data from MALDE and NAYAK.

CP-even fraction in D<sup>0</sup> → π<sup>+</sup>π<sup>-</sup>π<sup>+</sup>π<sup>-</sup> decays

Table with 4 columns: VALUE (%), DOCUMENT ID, TECN, COMMENT. Includes data from HARNEW, DARGENT, and MALDE.

CP-even fraction in D<sup>0</sup> → K<sub>S</sub><sup>0</sup>π<sup>+</sup>π<sup>-</sup>π<sup>0</sup> decays

Table with 3 columns: VALUE (%), DOCUMENT ID, COMMENT. Includes data from RESMI.

CP-even fraction in D<sup>0</sup> → K<sup>+</sup>K<sup>-</sup>π<sup>+</sup>π<sup>-</sup> decays

Table with 3 columns: VALUE (%), DOCUMENT ID, COMMENT. Includes data from DARGENT.

D<sup>0</sup> CP-VIOLATING ASYMMETRY DIFFERENCES

ΔA<sub>CP</sub> = A<sub>CP</sub>(K<sup>+</sup>K<sup>-</sup>) - A<sub>CP</sub>(π<sup>+</sup>π<sup>-</sup>)

CP violation in these modes can come from the decay amplitudes (direct) and/or from mixing or interference of mixing and decay (indirect).

Table with 5 columns: VALUE (%), EVTS, DOCUMENT ID, TECN, COMMENT. Includes data from AAIJ, LHCb, and AALTONEN.

Calculated from the AUBERT 08M values of A<sub>CP</sub>(K<sup>+</sup>K<sup>-</sup>) and A<sub>CP</sub>(π<sup>+</sup>π<sup>-</sup>). The systematic error here combines the systematic errors in quadrature, and therefore somewhat over-estimates it.

# Meson Particle Listings

## $D^0$

### $D^0$ TESTS OF LOCAL CP-VIOLATION (CPV)

We list model-independent searches for local CP violation in phase-space distributions of multi-body decays.

Most of these searches divide phase space (Dalitz plot for 3-body decays, five-dimensional equivalent for 4-body decays) into bins, and perform a  $\chi^2$  test comparing normalised yields  $N_i, \bar{N}_i$  in CP-conjugate bin pairs  $i$ :  $\chi^2 = \sum_i (N_i - \alpha \bar{N}_i) / \sigma(N_i - \alpha \bar{N}_i)$ . The factor  $\alpha = (\sum_i N_i) / (\sum_i \bar{N}_i)$  removes the dependence on phase-space-integrated rate asymmetries. The result is used to obtain the probability (p-value) to obtain the measured  $\chi^2$  or larger under the assumption of CP conservation [AUBERT 08AO, BEDIAGA 09]. Alternative methods obtain p-values from other test variables based on unbinned analyses [WILLIAMS 11, AAIJ 14c]. Results can be combined using Fisher's method [MOSTELLER 48].

#### Local CPV in $D^0, \bar{D}^0 \rightarrow \pi^+ \pi^- \pi^0$

p-value (%)	EVTS	DOCUMENT ID	TECN	COMMENT
<b>4.9 OUR EVALUATION</b>				
2.6	566k	1 AAIJ	15A LHCb	unbinned method
32.8	82k	AUBERT	08AO BABR	$\chi^2$

<sup>1</sup> Unusually, AAIJ 15A assigns an uncertainty on the p value of  $\pm 0.5\%$ . This results from limited test statistics.

#### Local CPV in $D^0, \bar{D}^0 \rightarrow \pi^+ \pi^- \pi^+ \pi^-$

p-value (%)	EVTS	DOCUMENT ID	TECN	COMMENT
<b>0.6 ± 0.2</b>				
• • • We do not use the following data for averages, fits, limits, etc. • • •	1.0M	1 AAIJ	17AE LHCb	unbinned, P-odd
4.6 ± 0.5	1.0M	2,3 AAIJ	17AE LHCb	unbinned, P-even
41	330k	2,4 AAIJ	13BR LHCb	$\chi^2$ , P-even

<sup>1</sup> This AAIJ 17AE value tests CP Violation in P-odd variables.  
<sup>2</sup> This value tests CP Violation in P-even variables.  
<sup>3</sup> Not included in average as correlation to P-odd measurement using the same data is unclear.  
<sup>4</sup> See AAIJ 17AE.

#### Local CPV in $D^0, \bar{D}^0 \rightarrow K_S^0 \pi^+ \pi^-$

p-value (%)	EVTS	DOCUMENT ID	TECN	COMMENT
<b>96</b>	350k	AALTONEN	12AD CDF	$\chi^2$

#### Local CPV in $D^0, \bar{D}^0 \rightarrow K^+ K^- \pi^0$

p-value (%)	EVTS	DOCUMENT ID	TECN	COMMENT
<b>16.6</b>	11k	AUBERT	08AO BABR	$\chi^2$

#### Local CPV in $D^0, \bar{D}^0 \rightarrow K^+ K^- \pi^+ \pi^-$

p-value (%)	EVTS	DOCUMENT ID	TECN	COMMENT
<b>9.1</b>	57k	AAIJ	13BR LHCb	$\chi^2$

### CP VIOLATING ASYMMETRIES OF P-ODD (T-ODD) MOMENTS

The CP-sensitive P-odd (T-odd) correlation in  $D^0, \bar{D}^0$  decays. The  $D^0$  and  $\bar{D}^0$  are distinguished by the charge of the parent  $D^*$ :  $D^{*+} \rightarrow D^0 \pi^+$  and  $D^{*-} \rightarrow \bar{D}^0 \pi^-$ .

#### $A_{Tviol}(K^+ K^- \pi^+ \pi^-)$ in $D^0, \bar{D}^0 \rightarrow K^+ K^- \pi^+ \pi^-$

$C_T \equiv \vec{p}_{K^+} \cdot (\vec{p}_{\pi^+} \times \vec{p}_{\pi^-})$  is a parity-odd correlation of the  $K^+, \pi^+$ , and  $\pi^-$  momenta (evaluated in the  $D^0$  rest frame) for the  $D^0$ .  $\bar{C}_T \equiv \vec{p}_{K^-} \cdot (\vec{p}_{\pi^-} \times \vec{p}_{\pi^+})$  is the corresponding quantity for the  $\bar{D}^0$ . Then  $A_T \equiv [\Gamma(C_T > 0) - \Gamma(C_T < 0)] / [\Gamma(C_T > 0) + \Gamma(C_T < 0)]$ , and  $\bar{A}_T \equiv [\Gamma(-\bar{C}_T > 0) - \Gamma(-\bar{C}_T < 0)] / [\Gamma(-\bar{C}_T > 0) + \Gamma(-\bar{C}_T < 0)]$ , and  $A_{Tviol} \equiv \frac{1}{2}(A_T - \bar{A}_T)$ .  $C_T$  and  $\bar{C}_T$  are commonly referred to as T-odd moments, because they are odd under T reversal. However, the T-conjugate process  $K^+ K^- \pi^+ \pi^- \rightarrow D^0$  is not accessible, while the P-conjugate process is.

VALUE (units $10^{-3}$ )	EVTS	DOCUMENT ID	TECN	COMMENT
<b>2.9 ± 2.2 OUR AVERAGE</b>				
5.2 ± 3.7 ± 0.7	110k	1 KIM	19 BELL	$e^+ e^-$ at $\Upsilon(1S) - \Upsilon(6S)$
1.8 ± 2.9 ± 0.4	171k	AAIJ	14BC LHCb	$B \rightarrow D^0 \mu^- X$
1.0 ± 5.1 ± 4.4	47k	DEL-AMO-SA...10	BABR	$e^+ e^- \approx 10.6$ GeV
• • • We do not use the following data for averages, fits, limits, etc. • • •				
10 ± 57 ± 37	0.8k	LINK	05E FOCS	$\gamma A, \bar{E}_\gamma \approx 180$ GeV

<sup>1</sup> KIM 19 also study CP-violating asymmetries in several other kinematic variables. No evidence for CP violation is found in any of them.

#### $A_{Tviol}(K_S \pi^+ \pi^- \pi^0)$ in $D^0, \bar{D}^0 \rightarrow K_S \pi^+ \pi^- \pi^0$

VALUE (units $10^{-3}$ )	EVTS	DOCUMENT ID	TECN	COMMENT
<b>-0.20 ± 1.38<sup>+0.23</sup><sub>-0.76</sub></b>	745k	1 PRASANTH	17 BELL	$e^+ e^-$ at $\Upsilon(nS)$ 's

<sup>1</sup> PRASANTH 17 also measures  $A_{Tviol}$  in sub-regions of the  $D^0 \rightarrow K_S \pi^+ \pi^- \pi^0$  phase-space. No evidence of T violation is found.

### $D^0$ CPT-VIOLATING DECAY-RATE ASYMMETRIES

#### $A_{CPT}(K^\mp \pi^\pm)$ in $D^0 \rightarrow K^- \pi^+, \bar{D}^0 \rightarrow K^+ \pi^-$

$A_{CPT}(t)$  is defined in terms of the time-dependent decay probabilities  $P(D^0 \rightarrow K^- \pi^+)$  and  $P(\bar{D}^0 \rightarrow K^+ \pi^-)$  by  $A_{CPT}(t) = (P - \bar{P}) / (P + \bar{P})$ . For small mixing parameters  $x \equiv \Delta m / \Gamma$  and  $y \equiv \Delta \Gamma / 2\Gamma$  (as is the case), and times  $t$ ,  $A_{CPT}(t)$  reduces to  $[y \operatorname{Re} \xi - x \operatorname{Im} \xi] \Gamma t$ , where  $\xi$  is the CPT-violating parameter.

The following is actually  $y \operatorname{Re} \xi - x \operatorname{Im} \xi$ .

VALUE	DOCUMENT ID	TECN	COMMENT
<b>0.0083 ± 0.0065 ± 0.0041</b>	LINK	03B FOCS	$\gamma$ nucleus, $\bar{E}_\gamma \approx 180$ GeV

#### $D^0 \rightarrow K^*(892)^- \ell^+ \nu_\ell$ FORM FACTORS

##### $r_V \equiv V(0)/A_1(0)$ in $D^0 \rightarrow K^*(892)^- \ell^+ \nu_\ell$

VALUE	EVTS	DOCUMENT ID	TECN	COMMENT
<b>1.46 ± 0.07 OUR AVERAGE</b>				
1.46 ± 0.07 ± 0.02	3k	ABLIKIM	19G BES3	$K^*(892)^- e^+ \nu_e$
1.71 ± 0.68 ± 0.34		LINK	05B FOCS	$K^*(892)^- \mu^+ \nu_\mu$

##### $r_2 \equiv A_2(0)/A_1(0)$ in $D^0 \rightarrow K^*(892)^- \ell^+ \nu_\ell$

VALUE	EVTS	DOCUMENT ID	TECN	COMMENT
<b>0.68 ± 0.06 OUR AVERAGE</b>				
0.67 ± 0.06 ± 0.01	3k	ABLIKIM	19G BES3	$K^*(892)^- e^+ \nu_e$
0.91 ± 0.37 ± 0.10		LINK	05B FOCS	$K^*(892)^- \mu^+ \nu_\mu$

#### $D^0 \rightarrow K^- / \pi^- \ell^+ \nu_\ell$ FORM FACTORS

##### $f_+(0)$ in $D^0 \rightarrow K^- \ell^+ \nu_\ell$

VALUE	EVTS	DOCUMENT ID	TECN	COMMENT
<b>0.736 ± 0.004 OUR AVERAGE</b>				
0.7368 ± 0.0026 ± 0.0036	71k	ABLIKIM	15X BES3	$\ell=e$ , 2-parameter fit
0.727 ± 0.007 ± 0.009		AUBERT	07Bg BABR	$\ell=e$ , 2-parameter fit

##### $f_+(0)|V_{cd}|$ in $D^0 \rightarrow K^- \ell^+ \nu_\ell$

VALUE	EVTS	DOCUMENT ID	TECN	COMMENT
<b>0.7166 ± 0.0030 OUR AVERAGE</b>				
0.7133 ± 0.0038 ± 0.0029	47k	ABLIKIM	19B BES3	$\ell=\mu$ , 2-parameter fit
0.7172 ± 0.0025 ± 0.0035	71k	1 ABLIKIM	15X BES3	$\ell=e$ , 2-parameter fit
0.726 ± 0.008 ± 0.004		BESSION	09 CLEO	$\ell=e$ , 3-parameter fit

<sup>1</sup> The 3-parameter fit yields  $0.7195 \pm 0.0035 \pm 0.0041$ .

##### $r_1 \equiv a_1/a_0$ in $D^0 \rightarrow K^- \ell^+ \nu_\ell$

VALUE	EVTS	DOCUMENT ID	TECN	COMMENT
<b>-2.40 ± 0.16 OUR AVERAGE</b>				
-2.33 ± 0.16 ± 0.08	71k	1 ABLIKIM	15X BES3	$\ell=e$ , 3-parameter fit
-2.65 ± 0.34 ± 0.08		BESSION	09 CLEO	$\ell=e$ , 3-parameter fit

<sup>1</sup> The 2-parameter fit yields  $-2.23 \pm 0.09 \pm 0.06$ .

##### $r_2 \equiv a_2/a_0$ in $D^0 \rightarrow K^- \ell^+ \nu_\ell$

VALUE	EVTS	DOCUMENT ID	TECN	COMMENT
<b>5 ± 4 OUR AVERAGE</b>				
3.4 ± 3.9 ± 2.4	71k	ABLIKIM	15X BES3	$\ell=e$ , 3-parameter fit
13 ± 9 ± 1		BESSION	09 CLEO	$\ell=e$ , 3-parameter fit

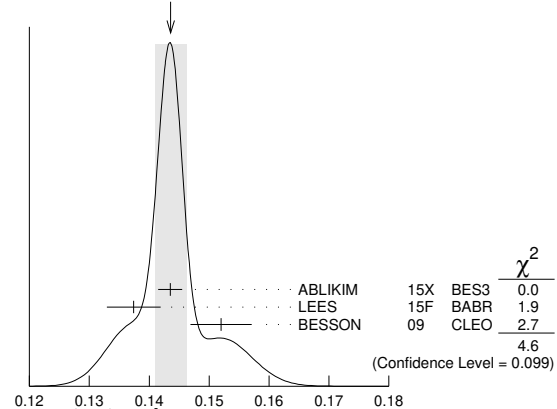
##### $f_+(0)$ in $D^0 \rightarrow \pi^- \ell^+ \nu_\ell$

VALUE	EVTS	DOCUMENT ID	TECN	COMMENT
<b>0.6372 ± 0.0080 ± 0.0044</b>				
0.6372 ± 0.0080 ± 0.0044	6.3k	ABLIKIM	15X BES3	$\ell=e$ , 2-parameter fit

##### $f_+(0)|V_{cd}|$ in $D^0 \rightarrow \pi^- \ell^+ \nu_\ell$

VALUE	EVTS	DOCUMENT ID	TECN	COMMENT
<b>0.1436 ± 0.0026 OUR AVERAGE</b>				
0.1435 ± 0.0018 ± 0.0009	6.3k	1 ABLIKIM	15X BES3	$\ell=e$ , 2-parameter fit
0.1374 ± 0.0038 ± 0.0024	5.3k	2 LEES	15F BABR	$\ell=e$ , 3-parameter fit
0.152 ± 0.005 ± 0.001		BESSION	09 CLEO	$\ell=e$ , 3-parameter fit

WEIGHTED AVERAGE  
 0.1436 ± 0.0026 (Error scaled by 1.5)



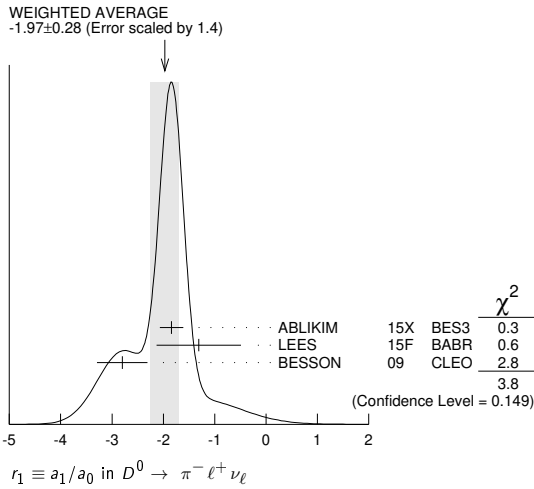
<sup>1</sup> The 3-parameter fit yields  $0.1420 \pm 0.0024 \pm 0.0010$ .

<sup>2</sup> LEES 15F reports a value  $0.1374 \pm 0.0038 \pm 0.0022 \pm 0.0009$ , where the last uncertainty is due to the uncertainties of the  $D^0 \rightarrow K^- \pi^+$  branching fraction.

$r_1 \equiv a_1/a_0$  in  $D^0 \rightarrow \pi^- \ell^+ \nu_\ell$

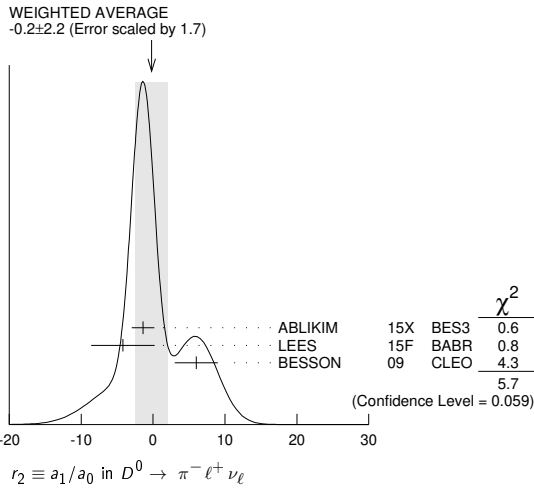
Table with columns: VALUE, EVTS, DOCUMENT ID, TECN, COMMENT. Includes entries for ABLIKIM, LEES, BESSON with their respective values and error bars.

<sup>1</sup> The 2-parameter fit yields  $-2.04 \pm 0.08 \pm 0.03$ .



$r_2 \equiv a_1/a_0$  in  $D^0 \rightarrow \pi^- \ell^+ \nu_\ell$

Table with columns: VALUE, EVTS, DOCUMENT ID, TECN, COMMENT. Includes entries for ABLIKIM, LEES, BESSON with their respective values and error bars.



Amplitude analyses

$D \rightarrow K\pi\pi\pi, D \rightarrow KK\pi\pi$  partial wave analyses

Amplitude analyses of  $D^0$  decays to a variety of 4-body kaon or pion final states, fitting simultaneously different partial wave components.

Table with columns: VALUE, DOCUMENT ID, TECN, COMMENT. Lists various experiments and their results for different decay channels.

<sup>1</sup> AAIJ 19c also provides measurements of CP violation in  $D^0 \rightarrow K^+ K^- \pi^+ \pi^-$ , with results compatible with CP symmetry.

D<sup>0</sup> REFERENCES

Extensive list of references for D0 decays, including authors, journal abbreviations, and publication years. Includes collaborations like LHCb, Belle, BABAR, etc.

Meson Particle Listings

$D^0, D^*(2007)^0$

Table listing meson particles with columns for name, codes, and references. Includes entries for D\*, D, and various other particles with their respective experimental collaborations and publication details.

OTHER RELATED PAPERS

D\*(2007)^0

(J^P) = 1/2(1^-)

J consistent with 1, value 0 ruled out (NGUYEN 77).

D\*(2007)^0 MASS

The fit includes D^pm, D^0, D\_s^pm, D^\*, D\_s^0, D\_s^pm, D\_1(2420)^0, D\_2^pm(2460)^0, and D\_{S1}(2536)^pm mass and mass difference measurements.

Table with columns: VALUE (MeV), DOCUMENT ID, TECN, COMMENT. Lists related publications like RICHMAN, ROSNER, and GOLDBABER with their values and fit parameters.

See key on page 999

Meson Particle Listings

$D^*(2007)^0, D^*(2010)^\pm$

$m_{D^*(2007)^0} - m_{D^0}$

The fit includes  $D^\pm, D^0, D_s^\pm, D^{*\pm}, D^{*0}, D_1(2420)^0, D_2^*(2460)^0$ , and  $D_{s1}(2536)^\pm$  mass and mass difference measurements.

VALUE (MeV)	EVTS	DOCUMENT ID	TECN	COMMENT
<b>142.014 ± 0.030 OUR FIT</b>	Error	includes scale factor of 1.5.		
<b>142.016 ± 0.030 OUR AVERAGE</b>	Error	includes scale factor of 1.5.		
142.007 ± 0.015 ± 0.014	10K	<sup>2</sup> TOMARADZE 15	CLEO	$e^+e^- \rightarrow$ hadrons
142.2 ± 0.3 ± 0.2	145	ALBRECHT 95F	ARG	$e^+e^- \rightarrow$ hadrons
142.12 ± 0.05 ± 0.05	1176	BORTOLETTO92B	CLE2	$e^+e^- \rightarrow$ hadrons
• • •	We do not use the following data for averages, fits, limits, etc. • • •			
142.2 ± 2.0		SADROZINSKI 80	CBAL	$D^{*0} \rightarrow D^0\pi^0$
142.7 ± 1.7		<sup>3</sup> GOLDHABER 77	MRK1	$e^+e^-$

<sup>2</sup> Obtained by analyzing CLEO-c data but not authored by the CLEO Collaboration. This value comes from the average of the results for two decay modes,  $D^0 \rightarrow K^-\pi^+$  and  $D^0 \rightarrow K^-\pi^+\pi^-\pi^+$ .  
<sup>3</sup> From simultaneous fit to  $D^*(2010)^+, D^*(2007)^0, D^+,$  and  $D^0$ .

$D^*(2007)^0$  WIDTH

VALUE (MeV)	CL%	DOCUMENT ID	TECN	COMMENT
<b>&lt;2.1</b>	90	<sup>4</sup> ABACHI 88B	HRS	$D^{*0} \rightarrow D^+\pi^-$

<sup>4</sup> Assuming  $m_{D^{*0}} = 2007.2 \pm 2.1$  MeV/c<sup>2</sup>.

$D^*(2007)^0$  DECAY MODES

$\bar{D}^*(2007)^0$  modes are charge conjugates of modes below.

Mode	Fraction ( $\Gamma_i/\Gamma$ )
$\Gamma_1$ $D^0\pi^0$	(64.7 ± 0.9) %
$\Gamma_2$ $D^0\gamma$	(35.3 ± 0.9) %

CONSTRAINED FIT INFORMATION

An overall fit to 2 branching ratios uses 5 measurements and one constraint to determine 2 parameters. The overall fit has a  $\chi^2 = 2.5$  for 4 degrees of freedom.

The following off-diagonal array elements are the correlation coefficients  $\langle \delta x_i \delta x_j \rangle / (\delta x_i \delta x_j)$ , in percent, from the fit to the branching fractions,  $x_i \equiv \Gamma_i/\Gamma_{\text{total}}$ . The fit constrains the  $x_i$  whose labels appear in this array to sum to one.

$$x_2 \begin{vmatrix} -100 \\ x_1 \end{vmatrix}$$

$D^*(2007)^0$  BRANCHING RATIOS

$\Gamma(D^0\pi^0)/\Gamma(D^0\gamma)$	$\Gamma_1/\Gamma_2$			
<b>1.83 ± 0.07 OUR FIT</b>	Error	includes scale factor of 1.1.		
<b>1.85 ± 0.07 OUR AVERAGE</b>				
1.90 ± 0.07 ± 0.05	4.9k	ABLIKIM 15B	BES3	10.6 $e^+e^- \rightarrow$ hadrons
1.74 ± 0.02 ± 0.13		AUBERT, BE 05G	BABR	10.6 $e^+e^- \rightarrow$ hadrons
$\Gamma(D^0\pi^0)/\Gamma_{\text{total}}$	$\Gamma_1/\Gamma$			
<b>0.647 ± 0.009 OUR FIT</b>				
• • •	We do not use the following data for averages, fits, limits, etc. • • •			
0.655 ± 0.008 ± 0.005	3.2k	<sup>5</sup> ABLIKIM 15B	BES3	$e^+e^- \rightarrow$ hadrons
0.635 ± 0.003 ± 0.017	69k	<sup>5</sup> AUBERT, BE 05G	BABR	10.6 $e^+e^- \rightarrow$ hadrons
0.596 ± 0.035 ± 0.028	858	<sup>6</sup> ALBRECHT 95F	ARG	$e^+e^- \rightarrow$ hadrons
0.636 ± 0.023 ± 0.033	1097	<sup>6</sup> BUTLER 92	CLE2	$e^+e^- \rightarrow$ hadrons
$\Gamma(D^0\gamma)/\Gamma_{\text{total}}$	$\Gamma_2/\Gamma$			
<b>0.353 ± 0.009 OUR FIT</b>				
<b>0.381 ± 0.029 OUR AVERAGE</b>				
0.404 ± 0.035 ± 0.028	456	<sup>6</sup> ALBRECHT 95F	ARG	$e^+e^- \rightarrow$ hadrons
0.364 ± 0.023 ± 0.033	621	<sup>6</sup> BUTLER 92	CLE2	$e^+e^- \rightarrow$ hadrons
0.37 ± 0.08 ± 0.08		ADLER 88D	MRK3	$e^+e^-$
• • •	We do not use the following data for averages, fits, limits, etc. • • •			
0.345 ± 0.008 ± 0.005	1.8k	<sup>5</sup> ABLIKIM 15B	BES3	$e^+e^- \rightarrow$ hadrons
0.365 ± 0.003 ± 0.017	68k	<sup>5</sup> AUBERT, BE 05G	BABR	10.6 $e^+e^- \rightarrow$ hadrons
0.47 ± 0.23		LOW 87	HRS	29 GeV $e^+e^-$
0.53 ± 0.13		BARTEL 85G	JADE	$e^+e^-$ , hadrons
0.47 ± 0.12		COLES 82	MRK2	$e^+e^-$
0.45 ± 0.15		GOLDHABER 77	MRK1	$e^+e^-$

<sup>5</sup> Derived from the ratio  $\Gamma(D^0\pi^0)/\Gamma(D^0\gamma)$  assuming that the branching fractions of  $D^{*0} \rightarrow D^0\pi^0$  and  $D^{*0} \rightarrow D^0\gamma$  decays sum to 100%  
<sup>6</sup> The BUTLER 92 and ALBRECHT 95F branching ratios are not independent, they have been constrained by the authors to sum to 100%.

$D^*(2007)^0$  REFERENCES

ABLIKIM 15B	PR D91 031101	M. Ablikim et al.	(BESIII Collab.)
TOMARADZE 15	PR D91 011102	A. Tomaradze et al.	(NWES)
AUBERT, BE 05G	PR D72 091101	B. Aubert et al.	(BABAR Collab.)
ALBRECHT 95F	ZPHY C66 63	H. Albrecht et al.	(ARGUS Collab.)
BORTOLETTO 92B	PRL 69 2046	D. Bortoletto et al.	(CLEO Collab.)
BUTLER 92	PRL 69 2041	F. Butler et al.	(CLEO Collab.)
ABACHI 88B	PL B212 533	S. Abachi et al.	(ANL, IND, MICH, PURD+)
ADLER 88D	PL B208 152	J. Adler et al.	(Mark III Collab.)
LOW 87	PL B183 232	E.H. Low et al.	(HRS Collab.)
BARTEL 85G	PL 161B 197	W. Bartel et al.	(JADE Collab.)
COLES 82	PR D26 2190	M.W. Coles et al.	(LBL, SLAC)
SADROZINSKI 80	Madison Conf. 681	H.F.W. Sadrozinski et al.	(PRIN, CIT+)
GOLDHABER 77	PL 69B 503	G. Goldhaber et al.	(Mark I Collab.)
NGUYEN 77	PRL 39 262	H.K. Nguyen et al.	(LBL, SLAC)

$D^*(2010)^\pm$

$I(J^P) = \frac{1}{2}(1^-)$   
 I, J, P need confirmation.

$D^*(2010)^\pm$  MASS

The fit includes  $D^\pm, D^0, D_s^\pm, D^{*\pm}, D^{*0}, D_s^{*\pm}, D_1(2420)^0, D_2^*(2460)^0$ , and  $D_{s1}(2536)^\pm$  mass and mass difference measurements.

VALUE (MeV)	DOCUMENT ID	TECN	CHG	COMMENT
<b>2010.26 ± 0.05 OUR FIT</b>				

• • • We do not use the following data for averages, fits, limits, etc. • • •  
 2008 ± 3 <sup>1</sup> GOLDHABER 77 MRK1 ±  $e^+e^-$   
 2008.6 ± 1.0 <sup>2</sup> PERUZZI 77 LGW ±  $e^+e^-$   
<sup>1</sup> From simultaneous fit to  $D^*(2010)^+, D^*(2007)^0, D^+,$  and  $D^0$ ; not independent of FELDMAN 77B mass difference below.  
<sup>2</sup> PERUZZI 77 mass not independent of FELDMAN 77B mass difference below and PERUZZI 77  $D^0$  mass value.

$m_{D^*(2010)^+} - m_{D^+}$

The fit includes  $D^\pm, D^0, D_s^\pm, D^{*\pm}, D^{*0}, D_s^{*\pm}, D_1(2420)^0, D_2^*(2460)^0$ , and  $D_{s1}(2536)^\pm$  mass and mass difference measurements.

VALUE (MeV)	EVTS	DOCUMENT ID	TECN	COMMENT
<b>140.603 ± 0.015 OUR FIT</b>				
<b>140.602 ± 0.014 OUR AVERAGE</b>				
140.6010 ± 0.0068 ± 0.0129	151k	LEES 17F	BABR	$e^+e^- \rightarrow$ hadrons
140.64 ± 0.08 ± 0.06	620	BORTOLETTO92B	CLE2	$e^+e^- \rightarrow$ hadrons

$m_{D^*(2010)^+} - m_{D^0}$

The fit includes  $D^\pm, D^0, D_s^\pm, D^{*\pm}, D^{*0}, D_s^{*\pm}, D_1(2420)^0, D_2^*(2460)^0$ , and  $D_{s1}(2536)^\pm$  mass and mass difference measurements.

VALUE (MeV)	EVTS	DOCUMENT ID	TECN	COMMENT
<b>145.4257 ± 0.0017 OUR FIT</b>				
<b>145.4258 ± 0.0020 OUR AVERAGE</b>				Error includes scale factor of 1.2.
145.4259 ± 0.0004 ± 0.0017	312.8k	LEES 13x	BABR	$D^{*\pm} \rightarrow D^0\pi^\pm \rightarrow (K\pi, K3\pi)\pi^\pm$
145.412 ± 0.002 ± 0.012		ANASTASSOV 02	CLE2	$D^{*\pm} \rightarrow D^0\pi^\pm \rightarrow (K\pi)\pi^\pm$
145.54 ± 0.08	611	<sup>3</sup> ADINOLFI 99	BEAT	$D^{*\pm} \rightarrow D^0\pi^\pm$
145.45 ± 0.02		<sup>3</sup> BREITWEG 99	ZEUS	$D^{*\pm} \rightarrow D^0\pi^\pm \rightarrow (K\pi)\pi^\pm$
145.42 ± 0.05		<sup>3</sup> BREITWEG 99	ZEUS	$D^{*\pm} \rightarrow D^0\pi^\pm \rightarrow (K^-\pi^+)\pi^\pm$
145.5 ± 0.15	103	<sup>4</sup> ADLOFF 97B	H1	$D^{*\pm} \rightarrow D^0\pi^\pm$
145.44 ± 0.08	152	<sup>4</sup> BREITWEG 97	ZEUS	$D^{*\pm} \rightarrow D^0\pi^\pm, D^0 \rightarrow K^-\pi^+$
145.42 ± 0.11	199	<sup>4</sup> BREITWEG 97	ZEUS	$D^{*\pm} \rightarrow D^0\pi^\pm, D^0 \rightarrow K^-\pi^+$
145.4 ± 0.2	48	<sup>4</sup> DERRICK 95	ZEUS	$D^{*\pm} \rightarrow D^0\pi^\pm$
145.39 ± 0.06 ± 0.03		BARLAG 92B	ACCM	$\pi^- 230$ GeV
145.5 ± 0.2	115	<sup>4</sup> ALEXANDER 91B	OPAL	$D^{*\pm} \rightarrow D^0\pi^\pm$
145.30 ± 0.06		<sup>4</sup> DECAMP 91J	ALEP	$D^{*\pm} \rightarrow D^0\pi^\pm$
145.40 ± 0.05 ± 0.10		ABACHI 88B	HRS	$D^{*\pm} \rightarrow D^0\pi^\pm$
145.46 ± 0.07 ± 0.03		ALBRECHT 85F	ARG	$D^{*\pm} \rightarrow D^0\pi^\pm$
145.5 ± 0.3	28	BAILEY 83	SPEC	$D^{*\pm} \rightarrow D^0\pi^\pm$
145.5 ± 0.3	60	FITCH 81	SPEC	$\pi^- A$
145.3 ± 0.5	30	FELDMAN 77B	MRK1	$D^{*+} \rightarrow D^0\pi^+$
• • •	We do not use the following data for averages, fits, limits, etc. • • •			
145.4256 ± 0.0006 ± 0.0017	138.5k	LEES 13x	BABR	$D^{*\pm} \rightarrow D^0\pi^\pm \rightarrow (K^-\pi^+)\pi^\pm$
145.4266 ± 0.0005 ± 0.0019	174.3k	LEES 13x	BABR	$D^{*\pm} \rightarrow D^0\pi^\pm \rightarrow (K^-2\pi^+\pi^-)\pi^\pm$
145.44 ± 0.09	122	<sup>4</sup> BREITWEG 97B	ZEUS	$D^{*\pm} \rightarrow D^0\pi^\pm, D^0 \rightarrow K^-\pi^+$
145.8 ± 1.5	16	AHLEN 83	HRS	$D^{*+} \rightarrow D^0\pi^+$
145.1 ± 1.8	12	BAILEY 83	SPEC	$D^{*+} \rightarrow D^0\pi^+$

# Meson Particle Listings

## $D^*(2010)^\pm, D_0^*(2300)^0$

VALUE	CL%	EVTS	DOCUMENT ID	TECN	COMMENT
145.1 ± 0.5		14	BAILEY 83	SPEC	$D^{*\pm} \rightarrow D^0 \pi^\pm$
145.5 ± 0.5		14	YELTON 82	MRK2	$29 e^+ e^- \rightarrow K^- \pi^+$
~ 145.5			VERY 80	SPEC	$\gamma A$
145.2 ± 0.6		2	BLIETSCHAU 79	BEBC	$\nu p$

<sup>3</sup> Statistical errors only.  
<sup>4</sup> Systematic error not evaluated.

### $m_{D^*(2010)^+} - m_{D^*(2007)^0}$

VALUE (MeV)	DOCUMENT ID	TECN	COMMENT
<b>2.6 ± 1.8</b>	<b>5 PERUZZI 77</b>	LGW	$e^+ e^-$

• • • We do not use the following data for averages, fits, limits, etc. • • •  
<sup>5</sup> Not independent of FELDMAN 77B mass difference above, PERUZZI 77  $D^0$  mass, and GOLDHABER 77  $D^*(2007)^0$  mass.

### $D^*(2010)^\pm$ WIDTH

VALUE (keV)	CL%	EVTS	DOCUMENT ID	TECN	COMMENT
<b>83.4 ± 1.8 ± 1.4</b>	<b>312.8k</b>		<b>6 LEES 13x</b>	BABR	$D^{*\pm} \rightarrow D^0 \pi^\pm \rightarrow (K \pi, K 3\pi) \pi^\pm$
96 ± 4 ± 22			6 ANASTASSOV 02	CLE2	$D^{*\pm} \rightarrow D^0 \pi^\pm \rightarrow (K \pi) \pi^\pm$
83.4 ± 1.7 ± 1.5	138.5k		6 LEES 13x	BABR	$D^{*\pm} \rightarrow D^0 \pi^\pm \rightarrow (K^- \pi^+) \pi^\pm$
83.2 ± 1.5 ± 2.6	174.3k		6 LEES 13x	BABR	$D^{*\pm} \rightarrow D^0 \pi^\pm \rightarrow (K^- 2\pi^+ \pi^-) \pi^\pm$
<131	90	110	BARLAG 92B	ACCM	$\pi^- 230 \text{ GeV}$

• • • We do not use the following data for averages, fits, limits, etc. • • •  
<sup>6</sup> Ignoring the electromagnetic contribution from  $D^{*\pm} \rightarrow D^\pm \gamma$ .

### $D^*(2010)^\pm$ DECAY MODES

$D^*(2010)^-$  modes are charge conjugates of the modes below.

Mode	Fraction ( $\Gamma_i/\Gamma$ )
$\Gamma_1 D^0 \pi^+$	(67.7 ± 0.5) %
$\Gamma_2 D^+ \pi^0$	(30.7 ± 0.5) %
$\Gamma_3 D^+ \gamma$	(1.6 ± 0.4) %

### CONSTRAINED FIT INFORMATION

An overall fit to 3 branching ratios uses 6 measurements and one constraint to determine 3 parameters. The overall fit has a  $\chi^2 = 0.3$  for 4 degrees of freedom.

The following *off-diagonal* array elements are the correlation coefficients  $\langle \delta x_i \delta x_j \rangle / (\delta x_i \delta x_j)$ , in percent, from the fit to the branching fractions,  $x_i \equiv \Gamma_i/\Gamma_{\text{total}}$ . The fit constrains the  $x_i$  whose labels appear in this array to sum to one.

$x_2$	-62	
$x_3$	-43	-44
	$x_1$	$x_2$

### $D^*(2010)^+$ BRANCHING RATIOS

$\Gamma(D^0 \pi^+)/\Gamma_{\text{total}}$	VALUE	DOCUMENT ID	TECN	COMMENT
<b>0.677 ± 0.005 OUR FIT</b>				
<b>0.677 ± 0.006 OUR AVERAGE</b>				
0.6759 ± 0.0029 ± 0.0064	7,8,9	BARTELT 98	CLE2	$e^+ e^-$
0.688 ± 0.024 ± 0.013		ALBRECHT 95F	ARG	$e^+ e^- \rightarrow$ hadrons
0.681 ± 0.010 ± 0.013		7 BUTLER 92	CLE2	$e^+ e^- \rightarrow$ hadrons
0.57 ± 0.04 ± 0.04		ADLER 88D	MRK3	$e^+ e^-$
0.44 ± 0.10		COLES 82	MRK2	$e^+ e^-$
0.6 ± 0.15		9 GOLDHABER 77	MRK1	$e^+ e^-$

• • • We do not use the following data for averages, fits, limits, etc. • • •

$\Gamma(D^+ \pi^0)/\Gamma_{\text{total}}$	VALUE	DOCUMENT ID	TECN	COMMENT
<b>0.307 ± 0.005 OUR FIT</b>				
<b>0.3073 ± 0.0013 ± 0.0062</b>				
0.312 ± 0.011 ± 0.008	1404	ALBRECHT 95F	ARG	$e^+ e^- \rightarrow$ hadrons
0.308 ± 0.004 ± 0.008	410	7 BUTLER 92	CLE2	$e^+ e^- \rightarrow$ hadrons
0.26 ± 0.02 ± 0.02		ADLER 88D	MRK3	$e^+ e^-$
0.34 ± 0.07		COLES 82	MRK2	$e^+ e^-$

• • • We do not use the following data for averages, fits, limits, etc. • • •

$\Gamma(D^+ \gamma)/\Gamma_{\text{total}}$	VALUE	CL%	EVTS	DOCUMENT ID	TECN	COMMENT
<b>0.016 ± 0.004 OUR FIT</b>						
<b>0.016 ± 0.005 OUR AVERAGE</b>						
0.0168 ± 0.0042 ± 0.0029				7,8 BARTELT 98	CLE2	$e^+ e^-$
0.011 ± 0.014 ± 0.016			12	7 BUTLER 92	CLE2	$e^+ e^- \rightarrow$ hadrons
<0.052			90	ALBRECHT 95F	ARG	$e^+ e^- \rightarrow$ hadrons
0.17 ± 0.05 ± 0.05				ADLER 88D	MRK3	$e^+ e^-$
0.22 ± 0.12				10 COLES 82	MRK2	$e^+ e^-$

• • • We do not use the following data for averages, fits, limits, etc. • • •  
<sup>7</sup> The branching ratios are not independent, they have been constrained by the authors to sum to 100%.  
<sup>8</sup> Systematic error includes theoretical error on the prediction of the ratio of hadronic modes.  
<sup>9</sup> Assuming that isospin is conserved in the decay.  
<sup>10</sup> Not independent of  $\Gamma(D^0 \pi^+)/\Gamma_{\text{total}}$  and  $\Gamma(D^+ \pi^0)/\Gamma_{\text{total}}$  measurement.

### $D^*(2010)^\pm$ REFERENCES

LEES 17F	PRL 119 202003	J.P. Lees et al.	(BABAR Collab.)
LEES 13X	PRL 111 111801	J.P. Lees et al.	(BABAR Collab.)
Also	PR D88 052003	J.P. Lees et al.	(BABAR Collab.)
Also	PR D88 079902 (err.)	J.P. Lees et al.	(BABAR Collab.)
ANASTASSOV 02	PR D65 032003	A. Anastassov et al.	(CLEO Collab.)
ADWOLFI 99	NP B54 7 3	M. Adloff et al.	(Belle Collab.)
BREITWEG 99	EPL C6 67	J. Breitweg et al.	(ZEUS Collab.)
BARTELT 98	PRL 80 3919	J. Bartelt et al.	(CLEO Collab.)
ADLOFF 97B	ZPHY C72 593	C. Adloff et al.	(HI Collab.)
BREITWEG 97	PL B401 192	J. Breitweg et al.	(ZEUS Collab.)
BREITWEG 97B	PL B407 402	J. Breitweg et al.	(ZEUS Collab.)
ALBRECHT 95F	ZPHY C66 63	H. Albrecht et al.	(ARGUS Collab.)
DERRICK 95	PL B349 225	M. Derrick et al.	(ZEUS Collab.)
BARLAG 92B	PL B278 480	S. Barlag et al.	(ACCMOR Collab.)
BORTOLETTO 92B	PRL 69 2046	D. Bortoletto et al.	(CLEO Collab.)
BUTLER 92	PRL 69 2041	F. Butler et al.	(CLEO Collab.)
ALEXANDER 91B	PL B262 341	G. Alexander et al.	(OPAL Collab.)
DECAMP 91J	PL B266 218	D. Decamp et al.	(ALEPH Collab.)
ABACHI 88B	PL B212 533	S. Abachi et al.	(ANL, IND, MICH, PURD+)
ADLER 88D	PL B208 152	J. Adler et al.	(ANL, IND, LBL+)
ALBRECHT 85F	PL 150B 235	H. Albrecht et al.	(ARGUS Collab.)
AHLEN 83	PRL 51 1147	S.P. Ahlen et al.	(ANL, IND, LBL+)
BAILEY 83	PL 132B 230	R. Bailey et al.	(AMST, BRIS, CERN, CRAC+)
COLES 82	PR D26 2190	M.W. Coles et al.	(LBL, SLAC)
YELTON 82	PRL 49 430	J.M. Yelton et al.	(SLAC, LBL, UCB+)
FITCH 81	PRL 46 761	V.L. Fitch et al.	(PRIN, SAcl, TORI+)
VERY 80	PRL 44 1309	P. Avery et al.	(ILL, FNAL, COLU)
BLIETSCHAU 79	PL B68 108	J. Blietschau et al.	(AACH3, BONN, CERN+)
FELDMAN 77B	PRL 38 1313	G.J. Feldman et al.	(Mark I Collab.)
GOLDHABER 77	PL 69B 503	G. Goldhaber et al.	(Mark I Collab.)
PERUZZI 77	PRL 39 1301	I. Peruzzi et al.	(LGW Collab.)

### $D_0^*(2300)^0$

$$I(J^P) = \frac{1}{2}(0^+)$$

was  $D_0^*(2400)^0$   
 $J^P = 0^+$  assignment favored (ABE 04D).

### $D_0^*(2300)^0$ MASS

VALUE (MeV)	EVTS	DOCUMENT ID	TECN	COMMENT
<b>2300 ± 19 OUR AVERAGE</b>				
2297 ± 8 ± 20	3.4k	AUBERT 09AB	BABR	$B^- \rightarrow D^+ \pi^- \pi^-$
2308 ± 17 ± 32		ABE 04D	BELL	$B^- \rightarrow D^+ \pi^- \pi^-$
2407 ± 21 ± 35	9.8k	1 LINK 04A	FOCS	$\gamma A$

• • • We do not use the following data for averages, fits, limits, etc. • • •  
<sup>1</sup> Possibly the feed-down from another state.

### $D_0^*(2300)^0$ WIDTH

VALUE (MeV)	EVTS	DOCUMENT ID	TECN	COMMENT
<b>274 ± 40 OUR AVERAGE</b>				
273 ± 12 ± 48	3.4k	AUBERT 09AB	BABR	$B^- \rightarrow D^+ \pi^- \pi^-$
276 ± 21 ± 63		ABE 04D	BELL	$B^- \rightarrow D^+ \pi^- \pi^-$
240 ± 55 ± 59	9.8k	2 LINK 04A	FOCS	$\gamma A$

• • • We do not use the following data for averages, fits, limits, etc. • • •  
<sup>2</sup> Possibly the feed-down from another state.

### $D_0^*(2300)^0$ DECAY MODES

Mode	Fraction ( $\Gamma_i/\Gamma$ )
$\Gamma_1 D^+ \pi^-$	seen

### $D_0^*(2300)^0$ REFERENCES

AUBERT 09AB	PR D79 112004	B. Aubert et al.	(BABAR Collab.)
ABE 04D	PR D69 112002	K. Abe et al.	(BELLE Collab.)
LINK 04A	PL B586 11	J.M. Link et al.	(FOCUS Collab.)

See key on page 999

Meson Particle Listings

$D_0^*(2300)^\pm, D_1(2420)^0$

$D_0^*(2300)^\pm$

$I(J^P) = \frac{1}{2}(0^+)$

OMITTED FROM SUMMARY TABLE  
was  $D_0^*(2400)^\pm$   
 $J, P$  need confirmation.

$D_0^*(2300)^\pm$  MASS

VALUE (MeV)	EVTS	DOCUMENT ID	TECN	COMMENT
<b>2349 ± 7 OUR AVERAGE</b>				
2360 ± 15 ± 30		<sup>1</sup> AAIJ	15X LHCb	$B^0 \rightarrow \bar{D}^0 K^+ \pi^-$
2349 ± 6 ± 4		<sup>2</sup> AAIJ	15Y LHCb	$B^0 \rightarrow \bar{D}^0 \pi^+ \pi^-$
• • • We do not use the following data for averages, fits, limits, etc. • • •				
2354 ± 7 ± 11		<sup>3</sup> AAIJ	15Y LHCb	$B^0 \rightarrow \bar{D}^0 \pi^+ \pi^-$
2403 ± 14 ± 35	18.8k	<sup>4</sup> LINK	04A FOCS	$\gamma A$
<sup>1</sup> From the Dalitz plot analysis including various $K^*$ and $D^{**}$ mesons as well as broad structures in the $K\pi$ S-wave and the $D\pi$ S- and P-waves. <sup>2</sup> Modeling the $\pi^+\pi^-$ S-wave with the isobar formalism. <sup>3</sup> Modeling the $\pi^+\pi^-$ S-wave with the K-matrix formalism. <sup>4</sup> Possibly the feed-down from another state.				

$D_0^*(2300)^\pm$  WIDTH

VALUE (MeV)	EVTS	DOCUMENT ID	TECN	COMMENT
<b>221 ± 18 OUR AVERAGE</b>				
255 ± 26 ± 51		<sup>1</sup> AAIJ	15X LHCb	$B^0 \rightarrow \bar{D}^0 K^+ \pi^-$
217 ± 13 ± 13		<sup>2</sup> AAIJ	15Y LHCb	$B^0 \rightarrow \bar{D}^0 \pi^+ \pi^-$
• • • We do not use the following data for averages, fits, limits, etc. • • •				
230 ± 15 ± 21		<sup>3</sup> AAIJ	15Y LHCb	$B^0 \rightarrow \bar{D}^0 \pi^+ \pi^-$
283 ± 24 ± 34	18.8k	<sup>4</sup> LINK	04A FOCS	$\gamma A$
<sup>1</sup> From the Dalitz plot analysis including various $K^*$ and $D^{**}$ mesons as well as broad structures in the $K\pi$ S-wave and the $D\pi$ S- and P-waves. <sup>2</sup> Modeling the $\pi^+\pi^-$ S-wave with the isobar formalism. <sup>3</sup> Modeling the $\pi^+\pi^-$ S-wave with the K-matrix formalism. <sup>4</sup> Possibly the feed-down from another state.				

$D_0^*(2300)^\pm$  DECAY MODES

Mode	Fraction ( $\Gamma_i/\Gamma$ )
$\Gamma_1 D^0 \pi^+$	seen

$D_0^*(2300)^\pm$  REFERENCES

AAIJ	15X	PR D92 012012	R. Aaij <i>et al.</i>	(LHCb Collab.)
AAIJ	15Y	PR D92 032002	R. Aaij <i>et al.</i>	(LHCb Collab.)
LINK	04A	PL B586 11	J.M. Link <i>et al.</i>	(FOCUS Collab.)

$D_1(2420)^0$

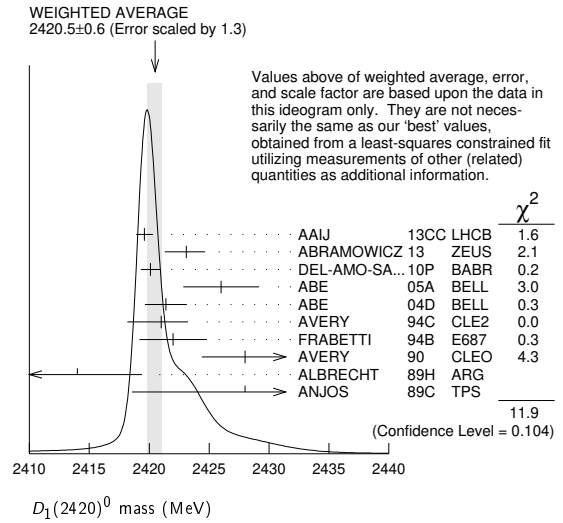
$I(J^P) = \frac{1}{2}(1^+)$

$D_1(2420)^0$  MASS

The fit includes  $D^\pm, D^0, D_s^\pm, D^{*\pm}, D^{*0}, D_s^{*\pm}, D_1(2420)^0, D_2^*(2460)^0,$  and  $D_{s1}(2536)^\pm$  mass and mass difference measurements.

VALUE (MeV)	EVTS	DOCUMENT ID	TECN	COMMENT
<b>2420.8 ± 0.5 OUR FIT</b> Error includes scale factor of 1.3.				
<b>2420.5 ± 0.6 OUR AVERAGE</b> Error includes scale factor of 1.3. See the ideogram below.				
2419.6 ± 0.1 ± 0.7	210k	AAIJ	13cc LHCb	$pp \rightarrow D^{*+} \pi^- X$
2423.1 ± 1.5 ± 0.4	2.7k	<sup>1</sup> ABRAMOWICZ13	ZEUS	$e^\pm p \rightarrow D^{(*)+} \pi^- X$
2420.1 ± 0.1 ± 0.8	103k	DEL-AMO-SA...10P	BABR	$e^+ e^- \rightarrow D^{*+} \pi^- X$
2426 ± 3 ± 1	151	ABE	05A BELL	$B^- \rightarrow D^0 \pi^+ \pi^- \pi^-$
2421.4 ± 1.5 ± 0.9		<sup>2</sup> ABE	04D BELL	$B^- \rightarrow D^{*+} \pi^- \pi^-$
2421 ± 1 ± 2	286	AVERY	94C CLE2	$e^+ e^- \rightarrow D^{*+} \pi^- X$
2422 ± 2 ± 2	51	FRABETTI	94B E687	$\gamma Be \rightarrow D^{*+} \pi^- X$
2428 ± 3 ± 2	279	AVERY	90 CLEO	$e^+ e^- \rightarrow D^{*+} \pi^- X$
2414 ± 2 ± 5	171	ALBRECHT	89H ARG	$e^+ e^- \rightarrow D^{*+} \pi^- X$
2428 ± 8 ± 5	171	ANJOS	89C TPS	$\gamma N \rightarrow D^{*+} \pi^- X$
• • • We do not use the following data for averages, fits, limits, etc. • • •				
2420.5 ± 2.1 ± 0.9	3110 ± 340	<sup>3</sup> CHEKANOV	09 ZEUS	$e^\pm p \rightarrow D^{*+} \pi^- X$
2421.7 ± 0.7 ± 0.6	7.5k	ABULENCIA	06A CDF	$1900 p\bar{p} \rightarrow D^{*+} \pi^- X$
2425 ± 3	235	<sup>4</sup> ABREU	98M DLPH	$e^+ e^-$
<sup>1</sup> From the combined fit of the $M(D^+ \pi^-)$ and $M(D^{*+} \pi^-)$ distributions. and $A_{D_2}$ fixed to the theoretical prediction of -1. <sup>2</sup> Fit includes the contribution from $D_1^*(2430)^0$ . <sup>3</sup> Calculated using the mass difference $m(D_1^0) - m(D^{*+})_{PDG}$ reported below and $m(D^{*+})_{PDG} = 2010.27 \pm 0.17$ MeV. The 0.17 MeV uncertainty of the PDG mass value should be added to the experimental uncertainty of 0.9 MeV.				

<sup>4</sup> No systematic error given.



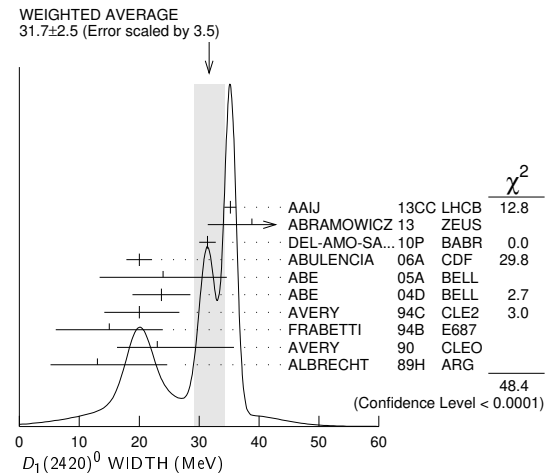
$m_{D_1^0} - m_{D^{*+}}$

The fit includes  $D^\pm, D^0, D_s^\pm, D^{*\pm}, D^{*0}, D_s^{*\pm}, D_1(2420)^0, D_2^*(2460)^0,$  and  $D_{s1}(2536)^\pm$  mass and mass difference measurements.

VALUE (MeV)	EVTS	DOCUMENT ID	TECN	COMMENT
<b>410.6 ± 0.5 OUR FIT</b> Error includes scale factor of 1.3.				
<b>411.5 ± 0.8 OUR AVERAGE</b>				
410.2 ± 2.1 ± 0.9	3110 ± 340	CHEKANOV	09 ZEUS	$e^\pm p \rightarrow D^{*+} \pi^- X$
411.7 ± 0.7 ± 0.4	7.5k	ABULENCIA	06A CDF	$1900 p\bar{p} \rightarrow D^{*+} \pi^- X$

$D_1(2420)^0$  WIDTH

VALUE (MeV)	EVTS	DOCUMENT ID	TECN	COMMENT
<b>31.7 ± 2.5 OUR AVERAGE</b> Error includes scale factor of 3.5. See the ideogram below.				
35.2 ± 0.4 ± 0.9	210k	AAIJ	13cc LHCb	$pp \rightarrow D^{*+} \pi^- X$
38.8 ± 5.0 ± 1.9	2.7k	<sup>1</sup> ABRAMOWICZ13	ZEUS	$e^\pm p \rightarrow D^{(*)+} \pi^- X$
31.4 ± 0.5 ± 1.3	103k	DEL-AMO-SA...10P	BABR	$e^+ e^- \rightarrow D^{*+} \pi^- X$
20.0 ± 1.7 ± 1.3	7.5k	ABULENCIA	06A CDF	$1900 p\bar{p} \rightarrow D^{*+} \pi^- X$
24 ± 7 ± 8	151	ABE	05A BELL	$B^- \rightarrow D^0 \pi^+ \pi^- \pi^-$
23.7 ± 2.7 ± 4.0		<sup>2</sup> ABE	04D BELL	$B^- \rightarrow D^{*+} \pi^- \pi^-$
20 ± 6 ± 3	286	AVERY	94C CLE2	$e^+ e^- \rightarrow D^{*+} \pi^- X$
15 ± 8 ± 4	51	FRABETTI	94B E687	$\gamma Be \rightarrow D^{*+} \pi^- X$
23 ± 8 ± 10	279	AVERY	90 CLEO	$e^+ e^- \rightarrow D^{*+} \pi^- X$
13 ± 6 ± 10	171	ALBRECHT	89H ARG	$e^+ e^- \rightarrow D^{*+} \pi^- X$
• • • We do not use the following data for averages, fits, limits, etc. • • •				
53.2 ± 7.2 ± 3.3	3110 ± 340	CHEKANOV	09 ZEUS	$e^\pm p \rightarrow D^{*+} \pi^- X$
58 ± 14 ± 10	171	ANJOS	89C TPS	$\gamma N \rightarrow D^{*+} \pi^- X$



<sup>1</sup> From the combined fit of the  $M(D^+ \pi^-)$  and  $M(D^{*+} \pi^-)$  distributions. and  $A_{D_2}$  fixed to the theoretical prediction of -1.



# Meson Particle Listings

## $D_1(2420)^0, D_1(2420)^\pm$

<sup>2</sup>Fit includes the contribution from  $D_1^*(2430)^0$ .

### $D_1(2420)^0$ DECAY MODES

$\bar{D}_1(2420)^0$  modes are charge conjugates of modes below.

Mode	Fraction ( $\Gamma_i/\Gamma$ )
$\Gamma_1$ $D^*(2010)^+ \pi^-$	seen
$\Gamma_2$ $D^0 \pi^+ \pi^-$	seen
$\Gamma_3$ $D^0 \rho^0$	
$\Gamma_4$ $D^0 f_0(500)$	
$\Gamma_5$ $D_0^*(2300)^+ \pi^-$	
$\Gamma_6$ $D^+ \pi^-$	not seen
$\Gamma_7$ $D^{*0} \pi^+ \pi^-$	not seen

### $D_1(2420)^0$ BRANCHING RATIOS

$\Gamma(D^*(2010)^+ \pi^-)/\Gamma_{\text{total}}$				$\Gamma_1/\Gamma$
VALUE	DOCUMENT ID	TECN	COMMENT	
seen	ACKERSTAFF 97W	OPAL	$e^+ e^- \rightarrow D^{*+} \pi^- X$	
seen	AVERY 90	CLEO	$e^+ e^- \rightarrow D^{*+} \pi^- X$	
seen	ALBRECHT 89H	ARG	$e^+ e^- \rightarrow D^* \pi^- X$	
seen	ANJOS 89c	TPS	$\gamma N \rightarrow D^{*+} \pi^- X$	

$\Gamma(D^+ \pi^-)/\Gamma(D^*(2010)^+ \pi^-)$				$\Gamma_6/\Gamma_1$
VALUE	CL%	DOCUMENT ID	TECN	COMMENT
<0.24	90	AVERY 90	CLEO	$e^+ e^- \rightarrow D^+ \pi^- X$

### $D_1(2420)^0$ POLARIZATION AMPLITUDE $A_{D_1}$

A polarization amplitude  $A_{D_1}$  is a parameter that depends on the initial polarization of the  $D_1$  and is sensitive to a possible S-wave contribution to its decay. For  $D_1$  decays the helicity angle,  $\theta_h$ , distribution varies like  $1 + A_{D_1} \cos^2 \theta_h$ , where  $\theta_h$  is the angle in the  $D^*$  rest frame between the two pions emitted by the  $D_1 \rightarrow D^* \pi$  and the  $D^* \rightarrow D \pi$ .

Unpolarized  $D_1$  decaying purely via D-wave is predicted to give  $A_{D_1} = 3$ .

VALUE	EVTS	DOCUMENT ID	TECN	COMMENT
<b>5.73 ± 0.25 OUR AVERAGE</b>				
7.8 <sup>+6.7</sup> <sub>-2.7</sub> <sup>+4.6</sup> <sub>-1.8</sub>	2.7k	1 ABRAMOWICZ13	ZEUS	$e^\pm p \rightarrow D^{(*)+} \pi^- X$
5.72 ± 0.25	103k	DEL-AMO-SA...10P	BABR	$e^+ e^- \rightarrow D^{*+} \pi^- X$
5.9 <sup>+3.0</sup> <sub>-1.7</sub> <sup>+2.4</sup> <sub>-1.0</sub>		CHEKANOV 09	ZEUS	$e^\pm p \rightarrow D^{*+} \pi^- X$
• • • We do not use the following data for averages, fits, limits, etc. • • •				
3.30 ± 0.48	210k	2 AAIJ	13CC LHCb	$pp \rightarrow D^{*+} \pi^- X$
3.8 ± 0.6 ± 0.8		3 AUBERT	09Y BABR	$B^+ \rightarrow D_1^0 \ell^+ \nu_\ell$
2.74 <sup>+1.40</sup> <sub>-0.93</sub>		4 AVERY	94c CLE2	$e^+ e^- \rightarrow D^{*+} \pi^- X$

- From the combined fit of the  $M(D^+ \pi^-)$  and  $M(D^{*+} \pi^-)$  distributions. and  $A_{D_2}$  fixed to the theoretical prediction of  $-1$ . A pure D-wave not excluded although some S-wave mixing possible.
- Systematic uncertainty not estimated. Resonance parameters fixed.
- Assuming  $\Gamma(\Upsilon(4S) \rightarrow B^+ B^-) / \Gamma(\Upsilon(4S) \rightarrow B^0 \bar{B}^0) = 1.065 \pm 0.026$  and equal partial widths and helicity angle distributions for charged and neutral  $D_1$  mesons.
- Systematic uncertainties not estimated.

### $D_1(2420)^0$ REFERENCES

AAIJ 13CC	JHEP 1309 145	R. Aaij et al.	(LHCb Collab.)
ABRAMOWICZ 13 NP	B866 229	H. Abramowicz et al.	(ZEUS Collab.)
DEL-AMO-SA...10P	PR D82 111101	P. del Amo Sanchez et al.	(BABAR Collab.)
AUBERT 09Y	PRL 103 051803	B. Aubert et al.	(BABAR Collab.)
CHEKANOV 09	EPJ C60 25	S. Chekanov et al.	(ZEUS Collab.)
ABUENCIA 06A	PR D73 051104	A. Abulencia et al.	(CDF Collab.)
ABE 05A	PRL 94 221805	K. Abe et al.	(BELLE Collab.)
ABE 04D	PR D69 112002	K. Abe et al.	(BELLE Collab.)
ABREU 98M	PL B426 231	P. Abreu et al.	(DELPHI Collab.)
ACKERSTAFF 97W	ZPHY C76 425	K. Ackerstaff et al.	(OPAL Collab.)
AVERY 94C	PL B331 236	P. Avery et al.	(CLEO Collab.)
FRABETTI 94B	PRL 72 324	P.L. Frabetti et al.	(FNAL E687 Collab.)
AVERY 90	PR D41 774	P. Avery, D. Besson	(CLEO Collab.)
ALBRECHT 89H	PL B232 398	H. Albrecht et al.	(ARGUS Collab.) JP
ANJOS 89c	PRL 62 1717	J.C. Anjos et al.	(FNAL E691 Collab.)

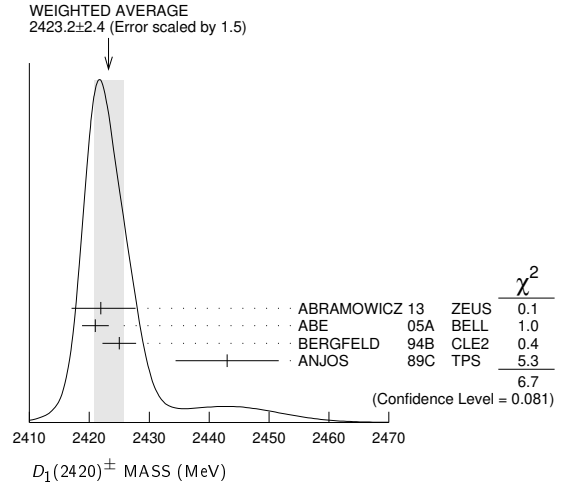
$D_1(2420)^\pm$   $I(J^P) = \frac{1}{2}(?)^?$   
I needs confirmation.

OMITTED FROM SUMMARY TABLE  
Seen in  $D^*(2007)^0 \pi^+$ .  $J^P = 0^+$  ruled out.

### $D_1(2420)^\pm$ MASS

VALUE (MeV)	EVTS	DOCUMENT ID	TECN	COMMENT
<b>2423.2 ± 2.4 OUR AVERAGE</b>				Error includes scale factor of 1.5. See the ideogram below.
2421.9 ± 4.7 <sup>+3.4</sup> <sub>-1.2</sub>	759	1 ABRAMOWICZ13	ZEUS	$e^\pm p \rightarrow D^{(*)0} \pi^+ X$
2421 ± 2 ± 1	124	ABE 05A	BELL	$\bar{B}^0 \rightarrow D^+ \pi^+ \pi^- \pi^-$
2425 ± 2 ± 2	146	BERGFELD 94B	CLE2	$e^+ e^- \rightarrow D^{*0} \pi^+ X$
2443 ± 7 ± 5	190	ANJOS 89c	TPS	$\gamma N \rightarrow D^0 \pi^+ X^0$

<sup>1</sup> From the fit of the  $M(D^0 \pi^+)$  distribution. The widths of the  $D_1^+$  and  $D_2^+$  are fixed to 25 MeV and 37 MeV, and  $A_{D_1}$  and  $A_{D_2}$  are fixed to the theoretical predictions of 3 and  $-1$ , respectively.



### $m_{D_1^*(2420)^\pm} - m_{D_1(2420)^0}$

VALUE (MeV)	DOCUMENT ID	TECN	COMMENT
<b>4 <sup>+2</sup> <sub>-3</sub> ± 3</b>	BERGFELD 94B	CLE2	$e^+ e^- \rightarrow \text{hadrons}$

### $D_1(2420)^\pm$ WIDTH

VALUE (MeV)	EVTS	DOCUMENT ID	TECN	COMMENT
<b>25 ± 6 OUR AVERAGE</b>				
21 ± 5 ± 8	124	ABE 05A	BELL	$\bar{B}^0 \rightarrow D^+ \pi^+ \pi^- \pi^-$
26 <sup>+8</sup> <sub>-7</sub> ± 4	146	BERGFELD 94B	CLE2	$e^+ e^- \rightarrow D^{*0} \pi^+ X$
41 ± 19 ± 8	190	ANJOS 89c	TPS	$\gamma N \rightarrow D^0 \pi^+ X^0$

### $D_1(2420)^\pm$ DECAY MODES

$D_1^*(2420)^-$  modes are charge conjugates of modes below.

Mode	Fraction ( $\Gamma_i/\Gamma$ )
$\Gamma_1$ $D^*(2007)^0 \pi^+$	seen
$\Gamma_2$ $D^+ \pi^+ \pi^-$	seen
$\Gamma_3$ $D^+ \rho^0$	
$\Gamma_4$ $D^+ f_0(500)$	
$\Gamma_5$ $D_0^*(2300)^0 \pi^+$	
$\Gamma_6$ $D^0 \pi^+$	not seen
$\Gamma_7$ $D^{*+} \pi^+ \pi^-$	not seen

### $D_1(2420)^\pm$ BRANCHING RATIOS

$\Gamma(D^*(2007)^0 \pi^+)/\Gamma_{\text{total}}$				$\Gamma_1/\Gamma$
VALUE	DOCUMENT ID	TECN	COMMENT	
seen	ANJOS 89c	TPS	$\gamma N \rightarrow D^0 \pi^+ X^0$	

$\Gamma(D^0 \pi^+)/\Gamma(D^*(2007)^0 \pi^+)$				$\Gamma_6/\Gamma_1$
VALUE	CL%	DOCUMENT ID	TECN	COMMENT
<0.18	90	BERGFELD 94B	CLE2	$e^+ e^- \rightarrow \text{hadrons}$

### $D_1(2420)^\pm$ POLARIZATION AMPLITUDE $A_{D_1}$

A polarization amplitude  $A_{D_1}$  is a parameter that depends on the initial polarization of the  $D_1$  and is sensitive to a possible S-wave contribution to its decay. For  $D_1$  decays the helicity angle,  $\theta_h$ , distribution varies like

See key on page 999

Meson Particle Listings

$D_1(2420)^\pm, D_1(2430)^0, D_2^*(2460)^0$

$1 + A_{D_1} \cos^2 \theta_h$ , where  $\theta_h$  is the angle in the  $D^*$  rest frame between the two pions emitted by the  $D_1 \rightarrow D^* \pi$  and the  $D^* \rightarrow D \pi$ .

Unpolarized  $D_1$  decaying purely via  $D$ -wave is predicted to give  $A_{D_1} = 3$ .

VALUE	DOCUMENT ID	TECN	COMMENT
$3.8 \pm 0.6 \pm 0.8$	<sup>2</sup> AUBERT	09Y	BABR $B^0 \rightarrow D_1^- \ell^+ \nu_\ell$
<sup>2</sup> Assuming $\Gamma(\Upsilon(4S) \rightarrow B^+ B^-) / \Gamma(\Upsilon(4S) \rightarrow B^0 \bar{B}^0) = 1.065 \pm 0.026$ and equal partial widths and helicity angle distributions for charged and neutral $D_1$ mesons.			

$D_1(2420)^\pm$  REFERENCES

ABRAMOWICZ 13	NP B866 229	H. Abramowicz et al.	(ZEUS Collab.)
AUBERT 09Y	PRL 103 051803	B. Aubert et al.	(BABAR Collab.)
ABE 05A	PRL 94 221805	K. Abe et al.	(BELLE Collab.)
BERGFELD 94B	PL B340 194	T. Bergfeld et al.	(CLEO Collab.)
ANJOS 89C	PRL 62 1717	J.C. Anjos et al.	(FNAL E691 Collab.)

$D_1(2430)^0$

$I(J^P) = \frac{1}{2}(1^+)$

OMITTED FROM SUMMARY TABLE  
 $J = 1^+$  assignment favored (ABE 04D).

$D_1(2430)^0$  MASS

VALUE (MeV)	DOCUMENT ID	TECN	COMMENT
$2427 \pm 26 \pm 25$	ABE	04D	BELL $B^- \rightarrow D^{*+} \pi^- \pi^-$
$2477 \pm 28$	<sup>1</sup> AUBERT	06L	BABR $\bar{B}^0 \rightarrow D^{*+} \omega \pi^-$
<sup>1</sup> Systematic errors not estimated.			

$D_1(2430)^0$  WIDTH

VALUE (MeV)	DOCUMENT ID	TECN	COMMENT
$384_{-107}^{+107} \pm 74$	ABE	04D	BELL $B^- \rightarrow D^{*+} \pi^- \pi^-$
$266 \pm 97$	<sup>2</sup> AUBERT	06L	BABR $\bar{B}^0 \rightarrow D^{*+} \omega \pi^-$
<sup>2</sup> Systematic errors not estimated.			

$D_1(2430)^0$  DECAY MODES

Mode	Fraction ( $\Gamma_i/\Gamma$ )
$\Gamma_1$ $D^*(2010)^+ \pi^-$	seen

$D_1(2430)^0$  REFERENCES

AUBERT 06L	PR D74 012001	B. Aubert et al.	(BABAR Collab.)
ABE 04D	PR D69 112002	K. Abe et al.	(BELLE Collab.)

$D_2^*(2460)^0$

$I(J^P) = \frac{1}{2}(2^+)$

$J^P = 2^+$  assignment strongly favored (ALBRECHT 89B, ALBRECHT 89H), natural parity confirmed by the helicity analysis (DEL-AMO-SANCHEZ 10P). AAIJ 13CC confirms  $J^P = 2^+$  and natural parity.

$D_2^*(2460)^0$  MASS

The fit includes  $D^\pm, D^0, D_s^\pm, D^{*+}, D^{*0}, D_s^{*+}, D_1(2420)^0, D_2^*(2460)^0$ , and  $D_{s1}(2536)^\pm$  mass and mass difference measurements.

VALUE (MeV)	EVTS	DOCUMENT ID	TECN	COMMENT
<b>2460.7 ± 0.4 ± 1.2</b>	OUR FIT	Error includes scale factor of 3.1.		
<b>2460.56 ± 0.35</b>	OUR AVERAGE	Error includes scale factor of 2.6. See the ideogram below.		
$2463.7 \pm 0.4 \pm 0.7$	28k	<sup>1</sup> AAIJ	16AH LHCB	$B^- \rightarrow D^+ \pi^- \pi^-$
$2460.4 \pm 0.4 \pm 1.2$	82k	AAIJ	13CC LHCB	$pp \rightarrow D^{*+} \pi^- X$
$2460.4 \pm 0.1 \pm 0.1$	675k	AAIJ	13CC LHCB	$pp \rightarrow D^+ \pi^- X$
$2462.5 \pm 2.4 \pm 1.3_{-1.1}^+$	2.3k	<sup>2</sup> ABRAMOWICZ13	ZEUS	$e^\pm p \rightarrow D^*(*) \pi^- X$
$2462.2 \pm 0.1 \pm 0.8$	243k	DEL-AMO-SA...10P	BABR	$e^+ e^- \rightarrow D^+ \pi^- X$
$2460.4 \pm 1.2 \pm 2.2$	3.4k	AUBERT	09AB BABR	$B^- \rightarrow D^+ \pi^- \pi^-$
$2461.6 \pm 2.1 \pm 3.3$		<sup>3</sup> ABE	04D BELL	$B^- \rightarrow D^+ \pi^- \pi^-$
$2464.5 \pm 1.1 \pm 1.9$	5.8k	<sup>3</sup> LINK	04A FOCUS	$\gamma A$
$2465 \pm 3 \pm 3$	486	AVERY	94C CLE2	$e^+ e^- \rightarrow D^+ \pi^- X$
$2453 \pm 3 \pm 2$	128	FRABETTI	94B E687	$\gamma Be \rightarrow D^+ \pi^- X$
$2461 \pm 3 \pm 1$	440	AVERY	90 CLEO	$e^+ e^- \rightarrow D^{*+} \pi^- X$
$2455 \pm 3 \pm 5$	337	ALBRECHT	89B ARG	$e^+ e^- \rightarrow D^+ \pi^- X$
$2459 \pm 3 \pm 2$	153	ANJOS	89C TPS	$\gamma N \rightarrow D^+ \pi^- X$

• • • We do not use the following data for averages, fits, limits, etc. • • •

$2469.1 \pm 3.7 \pm 1.2_{-1.3}^+$	1.5k	<sup>4</sup> CHEKANOV	09 ZEUS	$e^\pm p \rightarrow D^*(*) \pi^- X$
$2463.3 \pm 0.6 \pm 0.8$	20k	ABULENCIA	06A CDF	$1900 p\bar{p} \rightarrow D^+ \pi^- X$
$2461 \pm 6$	126	<sup>5</sup> ABREU	98M DLPH	$e^+ e^-$
$2466 \pm 7$	1	ASRATYAN	95 BEBC	$53,40 \nu(\bar{\nu}) \rightarrow pX, dX$

<sup>1</sup> From the amplitude analysis in the model describing the  $D^+ \pi^-$  wave together with virtual contributions from the  $D^*(2007)^0$  and  $B^{*0}$  states, and components corresponding to the  $D_2^*(2460)^0, D_1^*(2680)^0, D_3^*(2760)^0$ , and  $D_2^*(3000)^0$  resonances.

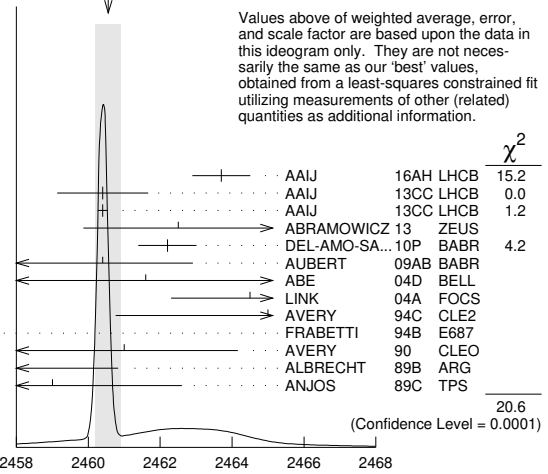
<sup>2</sup> From the combined fit of the  $M(D^+ \pi^-)$  and  $M(D^{*+} \pi^-)$  distributions. and  $A_{D_2}$  fixed to the theoretical prediction of  $-1$ .

<sup>3</sup> Fit includes the contribution from  $D_0^*(2400)^0$ .

<sup>4</sup> Calculated using the mass difference  $m(D_2^{*0}) - m(D^{*+})_{PDG}$  reported below and  $m(D^{*+})_{PDG} = 2010.27 \pm 0.17$  MeV. The 0.17 MeV uncertainty of the PDG mass value should be added to the experimental uncertainty of  $+1.2$  MeV.

<sup>5</sup> No systematic error given.

WEIGHTED AVERAGE  
 $2460.56 \pm 0.35$  (Error scaled by 2.6)



$D_2^*(2460)^0$  mass (MeV)

$m_{D_2^{*0}} - m_{D^+}$

The fit includes  $D^\pm, D^0, D_s^\pm, D^{*+}, D^{*0}, D_s^{*+}, D_1(2420)^0, D_2^*(2460)^0$ , and  $D_{s1}(2536)^\pm$  mass and mass difference measurements.

VALUE (MeV)	EVTS	DOCUMENT ID	TECN	COMMENT
<b>591.0 ± 0.4</b>	OUR FIT	Error includes scale factor of 2.9.		
<b>593.9 ± 0.6 ± 0.5</b>	20k	ABULENCIA	06A CDF	$1900 p\bar{p} \rightarrow D^+ \pi^- X$

$m_{D_2^{*0}} - m_{D^{*+}}$

The fit includes  $D^\pm, D^0, D_s^\pm, D^{*+}, D^{*0}, D_s^{*+}, D_1(2420)^0, D_2^*(2460)^0$ , and  $D_{s1}(2536)^\pm$  mass and mass difference measurements.

VALUE (MeV)	EVTS	DOCUMENT ID	TECN	COMMENT
<b>450.4 ± 0.4</b>	OUR FIT	Error includes scale factor of 2.9.		
<b>458.8 ± 3.7 ± 1.2_{-1.3}^+</b>	1560 ± 230	CHEKANOV	09 ZEUS	$e^\pm p \rightarrow D^*(*) \pi^- X$

$D_2^*(2460)^0$  WIDTH

VALUE (MeV)	EVTS	DOCUMENT ID	TECN	COMMENT	
<b>47.5 ± 1.1</b>	OUR AVERAGE	Error includes scale factor of 1.8. See the ideogram below.			
$47.0 \pm 0.8 \pm 1.0$	28k	<sup>6</sup> AAIJ	16AH LHCB	$B^- \rightarrow D^+ \pi^- \pi^-$	
$43.2 \pm 1.2 \pm 3.0$	82k	AAIJ	13CC LHCB	$pp \rightarrow D^{*+} \pi^- X$	
$45.6 \pm 0.4 \pm 1.1$	675k	AAIJ	13CC LHCB	$pp \rightarrow D^+ \pi^- X$	
$46.6 \pm 8.1 \pm 5.9_{-3.8}^+$	2.3k	<sup>7</sup> ABRAMOWICZ13	ZEUS	$e^\pm p \rightarrow D^*(*) \pi^- X$	
$50.5 \pm 0.6 \pm 0.7$	243k	DEL-AMO-SA...10P	BABR	$e^+ e^- \rightarrow D^+ \pi^- X$	
$41.8 \pm 2.5 \pm 2.9$	3.4k	AUBERT	09AB BABR	$B^- \rightarrow D^+ \pi^- \pi^-$	
$49.2 \pm 2.3 \pm 1.3$	20k	ABULENCIA	06A CDF	$1900 p\bar{p} \rightarrow D^+ \pi^- X$	
$45.6 \pm 4.4 \pm 6.7$		<sup>8</sup> ABE	04D BELL	$B^- \rightarrow D^+ \pi^- \pi^-$	
$38.7 \pm 5.3 \pm 2.9$	5.8k	<sup>8</sup> LINK	04A FOCUS	$\gamma A$	
$28 \pm 8_{-7}^+$	± 6	486	AVERY	94C CLE2	$e^+ e^- \rightarrow D^+ \pi^- X$
$25 \pm 10 \pm 5$	128	FRABETTI	94B E687	$\gamma Be \rightarrow D^+ \pi^- X$	
$20 \pm 9 \pm 9_{-12}^+$	440	AVERY	90 CLEO	$e^+ e^- \rightarrow D^{*+} \pi^- X$	

# Meson Particle Listings

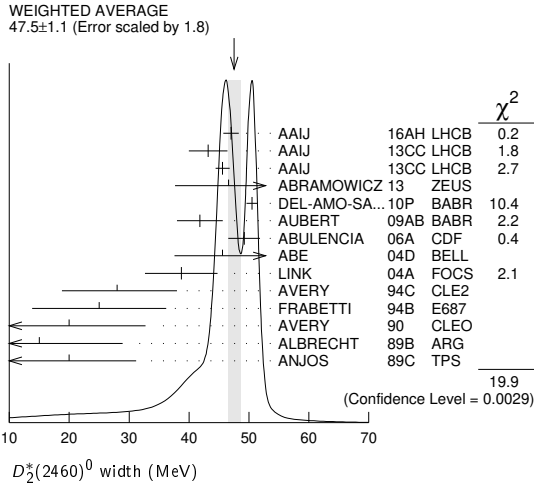
## $D_2^*(2460)^0, D_2^*(2460)^\pm$

15	$+^{13}_{-10}$	$+^5_{-10}$	337	ALBRECHT	89B	ARG	$e^+e^- \rightarrow D^+\pi^-X$
20	$\pm 10$	$\pm 5$	153	ANJOS	89C	TPS	$\gamma N \rightarrow D^+\pi^-X$

<sup>6</sup> From the amplitude analysis in the model describing the  $D^+\pi^-$  wave together with virtual contributions from the  $D^*(2007)^0$  and  $B^{*0}$  states, and components corresponding to the  $D_2^*(2460)^0, D_1^*(2680)^0, D_3^*(2760)^0$ , and  $D_2^*(3000)^0$  resonances.

<sup>7</sup> From the combined fit of the  $M(D^+\pi^-)$  and  $M(D^{*+}\pi^-)$  distributions. and  $A_{D_2}$  fixed to the theoretical prediction of  $-1$ .

<sup>8</sup> Fit includes the contribution from  $D_0^*(2400)^0$ .



### $D_2^*(2460)^0$ DECAY MODES

$\bar{D}_2^*(2460)^0$  modes are charge conjugates of modes below.

Mode	Fraction ( $\Gamma_i/\Gamma$ )
$\Gamma_1$ $D^+\pi^-$	seen
$\Gamma_2$ $D^*(2010)^+\pi^-$	seen
$\Gamma_3$ $D^0\pi^+\pi^-$	not seen
$\Gamma_4$ $D^{*0}\pi^+\pi^-$	not seen

### $D_2^*(2460)^0$ BRANCHING RATIOS

$\Gamma(D^+\pi^-)/\Gamma_{total}$	$\Gamma_1/\Gamma$
seen	3.4k
seen	337
seen	

$\Gamma(D^*(2010)^+\pi^-)/\Gamma_{total}$	$\Gamma_2/\Gamma$
seen	
seen	
seen	

$\Gamma(D^+\pi^-)/[\Gamma(D^+\pi^-) + \Gamma(D^*(2010)^+\pi^-)]$	$\Gamma_1/(\Gamma_1 + \Gamma_2)$
1.4 ± 0.3 ± 0.3	2.3k
1.47 ± 0.03 ± 0.16	379k
2.8 ± 0.8 $+^{0.5}_{-0.6}$	1560 ± 230
2.2 ± 0.7 ± 0.6	
2.3 ± 0.8	
3.0 ± 1.1 ± 1.5	

••• We do not use the following data for averages, fits, limits, etc. •••

<sup>9</sup> From the combined fit of the  $M(D^+\pi^-)$  and  $M(D^{*+}\pi^-)$  distributions. and  $A_{D_2}$  fixed to the theoretical prediction of  $-1$ .

$\Gamma(D^+\pi^-)/[\Gamma(D^+\pi^-) + \Gamma(D^*(2010)^+\pi^-)]$	$\Gamma_1/(\Gamma_1 + \Gamma_2)$
0.62 ± 0.03 ± 0.02	8414

••• We do not use the following data for averages, fits, limits, etc. •••

<sup>10</sup> Assuming  $\Gamma(\Upsilon(4S) \rightarrow B^+B^-) / \Gamma(\Upsilon(4S) \rightarrow B^0\bar{B}^0) = 1.065 \pm 0.026$  and equal partial widths for charged and neutral  $D_2^*$  mesons.

### $D_2^*(2460)^0$ POLARIZATION AMPLITUDE $A_{D_2}$

A polarization amplitude  $A_{D_2}$  is a parameter that depends on the initial polarization of the  $D_2$ . For  $D_2$  decays the helicity angle,  $\theta_H$ , distribution varies like  $1 + A_{D_2} \cos^2(\theta_H)$ , where  $\theta_H$  is the angle in the  $D^*$  rest frame between the two pions emitted by the  $D_2 \rightarrow D^*\pi$  and  $D^* \rightarrow D\pi$ .

VALUE	EVTS	DOCUMENT ID	TECN	COMMENT
••• We do not use the following data for averages, fits, limits, etc. •••				
$-1.16 \pm 0.35$	2.3k	<sup>11</sup> ABRAMOWICZ13	ZEUS	$e^\pm p \rightarrow D^{(*)+}\pi^-X$
consistent with $-1$	243k	DEL-AMO-SA...10P	BABR	$e^+e^- \rightarrow D^+\pi^-X$
$-0.74 \pm 0.49$		<sup>12</sup> AVERY	94C CLE2	$e^+e^- \rightarrow D^{*+}\pi^-X$
$-0.38$				

<sup>11</sup> From the combined fit of the  $M(D^+\pi^-)$  and  $M(D^{*+}\pi^-)$  distributions.  
<sup>12</sup> Systematic uncertainties not estimated.

### $D_2^*(2460)^0$ REFERENCES

AAIJ 16AH PR D94 072001	R. Aaij et al.	(LHCb Collab.)
AAIJ 13CC JHEP 1309 145	R. Aaij et al.	(LHCb Collab.)
ABRAMOWICZ 13 NP B866 229	H. Abramowicz et al.	(ZEUS Collab.)
DEL-AMO-SA...10P PR D52 111101	P. del Amo Sanchez et al.	(BABAR Collab.)
AUBERT 09AB PR D79 112004	B. Aubert et al.	(BABAR Collab.)
AUBERT 09Y PRL 103 051803	B. Aubert et al.	(BABAR Collab.)
CHEKANOV 09 EPJ C60 25	S. Chekanov et al.	(ZEUS Collab.)
ABULENCIA 06A PR D73 051104	A. Abulencia et al.	(CDF Collab.)
ABE 04D PR D69 112002	K. Abe et al.	(BELLE Collab.)
LINK 04A PL B586 11	J.M. Link et al.	(FOCUS Collab.)
ABREU 98M PL B426 231	P. Abreu et al.	(DELPHI Collab.)
ACKERSTAFF 97W ZPHY C76 425	K. Ackerstaff et al.	(OPAL Collab.)
ASRATYAN 95 ZPHY C68 43	A.E. Asratyan et al.	(BIRM, BELG, CERN+)
AVERY 94C PL B331 236	P. Avery et al.	(CLEO Collab.)
FRABETTI 94B PRL 72 324	P.L. Frabetti et al.	(FNAL E687 Collab.)
AVERY 90 PR D41 374	P. Avery, D. Besson	(CLEO Collab.)
ALBRECHT 89B PL B221 422	H. Albrecht et al.	(ARGUS Collab.) JP
ALBRECHT 89H PL B232 398	H. Albrecht et al.	(ARGUS Collab.) JP
ANJOS 89C PRL 62 1717	J.C. Anjos et al.	(FNAL E691 Collab.)

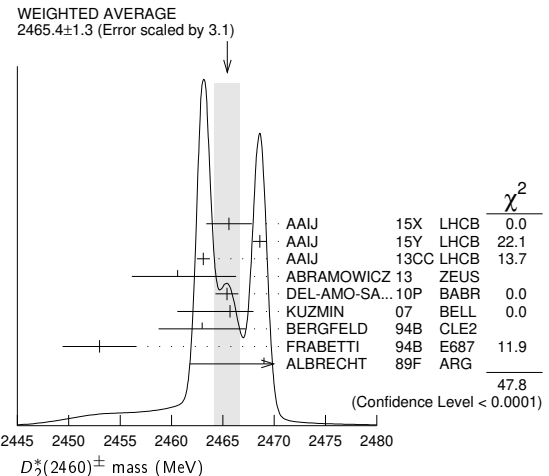
### $D_2^*(2460)^\pm$

$$J(P) = \frac{1}{2}(2^+)$$

$J^P = 2^+$  assignment strongly favored (ALBRECHT 89B).

### $D_2^*(2460)^\pm$ MASS

VALUE (MeV)	EVTS	DOCUMENT ID	TECN	COMMENT
<b>2465.4 ± 1.3 OUR AVERAGE</b>				Error includes scale factor of 3.1. See the ideogram below.
2465.6 ± 1.8 ± 1.3		<sup>1</sup> AAIJ	15X LHCB	$B^0 \rightarrow \bar{D}^0 K^+\pi^-$
2468.6 ± 0.6 ± 0.3		<sup>2</sup> AAIJ	15Y LHCB	$B^0 \rightarrow \bar{D}^0 \pi^+\pi^-$
2463.1 ± 0.2 ± 0.6	342k	AAIJ	13CC LHCB	$pp \rightarrow D^0 \pi^+ X$
2460.6 ± 4.4 $+^{3.6}_{-0.8}$	1371	<sup>3</sup> ABRAMOWICZ13	ZEUS	$e^\pm p \rightarrow D^{(*)0} \pi^+ X$
2465.4 ± 0.2 ± 1.1	111k	<sup>4</sup> DEL-AMO-SA...10P	BABR	$e^+e^- \rightarrow D^0 \pi^+ X$
2465.7 ± 1.8 $+^{1.4}_{-4.8}$	2909	KUZMIN	07 BELL	$e^+e^- \rightarrow$ hadrons
2463 ± 3 ± 3	310	BERGFELD	94B CLE2	$e^+e^- \rightarrow D^0 \pi^+ X$
2453 ± 3 ± 2	185	FRABETTI	94B E687	$\gamma Be \rightarrow D^0 \pi^+ X$
2469 ± 4 ± 6		ALBRECHT	89F ARG	$e^+e^- \rightarrow D^0 \pi^+ X$
••• We do not use the following data for averages, fits, limits, etc. •••				
2468.1 ± 0.6 ± 0.5		<sup>5</sup> AAIJ	15Y LHCB	$B^0 \rightarrow \bar{D}^0 \pi^+ \pi^-$
2467.6 ± 1.5 ± 0.8	3.5k	<sup>6</sup> LINK	04A FOCUS	$\gamma A$



<sup>1</sup> From the Dalitz plot analysis including various  $K^*$  and  $D^{**}$  mesons as well as broad structures in the  $K\pi$  S-wave and the  $D\pi$  S- and P-waves.  
<sup>2</sup> Modeling the  $\pi^+\pi^-$  S-wave with the isobar formalism.

See key on page 999

Meson Particle Listings

$D_2^*(2460)^\pm, D(2550)^0, D_J^*(2600)$

<sup>3</sup> From the fit of the  $M(D^0 \pi^+)$  distribution. The widths of the  $D_1^+$  and  $D_2^{*+}$  are fixed to 25 MeV and 37 MeV, and  $A_{D_1}$  and  $A_{D_2}$  are fixed to the theoretical predictions of 3 and  $-1$ , respectively.

<sup>4</sup> At a fixed width of 50.5 MeV.

<sup>5</sup> Modeling the  $\pi^+ \pi^-$  S-wave with the K-matrix formalism.

<sup>6</sup> Fit includes the contribution from  $D_0^*(2400)^\pm$ . Not independent of the corresponding mass difference measurement,  $(m_{D_2^*(2460)^\pm} - m_{D_2^*(2460)^0})$ .

$m_{D_2^*(2460)^\pm} - m_{D_2^*(2460)^0}$

VALUE (MeV)	DOCUMENT ID	TECN	COMMENT
<b>2.4 ± 1.7 OUR AVERAGE</b>			
3.1 ± 1.9 ± 0.9	LINK	04A	FOCS $\gamma A$
- 2 ± 4 ± 4	BERGFELD	94B	CLE2 $e^+ e^- \rightarrow$ hadrons
0 ± 4	FRABETTI	94B	E687 $\gamma Be \rightarrow D \pi X$
14 ± 5 ± 8	ALBRECHT	89F	ARG $e^+ e^- \rightarrow D^0 \pi^+ X$

$D_2^*(2460)^\pm$  WIDTH

VALUE (MeV)	EVTS	DOCUMENT ID	TECN	COMMENT
<b>46.7 ± 1.2 OUR AVERAGE</b>				
46.0 ± 3.4 ± 3.2		<sup>1</sup> AAIJ	15X	LHCB $B^0 \rightarrow \bar{D}^0 K^+ \pi^-$
47.3 ± 1.5 ± 0.7		<sup>2</sup> AAIJ	15Y	LHCB $B^0 \rightarrow \bar{D}^0 \pi^+ \pi^-$
48.6 ± 1.3 ± 1.9	342k	AAIJ	13CC	LHCB $pp \rightarrow D^0 \pi^+ X$
49.7 ± 3.8 ± 6.4	2909	KUZMIN	07	BELL $e^+ e^- \rightarrow$ hadrons
34.1 ± 6.5 ± 4.2	3.5k	<sup>3</sup> LINK	04A	FOCS $\gamma A$
27 <sup>+11</sup> <sub>-8</sub> ± 5	310	BERGFELD	94B	CLE2 $e^+ e^- \rightarrow D^0 \pi^+ X$
23 ± 9 ± 5	185	FRABETTI	94B	E687 $\gamma Be \rightarrow D^0 \pi^+ X$
46.0 ± 1.4 ± 1.8		<sup>4</sup> AAIJ	15Y	LHCB $B^0 \rightarrow \bar{D}^0 \pi^+ \pi^-$

<sup>1</sup> From the Dalitz plot analysis including various  $K^*$  and  $D^{**}$  mesons as well as broad structures in the  $K \pi$  S-wave and the  $D \pi$  S- and P-waves.

<sup>2</sup> Modeling the  $\pi^+ \pi^-$  S-wave with the isobar formalism.

<sup>3</sup> Fit includes the contribution from  $D_0^*(2400)^\pm$ .

<sup>4</sup> Modeling the  $\pi^+ \pi^-$  S-wave with the K-matrix formalism.

$D_2^*(2460)^\pm$  DECAY MODES

$D_2^*(2460)^\pm$  modes are charge conjugates of modes below.

Mode	Fraction ( $\Gamma_i/\Gamma$ )
$\Gamma_1$ $D^0 \pi^+$	seen
$\Gamma_2$ $D^{*0} \pi^+$	seen
$\Gamma_3$ $D^+ \pi^+ \pi^-$	not seen
$\Gamma_4$ $D^{*+} \pi^+ \pi^-$	not seen

$D_2^*(2460)^\pm$  BRANCHING RATIOS

$\Gamma(D^0 \pi^+)/\Gamma_{total}$	$\Gamma_1/\Gamma$
seen	ALBRECHT 89F ARG $e^+ e^- \rightarrow D^0 \pi^+ X$

$\Gamma(D^0 \pi^+)/\Gamma(D^{*0} \pi^+)$	$\Gamma_1/\Gamma_2$
<b>1.2 ± 0.4 OUR AVERAGE</b>	
1.1 ± 0.4 <sup>+0.3</sup> <sub>-0.2</sub>	1371 <sup>1</sup> ABRAMOWICZ13 ZEUS $e^\pm p \rightarrow D^{(*)0} \pi^+ X$
1.9 ± 1.1 ± 0.3	BERGFELD 94B CLE2 $e^+ e^- \rightarrow$ hadrons

<sup>1</sup> From the fit of the  $M(D^0 \pi^+)$  distribution. The widths of the  $D_1^+$  and  $D_2^{*+}$  are fixed to 25 MeV and 37 MeV, and  $A_{D_1}$  and  $A_{D_2}$  are fixed to the theoretical predictions of 3 and  $-1$ , respectively.

$\Gamma(D^0 \pi^+)/[\Gamma(D^0 \pi^+) + \Gamma(D^{*0} \pi^+)]$	$\Gamma_1/(\Gamma_1 + \Gamma_2)$
0.62 ± 0.03 ± 0.02	3361 <sup>1</sup> AUBERT 09Y BABR $\bar{B}^0 \rightarrow D_2^{*+} \ell^- \nu_\ell$

<sup>1</sup> Assuming  $\Gamma(\Upsilon(4S) \rightarrow B^+ B^-) / \Gamma(\Upsilon(4S) \rightarrow B^0 \bar{B}^0) = 1.065 \pm 0.026$  and equal partial widths for charged and neutral  $D_2^*$  mesons.

$D_2^*(2460)^\pm$  REFERENCES

AAIJ 15X	PR D92 012012	R. Aaij et al.	(LHCb Collab.)
AAIJ 15Y	PR D92 032002	R. Aaij et al.	(LHCb Collab.)
AAIJ 13CC	JHEP 1309 145	R. Aaij et al.	(LHCb Collab.)
ABRAMOWICZ 13	NP B866 229	H. Abramowicz et al.	(ZEUS Collab.)
DEL-AMO-SA...10P	PR D82 111101	P. del Amo Sanchez et al.	(BABAR Collab.)
AUBERT 09Y	PRL 103 051803	B. Aubert et al.	(BABAR Collab.)
KUZMIN 07	PR D76 012006	A. Kuzmin et al.	(BELLE Collab.)
LINK 04A	PL B586 11	J.M. Link et al.	(FOCUS Collab.)
BERGFELD 94B	PL B340 194	T. Bergfeld et al.	(CLEO Collab.)
FRABETTI 94B	PRL 72 324	P.L. Frabetti et al.	(FNAL E687 Collab.)
ALBRECHT 89B	PL B221 422	H. Albrecht et al.	(ARGUS Collab.)
ALBRECHT 89F	PL B231 208	H. Albrecht et al.	(ARGUS Collab.)

$D(2550)^0$

$I(J^P) = \frac{1}{2}(?^?)$

OMITTED FROM SUMMARY TABLE

Unnatural parity according to the helicity analysis of DEL-AMO-SANCHEZ 10P and AAIJ 13CC. DEL-AMO-SANCHEZ 10P suggests  $J^P = 0^-$ .

$D(2550)^0$  MASS

VALUE (MeV)	EVTS	DOCUMENT ID	TECN	COMMENT
<b>2564 ± 20 OUR AVERAGE</b>				Error includes scale factor of 3.9.
2579.5 ± 3.4 ± 5.5	60k	AAIJ	13cc	LHCB $pp \rightarrow D^{*+} \pi^- X$
2539.4 ± 4.5 ± 6.8	34k	DEL-AMO-SA...10P	BABR	$e^+ e^- \rightarrow D^{*+} \pi^- X$

$D(2550)^0$  WIDTH

VALUE (MeV)	EVTS	DOCUMENT ID	TECN	COMMENT
<b>135 ± 17 OUR AVERAGE</b>				
177.5 ± 17.8 ± 46.0	60k	AAIJ	13cc	LHCB $pp \rightarrow D^{*+} \pi^- X$
130 ± 12 ± 13	34k	DEL-AMO-SA...10P	BABR	$e^+ e^- \rightarrow D^{*+} \pi^- X$

$D(2550)^0$  DECAY MODES

Mode	Fraction ( $\Gamma_i/\Gamma$ )
$\Gamma_1$ $D^{*+} \pi^-$	seen

$D(2550)^0$  POLARIZATION AMPLITUDE  $A_{D_J}$

A polarization amplitude  $A_{D_J}$  is a parameter that depends on the initial polarization of the  $D_J$ . For  $D_J$  decays the helicity angle,  $\theta_H$ , distribution varies like  $1 + A_{D_J} \cos^2(\theta_H)$ , where  $\theta_H$  is the angle in the  $D_J$  rest frame between the two pions emitted in the  $D_J \rightarrow D^* \pi$  and  $D^* \rightarrow D \pi$  decays.

VALUE	EVTS	DOCUMENT ID	TECN	COMMENT
4.2 ± 1.3	60k	<sup>1</sup> AAIJ	13cc	LHCB $pp \rightarrow D^{*+} \pi^- X$
				<sup>1</sup> Systematic uncertainty not estimated.

$D(2550)^0$  REFERENCES

AAIJ 13CC	JHEP 1309 145	R. Aaij et al.	(LHCb Collab.)
DEL-AMO-SA...10P	PR D82 111101	P. del Amo Sanchez et al.	(BABAR Collab.)

$D_J^*(2600)$

$I(J^P) = \frac{1}{2}(?^?)$

OMITTED FROM SUMMARY TABLE

was  $D(2600)$

$J^P$  consistent with natural parity (DEL-AMO-SANCHEZ 10P, AAIJ 13CC).

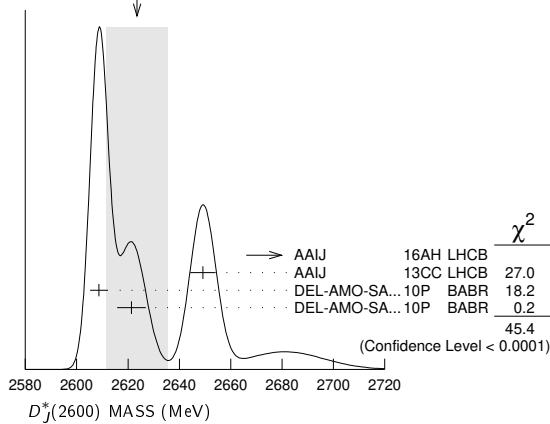
$D_J^*(2600)$  MASS

VALUE (MeV)	EVTS	DOCUMENT ID	TECN	CHG	COMMENT
<b>2623 ± 12 OUR AVERAGE</b>					Error includes scale factor of 4.8. See the ideogram below.
2681.1 ± 5.6 ± 14.0	28k	<sup>1</sup> AAIJ	16AH	LHCB	$B^- \rightarrow D^+ \pi^- \pi^-$
2649.2 ± 3.5 ± 3.5	51k	AAIJ	13cc	LHCB	$pp \rightarrow D^{*+} \pi^- X$
2608.7 ± 2.4 ± 2.5	26k	DEL-AMO-SA...10P	BABR	0	$e^+ e^- \rightarrow D^+ \pi^- X$
2621.3 ± 3.7 ± 4.2	13k	<sup>2</sup> DEL-AMO-SA...10P	BABR	+	$e^+ e^- \rightarrow D^0 \pi^+ X$

<sup>1</sup> From the amplitude analysis in the model describing the  $D^+ \pi^-$  wave together with virtual contributions from the  $D^{*+}(2007)^0$  and  $B^{*0}$  states, and components corresponding to the  $D_2^*(2460)^0, D_1^*(2680)^0, D_3^*(2760)^0$ , and  $D_2^*(3000)^0$  resonances.

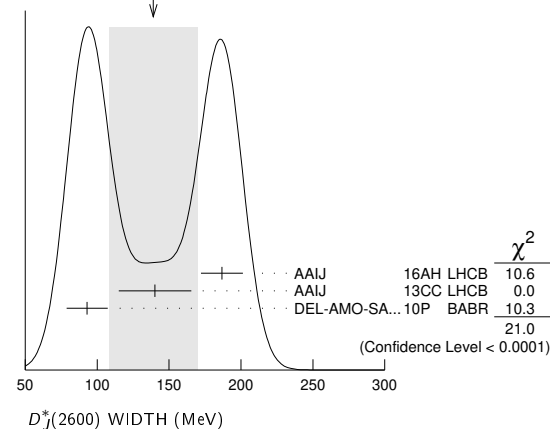
<sup>2</sup> At a fixed width of 93 MeV.

## Meson Particle Listings

 $D_J^*(2600)$ ,  $D^*(2640)^\pm$ ,  $D(2740)^0$ ,  $D_3^*(2750)$ WEIGHTED AVERAGE  
2623±12 (Error scaled by 4.8) $D_J^*(2600)$  WIDTH

VALUE (MeV)	EVTS	DOCUMENT ID	TECN	COMMENT
<b>139 ± 31</b>	<b>OUR AVERAGE</b>	Error includes scale factor of 3.2. See the ideogram below.		
186.7 ± 8.5 ± 11.9	28k	<sup>3</sup> AAIJ	16AH LHCB	$B^- \rightarrow D^+ \pi^- \pi^-$
140.2 ± 17.1 ± 18.6	51k	AAIJ	13CC LHCB	$pp \rightarrow D^{*+} \pi^- X$
93 ± 6 ± 13	26k	DEL-AMO-SA...10P	BABR	$e^+ e^- \rightarrow D^+ \pi^- X$

<sup>3</sup>From the amplitude analysis in the model describing the  $D^+ \pi^-$  wave together with virtual contributions from the  $D^*(2007)^0$  and  $B^{*0}$  states, and components corresponding to the  $D_2^*(2460)^0$ ,  $D_1^*(2680)^0$ ,  $D_3^*(2760)^0$ , and  $D_2^*(3000)^0$  resonances.

WEIGHTED AVERAGE  
139±31 (Error scaled by 3.2) $D_J^*(2600)$  DECAY MODES

Mode	Fraction ( $\Gamma_i/\Gamma$ )
$\Gamma_1$ $D \pi$	seen
$\Gamma_2$ $D^+ \pi^-$	seen
$\Gamma_3$ $D^0 \pi^\pm$	seen
$\Gamma_4$ $D^* \pi$	seen
$\Gamma_5$ $D^{*+} \pi^-$	seen

 $D_J^*(2600)$  BRANCHING RATIOS

$\Gamma(D^+ \pi^-)/\Gamma(D^{*+} \pi^-)$	VALUE	EVTS	DOCUMENT ID	TECN	COMMENT	$\Gamma_2/\Gamma_5$
	<b>0.32 ± 0.02 ± 0.09</b>	76k	DEL-AMO-SA...10P	BABR	$e^+ e^- \rightarrow D^{(*)+} \pi^- X$	

 $D_J^*(2600)$  REFERENCES

AAIJ	16AH	PR D94 072001	R. Aaij et al.	(LHCb Collab.)
AAIJ	13CC	JHEP 1309 145	R. Aaij et al.	(LHCb Collab.)
DEL-AMO-SA...10P	PR	D82 111101	P. del Amo Sanchez et al.	(BABAR Collab.)

 $D^*(2640)^\pm$ 

$$I(J^P) = \frac{1}{2}(??)$$

OMITTED FROM SUMMARY TABLE

Seen in  $Z$  decays by ABREU 98M. Not seen by ABBIENDI 01N and CHEKANOV 09. Needs confirmation. $D^*(2640)^\pm$  MASS

VALUE (MeV)	EVTS	DOCUMENT ID	TECN	COMMENT
<b>2637 ± 2 ± 6</b>	66 ± 14	ABREU	98M DLPH	$e^+ e^- \rightarrow D^{*+} \pi^+ \pi^- X$

 $D^*(2640)^\pm$  WIDTH

VALUE (MeV)	CL%	DOCUMENT ID	TECN	COMMENT
<b>&lt;15</b>	95	ABREU	98M DLPH	$e^+ e^- \rightarrow D^{*+} \pi^+ \pi^- X$

 $D^*(2640)^+$  DECAY MODES $D^*(2640)^-$  modes are charge conjugates of modes below.

Mode	Fraction ( $\Gamma_i/\Gamma$ )
$\Gamma_1$ $D^*(2010)^+ \pi^+ \pi^-$	seen

 $D^*(2640)^\pm$  REFERENCES

CHEKANOV	09	EPJ C60 25	S. Chekanov et al.	(ZEUS Collab.)
ABBIENDI	01N	EPJ C20 445	G. Abbiendi et al.	(OPAL Collab.)
ABREU	98M	PL B426 231	P. Abreu et al.	(DELPHI Collab.)

 $D(2740)^0$ 

$$I(J^P) = \frac{1}{2}(??)$$

OMITTED FROM SUMMARY TABLE

 $J^P$  consistent with unnatural parity (AAIJ 13CC). $D(2740)^0$  MASS

VALUE (MeV)	EVTS	DOCUMENT ID	TECN	COMMENT
<b>2737.0 ± 3.5 ± 11.2</b>	7.7k	AAIJ	13CC LHCB	$pp \rightarrow D^+ \pi^- X$

 $D(2740)^0$  WIDTH

VALUE (MeV)	EVTS	DOCUMENT ID	TECN	COMMENT
<b>73.2 ± 13.4 ± 25.0</b>	7.7k	AAIJ	13CC LHCB	$pp \rightarrow D^+ \pi^- X$

 $D(2740)^0$  DECAY MODES

Mode	Fraction ( $\Gamma_i/\Gamma$ )
$\Gamma_1$ $D^* \pi^-$	seen

 $D(2740)^0$  POLARIZATION AMPLITUDE  $A_{D_J}$ 

A polarization amplitude  $A_{D_J}$  is a parameter that depends on the initial polarization of the  $D_J$ . For  $D_J$  decays the helicity angle,  $\theta_H$ , distribution varies like  $1 + A_{D_J} \cos^2(\theta_H)$ , where  $\theta_H$  is the angle in the  $D_J$  rest frame between the two pions emitted in the  $D_J \rightarrow D^* \pi$  and  $D^* \rightarrow D \pi$  decays.

VALUE	EVTS	DOCUMENT ID	TECN	COMMENT
• • • We do not use the following data for averages, fits, limits, etc. • • •				
3.1 ± 2.2	7.7k	<sup>1</sup> AAIJ	13CC LHCB	$pp \rightarrow D^+ \pi^- X$
<sup>1</sup> Systematic uncertainty not estimated.				

 $D(2740)^0$  REFERENCES

AAIJ	13CC	JHEP 1309 145	R. Aaij et al.	(LHCb Collab.)
------	------	---------------	----------------	----------------

 $D_3^*(2750)$ 

$$I(J^P) = \frac{1}{2}(3^-)$$

OMITTED FROM SUMMARY TABLE

 $J^P$  determined by AAIJ 15Y from the Dalitz plot analysis of  $B^0 \rightarrow \bar{D}^0 \pi^+ \pi^-$  decays.  $J^P$  consistent with natural parity (AAIJ 13CC).

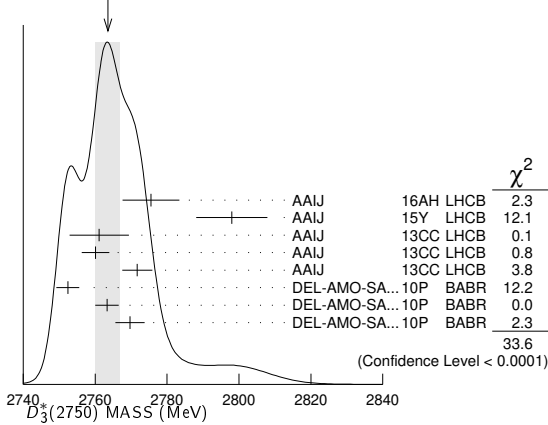
$D_3^*(2750)$ ,  $D(3000)^0$

$D_3^*(2750)$  MASS

VALUE (MeV)	EVTS	DOCUMENT ID	TECN	CHG	COMMENT
<b>2763.5 ± 3.4 OUR AVERAGE</b>		Error includes scale factor of 2.2. See the ideogram below.			
2775.5 ± 4.5 ± 6.5	28k	<sup>1</sup> AAIJ	16AH	LHCB	$B^- \rightarrow D^+ \pi^- \pi^-$
2798 ± 7 ± 7		<sup>2</sup> AAIJ	15Y	LHCB	$B^0 \rightarrow \bar{D}^0 \pi^+ \pi^-$
2761.1 ± 5.1 ± 6.5	14k	AAIJ	13CC	LHCB 0	$pp \rightarrow D^{*+} \pi^- X$
2760.1 ± 1.1 ± 3.7	56k	AAIJ	13CC	LHCB 0	$pp \rightarrow D^+ \pi^- X$
2771.7 ± 1.7 ± 3.8	20k	AAIJ	13CC	LHCB +	$pp \rightarrow D^0 \pi^+ X$
2752.4 ± 1.7 ± 2.7	23.5k	<sup>3</sup> DEL-AMO-SA...10P	BABR	0	$e^+ e^- \rightarrow D^{*+} \pi^- X$
2763.3 ± 2.3 ± 2.3	11.3k	<sup>3</sup> DEL-AMO-SA...10P	BABR	0	$e^+ e^- \rightarrow D^+ \pi^- X$
2769.7 ± 3.8 ± 1.5	5.7k	<sup>3,4</sup> DEL-AMO-SA...10P	BABR	+	$e^+ e^- \rightarrow D^0 \pi^+ X$
• • • We do not use the following data for averages, fits, limits, etc. • • •					
2802 ± 11 ± 10		<sup>5</sup> AAIJ	15Y	LHCB	$B^0 \rightarrow \bar{D}^0 \pi^+ \pi^-$

- <sup>1</sup> From the amplitude analysis in the model describing the  $D^+ \pi^-$  wave together with virtual contributions from the  $D^*(2007)^0$  and  $B^{*0}$  states, and components corresponding to the  $D_2^*(2460)^0$ ,  $D_1^*(2680)^0$ ,  $D_3^*(2760)^0$ , and  $D_2^*(3000)^0$  resonances.  
<sup>2</sup> Modeling the  $\pi^+ \pi^-$  S-wave with the Isobar formalism.  
<sup>3</sup> The states observed in the  $D^* \pi$  and  $D \pi$  final states are not necessarily the same.  
<sup>4</sup> At a fixed width of 60.9 MeV.  
<sup>5</sup> Modeling the  $\pi^+ \pi^-$  S-wave with the K-matrix formalism.

WEIGHTED AVERAGE  
2763.5±3.4 (Error scaled by 2.2)



$D_3^*(2750)$  WIDTH

VALUE (MeV)	EVTS	DOCUMENT ID	TECN	CHG	COMMENT
<b>66 ± 5 OUR AVERAGE</b>					
95.3 ± 9.6 ± 34.0	28k	<sup>6</sup> AAIJ	16AH	LHCB	$B^- \rightarrow D^+ \pi^- \pi^-$
105 ± 18 ± 24		<sup>7</sup> AAIJ	15Y	LHCB	$B^0 \rightarrow \bar{D}^0 \pi^+ \pi^-$
74.4 ± 3.4 ± 37.0	14k	AAIJ	13CC	LHCB 0	$pp \rightarrow D^{*+} \pi^- X$
74.4 ± 3.4 ± 19.1	56k	AAIJ	13CC	LHCB 0	$pp \rightarrow D^+ \pi^- X$
66.7 ± 6.6 ± 10.5	20k	AAIJ	13CC	LHCB +	$pp \rightarrow D^0 \pi^+ X$
71 ± 6 ± 11	23.5k	<sup>8</sup> DEL-AMO-SA...10P	BABR	0	$e^+ e^- \rightarrow D^{*+} \pi^- X$
60.9 ± 5.1 ± 3.6	11.3k	<sup>8</sup> DEL-AMO-SA...10P	BABR	0	$e^+ e^- \rightarrow D^+ \pi^- X$
• • • We do not use the following data for averages, fits, limits, etc. • • •					
154 ± 27 ± 16		<sup>9</sup> AAIJ	15Y	LHCB	$B^0 \rightarrow \bar{D}^0 \pi^+ \pi^-$

- <sup>6</sup> From the amplitude analysis in the model describing the  $D^+ \pi^-$  wave together with virtual contributions from the  $D^*(2007)^0$  and  $B^{*0}$  states, and components corresponding to the  $D_2^*(2460)^0$ ,  $D_1^*(2680)^0$ ,  $D_3^*(2760)^0$ , and  $D_2^*(3000)^0$  resonances.  
<sup>7</sup> Modeling the  $\pi^+ \pi^-$  S-wave with the Isobar formalism.  
<sup>8</sup> The states observed in the  $D^* \pi$  and  $D \pi$  final states are not necessarily the same.  
<sup>9</sup> Modeling the  $\pi^+ \pi^-$  S-wave with the K-matrix formalism.

$D_3^*(2750)$  DECAY MODES

Mode	Fraction ( $\Gamma_i/\Gamma$ )
$\Gamma_1$ $D \pi$	seen
$\Gamma_2$ $D^+ \pi^-$	seen
$\Gamma_3$ $D^0 \pi^\pm$	seen
$\Gamma_4$ $D^* \pi$	seen
$\Gamma_5$ $D^{*+} \pi^-$	seen

$D_3^*(2750)$  BRANCHING RATIOS

$\Gamma(D^+ \pi^-)/\Gamma(D^{*+} \pi^-)$	VALUE	EVTS	DOCUMENT ID	TECN	COMMENT	$\Gamma_2/\Gamma_5$
	<b>0.42 ± 0.05 ± 0.11</b>	34.8k	<sup>10</sup> DEL-AMO-SA...10P	BABR	$e^+ e^- \rightarrow D^{*+} \pi^- X$	

<sup>10</sup> The states observed in the  $D^* \pi$  and  $D \pi$  final states are not necessarily the same.

$D_3^*(2750)$  POLARIZATION AMPLITUDE  $A_D$

A polarization amplitude  $A_D$  is a parameter that depends on the initial polarization of the  $D_3^*(2750)$ . For  $D_3^*(2750)$  decays the helicity angle,  $\theta_H$ , distribution varies like  $1 + A_D \cos(\theta_H)$ , where  $\theta_H$  is the angle in the  $D^*$  rest frame between the two pions emitted by the  $D_3^*(2750) \rightarrow D^* \pi$  and  $D^* \rightarrow D \pi$ .

VALUE	EVTS	DOCUMENT ID	TECN	COMMENT
• • • We do not use the following data for averages, fits, limits, etc. • • •				
-0.33 ± 0.28	23.5k	<sup>11</sup> DEL-AMO-SA...10P	BABR	$e^+ e^- \rightarrow D^{*+} \pi^- X$
<sup>11</sup> Systematic uncertainties not estimated. The states observed in the $D^* \pi$ and $D \pi$ final states are not necessarily the same.				

$D_3^*(2750)$  REFERENCES

AAIJ	16AH	PR D94 072001	R. Aaij et al.	(LHCb Collab.)
AAIJ	15Y	PR D52 032002	R. Aaij et al.	(LHCb Collab.) JP
AAIJ	13CC	JHEP 1309 145	R. Aaij et al.	(LHCb Collab.)
DEL-AMO-SA...10P	PR	D82 111101	P. del Amo Sanchez et al.	(BABAR Collab.)

$D(3000)^0$

$I(J^P) = \frac{1}{2}(??)$

OMITTED FROM SUMMARY TABLE

Both natural- and unnatural-parity components observed depending on the decay mode (AAIJ 13CC).

$D(3000)^0$  MASS

VALUE (MeV)	EVTS	DOCUMENT ID	TECN	COMMENT
<b>3214 ± 29 ± 49</b>	28k	<sup>1</sup> AAIJ	16AH	LHCB $B^- \rightarrow D^+ \pi^- \pi^-$
• • • We do not use the following data for averages, fits, limits, etc. • • •				
2971.8 ± 8.7	9.5k	<sup>2,3</sup> AAIJ	13CC	LHCB $pp \rightarrow D^{*+} \pi^- X$
3008.1 ± 4.0	17.6k	<sup>2,4</sup> AAIJ	13CC	LHCB $pp \rightarrow D^+ \pi^- X$

- <sup>1</sup> From the amplitude analysis in the model describing the  $D^+ \pi^-$  wave together with virtual contributions from the  $D^*(2007)^0$  and  $B^{*0}$  states, and components corresponding to the  $D_2^*(2460)^0$ ,  $D_1^*(2680)^0$ ,  $D_3^*(2760)^0$ , and  $D_2^*(3000)^0$  resonances.  
<sup>2</sup> Systematic uncertainty not estimated.  
<sup>3</sup> Unnatural parity preferred.  
<sup>4</sup> Natural parity state. A state  $D(3000)^+$  is possibly seen in  $D^0 \pi^+$  final state.

$D(3000)^0$  WIDTH

VALUE (MeV)	EVTS	DOCUMENT ID	TECN	COMMENT
<b>186 ± 38 ± 72</b>	28k	<sup>5</sup> AAIJ	16AH	LHCB $B^- \rightarrow D^+ \pi^- \pi^-$
• • • We do not use the following data for averages, fits, limits, etc. • • •				
188.1 ± 44.8	9.5k	<sup>6,7</sup> AAIJ	13CC	LHCB $pp \rightarrow D^{*+} \pi^- X$
110.5 ± 11.5	17.6k	<sup>6,8</sup> AAIJ	13CC	LHCB $pp \rightarrow D^+ \pi^- X$

- <sup>5</sup> From the amplitude analysis in the model describing the  $D^+ \pi^-$  wave together with virtual contributions from the  $D^*(2007)^0$  and  $B^{*0}$  states, and components corresponding to the  $D_2^*(2460)^0$ ,  $D_1^*(2680)^0$ ,  $D_3^*(2760)^0$ , and  $D_2^*(3000)^0$  resonances.  
<sup>6</sup> Systematic uncertainty not estimated.  
<sup>7</sup> Unnatural parity preferred.  
<sup>8</sup> Natural parity state. A state  $D(3000)^+$  is possibly seen in  $D^0 \pi^+$  final state.

$D(3000)^0$  DECAY MODES

Mode	Fraction ( $\Gamma_i/\Gamma$ )
$\Gamma_1$ $D^{*+} \pi^-$	seen

$D(3000)^0$  POLARIZATION AMPLITUDE  $A_{D_J}$

A polarization amplitude  $A_{D_J}$  is a parameter that depends on the initial polarization of the  $D_J$ . For  $D_J$  decays the helicity angle,  $\theta_H$ , distribution varies like  $1 + A_{D_J} \cos^2(\theta_H)$ , where  $\theta_H$  is the angle in the  $D_J$  rest frame between the two pions emitted in the  $D_J \rightarrow D^* \pi$  and  $D^* \rightarrow D \pi$  decays.

VALUE	EVTS	DOCUMENT ID	TECN	COMMENT
• • • We do not use the following data for averages, fits, limits, etc. • • •				
1.5 ± 0.9	9.5k	<sup>9</sup> AAIJ	13CC	LHCB $pp \rightarrow D^{*+} \pi^- X$
<sup>9</sup> Systematic uncertainty not estimated.				

$D(3000)^0$  REFERENCES

AAIJ	16AH	PR D94 072001	R. Aaij et al.	(LHCb Collab.)
AAIJ	13CC	JHEP 1309 145	R. Aaij et al.	(LHCb Collab.)

# Meson Particle Listings

$D_s^\pm$

## CHARMED, STRANGE MESONS ( $C = S = \pm 1$ )

$$D_s^+ = c\bar{s}, D_s^- = \bar{c}s, \text{ similarly for } D_s^{*\pm}$$

$D_s^\pm$

$$J(P) = 0(0^-)$$

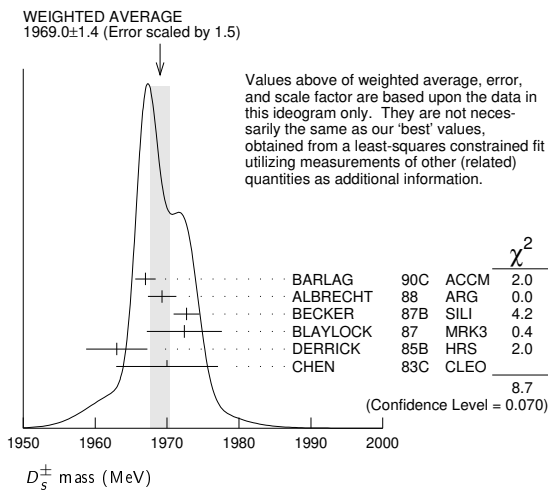
The angular distributions of the decays of the  $\phi$  and  $\bar{K}^*(892)^0$  in the  $\phi\pi^+$  and  $K^+\bar{K}^*(892)^0$  modes strongly indicate that the spin is zero. The parity given is that expected of a  $c\bar{s}$  ground state.

### $D_s^\pm$ MASS

The fit includes  $D_s^\pm, D^0, D_s^{*\pm}, D^{*0}, D_s^{*+}, D_1(2420)^0, D_2^*(2460)^0,$  and  $D_{s1}(2536)^\pm$  mass and mass difference measurements. Measurements of the  $D_s^\pm$  mass with an error greater than 10 MeV are omitted from the fit and average. A number of early measurements have been omitted altogether.

VALUE (MeV)	EVTS	DOCUMENT ID	TECN	COMMENT
<b>1968.34 ± 0.07 OUR FIT</b>				
<b>1969.0 ± 1.4 OUR AVERAGE</b>				Error includes scale factor of 1.5. See the ideogram below.
1967.0 ± 1.0 ± 1.0	54	BARLAG	90c	ACCM $\pi^-$ Cu 230 GeV
1969.3 ± 1.4 ± 1.4		ALBRECHT	88	ARG $e^+e^-$ 9.4–10.6 GeV
1972.7 ± 1.5 ± 1.0	21	BECKER	87B	SILI 200 GeV $\pi, K, p$
1972.4 ± 3.7 ± 3.7	27	BLAYLOCK	87	MRK3 $e^+e^-$ 4.14 GeV
1963 ± 3 ± 3	30	DERRICK	85B	HRS $e^+e^-$ 29 GeV
1970 ± 5 ± 5	104	CHEN	83c	CLEO $e^+e^-$ 10.5 GeV
••• We do not use the following data for averages, fits, limits, etc. •••				
1968.3 ± 0.7 ± 0.7	290	<sup>1</sup> ANJOS	88	E691 Photoproduction
1980 ± 15	6	USHIDA	86	EMUL $\nu$ wideband
1973.6 ± 2.6 ± 3.0	163	ALBRECHT	85D	ARG $e^+e^-$ 10 GeV
1948 ± 28 ± 10	65	AIHARA	84D	TPC $e^+e^-$ 29 GeV
1975 ± 9 ± 10	49	ALTHOFF	84	TASS $e^+e^-$ 14–25 GeV
1975 ± 4	3	BAILEY	84	ACCM hadron <sup>+</sup> Be → $\phi\pi^+ X$

<sup>1</sup> ANJOS 88 enters the fit via  $m_{D_s^\pm} - m_{D^\pm}$  (see below).



$$m_{D_s^\pm} - m_{D^\pm}$$

The fit includes  $D_s^\pm, D^0, D_s^{*\pm}, D^{*0}, D_s^{*+}, D_1(2420)^0, D_2^*(2460)^0,$  and  $D_{s1}(2536)^\pm$  mass and mass difference measurements.

VALUE (MeV)	EVTS	DOCUMENT ID	TECN	COMMENT
<b>98.69 ± 0.05 OUR FIT</b>				
<b>98.69 ± 0.05 OUR AVERAGE</b>				
98.68 ± 0.03 ± 0.04		AAIJ	13v	LHCB $D_s^+ \rightarrow K^+ K^- \pi^+$
99.41 ± 0.38 ± 0.21		ACOSTA	03D	CDF2 $\bar{p}p, \sqrt{s} = 1.96$ TeV
98.4 ± 0.1 ± 0.3	48k	AUBERT	02c	BABR $e^+e^- \approx \Upsilon(4S)$
99.5 ± 0.6 ± 0.3		BROWN	94	CLE2 $e^+e^- \approx \Upsilon(4S)$
98.5 ± 1.5	555	CHEN	89	CLEO $e^+e^-$ 10.5 GeV
99.0 ± 0.8	290	ANJOS	88	E691 Photoproduction

### $D_s^\pm$ MEAN LIFE

Measurements with an error greater than  $100 \times 10^{-15}$  s or with fewer than 100 events have been omitted from the Listings.

VALUE ( $10^{-15}$ s)	EVTS	DOCUMENT ID	TECN	COMMENT
<b>504 ± 4 OUR AVERAGE</b>				Error includes scale factor of 1.2.
506.4 ± 3.0 ± 1.7 ± 1.7		<sup>1</sup> AAIJ	17AN	LHCB $pp$ at 7, 8 TeV
507.4 ± 5.5 ± 5.1	13.6k	LINK	05J	FOCS $\phi\pi^+$ and $\bar{K}^{*0} K^+$
472.5 ± 17.2 ± 6.6	760	IORI	01	SELX 600 GeV $\Sigma^-, \pi^-, p$
518 ± 14 ± 7	1662	AITALA	99	E791 $\pi^-$ nucleus, 500 GeV
486.3 ± 15.0 ± 4.9 ± 5.1	2167	<sup>2</sup> BONVICINI	99	CLE2 $e^+e^- \approx \Upsilon(4S)$
475 ± 20 ± 7	900	FRABETTI	93F	E687 $\gamma$ Be, $\phi\pi^+$
500 ± 60 ± 30	104	FRABETTI	90	E687 $\gamma$ Be, $\phi\pi^+$
470 ± 40 ± 20	228	RAAB	88	E691 Photoproduction

<sup>1</sup> This AAIJ 17AN value is derived from the difference between the  $D_s^-$  and  $D^-$  widths.

The 3rd uncertainty,  $\pm 1.7 \times 10^{-15}$  s, arises from the uncertainty of the  $D^-$  width.

<sup>2</sup> BONVICINI 99 obtains  $1.19 \pm 0.04$  for the ratio of  $D_s^\pm$  to  $D^0$  lifetimes.

### $D_s^\pm$ DECAY MODES

Unless otherwise noted, the branching fractions for modes with a resonance in the final state include all the decay modes of the resonance.  $D_s^\pm$  modes are charge conjugates of the modes below.

Mode	Fraction ( $\Gamma_i/\Gamma$ )	Scale factor/Confidence level
<b>Inclusive modes</b>		
$\Gamma_1$ $e^+$ semileptonic	[a] ( 6.5 ± 0.4 ) %	
$\Gamma_2$ $\pi^+$ anything	(119.3 ± 1.4 ) %	
$\Gamma_3$ $\pi^-$ anything	( 43.2 ± 0.9 ) %	
$\Gamma_4$ $\pi^0$ anything	(123 ± 7 ) %	
$\Gamma_5$ $K^-$ anything	( 18.7 ± 0.5 ) %	
$\Gamma_6$ $K^+$ anything	( 28.9 ± 0.7 ) %	
$\Gamma_7$ $K_S^0$ anything	( 19.0 ± 1.1 ) %	
$\Gamma_8$ $\eta$ anything	[b] ( 29.9 ± 2.8 ) %	
$\Gamma_9$ $\omega$ anything	( 6.1 ± 1.4 ) %	
$\Gamma_{10}$ $\eta'$ anything	[c] ( 10.3 ± 1.4 ) %	S=1.1
$\Gamma_{11}$ $f_0(980)$ anything, $f_0 \rightarrow \pi^+\pi^-$	< 1.3 %	CL=90%
$\Gamma_{12}$ $\phi$ anything	( 15.7 ± 1.0 ) %	
$\Gamma_{13}$ $K^+ K^-$ anything	( 15.8 ± 0.7 ) %	
$\Gamma_{14}$ $K_S^0 K^+$ anything	( 5.8 ± 0.5 ) %	
$\Gamma_{15}$ $K_S^0 K^-$ anything	( 1.9 ± 0.4 ) %	
$\Gamma_{16}$ $2K^0$ anything	( 1.70 ± 0.32 ) %	
$\Gamma_{17}$ $2K^+$ anything	< 2.6 × 10 <sup>-3</sup>	CL=90%
$\Gamma_{18}$ $2K^-$ anything	< 6 × 10 <sup>-4</sup>	CL=90%
<b>Leptonic and semileptonic modes</b>		
$\Gamma_{19}$ $e^+ \nu_e$	< 8.3 × 10 <sup>-5</sup>	CL=90%
$\Gamma_{20}$ $\mu^+ \nu_\mu$	( 5.49 ± 0.16 ) × 10 <sup>-3</sup>	
$\Gamma_{21}$ $\tau^+ \nu_\tau$	( 5.48 ± 0.23 ) %	
$\Gamma_{22}$ $\gamma e^+ \nu_e$	< 1.3 × 10 <sup>-4</sup>	CL=90%
$\Gamma_{23}$ $K^+ K^- e^+ \nu_e$	—	
$\Gamma_{24}$ $\phi e^+ \nu_e$	[d] ( 2.39 ± 0.16 ) %	S=1.3
$\Gamma_{25}$ $\phi \mu^+ \nu_\mu$	( 1.9 ± 0.5 ) %	
$\Gamma_{26}$ $\eta e^+ \nu_e + \eta'(958) e^+ \nu_e$	[d] ( 3.03 ± 0.24 ) %	
$\Gamma_{27}$ $\eta e^+ \nu_e$	[d] ( 2.32 ± 0.08 ) %	
$\Gamma_{28}$ $\eta'(958) e^+ \nu_e$	[d] ( 8.0 ± 0.7 ) × 10 <sup>-3</sup>	
$\Gamma_{29}$ $\eta \mu^+ \nu_\mu$	( 2.4 ± 0.5 ) %	
$\Gamma_{30}$ $\eta'(958) \mu^+ \nu_\mu$	( 1.1 ± 0.5 ) %	
$\Gamma_{31}$ $\omega e^+ \nu_e$	[e] < 2.0 × 10 <sup>-3</sup>	CL=90%
$\Gamma_{32}$ $K^0 e^+ \nu_e$	( 3.4 ± 0.4 ) × 10 <sup>-3</sup>	
$\Gamma_{33}$ $K^*(892)^0 e^+ \nu_e$	[d] ( 2.15 ± 0.28 ) × 10 <sup>-3</sup>	S=1.1
$\Gamma_{34}$ $f_0(980) e^+ \nu_e, f_0 \rightarrow \pi^+\pi^-$		
<b>Hadronic modes with a <math>K\bar{K}</math> pair</b>		
$\Gamma_{35}$ $K^+ K_S^0$	( 1.46 ± 0.04 ) %	S=1.1
$\Gamma_{36}$ $K^+ K^0$	( 1.49 ± 0.06 ) %	
$\Gamma_{37}$ $K^+ \bar{K}^0$	( 2.95 ± 0.14 ) %	
$\Gamma_{38}$ $K^+ K^- \pi^+$	[f] ( 5.39 ± 0.15 ) %	S=1.2
$\Gamma_{39}$ $\phi\pi^+$	[d,g] ( 4.5 ± 0.4 ) %	
$\Gamma_{40}$ $\phi\pi^+, \phi \rightarrow K^+ K^-$	[g] ( 2.24 ± 0.08 ) %	
$\Gamma_{41}$ $K^+ \bar{K}^*(892)^0, \bar{K}^{*0} \rightarrow K^- \pi^+$	( 2.58 ± 0.08 ) %	
$\Gamma_{42}$ $f_0(980)\pi^+, f_0 \rightarrow K^+ K^-$	( 1.14 ± 0.31 ) %	
$\Gamma_{43}$ $f_0(1370)\pi^+, f_0 \rightarrow K^+ K^-$	( 7 ± 5 ) × 10 <sup>-4</sup>	
$\Gamma_{44}$ $f_0(1710)\pi^+, f_0 \rightarrow K^+ K^-$	( 6.6 ± 2.8 ) × 10 <sup>-4</sup>	

$\Gamma_{45}$	$K^+ \bar{K}_0^*(1430)^0, \bar{K}_0^+ \rightarrow$	$(1.8 \pm 0.4) \times 10^{-3}$	
$\Gamma_{46}$	$K^+ K_S^0 \pi^+$	$(1.52 \pm 0.22) \%$	
$\Gamma_{47}$	$2K_S^0 \pi^+$	$(7.7 \pm 0.6) \times 10^{-3}$	
$\Gamma_{48}$	$K^0 \bar{K}^0 \pi^+$	—	
$\Gamma_{49}$	$K^*(892)^+ \bar{K}^0$	[d] $(5.4 \pm 1.2) \%$	
$\Gamma_{50}$	$K^+ K^- \pi^+ \pi^0$	$(6.2 \pm 0.6) \%$	S=1.1
$\Gamma_{51}$	$\phi \rho^+$	[d] $(8.4 \pm_{-2.3}^{+1.9}) \%$	
$\Gamma_{52}$	$K_S^0 K^- 2\pi^+$	$(1.65 \pm 0.10) \%$	
$\Gamma_{53}$	$K^*(892)^+ \bar{K}^*(892)^0$	[d] $(7.2 \pm 2.6) \%$	
$\Gamma_{54}$	$K^+ K_S^0 \pi^+ \pi^-$	$(9.9 \pm 0.8) \times 10^{-3}$	
$\Gamma_{55}$	$K^+ K^- 2\pi^+ \pi^-$	$(8.6 \pm 1.5) \times 10^{-3}$	
$\Gamma_{56}$	$\phi 2\pi^+ \pi^-$	[d] $(1.21 \pm 0.16) \%$	
$\Gamma_{57}$	$\phi \rho^0 \pi^+, \phi \rightarrow K^+ K^-$	$(6.5 \pm 1.3) \times 10^{-3}$	
$\Gamma_{58}$	$\phi a_1(1260)^+, \phi \rightarrow$ $K^+ K^-, a_1^+ \rightarrow$ $\rho^0 \pi^+$	$(7.4 \pm 1.2) \times 10^{-3}$	
$\Gamma_{59}$	$\phi 2\pi^+ \pi^-$ non- $\rho, \phi \rightarrow$ $K^+ K^-$	$(1.8 \pm 0.7) \times 10^{-3}$	
$\Gamma_{60}$	$K^+ K^- \rho^0 \pi^+$ non- $\phi$	$< 2.6 \times 10^{-4}$	CL=90%
$\Gamma_{61}$	$K^+ K^- 2\pi^+ \pi^-$ nonresonant	$(9 \pm 7) \times 10^{-4}$	
$\Gamma_{62}$	$2K_S^0 2\pi^+ \pi^-$	$(8.4 \pm 3.5) \times 10^{-4}$	
<b>Hadronic modes without <math>K</math>'s</b>			
$\Gamma_{63}$	$\pi^+ \pi^0$	$< 3.4 \times 10^{-4}$	CL=90%
$\Gamma_{64}$	$2\pi^+ \pi^-$	$(1.08 \pm 0.04) \%$	S=1.1
$\Gamma_{65}$	$\rho^0 \pi^+$	$(1.9 \pm 1.2) \times 10^{-4}$	
$\Gamma_{66}$	$\pi^+(\pi^+ \pi^-)_{S\text{-wave}}$	[h] $(9.0 \pm 0.4) \times 10^{-3}$	
$\Gamma_{67}$	$f_0(980) \pi^+, f_0 \rightarrow \pi^+ \pi^-$		
$\Gamma_{68}$	$f_0(1370) \pi^+, f_0 \rightarrow \pi^+ \pi^-$		
$\Gamma_{69}$	$f_0(1500) \pi^+, f_0 \rightarrow \pi^+ \pi^-$		
$\Gamma_{70}$	$f_2(1270) \pi^+, f_2 \rightarrow \pi^+ \pi^-$	$(1.09 \pm 0.20) \times 10^{-3}$	
$\Gamma_{71}$	$\rho(1450)^0 \pi^+, \rho^0 \rightarrow \pi^+ \pi^-$	$(3.0 \pm 1.9) \times 10^{-4}$	
$\Gamma_{72}$	$\pi^+ 2\pi^0$	$(6.5 \pm 1.3) \times 10^{-3}$	
$\Gamma_{73}$	$2\pi^+ \pi^- \pi^0$	—	
$\Gamma_{74}$	$\eta \pi^+$	[d] $(1.68 \pm 0.10) \%$	S=1.2
$\Gamma_{75}$	$\omega \pi^+$	[d] $(1.92 \pm 0.30) \times 10^{-3}$	
$\Gamma_{76}$	$3\pi^+ 2\pi^-$	$(7.9 \pm 0.8) \times 10^{-3}$	
$\Gamma_{77}$	$2\pi^+ \pi^- 2\pi^0$	—	
$\Gamma_{78}$	$\eta \rho^+$	[d] $(8.9 \pm 0.8) \%$	
$\Gamma_{79}$	$\eta \pi^+ \pi^0$	$(9.5 \pm 0.5) \%$	
$\Gamma_{80}$	$\eta(\pi^+ \pi^0)_{P\text{-wave}}$	$(5.1 \pm 3.1) \times 10^{-3}$	
$\Gamma_{81}$	$a_0(980)^+ \pi^0, a_0(980)^+ \rightarrow \eta \pi^+$	$(2.2 \pm 0.4) \%$	
$\Gamma_{82}$	$\omega \pi^+ \pi^0$	[d] $(2.8 \pm 0.7) \%$	
$\Gamma_{83}$	$3\pi^+ 2\pi^- \pi^0$	$(4.9 \pm 3.2) \%$	
$\Gamma_{84}$	$\omega 2\pi^+ \pi^-$	[d] $(1.6 \pm 0.5) \%$	
$\Gamma_{85}$	$\eta'(958) \pi^+$	[c,d] $(3.94 \pm 0.25) \%$	
$\Gamma_{86}$	$3\pi^+ 2\pi^- 2\pi^0$	—	
$\Gamma_{87}$	$\omega \eta \pi^+$	[d] $< 2.13 \%$	CL=90%
$\Gamma_{88}$	$\eta'(958) \rho^+$	[c,d] $(5.8 \pm 1.5) \%$	
$\Gamma_{89}$	$\eta'(958) \pi^+ \pi^0$	$(5.6 \pm 0.8) \%$	
$\Gamma_{90}$	$\eta'(958) \pi^+ \pi^0$ nonresonant	$< 5.1 \%$	CL=90%
<b>Modes with one or three <math>K</math>'s</b>			
$\Gamma_{91}$	$K^+ \pi^0$	$(6.1 \pm 2.1) \times 10^{-4}$	
$\Gamma_{92}$	$K_S^0 \pi^+$	$(1.19 \pm 0.05) \times 10^{-3}$	
$\Gamma_{93}$	$K^+ \eta$	[d] $(1.72 \pm 0.34) \times 10^{-3}$	
$\Gamma_{94}$	$K^+ \omega$	[d] $(8.7 \pm 2.5) \times 10^{-4}$	
$\Gamma_{95}$	$K^+ \eta'(958)$	[d] $(1.7 \pm 0.5) \times 10^{-3}$	
$\Gamma_{96}$	$K^+ \pi^+ \pi^-$	$(6.5 \pm 0.4) \times 10^{-3}$	
$\Gamma_{97}$	$K^+ \rho^0$	$(2.5 \pm 0.4) \times 10^{-3}$	
$\Gamma_{98}$	$K^+ \rho(1450)^0, \rho^0 \rightarrow \pi^+ \pi^-$	$(6.9 \pm 2.4) \times 10^{-4}$	
$\Gamma_{99}$	$K^*(892)^0 \pi^+, K^{*0} \rightarrow K^+ \pi^-$	$(1.41 \pm 0.24) \times 10^{-3}$	
$\Gamma_{100}$	$K^*(1410)^0 \pi^+, K^{*0} \rightarrow$ $K^+ \pi^-$	$(1.23 \pm 0.28) \times 10^{-3}$	
$\Gamma_{101}$	$K^*(1430)^0 \pi^+, K^{*0} \rightarrow$ $K^+ \pi^-$	$(5.0 \pm 3.5) \times 10^{-4}$	
$\Gamma_{102}$	$K^+ \pi^+ \pi^-$ nonresonant	$(1.03 \pm 0.34) \times 10^{-3}$	
$\Gamma_{103}$	$K^0 \pi^+ \pi^0$	$(1.00 \pm 0.18) \%$	
$\Gamma_{104}$	$K_S^0 2\pi^+ \pi^-$	$(3.0 \pm 1.1) \times 10^{-3}$	
$\Gamma_{105}$	$K^+ \omega \pi^0$	[d] $< 8.2 \times 10^{-3}$	CL=90%
$\Gamma_{106}$	$K^+ \omega \pi^+ \pi^-$	[d] $< 5.4 \times 10^{-3}$	CL=90%
$\Gamma_{107}$	$K^+ \omega \eta$	[d] $< 7.9 \times 10^{-3}$	CL=90%
$\Gamma_{108}$	$2K^+ K^-$	$(2.16 \pm 0.20) \times 10^{-4}$	
$\Gamma_{109}$	$\phi K^+, \phi \rightarrow K^+ K^-$	$(8.8 \pm 2.0) \times 10^{-5}$	

**Doubly Cabibbo-suppressed modes**

$\Gamma_{110}$	$2K^+ \pi^-$	$(1.28 \pm 0.04) \times 10^{-4}$
$\Gamma_{111}$	$K^+ K^*(892)^0, K^{*0} \rightarrow$ $K^+ \pi^-$	$(6.0 \pm 3.4) \times 10^{-5}$

**Baryon-antibaryon mode**

$\Gamma_{112}$	$\rho \bar{\rho}$	$(1.22 \pm 0.11) \times 10^{-3}$	
$\Gamma_{113}$	$\rho \bar{\rho} e^+ \nu_e$	$< 2.0 \times 10^{-4}$	CL=90%

**$\Delta C = 1$  weak neutral current (C1) modes,  
Lepton family number (LF), or  
Lepton number (L) violating modes**

$\Gamma_{114}$	$\pi^+ e^+ e^-$	[j] $< 1.3 \times 10^{-5}$	CL=90%
$\Gamma_{115}$	$\pi^+ \phi, \phi \rightarrow e^+ e^-$	[j] $(6 \pm_{-4}^{+8}) \times 10^{-6}$	
$\Gamma_{116}$	$\pi^+ \mu^+ \mu^-$	[i] $< 4.1 \times 10^{-7}$	CL=90%
$\Gamma_{117}$	$K^+ e^+ e^-$	CI $< 3.7 \times 10^{-6}$	CL=90%
$\Gamma_{118}$	$K^+ \mu^+ \mu^-$	CI $< 2.1 \times 10^{-5}$	CL=90%
$\Gamma_{119}$	$K^*(892)^+ \mu^+ \mu^-$	CI $< 1.4 \times 10^{-3}$	CL=90%
$\Gamma_{120}$	$\pi^+ e^+ \mu^-$	LF $< 1.2 \times 10^{-5}$	CL=90%
$\Gamma_{121}$	$\pi^+ e^- \mu^+$	LF $< 2.0 \times 10^{-5}$	CL=90%
$\Gamma_{122}$	$K^+ e^- \mu^+$	LF $< 1.4 \times 10^{-5}$	CL=90%
$\Gamma_{123}$	$K^+ e^- \mu^+$	LF $< 9.7 \times 10^{-6}$	CL=90%
$\Gamma_{124}$	$\pi^- 2e^+$	L $< 4.1 \times 10^{-6}$	CL=90%
$\Gamma_{125}$	$\pi^- 2\mu^+$	L $< 1.2 \times 10^{-7}$	CL=90%
$\Gamma_{126}$	$\pi^- e^+ \mu^+$	L $< 8.4 \times 10^{-6}$	CL=90%
$\Gamma_{127}$	$K^- 2e^+$	L $< 5.2 \times 10^{-6}$	CL=90%
$\Gamma_{128}$	$K^- 2\mu^+$	L $< 1.3 \times 10^{-5}$	CL=90%
$\Gamma_{129}$	$K^- e^+ \mu^+$	L $< 6.1 \times 10^{-6}$	CL=90%
$\Gamma_{130}$	$K^*(892)^- 2\mu^+$	L $< 1.4 \times 10^{-3}$	CL=90%

[a] This is the purely  $e^+$  semileptonic branching fraction: the  $e^+$  fraction from  $\tau^+$  decays has been subtracted off. The sum of our (non- $\tau$ )  $e^+$  exclusive fractions — an  $e^+ \nu_e$  with an  $\eta, \eta', \phi, K^0$ , or  $K^{*0}$  — is  $5.99 \pm 0.31 \%$ .

[b] This fraction includes  $\eta$  from  $\eta'$  decays.

[c] The sum of our exclusive  $\eta'$  fractions —  $\eta' e^+ \nu_e, \eta' \mu^+ \nu_\mu, \eta' \pi^+, \eta' \rho^+$ , and  $\eta' K^+$  — is  $11.8 \pm 1.6 \%$ .

[d] This branching fraction includes all the decay modes of the final-state resonance.

[e] A test for  $u\bar{u}$  or  $d\bar{d}$  content in the  $D_s^+$ . Neither Cabibbo-favored nor Cabibbo-suppressed decays can contribute, and  $\omega$ - $\phi$  mixing is an unlikely explanation for any fraction above about  $2 \times 10^{-4}$ .

[f] The branching fraction for this mode may differ from the sum of the submodes that contribute to it, due to interference effects. See the relevant papers.

[g] We decouple the  $D_s^+ \rightarrow \phi \pi^+$  branching fraction obtained from mass projections (and used to get some of the other branching fractions) from the  $D_s^+ \rightarrow \phi \pi^+, \phi \rightarrow K^+ K^-$  branching fraction obtained from the Dalitz-plot analysis of  $D_s^+ \rightarrow K^+ K^- \pi^+$ . That is, the ratio of these two branching fractions is not exactly the  $\phi \rightarrow K^+ K^-$  branching fraction 0.491.

[h] This is the average of a model-independent and a  $K$ -matrix parametrization of the  $\pi^+ \pi^-$  S-wave and is a sum over several  $f_0$  mesons.

[i] This mode is not a useful test for a  $\Delta C=1$  weak neutral current because both quarks must change flavor in this decay.

[j] This is *not* a test for the  $\Delta C=1$  weak neutral current, but leads to the  $\pi^+ \ell^+ \ell^-$  final state.

**CONSTRAINED FIT INFORMATION**

An overall fit to 13 branching ratios uses 18 measurements and one constraint to determine 10 parameters. The overall fit has a  $\chi^2 = 6.8$  for 9 degrees of freedom.

The following *off-diagonal* array elements are the correlation coefficients  $\langle \delta x_i \delta x_j \rangle / (\delta x_i \delta x_j)$ , in percent, from the fit to the branching fractions,  $x_i \equiv \Gamma_i / \Gamma_{\text{total}}$ . The fit constrains the  $x_i$  whose labels appear in this array to sum to one.



## Meson Particle Listings

 $D_S^\pm$ 

X38	51								
X50	22	29							
X52	28	30	11						
X54	23	25	13	38					
X64	34	50	19	19	17				
X74	-7	-7	-15	1	-7	-7			
X75	0	0	-1	0	0	0	4		
X96	5	12	-6	7	1	3	16	1	
	X35	X38	X50	X52	X54	X64	X74	X75	

See the related review(s):

[D<sub>S</sub><sup>±</sup> Branching Fractions](#)**D<sub>S</sub><sup>±</sup> BRANCHING RATIOS**

A number of older, now obsolete results have been omitted. They may be found in earlier editions.

**Inclusive modes**

$\Gamma(e^+ \text{ semileptonic})/\Gamma_{\text{total}}$		$\Gamma_1/\Gamma$	
VALUE (%)	EVTS	DOCUMENT ID	TECN COMMENT
<b>6.52 ± 0.39 ± 0.15</b>	536 ± 29	<sup>1</sup> ASNER	10 CLEO e <sup>+</sup> e <sup>-</sup> at 3774 MeV

<sup>1</sup>Using the  $D_S^+$  and  $D_S^0$  lifetimes, ASNER 10 finds that the ratio of the  $D_S^+$  and  $D_S^0$  semileptonic widths is  $0.828 \pm 0.051 \pm 0.025$ .

$\Gamma(\pi^+ \text{ anything})/\Gamma_{\text{total}}$		$\Gamma_2/\Gamma$	
VALUE (%)	DOCUMENT ID	TECN	COMMENT
<b>119.3 ± 1.2 ± 0.7</b>	DOBBS	09 CLEO	e <sup>+</sup> e <sup>-</sup> at 4170 MeV

$\Gamma(\pi^- \text{ anything})/\Gamma_{\text{total}}$		$\Gamma_3/\Gamma$	
VALUE (%)	DOCUMENT ID	TECN	COMMENT
<b>43.2 ± 0.9 ± 0.3</b>	DOBBS	09 CLEO	e <sup>+</sup> e <sup>-</sup> at 4170 MeV

$\Gamma(\pi^0 \text{ anything})/\Gamma_{\text{total}}$		$\Gamma_4/\Gamma$	
VALUE (%)	DOCUMENT ID	TECN	COMMENT
<b>123.4 ± 3.8 ± 5.3</b>	DOBBS	09 CLEO	e <sup>+</sup> e <sup>-</sup> at 4170 MeV

$\Gamma(K^- \text{ anything})/\Gamma_{\text{total}}$		$\Gamma_5/\Gamma$	
VALUE (%)	DOCUMENT ID	TECN	COMMENT
<b>18.7 ± 0.5 ± 0.2</b>	DOBBS	09 CLEO	e <sup>+</sup> e <sup>-</sup> at 4170 MeV

$\Gamma(K^+ \text{ anything})/\Gamma_{\text{total}}$		$\Gamma_6/\Gamma$	
VALUE (%)	DOCUMENT ID	TECN	COMMENT
<b>28.9 ± 0.6 ± 0.3</b>	DOBBS	09 CLEO	e <sup>+</sup> e <sup>-</sup> at 4170 MeV

$\Gamma(K_S^0 \text{ anything})/\Gamma_{\text{total}}$		$\Gamma_7/\Gamma$	
VALUE (%)	DOCUMENT ID	TECN	COMMENT
<b>19.0 ± 1.0 ± 0.4</b>	DOBBS	09 CLEO	e <sup>+</sup> e <sup>-</sup> at 4170 MeV

$\Gamma(\eta \text{ anything})/\Gamma_{\text{total}}$		$\Gamma_8/\Gamma$	
VALUE (%)	EVTS	DOCUMENT ID	TECN COMMENT
<b>29.9 ± 2.2 ± 1.7</b>		DOBBS	09 CLEO e <sup>+</sup> e <sup>-</sup> at 4170 MeV
••• We do not use the following data for averages, fits, limits, etc. •••			
23.5 ± 3.1 ± 2.0	674 ± 91	HUANG	06B CLEO See DOBBS 09

$\Gamma(\omega \text{ anything})/\Gamma_{\text{total}}$		$\Gamma_9/\Gamma$	
VALUE (%)	DOCUMENT ID	TECN	COMMENT
<b>6.1 ± 1.4 ± 0.3</b>	DOBBS	09 CLEO	e <sup>+</sup> e <sup>-</sup> at 4170 MeV

$\Gamma(\eta' \text{ anything})/\Gamma_{\text{total}}$		$\Gamma_{10}/\Gamma$	
VALUE (%)	EVTS	DOCUMENT ID	TECN COMMENT
<b>10.3 ± 1.4 OUR AVERAGE</b>	Error includes scale factor of 1.1.		
8.8 ± 1.8 ± 0.5	68	ABLIKIM	15z BES3 482 pb <sup>-1</sup> , 4009 MeV
11.7 ± 1.7 ± 0.7		DOBBS	09 CLEO e <sup>+</sup> e <sup>-</sup> at 4170 MeV
••• We do not use the following data for averages, fits, limits, etc. •••			
8.7 ± 1.9 ± 0.8	68	HUANG	06B CLEO See DOBBS 09

$\Gamma(f_0(980) \text{ anything}, f_0 \rightarrow \pi^+ \pi^-)/\Gamma_{\text{total}}$		$\Gamma_{11}/\Gamma$	
VALUE (%)	CL%	DOCUMENT ID	TECN COMMENT
<b>&lt;1.3</b>	90	DOBBS	09 CLEO e <sup>+</sup> e <sup>-</sup> at 4170 MeV

$\Gamma(\phi \text{ anything})/\Gamma_{\text{total}}$		$\Gamma_{12}/\Gamma$	
VALUE (%)	EVTS	DOCUMENT ID	TECN COMMENT
<b>15.7 ± 0.8 ± 0.6</b>		DOBBS	09 CLEO e <sup>+</sup> e <sup>-</sup> at 4170 MeV
••• We do not use the following data for averages, fits, limits, etc. •••			
16.1 ± 1.2 ± 1.1	398 ± 27	HUANG	06B CLEO See DOBBS 09

$\Gamma(K^+ K^- \text{ anything})/\Gamma_{\text{total}}$		$\Gamma_{13}/\Gamma$	
VALUE (%)	DOCUMENT ID	TECN	COMMENT
<b>15.8 ± 0.6 ± 0.3</b>	DOBBS	09 CLEO	e <sup>+</sup> e <sup>-</sup> at 4170 MeV

$\Gamma(K_S^0 K^+ \text{ anything})/\Gamma_{\text{total}}$		$\Gamma_{14}/\Gamma$	
VALUE (%)	DOCUMENT ID	TECN	COMMENT
<b>5.8 ± 0.5 ± 0.1</b>	DOBBS	09 CLEO	e <sup>+</sup> e <sup>-</sup> at 4170 MeV

$\Gamma(K_S^0 K^- \text{ anything})/\Gamma_{\text{total}}$		$\Gamma_{15}/\Gamma$	
VALUE (%)	DOCUMENT ID	TECN	COMMENT
<b>1.9 ± 0.4 ± 0.1</b>	DOBBS	09 CLEO	e <sup>+</sup> e <sup>-</sup> at 4170 MeV

$\Gamma(2K_S^0 \text{ anything})/\Gamma_{\text{total}}$		$\Gamma_{16}/\Gamma$	
VALUE (%)	DOCUMENT ID	TECN	COMMENT
<b>1.7 ± 0.3 ± 0.1</b>	DOBBS	09 CLEO	e <sup>+</sup> e <sup>-</sup> at 4170 MeV

$\Gamma(2K^+ \text{ anything})/\Gamma_{\text{total}}$		$\Gamma_{17}/\Gamma$	
VALUE (%)	DOCUMENT ID	TECN	COMMENT
<b>&lt;0.26</b>	90	DOBBS	09 CLEO e <sup>+</sup> e <sup>-</sup> at 4170 MeV

$\Gamma(2K^- \text{ anything})/\Gamma_{\text{total}}$		$\Gamma_{18}/\Gamma$	
VALUE (%)	DOCUMENT ID	TECN	COMMENT
<b>&lt;0.06</b>	90	DOBBS	09 CLEO e <sup>+</sup> e <sup>-</sup> at 4170 MeV

**Leptonic and semileptonic modes**

See the related review(s):

[Leptonic Decays of Charged Pseudoscalar Mesons](#)

$\Gamma(e^+ \nu_e)/\Gamma_{\text{total}}$		$\Gamma_{19}/\Gamma$	
VALUE	CL%	DOCUMENT ID	TECN COMMENT
<b>&lt;0.83 × 10<sup>-4</sup></b>	90	<sup>1</sup> ZUPANC	13 BELL e <sup>+</sup> e <sup>-</sup> at $\Upsilon(4S), \Upsilon(5S)$
••• We do not use the following data for averages, fits, limits, etc. •••			
<2.3 × 10 <sup>-4</sup>	90	DEL-AMO-SA...10j	BABR e <sup>+</sup> e <sup>-</sup> , 10.58 GeV
<1.2 × 10 <sup>-4</sup>	90	ALEXANDER	09 CLEO e <sup>+</sup> e <sup>-</sup> at 4170 MeV
<1.3 × 10 <sup>-4</sup>	90	PEDLAR	07A CLEO See ALEXANDER 09
<sup>1</sup> ZUPANC 13 also gives the limit as <1.0 × 10 <sup>-4</sup> at 95% CL.			

$\Gamma(\mu^+ \nu_\mu)/\Gamma_{\text{total}}$		$\Gamma_{20}/\Gamma$	
VALUE (units 10 <sup>-3</sup> )	EVTS	DOCUMENT ID	TECN COMMENT
<b>5.49 ± 0.16 OUR AVERAGE</b>			
5.49 ± 0.16 ± 0.15	1.1k	ABLIKIM	19E BES3 e <sup>+</sup> e <sup>-</sup> at 4178 MeV
4.95 ± 0.67 ± 0.26	69	<sup>1</sup> ABLIKIM	16o BES3 e <sup>+</sup> e <sup>-</sup> at 4.009 GeV
5.31 ± 0.28 ± 0.20	492 ± 26	<sup>2</sup> ZUPANC	13 BELL e <sup>+</sup> e <sup>-</sup> at $\Upsilon(4S), \Upsilon(5S)$
6.02 ± 0.38 ± 0.34	275 ± 17	<sup>3</sup> DEL-AMO-SA...10j	BABR e <sup>+</sup> e <sup>-</sup> , 10.58 GeV
5.65 ± 0.45 ± 0.17	235 ± 14	ALEXANDER	09 CLEO e <sup>+</sup> e <sup>-</sup> at 4170 MeV
••• We do not use the following data for averages, fits, limits, etc. •••			
6.44 ± 0.76 ± 0.57	169 ± 18	<sup>4</sup> WIDHALM	08 BELL See ZUPANC 13
5.94 ± 0.66 ± 0.31	88	<sup>5</sup> PEDLAR	07A CLEO See ALEXANDER 09
6.8 ± 1.1 ± 1.8	553	<sup>6</sup> HEISTER	02i ALEP Z decays

<sup>1</sup>ABLIKIM 16o value is constrained by the Standard Model ratio of  $\Gamma(D_S^+ \rightarrow \tau^+ \nu_\tau)/\Gamma(D_S^+ \rightarrow \mu^+ \nu_\mu) = 9.76$ ; the unconstrained value is  $(0.517 \pm 0.075 \pm 0.021)\%$ . The constrained value is used to obtain the decay constant,  $f_{D_S^+} = (241.0 \pm 16.3 \pm 6.6)$  MeV.

<sup>2</sup>ZUPANC 13 uses both  $\mu^+ \nu$  and  $\tau^+ \nu$  events to get  $f_{D_S} = (255.5 \pm 4.2 \pm 5.1)$  MeV.

<sup>3</sup>DEL-AMO-SANCHEZ 10j uses  $\mu^+ \nu_\mu$  and  $\tau^+ \nu_\tau$  events together to get  $f_{D_S} = (258.6 \pm 6.4 \pm 7.5)$  MeV.

<sup>4</sup>WIDHALM 08 gets  $f_{D_S} = (275 \pm 16 \pm 12)$  MeV from the branching fraction.

<sup>5</sup>PEDLAR 07A also fits  $\mu^+$  and  $\tau^+$  events together and gets an effective  $\mu^+ \nu_\mu$  branching fraction of  $(6.38 \pm 0.59 \pm 0.33) \times 10^{-3}$ .

<sup>6</sup>This HEISTER 02i result is not actually an independent measurement of the absolute  $\mu^+ \nu_\mu$  branching fraction, but is in fact based on our  $\phi\pi^+$  branching fraction of 3.6 ± 0.9%, so it cannot be included in our overall fit. HEISTER 02i combines its  $D_S^+ \rightarrow \tau^+ \nu_\tau$  and  $\mu^+ \nu_\mu$  branching fractions to get  $f_{D_S} = (285 \pm 19 \pm 40)$  MeV.

$\Gamma(\mu^+ \nu_\mu)/\Gamma(\phi\pi^+)$		$\Gamma_{20}/\Gamma_{39}$	
VALUE	EVTS	DOCUMENT ID	TECN COMMENT
••• We do not use the following data for averages, fits, limits, etc. •••			
0.143 ± 0.018 ± 0.006	489 ± 55	<sup>1</sup> AUBERT	07v BABR e <sup>+</sup> e <sup>-</sup> ≈ $\Upsilon(4S)$
0.23 ± 0.06 ± 0.04	18	<sup>2</sup> ALEXANDROV	00 BEAT $\pi^-$ nucleus, 350 GeV

- 0.173±0.023±0.035 182 <sup>3</sup> CHADHA 98 CLE2  $e^+e^- \approx \Upsilon(4S)$   
 0.245±0.052±0.074 39 <sup>4</sup> ACOSTA 94 CLE2 See CHADHA 98
- <sup>1</sup> AUBERT 07v gets  $f_{D_s^+} = (283 \pm 17 \pm 16)$  MeV, using  $\Gamma(D_s^+ \rightarrow \phi\pi^+)/\Gamma(\text{total}) = (4.71 \pm 0.46)\%$ .  
<sup>2</sup> ALEXANDROV 00 uses  $f_D^2/f_{D_s}^2 = 0.82 \pm 0.09$  from a lattice-gauge-theory calculation to get the relative numbers of  $D^+ \rightarrow \mu^+\nu_\mu$  and  $D_s^+ \rightarrow \mu^+\nu_\mu$  events. The present result leads to  $f_{D_s} = (323 \pm 44 \pm 36)$  MeV.  
<sup>3</sup> CHADHA 98 obtains  $f_{D_s} = (280 \pm 19 \pm 28 \pm 34)$  MeV from this measurement, using  $\Gamma(D_s^+ \rightarrow \phi\pi^+)/\Gamma(\text{total}) = 0.036 \pm 0.009$ .  
<sup>4</sup> ACOSTA 94 obtains  $f_{D_s} = (344 \pm 37 \pm 52 \pm 42)$  MeV from this measurement, using  $\Gamma(D_s^+ \rightarrow \phi\pi^+)/\Gamma(\text{total}) = 0.037 \pm 0.009$ .

$\Gamma(\tau^+\nu_\tau)/\Gamma_{\text{total}}$   $\Gamma_{21}/\Gamma$   
 See the note on "Decay Constants of Charged Pseudoscalar Mesons" above.

VALUE (%)	EVTS	DOCUMENT ID	TECN	COMMENT
<b>5.48±0.23 OUR AVERAGE</b>				
4.83±0.65±0.26	33	1 ABLIKIM	160 BES3	$e^+e^-$ at 4.009 GeV
5.70±0.21±0.31 -0.30	2.2k	2 ZUPANC	13 BELL	$e^+e^-$ at $\Upsilon(4S)$ , $\Upsilon(5S)$
4.96±0.37±0.57	748±53	<sup>3</sup> DEL-AMO-SA..10j	BABR	$e^- \bar{\nu}_e \nu_\tau, \mu^- \bar{\nu}_\mu \nu_\tau$
6.42±0.81±0.18	126±16	<sup>4</sup> ALEXANDER	09 CLEO	$\tau^+ \rightarrow \pi^+ \bar{\nu}_\tau$
5.52±0.57±0.21	155±17	<sup>4</sup> NAIK	09A CLEO	$\tau^+ \rightarrow \rho^+ \bar{\nu}_\tau$
5.30±0.47±0.22	181±16	<sup>4</sup> ONYISI	09 CLEO	$\tau^+ \rightarrow e^+ \nu_e \bar{\nu}_\tau$
••• We do not use the following data for averages, fits, limits, etc. •••				
6.17±0.71±0.34	102	<sup>5</sup> ECKLUND	08 CLEO	See ONYISI 09
8.0 ±1.3 ±0.4	47	<sup>5</sup> PEDLAR	07A CLEO	See ALEXANDER 09
5.79±0.77±1.84	881	<sup>6</sup> HEISTER	02i ALEP	Z decays
7.0 ±2.1 ±2.0	22	<sup>7</sup> ABBIENDI	01L OPAL	$D_s^{*+} \rightarrow \gamma D_s^+$ from Z's
7.4 ±2.8 ±2.4	16	<sup>8</sup> ACCIARRI	97F L3	$D_s^{*+} \rightarrow \gamma D_s^+$ from Z's

- <sup>1</sup> ABLIKIM 160 value is constrained by the Standard Model ratio of  $\Gamma(D_s^+ \rightarrow \tau^+\nu_\tau)/\Gamma(D_s^+ \rightarrow \mu^+\nu_\mu) = 9.76$ ; the unconstrained value is  $(3.28 \pm 1.83 \pm 0.37)\%$ .  
<sup>2</sup> ZUPANC 13 uses both  $\mu^+\nu$  and  $\tau^+\nu$  events to get  $f_{D_s} = (255.5 \pm 4.2 \pm 5.1)$  MeV.  
<sup>3</sup> DEL-AMO-SANCHEZ 10j (with a small correction; see LEES 15d) uses  $\mu^+\nu_\mu$  and  $\tau^+\nu_\tau$  events together to get  $f_{D_s} = (259.9 \pm 6.6 \pm 7.6)$  MeV.  
<sup>4</sup> ALEXANDER 09, NAIK 09A, and ONYISI 09 use different  $\tau$  decay modes and are independent. The three papers combined give  $f_{D_s} = (259.7 \pm 7.8 \pm 3.4)$  MeV.  
<sup>5</sup> ECKLUND 08 and PEDLAR 07A are independent: ECKLUND 08 uses  $\tau^+ \rightarrow e^+\nu_e \bar{\nu}_\tau$  events, PEDLAR 07A uses  $\tau^+ \rightarrow \pi^+ \bar{\nu}_\tau$  events.  
<sup>6</sup> HEISTER 02i combines its  $D_s^+ \rightarrow \tau^+\nu_\tau$  and  $\mu^+\nu_\mu$  branching fractions to get  $f_{D_s} = (285 \pm 19 \pm 40)$  MeV.  
<sup>7</sup> This ABBIENDI 01L value gives a decay constant  $f_{D_s}$  of  $(286 \pm 44 \pm 41)$  MeV.  
<sup>8</sup> The second ACCIARRI 97F error here combines in quadrature systematic (0.016) and normalization (0.018) errors. The branching fraction gives  $f_{D_s} = (309 \pm 58 \pm 33 \pm 38)$  MeV.

$\Gamma(\tau^+\nu_\tau)/\Gamma(\mu^+\nu_\mu)$   $\Gamma_{21}/\Gamma_{20}$

••• We do not use the following data for averages, fits, limits, etc. •••

VALUE	EVTS	DOCUMENT ID	TECN	COMMENT
10.73±0.69±0.56 -0.53	2.2k/492	1 ZUPANC	13 BELL	$e^+e^-$ at $\Upsilon(4S)$ , $\Upsilon(5S)$
11.0 ±1.4 ±0.6	102	<sup>2</sup> ECKLUND	08 CLEO	See ONYISI 09

<sup>1</sup> This ZUPANC 13 ratio is not independent of the separate  $\tau\nu$  and  $\mu\nu$  fractions listed above.  
<sup>2</sup> This ECKLUND 08 value also uses results from PEDLAR 07A, and it is not independent of other results in these Listings. Combined with earlier CLEO results, the decay constant  $f_{D_s}$  is  $274 \pm 10 \pm 5$  MeV.

$\Gamma(\gamma e^+\nu_e)/\Gamma_{\text{total}}$   $\Gamma_{22}/\Gamma$

VALUE	CL%	DOCUMENT ID	TECN	COMMENT
<b>&lt;1.3 × 10<sup>-4</sup></b>	90	ABLIKIM	19AD BES3	for $E_\gamma > 10$ MeV

$\Gamma(K^+K^-e^+\nu_e)/\Gamma(K^+K^-\pi^+)$   $\Gamma_{23}/\Gamma_{38}$

••• We do not use the following data for averages, fits, limits, etc. •••

VALUE	DOCUMENT ID	TECN	COMMENT
0.558±0.007±0.016	<sup>1</sup> AUBERT 08AN BABR		$e^+e^-$ at $\Upsilon(4S)$

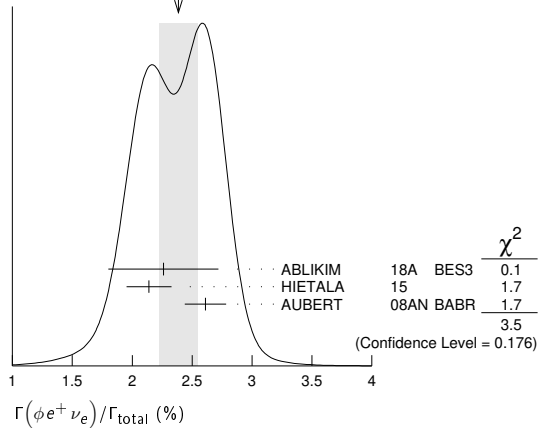
- <sup>1</sup> This AUBERT 08AN ratio is only for the  $K^+K^-$  mass in the range 1.01–to–1.03 GeV in the numerator and 1.0095–to–1.0295 GeV in the denominator.

$\Gamma(\phi e^+\nu_e)/\Gamma_{\text{total}}$   $\Gamma_{24}/\Gamma$

See the end of the  $D_s^+$  Listings for measurements of  $D_s^+ \rightarrow \phi e^+\nu_e$  form factors. Unseen decay modes of the  $\phi$  are included.

VALUE (%)	EVTS	DOCUMENT ID	TECN	COMMENT
<b>2.39±0.16 OUR AVERAGE</b> Error includes scale factor of 1.3. See the ideogram below.				
2.26±0.45±0.09	26	ABLIKIM	18A BES3	$e^+e^-$ at 4.009 GeV
2.14±0.17±0.08	207	HIETALA	15	Uses CLEO data
2.61±0.03±0.17	25k	AUBERT	08AN BABR	$e^+e^-$ at $\Upsilon(4S)$
••• We do not use the following data for averages, fits, limits, etc. •••				
2.36±0.23±0.13	106	ECKLUND	09 CLEO	See HIETALA 15
2.29±0.37±0.11	45	YELTON	09 CLEO	See ECKLUND 09

WEIGHTED AVERAGE  
2.39±0.16 (Error scaled by 1.3)



$\Gamma(\phi e^+\nu_e)/\Gamma(\phi\pi^+)$   $\Gamma_{24}/\Gamma_{39}$

As noted in the comment column, most of these measurements use  $\phi\mu^+\nu_\mu$  events in addition to or instead of  $\phi e^+\nu_e$  events.

••• We do not use the following data for averages, fits, limits, etc. •••

VALUE	EVTS	DOCUMENT ID	TECN	COMMENT
0.540±0.033±0.048	793	LINK	02j FOCUS	Uses $\phi\mu^+\nu_\mu$
0.54 ±0.05 ±0.04	367	BUTLER	94 CLE2	Uses $\phi e^+\nu_e$ and $\phi\mu^+\nu_\mu$
0.58 ±0.17 ±0.07	97	FRABETTI	93c E687	Uses $\phi\mu^+\nu_\mu$
0.57 ±0.15 ±0.15	104	ALBRECHT	91 ARG	Uses $\phi e^+\nu_e$
0.49 ±0.10 ±0.10 -0.14	54	ALEXANDER	90b CLEO	Uses $\phi e^+\nu_e$ and $\phi\mu^+\nu_\mu$

$\Gamma(\phi\mu^+\nu_\mu)/\Gamma_{\text{total}}$   $\Gamma_{25}/\Gamma$

VALUE (%)	EVTS	DOCUMENT ID	TECN	COMMENT
<b>1.94±0.53±0.09</b>	22	ABLIKIM	18A BES3	$e^+e^-$ at 4.009 GeV

$\Gamma(\eta e^+\nu_e)/\Gamma_{\text{total}}$   $\Gamma_{27}/\Gamma$

Unseen decay modes of the  $\eta$  are included.

VALUE (%)	EVTS	DOCUMENT ID	TECN	COMMENT
<b>2.32 ±0.08 OUR AVERAGE</b>				
2.323±0.063±0.063	1.8k	ABLIKIM	19s BES3	$e^+e^-$ at 4178 MeV
2.30 ±0.31 ±0.08	63	ABLIKIM	16T BES3	$e^+e^-$ at 4.009 GeV
2.28 ±0.14 ±0.19	358	<sup>1</sup> HIETALA	15	Uses CLEO data
••• We do not use the following data for averages, fits, limits, etc. •••				
2.48 ±0.29 ±0.13	82	YELTON	09 CLEO	See HIETALA 15

<sup>1</sup> Obtained by analyzing CLEO-c data but not authored by the CLEO Collaboration.

$\Gamma(\eta e^+\nu_e)/\Gamma(\phi e^+\nu_e)$   $\Gamma_{27}/\Gamma_{24}$

Unseen decay modes of the  $\eta$  and the  $\phi$  are included.

VALUE	EVTS	DOCUMENT ID	TECN	COMMENT
••• We do not use the following data for averages, fits, limits, etc. •••				
1.24±0.12±0.15	440	<sup>1</sup> BRANDENB...	95 CLE2	See HIETALA 15

<sup>1</sup> BRANDENBURG 95 uses both  $e^+$  and  $\mu^+$  events and makes a phase-space adjustment to use the  $\mu^+$  events as  $e^+$  events.

$\Gamma(\eta'(958) e^+\nu_e)/\Gamma_{\text{total}}$   $\Gamma_{28}/\Gamma$

Unseen decay modes of the  $\eta'(958)$  are included.

VALUE (%)	EVTS	DOCUMENT ID	TECN	COMMENT
<b>0.80 ±0.07 OUR AVERAGE</b>				
0.824±0.073±0.027	261	ABLIKIM	19s BES3	$e^+e^-$ at 4178 MeV
0.93 ±0.30 ±0.05	14	ABLIKIM	16T BES3	$e^+e^-$ at 4009 MeV
0.68 ±0.15 ±0.06	20	<sup>1</sup> HIETALA	15	Uses CLEO data
••• We do not use the following data for averages, fits, limits, etc. •••				
0.91 ±0.33 ±0.05	7.5	YELTON	09 CLEO	See HIETALA 15

<sup>1</sup> Obtained by analyzing CLEO-c data but not authored by the CLEO Collaboration.

$\Gamma(\eta'(958) e^+\nu_e)/\Gamma(\phi e^+\nu_e)$   $\Gamma_{28}/\Gamma_{24}$

Unseen decay modes of the resonances are included.

VALUE	EVTS	DOCUMENT ID	TECN	COMMENT
••• We do not use the following data for averages, fits, limits, etc. •••				
0.43±0.11±0.07	29	<sup>1</sup> BRANDENB...	95 CLE2	See HIETALA 15

<sup>1</sup> BRANDENBURG 95 uses both  $e^+$  and  $\mu^+$  events and makes a phase-space adjustment to use the  $\mu^+$  events as  $e^+$  events.

$[\Gamma(\eta e^+\nu_e) + \Gamma(\eta'(958) e^+\nu_e)]/\Gamma(\phi e^+\nu_e)$   $\Gamma_{26}/\Gamma_{24} = (\Gamma_{27} + \Gamma_{28})/\Gamma_{24}$

Unseen decay modes of the resonances are included.

VALUE	DOCUMENT ID	TECN	COMMENT
••• We do not use the following data for averages, fits, limits, etc. •••			
1.67±0.17±0.17	<sup>1</sup> BRANDENB...	95 CLE2	See HIETALA 15

<sup>1</sup> This BRANDENBURG 95 data is redundant with data in previous blocks.

# Meson Particle Listings

$D_s^\pm$

$\Gamma(\eta\mu^+\nu_\mu)/\Gamma_{total}$	EVTS	DOCUMENT ID	TECN	COMMENT	$\Gamma_{29}/\Gamma$
<b>2.42 ± 0.46 ± 0.11</b>	44	ABLIKIM	18A	BES3	$e^+e^-$ at 4.009 GeV

$\Gamma(\eta'(958)\mu^+\nu_\mu)/\Gamma_{total}$	EVTS	DOCUMENT ID	TECN	COMMENT	$\Gamma_{30}/\Gamma$
<b>1.06 ± 0.54 ± 0.07</b>	10	ABLIKIM	18A	BES3	$e^+e^-$ at 4.009 GeV

$\Gamma(\omega e^+\nu_e)/\Gamma_{total}$	CL%	DOCUMENT ID	TECN	COMMENT	$\Gamma_{31}/\Gamma$
<b>&lt;0.20</b>	90	MARTIN	11	CLEO	$e^+e^-$ at 4170 MeV

A test for  $u\bar{u}$  or  $d\bar{d}$  content in the  $D_s^+$ . Neither Cabibbo-favored nor Cabibbo-suppressed decays can contribute, and  $\omega - \phi$  mixing is an unlikely explanation for any fraction above about  $2 \times 10^{-4}$ .

$\Gamma(K^0 e^+\nu_e)/\Gamma_{total}$	EVTS	DOCUMENT ID	TECN	COMMENT	$\Gamma_{32}/\Gamma$
<b>0.34 ± 0.04 OUR AVERAGE</b>					
0.325 ± 0.038 ± 0.016	117	<sup>1</sup> ABLIKIM	19D	BES3	$e^+e^-$ at 4178 MeV
0.39 ± 0.08 ± 0.03	42	HIETALA	15		Uses CLEO data
• • • We do not use the following data for averages, fits, limits, etc. • • •					
0.37 ± 0.10 ± 0.02	14	YELTON	09	CLEO	See HIETALA 15
<sup>1</sup> $K^0$ reconstructed via $K^0 \rightarrow K_S^0 \rightarrow \pi^+\pi^-$ decays.					

$\Gamma(K^*(892)^0 e^+\nu_e)/\Gamma_{total}$	EVTS	DOCUMENT ID	TECN	COMMENT	$\Gamma_{33}/\Gamma$
<b>0.215 ± 0.028 OUR AVERAGE</b>					
0.237 ± 0.026 ± 0.020	155	ABLIKIM	19D	BES3	$e^+e^-$ at 4178 MeV
0.18 ± 0.04 ± 0.01	32	<sup>1</sup> HIETALA	15		$e^+e^-$ at 4.170 GeV
• • • We do not use the following data for averages, fits, limits, etc. • • •					
0.18 ± 0.07 ± 0.01	7.5	YELTON	09	CLEO	See HIETALA 15
<sup>1</sup> Uses CLEO data, but not authored by the CLEO collaboration					

$\Gamma(f_0(980) e^+\nu_e, f_0 \rightarrow \pi^+\pi^-)/\Gamma_{total}$	EVTS	DOCUMENT ID	TECN	COMMENT	$\Gamma_{34}/\Gamma$
<b>0.13 ± 0.03 ± 0.01</b>	42	<sup>1</sup> HIETALA	15		Uses CLEO data
0.20 ± 0.03 ± 0.01	44	ECKLUND	09	CLEO	See HIETALA 15
0.13 ± 0.04 ± 0.01	13	YELTON	09	CLEO	See ECKLUND 09
<sup>1</sup> HIETALA 15 uses a tighter cut on the reconstructed $\pi^+\pi^-$ mass ( $\pm 60$ MeV around the $f^0$ ) than ECKLUND 09. It finds that applying the same tight cut to both analyses gives consistent results.					

Hadronic modes with a  $K\bar{K}$  pair

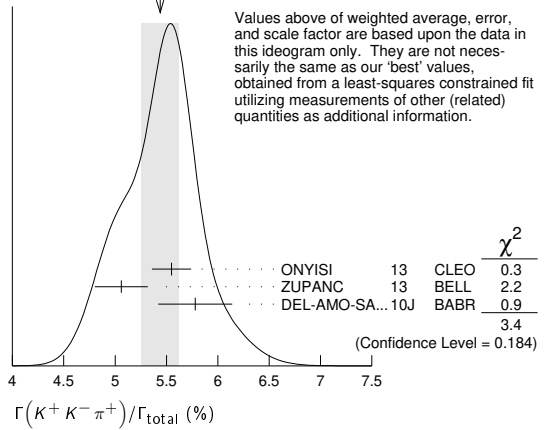
$\Gamma(K^+K_S^0)/\Gamma_{total}$	EVTS	DOCUMENT ID	TECN	COMMENT	$\Gamma_{35}/\Gamma$
<b>1.46 ± 0.04 OUR FIT</b>					
<b>1.46 ± 0.05 OUR AVERAGE</b>					
1.425 ± 0.038 ± 0.031	1.8k	ABLIKIM	19AMBES3		$e^+e^-$ at 4178 MeV
1.52 ± 0.05 ± 0.03		ONYISI	13	CLEO	$e^+e^-$ at 4.17 GeV
• • • We do not use the following data for averages, fits, limits, etc. • • •					
1.49 ± 0.07 ± 0.05		<sup>1</sup> ALEXANDER	08	CLEO	See ONYISI 13
<sup>1</sup> ALEXANDER 08 uses single- and double-tagged events in an overall fit.					

$\Gamma(K^+K_0^0)/\Gamma_{total}$	EVTS	DOCUMENT ID	TECN	COMMENT	$\Gamma_{36}/\Gamma$
<b>1.485 ± 0.039 ± 0.046</b>	2.3k	ABLIKIM	19AMBES3		$e^+e^-$ at 4178 MeV

$\Gamma(K^+\bar{K}^0)/\Gamma_{total}$	EVTS	DOCUMENT ID	TECN	COMMENT	$\Gamma_{37}/\Gamma$
<b>2.95 ± 0.11 ± 0.09</b>	2.0k	<sup>1</sup> ZUPANC	13	BELL	$e^+e^-$ at $\Upsilon(4S), \Upsilon(5S)$
<sup>1</sup> ZUPANC 13 finds the $\bar{K}^0$ from its missing-mass squared, not from $K_S^0 \rightarrow \pi^+\pi^-$ .					
The DCS ( $D_s^+ \rightarrow K^+K^0$ ) contribution to this fraction is estimated to be an order of magnitude below the statistical uncertainty.					

$\Gamma(K^+K^-\pi^+)/\Gamma_{total}$	EVTS	DOCUMENT ID	TECN	COMMENT	$\Gamma_{38}/\Gamma$
<b>5.39 ± 0.15 OUR FIT</b>					
<b>5.44 ± 0.18 OUR AVERAGE</b>					
5.55 ± 0.14 ± 0.13		ONYISI	13	CLEO	$e^+e^-$ at 4.17 GeV
5.06 ± 0.15 ± 0.21	4.1k	ZUPANC	13	BELL	$e^+e^-$ at $\Upsilon(4S), \Upsilon(5S)$
5.78 ± 0.20 ± 0.30		DEL-AMO-SA...10J		BABR	$e^+e^-$ , 10.58 GeV
• • • We do not use the following data for averages, fits, limits, etc. • • •					
5.50 ± 0.23 ± 0.16		<sup>1</sup> ALEXANDER	08	CLEO	See ONYISI 13
<sup>1</sup> ALEXANDER 08 uses single- and double-tagged events in an overall fit.					

WEIGHTED AVERAGE  
5.44 ± 0.18 (Error scaled by 1.3)



$\Gamma(\phi\pi^+)/\Gamma_{total}$	EVTS	DOCUMENT ID	TECN	COMMENT	$\Gamma_{39}/\Gamma$
<b>4.5 ± 0.4 OUR AVERAGE</b>					
4.62 ± 0.36 ± 0.51		<sup>1</sup> AUBERT	06N	BABR	$e^+e^-$ at $\Upsilon(4S)$
4.81 ± 0.52 ± 0.38	212 ± 19	<sup>2</sup> AUBERT	05v	BABR	$e^+e^- \approx \Upsilon(4S)$
3.59 ± 0.77 ± 0.48		<sup>3</sup> ARTUSO	96	CLE2	$e^+e^-$ at $\Upsilon(4S)$
• • • We do not use the following data for averages, fits, limits, etc. • • •					
3.9 <sup>+5.1 +1.8</sup> <sub>-1.9 -1.1</sub>		<sup>4</sup> BAI		95c BES	$e^+e^-$ 4.03 GeV

The results here are model-independent. For earlier, model-dependent results, see our PDG 06 edition. We decouple the  $D_s^+ \rightarrow \phi\pi^+$  branching fraction obtained from mass projections (and used to get some of the other branching fractions) from the  $D_s^+ \rightarrow \phi\pi^+, \phi \rightarrow K^+K^-$  branching fraction obtained from the Dalitz-plot analysis of  $D_s^+ \rightarrow K^+K^-\pi^+$ . That is, the ratio of these two branching fractions is not exactly the  $\phi \rightarrow K^+K^-$  branching fraction 0.491.

- <sup>1</sup> This AUBERT 06N measurement uses  $\bar{B}^0 \rightarrow D_s^{(*)-}D^{(*)+}$  and  $B^- \rightarrow D_s^{(*)-}D^{(*)+}$  decays, including some from other papers. However, the result is independent of AUBERT 05v.
- <sup>2</sup> AUBERT 05v uses the ratio of  $B^0 \rightarrow D^{*-}D_s^{*+}$  events seen in two different ways, in both of which the  $D^{*-} \rightarrow \bar{D}^0\pi^-$  decay is fully reconstructed: (1) The  $D_s^{*+} \rightarrow D_s^+\gamma, D_s^+ \rightarrow \phi\pi^+$  decay is fully reconstructed. (2) The number of events in the  $D_s^+$  peak in the missing mass spectrum against the  $D^{*-}\gamma$  is measured.
- <sup>3</sup> ARTUSO 96 uses partially reconstructed  $\bar{B}^0 \rightarrow D^{*+}D_s^{*-}$  decays to get a model-independent value for  $\Gamma(D_s^- \rightarrow \phi\pi^-)/\Gamma(D^0 \rightarrow K^-\pi^+)$  of  $0.92 \pm 0.20 \pm 0.11$ .
- <sup>4</sup> BAI 95c uses  $e^+e^- \rightarrow D_s^+D_s^-$  events in which one or both of the  $D_s^\pm$  are observed to obtain the first model-independent measurement of the  $D_s^+ \rightarrow \phi\pi^+$  branching fraction, without assumptions about  $\sigma(D_s^\pm)$ . However, with only two "doubly-tagged" events, the statistical error is very large.

$\Gamma(\phi\pi^+, \phi \rightarrow K^+K^-)/\Gamma(K^+K^-\pi^+)$	EVTS	DOCUMENT ID	TECN	COMMENT	$\Gamma_{40}/\Gamma_{38}$
<b>41.6 ± 0.8 OUR AVERAGE</b>					
41.4 ± 0.8 ± 0.5		DEL-AMO-SA...11G		BABR	Dalitz fit, 96k ± 369 evts
42.2 ± 1.6 ± 0.3		MITCHELL	09A	CLEO	Dalitz fit, 12k evts
• • • We do not use the following data for averages, fits, limits, etc. • • •					
39.6 ± 3.3 ± 4.7		FRABETTI	95B	E687	Dalitz fit, 701 evts

$\Gamma(K^+\bar{K}^*(892)^0, \bar{K}^{*0} \rightarrow K^-\pi^+)/\Gamma(K^+K^-\pi^+)$	EVTS	DOCUMENT ID	TECN	COMMENT	$\Gamma_{41}/\Gamma_{38}$
<b>47.8 ± 0.6 OUR AVERAGE</b>					
47.9 ± 0.5 ± 0.5		DEL-AMO-SA...11G		BABR	Dalitz fit, 96k ± 369 evts
47.4 ± 1.5 ± 0.4		MITCHELL	09A	CLEO	Dalitz fit, 12k evts
• • • We do not use the following data for averages, fits, limits, etc. • • •					
47.8 ± 4.6 ± 4.0		FRABETTI	95B	E687	Dalitz fit, 701 evts

$\Gamma(f_0(980)\pi^+, f_0 \rightarrow K^+K^-)/\Gamma(K^+K^-\pi^+)$	EVTS	DOCUMENT ID	TECN	COMMENT	$\Gamma_{42}/\Gamma_{38}$
<b>21 ± 6 OUR AVERAGE</b>					
16.4 ± 0.7 ± 2.0		DEL-AMO-SA...11G		BABR	Dalitz fit, 96k ± 369 evts
28.2 ± 1.9 ± 1.8		MITCHELL	09A	CLEO	Dalitz fit, 12k evts
• • • We do not use the following data for averages, fits, limits, etc. • • •					
11.0 ± 3.5 ± 2.6		FRABETTI	95B	E687	Dalitz fit, 701 evts

$\Gamma(f_0(1370)\pi^+, f_0 \rightarrow K^+ K^-)/\Gamma(K^+ K^- \pi^+)$   $\Gamma_{43}/\Gamma_{38}$   
This is the "fit fraction" from the Dalitz-plot analysis.

VALUE (units $10^{-2}$ )	DOCUMENT ID	TECN	COMMENT
<b>1.3 ± 0.8 OUR AVERAGE</b>	Error	includes scale factor of 3.9.	
1.1 ± 0.1 ± 0.2	DEL-AMO-SA...11G	BABR	Dalitz fit, 96k ± 369 evts
4.3 ± 0.6 ± 0.5	MITCHELL 09A	CLEO	Dalitz fit, 12k evts

$\Gamma(f_0(1710)\pi^+, f_0 \rightarrow K^+ K^-)/\Gamma(K^+ K^- \pi^+)$   $\Gamma_{44}/\Gamma_{38}$   
This is the "fit fraction" from the Dalitz-plot analysis.

VALUE (units $10^{-2}$ )	DOCUMENT ID	TECN	COMMENT
<b>1.2 ± 0.5 OUR AVERAGE</b>	Error	includes scale factor of 3.8.	
1.1 ± 0.1 ± 0.1	DEL-AMO-SA...11G	BABR	Dalitz fit, 96k ± 369 evts
3.4 ± 0.5 ± 0.3	MITCHELL 09A	CLEO	Dalitz fit, 12k evts
• • • We do not use the following data for averages, fits, limits, etc. • • •			
3.4 ± 2.3 ± 3.5	FRABETTI 95B	E687	Dalitz fit, 701 evts

$\Gamma(K^+ K_S^0(1430)^0, \bar{K}_S^0 \rightarrow K^- \pi^+)/\Gamma(K^+ K^- \pi^+)$   $\Gamma_{45}/\Gamma_{38}$   
This is the "fit fraction" from the Dalitz-plot analysis.

VALUE (units $10^{-2}$ )	DOCUMENT ID	TECN	COMMENT
<b>3.4 ± 0.7 OUR AVERAGE</b>	Error	includes scale factor of 1.2.	
2.4 ± 0.3 ± 1.0	DEL-AMO-SA...11G	BABR	Dalitz fit, 96k ± 369 evts
3.9 ± 0.5 ± 0.5	MITCHELL 09A	CLEO	Dalitz fit, 12k evts
• • • We do not use the following data for averages, fits, limits, etc. • • •			
9.3 ± 3.2 ± 3.2	FRABETTI 95B	E687	Dalitz fit, 701 evts

$\Gamma(K^+ K_S^0 \pi^0)/\Gamma_{total}$   $\Gamma_{46}/\Gamma$

VALUE (%)	DOCUMENT ID	TECN	COMMENT
<b>1.52 ± 0.09 ± 0.20</b>	ONYISI 13	CLEO	$e^+ e^-$ at 4.17 GeV

$\Gamma(2K_S^0 \pi^+)/\Gamma_{total}$   $\Gamma_{47}/\Gamma$

VALUE (%)	DOCUMENT ID	TECN	COMMENT
<b>0.77 ± 0.05 ± 0.03</b>	ONYISI 13	CLEO	$e^+ e^-$ at 4.17 GeV

$\Gamma(K^*(892) + \bar{K}^0)/\Gamma(\phi \pi^+)$   $\Gamma_{49}/\Gamma_{39}$   
Unseen decay modes of the resonances are included.

VALUE	DOCUMENT ID	TECN	COMMENT
<b>1.20 ± 0.21 ± 0.13</b>	CHEN 89	CLEO	$e^+ e^-$ 10 GeV

$\Gamma(K^+ K^- \pi^+ \pi^0)/\Gamma_{total}$   $\Gamma_{50}/\Gamma$

VALUE (%)	DOCUMENT ID	TECN	COMMENT
<b>6.2 ± 0.6 OUR FIT</b>	Error	includes scale factor of 1.1.	
<b>6.37 ± 0.21 ± 0.56</b>	ONYISI 13	CLEO	$e^+ e^-$ at 4.17 GeV
• • • We do not use the following data for averages, fits, limits, etc. • • •			
5.65 ± 0.29 ± 0.40	<sup>1</sup> ALEXANDER 08	CLEO	See ONYISI 13
<sup>1</sup> ALEXANDER 08 uses single- and double-tagged events in an overall fit.			

$\Gamma(\phi \rho^+)/\Gamma(\phi \pi^+)$   $\Gamma_{51}/\Gamma_{39}$

VALUE	EVTS	DOCUMENT ID	TECN	COMMENT
<b>1.86 ± 0.26 ± 0.29 ± 0.40</b>	253	AVERY 92	CLE2	$e^+ e^- \approx 10.5$ GeV

$\Gamma(K_S^0 K^- 2\pi^+)/\Gamma_{total}$   $\Gamma_{52}/\Gamma$

VALUE (%)	DOCUMENT ID	TECN	COMMENT
<b>1.65 ± 0.10 OUR FIT</b>			
<b>1.69 ± 0.07 ± 0.08</b>	ONYISI 13	CLEO	$e^+ e^-$ at 4.17 GeV
• • • We do not use the following data for averages, fits, limits, etc. • • •			
1.64 ± 0.10 ± 0.07	<sup>1</sup> ALEXANDER 08	CLEO	See ONYISI 13
<sup>1</sup> ALEXANDER 08 uses single- and double-tagged events in an overall fit.			

$\Gamma(K^*(892) + \bar{K}^*(892)^0)/\Gamma(\phi \pi^+)$   $\Gamma_{53}/\Gamma_{39}$   
Unseen decay modes of the resonances are included.

VALUE	DOCUMENT ID	TECN	COMMENT
<b>1.6 ± 0.4 ± 0.4</b>	ALBRECHT 92b	ARG	$e^+ e^- \approx 10.4$ GeV

$\Gamma(K^+ K_S^0 \pi^+ \pi^-)/\Gamma_{total}$   $\Gamma_{54}/\Gamma$

VALUE (%)	DOCUMENT ID	TECN	COMMENT
<b>0.99 ± 0.08 OUR FIT</b>			
<b>1.03 ± 0.06 ± 0.08</b>	ONYISI 13	CLEO	$e^+ e^-$ at 4.17 GeV

$\Gamma(K^+ K_S^0 \pi^+ \pi^-)/\Gamma(K_S^0 K^- 2\pi^+)$   $\Gamma_{54}/\Gamma_{52}$

VALUE	EVTS	DOCUMENT ID	TECN	COMMENT
<b>0.60 ± 0.05 OUR FIT</b>				
<b>0.586 ± 0.052 ± 0.043</b>	476	LINK 01c	FOCS	$\gamma$ A, $\bar{E}_\gamma \approx 180$ GeV

$\Gamma(K^+ K^- 2\pi^+ \pi^-)/\Gamma(K^+ K^- \pi^+)$   $\Gamma_{55}/\Gamma_{38}$

VALUE	EVTS	DOCUMENT ID	TECN	COMMENT
<b>0.160 ± 0.027 OUR AVERAGE</b>				
0.150 ± 0.019 ± 0.025	240	LINK	03D	FOCS $\gamma$ A, $\bar{E}_\gamma \approx 180$ GeV
0.188 ± 0.036 ± 0.040	75	FRABETTI 97c	E687	$\gamma$ Be, $\bar{E}_\gamma \approx 200$ GeV

$\Gamma(\phi 2\pi^+ \pi^-)/\Gamma(\phi \pi^+)$   $\Gamma_{56}/\Gamma_{39}$

VALUE	EVTS	DOCUMENT ID	TECN	COMMENT
<b>0.269 ± 0.027 OUR AVERAGE</b>				
0.249 ± 0.024 ± 0.021	136	LINK	03D	FOCS $\gamma$ A, $\bar{E}_\gamma \approx 180$ GeV
0.28 ± 0.06 ± 0.01	40	FRABETTI 97c	E687	$\gamma$ Be, $\bar{E}_\gamma \approx 200$ GeV
0.58 ± 0.21 ± 0.10	21	FRABETTI 92	E687	$\gamma$ Be
0.42 ± 0.13 ± 0.07	19	ANJOS 88	E691	Photoproduction
1.11 ± 0.37 ± 0.28	62	ALBRECHT 85D	ARG	$e^+ e^- 10$ GeV

$\Gamma(K^+ K^- \rho^0 \pi^+ \text{non-}\phi)/\Gamma(K^+ K^- 2\pi^+ \pi^-)$   $\Gamma_{60}/\Gamma_{55}$

VALUE	CL%	DOCUMENT ID	TECN	COMMENT
<b>&lt;0.03</b>	90	LINK	03D	FOCS $\gamma$ A, $\bar{E}_\gamma \approx 180$ GeV

$\Gamma(\phi \rho^0 \pi^+, \phi \rightarrow K^+ K^-)/\Gamma(K^+ K^- 2\pi^+ \pi^-)$   $\Gamma_{57}/\Gamma_{55}$

VALUE	DOCUMENT ID	TECN	COMMENT
<b>0.75 ± 0.06 ± 0.04</b>	LINK	03D	FOCS $\gamma$ A, $\bar{E}_\gamma \approx 180$ GeV

$\Gamma(\phi a_1(1260)^+, \phi \rightarrow K^+ K^-, a_1^+ \rightarrow \rho^0 \pi^+)/\Gamma(K^+ K^- \pi^+)$   $\Gamma_{58}/\Gamma_{38}$

VALUE	DOCUMENT ID	TECN	COMMENT
<b>0.137 ± 0.019 ± 0.011</b>	LINK	03D	FOCS $\gamma$ A, $\bar{E}_\gamma \approx 180$ GeV

$\Gamma(K^+ K^- 2\pi^+ \pi^- \text{nonresonant})/\Gamma(K^+ K^- 2\pi^+ \pi^-)$   $\Gamma_{61}/\Gamma_{55}$

VALUE	DOCUMENT ID	TECN	COMMENT
<b>0.10 ± 0.06 ± 0.05</b>	LINK	03D	FOCS $\gamma$ A, $\bar{E}_\gamma \approx 180$ GeV

$\Gamma(\phi 2\pi^+ \pi^- \text{non-}\rho, \phi \rightarrow K^+ K^-)/\Gamma(K^+ K^- 2\pi^+ \pi^-)$   $\Gamma_{59}/\Gamma_{55}$

VALUE	DOCUMENT ID	TECN	COMMENT
<b>0.21 ± 0.05 ± 0.06</b>	LINK	03D	FOCS $\gamma$ A, $\bar{E}_\gamma \approx 180$ GeV

$\Gamma(2K_S^0 2\pi^+ \pi^-)/\Gamma(K_S^0 K^- 2\pi^+)$   $\Gamma_{62}/\Gamma_{52}$

VALUE	EVTS	DOCUMENT ID	TECN	COMMENT
<b>0.051 ± 0.015 ± 0.015</b>	37 ± 10	LINK	04D	FOCS $\gamma$ A, $\bar{E}_\gamma \approx 180$ GeV

**Pionic modes**

$\Gamma(\pi^+ \pi^0)/\Gamma(K^+ K_S^0)$   $\Gamma_{63}/\Gamma_{35}$

VALUE (units $10^{-2}$ )	CL%	DOCUMENT ID	TECN	COMMENT
<b>&lt;2.3</b>	90	MENDEZ 10	CLEO	$e^+ e^-$ at 4170 MeV
• • • We do not use the following data for averages, fits, limits, etc. • • •				
<4.1	90	ADAMS 07A	CLEO	See MENDEZ 10

$\Gamma(2\pi^+ \pi^-)/\Gamma_{total}$   $\Gamma_{64}/\Gamma$

VALUE (%)	DOCUMENT ID	TECN	COMMENT
<b>1.08 ± 0.04 OUR FIT</b>	Error	includes scale factor of 1.1.	
<b>1.11 ± 0.04 ± 0.04</b>	ONYISI 13	CLEO	$e^+ e^-$ at 4.17 GeV
• • • We do not use the following data for averages, fits, limits, etc. • • •			
1.11 ± 0.07 ± 0.04	<sup>1</sup> ALEXANDER 08	CLEO	See ONYISI 13
<sup>1</sup> ALEXANDER 08 uses single- and double-tagged events in an overall fit.			

$\Gamma(2\pi^+ \pi^-)/\Gamma(K^+ K^- \pi^+)$   $\Gamma_{64}/\Gamma_{38}$

VALUE	EVTS	DOCUMENT ID	TECN	COMMENT
<b>0.201 ± 0.007 OUR FIT</b>				
<b>0.199 ± 0.004 ± 0.009</b>	$\approx 10.5$ k	AUBERT 09o	BABR	$e^+ e^- \approx 10.6$ GeV
• • • We do not use the following data for averages, fits, limits, etc. • • •				
0.265 ± 0.041 ± 0.031	98	FRABETTI 97D	E687	$\gamma$ Be $\approx 200$ GeV

$\Gamma(\rho^0 \pi^+)/\Gamma(2\pi^+ \pi^-)$   $\Gamma_{65}/\Gamma_{64}$

VALUE	CL%	DOCUMENT ID	TECN	COMMENT
<b>0.018 ± 0.005 ± 0.010</b>		AUBERT 09o	BABR	Dalitz fit, $\approx 10.5$ k evts
• • • We do not use the following data for averages, fits, limits, etc. • • •				
not seen		LINK 04	FOCS	Dalitz fit, 1475 ± 50 evts
0.058 ± 0.023 ± 0.037		AITALA 01A	E791	Dalitz fit, 848 evts
<0.073	90	FRABETTI 97D	E687	$\gamma$ Be $\approx 200$ GeV

$\Gamma(\pi^+ (\pi^+ \pi^-)_{S\text{-wave}})/\Gamma(2\pi^+ \pi^-)$   $\Gamma_{66}/\Gamma_{64}$   
This is the "fit fraction" from the Dalitz-plot analysis. See also KLEMPPT 08, which uses 568  $D_s^\pm \rightarrow 3\pi$  decays (over 280 background events) from FNAL E791 to study various parametrizations of the decay amplitudes. The emphasis there is more on S-wave  $\pi\pi$  decay products — 20 different solutions are given — than on  $D_s^\pm$  fit fractions.

VALUE	DOCUMENT ID	TECN	COMMENT
<b>0.833 ± 0.020 OUR AVERAGE</b>			
0.830 ± 0.009 ± 0.019	<sup>1</sup> AUBERT 09o	09o	BABR Dalitz fit, $\approx 10.5$ k evts
0.8704 ± 0.0560 ± 0.0438	<sup>2</sup> LINK 04	FOCS	Dalitz fit, 1475 ± 50 evts
<sup>1</sup> AUBERT 09o gives the amplitude and phase of the $\pi^+ \pi^-$ S-wave in 29 $\pi^+ \pi^-$ invariant-mass bins.			
<sup>2</sup> LINK 04 borrows a K-matrix parametrization from ANISOVICH 03 of the full $\pi-\pi$ S-wave isoscalar scattering amplitude to describe the $\pi^+ \pi^-$ S-wave component of the $\pi^+ \pi^+ \pi^-$ state. The fit fraction given above is a sum over five $f_0$ mesons, the $f_0(980)$ , $f_0(1300)$ , $f_0(1200-1600)$ , $f_0(1500)$ , and $f_0(1750)$ . See LINK 04 for details and discussion.			

Downloaded from https://academic.oup.com/ptep/article/2020/8/083C01/5891211 by guest on 12 November 2020



$D_s^\pm$

$\Gamma(\omega\eta\pi^+)/\Gamma_{total}$   $\Gamma_{87}/\Gamma$   
Unseen decay modes of the  $\omega$  and  $\eta$  are included.  

VALUE	CL%	DOCUMENT ID	TECN	COMMENT
$<2.13 \times 10^{-2}$	90	GE	09A	CLEO $e^+e^-$ at 4170 MeV

$\Gamma(\eta'(958)\rho^+)/\Gamma_{total}$   $\Gamma_{88}/\Gamma$   

VALUE (%)	DOCUMENT ID	TECN	COMMENT
$5.8 \pm 1.4 \pm 0.4$	ABLIIKIM	15Z	BES3 $482 \text{ pb}^{-1}$ , 4009 MeV

$\Gamma(\eta'(958)\rho^+)/\Gamma(\phi\pi^+)$   $\Gamma_{88}/\Gamma_{39}$   
Unseen decay modes of the resonances are included.  

VALUE	EVTs	DOCUMENT ID	TECN	COMMENT
•••				We do not use the following data for averages, fits, limits, etc. •••
$2.78 \pm 0.28 \pm 0.30$	137	<sup>1</sup> JESSOP	98	CLE2 $e^+e^- \approx \Upsilon(4S)$
$3.44 \pm 0.62_{-0.46}^{+0.44}$	68	AVERY	92	CLE2 See JESSOP 98

<sup>1</sup>This JESSOP 98 fraction, when combined with other  $\eta'$  fractions, greatly overshoots the inclusive  $\eta'$  fraction. See the measurement just above, which fits nicely.

$\Gamma(\eta'(958)\pi^+\pi^0)/\Gamma_{total}$   $\Gamma_{89}/\Gamma$   

VALUE (%)	DOCUMENT ID	TECN	COMMENT
$5.6 \pm 0.5 \pm 0.6$	ONYISI	13	CLEO $e^+e^-$ at 4.17 GeV

$\Gamma(\eta'(958)\pi^+\pi^0 \text{ nonresonant})/\Gamma_{total}$   $\Gamma_{90}/\Gamma$   

VALUE	CL%	DOCUMENT ID	TECN	COMMENT
$<5.1 \times 10^{-2}$	90	ABLIIKIM	15Z	BES3 $482 \text{ pb}^{-1}$ , 4009 MeV

———— Modes with one or three K's ————

$\Gamma(K^+\pi^0)/\Gamma(K^+K_S^0)$   $\Gamma_{91}/\Gamma_{35}$   

VALUE (units $10^{-2}$ )	EVTs	DOCUMENT ID	TECN	COMMENT
$4.2 \pm 1.4 \pm 0.2$	202 ± 70	MENDEZ	10	CLEO $e^+e^-$ at 4170 MeV
•••				We do not use the following data for averages, fits, limits, etc. •••
$5.5 \pm 1.3 \pm 0.7$	141 ± 34	ADAMS	07A	CLEO See MENDEZ 10

$\Gamma(K_S^0\pi^+)/\Gamma(K^+K_S^0)$   $\Gamma_{92}/\Gamma_{35}$   

VALUE (units $10^{-2}$ )	EVTs	DOCUMENT ID	TECN	COMMENT
<b>8.12 ± 0.28 OUR AVERAGE</b>				
$8.5 \pm 0.7 \pm 0.2$	393 ± 33	MENDEZ	10	CLEO $e^+e^-$ at 4170 MeV
$8.03 \pm 0.24 \pm 0.19$	17.6k ± 481	WON	09	BELL $e^+e^-$ at $\Upsilon(4S)$
$10.4 \pm 2.4 \pm 1.4$	113 ± 26	LINK	08	FOCS $\gamma A, \bar{E}_\gamma \approx 180 \text{ GeV}$
•••				We do not use the following data for averages, fits, limits, etc. •••
$8.2 \pm 0.9 \pm 0.2$	206 ± 22	ADAMS	07A	CLEO See MENDEZ 10

$\Gamma(K^+\eta)/\Gamma(K^+K_S^0)$   $\Gamma_{93}/\Gamma_{35}$   
Unseen decay modes of the  $\eta$  are included.  

VALUE (units $10^{-2}$ )	EVTs	DOCUMENT ID	TECN	COMMENT
$11.8 \pm 2.2 \pm 0.6$	222 ± 41	MENDEZ	10	CLEO $e^+e^-$ at 4170 MeV

$\Gamma(K^+\eta)/\Gamma(\eta\pi^+)$   $\Gamma_{93}/\Gamma_{74}$   

VALUE (units $10^{-2}$ )	EVTs	DOCUMENT ID	TECN	COMMENT
•••				We do not use the following data for averages, fits, limits, etc. •••
$8.9 \pm 1.5 \pm 0.4$	113 ± 18	ADAMS	07A	CLEO See MENDEZ 10

$\Gamma(K^+\omega)/\Gamma_{total}$   $\Gamma_{94}/\Gamma$   
Unseen decay modes of the  $\omega$  are included.  

VALUE (units $10^{-4}$ )	CL%	EVTs	DOCUMENT ID	TECN	COMMENT
$8.7 \pm 2.4 \pm 0.8$		29	<sup>1</sup> ABLIIKIM	19AH	BES3 $e^+e^-$ at 4.178 GeV
•••					We do not use the following data for averages, fits, limits, etc. •••
<24		90	GE	09A	CLEO $e^+e^-$ at 4170 MeV

<sup>1</sup>Evidence for mode at 4.4σ.

$\Gamma(K^+\eta(958))/\Gamma(K^+K_S^0)$   $\Gamma_{95}/\Gamma_{35}$   
Unseen decay modes of the  $\eta'(958)$  are included.  

VALUE (units $10^{-2}$ )	EVTs	DOCUMENT ID	TECN	COMMENT
$11.8 \pm 3.6 \pm 0.7$	56 ± 17	MENDEZ	10	CLEO $e^+e^-$ at 4170 MeV

$\Gamma(K^+\eta(958))/\Gamma(\eta'(958)\pi^+)$   $\Gamma_{95}/\Gamma_{85}$   

VALUE (units $10^{-2}$ )	EVTs	DOCUMENT ID	TECN	COMMENT
•••				We do not use the following data for averages, fits, limits, etc. •••
$4.2 \pm 1.3 \pm 0.3$	28 ± 9	ADAMS	07A	CLEO See MENDEZ 10

$\Gamma(K^+\pi^+\pi^-)/\Gamma_{total}$   $\Gamma_{96}/\Gamma$   

VALUE (%)	DOCUMENT ID	TECN	COMMENT	
<b>0.65 ± 0.04 OUR FIT</b>				
$0.654 \pm 0.033 \pm 0.025$	ONYISI	13	CLEO $e^+e^-$ at 4.17 GeV	
•••				We do not use the following data for averages, fits, limits, etc. •••
$0.69 \pm 0.05 \pm 0.03$	<sup>1</sup> ALEXANDER	08	CLEO See ONYISI 13	

<sup>1</sup>ALEXANDER 08 uses single- and double-tagged events in an overall fit.

$\Gamma(K^+\pi^+\pi^-)/\Gamma(K^+K^-\pi^+)$   $\Gamma_{96}/\Gamma_{38}$   

VALUE	EVTs	DOCUMENT ID	TECN	COMMENT
$0.121 \pm 0.008$	OUR FIT			Error includes scale factor of 1.1.
$0.127 \pm 0.007 \pm 0.014$	567 ± 31	LINK	04F	FOCS $\gamma A, \bar{E}_\gamma \approx 180 \text{ GeV}$

$\Gamma(K^+\rho^0)/\Gamma(K^+\pi^+\pi^-)$   $\Gamma_{97}/\Gamma_{96}$   
This is the “fit fraction” from the Dalitz-plot analysis.  

VALUE	DOCUMENT ID	TECN	COMMENT
$0.3883 \pm 0.0531 \pm 0.0261$	LINK	04F	FOCS Dalitz fit, 567 evts

$\Gamma(K^+\rho(1450)^0, \rho^0 \rightarrow \pi^+\pi^-)/\Gamma(K^+\pi^+\pi^-)$   $\Gamma_{98}/\Gamma_{96}$   
This is the “fit fraction” from the Dalitz-plot analysis.  

VALUE	DOCUMENT ID	TECN	COMMENT
$0.1062 \pm 0.0351 \pm 0.0104$	LINK	04F	FOCS Dalitz fit, 567 evts

$\Gamma(K^*(892)^0\pi^+, K^{*0} \rightarrow K^+\pi^-)/\Gamma(K^+\pi^+\pi^-)$   $\Gamma_{99}/\Gamma_{96}$   
This is the “fit fraction” from the Dalitz-plot analysis.  

VALUE	DOCUMENT ID	TECN	COMMENT
$0.2164 \pm 0.0321 \pm 0.0114$	LINK	04F	FOCS Dalitz fit, 567 evts

$\Gamma(K^*(1410)^0\pi^+, K^{*0} \rightarrow K^+\pi^-)/\Gamma(K^+\pi^+\pi^-)$   $\Gamma_{100}/\Gamma_{96}$   
This is the “fit fraction” from the Dalitz-plot analysis.  

VALUE	DOCUMENT ID	TECN	COMMENT
$0.1882 \pm 0.0403 \pm 0.0122$	LINK	04F	FOCS Dalitz fit, 567 evts

$\Gamma(K^*(1430)^0\pi^+, K^{*0} \rightarrow K^+\pi^-)/\Gamma(K^+\pi^+\pi^-)$   $\Gamma_{101}/\Gamma_{96}$   
This is the “fit fraction” from the Dalitz-plot analysis.  

VALUE	DOCUMENT ID	TECN	COMMENT
$0.0765 \pm 0.0500 \pm 0.0170$	LINK	04F	FOCS Dalitz fit, 567 evts

$\Gamma(K^+\pi^+\pi^- \text{ nonresonant})/\Gamma(K^+\pi^+\pi^-)$   $\Gamma_{102}/\Gamma_{96}$   
This is the “fit fraction” from the Dalitz-plot analysis.  

VALUE	DOCUMENT ID	TECN	COMMENT
$0.1588 \pm 0.0492 \pm 0.0153$	LINK	04F	FOCS Dalitz fit, 567 evts

$\Gamma(K^0\pi^+\pi^0)/\Gamma_{total}$   $\Gamma_{103}/\Gamma$   

VALUE (%)	EVTs	DOCUMENT ID	TECN	COMMENT
$1.00 \pm 0.18 \pm 0.04$	44 ± 8	NAIK	09A	CLEO $e^+e^-$ at 4170 MeV

$\Gamma(K_S^0 2\pi^+\pi^-)/\Gamma(K_S^0 K^- 2\pi^+)$   $\Gamma_{104}/\Gamma_{52}$   

VALUE	EVTs	DOCUMENT ID	TECN	COMMENT
$0.18 \pm 0.04 \pm 0.05$	179 ± 36	LINK	08	FOCS $\gamma A, \bar{E}_\gamma \approx 180 \text{ GeV}$

$\Gamma(K^+\omega\pi^0)/\Gamma_{total}$   $\Gamma_{105}/\Gamma$   
Unseen decay modes of the  $\omega$  are included.  

VALUE (%)	CL%	DOCUMENT ID	TECN	COMMENT
<0.82	90	GE	09A	CLEO $e^+e^-$ at 4170 MeV

$\Gamma(K^+\omega\pi^+\pi^-)/\Gamma_{total}$   $\Gamma_{106}/\Gamma$   
Unseen decay modes of the  $\omega$  are included.  

VALUE (%)	CL%	DOCUMENT ID	TECN	COMMENT
<0.54	90	GE	09A	CLEO $e^+e^-$ at 4170 MeV

$\Gamma(K^+\omega\eta)/\Gamma_{total}$   $\Gamma_{107}/\Gamma$   
Unseen decay modes of the  $\omega$  and  $\eta$  are included.  

VALUE (%)	CL%	DOCUMENT ID	TECN	COMMENT
<0.79	90	GE	09A	CLEO $e^+e^-$ at 4170 MeV

$\Gamma(K^+K^-)/\Gamma(K^+K^-\pi^+)$   $\Gamma_{108}/\Gamma_{38}$   

VALUE (units $10^{-3}$ )	EVTs	DOCUMENT ID	TECN	COMMENT
$4.0 \pm 0.3 \pm 0.2$	748 ± 60	DEL-AMO-SA..11g	BABR	$e^+e^- \approx \Upsilon(4S)$
•••				We do not use the following data for averages, fits, limits, etc. •••
$8.95 \pm 2.12_{-2.31}^{+2.24}$	31	LINK	02i	FOCS $\gamma A, \approx 180 \text{ GeV}$

$\Gamma(\phi K^+, \phi \rightarrow K^+K^-)/\Gamma(2K^+K^-)$   $\Gamma_{109}/\Gamma_{108}$   

VALUE	DOCUMENT ID	TECN	COMMENT
$0.41 \pm 0.08 \pm 0.03$	DEL-AMO-SA..11g	BABR	$e^+e^- \approx \Upsilon(4S)$

———— Doubly Cabibbo-suppressed modes ————

$\Gamma(2K^+\pi^-)/\Gamma(K^+K^-\pi^+)$   $\Gamma_{110}/\Gamma_{38}$   

VALUE (units $10^{-3}$ )	EVTs	DOCUMENT ID	TECN	COMMENT
<b>2.371 ± 0.034 OUR AVERAGE</b>				
$2.372 \pm 0.024 \pm 0.025$	67k	AAIJ	19g	LHCB $pp$ at 8 TeV
$2.3 \pm 0.3 \pm 0.2$	356 ± 52	DEL-AMO-SA..11g	BABR	$e^+e^- \approx \Upsilon(4S)$
$2.29 \pm 0.28 \pm 0.12$	281 ± 34	KO	09	BELL $e^+e^-$ at $\Upsilon(4S)$
$5.2 \pm 1.7 \pm 1.1$	27 ± 9	LINK	05k	FOCS <0.78%, CL = 90%

$\Gamma(K^+K^*(892)^0, K^{*0} \rightarrow K^+\pi^-)/\Gamma(2K^+\pi^-)$   $\Gamma_{111}/\Gamma_{110}$   

VALUE	DOCUMENT ID	TECN	COMMENT
$0.47 \pm 0.22 \pm 0.15$	DEL-AMO-SA..11g	BABR	$e^+e^- \approx \Upsilon(4S)$

## Meson Particle Listings

 $D_s^\pm$ 

## Baryon-antibaryon mode

$\Gamma(p\bar{p})/\Gamma_{\text{total}}$   $\Gamma_{112}/\Gamma$   
 This is the only baryonic mode allowed kinematically.

VALUE (units $10^{-3}$ )	EVTS	DOCUMENT ID	TECN	COMMENT
<b>1.22 ± 0.11 OUR AVERAGE</b>				
1.21 ± 0.10 ± 0.05	193 ± 17	ABLIKIM	19oBES3	$e^+e^-$ , $E_{\text{cm}} = 4178$ MeV
1.30 ± 0.36 $^{+0.12}_{-0.16}$	13.0 ± 3.6	ATHAR	08 CLEO	$e^+e^-$ , $E_{\text{cm}} \approx 4170$ MeV

$\Gamma(p\bar{p}e^+\nu_e)/\Gamma_{\text{total}}$   $\Gamma_{113}/\Gamma$   
 VALUE CL% DOCUMENT ID TECN COMMENT  
**<2.0 × 10<sup>-4</sup>** 90 ABLIKIM 19bD BES3  $e^+e^-$  at 4178 MeV

## Rare or forbidden modes

$\Gamma(\pi^+e^+e^-)/\Gamma_{\text{total}}$   $\Gamma_{114}/\Gamma$   
 This mode is not a useful test for a  $\Delta C=1$  weak neutral current because both quarks must change flavor in this decay.

VALUE	CL%	DOCUMENT ID	TECN	COMMENT
<b>&lt;13 × 10<sup>-6</sup></b>	90	LEES	11G BABR	$e^+e^- \approx \Upsilon(4S)$
••• We do not use the following data for averages, fits, limits, etc. •••				
< 2.2 × 10 <sup>-5</sup>	90	<sup>1</sup> RUBIN	10 CLEO	$e^+e^-$ at 4170 MeV
<27 × 10 <sup>-5</sup>	90	AITALA	99G E791	$\pi^- N$ 500 GeV

<sup>1</sup>This RUBIN 10 limit is for the  $e^+e^-$  mass in the continuum away from the  $\phi(1020)$ . See the next data block.

$\Gamma(\pi^+\phi, \phi \rightarrow e^+e^-)/\Gamma_{\text{total}}$   $\Gamma_{115}/\Gamma$   
 This is not a test for the  $\Delta C=1$  weak neutral current, but leads to the  $\pi^+e^+e^-$  final state.  
 VALUE EVTS DOCUMENT ID TECN COMMENT  
**(6 $^{+8}_{-4} \pm 1$ ) × 10<sup>-6</sup>** 3 RUBIN 10 CLEO  $e^+e^-$  at 4170 MeV

$\Gamma(\pi^+\mu^+\mu^-)/\Gamma_{\text{total}}$   $\Gamma_{116}/\Gamma$   
 This mode is not a useful test for a  $\Delta C=1$  weak neutral current because both quarks must change flavor in this decay.  
 VALUE CL% DOCUMENT ID TECN COMMENT  
**<4.1 × 10<sup>-7</sup>** 90 AAIJ 13AF LHCB  $p\bar{p}$  at 7 TeV  
 ••• We do not use the following data for averages, fits, limits, etc. •••  
 <4.3 × 10<sup>-5</sup> 90 LEES 11G BABR  $e^+e^- \approx \Upsilon(4S)$   
 <2.6 × 10<sup>-5</sup> 90 LINK 03F FOCS  $\gamma A, \bar{E}_\gamma \approx 180$  GeV  
 <1.4 × 10<sup>-4</sup> 90 AITALA 99G E791  $\pi^- N$  500 GeV  
 <4.3 × 10<sup>-4</sup> 90 KODAMA 95 E653  $\pi^-$  emulsion 600 GeV

$\Gamma(K^+e^+e^-)/\Gamma_{\text{total}}$   $\Gamma_{117}/\Gamma$   
 A test for the  $\Delta C=1$  weak neutral current. Allowed by higher-order electroweak interactions.  
 VALUE CL% DOCUMENT ID TECN COMMENT  
**<3.7 × 10<sup>-6</sup>** 90 LEES 11G BABR  $e^+e^- \approx \Upsilon(4S)$   
 ••• We do not use the following data for averages, fits, limits, etc. •••  
 <5.2 × 10<sup>-5</sup> 90 RUBIN 10 CLEO  $e^+e^-$  at 4170 MeV  
 <1.6 × 10<sup>-3</sup> 90 AITALA 99G E791  $\pi^- N$  500 GeV

$\Gamma(K^+\mu^+\mu^-)/\Gamma_{\text{total}}$   $\Gamma_{118}/\Gamma$   
 A test for the  $\Delta C=1$  weak neutral current. Allowed by higher-order electroweak interactions.  
 VALUE CL% DOCUMENT ID TECN COMMENT  
**<21 × 10<sup>-6</sup>** 90 LEES 11G BABR  $e^+e^- \approx \Upsilon(4S)$   
 ••• We do not use the following data for averages, fits, limits, etc. •••  
 < 3.6 × 10<sup>-5</sup> 90 LINK 03F FOCS  $\gamma A, \bar{E}_\gamma \approx 180$  GeV  
 < 1.4 × 10<sup>-4</sup> 90 AITALA 99G E791  $\pi^- N$  500 GeV  
 < 5.9 × 10<sup>-4</sup> 90 KODAMA 95 E653  $\pi^-$  emulsion 600 GeV

$\Gamma(K^*(892)^+\mu^+\mu^-)/\Gamma_{\text{total}}$   $\Gamma_{119}/\Gamma$   
 A test for the  $\Delta C=1$  weak neutral current. Allowed by higher-order electroweak interactions.  
 VALUE CL% DOCUMENT ID TECN COMMENT  
**<1.4 × 10<sup>-3</sup>** 90 KODAMA 95 E653  $\pi^-$  emulsion 600 GeV

$\Gamma(\pi^+e^+\mu^-)/\Gamma_{\text{total}}$   $\Gamma_{120}/\Gamma$   
 A test of lepton-family-number conservation.  
 VALUE CL% DOCUMENT ID TECN COMMENT  
**<12 × 10<sup>-6</sup>** 90 LEES 11G BABR  $e^+e^- \approx \Upsilon(4S)$

$\Gamma(\pi^+e^+\mu^+)/\Gamma_{\text{total}}$   $\Gamma_{121}/\Gamma$   
 A test of lepton-family-number conservation.  
 VALUE CL% DOCUMENT ID TECN COMMENT  
**<20 × 10<sup>-6</sup>** 90 LEES 11G BABR  $e^+e^- \approx \Upsilon(4S)$

$\Gamma(K^+e^+\mu^-)/\Gamma_{\text{total}}$   $\Gamma_{122}/\Gamma$   
 A test of lepton-family-number conservation.  
 VALUE CL% DOCUMENT ID TECN COMMENT  
**<14 × 10<sup>-6</sup>** 90 LEES 11G BABR  $e^+e^- \approx \Upsilon(4S)$

$\Gamma(K^+e^-\mu^+)/\Gamma_{\text{total}}$   $\Gamma_{123}/\Gamma$   
 A test of lepton-family-number conservation.  
 VALUE CL% DOCUMENT ID TECN COMMENT  
**<9.7 × 10<sup>-6</sup>** 90 LEES 11G BABR  $e^+e^- \approx \Upsilon(4S)$

$\Gamma(\pi^-2e^+)/\Gamma_{\text{total}}$   $\Gamma_{124}/\Gamma$   
 A test of lepton-number conservation.  
 VALUE CL% DOCUMENT ID TECN COMMENT  
**< 4.1 × 10<sup>-6</sup>** 90 LEES 11G BABR  $e^+e^- \approx \Upsilon(4S)$   
 ••• We do not use the following data for averages, fits, limits, etc. •••  
 < 1.8 × 10<sup>-5</sup> 90 RUBIN 10 CLEO  $e^+e^-$  at 4170 MeV  
 <69 × 10<sup>-5</sup> 90 AITALA 99G E791  $\pi^- N$  500 GeV

$\Gamma(\pi^-2\mu^+)/\Gamma_{\text{total}}$   $\Gamma_{125}/\Gamma$   
 A test of lepton-number conservation.  
 VALUE CL% DOCUMENT ID TECN COMMENT  
**<1.2 × 10<sup>-7</sup>** 90 AAIJ 13AF LHCB  $p\bar{p}$  at 7 TeV  
 ••• We do not use the following data for averages, fits, limits, etc. •••  
 <1.4 × 10<sup>-5</sup> 90 LEES 11G BABR  $e^+e^- \approx \Upsilon(4S)$   
 <2.9 × 10<sup>-5</sup> 90 LINK 03F FOCS  $\gamma A, \bar{E}_\gamma \approx 180$  GeV  
 <8.2 × 10<sup>-5</sup> 90 AITALA 99G E791  $\pi^- N$  500 GeV  
 <4.3 × 10<sup>-4</sup> 90 KODAMA 95 E653  $\pi^-$  emulsion 600 GeV

$\Gamma(\pi^-e^+\mu^+)/\Gamma_{\text{total}}$   $\Gamma_{126}/\Gamma$   
 A test of lepton-number conservation.  
 VALUE CL% DOCUMENT ID TECN COMMENT  
**<8.4 × 10<sup>-6</sup>** 90 LEES 11G BABR  $e^+e^- \approx \Upsilon(4S)$   
 ••• We do not use the following data for averages, fits, limits, etc. •••  
 <7.3 × 10<sup>-4</sup> 90 AITALA 99G E791  $\pi^- N$  500 GeV

$\Gamma(K^-2e^+)/\Gamma_{\text{total}}$   $\Gamma_{127}/\Gamma$   
 A test of lepton-number conservation.  
 VALUE CL% DOCUMENT ID TECN COMMENT  
**< 5.2 × 10<sup>-6</sup>** 90 LEES 11G BABR  $e^+e^- \approx \Upsilon(4S)$   
 ••• We do not use the following data for averages, fits, limits, etc. •••  
 < 1.7 × 10<sup>-5</sup> 90 RUBIN 10 CLEO  $e^+e^-$  at 4170 MeV  
 <63 × 10<sup>-5</sup> 90 AITALA 99G E791  $\pi^- N$  500 GeV

$\Gamma(K^-2\mu^+)/\Gamma_{\text{total}}$   $\Gamma_{128}/\Gamma$   
 A test of lepton-number conservation.  
 VALUE CL% DOCUMENT ID TECN COMMENT  
**<1.3 × 10<sup>-5</sup>** 90 LEES 11G BABR  $e^+e^- \approx \Upsilon(4S)$   
**<1.3 × 10<sup>-5</sup>** 90 LINK 03F FOCS  $\gamma A, \bar{E}_\gamma \approx 180$  GeV  
 ••• We do not use the following data for averages, fits, limits, etc. •••  
 <1.8 × 10<sup>-4</sup> 90 AITALA 99G E791  $\pi^- N$  500 GeV  
 <5.9 × 10<sup>-4</sup> 90 KODAMA 95 E653  $\pi^-$  emulsion 600 GeV

$\Gamma(K^-e^+\mu^+)/\Gamma_{\text{total}}$   $\Gamma_{129}/\Gamma$   
 A test of lepton-number conservation.  
 VALUE CL% DOCUMENT ID TECN COMMENT  
**<6.1 × 10<sup>-6</sup>** 90 LEES 11G BABR  $e^+e^- \approx \Upsilon(4S)$   
 ••• We do not use the following data for averages, fits, limits, etc. •••  
 <6.8 × 10<sup>-4</sup> 90 AITALA 99G E791  $\pi^- N$  500 GeV

$\Gamma(K^*(892)^-2\mu^+)/\Gamma_{\text{total}}$   $\Gamma_{130}/\Gamma$   
 A test of lepton-number conservation.  
 VALUE CL% DOCUMENT ID TECN COMMENT  
**<1.4 × 10<sup>-3</sup>** 90 KODAMA 95 E653  $\pi^-$  emulsion 600 GeV

 $D_s^+ - D_s^-$  CP-VIOLATING DECAY-RATE ASYMMETRIES

This is the difference between  $D_s^+$  and  $D_s^-$  partial widths for the decay to state  $f$ , divided by the sum of the widths:

$$A_{CP}(f) = [\Gamma(D_s^+ \rightarrow f) - \Gamma(D_s^- \rightarrow \bar{f})] / [\Gamma(D_s^+ \rightarrow f) + \Gamma(D_s^- \rightarrow \bar{f})].$$

$A_{CP}(\mu^\pm\nu)$  in  $D_s^+ \rightarrow \mu^+\nu, D_s^- \rightarrow \mu^-\bar{\nu}_\mu$   
 VALUE (%) DOCUMENT ID TECN COMMENT  
**4.8 ± 6.1** ALEXANDER 09 CLEO  $e^+e^-$  at 4170 MeV

$A_{CP}(K^\pm K_S^0)$  in  $D_s^\pm \rightarrow K^\pm K_S^0$   
 VALUE (%) EVTS DOCUMENT ID TECN COMMENT  
**0.09 ± 0.26 OUR AVERAGE**  
 0.6 ± 2.8 ± 0.6 1.8k ABLIKIM 19AMBES3  $e^+e^-$  at 4178 MeV  
 -0.05 ± 0.23 ± 0.24 288k <sup>1</sup>LEES 13E BABR  $e^+e^-$  at  $\Upsilon(4S)$   
 2.6 ± 1.5 ± 0.6 ONYISI 13 CLEO  $e^+e^-$  at 4.17 GeV  
 0.12 ± 0.36 ± 0.22 KO 10 BELL  $e^+e^- \approx \Upsilon(4S)$   
 ••• We do not use the following data for averages, fits, limits, etc. •••  
 4.7 ± 1.8 ± 0.9 4.0k MENDEZ 10 CLEO See ONYISI 13  
 4.9 ± 2.1 ± 0.9 ALEXANDER 08 CLEO See MENDEZ 10  
<sup>1</sup>LEES 13E finds that after subtracting the contribution due to  $K^0 - \bar{K}^0$  mixing, the CP asymmetry is (+0.28 ± 0.23 ± 0.24)%.

See key on page 999

## Meson Particle Listings

 $D_s^\pm$  $A_{CP}(K^\pm K_L^0)$  in  $D_s^\pm \rightarrow K^\pm K_L^0$ 

VALUE (units $10^{-2}$ )	EVTS	DOCUMENT ID	TECN	COMMENT
$-1.1 \pm 2.6 \pm 0.6$	2.3k	ABLKIM	19AMBES3	$e^+e^-$ at 4178 MeV

 $A_{CP}(K^+K^-\pi^\pm)$  in  $D_s^\pm \rightarrow K^+K^-\pi^\pm$ 

VALUE (%)	DOCUMENT ID	TECN	COMMENT
$-0.5 \pm 0.8 \pm 0.4$	ONYISI	13	CLEO $e^+e^-$ at 4.17 GeV
••• We do not use the following data for averages, fits, limits, etc. •••			
$0.3 \pm 1.1 \pm 0.8$	ALEXANDER	08	CLEO See ONYISI 13

 $A_{CP}(\phi\pi^\pm)$  in  $D_s^\pm \rightarrow \phi\pi^\pm$ 

VALUE (%)	DOCUMENT ID	TECN	COMMENT
$-0.38 \pm 0.26 \pm 0.08$	ABAZOV	14B	D0 $p\bar{p}$ at 1.96 TeV

 $A_{CP}(K^\pm K_S^0 \pi^0)$  in  $D_s^\pm \rightarrow K^\pm K_S^0 \pi^0$ 

VALUE (%)	DOCUMENT ID	TECN	COMMENT
$-1.6 \pm 6.0 \pm 1.1$	ONYISI	13	CLEO $e^+e^-$ at 4.17 GeV

 $A_{CP}(2K_S^0 \pi^\pm)$  in  $D_s^\pm \rightarrow 2K_S^0 \pi^\pm$ 

VALUE (%)	DOCUMENT ID	TECN	COMMENT
$3.1 \pm 5.2 \pm 0.6$	ONYISI	13	CLEO $e^+e^-$ at 4.17 GeV

 $A_{CP}(K^+K^-\pi^\pm\pi^0)$  in  $D_s^\pm \rightarrow K^+K^-\pi^\pm\pi^0$ 

VALUE (%)	DOCUMENT ID	TECN	COMMENT
$0.0 \pm 2.7 \pm 1.2$	ONYISI	13	CLEO $e^+e^-$ at 4.17 GeV
••• We do not use the following data for averages, fits, limits, etc. •••			
$-5.9 \pm 4.2 \pm 1.2$	ALEXANDER	08	CLEO See ONYISI 13

 $A_{CP}(K^\pm K_S^0 \pi^+ \pi^-)$  in  $D_s^\pm \rightarrow K^\pm K_S^0 \pi^+ \pi^-$ 

VALUE (%)	DOCUMENT ID	TECN	COMMENT
$-5.7 \pm 5.3 \pm 0.9$	ONYISI	13	CLEO $e^+e^-$ at 4.17 GeV

 $A_{CP}(K_S^0 K^\mp 2\pi^\pm)$  in  $D_s^\pm \rightarrow K_S^0 K^\mp 2\pi^\pm$ 

VALUE (%)	DOCUMENT ID	TECN	COMMENT
$4.1 \pm 2.7 \pm 0.9$	ONYISI	13	CLEO $e^+e^-$ at 4.17 GeV
••• We do not use the following data for averages, fits, limits, etc. •••			
$-0.7 \pm 3.6 \pm 1.1$	ALEXANDER	08	CLEO See ONYISI 13

 $A_{CP}(\pi^+ \pi^- \pi^\pm)$  in  $D_s^\pm \rightarrow \pi^+ \pi^- \pi^\pm$ 

VALUE (%)	DOCUMENT ID	TECN	COMMENT
$-0.7 \pm 3.0 \pm 0.6$	ONYISI	13	CLEO $e^+e^-$ at 4.17 GeV
••• We do not use the following data for averages, fits, limits, etc. •••			
$2.0 \pm 4.6 \pm 0.7$	ALEXANDER	08	CLEO See ONYISI 13

 $A_{CP}(\pi^\pm \eta)$  in  $D_s^\pm \rightarrow \pi^\pm \eta$ 

VALUE (%)	EVTS	DOCUMENT ID	TECN	COMMENT
$1.1 \pm 3.0 \pm 0.8$		ONYISI	13	CLEO $e^+e^-$ at 4.17 GeV
••• We do not use the following data for averages, fits, limits, etc. •••				
$-4.6 \pm 2.9 \pm 0.3$	2.5k	MENDEZ	10	CLEO See ONYISI 13
$-8.2 \pm 5.2 \pm 0.8$		ALEXANDER	08	CLEO See MENDEZ 10

 $A_{CP}(\pi^\pm \eta')$  in  $D_s^\pm \rightarrow \pi^\pm \eta'$ 

VALUE (%)	EVTS	DOCUMENT ID	TECN	COMMENT
$-0.9 \pm 0.5$	<b>OUR AVERAGE</b>			
$-0.82 \pm 0.36 \pm 0.35$	152k	AAIJ	17AF	LHCb $p\bar{p}$ at 7, 8 TeV
$-2.2 \pm 2.2 \pm 0.6$		ONYISI	13	CLEO $e^+e^-$ at 4.17 GeV
••• We do not use the following data for averages, fits, limits, etc. •••				
$-6.1 \pm 3.0 \pm 0.3$	1.4k	MENDEZ	10	CLEO See ONYISI 13
$-5.5 \pm 3.7 \pm 1.2$		ALEXANDER	08	CLEO See MENDEZ 10

 $A_{CP}(\eta\pi^\pm\pi^0)$  in  $D_s^\pm \rightarrow \eta\pi^\pm\pi^0$ 

VALUE (%)	DOCUMENT ID	TECN	COMMENT
$-0.5 \pm 3.9 \pm 2.0$	ONYISI	13	CLEO $e^+e^-$ at 4.17 GeV

 $A_{CP}(\eta'\pi^\pm\pi^0)$  in  $D_s^\pm \rightarrow \eta'\pi^\pm\pi^0$ 

VALUE (%)	DOCUMENT ID	TECN	COMMENT
$-0.4 \pm 7.4 \pm 1.9$	ONYISI	13	CLEO $e^+e^-$ at 4.17 GeV

 $A_{CP}(K^\pm\pi^0)$  in  $D_s^\pm \rightarrow K^\pm\pi^0$ 

VALUE (%)	EVTS	DOCUMENT ID	TECN	COMMENT
$-26.6 \pm 23.8 \pm 0.9$	202 ± 70	MENDEZ	10	CLEO $e^+e^-$ at 4170 MeV
••• We do not use the following data for averages, fits, limits, etc. •••				
$2 \pm 29$		ADAMS	07A	CLEO See MENDEZ 10

 $A_{CP}(K^0/K^0\pi^\pm)$  in  $D_s^\pm \rightarrow K^0\pi^\pm, D_s^- \rightarrow K^0\pi^-$ 

VALUE (%)	EVTS	DOCUMENT ID	TECN	COMMENT
$0.4 \pm 0.5$	<b>OUR AVERAGE</b>			
$0.38 \pm 0.46 \pm 0.17$	121k	<sup>1</sup> AAIJ	14BD	LHCb $p\bar{p}$ at 7, 8 TeV
$0.3 \pm 2.0 \pm 0.3$	14k	LEES	13E	BABR $e^+e^-$ at $\Upsilon(4S)$
••• We do not use the following data for averages, fits, limits, etc. •••				
$0.61 \pm 0.83 \pm 0.14$	26k	AAIJ	13W	LHCb See AAJJ 14BD
<sup>1</sup> AAIJ 14BD reports its result as $A_{CP}(D_s^\pm \rightarrow K_S^0 K^\pm)$ with CP-violation effects in the $K^0 - \bar{K}^0$ system subtracted. It also measures $A_{CP}(D^\pm \rightarrow \bar{K}^0/K^0 K^\pm) + A_{CP}(D_s^\pm \rightarrow \bar{K}^0/K^0 \pi^\pm) = (0.41 \pm 0.49 \pm 0.26)\%$ .				

 $A_{CP}(K_S^0\pi^\pm)$  in  $D_s^\pm \rightarrow K_S^0\pi^\pm$ 

VALUE (%)	EVTS	DOCUMENT ID	TECN	COMMENT
$0.20 \pm 0.18$	<b>OUR AVERAGE</b>			
$0.16 \pm 0.17 \pm 0.05$	721k	AAIJ	19T	LHCb $p\bar{p}$ at 7, 8, 13 TeV
$0.6 \pm 2.0 \pm 0.3$	14k	LEES	13E	BABR $e^+e^-$ at $\Upsilon(4S)$
$5.45 \pm 2.50 \pm 0.33$		KO	10	BELL $e^+e^- \approx \Upsilon(4S)$
$16.3 \pm 7.3 \pm 0.3$	0.4k	MENDEZ	10	CLEO $e^+e^-$ at 4170 MeV
••• We do not use the following data for averages, fits, limits, etc. •••				
$27 \pm 11$		ADAMS	07A	CLEO See MENDEZ 10

 $A_{CP}(K^\pm\pi^+\pi^-)$  in  $D_s^\pm \rightarrow K^\pm\pi^+\pi^-$ 

VALUE (%)	DOCUMENT ID	TECN	COMMENT
$4.5 \pm 4.8 \pm 0.6$	ONYISI	13	CLEO $e^+e^-$ at 4.17 GeV
••• We do not use the following data for averages, fits, limits, etc. •••			
$11.2 \pm 7.0 \pm 0.9$	ALEXANDER	08	CLEO See ONYISI 13

 $A_{CP}(K^\pm\eta)$  in  $D_s^\pm \rightarrow K^\pm\eta$ 

VALUE (%)	EVTS	DOCUMENT ID	TECN	COMMENT
$9.3 \pm 15.2 \pm 0.9$	222 ± 41	MENDEZ	10	CLEO $e^+e^-$ at 4170 MeV
••• We do not use the following data for averages, fits, limits, etc. •••				
$-20 \pm 18$		ADAMS	07A	CLEO See MENDEZ 10

 $A_{CP}(K^\pm\eta'(958))$  in  $D_s^\pm \rightarrow K^\pm\eta'(958)$ 

VALUE (%)	EVTS	DOCUMENT ID	TECN	COMMENT
$6.0 \pm 18.9 \pm 0.9$	56 ± 17	MENDEZ	10	CLEO $e^+e^-$ at 4170 MeV
••• We do not use the following data for averages, fits, limits, etc. •••				
$-17 \pm 37$		ADAMS	07A	CLEO See MENDEZ 10

## CP VIOLATING ASYMMETRIES OF P-ODD (T-ODD) MOMENTS

 $A_{Tviol}(K_S^0 K^\pm \pi^+ \pi^-)$  in  $D_s^\pm \rightarrow K_S^0 K^\pm \pi^+ \pi^-$ 

$C_T \equiv \bar{p}_{K^+} \cdot (\bar{p}_{\pi^+} \times \bar{p}_{\pi^-})$  is a parity-odd correlation of the  $K^+$ ,  $\pi^+$ , and  $\pi^-$  momenta for the  $D_s^+$ .  $\bar{C}_T \equiv \bar{p}_{K^-} \cdot (\bar{p}_{\pi^-} \times \bar{p}_{\pi^+})$  is the corresponding quantity for the  $D_s^-$ . Then

$A_T \equiv [\Gamma(C_T > 0) - \Gamma(C_T < 0)] / [\Gamma(C_T > 0) + \Gamma(C_T < 0)]$ , and

$\bar{A}_T \equiv [\Gamma(-\bar{C}_T > 0) - \Gamma(-\bar{C}_T < 0)] / [\Gamma(-\bar{C}_T > 0) + \Gamma(-\bar{C}_T < 0)]$ , and

$A_{Tviol} \equiv \frac{1}{2}(A_T - \bar{A}_T)$ .  $C_T$  and  $\bar{C}_T$  are commonly referred to as  $T$ -odd moments, because they are odd under  $T$  reversal. However, the  $T$ -conjugate process  $K_S^0 K^\pm \pi^+ \pi^- \rightarrow D_s^\pm$  is not accessible, while the  $P$ -conjugate process is.

VALUE (units $10^{-3}$ )	EVTS	DOCUMENT ID	TECN	COMMENT
$-13.6 \pm 7.7 \pm 3.4$	29.8 ± 0.3k	LEES	11E	BABR $e^+e^- \approx \Upsilon(4S)$
••• We do not use the following data for averages, fits, limits, etc. •••				
$-36 \pm 67 \pm 23$	508 ± 34	LINK	05E	FOCS $\gamma A, \bar{E}_\gamma \approx 180$ GeV

 $D_s^\pm$  Semileptonic Form Factors and Decay Constants $r_2 \equiv A_2(0)/A_1(0)$  in  $D_s^\pm \rightarrow \phi\ell^+\nu_\ell$ 

VALUE	EVTS	DOCUMENT ID	TECN	COMMENT
$0.84 \pm 0.11$	<b>OUR AVERAGE</b>			Error includes scale factor of 2.4.
$0.816 \pm 0.036 \pm 0.030$	25 ± 0.5k	<sup>1</sup> AUBERT	08AN	BABR $\phi e^+ \nu_e$
$0.713 \pm 0.202 \pm 0.284$	793	LINK	04C	FOCS $\phi\mu^+ \nu_\mu$
$1.57 \pm 0.25 \pm 0.19$	271	AITALA	99D	E791 $\phi e^+ \nu_e, \phi\mu^+ \nu_\mu$
$1.4 \pm 0.5 \pm 0.3$	308	AVERY	94B	CLE2 $\phi e^+ \nu_e$
$1.1 \pm 0.8 \pm 0.1$	90	FRABETTI	94F	E687 $\phi\mu^+ \nu_\mu$
$2.1 \pm 0.6 \pm 0.2$	19	KODAMA	93	E653 $\phi\mu^+ \nu_\mu$

<sup>1</sup>To compare with previous measurements, this AUBERT 08AN value is from a fit that fixes the pole masses at  $m_A = 2.5$  GeV/ $c^2$  and  $m_V = 2.1$  GeV/ $c^2$ . A simultaneous fit to  $r_2, r_V, r_0$  (a significant  $s$ -wave contribution) and  $m_A$ , gives  $r_2 = 0.763 \pm 0.071 \pm 0.065$ .





See key on page 999

Meson Particle Listings

$D_s^{*\pm}, D_{s0}^*(2317)^\pm$

$m_{D_s^{*\pm}} - m_{D_s^\pm}$

The fit includes  $D^\pm, D^0, D_s^\pm, D^{*\pm}, D^{*0}, D_s^{*\pm}, D_1(2420)^0, D_2^*(2460)^0,$  and  $D_{s1}(2536)^\pm$  mass and mass difference measurements.

VALUE (MeV)	EVTS	DOCUMENT ID	TECN	COMMENT
<b>143.8 ± 0.4 OUR FIT</b>				
<b>143.9 ± 0.4 OUR AVERAGE</b>				
143.76 ± 0.39 ± 0.40		GRONBERG 95	CLE2	$e^+ e^-$
144.22 ± 0.47 ± 0.37		BROWN 94	CLE2	$e^+ e^-$
142.5 ± 0.8 ± 1.5		2 ALBRECHT 88	ARG	$e^+ e^- \rightarrow D_s^\pm \gamma X$
139.5 ± 8.3 ± 9.7	60	AIHARA 84D	TPC	$e^+ e^- \rightarrow$ hadrons
• • • We do not use the following data for averages, fits, limits, etc. • • •				
143.0 ± 18.0	8	ASRATYAN 85	HLBC	FNAL 15-ft, $\nu$ - $^2$ H
110 ± 46		BRANDELIK 79	DASP	$e^+ e^- \rightarrow D_s^\pm \gamma X$
2 Result includes data of ALBRECHT 84B.				

$D_s^{*\pm}$  WIDTH

VALUE (MeV)	CL%	DOCUMENT ID	TECN	COMMENT
< 1.9	90	GRONBERG 95	CLE2	$e^+ e^-$
< 4.5	90	ALBRECHT 88	ARG	$E_{cm}^{ee} = 10.2$ GeV
• • • We do not use the following data for averages, fits, limits, etc. • • •				
< 4.9	90	BROWN 94	CLE2	$e^+ e^-$
< 22	90	BLAYLOCK 87	MRK3	$e^+ e^- \rightarrow D_s^\pm \gamma X$

$D_s^{*+}$  DECAY MODES

$D_s^{*-}$  modes are charge conjugates of the modes below.

Mode	Fraction ( $\Gamma_j/\Gamma$ )
$\Gamma_1 D_s^+ \gamma$	(93.5 ± 0.7) %
$\Gamma_2 D_s^+ \pi^0$	( 5.8 ± 0.7) %
$\Gamma_3 D_s^+ e^+ e^-$	( 6.7 ± 1.6) × 10 <sup>-3</sup>

CONSTRAINED FIT INFORMATION

An overall fit to 2 branching ratios uses 3 measurements and one constraint to determine 3 parameters. The overall fit has a  $\chi^2 = 0.0$  for 1 degrees of freedom.

The following *off-diagonal* array elements are the correlation coefficients  $\langle \delta x_i \delta x_j \rangle / (\delta x_i \delta x_j)$ , in percent, from the fit to the branching fractions,  $x_i \equiv \Gamma_i / \Gamma_{total}$ . The fit constrains the  $x_i$  whose labels appear in this array to sum to one.

$x_2$	-97	
$x_3$	-19	-4
	$x_1$	$x_2$

$D_s^{*+}$  BRANCHING RATIOS

$\Gamma(D_s^{*+} \gamma) / \Gamma_{total}$	$\Gamma_1 / \Gamma$
<b>0.935 ± 0.007 OUR FIT</b>	
• • • We do not use the following data for averages, fits, limits, etc. • • •	
seen	ASRATYAN 91 HLBC $\bar{\nu}_\mu$ Ne
seen	ALBRECHT 88 ARG $e^+ e^- \rightarrow D_s^{*+} \gamma X$
seen	AIHARA 84D
seen	ALBRECHT 84B
seen	BRANDELIK 79

$\Gamma(D_s^{*+} \pi^0) / \Gamma(D_s^{*+} \gamma)$	$\Gamma_2 / \Gamma_1$
<b>0.062 ± 0.008 OUR FIT</b>	
<b>0.062 ± 0.008 OUR AVERAGE</b>	
0.062 ± 0.005 ± 0.006	AUBERT, BE 05G BABR 10.6 $e^+ e^- \rightarrow$ hadrons
0.062 ± 0.020 ± 0.022	GRONBERG 95 CLE2 $e^+ e^-$

$\Gamma(D_s^{*+} e^+ e^-) / \Gamma(D_s^{*+} \gamma)$	$\Gamma_3 / \Gamma_1$
<b>7.2 ± 1.7 OUR FIT</b>	
<b>7.2 ± 1.5 ± 1.0</b>	38 CRONIN-HEN.12 CLEO 4.17 $e^+ e^- \rightarrow$ hadrons

$D_s^{*\pm}$  REFERENCES

CRONIN-HEN.12	PR D86 072005	D. Cronin-Hennessey et al.	(CLEO Collab.)
AUBERT, BE 05G	PR D72 091101	B. Aubert et al.	(BABAR Collab.)
GRONBERG 95	PRL 75 3232	J. Gronberg et al.	(CLEO Collab.)
BROWN 94	PR D50 1884	D. Brown et al.	(CLEO Collab.)
ASRATYAN 91	PL B257 525	A.E. Asratyan et al.	(ITEP, BELG, SACL+)
ALBRECHT 88	PL B207 349	H. Albrecht et al.	(ARGUS Collab.)
BLAYLOCK 87	PRL 58 2171	G.T. Blaylock et al.	(Mark III Collab.)
ASRATYAN 85	PL 156B 441	A.E. Asratyan et al.	(ITEP, SERP)
AIHARA 84D	PRL 53 2465	H. Aihara et al.	(TPC Collab.)
ALBRECHT 84B	PL 146B 111	H. Albrecht et al.	(ARGUS Collab.)
BRANDELIK 79	PL 80B 412	R. Brandelik et al.	(DASP Collab.)

$D_{s0}^*(2317)^\pm$

$I(J^P) = 0(0^+)$   
 $J, P$  need confirmation.

AUBERT 06P and CHOI 15A do not observe neutral and doubly charged partners of the  $D_{s0}^*(2317)^\pm$ .

$D_{s0}^*(2317)^\pm$  MASS

The fit includes  $D^\pm, D^0, D_s^\pm, D^{*\pm}, D^{*0}, D_s^{*\pm}, D_1(2420)^0, D_2^*(2460)^0,$  and  $D_{s1}(2536)^\pm$  mass and mass difference measurements.

VALUE (MeV)	EVTS	DOCUMENT ID	TECN	COMMENT
<b>2317.8 ± 0.5 OUR FIT</b>				
<b>2318.0 ± 0.7 OUR AVERAGE</b>				
2318.3 ± 1.2 ± 1.2	115	1 ABLIKIM 18J BES3		4.6 $e^+ e^- \rightarrow D_s^{*\pm} D_{s0}^*(2317)^\mp$
2319.6 ± 0.2 ± 1.4	3.1k	AUBERT 06P BABR	B	10.6 $e^+ e^- \rightarrow D_s^+ \pi^0 X$
2317.3 ± 0.4 ± 0.8	1.0k	2 AUBERT 04E BABR		10.6 $e^+ e^-$
• • • We do not use the following data for averages, fits, limits, etc. • • •				
2317.2 ± 1.3	88	3 AUBERT, B 04s BABR	B	$D_{s0}^*(2317) + \bar{D}^{(*)}$
2317.2 ± 0.5 ± 0.9	761	4 MIKAMI 04 BELL		10.6 $e^+ e^-$
2316.8 ± 0.4 ± 3.0	1.2k	4,5 AUBERT 03G BABR		10.6 $e^+ e^-$
2317.6 ± 1.3	273	4,6 AUBERT 03G BABR		10.6 $e^+ e^-$
2319.8 ± 2.1 ± 2.0	24	4 KROKOVNY 03B BELL		10.6 $e^+ e^-$

- 1 From a fit of the  $D_s^{*+}$  recoil mass where the  $D_{s0}^*(2317)$  signal is described with a Crystal Ball function convolved with a Gaussian function.
- 2 Supersedes AUBERT 03G.
- 3 Systematic errors not evaluated.
- 4 Not independent of the corresponding  $m_{D_{s0}^*(2317)} - m_{D_s^\pm}$ .
- 5 From  $D_s^+ \rightarrow K^+ K^- \pi^+$  decay.
- 6 From  $D_s^+ \rightarrow K^+ K^- \pi^+ \pi^0$  decay.

$m_{D_{s0}^*(2317)^\pm} - m_{D_s^\pm}$

The fit includes  $D^\pm, D^0, D_s^\pm, D^{*\pm}, D^{*0}, D_s^{*\pm}, D_1(2420)^0, D_2^*(2460)^0,$  and  $D_{s1}(2536)^\pm$  mass and mass difference measurements.

VALUE (MeV)	EVTS	DOCUMENT ID	TECN	COMMENT
<b>349.4 ± 0.5 OUR FIT</b>				
<b>349.2 ± 0.7 OUR AVERAGE</b>				
348.7 ± 0.5 ± 0.7	761	MIKAMI 04 BELL		10.6 $e^+ e^-$
350.0 ± 1.2 ± 1.0	135	BESSION 03 CLE2		10.6 $e^+ e^-$
351.3 ± 2.1 ± 1.9	24	7 KROKOVNY 03B BELL		10.6 $e^+ e^-$
• • • We do not use the following data for averages, fits, limits, etc. • • •				
349.6 ± 0.4 ± 3.0	1267	8,9 AUBERT 03G BABR		10.6 $e^+ e^-$
350.2 ± 1.3	273	10,11 AUBERT 03G BABR		10.6 $e^+ e^-$
7 Recalculated by us using $m_{D_s^\pm} = 1968.5 \pm 0.6$ MeV.				
8 From $D_s^+ \rightarrow K^+ K^- \pi^+$ decay.				
9 Recalculated by us using $m_{D_s^\pm} = 1967.20 \pm 0.03$ MeV.				
10 From $D_s^+ \rightarrow K^+ K^- \pi^+ \pi^0$ decay.				
11 Recalculated by us using $m_{D_s^\pm} = 1967.4 \pm 0.2$ MeV. Systematic errors not estimated.				

$D_{s0}^*(2317)^\pm$  WIDTH

VALUE (MeV)	CL%	EVTS	DOCUMENT ID	TECN	COMMENT
< 3.8	95	3180	AUBERT 06P BABR		10.6 $e^+ e^- \rightarrow D_s^+ \pi^0 X$
• • • We do not use the following data for averages, fits, limits, etc. • • •					
< 4.6	90	761	MIKAMI 04 BELL		10.6 $e^+ e^-$
< 10			AUBERT 03G BABR		10.6 $e^+ e^-$
< 7	90	135	BESSION 03 CLE2		10.6 $e^+ e^-$

# Meson Particle Listings

## $D_{s0}^*(2317)^\pm, D_{s1}(2460)^\pm$

### $D_{s0}^*(2317)^\pm$ DECAY MODES

$D_{s0}^*(2317)^-$  modes are charge conjugates of modes below.

Mode	Fraction ( $\Gamma_i/\Gamma$ )	Confidence level
$\Gamma_1 D_s^+ \pi^0$	$(100^{+0}_{-20})\%$	
$\Gamma_2 D_s^+ \gamma$	$< 5\%$	90%
$\Gamma_3 D_s^*(2112)^+ \gamma$	$< 6\%$	90%
$\Gamma_4 D_s^+ \gamma \gamma$	$< 18\%$	95%
$\Gamma_5 D_s^*(2112)^+ \pi^0$	$< 11\%$	90%
$\Gamma_6 D_s^+ \pi^+ \pi^-$	$< 4 \times 10^{-3}$	90%
$\Gamma_7 D_s^+ \pi^0 \pi^0$	not seen	

### $D_{s0}^*(2317)^\pm$ BRANCHING RATIOS

$\Gamma(D_s^+ \pi^0)/\Gamma_{\text{total}}$	$\Gamma_1/\Gamma$				
VALUE	EVTS	DOCUMENT ID	TECN	COMMENT	
$1.00^{+0.00+0.00}_{-0.14-0.14}$	47	ABLIKIM	18J	BES3	$4.6 e^+ e^- \rightarrow D_{s0}^{*\pm} D_{s0}^*(2317)^\mp$

• • • We do not use the following data for averages, fits, limits, etc. • • •  
 seen 1.5k AUBERT 03G BABR  $10.6 e^+ e^-$

$\Gamma(D_s^+ \gamma)/\Gamma(D_s^+ \pi^0)$	$\Gamma_2/\Gamma_1$				
VALUE	CL%	DOCUMENT ID	TECN	COMMENT	
$< 0.05$	90	MIKAMI	04	BELL	$10.6 e^+ e^-$
$< 0.14$	95	AUBERT	06P	BABR	$10.6 e^+ e^-$
$< 0.052$	90	BESSION	03	CLE2	$10.6 e^+ e^-$

$\Gamma(D_s^*(2112)^+ \gamma)/\Gamma(D_s^+ \pi^0)$	$\Gamma_3/\Gamma_1$				
VALUE	CL%	DOCUMENT ID	TECN	COMMENT	
$< 0.059$	90	BESSION	03	CLE2	$10.6 e^+ e^-$
$< 0.16$	95	AUBERT	06P	BABR	$10.6 e^+ e^-$
$< 0.18$	90	MIKAMI	04	BELL	$10.6 e^+ e^-$

$\Gamma(D_s^+ \gamma \gamma)/\Gamma(D_s^+ \pi^0)$	$\Gamma_4/\Gamma_1$				
VALUE	CL%	DOCUMENT ID	TECN	COMMENT	
$< 0.18$	95	AUBERT	06P	BABR	$10.6 e^+ e^-$
not seen		AUBERT	03G	BABR	$10.6 e^+ e^-$

$\Gamma(D_s^*(2112)^+ \pi^0)/\Gamma(D_s^+ \pi^0)$	$\Gamma_5/\Gamma_1$				
VALUE	CL%	DOCUMENT ID	TECN	COMMENT	
$< 0.11$	90	BESSION	03	CLE2	$10.6 e^+ e^-$

$\Gamma(D_s^+ \pi^+ \pi^-)/\Gamma(D_s^+ \pi^0)$	$\Gamma_6/\Gamma_1$				
VALUE	CL%	DOCUMENT ID	TECN	COMMENT	
$< 0.004$	90	MIKAMI	04	BELL	$10.6 e^+ e^-$
$< 0.005$	95	AUBERT	06P	BABR	$10.6 e^+ e^-$
$< 0.019$	90	BESSION	03	CLE2	$10.6 e^+ e^-$

$\Gamma(D_s^+ \pi^0 \pi^0)/\Gamma(D_s^+ \pi^0)$	$\Gamma_7/\Gamma_1$				
VALUE	CL%	DOCUMENT ID	TECN	COMMENT	
$< 0.25$	95	AUBERT	06P	BABR	$10.6 e^+ e^-$

### $D_{s0}^*(2317)^\pm$ REFERENCES

ABLIKIM	18J	PR D97 051103	M. Ablikim et al.	(BESIII Collab.)
CHOI	15A	PR D91 092011	S.-K. Choi et al.	(BELLE Collab.)
AUBERT	06P	PR D74 032007	B. Aubert et al.	(BABAR Collab.)
AUBERT	04E	PR D69 031101	B. Aubert et al.	(BABAR Collab.)
AUBERT,B	04S	PRL 93 181801	B. Aubert et al.	(BABAR Collab.)
MIKAMI	04	PRL 92 012002	Y. Mikami et al.	(BELLE Collab.)
AUBERT	03G	PRL 90 242001	B. Aubert et al.	(BABAR Collab.)
BESSION	03	PR D68 032002	D. Besson et al.	(CLEO Collab.)
KROKOVNY	03B	PRL 91 262002	P. Krokovny et al.	(BELLE Collab.)

## $D_{s1}(2460)^\pm$

$$I(J^P) = 0(1^+)$$

### $D_{s1}(2460)^\pm$ MASS

The fit includes  $D^\pm, D^0, D_s^\pm, D^{*\pm}, D^{*0}, D_s^{*\pm}, D_1(2420)^0, D_2^*(2460)^0$ , and  $D_{s1}(2536)^\pm$  mass and mass difference measurements.

VALUE (MeV)	EVTS	DOCUMENT ID	TECN	COMMENT	
<b><math>2459.5 \pm 0.6</math> OUR FIT</b>		Error includes scale factor of 1.1.			
<b><math>2459.6 \pm 0.9</math> OUR AVERAGE</b>		Error includes scale factor of 1.3.			
$2460.1 \pm 0.2 \pm 0.8$		<sup>1</sup> AUBERT	06P	BABR	$10.6 e^+ e^-$
$2458.0 \pm 1.0 \pm 1.0$	195	AUBERT	04E	BABR	$10.6 e^+ e^-$
• • • We do not use the following data for averages, fits, limits, etc. • • •					
$2459.5 \pm 1.2 \pm 3.7$	920	AUBERT	06P	BABR	$10.6 e^+ e^- \rightarrow D_s^+ \gamma X$
$2458.6 \pm 1.0 \pm 2.5$	560	AUBERT	06P	BABR	$10.6 e^+ e^- \rightarrow D_s^+ \pi^0 \gamma X$
$2460.2 \pm 0.2 \pm 0.8$	123	AUBERT	06P	BABR	$10.6 e^+ e^- \rightarrow D_s^+ \pi^+ \pi^- X$
$2458.9 \pm 1.5$	112	<sup>2</sup> AUBERT,B	04S	BABR	$B \rightarrow D_{s1}(2460)^+ \bar{D}^{(*)}$
$2461.1 \pm 1.6$	139	<sup>3</sup> AUBERT,B	04S	BABR	$B \rightarrow D_{s1}(2460)^+ \bar{D}^{(*)}$
$2456.5 \pm 1.3 \pm 1.3$	126	<sup>4,5</sup> MIKAMI	04	BELL	$10.6 e^+ e^-$
$2459.5 \pm 1.3 \pm 2.0$	152	<sup>6,7</sup> MIKAMI	04	BELL	$10.6 e^+ e^-$
$2459.9 \pm 0.9 \pm 1.6$	60	<sup>6,7</sup> MIKAMI	04	BELL	$10.6 e^+ e^-$
$2459.2 \pm 1.6 \pm 2.0$	57	KROKOVNY	03B	BELL	$10.6 e^+ e^-$

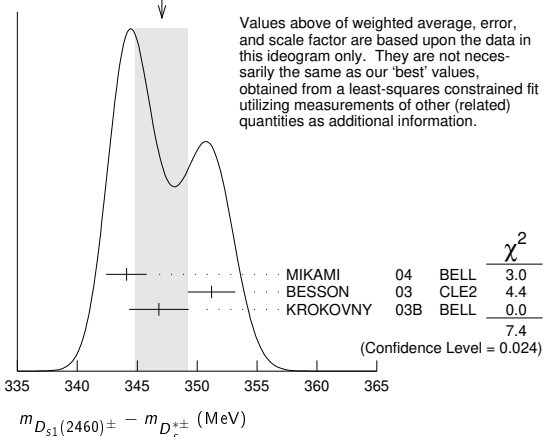
- The average of the values obtained from the  $D_s^+ \gamma, D_s^+ \pi^0 \gamma, D_s^+ \pi^+ \pi^-$  final state.
- Systematic errors not evaluated. From the decay to  $D_s^+ \pi^0$ .
- Systematic errors not evaluated. From the decay to  $D_s^+ \gamma$ .
- Not independent of the corresponding  $m_{D_{s1}(2460)^\pm} - m_{D_s^{*\pm}}$ .
- Using  $m_{D_s^{*+}} = 2112.4 \pm 0.7$  MeV.
- Not independent of the corresponding  $m_{D_{s1}(2460)^\pm} - m_{D_s^\pm}$ .
- Using  $m_{D_s^+} = 1968.5 \pm 0.6$  MeV.

### $m_{D_{s1}(2460)^\pm} - m_{D_s^{*\pm}}$

The fit includes  $D^\pm, D^0, D_s^\pm, D^{*\pm}, D^{*0}, D_s^{*\pm}, D_1(2420)^0, D_2^*(2460)^0$ , and  $D_{s1}(2536)^\pm$  mass and mass difference measurements.

VALUE (MeV)	EVTS	DOCUMENT ID	TECN	COMMENT	
<b><math>347.3 \pm 0.7</math> OUR FIT</b>		Error includes scale factor of 1.2.			
<b><math>347.1 \pm 2.2</math> OUR AVERAGE</b>		Error includes scale factor of 1.9. See the ideogram below.			
$344.1 \pm 1.3 \pm 1.1$	126	MIKAMI	04	BELL	$10.6 e^+ e^-$
$351.2 \pm 1.7 \pm 1.0$	41	BESSION	03	CLE2	$10.6 e^+ e^-$
$346.8 \pm 1.6 \pm 1.9$	57	<sup>8</sup> KROKOVNY	03B	BELL	$10.6 e^+ e^-$
<sup>8</sup> Recalculated by us using $m_{D_s^{*+}} = 2112.4 \pm 0.7$ MeV.					

WEIGHTED AVERAGE  
 $347.1 \pm 2.2$  (Error scaled by 1.9)



### $m_{D_{s1}(2460)^\pm} - m_{D_s^\pm}$

The fit includes  $D^\pm, D^0, D_s^\pm, D^{*\pm}, D^{*0}, D_s^{*\pm}, D_1(2420)^0, D_2^*(2460)^0$ , and  $D_{s1}(2536)^\pm$  mass and mass difference measurements.

VALUE (MeV)	EVTS	DOCUMENT ID	TECN	COMMENT	
<b><math>491.2 \pm 0.6</math> OUR FIT</b>		Error includes scale factor of 1.1.			
<b><math>491.3 \pm 1.4</math> OUR AVERAGE</b>					
$491.0 \pm 1.3 \pm 1.9$	152	<sup>9</sup> MIKAMI	04	BELL	$10.6 e^+ e^-$
$491.4 \pm 0.9 \pm 1.5$	60	<sup>10</sup> MIKAMI	04	BELL	$10.6 e^+ e^-$

$D_{s1}(2460)^\pm, D_{s1}(2536)^\pm$

<sup>9</sup>From the decay to  $D_s^+ \gamma$ .  
<sup>10</sup>From the decay to  $D_s^+ \pi^+ \pi^-$ .

$D_{s1}(2460)^\pm$  WIDTH

VALUE (MeV)	CL%	EVTS	DOCUMENT ID	TECN	COMMENT
< 3.5	95	123	AUBERT	06P BABR	$10.6 e^+ e^- \rightarrow D_s^+ \pi^+ \pi^- X$
• • • We do not use the following data for averages, fits, limits, etc. • • •					
< 6.3	95	560	AUBERT	06P BABR	$10.6 e^+ e^- \rightarrow D_s^+ \pi^0 \gamma X$
< 10		195	AUBERT	04E BABR	$10.6 e^+ e^-$
< 5.5	90	126	MIKAMI	04 BELL	$10.6 e^+ e^-$
< 7	90	41	BESSION	03 CLE2	$10.6 e^+ e^-$

$D_{s1}(2460)^+$  DECAY MODES

$D_{s1}(2460)^-$  modes are charge conjugates of the modes below.

Mode	Fraction ( $\Gamma_i/\Gamma$ )	Scale factor/ Confidence level
$\Gamma_1 D_s^{*+} \pi^0$	(48 ± 11) %	
$\Gamma_2 D_s^+ \gamma$	(18 ± 4) %	
$\Gamma_3 D_s^+ \pi^+ \pi^-$	(4.3 ± 1.3) %	S=1.1
$\Gamma_4 D_s^+ \gamma$	< 8 %	CL=90%
$\Gamma_5 D_{s0}^*(2317)^+ \gamma$	(3.7 ± 5.0, 2.4) %	
$\Gamma_6 D_s^+ \pi^0$		
$\Gamma_7 D_s^+ \pi^0 \pi^0$		
$\Gamma_8 D_s^+ \gamma \gamma$		

CONSTRAINED FIT INFORMATION

An overall fit to 7 branching ratios uses 8 measurements and one constraint to determine 5 parameters. The overall fit has a  $\chi^2 = 3.4$  for 4 degrees of freedom.

The following *off-diagonal* array elements are the correlation coefficients  $\langle \delta x_i \delta x_j \rangle / (\delta x_i \delta x_j)$ , in percent, from the fit to the branching fractions,  $x_i \equiv \Gamma_i / \Gamma_{\text{total}}$ . The fit constrains the  $x_i$  whose labels appear in this array to sum to one.

$x_2$	80		
$x_3$	68	62	
$x_5$	-3	25	26
	$x_1$	$x_2$	$x_3$

$D_{s1}(2460)^\pm$  BRANCHING RATIOS

$\Gamma(D_s^{*+} \pi^0) / \Gamma_{\text{total}}$	CL%	EVTS	DOCUMENT ID	TECN	COMMENT
<b>0.48 ± 0.11 OUR FIT</b>					
<b>0.56 ± 0.13 ± 0.09</b>			<sup>11</sup> AUBERT	06N BABR	$B \rightarrow D_{s1}(2460)^- \bar{D}^{(*)}$
• • • We do not use the following data for averages, fits, limits, etc. • • •					
seen		41	BESSION	03 CLE2	$10.6 e^+ e^-$

<sup>11</sup> Evaluated in AUBERT 06N including measurements from AUBERT,B 04s.

$\Gamma(D_s^+ \gamma) / \Gamma_{\text{total}}$	CL%	EVTS	DOCUMENT ID	TECN	COMMENT
<b>0.18 ± 0.04 OUR FIT</b>					
<b>0.16 ± 0.04 ± 0.03</b>			<sup>12</sup> AUBERT	06N BABR	$B \rightarrow D_{s1}(2460)^- \bar{D}^{(*)}$
<sup>12</sup> Evaluated in AUBERT 06N including measurements from AUBERT,B 04s.					

$\Gamma(D_s^+ \gamma) / \Gamma(D_s^{*+} \pi^0)$	CL%	EVTS	DOCUMENT ID	TECN	COMMENT
<b>0.38 ± 0.05 OUR FIT</b>					
<b>0.44 ± 0.09 OUR AVERAGE</b>					
0.55 ± 0.13 ± 0.08		152	MIKAMI	04 BELL	$10.6 e^+ e^-$
0.38 ± 0.11 ± 0.04		38	KROKOVNY	03B BELL	$10.6 e^+ e^-$
• • • We do not use the following data for averages, fits, limits, etc. • • •					
0.274 ± 0.045 ± 0.020		251	<sup>13</sup> AUBERT,B	04s BABR	$B \rightarrow D_{s1}(2460)^+ \bar{D}^{(*)}$
< 0.49		90	BESSION	03 CLE2	$10.6 e^+ e^-$
<sup>13</sup> Used by AUBERT 06N in their measurement of $B(D_s^{*-} \pi^0)$ and $B(D_s^- \gamma)$ .					

$\Gamma(D_s^+ \pi^+ \pi^-) / \Gamma(D_s^{*+} \pi^0)$	CL%	EVTS	DOCUMENT ID	TECN	COMMENT
<b>0.090 ± 0.020 OUR FIT</b>					Error includes scale factor of 1.2.
<b>0.14 ± 0.04 ± 0.02</b>		60	MIKAMI	04 BELL	$10.6 e^+ e^-$
• • • We do not use the following data for averages, fits, limits, etc. • • •					
< 0.08		90	BESSION	03 CLE2	$10.6 e^+ e^-$

$\Gamma(D_s^{*+} \gamma) / \Gamma(D_s^{*+} \pi^0)$	CL%	DOCUMENT ID	TECN	COMMENT	
<b>&lt; 0.16</b>		90	BESSION	03 CLE2	$10.6 e^+ e^-$
• • • We do not use the following data for averages, fits, limits, etc. • • •					
< 0.31		90	MIKAMI	04 BELL	$10.6 e^+ e^-$

$\Gamma(D_{s0}^*(2317)^+ \gamma) / \Gamma(D_s^{*+} \pi^0)$	CL%	DOCUMENT ID	TECN	COMMENT	
<b>&lt; 0.22</b>		95	AUBERT	04E BABR	$10.6 e^+ e^-$
• • • We do not use the following data for averages, fits, limits, etc. • • •					
< 0.58		90	BESSION	03 CLE2	$10.6 e^+ e^-$

$\Gamma(D_s^{*+} \pi^0) / [\Gamma(D_s^{*+} \pi^0) + \Gamma(D_{s0}^*(2317)^+ \gamma)]$	CL%	DOCUMENT ID	TECN	COMMENT	
<b>0.93 ± 0.09 OUR FIT</b>					
<b>0.97 ± 0.09 ± 0.05</b>			AUBERT	06P BABR	$10.6 e^+ e^-$

$\Gamma(D_s^+ \gamma) / [\Gamma(D_s^{*+} \pi^0) + \Gamma(D_{s0}^*(2317)^+ \gamma)]$	CL%	DOCUMENT ID	TECN	COMMENT	
<b>0.35 ± 0.04 OUR FIT</b>					
<b>0.337 ± 0.036 ± 0.038</b>			AUBERT	06P BABR	$10.6 e^+ e^-$

$\Gamma(D_s^+ \pi^+ \pi^-) / [\Gamma(D_s^{*+} \pi^0) + \Gamma(D_{s0}^*(2317)^+ \gamma)]$	CL%	DOCUMENT ID	TECN	COMMENT	
<b>0.083 ± 0.017 OUR FIT</b>				Error includes scale factor of 1.2.	
<b>0.077 ± 0.013 ± 0.008</b>			AUBERT	06P BABR	$10.6 e^+ e^-$

$\Gamma(D_s^{*+} \gamma) / [\Gamma(D_s^{*+} \pi^0) + \Gamma(D_{s0}^*(2317)^+ \gamma)]$	CL%	DOCUMENT ID	TECN	COMMENT	
<b>&lt; 0.24</b>		95	AUBERT	06P BABR	$10.6 e^+ e^-$

$\Gamma(D_{s0}^*(2317)^+ \gamma) / [\Gamma(D_s^{*+} \pi^0) + \Gamma(D_{s0}^*(2317)^+ \gamma)]$	CL%	DOCUMENT ID	TECN	COMMENT	
<b>&lt; 0.25</b>		95	AUBERT	06P BABR	$10.6 e^+ e^-$

$\Gamma(D_s^+ \pi^0) / [\Gamma(D_s^{*+} \pi^0) + \Gamma(D_{s0}^*(2317)^+ \gamma)]$	CL%	DOCUMENT ID	TECN	COMMENT	
<b>&lt; 0.042</b>		95	AUBERT	06P BABR	$10.6 e^+ e^-$

$\Gamma(D_s^+ \pi^0 \pi^0) / [\Gamma(D_s^{*+} \pi^0) + \Gamma(D_{s0}^*(2317)^+ \gamma)]$	CL%	DOCUMENT ID	TECN	COMMENT	
<b>&lt; 0.68</b>		95	AUBERT	06P BABR	$10.6 e^+ e^-$

$\Gamma(D_s^+ \gamma \gamma) / [\Gamma(D_s^{*+} \pi^0) + \Gamma(D_{s0}^*(2317)^+ \gamma)]$	CL%	DOCUMENT ID	TECN	COMMENT	
<b>&lt; 0.33</b>		95	AUBERT	06P BABR	$10.6 e^+ e^-$

$D_{s1}(2460)^\pm$  REFERENCES

AUBERT 06N PR D74 031103	B. Aubert et al.	(BABAR Collab.)
AUBERT 06P PR D74 032002	B. Aubert et al.	(BABAR Collab.)
AUBERT 04E PR D69 031101	B. Aubert et al.	(BABAR Collab.)
AUBERT,B 04S PRL 93 181801	B. Aubert et al.	(BABAR Collab.)
MIKAMI 04 PRL 92 012002	Y. Mikami et al.	(BELLE Collab.)
BESSION 03 PR D68 032002	D. Besson et al.	(CLEO Collab.)
KROKOVNY 03B PRL 91 262002	P. Krokovny et al.	(BELLE Collab.)

$D_{s1}(2536)^\pm$

$I(J^P) = 0(1^+)$   
 $J, P$  need confirmation.

Seen in  $D^*(2010)^+ K^0, D^*(2007)^0 K^+$ , and  $D_s^+ \pi^+ \pi^-$ . Not seen in  $D^+ K^0$  or  $D^0 K^+$ .  $J^P = 1^+$  assignment strongly favored.

$D_{s1}(2536)^\pm$  MASS

The fit includes  $D^\pm, D^0, D_s^\pm, D^{*+}, D^{*0}, D_s^{*\pm}, D_1(2420)^0, D_2^*(2460)^0$ , and  $D_{s1}(2536)^\pm$  mass and mass difference measurements.

VALUE (MeV)	CL%	EVTS	DOCUMENT ID	TECN	COMMENT
<b>2535.11 ± 0.06 OUR FIT</b>					
<b>2535.21 ± 0.28 OUR AVERAGE</b>					
2537.7 ± 0.5 ± 3.1		24	<sup>1</sup> ABLIKIM	19P BES3	$4.6 e^+ e^- \rightarrow D_s^+ \bar{D}^0 K^-$
2535.7 ± 0.6 ± 0.5		46	<sup>2</sup> ABAZOV	09G D0	$B_s^0 \rightarrow D_{s1}^- \mu^+ \nu_\mu X$
2534.78 ± 0.31 ± 0.40		182	AUBERT	08B BABR	$B \rightarrow \bar{D}^{(*)} D^* K$
2534.6 ± 0.3 ± 0.7		193	AUBERT	06P BABR	$10.6 e^+ e^- \rightarrow D_s^+ \pi^+ \pi^- X$
2535.3 ± 0.7		92	<sup>3</sup> HEISTER	02B ALEP	$e^+ e^- \rightarrow D^{*+} K^0 X, D^{*0} K^+ X$
2534.2 ± 1.2		9	ASRATYAN	94 BEBC	$\nu N \rightarrow D^{*+} K^0 X, D^{*0} K^+ X$
2535 ± 0.6 ± 1		75	FRABETTI	94B E687	$\gamma Be \rightarrow D^{*+} K^0 X, D^{*0} K^+ X$
2535.2 ± 0.5 ± 1.5		28	ALBRECHT	92R ARG	$10.4 e^+ e^- \rightarrow D^{*+} K^0 X, D^{*0} K^+ X$
2536.6 ± 0.7 ± 0.4			AVERY	90 CLEO	$e^+ e^- \rightarrow D^{*+} K^0 X$
2535.9 ± 0.6 ± 0.2			ALBRECHT	89E ARG	$D_{s1}^* \rightarrow D^*(2010) K^0$



See key on page 999

Meson Particle Listings

$D_{s2}^*(2573), D_{s1}^*(2700)^\pm$

$D_{s2}^*(2573)$

$I(J^P) = 0(2^+)$

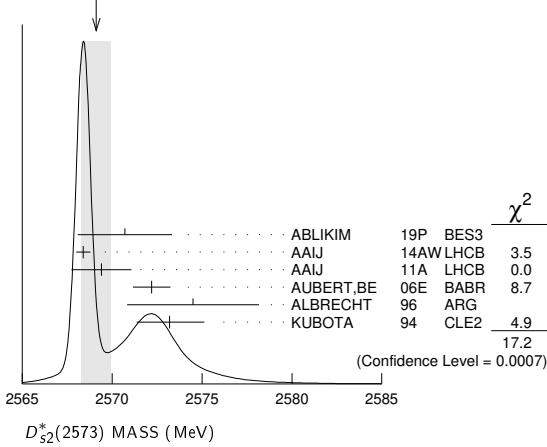
$J^P$  is natural, width and decay modes consistent with  $2^+$ .  
AAIJ 14AW confirms  $J^P = 2^+$ .

$D_{s2}^*(2573)$  MASS

VALUE (MeV)	EVTs	DOCUMENT ID	TECN	COMMENT
<b>2569.1 ± 0.8</b>	<b>OUR AVERAGE</b>	Error includes scale factor of 2.4. See the ideogram below.		
2570.7 ± 2.0 ± 1.7	62	<sup>1</sup> ABLIKIM 19P BES3	4.6	$e^+e^- \rightarrow D_s^+ \bar{D}^0 K^-$
2568.39 ± 0.29 ± 0.26		AAIJ 14AW LHCb	$B_s^0 \rightarrow \bar{D}^0 K^- \pi^+$	
2569.4 ± 1.6 ± 0.5	82	AAIJ 11A LHCb	$B_s \rightarrow D_{s2}^*(2573) \mu \bar{\nu} X$	
2572.2 ± 0.3 ± 1.0		AUBERT, BE 06E BABR	$e^+e^- \rightarrow DKX$	
2574.5 ± 3.3 ± 1.6		ALBRECHT 96 ARG	$e^+e^- \rightarrow D^0 K^+ X$	
2573.2 <sup>+1.7</sup> / <sub>-1.6</sub> ± 0.9	217	KUBOTA 94 CLE2	$e^+e^- \sim 10.5$ GeV	
• • •	We do not use the following data for averages, fits, limits, etc. • • •			
2570.0 ± 4.3	25	<sup>2</sup> EVDOKIMOV 04 SELX	600	$\Sigma^- A \rightarrow D^0 K^+ X$
2568.6 ± 3.2	64	<sup>3</sup> HEISTER 02B ALEP		$e^+e^- \rightarrow D^0 K^+ X$

- <sup>1</sup> From a fit of the  $D_s^+$  recoil mass distribution.
- <sup>2</sup> Not independent of the mass difference below.
- <sup>3</sup> Calculated using  $m_{D^0} = 1864.5 \pm 0.5$  MeV and the mass difference below.

WEIGHTED AVERAGE  
2569.1 ± 0.8 (Error scaled by 2.4)



$m_{D_{s2}^*(2573)} - m_{D^0}$

VALUE (MeV)	EVTs	DOCUMENT ID	TECN	COMMENT
<b>704 ± 3 ± 1</b>	64	HEISTER 02B ALEP		$e^+e^- \rightarrow D^0 K^+ X$
• • •	We do not use the following data for averages, fits, limits, etc. • • •			
705.4 ± 4.3	25	<sup>1</sup> EVDOKIMOV 04 SELX	600	$\Sigma^- A \rightarrow D^0 K^+ X$

<sup>1</sup> Systematic errors not estimated.

$D_{s2}^*(2573)$  WIDTH

VALUE (MeV)	EVTs	DOCUMENT ID	TECN	COMMENT
<b>16.9 ± 0.7</b>	<b>OUR AVERAGE</b>			
17.2 ± 3.6 ± 1.1	62	<sup>1</sup> ABLIKIM 19P BES3	4.6	$e^+e^- \rightarrow D_s^+ \bar{D}^0 K^-$
16.9 ± 0.5 ± 0.6		AAIJ 14AW LHCb	$B_s^0 \rightarrow \bar{D}^0 K^- \pi^+$	
12.1 ± 4.5 ± 1.6	82	AAIJ 11A LHCb	$B_s \rightarrow D_{s2}^*(2573) \mu \bar{\nu} X$	
27.1 ± 0.6 ± 5.6		AUBERT, BE 06E BABR	$e^+e^- \rightarrow DKX$	
10.4 ± 8.3 ± 3.0		ALBRECHT 96 ARG	$e^+e^- \rightarrow D^0 K^+ X$	
16 <sup>+5</sup> / <sub>-4</sub> ± 3	217	KUBOTA 94 CLE2	$e^+e^- \sim 10.5$ GeV	
• • •	We do not use the following data for averages, fits, limits, etc. • • •			
14 <sup>+9</sup> / <sub>-6</sub>	25	<sup>2</sup> EVDOKIMOV 04 SELX	600	$\Sigma^- A \rightarrow D^0 K^+ X$

- <sup>1</sup> From a fit of the  $D_s^+$  recoil mass distribution.
- <sup>2</sup> Systematic errors not estimated.

$D_{s2}^*(2573)^+$  DECAY MODES

$D_{s2}^*(2573)^-$  modes are charge conjugates of the modes below.

Mode	Fraction ( $\Gamma_i/\Gamma$ )
$\Gamma_1$ $D^0 K^+$	seen
$\Gamma_2$ $D^*(2007)^0 K^+$	not seen

$D_{s2}^*(2573)^+$  BRANCHING RATIOS

VALUE	EVTs	DOCUMENT ID	TECN	CHG	COMMENT	$\Gamma_1/\Gamma$
<b>seen</b>	217	KUBOTA 94 CLE2		±	$e^+e^- \sim 10.5$ GeV	

$\Gamma(D^* K^+)/\Gamma_{total}$

VALUE	CL%	DOCUMENT ID	TECN	CHG	COMMENT	$\Gamma_2/\Gamma_1$
<b>&lt; 0.33</b>	90	KUBOTA 94 CLE2		+	$e^+e^- \sim 10.5$ GeV	

$D_{s2}^*(2573)$  REFERENCES

ABLIKIM 19P CP C43 031001	M. Ablikim et al.	(BESIII Collab.)
AAIJ 14AW PRL 113 162001	R. Aaij et al.	(LHCb Collab.) JP
AAIJ 11A PL B698 34	R. Aaij et al.	(LHCb Collab.)
AUBERT, BE 06E PRL 97 222001	B. Aubert et al.	(BABAR Collab.)
EVDOKIMOV 04 PRL 93 242001	A.V. Evdokimov et al.	(SELEX Collab.)
HEISTER 02B PL B526 34	A. Heister et al.	(ALEPH Collab.)
ALBRECHT 96 ZPHY C69 405	H. Albrecht et al.	(ARGUS Collab.)
KUBOTA 94 PRL 72 1972	Y. Kubota et al.	(CLEO Collab.)

$D_{s1}^*(2700)^\pm$

$I(J^P) = 0(1^-)$

$D_{s1}^*(2700)^+$  MASS

VALUE (MeV)	EVTs	DOCUMENT ID	TECN	COMMENT
<b>2708.3 <sup>+4.0</sup>/<sub>-3.4</sub></b>	<b>OUR AVERAGE</b>			
2699 <sup>+14</sup> / <sub>-7</sub>		<sup>1</sup> LEES 15c BABR	$B \rightarrow D D^0 K^+$	
2709.2 ± 1.9 ± 4.5	52k	<sup>2</sup> AAIJ 12AU LHCb	$pp \rightarrow (DK)^+ X$ at 7 TeV	
2710 ± 2 <sup>+12</sup> / <sub>-7</sub>	10.4k	<sup>3</sup> AUBERT 09AR BABR	$e^+e^- \rightarrow D^{(*)} K X$	
2708 ± 9 <sup>+11</sup> / <sub>-10</sub>	182	BRODZICKA 08 BELL	$B^+ \rightarrow D^0 \bar{D}^0 K^+$	
• • •	We do not use the following data for averages, fits, limits, etc. • • •			
2694 ± 8 <sup>+13</sup> / <sub>-3</sub>		LEES 15c BABR	$B^0 \rightarrow D^- D^0 K^+$	
2707 ± 8 ± 8		LEES 15c BABR	$B^+ \rightarrow \bar{D}^0 D^0 K^+$	
2688 ± 4 ± 3		<sup>4</sup> AUBERT, BE 06E BABR	10.6 $e^+e^- \rightarrow DKX$	

- <sup>1</sup> From a combined analysis of  $B^0 \rightarrow D^- D^0 K^+$  and  $B^+ \rightarrow \bar{D}^0 D^0 K^+$ .
- <sup>2</sup> From the combined fit of the  $D^+ K_S^0$  and  $D^0 K^+$  modes in the model including the  $D_{s2}^*(2573)^+$ ,  $D_{s1}^*(2700)^+$  and spin-0  $D_{s,J}^*(2860)^+$ .
- <sup>3</sup> From simultaneous fits to the two  $DK$  mass spectra and to the total  $D^* K$  mass spectrum.
- <sup>4</sup> Superseded by AUBERT 09AR.

$D_{s1}^*(2700)^+$  WIDTH

VALUE (MeV)	EVTs	DOCUMENT ID	TECN	COMMENT
<b>120 ± 11</b>	<b>OUR AVERAGE</b>			
127 <sup>+24</sup> / <sub>-19</sub>		<sup>5</sup> LEES 15c BABR	$B \rightarrow D D^0 K^+$	
115.8 ± 7.3 ± 12.1	52k	<sup>6</sup> AAIJ 12AU LHCb	$pp \rightarrow (DK)^+ X$ at 7 TeV	
149 ± 7 <sup>+39</sup> / <sub>-52</sub>	10.4k	<sup>7</sup> AUBERT 09AR BABR	$e^+e^- \rightarrow D^{(*)} K X$	
108 ± 23 <sup>+36</sup> / <sub>-31</sub>	182	BRODZICKA 08 BELL	$B^+ \rightarrow D^0 \bar{D}^0 K^+$	
• • •	We do not use the following data for averages, fits, limits, etc. • • •			
145 ± 24 <sup>+22</sup> / <sub>-14</sub>		LEES 15c BABR	$B^0 \rightarrow D^- D^0 K^+$	
113 ± 21 <sup>+20</sup> / <sub>-16</sub>		LEES 15c BABR	$B^+ \rightarrow \bar{D}^0 D^0 K^+$	
112 ± 7 ± 36		<sup>8</sup> AUBERT, BE 06E BABR	10.6 $e^+e^- \rightarrow DKX$	

- <sup>5</sup> From a combined analysis of  $B^0 \rightarrow D^- D^0 K^+$  and  $B^+ \rightarrow \bar{D}^0 D^0 K^+$ .
- <sup>6</sup> From the combined fit of the  $D^+ K_S^0$  and  $D^0 K^+$  modes in the model including the  $D_{s2}^*(2573)^+$ ,  $D_{s1}^*(2700)^+$  and spin-0  $D_{s,J}^*(2860)^+$ .
- <sup>7</sup> From simultaneous fits to the two  $DK$  mass spectra and to the total  $D^* K$  mass spectrum.
- <sup>8</sup> Superseded by AUBERT 09AR.

$D_{s1}^*(2700)^\pm$  DECAY MODES

Mode
$\Gamma_1$ $DK$
$\Gamma_2$ $D^0 K^+$
$\Gamma_3$ $D^+ K_S^0$
$\Gamma_4$ $D^* K$
$\Gamma_5$ $D^{*0} K^+$
$\Gamma_6$ $D^{*+} K_S^0$

## Meson Particle Listings

 $D_{s1}^*(2700)^\pm, D_{s1}^*(2860)^\pm, D_{s3}^*(2860)^\pm, D_{sJ}(3040)^\pm$ 
 $D_{s1}^*(2700)^\pm$  BRANCHING RATIOS

$\Gamma(D^*K)/\Gamma(DK)$	VALUE	EVTS	DOCUMENT ID	TECN	COMMENT	$\Gamma_4/\Gamma_1$
$0.91 \pm 0.13 \pm 0.12$	10.4k	9	AUBERT	09AR BABR	$e^+e^- \rightarrow D^{(*)}KX$	
<sup>9</sup> From the average of the corresponding ratios with $D^{(*)0}K^+$ and $D^{(*)+}K_S^0$ .						

$\Gamma(D^{*0}K^+)/\Gamma(D^0K^+)$	VALUE	EVTS	DOCUMENT ID	TECN	COMMENT	$\Gamma_5/\Gamma_2$
$0.88 \pm 0.14 \pm 0.14$	7716	10	AUBERT	09AR BABR	$e^+e^- \rightarrow D^{(*)}KX$	
<sup>10</sup> From the $D^{*0}K^+$ and $D^0K^+$ , where $D^{*0} \rightarrow D^0\pi^0$ .						

$\Gamma(D^{*+}K_S^0)/\Gamma(D^+K_S^0)$	VALUE	EVTS	DOCUMENT ID	TECN	COMMENT	$\Gamma_6/\Gamma_3$
$1.14 \pm 0.39 \pm 0.23$	2700	11	AUBERT	09AR BABR	$e^+e^- \rightarrow D^{(*)}KX$	
<sup>11</sup> From the $D^{*+}K_S^0$ and $D^+K_S^0$ , where $D^{*+} \rightarrow D^+\pi^0$ .						

 $D_{s1}^*(2700)^\pm$  REFERENCES

LEES	15C	PR D91 052002	J.P. Lees et al.	(BABAR Collab.)
AAIJ	12AU	JHEP 1210 151	R. Aaij et al.	(LHCb Collab.)
AUBERT	09AR	PR D80 092003	B. Aubert et al.	(BABAR Collab.)
BRODZICKA	08	PRL 100 092001	J. Brodzicka et al.	(BELLE Collab.)
AUBERT,BE	06E	PRL 97 222001	B. Aubert et al.	(BABAR Collab.)

$D_{s1}^*(2860)^\pm$   $I(J^P) = 0(1^-)$

OMITTED FROM SUMMARY TABLE  
 $J^P$  consistent with  $1^-$  from angular analysis of AAIJ 14AW. Observed by AUBERT,BE 06E and AUBERT 09AR in inclusive production of  $DK$  and  $D^*K$  in  $e^+e^-$  annihilation.

 $D_{s1}^*(2860)^\pm$  MASS

VALUE (MeV)	EVTS	DOCUMENT ID	TECN	COMMENT
$2859 \pm 12 \pm 24$		1 AAIJ	14AW LHCb	$B_S^0 \rightarrow \bar{D}^0 K^- \pi^+$
••• We do not use the following data for averages, fits, limits, etc. •••				
$2866.1 \pm 1.0 \pm 6.3$	36k	2,3 AAIJ	12AU LHCb	$pp \rightarrow (DK)^+X$ at 7 TeV
$2862 \pm 2 \pm \frac{5}{2}$	3122	3,4 AUBERT	09AR BABR	$e^+e^- \rightarrow D^{(*)}KX$
$2856.6 \pm 1.5 \pm 5.0$		5 AUBERT,BE	06E BABR	$e^+e^- \rightarrow DKX$

- <sup>1</sup> Separated from the spin-3 component  $D_{s3}^*(2860)^-$  by a fit of the helicity angle of the  $\bar{D}^0 K^-$  system, with a statistical significance of the spin-3 and spin-1 components in excess of  $10\sigma$ .
- <sup>2</sup> From the combined fit of the  $D^+K_S^0$  and  $D^0K^+$  modes in the model including the  $D_{s2}^*(2573)^+$ ,  $D_{s1}^*(2700)^+$  and spin-0  $D_{sJ}(2860)^+$ .
- <sup>3</sup> Possible contribution from the  $D_{s3}^*(2860)$  state.
- <sup>4</sup> From simultaneous fits to the two  $DK$  mass spectra and to the total  $D^*K$  mass spectrum.
- <sup>5</sup> Superseded by AUBERT 09AR.

 $D_{s1}^*(2860)^\pm$  WIDTH

VALUE (MeV)	EVTS	DOCUMENT ID	TECN	COMMENT
$159 \pm 23 \pm 77$		1 AAIJ	14AW LHCb	$B_S^0 \rightarrow \bar{D}^0 K^- \pi^+$
••• We do not use the following data for averages, fits, limits, etc. •••				
$69.9 \pm 3.2 \pm 6.6$	36k	2,3 AAIJ	12AU LHCb	$pp \rightarrow (DK)^+X$ at 7 TeV
$48 \pm 3 \pm 6$	3122	3,4 AUBERT	09AR BABR	$e^+e^- \rightarrow D^{(*)}KX$
$47 \pm 7 \pm 10$		5 AUBERT,BE	06E BABR	$e^+e^- \rightarrow DKX$

- <sup>1</sup> Separated from the spin-3 component  $D_{s3}^*(2860)^-$  by a fit of the helicity angle of the  $\bar{D}^0 K^-$  system, with a statistical significance of the spin-3 and spin-1 components in excess of  $10\sigma$ .
- <sup>2</sup> From the combined fit of the  $D^+K_S^0$  and  $D^0K^+$  modes in the model including the  $D_{s2}^*(2573)^+$ ,  $D_{s1}^*(2700)^+$  and spin-0  $D_{sJ}(2860)^+$ .
- <sup>3</sup> Possible contribution from the  $D_{s3}^*(2860)$  state.
- <sup>4</sup> From simultaneous fits to the two  $DK$  mass spectra and to the total  $D^*K$  mass spectrum.
- <sup>5</sup> Superseded by AUBERT 09AR.

 $D_{s1}^*(2860)^\pm$  DECAY MODES

Mode
$\Gamma_1$ $DK$
$\Gamma_2$ $D^0K^+$
$\Gamma_3$ $D^+K_S^0$
$\Gamma_4$ $D^*K$
$\Gamma_5$ $D^{*0}K^+$
$\Gamma_6$ $D^{*+}K_S^0$

 $D_{s1}^*(2860)^\pm$  BRANCHING RATIOS

$\Gamma(D^*K)/\Gamma(DK)$	VALUE	EVTS	DOCUMENT ID	TECN	COMMENT	$\Gamma_4/\Gamma_1$
$1.10 \pm 0.15 \pm 0.19$	3122	1	AUBERT	09AR BABR	$e^+e^- \rightarrow D^{(*)}KX$	
<sup>1</sup> From the average of the corresponding ratios with $D^{(*)0}K^+$ and $D^{(*)+}K_S^0$ .						

$\Gamma(D^{*0}K^+)/\Gamma(D^0K^+)$	VALUE	EVTS	DOCUMENT ID	TECN	COMMENT	$\Gamma_5/\Gamma_2$
$1.04 \pm 0.17 \pm 0.20$	2241	1	AUBERT	09AR BABR	$e^+e^- \rightarrow D^{(*)}KX$	
<sup>1</sup> From the $D^{*0}K^+$ and $D^0K^+$ , where $D^{*0} \rightarrow D^0\pi^0$ .						

$\Gamma(D^{*+}K_S^0)/\Gamma(D^+K_S^0)$	VALUE	EVTS	DOCUMENT ID	TECN	COMMENT	$\Gamma_6/\Gamma_3$
$1.38 \pm 0.35 \pm 0.49$	881	1	AUBERT	09AR BABR	$e^+e^- \rightarrow D^{(*)}KX$	
<sup>1</sup> From the $D^{*+}K_S^0$ and $D^+K_S^0$ , where $D^{*+} \rightarrow D^+\pi^0$ .						

 $D_{s1}^*(2860)^\pm$  REFERENCES

AAIJ	14AW	PRL 113 162001	R. Aaij et al.	(LHCb Collab.)JP
AAIJ	12AU	JHEP 1210 151	R. Aaij et al.	(LHCb Collab.)
AUBERT	09AR	PR D80 092003	B. Aubert et al.	(BABAR Collab.)
AUBERT,BE	06E	PRL 97 222001	B. Aubert et al.	(BABAR Collab.)

$D_{s3}^*(2860)^\pm$   $I(J^P) = 0(3^-)$

OMITTED FROM SUMMARY TABLE  
 $J^P$  consistent with  $3^-$  from angular analysis of AAIJ 14AW.

 $D_{s3}^*(2860)^\pm$  MASS

VALUE (MeV)	DOCUMENT ID	TECN	COMMENT
$2860.5 \pm 2.6 \pm 6.5$	1 AAIJ	14AW LHCb	$B_S^0 \rightarrow \bar{D}^0 K^- \pi^+$
<sup>1</sup> Separated from the spin-1 component $D_{s1}^*(2860)^-$ by a fit of the helicity angle of the $\bar{D}^0 K^-$ system, with a statistical significance of the spin-3 and spin-1 components in excess of $10\sigma$ .			

 $D_{s3}^*(2860)^\pm$  WIDTH

VALUE (MeV)	DOCUMENT ID	TECN	COMMENT
$53 \pm 7 \pm 7$	1 AAIJ	14AW LHCb	$B_S^0 \rightarrow \bar{D}^0 K^- \pi^+$
<sup>1</sup> Separated from the spin-1 component $D_{s1}^*(2860)^-$ by a fit of the helicity angle of the $\bar{D}^0 K^-$ system, with a statistical significance of the spin-3 and spin-1 components in excess of $10\sigma$ .			

 $D_{s3}^*(2860)^\pm$  REFERENCES

AAIJ	14AW	PRL 113 162001	R. Aaij et al.	(LHCb Collab.)JP
------	------	----------------	----------------	------------------

$D_{sJ}(3040)^\pm$   $I(J^P) = 0(?^?)$

OMITTED FROM SUMMARY TABLE  
 Observed by AUBERT 09AR in inclusive production of  $D^*K$  in  $e^+e^-$  annihilation.

 $D_{sJ}(3040)^\pm$  MASS

VALUE (MeV)	DOCUMENT ID	TECN	COMMENT
$3044 \pm 8 \pm \frac{30}{5}$	AUBERT	09AR BABR	$e^+e^- \rightarrow D^*KX$

 $D_{sJ}(3040)^\pm$  WIDTH

VALUE (MeV)	DOCUMENT ID	TECN	COMMENT
$239 \pm 35 \pm \frac{46}{42}$	AUBERT	09AR BABR	$e^+e^- \rightarrow D^*KX$

 $D_{sJ}(3040)^\pm$  DECAY MODES

Mode
$\Gamma_1$ $D^*K$
$\Gamma_2$ $D^{*0}K^+$
$\Gamma_3$ $D^{*+}K_S^0$

 $D_{sJ}(3040)^\pm$  REFERENCES

AUBERT	09AR	PR D80 092003	B. Aubert et al.	(BABAR Collab.)
--------	------	---------------	------------------	-----------------

**BOTTOM MESONS****( $B = \pm 1$ )** $B^+ = u\bar{b}$ ,  $B^0 = d\bar{b}$ ,  $\bar{B}^0 = \bar{d}b$ ,  $B^- = \bar{u}b$ , similarly for  $B^{*s}$ **B-particle organization**

Many measurements of  $B$  decays involve admixtures of  $B$  hadrons. Previously we arbitrarily included such admixtures in the  $B^\pm$  section, but because of their importance we have created two new sections: “ $B^\pm/B^0$  Admixture” for  $\Upsilon(4S)$  results and “ $B^\pm/B^0/B_s^0/b$ -baryon Admixture” for results at higher energies. Most inclusive decay branching fractions and  $\chi_b$  at high energy are found in the Admixture sections.  $B^0\bar{B}^0$  mixing data are found in the  $B^0$  section, while  $B_s^0\bar{B}_s^0$  mixing data and  $B\bar{B}$  mixing data for a  $B^0/B_s^0$  admixture are found in the  $B_s^0$  section.  $CP$ -violation data are found in the  $B^\pm$ ,  $B^0$ , and  $B^\pm/B^0$  Admixture sections.  $b$ -baryons are found near the end of the Baryon section. Recently, we also created a new section: “ $V_{cb}$  and  $V_{ub}$  CKM Matrix Elements.”

The organization of the  $B$  sections is now as follows, where bullets indicate particle sections and brackets indicate reviews.

[Production and Decay of *b*-flavored Hadrons]

[A Short Note on HFLAV Activities]

- $B^\pm$ 
  - mass, mean life
  - branching fractions
  - polarization in  $B^\pm$  decay
  - $CP$  violation
- $B^0$ 
  - mass, mean life
  - branching fractions
  - [Polarization in  $B$  decay]
  - polarization in  $B^0$  decay
  - [ $B\bar{B}$  Mixing]
  - $B^0\bar{B}^0$  mixing
  - $CP$  violation
- $B^\pm/B^0$  Admixture
  - branching fractions,  $CP$  violation
  - $CP$  violation
- $B^\pm/B^0/B_s^0/b$ -baryon Admixture
  - mean life
  - production fractions
  - branching fractions
  - $\chi_b$  at high energy
  - production fractions in hadronic  $Z$  decay
- $V_{cb}$  and  $V_{ub}$  CKM Matrix Elements
  - [Determination of  $V_{cb}$  and  $V_{ub}$ ]
- $B^*$ 
  - mass
- $B_1(5721)^0$ 
  - mass
- $B_J^*(5732)$ 
  - mass, width
- $B_2(5747)^0$ 
  - mass
- $B_s^0$ 
  - mass, mean life
  - branching fractions
  - polarization in  $B_s^0$  decay
  - $B_s^0\bar{B}_s^0$  mixing
- $B_s^*$ 
  - mass
- $B_{s,J}^*(5850)$ 
  - mass, width
- $B_c^\pm$ 
  - mass, mean life
  - branching fractions

At the end of Baryon Listings:

- $\Lambda_b$ 
  - mass, mean life
  - branching fractions
- $\Sigma_b^*$ ,  $\Sigma_b^{*s}$ 
  - mass
- $\Xi_b^0$ ,  $\Xi_b^-$ 
  - mean life
- $\Omega_b^-$ 
  - mass, mean life
  - branching fractions
- $b$ -baryon Admixture
  - mean life
  - branching fractions

**See the related review(s):****Production and Decay of *b*-flavored Hadrons****HEAVY FLAVOR AVERAGING GROUP**

Revised August 2019 by U. Egede (Monash University) and A. Soffer (Tel Aviv University)

The Heavy Flavor Averaging Group (HFLAV)\* is an international collaboration of physicists from experiments measuring properties of heavy flavored particles, *i.e.*, hadrons containing  $b$  and  $c$  quarks, and  $\tau$  leptons. HFLAV calculates and publishes [1] world average values of quantities such as lifetimes, branching fractions, form factors, mixing parameters, and  $CP$ -violating asymmetries. Most parameters concern decays of  $B$  and  $D$  mesons, and many are related to elements of the Cabibbo-Kobayashi-Maskawa (CKM) quark mixing matrix [2], [3].

HFLAV was originally formed in 2002 to continue the activities of the LEP Heavy Flavor Steering group. Since its inception, a wide range of results have become available from increasingly larger data sets. Consequently, HFLAV has expanded to include seven subgroups:

- $b$ -hadron lifetimes and oscillations, including parameters of  $CP$  violation in  $b$  mixing;
- decay-time-dependent  $CP$  violation in  $B$  decays, and angles of the CKM Unitarity Triangle;
- semileptonic decays of  $b$ -hadrons ( $B \rightarrow X\ell\nu$ ,  $\ell = e, \mu, \tau$ ), including determinations of the CKM matrix elements  $|V_{cb}|$  and  $|V_{ub}|$ ;
- $b$ -hadron decays to hadronic final states containing  $c$ -quarks (open charm and charmonium);
- (rarer)  $b$ -hadron decays to final states not containing  $c$ -quarks, including fully hadronic, semileptonic ( $B \rightarrow X\ell\ell, X\nu\bar{\nu}$ ), leptonic, and radiative decays;
- $c$ -hadron physics including branching fractions,  $CP$ - and  $T$ -violating asymmetries,  $D^0\bar{D}^0$  mixing, semileptonic decays, and properties of excited  $D$  states and charm baryons;
- $\tau$ -lepton physics including branching fractions, tests of lepton universality, determination of the CKM matrix element  $|V_{us}|$ , and searches for lepton flavor violation.

\* The group was originally referred to as “HFAG.” This acronym was changed to “HFLAV” in 2017.



# Meson Particle Listings

## $b$ -flavored hadrons, $B^\pm$

Each subgroup has one or two conveners and typically a half-dozen members representing experiments that conduct measurements in that area. Most groups contain representatives from the BABAR, Belle, Belle II and LHCb experiments, and some groups have representatives from the ATLAS, BESIII, CLEO(c), CDF, CMS and D0 experiments. Members of HFLAV are appointed by their respective experimental collaborations. HFLAV has two co-leaders, who are appointed by the managements of Belle II and LHCb.

The averaging procedures used by HFLAV are similar to those of the PDG [4]. When calculating world averages, common parameters used for different input measurements are adjusted (rescaled) to common values. The confidence level of the fit is provided to indicate the consistency of the measurements included in the average. However, unlike the PDG, when obtaining a world average with a small confidence level (*i.e.*, a large  $\chi^2$  per degree of freedom), HFLAV does not usually scale the resulting uncertainty. Rather, the systematic uncertainties of the measurements are reviewed with experts from the experiments to understand the discrepancy. Unless inconsistencies among measurements are found, no correction is made to the calculated uncertainty. Close communication between representatives of the experiments and HFLAV members who perform averages helps ensure that measurement uncertainties, known correlations, and systematic effects are properly accounted for. If a special treatment is needed to calculate an average, or if an approximation used in an average calculation might not be sufficiently accurate (*e.g.*, assuming Gaussian uncertainties when the likelihood function is non-Gaussian), a note is included in the HFLAV publication and online documentation to describe this.

In general, HFLAV uses all publicly available results that have written documentation such as a journal publication, preprint, or conference note. These include preliminary results presented at conferences and workshops. However, preliminary results that remain unpublished for an extended period of time, or for which no publication is planned, are not included. A special subset of HFLAV averages are included in the PDG listings; for these averages, only measurements that are published or accepted for publication are used. The averages provided by HFLAV are listed by the PDG as “OUR EVALUATION” with a corresponding note.

All HFLAV averages and input measurements are documented in an approximately biennial journal paper or preprint; the most recent version is Ref. [1]. The latest results and plots are posted on an extensive set of webpages that are updated several times per year; these are available at

<https://hflav.web.cern.ch>.

### References:

1. Y. Amhis *et al.* (Heavy Flavor Averaging Group) (2018), [arXiv:1909.12524], updated results and plots available at <https://hflav.web.cern.ch/>.
2. N. Cabibbo, Phys. Rev. Lett. **10**, 531 (1963).

3. M. Kobayashi and T. Maskawa, Prog. Theor. Phys. **49**, 652 (1973).
4. See Section 5 of the “Introduction” to this *Review*.

$B^\pm$

$$I(J^P) = \frac{1}{2}(0^-)$$

Quantum numbers not measured. Values shown are quark-model predictions.

See also the  $B^\pm/B^0$  ADMIXTURE and  $B^\pm/B^0/B_s^0/b$ -baryon ADMIXTURE sections.

### $B^\pm$ MASS

The fit uses  $m_{B^\pm}$ , ( $m_{B^0} - m_{B^\pm}$ ), and  $m_{B^0}$  to determine  $m_{B^\pm}$ ,  $m_{B^0}$ , and the mass difference.

VALUE (MeV)	EVTs	DOCUMENT ID	TECN	COMMENT
<b>5279.34 ± 0.12 OUR FIT</b>				
<b>5279.25 ± 0.26 OUR AVERAGE</b>				
5279.38 ± 0.11 ± 0.33		1 AAIJ	12E LHCb	$p\bar{p}$ at 7 TeV
5279.10 ± 0.41 ± 0.36		2 ACOSTA	06 CDF	$p\bar{p}$ at 1.96 TeV
5279.1 ± 0.4 ± 0.4	526	3 CSORNA	00 CLE2	$e^+e^- \rightarrow \Upsilon(4S)$
5279.1 ± 1.7 ± 1.4	147	ABE	96B CDF	$p\bar{p}$ at 1.8 TeV
••• We do not use the following data for averages, fits, limits, etc. •••				
5278.8 ± 0.54 ± 2.0	362	ALAM	94 CLE2	$e^+e^- \rightarrow \Upsilon(4S)$
5278.3 ± 0.4 ± 2.0		BORTOLETTI	092 CLEO	$e^+e^- \rightarrow \Upsilon(4S)$
5280.5 ± 1.0 ± 2.0		4 ALBRECHT	90J ARG	$e^+e^- \rightarrow \Upsilon(4S)$
5275.8 ± 1.3 ± 3.0	32	ALBRECHT	87C ARG	$e^+e^- \rightarrow \Upsilon(4S)$
5278.2 ± 1.8 ± 3.0	12	5 ALBRECHT	87D ARG	$e^+e^- \rightarrow \Upsilon(4S)$
5278.6 ± 0.8 ± 2.0		BEBEK	87 CLEO	$e^+e^- \rightarrow \Upsilon(4S)$

<sup>1</sup> Uses  $B^+ \rightarrow J/\psi K^+$  fully reconstructed decays.

<sup>2</sup> Uses exclusively reconstructed final states containing a  $J/\psi \rightarrow \mu^+\mu^-$  decays.

<sup>3</sup> CSORNA 00 uses fully reconstructed 526  $B^+ \rightarrow J/\psi(\ell) K^+$  events and invariant masses without beam constraint.

<sup>4</sup> ALBRECHT 90J assumes 10580 for  $\Upsilon(4S)$  mass. Supersedes ALBRECHT 87C and ALBRECHT 87D.

<sup>5</sup> Found using fully reconstructed decays with  $J/\psi(1S)$ . ALBRECHT 87D assume  $m_{\Upsilon(4S)} = 10577$  MeV.

### $B^\pm$ MEAN LIFE

See  $B^\pm/B^0/B_s^0/b$ -baryon ADMIXTURE section for data on  $B$ -hadron mean life averaged over species of bottom particles.

“OUR EVALUATION” is an average using rescaled values of the data listed below. The average and rescaling were performed by the Heavy Flavor Averaging Group (HFLAV) and are described at <https://hflav.web.cern.ch/>. The averaging/rescaling procedure takes into account correlations between the measurements and asymmetric lifetime errors.

VALUE ( $10^{-12}$ s)	EVTs	DOCUMENT ID	TECN	COMMENT
<b>1.638 ± 0.004 OUR EVALUATION</b>				
1.637 ± 0.004 ± 0.003		AAIJ	14E LHCb	$p\bar{p}$ at 7 TeV
1.639 ± 0.009 ± 0.009		1 AALTONEN	11 CDF	$p\bar{p}$ at 1.96 TeV
1.663 ± 0.023 ± 0.015		2 AALTONEN	11B CDF	$p\bar{p}$ at 1.96 TeV
1.635 ± 0.011 ± 0.011		3 ABE	05B BELL	$e^+e^- \rightarrow \Upsilon(4S)$
1.624 ± 0.014 ± 0.018		4 ABDALLAH	04E DLPH	$e^+e^- \rightarrow Z$
1.636 ± 0.058 ± 0.025		5 ACOSTA	02C CDF	$p\bar{p}$ at 1.8 TeV
1.673 ± 0.032 ± 0.023		6 AUBERT	01F BABR	$e^+e^- \rightarrow \Upsilon(4S)$
1.648 ± 0.049 ± 0.035		7 BARATE	00R ALEP	$e^+e^- \rightarrow Z$
1.643 ± 0.037 ± 0.025		8 ABBIENDI	99J OPAL	$e^+e^- \rightarrow Z$
1.637 ± 0.058 $^{+0.045}_{-0.043}$		7 ABE	98Q CDF	$p\bar{p}$ at 1.8 TeV
1.66 ± 0.06 ± 0.03		8 ACCIARRI	98S L3	$e^+e^- \rightarrow Z$
1.66 ± 0.06 ± 0.05		8 ABE	97J SLD	$e^+e^- \rightarrow Z$
1.58 $^{+0.21}_{-0.18}$ $^{+0.04}_{-0.03}$	94	5 BUSKULIC	96J ALEP	$e^+e^- \rightarrow Z$
1.61 ± 0.16 ± 0.12		7,9 ABREU	95Q DLPH	$e^+e^- \rightarrow Z$
1.72 ± 0.08 ± 0.06		10 ADAM	95 DLPH	$e^+e^- \rightarrow Z$
1.52 ± 0.14 ± 0.09		7 AKERS	95T OPAL	$e^+e^- \rightarrow Z$
••• We do not use the following data for averages, fits, limits, etc. •••				
1.695 ± 0.026 ± 0.015		6 ABE	02H BELL	Repl. by ABE 05B
1.68 ± 0.07 ± 0.02		5 ABE	98B CDF	Repl. by ACOSTA 02C
1.56 ± 0.13 ± 0.06		7 ABE	96C CDF	Repl. by ABE 98Q
1.58 ± 0.09 ± 0.03		11 BUSKULIC	96J ALEP	$e^+e^- \rightarrow Z$
1.58 ± 0.09 ± 0.04		7 BUSKULIC	96J ALEP	Repl. by BARATE 00R
1.70 ± 0.09		12 ADAM	95 DLPH	$e^+e^- \rightarrow Z$
1.61 ± 0.16 ± 0.05	148	5 ABE	94D CDF	Repl. by ABE 98B
1.30 $^{+0.33}_{-0.29}$ ± 0.16	92	7 ABREU	93D DLPH	Sup. by ABREU 95Q
1.56 ± 0.19 ± 0.13	134	10 ABREU	93G DLPH	Sup. by ADAM 95
1.51 $^{+0.30}_{-0.28}$ $^{+0.12}_{-0.14}$	59	7 ACTON	93C OPAL	Sup. by AKERS 95T
1.47 $^{+0.22}_{-0.19}$ $^{+0.15}_{-0.14}$	77	7 BUSKULIC	93D ALEP	Sup. by BUSKULIC 96J

- <sup>1</sup> Measured mean life using fully reconstructed decays ( $J/\psi K^{(*)}$ ).
- <sup>2</sup> Measured using  $B^- \rightarrow D^0 \pi^-$  with  $D^0 \rightarrow K^- \pi^+$  events that were selected using a silicon vertex trigger.
- <sup>3</sup> Measurement performed using a combined fit of  $CP$ -violation, mixing and lifetimes.
- <sup>4</sup> Measurement performed using an inclusive reconstruction and  $B$  flavor identification technique.
- <sup>5</sup> Measured mean life using fully reconstructed decays.
- <sup>6</sup> Events are selected in which one  $B$  meson is fully reconstructed while the second  $B$  meson is reconstructed inclusively.
- <sup>7</sup> Data analyzed using  $D/D^* \ell X$  event vertices.
- <sup>8</sup> Data analyzed using charge of secondary vertex.
- <sup>9</sup> ABREU 95q assumes  $B(B^0 \rightarrow D^{*-} \ell^+ \nu_\ell) = 3.2 \pm 1.7\%$ .
- <sup>10</sup> Data analyzed using vertex-charge technique to tag  $B$  charge.
- <sup>11</sup> Combined result of  $D/D^* \ell X$  analysis and fully reconstructed  $B$  analysis.
- <sup>12</sup> Combined ABREU 95q and ADAM 95 result.

$\tau_{B^+}/\tau_{B^-}$	DOCUMENT ID	TECN	COMMENT
<b>1.002 ± 0.004 ± 0.002</b>	<sup>1</sup> AAIJ	14E LHCB	$pp$ at 7 TeV

<sup>1</sup> Measured using  $B^\pm \rightarrow J/\psi K^\pm$  decays.

**$B^+$  DECAY MODES**

$B^-$  modes are charge conjugates of the modes below. Modes which do not identify the charge state of the  $B$  are listed in the  $B^\pm/B^0$  ADMIXTURE section.

The branching fractions listed below assume 50%  $B^0 \bar{B}^0$  and 50%  $B^+ B^-$  production at the  $\Upsilon(4S)$ . We have attempted to bring older measurements up to date by rescaling their assumed  $\Upsilon(4S)$  production ratio to 50:50 and their assumed  $D, D_s, D^*$ , and  $\psi$  branching ratios to current values whenever this would affect our averages and best limits significantly.

Indentation is used to indicate a subchannel of a previous reaction. All resonant subchannels have been corrected for resonance branching fractions to the final state so the sum of the subchannel branching fractions can exceed that of the final state.

For inclusive branching fractions, e.g.,  $B \rightarrow D^\pm X$ , the values usually are multiplicities, not branching fractions. They can be greater than one.

Mode	Fraction ( $\Gamma_i/\Gamma$ )	Scale factor/ Confidence level
<b>Semileptonic and leptonic modes</b>		
$\Gamma_1 \ell^+ \nu_\ell X$	[a] ( 10.99 ± 0.28 ) %	
$\Gamma_2 e^+ \nu_e X_c$	( 10.8 ± 0.4 ) %	
$\Gamma_3 D \ell^+ \nu_\ell X$	( 9.7 ± 0.7 ) %	
$\Gamma_4 \bar{D}^0 \ell^+ \nu_\ell$	[a] ( 2.35 ± 0.09 ) %	
$\Gamma_5 \bar{D}^0 \tau^+ \nu_\tau$	( 7.7 ± 2.5 ) × 10 <sup>-3</sup>	
$\Gamma_6 \bar{D}^*(2007)^0 \ell^+ \nu_\ell$	[a] ( 5.66 ± 0.22 ) %	
$\Gamma_7 \bar{D}^*(2007)^0 \tau^+ \nu_\tau$	( 1.88 ± 0.20 ) %	
$\Gamma_8 D^- \pi^+ \ell^+ \nu_\ell$	( 4.4 ± 0.4 ) × 10 <sup>-3</sup>	
$\Gamma_9 \bar{D}_0^*(2420)^0 \ell^+ \nu_\ell, \bar{D}_0^{*0} \rightarrow$	( 2.5 ± 0.5 ) × 10 <sup>-3</sup>	
$\Gamma_{10} \bar{D}_2^*(2460)^0 \ell^+ \nu_\ell, \bar{D}_2^{*0} \rightarrow$	( 1.53 ± 0.16 ) × 10 <sup>-3</sup>	
$\Gamma_{11} D^{(*)} n \pi \ell^+ \nu_\ell (n \geq 1)$	( 1.88 ± 0.25 ) %	
$\Gamma_{12} D^{*-} \pi^+ \ell^+ \nu_\ell$	( 6.0 ± 0.4 ) × 10 <sup>-3</sup>	
$\Gamma_{13} \bar{D}_1^*(2420)^0 \ell^+ \nu_\ell, \bar{D}_1^{*0} \rightarrow$	( 3.03 ± 0.20 ) × 10 <sup>-3</sup>	
$\Gamma_{14} \bar{D}_1^{*-} \pi^+ \ell^+ \nu_\ell, \bar{D}_1^{*0} \rightarrow$	( 2.7 ± 0.6 ) × 10 <sup>-3</sup>	
$\Gamma_{15} \bar{D}_2^{*-} \pi^+ \ell^+ \nu_\ell, \bar{D}_2^{*0} \rightarrow$	( 1.01 ± 0.24 ) × 10 <sup>-3</sup>	S=2.0
$\Gamma_{16} \bar{D}^0 \pi^+ \pi^- \ell^+ \nu_\ell$	( 1.7 ± 0.4 ) × 10 <sup>-3</sup>	
$\Gamma_{17} \bar{D}^{*0} \pi^+ \pi^- \ell^+ \nu_\ell$	( 8 ± 5 ) × 10 <sup>-4</sup>	
$\Gamma_{18} D_s^{(*)-} K^+ \ell^+ \nu_\ell$	( 6.1 ± 1.0 ) × 10 <sup>-4</sup>	
$\Gamma_{19} D_s^- K^+ \ell^+ \nu_\ell$	( 3.0 ± 1.4 ) × 10 <sup>-4</sup>	
$\Gamma_{20} D_s^{*-} K^+ \ell^+ \nu_\ell$	( 2.9 ± 1.9 ) × 10 <sup>-4</sup>	
$\Gamma_{21} \pi^0 \ell^+ \nu_\ell$	( 7.80 ± 0.27 ) × 10 <sup>-5</sup>	
$\Gamma_{22} \pi^0 e^+ \nu_e$		
$\Gamma_{23} \eta \ell^+ \nu_\ell$	( 3.9 ± 0.5 ) × 10 <sup>-5</sup>	
$\Gamma_{24} \eta' \ell^+ \nu_\ell$	( 2.3 ± 0.8 ) × 10 <sup>-5</sup>	
$\Gamma_{25} \omega \ell^+ \nu_\ell$	[a] ( 1.19 ± 0.09 ) × 10 <sup>-4</sup>	
$\Gamma_{26} \omega \mu^+ \nu_\mu$		
$\Gamma_{27} \rho^0 \ell^+ \nu_\ell$	[a] ( 1.58 ± 0.11 ) × 10 <sup>-4</sup>	
$\Gamma_{28} p \bar{p} \ell^+ \nu_\ell$	( 5.8 ± 2.6 ) × 10 <sup>-6</sup>	
$\Gamma_{29} p \bar{p} \mu^+ \nu_\mu$	< 8.5 × 10 <sup>-6</sup>	CL=90%

$\Gamma_{30} p \bar{p} e^+ \nu_e$	( 8.2 ± 4.0 ) × 10 <sup>-6</sup>	
$\Gamma_{31} e^+ \nu_e$	< 9.8 × 10 <sup>-7</sup>	CL=90%
$\Gamma_{32} \mu^+ \nu_\mu$	2.90 × 10 <sup>-07</sup> to 1.07 × 10 <sup>-06</sup>	CL=90%
$\Gamma_{33} \tau^+ \nu_\tau$	( 1.09 ± 0.24 ) × 10 <sup>-4</sup>	S=1.2
$\Gamma_{34} \ell^+ \nu_\ell \gamma$	< 3.0 × 10 <sup>-6</sup>	CL=90%
$\Gamma_{35} e^+ \nu_e \gamma$	< 4.3 × 10 <sup>-6</sup>	CL=90%
$\Gamma_{36} \mu^+ \nu_\mu \gamma$	< 3.4 × 10 <sup>-6</sup>	CL=90%
$\Gamma_{37} \mu^+ \mu^- \mu^+ \nu_\mu$	< 1.6 × 10 <sup>-8</sup>	CL=95%

**Inclusive modes**

$\Gamma_{38} D^0 X$	( 8.6 ± 0.7 ) %
$\Gamma_{39} \bar{D}^0 X$	( 79 ± 4 ) %
$\Gamma_{40} D^+ X$	( 2.5 ± 0.5 ) %
$\Gamma_{41} D^- X$	( 9.9 ± 1.2 ) %
$\Gamma_{42} D_s^+ X$	( 7.9 ± 1.4 ) %
$\Gamma_{43} D_s^- X$	( 1.10 ± 0.40 ) %
$\Gamma_{44} \Lambda_c^+ X$	( 2.1 ± 0.9 ) %
$\Gamma_{45} \bar{\Lambda}_c^- X$	( 2.8 ± 1.1 ) %
$\Gamma_{46} \bar{c} X$	( 97 ± 4 ) %
$\Gamma_{47} c X$	( 23.4 ± 2.2 ) %
$\Gamma_{48} c / \bar{c} X$	( 120 ± 6 ) %

**$D, D^*$ , or  $D_s$  modes**

$\Gamma_{49} \bar{D}^0 \pi^+$	( 4.68 ± 0.13 ) × 10 <sup>-3</sup>
$\Gamma_{50} D_{CP(+1)} \pi^+$	[b] ( 2.05 ± 0.18 ) × 10 <sup>-3</sup>
$\Gamma_{51} D_{CP(-1)} \pi^+$	[b] ( 2.0 ± 0.4 ) × 10 <sup>-3</sup>
$\Gamma_{52} \bar{D}^0 \rho^+$	( 1.34 ± 0.18 ) %
$\Gamma_{53} \bar{D}^0 K^+$	( 3.63 ± 0.12 ) × 10 <sup>-4</sup>
$\Gamma_{54} D_{CP(+1)} K^+$	[b] ( 1.80 ± 0.07 ) × 10 <sup>-4</sup>
$\Gamma_{55} D_{CP(-1)} K^+$	[b] ( 1.96 ± 0.18 ) × 10 <sup>-4</sup>
$\Gamma_{56} D^0 K^+$	( 3.57 ± 0.35 ) × 10 <sup>-6</sup>
$\Gamma_{57} [K^- \pi^+]_D K^+$	[c] < 2.8 × 10 <sup>-7</sup>
$\Gamma_{58} [K^+ \pi^-]_D K^+$	[c] < 1.5 × 10 <sup>-5</sup>
$\Gamma_{59} [K^- \pi^+ \pi^0]_D K^+$	seen
$\Gamma_{60} [K^+ \pi^- \pi^0]_D K^+$	seen
$\Gamma_{61} [K^- \pi^+ \pi^+ \pi^-]_D K^+$	seen
$\Gamma_{62} [K^+ \pi^- \pi^+ \pi^-]_D K^+$	seen
$\Gamma_{63} [\pi^+ \pi^+ \pi^- \pi^-] K^+$	
$\Gamma_{64} [\pi^+ \pi^- \pi^+ \pi^-]_D K^*(892)^+$	
$\Gamma_{65} [K^- \pi^+]_D K^*(892)^+$	[c]
$\Gamma_{66} [K^+ \pi^-]_D K^*(892)^+$	[c]
$\Gamma_{67} [K^- \pi^+ \pi^- \pi^+]_D K^*(892)^+$	
$\Gamma_{68} [K^+ \pi^- \pi^+ \pi^-]_D K^*(892)^+$	
$\Gamma_{69} [K^- \pi^+]_D \pi^+$	[c] ( 6.3 ± 1.1 ) × 10 <sup>-7</sup>
$\Gamma_{70} [K^+ \pi^-]_D \pi^+$	( 1.78 ± 0.32 ) × 10 <sup>-4</sup>
$\Gamma_{71} [K^- \pi^+ \pi^0]_D \pi^+$	seen
$\Gamma_{72} [K^+ \pi^- \pi^0]_D \pi^+$	seen
$\Gamma_{73} [K^- \pi^+ \pi^+ \pi^-]_D \pi^+$	seen
$\Gamma_{74} [K^+ \pi^- \pi^+ \pi^-]_D \pi^+$	seen
$\Gamma_{75} [K^- \pi^+]_{(D\pi)} \pi^+$	
$\Gamma_{76} [K^+ \pi^-]_{(D\pi)} \pi^+$	
$\Gamma_{77} [K^- \pi^+]_{(D\gamma)} \pi^+$	
$\Gamma_{78} [K^+ \pi^-]_{(D\gamma)} \pi^+$	
$\Gamma_{79} [K^- \pi^+]_{(D\pi)} K^+$	
$\Gamma_{80} [K^+ \pi^-]_{(D\pi)} K^+$	
$\Gamma_{81} [K^- \pi^+]_{(D\gamma)} K^+$	
$\Gamma_{82} [K^+ \pi^-]_{(D\gamma)} K^+$	
$\Gamma_{83} [\pi^+ \pi^- \pi^0]_D K^-$	( 4.6 ± 0.9 ) × 10 <sup>-6</sup>
$\Gamma_{84} [K_S^0 K^+ \pi^-]_D K^+$	seen
$\Gamma_{85} [K_S^0 K^- \pi^+]_D K^+$	seen
$\Gamma_{86} [K^*(892)^+ K^-]_D K^+$	seen
$\Gamma_{87} [K_S^0 K^- \pi^+]_D \pi^+$	seen
$\Gamma_{88} [K^*(892)^+ K^-]_D \pi^+$	seen
$\Gamma_{89} [K_S^0 K^+ \pi^-]_D \pi^+$	seen
$\Gamma_{90} [K^*(892)^- K^+]_D \pi^+$	seen
$\Gamma_{91} [K^+ K^- \pi^0]_D K^+$	
$\Gamma_{92} [K^+ K^- \pi^0]_D \pi^+$	
$\Gamma_{93} [\pi^+ \pi^- \pi^0]_D K^+$	
$\Gamma_{94} [\pi^+ \pi^- \pi^0]_D \pi^+$	
$\Gamma_{95} \bar{D}^0 K^*(892)^+$	( 5.3 ± 0.4 ) × 10 <sup>-4</sup>

## Meson Particle Listings

 $B^\pm$ 

$\Gamma_{96}$	$D_{CP(-)} K^*(892)^+$	[b]	$(2.7 \pm 0.8) \times 10^{-4}$	$\Gamma_{154}$	$\bar{D}_2^*(2462)^0 \pi^+$		$(1.8 \pm 0.5) \times 10^{-4}$
$\Gamma_{97}$	$D_{CP(+)} K^*(892)^+$	[b]	$(6.2 \pm 0.7) \times 10^{-4}$		$\times B(\bar{D}_3^*(2462)^0 \rightarrow D^{*-} \pi^+)$		
$\Gamma_{98}$	$D^0 K^*(892)^+$		$(3.1 \pm 1.6) \times 10^{-6}$	$\Gamma_{155}$	$\bar{D}_1^*(2427)^0 \pi^+$		$(5.0 \pm 1.2) \times 10^{-4}$
$\Gamma_{99}$	$\bar{D}^0 K^+ \pi^+ \pi^-$		$(5.2 \pm 2.1) \times 10^{-4}$		$\times B(\bar{D}_1^*(2427)^0 \rightarrow D^{*-} \pi^+)$		
$\Gamma_{100}$	$[K^+ \pi^-]_D K^+ \pi^- \pi^+$			$\Gamma_{156}$	$\bar{D}_1(2420)^0 \pi^+ \times B(\bar{D}_1^0 \rightarrow$	$< 6$	$\times 10^{-6}$ CL=90%
$\Gamma_{101}$	$[K^- \pi^+]_D K^+ \pi^- \pi^+$				$\bar{D}^{*0} \pi^+ \pi^-)$		
$\Gamma_{102}$	$D_{CP(+)} K^+ \pi^- \pi^+$			$\Gamma_{157}$	$\bar{D}_1^*(2420)^0 \rho^+$	$< 1.4$	$\times 10^{-3}$ CL=90%
$\Gamma_{103}$	$\bar{D}^0 K^+ \bar{K}^0$		$(5.5 \pm 1.6) \times 10^{-4}$	$\Gamma_{158}$	$\bar{D}_2^*(2460)^0 \pi^+$	$< 1.3$	$\times 10^{-3}$ CL=90%
$\Gamma_{104}$	$\bar{D}^0 K^+ \bar{K}^*(892)^0$		$(7.5 \pm 1.7) \times 10^{-4}$	$\Gamma_{159}$	$\bar{D}_2^*(2460)^0 \pi^+ \times B(\bar{D}_2^{*0} \rightarrow$	$< 2.2$	$\times 10^{-5}$ CL=90%
$\Gamma_{105}$	$\bar{D}^0 \pi^+ \pi^+ \pi^-$		$(5.6 \pm 2.1) \times 10^{-3}$		$\bar{D}^{*0} \pi^+ \pi^-)$		
$\Gamma_{106}$	$[K^- \pi^+]_D \pi^+ \pi^- \pi^+$			$\Gamma_{160}$	$\bar{D}_1^*(2680)^0 \pi^+, \bar{D}_1^*(2680)^0 \rightarrow$	$(8.4 \pm 2.1) \times 10^{-5}$	
$\Gamma_{107}$	$\bar{D}^0 \pi^+ \pi^+ \pi^-$ nonresonant		$(5 \pm 4) \times 10^{-3}$		$D^- \pi^+$		
$\Gamma_{108}$	$\bar{D}^0 \pi^+ \rho^0$		$(4.2 \pm 3.0) \times 10^{-3}$	$\Gamma_{161}$	$\bar{D}_3^*(2760)^0 \pi^+,$	$(1.00 \pm 0.22) \times 10^{-5}$	
$\Gamma_{109}$	$\bar{D}^0 a_1(1260)^+$		$(4 \pm 4) \times 10^{-3}$		$\bar{D}_3^*(2760)^0 \pi^+ \rightarrow D^- \pi^+$		
$\Gamma_{110}$	$\bar{D}^0 \omega \pi^+$		$(4.1 \pm 0.9) \times 10^{-3}$	$\Gamma_{162}$	$\bar{D}_2^*(3000)^0 \pi^+,$	$(2.0 \pm 1.4) \times 10^{-6}$	
$\Gamma_{111}$	$D^*(2010)^- \pi^+ \pi^+$		$(1.35 \pm 0.22) \times 10^{-3}$		$\bar{D}_2^*(3000)^0 \pi^+ \rightarrow D^- \pi^+$		
$\Gamma_{112}$	$D^*(2010)^- K^+ \pi^+$		$(8.2 \pm 1.4) \times 10^{-5}$	$\Gamma_{163}$	$\bar{D}_2^*(2460)^0 \rho^+$	$< 4.7$	$\times 10^{-3}$ CL=90%
$\Gamma_{113}$	$\bar{D}_1(2420)^0 \pi^+, \bar{D}_1^0 \rightarrow$		$(5.2 \pm 2.2) \times 10^{-4}$	$\Gamma_{164}$	$\bar{D}^0 D_s^+$	$(9.0 \pm 0.9) \times 10^{-3}$	
	$D^*(2010)^- \pi^+$			$\Gamma_{165}$	$D_{s0}^*(2317)^+ \bar{D}^0, D_{s0}^{*+} \rightarrow$	$(8.0 \pm \begin{matrix} 1.6 \\ -1.3 \end{matrix}) \times 10^{-4}$	
					$D_s^+ \pi^0$		
$\Gamma_{114}$	$D^- \pi^+ \pi^+$		$(1.07 \pm 0.05) \times 10^{-3}$	$\Gamma_{166}$	$D_{s0}(2317)^+ \bar{D}^0 \times$	$< 7.6$	$\times 10^{-4}$ CL=90%
$\Gamma_{115}$	$D^- K^+ \pi^+$		$(7.7 \pm 0.5) \times 10^{-5}$		$B(D_{s0}(2317)^+ \rightarrow D_s^{*+} \gamma)$		
$\Gamma_{116}$	$D_0^*(2300)^0 K^+, D_0^{*0} \rightarrow$		$(6.1 \pm 2.4) \times 10^{-6}$	$\Gamma_{167}$	$D_{s0}(2317)^+ \bar{D}^*(2007)^0 \times$	$(9 \pm 7) \times 10^{-4}$	
					$B(D_{s0}(2317)^+ \rightarrow D_s^+ \pi^0)$		
$\Gamma_{117}$	$D_2^*(2460)^0 K^+, D_2^{*0} \rightarrow$		$(2.32 \pm 0.23) \times 10^{-5}$	$\Gamma_{168}$	$D_{sJ}(2457)^+ \bar{D}^0$	$(3.1 \pm \begin{matrix} 1.0 \\ 0.9 \end{matrix}) \times 10^{-3}$	
$\Gamma_{118}$	$D_1^*(2760)^0 K^+, D_1^{*0} \rightarrow$		$(3.6 \pm 1.2) \times 10^{-6}$	$\Gamma_{169}$	$D_{sJ}(2457)^+ \bar{D}^0 \times$	$(4.6 \pm \begin{matrix} 1.3 \\ -1.1 \end{matrix}) \times 10^{-4}$	
					$B(D_{sJ}(2457)^+ \rightarrow D_s^+ \gamma)$		
$\Gamma_{119}$	$D^+ K^0$		$< 2.9$	$\Gamma_{170}$	$D_{sJ}(2457)^+ \bar{D}^0 \times$	$< 2.2$	$\times 10^{-4}$ CL=90%
$\Gamma_{120}$	$D^+ K^+ \pi^-$		$(5.6 \pm 1.1) \times 10^{-6}$		$B(D_{sJ}(2457)^+ \rightarrow$		
$\Gamma_{121}$	$D_2^*(2460)^0 K^+, D_2^{*0} \rightarrow$		$< 6.3$		$D_s^+ \pi^+ \pi^-)$		
				$\Gamma_{171}$	$D_{sJ}(2457)^+ \bar{D}^0 \times$	$< 2.7$	$\times 10^{-4}$ CL=90%
					$B(D_{sJ}(2457)^+ \rightarrow D_s^+ \pi^0)$		
$\Gamma_{122}$	$D^+ K^{*0}$		$< 4.9$	$\Gamma_{172}$	$D_{sJ}(2457)^+ \bar{D}^0 \times$	$< 9.8$	$\times 10^{-4}$ CL=90%
$\Gamma_{123}$	$D^+ \bar{K}^{*0}$		$< 1.4$		$B(D_{sJ}(2457)^+ \rightarrow D_s^{*+} \gamma)$		
$\Gamma_{124}$	$\bar{D}^*(2007)^0 \pi^+$		$(4.90 \pm 0.17) \times 10^{-3}$	$\Gamma_{173}$	$D_{sJ}(2457)^+ \bar{D}^*(2007)^0$	$(1.20 \pm 0.30) \%$	
$\Gamma_{125}$	$\bar{D}_{CP(+)}^0 \pi^+$	[d]	$(2.7 \pm 0.6) \times 10^{-3}$	$\Gamma_{174}$	$D_{sJ}(2457)^+ \bar{D}^*(2007)^0 \times$	$(1.4 \pm \begin{matrix} 0.7 \\ 0.6 \end{matrix}) \times 10^{-3}$	
$\Gamma_{126}$	$\bar{D}_{CP(-)}^0 \pi^+$	[d]	$(2.4 \pm 0.9) \times 10^{-3}$		$B(D_{sJ}(2457)^+ \rightarrow D_s^+ \gamma)$		
$\Gamma_{127}$	$\bar{D}^*(2007)^0 \omega \pi^+$		$(4.5 \pm 1.2) \times 10^{-3}$	$\Gamma_{175}$	$\bar{D}^0 D_{s1}(2536)^+ \times$	$(4.0 \pm 1.0) \times 10^{-4}$	
$\Gamma_{128}$	$\bar{D}^*(2007)^0 \rho^+$		$(9.8 \pm 1.7) \times 10^{-3}$		$B(D_{s1}(2536)^+ \rightarrow$		
$\Gamma_{129}$	$\bar{D}^*(2007)^0 K^+$		$(3.97 \pm \begin{matrix} 0.31 \\ 0.28 \end{matrix}) \times 10^{-4}$		$D^*(2007)^0 K^+ +$		
					$D^*(2010)^+ K^0)$		
$\Gamma_{130}$	$\bar{D}_{CP(+)}^0 K^+$	[d]	$(2.60 \pm 0.33) \times 10^{-4}$	$\Gamma_{176}$	$\bar{D}^0 D_{s1}(2536)^+ \times$	$(2.2 \pm 0.7) \times 10^{-4}$	
$\Gamma_{131}$	$\bar{D}_{CP(-)}^0 K^+$	[d]	$(2.19 \pm 0.30) \times 10^{-4}$		$B(D_{s1}(2536)^+ \rightarrow$		
$\Gamma_{132}$	$D^*(2007)^0 K^+$		$(7.8 \pm 2.2) \times 10^{-6}$		$D^*(2007)^0 K^+ +$		
$\Gamma_{133}$	$\bar{D}^*(2007)^0 K^*(892)^+$		$(8.1 \pm 1.4) \times 10^{-4}$		$D^*(2010)^+ K^0)$		
$\Gamma_{134}$	$\bar{D}^*(2007)^0 K^+ \bar{K}^0$		$< 1.06$	$\Gamma_{177}$	$\bar{D}^*(2007)^0 D_{s1}(2536)^+ \times$	$(5.5 \pm 1.6) \times 10^{-4}$	
$\Gamma_{135}$	$\bar{D}^*(2007)^0 K^+ \bar{K}^*(892)^0$		$(1.5 \pm 0.4) \times 10^{-3}$		$B(D_{s1}(2536)^+ \rightarrow$		
$\Gamma_{136}$	$\bar{D}^*(2007)^0 \pi^+ \pi^+ \pi^-$		$(1.03 \pm 0.12) \%$		$D^*(2007)^0 K^+)$		
$\Gamma_{137}$	$\bar{D}^*(2007)^0 a_1(1260)^+$		$(1.9 \pm 0.5) \%$	$\Gamma_{178}$	$\bar{D}^0 D_{s1}(2536)^+ \times$	$(2.3 \pm 1.1) \times 10^{-4}$	
$\Gamma_{138}$	$\bar{D}^*(2007)^0 \pi^- \pi^+ \pi^+ \pi^0$		$(1.8 \pm 0.4) \%$		$B(D_{s1}(2536)^+ \rightarrow D^{*+} K^0)$		
$\Gamma_{139}$	$\bar{D}^{*0} 3\pi^+ 2\pi^-$		$(5.7 \pm 1.2) \times 10^{-3}$	$\Gamma_{179}$	$\bar{D}^0 D_{sJ}(2700)^+ \times$	$(5.6 \pm 1.8) \times 10^{-4}$	S=1.7
$\Gamma_{140}$	$D^*(2010)^+ \pi^0$		$< 3.6$		$B(D_{sJ}(2700)^+ \rightarrow D^0 K^+)$		
$\Gamma_{141}$	$D^*(2010)^+ K^0$		$< 9.0$	$\Gamma_{180}$	$\bar{D}^{*0} D_{s1}(2536)^+, D_{s1}^+ \rightarrow$	$(3.9 \pm 2.6) \times 10^{-4}$	
$\Gamma_{142}$	$D^*(2010)^- \pi^+ \pi^+ \pi^0$		$(1.5 \pm 0.7) \%$		$D^{*+} K^0$		
$\Gamma_{143}$	$D^*(2010)^- \pi^+ \pi^+ \pi^+ \pi^-$		$(2.6 \pm 0.4) \times 10^{-3}$	$\Gamma_{181}$	$\bar{D}^0 D_{sJ}(2573)^+, D_{sJ}^+ \rightarrow$	$(8 \pm 15) \times 10^{-6}$	
$\Gamma_{144}$	$\bar{D}^{*0} \pi^+$	[e]	$(5.7 \pm 1.2) \times 10^{-3}$		$D^0 K^+$		
$\Gamma_{145}$	$\bar{D}_1^*(2420)^0 \pi^+$		$(1.5 \pm 0.6) \times 10^{-3}$	$\Gamma_{182}$	$\bar{D}^{*0} D_{sJ}(2573), D_{sJ}^+ \rightarrow D^0 K^+$	$< 2$	$\times 10^{-4}$ CL=90%
				$\Gamma_{183}$	$\bar{D}^*(2007)^0 D_{sJ}(2573), D_{sJ}^+ \rightarrow$	$< 5$	$\times 10^{-4}$ CL=90%
$\Gamma_{146}$	$\bar{D}_1(2420)^0 \pi^+ \times B(\bar{D}_1^0 \rightarrow$		$(2.5 \pm \begin{matrix} 1.6 \\ -1.4 \end{matrix}) \times 10^{-4}$		$D^0 K^+$		
	$\bar{D}^0 \pi^+ \pi^-)$			$\Gamma_{184}$	$\bar{D}^0 D_s^{*+}$	$(7.6 \pm 1.6) \times 10^{-3}$	
$\Gamma_{147}$	$\bar{D}_1(2420)^0 \pi^+ \times B(\bar{D}_1^0 \rightarrow$		$(2.2 \pm 1.0) \times 10^{-4}$	$\Gamma_{185}$	$\bar{D}^*(2007)^0 D_s^+$	$(8.2 \pm 1.7) \times 10^{-3}$	
	$\bar{D}^0 \pi^+ \pi^-$ (nonresonant))			$\Gamma_{186}$	$\bar{D}^*(2007)^0 D_s^{*+}$	$(1.71 \pm 0.24) \%$	
$\Gamma_{148}$	$\bar{D}_2^*(2462)^0 \pi^+$		$(3.56 \pm 0.24) \times 10^{-4}$	$\Gamma_{187}$	$D_s^{(*)+} \bar{D}^{*0}$	$(2.7 \pm 1.2) \%$	
				$\Gamma_{188}$	$\bar{D}^*(2007)^0 D^*(2010)^+$	$(8.1 \pm 1.7) \times 10^{-4}$	
$\Gamma_{149}$	$\times B(\bar{D}_3^*(2462)^0 \rightarrow D^- \pi^+)$			$\Gamma_{189}$	$\bar{D}^0 D^*(2010)^+ +$	$< 1.30$	$\%$ CL=90%
$\Gamma_{150}$	$\bar{D}_2^*(2462)^0 \pi^+ \times B(\bar{D}_2^{*0} \rightarrow$		$(2.2 \pm 1.0) \times 10^{-4}$		$\bar{D}^*(2007)^0 D^+$		
	$\bar{D}^0 \pi^- \pi^+)$			$\Gamma_{190}$	$\bar{D}^0 D^*(2010)^+$	$(3.9 \pm 0.5) \times 10^{-4}$	
$\Gamma_{151}$	$\bar{D}_2^*(2462)^0 \pi^+ \times B(\bar{D}_2^{*0} \rightarrow$		$(2.2 \pm 1.1) \times 10^{-4}$	$\Gamma_{191}$	$\bar{D}^0 D^+$	$(3.8 \pm 0.4) \times 10^{-4}$	
	$D^*(2010)^- \pi^+)$			$\Gamma_{192}$	$\bar{D}^0 D + K^0$	$(1.55 \pm 0.21) \times 10^{-3}$	
$\Gamma_{152}$	$\bar{D}_0^*(2400)^0 \pi^+$		$(6.4 \pm 1.4) \times 10^{-4}$	$\Gamma_{193}$	$D^+ \bar{D}^*(2007)^0$	$(6.3 \pm 1.7) \times 10^{-4}$	
	$\times B(\bar{D}_0^{*0}(2400)^0 \rightarrow D^- \pi^+)$			$\Gamma_{194}$	$\bar{D}^*(2007)^0 D^+ K^0$	$(2.1 \pm 0.5) \times 10^{-3}$	
$\Gamma_{153}$	$\bar{D}_1(2421)^0 \pi^+$		$(6.8 \pm 1.5) \times 10^{-4}$				
	$\times B(\bar{D}_1(2421)^0 \rightarrow D^{*-} \pi^+)$						





Γ <sub>430</sub>	$K^*(892)^+ K^+ K^-$	( 3.6 ± 0.5 ) × 10 <sup>-5</sup>	
Γ <sub>431</sub>	$K^*(892)^+ \phi$	( 10.0 ± 2.0 ) × 10 <sup>-6</sup>	S=1.7
Γ <sub>432</sub>	$\phi(K\pi)^{*+}$	( 8.3 ± 1.6 ) × 10 <sup>-6</sup>	
Γ <sub>433</sub>	$\phi K_1(1270)^+$	( 6.1 ± 1.9 ) × 10 <sup>-6</sup>	
Γ <sub>434</sub>	$\phi K_1(1400)^+$	< 3.2	× 10 <sup>-6</sup> CL=90%
Γ <sub>435</sub>	$\phi K^*(1410)^+$	< 4.3	× 10 <sup>-6</sup> CL=90%
Γ <sub>436</sub>	$\phi K_0^*(1430)^+$	( 7.0 ± 1.6 ) × 10 <sup>-6</sup>	
Γ <sub>437</sub>	$\phi K_2^*(1430)^+$	( 8.4 ± 2.1 ) × 10 <sup>-6</sup>	
Γ <sub>438</sub>	$\phi K_2^*(1770)^+$	< 1.50	× 10 <sup>-5</sup> CL=90%
Γ <sub>439</sub>	$\phi K_2^*(1820)^+$	< 1.63	× 10 <sup>-5</sup> CL=90%
Γ <sub>440</sub>	$a_1^+ K^{*0}$	< 3.6	× 10 <sup>-6</sup> CL=90%
Γ <sub>441</sub>	$K^+ \phi$	( 5.0 ± 1.2 ) × 10 <sup>-6</sup>	S=2.3
Γ <sub>442</sub>	$\eta' \eta' K^+$	< 2.5	× 10 <sup>-5</sup> CL=90%
Γ <sub>443</sub>	$\omega \phi K^+$	< 1.9	× 10 <sup>-6</sup> CL=90%
Γ <sub>444</sub>	$X(1812) K^+ \times B(X \rightarrow \omega \phi)$	< 3.2	× 10 <sup>-7</sup> CL=90%
Γ <sub>445</sub>	$K^*(892)^+ \gamma$	( 3.92 ± 0.22 ) × 10 <sup>-5</sup>	S=1.7
Γ <sub>446</sub>	$K_1(1270)^+ \gamma$	( 4.4 ± 0.7 ) × 10 <sup>-5</sup>	
Γ <sub>447</sub>	$\eta K^+ \gamma$	( 7.9 ± 0.9 ) × 10 <sup>-6</sup>	
Γ <sub>448</sub>	$\eta' K^+ \gamma$	( 2.9 ± 1.0 ) × 10 <sup>-6</sup>	
Γ <sub>449</sub>	$\phi K^+ \gamma$	( 2.7 ± 0.4 ) × 10 <sup>-6</sup>	S=1.2
Γ <sub>450</sub>	$K^+ \pi^- \pi^+ \gamma$	( 2.58 ± 0.15 ) × 10 <sup>-5</sup>	S=1.3
Γ <sub>451</sub>	$K^*(892)^0 \pi^+ \gamma$	( 2.33 ± 0.12 ) × 10 <sup>-5</sup>	
Γ <sub>452</sub>	$K^+ \rho^0 \gamma$	( 8.2 ± 0.9 ) × 10 <sup>-6</sup>	
Γ <sub>453</sub>	$(K^+ \pi^-)_{NR} \pi^+ \gamma$	( 9.9 ± 1.7 ) × 10 <sup>-6</sup>	
Γ <sub>454</sub>	$K^0 \pi^+ \pi^0 \gamma$	( 4.6 ± 0.5 ) × 10 <sup>-5</sup>	
Γ <sub>455</sub>	$K_1(1400)^+ \gamma$	( 10 ± 5 ) × 10 <sup>-6</sup>	
Γ <sub>456</sub>	$K^*(1410)^+ \gamma$	( 2.7 ± 0.8 ) × 10 <sup>-5</sup>	
Γ <sub>457</sub>	$K_0^*(1430)^0 \pi^+ \gamma$	( 1.32 ± 0.26 ) × 10 <sup>-6</sup>	
Γ <sub>458</sub>	$K_2^*(1430)^+ \gamma$	( 1.4 ± 0.4 ) × 10 <sup>-5</sup>	
Γ <sub>459</sub>	$K^*(1680)^+ \gamma$	( 6.7 ± 1.7 ) × 10 <sup>-5</sup>	
Γ <sub>460</sub>	$K_3^*(1780)^+ \gamma$	< 3.9	× 10 <sup>-5</sup> CL=90%
Γ <sub>461</sub>	$K_4^*(2045)^+ \gamma$	< 9.9	× 10 <sup>-3</sup> CL=90%

Light unflavored meson modes

Γ <sub>462</sub>	$\rho^+ \gamma$	( 9.8 ± 2.5 ) × 10 <sup>-7</sup>	
Γ <sub>463</sub>	$\pi^+ \pi^0$	( 5.5 ± 0.4 ) × 10 <sup>-6</sup>	S=1.2
Γ <sub>464</sub>	$\pi^+ \pi^+ \pi^-$	( 1.52 ± 0.14 ) × 10 <sup>-5</sup>	
Γ <sub>465</sub>	$\rho^0 \pi^+$	( 8.3 ± 1.2 ) × 10 <sup>-6</sup>	
Γ <sub>466</sub>	$\pi^+ f_0(980), f_0 \rightarrow \pi^+ \pi^-$	< 1.5	× 10 <sup>-6</sup> CL=90%
Γ <sub>467</sub>	$\pi^+ f_2(1270)$	( 2.2 ± 0.7 ) × 10 <sup>-6</sup>	
Γ <sub>468</sub>	$\rho(1450)^0 \pi^+, \rho^0 \rightarrow \pi^+ \pi^-$	( 1.4 ± 0.6 ) × 10 <sup>-6</sup>	
Γ <sub>469</sub>	$\rho(1450)^0 \pi^+, \rho^0 \rightarrow K^+ K^-$	( 1.60 ± 0.14 ) × 10 <sup>-6</sup>	
Γ <sub>470</sub>	$f_0(1370) \pi^+, f_0 \rightarrow \pi^+ \pi^-$	< 4.0	× 10 <sup>-6</sup> CL=90%
Γ <sub>471</sub>	$f_0(500) \pi^+, f_0 \rightarrow \pi^+ \pi^-$	< 4.1	× 10 <sup>-6</sup> CL=90%
Γ <sub>472</sub>	$\pi^+ \pi^- \pi^+$ nonresonant	( 5.3 ± 1.5 ) × 10 <sup>-6</sup>	
Γ <sub>473</sub>	$\pi^+ \pi^0 \pi^0$	< 8.9	× 10 <sup>-4</sup> CL=90%
Γ <sub>474</sub>	$\rho^+ \pi^0$	( 1.09 ± 0.14 ) × 10 <sup>-5</sup>	
Γ <sub>475</sub>	$\pi^+ \pi^- \pi^+ \pi^0$	< 4.0	× 10 <sup>-3</sup> CL=90%
Γ <sub>476</sub>	$\rho^+ \rho^0$	( 2.40 ± 0.19 ) × 10 <sup>-5</sup>	
Γ <sub>477</sub>	$\rho^+ f_0(980), f_0 \rightarrow \pi^+ \pi^-$	< 2.0	× 10 <sup>-6</sup> CL=90%
Γ <sub>478</sub>	$a_1(1260)^+ \pi^0$	( 2.6 ± 0.7 ) × 10 <sup>-5</sup>	
Γ <sub>479</sub>	$a_1(1260)^0 \pi^+$	( 2.0 ± 0.6 ) × 10 <sup>-5</sup>	
Γ <sub>480</sub>	$\omega \pi^+$	( 6.9 ± 0.5 ) × 10 <sup>-6</sup>	
Γ <sub>481</sub>	$\omega \rho^+$	( 1.59 ± 0.21 ) × 10 <sup>-5</sup>	
Γ <sub>482</sub>	$\eta \pi^+$	( 4.02 ± 0.27 ) × 10 <sup>-6</sup>	
Γ <sub>483</sub>	$\eta \rho^+$	( 7.0 ± 2.9 ) × 10 <sup>-6</sup>	S=2.8
Γ <sub>484</sub>	$\eta' \pi^+$	( 2.7 ± 0.9 ) × 10 <sup>-6</sup>	S=1.9
Γ <sub>485</sub>	$\eta' \rho^+$	( 9.7 ± 2.2 ) × 10 <sup>-6</sup>	
Γ <sub>486</sub>	$\phi \pi^+$	( 3.2 ± 1.5 ) × 10 <sup>-8</sup>	
Γ <sub>487</sub>	$\phi \rho^+$	< 3.0	× 10 <sup>-6</sup> CL=90%
Γ <sub>488</sub>	$a_0(980)^0 \pi^+, a_0^0 \rightarrow \eta \pi^0$	< 5.8	× 10 <sup>-6</sup> CL=90%
Γ <sub>489</sub>	$a_0(980)^+ \pi^0, a_0^+ \rightarrow \eta \pi^+$	< 1.4	× 10 <sup>-6</sup> CL=90%
Γ <sub>490</sub>	$\pi^+ \pi^+ \pi^+ \pi^-$	< 8.6	× 10 <sup>-4</sup> CL=90%
Γ <sub>491</sub>	$\rho^0 a_1(1260)^+$	< 6.2	× 10 <sup>-4</sup> CL=90%
Γ <sub>492</sub>	$\rho^0 a_2(1320)^+$	< 7.2	× 10 <sup>-4</sup> CL=90%
Γ <sub>493</sub>	$b_1^0 \pi^+, b_1^0 \rightarrow \omega \pi^0$	( 6.7 ± 2.0 ) × 10 <sup>-6</sup>	
Γ <sub>494</sub>	$b_1^+ \pi^0, b_1^+ \rightarrow \omega \pi^+$	< 3.3	× 10 <sup>-6</sup> CL=90%
Γ <sub>495</sub>	$\pi^+ \pi^+ \pi^+ \pi^- \pi^- \pi^0$	< 6.3	× 10 <sup>-3</sup> CL=90%

Γ <sub>496</sub>	$b_1^+ \rho^0, b_1^+ \rightarrow \omega \pi^+$	< 5.2	× 10 <sup>-6</sup> CL=90%
Γ <sub>497</sub>	$a_1(1260)^+ a_1(1260)^0$	< 1.3	% CL=90%
Γ <sub>498</sub>	$b_1^0 \rho^+, b_1^0 \rightarrow \omega \pi^0$	< 3.3	× 10 <sup>-6</sup> CL=90%

Charged particle (h±) modes

$h^\pm = K^\pm \text{ or } \pi^\pm$			
Γ <sub>499</sub>	$h^+ \pi^0$	( 1.6 ± 0.7 ) × 10 <sup>-5</sup>	
Γ <sub>500</sub>	$\omega h^+$	( 1.38 ± 0.27 ) × 10 <sup>-5</sup>	
Γ <sub>501</sub>	$h^+ \chi^0(\text{Familon})$	< 4.9	× 10 <sup>-5</sup> CL=90%
Γ <sub>502</sub>	$K^+ \chi^0, \chi^0 \rightarrow \mu^+ \mu^-$	< 1	× 10 <sup>-7</sup> CL=95%

Baryon modes

Γ <sub>503</sub>	$p \bar{p} \pi^+$	( 1.62 ± 0.20 ) × 10 <sup>-6</sup>	
Γ <sub>504</sub>	$p \bar{p} \pi^+$ nonresonant	< 5.3	× 10 <sup>-5</sup> CL=90%
Γ <sub>505</sub>	$p \bar{p} \pi^+ \pi^-$		
Γ <sub>506</sub>	$p \bar{p} K^+$	( 5.9 ± 0.5 ) × 10 <sup>-6</sup>	S=1.5
Γ <sub>507</sub>	$\Theta(1710)^{++} \bar{p}, \Theta^{++} \rightarrow p K^+$	[g] < 9.1	× 10 <sup>-8</sup> CL=90%
Γ <sub>508</sub>	$f_J(2220) K^+, f_J \rightarrow p \bar{p}$	[g] < 4.1	× 10 <sup>-7</sup> CL=90%
Γ <sub>509</sub>	$\rho \bar{\Lambda}(1520)$	( 3.1 ± 0.6 ) × 10 <sup>-7</sup>	
Γ <sub>510</sub>	$p \bar{p} K^+$ nonresonant	< 8.9	× 10 <sup>-5</sup> CL=90%
Γ <sub>511</sub>	$p \bar{p} K^*(892)^+$	( 3.6 ± 0.8 ) × 10 <sup>-6</sup>	
Γ <sub>512</sub>	$f_J(2220) K^{*+}, f_J \rightarrow p \bar{p}$	< 7.7	× 10 <sup>-7</sup> CL=90%
Γ <sub>513</sub>	$\rho \bar{\Lambda}$	( 2.4 ± 1.0 ) × 10 <sup>-7</sup>	
Γ <sub>514</sub>	$\rho \bar{\Lambda} \gamma$	( 2.4 ± 0.5 ) × 10 <sup>-6</sup>	
Γ <sub>515</sub>	$\rho \bar{\Lambda} \pi^0$	( 3.0 ± 0.7 ) × 10 <sup>-6</sup>	
Γ <sub>516</sub>	$\rho \bar{\Sigma}(1385)^0$	< 4.7	× 10 <sup>-7</sup> CL=90%
Γ <sub>517</sub>	$\Delta^+ \bar{\Lambda}$	< 8.2	× 10 <sup>-7</sup> CL=90%
Γ <sub>518</sub>	$\rho \bar{\Sigma} \gamma$	< 4.6	× 10 <sup>-6</sup> CL=90%
Γ <sub>519</sub>	$\rho \bar{\Lambda} \pi^+ \pi^-$	( 1.13 ± 0.13 ) × 10 <sup>-5</sup>	
Γ <sub>520</sub>	$\rho \bar{\Lambda} \pi^+ \pi^-$ nonresonant	( 5.9 ± 1.1 ) × 10 <sup>-6</sup>	
Γ <sub>521</sub>	$\rho \bar{\Lambda} \rho^0, \rho^0 \rightarrow \pi^+ \pi^-$	( 4.8 ± 0.9 ) × 10 <sup>-6</sup>	
Γ <sub>522</sub>	$\rho \bar{\Lambda} f_2(1270), f_2 \rightarrow \pi^+ \pi^-$	( 2.0 ± 0.8 ) × 10 <sup>-6</sup>	
Γ <sub>523</sub>	$\rho \bar{\Lambda} K^+ K^-$	( 4.1 ± 0.7 ) × 10 <sup>-6</sup>	
Γ <sub>524</sub>	$\rho \bar{\Lambda} \phi$	( 8.0 ± 2.2 ) × 10 <sup>-7</sup>	
Γ <sub>525</sub>	$\bar{p} \bar{\Lambda} K^+ K^-$	( 3.7 ± 0.6 ) × 10 <sup>-6</sup>	
Γ <sub>526</sub>	$\bar{\Lambda} \bar{\Lambda} \pi^+$	< 9.4	× 10 <sup>-7</sup> CL=90%
Γ <sub>527</sub>	$\bar{\Lambda} \bar{\Lambda} K^+$	( 3.4 ± 0.6 ) × 10 <sup>-6</sup>	
Γ <sub>528</sub>	$\bar{\Lambda} \bar{\Lambda} K^{*+}$	( 2.2 ± 1.2 ) × 10 <sup>-6</sup>	
Γ <sub>529</sub>	$\Lambda(1520) \bar{\Lambda} K^+$	( 2.2 ± 0.7 ) × 10 <sup>-6</sup>	
Γ <sub>530</sub>	$\bar{\Lambda} \bar{\Lambda}(1520) K^+$	< 2.08	× 10 <sup>-6</sup>
Γ <sub>531</sub>	$\bar{\Delta}^0 \rho$	< 1.38	× 10 <sup>-6</sup> CL=90%
Γ <sub>532</sub>	$\bar{\Delta}^{++} \bar{p}$	< 1.4	× 10 <sup>-7</sup> CL=90%
Γ <sub>533</sub>	$D^+ p \bar{p}$	< 1.5	× 10 <sup>-5</sup> CL=90%
Γ <sub>534</sub>	$D^*(2010)^+ p \bar{p}$	< 1.5	× 10 <sup>-5</sup> CL=90%
Γ <sub>535</sub>	$\bar{D}^0 p \bar{p} \pi^+$	( 3.72 ± 0.27 ) × 10 <sup>-4</sup>	
Γ <sub>536</sub>	$\bar{D}^{*0} p \bar{p} \pi^+$	( 3.73 ± 0.32 ) × 10 <sup>-4</sup>	
Γ <sub>537</sub>	$D^- p \bar{p} \pi^+ \pi^-$	( 1.66 ± 0.30 ) × 10 <sup>-4</sup>	
Γ <sub>538</sub>	$D^{*-} p \bar{p} \pi^+ \pi^-$	( 1.86 ± 0.25 ) × 10 <sup>-4</sup>	
Γ <sub>539</sub>	$\rho \bar{\Lambda}^0 \bar{D}^0$	( 1.43 ± 0.32 ) × 10 <sup>-5</sup>	
Γ <sub>540</sub>	$\rho \bar{\Lambda}^0 \bar{D}^*(2007)^0$	< 5	× 10 <sup>-5</sup> CL=90%
Γ <sub>541</sub>	$\bar{\Lambda}_c^- p \pi^+$	( 2.3 ± 0.4 ) × 10 <sup>-4</sup>	S=2.2
Γ <sub>542</sub>	$\bar{\Lambda}_c^- \Delta(1232)^{++}$	< 1.9	× 10 <sup>-5</sup> CL=90%
Γ <sub>543</sub>	$\bar{\Lambda}_c^- \Delta_X(1600)^{++}$	( 4.7 ± 1.0 ) × 10 <sup>-5</sup>	
Γ <sub>544</sub>	$\bar{\Lambda}_c^- \Delta_X(2420)^{++}$	( 3.7 ± 0.8 ) × 10 <sup>-5</sup>	
Γ <sub>545</sub>	$(\bar{\Lambda}_c^- p)_s \pi^+$	[h] ( 3.1 ± 0.7 ) × 10 <sup>-5</sup>	
Γ <sub>546</sub>	$\bar{\Sigma}_c(2520)^0 p$	< 3	× 10 <sup>-6</sup> CL=90%
Γ <sub>547</sub>	$\bar{\Sigma}_c(2800)^0 p$	( 2.6 ± 0.9 ) × 10 <sup>-5</sup>	
Γ <sub>548</sub>	$\bar{\Lambda}_c^- p \pi^+ \pi^0$	( 1.8 ± 0.6 ) × 10 <sup>-3</sup>	
Γ <sub>549</sub>	$\bar{\Lambda}_c^- p \pi^+ \pi^+ \pi^-$	( 2.2 ± 0.7 ) × 10 <sup>-3</sup>	
Γ <sub>550</sub>	$\bar{\Lambda}_c^- p \pi^+ \pi^+ \pi^- \pi^0$	< 1.34	% CL=90%
Γ <sub>551</sub>	$\Lambda_c^+ \bar{\Lambda}_c^- K^+$	( 4.9 ± 0.7 ) × 10 <sup>-4</sup>	
Γ <sub>552</sub>	$\Xi_c(2930) \Lambda_c^+, \Xi_c \rightarrow K^+ \bar{\Lambda}_c^-$	( 1.7 ± 0.5 ) × 10 <sup>-4</sup>	
Γ <sub>553</sub>	$\bar{\Sigma}_c(2455)^0 p$	( 2.9 ± 0.7 ) × 10 <sup>-5</sup>	
Γ <sub>554</sub>	$\bar{\Sigma}_c(2455)^0 p \pi^0$	( 3.5 ± 1.1 ) × 10 <sup>-4</sup>	
Γ <sub>555</sub>	$\bar{\Sigma}_c(2455)^0 p \pi^- \pi^+$	( 3.5 ± 1.1 ) × 10 <sup>-4</sup>	
Γ <sub>556</sub>	$\bar{\Sigma}_c(2455)^- p \pi^+ \pi^+$	( 2.37 ± 0.20 ) × 10 <sup>-4</sup>	
Γ <sub>557</sub>	$\bar{\Lambda}_c(2593)^- / \bar{\Lambda}_c(2625)^- p \pi^+$	< 1.9	× 10 <sup>-4</sup> CL=90%
Γ <sub>558</sub>	$\Xi_c^0 \Lambda_c^+$	( 9.5 ± 2.3 ) × 10 <sup>-4</sup>	
Γ <sub>559</sub>	$\Xi_c^0 \Lambda_c^+, \Xi_c^0 \rightarrow \Xi^+ \pi^-$	( 1.76 ± 0.29 ) × 10 <sup>-5</sup>	



$\Gamma(\overline{D}^0 \ell^+ \nu_\ell)/\Gamma_{\text{total}}$   $\Gamma_4/\Gamma$   
 "OUR EVALUATION" is an average using rescaled values of the data listed below. The average and rescaling were performed by the Heavy Flavor Averaging Group (HFLAV) and are described at <https://hflav.web.cern.ch/>. The averaging/rescaling procedure takes into account correlations between the measurements.  $\ell = e$  or  $\mu$ , not sum over  $e$  and  $\mu$  modes.

VALUE (%) DOCUMENT ID TECN COMMENT  
**2.35 ± 0.03 ± 0.09 OUR EVALUATION**  
**2.29 ± 0.08 OUR AVERAGE**

2.29 ± 0.08 ± 0.09	<sup>1</sup> AUBERT	10	BABR	$e^+e^- \rightarrow \Upsilon(4S)$
2.34 ± 0.03 ± 0.13	AUBERT	09A	BABR	$e^+e^- \rightarrow \Upsilon(4S)$
2.21 ± 0.13 ± 0.19	<sup>2</sup> BARTELT	99	CLE2	$e^+e^- \rightarrow \Upsilon(4S)$
1.6 ± 0.6 ± 0.3	<sup>3</sup> FULTON	91	CLEO	$e^+e^- \rightarrow \Upsilon(4S)$
2.33 ± 0.09 ± 0.09	<sup>1</sup> AUBERT	08Q	BABR	Repl. by AUBERT 09A
1.94 ± 0.15 ± 0.34	<sup>4</sup> ATHANAS	97	CLE2	Repl. by BARTELT 99

- • • We do not use the following data for averages, fits, limits, etc. • • •
- <sup>1</sup> Uses a fully reconstructed  $B$  meson as a tag on the recoil side.
- <sup>2</sup> Assumes equal production of  $B^+$  and  $B^0$  at the  $\Upsilon(4S)$ .
- <sup>3</sup> FULTON 91 assumes equal production of  $B^0\overline{B}^0$  and  $B^+B^-$  at the  $\Upsilon(4S)$ .
- <sup>4</sup> ATHANAS 97 uses missing energy and missing momentum to reconstruct neutrino.

$\Gamma(\overline{D}^0 \ell^+ \nu_\ell)/\Gamma(\ell^+ \nu_\ell X)$   $\Gamma_4/\Gamma_1$

VALUE	DOCUMENT ID	TECN	COMMENT	$\chi^2$
<b>0.255 ± 0.009 ± 0.009</b>	<sup>1</sup> AUBERT	10	BABR $e^+e^- \rightarrow \Upsilon(4S)$	0.8
				0.0
				3.7
				4.5

- <sup>1</sup> Uses a fully reconstructed  $B$  meson on the recoil side.

$\Gamma(\overline{D}^0 \ell^+ \nu_\ell)/\Gamma(D \ell^+ \nu_\ell X)$   $\Gamma_4/\Gamma_3$

VALUE	DOCUMENT ID	TECN	COMMENT
<b>0.230 ± 0.020 OUR AVERAGE</b>			
0.25 ± 0.06	<sup>1</sup> AAIJ	19AC	LHCB $pp$ at 7 and 8 TeV
0.227 ± 0.014 ± 0.016	<sup>2</sup> AUBERT	07AN	BABR $e^+e^- \rightarrow \Upsilon(4S)$

- <sup>1</sup> The relative branching fractions of  $B^- \rightarrow D^0, D^{*0}, D^{*0}$  in the  $B^- \rightarrow D^0 X \mu^- \overline{\nu}$  channel are determined by fitting the distribution of the missing mass in  $\overline{B}_s^{*0} \rightarrow B^- K^+$  decays.
- <sup>2</sup> Uses a fully reconstructed  $B$  meson on the recoil side.

$\Gamma(\overline{D}^0 \tau^+ \nu_\tau)/\Gamma_{\text{total}}$   $\Gamma_5/\Gamma$

VALUE (units $10^{-2}$ )	DOCUMENT ID	TECN	COMMENT
<b>0.77 ± 0.22 ± 0.12</b>	<sup>1</sup> BOZEK	10	BELL $e^+e^- \rightarrow \Upsilon(4S)$
0.67 ± 0.37 ± 0.13	<sup>2</sup> AUBERT	08N	BABR Repl. by AUBERT 09s

- • • We do not use the following data for averages, fits, limits, etc. • • •
- <sup>1</sup> Assumes equal production of  $B^+$  and  $B^0$  at the  $\Upsilon(4S)$ .
- <sup>2</sup> Uses a fully reconstructed  $B$  meson as a tag on the recoil side.

$\Gamma(\overline{D}^0 \tau^+ \nu_\tau)/\Gamma(\overline{D}^0 \ell^+ \nu_\ell)$   $\Gamma_5/\Gamma_4$

VALUE	DOCUMENT ID	TECN	COMMENT
<b>0.429 ± 0.082 ± 0.052</b>	<sup>1,2</sup> LEES	12D	BABR $e^+e^- \rightarrow \Upsilon(4S)$
0.314 ± 0.170 ± 0.049	<sup>1</sup> AUBERT	09s	BABR Repl. by LEES 12D

- <sup>1</sup> Uses a fully reconstructed  $B$  meson as a tag on the recoil side.
- <sup>2</sup> Uses  $\tau^+ \rightarrow e^+ \nu_e \overline{\nu}_\tau$  and  $\tau^+ \rightarrow \mu^+ \nu_\mu \overline{\nu}_\tau$  and  $e^+$  or  $\mu^+$  as  $\ell^+$ .

$\Gamma(\overline{D}^*(2007)^0 \ell^+ \nu_\ell)/\Gamma_{\text{total}}$   $\Gamma_6/\Gamma$

"OUR EVALUATION" is an average using rescaled values of the data listed below. The average and rescaling were performed by the Heavy Flavor Averaging Group (HFLAV) and are described at <https://hflav.web.cern.ch/>. The averaging/rescaling procedure takes into account correlations between the measurements.  $\ell = e$  or  $\mu$ , not sum over  $e$  and  $\mu$  modes.

VALUE (%) EVTS DOCUMENT ID TECN COMMENT  
**5.66 ± 0.07 ± 0.21 OUR EVALUATION**

**5.60 ± 0.26 OUR FIT** Error includes scale factor of 1.5.  
**5.58 ± 0.26 OUR AVERAGE** Error includes scale factor of 1.5. See the ideogram below.

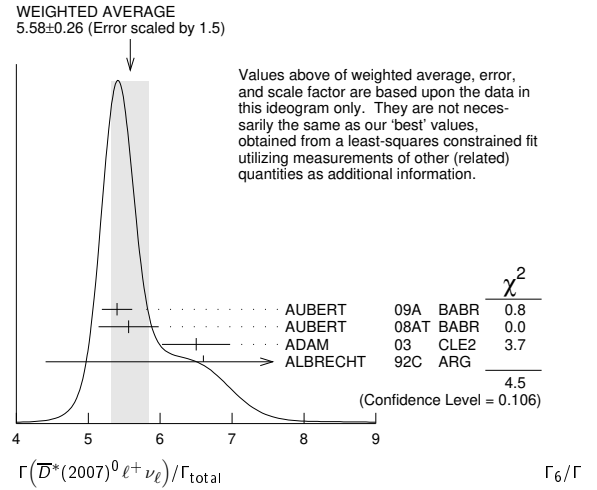
5.40 ± 0.02 ± 0.21	AUBERT	09A	BABR	$e^+e^- \rightarrow \Upsilon(4S)$
5.56 ± 0.08 ± 0.41	<sup>1</sup> AUBERT	08AT	BABR	$e^+e^- \rightarrow \Upsilon(4S)$
6.50 ± 0.20 ± 0.43	<sup>2</sup> ADAM	03	CLE2	$e^+e^- \rightarrow \Upsilon(4S)$
6.6 ± 1.6 ± 1.5	<sup>3</sup> ALBRECHT	92C	ARG	$e^+e^- \rightarrow \Upsilon(4S)$
5.83 ± 0.15 ± 0.30	<sup>4</sup> AUBERT	08Q	BABR	Repl. by AUBERT 09A
6.50 ± 0.20 ± 0.43	<sup>5</sup> BRIERE	02	CLE2	$e^+e^- \rightarrow \Upsilon(4S)$
5.13 ± 0.54 ± 0.64	<sup>6</sup> BARISH	95	CLE2	Repl. by ADAM 03
seen	<sup>7</sup> SANGHERA	93	CLE2	$e^+e^- \rightarrow \Upsilon(4S)$
4.1 ± 0.8 ± 0.8	<sup>8</sup> FULTON	91	CLEO	$e^+e^- \rightarrow \Upsilon(4S)$
7.0 ± 1.8 ± 1.4	<sup>9</sup> ANTREASYAN	90B	CBAL	$e^+e^- \rightarrow \Upsilon(4S)$

- • • We do not use the following data for averages, fits, limits, etc. • • •
- <sup>1</sup> Measured using the dependence of  $B^- \rightarrow D^{*0} e^- \overline{\nu}_e$  decay differential rate and the form factor description by CAPRINI 98.
- <sup>2</sup> Simultaneous measurements of both  $B^0 \rightarrow D^*(2010)^- \ell \nu$  and  $B^+ \rightarrow \overline{D}^*(2007)^0 \ell \nu$ .
- <sup>3</sup> ALBRECHT 92C reports  $0.058 \pm 0.014 \pm 0.013$ . We rescale using the method described in STONE 94 but with the updated PDG 94  $B(D^0 \rightarrow K^- \pi^+)$ . Assumes equal production of  $B^0\overline{B}^0$  and  $B^+B^-$  at the  $\Upsilon(4S)$ .
- <sup>4</sup> Uses a fully reconstructed  $B$  meson as a tag on the recoil side.
- <sup>5</sup> The results are based on the same analysis and data sample reported in ADAM 03.
- <sup>6</sup> BARISH 95 use  $B(D^0 \rightarrow K^- \pi^+) = (3.91 \pm 0.08 \pm 0.17)\%$  and  $B(D^{*0} \rightarrow D^0 \pi^0) = (63.6 \pm 2.3 \pm 3.3)\%$ .

<sup>7</sup> Combining  $\overline{D}^{*0} \ell^+ \nu_\ell$  and  $\overline{D}^{*-} \ell^+ \nu_\ell$  SANGHERA 93 test  $V-A$  structure and fit the decay angular distributions to obtain  $A_{FB} = 3/4 * (\Gamma^- - \Gamma^+)/\Gamma = 0.14 \pm 0.06 \pm 0.03$ . Assuming a value of  $V_{cb}$ , they measure  $V, A_1,$  and  $A_2$ , the three form factors for the  $D^* \ell \nu_\ell$  decay, where results are slightly dependent on model assumptions.

<sup>8</sup> Assumes equal production of  $B^0\overline{B}^0$  and  $B^+B^-$  at the  $\Upsilon(4S)$ . Uncorrected for  $D$  and  $D^*$  branching ratio assumptions.

<sup>9</sup> ANTREASYAN 90B is average over  $B$  and  $\overline{D}^*(2010)$  charge states.



$\Gamma(\overline{D}^*(2007)^0 \ell^+ \nu_\ell)/\Gamma(D \ell^+ \nu_\ell X)$   $\Gamma_6/\Gamma_3$

VALUE	DOCUMENT ID	TECN	COMMENT
<b>0.582 ± 0.018 ± 0.030</b>	<sup>1</sup> AUBERT	07AN	BABR $e^+e^- \rightarrow \Upsilon(4S)$

- <sup>1</sup> Uses a fully reconstructed  $B$  meson on the recoil side.

$\Gamma(\overline{D}^*(2007)^0 \tau^+ \nu_\tau)/\Gamma_{\text{total}}$   $\Gamma_7/\Gamma$

VALUE (units $10^{-2}$ )	DOCUMENT ID	TECN	COMMENT
<b>1.88 ± 0.20 OUR FIT</b>			
<b>2.12 ± 0.28 ± 0.29</b>	<sup>1</sup> BOZEK	10	BELL $e^+e^- \rightarrow \Upsilon(4S)$

- • • We do not use the following data for averages, fits, limits, etc. • • •
- 2.25 ± 0.48 ± 0.28 <sup>2</sup> AUBERT 08N BABR Repl. by AUBERT 09s
- <sup>1</sup> Assumes equal production of  $B^+$  and  $B^0$  at the  $\Upsilon(4S)$ .
- <sup>2</sup> Uses a fully reconstructed  $B$  meson as a tag on the recoil side.

$\Gamma(\overline{D}^*(2007)^0 \tau^+ \nu_\tau)/\Gamma(\overline{D}^*(2007)^0 \ell^+ \nu_\ell)$   $\Gamma_7/\Gamma_6$

VALUE	DOCUMENT ID	TECN	COMMENT
<b>0.335 ± 0.034 OUR FIT</b>			
<b>0.322 ± 0.032 ± 0.022</b>	<sup>1,2</sup> LEES	12D	BABR $e^+e^- \rightarrow \Upsilon(4S)$
0.346 ± 0.073 ± 0.034	<sup>1</sup> AUBERT	09s	BABR Repl. by LEES 12D

- • • We do not use the following data for averages, fits, limits, etc. • • •
- <sup>1</sup> Uses a fully reconstructed  $B$  meson as a tag on the recoil side.
- <sup>2</sup> Uses  $\tau^+ \rightarrow e^+ \nu_e \overline{\nu}_\tau$  and  $\tau^+ \rightarrow \mu^+ \nu_\mu \overline{\nu}_\tau$  and  $e^+$  or  $\mu^+$  as  $\ell^+$ .

$\Gamma(D^- \pi^+ \ell^+ \nu_\ell)/\Gamma_{\text{total}}$   $\Gamma_8/\Gamma$

VALUE (units $10^{-3}$ )	DOCUMENT ID	TECN	COMMENT
<b>4.4 ± 0.4 OUR AVERAGE</b>			
4.55 ± 0.27 ± 0.39	VOSSEN	18	BELL $e^+e^- \rightarrow \Upsilon(4S)$
4.2 ± 0.6 ± 0.3	<sup>1</sup> AUBERT	08Q	BABR $e^+e^- \rightarrow \Upsilon(4S)$

- • • We do not use the following data for averages, fits, limits, etc. • • •
- 4.4 ± 0.6 ± 0.2 <sup>1,2</sup> LIVENTSEV 08 BELL Repl. by VOSSEN 18
- 5.8 ± 1.0 ± 0.2 <sup>3</sup> LIVENTSEV 05 BELL Repl. by LIVENTSEV 08
- <sup>1</sup> Uses a fully reconstructed  $B$  meson as a tag on the recoil side.
- <sup>2</sup> LIVENTSEV 08 reports  $(4.0 \pm 0.4 \pm 0.6) \times 10^{-3}$  from a measurement of  $[\Gamma(B^+ \rightarrow D^- \pi^+ \ell^+ \nu_\ell)/\Gamma_{\text{total}}] / [B(B^+ \rightarrow \overline{D}^0 \ell^+ \nu_\ell)]$  assuming  $B(B^+ \rightarrow \overline{D}^0 \ell^+ \nu_\ell) = (2.15 \pm 0.22) \times 10^{-2}$ , which we rescale to our best value  $B(B^+ \rightarrow \overline{D}^0 \ell^+ \nu_\ell) = (2.35 \pm 0.09) \times 10^{-2}$ . Our first error is their experiment's error and our second error is the systematic error from using our best value.
- <sup>3</sup> LIVENTSEV 05 reports  $[\Gamma(B^+ \rightarrow D^- \pi^+ \ell^+ \nu_\ell)/\Gamma_{\text{total}}] / [B(B^0 \rightarrow D^- \ell^+ \nu_\ell)] = 0.25 \pm 0.03 \pm 0.03$  which we multiply by our best value  $B(B^0 \rightarrow D^- \ell^+ \nu_\ell) = (2.31 \pm 0.10) \times 10^{-2}$ . Our first error is their experiment's error and our second error is the systematic error from using our best value.

$\Gamma(\overline{D}_s^*(2420)^0 \ell^+ \nu_\ell, \overline{D}_s^{*0} \rightarrow D^- \pi^+)/\Gamma_{\text{total}}$   $\Gamma_9/\Gamma$

VALUE (units $10^{-3}$ )	DOCUMENT ID	TECN	COMMENT
<b>2.5 ± 0.5 OUR AVERAGE</b>			
2.6 ± 0.5 ± 0.4	<sup>1</sup> AUBERT	08BL	BABR $e^+e^- \rightarrow \Upsilon(4S)$
2.4 ± 0.4 ± 0.6	<sup>1</sup> LIVENTSEV	08	BELL $e^+e^- \rightarrow \Upsilon(4S)$

- <sup>1</sup> Uses a fully reconstructed  $B$  meson as a tag on the recoil side.



## Meson Particle Listings

 $B^\pm$  $\Gamma(\bar{D}_2^*(2460)^0 \ell^+ \nu_\ell, \bar{D}_2^{*0} \rightarrow D^- \pi^+) / \Gamma_{\text{total}}$   $\Gamma_{10} / \Gamma$ 

VALUE (units $10^{-3}$ )	DOCUMENT ID	TECN	COMMENT
<b>1.53 ± 0.16 OUR AVERAGE</b>			
1.42 ± 0.15 ± 0.15	<sup>1</sup> AUBERT	09Y	BABR $e^+ e^- \rightarrow \Upsilon(4S)$
1.5 ± 0.2 ± 0.2	<sup>2</sup> AUBERT	08BL	BABR $e^+ e^- \rightarrow \Upsilon(4S)$
2.2 ± 0.3 ± 0.4	<sup>2</sup> LIVENTSEV	08	BELL $e^+ e^- \rightarrow \Upsilon(4S)$

- <sup>1</sup> Uses a simultaneous fit of all  $B$  semileptonic decays without full reconstruction of events. AUBERT 09Y reports  $B(B^+ \rightarrow \bar{D}_2^*(2460)^0 \ell^+ \nu_\ell) \cdot B(\bar{D}_2^*(2460)^0 \rightarrow D^{(*)-} \pi^+) = (2.29 \pm 0.23 \pm 0.21) \times 10^{-3}$  and the authors have provided us the individual measurement.
- <sup>2</sup> Uses a fully reconstructed  $B$  meson as a tag on the recoil side.

 $\Gamma(D^{(*)-} n \pi \ell^+ \nu_\ell (n \geq 1)) / \Gamma(D \ell^+ \nu_\ell X)$   $\Gamma_{11} / \Gamma_3$ 

VALUE	DOCUMENT ID	TECN	COMMENT
<b>0.193 ± 0.022 OUR AVERAGE</b>			
0.21 ± 0.07	<sup>1,2</sup> AAIJ	19AC	LHCB $pp$ at 7 and 8 TeV
0.191 ± 0.013 ± 0.019	<sup>3</sup> AUBERT	07AN	BABR $e^+ e^- \rightarrow \Upsilon(4S)$

- <sup>1</sup> The relative branching fractions of  $B^- \rightarrow D^0, D^{*0}, D^{*0}$  in the  $B^- \rightarrow D^0 X \mu^- \bar{\nu}$  channel are determined by fitting the distribution of the missing mass in  $\bar{B}_s^0 \rightarrow B^- K^+$  decays.
- <sup>2</sup> In this measurement of  $f_{D^{*0}} = B(B^- \rightarrow (D^{*0} \rightarrow D^0 X) \mu^- \bar{\nu}) / B(B^- \rightarrow D^0 X \mu^- \bar{\nu})$ ,  $D^{*0}$  refers collectively to L = 1 states  $D_0^*(2400), D_1^*(2420), D_1^*(2430)$ , and  $D_2^*(2460)$ , as well as other resonances such as radially excited  $D$  mesons, and to nonresonant contributions with additional pions.
- <sup>3</sup> Uses a fully reconstructed  $B$  meson on the recoil side.

 $\Gamma(D^{*-} \pi^+ \ell^+ \nu_\ell) / \Gamma_{\text{total}}$   $\Gamma_{12} / \Gamma$ 

VALUE (units $10^{-3}$ )	DOCUMENT ID	TECN	COMMENT
<b>6.0 ± 0.4 OUR AVERAGE</b>			
6.03 ± 0.43 ± 0.38		VOSSEN	18 BELL $e^+ e^- \rightarrow \Upsilon(4S)$
5.9 ± 0.5 ± 0.4	<sup>1</sup> AUBERT	08Q	BABR $e^+ e^- \rightarrow \Upsilon(4S)$

- • • We do not use the following data for averages, fits, limits, etc. • • •
- 7.0 ± 1.1 ± 0.3 <sup>1,2</sup> LIVENTSEV 08 BELL Repl. by VOSSEN 18
- 6.1 ± 1.4 ± 0.2 <sup>3,4</sup> LIVENTSEV 05 BELL Repl. by LIVENTSEV 08
- <sup>1</sup> Uses a fully reconstructed  $B$  meson as a tag on the recoil side.
- <sup>2</sup> LIVENTSEV 08 reports  $(6.4 \pm 0.8 \pm 0.9) \times 10^{-3}$  from a measurement of  $[\Gamma(B^+ \rightarrow D^{*-} \pi^+ \ell^+ \nu_\ell) / \Gamma_{\text{total}}] / [B(B^+ \rightarrow \bar{D}^0 \ell^+ \nu_\ell)]$  assuming  $B(B^+ \rightarrow \bar{D}^0 \ell^+ \nu_\ell) = (2.15 \pm 0.22) \times 10^{-2}$ , which we rescale to our best value  $B(B^+ \rightarrow \bar{D}^0 \ell^+ \nu_\ell) = (2.35 \pm 0.09) \times 10^{-2}$ . Our first error is their experiment's error and our second error is the systematic error from using our best value.
- <sup>3</sup> Excludes  $D^{*+}$  contribution to  $D$  modes.
- <sup>4</sup> LIVENTSEV 05 reports  $[\Gamma(B^+ \rightarrow D^{*-} \pi^+ \ell^+ \nu_\ell) / \Gamma_{\text{total}}] / [B(B^0 \rightarrow D^*(2010)^- \ell^+ \nu_\ell)] = 0.12 \pm 0.02 \pm 0.02$  which we multiply by our best value  $B(B^0 \rightarrow D^*(2010)^- \ell^+ \nu_\ell) = (5.05 \pm 0.14) \times 10^{-2}$ . Our first error is their experiment's error and our second error is the systematic error from using our best value.

 $\Gamma(\bar{D}_1(2420)^0 \ell^+ \nu_\ell, \bar{D}_1^0 \rightarrow D^{*-} \pi^+) / \Gamma_{\text{total}}$   $\Gamma_{13} / \Gamma$ 

VALUE (units $10^{-3}$ )	DOCUMENT ID	TECN	COMMENT
<b>3.03 ± 0.20 OUR AVERAGE</b>			
2.97 ± 0.17 ± 0.17	<sup>1</sup> AUBERT	09Y	BABR $e^+ e^- \rightarrow \Upsilon(4S)$
2.9 ± 0.3 ± 0.3	<sup>2</sup> AUBERT	08BL	BABR $e^+ e^- \rightarrow \Upsilon(4S)$
4.2 ± 0.7 ± 0.7	<sup>2</sup> LIVENTSEV	08	BELL $e^+ e^- \rightarrow \Upsilon(4S)$
3.73 ± 0.85 ± 0.57	<sup>3</sup> ANASTASSOV	98	CLE2 $e^+ e^- \rightarrow \Upsilon(4S)$

- <sup>1</sup> Uses a simultaneous measurement of all  $B$  semileptonic decays without full reconstruction of events.
- <sup>2</sup> Uses a fully reconstructed  $B$  meson as a tag on the recoil side.
- <sup>3</sup> Assumes equal production of  $B^+$  and  $B^0$  at the  $\Upsilon(4S)$ .

 $\Gamma(\bar{D}_1^*(2430)^0 \ell^+ \nu_\ell, \bar{D}_1^{*0} \rightarrow D^{*-} \pi^+) / \Gamma_{\text{total}}$   $\Gamma_{14} / \Gamma$ 

VALUE (units $10^{-3}$ )	CL%	DOCUMENT ID	TECN	COMMENT
<b>2.7 ± 0.4 ± 0.5</b>		<sup>1</sup> AUBERT	08BL	BABR $e^+ e^- \rightarrow \Upsilon(4S)$
<0.7	90	<sup>1</sup> LIVENTSEV	08	BELL $e^+ e^- \rightarrow \Upsilon(4S)$

- <sup>1</sup> Uses a fully reconstructed  $B$  meson as a tag on the recoil side.

 $\Gamma(\bar{D}_2^*(2460)^0 \ell^+ \nu_\ell, \bar{D}_2^{*0} \rightarrow D^{*-} \pi^+) / \Gamma_{\text{total}}$   $\Gamma_{15} / \Gamma$ 

VALUE (units $10^{-3}$ )	CL%	DOCUMENT ID	TECN	COMMENT
<b>1.01 ± 0.24 OUR AVERAGE</b>				Error includes scale factor of 2.0.
0.87 ± 0.11 ± 0.07		<sup>1</sup> AUBERT	09Y	BABR $e^+ e^- \rightarrow \Upsilon(4S)$
1.5 ± 0.2 ± 0.2		<sup>2</sup> AUBERT	08BL	BABR $e^+ e^- \rightarrow \Upsilon(4S)$
1.8 ± 0.6 ± 0.3		<sup>2</sup> LIVENTSEV	08	BELL $e^+ e^- \rightarrow \Upsilon(4S)$

- • • We do not use the following data for averages, fits, limits, etc. • • •
- <1.6 90 <sup>3</sup> ANASTASSOV 98 CLE2  $e^+ e^- \rightarrow \Upsilon(4S)$
- <sup>1</sup> Uses a simultaneous fit of all  $B$  semileptonic decays without full reconstruction of events. AUBERT 09Y reports  $B(B^+ \rightarrow \bar{D}_2^*(2460)^0 \ell^+ \nu_\ell) \cdot B(\bar{D}_2^*(2460)^0 \rightarrow D^{(*)-} \pi^+) = (2.29 \pm 0.23 \pm 0.21) \times 10^{-3}$  and the authors have provided us the individual measurement.
- <sup>2</sup> Uses a fully reconstructed  $B$  meson as a tag on the recoil side.
- <sup>3</sup> Assumes equal production of  $B^+$  and  $B^0$  at the  $\Upsilon(4S)$ .

 $\Gamma(\bar{D}^0 \pi^+ \pi^- \ell^+ \nu_\ell) / \Gamma(\bar{D}^0 \ell^+ \nu_\ell)$   $\Gamma_{16} / \Gamma_4$ 

VALUE (units $10^{-2}$ )	DOCUMENT ID	TECN	COMMENT
<b>7.1 ± 1.3 ± 0.8</b>	<sup>1</sup> LEES	16	BABR $e^+ e^- \rightarrow \Upsilon(4S)$

- <sup>1</sup> Measurement used electrons and muons as leptons.

 $\Gamma(\bar{D}^{*0} \pi^+ \pi^- \ell^+ \nu_\ell) / \Gamma(\bar{D}^{*0} (2007)^0 \ell^+ \nu_\ell)$   $\Gamma_{17} / \Gamma_6$ 

VALUE (units $10^{-2}$ )	DOCUMENT ID	TECN	COMMENT
<b>1.4 ± 0.7 ± 0.4</b>	<sup>1</sup> LEES	16	BABR $e^+ e^- \rightarrow \Upsilon(4S)$

- <sup>1</sup> Measurement used electrons and muons as leptons.

 $\Gamma(D_s^{(*)-} K^+ \ell^+ \nu_\ell) / \Gamma_{\text{total}}$   $\Gamma_{18} / \Gamma$ 

VALUE (units $10^{-4}$ )	DOCUMENT ID	TECN	COMMENT
<b>6.1 ± 1.0 OUR AVERAGE</b>			
5.9 ± 1.2 ± 1.5	<sup>1</sup> STYPULA	12	BELL $e^+ e^- \rightarrow \Upsilon(4S)$
6.13 <sup>+1.04</sup> <sub>-1.03</sub> ± 0.67	<sup>1</sup> DEL-AMO-SA..11L	BABR	$e^+ e^- \rightarrow \Upsilon(4S)$

- <sup>1</sup> Assumes equal production of  $B^+$  and  $B^0$  at the  $\Upsilon(4S)$ .

 $\Gamma(D_s^- K^+ \ell^+ \nu_\ell) / \Gamma_{\text{total}}$   $\Gamma_{19} / \Gamma$ 

VALUE (units $10^{-4}$ )	DOCUMENT ID	TECN	COMMENT
<b>3.0 ± 0.9<sup>+1.1</sup><sub>-0.8</sub></b>	<sup>1</sup> STYPULA	12	BELL $e^+ e^- \rightarrow \Upsilon(4S)$

- <sup>1</sup> Assumes equal production of  $B^+$  and  $B^0$  at the  $\Upsilon(4S)$ .

 $\Gamma(D_s^{*-} K^+ \ell^+ \nu_\ell) / \Gamma_{\text{total}}$   $\Gamma_{20} / \Gamma$ 

VALUE (units $10^{-4}$ )	DOCUMENT ID	TECN	COMMENT
<b>2.9 ± 1.6<sup>+1.1</sup><sub>-1.0</sub></b>	<sup>1,2</sup> STYPULA	12	BELL $e^+ e^- \rightarrow \Upsilon(4S)$

- <sup>1</sup> Assumes equal production of  $B^+$  and  $B^0$  at the  $\Upsilon(4S)$ .
- <sup>2</sup> STYPULA 12 provides also an upper limit of  $0.56 \times 10^{-3}$  at 90% CL for the same data. Also measures branching fraction of the combined modes of  $D_s^- K^+ \ell^+ \nu_\ell$  and  $D_s^{*-} K^+ \ell^+ \nu_\ell$  as  $B(B^+ \rightarrow D_s^{*-} K^+ \ell^+ \nu_\ell) = (5.9 \pm 1.2 \pm 1.5) \times 10^{-4}$ .

 $\Gamma(\pi^0 \ell^+ \nu_\ell) / \Gamma_{\text{total}}$   $\Gamma_{21} / \Gamma$ 

"OUR EVALUATION" is an average using rescaled values of the data listed below. The average and rescaling were performed by the Heavy Flavor Averaging Group (HFLAV) and are described at <https://hflav.web.cern.ch/>. The averaging/rescaling procedure takes into account correlations between the measurements.

VALUE (units $10^{-4}$ )	DOCUMENT ID	TECN	COMMENT
<b>0.780 ± 0.027 OUR EVALUATION</b>			
<b>0.748 ± 0.029 OUR AVERAGE</b>			

- 0.80 ± 0.08 ± 0.04 <sup>1</sup> SIBIDANOV 13 BELL  $e^+ e^- \rightarrow \Upsilon(4S)$
- 0.77 ± 0.04 ± 0.03 <sup>2</sup> LEES 12AA BABR  $e^+ e^- \rightarrow \Upsilon(4S)$
- 0.705 ± 0.025 ± 0.035 <sup>3</sup> DEL-AMO-SA..11c BABR  $e^+ e^- \rightarrow \Upsilon(4S)$
- 0.82 ± 0.09 ± 0.05 <sup>3</sup> AUBERT 08AV BABR  $e^+ e^- \rightarrow \Upsilon(4S)$
- 0.77 ± 0.14 ± 0.08 <sup>4</sup> HOKUUE 07 BELL  $e^+ e^- \rightarrow \Upsilon(4S)$
- • • We do not use the following data for averages, fits, limits, etc. • • •
- 0.74 ± 0.05 ± 0.10 <sup>5</sup> AUBERT,B 05o BABR Repl. by DEL-AMO-SANCHEZ 11c

- <sup>1</sup> The signal events are tagged by a second  $B$  meson reconstructed in the fully hadronic decays.

- <sup>2</sup> Uses loose neutrino reconstruction technique. Assumes  $B(Y(4S) \rightarrow B^+ B^-) = (51.6 \pm 0.6)\%$  and  $B(Y(4S) \rightarrow B^0 \bar{B}^0) = (48.4 \pm 0.6)\%$ .

- <sup>3</sup> Using the isospin symmetry relation,  $B^+$  and  $B^0$  branching fractions are combined.

- <sup>4</sup> The signal events are tagged by a second  $B$  meson reconstructed in the semileptonic mode  $B \rightarrow D^{(*)} \ell \nu_\ell$ .

- <sup>5</sup>  $B^+$  and  $B^0$  decays combined assuming isospin symmetry. Systematic errors include both experimental and form-factor uncertainties.

 $\Gamma(\pi^0 e^+ \nu_e) / \Gamma_{\text{total}}$   $\Gamma_{22} / \Gamma$ 

VALUE (units $10^{-4}$ )	CL%	DOCUMENT ID	TECN	COMMENT
<b>0.9 ± 0.2 ± 0.2</b>		<sup>1</sup> ALEXANDER	96T	CLE2 $e^+ e^- \rightarrow \Upsilon(4S)$
<2.2	90	ANTREASNYAN	90B	CBAL $e^+ e^- \rightarrow \Upsilon(4S)$

- <sup>1</sup> Derived based in the reported  $B^0$  result by assuming isospin symmetry:  $\Gamma(B^0 \rightarrow \pi^- \ell^+ \nu) = 2\Gamma(B^+ \rightarrow \pi^0 \ell^+ \nu)$ .

 $\Gamma(\eta \ell^+ \nu_\ell) / \Gamma_{\text{total}}$   $\Gamma_{23} / \Gamma$ 

VALUE (units $10^{-4}$ )	CL%	DOCUMENT ID	TECN	COMMENT
<b>0.39 ± 0.05 OUR AVERAGE</b>				
0.42 ± 0.11 ± 0.03		<sup>1</sup> BELENO	17	BELL $e^+ e^- \rightarrow \Upsilon(4S)$
0.38 ± 0.05 ± 0.05		<sup>2</sup> LEES	12AA	BABR $e^+ e^- \rightarrow \Upsilon(4S)$
0.31 ± 0.06 ± 0.08		<sup>2</sup> AUBERT	09Q	BABR $e^+ e^- \rightarrow \Upsilon(4S)$
0.64 ± 0.20 ± 0.03		<sup>3</sup> AUBERT	08AV	BABR $e^+ e^- \rightarrow \Upsilon(4S)$

• • • We do not use the following data for averages, fits, limits, etc. • • •

Table with 5 columns: VALUE (units 10^-4), CL%, DOCUMENT ID, TECN, COMMENT. Includes entries like DEL-AMO-SA...11F BABR Repl. by LEES 12AA.

- 1 Uses missing-mass technique by fully reconstructing the hadronic decay chain of the accompanying B.
2 Uses loose neutrino reconstruction technique. Assumes B(T(4S) -> B+ B-) = (51.6 +/- 0.6)% and B(T(4S) -> B0 B0) = (48.4 +/- 0.6)%.
3 Assumes equal production of B+ and B0 at the T(4S).
4 The B0 and B+ results are combined assuming the isospin, B lifetimes, and relative charged/neutral B production at the T(4S).
5 ATHAR 03 reports systematic errors 0.16 +/- 0.09, which are experimental systematic and systematic due to model dependence. We combine these in quadrature.

Gamma(rho0 l+ nu\_l) / Gamma\_total

Table with 5 columns: VALUE (units 10^-4), CL%, DOCUMENT ID, TECN, COMMENT. Includes 'OUR AVERAGE' and various experimental results.

• • • We do not use the following data for averages, fits, limits, etc. • • •

Table with 5 columns: VALUE (units 10^-4), CL%, DOCUMENT ID, TECN, COMMENT. Includes BELENO 17 BELL e+ e- -> T(4S).

- 1 Uses loose neutrino reconstruction technique. Assumes B(Y(4S) -> B+ B-) = (51.6 +/- 0.6)% and B(Y(4S) -> B0 B0) = (48.4 +/- 0.6)%.
2 Assumes equal production of B+ and B0 at the T(4S).
3 The B0 and B+ results are combined assuming the isospin, B lifetimes, and relative charged/neutral B production at the T(4S). Corresponds to 90% CL interval (1.20-4.46) x 10^-4.
4 Uses missing-mass technique by fully reconstructing the hadronic decay chain of the accompanying B.

Gamma(omega l+ nu\_l) / Gamma\_total

Table with 5 columns: VALUE (units 10^-4), CL%, DOCUMENT ID, TECN, COMMENT. Includes 'OUR AVERAGE' and various experimental results.

• • • We do not use the following data for averages, fits, limits, etc. • • •

Table with 5 columns: VALUE (units 10^-4), CL%, DOCUMENT ID, TECN, COMMENT. Includes AUBERT 09Q BABR Repl. by LEES 13A.

- 1 LEES 13A reports (1.21 +/- 0.14 +/- 0.08) x 10^-4 from a measurement of [Gamma(B+ -> omega l+ nu\_l) / Gamma\_total] x [B(omega(782) -> pi+ pi- pi0)] assuming B(omega(782) -> pi+ pi- pi0) = (89.2 +/- 0.7) x 10^-2, which we rescale to our best value B(omega(782) -> pi+ pi- pi0) = (89.3 +/- 0.6) x 10^-2. Our first error is their experiment's error and our second error is the systematic error from using our best value.
2 Uses B(T(4S) -> B+ B-) = (51.6 +/- 0.6)% and B(T(4S) -> B0 B0) = (48.4 +/- 0.6)%.
3 Uses semileptonic tagging. Assumes B(omega -> pi+ pi- pi0) = (89.2 +/- 0.7)% and that the production ratio of B+ B- to B0 B0 from T(4S) is 1.056 +/- 0.028. The partial branching fractions in three bins of q^2 are also reported.
4 The signal events are tagged by a second B meson reconstructed in the fully hadronic decays.
5 Uses loose neutrino reconstruction technique.
6 Assumes equal production of B+ and B0 at the T(4S).
7 BEAN 93B limit set using ISGW Model. Using isospin and the quark model to combine Gamma(rho0 l+ nu\_l) and Gamma(rho- l+ nu\_l) with this result, they obtain a limit <(1.6-2.7) x 10^-4 at 90% CL for B+ -> omega l+ nu\_l. The range corresponds to the ISGW, WSB, and KS models. An upper limit on |V\_ub/V\_cb| < 0.8-0.13 at 90% CL is derived as well.

- 1 LEES 13A reports (1.21 +/- 0.14 +/- 0.08) x 10^-4 from a measurement of [Gamma(B+ -> omega l+ nu\_l) / Gamma\_total] x [B(omega(782) -> pi+ pi- pi0)] assuming B(omega(782) -> pi+ pi- pi0) = (89.2 +/- 0.7) x 10^-2, which we rescale to our best value B(omega(782) -> pi+ pi- pi0) = (89.3 +/- 0.6) x 10^-2. Our first error is their experiment's error and our second error is the systematic error from using our best value.
2 Uses B(T(4S) -> B+ B-) = (51.6 +/- 0.6)% and B(T(4S) -> B0 B0) = (48.4 +/- 0.6)%.
3 Uses semileptonic tagging. Assumes B(omega -> pi+ pi- pi0) = (89.2 +/- 0.7)% and that the production ratio of B+ B- to B0 B0 from T(4S) is 1.056 +/- 0.028. The partial branching fractions in three bins of q^2 are also reported.
4 The signal events are tagged by a second B meson reconstructed in the fully hadronic decays.
5 Uses loose neutrino reconstruction technique.
6 Assumes equal production of B+ and B0 at the T(4S).
7 BEAN 93B limit set using ISGW Model. Using isospin and the quark model to combine Gamma(rho0 l+ nu\_l) and Gamma(rho- l+ nu\_l) with this result, they obtain a limit <(1.6-2.7) x 10^-4 at 90% CL for B+ -> omega l+ nu\_l. The range corresponds to the ISGW, WSB, and KS models. An upper limit on |V\_ub/V\_cb| < 0.8-0.13 at 90% CL is derived as well.

Gamma(omega mu+ nu\_mu) / Gamma\_total

Table with 5 columns: VALUE (units 10^-4), CL%, DOCUMENT ID, TECN, COMMENT. Includes ALBRECHT 91C ARG.

- 1 In ALBRECHT 91C, one event is fully reconstructed providing evidence for the b -> u transition.

Gamma(rho0 l+ nu\_l) / Gamma\_total

OUR EVALUATION is an average using rescaled values of the data listed below. The average and rescaling were performed by the Heavy Flavor Averaging Group (HFLAV) and are described at https://hflav.web.cern.ch/. The averaging/rescaling procedure takes into account correlations between the measurements and asymmetric lifetime errors.

Table with 5 columns: VALUE (units 10^-4), CL%, DOCUMENT ID, TECN, COMMENT. Includes 'OUR EVALUATION' and various experimental results.

• • • We do not use the following data for averages, fits, limits, etc. • • •

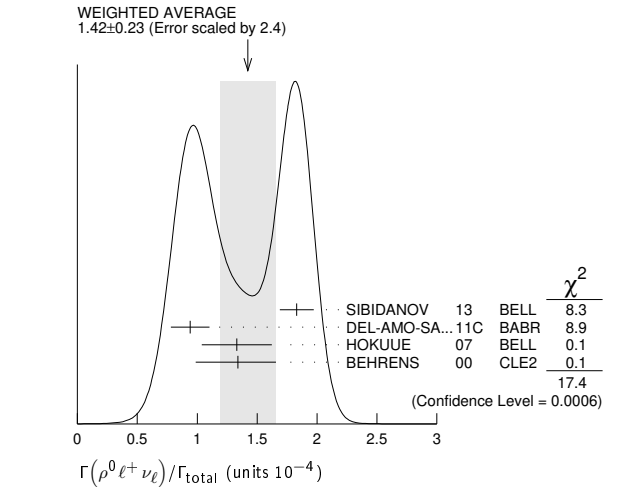
Table with 5 columns: VALUE (units 10^-4), CL%, DOCUMENT ID, TECN, COMMENT. Includes AUBERT,B 05O BABR Repl. by DEL-AMO-SANCHEZ 11c.

Table with 5 columns: VALUE (units 10^-4), CL%, DOCUMENT ID, TECN, COMMENT. Includes BEHRENS 00 CLE2 e+ e- -> T(4S).

- 1 The signal events are tagged by a second B meson reconstructed in the fully hadronic decays.
2 B+ and B0 decays combined assuming isospin symmetry. Systematic errors include both experimental and form-factor uncertainties.

- 3 The signal events are tagged by a second B meson reconstructed in the semileptonic mode B -> D(\*) l nu\_l.
4 Derived based in the reported B0 result by assuming isospin symmetry: Gamma(B0 -> rho- l+ nu) = 2Gamma(B+ -> rho0 l+ nu) approx 2Gamma(B+ -> omega l+ nu).

- 5 BEAN 93B limit set using ISGW Model. Using isospin and the quark model to combine Gamma(omega0 l+ nu\_l) and Gamma(rho- l+ nu\_l) with this result, they obtain a limit <(1.6-2.7) x 10^-4 at 90% CL for B+ -> rho0 l+ nu\_l. The range corresponds to the ISGW, WSB, and KS models. An upper limit on |V\_ub/V\_cb| < 0.8-0.13 at 90% CL is derived as well.



Gamma(rho0 l+ nu\_l) / Gamma\_total

Table with 5 columns: VALUE (units 10^-6), CL%, DOCUMENT ID, TECN, COMMENT. Includes TIEN 14 BELL e+ e- -> T(4S).

- 1 Assumes equal production of B+ and B0 at the T(4S).

Gamma(rho0 l+ nu\_l) / Gamma\_total

Table with 5 columns: VALUE (units 10^-6), CL%, DOCUMENT ID, TECN, COMMENT. Includes TIEN 14 BELL e+ e- -> T(4S).

- 1 Assumes equal production of B+ and B0 at the T(4S).

Gamma(rho0 l+ nu\_l) / Gamma\_total

Table with 5 columns: VALUE (units 10^-6), CL%, DOCUMENT ID, TECN, COMMENT. Includes TIEN 14 BELL e+ e- -> T(4S).

• • • We do not use the following data for averages, fits, limits, etc. • • •

- 1 Assumes equal production of B+ and B0 at the T(4S).
2 Based on phase-space model; if V-A model is used, the 90% CL upper limit becomes < 1.2 x 10^-3.

Gamma(e+ nu\_e) / Gamma\_total

Table with 5 columns: VALUE (units 10^-6), CL%, DOCUMENT ID, TECN, COMMENT. Includes SATOYAMA 07 BELL e+ e- -> T(4S).

• • • We do not use the following data for averages, fits, limits, etc. • • •

Table with 5 columns: VALUE (units 10^-6), CL%, DOCUMENT ID, TECN, COMMENT. Includes YOOK 15 BELL e+ e- -> T(4S), AUBERT 10E BABR e+ e- -> T(4S), AUBERT 09V BABR e+ e- -> T(4S), AUBERT 08AD BABR e+ e- -> T(4S), ARTUSO 95 CLE2 e+ e- -> T(4S).

- 1 Assumes equal production of B+ and B0 at the T(4S).

- 2 Assumes B(T(4S) -> B+ B-) = 0.513 +/- 0.006.

## Meson Particle Listings

 $B^\pm$  $\Gamma(\mu^+\nu_\mu)/\Gamma_{\text{total}}$   $\Gamma_{32}/\Gamma$ 

VALUE (units $10^{-6}$ )	CL%	DOCUMENT ID	TECN	COMMENT
<b>0.29 to 1.07</b>	90	<sup>1</sup> SIBIDANOV	18 BELL	$e^+e^- \rightarrow \Upsilon(4S)$
$< 2.7$	90	<sup>2</sup> YOOK	15 BELL	$e^+e^- \rightarrow \Upsilon(4S)$
$< 11$	90	<sup>3</sup> AUBERT	10E BABR	$e^+e^- \rightarrow \Upsilon(4S)$
$< 1.0$	90	<sup>3</sup> AUBERT	09V BABR	$e^+e^- \rightarrow \Upsilon(4S)$
$< 5.6$	90	<sup>3</sup> AUBERT	08AD BABR	$e^+e^- \rightarrow \Upsilon(4S)$
$< 1.7$	90	<sup>3,4</sup> SATOYAMA	07 BELL	$e^+e^- \rightarrow \Upsilon(4S)$
$< 6.6$	90	AUBERT	04o BABR	Repl. by AUBERT 09V
$< 21$	90	ARTUSO	95 CLE2	$e^+e^- \rightarrow \Upsilon(4S)$

<sup>1</sup> This is a 90% confidence interval in the frequentist approach. A 2.4 standard deviation signal above the background is found, with a measured branching fraction  $(6.46 \pm 2.22 \pm 1.60) \times 10^{-7}$ .

<sup>2</sup> Assumes  $B(\Upsilon(4S) \rightarrow B^+B^-) = 0.513 \pm 0.006$ .

<sup>3</sup> Assumes equal production of  $B^+$  and  $B^0$  at the  $\Upsilon(4S)$ .

<sup>4</sup> Superseded by SIBIDANOV 18.

 $\Gamma(\tau^+\nu_\tau)/\Gamma_{\text{total}}$   $\Gamma_{33}/\Gamma$ 

See the note on "Decay Constants of Charged Pseudoscalar Mesons" in the  $D_s^\pm$  Listings.

VALUE (units $10^{-4}$ )	CL%	DOCUMENT ID	TECN	COMMENT
<b>1.09 ± 0.24 OUR AVERAGE</b>		Error includes scale factor of 1.2.		
$1.25 \pm 0.28 \pm 0.27$		<sup>1,2</sup> KRONENBIT...	15 BELL	$e^+e^- \rightarrow \Upsilon(4S)$
$0.72_{-0.25}^{+0.27} \pm 0.11$		<sup>3</sup> HARA	13 BELL	$e^+e^- \rightarrow \Upsilon(4S)$
$1.83_{-0.49}^{+0.53} \pm 0.24$		<sup>2,4</sup> LEES	13k BABR	$e^+e^- \rightarrow \Upsilon(4S)$
$1.7 \pm 0.8 \pm 0.2$		<sup>2,5</sup> AUBERT	10E BABR	$e^+e^- \rightarrow \Upsilon(4S)$
$1.54_{-0.37}^{+0.38} \pm 0.29$		<sup>2,6</sup> HARA	10 BELL	Repl. by KRONENBIT-TER 15
$1.8_{-0.8}^{+0.9} \pm 0.45$		<sup>2,7</sup> AUBERT	08D BABR	Repl. by LEES 13k
$0.9 \pm 0.6 \pm 0.1$		<sup>2,5</sup> AUBERT	07AL BABR	Repl. by AUBERT 10E
$< 2.6$	90	<sup>2</sup> AUBERT	06K BABR	$e^+e^- \rightarrow \Upsilon(4S)$
$1.79_{-0.49}^{+0.56} \pm 0.46$		<sup>2,7</sup> IKADO	06 BELL	Repl. by HARA 13
$< 4.2$	90	<sup>2</sup> AUBERT,B	05B BABR	Repl. by AUBERT 06k
$< 8.3$	90	<sup>8</sup> BARATE	01E ALEP	$e^+e^- \rightarrow Z$
$< 8.4$	90	<sup>2</sup> BROWDER	01 CLE2	$e^+e^- \rightarrow \Upsilon(4S)$
$< 5.7$	90	<sup>9</sup> ACCIARRI	97F L3	$e^+e^- \rightarrow Z$
$< 104$	90	<sup>10</sup> ALBRECHT	95D ARG	$e^+e^- \rightarrow \Upsilon(4S)$
$< 22$	90	ARTUSO	95 CLE2	$e^+e^- \rightarrow \Upsilon(4S)$
$< 18$	90	<sup>11</sup> BUSKULIC	95 ALEP	$e^+e^- \rightarrow Z$

<sup>1</sup> Requires one reconstructed semileptonic  $B$  decay  $B^- \rightarrow D^{(*)0} \ell^- \bar{\nu}_\ell$  in the recoil.

<sup>2</sup> Assumes equal production of  $B^+$  and  $B^0$  at the  $\Upsilon(4S)$ .

<sup>3</sup> The authors combine their result with that from HARA 10 obtaining  $B(B^- \rightarrow \tau^- \bar{\nu}_\tau) = (0.96 \pm 0.26) \times 10^{-4}$  and deriving  $f_B |V_{ub}| = (7.4 \pm 0.8 \pm 0.5) \times 10^{-4}$  GeV.

<sup>4</sup> Requires a fully reconstructed hadronic  $B$ -decay in the recoil. Reports that this result combined with AUBERT 10E value gives  $B(B^- \rightarrow \tau^- \bar{\nu}_\tau) = (1.79 \pm 0.48) \times 10^{-4}$ .

<sup>5</sup> Requires one reconstructed semileptonic  $B$  decay  $B^- \rightarrow D^0 \ell^- \bar{\nu}_\ell X$  in the recoil.

<sup>6</sup> Requires one reconstructed semileptonic  $B$  decay  $B^- \rightarrow D^{(*)0} \ell^- \bar{\nu}_\ell X$  in the recoil.

<sup>7</sup> The analysis is based on a sample of events with one fully reconstructed tag  $B$  in a hadronic decay mode  $B^- \rightarrow D^{(*)0} X^-$ .

<sup>8</sup> The energy-flow and  $b$ -tagging algorithms were used.

<sup>9</sup> ACCIARRI 97F uses missing-energy technique and  $f(b \rightarrow B^-) = (38.2 \pm 2.5)\%$ .

<sup>10</sup> ALBRECHT 95D uses full reconstruction of one  $B$  decay as tag.

<sup>11</sup> BUSKULIC 95 uses same missing-energy technique as in  $\bar{b} \rightarrow \tau^+ \nu_\tau X$ , but analysis is restricted to endpoint region of missing-energy distribution.

 $\Gamma(\ell^+\nu_\ell)/\Gamma_{\text{total}}$   $\Gamma_{34}/\Gamma$ 

VALUE	CL%	DOCUMENT ID	TECN	COMMENT
<b><math>&lt; 3.0 \times 10^{-6}</math></b>	90	<sup>1,2</sup> GELB	18 BELL	$e^+e^- \rightarrow \Upsilon(4S)$
$< 3.5 \times 10^{-6}$	90	<sup>2,3</sup> HELLER	15 BELL	$e^+e^- \rightarrow \Upsilon(4S)$
$< 15.6 \times 10^{-6}$	90	<sup>2</sup> AUBERT	09AT BABR	$e^+e^- \rightarrow \Upsilon(4S)$

<sup>1</sup> Supersedes HELLER 15.

<sup>2</sup> Assumes equal production of  $B^+$  and  $B^0$  at the  $\Upsilon(4S)$ .

<sup>3</sup> Superseded by GELB 18.

 $\Gamma(e^+\nu_e)/\Gamma_{\text{total}}$   $\Gamma_{35}/\Gamma$ 

VALUE	CL%	DOCUMENT ID	TECN	COMMENT
<b><math>&lt; 4.3 \times 10^{-6}</math></b>	90	<sup>1,2</sup> GELB	18 BELL	$e^+e^- \rightarrow \Upsilon(4S)$
$< 6.1 \times 10^{-6}$	90	<sup>2,3</sup> HELLER	15 BELL	$e^+e^- \rightarrow \Upsilon(4S)$
$< 17 \times 10^{-6}$	90	<sup>2</sup> AUBERT	09AT BABR	$e^+e^- \rightarrow \Upsilon(4S)$
$< 200 \times 10^{-6}$	90	<sup>4</sup> BROWDER	97 CLE2	$e^+e^- \rightarrow \Upsilon(4S)$

<sup>1</sup> Supersedes HELLER 15.

<sup>2</sup> Assumes equal production of  $B^+$  and  $B^0$  at the  $\Upsilon(4S)$ .

<sup>3</sup> Superseded by GELB 18.

<sup>4</sup> BROWDER 97 uses the hermiticity of the CLEOII detector to reconstruct the neutrino energy and momentum.

 $\Gamma(\mu^+\nu_\mu\gamma)/\Gamma_{\text{total}}$   $\Gamma_{36}/\Gamma$ 

VALUE	CL%	DOCUMENT ID	TECN	COMMENT
<b><math>&lt; 3.4 \times 10^{-6}</math></b>	90	<sup>1,2</sup> GELB	18 BELL	$e^+e^- \rightarrow \Upsilon(4S)$
$< 3.4 \times 10^{-6}$	90	<sup>2,3</sup> HELLER	15 BELL	$e^+e^- \rightarrow \Upsilon(4S)$
$< 24 \times 10^{-6}$	90	<sup>2,4</sup> AUBERT	09AT BABR	$e^+e^- \rightarrow \Upsilon(4S)$
$< 52 \times 10^{-6}$	90	<sup>5</sup> BROWDER	97 CLE2	$e^+e^- \rightarrow \Upsilon(4S)$

<sup>1</sup> Supersedes HELLER 15.

<sup>2</sup> Assumes equal production of  $B^+$  and  $B^0$  at the  $\Upsilon(4S)$ .

<sup>3</sup> Superseded by GELB 18.

<sup>4</sup> Note that the value given by AUBERT 09AT is  $24 \times 10^{-6}$  in the paper abstract, and  $26 \times 10^{-6}$  in the paper itself (Table I).

<sup>5</sup> BROWDER 97 uses the hermiticity of the CLEOII detector to reconstruct the neutrino energy and momentum.

 $\Gamma(\mu^+\mu^-\mu^+\nu_\mu)/\Gamma_{\text{total}}$   $\Gamma_{37}/\Gamma$ 

VALUE	CL%	DOCUMENT ID	TECN	COMMENT
<b><math>&lt; 1.6 \times 10^{-8}</math></b>	95	<sup>1</sup> AAIJ	19P LHCB	$pp$ at 7, 8, 13 TeV

<sup>1</sup> AAIJ 19P limit established for the kinematic region where the lower of the two  $M(\mu^+\mu^-)$  is less than 980 MeV/ $c^2$ .

 $\Gamma(D^0X)/\Gamma_{\text{total}}$   $\Gamma_{38}/\Gamma$ 

VALUE	DOCUMENT ID	TECN	COMMENT
<b>0.086 ± 0.006 ± 0.004</b>	<sup>1</sup> AUBERT	07N BABR	$e^+e^- \rightarrow \Upsilon(4S)$
$0.098 \pm 0.009 \pm 0.006$	<sup>1</sup> AUBERT, BE	04B BABR	Repl. by AUBERT 07N

<sup>1</sup> Events are selected by completely reconstructing one  $B$  and searching for a reconstructed charmed particle in the rest of the event. The last error includes systematic and charm branching ratio uncertainties.

 $\Gamma(\bar{D}^0X)/\Gamma_{\text{total}}$   $\Gamma_{39}/\Gamma$ 

VALUE	DOCUMENT ID	TECN	COMMENT
<b>0.786 ± 0.016 +0.034 -0.033</b>	<sup>1</sup> AUBERT	07N BABR	$e^+e^- \rightarrow \Upsilon(4S)$
$0.793 \pm 0.025 +0.045 -0.044$	<sup>1</sup> AUBERT, BE	04B BABR	Repl. by AUBERT 07N

<sup>1</sup> Events are selected by completely reconstructing one  $B$  and searching for a reconstructed charmed particle in the rest of the event. The last error includes systematic and charm branching ratio uncertainties.

 $\Gamma(D^0X)/[\Gamma(D^0X) + \Gamma(\bar{D}^0X)]$   $\Gamma_{38}/(\Gamma_{38} + \Gamma_{39})$ 

VALUE	DOCUMENT ID	TECN	COMMENT
<b>0.098 ± 0.007 ± 0.001</b>	AUBERT	07N BABR	$e^+e^- \rightarrow \Upsilon(4S)$
$0.110 \pm 0.010 \pm 0.003$	AUBERT, BE	04B BABR	Repl. by AUBERT 07N

<sup>1</sup> We do not use the following data for averages, fits, limits, etc. ● ● ●

<sup>1</sup> AUBERT, BE 04B BABR Repl. by AUBERT 07N

<sup>1</sup> AUBERT 07N BABR  $e^+e^- \rightarrow \Upsilon(4S)$

<sup>1</sup> AUBERT, BE 04B BABR Repl. by AUBERT 07N

<sup>1</sup> AUBERT, BE 04B BABR Repl. by AUBERT 07N

<sup>1</sup> Events are selected by completely reconstructing one  $B$  and searching for a reconstructed charmed particle in the rest of the event. The last error includes systematic and charm branching ratio uncertainties.

 $\Gamma(D^+X)/\Gamma_{\text{total}}$   $\Gamma_{40}/\Gamma$ 

VALUE	DOCUMENT ID	TECN	COMMENT
<b>0.025 ± 0.005 ± 0.002</b>	<sup>1</sup> AUBERT	07N BABR	$e^+e^- \rightarrow \Upsilon(4S)$
$0.038 \pm 0.009 \pm 0.005$	<sup>1</sup> AUBERT, BE	04B BABR	Repl. by AUBERT 07N

<sup>1</sup> Events are selected by completely reconstructing one  $B$  and searching for a reconstructed charmed particle in the rest of the event. The last error includes systematic and charm branching ratio uncertainties.

 $\Gamma(D^+X)/[\Gamma(D^+X) + \Gamma(D^-X)]$   $\Gamma_{40}/(\Gamma_{40} + \Gamma_{41})$ 

VALUE	DOCUMENT ID	TECN	COMMENT
<b>0.204 ± 0.035 ± 0.001</b>	AUBERT	07N BABR	$e^+e^- \rightarrow \Upsilon(4S)$
$0.278 \pm 0.052 \pm 0.009$	AUBERT, BE	04B BABR	Repl. by AUBERT 07N

<sup>1</sup> AUBERT 07N BABR  $e^+e^- \rightarrow \Upsilon(4S)$

<sup>1</sup> AUBERT, BE 04B BABR Repl. by AUBERT 07N

<sup>1</sup> AUBERT 07N BABR  $e^+e^- \rightarrow \Upsilon(4S)$

<sup>1</sup> We do not use the following data for averages, fits, limits, etc. ● ● ●

<sup>1</sup> AUBERT, BE 04B BABR Repl. by AUBERT 07N

<sup>1</sup> AUBERT, BE 04B BABR Repl. by AUBERT 07N

<sup>1</sup> Events are selected by completely reconstructing one  $B$  and searching for a reconstructed charmed particle in the rest of the event. The last error includes systematic and charm branching ratio uncertainties.

$\Gamma(D_s^- X)/\Gamma_{total}$					$\Gamma_{43}/\Gamma$
VALUE	CL%	DOCUMENT ID	TECN	COMMENT	

$0.011 \pm 0.004 + 0.002$ $-0.003 - 0.001$		1 AUBERT	07N	BABR $e^+e^- \rightarrow \Upsilon(4S)$	
<0.022	90	1 AUBERT, BE	04B	BABR Repl. by AUBERT 07N	

• • • We do not use the following data for averages, fits, limits, etc. • • •  
 1 Events are selected by completely reconstructing one  $B$  and searching for a reconstructed charmed particle in the rest of the event. The last error includes systematic and charm branching ratio uncertainties.

$\Gamma(D_s^+ X)/[\Gamma(D_s^+ X) + \Gamma(D_s^- X)]$					$\Gamma_{42}/(\Gamma_{42} + \Gamma_{43})$
VALUE	CL%	DOCUMENT ID	TECN	COMMENT	

$0.884 \pm 0.038 \pm 0.002$		AUBERT	07N	BABR $e^+e^- \rightarrow \Upsilon(4S)$	
$0.966 \pm 0.039 \pm 0.012$		AUBERT, BE	04B	BABR Repl. by AUBERT 07N	

$\Gamma(D_s^- X)/[\Gamma(D_s^+ X) + \Gamma(D_s^- X)]$					$\Gamma_{43}/(\Gamma_{42} + \Gamma_{43})$
VALUE	CL%	DOCUMENT ID	TECN	COMMENT	

<0.126	90	AUBERT, BE	04B	BABR $e^+e^- \rightarrow \Upsilon(4S)$	
--------	----	------------	-----	--	--

$\Gamma(A_c^+ X)/\Gamma_{total}$					$\Gamma_{44}/\Gamma$
VALUE	CL%	DOCUMENT ID	TECN	COMMENT	

$0.021 \pm 0.005 + 0.008$ $-0.004$		1 AUBERT	07N	BABR $e^+e^- \rightarrow \Upsilon(4S)$	
$0.029 \pm 0.008 + 0.011$ $-0.007$		1 AUBERT, BE	04B	BABR Repl. by AUBERT 07N	

• • • We do not use the following data for averages, fits, limits, etc. • • •  
 1 Events are selected by completely reconstructing one  $B$  and searching for a reconstructed charmed particle in the rest of the event. The last error includes systematic and charm branching ratio uncertainties.

$\Gamma(\bar{A}_c^+ X)/\Gamma_{total}$					$\Gamma_{45}/\Gamma$
VALUE	CL%	DOCUMENT ID	TECN	COMMENT	

$0.028 \pm 0.005 + 0.010$ $-0.007$		1 AUBERT	07N	BABR $e^+e^- \rightarrow \Upsilon(4S)$	
$0.035 \pm 0.008 + 0.013$ $-0.009$		1 AUBERT, BE	04B	BABR Repl. by AUBERT 07N	

• • • We do not use the following data for averages, fits, limits, etc. • • •  
 1 Events are selected by completely reconstructing one  $B$  and searching for a reconstructed charmed particle in the rest of the event. The last error includes systematic and charm branching ratio uncertainties.

$\Gamma(A_c^+ X)/[\Gamma(A_c^+ X) + \Gamma(\bar{A}_c^+ X)]$					$\Gamma_{44}/(\Gamma_{44} + \Gamma_{45})$
VALUE	CL%	DOCUMENT ID	TECN	COMMENT	

$0.427 \pm 0.071 \pm 0.001$		AUBERT	07N	BABR $e^+e^- \rightarrow \Upsilon(4S)$	
$0.452 \pm 0.090 \pm 0.003$		AUBERT, BE	04B	BABR Repl. by AUBERT 07N	

$\Gamma(\bar{c} X)/\Gamma_{total}$					$\Gamma_{46}/\Gamma$
VALUE	CL%	DOCUMENT ID	TECN	COMMENT	

$0.968 \pm 0.019 + 0.041$ $-0.039$		1 AUBERT	07N	BABR $e^+e^- \rightarrow \Upsilon(4S)$	
$0.983 \pm 0.030 + 0.054$ $-0.051$		1 AUBERT, BE	04B	BABR Repl. by AUBERT 07N	

• • • We do not use the following data for averages, fits, limits, etc. • • •  
 1 Events are selected by completely reconstructing one  $B$  and searching for a reconstructed charmed particle in the rest of the event. The last error includes systematic and charm branching ratio uncertainties.

$\Gamma(c X)/\Gamma_{total}$					$\Gamma_{47}/\Gamma$
VALUE	CL%	DOCUMENT ID	TECN	COMMENT	

$0.234 \pm 0.012 + 0.018$ $-0.014$		1 AUBERT	07N	BABR $e^+e^- \rightarrow \Upsilon(4S)$	
$0.330 \pm 0.022 + 0.055$ $-0.037$		1 AUBERT, BE	04B	BABR Repl. by AUBERT 07N	

• • • We do not use the following data for averages, fits, limits, etc. • • •  
 1 Events are selected by completely reconstructing one  $B$  and searching for a reconstructed charmed particle in the rest of the event. The last error includes systematic and charm branching ratio uncertainties.

$\Gamma(c/\bar{c} X)/\Gamma_{total}$					$\Gamma_{48}/\Gamma$
VALUE	CL%	DOCUMENT ID	TECN	COMMENT	

$1.202 \pm 0.023 + 0.053$ $-0.049$		1 AUBERT	07N	BABR $e^+e^- \rightarrow \Upsilon(4S)$	
$1.313 \pm 0.037 + 0.088$ $-0.075$		1 AUBERT, BE	04B	BABR Repl. by AUBERT 07N	

• • • We do not use the following data for averages, fits, limits, etc. • • •  
 1 Events are selected by completely reconstructing one  $B$  and searching for a reconstructed charmed particle in the rest of the event. The last error includes systematic and charm branching ratio uncertainties.

$\Gamma(D^0 \pi^+)/\Gamma_{total}$					$\Gamma_{49}/\Gamma$
VALUE (units $10^{-3}$ )	EVTs	DOCUMENT ID	TECN	COMMENT	

$4.68 \pm 0.13$ OUR FIT					
$4.70 \pm 0.13$ OUR AVERAGE					
$4.34 \pm 0.10 \pm 0.23$		1 KATO	18	BELL $e^+e^- \rightarrow \Upsilon(4S)$	
$4.90 \pm 0.07 \pm 0.22$		2 AUBERT	07H	BABR $e^+e^- \rightarrow \Upsilon(4S)$	

$5.0 \pm 0.6 \pm 0.3$		3 ABULENCIA	06J	CDF $p\bar{p}$ at 1.96 TeV	
$4.49 \pm 0.21 \pm 0.23$		4 AUBERT, BE	06J	BABR $e^+e^- \rightarrow \Upsilon(4S)$	
$4.97 \pm 0.12 \pm 0.29$		2,5 AHMED	02B	CLE2 $e^+e^- \rightarrow \Upsilon(4S)$	
$5.0 \pm 0.7 \pm 0.6$	54	6 BORTOLETTO	92	CLEO $e^+e^- \rightarrow \Upsilon(4S)$	
$5.4 + 1.8 + 1.2$ $-1.5 - 0.9$	14	7 BEBEK	87	CLEO $e^+e^- \rightarrow \Upsilon(4S)$	

• • • We do not use the following data for averages, fits, limits, etc. • • •  
 1 Measures absolute branching fractions using a missing-mass technique.  
 2 Assumes equal production of  $B^+$  and  $B^0$  at the  $\Upsilon(4S)$ .  
 3 ABULENCIA 06J reports  $[\Gamma(B^+ \rightarrow \bar{D}^0 \pi^+)/\Gamma_{total}] / [B(B^0 \rightarrow D^- \pi^+)] = 1.97 \pm 0.10 \pm 0.21$  which we multiply by our best value  $B(B^0 \rightarrow D^- \pi^+) = (2.52 \pm 0.13) \times 10^{-3}$ . Our first error is their experiment's error and our second error is the systematic error from using our best value.  
 4 Uses a missing-mass method. Does not depend on  $D$  branching fractions or  $B^+/B^0$  production rates.  
 5 AHMED 02B reports an additional uncertainty on the branching ratios to account for 4.5% uncertainty on relative production of  $B^0$  and  $B^+$ , which is not included here.  
 6 Assumes equal production of  $B^+$  and  $B^0$  at the  $\Upsilon(4S)$  and uses the Mark III branching fractions for the  $D$ .  
 7 BEBEK 87 value has been updated in BERKELMAN 91 to use same assumptions as noted for BORTOLETTO 92.  
 8 AUBERT, B 04P reports  $[\Gamma(B^+ \rightarrow \bar{D}^0 \pi^+)/\Gamma_{total}] \times [B(D^0 \rightarrow K^- \pi^+)] = (1.846 \pm 0.032 \pm 0.097) \times 10^{-4}$  which we divide by our best value  $B(D^0 \rightarrow K^- \pi^+) = (3.950 \pm 0.031) \times 10^{-2}$ . Our first error is their experiment's error and our second error is the systematic error from using our best value.  
 9 ALAM 94 assume equal production of  $B^+$  and  $B^0$  at the  $\Upsilon(4S)$  and use the CLEO II absolute  $B(D^0 \rightarrow K^- \pi^+)$  and the PDG 1992  $B(D^0 \rightarrow K^- \pi^+ \pi^0)/B(D^0 \rightarrow K^- \pi^+)$  and  $B(D^0 \rightarrow K^- 2\pi^+ \pi^-)/B(D^0 \rightarrow K^- \pi^+)$ .  
 10 ALBRECHT 88k assumes  $B^0 \bar{B}^0, B^+ B^-$  ratio is 45:55. Superseded by ALBRECHT 90J.

$\Gamma(D^0 \rho^+)/\Gamma_{total}$					$\Gamma_{52}/\Gamma$
VALUE	EVTs	DOCUMENT ID	TECN	COMMENT	

$0.0134 \pm 0.0018$ OUR AVERAGE					
$0.0135 \pm 0.0012 \pm 0.0015$	212	1 ALAM	94	CLE2 $e^+e^- \rightarrow \Upsilon(4S)$	
$0.013 \pm 0.004 \pm 0.004$	19	2 ALBRECHT	90J	ARG $e^+e^- \rightarrow \Upsilon(4S)$	
$0.021 \pm 0.008 \pm 0.009$	10	3 ALBRECHT	88k	ARG $e^+e^- \rightarrow \Upsilon(4S)$	

• • • We do not use the following data for averages, fits, limits, etc. • • •  
 1 ALAM 94 assume equal production of  $B^+$  and  $B^0$  at the  $\Upsilon(4S)$  and use the CLEO II absolute  $B(D^0 \rightarrow K^- \pi^+)$  and the PDG 1992  $B(D^0 \rightarrow K^- \pi^+ \pi^0)/B(D^0 \rightarrow K^- \pi^+)$  and  $B(D^0 \rightarrow K^- 2\pi^+ \pi^-)/B(D^0 \rightarrow K^- \pi^+)$ .  
 2 Assumes equal production of  $B^+$  and  $B^0$  at the  $\Upsilon(4S)$  and uses the Mark III branching fractions for the  $D$ .  
 3 ALBRECHT 88k assumes  $B^0 \bar{B}^0, B^+ B^-$  ratio is 45:55.

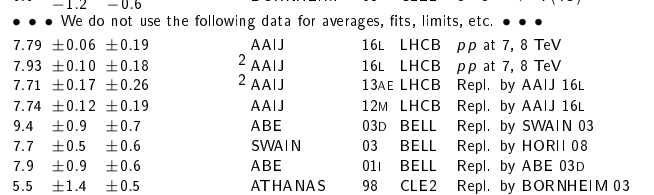
$\Gamma(D^0 K^+)/\Gamma(D^0 \pi^+)$					$\Gamma_{53}/\Gamma_{49}$
VALUE (units $10^{-2}$ )	EVTs	DOCUMENT ID	TECN	COMMENT	

$7.75 \pm 0.15$ OUR AVERAGE					
$7.768 \pm 0.038 \pm 0.066$		1 AAIJ	18A	LHCB $p\bar{p}$ at 7, 8, 13 TeV	
$6.77 \pm 0.23 \pm 0.30$		HORII	08	BELL $e^+e^- \rightarrow \Upsilon(4S)$	
$8.31 \pm 0.35 \pm 0.20$		AUBERT	04N	BABR $e^+e^- \rightarrow \Upsilon(4S)$	
$9.9 + 1.4 + 0.7$ $-1.2 - 0.6$		BORNHEIM	03	CLE2 $e^+e^- \rightarrow \Upsilon(4S)$	

• • • We do not use the following data for averages, fits, limits, etc. • • •  
 1 AAIJ 16L reports  $\chi^2 = 0.0$  for the fit. Error includes scale factor of 2.1. See the ideogram below.  
 2 AAIJ 16L reports  $\chi^2 = 6.8$  for the fit.  
 2 AAIJ 13AE reports  $\chi^2 = 1.9$  for the fit.  
 3 ALBRECHT 88k assumes  $B^0 \bar{B}^0, B^+ B^-$  ratio is 45:55.

$\Gamma(D^0 \pi^+)/\Gamma_{total}$					$\chi^2$
VALUE (units $10^{-2}$ )	EVTs	DOCUMENT ID	TECN	COMMENT	

$7.79 \pm 0.06 \pm 0.19$		AAIJ	16L	LHCB $p\bar{p}$ at 7, 8 TeV	0.0
$7.93 \pm 0.10 \pm 0.18$		AAIJ	16L	LHCB $p\bar{p}$ at 7, 8 TeV	6.8
$7.71 \pm 0.17 \pm 0.26$		AAIJ	13AE	LHCB Repl. by AAIJ 16L	1.9
$7.74 \pm 0.12 \pm 0.19$		AAIJ	12M	LHCB Repl. by AAIJ 16L	8.7
$9.4 \pm 0.9 \pm 0.7$		ABE	03D	BELL Repl. by SWAIN 03	
$7.7 \pm 0.5 \pm 0.6$		SWAIN	03	BELL Repl. by HORII 08	
$7.9 \pm 0.9 \pm 0.6$		ABE	01I	BELL Repl. by ABE 03D	
$5.5 \pm 1.4 \pm 0.5$		ATHANAS	98	CLE2 Repl. by BORNHEIM 03	



WEIGHTED AVERAGE  
 7.75±0.15 (Error scaled by 2.1)  
 1 Supersedes AAIJ 16L.



See key on page 999

# Meson Particle Listings

$B^\pm$

••• We do not use the following data for averages, fits, limits, etc. •••

$4.10 \pm 0.25 \pm 0.05$	AAIJ	12M	LHCB	Repl. by AAIJ 16L		
$3.40^{+0.55+0.15}_{-0.53-0.22}$	HORII	08	BELL	Repl. by HORII 11		
$3.5^{+1.0}_{-0.9} \pm 0.2$	SAIGO	05	BELL	Repl. by HORII 08		

<sup>1</sup> AALTONEN 11AJ also measures the ratio separately for  $B^+$  ( $R^+(\pi)$ ) and  $B^-$  ( $R^-(\pi)$ ) and obtains:  $R^+(\pi) = (2.4 \pm 1.0 \pm 0.4) \times 10^{-3}$ ,  $R^-(\pi) = (3.1 \pm 1.1 \pm 0.4) \times 10^{-3}$ .

**$\Gamma([K^-\pi^+\pi^0]_{D\pi^+})/\Gamma([K^+\pi^-\pi^0]_{D\pi^+})$   $\Gamma_{71}/\Gamma_{72}$**

VALUE (units $10^{-3}$ )	DOCUMENT ID	TECN	COMMENT
<b><math>2.2 \pm 0.4</math> OUR AVERAGE</b>			
$2.35 \pm 0.49 \pm 0.06$	<sup>1</sup> AAIJ	15w	LHCB <i>pp</i> at 7, 8 TeV
$1.89 \pm 0.54^{+0.22}_{-0.25}$	NAYAK	13	BELL $e^+e^- \rightarrow \Upsilon(4S)$

<sup>1</sup> Uses  $D^0 \rightarrow K^-\pi^+\pi^0$  for the favored mode, and  $D^0 \rightarrow K^+\pi^-\pi^0$  for the suppressed mode.

**$\Gamma([K^-\pi^+\pi^+ \pi^-]_{D\pi^+})/\Gamma([K^+\pi^-\pi^+ \pi^-]_{D\pi^+})$   $\Gamma_{73}/\Gamma_{74}$**

VALUE (units $10^{-3}$ )	DOCUMENT ID	TECN	COMMENT
<b><math>3.77 \pm 0.18 \pm 0.06</math></b>	AAIJ	16L	LHCB <i>pp</i> at 7, 8 TeV

••• We do not use the following data for averages, fits, limits, etc. •••

$3.7 \pm 0.4$	AAIJ	13AE	LHCB	Repl. by AAIJ 16L
---------------	------	------	------	-------------------

**$\Gamma([K^-\pi^+]_{(D\pi)K^+})/\Gamma([K^+\pi^-]_{(D\pi)K^+})$   $\Gamma_{75}/\Gamma_{76}$**

VALUE (units $10^{-3}$ )	DOCUMENT ID	TECN	COMMENT
<b><math>3.2 \pm 0.9 \pm 0.8</math></b>	DEL-AMO-SA..10H	BABR	$e^+e^- \rightarrow \Upsilon(4S)$

**$\Gamma([K^-\pi^+]_{(D\gamma)K^+})/\Gamma([K^+\pi^-]_{(D\gamma)K^+})$   $\Gamma_{77}/\Gamma_{78}$**

VALUE (units $10^{-3}$ )	DOCUMENT ID	TECN	COMMENT
<b><math>2.7 \pm 1.4 \pm 2.2</math></b>	DEL-AMO-SA..10H	BABR	$e^+e^- \rightarrow \Upsilon(4S)$

**$\Gamma([K^-\pi^+]_{(D\pi)K^+})/\Gamma([K^+\pi^-]_{(D\pi)K^+})$   $\Gamma_{79}/\Gamma_{80}$**

VALUE (units $10^{-3}$ )	DOCUMENT ID	TECN	COMMENT
<b><math>1.8 \pm 0.9 \pm 0.4</math></b>	DEL-AMO-SA..10H	BABR	$e^+e^- \rightarrow \Upsilon(4S)$

**$\Gamma([K^-\pi^+]_{(D\gamma)K^+})/\Gamma([K^+\pi^-]_{(D\gamma)K^+})$   $\Gamma_{81}/\Gamma_{82}$**

VALUE (units $10^{-3}$ )	DOCUMENT ID	TECN	COMMENT
<b><math>1.3 \pm 1.4 \pm 0.8</math></b>	DEL-AMO-SA..10H	BABR	$e^+e^- \rightarrow \Upsilon(4S)$

**$\Gamma([\pi^+\pi^-\pi^0]_{D K^-})/\Gamma_{total}$   $\Gamma_{83}/\Gamma$**

VALUE (units $10^{-6}$ )	DOCUMENT ID	TECN	COMMENT
<b><math>4.6 \pm 0.8 \pm 0.4</math></b>	<sup>1</sup> AUBERT	07BJ	BABR $e^+e^- \rightarrow \Upsilon(4S)$

••• We do not use the following data for averages, fits, limits, etc. •••

$5.5 \pm 1.0 \pm 0.7$	<sup>1</sup> AUBERT,B	05T	BABR	Repl. by AUBERT 07BJ
-----------------------	-----------------------	-----	------	----------------------

<sup>1</sup> Assumes equal production of  $B^+$  and  $B^0$  at the  $\Upsilon(4S)$ .

**$\Gamma([K_S^0 K^+\pi^-]_{D K^+})/\Gamma([K_S^0 K^+\pi^-]_{D\pi^+})$   $\Gamma_{84}/\Gamma_{89}$**

VALUE	DOCUMENT ID	TECN	COMMENT
<b><math>0.092 \pm 0.009 \pm 0.004</math></b>	<sup>1</sup> AAIJ	14v	LHCB <i>pp</i> at 7, 8 TeV

<sup>1</sup> The analysis uses all of  $D \rightarrow K_S^0 K \pi$  Dalitz decays.

**$\Gamma([K_S^0 K^-\pi^+]_{D K^+})/\Gamma([K_S^0 K^-\pi^+]_{D\pi^+})$   $\Gamma_{85}/\Gamma_{87}$**

VALUE	DOCUMENT ID	TECN	COMMENT
<b><math>0.066 \pm 0.009 \pm 0.002</math></b>	<sup>1</sup> AAIJ	14v	LHCB <i>pp</i> at 7, 8 TeV

<sup>1</sup> The analysis uses all of  $D \rightarrow K_S^0 K \pi$  Dalitz decays.

**$\Gamma([K_S^0 K^-\pi^+]_{D K^+})/\Gamma([K_S^0 K^+\pi^-]_{D\pi^+})$   $\Gamma_{85}/\Gamma_{89}$**

VALUE	DOCUMENT ID	TECN	COMMENT
<b><math>0.084 \pm 0.011 \pm 0.003</math></b>	<sup>1</sup> AAIJ	14v	LHCB <i>pp</i> at 7, 8 TeV

<sup>1</sup> The Analysis uses  $D \rightarrow K^*(892) K \rightarrow K_S^0 K \pi$  decays.

**$\Gamma([K^*(892)^+K^-]_{D K^+})/\Gamma([K^*(892)^-K^+]_{D\pi^+})$   $\Gamma_{86}/\Gamma_{90}$**

VALUE	DOCUMENT ID	TECN	COMMENT
<b><math>0.056 \pm 0.013 \pm 0.002</math></b>	<sup>1</sup> AAIJ	14v	LHCB <i>pp</i> at 7, 8 TeV

<sup>1</sup> The Analysis uses  $D \rightarrow K^*(892) K \rightarrow K_S^0 K \pi$  decays.

**$\Gamma([K^+K^-\pi^0]_{D K^+})/\Gamma([K^+K^-\pi^0]_{D\pi^+})$   $\Gamma_{91}/\Gamma_{92}$**

VALUE	DOCUMENT ID	TECN	COMMENT
<b><math>0.95 \pm 0.22 \pm 0.05</math></b>	<sup>1</sup> AAIJ	15w	LHCB <i>pp</i> at 7, 8 TeV

<sup>1</sup> Uses  $D \rightarrow K^+K^-\pi^0$  mode.

**$\Gamma([\pi^+\pi^-\pi^0]_{D K^+})/\Gamma([\pi^+\pi^-\pi^0]_{D\pi^+})$   $\Gamma_{93}/\Gamma_{94}$**

VALUE	DOCUMENT ID	TECN	COMMENT
<b><math>0.98 \pm 0.11 \pm 0.05</math></b>	<sup>1</sup> AAIJ	15w	LHCB <i>pp</i> at 7, 8 TeV

<sup>1</sup> Uses  $D \rightarrow \pi^+\pi^-\pi^0$  mode.

**$\Gamma([K_S^0 K^+\pi^-]_{D\pi^+})/\Gamma([K_S^0 K^+\pi^-]_{D\pi^+})$   $\Gamma_{89}/\Gamma_{87}$**

VALUE	DOCUMENT ID	TECN	COMMENT
<b><math>1.528 \pm 0.058 \pm 0.025</math></b>	<sup>1</sup> AAIJ	14v	LHCB <i>pp</i> at 7, 8 TeV

<sup>1</sup> The analysis uses all of  $D \rightarrow K_S^0 K \pi$  Dalitz decays.

**$\Gamma([K^*(892)^-K^+]_{D\pi^+})/\Gamma([K^*(892)^+K^-]_{D\pi^+})$   $\Gamma_{90}/\Gamma_{88}$**

VALUE	DOCUMENT ID	TECN	COMMENT
<b><math>2.57 \pm 0.13 \pm 0.06</math></b>	<sup>1</sup> AAIJ	14v	LHCB <i>pp</i> at 7, 8 TeV

<sup>1</sup> The Analysis uses  $D \rightarrow K^*(892) K \rightarrow K_S^0 K \pi$  decays.

**$\Gamma(\overline{D^0} K^*(892)^+)/\Gamma_{total}$   $\Gamma_{95}/\Gamma$**

VALUE (units $10^{-4}$ )	DOCUMENT ID	TECN	COMMENT
<b><math>5.3 \pm 0.4</math> OUR AVERAGE</b>			
$5.29 \pm 0.30 \pm 0.34$	<sup>1</sup> AUBERT	06z	BABR $e^+e^- \rightarrow \Upsilon(4S)$
$6.1 \pm 1.6 \pm 1.7$	<sup>1</sup> MAHAPATRA	02	CLE2 $e^+e^- \rightarrow \Upsilon(4S)$

••• We do not use the following data for averages, fits, limits, etc. •••

$6.3 \pm 0.7 \pm 0.5$	<sup>1</sup> AUBERT	04q	BABR	Repl. by AUBERT 06z
-----------------------	---------------------	-----	------	---------------------

<sup>1</sup> Assumes equal production of  $B^+$  and  $B^0$  at the  $\Upsilon(4S)$ .

**$\Gamma(D_{CP(-)} K^*(892)^+)/\Gamma(\overline{D^0} K^*(892)^+)$   $\Gamma_{96}/\Gamma_{95}$**

VALUE	DOCUMENT ID	TECN	COMMENT
<b><math>0.515 \pm 0.135 \pm 0.065</math></b>	<sup>1</sup> AUBERT	09AJ	BABR $e^+e^- \rightarrow \Upsilon(4S)$

••• We do not use the following data for averages, fits, limits, etc. •••

$0.325 \pm 0.13 \pm 0.04$	<sup>2</sup> AUBERT,B	05U	BABR	Repl. by AUBERT 09AJ
---------------------------	-----------------------	-----	------	----------------------

<sup>1</sup> The authors report  $R_{CP-} = 1.03 \pm 0.27 \pm 0.13$  which is, assuming *CP* conservation, twice the value of the quoted above branching ratio,  
<sup>2</sup> The authors report  $R_{CP-} = 0.65 \pm 0.26 \pm 0.08$  which is, assuming *CP* conservation, twice the value of the quoted above branching ratio.

**$\Gamma(D_{CP(+)} K^*(892)^+)/\Gamma(\overline{D^0} K^*(892)^+)$   $\Gamma_{97}/\Gamma_{95}$**

VALUE	DOCUMENT ID	TECN	COMMENT
<b><math>1.16 \pm 0.08</math> OUR AVERAGE</b>			
$1.18 \pm 0.08 \pm 0.02$	<sup>1</sup> AAIJ	18x	LHCB <i>pp</i> at 7, 8, 13 TeV
$1.085 \pm 0.175 \pm 0.045$	<sup>2</sup> AUBERT	09AJ	BABR $e^+e^- \rightarrow \Upsilon(4S)$

••• We do not use the following data for averages, fits, limits, etc. •••

$1.18 \pm 0.08 \pm 0.01$	<sup>3</sup> AAIJ	17B0	LHCB	Repl. by AAIJ 18x
$0.98 \pm 0.20 \pm 0.055$	<sup>4</sup> AUBERT,B	05U	BABR	Repl. by AUBERT 09AJ

<sup>1</sup> Measures the ratio separately for  $K^+K^-$  and  $\pi^+\pi^-$  final states,  $R_{KK} = 1.22 \pm 0.09 \pm 0.02$  and  $R_{\pi\pi} = 1.08 \pm 0.14 \pm 0.03$ , and combines the two results.  
<sup>2</sup> The authors report  $R_{CP+} = 2.17 \pm 0.35 \pm 0.09$  which is, assuming *CP* conservation, twice the value of the quoted above branching ratio,  
<sup>3</sup> Measures the ratio separately for  $K^+K^-$  and  $\pi^+\pi^-$  final states,  $R_{KK} = 1.22 \pm 0.09 \pm 0.01$  and  $R_{\pi\pi} = 1.08 \pm 0.14 \pm 0.03$ , and combines the two results.  
<sup>4</sup> The authors report  $R_{CP+} = 1.96 \pm 0.40 \pm 0.11$  which is, assuming *CP* conservation, twice the value of the quoted above branching ratio.

**$\Gamma(\overline{D^0} K^*(892)^+)/\Gamma(\overline{D^0} K^*(892)^+)$   $\Gamma_{98}/\Gamma_{95}$**

"OUR EVALUATION" is derived from  $\Gamma_B(B^+ \rightarrow \overline{D^0} K^+)$  data block listed in "CP violation parameters" section.

VALUE (units $10^{-3}$ )	DOCUMENT ID
<b><math>5.8 \pm 3.0</math> OUR EVALUATION</b>	

**$\Gamma(\overline{D^0} K^+\pi^+\pi^-)/\Gamma(\overline{D^0} \pi^+\pi^+\pi^-)$   $\Gamma_{99}/\Gamma_{105}$**

VALUE (units $10^{-2}$ )	DOCUMENT ID	TECN	COMMENT
<b><math>9.4 \pm 1.3 \pm 0.9</math></b>	AAIJ	12T	LHCB <i>pp</i> at 7 TeV

**$\Gamma(D_{CP(+)} K^+\pi^+\pi^-)/\Gamma([K^+\pi^-]_{D K^+} \pi^+\pi^-)$   $\Gamma_{102}/\Gamma_{100}$**

VALUE	DOCUMENT ID	TECN	COMMENT
<b><math>1.040 \pm 0.064</math></b>	AAIJ	15Bc	LHCB <i>pp</i> at 7, 8 TeV

**$\Gamma([K^-\pi^+]_{D K^+} \pi^+\pi^-)/\Gamma([K^+\pi^-]_{D K^+} \pi^+\pi^-)$   $\Gamma_{101}/\Gamma_{100}$**

VALUE (units $10^{-4}$ )	DOCUMENT ID	TECN	COMMENT
<b><math>85^{+36}_{-33}</math></b>	AAIJ	15Bc	LHCB <i>pp</i> at 7, 8 TeV

**$\Gamma(\overline{D^0} K^+\overline{K}^0)/\Gamma_{total}$   $\Gamma_{103}/\Gamma$**

VALUE (units $10^{-4}$ )	DOCUMENT ID	TECN	COMMENT
<b><math>5.5 \pm 1.4 \pm 0.8</math></b>	<sup>1</sup> DRUTSKOY	02	BELL $e^+e^- \rightarrow \Upsilon(4S)$

<sup>1</sup> Assumes equal production of  $B^+$  and  $B^0$  at the  $\Upsilon(4S)$ .

**$\Gamma(\overline{D^0} K^+\overline{K}^0(892)^0)/\Gamma_{total}$   $\Gamma_{104}/\Gamma$**

VALUE (units $10^{-4}$ )	DOCUMENT ID	TECN	COMMENT
<b><math>7.5 \pm 1.3 \pm 1.1</math></b>	<sup>1</sup> DRUTSKOY	02	BELL $e^+e^- \rightarrow \Upsilon(4S)$

<sup>1</sup> Assumes equal production of  $B^+$  and  $B^0$  at the  $\Upsilon(4S)$ .

**$\Gamma(\overline{D^0} \pi^+\pi^+\pi^-)/\Gamma_{total}$   $\Gamma_{105}/\Gamma$**

VALUE	DOCUMENT ID	TECN	COMMENT
<b><math>0.0056 \pm 0.0021</math> OUR FIT</b>			Error includes scale factor of 3.6.
<b><math>0.0115 \pm 0.0029 \pm 0.0021</math></b>	<sup>1</sup> BORTOLETTO92	CLEO	$e^+e^- \rightarrow \Upsilon(4S)$

<sup>1</sup> BORTOLETTO 92 assumes equal production of  $B^+$  and  $B^0$  at the  $\Upsilon(4S)$  and uses Mark III branching fractions for the *D*.

**$\Gamma(\overline{D^0} \pi^+\pi^+\pi^-)/\Gamma(\overline{D^0} \pi^+)$   $\Gamma_{105}/\Gamma_{49}$**

VALUE	DOCUMENT ID	TECN	COMMENT
<b><math>1.2 \pm 0.4</math> OUR FIT</b>			Error includes scale factor of 3.7.
<b><math>1.27 \pm 0.06 \pm 0.11</math></b>	AAIJ	11E	LHCB <i>pp</i> at 7 TeV



See key on page 999

## Meson Particle Listings

 $B^\pm$ 

<sup>4</sup> Uses a missing-mass method. Does not depend on  $D$  branching fractions or  $B^+/B^0$  production rates.

<sup>5</sup> BRANDENBURG 98 assume equal production of  $B^+$  and  $B^0$  at  $\Upsilon(4S)$  and use the  $D^*$  reconstruction technique. The first error is their experiment's error and the second error is the systematic error from the PDG 96 value of  $B(D^* \rightarrow D\pi)$ .

<sup>6</sup> ALAM 94 assume equal production of  $B^+$  and  $B^0$  at the  $\Upsilon(4S)$  and use the CLEO II  $B(D^*(2007)^0 \rightarrow D^0\pi^0)$  and absolute  $B(D^0 \rightarrow K^-\pi^+)$  and the PDG 1992  $B(D^0 \rightarrow K^-\pi^+\pi^0)/B(D^0 \rightarrow K^-\pi^+)$  and  $B(D^0 \rightarrow K^-2\pi^+\pi^-)/B(D^0 \rightarrow K^-\pi^+)$ .

<sup>7</sup> Assumes equal production of  $B^+$  and  $B^0$  at the  $\Upsilon(4S)$  and uses MarkIII branching fractions for the  $D$  and  $D^*(2010)$ .

<sup>8</sup> This is a derived branching ratio, using the inclusive pion spectrum and other two-body  $B$  decays. BEBEK 87 assume the  $\Upsilon(4S)$  decays 43% to  $B^0\bar{B}^0$ .

$\Gamma(\bar{D}^*(2007)^0 \omega \pi^+)/\Gamma_{\text{total}}$   $\Gamma_{127}/\Gamma$   

VALUE	DOCUMENT ID	TECN	COMMENT
<b>0.0045 ± 0.0010 ± 0.0007</b>	<sup>1</sup> ALEXANDER 01B	CLE2	$e^+e^- \rightarrow \Upsilon(4S)$

<sup>1</sup> Assumes equal production of  $B^+$  and  $B^0$  at the  $\Upsilon(4S)$ . The signal is consistent with all observed  $\omega\pi^+$  having proceeded through the  $\rho^+$  resonance at mass  $1349 \pm 25^{+10}_{-5}$  MeV and width  $547 \pm 86^{+46}_{-45}$  MeV.

$\Gamma(\bar{D}^*(2007)^0 \rho^+)/\Gamma_{\text{total}}$   $\Gamma_{128}/\Gamma$   

VALUE	DOCUMENT ID	TECN	COMMENT
<b>0.0098 ± 0.0017 OUR AVERAGE</b>			
0.0098 ± 0.0006 ± 0.0017	<sup>1</sup> CSORNA 03	CLE2	$e^+e^- \rightarrow \Upsilon(4S)$
0.010 ± 0.006 ± 0.004	<sup>2</sup> ALBRECHT 90J	ARG	$e^+e^- \rightarrow \Upsilon(4S)$

• • • We do not use the following data for averages, fits, limits, etc. • • •

0.0168 ± 0.0021 ± 0.0028  $\Gamma_{128}/\Gamma$   

VALUE	DOCUMENT ID	TECN	COMMENT
	<sup>3</sup> ALAM 94	CLE2	$e^+e^- \rightarrow \Upsilon(4S)$

<sup>1</sup> Assumes equal production of  $B^0$  and  $B^+$  at the  $\Upsilon(4S)$  resonance. The second error combines the systematic and theoretical uncertainties in quadrature. CSORNA 03 includes data used in ALAM 94. A full angular fit to three complex helicity amplitudes is performed.

<sup>2</sup> Assumes equal production of  $B^+$  and  $B^0$  at the  $\Upsilon(4S)$  and uses MarkIII branching fractions for the  $D$  and  $D^*(2010)$ .

<sup>3</sup> ALAM 94 assume equal production of  $B^+$  and  $B^0$  at the  $\Upsilon(4S)$  and use the CLEO II  $B(D^*(2007)^0 \rightarrow D^0\pi^0)$  and absolute  $B(D^0 \rightarrow K^-\pi^+)$  and the PDG 1992  $B(D^0 \rightarrow K^-\pi^+\pi^0)/B(D^0 \rightarrow K^-\pi^+)$  and  $B(D^0 \rightarrow K^-2\pi^+\pi^-)/B(D^0 \rightarrow K^-\pi^+)$ . The nonresonant  $\pi^+\pi^0$  contribution under the  $\rho^+$  is negligible.

$\Gamma(\bar{D}^*(2007)^0 K^+)/\Gamma_{\text{total}}$   $\Gamma_{129}/\Gamma$   

VALUE (units $10^{-4}$ )	DOCUMENT ID	TECN	COMMENT
<b>3.97 ± 0.31 ± 0.28 OUR AVERAGE</b>			
3.98 ± 0.28 ± 0.13	<sup>1</sup> AUBERT 05N	BABR	$e^+e^- \rightarrow \Upsilon(4S)$
3.8 ± 1.0 ± 0.1	<sup>2</sup> ABE 01i	BELL	$e^+e^- \rightarrow \Upsilon(4S)$

<sup>1</sup> AUBERT 05N reports  $[\Gamma(B^+ \rightarrow \bar{D}^*(2007)^0 K^+)/\Gamma_{\text{total}}] / [B(B^+ \rightarrow \bar{D}^*(2007)^0 \pi^+)] = 0.0813 \pm 0.0040^{+0.0042}_{-0.0031}$  which we multiply by our best value  $B(B^+ \rightarrow \bar{D}^*(2007)^0 \pi^+) = (4.90 \pm 0.17) \times 10^{-3}$ . Our first error is their experiment's error and our second error is the systematic error from using our best value.

<sup>2</sup> ABE 01i reports  $[\Gamma(B^+ \rightarrow \bar{D}^*(2007)^0 K^+)/\Gamma_{\text{total}}] / [B(B^+ \rightarrow \bar{D}^*(2007)^0 \pi^+)] = 0.078 \pm 0.019 \pm 0.009$  which we multiply by our best value  $B(B^+ \rightarrow \bar{D}^*(2007)^0 \pi^+) = (4.90 \pm 0.17) \times 10^{-3}$ . Our first error is their experiment's error and our second error is the systematic error from using our best value.

$\Gamma(\bar{D}^{*0}_{CP(1)} K^+)/\Gamma_{\text{total}}$   $\Gamma_{130}/\Gamma$   

VALUE (units $10^{-4}$ )	DOCUMENT ID	TECN	COMMENT
<b>2.60 ± 0.27 ± 0.20 ± 0.18</b>	<sup>1</sup> AUBERT 08BF	BABR	$e^+e^- \rightarrow \Upsilon(4S)$

<sup>1</sup> AUBERT 08BF reports  $[\Gamma(B^+ \rightarrow \bar{D}^{*0}_{CP(1)} K^+)/\Gamma_{\text{total}}] / [B(B^+ \rightarrow \bar{D}^*(2007)^0 K^+)] = 0.655 \pm 0.065 \pm 0.020$  which we multiply by our best value  $B(B^+ \rightarrow \bar{D}^*(2007)^0 K^+) = (3.97^{+0.31}_{-0.28}) \times 10^{-4}$ . Our first error is their experiment's error and our second error is the systematic error from using our best value.

$\Gamma(\bar{D}^*(2007)^0 K^+)/\Gamma(\bar{D}^*(2007)^0 \pi^+)$   $\Gamma_{129}/\Gamma_{124}$   

VALUE (units $10^{-2}$ )	DOCUMENT ID	TECN	COMMENT
<b>7.930 ± 0.110 ± 0.560</b>	AALJ	18A	LHCB $pp$ at 7, 8, 13 TeV

$\Gamma(\bar{D}^{*0}_{CP(1)} K^+)/\Gamma(\bar{D}^{*0}_{CP(1)} \pi^+)$   $\Gamma_{130}/\Gamma_{125}$   

VALUE	DOCUMENT ID	TECN	COMMENT
<b>0.095 ± 0.017 OUR AVERAGE</b>			
0.11 ± 0.02 ± 0.02	<sup>1</sup> ABE 06	BELL	$e^+e^- \rightarrow \Upsilon(4S)$
0.086 ± 0.021 ± 0.007	<sup>2</sup> AUBERT 05N	BABR	$e^+e^- \rightarrow \Upsilon(4S)$

<sup>1</sup> Reports a double ratio of  $B(B^+ \rightarrow D^{*0}_{CP(1)} K^+)/B(B^+ \rightarrow D^{*0}_{CP(1)} \pi^+)$  and  $B(B^+ \rightarrow \bar{D}^{*0} K^+)/B(B^+ \rightarrow \bar{D}^{*0} \pi^+)$ ,  $1.41 \pm 0.25 \pm 0.06$ . We multiply by our best value of  $B(B^+ \rightarrow \bar{D}^{*0} K^+)/B(B^+ \rightarrow \bar{D}^{*0} \pi^+) = 0.080 \pm 0.011$ . Our first error is their experiment's error and the second error is systematic error from using our best value.

<sup>2</sup> Uses  $D^{*0} \rightarrow D^0\pi^0$  with  $D^0$  reconstructed in the  $CP$ -even eigenstates  $K^+K^-$  and  $\pi^+\pi^-$ .

$\Gamma(\bar{D}^{*0}_{CP(-1)} K^+)/\Gamma_{\text{total}}$   $\Gamma_{131}/\Gamma$   

VALUE (units $10^{-4}$ )	DOCUMENT ID	TECN	COMMENT
<b>2.19 ± 0.25 ± 0.17 ± 0.15</b>	<sup>1</sup> AUBERT 08BF	BABR	$e^+e^- \rightarrow \Upsilon(4S)$

<sup>1</sup> AUBERT 08BF reports  $[\Gamma(B^+ \rightarrow \bar{D}^{*0}_{CP(-1)} K^+)/\Gamma_{\text{total}}] / [B(B^+ \rightarrow \bar{D}^*(2007)^0 K^+)] = 0.55 \pm 0.06 \pm 0.02$  which we multiply by our best value  $B(B^+ \rightarrow \bar{D}^*(2007)^0 K^+) = (3.97^{+0.31}_{-0.28}) \times 10^{-4}$ . Our first error is their experiment's error and our second error is the systematic error from using our best value.

$\Gamma(\bar{D}^{*0}_{CP(-1)} K^+)/\Gamma(D^{*0}_{CP(-1)} \pi^+)$   $\Gamma_{131}/\Gamma_{126}$   

VALUE	DOCUMENT ID	TECN	COMMENT
<b>0.09 ± 0.03 ± 0.01</b>	<sup>1</sup> ABE 06	BELL	$e^+e^- \rightarrow \Upsilon(4S)$

<sup>1</sup> Reports a double ratio of  $B(B^+ \rightarrow (D^{*0}_{CP(-1)})^0 K^+)/B(B^+ \rightarrow (D^{*0}_{CP(-1)})^0 \pi^+)$  and  $B(B^+ \rightarrow \bar{D}^{*0} K^+)/B(B^+ \rightarrow \bar{D}^{*0} \pi^+)$ ,  $1.15 \pm 0.31 \pm 0.12$ . We multiply by our best value of  $B(B^+ \rightarrow \bar{D}^{*0} K^+)/B(B^+ \rightarrow \bar{D}^{*0} \pi^+) = 0.080 \pm 0.011$ . Our first error is their experiment's error and the second error is systematic error from using our best value.

$\Gamma(D^*(2007)^0 K^+)/\Gamma(\bar{D}^*(2007)^0 K^+)$   $\Gamma_{132}/\Gamma_{129}$   

"OUR EVALUATION" is derived from  $\Gamma_{B^+ \rightarrow D^{*0} K^+}$  data block listed in "CP violation parameters" section.

$\Gamma(D^*(2007)^0 K^+)/\Gamma_{\text{total}}$   $\Gamma_{133}/\Gamma$   

VALUE (units $10^{-2}$ )	DOCUMENT ID	TECN	COMMENT
<b>1.96 ± 0.53 OUR EVALUATION</b>			

$\Gamma(\bar{D}^*(2007)^0 K^*(892)^+)/\Gamma_{\text{total}}$   $\Gamma_{133}/\Gamma$   

VALUE (units $10^{-4}$ )	DOCUMENT ID	TECN	COMMENT
<b>8.1 ± 1.4 OUR AVERAGE</b>			
8.3 ± 1.1 ± 1.0	<sup>1</sup> AUBERT 04k	BABR	$e^+e^- \rightarrow \Upsilon(4S)$
7.2 ± 2.2 ± 2.6	<sup>2</sup> MAHAPATRA 02	CLE2	$e^+e^- \rightarrow \Upsilon(4S)$

<sup>1</sup> Assumes equal production of  $B^+$  and  $B^0$  at the  $\Upsilon(4S)$ .

<sup>2</sup> Assumes equal production of  $B^+$  and  $B^0$  at the  $\Upsilon(4S)$  and an unpolarized final state.

$\Gamma(\bar{D}^*(2007)^0 K^+ \bar{K}^0)/\Gamma_{\text{total}}$   $\Gamma_{134}/\Gamma$   

VALUE (units $10^{-4}$ )	CL%	DOCUMENT ID	TECN	COMMENT
<b>&lt;10.6</b>	90	<sup>1</sup> DRUTSKOY 02	BELL	$e^+e^- \rightarrow \Upsilon(4S)$

<sup>1</sup> Assumes equal production of  $B^+$  and  $B^0$  at the  $\Upsilon(4S)$ .

$\Gamma(\bar{D}^*(2007)^0 K^+ \bar{K}^*(892)^0)/\Gamma_{\text{total}}$   $\Gamma_{135}/\Gamma$   

VALUE (units $10^{-4}$ )	DOCUMENT ID	TECN	COMMENT
<b>15.3 ± 3.1 ± 2.9</b>	<sup>1</sup> DRUTSKOY 02	BELL	$e^+e^- \rightarrow \Upsilon(4S)$

<sup>1</sup> Assumes equal production of  $B^+$  and  $B^0$  at the  $\Upsilon(4S)$ .

$\Gamma(\bar{D}^*(2007)^0 \pi^+ \pi^+ \pi^-)/\Gamma_{\text{total}}$   $\Gamma_{136}/\Gamma$   

VALUE (units $10^{-2}$ )	EVTS	DOCUMENT ID	TECN	COMMENT
<b>1.03 ± 0.12 OUR AVERAGE</b>				
1.055 ± 0.047 ± 0.129		<sup>1</sup> MAJUMDER 04	BELL	$e^+e^- \rightarrow \Upsilon(4S)$
0.94 ± 0.20 ± 0.17	48	<sup>2,3</sup> ALAM 94	CLE2	$e^+e^- \rightarrow \Upsilon(4S)$

<sup>1</sup> Assumes equal production of  $B^+$  and  $B^0$  at the  $\Upsilon(4S)$ .

<sup>2</sup> ALAM 94 assume equal production of  $B^+$  and  $B^0$  at the  $\Upsilon(4S)$  and use the CLEO II  $B(D^*(2007)^0 \rightarrow D^0\pi^0)$  and absolute  $B(D^0 \rightarrow K^-\pi^+)$  and the PDG 1992  $B(D^0 \rightarrow K^-\pi^+\pi^0)/B(D^0 \rightarrow K^-\pi^+)$  and  $B(D^0 \rightarrow K^-2\pi^+\pi^-)/B(D^0 \rightarrow K^-\pi^+)$ .

<sup>3</sup> The three pion mass is required to be between 1.0 and 1.6 GeV consistent with an  $a_1$  meson. (If this channel is dominated by  $a_1^+$ , the branching ratio for  $\bar{D}^{*0} a_1^+$  is twice that for  $\bar{D}^{*0} \pi^+ \pi^+ \pi^-$ .)

$\Gamma(\bar{D}^*(2007)^0 a_1(1260)^+)/\Gamma_{\text{total}}$   $\Gamma_{137}/\Gamma$   

VALUE	DOCUMENT ID	TECN	COMMENT
<b>0.0188 ± 0.0040 ± 0.0034</b>	<sup>1,2</sup> ALAM 94	CLE2	$e^+e^- \rightarrow \Upsilon(4S)$

<sup>1</sup> ALAM 94 value is twice their  $\Gamma(\bar{D}^*(2007)^0 \pi^+ \pi^+ \pi^-)/\Gamma_{\text{total}}$  value based on their observation that the three pions are dominantly in the  $a_1(1260)$  mass range 1.0 to 1.6 GeV.

<sup>2</sup> ALAM 94 assume equal production of  $B^+$  and  $B^0$  at the  $\Upsilon(4S)$  and use the CLEO II  $B(D^*(2007)^0 \rightarrow D^0\pi^0)$  and absolute  $B(D^0 \rightarrow K^-\pi^+)$  and the PDG 1992  $B(D^0 \rightarrow K^-\pi^+\pi^0)/B(D^0 \rightarrow K^-\pi^+)$  and  $B(D^0 \rightarrow K^-2\pi^+\pi^-)/B(D^0 \rightarrow K^-\pi^+)$ .

$\Gamma(\bar{D}^*(2007)^0 \pi^- \pi^+ \pi^0)/\Gamma_{\text{total}}$   $\Gamma_{138}/\Gamma$   

VALUE	DOCUMENT ID	TECN	COMMENT
<b>0.0180 ± 0.0024 ± 0.0027</b>	<sup>1</sup> ALEXANDER 01B	CLE2	$e^+e^- \rightarrow \Upsilon(4S)$

<sup>1</sup> Assumes equal production of  $B^+$  and  $B^0$  at the  $\Upsilon(4S)$ . The signal is consistent with all observed  $\omega\pi^+$  having proceeded through the  $\rho^+$  resonance at mass  $1349 \pm 25^{+10}_{-5}$  MeV and width  $547 \pm 86^{+46}_{-45}$  MeV.

$\Gamma(\bar{D}^{*0} 3\pi^+ 2\pi^-)/\Gamma_{\text{total}}$   $\Gamma_{139}/\Gamma$   

VALUE (units $10^{-3}$ )	DOCUMENT ID	TECN	COMMENT
<b>5.67 ± 0.91 ± 0.85</b>	<sup>1</sup> MAJUMDER 04	BELL	$e^+e^- \rightarrow \Upsilon(4S)$

<sup>1</sup> Assumes equal production of  $B^+$  and  $B^0$  at the  $\Upsilon(4S)$ .





See key on page 999

# Meson Particle Listings

$B^\pm$

$\Gamma(\overline{D}_s^*(2460)^0 \pi^+ \times B(\overline{D}_s^{*0} \rightarrow \overline{D}^{*0} \pi^+ \pi^-))/\Gamma_{\text{total}}$ <span style="float:right"><math>\Gamma_{159}/\Gamma</math></span>				
VALUE (units $10^{-4}$ )	CL%	DOCUMENT ID	TECN	COMMENT
<b>&lt;0.22</b>	90	1 ABE	05A BELL	$e^+ e^- \rightarrow \Upsilon(4S)$

<sup>1</sup> Assumes equal production of  $B^+$  and  $B^0$  at the  $\Upsilon(4S)$ .

$\Gamma(\overline{D}_s^*(2460)^0 \rho^+)/\Gamma_{\text{total}}$ <span style="float:right"><math>\Gamma_{163}/\Gamma</math></span>				
VALUE	CL%	DOCUMENT ID	TECN	COMMENT
<b>&lt;0.0047</b>	90	1 ALAM	94 CLE2	$e^+ e^- \rightarrow \Upsilon(4S)$
<0.005	90	2 ALAM	94 CLE2	$e^+ e^- \rightarrow \Upsilon(4S)$

<sup>1</sup> ALAM 94 assume equal production of  $B^+$  and  $B^0$  at the  $\Upsilon(4S)$  and use the Mark III  $B(D^+ \rightarrow K^- 2\pi^+)$  and  $B(D_s^*(2460)^0 \rightarrow D^+ \pi^-) = 30\%$ .

<sup>2</sup> ALAM 94 assume equal production of  $B^+$  and  $B^0$  at the  $\Upsilon(4S)$  and use the Mark III  $B(D^+ \rightarrow K^- 2\pi^+)$ , the CLEO II  $B(D^*(2010)^+ \rightarrow D^0 \pi^+)$  and  $B(D_s^*(2460)^0 \rightarrow D^*(2010)^+ \pi^-) = 20\%$ .

$\Gamma(\overline{D}_s^*(2680)^0 \pi^+, \overline{D}_s^*(2680)^0 \rightarrow D^- \pi^+)/\Gamma_{\text{total}}$ <span style="float:right"><math>\Gamma_{160}/\Gamma</math></span>				
VALUE (units $10^{-4}$ )	CL%	DOCUMENT ID	TECN	COMMENT
<b>0.84 ± 0.06 ± 0.20</b>		1 AAIJ	16AH LHCB	$pp$ at 7, 8 TeV

<sup>1</sup> Measured using a Dalitz plot analysis of  $B^+ \rightarrow D^- \pi^+ \pi^+$  decays.

$\Gamma(\overline{D}_s^*(2760)^0 \pi^+, \overline{D}_s^*(2760)^0 \pi^+ \rightarrow D^- \pi^+)/\Gamma_{\text{total}}$ <span style="float:right"><math>\Gamma_{161}/\Gamma</math></span>				
VALUE (units $10^{-5}$ )	CL%	DOCUMENT ID	TECN	COMMENT
<b>1.0 ± 0.1 ± 0.2</b>		1 AAIJ	16AH LHCB	$pp$ at 7, 8 TeV

<sup>1</sup> Measured using a Dalitz plot analysis of  $B^+ \rightarrow D^- \pi^+ \pi^+$  decays.

$\Gamma(\overline{D}_s^*(3000)^0 \pi^+, \overline{D}_s^*(3000)^0 \pi^+ \rightarrow D^- \pi^+)/\Gamma_{\text{total}}$ <span style="float:right"><math>\Gamma_{162}/\Gamma</math></span>				
VALUE (units $10^{-6}$ )	CL%	DOCUMENT ID	TECN	COMMENT
<b>2 ± 1 ± 1</b>		1 AAIJ	16AH LHCB	$pp$ at 7, 8 TeV

<sup>1</sup> Measured using a Dalitz plot analysis of  $B^+ \rightarrow D^- \pi^+ \pi^+$  decays.

$\Gamma(D^0 D_s^+)/\Gamma_{\text{total}}$ <span style="float:right"><math>\Gamma_{164}/\Gamma</math></span>				
VALUE (units $10^{-3}$ )	CL%	DOCUMENT ID	TECN	COMMENT
<b>9.0 ± 0.9 OUR AVERAGE</b>				
8.6 ± 0.2 ± 1.1		1 AAIJ	13AP LHCB	$pp$ at 7 TeV
9.5 ± 2.0 ± 0.8		2 AUBERT	06N BABR	$e^+ e^- \rightarrow \Upsilon(4S)$
9.8 ± 2.6 ± 0.9		3 GIBAUT	96 CLE2	$e^+ e^- \rightarrow \Upsilon(4S)$
14 ± 8 ± 1		4 ALBRECHT	92G ARG	$e^+ e^- \rightarrow \Upsilon(4S)$
13 ± 6 ± 1		5 BORTOLETTO	090 CLEO	$e^+ e^- \rightarrow \Upsilon(4S)$

<sup>1</sup> Uses  $B(B^0 \rightarrow D^- D_s^+) = (7.2 \pm 0.8) \times 10^{-3}$ .

<sup>2</sup> AUBERT 06N reports  $(0.92 \pm 0.14 \pm 0.18) \times 10^{-2}$  from a measurement of  $[\Gamma(B^+ \rightarrow \overline{D}^0 D_s^+)/\Gamma_{\text{total}}] \times [B(D_s^+ \rightarrow \phi \pi^+)]$  assuming  $B(D_s^+ \rightarrow \phi \pi^+) = 0.0462 \pm 0.0062$ , which we rescale to our best value  $B(D_s^+ \rightarrow \phi \pi^+) = (4.5 \pm 0.4) \times 10^{-2}$ . Our first error is their experiment's error and our second error is the systematic error from using our best value.

<sup>3</sup> GIBAUT 96 reports  $0.0126 \pm 0.0022 \pm 0.0025$  from a measurement of  $[\Gamma(B^+ \rightarrow \overline{D}^0 D_s^+)/\Gamma_{\text{total}}] \times [B(D_s^+ \rightarrow \phi \pi^+)]$  assuming  $B(D_s^+ \rightarrow \phi \pi^+) = 0.035$ , which we rescale to our best value  $B(D_s^+ \rightarrow \phi \pi^+) = (4.5 \pm 0.4) \times 10^{-2}$ . Our first error is their experiment's error and our second error is the systematic error from using our best value.

<sup>4</sup> ALBRECHT 92G reports  $0.024 \pm 0.012 \pm 0.004$  from a measurement of  $[\Gamma(B^+ \rightarrow \overline{D}^0 D_s^+)/\Gamma_{\text{total}}] \times [B(D_s^+ \rightarrow \phi \pi^+)]$  assuming  $B(D_s^+ \rightarrow \phi \pi^+) = 0.027$ , which we rescale to our best value  $B(D_s^+ \rightarrow \phi \pi^+) = (4.5 \pm 0.4) \times 10^{-2}$ . Our first error is their experiment's error and our second error is the systematic error from using our best value. Assumes PDG 1990  $D^0$  branching ratios, e.g.,  $B(D^0 \rightarrow K^- \pi^+) = 3.71 \pm 0.25\%$ .

<sup>5</sup> BORTOLETTO 90 reports  $0.029 \pm 0.013$  from a measurement of  $[\Gamma(B^+ \rightarrow \overline{D}^0 D_s^+)/\Gamma_{\text{total}}] \times [B(D_s^+ \rightarrow \phi \pi^+)]$  assuming  $B(D_s^+ \rightarrow \phi \pi^+) = 0.02$ , which we rescale to our best value  $B(D_s^+ \rightarrow \phi \pi^+) = (4.5 \pm 0.4) \times 10^{-2}$ . Our first error is their experiment's error and our second error is the systematic error from using our best value.

$\Gamma(D_{s0}^*(2317)^+ \overline{D}^0, D_{s0}^*(2317)^+ \rightarrow D_s^+ \pi^0)/\Gamma_{\text{total}}$ <span style="float:right"><math>\Gamma_{165}/\Gamma</math></span>				
VALUE (units $10^{-3}$ )	CL%	DOCUMENT ID	TECN	COMMENT
<b>0.80 ± 0.16 ± 0.13 OUR AVERAGE</b>				

0.80 ± 0.17 ± 0.16 ± 0.02      1,2 CHOI      15A BELL       $e^+ e^- \rightarrow \Upsilon(4S)$

0.80 ± 0.35 ± 0.21 ± 0.07      2,3 AUBERT,B      04s BABR       $e^+ e^- \rightarrow \Upsilon(4S)$

• • • We do not use the following data for averages, fits, limits, etc. • • •

0.65 ± 0.26 ± 0.24 ± 0.06      2,4 KROKOVNY      03b BELL      Repl. by CHOI 15A

<sup>1</sup> CHOI 15A reports  $(8.0^{+1.3}_{-1.2} \pm 1.1 \pm 0.4) \times 10^{-4}$  from a measurement of  $[\Gamma(B^+ \rightarrow D_{s0}^*(2317)^+ \overline{D}^0, D_{s0}^*(2317)^+ \rightarrow D_s^+ \pi^0)/\Gamma_{\text{total}}] \times [B(D_s^+ \rightarrow K^+ K^- \pi^+)]$  assuming  $B(D_s^+ \rightarrow K^+ K^- \pi^+) = (5.39 \pm 0.21) \times 10^{-2}$ , which we rescale to our best value  $B(D_s^+ \rightarrow K^+ K^- \pi^+) = (5.39 \pm 0.15) \times 10^{-2}$ . Our first error is their experiment's error and our second error is the systematic error from using our best value.

<sup>2</sup> Assumes equal production of  $B^+$  and  $B^0$  at the  $\Upsilon(4S)$ .

<sup>3</sup> AUBERT,B 04s reports  $(1.0 \pm 0.3^{+0.4}_{-0.2}) \times 10^{-3}$  from a measurement of  $[\Gamma(B^+ \rightarrow D_{s0}^*(2317)^+ \overline{D}^0, D_{s0}^*(2317)^+ \rightarrow D_s^+ \pi^0)/\Gamma_{\text{total}}] \times [B(D_s^+ \rightarrow \phi \pi^+)]$  assuming  $B(D_s^+ \rightarrow \phi \pi^+) = 0.036 \pm 0.009$ , which we rescale to our best value  $B(D_s^+ \rightarrow \phi \pi^+) = (4.5 \pm 0.4) \times 10^{-2}$ . Our first error is their experiment's error and our second error is the systematic error from using our best value.

$0.4) \times 10^{-2}$ . Our first error is their experiment's error and our second error is the systematic error from using our best value.

<sup>4</sup> KROKOVNY 03b reports  $(0.81^{+0.30}_{-0.27} \pm 0.24) \times 10^{-3}$  from a measurement of  $[\Gamma(B^+ \rightarrow D_{s0}^*(2317)^+ \overline{D}^0, D_{s0}^*(2317)^+ \rightarrow D_s^+ \pi^0)/\Gamma_{\text{total}}] \times [B(D_s^+ \rightarrow \phi \pi^+)]$  assuming  $B(D_s^+ \rightarrow \phi \pi^+) = 0.036 \pm 0.009$ , which we rescale to our best value  $B(D_s^+ \rightarrow \phi \pi^+) = (4.5 \pm 0.4) \times 10^{-2}$ . Our first error is their experiment's error and our second error is the systematic error from using our best value.

$\Gamma(D_{s0}(2317)^+ \overline{D}^0 \times B(D_{s0}(2317)^+ \rightarrow D_s^+ \gamma))/\Gamma_{\text{total}}$ <span style="float:right"><math>\Gamma_{166}/\Gamma</math></span>				
VALUE (units $10^{-3}$ )	CL%	DOCUMENT ID	TECN	COMMENT
<b>&lt;0.76</b>	90	1 KROKOVNY	03b BELL	$e^+ e^- \rightarrow \Upsilon(4S)$

<sup>1</sup> Assumes equal production of  $B^+$  and  $B^0$  at the  $\Upsilon(4S)$ .

$\Gamma(D_{s0}(2317)^+ \overline{D}^*(2007)^0 \times B(D_{s0}(2317)^+ \rightarrow D_s^+ \pi^0))/\Gamma_{\text{total}}$ <span style="float:right"><math>\Gamma_{167}/\Gamma</math></span>				
VALUE (units $10^{-3}$ )	CL%	DOCUMENT ID	TECN	COMMENT
<b>0.9 ± 0.6 ± 0.4 ± 0.3</b>		1 AUBERT,B	04s BABR	$e^+ e^- \rightarrow \Upsilon(4S)$

<sup>1</sup> Assumes equal production of  $B^+$  and  $B^0$  at the  $\Upsilon(4S)$ .

$\Gamma(D_{sJ}(2457)^+ \overline{D}^0)/\Gamma_{\text{total}}$ <span style="float:right"><math>\Gamma_{168}/\Gamma</math></span>				
VALUE (units $10^{-3}$ )	CL%	DOCUMENT ID	TECN	COMMENT
<b>3.1 ± 1.0 ± 0.9 OUR AVERAGE</b>				

4.3 ± 1.6 ± 1.3      1 AUBERT      06N BABR       $e^+ e^- \rightarrow \Upsilon(4S)$

4.6 ± 1.8 ± 1.0      2,3 AUBERT,B      04s BABR       $e^+ e^- \rightarrow \Upsilon(4S)$

2.1 ± 1.1 ± 0.9 ± 0.5      2,4 KROKOVNY      03b BELL       $e^+ e^- \rightarrow \Upsilon(4S)$

<sup>1</sup> Uses a missing-mass method in the events that one of the  $B$  mesons is fully reconstructed.

<sup>2</sup> Assumes equal production of  $B^+$  and  $B^0$  at the  $\Upsilon(4S)$ .

<sup>3</sup> AUBERT,B 04s reports  $[\Gamma(B^+ \rightarrow D_{sJ}(2457)^+ \overline{D}^0)/\Gamma_{\text{total}}] \times [B(D_{s1}(2460)^+ \rightarrow D_s^+ \pi^0)] = (2.2^{+0.8}_{-0.7} \pm 0.3) \times 10^{-3}$  which we divide by our best value  $B(D_{s1}(2460)^+ \rightarrow D_s^+ \pi^0) = (48 \pm 11) \times 10^{-2}$ . Our first error is their experiment's error and our second error is the systematic error from using our best value.

<sup>4</sup> KROKOVNY 03b reports  $[\Gamma(B^+ \rightarrow D_{sJ}(2457)^+ \overline{D}^0)/\Gamma_{\text{total}}] \times [B(D_{s1}(2460)^+ \rightarrow D_s^+ \pi^0)] = (1.0^{+0.5}_{-0.4} \pm 0.1) \times 10^{-3}$  which we divide by our best value  $B(D_{s1}(2460)^+ \rightarrow D_s^+ \pi^0) = (48 \pm 11) \times 10^{-2}$ . Our first error is their experiment's error and our second error is the systematic error from using our best value.

$\Gamma(D_{sJ}(2457)^+ \overline{D}^0 \times B(D_{sJ}(2457)^+ \rightarrow D_s^+ \gamma))/\Gamma_{\text{total}}$ <span style="float:right"><math>\Gamma_{169}/\Gamma</math></span>				
VALUE (units $10^{-3}$ )	CL%	DOCUMENT ID	TECN	COMMENT
<b>0.46 ± 0.13 ± 0.11 OUR AVERAGE</b>				

0.48 ± 0.19 ± 0.13 ± 0.04      1,2 AUBERT,B      04s BABR       $e^+ e^- \rightarrow \Upsilon(4S)$

0.45 ± 0.15 ± 0.14 ± 0.04      1,3 KROKOVNY      03b BELL       $e^+ e^- \rightarrow \Upsilon(4S)$

<sup>1</sup> Assumes equal production of  $B^+$  and  $B^0$  at the  $\Upsilon(4S)$ .

<sup>2</sup> AUBERT,B 04s reports  $(0.6 \pm 0.2^{+0.2}_{-0.1}) \times 10^{-3}$  from a measurement of  $[\Gamma(B^+ \rightarrow D_{sJ}(2457)^+ \overline{D}^0 \times B(D_{sJ}(2457)^+ \rightarrow D_s^+ \gamma))/\Gamma_{\text{total}}] \times [B(D_s^+ \rightarrow \phi \pi^+)]$  assuming  $B(D_s^+ \rightarrow \phi \pi^+) = 0.036 \pm 0.009$ , which we rescale to our best value  $B(D_s^+ \rightarrow \phi \pi^+) = (4.5 \pm 0.4) \times 10^{-2}$ . Our first error is their experiment's error and our second error is the systematic error from using our best value.

<sup>3</sup> KROKOVNY 03b reports  $(0.56^{+0.16}_{-0.15} \pm 0.17) \times 10^{-3}$  from a measurement of  $[\Gamma(B^+ \rightarrow D_{sJ}(2457)^+ \overline{D}^0 \times B(D_{sJ}(2457)^+ \rightarrow D_s^+ \gamma))/\Gamma_{\text{total}}] \times [B(D_s^+ \rightarrow \phi \pi^+)]$  assuming  $B(D_s^+ \rightarrow \phi \pi^+) = 0.036 \pm 0.009$ , which we rescale to our best value  $B(D_s^+ \rightarrow \phi \pi^+) = (4.5 \pm 0.4) \times 10^{-2}$ . Our first error is their experiment's error and our second error is the systematic error from using our best value.

$\Gamma(D_{sJ}(2457)^+ \overline{D}^0 \times B(D_{sJ}(2457)^+ \rightarrow D_s^+ \pi^+ \pi^-))/\Gamma_{\text{total}}$ <span style="float:right"><math>\Gamma_{170}/\Gamma</math></span>				
VALUE (units $10^{-3}$ )	CL%	DOCUMENT ID	TECN	COMMENT
<b>&lt;0.22</b>	90	1 KROKOVNY	03b BELL	$e^+ e^- \rightarrow \Upsilon(4S)$

<sup>1</sup> Assumes equal production of  $B^+$  and  $B^0$  at the  $\Upsilon(4S)$ .

$\Gamma(D_{sJ}(2457)^+ \overline{D}^0 \times B(D_{sJ}(2457)^+ \rightarrow D_s^+ \pi^0))/\Gamma_{\text{total}}$ <span style="float:right"><math>\Gamma_{171}/\Gamma</math></span>				
VALUE (units $10^{-3}$ )	CL%	DOCUMENT ID	TECN	COMMENT
<b>&lt;0.27</b>	90	1 KROKOVNY	03b BELL	$e^+ e^- \rightarrow \Upsilon(4S)$

<sup>1</sup> Assumes equal production of  $B^+$  and  $B^0$  at the  $\Upsilon(4S)$ .

$\Gamma(D_{sJ}(2457)^+ \overline{D}^0 \times B(D_{sJ}(2457)^+ \rightarrow D_s^+ \gamma))/\Gamma_{\text{total}}$ <span style="float:right"><math>\Gamma_{172}/\Gamma</math></span>				
VALUE (units $10^{-3}$ )	CL%	DOCUMENT ID	TECN	COMMENT
<b>&lt;0.98</b>	90	1 KROKOVNY	03b BELL	$e^+ e^- \rightarrow \Upsilon(4S)$

<sup>1</sup> Assumes equal production of  $B^+$  and  $B^0$  at the  $\Upsilon(4S)$ .

# Meson Particle Listings

$B^\pm$

$\Gamma(D_{sJ}(2457)^+ \bar{D}^*(2007)^0)/\Gamma_{\text{total}}$		$\Gamma_{173}/\Gamma$	
VALUE (units $10^{-3}$ )	DOCUMENT ID	TECN	COMMENT
<b>12.0 ± 3.0 OUR AVERAGE</b>			
11.2 ± 2.6 ± 2.0	<sup>1</sup> AUBERT	06N	BABR $e^+e^- \rightarrow \Upsilon(4S)$
16 $^{+8}_{-6} \pm 4$	<sup>2,3</sup> AUBERT,B	04s	BABR $e^+e^- \rightarrow \Upsilon(4S)$

<sup>1</sup> Uses a missing-mass method in the events that one of the  $B$  mesons is fully reconstructed.  
<sup>2</sup> AUBERT,B 04s reports  $[\Gamma(B^+ \rightarrow D_{sJ}(2457)^+ \bar{D}^*(2007)^0)/\Gamma_{\text{total}}] \times [B(D_{s1}(2460)^+ \rightarrow D_s^{*+} \pi^0)] = (7.6 \pm 1.7^{+3.2}_{-2.4}) \times 10^{-3}$  which we divide by our best value  $B(D_{s1}(2460)^+ \rightarrow D_s^{*+} \pi^0) = (48 \pm 11) \times 10^{-2}$ . Our first error is their experiment's error and our second error is the systematic error from using our best value.  
<sup>3</sup> Assumes equal production of  $B^+$  and  $B^0$  at the  $\Upsilon(4S)$ .

$\Gamma(D_{sJ}(2457)^+ \bar{D}^*(2007)^0 \times B(D_{sJ}(2457)^+ \rightarrow D_s^{*+} \gamma))/\Gamma_{\text{total}}$		$\Gamma_{174}/\Gamma$	
VALUE (units $10^{-3}$ )	DOCUMENT ID	TECN	COMMENT
<b>1.4 ± 0.4 <math>^{+0.6}_{-0.4}</math></b>	<sup>1</sup> AUBERT,B	04s	BABR $e^+e^- \rightarrow \Upsilon(4S)$

<sup>1</sup> Assumes equal production of  $B^+$  and  $B^0$  at the  $\Upsilon(4S)$ .

$\Gamma(\bar{D}^0 D_{s1}(2536)^+ \times B(D_{s1}(2536)^+ \rightarrow D^*(2007)^0 K^+))/\Gamma_{\text{total}}$		$\Gamma_{176}/\Gamma$	
VALUE (units $10^{-4}$ )	CL%	DOCUMENT ID	TECN COMMENT
<b>2.16 ± 0.52 ± 0.45</b>		<sup>1</sup> AUBERT	08B BABR $e^+e^- \rightarrow \Upsilon(4S)$
• • • We do not use the following data for averages, fits, limits, etc. • • •			
< 7	90	AUBERT	03x BABR Repl. by AUBERT 08B

<sup>1</sup> Assumes equal production of  $B^+$  and  $B^0$  at the  $\Upsilon(4S)$ .

$\Gamma(\bar{D}^0 D_{s1}(2536)^+ \times B(D_{s1}(2536)^+ \rightarrow D^*(2007)^0 K^+ + D^*(2010)^+ K^0))/\Gamma_{\text{total}}$		$\Gamma_{175}/\Gamma$	
VALUE (units $10^{-4}$ )	DOCUMENT ID	TECN	COMMENT
<b>3.97 ± 0.85 ± 0.56</b>	<sup>1,2</sup> AUSHEV	11	BELL $e^+e^- \rightarrow \Upsilon(4S)$

<sup>1</sup> Uses  $\Gamma(D^*(2007)^0 \rightarrow D^0 \pi^0) / \Gamma(D^*(2007)^0 \rightarrow D^0 \gamma) = 1.74 \pm 0.13$  and  $\Gamma(D_{s1}(2536)^+ \rightarrow D^*(2007)^0 K^+) / \Gamma(D_{s1}(2536)^+ \rightarrow D^*(2010)^+ K^0) = 1.36 \pm 0.2$ .  
<sup>2</sup> Assumes equal production of  $B^+$  and  $B^0$  at the  $\Upsilon(4S)$ .

$\Gamma(\bar{D}^*(2007)^0 D_{s1}(2536)^+ \times B(D_{s1}(2536)^+ \rightarrow D^*(2007)^0 K^+))/\Gamma_{\text{total}}$		$\Gamma_{177}/\Gamma$	
VALUE (units $10^{-4}$ )	CL%	DOCUMENT ID	TECN COMMENT
<b>5.46 ± 1.17 ± 1.04</b>		<sup>1</sup> AUBERT	08B BABR $e^+e^- \rightarrow \Upsilon(4S)$
• • • We do not use the following data for averages, fits, limits, etc. • • •			
< 7	90	AUBERT	03x BABR Repl. by AUBERT 08B

<sup>1</sup> Assumes equal production of  $B^+$  and  $B^0$  at the  $\Upsilon(4S)$ .

$\Gamma(\bar{D}^0 D_{s1}(2536)^+ \times B(D_{s1}(2536)^+ \rightarrow D^{*+} K^0))/\Gamma_{\text{total}}$		$\Gamma_{178}/\Gamma$	
VALUE (units $10^{-4}$ )	DOCUMENT ID	TECN	COMMENT
<b>2.30 ± 0.98 ± 0.43</b>	<sup>1</sup> AUBERT	08B	BABR $e^+e^- \rightarrow \Upsilon(4S)$

<sup>1</sup> Assumes equal production of  $B^+$  and  $B^0$  at the  $\Upsilon(4S)$ .

$\Gamma(\bar{D}^0 D_{sJ}(2700)^+ \times B(D_{sJ}(2700)^+ \rightarrow D^0 K^+))/\Gamma_{\text{total}}$		$\Gamma_{179}/\Gamma$	
VALUE (units $10^{-4}$ )	DOCUMENT ID	TECN	COMMENT
<b>5.6 ± 1.8 OUR AVERAGE</b>	Error includes scale factor of 1.7.		
5.02 ± 0.71 ± 0.93	<sup>1</sup> LEES	15c	BABR $e^+e^- \rightarrow \Upsilon(4S)$
11.3 ± 2.2 $^{+1.4}_{-2.8}$	<sup>1</sup> BRODZICKA	08	BELL $e^+e^- \rightarrow \Upsilon(4S)$

<sup>1</sup> Assumes equal production of  $B^+$  and  $B^0$  at the  $\Upsilon(4S)$ .

$\Gamma(\bar{D}^*(2007)^0 D_{s1}(2536)^+, D_{s1}^+ \rightarrow D^{*+} K^0)/\Gamma_{\text{total}}$		$\Gamma_{180}/\Gamma$	
VALUE (units $10^{-4}$ )	DOCUMENT ID	TECN	COMMENT
<b>3.92 ± 2.46 ± 0.83</b>	<sup>1</sup> AUBERT	08B	BABR $e^+e^- \rightarrow \Upsilon(4S)$

<sup>1</sup> Assumes equal production of  $B^+$  and  $B^0$  at the  $\Upsilon(4S)$ .

$\Gamma(\bar{D}^0 D_{sJ}(2573)^+, D_{sJ}^+ \rightarrow D^0 K^+)/\Gamma_{\text{total}}$		$\Gamma_{181}/\Gamma$	
VALUE (units $10^{-4}$ )	DOCUMENT ID	TECN	COMMENT
<b>0.08 ± 0.14 ± 0.05</b>	<sup>1</sup> LEES	15c	BABR $e^+e^- \rightarrow \Upsilon(4S)$

<sup>1</sup> Assumes equal production of  $B^+$  and  $B^0$  at the  $\Upsilon(4S)$ .

$\Gamma(\bar{D}^*(2007)^0 D_{sJ}(2573), D_{sJ}^+ \rightarrow D^0 K^+)/\Gamma_{\text{total}}$		$\Gamma_{182}/\Gamma$	
VALUE (units $10^{-4}$ )	CL%	DOCUMENT ID	TECN COMMENT
< 2	90	AUBERT	03x BABR $e^+e^- \rightarrow \Upsilon(4S)$

$\Gamma(\bar{D}^*(2007)^0 D_{sJ}(2573), D_{sJ}^+ \rightarrow D^0 K^+)/\Gamma_{\text{total}}$		$\Gamma_{183}/\Gamma$	
VALUE (units $10^{-4}$ )	CL%	DOCUMENT ID	TECN COMMENT
< 5	90	AUBERT	03x BABR $e^+e^- \rightarrow \Upsilon(4S)$

$\Gamma(\bar{D}^0 D_s^{*+})/\Gamma_{\text{total}}$		$\Gamma_{184}/\Gamma$	
VALUE	DOCUMENT ID	TECN	COMMENT
<b>0.0076 ± 0.0016 OUR AVERAGE</b>			
0.0079 ± 0.0017 ± 0.0007	<sup>1</sup> AUBERT	06N	BABR $e^+e^- \rightarrow \Upsilon(4S)$
0.0068 ± 0.0025 ± 0.0006	<sup>2</sup> GIBAUT	96	CLE2 $e^+e^- \rightarrow \Upsilon(4S)$
0.010 ± 0.007 ± 0.001	<sup>3</sup> ALBRECHT	92G	ARG $e^+e^- \rightarrow \Upsilon(4S)$

<sup>1</sup> AUBERT 06N reports  $(0.77 \pm 0.15 \pm 0.13) \times 10^{-2}$  from a measurement of  $[\Gamma(B^+ \rightarrow \bar{D}^0 D_s^{*+})/\Gamma_{\text{total}}] \times [B(D_s^+ \rightarrow \phi \pi^+)]$  assuming  $B(D_s^+ \rightarrow \phi \pi^+) = 0.0462 \pm 0.0062$ , which we rescale to our best value  $B(D_s^+ \rightarrow \phi \pi^+) = (4.5 \pm 0.4) \times 10^{-2}$ . Our first error is their experiment's error and our second error is the systematic error from using our best value.  
<sup>2</sup> GIBAUT 96 reports  $0.0087 \pm 0.0027 \pm 0.0017$  from a measurement of  $[\Gamma(B^+ \rightarrow \bar{D}^0 D_s^{*+})/\Gamma_{\text{total}}] \times [B(D_s^+ \rightarrow \phi \pi^+)]$  assuming  $B(D_s^+ \rightarrow \phi \pi^+) = 0.035$ , which we rescale to our best value  $B(D_s^+ \rightarrow \phi \pi^+) = (4.5 \pm 0.4) \times 10^{-2}$ . Our first error is their experiment's error and our second error is the systematic error from using our best value.  
<sup>3</sup> ALBRECHT 92G reports  $0.016 \pm 0.012 \pm 0.003$  from a measurement of  $[\Gamma(B^+ \rightarrow \bar{D}^0 D_s^{*+})/\Gamma_{\text{total}}] \times [B(D_s^+ \rightarrow \phi \pi^+)]$  assuming  $B(D_s^+ \rightarrow \phi \pi^+) = 0.027$ , which we rescale to our best value  $B(D_s^+ \rightarrow \phi \pi^+) = (4.5 \pm 0.4) \times 10^{-2}$ . Our first error is their experiment's error and our second error is the systematic error from using our best value. Assumes PDG 1990  $D^0$  branching ratios, e.g.,  $B(D^0 \rightarrow K^- \pi^+) = 3.71 \pm 0.25\%$ .

$\Gamma(\bar{D}^*(2007)^0 D_s^+)/\Gamma_{\text{total}}$		$\Gamma_{185}/\Gamma$	
VALUE	DOCUMENT ID	TECN	COMMENT
<b>0.0082 ± 0.0017 OUR AVERAGE</b>			
0.0078 ± 0.0018 ± 0.0007	<sup>1</sup> AUBERT	06N	BABR $e^+e^- \rightarrow \Upsilon(4S)$
0.011 ± 0.004 ± 0.001	<sup>2</sup> GIBAUT	96	CLE2 $e^+e^- \rightarrow \Upsilon(4S)$
0.008 ± 0.006 ± 0.001	<sup>3</sup> ALBRECHT	92G	ARG $e^+e^- \rightarrow \Upsilon(4S)$

<sup>1</sup> AUBERT 06N reports  $(0.76 \pm 0.15 \pm 0.13) \times 10^{-2}$  from a measurement of  $[\Gamma(B^+ \rightarrow \bar{D}^*(2007)^0 D_s^+)/\Gamma_{\text{total}}] \times [B(D_s^+ \rightarrow \phi \pi^+)]$  assuming  $B(D_s^+ \rightarrow \phi \pi^+) = 0.0462 \pm 0.0062$ , which we rescale to our best value  $B(D_s^+ \rightarrow \phi \pi^+) = (4.5 \pm 0.4) \times 10^{-2}$ . Our first error is their experiment's error and our second error is the systematic error from using our best value.  
<sup>2</sup> GIBAUT 96 reports  $0.0140 \pm 0.0043 \pm 0.0035$  from a measurement of  $[\Gamma(B^+ \rightarrow \bar{D}^*(2007)^0 D_s^+)/\Gamma_{\text{total}}] \times [B(D_s^+ \rightarrow \phi \pi^+)]$  assuming  $B(D_s^+ \rightarrow \phi \pi^+) = 0.035$ , which we rescale to our best value  $B(D_s^+ \rightarrow \phi \pi^+) = (4.5 \pm 0.4) \times 10^{-2}$ . Our first error is their experiment's error and our second error is the systematic error from using our best value.  
<sup>3</sup> ALBRECHT 92G reports  $0.013 \pm 0.009 \pm 0.002$  from a measurement of  $[\Gamma(B^+ \rightarrow \bar{D}^*(2007)^0 D_s^+)/\Gamma_{\text{total}}] \times [B(D_s^+ \rightarrow \phi \pi^+)]$  assuming  $B(D_s^+ \rightarrow \phi \pi^+) = 0.027$ , which we rescale to our best value  $B(D_s^+ \rightarrow \phi \pi^+) = (4.5 \pm 0.4) \times 10^{-2}$ . Our first error is their experiment's error and our second error is the systematic error from using our best value. Assumes PDG 1990  $D^0$  and  $D^*(2007)^0$  branching ratios, e.g.,  $B(D^0 \rightarrow K^- \pi^+) = 3.71 \pm 0.25\%$  and  $B(D^*(2007)^0 \rightarrow D^0 \pi^0) = 55 \pm 6\%$ .

$\Gamma(\bar{D}^*(2007)^0 D_s^{*+})/\Gamma_{\text{total}}$		$\Gamma_{186}/\Gamma$	
VALUE	DOCUMENT ID	TECN	COMMENT
<b>0.0171 ± 0.0024 OUR AVERAGE</b>			
0.0167 ± 0.0019 ± 0.0015	<sup>1</sup> AUBERT	06N	BABR $e^+e^- \rightarrow \Upsilon(4S)$
0.024 ± 0.009 ± 0.002	<sup>2</sup> GIBAUT	96	CLE2 $e^+e^- \rightarrow \Upsilon(4S)$
0.019 ± 0.010 ± 0.002	<sup>3</sup> ALBRECHT	92G	ARG $e^+e^- \rightarrow \Upsilon(4S)$

<sup>1</sup> AUBERT 06N reports  $(1.62 \pm 0.22 \pm 0.18) \times 10^{-2}$  from a measurement of  $[\Gamma(B^+ \rightarrow \bar{D}^*(2007)^0 D_s^{*+})/\Gamma_{\text{total}}] \times [B(D_s^+ \rightarrow \phi \pi^+)]$  assuming  $B(D_s^+ \rightarrow \phi \pi^+) = 0.0462 \pm 0.0062$ , which we rescale to our best value  $B(D_s^+ \rightarrow \phi \pi^+) = (4.5 \pm 0.4) \times 10^{-2}$ . Our first error is their experiment's error and our second error is the systematic error from using our best value.  
<sup>2</sup> GIBAUT 96 reports  $0.0310 \pm 0.0088 \pm 0.0065$  from a measurement of  $[\Gamma(B^+ \rightarrow \bar{D}^*(2007)^0 D_s^{*+})/\Gamma_{\text{total}}] \times [B(D_s^+ \rightarrow \phi \pi^+)]$  assuming  $B(D_s^+ \rightarrow \phi \pi^+) = 0.035$ , which we rescale to our best value  $B(D_s^+ \rightarrow \phi \pi^+) = (4.5 \pm 0.4) \times 10^{-2}$ . Our first error is their experiment's error and our second error is the systematic error from using our best value.  
<sup>3</sup> ALBRECHT 92G reports  $0.031 \pm 0.016 \pm 0.005$  from a measurement of  $[\Gamma(B^+ \rightarrow \bar{D}^*(2007)^0 D_s^{*+})/\Gamma_{\text{total}}] \times [B(D_s^+ \rightarrow \phi \pi^+)]$  assuming  $B(D_s^+ \rightarrow \phi \pi^+) = 0.027$ , which we rescale to our best value  $B(D_s^+ \rightarrow \phi \pi^+) = (4.5 \pm 0.4) \times 10^{-2}$ . Our first error is their experiment's error and our second error is the systematic error from using our best value. Assumes PDG 1990  $D^0$  and  $D^*(2007)^0$  branching ratios, e.g.,  $B(D^0 \rightarrow K^- \pi^+) = 3.71 \pm 0.25\%$  and  $B(D^*(2007)^0 \rightarrow D^0 \pi^0) = 55 \pm 6\%$ .

$\Gamma(D_s^{*+} \bar{D}^{*0})/\Gamma_{\text{total}}$		$\Gamma_{187}/\Gamma$	
VALUE	DOCUMENT ID	TECN	COMMENT
<b>(2.73 ± 0.93 ± 0.68) × 10<sup>-2</sup></b>	<sup>1</sup> AHMED	00B	CLE2 $e^+e^- \rightarrow \Upsilon(4S)$

<sup>1</sup> AHMED 00B reports their experiment's uncertainties  $(\pm 0.78 \pm 0.48 \pm 0.68)\%$ , where the first error is statistical, the second is systematic, and the third is the uncertainty in the  $D_s \rightarrow \phi \pi$  branching fraction. We combine the first two in quadrature.

$\Gamma(\bar{D}^*(2007)^0 D^*(2010)^+)/\Gamma_{\text{total}}$		$\Gamma_{188}/\Gamma$	
VALUE (units $10^{-4}$ )	CL%	DOCUMENT ID	TECN COMMENT
<b>8.1 ± 1.2 ± 1.2</b>		<sup>1</sup> AUBERT,B	06A BABR $e^+e^- \rightarrow \Upsilon(4S)$
• • • We do not use the following data for averages, fits, limits, etc. • • •			
< 110	90	BARATE	98Q ALEP $e^+e^- \rightarrow Z$

<sup>1</sup> Assumes equal production of  $B^+$  and  $B^0$  at the  $\Upsilon(4S)$ .

See key on page 999

Meson Particle Listings

$B^\pm$

$\Gamma(\bar{D}^0 D^*(2010)^+) + \Gamma(\bar{D}^*(2007)^0 D^+)/\Gamma_{total}$   $\Gamma_{189}/\Gamma$

VALUE (units $10^{-4}$ )	CL%	DOCUMENT ID	TECN	COMMENT
<130	90	BARATE	98Q	ALEP $e^+e^- \rightarrow Z$

$\Gamma(\bar{D}^0 D^*(2010)^+)/\Gamma_{total}$   $\Gamma_{190}/\Gamma$

VALUE (units $10^{-4}$ )	DOCUMENT ID	TECN	COMMENT
<b>3.9 ± 0.5 OUR AVERAGE</b>			
3.6 ± 0.5 ± 0.4	<sup>1</sup> AUBERT,B	06A	BABR $e^+e^- \rightarrow \Upsilon(4S)$
4.57 ± 0.71 ± 0.56	<sup>1</sup> MAJUMDER	05	BELL $e^+e^- \rightarrow \Upsilon(4S)$

<sup>1</sup> Assumes equal production of  $B^+$  and  $B^0$  at the  $\Upsilon(4S)$ .

$\Gamma(\bar{D}^0 D^+)/\Gamma_{total}$   $\Gamma_{191}/\Gamma$

VALUE (units $10^{-4}$ )	CL%	DOCUMENT ID	TECN	COMMENT
<b>3.8 ± 0.4 OUR AVERAGE</b>				
3.85 ± 0.31 ± 0.38		<sup>1</sup> ADACHI	08	BELL $e^+e^- \rightarrow \Upsilon(4S)$
3.8 ± 0.6 ± 0.5		<sup>1</sup> AUBERT,B	06A	BABR $e^+e^- \rightarrow \Upsilon(4S)$

••• We do not use the following data for averages, fits, limits, etc. •••

4.83 ± 0.78 ± 0.58		<sup>1</sup> MAJUMDER	05	BELL Repl. by ADACHI 08
<67	90	BARATE	98Q	ALEP $e^+e^- \rightarrow Z$

<sup>1</sup> Assumes equal production of  $B^+$  and  $B^0$  at the  $\Upsilon(4S)$ .

$\Gamma(\bar{D}^0 D^+ K^0)/\Gamma_{total}$   $\Gamma_{192}/\Gamma$

VALUE (units $10^{-3}$ )	CL%	DOCUMENT ID	TECN	COMMENT
<b>1.55 ± 0.17 ± 0.13</b>		<sup>1</sup> DEL-AMO-SA..11B	BABR	$e^+e^- \rightarrow \Upsilon(4S)$

••• We do not use the following data for averages, fits, limits, etc. •••

<2.8	90	<sup>1</sup> AUBERT	03X	BABR Repl. by DEL-AMO-SANCHEZ 11B
------	----	---------------------	-----	-----------------------------------

<sup>1</sup> Assumes equal production of  $B^+$  and  $B^0$  at the  $\Upsilon(4S)$ .

$\Gamma(D^+ \bar{D}^*(2007)^0)/\Gamma_{total}$   $\Gamma_{193}/\Gamma$

VALUE (units $10^{-4}$ )	DOCUMENT ID	TECN	COMMENT
<b>6.3 ± 1.4 ± 1.0</b>	<sup>1</sup> AUBERT,B	06A	BABR $e^+e^- \rightarrow \Upsilon(4S)$

<sup>1</sup> Assumes equal production of  $B^+$  and  $B^0$  at the  $\Upsilon(4S)$ .

$\Gamma(\bar{D}^*(2007)^0 D^+ K^0)/\Gamma_{total}$   $\Gamma_{194}/\Gamma$

VALUE (units $10^{-3}$ )	CL%	DOCUMENT ID	TECN	COMMENT
<b>2.06 ± 0.38 ± 0.30</b>		<sup>1</sup> DEL-AMO-SA..11B	BABR	$e^+e^- \rightarrow \Upsilon(4S)$

••• We do not use the following data for averages, fits, limits, etc. •••

<6.1	90	<sup>1</sup> AUBERT	03X	BABR Repl. by DEL-AMO-SANCHEZ 11B
------	----	---------------------	-----	-----------------------------------

<sup>1</sup> Assumes equal production of  $B^+$  and  $B^0$  at the  $\Upsilon(4S)$ .

$\Gamma(\bar{D}^0 D^*(2010)^+ K^0)/\Gamma_{total}$   $\Gamma_{195}/\Gamma$

VALUE (units $10^{-3}$ )	DOCUMENT ID	TECN	COMMENT
<b>3.81 ± 0.31 ± 0.23</b>	<sup>1</sup> DEL-AMO-SA..11B	BABR	$e^+e^- \rightarrow \Upsilon(4S)$

••• We do not use the following data for averages, fits, limits, etc. •••

5.2 $^{+1.0}_{-0.9}$ ± 0.7	<sup>1</sup> AUBERT	03X	BABR Repl. by DEL-AMO-SANCHEZ 11B
----------------------------	---------------------	-----	-----------------------------------

<sup>1</sup> Assumes equal production of  $B^+$  and  $B^0$  at the  $\Upsilon(4S)$ .

$\Gamma(\bar{D}^*(2007)^0 D^*(2010)^+ K^0)/\Gamma_{total}$   $\Gamma_{196}/\Gamma$

VALUE (units $10^{-3}$ )	DOCUMENT ID	TECN	COMMENT
<b>9.17 ± 0.83 ± 0.90</b>	<sup>1</sup> DEL-AMO-SA..11B	BABR	$e^+e^- \rightarrow \Upsilon(4S)$

••• We do not use the following data for averages, fits, limits, etc. •••

7.8 $^{+2.3}_{-2.1}$ ± 1.4	<sup>1</sup> AUBERT	03X	BABR Repl. by DEL-AMO-SANCHEZ 11B
----------------------------	---------------------	-----	-----------------------------------

<sup>1</sup> Assumes equal production of  $B^+$  and  $B^0$  at the  $\Upsilon(4S)$ .

$\Gamma(\bar{D}^0 D^0 K^+)/\Gamma_{total}$   $\Gamma_{197}/\Gamma$

VALUE (units $10^{-3}$ )	DOCUMENT ID	TECN	COMMENT
<b>1.45 ± 0.33 OUR AVERAGE</b>			
1.31 ± 0.07 ± 0.12	<sup>1</sup> DEL-AMO-SA..11B	BABR	$e^+e^- \rightarrow \Upsilon(4S)$
2.22 ± 0.22 $^{+0.26}_{-0.24}$	<sup>1</sup> BRODZICKA	08	BELL $e^+e^- \rightarrow \Upsilon(4S)$

••• We do not use the following data for averages, fits, limits, etc. •••

1.17 ± 0.21 ± 0.15	<sup>1</sup> CHISTOV	04	BELL Repl. by BRODZICKA 08
1.9 ± 0.3 ± 0.3	<sup>1</sup> AUBERT	03X	BABR Repl. by DEL-AMO-SANCHEZ 11B

<sup>1</sup> Assumes equal production of  $B^+$  and  $B^0$  at the  $\Upsilon(4S)$ .

$\Gamma(\bar{D}^*(2007)^0 D^0 K^+)/\Gamma_{total}$   $\Gamma_{198}/\Gamma$

VALUE (units $10^{-3}$ )	DOCUMENT ID	TECN	COMMENT
<b>2.26 ± 0.16 ± 0.17</b>	<sup>1</sup> DEL-AMO-SA..11B	BABR	$e^+e^- \rightarrow \Upsilon(4S)$

••• We do not use the following data for averages, fits, limits, etc. •••

<3.8	90	<sup>1</sup> AUBERT	03X	BABR Repl. by DEL-AMO-SANCHEZ 11B
------	----	---------------------	-----	-----------------------------------

<sup>1</sup> Assumes equal production of  $B^+$  and  $B^0$  at the  $\Upsilon(4S)$ .

$\Gamma(\bar{D}^0 D^*(2007)^0 K^+)/\Gamma_{total}$   $\Gamma_{199}/\Gamma$

VALUE (units $10^{-3}$ )	DOCUMENT ID	TECN	COMMENT
<b>6.32 ± 0.19 ± 0.45</b>	<sup>1</sup> DEL-AMO-SA..11B	BABR	$e^+e^- \rightarrow \Upsilon(4S)$

••• We do not use the following data for averages, fits, limits, etc. •••

4.7 ± 0.7 ± 0.7	<sup>1</sup> AUBERT	03X	BABR Repl. by DEL-AMO-SANCHEZ 11B
-----------------	---------------------	-----	-----------------------------------

<sup>1</sup> Assumes equal production of  $B^+$  and  $B^0$  at the  $\Upsilon(4S)$ .

$\Gamma(\bar{D}^*(2007)^0 D^*(2007)^0 K^+)/\Gamma_{total}$   $\Gamma_{200}/\Gamma$

VALUE (units $10^{-3}$ )	DOCUMENT ID	TECN	COMMENT
<b>11.23 ± 0.36 ± 1.26</b>	<sup>1</sup> DEL-AMO-SA..11B	BABR	$e^+e^- \rightarrow \Upsilon(4S)$

••• We do not use the following data for averages, fits, limits, etc. •••

5.3 $^{+1.1}_{-1.0}$ ± 1.2	<sup>1</sup> AUBERT	03X	BABR Repl. by DEL-AMO-SANCHEZ 11B
----------------------------	---------------------	-----	-----------------------------------

<sup>1</sup> Assumes equal production of  $B^+$  and  $B^0$  at the  $\Upsilon(4S)$ .

$\Gamma(D^- D^+ K^+)/\Gamma_{total}$   $\Gamma_{201}/\Gamma$

VALUE (units $10^{-3}$ )	CL%	DOCUMENT ID	TECN	COMMENT
<b>0.22 ± 0.05 ± 0.05</b>		<sup>1</sup> DEL-AMO-SA..11B	BABR	$e^+e^- \rightarrow \Upsilon(4S)$

••• We do not use the following data for averages, fits, limits, etc. •••

<0.90	90	<sup>1</sup> CHISTOV	04	BELL $e^+e^- \rightarrow \Upsilon(4S)$
<0.4	90	<sup>1</sup> AUBERT	03X	BABR Repl. by DEL-AMO-SANCHEZ 11B

<sup>1</sup> Assumes equal production of  $B^+$  and  $B^0$  at the  $\Upsilon(4S)$ .

$\Gamma(D^- D^*(2010)^+ K^+)/\Gamma_{total}$   $\Gamma_{202}/\Gamma$

VALUE (units $10^{-3}$ )	CL%	DOCUMENT ID	TECN	COMMENT
<b>0.63 ± 0.09 ± 0.06</b>		<sup>1</sup> DEL-AMO-SA..11B	BABR	$e^+e^- \rightarrow \Upsilon(4S)$

••• We do not use the following data for averages, fits, limits, etc. •••

<0.7	90	<sup>1</sup> AUBERT	03X	BABR Repl. by DEL-AMO-SANCHEZ 11B
------	----	---------------------	-----	-----------------------------------

<sup>1</sup> Assumes equal production of  $B^+$  and  $B^0$  at the  $\Upsilon(4S)$ .

$\Gamma(D^*(2010)^- D^+ K^+)/\Gamma_{total}$   $\Gamma_{203}/\Gamma$

VALUE (units $10^{-3}$ )	DOCUMENT ID	TECN	COMMENT
<b>0.60 ± 0.10 ± 0.08</b>	<sup>1</sup> DEL-AMO-SA..11B	BABR	$e^+e^- \rightarrow \Upsilon(4S)$

••• We do not use the following data for averages, fits, limits, etc. •••

1.5 ± 0.3 ± 0.2	<sup>1</sup> AUBERT	03X	BABR Repl. by DEL-AMO-SANCHEZ 11B
-----------------	---------------------	-----	-----------------------------------

<sup>1</sup> Assumes equal production of  $B^+$  and  $B^0$  at the  $\Upsilon(4S)$ .

$\Gamma(D^*(2010)^- D^*(2010)^+ K^+)/\Gamma_{total}$   $\Gamma_{204}/\Gamma$

VALUE (units $10^{-3}$ )	CL%	DOCUMENT ID	TECN	COMMENT
<b>1.32 ± 0.13 ± 0.12</b>		<sup>1</sup> DEL-AMO-SA..11B	BABR	$e^+e^- \rightarrow \Upsilon(4S)$

••• We do not use the following data for averages, fits, limits, etc. •••

<1.8	90	<sup>1</sup> AUBERT	03X	BABR Repl. by DEL-AMO-SANCHEZ 11B
------	----	---------------------	-----	-----------------------------------

<sup>1</sup> Assumes equal production of  $B^+$  and  $B^0$  at the  $\Upsilon(4S)$ .

$\Gamma((\bar{D}^+ \bar{D}^*)(D + D^*)K)/\Gamma_{total}$   $\Gamma_{205}/\Gamma$

VALUE (units $10^{-2}$ )	DOCUMENT ID	TECN	COMMENT
<b>4.05 ± 0.11 ± 0.28</b>	<sup>1</sup> DEL-AMO-SA..11B	BABR	$e^+e^- \rightarrow \Upsilon(4S)$

••• We do not use the following data for averages, fits, limits, etc. •••

3.5 ± 0.3 ± 0.5	<sup>1</sup> AUBERT	03X	BABR Repl. by DEL-AMO-SANCHEZ 11B
-----------------	---------------------	-----	-----------------------------------

<sup>1</sup> Assumes equal production of  $B^+$  and  $B^0$  at the  $\Upsilon(4S)$ .

$\Gamma(D_s^+ \pi^0)/\Gamma_{total}$   $\Gamma_{206}/\Gamma$

VALUE (units $10^{-5}$ )	CL%	DOCUMENT ID	TECN	COMMENT
<b>1.6 <math>^{+0.6}_{-0.5}</math> ± 0.1</b>		<sup>1</sup> AUBERT	07M	BABR $e^+e^- \rightarrow \Upsilon(4S)$

••• We do not use the following data for averages, fits, limits, etc. •••

<16	90	<sup>2</sup> ALEXANDER	93B	CLE2 $e^+e^- \rightarrow \Upsilon(4S)$
-----	----	------------------------	-----	--

<sup>1</sup> AUBERT 07M reports  $[\Gamma(B^+ \rightarrow D_s^+ \pi^0)/\Gamma_{total}] \times [B(D_s^+ \rightarrow \phi\pi^+)] = (7.0 \pm 2.4 + 0.6) \times 10^{-7}$  which we divide by our best value  $B(D_s^+ \rightarrow \phi\pi^+) = (4.5 \pm 0.4) \times 10^{-2}$ . Our first error is their experiment's error and our second error is the systematic error from using our best value.

<sup>2</sup> ALEXANDER 93B reports  $< 2.0 \times 10^{-4}$  from a measurement of  $[\Gamma(B^+ \rightarrow D_s^+ \pi^0)/\Gamma_{total}] \times [B(D_s^+ \rightarrow \phi\pi^+)]$  assuming  $B(D_s^+ \rightarrow \phi\pi^+) = 0.037$ , which we rescale to our best value  $B(D_s^+ \rightarrow \phi\pi^+) = 4.5 \times 10^{-2}$ .

$[\Gamma(D_s^+ \pi^0) + \Gamma(D_s^{*+} \pi^0)]/\Gamma_{total}$   $(\Gamma_{206} + \Gamma_{207})/\Gamma$

VALUE	CL%	DOCUMENT ID	TECN	COMMENT
<b>&lt;5 × 10<sup>-4</sup></b>		<sup>1</sup> ALBRECHT	93E	ARG $e^+e^- \rightarrow \Upsilon(4S)$

<sup>1</sup> ALBRECHT 93E reports  $< 0.9 \times 10^{-3}$  from a measurement of  $[\Gamma(B^+ \rightarrow D_s^+ \pi^0) + \Gamma(B^+ \rightarrow D_s^{*+} \pi^0)]/\Gamma_{total} \times [B(D_s^+ \rightarrow \phi\pi^+)]$  assuming  $B(D_s^+ \rightarrow \phi\pi^+) = 0.027$ , which we rescale to our best value  $B(D_s^+ \rightarrow \phi\pi^+) = 4.5 \times 10^{-2}$ .

## Meson Particle Listings

 $B^\pm$ 

$\Gamma(D_s^{*+}\pi^0)/\Gamma_{\text{total}}$					$\Gamma_{207}/\Gamma$
VALUE	CL%	DOCUMENT ID	TECN	COMMENT	
$<2.6 \times 10^{-4}$	90	<sup>1</sup> ALEXANDER 93B	CLE2	$e^+e^- \rightarrow \Upsilon(4S)$	
<sup>1</sup> ALEXANDER 93B reports $<3.2 \times 10^{-4}$ from a measurement of $[\Gamma(B^+ \rightarrow D_s^{*+}\pi^0)/\Gamma_{\text{total}}] \times [B(D_s^+ \rightarrow \phi\pi^+)]$ assuming $B(D_s^+ \rightarrow \phi\pi^+) = 0.037$ , which we rescale to our best value $B(D_s^+ \rightarrow \phi\pi^+) = 4.5 \times 10^{-2}$ .					

$\Gamma(D_s^{*+}\eta)/\Gamma_{\text{total}}$					$\Gamma_{208}/\Gamma$
VALUE	CL%	DOCUMENT ID	TECN	COMMENT	
$<4 \times 10^{-4}$	90	<sup>1</sup> ALEXANDER 93B	CLE2	$e^+e^- \rightarrow \Upsilon(4S)$	
<sup>1</sup> ALEXANDER 93B reports $<4.6 \times 10^{-4}$ from a measurement of $[\Gamma(B^+ \rightarrow D_s^{*+}\eta)/\Gamma_{\text{total}}] \times [B(D_s^+ \rightarrow \phi\pi^+)]$ assuming $B(D_s^+ \rightarrow \phi\pi^+) = 0.037$ , which we rescale to our best value $B(D_s^+ \rightarrow \phi\pi^+) = 4.5 \times 10^{-2}$ .					

$\Gamma(D_s^{*+}\eta)/\Gamma_{\text{total}}$					$\Gamma_{209}/\Gamma$
VALUE	CL%	DOCUMENT ID	TECN	COMMENT	
$<6 \times 10^{-4}$	90	<sup>1</sup> ALEXANDER 93B	CLE2	$e^+e^- \rightarrow \Upsilon(4S)$	
<sup>1</sup> ALEXANDER 93B reports $<7.5 \times 10^{-4}$ from a measurement of $[\Gamma(B^+ \rightarrow D_s^{*+}\eta)/\Gamma_{\text{total}}] \times [B(D_s^+ \rightarrow \phi\pi^+)]$ assuming $B(D_s^+ \rightarrow \phi\pi^+) = 0.037$ , which we rescale to our best value $B(D_s^+ \rightarrow \phi\pi^+) = 4.5 \times 10^{-2}$ .					

$\Gamma(D_s^{*+}\rho^0)/\Gamma_{\text{total}}$					$\Gamma_{210}/\Gamma$
VALUE	CL%	DOCUMENT ID	TECN	COMMENT	
$<3.0 \times 10^{-4}$	90	<sup>1</sup> ALEXANDER 93B	CLE2	$e^+e^- \rightarrow \Upsilon(4S)$	
<sup>1</sup> ALEXANDER 93B reports $<3.7 \times 10^{-4}$ from a measurement of $[\Gamma(B^+ \rightarrow D_s^{*+}\rho^0)/\Gamma_{\text{total}}] \times [B(D_s^+ \rightarrow \phi\pi^+)]$ assuming $B(D_s^+ \rightarrow \phi\pi^+) = 0.037$ , which we rescale to our best value $B(D_s^+ \rightarrow \phi\pi^+) = 4.5 \times 10^{-2}$ .					

$[\Gamma(D_s^{*+}\rho^0) + \Gamma(D_s^{*+}\bar{K}^*(892)^0)]/\Gamma_{\text{total}}$					$(\Gamma_{210} + \Gamma_{221})/\Gamma$
VALUE	CL%	DOCUMENT ID	TECN	COMMENT	
$<2.0 \times 10^{-3}$	90	<sup>1</sup> ALBRECHT 93E	ARG	$e^+e^- \rightarrow \Upsilon(4S)$	
<sup>1</sup> ALBRECHT 93E reports $<3.4 \times 10^{-3}$ from a measurement of $[\Gamma(B^+ \rightarrow D_s^{*+}\rho^0) + \Gamma(B^+ \rightarrow D_s^{*+}\bar{K}^*(892)^0)]/\Gamma_{\text{total}} \times [B(D_s^+ \rightarrow \phi\pi^+)]$ assuming $B(D_s^+ \rightarrow \phi\pi^+) = 0.027$ , which we rescale to our best value $B(D_s^+ \rightarrow \phi\pi^+) = 4.5 \times 10^{-2}$ .					

$\Gamma(D_s^{*+}\rho^0)/\Gamma_{\text{total}}$					$\Gamma_{211}/\Gamma$
VALUE	CL%	DOCUMENT ID	TECN	COMMENT	
$<4 \times 10^{-4}$	90	<sup>1</sup> ALEXANDER 93B	CLE2	$e^+e^- \rightarrow \Upsilon(4S)$	
<sup>1</sup> ALEXANDER 93B reports $<4.8 \times 10^{-4}$ from a measurement of $[\Gamma(B^+ \rightarrow D_s^{*+}\rho^0)/\Gamma_{\text{total}}] \times [B(D_s^+ \rightarrow \phi\pi^+)]$ assuming $B(D_s^+ \rightarrow \phi\pi^+) = 0.037$ , which we rescale to our best value $B(D_s^+ \rightarrow \phi\pi^+) = 4.5 \times 10^{-2}$ .					

$[\Gamma(D_s^{*+}\rho^0) + \Gamma(D_s^{*+}\bar{K}^*(892)^0)]/\Gamma_{\text{total}}$					$(\Gamma_{211} + \Gamma_{223})/\Gamma$
VALUE	CL%	DOCUMENT ID	TECN	COMMENT	
$<1.2 \times 10^{-3}$	90	<sup>1</sup> ALBRECHT 93E	ARG	$e^+e^- \rightarrow \Upsilon(4S)$	
<sup>1</sup> ALBRECHT 93E reports $<2.0 \times 10^{-3}$ from a measurement of $[\Gamma(B^+ \rightarrow D_s^{*+}\rho^0) + \Gamma(B^+ \rightarrow D_s^{*+}\bar{K}^*(892)^0)]/\Gamma_{\text{total}} \times [B(D_s^+ \rightarrow \phi\pi^+)]$ assuming $B(D_s^+ \rightarrow \phi\pi^+) = 0.027$ , which we rescale to our best value $B(D_s^+ \rightarrow \phi\pi^+) = 4.5 \times 10^{-2}$ .					

$\Gamma(D_s^{*+}\omega)/\Gamma_{\text{total}}$					$\Gamma_{212}/\Gamma$
VALUE	CL%	DOCUMENT ID	TECN	COMMENT	
$<4 \times 10^{-4}$	90	<sup>1</sup> ALEXANDER 93B	CLE2	$e^+e^- \rightarrow \Upsilon(4S)$	
••• We do not use the following data for averages, fits, limits, etc. •••					
$<2.0 \times 10^{-3}$	90	<sup>2</sup> ALBRECHT 93E	ARG	$e^+e^- \rightarrow \Upsilon(4S)$	
<sup>1</sup> ALEXANDER 93B reports $<4.8 \times 10^{-4}$ from a measurement of $[\Gamma(B^+ \rightarrow D_s^{*+}\omega)/\Gamma_{\text{total}}] \times [B(D_s^+ \rightarrow \phi\pi^+)]$ assuming $B(D_s^+ \rightarrow \phi\pi^+) = 0.037$ , which we rescale to our best value $B(D_s^+ \rightarrow \phi\pi^+) = 4.5 \times 10^{-2}$ .					
<sup>2</sup> ALBRECHT 93E reports $<3.4 \times 10^{-3}$ from a measurement of $[\Gamma(B^+ \rightarrow D_s^{*+}\omega)/\Gamma_{\text{total}}] \times [B(D_s^+ \rightarrow \phi\pi^+)]$ assuming $B(D_s^+ \rightarrow \phi\pi^+) = 0.027$ , which we rescale to our best value $B(D_s^+ \rightarrow \phi\pi^+) = 4.5 \times 10^{-2}$ .					

$\Gamma(D_s^{*+}\omega)/\Gamma_{\text{total}}$					$\Gamma_{213}/\Gamma$
VALUE	CL%	DOCUMENT ID	TECN	COMMENT	
$<6 \times 10^{-4}$	90	<sup>1</sup> ALEXANDER 93B	CLE2	$e^+e^- \rightarrow \Upsilon(4S)$	
••• We do not use the following data for averages, fits, limits, etc. •••					
$<1.1 \times 10^{-3}$	90	<sup>2</sup> ALBRECHT 93E	ARG	$e^+e^- \rightarrow \Upsilon(4S)$	
<sup>1</sup> ALEXANDER 93B reports $<6.8 \times 10^{-4}$ from a measurement of $[\Gamma(B^+ \rightarrow D_s^{*+}\omega)/\Gamma_{\text{total}}] \times [B(D_s^+ \rightarrow \phi\pi^+)]$ assuming $B(D_s^+ \rightarrow \phi\pi^+) = 0.037$ , which we rescale to our best value $B(D_s^+ \rightarrow \phi\pi^+) = 4.5 \times 10^{-2}$ .					
<sup>2</sup> ALBRECHT 93E reports $<1.9 \times 10^{-3}$ from a measurement of $[\Gamma(B^+ \rightarrow D_s^{*+}\omega)/\Gamma_{\text{total}}] \times [B(D_s^+ \rightarrow \phi\pi^+)]$ assuming $B(D_s^+ \rightarrow \phi\pi^+) = 0.027$ , which we rescale to our best value $B(D_s^+ \rightarrow \phi\pi^+) = 4.5 \times 10^{-2}$ .					

$\Gamma(D_s^{*+}a_1(1260)^0)/\Gamma_{\text{total}}$					$\Gamma_{214}/\Gamma$
VALUE	CL%	DOCUMENT ID	TECN	COMMENT	
$<1.8 \times 10^{-3}$	90	<sup>1</sup> ALBRECHT 93E	ARG	$e^+e^- \rightarrow \Upsilon(4S)$	
<sup>1</sup> ALBRECHT 93E reports $<3.0 \times 10^{-3}$ from a measurement of $[\Gamma(B^+ \rightarrow D_s^{*+}a_1(1260)^0)/\Gamma_{\text{total}}] \times [B(D_s^+ \rightarrow \phi\pi^+)]$ assuming $B(D_s^+ \rightarrow \phi\pi^+) = 0.027$ , which we rescale to our best value $B(D_s^+ \rightarrow \phi\pi^+) = 4.5 \times 10^{-2}$ .					

$\Gamma(D_s^{*+}a_1(1260)^0)/\Gamma_{\text{total}}$					$\Gamma_{215}/\Gamma$
VALUE	CL%	DOCUMENT ID	TECN	COMMENT	
$<1.3 \times 10^{-3}$	90	<sup>1</sup> ALBRECHT 93E	ARG	$e^+e^- \rightarrow \Upsilon(4S)$	
<sup>1</sup> ALBRECHT 93E reports $<2.2 \times 10^{-3}$ from a measurement of $[\Gamma(B^+ \rightarrow D_s^{*+}a_1(1260)^0)/\Gamma_{\text{total}}] \times [B(D_s^+ \rightarrow \phi\pi^+)]$ assuming $B(D_s^+ \rightarrow \phi\pi^+) = 0.027$ , which we rescale to our best value $B(D_s^+ \rightarrow \phi\pi^+) = 4.5 \times 10^{-2}$ .					

$\Gamma(D_s^+K^+K^-)/\Gamma(\bar{D}^0D_s^+)$					$\Gamma_{216}/\Gamma_{164}$
VALUE (units $10^{-4}$ )		DOCUMENT ID	TECN	COMMENT	
$8.0 \pm 0.9 \pm 0.1$		<sup>1</sup> AAIJ 18B	LHCB	$pp$ at 7, 8, 13 TeV	
<sup>1</sup> AAIJ 18B reports $[\Gamma(B^+ \rightarrow D_s^+K^+K^-)/\Gamma(B^+ \rightarrow \bar{D}^0D_s^+)] / [B(D^0 \rightarrow K^+K^-)] = 0.197 \pm 0.015 \pm 0.017$ which we multiply by our best value $B(D^0 \rightarrow K^+K^-) = (4.08 \pm 0.06) \times 10^{-3}$ . Our first error is their experiment's error and our second error is the systematic error from using our best value.					

$\Gamma(D_s^+\phi)/\Gamma_{\text{total}}$					$\Gamma_{217}/\Gamma$
VALUE (units $10^{-6}$ )	CL%	DOCUMENT ID	TECN	COMMENT	
$<0.42$	90	<sup>1</sup> AAIJ 18B	LHCB	$pp$ at 7, 8, 13 TeV	
••• We do not use the following data for averages, fits, limits, etc. •••					
$1.7^{+1.1}_{-0.7} \pm 0.2$		<sup>2</sup> AAIJ 13R	LHCB	Repl. by AAJ 18B	
$<1.9$	90	<sup>3</sup> AUBERT 06F	BABR	$e^+e^- \rightarrow \Upsilon(4S)$	
$<1000$	90	<sup>4</sup> ALBRECHT 93E	ARG	$e^+e^- \rightarrow \Upsilon(4S)$	
$<260$	90	<sup>5</sup> ALEXANDER 93B	CLE2	$e^+e^- \rightarrow \Upsilon(4S)$	

- AAIJ 18B uses  $B^+ \rightarrow D_s^+\bar{D}^0$  decays for normalization.
- AAIJ 13R reports  $(1.87^{+1.25}_{-0.73} \pm 0.19 \pm 0.32) \times 10^{-6}$  from a measurement of  $[\Gamma(B^+ \rightarrow D_s^+\phi)/\Gamma_{\text{total}}] / [B(B^+ \rightarrow \bar{D}^0D_s^+)]$  assuming  $B(B^+ \rightarrow \bar{D}^0D_s^+) = (10.0 \pm 1.7) \times 10^{-3}$ , which we rescale to our best value  $B(B^+ \rightarrow \bar{D}^0D_s^+) = (9.0 \pm 0.9) \times 10^{-3}$ . Our first error is their experiment's error and our second error is the systematic error from using our best value.
- Assumes equal production of  $B^+$  and  $B^0$  at the  $\Upsilon(4S)$ .
- ALBRECHT 93E reports  $<1.7 \times 10^{-3}$  from a measurement of  $[\Gamma(B^+ \rightarrow D_s^+\phi)/\Gamma_{\text{total}}] \times [B(D_s^+ \rightarrow \phi\pi^+)]$  assuming  $B(D_s^+ \rightarrow \phi\pi^+) = 0.027$ , which we rescale to our best value  $B(D_s^+ \rightarrow \phi\pi^+) = 4.5 \times 10^{-2}$ .
- ALEXANDER 93B reports  $<3.1 \times 10^{-4}$  from a measurement of  $[\Gamma(B^+ \rightarrow D_s^+\phi)/\Gamma_{\text{total}}] \times [B(D_s^+ \rightarrow \phi\pi^+)]$  assuming  $B(D_s^+ \rightarrow \phi\pi^+) = 0.037$ , which we rescale to our best value  $B(D_s^+ \rightarrow \phi\pi^+) = 4.5 \times 10^{-2}$ .

$\Gamma(D_s^{*+}\phi)/\Gamma_{\text{total}}$					$\Gamma_{218}/\Gamma$
VALUE	CL%	DOCUMENT ID	TECN	COMMENT	
$<1.2 \times 10^{-5}$	90	<sup>1</sup> AUBERT 06F	BABR	$e^+e^- \rightarrow \Upsilon(4S)$	
••• We do not use the following data for averages, fits, limits, etc. •••					
$<1.3 \times 10^{-3}$	90	<sup>2</sup> ALBRECHT 93E	ARG	$e^+e^- \rightarrow \Upsilon(4S)$	
$<3.5 \times 10^{-4}$	90	<sup>3</sup> ALEXANDER 93B	CLE2	$e^+e^- \rightarrow \Upsilon(4S)$	

- Assumes equal production of  $B^+$  and  $B^0$  at the  $\Upsilon(4S)$ .
- ALBRECHT 93E reports  $<2.1 \times 10^{-3}$  from a measurement of  $[\Gamma(B^+ \rightarrow D_s^{*+}\phi)/\Gamma_{\text{total}}] \times [B(D_s^+ \rightarrow \phi\pi^+)]$  assuming  $B(D_s^+ \rightarrow \phi\pi^+) = 0.027$ , which we rescale to our best value  $B(D_s^+ \rightarrow \phi\pi^+) = 4.5 \times 10^{-2}$ .
- ALEXANDER 93B reports  $<4.2 \times 10^{-4}$  from a measurement of  $[\Gamma(B^+ \rightarrow D_s^{*+}\phi)/\Gamma_{\text{total}}] \times [B(D_s^+ \rightarrow \phi\pi^+)]$  assuming  $B(D_s^+ \rightarrow \phi\pi^+) = 0.037$ , which we rescale to our best value  $B(D_s^+ \rightarrow \phi\pi^+) = 4.5 \times 10^{-2}$ .

$\Gamma(D_s^{*+}\bar{K}^0)/\Gamma_{\text{total}}$					$\Gamma_{219}/\Gamma$
VALUE	CL%	DOCUMENT ID	TECN	COMMENT	
$<8 \times 10^{-4}$	90	<sup>1</sup> ALEXANDER 93B	CLE2	$e^+e^- \rightarrow \Upsilon(4S)$	
••• We do not use the following data for averages, fits, limits, etc. •••					
$<1.5 \times 10^{-3}$	90	<sup>2</sup> ALBRECHT 93E	ARG	$e^+e^- \rightarrow \Upsilon(4S)$	

- ALEXANDER 93B reports  $<10.3 \times 10^{-4}$  from a measurement of  $[\Gamma(B^+ \rightarrow D_s^{*+}\bar{K}^0)/\Gamma_{\text{total}}] \times [B(D_s^+ \rightarrow \phi\pi^+)]$  assuming  $B(D_s^+ \rightarrow \phi\pi^+) = 0.037$ , which we rescale to our best value  $B(D_s^+ \rightarrow \phi\pi^+) = 4.5 \times 10^{-2}$ .
- ALBRECHT 93E reports  $<2.5 \times 10^{-3}$  from a measurement of  $[\Gamma(B^+ \rightarrow D_s^{*+}\bar{K}^0)/\Gamma_{\text{total}}] \times [B(D_s^+ \rightarrow \phi\pi^+)]$  assuming  $B(D_s^+ \rightarrow \phi\pi^+) = 0.027$ , which we rescale to our best value  $B(D_s^+ \rightarrow \phi\pi^+) = 4.5 \times 10^{-2}$ .

$\Gamma(D_s^{*+} \bar{K}^0)/\Gamma_{total}$   $\Gamma_{220}/\Gamma$

VALUE	CL%	DOCUMENT ID	TECN	COMMENT
$<9 \times 10^{-4}$	90	<sup>1</sup> ALEXANDER 93B	CLE2	$e^+e^- \rightarrow \Upsilon(4S)$
••• We do not use the following data for averages, fits, limits, etc. •••				
$<1.9 \times 10^{-3}$	90	<sup>2</sup> ALBRECHT 93E	ARG	$e^+e^- \rightarrow \Upsilon(4S)$
<sup>1</sup> ALEXANDER 93B reports $<10.9 \times 10^{-4}$ from a measurement of $[\Gamma(B^+ \rightarrow D_s^{*+} \bar{K}^0)/\Gamma_{total}] \times [B(D_s^+ \rightarrow \phi\pi^+)]$ assuming $B(D_s^+ \rightarrow \phi\pi^+) = 0.037$ , which we rescale to our best value $B(D_s^+ \rightarrow \phi\pi^+) = 4.5 \times 10^{-2}$ .				
<sup>2</sup> ALBRECHT 93E reports $<3.1 \times 10^{-3}$ from a measurement of $[\Gamma(B^+ \rightarrow D_s^{*+} \bar{K}^0)/\Gamma_{total}] \times [B(D_s^+ \rightarrow \phi\pi^+)]$ assuming $B(D_s^+ \rightarrow \phi\pi^+) = 0.027$ , which we rescale to our best value $B(D_s^+ \rightarrow \phi\pi^+) = 4.5 \times 10^{-2}$ .				

$\Gamma(D_s^+ \bar{K}^*(892)^0)/\Gamma_{total}$   $\Gamma_{221}/\Gamma$

VALUE	CL%	DOCUMENT ID	TECN	COMMENT
$<4.4 \times 10^{-6}$	90	AAIJ	13R	LHCB $pp$ at 7 TeV
••• We do not use the following data for averages, fits, limits, etc. •••				
$<4 \times 10^{-4}$	90	<sup>1</sup> ALEXANDER 93B	CLE2	$e^+e^- \rightarrow \Upsilon(4S)$
<sup>1</sup> ALEXANDER 93B reports $<4.4 \times 10^{-4}$ from a measurement of $[\Gamma(B^+ \rightarrow D_s^+ \bar{K}^*(892)^0)/\Gamma_{total}] \times [B(D_s^+ \rightarrow \phi\pi^+)]$ assuming $B(D_s^+ \rightarrow \phi\pi^+) = 0.037$ , which we rescale to our best value $B(D_s^+ \rightarrow \phi\pi^+) = 4.5 \times 10^{-2}$ .				

$\Gamma(D_s^+ K^*0)/\Gamma_{total}$   $\Gamma_{222}/\Gamma$

VALUE (units $10^{-6}$ )	CL%	DOCUMENT ID	TECN	COMMENT
$<3.5$	90	AAIJ	13R	LHCB $pp$ at 7 TeV

$\Gamma(D_s^{*+} \bar{K}^*(892)^0)/\Gamma_{total}$   $\Gamma_{223}/\Gamma$

VALUE	CL%	DOCUMENT ID	TECN	COMMENT
$<3.5 \times 10^{-4}$	90	<sup>1</sup> ALEXANDER 93B	CLE2	$e^+e^- \rightarrow \Upsilon(4S)$
<sup>1</sup> ALEXANDER 93B reports $<4.3 \times 10^{-4}$ from a measurement of $[\Gamma(B^+ \rightarrow D_s^{*+} \bar{K}^*(892)^0)/\Gamma_{total}] \times [B(D_s^+ \rightarrow \phi\pi^+)]$ assuming $B(D_s^+ \rightarrow \phi\pi^+) = 0.037$ , which we rescale to our best value $B(D_s^+ \rightarrow \phi\pi^+) = 4.5 \times 10^{-2}$ .				

$\Gamma(D_s^- \pi^+ K^+)/\Gamma_{total}$   $\Gamma_{224}/\Gamma$

VALUE (units $10^{-4}$ )	CL%	DOCUMENT ID	TECN	COMMENT
<b><math>1.80 \pm 0.22</math> OUR AVERAGE</b>				
$1.71^{+0.09}_{-0.07} \pm 0.25$		<sup>1</sup> WIECHCZYN...09	BELL	$e^+e^- \rightarrow \Upsilon(4S)$
$2.02 \pm 0.13 \pm 0.38$		<sup>1</sup> AUBERT 08G	BABR	$e^+e^- \rightarrow \Upsilon(4S)$
••• We do not use the following data for averages, fits, limits, etc. •••				
$<7$	90	<sup>2</sup> ALBRECHT 93E	ARG	$e^+e^- \rightarrow \Upsilon(4S)$
<sup>1</sup> Assumes equal production of $B^+$ and $B^0$ at the $\Upsilon(4S)$ .				
<sup>2</sup> ALBRECHT 93E reports $<1.1 \times 10^{-3}$ from a measurement of $[\Gamma(B^+ \rightarrow D_s^- \pi^+ K^+)/\Gamma_{total}] \times [B(D_s^+ \rightarrow \phi\pi^+)]$ assuming $B(D_s^+ \rightarrow \phi\pi^+) = 0.027$ , which we rescale to our best value $B(D_s^+ \rightarrow \phi\pi^+) = 4.5 \times 10^{-2}$ .				

$\Gamma(D_s^- \pi^+ K^+)/\Gamma_{total}$   $\Gamma_{225}/\Gamma$

VALUE (units $10^{-4}$ )	CL%	DOCUMENT ID	TECN	COMMENT
<b><math>1.45 \pm 0.24</math> OUR AVERAGE</b>				
$1.31^{+0.13}_{-0.12} \pm 0.28$		<sup>1</sup> WIECHCZYN...09	BELL	$e^+e^- \rightarrow \Upsilon(4S)$
$1.67 \pm 0.16 \pm 0.35$		<sup>1</sup> AUBERT 08G	BABR	$e^+e^- \rightarrow \Upsilon(4S)$
••• We do not use the following data for averages, fits, limits, etc. •••				
$<10$	90	<sup>2</sup> ALBRECHT 93E	ARG	$e^+e^- \rightarrow \Upsilon(4S)$
<sup>1</sup> Assumes equal production of $B^+$ and $B^0$ at the $\Upsilon(4S)$ .				
<sup>2</sup> ALBRECHT 93E reports $<1.6 \times 10^{-3}$ from a measurement of $[\Gamma(B^+ \rightarrow D_s^{*-} \pi^+ K^+)/\Gamma_{total}] \times [B(D_s^+ \rightarrow \phi\pi^+)]$ assuming $B(D_s^+ \rightarrow \phi\pi^+) = 0.027$ , which we rescale to our best value $B(D_s^+ \rightarrow \phi\pi^+) = 4.5 \times 10^{-2}$ .				

$\Gamma(D_s^- \pi^+ K^*(892)^+)/\Gamma_{total}$   $\Gamma_{226}/\Gamma$

VALUE	CL%	DOCUMENT ID	TECN	COMMENT
$<5 \times 10^{-3}$	90	<sup>1</sup> ALBRECHT 93E	ARG	$e^+e^- \rightarrow \Upsilon(4S)$
<sup>1</sup> ALBRECHT 93E reports $<8.6 \times 10^{-3}$ from a measurement of $[\Gamma(B^+ \rightarrow D_s^- \pi^+ K^*(892)^+)/\Gamma_{total}] \times [B(D_s^+ \rightarrow \phi\pi^+)]$ assuming $B(D_s^+ \rightarrow \phi\pi^+) = 0.027$ , which we rescale to our best value $B(D_s^+ \rightarrow \phi\pi^+) = 4.5 \times 10^{-2}$ .				

$\Gamma(D_s^{*-} \pi^+ K^*(892)^+)/\Gamma_{total}$   $\Gamma_{227}/\Gamma$

VALUE	CL%	DOCUMENT ID	TECN	COMMENT
$<7 \times 10^{-3}$	90	<sup>1</sup> ALBRECHT 93E	ARG	$e^+e^- \rightarrow \Upsilon(4S)$
<sup>1</sup> ALBRECHT 93E reports $<1.1 \times 10^{-2}$ from a measurement of $[\Gamma(B^+ \rightarrow D_s^{*-} \pi^+ K^*(892)^+)/\Gamma_{total}] \times [B(D_s^+ \rightarrow \phi\pi^+)]$ assuming $B(D_s^+ \rightarrow \phi\pi^+) = 0.027$ , which we rescale to our best value $B(D_s^+ \rightarrow \phi\pi^+) = 4.5 \times 10^{-2}$ .				

$\Gamma(D_s^- K^+ K^+)/\Gamma_{total}$   $\Gamma_{228}/\Gamma$

VALUE (units $10^{-5}$ )	DOCUMENT ID	TECN	COMMENT
<b><math>0.97 \pm 0.21</math> OUR AVERAGE</b>			
$0.93 \pm 0.22 \pm 0.10$	<sup>1</sup> WIECHCZYN...15	BELL	$e^+e^- \rightarrow \Upsilon(4S)$
$1.1 \pm 0.4 \pm 0.2$	<sup>1</sup> AUBERT 08G	BABR	$e^+e^- \rightarrow \Upsilon(4S)$
<sup>1</sup> Assumes equal production of $B^+$ and $B^0$ at the $\Upsilon(4S)$ .			

$\Gamma(D_s^- K^+ K^+)/\Gamma(D_s^- \pi^+ K^+)$   $\Gamma_{228}/\Gamma_{224}$

VALUE	DOCUMENT ID	TECN	COMMENT
<b><math>0.054 \pm 0.013 \pm 0.006</math></b>	WIECHCZYN...15	BELL	$e^+e^- \rightarrow \Upsilon(4S)$

$\Gamma(D_s^{*-} K^+ K^+)/\Gamma_{total}$   $\Gamma_{229}/\Gamma$

VALUE (units $10^{-4}$ )	CL%	DOCUMENT ID	TECN	COMMENT
$<0.15$	90	<sup>1</sup> AUBERT 08G	BABR	$e^+e^- \rightarrow \Upsilon(4S)$
<sup>1</sup> Assumes equal production of $B^+$ and $B^0$ at the $\Upsilon(4S)$ .				

$\Gamma(\eta_c K^+)/\Gamma_{total}$   $\Gamma_{230}/\Gamma$

VALUE (units $10^{-3}$ )	DOCUMENT ID	TECN	COMMENT
<b><math>1.06 \pm 0.09</math> OUR AVERAGE</b>	Error includes scale factor of 1.2.		
$0.74^{+0.09}_{-0.08} \pm 0.25$	<sup>1</sup> CHILIKIN 19	BELL	$e^+e^- \rightarrow \Upsilon(4S)$
$1.20 \pm 0.08 \pm 0.07$	<sup>2</sup> KATO 18	BELL	$e^+e^- \rightarrow \Upsilon(4S)$
$0.87 \pm 0.15$	<sup>2,3</sup> AUBERT 06E	BABR	$e^+e^- \rightarrow \Upsilon(4S)$
$1.24^{+0.25}_{-0.19} \pm 0.12$	<sup>4</sup> AUBERT,B 05L	BABR	$e^+e^- \rightarrow \Upsilon(4S)$
$1.25 \pm 0.14^{+0.39}_{-0.40}$	<sup>5</sup> FANG 03	BELL	$e^+e^- \rightarrow \Upsilon(4S)$
$0.69^{+0.26}_{-0.21} \pm 0.22$	<sup>6</sup> EDWARDS 01	CLE2	$e^+e^- \rightarrow \Upsilon(4S)$
••• We do not use the following data for averages, fits, limits, etc. •••			
$1.01 \pm 0.12 \pm 0.05$	<sup>3,7</sup> AUBERT,B 04B	BABR	$e^+e^- \rightarrow \Upsilon(4S)$

<sup>1</sup> CHILIKIN 19 reports  $[\Gamma(B^+ \rightarrow \eta_c K^+)/\Gamma_{total}] \times [B(\eta_c(1S) \rightarrow \pi^+ \pi^- \rho\bar{p})] = (39.4^{+4.1+2.2}_{-3.9-1.8}) \times 10^{-7}$  which we divide by our best value  $B(\eta_c(1S) \rightarrow \pi^+ \pi^- \rho\bar{p}) = (5.3 \pm 1.8) \times 10^{-3}$ . Our first error is their experiment's error and our second error is the systematic error from using our best value.

<sup>2</sup> Measures absolute branching fractions using a missing-mass technique.

<sup>3</sup> The ratio of  $B(B^\pm \rightarrow K^\pm \eta_c) B(\eta_c \rightarrow K\bar{K}\pi) = (7.4 \pm 0.5 \pm 0.7) \times 10^{-5}$  reported in AUBERT,B 04B and  $B(B^\pm \rightarrow K^\pm \eta_c) = (8.7 \pm 1.5) \times 10^{-3}$  reported in AUBERT 06E contribute to the determination of  $B(\eta_c \rightarrow K\bar{K}\pi)$ , which is used by others for normalization.

<sup>4</sup> AUBERT,B 05L reports  $[\Gamma(B^+ \rightarrow \eta_c K^+)/\Gamma_{total}] \times [B(\eta_c(1S) \rightarrow \rho\bar{p})] = (1.8^{+0.3}_{-0.2}) \times 10^{-6}$  which we divide by our best value  $B(\eta_c(1S) \rightarrow \rho\bar{p}) = (1.45 \pm 0.14) \times 10^{-3}$ . Our first error is their experiment's error and our second error is the systematic error from using our best value.

<sup>5</sup> Assumes equal production of  $B^+$  and  $B^0$  at the  $\Upsilon(4S)$ .

<sup>6</sup> EDWARDS 01 assumes equal production of  $B^0$  and  $B^+$  at the  $\Upsilon(4S)$ . The correlated uncertainties (28.3)% from  $B(J/\psi(1S) \rightarrow \gamma \eta_c)$  in those modes have been accounted for.

<sup>7</sup> AUBERT,B 04B reports  $[\Gamma(B^+ \rightarrow \eta_c K^+)/\Gamma_{total}] \times [B(\eta_c(1S) \rightarrow K\bar{K}\pi)] = (0.074 \pm 0.005 \pm 0.007) \times 10^{-3}$  which we divide by our best value  $B(\eta_c(1S) \rightarrow K\bar{K}\pi) = (7.3 \pm 0.4) \times 10^{-2}$ . Our first error is their experiment's error and our second error is the systematic error from using our best value.

$\Gamma(B^+ \rightarrow \eta_c K^+)/\Gamma_{total} \times \Gamma(\eta_c(1S) \rightarrow \gamma\gamma)/\Gamma_{total}$   $\Gamma_{230}/\Gamma \times \Gamma_{49}^{\eta_c(1S)}/\Gamma_{\eta_c(1S)}$

VALUE (units $10^{-6}$ )	DOCUMENT ID	TECN	COMMENT
<b><math>0.22^{+0.09+0.04}_{-0.07-0.02}</math></b>	<sup>1</sup> WICHT 08	BELL	$e^+e^- \rightarrow \Upsilon(4S)$
<sup>1</sup> Assumes equal production of $B^+$ and $B^0$ at the $\Upsilon(4S)$ .			

$\Gamma(\eta_c K^+, \eta_c \rightarrow K_S^0 K^\mp \pi^\pm)/\Gamma_{total}$   $\Gamma_{231}/\Gamma$

VALUE (units $10^{-6}$ )	DOCUMENT ID	TECN	COMMENT
<b><math>26.7 \pm 1.4^{+5.7}_{-5.5}</math></b>	<sup>1,2</sup> VINOKUROVA 11	BELL	$e^+e^- \rightarrow \Upsilon(4S)$
<sup>1</sup> Assumes equal production of $B^0$ and $B^+$ from Upsilon(4S) decays.			
<sup>2</sup> VINOKUROVA 11 reports $(26.7 \pm 1.4^{+2.9}_{-2.9} \pm 4.9) \times 10^{-6}$ , where the first uncertainty is statistical, the second is due to systematics, and the third comes from interference of $\eta_c(1S) \rightarrow K_S^0 K^\pm \pi^\mp$ with nonresonant $K_S^0 K^\pm \pi^\mp$ . We combined both systematic uncertainties to single values.			

$\Gamma(\eta_c K^*(892)^+)/\Gamma_{total}$   $\Gamma_{232}/\Gamma$

VALUE (units $10^{-3}$ )	DOCUMENT ID	TECN	COMMENT
<b><math>1.1^{+0.5}_{-0.4} \pm 0.1</math></b>	<sup>1,2</sup> AUBERT 07AV	BABR	$e^+e^- \rightarrow \Upsilon(4S)$
<sup>1</sup> AUBERT 07AV reports $[\Gamma(B^+ \rightarrow \eta_c K^*(892)^+)/\Gamma_{total}] \times [B(\eta_c(1S) \rightarrow \rho\bar{p})] = (1.57^{+0.56+0.45}_{-0.46-0.36}) \times 10^{-6}$ which we divide by our best value $B(\eta_c(1S) \rightarrow \rho\bar{p}) = (1.45 \pm 0.14) \times 10^{-3}$ . Our first error is their experiment's error and our second error is the systematic error from using our best value.			
<sup>2</sup> Assumes equal production of $B^+$ and $B^0$ at the $\Upsilon(4S)$ .			

$\Gamma(\eta_c K^+ \pi^+ \pi^-)/\Gamma_{total}$   $\Gamma_{233}/\Gamma$

VALUE	CL%	DOCUMENT ID	TECN	COMMENT
$<3.9 \times 10^{-4}$	90	VINOKUROVA 15	BELL	$e^+e^- \rightarrow \Upsilon(4S)$

# Meson Particle Listings

$B^\pm$

$\Gamma(\eta_c K^+ \omega(782))/\Gamma_{\text{total}}$				$\Gamma_{234}/\Gamma$
VALUE	CL%	DOCUMENT ID	TECN	COMMENT
$< 3.3 \times 10^{-4}$	90	VINOKUROVA 15	BELL	$e^+ e^- \rightarrow \Upsilon(4S)$

$\Gamma(\eta_c K^+ \eta)/\Gamma_{\text{total}}$				$\Gamma_{235}/\Gamma$
VALUE	CL%	DOCUMENT ID	TECN	COMMENT
$< 2.2 \times 10^{-4}$	90	VINOKUROVA 15	BELL	$e^+ e^- \rightarrow \Upsilon(4S)$

$\Gamma(\eta_c K^+ \pi^0)/\Gamma_{\text{total}}$				$\Gamma_{236}/\Gamma$
VALUE	CL%	DOCUMENT ID	TECN	COMMENT
$< 6.2 \times 10^{-5}$	90	VINOKUROVA 15	BELL	$e^+ e^- \rightarrow \Upsilon(4S)$

$\Gamma(\eta_c(2S) K^+)/\Gamma_{\text{total}}$				$\Gamma_{237}/\Gamma$
VALUE (units $10^{-4}$ )	CL%	DOCUMENT ID	TECN	COMMENT
<b>4.4 ± 1.0 OUR AVERAGE</b>				
4.8 ± 1.1 ± 0.3		1 KATO 18	BELL	$e^+ e^- \rightarrow \Upsilon(4S)$
3.4 ± 1.8 ± 0.3		1 AUBERT 06E	BABR	$e^+ e^- \rightarrow \Upsilon(4S)$

1 Measures absolute branching fractions using a missing-mass technique.

$\Gamma(\eta_c(2S) K^+, \eta_c \rightarrow p\bar{p})/\Gamma_{\text{total}}$				$\Gamma_{238}/\Gamma$
VALUE (units $10^{-8}$ )	CL%	DOCUMENT ID	TECN	COMMENT
<b>3.47 ± 0.72 ± 0.26</b>		1 AAIJ 17AD	LHCB	$pp$ at 7 and 8 TeV

• • • We do not use the following data for averages, fits, limits, etc. • • •  
 <10.6 95 2 AAIJ 13s LHCB Repl. by AAIJ 17AD

1 Measured relative to  $B^+ \rightarrow J/\psi K^+$  decay with charmonia reconstructed in  $p\bar{p}$  final state and using  $B(B^+ \rightarrow J/\psi K^+) \times B(J/\psi \rightarrow p\bar{p}) = (2.17 \pm 0.08) \times 10^{-6}$ . The last uncertainty includes the uncertainty of  $B(B^+ \rightarrow J/\psi K^+) \times B(J/\psi \rightarrow p\bar{p})$ .

2 Measured relative to  $B^+ \rightarrow J/\psi K^+$  decay with charmonia reconstructed in  $p\bar{p}$  final state and using  $B(B^+ \rightarrow J/\psi K^+) = (1.013 \pm 0.034) \times 10^{-3}$  and  $B(J/\psi \rightarrow p\bar{p}) = (2.17 \pm 0.07) \times 10^{-3}$ .

$\Gamma(\eta_c(2S) K^+, \eta_c \rightarrow p\bar{p}\pi^+\pi^-)/\Gamma_{\text{total}}$				$\Gamma_{240}/\Gamma$
VALUE (units $10^{-7}$ )	CL%	DOCUMENT ID	TECN	COMMENT
<b>11.2 ± 1.8 + 0.5 - 1.6 - 0.7</b>		CHILIKIN 19	BELL	$e^+ e^- \rightarrow \Upsilon(4S)$

$\Gamma(B^+ \rightarrow h_c(1P) K^+)/\Gamma_{\text{total}} \times \Gamma(h_c(1P) \rightarrow \gamma \eta_c(1S))/\Gamma_{\text{total}}$				$\Gamma_{340}/\Gamma \times \Gamma_{12}^{h_c(1P)}/\Gamma_{h_c(1P)}$
VALUE (units $10^{-4}$ )	CL%	DOCUMENT ID	TECN	COMMENT
<b>&lt; 0.48</b>	90	1 AUBERT 08AB	BABR	$e^+ e^- \rightarrow \Upsilon(4S)$

1 Uses the production ratio of  $(B^+ B^-)/(B^0 \bar{B}^0) = 1.026 \pm 0.032$  at  $\Upsilon(4S)$ .

$\Gamma(B^+ \rightarrow \eta_c(2S) K^+)/\Gamma_{\text{total}} \times \Gamma(\eta_c(2S) \rightarrow \gamma \gamma)/\Gamma_{\text{total}}$				$\Gamma_{237}/\Gamma \times \Gamma_{16}^{\eta_c(2S)}/\Gamma_{\eta_c(2S)}$
VALUE (units $10^{-6}$ )	CL%	DOCUMENT ID	TECN	COMMENT
<b>&lt; 0.18</b>	90	1 WICHT 08	BELL	$e^+ e^- \rightarrow \Upsilon(4S)$

1 Assumes equal production of  $B^+$  and  $B^0$  at the  $\Upsilon(4S)$ .

$\Gamma(\eta_c(2S) K^+, \eta_c \rightarrow K_S^0 K^\mp \pi^\pm)/\Gamma_{\text{total}}$				$\Gamma_{239}/\Gamma$
VALUE (units $10^{-6}$ )	CL%	DOCUMENT ID	TECN	COMMENT
<b>3.4 ± 2.2 + 0.5 - 1.5 - 0.4</b>		1,2 VINOKUROVA 11	BELL	$e^+ e^- \rightarrow \Upsilon(4S)$

1 Assumes equal production of  $B^0$  and  $B^+$  from Upsilon(4S) decays.  
 2 The first uncertainty includes both statistical and interference effects while the second is due to systematics.

$\Gamma(J/\psi(1S) K^+)/\Gamma_{\text{total}}$				$\Gamma_{275}/\Gamma$
VALUE (units $10^{-4}$ )	EVTS	DOCUMENT ID	TECN	COMMENT
<b>10.06 ± 0.27 OUR FIT</b>				
<b>9.97 ± 0.30 OUR AVERAGE</b>				

9.4 ± 0.7 ± 0.8		1 CHILIKIN 19	BELL	$e^+ e^- \rightarrow \Upsilon(4S)$
8.9 ± 0.6 ± 0.5		2 KATO 18	BELL	$e^+ e^- \rightarrow \Upsilon(4S)$
8.1 ± 1.3 ± 0.7		2 AUBERT 06E	BABR	$e^+ e^- \rightarrow \Upsilon(4S)$
10.61 ± 0.15 ± 0.48		3 AUBERT 05J	BABR	$e^+ e^- \rightarrow \Upsilon(4S)$
10.4 ± 1.1 ± 0.1		4 AUBERT,B 05L	BABR	$e^+ e^- \rightarrow \Upsilon(4S)$
10.1 ± 0.2 ± 0.7		3 ABE 03B	BELL	$e^+ e^- \rightarrow \Upsilon(4S)$
10.2 ± 0.8 ± 0.7		3 JESSOP 97	CLE2	$e^+ e^- \rightarrow \Upsilon(4S)$
9.24 ± 3.04 ± 0.05		5 BORTOLETTO 92	CLEO	$e^+ e^- \rightarrow \Upsilon(4S)$
8.09 ± 3.50 ± 0.04	6	6 ALBRECHT 90J	ARG	$e^+ e^- \rightarrow \Upsilon(4S)$

• • • We do not use the following data for averages, fits, limits, etc. • • •  
 10.1 ± 0.3 ± 0.5 3 AUBERT 02 BABR Repl. by AUBERT 05J  
 11.0 ± 1.5 ± 0.9 59 3 ALAM 94 CLE2 Repl. by JESSOP 97  
 22 ± 10 ± 2 BUSKULIC 92G ALEP  $e^+ e^- \rightarrow Z$   
 7 ± 4 3 7 ALBRECHT 87D ARG  $e^+ e^- \rightarrow \Upsilon(4S)$   
 10 ± 7 ± 2 3 8 BEBEK 87 CLEO  $e^+ e^- \rightarrow \Upsilon(4S)$   
 9 ± 5 3 9 ALAM 86 CLEO  $e^+ e^- \rightarrow \Upsilon(4S)$

1 CHILIKIN 19 reports  $[\Gamma(B^+ \rightarrow J/\psi(1S) K^+)/\Gamma_{\text{total}}] \times [B(J/\psi(1S) \rightarrow p\bar{p}\pi^+\pi^-)] = (56.4^{+3.3+2.7}_{-3.2-2.5}) \times 10^{-7}$  which we divide by our best value  $B(J/\psi(1S) \rightarrow p\bar{p}\pi^+\pi^-) = (6.0 \pm 0.5) \times 10^{-3}$ . Our first error is their experiment's error and our second error is the systematic error from using our best value.

2 Measures absolute branching fractions using a missing-mass technique.  
 3 Assumes equal production of  $B^+$  and  $B^0$  at the  $\Upsilon(4S)$ .  
 4 AUBERT,B 05L reports  $[\Gamma(B^+ \rightarrow J/\psi(1S) K^+)/\Gamma_{\text{total}}] \times [B(J/\psi(1S) \rightarrow p\bar{p})] = (2.2 \pm 0.2 \pm 0.1) \times 10^{-6}$  which we divide by our best value  $B(J/\psi(1S) \rightarrow p\bar{p}) = (2.121 \pm 0.029) \times 10^{-3}$ . Our first error is their experiment's error and our second error is the systematic error from using our best value.  
 5 BORTOLETTO 92 reports  $(8 \pm 2 \pm 2) \times 10^{-4}$  from a measurement of  $[\Gamma(B^+ \rightarrow J/\psi(1S) K^+)/\Gamma_{\text{total}}] \times [B(J/\psi(1S) \rightarrow e^+ e^-)]$  assuming  $B(J/\psi(1S) \rightarrow e^+ e^-) = 0.069 \pm 0.009$ , which we rescale to our best value  $B(J/\psi(1S) \rightarrow e^+ e^-) = (5.971 \pm 0.032) \times 10^{-2}$ . Our first error is their experiment's error and our second error is the systematic error from using our best value. Assumes equal production of  $B^+$  and  $B^0$  at the  $\Upsilon(4S)$ .  
 6 ALBRECHT 90J reports  $(7 \pm 3 \pm 1) \times 10^{-4}$  from a measurement of  $[\Gamma(B^+ \rightarrow J/\psi(1S) K^+)/\Gamma_{\text{total}}] \times [B(J/\psi(1S) \rightarrow e^+ e^-)]$  assuming  $B(J/\psi(1S) \rightarrow e^+ e^-) = 0.069 \pm 0.009$ , which we rescale to our best value  $B(J/\psi(1S) \rightarrow e^+ e^-) = (5.971 \pm 0.032) \times 10^{-2}$ . Our first error is their experiment's error and our second error is the systematic error from using our best value. Assumes equal production of  $B^+$  and  $B^0$  at the  $\Upsilon(4S)$ .  
 7 ALBRECHT 87D assume  $B^+ B^-/B^0 \bar{B}^0$  ratio is 55/45. Superseded by ALBRECHT 90J.  
 8 BEBEK 87 value has been updated in BERKELMAN 91 to use same assumptions as noted for BORTOLETTO 92.  
 9 ALAM 86 assumes  $B^\pm/B^0$  ratio is 60/40.

$\Gamma(\eta_c K^+)/\Gamma(J/\psi(1S) K^+)$				$\Gamma_{230}/\Gamma_{275}$
VALUE	CL%	DOCUMENT ID	TECN	COMMENT
<b>0.87 ± 0.10 OUR AVERAGE</b>				
0.84 ± 0.06 ± 0.08		1 AAIJ 13s	LHCB	$pp$ at 7 TeV
1.33 ± 0.10 ± 0.43		2 AUBERT,B 04B	BABR	$e^+ e^- \rightarrow \Upsilon(4S)$

1 AAIJ 13s reports  $[\Gamma(B^+ \rightarrow \eta_c K^+)/\Gamma(B^+ \rightarrow J/\psi(1S) K^+)] \times [B(\eta_c(1S) \rightarrow p\bar{p})] / [B(J/\psi(1S) \rightarrow p\bar{p})] = 0.578 \pm 0.035 \pm 0.026$  which we multiply or divide by our best values  $B(\eta_c(1S) \rightarrow p\bar{p}) = (1.45 \pm 0.14) \times 10^{-3}$ ,  $B(J/\psi(1S) \rightarrow p\bar{p}) = (2.121 \pm 0.029) \times 10^{-3}$ . Our first error is their experiment's error and our second error is the systematic error from using our best values.  
 2 Uses BABAR measurement of  $B(B^+ \rightarrow J/\psi K^+) = (10.1 \pm 0.3 \pm 0.5) \times 10^{-4}$ .

$\Gamma(B^+ \rightarrow J/\psi(1S) K^+)/\Gamma_{\text{total}} \times \Gamma(J/\psi(1S) \rightarrow \gamma \gamma)/\Gamma_{\text{total}}$				$\Gamma_{275}/\Gamma \times \Gamma_{303}^{J/\psi(1S)}/\Gamma_{J/\psi(1S)}$
VALUE (units $10^{-6}$ )	CL%	DOCUMENT ID	TECN	COMMENT
<b>&lt; 0.16</b>	90	1 WICHT 08	BELL	$e^+ e^- \rightarrow \Upsilon(4S)$

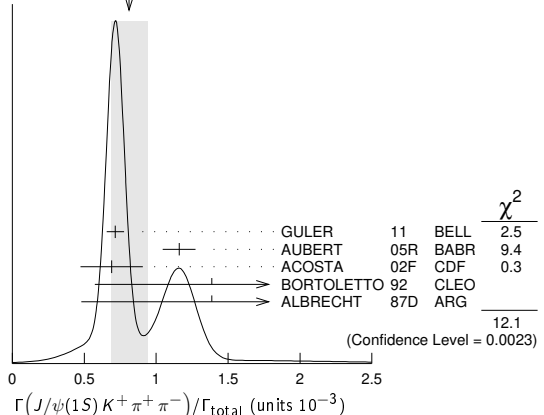
1 Assumes equal production of  $B^+$  and  $B^0$  at the  $\Upsilon(4S)$ .

$\Gamma(J/\psi(1S) K^+ \pi^+ \pi^-)/\Gamma_{\text{total}}$				$\Gamma_{277}/\Gamma$	
VALUE (units $10^{-3}$ )	CL%	EVTS	DOCUMENT ID	TECN	COMMENT
<b>0.81 ± 0.13 OUR AVERAGE</b>					Error includes scale factor of 2.5. See the ideogram below.

0.716 ± 0.010 ± 0.060		1 GULER 11	BELL	$e^+ e^- \rightarrow \Upsilon(4S)$
1.16 ± 0.07 ± 0.09		1 AUBERT 05R	BABR	$e^+ e^- \rightarrow \Upsilon(4S)$
0.69 ± 0.18 ± 0.12		2 ACOSTA 02F	CDF	$p\bar{p}$ 1.8 TeV
1.39 ± 0.81 ± 0.01		3 BORTOLETTO 92	CLEO	$e^+ e^- \rightarrow \Upsilon(4S)$
1.39 ± 0.91 ± 0.01	6	4 ALBRECHT 87D	ARG	$e^+ e^- \rightarrow \Upsilon(4S)$

• • • We do not use the following data for averages, fits, limits, etc. • • •  
 <1.8 90 5 ALBRECHT 90J ARG  $e^+ e^- \rightarrow \Upsilon(4S)$

WEIGHTED AVERAGE  
 0.81 ± 0.13 (Error scaled by 2.5)



1 Assumes equal production of  $B^+$  and  $B^0$  at the  $\Upsilon(4S)$ .  
 2 ACOSTA 02F uses as reference of  $B(B \rightarrow J/\psi(1S) K^+) = (10.1 \pm 0.6) \times 10^{-4}$ . The second error includes the systematic error and the uncertainties of the branching ratio.  
 3 BORTOLETTO 92 reports  $(1.2 \pm 0.6 \pm 0.4) \times 10^{-3}$  from a measurement of  $[\Gamma(B^+ \rightarrow J/\psi(1S) K^+ \pi^+ \pi^-)/\Gamma_{\text{total}}] \times [B(J/\psi(1S) \rightarrow e^+ e^-)]$  assuming  $B(J/\psi(1S) \rightarrow e^+ e^-) = 0.069 \pm 0.009$ , which we rescale to our best value

$B(J/\psi(1S) \rightarrow e^+e^-) = (5.971 \pm 0.032) \times 10^{-2}$ . Our first error is their experiment's error and our second error is the systematic error from using our best value. Assumes equal production of  $B^+$  and  $B^0$  at the  $\Upsilon(4S)$ .

<sup>4</sup>ALBRECHT 87D reports  $(1.2 \pm 0.8) \times 10^{-3}$  from a measurement of  $[\Gamma(B^+ \rightarrow J/\psi(1S) K^+ \pi^+ \pi^-)/\Gamma_{\text{total}}] \times [B(J/\psi(1S) \rightarrow e^+e^-)]$  assuming  $B(J/\psi(1S) \rightarrow e^+e^-) = 0.069 \pm 0.009$ , which we rescale to our best value  $B(J/\psi(1S) \rightarrow e^+e^-) = (5.971 \pm 0.032) \times 10^{-2}$ . Our first error is their experiment's error and our second error is the systematic error from using our best value. They actually report  $0.0011 \pm 0.0007$  assuming  $B^+ B^-/B^0 \bar{B}^0$  ratio is 55/45. We rescale to 50/50. Analysis explicitly removes  $B^+ \rightarrow \psi(2S) K^+$ .

<sup>5</sup>ALBRECHT 90J reports  $< 1.6 \times 10^{-3}$  from a measurement of  $[\Gamma(B^+ \rightarrow J/\psi(1S) K^+ \pi^+ \pi^-)/\Gamma_{\text{total}}] \times [B(J/\psi(1S) \rightarrow e^+e^-)]$  assuming  $B(J/\psi(1S) \rightarrow e^+e^-) = 0.069$ , which we rescale to our best value  $B(J/\psi(1S) \rightarrow e^+e^-) = 5.971 \times 10^{-2}$ . Assumes equal production of  $B^+$  and  $B^0$  at the  $\Upsilon(4S)$ .

$\Gamma(J/\psi(1S) K^+ K^- K^+)/\Gamma_{\text{total}}$		$\Gamma_{278}/\Gamma$	
VALUE (units $10^{-6}$ )	DOCUMENT ID	TECN	COMMENT
<b><math>33.7 \pm 2.5 \pm 1.4</math></b>	LEES	15	BABR $e^+e^- \rightarrow \Upsilon(4S)$

$\Gamma(h_c(1P) K^+, h_c \rightarrow J/\psi \pi^+ \pi^-)/\Gamma_{\text{total}}$		$\Gamma_{241}/\Gamma$	
VALUE	CL%	DOCUMENT ID	TECN COMMENT
<b><math>&lt; 3.4 \times 10^{-6}</math></b>	90	<sup>1</sup> AUBERT 05R	BABR $e^+e^- \rightarrow \Upsilon(4S)$
<sup>1</sup> Assumes equal production of $B^+$ and $B^0$ at the $\Upsilon(4S)$ .			

$\Gamma(X(3730)^0 K^+, X^0 \rightarrow \eta_c \eta)/\Gamma_{\text{total}}$		$\Gamma_{242}/\Gamma$	
VALUE	CL%	DOCUMENT ID	TECN COMMENT
<b><math>&lt; 4.6 \times 10^{-5}</math></b>	90	VINOKUROVA 15	BELL $e^+e^- \rightarrow \Upsilon(4S)$

$\Gamma(X(3730)^0 K^+, X^0 \rightarrow \eta_c \pi^0)/\Gamma_{\text{total}}$		$\Gamma_{243}/\Gamma$	
VALUE	CL%	DOCUMENT ID	TECN COMMENT
<b><math>&lt; 5.7 \times 10^{-6}</math></b>	90	VINOKUROVA 15	BELL $e^+e^- \rightarrow \Upsilon(4S)$

$\Gamma(\chi_{c1}(3872) K^+)/\Gamma_{\text{total}}$		$\Gamma_{244}/\Gamma$	
VALUE	CL%	DOCUMENT ID	TECN COMMENT
<b><math>&lt; 2.6 \times 10^{-4}</math></b>	90	<sup>1</sup> KATO 18	BELL $e^+e^- \rightarrow \Upsilon(4S)$
••• We do not use the following data for averages, fits, limits, etc. •••			
$< 3.2 \times 10^{-4}$	90	<sup>1</sup> AUBERT 06E	BABR $e^+e^- \rightarrow \Upsilon(4S)$
<sup>1</sup> Measures absolute branching fractions using a missing-mass technique.			

$\Gamma(B^+ \rightarrow \chi_{c1}(3872) K^+)/\Gamma_{\text{total}} \times \Gamma(\chi_{c1}(3872) \rightarrow \gamma\gamma)/\Gamma_{\text{total}}$		$\Gamma_{244}/\Gamma \times \Gamma_{\chi_{c1}(3872)}/\Gamma_{\chi_{c1}(3872)}$	
VALUE (units $10^{-6}$ )	CL%	DOCUMENT ID	TECN COMMENT
<b><math>&lt; 0.24</math></b>	90	<sup>1</sup> WICHT 08	BELL $e^+e^- \rightarrow \Upsilon(4S)$
<sup>1</sup> Assumes equal production of $B^+$ and $B^0$ at the $\Upsilon(4S)$ .			

$\Gamma(\chi_{c1}(3872) K^+, \chi_{c1} \rightarrow J/\psi \pi^+ \pi^-)/\Gamma_{\text{total}}$		$\Gamma_{246}/\Gamma$	
VALUE (units $10^{-6}$ )	DOCUMENT ID	TECN	COMMENT
<b><math>8.6 \pm 0.8</math> OUR AVERAGE</b>	Error includes scale factor of 1.1.		
$8.63 \pm 0.82 \pm 0.52$	<sup>1</sup> CHOI 11	BELL	$e^+e^- \rightarrow \Upsilon(4S)$
$8.4 \pm 1.5 \pm 0.7$	<sup>1</sup> AUBERT 08Y	BABR	$e^+e^- \rightarrow \Upsilon(4S)$
••• We do not use the following data for averages, fits, limits, etc. •••			
$10.1 \pm 2.5 \pm 1.0$	<sup>1</sup> AUBERT 06	BABR	Repl. by AUBERT 08Y
$12.8 \pm 4.1$	<sup>1</sup> AUBERT 05R	BABR	Repl. by AUBERT 06
$12.4 \pm 2.8 \pm 0.4$	<sup>2</sup> CHOI 03	BELL	Repl. by CHOI 11
<sup>1</sup> Assumes equal production of $B^+$ and $B^0$ at the $\Upsilon(4S)$ .			
<sup>2</sup> CHOI 03 reports $[\Gamma(B^+ \rightarrow \chi_{c1}(3872) K^+, \chi_{c1} \rightarrow J/\psi \pi^+ \pi^-)/\Gamma_{\text{total}}] / [B(B^+ \rightarrow \psi(2S) K^+)] = 0.0200 \pm 0.0038 \pm 0.0023$ which we multiply by our best value $B(B^+ \rightarrow \psi(2S) K^+) = (6.19 \pm 0.22) \times 10^{-4}$ . Our first error is their experiment's error and our second error is the systematic error from using our best value.			

$\Gamma(\chi_{c1}(3872) K^+, \chi_{c1} \rightarrow J/\psi \gamma)/\Gamma_{\text{total}}$		$\Gamma_{247}/\Gamma$	
VALUE (units $10^{-6}$ )	DOCUMENT ID	TECN	COMMENT
<b><math>2.1 \pm 0.4</math> OUR AVERAGE</b>	Error includes scale factor of 1.1.		
$1.78^{+0.48}_{-0.44} \pm 0.12$	<sup>1</sup> BHARDWAJ 11	BELL	$e^+e^- \rightarrow \Upsilon(4S)$
$2.8 \pm 0.8 \pm 0.1$	<sup>2</sup> AUBERT 09B	BABR	$e^+e^- \rightarrow \Upsilon(4S)$
••• We do not use the following data for averages, fits, limits, etc. •••			
$3.3 \pm 1.0 \pm 0.3$	<sup>1</sup> AUBERT, BE 06M	BABR	Repl. by AUBERT 09B
<sup>1</sup> Assumes equal production of $B^+$ and $B^0$ at the $\Upsilon(4S)$ .			
<sup>2</sup> Uses $B(\Upsilon(4S) \rightarrow B^+ B^-) = (51.6 \pm 0.6)\%$ and $B(\Upsilon(4S) \rightarrow B^0 \bar{B}^0) = (48.4 \pm 0.6)\%$ .			

$\Gamma(\chi_{c1}(3872) K^*(892)^+, \chi_{c1} \rightarrow J/\psi \gamma)/\Gamma_{\text{total}}$		$\Gamma_{265}/\Gamma$	
VALUE (units $10^{-6}$ )	CL%	DOCUMENT ID	TECN COMMENT
<b><math>&lt; 4.8</math></b>	90	<sup>1</sup> AUBERT 09B	BABR $e^+e^- \rightarrow \Upsilon(4S)$
<sup>1</sup> Uses $B(\Upsilon(4S) \rightarrow B^+ B^-) = (51.6 \pm 0.6)\%$ and $B(\Upsilon(4S) \rightarrow B^0 \bar{B}^0) = (48.4 \pm 0.6)\%$ .			

$\Gamma(\chi_{c1}(3872) K^+, \chi_{c1} \rightarrow \psi(2S) \gamma)/\Gamma_{\text{total}}$		$\Gamma_{248}/\Gamma$	
VALUE (units $10^{-6}$ )	CL%	DOCUMENT ID	TECN COMMENT
<b><math>4 \pm 4</math> OUR AVERAGE</b>	Error includes scale factor of 2.5.		
$0.83^{+1.98}_{-1.83} \pm 0.44$	1,2	BHARDWAJ 11	BELL $e^+e^- \rightarrow \Upsilon(4S)$
$9.5 \pm 2.7 \pm 0.6$	3	AUBERT 09B	BABR $e^+e^- \rightarrow \Upsilon(4S)$
<sup>1</sup> BHARDWAJ 11 measurement is equivalent to a limit of $< 3.45 \times 10^{-6}$ at 90% CL.			
<sup>2</sup> Assumes equal production of $B^+$ and $B^0$ at the $\Upsilon(4S)$ .			
<sup>3</sup> Uses $B(\Upsilon(4S) \rightarrow B^+ B^-) = (51.6 \pm 0.6)\%$ and $B(\Upsilon(4S) \rightarrow B^0 \bar{B}^0) = (48.4 \pm 0.6)\%$ .			

$\Gamma(\chi_{c1}(3872) K^*(892)^+, \chi_{c1} \rightarrow \psi(2S) \gamma)/\Gamma_{\text{total}}$		$\Gamma_{266}/\Gamma$	
VALUE (units $10^{-6}$ )	CL%	DOCUMENT ID	TECN COMMENT
<b><math>&lt; 28</math></b>	90	<sup>1</sup> AUBERT 09B	BABR $e^+e^- \rightarrow \Upsilon(4S)$
<sup>1</sup> Uses $B(\Upsilon(4S) \rightarrow B^+ B^-) = (51.6 \pm 0.6)\%$ and $B(\Upsilon(4S) \rightarrow B^0 \bar{B}^0) = (48.4 \pm 0.6)\%$ .			

$\Gamma(\chi_{c1}(3872) K^+, \chi_{c1} \rightarrow D^0 \bar{D}^0)/\Gamma_{\text{total}}$		$\Gamma_{250}/\Gamma$	
VALUE	CL%	DOCUMENT ID	TECN COMMENT
<b><math>&lt; 6.0 \times 10^{-5}</math></b>	90	<sup>1</sup> CHISTOV 04	BELL $e^+e^- \rightarrow \Upsilon(4S)$
<sup>1</sup> Assumes equal production of $B^+$ and $B^0$ at the $\Upsilon(4S)$ .			

$\Gamma(\chi_{c1}(3872) K^+, \chi_{c1} \rightarrow D^+ D^-)/\Gamma_{\text{total}}$		$\Gamma_{251}/\Gamma$	
VALUE	CL%	DOCUMENT ID	TECN COMMENT
<b><math>&lt; 4.0 \times 10^{-5}</math></b>	90	<sup>1</sup> CHISTOV 04	BELL $e^+e^- \rightarrow \Upsilon(4S)$
<sup>1</sup> Assumes equal production of $B^+$ and $B^0$ at the $\Upsilon(4S)$ .			

$\Gamma(\chi_{c1}(3872) K^+, \chi_{c1} \rightarrow D^0 \bar{D}^0 \pi^0)/\Gamma_{\text{total}}$		$\Gamma_{252}/\Gamma$	
VALUE (units $10^{-4}$ )	CL%	DOCUMENT ID	TECN COMMENT
<b><math>1.02 \pm 0.31^{+0.21}_{-0.29}</math></b>	1	GOKHROO 06	BELL $e^+e^- \rightarrow \Upsilon(4S)$
••• We do not use the following data for averages, fits, limits, etc. •••			
$< 0.6$	90	<sup>2</sup> CHISTOV 04	BELL Repl. by GOKHROO 06
<sup>1</sup> Measure the near-threshold enhancements in the $(D^0 \bar{D}^0 \pi^0)$ system at a mass $3875.2 \pm 0.7^{+0.3}_{-1.6} \pm 0.8$ MeV/c <sup>2</sup> .			
<sup>2</sup> Assumes equal production of $B^+$ and $B^0$ at the $\Upsilon(4S)$ .			

$\Gamma(\chi_{c1}(3872) K^+, \chi_{c1} \rightarrow \bar{D}^{*0} D^0)/\Gamma_{\text{total}}$		$\Gamma_{253}/\Gamma$	
VALUE (units $10^{-4}$ )	CL%	DOCUMENT ID	TECN COMMENT
<b><math>0.85 \pm 0.26</math> OUR AVERAGE</b>	Error includes scale factor of 1.4.		
$0.77 \pm 0.16 \pm 0.10$	<sup>1</sup> AUSHEV 10	BELL	$e^+e^- \rightarrow \Upsilon(4S)$
$1.67 \pm 0.36 \pm 0.47$	<sup>1</sup> AUBERT 08B	BABR	$e^+e^- \rightarrow \Upsilon(4S)$
<sup>1</sup> Assumes equal production of $B^+$ and $B^0$ at the $\Upsilon(4S)$ .			

$\Gamma(\chi_{c1}(3872)^0 K^+, \chi_{c1}^0 \rightarrow \eta_c \pi^+ \pi^-)/\Gamma_{\text{total}}$		$\Gamma_{254}/\Gamma$	
VALUE	CL%	DOCUMENT ID	TECN COMMENT
<b><math>&lt; 3.0 \times 10^{-5}</math></b>	90	VINOKUROVA 15	BELL $e^+e^- \rightarrow \Upsilon(4S)$

$\Gamma(\chi_{c1}(3872)^0 K^+, \chi_{c1}^0 \rightarrow \eta_c \omega(782))/\Gamma_{\text{total}}$		$\Gamma_{255}/\Gamma$	
VALUE	CL%	DOCUMENT ID	TECN COMMENT
<b><math>&lt; 6.9 \times 10^{-5}</math></b>	90	VINOKUROVA 15	BELL $e^+e^- \rightarrow \Upsilon(4S)$

$\Gamma(\chi_{c1}(3872) K^+, \chi_{c1} \rightarrow \chi_{c1}(1P) \pi^+ \pi^-)/\Gamma_{\text{total}}$		$\Gamma_{256}/\Gamma$	
VALUE	CL%	DOCUMENT ID	TECN COMMENT
<b><math>&lt; 1.5 \times 10^{-6}</math></b>	90	<sup>1</sup> BHARDWAJ 16	BELL $e^+e^- \rightarrow \Upsilon(4S)$
<sup>1</sup> Assumes equal production of $B^+$ and $B^0$ at the $\Upsilon(4S)$ .			

$\Gamma(\chi_{c1}(3872) K^+, \chi_{c1}(3872) \rightarrow \chi_{c1}(1P) \pi^0)/\Gamma_{\text{total}}$		$\Gamma_{257}/\Gamma$	
VALUE	CL%	DOCUMENT ID	TECN COMMENT
<b><math>&lt; 8.1 \times 10^{-6}</math></b>	90	<sup>1</sup> BHARDWAJ 19	BELL $e^+e^- \rightarrow \Upsilon(4S)$
<sup>1</sup> Assumes equal production of $B^+$ and $B^0$ at the $\Upsilon(4S)$ .			

$\Gamma(X(3915) K^+)/\Gamma_{\text{total}}$		$\Gamma_{258}/\Gamma$	
VALUE	CL%	DOCUMENT ID	TECN COMMENT
<b><math>&lt; 2.8 \times 10^{-4}</math></b>	90	<sup>1</sup> KATO 18	BELL $e^+e^- \rightarrow \Upsilon(4S)$
<sup>1</sup> Measures absolute branching fractions using a missing-mass technique.			

$\Gamma(X(3915)^0 K^+, X^0 \rightarrow \eta_c \eta)/\Gamma_{\text{total}}$		$\Gamma_{259}/\Gamma$	
VALUE	CL%	DOCUMENT ID	TECN COMMENT
<b><math>&lt; 4.7 \times 10^{-5}</math></b>	90	<sup>1</sup> VINOKUROVA 15	BELL $e^+e^- \rightarrow \Upsilon(4S)$
<sup>1</sup> Upper limit is corrected in the Erratum.			

$\Gamma(X(3915)^0 K^+, X^0 \rightarrow \eta_c \pi^0)/\Gamma_{\text{total}}$		$\Gamma_{260}/\Gamma$	
VALUE	CL%	DOCUMENT ID	TECN COMMENT
<b><math>&lt; 1.7 \times 10^{-5}</math></b>	90	<sup>1</sup> VINOKUROVA 15	BELL $e^+e^- \rightarrow \Upsilon(4S)$
<sup>1</sup> Upper limit is corrected in the Erratum.			

$\Gamma(X(4014)^0 K^+, X^0 \rightarrow \eta_c \eta)/\Gamma_{\text{total}}$		$\Gamma_{261}/\Gamma$	
VALUE	CL%	DOCUMENT ID	TECN COMMENT
<b><math>&lt; 3.9 \times 10^{-5}</math></b>	90	VINOKUROVA 15	BELL $e^+e^- \rightarrow \Upsilon(4S)$



## Meson Particle Listings

 $B^\pm$ 

$\Gamma(X(4014)^0 K^+, X^0 \rightarrow \eta_c \pi^0)/\Gamma_{\text{total}}$					$\Gamma_{262}/\Gamma$
VALUE	CL%	DOCUMENT ID	TECN	COMMENT	
$<1.2 \times 10^{-5}$	90	VINOKUROVA 15	BELL	$e^+ e^- \rightarrow \Upsilon(4S)$	

$\Gamma(Z_c(3900)^0 K^+, Z_c^0 \rightarrow \eta_c \pi^+ \pi^-)/\Gamma_{\text{total}}$					$\Gamma_{263}/\Gamma$
VALUE	CL%	DOCUMENT ID	TECN	COMMENT	
$<4.7 \times 10^{-5}$	90	VINOKUROVA 15	BELL	$e^+ e^- \rightarrow \Upsilon(4S)$	

$\Gamma(X(4020)^0 K^+, X^0 \rightarrow \eta_c \pi^+ \pi^-)/\Gamma_{\text{total}}$					$\Gamma_{264}/\Gamma$
VALUE	CL%	DOCUMENT ID	TECN	COMMENT	
$<1.6 \times 10^{-5}$	90	VINOKUROVA 15	BELL	$e^+ e^- \rightarrow \Upsilon(4S)$	

$\Gamma(\chi_{c1}(3872) K^+, \chi_{c1} \rightarrow J/\psi(1S)\eta)/\Gamma_{\text{total}}$					$\Gamma_{249}/\Gamma$
VALUE	CL%	DOCUMENT ID	TECN	COMMENT	
$<7.7 \times 10^{-6}$	90	<sup>1</sup> AUBERT 04Y	BABR	$e^+ e^- \rightarrow \Upsilon(4S)$	
<sup>1</sup> Assumes equal production of $B^+$ and $B^0$ at the $\Upsilon(4S)$ .					

$\Gamma(\chi_{c1}(3872) + K^0, \chi_{c1}^+ \rightarrow J/\psi(1S)\pi^+ \pi^0)/\Gamma_{\text{total}}$					$\Gamma_{267}/\Gamma$
VALUE (units $10^{-6}$ )	CL%	DOCUMENT ID	TECN	COMMENT	
$<6.1$	90	<sup>1,2</sup> CHOI 11	BELL	$e^+ e^- \rightarrow \Upsilon(4S)$	
• • • We do not use the following data for averages, fits, limits, etc. • • •					
$<22$	90	<sup>3</sup> AUBERT 05B	BABR	$e^+ e^- \rightarrow \Upsilon(4S)$	
<sup>1</sup> Assumes $\pi^+ \pi^0$ originates from $\rho^+$ .					
<sup>2</sup> Assumes equal production of $B^+$ and $B^0$ at the $\Upsilon(4S)$ .					
<sup>3</sup> Assumes equal production of $B^+$ and $B^0$ at the $\Upsilon(4S)$ . The isovector-X hypothesis is excluded with a likelihood test at $1 \times 10^{-4}$ level.					

$\Gamma(\chi_{c1}(3872) K^0 \pi^+, \chi_{c1} \rightarrow J/\psi(1S)\pi^+ \pi^-)/\Gamma_{\text{total}}$					$\Gamma_{268}/\Gamma$
VALUE (units $10^{-6}$ )	CL%	DOCUMENT ID	TECN	COMMENT	
$10.6 \pm 3.0 \pm 0.9$		BALA 15	BELL	$e^+ e^- \rightarrow \Upsilon(4S)$	

$\Gamma(Z_c(4430)^+ K^0, Z_c^+ \rightarrow J/\psi \pi^+)/\Gamma_{\text{total}}$					$\Gamma_{269}/\Gamma$
VALUE (units $10^{-5}$ )	CL%	DOCUMENT ID	TECN	COMMENT	
$<1.5$	95	<sup>1</sup> AUBERT 09AA	BABR	$e^+ e^- \rightarrow \Upsilon(4S)$	
<sup>1</sup> Assumes equal production of $B^+$ and $B^0$ at the $\Upsilon(4S)$ .					

$\Gamma(Z_c(4430)^+ K^0, Z_c^+ \rightarrow \psi(2S)\pi^+)/\Gamma_{\text{total}}$					$\Gamma_{270}/\Gamma$
VALUE (units $10^{-5}$ )	CL%	DOCUMENT ID	TECN	COMMENT	
$<4.7$	95	<sup>1</sup> AUBERT 09AA	BABR	$e^+ e^- \rightarrow \Upsilon(4S)$	
<sup>1</sup> Assumes equal production of $B^+$ and $B^0$ at the $\Upsilon(4S)$ .					

$\Gamma(\psi(4260)^0 K^+, \psi^0 \rightarrow J/\psi \pi^+ \pi^-)/\Gamma_{\text{total}}$					$\Gamma_{271}/\Gamma$
VALUE (units $10^{-6}$ )	CL%	DOCUMENT ID	TECN	COMMENT	
$<15.6$	95	<sup>1,2</sup> GARG 19	BELL	$e^+ e^- \rightarrow \Upsilon(4S)$	
• • • We do not use the following data for averages, fits, limits, etc. • • •					
$<29$	95	<sup>2</sup> AUBERT 06	BABR	$e^+ e^- \rightarrow \Upsilon(4S)$	
<sup>1</sup> Corresponds to a 90% CL upper limit of $<14 \times 10^{-6}$ .					
<sup>2</sup> Assumes equal production of $B^+$ and $B^0$ at the $\Upsilon(4S)$ .					

$\Gamma(X(3915) K^+, X \rightarrow J/\psi \gamma)/\Gamma_{\text{total}}$					$\Gamma_{272}/\Gamma$
VALUE (units $10^{-6}$ )	CL%	DOCUMENT ID	TECN	COMMENT	
$<14$	90	<sup>1</sup> AUBERT, BE 06M	BABR	$e^+ e^- \rightarrow \Upsilon(4S)$	
<sup>1</sup> Assumes equal production of $B^+$ and $B^0$ at the $\Upsilon(4S)$ .					

$\Gamma(X(3915) K^+, X \rightarrow \chi_{c1}(1P)\pi^0)/\Gamma_{\text{total}}$					$\Gamma_{273}/\Gamma$
VALUE	CL%	DOCUMENT ID	TECN	COMMENT	
$<3.8 \times 10^{-5}$	90	<sup>1</sup> BHARDWAJ 19	BELL	$e^+ e^- \rightarrow \Upsilon(4S)$	
<sup>1</sup> Assumes equal production of $B^+$ and $B^0$ at the $\Upsilon(4S)$ .					

$\Gamma(X(3930)^0 K^+, X^0 \rightarrow J/\psi \gamma)/\Gamma_{\text{total}}$					$\Gamma_{274}/\Gamma$
VALUE (units $10^{-6}$ )	CL%	DOCUMENT ID	TECN	COMMENT	
$<2.5$	90	<sup>1</sup> AUBERT, BE 06M	BABR	$e^+ e^- \rightarrow \Upsilon(4S)$	
<sup>1</sup> Assumes equal production of $B^+$ and $B^0$ at the $\Upsilon(4S)$ .					

$\Gamma(J/\psi(1S) K^0 \pi^+)/\Gamma_{\text{total}}$					$\Gamma_{276}/\Gamma$
VALUE (units $10^{-3}$ )	CL%	DOCUMENT ID	TECN	COMMENT	
$1.101 \pm 0.021$		<sup>1</sup> AUBERT 09AA	BABR	$e^+ e^- \rightarrow \Upsilon(4S)$	
<sup>1</sup> Does not report systematic uncertainties.					

$\Gamma(J/\psi(1S) K^*(892)^+)/\Gamma_{\text{total}}$					$\Gamma_{280}/\Gamma$
For polarization information see the Listings at the end of the " $B^0$ Branching Ratios" section.					
VALUE (units $10^{-3}$ )	CL%	DOCUMENT ID	TECN	COMMENT	

<b>1.43 ± 0.08 OUR FIT</b>					
<b>1.43 ± 0.08 OUR AVERAGE</b>					
$1.78^{+0.36}_{-0.32} \pm 0.02$		<sup>1,2</sup> AUBERT 07AV	BABR	$e^+ e^- \rightarrow \Upsilon(4S)$	
$1.454 \pm 0.047 \pm 0.097$		<sup>2</sup> AUBERT 05J	BABR	$e^+ e^- \rightarrow \Upsilon(4S)$	
$1.28 \pm 0.07 \pm 0.14$		<sup>2</sup> ABE 02N	BELL	$e^+ e^- \rightarrow \Upsilon(4S)$	
$1.41 \pm 0.23 \pm 0.24$		<sup>2</sup> JESSOP 97	CLE2	$e^+ e^- \rightarrow \Upsilon(4S)$	
$1.58 \pm 0.47 \pm 0.27$		<sup>3</sup> ABE 96H	CDF	$p\bar{p}$ at 1.8 TeV	
$1.50 \pm 1.08 \pm 0.01$		<sup>4</sup> BORTOLETTO 92	CLEO	$e^+ e^- \rightarrow \Upsilon(4S)$	
$1.85 \pm 1.30 \pm 0.01$		<sup>2,5</sup> ALBRECHT 90J	ARG	$e^+ e^- \rightarrow \Upsilon(4S)$	
• • • We do not use the following data for averages, fits, limits, etc. • • •					
$1.37 \pm 0.09 \pm 0.11$		<sup>2</sup> AUBERT 02	BABR	Repl. by AUBERT 05J	
$1.78 \pm 0.51 \pm 0.23$		<sup>13,2</sup> ALAM 94	CLE2	Sup. by JESSOP 97	

<sup>1</sup> AUBERT 07AV reports  $[\Gamma(B^+ \rightarrow J/\psi(1S) K^*(892)^+)/\Gamma_{\text{total}}] \times [B(J/\psi(1S) \rightarrow p\bar{p})] = (3.78^{+0.72+0.28}_{-0.64-0.23}) \times 10^{-6}$  which we divide by our best value  $B(J/\psi(1S) \rightarrow p\bar{p}) = (2.121 \pm 0.029) \times 10^{-3}$ . Our first error is their experiment's error and our second error is the systematic error from using our best value.

<sup>2</sup> Assumes equal production of  $B^+$  and  $B^0$  at the  $\Upsilon(4S)$ .

<sup>3</sup> ABE 96H assumes that  $B(B^+ \rightarrow J/\psi K^+) = (1.02 \pm 0.14) \times 10^{-3}$ .

<sup>4</sup> BORTOLETTO 92 reports  $(1.3 \pm 0.9 \pm 0.3) \times 10^{-3}$  from a measurement of  $[\Gamma(B^+ \rightarrow J/\psi(1S) K^*(892)^+)/\Gamma_{\text{total}}] \times [B(J/\psi(1S) \rightarrow e^+ e^-)]$  assuming  $B(J/\psi(1S) \rightarrow e^+ e^-) = 0.069 \pm 0.009$ , which we rescale to our best value  $B(J/\psi(1S) \rightarrow e^+ e^-) = (5.971 \pm 0.032) \times 10^{-2}$ . Our first error is their experiment's error and our second error is the systematic error from using our best value. Assumes equal production of  $B^+$  and  $B^0$  at the  $\Upsilon(4S)$ .

<sup>5</sup> ALBRECHT 90J reports  $(1.6 \pm 1.1 \pm 0.3) \times 10^{-3}$  from a measurement of  $[\Gamma(B^+ \rightarrow J/\psi(1S) K^*(892)^+)/\Gamma_{\text{total}}] \times [B(J/\psi(1S) \rightarrow e^+ e^-)]$  assuming  $B(J/\psi(1S) \rightarrow e^+ e^-) = 0.069 \pm 0.009$ , which we rescale to our best value  $B(J/\psi(1S) \rightarrow e^+ e^-) = (5.971 \pm 0.032) \times 10^{-2}$ . Our first error is their experiment's error and our second error is the systematic error from using our best value. Assumes equal production of  $B^+$  and  $B^0$  at the  $\Upsilon(4S)$ .

$\Gamma(J/\psi(1S) K^*(892)^+)/\Gamma(J/\psi(1S) K^+)$					$\Gamma_{280}/\Gamma_{275}$
VALUE	CL%	DOCUMENT ID	TECN	COMMENT	
<b>1.39 ± 0.09 OUR AVERAGE</b>					
$1.37 \pm 0.05 \pm 0.08$		AUBERT 05J	BABR	$e^+ e^- \rightarrow \Upsilon(4S)$	
$1.45 \pm 0.20 \pm 0.17$		<sup>1</sup> JESSOP 97	CLE2	$e^+ e^- \rightarrow \Upsilon(4S)$	
$1.92 \pm 0.60 \pm 0.17$		ABE 96Q	CDF	$p\bar{p}$	
• • • We do not use the following data for averages, fits, limits, etc. • • •					
$1.37 \pm 0.10 \pm 0.08$		<sup>2</sup> AUBERT 02	BABR	Repl. by AUBERT 05J	

<sup>1</sup> JESSOP 97 assumes equal production of  $B^+$  and  $B^0$  at the  $\Upsilon(4S)$ . The measurement is actually measured as an average over kaon charged and neutral states.

<sup>2</sup> Assumes equal production of  $B^+$  and  $B^0$  at the  $\Upsilon(4S)$ .

$\Gamma(J/\psi(1S) K(1270)^+)/\Gamma_{\text{total}}$					$\Gamma_{281}/\Gamma$
VALUE (units $10^{-3}$ )	CL%	DOCUMENT ID	TECN	COMMENT	
$1.80 \pm 0.34 \pm 0.39$		<sup>1</sup> ABE 01L	BELL	$e^+ e^- \rightarrow \Upsilon(4S)$	
<sup>1</sup> Uses the PDG value of $B(B^+ \rightarrow J/\psi(1S) K^+) = (1.00 \pm 0.10) \times 10^{-3}$ .					

$\Gamma(J/\psi(1S) K(1400)^+)/\Gamma(J/\psi(1S) K(1270)^+)$					$\Gamma_{282}/\Gamma_{281}$
VALUE	CL%	DOCUMENT ID	TECN	COMMENT	
$<0.30$	90	ABE 01L	BELL	$e^+ e^- \rightarrow \Upsilon(4S)$	

$\Gamma(J/\psi(1S) \eta K^+)/\Gamma_{\text{total}}$					$\Gamma_{283}/\Gamma$
VALUE (units $10^{-5}$ )	CL%	DOCUMENT ID	TECN	COMMENT	
<b>12.4 ± 1.4 OUR AVERAGE</b>					
$12.7 \pm 1.1 \pm 1.1$		<sup>1</sup> IWASHITA 14	BELL	$e^+ e^- \rightarrow \Upsilon(4S)$	
$10.8 \pm 2.3 \pm 2.4$		<sup>1</sup> AUBERT 04Y	BABR	$e^+ e^- \rightarrow \Upsilon(4S)$	
<sup>1</sup> Assumes equal production of $B^+$ and $B^0$ at the $\Upsilon(4S)$ .					

$\Gamma(\chi_{c1-odd}(3872) K^+, \chi_{c1-odd} \rightarrow J/\psi \eta)/\Gamma_{\text{total}}$					$\Gamma_{284}/\Gamma$
VALUE	CL%	DOCUMENT ID	TECN	COMMENT	
$<3.8 \times 10^{-6}$	90	IWASHITA 14	BELL	$e^+ e^- \rightarrow \Upsilon(4S)$	

$\Gamma(\psi(4160) K^+, \psi \rightarrow J/\psi \eta)/\Gamma_{\text{total}}$					$\Gamma_{285}/\Gamma$
VALUE	CL%	DOCUMENT ID	TECN	COMMENT	
$<7.4 \times 10^{-6}$	90	IWASHITA 14	BELL	$e^+ e^- \rightarrow \Upsilon(4S)$	

$\Gamma(J/\psi(1S) \eta' K^+)/\Gamma_{\text{total}}$					$\Gamma_{286}/\Gamma$
VALUE (units $10^{-5}$ )	CL%	DOCUMENT ID	TECN	COMMENT	
$<8.8$	90	<sup>1</sup> XIE 07	BELL	$e^+ e^- \rightarrow \Upsilon(4S)$	
<sup>1</sup> Assumes equal production of $B^+$ and $B^0$ at the $\Upsilon(4S)$ .					



## Meson Particle Listings

 $B^\pm$ 

$\Gamma(J/\psi(1S)\rho\bar{p}\pi^+)/\Gamma_{\text{total}}$					$\Gamma_{305}/\Gamma$
VALUE	CL%	DOCUMENT ID	TECN	COMMENT	
$<5.0 \times 10^{-7}$	90	1 AAIJ	13z	LHCB $pp$ at 7 TeV	
<sup>1</sup> Uses $B(B_S^0 \rightarrow J/\psi(1S)\pi^+\pi^-) = (1.98 \pm 0.20) \times 10^{-4}$ .					

$\Gamma(J/\psi(1S)\rho\bar{\Lambda})/\Gamma_{\text{total}}$					$\Gamma_{306}/\Gamma$
VALUE (units $10^{-6}$ )	CL%	DOCUMENT ID	TECN	COMMENT	
<b>14.6 ± 1.2 OUR AVERAGE</b>					
15.1 ± 0.8 ± 1.0		1 SIRUNYAN	19CM	CMS $pp$ at 8 TeV	
11.7 ± 2.8 $^{+1.8}_{-2.3}$		2 XIE	05	BELL $e^+e^- \rightarrow \Upsilon(4S)$	
12 $^{+9}_{-6}$		2 AUBERT	03k	BABR $e^+e^- \rightarrow \Upsilon(4S)$	

• • • We do not use the following data for averages, fits, limits, etc. • • •

<41					$\Gamma_{307}/\Gamma$
VALUE	CL%	DOCUMENT ID	TECN	COMMENT	
$<1.1 \times 10^{-5}$	90	1 XIE	05	BELL $e^+e^- \rightarrow \Upsilon(4S)$	
<sup>1</sup> Assumes equal production of $B^+$ and $B^0$ at the $\Upsilon(4S)$ .					

$\Gamma(J/\psi(1S)\rho\bar{\Lambda})/\Gamma_{\text{total}}$					$\Gamma_{308}/\Gamma$
VALUE (units $10^{-5}$ )	CL%	DOCUMENT ID	TECN	COMMENT	
<b>&lt;12</b>	90	1 AUBERT	05U	BABR $e^+e^- \rightarrow \Upsilon(4S)$	
<sup>1</sup> Assumes equal production of $B^+$ and $B^0$ at the $\Upsilon(4S)$ .					

$\Gamma(J/\psi(1S)\bar{D}^0\pi^+)/\Gamma_{\text{total}}$					$\Gamma_{309}/\Gamma$
VALUE (units $10^{-5}$ )	CL%	DOCUMENT ID	TECN	COMMENT	
<b>&lt;2.5</b>	90	1 ZHANG	05B	BELL $e^+e^- \rightarrow \Upsilon(4S)$	
• • • We do not use the following data for averages, fits, limits, etc. • • •					
<5.2	90	1 AUBERT	05R	BABR $e^+e^- \rightarrow \Upsilon(4S)$	
<sup>1</sup> Assumes equal production of $B^+$ and $B^0$ at the $\Upsilon(4S)$ .					

$\Gamma(\psi(2S)\pi^+)/\Gamma_{\text{total}}$					$\Gamma_{310}/\Gamma$
VALUE (units $10^{-5}$ )		DOCUMENT ID	TECN	COMMENT	
<b>2.44 ± 0.22 ± 0.20</b>		1 BHARDWAJ	08	BELL $e^+e^- \rightarrow \Upsilon(4S)$	
<sup>1</sup> Assumes equal production of $B^+$ and $B^0$ at the $\Upsilon(4S)$ .					

$\Gamma(\psi(2S)\pi^+)/\Gamma(\psi(2S)K^+)$					$\Gamma_{310}/\Gamma_{311}$
VALUE (units $10^{-2}$ )		DOCUMENT ID	TECN	COMMENT	
<b>3.97 ± 0.29 OUR AVERAGE</b>					
3.95 ± 0.40 ± 0.12		AAIJ	12Ac	LHCB $pp$ at 7 TeV	
3.99 ± 0.36 ± 0.17		BHARDWAJ	08	BELL $e^+e^- \rightarrow \Upsilon(4S)$	

$\Gamma(\psi(2S)K^+)/\Gamma_{\text{total}}$					$\Gamma_{311}/\Gamma$
VALUE (units $10^{-4}$ )	EVTS	DOCUMENT ID	TECN	COMMENT	
<b>6.19 ± 0.22 OUR FIT</b>					
<b>6.48 ± 0.34 OUR AVERAGE</b>					
6.4 ± 1.0 ± 0.4		1 KATO	18	BELL $e^+e^- \rightarrow \Upsilon(4S)$	
6.65 ± 0.17 ± 0.55		2 GULER	11	BELL $e^+e^- \rightarrow \Upsilon(4S)$	
4.9 ± 1.6 ± 0.4		1 AUBERT	06E	BABR $e^+e^- \rightarrow \Upsilon(4S)$	
6.17 ± 0.32 ± 0.44		2 AUBERT	05J	BABR $e^+e^- \rightarrow \Upsilon(4S)$	
7.8 ± 0.7 ± 0.9		2 RICHICHI	01	CLE2 $e^+e^- \rightarrow \Upsilon(4S)$	
18 ± 8 ± 4	5	2 ALBRECHT	90J	ARG $e^+e^- \rightarrow \Upsilon(4S)$	
• • • We do not use the following data for averages, fits, limits, etc. • • •					
6.9 ± 0.6		2 ABE	03B	BELL Repl. by GULER 11	
6.4 ± 0.5 ± 0.8		2 AUBERT	02	BABR Repl. by AUBERT 05J	
6.1 ± 2.3 ± 0.9	7	2 ALAM	94	CLE2 Repl. by RICHICHI 01	
<5 at 90% CL		2 BORTOLETTO	92	CLEO $e^+e^- \rightarrow \Upsilon(4S)$	
22 ± 17	3	3 ALBRECHT	87D	ARG $e^+e^- \rightarrow \Upsilon(4S)$	
<sup>1</sup> Measures absolute branching fractions using a missing-mass technique.					
<sup>2</sup> Assumes equal production of $B^+$ and $B^0$ at the $\Upsilon(4S)$ .					
<sup>3</sup> ALBRECHT 87D assume $B^+B^-/B^0\bar{B}^0$ ratio is 55/45. Superseded by ALBRECHT 90J.					

$\Gamma(\psi(2S)K^+)/\Gamma(J/\psi(1S)K^+)$					$\Gamma_{311}/\Gamma_{275}$
VALUE		DOCUMENT ID	TECN	COMMENT	
<b>0.616 ± 0.018 OUR FIT</b>					
<b>0.605 ± 0.021 OUR AVERAGE</b>					
0.58 ± 0.11 ± 0.02		1 AAIJ	13s	LHCB $pp$ at 7 TeV	
0.607 ± 0.018 ± 0.013		2,3 AAIJ	12L	LHCB $pp$ at 7 TeV	
0.63 ± 0.05 ± 0.08		ABAZOV	09Y	D0 $p\bar{p}$ at 1.96 TeV	
0.558 ± 0.082 ± 0.056		ABE	980	CDF $p\bar{p}$ 1.8 TeV	
• • • We do not use the following data for averages, fits, limits, etc. • • •					
0.64 ± 0.06 ± 0.07		4 AUBERT	02	BABR $e^+e^- \rightarrow \Upsilon(4S)$	
<sup>1</sup> AAIJ 13s reports $[\Gamma(B^+ \rightarrow \psi(2S)K^+)/\Gamma(B^+ \rightarrow J/\psi(1S)K^+)] \times [B(\psi(2S) \rightarrow \rho\bar{p})] / [B(J/\psi(1S) \rightarrow \rho\bar{p})] = 0.080 \pm 0.012 \pm 0.009$ which we multiply or divide by our best values $B(\psi(2S) \rightarrow \rho\bar{p}) = (2.94 \pm 0.08) \times 10^{-4}$ , $B(J/\psi(1S) \rightarrow \rho\bar{p}) =$					

$(2.121 \pm 0.029) \times 10^{-3}$ . Our first error is their experiment's error and our second error is the systematic error from using our best values.

<sup>2</sup> AAIJ 12L reports  $0.594 \pm 0.006 \pm 0.016 \pm 0.015$  from a measurement of  $[\Gamma(B^+ \rightarrow \psi(2S)K^+)/\Gamma(B^+ \rightarrow J/\psi(1S)K^+)] \times [B(J/\psi(1S) \rightarrow e^+e^-)] / [B(\psi(2S) \rightarrow e^+e^-)]$  assuming  $B(J/\psi(1S) \rightarrow e^+e^-) = (5.94 \pm 0.06) \times 10^{-2}$ ,  $B(\psi(2S) \rightarrow e^+e^-) = (7.72 \pm 0.17) \times 10^{-3}$ , which we rescale to our best values  $B(J/\psi(1S) \rightarrow e^+e^-) = (5.971 \pm 0.032) \times 10^{-2}$ ,  $B(\psi(2S) \rightarrow e^+e^-) = (7.93 \pm 0.17) \times 10^{-3}$ . Our first error is their experiment's error and our second error is the systematic error from using our best values.

<sup>3</sup> Assumes  $B(J/\psi \rightarrow \mu^+\mu^-) / B(\psi(2S) \rightarrow \mu^+\mu^-) = B(J/\psi \rightarrow e^+e^-) / B(\psi(2S) \rightarrow e^+e^-) = 7.69 \pm 0.19$ .

<sup>4</sup> Assumes equal production of  $B^+$  and  $B^0$  at the  $\Upsilon(4S)$ .

$\Gamma(\psi(2S)K^*(892^+)/\Gamma_{\text{total}}$					$\Gamma_{312}/\Gamma$
VALUE (units $10^{-4}$ )	CL%	DOCUMENT ID	TECN	COMMENT	
<b>6.7 ± 1.4 OUR AVERAGE</b>					
5.92 ± 0.85 ± 0.89		1 AUBERT	05J	BABR $e^+e^- \rightarrow \Upsilon(4S)$	
9.2 ± 1.9 ± 1.2		1 RICHICHI	01	CLE2 $e^+e^- \rightarrow \Upsilon(4S)$	
• • • We do not use the following data for averages, fits, limits, etc. • • •					
<30	90	1 ALAM	94	CLE2 Repl. by RICHICHI 01	
<35	90	1 BORTOLETTO	092	CLEO $e^+e^- \rightarrow \Upsilon(4S)$	
<49	90	1 ALBRECHT	90J	ARG $e^+e^- \rightarrow \Upsilon(4S)$	
<sup>1</sup> Assumes equal production of $B^+$ and $B^0$ at the $\Upsilon(4S)$ .					

$\Gamma(\psi(2S)K^*(892^+)/\Gamma(\psi(2S)K^+)$					$\Gamma_{312}/\Gamma_{311}$
VALUE		DOCUMENT ID	TECN	COMMENT	
<b>0.96 ± 0.15 ± 0.09</b>		AUBERT	05J	BABR $e^+e^- \rightarrow \Upsilon(4S)$	

$\Gamma(\psi(2S)K^0\pi^+)/\Gamma_{\text{total}}$					$\Gamma_{313}/\Gamma$
VALUE (units $10^{-3}$ )		DOCUMENT ID	TECN	COMMENT	
<b>0.588 ± 0.034</b>		1 AUBERT	09AA	BABR $e^+e^- \rightarrow \Upsilon(4S)$	
• • • We do not use the following data for averages, fits, limits, etc. • • •					
<sup>1</sup> Does not report systematic uncertainties.					

$\Gamma(\psi(2S)K^+\pi^-\pi^-)/\Gamma_{\text{total}}$					$\Gamma_{314}/\Gamma$
VALUE (units $10^{-4}$ )	EVTS	DOCUMENT ID	TECN	COMMENT	
<b>4.3 ± 0.5 OUR AVERAGE</b>					
4.31 ± 0.20 ± 0.50		1 GULER	11	BELL $e^+e^- \rightarrow \Upsilon(4S)$	
19 ± 11 ± 4	3	1 ALBRECHT	90J	ARG $e^+e^- \rightarrow \Upsilon(4S)$	
<sup>1</sup> Assumes equal production of $B^+$ and $B^0$ at the $\Upsilon(4S)$ .					

$\Gamma(\psi(2S)\phi(1020)K^+)/\Gamma_{\text{total}}$					$\Gamma_{315}/\Gamma$
VALUE (units $10^{-6}$ )		DOCUMENT ID	TECN	COMMENT	
<b>4.0 ± 0.4 ± 0.6</b>		1,2 KHACHATRYAN	17c	CMS $pp$ at 8 TeV	
<sup>1</sup> Measured using $B^+ \rightarrow \psi(2S)K^+$ as a normalization channel. The second error represents total systematic uncertainties including those from branching fractions which were taken from PDG 16 as $B(\phi \rightarrow K^+K^-) = 0.489 \pm 0.005$ and $B(B^+ \rightarrow \psi(2S)K^+) = (6.26 \pm 0.24) \times 10^{-4}$ .					
<sup>2</sup> An upper limit on the fraction of the non- $\phi$ component in $B^+ \rightarrow \psi(2S)K^+K^-K^+$ decays is set as 0.26 at the 95% confidence level.					

$\Gamma(\psi(3770)K^+)/\Gamma_{\text{total}}$					$\Gamma_{316}/\Gamma$
VALUE (units $10^{-3}$ )	CL%	DOCUMENT ID	TECN	COMMENT	
<b>0.49 ± 0.13 OUR AVERAGE</b>					
3.5 ± 2.5 ± 0.3		1 AUBERT	06E	BABR $e^+e^- \rightarrow \Upsilon(4S)$	
0.48 ± 0.11 ± 0.07		2 CHISTOV	04	BELL $e^+e^- \rightarrow \Upsilon(4S)$	
• • • We do not use the following data for averages, fits, limits, etc. • • •					
<0.23	90	1 KATO	18	BELL $e^+e^- \rightarrow \Upsilon(4S)$	
<sup>1</sup> Measures absolute branching fractions using a missing-mass technique.					
<sup>2</sup> Assumes equal production of $B^+$ and $B^0$ at the $\Upsilon(4S)$ .					

$\Gamma(\psi(3770)K^+, \psi \rightarrow D^0\bar{D}^0)/\Gamma_{\text{total}}$					$\Gamma_{317}/\Gamma$
VALUE (units $10^{-4}$ )		DOCUMENT ID	TECN	COMMENT	
<b>1.5 ± 0.5 OUR AVERAGE</b>					
1.18 ± 0.41 ± 0.15		1 LEES	15c	BABR $e^+e^- \rightarrow \Upsilon(4S)$	
2.2 ± 0.5 ± 0.3		1 BRODZICKA	08	BELL $e^+e^- \rightarrow \Upsilon(4S)$	
• • • We do not use the following data for averages, fits, limits, etc. • • •					
1.41 ± 0.30 ± 0.22		1 AUBERT	08B	BABR Repl. by LEES 15c	
3.4 ± 0.8 ± 0.5		1 CHISTOV	04	BELL Repl. by BRODZICKA 08	
<sup>1</sup> Assumes equal production of $B^+$ and $B^0$ at the $\Upsilon(4S)$ .					

$\Gamma(\psi(3770)K^+, \psi \rightarrow D^+D^-)/\Gamma_{\text{total}}$					$\Gamma_{318}/\Gamma$
VALUE (units $10^{-4}$ )		DOCUMENT ID	TECN	COMMENT	
<b>0.94 ± 0.35 OUR AVERAGE</b>					
0.84 ± 0.32 ± 0.21		1 AUBERT	08B	BABR $e^+e^- \rightarrow \Upsilon(4S)$	
1.4 ± 0.8 ± 0.2		1 CHISTOV	04	BELL $e^+e^- \rightarrow \Upsilon(4S)$	
<sup>1</sup> Assumes equal production of $B^+$ and $B^0$ at the $\Upsilon(4S)$ .					

$\Gamma(\psi(3770)K^+, \psi \rightarrow \rho\bar{p})/\Gamma_{\text{total}}$					$\Gamma_{319}/\Gamma$
VALUE	CL%	DOCUMENT ID	TECN	COMMENT	
<b>&lt;2 × 10<sup>-7</sup></b>	95	1 AAIJ	17Ad	LHCB $pp$ at 7 and 8 TeV	
<sup>1</sup> Measured relative to $B^+ \rightarrow J/\psi K^+$ decay with charmonia reconstructed in $p\bar{p}$ final state and using $B(B^+ \rightarrow J/\psi K^+) \times B(J/\psi \rightarrow \rho\bar{p}) = (2.17 \pm 0.08) \times 10^{-6}$ .					

See key on page 999

# Meson Particle Listings

$B^\pm$

## $\Gamma(\psi(4040) K^+)/\Gamma_{\text{total}}$ $\Gamma_{320}/\Gamma$

VALUE	CL%	DOCUMENT ID	TECN	COMMENT
$<1.3 \times 10^{-4}$	90	AAIJ	13bc LHCB	$pp$ at 7, 8 TeV
••• We do not use the following data for averages, fits, limits, etc. •••				
$<3.0 \times 10^{-3}$	90	<sup>1</sup> IWASHITA	14 BELL	$e^+e^- \rightarrow \Upsilon(4S)$
<sup>1</sup> IWASHITA 14 reports $[\Gamma(B^+ \rightarrow \psi(4040) K^+)/\Gamma_{\text{total}}] \times [B(\psi(4040) \rightarrow J/\psi\eta)] < 15.5 \times 10^{-6}$ which we divide by our best value $B(\psi(4040) \rightarrow J/\psi\eta) = 5.2 \times 10^{-3}$ .				

## $\Gamma(\psi(4160) K^+)/\Gamma_{\text{total}}$ $\Gamma_{321}/\Gamma$

VALUE (units $10^{-4}$ )	DOCUMENT ID	TECN	COMMENT
$5.1^{+1.3+2.5}_{-1.2-2.4}$	<sup>1</sup> AAIJ	13bc LHCB	$pp$ at 7, 8 TeV
<sup>1</sup> AAIJ 13bc reports $[\Gamma(B^+ \rightarrow \psi(4160) K^+)/\Gamma_{\text{total}}] \times B(\psi(4160) \rightarrow \mu^+\mu^-) = (3.5^{+0.9}_{-0.8}) \times 10^{-9}$ which we divide by our best value $B(\psi(4160) \rightarrow e^+e^-) = (6.9 \pm 3.3) \times 10^{-6}$ assuming lepton universality. Our first error is their experiment's error and our second error is the systematic error from using our best value.			

## $\Gamma(\psi(4160) K^+, \psi \rightarrow \bar{D}^0 D^0)/\Gamma_{\text{total}}$ $\Gamma_{322}/\Gamma$

VALUE (units $10^{-4}$ )	DOCUMENT ID	TECN	COMMENT
$0.84 \pm 0.41 \pm 0.33$	<sup>1</sup> LEES	15c BABR	$e^+e^- \rightarrow \Upsilon(4S)$
<sup>1</sup> Assumes equal production of $B^+$ and $B^0$ at the $\Upsilon(4S)$ .			

## $\Gamma(\chi_{c0} \pi^+, \chi_{c0} \rightarrow \pi^+ \pi^-)/\Gamma_{\text{total}}$ $\Gamma_{323}/\Gamma$

VALUE (units $10^{-6}$ )	CL%	DOCUMENT ID	TECN	COMMENT
$<0.1$	90	<sup>1</sup> AUBERT	09L BABR	$e^+e^- \rightarrow \Upsilon(4S)$
••• We do not use the following data for averages, fits, limits, etc. •••				
$<0.3$	90	<sup>1</sup> AUBERT,B	05G BABR	Repl. by AUBERT 09L
<sup>1</sup> Assumes equal production of $B^+$ and $B^0$ at the $\Upsilon(4S)$ .				

## $\Gamma(\chi_{c0} K^+)/\Gamma_{\text{total}}$ $\Gamma_{324}/\Gamma$

VALUE (units $10^{-4}$ )	CL%	DOCUMENT ID	TECN	COMMENT
$1.50^{+0.15}_{-0.13}$ OUR AVERAGE				
$1.8^{+0.6}_{-0.5} \pm 0.6$		<sup>1</sup> CHILIKIN	19 BELL	$e^+e^- \rightarrow \Upsilon(4S)$
$1.84 \pm 0.25 \pm 0.14$		<sup>2,3</sup> LEES	12o BABR	$e^+e^- \rightarrow \Upsilon(4S)$
$1.68 \pm 0.32 \pm 0.16$		<sup>2,4</sup> LEES	12o BABR	$e^+e^- \rightarrow \Upsilon(4S)$
$1.8 \pm 0.8 \pm 0.1$		<sup>5</sup> LEES	11i BABR	$e^+e^- \rightarrow \Upsilon(4S)$
$1.23^{+0.28}_{-0.25} \pm 0.05$		<sup>2,6</sup> AUBERT	08ai BABR	$e^+e^- \rightarrow \Upsilon(4S)$
$4.3 \pm 2.0 \pm 0.2$		<sup>7</sup> AUBERT,BE	06M BABR	$e^+e^- \rightarrow \Upsilon(4S)$
$1.12 \pm 0.12^{+0.30}_{-0.20}$		<sup>2</sup> GARMASH	06 BELL	$e^+e^- \rightarrow \Upsilon(4S)$
••• We do not use the following data for averages, fits, limits, etc. •••				
$<3.3$	90	<sup>8</sup> KATO	18 BELL	$e^+e^- \rightarrow \Upsilon(4S)$
$<2.7$	95	<sup>9</sup> AAIJ	13s LHCB	$pp$ at 7 TeV
$<5$	90	<sup>2,10</sup> WICHT	08 BELL	$e^+e^- \rightarrow \Upsilon(4S)$
$<1.8$	90	<sup>8</sup> AUBERT	06E BABR	$e^+e^- \rightarrow \Upsilon(4S)$
$1.84 \pm 0.32 \pm 0.31$		<sup>2,11</sup> AUBERT	06o BABR	Repl. by LEES 12o
$<8.9$	90	<sup>2</sup> AUBERT	05k BABR	$e^+e^- \rightarrow \Upsilon(4S)$
$1.39 \pm 0.49 \pm 0.11$		<sup>12</sup> AUBERT,B	05N BABR	Repl. by AUBERT 08ai
$1.96 \pm 0.35^{+2.00}_{-0.42}$		<sup>2</sup> GARMASH	05 BELL	Repl. by GARMASH 06
$2.7 \pm 0.7$		<sup>13</sup> AUBERT	04t BABR	Repl. by AUBERT,B 04P
$3.0 \pm 0.8 \pm 0.3$		<sup>14</sup> AUBERT,B	04P BABR	Repl. by AUBERT,B 05N
$6.0^{+2.1}_{-1.8} \pm 1.1$		<sup>15</sup> ABE	02b BELL	Repl. by GARMASH 05
$<4.8$	90	<sup>16</sup> EDWARDS	01 CLE2	$e^+e^- \rightarrow \Upsilon(4S)$

- <sup>1</sup> CHILIKIN 19 reports  $[\Gamma(B^+ \rightarrow \chi_{c0} K^+)/\Gamma_{\text{total}}] \times [B(\chi_{c0}(1P) \rightarrow p\bar{p}\pi^+\pi^-)] = (3.7^{+1.2+0.2}_{-1.0-0.3}) \times 10^{-7}$  which we divide by our best value  $B(\chi_{c0}(1P) \rightarrow p\bar{p}\pi^+\pi^-) = (2.1 \pm 0.7) \times 10^{-3}$ . Our first error is their experiment's error and our second error is the systematic error from using our best value.
- <sup>2</sup> Assumes equal production of  $B^+$  and  $B^0$  at the  $\Upsilon(4S)$ .
- <sup>3</sup> Measured in the  $B^+ \rightarrow K^+ K^- K^+$  decay.
- <sup>4</sup> Measured in the  $B^+ \rightarrow K^+ K_S^0 K_S^0$  decay.
- <sup>5</sup> LEES 11i reports  $[\Gamma(B^+ \rightarrow \chi_{c0} K^+)/\Gamma_{\text{total}}] \times [B(\chi_{c0}(1P) \rightarrow \pi\pi)] = (1.53 \pm 0.66 \pm 0.27) \times 10^{-6}$  which we divide by our best value  $B(\chi_{c0}(1P) \rightarrow \pi\pi) = (8.51 \pm 0.33) \times 10^{-3}$ . Our first error is their experiment's error and our second error is the systematic error from using our best value.
- <sup>6</sup> AUBERT 08ai reports  $(0.70 \pm 0.10^{+0.13}_{-0.10}) \times 10^{-6}$  for  $B(B^+ \rightarrow \chi_{c0} K^+) \times B(\chi_{c0} \rightarrow \pi^+ \pi^-)$ . We compute  $B(B^+ \rightarrow \chi_{c0} K^+)$  using the PDG value  $B(\chi_{c0} \rightarrow \pi\pi) = (8.51 \pm 0.33) \times 10^{-3}$  and 2/3 for the  $\pi^+ \pi^-$  fraction. Our first error is their experiment's error and the second error is systematic error from using our best value.
- <sup>7</sup> AUBERT,BE 06M reports  $[\Gamma(B^+ \rightarrow \chi_{c0} K^+)/\Gamma_{\text{total}}] \times [B(\chi_{c0}(1P) \rightarrow \gamma J/\psi(1S))] = (6.1 \pm 2.6 \pm 1.1) \times 10^{-6}$  which we divide by our best value  $B(\chi_{c0}(1P) \rightarrow \gamma J/\psi(1S)) = (1.40 \pm 0.05) \times 10^{-2}$ . Our first error is their experiment's error and our second error is the systematic error from using our best value. The significance of the observed signal is 2.4  $\sigma$ .
- <sup>8</sup> Measures absolute branching fractions using a missing-mass technique.
- <sup>9</sup> AAIJ 13s reports  $[\Gamma(B^+ \rightarrow \chi_{c0} K^+)/\Gamma_{\text{total}}] \times [B(\chi_{c0}(1P) \rightarrow p\bar{p})] < 6 \times 10^{-8}$  which we divide by our best value  $B(\chi_{c0}(1P) \rightarrow p\bar{p}) = 2.21 \times 10^{-4}$ .
- <sup>10</sup> WICHT 08 reports  $[\Gamma(B^+ \rightarrow \chi_{c0} K^+)/\Gamma_{\text{total}}] \times [B(\chi_{c0}(1P) \rightarrow \gamma\gamma)] < 0.11 \times 10^{-6}$  which we divide by our best value  $B(\chi_{c0}(1P) \rightarrow \gamma\gamma) = 2.04 \times 10^{-4}$ .

- <sup>11</sup> Measured in the  $B^+ \rightarrow K^+ K^- K^+$  decay.
- <sup>12</sup> AUBERT,B 05N reports  $(0.66 \pm 0.22 \pm 0.08) \times 10^{-6}$  for  $B(B^+ \rightarrow \chi_{c0}^0 K^+) \times B(\chi_{c0}^0 \rightarrow \pi^+ \pi^-)$ . We compute  $B(B^+ \rightarrow \chi_{c0}^0 K^+)$  using the PDG value  $B(\chi_{c0}^0 \rightarrow \pi^+ \pi^-) = (7.1 \pm 0.6) \times 10^{-3}$  and 2/3 for the  $\pi^+ \pi^-$  fraction.
- <sup>13</sup> The measurement performed using decay channels  $\chi_{c0} \rightarrow \pi^+ \pi^-$  and  $\chi_{c0} \rightarrow K^+ K^-$ . The ratio of the branching ratios for these channels is found to be consistent with world average.
- <sup>14</sup> AUBERT 04P reports  $B(B^+ \rightarrow \chi_{c0} K^+) \times B(\chi_{c0} \rightarrow \pi^+ \pi^-) = (1.5 \pm 0.4 \pm 0.1) \times 10^{-6}$  and used PDG value of  $B(\chi_{c0} \rightarrow \pi\pi) = (7.4 \pm 0.8) \times 10^{-3}$  and Clebsh-Gordan coefficient to compute  $B(B^+ \rightarrow \chi_{c0} K^+)$ .
- <sup>15</sup> ABE 02b measures the ratio of  $B(B^+ \rightarrow \chi_{c0} K^+)/B(B^+ \rightarrow J/\psi(1S) K^+) = 0.60 \pm 0.21 - 0.18 \pm 0.05 \pm 0.08$ , where the third error is due to the uncertainty in the  $B(\chi_{c0} \rightarrow \pi^+ \pi^-)$ , and uses  $B(B^+ \rightarrow J/\psi(1S) K^+) = (10.0 \pm 1.0) \times 10^{-4}$  to obtain the result.
- <sup>16</sup> EDWARDS 01 assumes equal production of  $B^0$  and  $B^+$  at the  $\Upsilon(4S)$ . The correlated uncertainties (28.3)% from  $B(J/\psi(1S) \rightarrow \gamma\eta_c)$  in those modes have been accounted for.

## $\Gamma(\chi_{c0} K^*(892^+)/\Gamma_{\text{total}}$ $\Gamma_{325}/\Gamma$

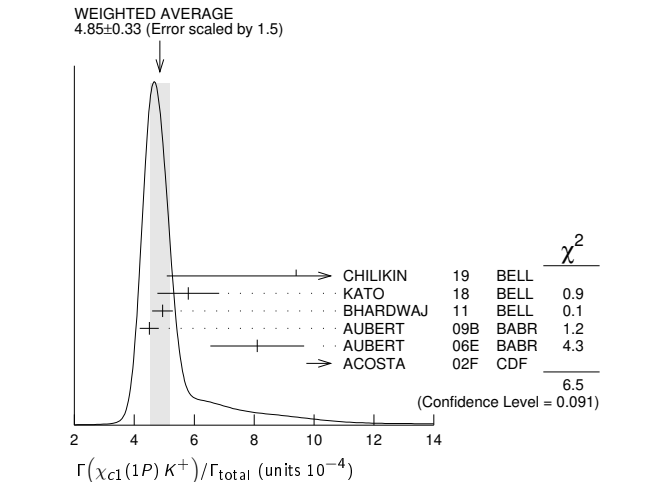
VALUE (units $10^{-4}$ )	CL%	DOCUMENT ID	TECN	COMMENT
$< 2.1$	90	<sup>1</sup> AUBERT	08bd BABR	$e^+e^- \rightarrow \Upsilon(4S)$
••• We do not use the following data for averages, fits, limits, etc. •••				
$<28.6$	90	<sup>1</sup> AUBERT	05k BABR	Repl. by AUBERT 08bd
<sup>1</sup> Assumes equal production of $B^+$ and $B^0$ at the $\Upsilon(4S)$ .				

## $\Gamma(\chi_{c1}(1P) \pi^+)/\Gamma_{\text{total}}$ $\Gamma_{326}/\Gamma$

VALUE (units $10^{-5}$ )	DOCUMENT ID	TECN	COMMENT
$2.2 \pm 0.4 \pm 0.3$	<sup>1</sup> KUMAR	06 BELL	$e^+e^- \rightarrow \Upsilon(4S)$
<sup>1</sup> Assumes equal production of $B^+$ and $B^0$ at the $\Upsilon(4S)$ .			

## $\Gamma(\chi_{c1}(1P) K^+)/\Gamma_{\text{total}}$ $\Gamma_{327}/\Gamma$

VALUE (units $10^{-4}$ )	EVTS	DOCUMENT ID	TECN	COMMENT
<b><math>4.85 \pm 0.33</math> OUR AVERAGE</b>		Error includes scale factor of 1.5. See the ideogram below.		
$9^{+3}_{-2} \pm 4$		<sup>1</sup> CHILIKIN	19 BELL	$e^+e^- \rightarrow \Upsilon(4S)$
$5.8 \pm 0.9 \pm 0.5$		<sup>2</sup> KATO	18 BELL	$e^+e^- \rightarrow \Upsilon(4S)$
$4.94 \pm 0.11 \pm 0.33$		<sup>3</sup> BHARDWAJ	11 BELL	$e^+e^- \rightarrow \Upsilon(4S)$
$4.5 \pm 0.1 \pm 0.3$		<sup>4</sup> AUBERT	09b BABR	$e^+e^- \rightarrow \Upsilon(4S)$
$8.1 \pm 1.4 \pm 0.7$		<sup>2</sup> AUBERT	06E BABR	$e^+e^- \rightarrow \Upsilon(4S)$
$15.5 \pm 5.4 \pm 2.0$		<sup>5</sup> ACOSTA	02F CDF	$p\bar{p}$ 1.8 TeV
••• We do not use the following data for averages, fits, limits, etc. •••				
$5.1 \pm 0.4 \pm 0.1$		<sup>6</sup> AUBERT,BE	06M BABR	Repl. by AUBERT 09b
$4.49 \pm 0.19 \pm 0.53$		<sup>3</sup> SONI	06 BELL	Repl. by BHARDWAJ 11
$5.79 \pm 0.26 \pm 0.65$		<sup>3</sup> AUBERT	05J BABR	Repl. by AUBERT,BE 06M
$6.0 \pm 0.9 \pm 0.2$		<sup>7</sup> AUBERT	02 BABR	Repl. by AUBERT 05J
$9.7 \pm 4.0 \pm 0.9$		<sup>3</sup> ALAM	94 CLE2	$e^+e^- \rightarrow \Upsilon(4S)$
$19 \pm 13 \pm 6$		<sup>8</sup> ALBRECHT	92E ARG	$e^+e^- \rightarrow \Upsilon(4S)$



- <sup>1</sup> CHILIKIN 19 reports  $[\Gamma(B^+ \rightarrow \chi_{c1}(1P) K^+)/\Gamma_{\text{total}}] \times [B(\chi_{c1}(1P) \rightarrow p\bar{p}\pi^+\pi^-)] = (4.7^{+1.3+0.4}_{-1.2-0.2}) \times 10^{-7}$  which we divide by our best value  $B(\chi_{c1}(1P) \rightarrow p\bar{p}\pi^+\pi^-) = (5.0 \pm 1.9) \times 10^{-4}$ . Our first error is their experiment's error and our second error is the systematic error from using our best value.
- <sup>2</sup> Measures absolute branching fractions using a missing-mass technique.
- <sup>3</sup> Assumes equal production of  $B^+$  and  $B^0$  at the  $\Upsilon(4S)$ .
- <sup>4</sup> Uses  $\chi_{c1,2} \rightarrow J/\psi\gamma$ . Assumes  $B(\Upsilon(4S) \rightarrow B^+ B^-) = (51.6 \pm 0.6)\%$  and  $B(\Upsilon(4S) \rightarrow B^0 \bar{B}^0) = (48.4 \pm 0.6)\%$ .
- <sup>5</sup> ACOSTA 02F uses as reference of  $B(B \rightarrow J/\psi(1S) K^+) = (10.1 \pm 0.6) \times 10^{-4}$ . The second error includes the systematic error and the uncertainties of the branching ratio.

# Meson Particle Listings

## B±

<sup>6</sup> AUBERT, BE 06M reports  $[\Gamma(B^+ \rightarrow \chi_{c1}(1P)K^+)/\Gamma_{total}] \times [B(\chi_{c1}(1P) \rightarrow \gamma J/\psi(1S))] = (1.76 \pm 0.07 \pm 0.12) \times 10^{-4}$  which we divide by our best value  $B(\chi_{c1}(1P) \rightarrow \gamma J/\psi(1S)) = (34.3 \pm 1.0) \times 10^{-2}$ . Our first error is their experiment's error and our second error is the systematic error from using our best value.

<sup>7</sup> AUBERT 02 reports  $(7.5 \pm 0.9 \pm 0.8) \times 10^{-4}$  from a measurement of  $[\Gamma(B^+ \rightarrow \chi_{c1}(1P)K^+)/\Gamma_{total}] \times [B(\chi_{c1}(1P) \rightarrow \gamma J/\psi(1S))]$  assuming  $B(\chi_{c1}(1P) \rightarrow \gamma J/\psi(1S)) = 0.273 \pm 0.016$ , which we rescale to our best value  $B(\chi_{c1}(1P) \rightarrow \gamma J/\psi(1S)) = (34.3 \pm 1.0) \times 10^{-2}$ . Our first error is their experiment's error and our second error is the systematic error from using our best value. Assumes equal production of  $B^+$  and  $B^0$  at the  $\Upsilon(4S)$ .

<sup>8</sup> ALBRECHT 92E assumes no  $\chi_{c2}(1P)$  production and  $B(\Upsilon(4S) \rightarrow B^+B^-) = 50\%$ .

$\Gamma(\chi_{c1}(1P)K^+)/\Gamma(J/\psi(1S)K^+)$		$\Gamma_{327}/\Gamma_{275}$	
VALUE	DOCUMENT ID	TECN	COMMENT
<b>0.60 ± 0.07 ± 0.02</b>	<sup>1</sup> AUBERT	02	BABR $e^+e^- \rightarrow \Upsilon(4S)$

<sup>1</sup> AUBERT 02 reports  $0.75 \pm 0.08 \pm 0.05$  from a measurement of  $[\Gamma(B^+ \rightarrow \chi_{c1}(1P)K^+)/\Gamma(B^+ \rightarrow J/\psi(1S)K^+)] \times [B(\chi_{c1}(1P) \rightarrow \gamma J/\psi(1S))]$  assuming  $B(\chi_{c1}(1P) \rightarrow \gamma J/\psi(1S)) = 0.273 \pm 0.016$ , which we rescale to our best value  $B(\chi_{c1}(1P) \rightarrow \gamma J/\psi(1S)) = (34.3 \pm 1.0) \times 10^{-2}$ . Our first error is their experiment's error and our second error is the systematic error from using our best value. Assumes equal production of  $B^+$  and  $B^0$  at the  $\Upsilon(4S)$ .

$\Gamma(\chi_{c1}(1P)\pi^+)/\Gamma(\chi_{c1}(1P)K^+)$		$\Gamma_{326}/\Gamma_{327}$	
VALUE	DOCUMENT ID	TECN	COMMENT
<b>0.043 ± 0.008 ± 0.003</b>	<sup>1</sup> KUMAR	06	BELL $e^+e^- \rightarrow \Upsilon(4S)$

<sup>1</sup> Assumes equal production of  $B^+$  and  $B^0$  at the  $\Upsilon(4S)$ .

$\Gamma(\chi_{c1}(1P)K^*(892)^+)/\Gamma_{total}$		$\Gamma_{328}/\Gamma$		
VALUE (units $10^{-4}$ )	CL%	DOCUMENT ID	TECN	COMMENT
<b>3.0 ± 0.6 OUR AVERAGE</b>				Error includes scale factor of 1.1.
2.6 ± 0.5 ± 0.4		<sup>1</sup> AUBERT	09B	BABR $e^+e^- \rightarrow \Upsilon(4S)$
4.05 ± 0.59 ± 0.95		<sup>2</sup> SONI	06	BELL $e^+e^- \rightarrow \Upsilon(4S)$

• • • We do not use the following data for averages, fits, limits, etc. • • •

2.94 ± 0.95 ± 0.98		<sup>2</sup> AUBERT	05J	BABR Repl. by AUBERT 09B
< 21	90	<sup>2</sup> ALAM	94	CLE2 $e^+e^- \rightarrow \Upsilon(4S)$

<sup>1</sup> Uses  $\chi_{c1,2} \rightarrow J/\psi\gamma$ . Assumes  $B(\Upsilon(4S) \rightarrow B^+B^-) = (51.6 \pm 0.6)\%$  and  $B(\Upsilon(4S) \rightarrow B^0\bar{B}^0) = (48.4 \pm 0.6)\%$ .

<sup>2</sup> Assumes equal production of  $B^+$  and  $B^0$  at the  $\Upsilon(4S)$ .

$\Gamma(\chi_{c1}(1P)K^*(892)^+)/\Gamma(\chi_{c1}(1P)K^+)$		$\Gamma_{328}/\Gamma_{327}$	
VALUE	DOCUMENT ID	TECN	COMMENT
<b>0.51 ± 0.17 ± 0.16</b>	AUBERT	05J	BABR $e^+e^- \rightarrow \Upsilon(4S)$

$\Gamma(\chi_{c1}(1P)K^0\pi^+)/\Gamma_{total}$		$\Gamma_{329}/\Gamma$		
VALUE (units $10^{-4}$ )	CL%	DOCUMENT ID	TECN	COMMENT
<b>5.75 ± 0.26 ± 0.32</b>		<sup>1</sup> BHARDWAJ	16	BELL $e^+e^- \rightarrow \Upsilon(4S)$

<sup>1</sup> Assumes equal production of  $B^+$  and  $B^0$  at the  $\Upsilon(4S)$ .

$\Gamma(\chi_{c1}(1P)K^0\pi^+)/\Gamma(J/\psi(1S)K^0\pi^+)$		$\Gamma_{329}/\Gamma_{276}$	
VALUE	DOCUMENT ID	TECN	COMMENT
<b>0.503 ± 0.030 ± 0.014</b>	<sup>1</sup> LEES	12B	BABR $e^+e^- \rightarrow \Upsilon(4S)$

<sup>1</sup> LEES 12B reports  $0.501 \pm 0.024 \pm 0.028$  from a measurement of  $[\Gamma(B^+ \rightarrow \chi_{c1}(1P)K^0\pi^+)/\Gamma(B^+ \rightarrow J/\psi(1S)K^0\pi^+)] \times [B(\chi_{c1}(1P) \rightarrow \gamma J/\psi(1S))]$  assuming  $B(\chi_{c1}(1P) \rightarrow \gamma J/\psi(1S)) = (34.4 \pm 1.5) \times 10^{-2}$ , which we rescale to our best value  $B(\chi_{c1}(1P) \rightarrow \gamma J/\psi(1S)) = (34.3 \pm 1.0) \times 10^{-2}$ . Our first error is their experiment's error and our second error is the systematic error from using our best value.

$\Gamma(\chi_{c1}(1P)K^+\pi^0)/\Gamma_{total}$		$\Gamma_{330}/\Gamma$		
VALUE (units $10^{-4}$ )	CL%	DOCUMENT ID	TECN	COMMENT
<b>3.29 ± 0.29 ± 0.19</b>		<sup>1</sup> BHARDWAJ	16	BELL $e^+e^- \rightarrow \Upsilon(4S)$

<sup>1</sup> Assumes equal production of  $B^+$  and  $B^0$  at the  $\Upsilon(4S)$ .

$\Gamma(\chi_{c1}(1P)K^+\pi^-\pi^-)/\Gamma_{total}$		$\Gamma_{331}/\Gamma$		
VALUE (units $10^{-4}$ )	CL%	DOCUMENT ID	TECN	COMMENT
<b>3.74 ± 0.18 ± 0.24</b>		<sup>1</sup> BHARDWAJ	16	BELL $e^+e^- \rightarrow \Upsilon(4S)$

<sup>1</sup> Assumes equal production of  $B^+$  and  $B^0$  at the  $\Upsilon(4S)$ .

$\Gamma(\chi_{c1}(2P)K^+, \chi_{c1}(2P) \rightarrow \pi^+\pi^-\chi_{c1}(1P))/\Gamma_{total}$		$\Gamma_{332}/\Gamma$		
VALUE	CL%	DOCUMENT ID	TECN	COMMENT
<b>&lt; 1.1 × 10<sup>-5</sup></b>	90	<sup>1,2</sup> BHARDWAJ	16	BELL $e^+e^- \rightarrow \Upsilon(4S)$

<sup>1</sup> BHARDWAJ 16 analysis fixes mass and width of the  $\chi_{c1}(2P)$  state to 3920 MeV and 20 MeV.

<sup>2</sup> Assumes equal production of  $B^+$  and  $B^0$  at the  $\Upsilon(4S)$ .

$\Gamma(\chi_{c2}K^+)/\Gamma_{total}$		$\Gamma_{333}/\Gamma$		
VALUE (units $10^{-5}$ )	CL%	DOCUMENT ID	TECN	COMMENT
<b>1.11 + 0.36 - 0.34 ± 0.09</b>		<sup>1</sup> BHARDWAJ	11	BELL $e^+e^- \rightarrow \Upsilon(4S)$

• • • We do not use the following data for averages, fits, limits, etc. • • •

< 1.8	90	<sup>2</sup> AUBERT	09B	BABR $e^+e^- \rightarrow \Upsilon(4S)$
< 2.0	90	<sup>3</sup> AUBERT	06E	BABR $e^+e^- \rightarrow \Upsilon(4S)$
< 2.9	90	<sup>1</sup> SONI	06	BELL Repl. by BHARDWAJ 11
< 3.0	90	<sup>1</sup> AUBERT	05K	BABR Repl. by AUBERT 06E

<sup>1</sup> Assumes equal production of  $B^+$  and  $B^0$  at the  $\Upsilon(4S)$ .

<sup>2</sup> Uses  $\chi_{c1,2} \rightarrow J/\psi\gamma$ . Assumes  $B(\Upsilon(4S) \rightarrow B^+B^-) = (51.6 \pm 0.6)\%$  and  $B(\Upsilon(4S) \rightarrow B^0\bar{B}^0) = (48.4 \pm 0.6)\%$ .

<sup>3</sup> Perform measurements of absolute branching fractions using a missing mass technique.

$\Gamma(\chi_{c2}K^+, \chi_{c2} \rightarrow p\bar{p}\pi^+\pi^-)/\Gamma_{total}$		$\Gamma_{334}/\Gamma$	
VALUE	DOCUMENT ID	TECN	COMMENT
<b>&lt; 1.9 × 10<sup>-7</sup></b>	CHILIKIN	19	BELL $e^+e^- \rightarrow \Upsilon(4S)$

$\Gamma(B^+ \rightarrow \chi_{c2}K^+)/\Gamma_{total} \times \Gamma(\chi_{c2}(1P) \rightarrow \gamma\gamma)/\Gamma_{total}$		$\Gamma_{333}/\Gamma \times \Gamma_{93}^{\chi_{c2}(1P)}/\Gamma_{\chi_{c2}(1P)}$		
VALUE (units $10^{-6}$ )	CL%	DOCUMENT ID	TECN	COMMENT
<b>&lt; 0.09</b>	90	<sup>1</sup> WICHT	08	BELL $e^+e^- \rightarrow \Upsilon(4S)$

<sup>1</sup> Assumes equal production of  $B^+$  and  $B^0$  at the  $\Upsilon(4S)$ .

$\Gamma(\chi_{c2}K^*(892)^+)/\Gamma_{total}$		$\Gamma_{335}/\Gamma$		
VALUE	CL%	DOCUMENT ID	TECN	COMMENT
<b>&lt; 12 × 10<sup>-5</sup></b>	90	<sup>1</sup> AUBERT	09B	BABR $e^+e^- \rightarrow \Upsilon(4S)$

• • • We do not use the following data for averages, fits, limits, etc. • • •

< 12.7 × 10 <sup>-5</sup>	90	<sup>2</sup> SONI	06	BELL $e^+e^- \rightarrow \Upsilon(4S)$
< 1.2 × 10 <sup>-5</sup>	90	<sup>2</sup> AUBERT	05K	BABR Repl. by AUBERT 09B

<sup>1</sup> Uses  $\chi_{c1,2} \rightarrow J/\psi\gamma$ . Assumes  $B(\Upsilon(4S) \rightarrow B^+B^-) = (51.6 \pm 0.6)\%$  and  $B(\Upsilon(4S) \rightarrow B^0\bar{B}^0) = (48.4 \pm 0.6)\%$ .

<sup>2</sup> Assumes equal production of  $B^+$  and  $B^0$  at the  $\Upsilon(4S)$ .

$\Gamma(\chi_{c2}K^0\pi^+)/\Gamma_{total}$		$\Gamma_{336}/\Gamma$		
VALUE (units $10^{-4}$ )	CL%	DOCUMENT ID	TECN	COMMENT
<b>1.16 ± 0.22 ± 0.12</b>		<sup>1</sup> BHARDWAJ	16	BELL $e^+e^- \rightarrow \Upsilon(4S)$

<sup>1</sup> Assumes equal production of  $B^+$  and  $B^0$  at the  $\Upsilon(4S)$ .

$\Gamma(\chi_{c2}K^+\pi^0)/\Gamma_{total}$		$\Gamma_{337}/\Gamma$		
VALUE	CL%	DOCUMENT ID	TECN	COMMENT
<b>&lt; 0.62 × 10<sup>-4</sup></b>	90	<sup>1</sup> BHARDWAJ	16	BELL $e^+e^- \rightarrow \Upsilon(4S)$

<sup>1</sup> Assumes equal production of  $B^+$  and  $B^0$  at the  $\Upsilon(4S)$ .

$\Gamma(\chi_{c2}K^+\pi^-\pi^-)/\Gamma_{total}$		$\Gamma_{338}/\Gamma$		
VALUE (units $10^{-4}$ )	CL%	DOCUMENT ID	TECN	COMMENT
<b>1.34 ± 0.17 ± 0.09</b>		<sup>1</sup> BHARDWAJ	16	BELL $e^+e^- \rightarrow \Upsilon(4S)$

<sup>1</sup> Assumes equal production of  $B^+$  and  $B^0$  at the  $\Upsilon(4S)$ .

$\Gamma(\chi_{c2}(3930)\pi^+, \chi_{c2} \rightarrow \pi^+\pi^-)/\Gamma_{total}$		$\Gamma_{339}/\Gamma$		
VALUE (units $10^{-6}$ )	CL%	DOCUMENT ID	TECN	COMMENT
<b>&lt; 0.1</b>	90	<sup>1</sup> AUBERT	09L	BABR $e^+e^- \rightarrow \Upsilon(4S)$

<sup>1</sup> Assumes equal production of  $B^+$  and  $B^0$  at the  $\Upsilon(4S)$ .

$\Gamma(h_c(1P)K^+)/\Gamma_{total}$		$\Gamma_{340}/\Gamma$		
VALUE (units $10^{-5}$ )	CL%	DOCUMENT ID	TECN	COMMENT
<b>3.7 + 1.0 + 0.8 - 0.9 - 0.8</b>		CHILIKIN	19	BELL $e^+e^- \rightarrow \Upsilon(4S)$

• • • We do not use the following data for averages, fits, limits, etc. • • •

< 3.8	90	<sup>1</sup> FANG	06	BELL $e^+e^- \rightarrow \Upsilon(4S)$
-------	----	-------------------	----	--

<sup>1</sup> Assumes equal production of  $B^+$  and  $B^0$  at the  $\Upsilon(4S)$  and  $B(h_c \rightarrow \eta_c\gamma) = 50\%$ .

$\Gamma(h_c(1P)K^+, h_c \rightarrow p\bar{p})/\Gamma_{total}$		$\Gamma_{341}/\Gamma$		
VALUE	CL%	DOCUMENT ID	TECN	COMMENT
<b>&lt; 6.4 × 10<sup>-8</sup></b>	95	<sup>1</sup> AAIJ	13S	LHCb $pp$ at 7 TeV

<sup>1</sup> Measured relative to  $B^+ \rightarrow J/\psi K^+$  decay with charmonia reconstructed in  $p\bar{p}$  final state and using  $B(B^+ \rightarrow J/\psi K^+) = (1.013 \pm 0.034) \times 10^{-3}$  and  $B(J/\psi \rightarrow p\bar{p}) = (2.17 \pm 0.07) \times 10^{-3}$ .

$\Gamma(K^0\pi^+)/\Gamma_{total}$		$\Gamma_{342}/\Gamma$		
VALUE (units $10^{-6}$ )	CL%	DOCUMENT ID	TECN	COMMENT
<b>23.7 ± 0.8 OUR FIT</b>				
<b>23.8 ± 0.7 OUR AVERAGE</b>				
23.97 ± 0.53 ± 0.71		<sup>1</sup> DUH	13	BELL $e^+e^- \rightarrow \Upsilon(4S)$
23.9 ± 1.1 ± 1.0		<sup>1</sup> AUBERT, BE	06C	BABR $e^+e^- \rightarrow \Upsilon(4S)$
18.8 + 3.7 + 2.1 - 3.3 - 1.8		<sup>1</sup> BORNHEIM	03	CLE2 $e^+e^- \rightarrow \Upsilon(4S)$

• • • We do not use the following data for averages, fits, limits, etc. • • •

Table with columns: VALUE (units 10^-6), CL%, DOCUMENT ID, TECN, COMMENT. Rows include LIN 07 BELL, AUBERT, BE 05E BABR, AUBERT 04M BABR, CHAO 04 BELL, CASEY 02 BELL, ABE 01H BELL, AUBERT 01E BABR, CRONIN-HEN.00 CLE2, GODANG 98 CLE2, ASNER 96 CLE2, ALBRECHT 91B ARG, AVERY 89B CLE0, AVERY 87 CLE0.

1 Assumes equal production of B+ and B0 at the T(4S).
2 AVERY 89B reports < 9 x 10^-5 assuming the T(4S) decays 43% to B0 B0. We rescale to 50%.

Gamma(K+ pi0)/Gamma total F343/Gamma

Table with columns: VALUE (units 10^-6), CL%, DOCUMENT ID, TECN, COMMENT. Rows include DUH 13 BELL, AUBERT 07bc BABR, BORNHEIM 03 CLE2.

• • • We do not use the following data for averages, fits, limits, etc. • • •

Table with columns: VALUE (units 10^-6), CL%, DOCUMENT ID, TECN, COMMENT. Rows include LIN 07A BELL, AUBERT 05L BABR, CHAO 04 BELL, AUBERT 03L BABR, CASEY 02 BELL, ABE 01H BELL, AUBERT 01E BABR, CRONIN-HEN.00 CLE2, GODANG 98 CLE2, ASNER 96 CLE2.

1 Assumes equal production of B+ and B0 at the T(4S).

Gamma(K+ pi0)/Gamma(K0 pi+) F343/Gamma342

Table with columns: VALUE, DOCUMENT ID, TECN, COMMENT. Rows include LIN 07A BELL, ABE 01H BELL.

• • • We do not use the following data for averages, fits, limits, etc. • • •

Gamma(eta K+)/Gamma total F344/Gamma

Table with columns: VALUE (units 10^-6), DOCUMENT ID, TECN, COMMENT. Rows include AUBERT 09Av BABR, WICHT 08 BELL, SCHUEMANN 06 BELL, RICHICHI 00 CLE2.

• • • We do not use the following data for averages, fits, limits, etc. • • •

Table with columns: VALUE (units 10^-6), DOCUMENT ID, TECN, COMMENT. Rows include AUBERT 07AE BABR, AUBERT 05M BABR, AUBERT 03W BABR, ABE 01M BELL, AUBERT 01G BABR, BEHRENS 98 CLE2.

1 Assumes equal production of B+ and B0 at the T(4S).
2 WICHT 08 reports [Gamma(B+ -> eta K+)/Gamma total] x [B(eta(958) -> gamma)] = (1.40 +0.16 +0.15 -0.12) x 10^-6 which we divide by our best value B(eta(958) -> gamma) = (2.307 +/- 0.33) x 10^-2. Our first error is their experiment's error and our second error is the systematic error from using our best value.

Gamma(eta K\*(892))/Gamma total F345/Gamma

Table with columns: VALUE (units 10^-6), CL%, DOCUMENT ID, TECN, COMMENT. Row includes DEL-AMO-SA...10A BABR.

• • • We do not use the following data for averages, fits, limits, etc. • • •

Table with columns: VALUE (units 10^-6), CL%, DOCUMENT ID, TECN, COMMENT. Rows include AUBERT 07E BABR, SCHUEMANN 07 BELL, AUBERT, B 04D BABR, RICHICHI 00 CLE2, BEHRENS 98 CLE2.

1 Assumes equal production of B+ and B0 at the T(4S).

Gamma(eta K\*(1430)+)/Gamma total F346/Gamma

Table with columns: VALUE (units 10^-6), DOCUMENT ID, TECN, COMMENT. Row includes DEL-AMO-SA...10A BABR.

1 Assumes equal production of B+ and B0 at the T(4S).

Gamma(eta K\*(1430)+)/Gamma total F347/Gamma

Table with columns: VALUE (units 10^-6), DOCUMENT ID, TECN, COMMENT. Row includes DEL-AMO-SA...10A BABR.

1 Assumes equal production of B+ and B0 at the T(4S).

Gamma(K+)/Gamma total F348/Gamma

Table with columns: VALUE (units 10^-6), CL%, DOCUMENT ID, TECN, COMMENT. Rows include HOI 12 BELL, AUBERT 09Av BABR, RICHICHI 00 CLE2.

• • • We do not use the following data for averages, fits, limits, etc. • • •

Table with columns: VALUE (units 10^-6), CL%, DOCUMENT ID, TECN, COMMENT. Rows include WICHT 08 BELL, AUBERT 07AE BABR, CHANG 07B BELL, AUBERT, B 05K BABR, CHANG 05A BELL, AUBERT 04H BABR, BEHRENS 98 CLE2.

1 Assumes equal production of B+ and B0 at the T(4S).
2 WICHT 08 reports [Gamma(B+ -> eta K+)/Gamma total] x [B(eta -> 2 gamma)] = (0.87 +0.16 +0.10 -0.15 -0.07) x 10^-6 which we divide by our best value B(eta -> 2 gamma) = (39.41 +/- 0.20) x 10^-2. Our first error is their experiment's error and our second error is the systematic error from using our best value.

Gamma(eta K\*(892)+)/Gamma total F349/Gamma

Table with columns: VALUE (units 10^-6), CL%, DOCUMENT ID, TECN, COMMENT. Rows include WANG 07B BELL, AUBERT, B 06H BABR, RICHICHI 00 CLE2.

• • • We do not use the following data for averages, fits, limits, etc. • • •

Table with columns: VALUE (units 10^-6), DOCUMENT ID, TECN, COMMENT. Rows include AUBERT, B 04D BABR, BEHRENS 98 CLE2.

1 Assumes equal production of B+ and B0 at the T(4S).

Gamma(eta K\*(1430)+)/Gamma total F350/Gamma

Table with columns: VALUE (units 10^-6), DOCUMENT ID, TECN, COMMENT. Row includes AUBERT, B 06H BABR.

1 Assumes equal production of B+ and B0 at the T(4S).

Gamma(eta K\*(1430)+)/Gamma total F351/Gamma

Table with columns: VALUE (units 10^-6), DOCUMENT ID, TECN, COMMENT. Row includes AUBERT, B 06H BABR.

1 Assumes equal production of B+ and B0 at the T(4S).

Gamma(eta(1295) K+ x B(eta(1295) -> eta pi pi))/Gamma total F352/Gamma

Table with columns: VALUE (units 10^-6), DOCUMENT ID, TECN, COMMENT. Row includes AUBERT 08x BABR.

1 Assumes equal production of B+ and B0 at the T(4S).

Gamma(eta(1405) K+ x B(eta(1405) -> eta pi pi))/Gamma total F353/Gamma

Table with columns: VALUE (units 10^-6), CL%, DOCUMENT ID, TECN, COMMENT. Row includes AUBERT 08x BABR.

1 Assumes equal production of B+ and B0 at the T(4S).

Gamma(eta(1405) K+ x B(eta(1405) -> K\* K))/Gamma total F354/Gamma

Table with columns: VALUE (units 10^-6), CL%, DOCUMENT ID, TECN, COMMENT. Row includes AUBERT 08x BABR.

1 Assumes equal production of B+ and B0 at the T(4S).

Downloaded from https://academic.oup.com/ptep/article/2020/8/083C01/5891211 by guest on 12 November 2020

## Meson Particle Listings

 $B^\pm$  $\Gamma(\eta(1475) K^+ \times B(\eta(1475) \rightarrow K^* K)) / \Gamma_{\text{total}}$   $\Gamma_{355} / \Gamma$ 

VALUE (units $10^{-6}$ )	CL%	DOCUMENT ID	TECN	COMMENT
$13.8^{+1.8+1.0}_{-1.7-0.6}$		1 AUBERT	08x BABR	$e^+ e^- \rightarrow \Upsilon(4S)$

<sup>1</sup> Assumes equal production of  $B^+$  and  $B^0$  at the  $\Upsilon(4S)$ .

 $\Gamma(f_1(1285) K^+) / \Gamma_{\text{total}}$   $\Gamma_{356} / \Gamma$ 

VALUE (units $10^{-6}$ )	CL%	DOCUMENT ID	TECN	COMMENT
$<2.0$	90	1 AUBERT	08x BABR	$e^+ e^- \rightarrow \Upsilon(4S)$

<sup>1</sup> Assumes equal production of  $B^+$  and  $B^0$  at the  $\Upsilon(4S)$ .

 $\Gamma(f_1(1420) K^+ \times B(f_1(1420) \rightarrow \eta \pi \pi)) / \Gamma_{\text{total}}$   $\Gamma_{357} / \Gamma$ 

VALUE (units $10^{-6}$ )	CL%	DOCUMENT ID	TECN	COMMENT
$<2.9$	90	1 AUBERT	08x BABR	$e^+ e^- \rightarrow \Upsilon(4S)$

<sup>1</sup> Assumes equal production of  $B^+$  and  $B^0$  at the  $\Upsilon(4S)$ .

 $\Gamma(f_1(1420) K^+ \times B(f_1(1420) \rightarrow K^* K)) / \Gamma_{\text{total}}$   $\Gamma_{358} / \Gamma$ 

VALUE (units $10^{-6}$ )	CL%	DOCUMENT ID	TECN	COMMENT
$<4.1$	90	1 AUBERT	08x BABR	$e^+ e^- \rightarrow \Upsilon(4S)$

<sup>1</sup> Assumes equal production of  $B^+$  and  $B^0$  at the  $\Upsilon(4S)$ .

 $\Gamma(\phi(1680) K^+ \times B(\phi(1680) \rightarrow K^* K)) / \Gamma_{\text{total}}$   $\Gamma_{359} / \Gamma$ 

VALUE (units $10^{-6}$ )	CL%	DOCUMENT ID	TECN	COMMENT
$<3.4$	90	1 AUBERT	08x BABR	$e^+ e^- \rightarrow \Upsilon(4S)$

<sup>1</sup> Assumes equal production of  $B^+$  and  $B^0$  at the  $\Upsilon(4S)$ .

 $\Gamma(f_0(1500) K^+) / \Gamma_{\text{total}}$   $\Gamma_{360} / \Gamma$ 

VALUE (units $10^{-6}$ )	CL%	DOCUMENT ID	TECN	COMMENT
$3.7 \pm 2.2$ OUR AVERAGE				
$17 \pm 4 \pm 12$		1 LEES	12o BABR	$e^+ e^- \rightarrow \Upsilon(4S)$
$20 \pm 10 \pm 27$		2 LEES	12o BABR	$e^+ e^- \rightarrow \Upsilon(4S)$
$3.2^{+2.3}_{-2.3} \pm 0.2$		3,4 AUBERT	08A1 BABR	$e^+ e^- \rightarrow \Upsilon(4S)$

• • • We do not use the following data for averages, fits, limits, etc. • • •

VALUE (units $10^{-6}$ )	CL%	DOCUMENT ID	TECN	COMMENT
$<19$	90	4,5 AUBERT,B	05N BABR	Repl. by AUBERT 08A1

<sup>1</sup> Measured in the  $B^+ \rightarrow K^+ K^- K^+$  decay.<sup>2</sup> Measured in the  $B^+ \rightarrow K^+ K_S^0 K_S^0$  decay.<sup>3</sup> AUBERT 08A1 reports  $B(B^+ \rightarrow f_0(1500) K^+) \cdot B(f_0(1500) \rightarrow \pi^+ \pi^-) = (0.73 \pm 0.21_{-0.48}^{+0.47}) \times 10^{-6}$ . We divide this result by our best value of  $B(f_0(1500) \rightarrow \pi \pi) = (34.5 \pm 2.2) \times 10^{-2}$  multiplied by 2/3 to account for the  $\pi^+ \pi^-$  fraction. Our first quoted uncertainty is the combined experiment's uncertainty and our second is the systematic uncertainty from using our best value.<sup>4</sup> Assumes equal production of  $B^+$  and  $B^0$  at the  $\Upsilon(4S)$ .<sup>5</sup> AUBERT,B 05N reports  $B(B^+ \rightarrow f_0(1500) K^+) \cdot B(f_0(1500) \rightarrow \pi^+ \pi^-) < 4.4 \times 10^{-6}$ . We divide this result by our best value of  $B(f_0(1500) \rightarrow \pi \pi) = (34.5 \pm 2.2) \times 10^{-2}$  multiplied by 2/3 to account for the  $\pi^+ \pi^-$  fraction. Our first quoted uncertainty is the combined experiment's uncertainty and our second is the systematic uncertainty from using our best value. $\Gamma(\omega K^+) / \Gamma_{\text{total}}$   $\Gamma_{361} / \Gamma$ 

VALUE (units $10^{-6}$ )	CL%	DOCUMENT ID	TECN	COMMENT
$6.5 \pm 0.4$ OUR AVERAGE				
$6.8 \pm 0.4 \pm 0.4$		1 CHOBANOVA	14 BELL	$e^+ e^- \rightarrow \Upsilon(4S)$
$6.3 \pm 0.5 \pm 0.3$		1 AUBERT	07AE BABR	$e^+ e^- \rightarrow \Upsilon(4S)$
$3.2^{+2.4}_{-1.9} \pm 0.8$		1 JESSOP	00 CLE2	$e^+ e^- \rightarrow \Upsilon(4S)$

• • • We do not use the following data for averages, fits, limits, etc. • • •

VALUE (units $10^{-6}$ )	CL%	DOCUMENT ID	TECN	COMMENT
$6.1 \pm 0.6 \pm 0.4$		1 AUBERT,B	06E BABR	AUBERT 07AE
$8.1 \pm 0.6 \pm 0.6$		1 JEN	06 BELL	Repl. by CHOBANOVA 14
$4.8 \pm 0.8 \pm 0.4$		1 AUBERT	04H BABR	Repl. by AUBERT,B 06E
$6.5^{+1.3}_{-1.2} \pm 0.6$		1 WANG	04A BELL	Repl. by JEN 06
$9.2^{+2.6}_{-2.3} \pm 1.0$		1 LU	02 BELL	Repl. by WANG 04A
$<4$	90	1 AUBERT	01G BABR	$e^+ e^- \rightarrow \Upsilon(4S)$
$1.5^{+7}_{-6} \pm 2$		1 BERGFELD	98 CLE2	Repl. by JESSOP 00

<sup>1</sup> Assumes equal production of  $B^+$  and  $B^0$  at the  $\Upsilon(4S)$ .

 $\Gamma(\omega K^*(892)^+) / \Gamma_{\text{total}}$   $\Gamma_{362} / \Gamma$ 

VALUE (units $10^{-6}$ )	CL%	DOCUMENT ID	TECN	COMMENT
$<7.4$	90	1 AUBERT	09H BABR	$e^+ e^- \rightarrow \Upsilon(4S)$

• • • We do not use the following data for averages, fits, limits, etc. • • •

VALUE (units $10^{-6}$ )	CL%	DOCUMENT ID	TECN	COMMENT
$<3.4$	90	1 AUBERT,B	06T BABR	Repl. by AUBERT 09H
$<7.4$	90	1 AUBERT	05o BABR	Repl. by AUBERT,B 06T
$<87$	90	1 BERGFELD	98 CLE2	

<sup>1</sup> Assumes equal production of  $B^+$  and  $B^0$  at the  $\Upsilon(4S)$ .

 $\Gamma(\omega(K\pi)_0^{*+}) / \Gamma_{\text{total}}$   $\Gamma_{363} / \Gamma$ 

( $K\pi$ )<sub>0</sub><sup>\*+</sup> is the total S-wave composed of  $K_0^*(1430)$  and nonresonant that are described using LASS shape.

VALUE (units $10^{-6}$ )	CL%	DOCUMENT ID	TECN	COMMENT
$27.5 \pm 3.0 \pm 2.6$		1 AUBERT	09H BABR	$e^+ e^- \rightarrow \Upsilon(4S)$

<sup>1</sup> Assumes equal production of  $B^+$  and  $B^0$  at the  $\Upsilon(4S)$ .

 $\Gamma(\omega K_0^*(1430)^+) / \Gamma_{\text{total}}$   $\Gamma_{364} / \Gamma$ 

VALUE (units $10^{-6}$ )	CL%	DOCUMENT ID	TECN	COMMENT
$24.0 \pm 2.6 \pm 4.4$		1 AUBERT	09H BABR	$e^+ e^- \rightarrow \Upsilon(4S)$

<sup>1</sup> Assumes equal production of  $B^+$  and  $B^0$  at the  $\Upsilon(4S)$ .

 $\Gamma(\omega K_2^*(1430)^+) / \Gamma_{\text{total}}$   $\Gamma_{365} / \Gamma$ 

VALUE (units $10^{-6}$ )	CL%	DOCUMENT ID	TECN	COMMENT
$21.5 \pm 3.6 \pm 2.4$		1 AUBERT	09H BABR	$e^+ e^- \rightarrow \Upsilon(4S)$

<sup>1</sup> Assumes equal production of  $B^+$  and  $B^0$  at the  $\Upsilon(4S)$ .

 $\Gamma(a_0(980)^0 K^+ \times B(a_0(980)^0 \rightarrow \eta \pi^0)) / \Gamma_{\text{total}}$   $\Gamma_{367} / \Gamma$ 

VALUE (units $10^{-6}$ )	CL%	DOCUMENT ID	TECN	COMMENT
$<2.5$	90	1 AUBERT,BE	04 BABR	$e^+ e^- \rightarrow \Upsilon(4S)$

<sup>1</sup> Assumes equal production of charged and neutral  $B$  mesons from  $\Upsilon(4S)$  decays.

 $\Gamma(a_0(980)^+ K^0 \times B(a_0(980)^+ \rightarrow \eta \pi^+)) / \Gamma_{\text{total}}$   $\Gamma_{366} / \Gamma$ 

VALUE (units $10^{-6}$ )	CL%	DOCUMENT ID	TECN	COMMENT
$<3.9$	90	1 AUBERT,BE	04 BABR	$e^+ e^- \rightarrow \Upsilon(4S)$

<sup>1</sup> Assumes equal production of charged and neutral  $B$  mesons from  $\Upsilon(4S)$  decays.

 $\Gamma(K^*(892)^0 \pi^+) / \Gamma_{\text{total}}$   $\Gamma_{368} / \Gamma$ 

VALUE (units $10^{-6}$ )	CL%	DOCUMENT ID	TECN	COMMENT
$10.1 \pm 0.8$ OUR AVERAGE				
$10.1 \pm 1.7 \pm 1.0$		1 LEES	17G BABR	$e^+ e^- \rightarrow \Upsilon(4S)$
$10.8 \pm 0.6^{+1.2}_{-1.4}$		2 AUBERT	08A1 BABR	$e^+ e^- \rightarrow \Upsilon(4S)$
$9.67 \pm 0.64^{+0.81}_{-0.89}$		2 GARMASH	06 BELL	$e^+ e^- \rightarrow \Upsilon(4S)$

• • • We do not use the following data for averages, fits, limits, etc. • • •

VALUE (units $10^{-6}$ )	CL%	DOCUMENT ID	TECN	COMMENT
$13.5 \pm 1.2^{+0.8}_{-0.9}$		2 AUBERT,B	05N BABR	Repl. by AUBERT 08A1
$9.8 \pm 0.9^{+1.1}_{-1.2}$		2 GARMASH	05 BELL	Repl. by GARMASH 06
$15.5 \pm 1.8^{+1.5}_{-4.0}$		2,3 AUBERT,B	04P BABR	Repl. by AUBERT,B 05N
$19.4^{+4.2}_{-3.9}^{+4.1}_{-7.1}$		4 GARMASH	02 BELL	Repl. by GARMASH 05
$<119$	90	5 ABE	00C SLD	$e^+ e^- \rightarrow Z$
$<16$	90	2 JESSOP	00 CLE2	$e^+ e^- \rightarrow \Upsilon(4S)$
$<390$	90	6 ADAM	96D DLPH	$e^+ e^- \rightarrow Z$
$<41$	90	ASNER	96 CLE2	Repl. by JESSOP 00
$<480$	90	6 ABREU	95N DLPH	Sup. by ADAM 96D
$<170$	90	ALBRECHT	91B ARG	$e^+ e^- \rightarrow \Upsilon(4S)$
$<150$	90	7 AVERY	89B CLEO	$e^+ e^- \rightarrow \Upsilon(4S)$
$<260$	90	AVERY	87 CLEO	$e^+ e^- \rightarrow \Upsilon(4S)$

<sup>1</sup> Obtains the result from a Dalitz analysis of  $B^+ \rightarrow K_S^0 \pi^+ \pi^0$  decays. The first error is statistical, the second combines all the systematic uncertainties reported in the paper, including signal modelling.<sup>2</sup> Assumes equal production of  $B^+$  and  $B^0$  at the  $\Upsilon(4S)$ .<sup>3</sup> AUBERT 04P also report a branching ratio for  $B^+ \rightarrow$  "higher  $K^*$  resonances"  $\pi^+$ ,  $K^* \rightarrow K^+ \pi^-$ ,  $(25.1 \pm 2.0^{+11.0}_{-5.7}) \times 10^{-6}$ .<sup>4</sup> Uses a reference decay mode  $B^+ \rightarrow \bar{D}^0 \pi^+$  and  $\bar{D}^0 \rightarrow K^+ \pi^-$  with  $B(B^+ \rightarrow \bar{D}^0 \pi^+) \cdot B(\bar{D}^0 \rightarrow K^+ \pi^-) = (20.3 \pm 2.0) \times 10^{-5}$ .<sup>5</sup> ABE 00c assumes  $B(Z \rightarrow b\bar{b}) = (21.7 \pm 0.1)\%$  and the  $B$  fractions  $f_{B^0} = f_{B^+} = (39.7^{+1.8}_{-2.2})\%$  and  $f_{B_S} = (10.5^{+1.8}_{-2.2})\%$ .<sup>6</sup> Assumes a  $B^0, B^-$  production fraction of 0.39 and a  $B_S$  production fraction of 0.12.<sup>7</sup> AVERY 89B reports  $< 1.3 \times 10^{-4}$  assuming the  $\Upsilon(4S)$  decays 43% to  $B^0 \bar{B}^0$ . We rescale to 50%. $\Gamma(K^*(892)^+ \pi^0) / \Gamma_{\text{total}}$   $\Gamma_{369} / \Gamma$ 

VALUE (units $10^{-6}$ )	CL%	DOCUMENT ID	TECN	COMMENT
$6.8 \pm 0.9$ OUR AVERAGE				
$6.4 \pm 0.9^{+0.4}_{-0.5}$		1 LEES	17G BABR	$e^+ e^- \rightarrow \Upsilon(4S)$
$8.2 \pm 1.5 \pm 1.1$		2 LEES	11i BABR	$e^+ e^- \rightarrow \Upsilon(4S)$

• • • We do not use the following data for averages, fits, limits, etc. • • •

VALUE (units $10^{-6}$ )	CL%	DOCUMENT ID	TECN	COMMENT
$6.9 \pm 2.0 \pm 1.3$		2 AUBERT	05x BABR	Repl. by LEES 11i
$<31$	90	2 JESSOP	00 CLE2	$e^+ e^- \rightarrow \Upsilon(4S)$
$<99$	90	ASNER	96 CLE2	Repl. by JESSOP 00

<sup>1</sup> Obtains the result from a Dalitz analysis of  $B^+ \rightarrow K_S^0 \pi^+ \pi^0$  decays. The first error is statistical, the second combines all the systematic uncertainties reported in the paper, including signal modelling.<sup>2</sup> Assumes equal production of  $B^+$  and  $B^0$  at the  $\Upsilon(4S)$ .

$\Gamma(K^+ \pi^- \pi^+)/\Gamma_{total}$		$\Gamma_{370}/\Gamma$		
VALUE (units $10^{-6}$ )		DOCUMENT ID	TECN	COMMENT
<b>51.0 ± 2.9 OUR AVERAGE</b>				
54.4 ± 1.1 ± 4.6	1	AUBERT	08AI	BABR $e^+e^- \rightarrow \Upsilon(4S)$
48.8 ± 1.1 ± 3.6	1	GARMASH	06	BELL $e^+e^- \rightarrow \Upsilon(4S)$
• • • We do not use the following data for averages, fits, limits, etc. • • •				
64.1 ± 2.4 ± 4.0	1	AUBERT,B	05N	BABR Repl. by AUBERT 08AI
46.6 ± 2.1 ± 4.3	1	GARMASH	05	BELL Repl. by GARMASH 06
53.6 ± 3.1 ± 5.1	1	GARMASH	04	BELL Repl. by GARMASH 05
59.1 ± 3.8 ± 3.2	2	AUBERT	03M	BABR Repl. by AUBERT,B 05N
55.6 ± 5.8 ± 7.7	3	GARMASH	02	BELL Repl. by GARMASH 04

- <sup>1</sup> Assumes equal production of  $B^+$  and  $B^0$  at the  $\Upsilon(4S)$ .
- <sup>2</sup> Assumes equal production of  $B^0$  and  $B^+$  at the  $\Upsilon(4S)$ ; charm and charmonium contributions are subtracted, otherwise no assumptions about intermediate resonances.
- <sup>3</sup> Uses a reference decay mode  $B^+ \rightarrow \bar{D}^0 \pi^+$  and  $\bar{D}^0 \rightarrow K^+ \pi^-$  with  $B(B^+ \rightarrow \bar{D}^0 \pi^+) \cdot B(\bar{D}^0 \rightarrow K^+ \pi^-) = (20.3 \pm 2.0) \times 10^{-5}$ .

$\Gamma(K^+ \pi^- \pi^+ \text{ nonresonant})/\Gamma_{total}$		$\Gamma_{371}/\Gamma$			
VALUE (units $10^{-6}$ )	CL%	DOCUMENT ID	TECN	COMMENT	
<b>16.3<sup>+2.1</sup>-1.5 OUR AVERAGE</b>					
9.3 ± 1.0 <sup>+6.9</sup> -1.7		1,2	AUBERT	08AI	BABR $e^+e^- \rightarrow \Upsilon(4S)$
16.9 ± 1.3 ± 1.7	1.6	1	GARMASH	06	BELL $e^+e^- \rightarrow \Upsilon(4S)$
• • • We do not use the following data for averages, fits, limits, etc. • • •					
2.9 ± 0.6 ± 0.5		1	AUBERT,B	05N	BABR Repl. by AUBERT 08AI
17.3 ± 1.7 ± 17.2	8.0	1	GARMASH	05	BELL Repl. by GARMASH 06
< 17	90	1	AUBERT,B	04P	BABR Repl. by AUBERT,B 05N
< 330	90	3	ADAM	96D	DLPH $e^+e^- \rightarrow Z$
< 28	90		BERGFELD	96B	CLE2 $e^+e^- \rightarrow \Upsilon(4S)$
< 400	90	3	ABREU	95N	DLPH Sup. by ADAM 96D
< 330	90		ALBRECHT	91E	ARG $e^+e^- \rightarrow \Upsilon(4S)$
< 190	90	4	AVERY	89B	CLEO $e^+e^- \rightarrow \Upsilon(4S)$

- <sup>1</sup> Assumes equal production of  $B^+$  and  $B^0$  at the  $\Upsilon(4S)$ .
- <sup>2</sup> Calculate the total nonresonant contribution by combining the S-wave composed of  $K_0^*(1430)$  and nonresonant that are described using LASS shape.
- <sup>3</sup> Assumes a  $B^0, B^-$  production fraction of 0.39 and a  $B_s$  production fraction of 0.12.
- <sup>4</sup> AVERY 89B reports  $< 1.7 \times 10^{-4}$  assuming the  $\Upsilon(4S)$  decays 43% to  $B^0 \bar{B}^0$ . We rescale to 50%.

$\Gamma(\omega(782) K^+)/\Gamma_{total}$		$\Gamma_{372}/\Gamma$		
VALUE (units $10^{-6}$ )		DOCUMENT ID	TECN	COMMENT
<b>5.9<sup>+8.8</sup>-9.0 ± 0.2</b>				
	1,2	AUBERT	08AI	BABR $e^+e^- \rightarrow \Upsilon(4S)$
• • • We do not use the following data for averages, fits, limits, etc. • • •				
	1	AUBERT,B	05N	BABR Repl. by AUBERT 08AI
	1	GARMASH	05	BELL Repl. by GARMASH 06
	1	AUBERT,B	04P	BABR Repl. by AUBERT,B 05N
	3	ADAM	96D	DLPH $e^+e^- \rightarrow Z$
	90	BERGFELD	96B	CLE2 $e^+e^- \rightarrow \Upsilon(4S)$
	90	ABREU	95N	DLPH Sup. by ADAM 96D
	90	ALBRECHT	91E	ARG $e^+e^- \rightarrow \Upsilon(4S)$
	90	AVERY	89B	CLEO $e^+e^- \rightarrow \Upsilon(4S)$

- <sup>1</sup> Assumes equal production of  $B^+$  and  $B^0$  at the  $\Upsilon(4S)$ .
- <sup>2</sup> AUBERT 08AI reports  $[\Gamma(B^+ \rightarrow \omega(782) K^+)/\Gamma_{total}] \times [B(\omega(782) \rightarrow \pi^+ \pi^-)] = (0.09 \pm 0.13 \pm 0.036) \times 10^{-6}$  which we divide by our best value  $B(\omega(782) \rightarrow \pi^+ \pi^-) = (1.53 \pm 0.06) \times 10^{-2}$ . Our first error is their experiment's error and our second error is the systematic error from using our best value.

$\Gamma(K^+ \bar{f}_0(980) \times B(\bar{f}_0(980) \rightarrow \pi^+ \pi^-))/\Gamma_{total}$		$\Gamma_{373}/\Gamma$			
VALUE (units $10^{-6}$ )	CL%	DOCUMENT ID	TECN	COMMENT	
<b>9.4<sup>+1.0</sup>-1.2 OUR AVERAGE</b>					
10.3 ± 0.5 ± 2.0	1.4	1	AUBERT	08AI	BABR $e^+e^- \rightarrow \Upsilon(4S)$
8.78 ± 0.82 ± 0.85	1.76	1	GARMASH	06	BELL $e^+e^- \rightarrow \Upsilon(4S)$
• • • We do not use the following data for averages, fits, limits, etc. • • •					
9.47 ± 0.97 ± 0.62	0.88	1	AUBERT,B	05N	BABR Repl. by AUBERT 08AI
7.55 ± 1.24 ± 1.63	1.18	1	GARMASH	05	BELL Repl. by GARMASH 06
9.2 ± 1.2 ± 2.1	2.6	2	AUBERT,B	04P	BABR Repl. by AUBERT,B 05N
9.6 ± 2.5 ± 3.7	2.3	3	GARMASH	02	BELL Repl. by GARMASH 05
< 80	90	4	AVERY	89B	CLEO $e^+e^- \rightarrow \Upsilon(4S)$

- <sup>1</sup> Assumes equal production of  $B^+$  and  $B^0$  at the  $\Upsilon(4S)$ .
- <sup>2</sup> AUBERT,B 04P also reports  $B(B^+ \rightarrow \text{"higher } f_0 \text{ resonances"} \pi^+, f(980)^0 \rightarrow \pi^+ \pi^-) = (3.2 \pm 1.2 \pm 6.0) \times 10^{-6}$ .
- <sup>3</sup> Uses a reference decay mode  $B^+ \rightarrow \bar{D}^0 \pi^+$  and  $\bar{D}^0 \rightarrow K^+ \pi^-$  with  $B(B^+ \rightarrow \bar{D}^0 \pi^+) \cdot B(\bar{D}^0 \rightarrow K^+ \pi^-) = (20.3 \pm 2.0) \times 10^{-5}$ . Only charged pions from the  $f_0(980)$  are used.
- <sup>4</sup> AVERY 89B reports  $< 7 \times 10^{-5}$  assuming the  $\Upsilon(4S)$  decays 43% to  $B^0 \bar{B}^0$ . We rescale to 50%.

$\Gamma(f_2(1270)^0 K^+)/\Gamma_{total}$		$\Gamma_{374}/\Gamma$			
VALUE (units $10^{-6}$ )	CL%	DOCUMENT ID	TECN	COMMENT	
<b>1.07 ± 0.27 OUR AVERAGE</b>					
0.89 <sup>+0.38+0.01</sup> <sub>-0.33-0.03</sub>		1,2	AUBERT	08AI	BABR $e^+e^- \rightarrow \Upsilon(4S)$
1.33 ± 0.30 ± 0.23	0.34	1	GARMASH	06	BELL $e^+e^- \rightarrow \Upsilon(4S)$
• • • We do not use the following data for averages, fits, limits, etc. • • •					
< 16	90	3	AUBERT,B	05N	BABR Repl. by AUBERT 08AI
< 2.3	90	4	GARMASH	05	BELL Repl. by GARMASH 06

- <sup>1</sup> Assumes equal production of  $B^+$  and  $B^0$  at the  $\Upsilon(4S)$ .
- <sup>2</sup> AUBERT 08AI reports  $(0.50 \pm 0.15 \pm 0.15) \times 10^{-6}$  for  $B(B^+ \rightarrow f_2(1270) K^+) \times B(f_2 \rightarrow \pi^+ \pi^-)$ . We compute  $B(B^+ \rightarrow f_2(1270) K^+)$  using the PDG value  $B(f_2(1270) \rightarrow \pi\pi) = (84.2 \pm 2.9) \times 10^{-2}$  and 2/3 for the  $\pi^+ \pi^-$  fraction. Our first error is their experiment's error and the second error is systematic error from using our best value.
- <sup>3</sup> AUBERT,B 05N reports  $8.9 \times 10^{-6}$  at 90% CL for  $B(B^+ \rightarrow f_2(1270) K^+) \times B(f_2(1270) \rightarrow \pi^+ \pi^-)$ . We rescaled it using the PDG value  $B(f_2(1270) \rightarrow \pi\pi) = 84.7\%$  and 2/3 for the  $\pi^+ \pi^-$  fraction.
- <sup>4</sup> GARMASH 05 reports  $1.3 \times 10^{-6}$  at 90% CL for  $B(B^+ \rightarrow f_2(1270) K^+) \times B(f_2(1270) \rightarrow \pi^+ \pi^-)$ . We rescaled it using the PDG value  $B(f_2(1270) \rightarrow \pi\pi) = 84.7\%$  and 2/3 for the  $\pi^+ \pi^-$  fraction.

$\Gamma(\bar{f}_0(1370)^0 K^+ \times B(\bar{f}_0(1370)^0 \rightarrow \pi^+ \pi^-))/\Gamma_{total}$		$\Gamma_{375}/\Gamma$			
VALUE	CL%	DOCUMENT ID	TECN	COMMENT	
<b>&lt; 10.7 × 10<sup>-6</sup></b>					
	90	1	AUBERT,B	05N	BABR $e^+e^- \rightarrow \Upsilon(4S)$
• • • We do not use the following data for averages, fits, limits, etc. • • •					
<sup>1</sup> Assumes equal production of $B^+$ and $B^0$ at the $\Upsilon(4S)$ .					

$\Gamma(\rho^0(1450) K^+ \times B(\rho^0(1450) \rightarrow \pi^+ \pi^-))/\Gamma_{total}$		$\Gamma_{376}/\Gamma$			
VALUE	CL%	DOCUMENT ID	TECN	COMMENT	
<b>&lt; 11.7 × 10<sup>-6</sup></b>					
	90	1	AUBERT,B	05N	BABR $e^+e^- \rightarrow \Upsilon(4S)$
• • • We do not use the following data for averages, fits, limits, etc. • • •					
<sup>1</sup> Assumes equal production of $B^+$ and $B^0$ at the $\Upsilon(4S)$ .					

$\Gamma(f_2'(1525) K^+ \times B(f_2'(1525) \rightarrow \pi^+ \pi^-))/\Gamma_{total}$		$\Gamma_{377}/\Gamma$			
VALUE	CL%	DOCUMENT ID	TECN	COMMENT	
<b>&lt; 3.4 × 10<sup>-6</sup></b>					
	90	1	AUBERT,B	05N	BABR $e^+e^- \rightarrow \Upsilon(4S)$
• • • We do not use the following data for averages, fits, limits, etc. • • •					
<sup>1</sup> Assumes equal production of $B^+$ and $B^0$ at the $\Upsilon(4S)$ .					

$\Gamma(K^+ \rho^0)/\Gamma_{total}$		$\Gamma_{378}/\Gamma$			
VALUE (units $10^{-6}$ )	CL%	DOCUMENT ID	TECN	COMMENT	
<b>3.7 ± 0.5 OUR AVERAGE</b>					
3.56 ± 0.45 ± 0.57	0.46	1	AUBERT	08AI	BABR $e^+e^- \rightarrow \Upsilon(4S)$
3.89 ± 0.47 ± 0.43	0.41	1	GARMASH	06	BELL $e^+e^- \rightarrow \Upsilon(4S)$
• • • We do not use the following data for averages, fits, limits, etc. • • •					
5.07 ± 0.75 ± 0.55	0.88	1	AUBERT,B	05N	BABR Repl. by AUBERT 08AI
4.78 ± 0.75 ± 1.01	0.97	1	GARMASH	05	BELL Repl. by GARMASH 06
< 6.2	90	2	AUBERT,B	04P	BABR Repl. by AUBERT,B 05N
< 12	90	3	GARMASH	02	BELL $e^+e^- \rightarrow \Upsilon(4S)$
< 86	90	4	ABE	00C	SLD $e^+e^- \rightarrow Z$
< 17	90	1	JESSOP	00	CLE2 $e^+e^- \rightarrow \Upsilon(4S)$
< 120	90	5	ADAM	96D	DLPH $e^+e^- \rightarrow Z$
< 19	90		ASNER	96	CLE2 Repl. by JESSOP 00
< 190	90	5	ABREU	95N	DLPH Sup. by ADAM 96D
< 180	90		ALBRECHT	91B	ARG $e^+e^- \rightarrow \Upsilon(4S)$
< 80	90	6	AVERY	89B	CLEO $e^+e^- \rightarrow \Upsilon(4S)$
< 260	90		AVERY	87	CLEO $e^+e^- \rightarrow \Upsilon(4S)$

- <sup>1</sup> Assumes equal production of  $B^+$  and  $B^0$  at the  $\Upsilon(4S)$ .
- <sup>2</sup> AUBERT 04P reports a central value of  $(3.9 \pm 1.2 \pm 1.3) \times 10^{-6}$  for this branching ratio.
- <sup>3</sup> Uses a reference decay mode  $B^+ \rightarrow \bar{D}^0 \pi^+$  and  $\bar{D}^0 \rightarrow K^+ \pi^-$  with  $B(B^+ \rightarrow \bar{D}^0 \pi^+) \cdot B(\bar{D}^0 \rightarrow K^+ \pi^-) = (20.3 \pm 2.0) \times 10^{-5}$ .
- <sup>4</sup> ABE 00C assumes  $B(Z \rightarrow b\bar{b}) = (21.7 \pm 0.1)\%$  and the  $B$  fractions  $f_{B^0} = f_{B^+} = (39.7 \pm 2.2)\%$  and  $f_{B_s} = (10.5 \pm 2.2)\%$ .
- <sup>5</sup> Assumes production fractions  $f_{B^0} = f_{B^-} = 0.39$  and  $f_{B_s} = 0.12$ .
- <sup>6</sup> AVERY 89B reports  $< 7 \times 10^{-5}$  assuming the  $\Upsilon(4S)$  decays 43% to  $B^0 \bar{B}^0$ . We rescale to 50%.

$\Gamma(K_0^*(1430)^0 \pi^+)/\Gamma_{total}$		$\Gamma_{379}/\Gamma$			
VALUE (units $10^{-6}$ )		DOCUMENT ID	TECN	COMMENT	
<b>39<sup>+6</sup>-5 OUR AVERAGE</b> Error includes scale factor of 1.4. See the ideogram below.					
34.6 ± 3.3 ± 4.6		1	LEES	17G	BABR $e^+e^- \rightarrow \Upsilon(4S)$
32.0 ± 1.2 ± 10.8	6.0	2	AUBERT	08AI	BABR $e^+e^- \rightarrow \Upsilon(4S)$
51.6 ± 1.7 ± 7.0	7.5	2	GARMASH	06	BELL $e^+e^- \rightarrow \Upsilon(4S)$

Downloaded from https://academic.oup.com/ptep/article/2020/8/083C01/5891211 by guest on 12 November 2020



## Meson Particle Listings

 $B^\pm$ 

• • • We do not use the following data for averages, fits, limits, etc. • • •

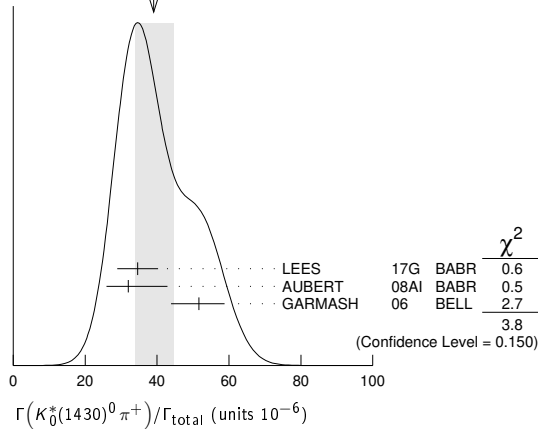
$44.4 \pm 2.2 \pm 5.3$	<sup>2,3</sup> AUBERT,B	05N	BABR	Repl. by AUBERT 08A1
$45.0 \pm 2.9 \pm 15.0$ $-10.7$	<sup>2</sup> GARMASH	05	BELL	Repl. by GARMASH 06

<sup>1</sup> Obtains the result from a Dalitz analysis of  $B^+ \rightarrow K_S^0 \pi^+ \pi^0$  decays. The first error is statistical, the second combines all the systematic uncertainties reported in the paper, including signal modelling.

<sup>2</sup> Assumes equal production of  $B^+$  and  $B^0$  at the  $\Upsilon(4S)$ .

<sup>3</sup> See erratum: AUBERT,BE 06a.

WEIGHTED AVERAGE  
39+6-5 (Error scaled by 1.4)



### $\Gamma(K_S^*(1430)^0 \pi^+) / \Gamma_{\text{total}}$ Γ381/Γ

VALUE (units $10^{-6}$ )	CL%	DOCUMENT ID	TECN	COMMENT
$5.6 \pm 2.2 \pm 0.1$		<sup>1,2</sup> AUBERT	08A1	BABR $e^+ e^- \rightarrow \Upsilon(4S)$

• • • We do not use the following data for averages, fits, limits, etc. • • •

$< 23$	90	<sup>3</sup> AUBERT,B	05N	BABR Repl. by AUBERT 08A1
$< 6.9$	90	<sup>4</sup> GARMASH	05	BELL $e^+ e^- \rightarrow \Upsilon(4S)$
$< 680$	90	ALBRECHT	91B	ARG $e^+ e^- \rightarrow \Upsilon(4S)$

<sup>1</sup> Assumes equal production of  $B^+$  and  $B^0$  at the  $\Upsilon(4S)$ .

<sup>2</sup> AUBERT 08A1 reports  $(1.85 \pm 0.41 \pm 0.61) \times 10^{-6}$  for  $B(B^+ \rightarrow K_S^*(1430)^0 \pi^+) \times B(K_S^*(1430)^0 \rightarrow K^+ \pi^-)$ . We compute  $B(B^+ \rightarrow K_S^*(1430)^0 \pi^+)$  using the PDG value  $B(K_S^*(1430)^0 \rightarrow K\pi) = (49.9 \pm 1.2) \times 10^{-2}$  and 2/3 for the  $K^+ \pi^-$  fraction. Our first error is their experiment's error and the second error is systematic error from using our best value.

<sup>3</sup> AUBERT,B 05N reports  $7.7 \times 10^{-6}$  at 90% CL for  $B(B^+ \rightarrow K_S^*(1430)^0 \pi^+) \times B(K_S^*(1430)^0 \rightarrow K^+ \pi^-)$ . We rescaled it using the PDG value  $B(K_S^*(1430)^0 \rightarrow K\pi) = 49.9\%$  and 2/3 for the  $K^+ \pi^-$  fraction.

<sup>4</sup> GARMASH 05 reports  $2.3 \times 10^{-6}$  at 90% CL for  $B(B^+ \rightarrow K_S^*(1430)^0 \pi^+) \times B(K_S^*(1430)^0 \rightarrow K^+ \pi^-)$ . We rescaled it using the PDG value  $B(K_S^*(1430)^0 \rightarrow K\pi) = 49.9\%$  and 2/3 for the  $K^+ \pi^-$  mode.

### $\Gamma(K_S^*(1430)^+ \pi^+) / \Gamma_{\text{total}}$ Γ380/Γ

VALUE (units $10^{-6}$ )	CL%	DOCUMENT ID	TECN	COMMENT
$11.9 \pm 1.7 \pm 1.0$ $-1.6$		<sup>1</sup> LEES	17G	BABR $e^+ e^- \rightarrow \Upsilon(4S)$

<sup>1</sup> Obtains the result from a Dalitz analysis of  $B^+ \rightarrow K_S^0 \pi^+ \pi^0$  decays. The first error is statistical, the second combines all the systematic uncertainties reported in the paper, including signal modelling.

### $\Gamma(K^*(1410)^0 \pi^+) / \Gamma_{\text{total}}$ Γ382/Γ

VALUE (units $10^{-6}$ )	CL%	DOCUMENT ID	TECN	COMMENT
$< 45$	90	<sup>1</sup> GARMASH	05	BELL $e^+ e^- \rightarrow \Upsilon(4S)$

<sup>1</sup> GARMASH 05 reports  $2.0 \times 10^{-6}$  at 90% CL for  $B(B^+ \rightarrow K^*(1410)^0 \pi^+) \times B(K^*(1410)^0 \rightarrow K^+ \pi^-)$ . We rescaled it using the PDG value  $B(K^*(1410)^0 \rightarrow K\pi) = 6.6\%$  and 2/3 for the  $K^+ \pi^-$  mode.

### $\Gamma(K^*(1680)^0 \pi^+) / \Gamma_{\text{total}}$ Γ383/Γ

VALUE (units $10^{-6}$ )	CL%	DOCUMENT ID	TECN	COMMENT
$< 12$	90	<sup>1</sup> GARMASH	05	BELL $e^+ e^- \rightarrow \Upsilon(4S)$

• • • We do not use the following data for averages, fits, limits, etc. • • •

$< 15$	90	<sup>2</sup> AUBERT,B	05N	BABR $e^+ e^- \rightarrow \Upsilon(4S)$
--------	----	-----------------------	-----	---

<sup>1</sup> GARMASH 05 reports  $3.1 \times 10^{-6}$  at 90% CL for  $B(B^+ \rightarrow K^*(1680)^0 \pi^+) \times B(K^*(1680)^0 \rightarrow K^+ \pi^-)$ . We rescaled it using the PDG value  $B(K^*(1680)^0 \rightarrow K\pi) = 38.7\%$  and 2/3 for the  $K^+ \pi^-$  mode.

<sup>2</sup> AUBERT,B 05N reports  $3.8 \times 10^{-6}$  at 90% CL for  $B(B^+ \rightarrow K^*(1680)^0 \pi^+) \times B(K^*(1680)^0 \rightarrow K^+ \pi^-)$ . We rescaled it using the PDG value  $B(K^*(1680)^0 \rightarrow K\pi) = 38.7\%$  and 2/3 for the  $K^+ \pi^-$  fraction.

### $\Gamma(K^+ \pi^0 \pi^0) / \Gamma_{\text{total}}$ Γ384/Γ

VALUE (units $10^{-6}$ )	CL%	DOCUMENT ID	TECN	COMMENT
$16.2 \pm 1.2 \pm 1.5$		<sup>1</sup> LEES	11I	BABR $e^+ e^- \rightarrow \Upsilon(4S)$

<sup>1</sup> Assumes equal production of  $B^+$  and  $B^0$  at the  $\Upsilon(4S)$ .

### $\Gamma(\eta(980) K^+ \times B(\eta_0 \rightarrow \pi^0 \pi^0)) / \Gamma_{\text{total}}$ Γ385/Γ

VALUE (units $10^{-6}$ )	CL%	DOCUMENT ID	TECN	COMMENT
$2.8 \pm 0.6 \pm 0.5$		<sup>1</sup> LEES	11I	BABR $e^+ e^- \rightarrow \Upsilon(4S)$

<sup>1</sup> Assumes equal production of  $B^+$  and  $B^0$  at the  $\Upsilon(4S)$ .

### $\Gamma(K^- \pi^+ \pi^+) / \Gamma_{\text{total}}$ Γ386/Γ

VALUE	CL%	DOCUMENT ID	TECN	COMMENT
$< 4.6 \times 10^{-8}$	90	AAIJ	17E	LHCB $pp$ at 7, 8 TeV

• • • We do not use the following data for averages, fits, limits, etc. • • •

$< 9.5 \times 10^{-7}$	90	<sup>1</sup> AUBERT	08BE	BABR $e^+ e^- \rightarrow \Upsilon(4S)$
$< 4.5 \times 10^{-6}$	90	<sup>1</sup> GARMASH	04	BELL $e^+ e^- \rightarrow \Upsilon(4S)$
$< 1.8 \times 10^{-6}$	90	<sup>2</sup> AUBERT	03M	BABR Repl. by AUBERT 08BE
$< 7.0 \times 10^{-6}$	90	<sup>3</sup> GARMASH	02	BELL $e^+ e^- \rightarrow \Upsilon(4S)$

<sup>1</sup> Assumes equal production of  $B^+$  and  $B^0$  at the  $\Upsilon(4S)$ .

<sup>2</sup> Assumes equal production of  $B^0$  and  $B^+$  at the  $\Upsilon(4S)$ ; charm and charmonium contributions are subtracted, otherwise no assumptions about intermediate resonances.

<sup>3</sup> Uses a reference decay mode  $B^+ \rightarrow \bar{D}^0 \pi^+$  and  $\bar{D}^0 \rightarrow K^+ \pi^-$  with  $B(B^+ \rightarrow \bar{D}^0 \pi^+) \cdot B(\bar{D}^0 \rightarrow K^+ \pi^-) = (20.3 \pm 2.0) \times 10^{-5}$ .

### $\Gamma(K^- \pi^+ \pi^+ \text{nonresonant}) / \Gamma_{\text{total}}$ Γ387/Γ

VALUE (units $10^{-6}$ )	CL%	DOCUMENT ID	TECN	COMMENT
$< 56$	90	BERGFELD	96B	CLE2 $e^+ e^- \rightarrow \Upsilon(4S)$

### $\Gamma(K_1(1270)^0 \pi^+) / \Gamma_{\text{total}}$ Γ388/Γ

VALUE	CL%	DOCUMENT ID	TECN	COMMENT
$< 4.0 \times 10^{-5}$	90	<sup>1</sup> AUBERT	10D	BABR $e^+ e^- \rightarrow \Upsilon(4S)$

<sup>1</sup> Assumes equal production of  $B^+$  and  $B^0$  at the  $\Upsilon(4S)$ .

### $\Gamma(K_1(1400)^0 \pi^+) / \Gamma_{\text{total}}$ Γ389/Γ

VALUE	CL%	DOCUMENT ID	TECN	COMMENT
$< 3.9 \times 10^{-5}$	90	<sup>1</sup> AUBERT	10D	BABR $e^+ e^- \rightarrow \Upsilon(4S)$

• • • We do not use the following data for averages, fits, limits, etc. • • •

$< 2.6 \times 10^{-3}$	90	ALBRECHT	91B	ARG $e^+ e^- \rightarrow \Upsilon(4S)$
------------------------	----	----------	-----	--

<sup>1</sup> Assumes equal production of  $B^+$  and  $B^0$  at the  $\Upsilon(4S)$ .

### $\Gamma(K^0 \pi^+ \pi^0) / \Gamma_{\text{total}}$ Γ390/Γ

VALUE (units $10^{-6}$ )	CL%	DOCUMENT ID	TECN	COMMENT
$31.8 \pm 1.8 \pm 5.3$ $-2.1$		<sup>1</sup> LEES	17G	BABR $e^+ e^- \rightarrow \Upsilon(4S)$
$< 66$	90	<sup>2</sup> ECKHART	02	CLE2 $e^+ e^- \rightarrow \Upsilon(4S)$

<sup>1</sup> Obtains the result from a Dalitz analysis of  $B^+ \rightarrow K_S^0 \pi^+ \pi^0$  decays. The first error is statistical, the second combines all the systematic uncertainties reported in the paper, including signal modelling.

<sup>2</sup> Assumes equal production of  $B^+$  and  $B^0$  at the  $\Upsilon(4S)$ .

### $\Gamma(K^0 \rho^+) / \Gamma_{\text{total}}$ Γ391/Γ

VALUE (units $10^{-6}$ )	CL%	DOCUMENT ID	TECN	COMMENT
$7.3 \pm 1.0$ $-1.2$ OUR AVERAGE				

$6.5 \pm 1.1 \pm 0.8$ $-1.9$		<sup>1</sup> LEES	17G	BABR $e^+ e^- \rightarrow \Upsilon(4S)$
---------------------------------	--	-------------------	-----	---

$8.0 \pm 1.4 \pm 0.6$ $-1.3$		AUBERT	07Z	BABR $e^+ e^- \rightarrow \Upsilon(4S)$
---------------------------------	--	--------	-----	---

• • • We do not use the following data for averages, fits, limits, etc. • • •

$< 48$	90	ASNER	96	CLE2 $e^+ e^- \rightarrow \Upsilon(4S)$
--------	----	-------	----	---

<sup>1</sup> Obtains the result from a Dalitz analysis of  $B^+ \rightarrow K_S^0 \pi^+ \pi^0$  decays. The first error is statistical, the second combines all the systematic uncertainties reported in the paper, including signal modelling.

### $\Gamma(K^*(892)^+ \pi^+ \pi^-) / \Gamma_{\text{total}}$ Γ392/Γ

VALUE (units $10^{-6}$ )	CL%	DOCUMENT ID	TECN	COMMENT
$75.3 \pm 6.0 \pm 8.1$		<sup>1</sup> AUBERT,B	06U	BABR $e^+ e^- \rightarrow \Upsilon(4S)$

• • • We do not use the following data for averages, fits, limits, etc. • • •

$< 1100$	90	ALBRECHT	91E	ARG $e^+ e^- \rightarrow \Upsilon(4S)$
----------	----	----------	-----	--

<sup>1</sup> Assumes equal production of  $B^+$  and  $B^0$  at the  $\Upsilon(4S)$ .

### $\Gamma(K^*(892)^+ \rho^0) / \Gamma_{\text{total}}$ Γ393/Γ

VALUE (units $10^{-6}$ )	CL%	DOCUMENT ID	TECN	COMMENT
$4.6 \pm 1.0 \pm 0.4$		<sup>1</sup> DEL-AMO-SA...11D	BABR	$e^+ e^- \rightarrow \Upsilon(4S)$

• • • We do not use the following data for averages, fits, limits, etc. • • •

$< 6.1$	90	<sup>1</sup> AUBERT,B	06G	BABR Repl. by DEL-AMO-SANCHEZ 11D
---------	----	-----------------------	-----	-----------------------------------

$10.6 \pm 3.0 \pm 2.4$ $-2.6$		<sup>1</sup> AUBERT	03V	BABR Repl. by AUBERT,B 06G
----------------------------------	--	---------------------	-----	----------------------------

<sup>1</sup> Assumes equal production of  $B^+$  and  $B^0$  at the  $\Upsilon(4S)$ .

<sup>2</sup> Assumes a helicity 00 configuration. For a helicity 11 configuration, the limit decreases to  $4.9 \times 10^{-5}$ .



## Meson Particle Listings

 $B^\pm$  $\Gamma(K^+ \bar{K}_0^*(1430)^0)/\Gamma_{\text{total}}$   $\Gamma_{413}/\Gamma$ 

VALUE (units $10^{-6}$ )	CL%	DOCUMENT ID	TECN	COMMENT
<b>0.38 ± 0.12 ± 0.05</b>		<sup>1</sup> AAIJ	19AL LHCb	$pp$ at 7, 8 TeV

• • • We do not use the following data for averages, fits, limits, etc. • • •

<2.2	90	<sup>2</sup> AUBERT	07AR BABR	$e^+e^- \rightarrow \Upsilon(4S)$
------	----	---------------------	-----------	-----------------------------------

<sup>1</sup> AAIJ 19AL reports  $(4.5 \pm 0.7 \pm 1.2) \times 10^{-2}$  for fit fraction for  $B^+ \rightarrow K^+ \bar{K}_0^*(1430)^0$  from the amplitude analysis of  $B^\pm \rightarrow \pi^\pm K^+ K^-$  decays. We use the PDG 19 value  $B(B^+ \rightarrow K^+ K^- \pi^+) = (5.2 \pm 0.4) \times 10^{-6}$  to obtain  $B(B^+ \rightarrow K^+ \bar{K}_0^*(1430)^0, \bar{K}_0^*(1430)^0 \rightarrow K^+ \pi^-)$ . We compute  $B(B^+ \rightarrow K^+ \bar{K}_0^*(1430)^0)$  using 2/3 of PDG 19 value  $B(K_0^*(1430)^0 \rightarrow K\pi) = (93 \pm 10)\%$  for the  $K^+ \pi^-$  fraction. Our first error is the experiment's error and the second error is systematic error from using our best value. <sup>2</sup> Assumes equal production of  $B^+$  and  $B^0$  at the  $\Upsilon(4S)$ .

 $\Gamma(\rho(1450)^0 \pi^+, \rho^0 \rightarrow K^+ K^-)/\Gamma_{\text{total}}$   $\Gamma_{469}/\Gamma$ 

VALUE (units $10^{-6}$ )	CL%	DOCUMENT ID	TECN	COMMENT
<b>1.60 ± 0.08 ± 0.12</b>		<sup>1</sup> AAIJ	19AL LHCb	$pp$ at 7, 8 TeV

<sup>1</sup> AAIJ 19AL reports  $0.307 \pm 0.012 \pm 0.009$  fit fraction for  $B^+ \rightarrow \rho(1450)^0 \pi^+$  from the amplitude analysis of  $B^\pm \rightarrow \pi^\pm K^+ K^-$  decays. We use the PDG 19 value  $B(B^+ \rightarrow K^+ K^- \pi^+) = (5.2 \pm 0.4) \times 10^{-6}$  to obtain  $B(B^+ \rightarrow \rho(1450)^0 \pi^+, \rho(1450)^0 \rightarrow K^+ K^-)$ . Our first error is the experiment's error and the second error is systematic error from using our best value.

 $\Gamma(\pi^+(K^+ K^-)_{S\text{-wave}})/\Gamma_{\text{total}}$   $\Gamma_{414}/\Gamma$ 

VALUE (units $10^{-7}$ )	CL%	DOCUMENT ID	TECN	COMMENT
<b>8.53 ± 0.67 ± 0.66</b>		<sup>1</sup> AAIJ	19AL LHCb	$pp$ at 7, 8 TeV

<sup>1</sup> AAIJ 19AL reports  $0.164 \pm 0.008 \pm 0.011$  fit fraction for  $B^+ \rightarrow \pi^+(K^+ K^-)_{S\text{-wave}}$  in the region of  $0.95 < m(K^+ K^-) < 1.42$  GeV/ $c^2$  from the amplitude analysis of  $B^\pm \rightarrow \pi^\pm K^+ K^-$  decays. We use the PDG 19 value  $B(B^+ \rightarrow K^+ K^- \pi^+) = (5.2 \pm 0.4) \times 10^{-6}$  to obtain  $B(B^+ \rightarrow \pi^+(K^+ K^-)_{S\text{-wave}})$ . Our first error is the experiment's error and the second error is systematic error from using our best value.

 $\Gamma(K^+ K^+ \pi^-)/\Gamma_{\text{total}}$   $\Gamma_{415}/\Gamma$ 

VALUE	CL%	DOCUMENT ID	TECN	COMMENT
<b>&lt;1.1 × 10<sup>-8</sup></b>	90	AAIJ	17E LHCb	$pp$ at 7, 8 TeV

• • • We do not use the following data for averages, fits, limits, etc. • • •

<1.6 × 10 <sup>-7</sup>	90	<sup>1</sup> AUBERT	08BE BABR	$e^+e^- \rightarrow \Upsilon(4S)$
<2.4 × 10 <sup>-6</sup>	90	<sup>1</sup> GARMASH	04 BELL	$e^+e^- \rightarrow \Upsilon(4S)$
<1.3 × 10 <sup>-6</sup>	90	<sup>2</sup> AUBERT	03M BABR	Repl. by AUBERT 08BE
<3.2 × 10 <sup>-6</sup>	90	<sup>3</sup> GARMASH	02 BELL	$e^+e^- \rightarrow \Upsilon(4S)$

<sup>1</sup> Assumes equal production of  $B^+$  and  $B^0$  at the  $\Upsilon(4S)$ .  
<sup>2</sup> Assumes equal production of  $B^0$  and  $B^+$  at the  $\Upsilon(4S)$ ; charm and charmonium contributions are subtracted, otherwise no assumptions about intermediate resonances.  
<sup>3</sup> Uses a reference decay mode  $B^+ \rightarrow \bar{D}^0 \pi^+$  and  $\bar{D}^0 \rightarrow K^+ \pi^-$  with  $B(B^+ \rightarrow \bar{D}^0 \pi^+) \cdot B(\bar{D}^0 \rightarrow K^+ \pi^-) = (20.3 \pm 2.0) \times 10^{-5}$ .

 $\Gamma(K^+ K^+ \pi^- \text{nonresonant})/\Gamma_{\text{total}}$   $\Gamma_{416}/\Gamma$ 

VALUE (units $10^{-6}$ )	CL%	DOCUMENT ID	TECN	COMMENT
<b>&lt;87.9</b>	90	ABBIENDI	00B OPAL	$e^+e^- \rightarrow Z$

 $\Gamma(f_2'(1525) K^+)/\Gamma_{\text{total}}$   $\Gamma_{417}/\Gamma$ 

VALUE (units $10^{-6}$ )	CL%	DOCUMENT ID	TECN	COMMENT
<b>1.8 ± 0.5 OUR AVERAGE</b>		Error includes scale factor of 1.1.		

1.56 ± 0.36 ± 0.30		<sup>1,2</sup> LEES	12o BABR	$e^+e^- \rightarrow \Upsilon(4S)$
2.8 ± 0.9 <sup>+0.5</sup> / <sub>-0.4</sub>		<sup>1,3</sup> LEES	12o BABR	$e^+e^- \rightarrow \Upsilon(4S)$

• • • We do not use the following data for averages, fits, limits, etc. • • •

<8	90	<sup>1,4</sup> GARMASH	05 BELL	$e^+e^- \rightarrow \Upsilon(4S)$
----	----	------------------------	---------	-----------------------------------

<sup>1</sup> Assumes equal production of  $B^+$  and  $B^0$  at the  $\Upsilon(4S)$ .  
<sup>2</sup> Measured in the  $B^+ \rightarrow K^+ K^- K^+$  decay.  
<sup>3</sup> Measured in the  $B^+ \rightarrow K^+ K_S^0 K_S^0$  decay.  
<sup>4</sup> GARMASH 05 reports  $B(B^+ \rightarrow f_2'(1525) K^+) \cdot B(f_2'(1525) \rightarrow K^+ K^-) < 4.9 \times 10^{-6}$  at 90% CL. We divide this result by our best value of  $B(f_2'(1525) \rightarrow K\bar{K}) = 87.6 \times 10^{-2}$  multiplied by 2/3 to account for the  $K^+ K^-$  fraction.

 $\Gamma(K^+ f_J(2220))/\Gamma_{\text{total}}$   $\Gamma_{418}/\Gamma$ 

VALUE (units $10^{-6}$ )	CL%	DOCUMENT ID	TECN	COMMENT
not seen		<sup>1</sup> HUANG	03 BELL	$e^+e^- \rightarrow \Upsilon(4S)$

<sup>1</sup> No evidence is found for such decay and set a limit on  $B(B^+ \rightarrow f_J(2220)) \times B(f_J(2220) \rightarrow \phi\phi) < 1.2 \times 10^{-6}$  at 90%CL where the  $f_J(2220)$  is a possible glueball state.

 $\Gamma(K^* \pi^+ K^-)/\Gamma_{\text{total}}$   $\Gamma_{419}/\Gamma$ 

VALUE (units $10^{-6}$ )	CL%	DOCUMENT ID	TECN	COMMENT
<b>&lt;11.8</b>	90	<sup>1</sup> AUBERT,B	06u BABR	$e^+e^- \rightarrow \Upsilon(4S)$

<sup>1</sup> Assumes equal production of  $B^+$  and  $B^0$  at the  $\Upsilon(4S)$ .

 $\Gamma(K^*(892) + K^*(892)^0)/\Gamma_{\text{total}}$   $\Gamma_{420}/\Gamma$ 

VALUE (units $10^{-6}$ )	CL%	DOCUMENT ID	TECN	COMMENT
<b>0.91 ± 0.29 OUR AVERAGE</b>				

0.77 <sup>+0.35</sup> / <sub>-0.30</sub> ± 0.12		<sup>1</sup> GOH	15 BELL	$e^+e^- \rightarrow \Upsilon(4S)$
1.2 ± 0.5 ± 0.1		<sup>2</sup> AUBERT	09F BABR	$e^+e^- \rightarrow \Upsilon(4S)$

• • • We do not use the following data for averages, fits, limits, etc. • • •

<71	90	<sup>3</sup> GODANG	02 CLE2	$e^+e^- \rightarrow \Upsilon(4S)$
-----	----	---------------------	---------	-----------------------------------

<sup>1</sup> Signal significance is 2.7 standard deviations. This measurement corresponds to an upper limit of  $< 1.31 \times 10^{-6}$  at 90% CL.  
<sup>2</sup> Signal significance is 3.7 standard deviations.  
<sup>3</sup> Assumes a helicity 00 configuration. For a helicity 11 configuration, the limit decreases to  $4.8 \times 10^{-5}$ .

 $\Gamma(K^* K^+ \pi^-)/\Gamma_{\text{total}}$   $\Gamma_{421}/\Gamma$ 

VALUE (units $10^{-6}$ )	CL%	DOCUMENT ID	TECN	COMMENT
<b>&lt;6.1</b>	90	<sup>1</sup> AUBERT,B	06u BABR	$e^+e^- \rightarrow \Upsilon(4S)$

<sup>1</sup> Assumes equal production of  $B^+$  and  $B^0$  at the  $\Upsilon(4S)$ .

 $\Gamma(K^+ K^- K^+)/\Gamma_{\text{total}}$   $\Gamma_{422}/\Gamma$ 

VALUE (units $10^{-6}$ )	CL%	DOCUMENT ID	TECN	COMMENT
<b>34.0 ± 1.4 OUR AVERAGE</b>		Error includes scale factor of 1.4.		

34.6 ± 0.6 ± 0.9		<sup>1,2</sup> LEES	12o BABR	$e^+e^- \rightarrow \Upsilon(4S)$
30.6 ± 1.2 ± 2.3		<sup>1</sup> GARMASH	05 BELL	$e^+e^- \rightarrow \Upsilon(4S)$

• • • We do not use the following data for averages, fits, limits, etc. • • •

35.2 ± 0.9 ± 1.6		<sup>1</sup> AUBERT	06o BABR	Repl. by LEES 12o
32.8 ± 1.8 ± 2.8		<sup>1</sup> GARMASH	04 BELL	Repl. by GARMASH 05
29.6 ± 2.1 ± 1.6		<sup>3</sup> AUBERT	03M BABR	Repl. by AUBERT 06o
35.3 ± 3.7 ± 4.5		<sup>4</sup> GARMASH	02 BELL	Repl. by GARMASH 04
<200	90	<sup>5</sup> ADAM	96D DLPH	$e^+e^- \rightarrow Z$
<320	90	<sup>5</sup> ABREU	95N DLPH	Sup. by ADAM 96D
<350	90	ALBRECHT	91E ARG	$e^+e^- \rightarrow \Upsilon(4S)$

<sup>1</sup> Assumes equal production of  $B^+$  and  $B^0$  at the  $\Upsilon(4S)$ .  
<sup>2</sup> All intermediate charmonium and charm resonances are removed, except of  $\chi_{c0}$ .  
<sup>3</sup> Assumes equal production of  $B^0$  and  $B^+$  at the  $\Upsilon(4S)$ ; charm and charmonium contributions are subtracted, otherwise no assumptions about intermediate resonances.  
<sup>4</sup> Uses a reference decay mode  $B^+ \rightarrow \bar{D}^0 \pi^+$  and  $\bar{D}^0 \rightarrow K^+ \pi^-$  with  $B(B^+ \rightarrow \bar{D}^0 \pi^+) \cdot B(\bar{D}^0 \rightarrow K^+ \pi^-) = (20.3 \pm 2.0) \times 10^{-5}$ .  
<sup>5</sup> Assumes  $B^0$  and  $B^-$  production fractions of 0.39, and  $B_S$  production fraction of 0.12.

 $\Gamma(K^+ \phi)/\Gamma_{\text{total}}$   $\Gamma_{423}/\Gamma$ 

VALUE (units $10^{-6}$ )	CL%	DOCUMENT ID	TECN	COMMENT
<b>8.8 <sup>+0.7</sup>/<sub>-0.6</sub> OUR AVERAGE</b>		Error includes scale factor of 1.1.		

9.2 ± 0.4 <sup>+0.7</sup> / <sub>-0.5</sub>		<sup>1</sup> LEES	12o BABR	$e^+e^- \rightarrow \Upsilon(4S)$
7.6 ± 1.3 ± 0.6		<sup>2</sup> ACOSTA	05J CDF	$p\bar{p}$ at 1.96 TeV
9.60 ± 0.92 <sup>+1.05</sup> / <sub>-0.85</sub>		<sup>1</sup> GARMASH	05 BELL	$e^+e^- \rightarrow \Upsilon(4S)$

5.5 <sup>+2.1</sup> / <sub>-1.8</sub> ± 0.6		<sup>1</sup> BRIERE	01 CLE2	$e^+e^- \rightarrow \Upsilon(4S)$
---	--	---------------------	---------	-----------------------------------

• • • We do not use the following data for averages, fits, limits, etc. • • •

8.4 ± 0.7 ± 0.7		<sup>1</sup> AUBERT	06o BABR	Repl. by LEES 12o
10.0 <sup>+0.9</sup> / <sub>-0.8</sub> ± 0.5		<sup>1</sup> AUBERT	04A BABR	Repl. by AUBERT 06o
9.4 ± 1.1 ± 0.7		<sup>1</sup> CHEN	03B BELL	Repl. by GARMASH 05
14.6 <sup>+3.0</sup> / <sub>-2.8</sub> ± 2.0		<sup>3</sup> GARMASH	02 BELL	Repl. by CHEN 03B

7.7 <sup>+1.6</sup> / <sub>-1.4</sub> ± 0.8		<sup>1</sup> AUBERT	01D BABR	$e^+e^- \rightarrow \Upsilon(4S)$
---	--	---------------------	----------	-----------------------------------

<144	90	<sup>4</sup> ABE	00C SLD	$e^+e^- \rightarrow Z$
<5	90	<sup>1</sup> BERGFELD	98 CLE2	
<280	90	<sup>5</sup> ADAM	96D DLPH	$e^+e^- \rightarrow Z$
<12	90	ASNEN	96 CLE2	$e^+e^- \rightarrow \Upsilon(4S)$
<440	90	<sup>6</sup> ABREU	95N DLPH	Sup. by ADAM 96D
<180	90	ALBRECHT	91B ARG	$e^+e^- \rightarrow \Upsilon(4S)$
<90	90	<sup>7</sup> AVERY	89B CLEO	$e^+e^- \rightarrow \Upsilon(4S)$
<210	90	AVERY	87 CLEO	$e^+e^- \rightarrow \Upsilon(4S)$

<sup>1</sup> Assumes equal production of  $B^+$  and  $B^0$  at the  $\Upsilon(4S)$ .  
<sup>2</sup> Uses  $B(B^+ \rightarrow J/\psi K^+) = (1.00 \pm 0.04) \times 10^{-3}$  and  $B(J/\psi \rightarrow \mu^+ \mu^-) = 0.0588 \pm 0.0010$ .  
<sup>3</sup> Uses a reference decay mode  $B^+ \rightarrow \bar{D}^0 \pi^+$  and  $\bar{D}^0 \rightarrow K^+ \pi^-$  with  $B(B^+ \rightarrow \bar{D}^0 \pi^+) \cdot B(\bar{D}^0 \rightarrow K^+ \pi^-) = (20.3 \pm 2.0) \times 10^{-5}$ .  
<sup>4</sup> ABE 00C assumes  $B(Z \rightarrow b\bar{b}) = (21.7 \pm 0.1)\%$  and the  $B$  fractions  $f_{B^0} = f_{B^+} = (39.7 \pm 1.8)\%$  and  $f_{B_S} = (10.5 \pm 1.8)\%$ .  
<sup>5</sup> ADAM 96D assumes  $f_{B^0} = f_{B^-} = 0.39$  and  $f_{B_S} = 0.12$ .  
<sup>6</sup> Assumes a  $B^0, B^-$  production fraction of 0.39 and a  $B_S$  production fraction of 0.12.  
<sup>7</sup> AVERY 89B reports  $< 8 \times 10^{-5}$  assuming the  $\Upsilon(4S)$  decays 43% to  $B^0 \bar{B}^0$ . We rescale to 50%.

See key on page 999

Meson Particle Listings

$B^\pm$

$\Gamma(\phi_0(980) K^+ \times B(\phi_0(980) \rightarrow K^+ K^-))/\Gamma_{total}$   $\Gamma_{424}/\Gamma$

VALUE (units $10^{-6}$ )	CL%	DOCUMENT ID	TECN	COMMENT
<b>9.4 ± 1.6 ± 2.8</b>		<sup>1</sup> LEES	120	BABR $e^+e^- \rightarrow \Upsilon(4S)$
• • • We do not use the following data for averages, fits, limits, etc. • • •				
6.5 ± 2.5 ± 1.6		<sup>1</sup> AUBERT	060	BABR $e^+e^- \rightarrow \Upsilon(4S)$
<2.9	90	<sup>1</sup> GARMASH	05	BELL $e^+e^- \rightarrow \Upsilon(4S)$
<sup>1</sup> Assumes equal production of $B^+$ and $B^0$ at the $\Upsilon(4S)$ .				

$\Gamma(a_2(1320) K^+ \times B(a_2(1320) \rightarrow K^+ K^-))/\Gamma_{total}$   $\Gamma_{425}/\Gamma$

VALUE	CL%	DOCUMENT ID	TECN	COMMENT
<b>&lt;1.1 × 10<sup>-6</sup></b>	90	<sup>1</sup> GARMASH	05	BELL $e^+e^- \rightarrow \Upsilon(4S)$
<sup>1</sup> Assumes equal production of $B^+$ and $B^0$ at the $\Upsilon(4S)$ .				

$\Gamma(X_0(1550) K^+ \times B(X_0(1550) \rightarrow K^+ K^-))/\Gamma_{total}$   $\Gamma_{426}/\Gamma$

$X_0(1550)$  is a possible spin zero state near 1.55 GeV/c<sup>2</sup> invariant mass of  $K^+ K^-$ .

VALUE (units $10^{-6}$ )	DOCUMENT ID	TECN	COMMENT
<b>4.3 ± 0.6 ± 0.3</b>	<sup>1</sup> AUBERT	060	BABR $e^+e^- \rightarrow \Upsilon(4S)$
<sup>1</sup> Assumes equal production of $B^+$ and $B^0$ at the $\Upsilon(4S)$ .			

$\Gamma(\phi(1680) K^+ \times B(\phi(1680) \rightarrow K^+ K^-))/\Gamma_{total}$   $\Gamma_{427}/\Gamma$

VALUE	CL%	DOCUMENT ID	TECN	COMMENT
<b>&lt;0.8 × 10<sup>-6</sup></b>	90	<sup>1</sup> GARMASH	05	BELL $e^+e^- \rightarrow \Upsilon(4S)$
<sup>1</sup> Assumes equal production of $B^+$ and $B^0$ at the $\Upsilon(4S)$ .				

$\Gamma(\phi_0(1710) K^+ \times B(\phi_0(1710) \rightarrow K^+ K^-))/\Gamma_{total}$   $\Gamma_{428}/\Gamma$

VALUE (units $10^{-6}$ )	DOCUMENT ID	TECN	COMMENT
<b>1.12 ± 0.25 ± 0.50</b>	<sup>1</sup> LEES	120	BABR $e^+e^- \rightarrow \Upsilon(4S)$
• • • We do not use the following data for averages, fits, limits, etc. • • •			
1.7 ± 1.0 ± 0.3	<sup>1</sup> AUBERT	060	BABR Repl. by LEES 120
<sup>1</sup> Assumes equal production of $B^+$ and $B^0$ at the $\Upsilon(4S)$ .			

$\Gamma(K^+ K^- K^+ \text{ nonresonant})/\Gamma_{total}$   $\Gamma_{429}/\Gamma$

VALUE (units $10^{-6}$ )	CL%	DOCUMENT ID	TECN	COMMENT
<b>23.8 ± 2.8 OUR AVERAGE</b>				
22.8 ± 2.7 ± 7.6		<sup>1</sup> LEES	120	BABR $e^+e^- \rightarrow \Upsilon(4S)$
24.0 ± 1.5 ± 2.6		<sup>1</sup> GARMASH	05	BELL $e^+e^- \rightarrow \Upsilon(4S)$
• • • We do not use the following data for averages, fits, limits, etc. • • •				
50.0 ± 6.0 ± 4.0		<sup>1</sup> AUBERT	060	BABR Repl. by LEES 120
<38	90	BERGFELD	96B	CLE2 $e^+e^- \rightarrow \Upsilon(4S)$
<sup>1</sup> Assumes equal production of $B^+$ and $B^0$ at the $\Upsilon(4S)$ .				

$\Gamma(K^*(892) K^+ K^-)/\Gamma_{total}$   $\Gamma_{430}/\Gamma$

VALUE (units $10^{-6}$ )	CL%	DOCUMENT ID	TECN	COMMENT
<b>36.2 ± 3.3 ± 3.6</b>				
• • • We do not use the following data for averages, fits, limits, etc. • • •				
<1600	90	ALBRECHT	91E	ARG $e^+e^- \rightarrow \Upsilon(4S)$
<sup>1</sup> Assumes equal production of $B^+$ and $B^0$ at the $\Upsilon(4S)$ .				

$\Gamma(K^*(892) \phi)/\Gamma_{total}$   $\Gamma_{431}/\Gamma$

VALUE (units $10^{-6}$ )	CL%	DOCUMENT ID	TECN	COMMENT
<b>10.0 ± 2.0 OUR AVERAGE</b> Error includes scale factor of 1.7.				
11.2 ± 1.0 ± 0.9		<sup>1</sup> AUBERT	07BA	BABR $e^+e^- \rightarrow \Upsilon(4S)$
6.7 ± 2.1 ± 0.7		<sup>1</sup> CHEN	03B	BELL $e^+e^- \rightarrow \Upsilon(4S)$
• • • We do not use the following data for averages, fits, limits, etc. • • •				
12.7 ± 2.2		<sup>1</sup> AUBERT	03V	BABR Repl. by AUBERT 07BA
-2.0 ± 1.1				
9.7 ± 4.2		<sup>1</sup> AUBERT	01D	BABR Repl. by AUBERT 03V
-3.4 ± 1.7				
< 22.5	90	<sup>1</sup> BRIERE	01	CLE2 $e^+e^- \rightarrow \Upsilon(4S)$
< 41	90	<sup>1</sup> BERGFELD	98	CLE2
< 70	90	ASNER	96	CLE2 $e^+e^- \rightarrow \Upsilon(4S)$
<1300	90	ALBRECHT	91B	ARG $e^+e^- \rightarrow \Upsilon(4S)$
<sup>1</sup> Assumes equal production of $B^+$ and $B^0$ at the $\Upsilon(4S)$ .				

$\Gamma(\phi(K\pi)_0^{*+})/\Gamma_{total}$   $\Gamma_{432}/\Gamma$

$(K\pi)_0^{*+}$  is the total S-wave composed of  $K_0^*(1430)$  and nonresonant that are described using LA SS shape.

VALUE (units $10^{-6}$ )	DOCUMENT ID	TECN	COMMENT
<b>8.3 ± 1.4 ± 0.8</b>	<sup>1</sup> AUBERT	08B1	BABR $e^+e^- \rightarrow \Upsilon(4S)$
<sup>1</sup> Assumes equal production of $B^+$ and $B^0$ at the $\Upsilon(4S)$ .			

$\Gamma(\phi K_1(1270)^+)/\Gamma_{total}$   $\Gamma_{433}/\Gamma$

VALUE (units $10^{-6}$ )	DOCUMENT ID	TECN	COMMENT
<b>6.1 ± 1.6 ± 1.1</b>	<sup>1</sup> AUBERT	08B1	BABR $e^+e^- \rightarrow \Upsilon(4S)$
<sup>1</sup> Assumes equal production of $B^+$ and $B^0$ at the $\Upsilon(4S)$ .			

$\Gamma(\phi K_1(1400)^+)/\Gamma_{total}$   $\Gamma_{434}/\Gamma$

VALUE (units $10^{-6}$ )	CL%	DOCUMENT ID	TECN	COMMENT
<b>&lt; 3.2</b>	90	<sup>1</sup> AUBERT	08B1	BABR $e^+e^- \rightarrow \Upsilon(4S)$
• • • We do not use the following data for averages, fits, limits, etc. • • •				
<1100	90	ALBRECHT	91B	ARG $e^+e^- \rightarrow \Upsilon(4S)$
<sup>1</sup> Assumes equal production of $B^+$ and $B^0$ at the $\Upsilon(4S)$ .				

$\Gamma(\phi K^*(1410)^+)/\Gamma_{total}$   $\Gamma_{435}/\Gamma$

VALUE (units $10^{-6}$ )	CL%	DOCUMENT ID	TECN	COMMENT
<b>&lt;4.3</b>	90	<sup>1</sup> AUBERT	08B1	BABR $e^+e^- \rightarrow \Upsilon(4S)$
<sup>1</sup> Assumes equal production of $B^+$ and $B^0$ at the $\Upsilon(4S)$ .				

$\Gamma(\phi K_0^*(1430)^+)/\Gamma_{total}$   $\Gamma_{436}/\Gamma$

VALUE (units $10^{-6}$ )	DOCUMENT ID	TECN	COMMENT
<b>7.0 ± 1.3 ± 0.9</b>	<sup>1</sup> AUBERT	08B1	BABR $e^+e^- \rightarrow \Upsilon(4S)$
<sup>1</sup> Assumes equal production of $B^+$ and $B^0$ at the $\Upsilon(4S)$ .			

$\Gamma(\phi K_2^*(1430)^+)/\Gamma_{total}$   $\Gamma_{437}/\Gamma$

VALUE (units $10^{-6}$ )	CL%	DOCUMENT ID	TECN	COMMENT
<b>8.4 ± 1.8 ± 1.0</b>		<sup>1</sup> AUBERT	08B1	BABR $e^+e^- \rightarrow \Upsilon(4S)$
• • • We do not use the following data for averages, fits, limits, etc. • • •				
<3400	90	ALBRECHT	91B	ARG $e^+e^- \rightarrow \Upsilon(4S)$
<sup>1</sup> Assumes equal production of $B^+$ and $B^0$ at the $\Upsilon(4S)$ .				

$\Gamma(\phi K_2^*(1770)^+)/\Gamma_{total}$   $\Gamma_{438}/\Gamma$

VALUE (units $10^{-6}$ )	CL%	DOCUMENT ID	TECN	COMMENT
<b>&lt;15.0</b>	90	<sup>1</sup> AUBERT	08B1	BABR $e^+e^- \rightarrow \Upsilon(4S)$
<sup>1</sup> Assumes equal production of $B^+$ and $B^0$ at the $\Upsilon(4S)$ .				

$\Gamma(\phi K_2^*(1820)^+)/\Gamma_{total}$   $\Gamma_{439}/\Gamma$

VALUE (units $10^{-6}$ )	CL%	DOCUMENT ID	TECN	COMMENT
<b>&lt;16.3</b>	90	<sup>1</sup> AUBERT	08B1	BABR $e^+e^- \rightarrow \Upsilon(4S)$
<sup>1</sup> Assumes equal production of $B^+$ and $B^0$ at the $\Upsilon(4S)$ .				

$\Gamma(a_1^{*+} K^0)/\Gamma_{total}$   $\Gamma_{440}/\Gamma$

VALUE (units $10^{-6}$ )	CL%	DOCUMENT ID	TECN	COMMENT
<b>&lt;3.6</b>	90	<sup>1,2</sup> DEL-AMO-SA...	10I	BABR $e^+e^- \rightarrow \Upsilon(4S)$
<sup>1</sup> Assumes $B(a_1^\pm \rightarrow \pi^\pm \pi^+ \pi^-) = 0.5$				
<sup>2</sup> Assumes equal production of $B^+$ and $B^0$ at the $\Upsilon(4S)$ .				

$\Gamma(K^+ \phi)/\Gamma_{total}$   $\Gamma_{441}/\Gamma$

VALUE (units $10^{-6}$ )	DOCUMENT ID	TECN	COMMENT
<b>5.0 ± 1.2 OUR AVERAGE</b> Error includes scale factor of 2.3.			
5.6 ± 0.5 ± 0.3	<sup>1</sup> LEES	11A	BABR $e^+e^- \rightarrow \Upsilon(4S)$
2.6 ± 1.1	<sup>1</sup> HUANG	03	BELL $e^+e^- \rightarrow \Upsilon(4S)$
-0.9 ± 0.3			
• • • We do not use the following data for averages, fits, limits, etc. • • •			
7.5 ± 1.0 ± 0.7	<sup>1</sup> AUBERT, BE	06H	BABR Repl. by LEES 11A
<sup>1</sup> Assumes equal production of $B^0$ and $B^+$ at the $\Upsilon(4S)$ and for a $\phi$ invariant mass below 2.85 GeV/c <sup>2</sup> .			

$\Gamma(\eta'/\eta K^+)/\Gamma_{total}$   $\Gamma_{442}/\Gamma$

VALUE (units $10^{-6}$ )	CL%	DOCUMENT ID	TECN	COMMENT
<b>&lt;25</b>	90	<sup>1</sup> AUBERT, B	06P	BABR $e^+e^- \rightarrow \Upsilon(4S)$
<sup>1</sup> Assumes equal production of $B^+$ and $B^0$ at the $\Upsilon(4S)$ .				

$\Gamma(\omega \phi K^+)/\Gamma_{total}$   $\Gamma_{443}/\Gamma$

VALUE (units $10^{-6}$ )	CL%	DOCUMENT ID	TECN	COMMENT
<b>&lt;1.9</b>	90	<sup>1</sup> LIU	09	BELL $e^+e^- \rightarrow \Upsilon(4S)$
<sup>1</sup> Assumes equal production of $B^+$ and $B^0$ at the $\Upsilon(4S)$ .				

$\Gamma(X(1812) K^+ \times B(X \rightarrow \omega \phi))/\Gamma_{total}$   $\Gamma_{444}/\Gamma$

VALUE (units $10^{-6}$ )	CL%	DOCUMENT ID	TECN	COMMENT
<b>&lt;0.32</b>	90	<sup>1</sup> LIU	09	BELL $e^+e^- \rightarrow \Upsilon(4S)$
<sup>1</sup> Assumes equal production of $B^+$ and $B^0$ at the $\Upsilon(4S)$ .				

$\Gamma(K^*(892) \gamma)/\Gamma_{total}$   $\Gamma_{445}/\Gamma$

VALUE (units $10^{-5}$ )	CL%	DOCUMENT ID	TECN	COMMENT
<b>3.92 ± 0.22 OUR AVERAGE</b> Error includes scale factor of 1.7.				
3.76 ± 0.10 ± 0.12		<sup>1</sup> HORIGUCHI	17	BELL $e^+e^- \rightarrow \Upsilon(4S)$
4.22 ± 0.14 ± 0.16		<sup>2</sup> AUBERT	09a0	BABR $e^+e^- \rightarrow \Upsilon(4S)$
3.76 ± 0.89		<sup>3</sup> COAN	00	CLE2 $e^+e^- \rightarrow \Upsilon(4S)$
-0.83 ± 0.28				

# Meson Particle Listings

## $B^\pm$

- • • We do not use the following data for averages, fits, limits, etc. • • •

3.87 ± 0.28 ± 0.26	4	AUBERT,BE	04A	BABR	Repl. by AUBERT 09A0
4.25 ± 0.31 ± 0.24	3	NAKAO	04	BELL	Repl. by HORIGUCHI 17
3.83 ± 0.62 ± 0.22	3	AUBERT	02c	BABR	Repl. by AUBERT,BE 04A
5.7 ± 3.1 ± 1.1	5	AMMAR	93	CLE2	Repl. by COAN 00
< 55	90	6	ALBRECHT	89G	ARG $e^+e^- \rightarrow \Upsilon(4S)$
< 55	90	6	AVERY	89B	CLEO $e^+e^- \rightarrow \Upsilon(4S)$
< 180	90	6	AVERY	87	CLEO $e^+e^- \rightarrow \Upsilon(4S)$

  - 1 Uses  $B(\Upsilon(4S) \rightarrow B^+B^-) = (51.4 \pm 0.6)\%$  and  $B(\Upsilon(4S) \rightarrow B^0\bar{B}^0) = (48.6 \pm 0.6)\%$ .
  - 2 Uses  $B(\Upsilon(4S) \rightarrow B^+B^-) = (51.6 \pm 0.6)\%$  and  $B(\Upsilon(4S) \rightarrow B^0\bar{B}^0) = (48.4 \pm 0.6)\%$ .
  - 3 Assumes equal production of  $B^+$  and  $B^0$  at the  $\Upsilon(4S)$ .
  - 4 Uses the production ratio of charged and neutral B from  $\Upsilon(4S)$  decays  $R^{+0} = 1.006 \pm 0.048$ .
  - 5 AMMAR 93 observed  $4.1 \pm 2.3$  events above background.
  - 6 Assumes the  $\Upsilon(4S)$  decays 43% to  $B^0\bar{B}^0$ .

$\Gamma(K_1(1270)^+\gamma)/\Gamma_{total}$   $\Gamma_{446}/\Gamma$

VALUE (units $10^{-5}$ )	CL%	DOCUMENT ID	TECN	COMMENT
<b>4.4 <math>\pm_{-0.6}^{+0.7}</math> OUR AVERAGE</b>				
4.41 $\pm_{-0.44}^{+0.63} \pm 0.58$	1,2	DEL-AMO-SA...16	BABR	$e^+e^- \rightarrow \Upsilon(4S)$
4.3 $\pm 0.9 \pm 0.9$	3	YANG	05	BELL $e^+e^- \rightarrow \Upsilon(4S)$

- • • We do not use the following data for averages, fits, limits, etc. • • •

< 9.9	90	3	NISHIDA	02	BELL	Repl. by YANG 05
< 730	90	4	ALBRECHT	89G	ARG	$e^+e^- \rightarrow \Upsilon(4S)$

  - 1 Requires  $M_{K\pi\pi} < 1.8 \text{ GeV}/c^2$ .
  - 2 Uses  $B(\Upsilon(4S) \rightarrow B^+B^-) = 0.513 \pm 0.006$ .
  - 3 Assumes equal production of  $B^+$  and  $B^0$  at the  $\Upsilon(4S)$ .
  - 4 ALBRECHT 89G reports  $< 0.0066$  assuming the  $\Upsilon(4S)$  decays 45% to  $B^0\bar{B}^0$ . We rescale to 50%.

$\Gamma(\eta K^+\gamma)/\Gamma_{total}$   $\Gamma_{447}/\Gamma$

VALUE (units $10^{-6}$ )	DOCUMENT ID	TECN	COMMENT
<b>7.9 ± 0.9 OUR AVERAGE</b>			
7.7 ± 1.0 ± 0.4	1,2	AUBERT	09 BABR $e^+e^- \rightarrow \Upsilon(4S)$
8.4 ± 1.5 $\pm_{-0.9}^{+1.2}$	2,3	NISHIDA	05 BELL $e^+e^- \rightarrow \Upsilon(4S)$

- • • We do not use the following data for averages, fits, limits, etc. • • •

10.0 ± 1.3 ± 0.5	1,2	AUBERT,B	06M BABR	Repl. by AUBERT 09
------------------	-----	----------	----------	--------------------

  - 1  $m_{\eta K} < 3.25 \text{ GeV}/c^2$ .
  - 2 Assumes equal production of  $B^+$  and  $B^0$  at the  $\Upsilon(4S)$ .
  - 3  $m_{\eta K} < 2.4 \text{ GeV}/c^2$ .

$\Gamma(\eta' K^+\gamma)/\Gamma_{total}$   $\Gamma_{448}/\Gamma$

VALUE (units $10^{-6}$ )	DOCUMENT ID	TECN	COMMENT
<b>2.9 <math>\pm_{-0.9}^{+1.0}</math> OUR AVERAGE</b>			
3.6 ± 1.2 ± 0.4	1,2	WEDD	10 BELL $e^+e^- \rightarrow \Upsilon(4S)$
1.9 $\pm_{-1.2}^{+1.5} \pm 0.1$	1,3	AUBERT,B	06M BABR $e^+e^- \rightarrow \Upsilon(4S)$

- 1 Assumes equal production of  $B^+$  and  $B^0$  at the  $\Upsilon(4S)$ .
- 2  $m_{\eta' K} < 3.4 \text{ GeV}/c^2$ .
- 3 Set the upper limit of  $4.2 \times 10^{-6}$  at 90% CL with  $m_{\eta' K} < 3.25 \text{ GeV}/c^2$ .

$\Gamma(\phi K^+\gamma)/\Gamma_{total}$   $\Gamma_{449}/\Gamma$

VALUE (units $10^{-6}$ )	DOCUMENT ID	TECN	COMMENT
<b>2.7 ± 0.4 OUR AVERAGE</b>			Error includes scale factor of 1.2.
2.48 ± 0.30 ± 0.24	1	SAHOO	11A BELL $e^+e^- \rightarrow \Upsilon(4S)$
3.5 ± 0.6 ± 0.4	1	AUBERT	07Q BABR $e^+e^- \rightarrow \Upsilon(4S)$

- • • We do not use the following data for averages, fits, limits, etc. • • •

3.4 ± 0.9 ± 0.4	1	DRUTSKOY	04 BELL	Repl. by SAHOO 11A
-----------------	---	----------	---------	--------------------

  - 1 Assumes equal production of  $B^+$  and  $B^0$  at  $\Upsilon(4S)$ .

$\Gamma(K^+\pi^-\pi^+\gamma)/\Gamma_{total}$   $\Gamma_{450}/\Gamma$

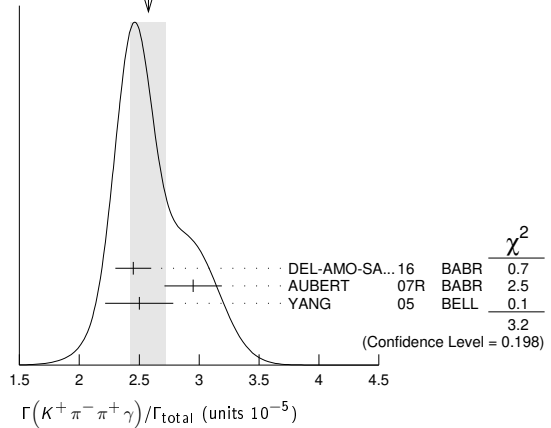
VALUE (units $10^{-5}$ )	DOCUMENT ID	TECN	COMMENT
<b>2.58 ± 0.15 OUR AVERAGE</b>			Error includes scale factor of 1.3. See the ideogram below.
2.45 ± 0.09 ± 0.12	1,2	DEL-AMO-SA...16	BABR $e^+e^- \rightarrow \Upsilon(4S)$
2.95 ± 0.13 ± 0.20	1,3	AUBERT	07R BABR $e^+e^- \rightarrow \Upsilon(4S)$
2.50 ± 0.18 ± 0.22	3,4	YANG	05 BELL $e^+e^- \rightarrow \Upsilon(4S)$

- • • We do not use the following data for averages, fits, limits, etc. • • •

2.4 ± 0.5 $\pm_{-0.2}^{+0.4}$	3,5	NISHIDA	02 BELL	Repl. by YANG 05
-------------------------------	-----	---------	---------	------------------

  - 1  $M_{K\pi\pi} < 1.8 \text{ GeV}/c^2$ .
  - 2 Uses  $B(\Upsilon(4S) \rightarrow B^+B^-) = 0.513 \pm 0.006$ .
  - 3 Assumes equal production of  $B^+$  and  $B^0$  at the  $\Upsilon(4S)$ .
  - 4  $M_{K\pi\pi} < 2.0 \text{ GeV}/c^2$ .
  - 5  $M_{K\pi\pi} < 2.4 \text{ GeV}/c^2$ .

WEIGHTED AVERAGE  
2.58 ± 0.15 (Error scaled by 1.3)



$\Gamma(K^*(892)^0\pi^+\gamma)/\Gamma_{total}$   $\Gamma_{451}/\Gamma$

VALUE (units $10^{-5}$ )	DOCUMENT ID	TECN	COMMENT
<b>2.33 ± 0.12 OUR AVERAGE</b>			
2.34 ± 0.09 $\pm_{-0.07}^{+0.08}$	1,2	DEL-AMO-SA...16	BABR $e^+e^- \rightarrow \Upsilon(4S)$
2.0 $\pm_{-0.6}^{+0.7} \pm 0.2$	3,4	NISHIDA	02 BELL $e^+e^- \rightarrow \Upsilon(4S)$

- 1 Requires  $M_{K\pi\pi} < 1.8 \text{ GeV}/c^2$ .
- 2 Uses  $B(\Upsilon(4S) \rightarrow B^+B^-) = 0.513 \pm 0.006$ .
- 3 Assumes equal production of  $B^+$  and  $B^0$  at the  $\Upsilon(4S)$ .
- 4  $M_{K\pi\pi} < 2.4 \text{ GeV}/c^2$ .

$\Gamma(K^+\rho^0\gamma)/\Gamma_{total}$   $\Gamma_{452}/\Gamma$

VALUE (units $10^{-6}$ )	DOCUMENT ID	TECN	COMMENT
<b>8.2 ± 0.4 ± 0.8</b>	1,2	DEL-AMO-SA...16	BABR $e^+e^- \rightarrow \Upsilon(4S)$

- • • We do not use the following data for averages, fits, limits, etc. • • •

< 20	90	3,4	NISHIDA	02 BELL	$e^+e^- \rightarrow \Upsilon(4S)$
------	----	-----	---------	---------	-----------------------------------

  - 1 Requires  $M_{K\pi\pi} < 1.8 \text{ GeV}/c^2$ .
  - 2 Uses  $B(\Upsilon(4S) \rightarrow B^+B^-) = 0.513 \pm 0.006$ .
  - 3 Assumes equal production of  $B^+$  and  $B^0$  at the  $\Upsilon(4S)$ .
  - 4  $M_{K\pi\pi} < 2.4 \text{ GeV}/c^2$ .

$\Gamma((K^+\pi^-)NR\pi^+\gamma)/\Gamma_{total}$   $\Gamma_{453}/\Gamma$

VALUE (units $10^{-6}$ )	DOCUMENT ID	TECN	COMMENT
<b>9.9 ± 0.7 <math>\pm_{-1.9}^{+1.5}</math></b>	1,2	DEL-AMO-SA...16	BABR $e^+e^- \rightarrow \Upsilon(4S)$

- • • We do not use the following data for averages, fits, limits, etc. • • •

< 9.2	90	3,4	NISHIDA	02 BELL	$e^+e^- \rightarrow \Upsilon(4S)$
-------	----	-----	---------	---------	-----------------------------------

  - 1 Requires  $M_{K\pi\pi} < 1.8 \text{ GeV}/c^2$ .
  - 2 Uses  $B(\Upsilon(4S) \rightarrow B^+B^-) = 0.513 \pm 0.006$ .
  - 3 Assumes equal production of  $B^+$  and  $B^0$  at the  $\Upsilon(4S)$ .
  - 4  $M_{K\pi\pi} < 2.4 \text{ GeV}/c^2$ .

$\Gamma(K^0\pi^+\pi^0\gamma)/\Gamma_{total}$   $\Gamma_{454}/\Gamma$

VALUE (units $10^{-5}$ )	DOCUMENT ID	TECN	COMMENT
<b>4.56 ± 0.42 ± 0.31</b>	1,2	AUBERT	07R BABR $e^+e^- \rightarrow \Upsilon(4S)$

- 1  $M_{K\pi\pi} < 1.8 \text{ GeV}/c^2$ .
- 2 Assumes equal production of  $B^+$  and  $B^0$  at the  $\Upsilon(4S)$ .

$\Gamma(K_1(1400)^+\gamma)/\Gamma_{total}$   $\Gamma_{455}/\Gamma$

VALUE (units $10^{-6}$ )	DOCUMENT ID	TECN	COMMENT
<b>9.7 <math>\pm_{-2.4}^{+4.6} \pm_{-2.4}^{+2.9}</math></b>	1,2	DEL-AMO-SA...16	BABR $e^+e^- \rightarrow \Upsilon(4S)$

- • • We do not use the following data for averages, fits, limits, etc. • • •

< 15	90	3	YANG	05 BELL	$e^+e^- \rightarrow \Upsilon(4S)$
< 50	90	3	NISHIDA	02 BELL	Repl. by YANG 05
< 2200	90	4	ALBRECHT	89G ARG	$e^+e^- \rightarrow \Upsilon(4S)$

  - 1 Requires  $M_{K\pi\pi} < 1.8 \text{ GeV}/c^2$ .
  - 2 Uses  $B(\Upsilon(4S) \rightarrow B^+B^-) = 0.513 \pm 0.006$ .
  - 3 Assumes equal production of  $B^+$  and  $B^0$  at the  $\Upsilon(4S)$ .
  - 4 ALBRECHT 89G reports  $< 0.0020$  assuming the  $\Upsilon(4S)$  decays 45% to  $B^0\bar{B}^0$ . We rescale to 50%.

$\Gamma(K^*(1410)^+\gamma)/\Gamma_{total}$   $\Gamma_{456}/\Gamma$

VALUE (units $10^{-5}$ )	DOCUMENT ID	TECN	COMMENT
<b>2.71 <math>\pm_{-0.48}^{+0.54} \pm 0.59</math></b>	1,2	DEL-AMO-SA...16	BABR $e^+e^- \rightarrow \Upsilon(4S)$

- 1 Requires  $M_{K\pi\pi} < 1.8 \text{ GeV}/c^2$ .
- 2 Uses  $B(\Upsilon(4S) \rightarrow B^+B^-) = 0.513 \pm 0.006$ .

See key on page 999

Meson Particle Listings

$B^\pm$

$\Gamma(K_S^*(1430)^0 \pi^+ \gamma) / \Gamma_{total}$   $\Gamma_{457} / \Gamma$

VALUE (units $10^{-6}$ )	DOCUMENT ID	TECN	COMMENT
$1.32^{+0.09+0.24}_{-0.10-0.30}$	1,2 DEL-AMO-SA...16	BABR	$e^+ e^- \rightarrow \Upsilon(4S)$

1 Requires  $M_{K\pi\pi} < 1.8 \text{ GeV}/c^2$ .  
 2 Uses  $B(\Upsilon(4S) \rightarrow B^+ B^-) = 0.513 \pm 0.006$ .

$\Gamma(K_S^*(1430)^+ \gamma) / \Gamma_{total}$   $\Gamma_{458} / \Gamma$

VALUE (units $10^{-5}$ )	CL%	DOCUMENT ID	TECN	COMMENT
$1.4 \pm 0.4$	OUR AVERAGE			
$0.87^{+0.70+0.87}_{-0.53-1.04}$		1,2 DEL-AMO-SA...16	BABR	$e^+ e^- \rightarrow \Upsilon(4S)$
$1.45 \pm 0.40 \pm 0.15$		3 AUBERT,B	04U	BABR $e^+ e^- \rightarrow \Upsilon(4S)$

• • • We do not use the following data for averages, fits, limits, etc. • • •

<140	90	4 ALBRECHT	89G	ARG $e^+ e^- \rightarrow \Upsilon(4S)$
------	----	------------	-----	--

1 Requires  $M_{K\pi\pi} < 1.8 \text{ GeV}/c^2$ .  
 2 Uses  $B(\Upsilon(4S) \rightarrow B^+ B^-) = 0.513 \pm 0.006$ .  
 3 Assumes equal production of  $B^+$  and  $B^0$  at the  $\Upsilon(4S)$ .  
 4 ALBRECHT 89G reports  $< 0.0013$  assuming the  $\Upsilon(4S)$  decays 45% to  $B^0 \bar{B}^0$ . We rescale to 50%.

$\Gamma(K^*(1680)^+ \gamma) / \Gamma_{total}$   $\Gamma_{459} / \Gamma$

VALUE (units $10^{-5}$ )	CL%	DOCUMENT ID	TECN	COMMENT
$6.67^{+0.93+1.44}_{-0.76-1.14}$		1,2 DEL-AMO-SA...16	BABR	$e^+ e^- \rightarrow \Upsilon(4S)$

• • • We do not use the following data for averages, fits, limits, etc. • • •

<190	90	3 ALBRECHT	89G	ARG $e^+ e^- \rightarrow \Upsilon(4S)$
------	----	------------	-----	--

1 Requires  $M_{K\pi\pi} < 1.8 \text{ GeV}/c^2$ .  
 2 Uses  $B(\Upsilon(4S) \rightarrow B^+ B^-) = 0.513 \pm 0.006$ .  
 3 ALBRECHT 89G reports  $< 0.0017$  assuming the  $\Upsilon(4S)$  decays 45% to  $B^0 \bar{B}^0$ . We rescale to 50%.

$\Gamma(K_S^*(1780)^+ \gamma) / \Gamma_{total}$   $\Gamma_{460} / \Gamma$

VALUE (units $10^{-6}$ )	CL%	DOCUMENT ID	TECN	COMMENT
< 39	90	1,2 NISHIDA	05	BELL $e^+ e^- \rightarrow \Upsilon(4S)$

• • • We do not use the following data for averages, fits, limits, etc. • • •

<5500	90	3 ALBRECHT	89G	ARG $e^+ e^- \rightarrow \Upsilon(4S)$
-------	----	------------	-----	--

1 Assumes equal production of  $B^+$  and  $B^0$  at the  $\Upsilon(4S)$ .  
 2 Uses  $B(K_S^*(1780) \rightarrow \eta K) = 0.11^{+0.05}_{-0.04}$ .  
 3 ALBRECHT 89G reports  $< 0.005$  assuming the  $\Upsilon(4S)$  decays 45% to  $B^0 \bar{B}^0$ . We rescale to 50%.

$\Gamma(K_S^*(2045)^+ \gamma) / \Gamma_{total}$   $\Gamma_{461} / \Gamma$

VALUE	CL%	DOCUMENT ID	TECN	COMMENT
<0.0099	90	1 ALBRECHT	89G	ARG $e^+ e^- \rightarrow \Upsilon(4S)$

1 ALBRECHT 89G reports  $< 0.0090$  assuming the  $\Upsilon(4S)$  decays 45% to  $B^0 \bar{B}^0$ . We rescale to 50%.

$\Gamma(\rho^+ \gamma) / \Gamma_{total}$   $\Gamma_{462} / \Gamma$

VALUE (units $10^{-6}$ )	CL%	DOCUMENT ID	TECN	COMMENT
$0.98 \pm 0.25$	OUR AVERAGE			
$1.20^{+0.42+0.20}_{-0.37-0.10}$		1 AUBERT	08BH	BABR $e^+ e^- \rightarrow \Upsilon(4S)$
$0.87^{+0.29+0.09}_{-0.27-0.11}$		1 TANIGUCHI	08	BELL $e^+ e^- \rightarrow \Upsilon(4S)$

• • • We do not use the following data for averages, fits, limits, etc. • • •

$1.10^{+0.37+0.09}_{-0.33-0.09}$		1 AUBERT	07L	BABR Repl. by AUBERT 08BH
$0.55^{+0.42+0.09}_{-0.36-0.08}$		1 MOHAPATRA	06	BELL Repl. by TANIGUCHI 08
$0.9^{+0.6}_{-0.5} \pm 0.1$	90	1 AUBERT	05	BABR Repl. by AUBERT 07L
< 2.2	90	1 MOHAPATRA	05	BELL $e^+ e^- \rightarrow \Upsilon(4S)$
< 2.1	90	1 AUBERT	04c	BABR $e^+ e^- \rightarrow \Upsilon(4S)$
<13	90	1,2 COAN	00	CLE2 $e^+ e^- \rightarrow \Upsilon(4S)$

1 Assumes equal production of  $B^+$  and  $B^0$  at  $\Upsilon(4S)$ .  
 2 No evidence for a nonresonant  $K\pi\gamma$  contamination was seen; the central value assumes no contamination.

$\Gamma(\pi^+ \pi^0) / \Gamma_{total}$   $\Gamma_{463} / \Gamma$

VALUE (units $10^{-6}$ )	CL%	DOCUMENT ID	TECN	COMMENT
$5.5 \pm 0.4$	OUR AVERAGE			Error includes scale factor of 1.2.
$5.86 \pm 0.26 \pm 0.38$		1 DUH	13	BELL $e^+ e^- \rightarrow \Upsilon(4S)$
$5.02 \pm 0.46 \pm 0.29$		1 AUBERT	07bc	BABR $e^+ e^- \rightarrow \Upsilon(4S)$
$4.6^{+1.8+0.6}_{-1.6-0.7}$		1 BORNHEIM	03	CLE2 $e^+ e^- \rightarrow \Upsilon(4S)$

• • • We do not use the following data for averages, fits, limits, etc. • • •

$6.5 \pm 0.4 \pm 0.4$		1 LIN	07A	BELL Repl. by DUH 13
$5.8 \pm 0.6 \pm 0.4$		1 AUBERT	05L	BABR Repl. by AUBERT 07bc
$5.0 \pm 1.2 \pm 0.5$		1 CHAO	04	BELL Repl. by LIN 07A
$5.5^{+1.0}_{-1.9} \pm 0.6$		1 AUBERT	03L	BABR Repl. by AUBERT 05L
$7.4^{+2.3}_{-2.2} \pm 0.9$		1 CASEY	02	BELL Repl. by CHAO 04
< 13.4	90	1 ABE	01H	BELL $e^+ e^- \rightarrow \Upsilon(4S)$

< 9.6	90	1 AUBERT	01E	BABR $e^+ e^- \rightarrow \Upsilon(4S)$
< 12.7	90	1 CRONIN-HEN.	00	CLE2 $e^+ e^- \rightarrow \Upsilon(4S)$
< 20	90	GODANG	98	CLE2 Repl. by CRONIN-HENNESSY 00
< 17	90	ASNER	96	CLE2 Repl. by GODANG 98
< 240	90	1 ALBRECHT	90b	ARG $e^+ e^- \rightarrow \Upsilon(4S)$
<2300	90	2 BEBEK	87	CLEO $e^+ e^- \rightarrow \Upsilon(4S)$

1 Assumes equal production of  $B^+$  and  $B^0$  at the  $\Upsilon(4S)$ .  
 2 BEBEK 87 assume the  $\Upsilon(4S)$  decays 43% to  $B^0 \bar{B}^0$ .

$\Gamma(\pi^+ \pi^0) / \Gamma(K^0 \pi^+)$   $\Gamma_{463} / \Gamma_{342}$

VALUE	DOCUMENT ID	TECN	COMMENT
$0.285 \pm 0.02 \pm 0.02$	LIN	07A	BELL $e^+ e^- \rightarrow \Upsilon(4S)$

$\Gamma(\pi^+ \pi^+ \pi^-) / \Gamma_{total}$   $\Gamma_{464} / \Gamma$

VALUE (units $10^{-6}$ )	CL%	DOCUMENT ID	TECN	COMMENT
$15.2 \pm 0.6^{+1.3}_{-1.2}$		1 AUBERT	09L	BABR $e^+ e^- \rightarrow \Upsilon(4S)$

• • • We do not use the following data for averages, fits, limits, etc. • • •

$16.2 \pm 1.2 \pm 0.9$		1 AUBERT,B	05G	BABR Repl. by AUBERT 09L
$10.9 \pm 3.3 \pm 1.6$		1 AUBERT	03m	BABR Repl. by AUBERT 05G
<130	90	2 ADAM	96D	DLPH $e^+ e^- \rightarrow Z$
<220	90	3 ABREU	95N	DLPH Sup. by ADAM 96D
<450	90	4 ALBRECHT	90B	ARG $e^+ e^- \rightarrow \Upsilon(4S)$
<190	90	5 BORTOLETTO	89	CLEO $e^+ e^- \rightarrow \Upsilon(4S)$

1 Assumes equal production of  $B^0$  and  $B^+$  at the  $\Upsilon(4S)$ ; charm and charmonium contributions are subtracted, otherwise no assumptions about intermediate resonances.  
 2 ADAM 96D assumes  $f_{B^0} = f_{B^-} = 0.39$  and  $f_{B_s} = 0.12$ .  
 3 Assumes a  $B^0, B^-$  production fraction of 0.39 and a  $B_s$  production fraction of 0.12.  
 4 ALBRECHT 90B limit assumes equal production of  $B^0 \bar{B}^0$  and  $B^+ B^-$  at  $\Upsilon(4S)$ .  
 5 BORTOLETTO 89 reports  $< 1.7 \times 10^{-4}$  assuming the  $\Upsilon(4S)$  decays 43% to  $B^0 \bar{B}^0$ . We rescale to 50%.

$\Gamma(\rho^0 \pi^+) / \Gamma_{total}$   $\Gamma_{465} / \Gamma$

VALUE (units $10^{-6}$ )	CL%	DOCUMENT ID	TECN	COMMENT
$8.3 \pm 1.2$	OUR AVERAGE			
$8.1 \pm 0.7^{+1.3}_{-1.6}$		1 AUBERT	09L	BABR $e^+ e^- \rightarrow \Upsilon(4S)$
$8.0^{+2.3}_{-2.0} \pm 0.7$		1 GORDON	02	BELL $e^+ e^- \rightarrow \Upsilon(4S)$
$10.4^{+3.3}_{-3.4} \pm 2.1$		1 JESSOP	00	CLE2 $e^+ e^- \rightarrow \Upsilon(4S)$

• • • We do not use the following data for averages, fits, limits, etc. • • •

$8.8 \pm 1.0^{+0.6}_{-0.9}$		1 AUBERT,B	05G	BABR Repl. by AUBERT 09L
$9.5 \pm 1.1 \pm 0.9$		1 AUBERT	04z	BABR Repl. by AUBERT 05G
< 83	90	2 ABE	00c	SLD $e^+ e^- \rightarrow Z$
<160	90	3 ADAM	96D	DLPH $e^+ e^- \rightarrow Z$
< 43	90	ASNER	96	CLE2 Repl. by JESSOP 00
<260	90	4 ABREU	95N	DLPH Sup. by ADAM 96D
<150	90	1 ALBRECHT	90B	ARG $e^+ e^- \rightarrow \Upsilon(4S)$
<170	90	5 BORTOLETTO	89	CLEO $e^+ e^- \rightarrow \Upsilon(4S)$
<230	90	5 BEBEK	87	CLEO $e^+ e^- \rightarrow \Upsilon(4S)$
<600	90	GILES	84	CLEO Repl. by BEBEK 87

1 Assumes equal production of  $B^+$  and  $B^0$  at the  $\Upsilon(4S)$ .  
 2 ABE 00c assumes  $B(Z \rightarrow b\bar{b}) = (21.7 \pm 0.1)\%$  and the  $B$  fractions  $f_{B^0} = f_{B^+} = (39.7^{+1.8}_{-2.2})\%$  and  $f_{B_s} = (10.5^{+1.8}_{-2.2})\%$ .  
 3 ADAM 96D assumes  $f_{B^0} = f_{B^-} = 0.39$  and  $f_{B_s} = 0.12$ .  
 4 Assumes a  $B^0, B^-$  production fraction of 0.39 and a  $B_s$  production fraction of 0.12.  
 5 Papers assume the  $\Upsilon(4S)$  decays 43% to  $B^0 \bar{B}^0$ . We rescale to 50%.

$[\Gamma(K^*(892)^0 \pi^+) + \Gamma(\rho^0 \pi^+)] / \Gamma_{total}$   $(\Gamma_{368} + \Gamma_{465}) / \Gamma$

VALUE (units $10^{-6}$ )	DOCUMENT ID	TECN	COMMENT
$170^{+120}_{-80} \pm 20$	1 ADAM	96D	DLPH $e^+ e^- \rightarrow Z$

1 ADAM 96D assumes  $f_{B^0} = f_{B^-} = 0.39$  and  $f_{B_s} = 0.12$ .

$\Gamma(\pi^+ f_0(980), f_0 \rightarrow \pi^+ \pi^-) / \Gamma_{total}$   $\Gamma_{466} / \Gamma$

VALUE (units $10^{-6}$ )	CL%	DOCUMENT ID	TECN	COMMENT
< 1.5	90	1 AUBERT	09L	BABR $e^+ e^- \rightarrow \Upsilon(4S)$

• • • We do not use the following data for averages, fits, limits, etc. • • •

< 3.0	90	1 AUBERT,B	05G	BABR Repl. by AUBERT 09L
<140	90	2 BORTOLETTO	89	CLEO $e^+ e^- \rightarrow \Upsilon(4S)$

1 Assumes equal production of  $B^+$  and  $B^0$  at the  $\Upsilon(4S)$ .  
 2 BORTOLETTO 89 reports  $< 1.2 \times 10^{-4}$  assuming the  $\Upsilon(4S)$  decays 43% to  $B^0 \bar{B}^0$ . We rescale to 50%.

Downloaded from https://academic.oup.com/ptep/article/2020/8/083C01/5891211 by guest on 12 November 2020



See key on page 999

Meson Particle Listings

B±

Γ(ηρ+)/Γtotal Γ483/Γ

Table with columns: VALUE (units 10^-6), CL%, DOCUMENT ID, TECN, COMMENT. Includes data for AUBERT, WANG, AUBERT,B, RICHICHI, BEHRENS and a note about equal production of B+ and B0.

Γ(η'π+)/Γtotal Γ484/Γ

Table with columns: VALUE (units 10^-6), CL%, DOCUMENT ID, TECN, COMMENT. Includes data for AUBERT, SCHUEMANN, AUBERT, AUBERT,B, ABE, AUBERT, RICHICHI, BEHRENS and a note about equal production of B+ and B0.

Γ(η'ρ+)/Γtotal Γ485/Γ

Table with columns: VALUE (units 10^-6), CL%, DOCUMENT ID, TECN, COMMENT. Includes data for DEL-AMO-SA..10A, AUBERT, SCHUEMANN, AUBERT,B, RICHICHI, BEHRENS and a note about equal production of B+ and B0.

Γ(φπ+)/Γtotal Γ486/Γ

Table with columns: VALUE (units 10^-8), CL%, DOCUMENT ID, TECN, COMMENT. Includes data for AAIJ, AAIJ, KIM, AUBERT,B, AUBERT, ABE, BERGFELD and a note about fit fraction for B+ to phi(1020)pi+.

Γ(φρ+)/Γtotal Γ487/Γ

Table with columns: VALUE (units 10^-6), CL%, DOCUMENT ID, TECN, COMMENT. Includes data for AUBERT, BERGFELD and a note about equal production of B+ and B0.

Γ(a0(980)0π+, a00 → ηπ0)/Γtotal Γ488/Γ

Table with columns: VALUE (units 10^-6), CL%, DOCUMENT ID, TECN, COMMENT. Includes data for AUBERT, BE and a note about equal production of charged and neutral B mesons.

Γ(a0(980)+π0, a0+ → ηπ+)/Γtotal Γ489/Γ

Table with columns: VALUE (units 10^-6), CL%, DOCUMENT ID, TECN, COMMENT. Includes data for AUBERT and a note about equal production of B+ and B0.

Γ(π+π+π+π-π-)/Γtotal Γ490/Γ

Table with columns: VALUE, CL%, DOCUMENT ID, TECN, COMMENT. Includes data for ALBRECHT and a note about equal production of B0B0 and B+B-.

Γ(ρ0a1(1260)+)/Γtotal Γ491/Γ

Table with columns: VALUE, CL%, DOCUMENT ID, TECN, COMMENT. Includes data for BORTOLETTO89, ALBRECHT, BEBEK and a note about B0B0 decays.

Γ(ρ0a2(1320)+)/Γtotal Γ492/Γ

Table with columns: VALUE, CL%, DOCUMENT ID, TECN, COMMENT. Includes data for BORTOLETTO89, BEBEK and a note about B0B0 decays.

Γ(b10π+, b10 → ωπ0)/Γtotal Γ493/Γ

Table with columns: VALUE (units 10^-6), CL%, DOCUMENT ID, TECN, COMMENT. Includes data for AUBERT and a note about equal production of B+ and B0.

Γ(b1+π0, b1+ → ωπ+)/Γtotal Γ494/Γ

Table with columns: VALUE (units 10^-6), CL%, DOCUMENT ID, TECN, COMMENT. Includes data for AUBERT and a note about equal production of B+ and B0.

Γ(π+π+π+π-π-π0)/Γtotal Γ495/Γ

Table with columns: VALUE, CL%, DOCUMENT ID, TECN, COMMENT. Includes data for ALBRECHT and a note about equal production of B0B0 and B+B-.

Γ(b1+ρ0, b1+ → ωπ+)/Γtotal Γ496/Γ

Table with columns: VALUE, CL%, DOCUMENT ID, TECN, COMMENT. Includes data for AUBERT and a note about equal production of B+ and B0.

Γ(b10ρ+, b10 → ωπ0)/Γtotal Γ498/Γ

Table with columns: VALUE, CL%, DOCUMENT ID, TECN, COMMENT. Includes data for AUBERT and a note about equal production of B+ and B0.

Γ(a1(1260)0a1(1260)0)/Γtotal Γ497/Γ

Table with columns: VALUE, CL%, DOCUMENT ID, TECN, COMMENT. Includes data for ALBRECHT and a note about equal production of B0B0 and B+B-.

Γ(h+π0)/Γtotal Γ499/Γ

Table with columns: VALUE (units 10^-6), CL%, DOCUMENT ID, TECN, COMMENT. Includes data for GODANG and a note about h+ = K+ or pi+.

Γ(ωh+)/Γtotal Γ500/Γ

Table with columns: VALUE (units 10^-6), CL%, DOCUMENT ID, TECN, COMMENT. Includes data for LU, JESSOP and a note about h+ = K+ or pi+.

Γ(h+X0(Familon))/Γtotal Γ501/Γ

Table with columns: VALUE (units 10^-6), CL%, DOCUMENT ID, TECN, COMMENT. Includes data for AMMAR and a note about feebly-interacting particle X0.



# Meson Particle Listings

## $B^\pm$

### $\Gamma(K^+ X^0, X^0 \rightarrow \mu^+ \mu^-)/\Gamma_{\text{total}}$ $\Gamma_{502}/\Gamma$

$X^0$  stands here for a long-lived scalar particle.

VALUE	CL%	DOCUMENT ID	TECN	COMMENT
$<1 \times 10^{-7}$	95	<sup>1</sup> AAIJ	17AQ LHCb	$pp$ at 7, 8 TeV

<sup>1</sup> AAIJ 17AQ searched for a long-lived scalar particle  $X^0 \rightarrow \mu^+ \mu^-$  in the mass range 250–4700 MeV and lifetime range 0.1–1000 ps. The limit is between  $10^{-7}$  and  $2 \times 10^{-10}$  in these ranges except in vetoed mass regions around  $K_S^0, J/\psi, \psi(2S),$  and  $\psi(3770)$ .

### $\Gamma(p\bar{p}\pi^+)/\Gamma_{\text{total}}$ $\Gamma_{503}/\Gamma$

VALUE (units $10^{-6}$ )	CL%	DOCUMENT ID	TECN	COMMENT
<b>1.62 ± 0.20 OUR AVERAGE</b>				
$1.60^{+0.22}_{-0.19} \pm 0.12$		<sup>1,2,3</sup> WEI	08 BELL	$e^+ e^- \rightarrow \Upsilon(4S)$
$1.69 \pm 0.29 \pm 0.26$		<sup>1</sup> AUBERT	07AV BABR	$e^+ e^- \rightarrow \Upsilon(4S)$

• • • We do not use the following data for averages, fits, limits, etc. • • •

$1.07 \pm 0.11 \pm 0.11$		<sup>4</sup> AAIJ	14AF LHCb	$pp$ at 7, 8 TeV
$3.06^{+0.73}_{-0.62} \pm 0.37$		<sup>1,3</sup> WANG	04 BELL	Repl. by WEI 08
$< 3.7$	90	<sup>1,2</sup> ABE	02K BELL	Repl. by WANG 04
$< 500$	90	<sup>5</sup> ABBEU	95N DLPB	Repl. by ADAM 96D
$< 160$	90	<sup>6</sup> BEBEK	89 CLEO	$e^+ e^- \rightarrow \Upsilon(4S)$
$570 \pm 150 \pm 210$		<sup>7</sup> ALBRECHT	88F ARG	$e^+ e^- \rightarrow \Upsilon(4S)$

<sup>1</sup> Assumes equal production of  $B^+$  and  $B^0$  at the  $\Upsilon(4S)$ .  
<sup>2</sup> Explicitly vetoes resonant production of  $p\bar{p}$  from Charmonium states.  
<sup>3</sup> Also provides results with  $m_{p\bar{p}} < 2.85$  GeV/ $c^2$  and angular asymmetry of  $p\bar{p}$  system.  
<sup>4</sup> Requires  $m_{p\bar{p}} < 2.85$  GeV/ $c^2$ .  
<sup>5</sup> Assumes a  $B^0, B^-$  production fraction of 0.39 and a  $B_S$  production fraction of 0.12.  
<sup>6</sup> BEBEK 89 reports  $< 1.4 \times 10^{-4}$  assuming the  $\Upsilon(4S)$  decays 43% to  $B^0 \bar{B}^0$ . We rescale to 50%.  
<sup>7</sup> ALBRECHT 88F reports  $(5.2 \pm 1.4 \pm 1.9) \times 10^{-4}$  assuming the  $\Upsilon(4S)$  decays 45% to  $B^0 \bar{B}^0$ . We rescale to 50%.

### $\Gamma(p\bar{p}\pi^+ \text{nonresonant})/\Gamma_{\text{total}}$ $\Gamma_{504}/\Gamma$

VALUE (units $10^{-6}$ )	CL%	DOCUMENT ID	TECN	COMMENT
<b>&lt; 53</b>	90	BERGFELD	96B CLE2	$e^+ e^- \rightarrow \Upsilon(4S)$

### $\Gamma(p\bar{p}\pi^+ \pi^+ \pi^-)/\Gamma_{\text{total}}$ $\Gamma_{505}/\Gamma$

• • • We do not use the following data for averages, fits, limits, etc. • • •

VALUE	CL%	DOCUMENT ID	TECN	COMMENT
$< 5.2 \times 10^{-4}$	90	<sup>1</sup> ALBRECHT	88F ARG	$e^+ e^- \rightarrow \Upsilon(4S)$

<sup>1</sup> ALBRECHT 88F reports  $< 4.7 \times 10^{-4}$  assuming the  $\Upsilon(4S)$  decays 45% to  $B^0 \bar{B}^0$ . We rescale to 50%.

### $\Gamma(p\bar{p}K^+)/\Gamma_{\text{total}}$ $\Gamma_{506}/\Gamma$

VALUE (units $10^{-6}$ )	CL%	DOCUMENT ID	TECN	COMMENT
<b>5.9 ± 0.5 OUR AVERAGE</b>				Error includes scale factor of 1.5.
$5.54^{+0.27}_{-0.25} \pm 0.36$		<sup>1,2,3</sup> WEI	08 BELL	$e^+ e^- \rightarrow \Upsilon(4S)$
$6.7 \pm 0.5 \pm 0.4$		<sup>1,3</sup> AUBERT,B	05L BABR	$e^+ e^- \rightarrow \Upsilon(4S)$

• • • We do not use the following data for averages, fits, limits, etc. • • •

$4.59^{+0.38}_{-0.34} \pm 0.50$		<sup>1,2,3</sup> WANG	05A BELL	Repl. by WEI 08
$5.66^{+0.67}_{-0.57} \pm 0.62$		<sup>1,2,3</sup> WANG	04 BELL	Repl. by WANG 05A
$4.3^{+1.1}_{-0.9} \pm 0.5$		<sup>1,2</sup> ABE	02K BELL	Repl. by WANG 04

<sup>1</sup> Assumes equal production of  $B^+$  and  $B^0$  at the  $\Upsilon(4S)$ .  
<sup>2</sup> Explicitly vetoes resonant production of  $p\bar{p}$  from Charmonium states.  
<sup>3</sup> Provides also results with  $m_{p\bar{p}} < 2.85$  GeV/ $c^2$  and angular asymmetry of  $p\bar{p}$  system.

### $\Gamma(p\bar{p}K^+)/\Gamma(J/\psi(1S)K^+)$ $\Gamma_{506}/\Gamma_{275}$

VALUE	DOCUMENT ID	TECN	COMMENT
<b>0.0104 ± 0.0005 ± 0.0001</b>	<sup>1,2</sup> AAIJ	13S LHCb	$pp$ at 7 TeV

<sup>1</sup> AAIJ 13S reports  $[\Gamma(B^+ \rightarrow p\bar{p}K^+)/\Gamma(B^+ \rightarrow J/\psi(1S)K^+)] / [B(J/\psi(1S) \rightarrow p\bar{p})] = 4.91 \pm 0.19 \pm 0.14$  which we multiply by our best value  $B(J/\psi(1S) \rightarrow p\bar{p}) = (2.121 \pm 0.029) \times 10^{-3}$ . Our first error is their experiment's error and our second error is the systematic error from using our best value.

<sup>2</sup> Measurement includes contribution where  $p\bar{p}$  is produced in charmonia decays.

### $\Gamma(\Theta(1710)^{++}, \Theta^{++} \rightarrow pK^+)/\Gamma_{\text{total}}$ $\Gamma_{507}/\Gamma$

VALUE (units $10^{-6}$ )	CL%	DOCUMENT ID	TECN	COMMENT
<b>&lt; 0.091</b>	90	<sup>1</sup> WANG	05A BELL	$e^+ e^- \rightarrow \Upsilon(4S)$

• • • We do not use the following data for averages, fits, limits, etc. • • •

$< 0.1$	90	<sup>1,2</sup> AUBERT,B	05L BABR	$e^+ e^- \rightarrow \Upsilon(4S)$
---------	----	-------------------------	----------	------------------------------------

<sup>1</sup> Assumes equal production of  $B^+$  and  $B^0$  at the  $\Upsilon(4S)$ .  
<sup>2</sup> Provides upper limits depending on the pentaquark masses between 1.43 to 2.0 GeV/ $c^2$ .

### $\Gamma(f_J(2220)K^+, f_J \rightarrow p\bar{p})/\Gamma_{\text{total}}$ $\Gamma_{508}/\Gamma$

VALUE (units $10^{-6}$ )	CL%	DOCUMENT ID	TECN	COMMENT
<b>&lt; 0.41</b>	90	<sup>1</sup> WANG	05A BELL	$e^+ e^- \rightarrow \Upsilon(4S)$

<sup>1</sup> Assumes equal production of  $B^+$  and  $B^0$  at the  $\Upsilon(4S)$ .

### $\Gamma(p\bar{\Lambda}(1520))/\Gamma_{\text{total}}$ $\Gamma_{509}/\Gamma$

VALUE (units $10^{-7}$ )	CL%	DOCUMENT ID	TECN	COMMENT
<b>3.15 ± 0.48 ± 0.27</b>		<sup>1</sup> AAIJ	14AF LHCb	$pp$ at 7, 8 TeV

• • • We do not use the following data for averages, fits, limits, etc. • • •

$3.9^{+1.0}_{-0.9} \pm 0.3$		<sup>1</sup> AAIJ	13AU LHCb	Repl. by AAIJ 14AF
$< 1.5$	90	<sup>2</sup> AUBERT,B	05L BABR	$e^+ e^- \rightarrow \Upsilon(4S)$

<sup>1</sup> Uses  $B(B^+ \rightarrow J/\psi K^+) = (1.016 \pm 0.033) \times 10^{-3}$ ,  $B(J/\psi \rightarrow p\bar{p}) = (2.17 \pm 0.07) \times 10^{-3}$  and  $B(\Lambda(1520) \rightarrow K^- p) = 0.234 \pm 0.016$ .  
<sup>2</sup> Assumes equal production of  $B^+$  and  $B^0$  at the  $\Upsilon(4S)$ .

### $\Gamma(p\bar{p}K^+ \text{nonresonant})/\Gamma_{\text{total}}$ $\Gamma_{510}/\Gamma$

VALUE (units $10^{-6}$ )	CL%	DOCUMENT ID	TECN	COMMENT
<b>&lt; 89</b>	90	BERGFELD	96B CLE2	$e^+ e^- \rightarrow \Upsilon(4S)$

### $\Gamma(p\bar{p}K^*(892)^+)/\Gamma_{\text{total}}$ $\Gamma_{511}/\Gamma$

VALUE (units $10^{-6}$ )	CL%	DOCUMENT ID	TECN	COMMENT
<b>3.6 + 0.8 - 0.7 OUR AVERAGE</b>				
$3.38^{+0.73}_{-0.60} \pm 0.39$		<sup>1,2</sup> CHEN	08c BELL	$e^+ e^- \rightarrow \Upsilon(4S)$
$5.3 \pm 1.5 \pm 1.3$		<sup>2</sup> AUBERT	07AV BABR	$e^+ e^- \rightarrow \Upsilon(4S)$

• • • We do not use the following data for averages, fits, limits, etc. • • •

$10.3^{+3.6}_{-2.8} \pm 1.3$		<sup>2,3</sup> WANG	04 BELL	Repl. by CHEN 08c
------------------------------	--	---------------------	---------	-------------------

<sup>1</sup> Explicitly vetoes resonant production of  $p\bar{p}$  from charmonium states.  
<sup>2</sup> Assumes equal production of  $B^+$  and  $B^0$  at the  $\Upsilon(4S)$ .  
<sup>3</sup> Explicitly vetoes resonant production of  $p\bar{p}$  from charmonium states. The branching fraction for  $M_{p\bar{p}} < 2.85$  GeV/ $c^2$  is also reported.

### $\Gamma(f_J(2220)K^{*+}, f_J \rightarrow p\bar{p})/\Gamma_{\text{total}}$ $\Gamma_{512}/\Gamma$

VALUE (units $10^{-6}$ )	CL%	DOCUMENT ID	TECN	COMMENT
<b>&lt; 0.77</b>	90	<sup>1</sup> AUBERT	07AV BABR	$e^+ e^- \rightarrow \Upsilon(4S)$

<sup>1</sup> Assumes equal production of  $B^+$  and  $B^0$  at the  $\Upsilon(4S)$ .

### $\Gamma(p\bar{\Lambda})/\Gamma_{\text{total}}$ $\Gamma_{513}/\Gamma$

VALUE (units $10^{-6}$ )	CL%	DOCUMENT ID	TECN	COMMENT
<b>0.24 + 0.10 - 0.08 ± 0.03</b>		<sup>1</sup> AAIJ	17R LHCb	$pp$ at 7, 8 TeV

• • • We do not use the following data for averages, fits, limits, etc. • • •

$< 0.32$	90	<sup>2</sup> TSAI	07 BELL	$e^+ e^- \rightarrow \Upsilon(4S)$
$< 0.49$	90	<sup>2</sup> CHANG	05 BELL	Repl. by TSAI 07
$< 1.5$	90	<sup>2</sup> BORNHEIM	03 CLE2	$e^+ e^- \rightarrow \Upsilon(4S)$
$< 2.2$	90	<sup>2</sup> ABE	02b BELL	$e^+ e^- \rightarrow \Upsilon(4S)$
$< 2.6$	90	<sup>2</sup> COAN	99 CLE2	$e^+ e^- \rightarrow \Upsilon(4S)$
$< 60$	90	<sup>3</sup> AVERY	89B CLEO	$e^+ e^- \rightarrow \Upsilon(4S)$
$< 93$	90	<sup>4</sup> ALBRECHT	88F ARG	$e^+ e^- \rightarrow \Upsilon(4S)$

<sup>1</sup> Statistical significance of the signal is 4.1 standard deviations where the normalisation is based on  $B(B^+ \rightarrow K_S^0 \pi^+) = (11.895 \pm 0.375) \times 10^{-6}$ .  
<sup>2</sup> Assumes equal production of  $B^+$  and  $B^0$  at the  $\Upsilon(4S)$ .  
<sup>3</sup> AVERY 89b reports  $< 5 \times 10^{-5}$  assuming the  $\Upsilon(4S)$  decays 43% to  $B^0 \bar{B}^0$ . We rescale to 50%.  
<sup>4</sup> ALBRECHT 88F reports  $< 8.5 \times 10^{-5}$  assuming the  $\Upsilon(4S)$  decays 45% to  $B^0 \bar{B}^0$ . We rescale to 50%.

### $\Gamma(p\bar{\Lambda}\gamma)/\Gamma_{\text{total}}$ $\Gamma_{514}/\Gamma$

VALUE (units $10^{-6}$ )	CL%	DOCUMENT ID	TECN	COMMENT
<b>2.45 + 0.44 - 0.38 ± 0.22</b>		<sup>1</sup> WANG	07c BELL	$e^+ e^- \rightarrow \Upsilon(4S)$

• • • We do not use the following data for averages, fits, limits, etc. • • •

$2.16^{+0.58}_{-0.53} \pm 0.20$		<sup>1</sup> LEE	05 BELL	Repl. by WANG 07c
$< 3.9$	90	<sup>2</sup> EDWARDS	03 CLE2	$e^+ e^- \rightarrow \Upsilon(4S)$

<sup>1</sup> Assumes equal production of  $B^+$  and  $B^0$  at the  $\Upsilon(4S)$ .  
<sup>2</sup> Corresponds to  $E_\gamma > 1.5$  GeV. The limit changes to  $3.3 \times 10^{-6}$  for  $E_\gamma > 2.0$  GeV.

### $\Gamma(p\bar{\Lambda}\pi^0)/\Gamma_{\text{total}}$ $\Gamma_{515}/\Gamma$

VALUE (units $10^{-6}$ )	CL%	DOCUMENT ID	TECN	COMMENT
<b>3.00 + 0.61 - 0.53 ± 0.33</b>		<sup>1</sup> WANG	07c BELL	$e^+ e^- \rightarrow \Upsilon(4S)$

<sup>1</sup> Assumes equal production of  $B^+$  and  $B^0$  at the  $\Upsilon(4S)$ .

### $\Gamma(p\bar{\Sigma}^-(1385)^0)/\Gamma_{\text{total}}$ $\Gamma_{516}/\Gamma$

VALUE (units $10^{-6}$ )	CL%	DOCUMENT ID	TECN	COMMENT
<b>&lt; 0.47</b>	90	<sup>1</sup> WANG	07c BELL	$e^+ e^- \rightarrow \Upsilon(4S)$

<sup>1</sup> Assumes equal production of  $B^+$  and  $B^0$  at the  $\Upsilon(4S)$ .

### $\Gamma(\Delta^+ \bar{\Lambda})/\Gamma_{\text{total}}$ $\Gamma_{517}/\Gamma$

VALUE (units $10^{-6}$ )	CL%	DOCUMENT ID	TECN	COMMENT
<b>&lt; 0.82</b>	90	<sup>1</sup> WANG	07c BELL	$e^+ e^- \rightarrow \Upsilon(4S)$

<sup>1</sup> Assumes equal production of  $B^+$  and  $B^0$  at the  $\Upsilon(4S)$ .

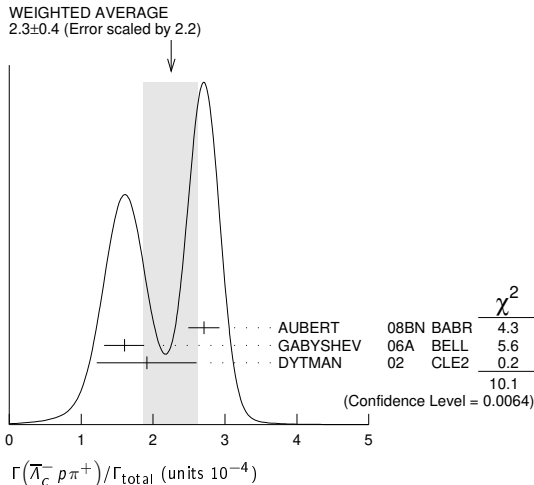


# Meson Particle Listings

$B^\pm$

$\Gamma(\bar{A}_c^- \rho \pi^+)/\Gamma_{\text{total}}$	$\Gamma_{541}/\Gamma$		
VALUE (units $10^{-4}$ )	DOCUMENT ID	TECN	COMMENT
<b><math>2.3 \pm 0.4</math> OUR AVERAGE</b>	Error includes scale factor of 2.2. See the ideogram below.		
$2.71 \pm 0.16 \pm 0.14$	1,2 AUBERT	08BN BABR	$e^+ e^- \rightarrow \Upsilon(4S)$
$1.60 \pm 0.20 \pm 0.08$	1,3 GABYSHEV	06A BELL	$e^+ e^- \rightarrow \Upsilon(4S)$
$1.9 \pm 0.5 \pm 0.1$	1,4 DYTMAN	02 CLE2	$e^+ e^- \rightarrow \Upsilon(4S)$

- • • We do not use the following data for averages, fits, limits, etc. • • •
  - 1.5  $\pm 0.4 \pm 0.1$  1,5 GABYSHEV 02 BELL Repl. by GABYSHEV 06A
  - 6.2  $\pm 2.3 \pm 1.6$  1,6 FU 97 CLE2 Repl. by DYTMAN 02
- 1 Assumes equal production of  $B^+$  and  $B^0$  at the  $\Upsilon(4S)$ .
- 2 AUBERT 08BN reports  $(3.4 \pm 0.1 \pm 0.9) \times 10^{-4}$  from a measurement of  $[\Gamma(B^+ \rightarrow \bar{A}_c^- \rho \pi^+)/\Gamma_{\text{total}}] \times [B(\Lambda_c^+ \rightarrow p K^- \pi^+)]$  assuming  $B(\Lambda_c^+ \rightarrow p K^- \pi^+) = (5.0 \pm 1.3) \times 10^{-2}$ , which we rescale to our best value  $B(\Lambda_c^+ \rightarrow p K^- \pi^+) = (6.28 \pm 0.32) \times 10^{-2}$ . Our first error is their experiment's error and our second error is the systematic error from using our best value.
- 3 GABYSHEV 06A reports  $(2.01 \pm 0.15 \pm 0.20) \times 10^{-4}$  from a measurement of  $[\Gamma(B^+ \rightarrow \bar{A}_c^- \rho \pi^+)/\Gamma_{\text{total}}] \times [B(\Lambda_c^+ \rightarrow p K^- \pi^+)]$  assuming  $B(\Lambda_c^+ \rightarrow p K^- \pi^+) = 0.05$ , which we rescale to our best value  $B(\Lambda_c^+ \rightarrow p K^- \pi^+) = (6.28 \pm 0.32) \times 10^{-2}$ . Our first error is their experiment's error and our second error is the systematic error from using our best value.
- 4 DYTMAN 02 reports  $(2.4 \pm 0.63 \pm 0.62) \times 10^{-4}$  from a measurement of  $[\Gamma(B^+ \rightarrow \bar{A}_c^- \rho \pi^+)/\Gamma_{\text{total}}] \times [B(\Lambda_c^+ \rightarrow p K^- \pi^+)]$  assuming  $B(\Lambda_c^+ \rightarrow p K^- \pi^+) = 0.05$ , which we rescale to our best value  $B(\Lambda_c^+ \rightarrow p K^- \pi^+) = (6.28 \pm 0.32) \times 10^{-2}$ . Our first error is their experiment's error and our second error is the systematic error from using our best value.
- 5 GABYSHEV 02 reports  $(1.87 \pm 0.51 \pm 0.49) \times 10^{-4}$  from a measurement of  $[\Gamma(B^+ \rightarrow \bar{A}_c^- \rho \pi^+)/\Gamma_{\text{total}}] \times [B(\Lambda_c^+ \rightarrow p K^- \pi^+)]$  assuming  $B(\Lambda_c^+ \rightarrow p K^- \pi^+) = 0.05$ , which we rescale to our best value  $B(\Lambda_c^+ \rightarrow p K^- \pi^+) = (6.28 \pm 0.32) \times 10^{-2}$ . Our first error is their experiment's error and our second error is the systematic error from using our best value.
- 6 FU 97 uses PDG 96 values of  $\Lambda_c$  branching fraction.



$\Gamma(\bar{A}_c^- \Delta(1232)^+)/\Gamma_{\text{total}}$	$\Gamma_{542}/\Gamma$		
VALUE (units $10^{-5}$ )	DOCUMENT ID	TECN	COMMENT
<b><math>&lt;1.9</math></b>	90	GABYSHEV 06A BELL	$e^+ e^- \rightarrow \Upsilon(4S)$

$\Gamma(\bar{A}_c^- \Delta_X(1600)^+)/\Gamma_{\text{total}}$	$\Gamma_{543}/\Gamma$		
VALUE (units $10^{-5}$ )	DOCUMENT ID	TECN	COMMENT
<b><math>4.7 \pm 0.9 \pm 0.2</math></b>	1 GABYSHEV 06A BELL	$e^+ e^- \rightarrow \Upsilon(4S)$	

1 GABYSHEV 06A reports  $(5.9 \pm 1.0 \pm 0.6) \times 10^{-5}$  from a measurement of  $[\Gamma(B^+ \rightarrow \bar{A}_c^- \Delta_X(1600)^+)/\Gamma_{\text{total}}] \times [B(\Lambda_c^+ \rightarrow p K^- \pi^+)]$  assuming  $B(\Lambda_c^+ \rightarrow p K^- \pi^+) = 0.05$ , which we rescale to our best value  $B(\Lambda_c^+ \rightarrow p K^- \pi^+) = (6.28 \pm 0.32) \times 10^{-2}$ . Our first error is their experiment's error and our second error is the systematic error from using our best value.

$\Gamma(\bar{A}_c^- \Delta_X(2420)^+)/\Gamma_{\text{total}}$	$\Gamma_{544}/\Gamma$		
VALUE (units $10^{-5}$ )	DOCUMENT ID	TECN	COMMENT
<b><math>3.7 \pm 0.9 \pm 0.2</math></b>	1 GABYSHEV 06A BELL	$e^+ e^- \rightarrow \Upsilon(4S)$	

1 GABYSHEV 06A reports  $(4.7 \pm 1.0 \pm 0.9) \times 10^{-5}$  from a measurement of  $[\Gamma(B^+ \rightarrow \bar{A}_c^- \Delta_X(2420)^+)/\Gamma_{\text{total}}] \times [B(\Lambda_c^+ \rightarrow p K^- \pi^+)]$  assuming  $B(\Lambda_c^+ \rightarrow p K^- \pi^+) = 0.05$ , which we rescale to our best value  $B(\Lambda_c^+ \rightarrow p K^- \pi^+) = (6.28 \pm 0.32) \times 10^{-2}$ . Our first error is their experiment's error and our second error is the systematic error from using our best value.

$\Gamma(\bar{A}_c^- \rho_s \pi^+)/\Gamma_{\text{total}}$	$\Gamma_{545}/\Gamma$		
VALUE (units $10^{-5}$ )	DOCUMENT ID	TECN	COMMENT
<b><math>3.1 \pm 0.7 \pm 0.2</math></b>	1 GABYSHEV 06A BELL	$e^+ e^- \rightarrow \Upsilon(4S)$	

$(\bar{A}_c^- \rho)_s$  denotes a low-mass enhancement near 3.35 GeV/c<sup>2</sup>.

1 GABYSHEV 06A reports  $(3.9 \pm 0.8 \pm 0.4) \times 10^{-5}$  from a measurement of  $[\Gamma(B^+ \rightarrow \bar{A}_c^- \rho_s \pi^+)/\Gamma_{\text{total}}] \times [B(\Lambda_c^+ \rightarrow p K^- \pi^+)]$  assuming  $B(\Lambda_c^+ \rightarrow p K^- \pi^+) = 0.05$ , which we rescale to our best value  $B(\Lambda_c^+ \rightarrow p K^- \pi^+) = (6.28 \pm 0.32) \times 10^{-2}$ . Our first error is their experiment's error and our second error is the systematic error from using our best value.

$\Gamma(\Sigma_c(2520)^0 \rho)/\Gamma_{\text{total}}$	$\Gamma_{546}/\Gamma$			
VALUE (units $10^{-5}$ )	CL%	DOCUMENT ID	TECN	COMMENT
<b><math>&lt;0.3</math></b>	90	1,2 AUBERT 08BN BABR	$e^+ e^- \rightarrow \Upsilon(4S)$	
$<2.7$	90	1,2 GABYSHEV 06A BELL	$e^+ e^- \rightarrow \Upsilon(4S)$	
$<4.6$	90	1,2 GABYSHEV 02 BELL	Repl. by GABYSHEV 06A	

- • • We do not use the following data for averages, fits, limits, etc. • • •
- 1 Assumes equal production of  $B^+$  and  $B^0$  at the  $\Upsilon(4S)$ .
- 2 Uses the value for  $\Lambda_c \rightarrow p K^- \pi^+$  branching ratio  $(5.0 \pm 1.3)\%$ .

$\Gamma(\Sigma_c(2520)^0 \rho)/\Gamma(\bar{A}_c^- \rho \pi^+)$	$\Gamma_{546}/\Gamma_{541}$			
VALUE (units $10^{-3}$ )	CL%	DOCUMENT ID	TECN	COMMENT
<b><math>&lt;9</math></b>	90	AUBERT 08BN BABR	$e^+ e^- \rightarrow \Upsilon(4S)$	

$\Gamma(\Sigma_c(2800)^0 \rho)/\Gamma_{\text{total}}$	$\Gamma_{547}/\Gamma$		
VALUE (units $10^{-5}$ )	DOCUMENT ID	TECN	COMMENT
<b><math>2.6 \pm 0.7 \pm 0.4</math></b>	1 AUBERT 08BN BABR	$e^+ e^- \rightarrow \Upsilon(4S)$	

1 AUBERT 08BN reports  $[\Gamma(B^+ \rightarrow \Sigma_c(2800)^0 \rho)/\Gamma_{\text{total}}] / [B(B^+ \rightarrow \bar{A}_c^- \rho \pi^+)] = 0.117 \pm 0.023 \pm 0.024$  which we multiply by our best value  $B(B^+ \rightarrow \bar{A}_c^- \rho \pi^+) = (2.3 \pm 0.4) \times 10^{-4}$ . Our first error is their experiment's error and our second error is the systematic error from using our best value.

$\Gamma(\bar{A}_c^- \rho \pi^+ \pi^0)/\Gamma_{\text{total}}$	$\Gamma_{548}/\Gamma$			
VALUE (units $10^{-3}$ )	CL%	DOCUMENT ID	TECN	COMMENT
<b><math>1.81 \pm 0.29 \pm 0.52 \pm 0.50</math></b>	1,2	DYTMAN 02 CLE2	$e^+ e^- \rightarrow \Upsilon(4S)$	

- • • We do not use the following data for averages, fits, limits, etc. • • •
- $<3.12$  90 3 FU 97 CLE2  $e^+ e^- \rightarrow \Upsilon(4S)$
- 1 Assumes equal production of  $B^+$  and  $B^0$  at the  $\Upsilon(4S)$ .
- 2 DYTMAN 02 measurement uses  $B(\Lambda_c^- \rightarrow \bar{p} K^+ \pi^-) = 5.0 \pm 1.3\%$ . The second error includes the systematic and the uncertainty of the branching ratio.
- 3 FU 97 uses PDG 96 values of  $\Lambda_c$  branching ratio.

$\Gamma(\bar{A}_c^- \rho \pi^+ \pi^+ \pi^-)/\Gamma_{\text{total}}$	$\Gamma_{549}/\Gamma$			
VALUE (units $10^{-3}$ )	CL%	DOCUMENT ID	TECN	COMMENT
<b><math>2.25 \pm 0.25 \pm 0.63 \pm 0.61</math></b>	1,2	DYTMAN 02 CLE2	$e^+ e^- \rightarrow \Upsilon(4S)$	

- • • We do not use the following data for averages, fits, limits, etc. • • •
- $<1.46$  90 3 FU 97 CLE2  $e^+ e^- \rightarrow \Upsilon(4S)$
- 1 Assumes equal production of  $B^+$  and  $B^0$  at the  $\Upsilon(4S)$ .
- 2 DYTMAN 02 measurement uses  $B(\Lambda_c^- \rightarrow \bar{p} K^+ \pi^-) = 5.0 \pm 1.3\%$ . The second error includes the systematic and the uncertainty of the branching ratio.
- 3 FU 97 uses PDG 96 values of  $\Lambda_c$  branching ratio.

$\Gamma(\bar{A}_c^- \rho \pi^+ \pi^+ \pi^- \pi^0)/\Gamma_{\text{total}}$	$\Gamma_{550}/\Gamma$			
VALUE	CL%	DOCUMENT ID	TECN	COMMENT
<b><math>&lt;1.34 \times 10^{-2}</math></b>	90	1 FU 97 CLE2	$e^+ e^- \rightarrow \Upsilon(4S)$	

- 1 FU 97 uses PDG 96 values of  $\Lambda_c$  branching ratio.

$\Gamma(A_c^+ \Lambda_c^- K^+)/\Gamma_{\text{total}}$	$\Gamma_{551}/\Gamma$		
VALUE (units $10^{-4}$ )	DOCUMENT ID	TECN	COMMENT
<b><math>4.9 \pm 0.7</math> OUR AVERAGE</b>			
$4.80 \pm 0.43 \pm 0.60$	LI 18A BELL	$e^+ e^- \rightarrow \Upsilon(4S)$	
$9.1 \pm 4.5 \pm 0.5$	1,2 AUBERT 08H BABR	$e^+ e^- \rightarrow \Upsilon(4S)$	

- • • We do not use the following data for averages, fits, limits, etc. • • •
- $6.3 \pm 2.5 \pm 0.3$  2,3 GABYSHEV 06 BELL Repl. by LI 18A.

1 AUBERT 08H reports  $(1.14 \pm 0.15 \pm 0.62) \times 10^{-3}$  from a measurement of  $[\Gamma(B^+ \rightarrow A_c^+ \Lambda_c^- K^+)/\Gamma_{\text{total}}] \times [B(\Lambda_c^+ \rightarrow p K^- \pi^+)]$  assuming  $B(\Lambda_c^+ \rightarrow p K^- \pi^+) = (5.0 \pm 1.3) \times 10^{-2}$ , which we rescale to our best value  $B(\Lambda_c^+ \rightarrow p K^- \pi^+) = (6.28 \pm 0.32) \times 10^{-2}$ . Our first error is their experiment's error and our second error is the systematic error from using our best value.

2 Assumes equal production of  $B^+$  and  $B^0$  at the  $\Upsilon(4S)$ .

3 GABYSHEV 06 reports  $(7.9 \pm 1.0 \pm 3.6) \times 10^{-4}$  from a measurement of  $[\Gamma(B^+ \rightarrow A_c^+ \Lambda_c^- K^+)/\Gamma_{\text{total}}] \times [B(\Lambda_c^+ \rightarrow p K^- \pi^+)]$  assuming  $B(\Lambda_c^+ \rightarrow p K^- \pi^+) = (5.0 \pm 1.3) \times 10^{-2}$ , which we rescale to our best value  $B(\Lambda_c^+ \rightarrow p K^- \pi^+) = (6.28 \pm 0.32) \times 10^{-2}$ . Our first error is their experiment's error and our second error is the systematic error from using our best value.

See key on page 999

Meson Particle Listings

$B^{\pm}$

$\Gamma(\Xi_c(2930)\Lambda_c^+ \Xi_c \rightarrow K^+\Lambda_c^-)/\Gamma_{total}$	$\Gamma_{552}/\Gamma$		
VALUE (units $10^{-4}$ )	DOCUMENT ID	TECN	COMMENT
<b>1.73 ± 0.45 ± 0.21</b>	1 LI	18A BELL	$e^+e^- \rightarrow \Upsilon(4S)$

<sup>1</sup> The  $\Xi_c(2930)$  is found in its decay to  $K^-\Lambda_c^+$  in  $B^- \rightarrow K^-\Lambda_c^+\Lambda_c^+$  with a significance more than 5 sigma.

$\Gamma(\Xi_c(2455)^0 \rho)/\Gamma_{total}$	$\Gamma_{553}/\Gamma$		
VALUE (units $10^{-5}$ )	CL%	DOCUMENT ID	TECN COMMENT
<b>2.9 ± 0.6 ± 0.2</b> <b>0.1</b>		1,2 GABYSHEV 06A BELL	$e^+e^- \rightarrow \Upsilon(4S)$

••• We do not use the following data for averages, fits, limits, etc. •••  
 <8 90 <sup>1,3</sup> DYTMAN 02 CLE2  $e^+e^- \rightarrow \Upsilon(4S)$   
 <9.3 90 <sup>1,4</sup> GABYSHEV 02 BELL Repl. by GABYSHEV 06A

<sup>1</sup> Assumes equal production of  $B^+$  and  $B^0$  at the  $\Upsilon(4S)$ .  
<sup>2</sup> GABYSHEV 06A reports  $(3.7 \pm 0.7 \pm 0.4) \times 10^{-5}$  from a measurement of  $[\Gamma(B^+ \rightarrow \Xi_c(2455)^0 \rho)/\Gamma_{total}] \times [B(\Lambda_c^+ \rightarrow pK^-\pi^+)]$  assuming  $B(\Lambda_c^+ \rightarrow pK^-\pi^+) = 0.05$ , which we rescale to our best value  $B(\Lambda_c^+ \rightarrow pK^-\pi^+) = (6.28 \pm 0.32) \times 10^{-2}$ . Our first error is their experiment's error and our second error is the systematic error from using our best value.  
<sup>3</sup> DYTMAN 02 measurement uses  $B(\Lambda_c^- \rightarrow \bar{p}K^+\pi^-) = 5.0 \pm 1.3\%$ . The second error includes the systematic and the uncertainty of the branching ratio.  
<sup>4</sup> Uses the value for  $\Lambda_c \rightarrow pK^-\pi^+$  branching ratio (5.0 ± 1.3)%.

$\Gamma(\Xi_c(2455)^0 \rho)/\Gamma(\Lambda_c^- \rho \pi^+)$	$\Gamma_{553}/\Gamma_{541}$		
VALUE	DOCUMENT ID	TECN	COMMENT
<b>0.123 ± 0.012 ± 0.008</b>	1 AUBERT	08BN BABR	$e^+e^- \rightarrow \Upsilon(4S)$

<sup>1</sup> Assumes equal production of  $B^+$  and  $B^0$  at the  $\Upsilon(4S)$ .

$\Gamma(\Xi_c(2455)^0 \rho \pi^0)/\Gamma_{total}$	$\Gamma_{554}/\Gamma$		
VALUE (units $10^{-4}$ )	DOCUMENT ID	TECN	COMMENT
<b>3.5 ± 1.1 ± 0.2</b>	1,2 DYTMAN 02	CLE2	$e^+e^- \rightarrow \Upsilon(4S)$

<sup>1</sup> DYTMAN 02 reports  $(4.4 \pm 1.4) \times 10^{-4}$  from a measurement of  $[\Gamma(B^+ \rightarrow \Xi_c(2455)^0 \rho \pi^0)/\Gamma_{total}] \times [B(\Lambda_c^+ \rightarrow pK^-\pi^+)]$  assuming  $B(\Lambda_c^+ \rightarrow pK^-\pi^+) = 0.05$ , which we rescale to our best value  $B(\Lambda_c^+ \rightarrow pK^-\pi^+) = (6.28 \pm 0.32) \times 10^{-2}$ . Our first error is their experiment's error and our second error is the systematic error from using our best value.  
<sup>2</sup> Assumes equal production of  $B^+$  and  $B^0$  at the  $\Upsilon(4S)$ .

$\Gamma(\Xi_c(2455)^0 \rho \pi^+ \pi^+)/\Gamma_{total}$	$\Gamma_{555}/\Gamma$		
VALUE (units $10^{-4}$ )	DOCUMENT ID	TECN	COMMENT
<b>3.5 ± 1.0 ± 0.2</b>	1,2 DYTMAN 02	CLE2	$e^+e^- \rightarrow \Upsilon(4S)$

<sup>1</sup> DYTMAN 02 reports  $(4.4 \pm 1.3) \times 10^{-4}$  from a measurement of  $[\Gamma(B^+ \rightarrow \Xi_c(2455)^0 \rho \pi^+ \pi^+)/\Gamma_{total}] \times [B(\Lambda_c^+ \rightarrow pK^-\pi^+)]$  assuming  $B(\Lambda_c^+ \rightarrow pK^-\pi^+) = 0.05$ , which we rescale to our best value  $B(\Lambda_c^+ \rightarrow pK^-\pi^+) = (6.28 \pm 0.32) \times 10^{-2}$ . Our first error is their experiment's error and our second error is the systematic error from using our best value.  
<sup>2</sup> Assumes equal production of  $B^+$  and  $B^0$  at the  $\Upsilon(4S)$ .

$\Gamma(\Xi_c(2455)^- \rho \pi^+ \pi^+)/\Gamma_{total}$	$\Gamma_{556}/\Gamma$		
VALUE (units $10^{-4}$ )	DOCUMENT ID	TECN	COMMENT
<b>2.37 ± 0.20 OUR AVERAGE</b>			

2.37 ± 0.16 ± 0.13 -0.12	1,2 LEES	12Z BABR	$e^+e^- \rightarrow \Upsilon(4S)$
2.2 ± 0.8 ± 0.1	1,3 DYTMAN 02	CLE2	$e^+e^- \rightarrow \Upsilon(4S)$

<sup>1</sup> Assumes equal production of  $B^+$  and  $B^0$  at the  $\Upsilon(4S)$ .  
<sup>2</sup> LEES 12Z reports  $(2.98 \pm 0.16 \pm 0.15 \pm 0.77) \times 10^{-4}$  from a measurement of  $[\Gamma(B^+ \rightarrow \Xi_c(2455)^- \rho \pi^+ \pi^+)/\Gamma_{total}] \times [B(\Lambda_c^+ \rightarrow pK^-\pi^+)]$  assuming  $B(\Lambda_c^+ \rightarrow pK^-\pi^+) = (5.0 \pm 1.3) \times 10^{-2}$ , which we rescale to our best value  $B(\Lambda_c^+ \rightarrow pK^-\pi^+) = (6.28 \pm 0.32) \times 10^{-2}$ . Our first error is their experiment's error and our second error is the systematic error from using our best value.  
<sup>3</sup> DYTMAN 02 reports  $(2.8 \pm 0.9 \pm 0.5 \pm 0.7) \times 10^{-4}$  from a measurement of  $[\Gamma(B^+ \rightarrow \Xi_c(2455)^- \rho \pi^+ \pi^+)/\Gamma_{total}] \times [B(\Lambda_c^+ \rightarrow pK^-\pi^+)]$  assuming  $B(\Lambda_c^+ \rightarrow pK^-\pi^+) = (5.0 \pm 1.3) \times 10^{-2}$ , which we rescale to our best value  $B(\Lambda_c^+ \rightarrow pK^-\pi^+) = (6.28 \pm 0.32) \times 10^{-2}$ . Our first error is their experiment's error and our second error is the systematic error from using our best value.

$\Gamma(\Lambda_c(2593)^- / \Lambda_c(2625)^- \rho \pi^+)/\Gamma_{total}$	$\Gamma_{557}/\Gamma$		
VALUE	CL%	DOCUMENT ID	TECN COMMENT
<b>&lt; 1.9 × 10<sup>-4</sup></b>	90	1,2 DYTMAN 02	CLE2 $e^+e^- \rightarrow \Upsilon(4S)$

<sup>1</sup> Assumes equal production of  $B^+$  and  $B^0$  at the  $\Upsilon(4S)$ .  
<sup>2</sup> DYTMAN 02 measurement uses  $B(\Lambda_c^- \rightarrow \bar{p}K^+\pi^-) = 5.0 \pm 1.3\%$ . The second error includes the systematic and the uncertainty of the branching ratio.

$\Gamma(\Xi_c^0 \Lambda_c^+)/\Gamma_{total}$	$\Gamma_{558}/\Gamma$		
VALUE (units $10^{-4}$ )	DOCUMENT ID	TECN	COMMENT
<b>9.51 ± 2.10 ± 0.88</b>	1 LI	19A BELL	$e^+e^- \rightarrow \Upsilon(4S)$

<sup>1</sup> First measured the absolute branching fraction using a missing-mass technique.

$\Gamma(\Xi_c^0 \Lambda_c^+, \Xi_c^0 \rightarrow \Xi^+ \pi^-)/\Gamma_{total}$	$\Gamma_{559}/\Gamma$		
VALUE (units $10^{-5}$ )	DOCUMENT ID	TECN	COMMENT
<b>1.76 ± 0.29 OUR AVERAGE</b>			

1.71 ± 0.28 ± 0.15	1 LI	19A BELL	$e^+e^- \rightarrow \Upsilon(4S)$
2.0 ± 0.7 ± 0.1	2,3 AUBERT	08H BABR	$e^+e^- \rightarrow \Upsilon(4S)$
4.5 <sup>+1.8</sup> <sub>-1.5</sub> ± 0.2	3,4 CHISTOV	06A BELL	Repl. by LI 19A

<sup>1</sup> Using a hadronic  $B$ -tagging method based on a full reconstruction.  
<sup>2</sup> AUBERT 08H reports  $(2.51 \pm 0.89 \pm 0.61) \times 10^{-5}$  from a measurement of  $[\Gamma(B^+ \rightarrow \Xi_c^0 \Lambda_c^+, \Xi_c^0 \rightarrow \Xi^+ \pi^-)/\Gamma_{total}] \times [B(\Lambda_c^+ \rightarrow pK^-\pi^+)]$  assuming  $B(\Lambda_c^+ \rightarrow pK^-\pi^+) = (5.0 \pm 1.3) \times 10^{-2}$ , which we rescale to our best value  $B(\Lambda_c^+ \rightarrow pK^-\pi^+) = (6.28 \pm 0.32) \times 10^{-2}$ . Our first error is their experiment's error and our second error is the systematic error from using our best value.  
<sup>3</sup> Assumes equal production of  $B^+$  and  $B^0$  at the  $\Upsilon(4S)$ .  
<sup>4</sup> CHISTOV 06A reports  $(5.6 <sup>+1.9</sup><sub>-1.5</sub>) \times 10^{-5}$  from a measurement of  $[\Gamma(B^+ \rightarrow \Xi_c^0 \Lambda_c^+, \Xi_c^0 \rightarrow \Xi^+ \pi^-)/\Gamma_{total}] \times [B(\Lambda_c^+ \rightarrow pK^-\pi^+)]$  assuming  $B(\Lambda_c^+ \rightarrow pK^-\pi^+) = (5.0 \pm 1.3) \times 10^{-2}$ , which we rescale to our best value  $B(\Lambda_c^+ \rightarrow pK^-\pi^+) = (6.28 \pm 0.32) \times 10^{-2}$ . Our first error is their experiment's error and our second error is the systematic error from using our best value.

$\Gamma(\Xi_c^0 \Lambda_c^+, \Xi_c^0 \rightarrow \Lambda K^+ \pi^-)/\Gamma_{total}$	$\Gamma_{560}/\Gamma$		
VALUE (units $10^{-5}$ )	DOCUMENT ID	TECN	COMMENT
<b>1.14 ± 0.26 OUR AVERAGE</b>			

1.11 ± 0.26 ± 0.10	1 LI	19A BELL	$e^+e^- \rightarrow \Upsilon(4S)$
1.4 ± 0.8 ± 0.1	2,3 AUBERT	08H BABR	$e^+e^- \rightarrow \Upsilon(4S)$
3.2 <sup>+1.1</sup> <sub>-0.9</sub> ± 0.2	3,4 CHISTOV	06A BELL	Repl. by LI 19A

<sup>1</sup> Using a hadronic  $B$ -tagging method based on a full reconstruction.  
<sup>2</sup> AUBERT 08H reports  $(1.70 \pm 0.93 \pm 0.53) \times 10^{-5}$  from a measurement of  $[\Gamma(B^+ \rightarrow \Xi_c^0 \Lambda_c^+, \Xi_c^0 \rightarrow \Lambda K^+ \pi^-)/\Gamma_{total}] \times [B(\Lambda_c^+ \rightarrow pK^-\pi^+)]$  assuming  $B(\Lambda_c^+ \rightarrow pK^-\pi^+) = (5.0 \pm 1.3) \times 10^{-2}$ , which we rescale to our best value  $B(\Lambda_c^+ \rightarrow pK^-\pi^+) = (6.28 \pm 0.32) \times 10^{-2}$ . Our first error is their experiment's error and our second error is the systematic error from using our best value.  
<sup>3</sup> Assumes equal production of  $B^+$  and  $B^0$  at the  $\Upsilon(4S)$ .  
<sup>4</sup> CHISTOV 06A reports  $(4.0 <sup>+1.1</sup><sub>-0.9</sub>) \times 10^{-5}$  from a measurement of  $[\Gamma(B^+ \rightarrow \Xi_c^0 \Lambda_c^+, \Xi_c^0 \rightarrow \Lambda K^+ \pi^-)/\Gamma_{total}] \times [B(\Lambda_c^+ \rightarrow pK^-\pi^+)]$  assuming  $B(\Lambda_c^+ \rightarrow pK^-\pi^+) = (5.0 \pm 1.3) \times 10^{-2}$ , which we rescale to our best value  $B(\Lambda_c^+ \rightarrow pK^-\pi^+) = (6.28 \pm 0.32) \times 10^{-2}$ . Our first error is their experiment's error and our second error is the systematic error from using our best value.

$\Gamma(\Xi_c^0 \Lambda_c^+, \Xi_c^0 \rightarrow \rho K^- K^+ \pi^+)/\Gamma_{total}$	$\Gamma_{561}/\Gamma$		
VALUE (units $10^{-6}$ )	DOCUMENT ID	TECN	COMMENT
<b>5.47 ± 1.78 ± 0.57</b>	1 LI	19A BELL	$e^+e^- \rightarrow \Upsilon(4S)$

<sup>1</sup> Using a hadronic  $B$ -tagging method based on a full reconstruction.

$\Gamma(\Lambda_c^+ \Xi_c^0)/\Gamma_{total}$	$\Gamma_{562}/\Gamma$		
VALUE	CL%	DOCUMENT ID	TECN COMMENT
<b>&lt; 6.5 × 10<sup>-4</sup></b>	90	1 LI	19G BELL $e^+e^- \rightarrow \Upsilon(4S)$

<sup>1</sup> Uses fully reconstructed  $B^+$  meson on tag side and recoil against  $\Lambda_c^+$  on signal side.

$\Gamma(\Lambda_c^+ \Xi_c(2645)^0)/\Gamma_{total}$	$\Gamma_{563}/\Gamma$		
VALUE	CL%	DOCUMENT ID	TECN COMMENT
<b>&lt; 7.9 × 10<sup>-4</sup></b>	90	1 LI	19G BELL $e^+e^- \rightarrow \Upsilon(4S)$

<sup>1</sup> Uses fully reconstructed  $B^+$  meson on tag side and recoil against  $\Lambda_c^+$  on signal side.

$\Gamma(\Lambda_c^+ \Xi_c(2790)^0)/\Gamma_{total}$	$\Gamma_{564}/\Gamma$		
VALUE (units $10^{-3}$ )	DOCUMENT ID	TECN	COMMENT
<b>1.1 ± 0.4 ± 0.2</b>	1 LI	19G BELL	$e^+e^- \rightarrow \Upsilon(4S)$

<sup>1</sup> Uses fully reconstructed  $B^+$  meson on tag side and recoil against  $\Lambda_c^+$  on signal side.

$\Gamma(\pi^+ \ell^+ \ell^-)/\Gamma_{total}$	$\Gamma_{565}/\Gamma$		
VALUE	CL%	DOCUMENT ID	TECN COMMENT
<b>&lt; 4.9 × 10<sup>-8</sup></b>	90	1 WEI	08A BELL $e^+e^- \rightarrow \Upsilon(4S)$

••• We do not use the following data for averages, fits, limits, etc. •••  
 <6.6 × 10<sup>-8</sup> 90 <sup>1</sup> LEES 13M BABR  $e^+e^- \rightarrow \Upsilon(4S)$   
 <1.2 × 10<sup>-7</sup> 90 <sup>1</sup> AUBERT 07AG BABR  $e^+e^- \rightarrow \Upsilon(4S)$   
<sup>1</sup> Assumes equal production of  $B^+$  and  $B^0$  at the  $\Upsilon(4S)$ .

$\Gamma(\pi^+ e^+ e^-)/\Gamma_{total}$	$\Gamma_{566}/\Gamma$		
VALUE	CL%	DOCUMENT ID	TECN COMMENT
<b>&lt; 8.0 × 10<sup>-8</sup></b>	90	1 WEI	08A BELL $e^+e^- \rightarrow \Upsilon(4S)$

••• We do not use the following data for averages, fits, limits, etc. •••  
 <12.5 × 10<sup>-8</sup> 90 <sup>1</sup> LEES 13M BABR  $e^+e^- \rightarrow \Upsilon(4S)$   
 <18 × 10<sup>-8</sup> 90 <sup>1</sup> AUBERT 07AG BABR  $e^+e^- \rightarrow \Upsilon(4S)$   
 < 3.9 × 10<sup>-3</sup> 90 <sup>2</sup> WEIR 90B MRK2  $e^+e^-$  29 GeV  
<sup>1</sup> Assumes equal production of  $B^+$  and  $B^0$  at the  $\Upsilon(4S)$ .  
<sup>2</sup> WEIR 90B assumes  $B^+$  production cross section from LUND.

# Meson Particle Listings

$B^\pm$

## $\Gamma(\pi^+ \mu^+ \mu^-) / \Gamma_{\text{total}}$ Γ<sub>567</sub>/Γ

Test for  $\Delta B=1$  weak neutral current. Allowed by higher-order electroweak interactions.

VALUE (units $10^{-8}$ )	CL%	DOCUMENT ID	TECN	COMMENT
<b>1.75 ± 0.22 ± 0.05</b>		<sup>1</sup> AAIJ	15AR LHCb	$pp$ at 7, 8 TeV
< 5.5	90	<sup>2</sup> LEES	13M BABR	$e^+e^- \rightarrow \Upsilon(4S)$
2.3 ± 0.6 ± 0.1		AAIJ	12AY LHCb	Repl. by AAIJ 15AR
< 6.9	90	<sup>2</sup> WEI	08A BELL	$e^+e^- \rightarrow \Upsilon(4S)$
< 28	90	<sup>2</sup> AUBERT	07AG BABR	$e^+e^- \rightarrow \Upsilon(4S)$

<sup>1</sup> AAIJ 15AR reports  $(1.83 \pm 0.24 \pm 0.05) \times 10^{-8}$  from a measurement of  $[\Gamma(B^+ \rightarrow \pi^+ \mu^+ \mu^-) / \Gamma_{\text{total}}] / [B(B^+ \rightarrow J/\psi(1S) K^+) / [B(J/\psi(1S) \rightarrow \mu^+ \mu^-)]]$  assuming  $B(B^+ \rightarrow J/\psi(1S) K^+) = (1.05 \pm 0.05) \times 10^{-3}$ ,  $B(J/\psi(1S) \rightarrow \mu^+ \mu^-) = (5.961 \pm 0.033) \times 10^{-2}$ , which we rescale to our best values  $B(B^+ \rightarrow J/\psi(1S) K^+) = (1.006 \pm 0.027) \times 10^{-3}$ ,  $B(J/\psi(1S) \rightarrow \mu^+ \mu^-) = (5.961 \pm 0.033) \times 10^{-2}$ . Our first error is their experiment's error and our second error is the systematic error from using our best values.

<sup>2</sup> Assumes equal production of  $B^+$  and  $B^0$  at the  $\Upsilon(4S)$ .

## $\Gamma(\pi^+ \mu^+ \mu^-) / \Gamma(K^+ \mu^+ \mu^-)$ Γ<sub>567</sub>/Γ<sub>571</sub>

VALUE	DOCUMENT ID	TECN	COMMENT
0.053 ± 0.014 ± 0.001	AAIJ	12AY LHCb	Repl. by AAIJ 15AR

## $\Gamma(\pi^+ \nu \bar{\nu}) / \Gamma_{\text{total}}$ Γ<sub>568</sub>/Γ

Test for  $\Delta B=1$  weak neutral current. Allowed by higher-order electroweak interactions.

VALUE	CL%	DOCUMENT ID	TECN	COMMENT
<b>&lt; 1.4 × 10<sup>-5</sup></b>	90	<sup>1</sup> GRYGIER	17 BELL	$e^+e^- \rightarrow \Upsilon(4S)$
< 9.8 × 10 <sup>-5</sup>	90	<sup>1</sup> LUTZ	13 BELL	$e^+e^- \rightarrow \Upsilon(4S)$
< 1.7 × 10 <sup>-4</sup>	90	<sup>1</sup> CHEN	07D BELL	$e^+e^- \rightarrow \Upsilon(4S)$
< 1.0 × 10 <sup>-4</sup>	90	<sup>1</sup> AUBERT	05H BABR	$e^+e^- \rightarrow \Upsilon(4S)$

<sup>1</sup> Assumes equal production of  $B^+$  and  $B^0$  at the  $\Upsilon(4S)$ .

## $\Gamma(K^+ \ell^+ \ell^-) / \Gamma_{\text{total}}$ Γ<sub>569</sub>/Γ

Test for  $\Delta B=1$  weak neutral current. Allowed by higher-order electroweak interactions.

VALUE (units $10^{-7}$ )	DOCUMENT ID	TECN	COMMENT
<b>4.51 ± 0.23 OUR AVERAGE</b>	Error includes scale factor of 1.1.		
4.36 ± 0.15 ± 0.18	<sup>1</sup> AAIJ	13H LHCb	$pp$ at 7 TeV
4.8 ± 0.9 ± 0.2	<sup>2</sup> AUBERT	09T BABR	$e^+e^- \rightarrow \Upsilon(4S)$
5.3 <sup>+0.6</sup> / <sub>-0.5</sub> ± 0.3	<sup>2</sup> WEI	09A BELL	$e^+e^- \rightarrow \Upsilon(4S)$

<sup>1</sup> Uses  $B(B^+ \rightarrow J/\psi K^+ \rightarrow \mu^+ \mu^- K^+) = (6.01 \pm 0.21) \times 10^{-5}$ .

<sup>2</sup> Assumes equal production of  $B^+$  and  $B^0$  at the  $\Upsilon(4S)$ .

## $\Gamma(K^+ e^+ e^-) / \Gamma_{\text{total}}$ Γ<sub>570</sub>/Γ

Test for  $\Delta B=1$  weak neutral current. Allowed by higher-order electroweak interactions.

VALUE (units $10^{-7}$ )	CL%	DOCUMENT ID	TECN	COMMENT
<b>5.5 ± 0.7 OUR AVERAGE</b>				
5.1 <sup>+1.2</sup> / <sub>-1.1</sub> ± 0.2		<sup>1</sup> AUBERT	09T BABR	$e^+e^- \rightarrow \Upsilon(4S)$
5.7 <sup>+0.9</sup> / <sub>-0.8</sub> ± 0.3		<sup>1</sup> WEI	09A BELL	$e^+e^- \rightarrow \Upsilon(4S)$
< 14	90	<sup>1</sup> AUBERT,B	06J BABR	Repl. by AUBERT 09T
< 9	90	<sup>1</sup> AUBERT	03U BABR	Repl. by AUBERT,B 06J
< 24	90	<sup>3</sup> ANDERSON	01B CLE2	$e^+e^- \rightarrow \Upsilon(4S)$
< 990	90	<sup>4</sup> ALBRECHT	91E ARG	$e^+e^- \rightarrow \Upsilon(4S)$
< 68000	90	<sup>5</sup> WEIR	90B MRK2	$e^+e^-$ 29 GeV
< 600	90	<sup>6</sup> AVERY	89B CLEO	$e^+e^- \rightarrow \Upsilon(4S)$
< 2500	90	<sup>7</sup> AVERY	87 CLEO	$e^+e^- \rightarrow \Upsilon(4S)$

<sup>1</sup> Assumes equal production of  $B^+$  and  $B^0$  at the  $\Upsilon(4S)$ .

<sup>2</sup> Assumes equal production of  $B^0$  and  $B^+$  at  $\Upsilon(4S)$ . The second error is a total of systematic uncertainties including model dependence.

<sup>3</sup> The result is for di-lepton masses above 0.5 GeV.

<sup>4</sup> ALBRECHT 91E reports  $< 9.0 \times 10^{-5}$  assuming the  $\Upsilon(4S)$  decays 45% to  $B^0 \bar{B}^0$ . We rescale to 50%.

<sup>5</sup> WEIR 90B assumes  $B^+$  production cross section from LUND.

<sup>6</sup> AVERY 89B reports  $< 5 \times 10^{-5}$  assuming the  $\Upsilon(4S)$  decays 43% to  $B^0 \bar{B}^0$ . We rescale to 50%.

<sup>7</sup> AVERY 87 reports  $< 2.1 \times 10^{-4}$  assuming the  $\Upsilon(4S)$  decays 40% to  $B^0 \bar{B}^0$ . We rescale to 50%.

## $\Gamma(K^+ \mu^+ \mu^-) / \Gamma_{\text{total}}$ Γ<sub>571</sub>/Γ

Test for  $\Delta B=1$  weak neutral current. Allowed by higher-order electroweak interactions.

VALUE (units $10^{-7}$ )	CL%	DOCUMENT ID	TECN	COMMENT
<b>4.41 ± 0.22 OUR FIT</b>		Error includes scale factor of 1.2.		
<b>4.36 ± 0.27 OUR AVERAGE</b>		Error includes scale factor of 1.3.		
4.29 ± 0.07 ± 0.21		<sup>1</sup> AAIJ	14M LHCb	$pp$ at 7, 8 TeV
4.1 <sup>+1.6</sup> / <sub>-1.5</sub> ± 0.2		<sup>2</sup> AUBERT	09T BABR	$e^+e^- \rightarrow \Upsilon(4S)$
5.3 <sup>+0.8</sup> / <sub>-0.7</sub> ± 0.3		<sup>2</sup> WEI	09A BELL	$e^+e^- \rightarrow \Upsilon(4S)$
< 12	90	<sup>2</sup> AUBERT	02L BABR	$e^+e^- \rightarrow \Upsilon(4S)$
< 36.8	90	<sup>5</sup> ANDERSON	01B CLE2	$e^+e^- \rightarrow \Upsilon(4S)$
< 52	90	<sup>6</sup> AFFOLDER	99B CDF	$p\bar{p}$ at 1.8 TeV
< 100	90	<sup>7</sup> ABE	96L CDF	Repl. by AFFOLDER 99B
< 2400	90	<sup>8</sup> ALBRECHT	91E ARG	$e^+e^- \rightarrow \Upsilon(4S)$
< 64000	90	<sup>9</sup> WEIR	90B MRK2	$e^+e^-$ 29 GeV
< 1700	90	<sup>10</sup> AVERY	89B CLEO	$e^+e^- \rightarrow \Upsilon(4S)$
< 3800	90	<sup>11</sup> AVERY	87 CLEO	$e^+e^- \rightarrow \Upsilon(4S)$

<sup>1</sup> Uses  $B(B^+ \rightarrow J/\psi(1S) K^+) = (0.998 \pm 0.014 \pm 0.040) \times 10^{-3}$  for normalization.

<sup>2</sup> Assumes equal production of  $B^+$  and  $B^0$  at the  $\Upsilon(4S)$ .

<sup>3</sup> Uses  $B(B^+ \rightarrow J/\psi K^+ \rightarrow \mu^+ \mu^- K^+) = (6.01 \pm 0.21) \times 10^{-5}$ .

<sup>4</sup> Assumes equal production of  $B^0$  and  $B^+$  at  $\Upsilon(4S)$ . The second error is a total of systematic uncertainties including model dependence.

<sup>5</sup> The result is for di-lepton masses above 0.5 GeV.

<sup>6</sup> AFFOLDER 99B measured relative to  $B^+ \rightarrow J/\psi(1S) K^+$ .

<sup>7</sup> ABE 96L measured relative to  $B^+ \rightarrow J/\psi(1S) K^+$  using PDG 94 branching ratios.

<sup>8</sup> ALBRECHT 91E reports  $< 2.2 \times 10^{-4}$  assuming the  $\Upsilon(4S)$  decays 45% to  $B^0 \bar{B}^0$ . We rescale to 50%.

<sup>9</sup> WEIR 90B assumes  $B^+$  production cross section from LUND.

<sup>10</sup> AVERY 89B reports  $< 1.5 \times 10^{-4}$  assuming the  $\Upsilon(4S)$  decays 43% to  $B^0 \bar{B}^0$ . We rescale to 50%.

<sup>11</sup> AVERY 87 reports  $< 3.2 \times 10^{-4}$  assuming the  $\Upsilon(4S)$  decays 40% to  $B^0 \bar{B}^0$ . We rescale to 50%.

## $\Gamma(K^+ \mu^+ \mu^- \text{ nonresonant}) / \Gamma_{\text{total}}$ Γ<sub>572</sub>/Γ

VALUE (units $10^{-7}$ )	DOCUMENT ID	TECN	COMMENT
<b>4.37 ± 0.15 ± 0.23</b>	<sup>1</sup> AAIJ	17Y LHCb	$pp$ at 7, 8 TeV

<sup>1</sup> Measured in amplitude analysis using model including short-distance  $K^+ \mu^+ \mu^-$  and  $\rho(770)$ ,  $\omega(782)$ ,  $\phi(1020)$ ,  $J/\psi$ ,  $\psi(2S)$ ,  $\psi(3770)$ ,  $\psi(4040)$ ,  $\psi(4160)$ , and  $\psi(4415)$  contributions.

## $\Gamma(K^+ \tau^+ \tau^-) / \Gamma_{\text{total}}$ Γ<sub>573</sub>/Γ

VALUE	CL%	DOCUMENT ID	TECN	COMMENT
<b>&lt; 2.25 × 10<sup>-3</sup></b>	90	<sup>1,2</sup> LEES	17 BABR	$e^+e^- \rightarrow \Upsilon(4S)$

<sup>1</sup> Uses only leptonic decays of  $\tau$  and the quoted limit combines the final states  $K^+ e^+ e^-$ ,  $K^+ \mu^+ \mu^-$ , and  $K^+ e^\pm \mu^\mp$ .

<sup>2</sup> If observed events are interpreted as a signal the branching fraction measurement becomes  $(1.31^{+0.66+0.35}_{-0.61-0.25}) \times 10^{-3}$ .

## $\Gamma(K^+ \mu^+ \mu^-) / \Gamma(J/\psi(1S) K^+)$ Γ<sub>571</sub>/Γ<sub>275</sub>

VALUE (units $10^{-3}$ )	DOCUMENT ID	TECN	COMMENT
<b>0.439 ± 0.024 OUR FIT</b>	Error includes scale factor of 1.1.		
<b>0.46 ± 0.04 ± 0.02</b>	AALTONEN	11A CDF	$p\bar{p}$ at 1.96 TeV
< 0.38 ± 0.05 ± 0.02	AALTONEN	11L CDF	Repl. by AALTONEN 11A
0.59 ± 0.15 ± 0.03	AALTONEN	09B CDF	Repl. by AALTONEN 11L

## $\Gamma(K^+ \nu \bar{\nu}) / \Gamma_{\text{total}}$ Γ<sub>574</sub>/Γ

Test for  $\Delta B=1$  weak neutral current. Allowed by higher-order electroweak interactions.

VALUE	CL%	DOCUMENT ID	TECN	COMMENT
<b>&lt; 1.6 × 10<sup>-5</sup></b>	90	<sup>1,2</sup> LEES	13I BABR	$e^+e^- \rightarrow \Upsilon(4S)$
< 1.9 × 10 <sup>-5</sup>	90	<sup>1,3</sup> GRYGIER	17 BELL	$e^+e^- \rightarrow \Upsilon(4S)$
< 5.5 × 10 <sup>-5</sup>	90	<sup>1</sup> LUTZ	13 BELL	$e^+e^- \rightarrow \Upsilon(4S)$
< 1.3 × 10 <sup>-5</sup>	90	<sup>1</sup> DEL-AMO-SAL0Q	BABR	Repl. by LEES 13I
< 1.4 × 10 <sup>-5</sup>	90	<sup>1</sup> CHEN	07D BELL	$e^+e^- \rightarrow \Upsilon(4S)$
< 5.2 × 10 <sup>-5</sup>	90	<sup>1</sup> AUBERT	05H BABR	$e^+e^- \rightarrow \Upsilon(4S)$
< 2.4 × 10 <sup>-4</sup>	90	<sup>1</sup> BROWDER	01 CLE2	$e^+e^- \rightarrow \Upsilon(4S)$

<sup>1</sup> Assumes equal production of  $B^+$  and  $B^0$  at the  $\Upsilon(4S)$ .

<sup>2</sup> Also reported a limit  $< 3.7 \times 10^{-5}$  at 90% CL obtained using a fully reconstructed hadronic  $B$ -tag events.

<sup>3</sup> The result was reported in arXiv:1702.03224, but missing from the publication by mistake.

Γ(ρ±ν̄)/Γtotal Γ575/Γ

Table with columns: VALUE (units 10^-7), CL%, DOCUMENT ID, TECN, COMMENT. Includes entries for GRYGIER, BELL, LUTZ, CHEN and a note about equal production of B+ and B0.

Γ(K\*(892)+ℓ+ℓ-)/Γtotal Γ576/Γ

Table with columns: VALUE (units 10^-7), CL%, DOCUMENT ID, TECN, COMMENT. Includes OUR AVERAGE and entries for AAIJ, AUBERT, WEI, AAIJ, AUBERT, ISHIKAWA.

Γ(K\*(892)+e+e-)/Γtotal Γ577/Γ

Table with columns: VALUE (units 10^-7), CL%, DOCUMENT ID, TECN, COMMENT. Includes OUR AVERAGE and entries for AUBERT, WEI, AUBERT, ISHIKAWA, ABE, AUBERT, ALBRECHT.

Γ(K\*(892)+μ+μ-)/Γtotal Γ578/Γ

Table with columns: VALUE (units 10^-7), CL%, DOCUMENT ID, TECN, COMMENT. Includes OUR FIT and OUR AVERAGE, and entries for AAIJ, AUBERT, WEI, AAIJ, AUBERT, AUBERT, ISHIKAWA, ABE, AUBERT.

Γ(K\*(892)+μ+μ-)/Γ(J/ψ(1S)K\*(892)+) Γ578/Γ280

Table with columns: VALUE (units 10^-3), DOCUMENT ID, TECN, COMMENT. Includes OUR FIT and entry for AALTONEN.

Γ(K\*(892)+ν̄)/Γtotal Γ579/Γ

Table with columns: VALUE (units 10^-4), CL%, DOCUMENT ID, TECN, COMMENT. Includes entries for LUTZ, GRYGIER, LEES, AUBERT, CHEN and a note about equal production of B+ and B0.

Γ(K+π+π-μ+μ-)/Γ(ψ(2S)K+) Γ580/Γ311

Table with columns: VALUE (units 10^-4), DOCUMENT ID, TECN, COMMENT. Includes entry for AAIJ.

Γ(φK+μ+μ-)/Γ(J/ψ(1S)φK+) Γ581/Γ287

Table with columns: VALUE (units 10^-3), DOCUMENT ID, TECN, COMMENT. Includes entry for AAIJ.

Γ(Λ̄pν̄)/Γtotal Γ582/Γ

Table with columns: VALUE (units 10^-5), CL%, DOCUMENT ID, TECN, COMMENT. Includes entry for LEES and a note about signal candidates.

Γ(π+e+μ-)/Γtotal Γ583/Γ

Table with columns: VALUE (units 10^-6), CL%, DOCUMENT ID, TECN, COMMENT. Includes entry for WEIR and a note about production cross section.

Γ(π+e-μ+)/Γtotal Γ584/Γ

Table with columns: VALUE (units 10^-6), CL%, DOCUMENT ID, TECN, COMMENT. Includes entry for WEIR and a note about production cross section.

Γ(π+e±μ∓)/Γtotal Γ585/Γ

Table with columns: VALUE (units 10^-7), CL%, DOCUMENT ID, TECN, COMMENT. Includes entry for AUBERT and a note about equal production of B+ and B0.

Γ(π+e+τ-)/Γtotal Γ586/Γ

Table with columns: VALUE (units 10^-6), CL%, DOCUMENT ID, TECN, COMMENT. Includes entry for LEES and a note about fully reconstructed hadronic B decay.

Γ(π+e-τ+)/Γtotal Γ587/Γ

Table with columns: VALUE (units 10^-6), CL%, DOCUMENT ID, TECN, COMMENT. Includes entry for LEES and a note about fully reconstructed hadronic B decay.

Γ(π+e±τ∓)/Γtotal Γ588/Γ

Table with columns: VALUE (units 10^-6), CL%, DOCUMENT ID, TECN, COMMENT. Includes entry for LEES and notes about B(B+ to h+ℓ+τ-) and fully reconstructed hadronic B decay.

Γ(π+μ+τ-)/Γtotal Γ589/Γ

Table with columns: VALUE (units 10^-6), CL%, DOCUMENT ID, TECN, COMMENT. Includes entry for LEES and a note about fully reconstructed hadronic B decay.

Γ(π+μ-τ+)/Γtotal Γ590/Γ

Table with columns: VALUE (units 10^-6), CL%, DOCUMENT ID, TECN, COMMENT. Includes entry for LEES and a note about fully reconstructed hadronic B decay.

Γ(π+μ±τ∓)/Γtotal Γ591/Γ

Table with columns: VALUE (units 10^-6), CL%, DOCUMENT ID, TECN, COMMENT. Includes entry for LEES and notes about B(B+ to h+ℓ+τ-) and fully reconstructed hadronic B decay.

Downloaded from https://academic.oup.com/ptep/article/2020/8/083C01/5891211 by guest on 12 November 2020

## Meson Particle Listings

 $B^\pm$  $\Gamma(K^+ e^+ \mu^-)/\Gamma_{\text{total}}$   $\Gamma_{592}/\Gamma$ 

Test of lepton family number conservation.

VALUE	CL%	DOCUMENT ID	TECN	COMMENT
$<7.0 \times 10^{-9}$	90	AAIJ	19AMLHCB	$pp$ at 7, 8 TeV
••• We do not use the following data for averages, fits, limits, etc. •••				
$<0.91 \times 10^{-7}$	90	<sup>1</sup> AUBERT,B	06J BABR	$e^+ e^- \rightarrow \Upsilon(4S)$
$<8 \times 10^{-7}$	90	<sup>1</sup> AUBERT	02L BABR	Repl. by AUBERT,B 06J
$<6.4 \times 10^{-3}$	90	<sup>2</sup> WEIR	90B MRK2	$e^+ e^-$ 29 GeV

<sup>1</sup> Assumes equal production of  $B^+$  and  $B^0$  at the  $\Upsilon(4S)$ .  
<sup>2</sup> WEIR 90B assumes  $B^+$  production cross section from LUND.

 $\Gamma(K^+ e^- \mu^+)/\Gamma_{\text{total}}$   $\Gamma_{593}/\Gamma$ 

Test of lepton family number conservation.

VALUE	CL%	DOCUMENT ID	TECN	COMMENT
$<6.4 \times 10^{-9}$	90	AAIJ	19AMLHCB	$pp$ at 7, 8 TeV
••• We do not use the following data for averages, fits, limits, etc. •••				
$<1.3 \times 10^{-7}$	90	<sup>1</sup> AUBERT,B	06J BABR	$e^+ e^- \rightarrow \Upsilon(4S)$
$<6.4 \times 10^{-3}$	90	<sup>2</sup> WEIR	90B MRK2	$e^+ e^-$ 29 GeV

<sup>1</sup> Assumes equal production of  $B^+$  and  $B^0$  at the  $\Upsilon(4S)$ .  
<sup>2</sup> WEIR 90B assumes  $B^+$  production cross section from LUND.

 $\Gamma(K^+ e^\pm \mu^\mp)/\Gamma_{\text{total}}$   $\Gamma_{594}/\Gamma$ 

Test of lepton family number conservation.

VALUE (units $10^{-7}$ )	CL%	DOCUMENT ID	TECN	COMMENT
$<0.91$	90	<sup>1</sup> AUBERT,B	06J BABR	$e^+ e^- \rightarrow \Upsilon(4S)$

<sup>1</sup> Assumes equal production of  $B^+$  and  $B^0$  at the  $\Upsilon(4S)$ .

 $\Gamma(K^+ e^+ \tau^-)/\Gamma_{\text{total}}$   $\Gamma_{595}/\Gamma$ 

Test of lepton family number conservation.

VALUE (units $10^{-6}$ )	CL%	DOCUMENT ID	TECN	COMMENT
$<43$	90	<sup>1</sup> LEES	12P BABR	$e^+ e^- \rightarrow \Upsilon(4S)$

<sup>1</sup> Uses a fully reconstructed hadronic  $B$  decay as a tag on the recoil side.

 $\Gamma(K^+ e^- \tau^+)/\Gamma_{\text{total}}$   $\Gamma_{596}/\Gamma$ 

Test of lepton family number conservation.

VALUE (units $10^{-6}$ )	CL%	DOCUMENT ID	TECN	COMMENT
$<15$	90	<sup>1</sup> LEES	12P BABR	$e^+ e^- \rightarrow \Upsilon(4S)$

<sup>1</sup> Uses a fully reconstructed hadronic  $B$  decay as a tag on the recoil side.

 $\Gamma(K^+ e^\pm \tau^\mp)/\Gamma_{\text{total}}$   $\Gamma_{597}/\Gamma$ 

Test of lepton family number conservation.

VALUE (units $10^{-6}$ )	CL%	DOCUMENT ID	TECN	COMMENT
$<30$	90	<sup>1,2</sup> LEES	12P BABR	$e^+ e^- \rightarrow \Upsilon(4S)$

<sup>1</sup> Assumes  $B(B^+ \rightarrow h^+ \ell^+ \tau^-) = B(B^+ \rightarrow h^+ \ell^- \tau^+)$ .  
<sup>2</sup> Uses a fully reconstructed hadronic  $B$  decay as a tag on the recoil side.

 $\Gamma(K^+ \mu^+ \tau^-)/\Gamma_{\text{total}}$   $\Gamma_{598}/\Gamma$ 

Test of lepton family number conservation.

VALUE (units $10^{-6}$ )	CL%	DOCUMENT ID	TECN	COMMENT
$<45$	90	<sup>1</sup> LEES	12P BABR	$e^+ e^- \rightarrow \Upsilon(4S)$

<sup>1</sup> Uses a fully reconstructed hadronic  $B$  decay as a tag on the recoil side.

 $\Gamma(K^+ \mu^- \tau^+)/\Gamma_{\text{total}}$   $\Gamma_{599}/\Gamma$ 

Test of lepton family number conservation.

VALUE (units $10^{-6}$ )	CL%	DOCUMENT ID	TECN	COMMENT
$<28$	90	<sup>1</sup> LEES	12P BABR	$e^+ e^- \rightarrow \Upsilon(4S)$

<sup>1</sup> Uses a fully reconstructed hadronic  $B$  decay as a tag on the recoil side.

 $\Gamma(K^+ \mu^\pm \tau^\mp)/\Gamma_{\text{total}}$   $\Gamma_{600}/\Gamma$ 

Test of lepton family number conservation.

VALUE (units $10^{-6}$ )	CL%	DOCUMENT ID	TECN	COMMENT
$<48$	90	<sup>1,2</sup> LEES	12P BABR	$e^+ e^- \rightarrow \Upsilon(4S)$
••• We do not use the following data for averages, fits, limits, etc. •••				
$<77$	90	<sup>1</sup> AUBERT	07AZ BABR	Repl. by LEES 12P

<sup>1</sup> Uses a fully reconstructed hadronic  $B$  decay as a tag on the recoil side.  
<sup>2</sup> Assumes  $B(B^+ \rightarrow h^+ \ell^+ \tau^-) = B(B^+ \rightarrow h^+ \ell^- \tau^+)$ .

 $\Gamma(K^*(892)^+ e^+ \mu^-)/\Gamma_{\text{total}}$   $\Gamma_{601}/\Gamma$ 

Test of lepton family number conservation.

VALUE (units $10^{-7}$ )	CL%	DOCUMENT ID	TECN	COMMENT
$<13$	90	<sup>1</sup> AUBERT,B	06J BABR	$e^+ e^- \rightarrow \Upsilon(4S)$

<sup>1</sup> Assumes equal production of  $B^+$  and  $B^0$  at the  $\Upsilon(4S)$ .

 $\Gamma(K^*(892)^+ e^- \mu^+)/\Gamma_{\text{total}}$   $\Gamma_{602}/\Gamma$ 

Test of lepton family number conservation.

VALUE (units $10^{-7}$ )	CL%	DOCUMENT ID	TECN	COMMENT
$<9.9$	90	<sup>1</sup> AUBERT,B	06J BABR	$e^+ e^- \rightarrow \Upsilon(4S)$

<sup>1</sup> Assumes equal production of  $B^+$  and  $B^0$  at the  $\Upsilon(4S)$ .

 $\Gamma(K^*(892)^+ e^\pm \mu^\mp)/\Gamma_{\text{total}}$   $\Gamma_{603}/\Gamma$ 

Test of lepton family number conservation.

VALUE	CL%	DOCUMENT ID	TECN	COMMENT
$<1.4 \times 10^{-6}$	90	<sup>1</sup> AUBERT,B	06J BABR	$e^+ e^- \rightarrow \Upsilon(4S)$
••• We do not use the following data for averages, fits, limits, etc. •••				
$<7.9 \times 10^{-6}$	90	<sup>1</sup> AUBERT	02L BABR	Repl. by AUBERT,B 06J

<sup>1</sup> Assumes equal production of  $B^+$  and  $B^0$  at the  $\Upsilon(4S)$ .

 $\Gamma(\pi^- e^+ e^+)/\Gamma_{\text{total}}$   $\Gamma_{604}/\Gamma$ 

Test of total lepton number conservation.

VALUE	CL%	DOCUMENT ID	TECN	COMMENT
$<2.3 \times 10^{-8}$	90	<sup>1</sup> LEES	12J BABR	$e^+ e^- \rightarrow \Upsilon(4S)$
••• We do not use the following data for averages, fits, limits, etc. •••				
$<1.6 \times 10^{-6}$	90	<sup>1</sup> EDWARDS	02B CLE2	$e^+ e^- \rightarrow \Upsilon(4S)$
$<0.0039$	90	<sup>2</sup> WEIR	90B MRK2	$e^+ e^-$ 29 GeV

<sup>1</sup> Assumes equal production of  $B^+$  and  $B^0$  at the  $\Upsilon(4S)$ .  
<sup>2</sup> WEIR 90B assumes  $B^+$  production cross section from LUND.

 $\Gamma(\pi^- \mu^+ \mu^+)/\Gamma_{\text{total}}$   $\Gamma_{605}/\Gamma$ 

Test of total lepton number conservation.

VALUE	CL%	DOCUMENT ID	TECN	COMMENT
$<4.0 \times 10^{-9}$	95	<sup>1</sup> AAIJ	14AC LHCb	$pp$ at 7, 8 TeV
••• We do not use the following data for averages, fits, limits, etc. •••				
$<1.3 \times 10^{-8}$	95	<sup>2</sup> AAIJ	12AD LHCb	Repl. by AAIJ 14AC
$<4.4 \times 10^{-8}$	90	AAIJ	12c LHCb	$pp$ at 7 TeV
$<10.7 \times 10^{-8}$	90	<sup>3</sup> LEES	12J BABR	$e^+ e^- \rightarrow \Upsilon(4S)$
$<1.4 \times 10^{-6}$	90	<sup>3</sup> EDWARDS	02B CLE2	$e^+ e^- \rightarrow \Upsilon(4S)$
$<9.1 \times 10^{-3}$	90	<sup>4</sup> WEIR	90B MRK2	$e^+ e^-$ 29 GeV

<sup>1</sup> Uses  $B^+ \rightarrow J/\psi K^+$ ,  $J/\psi \rightarrow \mu^+ \mu^-$  mode for normalization. Obtains neutrino-mass-dependent upper limits in the range  $0.4\text{--}4.0 \times 10^{-9}$ . This limit is applicable for Majorana neutrino lifetime  $< 1$  ps.  
<sup>2</sup> Uses  $B^+ \rightarrow J/\psi K^+$ ,  $J/\psi \rightarrow \mu^+ \mu^-$  mode for normalization. Obtains neutrino-mass-dependent upper limits in the range  $0.4\text{--}1.0 \times 10^{-8}$ .  
<sup>3</sup> Assumes equal production of  $B^+$  and  $B^0$  at the  $\Upsilon(4S)$ .  
<sup>4</sup> WEIR 90B assumes  $B^+$  production cross section from LUND.

 $\Gamma(\pi^- e^+ \mu^+)/\Gamma_{\text{total}}$   $\Gamma_{606}/\Gamma$ 

Test of total lepton number conservation.

VALUE	CL%	DOCUMENT ID	TECN	COMMENT
$<1.5 \times 10^{-7}$	90	<sup>1</sup> LEES	14A BABR	$e^+ e^- \rightarrow \Upsilon(4S)$
••• We do not use the following data for averages, fits, limits, etc. •••				
$<1.3 \times 10^{-6}$	90	<sup>1</sup> EDWARDS	02B CLE2	$e^+ e^- \rightarrow \Upsilon(4S)$
$<0.0064$	90	<sup>2</sup> WEIR	90B MRK2	$e^+ e^-$ 29 GeV

<sup>1</sup> Assumes equal production of  $B^+$  and  $B^0$  at the  $\Upsilon(4S)$ .  
<sup>2</sup> WEIR 90B assumes  $B^+$  production cross section from LUND.

 $\Gamma(\rho^- e^+ e^+)/\Gamma_{\text{total}}$   $\Gamma_{607}/\Gamma$ 

Test of total lepton number conservation.

VALUE (units $10^{-6}$ )	CL%	DOCUMENT ID	TECN	COMMENT
$<0.17$	90	<sup>1</sup> LEES	14A BABR	$e^+ e^- \rightarrow \Upsilon(4S)$
••• We do not use the following data for averages, fits, limits, etc. •••				
$<2.6$	90	<sup>1</sup> EDWARDS	02B CLE2	$e^+ e^- \rightarrow \Upsilon(4S)$

<sup>1</sup> Assumes equal production of  $B^+$  and  $B^0$  at the  $\Upsilon(4S)$ .

 $\Gamma(\rho^- \mu^+ \mu^+)/\Gamma_{\text{total}}$   $\Gamma_{608}/\Gamma$ 

Test of total lepton number conservation.

VALUE (units $10^{-6}$ )	CL%	DOCUMENT ID	TECN	COMMENT
$<0.42$	90	LEES	14A BABR	$e^+ e^- \rightarrow \Upsilon(4S)$
••• We do not use the following data for averages, fits, limits, etc. •••				
$<5.0$	90	<sup>1</sup> EDWARDS	02B CLE2	$e^+ e^- \rightarrow \Upsilon(4S)$

<sup>1</sup> Assumes equal production of  $B^+$  and  $B^0$  at the  $\Upsilon(4S)$ .

 $\Gamma(\rho^- e^+ \mu^+)/\Gamma_{\text{total}}$   $\Gamma_{609}/\Gamma$ 

Test of total lepton number conservation.

VALUE (units $10^{-6}$ )	CL%	DOCUMENT ID	TECN	COMMENT
$<0.47$	90	<sup>1</sup> LEES	14A BABR	$e^+ e^- \rightarrow \Upsilon(4S)$
••• We do not use the following data for averages, fits, limits, etc. •••				
$<3.3$	90	<sup>1</sup> EDWARDS	02B CLE2	$e^+ e^- \rightarrow \Upsilon(4S)$

<sup>1</sup> Assumes equal production of  $B^+$  and  $B^0$  at the  $\Upsilon(4S)$ .

 $\Gamma(K^- e^+ e^+)/\Gamma_{\text{total}}$   $\Gamma_{610}/\Gamma$ 

Test of total lepton number conservation.

VALUE	CL%	DOCUMENT ID	TECN	COMMENT
$<3.0 \times 10^{-8}$	90	<sup>1</sup> LEES	12J BABR	$e^+ e^- \rightarrow \Upsilon(4S)$
••• We do not use the following data for averages, fits, limits, etc. •••				
$<1.0 \times 10^{-6}$	90	<sup>1</sup> EDWARDS	02B CLE2	$e^+ e^- \rightarrow \Upsilon(4S)$
$<0.0039$	90	<sup>2</sup> WEIR	90B MRK2	$e^+ e^-$ 29 GeV

<sup>1</sup> Assumes equal production of  $B^+$  and  $B^0$  at the  $\Upsilon(4S)$ .  
<sup>2</sup> WEIR 90B assumes  $B^+$  production cross section from LUND.

$\Gamma(K^- e^+ \mu^+)/\Gamma_{total}$   $\Gamma_{611}/\Gamma$   
 Test of total lepton number conservation.

VALUE	CL%	DOCUMENT ID	TECN	COMMENT
$<4.1 \times 10^{-8}$	90	AAIJ	12c	LHCB $pp$ at 7 TeV
• • • We do not use the following data for averages, fits, limits, etc. • • •				
$<6.7 \times 10^{-8}$	90	<sup>1</sup> LEES	12j	BABR $e^+e^- \rightarrow \Upsilon(4S)$
$<1.8 \times 10^{-6}$	90	<sup>1</sup> EDWARDS	02b	CLE2 $e^+e^- \rightarrow \Upsilon(4S)$
$<9.1 \times 10^{-3}$	90	<sup>2</sup> WEIR	90b	MRK2 $e^+e^-$ 29 GeV

<sup>1</sup> Assumes equal production of  $B^+$  and  $B^0$  at the  $\Upsilon(4S)$ .  
<sup>2</sup> WEIR 90b assumes  $B^+$  production cross section from LUND.

$\Gamma(K^- e^+ \mu^+)/\Gamma_{total}$   $\Gamma_{612}/\Gamma$   
 Test of total lepton number conservation.

VALUE	CL%	DOCUMENT ID	TECN	COMMENT
$<1.6 \times 10^{-7}$	90	<sup>1</sup> LEES	14a	BABR $e^+e^- \rightarrow \Upsilon(4S)$
• • • We do not use the following data for averages, fits, limits, etc. • • •				
$<2.0 \times 10^{-6}$	90	<sup>1</sup> EDWARDS	02b	CLE2 $e^+e^- \rightarrow \Upsilon(4S)$
$<0.0064$	90	<sup>2</sup> WEIR	90b	MRK2 $e^+e^-$ 29 GeV

<sup>1</sup> Assumes equal production of  $B^+$  and  $B^0$  at the  $\Upsilon(4S)$ .  
<sup>2</sup> WEIR 90b assumes  $B^+$  production cross section from LUND.

$\Gamma(K^*(892)^- e^+ e^+)/\Gamma_{total}$   $\Gamma_{613}/\Gamma$   
 Test of total lepton number conservation.

VALUE (units $10^{-6}$ )	CL%	DOCUMENT ID	TECN	COMMENT
$<0.40$	90	<sup>1</sup> LEES	14a	BABR $e^+e^- \rightarrow \Upsilon(4S)$
• • • We do not use the following data for averages, fits, limits, etc. • • •				
$<2.8$	90	<sup>1</sup> EDWARDS	02b	CLE2 $e^+e^- \rightarrow \Upsilon(4S)$

<sup>1</sup> Assumes equal production of  $B^+$  and  $B^0$  at the  $\Upsilon(4S)$ .

$\Gamma(K^*(892)^- \mu^+ \mu^+)/\Gamma_{total}$   $\Gamma_{614}/\Gamma$   
 Test of total lepton number conservation.

VALUE (units $10^{-6}$ )	CL%	DOCUMENT ID	TECN	COMMENT
$<0.59$	90	<sup>1</sup> LEES	14a	BABR $e^+e^- \rightarrow \Upsilon(4S)$
• • • We do not use the following data for averages, fits, limits, etc. • • •				
$<8.3$	90	<sup>1</sup> EDWARDS	02b	CLE2 $e^+e^- \rightarrow \Upsilon(4S)$

<sup>1</sup> Assumes equal production of  $B^+$  and  $B^0$  at the  $\Upsilon(4S)$ .

$\Gamma(K^*(892)^- e^+ \mu^+)/\Gamma_{total}$   $\Gamma_{615}/\Gamma$   
 Test of total lepton number conservation.

VALUE (units $10^{-6}$ )	CL%	DOCUMENT ID	TECN	COMMENT
$<0.30$	90	<sup>1</sup> LEES	14a	BABR $e^+e^- \rightarrow \Upsilon(4S)$
• • • We do not use the following data for averages, fits, limits, etc. • • •				
$<4.4$	90	<sup>1</sup> EDWARDS	02b	CLE2 $e^+e^- \rightarrow \Upsilon(4S)$

<sup>1</sup> Assumes equal production of  $B^+$  and  $B^0$  at the  $\Upsilon(4S)$ .

$\Gamma(D^- e^+ e^+)/\Gamma_{total}$   $\Gamma_{616}/\Gamma$

VALUE	CL%	DOCUMENT ID	TECN	COMMENT
$<2.6 \times 10^{-6}$	90	<sup>1</sup> LEES	14a	BABR $e^+e^- \rightarrow \Upsilon(4S)$
$2.6 \times 10^{-6}$	90	<sup>1,2</sup> SEON	11	BELL $e^+e^- \rightarrow \Upsilon(4S)$

<sup>1</sup> Assumes equal production of  $B^0$  and  $B^+$  from Upsilon(4S) decays.  
<sup>2</sup> Uses  $D^- \rightarrow K^+ \pi^- \pi^-$  mode and 3-body phase-space hypothesis for the signal decays.

$\Gamma(D^- e^+ \mu^+)/\Gamma_{total}$   $\Gamma_{617}/\Gamma$

VALUE	CL%	DOCUMENT ID	TECN	COMMENT
$<1.8 \times 10^{-6}$	90	<sup>1,2</sup> SEON	11	BELL $e^+e^- \rightarrow \Upsilon(4S)$
• • • We do not use the following data for averages, fits, limits, etc. • • •				
$<2.1 \times 10^{-6}$	90	<sup>1</sup> LEES	14a	BABR $e^+e^- \rightarrow \Upsilon(4S)$

<sup>1</sup> Assumes equal production of  $B^0$  and  $B^+$  from Upsilon(4S) decays.  
<sup>2</sup> Uses  $D^- \rightarrow K^+ \pi^- \pi^-$  mode and 3-body phase-space hypothesis for the signal decays.

$\Gamma(D^- \mu^+ \mu^+)/\Gamma_{total}$   $\Gamma_{618}/\Gamma$

VALUE	CL%	DOCUMENT ID	TECN	COMMENT
$<6.9 \times 10^{-7}$	95	<sup>1</sup> AAIJ	12Ad	LHCB $pp$ at 7 TeV
• • • We do not use the following data for averages, fits, limits, etc. • • •				
$<17 \times 10^{-7}$	90	<sup>2</sup> LEES	14a	BABR $e^+e^- \rightarrow \Upsilon(4S)$
$<1.1 \times 10^{-6}$	90	<sup>2,3</sup> SEON	11	BELL $e^+e^- \rightarrow \Upsilon(4S)$

<sup>1</sup> Uses  $B^+ \rightarrow \psi(2S) K^+$ ,  $\psi(2S) \rightarrow J/\psi \pi^+ \pi^-$  mode for normalization.  
<sup>2</sup> Assumes equal production of  $B^0$  and  $B^+$  from Upsilon(4S) decays.  
<sup>3</sup> Uses  $D^- \rightarrow K^+ \pi^- \pi^-$  mode and 3-body phase-space hypothesis for the signal decays.

$\Gamma(D^{*-} \mu^+ \mu^+)/\Gamma_{total}$   $\Gamma_{619}/\Gamma$

VALUE	CL%	DOCUMENT ID	TECN	COMMENT
$<2.4 \times 10^{-6}$	95	<sup>1</sup> AAIJ	12Ad	LHCB $pp$ at 7 TeV

<sup>1</sup> Uses  $B^+ \rightarrow \psi(2S) K^+$ ,  $\psi(2S) \rightarrow J/\psi \pi^+ \pi^-$  mode for normalization.

$\Gamma(D_s^- \mu^+ \mu^+)/\Gamma_{total}$   $\Gamma_{620}/\Gamma$

VALUE	CL%	DOCUMENT ID	TECN	COMMENT
$<5.8 \times 10^{-7}$	95	<sup>1</sup> AAIJ	12Ad	LHCB $pp$ at 7 TeV

<sup>1</sup> Uses  $B^+ \rightarrow \psi(2S) K^+$ ,  $\psi(2S) \rightarrow J/\psi \pi^+ \pi^-$  mode for normalization. Obtains neutrino-mass-dependent upper limits in the range  $1.5-8.0 \times 10^{-7}$ .

$\Gamma(\bar{D}^0 \pi^- \mu^+ \mu^+)/\Gamma_{total}$   $\Gamma_{621}/\Gamma$

VALUE	CL%	DOCUMENT ID	TECN	COMMENT
$<1.5 \times 10^{-6}$	95	<sup>1</sup> AAIJ	12Ad	LHCB $pp$ at 7 TeV

<sup>1</sup> Uses  $B^+ \rightarrow \psi(2S) K^+$ ,  $\psi(2S) \rightarrow J/\psi \pi^+ \pi^-$  mode for normalization. Obtains neutrino-mass-dependent upper limits in the range  $0.3-1.5 \times 10^{-6}$ .

$\Gamma(\Lambda^0 \mu^+)/\Gamma_{total}$   $\Gamma_{622}/\Gamma$

VALUE	CL%	DOCUMENT ID	TECN	COMMENT
$<6 \times 10^{-8}$	90	<sup>1,2</sup> DEL-AMO-SAN...	11k	BABR $e^+e^- \rightarrow \Upsilon(4S)$

<sup>1</sup> DEL-AMO-SANCHEZ 11k reports  $<6.1 \times 10^{-8}$  from a measurement of  $[\Gamma(B^+ \rightarrow \Lambda^0 \mu^+)/\Gamma_{total}] \times [B(\Lambda \rightarrow p \pi^-)]$  assuming  $B(\Lambda \rightarrow p \pi^-) = (63.9 \pm 0.5) \times 10^{-2}$ .  
<sup>2</sup> Uses  $B(\Upsilon(4S) \rightarrow B^0 \bar{B}^0) = (51.6 \pm 0.6)\%$  and  $B(\Upsilon(4S) \rightarrow B^+ B^-) = (48.4 \pm 0.6)\%$ .

$\Gamma(\Lambda^0 e^+)/\Gamma_{total}$   $\Gamma_{623}/\Gamma$

VALUE	CL%	DOCUMENT ID	TECN	COMMENT
$<3.2 \times 10^{-8}$	90	<sup>1,2</sup> DEL-AMO-SA...	11k	BABR $e^+e^- \rightarrow \Upsilon(4S)$

<sup>1</sup> DEL-AMO-SANCHEZ 11k reports  $<3.2 \times 10^{-8}$  from a measurement of  $[\Gamma(B^+ \rightarrow \Lambda^0 e^+)/\Gamma_{total}] \times [B(\Lambda \rightarrow p \pi^-)]$  assuming  $B(\Lambda \rightarrow p \pi^-) = (63.9 \pm 0.5) \times 10^{-2}$ .  
<sup>2</sup> Uses  $B(\Upsilon(4S) \rightarrow B^0 \bar{B}^0) = (51.6 \pm 0.6)\%$  and  $B(\Upsilon(4S) \rightarrow B^+ B^-) = (48.4 \pm 0.6)\%$ .

$\Gamma(\bar{\Lambda}^0 \mu^+)/\Gamma_{total}$   $\Gamma_{624}/\Gamma$

VALUE	CL%	DOCUMENT ID	TECN	COMMENT
$<6 \times 10^{-8}$	90	<sup>1,2</sup> DEL-AMO-SA...	11k	BABR $e^+e^- \rightarrow \Upsilon(4S)$

<sup>1</sup> DEL-AMO-SANCHEZ 11k reports  $<6.2 \times 10^{-8}$  from a measurement of  $[\Gamma(B^+ \rightarrow \bar{\Lambda}^0 \mu^+)/\Gamma_{total}] \times [B(\Lambda \rightarrow p \pi^-)]$  assuming  $B(\Lambda \rightarrow p \pi^-) = (63.9 \pm 0.5) \times 10^{-2}$ .  
<sup>2</sup> Uses  $B(\Upsilon(4S) \rightarrow B^0 \bar{B}^0) = (51.6 \pm 0.6)\%$  and  $B(\Upsilon(4S) \rightarrow B^+ B^-) = (48.4 \pm 0.6)\%$ .

$\Gamma(\bar{\Lambda}^0 e^+)/\Gamma_{total}$   $\Gamma_{625}/\Gamma$

VALUE	CL%	DOCUMENT ID	TECN	COMMENT
$<8 \times 10^{-8}$	90	<sup>1,2</sup> DEL-AMO-SA...	11k	BABR $e^+e^- \rightarrow \Upsilon(4S)$

<sup>1</sup> DEL-AMO-SANCHEZ 11k reports  $<8.1 \times 10^{-8}$  from a measurement of  $[\Gamma(B^+ \rightarrow \bar{\Lambda}^0 e^+)/\Gamma_{total}] \times [B(\Lambda \rightarrow p \pi^-)]$  assuming  $B(\Lambda \rightarrow p \pi^-) = (63.9 \pm 0.5) \times 10^{-2}$ .  
<sup>2</sup> Uses  $B(\Upsilon(4S) \rightarrow B^0 \bar{B}^0) = (51.6 \pm 0.6)\%$  and  $B(\Upsilon(4S) \rightarrow B^+ B^-) = (48.4 \pm 0.6)\%$ .

**POLARIZATION IN  $B^+$  DECAY**

In decays involving two vector mesons, one can distinguish among the states in which meson polarizations are both longitudinal ( $L$ ) or both are transverse and parallel ( $\parallel$ ) or perpendicular ( $\perp$ ) to each other with the parameters  $\Gamma_L/\Gamma$ ,  $\Gamma_{\perp}/\Gamma$ , and the relative phases  $\phi_{\parallel}$  and  $\phi_{\perp}$ . See the definitions in the note on "Polarization in  $B$  Decays" review in the  $B^0$  Particle Listings.

$\Gamma_L/\Gamma$  in  $B^+ \rightarrow \bar{D}^{*0} \rho^+$

VALUE	DOCUMENT ID	TECN	COMMENT
$0.892 \pm 0.018 \pm 0.016$	CSORNA	03	CLE2 $e^+e^- \rightarrow \Upsilon(4S)$

$\Gamma_L/\Gamma$  in  $B^+ \rightarrow \bar{D}^{*0} K^{*+}$

VALUE	DOCUMENT ID	TECN	COMMENT
$0.86 \pm 0.06 \pm 0.03$	AUBERT	04k	BABR $e^+e^- \rightarrow \Upsilon(4S)$

$\Gamma_L/\Gamma$  in  $B^+ \rightarrow J/\psi K^{*+}$

VALUE	DOCUMENT ID	TECN	COMMENT
$0.604 \pm 0.015 \pm 0.018$	ITOH	05	BELL $e^+e^- \rightarrow \Upsilon(4S)$

$\Gamma_{\perp}/\Gamma$  in  $B^+ \rightarrow J/\psi K^{*+}$

VALUE	DOCUMENT ID	TECN	COMMENT
$0.180 \pm 0.014 \pm 0.010$	ITOH	05	BELL $e^+e^- \rightarrow \Upsilon(4S)$

$\Gamma_L/\Gamma$  in  $B^+ \rightarrow \omega K^{*+}$

VALUE	DOCUMENT ID	TECN	COMMENT
$0.41 \pm 0.18 \pm 0.05$	AUBERT	09h	BABR $e^+e^- \rightarrow \Upsilon(4S)$

$\Gamma_L/\Gamma$  in  $B^+ \rightarrow \omega K_2^*(1430)^+$

VALUE	DOCUMENT ID	TECN	COMMENT
$0.56 \pm 0.10 \pm 0.04$	AUBERT	09h	BABR $e^+e^- \rightarrow \Upsilon(4S)$

$\Gamma_L/\Gamma$  in  $B^+ \rightarrow K^{*+} \bar{K}^{*0}$

VALUE	DOCUMENT ID	TECN	COMMENT
$0.82^{+0.15}_{-0.21}$ OUR AVERAGE			
$1.06 \pm 0.30 \pm 0.14$	<sup>1</sup> GOH	15	BELL $e^+e^- \rightarrow \Upsilon(4S)$
$0.75^{+0.16}_{-0.26} \pm 0.03$	<sup>2,3</sup> AUBERT	09f	BABR $e^+e^- \rightarrow \Upsilon(4S)$

<sup>1</sup> Signal significance 2.7 standard deviations.  
<sup>2</sup> Signal significance 3.7 standard deviations.  
<sup>3</sup> Assumes equal production of  $B^+$  and  $B^0$  at the  $\Upsilon(4S)$ .

$\Gamma_L/\Gamma$  in  $B^+ \rightarrow \phi K^*(892)^+$

VALUE	DOCUMENT ID	TECN	COMMENT
$0.50 \pm 0.05$ OUR AVERAGE			
$0.49 \pm 0.05 \pm 0.03$	AUBERT	07Ba	BABR $e^+e^- \rightarrow \Upsilon(4S)$
$0.52 \pm 0.08 \pm 0.03$	CHEN	05A	BELL $e^+e^- \rightarrow \Upsilon(4S)$
• • • We do not use the following data for averages, fits, limits, etc. • • •			
$0.46 \pm 0.12 \pm 0.03$	AUBERT	03v	BABR Repl. by AUBERT 07Ba



# Meson Particle Listings

## $B^\pm$

### $\Gamma_\perp/\Gamma$ in $B^+ \rightarrow \phi K^{*+}$

VALUE	DOCUMENT ID	TECN	COMMENT
<b>0.20 ± 0.05 OUR AVERAGE</b>			
0.21 ± 0.05 ± 0.02	AUBERT	07BA	BABR $e^+e^- \rightarrow \Upsilon(4S)$
0.19 ± 0.08 ± 0.02	CHEN	05A	BELL $e^+e^- \rightarrow \Upsilon(4S)$

### $\phi_\parallel$ in $B^+ \rightarrow \phi K^{*+}$

VALUE (°)	DOCUMENT ID	TECN	COMMENT
<b>2.34 ± 0.18 OUR AVERAGE</b>			
2.47 ± 0.20 ± 0.07	AUBERT	07BA	BABR $e^+e^- \rightarrow \Upsilon(4S)$
2.10 ± 0.28 ± 0.04	CHEN	05A	BELL $e^+e^- \rightarrow \Upsilon(4S)$

### $\phi_\perp$ in $B^+ \rightarrow \phi K^{*+}$

VALUE (°)	DOCUMENT ID	TECN	COMMENT
<b>2.58 ± 0.17 OUR AVERAGE</b>			
2.69 ± 0.20 ± 0.03	AUBERT	07BA	BABR $e^+e^- \rightarrow \Upsilon(4S)$
2.31 ± 0.30 ± 0.07	CHEN	05A	BELL $e^+e^- \rightarrow \Upsilon(4S)$

### $\delta_0(B^+ \rightarrow \phi K^{*+})$

VALUE (rad)	DOCUMENT ID	TECN	COMMENT
<b>3.07 ± 0.18 ± 0.06</b>			
	AUBERT	07BA	BABR $e^+e^- \rightarrow \Upsilon(4S)$

### $A_{CP}^0(B^+ \rightarrow \phi K^{*+})$

VALUE	DOCUMENT ID	TECN	COMMENT
<b>0.17 ± 0.11 ± 0.02</b>			
	AUBERT	07BA	BABR $e^+e^- \rightarrow \Upsilon(4S)$

### $A_{CP}^\perp(B^+ \rightarrow \phi K^{*+})$

VALUE	DOCUMENT ID	TECN	COMMENT
<b>0.22 ± 0.24 ± 0.08</b>			
	AUBERT	07BA	BABR $e^+e^- \rightarrow \Upsilon(4S)$

### $\Delta\phi_\parallel(B^+ \rightarrow \phi K^{*+})$

VALUE (rad)	DOCUMENT ID	TECN	COMMENT
<b>0.07 ± 0.20 ± 0.05</b>			
	AUBERT	07BA	BABR $e^+e^- \rightarrow \Upsilon(4S)$

### $\Delta\phi_\perp(B^+ \rightarrow \phi K^{*+})$

VALUE (rad)	DOCUMENT ID	TECN	COMMENT
<b>0.19 ± 0.20 ± 0.07</b>			
	AUBERT	07BA	BABR $e^+e^- \rightarrow \Upsilon(4S)$

### $\Delta\delta_0(B^+ \rightarrow \phi K^{*+})$

VALUE (rad)	DOCUMENT ID	TECN	COMMENT
<b>0.20 ± 0.18 ± 0.03</b>			
	AUBERT	07BA	BABR $e^+e^- \rightarrow \Upsilon(4S)$

### $\Gamma_L/\Gamma$ in $B^+ \rightarrow \phi K_1(1270)^+$

VALUE	DOCUMENT ID	TECN	COMMENT
<b>0.46<sup>+0.12+0.06</sup><sub>-0.13-0.07</sub></b>			
	AUBERT	08B1	BABR $e^+e^- \rightarrow \Upsilon(4S)$

### $\Gamma_L/\Gamma$ in $B^+ \rightarrow \phi K_2^*(1430)^+$

VALUE	DOCUMENT ID	TECN	COMMENT
<b>0.80<sup>+0.09</sup><sub>-0.10</sub> ± 0.03</b>			
	AUBERT	08B1	BABR $e^+e^- \rightarrow \Upsilon(4S)$

### $\delta_0(B^+ \rightarrow \phi K_2^*(1430)^+)$

VALUE (rad)	DOCUMENT ID	TECN	COMMENT
<b>3.59 ± 0.19 ± 0.12</b>			
	AUBERT	08B1	BABR $e^+e^- \rightarrow \Upsilon(4S)$

### $\Delta\delta_0(B^+ \rightarrow \phi K_2^*(1430)^+)$

VALUE (rad)	DOCUMENT ID	TECN	COMMENT
<b>-0.05 ± 0.19 ± 0.06</b>			
	AUBERT	08B1	BABR $e^+e^- \rightarrow \Upsilon(4S)$

### $\Gamma_L/\Gamma$ in $B^+ \rightarrow \rho^0 K^*(892)^+$

VALUE	DOCUMENT ID	TECN	COMMENT
<b>0.78 ± 0.12 ± 0.03</b>			
	DEL-AMO-SA...11d	BABR	$e^+e^- \rightarrow \Upsilon(4S)$

• • • We do not use the following data for averages, fits, limits, etc. • • •

0.96 <sup>+0.04</sup> <sub>-0.15</sub> ± 0.04	AUBERT	03v	BABR Repl. by DEL-A-MO-SANCHEZ 11d
---	--------	-----	------------------------------------

### $\Gamma_L/\Gamma(B^+ \rightarrow K^*(892)^0 \rho^+)$

VALUE	DOCUMENT ID	TECN	COMMENT
<b>0.48 ± 0.08 OUR AVERAGE</b>			
0.52 ± 0.10 ± 0.04	AUBERT,B	06G	BABR $e^+e^- \rightarrow \Upsilon(4S)$
0.43 ± 0.11 <sup>+0.05</sup> <sub>-0.02</sub>	ZHANG	05D	BELL $e^+e^- \rightarrow \Upsilon(4S)$

### $\Gamma_L/\Gamma$ in $B^+ \rightarrow \rho^+ \rho^0$

VALUE	DOCUMENT ID	TECN	COMMENT
<b>0.950 ± 0.016 OUR AVERAGE</b>			
0.950 ± 0.015 ± 0.006	AUBERT	09G	BABR $e^+e^- \rightarrow \Upsilon(4S)$
0.948 ± 0.106 ± 0.021	ZHANG	03B	BELL $e^+e^- \rightarrow \Upsilon(4S)$

• • • We do not use the following data for averages, fits, limits, etc. • • •

0.905 ± 0.042 <sup>+0.023</sup> <sub>-0.027</sub>	AUBERT,BE	06G	BABR Repl. by AUBERT 09G
0.97 <sup>+0.03</sup> <sub>-0.07</sub> ± 0.04	AUBERT	03v	BABR Repl. by AUBERT,BE 06G

### $\Gamma_L/\Gamma$ in $B^+ \rightarrow \omega \rho^+$

VALUE	DOCUMENT ID	TECN	COMMENT
<b>0.90 ± 0.05 ± 0.03</b>			
	AUBERT	09H	BABR $e^+e^- \rightarrow \Upsilon(4S)$

• • • We do not use the following data for averages, fits, limits, etc. • • •

0.82 ± 0.11 ± 0.02	AUBERT,B	06T	BABR Repl. by AUBERT 09H
0.88 <sup>+0.12</sup> <sub>-0.15</sub> ± 0.03	AUBERT	05o	BABR Repl. by AUBERT,B 06T

### $\Gamma_L/\Gamma$ in $B^+ \rightarrow \rho \bar{p} K^*(892)^+$

VALUE	DOCUMENT ID	TECN	COMMENT
<b>0.32 ± 0.17 ± 0.09</b>			
	CHEN	08c	BELL $e^+e^- \rightarrow \Upsilon(4S)$

### CP VIOLATION

$A_{CP}$  is defined as

$$\frac{B(B^- \rightarrow \bar{f}) - B(B^+ \rightarrow f)}{B(B^- \rightarrow \bar{f}) + B(B^+ \rightarrow f)}$$

the CP-violation charge asymmetry of exclusive  $B^-$  and  $B^+$  decay.

### $A_{CP}(B^+ \rightarrow J/\psi(1S)K^+)$

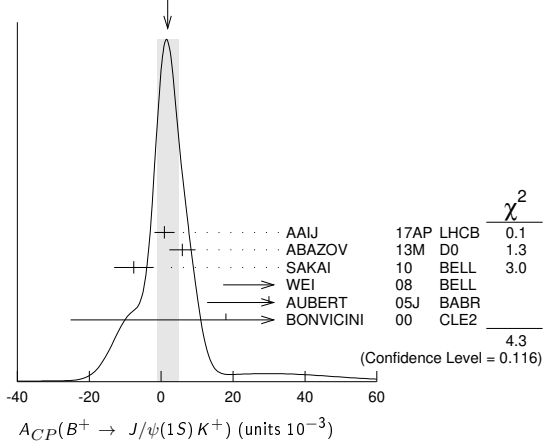
VALUE (units $10^{-3}$ )	DOCUMENT ID	TECN	COMMENT
<b>1.8 ± 3.0 OUR AVERAGE</b>			Error includes scale factor of 1.5. See the ideogram below.
0.9 ± 2.7 ± 0.7	AAIJ	17AP	LHCB $pp$ at 7, 8 TeV
5.9 ± 3.6 ± 0.7	ABAZOV	13M	D0 $p\bar{p}$ at 1.96 TeV
-7.6 ± 5.0 ± 2.2	SAKAI	10	BELL $e^+e^- \rightarrow \Upsilon(4S)$
90 ± 70 ± 20	<sup>1</sup> WEI	08	BELL $e^+e^- \rightarrow \Upsilon(4S)$
30 ± 14 ± 10	<sup>2</sup> AUBERT	05J	BABR $e^+e^- \rightarrow \Upsilon(4S)$
18 ± 43 ± 4	<sup>3</sup> BONVICINI	00	CLE2 $e^+e^- \rightarrow \Upsilon(4S)$

• • • We do not use the following data for averages, fits, limits, etc. • • •

7.5 ± 6.1 ± 3.0	<sup>4</sup> ABAZOV	08o	D0 Repl. by ABAZOV 13M
30 ± 15 ± 6	AUBERT	04P	BABR Repl. by AUBERT 05J
-26 ± 22 ± 17	ABE	03B	BELL Repl. by SAKAI 10
3 ± 30 ± 4	AUBERT	02F	BABR Repl. by AUBERT 04P

- Uses  $B^+ \rightarrow J/\psi K^+$ , where  $J/\psi \rightarrow p\bar{p}$ .
- The result reported corresponds to  $-A_{CP}$ .
- A +0.3% correction is applied due to a slightly higher reconstruction efficiency for the positive kaons.
- Uses  $J/\psi \rightarrow \mu^+ \mu^-$  decay.

WEIGHTED AVERAGE  
1.8 ± 3.0 (Error scaled by 1.5)



### $A_{CP}(B^+ \rightarrow J/\psi(1S)\pi^+)$

VALUE (units $10^{-2}$ )	DOCUMENT ID	TECN	COMMENT
<b>1.8 ± 1.2 OUR AVERAGE</b>			Error includes scale factor of 1.3.
1.91 ± 0.89 ± 0.16	<sup>1</sup> AAIJ	17o	LHCB $pp$ at 7, 8 TeV
-4.2 ± 4.4 ± 0.9	ABAZOV	13M	D0 $p\bar{p}$ at 1.96 TeV
12.3 ± 8.5 ± 0.4	AUBERT	04P	BABR $e^+e^- \rightarrow \Upsilon(4S)$
-2.3 ± 16.4 ± 1.5	ABE	03B	BELL $e^+e^- \rightarrow \Upsilon(4S)$

• • • We do not use the following data for averages, fits, limits, etc. • • •

0.5 ± 2.7 ± 1.1	<sup>2</sup> AAIJ	12Ac	LHCB Repl. by AAIJ 17o
-9 ± 8 ± 3	<sup>3</sup> ABAZOV	08o	D0 Repl. by ABAZOV 13M
1 ± 22 ± 1	AUBERT	02F	BABR Repl. by AUBERT 04P

- Obtained by using LHCb measurement of  $A_{CP}(B^+ \rightarrow J/\psi K^+) = (0.09 \pm 0.27 \pm 0.07) \times 10^{-2}$  of AAIJ 17AP.
- Uses  $A_{CP}(B^+ \rightarrow J/\psi K^+) = 0.001 \pm 0.007$  to extract production asymmetry.
- Uses  $J/\psi \rightarrow \mu^+ \mu^-$  decay.

### $A_{CP}(B^+ \rightarrow J/\psi \rho^+)$

VALUE	DOCUMENT ID	TECN	COMMENT
<b>-0.05 ± 0.05 OUR AVERAGE</b>			
-0.045 <sup>+0.056</sup> <sub>-0.057</sub> ± 0.008	AAIJ	19o	LHCB $pp$ at 7 and 8 TeV
-0.11 ± 0.12 ± 0.08	AUBERT	07Ac	BABR $e^+e^- \rightarrow \Upsilon(4S)$

**A<sub>CP</sub>(B<sup>+</sup> → J/ψK\*(892)<sup>+</sup>)**

VALUE	DOCUMENT ID	TECN	COMMENT
<b>-0.048 ± 0.029 ± 0.016</b>	<sup>1</sup> AUBERT	05J	BABR e <sup>+</sup> e <sup>-</sup> → T(4S)

<sup>1</sup> The result reported corresponds to -A<sub>CP</sub>.

**A<sub>CP</sub>(B<sup>+</sup> → η<sub>c</sub>K<sup>+</sup>)**

VALUE	DOCUMENT ID	TECN	COMMENT
<b>0.01 ± 0.07 OUR AVERAGE</b>	Error includes scale factor of 2.2.		
0.040 ± 0.034 ± 0.004	<sup>1</sup> AAIJ	14AF	LHCB pp at 7, 8 TeV
-0.16 ± 0.08 ± 0.02	<sup>1</sup> WEI	08	BELL e <sup>+</sup> e <sup>-</sup> → T(4S)
• • • We do not use the following data for averages, fits, limits, etc. • • •			
0.046 ± 0.057 ± 0.007	<sup>1</sup> AAIJ	13AU	LHCB Repl. by AAIJ 14AF

<sup>1</sup> Uses B<sup>+</sup> → η<sub>c</sub>K<sup>+</sup>, where η<sub>c</sub> → p $\bar{p}$ .

**A<sub>CP</sub>(B<sup>+</sup> → ψ(2S)π<sup>+</sup>)**

VALUE	DOCUMENT ID	TECN	COMMENT
<b>0.03 ± 0.06 OUR AVERAGE</b>			
0.048 ± 0.090 ± 0.011	<sup>1</sup> AAIJ	12AC	LHCB pp at 7 TeV
0.022 ± 0.085 ± 0.016	BHARDWAJ	08	BELL e <sup>+</sup> e <sup>-</sup> → T(4S)

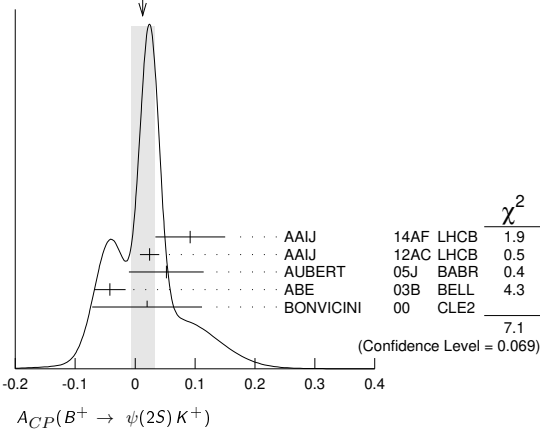
<sup>1</sup> Uses A<sub>CP</sub>(B<sup>+</sup> → J/ψK<sup>+</sup>) = 0.001 ± 0.007 to extract production asymmetry.

**A<sub>CP</sub>(B<sup>+</sup> → ψ(2S)K<sup>+</sup>)**

VALUE	DOCUMENT ID	TECN	COMMENT
<b>0.012 ± 0.020 OUR AVERAGE</b>	Error includes scale factor of 1.5. See the ideogram below.		
0.092 ± 0.058 ± 0.004	<sup>1</sup> AAIJ	14AF	LHCB pp at 7, 8 TeV
0.024 ± 0.014 ± 0.008	<sup>2</sup> AAIJ	12AC	LHCB pp at 7 TeV
0.052 ± 0.059 ± 0.020	AUBERT	05J	BABR e <sup>+</sup> e <sup>-</sup> → T(4S)
-0.042 ± 0.020 ± 0.017	ABE	03B	BELL e <sup>+</sup> e <sup>-</sup> → T(4S)
0.02 ± 0.091 ± 0.01	<sup>3</sup> BONVICINI	00	CLE2 e <sup>+</sup> e <sup>-</sup> → T(4S)
• • • We do not use the following data for averages, fits, limits, etc. • • •			
-0.002 ± 0.123 ± 0.012	<sup>1,2</sup> AAIJ	13AU	LHCB Repl. by AAIJ 14AF

<sup>1</sup> Uses ψ(2S) → p $\bar{p}$  decays.  
<sup>2</sup> Uses A<sub>CP</sub>(B<sup>+</sup> → J/ψK<sup>+</sup>) = 0.001 ± 0.007 to extract production asymmetry.  
<sup>3</sup> A + 0.3% correction is applied due to a slightly higher reconstruction efficiency for the positive kaons.

WEIGHTED AVERAGE  
0.012 ± 0.020 (Error scaled by 1.5)



**A<sub>CP</sub>(B<sup>+</sup> → ψ(2S)K\*(892)<sup>+</sup>)**

VALUE	DOCUMENT ID	TECN	COMMENT
<b>0.077 ± 0.207 ± 0.051</b>	<sup>1</sup> AUBERT	05J	BABR e <sup>+</sup> e <sup>-</sup> → T(4S)

<sup>1</sup> The result reported corresponds to -A<sub>CP</sub>.

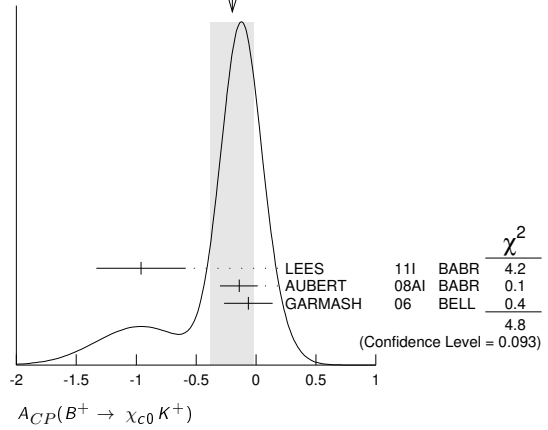
**A<sub>CP</sub>(B<sup>+</sup> → χ<sub>01</sub>(1P)π<sup>+</sup>)**

VALUE	DOCUMENT ID	TECN	COMMENT
<b>0.07 ± 0.18 ± 0.02</b>	KUMAR	06	BELL e <sup>+</sup> e <sup>-</sup> → T(4S)

**A<sub>CP</sub>(B<sup>+</sup> → χ<sub>00</sub>K<sup>+</sup>)**

VALUE	DOCUMENT ID	TECN	COMMENT
<b>-0.20 ± 0.18 OUR AVERAGE</b>	Error includes scale factor of 1.5. See the ideogram below.		
-0.96 ± 0.37 ± 0.04	LEES	11I	BABR e <sup>+</sup> e <sup>-</sup> → T(4S)
-0.14 ± 0.15 <sup>+0.03</sup> <sub>-0.06</sub>	AUBERT	08AI	BABR e <sup>+</sup> e <sup>-</sup> → T(4S)
-0.065 ± 0.20 <sup>+0.035</sup> <sub>-0.024</sub>	GARMASH	06	BELL e <sup>+</sup> e <sup>-</sup> → T(4S)

WEIGHTED AVERAGE  
-0.20 ± 0.18 (Error scaled by 1.5)



**A<sub>CP</sub>(B<sup>+</sup> → χ<sub>01</sub>K<sup>+</sup>)**

VALUE	DOCUMENT ID	TECN	COMMENT
<b>-0.009 ± 0.033 OUR AVERAGE</b>			
-0.01 ± 0.03 ± 0.02	KUMAR	06	BELL e <sup>+</sup> e <sup>-</sup> → T(4S)
-0.003 ± 0.076 ± 0.017	<sup>1</sup> AUBERT	05J	BABR e <sup>+</sup> e <sup>-</sup> → T(4S)

<sup>1</sup> The result reported corresponds to -A<sub>CP</sub>.

**A<sub>CP</sub>(B<sup>+</sup> → χ<sub>01</sub>K\*(892)<sup>+</sup>)**

VALUE	DOCUMENT ID	TECN	COMMENT
<b>0.471 ± 0.378 ± 0.268</b>	<sup>1</sup> AUBERT	05J	BABR e <sup>+</sup> e <sup>-</sup> → T(4S)

<sup>1</sup> The result reported corresponds to -A<sub>CP</sub>.

**A<sub>CP</sub>(B<sup>+</sup> → D<sup>0</sup>ℓ<sup>+</sup>ν<sub>ℓ</sub>)**

VALUE (units 10 <sup>-2</sup> )	DOCUMENT ID	TECN	COMMENT
<b>-0.14 ± 0.14 ± 0.14</b>	<sup>1</sup> ABZOV	17A	D0 p $\bar{p}$ at 1.96 TeV

<sup>1</sup> Uses D<sup>0</sup> → K<sup>-</sup>π<sup>+</sup> decays and f(B<sup>+</sup>) = 0.56 ± 0.01 from 10.4 fb<sup>-1</sup> of Run II data.

**A<sub>CP</sub>(B<sup>+</sup> → D<sup>0</sup>π<sup>+</sup>)**

VALUE	DOCUMENT ID	TECN	COMMENT
<b>-0.007 ± 0.007 OUR AVERAGE</b>			
-0.006 ± 0.005 ± 0.010	<sup>1</sup> AAIJ	13AE	LHCB pp at 7 TeV
-0.008 ± 0.008	ABE	06	BELL e <sup>+</sup> e <sup>-</sup> → T(4S)

<sup>1</sup> Uses B<sup>±</sup> → [K<sup>±</sup>π<sup>∓</sup>π<sup>±</sup>π<sup>-</sup>]<sub>D</sub>h<sup>±</sup> mode.

**A<sub>CP</sub>(B<sup>+</sup> → D<sub>CP(+1)</sub>π<sup>+</sup>)**

VALUE	DOCUMENT ID	TECN	COMMENT
<b>-0.0080 ± 0.0026 OUR AVERAGE</b>			
-0.008 ± 0.003 ± 0.002	<sup>1</sup> AAIJ	18A	LHCB pp at 7, 8, 13 TeV
-0.008 ± 0.006 ± 0.002	<sup>2</sup> AAIJ	18A	LHCB pp at 7, 8, 13 TeV
-0.0098 ± 0.0043 ± 0.0021	AAIJ	16L	LHCB pp at 7, 8 TeV
0.035 ± 0.024	ABE	06	BELL e <sup>+</sup> e <sup>-</sup> → T(4S)

<sup>1</sup> Uses D → K<sup>+</sup>K<sup>-</sup> decay mode.  
<sup>2</sup> Uses D → π<sup>+</sup>π<sup>-</sup> decay mode.

**A<sub>CP</sub>(B<sup>+</sup> → D<sub>CP(-1)</sub>π<sup>+</sup>)**

VALUE	DOCUMENT ID	TECN	COMMENT
<b>0.017 ± 0.026</b>	ABE	06	BELL e <sup>+</sup> e <sup>-</sup> → T(4S)

**A<sub>CP</sub>([K<sup>∓</sup>π<sup>±</sup>π<sup>±</sup>π<sup>-</sup>]<sub>D</sub>π<sup>+</sup>)**

VALUE	DOCUMENT ID	TECN	COMMENT
<b>0.023 ± 0.048 ± 0.005</b>	AAIJ	16L	LHCB pp at 7, 8 TeV
• • • We do not use the following data for averages, fits, limits, etc. • • •			
0.13 ± 0.10	AAIJ	13AE	LHCB Repl. by AAIJ 16L

**A<sub>CP</sub>(B<sup>+</sup> → [π<sup>+</sup>π<sup>+</sup>π<sup>-</sup>π<sup>-</sup>]<sub>D</sub>K<sup>+</sup>)**

VALUE	DOCUMENT ID	TECN	COMMENT
<b>0.100 ± 0.034 ± 0.018</b>	AAIJ	16L	LHCB pp at 7, 8 TeV

**A<sub>CP</sub>(B<sup>+</sup> → [π<sup>+</sup>π<sup>-</sup>π<sup>+</sup>π<sup>-</sup>]<sub>D</sub>K\*(892)<sup>+</sup>)**

VALUE	DOCUMENT ID	TECN	COMMENT
<b>0.02 ± 0.11 ± 0.01</b>	AAIJ	17Bo	LHCB pp at 7, 8, 13 TeV

**A<sub>CP</sub>(B<sup>+</sup> → D<sup>0</sup>K<sup>+</sup>)**

VALUE	DOCUMENT ID	TECN	COMMENT
<b>-0.017 ± 0.005 OUR AVERAGE</b>			
-0.019 ± 0.005 ± 0.002	<sup>1</sup> AAIJ	18A	LHCB pp at 7, 8, 13 TeV
-0.0194 ± 0.0072 ± 0.0060	AAIJ	16L	LHCB pp at 7, 8 TeV
0.010 ± 0.026 ± 0.005	<sup>2</sup> AAIJ	15W	LHCB pp at 7, 8 TeV
0.066 ± 0.036	ABE	06	BELL e <sup>+</sup> e <sup>-</sup> → T(4S)

# Meson Particle Listings

## $B^\pm$

- • • We do not use the following data for averages, fits, limits, etc. • • •

0.000 ± 0.012 ± 0.002	<sup>3</sup> AAIJ	16L	LHCB	$p\bar{p}$ at 7, 8 TeV
-0.029 ± 0.020 ± 0.018	<sup>3</sup> AAIJ	13AE	LHCB	Repl. by AAJ 16L
0.003 ± 0.080 ± 0.037	<sup>4</sup> ABE	03D	BELL	Repl. by SWAIN 03
0.04 ± 0.06 ± 0.03	<sup>5</sup> SWAIN	03	BELL	Repl. by ABE 06

  - Supersedes AAJ 16L.
  - Uses  $D^0 \rightarrow K^- \pi^+ \pi^0$  for the favored mode, and  $D^0 \rightarrow K^+ \pi^- \pi^0$  for the suppressed mode.
  - Uses  $B^\pm \rightarrow [K^\pm \pi^\mp \pi^\pm \pi^\mp]_D h^\pm$  mode.
  - Corresponds to 90% confidence range  $-0.15 < A_{CP} < 0.16$ .
  - Corresponds to 90% confidence range  $-0.07 < A_{CP} < 0.15$ .

$A_{CP}([K^\mp \pi^\pm \pi^\pm \pi^\mp]_D K^+)$

VALUE	DOCUMENT ID	TECN	COMMENT
<b>-0.313 ± 0.102 ± 0.038</b>	AAIJ	16L	LHCB $p\bar{p}$ at 7, 8 TeV
• • • We do not use the following data for averages, fits, limits, etc. • • •			
-0.42 ± 0.22	AAIJ	13AE	LHCB Repl. by AAJ 16L

$A_{CP}(B^+ \rightarrow [\pi^+ \pi^+ \pi^- \pi^-]_D \pi^+)$

VALUE (units $10^{-3}$ )	DOCUMENT ID	TECN	COMMENT
<b>-4.1 ± 7.9 ± 2.4</b>	AAIJ	16L	LHCB $p\bar{p}$ at 7, 8 TeV

$A_{CP}(B^+ \rightarrow [K^- \pi^+]_D K^+)$

VALUE	DOCUMENT ID	TECN	COMMENT
<b>-0.58 ± 0.21 OUR AVERAGE</b>			
-0.82 ± 0.44 ± 0.09	AALTONEN	11AJ	CDF $p\bar{p}$ at 1.96 TeV
-0.39 ± 0.26 ± 0.04	HORII	11	BELL $e^+ e^- \rightarrow \Upsilon(4S)$
-0.28 ± 0.03			
-0.86 ± 0.47 ± 0.12	DEL-AMO-SA...10H	BABR	$e^+ e^- \rightarrow \Upsilon(4S)$
-0.16 ± 0.16			
• • • We do not use the following data for averages, fits, limits, etc. • • •			
-0.1 ± 0.8 ± 0.4	HORII	08	BELL Repl. by HORII 11
+0.88 ± 0.77 ± 0.06	SAIGO	05	BELL Repl. by HORII 08

$A_{CP}(B^+ \rightarrow [K^- \pi^+ \pi^0]_D K^+)$

VALUE	DOCUMENT ID	TECN	COMMENT
<b>0.07 ± 0.30 OUR AVERAGE</b>			Error includes scale factor of 1.5.
-0.20 ± 0.27 ± 0.04	<sup>1</sup> AAIJ	15W	LHCB $p\bar{p}$ at 7, 8 TeV
0.41 ± 0.30 ± 0.05	NAYAK	13	BELL $e^+ e^- \rightarrow \Upsilon(4S)$
<sup>1</sup> Uses $D^0 \rightarrow K^- \pi^+ \pi^0$ for the favored mode, and $D^0 \rightarrow K^+ \pi^- \pi^0$ for the suppressed mode.			

$A_{CP}(B^+ \rightarrow [K^+ K^- \pi^0]_D K^+)$

VALUE	DOCUMENT ID	TECN	COMMENT
<b>0.30 ± 0.20 ± 0.02</b>	<sup>1</sup> AAIJ	15W	LHCB $p\bar{p}$ at 7, 8 TeV
<sup>1</sup> Uses $D \rightarrow K^+ K^- \pi^0$ mode.			

$A_{CP}(B^+ \rightarrow [\pi^+ \pi^- \pi^0]_D K^+)$

VALUE	DOCUMENT ID	TECN	COMMENT
<b>0.054 ± 0.091 ± 0.011</b>	<sup>1</sup> AAIJ	15W	LHCB $p\bar{p}$ at 7, 8 TeV
<sup>1</sup> Uses $D \rightarrow \pi^+ \pi^- \pi^0$ mode.			

$A_{CP}(B^+ \rightarrow \bar{D}^0 K^*(892)^+)$

VALUE	DOCUMENT ID	TECN	COMMENT
<b>-0.007 ± 0.019 OUR AVERAGE</b>			
-0.004 ± 0.023 ± 0.008	<sup>1</sup> AAIJ	17B0	LHCB $p\bar{p}$ at 7, 8, 13 TeV
-0.013 ± 0.031 ± 0.009	<sup>2</sup> AAIJ	17B0	LHCB $p\bar{p}$ at 7, 8, 13 TeV
<sup>1</sup> Uses $B^\pm \rightarrow [K^\pm \pi^\mp]_D K^*(892)^\pm$ decay mode.			
<sup>2</sup> Uses $B^\pm \rightarrow [K^\pm \pi^\mp \pi^\pm \pi^\mp]_D K^*(892)^\pm$ decay mode.			

$A_{CP}(B^+ \rightarrow [K^- \pi^+]_D K^*(892)^+)$

VALUE	DOCUMENT ID	TECN	COMMENT
<b>-0.75 ± 0.16 OUR AVERAGE</b>			
-0.81 ± 0.17 ± 0.04	AAIJ	17B0	LHCB $p\bar{p}$ at 7, 8, 13 TeV
-0.34 ± 0.43 ± 0.16	AUBERT	09AJ	BABR $e^+ e^- \rightarrow \Upsilon(4S)$
• • • We do not use the following data for averages, fits, limits, etc. • • •			
-0.22 ± 0.61 ± 0.17	AUBERT,B	05V	BABR Repl. by AUBERT 09AJ

$A_{CP}(B^+ \rightarrow [K^- \pi^+ \pi^- \pi^+]_D K^*(892)^+)$

VALUE	DOCUMENT ID	TECN	COMMENT
<b>-0.45 ± 0.21 ± 0.14</b>	AAIJ	17B0	LHCB $p\bar{p}$ at 7, 8, 13 TeV

$A_{CP}(B^+ \rightarrow [K^- \pi^+]_D \pi^+)$

VALUE	DOCUMENT ID	TECN	COMMENT
<b>0.00 ± 0.09 OUR AVERAGE</b>			
0.13 ± 0.25 ± 0.02	AALTONEN	11AJ	CDF $p\bar{p}$ at 1.96 TeV
-0.04 ± 0.11 ± 0.02	HORII	11	BELL $e^+ e^- \rightarrow \Upsilon(4S)$
-0.01 ± 0.01			
0.03 ± 0.17 ± 0.04	DEL-AMO-SA...10H	BABR	$e^+ e^- \rightarrow \Upsilon(4S)$
• • • We do not use the following data for averages, fits, limits, etc. • • •			
-0.02 ± 0.15 ± 0.04	HORII	08	BELL Repl. by HORII 11
+0.30 ± 0.29 ± 0.06	SAIGO	05	BELL Repl. by HORII 08

$A_{CP}(B^+ \rightarrow [K^- \pi^+ \pi^0]_D \pi^+)$

VALUE	DOCUMENT ID	TECN	COMMENT
<b>0.35 ± 0.16 OUR AVERAGE</b>			
0.438 ± 0.190 ± 0.011	<sup>1</sup> AAIJ	15W	LHCB $p\bar{p}$ at 7, 8 TeV
0.16 ± 0.27 ± 0.03	NAYAK	13	BELL $e^+ e^- \rightarrow \Upsilon(4S)$
-0.04 ± 0.04			
<sup>1</sup> Uses $D^0 \rightarrow K^- \pi^+ \pi^0$ for the favored mode, and $D^0 \rightarrow K^+ \pi^- \pi^0$ for the suppressed mode.			

$A_{CP}(B^+ \rightarrow [K^+ K^- \pi^0]_D \pi^+)$

VALUE	DOCUMENT ID	TECN	COMMENT
<b>-0.030 ± 0.040 ± 0.005</b>	<sup>1</sup> AAIJ	15W	LHCB $p\bar{p}$ at 7, 8 TeV
<sup>1</sup> Uses $D \rightarrow K^+ K^-$ mode.			

$A_{CP}(B^+ \rightarrow [\pi^+ \pi^- \pi^0]_D \pi^+)$

VALUE	DOCUMENT ID	TECN	COMMENT
<b>-0.016 ± 0.020 ± 0.004</b>	<sup>1</sup> AAIJ	15W	LHCB $p\bar{p}$ at 7, 8 TeV
<sup>1</sup> Uses $D \rightarrow \pi^+ \pi^-$ mode.			

$A_{CP}(B^+ \rightarrow [K^- \pi^+]_{(D\pi)} \pi^+)$

VALUE	DOCUMENT ID	TECN	COMMENT
<b>-0.09 ± 0.27 ± 0.05</b>	DEL-AMO-SA...10H	BABR	$e^+ e^- \rightarrow \Upsilon(4S)$

$A_{CP}(B^+ \rightarrow [K^- \pi^+]_{(D\gamma)} \pi^+)$

VALUE	DOCUMENT ID	TECN	COMMENT
<b>-0.65 ± 0.55 ± 0.22</b>	DEL-AMO-SA...10H	BABR	$e^+ e^- \rightarrow \Upsilon(4S)$

$A_{CP}(B^+ \rightarrow [K^- \pi^+]_{(D\pi)} K^+)$

VALUE	DOCUMENT ID	TECN	COMMENT
<b>0.77 ± 0.35 ± 0.12</b>	DEL-AMO-SA...10H	BABR	$e^+ e^- \rightarrow \Upsilon(4S)$

$A_{CP}(B^+ \rightarrow [K^- \pi^+]_{(D\gamma)} K^+)$

VALUE	DOCUMENT ID	TECN	COMMENT
<b>0.36 ± 0.94 ± 0.25</b>	DEL-AMO-SA...10H	BABR	$e^+ e^- \rightarrow \Upsilon(4S)$
-0.41 ± 0.41			

$A_{CP}(B^+ \rightarrow [\pi^+ \pi^- \pi^0]_D K^+)$

VALUE	DOCUMENT ID	TECN	COMMENT
<b>-0.02 ± 0.15 ± 0.03</b>	<sup>1</sup> AUBERT	07BJ	BABR $e^+ e^- \rightarrow \Upsilon(4S)$
• • • We do not use the following data for averages, fits, limits, etc. • • •			
-0.02 ± 0.16 ± 0.03	AUBERT,B	05T	BABR Repl. by AUBERT 07BJ
<sup>1</sup> Uses a Dalitz plot analysis of $D^0 \rightarrow \pi^+ \pi^- \pi^0$ . Also reports the one-sigma regions: $0.06 < r_B < 0.78$ , $-30^\circ < \gamma < 76^\circ$ , and $-27^\circ < \delta < 78^\circ$ .			

$A_{CP}(B^+ \rightarrow [K_S^0 K^+ \pi^-]_D K^+)$

VALUE	DOCUMENT ID	TECN	COMMENT
<b>0.040 ± 0.091 ± 0.018</b>	<sup>1</sup> AAIJ	14V	LHCB $p\bar{p}$ at 7, 8 TeV
<sup>1</sup> The analysis uses all of $D \rightarrow K_S^0 K \pi$ Dalitz decays.			

$A_{CP}(B^+ \rightarrow [K_S^0 K^- \pi^+]_D K^+)$

VALUE	DOCUMENT ID	TECN	COMMENT
<b>0.233 ± 0.129 ± 0.024</b>	<sup>1</sup> AAIJ	14V	LHCB $p\bar{p}$ at 7, 8 TeV
<sup>1</sup> The analysis uses all of $D \rightarrow K_S^0 K \pi$ Dalitz decays.			

$A_{CP}(B^+ \rightarrow [K_S^0 K^- \pi^+]_D \pi^+)$

VALUE	DOCUMENT ID	TECN	COMMENT
<b>-0.052 ± 0.029 ± 0.017</b>	<sup>1</sup> AAIJ	14V	LHCB $p\bar{p}$ at 7, 8 TeV
<sup>1</sup> The analysis uses all of $D \rightarrow K_S^0 K \pi$ Dalitz decays.			

$A_{CP}(B^+ \rightarrow [K_S^0 K^+ \pi^-]_D \pi^+)$

VALUE	DOCUMENT ID	TECN	COMMENT
<b>-0.025 ± 0.024 ± 0.010</b>	<sup>1</sup> AAIJ	14V	LHCB $p\bar{p}$ at 7, 8 TeV
<sup>1</sup> The analysis uses all of $D \rightarrow K_S^0 K \pi$ Dalitz decays.			

$A_{CP}(B^+ \rightarrow [K^*(892)^- K^+]_D K^+)$

VALUE	DOCUMENT ID	TECN	COMMENT
<b>0.026 ± 0.109 ± 0.029</b>	<sup>1</sup> AAIJ	14V	LHCB $p\bar{p}$ at 7, 8 TeV
<sup>1</sup> The Analysis uses $D \rightarrow K^*(892) K \rightarrow K_S^0 K \pi$ decays.			

$A_{CP}(B^+ \rightarrow [K^*(892)^+ K^-]_D K^+)$

VALUE	DOCUMENT ID	TECN	COMMENT
<b>0.336 ± 0.208 ± 0.026</b>	<sup>1</sup> AAIJ	14V	LHCB $p\bar{p}$ at 7, 8 TeV
<sup>1</sup> The Analysis uses $D \rightarrow K^*(892) K \rightarrow K_S^0 K \pi$ decays.			

$A_{CP}(B^+ \rightarrow [K^*(892)^+ K^-]_D \pi^+)$

VALUE	DOCUMENT ID	TECN	COMMENT
<b>-0.054 ± 0.043 ± 0.017</b>	<sup>1</sup> AAIJ	14V	LHCB $p\bar{p}$ at 7, 8 TeV
<sup>1</sup> The Analysis uses $D \rightarrow K^*(892) K \rightarrow K_S^0 K \pi$ decays.			

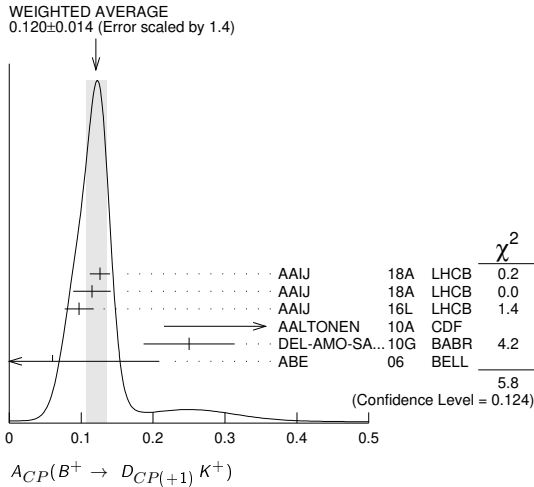
$A_{CP}(B^+ \rightarrow [K^*(892)^- K^+]_D \pi^+)$

VALUE	DOCUMENT ID	TECN	COMMENT
<b>-0.012 ± 0.028 ± 0.010</b>	<sup>1</sup> AAIJ	14V	LHCB $p\bar{p}$ at 7, 8 TeV
<sup>1</sup> The Analysis uses $D \rightarrow K^*(892) K \rightarrow K_S^0 K \pi$ decays.			

**$A_{CP}(B^+ \rightarrow D_{CP(+)}K^+)$**

VALUE	DOCUMENT ID	TECN	COMMENT
<b>0.120±0.014 OUR AVERAGE</b>	Error includes scale factor of 1.4. See the ideogram below.		
0.126±0.014±0.002	<sup>1</sup> AAIJ	18A LHCb	pp at 7, 8, 13 TeV
0.115±0.025±0.007	<sup>2</sup> AAIJ	18A LHCb	pp at 7, 8, 13 TeV
0.097±0.018±0.009	AAIJ	16L LHCb	pp at 7, 8 TeV
0.39 ±0.17 ±0.04	AALTONEN	10A CDF	p $\bar{p}$ at 1.96 TeV
0.25 ±0.06 ±0.02	<sup>3</sup> DEL-AMO-SA...	10G BABR	e <sup>+</sup> e <sup>-</sup> → $\Upsilon(4S)$
0.06 ±0.14 ±0.05	ABE	06 BELL	e <sup>+</sup> e <sup>-</sup> → $\Upsilon(4S)$
••• We do not use the following data for averages, fits, limits, etc. •••			
0.145±0.032±0.010	<sup>4</sup> AAIJ	12M LHCb	Repl. by AAIJ 16L
0.27 ±0.09 ±0.04	AUBERT	08AA BABR	Repl. by DEL-AMO-SANCHEZ 10G
0.35 ±0.13 ±0.04	AUBERT	06J BABR	Repl. by AUBERT 08AA
0.07 ±0.17 ±0.06	AUBERT	04N BABR	Repl. by AUBERT 06J
0.29 ±0.26 ±0.05	<sup>5</sup> ABE	03D BELL	Repl. by SWAIN 03
0.06 ±0.19 ±0.04	<sup>6</sup> SWAIN	03 BELL	Repl. by ABE 06

- <sup>1</sup> Uses D → K<sup>+</sup>K<sup>-</sup> decay mode.
- <sup>2</sup> Uses D → π<sup>+</sup>π<sup>-</sup> decay mode.
- <sup>3</sup> Reports the first evidence for direct CP violation in B → DK decays with 3.6 standard deviations.
- <sup>4</sup> AAIJ 12M reports an evidence of direct CP violation in B<sup>±</sup> → DK<sup>±</sup> decays with a total significance of 5.8 σ.
- <sup>5</sup> Corresponds to 90% confidence range -0.14 < A<sub>CP</sub> < 0.73.
- <sup>6</sup> Corresponds to 90% confidence range -0.26 < A<sub>CP</sub> < 0.38.



**$A_{ADS}(B^+ \rightarrow DK^+)$**

$$A_{ADS}(B^+ \rightarrow DK^+) = \frac{(R_K^- - R_K^+)}{(R_K^- + R_K^+)}$$

where

$$R_K^- = \Gamma(B^- \rightarrow [K^-\pi^-]_D K^-) / \Gamma(B^- \rightarrow [K^-\pi^+]_D K^-)$$

$$R_K^+ = \Gamma(B^+ \rightarrow [K^-\pi^+]_D K^+) / \Gamma(B^+ \rightarrow [K^+\pi^-]_D K^+)$$

VALUE	DOCUMENT ID	TECN	COMMENT
<b>-0.403±0.056±0.011</b>	AAIJ	16L LHCb	pp at 7, 8 TeV
••• We do not use the following data for averages, fits, limits, etc. •••			
-0.52 ±0.15 ±0.02	AAIJ	12M LHCb	Repl. by AAIJ 16L

**$A_{ADS}(B^+ \rightarrow D\pi^+)$**

$$A_{ADS}(B^+ \rightarrow D\pi^+) = \frac{(R_\pi^- - R_\pi^+)}{(R_\pi^- + R_\pi^+)}$$

where

$$R_\pi^- = \Gamma(B^- \rightarrow [K^+\pi^-]_D \pi^-) / \Gamma(B^- \rightarrow [K^-\pi^+]_D \pi^-)$$

$$R_\pi^+ = \Gamma(B^+ \rightarrow [K^-\pi^+]_D \pi^+) / \Gamma(B^+ \rightarrow [K^+\pi^-]_D \pi^+)$$

VALUE	DOCUMENT ID	TECN	COMMENT
<b>0.100±0.031±0.009</b>	AAIJ	16L LHCb	pp at 7, 8 TeV
••• We do not use the following data for averages, fits, limits, etc. •••			
0.143±0.062±0.011	AAIJ	12M LHCb	Repl. by AAIJ 16L

**$A_{ADS}(B^+ \rightarrow [K^-\pi^+]_D K^+\pi^-\pi^+)$**

VALUE	DOCUMENT ID	TECN	COMMENT
<b>-0.33<sup>+0.36</sup><sub>-0.34</sub></b>	AAIJ	15Bc LHCb	pp at 7, 8 TeV

**$A_{ADS}(B^+ \rightarrow [K^-\pi^+]_D \pi^+\pi^-\pi^+)$**

VALUE	DOCUMENT ID	TECN	COMMENT
<b>-0.013±0.087</b>	AAIJ	15Bc LHCb	pp at 7, 8 TeV

**$A_{CP}(B^+ \rightarrow D_{CP(-)}K^+)$**

VALUE	DOCUMENT ID	TECN	COMMENT
<b>-0.10±0.07 OUR AVERAGE</b>	Error includes scale factor of 1.4. See the ideogram below.		
-0.09±0.07±0.02	DEL-AMO-SA...	10G BABR	e <sup>+</sup> e <sup>-</sup> → $\Upsilon(4S)$
-0.12±0.14±0.05	ABE	06 BELL	e <sup>+</sup> e <sup>-</sup> → $\Upsilon(4S)$
••• We do not use the following data for averages, fits, limits, etc. •••			
-0.09±0.09±0.02	AUBERT	08AA BABR	Repl. by DEL-AMO-SANCHEZ 10G
-0.06±0.13±0.04	AUBERT	06J BABR	Repl. by AUBERT 08AA
-0.22±0.24±0.04	<sup>1</sup> ABE	03D BELL	Repl. by SWAIN 03
-0.19±0.17±0.05	<sup>2</sup> SWAIN	03 BELL	Repl. by ABE 06
<sup>1</sup> Corresponds to 90% confidence range -0.62 < A <sub>CP</sub> < 0.18.			
<sup>2</sup> Corresponds to 90% confidence range -0.47 < A <sub>CP</sub> < 0.11.			

**$A_{CP}(B^+ \rightarrow [K^+K^-]_D K^+\pi^-\pi^+)$**

VALUE	DOCUMENT ID	TECN	COMMENT
<b>-0.045±0.064±0.011</b>	AAIJ	15Bc LHCb	pp at 7, 8 TeV

**$A_{CP}(B^+ \rightarrow [\pi^+\pi^-]_D K^+\pi^-\pi^+)$**

VALUE	DOCUMENT ID	TECN	COMMENT
<b>-0.054±0.101±0.011</b>	AAIJ	15Bc LHCb	pp at 7, 8 TeV

**$A_{CP}(B^+ \rightarrow [K^-\pi^+]_D K^+\pi^-\pi^+)$**

VALUE	DOCUMENT ID	TECN	COMMENT
<b>0.013±0.019±0.013</b>	AAIJ	15Bc LHCb	pp at 7, 8 TeV

**$A_{CP}(B^+ \rightarrow [K^+K^-]_D \pi^+\pi^-\pi^+)$**

VALUE	DOCUMENT ID	TECN	COMMENT
<b>-0.019±0.011±0.010</b>	AAIJ	15Bc LHCb	pp at 7, 8 TeV

**$A_{CP}(B^+ \rightarrow [\pi^+\pi^-]_D \pi^+\pi^-\pi^+)$**

VALUE	DOCUMENT ID	TECN	COMMENT
<b>-0.013±0.016±0.010</b>	AAIJ	15Bc LHCb	pp at 7, 8 TeV

**$A_{CP}(B^+ \rightarrow [K^-\pi^+]_D \pi^+\pi^-\pi^+)$**

VALUE	DOCUMENT ID	TECN	COMMENT
<b>-0.002±0.003±0.011</b>	AAIJ	15Bc LHCb	pp at 7, 8 TeV

**$A_{CP}(B^+ \rightarrow \bar{D}^{*0}\pi^+)$**

VALUE	DOCUMENT ID	TECN	COMMENT
<b>0.0010±0.0028 OUR AVERAGE</b>	Error includes scale factor of 1.2.		
0.000 ±0.006 ±0.001	<sup>1</sup> AAIJ	18A LHCb	pp at 7, 8, 13 TeV
0.002 ±0.003 ±0.001	<sup>2</sup> AAIJ	18A LHCb	pp at 7, 8, 13 TeV
-0.014 ±0.015	ABE	06 BELL	e <sup>+</sup> e <sup>-</sup> → $\Upsilon(4S)$
<sup>1</sup> Uses D <sup>*0</sup> → D <sup>0</sup> γ decay mode.			
<sup>2</sup> Uses D <sup>*0</sup> → D <sup>0</sup> π <sup>0</sup> decay mode.			

**$A_{CP}(B^+ \rightarrow (D_{CP(+)}^*)^0\pi^+)$**

VALUE	DOCUMENT ID	TECN	COMMENT
<b>0.016±0.010 OUR AVERAGE</b>	Error includes scale factor of 1.2.		
-0.003±0.017±0.002	<sup>1</sup> AAIJ	18A LHCb	pp at 7, 8, 13 TeV
0.025±0.010±0.003	<sup>2</sup> AAIJ	18A LHCb	pp at 7, 8, 13 TeV
-0.021±0.045	ABE	06 BELL	e <sup>+</sup> e <sup>-</sup> → $\Upsilon(4S)$
<sup>1</sup> Uses D <sup>*0</sup> → D <sup>0</sup> γ decay mode.			
<sup>2</sup> Uses D <sup>*0</sup> → D <sup>0</sup> π <sup>0</sup> decay mode.			

**$A_{CP}(B^+ \rightarrow (D_{CP(-)}^*)^0\pi^+)$**

VALUE	DOCUMENT ID	TECN	COMMENT
<b>-0.090±0.051</b>	ABE	06 BELL	e <sup>+</sup> e <sup>-</sup> → $\Upsilon(4S)$

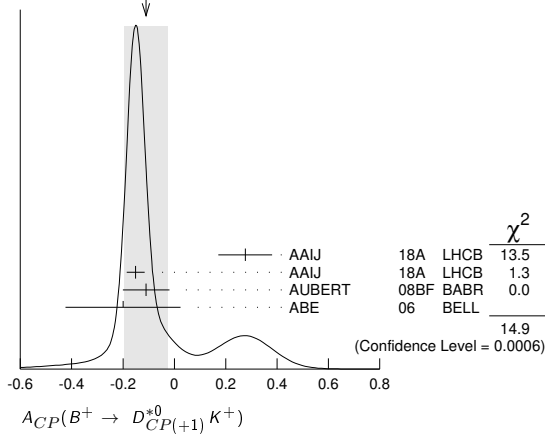
**$A_{CP}(B^+ \rightarrow D^{*0}K^+)$**

VALUE	DOCUMENT ID	TECN	COMMENT
<b>-0.001±0.011 OUR AVERAGE</b>	Error includes scale factor of 1.1.		
0.001±0.021±0.007	<sup>1</sup> AAIJ	18A LHCb	pp at 7, 8, 13 TeV
0.006±0.012±0.004	<sup>2</sup> AAIJ	18A LHCb	pp at 7, 8, 13 TeV
-0.06 ±0.04 ±0.01	AUBERT	08BF BABR	e <sup>+</sup> e <sup>-</sup> → $\Upsilon(4S)$
-0.089±0.086	ABE	06 BELL	e <sup>+</sup> e <sup>-</sup> → $\Upsilon(4S)$
<sup>1</sup> Uses D <sup>*0</sup> → D <sup>0</sup> γ decay mode.			
<sup>2</sup> Uses D <sup>*0</sup> → D <sup>0</sup> π <sup>0</sup> decay mode.			

**$A_{CP}(B^+ \rightarrow D_{CP(+)}^{*0}K^+)$**

VALUE	DOCUMENT ID	TECN	COMMENT
<b>-0.11 ±0.08 OUR AVERAGE</b>	Error includes scale factor of 2.7. See the ideogram below.		
0.276±0.094±0.047	<sup>1</sup> AAIJ	18A LHCb	pp at 7, 8, 13 TeV
-0.151±0.033±0.011	<sup>2</sup> AAIJ	18A LHCb	pp at 7, 8, 13 TeV
-0.11 ±0.09 ±0.01	AUBERT	08BF BABR	e <sup>+</sup> e <sup>-</sup> → $\Upsilon(4S)$
-0.20 ±0.22 ±0.04	ABE	06 BELL	e <sup>+</sup> e <sup>-</sup> → $\Upsilon(4S)$
••• We do not use the following data for averages, fits, limits, etc. •••			
-0.10 ±0.23 <sup>+0.03</sup> <sub>-0.04</sub>	AUBERT	05N BABR	Repl. by AUBERT 08BF
<sup>1</sup> Uses D <sup>*0</sup> → D <sup>0</sup> γ decay mode.			
<sup>2</sup> Uses D <sup>*0</sup> → D <sup>0</sup> π <sup>0</sup> decay mode.			

## Meson Particle Listings

 $B^\pm$ WEIGHTED AVERAGE  
-0.11±0.08 (Error scaled by 2.7) $A_{CP}(B^+ \rightarrow D_{CP(-)}^* K^+)$ 

VALUE	DOCUMENT ID	TECN	COMMENT
<b>0.07±0.10 OUR AVERAGE</b>			
+0.06±0.10±0.02	AUBERT	08BF BABR	$e^+e^- \rightarrow \Upsilon(4S)$
+0.13±0.30±0.08	ABE	06 BELL	$e^+e^- \rightarrow \Upsilon(4S)$

 $A_{CP}(B^+ \rightarrow D_{CP(+)} K^*(892)^+)$ 

VALUE	DOCUMENT ID	TECN	COMMENT
<b>0.08±0.06 OUR AVERAGE</b>			
0.08±0.06±0.01	<sup>1</sup> AAIJ	17B0 LHCB	$pp$ at 7, 8, 13 TeV
0.09±0.13±0.06	AUBERT	09AJ BABR	$e^+e^- \rightarrow \Upsilon(4S)$
••• We do not use the following data for averages, fits, limits, etc. •••			
-0.08±0.19±0.08	AUBERT,B	05U BABR	Repl. by AUBERT 09AJ

<sup>1</sup> Measures the asymmetry separately for  $K^+K^-$  and  $\pi^+\pi^-$  final states,  $A(KK) = 0.06 \pm 0.07 \pm 0.01$  and  $A(\pi\pi) = 0.15 \pm 0.13 \pm 0.01$ , and combines the two results. The value of  $A(\pi\pi)$  was updated in AAIJ 18x.

 $A_{CP}(B^+ \rightarrow D_{CP(-)} K^*(892)^+)$ 

VALUE	DOCUMENT ID	TECN	COMMENT
<b>-0.23±0.21±0.07</b>	AUBERT	09AJ BABR	$e^+e^- \rightarrow \Upsilon(4S)$
••• We do not use the following data for averages, fits, limits, etc. •••			
-0.26±0.40±0.12	AUBERT,B	05U BABR	Repl. by AUBERT 09AJ

 $A_{CP}(B^+ \rightarrow D_s^+ \phi)$ 

VALUE	DOCUMENT ID	TECN	COMMENT
<b>-0.01±0.41±0.03</b>	AAIJ	13R LHCB	$pp$ at 7 TeV

 $A_{CP}(B^+ \rightarrow D_s^+ \bar{D}^0)$ 

VALUE (%)	DOCUMENT ID	TECN	COMMENT
<b>-0.4±0.5±0.5</b>	AAIJ	18W LHCB	$pp$ at 7, 8 TeV

 $A_{CP}(B^+ \rightarrow D^{*+} \bar{D}^{*0})$ 

VALUE	DOCUMENT ID	TECN	COMMENT
<b>-0.15±0.11±0.02</b>	AUBERT,B	06A BABR	$e^+e^- \rightarrow \Upsilon(4S)$

 $A_{CP}(B^+ \rightarrow D^{*+} \bar{D}^0)$ 

VALUE	DOCUMENT ID	TECN	COMMENT
<b>-0.06±0.13±0.02</b>	AUBERT,B	06A BABR	$e^+e^- \rightarrow \Upsilon(4S)$

 $A_{CP}(B^+ \rightarrow D^+ \bar{D}^{*0})$ 

VALUE	DOCUMENT ID	TECN	COMMENT
<b>0.13±0.18±0.04</b>	AUBERT,B	06A BABR	$e^+e^- \rightarrow \Upsilon(4S)$

 $A_{CP}(B^+ \rightarrow D^+ \bar{D}^0)$ 

VALUE	DOCUMENT ID	TECN	COMMENT
<b>0.016±0.025 OUR AVERAGE</b>			
0.023±0.027±0.004	AAIJ	18W LHCB	$pp$ at 7, 8 TeV
0.00±0.08±0.02	ADACHI	08 BELL	$e^+e^- \rightarrow \Upsilon(4S)$
-0.13±0.14±0.02	AUBERT,B	06A BABR	$e^+e^- \rightarrow \Upsilon(4S)$

 $A_{CP}(B^+ \rightarrow K_S^0 \pi^+)$ 

VALUE	DOCUMENT ID	TECN	COMMENT
<b>-0.017±0.016 OUR AVERAGE</b>			
-0.022±0.025±0.010	AAIJ	13Bs LHCB	$pp$ at 7 TeV
-0.011±0.021±0.006	DUH	13 BELL	$e^+e^- \rightarrow \Upsilon(4S)$
-0.029±0.039±0.010	<sup>1</sup> AUBERT,BE	06c BABR	$e^+e^- \rightarrow \Upsilon(4S)$
0.18±0.24	<sup>2</sup> CHEN	00 CLE2	$e^+e^- \rightarrow \Upsilon(4S)$

••• We do not use the following data for averages, fits, limits, etc. •••

0.03±0.03±0.01	LIN	07 BELL	Repl. by DUH 13
-0.09±0.05±0.01	<sup>3</sup> AUBERT,BE	05E BABR	Repl. by AUBERT,BE 06c
0.05±0.05±0.01	<sup>4</sup> CHAO	05A BELL	Repl. by LIN 07
-0.05±0.08±0.01	<sup>5</sup> AUBERT	04M BABR	Repl. by AUBERT,BE 05E
0.07+0.09+0.01 -0.08-0.03	<sup>6</sup> UNNO	03 BELL	Repl. by CHAO 05A
0.46±0.15±0.02	<sup>7</sup> CASEY	02 BELL	Repl. by UNNO 03
0.098+0.430+0.020 -0.343-0.063	<sup>8</sup> ABE	01K BELL	Repl. by CASEY 02
-0.21±0.18±0.03	<sup>9</sup> AUBERT	01E BABR	Repl. by AUBERT 04M

<sup>1</sup> Corresponds to 90% confidence range  $-0.092 < A_{CP} < 0.036$ .<sup>2</sup> Corresponds to 90% confidence range  $-0.22 < A_{CP} < 0.56$ .<sup>3</sup> Corresponds to 90% confidence range  $-0.16 < A_{CP} < -0.02$ .<sup>4</sup> Corresponds to 90% confidence range  $-0.04 < A_{CP} < 0.13$ .<sup>5</sup> Corresponds to 90% confidence range  $-0.18 < A_{CP} < 0.08$ .<sup>6</sup> Corresponds to 90% confidence range  $-0.10 < A_{CP} < +0.22$ .<sup>7</sup> Corresponds to 90% confidence range  $+0.19 < A_{CP} < +0.72$ .<sup>8</sup> Corresponds to 90% confidence range  $-0.53 < A_{CP} < 0.82$ .<sup>9</sup> Corresponds to 90% confidence range  $-0.51 < A_{CP} < 0.09$ . $A_{CP}(B^+ \rightarrow K^+ \pi^0)$ 

VALUE	DOCUMENT ID	TECN	COMMENT
<b>0.037±0.021 OUR AVERAGE</b>			
0.043±0.024±0.002	DUH	13 BELL	$e^+e^- \rightarrow \Upsilon(4S)$
0.030±0.039±0.010	AUBERT	07Bc BABR	$e^+e^- \rightarrow \Upsilon(4S)$
-0.29±0.23	<sup>1</sup> CHEN	00 CLE2	$e^+e^- \rightarrow \Upsilon(4S)$

••• We do not use the following data for averages, fits, limits, etc. •••

0.07±0.03±0.01	LIN	08 BELL	Repl. by DUH 13
0.06±0.06±0.01	<sup>2</sup> AUBERT	05L BABR	Repl. by AUBERT 07Bc
0.06±0.06±0.02	<sup>2</sup> CHAO	05A BELL	Repl. by CHAO 04B
0.04±0.05±0.02	<sup>3</sup> CHAO	04B BELL	Repl. by LIN 08
-0.09±0.09±0.01	<sup>4</sup> AUBERT	03L BABR	Repl. by AUBERT 05L
-0.02±0.19±0.02	<sup>5</sup> CASEY	02 BELL	Repl. by CHAO 04B
-0.059+0.222+0.055 -0.196-0.017	<sup>6</sup> ABE	01K BELL	Repl. by CASEY 02
0.00±0.18±0.04	<sup>7</sup> AUBERT	01E BABR	Repl. by AUBERT 03L

<sup>1</sup> Corresponds to 90% confidence range  $-0.67 < A_{CP} < 0.09$ .<sup>2</sup> Corresponds to a 90% CL interval of  $-0.06 < A_{CP} < 0.18$ .<sup>3</sup> Corresponds to 90% CL interval of  $-0.05 < A_{CP} < 0.13$ .<sup>4</sup> Corresponds to 90% confidence range  $-0.24 < A_{CP} < 0.06$ .<sup>5</sup> Corresponds to 90% confidence range  $-0.35 < A_{CP} < +0.30$ .<sup>6</sup> Corresponds to 90% confidence range  $-0.40 < A_{CP} < 0.36$ .<sup>7</sup> Corresponds to 90% confidence range  $-0.30 < A_{CP} < +0.30$ . $A_{CP}(B^+ \rightarrow \eta' K^+)$ 

VALUE	DOCUMENT ID	TECN	COMMENT
<b>0.004±0.011 OUR AVERAGE</b>			
-0.002±0.012±0.006	<sup>1</sup> AAIJ	15o LHCB	$pp$ at 7, 8 TeV
0.008+0.017+0.009 -0.018-0.018	AUBERT	09AV BABR	$e^+e^- \rightarrow \Upsilon(4S)$
0.028±0.028±0.021	SCHUEMANN	06 BELL	$e^+e^- \rightarrow \Upsilon(4S)$
0.03±0.12	<sup>2</sup> CHEN	00 CLE2	$e^+e^- \rightarrow \Upsilon(4S)$

••• We do not use the following data for averages, fits, limits, etc. •••

0.010±0.022±0.006	AUBERT	07AE BABR	Repl. by AUBERT 09AV
0.033±0.028±0.005	<sup>3</sup> AUBERT	05M BABR	Repl. by AUBERT 07AE
0.037±0.045±0.011	<sup>4</sup> AUBERT	03W BABR	Repl. by AUBERT 05M
-0.11±0.11±0.02	<sup>5</sup> AUBERT	02E BABR	Repl. by AUBERT 05M
-0.015±0.070±0.009	<sup>6</sup> CHEN	02B BELL	Repl. by SCHUEMANN 06
0.06±0.15±0.01	<sup>7</sup> ABE	01M BELL	Repl. by CHEN 02B

<sup>1</sup> Obtained using  $A_{CP}(B^\pm \rightarrow J/\psi K^\pm) = (0.3 \pm 0.6) \times 10^{-2}$ .<sup>2</sup> Corresponds to 90% confidence range  $-0.17 < A_{CP} < 0.23$ .<sup>3</sup> Corresponds to 90% confidence range  $-0.012 < A_{CP} < 0.078$ .<sup>4</sup> Corresponds to 90% confidence range  $-0.04 < A_{CP} < 0.11$ .<sup>5</sup> Corresponds to 90% confidence range  $-0.28 < A_{CP} < 0.07$ .<sup>6</sup> Corresponds to 90% confidence range  $-0.13 < A_{CP} < 0.10$ .<sup>7</sup> Corresponds to 90% confidence range  $-0.20 < A_{CP} < 0.32$ . $A_{CP}(B^+ \rightarrow \eta' K^*(892)^+)$ 

VALUE	DOCUMENT ID	TECN	COMMENT
<b>-0.26±0.27±0.02</b>	DEL-AMO-SA..10A	BABR	$e^+e^- \rightarrow \Upsilon(4S)$

••• We do not use the following data for averages, fits, limits, etc. •••

-0.30+0.33-0.37±0.02	<sup>1</sup> AUBERT	07E BABR	Repl. by DEL-AMO-SANCHEZ 10A
----------------------	---------------------	----------	------------------------------

<sup>1</sup> Reports  $A_{CP}$  with the opposite sign convention. $A_{CP}(B^+ \rightarrow \eta' K_0^*(1430)^+)$ 

VALUE	DOCUMENT ID	TECN	COMMENT
<b>0.06±0.20±0.02</b>	DEL-AMO-SA..10A	BABR	$e^+e^- \rightarrow \Upsilon(4S)$

 $A_{CP}(B^+ \rightarrow \eta' K_2^*(1430)^+)$ 

VALUE	DOCUMENT ID	TECN	COMMENT
<b>0.15±0.13±0.02</b>	DEL-AMO-SA..10A	BABR	$e^+e^- \rightarrow \Upsilon(4S)$

$A_{CP}(B^+ \rightarrow \eta K^+)$ 

VALUE	DOCUMENT ID	TECN	COMMENT
<b><math>-0.37 \pm 0.08</math> OUR AVERAGE</b>			
$-0.38 \pm 0.11 \pm 0.01$	HOI	12 BELL	$e^+ e^- \rightarrow \Upsilon(4S)$
$-0.36 \pm 0.11 \pm 0.03$	AUBERT	09AV BABR	$e^+ e^- \rightarrow \Upsilon(4S)$
• • • We do not use the following data for averages, fits, limits, etc. • • •			
$-0.22 \pm 0.11 \pm 0.01$	AUBERT	07AE BABR	Repl. by AUBERT 09AV
$-0.39 \pm 0.16 \pm 0.03$	CHANG	07B BELL	Repl. by HOI 12
$-0.20 \pm 0.15 \pm 0.01$	AUBERT,B	05K BABR	Repl. by AUBERT 07AE
$-0.49 \pm 0.31 \pm 0.07$	CHANG	05A BELL	Repl. by CHANG 07B
$-0.52 \pm 0.24 \pm 0.01$	AUBERT	04H BABR	Repl. by AUBERT,B 05K

 $A_{CP}(B^+ \rightarrow \eta K^*(892)^+)$ 

VALUE	DOCUMENT ID	TECN	COMMENT
<b><math>0.02 \pm 0.06</math> OUR AVERAGE</b>			
$0.03 \pm 0.10 \pm 0.01$	WANG	07B BELL	$e^+ e^- \rightarrow \Upsilon(4S)$
$0.01 \pm 0.08 \pm 0.02$	AUBERT,B	06H BABR	$e^+ e^- \rightarrow \Upsilon(4S)$
• • • We do not use the following data for averages, fits, limits, etc. • • •			
$0.13 \pm 0.14 \pm 0.02$	AUBERT,B	04D BABR	Repl. by AUBERT,B 06H

 $A_{CP}(B^+ \rightarrow \eta K_0^*(1430)^+)$ 

VALUE	DOCUMENT ID	TECN	COMMENT
<b><math>0.05 \pm 0.13 \pm 0.02</math></b>			
	AUBERT,B	06H BABR	$e^+ e^- \rightarrow \Upsilon(4S)$

 $A_{CP}(B^+ \rightarrow \eta K_2^*(1430)^+)$ 

VALUE	DOCUMENT ID	TECN	COMMENT
<b><math>-0.45 \pm 0.30 \pm 0.02</math></b>			
	AUBERT,B	06H BABR	$e^+ e^- \rightarrow \Upsilon(4S)$

 $A_{CP}(B^+ \rightarrow \omega K^+)$ 

VALUE	DOCUMENT ID	TECN	COMMENT
<b><math>-0.02 \pm 0.04</math> OUR AVERAGE</b>			
$-0.03 \pm 0.04 \pm 0.01$	CHOBANOVA	14 BELL	$e^+ e^- \rightarrow \Upsilon(4S)$
$-0.01 \pm 0.07 \pm 0.01$	AUBERT	07AE BABR	$e^+ e^- \rightarrow \Upsilon(4S)$
• • • We do not use the following data for averages, fits, limits, etc. • • •			
$0.05 \pm 0.09 \pm 0.01$	AUBERT,B	06E BABR	Repl. by AUBERT 07AE
$0.05 \pm 0.08 \pm 0.01$	JEN	06 BELL	Repl. by CHOBANOVA 14
$-0.09 \pm 0.17 \pm 0.01$	AUBERT	04H BABR	Repl. by AUBERT,B 06E
$0.06 \pm 0.21 \pm 0.01$	<sup>1</sup> WANG	04A BELL	Repl. by JEN 06
$-0.21 \pm 0.28 \pm 0.03$	<sup>2</sup> LU	02 BELL	Repl. by WANG 04A

<sup>1</sup> Corresponds to 90% CL interval  $0.15 < A_{CP} < 0.90$ <sup>2</sup> Corresponds to 90% confidence range  $-0.70 < A_{CP} < +0.38$ . $A_{CP}(B^+ \rightarrow \omega K^{*+})$ 

VALUE	DOCUMENT ID	TECN	COMMENT
<b><math>+0.29 \pm 0.35 \pm 0.02</math></b>			
	AUBERT	09H BABR	$e^+ e^- \rightarrow \Upsilon(4S)$

 $A_{CP}(B^+ \rightarrow \omega(K\pi)_0^{*+})$ 

VALUE	DOCUMENT ID	TECN	COMMENT
<b><math>-0.10 \pm 0.09 \pm 0.02</math></b>			
	AUBERT	09H BABR	$e^+ e^- \rightarrow \Upsilon(4S)$

 $A_{CP}(B^+ \rightarrow \omega K_2^*(1430)^+)$ 

VALUE	DOCUMENT ID	TECN	COMMENT
<b><math>+0.14 \pm 0.15 \pm 0.02</math></b>			
	AUBERT	09H BABR	$e^+ e^- \rightarrow \Upsilon(4S)$

 $A_{CP}(B^+ \rightarrow K^{*0} \pi^+)$ 

VALUE	DOCUMENT ID	TECN	COMMENT
<b><math>-0.04 \pm 0.09</math> OUR AVERAGE</b>			
$-0.12 \pm 0.21 \pm 0.08$	<sup>1</sup> LEES	17G BABR	$e^+ e^- \rightarrow \Upsilon(4S)$
$0.032 \pm 0.052 \pm 0.016$	AUBERT	08A1 BABR	$e^+ e^- \rightarrow \Upsilon(4S)$
$-0.149 \pm 0.064 \pm 0.022$	GARMASH	06 BELL	$e^+ e^- \rightarrow \Upsilon(4S)$
• • • We do not use the following data for averages, fits, limits, etc. • • •			
$0.068 \pm 0.078 \pm 0.070$	AUBERT,B	05N BABR	Repl. by AUBERT 08A1

<sup>1</sup> Obtains the result from a Dalitz analysis of  $B^+ \rightarrow K_S^0 \pi^+ \pi^0$  decays. The first error is statistical, the second combines all the systematic uncertainties reported in the paper, including signal modelling. $A_{CP}(B^+ \rightarrow K^*(892)^+ \pi^0)$ 

VALUE	DOCUMENT ID	TECN	COMMENT
<b><math>-0.39 \pm 0.21</math> OUR AVERAGE</b>			
$-0.52 \pm 0.14 \pm 0.06$	<sup>1</sup> LEES	17G BABR	$e^+ e^- \rightarrow \Upsilon(4S)$
$-0.06 \pm 0.24 \pm 0.04$	LEES	11I BABR	$e^+ e^- \rightarrow \Upsilon(4S)$
• • • We do not use the following data for averages, fits, limits, etc. • • •			
$0.04 \pm 0.29 \pm 0.05$	AUBERT	05X BABR	Repl. by LEES 11I

<sup>1</sup> Obtains the result from a Dalitz analysis of  $B^+ \rightarrow K_S^0 \pi^+ \pi^0$  decays. The first error is statistical, the second combines all the systematic uncertainties reported in the paper, including signal modelling. $A_{CP}(B^+ \rightarrow K^+ \pi^- \pi^+)$ 

VALUE	DOCUMENT ID	TECN	COMMENT
<b><math>0.027 \pm 0.008</math> OUR AVERAGE</b>			
$0.025 \pm 0.004 \pm 0.008$	<sup>1</sup> AAIJ	14B0 LHCB	$pp$ at 7, 8 TeV
$0.028 \pm 0.020 \pm 0.023$	AUBERT	08A1 BABR	$e^+ e^- \rightarrow \Upsilon(4S)$
$0.049 \pm 0.026 \pm 0.020$	GARMASH	06 BELL	$e^+ e^- \rightarrow \Upsilon(4S)$
• • • We do not use the following data for averages, fits, limits, etc. • • •			
$0.032 \pm 0.008 \pm 0.008$	AAIJ	13AZ LHCB	Repl. by AAIJ 14B0
$-0.013 \pm 0.037 \pm 0.011$	AUBERT,B	05N BABR	Repl. by AUBERT 08A1
$0.01 \pm 0.07 \pm 0.03$	AUBERT	03M BABR	Repl. by AUBERT,B 05N
<sup>1</sup> AAIJ 14B0 reports also $CP$ asymmetries in restricted regions of phase space.			

 $A_{CP}(B^+ \rightarrow K^+ K^- K^+ \text{nonresonant})$ 

VALUE	DOCUMENT ID	TECN	COMMENT
<b><math>0.060 \pm 0.044 \pm 0.019</math></b>			
	LEES	12O BABR	$e^+ e^- \rightarrow \Upsilon(4S)$

 $A_{CP}(B^+ \rightarrow f(980)^0 K^+)$ 

VALUE	DOCUMENT ID	TECN	COMMENT
<b><math>-0.08 \pm 0.08 \pm 0.04</math></b>			
	<sup>1</sup> LEES	12O BABR	$e^+ e^- \rightarrow \Upsilon(4S)$
<sup>1</sup> Measured in the $B^+ \rightarrow K^+ K^- K^+$ decay.			

 $A_{CP}(B^+ \rightarrow f_2(1270) K^+)$ 

VALUE	DOCUMENT ID	TECN	COMMENT
<b><math>-0.68 \pm 0.19</math> OUR AVERAGE</b>			
$-0.85 \pm 0.22 \pm 0.26$	AUBERT	08A1 BABR	$e^+ e^- \rightarrow \Upsilon(4S)$
$-0.59 \pm 0.22 \pm 0.036$	GARMASH	06 BELL	$e^+ e^- \rightarrow \Upsilon(4S)$

 $A_{CP}(B^+ \rightarrow f_0(1500) K^+)$ 

VALUE	DOCUMENT ID	TECN	COMMENT
<b><math>0.28 \pm 0.26 \pm 0.15</math></b>			
	AUBERT	08A1 BABR	$e^+ e^- \rightarrow \Upsilon(4S)$

 $A_{CP}(B^+ \rightarrow f_2'(1525)^0 K^+)$ 

VALUE	DOCUMENT ID	TECN	COMMENT
<b><math>-0.08 \pm 0.05</math> OUR AVERAGE</b>			
$0.18 \pm 0.18 \pm 0.04$	<sup>1</sup> LEES	11I BABR	$e^+ e^- \rightarrow \Upsilon(4S)$
$-0.106 \pm 0.050 \pm 0.036$	AUBERT	08A1 BABR	$e^+ e^- \rightarrow \Upsilon(4S)$
$-0.077 \pm 0.065 \pm 0.046$	GARMASH	06 BELL	$e^+ e^- \rightarrow \Upsilon(4S)$
• • • We do not use the following data for averages, fits, limits, etc. • • •			
$-0.14 \pm 0.10 \pm 0.04$	<sup>2</sup> LEES	12O BABR	$e^+ e^- \rightarrow \Upsilon(4S)$
$0.31 \pm 0.25 \pm 0.08$	<sup>3</sup> AUBERT	06O BABR	Repl. by LEES 12O
$0.088 \pm 0.095 \pm 0.097$	AUBERT,B	05N BABR	Repl. by AUBERT 08A1

<sup>1</sup> Measured in  $B^+ \rightarrow f_0 K^+$  with  $f_0 \rightarrow \pi^0 \pi^0$  decay.<sup>2</sup> Measured in the  $B^+ \rightarrow K^+ K^- K^+$  decay assuming  $A_{CP}(B^+ \rightarrow f_2'(1525)^0 K^+) = A_{CP}(B^+ \rightarrow f_0(1500)^0 K^+) = A_{CP}(B^+ \rightarrow f_0(1710)^0 K^+)$ <sup>3</sup> Measured in the  $B^+ \rightarrow K^+ K^- K^+$  decay. $A_{CP}(B^+ \rightarrow \rho^0 K^+)$ 

VALUE	DOCUMENT ID	TECN	COMMENT
<b><math>0.37 \pm 0.10</math> OUR AVERAGE</b>			
$0.44 \pm 0.10 \pm 0.06$	AUBERT	08A1 BABR	$e^+ e^- \rightarrow \Upsilon(4S)$
$0.30 \pm 0.11 \pm 0.11$	GARMASH	06 BELL	$e^+ e^- \rightarrow \Upsilon(4S)$
• • • We do not use the following data for averages, fits, limits, etc. • • •			
$0.32 \pm 0.13 \pm 0.10$	AUBERT,B	05N BABR	Repl. by AUBERT 08A1

 $A_{CP}(B^+ \rightarrow K^0 \pi^+ \pi^0)$ 

VALUE	DOCUMENT ID	TECN	COMMENT
<b><math>0.07 \pm 0.05 \pm 0.04</math></b>			
	<sup>1</sup> LEES	17G BABR	$e^+ e^- \rightarrow \Upsilon(4S)$
<sup>1</sup> Obtains the result from a Dalitz analysis of $B^+ \rightarrow K_S^0 \pi^+ \pi^0$ decays. The first error is statistical, the second combines all the systematic uncertainties reported in the paper, including signal modelling.			

 $A_{CP}(B^+ \rightarrow K_0^*(1430)^0 \pi^+)$ 

VALUE	DOCUMENT ID	TECN	COMMENT
<b><math>0.061 \pm 0.032</math> OUR AVERAGE</b>			
$0.14 \pm 0.10 \pm 0.14$	<sup>1</sup> LEES	17G BABR	$e^+ e^- \rightarrow \Upsilon(4S)$
$0.032 \pm 0.035 \pm 0.034$	AUBERT	08A1 BABR	$e^+ e^- \rightarrow \Upsilon(4S)$
$0.076 \pm 0.038 \pm 0.028$	GARMASH	06 BELL	$e^+ e^- \rightarrow \Upsilon(4S)$
• • • We do not use the following data for averages, fits, limits, etc. • • •			
$-0.064 \pm 0.032 \pm 0.023$	AUBERT,B	05N BABR	Repl. by AUBERT 08A1

<sup>1</sup> Obtains the result from a Dalitz analysis of  $B^+ \rightarrow K_S^0 \pi^+ \pi^0$  decays. The first error is statistical, the second combines all the systematic uncertainties reported in the paper, including signal modelling.

## Meson Particle Listings

 $B^\pm$  $A_{CP}(B^+ \rightarrow K_S^0(1430)^+ \pi^0)$ 

VALUE	DOCUMENT ID	TECN	COMMENT
$0.26 \pm 0.12 \pm 0.14_{-0.08}$	<sup>1</sup> LEES	17G	BABR $e^+e^- \rightarrow \Upsilon(4S)$

<sup>1</sup> Obtains the result from a Dalitz analysis of  $B^+ \rightarrow K_S^0 \pi^+ \pi^0$  decays. The first error is statistical, the second combines all the systematic uncertainties reported in the paper, including signal modelling.

 $A_{CP}(B^+ \rightarrow K_S^*(1430)^0 \pi^+)$ 

VALUE	DOCUMENT ID	TECN	COMMENT
$0.05 \pm 0.23 \pm 0.18_{-0.08}$	AUBERT	08A1	BABR $e^+e^- \rightarrow \Upsilon(4S)$

 $A_{CP}(B^+ \rightarrow K^+ \pi^0 \pi^0)$ 

VALUE	DOCUMENT ID	TECN	COMMENT
$-0.06 \pm 0.06 \pm 0.04$	LEES	11i	BABR $e^+e^- \rightarrow \Upsilon(4S)$

 $A_{CP}(B^+ \rightarrow K^0 \rho^+)$ 

VALUE	DOCUMENT ID	TECN	COMMENT
$-0.03 \pm 0.15$ OUR AVERAGE			

$0.21 \pm 0.19 \pm 0.24_{-0.20}$	<sup>1</sup> LEES	17G	BABR $e^+e^- \rightarrow \Upsilon(4S)$
$-0.12 \pm 0.17 \pm 0.02$	AUBERT	07Z	BABR $e^+e^- \rightarrow \Upsilon(4S)$

<sup>1</sup> Obtains the result from a Dalitz analysis of  $B^+ \rightarrow K_S^0 \pi^+ \pi^0$  decays. The first error is statistical, the second combines all the systematic uncertainties reported in the paper, including signal modelling.

 $A_{CP}(B^+ \rightarrow K^{*+} \pi^+ \pi^-)$ 

VALUE	DOCUMENT ID	TECN	COMMENT
$0.07 \pm 0.07 \pm 0.04$	AUBERT,B	06U	BABR $e^+e^- \rightarrow \Upsilon(4S)$

 $A_{CP}(B^+ \rightarrow \rho^0 K^*(892)^+)$ 

VALUE	DOCUMENT ID	TECN	COMMENT
$0.31 \pm 0.13 \pm 0.03$	DEL-AMO-SA...11D	BABR	$e^+e^- \rightarrow \Upsilon(4S)$

••• We do not use the following data for averages, fits, limits, etc. •••

$0.20 \pm 0.32 \pm 0.04_{-0.29}$	AUBERT	03V	BABR Repl. by DEL-A MO-SANCHEZ 11D
----------------------------------	--------	-----	------------------------------------

 $A_{CP}(B^+ \rightarrow K^*(892)^+ f_0(980))$ 

VALUE	DOCUMENT ID	TECN	COMMENT
$-0.15 \pm 0.12 \pm 0.03$	DEL-AMO-SA...11D	BABR	$e^+e^- \rightarrow \Upsilon(4S)$

••• We do not use the following data for averages, fits, limits, etc. •••

$-0.34 \pm 0.21 \pm 0.03$	AUBERT,B	06G	BABR Repl. by DEL-AMO-SANCHEZ 11D
---------------------------	----------	-----	-----------------------------------

 $A_{CP}(B^+ \rightarrow a_1^+ K^0)$ 

VALUE	DOCUMENT ID	TECN	COMMENT
$+0.12 \pm 0.11 \pm 0.02$	AUBERT	08F	BABR $e^+e^- \rightarrow \Upsilon(4S)$

 $A_{CP}(B^+ \rightarrow b_1^+ K^0)$ 

VALUE	DOCUMENT ID	TECN	COMMENT
$-0.03 \pm 0.15 \pm 0.02$	AUBERT	08AG	BABR $e^+e^- \rightarrow \Upsilon(4S)$

 $A_{CP}(B^+ \rightarrow K^*(892)^0 \rho^+)$ 

VALUE	DOCUMENT ID	TECN	COMMENT
$-0.01 \pm 0.16 \pm 0.02$	AUBERT,B	06G	BABR $e^+e^- \rightarrow \Upsilon(4S)$

 $A_{CP}(B^+ \rightarrow b_1^0 K^+)$ 

VALUE	DOCUMENT ID	TECN	COMMENT
$-0.46 \pm 0.20 \pm 0.02$	AUBERT	07Bi	BABR $e^+e^- \rightarrow \Upsilon(4S)$

 $A_{CP}(B^+ \rightarrow K^0 K^+)$ 

VALUE	DOCUMENT ID	TECN	COMMENT
$0.04 \pm 0.14$ OUR AVERAGE			

$0.014 \pm 0.168 \pm 0.002$	DUH	13	BELL $e^+e^- \rightarrow \Upsilon(4S)$
$0.10 \pm 0.26 \pm 0.03$	<sup>1</sup> AUBERT,BE	06c	BABR $e^+e^- \rightarrow \Upsilon(4S)$

••• We do not use the following data for averages, fits, limits, etc. •••

$0.13 \pm 0.23 \pm 0.02_{-0.24}$	LIN	07	BELL Repl. by DUH 13
$0.15 \pm 0.33 \pm 0.03$	<sup>2</sup> AUBERT,BE	05E	BABR Repl. by AUBERT,BE 06c

<sup>1</sup> Corresponds to 90% confidence range  $-0.31 < A_{CP} < 0.54$ .  
<sup>2</sup> Corresponds to 90% confidence range  $-0.43 < A_{CP} < 0.68$ .

 $A_{CP}(B^+ \rightarrow K_S^0 K^+)$ 

VALUE	DOCUMENT ID	TECN	COMMENT
$-0.21 \pm 0.14 \pm 0.01$	AAIJ	13Bs	LHCB $pp$ at 7 TeV

 $A_{CP}(B^+ \rightarrow K^+ K_S^0 K_S^0)$ 

VALUE	DOCUMENT ID	TECN	COMMENT
$0.025 \pm 0.031$ OUR AVERAGE			

$0.016 \pm 0.039 \pm 0.009$	KALIYAR	19	BELL $e^+e^- \rightarrow \Upsilon(4S)$
$0.04 \pm 0.04 \pm 0.02_{-0.05}$	LEES	12o	BABR $e^+e^- \rightarrow \Upsilon(4S)$

••• We do not use the following data for averages, fits, limits, etc. •••

$-0.04 \pm 0.11 \pm 0.02$	<sup>1</sup> AUBERT,B	04V	BABR Repl. by LEES 12o
---------------------------	-----------------------	-----	------------------------

<sup>1</sup> Corresponds to 90% confidence range  $-0.23 < A_{CP} < 0.15$ .

 $A_{CP}(B^+ \rightarrow K^+ K^- \pi^+)$ 

VALUE	DOCUMENT ID	TECN	COMMENT
$-0.122 \pm 0.021$ OUR AVERAGE			
$-0.170 \pm 0.073 \pm 0.017$	<sup>1</sup> HSU	17	BELL $e^+e^- \rightarrow \Upsilon(4S)$
$-0.123 \pm 0.017 \pm 0.014$	<sup>2</sup> AAIJ	14Bo	LHCB $pp$ at 7, 8 TeV
$0.00 \pm 0.10 \pm 0.03$	AUBERT	07Bb	BABR $e^+e^- \rightarrow \Upsilon(4S)$

••• We do not use the following data for averages, fits, limits, etc. •••

$-0.141 \pm 0.040 \pm 0.019$	<sup>3</sup> AAIJ	14	LHCB Repl. by AAIJ 14Bo
<sup>1</sup> HSU 17 provides also measurement as a function of $K^+ K^-$ invariant mass.			
<sup>2</sup> AAIJ 14Bo reports also $CP$ asymmetries in restricted regions of phase space.			
<sup>3</sup> AAIJ 14 reports $A_{CP}(B^+ \rightarrow K^+ K^- \pi^+) = -0.648 \pm 0.070 \pm 0.013 \pm 0.007$ in the Dalitz plot region of $m_{K^+ K^-}^2 < 1.5 \text{ GeV}^2/c^4$ . The third uncertainty is due to the $CP$ asymmetry of the $B^\pm \rightarrow J/\psi K^\pm$ reference mode uncertainty.			

 $A_{CP}(B^+ \rightarrow K^+ K^- \pi^+ \text{ nonresonant})$ 

VALUE	DOCUMENT ID	TECN	COMMENT
$-0.107 \pm 0.053 \pm 0.035$	<sup>1</sup> AAIJ	19AL	LHCB $pp$ at 7, 8 TeV

<sup>1</sup> Uses amplitude analysis of  $B^\pm \rightarrow \pi^\pm K^+ K^-$  decays.

 $A_{CP}(B^+ \rightarrow K^+ \bar{K}^*(892)^0)$ 

VALUE	DOCUMENT ID	TECN	COMMENT
$0.123 \pm 0.087 \pm 0.045$	<sup>1</sup> AAIJ	19AL	LHCB $pp$ at 7, 8 TeV

<sup>1</sup> Uses amplitude analysis of  $B^\pm \rightarrow \pi^\pm K^+ K^-$  decays.

 $A_{CP}(B^+ \rightarrow K^+ \bar{K}_S^0(1430)^0)$ 

VALUE	DOCUMENT ID	TECN	COMMENT
$0.104 \pm 0.149 \pm 0.088$	<sup>1</sup> AAIJ	19AL	LHCB $pp$ at 7, 8 TeV

<sup>1</sup> Uses amplitude analysis of  $B^\pm \rightarrow \pi^\pm K^+ K^-$  decays.

 $A_{CP}(B^+ \rightarrow \phi \pi^+)$ 

VALUE	DOCUMENT ID	TECN	COMMENT
$0.098 \pm 0.436 \pm 0.266$	<sup>1</sup> AAIJ	19AL	LHCB $pp$ at 7, 8 TeV

<sup>1</sup> Uses amplitude analysis of  $B^\pm \rightarrow \pi^\pm K^+ K^-$  decays.

 $A_{CP}(B^+ \rightarrow \pi^+(K^+ K^-)_{S\text{-wave}})$ 

VALUE	DOCUMENT ID	TECN	COMMENT
$-0.664 \pm 0.038 \pm 0.019$	<sup>1</sup> AAIJ	19AL	LHCB $pp$ at 7, 8 TeV

<sup>1</sup> Uses amplitude analysis of  $B^\pm \rightarrow \pi^\pm K^+ K^-$  decays in the  $\pi\pi - KK$  rescattering mass region of  $0.95 < m(K^+ K^-) < 1.42 \text{ GeV}/c^2$ .

 $A_{CP}(B^+ \rightarrow K^+ K^- K^+)$ 

VALUE	DOCUMENT ID	TECN	COMMENT
$-0.033 \pm 0.008$ OUR AVERAGE			
$-0.036 \pm 0.004 \pm 0.007$	<sup>1</sup> AAIJ	14Bo	LHCB $pp$ at 7, 8 TeV
$-0.017 \pm 0.019_{-0.014} \pm 0.014$	<sup>2</sup> LEES	12o	BABR $e^+e^- \rightarrow \Upsilon(4S)$

••• We do not use the following data for averages, fits, limits, etc. •••

$-0.043 \pm 0.009 \pm 0.008$	AAIJ	13Az	LHCB Repl. by AAIJ 14Bo
$-0.017 \pm 0.026 \pm 0.015$	AUBERT	06o	BABR Repl. by LEES 12o
$0.02 \pm 0.07 \pm 0.03$	AUBERT	03M	BABR Repl. by AUBERT 06o

<sup>1</sup> AAIJ 14Bo reports also  $CP$  asymmetries in restricted regions of phase space.

<sup>2</sup> All intermediate charmonium and charm resonances are removed, except of  $\chi_{c0}$ .

 $A_{CP}(B^+ \rightarrow \phi K^+)$ 

VALUE	DOCUMENT ID	TECN	COMMENT
$0.024 \pm 0.028$ OUR AVERAGE			Error includes scale factor of 2.3.
$0.017 \pm 0.011 \pm 0.006$	<sup>1</sup> AAIJ	15o	LHCB $pp$ at 7, 8 TeV
$0.128 \pm 0.044 \pm 0.013$	LEES	12o	BABR $e^+e^- \rightarrow \Upsilon(4S)$

$-0.07 \pm 0.17 \pm 0.03_{-0.02}$	ACOSTA	05J	CDF $p\bar{p}$ at 1.96 TeV
$0.01 \pm 0.12 \pm 0.05$	<sup>2</sup> CHEN	03B	BELL $e^+e^- \rightarrow \Upsilon(4S)$

••• We do not use the following data for averages, fits, limits, etc. •••

$0.022 \pm 0.021 \pm 0.009$	AAIJ	14A	LHCB Repl. by AAIJ 15o
$0.00 \pm 0.08 \pm 0.02$	AUBERT	06o	BABR Repl. by LEES 12o
$0.04 \pm 0.09 \pm 0.01$	<sup>3</sup> AUBERT	04A	BABR Repl. by AUBERT 06o
$-0.05 \pm 0.20 \pm 0.03$	<sup>4</sup> AUBERT	02E	BABR $e^+e^- \rightarrow \Upsilon(4S)$

<sup>1</sup> Obtained using  $A_{CP}(B^\pm \rightarrow J/\psi K^\pm) = (0.3 \pm 0.6) \times 10^{-2}$ .

<sup>2</sup> Corresponds to 90% confidence range  $-0.20 < A_{CP} < 0.22$ .

<sup>3</sup> Corresponds to 90% confidence range  $-0.10 < A_{CP} < 0.18$ .

<sup>4</sup> Corresponds to 90% confidence range  $-0.37 < A_{CP} < 0.28$ .

 $A_{CP}(B^+ \rightarrow X_0(1550) K^+)$ 

VALUE	DOCUMENT ID	TECN	COMMENT
$-0.04 \pm 0.07 \pm 0.02$	<sup>1</sup> AUBERT	06o	BABR $e^+e^- \rightarrow \Upsilon(4S)$

<sup>1</sup> Measured in the  $B^+ \rightarrow K^+ K^- K^+$  decay.

 $A_{CP}(B^+ \rightarrow K^{*+} K^+ K^-)$ 

VALUE	DOCUMENT ID	TECN	COMMENT
$0.11 \pm 0.08 \pm 0.03$	AUBERT,B	06U	BABR $e^+e^- \rightarrow \Upsilon(4S)$

ACP(B+ → ϕK\*(892)±)

Table with columns: VALUE, DOCUMENT ID, TECN, COMMENT. Rows include experimental data points and averages, with footnotes explaining confidence ranges.

ACP(B+ → ϕ(Kπ)0±)

Table with columns: VALUE, DOCUMENT ID, TECN, COMMENT. Row includes experimental data point.

ACP(B+ → ϕK1(1270)±)

Table with columns: VALUE, DOCUMENT ID, TECN, COMMENT. Row includes experimental data point.

ACP(B+ → ϕK2(1430)±)

Table with columns: VALUE, DOCUMENT ID, TECN, COMMENT. Row includes experimental data point.

ACP(B+ → K+ ϕϕ)

Table with columns: VALUE, DOCUMENT ID, TECN, COMMENT. Row includes experimental data point.

ACP(B+ → K+[ϕϕ]ηc)

Table with columns: VALUE, DOCUMENT ID, TECN, COMMENT. Row includes experimental data point.

ACP(B+ → K\*(892)±γ)

Table with columns: VALUE, DOCUMENT ID, TECN, COMMENT. Rows include experimental data points and a note about branching ratios.

ACP(B+ → Xsγ)

Table with columns: VALUE, DOCUMENT ID, TECN, COMMENT. Row includes experimental data point and a note about technique.

ACP(B+ → ηK+γ)

Table with columns: VALUE, DOCUMENT ID, TECN, COMMENT. Rows include experimental data points and notes about mass values.

ACP(B+ → ϕK+γ)

Table with columns: VALUE, DOCUMENT ID, TECN, COMMENT. Rows include experimental data points and a note about scale factor.

ACP(B+ → ρ+γ)

Table with columns: VALUE, DOCUMENT ID, TECN, COMMENT. Row includes experimental data point.

ACP(B+ → π+π0)

Table with columns: VALUE, DOCUMENT ID, TECN, COMMENT. Rows include experimental data points and footnotes.

1 Corresponds to a 90% CL interval of -0.19 < ACP < 0.21.
2 Corresponds to a 90% CL interval of -0.17 < ACP < 0.16.
3 This corresponds to 90% CL interval of -0.18 < ACP < 0.14.
4 Corresponds to 90% confidence range -0.32 < ACP < 0.27.
5 Corresponds to 90% confidence range -0.23 < ACP < +0.86.

ACP(B+ → π+π-π+)

Table with columns: VALUE, DOCUMENT ID, TECN, COMMENT. Rows include experimental data points and notes about phase space and uncertainty.

ACP(B+ → ρ0π+)

Table with columns: VALUE, DOCUMENT ID, TECN, COMMENT. Rows include experimental data points and notes about amplitude analysis.

ACP(B+ → f2(1270)π+)

Table with columns: VALUE, DOCUMENT ID, TECN, COMMENT. Rows include experimental data points and notes about amplitude analysis.

1 This result is obtained with an amplitude analysis of B+ → π+π+π- decays, using the isobar model within the mass range 1.0 < m(π+π-) < 1.5 GeV to describe the π+π- S-wave contribution.
2 Uses amplitude analysis of B± → π±K+K- decays.

ACP(B+ → ρ0(1450)π+)

Table with columns: VALUE, DOCUMENT ID, TECN, COMMENT. Rows include experimental data points and notes about amplitude analysis.

ACP(B+ → ρ3(1690)π+)

Table with columns: VALUE, DOCUMENT ID, TECN, COMMENT. Row includes experimental data point and a note about amplitude analysis.

ACP(B+ → f0(1370)π+)

Table with columns: VALUE, DOCUMENT ID, TECN, COMMENT. Row includes experimental data point.

ACP(B+ → π+π-π+ nonresonant)

Table with columns: VALUE, DOCUMENT ID, TECN, COMMENT. Row includes experimental data point.

ACP(B+ → ρ+π0)

Table with columns: VALUE, DOCUMENT ID, TECN, COMMENT. Rows include experimental data points and notes about amplitude analysis.

ACP(B+ → ρ+ρ0)

Table with columns: VALUE, DOCUMENT ID, TECN, COMMENT. Rows include experimental data points and notes about amplitude analysis.

1 Corresponds to a 90% CL interval of -0.19 < ACP < 0.21.
2 Corresponds to a 90% CL interval of -0.17 < ACP < 0.16.
3 This corresponds to 90% CL interval of -0.18 < ACP < 0.14.
4 Corresponds to 90% confidence range -0.32 < ACP < 0.27.
5 Corresponds to 90% confidence range -0.23 < ACP < +0.86.



## Meson Particle Listings

 $B^\pm$  $A_{CP}(B^+ \rightarrow \omega\pi^+)$ 

VALUE	DOCUMENT ID	TECN	COMMENT
<b><math>-0.04 \pm 0.05</math> OUR AVERAGE</b>			
$-0.048 \pm 0.065 \pm 0.038$	<sup>1</sup> AAIJ	20A	LHCB $pp$ at 7, 8 TeV
$-0.02 \pm 0.08 \pm 0.01$	AUBERT	07AE	BABR $e^+e^- \rightarrow \Upsilon(4S)$
$-0.02 \pm 0.09 \pm 0.01$	JEN	06	BELL $e^+e^- \rightarrow \Upsilon(4S)$
$-0.34 \pm 0.25$	<sup>2</sup> CHEN	00	CLE2 $e^+e^- \rightarrow \Upsilon(4S)$
••• We do not use the following data for averages, fits, limits, etc. •••			
$-0.01 \pm 0.10 \pm 0.01$	AUBERT,B	06E	BABR Repl. by AUBERT 07AE
$0.03 \pm 0.16 \pm 0.01$	AUBERT	04H	BABR Repl. by AUBERT,B 06E
$0.50 \pm 0.23 \pm 0.02$	<sup>3</sup> WANG	04A	BELL Repl. by JEN 06
$-0.01 \pm 0.29 \pm 0.03$	<sup>4</sup> AUBERT	02E	BABR Repl. by AUBERT 04H

<sup>1</sup> This result is obtained with an amplitude analysis of  $B^+ \rightarrow \pi^+\pi^+\pi^-$  decays, using the isobar model within the mass range  $1.0 < m(\pi^+\pi^-) < 1.5$  GeV to describe the  $\pi^+\pi^-$  S-wave contribution.

<sup>2</sup> Corresponds to 90% confidence range  $-0.75 < A_{CP} < 0.07$ .

<sup>3</sup> Corresponds to 90% CL interval  $-0.25 < A_{CP} < 0.41$

<sup>4</sup> Corresponds to 90% confidence range  $-0.50 < A_{CP} < 0.46$ .

 $A_{CP}(B^+ \rightarrow \omega\rho^+)$ 

VALUE	DOCUMENT ID	TECN	COMMENT
<b><math>-0.20 \pm 0.09 \pm 0.02</math></b>			
$0.04 \pm 0.18 \pm 0.02$	AUBERT,B	06T	BABR Repl. by AUBERT 09H
$0.05 \pm 0.26 \pm 0.02$	AUBERT	05o	BABR Repl. by AUBERT,B 06T

 $A_{CP}(B^+ \rightarrow \eta\pi^+)$ 

VALUE	DOCUMENT ID	TECN	COMMENT
<b><math>-0.14 \pm 0.07</math> OUR AVERAGE</b>			Error includes scale factor of 1.4.
$-0.19 \pm 0.06 \pm 0.01$	HOI	12	BELL $e^+e^- \rightarrow \Upsilon(4S)$
$-0.03 \pm 0.09 \pm 0.03$	AUBERT	09AV	BABR $e^+e^- \rightarrow \Upsilon(4S)$
••• We do not use the following data for averages, fits, limits, etc. •••			
$-0.08 \pm 0.10 \pm 0.01$	AUBERT	07AE	BABR Repl. by AUBERT 09AV
$-0.23 \pm 0.09 \pm 0.02$	CHANG	07b	BELL Repl. by HOI 12
$-0.13 \pm 0.12 \pm 0.01$	AUBERT,B	05K	BABR Repl. by AUBERT 07AE
$0.07 \pm 0.15 \pm 0.03$	CHANG	05A	BELL Repl. by CHANG 07b
$-0.44 \pm 0.18 \pm 0.01$	AUBERT	04H	BABR Repl. by AUBERT,B 05K

 $A_{CP}(B^+ \rightarrow \eta\rho^+)$ 

VALUE	DOCUMENT ID	TECN	COMMENT
<b><math>0.11 \pm 0.11</math> OUR AVERAGE</b>			
$0.13 \pm 0.11 \pm 0.02$	AUBERT	08AH	BABR $e^+e^- \rightarrow \Upsilon(4S)$
$-0.04 \pm 0.34 \pm 0.01$	WANG	07B	BELL $e^+e^- \rightarrow \Upsilon(4S)$
••• We do not use the following data for averages, fits, limits, etc. •••			
$0.02 \pm 0.18 \pm 0.02$	AUBERT,B	05K	BABR Repl. by AUBERT 08AH

 $A_{CP}(B^+ \rightarrow \eta'\pi^+)$ 

VALUE	DOCUMENT ID	TECN	COMMENT
<b><math>0.06 \pm 0.16</math> OUR AVERAGE</b>			
$0.03 \pm 0.17 \pm 0.02$	AUBERT	09AV	BABR $e^+e^- \rightarrow \Upsilon(4S)$
$0.20 \pm 0.37 \pm 0.04$	SCHUEMANN	06	BELL $e^+e^- \rightarrow \Upsilon(4S)$
••• We do not use the following data for averages, fits, limits, etc. •••			
$0.21 \pm 0.17 \pm 0.01$	AUBERT	07AE	BABR Repl. by AUBERT 09AV
$0.14 \pm 0.16 \pm 0.01$	AUBERT,B	05K	BABR Repl. by AUBERT 07AE

 $A_{CP}(B^+ \rightarrow \eta'\rho^+)$ 

VALUE	DOCUMENT ID	TECN	COMMENT
<b><math>0.26 \pm 0.17 \pm 0.02</math></b>			
$0.04 \pm 0.28 \pm 0.02$	<sup>1</sup> AUBERT	07E	BABR Repl. by DEL-AMO-SANCHEZ 10A

<sup>1</sup> Reports  $A_{CP}$  with the opposite sign convention.

 $A_{CP}(B^+ \rightarrow b_1^0\pi^+)$ 

VALUE	DOCUMENT ID	TECN	COMMENT
<b><math>+0.05 \pm 0.16 \pm 0.02</math></b>			
$0.05 \pm 0.16 \pm 0.02$	AUBERT	07Bi	BABR $e^+e^- \rightarrow \Upsilon(4S)$

 $A_{CP}(B^+ \rightarrow \rho\bar{\rho}\pi^+)$ 

VALUE	DOCUMENT ID	TECN	COMMENT
<b><math>0.00 \pm 0.04</math> OUR AVERAGE</b>			
$-0.02 \pm 0.05 \pm 0.02$	<sup>1</sup> WEI	08	BELL $e^+e^- \rightarrow \Upsilon(4S)$
$+0.04 \pm 0.07 \pm 0.04$	AUBERT	07AV	BABR $e^+e^- \rightarrow \Upsilon(4S)$
••• We do not use the following data for averages, fits, limits, etc. •••			
$-0.16 \pm 0.22 \pm 0.01$	WANG	04	BELL Repl. by WEI 08

<sup>1</sup> Requires  $m_{\rho\bar{\rho}} < 2.85$  GeV/c<sup>2</sup>.

 $A_{CP}(B^+ \rightarrow \rho\bar{K}K^+)$ 

VALUE	DOCUMENT ID	TECN	COMMENT
<b><math>0.00 \pm 0.04</math> OUR AVERAGE</b>			Error includes scale factor of 2.2.
$0.021 \pm 0.020 \pm 0.004$	<sup>1</sup> AAIJ	14AF	LHCB $pp$ at 7, 8 TeV
$-0.17 \pm 0.10 \pm 0.02$	<sup>1</sup> WEI	08	BELL $e^+e^- \rightarrow \Upsilon(4S)$
$-0.16 \pm 0.07 \pm 0.04$	<sup>1</sup> AUBERT,B	05L	BABR $e^+e^- \rightarrow \Upsilon(4S)$
••• We do not use the following data for averages, fits, limits, etc. •••			
$-0.047 \pm 0.036 \pm 0.007$	<sup>1</sup> AAIJ	13AF	LHCB Repl. by AAIJ 14AF
$-0.05 \pm 0.11 \pm 0.01$	WANG	04	BELL Repl. by WEI 08
<sup>1</sup> Requires $m_{\rho\bar{\rho}} < 2.85$ GeV/c <sup>2</sup> .			

 $A_{CP}(B^+ \rightarrow \rho\bar{K}K^*(892)^+)$ 

VALUE	DOCUMENT ID	TECN	COMMENT
<b><math>0.21 \pm 0.16</math> OUR AVERAGE</b>			Error includes scale factor of 1.4.
$-0.01 \pm 0.19 \pm 0.02$	CHEN	08c	BELL $e^+e^- \rightarrow \Upsilon(4S)$
$+0.32 \pm 0.13 \pm 0.05$	AUBERT	07AV	BABR $e^+e^- \rightarrow \Upsilon(4S)$

 $A_{CP}(B^+ \rightarrow \rho\bar{A}\gamma)$ 

VALUE	DOCUMENT ID	TECN	COMMENT
<b><math>+0.17 \pm 0.16 \pm 0.05</math></b>			
$0.17 \pm 0.16 \pm 0.05$	WANG	07c	BELL $e^+e^- \rightarrow \Upsilon(4S)$

 $A_{CP}(B^+ \rightarrow \rho\bar{A}\pi^0)$ 

VALUE	DOCUMENT ID	TECN	COMMENT
<b><math>+0.01 \pm 0.17 \pm 0.04</math></b>			
$0.01 \pm 0.17 \pm 0.04$	WANG	07c	BELL $e^+e^- \rightarrow \Upsilon(4S)$

 $A_{CP}(B^+ \rightarrow K^+\ell^+\ell^-)$ 

VALUE	DOCUMENT ID	TECN	COMMENT
<b><math>-0.02 \pm 0.08</math> OUR AVERAGE</b>			
$-0.03 \pm 0.14 \pm 0.01$	<sup>1</sup> LEES	12s	BABR $e^+e^- \rightarrow \Upsilon(4S)$
$-0.18 \pm 0.18 \pm 0.01$	AUBERT	09T	BABR $e^+e^- \rightarrow \Upsilon(4S)$
$+0.04 \pm 0.10 \pm 0.02$	WEI	09A	BELL $e^+e^- \rightarrow \Upsilon(4S)$
••• We do not use the following data for averages, fits, limits, etc. •••			
$-0.07 \pm 0.22 \pm 0.02$	AUBERT,B	06J	BABR Repl. by AUBERT 09T
<sup>1</sup> Measured in the union of $0.10 < q^2 < 8.12$ GeV <sup>2</sup> /c <sup>4</sup> and $q^2 > 10.11$ GeV <sup>2</sup> /c <sup>4</sup> . LEES 12s reports also individual measurements $A_{CP}(B^+ \rightarrow K^+\ell^+\ell^-) = 0.02 \pm 0.18 \pm 0.01$ for $0.10 < q^2 < 8.12$ GeV <sup>2</sup> /c <sup>4</sup> and $A_{CP}(B^+ \rightarrow K^+\ell^+\ell^-) = -0.06 \pm 0.22 \pm 0.01$ for $q^2 > 10.11$ GeV <sup>2</sup> /c <sup>4</sup> .			

 $A_{CP}(B^+ \rightarrow K^+e^+e^-)$ 

VALUE	DOCUMENT ID	TECN	COMMENT
<b><math>+0.14 \pm 0.14 \pm 0.03</math></b>			
$0.14 \pm 0.14 \pm 0.03$	WEI	09A	BELL $e^+e^- \rightarrow \Upsilon(4S)$

 $A_{CP}(B^+ \rightarrow K^+\mu^+\mu^-)$ 

VALUE	DOCUMENT ID	TECN	COMMENT
<b><math>0.011 \pm 0.017</math> OUR AVERAGE</b>			
$0.012 \pm 0.017 \pm 0.001$	AAIJ	14AN	LHCB $pp$ at 7, 8 TeV
$-0.05 \pm 0.13 \pm 0.03$	WEI	09A	BELL $e^+e^- \rightarrow \Upsilon(4S)$
••• We do not use the following data for averages, fits, limits, etc. •••			
$0.000 \pm 0.033 \pm 0.009$	AAIJ	13BN	LHCB Repl. by AAIJ 14AN

 $A_{CP}(B^+ \rightarrow \pi^+\mu^+\mu^-)$ 

VALUE	DOCUMENT ID	TECN	COMMENT
<b><math>-0.11 \pm 0.12 \pm 0.01</math></b>			
$-0.11 \pm 0.12 \pm 0.01$	AAIJ	15AR	LHCB $pp$ at 7, 8 TeV

 $A_{CP}(B^+ \rightarrow K^*+\ell^+\ell^-)$ 

VALUE	DOCUMENT ID	TECN	COMMENT
<b><math>-0.09 \pm 0.14</math> OUR AVERAGE</b>			
$0.01 \pm 0.26 \pm 0.02$	AUBERT	09T	BABR $e^+e^- \rightarrow \Upsilon(4S)$
$-0.13 \pm 0.17 \pm 0.01$	WEI	09A	BELL $e^+e^- \rightarrow \Upsilon(4S)$
••• We do not use the following data for averages, fits, limits, etc. •••			
$0.03 \pm 0.23 \pm 0.03$	AUBERT,B	06J	BABR Repl. by AUBERT 09T

 $A_{CP}(B^+ \rightarrow K^*e^+e^-)$ 

VALUE	DOCUMENT ID	TECN	COMMENT
<b><math>-0.14 \pm 0.23 \pm 0.02</math></b>			
$-0.14 \pm 0.23 \pm 0.02$	WEI	09A	BELL $e^+e^- \rightarrow \Upsilon(4S)$

 $A_{CP}(B^+ \rightarrow K^*\mu^+\mu^-)$ 

VALUE	DOCUMENT ID	TECN	COMMENT
<b><math>-0.12 \pm 0.24 \pm 0.02</math></b>			
$-0.12 \pm 0.24 \pm 0.02$	WEI	09A	BELL $e^+e^- \rightarrow \Upsilon(4S)$

CP VIOLATION PARAMETERS IN  $B^+ \rightarrow DK^+$  AND SIMILAR DECAYS

The parameters  $r_{B^+}$  and  $\delta_{B^+}$  are the magnitude ratio and strong phase difference between the amplitudes of  $A(B^+ \rightarrow \bar{D}^{(*)0}K^{(*)+})$  and  $A(B^+ \rightarrow D^{(*)0}K^{(*)+})$ . The measured observables are defined as  $x_{\pm} = r_{B^+} \cos(\delta_{B^+} \pm \gamma)$  and  $y_{\pm} = r_{B^+} \sin(\delta_{B^+} \pm \gamma)$ , and can be used to measure the CKM angle  $\gamma$ .

"OUR EVALUATION" is provided by the Heavy Flavor Averaging Group (HFLAV). It is derived from combinations of their results on  $B^+ \rightarrow DK^+$  and related processes.

$\gamma$  For angle  $\gamma(\phi_3)$  of the CKM unitarity triangle, see the review on “CP Violation” in the Reviews section.  
 “OUR EVALUATION” is provided by the Heavy Flavor Averaging Group (HFLAV).

VALUE (°)	CL%	DOCUMENT ID	TECN	COMMENT
$71.1^{+4.6}_{-5.3}$		<b>OUR EVALUATION</b>		
$5.7^{+10.2}_{-8.8} \pm 6.7$		1 RESM1	19 BELL	$e^+e^- \rightarrow \Upsilon(4S)$
$87^{+11}_{-12}$		2 AAIJ	18AD LHCB	$pp$ at 13 TeV
$128^{+17}_{-22}$		3 AAIJ	18U LHCB	$pp$ at 7, 8 TeV
$5-86$ or $185-266$		4 AAIJ	18Z LHCB	$pp$ at 7, 8 TeV
$80^{+21}_{-22}$		5 AAIJ	16AA LHCB	Repl. by AAIJ 16Z
$72.2^{+6.8}_{-7.3}$		6 AAIJ	16AQ LHCB	$pp$ at 7, 8 TeV
$71 \pm 20$		7,8 AAIJ	16Z LHCB	$pp$ at 7, 8 TeV
$74^{+20}_{-19}$		AAIJ	15BC LHCB	$pp$ at 7, 8 TeV
$63.5^{+7.2}_{-6.7}$		9,10 AAIJ	15K LHCB	$pp$ at 7, 8 TeV
$62^{+15}_{-14}$		11 AAIJ	14BA LHCB	$pp$ at 7, 8 TeV
$84^{+49}_{-42}$		12 AAIJ	14BE LHCB	Repl. by AAIJ 14BA
$115^{+28}_{-43}$		13 AAIJ	14BF LHCB	Repl. by AAIJ 18U
$72.6^{+9.7}_{-17.2}$		14 AAIJ	13AK LHCB	$pp$ at 7 TeV
$69^{+17}_{-16}$		15 LEES	13B BABR	$e^+e^- \rightarrow \Upsilon(4S)$
$44^{+43}_{-38}$		16,17 AAIJ	12AQ LHCB	Repl. by AAIJ 13AK
$77.3^{+15.1}_{-14.9} \pm 5.9$		17,18 AIHARA	12 BELL	$e^+e^- \rightarrow \Upsilon(4S)$
$68 \pm 14 \pm 5$		19 DEL-AMO-SA..10F	BABR	Repl. by LEES 13B
$7$ to $173$	95	20 DEL-AMO-SA..10G	BABR	$e^+e^- \rightarrow \Upsilon(4S)$
$78.4^{+10.8}_{-11.6} \pm 9.6$		21 POLUEKTOV	10 BELL	$e^+e^- \rightarrow \Upsilon(4S)$
$162 \pm 56$		22 AUBERT	09R BABR	$e^+e^- \rightarrow \Upsilon(4S)$
$76^{+22}_{-23} \pm 7.1$		23 AUBERT	08AL BABR	Repl. by DEL-AMO-SANCHEZ 10F
$53^{+15}_{-18} \pm 10$		24 POLUEKTOV	06 BELL	Repl. by POLUEKTOV 10
$70 \pm 31^{+18}_{-15}$		25 AUBERT,B	05Y BABR	Repl. by AUBERT 08AL
$77^{+17}_{-19} \pm 17$		26 POLUEKTOV	04 BELL	Repl. by POLUEKTOV 06

- Uses binned analysis of  $D \rightarrow K_S^0 \pi^+ \pi^- \pi^0$  from  $B^\pm \rightarrow DK^\pm$  modes over the phase space. Strong phase measurements from RESM1 18 analysis of CLEO-c data of the  $D$  decay over the phase space binning are used as input.
- Uses binned Dalitz plot analysis of  $D \rightarrow K_S^0 \pi^+ \pi^-$  and  $K_S^0 K^+ K^-$  from  $B^\pm \rightarrow DK^\pm$  modes. Strong phase measurements from CLEO-c of the  $D$  decay over the Dalitz plot are used as input.
- Measured in  $B_S^0 \rightarrow D_S^\mp K^\pm$  decays, constraining  $-2\beta_S$  by the measurement of  $\phi_S = 0.030 \pm 0.033$  from HFLAV. The value is modulo  $180^\circ$ .
- AAIJ 18Z reports the intervals  $(5-86)^\circ$  or  $(185-266)^\circ$  at 68% C.L. The extraction uses the time dependent CP violation measurement in  $B^0 \rightarrow D^\mp \pi^\pm$  decays with external input and some theoretical assumptions.
- Uses Dalitz plot analysis of  $D \rightarrow K_S^0 \pi^+ \pi^-$  decays coming from  $B^0 \rightarrow DK^*(892)^0$  modes. Measures  $r_{B^0} = 0.39 \pm 0.13$ , and  $\delta_{B^0} = 197^{+24}_{-20}$  degrees.
- A combination of measurements from analyses of time-integrated  $B^+ \rightarrow DK^+$ ,  $B^0 \rightarrow DK^*(892)^0$ ,  $B^0 \rightarrow DK^+ \pi^-$ , and  $B^+ \rightarrow DK^+ \pi^+ \pi^-$  tree-level decays. In addition, results from a time-dependent analysis of  $B_S^0 \rightarrow D_S K$  decays are included.
- A model-independent binned Dalitz plot analysis of the decays  $B^0 \rightarrow DK^*(892)^0$ , with  $D \rightarrow K_S^0 \pi^+ \pi^-$  and  $D \rightarrow K_S^0 K^+ K^-$ . The results cannot be combined with the model-dependent analysis of the same dataset reported in AAIJ 16AA.
- Angle  $\gamma$  required to satisfy  $0 < \gamma < 180$  degrees.
- Obtained by measuring time-dependent CP asymmetry in  $B_S^0 \rightarrow K^+ K^-$  and using a U-spin relation between  $B_S^0 \rightarrow K^+ K^-$  and  $B^0 \rightarrow \pi^+ \pi^-$ .
- Results are also presented using additional inputs on  $B^0 \rightarrow \pi^0 \pi^0$  and  $B^+ \rightarrow \pi^+ \pi^0$  decays from other experiments and isospin symmetry assumptions. The dependence of the results on the maximum allowed amount of U-spin breaking up to 50% is also included.
- Uses binned Dalitz plot analysis of  $B^+ \rightarrow DK^+$  decays, with  $D \rightarrow K_S^0 \pi^+ \pi^-$  and  $D \rightarrow K_S^0 K^+ K^-$ . Strong phase measurements from CLEO-c (LIBBY 10) of the  $D$  decay over the Dalitz plot are used as input. Solution that satisfies  $0 < \gamma < 180$  is chosen.
- AAIJ 14BE uses model-dependent analysis of  $D \rightarrow K_S^0 \pi^+ \pi^-$  amplitudes. The model is the same as in DEL-AMO-SANCHEZ 10F.
- Measured in  $B_S^0 \rightarrow D_S^\mp K^\pm$  decays, constraining  $-2\beta_S$  by the measurement of  $\phi_S = 0.01 \pm 0.07 \pm 0.0$  from AAIJ 13AR. The value is modulo  $180^\circ$  at 68% CL.
- Presents a confidence region  $55.4^\circ < \gamma < 82.3^\circ$  at 68% CL with best fit value  $72.6^\circ$  and includes both statistical and systematic uncertainties. The corresponding 95% CL is  $40.2^\circ < \gamma < 92.7^\circ$ . The value is determined from combination of measurements using  $D$  meson decaying to  $K^+ K^-$ ,  $\pi^+ \pi^-$ ,  $K^\pm \pi^\mp$ ,  $K_S^0 \pi^+ \pi^-$ ,  $K_S^0 K^+ K^-$ , and  $K^\pm \pi^\mp \pi^\pm \pi^\mp$ . Combines  $B^\pm \rightarrow DK^\pm$  and  $B^\pm \rightarrow D\pi^\pm$ .

- Reports combination of published measurements using GGSZ, GLW, and ADS methods. Reports also  $2\sigma$  range of  $41-102^\circ$  and a  $5.9\sigma$  significance for  $\gamma(B^+ \rightarrow D^{(*)0} K^{(*)+}) \neq 0$  hypothesis.
- Reports combined statistical and systematic uncertainties.
- Uses binned Dalitz plot of  $\overline{D}^0 \rightarrow K_S^0 \pi^+ \pi^-$  decays from  $B^+ \rightarrow \overline{D}^0 K^+$ . Measurement of strong phases in  $\overline{D}^0 \rightarrow K_S^0 \pi^+ \pi^-$  Dalitz plot from LIBBY 10 is used as input.
- We combined the systematics in quadrature. The authors report separately the contribution to the systematic uncertainty due to the uncertainty on the bin-averaged strong phase difference between  $D^0$  and  $\overline{D}^0$  amplitudes.
- Uses Dalitz plot analysis of  $\overline{D}^0 \rightarrow K_S^0 \pi^+ \pi^-$ ,  $K_S^0 K^+ K^-$  decays from  $B^+ \rightarrow D^{(*)} K^+$ ,  $D K^{*+}$  modes. The corresponding two standard deviation interval for  $\gamma$  is  $39^\circ < \gamma < 98^\circ$ . CP conservation in the combined result is ruled out with a significance of 3.5 standard deviations.
- Reports confidence intervals for the CKM angle  $\gamma$  from the measured values of the GLW parameters using  $B^\pm \rightarrow DK^\pm$  decays with  $D$  mesons decaying to non-CP( $K\pi$ ), CP-even ( $K^+ K^-$ ,  $\pi^+ \pi^-$ ), and CP-odd ( $K_S^0 \pi^0$ ,  $K_S^0 \omega$ ) states.
- Uses Dalitz plot analysis of  $\overline{D}^0 \rightarrow K_S^0 \pi^+ \pi^-$  decays from  $B^+ \rightarrow D^{(*)} K^+$  modes. The corresponding two standard deviation interval for  $\gamma$  is  $54.2^\circ < \gamma < 100.5^\circ$ . CP conservation in the combined result is ruled out with a significance of 3.5 standard deviations.
- Uses Dalitz plot analysis of  $D^0 \rightarrow K_S^0 \pi^+ \pi^-$  decays coming from  $B^0 \rightarrow D^0 K^{*0}$  modes. The corresponding 95% CL interval is  $77^\circ < \gamma < 247^\circ$ . A 180 degree ambiguity is implied.
- Uses Dalitz plot analysis of  $\overline{D}^0 \rightarrow K_S^0 \pi^+ \pi^-$  and  $\overline{D}^0 \rightarrow K_S^0 K^+ K^-$  decays coming from  $B^\pm \rightarrow D^{(*)} K^{(\pm)}$  modes. The corresponding two standard deviation interval is  $29^\circ < \gamma < 122^\circ$ .
- Uses a Dalitz plot analysis of the  $\overline{D}^0 \rightarrow K_S^0 \pi^+ \pi^-$  decays; Combines the  $D K^+$ ,  $D^* K^+$  and  $D K^{*+}$  modes. The corresponding two standard deviations interval for gamma is  $8^\circ < \gamma < 111^\circ$ .
- Uses a Dalitz plot analysis of neutral  $D \rightarrow K_S^0 \pi^+ \pi^-$  decays coming from  $B^\pm \rightarrow DK^\pm$  and  $B^\pm \rightarrow D^* K^\pm$  followed by  $D^{*0} \rightarrow D\pi^0$ ,  $D\gamma$ . The corresponding two standard deviations interval for gamma is  $12^\circ < \gamma < 137^\circ$ . AUBERT,B 05Y also reports the amplitude ratios and the strong phases.
- Uses a Dalitz plot analysis of the 3-body  $D \rightarrow K_S^0 \pi^+ \pi^-$  decays coming from  $B^\pm \rightarrow DK^\pm$  and  $B^\pm \rightarrow D^* K^\pm$  followed by  $D^* \rightarrow D\pi^0$ ; here we use  $D$  to denote that the neutral  $D$  meson produced in the decay is an admixture of  $D^0$  and  $\overline{D}^0$ . The corresponding two standard deviations interval for  $\gamma$  is  $26^\circ < \gamma < 126^\circ$ . POLUEKTOV 04 also reports the amplitude ratios and the strong phases.

$r_B(B^+ \rightarrow D^0 K^+)$

$r_B$  and  $\delta_B$  are the amplitude ratio and relative strong phase between the amplitudes of  $A(B^+ \rightarrow D^0 K^+)$  and  $A(B^+ \rightarrow \overline{D}^0 K^+)$ ,

“OUR EVALUATION” is provided by the Heavy Flavor Averaging Group (HFLAV).

VALUE	CL%	DOCUMENT ID	TECN	COMMENT
$0.0993 \pm 0.0046$		<b>OUR EVALUATION</b>		
$0.323 \pm 0.147 \pm 0.056$		1 RESM1	19 BELL	$e^+e^- \rightarrow \Upsilon(4S)$
$0.086^{+0.013}_{-0.014}$		2 AAIJ	18AD LHCB	$pp$ at 13 TeV
$0.080^{+0.019}_{-0.021}$		3 AAIJ	14BA LHCB	$pp$ at 7, 8 TeV
$0.06 \pm 0.04$		4 AAIJ	14BE LHCB	Repl. by AAIJ 14BA
$0.097 \pm 0.011$		5 AAIJ	13AE LHCB	$pp$ at 7 TeV
$0.092^{+0.013}_{-0.012}$		6 LEES	13B BABR	$e^+e^- \rightarrow \Upsilon(4S)$
$0.07 \pm 0.04$		7,8 AAIJ	12AQ LHCB	$pp$ at 7 TeV
$0.145 \pm 0.030 \pm 0.015$		8,9 AIHARA	12 BELL	$e^+e^- \rightarrow \Upsilon(4S)$
$< 0.13$	90	10 LEES	11D BABR	$e^+e^- \rightarrow \Upsilon(4S)$
$0.096 \pm 0.029 \pm 0.006$		11 DEL-AMO-SA..10F	BABR	Repl. by LEES 13B
$0.095^{+0.051}_{-0.041}$		12 DEL-AMO-SA..10H	BABR	Repl. by LEES 13B
$0.160^{+0.040}_{-0.038} \pm 0.051 \pm 0.015$		13 POLUEKTOV	10 BELL	$e^+e^- \rightarrow \Upsilon(4S)$
$0.086 \pm 0.032 \pm 0.015$		14 AUBERT	08AL BABR	Repl. by DEL-AMO-SANCHEZ 10F
$< 0.19$	90	HORII	08 BELL	$e^+e^- \rightarrow \Upsilon(4S)$
$0.159^{+0.054}_{-0.050} \pm 0.050$		15 POLUEKTOV	06 BELL	Repl. by POLUEKTOV 10
$0.12 \pm 0.08 \pm 0.05$		16 AUBERT,B	05Y BABR	Repl. by AUBERT 08AL

- Uses binned analysis of  $D \rightarrow K_S^0 \pi^+ \pi^- \pi^0$  from  $B^\pm \rightarrow DK^\pm$  modes over the phase space. Strong phase measurements from RESM1 18 analysis of CLEO-c data of the  $D$  decay over the phase space binning are used as input.
- Uses binned Dalitz plot analysis of  $D \rightarrow K_S^0 \pi^+ \pi^-$  and  $K_S^0 K^+ K^-$  from  $B^\pm \rightarrow DK^\pm$  modes. Strong phase measurements from CLEO-c of the  $D$  decay over the Dalitz plot are used as input.
- Uses binned Dalitz plot analysis of  $B^+ \rightarrow DK^+$  decays, with  $D \rightarrow K_S^0 \pi^+ \pi^-$  and  $D \rightarrow K_S^0 K^+ K^-$ . Strong phase measurements from CLEO-c (LIBBY 10) of the  $D$  decay over the Dalitz plot are used as input.
- AAIJ 14BE uses model-dependent analysis of  $D \rightarrow K_S^0 \pi^+ \pi^-$  amplitudes. The model is the same as in DEL-AMO-SANCHEZ 10F.
- Uses  $B^\pm \rightarrow [K^\pm \pi^\mp \pi^\pm \pi^\mp]_D h^\pm$  mode.
- Reports combination of published measurements using GGSZ, GLW, and ADS methods.
- Reports combined statistical and systematic uncertainties.
- Uses binned Dalitz plot of  $\overline{D}^0 \rightarrow K_S^0 \pi^+ \pi^-$  decays from  $B^+ \rightarrow \overline{D}^0 K^+$ . Measurement of strong phases in  $\overline{D}^0 \rightarrow K_S^0 \pi^+ \pi^-$  Dalitz plot from LIBBY 10 is used as input.

## Meson Particle Listings

 $B^\pm$ 

<sup>9</sup>We combined the systematics in quadrature. The authors report separately the contribution to the systematic uncertainty due to the uncertainty on the bin-averaged strong phase difference between  $D^0$  and  $\bar{D}^0$  amplitudes.

- <sup>10</sup>Uses decays of neutral  $D$  to  $K^-\pi^+\pi^0$ .
- <sup>11</sup>Uses Dalitz plot analysis of  $\bar{D}^0 \rightarrow K_S^0\pi^+\pi^-$ ,  $K_S^0K^+K^-$  decays from  $B^+ \rightarrow D^{(*)}K^{(*)+}$  modes. The corresponding two standard deviation interval is  $0.037 < r_B < 0.155$ .
- <sup>12</sup>Uses the Cabibbo suppressed decay of  $B^+ \rightarrow \bar{D}^0K^+$  followed by  $\bar{D}^0 \rightarrow K^-\pi^+$ .
- <sup>13</sup>Uses Dalitz plot analysis of  $\bar{D}^0 \rightarrow K_S^0\pi^+\pi^-$  decays from  $B^+ \rightarrow D^0K^+$  modes. The corresponding two standard deviation interval is  $0.084 < r_B < 0.239$ .
- <sup>14</sup>Uses Dalitz plot analysis of  $\bar{D}^0 \rightarrow K_S^0\pi^+\pi^-$  and  $\bar{D}^0 \rightarrow K_S^0K^+K^-$  decays coming from  $B^\pm \rightarrow D^{(*)}K^{(*)\pm}$  modes.
- <sup>15</sup>Uses a Dalitz plot analysis of the  $\bar{D}^0 \rightarrow K_S^0\pi^+\pi^-$  decays; Combines the  $DK^+$ ,  $D^*K^+$  and  $DK^{*+}$  modes.
- <sup>16</sup>Uses a Dalitz analysis of neutral  $D$  decays to  $K_S^0\pi^+\pi^-$  in the processes  $B^\pm \rightarrow D^{(*)}K^\pm$ ,  $D^* \rightarrow D\pi^0$ ,  $D\gamma$ .

 $\delta_B(B^+ \rightarrow D^0K^+)$ 

"OUR EVALUATION" is provided by the Heavy Flavor Averaging Group (HFLAV).

VALUE (°)	DOCUMENT ID	TECN	COMMENT
-----------	-------------	------	---------

**129.6<sup>+5.0</sup><sub>-6.0</sub> OUR EVALUATION**

• • • We do not use the following data for averages, fits, limits, etc. • • •

83.4 <sup>+18.3</sup> <sub>-16.6</sub> ± 5.1	<sup>1</sup> RESMI	19 BELL	$e^+e^- \rightarrow \Upsilon(4S)$
101 ± 11	<sup>2</sup> AAIJ	18AD LHCB	$pp$ at 13 TeV
134 <sup>+14</sup> <sub>-15</sub>	<sup>3</sup> AAIJ	14BA LHCB	$pp$ at 7, 8 TeV
115 <sup>+41</sup> <sub>-51</sub>	<sup>4</sup> AAIJ	14BE LHCB	Repl. by AAIJ 14BA
105 <sup>+16</sup> <sub>-17</sub>	<sup>5</sup> LEES	13B BABR	$e^+e^- \rightarrow \Upsilon(4S)$
137 <sup>+35</sup> <sub>-46</sub>	<sup>6,7</sup> AAIJ	12AQ LHCB	$pp$ at 7 TeV
129.9 ± 15.0 ± 6.0	<sup>7,8</sup> AIHARA	12 BELL	$e^+e^- \rightarrow \Upsilon(4S)$
119 <sup>+19</sup> <sub>-20</sub> ± 4	<sup>9</sup> DEL-AMO-SA..10F	BABR	Repl. by LEES 13B
136.7 <sup>+13.0</sup> <sub>-15.8</sub> ± 23.2	<sup>10</sup> POLUEKTOV	10 BELL	$e^+e^- \rightarrow \Upsilon(4S)$
109 <sup>+27</sup> <sub>-30</sub> ± 8	<sup>11</sup> AUBERT	08AL BABR	Repl. by DEL-AMO-SANCHEZ 10F
145.7 <sup>+19.0</sup> <sub>-19.7</sub> ± 23.1	<sup>12</sup> POLUEKTOV	06 BELL	Repl. by POLUEKTOV 10
104 ± 45 <sup>+23</sup> <sub>-32</sub>	<sup>13</sup> AUBERT,B	05Y BABR	Repl. by AUBERT 08AL

- <sup>1</sup>Uses binned analysis of  $D \rightarrow K_S^0\pi^+\pi^-$  from  $B^\pm \rightarrow DK^\pm$  modes over the phase space. Strong phase measurements from RESMI 18 analysis of CLEO-c data of the  $D$  decay over the phase space binning are used as input.
- <sup>2</sup>Uses binned Dalitz plot analysis of  $D \rightarrow K_S^0\pi^+\pi^-$  and  $K_S^0K^+K^-$  from  $B^\pm \rightarrow DK^\pm$  modes. Strong phase measurements from CLEO-c of the  $D$  decay over the Dalitz plot are used as input.
- <sup>3</sup>Uses binned Dalitz plot analysis of  $B^+ \rightarrow DK^+$  decays, with  $D \rightarrow K_S^0\pi^+\pi^-$  and  $D \rightarrow K_S^0K^+K^-$ . Strong phase measurements from CLEO-c (LIBBY 10) of the  $D$  decay over the Dalitz plot are used as input.
- <sup>4</sup>AAIJ 14BE uses model-dependent analysis of  $D \rightarrow K_S^0\pi^+\pi^-$  amplitudes. The model is the same as in DEL-AMO-SANCHEZ 10F.
- <sup>5</sup>Reports combination of published measurements using GGSZ, GLW, and ADS methods.
- <sup>6</sup>Reports combined statistical and systematic uncertainties.
- <sup>7</sup>Uses binned Dalitz plot of  $\bar{D}^0 \rightarrow K_S^0\pi^+\pi^-$  decays from  $B^+ \rightarrow \bar{D}^0K^+$ . Measurement of strong phases in  $\bar{D}^0 \rightarrow K_S^0\pi^+\pi^-$  Dalitz plot from LIBBY 10 is used as input.
- <sup>8</sup>We combined the systematics in quadrature. The authors report separately the contribution to the systematic uncertainty due to the uncertainty on the bin-averaged strong phase difference between  $D^0$  and  $\bar{D}^0$  amplitudes.
- <sup>9</sup>Uses Dalitz plot analysis of  $\bar{D}^0 \rightarrow K_S^0\pi^+\pi^-$ ,  $K_S^0K^+K^-$  decays from  $B^+ \rightarrow D^{(*)}K^{(*)+}$  modes. The corresponding two standard deviation interval is  $75^\circ < \delta_B < 157^\circ$ .
- <sup>10</sup>Uses Dalitz plot analysis of  $\bar{D}^0 \rightarrow K_S^0\pi^+\pi^-$  decays from  $B^+ \rightarrow \bar{D}^0K^+$  modes. The corresponding two standard deviation interval is  $102.2^\circ < \delta_B < 162.3^\circ$ .
- <sup>11</sup>Uses Dalitz plot analysis of  $\bar{D}^0 \rightarrow K_S^0\pi^+\pi^-$  and  $\bar{D}^0 \rightarrow K_S^0K^+K^-$  decays coming from  $B^\pm \rightarrow D^{(*)}K^{(*)\pm}$  modes.
- <sup>12</sup>Uses a Dalitz plot analysis of the  $\bar{D}^0 \rightarrow K_S^0\pi^+\pi^-$  decays; Combines the  $DK^+$ ,  $D^*K^+$  and  $DK^{*+}$  modes.
- <sup>13</sup>Uses a Dalitz analysis of neutral  $D$  decays to  $K_S^0\pi^+\pi^-$  in the processes  $B^\pm \rightarrow D^{(*)}K^\pm$ ,  $D^* \rightarrow D\pi^0$ ,  $D\gamma$ .

 $r_B(B^+ \rightarrow D^0K^{*+})$ 

$r_B$  and  $\delta_B$  are the amplitude ratio and relative strong phase between the amplitudes of  $A_{CP}(B^+ \rightarrow D^0K^{*+})$  and  $A_{CP}(B^+ \rightarrow \bar{D}^0K^{*+})$ .

"OUR EVALUATION" is provided by the Heavy Flavor Averaging Group (HFLAV).

VALUE	DOCUMENT ID	TECN	COMMENT
-------	-------------	------	---------

**0.076 ± 0.020 OUR EVALUATION**

• • • We do not use the following data for averages, fits, limits, etc. • • •

0.143 <sup>+0.048</sup> <sub>-0.049</sub>	<sup>1</sup> LEES	13B BABR	$e^+e^- \rightarrow \Upsilon(4S)$
0.166 <sup>+0.073</sup> <sub>-0.069</sub>	<sup>2</sup> DEL-AMO-SA..10F	BABR	Repl. by LEES 13B
0.31 ± 0.07	<sup>3</sup> AUBERT	09AJ BABR	Repl. by LEES 13B
0.181 <sup>+0.088</sup> <sub>-0.108</sub> ± 0.042	<sup>4</sup> AUBERT	08AL BABR	Repl. by AUBERT 09AJ
0.564 <sup>+0.216</sup> <sub>-0.155</sub> ± 0.093	<sup>5</sup> POLUEKTOV	06 BELL	$e^+e^- \rightarrow \Upsilon(4S)$

<sup>1</sup>Reports combination of published measurements using GGSZ, GLW, and ADS methods.

<sup>2</sup>DEL-AMO-SANCHEZ 10F reports  $r_B \cdot k = 0.149^{+0.066}_{-0.062}$  for  $k = 0.9$ .

<sup>3</sup>Obtained by combining the GLW and ADS methods. The 2-sigma range corresponds to [0.17, 0.43].

<sup>4</sup>Uses Dalitz plot analysis of  $\bar{D}^0 \rightarrow K_S^0\pi^+\pi^-$  and  $\bar{D}^0 \rightarrow K_S^0K^+K^-$  decays coming from  $B^\pm \rightarrow D^{(*)}K^{(*)\pm}$  modes.

<sup>5</sup>Uses a Dalitz plot analysis of the  $\bar{D}^0 \rightarrow K_S^0\pi^+\pi^-$  decays; Combines the  $DK^+$ ,  $D^*K^+$  and  $DK^{*+}$  modes.

 $\delta_B(B^+ \rightarrow D^0K^{*+})$ 

"OUR EVALUATION" is provided by the Heavy Flavor Averaging Group (HFLAV).

VALUE (°)	DOCUMENT ID	TECN	COMMENT
-----------	-------------	------	---------

**98<sup>+18</sup><sub>-37</sub> OUR EVALUATION**

• • • We do not use the following data for averages, fits, limits, etc. • • •

101 ± 43	<sup>1</sup> LEES	13B BABR	$e^+e^- \rightarrow \Upsilon(4S)$
111 ± 32	DEL-AMO-SA..10F	BABR	Repl. by LEES 13B
104 <sup>+39</sup> <sub>-37</sub> ± 18	<sup>2</sup> AUBERT	08AL BABR	Repl. by LEES 13B
242.6 <sup>+20.2</sup> <sub>-23.2</sub> ± 49.4	<sup>3</sup> POLUEKTOV	06 BELL	$e^+e^- \rightarrow \Upsilon(4S)$

<sup>1</sup>Reports combination of published measurements using GGSZ, GLW, and ADS methods.

<sup>2</sup>Uses Dalitz plot analysis of  $\bar{D}^0 \rightarrow K_S^0\pi^+\pi^-$  and  $\bar{D}^0 \rightarrow K_S^0K^+K^-$  decays coming from  $B^\pm \rightarrow D^{(*)}K^{(*)\pm}$  modes.

<sup>3</sup>Uses a Dalitz plot analysis of the  $\bar{D}^0 \rightarrow K_S^0\pi^+\pi^-$  decays; Combines the  $DK^+$ ,  $D^*K^+$  and  $DK^{*+}$  modes.

 $r_B(B^+ \rightarrow D^{*0}K^+)$ 

$r_B$  and  $\delta_B$  are the amplitude ratio and relative strong phase between the amplitudes of  $A(B^+ \rightarrow D^{*0}K^+)$  and  $A(B^+ \rightarrow \bar{D}^{*0}K^+)$ .

"OUR EVALUATION" is provided by the Heavy Flavor Averaging Group (HFLAV).

VALUE	DOCUMENT ID	TECN	COMMENT
-------	-------------	------	---------

**0.140 ± 0.019 OUR EVALUATION**

• • • We do not use the following data for averages, fits, limits, etc. • • •

0.106 <sup>+0.019</sup> <sub>-0.036</sub>	<sup>1</sup> LEES	13B BABR	$e^+e^- \rightarrow \Upsilon(4S)$
0.133 <sup>+0.042</sup> <sub>-0.039</sub> ± 0.013	<sup>2</sup> DEL-AMO-SA..10F	BABR	Repl. by LEES 13B
0.096 <sup>+0.035</sup> <sub>-0.051</sub>	<sup>3</sup> DEL-AMO-SA..10H	BABR	Repl. by LEES 13B
0.196 <sup>+0.072+0.064</sup> <sub>-0.069-0.017</sub>	<sup>4</sup> POLUEKTOV	10 BELL	$e^+e^- \rightarrow \Upsilon(4S)$
0.135 ± 0.050 ± 0.012	<sup>5</sup> AUBERT	08AL BABR	Repl. by DEL-AMO-SANCHEZ 10F
0.175 <sup>+0.108</sup> <sub>-0.099</sub> ± 0.050	<sup>6</sup> POLUEKTOV	06 BELL	Repl. by POLUEKTOV 10
0.17 ± 0.10 ± 0.04	<sup>7</sup> AUBERT,B	05Y BABR	Repl. by AUBERT 08AL

<sup>1</sup>Reports combination of published measurements using GGSZ, GLW, and ADS methods.

<sup>2</sup>Uses Dalitz plot analysis of  $\bar{D}^0 \rightarrow K_S^0\pi^+\pi^-$ ,  $K_S^0K^+K^-$  decays from  $B^+ \rightarrow D^{(*)}K^{(*)+}$  modes. The corresponding two standard deviation interval is  $0.049 < r_B < 0.215$ .

<sup>3</sup>Uses the Cabibbo suppressed decay of  $B^+ \rightarrow \bar{D}^{*0}K^+$  followed by  $\bar{D}^{*0} \rightarrow \bar{D}\pi^0$  or  $\bar{D}\gamma$ , and  $\bar{D} \rightarrow K^-\pi^+$ .

<sup>4</sup>Uses Dalitz plot analysis of  $\bar{D}^0 \rightarrow K_S^0\pi^+\pi^-$  decays from  $B^+ \rightarrow D^{*0}K^+$  modes. The corresponding two standard deviation interval is  $0.061 < r_B < 0.271$ .

<sup>5</sup>Uses Dalitz plot analysis of  $\bar{D}^0 \rightarrow K_S^0\pi^+\pi^-$  and  $\bar{D}^0 \rightarrow K_S^0K^+K^-$  decays coming from  $B^\pm \rightarrow D^{(*)}K^{(*)\pm}$  modes.

<sup>6</sup>Uses a Dalitz plot analysis of the  $\bar{D}^0 \rightarrow K_S^0\pi^+\pi^-$  decays; Combines the  $DK^+$ ,  $D^*K^+$  and  $DK^{*+}$  modes.

<sup>7</sup>Uses a Dalitz analysis of neutral  $D$  decays to  $K_S^0\pi^+\pi^-$  in the processes  $B^\pm \rightarrow D^{(*)}K^\pm$ ,  $D^* \rightarrow D\pi^0$ ,  $D\gamma$ .

 $\delta_B(B^+ \rightarrow D^{*0}K^+)$ 

"OUR EVALUATION" is provided by the Heavy Flavor Averaging Group (HFLAV).

VALUE (°)	DOCUMENT ID	TECN	COMMENT
-----------	-------------	------	---------

**319.2<sup>+7.7</sup><sub>-8.7</sub> OUR EVALUATION**

• • • We do not use the following data for averages, fits, limits, etc. • • •

294 <sup>+21</sup> <sub>-31</sub>	<sup>1</sup> LEES	13B BABR	$e^+e^- \rightarrow \Upsilon(4S)$
278 ± 21 ± 6	<sup>2</sup> DEL-AMO-SA..10F	BABR	Repl. by LEES 13B
341.9 <sup>+18.0</sup> <sub>-19.6</sub> ± 23.1	<sup>3</sup> POLUEKTOV	10 BELL	$e^+e^- \rightarrow \Upsilon(4S)$
297 <sup>+27</sup> <sub>-29</sub> ± 6.4	<sup>4</sup> AUBERT	08AL BABR	Repl. by DEL-AMO-SANCHEZ 10F
302.0 <sup>+33.8</sup> <sub>-35.1</sub> ± 23.7	<sup>5</sup> POLUEKTOV	06 BELL	Repl. by POLUEKTOV 10
296 ± 41 <sup>+20</sup> <sub>-19</sub>	<sup>6</sup> AUBERT,B	05Y BABR	Repl. by AUBERT 08AL

<sup>1</sup>Reports combination of published measurements using GGSZ, GLW, and ADS methods. We added  $360^\circ$  to the value of  $(-66^{+21}_{-31})^\circ$  quoted by LEES 13B.

<sup>2</sup>Uses Dalitz plot analysis of  $\bar{D}^0 \rightarrow K_S^0\pi^+\pi^-$ ,  $K_S^0K^+K^-$  decays from  $B^+ \rightarrow D^{(*)}K^{(*)+}$  modes. The corresponding two standard deviation interval is  $236^\circ < \delta_B^* < 322^\circ$ .

- <sup>3</sup> Uses Dalitz plot analysis of  $\bar{D}^0 \rightarrow K_S^0 \pi^+ \pi^-$  decays from  $B^+ \rightarrow D^* K^+$  modes. The corresponding two standard deviation interval is  $296.5^\circ < \delta_B^* < 382.7^\circ$ .
- <sup>4</sup> Uses Dalitz plot analysis of  $\bar{D}^0 \rightarrow K_S^0 \pi^+ \pi^-$  and  $\bar{D}^0 \rightarrow K_S^0 K^+ K^-$  decays coming from  $B^\pm \rightarrow D^{(*)} K^{(*)\pm}$  modes.
- <sup>5</sup> Uses a Dalitz plot analysis of the  $\bar{D}^0 \rightarrow K_S^0 \pi^+ \pi^-$  decays; Combines the  $D K^+$ ,  $D^* K^+$  and  $D K^{*+}$  modes.
- <sup>6</sup> Uses a Dalitz analysis of neutral  $D$  decays to  $K_S^0 \pi^+ \pi^-$  in the processes  $B^\pm \rightarrow D^{(*)} K^\pm, D^* \rightarrow D \pi^0, D \gamma$ .

PARTIAL BRANCHING FRACTIONS

$B(B^+ \rightarrow K^{*+} \ell^+ \ell^-) (q^2 < 2.0 \text{ GeV}^2/c^4)$

VALUE (units $10^{-7}$ )	DOCUMENT ID	TECN	COMMENT
<b>1.4 ± 0.5 OUR AVERAGE</b>			
$1.37^{+0.60}_{-0.58}$	AAIJ	12AH LHCb	$pp$ at 7 TeV
$1.30 \pm 0.98 \pm 0.14$	AALTONEN	11AI CDF	$p\bar{p}$ at 1.96 TeV

$B(B^+ \rightarrow K^{*+} \ell^+ \ell^-) (2.0 < q^2 < 4.3 \text{ GeV}^2/c^4)$

VALUE (units $10^{-7}$ )	DOCUMENT ID	TECN	COMMENT
<b>1.1 ± 0.5 OUR AVERAGE</b>			
$1.24^{+0.60}_{-0.55}$	AAIJ	12AH LHCb	$pp$ at 7 TeV
$0.71 \pm 1.00 \pm 0.15$	AALTONEN	11AI CDF	$p\bar{p}$ at 1.96 TeV

$B(B^+ \rightarrow K^{*+} \ell^+ \ell^-) (4.3 < q^2 < 8.68 \text{ GeV}^2/c^4)$

VALUE (units $10^{-7}$ )	DOCUMENT ID	TECN	COMMENT
<b>2.4 <math>^{+0.8}_{-0.7}</math> OUR AVERAGE</b>			
$2.50^{+0.88}_{-0.74}$	AAIJ	12AH LHCb	$pp$ at 7 TeV
$1.71 \pm 1.58 \pm 0.49$	AALTONEN	11AI CDF	$p\bar{p}$ at 1.96 TeV

$B(B^+ \rightarrow K^{*+} \ell^+ \ell^-) (10.09 < q^2 < 12.86 \text{ GeV}^2/c^4)$

VALUE (units $10^{-7}$ )	DOCUMENT ID	TECN	COMMENT
<b>2.1 ± 0.6 OUR AVERAGE</b>			
$2.13^{+0.72}_{-0.66}$	AAIJ	12AH LHCb	$pp$ at 7 TeV
$1.97 \pm 0.99 \pm 0.22$	AALTONEN	11AI CDF	$p\bar{p}$ at 1.96 TeV

$B(B^+ \rightarrow K^{*+} \ell^+ \ell^-) (14.18 < q^2 < 16.0 \text{ GeV}^2/c^4)$

VALUE (units $10^{-7}$ )	DOCUMENT ID	TECN	COMMENT
<b>0.86 <math>^{+0.40}_{-0.32}</math> OUR AVERAGE</b>			
$1.00^{+0.47}_{-0.38}$	AAIJ	12AH LHCb	$pp$ at 7 TeV
$0.52 \pm 0.61 \pm 0.09$	AALTONEN	11AI CDF	$p\bar{p}$ at 1.96 TeV

$B(B^+ \rightarrow K^{*+} \ell^+ \ell^-) (15.0 < q^2 < 19.0 \text{ GeV}^2/c^4)$

VALUE (units $10^{-7}$ )	DOCUMENT ID	TECN	COMMENT
<b>1.50 <math>^{+0.32}_{-0.25} \pm 0.11</math></b>	<sup>1</sup> AAIJ	14M LHCb	$pp$ at 7, 8 TeV

<sup>1</sup> Uses  $B(B^+ \rightarrow J/\psi(1S) K^*(892)^+) = (1.431 \pm 0.027 \pm 0.090) \times 10^{-3}$  for normalization and  $\mu^+ \mu^-$  as a lepton pair.

$B(B^+ \rightarrow K^{*+} \ell^+ \ell^-) (q^2 > 16.0 \text{ GeV}^2/c^4)$

VALUE (units $10^{-7}$ )	DOCUMENT ID	TECN	COMMENT
<b>1.3 ± 0.4 OUR AVERAGE</b>			
$1.25 \pm 0.46$	AAIJ	12AH LHCb	$pp$ at 7 TeV
$1.57 \pm 0.96 \pm 0.17$	AALTONEN	11AI CDF	$p\bar{p}$ at 1.96 TeV

$B(B^+ \rightarrow K^{*+} \ell^+ \ell^-) (1.0 < q^2 < 6.0 \text{ GeV}^2/c^4)$

VALUE (units $10^{-7}$ )	DOCUMENT ID	TECN	COMMENT
<b>1.8 ± 0.4 OUR AVERAGE</b>			
$1.79^{+0.41}_{-0.37} \pm 0.13$	<sup>1</sup> AAIJ	14M LHCb	$pp$ at 7, 8 TeV
$2.57 \pm 1.61 \pm 0.40$	AALTONEN	11AI CDF	$p\bar{p}$ at 1.96 TeV
• • • We do not use the following data for averages, fits, limits, etc. • • •			
$2.90^{+0.90}_{-0.85}$	AAIJ	12AH LHCb	Repl. by AAIJ 14M

<sup>1</sup> Uses  $B(B^+ \rightarrow J/\psi(1S) K^*(892)^+) = (1.431 \pm 0.027 \pm 0.090) \times 10^{-3}$  for normalization and  $\mu^+ \mu^-$  as a lepton pair. Measured in  $1.1 < q^2 < 6.0 \text{ GeV}^2/c^4$ .

$B(B^+ \rightarrow K^{*+} \ell^+ \ell^-) (0.0 < q^2 < 4.3 \text{ GeV}^2/c^4)$

VALUE (units $10^{-7}$ )	DOCUMENT ID	TECN	COMMENT
<b>2.01 ± 1.39 ± 0.27</b>	AALTONEN	11AI CDF	$p\bar{p}$ at 1.96 TeV

$B(B^+ \rightarrow K^+ \ell^+ \ell^-) (q^2 < 2.0 \text{ GeV}^2/c^4)$

VALUE (units $10^{-7}$ )	DOCUMENT ID	TECN	COMMENT
<b>0.51 ± 0.08 OUR AVERAGE</b>			Error includes scale factor of 1.5.
$0.556 \pm 0.053 \pm 0.027$	<sup>1</sup> AAIJ	13H LHCb	$pp$ at 7 TeV
$0.36 \pm 0.11 \pm 0.03$	AALTONEN	11AI CDF	$p\bar{p}$ at 1.96 TeV

<sup>1</sup> Measured in  $0.05 < q^2 < 2.0 \text{ GeV}^2/c^4$  range.

$B(B^+ \rightarrow K^+ \ell^+ \ell^-) (2.0 < q^2 < 4.3 \text{ GeV}^2/c^4)$

VALUE (units $10^{-7}$ )	DOCUMENT ID	TECN	COMMENT
<b>0.60 ± 0.07 OUR AVERAGE</b>			Error includes scale factor of 1.3.
$0.573 \pm 0.053 \pm 0.023$	AAIJ	13H LHCb	$pp$ at 7 TeV
$0.80 \pm 0.15 \pm 0.05$	AALTONEN	11AI CDF	$p\bar{p}$ at 1.96 TeV

$B(B^+ \rightarrow K^+ \ell^+ \ell^-) (4.3 < q^2 < 8.68 \text{ GeV}^2/c^4)$

VALUE (units $10^{-7}$ )	DOCUMENT ID	TECN	COMMENT
<b>1.03 ± 0.07 OUR AVERAGE</b>			
$1.003 \pm 0.070 \pm 0.039$	AAIJ	13H LHCb	$pp$ at 7 TeV
$1.18 \pm 0.19 \pm 0.09$	AALTONEN	11AI CDF	$p\bar{p}$ at 1.96 TeV

$B(B^+ \rightarrow K^+ \ell^+ \ell^-) (10.09 < q^2 < 12.86 \text{ GeV}^2/c^4)$

VALUE (units $10^{-7}$ )	DOCUMENT ID	TECN	COMMENT
<b>0.58 ± 0.05 OUR AVERAGE</b>			
$0.565 \pm 0.050 \pm 0.022$	AAIJ	13H LHCb	$pp$ at 7 TeV
$0.68 \pm 0.12 \pm 0.05$	AALTONEN	11AI CDF	$p\bar{p}$ at 1.96 TeV

$B(B^+ \rightarrow K^+ \ell^+ \ell^-) (14.18 < q^2 < 16.0 \text{ GeV}^2/c^4)$

VALUE (units $10^{-7}$ )	DOCUMENT ID	TECN	COMMENT
<b>0.40 ± 0.05 OUR AVERAGE</b>			Error includes scale factor of 1.4.
$0.377 \pm 0.036 \pm 0.015$	AAIJ	13H LHCb	$pp$ at 7 TeV
$0.53 \pm 0.10 \pm 0.03$	AALTONEN	11AI CDF	$p\bar{p}$ at 1.96 TeV

$B(B^+ \rightarrow K^+ \ell^+ \ell^-) (16.0 < q^2 < 18.0 \text{ GeV}^2/c^4)$

VALUE (units $10^{-7}$ )	DOCUMENT ID	TECN	COMMENT
<b>0.354 ± 0.036 ± 0.018</b>	AAIJ	13H LHCb	$pp$ at 7 TeV

$B(B^+ \rightarrow K^+ \ell^+ \ell^-) (18.0 < q^2 < 22.0 \text{ GeV}^2/c^4)$

$F_H$  is a fractional contribution of (pseudo) scalar and tensor amplitudes to the decay width in the massless muon approximation.

VALUE (units $10^{-7}$ )	DOCUMENT ID	TECN	COMMENT
<b>0.312 ± 0.040 ± 0.016</b>	AAIJ	13H LHCb	$pp$ at 7 TeV

$B(B^+ \rightarrow K^+ \ell^+ \ell^-) (15.0 < q^2 < 22.0 \text{ GeV}^2/c^4)$

VALUE (units $10^{-7}$ )	DOCUMENT ID	TECN	COMMENT
<b>0.85 ± 0.03 ± 0.04</b>	<sup>1</sup> AAIJ	14M LHCb	$pp$ at 7, 8 TeV

<sup>1</sup> Uses  $B(B^+ \rightarrow J/\psi(1S) K^+) = (0.998 \pm 0.014 \pm 0.040) \times 10^{-3}$  for normalization and  $\mu^+ \mu^-$  as a lepton pair.

$B(B^+ \rightarrow K^+ \ell^+ \ell^-) (16.0 < q^2 < 18.0 \text{ GeV}^2/c^4)$

VALUE (units $10^{-7}$ )	DOCUMENT ID	TECN	COMMENT
<b>0.48 ± 0.11 ± 0.03</b>	AALTONEN	11AI CDF	$p\bar{p}$ at 1.96 TeV

$B(B^+ \rightarrow K^+ \ell^+ \ell^-) (1.0 < q^2 < 6.0 \text{ GeV}^2/c^4)$

VALUE (units $10^{-7}$ )	DOCUMENT ID	TECN	COMMENT
<b>1.21 ± 0.06 OUR AVERAGE</b>			
$1.40^{+0.98}_{-0.34} \pm 0.69$	<sup>1</sup> AAIJ	19S LHCb	$pp$ at 7, 8, 13 TeV
$1.19 \pm 0.034 \pm 0.059$	<sup>2</sup> AAIJ	14M LHCb	$pp$ at 7, 8 TeV
$1.41 \pm 0.20 \pm 0.10$	AALTONEN	11AI CDF	$p\bar{p}$ at 1.96 TeV

• • • We do not use the following data for averages, fits, limits, etc. • • •

VALUE (units $10^{-7}$ )	DOCUMENT ID	TECN	COMMENT
$1.56^{+0.19}_{-0.15} \pm 0.06$	<sup>3</sup> AAIJ	14AR LHCb	$pp$ at 7, 8 TeV
$1.205 \pm 0.085 \pm 0.070$	AAIJ	13H LHCb	Repl. by AAIJ 14M

<sup>1</sup> Measured by taking the ratio of the branching fraction from  $B^+ \rightarrow K^+ e^+ e^-$  and  $B^+ \rightarrow J/\psi(e^+ e^-) K^+$  decays and multiplying it by the measured value of  $B^+ \rightarrow J/\psi K^+$  and  $J/\psi \rightarrow e^+ e^-$  as in PDG 18. The branching fraction of  $B^+ \rightarrow K^+ e^+ e^-$  is determined in the region  $1.1 < q^2 < 6 \text{ GeV}^2/c^4$ .

<sup>2</sup> Uses  $B(B^+ \rightarrow J/\psi(1S) K^+) = (0.998 \pm 0.014 \pm 0.040) \times 10^{-3}$  for normalization and  $\mu^+ \mu^-$  for leptons. Measured for  $1.1 < q^2 < 6.0 \text{ GeV}^2/c^4$ .

<sup>3</sup> Measured by taking the ratio of the branching fraction from  $B^+ \rightarrow K^+ e^+ e^-$  and  $B^+ \rightarrow J/\psi(e^+ e^-) K^+$  decays and multiplying it by the measured value of  $B^+ \rightarrow J/\psi K^+$  and  $J/\psi \rightarrow e^+ e^-$  as in PDG 12. The branching fraction of  $B^+ \rightarrow K^+ e^+ e^-$  is determined in the region  $1 < q^2 < 6 \text{ GeV}^2/c^4$ .

$B(B^+ \rightarrow K^+ \mu^+ \mu^-) / B(B^+ \rightarrow K^+ e^+ e^-) (1.0 < q^2 < 6.0 \text{ GeV}^2/c^4)$

VALUE	DOCUMENT ID	TECN	COMMENT
<b>0.846 <math>^{+0.060}_{-0.054} \pm 0.016</math></b>	<sup>1</sup> AAIJ	19S LHCb	$pp$ at 7, 8, 13 TeV

• • • We do not use the following data for averages, fits, limits, etc. • • •

VALUE	DOCUMENT ID	TECN	COMMENT
$0.745^{+0.090}_{-0.074} \pm 0.036$	<sup>2</sup> AAIJ	14AR LHCb	$pp$ at 7, 8 TeV

<sup>1</sup> The ratio is determined using the relative branching fractions of the decays  $B^+ \rightarrow K^+ \ell^+ \ell^-$  and  $B^+ \rightarrow J/\psi(\ell^+ \ell^-) K^+$ , with  $\ell = e, \mu$ . Measured for the region  $1.1 < q^2 < 6.0 \text{ GeV}^2/c^4$ .

<sup>2</sup> The ratio is determined using the relative branching fractions of the decays  $B^+ \rightarrow K^+ \ell^+ \ell^-$  and  $B^+ \rightarrow J/\psi(\ell^+ \ell^-) K^+$ , with  $\ell = e, \mu$ .

$B(B^+ \rightarrow K^+ \ell^+ \ell^-) (0.0 < q^2 < 4.3 \text{ GeV}^2/c^4)$

VALUE (units $10^{-7}$ )	DOCUMENT ID	TECN	COMMENT
<b>1.13 ± 0.19 ± 0.08</b>	AALTONEN	11AI CDF	$p\bar{p}$ at 1.96 TeV







See key on page 999

Meson Particle Listings
B±, B0

Table with 5 columns: Author, Year, Document ID, Technique, Comment. Lists various meson decays and experiments like ASNER, BARISH, BERGFELD, etc.

5 CSORNA 00 uses fully reconstructed 135 B0 -> J/psi(l) K\_S^0 events and invariant masses without beam constraint.
6 ALBRECHT 90J assumes 10580 for T(4S) mass. Supersedes ALBRECHT 87c and ALBRECHT 87D.
7 Found using fully reconstructed decays with J/psi. ALBRECHT 87D assume m\_T(4S) = 10577 MeV.

m\_B0 - m\_B+

Table with 4 columns: VALUE (MeV), DOCUMENT ID, TECN, COMMENT. Shows results for m\_B0 - m\_B+ with our fit and average values.

1 Uses exclusively reconstructed final states containing a J/psi -> mu+ mu- decay.
2 Uses the B-momentum distributions in the e+ e- rest frame.
3 Uses exclusively reconstructed final states containing a J/psi -> mu+ mu- decays.
4 BEBEK 87 actually measure the difference between half of E\_cm and the B± or B0 mass, so the m\_B0 - m\_B± is more accurate. Assume m\_T(4S) = 10580 MeV.

m\_BH^0 - m\_BL^0

See the B0-B0 MIXING PARAMETERS section near the end of these B0 Listings.

B0 MEAN LIFE

See B±/B0/Bs^0/b-baryon ADMIXTURE section for data on B-hadron mean life averaged over species of bottom particles.

“OUR EVALUATION” is an average using rescaled values of the data listed below. The average and rescaling were performed by the Heavy Flavor Averaging Group (HFLAV) and are described at https://hflav.web.cern.ch/. The averaging/rescaling procedure takes into account correlations between the measurements and asymmetric lifetime errors.

Table with 5 columns: VALUE (10^-12 s), EVTS, DOCUMENT ID, TECN, COMMENT. Lists B0 mean life measurements from various experiments.

B0

I(JP) = 1/2(0-)

Quantum numbers not measured. Values shown are quark-model predictions.

See also the B±/B0 ADMIXTURE and B±/B0/Bs^0/b-baryon ADMIXTURE sections.

See the Note “Production and Decay of b-flavored Hadrons” at the beginning of the B± Particle Listings and the Note on “B0-B0 Mixing” near the end of the B0 Particle Listings.

B0 MASS

The fit uses m\_B+, (m\_B0 - m\_B+), and m\_B0 to determine m\_B+, m\_B0, and the mass difference.

Table with 5 columns: VALUE (MeV), EVTS, DOCUMENT ID, TECN, COMMENT. Shows B0 mass fit results and our fit/average values.

1 Uses B0 -> J/psi p pbar decays.
2 Measured with B0 -> J/psi(mu+ mu-) K\_S^0(pi+ pi-) decays.
3 Uses B0 -> J/psi K^0 fully reconstructed decays.
4 Uses exclusively reconstructed final states containing a J/psi -> mu+ mu- decays.

Downloaded from https://academic.oup.com/ptep/article/2020/8/083C01/5891211 by guest on 12 November 2020



## Meson Particle Listings

 $B^0$ 

1.54 ± 0.08 ± 0.06	17	ABE	96c	CDF	Repl. by ABE 98Q	
1.55 ± 0.06 ± 0.03	25	BUSKULIC	96J	ALEP	$e^+e^- \rightarrow Z$	
1.61 ± 0.07 ± 0.04	17	BUSKULIC	96J	ALEP	Repl. by BARATE 00R	
1.62 ± 0.12	26	ADAM	95	DLPH	$e^+e^- \rightarrow Z$	
1.57 ± 0.18 ± 0.08	121	14	ABE	94D	CDF	Repl. by ABE 98B
1.17 $^{+0.29}_{-0.23}$ ± 0.16	96	17	ABREU	93D	DLPH	Sup. by ABREU 95Q
1.55 ± 0.25 ± 0.18	76	22	ABREU	93G	DLPH	Sup. by ADAM 95
1.51 $^{+0.24}_{-0.23}$ ± 0.12	78	17	ACTON	93c	OPAL	Sup. by AKERS 95T
1.52 $^{+0.20}_{-0.18}$ ± 0.07	77	17	BUSKULIC	93D	ALEP	Sup. by BUSKULIC 96J
1.20 $^{+0.52}_{-0.36}$ ± 0.16	15	27	WAGNER	90	MRK2	$E_{\text{cm}}^{\text{ee}} = 29$ GeV
0.82 $^{+0.57}_{-0.37}$ ± 0.27		28	AVERRILL	89	HRS	$E_{\text{cm}}^{\text{ee}} = 29$ GeV

- Measured using  $B^0 \rightarrow J/\psi K^*(892)^0$  and  $B^0 \rightarrow J/\psi K_S^0$  decays.
- Measured using  $B^0 \rightarrow D^-\mu^+\nu X$  decays.
- Measured mean life using  $B^0 \rightarrow J/\psi K_S^0$  decays.
- Measured using  $B^0 \rightarrow J/\psi K^*0$  decays.
- Measured using  $B^0 \rightarrow K^+\pi^-$  decays.
- Measured with  $B_d^0 \rightarrow J/\psi(\mu^+\mu^-)K_S^0(\pi^+\pi^-)$  decays.
- Measured mean life using fully reconstructed decays ( $J/\psi K^*$ ).
- Measured mean life using  $B^0 \rightarrow J/\psi K^*0$  decays.
- Measured using a simultaneous fit of the  $B^0$  lifetime and  $\bar{B}^0 B^0$  oscillation frequency  $\Delta m_d$  in the partially reconstructed  $B^0 \rightarrow D^{*-}\ell\nu$  decays.
- Measurement performed using a combined fit of  $CP$ -violation, mixing and lifetimes.
- Measurement performed using an inclusive reconstruction and  $B$  flavor identification technique.
- AUBERT 03c uses a sample of approximately 14,000 exclusively reconstructed  $B^0 \rightarrow D^*(2010)^-\ell\nu$  and simultaneously measures the lifetime and oscillation frequency.
- Measurement performed with decays  $B^0 \rightarrow D^{*-}\pi^+$  and  $B^0 \rightarrow D^{*-}\rho^+$  using a partial reconstruction technique.
- Measured mean life using fully reconstructed decays.
- Data analyzed using partially reconstructed  $\bar{B}^0 \rightarrow D^{*+}\ell^-\bar{\nu}$  decays.
- Events are selected in which one  $B$  meson is fully reconstructed while the second  $B$  meson is reconstructed inclusively.
- Data analyzed using  $D/D^* \ell X$  event vertices.
- Data analyzed using charge of secondary vertex.
- Data analyzed using inclusive  $D/D^* \ell X$ .
- Measured mean life using partially reconstructed  $D^{*-}\pi^+ X$  vertices.
- ABREU 95Q assumes  $B(B^0 \rightarrow D^{*-}\ell^+\nu_\ell) = 3.2 \pm 1.7\%$ .
- Data analyzed using vertex-charge technique to tag  $B$  charge.
- AKERS 95T assumes  $B(B^0 \rightarrow D_s^{*+}D^0(*)^0) = 5.0 \pm 0.9\%$  to find  $B^+ / B^0$  yield.
- Measured using the time-dependent angular analysis of  $B_d^0 \rightarrow J/\psi K^*0$  decays.
- Combined result of  $D/D^* \ell X$  analysis, fully reconstructed  $B$  analysis, and partially reconstructed  $D^{*-}\pi^+ X$  analysis.
- Combined ABREU 95Q and ADAM 95 result.
- WAGNER 90 tagged  $B^0$  mesons by their decays into  $D^{*-}e^+\nu$  and  $D^{*-}\mu^+\nu$  where the  $D^{*-}$  is tagged by its decay into  $\pi^-\bar{D}^0$ .
- AVERRILL 89 is an estimate of the  $B^0$  mean lifetime assuming that  $B^0 \rightarrow D^{*+} + X$  always.

 $\tau_{B^0} / \tau_{\bar{B}^0}$ 

VALUE	DOCUMENT ID	TECN	COMMENT
<b>1.000 ± 0.008 ± 0.009</b>	1 AAIJ	14E	LHCB $pp$ at 7 TeV

- Measured using  $B^0 \rightarrow J/\psi K^*0$  decays.

MEAN LIFE RATIO  $\tau_{B^+} / \tau_{B^0}$  $\tau_{B^+} / \tau_{B^0}$  (direct measurements)

"OUR EVALUATION" is an average using rescaled values of the data listed below. The average and rescaling were performed by the Heavy Flavor Averaging Group (HFLAV) and are described at <https://hflav.web.cern.ch/>. The averaging/rescaling procedure takes into account correlations between the measurements and asymmetric lifetime errors.

VALUE	EVTS	DOCUMENT ID	TECN	COMMENT
<b>1.076 ± 0.004 OUR EVALUATION</b>				
1.074 ± 0.005 ± 0.003	1	AAIJ	14E	LHCB $pp$ at 7 TeV
1.088 ± 0.009 ± 0.004	2	AALTONEN	11	CDF $p\bar{p}$ at 1.96 TeV
1.080 ± 0.016 ± 0.014	3	ABAZOV	05D	D0 $p\bar{p}$ at 1.96 TeV
1.066 ± 0.008 ± 0.008	4	ABE	05B	BELL $e^+e^- \rightarrow \Upsilon(4S)$
1.060 ± 0.021 ± 0.024	5	ABDALLAH	04E	DLPH $e^+e^- \rightarrow Z$
1.093 ± 0.066 ± 0.028	6	ACOSTA	02c	CDF $p\bar{p}$ at 1.8 TeV
1.082 ± 0.026 ± 0.012	7	AUBERT	01F	BABR $e^+e^- \rightarrow \Upsilon(4S)$
1.085 ± 0.059 ± 0.018	3	BARATE	00R	ALEP $e^+e^- \rightarrow Z$
1.079 ± 0.064 ± 0.041	8	ABBIENDI	99J	OPAL $e^+e^- \rightarrow Z$
1.110 ± 0.056 $^{+0.033}_{-0.030}$	3	ABE	98Q	CDF $p\bar{p}$ at 1.8 TeV
1.09 ± 0.07 ± 0.03	8	ACCIARRI	98S	L3 $e^+e^- \rightarrow Z$
1.01 ± 0.07 ± 0.06	8	ABE	97J	SLD $e^+e^- \rightarrow Z$
1.27 $^{+0.23}_{-0.19}$ ± 0.03	6	BUSKULIC	96J	ALEP $e^+e^- \rightarrow Z$
1.00 $^{+0.17}_{-0.15}$ ± 0.10	3,9	ABREU	95Q	DLPH $e^+e^- \rightarrow Z$
1.06 $^{+0.13}_{-0.11}$ ± 0.10	10	ADAM	95	DLPH $e^+e^- \rightarrow Z$
0.99 ± 0.14 $^{+0.05}_{-0.04}$	3,11	AKERS	95T	OPAL $e^+e^- \rightarrow Z$

• • • We do not use the following data for averages, fits, limits, etc. • • •

1.091 ± 0.023 ± 0.014	7	ABE	02H	BELL	Repl. by ABE 05B	
1.06 ± 0.07 ± 0.02	6	ABE	98B	CDF	Repl. by ACOSTA 02c	
1.01 ± 0.11 ± 0.02	3	ABE	96C	CDF	Repl. by ABE 98Q	
1.03 ± 0.08 ± 0.02	12	BUSKULIC	96J	ALEP	$e^+e^- \rightarrow Z$	
0.98 ± 0.08 ± 0.03	3	BUSKULIC	96J	ALEP	Repl. by BARATE 00R	
1.02 ± 0.16 ± 0.05	269	6	ABE	94D	CDF	Repl. by ABE 98B
1.11 $^{+0.51}_{-0.39}$ ± 0.11	188	3	ABREU	93D	DLPH	Sup. by ABREU 95Q
1.01 $^{+0.29}_{-0.22}$ ± 0.12	253	10	ABREU	93G	DLPH	Sup. by ADAM 95
1.0 $^{+0.33}_{-0.25}$ ± 0.08	130		ACTON	93c	OPAL	Sup. by AKERS 95T
0.96 $^{+0.19}_{-0.15}$ ± 0.18	154	3	BUSKULIC	93D	ALEP	Sup. by BUSKULIC 96J

- Measured using  $B \rightarrow J/\psi K^*$  decays.
- Measured mean life using fully reconstructed decays ( $J/\psi K^*$ ).
- Data analyzed using  $D/D^* \mu X$  vertices.
- Measurement performed using a combined fit of  $CP$ -violation, mixing and lifetimes.
- Measurement performed using an inclusive reconstruction and  $B$  flavor identification technique.
- Measured using fully reconstructed decays.
- Events are selected in which one  $B$  meson is fully reconstructed while the second  $B$  meson is reconstructed inclusively.
- Data analyzed using charge of secondary vertex.
- ABREU 95Q assumes  $B(B^0 \rightarrow D^{*-}\ell^+\nu_\ell) = 3.2 \pm 1.7\%$ .
- Data analyzed using vertex-charge technique to tag  $B$  charge.
- AKERS 95T assumes  $B(B^0 \rightarrow D_s^{*+}D^0(*)^0) = 5.0 \pm 0.9\%$  to find  $B^+ / B^0$  yield.
- Combined result of  $D/D^* \ell X$  analysis and fully reconstructed  $B$  analysis.

 $\tau_{B^+} / \tau_{B^0}$  (inferred from branching fractions)

These measurements are inferred from the branching fractions for semileptonic decay or other spectator-dominated decays by assuming that the rates for such decays are equal for  $B^0$  and  $B^+$ . We do not use measurements which assume equal production of  $B^0$  and  $B^+$  because of the large uncertainty in the production ratio.

"OUR EVALUATION" has been obtained by the Heavy Flavor Averaging Group (HFLAV) by taking into account correlations between measurements.

VALUE	CL%	EVTS	DOCUMENT ID	TECN	COMMENT		
<b>1.076 ± 0.034 OUR EVALUATION</b>							
<b>1.07 ± 0.04 OUR AVERAGE</b>							
1.07 ± 0.04 ± 0.03			URQUIJO	07	BELL $e^+e^- \rightarrow \Upsilon(4S)$		
1.067 ± 0.041 ± 0.033			AUBERT,B	06Y	BABR $e^+e^- \rightarrow \Upsilon(4S)$		
• • • We do not use the following data for averages, fits, limits, etc. • • •							
0.95 $^{+0.117}_{-0.080}$ ± 0.091			1	ARTUSO	97	CLE2 $e^+e^- \rightarrow \Upsilon(4S)$	
1.15 ± 0.17 ± 0.06			2	JESSOP	97	CLE2 $e^+e^- \rightarrow \Upsilon(4S)$	
0.93 ± 0.18 ± 0.12			3	ATHANAS	94	CLE2	Sup. by ARTUSO 97
0.91 ± 0.27 ± 0.21			4	ALBRECHT	92c	ARG	$e^+e^- \rightarrow \Upsilon(4S)$
1.0 ± 0.4		29	4,5	ALBRECHT	92G	ARG	$e^+e^- \rightarrow \Upsilon(4S)$
0.89 ± 0.19 ± 0.13			4	FULTON	91	CLEO	$e^+e^- \rightarrow \Upsilon(4S)$
1.00 ± 0.23 ± 0.14			4	ALBRECHT	89L	ARG	$e^+e^- \rightarrow \Upsilon(4S)$
0.49 to 2.3		90	6	BEAN	87B	CLEO	$e^+e^- \rightarrow \Upsilon(4S)$

- ARTUSO 97 uses partial reconstruction of  $B \rightarrow D^* \ell \nu_\ell$  and independent of  $B^0$  and  $B^+$  production fraction.
- Assumes equal production of  $B^+$  and  $B^0$  at the  $\Upsilon(4S)$ .
- ATHANAS 94 uses events tagged by fully reconstructed  $B^-$  decays and partially or fully reconstructed  $B^0$  decays.
- Assumes equal production of  $B^0$  and  $B^+$ .
- ALBRECHT 92G data analyzed using  $B \rightarrow D_s \bar{D}, D_s \bar{D}^*, D_s^* \bar{D}, D_s^* \bar{D}^*$  events.
- BEAN 87B assume the fraction of  $B^0 \bar{B}^0$  events at the  $\Upsilon(4S)$  is 0.41.

 $\Delta\Gamma_{B_d^0} / \Gamma_{B_d^0}$ 

$\Gamma_{B_d^0}$  and  $\Delta\Gamma_{B_d^0}$  are the decay rate average and difference between two  $B_d^0$   $CP$  eigenstates (light – heavy). The  $\lambda_{CP}$  characterizes  $B^0$  and  $\bar{B}^0$  decays to states of charmonium plus  $K_L^0$ , see the review on "CP Violation" in the reviews section.

"OUR EVALUATION" has been obtained by the Heavy Flavor Averaging Group (HFLAV) by taking into account correlations between measurements.

VALUE (units $10^{-2}$ )	CL%	DOCUMENT ID	TECN	COMMENT	
<b>0.1 ± 1.0 OUR EVALUATION</b>					
<b>0.1 ± 1.0 OUR AVERAGE</b>					
3.4 ± 2.3 ± 2.4		1	SIRUNYAN	18BY	CMS $pp$ at 8 TeV
– 0.1 ± 1.1 ± 0.9		2	AABOUD	16G	ATLS $pp$ at 7, 8 TeV
– 4.4 ± 2.5 ± 1.1		3	AAIJ	14E	LHCB $pp$ at 7 TeV
1.7 ± 1.8 ± 1.1		4	HIGUCHI	12	BELL $e^+e^- \rightarrow \Upsilon(4S)$
0.8 ± 3.7 ± 1.8		5	AUBERT,B	04C	BABR $e^+e^- \rightarrow \Upsilon(4S)$
0 ± 0.9		6	ABDALLAH	03B	DLPH $e^+e^- \rightarrow Z$

• • • We do not use the following data for averages, fits, limits, etc. • • •  
 0.50 ± 1.38 ABAZOV 14 D0  $p\bar{p}$  at 1.96 TeV  
 < 80 95 7 BEHRENS 00B CLE2  $e^+e^- \rightarrow \Upsilon(4S)$   
<sup>1</sup> Measured using  $B^0 \rightarrow J/\psi K^*(892)^0$  and  $B^0 \rightarrow J/\psi K_S^0$  decays, and assuming  $\beta = 21.9 \pm 0.7$  degrees.  
<sup>2</sup> Measured from the ratio of decay time distributions of  $B^0 \rightarrow J/\psi K_S^0$  and  $B^0 \rightarrow J/\psi K^{*0}$  decays.  
<sup>3</sup> Measured using the effective lifetimes of  $B^0 \rightarrow J/\psi K_S^0$  and  $B^0 \rightarrow J/\psi K^{*0}$  decays.  
<sup>4</sup> Reports  $-\Delta\Gamma_d/\Gamma_d$  using  $B^0 \rightarrow J/\psi K_S^0, J/\psi K_L^0, D^-\pi^+, D^{*-}\pi^+, D^{*-}\rho^+$ , and  $D^{*-}\ell^+\nu$  decays.  
<sup>5</sup> Corresponds to 90% confidence range [-0.084, 0.068].  
<sup>6</sup> Used the measured  $\tau_{B^0} = 1.55 \pm 0.03$  ps. Corresponds to an upper limit of < 0.18 at 95% C.L.  
<sup>7</sup> BEHRENS 00B uses high-momentum lepton tags and partially reconstructed  $\bar{B}^0 \rightarrow D^{*+}\pi^-, \rho^-$  decays to determine the flavor of the  $B$  meson. Assumes  $\Delta_{md} = 0.478 \pm 0.018$  ps<sup>-1</sup> and  $\tau_{B^0} = 1.548 \pm 0.032$  ps.

**$B^0$  DECAY MODES**

$\bar{B}^0$  modes are charge conjugates of the modes below. Reactions indicate the weak decay vertex and do not include mixing. Modes which do not identify the charge state of the  $B$  are listed in the  $B^\pm/B^0$  ADMIXTURE section.

The branching fractions listed below assume 50%  $B^0\bar{B}^0$  and 50%  $B^+B^-$  production at the  $\Upsilon(4S)$ . We have attempted to bring older measurements up to date by rescaling their assumed  $\Upsilon(4S)$  production ratio to 50:50 and their assumed  $D, D_s, D^*$ , and  $\psi$  branching ratios to current values whenever this would affect our averages and best limits significantly.

Indentation is used to indicate a subchannel of a previous reaction. All resonant subchannels have been corrected for resonance branching fractions to the final state so the sum of the subchannel branching fractions can exceed that of the final state.

For inclusive branching fractions, e.g.,  $B \rightarrow D^\pm X$ , the values usually are multiplicities, not branching fractions. They can be greater than one.

Mode	Fraction ( $\Gamma_i/\Gamma$ )	Scale factor/ Confidence level
$\Gamma_1 \ell^+ \nu_\ell X$	[a] ( 10.33 ± 0.28 ) %	
$\Gamma_2 e^+ \nu_e X_c$	( 10.1 ± 0.4 ) %	
$\Gamma_3 D \ell^+ \nu_\ell X$	( 9.4 ± 0.9 ) %	
$\Gamma_4 D^- \ell^+ \nu_\ell$	[a] ( 2.31 ± 0.10 ) %	
$\Gamma_5 D^- \tau^+ \nu_\tau$	( 1.08 ± 0.23 ) %	
$\Gamma_6 D^*(2010)^- \ell^+ \nu_\ell$	[a] ( 5.05 ± 0.14 ) %	
$\Gamma_7 D^*(2010)^- \tau^+ \nu_\tau$	( 1.57 ± 0.09 ) %	S=1.1
$\Gamma_8 \bar{D}^0 \pi^- \ell^+ \nu_\ell$	( 4.1 ± 0.5 ) × 10 <sup>-3</sup>	
$\Gamma_9 D_0^*(2300)^- \ell^+ \nu_\ell, D_0^{*-} \rightarrow \bar{D}^0 \pi^-$	( 3.0 ± 1.2 ) × 10 <sup>-3</sup>	S=1.8
$\Gamma_{10} D_2^*(2460)^- \ell^+ \nu_\ell, D_2^{*-} \rightarrow \bar{D}^0 \pi^-$	( 1.21 ± 0.33 ) × 10 <sup>-3</sup>	S=1.8
$\Gamma_{11} \bar{D}^{(*)0} n \pi \ell^+ \nu_\ell (n \geq 1)$	( 2.3 ± 0.5 ) %	
$\Gamma_{12} \bar{D}^{*0} \pi^- \ell^+ \nu_\ell$	( 5.8 ± 0.8 ) × 10 <sup>-3</sup>	S=1.4
$\Gamma_{13} D_1(2420)^- \ell^+ \nu_\ell, D_1^- \rightarrow \bar{D}^{*0} \pi^-$	( 2.80 ± 0.28 ) × 10 <sup>-3</sup>	
$\Gamma_{14} D_1'(2430)^- \ell^+ \nu_\ell, D_1'^- \rightarrow \bar{D}^{*0} \pi^-$	( 3.1 ± 0.9 ) × 10 <sup>-3</sup>	
$\Gamma_{15} D_2^*(2460)^- \ell^+ \nu_\ell, D_2^{*-} \rightarrow \bar{D}^{*0} \pi^-$	( 6.8 ± 1.2 ) × 10 <sup>-4</sup>	
$\Gamma_{16} D^- \pi^+ \pi^- \ell^+ \nu_\ell$	( 1.3 ± 0.5 ) × 10 <sup>-3</sup>	
$\Gamma_{17} D^{*-} \pi^+ \pi^- \ell^+ \nu_\ell$	( 1.4 ± 0.5 ) × 10 <sup>-3</sup>	
$\Gamma_{18} \rho^- \ell^+ \nu_\ell$	[a] ( 2.94 ± 0.21 ) × 10 <sup>-4</sup>	
$\Gamma_{19} \pi^- \ell^+ \nu_\ell$	[a] ( 1.50 ± 0.06 ) × 10 <sup>-4</sup>	
$\Gamma_{20} \pi^- \mu^+ \nu_\mu$		
$\Gamma_{21} \pi^- \tau^+ \nu_\tau$	< 2.5 × 10 <sup>-4</sup>	CL=90%
<b>Inclusive modes</b>		
$\Gamma_{22} K^\pm X$	( 78 ± 8 ) %	
$\Gamma_{23} D^0 X$	( 8.1 ± 1.5 ) %	
$\Gamma_{24} \bar{D}^0 X$	( 47.4 ± 2.8 ) %	
$\Gamma_{25} D^+ X$	< 3.9 %	CL=90%
$\Gamma_{26} D^- X$	( 36.9 ± 3.3 ) %	
$\Gamma_{27} D_s^+ X$	( 10.3 ± 2.1 / 1.8 ) %	
$\Gamma_{28} D_s^- X$	< 2.6 %	CL=90%
$\Gamma_{29} \Lambda_c^+ X$	< 3.1 %	CL=90%
$\Gamma_{30} \bar{\Lambda}_c^- X$	( 5.0 ± 2.1 / 1.5 ) %	
$\Gamma_{31} \bar{c} X$	( 95 ± 5 ) %	
$\Gamma_{32} c X$	( 24.6 ± 3.1 ) %	
$\Gamma_{33} \bar{c}/c X$	( 119 ± 6 ) %	

**$D, D^*$ , or  $D_s$  modes**

$\Gamma_{34} D^- \pi^+$	( 2.52 ± 0.13 ) × 10 <sup>-3</sup>	S=1.1
$\Gamma_{35} D^- \rho^+$	( 7.6 ± 1.2 ) × 10 <sup>-3</sup>	
$\Gamma_{36} D^- K^0 \pi^+$	( 4.9 ± 0.9 ) × 10 <sup>-4</sup>	
$\Gamma_{37} D^- K^*(892)^+$	( 4.5 ± 0.7 ) × 10 <sup>-4</sup>	
$\Gamma_{38} D^- \omega \pi^+$	( 2.8 ± 0.6 ) × 10 <sup>-3</sup>	
$\Gamma_{39} D^- K^+$	( 1.86 ± 0.20 ) × 10 <sup>-4</sup>	
$\Gamma_{40} D^- K^+ \pi^+ \pi^-$	( 3.5 ± 0.8 ) × 10 <sup>-4</sup>	
$\Gamma_{41} D^- K^+ \bar{K}^0$	< 3.1 × 10 <sup>-4</sup>	CL=90%
$\Gamma_{42} D^- K^+ \bar{K}^*(892)^0$	( 8.8 ± 1.9 ) × 10 <sup>-4</sup>	
$\Gamma_{43} \bar{D}^0 \pi^+ \pi^-$	( 8.8 ± 0.5 ) × 10 <sup>-4</sup>	
$\Gamma_{44} D^*(2010)^- \pi^+$	( 2.74 ± 0.13 ) × 10 <sup>-3</sup>	
$\Gamma_{45} \bar{D}^0 K^+ K^-$	( 5.9 ± 0.5 ) × 10 <sup>-5</sup>	
$\Gamma_{46} D^- \pi^+ \pi^+ \pi^-$	( 6.0 ± 0.7 ) × 10 <sup>-3</sup>	S=1.1
$\Gamma_{47} (D^- \pi^+ \pi^+ \pi^-)$ nonresonant	( 3.9 ± 1.9 ) × 10 <sup>-3</sup>	
$\Gamma_{48} D^- \pi^+ \rho^0$	( 1.1 ± 1.0 ) × 10 <sup>-3</sup>	
$\Gamma_{49} D^- a_1(1260)^+$	( 6.0 ± 3.3 ) × 10 <sup>-3</sup>	
$\Gamma_{50} D^*(2010)^- \pi^+ \pi^0$	( 1.5 ± 0.5 ) %	
$\Gamma_{51} D^*(2010)^- \rho^+$	( 6.8 ± 0.9 ) × 10 <sup>-3</sup>	
$\Gamma_{52} D^*(2010)^- K^+$	( 2.12 ± 0.15 ) × 10 <sup>-4</sup>	
$\Gamma_{53} D^*(2010)^- K^0 \pi^+$	( 3.0 ± 0.8 ) × 10 <sup>-4</sup>	
$\Gamma_{54} D^*(2010)^- K^*(892)^+$	( 3.3 ± 0.6 ) × 10 <sup>-4</sup>	
$\Gamma_{55} D^*(2010)^- K^+ \bar{K}^0$	< 4.7 × 10 <sup>-4</sup>	CL=90%
$\Gamma_{56} D^*(2010)^- K^+ \bar{K}^*(892)^0$	( 1.29 ± 0.33 ) × 10 <sup>-3</sup>	
$\Gamma_{57} D^*(2010)^- \pi^+ \pi^+ \pi^-$	( 7.21 ± 0.29 ) × 10 <sup>-3</sup>	
$\Gamma_{58} (D^*(2010)^- \pi^+ \pi^+ \pi^-)$ non-resonant	( 0.0 ± 2.5 ) × 10 <sup>-3</sup>	
$\Gamma_{59} D^*(2010)^- \pi^+ \rho^0$	( 5.7 ± 3.2 ) × 10 <sup>-3</sup>	
$\Gamma_{60} D^*(2010)^- a_1(1260)^+$	( 1.30 ± 0.27 ) %	
$\Gamma_{61} \bar{D}_1(2420)^0 \pi^- \pi^+, \bar{D}_1^0 \rightarrow D^{*-} \pi^+$	( 1.47 ± 0.35 ) × 10 <sup>-4</sup>	
$\Gamma_{62} D^*(2010)^- K^+ \pi^- \pi^+$	( 4.7 ± 0.4 ) × 10 <sup>-4</sup>	
$\Gamma_{63} D^*(2010)^- \pi^+ \pi^+ \pi^- \pi^0$	( 1.76 ± 0.27 ) %	
$\Gamma_{64} D^{*-} 3\pi^+ 2\pi^-$	( 4.7 ± 0.9 ) × 10 <sup>-3</sup>	
$\Gamma_{65} D^*(2010)^- \omega \pi^+$	( 2.46 ± 0.18 ) × 10 <sup>-3</sup>	S=1.2
$\Gamma_{66} \bar{D}_1(2430)^0 \omega, \bar{D}_1^0 \rightarrow D^{*-} \pi^+$	( 2.7 ± 0.8 / 0.4 ) × 10 <sup>-4</sup>	
$\Gamma_{67} D^{*-} \rho(1450)^+, \rho^+ \rightarrow \omega \pi^+$	( 1.07 ± 0.40 / 0.34 ) × 10 <sup>-3</sup>	
$\Gamma_{68} \bar{D}_1(2420)^0 \omega, \bar{D}_1^0 \rightarrow D^{*-} \pi^+$	( 7.0 ± 2.2 ) × 10 <sup>-5</sup>	
$\Gamma_{69} \bar{D}_2^*(2460)^0 \omega, \bar{D}_2^0 \rightarrow D^{*-} \pi^+$	( 4.0 ± 1.4 ) × 10 <sup>-5</sup>	
$\Gamma_{70} D^{*-} b_1(1235)^+, b_1^+ \rightarrow \omega \pi^+$	< 7 × 10 <sup>-5</sup>	CL=90%
$\Gamma_{71} \bar{D}^{*-} \pi^+$	[b] ( 1.9 ± 0.9 ) × 10 <sup>-3</sup>	
$\Gamma_{72} D_1(2420)^- \pi^+, D_1^- \rightarrow D^{*-} \pi^+$	( 9.9 ± 2.0 / 2.5 ) × 10 <sup>-5</sup>	
$\Gamma_{73} D_1(2420)^- \pi^+, D_1^- \rightarrow D^{*-} \pi^+ \pi^-$	< 3.3 × 10 <sup>-5</sup>	CL=90%
$\Gamma_{74} \bar{D}_2^*(2460)^- \pi^+, (D_2^*)^- \rightarrow D^{*0} \pi^-$	( 2.38 ± 0.16 ) × 10 <sup>-4</sup>	
$\Gamma_{75} \bar{D}_0^*(2400)^- \pi^+, (D_0^*)^- \rightarrow D^{*0} \pi^-$	( 7.6 ± 0.8 ) × 10 <sup>-5</sup>	
$\Gamma_{76} D_2^*(2460)^- \pi^+, (D_2^*)^- \rightarrow D^{*0} \pi^-$	< 2.4 × 10 <sup>-5</sup>	CL=90%
$\Gamma_{77} \bar{D}_2^*(2460)^- \rho^+$	< 4.9 × 10 <sup>-3</sup>	CL=90%
$\Gamma_{78} D^0 \bar{D}^0$	( 1.4 ± 0.7 ) × 10 <sup>-5</sup>	
$\Gamma_{79} D^{*0} \bar{D}^0$	< 2.9 × 10 <sup>-4</sup>	CL=90%
$\Gamma_{80} D^- D^+$	( 2.11 ± 0.18 ) × 10 <sup>-4</sup>	
$\Gamma_{81} D^\pm D^{*\mp}$ ( $CP$ -averaged)	( 6.1 ± 0.6 ) × 10 <sup>-4</sup>	
$\Gamma_{82} D^- D_s^+$	( 7.2 ± 0.8 ) × 10 <sup>-3</sup>	
$\Gamma_{83} D^*(2010)^- D_s^+$	( 8.0 ± 1.1 ) × 10 <sup>-3</sup>	
$\Gamma_{84} D^- D_s^{*+}$	( 7.4 ± 1.6 ) × 10 <sup>-3</sup>	
$\Gamma_{85} D^*(2010)^- D_s^{*+}$	( 1.77 ± 0.14 ) %	
$\Gamma_{86} D_{s0}(2317)^- K^+, D_{s0}^- \rightarrow D_s^- \pi^0$	( 4.2 ± 1.4 ) × 10 <sup>-5</sup>	
$\Gamma_{87} D_{s0}(2317)^- \pi^+, D_{s0}^- \rightarrow D_s^- \pi^0$	< 2.5 × 10 <sup>-5</sup>	CL=90%
$\Gamma_{88} D_{s,J}(2457)^- K^+, D_{s,J}^- \rightarrow D_s^- \pi^0$	< 9.4 × 10 <sup>-6</sup>	CL=90%
$\Gamma_{89} D_{s,J}(2457)^- \pi^+, D_{s,J}^- \rightarrow D_s^- \pi^0$	< 4.0 × 10 <sup>-6</sup>	CL=90%
$\Gamma_{90} D_s^- D_s^+$	< 3.6 × 10 <sup>-5</sup>	CL=90%
$\Gamma_{91} D_s^{*-} D_s^+$	< 1.3 × 10 <sup>-4</sup>	CL=90%
$\Gamma_{92} D_s^{*0} D_s^{*+}$	< 2.4 × 10 <sup>-4</sup>	CL=90%
$\Gamma_{93} D_{s0}^+(2317)^+ D^-, D_{s0}^+ \rightarrow D_s^+ \pi^0$	( 1.06 ± 0.16 ) × 10 <sup>-3</sup>	S=1.1





# Meson Particle Listings

## B<sup>0</sup>

Light unflavored meson modes		
Γ <sub>335</sub> K*(892) <sup>+</sup> ρ <sup>-</sup>	( 1.03 ± 0.26 ) × 10 <sup>-5</sup>	
Γ <sub>336</sub> K <sub>S</sub> <sup>0</sup> (1430) <sup>+</sup> ρ <sup>-</sup>	( 2.8 ± 1.2 ) × 10 <sup>-5</sup>	
Γ <sub>337</sub> K <sub>1</sub> (1400) <sup>0</sup> ρ <sup>0</sup>	< 3.0 × 10 <sup>-3</sup>	CL=90%
Γ <sub>338</sub> K <sub>S</sub> <sup>0</sup> (1430) <sup>0</sup> ρ <sup>0</sup>	( 2.7 ± 0.6 ) × 10 <sup>-5</sup>	
Γ <sub>339</sub> K <sub>S</sub> <sup>0</sup> (1430) <sup>0</sup> f <sub>0</sub> (980), f <sub>0</sub> → ππ	( 2.7 ± 0.9 ) × 10 <sup>-6</sup>	
Γ <sub>340</sub> K <sub>S</sub> <sup>0</sup> (1430) <sup>0</sup> f <sub>0</sub> (980), f <sub>0</sub> → ππ	( 8.6 ± 2.0 ) × 10 <sup>-6</sup>	
Γ <sub>341</sub> K <sup>+</sup> K <sup>-</sup>	( 7.8 ± 1.5 ) × 10 <sup>-8</sup>	
Γ <sub>342</sub> K <sup>0</sup> K <sup>0</sup>	( 1.21 ± 0.16 ) × 10 <sup>-6</sup>	
Γ <sub>343</sub> K <sup>0</sup> K <sup>-</sup> π <sup>+</sup>	( 6.7 ± 0.5 ) × 10 <sup>-6</sup>	
Γ <sub>344</sub> K*(892) <sup>±</sup> K <sup>∓</sup>	< 4 × 10 <sup>-7</sup>	CL=90%
Γ <sub>345</sub> K <sup>0</sup> K <sup>0</sup> + K* <sup>0</sup> K <sup>0</sup>	< 9.6 × 10 <sup>-7</sup>	CL=90%
Γ <sub>346</sub> K <sup>+</sup> K <sup>-</sup> π <sup>0</sup>	( 2.2 ± 0.6 ) × 10 <sup>-6</sup>	
Γ <sub>347</sub> K <sub>S</sub> <sup>0</sup> K <sub>S</sub> <sup>0</sup> π <sup>0</sup>	< 9 × 10 <sup>-7</sup>	CL=90%
Γ <sub>348</sub> K <sub>S</sub> <sup>0</sup> K <sub>S</sub> <sup>0</sup> η	< 1.0 × 10 <sup>-6</sup>	CL=90%
Γ <sub>349</sub> K <sub>S</sub> <sup>0</sup> K <sub>S</sub> <sup>0</sup> η'	< 2.0 × 10 <sup>-6</sup>	CL=90%
Γ <sub>350</sub> K <sup>0</sup> K <sup>+</sup> K <sup>-</sup>	( 2.68 ± 0.11 ) × 10 <sup>-5</sup>	
Γ <sub>351</sub> K <sup>0</sup> φ	( 7.3 ± 0.7 ) × 10 <sup>-6</sup>	
Γ <sub>352</sub> f <sub>0</sub> (980)K <sup>0</sup> , f <sub>0</sub> → K <sup>+</sup> K <sup>-</sup>	( 7.0 ± 3.5 / 3.0 ) × 10 <sup>-6</sup>	
Γ <sub>353</sub> f <sub>0</sub> (1500)K <sup>0</sup>	( 1.3 ± 0.7 / 0.5 ) × 10 <sup>-5</sup>	
Γ <sub>354</sub> f <sub>2</sub> (1525) <sup>0</sup> K <sup>0</sup>	( 3 ± 5 / 4 ) × 10 <sup>-7</sup>	
Γ <sub>355</sub> f <sub>0</sub> (1710)K <sup>0</sup> , f <sub>0</sub> → K <sup>+</sup> K <sup>-</sup>	( 4.4 ± 0.9 ) × 10 <sup>-6</sup>	
Γ <sub>356</sub> K <sup>0</sup> K <sup>+</sup> K <sup>-</sup> nonresonant	( 3.3 ± 1.0 ) × 10 <sup>-5</sup>	
Γ <sub>357</sub> K <sub>S</sub> <sup>0</sup> K <sub>S</sub> <sup>0</sup> K <sub>S</sub> <sup>0</sup>	( 6.0 ± 0.5 ) × 10 <sup>-6</sup>	S=1.1
Γ <sub>358</sub> f <sub>0</sub> (980)K <sup>0</sup> , f <sub>0</sub> → K <sub>S</sub> <sup>0</sup> K <sub>S</sub> <sup>0</sup>	( 2.7 ± 1.8 ) × 10 <sup>-6</sup>	
Γ <sub>359</sub> f <sub>0</sub> (1710)K <sup>0</sup> , f <sub>0</sub> → K <sub>S</sub> <sup>0</sup> K <sub>S</sub> <sup>0</sup>	( 5.0 ± 5.0 / 2.6 ) × 10 <sup>-7</sup>	
Γ <sub>360</sub> f <sub>2</sub> (2010)K <sup>0</sup> , f <sub>2</sub> → K <sub>S</sub> <sup>0</sup> K <sub>S</sub> <sup>0</sup>	( 5 ± 6 ) × 10 <sup>-7</sup>	
Γ <sub>361</sub> K <sub>S</sub> <sup>0</sup> K <sub>S</sub> <sup>0</sup> K <sub>S</sub> <sup>0</sup> nonresonant	( 1.33 ± 0.31 ) × 10 <sup>-5</sup>	
Γ <sub>362</sub> K <sub>S</sub> <sup>0</sup> K <sub>S</sub> <sup>0</sup> K <sub>L</sub> <sup>0</sup>	< 1.6 × 10 <sup>-5</sup>	CL=90%
Γ <sub>363</sub> K*(892) <sup>0</sup> K <sup>+</sup> K <sup>-</sup>	( 2.75 ± 0.26 ) × 10 <sup>-5</sup>	
Γ <sub>364</sub> K*(892) <sup>0</sup> φ	( 1.00 ± 0.05 ) × 10 <sup>-5</sup>	
Γ <sub>365</sub> K <sup>+</sup> K <sup>-</sup> π <sup>+</sup> π <sup>-</sup> nonresonant	< 7.17 × 10 <sup>-5</sup>	CL=90%
Γ <sub>366</sub> K*(892) <sup>0</sup> K <sup>-</sup> π <sup>+</sup>	( 4.5 ± 1.3 ) × 10 <sup>-6</sup>	
Γ <sub>367</sub> K*(892) <sup>0</sup> K <sup>+</sup> π <sup>-</sup>	( 8.3 ± 2.4 ) × 10 <sup>-7</sup>	S=1.5
Γ <sub>368</sub> K <sup>+</sup> K <sup>+</sup> π <sup>-</sup> π <sup>-</sup> nonresonant	< 6.0 × 10 <sup>-6</sup>	CL=90%
Γ <sub>369</sub> K*(892) <sup>0</sup> K <sup>+</sup> π <sup>-</sup>	< 2.2 × 10 <sup>-6</sup>	CL=90%
Γ <sub>370</sub> K*(892) <sup>0</sup> K*(892) <sup>0</sup>	< 2 × 10 <sup>-7</sup>	CL=90%
Γ <sub>371</sub> K*(892) <sup>+</sup> K*(892) <sup>-</sup>	< 2.0 × 10 <sup>-6</sup>	CL=90%
Γ <sub>372</sub> K <sub>1</sub> (1400) <sup>0</sup> φ	< 5.0 × 10 <sup>-3</sup>	CL=90%
Γ <sub>373</sub> φ(Kπ) <sup>0</sup>	( 4.3 ± 0.4 ) × 10 <sup>-6</sup>	
Γ <sub>374</sub> φ(Kπ) <sup>0</sup> (1.60 < m <sub>Kπ</sub> < 2.15) [f]	< 1.7 × 10 <sup>-6</sup>	CL=90%
Γ <sub>375</sub> K <sub>S</sub> <sup>0</sup> (1430) <sup>0</sup> K <sup>-</sup> π <sup>+</sup>	< 3.18 × 10 <sup>-5</sup>	CL=90%
Γ <sub>376</sub> K <sub>S</sub> <sup>0</sup> (1430) <sup>0</sup> K <sup>+</sup> π <sup>-</sup>	< 3.3 × 10 <sup>-6</sup>	CL=90%
Γ <sub>377</sub> K <sub>S</sub> <sup>0</sup> (1430) <sup>0</sup> K <sub>S</sub> <sup>0</sup> (1430) <sup>0</sup>	< 8.4 × 10 <sup>-6</sup>	CL=90%
Γ <sub>378</sub> K <sub>S</sub> <sup>0</sup> (1430) <sup>0</sup> φ	( 3.9 ± 0.8 ) × 10 <sup>-6</sup>	
Γ <sub>379</sub> K <sub>S</sub> <sup>0</sup> (1430) <sup>0</sup> K*(892) <sup>0</sup>	< 1.7 × 10 <sup>-6</sup>	CL=90%
Γ <sub>380</sub> K <sub>S</sub> <sup>0</sup> (1430) <sup>0</sup> K <sub>S</sub> <sup>0</sup> (1430) <sup>0</sup>	< 4.7 × 10 <sup>-6</sup>	CL=90%
Γ <sub>381</sub> K*(1680) <sup>0</sup> φ	< 3.5 × 10 <sup>-6</sup>	CL=90%
Γ <sub>382</sub> K*(1780) <sup>0</sup> φ	< 2.7 × 10 <sup>-6</sup>	CL=90%
Γ <sub>383</sub> K*(2045) <sup>0</sup> φ	< 1.53 × 10 <sup>-5</sup>	CL=90%
Γ <sub>384</sub> K <sub>S</sub> <sup>0</sup> (1430) <sup>0</sup> ρ <sup>0</sup>	< 1.1 × 10 <sup>-3</sup>	CL=90%
Γ <sub>385</sub> K <sub>S</sub> <sup>0</sup> (1430) <sup>0</sup> φ	( 6.8 ± 0.9 ) × 10 <sup>-6</sup>	S=1.2
Γ <sub>386</sub> K <sup>0</sup> φφ	( 4.5 ± 0.9 ) × 10 <sup>-6</sup>	
Γ <sub>387</sub> η'η'K <sup>0</sup>	< 3.1 × 10 <sup>-5</sup>	CL=90%
Γ <sub>388</sub> ηK <sup>0</sup> γ	( 7.6 ± 1.8 ) × 10 <sup>-6</sup>	
Γ <sub>389</sub> η'K <sup>0</sup> γ	< 6.4 × 10 <sup>-6</sup>	CL=90%
Γ <sub>390</sub> K <sup>0</sup> φγ	( 2.7 ± 0.7 ) × 10 <sup>-6</sup>	
Γ <sub>391</sub> K <sup>+</sup> π <sup>-</sup> γ	( 4.6 ± 1.4 ) × 10 <sup>-6</sup>	
Γ <sub>392</sub> K*(892) <sup>0</sup> γ	( 4.18 ± 0.25 ) × 10 <sup>-5</sup>	S=2.1
Γ <sub>393</sub> K*(1410)γ	< 1.3 × 10 <sup>-4</sup>	CL=90%
Γ <sub>394</sub> K <sup>+</sup> π <sup>-</sup> γ nonresonant	< 2.6 × 10 <sup>-6</sup>	CL=90%
Γ <sub>395</sub> K*(892) <sup>0</sup> X(214), X → μ <sup>+</sup> μ <sup>-</sup> [g]	< 2.26 × 10 <sup>-8</sup>	CL=90%
Γ <sub>396</sub> K <sup>0</sup> π <sup>+</sup> π <sup>-</sup> γ	( 1.99 ± 0.18 ) × 10 <sup>-5</sup>	
Γ <sub>397</sub> K <sup>+</sup> π <sup>-</sup> π <sup>0</sup> γ	( 4.1 ± 0.4 ) × 10 <sup>-5</sup>	
Γ <sub>398</sub> K <sub>1</sub> (1270) <sup>0</sup> γ	< 5.8 × 10 <sup>-5</sup>	CL=90%
Γ <sub>399</sub> K <sub>1</sub> (1400) <sup>0</sup> γ	< 1.2 × 10 <sup>-5</sup>	CL=90%
Γ <sub>400</sub> K <sub>S</sub> <sup>0</sup> (1430) <sup>0</sup> γ	( 1.24 ± 0.24 ) × 10 <sup>-5</sup>	
Γ <sub>401</sub> K*(1680) <sup>0</sup> γ	< 2.0 × 10 <sup>-3</sup>	CL=90%
Γ <sub>402</sub> K <sub>S</sub> <sup>0</sup> (1780) <sup>0</sup> γ	< 8.3 × 10 <sup>-5</sup>	CL=90%
Γ <sub>403</sub> K <sub>S</sub> <sup>0</sup> (2045) <sup>0</sup> γ	< 4.3 × 10 <sup>-3</sup>	CL=90%
Γ <sub>404</sub> ρ <sup>0</sup> γ	( 8.6 ± 1.5 ) × 10 <sup>-7</sup>	
Γ <sub>405</sub> ρ <sup>0</sup> X(214), X → μ <sup>+</sup> μ <sup>-</sup> [g]	< 1.73 × 10 <sup>-8</sup>	CL=90%
Γ <sub>406</sub> ωγ	( 4.4 ± 1.8 / 1.6 ) × 10 <sup>-7</sup>	
Γ <sub>407</sub> φγ	< 1.0 × 10 <sup>-7</sup>	CL=90%
Γ <sub>408</sub> π <sup>+</sup> π <sup>-</sup>	( 5.12 ± 0.19 ) × 10 <sup>-6</sup>	
Γ <sub>409</sub> π <sup>0</sup> π <sup>0</sup>	( 1.59 ± 0.26 ) × 10 <sup>-6</sup>	S=1.4
Γ <sub>410</sub> ηπ <sup>0</sup>	( 4.1 ± 1.7 ) × 10 <sup>-7</sup>	
Γ <sub>411</sub> ηη	< 1.0 × 10 <sup>-6</sup>	CL=90%
Γ <sub>412</sub> η'π <sup>0</sup>	( 1.2 ± 0.6 ) × 10 <sup>-6</sup>	S=1.7
Γ <sub>413</sub> η'η'	< 1.7 × 10 <sup>-6</sup>	CL=90%
Γ <sub>414</sub> η'η	< 1.2 × 10 <sup>-6</sup>	CL=90%
Γ <sub>415</sub> η'ρ <sup>0</sup>	< 1.3 × 10 <sup>-6</sup>	CL=90%
Γ <sub>416</sub> η'f <sub>0</sub> (980), f <sub>0</sub> → π <sup>+</sup> π <sup>-</sup>	< 9 × 10 <sup>-7</sup>	CL=90%
Γ <sub>417</sub> ηρ <sup>0</sup>	< 1.5 × 10 <sup>-6</sup>	CL=90%
Γ <sub>418</sub> ηf <sub>0</sub> (980), f <sub>0</sub> → π <sup>+</sup> π <sup>-</sup>	< 4 × 10 <sup>-7</sup>	CL=90%
Γ <sub>419</sub> ωη	( 9.4 ± 4.0 / 3.1 ) × 10 <sup>-7</sup>	
Γ <sub>420</sub> ωη'	( 1.0 ± 0.5 / 0.4 ) × 10 <sup>-6</sup>	
Γ <sub>421</sub> ωρ <sup>0</sup>	< 1.6 × 10 <sup>-6</sup>	CL=90%
Γ <sub>422</sub> ωf <sub>0</sub> (980), f <sub>0</sub> → π <sup>+</sup> π <sup>-</sup>	< 1.5 × 10 <sup>-6</sup>	CL=90%
Γ <sub>423</sub> ωω	( 1.2 ± 0.4 ) × 10 <sup>-6</sup>	
Γ <sub>424</sub> φπ <sup>0</sup>	< 1.5 × 10 <sup>-7</sup>	CL=90%
Γ <sub>425</sub> φη	< 5 × 10 <sup>-7</sup>	CL=90%
Γ <sub>426</sub> φη'	< 5 × 10 <sup>-7</sup>	CL=90%
Γ <sub>427</sub> φπ <sup>+</sup> π <sup>-</sup>	( 1.8 ± 0.5 ) × 10 <sup>-7</sup>	
Γ <sub>428</sub> φρ <sup>0</sup>	< 3.3 × 10 <sup>-7</sup>	CL=90%
Γ <sub>429</sub> φf <sub>0</sub> (980), f <sub>0</sub> → π <sup>+</sup> π <sup>-</sup>	< 3.8 × 10 <sup>-7</sup>	CL=90%
Γ <sub>430</sub> φω	< 7 × 10 <sup>-7</sup>	CL=90%
Γ <sub>431</sub> φφ	< 2.7 × 10 <sup>-8</sup>	CL=90%
Γ <sub>432</sub> a <sub>0</sub> (980)π <sup>±</sup> π <sup>∓</sup> , a <sub>0</sub> <sup>±</sup> → ηπ <sup>±</sup>	< 3.1 × 10 <sup>-6</sup>	CL=90%
Γ <sub>433</sub> a <sub>0</sub> (1450)π <sup>±</sup> π <sup>∓</sup> , a <sub>0</sub> <sup>±</sup> → ηπ <sup>±</sup>	< 2.3 × 10 <sup>-6</sup>	CL=90%
Γ <sub>434</sub> π <sup>+</sup> π <sup>-</sup> π <sup>0</sup>	< 7.2 × 10 <sup>-4</sup>	CL=90%
Γ <sub>435</sub> ρ <sup>0</sup> π <sup>0</sup>	( 2.0 ± 0.5 ) × 10 <sup>-6</sup>	
Γ <sub>436</sub> ρ <sup>∓</sup> π <sup>±</sup>	[h] ( 2.30 ± 0.23 ) × 10 <sup>-5</sup>	
Γ <sub>437</sub> π <sup>+</sup> π <sup>-</sup> π <sup>+</sup> π <sup>-</sup>	< 1.12 × 10 <sup>-5</sup>	CL=90%
Γ <sub>438</sub> ρ <sup>0</sup> π <sup>+</sup> π <sup>-</sup>	< 8.8 × 10 <sup>-6</sup>	CL=90%
Γ <sub>439</sub> ρ <sup>0</sup> ρ <sup>0</sup>	( 9.6 ± 1.5 ) × 10 <sup>-7</sup>	
Γ <sub>440</sub> f <sub>0</sub> (980)π <sup>+</sup> π <sup>-</sup> , f <sub>0</sub> → π <sup>+</sup> π <sup>-</sup>	< 3.0 × 10 <sup>-6</sup>	CL=90%
Γ <sub>441</sub> ρ <sup>0</sup> f <sub>0</sub> (980), f <sub>0</sub> → π <sup>+</sup> π <sup>-</sup>	( 7.8 ± 2.5 ) × 10 <sup>-7</sup>	
Γ <sub>442</sub> f <sub>0</sub> (980)f <sub>0</sub> (980), f <sub>0</sub> → π <sup>+</sup> π <sup>-</sup> , f <sub>0</sub> → π <sup>+</sup> π <sup>-</sup>	< 1.9 × 10 <sup>-7</sup>	CL=90%
Γ <sub>443</sub> f <sub>0</sub> (980)f <sub>0</sub> (980), f <sub>0</sub> → π <sup>+</sup> π <sup>-</sup> , f <sub>0</sub> → K <sup>+</sup> K <sup>-</sup>	< 2.3 × 10 <sup>-7</sup>	CL=90%
Γ <sub>444</sub> a <sub>1</sub> (1260)π <sup>±</sup> π <sup>±</sup>	[h] ( 2.6 ± 0.5 ) × 10 <sup>-5</sup>	S=1.9
Γ <sub>445</sub> a <sub>2</sub> (1320)π <sup>±</sup> π <sup>±</sup>	[h] < 6.3 × 10 <sup>-6</sup>	CL=90%
Γ <sub>446</sub> π <sup>+</sup> π <sup>-</sup> π <sup>0</sup> π <sup>0</sup>	< 3.1 × 10 <sup>-3</sup>	CL=90%
Γ <sub>447</sub> ρ <sup>+</sup> ρ <sup>-</sup>	( 2.77 ± 0.19 ) × 10 <sup>-5</sup>	
Γ <sub>448</sub> a <sub>1</sub> (1260) <sup>0</sup> π <sup>0</sup>	< 1.1 × 10 <sup>-3</sup>	CL=90%
Γ <sub>449</sub> ωπ <sup>0</sup>	< 5 × 10 <sup>-7</sup>	CL=90%
Γ <sub>450</sub> π <sup>+</sup> π <sup>+</sup> π <sup>-</sup> π <sup>-</sup> π <sup>0</sup>	< 9.0 × 10 <sup>-3</sup>	CL=90%
Γ <sub>451</sub> a <sub>1</sub> (1260) <sup>+</sup> ρ <sup>-</sup>	< 6.1 × 10 <sup>-5</sup>	CL=90%
Γ <sub>452</sub> a <sub>1</sub> (1260) <sup>0</sup> ρ <sup>0</sup>	< 2.4 × 10 <sup>-3</sup>	CL=90%
Γ <sub>453</sub> b <sub>1</sub> <sup>∓</sup> π <sup>±</sup> , b <sub>1</sub> <sup>∓</sup> → ωπ <sup>∓</sup>	( 1.09 ± 0.15 ) × 10 <sup>-5</sup>	
Γ <sub>454</sub> b <sub>1</sub> <sup>0</sup> π <sup>0</sup> , b <sub>1</sub> <sup>0</sup> → ωπ <sup>0</sup>	< 1.9 × 10 <sup>-6</sup>	CL=90%
Γ <sub>455</sub> b <sub>1</sub> <sup>-</sup> ρ <sup>+</sup> , b <sub>1</sub> <sup>-</sup> → ωπ <sup>-</sup>	< 1.4 × 10 <sup>-6</sup>	CL=90%
Γ <sub>456</sub> b <sub>1</sub> <sup>0</sup> ρ <sup>0</sup> , b <sub>1</sub> <sup>0</sup> → ωπ <sup>0</sup>	< 3.4 × 10 <sup>-6</sup>	CL=90%
Γ <sub>457</sub> π <sup>+</sup> π <sup>+</sup> π <sup>+</sup> π <sup>-</sup> π <sup>-</sup> π <sup>-</sup>	< 3.0 × 10 <sup>-3</sup>	CL=90%
Γ <sub>458</sub> a <sub>1</sub> (1260) <sup>+</sup> a <sub>1</sub> (1260) <sup>-</sup> , a <sub>1</sub> <sup>+</sup> → 2π <sup>+</sup> π <sup>-</sup> , a <sub>1</sub> <sup>-</sup> → 2π <sup>-</sup> π <sup>+</sup>	( 1.18 ± 0.31 ) × 10 <sup>-5</sup>	
Γ <sub>459</sub> π <sup>+</sup> π <sup>+</sup> π <sup>+</sup> π <sup>-</sup> π <sup>-</sup> π <sup>-</sup> π <sup>0</sup>	< 1.1 %	CL=90%
Baryon modes		
Γ <sub>460</sub> p p̄	( 1.25 ± 0.32 ) × 10 <sup>-8</sup>	
Γ <sub>461</sub> p p̄π <sup>+</sup> π <sup>-</sup>	( 2.87 ± 0.19 ) × 10 <sup>-6</sup>	
Γ <sub>462</sub> p p̄K <sup>+</sup> K <sup>-</sup>	( 6.3 ± 0.5 ) × 10 <sup>-6</sup>	
Γ <sub>463</sub> p p̄K <sup>0</sup>	( 2.66 ± 0.32 ) × 10 <sup>-6</sup>	
Γ <sub>464</sub> Θ(1540) <sup>+</sup> p̄, Θ <sup>+</sup> → pK <sub>S</sub> <sup>0</sup> [l]	< 5 × 10 <sup>-8</sup>	CL=90%
Γ <sub>465</sub> f <sub>J</sub> (2220)K <sup>0</sup> , f <sub>J</sub> → p p̄	< 4.5 × 10 <sup>-7</sup>	CL=90%
Γ <sub>466</sub> p p̄K*(892) <sup>0</sup>	( 1.24 ± 0.28 / 0.25 ) × 10 <sup>-6</sup>	
Γ <sub>467</sub> f <sub>J</sub> (2220)K <sub>S</sub> <sup>0</sup> , f <sub>J</sub> → p p̄	< 1.5 × 10 <sup>-7</sup>	CL=90%
Γ <sub>468</sub> p p̄K <sup>+</sup> K <sup>-</sup>	( 1.21 ± 0.32 ) × 10 <sup>-7</sup>	
Γ <sub>469</sub> p p̄π <sup>0</sup>	( 5.0 ± 1.9 ) × 10 <sup>-7</sup>	

Downloaded from https://academic.oup.com/ptep/article/2020/8/083C01/5891211 by guest on 12 November 2020

See key on page 999

Meson Particle Listings

$B^0$

$\Gamma_{470}$	$p\bar{p}\bar{p}$	$< 2.0 \times 10^{-7}$	CL=90%
$\Gamma_{471}$	$p\bar{\Lambda}\pi^-$	$(3.14 \pm 0.29) \times 10^{-6}$	
$\Gamma_{472}$	$p\bar{\Lambda}\pi^-\gamma$	$< 6.5 \times 10^{-7}$	CL=90%
$\Gamma_{473}$	$p\bar{\Sigma}^-(1385)^-$	$< 2.6 \times 10^{-7}$	CL=90%
$\Gamma_{474}$	$\Delta(1232)^+\bar{p} + \Delta(1232)^-\rho$	$< 1.6 \times 10^{-6}$	
$\Gamma_{475}$	$\Delta^0\bar{\Lambda}$	$< 9.3 \times 10^{-7}$	CL=90%
$\Gamma_{476}$	$p\bar{\Lambda}K^-$	$< 8.2 \times 10^{-7}$	CL=90%
$\Gamma_{477}$	$p\bar{\Lambda}D^-$	$(2.5 \pm 0.4) \times 10^{-5}$	
$\Gamma_{478}$	$p\bar{\Lambda}D^{*-}$	$(3.4 \pm 0.8) \times 10^{-5}$	
$\Gamma_{479}$	$p\bar{\Sigma}^0\pi^-$	$< 3.8 \times 10^{-6}$	CL=90%
$\Gamma_{480}$	$\bar{\Lambda}\Lambda$	$< 3.2 \times 10^{-7}$	CL=90%
$\Gamma_{481}$	$\bar{\Lambda}\Lambda K^0$	$(4.8 \pm 1.0 \pm 0.9) \times 10^{-6}$	
$\Gamma_{482}$	$\bar{\Lambda}\Lambda K^{*0}$	$(2.5 \pm 0.9) \times 10^{-6}$	
$\Gamma_{483}$	$\bar{\Lambda}\Lambda D^0$	$(1.00 \pm 0.30 \pm 0.26) \times 10^{-5}$	
$\Gamma_{484}$	$D^0\Sigma^0\bar{\Lambda} + c.c.$	$< 3.1 \times 10^{-5}$	CL=90%
$\Gamma_{485}$	$\Delta^0\bar{\Delta}^0$	$< 1.5 \times 10^{-3}$	CL=90%
$\Gamma_{486}$	$\Delta^{++}\bar{\Delta}^{--}$	$< 1.1 \times 10^{-4}$	CL=90%
$\Gamma_{487}$	$\bar{D}^0 p\bar{p}$	$(1.04 \pm 0.07) \times 10^{-4}$	
$\Gamma_{488}$	$D_c^-\bar{\Lambda}p$	$(2.8 \pm 0.9) \times 10^{-5}$	
$\Gamma_{489}$	$\bar{D}^*(2007)^0 p\bar{p}$	$(9.9 \pm 1.1) \times 10^{-5}$	
$\Gamma_{490}$	$D^*(2010)^-\rho\bar{p}$	$(1.4 \pm 0.4) \times 10^{-3}$	
$\Gamma_{491}$	$D^-\rho\bar{p}\pi^+$	$(3.32 \pm 0.31) \times 10^{-4}$	
$\Gamma_{492}$	$D^*(2010)^-\rho\bar{p}\pi^+$	$(4.7 \pm 0.5) \times 10^{-4}$	S=1.2
$\Gamma_{493}$	$\bar{D}^0 p\bar{p}\pi^+\pi^-$	$(3.0 \pm 0.5) \times 10^{-4}$	
$\Gamma_{494}$	$\bar{D}^{*0} p\bar{p}\pi^+\pi^-$	$(1.9 \pm 0.5) \times 10^{-4}$	
$\Gamma_{495}$	$\Theta_c\bar{p}\pi^+, \Theta_c \rightarrow D^-p$	$< 9 \times 10^{-6}$	CL=90%
$\Gamma_{496}$	$\Theta_c\bar{p}\pi^+, \Theta_c \rightarrow D^{*-}p$	$< 1.4 \times 10^{-5}$	CL=90%
$\Gamma_{497}$	$\bar{\Sigma}_c^-\Delta^{++}$	$< 8 \times 10^{-4}$	CL=90%
$\Gamma_{498}$	$\bar{\Lambda}_c^-\rho\pi^+\pi^-$	$(1.02 \pm 0.14) \times 10^{-3}$	S=1.3
$\Gamma_{499}$	$\bar{\Lambda}_c^-\rho$	$(1.54 \pm 0.18) \times 10^{-5}$	
$\Gamma_{500}$	$\bar{\Lambda}_c^-\rho\pi^0$	$(1.55 \pm 0.19) \times 10^{-4}$	
$\Gamma_{501}$	$\bar{\Sigma}_c(2455)^-\rho$	$< 2.4 \times 10^{-5}$	
$\Gamma_{502}$	$\bar{\Lambda}_c^-\rho\pi^+\pi^-\pi^0$	$< 5.07 \times 10^{-3}$	CL=90%
$\Gamma_{503}$	$\bar{\Lambda}_c^-\rho\pi^+\pi^-\pi^+\pi^-$	$< 2.74 \times 10^{-3}$	CL=90%
$\Gamma_{504}$	$\bar{\Lambda}_c^-\rho\pi^+\pi^-$ (nonresonant)	$(5.5 \pm 1.0) \times 10^{-4}$	S=1.3
$\Gamma_{505}$	$\bar{\Sigma}_c(2520)^-\rho\pi^+$	$(1.02 \pm 0.18) \times 10^{-4}$	
$\Gamma_{506}$	$\bar{\Sigma}_c(2520)^0\rho\pi^-$	$< 3.1 \times 10^{-5}$	CL=90%
$\Gamma_{507}$	$\bar{\Sigma}_c(2455)^0\rho\pi^-$	$(1.08 \pm 0.16) \times 10^{-4}$	
$\Gamma_{508}$	$\bar{\Sigma}_c(2455)^0 N^0, N^0 \rightarrow \rho\pi^-$	$(6.4 \pm 1.7) \times 10^{-5}$	
$\Gamma_{509}$	$\bar{\Sigma}_c(2455)^-\rho\pi^+$	$(1.83 \pm 0.24) \times 10^{-4}$	
$\Gamma_{510}$	$\bar{\Lambda}_c^-\rho K^+\pi^-$	$(3.4 \pm 0.7) \times 10^{-5}$	
$\Gamma_{511}$	$\bar{\Sigma}_c(2455)^-\rho K^+, \bar{\Sigma}_c^{*-} \rightarrow \bar{\Lambda}_c^-\pi^-$	$(8.8 \pm 2.5) \times 10^{-6}$	
$\Gamma_{512}$	$\bar{\Lambda}_c^-\rho K^*(892)^0$	$< 2.42 \times 10^{-5}$	CL=90%
$\Gamma_{513}$	$\bar{\Lambda}_c^-\rho K^+K^-$	$(2.0 \pm 0.4) \times 10^{-5}$	
$\Gamma_{514}$	$\bar{\Lambda}_c^-\rho\phi$	$< 1.0 \times 10^{-5}$	CL=90%
$\Gamma_{515}$	$\bar{\Lambda}_c^-\rho\bar{p}p$	$< 2.8 \times 10^{-6}$	
$\Gamma_{516}$	$\bar{\Lambda}_c^-\Lambda K^+$	$(4.8 \pm 1.1) \times 10^{-5}$	
$\Gamma_{517}$	$\bar{\Lambda}_c^-\Lambda_c^+$	$< 1.6 \times 10^{-5}$	CL=95%
$\Gamma_{518}$	$\bar{\Lambda}_c^-(2593)^- / \bar{\Lambda}_c^-(2625)^-\rho$	$< 1.1 \times 10^{-4}$	CL=90%
$\Gamma_{519}$	$\bar{\Xi}_c^-\Lambda_c^+$	$(1.2 \pm 0.8) \times 10^{-3}$	
$\Gamma_{520}$	$\bar{\Xi}_c^-\Lambda_c^+, \bar{\Xi}_c^- \rightarrow \bar{\Xi}^+\pi^-\pi^-$	$(2.4 \pm 1.1) \times 10^{-5}$	S=1.8
$\Gamma_{521}$	$\bar{\Xi}_c^-\Lambda_c^+, \bar{\Xi}_c^- \rightarrow \bar{p}K^+\pi^-$	$(5.3 \pm 1.7) \times 10^{-6}$	
$\Gamma_{522}$	$\bar{\Xi}_c^-\Lambda_c^+ K^0$	$(4.0 \pm 0.9) \times 10^{-4}$	
$\Gamma_{523}$	$\bar{\Xi}_c^-(2930)^-\Lambda_c^+, \bar{\Xi}_c^- \rightarrow \bar{\Lambda}_c^+ K^0$	$(2.4 \pm 0.6) \times 10^{-4}$	

Lepton Family number (LF) or Lepton number (L) or Baryon number (B) violating modes, or/and  $\Delta B = 1$  weak neutral current (BI) modes

$\Gamma_{524}$	$\gamma\gamma$	B1	$< 3.2 \times 10^{-7}$	CL=90%
$\Gamma_{525}$	$e^+e^-$	B1	$< 8.3 \times 10^{-8}$	CL=90%
$\Gamma_{526}$	$e^+e^-\gamma$	B1	$< 1.2 \times 10^{-7}$	CL=90%
$\Gamma_{527}$	$\mu^+\mu^-$	B1	$(1.1 \pm 1.4 \pm 1.3) \times 10^{-10}$	S=1.6
$\Gamma_{528}$	$\mu^+\mu^-\gamma$	B1	$< 1.6 \times 10^{-7}$	CL=90%
$\Gamma_{529}$	$\mu^+\mu^-\mu^+\mu^-$	B1	$< 6.9 \times 10^{-10}$	CL=95%
$\Gamma_{530}$	$SP, S \rightarrow \mu^+\mu^-, P \rightarrow \mu^+\mu^-$	B1 [j]	$< 6.0 \times 10^{-10}$	CL=95%

$\Gamma_{531}$	$\tau^+\tau^-$	B1	$< 2.1 \times 10^{-3}$	CL=95%
$\Gamma_{532}$	$\pi^0\ell^+\ell^-$	B1	$< 5.3 \times 10^{-8}$	CL=90%
$\Gamma_{533}$	$\pi^0e^+e^-$	B1	$< 8.4 \times 10^{-8}$	CL=90%
$\Gamma_{534}$	$\pi^0\mu^+\mu^-$	B1	$< 6.9 \times 10^{-8}$	CL=90%
$\Gamma_{535}$	$\eta\ell^+\ell^-$	B1	$< 6.4 \times 10^{-8}$	CL=90%
$\Gamma_{536}$	$\eta e^+e^-$	B1	$< 1.08 \times 10^{-7}$	CL=90%
$\Gamma_{537}$	$\eta\mu^+\mu^-$	B1	$< 1.12 \times 10^{-7}$	CL=90%
$\Gamma_{538}$	$\pi^0\nu\bar{\nu}$	B1	$< 9 \times 10^{-6}$	CL=90%
$\Gamma_{539}$	$K^0\ell^+\ell^-$	B1 [a]	$(3.1 \pm 0.8 \pm 0.7) \times 10^{-7}$	
$\Gamma_{540}$	$K^0e^+e^-$	B1	$(1.6 \pm 1.0 \pm 0.8) \times 10^{-7}$	
$\Gamma_{541}$	$K^0\mu^+\mu^-$	B1	$(3.39 \pm 0.34) \times 10^{-7}$	
$\Gamma_{542}$	$K^0\nu\bar{\nu}$	B1	$< 2.6 \times 10^{-5}$	CL=90%
$\Gamma_{543}$	$\rho^0\nu\bar{\nu}$	B1	$< 4.0 \times 10^{-5}$	CL=90%
$\Gamma_{544}$	$K^*(892)^0\ell^+\ell^-$	B1 [a]	$(9.9 \pm 1.2 \pm 1.1) \times 10^{-7}$	
$\Gamma_{545}$	$K^*(892)^0e^+e^-$	B1	$(1.03 \pm 0.19 \pm 0.17) \times 10^{-6}$	
$\Gamma_{546}$	$K^*(892)^0\mu^+\mu^-$	B1	$(9.4 \pm 0.5) \times 10^{-7}$	
$\Gamma_{547}$	$K^*(892)^0\chi, \chi \rightarrow \mu^+\mu^-$			
$\Gamma_{548}$	$\pi^+\pi^-\mu^+\mu^-$	B1	$(2.1 \pm 0.5) \times 10^{-8}$	
$\Gamma_{549}$	$K^*(892)^0\nu\bar{\nu}$	B1	$< 1.8 \times 10^{-5}$	CL=90%
$\Gamma_{550}$	invisible	B1	$< 2.4 \times 10^{-5}$	CL=90%
$\Gamma_{551}$	$\nu\bar{\nu}\gamma$	B1	$< 1.7 \times 10^{-5}$	CL=90%
$\Gamma_{552}$	$\phi\nu\bar{\nu}$	B1	$< 1.27 \times 10^{-4}$	CL=90%
$\Gamma_{553}$	$e^\pm\mu^\mp$	LF [h]	$< 1.0 \times 10^{-9}$	CL=90%
$\Gamma_{554}$	$\pi^0e^\pm\mu^\mp$	LF	$< 1.4 \times 10^{-7}$	CL=90%
$\Gamma_{555}$	$K^0e^\pm\mu^\mp$	LF	$< 2.7 \times 10^{-7}$	CL=90%
$\Gamma_{556}$	$K^*(892)^0e^+\mu^-$	LF	$< 1.6 \times 10^{-7}$	CL=90%
$\Gamma_{557}$	$K^*(892)^0e^-\mu^+$	LF	$< 1.2 \times 10^{-7}$	CL=90%
$\Gamma_{558}$	$K^*(892)^0e^\pm\mu^\mp$	LF	$< 1.8 \times 10^{-7}$	CL=90%
$\Gamma_{559}$	$e^\pm\tau^\mp$	LF [h]	$< 2.8 \times 10^{-5}$	CL=90%
$\Gamma_{560}$	$\mu^\pm\tau^\mp$	LF [h]	$< 1.4 \times 10^{-5}$	CL=95%
$\Gamma_{561}$	$\Lambda_c^+\mu^-$	L,B	$< 1.4 \times 10^{-6}$	CL=90%
$\Gamma_{562}$	$\Lambda_c^+e^-$	L,B	$< 4 \times 10^{-6}$	CL=90%

- [a] An  $\ell$  indicates an  $e$  or a  $\mu$  mode, not a sum over these modes.
- [b]  $\bar{D}^{*0}$  represents an excited state with mass  $2.2 < M < 2.8$  GeV/ $c^2$ .
- [c]  $\chi_{c1}(3872)^+$  is a hypothetical charged partner of the  $\chi_{c1}(3872)$ .
- [d] Stands for the possible candidates of  $K^*(1410)$ ,  $K_0^*(1430)$  and  $K_2^*(1430)$ .
- [e]  $B^0$  and  $B_s^0$  contributions not separated. Limit is on weighted average of the two decay rates.
- [f] This decay refers to the coherent sum of resonant and nonresonant  $J^P = 0^+ K\pi$  components with  $1.60 < m_{K\pi} < 2.15$  GeV/ $c^2$ .
- [g]  $X(214)$  is a hypothetical particle of mass 214 MeV/ $c^2$  reported by the HyperCP experiment, Physical Review Letters **94** 021801 (2005)
- [h] The value is for the sum of the charge states or particle/antiparticle states indicated.
- [i]  $\Theta(1540)^+$  denotes a possible narrow pentaquark state.
- [j] Here  $S$  and  $P$  are the hypothetical scalar and pseudoscalar particles with masses of 2.5 GeV/ $c^2$  and 214.3 MeV/ $c^2$ , respectively.

CONSTRAINED FIT INFORMATION

An overall fit to 34 branching ratios uses 89 measurements and one constraint to determine 22 parameters. The overall fit has a  $\chi^2 = 64.3$  for 68 degrees of freedom.

The following off-diagonal array elements are the correlation coefficients  $\langle \delta x_i \delta x_j \rangle / (\delta x_i \delta x_j)$ , in percent, from the fit to the branching fractions,  $x_i \equiv \Gamma_i / \Gamma_{\text{total}}$ . The fit constrains the  $x_i$  whose labels appear in this array to sum to one.



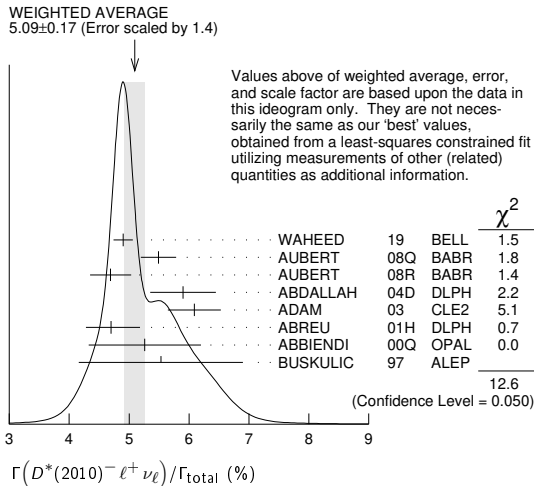
See key on page 999

# Meson Particle Listings

$B^0$

4.5 ± 0.3 ± 0.4	16	ALBRECHT	94	ARG	$e^+e^- \rightarrow \Upsilon(4S)$	
4.7 ± 0.5 ± 0.5	235	17	ALBRECHT	93	ARG	$e^+e^- \rightarrow \Upsilon(4S)$
seen	398	18	SANGHERA	93	CLE2	$e^+e^- \rightarrow \Upsilon(4S)$
7.0 ± 1.8 ± 1.4		19	ANTREASIAN	90B	CBAL	$e^+e^- \rightarrow \Upsilon(4S)$
		20	ALBRECHT	89c	ARG	$e^+e^- \rightarrow \Upsilon(4S)$
6.0 ± 1.0 ± 1.4		21	ALBRECHT	89j	ARG	$e^+e^- \rightarrow \Upsilon(4S)$
4.0 ± 0.4 ± 0.6		22	BORTOLETTO	89B	CLEO	$e^+e^- \rightarrow \Upsilon(4S)$
7.0 ± 1.2 ± 1.9	47	23	ALBRECHT	87j	ARG	$e^+e^- \rightarrow \Upsilon(4S)$

- Uses fully reconstructed  $D^{*-}\ell^+\nu$  events ( $\ell = e$  or  $\mu$ ).
- Uses a fully reconstructed  $B$  meson as a tag on the recoil side.
- Measured using fully reconstructed  $D^*$  sample and a simultaneous fit to the Caprini-Lellouch-Neubert form factor parameters:  $\rho^2 = 1.191 \pm 0.048 \pm 0.028$ ,  $R_1(1) = 1.429 \pm 0.061 \pm 0.044$ , and  $R_2(1) = 0.827 \pm 0.038 \pm 0.022$ .
- Measured using fully reconstructed  $D^*$  sample.
- Uses the combined fit of both  $B^0 \rightarrow D^*(2010)^-\ell\nu$  and  $B^+ \rightarrow \overline{D}(2007)^0\ell\nu$  samples.
- ABREU 01H measured using about 5000 partial reconstructed  $D^*$  sample.
- ABBIENDI 00Q assumes the fraction  $B(b \rightarrow B^0) = (39.7_{-2.2}^{+1.8})\%$ . This result is an average of two methods using exclusive and partial  $D^*$  reconstruction.
- BUSKULIC 97 assumes fraction ( $B^+$ ) = fraction ( $B^0$ ) =  $(37.8 \pm 2.2)\%$  and PDG 96 values for  $B$  lifetime and  $D^*$  and  $D$  branching fractions.
- Combines with previous partial reconstructed  $D^*$  measurement.
- Assumes equal production of  $B^+$  and  $B^0$  at the  $\Upsilon(4S)$ .
- The results are based on the same analysis and data sample reported in ADAM 03.
- ACKERSTAFF 97G assumes fraction ( $B^+$ ) = fraction ( $B^0$ ) =  $(37.8 \pm 2.2)\%$  and PDG 96 values for  $B$  lifetime and branching ratio of  $D^*$  and  $D$  decays.
- ABREU 96P result is the average of two methods using exclusive and partial  $D^*$  reconstruction.
- BARISH 95 use  $B(D^0 \rightarrow K^-\pi^+) = (3.91 \pm 0.08 \pm 0.17)\%$  and  $B(D^{*+} \rightarrow D^0\pi^+) = (68.1 \pm 1.0 \pm 1.3)\%$ .
- BUSKULIC 95N assumes fraction ( $B^+$ ) = fraction ( $B^0$ ) =  $38.2 \pm 1.3 \pm 2.2\%$  and  $\tau_{B^0} = 1.58 \pm 0.06$  ps.  $\Gamma(D^{*-}\ell^+\nu_\ell)/\text{total} = [5.18 - 0.13(\text{fraction}(B^0) - 38.2) - 1.5(\tau_{B^0} - 1.58)]\%$ .
- ALBRECHT 94 assumes  $B(D^{*+} \rightarrow D^0\pi^+) = 68.1 \pm 1.0 \pm 1.3\%$ . Uses partial reconstruction of  $D^{*+}$  and is independent of  $D^0$  branching ratios.
- ALBRECHT 93 reports  $0.052 \pm 0.005 \pm 0.006$ . We rescale using the method described in STONE 94 but with the updated PDG 94  $B(D^0 \rightarrow K^-\pi^+)$ . We have taken their average  $e$  and  $\mu$  value. They also obtain  $\alpha = 2\Gamma^0/(\Gamma^- + \Gamma^+) - 1 = 1.1 \pm 0.4 \pm 0.2$ ,  $A_{AF} = 3/4 * (\Gamma^- - \Gamma^+)/\Gamma = 0.2 \pm 0.08 \pm 0.06$  and a value of  $|V_{cb}| = 0.036 - 0.045$  depending on model assumptions.
- Combining  $\overline{D}^{*0}\ell^+\nu_\ell$  and  $\overline{D}^{*-}\ell^+\nu_\ell$  SANGHERA 93 test  $V-A$  structure and fit the decay angular distributions to obtain  $A_{FB} = 3/4 * (\Gamma^- - \Gamma^+)/\Gamma = 0.14 \pm 0.06 \pm 0.03$ . Assuming a value of  $V_{cb}$ , they measure  $V$ ,  $A_1$ , and  $A_2$ , the three form factors for the  $D^*\ell\nu_\ell$  decay, where results are slightly dependent on model assumptions.
- ANTREASIAN 90B is average over  $B$  and  $\overline{D}^*(2010)$  charge states.
- The measurement of ALBRECHT 89c suggests a  $D^*$  polarization  $\gamma_L/\gamma_T$  of  $0.85 \pm 0.45$ , or  $\alpha = 0.7 \pm 0.9$ .
- ALBRECHT 89j is ALBRECHT 87j value rescaled using  $B(D^*(2010)^- \rightarrow D^0\pi^-) = 0.57 \pm 0.04 \pm 0.04$ . Superseded by ALBRECHT 93.
- We have taken average of the the BORTOLETTO 89B values for electrons and muons,  $0.046 \pm 0.005 \pm 0.007$ . We rescale using the method described in STONE 94 but with the updated PDG 94  $B(D^0 \rightarrow K^-\pi^+)$ . The measurement suggests a  $D^*$  polarization parameter value  $\alpha = 0.65 \pm 0.66 \pm 0.25$ .
- ALBRECHT 87j assume  $\mu$ - $e$  universality, the  $B(\Upsilon(4S) \rightarrow B^0\overline{B}^0) = 0.45$ , the  $B(D^0 \rightarrow K^-\pi^+) = (0.042 \pm 0.004 \pm 0.004)$ , and the  $B(D^*(2010)^- \rightarrow D^0\pi^-) = 0.49 \pm 0.08$ . Superseded by ALBRECHT 89j.



$\Gamma(D^*(2010)^-\ell^+\nu_\ell)/\Gamma(D\ell^+\nu_\ell X)$				$\Gamma_6/\Gamma_3$
VALUE	DOCUMENT ID	TECN	COMMENT	
<b>0.537 ± 0.031 ± 0.036</b>	1	AUBERT	07AN BABR	$e^+e^- \rightarrow \Upsilon(4S)$

<sup>1</sup> Uses a fully reconstructed  $B$  meson on the recoil side.

$\Gamma(D^*(2010)^-\tau^+\nu_\tau)/\Gamma_{\text{total}}$				$\Gamma_7/\Gamma$
VALUE (units $10^{-2}$ )	DOCUMENT ID	TECN	COMMENT	
<b>1.57 ± 0.09 OUR FIT</b>	Error includes scale factor of 1.1.			
<b>1.48 ± 0.18 OUR AVERAGE</b>	Error includes scale factor of 1.1.			
1.42 ± 0.094 ± 0.140	1	AAIJ	18D LHCb	$pp$ at 7, 8 TeV
2.02 <sup>+0.40</sup> <sub>-0.37</sub> ± 0.37	2	MATYJA	07 BELL	$e^+e^- \rightarrow \Upsilon(4S)$
• • • We do not use the following data for averages, fits, limits, etc. • • •				
1.11 ± 0.51 ± 0.06	3	AUBERT	08N BABR	Repl. by AUBERT 09s
<sup>1</sup> Normalizes to $B(B^0 \rightarrow D^*(2010)^-\pi^+\pi^-) = (7.214 \pm 0.28) \times 10^{-3}$ .				
<sup>2</sup> Observed in the recoil of the accompanying $B$ meson.				
<sup>3</sup> Uses a fully reconstructed $B$ meson as a tag on the recoil side.				

$\Gamma(D^*(2010)^-\tau^+\nu_\tau)/\Gamma(D^*(2010)^-\ell^+\nu_\ell)$				$\Gamma_7/\Gamma_6$
VALUE	DOCUMENT ID	TECN	COMMENT	
<b>0.309 ± 0.016 OUR FIT</b>				
<b>0.315 ± 0.018 OUR AVERAGE</b>				
0.291 ± 0.019 ± 0.029	1	AAIJ	18D LHCb	$pp$ at 7, 8 TeV
0.302 ± 0.030 ± 0.011	2	SATO	16B BELL	$e^+e^- \rightarrow \Upsilon(4S)$
0.336 ± 0.027 ± 0.030	3	AAIJ	15Q LHCb	$pp$ at 7, 8 TeV
0.355 ± 0.039 ± 0.021	4.5	LEES	12D BABR	$e^+e^- \rightarrow \Upsilon(4S)$
• • • We do not use the following data for averages, fits, limits, etc. • • •				
0.207 ± 0.095 ± 0.008	4	AUBERT	09s BABR	Repl. by LEES 12d
<sup>1</sup> Uses $\tau^+ \rightarrow \pi^+\pi^-\pi^+\overline{\nu}_\tau$ and $\tau^+ \rightarrow \pi^+\pi^-\pi^0\overline{\nu}_\tau$ , and $\mu^+$ as $\ell^+$ .				
<sup>2</sup> Uses semileptonic $B$ decay events for tagging and $\tau^+ \rightarrow \ell^+\nu_\ell\overline{\nu}_\tau$ mode.				
<sup>3</sup> Uses $\tau^+ \rightarrow \mu^+\nu_\mu\overline{\nu}_\tau$ and $\mu^+$ as $\ell^+$ .				
<sup>4</sup> Uses a fully reconstructed $B$ meson as a tag on the recoil side.				
<sup>5</sup> Uses $\tau^+ \rightarrow e^+\nu_e\overline{\nu}_\tau$ and $\tau^+ \rightarrow \mu^+\nu_\mu\overline{\nu}_\tau$ and $e^+$ or $\mu^+$ as $\ell^+$ .				

$\Gamma(D^*(2010)^-\tau^+\nu_\tau)/\Gamma(D^*(2010)^-\pi^+\pi^-\pi^-)$				$\Gamma_7/\Gamma_{57}$
VALUE	DOCUMENT ID	TECN	COMMENT	
<b>1.97 ± 0.13 ± 0.18</b>	1	AAIJ	18D LHCb	$pp$ at 7, 8 TeV
<sup>1</sup> Uses $\tau^+ \rightarrow \pi^+\pi^-\pi^+\overline{\nu}_\tau$ and $\tau^+ \rightarrow \pi^+\pi^-\pi^0\overline{\nu}_\tau$ modes.				

$\Gamma(\overline{D}^0\pi^-\ell^+\nu_\ell)/\Gamma_{\text{total}}$				$\Gamma_8/\Gamma$
VALUE (units $10^{-3}$ )	DOCUMENT ID	TECN	COMMENT	
<b>4.1 ± 0.5 OUR AVERAGE</b>				
4.05 ± 0.36 ± 0.41		VOSSEN	18 BELL	$e^+e^- \rightarrow \Upsilon(4S)$
4.3 ± 0.8 ± 0.3	1	AUBERT	08Q BABR	$e^+e^- \rightarrow \Upsilon(4S)$
• • • We do not use the following data for averages, fits, limits, etc. • • •				
4.6 ± 0.9 ± 0.2	1,2	LIVENTSEV	08 BELL	Repl. by VOSSEN 18
3.5 ± 1.0 ± 0.1	3	LIVENTSEV	05 BELL	Repl. by LIVENTSEV 08
<sup>1</sup> Uses a fully reconstructed $B$ meson as a tag on the recoil side.				
<sup>2</sup> LIVENTSEV 08 reports $(4.2 \pm 0.7 \pm 0.6) \times 10^{-3}$ from a measurement of $[\Gamma(B^0 \rightarrow \overline{D}^0\pi^-\ell^+\nu_\ell)/\Gamma_{\text{total}}] / [B(B^0 \rightarrow D^-\ell^+\nu_\ell)]$ assuming $B(B^0 \rightarrow D^-\ell^+\nu_\ell) = (2.12 \pm 0.20) \times 10^{-2}$ , which we rescale to our best value $B(B^0 \rightarrow D^-\ell^+\nu_\ell) = (2.31 \pm 0.10) \times 10^{-2}$ . Our first error is their experiment's error and our second error is the systematic error from using our best value.				
<sup>3</sup> LIVENTSEV 05 reports $[\Gamma(B^0 \rightarrow \overline{D}^0\pi^-\ell^+\nu_\ell)/\Gamma_{\text{total}}] / [B(B^+ \rightarrow \overline{D}^0\ell^+\nu_\ell)] = 0.15 \pm 0.03 \pm 0.03$ which we multiply by our best value $B(B^+ \rightarrow \overline{D}^0\ell^+\nu_\ell) = (2.35 \pm 0.09) \times 10^{-2}$ . Our first error is their experiment's error and our second error is the systematic error from using our best value.				

$\Gamma(D_2^*(2300)^-\ell^+\nu_\ell, D_2^{*-} \rightarrow \overline{D}^0\pi^-)/\Gamma_{\text{total}}$				$\Gamma_9/\Gamma$
VALUE (units $10^{-3}$ )	DOCUMENT ID	TECN	COMMENT	
<b>3.0 ± 1.2 OUR AVERAGE</b>	Error includes scale factor of 1.8.			
4.4 ± 0.8 ± 0.6	1	AUBERT	08BL BABR	$e^+e^- \rightarrow \Upsilon(4S)$
2.0 ± 0.7 ± 0.5	1	LIVENTSEV	08 BELL	$e^+e^- \rightarrow \Upsilon(4S)$
<sup>1</sup> Uses a fully reconstructed $B$ meson as a tag on the recoil side.				

$\Gamma(D_2^*(2460)^-\ell^+\nu_\ell, D_2^{*-} \rightarrow \overline{D}^0\pi^-)/\Gamma_{\text{total}}$				$\Gamma_{10}/\Gamma$
VALUE (units $10^{-3}$ )	DOCUMENT ID	TECN	COMMENT	
<b>1.21 ± 0.33 OUR AVERAGE</b>	Error includes scale factor of 1.8.			
1.10 ± 0.17 ± 0.08	1	AUBERT	09Y BABR	$e^+e^- \rightarrow \Upsilon(4S)$
2.2 ± 0.4 ± 0.4	2	LIVENTSEV	08 BELL	$e^+e^- \rightarrow \Upsilon(4S)$
<sup>1</sup> Uses a simultaneous fit of all $B$ semileptonic decays without full reconstruction of events. AUBERT 09Y reports $B(B^0 \rightarrow \overline{D}_2^*(2460)^-\ell^+\nu_\ell) \cdot B(\overline{D}_2^*(2460)^- \rightarrow \overline{D}^{(*)0}\pi^-) = (1.77 \pm 0.26 \pm 0.11) \times 10^{-3}$ and the authors have provided us the individual measurement.				
<sup>2</sup> Uses a fully reconstructed $B$ meson as a tag on the recoil side.				

$\Gamma(\overline{D}^{*+}n\pi\ell^+\nu_\ell (n \geq 1))/\Gamma(D\ell^+\nu_\ell X)$				$\Gamma_{11}/\Gamma_3$
VALUE	DOCUMENT ID	TECN	COMMENT	
<b>0.248 ± 0.032 ± 0.030</b>	1	AUBERT	07AN BABR	$e^+e^- \rightarrow \Upsilon(4S)$
<sup>1</sup> Uses a fully reconstructed $B$ meson on the recoil side.				



# Meson Particle Listings

## $B^0$

### $\Gamma(\bar{D}^{*0} \pi^- \ell^+ \nu_\ell) / \Gamma_{\text{total}}$ $\Gamma_{12} / \Gamma$

VALUE (units $10^{-3}$ )	DOCUMENT ID	TECN	COMMENT
<b>5.8 ± 0.8 OUR AVERAGE</b>	Error includes scale factor of 1.4.		
6.46 ± 0.53 ± 0.52	VOSSEN 18	BELL	$e^+ e^- \rightarrow \Upsilon(4S)$
4.8 ± 0.8 ± 0.4	1 AUBERT 08Q	BABR	$e^+ e^- \rightarrow \Upsilon(4S)$
••• We do not use the following data for averages, fits, limits, etc. •••			
6.1 ± 2.4 ± 0.3	1,2 LIVENTSEV 08	BELL	Repl. by VOSSEN 18
5.7 ± 1.3 ± 0.2	3,4 LIVENTSEV 05	BELL	Repl. by LIVENTSEV 08

<sup>1</sup> Uses a fully reconstructed  $B$  meson as a tag on the recoil side.  
<sup>2</sup> LIVENTSEV 08 reports  $(5.6 \pm 2.1 \pm 0.8) \times 10^{-3}$  from a measurement of  $[\Gamma(B^0 \rightarrow \bar{D}^{*0} \pi^- \ell^+ \nu_\ell) / \Gamma_{\text{total}}] / [B(B^0 \rightarrow D^- \ell^+ \nu_\ell)]$  assuming  $B(B^0 \rightarrow D^- \ell^+ \nu_\ell) = (2.12 \pm 0.20) \times 10^{-2}$ , which we rescale to our best value  $B(B^0 \rightarrow D^- \ell^+ \nu_\ell) = (2.31 \pm 0.10) \times 10^{-2}$ . Our first error is their experiment's error and our second error is the systematic error from using our best value.  
<sup>3</sup> Excludes  $D^{*+}$  contribution to  $D \pi$  modes.  
<sup>4</sup> LIVENTSEV 05 reports  $[\Gamma(B^0 \rightarrow \bar{D}^{*0} \pi^- \ell^+ \nu_\ell) / \Gamma_{\text{total}}] / [B(B^+ \rightarrow \bar{D}^{*0} \ell^+ \nu_\ell)] = 0.10 \pm 0.02 \pm 0.01$  which we multiply by our best value  $B(B^+ \rightarrow \bar{D}^{*0} \ell^+ \nu_\ell) = (5.66 \pm 0.22) \times 10^{-2}$ . Our first error is their experiment's error and our second error is the systematic error from using our best value.

### $\Gamma(D_1(2420)^- \ell^+ \nu_\ell, D_1^- \rightarrow \bar{D}^{*0} \pi^-) / \Gamma_{\text{total}}$ $\Gamma_{13} / \Gamma$

VALUE (units $10^{-3}$ )	DOCUMENT ID	TECN	COMMENT
<b>2.80 ± 0.28 OUR AVERAGE</b>			
2.78 ± 0.24 ± 0.25	1 AUBERT 09Y	BABR	$e^+ e^- \rightarrow \Upsilon(4S)$
2.7 ± 0.4 ± 0.3	2 AUBERT 08BL	BABR	$e^+ e^- \rightarrow \Upsilon(4S)$
5.4 ± 1.9 ± 0.9	2 LIVENTSEV 08	BELL	$e^+ e^- \rightarrow \Upsilon(4S)$

<sup>1</sup> Uses a simultaneous measurement of all  $B$  semileptonic decays without full reconstruction of events.  
<sup>2</sup> Uses a fully reconstructed  $B$  meson as a tag on the recoil side.

### $\Gamma(D_1'(2430)^- \ell^+ \nu_\ell, D_1'^- \rightarrow \bar{D}^{*0} \pi^-) / \Gamma_{\text{total}}$ $\Gamma_{14} / \Gamma$

VALUE (units $10^{-3}$ )	CL%	DOCUMENT ID	TECN	COMMENT
<b>3.1 ± 0.7 ± 0.5</b>		1 AUBERT 08BL	BABR	$e^+ e^- \rightarrow \Upsilon(4S)$
••• We do not use the following data for averages, fits, limits, etc. •••				
<5.0	90	1 LIVENTSEV 08	BELL	$e^+ e^- \rightarrow \Upsilon(4S)$

<sup>1</sup> Uses a fully reconstructed  $B$  meson as a tag on the recoil side.

### $\Gamma(D_2^*(2460)^- \ell^+ \nu_\ell, D_2^{*-} \rightarrow \bar{D}^{*0} \pi^-) / \Gamma_{\text{total}}$ $\Gamma_{15} / \Gamma$

VALUE (units $10^{-3}$ )	CL%	DOCUMENT ID	TECN	COMMENT
<b>0.68 ± 0.12 OUR AVERAGE</b>				
0.67 ± 0.12 ± 0.05		1 AUBERT 09Y	BABR	$e^+ e^- \rightarrow \Upsilon(4S)$
0.7 ± 0.2 ± 0.2		2 AUBERT 08BL	BABR	$e^+ e^- \rightarrow \Upsilon(4S)$
••• We do not use the following data for averages, fits, limits, etc. •••				
<3.0	90	2 LIVENTSEV 08	BELL	$e^+ e^- \rightarrow \Upsilon(4S)$

<sup>1</sup> Uses a simultaneous fit of all  $B$  semileptonic decays without full reconstruction of events. AUBERT 09Y reports  $B(B^0 \rightarrow \bar{D}_2^{*0} \ell^+ \nu_\ell) \cdot B(\bar{D}_2^{*0} \ell^+ \nu_\ell \rightarrow \bar{D}^{*0} \pi^-) = (1.77 \pm 0.26 \pm 0.11) \times 10^{-3}$  and the authors have provided us the individual measurement.  
<sup>2</sup> Uses a fully reconstructed  $B$  meson as a tag on the recoil side.

### $\Gamma(D^- \pi^+ \pi^- \ell^+ \nu_\ell) / \Gamma(D^- \ell^+ \nu_\ell)$ $\Gamma_{16} / \Gamma_4$

VALUE (units $10^{-2}$ )	DOCUMENT ID	TECN	COMMENT
<b>5.8 ± 1.8 ± 1.2</b>	1 LEES 16	BABR	$e^+ e^- \rightarrow \Upsilon(4S)$

<sup>1</sup> Measurement used electrons and muons as leptons.

### $\Gamma(D^{*-} \pi^+ \pi^- \ell^+ \nu_\ell) / \Gamma(D^{*0}(2010)^- \ell^+ \nu_\ell)$ $\Gamma_{17} / \Gamma_6$

VALUE (units $10^{-2}$ )	DOCUMENT ID	TECN	COMMENT
<b>2.8 ± 0.8 ± 0.6</b>	1 LEES 16	BABR	$e^+ e^- \rightarrow \Upsilon(4S)$

<sup>1</sup> Measurement used electrons and muons as leptons.

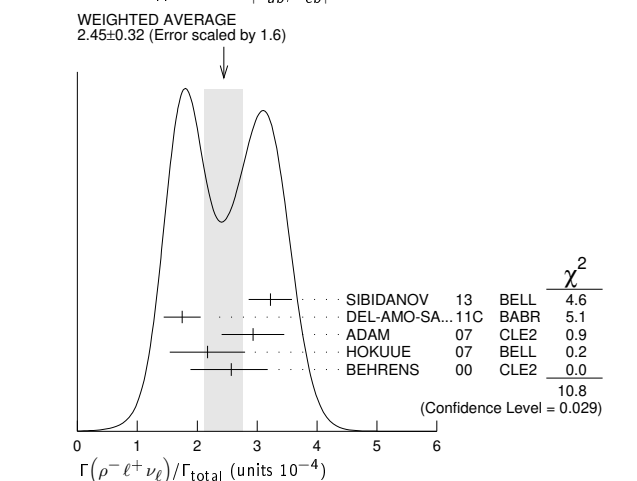
### $\Gamma(\rho^- \ell^+ \nu_\ell) / \Gamma_{\text{total}}$ $\Gamma_{18} / \Gamma$

$\ell = e$  or  $\mu$ , not sum over  $e$  and  $\mu$  modes.  
 "OUR EVALUATION" has been obtained by the Heavy Flavor Averaging Group (HFLAV) by including both  $B^0$  and  $B^+$  decays. The average assumes equality of the semileptonic decay width for these isospin conjugate states.

VALUE (units $10^{-4}$ )	CL%	DOCUMENT ID	TECN	COMMENT
<b>2.94 ± 0.11 ± 0.18 OUR EVALUATION</b>				
<b>2.45 ± 0.32 OUR AVERAGE</b>		Error includes scale factor of 1.6. See the ideogram below.		
3.22 ± 0.27 ± 0.24		1 SIBIDANOV 13	BELL	$e^+ e^- \rightarrow \Upsilon(4S)$
1.75 ± 0.15 ± 0.27		2 DEL-AMO-SA...11c	BABR	$e^+ e^- \rightarrow \Upsilon(4S)$
2.93 ± 0.37 ± 0.37		3 ADAM 07	CLE2	$e^+ e^- \rightarrow \Upsilon(4S)$
2.17 ± 0.54 ± 0.32		4 HOKUUE 07	BELL	$e^+ e^- \rightarrow \Upsilon(4S)$
2.57 ± 0.29 $^{+0.53}_{-0.62}$		5 BEHRENS 00	CLE2	$e^+ e^- \rightarrow \Upsilon(4S)$

2.14 ± 0.21 ± 0.56	2 AUBERT,B	05o	BABR	Repl. by DEL-AMO-SANCHEZ 11c
2.17 ± 0.34 $^{+0.62}_{-0.68}$	6 ATHAR 03	CLE2		Repl. by ADAM 07
3.29 ± 0.42 ± 0.72	7 AUBERT 03E	BABR		Repl. by AUBERT,B 05o
2.69 ± 0.41 $^{+0.61}_{-0.64}$	8 BEHRENS 00	CLE2		$e^+ e^- \rightarrow \Upsilon(4S)$
2.5 ± 0.4 $^{+0.7}_{-0.9}$	9 ALEXANDER 96T	CLE2		Repl. by BEHRENS 00
<4.1	90	10 BEAN 93B	CLE2	$e^+ e^- \rightarrow \Upsilon(4S)$

<sup>1</sup> The signal events are tagged by a second  $B$  meson reconstructed in the fully hadronic decays.  
<sup>2</sup>  $B^+$  and  $B^0$  decays combined assuming isospin symmetry. Systematic errors include both experimental and form-factor uncertainties.  
<sup>3</sup> The  $B^0$  and  $B^+$  results are combined assuming the isospin,  $B$  lifetimes, and relative charged/neutral  $B$  production at the  $\Upsilon(4S)$ .  
<sup>4</sup> The signal events are tagged by a second  $B$  meson reconstructed in the semileptonic mode  $B \rightarrow D^{(*)} \ell \nu_\ell$ .  
<sup>5</sup> Averaging with ALEXANDER 96T results including experimental and theoretical correlations considered, BEHRENS 00 reports systematic errors  $^{+0.33}_{-0.46} \pm 0.41$ , where the second error is theoretical model dependence. We combine these in quadrature.  
<sup>6</sup> ATHAR 03 reports systematic errors  $^{+0.47}_{-0.50} \pm 0.41 \pm 0.01$ , which are experimental systematic, systematic due to residual form-factor uncertainties in the signal, and systematic due to residual form-factor uncertainties in the cross-feed modes, respectively. We combine these in quadrature.  
<sup>7</sup> Uses isospin constraints and extrapolation to all electron energies according to five different form-factor calculations. The second error combines the systematic and theoretical uncertainties in quadrature.  
<sup>8</sup> BEHRENS 00 reports  $^{+0.35}_{-0.40} \pm 0.50$ , where the second error is the theoretical model dependence. We combine these in quadrature.  $B^+$  and  $B^0$  decays combined using isospin symmetry:  $\Gamma(B^0 \rightarrow \rho^- \ell^+ \nu) = 2\Gamma(B^+ \rightarrow \rho^0 \ell^+ \nu) \approx 2\Gamma(B^+ \rightarrow \omega \ell^+ \nu)$ . No evidence for  $\omega \ell \nu$  is reported.  
<sup>9</sup> ALEXANDER 96T reports  $^{+0.5}_{-0.7} \pm 0.5$  where the second error is the theoretical model dependence. We combine these in quadrature.  $B^+$  and  $B^0$  decays combined using isospin symmetry:  $\Gamma(B^0 \rightarrow \rho^- \ell^+ \nu) = 2\Gamma(B^+ \rightarrow \rho^0 \ell^+ \nu) \approx 2\Gamma(B^+ \rightarrow \omega \ell^+ \nu)$ . No evidence for  $\omega \ell \nu$  is reported.  
<sup>10</sup> BEAN 93B limit set using ISGW Model. Using isospin and the quark model to combine  $\Gamma(\rho^0 \ell^+ \nu_\ell)$  and  $\Gamma(\omega \ell^+ \nu_\ell)$  with this result, they obtain a limit  $<(1.6-2.7) \times 10^{-4}$  at 90% CL for  $B^+ \rightarrow (\omega \text{ or } \rho^0) \ell^+ \nu_\ell$ . The range corresponds to the ISGW, WSB, and KS models. An upper limit on  $|V_{ub}/V_{cb}| < 0.08-0.13$  at 90% CL is derived as well.



### $\Gamma(\pi^- \ell^+ \nu_\ell) / \Gamma_{\text{total}}$ $\Gamma_{19} / \Gamma$

"OUR EVALUATION" is provided by the Heavy Flavor Averaging Group (HFLAV) and the procedure is described at <https://hflav.web.cern.ch/>.

VALUE (units $10^{-4}$ )	DOCUMENT ID	TECN	COMMENT
<b>1.50 ± 0.06 OUR EVALUATION</b>			
<b>1.46 ± 0.04 OUR AVERAGE</b>			
1.49 ± 0.09 ± 0.07	1 SIBIDANOV 13	BELL	$e^+ e^- \rightarrow \Upsilon(4S)$
1.47 ± 0.05 ± 0.06	2,3 LEES 12AA	BABR	$e^+ e^- \rightarrow \Upsilon(4S)$
1.41 ± 0.05 ± 0.07	4 DEL-AMO-SA...11c	BABR	$e^+ e^- \rightarrow \Upsilon(4S)$
1.49 ± 0.04 ± 0.07	2 HA 11	BELL	$e^+ e^- \rightarrow \Upsilon(4S)$
1.54 ± 0.17 ± 0.09	4 AUBERT 08AV	BABR	$e^+ e^- \rightarrow \Upsilon(4S)$
1.37 ± 0.15 ± 0.11	5,6 ADAM 07	CLE2	$e^+ e^- \rightarrow \Upsilon(4S)$
1.38 ± 0.19 ± 0.14	7 HOKUUE 07	BELL	$e^+ e^- \rightarrow \Upsilon(4S)$

• • • We do not use the following data for averages, fits, limits, etc. • • •

1.42±0.05±0.08	<sup>2</sup> DEL-AMO-SA..11F	BABR	Repl. by LEES 12AA
1.46±0.07±0.08	<sup>8</sup> AUBERT	07J BABR	Repl. by DEL-AMO-SANCHEZ 11F
1.33±0.17±0.11	<sup>9</sup> AUBERT,B	06K BABR	Repl. by AUBERT 08AV
1.38±0.10±0.18	<sup>10</sup> AUBERT,B	05O BABR	Repl. by DEL-AMO-SANCHEZ 11C
1.33±0.18±0.13	<sup>11</sup> ATHAR	03 CLE2	Repl. by ADAM 07
1.8 ±0.4 ±0.4	<sup>12</sup> ALEXANDER	96T CLE2	Repl. by ATHAR 03

- The signal events are tagged by a second *B* meson reconstructed in the fully hadronic decays.
- Uses loose neutrino reconstruction technique. Assumes  $B(\Upsilon(4S) \rightarrow B^+ B^-) = (51.6 \pm 0.6)\%$  and  $B(\Upsilon(4S) \rightarrow B^0 \bar{B}^0) = (48.4 \pm 0.6)\%$ .
- Reports also a branching fraction value  $B(B^0 \rightarrow \pi^- \ell^+ \nu) = (1.45 \pm 0.04 \pm 0.06) \times 10^{-4}$  from the decays of  $B^+$  and  $B^0$  that are combined using the isospin symmetry relation.
- Using the isospin symmetry relation,  $B^+$  and  $B^0$  branching fractions are combined.
- The  $B^0$  and  $B^+$  results are combined assuming the isospin, *B* lifetimes, and relative charged/neutral *B* production at the  $\Upsilon(4S)$ .
- Also report the rate for  $q^2 > 16 \text{ GeV}^2$  of  $(0.41 \pm 0.08 \pm 0.04) \times 10^{-4}$  from which they obtain  $|V_{ub}| = 3.6 \pm 0.4 \pm 0.2^{+0.6}_{-0.4}$  (last error is from theory).
- The signal events are tagged by a second *B* meson reconstructed in the semileptonic mode  $B \rightarrow D^{(*)} \ell \nu_\ell$ .
- The analysis uses events in which the signal *B* decays are reconstructed with an innovative loose neutrino reconstruction technique.
- The signals are tagged by a second *B* meson reconstructed in a semileptonic or hadronic decay. The  $B^0$  and  $B^+$  results are combined assuming the isospin symmetry.
- $B^+$  and  $B^0$  decays combined assuming isospin symmetry. Systematic errors include both experimental and form-factor uncertainties.
- ATHAR 03 reports systematic errors  $0.11 \pm 0.01 \pm 0.07$ , which are experimental systematic, systematic due to residual form-factor uncertainties in the signal, and systematic due to residual form-factor uncertainties in the cross-feed modes, respectively. We combine these in quadrature.
- ALEXANDER 96T gives systematic errors  $\pm 0.3 \pm 0.2$  where the second error reflects the estimated model dependence. We combine these in quadrature. Assumes isospin symmetry:  $\Gamma(B^0 \rightarrow \pi^- \ell^+ \nu) = 2 \times \Gamma(B^+ \rightarrow \pi^0 \ell^+ \nu)$ .

$\Gamma(\pi^- \mu^+ \nu_\mu)/\Gamma_{\text{total}}$   **$\Gamma_{20}/\Gamma$**

VALUE	DOCUMENT ID	TECN	COMMENT
• • • We do not use the following data for averages, fits, limits, etc. • • •			
seen	<sup>1</sup> ALBRECHT	91c ARG	

- In ALBRECHT 91c, one event is fully reconstructed providing evidence for the *b* → *u* transition.

$\Gamma(\pi^- \tau^+ \nu_\tau)/\Gamma_{\text{total}}$   **$\Gamma_{21}/\Gamma$**

VALUE	CL%	DOCUMENT ID	TECN	COMMENT
$<2.5 \times 10^{-4}$	90	<sup>1</sup> HAMER	16 BELL	$e^+ e^- \rightarrow \Upsilon(4S)$

$\Gamma(K^\pm X)/\Gamma_{\text{total}}$   **$\Gamma_{22}/\Gamma$**

VALUE	DOCUMENT ID	TECN	COMMENT
<b><math>0.78 \pm 0.08</math></b>	<sup>1</sup> ALBRECHT	96D ARG	$e^+ e^- \rightarrow \Upsilon(4S)$

$\Gamma(D^0 X)/\Gamma_{\text{total}}$   **$\Gamma_{23}/\Gamma$**

VALUE	DOCUMENT ID	TECN	COMMENT
<b><math>0.081 \pm 0.014 \pm 0.005</math></b>	<sup>1</sup> AUBERT	07N BABR	$e^+ e^- \rightarrow \Upsilon(4S)$

- • • We do not use the following data for averages, fits, limits, etc. • • •
- |                   |                        |          |                     |
|-------------------|------------------------|----------|---------------------|
| 0.063±0.019±0.005 | <sup>1</sup> AUBERT,BE | 04B BABR | Repl. by AUBERT 07N |
|-------------------|------------------------|----------|---------------------|

$\Gamma(\bar{D}^0 X)/\Gamma_{\text{total}}$   **$\Gamma_{24}/\Gamma$**

VALUE	DOCUMENT ID	TECN	COMMENT
<b><math>0.474 \pm 0.020^{+0.020}_{-0.019}</math></b>	<sup>1</sup> AUBERT	07N BABR	$e^+ e^- \rightarrow \Upsilon(4S)$

- • • We do not use the following data for averages, fits, limits, etc. • • •
- |                   |                        |          |                     |
|-------------------|------------------------|----------|---------------------|
| 0.511±0.031±0.028 | <sup>1</sup> AUBERT,BE | 04B BABR | Repl. by AUBERT 07N |
|-------------------|------------------------|----------|---------------------|

$\Gamma(D^0 X)/[\Gamma(D^0 X) + \Gamma(\bar{D}^0 X)]$   **$\Gamma_{23}/(\Gamma_{23} + \Gamma_{24})$**

VALUE	DOCUMENT ID	TECN	COMMENT
<b><math>0.146 \pm 0.022 \pm 0.006</math></b>	AUBERT	07N BABR	$e^+ e^- \rightarrow \Upsilon(4S)$

$\Gamma(D^+ X)/\Gamma_{\text{total}}$   **$\Gamma_{25}/\Gamma$**

VALUE	CL%	DOCUMENT ID	TECN	COMMENT
<b><math>&lt;0.039</math></b>	90	<sup>1</sup> AUBERT	07N BABR	$e^+ e^- \rightarrow \Upsilon(4S)$

- • • We do not use the following data for averages, fits, limits, etc. • • •
- |          |    |                        |          |                     |
|----------|----|------------------------|----------|---------------------|
| $<0.051$ | 90 | <sup>1</sup> AUBERT,BE | 04B BABR | Repl. by AUBERT 07N |
|----------|----|------------------------|----------|---------------------|

$\Gamma(D^- X)/\Gamma_{\text{total}}$   **$\Gamma_{26}/\Gamma$**

VALUE	DOCUMENT ID	TECN	COMMENT
<b><math>0.369 \pm 0.016^{+0.030}_{-0.027}</math></b>	<sup>1</sup> AUBERT	07N BABR	$e^+ e^- \rightarrow \Upsilon(4S)$

- • • We do not use the following data for averages, fits, limits, etc. • • •
- |                               |                        |          |                     |
|-------------------------------|------------------------|----------|---------------------|
| 0.397±0.030±0.040<br>$-0.038$ | <sup>1</sup> AUBERT,BE | 04B BABR | Repl. by AUBERT 07N |
|-------------------------------|------------------------|----------|---------------------|

$\Gamma(D^+ X)/[\Gamma(D^+ X) + \Gamma(D^- X)]$   **$\Gamma_{25}/(\Gamma_{25} + \Gamma_{26})$**

VALUE	DOCUMENT ID	TECN	COMMENT
<b><math>0.058 \pm 0.028 \pm 0.006</math></b>	AUBERT	07N BABR	$e^+ e^- \rightarrow \Upsilon(4S)$

$\Gamma(D_s^+ X)/\Gamma_{\text{total}}$   **$\Gamma_{27}/\Gamma$**

VALUE	DOCUMENT ID	TECN	COMMENT
<b><math>0.103 \pm 0.012^{+0.017}_{-0.014}</math></b>	<sup>1</sup> AUBERT	07N BABR	$e^+ e^- \rightarrow \Upsilon(4S)$

- • • We do not use the following data for averages, fits, limits, etc. • • •
- |                               |                        |          |                     |
|-------------------------------|------------------------|----------|---------------------|
| 0.109±0.021±0.039<br>$-0.024$ | <sup>1</sup> AUBERT,BE | 04B BABR | Repl. by AUBERT 07N |
|-------------------------------|------------------------|----------|---------------------|

$\Gamma(D_s^- X)/\Gamma_{\text{total}}$   **$\Gamma_{28}/\Gamma$**

VALUE	CL%	DOCUMENT ID	TECN	COMMENT
<b><math>&lt;0.026</math></b>	90	<sup>1</sup> AUBERT	07N BABR	$e^+ e^- \rightarrow \Upsilon(4S)$

$\Gamma(D_s^+ X)/[\Gamma(D_s^+ X) + \Gamma(D_s^- X)]$   **$\Gamma_{27}/(\Gamma_{27} + \Gamma_{28})$**

VALUE	DOCUMENT ID	TECN	COMMENT
<b><math>0.879 \pm 0.066 \pm 0.005</math></b>	AUBERT	07N BABR	$e^+ e^- \rightarrow \Upsilon(4S)$

$\Gamma(A_c^+ X)/\Gamma_{\text{total}}$   **$\Gamma_{29}/\Gamma$**

VALUE	CL%	DOCUMENT ID	TECN	COMMENT
<b><math>&lt;0.031</math></b>	90	<sup>1</sup> AUBERT	07N BABR	$e^+ e^- \rightarrow \Upsilon(4S)$

- • • We do not use the following data for averages, fits, limits, etc. • • •
- |          |    |                        |          |                     |
|----------|----|------------------------|----------|---------------------|
| $<0.038$ | 90 | <sup>1</sup> AUBERT,BE | 04B BABR | Repl. by AUBERT 07N |
|----------|----|------------------------|----------|---------------------|

$\Gamma(\bar{A}_c^- X)/\Gamma_{\text{total}}$   **$\Gamma_{30}/\Gamma$**

VALUE	DOCUMENT ID	TECN	COMMENT
<b><math>0.05 \pm 0.010^{+0.019}_{-0.011}</math></b>	<sup>1</sup> AUBERT	07N BABR	$e^+ e^- \rightarrow \Upsilon(4S)$

- • • We do not use the following data for averages, fits, limits, etc. • • •
- |                               |                        |          |                     |
|-------------------------------|------------------------|----------|---------------------|
| 0.049±0.017±0.018<br>$-0.011$ | <sup>1</sup> AUBERT,BE | 04B BABR | Repl. by AUBERT 07N |
|-------------------------------|------------------------|----------|---------------------|

$\Gamma(A_c^+ X)/[\Gamma(A_c^+ X) + \Gamma(\bar{A}_c^- X)]$   **$\Gamma_{29}/(\Gamma_{29} + \Gamma_{30})$**

VALUE	DOCUMENT ID	TECN	COMMENT
<b><math>0.243 \pm 0.119^{+0.003}_{-0.121}</math></b>	AUBERT	07N BABR	$e^+ e^- \rightarrow \Upsilon(4S)$

$\Gamma(\bar{X})/\Gamma_{\text{total}}$   **$\Gamma_{31}/\Gamma$**

VALUE	DOCUMENT ID	TECN	COMMENT
<b><math>0.947 \pm 0.030^{+0.045}_{-0.040}</math></b>	<sup>1</sup> AUBERT	07N BABR	$e^+ e^- \rightarrow \Upsilon(4S)$

- • • We do not use the following data for averages, fits, limits, etc. • • •
- |                               |                        |          |                     |
|-------------------------------|------------------------|----------|---------------------|
| 1.039±0.051±0.063<br>$-0.058$ | <sup>1</sup> AUBERT,BE | 04B BABR | Repl. by AUBERT 07N |
|-------------------------------|------------------------|----------|---------------------|

- Events are selected by completely reconstructing one *B* and searching for a reconstructed charmed particle in the rest of the event. The last error includes systematic and charm branching ratio uncertainties.

## Meson Particle Listings

 $B^0$ 

$\Gamma(cX)/\Gamma_{\text{total}}$   $\Gamma_{32}/\Gamma$   
 VALUE DOCUMENT ID TECN COMMENT

**$0.246 \pm 0.024^{+0.021}_{-0.017}$**  <sup>1</sup>AUBERT 07N BABR  $e^+e^- \rightarrow \Upsilon(4S)$

• • • We do not use the following data for averages, fits, limits, etc. • • •

$0.237 \pm 0.036^{+0.041}_{-0.027}$  <sup>1</sup>AUBERT,BE 04B BABR Repl. by AUBERT 07N

<sup>1</sup> Events are selected by completely reconstructing one  $B$  and searching for a reconstructed charmed particle in the rest of the event. The last error includes systematic and charm branching ratio uncertainties.

$\Gamma(\bar{c}X)/\Gamma_{\text{total}}$   $\Gamma_{33}/\Gamma$   
 VALUE DOCUMENT ID TECN COMMENT

**$1.193 \pm 0.030^{+0.053}_{-0.049}$**  <sup>1</sup>AUBERT 07N BABR  $e^+e^- \rightarrow \Upsilon(4S)$

• • • We do not use the following data for averages, fits, limits, etc. • • •

$1.276 \pm 0.062^{+0.088}_{-0.074}$  <sup>1</sup>AUBERT,BE 04B BABR Repl. by AUBERT 07N

<sup>1</sup> Events are selected by completely reconstructing one  $B$  and searching for a reconstructed charmed particle in the rest of the event. The last error includes systematic and charm branching ratio uncertainties.

$\Gamma(D^- \pi^+)/\Gamma_{\text{total}}$   $\Gamma_{34}/\Gamma$   
 VALUE (units  $10^{-3}$ ) EVTS DOCUMENT ID TECN COMMENT

**$2.52 \pm 0.13$  OUR FIT** Error includes scale factor of 1.1.

**$2.68 \pm 0.13$  OUR AVERAGE**

$2.55 \pm 0.05 \pm 0.16$  <sup>1</sup>AUBERT 07H BABR  $e^+e^- \rightarrow \Upsilon(4S)$

$3.03 \pm 0.23 \pm 0.23$  <sup>2</sup>AUBERT,BE 06J BABR  $e^+e^- \rightarrow \Upsilon(4S)$

$2.68 \pm 0.12 \pm 0.24$  <sup>1,3</sup>AHMED 02B CLE2  $e^+e^- \rightarrow \Upsilon(4S)$

$2.7 \pm 0.6 \pm 0.5$  <sup>4</sup>BORTOLETTO92 CLEO  $e^+e^- \rightarrow \Upsilon(4S)$

$4.8 \pm 1.1 \pm 1.1$  <sup>22</sup> <sup>5</sup>ALBRECHT 90J ARG  $e^+e^- \rightarrow \Upsilon(4S)$

$5.1^{+2.8}_{-2.5}^{+1.3}_{-1.2}$  <sup>4</sup> <sup>6</sup>BEBEK 87 CLEO  $e^+e^- \rightarrow \Upsilon(4S)$

• • • We do not use the following data for averages, fits, limits, etc. • • •

$2.73 \pm 0.19 \pm 0.05$  <sup>1,7</sup>AUBERT,B 04O BABR Repl. by AUBERT 07H

$2.83 \pm 0.42 \pm 0.05$  <sup>81</sup> <sup>8</sup>ALAM 94 CLE2 Repl. by AHMED 02B

$3.1 \pm 1.3 \pm 1.0$  <sup>7</sup> <sup>5</sup>ALBRECHT 88K ARG  $e^+e^- \rightarrow \Upsilon(4S)$

<sup>1</sup> Assumes equal production of  $B^+$  and  $B^0$  at the  $\Upsilon(4S)$ .

<sup>2</sup> Uses a missing-mass method. Does not depend on  $D$  branching fractions or  $B^{\pm}/B^0$  production rates.

<sup>3</sup> AHMED 02B reports an additional uncertainty on the branching ratios to account for 4.5% uncertainty on relative production of  $B^0$  and  $B^+$ , which is not included here.

<sup>4</sup> BORTOLETTO 92 assumes equal production of  $B^+$  and  $B^0$  at the  $\Upsilon(4S)$  and uses Mark III branching fractions for the  $D$ .

<sup>5</sup> ALBRECHT 88K assumes  $B^0\bar{B}^0:B^+B^-$  production ratio is 45:55. Superseded by ALBRECHT 90J which assumes 50:50.

<sup>6</sup> BEBEK 87 value has been updated in BERKELMAN 91 to use same assumptions as noted for BORTOLETTO 92.

<sup>7</sup> AUBERT,B 04O reports  $[\Gamma(B^0 \rightarrow D^- \pi^+)/\Gamma_{\text{total}}] \times [B(D^+ \rightarrow K_S^0 \pi^+)] = (42.7 \pm 2.1 \pm 2.2) \times 10^{-6}$  which we divide by our best value  $B(D^+ \rightarrow K_S^0 \pi^+) = (1.562 \pm 0.031) \times 10^{-2}$ . Our first error is their experiment's error and our second error is the systematic error from using our best value.

<sup>8</sup> ALAM 94 reports  $[\Gamma(B^0 \rightarrow D^- \pi^+)/\Gamma_{\text{total}}] \times [B(D^+ \rightarrow K^- 2\pi^+)] = (0.265 \pm 0.032 \pm 0.023) \times 10^{-3}$  which we divide by our best value  $B(D^+ \rightarrow K^- 2\pi^+) = (9.38 \pm 0.16) \times 10^{-2}$ . Our first error is their experiment's error and our second error is the systematic error from using our best value. Assumes equal production of  $B^+$  and  $B^0$  at the  $\Upsilon(4S)$ .

$\Gamma(D^- \ell^+ \nu_\ell)/\Gamma(D^- \pi^+)$   $\Gamma_4/\Gamma_{34}$   
 VALUE DOCUMENT ID TECN COMMENT

**$9.9 \pm 1.0 \pm 0.9$**  AALTONEN 09E CDF  $p\bar{p}$  at 1.96 TeV

$\Gamma(D^- \rho^+)/\Gamma_{\text{total}}$   $\Gamma_{35}/\Gamma$   
 VALUE EVTS DOCUMENT ID TECN COMMENT

**$0.0076 \pm 0.0012$  OUR AVERAGE**

$0.0075 \pm 0.0013 \pm 0.0001$  <sup>79</sup> <sup>1</sup>ALAM 94 CLE2  $e^+e^- \rightarrow \Upsilon(4S)$

$0.009 \pm 0.005 \pm 0.003$  <sup>9</sup> <sup>2</sup>ALBRECHT 90J ARG  $e^+e^- \rightarrow \Upsilon(4S)$

• • • We do not use the following data for averages, fits, limits, etc. • • •

$0.022 \pm 0.012 \pm 0.009$  <sup>6</sup> <sup>2</sup>ALBRECHT 88K ARG  $e^+e^- \rightarrow \Upsilon(4S)$

<sup>1</sup> ALAM 94 reports  $[\Gamma(B^0 \rightarrow D^- \rho^+)/\Gamma_{\text{total}}] \times [B(D^+ \rightarrow K^- 2\pi^+)] = 0.000704 \pm 0.000096 \pm 0.000070$  which we divide by our best value  $B(D^+ \rightarrow K^- 2\pi^+) = (9.38 \pm 0.16) \times 10^{-2}$ . Our first error is their experiment's error and our second error is the systematic error from using our best value. Assumes equal production of  $B^+$  and  $B^0$  at the  $\Upsilon(4S)$ .

<sup>2</sup> ALBRECHT 88K assumes  $B^0\bar{B}^0:B^+B^-$  production ratio is 45:55. Superseded by ALBRECHT 90J which assumes 50:50.

$\Gamma(D^- K^0 \pi^+)/\Gamma_{\text{total}}$   $\Gamma_{36}/\Gamma$   
 VALUE (units  $10^{-4}$ ) DOCUMENT ID TECN COMMENT

**$4.9 \pm 0.7 \pm 0.5$**  <sup>1</sup>AUBERT,BE 05B BABR  $e^+e^- \rightarrow \Upsilon(4S)$

<sup>1</sup> Assumes equal production of  $B^+$  and  $B^0$  at the  $\Upsilon(4S)$ .

$\Gamma(D^- K^*(892^+)/\Gamma_{\text{total}}$   $\Gamma_{37}/\Gamma$   
 VALUE (units  $10^{-4}$ ) DOCUMENT ID TECN COMMENT

**$4.5 \pm 0.7$  OUR AVERAGE**

$4.6 \pm 0.6 \pm 0.5$  <sup>1</sup>AUBERT,BE 05B BABR  $e^+e^- \rightarrow \Upsilon(4S)$

$3.7 \pm 1.5 \pm 1.0$  <sup>1</sup>MAHAPATRA 02 CLE2  $e^+e^- \rightarrow \Upsilon(4S)$

<sup>1</sup> Assumes equal production of  $B^+$  and  $B^0$  at the  $\Upsilon(4S)$ .

$\Gamma(D^- \omega \pi^+)/\Gamma_{\text{total}}$   $\Gamma_{38}/\Gamma$   
 VALUE DOCUMENT ID TECN COMMENT

**$0.0028 \pm 0.0005 \pm 0.0004$**  <sup>1</sup>ALEXANDER 01B CLE2  $e^+e^- \rightarrow \Upsilon(4S)$

<sup>1</sup> Assumes equal production of  $B^+$  and  $B^0$  at the  $\Upsilon(4S)$ . The signal is consistent with all observed  $\omega \pi^+$  having proceeded through the  $\rho^+$  resonance at mass  $1349 \pm 25^{+10}_{-5}$  MeV and width  $547 \pm 86^{+46}_{-45}$  MeV.

$\Gamma(D^- K^+)/\Gamma_{\text{total}}$   $\Gamma_{39}/\Gamma$   
 VALUE (units  $10^{-4}$ ) DOCUMENT ID TECN COMMENT

**$1.86 \pm 0.20$  OUR AVERAGE**

$1.89 \pm 0.19 \pm 0.10$  <sup>1</sup>AAIJ 11F LHCb  $pp$  at 7 TeV

$1.7 \pm 0.4 \pm 0.1$  <sup>2</sup>ABE 01I BELL  $e^+e^- \rightarrow \Upsilon(4S)$

<sup>1</sup> AAIJ 11F reports  $(2.01 \pm 0.18 \pm 0.14) \times 10^{-4}$  from a measurement of  $[\Gamma(B^0 \rightarrow D^- K^+)/\Gamma_{\text{total}}] / [B(B^0 \rightarrow D^- \pi^+)]$  assuming  $B(B^0 \rightarrow D^- \pi^+) = (2.68 \pm 0.13) \times 10^{-3}$ , which we rescale to our best value  $B(B^0 \rightarrow D^- \pi^+) = (2.52 \pm 0.13) \times 10^{-3}$ . Our first error is their experiment's error and our second error is the systematic error from using our best value.

<sup>2</sup> ABE 01I reports  $[\Gamma(B^0 \rightarrow D^- K^+)/\Gamma_{\text{total}}] / [B(B^0 \rightarrow D^- \pi^+)] = (6.8 \pm 1.5 \pm 0.7) \times 10^{-2}$  which we multiply by our best value  $B(B^0 \rightarrow D^- \pi^+) = (2.52 \pm 0.13) \times 10^{-3}$ . Our first error is their experiment's error and our second error is the systematic error from using our best value.

$\Gamma(D^- K^+)/\Gamma(D^- \pi^+)$   $\Gamma_{39}/\Gamma_{34}$   
 VALUE (units  $10^{-2}$ ) DOCUMENT ID TECN COMMENT

**$8.22 \pm 0.11 \pm 0.25$**  AAIJ 13P LHCb  $pp$  at 7 TeV

$\Gamma(D^- K^+ \pi^+ \pi^-)/\Gamma(D^- \pi^+ \pi^+ \pi^-)$   $\Gamma_{40}/\Gamma_{46}$   
 VALUE (units  $10^{-2}$ ) DOCUMENT ID TECN COMMENT

**$5.9 \pm 1.1 \pm 0.5$**  AAIJ 12T LHCb  $pp$  at 7 TeV

$\Gamma(D^- K^+ \bar{K}^0)/\Gamma_{\text{total}}$   $\Gamma_{41}/\Gamma$   
 VALUE (units  $10^{-4}$ ) CL% DOCUMENT ID TECN COMMENT

**$< 3.1$**  <sup>90</sup> <sup>1</sup>DRUTSKOY 02 BELL  $e^+e^- \rightarrow \Upsilon(4S)$

<sup>1</sup> Assumes equal production of  $B^+$  and  $B^0$  at the  $\Upsilon(4S)$ .

$\Gamma(D^- K^+ \bar{K}^*(892^0))/\Gamma_{\text{total}}$   $\Gamma_{42}/\Gamma$   
 VALUE (units  $10^{-4}$ ) DOCUMENT ID TECN COMMENT

**$8.8 \pm 1.1 \pm 1.5$**  <sup>1</sup>DRUTSKOY 02 BELL  $e^+e^- \rightarrow \Upsilon(4S)$

<sup>1</sup> Assumes equal production of  $B^+$  and  $B^0$  at the  $\Upsilon(4S)$ .

$\Gamma(\bar{D}^0 \pi^+ \pi^-)/\Gamma_{\text{total}}$   $\Gamma_{43}/\Gamma$   
 VALUE (units  $10^{-4}$ ) CL% EVTS DOCUMENT ID TECN COMMENT

**$8.8 \pm 0.5$  OUR AVERAGE**

$8.95 \pm 0.15 \pm 0.52$  <sup>1</sup>AAIJ 15Y LHCb  $pp$  at 7, 8 TeV

$8.4 \pm 0.4 \pm 0.8$  <sup>2</sup>KUZMIN 07 BELL  $e^+e^- \rightarrow \Upsilon(4S)$

• • • We do not use the following data for averages, fits, limits, etc. • • •

$8.0 \pm 0.6 \pm 1.5$  <sup>2,3</sup>SATPATHY 03 BELL Repl. by KUZMIN 07

$< 16$  <sup>90</sup> <sup>2</sup>ALAM 94 CLE2  $e^+e^- \rightarrow \Upsilon(4S)$

$< 70$  <sup>90</sup> <sup>4</sup>BORTOLETTO92 CLEO  $e^+e^- \rightarrow \Upsilon(4S)$

$< 340$  <sup>90</sup> <sup>5</sup>BEBEK 87 CLEO  $e^+e^- \rightarrow \Upsilon(4S)$

$700 \pm 500$  <sup>5</sup> <sup>6</sup>BEHRENDTS 83 CLEO  $e^+e^- \rightarrow \Upsilon(4S)$

<sup>1</sup> The second uncertainty combines in quadrature all systematic uncertainties quoted in the paper. AAIJ 15Y reports  $B(B^0 \rightarrow \bar{D}^0 \pi^+ \pi^-) = (8.46 \pm 0.14 \pm 0.49) \times 10^{-4}$  in the kinematic region  $m(\bar{D}^0 \pi^+) > 2.1$  GeV which we corrected to the full phase-space dividing by 0.945 from Belle.

<sup>2</sup> Assumes equal production of  $B^+$  and  $B^0$  at the  $\Upsilon(4S)$ .

<sup>3</sup> No assumption about the intermediate mechanism is made in the analysis.

<sup>4</sup> BORTOLETTO 92 assumes equal production of  $B^+$  and  $B^0$  at the  $\Upsilon(4S)$  and uses Mark III branching fractions for the  $D$ . The product branching fraction into  $D_1^*(2340)\pi$  followed by  $D_1^*(2340) \rightarrow D^0 \pi$  is  $< 0.0001$  at 90% CL and into  $D_2^*(2460)\pi$  followed by  $D_2^*(2460) \rightarrow D^0 \pi$  is  $< 0.0004$  at 90% CL.

<sup>5</sup> BEBEK 87 assume the  $\Upsilon(4S)$  decays 43% to  $B^0\bar{B}^0$ . We rescale to 50%.  $B(D^0 \rightarrow K^- \pi^+) = (4.2 \pm 0.4 \pm 0.4)\%$  and  $B(D^0 \rightarrow K^- \pi^+ \pi^+ \pi^-) = (9.1 \pm 0.8 \pm 0.8)\%$  were used.

<sup>6</sup> Corrected by us using assumptions:  $B(D^0 \rightarrow K^- \pi^+) = (0.042 \pm 0.006)$  and  $B(\Upsilon(4S) \rightarrow B^0\bar{B}^0) = 50\%$ . The product branching ratio is  $B(B^0 \rightarrow \bar{D}^0 \pi^+ \pi^-)B(\bar{D}^0 \rightarrow K^+ \pi^-) = (0.39 \pm 0.26) \times 10^{-2}$ .

$\Gamma(D^*(2010)^-\pi^+)/\Gamma_{total}$			$\Gamma_{44}/\Gamma$		
VALUE (units $10^{-3}$ )	EVTS	DOCUMENT ID	TECN	COMMENT	
<b>2.74 ± 0.13 OUR AVERAGE</b>					
2.79 ± 0.08 ± 0.17		1 AUBERT	07H	BABR	$e^+e^- \rightarrow \Upsilon(4S)$
2.50 ± 0.34 ± 0.13		2,3 AUBERT,BE	06J	BABR	$e^+e^- \rightarrow \Upsilon(4S)$
2.81 ± 0.24 ± 0.05		4 BRANDENB...	98	CLE2	$e^+e^- \rightarrow \Upsilon(4S)$
2.6 ± 0.3 ± 0.4	82	5 ALAM	94	CLE2	$e^+e^- \rightarrow \Upsilon(4S)$
3.37 ± 0.96 ± 0.02		6 BORIOLETT092	CLEO	$e^+e^- \rightarrow \Upsilon(4S)$	
2.36 ± 0.88 ± 0.02	12	7 ALBRECHT	90J	ARG	$e^+e^- \rightarrow \Upsilon(4S)$
2.36 $^{+1.50}_{-1.10}$ ± 0.02	5	8 BEBEK	87	CLEO	$e^+e^- \rightarrow \Upsilon(4S)$

• • • We do not use the following data for averages, fits, limits, etc. • • •

10 ± 4 ± 1	8	9 AKERS	94J	OPAL	$e^+e^- \rightarrow Z$
2.7 ± 1.4 ± 1.0	5	10 ALBRECHT	87c	ARG	$e^+e^- \rightarrow \Upsilon(4S)$
3.5 ± 2 ± 2		11 ALBRECHT	86F	ARG	$e^+e^- \rightarrow \Upsilon(4S)$
17 ± 5 ± 5	41	12 GILES	84	CLEO	$e^+e^- \rightarrow \Upsilon(4S)$

<sup>1</sup> Assumes equal production of  $B^+$  and  $B^0$  at the  $\Upsilon(4S)$ .

<sup>2</sup> AUBERT,BE 06J reports  $[\Gamma(B^0 \rightarrow D^*(2010)^-\pi^+)/\Gamma_{total}] / [B(B^0 \rightarrow D^-\pi^+)] = 0.99 \pm 0.11 \pm 0.08$  which we multiply by our best value  $B(B^0 \rightarrow D^-\pi^+) = (2.52 \pm 0.13) \times 10^{-3}$ . Our first error is their experiment's error and our second error is the systematic error from using our best value.

<sup>3</sup> Uses a missing-mass method. Does not depend on  $D$  branching fractions or  $B^+\pi^0$  production rates.

<sup>4</sup> BRANDENBURG 98 assume equal production of  $B^+$  and  $B^0$  at  $\Upsilon(4S)$  and use the  $D^*$  reconstruction technique. The first error is their experiment's error and the second error is the systematic error from the PDG 96 value of  $B(D^* \rightarrow D\pi)$ .

<sup>5</sup> ALAM 94 assume equal production of  $B^+$  and  $B^0$  at the  $\Upsilon(4S)$  and use the CLEO II  $B(D^*(2010)^+ \rightarrow D^0\pi^+)$  and absolute  $B(D^0 \rightarrow K^-\pi^+)$  and the PDG 1992  $B(D^0 \rightarrow K^-\pi^+\pi^0)/B(D^0 \rightarrow K^-\pi^+)$  and  $B(D^0 \rightarrow K^-2\pi^+\pi^-)/B(D^0 \rightarrow K^-\pi^+)$ .

<sup>6</sup> BORIOLETT092 reports  $(4.0 \pm 1.0 \pm 0.7) \times 10^{-3}$  from a measurement of  $[\Gamma(B^0 \rightarrow D^*(2010)^-\pi^+)/\Gamma_{total}] \times [B(D^*(2010)^+ \rightarrow D^0\pi^+)]$  assuming  $B(D^*(2010)^+ \rightarrow D^0\pi^+) = 0.57 \pm 0.06$ , which we rescale to our best value  $B(D^*(2010)^+ \rightarrow D^0\pi^+) = (67.7 \pm 0.5) \times 10^{-2}$ . Our first error is their experiment's error and our second error is the systematic error from using our best value. Assumes equal production of  $B^+$  and  $B^0$  at the  $\Upsilon(4S)$  and uses Mark III branching fractions for the  $D$ .

<sup>7</sup> ALBRECHT 90J reports  $(2.8 \pm 0.9 \pm 0.6) \times 10^{-3}$  from a measurement of  $[\Gamma(B^0 \rightarrow D^*(2010)^-\pi^+)/\Gamma_{total}] \times [B(D^*(2010)^+ \rightarrow D^0\pi^+)]$  assuming  $B(D^*(2010)^+ \rightarrow D^0\pi^+) = 0.57 \pm 0.06$ , which we rescale to our best value  $B(D^*(2010)^+ \rightarrow D^0\pi^+) = (67.7 \pm 0.5) \times 10^{-2}$ . Our first error is their experiment's error and our second error is the systematic error from using our best value. Assumes equal production of  $B^+$  and  $B^0$  at the  $\Upsilon(4S)$  and uses Mark III branching fractions for the  $D$ .

<sup>8</sup> BEBEK 87 reports  $(2.8  $^{+1.5+1.0}_{-1.2-0.6}$ ) \times 10^{-3}$  from a measurement of  $[\Gamma(B^0 \rightarrow D^*(2010)^-\pi^+)/\Gamma_{total}] \times [B(D^*(2010)^+ \rightarrow D^0\pi^+)]$  assuming  $B(D^*(2010)^+ \rightarrow D^0\pi^+) = 0.57 \pm 0.06$ , which we rescale to our best value  $B(D^*(2010)^+ \rightarrow D^0\pi^+) = (67.7 \pm 0.5) \times 10^{-2}$ . Our first error is their experiment's error and our second error is the systematic error from using our best value. Updated in BERKELMAN 91 to use same assumptions as noted for BORIOLETT092 and ALBRECHT 90J.

<sup>9</sup> Assumes  $B(Z \rightarrow b\bar{b}) = 0.217$  and 38%  $B_d$  production fraction.

<sup>10</sup> ALBRECHT 87c use PDG 86 branching ratios for  $D$  and  $D^*(2010)$  and assume  $B(\Upsilon(4S) \rightarrow B^+B^-) = 55\%$  and  $B(\Upsilon(4S) \rightarrow B^0\bar{B}^0) = 45\%$ . Superseded by ALBRECHT 90J.

<sup>11</sup> ALBRECHT 86F uses pseudomass that is independent of  $D^0$  and  $D^+$  branching ratios.

<sup>12</sup> Assumes  $B(D^*(2010)^+ \rightarrow D^0\pi^+) = 0.60  $^{+0.08}_{-0.15}$$ . Assumes  $B(\Upsilon(4S) \rightarrow B^0\bar{B}^0) = 0.40 \pm 0.02$ . Does not depend on  $D$  branching ratios.

$\Gamma(D^*(2010)^-\ell^+\nu_\ell)/\Gamma(D^*(2010)^-\pi^+)$			$\Gamma_6/\Gamma_{44}$		
VALUE	DOCUMENT ID	TECN	COMMENT		
<b>16.5 ± 2.3 ± 1.1</b>					
	AALTONEN	09E	CDF		$p\bar{p}$ at 1.96 TeV

$\Gamma(D^0 K^+ K^-)/\Gamma(D^0 \pi^+ \pi^-)$			$\Gamma_{45}/\Gamma_{43}$		
VALUE	DOCUMENT ID	TECN	COMMENT		
<b>0.067 ± 0.005 OUR AVERAGE</b>					
0.069 ± 0.004 ± 0.003	AALJ	18AZ	LHCB		$p\bar{p}$ at 7, 8 TeV
0.056 ± 0.011 ± 0.007	AALJ	12AMLHCB			$p\bar{p}$ at 7 TeV

$\Gamma(D^-\pi^+\pi^+\pi^-)/\Gamma_{total}$			$\Gamma_{46}/\Gamma$		
VALUE	DOCUMENT ID	TECN	COMMENT		
<b>0.0060 ± 0.0007 OUR FIT</b> Error includes scale factor of 1.1.					
<b>0.0080 ± 0.0021 ± 0.0014</b>					
	1 BORIOLETT092	CLEO	$e^+e^- \rightarrow \Upsilon(4S)$		
	<sup>1</sup> BORIOLETT092 assumes equal production of $B^+$ and $B^0$ at the $\Upsilon(4S)$ and uses Mark III branching fractions for the $D$ .				

$\Gamma(D^-\pi^+\pi^+\pi^-)/\Gamma(D^-\pi^+)$			$\Gamma_{46}/\Gamma_{34}$		
VALUE	DOCUMENT ID	TECN	COMMENT		
<b>2.39 ± 0.23 OUR FIT</b>					
<b>2.38 ± 0.11 ± 0.21</b>	AALJ	11E	LHCB		$p\bar{p}$ at 7 TeV

$\Gamma((D^-\pi^+\pi^+\pi^-)_{nonresonant})/\Gamma_{total}$			$\Gamma_{47}/\Gamma$		
VALUE	DOCUMENT ID	TECN	COMMENT		
<b>0.0039 ± 0.0014 ± 0.0013</b>					
	1 BORIOLETT092	CLEO	$e^+e^- \rightarrow \Upsilon(4S)$		

<sup>1</sup> BORIOLETT092 assumes equal production of  $B^+$  and  $B^0$  at the  $\Upsilon(4S)$  and uses Mark III branching fractions for the  $D$ .

$\Gamma(D^-\pi^+\rho^0)/\Gamma_{total}$			$\Gamma_{48}/\Gamma$		
VALUE	DOCUMENT ID	TECN	COMMENT		
<b>0.0011 ± 0.0009 ± 0.0004</b>					
	1 BORIOLETT092	CLEO	$e^+e^- \rightarrow \Upsilon(4S)$		
	<sup>1</sup> BORIOLETT092 assumes equal production of $B^+$ and $B^0$ at the $\Upsilon(4S)$ and uses Mark III branching fractions for the $D$ .				

$\Gamma(D^-\pi^+(1260)^+)/\Gamma_{total}$			$\Gamma_{49}/\Gamma$		
VALUE	DOCUMENT ID	TECN	COMMENT		
<b>0.0060 ± 0.0022 ± 0.0024</b>					
	1 BORIOLETT092	CLEO	$e^+e^- \rightarrow \Upsilon(4S)$		
	<sup>1</sup> BORIOLETT092 assumes equal production of $B^+$ and $B^0$ at the $\Upsilon(4S)$ and uses Mark III branching fractions for the $D$ .				

$\Gamma(D^*(2010)^-\pi^+\pi^0)/\Gamma_{total}$			$\Gamma_{50}/\Gamma$		
VALUE	DOCUMENT ID	TECN	COMMENT		
<b>0.0152 ± 0.0052 ± 0.0001</b>					
	51	1 ALBRECHT	90J	ARG	$e^+e^- \rightarrow \Upsilon(4S)$
0.015 ± 0.008 ± 0.008	8	2 ALBRECHT	87c	ARG	$e^+e^- \rightarrow \Upsilon(4S)$

<sup>1</sup> ALBRECHT 90J reports  $0.018 \pm 0.004 \pm 0.005$  from a measurement of  $[\Gamma(B^0 \rightarrow D^*(2010)^-\pi^+\pi^0)/\Gamma_{total}] \times [B(D^*(2010)^+ \rightarrow D^0\pi^+)]$  assuming  $B(D^*(2010)^+ \rightarrow D^0\pi^+) = 0.57 \pm 0.06$ , which we rescale to our best value  $B(D^*(2010)^+ \rightarrow D^0\pi^+) = (67.7 \pm 0.5) \times 10^{-2}$ . Our first error is their experiment's error and our second error is the systematic error from using our best value. Assumes equal production of  $B^+$  and  $B^0$  at the  $\Upsilon(4S)$  and uses Mark III branching fractions for the  $D$ .

<sup>2</sup> ALBRECHT 87c use PDG 86 branching ratios for  $D$  and  $D^*(2010)$  and assume  $B(\Upsilon(4S) \rightarrow B^+B^-) = 55\%$  and  $B(\Upsilon(4S) \rightarrow B^0\bar{B}^0) = 45\%$ . Superseded by ALBRECHT 90J.

$\Gamma(D^*(2010)^-\rho^+)/\Gamma_{total}$			$\Gamma_{51}/\Gamma$		
VALUE (units $10^{-3}$ )	EVTS	DOCUMENT ID	TECN	COMMENT	
<b>6.8 ± 0.9 OUR AVERAGE</b>					
6.8 ± 0.3 ± 0.9		1,2 CSORNA	03	CLE2	$e^+e^- \rightarrow \Upsilon(4S)$
16.0 ± 11.3 ± 0.1		3 BORIOLETT092	CLEO	$e^+e^- \rightarrow \Upsilon(4S)$	
5.89 ± 3.52 ± 0.04	19	4 ALBRECHT	90J	ARG	$e^+e^- \rightarrow \Upsilon(4S)$
		2,5 MATVIENKO	15	BELL	$e^+e^- \rightarrow \Upsilon(4S)$
7.4 ± 1.0 ± 1.4	76	6,7 ALAM	94	CLE2	$e^+e^- \rightarrow \Upsilon(4S)$
81 ± 29 $^{+59}_{-24}$	19	8 CHEN	85	CLEO	$e^+e^- \rightarrow \Upsilon(4S)$

<sup>1</sup> The second error combines the systematic and theoretical uncertainties in quadrature. CSORNA 03 includes data used in ALAM 94. A full angular fit to three complex helicity amplitudes is performed.

<sup>2</sup> Assumes equal production of  $B^0$  and  $B^+$  at the  $\Upsilon(4S)$  resonance.

<sup>3</sup> BORIOLETT092 reports  $0.019 \pm 0.008 \pm 0.011$  from a measurement of  $[\Gamma(B^0 \rightarrow D^*(2010)^-\rho^+)/\Gamma_{total}] \times [B(D^*(2010)^+ \rightarrow D^0\pi^+)]$  assuming  $B(D^*(2010)^+ \rightarrow D^0\pi^+) = 0.57 \pm 0.06$ , which we rescale to our best value  $B(D^*(2010)^+ \rightarrow D^0\pi^+) = (67.7 \pm 0.5) \times 10^{-2}$ . Our first error is their experiment's error and our second error is the systematic error from using our best value. Assumes equal production of  $B^+$  and  $B^0$  at the  $\Upsilon(4S)$  and uses Mark III branching fractions for the  $D$ .

<sup>4</sup> ALBRECHT 90J reports  $0.007 \pm 0.003 \pm 0.003$  from a measurement of  $[\Gamma(B^0 \rightarrow D^*(2010)^-\rho^+)/\Gamma_{total}] \times [B(D^*(2010)^+ \rightarrow D^0\pi^+)]$  assuming  $B(D^*(2010)^+ \rightarrow D^0\pi^+) = 0.57 \pm 0.06$ , which we rescale to our best value  $B(D^*(2010)^+ \rightarrow D^0\pi^+) = (67.7 \pm 0.5) \times 10^{-2}$ . Our first error is their experiment's error and our second error is the systematic error from using our best value. Assumes equal production of  $B^+$  and  $B^0$  at the  $\Upsilon(4S)$  and uses Mark III branching fractions for the  $D$ .

<sup>5</sup> MATVIENKO 15 reports  $B(B^0 \rightarrow D^*(2010)^-\rho^+, \rho^+ \rightarrow \omega\pi^+) = (1.48 \pm 0.27  $^{+0.15+0.21}_{-0.09-0.56}$ ) \times 10^{-3}$ . The last uncertainty is a model one.

<sup>6</sup> ALAM 94 assume equal production of  $B^+$  and  $B^0$  at the  $\Upsilon(4S)$  and use the CLEO II  $B(D^*(2010)^+ \rightarrow D^0\pi^+)$  and absolute  $B(D^0 \rightarrow K^-\pi^+)$  and the PDG 1992  $B(D^0 \rightarrow K^-\pi^+\pi^0)/B(D^0 \rightarrow K^-\pi^+)$  and  $B(D^0 \rightarrow K^-2\pi^+\pi^-)/B(D^0 \rightarrow K^-\pi^+)$ .

<sup>7</sup> This decay is nearly completely longitudinally polarized,  $\Gamma_L/\Gamma = (93 \pm 5 \pm 5)\%$ , as expected from the factorization hypothesis (ROSNER 90). The nonresonant  $\pi^+\pi^0$  contribution under the  $\rho^+$  is less than 9% at 90% CL.

<sup>8</sup> Uses  $B(D^* \rightarrow D^0\pi^+) = 0.6 \pm 0.15$  and  $B(\Upsilon(4S) \rightarrow B^0\bar{B}^0) = 0.4$ . Does not depend on  $D$  branching ratios.

$\Gamma(D^*(2010)^-K^+)/\Gamma_{total}$			$\Gamma_{52}/\Gamma$		
VALUE (units $10^{-4}$ )	DOCUMENT ID	TECN	COMMENT		
<b>2.12 ± 0.15 OUR AVERAGE</b>					
2.13 ± 0.12 ± 0.10		1 AUBERT	06A	BABR	$e^+e^- \rightarrow \Upsilon(4S)$
2.0 ± 0.4 ± 0.1		2 ABE	01I	BELL	$e^+e^- \rightarrow \Upsilon(4S)$

<sup>1</sup> AUBERT 06A reports  $[\Gamma(B^0 \rightarrow D^*(2010)^-K^+)/\Gamma_{total}] / [B(B^0 \rightarrow D^*(2010)^-\pi^+)] = 0.0776 \pm 0.0034 \pm 0.0029$  which we multiply by our best value  $B(B^0 \rightarrow D^*(2010)^-\pi^+) = (2.74 \pm 0.13) \times 10^{-3}$ . Our first error is their experiment's error and our second error is the systematic error from using our best value.

<sup>2</sup> ABE 01I reports  $[\Gamma(B^0 \rightarrow D^*(2010)^-K^+)/\Gamma_{total}] / [B(B^0 \rightarrow D^*(2010)^-\pi^+)] = 0.074 \pm 0.015 \pm 0.006$  which we multiply by our best value  $B(B^0 \rightarrow D^*(2010)^-\pi^+) = (2.74 \pm 0.13) \times 10^{-3}$ . Our first error is their experiment's error and our second error is the systematic error from using our best value.

$\Gamma(D^*(2010)^-K^+)/\Gamma(D^*(2010)^-\pi^+)$			$\Gamma_{52}/\Gamma_{44}$		
VALUE	DOCUMENT ID	TECN	COMMENT		
<b>(7.76 ± 0.34 ± 0.26) × 10<sup>-2</sup></b>					
	AALJ	13AO	LHCB		$p\bar{p}$ at 7 TeV

# Meson Particle Listings

## $B^0$

### $\Gamma(D^*(2010)^- K^0 \pi^+)/\Gamma_{total}$ $\Gamma_{53}/\Gamma$

VALUE (units $10^{-4}$ )	DOCUMENT ID	TECN	COMMENT
<b>3.0 ± 0.7 ± 0.3</b>	1 AUBERT, BE	05B	BABR $e^+e^- \rightarrow \Upsilon(4S)$
1 Assumes equal production of $B^+$ and $B^0$ at the $\Upsilon(4S)$ .			

### $\Gamma(D^*(2010)^- K^*(892)^+)/\Gamma_{total}$ $\Gamma_{54}/\Gamma$

VALUE (units $10^{-4}$ )	DOCUMENT ID	TECN	COMMENT
<b>3.3 ± 0.6 OUR AVERAGE</b>			
3.2 ± 0.6 ± 0.3	1 AUBERT, BE	05B	BABR $e^+e^- \rightarrow \Upsilon(4S)$
3.8 ± 1.3 ± 0.8	2 MAHAPATRA	02	CLE2 $e^+e^- \rightarrow \Upsilon(4S)$
1 Assumes equal production of $B^+$ and $B^0$ at the $\Upsilon(4S)$ .			
2 Assumes equal production of $B^+$ and $B^0$ at the $\Upsilon(4S)$ and an unpolarized final state.			

### $\Gamma(D^*(2010)^- K^+ \bar{K}^0)/\Gamma_{total}$ $\Gamma_{55}/\Gamma$

VALUE (units $10^{-4}$ )	CL%	DOCUMENT ID	TECN	COMMENT
<b>&lt;4.7</b>	90	1 DRUTSKOY	02	BELL $e^+e^- \rightarrow \Upsilon(4S)$
1 Assumes equal production of $B^+$ and $B^0$ at the $\Upsilon(4S)$ .				

### $\Gamma(D^*(2010)^- K^+ \bar{K}^*(892)^0)/\Gamma_{total}$ $\Gamma_{56}/\Gamma$

VALUE (units $10^{-4}$ )	DOCUMENT ID	TECN	COMMENT
<b>12.9 ± 2.2 ± 2.5</b>	1 DRUTSKOY	02	BELL $e^+e^- \rightarrow \Upsilon(4S)$
1 Assumes equal production of $B^+$ and $B^0$ at the $\Upsilon(4S)$ .			

### $\Gamma(D^*(2010)^- \pi^+ \pi^+ \pi^-)/\Gamma_{total}$ $\Gamma_{57}/\Gamma$

VALUE (units $10^{-3}$ )	CL%	DOCUMENT ID	TECN	COMMENT
<b>7.21 ± 0.29 OUR AVERAGE</b>				
7.26 ± 0.11 ± 0.31		1 LEES	16H	BABR $e^+e^- \rightarrow \Upsilon(4S)$
6.81 ± 0.23 ± 0.72		2 MAJUMDER	04	BELL $e^+e^- \rightarrow \Upsilon(4S)$
6.3 ± 1.0 ± 1.1		3,4 ALAM	94	CLE2 $e^+e^- \rightarrow \Upsilon(4S)$
13.4 ± 3.6 ± 0.1		5 BORTOLETTO	92	CLEO $e^+e^- \rightarrow \Upsilon(4S)$
10.1 ± 4.1 ± 0.1		6 ALBRECHT	90J	ARG $e^+e^- \rightarrow \Upsilon(4S)$
• • • We do not use the following data for averages, fits, limits, etc. • • •				
33 ± 9 ± 16		7 ALBRECHT	87c	ARG $e^+e^- \rightarrow \Upsilon(4S)$
<42	90	8 BEBEK	87	CLEO $e^+e^- \rightarrow \Upsilon(4S)$

- Assumes  $B(\Upsilon(4S) \rightarrow B^0 \bar{B}^0) = 0.486 \pm 0.006$ .
- Assumes equal production of  $B^+$  and  $B^0$  at the  $\Upsilon(4S)$ .
- ALAM 94 assume equal production of  $B^+$  and  $B^0$  at the  $\Upsilon(4S)$  and use the CLEO II  $B(D^*(2010)^+ \rightarrow D^0 \pi^+)$  and absolute  $B(D^0 \rightarrow K^- \pi^+)$  and the PDG 1992  $B(D^0 \rightarrow K^- \pi^+ \pi^0)/B(D^0 \rightarrow K^- \pi^+)$  and  $B(D^0 \rightarrow K^- 2\pi^+ \pi^-)/B(D^0 \rightarrow K^- \pi^+)$ .
- The three pion mass is required to be between 1.0 and 1.6 GeV consistent with an  $a_1$  meson. (If this channel is dominated by  $a_1^+$ , the branching ratio for  $\bar{D}^* a_1^+$  is twice that for  $\bar{D}^* \pi^+ \pi^+ \pi^-$ .)
- BORTOLETTO 92 reports  $0.0159 \pm 0.0028 \pm 0.0037$  from a measurement of  $[\Gamma(B^0 \rightarrow D^*(2010)^- \pi^+ \pi^+ \pi^-)/\Gamma_{total}] \times [B(D^*(2010)^+ \rightarrow D^0 \pi^+)]$  assuming  $B(D^*(2010)^+ \rightarrow D^0 \pi^+) = 0.57 \pm 0.06$ , which we rescale to our best value  $B(D^*(2010)^+ \rightarrow D^0 \pi^+) = (67.7 \pm 0.5) \times 10^{-2}$ . Our first error is their experiment's error and our second error is the systematic error from using our best value. Assumes equal production of  $B^+$  and  $B^0$  at the  $\Upsilon(4S)$  and uses Mark III branching fractions for the  $D$ .
- ALBRECHT 90J reports  $0.012 \pm 0.003 \pm 0.004$  from a measurement of  $[\Gamma(B^0 \rightarrow D^*(2010)^- \pi^+ \pi^+ \pi^-)/\Gamma_{total}] \times [B(D^*(2010)^+ \rightarrow D^0 \pi^+)]$  assuming  $B(D^*(2010)^+ \rightarrow D^0 \pi^+) = 0.57 \pm 0.06$ , which we rescale to our best value  $B(D^*(2010)^+ \rightarrow D^0 \pi^+) = (67.7 \pm 0.5) \times 10^{-2}$ . Our first error is their experiment's error and our second error is the systematic error from using our best value. Assumes equal production of  $B^+$  and  $B^0$  at the  $\Upsilon(4S)$  and uses Mark III branching fractions for the  $D$ .
- ALBRECHT 87c use PDG 86 branching ratios for  $D$  and  $D^*(2010)$  and assume  $B(\Upsilon(4S) \rightarrow B^+ B^-) = 55\%$  and  $B(\Upsilon(4S) \rightarrow B^0 \bar{B}^0) = 45\%$ . Superseded by ALBRECHT 90J.
- BEBEK 87 value has been updated in BERKELMAN 91 to use same assumptions as noted for BORTOLETTO 92.

### $\Gamma((D^*(2010)^- \pi^+ \pi^+ \pi^-) nonresonant)/\Gamma_{total}$ $\Gamma_{58}/\Gamma$

VALUE	DOCUMENT ID	TECN	COMMENT
<b>0.0000 ± 0.0019 ± 0.0016</b>	1 BORTOLETTO	92	CLEO $e^+e^- \rightarrow \Upsilon(4S)$
1 BORTOLETTO 92 assumes equal production of $B^+$ and $B^0$ at the $\Upsilon(4S)$ and uses Mark III branching fractions for the $D$ and $D^*(2010)$ .			

### $\Gamma(D^*(2010)^- \pi^+ \rho^0)/\Gamma_{total}$ $\Gamma_{59}/\Gamma$

VALUE	DOCUMENT ID	TECN	COMMENT
<b>0.00573 ± 0.00317 ± 0.00004</b>	1 BORTOLETTO	92	CLEO $e^+e^- \rightarrow \Upsilon(4S)$
1 BORTOLETTO 92 reports $0.0068 \pm 0.0032 \pm 0.0021$ from a measurement of $[\Gamma(B^0 \rightarrow D^*(2010)^- \pi^+ \rho^0)/\Gamma_{total}] \times [B(D^*(2010)^+ \rightarrow D^0 \pi^+)]$ assuming $B(D^*(2010)^+ \rightarrow D^0 \pi^+) = 0.57 \pm 0.06$ , which we rescale to our best value $B(D^*(2010)^+ \rightarrow D^0 \pi^+) = (67.7 \pm 0.5) \times 10^{-2}$ . Our first error is their experiment's error and our second error is the systematic error from using our best value. Assumes equal production of $B^+$ and $B^0$ at the $\Upsilon(4S)$ and uses Mark III branching fractions for the $D$ .			

### $\Gamma(D^*(2010)^- a_1(1260)^+)/\Gamma_{total}$ $\Gamma_{60}/\Gamma$

VALUE	DOCUMENT ID	TECN	COMMENT
<b>0.0130 ± 0.0027 OUR AVERAGE</b>			
0.0126 ± 0.0020 ± 0.0022	1,2 ALAM	94	CLE2 $e^+e^- \rightarrow \Upsilon(4S)$
0.0152 ± 0.0070 ± 0.0001	3 BORTOLETTO	92	CLEO $e^+e^- \rightarrow \Upsilon(4S)$

- ALAM 94 value is twice their  $\Gamma(D^*(2010)^- \pi^+ \pi^+ \pi^-)/\Gamma_{total}$  value based on their observation that the three pions are dominantly in the  $a_1(1260)$  mass range 1.0 to 1.6 GeV.
- ALAM 94 assume equal production of  $B^+$  and  $B^0$  at the  $\Upsilon(4S)$  and use the CLEO II  $B(D^*(2010)^+ \rightarrow D^0 \pi^+)$  and absolute  $B(D^0 \rightarrow K^- \pi^+)$  and the PDG 1992  $B(D^0 \rightarrow K^- \pi^+ \pi^0)/B(D^0 \rightarrow K^- \pi^+)$  and  $B(D^0 \rightarrow K^- 2\pi^+ \pi^-)/B(D^0 \rightarrow K^- \pi^+)$ .
- BORTOLETTO 92 reports  $0.018 \pm 0.006 \pm 0.006$  from a measurement of  $[\Gamma(B^0 \rightarrow D^*(2010)^- a_1(1260)^+)/\Gamma_{total}] \times [B(D^*(2010)^+ \rightarrow D^0 \pi^+)]$  assuming  $B(D^*(2010)^+ \rightarrow D^0 \pi^+) = 0.57 \pm 0.06$ , which we rescale to our best value  $B(D^*(2010)^+ \rightarrow D^0 \pi^+) = (67.7 \pm 0.5) \times 10^{-2}$ . Our first error is their experiment's error and our second error is the systematic error from using our best value. Assumes equal production of  $B^+$  and  $B^0$  at the  $\Upsilon(4S)$  and uses Mark III branching fractions for the  $D$ .

### $\Gamma(\bar{D}_1^0(2420)^0 \pi^- \pi^+, \bar{D}_1^0 \rightarrow D^{*-} \pi^+)/\Gamma(D^*(2010)^- \pi^+ \pi^+ \pi^-)$ $\Gamma_{61}/\Gamma_{57}$

VALUE	DOCUMENT ID	TECN	COMMENT
<b>(2.04 ± 0.42 ± 0.22) × 10<sup>-2</sup></b>	AAIJ	13a0	LHCb $pp$ at 7 TeV

### $\Gamma(D^*(2010)^- K^+ \pi^- \pi^+)/\Gamma(D^*(2010)^- \pi^+ \pi^+ \pi^-)$ $\Gamma_{62}/\Gamma_{57}$

VALUE	DOCUMENT ID	TECN	COMMENT
<b>(6.47 ± 0.37 ± 0.35) × 10<sup>-2</sup></b>	AAIJ	13a0	LHCb $pp$ at 7 TeV

### $\Gamma(D^*(2010)^- \pi^+ \pi^+ \pi^- \pi^0)/\Gamma_{total}$ $\Gamma_{63}/\Gamma$

VALUE	EVTs	DOCUMENT ID	TECN	COMMENT
<b>0.0176 ± 0.0027 OUR AVERAGE</b>				
0.0172 ± 0.0014 ± 0.0024		1 ALEXANDER	01B	CLE2 $e^+e^- \rightarrow \Upsilon(4S)$
0.0345 ± 0.0181 ± 0.0003	28	2 ALBRECHT	90J	ARG $e^+e^- \rightarrow \Upsilon(4S)$

- Assumes equal production of  $B^+$  and  $B^0$  at the  $\Upsilon(4S)$ . The signal is consistent with all observed  $\omega \pi^+$  having proceeded through the  $\rho^+$  resonance at mass  $1349 \pm 25^{+10}_{-5}$  MeV and width  $547 \pm 86^{+46}_{-45}$  MeV.
- ALBRECHT 90J reports  $0.041 \pm 0.015 \pm 0.016$  from a measurement of  $[\Gamma(B^0 \rightarrow D^*(2010)^- \pi^+ \pi^+ \pi^- \pi^0)/\Gamma_{total}] \times [B(D^*(2010)^+ \rightarrow D^0 \pi^+)]$  assuming  $B(D^*(2010)^+ \rightarrow D^0 \pi^+) = 0.57 \pm 0.06$ , which we rescale to our best value  $B(D^*(2010)^+ \rightarrow D^0 \pi^+) = (67.7 \pm 0.5) \times 10^{-2}$ . Our first error is their experiment's error and our second error is the systematic error from using our best value. Assumes equal production of  $B^+$  and  $B^0$  at the  $\Upsilon(4S)$  and uses Mark III branching fractions for the  $D$ .

### $\Gamma(D^{*-} 3\pi^+ 2\pi^-)/\Gamma_{total}$ $\Gamma_{64}/\Gamma$

VALUE (units $10^{-3}$ )	DOCUMENT ID	TECN	COMMENT
<b>4.72 ± 0.59 ± 0.71</b>	1 MAJUMDER	04	BELL $e^+e^- \rightarrow \Upsilon(4S)$
1 Assumes equal production of $B^+$ and $B^0$ at the $\Upsilon(4S)$ .			

### $\Gamma(D^*(2010)^- \omega \pi^+)/\Gamma_{total}$ $\Gamma_{65}/\Gamma$

VALUE (units $10^{-3}$ )	DOCUMENT ID	TECN	COMMENT
<b>2.46 ± 0.18 OUR AVERAGE</b>			Error includes scale factor of 1.2.
2.31 ± 0.11 ± 0.14	1 MATVIENKO	15	BELL $e^+e^- \rightarrow \Upsilon(4S)$
2.88 ± 0.21 ± 0.31	1 AUBERT	06L	BABR $e^+e^- \rightarrow \Upsilon(4S)$
2.9 ± 0.3 ± 0.4	1,2 ALEXANDER	01B	CLE2 $e^+e^- \rightarrow \Upsilon(4S)$

- Assumes equal production of  $B^+$  and  $B^0$  at the  $\Upsilon(4S)$ .
- The signal is consistent with all observed  $\omega \pi^+$  having proceeded through the  $\rho^+$  resonance at mass  $1349 \pm 25^{+10}_{-5}$  MeV and width  $547 \pm 86^{+46}_{-45}$  MeV.

### $\Gamma(\bar{D}_1^0(2430)^0 \omega, \bar{D}_1^0 \rightarrow D^{*-} \pi^+)/\Gamma_{total}$ $\Gamma_{66}/\Gamma$

VALUE (units $10^{-4}$ )	DOCUMENT ID	TECN	COMMENT
<b>2.7 ± 0.8 OUR AVERAGE</b>			

- |                       |               |     |  |
|-----------------------|---------------|-----|--|
| 2.5 ± 0.4 ± 0.8 ± 0.2 | 1,2 MATVIENKO | 15  | BELL $e^+e^- \rightarrow \Upsilon(4S)$ |
| 4.1 ± 1.2 ± 1.1       | 3 AUBERT      | 06L | BABR $e^+e^- \rightarrow \Upsilon(4S)$ |
- Assumes equal production of  $B^+$  and  $B^0$ .
  - The measurement is obtained by amplitude analysis of  $B^0 \rightarrow D^{*-} \omega \pi^+$ . The second uncertainty combines in quadrature experimental systematic and model uncertainties.
  - Obtained by fitting the events with  $\cos \theta_{D^*} < 0.5$  and scaling up the result by a factor of 4/3. No interference effects between  $B^0 \rightarrow D_1^0 \omega$  and  $D^* \omega \pi^+$  are assumed.

### $\Gamma(D^{*-} \rho(1450)^+, \rho^+ \rightarrow \omega \pi^+)/\Gamma_{total}$ $\Gamma_{67}/\Gamma$

VALUE (units $10^{-3}$ )	DOCUMENT ID	TECN	COMMENT
<b>1.07 ± 0.15 ± 0.40 ± 0.31 ± 0.13</b>	1,2 MATVIENKO	15	BELL $e^+e^- \rightarrow \Upsilon(4S)$

- Obtained by amplitude analysis of  $\bar{B}^0 \rightarrow D^{*-} \omega \pi^+$ . The second uncertainty combines in quadrature experimental systematic and model uncertainties.
- Assumes equal production of  $B^0$  and  $B^+$  at  $\Upsilon(4S)$ .

$\Gamma(\overline{D}_1^0(2420)^0 \omega, \overline{D}_1^0 \rightarrow D^{*-} \pi^+)/\Gamma_{\text{total}}$				$\Gamma_{68}/\Gamma$
VALUE (units $10^{-4}$ )	DOCUMENT ID	TECN	COMMENT	
<b><math>0.7 \pm 0.2 \pm 0.1</math></b>	1,2 MATVIENKO	15	BELL $e^+e^- \rightarrow \Upsilon(4S)$	

<sup>1</sup> Obtained by amplitude analysis of  $\overline{B}^0 \rightarrow D^{*-} \omega \pi^+$ . The second uncertainty combines in quadrature experimental systematic and model uncertainties.  
<sup>2</sup> Assumes equal production of  $B^0$  and  $B^+$  at  $\Upsilon(4S)$ .

$\Gamma(\overline{D}_2^*(2460)^0 \omega, \overline{D}_2^* \rightarrow D^{*-} \pi^+)/\Gamma_{\text{total}}$				$\Gamma_{69}/\Gamma$
VALUE (units $10^{-4}$ )	DOCUMENT ID	TECN	COMMENT	
<b><math>0.4 \pm 0.1 \pm 0.1</math></b>	1,2 MATVIENKO	15	BELL $e^+e^- \rightarrow \Upsilon(4S)$	

<sup>1</sup> Obtained by amplitude analysis of  $\overline{B}^0 \rightarrow D^{*-} \omega \pi^+$ . The second uncertainty combines in quadrature experimental systematic and model uncertainties.  
<sup>2</sup> Assumes equal production of  $B^0$  and  $B^+$  at  $\Upsilon(4S)$ .

$\Gamma(D^{*-} b_1(1235)^+, b_1^+ \rightarrow \omega \pi^+)/\Gamma_{\text{total}}$				$\Gamma_{70}/\Gamma$
VALUE	CL%	DOCUMENT ID	TECN	COMMENT
<b><math>&lt;0.7 \times 10^{-4}</math></b>	90	1 MATVIENKO	15	BELL $e^+e^- \rightarrow \Upsilon(4S)$

<sup>1</sup> Assumes equal production of  $B^0$  and  $B^+$  at  $\Upsilon(4S)$ .

$\Gamma(\overline{D}^{*-} \pi^+)/\Gamma_{\text{total}}$				$\Gamma_{71}/\Gamma$
$D^{*-}$ represents an excited state with mass $2.2 < M < 2.8$ GeV/ $c^2$ .				
VALUE (units $10^{-3}$ )	DOCUMENT ID	TECN	COMMENT	
<b><math>1.9 \pm 0.9 \pm 0.1</math></b>	1,2 AUBERT,BE	06J	BABR $e^+e^- \rightarrow \Upsilon(4S)$	

<sup>1</sup> AUBERT,BE 06J reports  $[\Gamma(\overline{B}^0 \rightarrow \overline{D}^{*-} \pi^+)/\Gamma_{\text{total}}] / [\Gamma(\overline{B}^0 \rightarrow D^- \pi^+)] = 0.77 \pm 0.22 \pm 0.29$  which we multiply by our best value  $\text{B}(B^0 \rightarrow D^- \pi^+) = (2.52 \pm 0.13) \times 10^{-3}$ . Our first error is their experiment's error and our second error is the systematic error from using our best value.  
<sup>2</sup> Uses a missing-mass method. Does not depend on  $D$  branching fractions or  $B^+/B^0$  production rates.

$\Gamma(D_1^-(2420)^- \pi^+, D_1^- \rightarrow D^- \pi^+ \pi^-)/\Gamma_{\text{total}}$				$\Gamma_{72}/\Gamma$
VALUE (units $10^{-4}$ )	DOCUMENT ID	TECN	COMMENT	
<b><math>0.99 \pm_{-0.25}^{+0.29}</math></b>	<b>OUR FIT</b>			
<b><math>0.89 \pm 0.15 \pm_{-0.32}^{+0.17}</math></b>	1 ABE	05A	BELL $e^+e^- \rightarrow \Upsilon(4S)$	

<sup>1</sup> Assumes equal production of  $B^+$  and  $B^0$  at the  $\Upsilon(4S)$ .

$\Gamma(D_1^-(2420)^- \pi^+, D_1^- \rightarrow D^- \pi^+ \pi^-)/\Gamma(D^- \pi^+ \pi^+ \pi^-)$				$\Gamma_{72}/\Gamma_{46}$
VALUE (units $10^{-2}$ )	DOCUMENT ID	TECN	COMMENT	
<b><math>1.65 \pm_{-0.40}^{+0.35}</math></b>	<b>OUR FIT</b>			
<b><math>2.1 \pm 0.5 \pm_{-0.5}^{+0.3}</math></b>	AAIJ	11E	LHCb $pp$ at 7 TeV	

$\Gamma(D_1^-(2420)^- \pi^+, D_1^- \rightarrow D^{*-} \pi^+ \pi^-)/\Gamma_{\text{total}}$				$\Gamma_{73}/\Gamma$
VALUE (units $10^{-4}$ )	CL%	DOCUMENT ID	TECN	COMMENT
<b><math>&lt;0.33</math></b>	90	1 ABE	05A	BELL $e^+e^- \rightarrow \Upsilon(4S)$

<sup>1</sup> Assumes equal production of  $B^+$  and  $B^0$  at the  $\Upsilon(4S)$ .

$\Gamma(D^*(2010)^- \pi^+ \pi^+ \pi^-)/\Gamma(D^*(2010)^- \pi^+)$				$\Gamma_{57}/\Gamma_{44}$
VALUE	DOCUMENT ID	TECN	COMMENT	
<b><math>2.64 \pm 0.04 \pm 0.13</math></b>	AAIJ	13A0	LHCb $pp$ at 7 TeV	

$\Gamma(\overline{D}_2^*(2460)^- \pi^+, (D_2^*)^- \rightarrow D^0 \pi^-)/\Gamma_{\text{total}}$				$\Gamma_{74}/\Gamma$
VALUE (units $10^{-4}$ )	CL%	DOCUMENT ID	TECN	COMMENT
<b><math>2.38 \pm 0.16</math></b>	<b>OUR AVERAGE</b>			
$2.44 \pm 0.07 \pm 0.16$	1 AAJJ	15Y	LHCb $pp$ at 7, 8 TeV	
$2.15 \pm 0.17 \pm 0.31$	2,3 KUZMIN	07	BELL $e^+e^- \rightarrow \Upsilon(4S)$	

• • • We do not use the following data for averages, fits, limits, etc. • • •  
 $<14.7$  90 2 ALAM 94 CLE2  $e^+e^- \rightarrow \Upsilon(4S)$   
<sup>1</sup> Result obtained using the isobar formalism. The second uncertainty combines in quadrature all systematic uncertainties quoted in the paper.  
<sup>2</sup> Assumes equal production of  $B^+$  and  $B^0$  at the  $\Upsilon(4S)$ .  
<sup>3</sup> Our second uncertainty combines systematics and model errors quoted in the paper.

$\Gamma(\overline{D}_0^*(2400)^- \pi^+, (D_0^*)^- \rightarrow D^0 \pi^-)/\Gamma_{\text{total}}$				$\Gamma_{75}/\Gamma$
VALUE (units $10^{-4}$ )	DOCUMENT ID	TECN	COMMENT	
<b><math>0.76 \pm 0.08</math></b>	<b>OUR AVERAGE</b>			
$0.77 \pm 0.05 \pm 0.06$	1 AAJJ	15Y	LHCb $pp$ at 7, 8 TeV	
$0.60 \pm 0.13 \pm 0.27$	2,3 KUZMIN	07	BELL $e^+e^- \rightarrow \Upsilon(4S)$	

<sup>1</sup> Result obtained using the isobar formalism. The second uncertainty combines in quadrature all systematic uncertainties quoted in the paper.  
<sup>2</sup> Assumes equal production of  $B^+$  and  $B^0$  at the  $\Upsilon(4S)$ .  
<sup>3</sup> Our second uncertainty combines systematics and model errors quoted in the paper.

$\Gamma(D_2^*(2460)^- \pi^+, (D_2^*)^- \rightarrow D^{*-} \pi^+ \pi^-)/\Gamma_{\text{total}}$				$\Gamma_{76}/\Gamma$
VALUE (units $10^{-4}$ )	CL%	DOCUMENT ID	TECN	COMMENT
<b><math>&lt;0.24</math></b>	90	1 ABE	05A	BELL $e^+e^- \rightarrow \Upsilon(4S)$

<sup>1</sup> Assumes equal production of  $B^+$  and  $B^0$  at the  $\Upsilon(4S)$ .

$\Gamma(\overline{D}_2^*(2460)^- \rho^+)/\Gamma_{\text{total}}$				$\Gamma_{77}/\Gamma$
VALUE	CL%	DOCUMENT ID	TECN	COMMENT
<b><math>&lt;0.0049</math></b>	90	1 ALAM	94	CLE2 $e^+e^- \rightarrow \Upsilon(4S)$

<sup>1</sup> ALAM 94 assumes equal production of  $B^+$  and  $B^0$  at the  $\Upsilon(4S)$  and use the CLEO II absolute  $\text{B}(D^0 \rightarrow K^- \pi^+)$  and  $\text{B}(D_2^*(2460)^+ \rightarrow D^0 \pi^+) = 30\%$ .

$\Gamma(D^0 \overline{D}^0)/\Gamma_{\text{total}}$				$\Gamma_{78}/\Gamma$
VALUE (units $10^{-4}$ )	CL%	DOCUMENT ID	TECN	COMMENT
<b><math>0.14 \pm 0.06 \pm 0.03</math></b>		1 AAJJ	13AP	LHCb $pp$ at 7 TeV
$<0.43$	90	2 ADACHI	08	BELL $e^+e^- \rightarrow \Upsilon(4S)$
$<0.6$	90	2 AUBERT,B	06A	BABR $e^+e^- \rightarrow \Upsilon(4S)$

• • • We do not use the following data for averages, fits, limits, etc. • • •  
<sup>1</sup> Uses  $\text{B}(B^0 \rightarrow D^- D^+) = (2.11 \pm 0.31) \times 10^{-4}$  and  $\text{B}(B^+ \rightarrow \overline{D}^0 D_s^+) = (10.1 \pm 1.7) \times 10^{-3}$ .  
<sup>2</sup> Assumes equal production of  $B^+$  and  $B^0$  at the  $\Upsilon(4S)$ .

$\Gamma(D^{*0} \overline{D}^0)/\Gamma_{\text{total}}$				$\Gamma_{79}/\Gamma$
VALUE (units $10^{-4}$ )	CL%	DOCUMENT ID	TECN	COMMENT
<b><math>&lt;2.9</math></b>	90	1 AUBERT,B	06A	BABR $e^+e^- \rightarrow \Upsilon(4S)$

<sup>1</sup> Assumes equal production of  $B^+$  and  $B^0$  at the  $\Upsilon(4S)$ .

$\Gamma(D^- D^+)/\Gamma_{\text{total}}$				$\Gamma_{80}/\Gamma$
VALUE (units $10^{-4}$ )	CL%	DOCUMENT ID	TECN	COMMENT
<b><math>2.11 \pm 0.18</math></b>	<b>OUR AVERAGE</b>			
$2.12 \pm 0.16 \pm 0.18$	1 ROHRKEN	12	BELL $e^+e^- \rightarrow \Upsilon(4S)$	
$1.97 \pm 0.20 \pm 0.20$	1 FRATINA	07	BELL $e^+e^- \rightarrow \Upsilon(4S)$	
$2.8 \pm 0.4 \pm 0.5$	1 AUBERT,B	06A	BABR $e^+e^- \rightarrow \Upsilon(4S)$	
$1.91 \pm 0.51 \pm 0.30$	1 MAJUMDER	05	BELL Repl. by FRATINA 07	
$<9.4$	90	1 LIPELES	00	CLE2 $e^+e^- \rightarrow \Upsilon(4S)$
$<59$	90	BARATE	98Q	ALEP $e^+e^- \rightarrow Z$
$<12$	90	ASNER	97	CLE2 $e^+e^- \rightarrow \Upsilon(4S)$

• • • We do not use the following data for averages, fits, limits, etc. • • •  
<sup>1</sup> Assumes equal production of  $B^+$  and  $B^0$  at the  $\Upsilon(4S)$ .

$\Gamma(D^\pm D^{*\mp} (CP\text{-averaged}))/\Gamma_{\text{total}}$				$\Gamma_{81}/\Gamma$
VALUE (units $10^{-4}$ )	DOCUMENT ID	TECN	COMMENT	
<b><math>6.14 \pm 0.29 \pm 0.50</math></b>	1 ROHRKEN	12	BELL $e^+e^- \rightarrow \Upsilon(4S)$	

<sup>1</sup> Assumes equal production of  $B^+$  and  $B^0$  at the  $\Upsilon(4S)$ .

$\Gamma(D^- D_s^+)/\Gamma_{\text{total}}$				$\Gamma_{82}/\Gamma$
VALUE	EVT%	DOCUMENT ID	TECN	COMMENT
<b><math>0.0072 \pm 0.0008</math></b>	<b>OUR AVERAGE</b>			
$0.0073 \pm 0.0004 \pm 0.0007$	1 ZUPANC	07	BELL $e^+e^- \rightarrow \Upsilon(4S)$	
$0.0066 \pm 0.0014 \pm 0.0006$	2 AUBERT	06N	BABR $e^+e^- \rightarrow \Upsilon(4S)$	
$0.0068 \pm 0.0024 \pm 0.0006$	3 GIBAUT	96	CLE2 $e^+e^- \rightarrow \Upsilon(4S)$	
$0.010 \pm 0.009 \pm 0.001$	4 ALBRECHT	92G	ARG $e^+e^- \rightarrow \Upsilon(4S)$	
$0.0053 \pm 0.0030 \pm 0.0005$	5 BORTOLETTO92	CLEO	$e^+e^- \rightarrow \Upsilon(4S)$	
$0.012 \pm 0.007$	3 6 BORTOLETTO90	CLEO	$e^+e^- \rightarrow \Upsilon(4S)$	

• • • We do not use the following data for averages, fits, limits, etc. • • •  
<sup>1</sup> ZUPANC 07 reports  $(7.5 \pm 0.2 \pm 1.1) \times 10^{-3}$  from a measurement of  $[\Gamma(B^0 \rightarrow D^- D_s^+)/\Gamma_{\text{total}}] \times [\text{B}(D_s^+ \rightarrow \phi \pi^+)]$  assuming  $\text{B}(D_s^+ \rightarrow \phi \pi^+) = (4.4 \pm 0.6) \times 10^{-2}$ , which we rescale to our best value  $\text{B}(D_s^+ \rightarrow \phi \pi^+) = (4.5 \pm 0.4) \times 10^{-2}$ . Our first error is their experiment's error and our second error is the systematic error from using our best value.  
<sup>2</sup> AUBERT 06N reports  $(0.64 \pm 0.13 \pm 0.10) \times 10^{-2}$  from a measurement of  $[\Gamma(B^0 \rightarrow D^- D_s^+)/\Gamma_{\text{total}}] \times [\text{B}(D_s^+ \rightarrow \phi \pi^+)]$  assuming  $\text{B}(D_s^+ \rightarrow \phi \pi^+) = 0.0462 \pm 0.0062$ , which we rescale to our best value  $\text{B}(D_s^+ \rightarrow \phi \pi^+) = (4.5 \pm 0.4) \times 10^{-2}$ . Our first error is their experiment's error and our second error is the systematic error from using our best value.  
<sup>3</sup> GIBAUT 96 reports  $0.0087 \pm 0.0024 \pm 0.0020$  from a measurement of  $[\Gamma(B^0 \rightarrow D^- D_s^+)/\Gamma_{\text{total}}] \times [\text{B}(D_s^+ \rightarrow \phi \pi^+)]$  assuming  $\text{B}(D_s^+ \rightarrow \phi \pi^+) = 0.035$ , which we rescale to our best value  $\text{B}(D_s^+ \rightarrow \phi \pi^+) = (4.5 \pm 0.4) \times 10^{-2}$ . Our first error is their experiment's error and our second error is the systematic error from using our best value.  
<sup>4</sup> ALBRECHT 92G reports  $0.017 \pm 0.013 \pm 0.006$  from a measurement of  $[\Gamma(B^0 \rightarrow D^- D_s^+)/\Gamma_{\text{total}}] \times [\text{B}(D_s^+ \rightarrow \phi \pi^+)]$  assuming  $\text{B}(D_s^+ \rightarrow \phi \pi^+) = 0.027$ , which we rescale to our best value  $\text{B}(D_s^+ \rightarrow \phi \pi^+) = (4.5 \pm 0.4) \times 10^{-2}$ . Our first error is their experiment's error and our second error is the systematic error from using our best value. Assumes PDG 1990  $D^+$  branching ratios, e.g.,  $\text{B}(D^+ \rightarrow K^- 2\pi^+) = 7.7 \pm 1.0\%$ .  
<sup>5</sup> BORTOLETTO 92 reports  $0.0080 \pm 0.0045 \pm 0.0030$  from a measurement of  $[\Gamma(B^0 \rightarrow D^- D_s^+)/\Gamma_{\text{total}}] \times [\text{B}(D_s^+ \rightarrow \phi \pi^+)]$  assuming  $\text{B}(D_s^+ \rightarrow \phi \pi^+) = 0.030 \pm 0.011$ , which we rescale to our best value  $\text{B}(D_s^+ \rightarrow \phi \pi^+) = (4.5 \pm 0.4) \times 10^{-2}$ . Our first error is their experiment's error and our second error is the systematic error from using our best value. Assumes equal production of  $B^+$  and  $B^0$  at the  $\Upsilon(4S)$  and uses Mark III branching fractions for the  $D$ .  
<sup>6</sup> BORTOLETTO 90 assume  $\text{B}(D_s \rightarrow \phi \pi^+) = 2\%$ . Superseded by BORTOLETTO 92.

# Meson Particle Listings

## $B^0$

### $\Gamma(D^*(2010)^- D_s^+)/\Gamma_{total}$ $\Gamma_{83}/\Gamma$

VALUE	EVTS	DOCUMENT ID	TECN	COMMENT
<b>0.0080 ± 0.0011 OUR AVERAGE</b>				
0.0073 ± 0.0013 ± 0.0007		1 AUBERT 06N	BABR	$e^+e^- \rightarrow \Upsilon(4S)$
0.0083 ± 0.0015 ± 0.0007		2 AUBERT 03i	BABR	$e^+e^- \rightarrow \Upsilon(4S)$
0.0088 ± 0.0017 ± 0.0008		3 AHMED 00b	CLE2	$e^+e^- \rightarrow \Upsilon(4S)$
0.008 ± 0.006 ± 0.001		4 ALBRECHT 92G	ARG	$e^+e^- \rightarrow \Upsilon(4S)$
0.011 ± 0.006 ± 0.001		5 BORTOLETTO92	CLEO	$e^+e^- \rightarrow \Upsilon(4S)$
••• We do not use the following data for averages, fits, limits, etc. •••				
0.0072 ± 0.0022 ± 0.0006		6 GIBAUT 96	CLE2	Repl. by AHMED 00b
0.024 ± 0.014	3	7 BORTOLETTO90	CLEO	$e^+e^- \rightarrow \Upsilon(4S)$

- AUBERT 06N reports  $(0.71 \pm 0.13 \pm 0.09) \times 10^{-2}$  from a measurement of  $[\Gamma(B^0 \rightarrow D^*(2010)^- D_s^+)/\Gamma_{total}] \times [B(D_s^+ \rightarrow \phi\pi^+)]$  assuming  $B(D_s^+ \rightarrow \phi\pi^+) = 0.0462 \pm 0.0062$ , which we rescale to our best value  $B(D_s^+ \rightarrow \phi\pi^+) = (4.5 \pm 0.4) \times 10^{-2}$ . Our first error is their experiment's error and our second error is the systematic error from using our best value.
- AUBERT 03i reports  $0.0103 \pm 0.0014 \pm 0.0013$  from a measurement of  $[\Gamma(B^0 \rightarrow D^*(2010)^- D_s^+)/\Gamma_{total}] \times [B(D_s^+ \rightarrow \phi\pi^+)]$  assuming  $B(D_s^+ \rightarrow \phi\pi^+) = 0.036$ , which we rescale to our best value  $B(D_s^+ \rightarrow \phi\pi^+) = (4.5 \pm 0.4) \times 10^{-2}$ . Our first error is their experiment's error and our second error is the systematic error from using our best value.
- AHMED 00b reports  $0.0110 \pm 0.0018 \pm 0.0011$  from a measurement of  $[\Gamma(B^0 \rightarrow D^*(2010)^- D_s^+)/\Gamma_{total}] \times [B(D_s^+ \rightarrow \phi\pi^+)]$  assuming  $B(D_s^+ \rightarrow \phi\pi^+) = 0.036$ , which we rescale to our best value  $B(D_s^+ \rightarrow \phi\pi^+) = (4.5 \pm 0.4) \times 10^{-2}$ . Our first error is their experiment's error and our second error is the systematic error from using our best value.
- ALBRECHT 92G reports  $0.014 \pm 0.010 \pm 0.003$  from a measurement of  $[\Gamma(B^0 \rightarrow D^*(2010)^- D_s^+)/\Gamma_{total}] \times [B(D_s^+ \rightarrow \phi\pi^+)]$  assuming  $B(D_s^+ \rightarrow \phi\pi^+) = 0.027$ , which we rescale to our best value  $B(D_s^+ \rightarrow \phi\pi^+) = (4.5 \pm 0.4) \times 10^{-2}$ . Our first error is their experiment's error and our second error is the systematic error from using our best value. Assumes PDG 1990  $D^+$  and  $D^*(2010)^+$  branching ratios, e.g.,  $B(D^0 \rightarrow K^-\pi^+) = 3.71 \pm 0.25\%$ ,  $B(D^+ \rightarrow K^-2\pi^+) = 7.1 \pm 1.0\%$ , and  $B(D^*(2010)^+ \rightarrow D^0\pi^+) = 55 \pm 4\%$ .
- BORTOLETTO 92 reports  $0.016 \pm 0.009 \pm 0.006$  from a measurement of  $[\Gamma(B^0 \rightarrow D^*(2010)^- D_s^+)/\Gamma_{total}] \times [B(D_s^+ \rightarrow \phi\pi^+)]$  assuming  $B(D_s^+ \rightarrow \phi\pi^+) = 0.030 \pm 0.011$ , which we rescale to our best value  $B(D_s^+ \rightarrow \phi\pi^+) = (4.5 \pm 0.4) \times 10^{-2}$ . Our first error is their experiment's error and our second error is the systematic error from using our best value. Assumes equal production of  $B^+$  and  $B^0$  at the  $\Upsilon(4S)$  and uses Mark III branching fractions for the  $D$  and  $D^*(2010)$ .
- GIBAUT 96 reports  $0.0093 \pm 0.0023 \pm 0.0016$  from a measurement of  $[\Gamma(B^0 \rightarrow D^*(2010)^- D_s^+)/\Gamma_{total}] \times [B(D_s^+ \rightarrow \phi\pi^+)]$  assuming  $B(D_s^+ \rightarrow \phi\pi^+) = 0.035$ , which we rescale to our best value  $B(D_s^+ \rightarrow \phi\pi^+) = (4.5 \pm 0.4) \times 10^{-2}$ . Our first error is their experiment's error and our second error is the systematic error from using our best value.
- BORTOLETTO 90 assume  $B(D_s \rightarrow \phi\pi^+) = 2\%$ . Superseded by BORTOLETTO 92.

### $\Gamma(D^- D_s^+)/\Gamma_{total}$ $\Gamma_{84}/\Gamma$

VALUE	DOCUMENT ID	TECN	COMMENT
<b>0.0074 ± 0.0016 OUR AVERAGE</b>			
0.0071 ± 0.0016 ± 0.0006	1 AUBERT 06N	BABR	$e^+e^- \rightarrow \Upsilon(4S)$
0.0078 ± 0.0032 ± 0.0007	2 GIBAUT 96	CLE2	$e^+e^- \rightarrow \Upsilon(4S)$
0.016 ± 0.012 ± 0.001	3 ALBRECHT 92G	ARG	$e^+e^- \rightarrow \Upsilon(4S)$

- AUBERT 06n reports  $(0.69 \pm 0.16 \pm 0.09) \times 10^{-2}$  from a measurement of  $[\Gamma(B^0 \rightarrow D^- D_s^+)/\Gamma_{total}] \times [B(D_s^+ \rightarrow \phi\pi^+)]$  assuming  $B(D_s^+ \rightarrow \phi\pi^+) = 0.0462 \pm 0.0062$ , which we rescale to our best value  $B(D_s^+ \rightarrow \phi\pi^+) = (4.5 \pm 0.4) \times 10^{-2}$ . Our first error is their experiment's error and our second error is the systematic error from using our best value.
- GIBAUT 96 reports  $0.0100 \pm 0.0035 \pm 0.0022$  from a measurement of  $[\Gamma(B^0 \rightarrow D^- D_s^+)/\Gamma_{total}] \times [B(D_s^+ \rightarrow \phi\pi^+)]$  assuming  $B(D_s^+ \rightarrow \phi\pi^+) = 0.035$ , which we rescale to our best value  $B(D_s^+ \rightarrow \phi\pi^+) = (4.5 \pm 0.4) \times 10^{-2}$ . Our first error is their experiment's error and our second error is the systematic error from using our best value.
- ALBRECHT 92G reports  $0.027 \pm 0.017 \pm 0.009$  from a measurement of  $[\Gamma(B^0 \rightarrow D^- D_s^+)/\Gamma_{total}] \times [B(D_s^+ \rightarrow \phi\pi^+)]$  assuming  $B(D_s^+ \rightarrow \phi\pi^+) = 0.027$ , which we rescale to our best value  $B(D_s^+ \rightarrow \phi\pi^+) = (4.5 \pm 0.4) \times 10^{-2}$ . Our first error is their experiment's error and our second error is the systematic error from using our best value. Assumes PDG 1990  $D^+$  branching ratios, e.g.,  $B(D^+ \rightarrow K^-2\pi^+) = 7.7 \pm 1.0\%$ .

### $\Gamma(D^*(2010)^- D_s^{*+})/\Gamma_{total}$ $\Gamma_{85}/\Gamma$

VALUE	DOCUMENT ID	TECN	COMMENT
<b>0.0177 ± 0.0014 OUR AVERAGE</b>			
0.0173 ± 0.0018 ± 0.0015	1 AUBERT 06N	BABR	$e^+e^- \rightarrow \Upsilon(4S)$
0.0188 ± 0.0009 ± 0.0017	2 AUBERT 05v	BABR	$e^+e^- \rightarrow \Upsilon(4S)$
0.0158 ± 0.0027 ± 0.0014	3 AUBERT 03i	BABR	$e^+e^- \rightarrow \Upsilon(4S)$
0.015 ± 0.004 ± 0.001	4 AHMED 00b	CLE2	$e^+e^- \rightarrow \Upsilon(4S)$
0.016 ± 0.009 ± 0.001	5 ALBRECHT 92G	ARG	$e^+e^- \rightarrow \Upsilon(4S)$
••• We do not use the following data for averages, fits, limits, etc. •••			
0.016 ± 0.005 ± 0.001	6 GIBAUT 96	CLE2	Repl. by AHMED 00b

- AUBERT 06N reports  $(1.68 \pm 0.21 \pm 0.19) \times 10^{-2}$  from a measurement of  $[\Gamma(B^0 \rightarrow D^*(2010)^- D_s^{*+})/\Gamma_{total}] \times [B(D_s^+ \rightarrow \phi\pi^+)]$  assuming  $B(D_s^+ \rightarrow \phi\pi^+) = 0.0462 \pm$

0.0062, which we rescale to our best value  $B(D_s^+ \rightarrow \phi\pi^+) = (4.5 \pm 0.4) \times 10^{-2}$ . Our first error is their experiment's error and our second error is the systematic error from using our best value.

- A partial reconstruction technique is used and the result is independent of the particle decay rate of  $D_s^+$  meson. It also provides a model-independent determination of  $B(D_s^+ \rightarrow \phi\pi^+) = (4.81 \pm 0.52 \pm 0.38)\%$ .
- AUBERT 03i reports  $0.0197 \pm 0.0015 \pm 0.0030$  from a measurement of  $[\Gamma(B^0 \rightarrow D^*(2010)^- D_s^{*+})/\Gamma_{total}] \times [B(D_s^+ \rightarrow \phi\pi^+)]$  assuming  $B(D_s^+ \rightarrow \phi\pi^+) = 0.036$ , which we rescale to our best value  $B(D_s^+ \rightarrow \phi\pi^+) = (4.5 \pm 0.4) \times 10^{-2}$ . Our first error is their experiment's error and our second error is the systematic error from using our best value.
- AHMED 00b reports  $0.0182 \pm 0.0037 \pm 0.0025$  from a measurement of  $[\Gamma(B^0 \rightarrow D^*(2010)^- D_s^{*+})/\Gamma_{total}] \times [B(D_s^+ \rightarrow \phi\pi^+)]$  assuming  $B(D_s^+ \rightarrow \phi\pi^+) = 0.036$ , which we rescale to our best value  $B(D_s^+ \rightarrow \phi\pi^+) = (4.5 \pm 0.4) \times 10^{-2}$ . Our first error is their experiment's error and our second error is the systematic error from using our best value.
- ALBRECHT 92G reports  $0.026 \pm 0.014 \pm 0.006$  from a measurement of  $[\Gamma(B^0 \rightarrow D^*(2010)^- D_s^{*+})/\Gamma_{total}] \times [B(D_s^+ \rightarrow \phi\pi^+)]$  assuming  $B(D_s^+ \rightarrow \phi\pi^+) = 0.027$ , which we rescale to our best value  $B(D_s^+ \rightarrow \phi\pi^+) = (4.5 \pm 0.4) \times 10^{-2}$ . Our first error is their experiment's error and our second error is the systematic error from using our best value. Assumes PDG 1990  $D^+$  and  $D^*(2010)^+$  branching ratios, e.g.,  $B(D^0 \rightarrow K^-\pi^+) = 3.71 \pm 0.25\%$ ,  $B(D^+ \rightarrow K^-2\pi^+) = 7.1 \pm 1.0\%$ , and  $B(D^*(2010)^+ \rightarrow D^0\pi^+) = 55 \pm 4\%$ .
- GIBAUT 96 reports  $0.0203 \pm 0.0050 \pm 0.0036$  from a measurement of  $[\Gamma(B^0 \rightarrow D^*(2010)^- D_s^{*+})/\Gamma_{total}] \times [B(D_s^+ \rightarrow \phi\pi^+)]$  assuming  $B(D_s^+ \rightarrow \phi\pi^+) = 0.035$ , which we rescale to our best value  $B(D_s^+ \rightarrow \phi\pi^+) = (4.5 \pm 0.4) \times 10^{-2}$ . Our first error is their experiment's error and our second error is the systematic error from using our best value.

### $[\Gamma(D^*(2010)^- D_s^+) + \Gamma(D^*(2010)^- D_s^{*+})]/\Gamma_{total}$ $(\Gamma_{83} + \Gamma_{85})/\Gamma$

VALUE (units $10^{-2}$ )	EVTS	DOCUMENT ID	TECN	COMMENT
<b>2.5 ± 0.4 OUR AVERAGE</b>				
2.40 ± 0.35 ± 0.22		1 AUBERT 03i	BABR	$e^+e^- \rightarrow \Upsilon(4S)$
3.3 ± 0.9 ± 0.3	22	2 BORTOLETTO90	CLEO	$e^+e^- \rightarrow \Upsilon(4S)$

- AUBERT 03i reports  $(3.00 \pm 0.19 \pm 0.39) \times 10^{-2}$  from a measurement of  $[\Gamma(B^0 \rightarrow D^*(2010)^- D_s^+) + \Gamma(B^0 \rightarrow D^*(2010)^- D_s^{*+})]/\Gamma_{total}] \times [B(D_s^+ \rightarrow \phi\pi^+)]$  assuming  $B(D_s^+ \rightarrow \phi\pi^+) = 0.036$ , which we rescale to our best value  $B(D_s^+ \rightarrow \phi\pi^+) = (4.5 \pm 0.4) \times 10^{-2}$ . Our first error is their experiment's error and our second error is the systematic error from using our best value.
- BORTOLETTO 90 reports  $(7.5 \pm 2.0) \times 10^{-2}$  from a measurement of  $[\Gamma(B^0 \rightarrow D^*(2010)^- D_s^+) + \Gamma(B^0 \rightarrow D^*(2010)^- D_s^{*+})]/\Gamma_{total}] \times [B(D_s^+ \rightarrow \phi\pi^+)]$  assuming  $B(D_s^+ \rightarrow \phi\pi^+) = 0.02$ , which we rescale to our best value  $B(D_s^+ \rightarrow \phi\pi^+) = (4.5 \pm 0.4) \times 10^{-2}$ . Our first error is their experiment's error and our second error is the systematic error from using our best value.

### $\Gamma(D_{s0}(2317)^- K^+, D_{s0}^- \rightarrow D_s^- \pi^0)/\Gamma_{total}$ $\Gamma_{86}/\Gamma$

VALUE (units $10^{-5}$ )	DOCUMENT ID	TECN	COMMENT
<b>4.2 ± 1.4 ± 0.4</b>			
	1 DRUTSKOY 05	BELL	$e^+e^- \rightarrow \Upsilon(4S)$

- DRUTSKOY 05 reports  $(5.3^{+1.5}_{-1.3} \pm 1.6) \times 10^{-5}$  from a measurement of  $[\Gamma(B^0 \rightarrow D_{s0}(2317)^- K^+, D_{s0}^- \rightarrow D_s^- \pi^0)/\Gamma_{total}] \times [B(D_s^+ \rightarrow \phi\pi^+)]$  assuming  $B(D_s^+ \rightarrow \phi\pi^+) = 0.036 \pm 0.009$ , which we rescale to our best value  $B(D_s^+ \rightarrow \phi\pi^+) = (4.5 \pm 0.4) \times 10^{-2}$ . Our first error is their experiment's error and our second error is the systematic error from using our best value.

### $\Gamma(D_{s0}(2317)^- \pi^+, D_{s0}^- \rightarrow D_s^- \pi^0)/\Gamma_{total}$ $\Gamma_{87}/\Gamma$

VALUE (units $10^{-5}$ )	CL%	DOCUMENT ID	TECN	COMMENT
<2.5	90	1 DRUTSKOY 05	BELL	$e^+e^- \rightarrow \Upsilon(4S)$

- Assumes equal production of  $B^+$  and  $B^0$  at the  $\Upsilon(4S)$ .

### $\Gamma(D_{sJ}(2457)^- K^+, D_{sJ}^- \rightarrow D_s^- \pi^0)/\Gamma_{total}$ $\Gamma_{88}/\Gamma$

VALUE (units $10^{-5}$ )	CL%	DOCUMENT ID	TECN	COMMENT
<0.94	90	1 DRUTSKOY 05	BELL	$e^+e^- \rightarrow \Upsilon(4S)$

- Assumes equal production of  $B^+$  and  $B^0$  at the  $\Upsilon(4S)$ .

### $\Gamma(D_{sJ}(2457)^- \pi^+, D_{sJ}^- \rightarrow D_s^- \pi^0)/\Gamma_{total}$ $\Gamma_{89}/\Gamma$

VALUE (units $10^{-5}$ )	CL%	DOCUMENT ID	TECN	COMMENT
<0.40	90	1 DRUTSKOY 05	BELL	$e^+e^- \rightarrow \Upsilon(4S)$

- Assumes equal production of  $B^+$  and  $B^0$  at the  $\Upsilon(4S)$ .

### $\Gamma(D_s^- D_s^+)/\Gamma_{total}$ $\Gamma_{90}/\Gamma$

VALUE	CL%	DOCUMENT ID	TECN	COMMENT
< 3.6 × 10 <sup>-5</sup>	90	1 ZUPANC 07	BELL	$e^+e^- \rightarrow \Upsilon(4S)$

- We do not use the following data for averages, fits, limits, etc. •••

VALUE	CL%	DOCUMENT ID	TECN	COMMENT
<10 × 10 <sup>-5</sup>	90	1 AUBERT,BE 05	BABR	$e^+e^- \rightarrow \Upsilon(4S)$

- Assumes equal production of  $B^+$  and  $B^0$  at the  $\Upsilon(4S)$ .

See key on page 999

$\Gamma(D_s^{*-} D_s^+)/\Gamma_{total}$   $\Gamma_{91}/\Gamma$

VALUE	CL%	DOCUMENT ID	TECN	COMMENT
$<1.3 \times 10^{-4}$	90	1 AUBERT,BE	05F	BABR $e^+e^- \rightarrow \Upsilon(4S)$

<sup>1</sup> Assumes equal production of  $B^+$  and  $B^0$  at the  $\Upsilon(4S)$ .

$\Gamma(D_s^{*+} D_s^+)/\Gamma_{total}$   $\Gamma_{92}/\Gamma$

VALUE	CL%	DOCUMENT ID	TECN	COMMENT
$<2.4 \times 10^{-4}$	90	1 AUBERT,BE	05F	BABR $e^+e^- \rightarrow \Upsilon(4S)$

<sup>1</sup> Assumes equal production of  $B^+$  and  $B^0$  at the  $\Upsilon(4S)$ .

$\Gamma(D_{s0}^*(2317)^+ D^- , D_{s0}^{*+} \rightarrow D_s^+ \pi^0)/\Gamma_{total}$   $\Gamma_{93}/\Gamma$

VALUE (units $10^{-3}$ )	DOCUMENT ID	TECN	COMMENT
<b><math>1.06 \pm 0.16</math> OUR AVERAGE</b>	Error includes scale factor of 1.1.		
$0.99_{-0.15}^{+0.16} \pm 0.03$	1,2 CHOI	15A	BELL $e^+e^- \rightarrow \Upsilon(4S)$
$1.4_{-0.4}^{+0.5} \pm 0.1$	2,3 AUBERT,B	04s	BABR $e^+e^- \rightarrow \Upsilon(4S)$

• • • We do not use the following data for averages, fits, limits, etc. • • •

$0.69_{-0.24}^{+0.29} \pm 0.06$  2,4 KROKOVNY 03B BELL Repl. by CHOI 15A

<sup>1</sup> CHOI 15A reports  $(10.2_{-1.2}^{+1.3} \pm 1.0 \pm 0.4) \times 10^{-4}$  from a measurement of  $[\Gamma(B^0 \rightarrow D_s^{*0}(2317)^+ D^- , D_s^{*+} \rightarrow D_s^+ \pi^0)/\Gamma_{total}] \times [B(D_s^+ \rightarrow K^+ K^- \pi^+)] \times [B(D^+ \rightarrow K^- 2\pi^+)]$  assuming  $B(D_s^+ \rightarrow K^+ K^- \pi^+) = (5.39 \pm 0.21) \times 10^{-2}$ ,  $B(D^+ \rightarrow K^- 2\pi^+) = (9.13 \pm 0.19) \times 10^{-2}$ , which we rescale to our best values  $B(D_s^+ \rightarrow K^+ K^- \pi^+) = (5.39 \pm 0.15) \times 10^{-2}$ ,  $B(D^+ \rightarrow K^- 2\pi^+) = (9.38 \pm 0.16) \times 10^{-2}$ . Our first error is their experiment's error and our second error is the systematic error from using our best values.

<sup>2</sup> Assumes equal production of  $B^+$  and  $B^0$  at the  $\Upsilon(4S)$ .

<sup>3</sup> AUBERT,B 04s reports  $(1.8 \pm 0.4_{-0.5}^{+0.7}) \times 10^{-3}$  from a measurement of  $[\Gamma(B^0 \rightarrow D_s^{*0}(2317)^+ D^- , D_s^{*+} \rightarrow D_s^+ \pi^0)/\Gamma_{total}] \times [B(D_s^+ \rightarrow \phi\pi^+)]$  assuming  $B(D_s^+ \rightarrow \phi\pi^+) = 0.036 \pm 0.009$ , which we rescale to our best value  $B(D_s^+ \rightarrow \phi\pi^+) = (4.5 \pm 0.4) \times 10^{-2}$ . Our first error is their experiment's error and our second error is the systematic error from using our best value.

<sup>4</sup> KROKOVNY 03B reports  $(0.86_{-0.26}^{+0.33} \pm 0.26) \times 10^{-3}$  from a measurement of  $[\Gamma(B^0 \rightarrow D_s^{*0}(2317)^+ D^- , D_s^{*+} \rightarrow D_s^+ \pi^0)/\Gamma_{total}] \times [B(D_s^+ \rightarrow \phi\pi^+)]$  assuming  $B(D_s^+ \rightarrow \phi\pi^+) = 0.036 \pm 0.009$ , which we rescale to our best value  $B(D_s^+ \rightarrow \phi\pi^+) = (4.5 \pm 0.4) \times 10^{-2}$ . Our first error is their experiment's error and our second error is the systematic error from using our best value.

$\Gamma(D_{s0}(2317)^+ D^- , D_{s0}^{*+} \rightarrow D_s^{*+} \gamma)/\Gamma_{total}$   $\Gamma_{94}/\Gamma$

VALUE (units $10^{-3}$ )	CL%	DOCUMENT ID	TECN	COMMENT
<b><math>&lt;0.95</math></b>	90	1 KROKOVNY 03B	BELL	$e^+e^- \rightarrow \Upsilon(4S)$

<sup>1</sup> Assumes equal production of  $B^+$  and  $B^0$  at the  $\Upsilon(4S)$ .

$\Gamma(D_{s0}(2317)^+ D^*(2010)^- , D_{s0}^{*+} \rightarrow D_s^+ \pi^0)/\Gamma_{total}$   $\Gamma_{95}/\Gamma$

VALUE (units $10^{-3}$ )	DOCUMENT ID	TECN	COMMENT
<b><math>1.5 \pm 0.4_{-0.4}^{+0.5}</math></b>	1 AUBERT,B	04s	BABR $e^+e^- \rightarrow \Upsilon(4S)$

<sup>1</sup> Assumes equal production of  $B^+$  and  $B^0$  at the  $\Upsilon(4S)$ .

$\Gamma(D_{sJ}(2457)^+ D^-)/\Gamma_{total}$   $\Gamma_{96}/\Gamma$

VALUE (units $10^{-3}$ )	DOCUMENT ID	TECN	COMMENT
<b><math>3.5 \pm 1.1</math> OUR AVERAGE</b>			
$2.6 \pm 1.5 \pm 0.7$	1 AUBERT	06N	BABR $e^+e^- \rightarrow \Upsilon(4S)$
$4.8_{-1.6}^{+2.2} \pm 1.1$	2,3 AUBERT,B	04s	BABR $e^+e^- \rightarrow \Upsilon(4S)$
$3.9_{-1.3}^{+1.5} \pm 0.9$	2,4 KROKOVNY	03B	BELL $e^+e^- \rightarrow \Upsilon(4S)$

<sup>1</sup> Uses a missing-mass method in the events that one of the  $B$  mesons is fully reconstructed.

<sup>2</sup> Assumes equal production of  $B^+$  and  $B^0$  at the  $\Upsilon(4S)$ .

<sup>3</sup> AUBERT,B 04s reports  $[\Gamma(B^0 \rightarrow D_{sJ}(2457)^+ D^-)/\Gamma_{total}] \times [B(D_{s1}(2460)^+ \rightarrow D_s^{*+} \pi^0)] = (2.3_{-0.7}^{+1.0} \pm 0.3) \times 10^{-3}$  which we divide by our best value  $B(D_{s1}(2460)^+ \rightarrow D_s^{*+} \pi^0) = (48 \pm 11) \times 10^{-2}$ . Our first error is their experiment's error and our second error is the systematic error from using our best value.

<sup>4</sup> KROKOVNY 03B reports  $[\Gamma(B^0 \rightarrow D_{sJ}(2457)^+ D^-)/\Gamma_{total}] \times [B(D_{s1}(2460)^+ \rightarrow D_s^{*+} \pi^0)] = (1.9_{-0.6}^{+0.7} \pm 0.2) \times 10^{-3}$  which we divide by our best value  $B(D_{s1}(2460)^+ \rightarrow D_s^{*+} \pi^0) = (48 \pm 11) \times 10^{-2}$ . Our first error is their experiment's error and our second error is the systematic error from using our best value.

$\Gamma(D_{sJ}(2457)^+ D^- , D_{sJ}^{*+} \rightarrow D_s^+ \gamma)/\Gamma_{total}$   $\Gamma_{97}/\Gamma$

VALUE (units $10^{-3}$ )	DOCUMENT ID	TECN	COMMENT
<b><math>0.65_{-0.14}^{+0.17}</math> OUR AVERAGE</b>			
$0.64_{-0.16}^{+0.24} \pm 0.06$	1,2 AUBERT,B	04s	BABR $e^+e^- \rightarrow \Upsilon(4S)$
$0.66_{-0.19}^{+0.21} \pm 0.06$	1,3 KROKOVNY	03B	BELL $e^+e^- \rightarrow \Upsilon(4S)$

<sup>1</sup> Assumes equal production of  $B^+$  and  $B^0$  at the  $\Upsilon(4S)$ .

<sup>2</sup> AUBERT,B 04s reports  $(0.8 \pm 0.2_{-0.2}^{+0.3}) \times 10^{-3}$  from a measurement of  $[\Gamma(B^0 \rightarrow D_{sJ}(2457)^+ D^- , D_{sJ}^{*+} \rightarrow D_s^+ \gamma)/\Gamma_{total}] \times [B(D_s^+ \rightarrow \phi\pi^+)]$  assuming  $B(D_s^+ \rightarrow \phi\pi^+) = 0.036 \pm 0.009$ , which we rescale to our best value  $B(D_s^+ \rightarrow \phi\pi^+) = (4.5 \pm 0.4) \times 10^{-2}$ . Our first error is their experiment's error and our second error is the systematic error from using our best value.

$\phi\pi^+) = 0.036 \pm 0.009$ , which we rescale to our best value  $B(D_s^+ \rightarrow \phi\pi^+) = (4.5 \pm 0.4) \times 10^{-2}$ . Our first error is their experiment's error and our second error is the systematic error from using our best value.

<sup>3</sup> KROKOVNY 03B reports  $(0.82_{-0.19}^{+0.22} \pm 0.25) \times 10^{-3}$  from a measurement of  $[\Gamma(B^0 \rightarrow D_{sJ}(2457)^+ D^- , D_{sJ}^{*+} \rightarrow D_s^+ \gamma)/\Gamma_{total}] \times [B(D_s^+ \rightarrow \phi\pi^+)]$  assuming  $B(D_s^+ \rightarrow \phi\pi^+) = 0.036 \pm 0.009$ , which we rescale to our best value  $B(D_s^+ \rightarrow \phi\pi^+) = (4.5 \pm 0.4) \times 10^{-2}$ . Our first error is their experiment's error and our second error is the systematic error from using our best value.

$\Gamma(D_{sJ}(2457)^+ D^- , D_{sJ}^{*+} \rightarrow D_s^{*+} \gamma)/\Gamma_{total}$   $\Gamma_{98}/\Gamma$

VALUE (units $10^{-3}$ )	CL%	DOCUMENT ID	TECN	COMMENT
<b><math>&lt;0.60</math></b>	90	1 KROKOVNY 03B	BELL	$e^+e^- \rightarrow \Upsilon(4S)$

<sup>1</sup> Assumes equal production of  $B^+$  and  $B^0$  at the  $\Upsilon(4S)$ .

$\Gamma(D_{sJ}(2457)^+ D^- , D_{sJ}^{*+} \rightarrow D_s^+ \pi^+ \pi^-)/\Gamma_{total}$   $\Gamma_{99}/\Gamma$

VALUE (units $10^{-3}$ )	CL%	DOCUMENT ID	TECN	COMMENT
<b><math>&lt;0.20</math></b>	90	1 KROKOVNY 03B	BELL	$e^+e^- \rightarrow \Upsilon(4S)$

<sup>1</sup> Assumes equal production of  $B^+$  and  $B^0$  at the  $\Upsilon(4S)$ .

$\Gamma(D_{sJ}(2457)^+ D^- , D_{sJ}^{*+} \rightarrow D_s^+ \pi^0)/\Gamma_{total}$   $\Gamma_{100}/\Gamma$

VALUE (units $10^{-3}$ )	CL%	DOCUMENT ID	TECN	COMMENT
<b><math>&lt;0.36</math></b>	90	1 KROKOVNY 03B	BELL	$e^+e^- \rightarrow \Upsilon(4S)$

<sup>1</sup> Assumes equal production of  $B^+$  and  $B^0$  at the  $\Upsilon(4S)$ .

$\Gamma(D^*(2010)^- D_{sJ}(2457)^+)/\Gamma_{total}$   $\Gamma_{101}/\Gamma$

VALUE (units $10^{-3}$ )	DOCUMENT ID	TECN	COMMENT
<b><math>9.3 \pm 2.2</math> OUR AVERAGE</b>			
$8.8 \pm 2.0 \pm 1.4$	1 AUBERT	06N	BABR $e^+e^- \rightarrow \Upsilon(4S)$
$11_{-4}^{+5} \pm 3$	2,3 AUBERT,B	04s	BABR $e^+e^- \rightarrow \Upsilon(4S)$

<sup>1</sup> Uses a missing-mass method in the events that one of the  $B$  mesons is fully reconstructed.

<sup>2</sup> AUBERT,B 04s reports  $[\Gamma(B^0 \rightarrow D^*(2010)^- D_{sJ}(2457)^+)/\Gamma_{total}] \times [B(D_{s1}(2460)^+ \rightarrow D_s^{*+} \pi^0)] = (5.5 \pm 1.2_{-1.6}^{+2.2}) \times 10^{-3}$  which we divide by our best value  $B(D_{s1}(2460)^+ \rightarrow D_s^{*+} \pi^0) = (48 \pm 11) \times 10^{-2}$ . Our first error is their experiment's error and our second error is the systematic error from using our best value.

<sup>3</sup> Assumes equal production of  $B^+$  and  $B^0$  at the  $\Upsilon(4S)$ .

$\Gamma(D_{sJ}(2457)^+ D^*(2010)^- , D_{sJ}^{*+} \rightarrow D_s^+ \gamma)/\Gamma_{total}$   $\Gamma_{102}/\Gamma$

VALUE (units $10^{-3}$ )	DOCUMENT ID	TECN	COMMENT
<b><math>2.3 \pm 0.3_{-0.6}^{+0.9}</math></b>	1 AUBERT,B	04s	BABR $e^+e^- \rightarrow \Upsilon(4S)$

<sup>1</sup> Assumes equal production of  $B^+$  and  $B^0$  at the  $\Upsilon(4S)$ .

$[\Gamma(D^- D_{s1}(2536)^+ , D_{s1}^{*+} \rightarrow D^{*0} K^+) + \Gamma(D^{*+} K^0)]/\Gamma_{total}$   $\Gamma_{103}/\Gamma = (\Gamma_{104} + \Gamma_{105})/\Gamma$

VALUE (units $10^{-4}$ )	DOCUMENT ID	TECN	COMMENT
<b><math>2.75 \pm 0.62 \pm 0.36</math></b>	1,2 AUSHEV	11	BELL $e^+e^- \rightarrow \Upsilon(4S)$

<sup>1</sup> Uses  $\Gamma(D^*(2007)^0 \rightarrow D^0 \pi^0) / \Gamma(D^*(2007)^0 \rightarrow D^0 \gamma) = 1.74 \pm 0.13$  and  $\Gamma(D_{s1}(2536)^+ \rightarrow D^*(2007)^0 K^+) / \Gamma(D_{s1}(2536)^+ \rightarrow D^*(2010)^+ K^0) = 1.36 \pm 0.2$ .

<sup>2</sup> Assumes equal production of  $B^+$  and  $B^0$  at the  $\Upsilon(4S)$ .

$\Gamma(D^- D_{s1}(2536)^+ , D_{s1}^{*+} \rightarrow D^{*0} K^+)/\Gamma_{total}$   $\Gamma_{104}/\Gamma$

VALUE (units $10^{-4}$ )	CL%	DOCUMENT ID	TECN	COMMENT
<b><math>1.71 \pm 0.48 \pm 0.32</math></b>	1 AUBERT	08B	BABR	$e^+e^- \rightarrow \Upsilon(4S)$

• • • We do not use the following data for averages, fits, limits, etc. • • •

$<5$  90 AUBERT 03X BABR Repl. by AUBERT 08B

<sup>1</sup> Assumes equal production of  $B^+$  and  $B^0$  at the  $\Upsilon(4S)$ .

$\Gamma(D^- D_{s1}(2536)^+ , D_{s1}^{*+} \rightarrow D^{*+} K^0)/\Gamma_{total}$   $\Gamma_{105}/\Gamma$

VALUE (units $10^{-4}$ )	DOCUMENT ID	TECN	COMMENT
<b><math>2.61 \pm 1.03 \pm 0.31</math></b>	1 AUBERT	08B	BABR $e^+e^- \rightarrow \Upsilon(4S)$

<sup>1</sup> Assumes equal production of  $B^+$  and  $B^0$  at the  $\Upsilon(4S)$ .

$[\Gamma(D^*(2010)^- D_{s1}(2536)^+ , D_{s1}^{*+} \rightarrow D^{*0} K^+) + \Gamma(D^{*+} K^0)]/\Gamma_{total}$   $\Gamma_{106}/\Gamma = (\Gamma_{107} + \Gamma_{108})/\Gamma$

VALUE (units $10^{-4}$ )	DOCUMENT ID	TECN	COMMENT
<b><math>5.01 \pm 1.21 \pm 0.70</math></b>	1,2 AUSHEV	11	BELL $e^+e^- \rightarrow \Upsilon(4S)$

<sup>1</sup> Uses  $\Gamma(D^*(2007)^0 \rightarrow D^0 \pi^0) / \Gamma(D^*(2007)^0 \rightarrow D^0 \gamma) = 1.74 \pm 0.13$  and  $\Gamma(D_{s1}(2536)^+ \rightarrow D^*(2007)^0 K^+) / \Gamma(D_{s1}(2536)^+ \rightarrow D^*(2010)^+ K^0) = 1.36 \pm 0.2$ .

<sup>2</sup> Assumes equal production of  $B^+$  and  $B^0$  at the  $\Upsilon(4S)$ .

$\Gamma(D^*(2010)^- D_{s1}(2536)^+ , D_{s1}^{*+} \rightarrow D^{*0} K^+)/\Gamma_{total}$   $\Gamma_{107}/\Gamma$

VALUE (units $10^{-4}$ )	CL%	DOCUMENT ID	TECN	COMMENT
<b><math>3.32 \pm 0.88 \pm 0.66</math></b>	1 AUBERT	08B	BABR	$e^+e^- \rightarrow \Upsilon(4S)$

• • • We do not use the following data for averages, fits, limits, etc. • • •

$<7$  90 AUBERT 03X BABR Repl. by AUBERT 08B

<sup>1</sup> Assumes equal production of  $B^+$  and  $B^0$  at the  $\Upsilon(4S)$ .



# Meson Particle Listings

## $B^0$

### $\Gamma(D^{*-} D_{s1}(2536)^+, D_{s1}^+ \rightarrow D^{*+} K^0)/\Gamma_{total}$ $\Gamma_{108}/\Gamma$

VALUE (units $10^{-4}$ )	CL%	DOCUMENT ID	TECN	COMMENT
<b>5.00 ± 1.51 ± 0.67</b>		1 AUBERT 08B	BABR	$e^+e^- \rightarrow \Upsilon(4S)$

<sup>1</sup> Assumes equal production of  $B^+$  and  $B^0$  at the  $\Upsilon(4S)$ .

### $\Gamma(D^- D_{sJ}(2573)^+, D_{sJ}^+ \rightarrow D^0 K^+)/\Gamma_{total}$ $\Gamma_{109}/\Gamma$

VALUE (units $10^{-5}$ )	CL%	DOCUMENT ID	TECN	COMMENT
<b>3.4 ± 1.7 ± 0.5</b>		1 LEES 15c	BABR	$e^+e^- \rightarrow \Upsilon(4S)$

• • • We do not use the following data for averages, fits, limits, etc. • • •

<10	90	AUBERT 03X	BABR	$e^+e^- \rightarrow \Upsilon(4S)$
-----	----	------------	------	-----------------------------------

<sup>1</sup> Assumes equal production of  $B^+$  and  $B^0$  at the  $\Upsilon(4S)$ .

### $\Gamma(D^{*+}(2010)^- D_{sJ}(2573)^+, D_{sJ}^+ \rightarrow D^0 K^+)/\Gamma_{total}$ $\Gamma_{110}/\Gamma$

VALUE (units $10^{-4}$ )	CL%	DOCUMENT ID	TECN	COMMENT
<b>&lt;2</b>	90	AUBERT 03X	BABR	$e^+e^- \rightarrow \Upsilon(4S)$

### $\Gamma(D^- D_{sJ}(2700)^+, D_{sJ}^+ \rightarrow D^0 K^+)/\Gamma_{total}$ $\Gamma_{111}/\Gamma$

VALUE (units $10^{-4}$ )	CL%	DOCUMENT ID	TECN	COMMENT
<b>7.14 ± 0.96 ± 0.69</b>		1 LEES 15c	BABR	$e^+e^- \rightarrow \Upsilon(4S)$

<sup>1</sup> Assumes equal production of  $B^+$  and  $B^0$  at the  $\Upsilon(4S)$ .

### $\Gamma(D^+ \pi^-)/\Gamma_{total}$ $\Gamma_{112}/\Gamma$

VALUE (units $10^{-7}$ )	CL%	DOCUMENT ID	TECN	COMMENT
<b>7.4 ± 1.2 ± 0.4</b>		1,2 DAS 10	BELL	$e^+e^- \rightarrow \Upsilon(4S)$

<sup>1</sup> DAS 10 reports  $[\Gamma(B^0 \rightarrow D^+ \pi^-)/\Gamma_{total}] / [B(B^0 \rightarrow D^+ \pi^-)] = (2.92 \pm 0.38 \pm 0.31) \times 10^{-4}$  which we multiply by our best value  $B(B^0 \rightarrow D^+ \pi^-) = (2.52 \pm 0.13) \times 10^{-3}$ . Our first error is their experiment's error and our second error is the systematic error from using our best value.

<sup>2</sup> Derived using  $\tan(\theta_C) f_D/f_{D_s} \sqrt{B(B^0 \rightarrow D_s^+ \pi^-)/B(B^0 \rightarrow D^+ \pi^-)}$  by assuming the flavor SU(3) symmetry, where  $\theta_C$  is the Cabibbo angle,  $f_D$  ( $f_{D_s}$ ) is the  $D$  ( $D_s$ ) meson decay constant.

### $\Gamma(D_s^+ \pi^-)/\Gamma_{total}$ $\Gamma_{113}/\Gamma$

VALUE (units $10^{-6}$ )	CL%	DOCUMENT ID	TECN	COMMENT
<b>21.6 ± 2.6 OUR AVERAGE</b>				
19.9 ± 2.6 ± 1.8		1 DAS 10	BELL	$e^+e^- \rightarrow \Upsilon(4S)$
25 ± 4 ± 2		1 AUBERT 08AJ	BABR	$e^+e^- \rightarrow \Upsilon(4S)$

• • • We do not use the following data for averages, fits, limits, etc. • • •

14.0 ± 3.5 ± 1.3		2 AUBERT 07K	BABR	Repl. by AUBERT 08AJ
25 ± 9 ± 2		3 AUBERT 03D	BABR	Repl. by AUBERT 07K
19 ± 9 ± 2		4 KROKOVNY 02	BELL	Repl. by DAS 10
< 220	90	5 ALEXANDER 93B	CLE2	$e^+e^- \rightarrow \Upsilon(4S)$
< 1300	90	6 BORTOLETTO 90	CLEO	$e^+e^- \rightarrow \Upsilon(4S)$

- <sup>1</sup> Assumes equal production of  $B^+$  and  $B^0$  at the  $\Upsilon(4S)$ .
- <sup>2</sup> AUBERT 07K reports  $[\Gamma(B^0 \rightarrow D_s^+ \pi^-)/\Gamma_{total}] \times [B(D_s^+ \rightarrow \phi \pi^+)] = (0.63 \pm 0.15 \pm 0.05) \times 10^{-6}$  which we divide by our best value  $B(D_s^+ \rightarrow \phi \pi^+) = (4.5 \pm 0.4) \times 10^{-2}$ . Our first error is their experiment's error and our second error is the systematic error from using our best value.
- <sup>3</sup> AUBERT 03D reports  $[\Gamma(B^0 \rightarrow D_s^+ \pi^-)/\Gamma_{total}] \times [B(D_s^+ \rightarrow \phi \pi^+)] = (1.13 \pm 0.33 \pm 0.21) \times 10^{-6}$  which we divide by our best value  $B(D_s^+ \rightarrow \phi \pi^+) = (4.5 \pm 0.4) \times 10^{-2}$ . Our first error is their experiment's error and our second error is the systematic error from using our best value.
- <sup>4</sup> KROKOVNY 02 reports  $[\Gamma(B^0 \rightarrow D_s^+ \pi^-)/\Gamma_{total}] \times [B(D_s^+ \rightarrow \phi \pi^+)] = (0.86^{+0.37}_{-0.30} \pm 0.11) \times 10^{-6}$  which we divide by our best value  $B(D_s^+ \rightarrow \phi \pi^+) = (4.5 \pm 0.4) \times 10^{-2}$ . Our first error is their experiment's error and our second error is the systematic error from using our best value.
- <sup>5</sup> ALEXANDER 93B reports  $< 270 \times 10^{-6}$  from a measurement of  $[\Gamma(B^0 \rightarrow D_s^+ \pi^-)/\Gamma_{total}] \times [B(D_s^+ \rightarrow \phi \pi^+)]$  assuming  $B(D_s^+ \rightarrow \phi \pi^+) = 0.037$ , which we rescale to our best value  $B(D_s^+ \rightarrow \phi \pi^+) = 4.5 \times 10^{-2}$ .
- <sup>6</sup> BORTOLETTO 90 assume  $B(D_s \rightarrow \phi \pi^+) = 2\%$ .

### $[\Gamma(D_s^+ \pi^-) + \Gamma(D_s^- K^+)]/\Gamma_{total}$ $(\Gamma_{113} + \Gamma_{123})/\Gamma$

VALUE	CL%	DOCUMENT ID	TECN	COMMENT
<b>&lt; 1.0 × 10<sup>-3</sup></b>	90	1 ALBRECHT 93E	ARG	$e^+e^- \rightarrow \Upsilon(4S)$

<sup>1</sup> ALBRECHT 93E reports  $< 1.7 \times 10^{-3}$  from a measurement of  $[\Gamma(B^0 \rightarrow D_s^+ \pi^-) + \Gamma(B^0 \rightarrow D_s^- K^+)]/\Gamma_{total} \times [B(D_s^+ \rightarrow \phi \pi^+)]$  assuming  $B(D_s^+ \rightarrow \phi \pi^+) = 0.027$ , which we rescale to our best value  $B(D_s^+ \rightarrow \phi \pi^+) = 4.5 \times 10^{-2}$ .

### $\Gamma(D_s^{*+} \pi^-)/\Gamma_{total}$ $\Gamma_{114}/\Gamma$

VALUE (units $10^{-5}$ )	CL%	DOCUMENT ID	TECN	COMMENT
<b>2.1 ± 0.4 OUR AVERAGE</b>				Error includes scale factor of 1.4.
1.75 ± 0.34 ± 0.20		1 JOSHI 10	BELL	$e^+e^- \rightarrow \Upsilon(4S)$
2.6 ± 0.5 ± 0.2		1 AUBERT 08AJ	BABR	$e^+e^- \rightarrow \Upsilon(4S)$

- • • We do not use the following data for averages, fits, limits, etc. • • •
- |                 |    |                 |      |                                   |
|-----------------|----|-----------------|------|-----------------------------------|
| 2.9 ± 0.7 ± 0.3 |    | 2 AUBERT 07K    | BABR | Repl. by AUBERT 08AJ              |
| < 4.1           | 90 | AUBERT 03D      | BABR | Repl. by AUBERT 07K               |
| < 40            | 90 | 3 ALEXANDER 93B | CLE2 | $e^+e^- \rightarrow \Upsilon(4S)$ |

- <sup>1</sup> Assumes equal production of  $B^+$  and  $B^0$  at the  $\Upsilon(4S)$ .
- <sup>2</sup> AUBERT 07K reports  $[\Gamma(B^0 \rightarrow D_s^{*+} \pi^-)/\Gamma_{total}] \times [B(D_s^+ \rightarrow \phi \pi^+)] = (1.32 \pm 0.27 \pm 0.15) \times 10^{-6}$  which we divide by our best value  $B(D_s^+ \rightarrow \phi \pi^+) = (4.5 \pm 0.4) \times 10^{-2}$ . Our first error is their experiment's error and our second error is the systematic error from using our best value.
- <sup>3</sup> ALEXANDER 93B reports  $< 44 \times 10^{-5}$  from a measurement of  $[\Gamma(B^0 \rightarrow D_s^{*+} \pi^-)/\Gamma_{total}] \times [B(D_s^+ \rightarrow \phi \pi^+)]$  assuming  $B(D_s^+ \rightarrow \phi \pi^+) = 0.037$ , which we rescale to our best value  $B(D_s^+ \rightarrow \phi \pi^+) = 4.5 \times 10^{-2}$ .

### $[\Gamma(D_s^{*+} \pi^-) + \Gamma(D_s^{*-} K^+)]/\Gamma_{total}$ $(\Gamma_{114} + \Gamma_{124})/\Gamma$

VALUE	CL%	DOCUMENT ID	TECN	COMMENT
<b>&lt; 7 × 10<sup>-4</sup></b>	90	1 ALBRECHT 93E	ARG	$e^+e^- \rightarrow \Upsilon(4S)$

<sup>1</sup> ALBRECHT 93E reports  $< 1.2 \times 10^{-3}$  from a measurement of  $[\Gamma(B^0 \rightarrow D_s^{*+} \pi^-) + \Gamma(B^0 \rightarrow D_s^{*-} K^+)]/\Gamma_{total} \times [B(D_s^+ \rightarrow \phi \pi^+)]$  assuming  $B(D_s^+ \rightarrow \phi \pi^+) = 0.027$ , which we rescale to our best value  $B(D_s^+ \rightarrow \phi \pi^+) = 4.5 \times 10^{-2}$ .

### $\Gamma(D_s^+ \rho^-)/\Gamma_{total}$ $\Gamma_{115}/\Gamma$

VALUE (units $10^{-5}$ )	CL%	DOCUMENT ID	TECN	COMMENT
<b>&lt; 2.4</b>	90	1 AUBERT 08AJ	BABR	$e^+e^- \rightarrow \Upsilon(4S)$

• • • We do not use the following data for averages, fits, limits, etc. • • •

< 130	90	2 ALBRECHT 93E	ARG	$e^+e^- \rightarrow \Upsilon(4S)$
< 50	90	3 ALEXANDER 93B	CLE2	$e^+e^- \rightarrow \Upsilon(4S)$

- <sup>1</sup> Assumes equal production of  $B^+$  and  $B^0$  at the  $\Upsilon(4S)$ .
- <sup>2</sup> ALBRECHT 93E reports  $< 2.2 \times 10^{-3}$  from a measurement of  $[\Gamma(B^0 \rightarrow D_s^+ \rho^-)/\Gamma_{total}] \times [B(D_s^+ \rightarrow \phi \pi^+)]$  assuming  $B(D_s^+ \rightarrow \phi \pi^+) = 0.027$ , which we rescale to our best value  $B(D_s^+ \rightarrow \phi \pi^+) = 4.5 \times 10^{-2}$ .
- <sup>3</sup> ALEXANDER 93B reports  $< 6.6 \times 10^{-4}$  from a measurement of  $[\Gamma(B^0 \rightarrow D_s^+ \rho^-)/\Gamma_{total}] \times [B(D_s^+ \rightarrow \phi \pi^+)]$  assuming  $B(D_s^+ \rightarrow \phi \pi^+) = 0.037$ , which we rescale to our best value  $B(D_s^+ \rightarrow \phi \pi^+) = 4.5 \times 10^{-2}$ .

### $\Gamma(D_s^{*+} \rho^-)/\Gamma_{total}$ $\Gamma_{116}/\Gamma$

VALUE (units $10^{-5}$ )	CL%	DOCUMENT ID	TECN	COMMENT
<b>4.1 ± 1.3 ± 0.4</b>		1 AUBERT 08AJ	BABR	$e^+e^- \rightarrow \Upsilon(4S)$

• • • We do not use the following data for averages, fits, limits, etc. • • •

< 150	90	2 ALBRECHT 93E	ARG	$e^+e^- \rightarrow \Upsilon(4S)$
< 60	90	3 ALEXANDER 93B	CLE2	$e^+e^- \rightarrow \Upsilon(4S)$

- <sup>1</sup> Assumes equal production of  $B^+$  and  $B^0$  at the  $\Upsilon(4S)$ .
- <sup>2</sup> ALBRECHT 93E reports  $< 2.5 \times 10^{-3}$  from a measurement of  $[\Gamma(B^0 \rightarrow D_s^{*+} \rho^-)/\Gamma_{total}] \times [B(D_s^+ \rightarrow \phi \pi^+)]$  assuming  $B(D_s^+ \rightarrow \phi \pi^+) = 0.027$ , which we rescale to our best value  $B(D_s^+ \rightarrow \phi \pi^+) = 4.5 \times 10^{-2}$ .
- <sup>3</sup> ALEXANDER 93B reports  $< 7.4 \times 10^{-4}$  from a measurement of  $[\Gamma(B^0 \rightarrow D_s^{*+} \rho^-)/\Gamma_{total}] \times [B(D_s^+ \rightarrow \phi \pi^+)]$  assuming  $B(D_s^+ \rightarrow \phi \pi^+) = 0.037$ , which we rescale to our best value  $B(D_s^+ \rightarrow \phi \pi^+) = 4.5 \times 10^{-2}$ .

### $\Gamma(D_s^+ a_0^-)/\Gamma_{total}$ $\Gamma_{117}/\Gamma$

VALUE (units $10^{-5}$ )	CL%	DOCUMENT ID	TECN	COMMENT
<b>&lt; 1.9</b>	90	1 AUBERT 06X	BABR	$e^+e^- \rightarrow \Upsilon(4S)$

<sup>1</sup> Assumes equal production of  $B^+$  and  $B^0$  at the  $\Upsilon(4S)$ .

### $\Gamma(D_s^{*+} a_0^-)/\Gamma_{total}$ $\Gamma_{118}/\Gamma$

VALUE (units $10^{-5}$ )	CL%	DOCUMENT ID	TECN	COMMENT
<b>&lt; 3.6</b>	90	1 AUBERT 06X	BABR	$e^+e^- \rightarrow \Upsilon(4S)$

<sup>1</sup> Assumes equal production of  $B^+$  and  $B^0$  at the  $\Upsilon(4S)$ .

### $\Gamma(D_s^+ a_1(1260)^-)/\Gamma_{total}$ $\Gamma_{119}/\Gamma$

VALUE	CL%	DOCUMENT ID	TECN	COMMENT
<b>&lt; 2.1 × 10<sup>-3</sup></b>	90	1 ALBRECHT 93E	ARG	$e^+e^- \rightarrow \Upsilon(4S)$

<sup>1</sup> ALBRECHT 93E reports  $< 3.5 \times 10^{-3}$  from a measurement of  $[\Gamma(B^0 \rightarrow D_s^+ a_1(1260)^-)/\Gamma_{total}] \times [B(D_s^+ \rightarrow \phi \pi^+)]$  assuming  $B(D_s^+ \rightarrow \phi \pi^+) = 0.027$ , which we rescale to our best value  $B(D_s^+ \rightarrow \phi \pi^+) = 4.5 \times 10^{-2}$ .

### $\Gamma(D_s^{*+} a_1(1260)^-)/\Gamma_{total}$ $\Gamma_{120}/\Gamma$

VALUE	CL%	DOCUMENT ID	TECN	COMMENT
<b>&lt; 1.7 × 10<sup>-3</sup></b>	90	1 ALBRECHT 93E	ARG	$e^+e^- \rightarrow \Upsilon(4S)$

<sup>1</sup> ALBRECHT 93E reports  $< 2.9 \times 10^{-3}$  from a measurement of  $[\Gamma(B^0 \rightarrow D_s^{*+} a_1(1260)^-)/\Gamma_{total}] \times [B(D_s^+ \rightarrow \phi \pi^+)]$  assuming  $B(D_s^+ \rightarrow \phi \pi^+) = 0.027$ , which we rescale to our best value  $B(D_s^+ \rightarrow \phi \pi^+) = 4.5 \times 10^{-2}$ .

$\Gamma(D_s^{*+} a_2^-)/\Gamma_{total}$					$\Gamma_{121}/\Gamma$
VALUE (units 10 <sup>-5</sup> )	CL%	DOCUMENT ID	TECN	COMMENT	
<19	90	<sup>1</sup> AUBERT	06x BABR	e <sup>+</sup> e <sup>-</sup> → $\Upsilon(4S)$	
<sup>1</sup> Assumes equal production of B <sup>+</sup> and B <sup>0</sup> at the $\Upsilon(4S)$ .					

$\Gamma(D_s^{*+} a_2^-)/\Gamma_{total}$					$\Gamma_{122}/\Gamma$
VALUE (units 10 <sup>-5</sup> )	CL%	DOCUMENT ID	TECN	COMMENT	
<20	90	<sup>1</sup> AUBERT	06x BABR	e <sup>+</sup> e <sup>-</sup> → $\Upsilon(4S)$	
<sup>1</sup> Assumes equal production of B <sup>+</sup> and B <sup>0</sup> at the $\Upsilon(4S)$ .					

$\Gamma(D_s^- K^+)/\Gamma_{total}$					$\Gamma_{123}/\Gamma$
VALUE (units 10 <sup>-6</sup> )	CL%	DOCUMENT ID	TECN	COMMENT	
<b>27 ± 5 OUR FIT</b>		Error includes scale factor of 2.7.			
<b>22 ± 5 OUR AVERAGE</b>		Error includes scale factor of 1.8.			
19.1 ± 2.4 ± 1.7		<sup>1</sup> DAS	10 BELL	e <sup>+</sup> e <sup>-</sup> → $\Upsilon(4S)$	
29 ± 4 ± 2		<sup>1</sup> AUBERT	08AJ BABR	e <sup>+</sup> e <sup>-</sup> → $\Upsilon(4S)$	
• • • We do not use the following data for averages, fits, limits, etc. • • •					
27 ± 5 ± 2		<sup>2</sup> AUBERT	07k BABR	Repl. by AUBERT 08AJ	
26 ± 10 ± 2		<sup>3</sup> AUBERT	03D BABR	Repl. by AUBERT 07k	
36 +11 ± 3		<sup>4</sup> KROKOVNY	02 BELL	Repl. by DAS 10	
< 190	90	<sup>5</sup> ALEXANDER	93B CLE2	e <sup>+</sup> e <sup>-</sup> → $\Upsilon(4S)$	
<1300	90	<sup>6</sup> BORTOLETTO	090 CLEO	e <sup>+</sup> e <sup>-</sup> → $\Upsilon(4S)$	

<sup>1</sup> Assumes equal production of B<sup>+</sup> and B<sup>0</sup> at the  $\Upsilon(4S)$ .  
<sup>2</sup> AUBERT 07k reports  $[\Gamma(B^0 \rightarrow D_s^- K^+)/\Gamma_{total}] \times [B(D_s^+ \rightarrow \phi\pi^+)] = (1.21 \pm 0.17 \pm 0.11) \times 10^{-6}$  which we divide by our best value  $B(D_s^+ \rightarrow \phi\pi^+) = (4.5 \pm 0.4) \times 10^{-2}$ . Our first error is their experiment's error and our second error is the systematic error from using our best value.  
<sup>3</sup> AUBERT 03D reports  $[\Gamma(B^0 \rightarrow D_s^- K^+)/\Gamma_{total}] \times [B(D_s^+ \rightarrow \phi\pi^+)] = (1.16 \pm 0.36 \pm 0.24) \times 10^{-6}$  which we divide by our best value  $B(D_s^+ \rightarrow \phi\pi^+) = (4.5 \pm 0.4) \times 10^{-2}$ . Our first error is their experiment's error and our second error is the systematic error from using our best value.  
<sup>4</sup> KROKOVNY 02 reports  $[\Gamma(B^0 \rightarrow D_s^- K^+)/\Gamma_{total}] \times [B(D_s^+ \rightarrow \phi\pi^+)] = (1.61 \pm 0.45 \pm 0.38 \pm 0.21) \times 10^{-6}$  which we divide by our best value  $B(D_s^+ \rightarrow \phi\pi^+) = (4.5 \pm 0.4) \times 10^{-2}$ . Our first error is their experiment's error and our second error is the systematic error from using our best value.  
<sup>5</sup> ALEXANDER 93B reports < 230 × 10<sup>-6</sup> from a measurement of  $[\Gamma(B^0 \rightarrow D_s^- K^+)/\Gamma_{total}] \times [B(D_s^+ \rightarrow \phi\pi^+)]$  assuming  $B(D_s^+ \rightarrow \phi\pi^+) = 0.037$ , which we rescale to our best value  $B(D_s^+ \rightarrow \phi\pi^+) = 4.5 \times 10^{-2}$ .  
<sup>6</sup> BORTOLETTO 90 assume  $B(D_s \rightarrow \phi\pi^+) = 2\%$ .

$\Gamma(D_s^{*-} K^+)/\Gamma_{total}$					$\Gamma_{124}/\Gamma$
VALUE (units 10 <sup>-5</sup> )	CL%	DOCUMENT ID	TECN	COMMENT	
<b>2.19 ± 0.30 OUR AVERAGE</b>					
2.02 ± 0.33 ± 0.22		<sup>1</sup> JOSHI	10 BELL	e <sup>+</sup> e <sup>-</sup> → $\Upsilon(4S)$	
2.4 ± 0.4 ± 0.2		<sup>1</sup> AUBERT	08AJ BABR	e <sup>+</sup> e <sup>-</sup> → $\Upsilon(4S)$	
• • • We do not use the following data for averages, fits, limits, etc. • • •					
2.2 ± 0.6 ± 0.2		<sup>2</sup> AUBERT	07k BABR	Repl. by AUBERT 08AJ	
< 2.5	90	AUBERT	03D BABR	Repl. by AUBERT 07k	
<14	90	<sup>3</sup> ALEXANDER	93B CLE2	e <sup>+</sup> e <sup>-</sup> → $\Upsilon(4S)$	

<sup>1</sup> Assumes equal production of B<sup>+</sup> and B<sup>0</sup> at the  $\Upsilon(4S)$ .  
<sup>2</sup> AUBERT 07k reports  $[\Gamma(B^0 \rightarrow D_s^{*-} K^+)/\Gamma_{total}] \times [B(D_s^+ \rightarrow \phi\pi^+)] = (0.97 \pm 0.24 \pm 0.12) \times 10^{-6}$  which we divide by our best value  $B(D_s^+ \rightarrow \phi\pi^+) = (4.5 \pm 0.4) \times 10^{-2}$ . Our first error is their experiment's error and our second error is the systematic error from using our best value.  
<sup>3</sup> ALEXANDER 93B reports < 17 × 10<sup>-5</sup> from a measurement of  $[\Gamma(B^0 \rightarrow D_s^{*-} K^+)/\Gamma_{total}] \times [B(D_s^+ \rightarrow \phi\pi^+)]$  assuming  $B(D_s^+ \rightarrow \phi\pi^+) = 0.037$ , which we rescale to our best value  $B(D_s^+ \rightarrow \phi\pi^+) = 4.5 \times 10^{-2}$ .

$\Gamma(D_s^- K^+)/\Gamma(D^- \pi^+)$					$\Gamma_{123}/\Gamma_{34}$
VALUE (units 10 <sup>-2</sup> )	CL%	DOCUMENT ID	TECN	COMMENT	
<b>1.09 ± 0.19 OUR FIT</b>		Error includes scale factor of 2.6.			
<b>1.29 ± 0.05 ± 0.08</b>		AAIJ	15Ac LHCb	pp at 7, 8 TeV	

$\Gamma(D_s^- K^*(892)^+)/\Gamma_{total}$					$\Gamma_{125}/\Gamma$
VALUE (units 10 <sup>-5</sup> )	CL%	DOCUMENT ID	TECN	COMMENT	
<b>3.5 ± 1.0 ± 0.9 ± 0.4</b>		<sup>1</sup> AUBERT	08AJ BABR	e <sup>+</sup> e <sup>-</sup> → $\Upsilon(4S)$	
• • • We do not use the following data for averages, fits, limits, etc. • • •					
<280	90	<sup>2</sup> ALBRECHT	93E ARG	e <sup>+</sup> e <sup>-</sup> → $\Upsilon(4S)$	
< 80	90	<sup>3</sup> ALEXANDER	93B CLE2	e <sup>+</sup> e <sup>-</sup> → $\Upsilon(4S)$	

<sup>1</sup> Assumes equal production of B<sup>+</sup> and B<sup>0</sup> at the  $\Upsilon(4S)$ .  
<sup>2</sup> ALBRECHT 93E reports < 4.6 × 10<sup>-3</sup> from a measurement of  $[\Gamma(B^0 \rightarrow D_s^- K^*(892)^+)/\Gamma_{total}] \times [B(D_s^+ \rightarrow \phi\pi^+)]$  assuming  $B(D_s^+ \rightarrow \phi\pi^+) = 0.027$ , which we rescale to our best value  $B(D_s^+ \rightarrow \phi\pi^+) = 4.5 \times 10^{-2}$ .  
<sup>3</sup> ALEXANDER 93B reports < 9.7 × 10<sup>-4</sup> from a measurement of  $[\Gamma(B^0 \rightarrow D_s^- K^*(892)^+)/\Gamma_{total}] \times [B(D_s^+ \rightarrow \phi\pi^+)]$  assuming  $B(D_s^+ \rightarrow \phi\pi^+) = 0.037$ , which we rescale to our best value  $B(D_s^+ \rightarrow \phi\pi^+) = 4.5 \times 10^{-2}$ .

$\Gamma(D_s^{*-} K^*(892)^+)/\Gamma_{total}$					$\Gamma_{126}/\Gamma$
VALUE (units 10 <sup>-5</sup> )	CL%	DOCUMENT ID	TECN	COMMENT	
<b>3.2 ± 1.4 ± 0.4</b>		<sup>1</sup> AUBERT	08AJ BABR	e <sup>+</sup> e <sup>-</sup> → $\Upsilon(4S)$	
• • • We do not use the following data for averages, fits, limits, etc. • • •					
<350	90	<sup>2</sup> ALBRECHT	93E ARG	e <sup>+</sup> e <sup>-</sup> → $\Upsilon(4S)$	
< 90	90	<sup>3</sup> ALEXANDER	93B CLE2	e <sup>+</sup> e <sup>-</sup> → $\Upsilon(4S)$	

<sup>1</sup> Assumes equal production of B<sup>+</sup> and B<sup>0</sup> at the  $\Upsilon(4S)$ .  
<sup>2</sup> ALBRECHT 93E reports < 5.8 × 10<sup>-3</sup> from a measurement of  $[\Gamma(B^0 \rightarrow D_s^{*-} K^*(892)^+)/\Gamma_{total}] \times [B(D_s^+ \rightarrow \phi\pi^+)]$  assuming  $B(D_s^+ \rightarrow \phi\pi^+) = 0.027$ , which we rescale to our best value  $B(D_s^+ \rightarrow \phi\pi^+) = 4.5 \times 10^{-2}$ .  
<sup>3</sup> ALEXANDER 93B reports < 11.0 × 10<sup>-4</sup> from a measurement of  $[\Gamma(B^0 \rightarrow D_s^{*-} K^*(892)^+)/\Gamma_{total}] \times [B(D_s^+ \rightarrow \phi\pi^+)]$  assuming  $B(D_s^+ \rightarrow \phi\pi^+) = 0.037$ , which we rescale to our best value  $B(D_s^+ \rightarrow \phi\pi^+) = 4.5 \times 10^{-2}$ .

$\Gamma(D_s^- \pi^+ K^0)/\Gamma_{total}$					$\Gamma_{127}/\Gamma$
VALUE (units 10 <sup>-4</sup> )	CL%	DOCUMENT ID	TECN	COMMENT	
<b>0.97 ± 0.14 OUR AVERAGE</b>					
0.94 ± 0.12 ± 0.10		<sup>1</sup> WIECHCZYN...	15 BELL	e <sup>+</sup> e <sup>-</sup> → $\Upsilon(4S)$	
1.10 ± 0.26 ± 0.20		<sup>1</sup> AUBERT	08G BABR	e <sup>+</sup> e <sup>-</sup> → $\Upsilon(4S)$	
• • • We do not use the following data for averages, fits, limits, etc. • • •					
<40	90	<sup>2</sup> ALBRECHT	93E ARG	e <sup>+</sup> e <sup>-</sup> → $\Upsilon(4S)$	

<sup>1</sup> Assumes equal production of B<sup>+</sup> and B<sup>0</sup> at the  $\Upsilon(4S)$ .  
<sup>2</sup> ALBRECHT 93E reports < 7.3 × 10<sup>-3</sup> from a measurement of  $[\Gamma(B^0 \rightarrow D_s^- \pi^+ K^0)/\Gamma_{total}] \times [B(D_s^+ \rightarrow \phi\pi^+)]$  assuming  $B(D_s^+ \rightarrow \phi\pi^+) = 0.027$ , which we rescale to our best value  $B(D_s^+ \rightarrow \phi\pi^+) = 4.5 \times 10^{-2}$ .

$\Gamma(D_s^{*-} \pi^+ K^0)/\Gamma_{total}$					$\Gamma_{128}/\Gamma$
VALUE (units 10 <sup>-4</sup> )	CL%	DOCUMENT ID	TECN	COMMENT	
< 1.10	90	<sup>1</sup> AUBERT	08G BABR	e <sup>+</sup> e <sup>-</sup> → $\Upsilon(4S)$	
• • • We do not use the following data for averages, fits, limits, etc. • • •					
<25	90	<sup>2</sup> ALBRECHT	93E ARG	e <sup>+</sup> e <sup>-</sup> → $\Upsilon(4S)$	

<sup>1</sup> Assumes equal production of B<sup>+</sup> and B<sup>0</sup> at the  $\Upsilon(4S)$ .  
<sup>2</sup> ALBRECHT 93E reports < 4.2 × 10<sup>-3</sup> from a measurement of  $[\Gamma(B^0 \rightarrow D_s^{*-} \pi^+ K^0)/\Gamma_{total}] \times [B(D_s^+ \rightarrow \phi\pi^+)]$  assuming  $B(D_s^+ \rightarrow \phi\pi^+) = 0.027$ , which we rescale to our best value  $B(D_s^+ \rightarrow \phi\pi^+) = 4.5 \times 10^{-2}$ .

$\Gamma(D_s^- K^+ \pi^+ \pi^-)/\Gamma_{total}$					$\Gamma_{129}/\Gamma$
VALUE (units 10 <sup>-4</sup> )	CL%	DOCUMENT ID	TECN	COMMENT	
<b>1.73 ± 0.32 ± 0.35</b>		<sup>1</sup> AAIJ	12Ax LHCb	pp at 7 TeV	

<sup>1</sup> AAIJ 12Ax reports  $[\Gamma(B^0 \rightarrow D_s^- K^+ \pi^+ \pi^-)/\Gamma_{total}] / [B(B_s^0 \rightarrow D_s^- K^+ \pi^+ \pi^-)] = 0.54 \pm 0.07 \pm 0.07$  which we multiply by our best value  $B(B_s^0 \rightarrow D_s^- K^+ \pi^+ \pi^-) = (3.2 \pm 0.6) \times 10^{-4}$ . Our first error is their experiment's error and our second error is the systematic error from using our best value.

$\Gamma(D_s^- \pi^+ K^*(892)^0)/\Gamma_{total}$					$\Gamma_{130}/\Gamma$
VALUE	CL%	DOCUMENT ID	TECN	COMMENT	
<b>&lt;3.0 × 10<sup>-3</sup></b>		<sup>1</sup> ALBRECHT	93E ARG	e <sup>+</sup> e <sup>-</sup> → $\Upsilon(4S)$	
<sup>1</sup> ALBRECHT 93E reports < 5.0 × 10 <sup>-3</sup> from a measurement of $[\Gamma(B^0 \rightarrow D_s^- \pi^+ K^*(892)^0)/\Gamma_{total}] \times [B(D_s^+ \rightarrow \phi\pi^+)]$ assuming $B(D_s^+ \rightarrow \phi\pi^+) = 0.027$ , which we rescale to our best value $B(D_s^+ \rightarrow \phi\pi^+) = 4.5 \times 10^{-2}$ .					

$\Gamma(D_s^{*-} \pi^+ K^*(892)^0)/\Gamma_{total}$					$\Gamma_{131}/\Gamma$
VALUE	CL%	DOCUMENT ID	TECN	COMMENT	
<b>&lt;1.6 × 10<sup>-3</sup></b>		<sup>1</sup> ALBRECHT	93E ARG	e <sup>+</sup> e <sup>-</sup> → $\Upsilon(4S)$	
<sup>1</sup> ALBRECHT 93E reports < 2.7 × 10 <sup>-3</sup> from a measurement of $[\Gamma(B^0 \rightarrow D_s^{*-} \pi^+ K^*(892)^0)/\Gamma_{total}] \times [B(D_s^+ \rightarrow \phi\pi^+)]$ assuming $B(D_s^+ \rightarrow \phi\pi^+) = 0.027$ , which we rescale to our best value $B(D_s^+ \rightarrow \phi\pi^+) = 4.5 \times 10^{-2}$ .					

$\Gamma(D^0 K^0)/\Gamma_{total}$					$\Gamma_{132}/\Gamma$
VALUE (units 10 <sup>-5</sup> )	CL%	DOCUMENT ID	TECN	COMMENT	
<b>5.2 ± 0.7 OUR AVERAGE</b>					
5.3 ± 0.7 ± 0.3		<sup>1</sup> AUBERT,B	06L BABR	e <sup>+</sup> e <sup>-</sup> → $\Upsilon(4S)$	
5.0 ± 1.3 ± 0.6		<sup>1</sup> KROKOVNY	03 BELL	e <sup>+</sup> e <sup>-</sup> → $\Upsilon(4S)$	
<sup>1</sup> Assumes equal production of B <sup>+</sup> and B <sup>0</sup> at the $\Upsilon(4S)$ .					

$\Gamma(D^0 K^+ \pi^-)/\Gamma_{total}$					$\Gamma_{133}/\Gamma$
VALUE (units 10 <sup>-6</sup> )	CL%	DOCUMENT ID	TECN	COMMENT	
<b>88 ± 15 ± 9</b>		<sup>1</sup> AUBERT	06A BABR	e <sup>+</sup> e <sup>-</sup> → $\Upsilon(4S)$	
<sup>1</sup> Assumes equal production of B <sup>+</sup> and B <sup>0</sup> at the $\Upsilon(4S)$ .					

$\Gamma(D^0 K^+ \pi^-)/\Gamma(D^0 \pi^+ \pi^-)$					$\Gamma_{133}/\Gamma_{43}$
VALUE	CL%	DOCUMENT ID	TECN	COMMENT	
<b>0.106 ± 0.007 ± 0.008</b>		AAIJ	13Aq LHCb	pp at 7 TeV	

# Meson Particle Listings

## B<sup>0</sup>

### $\Gamma(\overline{D}^0 K^*(892)^0)/\Gamma_{\text{total}}$ Γ<sub>134</sub>/Γ

VALUE (units 10 <sup>-5</sup> )	DOCUMENT ID	TECN	COMMENT
<b>4.5 ± 0.6 OUR AVERAGE</b>			
5.4 ± 0.3 ± 1.1	1,2 AAIJ	15X	LHCB <i>pp</i> at 7, 8 TeV
4.0 ± 0.7 ± 0.3	3 AUBERT,B	06L	BABR e <sup>+</sup> e <sup>-</sup> → γ(4S)
4.8 <sup>+1.1</sup> <sub>-1.0</sub> ± 0.5	3 KROKOVNY	03	BELL e <sup>+</sup> e <sup>-</sup> → γ(4S)

- • • We do not use the following data for averages, fits, limits, etc. • • •
- 5.7 ± 0.9 ± 0.6 <sup>3</sup>AUBERT 06A BABR Repl. by AUBERT,B 06L
- <sup>1</sup> AAIJ 15x reports (5.13 ± 0.20 ± 0.15 ± 0.24 ± 0.60) × 10<sup>-5</sup> from a measurement of [Γ(B<sup>0</sup> →  $\overline{D}^0 K^*(892)^0$ )/Γ<sub>total</sub>] × [B(B<sup>0</sup> →  $\overline{D}^0 K^+ \pi^-$ )] assuming B(B<sup>0</sup> →  $\overline{D}^0 K^+ \pi^-$ ) = (9.2 ± 0.6 ± 0.7 ± 0.6) × 10<sup>-5</sup>, which we rescale to our best value B(B<sup>0</sup> →  $\overline{D}^0 K^+ \pi^-$ ) = (8.8 ± 1.7) × 10<sup>-5</sup>. Our first error is their experiment's error and our second error is the systematic error from using our best value.
- <sup>2</sup> Measured via amplitude analysis of B<sup>0</sup> →  $\overline{D}^0 K^+ \pi^-$ , which excludes contribution from decay via D\*(2010)<sup>-</sup> resonance.
- <sup>3</sup> Assumes equal production of B<sup>+</sup> and B<sup>0</sup> at the γ(4S).

### $\Gamma(\overline{D}^0 K^*(1430)^0)/\Gamma_{\text{total}}$ Γ<sub>135</sub>/Γ

VALUE	CL%	DOCUMENT ID	TECN	COMMENT
<b>&lt; 6.7 × 10<sup>-5</sup></b>	90	1 AAIJ	15X	LHCB <i>pp</i> at 7, 8 TeV

- <sup>1</sup> Measured via amplitude analysis of B<sup>0</sup> →  $\overline{D}^0 K^+ \pi^-$ , which excludes contribution from decay via D\*(2010)<sup>-</sup> resonance.

### $\Gamma(\overline{D}^0 K_0^*(1430)^0)/\Gamma_{\text{total}}$ Γ<sub>136</sub>/Γ

VALUE (units 10 <sup>-5</sup> )	DOCUMENT ID	TECN	COMMENT
<b>0.7 ± 0.7 ± 0.1</b>	1,2 AAIJ	15X	LHCB <i>pp</i> at 7, 8 TeV

- <sup>1</sup> AAIJ 15x reports (0.71 ± 0.27 ± 0.33 ± 0.47 ± 0.08) × 10<sup>-5</sup> from a measurement of [Γ(B<sup>0</sup> →  $\overline{D}^0 K_0^*(1430)^0$ )/Γ<sub>total</sub>] × [B(B<sup>0</sup> →  $\overline{D}^0 K^+ \pi^-$ )] assuming B(B<sup>0</sup> →  $\overline{D}^0 K^+ \pi^-$ ) = (9.2 ± 0.6 ± 0.7 ± 0.6) × 10<sup>-5</sup>, which we rescale to our best value B(B<sup>0</sup> →  $\overline{D}^0 K^+ \pi^-$ ) = (8.8 ± 1.7) × 10<sup>-5</sup>. Our first error is their experiment's error and our second error is the systematic error from using our best value.
- <sup>2</sup> Measured via amplitude analysis of B<sup>0</sup> →  $\overline{D}^0 K^+ \pi^-$ , which excludes contribution from decay via D\*(2010)<sup>-</sup> resonance.

### $\Gamma(\overline{D}^0 K_2^*(1430)^0)/\Gamma_{\text{total}}$ Γ<sub>137</sub>/Γ

VALUE (units 10 <sup>-5</sup> )	DOCUMENT ID	TECN	COMMENT
<b>2.1 ± 0.8 ± 0.4</b>	1,2 AAIJ	15X	LHCB <i>pp</i> at 7, 8 TeV

- <sup>1</sup> AAIJ 15x reports (2.04 ± 0.45 ± 0.30 ± 0.54 ± 0.25) × 10<sup>-5</sup> from a measurement of [Γ(B<sup>0</sup> →  $\overline{D}^0 K_2^*(1430)^0$ )/Γ<sub>total</sub>] × [B(B<sup>0</sup> →  $\overline{D}^0 K^+ \pi^-$ )] assuming B(B<sup>0</sup> →  $\overline{D}^0 K^+ \pi^-$ ) = (9.2 ± 0.6 ± 0.7 ± 0.6) × 10<sup>-5</sup>, which we rescale to our best value B(B<sup>0</sup> →  $\overline{D}^0 K^+ \pi^-$ ) = (8.8 ± 1.7) × 10<sup>-5</sup>. Our first error is their experiment's error and our second error is the systematic error from using our best value.
- <sup>2</sup> Measured via amplitude analysis of B<sup>0</sup> →  $\overline{D}^0 K^+ \pi^-$ , which excludes contribution from decay via D\*(2010)<sup>-</sup> resonance.

### $\Gamma(D_0^{*+}(2300)^- K^+, D_0^{*-}(2300)^0 \pi^-)/\Gamma_{\text{total}}$ Γ<sub>138</sub>/Γ

VALUE (units 10 <sup>-5</sup> )	DOCUMENT ID	TECN	COMMENT
<b>1.9 ± 0.8 ± 0.4</b>	1,2 AAIJ	15X	LHCB <i>pp</i> at 7, 8 TeV

- <sup>1</sup> AAIJ 15x reports (1.77 ± 0.26 ± 0.19 ± 0.67 ± 0.20) × 10<sup>-5</sup> from a measurement of [Γ(B<sup>0</sup> → D<sub>0</sub><sup>\*+</sup>(2300)<sup>-</sup> K<sup>+</sup>, D<sub>0</sub><sup>\*-</sup>(2300)<sup>0</sup> π<sup>-</sup>)/Γ<sub>total</sub>] × [B(B<sup>0</sup> →  $\overline{D}^0 K^+ \pi^-$ )] assuming B(B<sup>0</sup> →  $\overline{D}^0 K^+ \pi^-$ ) = (9.2 ± 0.6 ± 0.7 ± 0.6) × 10<sup>-5</sup>, which we rescale to our best value B(B<sup>0</sup> →  $\overline{D}^0 K^+ \pi^-$ ) = (8.8 ± 1.7) × 10<sup>-5</sup>. Our first error is their experiment's error and our second error is the systematic error from using our best value.
- <sup>2</sup> Measured via amplitude analysis of B<sup>0</sup> →  $\overline{D}^0 K^+ \pi^-$ , which excludes contribution from decay via D\*(2010)<sup>-</sup> resonance.

### $\Gamma(D_2^{*+}(2460)^- K^+, D_2^{*-}(2460)^0 \pi^-)/\Gamma_{\text{total}}$ Γ<sub>139</sub>/Γ

VALUE (units 10 <sup>-6</sup> )	DOCUMENT ID	TECN	COMMENT
<b>20.3 ± 3.5 OUR AVERAGE</b>			
22 ± 2 ± 4	1,2 AAIJ	15X	LHCB <i>pp</i> at 7, 8 TeV
18.3 ± 4.0 ± 3.1	3 AUBERT	06A	BABR e <sup>+</sup> e <sup>-</sup> → γ(4S)

- <sup>1</sup> AAIJ 15x reports (2.12 ± 0.10 ± 0.11 ± 0.11 ± 0.25) × 10<sup>-5</sup> from a measurement of [Γ(B<sup>0</sup> → D<sub>2</sub><sup>\*+</sup>(2460)<sup>-</sup> K<sup>+</sup>, D<sub>2</sub><sup>\*-</sup>(2460)<sup>0</sup> π<sup>-</sup>)/Γ<sub>total</sub>] × [B(B<sup>0</sup> →  $\overline{D}^0 K^+ \pi^-$ )] assuming B(B<sup>0</sup> →  $\overline{D}^0 K^+ \pi^-$ ) = (9.2 ± 0.6 ± 0.7 ± 0.6) × 10<sup>-5</sup>, which we rescale to our best value B(B<sup>0</sup> →  $\overline{D}^0 K^+ \pi^-$ ) = (8.8 ± 1.7) × 10<sup>-5</sup>. Our first error is their experiment's error and our second error is the systematic error from using our best value.
- <sup>2</sup> Measured via amplitude analysis of B<sup>0</sup> →  $\overline{D}^0 K^+ \pi^-$ , which excludes contribution from decay via D\*(2010)<sup>-</sup> resonance.
- <sup>3</sup> Assumes equal production of B<sup>+</sup> and B<sup>0</sup> at the γ(4S).

### $\Gamma(D_3^{*+}(2760)^- K^+, D_3^{*-}(2760)^0 \pi^-)/\Gamma_{\text{total}}$ Γ<sub>140</sub>/Γ

VALUE	CL%	DOCUMENT ID	TECN	COMMENT
<b>&lt; 0.10 × 10<sup>-5</sup></b>	90	1 AAIJ	15X	LHCB <i>pp</i> at 7, 8 TeV

- <sup>1</sup> Measured via amplitude analysis of B<sup>0</sup> →  $\overline{D}^0 K^+ \pi^-$ , which excludes contribution from decay via D\*(2010)<sup>-</sup> resonance.

### $\Gamma(\overline{D}^0 K^+ \pi^- \text{ nonresonant})/\Gamma_{\text{total}}$ Γ<sub>141</sub>/Γ

VALUE (units 10 <sup>-6</sup> )	CL%	DOCUMENT ID	TECN	COMMENT
<b>&lt; 37</b>	90	1 AUBERT	06A	BABR e <sup>+</sup> e <sup>-</sup> → γ(4S)

- <sup>1</sup> Assumes equal production of B<sup>+</sup> and B<sup>0</sup> at the γ(4S).

### $\Gamma([\overline{K}^+ K^-]_D K^*(892)^0)/\Gamma(\overline{D}^0 K^*(892)^0)$ Γ<sub>142</sub>/Γ<sub>134</sub>

VALUE	DOCUMENT ID	TECN	COMMENT
<b>0.92 ± 0.10 ± 0.02</b>	AAIJ	19N	LHCB <i>pp</i> at 7, 8, 13 TeV

- • • We do not use the following data for averages, fits, limits, etc. • • •
- 1.05<sup>+0.17</sup><sub>-0.15</sub> ± 0.04 AAIJ 14BN LHCB Repl. by AAIJ 16s
- 1.36<sup>+0.37</sup><sub>-0.32</sub> ± 0.07 AAIJ 13L LHCB Repl. by AAIJ 14BN

### $\Gamma([\pi^+ \pi^-]_D K^*(892)^0)/\Gamma(\overline{D}^0 K^*(892)^0)$ Γ<sub>143</sub>/Γ<sub>134</sub>

VALUE	DOCUMENT ID	TECN	COMMENT
<b>1.32 ± 0.19 ± 0.03</b>	AAIJ	19N	LHCB <i>pp</i> at 7, 8, 13 TeV

- • • We do not use the following data for averages, fits, limits, etc. • • •
- 1.21<sup>+0.28</sup><sub>-0.25</sub> ± 0.05 AAIJ 14BN LHCB Repl. by AAIJ 16s

### $\Gamma([\pi^+ K^-]_D K^*(892)^0)/\Gamma([\overline{K}^+ \pi^-]_D K^*(892)^0)$ Γ<sub>144</sub>/Γ<sub>145</sub>

VALUE	DOCUMENT ID	TECN	COMMENT
<b>0.080 ± 0.015 ± 0.002</b>	AAIJ	19N	LHCB <i>pp</i> at 7, 8, 13 TeV

### $\Gamma([\pi^+ \pi^- \pi^+ \pi^-]_D K^*(892)^0)/\Gamma(\overline{D}^0 K^*(892)^0)$ Γ<sub>146</sub>/Γ<sub>134</sub>

VALUE	DOCUMENT ID	TECN	COMMENT
<b>1.01 ± 0.16 ± 0.04</b>	AAIJ	19N	LHCB <i>pp</i> at 7, 8, 13 TeV

### $\Gamma([\pi^+ K^- \pi^+ \pi^-]_D K^*(892)^0)/\Gamma([\overline{K}^+ \pi^- \pi^+ \pi^-]_D K^*(892)^0)$ Γ<sub>147</sub>/Γ<sub>148</sub>

VALUE	DOCUMENT ID	TECN	COMMENT
<b>0.073 ± 0.018 ± 0.002</b>	AAIJ	19N	LHCB <i>pp</i> at 7, 8, 13 TeV

### $\Gamma(\overline{D}^0 \rho^0)/\Gamma_{\text{total}}$ Γ<sub>149</sub>/Γ

VALUE (units 10 <sup>-4</sup> )	CL%	DOCUMENT ID	TECN	COMMENT
<b>2.63 ± 0.14 OUR AVERAGE</b>				

- 2.69 ± 0.09 ± 0.13 1 LEES 11M BABR e<sup>+</sup>e<sup>-</sup> → γ(4S)
- 2.25 ± 0.14 ± 0.35 1 BLYTH 06 BELL e<sup>+</sup>e<sup>-</sup> → γ(4S)
- 2.74<sup>+0.36</sup><sub>-0.32</sub> ± 0.55 1 COAN 02 CLE2 e<sup>+</sup>e<sup>-</sup> → γ(4S)
- • • We do not use the following data for averages, fits, limits, etc. • • •
- 2.9 ± 0.2 ± 0.3 1 AUBERT 04B BABR Repl. by LEES 11M
- 3.1 ± 0.4 ± 0.5 1 ABE 02J BELL Repl. by BLYTH 06
- < 1.2 90 2 NEMAT 98 CLE2 Repl. by COAN 02
- < 4.8 90 3 ALAM 94 CLE2 Repl. by NEMAT 98
- <sup>1</sup> Assumes equal production of B<sup>+</sup> and B<sup>0</sup> at the γ(4S).
- <sup>2</sup> NEMAT 98 assumes equal production of B<sup>+</sup> and B<sup>0</sup> at the γ(4S) and use the PDG 96 values for D<sup>0</sup>, D<sup>\*0</sup>, η, η', and ω branching fractions.
- <sup>3</sup> ALAM 94 assume equal production of B<sup>+</sup> and B<sup>0</sup> at the γ(4S) and use the CLEO II absolute B(D<sup>0</sup> → K<sup>-</sup>π<sup>+</sup>) and the PDG 1992 B(D<sup>0</sup> → K<sup>-</sup>π<sup>+</sup>π<sup>0</sup>)/B(D<sup>0</sup> → K<sup>-</sup>π<sup>+</sup>) and B(D<sup>0</sup> → K<sup>-</sup>2π<sup>+</sup>π<sup>-</sup>)/B(D<sup>0</sup> → K<sup>-</sup>π<sup>+</sup>).

### $\Gamma(\overline{D}^0 \rho^0)/\Gamma_{\text{total}}$ Γ<sub>150</sub>/Γ

VALUE (units 10 <sup>-4</sup> )	CL%	DOCUMENT ID	TECN	COMMENT
<b>3.21 ± 0.21 OUR AVERAGE</b>				

- 3.21 ± 0.10 ± 0.21 1 AAIJ 15Y LHCB *pp* at 7, 8 TeV
- 3.19 ± 0.20 ± 0.45 2,3 KUZMIN 07 BELL e<sup>+</sup>e<sup>-</sup> → γ(4S)
- • • We do not use the following data for averages, fits, limits, etc. • • •
- 2.9 ± 1.0 ± 0.4 2 SATPATHY 03 BELL Repl. by KUZMIN 07
- < 3.9 90 4 NEMAT 98 CLE2 e<sup>+</sup>e<sup>-</sup> → γ(4S)
- < 5.0 90 5 ALAM 94 CLE2 Repl. by NEMAT 98
- < 6.0 90 6 BORTOLETTO92 CLEO e<sup>+</sup>e<sup>-</sup> → γ(4S)
- < 27.0 90 7 ALBRECHT 88k ARG e<sup>+</sup>e<sup>-</sup> → γ(4S)

- <sup>1</sup> Measured using isobar formalism in the decay chain B<sup>0</sup> →  $\overline{D}^0 \rho(770)$ , ρ → π<sup>+</sup>π<sup>-</sup> assuming B(ρ(770) → π<sup>+</sup>π<sup>-</sup>) = 1. The second uncertainty combines in quadrature all systematic uncertainties quoted in the paper.
- <sup>2</sup> Assumes equal production of B<sup>+</sup> and B<sup>0</sup> at the γ(4S).
- <sup>3</sup> Our second uncertainty combines systematics and model errors quoted in the paper.
- <sup>4</sup> NEMAT 98 assumes equal production of B<sup>+</sup> and B<sup>0</sup> at the γ(4S) and use the PDG 96 values for D<sup>0</sup>, D<sup>\*0</sup>, η, η', and ω branching fractions.
- <sup>5</sup> ALAM 94 assume equal production of B<sup>+</sup> and B<sup>0</sup> at the γ(4S) and use the CLEO II absolute B(D<sup>0</sup> → K<sup>-</sup>π<sup>+</sup>) and the PDG 1992 B(D<sup>0</sup> → K<sup>-</sup>π<sup>+</sup>π<sup>0</sup>)/B(D<sup>0</sup> → K<sup>-</sup>π<sup>+</sup>) and B(D<sup>0</sup> → K<sup>-</sup>2π<sup>+</sup>π<sup>-</sup>)/B(D<sup>0</sup> → K<sup>-</sup>π<sup>+</sup>).
- <sup>6</sup> BORTOLETTO 92 assumes equal production of B<sup>+</sup> and B<sup>0</sup> at the γ(4S) and uses Mark III branching fractions for the D.
- <sup>7</sup> ALBRECHT 88k reports < 0.003 assuming B<sup>0</sup>  $\overline{B}^0$ : B<sup>+</sup>B<sup>-</sup> production ratio is 45:55. We rescale to 50%.

### $\Gamma(\overline{D}^0 f_2)/\Gamma_{\text{total}}$ Γ<sub>151</sub>/Γ

VALUE (units 10 <sup>-4</sup> )	DOCUMENT ID	TECN	COMMENT
<b>1.56 ± 0.21 OUR AVERAGE</b>			

- 1.68 ± 0.11 ± 0.21 1 AAIJ 15Y LHCB *pp* at 7, 8 TeV
- 1.20 ± 0.18 ± 0.38 2,3 KUZMIN 07 BELL e<sup>+</sup>e<sup>-</sup> → γ(4S)

- <sup>1</sup> Result obtained using the isobar formalism. The second uncertainty combines in quadrature all systematic uncertainties quoted in the paper. Measured in the decay chain B<sup>0</sup> →  $\overline{D}^0 f_2(1270)$ , f<sub>2</sub> → π<sup>+</sup>π<sup>-</sup>.
- <sup>2</sup> Assumes equal production of B<sup>+</sup> and B<sup>0</sup> at the γ(4S).
- <sup>3</sup> Our second uncertainty combines systematics and model errors quoted in the paper.

$\Gamma(\bar{D}^0 \eta)/\Gamma_{total}$   $\Gamma_{152}/\Gamma$

VALUE (units $10^{-4}$ )	CL%	DOCUMENT ID	TECN	COMMENT
<b>2.36 ± 0.32 OUR AVERAGE</b>		Error includes scale factor of 2.5.		
2.53 ± 0.09 ± 0.11		1 LEES	11M BABR	$e^+e^- \rightarrow \Upsilon(4S)$
1.77 ± 0.16 ± 0.21		1 BLYTH	06 BELL	$e^+e^- \rightarrow \Upsilon(4S)$
• • • We do not use the following data for averages, fits, limits, etc. • • •				
2.5 ± 0.2 ± 0.3		1 AUBERT	04B BABR	Repl. by LEES 11M
1.4 $^{+0.5}_{-0.4}$ ± 0.3		1 ABE	02J BELL	Repl. by BLYTH 06
<1.3	90	2 NEMAT1	98 CLE2	$e^+e^- \rightarrow \Upsilon(4S)$
<6.8	90	3 ALAM	94 CLE2	Repl. by NEMAT1 98

1 Assumes equal production of  $B^+$  and  $B^0$  at the  $\Upsilon(4S)$ .  
 2 NEMAT1 98 assumes equal production of  $B^+$  and  $B^0$  at the  $\Upsilon(4S)$  and use the PDG 96 values for  $D^0, D^{*0}, \eta, \eta',$  and  $\omega$  branching fractions.  
 3 ALAM 94 assume equal production of  $B^+$  and  $B^0$  at the  $\Upsilon(4S)$  and use the CLEO II absolute  $B(D^0 \rightarrow K^-\pi^+)$  and the PDG 1992  $B(D^0 \rightarrow K^-\pi^+\pi^0)/B(D^0 \rightarrow K^-\pi^+)$  and  $B(D^0 \rightarrow K^-\pi^+\pi^-)/B(D^0 \rightarrow K^-\pi^+)$ .

$\Gamma(\bar{D}^0 \eta')/\Gamma_{total}$   $\Gamma_{153}/\Gamma$

VALUE (units $10^{-4}$ )	CL%	DOCUMENT ID	TECN	COMMENT
<b>1.38 ± 0.16 OUR AVERAGE</b>		Error includes scale factor of 1.3.		
1.48 ± 0.13 ± 0.07		1 LEES	11M BABR	$e^+e^- \rightarrow \Upsilon(4S)$
1.14 ± 0.20 $^{+0.10}_{-0.13}$		1 SCHUMANN	05 BELL	$e^+e^- \rightarrow \Upsilon(4S)$
• • • We do not use the following data for averages, fits, limits, etc. • • •				
1.7 ± 0.4 ± 0.2		1 AUBERT	04B BABR	Repl. by LEES 11M
<9.4	90	2 NEMAT1	98 CLE2	$e^+e^- \rightarrow \Upsilon(4S)$
<8.6	90	3 ALAM	94 CLE2	Repl. by NEMAT1 98

1 Assumes equal production of  $B^+$  and  $B^0$  at the  $\Upsilon(4S)$ .  
 2 NEMAT1 98 assumes equal production of  $B^+$  and  $B^0$  at the  $\Upsilon(4S)$  and use the PDG 96 values for  $D^0, D^{*0}, \eta, \eta',$  and  $\omega$  branching fractions.  
 3 ALAM 94 assume equal production of  $B^+$  and  $B^0$  at the  $\Upsilon(4S)$  and use the CLEO II absolute  $B(D^0 \rightarrow K^-\pi^+)$  and the PDG 1992  $B(D^0 \rightarrow K^-\pi^+\pi^0)/B(D^0 \rightarrow K^-\pi^+)$  and  $B(D^0 \rightarrow K^-\pi^+\pi^-)/B(D^0 \rightarrow K^-\pi^+)$ .

$\Gamma(\bar{D}^0 \eta')/\Gamma(\bar{D}^0 \eta)$   $\Gamma_{153}/\Gamma_{152}$

VALUE	DOCUMENT ID	TECN	COMMENT
<b>0.54 ± 0.07 ± 0.01</b>	LEES	11M BABR	$e^+e^- \rightarrow \Upsilon(4S)$
• • • We do not use the following data for averages, fits, limits, etc. • • •			
0.7 ± 0.2 ± 0.1	AUBERT	04B BABR	Repl. by LEES 11M

$\Gamma(\bar{D}^0 \omega)/\Gamma_{total}$   $\Gamma_{154}/\Gamma$

VALUE (units $10^{-4}$ )	CL%	DOCUMENT ID	TECN	COMMENT
<b>2.54 ± 0.16 OUR AVERAGE</b>				
2.75 ± 0.72 ± 0.35		1 AAIJ	15Y LHCB	$pp$ at 7, 8 TeV
2.57 ± 0.11 ± 0.14		2 LEES	11M BABR	$e^+e^- \rightarrow \Upsilon(4S)$
2.37 ± 0.23 ± 0.28		2 BLYTH	06 BELL	$e^+e^- \rightarrow \Upsilon(4S)$
• • • We do not use the following data for averages, fits, limits, etc. • • •				
3.0 ± 0.3 ± 0.4		2 AUBERT	04B BABR	Repl. by LEES 11M
1.8 ± 0.5 $^{+0.4}_{-0.3}$		2 ABE	02J BELL	Repl. by BLYTH 06
<5.1	90	3 NEMAT1	98 CLE2	$e^+e^- \rightarrow \Upsilon(4S)$
<6.3	90	4 ALAM	94 CLE2	Repl. by NEMAT1 98

1 Result obtained using the isobar model. The second uncertainty combines in quadrature all systematic uncertainties quoted in the paper.  
 2 Assumes equal production of  $B^+$  and  $B^0$  at the  $\Upsilon(4S)$ .  
 3 NEMAT1 98 assumes equal production of  $B^+$  and  $B^0$  at the  $\Upsilon(4S)$  and use the PDG 96 values for  $D^0, D^{*0}, \eta, \eta',$  and  $\omega$  branching fractions.  
 4 ALAM 94 assume equal production of  $B^+$  and  $B^0$  at the  $\Upsilon(4S)$  and use the CLEO II absolute  $B(D^0 \rightarrow K^-\pi^+)$  and the PDG 1992  $B(D^0 \rightarrow K^-\pi^+\pi^0)/B(D^0 \rightarrow K^-\pi^+)$  and  $B(D^0 \rightarrow K^-\pi^+\pi^-)/B(D^0 \rightarrow K^-\pi^+)$ .

$\Gamma(D^0 \phi)/\Gamma_{total}$   $\Gamma_{155}/\Gamma$

VALUE	CL%	DOCUMENT ID	TECN	COMMENT
<b>&lt; 2.3 × 10<sup>-6</sup></b>	95	AAIJ	18AY LHCB	$pp$ at 7 and 8 TeV
• • • We do not use the following data for averages, fits, limits, etc. • • •				
<11.6 × 10 <sup>-6</sup>	90	1 AUBERT	07A0 BABR	$e^+e^- \rightarrow \Upsilon(4S)$
1 Assumes equal production of $B^+$ and $B^0$ at the $\Upsilon(4S)$ .				

$\Gamma(D^0 K^+\pi^-)/\Gamma_{total}$   $\Gamma_{156}/\Gamma$

VALUE (units $10^{-6}$ )	CL%	DOCUMENT ID	TECN	COMMENT
• • • We do not use the following data for averages, fits, limits, etc. • • •				
<19	90	1 AUBERT	06A BABR	Repl. by AUBERT 09AE
1 Assumes equal production of $B^+$ and $B^0$ at the $\Upsilon(4S)$ .				

$\Gamma(D^0 K^+\pi^-)/\Gamma(\bar{D}^0 K^+\pi^-)$   $\Gamma_{156}/\Gamma_{133}$

VALUE	DOCUMENT ID	TECN	COMMENT
<b>0.060 ± 0.034 OUR AVERAGE</b>			
0.045 $^{+0.056}_{-0.050}$ ± 0.028	1,2 NEGISHI	12 BELL	$e^+e^- \rightarrow \Upsilon(4S)$
0.068 ± 0.042	3 AUBERT	09AE BABR	$e^+e^- \rightarrow \Upsilon(4S)$

1 Assumes equal production of  $B^0$  and  $B^+$  at  $\Upsilon(4S)$ .  
 2 Uses  $D^0 \rightarrow K^-\pi^+$  mode. Restricts  $K^+\pi^-$  mass within ±50 MeV of the nominal  $K^*0$  mass. Corresponds to the upper limit, < 0.16 at 95% CL.  
 3 Reports a signal at the level of 2.5 standard deviations after combining results from  $D^0 \rightarrow K^+\pi^-, K^+\pi^-\pi^0,$  and  $K^+\pi^-\pi^+\pi^-$ .

$\Gamma(D^0 K^*(892)^0)/\Gamma_{total}$   $\Gamma_{157}/\Gamma$

VALUE (units $10^{-5}$ )	CL%	DOCUMENT ID	TECN	COMMENT
• • • We do not use the following data for averages, fits, limits, etc. • • •				
<1.1	90	1 AUBERT,B	06L BABR	$e^+e^- \rightarrow \Upsilon(4S)$
<1.8	90	1 KROKOVNY	03 BELL	$e^+e^- \rightarrow \Upsilon(4S)$
1 Assumes equal production of $B^+$ and $B^0$ at the $\Upsilon(4S)$ .				

$\Gamma(D^0 K^*(892)^0)/\Gamma(\bar{D}^0 K^*(892)^0)$   $\Gamma_{157}/\Gamma_{134}$

"OUR EVALUATION" is derived from  $r_{B^0}(B^0 \rightarrow D K^{*0})$  data block listed in "CP violation parameters" section.

VALUE (units $10^{-2}$ )	DOCUMENT ID
--------------------------	-------------

**4.84  $^{+1.80}_{-2.07}$  OUR EVALUATION**

$\Gamma(\bar{D}^{*0} \gamma)/\Gamma_{total}$   $\Gamma_{158}/\Gamma$

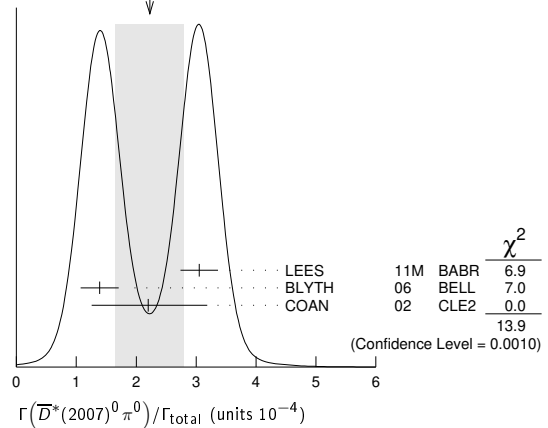
VALUE	CL%	DOCUMENT ID	TECN	COMMENT
<b>&lt;2.5 × 10<sup>-5</sup></b>	90	1 AUBERT,B	05Q BABR	$e^+e^- \rightarrow \Upsilon(4S)$
• • • We do not use the following data for averages, fits, limits, etc. • • •				
<5.0 × 10 <sup>-5</sup>	90	1 ARTUSO	00 CLE2	$e^+e^- \rightarrow \Upsilon(4S)$
1 Assumes equal production of $B^+$ and $B^0$ at the $\Upsilon(4S)$ .				

$\Gamma(\bar{D}^*(2007)^0 \pi^0)/\Gamma_{total}$   $\Gamma_{159}/\Gamma$

VALUE (units $10^{-4}$ )	CL%	DOCUMENT ID	TECN	COMMENT
<b>2.2 ± 0.6 OUR AVERAGE</b>		Error includes scale factor of 2.6. See the ideogram below.		
3.05 ± 0.14 ± 0.28		1 LEES	11M BABR	$e^+e^- \rightarrow \Upsilon(4S)$
1.39 ± 0.18 ± 0.26		1 BLYTH	06 BELL	$e^+e^- \rightarrow \Upsilon(4S)$
2.20 $^{+0.59}_{-0.52}$ ± 0.79		1 COAN	02 CLE2	$e^+e^- \rightarrow \Upsilon(4S)$
• • • We do not use the following data for averages, fits, limits, etc. • • •				
2.9 ± 0.4 ± 0.5		1 AUBERT	04B BABR	Repl. by LEES 11M
2.7 $^{+0.8}_{-0.7}$ ± 0.5		1 ABE	02J BELL	Repl. by BLYTH 06
<4.4	90	2 NEMAT1	98 CLE2	Repl. by COAN 02
<9.7	90	3 ALAM	94 CLE2	Repl. by NEMAT1 98

1 Assumes equal production of  $B^+$  and  $B^0$  at the  $\Upsilon(4S)$ .  
 2 NEMAT1 98 assumes equal production of  $B^+$  and  $B^0$  at the  $\Upsilon(4S)$  and use the PDG 96 values for  $D^0, D^{*0}, \eta, \eta',$  and  $\omega$  branching fractions.  
 3 ALAM 94 assume equal production of  $B^+$  and  $B^0$  at the  $\Upsilon(4S)$  and use the CLEO II  $B(D^*(2007)^0 \rightarrow D^0 \pi^0)$  and absolute  $B(D^0 \rightarrow K^-\pi^+)$  and the PDG 1992  $B(D^0 \rightarrow K^-\pi^+\pi^0)/B(D^0 \rightarrow K^-\pi^+)$  and  $B(D^0 \rightarrow K^-\pi^+\pi^-)/B(D^0 \rightarrow K^-\pi^+)$ .

WEIGHTED AVERAGE  
2.2±0.6 (Error scaled by 2.6)



$\Gamma(D^0 \pi^0)/\Gamma(\bar{D}^*(2007)^0 \pi^0)$   $\Gamma_{149}/\Gamma_{159}$

VALUE	DOCUMENT ID	TECN	COMMENT
<b>0.90 ± 0.08 OUR AVERAGE</b>			
0.88 ± 0.05 ± 0.06	LEES	11M BABR	$e^+e^- \rightarrow \Upsilon(4S)$
1.62 ± 0.23 ± 0.35	BLYTH	06 BELL	$e^+e^- \rightarrow \Upsilon(4S)$
• • • We do not use the following data for averages, fits, limits, etc. • • •			
1.0 ± 0.1 ± 0.2	AUBERT	04B BABR	Repl. by LEES 11M

$\Gamma(\bar{D}^*(2007)^0 \rho^0)/\Gamma_{total}$   $\Gamma_{160}/\Gamma$

VALUE	CL%	DOCUMENT ID	TECN	COMMENT
<b>&lt;5.1 × 10<sup>-4</sup></b>	90	1 SATPATHY	03 BELL	$e^+e^- \rightarrow \Upsilon(4S)$
• • • We do not use the following data for averages, fits, limits, etc. • • •				
<0.00056	90	2 NEMAT1	98 CLE2	$e^+e^- \rightarrow \Upsilon(4S)$
<0.00117	90	3 ALAM	94 CLE2	Repl. by NEMAT1 98

1 Assumes equal production of  $B^+$  and  $B^0$  at the  $\Upsilon(4S)$ .  
 2 NEMAT1 98 assumes equal production of  $B^+$  and  $B^0$  at the  $\Upsilon(4S)$  and use the PDG 96 values for  $D^0, D^{*0}, \eta, \eta',$  and  $\omega$  branching fractions.  
 3 ALAM 94 assume equal production of  $B^+$  and  $B^0$  at the  $\Upsilon(4S)$  and use the CLEO II  $B(D^*(2007)^0 \rightarrow D^0 \pi^0)$  and absolute  $B(D^0 \rightarrow K^-\pi^+)$  and the PDG 1992  $B(D^0 \rightarrow K^-\pi^+\pi^0)/B(D^0 \rightarrow K^-\pi^+)$  and  $B(D^0 \rightarrow K^-\pi^+\pi^-)/B(D^0 \rightarrow K^-\pi^+)$ .

## Meson Particle Listings

 $B^0$  $\Gamma(\bar{D}^*(2007)^0 \eta)/\Gamma_{\text{total}}$   $\Gamma_{161}/\Gamma$ 

VALUE (units $10^{-4}$ )	CL%	DOCUMENT ID	TECN	COMMENT
<b>2.3 ± 0.6 OUR AVERAGE</b>				Error includes scale factor of 2.8.
2.69 ± 0.14 ± 0.23		<sup>1</sup> LEES	11M BABR	$e^+e^- \rightarrow \Upsilon(4S)$
1.40 ± 0.28 ± 0.26		<sup>1</sup> BLYTH	06 BELL	$e^+e^- \rightarrow \Upsilon(4S)$
• • • We do not use the following data for averages, fits, limits, etc. • • •				
2.6 ± 0.4 ± 0.4		<sup>1</sup> AUBERT	04B BABR	Repl. by LEES 11M
<4.6	90	<sup>1</sup> ABE	02J BELL	$e^+e^- \rightarrow \Upsilon(4S)$
<2.6	90	<sup>2</sup> NEMAT1	98 CLE2	$e^+e^- \rightarrow \Upsilon(4S)$
<6.9	90	<sup>3</sup> ALAM	94 CLE2	Repl. by NEMAT1 98

- <sup>1</sup> Assumes equal production of  $B^+$  and  $B^0$  at the  $\Upsilon(4S)$ .  
<sup>2</sup> NEMAT1 98 assumes equal production of  $B^+$  and  $B^0$  at the  $\Upsilon(4S)$  and use the PDG 96 values for  $D^0$ ,  $D^{*0}$ ,  $\eta$ ,  $\eta'$ , and  $\omega$  branching fractions.  
<sup>3</sup> ALAM 94 assume equal production of  $B^+$  and  $B^0$  at the  $\Upsilon(4S)$  and use the CLEO II B( $D^*(2007)^0 \rightarrow D^0 \pi^0$ ) and absolute B( $D^0 \rightarrow K^- \pi^+$ ) and the PDG 1992 B( $D^0 \rightarrow K^- \pi^+ \pi^0$ )/B( $D^0 \rightarrow K^- \pi^+$ ) and B( $D^0 \rightarrow K^- 2\pi^+ \pi^-$ )/B( $D^0 \rightarrow K^- \pi^+$ ).

 $\Gamma(\bar{D}^0 \eta)/\Gamma(\bar{D}^*(2007)^0 \eta)$   $\Gamma_{152}/\Gamma_{161}$ 

VALUE	DOCUMENT ID	TECN	COMMENT
<b>0.99 ± 0.10 OUR AVERAGE</b>			
0.97 ± 0.07 ± 0.07	LEES	11M BABR	$e^+e^- \rightarrow \Upsilon(4S)$
1.27 ± 0.29 ± 0.25	BLYTH	06 BELL	$e^+e^- \rightarrow \Upsilon(4S)$
• • • We do not use the following data for averages, fits, limits, etc. • • •			
0.9 ± 0.2 ± 0.1	AUBERT	04B BABR	Repl. by LEES 11M

 $\Gamma(\bar{D}^*(2007)^0 \eta')/\Gamma(\bar{D}^*(2007)^0 \eta)$   $\Gamma_{162}/\Gamma_{161}$ 

VALUE	DOCUMENT ID	TECN	COMMENT
<b>0.61 ± 0.14 ± 0.02</b>	LEES	11M BABR	$e^+e^- \rightarrow \Upsilon(4S)$
• • • We do not use the following data for averages, fits, limits, etc. • • •			
0.5 ± 0.3 ± 0.1	AUBERT	04B BABR	Repl. by LEES 11M

 $\Gamma(\bar{D}^*(2007)^0 \eta')/\Gamma_{\text{total}}$   $\Gamma_{162}/\Gamma$ 

VALUE (units $10^{-4}$ )	CL%	DOCUMENT ID	TECN	COMMENT
<b>1.40 ± 0.22 OUR AVERAGE</b>				
1.48 ± 0.22 ± 0.13		<sup>1</sup> LEES	11M BABR	$e^+e^- \rightarrow \Upsilon(4S)$
1.21 ± 0.34 ± 0.22		<sup>1</sup> SCHUMANN	05 BELL	$e^+e^- \rightarrow \Upsilon(4S)$
• • • We do not use the following data for averages, fits, limits, etc. • • •				
1.3 ± 0.7 ± 0.2		<sup>1,2</sup> AUBERT	04B BABR	Repl. by LEES 11M
<14	90	BRANDENB...	98 CLE2	$e^+e^- \rightarrow \Upsilon(4S)$
<19	90	<sup>3</sup> NEMAT1	98 CLE2	$e^+e^- \rightarrow \Upsilon(4S)$
<27	90	<sup>4</sup> ALAM	94 CLE2	Repl. by NEMAT1 98

- <sup>1</sup> Assumes equal production of  $B^+$  and  $B^0$  at the  $\Upsilon(4S)$ .  
<sup>2</sup> Reports an upper limit  $< 2.6 \times 10^{-4}$  at 90% CL.  
<sup>3</sup> NEMAT1 98 assumes equal production of  $B^+$  and  $B^0$  at the  $\Upsilon(4S)$  and use the PDG 96 values for  $D^0$ ,  $D^{*0}$ ,  $\eta$ ,  $\eta'$ , and  $\omega$  branching fractions.  
<sup>4</sup> ALAM 94 assume equal production of  $B^+$  and  $B^0$  at the  $\Upsilon(4S)$  and use the CLEO II B( $D^*(2007)^0 \rightarrow D^0 \pi^0$ ) and absolute B( $D^0 \rightarrow K^- \pi^+$ ) and the PDG 1992 B( $D^0 \rightarrow K^- \pi^+ \pi^0$ )/B( $D^0 \rightarrow K^- \pi^+$ ) and B( $D^0 \rightarrow K^- 2\pi^+ \pi^-$ )/B( $D^0 \rightarrow K^- \pi^+$ ).

 $\Gamma(\bar{D}^0 \eta')/\Gamma(\bar{D}^*(2007)^0 \eta')$   $\Gamma_{153}/\Gamma_{162}$ 

VALUE	DOCUMENT ID	TECN	COMMENT
<b>0.96 ± 0.18 ± 0.06</b>	LEES	11M BABR	$e^+e^- \rightarrow \Upsilon(4S)$
• • • We do not use the following data for averages, fits, limits, etc. • • •			
1.3 ± 0.8 ± 0.2	AUBERT	04B BABR	Repl. by LEES 11M

 $\Gamma(\bar{D}^*(2007)^0 \pi^+ \pi^-)/\Gamma_{\text{total}}$   $\Gamma_{163}/\Gamma$ 

VALUE	DOCUMENT ID	TECN	COMMENT
<b>(6.2 ± 1.2 ± 1.8) × 10<sup>-4</sup></b>	<sup>1,2</sup> SATPATHY	03 BELL	$e^+e^- \rightarrow \Upsilon(4S)$
<sup>1</sup> Assumes equal production of $B^+$ and $B^0$ at the $\Upsilon(4S)$ .			
<sup>2</sup> No assumption about the intermediate mechanism is made in the analysis.			

 $\Gamma(\bar{D}^*(2007)^0 K^0)/\Gamma_{\text{total}}$   $\Gamma_{164}/\Gamma$ 

VALUE (units $10^{-5}$ )	CL%	DOCUMENT ID	TECN	COMMENT
<b>3.6 ± 1.2 ± 0.3</b>		<sup>1</sup> AUBERT,B	06L BABR	$e^+e^- \rightarrow \Upsilon(4S)$
• • • We do not use the following data for averages, fits, limits, etc. • • •				
<6.6	90	<sup>1</sup> KROKOVNY	03 BELL	$e^+e^- \rightarrow \Upsilon(4S)$
<sup>1</sup> Assumes equal production of $B^+$ and $B^0$ at the $\Upsilon(4S)$ .				

 $\Gamma(\bar{D}^*(2007)^0 K^*(892)^0)/\Gamma_{\text{total}}$   $\Gamma_{165}/\Gamma$ 

VALUE	CL%	DOCUMENT ID	TECN	COMMENT
<b>&lt;6.9 × 10<sup>-5</sup></b>	90	<sup>1</sup> KROKOVNY	03 BELL	$e^+e^- \rightarrow \Upsilon(4S)$
<sup>1</sup> Assumes equal production of $B^+$ and $B^0$ at the $\Upsilon(4S)$ .				

 $\Gamma(D^*(2007)^0 K^*(892)^0)/\Gamma_{\text{total}}$   $\Gamma_{166}/\Gamma$ 

VALUE	CL%	DOCUMENT ID	TECN	COMMENT
<b>&lt;4.0 × 10<sup>-5</sup></b>	90	<sup>1</sup> KROKOVNY	03 BELL	$e^+e^- \rightarrow \Upsilon(4S)$
<sup>1</sup> Assumes equal production of $B^+$ and $B^0$ at the $\Upsilon(4S)$ .				

 $\Gamma(D^*(2007)^0 \pi^+ \pi^+ \pi^- \pi^-)/\Gamma_{\text{total}}$   $\Gamma_{167}/\Gamma$ 

VALUE (units $10^{-3}$ )	DOCUMENT ID	TECN	COMMENT
<b>2.7 ± 0.5 OUR AVERAGE</b>			
2.60 ± 0.47 ± 0.37	<sup>1</sup> MAJUMDER	04 BELL	$e^+e^- \rightarrow \Upsilon(4S)$
3.0 ± 0.7 ± 0.6	<sup>1</sup> EDWARDS	02 CLE2	$e^+e^- \rightarrow \Upsilon(4S)$
<sup>1</sup> Assumes equal production of $B^+$ and $B^0$ at the $\Upsilon(4S)$ .			

 $\Gamma(D^*(2007)^0 \pi^+ \pi^+ \pi^- \pi^-)/\Gamma(D^*(2010)^- \pi^+ \pi^+ \pi^- \pi^0)$   $\Gamma_{167}/\Gamma_{63}$ 

VALUE	DOCUMENT ID	TECN	COMMENT
<b>0.17 ± 0.04 ± 0.02</b>	<sup>1</sup> EDWARDS	02 CLE2	$e^+e^- \rightarrow \Upsilon(4S)$
<sup>1</sup> Assumes equal production of $B^+$ and $B^0$ at the $\Upsilon(4S)$ .			

 $\Gamma(D^*(2010)^+ D^*(2010)^-)/\Gamma_{\text{total}}$   $\Gamma_{168}/\Gamma$ 

VALUE (units $10^{-4}$ )	CL%	DOCUMENT ID	TECN	COMMENT
<b>8.0 ± 0.6 OUR AVERAGE</b>				
7.82 ± 0.38 ± 0.63		<sup>1</sup> KRONENBIT...	12 BELL	$e^+e^- \rightarrow \Upsilon(4S)$
8.1 ± 0.6 ± 1.0		<sup>1</sup> AUBERT,B	06A BABR	$e^+e^- \rightarrow \Upsilon(4S)$
9.9 <sup>+4.2</sup> <sub>-3.3</sub> ± 1.2		<sup>1</sup> LIPELES	00 CLE2	$e^+e^- \rightarrow \Upsilon(4S)$
• • • We do not use the following data for averages, fits, limits, etc. • • •				
8.1 ± 0.8 ± 1.1		<sup>1</sup> MIYAKE	05 BELL	Repl. by KRONENBIT-TER 12
8.3 ± 1.6 ± 1.2		<sup>1,2</sup> AUBERT	02M BABR	Repl. by AUBERT,B 06B
6.2 <sup>+4.0</sup> <sub>-2.9</sub> ± 1.0		<sup>3</sup> ARTUSO	99 CLE2	Repl. by LIPELES 00
<61	90	<sup>4</sup> BARATE	98Q ALEP	$e^+e^- \rightarrow Z$
<22	90	<sup>5</sup> ASNER	97 CLE2	Repl. by ARTUSO 99

- <sup>1</sup> Assumes equal production of  $B^+$  and  $B^0$  at the  $\Upsilon(4S)$ .  
<sup>2</sup> AUBERT 02M also assumes the measured CP-odd fraction of the final states is  $0.22 \pm 0.18 \pm 0.03$ .  
<sup>3</sup> ARTUSO 99 uses B( $\Upsilon(4S) \rightarrow B^0 \bar{D}^0$ ) = (48 ± 4)%.  
<sup>4</sup> BARATE 98Q (ALEPH) observes 2 events with an expected background of  $0.10 \pm 0.03$  which corresponds to a branching ratio of  $(2.3 \pm 1.9 \pm 0.4) \times 10^{-3}$ .  
<sup>5</sup> ASNER 97 at CLEO observes 1 event with an expected background of  $0.022 \pm 0.011$ . This corresponds to a branching ratio of  $(5.3 \pm 7.1 \pm 1.0) \times 10^{-4}$ .

 $\Gamma(\bar{D}^*(2007)^0 \omega)/\Gamma_{\text{total}}$   $\Gamma_{169}/\Gamma$ 

VALUE (units $10^{-4}$ )	CL%	DOCUMENT ID	TECN	COMMENT
<b>3.6 ± 1.1 OUR AVERAGE</b>				Error includes scale factor of 3.1.
4.55 ± 0.24 ± 0.39		<sup>1</sup> LEES	11M BABR	$e^+e^- \rightarrow \Upsilon(4S)$
2.29 ± 0.39 ± 0.40		<sup>1</sup> BLYTH	06 BELL	$e^+e^- \rightarrow \Upsilon(4S)$
• • • We do not use the following data for averages, fits, limits, etc. • • •				
4.2 ± 0.7 ± 0.9	90	<sup>1</sup> AUBERT	04B BABR	Repl. by LEES 11M
< 7.9	90	<sup>1</sup> ABE	02J BELL	$e^+e^- \rightarrow \Upsilon(4S)$
< 7.4	90	<sup>2</sup> NEMAT1	98 CLE2	$e^+e^- \rightarrow \Upsilon(4S)$
<21	90	<sup>3</sup> ALAM	94 CLE2	Repl. by NEMAT1 98

- <sup>1</sup> Assumes equal production of  $B^+$  and  $B^0$  at the  $\Upsilon(4S)$ .  
<sup>2</sup> NEMAT1 98 assumes equal production of  $B^+$  and  $B^0$  at the  $\Upsilon(4S)$  and use the PDG 96 values for  $D^0$ ,  $D^{*0}$ ,  $\eta$ ,  $\eta'$ , and  $\omega$  branching fractions.  
<sup>3</sup> ALAM 94 assume equal production of  $B^+$  and  $B^0$  at the  $\Upsilon(4S)$  and use the CLEO II B( $D^*(2007)^0 \rightarrow D^0 \pi^0$ ) and absolute B( $D^0 \rightarrow K^- \pi^+$ ) and the PDG 1992 B( $D^0 \rightarrow K^- \pi^+ \pi^0$ )/B( $D^0 \rightarrow K^- \pi^+$ ) and B( $D^0 \rightarrow K^- 2\pi^+ \pi^-$ )/B( $D^0 \rightarrow K^- \pi^+$ ).

 $\Gamma(\bar{D}^0 \omega)/\Gamma(\bar{D}^*(2007)^0 \omega)$   $\Gamma_{154}/\Gamma_{169}$ 

VALUE	DOCUMENT ID	TECN	COMMENT
<b>0.58 ± 0.06 OUR AVERAGE</b>			
0.56 ± 0.04 ± 0.04	LEES	11M BABR	$e^+e^- \rightarrow \Upsilon(4S)$
1.04 ± 0.20 ± 0.17	BLYTH	06 BELL	$e^+e^- \rightarrow \Upsilon(4S)$
• • • We do not use the following data for averages, fits, limits, etc. • • •			
0.7 ± 0.1 ± 0.1	AUBERT	04B BABR	Repl. by LEES 11M

 $\Gamma(D^*(2010)^+ D^-)/\Gamma_{\text{total}}$   $\Gamma_{170}/\Gamma$ 

VALUE (units $10^{-4}$ )	CL%	DOCUMENT ID	TECN	COMMENT
<b>6.1 ± 1.5 OUR AVERAGE</b>				Error includes scale factor of 1.6.
5.7 ± 0.7 ± 0.7		<sup>1</sup> AUBERT,B	06A BABR	$e^+e^- \rightarrow \Upsilon(4S)$
11.7 ± 2.6 <sup>+2.2</sup> <sub>-2.5</sub>		<sup>1,2</sup> ABE	02Q BELL	$e^+e^- \rightarrow \Upsilon(4S)$
• • • We do not use the following data for averages, fits, limits, etc. • • •				
8.8 ± 1.0 ± 1.3		<sup>1</sup> AUBERT	03J BABR	Repl. by AUBERT,B 06B
14.8 ± 3.8 <sup>+2.8</sup> <sub>-3.1</sub>		<sup>1,3</sup> ABE	02Q BELL	$e^+e^- \rightarrow \Upsilon(4S)$
< 6.3	90	<sup>1</sup> LIPELES	00 CLE2	$e^+e^- \rightarrow \Upsilon(4S)$
<56	90	BARATE	98Q ALEP	$e^+e^- \rightarrow Z$
<18	90	ASNER	97 CLE2	$e^+e^- \rightarrow \Upsilon(4S)$

- <sup>1</sup> Assumes equal production of  $B^+$  and  $B^0$  at the  $\Upsilon(4S)$ .  
<sup>2</sup> The measurement is performed using fully reconstructed  $D^*$  and  $D^+$  decays.  
<sup>3</sup> The measurement is performed using a partial reconstruction technique for the  $D^*$  and fully reconstructed  $D^+$  decays as a cross check.

 $\Gamma(D^*(2007)^0 \bar{D}^*(2007)^0)/\Gamma_{\text{total}}$   $\Gamma_{171}/\Gamma$ 

VALUE (units $10^{-4}$ )	CL%	DOCUMENT ID	TECN	COMMENT
<b>&lt; 0.9</b>	90	<sup>1</sup> AUBERT,B	06A BABR	$e^+e^- \rightarrow \Upsilon(4S)$
• • • We do not use the following data for averages, fits, limits, etc. • • •				
<270	90	BARATE	98Q ALEP	$e^+e^- \rightarrow Z$
<sup>1</sup> Assumes equal production of $B^+$ and $B^0$ at the $\Upsilon(4S)$ .				

See key on page 999

Meson Particle Listings

$B^0$

$\Gamma(D^- D^0 K^+)/\Gamma_{total}$   $\Gamma_{172}/\Gamma$

VALUE (units $10^{-3}$ )	DOCUMENT ID	TECN	COMMENT
<b>1.07 ± 0.07 ± 0.09</b>	<sup>1</sup> DEL-AMO-SA..11B	BABR	$e^+ e^- \rightarrow \Upsilon(4S)$
• • • We do not use the following data for averages, fits, limits, etc. • • •			
1.7 ± 0.3 ± 0.3	<sup>1</sup> AUBERT	03x BABR	Repl. by DEL-AMO-SANCHEZ 11B

<sup>1</sup> Assumes equal production of  $B^+$  and  $B^0$  at the  $\Upsilon(4S)$ .

$\Gamma(D^- D^*(2007)^0 K^+)/\Gamma_{total}$   $\Gamma_{173}/\Gamma$

VALUE (units $10^{-3}$ )	DOCUMENT ID	TECN	COMMENT
<b>3.46 ± 0.18 ± 0.37</b>	<sup>1</sup> DEL-AMO-SA..11B	BABR	$e^+ e^- \rightarrow \Upsilon(4S)$
• • • We do not use the following data for averages, fits, limits, etc. • • •			
4.6 ± 0.7 ± 0.7	<sup>1</sup> AUBERT	03x BABR	Repl. by DEL-AMO-SANCHEZ 11B

<sup>1</sup> Assumes equal production of  $B^+$  and  $B^0$  at the  $\Upsilon(4S)$ .

$\Gamma(D^*(2010)^- D^0 K^+)/\Gamma_{total}$   $\Gamma_{174}/\Gamma$

VALUE (units $10^{-3}$ )	DOCUMENT ID	TECN	COMMENT
<b>2.47 ± 0.10 ± 0.18</b>	<sup>1</sup> DEL-AMO-SA..11B	BABR	$e^+ e^- \rightarrow \Upsilon(4S)$
• • • We do not use the following data for averages, fits, limits, etc. • • •			
3.1 $^{+0.4}_{-0.3}$ ± 0.4	<sup>1</sup> AUBERT	03x BABR	Repl. by DEL-AMO-SANCHEZ 11B

<sup>1</sup> Assumes equal production of  $B^+$  and  $B^0$  at the  $\Upsilon(4S)$ .

$\Gamma(D^*(2010)^- D^*(2007)^0 K^+)/\Gamma_{total}$   $\Gamma_{175}/\Gamma$

VALUE (units $10^{-3}$ )	DOCUMENT ID	TECN	COMMENT
<b>10.6 ± 0.33 ± 0.86</b>	<sup>1</sup> DEL-AMO-SA..11B	BABR	$e^+ e^- \rightarrow \Upsilon(4S)$
• • • We do not use the following data for averages, fits, limits, etc. • • •			
11.8 ± 1.0 ± 1.7	<sup>1</sup> AUBERT	03x BABR	Repl. by DEL-AMO-SANCHEZ 11B

<sup>1</sup> Assumes equal production of  $B^+$  and  $B^0$  at the  $\Upsilon(4S)$ .

$\Gamma(D^- D^+ K^0)/\Gamma_{total}$   $\Gamma_{176}/\Gamma$

VALUE (units $10^{-3}$ )	CL%	DOCUMENT ID	TECN	COMMENT
<b>0.75 ± 0.12 ± 0.12</b>		<sup>1</sup> DEL-AMO-SA..11B	BABR	$e^+ e^- \rightarrow \Upsilon(4S)$
• • • We do not use the following data for averages, fits, limits, etc. • • •				
<1.7	90	<sup>1</sup> AUBERT	03x BABR	Repl. by DEL-AMO-SANCHEZ 11B

<sup>1</sup> Assumes equal production of  $B^+$  and  $B^0$  at the  $\Upsilon(4S)$ .

$[\Gamma(D^*(2010)^- D^+ K^0) + \Gamma(D^- D^*(2010)^+ K^0)]/\Gamma_{total}$   $\Gamma_{177}/\Gamma$

VALUE (units $10^{-3}$ )	DOCUMENT ID	TECN	COMMENT
<b>6.41 ± 0.36 ± 0.39</b>	<sup>1</sup> DEL-AMO-SA..11B	BABR	$e^+ e^- \rightarrow \Upsilon(4S)$
• • • We do not use the following data for averages, fits, limits, etc. • • •			
6.5 ± 1.2 ± 1.0	<sup>1</sup> AUBERT	03x BABR	Repl. by DEL-AMO-SANCHEZ 11B

<sup>1</sup> Assumes equal production of  $B^+$  and  $B^0$  at the  $\Upsilon(4S)$ .

$\Gamma(D^*(2010)^- D^*(2010)^+ K^0)/\Gamma_{total}$   $\Gamma_{178}/\Gamma$

VALUE (units $10^{-3}$ )	DOCUMENT ID	TECN	COMMENT
<b>8.1 ± 0.7 OUR AVERAGE</b>			
8.26 ± 0.43 ± 0.67	<sup>1</sup> DEL-AMO-SA..11B	BABR	$e^+ e^- \rightarrow \Upsilon(4S)$
6.8 ± 0.8 ± 1.4	<sup>1,2</sup> DALSENO	07 BELL	$e^+ e^- \rightarrow \Upsilon(4S)$
8.8 ± 0.8 ± 1.4	<sup>1,2</sup> AUBERT,B	06q BABR	$e^+ e^- \rightarrow \Upsilon(4S)$
• • • We do not use the following data for averages, fits, limits, etc. • • •			
8.8 $^{+1.5}_{-1.4}$ ± 1.3	<sup>1</sup> AUBERT	03x BABR	Repl. by AUBERT,B 06q

<sup>1</sup> Assumes equal production of  $B^+$  and  $B^0$  at the  $\Upsilon(4S)$ .

<sup>2</sup> The result is rescaled by a factor of 2 to convert from  $K_S^0$  to  $K^0$ .

$\Gamma(D^{*-} D_{s1}(2536)^+, D_{s1}^+ \rightarrow D^{*+} K^0)/\Gamma_{total}$   $\Gamma_{179}/\Gamma$

VALUE (units $10^{-4}$ )	DOCUMENT ID	TECN	COMMENT
<b>8.0 ± 2.4 OUR AVERAGE</b>			
7.6 $^{+4.8+1.6}_{-4.2-1.4}$	<sup>1,2</sup> DALSENO	07 BELL	$e^+ e^- \rightarrow \Upsilon(4S)$
8.2 ± 2.6 ± 1.2	<sup>1,2</sup> AUBERT,B	06q BABR	$e^+ e^- \rightarrow \Upsilon(4S)$

<sup>1</sup> Assumes equal production of  $B^+$  and  $B^0$  at the  $\Upsilon(4S)$ .

<sup>2</sup> The result is rescaled by a factor of 2 to convert from  $K_S^0$  to  $K^0$ .

$\Gamma(D^0 D^0 K^0)/\Gamma_{total}$   $\Gamma_{180}/\Gamma$

VALUE (units $10^{-3}$ )	CL%	DOCUMENT ID	TECN	COMMENT
<b>0.27 ± 0.10 ± 0.05</b>		<sup>1</sup> DEL-AMO-SA..11B	BABR	$e^+ e^- \rightarrow \Upsilon(4S)$
• • • We do not use the following data for averages, fits, limits, etc. • • •				
<1.4	90	<sup>1</sup> AUBERT	03x BABR	Repl. by DEL-AMO-SANCHEZ 11B

<sup>1</sup> Assumes equal production of  $B^+$  and  $B^0$  at the  $\Upsilon(4S)$ .

$[\Gamma(\bar{D}^0 D^*(2007)^0 K^0) + \Gamma(\bar{D}^*(2007)^0 D^0 K^0)]/\Gamma_{total}$   $\Gamma_{181}/\Gamma$

VALUE (units $10^{-3}$ )	CL%	DOCUMENT ID	TECN	COMMENT
<b>1.08 ± 0.32 ± 0.36</b>		<sup>1</sup> DEL-AMO-SA..11B	BABR	$e^+ e^- \rightarrow \Upsilon(4S)$
• • • We do not use the following data for averages, fits, limits, etc. • • •				
<3.7	90	<sup>1</sup> AUBERT	03x BABR	Repl. by DEL-AMO-SANCHEZ 11B

<sup>1</sup> Assumes equal production of  $B^+$  and  $B^0$  at the  $\Upsilon(4S)$ .

$\Gamma(\bar{D}^*(2007)^0 D^*(2007)^0 K^0)/\Gamma_{total}$   $\Gamma_{182}/\Gamma$

VALUE (units $10^{-3}$ )	CL%	DOCUMENT ID	TECN	COMMENT
<b>2.40 ± 0.55 ± 0.67</b>		<sup>1</sup> DEL-AMO-SA..11B	BABR	$e^+ e^- \rightarrow \Upsilon(4S)$
• • • We do not use the following data for averages, fits, limits, etc. • • •				
<6.6	90	<sup>1</sup> AUBERT	03x BABR	Repl. by DEL-AMO-SANCHEZ 11B

<sup>1</sup> Assumes equal production of  $B^+$  and  $B^0$  at the  $\Upsilon(4S)$ .

$\Gamma((\bar{D} + \bar{D}^*)(D + D^*)K)/\Gamma_{total}$   $\Gamma_{183}/\Gamma$

VALUE (units $10^{-2}$ )	DOCUMENT ID	TECN	COMMENT
<b>3.68 ± 0.10 ± 0.24</b>	<sup>1</sup> DEL-AMO-SA..11B	BABR	$e^+ e^- \rightarrow \Upsilon(4S)$
• • • We do not use the following data for averages, fits, limits, etc. • • •			
4.3 ± 0.3 ± 0.6	<sup>1</sup> AUBERT	03x BABR	Repl. by DEL-AMO-SANCHEZ 11B

<sup>1</sup> Assumes equal production of  $B^+$  and  $B^0$  at the  $\Upsilon(4S)$ .

$\Gamma(\eta_c K^0)/\Gamma_{total}$   $\Gamma_{184}/\Gamma$

VALUE (units $10^{-3}$ )	DOCUMENT ID	TECN	COMMENT
<b>0.80 ± 0.11 OUR AVERAGE</b>			
0.71 $^{+0.12}_{-0.10}$ ± 0.24	<sup>1</sup> CHILIKIN	19 BELL	$e^+ e^- \rightarrow \Upsilon(4S)$
0.57 $^{+0.20}_{-0.18}$ ± 0.05	<sup>2,3</sup> AUBERT	07Av BABR	$e^+ e^- \rightarrow \Upsilon(4S)$
0.89 ± 0.15 ± 0.05	<sup>2,4</sup> AUBERT,B	04B BABR	$e^+ e^- \rightarrow \Upsilon(4S)$
1.23 ± 0.23 $^{+0.40}_{-0.41}$	<sup>2</sup> FANG	03 BELL	$e^+ e^- \rightarrow \Upsilon(4S)$
1.09 $^{+0.55}_{-0.42}$ ± 0.33	<sup>5</sup> EDWARDS	01 CLE2	$e^+ e^- \rightarrow \Upsilon(4S)$

<sup>1</sup> CHILIKIN 19 reports  $[\Gamma(B^0 \rightarrow \eta_c K^0)/\Gamma_{total}] \times [B(\eta_c(1S) \rightarrow \pi^+ \pi^- p\bar{p})] = (38.0^{+6.4+1.3}_{-2.9-4.7}) \times 10^{-7}$  which we divide by our best value  $B(\eta_c(1S) \rightarrow \pi^+ \pi^- p\bar{p}) = (5.3 \pm 1.8) \times 10^{-3}$ . Our first error is their experiment's error and our second error is the systematic error from using our best value.

<sup>2</sup> Assumes equal production of  $B^+$  and  $B^0$  at the  $\Upsilon(4S)$ .

<sup>3</sup> AUBERT 07Av reports  $[\Gamma(B^0 \rightarrow \eta_c K^0)/\Gamma_{total}] \times [B(\eta_c(1S) \rightarrow p\bar{p})] = (0.83^{+0.28}_{-0.26} \pm 0.05) \times 10^{-6}$  which we divide by our best value  $B(\eta_c(1S) \rightarrow p\bar{p}) = (1.45 \pm 0.14) \times 10^{-3}$ . Our first error is their experiment's error and our second error is the systematic error from using our best value.

<sup>4</sup> AUBERT,B 04B reports  $[\Gamma(B^0 \rightarrow \eta_c K^0)/\Gamma_{total}] \times [B(\eta_c(1S) \rightarrow K\bar{K}\pi)] = (0.0648 \pm 0.0085 \pm 0.0071) \times 10^{-3}$  which we divide by our best value  $B(\eta_c(1S) \rightarrow K\bar{K}\pi) = (7.3 \pm 0.4) \times 10^{-2}$ . Our first error is their experiment's error and our second error is the systematic error from using our best value.

<sup>5</sup> EDWARDS 01 assumes equal production of  $B^0$  and  $B^+$  at the  $\Upsilon(4S)$ . The correlated uncertainties (28.3)% from  $B(J/\psi(1S) \rightarrow \gamma\eta_c)$  in those modes have been accounted for.

$\Gamma(\eta_c K^0)/\Gamma(J/\psi(1S) K^0)$   $\Gamma_{184}/\Gamma_{198}$

VALUE	DOCUMENT ID	TECN	COMMENT
<b>1.39 ± 0.20 ± 0.45</b>	<sup>1</sup> AUBERT,B	04B BABR	$e^+ e^- \rightarrow \Upsilon(4S)$

<sup>1</sup> Uses BABAR measurement of  $B(B^0 \rightarrow J/\psi K^0) = (8.5 \pm 0.5 \pm 0.6) \times 10^{-4}$ .

$\Gamma(\eta_c(1S) K^+ \pi^-)/\Gamma(J/\psi(1S) K^+ \pi^-)$   $\Gamma_{185}/\Gamma_{199}$

VALUE	DOCUMENT ID	TECN	COMMENT
<b>0.52 ± 0.02 ± 0.05</b>	<sup>1</sup> AAIJ	18AN LHCB	$pp$ at 7, 8, 13 TeV

<sup>1</sup> AAIJ 18AN reports  $[\Gamma(B^0 \rightarrow \eta_c(1S) K^+ \pi^-)/\Gamma(B^0 \rightarrow J/\psi(1S) K^+ \pi^-)] \times [B(\eta_c(1S) \rightarrow p\bar{p})] / [B(J/\psi(1S) \rightarrow p\bar{p})] = 0.357 \pm 0.015 \pm 0.008$  which we multiply or divide by our best values  $B(\eta_c(1S) \rightarrow p\bar{p}) = (1.45 \pm 0.14) \times 10^{-3}$ ,  $B(J/\psi(1S) \rightarrow p\bar{p}) = (2.121 \pm 0.029) \times 10^{-3}$ . Our first error is their experiment's error and our second error is the systematic error from using our best values.

$\Gamma(\eta_c(1S) K^*(1410)^0)/\Gamma(\eta_c(1S) K^+ \pi^-)$   $\Gamma_{188}/\Gamma_{185}$

VALUE (units $10^{-2}$ )	DOCUMENT ID	TECN	COMMENT
<b>32 ± 24 ± 6</b>	<sup>1</sup> AAIJ	18AN LHCB	$pp$ at 7, 8, 13 TeV

<sup>1</sup> AAIJ 18AN reports  $[\Gamma(B^0 \rightarrow \eta_c(1S) K^*(1410)^0)/\Gamma(B^0 \rightarrow \eta_c(1S) K^+ \pi^-)] \times [B(K^*(1410) \rightarrow K\pi)] = 0.021 \pm 0.011 \pm 0.011$  which we divide by our best value  $B(K^*(1410) \rightarrow K\pi) = (6.6 \pm 1.3) \times 10^{-2}$ . Our first error is their experiment's error and our second error is the systematic error from using our best value.

$\Gamma(\eta_c(1S) K^+ \pi^- (NR))/\Gamma(\eta_c(1S) K^+ \pi^-)$   $\Gamma_{186}/\Gamma_{185}$

VALUE (units $10^{-2}$ )	DOCUMENT ID	TECN	COMMENT
<b>10.3 ± 1.4 <math>^{+1.0}_{-1.2}</math></b>	AAIJ	18AN LHCB	$pp$ at 7, 8, 13 TeV

# Meson Particle Listings

## $B^0$

### $\Gamma(\eta_c(1S)K_0^*(1430)^0)/\Gamma(\eta_c(1S)K^+\pi^-)$ $\Gamma_{189}/\Gamma_{185}$

VALUE (units $10^{-2}$ )	DOCUMENT ID	TECN	COMMENT
<b>27 ± 5 ± 3</b>	<sup>1</sup> AAIJ	18AN LHCB	pp at 7, 8, 13 TeV
<sup>1</sup> AAIJ 18AN reports $[\Gamma(B^0 \rightarrow \eta_c(1S)K_0^*(1430)^0)/\Gamma(B^0 \rightarrow \eta_c(1S)K^+\pi^-)] \times [B(K_0^*(1430) \rightarrow K\pi)] = 0.253 \pm 0.035^{+0.035}_{-0.028}$ which we divide by our best value $B(K_0^*(1430) \rightarrow K\pi) = (93 \pm 10) \times 10^{-2}$ . Our first error is their experiment's error and our second error is the systematic error from using our best value.			

### $\Gamma(\eta_c(1S)K_2^*(1430)^0)/\Gamma(\eta_c(1S)K^+\pi^-)$ $\Gamma_{190}/\Gamma_{185}$

VALUE (units $10^{-2}$ )	DOCUMENT ID	TECN	COMMENT
<b>8.2 ± 3.6 ± 0.2</b>	<sup>1</sup> AAIJ	18AN LHCB	pp at 7, 8, 13 TeV
<sup>1</sup> AAIJ 18AN reports $[\Gamma(B^0 \rightarrow \eta_c(1S)K_2^*(1430)^0)/\Gamma(B^0 \rightarrow \eta_c(1S)K^+\pi^-)] \times [B(K_2^*(1430) \rightarrow K\pi)] = 0.041 \pm 0.015^{+0.010}_{-0.016}$ which we divide by our best value $B(K_2^*(1430) \rightarrow K\pi) = (49.9 \pm 2.5) \times 10^{-2}$ . Our first error is their experiment's error and our second error is the systematic error from using our best value.			

### $\Gamma(\eta_c(1S)K^*(1680)^0)/\Gamma(\eta_c(1S)K^+\pi^-)$ $\Gamma_{191}/\Gamma_{185}$

VALUE (units $10^{-2}$ )	DOCUMENT ID	TECN	COMMENT
<b>5.7 ± 6.5 ± 0.4</b>	<sup>1</sup> AAIJ	18AN LHCB	pp at 7, 8, 13 TeV
<sup>1</sup> AAIJ 18AN reports $[\Gamma(B^0 \rightarrow \eta_c(1S)K^*(1680)^0)/\Gamma(B^0 \rightarrow \eta_c(1S)K^+\pi^-)] \times [B(K^*(1680) \rightarrow K\pi)] = 0.022 \pm 0.020^{+0.015}_{-0.017}$ which we divide by our best value $B(K^*(1680) \rightarrow K\pi) = (38.7 \pm 2.5) \times 10^{-2}$ . Our first error is their experiment's error and our second error is the systematic error from using our best value.			

### $\Gamma(\eta_c(1S)K_0^*(1950)^0)/\Gamma(\eta_c(1S)K^+\pi^-)$ $\Gamma_{192}/\Gamma_{185}$

VALUE (units $10^{-2}$ )	DOCUMENT ID	TECN	COMMENT
<b>7 ± 4 ± 2</b>	<sup>1</sup> AAIJ	18AN LHCB	pp at 7, 8, 13 TeV
<sup>1</sup> AAIJ 18AN reports $[\Gamma(B^0 \rightarrow \eta_c(1S)K_0^*(1950)^0)/\Gamma(B^0 \rightarrow \eta_c(1S)K^+\pi^-)] \times [B(K_0^*(1950) \rightarrow K^-\pi^+)] = 0.038 \pm 0.018^{+0.014}_{-0.025}$ which we divide by our best value $B(K_0^*(1950) \rightarrow K^-\pi^+) = (52 \pm 14) \times 10^{-2}$ . Our first error is their experiment's error and our second error is the systematic error from using our best value.			

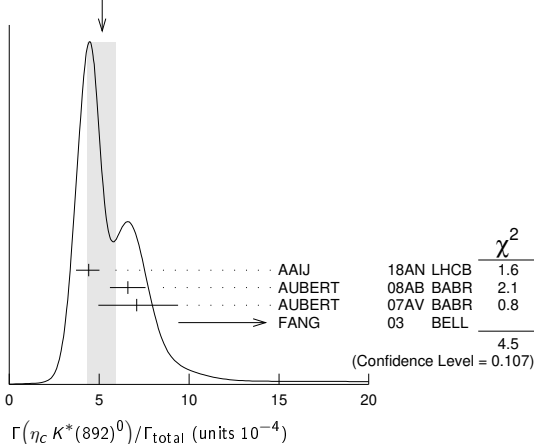
### $\Gamma(X(4100)^-K^+, X^- \rightarrow \eta_c\pi^-)/\Gamma(\eta_c(1S)K^+\pi^-)$ $\Gamma_{187}/\Gamma_{185}$

VALUE (units $10^{-2}$ )	DOCUMENT ID	TECN	COMMENT
<b>3.3 ± 1.1 ± 1.2 ± 1.1</b>	AAIJ	18AN LHCB	pp at 7, 8, 13 TeV

### $\Gamma(\eta_c K^*(892)^0)/\Gamma_{total}$ $\Gamma_{193}/\Gamma$

VALUE (units $10^{-4}$ )	DOCUMENT ID	TECN	COMMENT
<b>5.2 ± 0.7 ± 0.8</b> OUR AVERAGE	Error includes scale factor of 1.5. See the ideogram below.		
4.42 ± 0.24 ± 0.54 ± 0.66	<sup>1</sup> AAIJ	18AN LHCB	pp at 7, 8, 13 TeV
6.6 ± 0.8 ± 0.5	<sup>2,3</sup> AUBERT	08AB BABR	$e^+e^- \rightarrow \Upsilon(4S)$
7.1 ± 2.2 ± 0.7	<sup>4,5</sup> AUBERT	07AV BABR	$e^+e^- \rightarrow \Upsilon(4S)$
16.2 ± 3.2 ± 5.5 ± 6.0	<sup>5</sup> FANG	03 BELL	$e^+e^- \rightarrow \Upsilon(4S)$

WEIGHTED AVERAGE  
5.2 ± 0.7-0.8 (Error scaled by 1.5)



<sup>1</sup> AAIJ 18AN reports  $B(B^0 \rightarrow \eta_c K^*(892)^0, K^*(892)^0 \rightarrow K^+\pi^-) = (2.95 \pm 0.16^{+0.36}_{-0.44}) \times 10^{-4}$  using the fitted fraction of  $0.514 \pm 0.019^{+0.017}_{-0.048}$  from Dalitz decay of  $B(B^0 \rightarrow \eta_c K^+\pi^-) = (5.73 \pm 0.24 \pm 0.67) \times 10^{-4}$  and corrected for  $B(K^*(892)^0 \rightarrow K^+\pi^-) = 2/3$ .

<sup>2</sup> AUBERT 08AB reports  $[\Gamma(B^0 \rightarrow \eta_c K^*(892)^0)/\Gamma_{total}] / [B(B^+ \rightarrow \eta_c K^+)] = 0.62 \pm 0.06 \pm 0.05$  which we multiply by our best value  $B(B^+ \rightarrow \eta_c K^+) = (1.06 \pm 0.09) \times 10^{-3}$ . Our first error is their experiment's error and our second error is the systematic error from using our best value.

<sup>3</sup> Uses the production ratio of  $(B^+ B^-)/(B^0 \bar{B}^0) = 1.026 \pm 0.032$  at  $\Upsilon(4S)$ .

<sup>4</sup> AUBERT 07AV reports  $[\Gamma(B^0 \rightarrow \eta_c K^*(892)^0)/\Gamma_{total}] \times [B(\eta_c(1S) \rightarrow p\bar{p})] = (1.03^{+0.27}_{-0.24} \pm 0.17) \times 10^{-6}$  which we divide by our best value  $B(\eta_c(1S) \rightarrow p\bar{p}) = (1.45 \pm 0.14) \times 10^{-3}$ . Our first error is their experiment's error and our second error is the systematic error from using our best value.

<sup>5</sup> Assumes equal production of  $B^+$  and  $B^0$  at the  $\Upsilon(4S)$ .

### $\Gamma(\eta_c(2S)K_S^0, \eta_c \rightarrow p\bar{p}\pi^+\pi^-)/\Gamma_{total}$ $\Gamma_{194}/\Gamma$

VALUE (units $10^{-7}$ )	DOCUMENT ID	TECN	COMMENT
<b>4.2 ± 1.4 ± 0.3 ± 1.2 ± 0.3</b>	CHILIKIN	19 BELL	$e^+e^- \rightarrow \Upsilon(4S)$

### $\Gamma(\eta_c(2S)K^{*0})/\Gamma_{total}$ $\Gamma_{195}/\Gamma$

VALUE (units $10^{-4}$ )	CL%	DOCUMENT ID	TECN	COMMENT
<b>&lt; 3.9</b>	90	<sup>1</sup> AUBERT	08AB BABR	$e^+e^- \rightarrow \Upsilon(4S)$
<sup>1</sup> Uses the production ratio of $(B^+ B^-)/(B^0 \bar{B}^0) = 1.026 \pm 0.032$ at $\Upsilon(4S)$ .				

### $\Gamma(h_c(1P)K_S^0)/\Gamma_{total}$ $\Gamma_{196}/\Gamma$

VALUE	DOCUMENT ID	TECN	COMMENT
<b>&lt; 1.4 × 10<sup>-5</sup></b>	CHILIKIN	19 BELL	$e^+e^- \rightarrow \Upsilon(4S)$

### $\Gamma(B^0 \rightarrow h_c(1P)K^{*0})/\Gamma_{total} \times \Gamma(h_c(1P) \rightarrow \gamma\eta_c(1S))/\Gamma_{total}$ $\Gamma_{197}/\Gamma \times \Gamma_{12}^{h_c(1P)}/\Gamma_{h_c(1P)}$

VALUE (units $10^{-4}$ )	CL%	DOCUMENT ID	TECN	COMMENT
<b>&lt; 2.2</b>	90	<sup>1</sup> AUBERT	08AB BABR	$e^+e^- \rightarrow \Upsilon(4S)$
<sup>1</sup> Uses the production ratio of $(B^+ B^-)/(B^0 \bar{B}^0) = 1.026 \pm 0.032$ at $\Upsilon(4S)$ .				

### $\Gamma(\eta_c K^*(892)^0)/\Gamma(\eta_c K^0)$ $\Gamma_{193}/\Gamma_{184}$

VALUE	DOCUMENT ID	TECN	COMMENT
<b>1.33 ± 0.36 ± 0.24 ± 0.33</b>	FANG	03 BELL	$e^+e^- \rightarrow \Upsilon(4S)$

### $\Gamma(J/\psi(1S)K^0)/\Gamma_{total}$ $\Gamma_{198}/\Gamma$

VALUE (units $10^{-4}$ )	CL%	EVTS	DOCUMENT ID	TECN	COMMENT
<b>8.68 ± 0.30 OUR FIT</b>					
<b>8.67 ± 0.30 OUR AVERAGE</b>					
8.1 ± 0.9 ± 0.6			<sup>1</sup> CHILIKIN	19 BELL	$e^+e^- \rightarrow \Upsilon(4S)$
8.8 ± 1.4 ± 0.1			<sup>2,3</sup> AUBERT	07AV BABR	$e^+e^- \rightarrow \Upsilon(4S)$
8.69 ± 0.22 ± 0.30			<sup>3</sup> AUBERT	05J BABR	$e^+e^- \rightarrow \Upsilon(4S)$
7.9 ± 0.4 ± 0.9			<sup>3</sup> ABE	03B BELL	$e^+e^- \rightarrow \Upsilon(4S)$
9.5 ± 0.8 ± 0.6			<sup>3</sup> AVERY	00 CLE2	$e^+e^- \rightarrow \Upsilon(4S)$
11.5 ± 2.3 ± 1.7			<sup>4</sup> ABE	96H CDF	$p\bar{p}$ at 1.8 TeV
6.93 ± 4.07 ± 0.04			<sup>5</sup> BORTOLETTO	092 CLEO	$e^+e^- \rightarrow \Upsilon(4S)$
9.24 ± 7.21 ± 0.05			<sup>2</sup> 6 ALBRECHT	90J ARG	$e^+e^- \rightarrow \Upsilon(4S)$
••• We do not use the following data for averages, fits, limits, etc. •••					
8.3 ± 0.4 ± 0.5			<sup>3</sup> AUBERT	02 BABR	Repl. by AUBERT 05J
8.5 ± 1.4 ± 0.6			<sup>3</sup> JESSOP	97 CLE2	Repl. by AVERY 00
7.5 ± 2.4 ± 0.8		10	<sup>5</sup> ALAM	94 CLE2	Sup. by JESSOP 97
< 50	90		ALAM	86 CLEO	$e^+e^- \rightarrow \Upsilon(4S)$

<sup>1</sup> CHILIKIN 19 reports  $[\Gamma(B^0 \rightarrow J/\psi(1S)K^0)/\Gamma_{total}] \times [B(J/\psi(1S) \rightarrow p\bar{p}\pi^+\pi^-)] = (48.6 \pm 4.6^{+2.4}_{-2.6}) \times 10^{-7}$  which we divide by our best value  $B(J/\psi(1S) \rightarrow p\bar{p}\pi^+\pi^-) = (6.0 \pm 0.5) \times 10^{-3}$ . Our first error is their experiment's error and our second error is the systematic error from using our best value.

<sup>2</sup> AUBERT 07AV reports  $[\Gamma(B^0 \rightarrow J/\psi(1S)K^0)/\Gamma_{total}] \times [B(J/\psi(1S) \rightarrow p\bar{p})] = (1.87^{+0.28}_{-0.26} \pm 0.07) \times 10^{-6}$  which we divide by our best value  $B(J/\psi(1S) \rightarrow p\bar{p}) = (2.121 \pm 0.029) \times 10^{-3}$ . Our first error is their experiment's error and our second error is the systematic error from using our best value.

<sup>3</sup> Assumes equal production of  $B^+$  and  $B^0$  at the  $\Upsilon(4S)$ .

<sup>4</sup> ABE 96H assumes that  $B(B^+ \rightarrow J/\psi K^+) = (1.02 \pm 0.14) \times 10^{-3}$ .

<sup>5</sup> BORTOLETTO 92 reports  $(6 \pm 3 \pm 2) \times 10^{-4}$  from a measurement of  $[\Gamma(B^0 \rightarrow J/\psi(1S)K^0)/\Gamma_{total}] \times [B(J/\psi(1S) \rightarrow e^+e^-)]$  assuming  $B(J/\psi(1S) \rightarrow e^+e^-) = 0.069 \pm 0.009$ , which we rescale to our best value  $B(J/\psi(1S) \rightarrow e^+e^-) = (5.971 \pm 0.032) \times 10^{-2}$ . Our first error is their experiment's error and our second error is the systematic error from using our best value. Assumes equal production of  $B^+$  and  $B^0$  at the  $\Upsilon(4S)$ .

<sup>6</sup> ALBRECHT 90J reports  $(8 \pm 6 \pm 2) \times 10^{-4}$  from a measurement of  $[\Gamma(B^0 \rightarrow J/\psi(1S)K^0)/\Gamma_{total}] \times [B(J/\psi(1S) \rightarrow e^+e^-)]$  assuming  $B(J/\psi(1S) \rightarrow e^+e^-) = 0.069 \pm 0.009$ , which we rescale to our best value  $B(J/\psi(1S) \rightarrow e^+e^-) = (5.971 \pm 0.032) \times 10^{-2}$ . Our first error is their experiment's error and our second error is the systematic error from using our best value. Assumes equal production of  $B^+$  and  $B^0$  at the  $\Upsilon(4S)$ .

$\Gamma(J/\psi(1S)K^+\pi^-)/\Gamma_{total}$   $\Gamma_{199}/\Gamma$

VALUE (units $10^{-3}$ )	CL%	DOCUMENT ID	TECN	COMMENT
<b>1.15 ± 0.05 OUR AVERAGE</b>				
1.15 ± 0.01 ± 0.05		CHILIKIN 14	BELL	$\bar{B}^0 \rightarrow J/\psi K^-\pi^+$
1.16 ± 0.56 ± 0.01		<sup>1</sup> BORTOLETTO92	CLEO	$e^+e^- \rightarrow \Upsilon(4S)$

• • • We do not use the following data for averages, fits, limits, etc. • • •

1.079 ± 0.011

<1.3 90

<6.3 90

<sup>2</sup>AUBERT 09AA BABR  $e^+e^- \rightarrow \Upsilon(4S)$

<sup>3</sup>ALBRECHT 87D ARG  $e^+e^- \rightarrow \Upsilon(4S)$

<sup>4</sup>GILES 84 CLEO  $e^+e^- \rightarrow \Upsilon(4S)$

<sup>1</sup>BORTOLETTO 92 reports  $(1.0 \pm 0.4 \pm 0.3) \times 10^{-3}$  from a measurement of  $[\Gamma(B^0 \rightarrow J/\psi(1S)K^+\pi^-)/\Gamma_{total}] \times [B(J/\psi(1S) \rightarrow e^+e^-)]$  assuming  $B(J/\psi(1S) \rightarrow e^+e^-) = 0.069 \pm 0.009$ , which we rescale to our best value  $B(J/\psi(1S) \rightarrow e^+e^-) = (5.971 \pm 0.032) \times 10^{-2}$ . Our first error is their experiment's error and our second error is the systematic error from using our best value. Assumes equal production of  $B^+$  and  $B^0$  at the  $\Upsilon(4S)$ .

<sup>2</sup>Does not report systematic uncertainties.

<sup>3</sup>ALBRECHT 87D assume  $B^+B^-/B^0\bar{B}^0$  ratio is 55/45.  $K\pi$  system is specifically selected as nonresonant.

$\Gamma(J/\psi(1S)K^*(892)^0)/\Gamma_{total}$   $\Gamma_{200}/\Gamma$

VALUE (units $10^{-3}$ )	EVTS	DOCUMENT ID	TECN	COMMENT
<b>1.27 ± 0.05 OUR FIT</b>				
<b>1.28 ± 0.05 OUR AVERAGE</b>				
1.19 ± 0.01 ± 0.08		CHILIKIN 14	BELL	$\bar{B}^0 \rightarrow J/\psi K^-\pi^+$
1.33 $^{+0.22}_{-0.21}$ ± 0.02		<sup>1,2</sup> AUBERT 07AV	BABR	$e^+e^- \rightarrow \Upsilon(4S)$
1.309 ± 0.026 ± 0.077		<sup>2</sup> AUBERT 05J	BABR	$e^+e^- \rightarrow \Upsilon(4S)$
1.29 ± 0.05 ± 0.13		<sup>2</sup> ABE 02N	BELL	$e^+e^- \rightarrow \Upsilon(4S)$
1.74 ± 0.20 ± 0.18		<sup>3</sup> ABE 98O	CDF	$p\bar{p}$ 1.8 TeV
1.32 ± 0.17 ± 0.17		<sup>4</sup> JESSOP 97	CLE2	$e^+e^- \rightarrow \Upsilon(4S)$
1.27 ± 0.65 ± 0.01		<sup>5</sup> BORTOLETTO92	CLEO	$e^+e^- \rightarrow \Upsilon(4S)$
1.27 ± 0.60 ± 0.01	6	<sup>6</sup> ALBRECHT 90J	ARG	$e^+e^- \rightarrow \Upsilon(4S)$
4.04 ± 1.81 ± 0.02	5	<sup>7</sup> BEBEK 87	CLEO	$e^+e^- \rightarrow \Upsilon(4S)$

• • • We do not use the following data for averages, fits, limits, etc. • • •

1.24 ± 0.05 ± 0.09

1.36 ± 0.27 ± 0.22

1.69 ± 0.31 ± 0.18

29

<sup>2</sup>AUBERT 02 BABR Repl. by AUBERT 05J

<sup>8</sup>ABE 96H CDF Sup. by ABE 98O

<sup>9</sup>ALAM 94 CLE2 Sup. by JESSOP 97

<sup>10</sup>ALBRECHT 94G ARG  $e^+e^- \rightarrow \Upsilon(4S)$

<sup>11</sup>ALBAJAR 91E UA1  $E_{cm}^{pp} = 630$  GeV

<sup>12</sup>ALBRECHT 87D ARG  $e^+e^- \rightarrow \Upsilon(4S)$

<sup>13</sup>ALAM 86 CLEO Repl. by BEBEK 87

<sup>1</sup>AUBERT 07AV reports  $[\Gamma(B^0 \rightarrow J/\psi(1S)K^*(892)^0)/\Gamma_{total}] \times [B(J/\psi(1S) \rightarrow p\bar{p})] = (2.82^{+0.30+0.36}_{-0.28-0.35}) \times 10^{-6}$  which we divide by our best value  $B(J/\psi(1S) \rightarrow p\bar{p}) = (2.121 \pm 0.029) \times 10^{-3}$ . Our first error is their experiment's error and our second error is the systematic error from using our best value.

<sup>2</sup>Assumes equal production of  $B^+$  and  $B^0$  at the  $\Upsilon(4S)$ .

<sup>3</sup>ABE 98O reports  $[B(B^0 \rightarrow J/\psi(1S)K^*(892)^0)]/[B(B^+ \rightarrow J/\psi(1S)K^+)] = 1.76 \pm 0.14 \pm 0.15$ . We multiply by our best value  $B(B^+ \rightarrow J/\psi(1S)K^+) = (9.9 \pm 1.0) \times 10^{-4}$ . Our first error is their experiment's error and our second error is the systematic error from using our best value.

<sup>4</sup>Assumes equal production of  $B^+$  and  $B^0$  at the  $\Upsilon(4S)$ .

<sup>5</sup>BORTOLETTO 92 reports  $(1.1 \pm 0.5 \pm 0.3) \times 10^{-3}$  from a measurement of  $[\Gamma(B^0 \rightarrow J/\psi(1S)K^*(892)^0)/\Gamma_{total}] \times [B(J/\psi(1S) \rightarrow e^+e^-)]$  assuming  $B(J/\psi(1S) \rightarrow e^+e^-) = 0.069 \pm 0.009$ , which we rescale to our best value  $B(J/\psi(1S) \rightarrow e^+e^-) = (5.971 \pm 0.032) \times 10^{-2}$ . Our first error is their experiment's error and our second error is the systematic error from using our best value. Assumes equal production of  $B^+$  and  $B^0$  at the  $\Upsilon(4S)$ .

<sup>6</sup>ALBRECHT 90J reports  $(1.1 \pm 0.5 \pm 0.2) \times 10^{-3}$  from a measurement of  $[\Gamma(B^0 \rightarrow J/\psi(1S)K^*(892)^0)/\Gamma_{total}] \times [B(J/\psi(1S) \rightarrow e^+e^-)]$  assuming  $B(J/\psi(1S) \rightarrow e^+e^-) = 0.069 \pm 0.009$ , which we rescale to our best value  $B(J/\psi(1S) \rightarrow e^+e^-) = (5.971 \pm 0.032) \times 10^{-2}$ . Our first error is their experiment's error and our second error is the systematic error from using our best value. Assumes equal production of  $B^+$  and  $B^0$  at the  $\Upsilon(4S)$ .

<sup>7</sup>BEBEK 87 reports  $(3.5 \pm 1.6 \pm 0.3) \times 10^{-3}$  from a measurement of  $[\Gamma(B^0 \rightarrow J/\psi(1S)K^*(892)^0)/\Gamma_{total}] \times [B(J/\psi(1S) \rightarrow e^+e^-)]$  assuming  $B(J/\psi(1S) \rightarrow e^+e^-) = 0.069 \pm 0.009$ , which we rescale to our best value  $B(J/\psi(1S) \rightarrow e^+e^-) = (5.971 \pm 0.032) \times 10^{-2}$ . Our first error is their experiment's error and our second error is the systematic error from using our best value. Updated in BORTOLETTO 92 to use the same assumptions.

<sup>8</sup>ABE 96H assumes that  $B(B^+ \rightarrow J/\psi K^+) = (1.02 \pm 0.14) \times 10^{-3}$ .

<sup>9</sup>The neutral and charged  $B$  events together are predominantly longitudinally polarized,  $\Gamma_{\perp}/\Gamma = 0.080 \pm 0.08 \pm 0.05$ . This can be compared with a prediction using HQET, 0.73 (KRAMER 92). This polarization indicates that the  $B \rightarrow \psi K^*$  decay is dominated by the  $CP = -1$   $CP$  eigenstate. Assumes equal production of  $B^+$  and  $B^0$  at the  $\Upsilon(4S)$ .

<sup>10</sup>ALBRECHT 94G measures the polarization in the vector-vector decay to be predominantly longitudinal,  $\Gamma_T/\Gamma = 0.03 \pm 0.16 \pm 0.15$  making the neutral decay a  $CP$  eigenstate when the  $K^*0$  decays through  $K_S^0\pi^0$ .

<sup>11</sup>ALBAJAR 91E assumes  $B_S^0$  production fraction of 36%.

<sup>12</sup>ALBRECHT 87D assume  $B^+B^-/B^0\bar{B}^0$  ratio is 55/45. Superseded by ALBRECHT 90J.

<sup>13</sup>ALAM 86 assumes  $B^\pm/B^0$  ratio is 60/40. The observation of the decay  $B^+ \rightarrow J/\psi K^*(892)^+$  (HAAS 85) has been retracted in this paper.

$\Gamma(J/\psi(1S)K^*(892)^0)/\Gamma(J/\psi(1S)K^0)$   $\Gamma_{200}/\Gamma_{198}$

VALUE	DOCUMENT ID	TECN	COMMENT
<b>1.50 ± 0.09 OUR AVERAGE</b>			
1.51 ± 0.05 ± 0.08	AUBERT 05J	BABR	$e^+e^- \rightarrow \Upsilon(4S)$
1.39 ± 0.36 ± 0.10	ABE 96Q	CDF	$p\bar{p}$
1.49 ± 0.10 ± 0.08	<sup>1</sup> AUBERT 02	BABR	Repl. by AUBERT 05J

• • • We do not use the following data for averages, fits, limits, etc. • • •

<sup>1</sup>Assumes equal production of  $B^+$  and  $B^0$  at the  $\Upsilon(4S)$ .

$\Gamma(J/\psi(1S)\eta K_S^0)/\Gamma_{total}$   $\Gamma_{201}/\Gamma$

VALUE (units $10^{-5}$ )	DOCUMENT ID	TECN	COMMENT
<b>5.4 ± 0.9 OUR AVERAGE</b>			
5.22 ± 0.78 ± 0.49	<sup>1</sup> IWASHITA 14	BELL	$e^+e^- \rightarrow \Upsilon(4S)$
8.4 ± 2.6 ± 2.7	<sup>1</sup> AUBERT 04Y	BABR	$e^+e^- \rightarrow \Upsilon(4S)$

$\Gamma(J/\psi(1S)\eta' K_S^0)/\Gamma_{total}$   $\Gamma_{202}/\Gamma$

VALUE (units $10^{-5}$ )	CL%	DOCUMENT ID	TECN	COMMENT
<b>&lt;2.5</b>	90	<sup>1</sup> XIE 07	BELL	$e^+e^- \rightarrow \Upsilon(4S)$

<sup>1</sup>Assumes equal production of  $B^+$  and  $B^0$  at the  $\Upsilon(4S)$ .

$\Gamma(J/\psi(1S)\omega K^0)/\Gamma_{total}$   $\Gamma_{204}/\Gamma$

VALUE (units $10^{-4}$ )	DOCUMENT ID	TECN	COMMENT
<b>2.3 ± 0.3 ± 0.3</b>	<sup>1</sup> DEL-AMO-SA..10B	BABR	$e^+e^- \rightarrow \Upsilon(4S)$
3.1 ± 0.6 ± 0.3	<sup>1</sup> AUBERT 08W	BABR	Repl. by DEL-AMO-SANCHEZ 10B

• • • We do not use the following data for averages, fits, limits, etc. • • •

<sup>1</sup>Assumes equal production of  $B^+$  and  $B^0$  at the  $\Upsilon(4S)$ .

$\Gamma(\chi_{c1}(3872)K^0, \chi_{c1} \rightarrow J/\psi\omega)/\Gamma_{total}$   $\Gamma_{205}/\Gamma$

VALUE (units $10^{-5}$ )	DOCUMENT ID	TECN	COMMENT
<b>6 ± 3 ± 1</b>	<sup>1</sup> DEL-AMO-SA..10B	BABR	$e^+e^- \rightarrow \Upsilon(4S)$

<sup>1</sup>Assumes equal production of  $B^+$  and  $B^0$  at the  $\Upsilon(4S)$ .

$\Gamma(X(3915), X \rightarrow J/\psi\omega)/\Gamma_{total}$   $\Gamma_{206}/\Gamma$

VALUE (units $10^{-5}$ )	DOCUMENT ID	TECN	COMMENT
<b>2.1 ± 0.9 ± 0.3</b>	<sup>1</sup> DEL-AMO-SA..10B	BABR	$e^+e^- \rightarrow \Upsilon(4S)$
1.3 $^{+1.3}_{-1.1}$ ± 0.2	<sup>1,2</sup> AUBERT 08W	BABR	Repl. by DEL-AMO-SANCHEZ 10B

<sup>1</sup>Assumes equal production of  $B^+$  and  $B^0$  at the  $\Upsilon(4S)$ .

<sup>2</sup>Corresponds to upper limit of  $3.9 \times 10^{-5}$  at 90% CL.

$\Gamma(J/\psi(1S)\phi K^0)/\Gamma_{total}$   $\Gamma_{203}/\Gamma$

VALUE (units $10^{-5}$ )	DOCUMENT ID	TECN	COMMENT
<b>4.9 ± 1.0 OUR AVERAGE</b>			
4.43 ± 0.76 ± 0.19	LEES 15	BABR	$e^+e^- \rightarrow \Upsilon(4S)$
10.2 ± 3.8 ± 1.0	<sup>1</sup> AUBERT 03O	BABR	$e^+e^- \rightarrow \Upsilon(4S)$
8.8 $^{+3.5}_{-3.0}$ ± 1.3	<sup>2</sup> ANASTASSOV 00	CLE2	$e^+e^- \rightarrow \Upsilon(4S)$

<sup>1</sup>Assumes equal production of  $B^+$  and  $B^0$  at the  $\Upsilon(4S)$ .

<sup>2</sup>ANASTASSOV 00 finds 10 events on a background of  $0.5 \pm 0.2$ . Assumes equal production of  $B^0$  and  $B^+$  at the  $\Upsilon(4S)$ , a uniform Dalitz plot distribution, isotropic  $J/\psi(1S)$  and  $\phi$  decays, and  $B(B^+ \rightarrow J/\psi(1S)\phi K^+) = B(B^0 \rightarrow J/\psi(1S)\phi K^0)$ .

$\Gamma(J/\psi(1S)K(1270)^0)/\Gamma_{total}$   $\Gamma_{207}/\Gamma$

VALUE (units $10^{-3}$ )	DOCUMENT ID	TECN	COMMENT
<b>1.30 ± 0.34 ± 0.32</b>	<sup>1</sup> ABE 01L	BELL	$e^+e^- \rightarrow \Upsilon(4S)$

<sup>1</sup>Assumes equal production of  $B^+$  and  $B^0$  at the  $\Upsilon(4S)$  and uses the PDG value of  $B(B^+ \rightarrow J/\psi(1S)K^+) = (1.00 \pm 0.10) \times 10^{-3}$ .

$\Gamma(J/\psi(1S)\pi^0)/\Gamma_{total}$   $\Gamma_{208}/\Gamma$

VALUE (units $10^{-5}$ )	CL%	DOCUMENT ID	TECN	COMMENT
<b>1.66 ± 0.10 OUR AVERAGE</b>				
1.62 ± 0.11 ± 0.06		<sup>1</sup> PAL 18	BELL	$e^+e^- \rightarrow \Upsilon(4S)$
1.69 ± 0.14 ± 0.07		<sup>1</sup> AUBERT 08AU	BABR	$e^+e^- \rightarrow \Upsilon(4S)$
2.5 $^{+1.1}_{-0.9}$ ± 0.2		<sup>1</sup> AVERY 00	CLE2	$e^+e^- \rightarrow \Upsilon(4S)$

• • • We do not use the following data for averages, fits, limits, etc. • • •

1.94 ± 0.22 ± 0.17

2.3 ± 0.5 ± 0.2

2.0 ± 0.6 ± 0.2

< 2.0 90

< 5.8 90

< 690 90

<sup>1</sup>AUBERT,B 06B BABR Repl. by AUBERT 08AU

<sup>1</sup>ABE 03B BELL Repl. by PAL 18

<sup>1</sup>AUBERT 02 BABR Repl. by AUBERT,B 06B

<sup>2</sup>ACCIARRI 97C L3

<sup>1</sup>BISHAI 96 CLE2 Sup. by AVERY 00

<sup>1</sup>ALEXANDER 95 CLE2 Sup. by BISHAI 96

<sup>1</sup>Assumes equal production of  $B^+$  and  $B^0$  at the  $\Upsilon(4S)$ .

<sup>2</sup>ACCIARRI 97C assumes  $B_S^0$  production fraction (39.5 ± 4.0)% and  $B_S$  (12.0 ± 3.0)%.



# Meson Particle Listings

$B^0$

## $\Gamma(J/\psi(1S)\eta)/\Gamma_{total}$ $\Gamma_{209}/\Gamma$

VALUE (units $10^{-6}$ )	CL%	DOCUMENT ID	TECN	COMMENT
<b>10.8 ± 2.3 OUR AVERAGE</b>				Error includes scale factor of 1.5.
7.3 ± 2.5 ± 1.3		1 AAIJ	15D LHCb	$pp$ at 7, 8 TeV
12.3 <sup>+1.8</sup> ± 0.7		2,3 CHANG	12 BELL	$e^+e^- \rightarrow \Upsilon(4S)$

- • • We do not use the following data for averages, fits, limits, etc. • • •
- 9.5 ± 1.7 ± 0.8
- < 27
- < 1200
- 3 CHANG 07A BELL Repl. by CHANG 12
- 3 AUBERT 03B BABR  $e^+e^- \rightarrow \Upsilon(4S)$
- 4 ACCIARRI 97C L3
- 1 AAIJ 15D reports  $[\Gamma(B^0 \rightarrow J/\psi(1S)\eta)/\Gamma_{total}] / [B(B_S^0 \rightarrow J/\psi(1S)\eta)] = (1.85 \pm 0.61 \pm 0.14) \times 10^{-2}$  which we multiply by our best value  $B(B_S^0 \rightarrow J/\psi(1S)\eta) = (4.0 \pm 0.7) \times 10^{-4}$ . Our first error is their experiment's error and our second error is the systematic error from using our best value.
- 2 Reconstructs  $\eta$  in  $\gamma\gamma$  and  $\pi^+\pi^-\pi^0$  decays.
- 3 Assumes equal production of  $B^+$  and  $B^0$  at the  $\Upsilon(4S)$ .
- 4 ACCIARRI 97C assumes  $B^0$  production fraction  $(39.5 \pm 4.0\%)$  and  $B_S$   $(12.0 \pm 3.0\%)$ .

## $\Gamma(J/\psi(1S)\pi^+\pi^-)/\Gamma_{total}$ $\Gamma_{210}/\Gamma$

VALUE (units $10^{-5}$ )	CL%	DOCUMENT ID	TECN	COMMENT
<b>3.94 ± 0.17 OUR AVERAGE</b>				
3.92 ± 0.14 ± 0.11		1,2 AAIJ	13M LHCb	$pp$ at 7 TeV
4.6 ± 0.7 ± 0.6		3 AUBERT	03B BABR	$e^+e^- \rightarrow \Upsilon(4S)$

- 1 AAIJ 13M reports  $(3.97 \pm 0.09 \pm 0.11 \pm 0.16) \times 10^{-5}$  from a measurement of  $[\Gamma(B^0 \rightarrow J/\psi(1S)\pi^+\pi^-)/\Gamma_{total}] / [B(B^+ \rightarrow J/\psi(1S)K^+)]$  assuming  $B(B^+ \rightarrow J/\psi(1S)K^+) = (1.018 \pm 0.042) \times 10^{-3}$ , which we rescale to our best value  $B(B^+ \rightarrow J/\psi(1S)K^+) = (1.006 \pm 0.027) \times 10^{-3}$ . Our first error is their experiment's error and our second error is the systematic error from using our best value.
- 2 AAIJ 13M does not report correlations between various measurements of the  $J/\psi\pi\pi$  final state.
- 3 Assumes equal production of  $B^+$  and  $B^0$  at the  $\Upsilon(4S)$ .

## $\Gamma(J/\psi(1S)\pi^+\pi^- \text{ nonresonant})/\Gamma_{total}$ $\Gamma_{211}/\Gamma$

VALUE (units $10^{-5}$ )	CL%	DOCUMENT ID	TECN	COMMENT
<b>&lt; 1.2</b>		1 AUBERT	07Ac BABR	$e^+e^- \rightarrow \Upsilon(4S)$

- 1 Assumes equal production of  $B^+$  and  $B^0$  at the  $\Upsilon(4S)$ .

## $\Gamma(J/\psi(1S)f_0(500), f_0 \rightarrow \pi\pi)/\Gamma_{total}$ $\Gamma_{212}/\Gamma$

VALUE (units $10^{-6}$ )	CL%	DOCUMENT ID	TECN	COMMENT
<b>8.8 ± 0.5 ± 1.1</b>		1 AAIJ	14x LHCb	$pp$ at 7, 8 TeV

- • • We do not use the following data for averages, fits, limits, etc. • • •
- 6.4<sup>+2.5</sup> ± 0.3
- 1 AAIJ 14x uses Dalitz plot analysis of  $B^0 \rightarrow J/\psi\pi^+\pi^-$ .
- 2 AAIJ 13M reports  $(6.4 \pm 0.8 \pm 2.4) \times 10^{-6}$  from a measurement of  $[\Gamma(B^0 \rightarrow J/\psi(1S)f_0(500), f_0 \rightarrow \pi\pi)/\Gamma_{total}] / [B(B^0 \rightarrow J/\psi(1S)\pi^+\pi^-)]$  assuming  $B(B^0 \rightarrow J/\psi(1S)\pi^+\pi^-) = (3.97 \pm 0.09 \pm 0.11 \pm 0.16) \times 10^{-5}$ , which we rescale to our best value  $B(B^0 \rightarrow J/\psi(1S)\pi^+\pi^-) = (3.94 \pm 0.17) \times 10^{-5}$ . Our first error is their experiment's error and our second error is the systematic error from using our best value.
- 3 AAIJ 13M does not report correlations between various measurements of the  $J/\psi\pi\pi$  final state. Measured in Dalitz plot like analysis of  $B^0 \rightarrow J/\psi\pi^+\pi^-$ .

## $\Gamma(J/\psi(1S)f_2)/\Gamma_{total}$ $\Gamma_{213}/\Gamma$

VALUE (units $10^{-5}$ )	CL%	DOCUMENT ID	TECN	COMMENT
<b>0.33 ± 0.05 OUR AVERAGE</b>				Error includes scale factor of 1.5.
0.30 ± 0.03 ± 0.02		1 AAIJ	14x LHCb	$pp$ at 7, 8 TeV
0.41 ± 0.06 ± 0.02		2,3 AAIJ	13M LHCb	$pp$ at 7 TeV

- • • We do not use the following data for averages, fits, limits, etc. • • •
- < 0.5
- 1 AAIJ 14x uses Dalitz plot analysis of  $B^0 \rightarrow J/\psi\pi^+\pi^-$ .
- 2 AAIJ 13M reports  $[\Gamma(B^0 \rightarrow J/\psi(1S)f_2)/\Gamma_{total}] \times [B(f_2(1270) \rightarrow \pi\pi)] = (3.5 \pm 0.4 \pm 0.4) \times 10^{-6}$  from a measurement of  $[\Gamma(B^0 \rightarrow J/\psi(1S)f_2)/\Gamma_{total}] \times [B(f_2(1270) \rightarrow \pi\pi)] / [B(B^0 \rightarrow J/\psi(1S)\pi^+\pi^-)]$  assuming  $B(B^0 \rightarrow J/\psi(1S)\pi^+\pi^-) = (3.97 \pm 0.09 \pm 0.11 \pm 0.16) \times 10^{-5}$ , which we rescale to our best values  $B(f_2(1270) \rightarrow \pi\pi) = (84.2 \pm 2.9) \times 10^{-2}$ ,  $B(B^0 \rightarrow J/\psi(1S)\pi^+\pi^-) = (3.94 \pm 0.17) \times 10^{-5}$ . Our first error is their experiment's error and our second error is the systematic error from using our best values.
- 3 AAIJ 13M does not report correlations between various measurements of the  $J/\psi\pi\pi$  final state. Measured in Dalitz plot like analysis of  $B^0 \rightarrow J/\psi\pi^+\pi^-$ .
- 4 AUBERT 07Ac reports  $[\Gamma(B^0 \rightarrow J/\psi(1S)f_2)/\Gamma_{total}] \times [B(f_2(1270) \rightarrow \pi\pi)] < 0.46 \times 10^{-5}$  which we divide by our best value  $B(f_2(1270) \rightarrow \pi\pi) = 84.2 \times 10^{-2}$ .
- 5 Assumes equal production of  $B^+$  and  $B^0$  at the  $\Upsilon(4S)$ .

## $\Gamma(J/\psi(1S)\rho^0)/\Gamma_{total}$ $\Gamma_{214}/\Gamma$

VALUE (units $10^{-5}$ )	CL%	DOCUMENT ID	TECN	COMMENT
<b>2.55 ± 0.18</b>				
2.50 ± 0.10 ± 0.18		1 AAIJ	14x LHCb	$pp$ at 7, 8 TeV
2.7 ± 0.3 ± 0.2		2 AUBERT	07Ac BABR	$e^+e^- \rightarrow \Upsilon(4S)$

- • • We do not use the following data for averages, fits, limits, etc. • • •
- 2.47<sup>+0.22</sup> ± 0.11
- 1.6 ± 0.6 ± 0.4
- < 25
- 3,4 AAIJ
- 2 AUBERT
- 90 BISHAI
- 13M LHCb
- 03B BABR
- 96 CLE2
- Repl. by AAIJ 14x
- Repl. by AUBERT 07Ac
- $e^+e^- \rightarrow \Upsilon(4S)$
- 1 AAIJ 14x uses Dalitz plot analysis of  $B^0 \rightarrow J/\psi\pi^+\pi^-$ . We assume  $B(\rho(770)^0 \rightarrow \pi^+\pi^-) = 100\%$ .
- 2 Assumes equal production of  $B^+$  and  $B^0$  at the  $\Upsilon(4S)$ .
- 3 AAIJ 13M reports  $(2.49 \pm 0.20 \pm 0.16) \times 10^{-5}$  from a measurement of  $[\Gamma(B^0 \rightarrow J/\psi(1S)\rho^0)/\Gamma_{total}] / [B(B^0 \rightarrow J/\psi(1S)\pi^+\pi^-)]$  assuming  $B(B^0 \rightarrow J/\psi(1S)\pi^+\pi^-) = (3.97 \pm 0.09 \pm 0.11 \pm 0.16) \times 10^{-5}$ , which we rescale to our best value  $B(B^0 \rightarrow J/\psi(1S)\pi^+\pi^-) = (3.94 \pm 0.17) \times 10^{-5}$ . Our first error is their experiment's error and our second error is the systematic error from using our best value.
- 4 AAIJ 13M does not report correlations between various measurements of the  $J/\psi\pi\pi$  final state. Measured in Dalitz plot like analysis of  $B^0 \rightarrow J/\psi\pi^+\pi^-$ . Assumes  $B(\rho(770)^0 \rightarrow \pi\pi) = 100\%$ .

## $\Gamma(J/\psi(1S)f_0(980), f_0 \rightarrow \pi^+\pi^-)/\Gamma_{total}$ $\Gamma_{215}/\Gamma$

VALUE	CL%	DOCUMENT ID	TECN	COMMENT
<b>&lt; 1.1 × 10<sup>-6</sup></b>		1 AAIJ	13M LHCb	$pp$ at 7 TeV

- 1 AAIJ 13M does not provide correlations between various measurements of the  $J/\psi\pi^+\pi^-$  final state. The measurements were obtained from a Dalitz plot like analysis of  $B^0 \rightarrow J/\psi\pi^+\pi^-$ . Also reports  $\Gamma(J/\psi(1S)f_0(980), f_0 \rightarrow \pi^+\pi^-)/\Gamma_{total} = (6.1 \pm 3.1 \pm 1.7) \times 10^{-6}$ .

## $\Gamma(J/\psi(1S)\rho(1450)^0, \rho^0 \rightarrow \pi\pi)/\Gamma_{total}$ $\Gamma_{216}/\Gamma$

VALUE (units $10^{-6}$ )	CL%	DOCUMENT ID	TECN	COMMENT
<b>2.9 ± 1.6</b>				
4.6 ± 1.1 ± 1.9		1 AAIJ	14x LHCb	$pp$ at 7, 8 TeV
2.1 ± 2.4 ± 0.1		2,3 AAIJ	13M LHCb	$pp$ at 7 TeV

- 1 AAIJ 14x uses Dalitz plot analysis of  $B^0 \rightarrow J/\psi\pi^+\pi^-$ .
- 2 AAIJ 13M reports  $(2.1 \pm 1.0 \pm 2.2) \times 10^{-6}$  from a measurement of  $[\Gamma(B^0 \rightarrow J/\psi(1S)\rho(1450)^0, \rho^0 \rightarrow \pi\pi)/\Gamma_{total}] / [B(B^0 \rightarrow J/\psi(1S)\pi^+\pi^-)]$  assuming  $B(B^0 \rightarrow J/\psi(1S)\pi^+\pi^-) = (3.97 \pm 0.09 \pm 0.11 \pm 0.16) \times 10^{-5}$ , which we rescale to our best value  $B(B^0 \rightarrow J/\psi(1S)\pi^+\pi^-) = (3.94 \pm 0.17) \times 10^{-5}$ . Our first error is their experiment's error and our second error is the systematic error from using our best value.
- 3 AAIJ 13M does not report correlations between various measurements of the  $J/\psi\pi\pi$  final state. Measured in Dalitz plot like analysis of  $B^0 \rightarrow J/\psi\pi^+\pi^-$ .

## $\Gamma(J/\psi\rho(1700)^0, \rho^0 \rightarrow \pi^+\pi^-)/\Gamma_{total}$ $\Gamma_{217}/\Gamma$

VALUE (units $10^{-6}$ )	CL%	DOCUMENT ID	TECN	COMMENT
<b>2.0 ± 0.5 ± 1.2</b>		1 AAIJ	14x LHCb	$pp$ at 7, 8 TeV

- 1 AAIJ 14x uses Dalitz plot analysis of  $B^0 \rightarrow J/\psi\pi^+\pi^-$ .

## $\Gamma(J/\psi(1S)\omega)/\Gamma_{total}$ $\Gamma_{218}/\Gamma$

VALUE (units $10^{-5}$ )	CL%	DOCUMENT ID	TECN	COMMENT
<b>1.8 ± 0.7</b>				
1.8 <sup>+0.7</sup> ± 0.5		1 AAIJ	14x LHCb	$pp$ at 7, 8 TeV
< 27		90 BISHAI	96 CLE2	$e^+e^- \rightarrow \Upsilon(4S)$

- • • We do not use the following data for averages, fits, limits, etc. • • •
- 1 AAIJ 14x reports  $[\Gamma(B^0 \rightarrow J/\psi(1S)\omega)/\Gamma_{total}] \times [B(\omega(782) \rightarrow \pi^+\pi^-)] = (2.7 \pm 0.8 \pm 0.7) \times 10^{-7}$  which we divide by our best value  $B(\omega(782) \rightarrow \pi^+\pi^-) = (1.53 \pm 0.06) \times 10^{-2}$ . Our first error is their experiment's error and our second error is the systematic error from using our best value.

## $\Gamma(J/\psi(1S)\omega)/\Gamma(J/\psi(1S)\rho^0)$ $\Gamma_{218}/\Gamma_{214}$

VALUE	CL%	DOCUMENT ID	TECN	COMMENT
<b>0.61 ± 0.39</b>				
0.61 <sup>+0.39</sup> ± 0.21 ± 0.03		1,2 AAIJ	13M LHCb	$pp$ at 7 TeV

- 1 AAIJ 13M reports  $0.61 \pm 0.24 \pm 0.31$  from a measurement of  $[\Gamma(B^0 \rightarrow J/\psi(1S)\omega) / \Gamma(B^0 \rightarrow J/\psi(1S)\rho^0)] \times [B(\omega(782) \rightarrow \pi^+\pi^-)]$  assuming  $B(\omega(782) \rightarrow \pi^+\pi^-) = (1.53 \pm 0.11) \times 10^{-2}$ , which we rescale to our best value  $B(\omega(782) \rightarrow \pi^+\pi^-) = (1.53 \pm 0.06) \times 10^{-2}$ . Our first error is their experiment's error and our second error is the systematic error from using our best value.
- 2 AAIJ 13M does not report correlations between various measurements of the  $J/\psi\pi\pi$  final state. Measured in Dalitz plot like analysis of  $B^0 \rightarrow J/\psi\pi^+\pi^-$ . Assumes  $B(\rho(770)^0 \rightarrow \pi\pi) = 100\%$ .

## $\Gamma(J/\psi(1S)\omega)/\Gamma(J/\psi(1S)\rho^0)$ $\Gamma_{218}/\Gamma_{214}$

VALUE	CL%	DOCUMENT ID	TECN	COMMENT
<b>0.89 ± 0.19 ± 0.07</b>		AAIJ	13A LHCb	$pp$ at 7 TeV

## $\Gamma(J/\psi(1S)K^+K^-)/\Gamma_{total}$ $\Gamma_{219}/\Gamma$

VALUE (units $10^{-5}$ )	CL%	DOCUMENT ID	TECN	COMMENT
<b>2.50 ± 0.34 ± 0.07</b>		1 AAIJ	13BT LHCb	$pp$ at 7 TeV

- 1 AAIJ 13BT reports  $(2.53 \pm 0.31 \pm 0.19) \times 10^{-6}$  from a measurement of  $[\Gamma(B^0 \rightarrow J/\psi(1S)K^+K^-)/\Gamma_{total}] / [B(B^+ \rightarrow J/\psi(1S)K^+)]$  assuming  $B(B^+ \rightarrow J/\psi(1S)K^+) = (1.018 \pm 0.042) \times 10^{-3}$ , which we rescale to our best value  $B(B^+ \rightarrow J/\psi(1S)K^+) = (1.006 \pm 0.027) \times 10^{-3}$ . Our first error is their experiment's error and our second error is the systematic error from using our best value.

$\Gamma(J/\psi(1S) a_0(980), a_0 \rightarrow K^+ K^-) / \Gamma_{total}$   $\Gamma_{220} / \Gamma$

VALUE (units 10 <sup>-6</sup> )	DOCUMENT ID	TECN	COMMENT
<b>0.470 ± 0.331 ± 0.072</b>	<sup>1</sup> AAIJ	13BT LHCb	pp at 7 TeV

<sup>1</sup> AAIJ 13BT uses  $B(\bar{B}^0 \rightarrow J/\psi K^+ K^-) = (2.53 \pm 0.31 \pm 0.19) \times 10^{-6}$  to derive this result. It also reports the equivalent upper limit of  $< 9.0 \times 10^{-7}$  at 90% CL.

$\Gamma(J/\psi(1S) \phi) / \Gamma_{total}$   $\Gamma_{221} / \Gamma$

VALUE (units 10 <sup>-6</sup> )	CL%	DOCUMENT ID	TECN	COMMENT
<b>&lt; 0.19</b>	90	<sup>1</sup> AAIJ	13BT LHCb	pp at 7 TeV

• • • We do not use the following data for averages, fits, limits, etc. • • •

< 1.01	90	LEES	15 BABR	e <sup>+</sup> e <sup>-</sup> → $\Upsilon(4S)$
< 0.94	90	<sup>2</sup> LIU	08i BELL	e <sup>+</sup> e <sup>-</sup> → $\Upsilon(4S)$
< 9.2	90	<sup>2</sup> AUBERT	03o BABR	e <sup>+</sup> e <sup>-</sup> → $\Upsilon(4S)$

<sup>1</sup> AAIJ 13BT uses  $B(B^0 \rightarrow J/\psi(1S) K^+ K^-) = (2.53 \pm 0.31 \pm 0.19) \times 10^{-6}$  and  $B(\phi \rightarrow K^+ K^-) = (48.9 \pm 0.5)\%$  to obtain this result.  
<sup>2</sup> Assumes equal production of B<sup>+</sup> and B<sup>0</sup> at the  $\Upsilon(4S)$ .

$\Gamma(J/\psi(1S) \eta') / \Gamma_{total}$   $\Gamma_{222} / \Gamma$

VALUE (units 10 <sup>-6</sup> )	CL%	DOCUMENT ID	TECN	COMMENT
<b>7.6 ± 2.2 ± 1.0</b>		<sup>1</sup> AAIJ	15D LHCb	pp at 7, 8 TeV

• • • We do not use the following data for averages, fits, limits, etc. • • •

< 7.4	90	<sup>2,3</sup> CHANG	12 BELL	e <sup>+</sup> e <sup>-</sup> → $\Upsilon(4S)$
< 63	90	<sup>3</sup> AUBERT	03o BABR	e <sup>+</sup> e <sup>-</sup> → $\Upsilon(4S)$

<sup>1</sup> AAIJ 15D reports  $[\Gamma(B^0 \rightarrow J/\psi(1S) \eta') / \Gamma_{total}] / [B(B_S^0 \rightarrow J/\psi(1S) \eta')] = (2.28 \pm 0.65 \pm 0.16) \times 10^{-2}$  which we multiply by our best value  $B(B_S^0 \rightarrow J/\psi(1S) \eta') = (3.3 \pm 0.4) \times 10^{-4}$ . Our first error is their experiment's error and our second error is the systematic error from using our best value.  
<sup>2</sup> Reconstructs  $\eta'(985)$  in (etapi + pi)<sup>-</sup> and rho(770) decays.  
<sup>3</sup> Assumes equal production of B<sup>+</sup> and B<sup>0</sup> at the  $\Upsilon(4S)$ .

$\Gamma(J/\psi(1S) \eta) / \Gamma(J/\psi(1S) \eta'(958))$   $\Gamma_{209} / \Gamma_{222}$

VALUE	DOCUMENT ID	TECN	COMMENT
<b>1.111 ± 0.475 ± 0.062</b>	<sup>1</sup> AAIJ	15D LHCb	pp at 7, 8 TeV

<sup>1</sup> Uses  $J/\psi \rightarrow \mu^+ \mu^-$ ,  $\eta' \rightarrow \rho^0 \gamma$ , and  $\eta' \rightarrow \eta \pi^+ \pi^-$  decays.

$\Gamma(J/\psi(1S) K^0 \pi^+ \pi^-) / \Gamma(J/\psi(1S) K^0)$   $\Gamma_{223} / \Gamma_{198}$

VALUE	DOCUMENT ID	TECN	COMMENT
<b>0.50 ± 0.04 OUR AVERAGE</b>			
0.493 ± 0.034 ± 0.027	AAIJ	14L LHCb	pp at 7 TeV
1.24 ± 0.40 ± 0.15	AFFOLDER	02B CDF	p $\bar{p}$ 1.8 TeV

$\Gamma(J/\psi(1S) K^0 K^+ K^-) / \Gamma_{total}$   $\Gamma_{225} / \Gamma$

VALUE (units 10 <sup>-6</sup> )	DOCUMENT ID	TECN	COMMENT
<b>25 ± 7 OUR AVERAGE</b>			Error includes scale factor of 1.8.
34.9 ± 6.7 ± 1.5	LEES	15 BABR	e <sup>+</sup> e <sup>-</sup> → $\Upsilon(4S)$
20.2 ± 4.3 ± 1.9	<sup>1</sup> AAIJ	14L LHCb	pp at 7 TeV

<sup>1</sup> Measured with  $B(B^0 \rightarrow J/\psi K_S^0 K^+ K^-) / B(B^0 \rightarrow J/\psi K_S^0)$  using PDG 12 for the involved branching fractions.

$\Gamma(J/\psi(1S) K^0 K^- \pi^+ + c.c.) / \Gamma_{total}$   $\Gamma_{224} / \Gamma$

VALUE	CL%	DOCUMENT ID	TECN	COMMENT
<b>&lt; 21 × 10<sup>-6</sup></b>	90	<sup>1</sup> AAIJ	14L LHCb	pp at 7 TeV

<sup>1</sup> Measured with  $B(B^0 \rightarrow J/\psi K_S^0 K^\pm \pi^\mp) / B(B^0 \rightarrow J/\psi K_S^0 \pi^+ \pi^-)$  using PDG 12 values for the involved branching fractions.

$\Gamma(J/\psi(1S) K^0 \rho^0) / \Gamma_{total}$   $\Gamma_{227} / \Gamma$

VALUE (units 10 <sup>-4</sup> )	DOCUMENT ID	TECN	COMMENT
<b>5.4 ± 2.9 ± 0.9</b>	<sup>1</sup> AFFOLDER	02B CDF	p $\bar{p}$ 1.8 TeV

<sup>1</sup> Uses  $B^0 \rightarrow J/\psi(1S) K_S^0$  decay as a reference and  $B(B^0 \rightarrow J/\psi(1S) K^0) = 8.3 \times 10^{-4}$ .

$\Gamma(J/\psi(1S) K^*(892)^+ \pi^-) / \Gamma_{total}$   $\Gamma_{228} / \Gamma$

VALUE (units 10 <sup>-4</sup> )	DOCUMENT ID	TECN	COMMENT
<b>7.7 ± 4.1 ± 1.3</b>	<sup>1</sup> AFFOLDER	02B CDF	p $\bar{p}$ 1.8 TeV

<sup>1</sup> Uses  $B^0 \rightarrow J/\psi(1S) K_S^0$  decay as a reference and  $B(B^0 \rightarrow J/\psi(1S) K^0) = 8.3 \times 10^{-4}$ .

$\Gamma(J/\psi(1S) \pi^+ \pi^- \pi^+ \pi^-) / \Gamma(J/\psi(1S) \pi^+ \pi^-)$   $\Gamma_{229} / \Gamma_{210}$

VALUE	DOCUMENT ID	TECN	COMMENT
<b>0.361 ± 0.017 ± 0.021</b>	<sup>1</sup> AAIJ	14Y LHCb	pp at 7, 8 TeV

<sup>1</sup> Excludes contributions from  $\psi(2S)$  and  $\chi_{c1}(3872)$  decaying to  $J/\psi(1S) \pi^+ \pi^-$ .

$\Gamma(J/\psi(1S) f_1(1285)) / \Gamma_{total}$   $\Gamma_{230} / \Gamma$

VALUE (units 10 <sup>-6</sup> )	DOCUMENT ID	TECN	COMMENT
<b>8.4 ± 2.1 ± 0.5</b>	<sup>1</sup> AAIJ	14Y LHCb	pp at 7, 8 TeV

<sup>1</sup> AAIJ 14Y reports  $(8.37 \pm 1.95 \pm 0.71_{-0.66}^{+0.71} \pm 0.35) \times 10^{-6}$  from a measurement of  $[\Gamma(B^0 \rightarrow J/\psi(1S) f_1(1285)) / \Gamma_{total}] \times [B(f_1(1285) \rightarrow 2\pi^+ 2\pi^-)]$  assuming  $B(f_1(1285) \rightarrow 2\pi^+ 2\pi^-) = 0.11 \pm 0.007_{-0.006}^{+0.007}$  which we rescale to our best value  $B(f_1(1285) \rightarrow 2\pi^+ 2\pi^-) = (10.9 \pm 0.6) \times 10^{-2}$ . Our first error is their experiment's error and our second error is the systematic error from using our best value.

$\Gamma(J/\psi(1S) K^*(892)^0 \pi^+ \pi^-) / \Gamma_{total}$   $\Gamma_{231} / \Gamma$

VALUE (units 10 <sup>-4</sup> )	DOCUMENT ID	TECN	COMMENT
<b>6.6 ± 1.9 ± 1.1</b>	<sup>1</sup> AFFOLDER	02B CDF	p $\bar{p}$ 1.8 TeV

<sup>1</sup> Uses  $B^0 \rightarrow J/\psi(1S) K^*(892)^0$  decay as a reference and  $B(B^0 \rightarrow J/\psi(1S) K^0) = 12.4 \times 10^{-4}$ .

$\Gamma(\chi_{c1}(3872)^- K^+) / \Gamma_{total}$   $\Gamma_{232} / \Gamma$

VALUE	CL%	DOCUMENT ID	TECN	COMMENT
<b>&lt; 5 × 10<sup>-4</sup></b>	90	<sup>1</sup> AUBERT	06E BABR	e <sup>+</sup> e <sup>-</sup> → $\Upsilon(4S)$

<sup>1</sup> Perform measurements of absolute branching fractions using a missing mass technique.

$\Gamma(\chi_{c1}(3872)^- K^+, \chi_{c1}(3872)^- \rightarrow J/\psi(1S) \pi^- \pi^0) / \Gamma_{total}$   $\Gamma_{233} / \Gamma$

VALUE (units 10 <sup>-6</sup> )	CL%	DOCUMENT ID	TECN	COMMENT
<b>&lt; 4.2</b>	90	<sup>1,2</sup> CHOI	11 BELL	e <sup>+</sup> e <sup>-</sup> → $\Upsilon(4S)$

• • • We do not use the following data for averages, fits, limits, etc. • • •

< 5.4	90	<sup>2,3</sup> AUBERT	05B BABR	e <sup>+</sup> e <sup>-</sup> → $\Upsilon(4S)$
-------	----	-----------------------	----------	--

<sup>1</sup> Assumes  $\pi^+ \pi^0$  originates from  $\rho^+$ .  
<sup>2</sup> Assumes equal production of B<sup>+</sup> and B<sup>0</sup> at the  $\Upsilon(4S)$ .  
<sup>3</sup> The isovector-X hypothesis is excluded with a likelihood test at  $1 \times 10^{-4}$  level.

$\Gamma(\chi_{c1}(3872) K^0, \chi_{c1} \rightarrow J/\psi \pi^+ \pi^-) / \Gamma_{total}$   $\Gamma_{234} / \Gamma$

VALUE (units 10 <sup>-6</sup> )	CL%	DOCUMENT ID	TECN	COMMENT
<b>4.3 ± 1.2 ± 0.4</b>		<sup>1,2</sup> CHOI	11 BELL	e <sup>+</sup> e <sup>-</sup> → $\Upsilon(4S)$

• • • We do not use the following data for averages, fits, limits, etc. • • •

< 6.0	90	<sup>2</sup> AUBERT	08Y BABR	e <sup>+</sup> e <sup>-</sup> → $\Upsilon(4S)$
< 10.3	90	<sup>2,3</sup> AUBERT	06 BABR	Repl. by AUBERT 08Y

<sup>1</sup> CHOI 11 reports  $[\Gamma(B^0 \rightarrow \chi_{c1}(3872) K^0, \chi_{c1} \rightarrow J/\psi \pi^+ \pi^-) / \Gamma_{total}] / [B(B^+ \rightarrow \chi_{c1}(3872) K^+, \chi_{c1} \rightarrow J/\psi \pi^+ \pi^-)] = 0.50 \pm 0.14 \pm 0.04$  which we multiply by our best value  $B(B^+ \rightarrow \chi_{c1}(3872) K^+, \chi_{c1} \rightarrow J/\psi \pi^+ \pi^-) = (8.6 \pm 0.8) \times 10^{-6}$ . Our first error is their experiment's error and our second error is the systematic error from using our best value.  
<sup>2</sup> Assumes equal production of B<sup>+</sup> and B<sup>0</sup> at the  $\Upsilon(4S)$ .  
<sup>3</sup> The lower limit is also given to be  $1.34 \times 10^{-6}$  at 90% CL.

$\Gamma(\chi_{c1}(3872) K^0, \chi_{c1} \rightarrow J/\psi \gamma) / \Gamma_{total}$   $\Gamma_{235} / \Gamma$

VALUE (units 10 <sup>-6</sup> )	CL%	DOCUMENT ID	TECN	COMMENT
<b>&lt; 2.4</b>	90	<sup>1</sup> BHARDWAJ	11 BELL	e <sup>+</sup> e <sup>-</sup> → $\Upsilon(4S)$

• • • We do not use the following data for averages, fits, limits, etc. • • •

< 4.9	90	<sup>2</sup> AUBERT	09B BABR	e <sup>+</sup> e <sup>-</sup> → $\Upsilon(4S)$
-------	----	---------------------	----------	--

<sup>1</sup> Assumes equal production of B<sup>+</sup> and B<sup>0</sup> at the  $\Upsilon(4S)$ .  
<sup>2</sup> Uses  $B(\Upsilon(4S) \rightarrow B^+ B^-) = (51.6 \pm 0.6)\%$  and  $B(\Upsilon(4S) \rightarrow B^0 \bar{B}^0) = (48.4 \pm 0.6)\%$ .

$\Gamma(\chi_{c1}(3872) K^*(892)^0, \chi_{c1} \rightarrow J/\psi \gamma) / \Gamma_{total}$   $\Gamma_{236} / \Gamma$

VALUE (units 10 <sup>-6</sup> )	CL%	DOCUMENT ID	TECN	COMMENT
<b>&lt; 2.8</b>	90	<sup>1</sup> AUBERT	09B BABR	e <sup>+</sup> e <sup>-</sup> → $\Upsilon(4S)$

<sup>1</sup> Uses  $B(\Upsilon(4S) \rightarrow B^+ B^-) = (51.6 \pm 0.6)\%$  and  $B(\Upsilon(4S) \rightarrow B^0 \bar{B}^0) = (48.4 \pm 0.6)\%$ .

$\Gamma(\chi_{c1}(3872) K^0, \chi_{c1} \rightarrow \psi(2S) \gamma) / \Gamma_{total}$   $\Gamma_{237} / \Gamma$

VALUE (units 10 <sup>-6</sup> )	CL%	DOCUMENT ID	TECN	COMMENT
<b>&lt; 6.62</b>	90	<sup>1</sup> BHARDWAJ	11 BELL	e <sup>+</sup> e <sup>-</sup> → $\Upsilon(4S)$

• • • We do not use the following data for averages, fits, limits, etc. • • •

< 19	90	<sup>2</sup> AUBERT	09B BABR	e <sup>+</sup> e <sup>-</sup> → $\Upsilon(4S)$
------	----	---------------------	----------	--

<sup>1</sup> Assumes equal production of B<sup>+</sup> and B<sup>0</sup> at the  $\Upsilon(4S)$ .  
<sup>2</sup> Uses  $B(\Upsilon(4S) \rightarrow B^+ B^-) = (51.6 \pm 0.6)\%$  and  $B(\Upsilon(4S) \rightarrow B^0 \bar{B}^0) = (48.4 \pm 0.6)\%$ .

$\Gamma(\chi_{c1}(3872) K^*(892)^0, \chi_{c1} \rightarrow \psi(2S) \gamma) / \Gamma_{total}$   $\Gamma_{238} / \Gamma$

VALUE (units 10 <sup>-6</sup> )	CL%	DOCUMENT ID	TECN	COMMENT
<b>&lt; 4.4</b>	90	<sup>1</sup> AUBERT	09B BABR	e <sup>+</sup> e <sup>-</sup> → $\Upsilon(4S)$

<sup>1</sup> Uses  $B(\Upsilon(4S) \rightarrow B^+ B^-) = (51.6 \pm 0.6)\%$  and  $B(\Upsilon(4S) \rightarrow B^0 \bar{B}^0) = (48.4 \pm 0.6)\%$ .

$\Gamma(\chi_{c1}(3872) K^0, \chi_{c1} \rightarrow D^0 \bar{D}^0 \pi^0) / \Gamma_{total}$   $\Gamma_{239} / \Gamma$

VALUE (units 10 <sup>-4</sup> )	DOCUMENT ID	TECN	COMMENT
<b>1.66 ± 0.70 ± 0.32_{-0.37}^{+0.32}</b>	<sup>1</sup> GOKHROO	06 BELL	e <sup>+</sup> e <sup>-</sup> → $\Upsilon(4S)$

<sup>1</sup> Measure the near-threshold enhancements in the (D<sup>0</sup>  $\bar{D}^0$   $\pi^0$ ) system at a mass 3875.2 ± 0.7 ± 0.3 ± 0.8 MeV/c<sup>2</sup>.

$\Gamma(\chi_{c1}(3872) K^0, \chi_{c1} \rightarrow \bar{D}^{*0} D^0) / \Gamma_{total}$   $\Gamma_{240} / \Gamma$

VALUE (units 10 <sup>-4</sup> )	DOCUMENT ID	TECN	COMMENT
<b>1.2 ± 0.4 OUR AVERAGE</b>			
0.97 ± 0.46 ± 0.13	<sup>1</sup> AUSHEV	10 BELL	e <sup>+</sup> e <sup>-</sup> → $\Upsilon(4S)$
2.22 ± 1.05 ± 0.42	<sup>1,2</sup> AUBERT	08B BABR	e <sup>+</sup> e <sup>-</sup> → $\Upsilon(4S)$

<sup>1</sup> Assumes equal production of B<sup>+</sup> and B<sup>0</sup> at the  $\Upsilon(4S)$ .  
<sup>2</sup> This result is equivalent to the the 90% CL upper limit of  $4.37 \times 10^{-4}$ .

$\Gamma(\chi_{c1}(3872) K^+ \pi^-, \chi_{c1} \rightarrow J/\psi \pi^+ \pi^-) / \Gamma_{total}$   $\Gamma_{241} / \Gamma$

VALUE (units 10 <sup>-6</sup> )	DOCUMENT ID	TECN	COMMENT
<b>7.9 ± 1.3 ± 0.4</b>	<sup>1</sup> BALA	15 BELL	e <sup>+</sup> e <sup>-</sup> → $\Upsilon(4S)$

<sup>1</sup> Assumes equal production of B<sup>+</sup> and B<sup>0</sup> at the  $\Upsilon(4S)$ .

# Meson Particle Listings

$B^0$

$\Gamma(\chi_{c1}(3872)K^*(892)^0, \chi_{c1} \rightarrow J/\psi\pi^+\pi^-)/\Gamma_{total}$				$\Gamma_{242}/\Gamma$
VALUE (units $10^{-6}$ )	DOCUMENT ID	TECN	COMMENT	
$4.0 \pm 1.5 \pm 0.3$	BALA	15	BELL $e^+e^- \rightarrow \Upsilon(4S)$	

$\Gamma(\chi_{c1}(3872)\gamma, \chi_{c1} \rightarrow J/\psi\pi^+\pi^-)/\Gamma_{total}$				$\Gamma_{243}/\Gamma$
VALUE	CL%	DOCUMENT ID	TECN	COMMENT
$< 5.1 \times 10^{-7}$	90	1 CHOU	19	BELL $e^+e^- \rightarrow \Upsilon(4S)$

<sup>1</sup> Assumes equal production of  $B^+$  and  $B^0$  at  $\Upsilon(4S)$ .

$\Gamma(Z_c(4430)^\pm K^\mp, Z_c^\pm \rightarrow \psi(2S)\pi^\pm)/\Gamma_{total}$				$\Gamma_{244}/\Gamma$
VALUE (units $10^{-5}$ )	CL%	DOCUMENT ID	TECN	COMMENT
$6.0^{+1.7+2.5}_{-2.0-1.4}$		CHILIKIN	13	BELL $e^+e^- \rightarrow \Upsilon(4S)$

• • • We do not use the following data for averages, fits, limits, etc. • • •

$< 3.1$	95	1 AUBERT	09AA	BABR $e^+e^- \rightarrow \Upsilon(4S)$
$3.2^{+1.8+5.3}_{-0.9-1.6}$		1 MIZUK	09	BELL $e^+e^- \rightarrow \Upsilon(4S)$
$4.1 \pm 1.0 \pm 1.4$		1,2 CHOI	08	BELL Repl. by MIZUK 09

<sup>1</sup> Assumes equal production of  $B^+$  and  $B^0$  at the  $\Upsilon(4S)$ .  
<sup>2</sup> Establishes the  $(Z_c4430)^+$  with a significance of 6.5 sigma. Needs confirmation.

$\Gamma(Z_c(4430)^\pm K^\mp, Z_c^\pm \rightarrow J/\psi\pi^\pm)/\Gamma_{total}$				$\Gamma_{245}/\Gamma$
VALUE (units $10^{-6}$ )	CL%	DOCUMENT ID	TECN	COMMENT
$5.4^{+4.0+1.1}_{-1.0-0.6}$		CHILIKIN	14	BELL $\bar{B}^0 \rightarrow J/\psi K^- \pi^+$

• • • We do not use the following data for averages, fits, limits, etc. • • •

$< 4$	95	1 AUBERT	09AA	BABR $e^+e^- \rightarrow \Upsilon(4S)$
-------	----	----------	------	--

<sup>1</sup> Assumes equal production of  $B^+$  and  $B^0$  at the  $\Upsilon(4S)$ .

$\Gamma(Z_c(3900)^\pm K^\mp, Z_c^\pm \rightarrow J/\psi\pi^\pm)/\Gamma_{total}$				$\Gamma_{246}/\Gamma$
VALUE	CL%	DOCUMENT ID	TECN	COMMENT
$< 9 \times 10^{-7}$		CHILIKIN	14	BELL $\bar{B}^0 \rightarrow J/\psi K^- \pi^+$

$\Gamma(Z_c(4200)^\pm K^\mp, X^\pm \rightarrow J/\psi\pi^\pm)/\Gamma_{total}$				$\Gamma_{247}/\Gamma$
VALUE (units $10^{-5}$ )	CL%	DOCUMENT ID	TECN	COMMENT
$2.2^{+0.7+1.1}_{-0.5-0.6}$		CHILIKIN	14	BELL $\bar{B}^0 \rightarrow J/\psi K^- \pi^+$

$\Gamma(Z_c(3900)^\pm K^\mp, Z_c^\pm \rightarrow J/\psi\pi^\pm)/\Gamma(J/\psi(1S)K^*(892)^0)$				$\Gamma_{246}/\Gamma_{200}$
VALUE	CL%	DOCUMENT ID	TECN	COMMENT
$< 1.5 \times 10^{-2}$	90	ABAZOV	18B	D0 $p\bar{p}$ at 1.96 TeV

$\Gamma(J/\psi(1S)\rho\bar{\rho})/\Gamma_{total}$				$\Gamma_{248}/\Gamma$
VALUE (units $10^{-7}$ )	CL%	DOCUMENT ID	TECN	COMMENT
$4.51 \pm 0.40 \pm 0.44$		1 AAIJ	19U	LHCB $pp$ at 7, 8, 13 TeV

• • • We do not use the following data for averages, fits, limits, etc. • • •

$< 5.2$	90	2 AAIJ	13Z	LHCB Repl. by AAIJ 2019U
$< 8.3$	90	3 XIE	05	BELL $e^+e^- \rightarrow \Upsilon(4S)$
$< 19$	90	3 AUBERT	03K	BABR $e^+e^- \rightarrow \Upsilon(4S)$

<sup>1</sup> Measured relative to  $B_S^0 \rightarrow J/\psi\phi$  assuming  $B(B_S^0 \rightarrow J/\psi\phi) = (10.5 \pm 0.13 \pm 0.64) \times 10^{-4}$  and taking into account small  $K^+K^-$  S-wave contribution. Measurement assumes  $f_{s_c}/f_d = 0.259 \pm 0.015$  for 7, 8 TeV data and  $f_{s_c}/f_d$  multiplied by  $1.068 \pm 0.046$  for 13 TeV data.  
<sup>2</sup> Uses  $B(B_S^0 \rightarrow J/\psi(1S)\pi^+\pi^-) = (1.98 \pm 0.20) \times 10^{-4}$ .  
<sup>3</sup> Assumes equal production of  $B^+$  and  $B^0$  at the  $\Upsilon(4S)$ .

$\Gamma(J/\psi(1S)\gamma)/\Gamma_{total}$				$\Gamma_{249}/\Gamma$
VALUE (units $10^{-6}$ )	CL%	DOCUMENT ID	TECN	COMMENT
$< 1.5$	90	1 AAIJ	15BB	LHCB $pp$ at 7, 8 TeV

• • • We do not use the following data for averages, fits, limits, etc. • • •

$< 1.6$	90	2 AUBERT,B	04T	BABR $e^+e^- \rightarrow \Upsilon(4S)$
---------	----	------------	-----	--

<sup>1</sup> Branching fractions of normalization modes  $B^0 \rightarrow J/\psi\gamma X$  taken from PDG 14. Uses  $f_s/f_d = 0.259 \pm 0.015$ .  
<sup>2</sup> Assumes equal production of  $B^+$  and  $B^0$  at the  $\Upsilon(4S)$ .

$\Gamma(J/\psi(1S)\bar{D}^0)/\Gamma_{total}$				$\Gamma_{250}/\Gamma$
VALUE (units $10^{-5}$ )	CL%	DOCUMENT ID	TECN	COMMENT
$< 1.3$	90	1 AUBERT	05U	BABR $e^+e^- \rightarrow \Upsilon(4S)$

• • • We do not use the following data for averages, fits, limits, etc. • • •

$< 2.0$	90	1 ZHANG	05B	BELL $e^+e^- \rightarrow \Upsilon(4S)$
---------	----	---------	-----	--

<sup>1</sup> Assumes equal production of  $B^+$  and  $B^0$  at the  $\Upsilon(4S)$ .

$\Gamma(\psi(2S)\pi^0)/\Gamma_{total}$				$\Gamma_{251}/\Gamma$
VALUE (units $10^{-5}$ )	CL%	DOCUMENT ID	TECN	COMMENT
$1.17 \pm 0.17 \pm 0.08$		1 CHOBANOVA	16	BELL $e^+e^- \rightarrow \Upsilon(4S)$

<sup>1</sup> Assumes equal production of  $B^+$  and  $B^0$  at the  $\Upsilon(4S)$ .

$\Gamma(\psi(2S)K^0)/\Gamma_{total}$				$\Gamma_{252}/\Gamma$
VALUE (units $10^{-4}$ )	CL%	DOCUMENT ID	TECN	COMMENT
$5.8 \pm 0.5$		<b>OUR FIT</b>		
$5.8 \pm 0.5$		<b>OUR AVERAGE</b>		
$4.7 \pm 0.7 \pm 0.7$		1 AAIJ	14L	LHCB $pp$ at 7 TeV
$6.46 \pm 0.65 \pm 0.51$		2 AUBERT	05J	BABR $e^+e^- \rightarrow \Upsilon(4S)$
$6.7 \pm 1.1$		2 ABE	03B	BELL $e^+e^- \rightarrow \Upsilon(4S)$
$5.0 \pm 1.1 \pm 0.6$		2 RICHICHI	01	CLE2 $e^+e^- \rightarrow \Upsilon(4S)$

• • • We do not use the following data for averages, fits, limits, etc. • • •

$6.9 \pm 1.1 \pm 1.1$		2 AUBERT	02	BABR Repl. by AUBERT 05J
$< 8$	90	2 ALAM	94	CLE2 $e^+e^- \rightarrow \Upsilon(4S)$
$< 15$	90	2 BORTOLETTO	092	CLEO $e^+e^- \rightarrow \Upsilon(4S)$
$< 28$	90	2 ALBRECHT	90J	ARG $e^+e^- \rightarrow \Upsilon(4S)$

<sup>1</sup> Measured with  $B(B^0 \rightarrow \psi(2S)K_S^0) \times B(\psi(2S) \rightarrow J/\psi\pi^+\pi^-) / B(B^0 \rightarrow J/\psi K_S^0)$  using PDG 12 values for the involved branching fractions.  
<sup>2</sup> Assumes equal production of  $B^+$  and  $B^0$  at the  $\Upsilon(4S)$ .

$\Gamma(\psi(2S)K^0)/\Gamma(J/\psi(1S)K^0)$				$\Gamma_{252}/\Gamma_{198}$
VALUE	CL%	DOCUMENT ID	TECN	COMMENT
$0.82 \pm 0.13 \pm 0.12$		1 AUBERT	02	BABR $e^+e^- \rightarrow \Upsilon(4S)$

<sup>1</sup> Assumes equal production of  $B^+$  and  $B^0$  at the  $\Upsilon(4S)$ .

$\Gamma(\psi(3770)K^0, \psi \rightarrow \bar{D}^0 D^0)/\Gamma_{total}$				$\Gamma_{253}/\Gamma$
VALUE (units $10^{-4}$ )	CL%	DOCUMENT ID	TECN	COMMENT
$< 1.23$	90	1 AUBERT	08B	BABR $e^+e^- \rightarrow \Upsilon(4S)$

<sup>1</sup> Assumes equal production of  $B^+$  and  $B^0$  at the  $\Upsilon(4S)$ .

$\Gamma(\psi(3770)K^0, \psi \rightarrow D^- D^+)/\Gamma_{total}$				$\Gamma_{254}/\Gamma$
VALUE (units $10^{-4}$ )	CL%	DOCUMENT ID	TECN	COMMENT
$< 1.88$	90	1 AUBERT	08B	BABR $e^+e^- \rightarrow \Upsilon(4S)$

<sup>1</sup> Assumes equal production of  $B^+$  and  $B^0$  at the  $\Upsilon(4S)$ .

$\Gamma(\psi(2S)\pi^+\pi^-)/\Gamma(J/\psi(1S)\pi^+\pi^-)$				$\Gamma_{255}/\Gamma_{210}$
VALUE	CL%	DOCUMENT ID	TECN	COMMENT
$0.56 \pm 0.07 \pm 0.05$		1 AAIJ	13AA	LHCB $pp$ at 7 TeV

<sup>1</sup> Assuming lepton universality for dimuon decay modes of  $J/\psi$  and  $\psi(2S)$  mesons, the ratio  $B(J/\psi \rightarrow \mu^+\mu^-)/B(\psi(2S) \rightarrow \mu^+\mu^-) = B(J/\psi \rightarrow e^+e^-)/B(\psi(2S) \rightarrow e^+e^-) = 7.69 \pm 0.19$  was used.

$\Gamma(\psi(2S)K^+\pi^-)/\Gamma_{total}$				$\Gamma_{256}/\Gamma$
VALUE (units $10^{-4}$ )	CL%	DOCUMENT ID	TECN	COMMENT
$5.80 \pm 0.39$		1,2 CHILIKIN	13	BELL $e^+e^- \rightarrow \Upsilon(4S)$

• • • We do not use the following data for averages, fits, limits, etc. • • •

$5.57 \pm 0.16$		3 AUBERT	09AA	BABR $e^+e^- \rightarrow \Upsilon(4S)$
$5.68 \pm 0.13 \pm 0.42$		2 MIZUK	09	BELL $e^+e^- \rightarrow \Upsilon(4S)$
$< 10$	90	2 ALBRECHT	90J	ARG $e^+e^- \rightarrow \Upsilon(4S)$

<sup>1</sup> Combines measurements with  $\psi(2S) \rightarrow \ell^+\ell^-$  with measurement from MIZUK 09 which uses  $\psi(2S) \rightarrow J/\psi\pi^+\pi^-$ .  
<sup>2</sup> Assumes equal production of  $B^+$  and  $B^0$  at the  $\Upsilon(4S)$ .  
<sup>3</sup> Does not report systematic uncertainties.

$\Gamma(\psi(2S)K^*(892)^0)/\Gamma_{total}$				$\Gamma_{257}/\Gamma$
VALUE (units $10^{-4}$ )	CL%	DOCUMENT ID	TECN	COMMENT
$5.9 \pm 0.4$		<b>OUR FIT</b>		
$6.0^{+0.5}_{-0.7}$		<b>OUR AVERAGE</b>		
$5.55^{+0.22+0.41}_{-0.23-0.84}$		1 CHILIKIN	13	BELL $e^+e^- \rightarrow \Upsilon(4S)$
$6.49 \pm 0.59 \pm 0.97$		1 AUBERT	05J	BABR $e^+e^- \rightarrow \Upsilon(4S)$
$7.6 \pm 1.1 \pm 1.0$		1 RICHICHI	01	CLE2 $e^+e^- \rightarrow \Upsilon(4S)$
$9.0 \pm 2.2 \pm 0.9$		2 ABE	98O	CDF $p\bar{p}$ 1.8 TeV

• • • We do not use the following data for averages, fits, limits, etc. • • •

$5.52^{+0.35+0.53}_{-0.32-0.58}$		1 MIZUK	09	BELL $e^+e^- \rightarrow \Upsilon(4S)$
$< 19$	90	1 ALAM	94	CLE2 Repl. by RICHICHI 01
$14 \pm 8 \pm 4$		1 BORTOLETTO	92	CLEO $e^+e^- \rightarrow \Upsilon(4S)$
$< 23$	90	1 ALBRECHT	90J	ARG $e^+e^- \rightarrow \Upsilon(4S)$

<sup>1</sup> Assumes equal production of  $B^+$  and  $B^0$  at the  $\Upsilon(4S)$ .  
<sup>2</sup> ABE 98O reports  $[B(B^0 \rightarrow \psi(2S)K^*(892)^0)]/[B(B^+ \rightarrow J/\psi(1S)K^+)] = 0.908 \pm 0.194 \pm 0.10$ . We multiply by our best value  $B(B^+ \rightarrow J/\psi(1S)K^+) = (9.9 \pm 1.0) \times 10^{-4}$ . Our first error is their experiment's error and our second error is the systematic error from using our best value.

$\Gamma(\psi(2S)K^*(892)^0)/\Gamma(J/\psi(1S)K^*(892)^0)$				$\Gamma_{257}/\Gamma_{200}$
VALUE	CL%	DOCUMENT ID	TECN	COMMENT
$0.487 \pm 0.018 \pm 0.011$		1,2 AAIJ	12L	LHCB $pp$ at 7 TeV

<sup>1</sup> AAIJ 12L reports  $0.476 \pm 0.014 \pm 0.010 \pm 0.012$  from a measurement of  $[\Gamma(B^0 \rightarrow \psi(2S)K^*(892)^0)/\Gamma(B^0 \rightarrow J/\psi(1S)K^*(892)^0)] \times [B(J/\psi(1S) \rightarrow e^+e^-)] / [B(\psi(2S) \rightarrow e^+e^-)]$  assuming  $B(J/\psi(1S) \rightarrow e^+e^-) = (5.94 \pm 0.06) \times 10^{-2}$ ,  $B(\psi(2S) \rightarrow e^+e^-) = (7.72 \pm 0.17) \times 10^{-3}$ , which we rescale to our best values  $B(J/\psi(1S) \rightarrow e^+e^-) = (5.971 \pm 0.032) \times 10^{-2}$ ,  $B(\psi(2S) \rightarrow e^+e^-) = (7.93 \pm 0.17) \times 10^{-3}$ . Our first error is their experiment's error and our second error is the systematic error from using our best values.  
<sup>2</sup> Assumes  $B(J/\psi \rightarrow \mu^+\mu^-) / B(\psi(2S) \rightarrow \mu^+\mu^-) = B(J/\psi \rightarrow e^+e^-) / B(\psi(2S) \rightarrow e^+e^-) = 7.69 \pm 0.19$ .

See key on page 999

Meson Particle Listings

$B^0$

$\Gamma(\psi(2S) K^*(892)^0)/\Gamma(\psi(2S) K^0)$		$\Gamma_{257}/\Gamma_{252}$	
VALUE	DOCUMENT ID	TECN	COMMENT
<b>1.02±0.10 OUR FIT</b>			
<b>1.00±0.14±0.09</b>	AUBERT	05J	BABR $e^+e^- \rightarrow \Upsilon(4S)$

$\Gamma(\chi_{c0} K^0)/\Gamma_{total}$		$\Gamma_{258}/\Gamma$		
VALUE (units $10^{-6}$ )	CL%	DOCUMENT ID	TECN	COMMENT
<b>1.11<sup>+</sup><sub>-0.16</sub> ± 0.20 ± 0.14</b>		1 AAIJ	18F	LHCB $pp$ at 7, 8 TeV

- • • We do not use the following data for averages, fits, limits, etc. • • •

145	+103 -85	± 8	2,3	LEES	12l	BABR	$e^+e^- \rightarrow \Upsilon(4S)$
148	± 30	± 13	2,4	LEES	12o	BABR	$e^+e^- \rightarrow \Upsilon(4S)$
142	+55 -44	± 22	2,5	AUBERT	09AU	BABR	$e^+e^- \rightarrow \Upsilon(4S)$
< 113		90	5	GARMASH	07	BELL	$e^+e^- \rightarrow \Upsilon(4S)$
< 1240		90	2	AUBERT	05K	BABR	$e^+e^- \rightarrow \Upsilon(4S)$
< 500		90	6	EDWARDS	01	CLE2	$e^+e^- \rightarrow \Upsilon(4S)$

1 Uses Dalitz plot analysis of the  $B^0 \rightarrow K_S^0 \pi^+ \pi^-$  final state decays. For the branching fraction of the reference mode, the PDG 18 average  $B(B^0 \rightarrow K_S^0 \pi^+ \pi^-) = (4.96 \pm 0.20) \times 10^{-5}$  is used.  
 2 Assumes equal production of  $B^+$  and  $B^0$  at the  $\Upsilon(4S)$ .  
 3 LEES 12l reports  $[\Gamma(B^0 \rightarrow \chi_{c0} K^0)/\Gamma_{total}] \times [B(\chi_{c0}(1P) \rightarrow K_S^0 K_S^0)] = (0.46^{+0.25}_{-0.17} \pm 0.21) \times 10^{-6}$  which we divide by our best value  $B(\chi_{c0}(1P) \rightarrow K_S^0 K_S^0) = (3.16 \pm 0.17) \times 10^{-3}$ . Our first error is their experiment's error and our second error is the systematic error from using our best value.  
 4 Measured in the  $B^0 \rightarrow K_S^0 K^+ K^-$  decay.  
 5 Uses Dalitz plot analysis of the  $B^0 \rightarrow K^0 \pi^+ \pi^-$  final state decays.  
 6 EDWARDS 01 assumes equal production of  $B^0$  and  $B^+$  at the  $\Upsilon(4S)$ . The correlated uncertainties (28.3)% from  $B(J/\psi(1S) \rightarrow \gamma \eta_c)$  in those modes have been accounted for.

$\Gamma(\chi_{c0} K^*(892)^0)/\Gamma_{total}$		$\Gamma_{259}/\Gamma$		
VALUE (units $10^{-4}$ )	CL%	DOCUMENT ID	TECN	COMMENT
<b>1.7±0.3±0.2</b>		1 AUBERT	08BD	BABR $e^+e^- \rightarrow \Upsilon(4S)$
<7.7	90	1 AUBERT	05K	BABR Repl. by AUBERT 08BD

1 Assumes equal production of  $B^+$  and  $B^0$  at the  $\Upsilon(4S)$ .

$\Gamma(\chi_{c1} \pi^0)/\Gamma_{total}$		$\Gamma_{260}/\Gamma$		
VALUE (units $10^{-5}$ )	CL%	DOCUMENT ID	TECN	COMMENT
<b>1.12±0.25±0.12</b>		1 KUMAR	08	BELL $e^+e^- \rightarrow \Upsilon(4S)$

1 Assumes equal production of  $B^+$  and  $B^0$  at the  $\Upsilon(4S)$ .

$\Gamma(\chi_{c1} K^0)/\Gamma_{total}$		$\Gamma_{261}/\Gamma$					
VALUE (units $10^{-4}$ )	CL%	DOCUMENT ID	TECN	COMMENT			
<b>3.95±0.27 OUR AVERAGE</b>							
15	+5 -4	± 6	1	CHILIKIN	19	BELL	$e^+e^- \rightarrow \Upsilon(4S)$
3.78 <sup>+</sup> <sub>-0.16</sub> ± 0.17 ± 0.33		2	BHARDWAJ	11	BELL	$e^+e^- \rightarrow \Upsilon(4S)$	
4.2 ± 0.3 ± 0.3		3	AUBERT	09B	BABR	$e^+e^- \rightarrow \Upsilon(4S)$	
3.1 ± 1.5 ± 0.1		4	VERY	00	CLE2	$e^+e^- \rightarrow \Upsilon(4S)$	
<27	90	2	ALAM	94	CLE2	$e^+e^- \rightarrow \Upsilon(4S)$	

1 CHILIKIN 19 reports  $[\Gamma(B^0 \rightarrow \chi_{c1} K^0)/\Gamma_{total}] \times [B(\chi_{c1}(1P) \rightarrow p\bar{p}\pi^+\pi^-)] = (7.4^{+2.4+0.6}_{-2.0-0.4}) \times 10^{-7}$  which we divide by our best value  $B(\chi_{c1}(1P) \rightarrow p\bar{p}\pi^+\pi^-) = (5.0 \pm 1.9) \times 10^{-4}$ . Our first error is their experiment's error and our second error is the systematic error from using our best value.  
 2 Assumes equal production of  $B^+$  and  $B^0$  at the  $\Upsilon(4S)$ .  
 3 Uses  $\chi_{c1,2} \rightarrow J/\psi\gamma$ . Assumes  $B(\Upsilon(4S) \rightarrow B^+ B^-) = (51.6 \pm 0.6)\%$  and  $B(\Upsilon(4S) \rightarrow B^0 \bar{B}^0) = (48.4 \pm 0.6)\%$ .  
 4 VERY 00 reports  $(3.9^{+1.9}_{-1.3} \pm 0.4) \times 10^{-4}$  from a measurement of  $[\Gamma(B^0 \rightarrow \chi_{c1} K^0)/\Gamma_{total}] \times [B(\chi_{c1}(1P) \rightarrow \gamma J/\psi(1S))]$  assuming  $B(\chi_{c1}(1P) \rightarrow \gamma J/\psi(1S)) = 0.273 \pm 0.016$ , which we rescale to our best value  $B(\chi_{c1}(1P) \rightarrow \gamma J/\psi(1S)) = (34.3 \pm 1.0) \times 10^{-2}$ . Our first error is their experiment's error and our second error is the systematic error from using our best value. Assumes equal production of  $B^+$  and  $B^0$  at the  $\Upsilon(4S)$ .  
 5 AUBERT 02 reports  $(5.4 \pm 1.4 \pm 1.1) \times 10^{-4}$  from a measurement of  $[\Gamma(B^0 \rightarrow \chi_{c1} K^0)/\Gamma_{total}] \times [B(\chi_{c1}(1P) \rightarrow \gamma J/\psi(1S))]$  assuming  $B(\chi_{c1}(1P) \rightarrow \gamma J/\psi(1S)) = 0.273 \pm 0.016$ , which we rescale to our best value  $B(\chi_{c1}(1P) \rightarrow \gamma J/\psi(1S)) = (34.3 \pm 1.0) \times 10^{-2}$ . Our first error is their experiment's error and our second error is the systematic error from using our best value. Assumes equal production of  $B^+$  and  $B^0$  at the  $\Upsilon(4S)$ .

$\Gamma(\chi_{c1} K^0)/\Gamma(J/\psi(1S) K^0)$		$\Gamma_{261}/\Gamma_{198}$	
VALUE	DOCUMENT ID	TECN	COMMENT
<b>0.53±0.16±0.01</b>	1 AUBERT	02	BABR $e^+e^- \rightarrow \Upsilon(4S)$

1 AUBERT 02 reports  $0.66 \pm 0.11 \pm 0.17$  from a measurement of  $[\Gamma(B^0 \rightarrow \chi_{c1} K^0)/\Gamma(B^0 \rightarrow J/\psi(1S) K^0)] \times [B(\chi_{c1}(1P) \rightarrow \gamma J/\psi(1S))]$  assuming  $B(\chi_{c1}(1P) \rightarrow \gamma J/\psi(1S)) = 0.273 \pm 0.016$ , which we rescale to our best value  $B(\chi_{c1}(1P) \rightarrow \gamma J/\psi(1S)) = (34.3 \pm 1.0) \times 10^{-2}$ . Our first error is their experiment's error and our second error is the systematic error from using our best value. Assumes equal production of  $B^+$  and  $B^0$  at the  $\Upsilon(4S)$ .

$\Gamma(\chi_{c1} \pi^- K^+)/\Gamma_{total}$		$\Gamma_{262}/\Gamma$	
VALUE (units $10^{-4}$ )	DOCUMENT ID	TECN	COMMENT
<b>4.97±0.12±0.28</b>	1 BHARDWAJ	16	BELL $e^+e^- \rightarrow \Upsilon(4S)$
3.83±0.10±0.39	1 MIZUK	08	BELL Repl. by BHARDWAJ 16

1 Assumes equal production of  $B^+$  and  $B^0$  at the  $\Upsilon(4S)$ .

$\Gamma(\chi_{c1} \pi^- K^+)/\Gamma(J/\psi(1S) K^+ \pi^-)$		$\Gamma_{262}/\Gamma_{199}$	
VALUE	DOCUMENT ID	TECN	COMMENT
<b>0.476±0.021±0.013</b>	1 LEES	12B	BABR

1 LEES 12B reports  $0.474 \pm 0.013 \pm 0.026$  from a measurement of  $[\Gamma(B^0 \rightarrow \chi_{c1} \pi^- K^+)/\Gamma(B^0 \rightarrow J/\psi(1S) K^+ \pi^-)] \times [B(\chi_{c1}(1P) \rightarrow \gamma J/\psi(1S))]$  assuming  $B(\chi_{c1}(1P) \rightarrow \gamma J/\psi(1S)) = (34.4 \pm 1.5) \times 10^{-2}$ , which we rescale to our best value  $B(\chi_{c1}(1P) \rightarrow \gamma J/\psi(1S)) = (34.3 \pm 1.0) \times 10^{-2}$ . Our first error is their experiment's error and our second error is the systematic error from using our best value.

$\Gamma(\chi_{c1} K^*(892)^0)/\Gamma_{total}$		$\Gamma_{263}/\Gamma$		
VALUE (units $10^{-4}$ )	CL%	DOCUMENT ID	TECN	COMMENT
<b>2.38±0.19 OUR FIT</b>				Error includes scale factor of 1.2.
<b>2.22<sup>+</sup><sub>-0.31</sub> ± 0.40 ± 0.31</b>				Error includes scale factor of 1.6.
2.5 ± 0.2 ± 0.2		1 AUBERT	09B	BABR $e^+e^- \rightarrow \Upsilon(4S)$
1.73 <sup>+</sup> <sub>-0.12-0.22</sub> ± 0.15 ± 0.34		2 MIZUK	08	BELL $e^+e^- \rightarrow \Upsilon(4S)$
3.14±0.34±0.72		2 SONI	06	BELL Repl. by MIZUK 08
3.27±0.42±0.64		2 AUBERT	05J	BABR Repl. by AUBERT 09B
3.8 ± 1.3 ± 0.1		3 AUBERT	02	BABR Repl. by AUBERT 05J
<21	90	4 ALAM	94	CLE2 $e^+e^- \rightarrow \Upsilon(4S)$

1 Uses  $\chi_{c1,2} \rightarrow J/\psi\gamma$ . Assumes  $B(\Upsilon(4S) \rightarrow B^+ B^-) = (51.6 \pm 0.6)\%$  and  $B(\Upsilon(4S) \rightarrow B^0 \bar{B}^0) = (48.4 \pm 0.6)\%$ .  
 2 Assumes equal production of  $B^+$  and  $B^0$  at the  $\Upsilon(4S)$ .  
 3 AUBERT 02 reports  $(4.8 \pm 1.4 \pm 0.9) \times 10^{-4}$  from a measurement of  $[\Gamma(B^0 \rightarrow \chi_{c1} K^*(892)^0)/\Gamma_{total}] \times [B(\chi_{c1}(1P) \rightarrow \gamma J/\psi(1S))]$  assuming  $B(\chi_{c1}(1P) \rightarrow \gamma J/\psi(1S)) = 0.273 \pm 0.016$ , which we rescale to our best value  $B(\chi_{c1}(1P) \rightarrow \gamma J/\psi(1S)) = (34.3 \pm 1.0) \times 10^{-2}$ . Our first error is their experiment's error and our second error is the systematic error from using our best value. Assumes equal production of  $B^+$  and  $B^0$  at the  $\Upsilon(4S)$ .  
 4 BORTOLETTO 92 assumes equal production of  $B^+$  and  $B^0$  at the  $\Upsilon(4S)$ .

$\Gamma(\chi_{c1} K^*(892)^0)/\Gamma(J/\psi(1S) K^*(892)^0)$		$\Gamma_{263}/\Gamma_{200}$	
VALUE (units $10^{-2}$ )	DOCUMENT ID	TECN	COMMENT
<b>18.8±1.5 OUR FIT</b>			Error includes scale factor of 1.1.
<b>19.8±1.1±1.5</b>	1 AAIJ	13AC	LHCB $pp$ at 7 TeV

1 Uses  $B(\chi_{c1} \rightarrow J/\psi\gamma) = (34.4 \pm 1.5)\%$ .

$\Gamma(\chi_{c1} K^*(892)^0)/\Gamma(\chi_{c1} K^0)$		$\Gamma_{263}/\Gamma_{261}$	
VALUE	DOCUMENT ID	TECN	COMMENT
<b>0.72±0.11±0.12</b>	AUBERT	05J	BABR $e^+e^- \rightarrow \Upsilon(4S)$
0.89±0.34±0.17	1 AUBERT	02	BABR Repl. by AUBERT 05J

1 Assumes equal production of  $B^+$  and  $B^0$  at the  $\Upsilon(4S)$ .

$\Gamma(X(4051)^- K^+, X^- \rightarrow \chi_{c1} \pi^-)/\Gamma_{total}$		$\Gamma_{264}/\Gamma$		
VALUE (units $10^{-5}$ )	CL%	DOCUMENT ID	TECN	COMMENT
<b>3.0<sup>+</sup><sub>-0.8-1.6</sub> ± 1.5 ± 3.7</b>		1 MIZUK	08	BELL $e^+e^- \rightarrow \Upsilon(4S)$
<1.8	90	1,2	LEES	12B BABR

1 Assumes equal production of  $B^+$  and  $B^0$  at the  $\Upsilon(4S)$ .  
 2 Uses  $\chi_{c1} \rightarrow J/\psi\gamma$  mode. Uses  $\chi_{c1} \rightarrow J/\psi\gamma$  mode. Finds a good description of the data without this  $B^0 \rightarrow X(4051)^+ K^-$  decay mode in a fit.

$\Gamma(X(4248)^- K^+, X^- \rightarrow \chi_{c1} \pi^-)/\Gamma_{total}$		$\Gamma_{265}/\Gamma$		
VALUE (units $10^{-5}$ )	CL%	DOCUMENT ID	TECN	COMMENT
<b>4.0<sup>+</sup><sub>-0.9-0.5</sub> ± 2.3 ± 19.7</b>		1 MIZUK	08	BELL $e^+e^- \rightarrow \Upsilon(4S)$
<4.0	90	1,2	LEES	12B BABR

1 Assumes equal production of  $B^+$  and  $B^0$  at the  $\Upsilon(4S)$ .  
 2 Uses  $\chi_{c1} \rightarrow J/\psi\gamma$  mode. Finds a good description of the data without this  $B^0 \rightarrow X(4248)^+ K^-$  decay mode in a fit.

Downloaded from https://academic.oup.com/ptep/article/2020/8/083C01/5891211 by guest on 12 November 2020



See key on page 999

# Meson Particle Listings

## $B^0$

$\Gamma(\eta' K^0)/\Gamma_{total}$				$\Gamma_{277}/\Gamma$
VALUE (units $10^{-6}$ )	DOCUMENT ID	TECN	COMMENT	
<b>66 ± 4 OUR AVERAGE</b>	Error includes scale factor of 1.4.			
68.5 ± 2.2 ± 3.1	<sup>1</sup> AUBERT	09AV	BABR $e^+e^- \rightarrow \Upsilon(4S)$	
58.9 <sup>+3.5</sup> <sub>-3.5</sub> ± 4.3	<sup>1</sup> SCHUEMANN	06	BELL $e^+e^- \rightarrow \Upsilon(4S)$	
89 <sup>+18</sup> <sub>-16</sub> ± 9	<sup>1</sup> RICHICHI	00	CLE2 $e^+e^- \rightarrow \Upsilon(4S)$	
• • • We do not use the following data for averages, fits, limits, etc. • • •				
66.6 ± 2.6 ± 2.8	<sup>1</sup> AUBERT	07AE	BABR Repl. by AUBERT 09AV	
67.4 ± 3.3 ± 3.2	<sup>1</sup> AUBERT	05M	BABR AUBERT 07AE	
60.6 ± 5.6 ± 4.6	<sup>1</sup> AUBERT	03W	BABR Repl. by AUBERT 05M	
55 <sup>+19</sup> <sub>-16</sub> ± 8	<sup>1</sup> ABE	01M	BELL Repl. by SCHUEMANN 06	
42 <sup>+13</sup> <sub>-11</sub> ± 4	<sup>1</sup> AUBERT	01G	BABR Repl. by AUBERT 03W	
47 <sup>+27</sup> <sub>-20</sub> ± 9	BEHRENS	98	CLE2 Repl. by RICHICHI 00	

<sup>1</sup> Assumes equal production of  $B^+$  and  $B^0$  at the  $\Upsilon(4S)$ .

$\Gamma(\eta' K^*(892)^0)/\Gamma_{total}$				$\Gamma_{278}/\Gamma$
VALUE (units $10^{-6}$ )	DOCUMENT ID	TECN	COMMENT	
<b>2.8 ± 0.6 OUR AVERAGE</b>				
2.6 ± 0.7 ± 0.2	<sup>1</sup> SATO	14	BELL $e^+e^- \rightarrow \Upsilon(4S)$	
3.1 <sup>+0.9</sup> <sub>-0.8</sub> ± 0.3	<sup>1</sup> DEL-AMO-SA..10A	BABR	$e^+e^- \rightarrow \Upsilon(4S)$	
• • • We do not use the following data for averages, fits, limits, etc. • • •				
3.8 ± 1.1 ± 0.5	<sup>1</sup> AUBERT	07E	BABR Repl. by DEL-AMO-SANCHEZ 10A	
< 2.6	90	<sup>1</sup> SCHUEMANN	07 BELL $e^+e^- \rightarrow \Upsilon(4S)$	
< 7.6	90	<sup>1</sup> AUBERT,B	04D BABR Repl. by AUBERT 07E	
< 24	90	<sup>1</sup> RICHICHI	00 CLE2 $e^+e^- \rightarrow \Upsilon(4S)$	
< 39	90	BEHRENS	98 CLE2 Repl. by RICHICHI 00	

<sup>1</sup> Assumes equal production of  $B^+$  and  $B^0$  at the  $\Upsilon(4S)$ .

$\Gamma(\eta' K_0^*(1430)^0)/\Gamma_{total}$				$\Gamma_{279}/\Gamma$
VALUE (units $10^{-6}$ )	DOCUMENT ID	TECN	COMMENT	
<b>6.3 ± 1.3 ± 0.9</b>	<sup>1</sup> DEL-AMO-SA..10A	BABR	$e^+e^- \rightarrow \Upsilon(4S)$	

<sup>1</sup> Assumes equal production of  $B^+$  and  $B^0$  at the  $\Upsilon(4S)$ .

$\Gamma(\eta' K_2^*(1430)^0)/\Gamma_{total}$				$\Gamma_{280}/\Gamma$
VALUE (units $10^{-6}$ )	DOCUMENT ID	TECN	COMMENT	
<b>13.7<sup>+3.0</sup><sub>-2.9</sub> ± 1.2</b>	<sup>1</sup> DEL-AMO-SA..10A	BABR	$e^+e^- \rightarrow \Upsilon(4S)$	

<sup>1</sup> Assumes equal production of  $B^+$  and  $B^0$  at the  $\Upsilon(4S)$ .

$\Gamma(\eta K^0)/\Gamma_{total}$				$\Gamma_{281}/\Gamma$
VALUE (units $10^{-6}$ )	CL%	DOCUMENT ID	TECN	COMMENT
<b>1.23<sup>+0.27</sup><sub>-0.24</sub> OUR AVERAGE</b>				
1.27 <sup>+0.33</sup> <sub>-0.29</sub> ± 0.08		<sup>1</sup> HOI	12	BELL $e^+e^- \rightarrow \Upsilon(4S)$
1.15 <sup>+0.43</sup> <sub>-0.38</sub> ± 0.09		<sup>1</sup> AUBERT	09AV	BABR $e^+e^- \rightarrow \Upsilon(4S)$
• • • We do not use the following data for averages, fits, limits, etc. • • •				
< 1.9	90	<sup>1</sup> CHANG	07B	BELL Repl. by HOI 12
< 2.9	90	<sup>1</sup> AUBERT,B	06V	BABR $e^+e^- \rightarrow \Upsilon(4S)$
< 2.5	90	<sup>1</sup> AUBERT,B	05K	BABR $e^+e^- \rightarrow \Upsilon(4S)$
< 2.0	90	<sup>1</sup> CHANG	05A	BELL Repl. by CHANG 07B
< 5.2	90	<sup>1</sup> AUBERT	04H	BABR Repl. by AUBERT,B 05K
< 9.3	90	<sup>1</sup> RICHICHI	00	CLE2 $e^+e^- \rightarrow \Upsilon(4S)$
< 33	90	BEHRENS	98	CLE2 Repl. by RICHICHI 00

<sup>1</sup> Assumes equal production of  $B^+$  and  $B^0$  at the  $\Upsilon(4S)$ .

$\Gamma(\eta K^*(892)^0)/\Gamma_{total}$				$\Gamma_{282}/\Gamma$
VALUE (units $10^{-6}$ )	CL%	DOCUMENT ID	TECN	COMMENT
<b>15.9 ± 1.0 OUR AVERAGE</b>				
15.2 ± 1.2 ± 1.0		<sup>1</sup> WANG	07B	BELL $e^+e^- \rightarrow \Upsilon(4S)$
16.5 ± 1.1 ± 0.8		<sup>1</sup> AUBERT,B	06H	BABR $e^+e^- \rightarrow \Upsilon(4S)$
13.8 <sup>+5.5</sup> <sub>-4.6</sub> ± 1.6		<sup>1</sup> RICHICHI	00	CLE2 $e^+e^- \rightarrow \Upsilon(4S)$
• • • We do not use the following data for averages, fits, limits, etc. • • •				
18.6 ± 2.3 ± 1.2		<sup>1</sup> AUBERT,B	04D	BABR Repl. by AUBERT,B 06H
< 30	90	BEHRENS	98	CLE2 Repl. by RICHICHI 00

<sup>1</sup> Assumes equal production of  $B^+$  and  $B^0$  at the  $\Upsilon(4S)$ .

$\Gamma(\eta K_0^*(1430)^0)/\Gamma_{total}$				$\Gamma_{283}/\Gamma$
VALUE (units $10^{-6}$ )	CL%	DOCUMENT ID	TECN	COMMENT
<b>11.0 ± 1.6 ± 1.5</b>				
		<sup>1</sup> AUBERT,B	06H	BABR $e^+e^- \rightarrow \Upsilon(4S)$

<sup>1</sup> Assumes equal production of  $B^+$  and  $B^0$  at the  $\Upsilon(4S)$ .

$\Gamma(\eta K_2^*(1430)^0)/\Gamma_{total}$				$\Gamma_{284}/\Gamma$
VALUE (units $10^{-6}$ )	CL%	DOCUMENT ID	TECN	COMMENT
<b>9.6 ± 1.8 ± 1.1</b>				
		<sup>1</sup> AUBERT,B	06H	BABR $e^+e^- \rightarrow \Upsilon(4S)$

<sup>1</sup> Assumes equal production of  $B^+$  and  $B^0$  at the  $\Upsilon(4S)$ .

$\Gamma(\omega K^0)/\Gamma_{total}$				$\Gamma_{285}/\Gamma$
VALUE (units $10^{-6}$ )	CL%	DOCUMENT ID	TECN	COMMENT
<b>4.8 ± 0.4 OUR AVERAGE</b>				
4.5 ± 0.4 ± 0.3		<sup>1</sup> CHOBANOVA	14	BELL $e^+e^- \rightarrow \Upsilon(4S)$
5.4 ± 0.8 ± 0.3		<sup>1</sup> AUBERT	07AE	BABR $e^+e^- \rightarrow \Upsilon(4S)$
10.0 <sup>+5.4</sup> <sub>-4.2</sub> ± 1.4		<sup>1</sup> JESSOP	00	CLE2 $e^+e^- \rightarrow \Upsilon(4S)$
• • • We do not use the following data for averages, fits, limits, etc. • • •				
6.2 ± 1.0 ± 0.4		<sup>1</sup> AUBERT,B	06E	BABR Repl. by AUBERT 07AE
4.4 <sup>+0.8</sup> <sub>-0.7</sub> ± 0.4		<sup>1</sup> JEN	06	BELL Repl. by CHOBANOVA 14
5.9 <sup>+1.6</sup> <sub>-1.3</sub> ± 0.5		<sup>1</sup> AUBERT	04H	BABR Repl. by AUBERT,B 06E
4.0 <sup>+1.9</sup> <sub>-1.6</sub> ± 0.5		<sup>1</sup> WANG	04A	BELL Repl. by JEN 06
< 13	90	<sup>1</sup> AUBERT	01G	BABR Repl. by AUBERT 04H
< 57	90	<sup>1</sup> BERGFELD	98	CLE2 Repl. by JESSOP 00

<sup>1</sup> Assumes equal production of  $B^+$  and  $B^0$  at the  $\Upsilon(4S)$ .

$\Gamma(a_0(980)^0 K^0, a_0^0 \rightarrow \eta\pi^0)/\Gamma_{total}$				$\Gamma_{286}/\Gamma$
VALUE (units $10^{-6}$ )	CL%	DOCUMENT ID	TECN	COMMENT
<b>&lt; 7.8</b>	90	<sup>1</sup> AUBERT,BE	04	BABR $e^+e^- \rightarrow \Upsilon(4S)$

<sup>1</sup> Assumes equal production of charged and neutral  $B$  mesons at  $\Upsilon(4S)$ .

$\Gamma(b_1^0 K^0, b_1^0 \rightarrow \omega\pi^0)/\Gamma_{total}$				$\Gamma_{287}/\Gamma$
VALUE (units $10^{-6}$ )	CL%	DOCUMENT ID	TECN	COMMENT
<b>&lt; 7.8</b>	90	<sup>1</sup> AUBERT	08AG	BABR $e^+e^- \rightarrow \Upsilon(4S)$

<sup>1</sup> Assumes equal production of  $B^+$  and  $B^0$  at the  $\Upsilon(4S)$ .

$\Gamma(a_0(980)^\pm K^\mp, a_0^\pm \rightarrow \eta\pi^\pm)/\Gamma_{total}$				$\Gamma_{288}/\Gamma$
VALUE (units $10^{-6}$ )	CL%	DOCUMENT ID	TECN	COMMENT
<b>&lt; 1.9</b>	90	<sup>1</sup> AUBERT	07Y	BABR $e^+e^- \rightarrow \Upsilon(4S)$
• • • We do not use the following data for averages, fits, limits, etc. • • •				
< 2.1	90	<sup>1</sup> AUBERT,BE	04	BABR Repl. by AUBERT 07Y

<sup>1</sup> Assumes equal production of  $B^+$  and  $B^0$  at the  $\Upsilon(4S)$ .

$\Gamma(b_1^- K^+, b_1^- \rightarrow \omega\pi^-)/\Gamma_{total}$				$\Gamma_{289}/\Gamma$
VALUE (units $10^{-6}$ )	CL%	DOCUMENT ID	TECN	COMMENT
<b>7.4 ± 1.0 ± 1.0</b>				
		<sup>1</sup> AUBERT	07Bi	BABR $e^+e^- \rightarrow \Upsilon(4S)$

<sup>1</sup> Assumes equal production of  $B^+$  and  $B^0$  at the  $\Upsilon(4S)$ .

$\Gamma(b_1^0 K^{*0}, b_1^0 \rightarrow \omega\pi^0)/\Gamma_{total}$				$\Gamma_{290}/\Gamma$
VALUE	CL%	DOCUMENT ID	TECN	COMMENT
<b>&lt; 8.0 × 10<sup>-6</sup></b>	90	<sup>1</sup> AUBERT	09AF	BABR $e^+e^- \rightarrow \Upsilon(4S)$

<sup>1</sup> Assumes equal production of  $B^+$  and  $B^0$  at the  $\Upsilon(4S)$ .

$\Gamma(b_1^- K^{*+}, b_1^- \rightarrow \omega\pi^-)/\Gamma_{total}$				$\Gamma_{291}/\Gamma$
VALUE	CL%	DOCUMENT ID	TECN	COMMENT
<b>&lt; 5.0 × 10<sup>-6</sup></b>	90	<sup>1</sup> AUBERT	09AF	BABR $e^+e^- \rightarrow \Upsilon(4S)$

<sup>1</sup> Assumes equal production of  $B^+$  and  $B^0$  at the  $\Upsilon(4S)$ .

$\Gamma(a_0(1450)^\pm K^\mp, a_0^\pm \rightarrow \eta\pi^\pm)/\Gamma_{total}$				$\Gamma_{292}/\Gamma$
VALUE (units $10^{-6}$ )	CL%	DOCUMENT ID	TECN	COMMENT
<b>&lt; 3.1</b>	90	<sup>1</sup> AUBERT	07Y	BABR $e^+e^- \rightarrow \Upsilon(4S)$

<sup>1</sup> Assumes equal production of  $B^+$  and  $B^0$  at the  $\Upsilon(4S)$ .

$\Gamma(K_0^0 X^0 (\text{Familon}))/\Gamma_{total}$				$\Gamma_{293}/\Gamma$
VALUE (units $10^{-6}$ )	CL%	DOCUMENT ID	TECN	COMMENT
<b>&lt; 53</b>	90	<sup>1</sup> AMMAR	01B	CLE2 $e^+e^- \rightarrow \Upsilon(4S)$

<sup>1</sup> AMMAR 01B searched for the two-body decay of the  $B$  meson to a massless neutral feebly-interacting particle  $X^0$  such as the familon, the Nambu-Goldstone boson associated with a spontaneously broken global family symmetry.

$\Gamma(\omega K^*(892)^0)/\Gamma_{total}$				$\Gamma_{294}/\Gamma$
VALUE (units $10^{-6}$ )	CL%	DOCUMENT ID	TECN	COMMENT
<b>2.0 ± 0.5 OUR AVERAGE</b>				
2.2 ± 0.6 ± 0.2		<sup>1</sup> AUBERT	09H	BABR $e^+e^- \rightarrow \Upsilon(4S)$
1.8 ± 0.7 ± 0.3		<sup>1</sup> GOLDENZWE..08	BELL	$e^+e^- \rightarrow \Upsilon(4S)$
• • • We do not use the following data for averages, fits, limits, etc. • • •				
< 4.2	90	<sup>1</sup> AUBERT,B	06T	BABR Repl. by AUBERT 09H
< 6.0	90	<sup>1</sup> AUBERT	05o	BABR Repl. by AUBERT,B 06T
< 23	90	<sup>1</sup> BERGFELD	98	CLE2

<sup>1</sup> Assumes equal production of  $B^+$  and  $B^0$  at the  $\Upsilon(4S)$ .

$\Gamma(\omega(K\pi)_0^{*0})/\Gamma_{total}$				$\Gamma_{295}/\Gamma$
VALUE (units $10^{-6}$ )	CL%	DOCUMENT ID	TECN	COMMENT
<b>18.4 ± 1.8 ± 1.7</b>				
		<sup>1</sup> AUBERT	09H	BABR $e^+e^- \rightarrow \Upsilon(4S)$

<sup>1</sup> Assumes equal production of  $B^+$  and  $B^0$  at the  $\Upsilon(4S)$ .  
 $(K\pi)_0^{*0}$  is the total S-wave composed of  $K_0^*(1430)$  and nonresonant that are described using LASS shape.

Downloaded from https://academic.oup.com/ptep/article/2020/8/083C01/5891211 by guest on 12 November 2020

# Meson Particle Listings

## $B^0$

$\Gamma(\omega K_0^*(1430)^0)/\Gamma_{total}$	$\Gamma_{296}/\Gamma$		
VALUE (units $10^{-6}$ )	DOCUMENT ID	TECN	COMMENT
<b><math>16.0 \pm 1.6 \pm 3.0</math></b>	1 AUBERT	09H	BABR $e^+e^- \rightarrow \Upsilon(4S)$

<sup>1</sup> Assumes equal production of  $B^+$  and  $B^0$  at the  $\Upsilon(4S)$ .

$\Gamma(\omega K_2^*(1430)^0)/\Gamma_{total}$	$\Gamma_{297}/\Gamma$		
VALUE (units $10^{-6}$ )	DOCUMENT ID	TECN	COMMENT
<b><math>10.1 \pm 2.0 \pm 1.1</math></b>	1 AUBERT	09H	BABR $e^+e^- \rightarrow \Upsilon(4S)$

<sup>1</sup> Assumes equal production of  $B^+$  and  $B^0$  at the  $\Upsilon(4S)$ .

$\Gamma(\omega K^+\pi^-\text{nonresonant})/\Gamma_{total}$	$\Gamma_{298}/\Gamma$		
VALUE (units $10^{-6}$ )	DOCUMENT ID	TECN	COMMENT
<b><math>5.1 \pm 0.7 \pm 0.7</math></b>	1,2 GOLDENZWE..08	BELL	$e^+e^- \rightarrow \Upsilon(4S)$

<sup>1</sup> Assumes equal production of  $B^+$  and  $B^0$  at the  $\Upsilon(4S)$ .  
<sup>2</sup> For the  $K\pi$  mass range 0.755–1.250 GeV/ $c^2$ , excluding  $K^*(892)$ .

$\Gamma(K^+\pi^-\pi^0)/\Gamma_{total}$	$\Gamma_{299}/\Gamma$		
VALUE (units $10^{-6}$ )	DOCUMENT ID	TECN	COMMENT
<b><math>37.8 \pm 3.2</math> OUR AVERAGE</b>			
$38.5 \pm 1.0 \pm 3.9$	1,2 LEES	11	BABR $e^+e^- \rightarrow \Upsilon(4S)$
$36.6^{+4.2}_{-4.3} \pm 3.0$	1 CHANG	04	BELL $e^+e^- \rightarrow \Upsilon(4S)$

VALUE (units $10^{-6}$ )	DOCUMENT ID	TECN	COMMENT
$35.7^{+2.6}_{-1.5} \pm 2.2$	1 AUBERT	08AQ	BABR Repl. by LEES 11
<40	90	1 ECKHART	02 CLE2 $e^+e^- \rightarrow \Upsilon(4S)$

<sup>1</sup> Assumes equal production of  $B^+$  and  $B^0$  at the  $\Upsilon(4S)$ .  
<sup>2</sup> Uses Dalitz plot analysis of  $B^0 \rightarrow K^+\pi^-\pi^0$  decays.

$\Gamma(K^+\rho^-)/\Gamma_{total}$	$\Gamma_{300}/\Gamma$		
VALUE (units $10^{-6}$ )	DOCUMENT ID	TECN	COMMENT
<b><math>7.0 \pm 0.9</math> OUR AVERAGE</b>			
$6.6 \pm 0.5 \pm 0.8$	1,2 LEES	11	BABR $e^+e^- \rightarrow \Upsilon(4S)$
$15.1^{+3.4+2.4}_{-3.3-2.6}$	1 CHANG	04	BELL $e^+e^- \rightarrow \Upsilon(4S)$

VALUE (units $10^{-6}$ )	DOCUMENT ID	TECN	COMMENT
$8.0^{+0.8}_{-1.3} \pm 0.6$	1 AUBERT	08AQ	BABR Repl. by LEES 11
$7.3^{+1.3}_{-1.2} \pm 1.3$	1 AUBERT	03T	BABR Repl. by AUBERT 08AQ
<32	90	1 JESSOP	00 CLE2 $e^+e^- \rightarrow \Upsilon(4S)$
<35	90	ASNER	96 CLE2 Repl. by JESSOP 00

<sup>1</sup> Assumes equal production of  $B^+$  and  $B^0$  at the  $\Upsilon(4S)$ .  
<sup>2</sup> Uses Dalitz plot analysis of  $B^0 \rightarrow K^+\pi^-\pi^0$  decays.

$\Gamma(K^+\rho(1450)^-)/\Gamma_{total}$	$\Gamma_{301}/\Gamma$		
VALUE (units $10^{-6}$ )	DOCUMENT ID	TECN	COMMENT
<b><math>2.4 \pm 1.0 \pm 0.6</math></b>	1,2 LEES	11	BABR $e^+e^- \rightarrow \Upsilon(4S)$

VALUE (units $10^{-6}$ )	DOCUMENT ID	TECN	COMMENT
<2.1	90	1 AUBERT	08AQ BABR Repl. by LEES 11

<sup>1</sup> Assumes equal production of  $B^+$  and  $B^0$  at the  $\Upsilon(4S)$ .  
<sup>2</sup> Uses Dalitz plot analysis of  $B^0 \rightarrow K^+\pi^-\pi^0$  decays.

$\Gamma(K^+\rho(1700)^-)/\Gamma_{total}$	$\Gamma_{302}/\Gamma$		
VALUE (units $10^{-6}$ )	DOCUMENT ID	TECN	COMMENT
<b><math>0.6 \pm 0.6 \pm 0.4</math></b>	1,2 LEES	11	BABR $e^+e^- \rightarrow \Upsilon(4S)$

VALUE (units $10^{-6}$ )	DOCUMENT ID	TECN	COMMENT
<1.1	90	1 AUBERT	08AQ BABR Repl. by LEES 11

<sup>1</sup> Assumes equal production of  $B^+$  and  $B^0$  at the  $\Upsilon(4S)$ .  
<sup>2</sup> Uses Dalitz plot analysis of  $B^0 \rightarrow K^+\pi^-\pi^0$  decays.

$\Gamma((K^+\pi^-\pi^0)\text{nonresonant})/\Gamma_{total}$	$\Gamma_{303}/\Gamma$		
VALUE (units $10^{-6}$ )	DOCUMENT ID	TECN	COMMENT
<b><math>2.8 \pm 0.5 \pm 0.4</math></b>	1,2 LEES	11	BABR $e^+e^- \rightarrow \Upsilon(4S)$

VALUE (units $10^{-6}$ )	DOCUMENT ID	TECN	COMMENT
$4.4 \pm 0.9 \pm 0.5$	1 AUBERT	08AQ	BABR Repl. by LEES 11
<9.4	90	1 CHANG	04 BELL $e^+e^- \rightarrow \Upsilon(4S)$

<sup>1</sup> Assumes equal production of  $B^+$  and  $B^0$  at the  $\Upsilon(4S)$ .  
<sup>2</sup> Uses Dalitz plot analysis of  $B^0 \rightarrow K^+\pi^-\pi^0$  decays. The quoted value is only for the flat part of the non-resonant component.

$\Gamma((K\pi)_0^{*+}\pi^-, (K\pi)_0^{*+} \rightarrow K^+\pi^0)/\Gamma_{total}$	$\Gamma_{304}/\Gamma$		
VALUE (units $10^{-6}$ )	DOCUMENT ID	TECN	COMMENT
<b><math>34.2 \pm 2.4 \pm 4.1</math></b>	1,2 LEES	11	BABR $e^+e^- \rightarrow \Upsilon(4S)$

VALUE (units $10^{-6}$ )	DOCUMENT ID	TECN	COMMENT
$9.4^{+1.1+2.3}_{-1.3-2.1}$	1 AUBERT	08AQ	BABR Repl. by LEES 11

<sup>1</sup> Assumes equal production of  $B^+$  and  $B^0$  at the  $\Upsilon(4S)$ .  
<sup>2</sup> Uses Dalitz plot analysis of  $B^0 \rightarrow K^+\pi^-\pi^0$  decays.

$\Gamma((K\pi)_0^{*0}\pi^0, (K\pi)_0^{*0} \rightarrow K^+\pi^-)/\Gamma_{total}$	$\Gamma_{305}/\Gamma$		
VALUE (units $10^{-6}$ )	DOCUMENT ID	TECN	COMMENT
<b><math>8.6 \pm 1.1 \pm 1.3</math></b>	1,2 LEES	11	BABR $e^+e^- \rightarrow \Upsilon(4S)$

$(K\pi)_0^{*0}$  is the total S-wave composed of  $K_0^*(1430)$  and nonresonant that are described using LASS shape.  
 • • • We do not use the following data for averages, fits, limits, etc. • • •

VALUE (units $10^{-6}$ )	DOCUMENT ID	TECN	COMMENT
$8.7^{+1.1+2.8}_{-0.9-2.6}$	1 AUBERT	08AQ	BABR Repl. by LEES 11

<sup>1</sup> Assumes equal production of  $B^+$  and  $B^0$  at the  $\Upsilon(4S)$ .  
<sup>2</sup> Uses Dalitz plot analysis of  $B^0 \rightarrow K^+\pi^-\pi^0$  decays.

$\Gamma(K_2^*(1430)^0\pi^0)/\Gamma_{total}$	$\Gamma_{306}/\Gamma$		
VALUE (units $10^{-6}$ )	DOCUMENT ID	TECN	COMMENT
<b>&lt;4.0</b>	1 AUBERT	08AQ	BABR $e^+e^- \rightarrow \Upsilon(4S)$

<sup>1</sup> Assumes equal production of  $B^+$  and  $B^0$  at the  $\Upsilon(4S)$ .

$\Gamma(K^*(1680)^0\pi^0)/\Gamma_{total}$	$\Gamma_{307}/\Gamma$		
VALUE (units $10^{-6}$ )	DOCUMENT ID	TECN	COMMENT
<b>&lt;7.5</b>	90	1 AUBERT	08AQ BABR $e^+e^- \rightarrow \Upsilon(4S)$

<sup>1</sup> Assumes equal production of  $B^+$  and  $B^0$  at the  $\Upsilon(4S)$ .

$\Gamma(K_x^{*0}\pi^0)/\Gamma_{total}$	$\Gamma_{308}/\Gamma$		
VALUE (units $10^{-6}$ )	DOCUMENT ID	TECN	COMMENT
<b><math>6.1^{+1.6+0.5}_{-1.5-0.6}</math></b>	1 CHANG	04	BELL $e^+e^- \rightarrow \Upsilon(4S)$

<sup>1</sup> Assumes equal production of  $B^+$  and  $B^0$  at the  $\Upsilon(4S)$ .

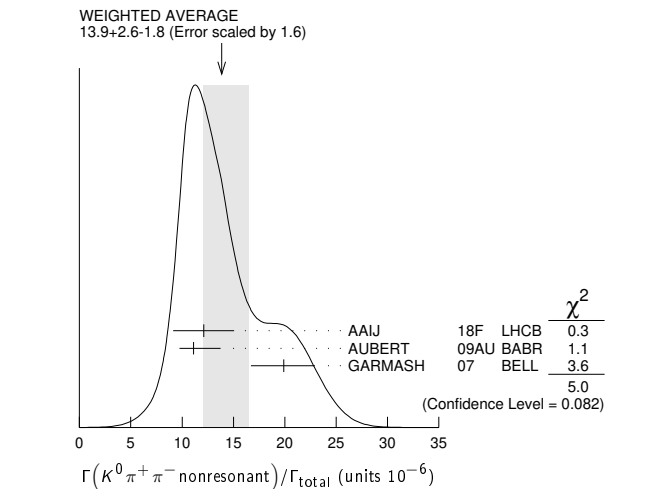
$\Gamma(K^0\pi^+\pi^-)/\Gamma_{total}$	$\Gamma_{309}/\Gamma$		
VALUE (units $10^{-6}$ )	DOCUMENT ID	TECN	COMMENT
<b><math>49.7 \pm 1.8</math> OUR FIT</b>			
<b><math>49.6 \pm 2.0</math> OUR AVERAGE</b>			
$50.2 \pm 1.5 \pm 1.8$	1 AUBERT	09AU	BABR $e^+e^- \rightarrow \Upsilon(4S)$
$47.5 \pm 2.4 \pm 3.7$	2 GARMASH	07	BELL $e^+e^- \rightarrow \Upsilon(4S)$
$50^{+10}_{-9} \pm 7$	1 ECKHART	02	CLE2 $e^+e^- \rightarrow \Upsilon(4S)$

VALUE (units $10^{-6}$ )	DOCUMENT ID	TECN	COMMENT
$43.0 \pm 2.3 \pm 2.3$	1 AUBERT	06I	BABR Repl. by AUBERT 09AU
$43.7 \pm 3.8 \pm 3.4$	1 AUBERT,B	04O	BABR Repl. by AUBERT 06I
$45.4 \pm 5.2 \pm 5.9$	1 GARMASH	04	BELL Repl. by GARMASH 07
<440	90	ALBRECHT	91E ARG $e^+e^- \rightarrow \Upsilon(4S)$

• • • We do not use the following data for averages, fits, limits, etc. • • •  
<sup>1</sup> Assumes equal production of  $B^+$  and  $B^0$  at the  $\Upsilon(4S)$ .  
<sup>2</sup> Uses Dalitz plot analysis of the  $B^0 \rightarrow K^0\pi^+\pi^-$  final state decays.

$\Gamma(K^0\pi^+\pi^-\text{nonresonant})/\Gamma_{total}$	$\Gamma_{310}/\Gamma$		
VALUE (units $10^{-6}$ )	DOCUMENT ID	TECN	COMMENT
<b><math>13.9^{+2.6}_{-1.8}</math> OUR AVERAGE</b>			Error includes scale factor of 1.6. See the ideogram below.
$12.1 \pm 0.6 \pm 2.9$	1 AAIJ	18F	LHCB $pp$ at 7, 8 TeV
$11.1^{+2.5}_{-1.0} \pm 0.9$	2 AUBERT	09AU	BABR $e^+e^- \rightarrow \Upsilon(4S)$
$19.9 \pm 2.5^{+1.7}_{-2.0}$	3 GARMASH	07	BELL $e^+e^- \rightarrow \Upsilon(4S)$

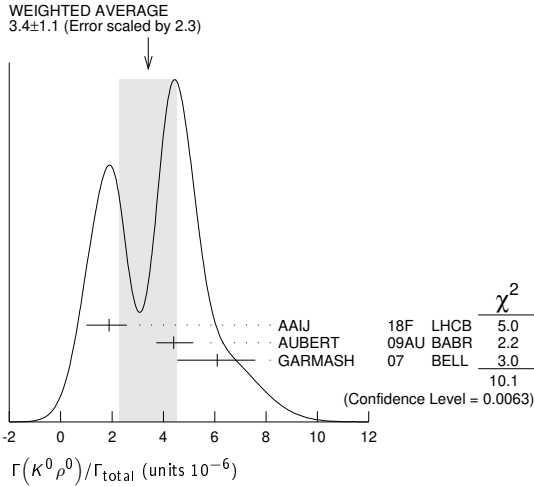
<sup>1</sup> Uses Dalitz plot analysis of the  $B^0 \rightarrow K_S^0\pi^+\pi^-$  final state decays. For the branching fraction of the reference mode, the PDG 18 average  $B(B^0 \rightarrow K_S^0\pi^+\pi^-) = (4.96 \pm 0.20) \times 10^{-5}$  is used.  
<sup>2</sup> Assumes equal production of  $B^+$  and  $B^0$  at the  $\Upsilon(4S)$ .  
<sup>3</sup> Uses Dalitz plot analysis of the  $B^0 \rightarrow K^0\pi^+\pi^-$  final state decays.



$\Gamma(K^0 \rho^0)/\Gamma_{total}$   $\Gamma_{311}/\Gamma$

VALUE (units 10 <sup>-6</sup> )	CL%	DOCUMENT ID	TECN	COMMENT
<b>3.4 ± 1.1 OUR AVERAGE</b>		Error includes scale factor of 2.3. See the ideogram below.		
1.89 <sup>+0.55</sup> <sub>-0.79</sub> ± 0.40		1 AAIJ	18F LHCB	pp at 7, 8 TeV
4.4 <sup>+0.7</sup> <sub>-0.6</sub> ± 0.3		2 AUBERT	09AU BABR	e <sup>+</sup> e <sup>-</sup> → $\Upsilon(4S)$
6.1 ± 1.0 <sup>+1.1</sup> <sub>-1.2</sub>		3 GARMASH	07 BELL	e <sup>+</sup> e <sup>-</sup> → $\Upsilon(4S)$
• • • We do not use the following data for averages, fits, limits, etc. • • •				
4.9 ± 0.8 ± 0.9		2 AUBERT	07F BABR	Repl. by AUBERT 09AU
< 39	90	ASNER	96 CLEO	e <sup>+</sup> e <sup>-</sup> → $\Upsilon(4S)$
< 320	90	ALBRECHT	91B ARG	e <sup>+</sup> e <sup>-</sup> → $\Upsilon(4S)$
< 500	90	4 AVERY	89B CLEO	e <sup>+</sup> e <sup>-</sup> → $\Upsilon(4S)$

- 1 Uses Dalitz plot analysis of the B<sup>0</sup> → K<sub>S</sub><sup>0</sup>π<sup>+</sup>π<sup>-</sup> final state decays. For the branching fraction of the reference mode, the PDG 18 average B(B<sup>0</sup> → K<sub>S</sub><sup>0</sup>π<sup>+</sup>π<sup>-</sup>) = (4.96 ± 0.20) × 10<sup>-5</sup> is used.
- 2 Assumes equal production of B<sup>+</sup> and B<sup>0</sup> at the  $\Upsilon(4S)$ .
- 3 Uses Dalitz plot analysis of the B<sup>0</sup> → K<sup>0</sup>π<sup>+</sup>π<sup>-</sup> final state decays.
- 4 AVERY 89B reports < 5.8 × 10<sup>-4</sup> assuming the  $\Upsilon(4S)$  decays 43% to B<sup>0</sup> $\bar{B}^0$ . We rescale to 50%.



$\Gamma(K^*(892)^+ \pi^-)/\Gamma_{total}$   $\Gamma_{312}/\Gamma$

VALUE (units 10 <sup>-6</sup> )	CL%	DOCUMENT ID	TECN	COMMENT
<b>7.5 ± 0.4 OUR AVERAGE</b>				
7.02 ± 0.30 ± 0.45		1 AAIJ	18F LHCB	pp at 7, 8 TeV
8.0 ± 1.1 ± 0.8		2,3 LEES	11 BABR	e <sup>+</sup> e <sup>-</sup> → $\Upsilon(4S)$
8.3 <sup>+0.9</sup> <sub>-0.8</sub> ± 0.8		3,4 AUBERT	09AU BABR	e <sup>+</sup> e <sup>-</sup> → $\Upsilon(4S)$
8.4 ± 1.1 <sup>+1.0</sup> <sub>-0.9</sub>		4 GARMASH	07 BELL	e <sup>+</sup> e <sup>-</sup> → $\Upsilon(4S)$
16 <sup>+6</sup> <sub>-5</sub> ± 2		3 ECKHART	02 CLE2	e <sup>+</sup> e <sup>-</sup> → $\Upsilon(4S)$
• • • We do not use the following data for averages, fits, limits, etc. • • •				
12.6 <sup>+2.7</sup> <sub>-1.6</sub> ± 0.9		2,3 AUBERT	08AQ BABR	Repl. by LEES 11
11.0 ± 1.5 ± 0.71		3 AUBERT	06i BABR	Repl. by AUBERT 09AU
12.9 ± 2.4 ± 1.4		3 AUBERT,B	04o BABR	Repl. by AUBERT 06i
14.8 <sup>+4.6</sup> <sub>-4.4</sub> ± 2.8		3 CHANG	04 BELL	Repl. by GARMASH 07
< 72	90	ASNER	96 CLE2	e <sup>+</sup> e <sup>-</sup> → $\Upsilon(4S)$
< 620	90	ALBRECHT	91B ARG	e <sup>+</sup> e <sup>-</sup> → $\Upsilon(4S)$
< 380	90	5 AVERY	89B CLEO	e <sup>+</sup> e <sup>-</sup> → $\Upsilon(4S)$
< 560	90	6 AVERY	87 CLEO	e <sup>+</sup> e <sup>-</sup> → $\Upsilon(4S)$

- 1 Uses Dalitz plot analysis of the B<sup>0</sup> → K<sub>S</sub><sup>0</sup>π<sup>+</sup>π<sup>-</sup> final state decays. For the branching fraction of the reference mode, the PDG 18 average B(B<sup>0</sup> → K<sub>S</sub><sup>0</sup>π<sup>+</sup>π<sup>-</sup>) = (4.96 ± 0.20) × 10<sup>-5</sup> is used.
- 2 Uses Dalitz plot analysis of B<sup>0</sup> → K<sup>+</sup>π<sup>-</sup>π<sup>0</sup> decays.
- 3 Assumes equal production of B<sup>+</sup> and B<sup>0</sup> at the  $\Upsilon(4S)$ .
- 4 Uses Dalitz plot analysis of the B<sup>0</sup> → K<sup>0</sup>π<sup>+</sup>π<sup>-</sup> final state decays.
- 5 AVERY 89B reports < 4.4 × 10<sup>-4</sup> assuming the  $\Upsilon(4S)$  decays 43% to B<sup>0</sup> $\bar{B}^0$ . We rescale to 50%.
- 6 AVERY 87 reports < 7 × 10<sup>-4</sup> assuming the  $\Upsilon(4S)$  decays 40% to B<sup>0</sup> $\bar{B}^0$ . We rescale to 50%.

$\Gamma(K_S^0(1430)^+ \pi^-)/\Gamma_{total}$   $\Gamma_{313}/\Gamma$

VALUE (units 10 <sup>-6</sup> )	DOCUMENT ID	TECN	COMMENT
<b>33 ± 7 OUR AVERAGE</b>	Error includes scale factor of 2.0.		
29.9 <sup>+2.3</sup> <sub>-1.7</sub> ± 3.6	1,2 AUBERT	09AU BABR	e <sup>+</sup> e <sup>-</sup> → $\Upsilon(4S)$
49.7 ± 3.8 <sup>+6.8</sup> <sub>-8.2</sub>	2 GARMASH	07 BELL	e <sup>+</sup> e <sup>-</sup> → $\Upsilon(4S)$
1 Assumes equal production of B <sup>+</sup> and B <sup>0</sup> at the $\Upsilon(4S)$ .			
2 Uses Dalitz plot analysis of the B <sup>0</sup> → K <sup>0</sup> π <sup>+</sup> π <sup>-</sup> final state decays.			

$\Gamma((K\pi)_0^{*+} \pi^-, (K\pi)_0^{*+} \rightarrow K^0 \pi^+)/\Gamma_{total}$   $\Gamma_{316}/\Gamma$

VALUE (units 10 <sup>-6</sup> )	DOCUMENT ID	TECN	COMMENT
<b>16.2 ± 0.69 ± 1.15</b>	1 AAIJ	18F LHCB	pp at 7, 8 TeV
1 Uses Dalitz plot analysis of the B <sup>0</sup> → K <sub>S</sub> <sup>0</sup> π <sup>+</sup> π <sup>-</sup> final state decays. (Kπ) <sub>0</sub> <sup>*+</sup> is the S-wave component of K <sup>0</sup> π <sup>+</sup> . For the branching fraction of the reference mode, the PDG 18 average B(B <sup>0</sup> → K <sub>S</sub> <sup>0</sup> π <sup>+</sup> π <sup>-</sup> ) = (4.96 ± 0.20) × 10 <sup>-5</sup> is used.			

$\Gamma(K_x^{*+} \pi^-)/\Gamma_{total}$   $\Gamma_{314}/\Gamma$

K<sub>x</sub><sup>\*+</sup> stands for the possible candidates of K<sup>\*</sup>(1410), K<sub>S</sub><sup>\*</sup>(1430) and K<sub>2</sub><sup>\*</sup>(1430).

VALUE (units 10 <sup>-6</sup> )	DOCUMENT ID	TECN	COMMENT
<b>5.1 ± 1.5 ± 0.6</b> <sub>-0.7</sub>	1 CHANG	04 BELL	e <sup>+</sup> e <sup>-</sup> → $\Upsilon(4S)$
1 Assumes equal production of B <sup>+</sup> and B <sup>0</sup> at the $\Upsilon(4S)$ .			

$\Gamma(K^*(1410)^+ \pi^-, K^{*+} \rightarrow K^0 \pi^+)/\Gamma_{total}$   $\Gamma_{315}/\Gamma$

VALUE (units 10 <sup>-6</sup> )	CL%	DOCUMENT ID	TECN	COMMENT
<b>&lt; 3.8</b>	90	1 GARMASH	07 BELL	e <sup>+</sup> e <sup>-</sup> → $\Upsilon(4S)$
1 Uses Dalitz plot analysis of the B <sup>0</sup> → K <sup>0</sup> π <sup>+</sup> π <sup>-</sup> final state decays.				

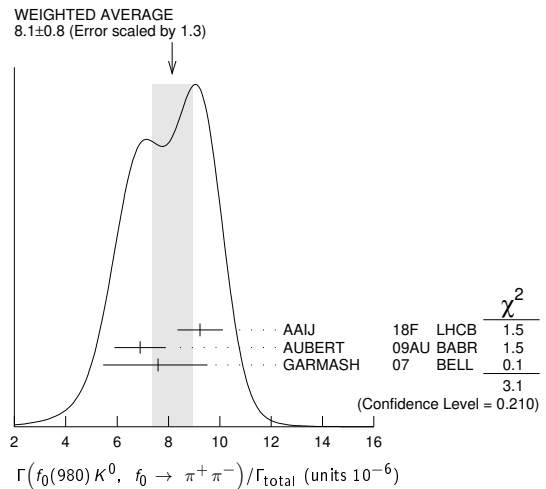
$\Gamma(K^0 f_0(500))/\Gamma_{total}$   $\Gamma_{318}/\Gamma$

VALUE (units 10 <sup>-6</sup> )	DOCUMENT ID	TECN	COMMENT
<b>0.16<sup>+0.20</sup><sub>-0.04</sub> ± 0.15</b>	1 AAIJ	18F LHCB	pp at 7, 8 TeV
1 Uses Dalitz plot analysis of the B <sup>0</sup> → K <sub>S</sub> <sup>0</sup> π <sup>+</sup> π <sup>-</sup> final state decays. For the branching fraction of the reference mode, the PDG 18 average B(B <sup>0</sup> → K <sub>S</sub> <sup>0</sup> π <sup>+</sup> π <sup>-</sup> ) = (4.96 ± 0.20) × 10 <sup>-5</sup> is used.			

$\Gamma(f_0(980) K^0, f_0 \rightarrow \pi^+ \pi^-)/\Gamma_{total}$   $\Gamma_{317}/\Gamma$

VALUE (units 10 <sup>-6</sup> )	CL%	DOCUMENT ID	TECN	COMMENT
<b>8.1 ± 0.8 OUR AVERAGE</b>	Error includes scale factor of 1.3. See the ideogram below.			
9.23 ± 0.40 ± 0.79		1 AAIJ	18F LHCB	pp at 7, 8 TeV
6.9 ± 0.8 ± 0.6		2 AUBERT	09AU BABR	e <sup>+</sup> e <sup>-</sup> → $\Upsilon(4S)$
7.6 ± 1.7 <sup>+0.9</sup> <sub>-1.3</sub>		3 GARMASH	07 BELL	e <sup>+</sup> e <sup>-</sup> → $\Upsilon(4S)$
• • • We do not use the following data for averages, fits, limits, etc. • • •				
5.5 ± 0.7 ± 0.6		2 AUBERT	06i BABR	Repl. by AUBERT 09AU
< 360	90	4 AVERY	89B CLEO	e <sup>+</sup> e <sup>-</sup> → $\Upsilon(4S)$

- 1 Uses Dalitz plot analysis of the B<sup>0</sup> → K<sub>S</sub><sup>0</sup>π<sup>+</sup>π<sup>-</sup> final state decays. For the branching fraction of the reference mode, the PDG 18 average B(B<sup>0</sup> → K<sub>S</sub><sup>0</sup>π<sup>+</sup>π<sup>-</sup>) = (4.96 ± 0.20) × 10<sup>-5</sup> is used.
- 2 Assumes equal production of B<sup>+</sup> and B<sup>0</sup> at the  $\Upsilon(4S)$ .
- 3 Uses Dalitz plot analysis of the B<sup>0</sup> → K<sup>0</sup>π<sup>+</sup>π<sup>-</sup> final state decays.
- 4 AVERY 89B reports < 4.2 × 10<sup>-4</sup> assuming the  $\Upsilon(4S)$  decays 43% to B<sup>0</sup> $\bar{B}^0$ . We rescale to 50%.





## Meson Particle Listings

 $B^0$ 

$\Gamma(f_2(1270)K^0)/\Gamma_{\text{total}}$   $\Gamma_{320}/\Gamma$

VALUE (units $10^{-6}$ )	CL%	DOCUMENT ID	TECN	COMMENT
$2.7^{+1.0}_{-0.8} \pm 0.9$		1 AUBERT	09AU BABR	$e^+e^- \rightarrow \Upsilon(4S)$

• • • We do not use the following data for averages, fits, limits, etc. • • •

<2.5	90	2 GARMASH	07 BELL	$e^+e^- \rightarrow \Upsilon(4S)$
------	----	-----------	---------	-----------------------------------

<sup>1</sup> Assumes equal production of  $B^+$  and  $B^0$  at the  $\Upsilon(4S)$ .  
<sup>2</sup> GARMASH 07 reports  $B(B^0 \rightarrow f_2(1270)K^0) \times B(f_2(1270) \rightarrow \pi^+\pi^-) < 1.4 \times 10^{-6}$  using Dalitz plot analysis. We compute  $B(B^0 \rightarrow f_2(1270)K^0)$  using the PDG value  $B(f_2(1270) \rightarrow \pi\pi) = 84.2 \times 10^{-2}$  and 2/3 for the  $\pi^+\pi^-$  fraction.

$\Gamma(f_x(1300)K^0, f_x \rightarrow \pi^+\pi^-)/\Gamma_{\text{total}}$   $\Gamma_{321}/\Gamma$

VALUE (units $10^{-6}$ )	CL%	DOCUMENT ID	TECN	COMMENT
$1.81^{+0.55}_{-0.45} \pm 0.48$		1 AUBERT	09AU BABR	$e^+e^- \rightarrow \Upsilon(4S)$

<sup>1</sup> Assumes equal production of  $B^+$  and  $B^0$  at the  $\Upsilon(4S)$ .

$\Gamma(K^0 f_0(1500))/\Gamma_{\text{total}}$   $\Gamma_{319}/\Gamma$

VALUE (units $10^{-6}$ )	CL%	DOCUMENT ID	TECN	COMMENT
$1.29 \pm 0.27 \pm 0.70$		1 AAIJ	18F LHCb	$pp$ at 7, 8 TeV

<sup>1</sup> Uses Dalitz plot analysis of the  $B^0 \rightarrow K_S^0 \pi^+ \pi^-$  final state decays. For the branching fraction of the reference mode, the PDG 18 average  $B(B^0 \rightarrow K_S^0 \pi^+ \pi^-) = (4.96 \pm 0.20) \times 10^{-5}$  is used.

$\Gamma(K^*(892)^0 \pi^0)/\Gamma_{\text{total}}$   $\Gamma_{322}/\Gamma$

VALUE (units $10^{-6}$ )	CL%	DOCUMENT ID	TECN	COMMENT
$3.3 \pm 0.5 \pm 0.4$		1,2 LEES	11 BABR	$e^+e^- \rightarrow \Upsilon(4S)$

• • • We do not use the following data for averages, fits, limits, etc. • • •

$3.6 \pm 0.7 \pm 0.4$		1,2 AUBERT	08AQ BABR	Repl. by LEES 11
< 3.5	90	2 CHANG	04 BELL	$e^+e^- \rightarrow \Upsilon(4S)$
< 3.6	90	JESSOP	00 CLE2	$e^+e^- \rightarrow \Upsilon(4S)$
< 28	90	ASNER	96 CLE2	Repl. by JESSOP 00

<sup>1</sup> Uses Dalitz plot analysis of  $B^0 \rightarrow K^+ \pi^- \pi^0$  decays.  
<sup>2</sup> Assumes equal production of  $B^+$  and  $B^0$  at the  $\Upsilon(4S)$ .

$\Gamma(K_2^*(1430)^+ \pi^-)/\Gamma_{\text{total}}$   $\Gamma_{323}/\Gamma$

VALUE (units $10^{-6}$ )	CL%	DOCUMENT ID	TECN	COMMENT
$3.65^{+0.15}_{-0.12} \pm 0.31$		1 AAIJ	18F LHCb	$pp$ at 7, 8 TeV

• • • We do not use the following data for averages, fits, limits, etc. • • •

< 16.2	90	2,3 AUBERT	08AQ BABR	$e^+e^- \rightarrow \Upsilon(4S)$
< 6	90	4 GARMASH	07 BELL	$e^+e^- \rightarrow \Upsilon(4S)$
< 18	90	3 GARMASH	04 BELL	Repl. by GARMASH 07
< 2600	90	ALBRECHT	91B ARG	$e^+e^- \rightarrow \Upsilon(4S)$

<sup>1</sup> Uses Dalitz plot analysis of the  $B^0 \rightarrow K_S^0 \pi^+ \pi^-$  final state decays. We compute  $B(B^0 \rightarrow K_2^*(1430)^+ \pi^-)$  using the PDG 18 value  $B(K_2^*(1430) \rightarrow K\pi) = 49.9 \times 10^{-2}$  and 2/3 for the  $K^0 \pi^+$  fraction. For the branching fraction of the reference mode, the PDG 18 average  $B(B^0 \rightarrow K_S^0 \pi^+ \pi^-) = (4.96 \pm 0.20) \times 10^{-5}$  is used.  
<sup>2</sup> Uses Dalitz plot analysis of  $B^0 \rightarrow K^+ \pi^- \pi^0$  decays.  
<sup>3</sup> Assumes equal production of  $B^+$  and  $B^0$  at the  $\Upsilon(4S)$ .  
<sup>4</sup> GARMASH 07 reports  $B(B^0 \rightarrow K_2^*(1430)^+ \pi^-) \times B(K_2^* \rightarrow K^0 \pi^+) < 2.1 \times 10^{-6}$  using Dalitz plot analysis. We compute  $B(B^0 \rightarrow K_2^*(1430)^+ \pi^-)$  using the PDG value  $B(K_2^*(1430) \rightarrow K\pi) = 49.9 \times 10^{-2}$  and 2/3 for the  $K^0 \pi^+$  fraction.

$\Gamma(K^*(1680)^+ \pi^-)/\Gamma_{\text{total}}$   $\Gamma_{324}/\Gamma$

VALUE (units $10^{-6}$ )	CL%	DOCUMENT ID	TECN	COMMENT
$14.1 \pm 0.58 \pm 0.84$		1 AAIJ	18F LHCb	$pp$ at 7, 8 TeV

• • • We do not use the following data for averages, fits, limits, etc. • • •

<25	90	2,3 AUBERT	08AQ BABR	$e^+e^- \rightarrow \Upsilon(4S)$
<10	90	4 GARMASH	07 BELL	$e^+e^- \rightarrow \Upsilon(4S)$

<sup>1</sup> Uses Dalitz plot analysis of the  $B^0 \rightarrow K_S^0 \pi^+ \pi^-$  final state decays. We compute  $B(B^0 \rightarrow K_2^*(1430)^+ \pi^-)$  using the PDG 18 value  $B(K_2^*(1430) \rightarrow K\pi) = (49.9 \pm 1.2) \times 10^{-2}$  and 2/3 for the  $K^0 \pi^+$  fraction. For the branching fraction of the reference mode, the PDG 18 average  $B(B^0 \rightarrow K_S^0 \pi^+ \pi^-) = (4.96 \pm 0.20) \times 10^{-5}$  is used.  
<sup>2</sup> Uses Dalitz plot analysis of  $B^0 \rightarrow K^+ \pi^- \pi^0$  decays.  
<sup>3</sup> Assumes equal production of  $B^+$  and  $B^0$  at the  $\Upsilon(4S)$ .  
<sup>4</sup> GARMASH 07 reports  $B(B^0 \rightarrow K^*(1680)^+ \pi^-) \times B(K^* \rightarrow K^0 \pi^+) < 2.6 \times 10^{-6}$  using Dalitz plot analysis. We compute  $B(B^0 \rightarrow K^*(1680)^+ \pi^-)$  using the PDG value  $B(K^*(1680) \rightarrow K\pi) = 38.7 \times 10^{-2}$  and 2/3 for the  $K^0 \pi^+$  fraction.

$\Gamma(K^+ \pi^- \pi^+ \pi^-)/\Gamma_{\text{total}}$   $\Gamma_{325}/\Gamma$

VALUE	CL%	DOCUMENT ID	TECN	COMMENT
$< 2.3 \times 10^{-4}$		1 ADAM	96D DLPH	$e^+e^- \rightarrow Z$

• • • We do not use the following data for averages, fits, limits, etc. • • •

< $1 \times 10^{-4}$	90	2 ABREU	95N DLPH	Sup. by ADAM 96D
----------------------	----	---------	----------	------------------

<sup>1</sup> ADAM 96D assumes  $f_{B^0} = f_{B^-} = 0.39$  and  $f_{B_S} = 0.12$ . Contributions from  $B^0$  and  $B_S$  decays cannot be separated. Limits are given for the weighted average of the decay rates for the two neutral  $B$  mesons.  
<sup>2</sup> Assumes a  $B^0, B^-$  production fraction of 0.39 and a  $B_S$  production fraction of 0.12. Contributions from  $B^0$  and  $B_S$  decays cannot be separated. Limits are given for the weighted average of the decay rates for the two neutral  $B$  mesons.

$\Gamma(\rho^0 K^+ \pi^-)/\Gamma_{\text{total}}$   $\Gamma_{326}/\Gamma$

VALUE (units $10^{-6}$ )	CL%	DOCUMENT ID	TECN	COMMENT
$2.8 \pm 0.5 \pm 0.5$		1,2 KYEONG	09 BELL	$e^+e^- \rightarrow \Upsilon(4S)$

<sup>1</sup> Assumes equal production of  $B^+$  and  $B^0$  at the  $\Upsilon(4S)$ .  
<sup>2</sup> Required  $0.75 < m_{K^+ \pi^-} < 1.20$  GeV/ $c^2$ .

$\Gamma(f_0(980)K^+ \pi^-, f_0 \rightarrow \pi\pi)/\Gamma_{\text{total}}$   $\Gamma_{327}/\Gamma$

VALUE (units $10^{-6}$ )	CL%	DOCUMENT ID	TECN	COMMENT
$1.4 \pm 0.4^{+0.3}_{-0.4}$		1,2 KYEONG	09 BELL	$e^+e^- \rightarrow \Upsilon(4S)$

<sup>1</sup> Assumes equal production of  $B^+$  and  $B^0$  at the  $\Upsilon(4S)$ .  
<sup>2</sup> Required  $0.75 < m_{K^+ K^-} < 1.2$  GeV/ $c^2$ .

$\Gamma(K^+ \pi^- \pi^+ \pi^- \text{ nonresonant})/\Gamma_{\text{total}}$   $\Gamma_{328}/\Gamma$

VALUE	CL%	DOCUMENT ID	TECN	COMMENT
$< 2.1 \times 10^{-6}$		1,2 KYEONG	09 BELL	$e^+e^- \rightarrow \Upsilon(4S)$

<sup>1</sup> Assumes equal production of  $B^+$  and  $B^0$  at the  $\Upsilon(4S)$ .  
<sup>2</sup> Required  $0.55 < m_{\pi^+ \pi^-} < 1.42$  and  $0.75 < m_{K^+ \pi^-} < 1.20$  GeV/ $c^2$ .

$\Gamma(K^*(892)^0 \pi^+ \pi^-)/\Gamma_{\text{total}}$   $\Gamma_{329}/\Gamma$

VALUE (units $10^{-6}$ )	CL%	DOCUMENT ID	TECN	COMMENT
$54.5 \pm 2.9 \pm 4.3$		1 AUBERT	07As BABR	$e^+e^- \rightarrow \Upsilon(4S)$

• • • We do not use the following data for averages, fits, limits, etc. • • •

$4.5^{+1.1+0.9}_{-1.0-1.6}$		1,2 KYEONG	09 BELL	$e^+e^- \rightarrow \Upsilon(4S)$
<1400	90	ALBRECHT	91E ARG	$e^+e^- \rightarrow \Upsilon(4S)$

<sup>1</sup> Assumes equal production of  $B^+$  and  $B^0$  at the  $\Upsilon(4S)$ .  
<sup>2</sup> Required  $0.55 < m_{\pi^+ \pi^-} < 1.42$  GeV/ $c^2$ .

$\Gamma(K^*(892)^0 \rho^0)/\Gamma_{\text{total}}$   $\Gamma_{330}/\Gamma$

VALUE (units $10^{-6}$ )	CL%	DOCUMENT ID	TECN	COMMENT
$3.9 \pm 1.3$ OUR AVERAGE		Error includes scale factor of 1.9.		

$5.1 \pm 0.6^{+0.6}_{-0.8}$		1 LEES	12k BABR	$e^+e^- \rightarrow \Upsilon(4S)$
$2.1^{+0.8+0.9}_{-0.7-0.5}$		1 KYEONG	09 BELL	$e^+e^- \rightarrow \Upsilon(4S)$

• • • We do not use the following data for averages, fits, limits, etc. • • •

$5.6 \pm 0.9 \pm 1.3$		1 AUBERT,B	06G BABR	Repl. by LEES 12k
< 34	90	2 GODANG	02 CLE2	$e^+e^- \rightarrow \Upsilon(4S)$
< 286	90	3 ABE	00c SLD	$e^+e^- \rightarrow Z$
< 460	90	ALBRECHT	91B ARG	$e^+e^- \rightarrow \Upsilon(4S)$
< 580	90	4 AVERY	89B CLEO	$e^+e^- \rightarrow \Upsilon(4S)$
< 960	90	5 AVERY	87 CLEO	$e^+e^- \rightarrow \Upsilon(4S)$

<sup>1</sup> Assumes equal production of  $B^+$  and  $B^0$  at the  $\Upsilon(4S)$ .  
<sup>2</sup> Assumes a helicity 00 configuration. For a helicity 11 configuration, the limit decreases to  $2.4 \times 10^{-5}$ .  
<sup>3</sup> ABE 00c assumes  $B(Z \rightarrow b\bar{b}) = (21.7 \pm 0.1)\%$  and the  $B$  fractions  $f_{B^0} = f_{B^+} = (39.7^{+1.8}_{-2.2})\%$  and  $f_{B_S} = (10.5^{+1.8}_{-2.2})\%$ .  
<sup>4</sup> AVERY 89B reports  $< 6.7 \times 10^{-4}$  assuming the  $\Upsilon(4S)$  decays 43% to  $B^0 \bar{B}^0$ . We rescale to 50%.  
<sup>5</sup> AVERY 87 reports  $< 1.2 \times 10^{-3}$  assuming the  $\Upsilon(4S)$  decays 40% to  $B^0 \bar{B}^0$ . We rescale to 50%.

$\Gamma(K^*(892)^0 f_0(980), f_0 \rightarrow \pi\pi)/\Gamma_{\text{total}}$   $\Gamma_{331}/\Gamma$

VALUE (units $10^{-6}$ )	CL%	DOCUMENT ID	TECN	COMMENT
$3.9^{+2.1}_{-1.8}$ OUR AVERAGE		Error includes scale factor of 3.9.		

$5.7 \pm 0.6 \pm 0.4$		1 LEES	12k BABR	$e^+e^- \rightarrow \Upsilon(4S)$
$1.4^{+0.6+0.6}_{-0.5-0.4}$		1,2 KYEONG	09 BELL	$e^+e^- \rightarrow \Upsilon(4S)$

• • • We do not use the following data for averages, fits, limits, etc. • • •

< 4.3	90	1 AUBERT,B	06G BABR	$e^+e^- \rightarrow \Upsilon(4S)$
< 170	90	3 AVERY	89B CLEO	$e^+e^- \rightarrow \Upsilon(4S)$

<sup>1</sup> Assumes equal production of  $B^+$  and  $B^0$  at the  $\Upsilon(4S)$ .  
<sup>2</sup> The upper limit is  $2.2 \times 10^{-6}$  at 90% CL.  
<sup>3</sup> AVERY 89B reports  $< 2.0 \times 10^{-4}$  assuming the  $\Upsilon(4S)$  decays 43% to  $B^0 \bar{B}^0$ . We rescale to 50%.

$\Gamma(K_1(1270)^+ \pi^-)/\Gamma_{\text{total}}$   $\Gamma_{332}/\Gamma$

VALUE	CL%	DOCUMENT ID	TECN	COMMENT
$< 3.0 \times 10^{-5}$		1 AUBERT	10d BABR	$e^+e^- \rightarrow \Upsilon(4S)$

<sup>1</sup> Assumes equal production of  $B^+$  and  $B^0$  at the  $\Upsilon(4S)$ .

$\Gamma(K_1(1400)^+ \pi^-)/\Gamma_{\text{total}}$   $\Gamma_{333}/\Gamma$

VALUE	CL%	DOCUMENT ID	TECN	COMMENT
$< 2.7 \times 10^{-5}$		1 AUBERT	10d BABR	$e^+e^- \rightarrow \Upsilon(4S)$

• • • We do not use the following data for averages, fits, limits, etc. • • •

< $1.1 \times 10^{-3}$	90	ALBRECHT	91B ARG	$e^+e^- \rightarrow \Upsilon(4S)$
------------------------	----	----------	---------	-----------------------------------

<sup>1</sup> Assumes equal production of  $B^+$  and  $B^0$  at the  $\Upsilon(4S)$ .

See key on page 999

# Meson Particle Listings

## $B^0$

### $\Gamma(a_1(1260)^- K^+)/\Gamma_{total}$ $\Gamma_{334}/\Gamma$

VALUE (units $10^{-6}$ )	CL%	DOCUMENT ID	TECN	COMMENT
<b>16.3 ± 2.9 ± 2.3</b>		1,2 AUBERT	08F BABR	$e^+e^- \rightarrow \Upsilon(4S)$
<230	90	3 ADAM	96D DLPH	$e^+e^- \rightarrow Z$
<390	90	4 ABREU	95N DLPH	Sup. by ADAM 96D

- • • We do not use the following data for averages, fits, limits, etc. • • •
- 1 Assumes equal production of  $B^+$  and  $B^0$  at the  $\Upsilon(4S)$ .
- 2 Assumes  $a_1^\pm$  decays only to  $3\pi$  and  $B(a_1^\pm \rightarrow \pi^\pm \pi^\mp \pi^\pm) = 0.5$ .
- 3 ADAM 96D assumes  $f_{B^0} = f_{B^-} = 0.39$  and  $f_{B_s} = 0.12$ . Contributions from  $B^0$  and  $B_s$  decays cannot be separated. Limits are given for the weighted average of the decay rates for the two neutral  $B$  mesons.
- 4 Assumes a  $B^0$ ,  $B^-$  production fraction of 0.39 and a  $B_s$  production fraction of 0.12. Contributions from  $B^0$  and  $B_s^0$  decays cannot be separated. Limits are given for the weighted average of the decay rates for the two neutral  $B$  mesons.

### $\Gamma(K^*(892)^+ \rho^-)/\Gamma_{total}$ $\Gamma_{335}/\Gamma$

VALUE (units $10^{-6}$ )	CL%	DOCUMENT ID	TECN	COMMENT
<b>10.3 ± 2.3 ± 1.3</b>		1 LEES	12K BABR	$e^+e^- \rightarrow \Upsilon(4S)$
<12.0	90	1 AUBERT,B	06G BABR	Repl. by LEES 12K

- • • We do not use the following data for averages, fits, limits, etc. • • •
- 1 Assumes equal production of  $B^+$  and  $B^0$  at the  $\Upsilon(4S)$ .

### $\Gamma(K_0^*(1430)^+ \rho^-)/\Gamma_{total}$ $\Gamma_{336}/\Gamma$

VALUE (units $10^{-6}$ )	CL%	DOCUMENT ID	TECN	COMMENT
<b>28 ± 10 ± 6</b>		1 LEES	12K BABR	$e^+e^- \rightarrow \Upsilon(4S)$

- 1 Assumes equal production of  $B^+$  and  $B^0$  at the  $\Upsilon(4S)$ .

### $\Gamma(K_1(1400)^0 \rho^0)/\Gamma_{total}$ $\Gamma_{337}/\Gamma$

VALUE	CL%	DOCUMENT ID	TECN	COMMENT
<b>&lt; 3.0 × 10<sup>-3</sup></b>	90	ALBRECHT	91B ARG	$e^+e^- \rightarrow \Upsilon(4S)$

### $\Gamma(K_0^*(1430)^0 \rho^0)/\Gamma_{total}$ $\Gamma_{338}/\Gamma$

VALUE (units $10^{-6}$ )	CL%	DOCUMENT ID	TECN	COMMENT
<b>27 ± 4 ± 4</b>		1 LEES	12K BABR	$e^+e^- \rightarrow \Upsilon(4S)$

- 1 Assumes equal production of  $B^+$  and  $B^0$  at the  $\Upsilon(4S)$ .

### $\Gamma(K_0^*(1430)^0 f_0(980), f_0 \rightarrow \pi\pi)/\Gamma_{total}$ $\Gamma_{339}/\Gamma$

VALUE (units $10^{-6}$ )	CL%	DOCUMENT ID	TECN	COMMENT
<b>2.7 ± 0.7 ± 0.6</b>		1 LEES	12K BABR	$e^+e^- \rightarrow \Upsilon(4S)$

- 1 Assumes equal production of  $B^+$  and  $B^0$  at the  $\Upsilon(4S)$ .

### $\Gamma(K_2^*(1430)^0 f_0(980), f_0 \rightarrow \pi\pi)/\Gamma_{total}$ $\Gamma_{340}/\Gamma$

VALUE (units $10^{-6}$ )	CL%	DOCUMENT ID	TECN	COMMENT
<b>8.6 ± 1.7 ± 1.0</b>		1 LEES	12K BABR	$e^+e^- \rightarrow \Upsilon(4S)$

- 1 Assumes equal production of  $B^+$  and  $B^0$  at the  $\Upsilon(4S)$ .

### $\Gamma(K^+ K^-)/\Gamma_{total}$ $\Gamma_{341}/\Gamma$

VALUE (units $10^{-8}$ )	CL%	DOCUMENT ID	TECN	COMMENT
<b>7.80 ± 1.27 ± 0.84</b>		1 AAIJ	17G LHCB	$pp$ at 7 and 8 TeV
10 ± 8 ± 4		2,3 DUH	13 BELL	$e^+e^- \rightarrow \Upsilon(4S)$
12 ± 8 ± 1		4 AAIJ	12AR LHCB	Repl. by AAIJ 17G
23 ± 10 ± 10		5 AALTONEN	12L CDF	$p\bar{p}$ at 1.96 TeV
< 70	90	6 AALTONEN	09c CDF	Repl. by AALTONEN 12L
< 50	90	3 AUBERT	07b BABR	$e^+e^- \rightarrow \Upsilon(4S)$
< 41	90	3 LIN	07 BELL	Repl. by DUH 13
< 180	90	7 ABULENCIA,A	06D CDF	Repl. by AALTONEN 09c
< 37	90	ABE	05G BELL	Repl. by LIN 07
< 70	90	CHAO	04 BELL	$e^+e^- \rightarrow \Upsilon(4S)$
< 80	90	3 BORNHEIM	03 CLE2	$e^+e^- \rightarrow \Upsilon(4S)$
< 60	90	3 AUBERT	02Q BABR	$e^+e^- \rightarrow \Upsilon(4S)$
< 90	90	3 CASEY	02 BELL	$e^+e^- \rightarrow \Upsilon(4S)$
< 270	90	3 ABE	01H BELL	$e^+e^- \rightarrow \Upsilon(4S)$
< 250	90	3 AUBERT	01c BABR	$e^+e^- \rightarrow \Upsilon(4S)$
< 6600	90	8 ABE	00c SLD	$e^+e^- \rightarrow Z$
< 190	90	3 CRONIN-HEN.	.00 CLE2	$e^+e^- \rightarrow \Upsilon(4S)$
< 430	90	GODANG	98 CLE2	Repl. by CRONIN-HENNESSY 00
< 4600		9 ADAM	96D DLPH	$e^+e^- \rightarrow Z$
< 400	90	ASNER	96 CLE2	Repl. by GODANG 98
< 1800	90	10 BUSKULIC	96V ALEP	$e^+e^- \rightarrow Z$
< 12000	90	11 ABREU	95N DLPH	Sup. by ADAM 96D
< 700	90	3 BATTLE	93 CLE2	$e^+e^- \rightarrow \Upsilon(4S)$

- 1 Supersedes results of AAIJ 12AR.
- 2 DUH 13 reports also for the same data  $B(B^0 \rightarrow K^+ K^-) < 0.20 \times 10^{-6}$  at 90% CL.
- 3 Assumes equal production of  $B^+$  and  $B^0$  at the  $\Upsilon(4S)$ .
- 4 AAIJ 12AR reports  $[\Gamma(B^0 \rightarrow K^+ K^-)/\Gamma_{total}] / [B(B_s^0 \rightarrow K^+ K^-)] / [\Gamma(\bar{b} \rightarrow B_s^0)/\Gamma(\bar{b} \rightarrow B^0)] = 0.018^{+0.008}_{-0.007} \pm 0.009$  which we multiply by our best values  $B(B_s^0 \rightarrow$

$K^+ K^-) = (2.66 \pm 0.22) \times 10^{-5}$ ,  $\Gamma(\bar{b} \rightarrow B_s^0)/\Gamma(\bar{b} \rightarrow B^0) = 0.246 \pm 0.023$ . Our first error is their experiment's error and our second error is the systematic error from using our best values.

- 5 Reported a central value of  $(0.23 \pm 0.10 \pm 0.10) \times 10^{-6}$  using  $B(B^0 \rightarrow K^+ \pi^-) = (19.4 \pm 0.6) \times 10^{-6}$ .
- 6 Obtains this result from  $B(K^+ K^-)/B(K^+ \pi^-) = 0.020 \pm 0.008 \pm 0.006$ , assuming  $B(B^0 \rightarrow K^+ \pi^-) = (19.4 \pm 0.6) \times 10^{-6}$ .
- 7 ABULENCIA,A 06D obtains this from  $\Gamma(K^+ K^-)/\Gamma(K^+ \pi^-) < 0.10$  at 90% CL, assuming  $B(B^0 \rightarrow K^+ \pi^-) = (18.9 \pm 0.7) \times 10^{-6}$ .
- 8 ABE 00c assumes  $B(Z \rightarrow b\bar{b}) = (21.7 \pm 0.1)\%$  and the  $B$  fractions  $f_{B^0} = f_{B^+} = (39.7^{+1.8}_{-2.2})\%$  and  $f_{B_s} = (10.5^{+1.8}_{-2.2})\%$ .
- 9 ADAM 96D assumes  $f_{B^0} = f_{B^-} = 0.39$  and  $f_{B_s} = 0.12$ . Contributions from  $B^0$  and  $B_s$  decays cannot be separated. Limits are given for the weighted average of the decay rates for the two neutral  $B$  mesons.
- 10 BUSKULIC 96v assumes PDG 96 production fractions for  $B^0$ ,  $B^+$ ,  $B_s$ ,  $b$  baryons.
- 11 Assumes a  $B^0$ ,  $B^-$  production fraction of 0.39 and a  $B_s$  production fraction of 0.12. Contributions from  $B^0$  and  $B_s^0$  decays cannot be separated. Limits are given for the weighted average of the decay rates for the two neutral  $B$  mesons.

### $\Gamma(K^0 \bar{K}^0)/\Gamma_{total}$ $\Gamma_{342}/\Gamma$

VALUE (units $10^{-6}$ )	CL%	DOCUMENT ID	TECN	COMMENT
<b>1.21 ± 0.16 OUR AVERAGE</b>				
1.26 ± 0.19 ± 0.05		1 DUH	13 BELL	$e^+e^- \rightarrow \Upsilon(4S)$
1.08 ± 0.28 ± 0.11		1 AUBERT,BE	06c BABR	$e^+e^- \rightarrow \Upsilon(4S)$
0.87 + 0.25 - 0.20 ± 0.09		1 LIN	07 BELL	Repl. by DUH 13
0.8 ± 0.3 ± 0.9		1 ABE	05G BELL	Repl. by LIN 07
1.19 + 0.40 - 0.35 ± 0.13		1 AUBERT,BE	05E BABR	Repl. by AUBERT,BE 06c
< 1.8	90	1 AUBERT	04M BABR	$e^+e^- \rightarrow \Upsilon(4S)$
< 1.5	90	1 CHAO	04 BELL	Repl. by ABE 05G
< 3.3	90	1 BORNHEIM	03 CLE2	$e^+e^- \rightarrow \Upsilon(4S)$
< 4.1	90	1 CASEY	02 BELL	$e^+e^- \rightarrow \Upsilon(4S)$
< 17	90	GODANG	98 CLE2	$e^+e^- \rightarrow \Upsilon(4S)$

- 1 Assumes equal production of  $B^+$  and  $B^0$  at the  $\Upsilon(4S)$ .

### $\Gamma(K^0 K^- \pi^+)/\Gamma_{total}$ $\Gamma_{343}/\Gamma$

VALUE (units $10^{-6}$ )	CL%	DOCUMENT ID	TECN	COMMENT
<b>6.7 ± 0.5 OUR FIT</b>				
<b>7.0 ± 0.6 OUR AVERAGE</b>				
7.2 ± 0.7 ± 0.3		1 LAI	19 BELL	$e^+e^- \rightarrow \Upsilon(4S)$
6.4 ± 1.0 ± 0.6		1 DEL-AMO-SA.	.10E BABR	$e^+e^- \rightarrow \Upsilon(4S)$
< 18	90	1 GARMASH	04 BELL	$e^+e^- \rightarrow \Upsilon(4S)$
< 21	90	1 ECKHART	02 CLE2	$e^+e^- \rightarrow \Upsilon(4S)$

- 1 Assumes equal production of  $B^+$  and  $B^0$  at the  $\Upsilon(4S)$ .

### $\Gamma(K^*(892)^\pm K^\mp)/\Gamma_{total}$ $\Gamma_{344}/\Gamma$

VALUE	CL%	DOCUMENT ID	TECN	COMMENT
<b>&lt; 0.4 × 10<sup>-6</sup></b>		90 AAIJ	14BMLHCB	$pp$ at 7 TeV

### $\Gamma(K^0 K^- \pi^+)/\Gamma(K^0 \pi^+ \pi^-)$ $\Gamma_{343}/\Gamma_{309}$

VALUE	CL%	DOCUMENT ID	TECN	COMMENT
<b>0.134 ± 0.011 OUR FIT</b>				
<b>0.123 ± 0.009 ± 0.015</b>				
0.128 ± 0.017 ± 0.009		AAIJ	17BP LHCB	$pp$ at 7, 8 TeV
		AAIJ	13BP LHCB	Repl. by AAIJ 17BP

- • • We do not use the following data for averages, fits, limits, etc. • • •

### $[\Gamma(\bar{K}^{*0} K^0) + \Gamma(K^{*0} \bar{K}^0)]/\Gamma_{total}$ $\Gamma_{345}/\Gamma$

VALUE (units $10^{-6}$ )	CL%	DOCUMENT ID	TECN	COMMENT
<b>&lt; 0.96</b>		90 1 AAIJ	16 LHCB	$pp$ at 7 TeV
< 1.9	90	2 AUBERT,BE	06N BABR	$e^+e^- \rightarrow \Upsilon(4S)$
				1 Assumes $B(B^0 \rightarrow K^0 \pi^+ \pi^-) = (4.96 \pm 0.20) \times 10^{-5}$ .
				2 Assumes equal production of $B^+$ and $B^0$ at the $\Upsilon(4S)$ .

### $\Gamma(K^+ K^- \pi^0)/\Gamma_{total}$ $\Gamma_{346}/\Gamma$

VALUE (units $10^{-6}$ )	CL%	DOCUMENT ID	TECN	COMMENT
<b>2.17 ± 0.60 ± 0.24</b>		1 GAUR	13 BELL	$e^+e^- \rightarrow \Upsilon(4S)$
< 19	90	1 ECKHART	02 CLE2	$e^+e^- \rightarrow \Upsilon(4S)$

- 1 Assumes equal production of  $B^+$  and  $B^0$  at the  $\Upsilon(4S)$ .

### $\Gamma(K_S^0 K_S^0 \pi^0)/\Gamma_{total}$ $\Gamma_{347}/\Gamma$

VALUE	CL%	DOCUMENT ID	TECN	COMMENT
<b>&lt; 0.9 × 10<sup>-6</sup></b>		90 1 AUBERT	09AD BABR	$e^+e^- \rightarrow \Upsilon(4S)$

- 1 Assumes equal production of  $B^+$  and  $B^0$  at the  $\Upsilon(4S)$ .

### $\Gamma(K_S^0 K_S^0 \eta)/\Gamma_{total}$ $\Gamma_{348}/\Gamma$

VALUE	CL%	DOCUMENT ID	TECN	COMMENT
<b>&lt; 1.0 × 10<sup>-6</sup></b>		90 1 AUBERT	09AD BABR	$e^+e^- \rightarrow \Upsilon(4S)$

- 1 Assumes equal production of  $B^+$  and  $B^0$  at the  $\Upsilon(4S)$ .

## Meson Particle Listings

 $B^0$ 

$\Gamma(K_S^0 K_S^0 \eta)/\Gamma_{\text{total}}$				$\Gamma_{349}/\Gamma$
VALUE	CL%	DOCUMENT ID	TECN	COMMENT
$<2.0 \times 10^{-6}$	90	<sup>1</sup> AUBERT	09AD BABR	$e^+e^- \rightarrow \Upsilon(4S)$
<sup>1</sup> Assumes equal production of $B^+$ and $B^0$ at the $\Upsilon(4S)$ .				

$\Gamma(K^0 K^+ K^-)/\Gamma_{\text{total}}$				$\Gamma_{350}/\Gamma$
VALUE (units $10^{-6}$ )	CL%	DOCUMENT ID	TECN	COMMENT
<b>26.8 ± 1.1 OUR FIT</b>				
<b>26.6 ± 1.2 OUR AVERAGE</b>				
26.5 ± 0.9 ± 0.8		<sup>1,2</sup> LEES	12o BABR	$e^+e^- \rightarrow \Upsilon(4S)$
28.3 ± 3.3 ± 4.0		<sup>1</sup> GARMASH	04 BELL	$e^+e^- \rightarrow \Upsilon(4S)$
• • • We do not use the following data for averages, fits, limits, etc. • • •				
23.8 ± 2.0 ± 1.6		<sup>1</sup> AUBERT,B	04v BABR	Repl. by LEES 12o
<1300	90	ALBRECHT	91E ARG	$e^+e^- \rightarrow \Upsilon(4S)$
<sup>1</sup> Assumes equal production of $B^+$ and $B^0$ at the $\Upsilon(4S)$ .				
<sup>2</sup> All intermediate charmonium and charm resonances are removed, except of $\chi_{c0}$ .				

$\Gamma(K^0 K^+ K^-)/\Gamma(K^0 \pi^+ \pi^-)$				$\Gamma_{350}/\Gamma_{309}$
VALUE	CL%	DOCUMENT ID	TECN	COMMENT
<b>0.539 ± 0.025 OUR FIT</b>				
<b>0.549 ± 0.018 ± 0.033</b>		AAIJ	17BP LHCB	$pp$ at 7, 8 TeV
• • • We do not use the following data for averages, fits, limits, etc. • • •				
0.385 ± 0.031 ± 0.023		AAIJ	13BP LHCB	Repl. by AAIJ 17BP

$\Gamma(K^0 \phi)/\Gamma_{\text{total}}$				$\Gamma_{351}/\Gamma$
VALUE (units $10^{-6}$ )	CL%	DOCUMENT ID	TECN	COMMENT
<b>7.3 ± 0.7 OUR AVERAGE</b>				
7.1 ± 0.6 ± 0.4		<sup>1</sup> LEES	12o BABR	$e^+e^- \rightarrow \Upsilon(4S)$
9.0 ± 2.2 ± 0.7		<sup>1</sup> CHEN	03B BELL	$e^+e^- \rightarrow \Upsilon(4S)$
• • • We do not use the following data for averages, fits, limits, etc. • • •				
8.4 ± 1.5 ± 0.5		<sup>1</sup> AUBERT	04A BABR	Repl. by LEES 12o
8.1 ± 3.1 ± 0.8		<sup>1</sup> AUBERT	01D BABR	$e^+e^- \rightarrow \Upsilon(4S)$
< 12.3	90	<sup>1</sup> BRIERE	01 CLE2	$e^+e^- \rightarrow \Upsilon(4S)$
< 31	90	<sup>1</sup> BERGFELD	98 CLE2	
< 88	90	ASNER	96 CLE2	$e^+e^- \rightarrow \Upsilon(4S)$
< 720	90	ALBRECHT	91B ARG	$e^+e^- \rightarrow \Upsilon(4S)$
< 420	90	<sup>2</sup> AVERY	89B CLEO	$e^+e^- \rightarrow \Upsilon(4S)$
<1000	90	<sup>3</sup> AVERY	87 CLEO	$e^+e^- \rightarrow \Upsilon(4S)$
<sup>1</sup> Assumes equal production of $B^+$ and $B^0$ at the $\Upsilon(4S)$ .				
<sup>2</sup> AVERY 89B reports $< 4.9 \times 10^{-4}$ assuming the $\Upsilon(4S)$ decays 43% to $B^0 \bar{B}^0$ . We rescale to 50%.				
<sup>3</sup> AVERY 87 reports $< 1.3 \times 10^{-3}$ assuming the $\Upsilon(4S)$ decays 40% to $B^0 \bar{B}^0$ . We rescale to 50%.				

$\Gamma(f_0(980) K^0, f_0 \rightarrow K^+ K^-)/\Gamma_{\text{total}}$				$\Gamma_{352}/\Gamma$
VALUE (units $10^{-6}$ )	CL%	DOCUMENT ID	TECN	COMMENT
<b>7.0 ± 2.6 ± 2.4</b>		<sup>1</sup> LEES	12o BABR	$e^+e^- \rightarrow \Upsilon(4S)$
<sup>1</sup> Assumes equal production of $B^+$ and $B^0$ at the $\Upsilon(4S)$ .				

$\Gamma(f_0(1500) K^0)/\Gamma_{\text{total}}$				$\Gamma_{353}/\Gamma$
VALUE (units $10^{-6}$ )	CL%	DOCUMENT ID	TECN	COMMENT
<b>13.3 ± 5.8 ± 3.2</b>		<sup>1</sup> LEES	12o BABR	$e^+e^- \rightarrow \Upsilon(4S)$
<sup>1</sup> Assumes equal production of $B^+$ and $B^0$ at the $\Upsilon(4S)$ .				

$\Gamma(f_2'(1525)^0 K^0)/\Gamma_{\text{total}}$				$\Gamma_{354}/\Gamma$
VALUE (units $10^{-6}$ )	CL%	DOCUMENT ID	TECN	COMMENT
<b>0.29 ± 0.27 ± 0.36</b>		<sup>1</sup> LEES	12o BABR	$e^+e^- \rightarrow \Upsilon(4S)$
<sup>1</sup> Assumes equal production of $B^+$ and $B^0$ at the $\Upsilon(4S)$ .				

$\Gamma(f_0(1710) K^0, f_0 \rightarrow K^+ K^-)/\Gamma_{\text{total}}$				$\Gamma_{355}/\Gamma$
VALUE (units $10^{-6}$ )	CL%	DOCUMENT ID	TECN	COMMENT
<b>4.4 ± 0.7 ± 0.5</b>		<sup>1</sup> LEES	12o BABR	$e^+e^- \rightarrow \Upsilon(4S)$
<sup>1</sup> Assumes equal production of $B^+$ and $B^0$ at the $\Upsilon(4S)$ .				

$\Gamma(K^0 K^+ K^- \text{ nonresonant})/\Gamma_{\text{total}}$				$\Gamma_{356}/\Gamma$
VALUE (units $10^{-6}$ )	CL%	DOCUMENT ID	TECN	COMMENT
<b>33 ± 5 ± 9</b>		<sup>1</sup> LEES	12o BABR	$e^+e^- \rightarrow \Upsilon(4S)$
<sup>1</sup> Assumes equal production of $B^+$ and $B^0$ at the $\Upsilon(4S)$ .				

$\Gamma(K_S^0 K_S^0 K_S^0)/\Gamma_{\text{total}}$				$\Gamma_{357}/\Gamma$
VALUE (units $10^{-6}$ )	CL%	DOCUMENT ID	TECN	COMMENT
<b>6.0 ± 0.5 OUR AVERAGE</b>				Error includes scale factor of 1.1.
6.19 ± 0.48 ± 0.19		<sup>1</sup> LEES	12i BABR	$e^+e^- \rightarrow \Upsilon(4S)$
4.2 ± 1.6 ± 0.8		<sup>1</sup> GARMASH	04 BELL	$e^+e^- \rightarrow \Upsilon(4S)$
• • • We do not use the following data for averages, fits, limits, etc. • • •				
6.9 ± 0.9 ± 0.6		<sup>1</sup> AUBERT,B	05 BABR	Repl. by LEES 12i
<sup>1</sup> Assumes equal production of $B^+$ and $B^0$ at the $\Upsilon(4S)$ .				

$\Gamma(f_0(980) K^0, f_0 \rightarrow K_S^0 K_S^0)/\Gamma_{\text{total}}$				$\Gamma_{358}/\Gamma$
VALUE (units $10^{-6}$ )	CL%	DOCUMENT ID	TECN	COMMENT
<b>2.7 ± 1.3 ± 1.3</b>		<sup>1,2</sup> LEES	12i BABR	$e^+e^- \rightarrow \Upsilon(4S)$
<sup>1</sup> Assumes equal production of $B^+$ and $B^0$ at the $\Upsilon(4S)$ .				
<sup>2</sup> Uses Dalitz plot analysis of the $B^0 \rightarrow K_S^0 K_S^0 K_S^0$ decay.				

$\Gamma(f_0(1710) K^0, f_0 \rightarrow K_S^0 K_S^0)/\Gamma_{\text{total}}$				$\Gamma_{359}/\Gamma$
VALUE (units $10^{-6}$ )	CL%	DOCUMENT ID	TECN	COMMENT
<b>0.50 ± 0.46 ± 0.11</b>		<sup>1,2</sup> LEES	12i BABR	$e^+e^- \rightarrow \Upsilon(4S)$
<sup>1</sup> Assumes equal production of $B^+$ and $B^0$ at the $\Upsilon(4S)$ .				
<sup>2</sup> Uses Dalitz plot analysis of the $B^0 \rightarrow K_S^0 K_S^0 K_S^0$ decay.				

$\Gamma(f_2(2010) K^0, f_2 \rightarrow K_S^0 K_S^0)/\Gamma_{\text{total}}$				$\Gamma_{360}/\Gamma$
VALUE (units $10^{-6}$ )	CL%	DOCUMENT ID	TECN	COMMENT
<b>0.54 ± 0.21 ± 0.52</b>		<sup>1,2</sup> LEES	12i BABR	$e^+e^- \rightarrow \Upsilon(4S)$
<sup>1</sup> Assumes equal production of $B^+$ and $B^0$ at the $\Upsilon(4S)$ .				
<sup>2</sup> Uses Dalitz plot analysis of the $B^0 \rightarrow K_S^0 K_S^0 K_S^0$ decay.				

$\Gamma(K_S^0 K_S^0 K_S^0 \text{ nonresonant})/\Gamma_{\text{total}}$				$\Gamma_{361}/\Gamma$
VALUE (units $10^{-6}$ )	CL%	DOCUMENT ID	TECN	COMMENT
<b>13.3 ± 2.2 ± 2.2</b>		<sup>1,2</sup> LEES	12i BABR	$e^+e^- \rightarrow \Upsilon(4S)$
<sup>1</sup> Assumes equal production of $B^+$ and $B^0$ at the $\Upsilon(4S)$ .				
<sup>2</sup> Uses Dalitz plot analysis of the $B^0 \rightarrow K_S^0 K_S^0 K_S^0$ decay.				

$\Gamma(K_S^0 K_S^0 K_L^0)/\Gamma_{\text{total}}$				$\Gamma_{362}/\Gamma$
VALUE (units $10^{-6}$ )	CL%	DOCUMENT ID	TECN	COMMENT
<b>&lt;16</b>	90	<sup>1</sup> AUBERT,B	06R BABR	$e^+e^- \rightarrow \Upsilon(4S)$
<sup>1</sup> Assumes equal production of $B^+$ and $B^0$ at the $\Upsilon(4S)$ .				

$\Gamma(K^*(892)^0 K^+ K^-)/\Gamma_{\text{total}}$				$\Gamma_{363}/\Gamma$
VALUE (units $10^{-6}$ )	CL%	DOCUMENT ID	TECN	COMMENT
<b>27.5 ± 1.3 ± 2.2</b>		<sup>1</sup> AUBERT	07As BABR	$e^+e^- \rightarrow \Upsilon(4S)$
• • • We do not use the following data for averages, fits, limits, etc. • • •				
<610	90	ALBRECHT	91E ARG	$e^+e^- \rightarrow \Upsilon(4S)$
<sup>1</sup> Assumes equal production of $B^+$ and $B^0$ at the $\Upsilon(4S)$ .				

$\Gamma(K^*(892)^0 \phi)/\Gamma_{\text{total}}$				$\Gamma_{364}/\Gamma$
VALUE (units $10^{-6}$ )	CL%	DOCUMENT ID	TECN	COMMENT
<b>10.0 ± 0.5 OUR FIT</b>				
<b>10.0 ± 0.5 OUR AVERAGE</b>				
10.4 ± 0.5 ± 0.6		<sup>1</sup> PRIM	13 BELL	$e^+e^- \rightarrow \Upsilon(4S)$
9.7 ± 0.5 ± 0.5		<sup>1</sup> AUBERT	08Bg BABR	$e^+e^- \rightarrow \Upsilon(4S)$
11.5 ± 4.5 ± 1.8		<sup>1</sup> BRIERE	01 CLE2	$e^+e^- \rightarrow \Upsilon(4S)$
• • • We do not use the following data for averages, fits, limits, etc. • • •				
9.2 ± 0.7 ± 0.6		<sup>1</sup> AUBERT	07D BABR	Repl. by AUBERT 08Bg
9.2 ± 0.9 ± 0.5		<sup>1</sup> AUBERT,B	04w BABR	Repl. by AUBERT 07D
11.2 ± 1.3 ± 0.8		<sup>1</sup> AUBERT	03v BABR	Repl. by AUBERT,B 04w
10.0 ± 1.6 ± 0.7		<sup>1</sup> CHEN	03B BELL	Repl. by PRIM 13
8.7 ± 2.5 ± 1.1		<sup>1</sup> AUBERT	01D BABR	Repl. by AUBERT 03v
<384	90	<sup>2</sup> ABE	00c SLD	$e^+e^- \rightarrow Z$
< 21	90	<sup>1</sup> BERGFELD	98 CLE2	
< 43	90	ASNER	96 CLE2	$e^+e^- \rightarrow \Upsilon(4S)$
<320	90	ALBRECHT	91B ARG	$e^+e^- \rightarrow \Upsilon(4S)$
<380	90	<sup>3</sup> AVERY	89B CLEO	$e^+e^- \rightarrow \Upsilon(4S)$
<380	90	<sup>4</sup> AVERY	87 CLEO	$e^+e^- \rightarrow \Upsilon(4S)$
<sup>1</sup> Assumes equal production of $B^+$ and $B^0$ at the $\Upsilon(4S)$ .				
<sup>2</sup> ABE 00c assumes $B(Z \rightarrow b\bar{b}) = (21.7 \pm 0.1)\%$ and the $B$ fractions $f_{B^0} = f_{B^+} = (39.7 \pm 2.2)\%$ and $f_{B_s} = (10.5 \pm 1.8)\%$ .				
<sup>3</sup> AVERY 89B reports $< 4.4 \times 10^{-4}$ assuming the $\Upsilon(4S)$ decays 43% to $B^0 \bar{B}^0$ . We rescale to 50%.				
<sup>4</sup> AVERY 87 reports $< 4.7 \times 10^{-4}$ assuming the $\Upsilon(4S)$ decays 40% to $B^0 \bar{B}^0$ . We rescale to 50%.				

$\Gamma(K^+ K^- \pi^+ \pi^- \text{ nonresonant})/\Gamma_{\text{total}}$				$\Gamma_{365}/\Gamma$
VALUE (units $10^{-6}$ )	CL%	DOCUMENT ID	TECN	COMMENT
<b>&lt;71.7</b>	90	<sup>1,2</sup> CHIANG	10 BELL	$e^+e^- \rightarrow \Upsilon(4S)$
<sup>1</sup> Measured in the range $0.7 < m_{K\pi} < 1.7$ and corrected using PS assumption for the full $K\pi$ mass range.				
<sup>2</sup> Assumes equal production of $B^+$ and $B^0$ at the $\Upsilon(4S)$ .				

See key on page 999

# Meson Particle Listings

## $B^0$

### $\Gamma(K^*(892)^0 K^- \pi^+)/\Gamma_{total}$ $\Gamma_{366}/\Gamma$

VALUE (units $10^{-6}$ )	CL%	DOCUMENT ID	TECN	COMMENT
<b>4.5 ± 1.3 OUR AVERAGE</b>				
2.11 <sup>+5.63+4.85</sup> <sub>-5.26-4.75</sub>		1,2 CHIANG	10	BELL $e^+e^- \rightarrow \Upsilon(4S)$
4.6 ± 1.1 ± 0.8		2 AUBERT	07As	BABR $e^+e^- \rightarrow \Upsilon(4S)$

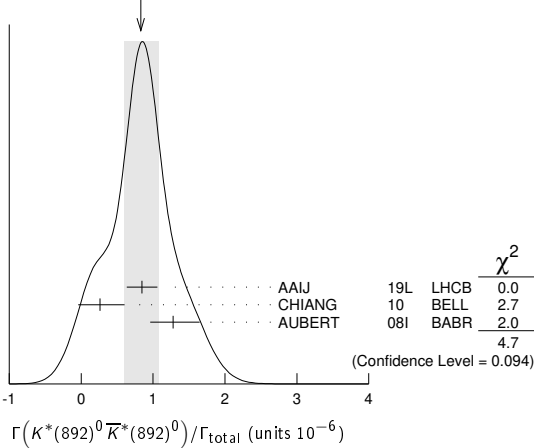
<sup>1</sup> Measured in the range  $0.7 < m_{K\pi} < 1.7$  and corrected using PS assumption for the full  $K\pi$  mass range. The quoted result is equivalent to the upper limit of  $< 13.9 \times 10^{-6}$  at 90% CL.  
<sup>2</sup> Assumes equal production of  $B^+$  and  $B^0$  at the  $\Upsilon(4S)$ .

### $\Gamma(K^*(892)^0 \bar{K}^*(892)^0)/\Gamma_{total}$ $\Gamma_{367}/\Gamma$

VALUE (units $10^{-6}$ )	CL%	DOCUMENT ID	TECN	COMMENT
<b>0.83 ± 0.24 OUR AVERAGE</b>				Error includes scale factor of 1.5. See the ideogram below.
0.85 ± 0.07 ± 0.20		1 AAIJ	19L	LHCB $pp$ at 7 and 8 TeV
0.26 <sup>+0.33+0.10</sup> <sub>-0.29-0.08</sub>		2,3 CHIANG	10	BELL $e^+e^- \rightarrow \Upsilon(4S)$
1.28 <sup>+0.35</sup> <sub>-0.30</sub> ± 0.11		3 AUBERT	08i	BABR $e^+e^- \rightarrow \Upsilon(4S)$

• • • We do not use the following data for averages, fits, limits, etc. • • •  
 $< 22$  90 4 GODANG 02 CLE2  $e^+e^- \rightarrow \Upsilon(4S)$   
 $< 469$  90 5 ABE 00c SLD  $e^+e^- \rightarrow Z$   
<sup>1</sup> AAIJ 19L reports  $[\Gamma(B^0 \rightarrow K^*(892)^0 \bar{K}^*(892)^0)/\Gamma_{total}] / [B(B_s^0 \rightarrow \bar{K}^*(892)^0 K^*(892)^0)] = 0.0758 \pm 0.0057 \pm 0.0030$  which we multiply by our best value  $B(B_s^0 \rightarrow \bar{K}^*(892)^0 K^*(892)^0) = (1.11 \pm 0.27) \times 10^{-5}$ . Our first error is their experiment's error and our second error is the systematic error from using our best value.  
<sup>2</sup> Measured in the range  $0.7 < m_{K\pi} < 1.7$  and corrected using PS assumption for the full  $K\pi$  mass range. The quoted result is equivalent to the upper limit of  $< 0.8 \times 10^{-6}$  at 90% CL.  
<sup>3</sup> Assumes equal production of  $B^+$  and  $B^0$  at the  $\Upsilon(4S)$ .  
<sup>4</sup> Assumes a helicity 00 configuration. For a helicity 11 configuration, the limit decreases to  $1.9 \times 10^{-5}$ .  
<sup>5</sup> ABE 00c assumes  $B(Z \rightarrow b\bar{b}) = (21.7 \pm 0.1)\%$  and the  $B$  fractions  $f_{B^0} = f_{B^+} = (39.7 \pm 2.2)\%$  and  $f_{B_s} = (10.5 \pm 1.8)\%$ .

WEIGHTED AVERAGE  
0.83±0.24 (Error scaled by 1.5)



### $\Gamma(K^+ K^+ \pi^- \pi^- \text{nonresonant})/\Gamma_{total}$ $\Gamma_{368}/\Gamma$

VALUE (units $10^{-6}$ )	CL%	DOCUMENT ID	TECN	COMMENT
<b>&lt; 6.0</b>	90	1 CHIANG	10	BELL $e^+e^- \rightarrow \Upsilon(4S)$

<sup>1</sup> Assumes equal production of  $B^+$  and  $B^0$  at the  $\Upsilon(4S)$ .

### $\Gamma(K^*(892)^0 K^+ \pi^-)/\Gamma_{total}$ $\Gamma_{369}/\Gamma$

VALUE (units $10^{-6}$ )	CL%	DOCUMENT ID	TECN	COMMENT
<b>&lt; 2.2</b>	90	1 AUBERT	07As	BABR $e^+e^- \rightarrow \Upsilon(4S)$
• • • We do not use the following data for averages, fits, limits, etc. • • •				
$< 7.6$	90	1 CHIANG	10	BELL $e^+e^- \rightarrow \Upsilon(4S)$

<sup>1</sup> Assumes equal production of  $B^+$  and  $B^0$  at the  $\Upsilon(4S)$ .

### $\Gamma(K^*(892)^0 K^*(892)^0)/\Gamma_{total}$ $\Gamma_{370}/\Gamma$

VALUE (units $10^{-6}$ )	CL%	DOCUMENT ID	TECN	COMMENT
<b>&lt; 0.2</b>	90	1 CHIANG	10	BELL $e^+e^- \rightarrow \Upsilon(4S)$
• • • We do not use the following data for averages, fits, limits, etc. • • •				
$< 0.41$	90	1 AUBERT	08i	BABR $e^+e^- \rightarrow \Upsilon(4S)$
$< 37$	90	2 GODANG	02	CLE2 $e^+e^- \rightarrow \Upsilon(4S)$

<sup>1</sup> Assumes equal production of  $B^+$  and  $B^0$  at the  $\Upsilon(4S)$ .  
<sup>2</sup> Assumes a helicity 00 configuration. For a helicity 11 configuration, the limit decreases to  $2.9 \times 10^{-5}$ .

### $\Gamma(K^*(892)^+ K^*(892)^-)/\Gamma_{total}$ $\Gamma_{371}/\Gamma$

VALUE (units $10^{-6}$ )	CL%	DOCUMENT ID	TECN	COMMENT
<b>&lt; 2.0</b>	90	1 AUBERT	08AP	BABR $e^+e^- \rightarrow \Upsilon(4S)$
• • • We do not use the following data for averages, fits, limits, etc. • • •				
$< 141$	90	2 GODANG	02	CLE2 $e^+e^- \rightarrow \Upsilon(4S)$

<sup>1</sup> Assumes equal production of  $B^+$  and  $B^0$  at the  $\Upsilon(4S)$ .  
<sup>2</sup> Assumes a helicity 00 configuration. For a helicity 11 configuration, the limit decreases to  $8.9 \times 10^{-5}$ .

### $\Gamma(K_1(1400)^0 \phi)/\Gamma_{total}$ $\Gamma_{372}/\Gamma$

VALUE (units $10^{-3}$ )	CL%	DOCUMENT ID	TECN	COMMENT
<b>&lt; 5.0 × 10<sup>-3</sup></b>	90	ALBRECHT	91B	ARG $e^+e^- \rightarrow \Upsilon(4S)$

### $\Gamma(\phi(K\pi)_0^0)/\Gamma_{total}$ $\Gamma_{373}/\Gamma$

This decay refers to the coherent sum of resonant and nonresonant  $J^P = 0^+ K\pi$  components with  $1.13 < m_{K\pi} < 1.53 \text{ GeV}/c^2$ .

VALUE (units $10^{-6}$ )	CL%	DOCUMENT ID	TECN	COMMENT
<b>4.3 ± 0.4 OUR AVERAGE</b>				
4.3 ± 0.4 ± 0.4		1 PRIM	13	BELL $e^+e^- \rightarrow \Upsilon(4S)$
4.3 ± 0.6 ± 0.4		1 AUBERT	08BG	BABR $e^+e^- \rightarrow \Upsilon(4S)$
• • • We do not use the following data for averages, fits, limits, etc. • • •				
5.0 ± 0.8 ± 0.3		1 AUBERT	07D	BABR Repl. by AUBERT 08Bg

<sup>1</sup> Assumes equal production of  $B^+$  and  $B^0$  at the  $\Upsilon(4S)$ .

### $\Gamma(\phi(K\pi)_0^0(1.60 < m_{K\pi} < 2.15))/\Gamma_{total}$ $\Gamma_{374}/\Gamma$

This decay refers to the coherent sum of resonant and nonresonant  $J^P = 0^+ K\pi$  components with  $1.60 < m_{K\pi} < 2.15 \text{ GeV}/c^2$ .

VALUE (units $10^{-6}$ )	CL%	DOCUMENT ID	TECN	COMMENT
<b>&lt; 1.7</b>	90	1 AUBERT	07Ao	BABR $e^+e^- \rightarrow \Upsilon(4S)$

<sup>1</sup> Assumes equal production of  $B^+$  and  $B^0$  at the  $\Upsilon(4S)$ .

### $\Gamma(K_0^*(1430)^0 K^- \pi^+)/\Gamma_{total}$ $\Gamma_{375}/\Gamma$

VALUE (units $10^{-6}$ )	CL%	DOCUMENT ID	TECN	COMMENT
<b>&lt; 31.8</b>	90	1,2 CHIANG	10	BELL $e^+e^- \rightarrow \Upsilon(4S)$

<sup>1</sup> Measured in the range  $0.7 < m_{K\pi} < 1.7$  and corrected using PS assumption for the full  $K\pi$  mass range.  
<sup>2</sup> Assumes equal production of  $B^+$  and  $B^0$  at the  $\Upsilon(4S)$ .

### $\Gamma(K_0^*(1430)^0 \bar{K}^*(892)^0)/\Gamma_{total}$ $\Gamma_{376}/\Gamma$

VALUE (units $10^{-6}$ )	CL%	DOCUMENT ID	TECN	COMMENT
<b>&lt; 3.3</b>	90	1,2 CHIANG	10	BELL $e^+e^- \rightarrow \Upsilon(4S)$

<sup>1</sup> Measured in the range  $0.7 < m_{K\pi} < 1.7$  and corrected using PS assumption for the full  $K\pi$  mass range.  
<sup>2</sup> Assumes equal production of  $B^+$  and  $B^0$  at the  $\Upsilon(4S)$ .

### $\Gamma(K_0^*(1430)^0 \bar{K}_0^*(1430)^0)/\Gamma_{total}$ $\Gamma_{377}/\Gamma$

VALUE (units $10^{-6}$ )	CL%	DOCUMENT ID	TECN	COMMENT
<b>&lt; 8.4</b>	90	1,2 CHIANG	10	BELL $e^+e^- \rightarrow \Upsilon(4S)$

<sup>1</sup> Measured in the range  $0.7 < m_{K\pi} < 1.7$  and corrected using PS assumption for the full  $K\pi$  mass range.  
<sup>2</sup> Assumes equal production of  $B^+$  and  $B^0$  at the  $\Upsilon(4S)$ .

### $\Gamma(K_0^*(1430)^0 \phi)/\Gamma_{total}$ $\Gamma_{378}/\Gamma$

VALUE (units $10^{-6}$ )	CL%	DOCUMENT ID	TECN	COMMENT
<b>3.9 ± 0.5 ± 0.6</b>		1 AUBERT	08BG	BABR $e^+e^- \rightarrow \Upsilon(4S)$
• • • We do not use the following data for averages, fits, limits, etc. • • •				
4.6 ± 0.7 ± 0.6		1 AUBERT	07D	BABR Repl. by AUBERT 08Bg
seen		2 AUBERT,B	04W	BABR Repl. by AUBERT 07D

<sup>1</sup> Assumes equal production of  $B^+$  and  $B^0$  at the  $\Upsilon(4S)$ .  
<sup>2</sup> Observed  $181 \pm 17$  events with statistical significance greater than  $10 \sigma$ .

### $\Gamma(K_0^*(1430)^0 K^*(892)^0)/\Gamma_{total}$ $\Gamma_{379}/\Gamma$

VALUE (units $10^{-6}$ )	CL%	DOCUMENT ID	TECN	COMMENT
<b>&lt; 1.7</b>	90	1 CHIANG	10	BELL $e^+e^- \rightarrow \Upsilon(4S)$

<sup>1</sup> Assumes equal production of  $B^+$  and  $B^0$  at the  $\Upsilon(4S)$ .

### $\Gamma(K_0^*(1430)^0 K_0^*(1430)^0)/\Gamma_{total}$ $\Gamma_{380}/\Gamma$

VALUE (units $10^{-6}$ )	CL%	DOCUMENT ID	TECN	COMMENT
<b>&lt; 4.7</b>	90	1 CHIANG	10	BELL $e^+e^- \rightarrow \Upsilon(4S)$

<sup>1</sup> Assumes equal production of  $B^+$  and  $B^0$  at the  $\Upsilon(4S)$ .

### $\Gamma(K^*(1680)^0 \phi)/\Gamma_{total}$ $\Gamma_{381}/\Gamma$

VALUE (units $10^{-6}$ )	CL%	DOCUMENT ID	TECN	COMMENT
<b>&lt; 3.5</b>	90	1 AUBERT	07Ao	BABR $e^+e^- \rightarrow \Upsilon(4S)$

<sup>1</sup> Assumes equal production of  $B^+$  and  $B^0$  at the  $\Upsilon(4S)$ .

### $\Gamma(K^*(1780)^0 \phi)/\Gamma_{total}$ $\Gamma_{382}/\Gamma$

VALUE (units $10^{-6}$ )	CL%	DOCUMENT ID	TECN	COMMENT
<b>&lt; 2.7</b>	90	1 AUBERT	07Ao	BABR $e^+e^- \rightarrow \Upsilon(4S)$

<sup>1</sup> Assumes equal production of  $B^+$  and  $B^0$  at the  $\Upsilon(4S)$ .

# Meson Particle Listings

## $B^0$

### $\Gamma(K^*(2045)^0 \phi) / \Gamma_{total}$ $\Gamma_{383} / \Gamma$

VALUE (units $10^{-6}$ )	CL%	DOCUMENT ID	TECN	COMMENT
<b>&lt;15.3</b>	90	<sup>1</sup> AUBERT	07A0 BABR	$e^+e^- \rightarrow \Upsilon(4S)$

<sup>1</sup> Assumes equal production of  $B^+$  and  $B^0$  at the  $\Upsilon(4S)$ .

### $\Gamma(K_2^*(1430)^0 \rho^0) / \Gamma_{total}$ $\Gamma_{384} / \Gamma$

VALUE (units $10^{-6}$ )	CL%	DOCUMENT ID	TECN	COMMENT
<b>&lt;1.1 <math>\times 10^3</math></b>	90	ALBRECHT	91B ARG	$e^+e^- \rightarrow \Upsilon(4S)$

### $\Gamma(K_2^*(1430)^0 \phi) / \Gamma_{total}$ $\Gamma_{385} / \Gamma$

VALUE (units $10^{-6}$ )	CL%	DOCUMENT ID	TECN	COMMENT
<b><math>6.8 \pm 0.9</math> OUR AVERAGE</b>		Error includes scale factor of 1.2.		
$5.5^{+0.9}_{-0.7} \pm 1.0$		<sup>1</sup> PRIM	13 BELL	$e^+e^- \rightarrow \Upsilon(4S)$
$7.5 \pm 0.9 \pm 0.5$		<sup>1</sup> AUBERT	08B0 BABR	$e^+e^- \rightarrow \Upsilon(4S)$
<b>•••</b> We do not use the following data for averages, fits, limits, etc. <b>••••</b>				
$7.8 \pm 1.1 \pm 0.6$		<sup>1</sup> AUBERT	07D BABR	Repl. by AUBERT 08B0
		<sup>2</sup> AUBERT,B	04W BABR	Repl. by AUBERT 07D
<1400	90	ALBRECHT	91B ARG	$e^+e^- \rightarrow \Upsilon(4S)$

<sup>1</sup> Assumes equal production of  $B^+$  and  $B^0$  at the  $\Upsilon(4S)$ .  
<sup>2</sup> The angular distribution of  $B \rightarrow \phi K^*(1430)$  provides evidence with statistical significance of 3.2  $\sigma$ .

### $\Gamma(K^0 \phi \phi) / \Gamma_{total}$ $\Gamma_{386} / \Gamma$

VALUE (units $10^{-6}$ )	CL%	DOCUMENT ID	TECN	COMMENT
<b><math>4.5 \pm 0.8 \pm 0.3</math></b>		<sup>1</sup> LEES	11A BABR	$e^+e^- \rightarrow \Upsilon(4S)$
<b>•••</b> We do not use the following data for averages, fits, limits, etc. <b>••••</b>				
$4.1^{+1.7}_{-1.4} \pm 0.4$		<sup>1</sup> AUBERT,BE	06H BABR	Repl. by LEES 11A

<sup>1</sup> Assumes equal production of  $B^0$  and  $B^+$  at the  $\Upsilon(4S)$  and for a  $\phi\phi$  invariant mass below 2.85 GeV/c<sup>2</sup>.

### $\Gamma(\eta' \eta' K^0) / \Gamma_{total}$ $\Gamma_{387} / \Gamma$

VALUE (units $10^{-6}$ )	CL%	DOCUMENT ID	TECN	COMMENT
<b>&lt;31</b>	90	<sup>1</sup> AUBERT,B	06P BABR	$e^+e^- \rightarrow \Upsilon(4S)$

<sup>1</sup> Assumes equal production of  $B^+$  and  $B^0$  at the  $\Upsilon(4S)$ .

### $\Gamma(\eta K^0 \gamma) / \Gamma_{total}$ $\Gamma_{388} / \Gamma$

VALUE (units $10^{-6}$ )	CL%	DOCUMENT ID	TECN	COMMENT
<b><math>7.6 \pm 1.8</math> OUR AVERAGE</b>				
$7.1^{+2.1}_{-2.0} \pm 0.4$		<sup>1,2</sup> AUBERT	09 BABR	$e^+e^- \rightarrow \Upsilon(4S)$
$8.7^{+3.1+1.9}_{-2.7-1.6}$		<sup>2,3</sup> NISHIDA	05 BELL	$e^+e^- \rightarrow \Upsilon(4S)$
<b>•••</b> We do not use the following data for averages, fits, limits, etc. <b>••••</b>				
$11.3^{+2.8}_{-1.6} \pm 0.6$		<sup>1,2</sup> AUBERT,B	06M BABR	Repl. by AUBERT 09

<sup>1</sup>  $m_{\eta K} < 3.25$  GeV/c<sup>2</sup>.  
<sup>2</sup> Assumes equal production of  $B^+$  and  $B^0$  at the  $\Upsilon(4S)$ .  
<sup>3</sup>  $m_{\eta K} < 2.4$  GeV/c<sup>2</sup>.

### $\Gamma(\eta' K^0 \gamma) / \Gamma_{total}$ $\Gamma_{389} / \Gamma$

VALUE (units $10^{-6}$ )	CL%	DOCUMENT ID	TECN	COMMENT
<b>&lt;6.4</b>	90	<sup>1,2</sup> WEDD	10 BELL	$e^+e^- \rightarrow \Upsilon(4S)$
<b>•••</b> We do not use the following data for averages, fits, limits, etc. <b>••••</b>				
<6.6	90	<sup>1,3</sup> AUBERT,B	06M BABR	$e^+e^- \rightarrow \Upsilon(4S)$

<sup>1</sup> Assumes equal production of  $B^+$  and  $B^0$  at the  $\Upsilon(4S)$ .  
<sup>2</sup>  $m_{\eta' K} < 3.4$  GeV/c<sup>2</sup>.  
<sup>3</sup>  $m_{\eta' K} < 3.25$  GeV/c<sup>2</sup>.

### $\Gamma(K^0 \phi \gamma) / \Gamma_{total}$ $\Gamma_{390} / \Gamma$

VALUE (units $10^{-6}$ )	CL%	DOCUMENT ID	TECN	COMMENT
<b><math>2.74 \pm 0.60 \pm 0.32</math></b>		<sup>1</sup> SAHO0	11A BELL	$e^+e^- \rightarrow \Upsilon(4S)$
<b>•••</b> We do not use the following data for averages, fits, limits, etc. <b>••••</b>				
<2.7	90	<sup>1</sup> AUBERT	07Q BABR	$e^+e^- \rightarrow \Upsilon(4S)$
<8.3	90	<sup>1</sup> DRUTSKOY	04 BELL	$e^+e^- \rightarrow \Upsilon(4S)$

<sup>1</sup> Assumes equal production of  $B^+$  and  $B^0$  at  $\Upsilon(4S)$ .

### $\Gamma(K^+ \pi^- \gamma) / \Gamma_{total}$ $\Gamma_{391} / \Gamma$

VALUE	CL%	DOCUMENT ID	TECN	COMMENT
<b><math>(4.6^{+1.3+0.5}_{-1.2-0.7}) \times 10^{-6}</math></b>		<sup>1,2</sup> NISHIDA	02 BELL	$e^+e^- \rightarrow \Upsilon(4S)$

<sup>1</sup> Assumes equal production of  $B^+$  and  $B^0$  at the  $\Upsilon(4S)$ .  
<sup>2</sup> 1.25 GeV/c<sup>2</sup> <  $M_{K\pi}$  < 1.6 GeV/c<sup>2</sup>

### $\Gamma(K^*(892)^0 \gamma) / \Gamma_{total}$ $\Gamma_{392} / \Gamma$

VALUE (units $10^{-6}$ )	CL%	DOCUMENT ID	TECN	COMMENT
<b><math>41.8 \pm 2.5</math> OUR AVERAGE</b>		Error includes scale factor of 2.1.		
$39.6 \pm 0.7 \pm 1.4$		<sup>1</sup> HORIGUCHI	17 BELL	$e^+e^- \rightarrow \Upsilon(4S)$
$44.7 \pm 1.0 \pm 1.6$		<sup>2</sup> AUBERT	09A0 BABR	$e^+e^- \rightarrow \Upsilon(4S)$
$45.5^{+7.2}_{-6.8} \pm 3.4$		<sup>3</sup> COAN	00 CLE2	$e^+e^- \rightarrow \Upsilon(4S)$
<b>•••</b> We do not use the following data for averages, fits, limits, etc. <b>••••</b>				
$39.2 \pm 2.0 \pm 2.4$		<sup>4</sup> AUBERT,BE	04A BABR	Repl. by AUBERT 09A0
$40.1 \pm 2.1 \pm 1.7$		<sup>5</sup> NAKAO	04 BELL	Repl. by HORIGUCHI 17
<110	90	ACOSTA	02G CDF	$p\bar{p}$ at 1.8 TeV
$42.3 \pm 4.0 \pm 2.2$		<sup>5</sup> AUBERT	02C BABR	Repl. by AUBERT,BE 04A
<210	90	<sup>6</sup> ADAM	96D DLPH	$e^+e^- \rightarrow Z$
$40 \pm 17 \pm 8$		<sup>7</sup> AMMAR	93 CLE2	Repl. by COAN 00
<420	90	ALBRECHT	89G ARG	$e^+e^- \rightarrow \Upsilon(4S)$
<240	90	<sup>8</sup> AVERY	89B CLEO	$e^+e^- \rightarrow \Upsilon(4S)$
<2100	90	AVERY	87 CLEO	$e^+e^- \rightarrow \Upsilon(4S)$

<sup>1</sup> Uses  $B(\Upsilon(4S) \rightarrow B^+ B^-) = (51.4 \pm 0.6)\%$  and  $B(\Upsilon(4S) \rightarrow B^0 \bar{B}^0) = (48.6 \pm 0.6)\%$ .  
<sup>2</sup> Uses  $B(\Upsilon(4S) \rightarrow B^+ B^-) = (51.6 \pm 0.6)\%$  and  $B(\Upsilon(4S) \rightarrow B^0 \bar{B}^0) = (48.4 \pm 0.6)\%$ .  
<sup>3</sup> Assumes equal production of  $B^+$  and  $B^0$  at the  $\Upsilon(4S)$ . No evidence for a nonresonant  $K\pi\gamma$  contamination was seen; the central value assumes no contamination.  
<sup>4</sup> Uses the production ratio of charged and neutral B from  $\Upsilon(4S)$  decays  $R^{+0} = 1.006 \pm 0.048$ .  
<sup>5</sup> Assumes equal production of  $B^+$  and  $B^0$  at the  $\Upsilon(4S)$ .  
<sup>6</sup> ADAM 96d assumes  $f_{B^0} = f_{B^-} = 0.39$  and  $f_{B_s} = 0.12$ .  
<sup>7</sup> AMMAR 93 observed 6.6  $\pm$  2.8 events above background.  
<sup>8</sup> AVERY 89b reports <  $2.8 \times 10^{-4}$  assuming the  $\Upsilon(4S)$  decays 43% to  $B^0 \bar{B}^0$ . We rescale to 50%.

### $\Gamma(K^*(1410)\gamma) / \Gamma_{total}$ $\Gamma_{393} / \Gamma$

VALUE	CL%	DOCUMENT ID	TECN	COMMENT
<b>&lt;1.3 <math>\times 10^{-4}</math></b>	90	<sup>1</sup> NISHIDA	02 BELL	$e^+e^- \rightarrow \Upsilon(4S)$

<sup>1</sup> Assumes equal production of  $B^+$  and  $B^0$  at the  $\Upsilon(4S)$ .

### $\Gamma(K^+ \pi^- \gamma \text{ nonresonant}) / \Gamma_{total}$ $\Gamma_{394} / \Gamma$

VALUE	CL%	DOCUMENT ID	TECN	COMMENT
<b>&lt;2.6 <math>\times 10^{-6}</math></b>	90	<sup>1,2</sup> NISHIDA	02 BELL	$e^+e^- \rightarrow \Upsilon(4S)$

<sup>1</sup> Assumes equal production of  $B^+$  and  $B^0$  at the  $\Upsilon(4S)$ .  
<sup>2</sup> 1.25 GeV/c<sup>2</sup> <  $M_{K\pi}$  < 1.6 GeV/c<sup>2</sup>

### $\Gamma(K^*(892)^0 X(214), X \rightarrow \mu^+ \mu^-) / \Gamma_{total}$ $\Gamma_{395} / \Gamma$

$X(214)$  is a hypothetical particle of mass 214 MeV/c<sup>2</sup> reported by the HyperCP experiment (PARK 05)

VALUE (units $10^{-8}$ )	CL%	DOCUMENT ID	TECN	COMMENT
<b>&lt;2.26</b>	90	<sup>1,2</sup> HYUN	10 BELL	$e^+e^- \rightarrow \Upsilon(4S)$

<sup>1</sup> Assumes equal production of  $B^+$  and  $B^0$  at the  $\Upsilon(4S)$ .  
<sup>2</sup> Based on scalar nature of X particle. With a vector X assumption, the upper limit is  $2.27 \times 10^{-8}$ .

### $\Gamma(K^0 \pi^+ \pi^- \gamma) / \Gamma_{total}$ $\Gamma_{396} / \Gamma$

VALUE (units $10^{-5}$ )	CL%	DOCUMENT ID	TECN	COMMENT
<b><math>1.99 \pm 0.18</math> OUR AVERAGE</b>				
$2.05 \pm 0.20^{+0.26}_{-0.22}$		<sup>1,2</sup> DEL-AMO-SA.	16 BABR	$e^+e^- \rightarrow \Upsilon(4S)$
$1.85 \pm 0.21 \pm 0.12$		<sup>1,3</sup> AUBERT	07R BABR	$e^+e^- \rightarrow \Upsilon(4S)$
$2.40 \pm 0.4 \pm 0.3$		<sup>3,4</sup> YANG	05 BELL	$e^+e^- \rightarrow \Upsilon(4S)$

<sup>1</sup>  $M_{K\pi\pi} < 1.8$  GeV/c<sup>2</sup>.  
<sup>2</sup> Uses  $B(\Upsilon(4S) \rightarrow B^+ B^-) = 0.513 \pm 0.006$ .  
<sup>3</sup> Assumes equal production of  $B^+$  and  $B^0$  at the  $\Upsilon(4S)$ .  
<sup>4</sup>  $M_{K\pi\pi} < 2.0$  GeV/c<sup>2</sup>.

### $\Gamma(K^+ \pi^- \pi^0 \gamma) / \Gamma_{total}$ $\Gamma_{397} / \Gamma$

VALUE (units $10^{-5}$ )	CL%	DOCUMENT ID	TECN	COMMENT
<b><math>4.07 \pm 0.22 \pm 0.31</math></b>		<sup>1,2</sup> AUBERT	07R BABR	$e^+e^- \rightarrow \Upsilon(4S)$

<sup>1</sup>  $M_{K\pi\pi} < 1.8$  GeV/c<sup>2</sup>.  
<sup>2</sup> Assumes equal production of  $B^+$  and  $B^0$  at the  $\Upsilon(4S)$ .

### $\Gamma(K_1(1270)^0 \gamma) / \Gamma_{total}$ $\Gamma_{398} / \Gamma$

VALUE (units $10^{-5}$ )	CL%	DOCUMENT ID	TECN	COMMENT
<b>&lt; 5.8</b>	90	<sup>1</sup> YANG	05 BELL	$e^+e^- \rightarrow \Upsilon(4S)$
<b>•••</b> We do not use the following data for averages, fits, limits, etc. <b>••••</b>				
<700	90	<sup>2</sup> ALBRECHT	89G ARG	$e^+e^- \rightarrow \Upsilon(4S)$

<sup>1</sup> Assumes equal production of  $B^+$  and  $B^0$  at the  $\Upsilon(4S)$ .  
<sup>2</sup> ALBRECHT 89g reports < 0.0078 assuming the  $\Upsilon(4S)$  decays 45% to  $B^0 \bar{B}^0$ . We rescale to 50%.

### $\Gamma(K_1(1400)^0 \gamma) / \Gamma_{total}$ $\Gamma_{399} / \Gamma$

VALUE (units $10^{-5}$ )	CL%	DOCUMENT ID	TECN	COMMENT
<b>&lt; 1.2</b>	90	<sup>1</sup> YANG	05 BELL	$e^+e^- \rightarrow \Upsilon(4S)$
<b>•••</b> We do not use the following data for averages, fits, limits, etc. <b>••••</b>				
<430	90	<sup>2</sup> ALBRECHT	89G ARG	$e^+e^- \rightarrow \Upsilon(4S)$

<sup>1</sup> Assumes equal production of  $B^+$  and  $B^0$  at the  $\Upsilon(4S)$ .  
<sup>2</sup> ALBRECHT 89g reports < 0.0048 assuming the  $\Upsilon(4S)$  decays 45% to  $B^0 \bar{B}^0$ . We rescale to 50%.

$\Gamma(K_S^0(1430)^0 \gamma) / \Gamma_{\text{total}}$   $\Gamma_{400} / \Gamma$ 

VALUE (units $10^{-5}$ )	CL%	DOCUMENT ID	TECN	COMMENT
<b>1.24 ± 0.24 OUR AVERAGE</b>				
1.22 ± 0.25 ± 0.10		<sup>1</sup> AUBERT,B	04U BABR	$e^+e^- \rightarrow \Upsilon(4S)$
1.3 ± 0.5 ± 0.1		<sup>1</sup> NISHIDA	02 BELL	$e^+e^- \rightarrow \Upsilon(4S)$
• • • We do not use the following data for averages, fits, limits, etc. • • •				
<40	90	<sup>2</sup> ALBRECHT	89G ARG	$e^+e^- \rightarrow \Upsilon(4S)$
<sup>1</sup> Assumes equal production of $B^+$ and $B^0$ at the $\Upsilon(4S)$ .				
<sup>2</sup> ALBRECHT 89G reports $< 4.4 \times 10^{-4}$ assuming the $\Upsilon(4S)$ decays 45% to $B^0 \bar{B}^0$ . We rescale to 50%.				

 $\Gamma(K^*(1680)^0 \gamma) / \Gamma_{\text{total}}$   $\Gamma_{401} / \Gamma$ 

VALUE	CL%	DOCUMENT ID	TECN	COMMENT
<b>&lt;0.0020</b>				
	90	<sup>1</sup> ALBRECHT	89G ARG	$e^+e^- \rightarrow \Upsilon(4S)$
<sup>1</sup> ALBRECHT 89G reports $< 0.0022$ assuming the $\Upsilon(4S)$ decays 45% to $B^0 \bar{B}^0$ . We rescale to 50%.				

 $\Gamma(K_S^0(1780)^0 \gamma) / \Gamma_{\text{total}}$   $\Gamma_{402} / \Gamma$ 

VALUE (units $10^{-6}$ )	CL%	DOCUMENT ID	TECN	COMMENT
<b>&lt; 83</b>				
	90	<sup>1,2</sup> NISHIDA	05 BELL	$e^+e^- \rightarrow \Upsilon(4S)$
• • • We do not use the following data for averages, fits, limits, etc. • • •				
<10000	90	<sup>3</sup> ALBRECHT	89G ARG	$e^+e^- \rightarrow \Upsilon(4S)$
<sup>1</sup> Assumes equal production of $B^+$ and $B^0$ at the $\Upsilon(4S)$ .				
<sup>2</sup> Uses $B(K_S^0(1780) \rightarrow \eta K) = 0.11^{+0.05}_{-0.04}$ .				
<sup>3</sup> ALBRECHT 89G reports $< 0.011$ assuming the $\Upsilon(4S)$ decays 45% to $B^0 \bar{B}^0$ . We rescale to 50%.				

 $\Gamma(K_S^0(2045)^0 \gamma) / \Gamma_{\text{total}}$   $\Gamma_{403} / \Gamma$ 

VALUE	CL%	DOCUMENT ID	TECN	COMMENT
<b>&lt;0.0043</b>				
	90	<sup>1</sup> ALBRECHT	89G ARG	$e^+e^- \rightarrow \Upsilon(4S)$
<sup>1</sup> ALBRECHT 89G reports $< 0.0048$ assuming the $\Upsilon(4S)$ decays 45% to $B^0 \bar{B}^0$ . We rescale to 50%.				

 $\Gamma(\rho^0 \gamma) / \Gamma_{\text{total}}$   $\Gamma_{404} / \Gamma$ 

VALUE (units $10^{-6}$ )	CL%	DOCUMENT ID	TECN	COMMENT
<b>0.86 ± 0.15 OUR AVERAGE</b>				
0.97 <sup>+0.24</sup> <sub>-0.22</sub> ± 0.06		<sup>1</sup> AUBERT	08BH BABR	$e^+e^- \rightarrow \Upsilon(4S)$
0.78 <sup>+0.17+0.09</sup> <sub>-0.16-0.10</sub>		<sup>1</sup> TANIGUCHI	08 BELL	$e^+e^- \rightarrow \Upsilon(4S)$
• • • We do not use the following data for averages, fits, limits, etc. • • •				
0.79 <sup>+0.22</sup> <sub>-0.20</sub> ± 0.06		<sup>1</sup> AUBERT	07L BABR	Repl. by AUBERT 08BH
1.25 <sup>+0.37+0.07</sup> <sub>-0.33-0.06</sub>		<sup>1</sup> MOHAPATRA	06 BELL	Repl. by TANIGUCHI 08
0.0 ± 0.2 ± 0.1	90	<sup>1</sup> AUBERT	05 BABR	Repl. by AUBERT 07L
< 0.8	90	<sup>1</sup> MOHAPATRA	05 BELL	$e^+e^- \rightarrow \Upsilon(4S)$
< 1.2	90	<sup>1</sup> AUBERT	04C BABR	$e^+e^- \rightarrow \Upsilon(4S)$
<17	90	<sup>1</sup> COAN	00 CLE2	$e^+e^- \rightarrow \Upsilon(4S)$
<sup>1</sup> Assumes equal production of $B^+$ and $B^0$ at the $\Upsilon(4S)$ .				

 $\Gamma(\rho^0 X(214), X \rightarrow \mu^+ \mu^-) / \Gamma_{\text{total}}$   $\Gamma_{405} / \Gamma$ 

$X(214)$  is a hypothetical particle of mass 214 MeV/ $c^2$  reported by the HyperCP experiment (PARK 05)

VALUE (units $10^{-8}$ )	CL%	DOCUMENT ID	TECN	COMMENT
<b>&lt;1.73</b>				
	90	<sup>1,2</sup> HYUN	10 BELL	$e^+e^- \rightarrow \Upsilon(4S)$
<sup>1</sup> Assumes equal production of $B^+$ and $B^0$ at the $\Upsilon(4S)$ .				
<sup>2</sup> The result is the same for a scalar or vector X particle.				

 $\Gamma(\rho^0 \gamma) / \Gamma(K^*(892)^0 \gamma)$   $\Gamma_{404} / \Gamma_{392}$ 

VALUE (units $10^{-2}$ )	DOCUMENT ID	TECN	COMMENT
<b>2.06<sup>+0.45+0.14</sup><sub>-0.43-0.16</sub></b>	TANIGUCHI	08 BELL	$e^+e^- \rightarrow \Upsilon(4S)$

 $\Gamma(\omega \gamma) / \Gamma_{\text{total}}$   $\Gamma_{406} / \Gamma$ 

VALUE (units $10^{-6}$ )	CL%	DOCUMENT ID	TECN	COMMENT
<b>0.44<sup>+0.18</sup><sub>-0.16</sub> OUR AVERAGE</b>				
0.50 <sup>+0.27</sup> <sub>-0.23</sub> ± 0.09		<sup>1</sup> AUBERT	08BH BABR	$e^+e^- \rightarrow \Upsilon(4S)$
0.40 <sup>+0.19</sup> <sub>-0.17</sub> ± 0.13		<sup>1</sup> TANIGUCHI	08 BELL	$e^+e^- \rightarrow \Upsilon(4S)$
• • • We do not use the following data for averages, fits, limits, etc. • • •				
0.40 <sup>+0.24</sup> <sub>-0.20</sub> ± 0.05		<sup>1</sup> AUBERT	07L BABR	Repl. by AUBERT 08BH
0.56 <sup>+0.34+0.05</sup> <sub>-0.27-0.10</sub>		<sup>1</sup> MOHAPATRA	06 BELL	Repl. by TANIGUCHI 08
<1.0	90	<sup>1</sup> AUBERT	05 BABR	Repl. by AUBERT 07L
<0.8	90	<sup>1</sup> MOHAPATRA	05 BELL	Repl. by MOHAPATRA 06
<1.0	90	<sup>1</sup> AUBERT	04C BABR	$e^+e^- \rightarrow \Upsilon(4S)$
<9.2	90	<sup>1</sup> COAN	00 CLE2	$e^+e^- \rightarrow \Upsilon(4S)$
<sup>1</sup> Assumes equal production of $B^+$ and $B^0$ at the $\Upsilon(4S)$ .				

 $\Gamma(\phi \gamma) / \Gamma_{\text{total}}$   $\Gamma_{407} / \Gamma$ 

VALUE	CL%	DOCUMENT ID	TECN	COMMENT
<b>&lt;1.0 × 10<sup>-7</sup></b>				
	90	<sup>1</sup> KING	16 BELL	$e^+e^- \rightarrow \Upsilon(4S)$
• • • We do not use the following data for averages, fits, limits, etc. • • •				
<8.5 × 10 <sup>-7</sup>	90	<sup>1</sup> AUBERT,BE	05C BABR	$e^+e^- \rightarrow \Upsilon(4S)$
<3.3 × 10 <sup>-6</sup>	90	<sup>1</sup> COAN	00 CLE2	$e^+e^- \rightarrow \Upsilon(4S)$
<sup>1</sup> Assumes equal production of $B^+$ and $B^0$ at the $\Upsilon(4S)$ .				

 $\Gamma(\pi^+ \pi^-) / \Gamma_{\text{total}}$   $\Gamma_{408} / \Gamma$ 

VALUE (units $10^{-6}$ )	CL%	DOCUMENT ID	TECN	COMMENT
<b>5.12 ± 0.19 OUR FIT</b>				
<b>5.13 ± 0.24 OUR AVERAGE</b>				
5.04 ± 0.21 ± 0.18		<sup>1</sup> DUH	13 BELL	$e^+e^- \rightarrow \Upsilon(4S)$
5.5 ± 0.4 ± 0.3		<sup>1</sup> AUBERT	07B BABR	$e^+e^- \rightarrow \Upsilon(4S)$
4.5 <sup>+1.4+0.5</sup> <sub>-1.2-0.4</sub>		<sup>1</sup> BORNHEIM	03 CLE2	$e^+e^- \rightarrow \Upsilon(4S)$
• • • We do not use the following data for averages, fits, limits, etc. • • •				
5.1 ± 0.2 ± 0.2		<sup>1</sup> LIN	07A BELL	Repl. by DUH 13
4.4 ± 0.6 ± 0.3		<sup>1</sup> CHAO	04 BELL	Repl. by LIN 07A
4.7 ± 0.6 ± 0.2		<sup>1</sup> AUBERT	02Q BABR	Repl. by AUBERT 07B
5.4 ± 1.2 ± 0.5		<sup>1</sup> CASEY	02 BELL	Repl. by CHAO 04
5.6 <sup>+2.3+0.4</sup> <sub>-2.0-0.5</sub>		<sup>1</sup> ABE	01H BELL	Repl. by CASEY 02
4.1 ± 1.0 ± 0.7		<sup>1</sup> AUBERT	01E BABR	Repl. by AUBERT 02Q
< 6.1	90	<sup>2</sup> ABE	00C SLD	$e^+e^- \rightarrow Z$
4.3 <sup>+1.6</sup> <sub>-1.4</sub> ± 0.5		<sup>1</sup> CRONIN-HEN..	00 CLE2	Repl. by BORNHEIM 03
< 15	90	GODANG	98 CLE2	Repl. by CRONIN-HENNESSY 00
< 45	90	<sup>3</sup> ADAM	96D DLPH	$e^+e^- \rightarrow Z$
< 20	90	ASNER	96 CLE2	Repl. by GODANG 98
< 41	90	<sup>4</sup> BUSKULIC	96V ALEP	$e^+e^- \rightarrow Z$
< 55	90	<sup>5</sup> ABREU	95N DLPH	Sup. by ADAM 96D
< 47	90	<sup>6</sup> AKERS	94L OPAL	$e^+e^- \rightarrow Z$
< 29	90	<sup>1</sup> BATTLE	93 CLE2	$e^+e^- \rightarrow \Upsilon(4S)$
<130	90	<sup>1</sup> ALBRECHT	90B ARG	$e^+e^- \rightarrow \Upsilon(4S)$
< 77	90	<sup>7</sup> BORTOLETTO	89 CLEO	$e^+e^- \rightarrow \Upsilon(4S)$
<260	90	<sup>7</sup> BEBEK	87 CLEO	$e^+e^- \rightarrow \Upsilon(4S)$
<500	90	GILES	84 CLEO	$e^+e^- \rightarrow \Upsilon(4S)$
<sup>1</sup> Assumes equal production of $B^+$ and $B^0$ at the $\Upsilon(4S)$ .				
<sup>2</sup> ABE 00C assumes $B(Z \rightarrow b\bar{b}) = (21.7 \pm 0.1)\%$ and the $B$ fractions $f_{B^0} = f_{B^+} = (39.7^{+1.8}_{-2.2})\%$ and $f_{B_s} = (10.5^{+1.8}_{-2.2})\%$ .				
<sup>3</sup> ADAM 96D assumes $f_{B^0} = f_{B^-} = 0.39$ and $f_{B_s} = 0.12$ .				
<sup>4</sup> BUSKULIC 96V assumes PDG 96 production fractions for $B^0, B^+, B_s, b$ baryons.				
<sup>5</sup> Assumes a $B^0, B^-$ production fraction of 0.39 and a $B_s$ production fraction of 0.12.				
<sup>6</sup> Assumes $B(Z \rightarrow b\bar{b}) = 0.217$ and $B_b^0(B_b^0)$ fraction 39.5% (12%).				
<sup>7</sup> Paper assumes the $\Upsilon(4S)$ decays 43% to $B^0 \bar{B}^0$ . We rescale to 50%.				

 $\Gamma(\pi^+ \pi^-) / \Gamma(K^+ \pi^-)$   $\Gamma_{408} / \Gamma_{275}$ 

VALUE	DOCUMENT ID	TECN	COMMENT
<b>0.261 ± 0.010 OUR FIT</b>			
<b>0.261 ± 0.015 OUR AVERAGE</b>			
0.262 ± 0.009 ± 0.017	AALJ	12AR LHCb	$pp$ at 7 TeV
0.259 ± 0.017 ± 0.016	AALTONEN	11N CDF	$p\bar{p}$ at 1.96 TeV
• • • We do not use the following data for averages, fits, limits, etc. • • •			
0.21 ± 0.05 ± 0.03	ABULENCIA,A	06D CDF	Repl. by AALTONEN 11N

 $\Gamma(\pi^0 \pi^0) / \Gamma_{\text{total}}$   $\Gamma_{409} / \Gamma$ 

VALUE (units $10^{-6}$ )	CL%	DOCUMENT ID	TECN	COMMENT
<b>1.59 ± 0.26 OUR AVERAGE</b>				
1.31 ± 0.19 ± 0.19		<sup>1</sup> JULIUS	17 BELL	$e^+e^- \rightarrow \Upsilon(4S)$
1.83 ± 0.21 ± 0.13		<sup>1</sup> LEES	13D BABR	$e^+e^- \rightarrow \Upsilon(4S)$
• • • We do not use the following data for averages, fits, limits, etc. • • •				
1.47 ± 0.25 ± 0.12		<sup>1</sup> AUBERT	07Bc BABR	Repl. by LEES 13D
1.17 ± 0.32 ± 0.10		<sup>1</sup> AUBERT	05L BABR	Repl. by AUBERT 07Bc
2.3 <sup>+0.4+0.2</sup> <sub>-0.5-0.3</sub>		<sup>1</sup> CHAO	05 BELL	Repl. by JULIUS 17
< 3.6	90	<sup>1</sup> AUBERT	03L BABR	$e^+e^- \rightarrow \Upsilon(4S)$
2.1 ± 0.6 ± 0.3		<sup>1</sup> AUBERT	03S BABR	Repl. by AUBERT 05L
< 4.4	90	<sup>1</sup> BORNHEIM	03 CLE2	$e^+e^- \rightarrow \Upsilon(4S)$
1.7 ± 0.6 ± 0.2		<sup>1</sup> LEE	03 BELL	Repl. by CHAO 05
< 5.7	90	<sup>1</sup> ASNER	02 CLE2	$e^+e^- \rightarrow \Upsilon(4S)$
< 6.4	90	<sup>1</sup> CASEY	02 BELL	$e^+e^- \rightarrow \Upsilon(4S)$
< 9.3	90	GODANG	98 CLE2	Repl. by ASNER 02
< 9.1	90	ASNER	96 CLE2	Repl. by GODANG 98
<60	90	<sup>2</sup> ACCIARRI	95H L3	$e^+e^- \rightarrow Z$
<sup>1</sup> Assumes equal production of $B^+$ and $B^0$ at the $\Upsilon(4S)$ .				
<sup>2</sup> ACCIARRI 95H assumes $f_{B^0} = 39.5 \pm 4.0$ and $f_{B_s} = 12.0 \pm 3.0\%$ .				

## Meson Particle Listings

 $B^0$ 

$\Gamma(\eta\pi^0)/\Gamma_{\text{total}}$	CL%	DOCUMENT ID	TECN	COMMENT	$\Gamma_{410}/\Gamma$
$0.41^{+0.17+0.05}_{-0.15-0.07}$		1,2 PAL	15	BELL $e^+e^- \rightarrow \Upsilon(4S)$	

••• We do not use the following data for averages, fits, limits, etc. •••

< 1.5	90	<sup>2</sup> AUBERT	08AH	BABR $e^+e^- \rightarrow \Upsilon(4S)$	
< 1.3	90	<sup>2</sup> AUBERT	06W	BABR Repl. by AUBERT 08AH	
< 2.5	90	<sup>2</sup> CHANG	05A	BELL Repl. by PAL 15	
< 2.5	90	<sup>2</sup> AUBERT,B	04D	BABR Repl. by AUBERT 06W	
< 2.9	90	<sup>2</sup> RICHICHI	00	CLE2 $e^+e^- \rightarrow \Upsilon(4S)$	
< 8	90	BEHRENS	98	CLE2 Repl. by RICHICHI 00	
< 250	90	<sup>3</sup> ACCIARRI	95H	L3 $e^+e^- \rightarrow Z$	
< 1800	90	<sup>2</sup> ALBRECHT	90B	ARG $e^+e^- \rightarrow \Upsilon(4S)$	

<sup>1</sup> PAL 15 signal significance is 3.0 standard deviations. The measurement corresponds to 90% CL upper limit of  $< 6.5 \times 10^{-7}$ .

<sup>2</sup> Assumes equal production of  $B^+$  and  $B^0$  at the  $\Upsilon(4S)$ .

<sup>3</sup> ACCIARRI 95H assumes  $f_{B^0} = 39.5 \pm 4.0$  and  $f_{B_s} = 12.0 \pm 3.0\%$ .

$\Gamma(\eta)/\Gamma_{\text{total}}$	CL%	DOCUMENT ID	TECN	COMMENT	$\Gamma_{411}/\Gamma$
< 1.0	90	<sup>1</sup> AUBERT	09AV	BABR $e^+e^- \rightarrow \Upsilon(4S)$	

••• We do not use the following data for averages, fits, limits, etc. •••

< 1.8	90	<sup>1</sup> AUBERT,B	06V	BABR Repl. by AUBERT 09AV	
< 2.0	90	<sup>1</sup> CHANG	05A	BELL $e^+e^- \rightarrow \Upsilon(4S)$	
< 2.8	90	<sup>1</sup> AUBERT,B	04X	BABR $e^+e^- \rightarrow \Upsilon(4S)$	
< 18	90	BEHRENS	98	CLE2 $e^+e^- \rightarrow \Upsilon(4S)$	
< 410	90	<sup>2</sup> ACCIARRI	95H	L3 $e^+e^- \rightarrow Z$	

<sup>1</sup> Assumes equal production of  $B^+$  and  $B^0$  at the  $\Upsilon(4S)$ .

<sup>2</sup> ACCIARRI 95H assumes  $f_{B^0} = 39.5 \pm 4.0$  and  $f_{B_s} = 12.0 \pm 3.0\%$ .

$\Gamma(\eta'\pi^0)/\Gamma_{\text{total}}$	CL%	DOCUMENT ID	TECN	COMMENT	$\Gamma_{412}/\Gamma$
$1.2 \pm 0.6$ OUR AVERAGE		Error includes scale factor of 1.7.			
$0.9 \pm 0.4 \pm 0.1$		<sup>1</sup> AUBERT	08AH	BABR $e^+e^- \rightarrow \Upsilon(4S)$	
$2.8 \pm 1.0 \pm 0.3$		<sup>1</sup> SCHUEMANN	06	BELL $e^+e^- \rightarrow \Upsilon(4S)$	

••• We do not use the following data for averages, fits, limits, etc. •••

$0.8^{+0.8}_{-0.6} \pm 0.1$		<sup>1</sup> AUBERT	06W	BABR Repl. by AUBERT 08AH	
$1.0^{+1.4}_{-1.0} \pm 0.8$	90	<sup>1</sup> AUBERT,B	04D	BABR Repl. by AUBERT 06W	
< 5.7	90	<sup>1</sup> RICHICHI	00	CLE2 $e^+e^- \rightarrow \Upsilon(4S)$	
< 11	90	BEHRENS	98	CLE2 Repl. by RICHICHI 00	

<sup>1</sup> Assumes equal production of  $B^+$  and  $B^0$  at the  $\Upsilon(4S)$ .

$\Gamma(\eta'\eta)/\Gamma_{\text{total}}$	CL%	DOCUMENT ID	TECN	COMMENT	$\Gamma_{413}/\Gamma$
< 1.7	90	<sup>1</sup> AUBERT	09AV	BABR $e^+e^- \rightarrow \Upsilon(4S)$	

••• We do not use the following data for averages, fits, limits, etc. •••

< 6.5	90	<sup>1</sup> SCHUEMANN	07	BELL $e^+e^- \rightarrow \Upsilon(4S)$	
< 2.4	90	<sup>1</sup> AUBERT,B	06V	BABR Repl. by AUBERT 09AV	
< 10	90	<sup>1</sup> AUBERT,B	04X	BABR Repl. by AUBERT,B 06V	
< 47	90	BEHRENS	98	CLE2 $e^+e^- \rightarrow \Upsilon(4S)$	

<sup>1</sup> Assumes equal production of  $B^+$  and  $B^0$  at the  $\Upsilon(4S)$ .

$\Gamma(\eta'\eta)/\Gamma_{\text{total}}$	CL%	DOCUMENT ID	TECN	COMMENT	$\Gamma_{414}/\Gamma$
< 1.2	90	<sup>1</sup> AUBERT	08AH	BABR $e^+e^- \rightarrow \Upsilon(4S)$	

••• We do not use the following data for averages, fits, limits, etc. •••

< 4.5	90	<sup>1</sup> SCHUEMANN	07	BELL $e^+e^- \rightarrow \Upsilon(4S)$	
< 1.7	90	<sup>1</sup> AUBERT	06W	BABR Repl. by AUBERT 08AH	
< 4.6	90	<sup>1</sup> AUBERT,B	04X	BABR $e^+e^- \rightarrow \Upsilon(4S)$	
< 27	90	BEHRENS	98	CLE2 $e^+e^- \rightarrow \Upsilon(4S)$	

<sup>1</sup> Assumes equal production of  $B^+$  and  $B^0$  at the  $\Upsilon(4S)$ .

$\Gamma(\eta'\rho^0)/\Gamma_{\text{total}}$	CL%	DOCUMENT ID	TECN	COMMENT	$\Gamma_{415}/\Gamma$
< 1.3	90	<sup>1</sup> SCHUEMANN	07	BELL $e^+e^- \rightarrow \Upsilon(4S)$	

••• We do not use the following data for averages, fits, limits, etc. •••

< 2.8	90	<sup>1</sup> DEL-AMO-SA..10A	BABR	$e^+e^- \rightarrow \Upsilon(4S)$	
< 3.7	90	AUBERT	07E	BABR Repl. by DEL-AMO-SANCHEZ 10A	
< 4.3	90	<sup>1</sup> AUBERT,B	04D	BABR Repl. by AUBERT 07E	
< 12	90	<sup>1</sup> RICHICHI	00	CLE2 $e^+e^- \rightarrow \Upsilon(4S)$	
< 23	90	BEHRENS	98	CLE2 Repl. by RICHICHI 00	

<sup>1</sup> Assumes equal production of  $B^+$  and  $B^0$  at the  $\Upsilon(4S)$ .

$\Gamma(\eta'\rho^0(980), f_0 \rightarrow \pi^+\pi^-)/\Gamma_{\text{total}}$	CL%	DOCUMENT ID	TECN	COMMENT	$\Gamma_{416}/\Gamma$
< 0.9	90	<sup>1</sup> DEL-AMO-SA..10A	BABR	$e^+e^- \rightarrow \Upsilon(4S)$	

••• We do not use the following data for averages, fits, limits, etc. •••

< 1.5	90	AUBERT	07E	BABR Repl. by DEL-AMO-SANCHEZ 10A	
-------	----	--------	-----	-----------------------------------	--

<sup>1</sup> Assumes equal production of  $B^+$  and  $B^0$  at the  $\Upsilon(4S)$ .

$\Gamma(\eta\rho^0)/\Gamma_{\text{total}}$	CL%	DOCUMENT ID	TECN	COMMENT	$\Gamma_{417}/\Gamma$
< 1.5	90	<sup>1</sup> AUBERT	07Y	BABR $e^+e^- \rightarrow \Upsilon(4S)$	

••• We do not use the following data for averages, fits, limits, etc. •••

< 1.9	90	<sup>1</sup> WANG	07B	BELL $e^+e^- \rightarrow \Upsilon(4S)$	
< 1.5	90	<sup>1</sup> AUBERT,B	04D	BABR Repl. by AUBERT 07Y	
< 10	90	<sup>1</sup> RICHICHI	00	CLE2 $e^+e^- \rightarrow \Upsilon(4S)$	
< 13	90	BEHRENS	98	CLE2 Repl. by RICHICHI 00	

<sup>1</sup> Assumes equal production of  $B^+$  and  $B^0$  at the  $\Upsilon(4S)$ .

$\Gamma(\eta f_0(980), f_0 \rightarrow \pi^+\pi^-)/\Gamma_{\text{total}}$	CL%	DOCUMENT ID	TECN	COMMENT	$\Gamma_{418}/\Gamma$
< 0.4	90	<sup>1</sup> AUBERT	07Y	BABR $e^+e^- \rightarrow \Upsilon(4S)$	

<sup>1</sup> Assumes equal production of  $B^+$  and  $B^0$  at the  $\Upsilon(4S)$ .

$\Gamma(\omega\eta)/\Gamma_{\text{total}}$	CL%	DOCUMENT ID	TECN	COMMENT	$\Gamma_{419}/\Gamma$
$0.94^{+0.35}_{-0.30} \pm 0.09$		<sup>1</sup> AUBERT	09AV	BABR $e^+e^- \rightarrow \Upsilon(4S)$	

••• We do not use the following data for averages, fits, limits, etc. •••

< 1.9	90	<sup>1</sup> AUBERT,B	05K	BABR Repl. by AUBERT 09AV	
$4.0^{+1.3}_{-1.2} \pm 0.4$		<sup>1</sup> AUBERT,B	04X	BABR Repl. by AUBERT,B 05K	
< 12	90	<sup>1</sup> BERGFELD	98	CLE2	

<sup>1</sup> Assumes equal production of  $B^+$  and  $B^0$  at the  $\Upsilon(4S)$ .

$\Gamma(\omega\eta')/\Gamma_{\text{total}}$	CL%	DOCUMENT ID	TECN	COMMENT	$\Gamma_{420}/\Gamma$
$1.01^{+0.46}_{-0.38} \pm 0.09$		<sup>1</sup> AUBERT	09AV	BABR $e^+e^- \rightarrow \Upsilon(4S)$	

••• We do not use the following data for averages, fits, limits, etc. •••

< 2.2	90	<sup>1</sup> SCHUEMANN	07	BELL $e^+e^- \rightarrow \Upsilon(4S)$	
< 2.8	90	<sup>1</sup> AUBERT,B	04X	BABR $e^+e^- \rightarrow \Upsilon(4S)$	
< 60	90	<sup>1</sup> BERGFELD	98	CLE2	

<sup>1</sup> Assumes equal production of  $B^+$  and  $B^0$  at the  $\Upsilon(4S)$ .

$\Gamma(\omega\rho^0)/\Gamma_{\text{total}}$	CL%	DOCUMENT ID	TECN	COMMENT	$\Gamma_{421}/\Gamma$
< 1.6	90	<sup>1</sup> AUBERT	09H	BABR $e^+e^- \rightarrow \Upsilon(4S)$	

••• We do not use the following data for averages, fits, limits, etc. •••

< 1.5	90	<sup>1</sup> AUBERT,B	06T	BABR Repl. by AUBERT 09H	
< 3.3	90	<sup>1</sup> AUBERT	05o	BABR Repl. by AUBERT,B 06T	
< 11	90	<sup>1</sup> BERGFELD	98	CLE2	

<sup>1</sup> Assumes equal production of  $B^+$  and  $B^0$  at the  $\Upsilon(4S)$ .

$\Gamma(\omega f_0(980), f_0 \rightarrow \pi^+\pi^-)/\Gamma_{\text{total}}$	CL%	DOCUMENT ID	TECN	COMMENT	$\Gamma_{422}/\Gamma$
< 1.5	90	<sup>1</sup> AUBERT	09H	BABR $e^+e^- \rightarrow \Upsilon(4S)$	

••• We do not use the following data for averages, fits, limits, etc. •••

< 1.5	90	<sup>1</sup> AUBERT,B	06T	BABR Repl. by AUBERT 09H	
-------	----	-----------------------	-----	--------------------------	--

<sup>1</sup> Assumes equal production of  $B^+$  and  $B^0$  at the  $\Upsilon(4S)$ .

$\Gamma(\omega\omega)/\Gamma_{\text{total}}$	CL%	DOCUMENT ID	TECN	COMMENT	$\Gamma_{423}/\Gamma$
$1.2 \pm 0.3^{+0.3}_{-0.2}$		<sup>1</sup> LEES	14	BABR $e^+e^- \rightarrow \Upsilon(4S)$	

••• We do not use the following data for averages, fits, limits, etc. •••

< 4.0	90	<sup>1</sup> AUBERT,B	06T	BABR Repl. by LEES 14	
< 19	90	<sup>1</sup> BERGFELD	98	CLE2	

<sup>1</sup> Assumes equal production of  $B^+$  and  $B^0$  at the  $\Upsilon(4S)$ .

$\Gamma(\phi\pi^0)/\Gamma_{\text{total}}$	CL%	DOCUMENT ID	TECN	COMMENT	$\Gamma_{424}/\Gamma$
< 0.15	90	<sup>1</sup> KIM	12A	BELL $e^+e^- \rightarrow \Upsilon(4S)$	

••• We do not use the following data for averages, fits, limits, etc. •••

< 0.28	90	<sup>1</sup> AUBERT,B	06c	BABR $e^+e^- \rightarrow \Upsilon(4S)$	
< 1.0	90	<sup>1</sup> AUBERT,B	04D	BABR Repl. by AUBERT,B 06c	
< 5	90	<sup>1</sup> BERGFELD	98	CLE2	

<sup>1</sup> Assumes equal production of  $B^+$  and  $B^0$  at the  $\Upsilon(4S)$ .

$\Gamma(\phi\eta)/\Gamma_{\text{total}}$	CL%	DOCUMENT ID	TECN	COMMENT	$\Gamma_{425}/\Gamma$
< 0.5	90	<sup>1</sup> AUBERT	09AV	BABR $e^+e^- \rightarrow \Upsilon(4S)$	

••• We do not use the following data for averages, fits, limits, etc. •••

< 0.6	90	<sup>1</sup> AUBERT,B	06V	BABR Repl. by AUBERT 09AV	
< 1.0	90	<sup>1</sup> AUBERT,B	04X	BABR Repl. by AUBERT,B 06V	
< 9	90	<sup>1</sup> BERGFELD	98	CLE2	

<sup>1</sup> Assumes equal production of  $B^+$  and  $B^0$  at the  $\Upsilon(4S)$ .

$\Gamma(\phi\eta)/\Gamma_{\text{total}}$   $\Gamma_{426}/\Gamma$

VALUE (units 10 <sup>-6</sup> )	CL%	DOCUMENT ID	TECN	COMMENT
< 0.5	90	1 SCHUEMANN 07	BELL	e <sup>+</sup> e <sup>-</sup> → $\Upsilon(4S)$
••• We do not use the following data for averages, fits, limits, etc. •••				
< 1.1	90	1 AUBERT 09AV	BABR	e <sup>+</sup> e <sup>-</sup> → $\Upsilon(4S)$
< 1.0	90	1 AUBERT,B 06V	BABR	Repl. by AUBERT 09AV
< 4.5	90	1 AUBERT,B 04X	BABR	Repl. by AUBERT,B 06V
<31	90	1 BERGFELD 98	CLE2	
1 Assumes equal production of B <sup>+</sup> and B <sup>0</sup> at the $\Upsilon(4S)$ .				

$\Gamma(\phi\pi^+\pi^-)/\Gamma_{\text{total}}$   $\Gamma_{427}/\Gamma$

VALUE (units 10 <sup>-7</sup> )	DOCUMENT ID	TECN	COMMENT
1.82 ± 0.25 ± 0.43	1 AAIJ 17A	LHCB	pp at 7, 8 TeV
1 Signal evidence is 4.5 standard deviations.			

$\Gamma(\phi\rho^0)/\Gamma_{\text{total}}$   $\Gamma_{428}/\Gamma$

VALUE (units 10 <sup>-6</sup> )	CL%	DOCUMENT ID	TECN	COMMENT
< 0.33	90	1 AUBERT 08BK	BABR	e <sup>+</sup> e <sup>-</sup> → $\Upsilon(4S)$
••• We do not use the following data for averages, fits, limits, etc. •••				
<156	90	2 ABE 00c	SLD	e <sup>+</sup> e <sup>-</sup> → Z
< 13	90	1 BERGFELD 98	CLE2	
1 Assumes equal production of B <sup>+</sup> and B <sup>0</sup> at the $\Upsilon(4S)$ .				
2 ABE 00c assumes B(Z → b $\bar{b}$ )=(21.7 ± 0.1)% and the B fractions f <sub>B<sup>0</sup></sub> =f <sub>B<sup>+</sup></sub> =(39.7 <sup>+1.8</sup> <sub>-2.2</sub> )% and f <sub>B<sub>s</sub></sub> =(10.5 <sup>+1.8</sup> <sub>-2.2</sub> )%.				

$\Gamma(\phi f_0(980), f_0 \rightarrow \pi^+\pi^-)/\Gamma_{\text{total}}$   $\Gamma_{429}/\Gamma$

VALUE (units 10 <sup>-6</sup> )	CL%	DOCUMENT ID	TECN	COMMENT
<0.38	90	1 AUBERT 08BK	BABR	e <sup>+</sup> e <sup>-</sup> → $\Upsilon(4S)$
1 Assumes equal production of B <sup>+</sup> and B <sup>0</sup> at the $\Upsilon(4S)$ .				

$\Gamma(\phi\omega)/\Gamma_{\text{total}}$   $\Gamma_{430}/\Gamma$

VALUE (units 10 <sup>-6</sup> )	CL%	DOCUMENT ID	TECN	COMMENT
< 0.7	90	1 LEES 14	BABR	e <sup>+</sup> e <sup>-</sup> → $\Upsilon(4S)$
••• We do not use the following data for averages, fits, limits, etc. •••				
< 1.2	90	1 AUBERT,B 06T	BABR	Repl. by LEES 14
<21	90	1 BERGFELD 98	CLE2	
1 Assumes equal production of B <sup>+</sup> and B <sup>0</sup> at the $\Upsilon(4S)$ .				

$\Gamma(\phi\phi)/\Gamma_{\text{total}}$   $\Gamma_{431}/\Gamma$

VALUE	CL%	DOCUMENT ID	TECN	COMMENT
<2.7 × 10 <sup>-8</sup>	90	AAIJ 19AP	LHCB	pp at 7, 8 and 13 TeV
••• We do not use the following data for averages, fits, limits, etc. •••				
<2.8 × 10 <sup>-8</sup>	90	AAIJ 15AS	LHCB	Repl. by AAIJ 19AP
<2 × 10 <sup>-7</sup>	90	1 AUBERT 08BK	BABR	e <sup>+</sup> e <sup>-</sup> → $\Upsilon(4S)$
<1.5 × 10 <sup>-6</sup>	90	1 AUBERT,B 04X	BABR	Repl. by AUBERT 08BK
<3.21 × 10 <sup>-4</sup>	90	2 ABE 00c	SLD	e <sup>+</sup> e <sup>-</sup> → Z
<1.2 × 10 <sup>-5</sup>	90	1 BERGFELD 98	CLE2	
<3.9 × 10 <sup>-5</sup>	90	ASNER 96	CLE2	e <sup>+</sup> e <sup>-</sup> → $\Upsilon(4S)$
1 Assumes equal production of B <sup>+</sup> and B <sup>0</sup> at the $\Upsilon(4S)$ .				
2 ABE 00c assumes B(Z → b $\bar{b}$ )=(21.7 ± 0.1)% and the B fractions f <sub>B<sup>0</sup></sub> =f <sub>B<sup>+</sup></sub> =(39.7 <sup>+1.8</sup> <sub>-2.2</sub> )% and f <sub>B<sub>s</sub></sub> =(10.5 <sup>+1.8</sup> <sub>-2.2</sub> )%.				

$\Gamma(a_0(980)\pm\pi^\mp, a_0^\pm \rightarrow \eta\pi^\pm)/\Gamma_{\text{total}}$   $\Gamma_{432}/\Gamma$

VALUE (units 10 <sup>-6</sup> )	CL%	DOCUMENT ID	TECN	COMMENT
<3.1	90	1 AUBERT 07Y	BABR	e <sup>+</sup> e <sup>-</sup> → $\Upsilon(4S)$
••• We do not use the following data for averages, fits, limits, etc. •••				
<5.1	90	1 AUBERT,BE 04	BABR	Repl. by AUBERT 07Y
1 Assumes equal production of B <sup>+</sup> and B <sup>0</sup> at the $\Upsilon(4S)$ .				

$\Gamma(a_0(1450)\pm\pi^\mp, a_0^\pm \rightarrow \eta\pi^\pm)/\Gamma_{\text{total}}$   $\Gamma_{433}/\Gamma$

VALUE (units 10 <sup>-6</sup> )	CL%	DOCUMENT ID	TECN	COMMENT
<2.3	90	1 AUBERT 07Y	BABR	e <sup>+</sup> e <sup>-</sup> → $\Upsilon(4S)$
1 Assumes equal production of B <sup>+</sup> and B <sup>0</sup> at the $\Upsilon(4S)$ .				

$\Gamma(\pi^+\pi^-\pi^0)/\Gamma_{\text{total}}$   $\Gamma_{434}/\Gamma$

VALUE	CL%	DOCUMENT ID	TECN	COMMENT
<7.2 × 10 <sup>-4</sup>	90	1 ALBRECHT 90B	ARG	e <sup>+</sup> e <sup>-</sup> → $\Upsilon(4S)$
1 ALBRECHT 90B limit assumes equal production of B <sup>0</sup> $\bar{B}^0$ and B <sup>+</sup> B <sup>-</sup> at $\Upsilon(4S)$ .				

$\Gamma(\rho^0\pi^0)/\Gamma_{\text{total}}$   $\Gamma_{435}/\Gamma$

VALUE (units 10 <sup>-6</sup> )	CL%	DOCUMENT ID	TECN	COMMENT
2.0 ± 0.5 OUR AVERAGE				
3.0 ± 0.5 ± 0.7		1,2 KUSAKA 08	BELL	e <sup>+</sup> e <sup>-</sup> → $\Upsilon(4S)$
1.4 ± 0.6 ± 0.3		1 AUBERT 04Z	BABR	e <sup>+</sup> e <sup>-</sup> → $\Upsilon(4S)$
1.6 <sup>+2.0</sup> <sub>-1.4</sub> ± 0.8		1 JESSOP 00	CLEO	e <sup>+</sup> e <sup>-</sup> → $\Upsilon(4S)$

••• We do not use the following data for averages, fits, limits, etc. •••

3.12 <sup>+0.88+0.60</sup> <sub>-0.82-0.76</sub>		1 DRAGIC 06	BELL	Repl. by KUSAKA 08
5.1 ± 1.6 ± 0.9		DRAGIC 04	BELL	Repl. by DRAGIC 06
< 5.3	90	1 GORDON 02	BELL	Repl. by DRAGIC 04
< 24	90	ASNER 96	CLEO	Repl. by JESSOP 00
<400	90	1 ALBRECHT 90B	ARG	e <sup>+</sup> e <sup>-</sup> → $\Upsilon(4S)$
1 Assumes equal production of B <sup>+</sup> and B <sup>0</sup> at the $\Upsilon(4S)$ .				
2 This is the first measurement that excludes contributions from $\rho(1450)$ and $\rho(1570)$ resonances.				

$\Gamma(\rho^\mp\pi^\pm)/\Gamma_{\text{total}}$   $\Gamma_{436}/\Gamma$

VALUE (units 10 <sup>-6</sup> )	CL%	DOCUMENT ID	TECN	COMMENT
23.0 ± 2.3 OUR AVERAGE				
22.6 ± 1.1 ± 4.4		1,2 KUSAKA 08	BELL	e <sup>+</sup> e <sup>-</sup> → $\Upsilon(4S)$
22.6 ± 1.8 ± 2.2		1 AUBERT 03T	BABR	e <sup>+</sup> e <sup>-</sup> → $\Upsilon(4S)$
27.6 <sup>+8.4</sup> <sub>-7.4</sub> ± 4.2		1 JESSOP 00	CLE2	e <sup>+</sup> e <sup>-</sup> → $\Upsilon(4S)$
••• We do not use the following data for averages, fits, limits, etc. •••				
20.8 <sup>+6.0+2.8</sup> <sub>-6.3-3.1</sub>		1 GORDON 02	BELL	Repl. by KUSAKA 08
< 88	90	ASNER 96	CLE2	Repl. by JESSOP 00
< 520	90	1 ALBRECHT 90B	ARG	e <sup>+</sup> e <sup>-</sup> → $\Upsilon(4S)$
<5200	90	3 BEBEK 87	CLEO	e <sup>+</sup> e <sup>-</sup> → $\Upsilon(4S)$
1 Assumes equal production of B <sup>+</sup> and B <sup>0</sup> at the $\Upsilon(4S)$ .				
2 This is the first measurement that excludes contributions from $\rho(1450)$ and $\rho(1570)$ resonances.				
3 BEBEK 87 reports < 6.1 × 10 <sup>-3</sup> assuming the $\Upsilon(4S)$ decays 43% to B <sup>0</sup> $\bar{B}^0$ . We rescale to 50%.				

1 Assumes equal production of B<sup>+</sup> and B<sup>0</sup> at the  $\Upsilon(4S)$ .  
 2 This is the first measurement that excludes contributions from  $\rho(1450)$  and  $\rho(1570)$  resonances.  
 3 BEBEK 87 reports < 6.1 × 10<sup>-3</sup> assuming the  $\Upsilon(4S)$  decays 43% to B<sup>0</sup> $\bar{B}^0$ . We rescale to 50%.

$\Gamma(\pi^+\pi^-\pi^+\pi^-)/\Gamma_{\text{total}}$   $\Gamma_{437}/\Gamma$

VALUE	CL%	DOCUMENT ID	TECN	COMMENT
<11.2 × 10 <sup>-6</sup>	90	1 VANHOEFER 14	BELL	e <sup>+</sup> e <sup>-</sup> → $\Upsilon(4S)$
••• We do not use the following data for averages, fits, limits, etc. •••				
<23.1 × 10 <sup>-6</sup>	90	1 AUBERT 08BB	BABR	e <sup>+</sup> e <sup>-</sup> → $\Upsilon(4S)$
<19.3 × 10 <sup>-6</sup>	90	1 CHIANG 08	BELL	Repl. by VANHOEFER 14
< 2.3 × 10 <sup>-4</sup>	90	2 ADAM 96D	DLPH	e <sup>+</sup> e <sup>-</sup> → Z
< 2.8 × 10 <sup>-4</sup>	90	3 ABREU 95N	DLPH	Sup. by ADAM 96D
< 6.7 × 10 <sup>-4</sup>	90	1 ALBRECHT 90B	ARG	e <sup>+</sup> e <sup>-</sup> → $\Upsilon(4S)$
1 Assumes equal production of B <sup>+</sup> and B <sup>0</sup> at the $\Upsilon(4S)$ .				
2 ADAM 96D assumes f <sub>B<sup>0</sup></sub> = f <sub>B<sup>-</sup></sub> = 0.39 and f <sub>B<sub>s</sub></sub> = 0.12.				
3 Assumes a B <sup>0</sup> , B <sup>-</sup> production fraction of 0.39 and a B <sub>s</sub> production fraction of 0.12.				

$\Gamma(\rho^0\pi^+\pi^-)/\Gamma_{\text{total}}$   $\Gamma_{438}/\Gamma$

VALUE (units 10 <sup>-6</sup> )	CL%	DOCUMENT ID	TECN	COMMENT
< 8.8	90	1 AUBERT 08BB	BABR	e <sup>+</sup> e <sup>-</sup> → $\Upsilon(4S)$
••• We do not use the following data for averages, fits, limits, etc. •••				
<12.0	90	1 VANHOEFER 14	BELL	e <sup>+</sup> e <sup>-</sup> → $\Upsilon(4S)$
<12.0	90	1 CHIANG 08	BELL	Repl. by VANHOEFER 14
1 Assumes equal production of B <sup>+</sup> and B <sup>0</sup> at the $\Upsilon(4S)$ .				

$\Gamma(\rho^0\rho^0)/\Gamma_{\text{total}}$   $\Gamma_{439}/\Gamma$

VALUE (units 10 <sup>-6</sup> )	CL%	DOCUMENT ID	TECN	COMMENT
0.96 ± 0.15 OUR FIT				
0.97 ± 0.24 OUR AVERAGE				
1.02 ± 0.30 ± 0.15		1,2 VANHOEFER 14	BELL	e <sup>+</sup> e <sup>-</sup> → $\Upsilon(4S)$
0.92 ± 0.32 ± 0.14		2 AUBERT 08BB	BABR	e <sup>+</sup> e <sup>-</sup> → $\Upsilon(4S)$
••• We do not use the following data for averages, fits, limits, etc. •••				
0.4 ± 0.4 <sup>+0.2</sup> <sub>-0.3</sub>		2 CHIANG 08	BELL	Repl. by VANHOEFER 14
1.07 ± 0.33 ± 0.19		2 AUBERT 07G	BABR	Repl. by AUBERT 08BB
< 1.1	90	2 AUBERT 05I	BABR	Repl. by AUBERT 07G
< 2.1	90	2 AUBERT 03V	BABR	Repl. by AUBERT 05I
< 18	90	3 GODANG 02	CLE2	e <sup>+</sup> e <sup>-</sup> → $\Upsilon(4S)$
<136	90	4 ABE 00c	SLD	e <sup>+</sup> e <sup>-</sup> → Z
<280	90	2 ALBRECHT 90B	ARG	e <sup>+</sup> e <sup>-</sup> → $\Upsilon(4S)$
<290	90	5 BORTOLETTO 089	CLEO	e <sup>+</sup> e <sup>-</sup> → $\Upsilon(4S)$
<430	90	5 BEBEK 87	CLEO	e <sup>+</sup> e <sup>-</sup> → $\Upsilon(4S)$

1 Signal significance 3.4 standard deviations.  
 2 Assumes equal production of B<sup>+</sup> and B<sup>0</sup> at the  $\Upsilon(4S)$ .  
 3 Assumes a helicity 00 configuration. For a helicity 11 configuration, the limit decreases to 1.4 × 10<sup>-5</sup>.  
 4 ABE 00c assumes B(Z → b $\bar{b}$ )=(21.7 ± 0.1)% and the B fractions f<sub>B<sup>0</sup></sub>=f<sub>B<sup>+</sup></sub>=(39.7<sup>+1.8</sup><sub>-2.2</sub>)% and f<sub>B<sub>s</sub></sub>=(10.5<sup>+1.8</sup><sub>-2.2</sub>)%.  
 5 Paper assumes the  $\Upsilon(4S)$  decays 43% to B<sup>0</sup> $\bar{B}^0$ . We rescale to 50%.

$\Gamma(\rho^0\rho^0)/\Gamma(K^*(892)^0\phi)$   $\Gamma_{439}/\Gamma_{364}$

VALUE (units 10 <sup>-2</sup> )	DOCUMENT ID	TECN	COMMENT
9.5 ± 1.5 OUR FIT			
9.4 ± 1.7 ± 0.9	AAIJ 15T	LHCB	pp at 7, 8 TeV





$\Gamma(p\bar{p})/\Gamma_{\text{total}}$		$\Gamma_{460}/\Gamma$		
VALUE (units 10 <sup>-8</sup> )	CL%	DOCUMENT ID	TECN	COMMENT
<b>1.25 ± 0.27 ± 0.18</b>		<sup>1</sup> AAIJ	17B LHCb	pp at 7 and 8 TeV
••• We do not use the following data for averages, fits, limits, etc. •••				
1.47 <sup>+0.62+0.35</sup> <sub>-0.51-0.14</sub>		<sup>2</sup> AAIJ	13Bq LHCb	Repl. by AAIJ 17Bj
< 11	90	<sup>3</sup> TSAI	07 BELL	e <sup>+</sup> e <sup>-</sup> → T(4S)
< 41	90	<sup>3</sup> CHANG	05 BELL	e <sup>+</sup> e <sup>-</sup> → T(4S)
< 27	90	<sup>3</sup> AUBERT	04U BABR	e <sup>+</sup> e <sup>-</sup> → T(4S)
< 140	90	<sup>3</sup> BORNHEIM	03 CLE2	e <sup>+</sup> e <sup>-</sup> → T(4S)
< 120	90	<sup>3</sup> ABE	02o BELL	e <sup>+</sup> e <sup>-</sup> → T(4S)
< 700	90	<sup>3</sup> COAN	99 CLE2	e <sup>+</sup> e <sup>-</sup> → T(4S)
< 1800	90	<sup>4</sup> BUSKULIC	96V ALEP	e <sup>+</sup> e <sup>-</sup> → Z
< 35000	90	<sup>5</sup> ABREU	95N DLPH	Sup. by ADAM 96D
< 3400	90	<sup>6</sup> BORTOLETTO	089 CLEO	e <sup>+</sup> e <sup>-</sup> → T(4S)
< 12000	90	<sup>7</sup> ALBRECHT	88F ARG	e <sup>+</sup> e <sup>-</sup> → T(4S)
< 17000	90	<sup>6</sup> BEBEK	87 CLEO	e <sup>+</sup> e <sup>-</sup> → T(4S)

- Uses normalization mode B(B<sup>0</sup> → K<sup>+</sup>π<sup>-</sup>) = (19.6 ± 0.5) × 10<sup>-6</sup>.
- Uses normalization mode B(B<sup>0</sup> → K<sup>+</sup>π<sup>-</sup>) = (19.55 ± 0.54) × 10<sup>-6</sup>.
- Assumes equal production of B<sup>+</sup> and B<sup>0</sup> at the T(4S).
- BUSKULIC 96V assumes PDG 96 production fractions for B<sup>0</sup>, B<sup>+</sup>, B<sub>s</sub>, b baryons.
- Assumes a B<sup>0</sup>, B<sup>-</sup> production fraction of 0.39 and a B<sub>s</sub> production fraction of 0.12.
- Paper assumes the T(4S) decays 43% to B<sup>0</sup>B<sup>0</sup>. We rescale to 50%.
- ALBRECHT 88F reports < 1.3 × 10<sup>-4</sup> assuming the T(4S) decays 45% to B<sup>0</sup>B<sup>0</sup>. We rescale to 50%.

$\Gamma(p\bar{p}\pi^+\pi^-)/\Gamma_{\text{total}}$		$\Gamma_{461}/\Gamma$		
VALUE (units 10 <sup>-6</sup> )	CL%	DOCUMENT ID	TECN	COMMENT
<b>2.87 ± 0.15 ± 0.11</b>		<sup>1,2</sup> AAIJ	17Bd LHCb	pp at 7, 8 TeV
••• We do not use the following data for averages, fits, limits, etc. •••				
< 950	90	<sup>3</sup> ABREU	95N DLPH	Sup. by ADAM 96D
< 250	90	<sup>4</sup> BEBEK	89 CLEO	e <sup>+</sup> e <sup>-</sup> → T(4S)
540 ± 180 ± 200		<sup>5</sup> ALBRECHT	88F ARG	e <sup>+</sup> e <sup>-</sup> → T(4S)

- AAIJ 17Bd reports  $[\Gamma(B^0 \rightarrow p\bar{p}\pi^+\pi^-)/\Gamma_{\text{total}}] / [B(B^0 \rightarrow J/\psi(1S)K^*(892)^0)] / [B(J/\psi(1S) \rightarrow p\bar{p})] / [B(K^*(892) \rightarrow (K\pi)^\pm)] = 1.07 \pm 0.04 \pm 0.04$  which we multiply by our best values B(B<sup>0</sup> → J/ψ(1S) K\*(892)<sup>0</sup>) = (1.27 ± 0.05) × 10<sup>-3</sup>, B(J/ψ(1S) → p $\bar{p}$ ) = (2.121 ± 0.029) × 10<sup>-3</sup>, B(K\*(892) → (Kπ)<sup>±</sup>) = (99.901 ± 0.009) × 10<sup>-2</sup>. Our first error is their experiment's error and our second error is the systematic error from using our best values.
- The branching ratio is given for m<sub>p $\bar{p}$</sub>  < 2.85 GeV.
- Assumes a B<sup>0</sup>, B<sup>-</sup> production fraction of 0.39 and a B<sub>s</sub> production fraction of 0.12.
- BEBEK 89 reports < 2.9 × 10<sup>-4</sup> assuming the T(4S) decays 43% to B<sup>0</sup>B<sup>0</sup>. We rescale to 50%.
- ALBRECHT 88F reports 6.0 ± 2.0 ± 2.2 assuming the T(4S) decays 45% to B<sup>0</sup>B<sup>0</sup>. We rescale to 50%.

$\Gamma(p\bar{p}\pi^+\pi^-)/\Gamma(p\bar{p}K^+\pi^-)$		$\Gamma_{461}/\Gamma_{462}$		
VALUE		DOCUMENT ID	TECN	COMMENT
••• We do not use the following data for averages, fits, limits, etc. •••				
0.46 ± 0.02 ± 0.02		<sup>1</sup> AAIJ	17Bd LHCb	pp at 7, 8 TeV
<sup>1</sup> The ratio is given for m <sub>p<math>\bar{p}</math></sub> < 2.85 GeV.				

$\Gamma(p\bar{p}K^0)/\Gamma_{\text{total}}$		$\Gamma_{463}/\Gamma$		
VALUE (units 10 <sup>-6</sup> )	CL%	DOCUMENT ID	TECN	COMMENT
<b>2.66 ± 0.32 OUR AVERAGE</b>				
2.51 <sup>+0.35</sup> <sub>-0.29</sub> ± 0.21		<sup>1,2</sup> CHEN	08c BELL	e <sup>+</sup> e <sup>-</sup> → T(4S)
3.0 ± 0.5 ± 0.3		<sup>2</sup> AUBERT	07AV BABR	e <sup>+</sup> e <sup>-</sup> → T(4S)
••• We do not use the following data for averages, fits, limits, etc. •••				
2.40 <sup>+0.64</sup> <sub>-0.44</sub> ± 0.28		<sup>2,3,4</sup> WANG	05A BELL	Repl. by CHEN 08c
1.88 <sup>+0.77</sup> <sub>-0.60</sub> ± 0.23		<sup>2,3,5</sup> WANG	04 BELL	Repl. by WANG 05A
< 7.2	90	<sup>2,3</sup> ABE	02k BELL	Repl. by WANG 04

- Explicitly vetoes resonant production of p $\bar{p}$  from charmonium states.
- Assumes equal production of B<sup>+</sup> and B<sup>0</sup> at the T(4S).
- Explicitly vetoes resonant production of p $\bar{p}$  from charmonium states and pK<sup>0</sup> production from Λ<sub>c</sub>.
- Provides also results with M<sub>p $\bar{p}$</sub>  < 2.85 GeV/c<sup>2</sup> and angular asymmetry of p $\bar{p}$  system.
- The branching fraction for M<sub>p $\bar{p}$</sub>  < 2.85 is also reported.

$\Gamma(\Theta(1540)^+\bar{p}, \Theta^+ \rightarrow pK_S^0)/\Gamma_{\text{total}}$		$\Gamma_{464}/\Gamma$		
VALUE (units 10 <sup>-6</sup> )	CL%	DOCUMENT ID	TECN	COMMENT
<b>&lt; 0.05</b>		<sup>1</sup> AUBERT	07AV BABR	e <sup>+</sup> e <sup>-</sup> → T(4S)
••• We do not use the following data for averages, fits, limits, etc. •••				
< 0.23	90	<sup>1</sup> WANG	05A BELL	e <sup>+</sup> e <sup>-</sup> → T(4S)
<sup>1</sup> Assumes equal production of B <sup>+</sup> and B <sup>0</sup> at the T(4S).				

$\Gamma(f_J(2220)K^0, f_J \rightarrow p\bar{p})/\Gamma_{\text{total}}$		$\Gamma_{465}/\Gamma$		
VALUE (units 10 <sup>-6</sup> )	CL%	DOCUMENT ID	TECN	COMMENT
<b>&lt; 0.45</b>		<sup>1</sup> AUBERT	07AV BABR	e <sup>+</sup> e <sup>-</sup> → T(4S)
<sup>1</sup> Assumes equal production of B <sup>+</sup> and B <sup>0</sup> at the T(4S).				

$\Gamma(p\bar{p}K^+\pi^-)/\Gamma_{\text{total}}$		$\Gamma_{462}/\Gamma$		
VALUE (units 10 <sup>-8</sup> )		DOCUMENT ID	TECN	COMMENT
<b>6.3 ± 0.5 ± 0.2</b>		<sup>1,2</sup> AAIJ	17Bd LHCb	pp at 7, 8 TeV
<sup>1</sup> AAIJ 17Bd reports $[\Gamma(B^0 \rightarrow p\bar{p}K^+\pi^-)/\Gamma_{\text{total}}] / [B(B^0 \rightarrow J/\psi(1S)K^*(892)^0)] / [B(J/\psi(1S) \rightarrow p\bar{p})] / [B(K^*(892) \rightarrow (K\pi)^\pm)] = 2.34 \pm 0.12 \pm 0.12$ which we multiply by our best values B(B <sup>0</sup> → J/ψ(1S) K*(892) <sup>0</sup> ) = (1.27 ± 0.05) × 10 <sup>-3</sup> , B(J/ψ(1S) → p $\bar{p}$ ) = (2.121 ± 0.029) × 10 <sup>-3</sup> , B(K*(892) → (Kπ) <sup>±</sup> ) = (99.901 ± 0.009) × 10 <sup>-2</sup> . Our first error is their experiment's error and our second error is the systematic error from using our best values.				
<sup>2</sup> The branching ratio is given for m <sub>p<math>\bar{p}</math></sub> < 2.85 GeV.				

$\Gamma(p\bar{p}K^*(892)^0)/\Gamma_{\text{total}}$		$\Gamma_{466}/\Gamma$		
VALUE (units 10 <sup>-6</sup> )	CL%	DOCUMENT ID	TECN	COMMENT
<b>1.24 ± 0.28 ± 0.25 OUR AVERAGE</b>				
1.18 <sup>+0.29</sup> <sub>-0.25</sub> ± 0.11		<sup>1,2</sup> CHEN	08c BELL	e <sup>+</sup> e <sup>-</sup> → T(4S)
1.47 ± 0.45 ± 0.40		<sup>2</sup> AUBERT	07AV BABR	e <sup>+</sup> e <sup>-</sup> → T(4S)
••• We do not use the following data for averages, fits, limits, etc. •••				
< 7.6	90	<sup>2</sup> WANG	04 BELL	e <sup>+</sup> e <sup>-</sup> → T(4S)
<sup>1</sup> Explicitly vetoes resonant production of p $\bar{p}$ from charmonium states.				
<sup>2</sup> Assumes equal production of B <sup>+</sup> and B <sup>0</sup> at the T(4S).				

$\Gamma(p\bar{p}\pi^0)/\Gamma_{\text{total}}$		$\Gamma_{469}/\Gamma$		
VALUE (units 10 <sup>-7</sup> )		DOCUMENT ID	TECN	COMMENT
<b>5.0 ± 1.8 ± 0.6</b>		PAL	19 BELL	e <sup>+</sup> e <sup>-</sup> → T(4S)

$\Gamma(f_J(2220)K_S^0, f_J \rightarrow p\bar{p})/\Gamma_{\text{total}}$		$\Gamma_{467}/\Gamma$		
VALUE (units 10 <sup>-6</sup> )	CL%	DOCUMENT ID	TECN	COMMENT
<b>&lt; 0.15</b>		<sup>1</sup> AUBERT	07AV BABR	e <sup>+</sup> e <sup>-</sup> → T(4S)
<sup>1</sup> Assumes equal production of B <sup>+</sup> and B <sup>0</sup> at the T(4S).				

$\Gamma(p\bar{p}K^+K^-)/\Gamma_{\text{total}}$		$\Gamma_{468}/\Gamma$		
VALUE (units 10 <sup>-8</sup> )		DOCUMENT ID	TECN	COMMENT
<b>12.1 ± 3.1 ± 0.5</b>		<sup>1,2</sup> AAIJ	17Bd LHCb	pp at 7, 8 TeV
<sup>1</sup> AAIJ 17Bd reports $[\Gamma(B^0 \rightarrow p\bar{p}K^+K^-)/\Gamma_{\text{total}}] / [B(B^0 \rightarrow J/\psi(1S)K^*(892)^0)] / [B(J/\psi(1S) \rightarrow p\bar{p})] / [B(K^*(892) \rightarrow (K\pi)^\pm)] = 0.045 \pm 0.011 \pm 0.004$ which we multiply by our best values B(B <sup>0</sup> → J/ψ(1S) K*(892) <sup>0</sup> ) = (1.27 ± 0.05) × 10 <sup>-3</sup> , B(J/ψ(1S) → p $\bar{p}$ ) = (2.121 ± 0.029) × 10 <sup>-3</sup> , B(K*(892) → (Kπ) <sup>±</sup> ) = (99.901 ± 0.009) × 10 <sup>-2</sup> . Our first error is their experiment's error and our second error is the systematic error from using our best values.				
<sup>2</sup> The branching ratio is given for m <sub>p<math>\bar{p}</math></sub> < 2.85 GeV.				

$\Gamma(p\bar{p}K^+K^-)/\Gamma(p\bar{p}K^+\pi^-)$		$\Gamma_{468}/\Gamma_{462}$		
VALUE (%)		DOCUMENT ID	TECN	COMMENT
••• We do not use the following data for averages, fits, limits, etc. •••				
1.9 ± 0.5 ± 0.2		<sup>1</sup> AAIJ	17Bd LHCb	pp at 7, 8 TeV
<sup>1</sup> The ratio is given for m <sub>p<math>\bar{p}</math></sub> < 2.85 GeV.				

$\Gamma(p\bar{p}p\bar{p})/\Gamma_{\text{total}}$		$\Gamma_{470}/\Gamma$		
VALUE	CL%	DOCUMENT ID	TECN	COMMENT
<b>&lt; 2.0 × 10<sup>-7</sup></b>		<sup>1</sup> LEES	18c BABR	e <sup>+</sup> e <sup>-</sup> → T(4S)
<sup>1</sup> Assumes equal production of B <sup>+</sup> and B <sup>0</sup> at the T(4S).				

$\Gamma(p\bar{\Lambda}\pi^-)/\Gamma_{\text{total}}$		$\Gamma_{471}/\Gamma$		
VALUE (units 10 <sup>-6</sup> )	CL%	DOCUMENT ID	TECN	COMMENT
<b>3.14 ± 0.29 OUR AVERAGE</b>				
3.07 ± 0.31 ± 0.23		<sup>1</sup> AUBERT	09Ac BABR	e <sup>+</sup> e <sup>-</sup> → T(4S)
3.23 <sup>+0.33</sup> <sub>-0.29</sub> ± 0.29		<sup>1</sup> WANG	07c BELL	e <sup>+</sup> e <sup>-</sup> → T(4S)
••• We do not use the following data for averages, fits, limits, etc. •••				
2.62 <sup>+0.44</sup> <sub>-0.40</sub> ± 0.31		<sup>1,2</sup> WANG	05A BELL	Repl. by WANG 07c
3.97 <sup>+1.00</sup> <sub>-0.80</sub> ± 0.56		<sup>1</sup> WANG	03 BELL	Repl. by WANG 05A
< 13	90	<sup>1</sup> COAN	99 CLE2	e <sup>+</sup> e <sup>-</sup> → T(4S)
< 180	90	<sup>3</sup> ALBRECHT	88F ARG	e <sup>+</sup> e <sup>-</sup> → T(4S)
<sup>1</sup> Assumes equal production of B <sup>+</sup> and B <sup>0</sup> at the T(4S).				
<sup>2</sup> Provides also results with M <sub>p<math>\bar{p}</math></sub> < 2.85 GeV/c <sup>2</sup> and angular asymmetry of p $\bar{\Lambda}$ system.				
<sup>3</sup> ALBRECHT 88F reports < 2.0 × 10 <sup>-4</sup> assuming the T(4S) decays 45% to B <sup>0</sup> B <sup>0</sup> . We rescale to 50%.				

$\Gamma(p\bar{\Lambda}\pi^-\gamma)/\Gamma_{\text{total}}$		$\Gamma_{472}/\Gamma$		
VALUE	CL%	DOCUMENT ID	TECN	COMMENT
<b>&lt; 6.5 × 10<sup>-7</sup></b>		<sup>1</sup> LAI	14 BELL	e <sup>+</sup> e <sup>-</sup> → T(4S)
<sup>1</sup> Assumes equal production of B <sup>+</sup> and B <sup>0</sup> at the T(4S).				

$\Gamma(p\bar{\Sigma}^-(1385^-)/\Gamma_{\text{total}}$		$\Gamma_{473}/\Gamma$		
VALUE (units 10 <sup>-6</sup> )	CL%	DOCUMENT ID	TECN	COMMENT
<b>&lt; 0.26</b>		<sup>1</sup> WANG	07c BELL	e <sup>+</sup> e <sup>-</sup> → T(4S)
<sup>1</sup> Assumes equal production of B <sup>+</sup> and B <sup>0</sup> at the T(4S).				

Downloaded from https://academic.oup.com/ptep/article/2020/8/083C01/5891211 by guest on 12 November 2020

## Meson Particle Listings

 $B^0$ 

$[\Gamma(\Delta(1232)^+\bar{p}) + \Gamma(\Delta(1232)^-p)]/\Gamma_{\text{total}}$					$\Gamma_{474}/\Gamma$
VALUE	DOCUMENT ID	TECN	COMMENT		
$<1.6 \times 10^{-6}$	PAL	19	BELL	$e^+e^- \rightarrow \Upsilon(4S)$	

$\Gamma(\Delta^0\bar{\Lambda})/\Gamma_{\text{total}}$					$\Gamma_{475}/\Gamma$
VALUE (units $10^{-6}$ )	CL%	DOCUMENT ID	TECN	COMMENT	
$<0.93$	90	<sup>1</sup> WANG	07c	BELL $e^+e^- \rightarrow \Upsilon(4S)$	
<sup>1</sup> Assumes equal production of $B^+$ and $B^0$ at the $\Upsilon(4S)$ .					

$\Gamma(p\bar{\Lambda}K^-)/\Gamma_{\text{total}}$					$\Gamma_{476}/\Gamma$
VALUE (units $10^{-6}$ )	CL%	DOCUMENT ID	TECN	COMMENT	
$<0.82$	90	<sup>1</sup> WANG	03	BELL $e^+e^- \rightarrow \Upsilon(4S)$	
<sup>1</sup> Assumes equal production of $B^+$ and $B^0$ at the $\Upsilon(4S)$ .					

$\Gamma(p\bar{\Lambda}D^-)/\Gamma_{\text{total}}$					$\Gamma_{477}/\Gamma$
VALUE (units $10^{-6}$ )	CL%	DOCUMENT ID	TECN	COMMENT	
$25.1 \pm 2.6 \pm 3.5$		<sup>1</sup> CHANG	15	BELL $e^+e^- \rightarrow \Upsilon(4S)$	
<sup>1</sup> Assumes equal production of $B^+$ and $B^0$ at the $\Upsilon(4S)$ .					

$\Gamma(p\bar{\Lambda}D^{*-})/\Gamma_{\text{total}}$					$\Gamma_{478}/\Gamma$
VALUE (units $10^{-6}$ )	CL%	DOCUMENT ID	TECN	COMMENT	
$33.6 \pm 6.3 \pm 4.4$		<sup>1</sup> CHANG	15	BELL $e^+e^- \rightarrow \Upsilon(4S)$	
<sup>1</sup> Assumes equal production of $B^+$ and $B^0$ at the $\Upsilon(4S)$ .					

$\Gamma(p\Sigma^0\pi^-)/\Gamma_{\text{total}}$					$\Gamma_{479}/\Gamma$
VALUE	CL%	DOCUMENT ID	TECN	COMMENT	
$<3.8 \times 10^{-6}$	90	<sup>1</sup> WANG	03	BELL $e^+e^- \rightarrow \Upsilon(4S)$	
<sup>1</sup> Assumes equal production of $B^+$ and $B^0$ at the $\Upsilon(4S)$ .					

$\Gamma(\bar{\Lambda})/\Gamma_{\text{total}}$					$\Gamma_{480}/\Gamma$
VALUE (units $10^{-6}$ )	CL%	DOCUMENT ID	TECN	COMMENT	
$<0.32$	90	<sup>1</sup> TSAI	07	BELL $e^+e^- \rightarrow \Upsilon(4S)$	
••• We do not use the following data for averages, fits, limits, etc. •••					
$<0.69$	90	<sup>1</sup> CHANG	05	BELL Repl. by TSAI 07	
$<1.2$	90	<sup>1</sup> BORNHEIM	03	CLE2 $e^+e^- \rightarrow \Upsilon(4S)$	
$<1.0$	90	<sup>1</sup> ABE	020	BELL Repl. by CHANG 05	
$<3.9$	90	<sup>1</sup> COAN	99	CLE2 $e^+e^- \rightarrow \Upsilon(4S)$	
<sup>1</sup> Assumes equal production of $B^+$ and $B^0$ at the $\Upsilon(4S)$ .					

$\Gamma(\bar{\Lambda}\Lambda K^0)/\Gamma_{\text{total}}$					$\Gamma_{481}/\Gamma$
VALUE (units $10^{-6}$ )	CL%	DOCUMENT ID	TECN	COMMENT	
$4.76 \pm 0.84 \pm 0.61$		<sup>1,2</sup> CHANG	09	BELL $e^+e^- \rightarrow \Upsilon(4S)$	
<sup>1</sup> Excluding charmonium events in $2.85 < m_{\Lambda\bar{\Lambda}} < 3.128$ GeV/ $c^2$ and $3.315 < m_{\Lambda\bar{\Lambda}} < 3.735$ GeV/ $c^2$ . Measurements in various $m_{\Lambda\bar{\Lambda}}$ bins are also reported.					
<sup>2</sup> Assumes equal production of $B^+$ and $B^0$ at the $\Upsilon(4S)$ .					

$\Gamma(\bar{\Lambda}\Lambda K^{*0})/\Gamma_{\text{total}}$					$\Gamma_{482}/\Gamma$
VALUE (units $10^{-6}$ )	CL%	DOCUMENT ID	TECN	COMMENT	
$2.46 \pm 0.87 \pm 0.72 \pm 0.34$		<sup>1,2</sup> CHANG	09	BELL $e^+e^- \rightarrow \Upsilon(4S)$	
<sup>1</sup> Excluding charmonium events in $2.85 < m_{\Lambda\bar{\Lambda}} < 3.128$ GeV/ $c^2$ and $3.315 < m_{\Lambda\bar{\Lambda}} < 3.735$ GeV/ $c^2$ . Measurements in various $m_{\Lambda\bar{\Lambda}}$ bins are also reported.					
<sup>2</sup> Assumes equal production of $B^+$ and $B^0$ at the $\Upsilon(4S)$ .					

$\Gamma(\bar{\Lambda}\Lambda D^0)/\Gamma_{\text{total}}$					$\Gamma_{483}/\Gamma$
VALUE (units $10^{-5}$ )	CL%	DOCUMENT ID	TECN	COMMENT	
$1.00 \pm 0.39 \pm 0.26$		<b>OUR AVERAGE</b>			
$0.90 \pm 0.29 \pm 0.19$		<sup>1,2</sup> LEES	14b	BABR $e^+e^- \rightarrow \Upsilon(4S)$	
$1.05 \pm 0.57 \pm 0.44$		<sup>2</sup> CHANG	09	BELL $e^+e^- \rightarrow \Upsilon(4S)$	
<sup>1</sup> Evidence for 3.4 st. dev. signal significance.					
<sup>2</sup> Assumes equal production of $B^+$ and $B^0$ at the $\Upsilon(4S)$ .					

$\Gamma(D^0\Sigma^0\bar{\Lambda} + \text{c.c.})/\Gamma_{\text{total}}$					$\Gamma_{484}/\Gamma$
VALUE	CL%	DOCUMENT ID	TECN	COMMENT	
$<3.1 \times 10^{-5}$	90	<sup>1,2</sup> LEES	14b	BABR $e^+e^- \rightarrow \Upsilon(4S)$	
<sup>1</sup> Here $\Sigma^0 \rightarrow \Lambda\gamma$ .					
<sup>2</sup> Assumes equal production of $B^+$ and $B^0$ at the $\Upsilon(4S)$ .					

$\Gamma(\Delta^0\bar{D}^0)/\Gamma_{\text{total}}$					$\Gamma_{485}/\Gamma$
VALUE	CL%	DOCUMENT ID	TECN	COMMENT	
$<0.0015$	90	<sup>1</sup> BORTOLETTO89	CLEO	$e^+e^- \rightarrow \Upsilon(4S)$	
<sup>1</sup> BORTOLETTO 89 reports $< 0.0018$ assuming $\Upsilon(4S)$ decays 43% to $B^0\bar{B}^0$ . We rescale to 50%.					

$\Gamma(D^{*+}\bar{D}^{*-})/\Gamma_{\text{total}}$					$\Gamma_{486}/\Gamma$
VALUE	CL%	DOCUMENT ID	TECN	COMMENT	
$<1.1 \times 10^{-4}$	90	<sup>1</sup> BORTOLETTO89	CLEO	$e^+e^- \rightarrow \Upsilon(4S)$	
<sup>1</sup> BORTOLETTO 89 reports $< 1.3 \times 10^{-4}$ assuming $\Upsilon(4S)$ decays 43% to $B^0\bar{B}^0$ . We rescale to 50%.					

$\Gamma(D^0\rho\rho)/\Gamma_{\text{total}}$					$\Gamma_{487}/\Gamma$
VALUE (units $10^{-4}$ )	CL%	DOCUMENT ID	TECN	COMMENT	
$1.04 \pm 0.07$		<b>OUR AVERAGE</b>			
$1.02 \pm 0.04 \pm 0.06$		<sup>1,2</sup> DEL-AMO-SA...12	BABR	$e^+e^- \rightarrow \Upsilon(4S)$	
$1.18 \pm 0.15 \pm 0.16$		<sup>2</sup> ABE	02w	BELL $e^+e^- \rightarrow \Upsilon(4S)$	
••• We do not use the following data for averages, fits, limits, etc. •••					
$1.13 \pm 0.06 \pm 0.08$		<sup>2</sup> AUBERT,B	06s	BABR Repl. by DEL-AMO-SANCHEZ 12	
<sup>1</sup> Uses the values of $D$ and $D^*$ branching fractions from PDG 08.					
<sup>2</sup> Assumes equal production of $B^+$ and $B^0$ at the $\Upsilon(4S)$ .					

$\Gamma(D_s^-\bar{\Lambda}\rho)/\Gamma_{\text{total}}$					$\Gamma_{488}/\Gamma$
VALUE (units $10^{-5}$ )	CL%	DOCUMENT ID	TECN	COMMENT	
$2.8 \pm 0.8 \pm 0.3$		<sup>1,2</sup> MEDVEDEVA	07	BELL $e^+e^- \rightarrow \Upsilon(4S)$	
<sup>1</sup> Assumes equal production of $B^+$ and $B^0$ at the $\Upsilon(4S)$ .					
<sup>2</sup> MEDVEDEVA 07 reports $(2.9 \pm 0.7 \pm 0.5 \pm 0.4) \times 10^{-5}$ from a measurement of $[\Gamma(B^0 \rightarrow D_s^-\bar{\Lambda}\rho)/\Gamma_{\text{total}}] \times [B(D_s^+ \rightarrow \phi\pi^+)]$ assuming $B(D_s^+ \rightarrow \phi\pi^+) = (4.4 \pm 0.6) \times 10^{-2}$ , which we rescale to our best value $B(D_s^+ \rightarrow \phi\pi^+) = (4.5 \pm 0.4) \times 10^{-2}$ . Our first error is their experiment's error and our second error is the systematic error from using our best value.					

$\Gamma(D^{*0}(2007)^0\rho\bar{\rho})/\Gamma_{\text{total}}$					$\Gamma_{489}/\Gamma$
VALUE (units $10^{-4}$ )	CL%	DOCUMENT ID	TECN	COMMENT	
$0.99 \pm 0.11$		<b>OUR AVERAGE</b>			
$0.97 \pm 0.07 \pm 0.09$		<sup>1,2</sup> DEL-AMO-SA...12	BABR	$e^+e^- \rightarrow \Upsilon(4S)$	
$1.20 \pm 0.33 \pm 0.21$		<sup>2</sup> ABE	02w	BELL $e^+e^- \rightarrow \Upsilon(4S)$	
••• We do not use the following data for averages, fits, limits, etc. •••					
$1.01 \pm 0.10 \pm 0.09$		<sup>2</sup> AUBERT,B	06s	BABR Repl. by DEL-AMO-SANCHEZ 12	
<sup>1</sup> Uses the values of $D$ and $D^*$ branching fractions from PDG 08.					
<sup>2</sup> Assumes equal production of $B^+$ and $B^0$ at the $\Upsilon(4S)$ .					

$\Gamma(D^{*0}(2010)^-\rho\bar{\rho})/\Gamma_{\text{total}}$					$\Gamma_{490}/\Gamma$
VALUE (units $10^{-4}$ )	CL%	DOCUMENT ID	TECN	COMMENT	
$14.5 \pm 3.4 \pm 2.7$		<sup>1</sup> ANDERSON	01	CLE2 $e^+e^- \rightarrow \Upsilon(4S)$	
<sup>1</sup> Assumes equal production of $B^+$ and $B^0$ at the $\Upsilon(4S)$ .					

$\Gamma(D^-\rho\bar{\rho}\pi^+)/\Gamma_{\text{total}}$					$\Gamma_{491}/\Gamma$
VALUE (units $10^{-4}$ )	CL%	DOCUMENT ID	TECN	COMMENT	
$3.32 \pm 0.10 \pm 0.29$		<sup>1,2</sup> DEL-AMO-SA...12	BABR	$e^+e^- \rightarrow \Upsilon(4S)$	
••• We do not use the following data for averages, fits, limits, etc. •••					
$3.38 \pm 0.14 \pm 0.29$		<sup>2</sup> AUBERT,B	06s	BABR Repl. by DEL-AMO-SANCHEZ 12	
<sup>1</sup> Uses the values of $D$ and $D^*$ branching fractions from PDG 08.					
<sup>2</sup> Assumes equal production of $B^+$ and $B^0$ at the $\Upsilon(4S)$ .					

$\Gamma(D^{*0}(2010)^-\rho\bar{\rho}\pi^+)/\Gamma_{\text{total}}$					$\Gamma_{492}/\Gamma$
VALUE (units $10^{-4}$ )	CL%	DOCUMENT ID	TECN	COMMENT	
$4.7 \pm 0.5$		<b>OUR AVERAGE</b>			
$4.55 \pm 0.16 \pm 0.39$		<sup>1,2</sup> DEL-AMO-SA...12	BABR	$e^+e^- \rightarrow \Upsilon(4S)$	
$6.5 \pm 1.3 \pm 1.0$		<sup>2</sup> ANDERSON	01	CLE2 $e^+e^- \rightarrow \Upsilon(4S)$	
••• We do not use the following data for averages, fits, limits, etc. •••					
$4.81 \pm 0.22 \pm 0.44$		<sup>2</sup> AUBERT,B	06s	BABR Repl. by DEL-AMO-SANCHEZ 12	
<sup>1</sup> Uses the values of $D$ and $D^*$ branching fractions from PDG 08.					
<sup>2</sup> Assumes equal production of $B^+$ and $B^0$ at the $\Upsilon(4S)$ .					

$\Gamma(D^0\rho\bar{\rho}\pi^+\pi^-)/\Gamma_{\text{total}}$					$\Gamma_{493}/\Gamma$
VALUE (units $10^{-4}$ )	CL%	DOCUMENT ID	TECN	COMMENT	
$2.99 \pm 0.21 \pm 0.45$		<sup>1,2</sup> DEL-AMO-SA...12	BABR	$e^+e^- \rightarrow \Upsilon(4S)$	
<sup>1</sup> Uses the values of $D$ and $D^*$ branching fractions from PDG 08.					
<sup>2</sup> Assumes equal production of $B^+$ and $B^0$ at the $\Upsilon(4S)$ .					

$\Gamma(D^{*0}\rho\bar{\rho}\pi^+\pi^-)/\Gamma_{\text{total}}$					$\Gamma_{494}/\Gamma$
VALUE (units $10^{-4}$ )	CL%	DOCUMENT ID	TECN	COMMENT	
$1.91 \pm 0.36 \pm 0.29$		<sup>1,2</sup> DEL-AMO-SA...12	BABR	$e^+e^- \rightarrow \Upsilon(4S)$	
<sup>1</sup> Uses the values of $D$ and $D^*$ branching fractions from PDG 08.					
<sup>2</sup> Assumes equal production of $B^+$ and $B^0$ at the $\Upsilon(4S)$ .					

$\Gamma(\Theta_c^-\bar{p}\pi^+, \Theta_c^- \rightarrow D^-\rho)/\Gamma_{\text{total}}$					$\Gamma_{495}/\Gamma$
VALUE (units $10^{-6}$ )	CL%	DOCUMENT ID	TECN	COMMENT	
$<9$	90	<sup>1</sup> AUBERT,B	06s	BABR $e^+e^- \rightarrow \Upsilon(4S)$	
<sup>1</sup> Assumes equal production of $B^+$ and $B^0$ at the $\Upsilon(4S)$ .					

See key on page 999

Meson Particle Listings

$B^0$

$\Gamma(\Theta_c \bar{p} \pi^+, \Theta_c \rightarrow D^{*-} p)/\Gamma_{total}$   $\Gamma_{496}/\Gamma$

VALUE (units $10^{-6}$ )	CL%	DOCUMENT ID	TECN	COMMENT
<14	90	<sup>1</sup> AUBERT,B	06s	BABR $e^+e^- \rightarrow \Upsilon(4S)$

<sup>1</sup> Assumes equal production of  $B^+$  and  $B^0$  at the  $\Upsilon(4S)$ .

$\Gamma(\Sigma_c^{--} \Delta^{++})/\Gamma_{total}$   $\Gamma_{497}/\Gamma$

VALUE	CL%	DOCUMENT ID	TECN	COMMENT
<8 × 10 <sup>-4</sup>	90	<sup>1</sup> PROCARIO	94	CLE2 $e^+e^- \rightarrow \Upsilon(4S)$

<sup>1</sup> PROCARIO 94 reports < 0.0012 from a measurement of  $[\Gamma(B^0 \rightarrow \Sigma_c^{--} \Delta^{++})/\Gamma_{total}] \times [B(\Lambda_c^+ \rightarrow p K^- \pi^+)]$  assuming  $B(\Lambda_c^+ \rightarrow p K^- \pi^+) = 0.043$ , which we rescale to our best value  $B(\Lambda_c^+ \rightarrow p K^- \pi^+) = 6.28 \times 10^{-2}$ .

$\Gamma(\bar{\Lambda}_c^- p \pi^+ \pi^-)/\Gamma_{total}$   $\Gamma_{498}/\Gamma$

VALUE (units $10^{-3}$ )	DOCUMENT ID	TECN	COMMENT
<b>1.02 ± 0.14 OUR AVERAGE</b>	Error includes scale factor of 1.3. See the ideogram below.		
1.23 ± 0.05 ± 0.33	<sup>1,2</sup> LEES	13H	BABR $e^+e^- \rightarrow \Upsilon(4S)$
0.89 ± 0.11 ± 0.05 -0.04	<sup>1,3</sup> PARK	07	BELL $e^+e^- \rightarrow \Upsilon(4S)$
1.33 ± 0.22 ± 0.07 -0.20	<sup>4</sup> DYTMAN	02	CLE2 $e^+e^- \rightarrow \Upsilon(4S)$

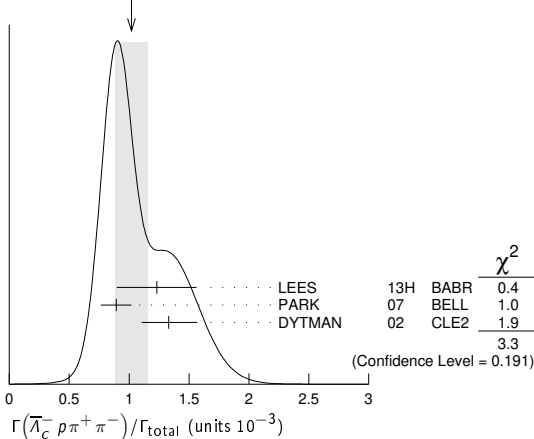
• • • We do not use the following data for averages, fits, limits, etc. • • •

0.88 ± 0.16 ± 0.05  
-0.04 <sup>5</sup> GABYSHEV 02 BELL Repl. by PARK 07

1.33 ± 0.46 ± 0.37 <sup>6</sup> FU 97 CLE2 Repl. by DYTMAN 02

<sup>1</sup> Assumes equal production of  $B^+$  and  $B^0$  at the  $\Upsilon(4S)$ .  
<sup>2</sup> Uses  $\Lambda_c^+ \rightarrow p K^- \pi^+$  mode. The second error includes the uncertainty of the branching fraction of the  $\Lambda_c$  decay,  $B(\Lambda_c^+ \rightarrow p K^- \pi^+) = (5.0 \pm 1.3)\%$ .  
<sup>3</sup> PARK 07 reports  $(11.2 \pm 0.5 \pm 3.2) \times 10^{-4}$  from a measurement of  $[\Gamma(B^0 \rightarrow \bar{\Lambda}_c^- p \pi^+ \pi^-)/\Gamma_{total}] \times [B(\Lambda_c^+ \rightarrow p K^- \pi^+)]$  assuming  $B(\Lambda_c^+ \rightarrow p K^- \pi^+) = (5.0 \pm 1.3) \times 10^{-2}$ , which we rescale to our best value  $B(\Lambda_c^+ \rightarrow p K^- \pi^+) = (6.28 \pm 0.32) \times 10^{-2}$ . Our first error is their experiment's error and our second error is the systematic error from using our best value.  
<sup>4</sup> DYTMAN 02 reports  $(1.67^{+0.27}_{-0.25}) \times 10^{-3}$  from a measurement of  $[\Gamma(B^0 \rightarrow \bar{\Lambda}_c^- p \pi^+ \pi^-)/\Gamma_{total}] \times [B(\Lambda_c^+ \rightarrow p K^- \pi^+)]$  assuming  $B(\Lambda_c^+ \rightarrow p K^- \pi^+) = 0.05$ , which we rescale to our best value  $B(\Lambda_c^+ \rightarrow p K^- \pi^+) = (6.28 \pm 0.32) \times 10^{-2}$ . Our first error is their experiment's error and our second error is the systematic error from using our best value.  
<sup>5</sup> GABYSHEV 02 reports  $(1.1 \pm 0.2) \times 10^{-3}$  from a measurement of  $[\Gamma(B^0 \rightarrow \bar{\Lambda}_c^- p \pi^+ \pi^-)/\Gamma_{total}] \times [B(\Lambda_c^+ \rightarrow p K^- \pi^+)]$  assuming  $B(\Lambda_c^+ \rightarrow p K^- \pi^+) = 0.05$ , which we rescale to our best value  $B(\Lambda_c^+ \rightarrow p K^- \pi^+) = (6.28 \pm 0.32) \times 10^{-2}$ . Our first error is their experiment's error and our second error is the systematic error from using our best value.  
<sup>6</sup> FU 97 uses PDG 96 values of  $\Lambda_c$  branching fraction.

WEIGHTED AVERAGE  
1.02 ± 0.14 (Error scaled by 1.3)



$\Gamma(\bar{\Lambda}_c^- p)/\Gamma_{total}$   $\Gamma_{499}/\Gamma$

VALUE (units $10^{-5}$ )	CL%	DOCUMENT ID	TECN	COMMENT
<b>1.54 ± 0.18 OUR AVERAGE</b>	Error includes scale factor of 1.3.			
1.51 ± 0.16 ± 0.08		<sup>1,2</sup> AUBERT	08BN	BABR $e^+e^- \rightarrow \Upsilon(4S)$
2.19 ± 0.56 ± 0.65 -0.49		<sup>1,3</sup> GABYSHEV	03	BELL $e^+e^- \rightarrow \Upsilon(4S)$

• • • We do not use the following data for averages, fits, limits, etc. • • •

2.10 ± 0.67 ± 0.77  
-0.55 - 0.46 <sup>1,4</sup> AUBERT 07AV BABR Repl. by AUBERT 08BN

< 9 90 <sup>1,5</sup> DYTMAN 02 CLE2  $e^+e^- \rightarrow \Upsilon(4S)$

< 3.1 90 <sup>1,4</sup> GABYSHEV 02 BELL  $e^+e^- \rightarrow \Upsilon(4S)$

< 21 90 <sup>6</sup> FU 97 CLE2  $e^+e^- \rightarrow \Upsilon(4S)$

<sup>1</sup> Assumes equal production of  $B^+$  and  $B^0$  at the  $\Upsilon(4S)$ .

<sup>2</sup> AUBERT 08BN reports  $(1.89 \pm 0.21 \pm 0.49) \times 10^{-5}$  from a measurement of  $[\Gamma(B^0 \rightarrow \bar{\Lambda}_c^- p)/\Gamma_{total}] \times [B(\Lambda_c^+ \rightarrow p K^- \pi^+)]$  assuming  $B(\Lambda_c^+ \rightarrow p K^- \pi^+) = (5.0 \pm 1.3) \times 10^{-2}$ , which we rescale to our best value  $B(\Lambda_c^+ \rightarrow p K^- \pi^+) = (6.28 \pm 0.32) \times 10^{-2}$ . Our first error is their experiment's error and our second error is the systematic error from using our best value.  
<sup>3</sup> The second error for GABYSHEV 03 includes the systematic and the error of  $\Lambda_c \rightarrow \bar{p} K^+ \pi^-$  decay branching fraction.

<sup>4</sup> Uses the value for  $\Lambda_c \rightarrow p K^- \pi^+$  branching ratio  $(5.0 \pm 1.3)\%$ .  
<sup>5</sup> DYTMAN 02 measurement uses  $B(\Lambda_c^- \rightarrow \bar{p} K^+ \pi^-) = 5.0 \pm 1.3\%$ . The second error includes the systematic and the uncertainty of the branching ratio.  
<sup>6</sup> FU 97 uses PDG 96 values of  $\Lambda_c$  branching ratio.

$\Gamma(\bar{\Lambda}_c^- p \pi^0)/\Gamma_{total}$   $\Gamma_{500}/\Gamma$

VALUE (units $10^{-4}$ )	CL%	DOCUMENT ID	TECN	COMMENT
<b>1.55 ± 0.17 ± 0.08</b>		<sup>1,2</sup> AUBERT	10H	BABR $e^+e^- \rightarrow \Upsilon(4S)$

• • • We do not use the following data for averages, fits, limits, etc. • • •

<5.9 90 <sup>3</sup> FU 97 CLE2  $e^+e^- \rightarrow \Upsilon(4S)$

<sup>1</sup> AUBERT 10H reports  $(1.94 \pm 0.17 \pm 0.52) \times 10^{-4}$  from a measurement of  $[\Gamma(B^0 \rightarrow \bar{\Lambda}_c^- p \pi^0)/\Gamma_{total}] \times [B(\Lambda_c^+ \rightarrow p K^- \pi^+)]$  assuming  $B(\Lambda_c^+ \rightarrow p K^- \pi^+) = (5.0 \pm 1.3) \times 10^{-2}$ , which we rescale to our best value  $B(\Lambda_c^+ \rightarrow p K^- \pi^+) = (6.28 \pm 0.32) \times 10^{-2}$ . Our first error is their experiment's error and our second error is the systematic error from using our best value.  
<sup>2</sup> Assumes equal production of  $B^+$  and  $B^0$  at the  $\Upsilon(4S)$ .  
<sup>3</sup> FU 97 uses PDG 96 values of  $\Lambda_c$  branching ratio.

$\Gamma(\bar{\Lambda}_c^- p K^+ K^-)/\Gamma_{total}$   $\Gamma_{513}/\Gamma$

VALUE (units $10^{-5}$ )	CL%	DOCUMENT ID	TECN	COMMENT
<b>2.0 ± 0.4 ± 0.1</b>		<sup>1,2</sup> LEES	15B	BABR $e^+e^- \rightarrow \Upsilon(4S)$

<sup>1</sup> LEES 15B reports  $[\Gamma(B^0 \rightarrow \bar{\Lambda}_c^- p K^+ K^-)/\Gamma_{total}] \times [B(\Lambda_c^+ \rightarrow p K^- \pi^+)] = (12.5 \pm 2.0 \pm 1.0) \times 10^{-7}$  which we divide by our best value  $B(\Lambda_c^+ \rightarrow p K^- \pi^+) = (6.28 \pm 0.32) \times 10^{-2}$ . Our first error is their experiment's error and our second error is the systematic error from using our best value.  
<sup>2</sup> Assumes equal production of  $B^+$  and  $B^0$  at the  $\Upsilon(4S)$ .

$\Gamma(\bar{\Lambda}_c^- p \phi)/\Gamma_{total}$   $\Gamma_{514}/\Gamma$

VALUE	CL%	DOCUMENT ID	TECN	COMMENT
<1.0 × 10 <sup>-5</sup>	90	<sup>1,2</sup> LEES	15B	BABR $e^+e^- \rightarrow \Upsilon(4S)$

<sup>1</sup> LEES 15B reports < 1.2 × 10<sup>-5</sup> from a measurement of  $[\Gamma(B^0 \rightarrow \bar{\Lambda}_c^- p \phi)/\Gamma_{total}] \times [B(\Lambda_c^+ \rightarrow p K^- \pi^+)]$  assuming  $B(\Lambda_c^+ \rightarrow p K^- \pi^+) = (5.0 \pm 1.3) \times 10^{-2}$ , which we rescale to our best value  $B(\Lambda_c^+ \rightarrow p K^- \pi^+) = 6.28 \times 10^{-2}$ .  
<sup>2</sup> Assumes equal production of  $B^+$  and  $B^0$  at the  $\Upsilon(4S)$ .

$\Gamma(\Sigma_c(2455)^- p)/\Gamma_{total}$   $\Gamma_{501}/\Gamma$

VALUE (units $10^{-6}$ )	CL%	DOCUMENT ID	TECN	COMMENT
<24		<sup>1,2</sup> AUBERT	10H	BABR $e^+e^- \rightarrow \Upsilon(4S)$

<sup>1</sup> AUBERT 10H reports  $[\Gamma(B^0 \rightarrow \Sigma_c(2455)^- p)/\Gamma_{total}] \times [B(\Lambda_c^+ \rightarrow p K^- \pi^+)] < 1.5 \times 10^{-6}$  which we divide by our best value  $B(\Lambda_c^+ \rightarrow p K^- \pi^+) = 6.28 \times 10^{-2}$ .  
<sup>2</sup> Assumes equal production of  $B^+$  and  $B^0$  at the  $\Upsilon(4S)$ .

$\Gamma(\bar{\Lambda}_c^- p \pi^+ \pi^- \pi^0)/\Gamma_{total}$   $\Gamma_{502}/\Gamma$

VALUE	CL%	DOCUMENT ID	TECN	COMMENT
<5.07 × 10 <sup>-3</sup>	90	<sup>1</sup> FU	97	CLE2 $e^+e^- \rightarrow \Upsilon(4S)$

<sup>1</sup> FU 97 uses PDG 96 values of  $\Lambda_c$  branching ratio.

$\Gamma(\bar{\Lambda}_c^- p \pi^+ \pi^- \pi^+ \pi^-)/\Gamma_{total}$   $\Gamma_{503}/\Gamma$

VALUE	CL%	DOCUMENT ID	TECN	COMMENT
<2.74 × 10 <sup>-3</sup>	90	<sup>1</sup> FU	97	CLE2 $e^+e^- \rightarrow \Upsilon(4S)$

<sup>1</sup> FU 97 uses PDG 96 values of  $\Lambda_c$  branching ratio.

$\Gamma(\bar{\Lambda}_c^- p \pi^+ \pi^- (\text{nonresonant}))/\Gamma_{total}$   $\Gamma_{504}/\Gamma$

VALUE (units $10^{-4}$ )	CL%	DOCUMENT ID	TECN	COMMENT
<b>5.5 ± 1.0 OUR AVERAGE</b>	Error includes scale factor of 1.3.			
7.9 ± 0.4 ± 2.0		<sup>1,2</sup> LEES	13H	BABR $e^+e^- \rightarrow \Upsilon(4S)$
5.1 ± 0.8 ± 0.3		<sup>1,3</sup> PARK	07	BELL $e^+e^- \rightarrow \Upsilon(4S)$

<sup>1</sup> Assumes equal production of  $B^+$  and  $B^0$  at the  $\Upsilon(4S)$ .  
<sup>2</sup> Uses  $\Lambda_c^+ \rightarrow p K^- \pi^+$  mode. The second error includes the uncertainty of the branching fraction of the  $\Lambda_c$  decay,  $B(\Lambda_c^+ \rightarrow p K^- \pi^+) = (5.0 \pm 1.3)\%$ .  
<sup>3</sup> PARK 07 reports  $(6.4 \pm 0.4 \pm 1.9) \times 10^{-4}$  from a measurement of  $[\Gamma(B^0 \rightarrow \bar{\Lambda}_c^- p \pi^+ \pi^- (\text{nonresonant}))/\Gamma_{total}] \times [B(\Lambda_c^+ \rightarrow p K^- \pi^+)]$  assuming  $B(\Lambda_c^+ \rightarrow p K^- \pi^+) = (5.0 \pm 1.3) \times 10^{-2}$ , which we rescale to our best value  $B(\Lambda_c^+ \rightarrow p K^- \pi^+) = (6.28 \pm 0.32) \times 10^{-2}$ . Our first error is their experiment's error and our second error is the systematic error from using our best value.

# Meson Particle Listings

## $B^0$

### $\Gamma(\overline{S}_C(2520)^{--} p \pi^+)/\Gamma_{\text{total}}$ $\Gamma_{505}/\Gamma$

VALUE (units $10^{-4}$ )	DOCUMENT ID	TECN	COMMENT
<b>1.02 ± 0.18 OUR AVERAGE</b>			
1.15 ± 0.10 ± 0.30	1,2 LEES	13H BABR	$e^+e^- \rightarrow \mathcal{T}(4S)$
0.96 ± 0.21 ± 0.05	1,3 PARK	07 BELL	$e^+e^- \rightarrow \mathcal{T}(4S)$

- • • We do not use the following data for averages, fits, limits, etc. • • •
- 1,3 ± 0.5 ± 0.1 <sup>4</sup>GABYSHEV 02 BELL Repl. by PARK 07
- <sup>1</sup>Assumes equal production of  $B^+$  and  $B^0$  at the  $\mathcal{T}(4S)$ .
- <sup>2</sup>Uses  $\Lambda_C^+ \rightarrow p K^- \pi^+$  mode. The second error includes the uncertainty of the branching fraction of the  $\Lambda_C$  decay,  $B(\Lambda_C^+ \rightarrow p K^- \pi^+) = (5.0 \pm 1.3)\%$ .
- <sup>3</sup>PARK 07 reports  $(1.2 \pm 0.1 \pm 0.4) \times 10^{-4}$  from a measurement of  $[\Gamma(B^0 \rightarrow \overline{S}_C(2520)^{--} p \pi^+)/\Gamma_{\text{total}}] \times [B(\Lambda_C^+ \rightarrow p K^- \pi^+)]$  assuming  $B(\Lambda_C^+ \rightarrow p K^- \pi^+) = (5.0 \pm 1.3) \times 10^{-2}$ , which we rescale to our best value  $B(\Lambda_C^+ \rightarrow p K^- \pi^+) = (6.28 \pm 0.32) \times 10^{-2}$ . Our first error is their experiment's error and our second error is the systematic error from using our best value.
- <sup>4</sup>GABYSHEV 02 reports  $(1.63_{-0.58}^{+0.64}) \times 10^{-4}$  from a measurement of  $[\Gamma(B^0 \rightarrow \overline{S}_C(2520)^{--} p \pi^+)/\Gamma_{\text{total}}] \times [B(\Lambda_C^+ \rightarrow p K^- \pi^+)]$  assuming  $B(\Lambda_C^+ \rightarrow p K^- \pi^+) = 0.05$ , which we rescale to our best value  $B(\Lambda_C^+ \rightarrow p K^- \pi^+) = (6.28 \pm 0.32) \times 10^{-2}$ . Our first error is their experiment's error and our second error is the systematic error from using our best value.

### $\Gamma(\overline{S}_C(2520)^0 p \pi^-)/\Gamma_{\text{total}}$ $\Gamma_{506}/\Gamma$

VALUE	CL%	DOCUMENT ID	TECN	COMMENT
<b>&lt;0.31 × 10<sup>-4</sup></b>	90	1,2 LEES	13H BABR	$e^+e^- \rightarrow \mathcal{T}(4S)$
<0.38 × 10 <sup>-4</sup>	90	1 PARK	07 BELL	$e^+e^- \rightarrow \mathcal{T}(4S)$
<1.21 × 10 <sup>-4</sup>	90	1,2 GABYSHEV	02 BELL	Repl. by PARK 07

- • • We do not use the following data for averages, fits, limits, etc. • • •
- <sup>1</sup>Assumes equal production of  $B^+$  and  $B^0$  at the  $\mathcal{T}(4S)$ .
- <sup>2</sup>Uses the value for  $\Lambda_C \rightarrow p K^- \pi^+$  branching ratio  $(5.0 \pm 1.3)\%$ .

### $\Gamma(\overline{S}_C(2455)^0 N^0, N^0 \rightarrow p \pi^-)/\Gamma_{\text{total}}$ $\Gamma_{508}/\Gamma$

$N^0$  is the  $N(1440) P_{11}$  or  $N(1535) S_{11}$  or an admixture of the two baryonic states.

VALUE (units $10^{-4}$ )	DOCUMENT ID	TECN	COMMENT
<b>0.64 ± 0.16 ± 0.03</b>	1,2 KIM	08 BELL	$e^+e^- \rightarrow \mathcal{T}(4S)$

- <sup>1</sup>Assumes equal production of  $B^+$  and  $B^0$  at the  $\mathcal{T}(4S)$ .
- <sup>2</sup>KIM 08 reports  $(0.80 \pm 0.15 \pm 0.25) \times 10^{-4}$  from a measurement of  $[\Gamma(B^0 \rightarrow \overline{S}_C(2455)^0 N^0, N^0 \rightarrow p \pi^-)/\Gamma_{\text{total}}] \times [B(\Lambda_C^+ \rightarrow p K^- \pi^+)]$  assuming  $B(\Lambda_C^+ \rightarrow p K^- \pi^+) = (5.0 \pm 1.3) \times 10^{-2}$ , which we rescale to our best value  $B(\Lambda_C^+ \rightarrow p K^- \pi^+) = (6.28 \pm 0.32) \times 10^{-2}$ . Our first error is their experiment's error and our second error is the systematic error from using our best value.

### $\Gamma(\overline{S}_C(2455)^0 p \pi^-)/\Gamma_{\text{total}}$ $\Gamma_{507}/\Gamma$

VALUE (units $10^{-4}$ )	CL%	DOCUMENT ID	TECN	COMMENT
<b>1.08 ± 0.16 OUR AVERAGE</b>				
0.91 ± 0.07 ± 0.24		1,2 LEES	13H BABR	$e^+e^- \rightarrow \mathcal{T}(4S)$
1.12 ± 0.21 ± 0.06		1,3 PARK	07 BELL	$e^+e^- \rightarrow \mathcal{T}(4S)$
1.8 ± 0.6 ± 0.1		4 DYTMAN	02 CLE2	$e^+e^- \rightarrow \mathcal{T}(4S)$
0.38 ± 0.37 ± 0.33 ± 0.02	90	5 GABYSHEV	02 BELL	Repl. by PARK 07

- • • We do not use the following data for averages, fits, limits, etc. • • •
- <sup>1</sup>Assumes equal production of  $B^+$  and  $B^0$  at the  $\mathcal{T}(4S)$ .
- <sup>2</sup>Uses  $\Lambda_C^+ \rightarrow p K^- \pi^+$  mode. The second error includes the uncertainty of the branching fraction of the  $\Lambda_C$  decay,  $B(\Lambda_C^+ \rightarrow p K^- \pi^+) = (5.0 \pm 1.3)\%$ .
- <sup>3</sup>PARK 07 reports  $(1.4 \pm 0.2 \pm 0.4) \times 10^{-4}$  from a measurement of  $[\Gamma(B^0 \rightarrow \overline{S}_C(2455)^0 p \pi^-)/\Gamma_{\text{total}}] \times [B(\Lambda_C^+ \rightarrow p K^- \pi^+)]$  assuming  $B(\Lambda_C^+ \rightarrow p K^- \pi^+) = (5.0 \pm 1.3) \times 10^{-2}$ , which we rescale to our best value  $B(\Lambda_C^+ \rightarrow p K^- \pi^+) = (6.28 \pm 0.32) \times 10^{-2}$ . Our first error is their experiment's error and our second error is the systematic error from using our best value.
- <sup>4</sup>DYTMAN 02 reports  $(2.2 \pm 0.7) \times 10^{-4}$  from a measurement of  $[\Gamma(B^0 \rightarrow \overline{S}_C(2455)^0 p \pi^-)/\Gamma_{\text{total}}] \times [B(\Lambda_C^+ \rightarrow p K^- \pi^+)]$  assuming  $B(\Lambda_C^+ \rightarrow p K^- \pi^+) = 0.05$ , which we rescale to our best value  $B(\Lambda_C^+ \rightarrow p K^- \pi^+) = (6.28 \pm 0.32) \times 10^{-2}$ . Our first error is their experiment's error and our second error is the systematic error from using our best value.
- <sup>5</sup>GABYSHEV 02 reports  $(0.48_{-0.41}^{+0.46}) \times 10^{-4}$  from a measurement of  $[\Gamma(B^0 \rightarrow \overline{S}_C(2455)^0 p \pi^-)/\Gamma_{\text{total}}] \times [B(\Lambda_C^+ \rightarrow p K^- \pi^+)]$  assuming  $B(\Lambda_C^+ \rightarrow p K^- \pi^+) = 0.05$ , which we rescale to our best value  $B(\Lambda_C^+ \rightarrow p K^- \pi^+) = (6.28 \pm 0.32) \times 10^{-2}$ . Our first error is their experiment's error and our second error is the systematic error from using our best value.

### $\Gamma(\overline{S}_C(2455)^{--} p \pi^+)/\Gamma_{\text{total}}$ $\Gamma_{509}/\Gamma$

VALUE (units $10^{-4}$ )	DOCUMENT ID	TECN	COMMENT
<b>1.83 ± 0.24 OUR AVERAGE</b>			
2.13 ± 0.10 ± 0.56	1,2 LEES	13H BABR	$e^+e^- \rightarrow \mathcal{T}(4S)$
1.67 ± 0.25 ± 0.09 ± 0.08	1,3 PARK	07 BELL	$e^+e^- \rightarrow \mathcal{T}(4S)$
2.9 ± 0.9 ± 0.2 ± 0.1	4 DYTMAN	02 CLE2	$e^+e^- \rightarrow \mathcal{T}(4S)$

- • • We do not use the following data for averages, fits, limits, etc. • • •

### 1.9 $_{-0.5}^{+0.6} \pm 0.1$ <sup>5</sup>GABYSHEV 02 BELL Repl. by PARK 07

- <sup>1</sup>Assumes equal production of  $B^+$  and  $B^0$  at the  $\mathcal{T}(4S)$ .
- <sup>2</sup>Uses  $\Lambda_C^+ \rightarrow p K^- \pi^+$  mode. The second error includes the uncertainty of the branching fraction of the  $\Lambda_C$  decay,  $B(\Lambda_C^+ \rightarrow p K^- \pi^+) = (5.0 \pm 1.3)\%$ .
- <sup>3</sup>PARK 07 reports  $(2.1 \pm 0.2 \pm 0.6) \times 10^{-4}$  from a measurement of  $[\Gamma(B^0 \rightarrow \overline{S}_C(2455)^{--} p \pi^+)/\Gamma_{\text{total}}] \times [B(\Lambda_C^+ \rightarrow p K^- \pi^+)]$  assuming  $B(\Lambda_C^+ \rightarrow p K^- \pi^+) = (5.0 \pm 1.3) \times 10^{-2}$ , which we rescale to our best value  $B(\Lambda_C^+ \rightarrow p K^- \pi^+) = (6.28 \pm 0.32) \times 10^{-2}$ . Our first error is their experiment's error and our second error is the systematic error from using our best value.
- <sup>4</sup>DYTMAN 02 reports  $(3.7 \pm 1.1) \times 10^{-4}$  from a measurement of  $[\Gamma(B^0 \rightarrow \overline{S}_C(2455)^{--} p \pi^+)/\Gamma_{\text{total}}] \times [B(\Lambda_C^+ \rightarrow p K^- \pi^+)]$  assuming  $B(\Lambda_C^+ \rightarrow p K^- \pi^+) = 0.05$ , which we rescale to our best value  $B(\Lambda_C^+ \rightarrow p K^- \pi^+) = (6.28 \pm 0.32) \times 10^{-2}$ . Our first error is their experiment's error and our second error is the systematic error from using our best value.
- <sup>5</sup>GABYSHEV 02 reports  $(2.38_{-0.69}^{+0.75}) \times 10^{-4}$  from a measurement of  $[\Gamma(B^0 \rightarrow \overline{S}_C(2455)^{--} p \pi^+)/\Gamma_{\text{total}}] \times [B(\Lambda_C^+ \rightarrow p K^- \pi^+)]$  assuming  $B(\Lambda_C^+ \rightarrow p K^- \pi^+) = 0.05$ , which we rescale to our best value  $B(\Lambda_C^+ \rightarrow p K^- \pi^+) = (6.28 \pm 0.32) \times 10^{-2}$ . Our first error is their experiment's error and our second error is the systematic error from using our best value.

### $\Gamma(\Lambda_C^- p K^+ \pi^-)/\Gamma_{\text{total}}$ $\Gamma_{510}/\Gamma$

VALUE (units $10^{-5}$ )	DOCUMENT ID	TECN	COMMENT
<b>3.4 ± 0.7 ± 0.2</b>	1,2 AUBERT	09AG BABR	$e^+e^- \rightarrow \mathcal{T}(4S)$

- <sup>1</sup>AUBERT 09AG reports  $(4.33 \pm 0.82 \pm 0.33 \pm 1.13) \times 10^{-5}$  from a measurement of  $[\Gamma(B^0 \rightarrow \Lambda_C^- p K^+ \pi^-)/\Gamma_{\text{total}}] \times [B(\Lambda_C^+ \rightarrow p K^- \pi^+)]$  assuming  $B(\Lambda_C^+ \rightarrow p K^- \pi^+) = (5.0 \pm 1.3) \times 10^{-2}$ , which we rescale to our best value  $B(\Lambda_C^+ \rightarrow p K^- \pi^+) = (6.28 \pm 0.32) \times 10^{-2}$ . Our first error is their experiment's error and our second error is the systematic error from using our best value.
- <sup>2</sup>Assumes equal production of  $B^+$  and  $B^0$  at the  $\mathcal{T}(4S)$ .

### $\Gamma(\overline{S}_C(2455)^{--} p K^+, \overline{S}_C^- \rightarrow \overline{\Lambda}_C^- \pi^-)/\Gamma_{\text{total}}$ $\Gamma_{511}/\Gamma$

VALUE (units $10^{-5}$ )	DOCUMENT ID	TECN	COMMENT
<b>0.88 ± 0.25 ± 0.05 ± 0.04</b>	1,2 AUBERT	09AG BABR	$e^+e^- \rightarrow \mathcal{T}(4S)$

- <sup>1</sup>AUBERT 09AG reports  $(1.11 \pm 0.30 \pm 0.09 \pm 0.29) \times 10^{-5}$  from a measurement of  $[\Gamma(B^0 \rightarrow \overline{S}_C(2455)^{--} p K^+, \overline{S}_C^- \rightarrow \overline{\Lambda}_C^- \pi^-)/\Gamma_{\text{total}}] \times [B(\Lambda_C^+ \rightarrow p K^- \pi^+)]$  assuming  $B(\Lambda_C^+ \rightarrow p K^- \pi^+) = (5.0 \pm 1.3) \times 10^{-2}$ , which we rescale to our best value  $B(\Lambda_C^+ \rightarrow p K^- \pi^+) = (6.28 \pm 0.32) \times 10^{-2}$ . Our first error is their experiment's error and our second error is the systematic error from using our best value.
- <sup>2</sup>Assumes equal production of  $B^+$  and  $B^0$  at the  $\mathcal{T}(4S)$ .

### $\Gamma(\Lambda_C^- p K^*(892)^0)/\Gamma_{\text{total}}$ $\Gamma_{512}/\Gamma$

VALUE (units $10^{-5}$ )	CL%	DOCUMENT ID	TECN	COMMENT
<b>&lt;2.42</b>	90	1 AUBERT	09AG BABR	$e^+e^- \rightarrow \mathcal{T}(4S)$

- <sup>1</sup>Assumes equal production of  $B^+$  and  $B^0$  at the  $\mathcal{T}(4S)$ .

### $\Gamma(\Lambda_C^- p \overline{p} p)/\Gamma_{\text{total}}$ $\Gamma_{515}/\Gamma$

VALUE (units $10^{-5}$ )	DOCUMENT ID	TECN	COMMENT
<b>&lt;2.8</b>	1 LEES	14c BABR	$e^+e^- \rightarrow \mathcal{T}(4S)$

- <sup>1</sup>Assumes equal production of  $B^+$  and  $B^0$  at the  $\mathcal{T}(4S)$  and  $B(\Lambda_C^+ \rightarrow p K^- \pi^+) = 0.050 \pm 0.013$ .

### $\Gamma(\overline{\Lambda}_C^- \Lambda K^+)/\Gamma_{\text{total}}$ $\Gamma_{516}/\Gamma$

VALUE (units $10^{-5}$ )	DOCUMENT ID	TECN	COMMENT
<b>4.8 ± 1.1 ± 0.2 ± 0.3</b>	1,2 LEES	11F BABR	$e^+e^- \rightarrow \mathcal{T}(4S)$

- <sup>1</sup>Assumes equal production of  $B^0$  and  $B^+$  from Upsilon(4S) decays.
- <sup>2</sup>LEES 11F reports  $(3.8 \pm 0.8 \pm 0.2 \pm 1.0) \times 10^{-5}$  from a measurement of  $[\Gamma(B^0 \rightarrow \overline{\Lambda}_C^- \Lambda K^+)/\Gamma_{\text{total}}] / [B(\Lambda_C^+ \rightarrow p K^- \pi^+)] / [B(\Lambda \rightarrow p \pi^-)]$  assuming  $B(\Lambda_C^+ \rightarrow p K^- \pi^+) = (5.0 \pm 1.3) \times 10^{-2}$ ,  $B(\Lambda \rightarrow p \pi^-) = (63.9 \pm 0.5) \times 10^{-2}$ , which we rescale to our best values  $B(\Lambda_C^+ \rightarrow p K^- \pi^+) = (6.28 \pm 0.32) \times 10^{-2}$ ,  $B(\Lambda \rightarrow p \pi^-) = (63.9 \pm 0.5) \times 10^{-2}$ . Our first error is their experiment's error and our second error is the systematic error from using our best values. The reported uncertainties are statistical, systematic, and  $\overline{\Lambda}_C^-$  branching fraction uncertainty.

### $\Gamma(\overline{\Lambda}_C^- \Lambda_C^+)/\Gamma_{\text{total}}$ $\Gamma_{517}/\Gamma$

VALUE (units $10^{-5}$ )	CL%	DOCUMENT ID	TECN	COMMENT
<b>&lt;1.6</b>	95	1 AAIJ	14AA LHCB	$pp$ at 7 TeV

- • • We do not use the following data for averages, fits, limits, etc. • • •
- <6.2 90 <sup>2</sup>UCHIDA 08 BELL  $e^+e^- \rightarrow \mathcal{T}(4S)$
- <sup>1</sup>Uses  $B(\overline{B}^0 \rightarrow D^+ D_s^-) = (7.2 \pm 0.8) \times 10^{-3}$ .
- <sup>2</sup>Assumes equal production of  $B^+$  and  $B^0$  at the  $\mathcal{T}(4S)$ .

See key on page 999

# Meson Particle Listings

## $B^0$

$\Gamma(\overline{A}_c(2593)^- / \overline{A}_c(2625)^- p) / \Gamma_{\text{total}}$					$\Gamma_{518} / \Gamma$
VALUE	CL%	DOCUMENT ID	TECN	COMMENT	
$< 1.1 \times 10^{-4}$	90	1,2 DYTMAN	02	CLE2 $e^+e^- \rightarrow \Upsilon(4S)$	

- <sup>1</sup> Assumes equal production of  $B^+$  and  $B^0$  at the  $\Upsilon(4S)$ .
- <sup>2</sup> DYTMAN 02 measurement uses  $B(\Lambda_c^- \rightarrow \overline{p}K^+\pi^-) = 5.0 \pm 1.3\%$ . The second error includes the systematic and the uncertainty of the branching ratio.

$\Gamma(\Xi_c^+ \Lambda_c^+) / \Gamma_{\text{total}}$					$\Gamma_{519} / \Gamma$
VALUE (units $10^{-3}$ )		DOCUMENT ID	TECN	COMMENT	
$1.2 \pm 0.7 \pm 0.3$		1,2 LI	19c	BELL $e^+e^- \rightarrow \Upsilon(4S)$	

- <sup>1</sup> Uses fully reconstructed  $B^0$  on tag side with recoil against  $\Lambda_c^+$ .
- <sup>2</sup> LI 19c reports  $(1.16 \pm 0.74 \pm 0.33) \times 10^{-3}$  from a measurement of  $[\Gamma(B^0 \rightarrow \Xi_c^+ \Lambda_c^+) / \Gamma_{\text{total}}] \times [B(\Lambda_c^+ \rightarrow pK^-\pi^+)]$  assuming  $B(\Lambda_c^+ \rightarrow pK^-\pi^+) = (6.28 \pm 0.32) \times 10^{-2}$ .

$\Gamma(\Xi_c^+ \Lambda_c^+, \Xi_c^- \rightarrow \Xi^+ \pi^- \pi^-) / \Gamma_{\text{total}}$					$\Gamma_{520} / \Gamma$
VALUE (units $10^{-3}$ )		DOCUMENT ID	TECN	COMMENT	
<b><math>2.4 \pm 1.1</math> OUR AVERAGE</b>		Error includes scale factor of 1.8.			
$3.3 \pm 0.7 \pm 0.3$		1 LI	19c	BELL $e^+e^- \rightarrow \Upsilon(4S)$	
$1.2 \pm 0.9 \pm 0.1$		2,3 AUBERT	08H	BABR $e^+e^- \rightarrow \Upsilon(4S)$	

- • • We do not use the following data for averages, fits, limits, etc. • • •
- $7.4^{+3.3}_{-2.7} \pm 0.4$       3,4 CHISTOV    06A    BELL    Repl. by LI 19c

- <sup>1</sup> LI 19c reports  $(3.32 \pm 0.74 \pm 0.33) \times 10^{-5}$  from a measurement of  $[\Gamma(B^0 \rightarrow \Xi_c^+ \Lambda_c^+, \Xi_c^- \rightarrow \Xi^+ \pi^- \pi^-) / \Gamma_{\text{total}}] \times [B(\Lambda_c^+ \rightarrow pK^-\pi^+)]$  assuming  $B(\Lambda_c^+ \rightarrow pK^-\pi^+) = (6.28 \pm 0.32) \times 10^{-2}$ .
- <sup>2</sup> AUBERT 08H reports  $(1.5 \pm 1.07 \pm 0.44) \times 10^{-5}$  from a measurement of  $[\Gamma(B^0 \rightarrow \Xi_c^+ \Lambda_c^+, \Xi_c^- \rightarrow \Xi^+ \pi^- \pi^-) / \Gamma_{\text{total}}] \times [B(\Lambda_c^+ \rightarrow pK^-\pi^+)]$  assuming  $B(\Lambda_c^+ \rightarrow pK^-\pi^+) = (5.0 \pm 1.3) \times 10^{-2}$ , which we rescale to our best value  $B(\Lambda_c^+ \rightarrow pK^-\pi^+) = (6.28 \pm 0.32) \times 10^{-2}$ . Our first error is their experiment's error and our second error is the systematic error from using our best value.
- <sup>3</sup> Assumes equal production of  $B^+$  and  $B^0$  at the  $\Upsilon(4S)$ .
- <sup>4</sup> CHISTOV 06A reports  $(9.3^{+3.7}_{-2.8} \pm 3.1) \times 10^{-5}$  from a measurement of  $[\Gamma(B^0 \rightarrow \Xi_c^+ \Lambda_c^+, \Xi_c^- \rightarrow \Xi^+ \pi^- \pi^-) / \Gamma_{\text{total}}] \times [B(\Lambda_c^+ \rightarrow pK^-\pi^+)]$  assuming  $B(\Lambda_c^+ \rightarrow pK^-\pi^+) = (5.0 \pm 1.3) \times 10^{-2}$ , which we rescale to our best value  $B(\Lambda_c^+ \rightarrow pK^-\pi^+) = (6.28 \pm 0.32) \times 10^{-2}$ . Our first error is their experiment's error and our second error is the systematic error from using our best value.

$\Gamma(\Xi_c^+ \Lambda_c^+, \Xi_c^- \rightarrow \overline{p}K^+\pi^-) / \Gamma_{\text{total}}$					$\Gamma_{521} / \Gamma$
VALUE (units $10^{-6}$ )		DOCUMENT ID	TECN	COMMENT	
<b><math>5.3 \pm 1.5 \pm 0.7</math></b>		1 LI	19c	BELL $e^+e^- \rightarrow \Upsilon(4S)$	

- <sup>1</sup> LI 19c reports  $(5.27 \pm 1.51 \pm 0.69) \times 10^{-6}$  from a measurement of  $[\Gamma(B^0 \rightarrow \Xi_c^+ \Lambda_c^+, \Xi_c^- \rightarrow \overline{p}K^+\pi^-) / \Gamma_{\text{total}}] \times [B(\Lambda_c^+ \rightarrow pK^-\pi^+)]$  assuming  $B(\Lambda_c^+ \rightarrow pK^-\pi^+) = (6.28 \pm 0.32) \times 10^{-2}$ .

$\Gamma(\Lambda_c^+ \Lambda_c^- K^0) / \Gamma_{\text{total}}$					$\Gamma_{522} / \Gamma$
VALUE (units $10^{-4}$ )		DOCUMENT ID	TECN	COMMENT	
<b><math>4.0 \pm 0.9</math> OUR AVERAGE</b>					
$3.99 \pm 0.76 \pm 0.51$		1 LI	18D	BELL $e^+e^- \rightarrow \Upsilon(4S)$	
$3.8 \pm 3.1 \pm 2.1$		2,3 AUBERT	08H	BABR $e^+e^- \rightarrow \Upsilon(4S)$	

- • • We do not use the following data for averages, fits, limits, etc. • • •
- $7.9^{+2.9}_{-2.3} \pm 4.3$       2,3 GABYSHEV    06    BELL    Repl. by LI 18D

- <sup>1</sup> Assumes  $B(\Upsilon(4S) \rightarrow B^0 \overline{B}^0) = 48.6 \pm 0.6\%$  and  $B(\Lambda_c^+ \rightarrow pK^-\pi^+) = 6.23 \pm 0.33\%$ .
- <sup>2</sup> Assumes  $B(\Lambda_c^+ \rightarrow pK^-\pi^+) = 5.0 \pm 1.3\%$ .
- <sup>3</sup> Assumes equal production of  $B^+$  and  $B^0$  at the  $\Upsilon(4S)$ .

$\Gamma(\Xi_c(2930)^- \Lambda_c^+, \Xi_c^- \rightarrow \Lambda_c^- K^0) / \Gamma_{\text{total}}$					$\Gamma_{523} / \Gamma$
VALUE (units $10^{-4}$ )		DOCUMENT ID	TECN	COMMENT	
<b><math>2.37 \pm 0.51 \pm 0.31</math></b>		1 LI	18D	BELL $e^+e^- \rightarrow \Upsilon(4S)$	

- <sup>1</sup> Assumes  $B(\Upsilon(4S) \rightarrow B^0 \overline{B}^0) = 48.6 \pm 0.6\%$  and  $B(\Lambda_c^+ \rightarrow pK^-\pi^+) = 6.23 \pm 0.33\%$ .

$\Gamma(\gamma\gamma) / \Gamma_{\text{total}}$					$\Gamma_{524} / \Gamma$
Test for $\Delta B=1$ weak neutral current. Allowed by higher-order electroweak interactions.					
VALUE	CL%	DOCUMENT ID	TECN	COMMENT	
$< 3.2 \times 10^{-7}$		90	1	DEL-AMO-SA...11A    BABR $e^+e^- \rightarrow \Upsilon(4S)$	

- • • We do not use the following data for averages, fits, limits, etc. • • •
- $< 6.2 \times 10^{-7}$       90      1    VILLA    06    BELL  $e^+e^- \rightarrow \Upsilon(4S)$   
 $< 1.7 \times 10^{-6}$       90      1    AUBERT    01    BABR  $e^+e^- \rightarrow \Upsilon(4S)$   
 $< 3.9 \times 10^{-5}$       90      2    ACCIARRI    95i    L3  $e^+e^- \rightarrow Z$

- <sup>1</sup> Assumes equal production of  $B^+$  and  $B^0$  at the  $\Upsilon(4S)$ .
- <sup>2</sup> ACCIARRI 95i assumes  $f_{B^0} = 39.5 \pm 4.0$  and  $f_{B_s} = 12.0 \pm 3.0\%$ .

$\Gamma(e^+e^-) / \Gamma_{\text{total}}$					$\Gamma_{525} / \Gamma$
Test for $\Delta B=1$ weak neutral current. Allowed by higher-order electroweak interactions.					
VALUE	CL%	DOCUMENT ID	TECN	COMMENT	
$< 8.3 \times 10^{-8}$		90		AALTONEN    09p    CDF $p\overline{p}$ at 1.96 TeV	

- • • We do not use the following data for averages, fits, limits, etc. • • •
- $< 11.3 \times 10^{-8}$       90      1    AUBERT    08p    BABR  $e^+e^- \rightarrow \Upsilon(4S)$   
 $< 6.1 \times 10^{-8}$       90      1    AUBERT    05w    BABR    Repl. by AUBERT 08p  
 $< 1.9 \times 10^{-7}$       90      1    CHANG    03    BELL  $e^+e^- \rightarrow \Upsilon(4S)$   
 $< 8.3 \times 10^{-7}$       90      1    BERGFELD    00b    CLE2  $e^+e^- \rightarrow \Upsilon(4S)$   
 $< 1.4 \times 10^{-5}$       90      2    ACCIARRI    97b    L3  $e^+e^- \rightarrow Z$   
 $< 5.9 \times 10^{-6}$       90      3    AMMAR    94    CLE2    Repl. by BERGFELD 00b  
 $< 2.6 \times 10^{-5}$       90      3    AVERY    89b    CLEO  $e^+e^- \rightarrow \Upsilon(4S)$   
 $< 7.6 \times 10^{-5}$       90      4    ALBRECHT    87d    ARG  $e^+e^- \rightarrow \Upsilon(4S)$   
 $< 6.4 \times 10^{-5}$       90      5    AVERY    87    CLEO  $e^+e^- \rightarrow \Upsilon(4S)$   
 $< 3 \times 10^{-4}$       90      6    GILES    84    CLEO    Repl. by AVERY 87

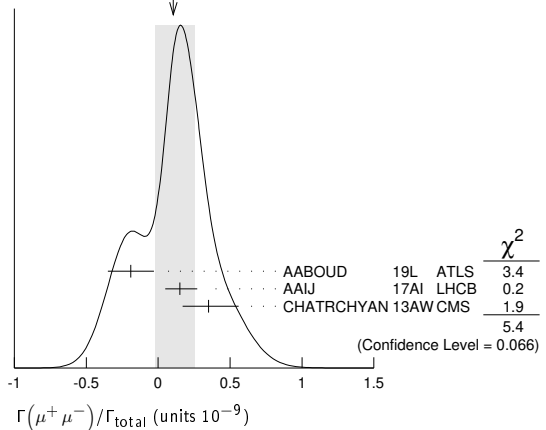
- <sup>1</sup> Assumes equal production of  $B^+$  and  $B^0$  at the  $\Upsilon(4S)$ .
- <sup>2</sup> ACCIARRI 97b assume PDG 96 production fractions for  $B^+$ ,  $B^0$ ,  $B_s$ , and  $\Lambda_b$ .
- <sup>3</sup> AVERY 89b reports  $< 3 \times 10^{-5}$  assuming the  $\Upsilon(4S)$  decays 43% to  $B^0 \overline{B}^0$ . We rescale to 50%.
- <sup>4</sup> ALBRECHT 87d reports  $< 8.5 \times 10^{-5}$  assuming the  $\Upsilon(4S)$  decays 45% to  $B^0 \overline{B}^0$ . We rescale to 50%.
- <sup>5</sup> AVERY 87 reports  $< 8 \times 10^{-5}$  assuming the  $\Upsilon(4S)$  decays 40% to  $B^0 \overline{B}^0$ . We rescale to 50%.

$\Gamma(e^+e^- \gamma) / \Gamma_{\text{total}}$					$\Gamma_{526} / \Gamma$
Test for $\Delta B=1$ weak neutral current. Allowed by higher-order electroweak interactions.					
VALUE	CL%	DOCUMENT ID	TECN	COMMENT	
$< 1.2 \times 10^{-7}$		90		AUBERT    08c    BABR $e^+e^- \rightarrow \Upsilon(4S)$	

$\Gamma(\mu^+ \mu^-) / \Gamma_{\text{total}}$					$\Gamma_{527} / \Gamma$
Test for $\Delta B=1$ weak neutral current. Allowed by higher-order electroweak interactions.					
VALUE (units $10^{-3}$ )	CL%	DOCUMENT ID	TECN	COMMENT	
<b><math>0.11^{+0.14}_{-0.13}</math> OUR AVERAGE</b>		Error includes scale factor of 1.6. See the ideogram below.			

- • • We do not use the following data for averages, fits, limits, etc. • • •
- $-0.19 \pm 0.16$       1,2 AABOUD    19L    ATLS  $p\overline{p}$  at 7, 8, 13 TeV  
 $0.15^{+0.12+0.02}_{-0.10-0.01}$       3    AAIJ    17Al    LHCB  $p\overline{p}$  at 7, 8, 13 TeV  
 $0.35^{+0.21}_{-0.18}$       4    CHATRCHYAN13AW    CMS  $p\overline{p}$  at 7, 8 TeV
- $-0.25 \pm 0.20$       5    AABOUD    16L    ATLS  $p\overline{p}$  at 7, 8 TeV, Repl. by AABOUD 16L
- $0.39^{+0.16}_{-0.14}$       6    KHACHATRY...15BE    LHC  $p\overline{p}$  at 7, 8 TeV
- $< 0.80$       90      7    AAIJ    13b    LHCB    Repl. by AAIJ 13BA  
 $< 0.63$       90      8    AAIJ    13BA    LHCB    Repl. by KHACHATRYAN 15BE
- $< 3.8$       90      9    AALTONEN    13F    CDF  $p\overline{p}$  at 1.96 TeV  
 $< 2.6$       90      7    AAIJ    12A    LHCB    Repl. by AAIJ 12W  
 $< 0.81$       90      10    AAIJ    12W    LHCB    Repl. by AAIJ 13B  
 $< 1.4$       90      10    CHATRCHYAN12A    CMS  $p\overline{p}$  at 7 TeV  
 $< 12$       90      11    AAIJ    11B    LHCB    Repl. by AAIJ 12A  
 $< 5.0$       90      10    AALTONEN    11Ag    CDF  $p\overline{p}$  at 1.96 TeV  
 $< 3.7$       90      10    CHATRCHYAN11T    CMS    Repl. by CHATRCHYAN 12A

WEIGHTED AVERAGE  
 $0.11 \pm 0.14 - 0.13$  (Error scaled by 1.6)



- <sup>1</sup> Corresponds to a 95% CL upper limit of  $< 2.1 \times 10^{-10}$ .
- <sup>2</sup> Uses normalization mode  $B(B^+ \rightarrow J/\psi K^+) = (1.010 \pm 0.029) \times 10^{-3}$  and  $B$  production ratio  $f(b \rightarrow B_s^0) / f(b \rightarrow B^0) = 0.256 \pm 0.013$ .
- <sup>3</sup> Corresponds to a 95% CL upper limit of  $< 3.4 \times 10^{-10}$ .
- <sup>4</sup> Reports also a limit of  $< 9.2 \times 10^{-10}$  at 90% CL, and uses  $B(B^+ \rightarrow J/\psi K^+ \rightarrow \mu^+ \mu^- K^+) = (6.0 \pm 0.2) \times 10^{-5}$  for normalization.

# Meson Particle Listings

## $B^0$

- <sup>5</sup> This value is obtained from a profile-likelihood fit, see Fig. 9. It corresponds to an upper limit of  $< 0.42 \times 10^{-9}$  at 95% C.L.
- <sup>6</sup> Derived from the combined fit to CMS and LHCb data. Uncertainty includes both statistical and systematic component. Also reports  $B(B^0 \rightarrow \mu^+ \mu^-)/B(B_s \rightarrow \mu^+ \mu^-) = 0.14^{+0.08}_{-0.06}$ .
- <sup>7</sup> Uses  $B(B^+ \rightarrow J/\psi K^+ \rightarrow \mu^+ \mu^- K^+) = (6.01 \pm 0.21) \times 10^{-5}$  and  $B(B^0 \rightarrow K^+ \pi^-) = (1.94 \pm 0.06) \times 10^{-5}$  for normalization.
- <sup>8</sup> Reports also a limit of  $< 7.4 \times 10^{-10}$  at 95% CL. Uses normalization modes  $B^+ \rightarrow J/\psi K^+ \rightarrow \mu^+ \mu^- K^+$  and  $B^0 \rightarrow K^+ \pi^-$ .
- <sup>9</sup> Uses normalization mode  $B(B^+ \rightarrow J/\psi K^+) = (10.22 \pm 0.35) \times 10^{-4}$ .
- <sup>10</sup> Uses  $B(B^+ \rightarrow J/\psi K^+ \rightarrow \mu^+ \mu^- K^+) = (6.01 \pm 0.21) \times 10^{-5}$ .
- <sup>11</sup> Uses  $B$  production ratio  $f(\bar{b} \rightarrow B^+)/f(\bar{b} \rightarrow B_s^0) = 3.71 \pm 0.47$  and three normalization modes.

**$\Gamma(\mu^+ \mu^- \gamma)/\Gamma_{total}$   $\Gamma_{528}/\Gamma$**   
 Test for  $\Delta B=1$  weak neutral current. Allowed by higher-order electroweak interactions.

VALUE	CL%	DOCUMENT ID	TECN	COMMENT
$<1.6 \times 10^{-7}$	90	AUBERT	08c	BABR $e^+ e^- \rightarrow \Upsilon(4S)$

**$\Gamma(\tau^+ \tau^-)/\Gamma_{total}$   $\Gamma_{531}/\Gamma$**   
 Test for  $\Delta B=1$  weak neutral current. Allowed by higher-order electroweak interactions.

VALUE	CL%	DOCUMENT ID	TECN	COMMENT
$<2.1 \times 10^{-3}$	95	1 AAIJ	17AJ	LHCB $pp$ at 7, 8 TeV
••• We do not use the following data for averages, fits, limits, etc. •••				
$<4.1 \times 10^{-3}$	90	2 AUBERT	06s	BABR $e^+ e^- \rightarrow \Upsilon(4S)$
1 Assuming no contribution from $B_s^0 \rightarrow \tau^+ \tau^-$ .				
2 Assumes equal production of $B^+$ and $B^0$ at the $\Upsilon(4S)$ .				

**$\Gamma(\mu^+ \mu^- \mu^+ \mu^-)/\Gamma_{total}$   $\Gamma_{529}/\Gamma$**

VALUE	CL%	DOCUMENT ID	TECN	COMMENT
$<6.9 \times 10^{-10}$	95	AAIJ	17N	LHCB $pp$ at 7, 8 TeV
••• We do not use the following data for averages, fits, limits, etc. •••				
$<5.3 \times 10^{-9}$	90	1 AAIJ	13AW	LHCB Repl. by AAIJ 17N
1 Also reports a limit of $< 6.6 \times 10^{-9}$ at 95% CL.				

**$\Gamma(S, P, S \rightarrow \mu^+ \mu^-, P \rightarrow \mu^+ \mu^-)/\Gamma_{total}$   $\Gamma_{530}/\Gamma$**   
 Here  $S$  and  $P$  are the hypothetical scalar and pseudoscalar particles with masses of 2.5 GeV/ $c^2$  and 214.3 MeV/ $c^2$ , respectively.

VALUE	CL%	DOCUMENT ID	TECN	COMMENT
$<6.0 \times 10^{-10}$	95	AAIJ	17N	LHCB $pp$ at 7, 8 TeV
••• We do not use the following data for averages, fits, limits, etc. •••				
$<5.1 \times 10^{-9}$	90	1 AAIJ	13AW	LHCB Repl. by AAIJ 17N
1 Also reports a limit of $< 6.3 \times 10^{-9}$ at 95% CL.				

**$\Gamma(\pi^0 \ell^+ \ell^-)/\Gamma_{total}$   $\Gamma_{532}/\Gamma$**

VALUE	CL%	DOCUMENT ID	TECN	COMMENT
$<5.3 \times 10^{-8}$	90	1 LEES	13M	BABR $e^+ e^- \rightarrow \Upsilon(4S)$
••• We do not use the following data for averages, fits, limits, etc. •••				
$<1.5 \times 10^{-7}$	90	1 WEI	08A	BELL $e^+ e^- \rightarrow \Upsilon(4S)$
$<1.2 \times 10^{-7}$	90	1 AUBERT	07AG	BABR Repl. by LEES 13M
1 Assumes equal production of $B^+$ and $B^0$ at the $\Upsilon(4S)$ .				

**$\Gamma(\pi^0 \nu \bar{\nu})/\Gamma_{total}$   $\Gamma_{538}/\Gamma$**   
 Test for  $\Delta B = 1$  weak neutral current. Allowed by higher-order electroweak interaction.

VALUE	CL%	DOCUMENT ID	TECN	COMMENT
$<0.9 \times 10^{-5}$	90	1 GRYGIER	17	BELL $e^+ e^- \rightarrow \Upsilon(4S)$
••• We do not use the following data for averages, fits, limits, etc. •••				
$<6.9 \times 10^{-5}$	90	1 LUTZ	13	BELL $e^+ e^- \rightarrow \Upsilon(4S)$
$<2.2 \times 10^{-4}$	90	1 CHEN	07D	BELL Repl. by LUTZ 13
1 Assumes equal production of $B^+$ and $B^0$ at the $\Upsilon(4S)$ .				

**$\Gamma(\pi^0 e^+ e^-)/\Gamma_{total}$   $\Gamma_{533}/\Gamma$**

VALUE	CL%	DOCUMENT ID	TECN	COMMENT
$<8.4 \times 10^{-8}$	90	1 LEES	13M	BABR $e^+ e^- \rightarrow \Upsilon(4S)$
••• We do not use the following data for averages, fits, limits, etc. •••				
$<2.3 \times 10^{-7}$	90	1 WEI	08A	BELL $e^+ e^- \rightarrow \Upsilon(4S)$
$<1.4 \times 10^{-7}$	90	1 AUBERT	07AG	BABR Repl. by LEES 13M
1 Assumes equal production of $B^+$ and $B^0$ at the $\Upsilon(4S)$ .				

**$\Gamma(\pi^0 \mu^+ \mu^-)/\Gamma_{total}$   $\Gamma_{534}/\Gamma$**

VALUE	CL%	DOCUMENT ID	TECN	COMMENT
$<6.9 \times 10^{-8}$	90	1 LEES	13M	BABR $e^+ e^- \rightarrow \Upsilon(4S)$
••• We do not use the following data for averages, fits, limits, etc. •••				
$<1.8 \times 10^{-7}$	90	1 WEI	08A	BELL $e^+ e^- \rightarrow \Upsilon(4S)$
$<5.1 \times 10^{-7}$	90	1 AUBERT	07AG	BABR $e^+ e^- \rightarrow \Upsilon(4S)$
1 Assumes equal production of $B^+$ and $B^0$ at the $\Upsilon(4S)$ .				

**$\Gamma(\eta \ell^+ \ell^-)/\Gamma_{total}$   $\Gamma_{535}/\Gamma$**

VALUE	CL%	DOCUMENT ID	TECN	COMMENT
$<6.4 \times 10^{-8}$	90	1 LEES	13M	BABR $e^+ e^- \rightarrow \Upsilon(4S)$
1 Assumes equal production of $B^+$ and $B^0$ at the $\Upsilon(4S)$ .				

**$\Gamma(\eta e^+ e^-)/\Gamma_{total}$   $\Gamma_{536}/\Gamma$**

VALUE	CL%	DOCUMENT ID	TECN	COMMENT
$<10.8 \times 10^{-8}$	90	1 LEES	13M	BABR $e^+ e^- \rightarrow \Upsilon(4S)$
1 Assumes equal production of $B^+$ and $B^0$ at the $\Upsilon(4S)$ .				

**$\Gamma(\eta \mu^+ \mu^-)/\Gamma_{total}$   $\Gamma_{537}/\Gamma$**

VALUE	CL%	DOCUMENT ID	TECN	COMMENT
$<11.2 \times 10^{-8}$	90	1 LEES	13M	BABR $e^+ e^- \rightarrow \Upsilon(4S)$
1 Assumes equal production of $B^+$ and $B^0$ at the $\Upsilon(4S)$ .				

**$\Gamma(K^0 \ell^+ \ell^-)/\Gamma_{total}$   $\Gamma_{539}/\Gamma$**

VALUE (units $10^{-7}$ )	CL%	DOCUMENT ID	TECN	COMMENT
<b>3.1 <math>\pm</math> 0.8 OUR AVERAGE</b>				
$2.1^{+1.5}_{-1.3} \pm 0.2$		1 AUBERT	09T	BABR $e^+ e^- \rightarrow \Upsilon(4S)$
$3.4^{+0.9}_{-0.8} \pm 0.2$		1 WEI	09A	BELL $e^+ e^- \rightarrow \Upsilon(4S)$
••• We do not use the following data for averages, fits, limits, etc. •••				
$2.9^{+1.6}_{-1.3} \pm 0.3$		1 AUBERT,B	06J	BABR Repl. by AUBERT 09T
$<6.8$	90	1 ISHIKAWA	03	BELL $e^+ e^- \rightarrow \Upsilon(4S)$
1 Assumes equal production of $B^0$ and $B^+$ at $\Upsilon(4S)$ .				

**$\Gamma(K^0 e^+ e^-)/\Gamma_{total}$   $\Gamma_{540}/\Gamma$**   
 Test for  $\Delta B=1$  weak neutral current. Allowed by higher-order electroweak interactions.

VALUE (units $10^{-7}$ )	CL%	DOCUMENT ID	TECN	COMMENT
<b>1.6 <math>\pm</math> 1.0 OUR AVERAGE</b>				
$0.8^{+1.5}_{-1.2} \pm 0.1$		1 AUBERT	09T	BABR $e^+ e^- \rightarrow \Upsilon(4S)$
$2.0^{+1.4}_{-1.0} \pm 0.1$		1 WEI	09A	BELL $e^+ e^- \rightarrow \Upsilon(4S)$
••• We do not use the following data for averages, fits, limits, etc. •••				
$1.3^{+1.6}_{-1.1} \pm 0.2$		1 AUBERT,B	06J	BABR Repl. by AUBERT 09T
$- 2.1^{+2.3}_{-1.6} \pm 0.8$		1 AUBERT	03U	BABR $e^+ e^- \rightarrow \Upsilon(4S)$
$< 5.4$	90	2 ISHIKAWA	03	BELL $e^+ e^- \rightarrow \Upsilon(4S)$
$< 27$	90	1 ABE	02	BELL Repl. by ISHIKAWA 03
$< 38$	90	1 AUBERT	02L	BABR $e^+ e^- \rightarrow \Upsilon(4S)$
$< 84.5$	90	3 ANDERSON	01B	CLE2 $e^+ e^- \rightarrow \Upsilon(4S)$
$< 3000$	90	1 ALBRECHT	91E	ARG $e^+ e^- \rightarrow \Upsilon(4S)$
$< 5200$	90	4 AVERY	87	CLEO $e^+ e^- \rightarrow \Upsilon(4S)$
1 Assumes equal production of $B^+$ and $B^0$ at the $\Upsilon(4S)$ .				
2 Assumes equal production of $B^0$ and $B^+$ at $\Upsilon(4S)$ .				
3 The result is for di-lepton masses above 0.5 GeV.				
4 AVERY 87 reports $< 6.5 \times 10^{-4}$ assuming the $\Upsilon(4S)$ decays 40% to $B^0 \bar{B}^0$ . We rescale to 50%.				

**$\Gamma(K^0 \nu \bar{\nu})/\Gamma_{total}$   $\Gamma_{542}/\Gamma$**   
 Test for  $\Delta B = 1$  weak neutral current. Allowed by higher-order electroweak interaction.

VALUE	CL%	DOCUMENT ID	TECN	COMMENT
$< 2.6 \times 10^{-5}$	90	1 GRYGIER	17	BELL $e^+ e^- \rightarrow \Upsilon(4S)$
••• We do not use the following data for averages, fits, limits, etc. •••				
$< 4.9 \times 10^{-5}$	90	1,2 LEES	13I	BABR $e^+ e^- \rightarrow \Upsilon(4S)$
$<19.4 \times 10^{-5}$	90	1 LUTZ	13	BELL $e^+ e^- \rightarrow \Upsilon(4S)$
$< 5.6 \times 10^{-5}$	90	1 DEL-AMO-SA...	10Q	BABR Repl. by LEES 13I
$< 1.6 \times 10^{-4}$	90	1 CHEN	07D	BELL $e^+ e^- \rightarrow \Upsilon(4S)$
1 Assumes equal production of $B^+$ and $B^0$ at the $\Upsilon(4S)$ .				
2 Also reported a limit $< 8.1 \times 10^{-5}$ at 90% CL obtained using a fully reconstructed hadronic $B$ -tag evnets.				

**$\Gamma(\rho^0 \nu \bar{\nu})/\Gamma_{total}$   $\Gamma_{543}/\Gamma$**   
 Test for  $\Delta B = 1$  weak neutral current. Allowed by higher-order electroweak interaction.

VALUE	CL%	DOCUMENT ID	TECN	COMMENT
$<4.0 \times 10^{-5}$	90	1 GRYGIER	17	BELL $e^+ e^- \rightarrow \Upsilon(4S)$
••• We do not use the following data for averages, fits, limits, etc. •••				
$<2.08 \times 10^{-4}$	90	1 LUTZ	13	BELL $e^+ e^- \rightarrow \Upsilon(4S)$
$<4.4 \times 10^{-4}$	90	1 CHEN	07D	BELL Repl. by LUTZ 13
1 Assumes equal production of $B^+$ and $B^0$ at the $\Upsilon(4S)$ .				

**$\Gamma(K^0 \mu^+ \mu^-)/\Gamma_{total}$   $\Gamma_{541}/\Gamma$**   
 Test for  $\Delta B=1$  weak neutral current. Allowed by higher-order electroweak interactions.

VALUE (units $10^{-7}$ )	CL%	DOCUMENT ID	TECN	COMMENT
<b>3.39 <math>\pm</math> 0.34 OUR FIT</b>				
<b>3.4 <math>\pm</math> 0.4 OUR AVERAGE</b>				
$3.27 \pm 0.34 \pm 0.17$		1 AAIJ	14M	LHCB $pp$ at 7, 8 TeV
$4.9^{+2.9}_{-2.5} \pm 0.3$		2 AUBERT	09T	BABR $e^+ e^- \rightarrow \Upsilon(4S)$
$4.4^{+1.3}_{-1.1} \pm 0.3$		2 WEI	09A	BELL $e^+ e^- \rightarrow \Upsilon(4S)$

• • • We do not use the following data for averages, fits, limits, etc. • • •

Table with columns: Value, Document ID, TECN, COMMENT. Rows include AAIJ, AUBERT, B, ISHIKAWA, ABE, AUBERT, ANDERSON, ALBRECHT, AVERY.

- 1 Uses B(B^0 -> J/psi(1S) K^0) = (0.928 +/- 0.013 +/- 0.037) x 10^-3 for normalization.
2 Assumes equal production of B+ and B0 at the T(4S).
3 Assumes equal production of B0 and B+ at T(4S). The second error is a total of systematic uncertainties including model dependence.
4 The result is for di-lepton masses above 0.5 GeV.
5 AVERY 87 reports < 4.5 x 10^-4 assuming the T(4S) decays 40% to B0 B0-bar. We rescale to 50%.

Gamma(K^0 mu+ mu-)/Gamma(J/psi(1S) K^0) Table with columns: VALUE, DOCUMENT ID, TECN, COMMENT. Includes OUR FIT and AALTONEN data.

Gamma(K\*(892)^0 l+ l-)/Gamma\_total Table with columns: VALUE, DOCUMENT ID, TECN, COMMENT. Includes OUR AVERAGE and AUBERT, WEI data.

Gamma(K\*(892)^0 e+ e-)/Gamma\_total Table with columns: VALUE, DOCUMENT ID, TECN, COMMENT. Includes OUR AVERAGE and AUBERT, WEI data.

Gamma(K\*(892)^0 e+ e-)/Gamma\_total Table with columns: VALUE, CL%, DOCUMENT ID, TECN, COMMENT. Includes OUR AVERAGE and AUBERT, WEI data.

- 1 Assumes equal production of B+ and B0 at the T(4S).
2 Assumes equal production of B0 and B+ at T(4S).

Gamma(K\*(892)^0 mu+ mu-)/Gamma\_total Table with columns: VALUE, CL%, DOCUMENT ID, TECN, COMMENT. Includes OUR FIT and OUR AVERAGE.

Gamma(K\*(892)^0 mu+ mu-)/Gamma\_total Table with columns: VALUE, CL%, DOCUMENT ID, TECN, COMMENT. Includes AAIJ, AUBERT, WEI, ISHIKAWA, ABE, AFFOLDER data.

- 1 Uses B(B^0 -> J/psi K\*(892)^0) = (1.19 +/- 0.01 +/- 0.08) x 10^-3. The second error is the total systematic uncertainty.
2 Assumes equal production of B+ and B0 at the T(4S).
3 Assumes equal production of B0 and B+ at T(4S). The second error is a total of systematic uncertainties including model dependence.
4 AFFOLDER 99b measured relative to B0 -> J/psi(1S) K\*(892)^0.

Gamma(K\*(892)^0 mu+ mu-)/Gamma(J/psi(1S) K\*(892)^0) Table with columns: VALUE, DOCUMENT ID, TECN, COMMENT. Includes OUR FIT and AALTONEN data.

- • • We do not use the following data for averages, fits, limits, etc. • • •
0.80 +/- 0.10 +/- 0.06 AALTONEN 11L CDF Repl. by AALTONEN 11A1
0.61 +/- 0.23 +/- 0.07 AALTONEN 09B CDF Repl. by AALTONEN 11L

Gamma(K\*(892)^0 chi -> mu+ mu-)/Gamma\_total Table with columns: VALUE, CL%, DOCUMENT ID, TECN, COMMENT. Includes AAIJ data.

- 1 The limit is obtained as a function of di-muon mass. A normalizing mode branching fraction value of B(B^0 -> K\*0 mu+ mu-) = (1.6 +/- 0.3) x 10^-7 is used.

Gamma(pi+ pi- mu+ mu-)/Gamma\_total Table with columns: VALUE, DOCUMENT ID, TECN, COMMENT. Includes AAIJ data.

- 1 AAIJ 15s reports (2.11 +/- 0.51 +/- 0.15 +/- 0.16) x 10^-8 from a measurement of [Gamma(B^0 -> pi+ pi- mu+ mu-)/Gamma\_total] / [Gamma(B^0 -> J/psi(1S) K\*(892)^0)] assuming B(B^0 -> J/psi(1S) K\*(892)^0) = (1.3 +/- 0.1) x 10^-3, which we rescale to our best value B(B^0 -> J/psi(1S) K\*(892)^0) = (1.27 +/- 0.05) x 10^-3. Our first error is their experiment's error and our second error is the systematic error from using our best value.

Gamma(K\*(892)^0 nu nu)/Gamma\_total Table with columns: VALUE, CL%, DOCUMENT ID, TECN, COMMENT. Includes GRYGIER data.

- • • We do not use the following data for averages, fits, limits, etc. • • •
< 1.2 x 10^-4 90 1,2 LEES 13i BABR e+ e- -> T(4S)
< 5.5 x 10^-5 90 1 LUTZ 13 BELL e+ e- -> T(4S)
< 1.2 x 10^-4 90 AUBERT 08b B BABR Repl. by LEES 13i
< 3.4 x 10^-4 90 1 CHEN 07D BELL e+ e- -> T(4S)
< 1.0 x 10^-3 90 3 ADAM 96D DLPH e+ e- -> Z
1 Assumes equal production of B+ and B0 at the T(4S).
2 Also reported a limit < 9.3 x 10^-5 at 90% CL obtained using a fully reconstructed hadronic B-tag evnets.
3 ADAM 96D assumes f\_B0 = f\_B- = 0.39 and f\_Bs = 0.12.

Gamma(invisible)/Gamma\_total Table with columns: VALUE, CL%, DOCUMENT ID, TECN, COMMENT. Includes LEES data.

- • • We do not use the following data for averages, fits, limits, etc. • • •
< 13 90 2 HSU 12 BELL e+ e- -> T(4S)
< 22 90 1 AUBERT,B 04J B BABR e+ e- -> T(4S)
1 Uses the fully reconstructed B0 -> D(\*)- l+ nu\_l events as a tag.
2 Identified by fully reconstructing a hadronic decay of the accompanying B meson and requiring no other particles in the event.

Gamma(nu nu gamma)/Gamma\_total Table with columns: VALUE, CL%, DOCUMENT ID, TECN, COMMENT. Includes LEES data.

- • • We do not use the following data for averages, fits, limits, etc. • • •
< 4.7 90 1 AUBERT,B 04J B BABR Repl. by LEES 12T
1 Uses the fully reconstructed B0 -> D(\*)- l+ nu\_l events as a tag.

Gamma(phi nu nu)/Gamma\_total Table with columns: VALUE, CL%, DOCUMENT ID, TECN, COMMENT. Includes LUTZ data.

- • • We do not use the following data for averages, fits, limits, etc. • • •
< 5.8 x 10^-5 90 1 CHEN 07D BELL Repl. by LUTZ 13
1 Assumes equal production of B+ and B0 at the T(4S).

Gamma(e+ e-)/Gamma\_total Table with columns: VALUE, CL%, DOCUMENT ID, TECN, COMMENT. Includes AAIJ data.

- • • We do not use the following data for averages, fits, limits, etc. • • •
< 2.8 x 10^-9 90 2 AAIJ 13BMLHCB Repl. by AAIJ 18T
< 6.4 x 10^-8 90 AALTONEN 09P CDF p p-bar at 1.96 TeV
< 9.2 x 10^-8 90 3 AUBERT 08P B BABR e+ e- -> T(4S)
< 1.8 x 10^-7 90 3 AUBERT 05W B BABR e+ e- -> T(4S)
< 1.7 x 10^-7 90 3 CHANG 03 BELL e+ e- -> T(4S)
< 15 x 10^-7 90 3 BERGFELD 00B CLE2 e+ e- -> T(4S)
< 3.5 x 10^-6 90 ABE 98V CDF p p-bar at 1.8 TeV
< 1.6 x 10^-5 90 4 ACCIARRI 97B L3 e+ e- -> Z
< 5.9 x 10^-6 90 AMMAR 94 CLE2 e+ e- -> T(4S)
< 3.4 x 10^-5 90 5 AVERY 89B CLEO e+ e- -> T(4S)
< 4.5 x 10^-5 90 6 ALBRECHT 87D ARG e+ e- -> T(4S)



# Meson Particle Listings

## $B^0$

$< 7.7 \times 10^{-5}$  90 7 AVERY 87 CLEO  $e^+e^- \rightarrow \Upsilon(4S)$   
 $< 3 \times 10^{-4}$  90 GILES 84 CLEO Repl. by AVERY 87

<sup>1</sup> AAIJ 18T uses normalization modes  $B(B^0 \rightarrow K^+\pi^-) = (19.6 \pm 0.5) \times 10^{-6}$  and  $B(B^+ \rightarrow J/\psi K^+) = (1.026 \pm 0.031) \times 10^{-3}$ .  
<sup>2</sup> Uses normalization mode  $B(B^0 \rightarrow K^+\pi^-) = (19.4 \pm 0.6) \times 10^{-6}$ .  
<sup>3</sup> Assumes equal production of  $B^+$  and  $B^0$  at the  $\Upsilon(4S)$ .  
<sup>4</sup> ACCIARRI 97B assume PDG 96 production fractions for  $B^+$ ,  $B^0$ ,  $B_s$ , and  $\Lambda_b$ .  
<sup>5</sup> Paper assumes the  $\Upsilon(4S)$  decays 43% to  $B^0\bar{B}^0$ . We rescale to 50%.  
<sup>6</sup> ALBRECHT 87D reports  $< 5 \times 10^{-5}$  assuming the  $\Upsilon(4S)$  decays 45% to  $B^0\bar{B}^0$ . We rescale to 50%.  
<sup>7</sup> AVERY 87 reports  $< 9 \times 10^{-5}$  assuming the  $\Upsilon(4S)$  decays 40% to  $B^0\bar{B}^0$ . We rescale to 50%.

$\Gamma(\pi^0 e^\pm \mu^\mp)/\Gamma_{total}$   $\Gamma_{554}/\Gamma$

VALUE	CL%	DOCUMENT ID	TECN	COMMENT
$< 1.4 \times 10^{-7}$	90	<sup>1</sup> AUBERT	07AG BABR	$e^+e^- \rightarrow \Upsilon(4S)$

<sup>1</sup> Assumes equal production of  $B^+$  and  $B^0$  at the  $\Upsilon(4S)$ .

$\Gamma(K^0 e^\pm \mu^\mp)/\Gamma_{total}$   $\Gamma_{555}/\Gamma$

Test of lepton family number conservation.

VALUE (units $10^{-7}$ )	CL%	DOCUMENT ID	TECN	COMMENT
$< 2.7$	90	<sup>1</sup> AUBERT,B	06J BABR	$e^+e^- \rightarrow \Upsilon(4S)$

• • • We do not use the following data for averages, fits, limits, etc. • • •

$< 40$	90	<sup>1</sup> AUBERT	02L BABR	Repl. by AUBERT,B 06J
--------	----	---------------------	----------	-----------------------

<sup>1</sup> Assumes equal production of  $B^+$  and  $B^0$  at the  $\Upsilon(4S)$ .

$\Gamma(K^*(892)^0 e^+ \mu^-)/\Gamma_{total}$   $\Gamma_{556}/\Gamma$

VALUE (units $10^{-7}$ )	CL%	DOCUMENT ID	TECN	COMMENT
$< 1.6$	90	<sup>1</sup> SANDILYA	18 BELL	$e^+e^- \rightarrow \Upsilon(4S)$

• • • We do not use the following data for averages, fits, limits, etc. • • •

$< 5.3$	90	<sup>2</sup> AUBERT,B	06J BABR	$e^+e^- \rightarrow \Upsilon(4S)$
---------	----	-----------------------	----------	-----------------------------------

<sup>1</sup> Uses  $B(\Upsilon(4S) \rightarrow B^0\bar{B}^0) = 0.486 \pm 0.006$ .  
<sup>2</sup> Assumes equal production of  $B^0$  and  $B^+$  at  $\Upsilon(4S)$ .

$\Gamma(K^*(892)^0 e^- \mu^+)/\Gamma_{total}$   $\Gamma_{557}/\Gamma$

VALUE (units $10^{-7}$ )	CL%	DOCUMENT ID	TECN	COMMENT
$< 1.2$	90	<sup>1</sup> SANDILYA	18 BELL	$e^+e^- \rightarrow \Upsilon(4S)$

• • • We do not use the following data for averages, fits, limits, etc. • • •

$< 3.4$	90	<sup>2</sup> AUBERT,B	06J BABR	$e^+e^- \rightarrow \Upsilon(4S)$
---------	----	-----------------------	----------	-----------------------------------

<sup>1</sup> Uses  $B(\Upsilon(4S) \rightarrow B^0\bar{B}^0) = 0.486 \pm 0.006$ .  
<sup>2</sup> Assumes equal production of  $B^0$  and  $B^+$  at  $\Upsilon(4S)$ .

$\Gamma(K^*(892)^0 e^\pm \mu^\mp)/\Gamma_{total}$   $\Gamma_{558}/\Gamma$

Test of lepton family number conservation.

VALUE (units $10^{-7}$ )	CL%	DOCUMENT ID	TECN	COMMENT
$< 1.8$	90	<sup>1</sup> SANDILYA	18 BELL	$e^+e^- \rightarrow \Upsilon(4S)$

• • • We do not use the following data for averages, fits, limits, etc. • • •

$< 5.8$	90	<sup>2</sup> AUBERT,B	06J BABR	$e^+e^- \rightarrow \Upsilon(4S)$
$< 34$	90	<sup>2</sup> AUBERT	02L BABR	Repl. by AUBERT,B 06J

<sup>1</sup> Uses  $B(\Upsilon(4S) \rightarrow B^0\bar{B}^0) = 0.486 \pm 0.006$ .  
<sup>2</sup> Assumes equal production of  $B^+$  and  $B^0$  at the  $\Upsilon(4S)$ .

$\Gamma(e^\pm \tau^\mp)/\Gamma_{total}$   $\Gamma_{559}/\Gamma$

Test of lepton family number conservation. Allowed by higher-order electroweak interactions.

VALUE	CL%	DOCUMENT ID	TECN	COMMENT
$< 2.8 \times 10^{-5}$	90	<sup>1</sup> AUBERT	08AD BABR	$e^+e^- \rightarrow \Upsilon(4S)$

• • • We do not use the following data for averages, fits, limits, etc. • • •

$< 1.1 \times 10^{-4}$	90	BORNHEIM	04 CLE2	$e^+e^- \rightarrow \Upsilon(4S)$
$< 5.3 \times 10^{-4}$	90	AMMAR	94 CLE2	Repl. by BORNHEIM 04

<sup>1</sup> Assumes equal production of  $B^+$  and  $B^0$  at the  $\Upsilon(4S)$ .

$\Gamma(\mu^\pm \tau^\mp)/\Gamma_{total}$   $\Gamma_{560}/\Gamma$

Test of lepton family number conservation. Allowed by higher-order electroweak interactions.

VALUE	CL%	DOCUMENT ID	TECN	COMMENT
$< 1.4 \times 10^{-5}$	95	<sup>1</sup> AAIJ	19AK LHCb	$pp$ at 7, 8 TeV

• • • We do not use the following data for averages, fits, limits, etc. • • •

$< 2.2 \times 10^{-5}$	90	<sup>2</sup> AUBERT	08AD BABR	$e^+e^- \rightarrow \Upsilon(4S)$
$< 3.8 \times 10^{-5}$	90	BORNHEIM	04 CLE2	$e^+e^- \rightarrow \Upsilon(4S)$
$< 8.3 \times 10^{-4}$	90	AMMAR	94 CLE2	Repl. by BORNHEIM 04

<sup>1</sup> Assuming no contribution from  $B_s^0 \rightarrow \mu^\pm \tau^\mp$ .  
<sup>2</sup> Assumes equal production of  $B^+$  and  $B^0$  at the  $\Upsilon(4S)$ .

$\Gamma(\Lambda_c^+ \mu^-)/\Gamma_{total}$   $\Gamma_{561}/\Gamma$

VALUE	CL%	DOCUMENT ID	TECN	COMMENT
$< 1.4 \times 10^{-6}$	90	<sup>1,2</sup> DEL-AMO-SA..11k	BABR	$e^+e^- \rightarrow \Upsilon(4S)$

<sup>1</sup> DEL-AMO-SANCHEZ 11k reports  $< 180 \times 10^{-8}$  from a measurement of  $[\Gamma(B^0 \rightarrow \Lambda_c^+ \mu^-)/\Gamma_{total}] \times [B(\Lambda_c^+ \rightarrow p K^- \pi^+)]$  assuming  $B(\Lambda_c^+ \rightarrow p K^- \pi^+) = (5.0 \pm 1.3) \times 10^{-2}$ , which we rescale to our best value  $B(\Lambda_c^+ \rightarrow p K^- \pi^+) = 6.28 \times 10^{-2}$ .  
<sup>2</sup> Uses  $B(\Upsilon(4S) \rightarrow B^0\bar{B}^0) = (51.6 \pm 0.6)\%$  and  $B(\Upsilon(4S) \rightarrow B^+B^-) = (48.4 \pm 0.6)\%$ .

$\Gamma(\Lambda_c^+ e^-)/\Gamma_{total}$   $\Gamma_{562}/\Gamma$

VALUE	CL%	DOCUMENT ID	TECN	COMMENT
$< 4 \times 10^{-6}$	90	<sup>1,2</sup> DEL-AMO-SA..11k	BABR	$e^+e^- \rightarrow \Upsilon(4S)$

<sup>1</sup> DEL-AMO-SANCHEZ 11k reports  $< 520 \times 10^{-8}$  from a measurement of  $[\Gamma(B^0 \rightarrow \Lambda_c^+ e^-)/\Gamma_{total}] \times [B(\Lambda_c^+ \rightarrow p K^- \pi^+)]$  assuming  $B(\Lambda_c^+ \rightarrow p K^- \pi^+) = (5.0 \pm 1.3) \times 10^{-2}$ , which we rescale to our best value  $B(\Lambda_c^+ \rightarrow p K^- \pi^+) = 6.28 \times 10^{-2}$ .  
<sup>2</sup> Uses  $B(\Upsilon(4S) \rightarrow B^0\bar{B}^0) = (51.6 \pm 0.6)\%$  and  $B(\Upsilon(4S) \rightarrow B^+B^-) = (48.4 \pm 0.6)\%$ .

### $B_s^0$ CROSS-PARTICLE BRANCHING RATIOS

$\Gamma([K^+ K^-]_D K^*(892)^0)/\Gamma_{total} \times B(B_s^0 \rightarrow [K^+ K^-]_D K^*(892)^0)$   $\Gamma_{142}/\Gamma \times B$

VALUE	DOCUMENT ID	TECN	COMMENT
$0.10 \pm 0.02 \pm 0.01$	AAIJ	14BN LHCb	$pp$ at 7, 8 TeV

$\Gamma([\pi^+ \pi^-]_D K^*(892)^0)/\Gamma_{total} \times B(B_s^0 \rightarrow [\pi^+ \pi^-]_D K^*(892)^0)$   $\Gamma_{143}/\Gamma \times B$

VALUE	DOCUMENT ID	TECN	COMMENT
$0.15 \pm 0.04 \pm 0.01$	AAIJ	14BN LHCb	$pp$ at 7, 8 TeV

See the related review(s):  
[Polarization in B Decays](#)

### POLARIZATION IN $B^0$ DECAY

In decays involving two vector mesons, one can distinguish among the states in which meson polarizations are both longitudinal ( $L$ ) or both are transverse and parallel ( $\parallel$ ) or perpendicular ( $\perp$ ) to each other with the parameters  $\Gamma_L/\Gamma$ ,  $\Gamma_\perp/\Gamma$ , and the relative phases  $\phi_\parallel$  and  $\phi_\perp$ . See the definitions in the note on "Polarization in B Decays" review in the  $B^0$  Particle Listings.

#### $\Gamma_L/\Gamma$ in $B^0 \rightarrow J/\psi(1S) K^*(892)^0$

VALUE	EVTs	DOCUMENT ID	TECN	COMMENT
$0.571 \pm 0.007$ OUR AVERAGE				
$0.572 \pm 0.006 \pm 0.014$		<sup>1</sup> AAIJ	13AT LHCb	$pp$ at 7 TeV
$0.587 \pm 0.011 \pm 0.013$		<sup>2</sup> ABAZOV	09E D0	$p\bar{p}$ at 1.96 TeV
$0.556 \pm 0.009 \pm 0.010$		<sup>3</sup> AUBERT	07AD BABR	$e^+e^- \rightarrow \Upsilon(4S)$
$0.562 \pm 0.026 \pm 0.018$		ACOSTA	05 CDF	$p\bar{p}$ at 1.96 TeV
$0.574 \pm 0.012 \pm 0.009$		ITOH	05 BELL	$e^+e^- \rightarrow \Upsilon(4S)$
$0.59 \pm 0.06 \pm 0.01$		<sup>4</sup> AFFOLDER	00N CDF	$p\bar{p}$ at 1.8 TeV
$0.52 \pm 0.07 \pm 0.04$		<sup>5</sup> JESSOP	97 CLE2	$e^+e^- \rightarrow \Upsilon(4S)$
$0.65 \pm 0.10 \pm 0.04$	65	ABE	95Z CDF	$p\bar{p}$ at 1.8 TeV
$0.97 \pm 0.16 \pm 0.15$	13	<sup>6</sup> ALBRECHT	94G ARG	$e^+e^- \rightarrow \Upsilon(4S)$

• • • We do not use the following data for averages, fits, limits, etc. • • •

$0.566 \pm 0.012 \pm 0.005$		<sup>7</sup> AUBERT	05P BABR	Repl. by AUBERT 07AD
$0.62 \pm 0.02 \pm 0.03$		<sup>7</sup> ABE	02N BELL	Repl. by ITOH 05
$0.597 \pm 0.028 \pm 0.024$		<sup>8</sup> AUBERT	01H BABR	Repl. by AUBERT 07AD
$0.80 \pm 0.08 \pm 0.05$	42	<sup>6</sup> ALAM	94 CLE2	Sup. by JESSOP 97

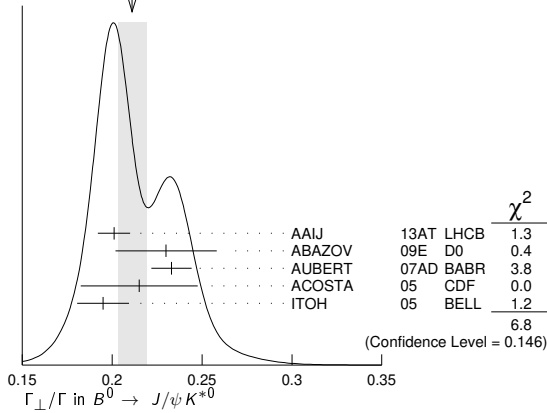
<sup>1</sup> AAIJ 13AT obtains  $\Gamma_\parallel/\Gamma = 0.227 \pm 0.004 \pm 0.011$ . The relation  $1 = (\Gamma_L + \Gamma_\perp + \Gamma_\parallel)/\Gamma$  is used to obtain  $\Gamma_L/\Gamma$ .  
<sup>2</sup> Measured the angular and lifetime parameters for the time-dependent angular untagged decays  $B_d^0 \rightarrow J/\psi K^{*0}$  and  $B_s^0 \rightarrow J/\psi \phi$ .  
<sup>3</sup> Obtained by combining the  $B^0$  and  $B^+$  modes.  
<sup>4</sup> AFFOLDER 00N measurements are based on 190  $B^0$  candidates obtained from a data sample of 89 pb<sup>-1</sup>. The  $P$ -wave fraction is found to be  $0.13_{-0.09}^{+0.12} \pm 0.06$ .  
<sup>5</sup> JESSOP 97 is the average over a mixture of  $B^0$  and  $B^+$  decays. The  $P$ -wave fraction is found to be  $0.16 \pm 0.08 \pm 0.04$ .  
<sup>6</sup> Averaged over an admixture of  $B^0$  and  $B^+$  decays.  
<sup>7</sup> Averaged over an admixture of  $B^0$  and  $B^+$  decays and the  $P$  wave fraction is  $(19 \pm 2 \pm 3)\%$ .  
<sup>8</sup> Averaged over an admixture of  $B^0$  and  $B^-$  decays and the  $P$  wave fraction is  $(16.0 \pm 3.2 \pm 1.4) \times 10^{-2}$ .

#### $\Gamma_\perp/\Gamma$ in $B^0 \rightarrow J/\psi K^{*0}$

VALUE	DOCUMENT ID	TECN	COMMENT
$0.211 \pm 0.008$ OUR AVERAGE	Error includes scale factor of 1.3. See the ideogram below.		
$0.201 \pm 0.004 \pm 0.008$	AAIJ	13AT LHCb	$pp$ at 7 TeV
$0.230 \pm 0.013 \pm 0.025$	<sup>1</sup> ABAZOV	09E D0	$p\bar{p}$ at 1.96 TeV
$0.233 \pm 0.010 \pm 0.005$	<sup>2</sup> AUBERT	07AD BABR	$e^+e^- \rightarrow \Upsilon(4S)$
$0.215 \pm 0.032 \pm 0.006$	ACOSTA	05 CDF	$p\bar{p}$ at 1.96 TeV
$0.195 \pm 0.012 \pm 0.008$	ITOH	05 BELL	$e^+e^- \rightarrow \Upsilon(4S)$

<sup>1</sup> Measured the angular and lifetime parameters for the time-dependent angular untagged decays  $B_d^0 \rightarrow J/\psi K^{*0}$  and  $B_s^0 \rightarrow J/\psi \phi$ .  
<sup>2</sup> Obtained by combining the  $B^0$  and  $B^+$  modes.

WEIGHTED AVERAGE  
0.211±0.008 (Error scaled by 1.3)

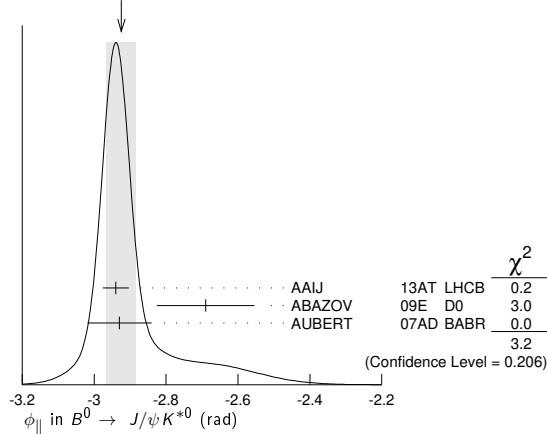


**φ<sub>||</sub> in B<sup>0</sup> → J/ψK\*<sup>0</sup>**

VALUE (rad)	DOCUMENT ID	TECN	COMMENT
<b>-2.92±0.04 OUR AVERAGE</b>	Error includes scale factor of 1.3. See the ideogram below.		
-2.94±0.02±0.03	AAIJ	13AT LHCb	pp at 7 TeV
-2.69±0.08±0.11	<sup>1</sup> ABAZOV	09E D0	p $\bar{p}$ at 1.96 TeV
-2.93±0.08±0.04	<sup>2</sup> AUBERT	07AD BABR	e <sup>+</sup> e <sup>-</sup> → T(4S)

<sup>1</sup> Obtained φ<sub>||</sub> as δ<sub>2</sub> - δ<sub>1</sub>, assuming they are uncorrelated.  
<sup>2</sup> Obtained by combining the B<sup>0</sup> and B<sup>+</sup> modes.

WEIGHTED AVERAGE  
-2.92±0.04 (Error scaled by 1.3)

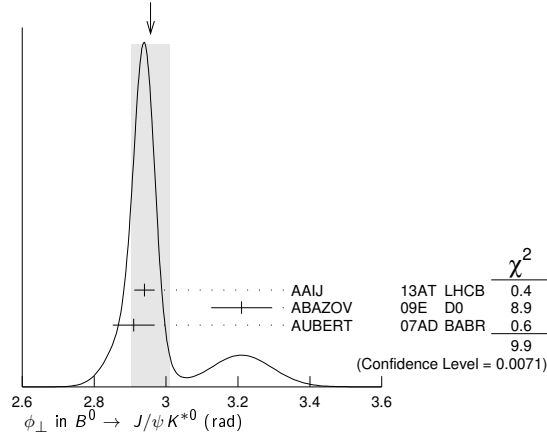


**φ<sub>⊥</sub> in B<sup>0</sup> → J/ψK\*<sup>0</sup>**

VALUE (rad)	DOCUMENT ID	TECN	COMMENT
<b>2.96±0.05 OUR AVERAGE</b>	Error includes scale factor of 2.2. See the ideogram below.		
2.94±0.02±0.02	AAIJ	13AT LHCb	pp at 7 TeV
3.21±0.06±0.06	ABAZOV	09E D0	p $\bar{p}$ at 1.96 TeV
2.91±0.05±0.03	<sup>1</sup> AUBERT	07AD BABR	e <sup>+</sup> e <sup>-</sup> → T(4S)

<sup>1</sup> Obtained by combining the B<sup>0</sup> and B<sup>+</sup> modes.

WEIGHTED AVERAGE  
2.96±0.05 (Error scaled by 2.2)



**Γ<sub>⊥</sub>/Γ in B<sup>0</sup> → ψ(2S)K\*(892)<sup>0</sup>**

VALUE	DOCUMENT ID	TECN	COMMENT
<b>0.463<sup>+0.028</sup><sub>-0.040</sub> OUR AVERAGE</b>			
0.455 <sup>+0.031+0.014</sup> <sub>-0.029-0.049</sub>	CHILIKIN	13 BELL	e <sup>+</sup> e <sup>-</sup> → T(4S)
0.48 ±0.05 ±0.02	<sup>1</sup> AUBERT	07AD BABR	e <sup>+</sup> e <sup>-</sup> → T(4S)
0.45 ±0.11 ±0.04	<sup>2</sup> RICHICHI	01 CLE2	e <sup>+</sup> e <sup>-</sup> → T(4S)
••• We do not use the following data for averages, fits, limits, etc. •••			
0.448 <sup>+0.040+0.040</sup> <sub>-0.027-0.053</sub>	MIZUK	09 BELL	e <sup>+</sup> e <sup>-</sup> → T(4S)

<sup>1</sup> Obtained by combining the B<sup>0</sup> and B<sup>+</sup> modes.  
<sup>2</sup> Averages between charged and neutral B mesons.

**Γ<sub>⊥</sub>/Γ in B<sup>0</sup> → ψ(2S)K\*<sup>0</sup>**

VALUE	DOCUMENT ID	TECN	COMMENT
<b>0.30±0.06±0.02</b>	<sup>1</sup> AUBERT	07AD BABR	e <sup>+</sup> e <sup>-</sup> → T(4S)

<sup>1</sup> Obtained by combining the B<sup>0</sup> and B<sup>+</sup> modes.

**φ<sub>||</sub> in B<sup>0</sup> → ψ(2S)K\*<sup>0</sup>**

VALUE (rad)	DOCUMENT ID	TECN	COMMENT
<b>-2.8±0.4±0.1</b>	<sup>1</sup> AUBERT	07AD BABR	e <sup>+</sup> e <sup>-</sup> → T(4S)

<sup>1</sup> Obtained by combining the B<sup>0</sup> and B<sup>+</sup> modes.

**φ<sub>⊥</sub> in B<sup>0</sup> → ψ(2S)K\*<sup>0</sup>**

VALUE (rad)	DOCUMENT ID	TECN	COMMENT
<b>2.8±0.3±0.1</b>	<sup>1</sup> AUBERT	07AD BABR	e <sup>+</sup> e <sup>-</sup> → T(4S)

<sup>1</sup> Obtained by combining the B<sup>0</sup> and B<sup>+</sup> modes.

**Γ<sub>⊥</sub>/Γ in B<sup>0</sup> → χ<sub>c1</sub>K\*(892)<sup>0</sup>**

VALUE	DOCUMENT ID	TECN	COMMENT
<b>0.83<sup>+0.06</sup><sub>-0.08</sub> OUR AVERAGE</b>	Error includes scale factor of 1.3.		
0.947 <sup>+0.038+0.046</sup> <sub>-0.048-0.099</sub>	MIZUK	08 BELL	e <sup>+</sup> e <sup>-</sup> → T(4S)
0.77 ±0.07 ±0.04	<sup>1</sup> AUBERT	07AD BABR	e <sup>+</sup> e <sup>-</sup> → T(4S)

<sup>1</sup> Obtained by combining the B<sup>0</sup> and B<sup>+</sup> modes.

**Γ<sub>⊥</sub>/Γ in B<sup>0</sup> → χ<sub>c1</sub>K\*(892)<sup>0</sup>**

VALUE	DOCUMENT ID	TECN	COMMENT
<b>0.03±0.04±0.02</b>	<sup>1</sup> AUBERT	07AD BABR	e <sup>+</sup> e <sup>-</sup> → T(4S)

<sup>1</sup> Obtained by combining the B<sup>0</sup> and B<sup>+</sup> modes.

**φ<sub>||</sub> in B<sup>0</sup> → χ<sub>c1</sub>K\*(892)<sup>0</sup>**

VALUE (rad)	DOCUMENT ID	TECN	COMMENT
<b>0.0±0.3±0.1</b>	<sup>1</sup> AUBERT	07AD BABR	e <sup>+</sup> e <sup>-</sup> → T(4S)

<sup>1</sup> Obtained by combining the B<sup>0</sup> and B<sup>+</sup> modes.

**Γ<sub>⊥</sub>/Γ in B<sup>0</sup> → D<sub>s</sub><sup>+</sup>D\*<sup>-</sup>**

VALUE	DOCUMENT ID	TECN	COMMENT
<b>0.52 ±0.05 OUR AVERAGE</b>			
0.519±0.050±0.028	<sup>1</sup> AUBERT	03i BABR	e <sup>+</sup> e <sup>-</sup> → T(4S)
0.506±0.139±0.036	AHMED	00b CLE2	e <sup>+</sup> e <sup>-</sup> → T(4S)

<sup>1</sup> Measurement performed using partial reconstruction of D\*<sup>-</sup> decay.

**Γ<sub>⊥</sub>/Γ in B<sup>0</sup> → D\*<sup>-</sup>ρ<sup>+</sup>**

VALUE	DOCUMENT ID	TECN	COMMENT
<b>0.885±0.016±0.012</b>	CSORNA	03 CLE2	e <sup>+</sup> e <sup>-</sup> → T(4S)
••• We do not use the following data for averages, fits, limits, etc. •••			
0.93 ±0.05 ±0.05	76 ALAM	94 CLE2	e <sup>+</sup> e <sup>-</sup> → T(4S)

**Γ<sub>⊥</sub>/Γ in B<sup>0</sup> → D<sub>s</sub><sup>+</sup>ρ<sup>-</sup>**

VALUE	DOCUMENT ID	TECN	COMMENT
<b>0.84<sup>+0.25</sup><sub>-0.28</sub> ±0.13</b>	<sup>1</sup> AUBERT	08AJ BABR	e <sup>+</sup> e <sup>-</sup> → T(4S)

<sup>1</sup> Assumes equal production of B<sup>+</sup> and B<sup>0</sup> at the T(4S).

**Γ<sub>⊥</sub>/Γ in B<sup>0</sup> → D<sub>s</sub><sup>+</sup>K\*<sup>-</sup>**

VALUE	DOCUMENT ID	TECN	COMMENT
<b>0.92<sup>+0.37</sup><sub>-0.31</sub> ±0.07</b>	<sup>1</sup> AUBERT	08AJ BABR	e <sup>+</sup> e <sup>-</sup> → T(4S)

<sup>1</sup> Assumes equal production of B<sup>+</sup> and B<sup>0</sup> at the T(4S).

**Γ<sub>⊥</sub>/Γ in B<sup>0</sup> → D\*<sup>+</sup>D\*<sup>-</sup>**

VALUE	DOCUMENT ID	TECN	COMMENT
<b>0.624±0.029±0.011</b>	KRONENBIT...12	BELL	e <sup>+</sup> e <sup>-</sup> → T(4S)
••• We do not use the following data for averages, fits, limits, etc. •••			
0.57 ±0.08 ±0.02	MIYAKE	05 BELL	Repl. by KRONENBITTER 12

# Meson Particle Listings

## $B^0$

### $\Gamma_{\perp}/\Gamma$ in $B^0 \rightarrow D^{*+}D^{*-}$

VALUE	DOCUMENT ID	TECN	COMMENT
<b>0.147 ± 0.019 OUR AVERAGE</b>			
0.138 ± 0.024 ± 0.006	KRONENBIT...12	BELL	$e^+e^- \rightarrow \Upsilon(4S)$
0.158 ± 0.028 ± 0.006	AUBERT 09c	BABR	$e^+e^- \rightarrow \Upsilon(4S)$
• • • We do not use the following data for averages, fits, limits, etc. • • •			
0.125 ± 0.043 ± 0.023	VERVINK 09	BELL	Repl. by KRONENBITTER 12
0.143 ± 0.034 ± 0.008	AUBERT 07b0	BABR	Repl. by AUBERT 09c
0.125 ± 0.044 ± 0.007	AUBERT, BE 05a	BABR	Repl. by AUBERT 07b0
0.19 ± 0.08 ± 0.01	MIYAKE 05	BELL	Repl. by VERVINK 09
0.063 ± 0.055 ± 0.009	AUBERT 03q	BABR	Repl. by AUBERT, BE 05a

### $\Gamma_{\perp}/\Gamma$ in $B^0 \rightarrow \bar{D}^{*0}\omega$

VALUE	DOCUMENT ID	TECN	COMMENT
<b>0.665 ± 0.047 ± 0.015</b>			
	LEES 11m	BABR	$e^+e^- \rightarrow \Upsilon(4S)$

### $\Gamma_{\perp}/\Gamma$ in $B^0 \rightarrow \bar{D}_1(2430)^0\omega$

VALUE (%)	DOCUMENT ID	TECN	COMMENT
<b>63.0 ± 9.1<sup>+5.5</sup><sub>-6.0</sub></b>	1,2 MATVIENKO 15	BELL	$e^+e^- \rightarrow \Upsilon(4S)$

<sup>1</sup> Obtained by amplitude analysis of  $\bar{B}^0 \rightarrow D^{*-}\omega\pi^+$ . The second uncertainty combines in quadrature experimental systematic and model uncertainties.

<sup>2</sup> Assumes equal production of  $B^0$  and  $B^+$  at  $\Upsilon(4S)$ .

### $\Gamma_{\perp}/\Gamma$ in $B^0 \rightarrow \bar{D}_1(2420)^0\omega$

VALUE (%)	DOCUMENT ID	TECN	COMMENT
<b>67.1 ± 11.7<sup>+2.3</sup><sub>-5.0</sub></b>	1,2 MATVIENKO 15	BELL	$e^+e^- \rightarrow \Upsilon(4S)$

<sup>1</sup> Obtained by amplitude analysis of  $\bar{B}^0 \rightarrow D^{*-}\omega\pi^+$ . The second uncertainty combines in quadrature experimental systematic and model uncertainties.

<sup>2</sup> Assumes equal production of  $B^0$  and  $B^+$  at  $\Upsilon(4S)$ .

### $\Gamma_{\perp}/\Gamma$ in $B^0 \rightarrow \bar{D}_2^*(2460)^0\omega$

VALUE (%)	DOCUMENT ID	TECN	COMMENT
<b>76.0<sup>+18.3+3.5</sup><sub>-8.5-2.8</sub></b>	1,2 MATVIENKO 15	BELL	$e^+e^- \rightarrow \Upsilon(4S)$

<sup>1</sup> Obtained by amplitude analysis of  $\bar{B}^0 \rightarrow D^{*-}\omega\pi^+$ . The second uncertainty combines in quadrature experimental systematic and model uncertainties.

<sup>2</sup> Assumes equal production of  $B^0$  and  $B^+$  at  $\Upsilon(4S)$ .

### $\Gamma_{\perp}/\Gamma$ in $B^0 \rightarrow D^{*-}\omega\pi^+$

VALUE	DOCUMENT ID	TECN	COMMENT
<b>0.654 ± 0.042 ± 0.016</b>	1 AUBERT 06l	BABR	$e^+e^- \rightarrow \Upsilon(4S)$

<sup>1</sup> Invariant mass of the  $[\omega\pi]$  system is restricted in the region 1.1 and 1.9 GeV.

### $\Gamma_{\perp}/\Gamma$ in $B^0 \rightarrow \omega K^{*0}$

VALUE	DOCUMENT ID	TECN	COMMENT
<b>0.69 ± 0.11 OUR AVERAGE</b>			
0.68 ± 0.17 ± 0.16	AAIJ 19j	LHCB	$pp$ at 7, 8 TeV
0.72 ± 0.14 ± 0.02	AUBERT 09h	BABR	$e^+e^- \rightarrow \Upsilon(4S)$
0.56 ± 0.29 <sup>+0.18</sup> <sub>-0.08</sub>	GOLDENZWE...08	BELL	$e^+e^- \rightarrow \Upsilon(4S)$

### $\Gamma_{\perp}/\Gamma$ in $B^0 \rightarrow \omega K^*(892)^0$

VALUE	DOCUMENT ID	TECN	COMMENT
<b>0.10 ± 0.09 ± 0.09</b>	AAIJ 19j	LHCB	$pp$ at 7, 8 TeV

### $A_{CP}^0$ in $B^0 \rightarrow \omega K^*(892)^0$

VALUE	DOCUMENT ID	TECN	COMMENT
<b>-0.13 ± 0.27 ± 0.13</b>	AAIJ 19j	LHCB	$pp$ at 7, 8 TeV

### $A_{CP}^{\perp}$ in $B^0 \rightarrow \omega K^*(892)^0$

VALUE	DOCUMENT ID	TECN	COMMENT
<b>0.3 ± 0.8 ± 0.4</b>	AAIJ 19j	LHCB	$pp$ at 7, 8 TeV

### $A_{CP}^{\parallel}$ in $B^0 \rightarrow \omega K^*(892)^0$

VALUE	DOCUMENT ID	TECN	COMMENT
<b>0.26 ± 0.55 ± 0.22</b>	AAIJ 19j	LHCB	$pp$ at 7, 8 TeV

### $\phi_0$ in $B^0 \rightarrow \omega K^*(892)^0$

VALUE	DOCUMENT ID	TECN	COMMENT
<b>-0.86 ± 0.29 ± 0.71</b>	AAIJ 19j	LHCB	$pp$ at 7, 8 TeV

### $\phi_{\perp}$ in $B^0 \rightarrow \omega K^*(892)^0$

VALUE	DOCUMENT ID	TECN	COMMENT
<b>1.6 ± 0.4 ± 0.6</b>	AAIJ 19j	LHCB	$pp$ at 7, 8 TeV

### $\phi_{\parallel}$ in $B^0 \rightarrow \omega K^*(892)^0$

VALUE	DOCUMENT ID	TECN	COMMENT
<b>-1.83 ± 0.29 ± 0.32</b>	AAIJ 19j	LHCB	$pp$ at 7, 8 TeV

### $\Gamma_{\perp}/\Gamma$ in $B^0 \rightarrow \omega K_2^*(1430)^0$

VALUE	DOCUMENT ID	TECN	COMMENT
<b>0.45 ± 0.12 ± 0.02</b>	AUBERT 09h	BABR	$e^+e^- \rightarrow \Upsilon(4S)$

### $\Gamma_{\perp}/\Gamma$ in $B^0 \rightarrow K^{*0}\bar{K}^{*0}$

VALUE	DOCUMENT ID	TECN	COMMENT
<b>0.74 ± 0.05 OUR AVERAGE</b>			
0.724 ± 0.051 ± 0.016	<sup>1</sup> AAIJ 19l	LHCB	$pp$ at 7 and 8 TeV
0.80 <sup>+0.10</sup> <sub>-0.12</sub> ± 0.06	AUBERT 08i	BABR	$e^+e^- \rightarrow \Upsilon(4S)$

<sup>1</sup> Untagged and time-integrated analysis within 150 MeV of the  $K^{*0}$  mass.

### $\Gamma_{\perp}/\Gamma$ in $B^0 \rightarrow \phi K^*(892)^0$

VALUE	DOCUMENT ID	TECN	COMMENT
<b>0.497 ± 0.017 OUR AVERAGE</b>			
0.497 ± 0.019 ± 0.015	AAIJ 14AM	LHCB	$pp$ at 7 TeV
0.499 ± 0.030 ± 0.018	PRIM 13	BELL	$e^+e^- \rightarrow \Upsilon(4S)$
0.494 ± 0.034 ± 0.013	AUBERT 08BG	BABR	$e^+e^- \rightarrow \Upsilon(4S)$
• • • We do not use the following data for averages, fits, limits, etc. • • •			
0.506 ± 0.040 ± 0.015	AUBERT 07D	BABR	Repl. by AUBERT 08BG
0.45 ± 0.05 ± 0.02	CHEN 05A	BELL	Repl. by PRIM 13
0.52 ± 0.05 ± 0.02	<sup>1</sup> AUBERT, B 04W	BABR	Repl. by AUBERT 07D
0.65 ± 0.07 ± 0.02	AUBERT 03V	BABR	Repl. by AUBERT, B 04W
0.41 ± 0.10 ± 0.04	CHEN 03B	BELL	Repl. by CHEN 05A

<sup>1</sup> AUBERT, B 04W also measures the fraction of parity-odd transverse contribution  $f_{\perp} = 0.22 \pm 0.05 \pm 0.02$  and the phases of the parity-even and parity-odd transverse amplitudes relative to the longitudinal amplitude.

### $\Gamma_{\perp}/\Gamma$ in $B^0 \rightarrow \phi K^*(892)^0$

VALUE	DOCUMENT ID	TECN	COMMENT
<b>0.224 ± 0.015 OUR AVERAGE</b>			
0.221 ± 0.016 ± 0.013	AAIJ 14AM	LHCB	$pp$ at 7 TeV
0.238 ± 0.026 ± 0.008	PRIM 13	BELL	$e^+e^- \rightarrow \Upsilon(4S)$
0.212 ± 0.032 ± 0.013	AUBERT 08BG	BABR	$e^+e^- \rightarrow \Upsilon(4S)$
• • • We do not use the following data for averages, fits, limits, etc. • • •			
0.227 ± 0.038 ± 0.013	AUBERT 07D	BABR	Repl. by AUBERT 08BG
0.31 <sup>+0.06</sup> <sub>-0.05</sub> ± 0.02	<sup>1</sup> CHEN 05A	BELL	Repl. by PRIM 13
0.22 ± 0.05 ± 0.02	AUBERT, B 04W	BABR	Repl. by AUBERT 07D

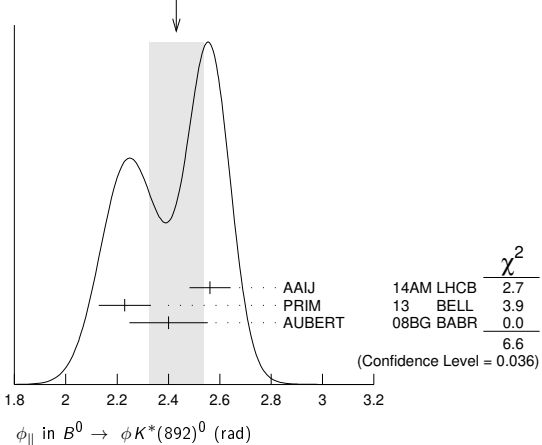
<sup>1</sup> This quantity was recalculated by the BELLE authors from numbers in the original paper.

### $\phi_{\parallel}$ in $B^0 \rightarrow \phi K^*(892)^0$

VALUE (rad)	DOCUMENT ID	TECN	COMMENT
<b>2.43 ± 0.11 OUR AVERAGE</b>			Error includes scale factor of 1.8. See the ideogram below.
2.562 ± 0.069 ± 0.040	AAIJ 14AM	LHCB	$pp$ at 7 TeV
2.23 ± 0.10 ± 0.02	PRIM 13	BELL	$e^+e^- \rightarrow \Upsilon(4S)$
2.40 ± 0.13 ± 0.08	AUBERT 08BG	BABR	$e^+e^- \rightarrow \Upsilon(4S)$
• • • We do not use the following data for averages, fits, limits, etc. • • •			
2.31 ± 0.14 ± 0.08	AUBERT 07D	BABR	Repl. by AUBERT 08BG
2.40 <sup>+0.28</sup> <sub>-0.24</sub> ± 0.07	<sup>1</sup> CHEN 05A	BELL	Repl. by PRIM 13
2.34 <sup>+0.23</sup> <sub>-0.20</sub> ± 0.05	AUBERT, B 04W	BABR	Repl. by AUBERT 07D

<sup>1</sup> This quantity was recalculated by the BELLE authors from numbers in the original paper.

WEIGHTED AVERAGE  
2.43 ± 0.11 (Error scaled by 1.8)



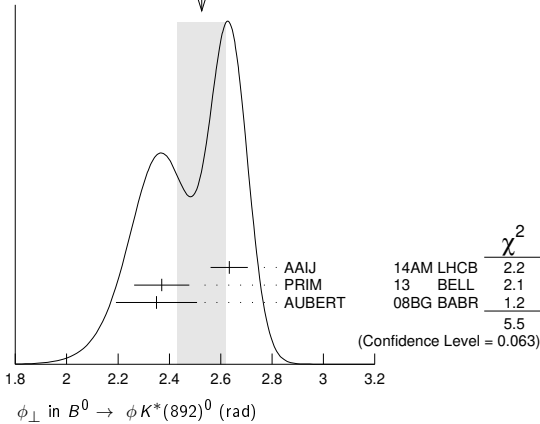
### $\phi_{\perp}$ in $B^0 \rightarrow \phi K^*(892)^0$

VALUE (rad)	DOCUMENT ID	TECN	COMMENT
<b>2.53 ± 0.09 OUR AVERAGE</b>			Error includes scale factor of 1.7. See the ideogram below.
2.633 ± 0.062 ± 0.037	AAIJ 14AM	LHCB	$pp$ at 7 TeV
2.37 ± 0.10 ± 0.04	PRIM 13	BELL	$e^+e^- \rightarrow \Upsilon(4S)$
2.35 ± 0.13 ± 0.09	AUBERT 08BG	BABR	$e^+e^- \rightarrow \Upsilon(4S)$

• • • We do not use the following data for averages, fits, limits, etc. • • •  
 2.24 ± 0.15 ± 0.09 AUBERT 07D BABR Repl. by AUBERT 08Bg  
 2.51 ± 0.25 ± 0.06 1 CHEN 05A BELL Repl. by PRIM 13  
 2.47 ± 0.25 ± 0.05 AUBERT,B 04W BABR Repl. by AUBERT 07D

<sup>1</sup> This quantity was recalculated by the BELLE authors from numbers in the original paper.

WEIGHTED AVERAGE  
2.53±0.09 (Error scaled by 1.7)



**$\delta_0(B^0 \rightarrow \phi K^*(892)^0)$**   
 VALUE (rad)  
**2.88 ± 0.10 OUR AVERAGE**

VALUE (rad)	DOCUMENT ID	TECN	COMMENT
2.91 ± 0.10 ± 0.08	PRIM	13	BELL e <sup>+</sup> e <sup>-</sup> → $\Upsilon(4S)$
2.82 ± 0.15 ± 0.09	AUBERT	08Bg	BABR e <sup>+</sup> e <sup>-</sup> → $\Upsilon(4S)$
• • • We do not use the following data for averages, fits, limits, etc. • • •			
2.78 ± 0.17 ± 0.09	AUBERT	07D	BABR Repl. by AUBERT 08Bg

**$A_{CP}^0$  in  $B^0 \rightarrow \phi K^*(892)^0$**   
 VALUE  
**-0.007 ± 0.030 OUR AVERAGE**

VALUE	DOCUMENT ID	TECN	COMMENT
-0.003 ± 0.038 ± 0.005	AAIJ	14AM	LHCb pp at 7 TeV
-0.030 ± 0.061 ± 0.007	PRIM	13	BELL e <sup>+</sup> e <sup>-</sup> → $\Upsilon(4S)$
0.01 ± 0.07 ± 0.02	AUBERT	08Bg	BABR e <sup>+</sup> e <sup>-</sup> → $\Upsilon(4S)$
• • • We do not use the following data for averages, fits, limits, etc. • • •			
-0.03 ± 0.08 ± 0.02	AUBERT	07D	BABR Repl. by AUBERT 08Bg
0.13 ± 0.12 ± 0.04	1 CHEN	05A	BELL Repl. by PRIM 13
-0.06 ± 0.10 ± 0.01	AUBERT,B	04W	BABR Repl. by AUBERT 07D

<sup>1</sup> This quantity was recalculated by the BELLE authors from numbers in the original paper.

**$A_{CP}^\perp$  in  $B^0 \rightarrow \phi K^*(892)^0$**   
 VALUE  
**-0.02 ± 0.06 OUR AVERAGE**

VALUE	DOCUMENT ID	TECN	COMMENT
0.047 ± 0.074 ± 0.009	AAIJ	14AM	LHCb pp at 7 TeV
-0.14 ± 0.11 ± 0.01	PRIM	13	BELL e <sup>+</sup> e <sup>-</sup> → $\Upsilon(4S)$
-0.04 ± 0.15 ± 0.06	AUBERT	08Bg	BABR e <sup>+</sup> e <sup>-</sup> → $\Upsilon(4S)$
• • • We do not use the following data for averages, fits, limits, etc. • • •			
-0.03 ± 0.16 ± 0.05	AUBERT	07D	BABR Repl. by AUBERT 08Bg
-0.20 ± 0.18 ± 0.04	1 CHEN	05A	BELL Repl. by PRIM 13
-0.10 ± 0.24 ± 0.05	AUBERT,B	04W	BABR Repl. by AUBERT 07D

<sup>1</sup> This quantity was recalculated by the BELLE authors from numbers in the original paper.

**$\Delta\phi_\parallel$  in  $B^0 \rightarrow \phi K^*(892)^0$**   
 VALUE (rad)  
**0.05 ± 0.05 OUR AVERAGE**

VALUE (rad)	DOCUMENT ID	TECN	COMMENT
0.045 ± 0.069 ± 0.015	AAIJ	14AM	LHCb pp at 7 TeV
-0.02 ± 0.10 ± 0.01	PRIM	13	BELL e <sup>+</sup> e <sup>-</sup> → $\Upsilon(4S)$
0.22 ± 0.12 ± 0.08	AUBERT	08Bg	BABR e <sup>+</sup> e <sup>-</sup> → $\Upsilon(4S)$
• • • We do not use the following data for averages, fits, limits, etc. • • •			
0.24 ± 0.14 ± 0.08	AUBERT	07D	BABR Repl. by AUBERT 08Bg
-0.32 ± 0.27 ± 0.07	1 CHEN	05A	BELL Repl. by PRIM 13
0.27 ± 0.20 ± 0.05	AUBERT,B	04W	BABR Repl. by AUBERT 07D

<sup>1</sup> This quantity was recalculated by the BELLE authors from numbers in the original paper.

**$\Delta\phi_\perp$  in  $B^0 \rightarrow \phi K^*(892)^0$**   
 VALUE (rad)  
**0.08 ± 0.05 OUR AVERAGE**

VALUE (rad)	DOCUMENT ID	TECN	COMMENT
0.062 ± 0.062 ± 0.005	AAIJ	14AM	LHCb pp at 7 TeV
0.05 ± 0.10 ± 0.02	PRIM	13	BELL e <sup>+</sup> e <sup>-</sup> → $\Upsilon(4S)$
0.21 ± 0.13 ± 0.08	AUBERT	08Bg	BABR e <sup>+</sup> e <sup>-</sup> → $\Upsilon(4S)$
• • • We do not use the following data for averages, fits, limits, etc. • • •			
0.19 ± 0.15 ± 0.08	AUBERT	07D	BABR Repl. by AUBERT 08Bg
-0.30 ± 0.25 ± 0.06	1 CHEN	05A	BELL Repl. by PRIM 13
0.36 ± 0.25 ± 0.05	AUBERT,B	04W	BABR Repl. by AUBERT 07D

<sup>1</sup> This quantity was recalculated by the BELLE authors from numbers in the original paper.

**$\Delta\delta_0(B^0 \rightarrow \phi K^*(892)^0)$**   
 VALUE (rad)  
**0.13 ± 0.09 OUR AVERAGE**

VALUE (rad)	DOCUMENT ID	TECN	COMMENT
0.08 ± 0.10 ± 0.01	PRIM	13	BELL e <sup>+</sup> e <sup>-</sup> → $\Upsilon(4S)$
0.27 ± 0.14 ± 0.08	AUBERT	08Bg	BABR e <sup>+</sup> e <sup>-</sup> → $\Upsilon(4S)$
• • • We do not use the following data for averages, fits, limits, etc. • • •			
0.21 ± 0.17 ± 0.08	AUBERT	07D	BABR Repl. by AUBERT 08Bg

**$\Delta\phi_{00}(B^0 \rightarrow \phi K_0^*(1430)^0)$**   
 VALUE (rad)  
**0.28 ± 0.42 ± 0.04**

VALUE (rad)	DOCUMENT ID	TECN	COMMENT
	AUBERT	08Bg	BABR e <sup>+</sup> e <sup>-</sup> → $\Upsilon(4S)$

**$\Gamma_\perp/\Gamma$  in  $B^0 \rightarrow \phi K_2^*(1430)^0$**   
 VALUE  
**0.913 +0.028 -0.050 OUR AVERAGE**

VALUE	DOCUMENT ID	TECN	COMMENT
0.918 +0.029 -0.060 ± 0.012	PRIM	13	BELL e <sup>+</sup> e <sup>-</sup> → $\Upsilon(4S)$
0.901 +0.046 -0.058 ± 0.037	AUBERT	08Bg	BABR e <sup>+</sup> e <sup>-</sup> → $\Upsilon(4S)$
• • • We do not use the following data for averages, fits, limits, etc. • • •			
0.853 +0.061 -0.069 ± 0.036	AUBERT	07D	BABR Repl. by AUBERT 08Bg

**$\Gamma_\parallel/\Gamma$  in  $B^0 \rightarrow \phi K_2^*(1430)^0$**   
 VALUE  
**0.027 +0.031 -0.025 OUR AVERAGE** Error includes scale factor of 1.1.

VALUE	DOCUMENT ID	TECN	COMMENT
0.056 +0.050 -0.035 ± 0.009	PRIM	13	BELL e <sup>+</sup> e <sup>-</sup> → $\Upsilon(4S)$
0.002 +0.018 -0.002 ± 0.031	AUBERT	08Bg	BABR e <sup>+</sup> e <sup>-</sup> → $\Upsilon(4S)$
• • • We do not use the following data for averages, fits, limits, etc. • • •			
0.045 +0.049 -0.040 ± 0.013	AUBERT	07D	BABR Repl. by AUBERT 08Bg

**$\phi_\parallel$  in  $B^0 \rightarrow \phi K_2^*(1430)^0$**   
 VALUE (rad)  
**4.0 ± 0.4 OUR AVERAGE**

VALUE (rad)	DOCUMENT ID	TECN	COMMENT
3.76 ± 2.88 ± 1.32	PRIM	13	BELL e <sup>+</sup> e <sup>-</sup> → $\Upsilon(4S)$
3.96 ± 0.38 ± 0.06	AUBERT	08Bg	BABR e <sup>+</sup> e <sup>-</sup> → $\Upsilon(4S)$
• • • We do not use the following data for averages, fits, limits, etc. • • •			
2.90 ± 0.39 ± 0.06	AUBERT	07D	BABR Repl. by AUBERT 08Bg

**$\phi_\perp$  in  $B^0 \rightarrow \phi K_2^*(1430)^0$**   
 VALUE (rad)  
**4.45 +0.43 -0.38 ± 0.13**

VALUE (rad)	DOCUMENT ID	TECN	COMMENT
	PRIM	13	BELL e <sup>+</sup> e <sup>-</sup> → $\Upsilon(4S)$
• • • We do not use the following data for averages, fits, limits, etc. • • •			
5.72 +0.55 -0.87 ± 0.11	AUBERT	07D	BABR Repl. by AUBERT 08Bg

**$\delta_0(B^0 \rightarrow \phi K_2^*(1430)^0)$**   
 VALUE (rad)  
**3.46 ± 0.14 OUR AVERAGE**

VALUE (rad)	DOCUMENT ID	TECN	COMMENT
3.53 ± 0.11 ± 0.19	PRIM	13	BELL e <sup>+</sup> e <sup>-</sup> → $\Upsilon(4S)$
3.41 ± 0.13 ± 0.13	AUBERT	08Bg	BABR e <sup>+</sup> e <sup>-</sup> → $\Upsilon(4S)$
• • • We do not use the following data for averages, fits, limits, etc. • • •			
3.54 +0.12 -0.14 ± 0.06	AUBERT	07D	BABR Repl. by AUBERT 08Bg

**$A_{CP}^0$  in  $B^0 \rightarrow \phi K_2^*(1430)^0$**   
 VALUE  
**-0.03 ± 0.04 OUR AVERAGE**

VALUE	DOCUMENT ID	TECN	COMMENT
-0.016 +0.066 -0.051 ± 0.008	PRIM	13	BELL e <sup>+</sup> e <sup>-</sup> → $\Upsilon(4S)$
-0.05 ± 0.06 ± 0.01	AUBERT	08Bg	BABR e <sup>+</sup> e <sup>-</sup> → $\Upsilon(4S)$

**$A_{CP}^\perp$  in  $B^0 \rightarrow \phi K_2^*(1430)^0$**   
 VALUE  
**-0.01 +0.85 -0.67 ± 0.09**

VALUE	DOCUMENT ID	TECN	COMMENT
	PRIM	13	BELL e <sup>+</sup> e <sup>-</sup> → $\Upsilon(4S)$

**$\Delta\phi_\parallel(B^0 \rightarrow \phi K_2^*(1430)^0)$**   
 VALUE (rad)  
**-0.9 ± 0.4 OUR AVERAGE**

VALUE (rad)	DOCUMENT ID	TECN	COMMENT
-0.02 ± 1.08 ± 0.10	PRIM	13	BELL e <sup>+</sup> e <sup>-</sup> → $\Upsilon(4S)$
-1.00 ± 0.38 ± 0.09	AUBERT	08Bg	BABR e <sup>+</sup> e <sup>-</sup> → $\Upsilon(4S)$

**$\Delta\phi_\perp(B^0 \rightarrow \phi K_2^*(1430)^0)$**   
 VALUE  
**-0.19 ± 0.42 ± 0.11**

VALUE	DOCUMENT ID	TECN	COMMENT
	PRIM	13	BELL e <sup>+</sup> e <sup>-</sup> → $\Upsilon(4S)$

**$\Delta\delta_0$  in  $B^0 \rightarrow \phi K_2^*(1430)^0$**   
 VALUE (rad)  
**0.08 ± 0.09 OUR AVERAGE**

VALUE (rad)	DOCUMENT ID	TECN	COMMENT
0.06 ± 0.11 ± 0.02	PRIM	13	BELL e <sup>+</sup> e <sup>-</sup> → $\Upsilon(4S)$
0.11 ± 0.13 ± 0.06	AUBERT	08Bg	BABR e <sup>+</sup> e <sup>-</sup> → $\Upsilon(4S)$

# Meson Particle Listings

## $B^0$

### $\Gamma_L/\Gamma$ in $B^0 \rightarrow K^*(892)^0 \rho^0$

VALUE	DOCUMENT ID	TECN	COMMENT
<b>0.173 ± 0.026 OUR AVERAGE</b>			
0.164 ± 0.015 ± 0.022	AAIJ	19j	LHCB $pp$ at 7, 8 TeV
0.40 ± 0.08 ± 0.11	LEES	12k	BABR $e^+e^- \rightarrow \Upsilon(4S)$
• • • We do not use the following data for averages, fits, limits, etc. • • •			
0.57 ± 0.09 ± 0.08	AUBERT,B	06g	BABR Repl. by LEES 12k

### $\Gamma_{\perp}/\Gamma$ in $B^0 \rightarrow K^*(892)^0 \rho^0$

VALUE	DOCUMENT ID	TECN	COMMENT
<b>0.401 ± 0.016 ± 0.037</b>	AAIJ	19j	LHCB $pp$ at 7, 8 TeV

### $A_{CP}^0$ in $B^0 \rightarrow K^*(892)^0 \rho^0$

VALUE	DOCUMENT ID	TECN	COMMENT
<b>-0.62 ± 0.09 ± 0.09</b>	AAIJ	19j	LHCB $pp$ at 7, 8 TeV

### $A_{CP}^{\perp}$ in $B^0 \rightarrow K^*(892)^0 \rho^0$

VALUE	DOCUMENT ID	TECN	COMMENT
<b>0.050 ± 0.039 ± 0.015</b>	AAIJ	19j	LHCB $pp$ at 7, 8 TeV

### $A_{CP}^{\parallel}$ in $B^0 \rightarrow K^*(892)^0 \rho^0$

VALUE	DOCUMENT ID	TECN	COMMENT
<b>0.188 ± 0.037 ± 0.022</b>	AAIJ	19j	LHCB $pp$ at 7, 8 TeV

### $\phi_0$ in $B^0 \rightarrow K^*(892)^0 \rho^0$

VALUE	DOCUMENT ID	TECN	COMMENT
<b>1.57 ± 0.08 ± 0.18</b>	AAIJ	19j	LHCB $pp$ at 7, 8 TeV

### $\phi_{\perp}$ in $B^0 \rightarrow K^*(892)^0 \rho^0$

VALUE	DOCUMENT ID	TECN	COMMENT
<b>-2.365 ± 0.032 ± 0.054</b>	AAIJ	19j	LHCB $pp$ at 7, 8 TeV

### $\phi_{\parallel}$ in $B^0 \rightarrow K^*(892)^0 \rho^0$

VALUE	DOCUMENT ID	TECN	COMMENT
<b>0.795 ± 0.030 ± 0.068</b>	AAIJ	19j	LHCB $pp$ at 7, 8 TeV

### $\Gamma_L/\Gamma$ in $B^0 \rightarrow K^{*+} \rho^-$

VALUE	DOCUMENT ID	TECN	COMMENT
<b>0.38 ± 0.13 ± 0.03</b>	LEES	12k	BABR $e^+e^- \rightarrow \Upsilon(4S)$

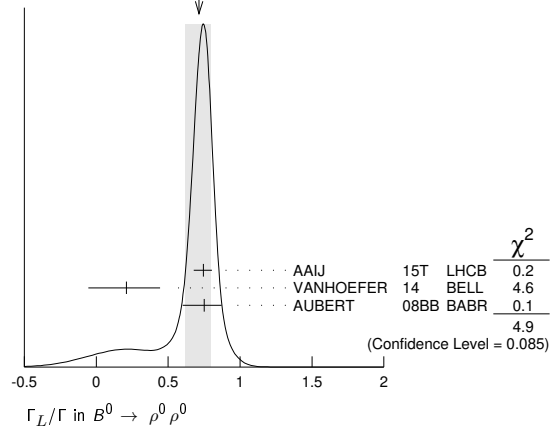
### $\Gamma_L/\Gamma$ in $B^0 \rightarrow \rho^+ \rho^-$

VALUE	DOCUMENT ID	TECN	COMMENT
<b>0.990 <sup>+0.021</sup> <sub>-0.019</sub> OUR AVERAGE</b>			
0.988 ± 0.012 ± 0.023	VANHOEFER	16	BELL $e^+e^- \rightarrow \Upsilon(4S)$
0.992 ± 0.024 <sup>+0.026</sup> <sub>-0.013</sub>	AUBERT	07BF	BABR $e^+e^- \rightarrow \Upsilon(4S)$
• • • We do not use the following data for averages, fits, limits, etc. • • •			
0.941 <sup>+0.034</sup> <sub>-0.040</sub> ± 0.030	SOMOV	06	BELL Repl. by VANHOEFER 16
0.978 ± 0.014 <sup>+0.021</sup> <sub>-0.029</sub>	AUBERT,B	05c	BABR Repl. by AUBERT 07BF
0.98 <sup>+0.02</sup> <sub>-0.08</sub> ± 0.03	AUBERT	04G	BABR Repl. by AUBERT,B 04R
0.99 ± 0.03 <sup>+0.04</sup> <sub>-0.03</sub>	AUBERT,B	04R	BABR Repl. by AUBERT,B 05c

### $\Gamma_L/\Gamma$ in $B^0 \rightarrow \rho^0 \rho^0$

VALUE	DOCUMENT ID	TECN	COMMENT
<b>0.71 <sup>+0.08</sup> <sub>-0.09</sub> OUR AVERAGE</b>			
Error includes scale factor of 1.6. See the ideogram below.			
0.745 <sup>+0.048</sup> <sub>-0.058</sub> ± 0.034	AAIJ	15T	LHCB $pp$ at 7, 8 TeV
0.21 <sup>+0.18</sup> <sub>-0.22</sub> ± 0.15	VANHOEFER	14	BELL $e^+e^- \rightarrow \Upsilon(4S)$
0.75 <sup>+0.11</sup> <sub>-0.14</sub> ± 0.05	AUBERT	08BB	BABR $e^+e^- \rightarrow \Upsilon(4S)$
• • • We do not use the following data for averages, fits, limits, etc. • • •			
0.87 ± 0.13 ± 0.04	AUBERT	07G	BABR Repl. by AUBERT 08BB

WEIGHTED AVERAGE  
0.71±0.08±0.09 (Error scaled by 1.6)



### $\Gamma_L/\Gamma$ in $B^0 \rightarrow a_1(1260)^+ a_1(1260)^-$

VALUE	DOCUMENT ID	TECN	COMMENT
<b>0.31 ± 0.22 ± 0.10</b>	AUBERT	09AL	BABR $e^+e^- \rightarrow \Upsilon(4S)$

### $\Gamma_L/\Gamma$ in $B^0 \rightarrow \rho^0 \bar{K}^*(892)^0$

VALUE	DOCUMENT ID	TECN	COMMENT
<b>1.01 ± 0.13 ± 0.03</b>	CHEN	08c	BELL $e^+e^- \rightarrow \Upsilon(4S)$

### $\Gamma_L/\Gamma$ in $B^0 \rightarrow \Lambda \bar{\Lambda} K^*(892)^0$

VALUE	DOCUMENT ID	TECN	COMMENT
<b>0.60 ± 0.22 ± 0.08</b>	CHANG	09	BELL $e^+e^- \rightarrow \Upsilon(4S)$

### $\Gamma_L/\Gamma$ in $B^0 \rightarrow K^*(892)^0 \mu^+ \mu^-$ ( $0.04 < q^2 < 6.0 \text{ GeV}^2/c^4$ )

VALUE	DOCUMENT ID	TECN	COMMENT
<b>0.50 ± 0.06 ± 0.04</b>	<sup>1</sup> AABOUD	18BY	ATLS $pp$ at 8 TeV

<sup>1</sup>A set of angular parameters obtained for this decay is also presented.

### $\Gamma_L/\Gamma$ in $B^0 \rightarrow K^*(892)^0 e^+ e^-$ ( $0.002 < q^2 < 1.120 \text{ GeV}^2/c^4$ )

VALUE	DOCUMENT ID	TECN	COMMENT
<b>0.16 ± 0.06 ± 0.03</b>	AAIJ	15z	LHCB $pp$ at 7, 8 TeV

### $A_T^{(2)}$ in $B^0 \rightarrow K^*(892)^0 e^+ e^-$ ( $0.002 < q^2 < 1.120 \text{ GeV}^2/c^4$ )

VALUE	DOCUMENT ID	TECN	COMMENT
<b>-0.23 ± 0.23 ± 0.05</b>	AAIJ	15z	LHCB $pp$ at 7, 8 TeV

### $A_T^{\perp}$ in $B^0 \rightarrow K^*(892)^0 e^+ e^-$ ( $0.002 < q^2 < 1.120 \text{ GeV}^2/c^4$ )

VALUE	DOCUMENT ID	TECN	COMMENT
<b>0.14 ± 0.22 ± 0.05</b>	AAIJ	15z	LHCB $pp$ at 7, 8 TeV

### $A_T^{\text{Re}}$ in $B^0 \rightarrow K^*(892)^0 e^+ e^-$ ( $0.002 < q^2 < 1.120 \text{ GeV}^2/c^4$ )

VALUE	DOCUMENT ID	TECN	COMMENT
<b>0.10 ± 0.18 ± 0.05</b>	AAIJ	15z	LHCB $pp$ at 7, 8 TeV

Related to  $A_{FB}^e, F_L$  by  $A_T^{\text{Re}} = (4/3) A_{FB}^e / (1 - F_L)$ .

## See the related review(s):

### $B^0 - \bar{B}^0$ Mixing

#### $B^0 - \bar{B}^0$ MIXING PARAMETERS

For a discussion of  $B^0 - \bar{B}^0$  mixing see the note on " $B^0 - \bar{B}^0$  Mixing" in the  $B^0$  Particle Listings above.

$\chi_d$  is a measure of the time-integrated  $B^0 - \bar{B}^0$  mixing probability that a produced  $B^0(\bar{B}^0)$  decays as a  $\bar{B}^0(B^0)$ . Mixing violates  $\Delta B \neq 2$  rule.

$$\chi_d = \frac{x_d^2}{2(1+x_d^2)}$$

$$\chi_d = \frac{\Delta m_{B^0}}{\Gamma_{B^0}} = (m_{B_H^0} - m_{B_L^0}) \tau_{B^0}$$

where  $H, L$  stand for heavy and light states of two  $B^0$   $CP$  eigenstates and  $\tau_{B^0} = \frac{1}{0.5(\Gamma_{B_H^0} + \Gamma_{B_L^0})}$ .

See key on page 999

Meson Particle Listings  
B<sup>0</sup>

**χ<sub>d</sub>** This B<sup>0</sup>-B<sup>0</sup> mixing parameter is the probability (integrated over time) that a produced B<sup>0</sup> (or B<sup>0</sup>) decays as a B<sup>0</sup> (or B<sup>0</sup>), e.g. for inclusive lepton decays  
χ<sub>d</sub> = Γ(B<sup>0</sup> → ℓ<sup>-</sup>X (via B<sup>0</sup>))/Γ(B<sup>0</sup> → ℓ<sup>±</sup>X)  
= Γ(B<sup>0</sup> → ℓ<sup>+</sup>X (via B<sup>0</sup>))/Γ(B<sup>0</sup> → ℓ<sup>±</sup>X)

Where experiments have measured the parameter r = χ/(1-χ), we have converted to χ. Mixing violates the ΔB ≠ 2 rule.

Note that the measurement of χ at energies higher than the T(4S) have not separated χ<sub>d</sub> from χ<sub>s</sub> where the subscripts indicate B<sup>0</sup>(B<sub>d</sub>) or B<sup>0</sup>(B<sub>s</sub>). They are listed in the B<sup>±</sup>/B<sup>0</sup>/B<sub>s</sub><sup>0</sup>/b-baryon ADMIXTURE section.

The experiments at T(4S) make an assumption about the B<sup>0</sup>B<sup>0</sup> fraction and about the ratio of the B<sup>±</sup> and B<sup>0</sup> semileptonic branching ratios (usually that it equals one).

“OUR EVALUATION” is an average using rescaled values of the data listed below. The average and rescaling were performed by the Heavy Flavor Averaging Group (HFLAV) and are described at <https://hflav.web.cern.ch/>. The averaging/rescaling procedure takes into account correlations between the measurements, includes χ<sub>d</sub> calculated from Δm<sub>B<sup>0</sup></sub> and τ<sub>B<sup>0</sup></sub>.

Table with columns: VALUE, CL%, DOCUMENT ID, TECN, COMMENT. Includes 'OUR EVALUATION' results and various experimental data points for χ<sub>d</sub>.

- 1 BEHRENS 00b uses high-momentum lepton tags and partially reconstructed B<sup>0</sup> → D\*+ π-, ρ- decays to determine the flavor of the B meson.
2 ALBRECHT 94 reports r=0.194 ± 0.062 ± 0.054. We convert to χ for comparison. Uses tagged events (lepton + pion from D\*).
3 BARTELT 93 analysis performed using tagged events (lepton+pion from D\*). Using dilepton events they obtain 0.157 ± 0.016 ± 0.033 ± 0.028.
4 ALBRECHT 92L is a combined measurement employing several lepton-based techniques. It uses all previous ARGUS data in addition to new data and therefore supersedes ALBRECHT 87L. A value of r = 20.6 ± 7.0% is directly measured. The value can be used to measure x = ΔM/Γ = 0.72 ± 0.15 for the B<sub>d</sub> meson. Assumes f<sub>+-</sub>/f<sub>0</sub> = 1.0 ± 0.05 and uses τ<sub>B<sup>±</sup></sub>/τ<sub>B<sup>0</sup></sub> = (0.95 ± 0.14) (f<sub>+-</sub>/f<sub>0</sub>).
5 Uses D\*+ K<sup>±</sup> correlations.
6 Uses (D\*+ ℓ-) K<sup>±</sup> correlations.
7 These experiments see a combination of B<sub>s</sub> and B<sub>d</sub> mesons.
8 ALBRECHT 87l is inclusive measurement with like-sign dileptons, with tagged B decays plus leptons, and one fully reconstructed event. Measures r=0.21 ± 0.08. We convert to χ for comparison. Superseded by ALBRECHT 92L.
9 BEAN 87B measured r < 0.24; we converted to χ.
10 Same-sign dilepton events. Limit assumes semileptonic BR for B<sup>+</sup> and B<sup>0</sup> equal. If B<sup>0</sup>/B<sup>±</sup> ratio < 0.58, no limit exists. The limit was corrected in BEAN 87B from r < 0.30 to r < 0.37. We converted this limit to χ.

Δm<sub>B<sup>0</sup></sub> = m<sub>B<sub>H</sub><sup>0</sup></sub> - m<sub>B<sub>L</sub><sup>0</sup></sub>

Δm<sub>B<sup>0</sup></sub> is a measure of 2π times the B<sup>0</sup>-B<sup>0</sup> oscillation frequency in time-dependent mixing experiments.

The second “OUR EVALUATION” is an average using rescaled values of the data listed below. The average and rescaling were performed by the Heavy Flavor Averaging Group (HFLAV) and are described at <https://hflav.web.cern.ch/>. The averaging/rescaling procedure takes into account correlations between the measurements.

The first “OUR EVALUATION”, also provided by the HFLAV, includes Δm<sub>d</sub> calculated from χ<sub>d</sub> measured at T(4S).

Table with columns: VALUE (10<sup>12</sup> h s<sup>-1</sup>), DOCUMENT ID, TECN, COMMENT. Lists various experimental measurements for Δm<sub>B<sup>0</sup></sub>.

Table with columns: Experiment ID, Experiment Name, Experiment Type, Decay Mode, Energy. Lists various experiments and their results for B<sup>0</sup> decays.

• • • We do not use the following data for averages, fits, limits, etc. • • •

Table with columns: Experiment ID, Experiment Name, Experiment Type, Decay Mode, Energy. Lists experiments not used for averages.

- 1 Uses semileptonic decays of B<sup>0</sup> → D- μ+ ν<sub>μ</sub>X and B<sup>0</sup> → D(\*)- μ+ ν<sub>μ</sub>X, where the D mesons are reconstructed in D- → K+ π- π- and D(\*)- → D<sup>0</sup> π- with D<sup>0</sup> → K+ π-.
2 Uses semileptonic decays of B<sup>0</sup> → D- μ+ ν<sub>μ</sub>X where the D- mesons are reconstructed in D- → K+ K- π-.
3 Measured using B<sup>0</sup> → D- π+ and B<sup>0</sup> → J/ψ K\*(892)0 decays.
4 Measured using B<sup>0</sup> → D- π+.
5 Uses opposite-side flavor-tagging with B → D(\*) μ ν<sub>μ</sub>X events.
6 Measured using a simultaneous fit of the B<sup>0</sup> lifetime and B<sup>0</sup>B<sup>0</sup> oscillation frequency Δm<sub>d</sub> in the partially reconstructed B<sup>0</sup> → D\* ℓ ν decays.
7 Measurement performed using a combined fit of CP-violation, mixing and lifetimes.
8 Events with a high transverse momentum lepton were removed and an inclusively reconstructed vertex was required.
9 AUBERT 03c uses a sample of approximately 14,000 exclusively reconstructed B<sup>0</sup> → D\*(2010)- ℓ ν and simultaneously measures the lifetime and oscillation frequency.
10 HASTINGS 03 measurement based on the time evolution of dilepton events. It also reports f<sub>+</sub>/f<sub>0</sub> = 1.01 ± 0.03 ± 0.09 and CPT violation parameters in B<sup>0</sup>-B<sup>0</sup> mixing.
11 ZHENG 03 data analyzed using partially reconstructed B<sup>0</sup> → D\* π+ decay and a flavor tag based on the charge of the lepton from the accompanying B decay.
12 Uses a tagged sample of fully-reconstructed neutral B decays at T(4S).
13 Measured based on the time evolution of dilepton events in T(4S) decays.
14 Data analyzed using partially reconstructed B<sup>0</sup> → D\*+ ℓ- D decay and a combination of flavor tags from the rest of the event.
15 Uses di-muon events.
16 Uses jet-charge and lepton-flavor tagging.
17 Uses ℓ- D\*+ ℓ events.
18 Uses π-B in the same side.
19 Uses ℓ-ℓ.
20 Uses ℓ-Q<sub>hem</sub>.
21 Uses ℓ-ℓ with impact parameters.
22 Uses D\*±-Q<sub>hem</sub>.
23 Uses π<sub>s</sub>± ℓ-Q<sub>hem</sub>.
24 Uses D\*±-ℓ/Q<sub>hem</sub>.
25 Uses D\*± ℓ-Q<sub>hem</sub>.
26 Uses D\*±-ℓ.
27 AUBERT 02N result based on the same analysis and data sample reported in AUBERT 02l.
28 Uses a tagged sample of B<sup>0</sup> decays reconstructed in the mode B<sup>0</sup> → D\* ℓ ν.
29 Uses a tagged sample of fully-reconstructed hadronic B<sup>0</sup> decays at T(4S).
30 ACCIARRI 98D combines results from ℓ-ℓ, ℓ-Q<sub>hem</sub>, and ℓ-ℓ with impact parameters.

# Meson Particle Listings

## $B^0$

- <sup>31</sup> ABREU 97N combines results from  $D^{*\pm}\text{-}Q_{\text{hem}}$ ,  $\ell\text{-}Q_{\text{hem}}$ ,  $\pi_S^{\pm}\ell\text{-}Q_{\text{hem}}$ , and  $\ell\text{-}\ell$ .
- <sup>32</sup> ACKERSTAFF 97V combines results from  $\ell\text{-}\ell$ ,  $\ell\text{-}Q_{\text{hem}}$ ,  $D^{*\pm}\ell\text{-}$ , and  $D^{*\pm}\text{-}Q_{\text{hem}}$ .
- <sup>33</sup> BUSKULIC 97D combines results from  $D^{*\pm}\ell\text{-}/Q_{\text{hem}}$ ,  $\ell\text{-}Q_{\text{hem}}$ , and  $\ell\text{-}\ell$ .
- <sup>34</sup> ABREU 96Q analysis performed using lepton, kaon, and jet-charge tags.
- <sup>35</sup> ALEXANDER 96V combines results from  $D^{*\pm}\ell\text{-}$  and  $D^{*\pm}\ell\text{-}Q_{\text{hem}}$ .
- <sup>36</sup> AKERS 95J combines results from charge measurement,  $D^{*\pm}\ell\text{-}Q_{\text{hem}}$  and  $\ell\text{-}\ell$ .

$$\chi_d = \Delta m_{B^0} / \Gamma_{B^0}$$

The second "OUR EVALUATION" is an average using rescaled values of the data listed below. The average and rescaling were performed by the Heavy Flavor Averaging Group (HFLAV) and are described at <https://hfav.web.cern.ch/>. The averaging/rescaling procedure takes into account correlations between the measurements.

The first "OUR EVALUATION", also provided by the HFLAV, includes  $\chi_d$  measured at  $\Upsilon(4S)$ .

VALUE	DOCUMENT ID
<b>0.769 ± 0.004 OUR EVALUATION</b>	First
<b>0.769 ± 0.004 OUR EVALUATION</b>	Second

### Re( $\lambda_{CP}$ / $|\lambda_{CP}|$ ) Re(z)

The  $\lambda_{CP}$  characterizes  $B^0$  and  $\bar{B}^0$  decays to states of charmonium plus  $K_S^0$ . Parameter z is used to describe CPT violation in mixing, see the review on "CPT Violation" in the reviews section.

VALUE	DOCUMENT ID	TECN	COMMENT
<b>0.047 ± 0.022 ± 0.003</b>	1 LEES	16E	BABR $e^+e^- \rightarrow \Upsilon(4S)$
• • • We do not use the following data for averages, fits, limits, etc. • • •			
0.014 ± 0.035 ± 0.034	2 AUBERT,B	04C	BABR Repl. by LEES 16E
1 The first uncertainty is the uncertainty from Re(z) and the second uncertainty is from Re( $\lambda$ / $ \lambda$ ).			
2 Corresponds to 90% confidence range [-0.072, 0.101].			

### $\Delta\Gamma$ Re(z)

VALUE	DOCUMENT ID	TECN	COMMENT
<b>-0.0071 ± 0.0039 ± 0.0020</b>	AUBERT	06T	BABR $e^+e^- \rightarrow \Upsilon(4S)$

### Re(z)

VALUE (units $10^{-2}$ )	DOCUMENT ID	TECN	COMMENT
<b>-4 ± 4 OUR AVERAGE</b>	Error	includes scale factor of 1.4.	
-6.5 ± 2.8 ± 1.4	1 LEES	16E	BABR $e^+e^- \rightarrow \Upsilon(4S)$
1.9 ± 3.7 ± 3.3	2 HIGUCHI	12	BELL $e^+e^- \rightarrow \Upsilon(4S)$
• • • We do not use the following data for averages, fits, limits, etc. • • •			
0 ± 12 ± 1	3 HASTINGS	03	BELL Repl. by HIGUCHI 12
1 Measurement uses decays $B^0/\bar{B}^0 \rightarrow c\bar{c}K_S^0/K_L^0$ .			
2 Measured using $B^0 \rightarrow J/\psi K_S^0, J/\psi K_L^0, D^-\pi^+, D^{*-}\pi^+, D^{*-}\rho^+$ , and $D^{*-}\ell^+\nu$ decays.			
3 Measured using inclusive dilepton events from $B^0$ decay.			

### Im(z)

VALUE (units $10^{-2}$ )	DOCUMENT ID	TECN	COMMENT
<b>-0.8 ± 0.4 OUR AVERAGE</b>			
1.0 ± 3.0 ± 1.3	1 LEES	16E	BABR $e^+e^- \rightarrow \Upsilon(4S)$
-0.57 ± 0.33 ± 0.33	2 HIGUCHI	12	BELL $e^+e^- \rightarrow \Upsilon(4S)$
-1.39 ± 0.73 ± 0.32	3 AUBERT	06T	BABR $e^+e^- \rightarrow \Upsilon(4S)$
• • • We do not use the following data for averages, fits, limits, etc. • • •			
3.8 ± 2.9 ± 2.5	4 AUBERT,B	04C	BABR Repl. by AUBERT 06T
-3 ± 1 ± 3	5 HASTINGS	03	BELL Repl. by HIGUCHI 12
1 Measurement uses decays $B^0/\bar{B}^0 \rightarrow c\bar{c}K_S^0/K_L^0$ .			
2 Measured using $B^0 \rightarrow J/\psi K_S^0, J/\psi K_L^0, D^-\pi^+, D^{*-}\pi^+, D^{*-}\rho^+$ , and $D^{*-}\ell^+\nu$ decays.			
3 Measurement uses $B^0/\bar{B}^0 \rightarrow \ell^+X/\ell^-X$ decays. Assuming $\Delta\Gamma = 0$ , the result becomes Im(z) = (-0.37 ± 0.54) × 10 <sup>-2</sup> .			
4 Corresponds to 90% confidence range [-0.028, 0.104].			
5 Measured using inclusive dilepton events from $B^0$ decay.			

## CP VIOLATION PARAMETERS

### Re( $\epsilon_{B^0}$ )/(1+ $|\epsilon_{B^0}|^2$ )

CP impurity in  $B_d^0$  system. It is obtained from either  $a_{\ell\ell}$ , the charge asymmetry in like-sign dilepton events or  $a_{CP}$ , the time-dependent asymmetry of inclusive  $B^0$  and  $\bar{B}^0$  decays.

"OUR EVALUATION" is an average obtained by the Heavy Flavor Averaging Group (HFLAV) and described at <https://hfav.web.cern.ch/>. It is the result of a fit to  $B_d$  and  $B_s$  CP asymmetries, which includes the  $B_d$  measurements listed below and the  $B_s$  measurements listed in the  $B_s$  section, taking into account correlations between those measurements.

VALUE (units $10^{-3}$ )	DOCUMENT ID	TECN	COMMENT
<b>-0.5 ± 0.4 OUR EVALUATION</b>			
<b>-0.1 ± 0.4 OUR AVERAGE</b>			
-0.05 ± 0.48 ± 0.75	1 AAIJ	15F	LHCB $pp$ at 7, 8 TeV
-0.975 ± 0.875 ± 0.475	2 LEES	15A	BABR $e^+e^- \rightarrow \Upsilon(4S)$
1.55 ± 1.05	3 ABAZOV	14	D0 $p\bar{p}$ at 1.96 TeV
0.15 ± 0.42 ± 0.94 ± 0.81	4 LEES	13N	BABR $e^+e^- \rightarrow \Upsilon(4S)$
-1.7 ± 1.1 ± 0.4	5 ABAZOV	12AC	D0 $p\bar{p}$ at 1.96 TeV
0.4 ± 1.3 ± 0.9	6 AUBERT	06T	BABR $e^+e^- \rightarrow \Upsilon(4S)$
-0.3 ± 2.0 ± 2.1	7 NAKANO	06	BELL $e^+e^- \rightarrow \Upsilon(4S)$
3.5 ± 10.3 ± 1.5	8 JAFFE	01	CLE2 $e^+e^- \rightarrow \Upsilon(4S)$

- • • We do not use the following data for averages, fits, limits, etc. • • •

-0.3 ± 1.3	9 ABAZOV	11U	D0 Repl. by ABAZOV 14
-2.3 ± 1.1 ± 0.8	10 ABAZOV	06S	D0 Repl. by ABAZOV 11U
-14.7 ± 6.7 ± 5.7	11 AUBERT,B	04C	BABR Repl. by AUBERT 06T
1.2 ± 2.9 ± 3.6	2 AUBERT	02K	BABR Repl. by LEES 15A
-3.2 ± 6.5	12 BARATE	01D	ALEP $e^+e^- \rightarrow Z$
4 ± 18 ± 3	13 BEHRENS	00B	CLE2 Repl. by JAFFE 01
1.2 ± 13.8 ± 3.2	14 ABBIENDI	99J	OPAL $e^+e^- \rightarrow Z$
2 ± 7 ± 3	15 ACKERSTAFF	97U	OPAL $e^+e^- \rightarrow Z$
< 45	16 BARTELT	93	CLE2 $e^+e^- \rightarrow \Upsilon(4S)$

- 1 AAIJ 15F uses semileptonic  $B^0$  decays in the inclusive final states  $D^-\mu^+$  and  $D^{*-}\mu^+$ , where the  $D^-$  meson decays into the  $K^+\pi^-\pi^-$  final state, and the  $D^{*-}$  meson into the  $\bar{D}^0(\rightarrow K^+\pi^-\pi^-)$  final state. Reports  $A_{SL}^d = (-0.02 \pm 0.19 \pm 0.30)\%$ , which equals to  $4\text{Re}(\epsilon_{B^0})/(1+|\epsilon_{B^0}|^2)$ .
- 2 Uses the charge asymmetry in like-sign dilepton events. LEES 15A reports  $A_{SL}^d = (-3.9 \pm 3.5 \pm 1.9) \times 10^{-3}$ .
- 3 ABAZOV 14 uses the dimuon charge asymmetry with different impact parameters from which it reports  $A_{SL}^d = (-0.62 \pm 0.42) \times 10^{-2}$ .
- 4 Uses  $B^0 \rightarrow D^{*-}X\ell^+\nu_\ell$  and a kaon-tagged sample which yields measurement of  $A_{SL}^d = (0.06 \pm 0.17_{-0.38}^{+0.32})\%$ , corresponding to  $\Delta_{CP} = 1-|q/p| = (0.29 \pm 0.84_{-1.88}^{+1.61}) \times 10^{-3}$ .
- 5 ABAZOV 12AC uses  $B^0 \rightarrow D^-\mu^+X$  and  $B^0 \rightarrow D^*(2010)^-\mu^+X$  decays without initial state flavor tagging which yields measurement of  $A_{SL}^d = (6.8 \pm 4.5 \pm 1.4) \times 10^{-3}$ .
- 6 AUBERT 06T reports  $|q/p|-1 = (-0.8 \pm 2.7 \pm 1.9) \times 10^{-3}$ . We convert to  $1-(|q/p|^2)/4$ .
- 7 Uses the charge asymmetry in like-sign dilepton events and reports  $|q/p| = 1.0005 \pm 0.0040 \pm 0.0043$ .
- 8 JAFFE 01 finds  $a_{\ell\ell} = 0.013 \pm 0.050 \pm 0.005$  and combines with the previous BEHRENS 00B independent measurement.
- 9 ABAZOV 11U uses the dimuon charge asymmetry with different impact parameters from which it reports  $A_{SL}^d = (-1.2 \pm 5.2) \times 10^{-3}$ .
- 10 Uses the dimuon charge asymmetry.
- 11 AUBERT 04C reports  $|q/p| = 1.029 \pm 0.013 \pm 0.011$  and we converted it to  $(1-|q/p|^2)/4$ .
- 12 BARATE 01D measured by investigating time-dependent asymmetries in semileptonic and fully inclusive  $B_d^0$  decays.
- 13 BEHRENS 00B uses high-momentum lepton tags and partially reconstructed  $\bar{B}^0 \rightarrow D^{*+}\pi^-, \rho^-$  decays to determine the flavor of the  $B$  meson.
- 14 Data analyzed using the time-dependent asymmetry of inclusive  $B^0$  decay. The production flavor of  $B^0$  mesons is determined using both the jet charge and the charge of secondary vertex in the opposite hemisphere.
- 15 ACKERSTAFF 97U assumes CPT and is based on measuring the charge asymmetry in a sample of  $B^0$  decays defined by lepton and  $Q_{\text{hem}}$  tags. If CPT is not invoked,  $\text{Re}(\epsilon_B) = -0.006 \pm 0.010 \pm 0.006$  is found. The indirect CPT violation parameter is determined to  $\text{Im}(\delta B) = -0.020 \pm 0.016 \pm 0.006$ .
- 16 BARTELT 93 finds  $a_{\ell\ell} = 0.031 \pm 0.096 \pm 0.032$  which corresponds to  $|a_{\ell\ell}| < 0.18$ , which yields the above  $|\text{Re}(\epsilon_{B^0})/(1+|\epsilon_{B^0}|^2)|$ .

### $A_{T/CP}$

$A_{T/CP}$  is defined as

$$\frac{P(\bar{B}^0 \rightarrow B^0) - P(B^0 \rightarrow \bar{B}^0)}{P(\bar{B}^0 \rightarrow B^0) + P(B^0 \rightarrow \bar{B}^0)}$$

the CPT invariant asymmetry between the oscillation probabilities  $P(\bar{B}^0 \rightarrow B^0)$  and  $P(B^0 \rightarrow \bar{B}^0)$ .

VALUE	DOCUMENT ID	TECN	COMMENT
<b>0.005 ± 0.012 ± 0.014</b>	1 AUBERT	02k	BABR $e^+e^- \rightarrow \Upsilon(4S)$

- 1 AUBERT 02k uses the charge asymmetry in like-sign dilepton events.

### $A_{CP}(B^0 \rightarrow D^*(2010)^+ D^-)$

$A_{CP}$  is defined as

$$\frac{B(\bar{B}^0 \rightarrow \bar{f}) - B(B^0 \rightarrow f)}{B(\bar{B}^0 \rightarrow \bar{f}) + B(B^0 \rightarrow f)}$$

the CP-violation charge asymmetry of exclusive  $B^0$  and  $\bar{B}^0$  decay.

VALUE	DOCUMENT ID	TECN	COMMENT
<b>0.037 ± 0.034 OUR AVERAGE</b>			
0.06 ± 0.05 ± 0.02	ROHRKEN	12	BELL $e^+e^- \rightarrow \Upsilon(4S)$
0.008 ± 0.048 ± 0.013	AUBERT	09c	BABR $e^+e^- \rightarrow \Upsilon(4S)$
0.07 ± 0.08 ± 0.04	1 AUSHEV	04	BELL $e^+e^- \rightarrow \Upsilon(4S)$
• • • We do not use the following data for averages, fits, limits, etc. • • •			
-0.12 ± 0.06 ± 0.02	AUBERT	07A1	BABR Repl. by AUBERT 09c
-0.03 ± 0.10 ± 0.02	AUBERT,B	06A	BABR Repl. by AUBERT 07A1
-0.03 ± 0.11 ± 0.05	AUBERT	03J	BABR Repl. by AUBERT,B 06B

- 1 Combines results from fully and partially reconstructed  $B^0 \rightarrow D^{*\pm}D^\mp$  decays.

### $A_{CP}(B^0 \rightarrow [K^+K^-]_D K^*(892)^0)$

VALUE	DOCUMENT ID	TECN	COMMENT
<b>-0.05 ± 0.10 ± 0.01</b>	AAIJ	19N	LHCB $pp$ at 7, 8, 13 TeV
• • • We do not use the following data for averages, fits, limits, etc. • • •			
-0.20 ± 0.15 ± 0.02	AAIJ	14B	LHCB Repl. by AAIJ 16S
-0.45 ± 0.23 ± 0.02	AAIJ	13L	LHCB Repl. by AAIJ 14B





## Meson Particle Listings

 $B^0$  $A_{CP}(B^0 \rightarrow K^+ \pi^- \pi^0 \text{ nonresonant})$ 

VALUE	DOCUMENT ID	TECN	COMMENT
$0.10 \pm 0.16 \pm 0.08$	<sup>1</sup> LEES	11	BABR $e^+ e^- \rightarrow \Upsilon(4S)$

••• We do not use the following data for averages, fits, limits, etc. •••

$0.23^{+0.19+0.11}_{-0.27-0.10}$	<sup>1</sup> AUBERT	08AQ	BABR Repl. by LEES 11
----------------------------------	---------------------	------	-----------------------

<sup>1</sup> Uses Dalitz plot analysis of  $B^0 \rightarrow K^+ \pi^- \pi^0$  decays. The quoted value is only for the flat part of the non-resonant component.

 $A_{CP}(B^0 \rightarrow K^0 \pi^+ \pi^-)$ 

VALUE	DOCUMENT ID	TECN	COMMENT
$-0.01 \pm 0.05 \pm 0.01$	<sup>1</sup> AUBERT	09AU	BABR $e^+ e^- \rightarrow \Upsilon(4S)$

<sup>1</sup> Uses Dalitz plot analysis of  $B^0 \rightarrow K^0 \pi^+ \pi^-$  decays and the first of two equivalent solutions is used.

 $A_{CP}(B^0 \rightarrow K^*(892)^+ \pi^-)$ 

VALUE	DOCUMENT ID	TECN	COMMENT
$-0.27 \pm 0.04$ OUR AVERAGE			

$-0.308 \pm 0.060 \pm 0.016$	<sup>1</sup> AAIJ	18F	LHCB $pp$ at 7, 8 TeV
$-0.29 \pm 0.11 \pm 0.02$	<sup>2</sup> LEES	11	BABR $e^+ e^- \rightarrow \Upsilon(4S)$
$-0.21 \pm 0.10 \pm 0.02$	<sup>3,4</sup> AUBERT	09AU	BABR $e^+ e^- \rightarrow \Upsilon(4S)$
$-0.21 \pm 0.11 \pm 0.07$	<sup>5</sup> DALSENO	09	BELL $e^+ e^- \rightarrow \Upsilon(4S)$
$0.26^{+0.33+0.10}_{-0.34-0.08}$	<sup>6</sup> EISENSTEIN	03	CLE2 $e^+ e^- \rightarrow \Upsilon(4S)$

••• We do not use the following data for averages, fits, limits, etc. •••

$-0.19^{+0.20}_{-0.15} \pm 0.04$	<sup>2</sup> AUBERT	08AQ	BABR Repl. by LEES 11
$-0.11 \pm 0.14 \pm 0.05$	<sup>3</sup> AUBERT	06I	BABR Repl. by AUBERT 09AU
$0.23 \pm 0.18^{+0.09}_{-0.06}$	AUBERT,B	04O	BABR Repl. by AUBERT 06I

<sup>1</sup> Uses Dalitz plot analysis of the  $B^0 \rightarrow K_S^0 \pi^+ \pi^-$  final state decays.  
<sup>2</sup> Uses Dalitz plot analysis of  $B^0 \rightarrow K^+ \pi^- \pi^0$  decays.  
<sup>3</sup> Uses Dalitz plot analysis of  $B^0 \rightarrow K^0 \pi^+ \pi^-$  decays.  
<sup>4</sup> The first of two equivalent solutions is used.  
<sup>5</sup> Uses Dalitz plot analysis of  $B^0 \rightarrow K^0 \pi^+ \pi^-$  decays and the first of two consistent solutions that may be preferred.  
<sup>6</sup> Corresponds to 90% confidence range  $-0.31 < A_{CP} < 0.78$ .

 $A_{CP}(B^0 \rightarrow (K\pi)_0^{*+} \pi^-)$ 

VALUE	DOCUMENT ID	TECN	COMMENT
$0.02 \pm 0.04$ OUR AVERAGE			

$-0.032 \pm 0.047 \pm 0.031$	<sup>1</sup> AAIJ	18F	LHCB $pp$ at 7, 8 TeV
$0.07 \pm 0.14 \pm 0.01$	<sup>2</sup> LEES	11	BABR $e^+ e^- \rightarrow \Upsilon(4S)$
$0.09 \pm 0.07 \pm 0.03$	<sup>3</sup> AUBERT	09AU	BABR $e^+ e^- \rightarrow \Upsilon(4S)$

••• We do not use the following data for averages, fits, limits, etc. •••

$0.17^{+0.11}_{-0.16} \pm 0.22$	<sup>2</sup> AUBERT	08AQ	BABR Repl. by LEES 11
---------------------------------	---------------------	------	-----------------------

<sup>1</sup> Uses Dalitz plot analysis of the  $B^0 \rightarrow K_S^0 \pi^+ \pi^-$  final states decays.  
<sup>2</sup> Uses Dalitz plot analysis of  $B^0 \rightarrow K^+ \pi^- \pi^0$  decays.  
<sup>3</sup> Uses Dalitz plot analysis of  $B^0 \rightarrow K^0 \pi^+ \pi^-$  decays and the first of two equivalent solutions is used.

 $A_{CP}(B^0 \rightarrow K_2^*(1430)^+ \pi^-)$ 

VALUE	DOCUMENT ID	TECN	COMMENT
$-0.29 \pm 0.22 \pm 0.09$	<sup>1</sup> AAIJ	18F	LHCB $pp$ at 7, 8 TeV

<sup>1</sup> Uses Dalitz plot analysis of the  $B^0 \rightarrow K_S^0 \pi^+ \pi^-$  final state decays.

 $A_{CP}(B^0 \rightarrow K^*(1680)^+ \pi^-)$ 

VALUE	DOCUMENT ID	TECN	COMMENT
$-0.07 \pm 0.13 \pm 0.04$	<sup>1</sup> AAIJ	18F	LHCB $pp$ at 7, 8 TeV

<sup>1</sup> Uses Dalitz plot analysis of the  $B^0 \rightarrow K_S^0 \pi^+ \pi^-$  final state decays.

 $A_{CP}(B^0 \rightarrow f_0(980) K_S^0)$ 

VALUE	DOCUMENT ID	TECN	COMMENT
$0.28 \pm 0.27 \pm 0.15$	<sup>1</sup> AAIJ	18F	LHCB $pp$ at 7, 8 TeV

<sup>1</sup> Uses Dalitz plot analysis of the  $B^0 \rightarrow K_S^0 \pi^+ \pi^-$  final state decays.

 $A_{CP}(B^0 \rightarrow (K\pi)_0^{*0} \pi^0)$ 

VALUE	DOCUMENT ID	TECN	COMMENT
$-0.15 \pm 0.10 \pm 0.04$	<sup>1</sup> LEES	11	BABR $e^+ e^- \rightarrow \Upsilon(4S)$

••• We do not use the following data for averages, fits, limits, etc. •••

$-0.22 \pm 0.12^{+0.30}_{-0.29}$	<sup>1</sup> AUBERT	08AQ	BABR Repl. by LEES 11
----------------------------------	---------------------	------	-----------------------

<sup>1</sup> Uses Dalitz plot analysis of  $B^0 \rightarrow K^+ \pi^- \pi^0$  decays.

 $A_{CP}(B^0 \rightarrow K^{*0} \pi^0)$ 

VALUE	DOCUMENT ID	TECN	COMMENT
$-0.15 \pm 0.12 \pm 0.04$	<sup>1</sup> LEES	11	BABR $e^+ e^- \rightarrow \Upsilon(4S)$

••• We do not use the following data for averages, fits, limits, etc. •••

$-0.09^{+0.21}_{-0.24} \pm 0.09$	<sup>1</sup> AUBERT	08AQ	BABR Repl. by LEES 11
----------------------------------	---------------------	------	-----------------------

<sup>1</sup> Uses Dalitz plot analysis of  $B^0 \rightarrow K^+ \pi^- \pi^0$  decays.

 $A_{CP}(B^0 \rightarrow K^*(892)^0 \pi^+ \pi^-)$ 

VALUE	DOCUMENT ID	TECN	COMMENT
$0.07 \pm 0.04 \pm 0.03$	AUBERT	07As	BABR $e^+ e^- \rightarrow \Upsilon(4S)$

 $A_{CP}(B^0 \rightarrow K^*(892)^0 \rho^0)$ 

VALUE	DOCUMENT ID	TECN	COMMENT
$-0.06 \pm 0.09 \pm 0.02$	LEES	12k	BABR $e^+ e^- \rightarrow \Upsilon(4S)$

••• We do not use the following data for averages, fits, limits, etc. •••

$0.09 \pm 0.19 \pm 0.02$	AUBERT,B	06G	BABR Repl. by LEES 12K
--------------------------	----------	-----	------------------------

 $A_{CP}(B^0 \rightarrow K^{*0} f_0(980))$ 

VALUE	DOCUMENT ID	TECN	COMMENT
$0.07 \pm 0.10 \pm 0.02$	LEES	12k	BABR $e^+ e^- \rightarrow \Upsilon(4S)$

••• We do not use the following data for averages, fits, limits, etc. •••

$-0.17 \pm 0.28 \pm 0.02$	AUBERT,B	06G	BABR Repl. by LEES 12K
---------------------------	----------	-----	------------------------

 $A_{CP}(B^0 \rightarrow K^{*+} \rho^-)$ 

VALUE	DOCUMENT ID	TECN	COMMENT
$0.21 \pm 0.15 \pm 0.02$	LEES	12k	BABR $e^+ e^- \rightarrow \Upsilon(4S)$

 $A_{CP}(B^0 \rightarrow K^*(892)^0 K^+ K^-)$ 

VALUE	DOCUMENT ID	TECN	COMMENT
$0.01 \pm 0.05 \pm 0.02$	AUBERT	07As	BABR $e^+ e^- \rightarrow \Upsilon(4S)$

 $A_{CP}(B^0 \rightarrow a_1^- K^+)$ 

VALUE	DOCUMENT ID	TECN	COMMENT
$-0.16 \pm 0.12 \pm 0.01$	AUBERT	08F	BABR $e^+ e^- \rightarrow \Upsilon(4S)$

 $A_{CP}(B^0 \rightarrow K^0 K^0)$ 

VALUE	DOCUMENT ID	TECN	COMMENT
$-0.58^{+0.73}_{-0.66} \pm 0.04$	LIN	07	BELL $e^+ e^- \rightarrow \Upsilon(4S)$

 $A_{CP}(B^0 \rightarrow K^*(892)^0 \phi)$ 

VALUE	DOCUMENT ID	TECN	COMMENT
$0.00 \pm 0.04$ OUR AVERAGE			

$-0.007 \pm 0.048 \pm 0.021$	PRIM	13	BELL $e^+ e^- \rightarrow \Upsilon(4S)$
------------------------------	------	----	---

$0.01 \pm 0.06 \pm 0.03$	AUBERT	08BG	BABR $e^+ e^- \rightarrow \Upsilon(4S)$
--------------------------	--------	------	---

••• We do not use the following data for averages, fits, limits, etc. •••

$-0.03 \pm 0.07 \pm 0.03$	AUBERT	07D	BABR Repl. by AUBERT 08BG
$0.02 \pm 0.09 \pm 0.02$	<sup>1</sup> CHEN	05A	BELL Repl. by PRIM 13
$-0.01 \pm 0.09 \pm 0.02$	AUBERT,B	04W	BABR Repl. by AUBERT 07D
$0.04 \pm 0.12 \pm 0.02$	AUBERT	03V	BABR Repl. by AUBERT 04W
$0.07 \pm 0.15^{+0.05}_{-0.03}$	<sup>2</sup> CHEN	03B	BELL Repl. by CHEN 05A
$0.00 \pm 0.27 \pm 0.03$	<sup>3</sup> AUBERT	02E	BABR Repl. by AUBERT 03V

<sup>1</sup> Corresponds to 90% confidence range  $-0.14 < A_{CP} < 0.17$ .

<sup>2</sup> Corresponds to 90% confidence range  $-0.18 < A_{CP} < 0.33$ .

<sup>3</sup> Corresponds to 90% confidence range  $-0.44 < A_{CP} < 0.44$ .

 $A_{CP}(B^0 \rightarrow K^*(892)^0 K^- \pi^+)$ 

VALUE	DOCUMENT ID	TECN	COMMENT
$0.22 \pm 0.33 \pm 0.20$	AUBERT	07As	BABR $e^+ e^- \rightarrow \Upsilon(4S)$

 $A_{CP}(B^0 \rightarrow \phi(K\pi)_0^{*0})$ 

VALUE	DOCUMENT ID	TECN	COMMENT
$0.12 \pm 0.08$ OUR AVERAGE			

$0.093 \pm 0.094 \pm 0.017$	PRIM	13	BELL $e^+ e^- \rightarrow \Upsilon(4S)$
-----------------------------	------	----	---

$0.20 \pm 0.14 \pm 0.06$	AUBERT	08BG	BABR $e^+ e^- \rightarrow \Upsilon(4S)$
--------------------------	--------	------	---

••• We do not use the following data for averages, fits, limits, etc. •••

$0.17 \pm 0.15 \pm 0.03$	AUBERT	07D	BABR Repl. by AUBERT 08BG
--------------------------	--------	-----	---------------------------

 $A_{CP}(B^0 \rightarrow \phi K_2^*(1430)^0)$ 

VALUE	DOCUMENT ID	TECN	COMMENT
$-0.11 \pm 0.10$ OUR AVERAGE			

$-0.155^{+0.152}_{-0.133} \pm 0.033$	PRIM	13	BELL $e^+ e^- \rightarrow \Upsilon(4S)$
--------------------------------------	------	----	---

$-0.08 \pm 0.12 \pm 0.05$	AUBERT	08BG	BABR $e^+ e^- \rightarrow \Upsilon(4S)$
---------------------------	--------	------	---

••• We do not use the following data for averages, fits, limits, etc. •••

$-0.12 \pm 0.14 \pm 0.04$	AUBERT	07D	BABR Repl. by AUBERT 08BG
---------------------------	--------	-----	---------------------------

 $A_{CP}(B^0 \rightarrow K^*(892)^0 \gamma)$ 

VALUE	DOCUMENT ID	TECN	COMMENT
$-0.006 \pm 0.011$ OUR AVERAGE			

$-0.013 \pm 0.017 \pm 0.004$	<sup>1</sup> HORIGUCHI	17	BELL $e^+ e^- \rightarrow \Upsilon(4S)$
------------------------------	------------------------	----	---

$0.008 \pm 0.017 \pm 0.009$	AAIJ	13	LHCB $pp$ at 7 TeV
-----------------------------	------	----	--------------------

$-0.016 \pm 0.022 \pm 0.007$	AUBERT	09AO	BABR $e^+ e^- \rightarrow \Upsilon(4S)$
------------------------------	--------	------	---

<sup>1</sup> Uses  $B(\Upsilon(4S) \rightarrow B^+ B^-) = (51.4 \pm 0.6)\%$  and  $B(\Upsilon(4S) \rightarrow B^0 \bar{B}^0) = (48.6 \pm 0.6)\%$ .

 $A_{CP}(B^0 \rightarrow K_2^*(1430)^0 \gamma)$ 

VALUE	DOCUMENT ID	TECN	COMMENT
$-0.08 \pm 0.15 \pm 0.01$	AUBERT,B	04U	BABR $e^+ e^- \rightarrow \Upsilon(4S)$

See key on page 999

# Meson Particle Listings

## $B^0$

### $A_{CP}(B^0 \rightarrow X_s \gamma)$

VALUE	DOCUMENT ID	TECN	COMMENT
$-0.0094 \pm 0.0174 \pm 0.0047$	<sup>1</sup> WATA NUKI	19 BELL	$e^+ e^- \rightarrow \Upsilon(4S)$

<sup>1</sup> Using a sum-of-exclusive technique with  $m_{X_s} < 2.8 \text{ GeV}/c^2$ .

### $A_{CP}(B^0 \rightarrow \rho^+ \pi^-)$

VALUE	DOCUMENT ID	TECN	COMMENT
<b><math>0.13 \pm 0.06</math> OUR AVERAGE</b>	Error includes scale factor of 1.1.		
$0.09^{+0.05}_{-0.06} \pm 0.04$	<sup>1</sup> LEES	13J BABR	$e^+ e^- \rightarrow \Upsilon(4S)$
$0.21 \pm 0.08 \pm 0.04$	<sup>1</sup> KUSAKA	07 BELL	$e^+ e^- \rightarrow \Upsilon(4S)$
• • • We do not use the following data for averages, fits, limits, etc. • • •			
$0.03 \pm 0.07 \pm 0.04$	AUBERT	07AA BABR	Repl. by LEES 13J
$-0.02 \pm 0.16^{+0.05}_{-0.02}$	WANG	05 BELL	Repl. by KUSAKA 07
$-0.18 \pm 0.08 \pm 0.03$	AUBERT	03T BABR	Repl. by AUBERT 07AA
<sup>1</sup> Uses time-dependent Dalitz plot analysis of $B^0 \rightarrow \pi^+ \pi^- \pi^0$ decays.			

### $A_{CP}(B^0 \rightarrow \rho^- \pi^+)$

VALUE	DOCUMENT ID	TECN	COMMENT
<b><math>-0.08 \pm 0.08</math> OUR AVERAGE</b>			
$-0.12 \pm 0.08^{+0.04}_{-0.05}$	<sup>1</sup> LEES	13J BABR	$e^+ e^- \rightarrow \Upsilon(4S)$
$0.08 \pm 0.16 \pm 0.11$	<sup>1</sup> KUSAKA	07 BELL	$e^+ e^- \rightarrow \Upsilon(4S)$
• • • We do not use the following data for averages, fits, limits, etc. • • •			
$-0.37 \pm 0.16^{+0.09}_{-0.10}$	AUBERT	07AA BABR	Repl. by LEES 13J
$-0.53 \pm 0.29^{+0.09}_{-0.04}$	WANG	05 BELL	Repl. by KUSAKA 07
<sup>1</sup> Uses time-dependent Dalitz plot analysis of $B^0 \rightarrow \pi^+ \pi^- \pi^0$ decays.			

### $A_{CP}(B^0 \rightarrow a_1(1260)^\pm \pi^\mp)$

VALUE	DOCUMENT ID	TECN	COMMENT
<b><math>-0.07 \pm 0.06</math> OUR AVERAGE</b>			
$-0.06 \pm 0.05 \pm 0.07$	DALSENO	12 BELL	$e^+ e^- \rightarrow \Upsilon(4S)$
$-0.07 \pm 0.07 \pm 0.02$	AUBERT	07o BABR	$e^+ e^- \rightarrow \Upsilon(4S)$

### $A_{CP}(B^0 \rightarrow b_1^- \pi^+)$

VALUE	DOCUMENT ID	TECN	COMMENT
<b><math>-0.05 \pm 0.10 \pm 0.02</math></b>	AUBERT	07Bi BABR	$e^+ e^- \rightarrow \Upsilon(4S)$

### $A_{CP}(B^0 \rightarrow p\bar{p}K^*(892)^0)$

VALUE	DOCUMENT ID	TECN	COMMENT
<b><math>0.05 \pm 0.12</math> OUR AVERAGE</b>			
$-0.08 \pm 0.20 \pm 0.02$	CHEN	08c BELL	$e^+ e^- \rightarrow \Upsilon(4S)$
$0.11 \pm 0.13 \pm 0.06$	AUBERT	07AV BABR	$e^+ e^- \rightarrow \Upsilon(4S)$

### $A_{CP}(B^0 \rightarrow \rho^0 \pi^+ \pi^-)$

VALUE	DOCUMENT ID	TECN	COMMENT
<b><math>0.04 \pm 0.07</math> OUR AVERAGE</b>			
$0.10 \pm 0.10 \pm 0.02$	AUBERT	09AC BABR	$e^+ e^- \rightarrow \Upsilon(4S)$
$-0.02 \pm 0.10 \pm 0.03$	WANG	07c BELL	$e^+ e^- \rightarrow \Upsilon(4S)$

### $A_{CP}(B^0 \rightarrow K^{*0} \ell^+ \ell^-)$

VALUE	DOCUMENT ID	TECN	COMMENT
<b><math>-0.05 \pm 0.10</math> OUR AVERAGE</b>			
$0.02 \pm 0.20 \pm 0.02$	AUBERT	09T BABR	$e^+ e^- \rightarrow \Upsilon(4S)$
$-0.08 \pm 0.12 \pm 0.02$	WEI	09A BELL	$e^+ e^- \rightarrow \Upsilon(4S)$

### $A_{CP}(B^0 \rightarrow K^{*0} e^+ e^-)$

VALUE	DOCUMENT ID	TECN	COMMENT
<b><math>-0.21 \pm 0.19 \pm 0.02</math></b>	WEI	09A BELL	$e^+ e^- \rightarrow \Upsilon(4S)$

### $A_{CP}(B^0 \rightarrow K^{*0} \mu^+ \mu^-)$

VALUE	DOCUMENT ID	TECN	COMMENT
<b><math>-0.034 \pm 0.024</math> OUR AVERAGE</b>			
$-0.035 \pm 0.024 \pm 0.003$	AAIJ	14AN LHCB	$pp$ at 7, 8 TeV
$0.00 \pm 0.15 \pm 0.03$	WEI	09A BELL	$e^+ e^- \rightarrow \Upsilon(4S)$
• • • We do not use the following data for averages, fits, limits, etc. • • •			
$-0.072 \pm 0.040 \pm 0.005$	AAIJ	13E LHCB	Repl. by AAIJ 14AN

### $C_{D^*(2010)^- D^+}(B^0 \rightarrow D^*(2010)^- D^+)$

VALUE	DOCUMENT ID	TECN	COMMENT
<b><math>-0.01 \pm 0.11</math> OUR AVERAGE</b>	Error includes scale factor of 1.6. See the ideogram below.		
$-0.13 \pm 0.16 \pm 0.05$	<sup>1</sup> ROHRKEN	12 BELL	$e^+ e^- \rightarrow \Upsilon(4S)$
$0.00 \pm 0.17 \pm 0.03$	AUBERT	09c BABR	$e^+ e^- \rightarrow \Upsilon(4S)$
$0.23 \pm 0.25 \pm 0.06$	<sup>2</sup> AUSHEV	04 BELL	$e^+ e^- \rightarrow \Upsilon(4S)$
• • • We do not use the following data for averages, fits, limits, etc. • • •			
$0.23 \pm 0.15 \pm 0.04$	AUBERT	07Ai BABR	Repl. by AUBERT 09c
$0.17 \pm 0.24 \pm 0.04$	AUBERT,B	05z BABR	Repl. by AUBERT 07Ai
$-0.22 \pm 0.37 \pm 0.10$	AUBERT	03j BABR	Repl. by AUBERT,B 05z

<sup>1</sup> ROHRKEN 12 reports the measurements of  $C = -0.01 \pm 0.11 \pm 0.04$  and  $\Delta C = 0.12 \pm 0.11 \pm 0.03$  such that  $C_{D^*(2010)^- D^+} = C - \Delta C$ .

<sup>2</sup> Combines results from fully and partially reconstructed  $B^0 \rightarrow D^{*\pm} D^\mp$  decays.

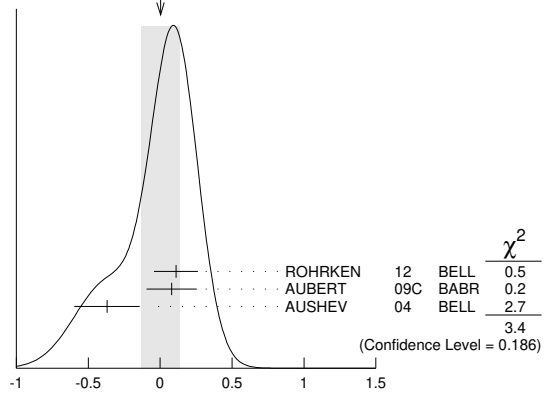
### $S_{D^*(2010)^- D^+}(B^0 \rightarrow D^*(2010)^- D^+)$

VALUE	DOCUMENT ID	TECN	COMMENT
<b><math>-0.72 \pm 0.15</math> OUR AVERAGE</b>	Error includes scale factor of 1.3. See the ideogram below.		
$-0.65 \pm 0.22 \pm 0.07$	<sup>1</sup> ROHRKEN	12 BELL	$e^+ e^- \rightarrow \Upsilon(4S)$
$-0.73 \pm 0.23 \pm 0.050$	AUBERT	09c BABR	$e^+ e^- \rightarrow \Upsilon(4S)$
$-0.96 \pm 0.43 \pm 0.12$	<sup>2</sup> AUSHEV	04 BELL	$e^+ e^- \rightarrow \Upsilon(4S)$
• • • We do not use the following data for averages, fits, limits, etc. • • •			
$-0.44 \pm 0.22 \pm 0.06$	AUBERT	07Ai BABR	Repl. by AUBERT 09c
$-0.29 \pm 0.33 \pm 0.07$	AUBERT,B	05z BABR	Repl. by AUBERT 07Ai
$-0.24 \pm 0.69 \pm 0.12$	AUBERT	03j BABR	Repl. by AUBERT,B 05z
<sup>1</sup> ROHRKEN 12 reports the measurements of $S = -0.78 \pm 0.15 \pm 0.05$ and $\Delta S = -0.13 \pm 0.15 \pm 0.04$ such that $S_{D^*(2010)^- D^+} = S - \Delta S$ .			
<sup>2</sup> Combines results from fully and partially reconstructed $B^0 \rightarrow D^{*\pm} D^\mp$ decays.			

### $C_{D^*(2010)^+ D^-}(B^0 \rightarrow D^*(2010)^+ D^-)$

VALUE	DOCUMENT ID	TECN	COMMENT
<b><math>0.00 \pm 0.13</math> OUR AVERAGE</b>	Error includes scale factor of 1.3. See the ideogram below.		
$0.11 \pm 0.14 \pm 0.06$	<sup>1</sup> ROHRKEN	12 BELL	$e^+ e^- \rightarrow \Upsilon(4S)$
$0.08 \pm 0.17 \pm 0.04$	AUBERT	09c BABR	$e^+ e^- \rightarrow \Upsilon(4S)$
$-0.37 \pm 0.22 \pm 0.06$	<sup>2</sup> AUSHEV	04 BELL	$e^+ e^- \rightarrow \Upsilon(4S)$
• • • We do not use the following data for averages, fits, limits, etc. • • •			
$0.18 \pm 0.15 \pm 0.04$	AUBERT	07Ai BABR	Repl. by AUBERT 09c
$0.09 \pm 0.25 \pm 0.06$	AUBERT,B	05z BABR	Repl. by AUBERT 07Ai
$-0.47 \pm 0.40 \pm 0.12$	AUBERT	03j BABR	Repl. by AUBERT,B 05z
<sup>1</sup> ROHRKEN 12 reports the measurements of $C = -0.01 \pm 0.11 \pm 0.04$ and $\Delta C = 0.12 \pm 0.11 \pm 0.03$ such that $C_{D^*(2010)^+ D^-} = C + \Delta C$ .			
<sup>2</sup> Combines results from fully and partially reconstructed $B^0 \rightarrow D^{*\pm} D^\mp$ decays.			

WEIGHTED AVERAGE  
0.00±0.13 (Error scaled by 1.3)



$C_{D^*(2010)^+ D^-}(B^0 \rightarrow D^*(2010)^+ D^-)$

### $S_{D^*(2010)^+ D^-}(B^0 \rightarrow D^*(2010)^+ D^-)$

VALUE	DOCUMENT ID	TECN	COMMENT
<b><math>-0.73 \pm 0.14</math> OUR AVERAGE</b>	Error includes scale factor of 1.6. See the ideogram below.		
$-0.90 \pm 0.21 \pm 0.07$	<sup>1</sup> ROHRKEN	12 BELL	$e^+ e^- \rightarrow \Upsilon(4S)$
$-0.62 \pm 0.21 \pm 0.03$	AUBERT	09c BABR	$e^+ e^- \rightarrow \Upsilon(4S)$
$-0.55 \pm 0.39 \pm 0.12$	<sup>2</sup> AUSHEV	04 BELL	$e^+ e^- \rightarrow \Upsilon(4S)$
• • • We do not use the following data for averages, fits, limits, etc. • • •			
$-0.79 \pm 0.21 \pm 0.06$	AUBERT	07Ai BABR	Repl. by AUBERT 09c
$-0.54 \pm 0.35 \pm 0.07$	AUBERT,B	05z BABR	Repl. by AUBERT 07Ai
$-0.82 \pm 0.75 \pm 0.14$	AUBERT	03j BABR	Repl. by AUBERT,B 05z
<sup>1</sup> ROHRKEN 12 reports the measurements of $S = -0.78 \pm 0.15 \pm 0.05$ and $\Delta S = -0.13 \pm 0.15 \pm 0.04$ such that $S_{D^*(2010)^+ D^-} = S + \Delta S$ .			
<sup>2</sup> Combines results from fully and partially reconstructed $B^0 \rightarrow D^{*\pm} D^\mp$ decays.			

### $C_{D^{*+} D^{*-}}(B^0 \rightarrow D^{*+} D^{*-})$

VALUE	DOCUMENT ID	TECN	COMMENT
<b><math>0.01 \pm 0.09</math> OUR AVERAGE</b>	Error includes scale factor of 1.6. See the ideogram below.		
$-0.15 \pm 0.08 \pm 0.04$	<sup>1,2</sup> KRONENBITTER	12 BELL	$e^+ e^- \rightarrow \Upsilon(4S)$
$+0.15 \pm 0.09 \pm 0.04$	<sup>3</sup> LEES	12AF BABR	$e^+ e^- \rightarrow \Upsilon(4S)$
$0.05 \pm 0.09 \pm 0.02$	AUBERT	09c BABR	$e^+ e^- \rightarrow \Upsilon(4S)$
• • • We do not use the following data for averages, fits, limits, etc. • • •			
$-0.15 \pm 0.13 \pm 0.04$	<sup>2</sup> VERVINK	09 BELL	Repl. by KRONENBITTER 12
$-0.02 \pm 0.11 \pm 0.02$	<sup>1</sup> AUBERT	07Bo BABR	Repl. by AUBERT 09c
$0.26 \pm 0.26 \pm 0.06$	<sup>2</sup> MIYAKE	05 BELL	Repl. by VERVINK 09
$0.28 \pm 0.23 \pm 0.02$	<sup>4</sup> AUBERT	03Q BABR	Repl. by AUBERT 07Bo

<sup>1</sup> Assumes both  $CP$ -even and  $CP$ -odd states having the  $CP$  asymmetry.

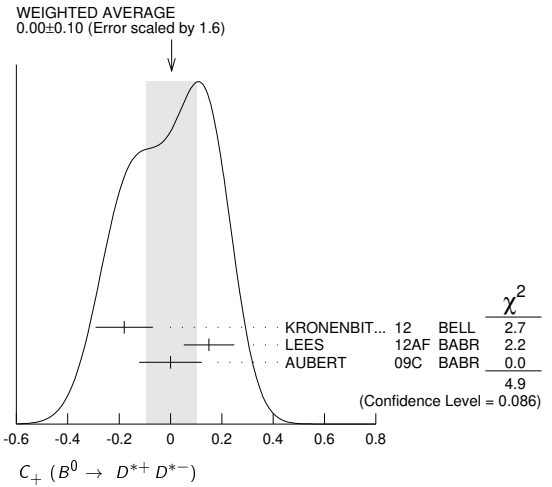
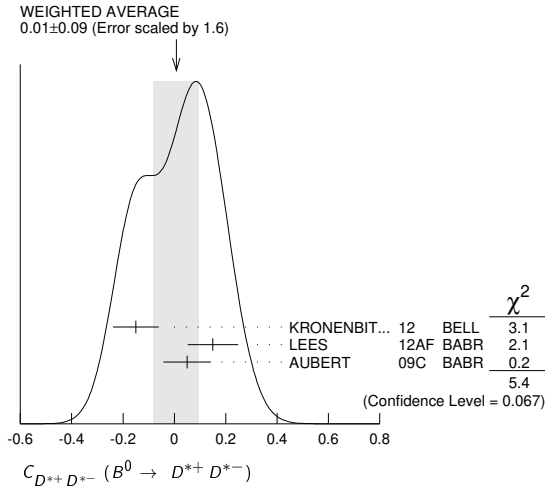
<sup>2</sup> Belle Collab. quotes  $A_{D^{*+} D^{*-}}$  which is equal to  $-C_{D^{*+} D^{*-}}$ .

<sup>3</sup> Measured partially reconstructed candidates when one  $D^0$  meson is not explicitly reconstructed. Analysis does not separate  $CP$ -even and  $CP$ -odd component.

# Meson Particle Listings

## $B^0$

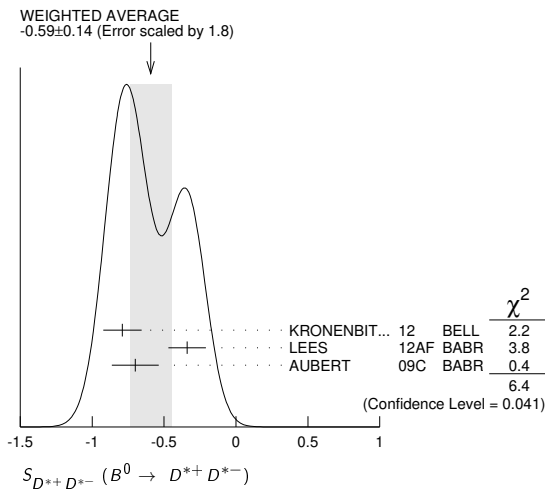
<sup>4</sup>AUBERT 03q reports  $|\lambda|=0.75 \pm 0.19 \pm 0.02$  and  $\text{Im}(\lambda)=0.05 \pm 0.29 \pm 0.10$ . We convert them to  $S$  and  $C$  parameters taking into account correlations.



### $S_{D^{*+}D^{*-}} (B^0 \rightarrow D^{*+}D^{*-})$

VALUE	DOCUMENT ID	TECN	COMMENT
<b>-0.59 ± 0.14 OUR AVERAGE</b>	Error includes scale factor of 1.8. See the ideogram below.		
-0.79 ± 0.13 ± 0.03	<sup>1</sup> KRONENBIT...12	BELL	$e^+e^- \rightarrow \Upsilon(4S)$
-0.34 ± 0.12 ± 0.05	<sup>2</sup> LEES	12AF BABR	$e^+e^- \rightarrow \Upsilon(4S)$
-0.70 ± 0.16 ± 0.03	<sup>1</sup> AUBERT	09c BABR	$e^+e^- \rightarrow \Upsilon(4S)$
• • • We do not use the following data for averages, fits, limits, etc. • • •			
-0.96 ± 0.25 ± 0.13	VERVINK	09 BELL	Repl. by KRONENBITTER 12
-0.66 ± 0.19 ± 0.04	<sup>1</sup> AUBERT	07B0 BABR	Repl. by AUBERT 09c
-0.75 ± 0.56 ± 0.12	MIYAKE	05 BELL	Repl. by VERVINK 09
0.06 ± 0.37 ± 0.13	<sup>3</sup> AUBERT	03q BABR	Repl. by AUBERT 07B0

<sup>1</sup>Assumes both  $CP$ -even and  $CP$ -odd states having the  $CP$  asymmetry.  
<sup>2</sup>Measured partially reconstructed candidates when one  $D^0$  meson is not explicitly reconstructed. Analysis does not separate  $CP$ -even and  $CP$ -odd component.  
<sup>3</sup>AUBERT 03q reports  $|\lambda|=0.75 \pm 0.19 \pm 0.02$  and  $\text{Im}(\lambda)=0.05 \pm 0.29 \pm 0.10$ . We convert them to  $S$  and  $C$  parameters taking into account correlations.



### $C_+ (B^0 \rightarrow D^{*+}D^{*-})$

See the note in the  $C_{\pi\pi}$  datablock, but for  $CP$  even final state.

VALUE	DOCUMENT ID	TECN	COMMENT
<b>0.00 ± 0.10 OUR AVERAGE</b>	Error includes scale factor of 1.6. See the ideogram below.		
-0.18 ± 0.10 ± 0.05	<sup>1</sup> KRONENBIT...12	BELL	$e^+e^- \rightarrow \Upsilon(4S)$
+0.15 ± 0.09 ± 0.04	<sup>2</sup> LEES	12AF BABR	$e^+e^- \rightarrow \Upsilon(4S)$
0.00 ± 0.12 ± 0.02	AUBERT	09c BABR	$e^+e^- \rightarrow \Upsilon(4S)$
• • • We do not use the following data for averages, fits, limits, etc. • • •			
-0.05 ± 0.14 ± 0.02	AUBERT	07B0 BABR	Repl. by AUBERT 09c
0.06 ± 0.17 ± 0.03	<sup>3</sup> AUBERT, BE	05A BABR	Repl. by AUBERT 07B0
<sup>1</sup> Belle Collab. quotes $A_{D^{*+}D^{*-}}$ which is equal to $-C_{D^{*+}D^{*-}}$ .			
<sup>2</sup> Measured partially reconstructed candidates when one $D^0$ meson is not explicitly reconstructed. Extracted under assumption of equal $C_+$ and $C_-$ .			
<sup>3</sup> AUBERT, BE 05A reports a $CP$ -odd fraction $R_{\perp} = 0.125 \pm 0.044 \pm 0.007$ .			

### $S_+ (B^0 \rightarrow D^{*+}D^{*-})$

See the note in the  $S_{\pi\pi}$  datablock, but for  $CP$  even final state.

VALUE	DOCUMENT ID	TECN	COMMENT
<b>-0.73 ± 0.09 OUR AVERAGE</b>	Error includes scale factor of 1.8. See the ideogram below.		
-0.81 ± 0.13 ± 0.03	KRONENBIT...12	BELL	$e^+e^- \rightarrow \Upsilon(4S)$
-0.49 ± 0.18 ± 0.08	<sup>1</sup> LEES	12AF BABR	$e^+e^- \rightarrow \Upsilon(4S)$
-0.76 ± 0.16 ± 0.04	AUBERT	09c BABR	$e^+e^- \rightarrow \Upsilon(4S)$
• • • We do not use the following data for averages, fits, limits, etc. • • •			
-0.72 ± 0.19 ± 0.05	AUBERT	07B0 BABR	Repl. by AUBERT 09c
-0.75 ± 0.25 ± 0.03	<sup>2</sup> AUBERT, BE	05A BABR	Repl. by AUBERT 07B0
<sup>1</sup> Measured partially reconstructed candidates when one $D^0$ meson is not explicitly reconstructed. Analysis does not separate $CP$ -even and $CP$ -odd component. Value is obtained from $S = -0.34 \pm 0.12 \pm 0.05$ using $S = S_+ (1 - 2R_{\perp})$ with $R_{\perp} = 0.158 \pm 0.029$ .			
<sup>2</sup> AUBERT, BE 05A reports a $CP$ -odd fraction $R_{\perp} = 0.125 \pm 0.044 \pm 0.007$ .			

### $C_- (B^0 \rightarrow D^{*+}D^{*-})$

See the note in the  $C_{\pi\pi}$  datablock, but for  $CP$  odd final state.

VALUE	DOCUMENT ID	TECN	COMMENT
<b>0.19 ± 0.31 OUR AVERAGE</b>	Error includes scale factor of 3.5.		
0.05 ± 0.39 ± 0.08	<sup>1</sup> KRONENBIT...12	BELL	$e^+e^- \rightarrow \Upsilon(4S)$
0.41 ± 0.49 ± 0.08	AUBERT	09c BABR	$e^+e^- \rightarrow \Upsilon(4S)$
• • • We do not use the following data for averages, fits, limits, etc. • • •			
0.23 ± 0.67 ± 0.10	AUBERT	07B0 BABR	Repl. by AUBERT 09c
-0.20 ± 0.96 ± 0.11	<sup>2</sup> AUBERT, BE	05A BABR	Repl. by AUBERT 07B0
<sup>1</sup> Belle Collab. quotes $A_{D^{*+}D^{*-}}$ which is equal to $-C_{D^{*+}D^{*-}}$ .			
<sup>2</sup> AUBERT, BE 05A reports a $CP$ -odd fraction $R_{\perp} = 0.125 \pm 0.044 \pm 0.007$ .			

### $S_- (B^0 \rightarrow D^{*+}D^{*-})$

See the note in the  $S_{\pi\pi}$  datablock, but for  $CP$  odd final state.

VALUE	DOCUMENT ID	TECN	COMMENT
<b>0.1 ± 1.6 OUR AVERAGE</b>	Error includes scale factor of 3.5.		
1.52 ± 0.62 ± 0.12	KRONENBIT...12	BELL	$e^+e^- \rightarrow \Upsilon(4S)$
-1.80 ± 0.70 ± 0.16	AUBERT	09c BABR	$e^+e^- \rightarrow \Upsilon(4S)$
• • • We do not use the following data for averages, fits, limits, etc. • • •			
-1.83 ± 1.04 ± 0.23	AUBERT	07B0 BABR	Repl. by AUBERT 09c
-1.75 ± 1.78 ± 0.22	<sup>1</sup> AUBERT, BE	05A BABR	Repl. by AUBERT 07B0
<sup>1</sup> AUBERT, BE 05A reports a $CP$ -odd fraction $R_{\perp} = 0.125 \pm 0.044 \pm 0.007$ .			

### $C (B^0 \rightarrow D^{*(2010)^+} D^{*(2010)^-} K_S^0)$

VALUE	DOCUMENT ID	TECN	COMMENT
<b>0.01 ± 0.28 ± 0.09</b>	<sup>1</sup> DALSENO	07 BELL	$e^+e^- \rightarrow \Upsilon(4S)$
<sup>1</sup> Reports value of $A$ which is equal to $-C$ .			

### $S (B^0 \rightarrow D^{*(2010)^+} D^{*(2010)^-} K_S^0)$

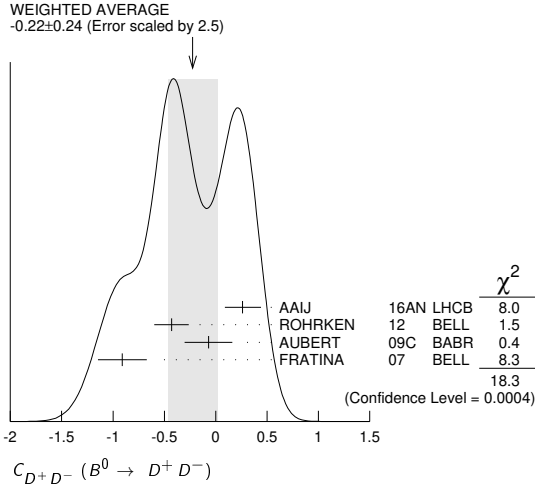
VALUE	DOCUMENT ID	TECN	COMMENT
<b>0.06 ± 0.45 ± 0.06</b>	<sup>1</sup> DALSENO	07 BELL	$e^+e^- \rightarrow \Upsilon(4S)$
<sup>1</sup> This value includes an unknown $CP$ dilution factor $D$ due to possible contributions from intermediate resonances and different partial waves.			

### $C_{D^+D^-} (B^0 \rightarrow D^+D^-)$

VALUE	DOCUMENT ID	TECN	COMMENT
<b>-0.22 ± 0.24 OUR AVERAGE</b>	Error includes scale factor of 2.5. See the ideogram below.		
0.26 ± 0.18 ± 0.02	AAIJ	16AN LHCB	$pp$ at 7, 8 TeV
-0.43 ± 0.16 ± 0.05	ROHRKEN	12 BELL	$e^+e^- \rightarrow \Upsilon(4S)$
-0.07 ± 0.23 ± 0.03	AUBERT	09c BABR	$e^+e^- \rightarrow \Upsilon(4S)$
-0.91 ± 0.23 ± 0.06	<sup>1</sup> FRATINA	07 BELL	$e^+e^- \rightarrow \Upsilon(4S)$

• • • We do not use the following data for averages, fits, limits, etc. • • •  
 0.11 ± 0.22 ± 0.07 AUBERT 07AI BABR Repl. by AUBERT 09c  
 0.11 ± 0.35 ± 0.06 AUBERT,B 05Z BABR Repl. by AUBERT 07AI

<sup>1</sup> The paper reports A, which is equal to -C.



**S<sub>D+D-</sub>(B<sup>0</sup> → D<sup>+</sup>D<sup>-</sup>)**

VALUE	DOCUMENT ID	TECN	COMMENT
<b>-0.76 ± 0.15 OUR AVERAGE</b>	Error includes scale factor of 1.2.		
-0.54 ± 0.17 ± 0.05	AAIJ	16AN LHCb	pp at 7, 8 TeV
-1.06 ± 0.21 ± 0.08	ROHRKEN	12 BELL	e <sup>+</sup> e <sup>-</sup> → γ(4S)
-0.63 ± 0.36 ± 0.05	AUBERT	09C BABR	e <sup>+</sup> e <sup>-</sup> → γ(4S)
-1.13 ± 0.37 ± 0.09	FRATINA	07 BELL	e <sup>+</sup> e <sup>-</sup> → γ(4S)
• • • We do not use the following data for averages, fits, limits, etc. • • •			
-0.54 ± 0.34 ± 0.06	AUBERT	07AI BABR	Repl. by AUBERT 09c
-0.29 ± 0.63 ± 0.06	AUBERT,B	05Z BABR	Repl. by AUBERT 07AI

**C<sub>J/ψ(1S)π<sup>0</sup></sub>(B<sup>0</sup> → J/ψ(1S)π<sup>0</sup>)**

VALUE	DOCUMENT ID	TECN	COMMENT
<b>0.03 ± 0.17 OUR AVERAGE</b>	Error includes scale factor of 1.5.		
0.15 ± 0.14 ± 0.04	<sup>1</sup> PAL	18 BELL	e <sup>+</sup> e <sup>-</sup> → γ(4S)
-0.20 ± 0.19 ± 0.03	AUBERT	08AU BABR	e <sup>+</sup> e <sup>-</sup> → γ(4S)
• • • We do not use the following data for averages, fits, limits, etc. • • •			
-0.08 ± 0.16 ± 0.05	<sup>1</sup> LEE	08A BELL	Repl. by PAL 18
-0.21 ± 0.26 ± 0.06	AUBERT,B	06B BABR	Repl. by AUBERT 08AU
0.01 ± 0.29 ± 0.03	<sup>1</sup> KATAOKA	04 BELL	Repl. by LEE 08A
0.38 ± 0.41 ± 0.09	AUBERT	03N BABR	Repl. by AUBERT,B 06B

<sup>1</sup> BELLE Collab. quotes A<sub>J/ψπ<sup>0</sup></sub> which is equal to -C<sub>J/ψπ<sup>0</sup></sub>.

**S<sub>J/ψ(1S)π<sup>0</sup></sub>(B<sup>0</sup> → J/ψ(1S)π<sup>0</sup>)**

VALUE	DOCUMENT ID	TECN	COMMENT
<b>-0.88 ± 0.32 OUR AVERAGE</b>	Error includes scale factor of 2.2.		
-0.59 ± 0.19 ± 0.03	PAL	18 BELL	e <sup>+</sup> e <sup>-</sup> → γ(4S)
-1.23 ± 0.21 ± 0.04	AUBERT	08AU BABR	e <sup>+</sup> e <sup>-</sup> → γ(4S)
• • • We do not use the following data for averages, fits, limits, etc. • • •			
-0.65 ± 0.21 ± 0.05	LEE	08A BELL	Repl. by PAL 18
-0.68 ± 0.30 ± 0.04	AUBERT,B	06B BABR	Repl. by AUBERT 08AU
-0.72 ± 0.42 ± 0.09	KATAOKA	04 BELL	Repl. by LEE 08A
0.05 ± 0.49 ± 0.16	AUBERT	03N BABR	Repl. by AUBERT,B 06B

**C(B<sup>0</sup> → J/ψ(1S)ρ<sup>0</sup>)**

VALUE	DOCUMENT ID	TECN	COMMENT
<b>-0.063 ± 0.056 ± 0.019 OUR AVERAGE</b>	Error includes scale factor of 1.5.		
	<sup>1</sup> AAIJ	15J LHCb	pp at 7, 8 TeV

<sup>1</sup> Time-dependent CP violation is measured in the B<sup>0</sup> → J/ψρ<sup>0</sup> and was used to limit the size of penguin amplitude contributions to φ<sub>S</sub> in B<sup>0</sup><sub>S</sub> → J/ψφ decays to be between [-1.05°, 1.18°] at 95% confidence level.

**S(B<sup>0</sup> → J/ψ(1S)ρ<sup>0</sup>)**

VALUE	DOCUMENT ID	TECN	COMMENT
<b>-0.66 ± 0.13 ± 0.09 OUR AVERAGE</b>	Error includes scale factor of 1.5.		
	<sup>1</sup> AAIJ	15J LHCb	pp at 7, 8 TeV

<sup>1</sup> Time-dependent CP violation is measured in the B<sup>0</sup> → J/ψρ<sup>0</sup> and was used to limit the size of penguin amplitude contributions to φ<sub>S</sub> in B<sup>0</sup><sub>S</sub> → J/ψφ decays to be between [-1.05°, 1.18°] at 95% confidence level.

**C<sub>D<sub>CP</sub><sup>(\*)</sup>h<sup>0</sup></sub>(B<sup>0</sup> → D<sub>CP</sub><sup>(\*)</sup>h<sup>0</sup>)**

VALUE	DOCUMENT ID	TECN	COMMENT
<b>-0.02 ± 0.07 ± 0.03</b>	<sup>1</sup> ABDESSALAM 15		e <sup>+</sup> e <sup>-</sup> → γ(4S)

• • • We do not use the following data for averages, fits, limits, etc. • • •  
 -0.23 ± 0.16 ± 0.04 AUBERT 07AJ BABR Repl. by ABDESSALAM 15  
<sup>1</sup> BABAR and BELLE combined analysis uses CP-eigenstate decay modes D<sup>0</sup> → K<sup>+</sup>K<sup>-</sup>, K<sub>S</sub><sup>0</sup>π<sup>0</sup>, K<sub>S</sub><sup>0</sup>ω, and h<sup>0</sup> = π<sup>0</sup>, η, ω.

**S<sub>D<sub>CP</sub><sup>(\*)</sup>h<sup>0</sup></sub>(B<sup>0</sup> → D<sub>CP</sub><sup>(\*)</sup>h<sup>0</sup>)**

VALUE	DOCUMENT ID	TECN	COMMENT
<b>-0.66 ± 0.10 ± 0.06</b>	<sup>1</sup> ABDESSALAM 15		e <sup>+</sup> e <sup>-</sup> → γ(4S)

• • • We do not use the following data for averages, fits, limits, etc. • • •  
 -0.56 ± 0.23 ± 0.05 AUBERT 07AJ BABR Repl. by ABDESSALAM 15  
<sup>1</sup> BABAR and BELLE combined analysis uses CP-eigenstate decay modes D<sup>0</sup> → K<sup>+</sup>K<sup>-</sup>, K<sub>S</sub><sup>0</sup>π<sup>0</sup>, K<sub>S</sub><sup>0</sup>ω, and h<sup>0</sup> = π<sup>0</sup>, η, ω.

**C<sub>K<sup>0</sup>π<sup>0</sup></sub>(B<sup>0</sup> → K<sup>0</sup>π<sup>0</sup>)**

VALUE	DOCUMENT ID	TECN	COMMENT
<b>0.00 ± 0.13 OUR AVERAGE</b>	Error includes scale factor of 1.4.		
-0.14 ± 0.13 ± 0.06	<sup>1</sup> FUJIKAWA	10A BELL	e <sup>+</sup> e <sup>-</sup> → γ(4S)
0.13 ± 0.13 ± 0.03	AUBERT	09I BABR	e <sup>+</sup> e <sup>-</sup> → γ(4S)

• • • We do not use the following data for averages, fits, limits, etc. • • •

0.24 ± 0.15 ± 0.03	AUBERT	08E BABR	Repl. by AUBERT 09I
0.05 ± 0.14 ± 0.05	<sup>1</sup> CHAO	07 BELL	Repl. by FUJIKAWA 10A
0.06 ± 0.18 ± 0.03	AUBERT	05Y BABR	Repl. by AUBERT 08E
-0.16 ± 0.29 ± 0.05	<sup>1,2</sup> CHAO	05A BELL	Repl. by CHEN 05B
0.11 ± 0.20 ± 0.09	<sup>1</sup> CHEN	05B BELL	Repl. by CHAO 07
-0.03 ± 0.36 ± 0.11	<sup>1</sup> AUBERT	04M BABR	Repl. by AUBERT,B 04M
0.40 ± 0.27 ± 0.09	<sup>3</sup> AUBERT,B	04M BABR	Repl. by AUBERT 05Y

<sup>1</sup> Reports A which is equal to -C.  
<sup>2</sup> Corresponds to a 90% CL interval of -0.33 < A<sub>CP</sub> < 0.64.  
<sup>3</sup> Based on a total signal yield of 122 ± 16 events.

**S<sub>K<sup>0</sup>π<sup>0</sup></sub>(B<sup>0</sup> → K<sup>0</sup>π<sup>0</sup>)**

VALUE	DOCUMENT ID	TECN	COMMENT
<b>0.58 ± 0.17 OUR AVERAGE</b>	Error includes scale factor of 1.4.		
0.67 ± 0.31 ± 0.08	FUJIKAWA	10A BELL	e <sup>+</sup> e <sup>-</sup> → γ(4S)
0.55 ± 0.20 ± 0.03	AUBERT	09I BABR	e <sup>+</sup> e <sup>-</sup> → γ(4S)

• • • We do not use the following data for averages, fits, limits, etc. • • •

0.40 ± 0.23 ± 0.03	AUBERT	08E BABR	Repl. by AUBERT 09I
0.33 ± 0.35 ± 0.08	CHAO	07 BELL	Repl. by FUJIKAWA 10A
0.35 ± 0.30 ± 0.04	AUBERT	05Y BABR	Repl. by AUBERT 08E
-0.33 ± 0.04			
0.32 ± 0.61 ± 0.13	CHEN	05B BELL	Repl. by CHAO 07
0.48 ± 0.37 ± 0.06	<sup>1</sup> AUBERT,B	04M BABR	Repl. by AUBERT 05Y

<sup>1</sup> Based on a total signal yield of 122 ± 16 events.

**C<sub>η(958)K<sub>S</sub><sup>0</sup></sub>(B<sup>0</sup> → η(958)K<sub>S</sub><sup>0</sup>)**

See updated measurements in C<sub>η'K<sub>S</sub><sup>0</sup></sub>

VALUE	DOCUMENT ID	TECN	COMMENT
<b>-0.04 ± 0.20 OUR AVERAGE</b>	Error includes scale factor of 2.5.		
-0.21 ± 0.10 ± 0.02	AUBERT	05M BABR	e <sup>+</sup> e <sup>-</sup> → γ(4S)
0.19 ± 0.11 ± 0.05	<sup>1</sup> CHEN	05B BELL	e <sup>+</sup> e <sup>-</sup> → γ(4S)

• • • We do not use the following data for averages, fits, limits, etc. • • •

-0.26 ± 0.22 ± 0.03	<sup>1</sup> ABE	03C BELL	Repl. by ABE 03H
0.01 ± 0.16 ± 0.04	<sup>1</sup> ABE	03H BELL	Repl. by CHEN 05B
0.10 ± 0.22 ± 0.04	AUBERT	03W BABR	Repl. by AUBERT 05M
-0.13 ± 0.32 ± 0.06	<sup>1</sup> CHEN	02B BELL	Repl. by ABE 03C

<sup>1</sup> BELLE Collab. quotes A<sub>η(958)K<sub>S</sub><sup>0</sup></sub> which is equal to -C<sub>η(958)K<sub>S</sub><sup>0</sup></sub>.

**S<sub>η(958)K<sub>S</sub><sup>0</sup></sub>(B<sup>0</sup> → η(958)K<sub>S</sub><sup>0</sup>)**

See updated measurements in S<sub>η'K<sub>S</sub><sup>0</sup></sub>

VALUE	DOCUMENT ID	TECN	COMMENT
<b>0.43 ± 0.17 OUR AVERAGE</b>	Error includes scale factor of 1.5.		
0.30 ± 0.14 ± 0.02	AUBERT	05M BABR	e <sup>+</sup> e <sup>-</sup> → γ(4S)
0.65 ± 0.18 ± 0.04	CHEN	05B BELL	e <sup>+</sup> e <sup>-</sup> → γ(4S)

• • • We do not use the following data for averages, fits, limits, etc. • • •

0.71 ± 0.37 ± 0.05	ABE	03C BELL	Repl. by ABE 03H
0.43 ± 0.27 ± 0.05	ABE	03H BELL	Repl. by CHEN 05B
0.02 ± 0.34 ± 0.03	AUBERT	03W BABR	Repl. by AUBERT 05M
0.28 ± 0.55 ± 0.07	CHEN	02B BELL	Repl. by ABE 03C

## Meson Particle Listings

 $B^0$  $C_{\eta K^0} (B^0 \rightarrow \eta K^0)$ 

VALUE	DOCUMENT ID	TECN	COMMENT
<b><math>-0.06 \pm 0.04</math> OUR AVERAGE</b>			
$-0.03 \pm 0.05 \pm 0.04$	<sup>1</sup> SANTELJ 14	BELL	$e^+ e^- \rightarrow \Upsilon(4S)$
$-0.08 \pm 0.06 \pm 0.02$	AUBERT 09i	BABR	$e^+ e^- \rightarrow \Upsilon(4S)$
• • • We do not use the following data for averages, fits, limits, etc. • • •			
$-0.16 \pm 0.07 \pm 0.03$	<sup>2</sup> AUBERT 07A	BABR	Repl. by AUBERT 09i
$0.01 \pm 0.07 \pm 0.05$	<sup>1,2</sup> CHEN 07	BELL	Repl. by SANTELJ 14

<sup>1</sup> The paper reports  $A$ , which is equal to  $-C$ .

<sup>2</sup> The mixing-induced  $CP$  violation is reported with a significance of more than 5 standard deviations in this  $b \rightarrow s$  penguin dominated mode.

 $S_{\eta K^0} (B^0 \rightarrow \eta K^0)$ 

VALUE	DOCUMENT ID	TECN	COMMENT
<b><math>0.63 \pm 0.06</math> OUR AVERAGE</b>			
$0.68 \pm 0.07 \pm 0.03$	SANTELJ 14	BELL	$e^+ e^- \rightarrow \Upsilon(4S)$
$0.57 \pm 0.08 \pm 0.02$	AUBERT 09i	BABR	$e^+ e^- \rightarrow \Upsilon(4S)$
• • • We do not use the following data for averages, fits, limits, etc. • • •			
$0.58 \pm 0.10 \pm 0.03$	<sup>1</sup> AUBERT 07A	BABR	Repl. by AUBERT 09i
$0.64 \pm 0.10 \pm 0.04$	<sup>1</sup> CHEN 07A	BELL	Repl. by SANTELJ 14

<sup>1</sup> The mixing-induced  $CP$  violation is reported with a significance of more than 5 standard deviations in this  $b \rightarrow s$  penguin dominated mode.

 $C_{\omega K_S^0} (B^0 \rightarrow \omega K_S^0)$ 

VALUE	DOCUMENT ID	TECN	COMMENT
<b><math>0.0 \pm 0.4</math> OUR AVERAGE</b>			Error includes scale factor of 3.0.
$0.36 \pm 0.19 \pm 0.05$	<sup>1</sup> CHOBANOVA 14	BELL	$e^+ e^- \rightarrow \Upsilon(4S)$
$-0.52 \pm 0.22 \pm 0.03$	AUBERT 09i	BABR	$e^+ e^- \rightarrow \Upsilon(4S)$
• • • We do not use the following data for averages, fits, limits, etc. • • •			
$0.09 \pm 0.29 \pm 0.06$	<sup>1</sup> CHAO 07	BELL	Repl. by CHOBANOVA 14
$-0.55 \pm 0.28 \pm 0.03$	AUBERT,B 06E	BABR	Repl. by AUBERT 09i
$-0.27 \pm 0.48 \pm 0.15$	<sup>1</sup> CHEN 05B	BELL	Repl. by CHAO 07

<sup>1</sup> Belle Collab. quotes  $A_{\omega K_S^0}$  which is equal to  $-C_{\omega K_S^0}$ .

 $S_{\omega K_S^0} (B^0 \rightarrow \omega K_S^0)$ 

VALUE	DOCUMENT ID	TECN	COMMENT
<b><math>0.70 \pm 0.21</math> OUR AVERAGE</b>			
$0.91 \pm 0.32 \pm 0.05$	CHOBANOVA 14	BELL	$e^+ e^- \rightarrow \Upsilon(4S)$
$0.55 \pm 0.26 \pm 0.02$	AUBERT 09i	BABR	$e^+ e^- \rightarrow \Upsilon(4S)$
• • • We do not use the following data for averages, fits, limits, etc. • • •			
$0.11 \pm 0.46 \pm 0.07$	CHAO 07	BELL	Repl. by CHOBANOVA 14
$0.51 \pm 0.35 \pm 0.02$	AUBERT,B 06E	BABR	Repl. by AUBERT 09i
$0.76 \pm 0.65 \pm 0.13$	CHEN 05B	BELL	Repl. by CHAO 07

 $C (B^0 \rightarrow K_S^0 \pi^0 \pi^0)$ 

VALUE	DOCUMENT ID	TECN	COMMENT
<b><math>-0.21 \pm 0.20</math> OUR AVERAGE</b>			
$-0.28 \pm 0.21 \pm 0.04$	<sup>1</sup> YUSA 19	BELL	$e^+ e^- \rightarrow \Upsilon(4S)$
$0.23 \pm 0.52 \pm 0.13$	AUBERT 07AQ	BABR	$e^+ e^- \rightarrow \Upsilon(4S)$

<sup>1</sup> Reports value of  $A$  which is equal to  $-C$ .

 $S (B^0 \rightarrow K_S^0 \pi^0 \pi^0)$ 

VALUE	DOCUMENT ID	TECN	COMMENT
<b><math>0.89 \pm 0.27</math> OUR AVERAGE</b>			
$0.92 \pm 0.27 \pm 0.11$	YUSA 19	BELL	$e^+ e^- \rightarrow \Upsilon(4S)$
$0.72 \pm 0.71 \pm 0.08$	AUBERT 07AQ	BABR	$e^+ e^- \rightarrow \Upsilon(4S)$

 $C_{\rho^0 K_S^0} (B^0 \rightarrow \rho^0 K_S^0)$ 

VALUE	DOCUMENT ID	TECN	COMMENT
<b><math>-0.04 \pm 0.20</math> OUR AVERAGE</b>			
$-0.05 \pm 0.26 \pm 0.10$	<sup>1</sup> AUBERT 09AU	BABR	$e^+ e^- \rightarrow \Upsilon(4S)$
$-0.03 \pm 0.24 \pm 0.15$	<sup>2,3</sup> DALSENO 09	BELL	$e^+ e^- \rightarrow \Upsilon(4S)$
• • • We do not use the following data for averages, fits, limits, etc. • • •			
$0.64 \pm 0.41 \pm 0.20$	AUBERT 07F	BABR	Repl. by AUBERT 09AU

<sup>1</sup> Uses Dalitz plot analysis of  $B^0 \rightarrow K^0 \pi^+ \pi^-$  decays and the first of two equivalent solutions is used.

<sup>2</sup> Quotes  $A_{\rho^0(K_S^0)}$  which is equal to  $-C_{\rho^0 K_S^0}$ .

<sup>3</sup> Uses Dalitz plot analysis of  $B^0 \rightarrow K^0 \pi^+ \pi^-$  decays and the first of two consistent solutions that may be preferred.

 $S_{\rho^0 K_S^0} (B^0 \rightarrow \rho^0 K_S^0)$ 

VALUE	DOCUMENT ID	TECN	COMMENT
<b><math>0.50 \pm 0.17</math> OUR AVERAGE</b>			
$0.35 \pm 0.26 \pm 0.07$	<sup>1</sup> AUBERT 09AU	BABR	$e^+ e^- \rightarrow \Upsilon(4S)$
$0.64 \pm 0.19 \pm 0.13$	<sup>2</sup> DALSENO 09	BELL	$e^+ e^- \rightarrow \Upsilon(4S)$
• • • We do not use the following data for averages, fits, limits, etc. • • •			
$0.20 \pm 0.52 \pm 0.24$	AUBERT 07F	BABR	Repl. by AUBERT 09AU
<sup>1</sup> Uses Dalitz plot analysis of $B^0 \rightarrow K^0 \pi^+ \pi^-$ decays and the first of two equivalent solutions is used.			
<sup>2</sup> Uses Dalitz plot analysis of $B^0 \rightarrow K^0 \pi^+ \pi^-$ decays and the first of two consistent solutions that may be preferred.			

 $C_{f_0(980) K_S^0} (B^0 \rightarrow f_0(980) K_S^0)$ 

VALUE	DOCUMENT ID	TECN	COMMENT
<b><math>0.29 \pm 0.20</math> OUR AVERAGE</b>			
$0.28 \pm 0.24 \pm 0.09$	<sup>1</sup> LEES 12o	BABR	$e^+ e^- \rightarrow \Upsilon(4S)$
$0.30 \pm 0.29 \pm 0.14$	<sup>2,3</sup> NAKAHAMA 10	BELL	$e^+ e^- \rightarrow \Upsilon(4S)$
• • • We do not use the following data for averages, fits, limits, etc. • • •			
$0.08 \pm 0.19 \pm 0.05$	<sup>4</sup> AUBERT 09AU	BABR	Repl. by LEES 12o
$0.06 \pm 0.17 \pm 0.11$	<sup>2,5</sup> DALSENO 09	BELL	Repl. by NAKAHAMA 10
$-0.41 \pm 0.23 \pm 0.07$	<sup>2</sup> AUBERT 07AX	BABR	Repl. by AUBERT 09AU
$0.15 \pm 0.15 \pm 0.07$	<sup>2</sup> CHAO 07	BELL	Repl. by DALSENO 09
$0.39 \pm 0.27 \pm 0.09$	<sup>2</sup> CHEN 05B	BELL	Repl. by CHAO 07
<sup>1</sup> Uses Dalitz plot analysis of the $B^0 \rightarrow K_S^0 K^+ K^-$ decay.			
<sup>2</sup> Quotes $A_{f_0(980) K_S^0}$ which is equal to $-C_{f_0(980) K_S^0}$ .			
<sup>3</sup> Uses Dalitz plot analysis of $B^0 \rightarrow K_S^0 K^+ K^-$ decays and the first of four consistent solutions that may be preferred.			
<sup>4</sup> Uses Dalitz plot analysis of $B^0 \rightarrow K^0 \pi^+ \pi^-$ decays and the first of two equivalent solutions is used.			
<sup>5</sup> Uses Dalitz plot analysis of $B^0 \rightarrow K^0 \pi^+ \pi^-$ decays and the first of two consistent solutions that may be preferred.			

 $S_{f_0(980) K_S^0} (B^0 \rightarrow f_0(980) K_S^0)$ 

VALUE	DOCUMENT ID	TECN	COMMENT
<b><math>-0.50 \pm 0.16</math> OUR AVERAGE</b>			
$-0.55 \pm 0.18 \pm 0.12$	<sup>1</sup> LEES 12o	BABR	$e^+ e^- \rightarrow \Upsilon(4S)$
$-0.43 \pm 0.22 \pm 0.14$	<sup>2</sup> DALSENO 09	BELL	$e^+ e^- \rightarrow \Upsilon(4S)$
• • • We do not use the following data for averages, fits, limits, etc. • • •			
$-0.96 \pm 0.21 \pm 0.04$	<sup>3</sup> AUBERT 09AU	BABR	Repl. by LEES 12o
$-0.25 \pm 0.26 \pm 0.10$	<sup>4</sup> AUBERT 07AX	BABR	Repl. by AUBERT 09AU
$0.18 \pm 0.23 \pm 0.11$	CHAO 07	BELL	Repl. by DALSENO 09
$0.47 \pm 0.41 \pm 0.08$	CHEN 05B	BELL	Repl. by CHAO 07
<sup>1</sup> Uses Dalitz plot analysis of the $B^0 \rightarrow K_S^0 K^+ K^-$ decay.			
<sup>2</sup> Uses Dalitz plot analysis of $B^0 \rightarrow K^0 \pi^+ \pi^-$ decays and the first of two consistent solutions that may be preferred.			
<sup>3</sup> Uses Dalitz plot analysis of $B^0 \rightarrow K^0 \pi^+ \pi^-$ decays and the first of two equivalent solutions is used.			
<sup>4</sup> Reports $\beta_{eff}$ . We quote $S$ obtained from epaps: E-PRLTAO-99-076741.			

 $S_{f_2(1270) K_S^0} (B^0 \rightarrow f_2(1270) K_S^0)$ 

VALUE	DOCUMENT ID	TECN	COMMENT
<b><math>-0.48 \pm 0.52 \pm 0.12</math></b>	<sup>1</sup> AUBERT 09AU	BABR	$e^+ e^- \rightarrow \Upsilon(4S)$
<sup>1</sup> Uses Dalitz plot analysis of $B^0 \rightarrow K^0 \pi^+ \pi^-$ decays and the first of two equivalent solutions is used.			

 $C_{f_2(1270) K_S^0} (B^0 \rightarrow f_2(1270) K_S^0)$ 

VALUE	DOCUMENT ID	TECN	COMMENT
<b><math>0.28 \pm 0.35</math> OUR AVERAGE</b>			
$0.28 \pm 0.35 \pm 0.11$	<sup>1</sup> AUBERT 09AU	BABR	$e^+ e^- \rightarrow \Upsilon(4S)$
<sup>1</sup> Uses Dalitz plot analysis of $B^0 \rightarrow K^0 \pi^+ \pi^-$ decays and the first of two equivalent solutions is used.			

 $S_{f_x(1300) K_S^0} (B^0 \rightarrow f_x(1300) K_S^0)$ 

VALUE	DOCUMENT ID	TECN	COMMENT
<b><math>-0.20 \pm 0.52 \pm 0.10</math></b>	<sup>1</sup> AUBERT 09AU	BABR	$e^+ e^- \rightarrow \Upsilon(4S)$
<sup>1</sup> Uses Dalitz plot analysis of $B^0 \rightarrow K^0 \pi^+ \pi^-$ decays and the first of two equivalent solutions is used.			

 $C_{f_x(1300) K_S^0} (B^0 \rightarrow f_x(1300) K_S^0)$ 

VALUE	DOCUMENT ID	TECN	COMMENT
<b><math>0.13 \pm 0.33</math> OUR AVERAGE</b>			
$0.13 \pm 0.33 \pm 0.10$	<sup>1</sup> AUBERT 09AU	BABR	$e^+ e^- \rightarrow \Upsilon(4S)$
<sup>1</sup> Uses Dalitz plot analysis of $B^0 \rightarrow K^0 \pi^+ \pi^-$ decays and the first of two equivalent solutions is used.			

 $S_{K^0 \pi^+ \pi^-} (B^0 \rightarrow K^0 \pi^+ \pi^- \text{ nonresonant})$ 

VALUE	DOCUMENT ID	TECN	COMMENT
<b><math>-0.01 \pm 0.31 \pm 0.10</math></b>	<sup>1</sup> AUBERT 09AU	BABR	$e^+ e^- \rightarrow \Upsilon(4S)$
<sup>1</sup> Uses Dalitz plot analysis of $B^0 \rightarrow K^0 \pi^+ \pi^-$ decays and the first of two equivalent solutions is used.			

$C_{K^0\pi^+\pi^-} (B^0 \rightarrow K^0\pi^+\pi^- \text{ nonresonant})$ 

VALUE	DOCUMENT ID	TECN	COMMENT
<b>0.01 ± 0.25 ± 0.08</b>	1 AUBERT	09AU BABR	$e^+e^- \rightarrow \Upsilon(4S)$

<sup>1</sup> Uses Dalitz plot analysis of  $B^0 \rightarrow K^0\pi^+\pi^-$  decays and the first of two equivalent solutions is used.

 $C_{K_S^0 K_S^0} (B^0 \rightarrow K_S^0 K_S^0)$ 

VALUE	DOCUMENT ID	TECN	COMMENT
<b>0.0 ± 0.4 OUR AVERAGE</b>	Error includes scale factor of 1.4.		
0.38 ± 0.38 ± 0.05	1 NAKAHAMA	08 BELL	$e^+e^- \rightarrow \Upsilon(4S)$
-0.40 ± 0.41 ± 0.06	AUBERT,BE	06C BABR	$e^+e^- \rightarrow \Upsilon(4S)$

<sup>1</sup> Reports  $A_{K_S^0 K_S^0}$  which equals to  $-C_{K_S^0 K_S^0}$ .

 $S_{K_S^0 K_S^0} (B^0 \rightarrow K_S^0 K_S^0)$ 

VALUE	DOCUMENT ID	TECN	COMMENT
<b>-0.8 ± 0.5 OUR AVERAGE</b>			
-0.38 <sup>+0.69</sup> <sub>-0.77</sub> ± 0.09	NAKAHAMA	08 BELL	$e^+e^- \rightarrow \Upsilon(4S)$
-1.28 <sup>+0.80</sup> <sub>-0.73</sub> ± 0.11	AUBERT,BE	06C BABR	$e^+e^- \rightarrow \Upsilon(4S)$

 $C_{K^+K^-K_S^0} (B^0 \rightarrow K^+K^-K_S^0 \text{ nonresonant})$ 

VALUE	DOCUMENT ID	TECN	COMMENT
<b>0.06 ± 0.08 OUR AVERAGE</b>			
0.02 ± 0.09 ± 0.03	1,2 LEES	12o BABR	$e^+e^- \rightarrow \Upsilon(4S)$
0.14 ± 0.11 ± 0.09	3,4 NAKAHAMA	10 BELL	$e^+e^- \rightarrow \Upsilon(4S)$
0.054 ± 0.102 ± 0.060	3,5 AUBERT	07AX BABR	Repl. by LEES 12o
0.09 ± 0.10 ± 0.05	3,5 CHAO	07 BELL	Repl. by NAKAHAMA 10
0.10 ± 0.14 ± 0.04	5 AUBERT	05T BABR	Repl. by AUBERT 07AX
0.09 ± 0.12 ± 0.07	3 CHEN	05B BELL	Repl. by CHAO 07
-0.10 ± 0.19 ± 0.10	5 AUBERT,B	04V BABR	Repl. by AUBERT 05T
0.40 ± 0.33 <sup>+0.28</sup> <sub>-0.10</sub>	3 ABE	03C BELL	Repl. by ABE 03H
0.17 ± 0.16 ± 0.04	3,5 ABE	03H BELL	Repl. by CHEN 05B

<sup>1</sup> Uses Dalitz plot analysis of the  $B^0 \rightarrow K_S^0 K^+ K^-$  decay.

<sup>2</sup> This measurement is performed on all the isobar components, excluding  $\phi K_S^0$  and  $f_0(980) K_S^0$ .

<sup>3</sup> Quotes  $A_{K^+K^-K_S^0}$  which is equal to  $-C_{K^+K^-K_S^0}$ .

<sup>4</sup> Uses Dalitz plot analysis of  $B^0 \rightarrow K_S^0 K^+ K^-$  decays and the first of four consistent solutions that may be preferred.

<sup>5</sup> Excludes the events from  $B^0 \rightarrow \phi K_S^0$  decay. The results are derived from a combined sample of  $K^+ K^- K_S^0$  and  $K^+ K^- K_L^0$  decays.

 $S_{K^+K^-K_S^0} (B^0 \rightarrow K^+K^-K_S^0 \text{ nonresonant})$ 

VALUE	DOCUMENT ID	TECN	COMMENT
<b>-0.66 ± 0.11 OUR AVERAGE</b>			
-0.65 ± 0.12 ± 0.03	1,2 LEES	12o BABR	$e^+e^- \rightarrow \Upsilon(4S)$
-0.68 ± 0.15 <sup>+0.21</sup> <sub>-0.13</sub>	3 CHAO	07 BELL	$e^+e^- \rightarrow \Upsilon(4S)$
-0.764 ± 0.111 <sup>+0.071</sup> <sub>-0.040</sub>	3,4 AUBERT	07AX BABR	Repl. by LEES 12o
-0.42 ± 0.17 ± 0.03	3,5 AUBERT	05T BABR	Repl. by AUBERT 07AX
-0.49 ± 0.18 ± 0.04	CHEN	05B BELL	Repl. by CHAO 07
-0.56 ± 0.25 ± 0.04	3,6 AUBERT,B	04V BABR	Repl. by AUBERT 05T
-0.49 ± 0.43 ± 0.11	ABE	03C BELL	Repl. by ABE 03H
-0.51 ± 0.26 ± 0.05	3,7 ABE	03H BELL	Repl. by CHEN 05B

<sup>1</sup> Uses Dalitz plot analysis of the  $B^0 \rightarrow K_S^0 K^+ K^-$  decay.

<sup>2</sup> This measurement is performed on all the isobar components, excluding  $\phi K_S^0$  and  $f_0(980) K_S^0$ . Note that the nonresonant component is not a  $CP$  eigenstate.

<sup>3</sup> Excludes events from  $B^0 \rightarrow \phi K_S^0$  decay. The results are derived from a combined sample of  $K^+ K^- K_S^0$  and  $K^+ K^- K_L^0$  decays.

<sup>4</sup> Reports  $\beta_{eff}$ . We quote  $S$  obtained from epaps: E-PRLTAO-99-076741.

<sup>5</sup> The measured  $CP$ -even final states fraction is  $0.89 \pm 0.08 \pm 0.06$ .

<sup>6</sup> The measured  $CP$ -even final states fraction is  $0.98 \pm 0.15 \pm 0.04$ .

<sup>7</sup> The measured  $CP$ -even final states fraction is  $1.03 \pm 0.15 \pm 0.05$ .

 $C_{K^+K^-K_S^0} (B^0 \rightarrow K^+K^-K_S^0 \text{ inclusive})$ 

VALUE	DOCUMENT ID	TECN	COMMENT
<b>0.015 ± 0.077 ± 0.053</b>	1,2 AUBERT	07AX BABR	$e^+e^- \rightarrow \Upsilon(4S)$

<sup>1</sup> Measured using full Dalitz plot fit including  $\phi$  component.

<sup>2</sup> The results are derived from a combined sample of  $K^+ K^- K_S^0$  and  $K^+ K^- K_L^0$  decays.

 $S_{K^+K^-K_S^0} (B^0 \rightarrow K^+K^-K_S^0 \text{ inclusive})$ 

VALUE	DOCUMENT ID	TECN	COMMENT
<b>-0.647 ± 0.116 ± 0.040</b>	1 AUBERT	07AX BABR	$e^+e^- \rightarrow \Upsilon(4S)$

<sup>1</sup> Measured using full Dalitz plot fit including  $\phi$  component.

 $C_{\phi K_S^0} (B^0 \rightarrow \phi K_S^0)$ 

VALUE	DOCUMENT ID	TECN	COMMENT
<b>0.01 ± 0.14 OUR AVERAGE</b>			
0.05 ± 0.18 ± 0.05	1 LEES	12o BABR	$e^+e^- \rightarrow \Upsilon(4S)$
-0.04 ± 0.20 ± 0.10	2,3 NAKAHAMA	10 BELL	$e^+e^- \rightarrow \Upsilon(4S)$
0.08 ± 0.18 ± 0.04	2,4 AUBERT	07AX BABR	Repl. by LEES 12o
-0.07 ± 0.15 ± 0.05	2,4 CHEN	07 BELL	Repl. by NAKAHAMA 10
0.00 ± 0.23 ± 0.05	4 AUBERT	05T BABR	Repl. by AUBERT 07AX
-0.08 ± 0.22 ± 0.09	2,4 CHEN	05B BELL	Repl. by CHEN 07
0.01 ± 0.33 ± 0.10	4 AUBERT,B	04G BABR	Repl. by AUBERT 05T
0.56 ± 0.41 ± 0.16	2 ABE	03C BELL	Repl. by ABE 03H
0.15 ± 0.29 ± 0.07	2 ABE	03H BELL	Repl. by CHEN 05B

<sup>1</sup> Uses Dalitz plot analysis of the  $B^0 \rightarrow K_S^0 K^+ K^-$  decay.

<sup>2</sup> Quotes  $A_{\phi K_S^0}$  which is equal to  $-C_{\phi K_S^0}$ .

<sup>3</sup> Uses Dalitz plot analysis of  $B^0 \rightarrow K_S^0 K^+ K^-$  decays and the first of four consistent solutions that may be preferred.

<sup>4</sup> Result combines  $B$ -meson final states  $\phi K_S^0$  and  $\phi K_L^0$  by assuming  $S_{\phi K_S^0} = -S_{\phi K_L^0}$ .

 $S_{\phi K_S^0} (B^0 \rightarrow \phi K_S^0)$ 

VALUE	DOCUMENT ID	TECN	COMMENT
<b>0.59 ± 0.14 OUR AVERAGE</b>			
0.66 ± 0.17 ± 0.07	1 LEES	12o BABR	$e^+e^- \rightarrow \Upsilon(4S)$
0.50 ± 0.21 ± 0.06	2 CHEN	07 BELL	$e^+e^- \rightarrow \Upsilon(4S)$
0.21 ± 0.26 ± 0.11	2,3 AUBERT	07AX BABR	Repl. by LEES 12o
0.50 ± 0.25 <sup>+0.07</sup> <sub>-0.04</sub>	2 AUBERT	05T BABR	Repl. by AUBERT 07AX
0.08 ± 0.33 ± 0.09	2 CHEN	05B BELL	Repl. by CHEN 07
0.47 ± 0.34 <sup>+0.08</sup> <sub>-0.06</sub>	2 AUBERT,B	04G BABR	Repl. by AUBERT 05T
-0.73 ± 0.64 ± 0.22	ABE	03C BELL	Repl. by ABE 03H
-0.96 ± 0.50 <sup>+0.09</sup> <sub>-0.11</sub>	ABE	03H BELL	Repl. by CHEN 05B

<sup>1</sup> Uses Dalitz plot analysis of the  $B^0 \rightarrow K_S^0 K^+ K^-$  decay.

<sup>2</sup> Result combines  $B$ -meson final states  $\phi K_S^0$  and  $\phi K_L^0$  by assuming  $S_{\phi K_S^0} = -S_{\phi K_L^0}$ .

<sup>3</sup> Reports  $\beta_{eff}$ . We quote  $S$  obtained from epaps: E-PRLTAO-99-076741.

 $C_{K_S^0 K_S^0 K_S^0} (B^0 \rightarrow K_S^0 K_S^0 K_S^0)$ 

VALUE	DOCUMENT ID	TECN	COMMENT
<b>-0.23 ± 0.14 OUR AVERAGE</b>			
-0.17 ± 0.18 ± 0.04	LEES	12i BABR	$e^+e^- \rightarrow \Upsilon(4S)$
-0.31 ± 0.20 ± 0.07	1 CHEN	07 BELL	$e^+e^- \rightarrow \Upsilon(4S)$
0.02 ± 0.21 ± 0.05	AUBERT	07AT BABR	Repl. by LEES 12i
-0.34 ± 0.28 <sup>+0.25</sup> <sub>-0.25</sub> ± 0.05	AUBERT,B	05 BABR	Repl. by AUBERT 07AT
-0.54 ± 0.34 ± 0.09	1 SUMISAWA	05 BELL	Repl. by CHEN 07

<sup>1</sup> Belle Collab. quotes  $A_{K_S^0 K_S^0 K_S^0}$  which is equal to  $-C_{K_S^0 K_S^0 K_S^0}$ .

 $S_{K_S^0 K_S^0 K_S^0} (B^0 \rightarrow K_S^0 K_S^0 K_S^0)$ 

VALUE	DOCUMENT ID	TECN	COMMENT
<b>-0.5 ± 0.6 OUR AVERAGE</b>	Error includes scale factor of 3.0.		
-0.94 ± 0.24 <sup>+0.21</sup> <sub>-0.21</sub> ± 0.06	LEES	12i BABR	$e^+e^- \rightarrow \Upsilon(4S)$
0.30 ± 0.32 ± 0.08	CHEN	07 BELL	$e^+e^- \rightarrow \Upsilon(4S)$
-0.71 ± 0.24 ± 0.04	AUBERT	07AT BABR	Repl. by LEES 12i
-0.71 ± 0.38 <sup>+0.32</sup> <sub>-0.32</sub> ± 0.04	AUBERT,B	05 BABR	Repl. by AUBERT 07AT
1.26 ± 0.68 ± 0.20	SUMISAWA	05 BELL	Repl. by CHEN 07.

 $C_{K_S^0 \pi^0 \gamma} (B^0 \rightarrow K_S^0 \pi^0 \gamma)$ 

VALUE	DOCUMENT ID	TECN	COMMENT
<b>0.36 ± 0.33 ± 0.04</b>	1 AUBERT	08BA BABR	$e^+e^- \rightarrow \Upsilon(4S)$
0.20 ± 0.20 ± 0.06	2,3 USHIRODA	06 BELL	$e^+e^- \rightarrow \Upsilon(4S)$
-1.0 ± 0.5 ± 0.2	1 AUBERT,B	05P BABR	Repl. by AUBERT 08BA
-0.03 ± 0.34 ± 0.11	3 USHIRODA	05 BELL	Repl. by USHIRODA 06

<sup>1</sup> Requires  $1.1 < M_{K_S^0 \pi^0} < 1.8 \text{ GeV}/c^2$ .

<sup>2</sup> Requires  $M_{K_S^0 \pi^0} < 1.8 \text{ GeV}/c^2$ .

<sup>3</sup> Reports  $A_{K_S^0 \pi^0 \gamma}$ , which is  $-C_{K_S^0 \pi^0 \gamma}$ .

## Meson Particle Listings

 $B^0$  $S_{K_S^0 \pi^0 \gamma} (B^0 \rightarrow K_S^0 \pi^0 \gamma)$ 

VALUE	DOCUMENT ID	TECN	COMMENT
$-0.78 \pm 0.59 \pm 0.09$	<sup>1</sup> AUBERT	08BA BABR	$e^+ e^- \rightarrow \Upsilon(4S)$
• • • We do not use the following data for averages, fits, limits, etc. • • •			
$-0.10 \pm 0.31 \pm 0.07$	<sup>2</sup> USHIRODA	06 BELL	$e^+ e^- \rightarrow \Upsilon(4S)$
$0.9 \pm 1.0 \pm 0.2$	<sup>1</sup> AUBERT,B	05P BABR	Repl. by AUBERT 08BA
$-0.58 \pm 0.46 \pm 0.11$	USHIRODA	05 BELL	Repl. by USHIRODA 06
<sup>1</sup> Requires $1.1 < M_{K_S^0 \pi^0} < 1.8 \text{ GeV}/c^2$ .			
<sup>2</sup> Requires $M_{K_S^0 \pi^0} < 1.8 \text{ GeV}/c^2$ .			

 $C_{K_S^0 \pi^+ \pi^- \gamma} (B^0 \rightarrow K_S^0 \pi^+ \pi^- \gamma)$ 

VALUE	DOCUMENT ID	TECN	COMMENT
$-0.39 \pm 0.20 \pm 0.03$	<sup>1</sup> DEL-AMO-SA...16	BABR	$e^+ e^- \rightarrow \Upsilon(4S)$
<sup>1</sup> Requires $M_{K \pi \pi} < 1.8 \text{ GeV}/c^2$ , $0.6 \text{ GeV}/c^2 < m_{\pi^+ \pi^-} < 0.9 \text{ GeV}/c^2$ , $m_{K \pi} < 0.845 \text{ GeV}/c^2$ or $m_{K \pi} > 0.945 \text{ GeV}/c^2$ .			

 $S_{K_S^0 \pi^+ \pi^- \gamma} (B^0 \rightarrow K_S^0 \pi^+ \pi^- \gamma)$ 

VALUE	DOCUMENT ID	TECN	COMMENT
$0.14 \pm 0.25 \pm 0.03$	<sup>1</sup> DEL-AMO-SA...16	BABR	$e^+ e^- \rightarrow \Upsilon(4S)$
<sup>1</sup> Requires $M_{K \pi \pi} < 1.8 \text{ GeV}/c^2$ , $0.6 \text{ GeV}/c^2 < m_{\pi^+ \pi^-} < 0.9 \text{ GeV}/c^2$ , $m_{K \pi} < 0.845 \text{ GeV}/c^2$ or $m_{K \pi} > 0.945 \text{ GeV}/c^2$ .			

 $C_{K^*(892)^0 \gamma} (B^0 \rightarrow K^*(892)^0 \gamma)$ 

VALUE	DOCUMENT ID	TECN	COMMENT
$-0.04 \pm 0.16$ OUR AVERAGE	Error includes scale factor of 1.2.		
$-0.14 \pm 0.16 \pm 0.03$	<sup>1</sup> AUBERT	08BA BABR	$e^+ e^- \rightarrow \Upsilon(4S)$
$0.20 \pm 0.24 \pm 0.05$	<sup>1,2</sup> USHIRODA	06 BELL	$e^+ e^- \rightarrow \Upsilon(4S)$
• • • We do not use the following data for averages, fits, limits, etc. • • •			
$-0.40 \pm 0.23 \pm 0.03$	AUBERT,B	05P BABR	Repl. by AUBERT 08BA
$-0.57 \pm 0.32 \pm 0.09$	<sup>3</sup> AUBERT,B	04Z BABR	Repl. by AUBERT,B 05P
<sup>1</sup> Requires $0.8 < M_{K_S^0 \pi^0} < 1.0 \text{ GeV}/c^2$ .			
<sup>2</sup> Reports value of A which is equal to $-C$ .			
<sup>3</sup> Based on a total signal of $105 \pm 14$ events with $K^*(892)^0 \rightarrow K_S^0 \pi^0$ only.			

 $S_{K^*(892)^0 \gamma} (B^0 \rightarrow K^*(892)^0 \gamma)$ 

VALUE	DOCUMENT ID	TECN	COMMENT
$-0.15 \pm 0.22$ OUR AVERAGE	Error includes scale factor of 1.4.		
$-0.03 \pm 0.29 \pm 0.03$	<sup>1</sup> AUBERT	08BA BABR	$e^+ e^- \rightarrow \Upsilon(4S)$
$-0.32 \pm 0.36 \pm 0.05$	<sup>1</sup> USHIRODA	06 BELL	$e^+ e^- \rightarrow \Upsilon(4S)$
• • • We do not use the following data for averages, fits, limits, etc. • • •			
$-0.21 \pm 0.40 \pm 0.05$	AUBERT,B	05P BABR	Repl. by AUBERT 08BA
$-0.79 \pm 0.63 \pm 0.10$	<sup>2</sup> USHIRODA	05 BELL	Repl. by USHIRODA 06
$0.25 \pm 0.63 \pm 0.14$	<sup>3</sup> AUBERT,B	04Z BABR	Repl. by AUBERT,B 05P
<sup>1</sup> Requires $0.8 < M_{K_S^0 \pi^0} < 1.0 \text{ GeV}/c^2$ .			
<sup>2</sup> Assumes $C(B^0 \rightarrow K^*(892)^0 \gamma) = 0$ .			
<sup>3</sup> Based on a total signal of $105 \pm 14$ events with $K^*(892)^0 \rightarrow K_S^0 \pi^0$ only.			

 $C_{\eta K^0 \gamma} (B^0 \rightarrow \eta K^0 \gamma)$ 

VALUE	DOCUMENT ID	TECN	COMMENT
$0.1 \pm 0.4$ OUR AVERAGE	Error includes scale factor of 1.4.		
$0.48 \pm 0.41 \pm 0.07$	<sup>1,2</sup> NAKANO	18 BELL	$e^+ e^- \rightarrow \Upsilon(4S)$
$-0.32 \pm 0.40 \pm 0.07$	<sup>3</sup> AUBERT	09 BABR	$e^+ e^- \rightarrow \Upsilon(4S)$
<sup>1</sup> Assuming $m_{\eta K_S^0} < 2.1 \text{ GeV}$ .			
<sup>2</sup> Reversed the sign for C=A.			
<sup>3</sup> Assuming $m_{\eta K} < 3.25 \text{ GeV}$ .			

 $S_{\eta K^0 \gamma} (B^0 \rightarrow \eta K^0 \gamma)$ 

VALUE	DOCUMENT ID	TECN	COMMENT
$-0.5 \pm 0.5$ OUR AVERAGE	Error includes scale factor of 1.2.		
$-1.32 \pm 0.77 \pm 0.36$	<sup>1</sup> NAKANO	18 BELL	$e^+ e^- \rightarrow \Upsilon(4S)$
$-0.18 \pm 0.49 \pm 0.12$	<sup>2</sup> AUBERT	09 BABR	$e^+ e^- \rightarrow \Upsilon(4S)$
<sup>1</sup> Assuming $m_{\eta K_S^0} < 2.1 \text{ GeV}$ .			
<sup>2</sup> Assuming $m_{\eta K} < 3.25 \text{ GeV}$ .			

 $C_{K^0 \phi \gamma} (B^0 \rightarrow K^0 \phi \gamma)$ 

VALUE	DOCUMENT ID	TECN	COMMENT
$-0.35 \pm 0.58 \pm 0.10$	<sup>1</sup> SAHOO	11A BELL	$e^+ e^- \rightarrow \Upsilon(4S)$
<sup>1</sup> Reports value of A, which is equal to $-C$ .			

 $S_{K^0 \phi \gamma} (B^0 \rightarrow K^0 \phi \gamma)$ 

VALUE	DOCUMENT ID	TECN	COMMENT
$0.74 \pm 0.72 \pm 0.10$	SAHOO	11A BELL	$e^+ e^- \rightarrow \Upsilon(4S)$
$-1.05 \pm 0.24$			

 $C(B^0 \rightarrow K_S^0 \rho^0 \gamma)$ 

VALUE	DOCUMENT ID	TECN	COMMENT
$-0.05 \pm 0.18 \pm 0.06$	<sup>1,2</sup> LI	08F BELL	$e^+ e^- \rightarrow \Upsilon(4S)$
<sup>1</sup> Requires $M_{K_S^0 \pi^+ \pi^-} < 1.8 \text{ GeV}/c^2$ and $0.6 < m_{\pi^+ \pi^-} < 0.9 \text{ GeV}/c^2$ .			
<sup>2</sup> Reports value of $A_{\text{eff}}$ which is equal to $-C$ , and includes the non-resonant $\pi^+ \pi^-$ contribution in the $\rho^0$ region.			

 $S(B^0 \rightarrow K_S^0 \rho^0 \gamma)$ 

VALUE	DOCUMENT ID	TECN	COMMENT
$-0.04 \pm 0.23$ OUR AVERAGE			
$-0.18 \pm 0.32 \pm 0.06$	<sup>1</sup> DEL-AMO-SA...16	BABR	$e^+ e^- \rightarrow \Upsilon(4S)$
$0.11 \pm 0.33 \pm 0.05$	<sup>2</sup> LI	08F BELL	$e^+ e^- \rightarrow \Upsilon(4S)$
<sup>1</sup> Requires $M_{K \pi \pi} < 1.8 \text{ GeV}/c^2$ , $0.6 \text{ GeV}/c^2 < m_{\pi^+ \pi^-} < 0.9 \text{ GeV}/c^2$ , $m_{K \pi} < 0.845 \text{ GeV}/c^2$ or $m_{K \pi} > 0.945 \text{ GeV}/c^2$ .			
<sup>2</sup> Requires $M_{K \pi \pi} < 1.8 \text{ GeV}/c^2$ .			

 $C(B^0 \rightarrow \rho^0 \gamma)$ 

VALUE	DOCUMENT ID	TECN	COMMENT
$0.44 \pm 0.49 \pm 0.14$	<sup>1</sup> USHIRODA	08 BELL	$e^+ e^- \rightarrow \Upsilon(4S)$
<sup>1</sup> Reports value of A which is equal to $-C$ .			

 $S(B^0 \rightarrow \rho^0 \gamma)$ 

VALUE	DOCUMENT ID	TECN	COMMENT
$-0.83 \pm 0.65 \pm 0.18$	USHIRODA	08 BELL	$e^+ e^- \rightarrow \Upsilon(4S)$

 $C_{\pi \pi} (B^0 \rightarrow \pi^+ \pi^-)$ 

$C_{\pi \pi}$  is defined as  $(1 - |\lambda|^2)/(1 + |\lambda|^2)$ , where the quantity  $\lambda = q/p \bar{A}_f/A_f$  is a phase convention independent observable quantity for the final state  $f$ . For details, see the review on "CP Violation" in the Reviews section.

VALUE	DOCUMENT ID	TECN	COMMENT
$-0.32 \pm 0.04$ OUR AVERAGE			
$-0.34 \pm 0.06 \pm 0.01$	AAIJ	18o LHCB	$pp$ at 7, 8 TeV
$-0.38 \pm 0.15 \pm 0.02$	AAIJ	13Bo LHCB	$pp$ at 7 TeV
$-0.33 \pm 0.06 \pm 0.03$	<sup>1</sup> DALSENO	13 BELL	$e^+ e^- \rightarrow \Upsilon(4S)$
$-0.25 \pm 0.08 \pm 0.02$	LEES	13D BABR	$e^+ e^- \rightarrow \Upsilon(4S)$
• • • We do not use the following data for averages, fits, limits, etc. • • •			
$-0.21 \pm 0.09 \pm 0.02$	AUBERT	07AF BABR	Repl. by LEES 13D
$-0.55 \pm 0.08 \pm 0.05$	<sup>1</sup> ISHINO	07 BELL	Repl. by DALSENO 13
$-0.56 \pm 0.12 \pm 0.06$	<sup>1</sup> ABE	05D BELL	Repl. by ISHINO 07
$-0.09 \pm 0.15 \pm 0.04$	AUBERT,BE	05 BABR	Repl. by AUBERT 07AF
$-0.58 \pm 0.15 \pm 0.07$	<sup>1</sup> ABE	04E BELL	Repl. by ABE 05D
$-0.77 \pm 0.27 \pm 0.08$	<sup>1</sup> ABE	03G BELL	Repl. by ABE 04E
$-0.94 \pm 0.31 \pm 0.25 \pm 0.09$	<sup>1</sup> ABE	02M BELL	Repl. by ABE 03G
$-0.25 \pm 0.45 \pm 0.47 \pm 0.14$	<sup>2</sup> AUBERT	02D BABR	Repl. by AUBERT 02Q
$-0.30 \pm 0.25 \pm 0.04$	<sup>3</sup> AUBERT	02Q BABR	Repl. by AUBERT,BE 05
<sup>1</sup> Paper reports $A_{\pi \pi}$ which equals to $-C_{\pi \pi}$ .			
<sup>2</sup> Corresponds to 90% confidence range $-1.0 < C_{\pi \pi} < 0.47$ .			
<sup>3</sup> Corresponds to 90% confidence range $-0.72 < C_{\pi \pi} < 0.12$ .			

 $S_{\pi \pi} (B^0 \rightarrow \pi^+ \pi^-)$ 

$S_{\pi \pi} = 2\text{Im}\lambda/(1 + |\lambda|^2)$ , see the note in the  $C_{\pi \pi}$  datablock above.

VALUE	DOCUMENT ID	TECN	COMMENT
$-0.65 \pm 0.04$ OUR AVERAGE			
$-0.63 \pm 0.05 \pm 0.01$	AAIJ	18o LHCB	$pp$ at 7, 8 TeV
$-0.71 \pm 0.13 \pm 0.02$	AAIJ	13Bo LHCB	$pp$ at 7 TeV
$-0.64 \pm 0.08 \pm 0.03$	<sup>1</sup> DALSENO	13 BELL	$e^+ e^- \rightarrow \Upsilon(4S)$
$-0.68 \pm 0.10 \pm 0.03$	LEES	13D BABR	$e^+ e^- \rightarrow \Upsilon(4S)$
• • • We do not use the following data for averages, fits, limits, etc. • • •			
$-0.60 \pm 0.11 \pm 0.03$	AUBERT	07AF BABR	Repl. by LEES 13D
$-0.61 \pm 0.10 \pm 0.04$	ISHINO	07 BELL	Repl. by DALSENO 13
$-0.67 \pm 0.16 \pm 0.06$	<sup>2</sup> ABE	05D BELL	Repl. by ISHINO 07
$-0.30 \pm 0.17 \pm 0.03$	AUBERT,BE	05 BABR	Repl. by AUBERT 07AF
$-1.00 \pm 0.21 \pm 0.07$	<sup>3</sup> ABE	04E BELL	Repl. by ABE 05D
$-1.23 \pm 0.41 \pm 0.08 \pm 0.27 \pm 0.13$	ABE	03G BELL	Repl. by ABE 04E
$-1.21 \pm 0.38 \pm 0.16 \pm 0.27 \pm 0.13$	ABE	02M BELL	Repl. by ABE 03G
$0.03 \pm 0.52 \pm 0.56 \pm 0.11$	<sup>4</sup> AUBERT	02D BABR	Repl. by AUBERT 02Q
$0.02 \pm 0.34 \pm 0.05$	<sup>5</sup> AUBERT	02Q BABR	Repl. by AUBERT,BE 05
<sup>1</sup> An isospin analysis using other BELLE measurements, disfavors the region of $23.8^\circ < \phi_2 < 66.8^\circ$ at 68% CL.			
<sup>2</sup> Rule out the CP-conserving case, $C_{\pi \pi} = S_{\pi \pi} = 0$ , at the 5.4 sigma level.			
<sup>3</sup> Rule out the CP-conserving case, $C_{\pi \pi} = S_{\pi \pi} = 0$ , at the 5.2 sigma level.			
<sup>4</sup> Corresponds to 90% confidence range $-0.89 < S_{\pi \pi} < 0.85$ .			
<sup>5</sup> Corresponds to 90% confidence range $-0.54 < S_{\pi \pi} < 0.58$ .			

C<sub>π<sup>0</sup>π<sup>0</sup></sub>(B<sup>0</sup> → π<sup>0</sup>π<sup>0</sup>)

Table with columns: VALUE, DOCUMENT ID, TECN, COMMENT. Includes OUR AVERAGE: -0.33 ± 0.22. Data points from JULIUS, LEES, AUBERT, CHAO.

1 BELLE Collab. quotes A<sub>π<sup>0</sup>π<sup>0</sup></sub> which is equal to -C<sub>π<sup>0</sup>π<sup>0</sup></sub>.  
2 Corresponds to a 90% CL interval of -0.88 < A<sub>CP</sub> < 0.64.

C<sub>ρ<sup>±</sup>π</sub>(B<sup>0</sup> → ρ<sup>±</sup>π<sup>-</sup>)

Table with columns: VALUE, DOCUMENT ID, TECN, COMMENT. Includes OUR AVERAGE: -0.03 ± 0.07. Data points from LEES, KUSAKA, AUBERT, WANG.

1 Uses time-dependent Dalitz plot analysis of B<sup>0</sup> → π<sup>±</sup>π<sup>-</sup>π<sup>0</sup> decays.

S<sub>ρ<sup>±</sup>π</sub>(B<sup>0</sup> → ρ<sup>±</sup>π<sup>-</sup>)

Table with columns: VALUE, DOCUMENT ID, TECN, COMMENT. Includes OUR AVERAGE: 0.05 ± 0.07. Data points from LEES, KUSAKA, AUBERT, WANG.

1 Uses time-dependent Dalitz plot analysis of B<sup>0</sup> → π<sup>±</sup>π<sup>-</sup>π<sup>0</sup> decays.

ΔC<sub>ρ<sup>±</sup>π</sub>(B<sup>0</sup> → ρ<sup>±</sup>π<sup>-</sup>)

ΔC<sub>ρ<sup>±</sup>π</sub> describes the asymmetry between the rates Γ(B<sup>0</sup> → ρ<sup>±</sup>π<sup>-</sup>) + Γ(B<sup>0</sup> → ρ<sup>-</sup>π<sup>+</sup>) and Γ(B<sup>0</sup> → ρ<sup>-</sup>π<sup>+</sup>) + Γ(B<sup>0</sup> → ρ<sup>±</sup>π<sup>-</sup>).

Table with columns: VALUE, DOCUMENT ID, TECN, COMMENT. Includes OUR AVERAGE: 0.27 ± 0.06. Data points from LEES, KUSAKA, AUBERT, WANG.

1 Uses time-dependent Dalitz plot analysis of B<sup>0</sup> → π<sup>±</sup>π<sup>-</sup>π<sup>0</sup> decays.

ΔS<sub>ρ<sup>±</sup>π</sub>(B<sup>0</sup> → ρ<sup>±</sup>π<sup>-</sup>)

ΔS<sub>ρ<sup>±</sup>π</sub> is related to the strong phase difference between the amplitudes contributing to B<sup>0</sup> → ρ<sup>±</sup>π<sup>-</sup>.

Table with columns: VALUE, DOCUMENT ID, TECN, COMMENT. Includes OUR AVERAGE: 0.01 ± 0.08. Data points from LEES, KUSAKA, AUBERT, WANG.

1 Uses time-dependent Dalitz plot analysis of B<sup>0</sup> → π<sup>±</sup>π<sup>-</sup>π<sup>0</sup> decays.

C<sub>ρ<sup>0</sup>π<sup>0</sup></sub>(B<sup>0</sup> → ρ<sup>0</sup>π<sup>0</sup>)

Table with columns: VALUE, DOCUMENT ID, TECN, COMMENT. Includes OUR AVERAGE: 0.27 ± 0.24. Data points from LEES, KUSAKA, AUBERT, DRAGIC.

1 Uses time-dependent Dalitz plot analysis of B<sup>0</sup> → π<sup>±</sup>π<sup>-</sup>π<sup>0</sup> decays.

2 Quotes A<sub>ρ<sup>0</sup>π<sup>0</sup></sub> which is equal to -C<sub>ρ<sup>0</sup>π<sup>0</sup></sub>.

S<sub>ρ<sup>0</sup>π<sup>0</sup></sub>(B<sup>0</sup> → ρ<sup>0</sup>π<sup>0</sup>)

Table with columns: VALUE, DOCUMENT ID, TECN, COMMENT. Includes OUR AVERAGE: -0.23 ± 0.34. Data points from LEES, KUSAKA, AUBERT.

1 Uses time-dependent Dalitz plot analysis of B<sup>0</sup> → π<sup>±</sup>π<sup>-</sup>π<sup>0</sup> decays.

C<sub>a<sub>1</sub>(1260)<sup>+</sup>π<sup>-</sup></sub>(B<sup>0</sup> → a<sub>1</sub>(1260)<sup>+</sup>π<sup>-</sup>)

Table with columns: VALUE, DOCUMENT ID, TECN, COMMENT. Includes OUR AVERAGE: -0.05 ± 0.11. Data points from DALSENO, AUBERT.

S<sub>a<sub>1</sub>(1260)<sup>+</sup>π<sup>-</sup></sub>(B<sup>0</sup> → a<sub>1</sub>(1260)<sup>+</sup>π<sup>-</sup>)

Table with columns: VALUE, DOCUMENT ID, TECN, COMMENT. Includes OUR AVERAGE: -0.2 ± 0.4. Error includes scale factor of 3.2. Data points from DALSENO, AUBERT.

ΔC<sub>a<sub>1</sub>(1260)<sup>+</sup>π<sup>-</sup></sub>(B<sup>0</sup> → a<sub>1</sub>(1260)<sup>+</sup>π<sup>-</sup>)

ΔC<sub>a<sub>1</sub>(1260)<sup>+</sup>π<sup>-</sup></sub> describes the asymmetry between the rates Γ(B<sup>0</sup> → a<sub>1</sub><sup>+</sup>π<sup>-</sup>) + Γ(B<sup>0</sup> → a<sub>1</sub><sup>-</sup>π<sup>+</sup>) and Γ(B<sup>0</sup> → a<sub>1</sub><sup>-</sup>π<sup>+</sup>) + Γ(B<sup>0</sup> → a<sub>1</sub><sup>+</sup>π<sup>-</sup>).

Table with columns: VALUE, DOCUMENT ID, TECN, COMMENT. Includes OUR AVERAGE: 0.43 ± 0.14. Error includes scale factor of 1.3. Data points from DALSENO, AUBERT.

ΔS<sub>a<sub>1</sub>(1260)<sup>+</sup>π<sup>-</sup></sub>(B<sup>0</sup> → a<sub>1</sub>(1260)<sup>+</sup>π<sup>-</sup>)

ΔS<sub>a<sub>1</sub>(1260)<sup>+</sup>π<sup>-</sup></sub> is related to the strong phase difference between the amplitudes contributing to B<sup>0</sup> → a<sub>1</sub>π decays.

Table with columns: VALUE, DOCUMENT ID, TECN, COMMENT. Includes OUR AVERAGE: -0.11 ± 0.12. Data points from DALSENO, AUBERT.

C(B<sup>0</sup> → b<sub>1</sub><sup>-</sup>K<sup>+</sup>)

Table with columns: VALUE, DOCUMENT ID, TECN, COMMENT. Includes OUR AVERAGE: -0.22 ± 0.23 ± 0.05. Data points from AUBERT.

ΔC(B<sup>0</sup> → b<sub>1</sub><sup>-</sup>π<sup>+</sup>)

Table with columns: VALUE, DOCUMENT ID, TECN, COMMENT. Includes OUR AVERAGE: -1.04 ± 0.23 ± 0.08. Data points from AUBERT.

C<sub>ρ<sup>0</sup>ρ<sup>0</sup></sub>(B<sup>0</sup> → ρ<sup>0</sup>ρ<sup>0</sup>)

Table with columns: VALUE, DOCUMENT ID, TECN, COMMENT. Includes OUR AVERAGE: 0.2 ± 0.8 ± 0.3. Data points from AUBERT.

S<sub>ρ<sup>0</sup>ρ<sup>0</sup></sub>(B<sup>0</sup> → ρ<sup>0</sup>ρ<sup>0</sup>)

Table with columns: VALUE, DOCUMENT ID, TECN, COMMENT. Includes OUR AVERAGE: 0.3 ± 0.7 ± 0.2. Data points from AUBERT.

C<sub>ρ<sup>±</sup>ρ<sup>-</sup></sub>(B<sup>0</sup> → ρ<sup>±</sup>ρ<sup>-</sup>)

Table with columns: VALUE, DOCUMENT ID, TECN, COMMENT. Includes OUR AVERAGE: 0.00 ± 0.09. Data points from VANHOEFER, AUBERT, SOMOV.

S<sub>ρ<sup>±</sup>ρ<sup>-</sup></sub>(B<sup>0</sup> → ρ<sup>±</sup>ρ<sup>-</sup>)

Table with columns: VALUE, DOCUMENT ID, TECN, COMMENT. Includes OUR AVERAGE: -0.14 ± 0.13. Data points from VANHOEFER, AUBERT, SOMOV.

|λ|(B<sup>0</sup> → J/ψK\*(892)<sup>0</sup>)

Table with columns: VALUE, CL%, DOCUMENT ID, TECN, COMMENT. Includes OUR AVERAGE: <0.25. Data points from AUBERT.

cos 2β(B<sup>0</sup> → J/ψK\*(892)<sup>0</sup>)

β(φ<sub>1</sub>) is one of the angles of CKM unitarity triangle, see the review on "CP" Violation in the Reviews section.

Table with columns: VALUE, DOCUMENT ID, TECN, COMMENT. Includes OUR AVERAGE: 1.7 ± 0.7 / -0.9. Data points from AUBERT, ITOH.

1 The measurement is obtained when sin 2β is fixed to 0.726 and the sign of cos 2β is positive with 86% confidence level.  
2 The measurement is obtained with sin 2β fixed to 0.731.



## Meson Particle Listings

 $B^0$  $\cos 2\beta (B^0 \rightarrow [K_S^0 \pi^+ \pi^-]_{D^{(*)}} h^0)$ 

VALUE	DOCUMENT ID	TECN	COMMENT
<b><math>0.91 \pm 0.22 \pm 0.11</math></b>	<sup>1</sup> ADACHI 18		$e^+ e^- \rightarrow \Upsilon(4S)$
$1.06 \pm 0.33 \pm 0.21$ $-0.15$	<sup>2</sup> VOROBYEV 16	BELL	$e^+ e^- \rightarrow \Upsilon(4S)$
$0.42 \pm 0.49 \pm 0.16$	<sup>3</sup> AUBERT 07BH	BABR	$e^+ e^- \rightarrow \Upsilon(4S)$
$1.87 \pm 0.40 \pm 0.22$ $-0.53 \pm 0.32$	<sup>4</sup> KROKOVNY 06	BELL	Repl. by VOROBYEV 16

<sup>1</sup> Analyzes joint data sample of Belle and BaBar using Dalitz plot analysis of  $D \rightarrow K_S^0 \pi^+ \pi^-$ ; the second error combines experimental systematic uncertainty and the Dalitz plot model uncertainty.

<sup>2</sup> A model-independent measurement uses the binned Dalitz plot technique.

<sup>3</sup> AUBERT 07BH evaluates the likelihoods for the positive and negative solutions assuming  $\sin(2\beta_{eff}) = 0.678$ . It quotes  $L_+ / (L_+ + L_-) = 0.86$  corresponding to a likelihood ratio of  $L_+ / L_- = 6.14$  in favor of the positive solution.

<sup>4</sup> KROKOVNY 06 evaluates the likelihoods for the positive and negative solutions assuming  $\sin(2\beta_{eff}) = 0.689$ . It quotes  $L_+ / (L_+ + L_-) = 0.983$  corresponding to a likelihood ratio of  $L_+ / L_- = 57.8$  in favor of the positive solution.

 $(S_+ + S_-)/2 (B^0 \rightarrow D^{*-} \pi^+)$ 

$$S_{\pm} = -\frac{2\text{Im}(\lambda_{\pm})}{1+|\lambda_{\pm}|^2} \text{ where } \lambda_+ \text{ and } \lambda_- \text{ are defined in the } C_{\pi\pi} \text{ datablock above for } B^0 \rightarrow D^{*-} \pi^+ \text{ and } \bar{B}^0 \rightarrow D^{*+} \pi^-.$$

VALUE	DOCUMENT ID	TECN	COMMENT
<b><math>-0.039 \pm 0.011</math> OUR AVERAGE</b>			
$-0.046 \pm 0.013 \pm 0.015$	<sup>1</sup> BAHINIPATI 11	BELL	$e^+ e^- \rightarrow \Upsilon(4S)$
$-0.040 \pm 0.023 \pm 0.010$	<sup>2</sup> AUBERT 06Y	BABR	$e^+ e^- \rightarrow \Upsilon(4S)$
$-0.034 \pm 0.014 \pm 0.009$	<sup>1</sup> AUBERT 05Z	BABR	$e^+ e^- \rightarrow \Upsilon(4S)$
$-0.039 \pm 0.020 \pm 0.013$	<sup>3</sup> RONGA 06	BELL	Repl. by BAHINIPATI 11
$-0.030 \pm 0.028 \pm 0.018$	<sup>1</sup> GERSHON 05	BELL	Repl. by RONGA 06
$-0.068 \pm 0.038 \pm 0.020$	<sup>2</sup> AUBERT 04V	BABR	Repl. by AUBERT 06Y
$-0.063 \pm 0.024 \pm 0.014$	<sup>1</sup> AUBERT 04W	BABR	Repl. by AUBERT 05Z
$0.060 \pm 0.040 \pm 0.019$	<sup>2</sup> SARANGI 04	BELL	Repl. by RONGA 06

<sup>1</sup> Uses partially reconstructed  $B^0 \rightarrow D^{*\pm} \pi^{\mp}$  decays.

<sup>2</sup> Uses fully reconstructed  $B^0 \rightarrow D^{*\pm} \pi^{\mp}$  decays.

<sup>3</sup> Combines the results from fully reconstructed and partially reconstructed  $D^{*\pm} \pi$  events by taking weighted averages. Assumes that systematic errors from physics parameters and fit biases in the two measurements are 100% correlated.

 $(S_- - S_+)/2 (B^0 \rightarrow D^{*-} \pi^+)$ 

VALUE	DOCUMENT ID	TECN	COMMENT
<b><math>-0.009 \pm 0.015</math> OUR AVERAGE</b>			
$-0.015 \pm 0.013 \pm 0.015$	<sup>1</sup> BAHINIPATI 11	BELL	$e^+ e^- \rightarrow \Upsilon(4S)$
$-0.049 \pm 0.042 \pm 0.015$	<sup>2</sup> AUBERT 06Y	BABR	$e^+ e^- \rightarrow \Upsilon(4S)$
$-0.019 \pm 0.022 \pm 0.013$	<sup>1</sup> AUBERT 05Z	BABR	$e^+ e^- \rightarrow \Upsilon(4S)$
$-0.011 \pm 0.020 \pm 0.013$	<sup>3</sup> RONGA 06	BELL	Repl. by BAHINIPATI 11
$-0.005 \pm 0.028 \pm 0.018$	<sup>1</sup> GERSHON 05	BELL	Repl. by RONGA 06
$0.031 \pm 0.070 \pm 0.033$	<sup>2</sup> AUBERT 04V	BABR	Repl. by AUBERT 06Y
$-0.004 \pm 0.037 \pm 0.014$	<sup>1</sup> AUBERT 04W	BABR	Repl. by AUBERT 05Z
$0.049 \pm 0.040 \pm 0.019$	<sup>2</sup> SARANGI 04	BELL	Repl. by RONGA 06

<sup>1</sup> Uses partially reconstructed  $B^0 \rightarrow D^{*\pm} \pi^{\mp}$  decays.

<sup>2</sup> Uses fully reconstructed  $B^0 \rightarrow D^{*\pm} \pi^{\mp}$  decays.

<sup>3</sup> Combines the results from fully reconstructed and partially reconstructed  $D^{*\pm} \pi$  events by taking weighted averages. Assumes that systematic errors from physics parameters and fit biases in the two measurements are 100% correlated.

 $(S_+ + S_-)/2 (B^0 \rightarrow D^- \pi^+)$ 

VALUE	DOCUMENT ID	TECN	COMMENT
<b><math>-0.046 \pm 0.023</math> OUR AVERAGE</b>			
$-0.010 \pm 0.023 \pm 0.07$	<sup>1</sup> AUBERT 06Y	BABR	$e^+ e^- \rightarrow \Upsilon(4S)$
$-0.050 \pm 0.021 \pm 0.012$	<sup>2</sup> RONGA 06	BELL	$e^+ e^- \rightarrow \Upsilon(4S)$
$-0.022 \pm 0.038 \pm 0.020$	<sup>1</sup> AUBERT 04V	BABR	Repl. by AUBERT 06Y
$-0.062 \pm 0.037 \pm 0.018$	<sup>1</sup> SARANGI 04	BELL	Repl. by RONGA 06

<sup>1</sup> Uses fully reconstructed  $B^0 \rightarrow D^{\pm} \pi^{\mp}$  decays.

<sup>2</sup> Combines the results from fully reconstructed and partially reconstructed  $D\pi$  events by taking weighted averages. Assumes that systematic errors from physics parameters and fit biases in the two measurements are 100% correlated.

 $(S_- - S_+)/2 (B^0 \rightarrow D^- \pi^+)$ 

VALUE	DOCUMENT ID	TECN	COMMENT
<b><math>-0.022 \pm 0.021</math> OUR AVERAGE</b>			
$-0.033 \pm 0.042 \pm 0.012$	<sup>1</sup> AUBERT 06Y	BABR	$e^+ e^- \rightarrow \Upsilon(4S)$
$-0.019 \pm 0.021 \pm 0.012$	<sup>2</sup> RONGA 06	BELL	$e^+ e^- \rightarrow \Upsilon(4S)$
$0.025 \pm 0.068 \pm 0.033$	<sup>1</sup> AUBERT 04V	BABR	Repl. by AUBERT 06Y
$-0.025 \pm 0.037 \pm 0.018$	<sup>1</sup> SARANGI 04	BELL	Repl. by RONGA 06

<sup>1</sup> Uses fully reconstructed  $B^0 \rightarrow D^{\pm} \pi^{\mp}$  decays.

<sup>2</sup> Combines the results from fully reconstructed and partially reconstructed  $D\pi$  events by taking weighted averages. Assumes that systematic errors from physics parameters and fit biases in the two measurements are 100% correlated.

 $S_+ (B^0 \rightarrow D^- \pi^+)$ 

VALUE	DOCUMENT ID	TECN	COMMENT
<b><math>0.058 \pm 0.020 \pm 0.011</math></b>	<sup>1</sup> AAIJ 18Z	LHCB	$pp$ at 7, 8 TeV
			<sup>1</sup> Measured in the simultaneous analysis of $B^0 \rightarrow D^{\mp} \pi^{\pm}$ decays. AAIJ 18Z reports a statistical (systematic) correlation of 0.6 (-0.41) with the measured value of $S_-(B^0 \rightarrow D^+ \pi^-)$ .

 $S_- (B^0 \rightarrow D^+ \pi^-)$ 

VALUE	DOCUMENT ID	TECN	COMMENT
<b><math>0.038 \pm 0.020 \pm 0.007</math></b>	<sup>1</sup> AAIJ 18Z	LHCB	$pp$ at 7, 8 TeV
			<sup>1</sup> Measured in the simultaneous analysis of $B^0 \rightarrow D^{\mp} \pi^{\pm}$ decays. AAIJ 18Z reports a statistical (systematic) correlation of 0.6 (-0.41) with the measured value of $S_+(B^0 \rightarrow D^- \pi^+)$ .

 $(S_+ + S_-)/2 (B^0 \rightarrow D^- \rho^+)$ 

VALUE	DOCUMENT ID	TECN	COMMENT
<b><math>-0.024 \pm 0.031 \pm 0.009</math></b>	<sup>1</sup> AUBERT 06Y	BABR	$e^+ e^- \rightarrow \Upsilon(4S)$
			<sup>1</sup> Uses fully reconstructed $B^0 \rightarrow D^- \rho^+$ decays.

 $(S_- - S_+)/2 (B^0 \rightarrow D^- \rho^+)$ 

VALUE	DOCUMENT ID	TECN	COMMENT
<b><math>-0.098 \pm 0.055 \pm 0.018</math></b>	<sup>1</sup> AUBERT 06Y	BABR	$e^+ e^- \rightarrow \Upsilon(4S)$
			<sup>1</sup> Uses fully reconstructed $B^0 \rightarrow D^- \rho^+$ decays.

 $C_{\eta_c K_S^0} (B^0 \rightarrow \eta_c K_S^0)$ 

VALUE	DOCUMENT ID	TECN	COMMENT
<b><math>0.080 \pm 0.124 \pm 0.029</math></b>	AUBERT 09K	BABR	$e^+ e^- \rightarrow \Upsilon(4S)$

 $S_{\eta_c K_S^0} (B^0 \rightarrow \eta_c K_S^0)$ 

VALUE	DOCUMENT ID	TECN	COMMENT
<b><math>0.925 \pm 0.160 \pm 0.057</math></b>	AUBERT 09K	BABR	$e^+ e^- \rightarrow \Upsilon(4S)$

 $C_{c\bar{c}K^{(*)0}} (B^0 \rightarrow c\bar{c}K^{(*)0})$ 

"OUR EVALUATION" is an average using rescaled values of the data listed below. The average and rescaling were performed by the Heavy Flavor Averaging Group (HFLAV) and are described at <https://hflav.web.cern.ch/>. The averaging/rescaling procedure takes into account correlations between the measurements.

VALUE (units $10^{-2}$ )	DOCUMENT ID	TECN	COMMENT
<b><math>0.5 \pm 1.7</math> OUR EVALUATION</b>			
<b><math>0.0 \pm 1.4</math> OUR AVERAGE</b>			
$-1.7 \pm 2.9$	<sup>1,2</sup> AAIJ	17BN LHCB	$pp$ at 7, 8 TeV
$-0.6 \pm 1.6 \pm 1.2$	<sup>3</sup> ADACHI 12A	BELL	$e^+ e^- \rightarrow \Upsilon(4S)$
$-29 \pm 53 \pm 6$	<sup>4</sup> AUBERT 09AU	BABR	$e^+ e^- \rightarrow \Upsilon(4S)$
$2.4 \pm 2.0 \pm 1.6$	<sup>5</sup> AUBERT 09K	BABR	$e^+ e^- \rightarrow \Upsilon(4S)$
$-4 \pm 7 \pm 5$	<sup>6</sup> SAHOO 08	BELL	Repl. by ADACHI 12A
$4.9 \pm 2.3 \pm 1.8$	<sup>5</sup> AUBERT 07AY	BABR	Repl. by AUBERT 09K
$-1.8 \pm 2.1 \pm 1.4$	<sup>7</sup> CHEN 07	BELL	Repl. by ADACHI 12A
$-0.7 \pm 4.1 \pm 3.3$	<sup>8</sup> ABE 05B	BELL	Repl. by CHEN 07
$5.1 \pm 3.2 \pm 1.4$	<sup>9</sup> AUBERT 05F	BABR	Repl. by AUBERT 07AY
$5.1 \pm 5.1 \pm 2.6$	<sup>10</sup> ABE 02Z	BELL	Repl. by ABE 05B
$5.3 \pm 5.4 \pm 3.2$	<sup>11</sup> AUBERT 02P	BABR	Repl. by AUBERT 05F

<sup>1</sup> Measurement based on  $B^0 \rightarrow J/\psi K_S^0, B^0 \rightarrow \psi(2S) K_S^0$  with  $J/\psi \rightarrow \mu^+ \mu^-, J/\psi \rightarrow e^+ e^-$  and  $\psi(2S) \rightarrow \mu^+ \mu^-$ .

<sup>2</sup> AAIJ 17BN provides the correlation coefficient  $\rho=0.42$  between the uncertainties of  $S_{B^0 \rightarrow c\bar{c}K^{(*)0}}$  and  $C_{c\bar{c}K^{(*)0}}$  ( $B^0 \rightarrow c\bar{c}K^{(*)0}$ ) measurements.

<sup>3</sup> Measurement based on  $B^0 \rightarrow J/\psi K_S^0, B^0 \rightarrow \psi(2S) K_S^0, B^0 \rightarrow J/\psi K_L^0$ , and  $B^0 \rightarrow \chi_{c1}(1P) K_S^0$  decays.

<sup>4</sup> Uses Dalitz plot analysis of  $B^0 \rightarrow K^0 \pi^+ \pi^-$  decays and the first of two equivalent solutions is used.

<sup>5</sup> Measurement based on  $B^0 \rightarrow c\bar{c}K^{(*)0}$  decays.

<sup>6</sup> Reports value of  $A$  of  $B^0 \rightarrow \psi(2S) K^0$  which is equal to  $-C$ .

<sup>7</sup> Reports value of  $A$  of  $B^0 \rightarrow J/\psi K^0$  which is equal to  $-C$ .

<sup>8</sup> Measurement based on  $15.2 \times 10^6 B\bar{B}$  pairs.

<sup>9</sup> Measurement based on  $227 \times 10^6 B\bar{B}$  pairs.

<sup>10</sup> Measured with both  $\eta_f = \pm 1$  samples.

<sup>11</sup> Measured with the high purity of  $\eta_f = -1$  samples.

 $\sin(2\beta)$ 

For a discussion of  $CP$  violation, see the review on "CP Violation" in the Reviews section.  $\sin(2\beta)$  is a measure of the  $CP$ -violating amplitude in the  $B^0_d \rightarrow J/\psi(1S) K_S^0$ .

"OUR EVALUATION" is an average using rescaled values of the data listed below. The average and rescaling were performed by the Heavy Flavor Averaging Group (HFLAV) and are described at <https://hflav.web.cern.ch/>. The averaging/rescaling procedure takes into account correlations between the measurements.

VALUE	DOCUMENT ID	TECN	COMMENT
<b><math>0.695 \pm 0.019</math> OUR EVALUATION</b>			
<b><math>0.698 \pm 0.027</math> OUR AVERAGE</b>			Error includes scale factor of 1.6. See the ideogram below.
$0.760 \pm 0.034$	<sup>1,2</sup> AAIJ	17BN LHCB	$pp$ at 7, 8 TeV
$0.667 \pm 0.023 \pm 0.012$	<sup>3</sup> ADACHI 12A	BELL	$e^+ e^- \rightarrow \Upsilon(4S)$
$0.57 \pm 0.58 \pm 0.06$	<sup>4</sup> SATO 12	BELL	$e^+ e^- \rightarrow \Upsilon(5S)$
$0.69 \pm 0.52 \pm 0.08$	<sup>5</sup> AUBERT 09AU	BABR	$e^+ e^- \rightarrow \Upsilon(4S)$

See key on page 999

# Meson Particle Listings

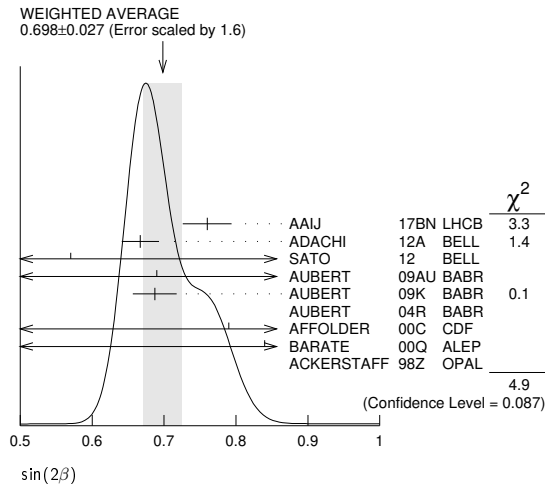
## $B^0$

$0.687 \pm 0.028 \pm 0.012$	6	AUBERT	09K	BABR	$e^+e^- \rightarrow \Upsilon(4S)$
$1.56 \pm 0.42 \pm 0.21$	7	AUBERT	04R	BABR	$e^+e^- \rightarrow \Upsilon(4S)$
$0.79 \begin{smallmatrix} +0.41 \\ -0.44 \end{smallmatrix}$	8	AFFOLDER	00C	CDF	$p\bar{p}$ at 1.8 TeV
$0.84 \begin{smallmatrix} +0.82 \\ -1.04 \end{smallmatrix} \pm 0.16$	9	BARATE	00Q	ALEP	$e^+e^- \rightarrow Z$
$3.2 \begin{smallmatrix} +1.8 \\ -2.0 \end{smallmatrix} \pm 0.5$	10	ACKERSTAFF	98Z	OPAL	$e^+e^- \rightarrow Z$

• • • We do not use the following data for averages, fits, limits, etc. • • •

$0.72 \pm 0.09 \pm 0.03$	11	SAHOO	08	BELL	Repl. by ADACHI 12A
$0.714 \pm 0.032 \pm 0.018$	6	AUBERT	07AY	BABR	Repl. by AUBERT 09K
$0.642 \pm 0.031 \pm 0.017$		CHEN	07	BELL	Repl. by ADACHI 12A
$0.728 \pm 0.056 \pm 0.023$	12	ABE	05B	BELL	Repl. by CHEN 07
$0.722 \pm 0.040 \pm 0.023$	13	AUBERT	05F	BABR	Repl. by AUBERT 07AY
$0.99 \pm 0.14 \pm 0.06$	14	ABE	02U	BELL	$e^+e^- \rightarrow \Upsilon(4S)$
$0.719 \pm 0.074 \pm 0.035$	15	ABE	02Z	BELL	Repl. by ABE 05B
$0.59 \pm 0.14 \pm 0.05$	16	AUBERT	02N	BABR	$e^+e^- \rightarrow \Upsilon(4S)$
$0.741 \pm 0.067 \pm 0.034$	17	AUBERT	02P	BABR	Repl. by AUBERT 05F
$0.58 \begin{smallmatrix} +0.32 \\ -0.34 \end{smallmatrix} \pm 0.09$		ABASHIAN	01	BELL	Repl. by ABE 01G
$0.99 \pm 0.14 \pm 0.06$	18	ABE	01G	BELL	Repl. by ABE 02Z
$0.34 \pm 0.20 \pm 0.05$		AUBERT	01	BABR	Repl. by AUBERT 01B
$0.59 \pm 0.14 \pm 0.05$	18	AUBERT	01B	BABR	Repl. by AUBERT 02P
$1.8 \pm 1.1 \pm 0.3$	19	ABE	98U	CDF	Repl. by AFFOLDER 00C

- Measurement based on  $B^0 \rightarrow J/\psi K_S^0$ ,  $B^0 \rightarrow \psi(2S) K_S^0$  with  $J/\psi \rightarrow \mu^+ \mu^-$ ,  $J/\psi \rightarrow e^+ e^-$  and  $\psi(2S) \rightarrow \mu^+ \mu^-$ .
- AAIJ 17BN provides the correlation coefficient  $\rho = 0.42$  between the uncertainties of  $\sin(2\beta)$  and  $\cos(2\beta)$  measurements.
- Measurement based on  $B^0 \rightarrow J/\psi K_S^0$ ,  $B^0 \rightarrow \psi(2S) K_S^0$ ,  $B^0 \rightarrow J/\psi K_L^0$ , and  $B^0 \rightarrow \chi_{c1}(1P) K_S^0$  decays.
- SATO 12 uses 121  $\text{fb}^{-1}$  data collected on  $\Upsilon(5S)$  resonance. Uses the " $B - \pi$  tagging" where  $B\pi^+$  and  $B\pi^-$  tagged  $J/\psi K_S^0$  events are compared.
- Uses Dalitz plot analysis of  $B^0 \rightarrow K^0 \pi^+ \pi^-$  decays and the first of two equivalent solutions.
- Measurement based on  $B^0 \rightarrow c\bar{c}K^*(*)0$  decays.
- Measurement in which the  $J/\psi$  decays to hadrons or to muons that do not satisfy the standard identification criteria.
- AFFOLDER 00C uses about 400  $B^0 \rightarrow J/\psi(1S) K_S^0$  events. The production flavor of  $B^0$  was determined using three tagging algorithms: a same-side tag, a jet-charge tag, and a soft-lepton tag.
- BARATE 00Q uses 23 candidates for  $B^0 \rightarrow J/\psi(1S) K_S^0$  decays. A combination of jet-charge, vertex-charge, and same-side tagging techniques were used to determine the  $B^0$  production flavor.
- ACKERSTAFF 98Z uses 24 candidates for  $B_d^0 \rightarrow J/\psi(1S) K_S^0$  decay. A combination of jet-charge and vertex-charge techniques were used to tag the  $B_d^0$  production flavor.
- Based on  $B^0 \rightarrow \psi(2S) K_S^0$  decays.
- Measurement based on  $152 \times 10^6 B\bar{B}$  pairs.
- Measurement based on  $227 \times 10^6 B\bar{B}$  pairs.
- ABE 02U result is based on the same analysis and data sample reported in ABE 01G.
- ABE 02Z result is based on  $85 \times 10^6 B\bar{B}$  pairs.
- AUBERT 02N result based on the same analysis and data sample reported in AUBERT 01B.
- AUBERT 02P result is based on  $88 \times 10^6 B\bar{B}$  pairs.
- First observation of CP violation in  $B^0$  meson system.
- ABE 98U uses  $198 \pm 17 B_d^0 \rightarrow J/\psi(1S) K^0$  events. The production flavor of  $B^0$  was determined using the same side tagging technique.



### $C_{J/\psi(nS)K^0} (B^0 \rightarrow J/\psi(nS)K^0)$

"OUR EVALUATION" is an average using rescaled values of the data listed below. The average and rescaling were performed by the Heavy Flavor Averaging Group (HFLAV) and are described at <https://hflav.web.cern.ch/>. The averaging/rescaling procedure takes into account correlations between the measurements.

VALUE (units $10^{-2}$ )	DOCUMENT ID	TECN	COMMENT
<b><math>0.5 \pm 2.0</math> OUR EVALUATION</b>			
<b><math>-0.5 \pm 1.6</math> OUR AVERAGE</b>			
$-1.7 \pm 2.9$	1,2	AAIJ	17BN LHCb $p\bar{p}$ at 7, 8 TeV
$1.5 \pm 2.1 \begin{smallmatrix} +2.3 \\ -4.5 \end{smallmatrix}$	3,4	ADACHI	12A BELL $e^+e^- \rightarrow \Upsilon(4S)$
$-10.4 \pm 5.5 \begin{smallmatrix} +2.7 \\ -4.7 \end{smallmatrix}$	4,5	ADACHI	12A BELL $e^+e^- \rightarrow \Upsilon(4S)$
$-1.9 \pm 2.6 \begin{smallmatrix} +4.1 \\ -1.7 \end{smallmatrix}$	4,6	ADACHI	12A BELL $e^+e^- \rightarrow \Upsilon(4S)$
$8.9 \pm 7.6 \pm 2.0$	5	AUBERT	09K BABR $e^+e^- \rightarrow \Upsilon(4S)$
$1.6 \pm 2.3 \pm 1.8$		AUBERT	09K BABR $e^+e^- \rightarrow \Upsilon(4S)$

• • • We do not use the following data for averages, fits, limits, etc. • • •

$-1.4 \pm 3.0$	7	AAIJ	17BN LHCb $p\bar{p}$ at 7, 8 TeV
$-5 \pm 10 \pm 1$	8	AAIJ	17BN LHCb $p\bar{p}$ at 7, 8 TeV
$-3.8 \pm 3.2 \pm 0.5$	9	AAIJ	15N LHCb Repl. by AAIJ 17BN
$3 \pm 9 \pm 1$	10	AAIJ	13K LHCb Repl. by AAIJ 15N
$-4 \pm 7 \pm 5$	4,5	SAHOO	08 BELL Repl. by ADACHI 12A
$-1.8 \pm 2.1 \pm 1.4$	4	CHEN	07 BELL Repl. by ADACHI 12A

- Measurement based on  $B^0 \rightarrow J/\psi K_S^0$ ,  $B^0 \rightarrow \psi(2S) K_S^0$  with  $J/\psi \rightarrow \mu^+ \mu^-$ ,  $J/\psi \rightarrow e^+ e^-$  and  $\psi(2S) \rightarrow \mu^+ \mu^-$ .
- AAIJ 17BN provides the correlation coefficient  $\rho = 0.42$  between the uncertainties of  $S_{J/\psi(nS)K^0} (B^0 \rightarrow J/\psi(nS)K^0)$  and  $C_{J/\psi(nS)K^0} (B^0 \rightarrow J/\psi(nS)K^0)$  measurements.
- Uses  $B^0 \rightarrow J/\psi K_S^0$  decays.
- The paper reports A, which is equal to  $-C$ .
- Uses  $B^0 \rightarrow \psi(2S) K_S^0$  decays.
- Uses  $B^0 \rightarrow J/\psi K_L^0$  decays.
- Measurement based on  $B^0 \rightarrow J/\psi K_S^0$  with  $J/\psi \rightarrow \mu^+ \mu^-$  and  $J/\psi \rightarrow e^+ e^-$ .
- Measurement based on  $B^0 \rightarrow \psi(2S) K_S^0$  with  $\psi(2S) \rightarrow \mu^+ \mu^-$ .
- AAIJ 15N uses 41,560 flavor-tagged  $B_d^0 \rightarrow J/\psi K_S^0$  events from  $3 \text{ fb}^{-1}$  of integrated luminosity. Provides the correlation coefficient  $\rho = 0.483$  between the statistical uncertainties of and measurements.
- AAIJ 13K uses 8200 flavor-tagged  $B_d^0 \rightarrow J/\psi K_S^0$  events from  $1 \text{ fb}^{-1}$  of integrated luminosity. Provides the correlation coefficient  $\rho = 0.42$  between the statistical uncertainties of  $S_{J/\psi(nS)K^0} (B^0 \rightarrow J/\psi(nS)K^0)$  and  $C_{J/\psi(nS)K^0} (B^0 \rightarrow J/\psi(nS)K^0)$  measurements.

### $S_{J/\psi(nS)K^0} (B^0 \rightarrow J/\psi(nS)K^0)$

"OUR EVALUATION" is an average using rescaled values of the data listed below. The average and rescaling were performed by the Heavy Flavor Averaging Group (HFLAV) and are described at <https://hflav.web.cern.ch/>. The averaging/rescaling procedure takes into account correlations between the measurements.

VALUE	DOCUMENT ID	TECN	COMMENT
<b><math>0.701 \pm 0.017</math> OUR EVALUATION</b>			
<b><math>0.698 \pm 0.024</math> OUR AVERAGE</b>			Error includes scale factor of 1.4. See the ideogram below.
$0.760 \pm 0.034$	1,2	AAIJ	17BN LHCb $p\bar{p}$ at 7, 8 TeV
$0.670 \pm 0.029 \pm 0.013$	3	ADACHI	12A BELL $e^+e^- \rightarrow \Upsilon(4S)$
$0.738 \pm 0.079 \pm 0.036$	4	ADACHI	12A BELL $e^+e^- \rightarrow \Upsilon(4S)$
$0.642 \pm 0.047 \pm 0.021$	5	ADACHI	12A BELL $e^+e^- \rightarrow \Upsilon(4S)$
$0.57 \pm 0.58 \pm 0.06$	6	SATO	12 BELL $e^+e^- \rightarrow \Upsilon(5S)$
$0.897 \pm 0.100 \pm 0.036$	4	AUBERT	09K BABR $e^+e^- \rightarrow \Upsilon(4S)$
$0.666 \pm 0.031 \pm 0.013$		AUBERT	09K BABR $e^+e^- \rightarrow \Upsilon(4S)$
$0.79 \begin{smallmatrix} +0.41 \\ -0.44 \end{smallmatrix}$	7	AFFOLDER	00C CDF $p\bar{p}$ at 1.8 TeV
$0.84 \begin{smallmatrix} +0.82 \\ -1.04 \end{smallmatrix} \pm 0.16$	8	BARATE	00Q ALEP $e^+e^- \rightarrow Z$
$3.2 \begin{smallmatrix} +1.8 \\ -2.0 \end{smallmatrix} \pm 0.5$	9	ACKERSTAFF	98Z OPAL $e^+e^- \rightarrow Z$

• • • We do not use the following data for averages, fits, limits, etc. • • •

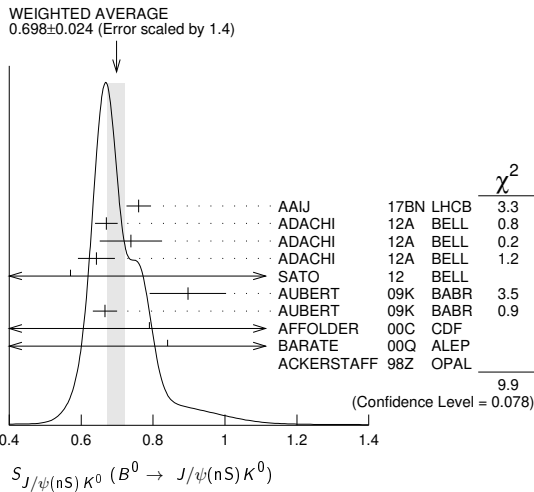
$0.75 \pm 0.04$	10	AAIJ	17BN LHCb $p\bar{p}$ at 7, 8 TeV
$0.84 \pm 0.10 \pm 0.01$	11	AAIJ	17BN LHCb $p\bar{p}$ at 7, 8 TeV
$0.731 \pm 0.035 \pm 0.020$	12	AAIJ	15N LHCb Repl. by AAIJ 17BN
$0.73 \pm 0.07 \pm 0.04$	13	AAIJ	13K LHCb Repl. by AAIJ 15N
$0.650 \pm 0.029 \pm 0.018$	14	SAHOO	08 BELL Repl. by ADACHI 12A
$0.72 \pm 0.09 \pm 0.03$	4	SAHOO	08 BELL Repl. by ADACHI 12A
$0.642 \pm 0.031 \pm 0.017$		CHEN	07 BELL Repl. by ADACHI 12A

- Measurement based on  $B^0 \rightarrow J/\psi K_S^0$ ,  $B^0 \rightarrow \psi(2S) K_S^0$  with  $J/\psi \rightarrow \mu^+ \mu^-$ ,  $J/\psi \rightarrow e^+ e^-$  and  $\psi(2S) \rightarrow \mu^+ \mu^-$ .
- AAIJ 17BN provides the correlation coefficient  $\rho = 0.42$  between the uncertainties of  $S_{J/\psi(nS)K^0} (B^0 \rightarrow J/\psi(nS)K^0)$  and  $C_{J/\psi(nS)K^0} (B^0 \rightarrow J/\psi(nS)K^0)$  measurements.
- Uses  $B^0 \rightarrow J/\psi K_S^0$  decays.
- Based on  $B^0 \rightarrow \psi(2S) K_S^0$  decays.
- Uses  $B^0 \rightarrow J/\psi K_L^0$  decays.
- SATO 12 uses 121  $\text{fb}^{-1}$  data collected at  $\Upsilon(5S)$  resonance. Uses the " $B - \pi$  tagging" where  $B\pi^+$  and  $B\pi^-$  tagged  $J/\psi K_S^0$  events are compared.
- AFFOLDER 00C uses about 400  $B^0 \rightarrow J/\psi(1S) K_S^0$  events. The production flavor of  $B^0$  was determined using three tagging algorithms: a same-side tag, a jet-charge tag, and a soft-lepton tag.

# Meson Particle Listings

## $B^0$

- <sup>8</sup> BARATE 00Q uses 23 candidates for  $B^0 \rightarrow J/\psi(1S)K_S^0$  decays. A combination of jet-charge, vertex-charge, and same-side tagging techniques were used to determine the  $B^0$  production flavor.
- <sup>9</sup> ACKERSTAFF 98Z uses 24 candidates for  $B^0 \rightarrow J/\psi(1S)K_S^0$  decay. A combination of jet-charge and vertex-charge techniques were used to tag the  $B^0$  production flavor.
- <sup>10</sup> Measurement based on  $B^0 \rightarrow J/\psi K_S^0$  with  $J/\psi \rightarrow \mu^+ \mu^-$  and  $J/\psi \rightarrow e^+ e^-$ .
- <sup>11</sup> Measurement based on  $B^0 \rightarrow \psi(2S)K_S^0$  with  $\psi(2S) \rightarrow \mu^+ \mu^-$ .
- <sup>12</sup> AAIJ 15N uses 41,560 flavor-tagged  $B_d \rightarrow J/\psi K_S^0$  events from 3 fb<sup>-1</sup> of integrated luminosity. Provides the correlation coefficient  $\rho = 0.483$  between the statistical uncertainties of and measurements.
- <sup>13</sup> AAIJ 13K uses 8200 flavor-tagged  $B_d \rightarrow J/\psi K_S^0$  events from 1 fb<sup>-1</sup> of integrated luminosity. Provides the correlation coefficient  $\rho = 0.42$  between the statistical uncertainties of  $S_{J/\psi(nS)K^0}$  ( $B^0 \rightarrow J/\psi(nS)K^0$ ) and  $C_{J/\psi(nS)K^0}$  ( $B^0 \rightarrow J/\psi(nS)K^0$ ) measurements.
- <sup>14</sup> Combined result of CHEN 07 and SAHOO 08.



$C_{J/\psi K^0}$  ( $B^0 \rightarrow J/\psi K^0$ )

VALUE	DOCUMENT ID	TECN	COMMENT
<b>0.025 ± 0.083 ± 0.054</b>	<sup>1</sup> AUBERT	09K	BABR $e^+ e^- \rightarrow \Upsilon(4S)$

<sup>1</sup> Based on  $B^0 \rightarrow J/\psi K^0, K^0 \rightarrow K_S^0 \pi^0$ .

$S_{J/\psi K^0}$  ( $B^0 \rightarrow J/\psi K^0$ )

VALUE	DOCUMENT ID	TECN	COMMENT
<b>0.601 ± 0.239 ± 0.087</b>	<sup>1,2</sup> AUBERT	09K	BABR $e^+ e^- \rightarrow \Upsilon(4S)$

<sup>1</sup> Based on  $B^0 \rightarrow J/\psi K^0, K^0 \rightarrow K_S^0 \pi^0$ .

<sup>2</sup> This  $S_{J/\psi K^0}$  value has been corrected for the dilution of the  $\sin(\Delta M \Delta t)$  coefficient of the CP asymmetry by a factor of  $1-R_{\perp}$ , which arises from the mixture of CP-even and CP-odd B decay amplitudes.

$C_{\chi_{c0} K_S^0}$  ( $B^0 \rightarrow \chi_{c0} K_S^0$ )

VALUE	DOCUMENT ID	TECN	COMMENT
<b>-0.29 ± 0.53 ± 0.06</b>	<sup>1</sup> AUBERT	09AU	BABR $e^+ e^- \rightarrow \Upsilon(4S)$

<sup>1</sup> Uses Dalitz plot analysis of  $B^0 \rightarrow K^0 \pi^+ \pi^-$  decays and the first of two equivalent solutions is used.

$S_{\chi_{c0} K_S^0}$  ( $B^0 \rightarrow \chi_{c0} K_S^0$ )

VALUE	DOCUMENT ID	TECN	COMMENT
<b>-0.69 ± 0.52 ± 0.08</b>	<sup>1</sup> AUBERT	09AU	BABR $e^+ e^- \rightarrow \Upsilon(4S)$

<sup>1</sup> Uses Dalitz plot analysis of  $B^0 \rightarrow K^0 \pi^+ \pi^-$  decays and the first of two equivalent solutions is used.

$C_{\chi_{c1} K_S^0}$  ( $B^0 \rightarrow \chi_{c1} K_S^0$ )

VALUE	DOCUMENT ID	TECN	COMMENT
<b>0.06 ± 0.07 OUR AVERAGE</b>			
0.017 ± 0.083 ± 0.026	ADACHI	12A	BELL $e^+ e^- \rightarrow \Upsilon(4S)$
0.129 ± 0.109 ± 0.025	AUBERT	09K	BABR $e^+ e^- \rightarrow \Upsilon(4S)$

$S_{\chi_{c1} K_S^0}$  ( $B^0 \rightarrow \chi_{c1} K_S^0$ )

VALUE	DOCUMENT ID	TECN	COMMENT
<b>0.63 ± 0.10 OUR AVERAGE</b>			
0.640 ± 0.117 ± 0.040	ADACHI	12A	BELL $e^+ e^- \rightarrow \Upsilon(4S)$
0.614 ± 0.160 ± 0.040	AUBERT	09K	BABR $e^+ e^- \rightarrow \Upsilon(4S)$

$\sin(2\beta_{\text{eff}})(B^0 \rightarrow \phi K^0)$

VALUE	DOCUMENT ID	TECN	COMMENT
<b>0.22 ± 0.27 ± 0.12</b>	AUBERT	07AX	BABR $e^+ e^- \rightarrow \Upsilon(4S)$

• • • We do not use the following data for averages, fits, limits, etc. • • •

0.50 ± 0.25 ± 0.07	<sup>1</sup> AUBERT	05T	BABR Repl. by AUBERT 07AX
--------------------	---------------------	-----	---------------------------

<sup>1</sup> Obtained by constraining C = 0.

$\sin(2\beta_{\text{eff}})(B^0 \rightarrow \phi K_0^*(1430)^0)$

VALUE	DOCUMENT ID	TECN	COMMENT
<b>0.97 ± 0.03</b>	<sup>1</sup> AUBERT	08BG	BABR $e^+ e^- \rightarrow \Upsilon(4S)$

• • • We do not use the following data for averages, fits, limits, etc. • • •

0.55 ± 0.22 ± 0.12	<sup>1</sup> AUBERT	05T	BABR Repl. by AUBERT 07AX
--------------------	---------------------	-----	---------------------------

<sup>1</sup> Measured using the CP-violation phase difference  $\Delta\phi_{00}$  between the B and  $\bar{B}$  decay amplitude.

$\sin(2\beta_{\text{eff}})(B^0 \rightarrow K^+ K^- K_S^0)$

VALUE	DOCUMENT ID	TECN	COMMENT
<b>0.77 ± 0.11 ± 0.07</b>	AUBERT	07AX	BABR $e^+ e^- \rightarrow \Upsilon(4S)$

• • • We do not use the following data for averages, fits, limits, etc. • • •

0.55 ± 0.22 ± 0.12	<sup>1</sup> AUBERT	05T	BABR Repl. by AUBERT 07AX
--------------------	---------------------	-----	---------------------------

<sup>1</sup> Obtained by constraining C = 0.

$\sin(2\beta_{\text{eff}})(B^0 \rightarrow [K_S^0 \pi^+ \pi^-]_{D^{(*)}} h^0)$

VALUE	DOCUMENT ID	TECN	COMMENT
<b>0.80 ± 0.14 ± 0.07</b>	<sup>1</sup> ADACHI	18	$e^+ e^- \rightarrow \Upsilon(4S)$

• • • We do not use the following data for averages, fits, limits, etc. • • •

0.43 ± 0.27 ± 0.08	<sup>2</sup> VOROBYEV	16	BELL $e^+ e^- \rightarrow \Upsilon(4S)$
0.29 ± 0.34 ± 0.06	AUBERT	07BH	BABR $e^+ e^- \rightarrow \Upsilon(4S)$
0.78 ± 0.44 ± 0.22	KROKOVNY	06	BELL Repl. by VOROBYEV 16

<sup>1</sup> Analyzes joint data sample of Belle and BaBar using Dalitz plot analysis of  $D \rightarrow K_S^0 \pi^+ \pi^-$ ; the second error combines experimental systematic uncertainty and the Dalitz plot model uncertainty.

<sup>2</sup> A model-independent measurement uses the binned Dalitz plot technique.

$\beta_{\text{eff}}(B^0 \rightarrow [K_S^0 \pi^+ \pi^-]_{D^{(*)}} h^0)$

VALUE (°)	DOCUMENT ID	TECN	COMMENT
<b>22.5 ± 4.4 ± 1.3</b>	<sup>1</sup> ADACHI	18	$e^+ e^- \rightarrow \Upsilon(4S)$

• • • We do not use the following data for averages, fits, limits, etc. • • •

11.7 ± 7.8 ± 2.1	<sup>2</sup> VOROBYEV	16	BELL $e^+ e^- \rightarrow \Upsilon(4S)$
------------------	-----------------------	----	---

<sup>1</sup> Analyzes joint data sample of Belle and BaBar using Dalitz plot analysis of  $D \rightarrow K_S^0 \pi^+ \pi^-$ ; the second error combines experimental systematic uncertainty and the Dalitz plot model uncertainty.

<sup>2</sup> A model-independent measurement uses the binned Dalitz plot technique.

$2\beta_{\text{eff}}(B^0 \rightarrow J/\psi \rho^0)$

VALUE (°)	DOCUMENT ID	TECN	COMMENT
<b>41.7 ± 9.6 + 2.8</b>	AAIJ	15J	LHCB $pp$ at 7, 8 TeV

$|\lambda|(B^0 \rightarrow [K_S^0 \pi^+ \pi^-]_{D^{(*)}} h^0)$

VALUE	DOCUMENT ID	TECN	COMMENT
<b>1.01 ± 0.08 ± 0.02</b>	AUBERT	07BH	BABR $e^+ e^- \rightarrow \Upsilon(4S)$

$|\sin(2\beta + \gamma)|$

$\beta$  ( $\phi_1$ ) and  $\gamma$  ( $\phi_3$ ) are angles of CKM unitarity triangle, see the review on "CP Violation" in the Reviews section.

VALUE	CL%	DOCUMENT ID	TECN	COMMENT
<b>&gt; 0.40</b>	90	<sup>1</sup> AUBERT	06Y	BABR $e^+ e^- \rightarrow \Upsilon(4S)$

• • • We do not use the following data for averages, fits, limits, etc. • • •

> 0.77	68	<sup>2</sup> AAIJ	18Z	LHCB $pp$ at 7, 8 TeV
> 0.13	95	<sup>3</sup> RONGA	06	BELL $e^+ e^- \rightarrow \Upsilon(4S)$
> 0.07	95	<sup>3</sup> RONGA	06	BELL $e^+ e^- \rightarrow \Upsilon(4S)$
> 0.35	90	<sup>4</sup> AUBERT	05Z	BABR $e^+ e^- \rightarrow \Upsilon(4S)$
> 0.69	68	<sup>5</sup> AUBERT	04V	BABR $e^+ e^- \rightarrow \Upsilon(4S)$
> 0.58	95	<sup>6</sup> AUBERT	04W	BABR Repl. by AUBERT 05Z

- <sup>1</sup> Uses fully reconstructed  $B^0 \rightarrow D^{(*)} \pi^+ \pi^-$  and  $D^{\pm} \rho^{\mp}$  decays and some theoretical assumptions.
- <sup>2</sup> Uses a time dependent CP violation measurement in  $B^0 \rightarrow D^{\mp} \pi^{\pm}$  decays with external input and some theoretical assumptions.
- <sup>3</sup> Combines the results from fully reconstructed and partially reconstructed  $D^{(*)} \pi$  events by taking weighted averages. Assumes that systematic errors from physics parameters and fit biases in the two measurements are 100% correlated.
- <sup>4</sup> Uses partially reconstructed  $B^0 \rightarrow D^{*} \pi^{\mp}$  decays and some theoretical assumptions.
- <sup>5</sup> Uses fully reconstructed  $B^0 \rightarrow D^{(*)} \pi^{\mp}$  decays and some theoretical assumptions, such as the SU(3) symmetry relation.
- <sup>6</sup> Combining this measurement with the results from AUBERT 04v for fully reconstructed  $B^0 \rightarrow D^{(*)} \pi^{\mp}$  and some theoretical assumptions, such as the SU(3) symmetry relation.

$2\beta + \gamma$

VALUE (°)	DOCUMENT ID	TECN	COMMENT
<b>83 ± 53 ± 20</b>	<sup>1</sup> AUBERT	08AC	BABR $e^+ e^- \rightarrow \Upsilon(4S)$

<sup>1</sup> Used a time-dependent Dalitz-plot analysis of  $B^0 \rightarrow D^{\mp} K^0 \pi^{\pm}$  assuming the ratio of the  $b \rightarrow u$  and  $b \rightarrow c$  decay amplitudes to be 0.3.

**α**  
For angle α(φ<sub>2</sub>) of the CKM unitarity triangle, see the review on “CP violation” in the reviews section.  
“OUR EVALUATION” is provided by the Heavy Flavor Averaging Group (HFLAV).

VALUE (°)	DOCUMENT ID	TECN	COMMENT
<b>84.9<sup>+5.1</sup><sub>-4.5</sub> OUR EVALUATION</b>			
93.7±10.6	<sup>1</sup> VANHOEFER 16	BELL	e <sup>+</sup> e <sup>-</sup> → T(4S)
84.9±13.5	<sup>1</sup> VANHOEFER 14	BELL	Repl. by VANHOEFER 16
79 ± 7 ± 11	<sup>2</sup> AUBERT 10d	BABR	e <sup>+</sup> e <sup>-</sup> → T(4S)
92.4 <sup>+6.0</sup> <sub>-6.5</sub>	<sup>1</sup> AUBERT 09g	BABR	e <sup>+</sup> e <sup>-</sup> → T(4S)
78.6± 7.3	<sup>3</sup> AUBERT 07o	BABR	e <sup>+</sup> e <sup>-</sup> → T(4S)
88 ± 17	<sup>4</sup> SOMOV 06	BELL	Repl. by VANHOEFER 14
100 ± 13	<sup>5</sup> AUBERT,B 05c	BABR	Repl. by AUBERT 09g
102 <sup>+16</sup> <sub>-12</sub> ± 14	<sup>6</sup> AUBERT,B 04r	BABR	Repl. by AUBERT,B 05c

- • • We do not use the following data for averages, fits, limits, etc. • • •
- <sup>1</sup> Based on an isospin analysis of the B → ρρ system.
- <sup>2</sup> Obtained using the time dependent analysis of B<sup>0</sup> → a<sub>1</sub>(1260)±π<sup>∓</sup> and branching fraction measurements of B → a<sub>1</sub>(1260)K and B → K<sub>1</sub>π. Uses SU(3) flavor relations.
- <sup>3</sup> The angle α<sub>eff</sub> is obtained using the measured CP parameters of B<sup>0</sup> → a<sub>1</sub>(1260)±π<sup>∓</sup> and choosing one of the four solutions that is compatible with the result of SM-based fits.
- <sup>4</sup> Obtained using isospin relation and selecting a solution closest to the CKM best fit average; the 90% CL allowed interval is 59° < φ<sub>2</sub> (≡ α) < 115°.
- <sup>5</sup> Obtained using isospin relation and selecting a solution closest to the CKM best fit average; 90% CL allowed interval is 79° < α < 123°.
- <sup>6</sup> Obtained from the measured CP parameters of the longitudinal polarization by selecting the solution closest to the CKM best fit central value of α = 95° - 98°.

**CP VIOLATION PARAMETERS IN B<sup>0</sup> → D<sup>0</sup>K<sup>∗0</sup> DECAY**

The parameters r<sub>B<sup>0</sup></sub> and δ<sub>B<sup>0</sup></sub> are the magnitude ratio and strong phase difference between the amplitudes of A(B<sup>0</sup> → D<sup>0</sup>K<sup>∗0</sup>) and A(B<sup>0</sup> → D<sup>0</sup>K<sup>∗0</sup>). The measured observables and are defined as x<sub>±</sub> = r<sub>B<sup>0</sup></sub> cos(δ<sub>B<sup>0</sup></sub> ± γ) and y<sub>±</sub> = r<sub>B<sup>0</sup></sub> sin(δ<sub>B<sup>0</sup></sub> ± γ) where γ is the CKM angle γ.

“OUR EVALUATION” is provided by the Heavy Flavor Averaging Group (HFLAV). The CKM angle γ is listed in the B<sup>+</sup> section for “CP VIOLATION PARAMETERS IN B<sup>+</sup> → D K<sup>+</sup> AND SIMILAR DECAYS.”

**x<sub>+</sub>(B<sup>0</sup> → DK<sup>∗0</sup>)**

VALUE	DOCUMENT ID	TECN	COMMENT
<b>0.04±0.17 OUR AVERAGE</b>			
0.04±0.16±0.11	<sup>1</sup> AAIJ 16s	LHCB	pp at 7, 8 TeV
0.05±0.35±0.02	AAIJ 16z	LHCB	pp at 7, 8 TeV
• • • We do not use the following data for averages, fits, limits, etc. • • •			
0.05±0.24±0.04	<sup>2</sup> AAIJ 16AA	LHCB	Repl. by AAIJ 16z
<sup>1</sup> Uses Dalitz plot of B <sup>0</sup> → DK <sup>+</sup> π <sup>-</sup> with D → K <sup>+</sup> K <sup>-</sup> , π <sup>+</sup> π <sup>-</sup> , or K <sup>+</sup> π <sup>-</sup> .			
<sup>2</sup> Uses Dalitz plot analysis of D → K <sub>S</sub> <sup>0</sup> π <sup>+</sup> π <sup>-</sup> decays coming from B <sup>0</sup> → DK <sup>∗</sup> (892) <sup>0</sup> modes.			

**x<sub>-</sub>(B<sup>0</sup> → DK<sup>∗0</sup>)**

VALUE	DOCUMENT ID	TECN	COMMENT
<b>-0.16±0.14 OUR AVERAGE</b>			
-0.02±0.13±0.14	<sup>1</sup> AAIJ 16s	LHCB	pp at 7, 8 TeV
-0.31±0.20±0.04	AAIJ 16z	LHCB	pp at 7, 8 TeV
• • • We do not use the following data for averages, fits, limits, etc. • • •			
-0.15±0.14±0.03	<sup>2</sup> AAIJ 16AA	LHCB	Repl. by AAIJ 16z
<sup>1</sup> Uses Dalitz plot of B <sup>0</sup> → DK <sup>+</sup> π <sup>-</sup> with D → K <sup>+</sup> K <sup>-</sup> , π <sup>+</sup> π <sup>-</sup> , or K <sup>+</sup> π <sup>-</sup> .			
<sup>2</sup> Uses Dalitz plot analysis of D → K <sub>S</sub> <sup>0</sup> π <sup>+</sup> π <sup>-</sup> decays coming from B <sup>0</sup> → DK <sup>∗</sup> (892) <sup>0</sup> modes.			

**y<sub>+</sub>(B<sup>0</sup> → DK<sup>∗0</sup>)**

VALUE	DOCUMENT ID	TECN	COMMENT
<b>-0.68±0.22 OUR AVERAGE</b>			
-0.47±0.28±0.22	<sup>1</sup> AAIJ 16s	LHCB	pp at 7, 8 TeV
-0.81±0.28±0.06	AAIJ 16z	LHCB	pp at 7, 8 TeV
• • • We do not use the following data for averages, fits, limits, etc. • • •			
-0.65 <sup>+0.24</sup> <sub>-0.23</sub> ± 0.08	<sup>2</sup> AAIJ 16AA	LHCB	Repl. by AAIJ 16z
<sup>1</sup> Uses Dalitz plot of B <sup>0</sup> → DK <sup>+</sup> π <sup>-</sup> with D → K <sup>+</sup> K <sup>-</sup> , π <sup>+</sup> π <sup>-</sup> , or K <sup>+</sup> π <sup>-</sup> .			
<sup>2</sup> Uses Dalitz plot analysis of D → K <sub>S</sub> <sup>0</sup> π <sup>+</sup> π <sup>-</sup> decays coming from B <sup>0</sup> → DK <sup>∗</sup> (892) <sup>0</sup> modes.			

**y<sub>-</sub>(B<sup>0</sup> → DK<sup>∗0</sup>)**

VALUE	DOCUMENT ID	TECN	COMMENT
<b>0.20±0.25 OUR AVERAGE</b>	Error includes scale factor of 1.2.		
-0.35±0.26±0.41	<sup>1</sup> AAIJ 16s	LHCB	pp at 7, 8 TeV
0.31±0.21±0.05	AAIJ 16z	LHCB	pp at 7, 8 TeV
• • • We do not use the following data for averages, fits, limits, etc. • • •			
0.25±0.15±0.06	<sup>2</sup> AAIJ 16AA	LHCB	Repl. by AAIJ 16z
<sup>1</sup> Uses Dalitz plot of B <sup>0</sup> → DK <sup>+</sup> π <sup>-</sup> with D → K <sup>+</sup> K <sup>-</sup> , π <sup>+</sup> π <sup>-</sup> , or K <sup>+</sup> π <sup>-</sup> .			
<sup>2</sup> Uses Dalitz plot analysis of D → K <sub>S</sub> <sup>0</sup> π <sup>+</sup> π <sup>-</sup> decays coming from B <sup>0</sup> → DK <sup>∗</sup> (892) <sup>0</sup> modes.			

**r<sub>B<sup>0</sup></sub>(B<sup>0</sup> → DK<sup>∗0</sup>)**

“OUR EVALUATION” is provided by the Heavy Flavor Averaging Group (HFLAV).

VALUE	DOCUMENT ID	TECN	COMMENT
<b>0.220<sup>+0.041</sup><sub>-0.047</sub> OUR EVALUATION</b>			
• • • We do not use the following data for averages, fits, limits, etc. • • •			
0.39 ± 0.13	<sup>1</sup> AAIJ 16AA	LHCB	Repl. by AAIJ 16z
0.56 ± 0.17	<sup>2</sup> AAIJ 16z	LHCB	pp at 7, 8 TeV
<sup>1</sup> Uses Dalitz plot analysis of D → K <sub>S</sub> <sup>0</sup> π <sup>+</sup> π <sup>-</sup> decays coming from B <sup>0</sup> → DK <sup>∗</sup> (892) <sup>0</sup> modes.			
<sup>2</sup> Measurement is performed with K <sup>+</sup> π <sup>-</sup> masses within 50 MeV of the K <sup>∗0</sup> mass and an absolute value of the cosine of the K <sup>∗0</sup> helicity angle greater than 0.4. Angle γ is required to satisfy 0 < γ < 180 degrees.			

**δ<sub>B<sup>0</sup></sub>(B<sup>0</sup> → DK<sup>∗0</sup>)**

“OUR EVALUATION” is provided by the Heavy Flavor Averaging Group (HFLAV).

VALUE (°)	DOCUMENT ID	TECN	COMMENT
<b>194<sup>+30</sup><sub>-22</sub> OUR EVALUATION</b>			
• • • We do not use the following data for averages, fits, limits, etc. • • •			
197 <sup>+24</sup> <sub>-20</sub>	<sup>1</sup> AAIJ 16AA	LHCB	Repl. by AAIJ 16z
204 <sup>+21</sup> <sub>-20</sub>	<sup>2</sup> AAIJ 16z	LHCB	pp at 7, 8 TeV
<sup>1</sup> Uses Dalitz plot analysis of D → K <sub>S</sub> <sup>0</sup> π <sup>+</sup> π <sup>-</sup> decays coming from B <sup>0</sup> → DK <sup>∗</sup> (892) <sup>0</sup> modes.			
<sup>2</sup> Measurement is performed with K <sup>+</sup> π <sup>-</sup> masses within 50 MeV of the K <sup>∗0</sup> mass and an absolute value of the cosine of the K <sup>∗0</sup> helicity angle greater than 0.4. Angle γ is required to satisfy 0 < γ < 180 degrees.			

**T and CPT VIOLATION PARAMETERS**

Measured values of the T-, CP-, and CPT-asymmetry parameters, defined as the differences in S<sub>α,β</sub><sup>±</sup> and C<sub>α,β</sub><sup>±</sup> between symmetry-transformed transitions. The indices α = ℓ<sup>+</sup>, ℓ<sup>-</sup> and β = K<sub>S</sub><sup>0</sup>, K<sub>L</sub><sup>0</sup> stand for reconstructed the flavor final state and the CP final states from T(4S) decay. The sign ± indicates whether the decay to the flavor final state α occurs before or after the decay to the CP final state.

Alternatively, violations of CPT symmetry and Lorentz invariance are searched for by studying interference effects in B<sup>0</sup> mixing. Results are expressed in terms of the standard model extension parameter Δa, which describes the difference between the couplings of the valence quarks within B<sup>0</sup> meson with the Lorentz-violating fields.

**ΔS<sub>T</sub><sup>±</sup>(S<sub>ℓ<sup>-</sup>,K<sub>S</sub><sup>0</sup></sub> - S<sub>ℓ<sup>+</sup>,K<sub>S</sub><sup>0</sup></sub>)**

VALUE	DOCUMENT ID	TECN	COMMENT
<b>-1.37±0.14±0.06</b>	LEES 12w	BABR	e <sup>+</sup> e <sup>-</sup> → T(4S)

**ΔS<sub>T</sub><sup>-</sup>(S<sub>ℓ<sup>-</sup>,K<sub>S</sub><sup>0</sup></sub> - S<sub>ℓ<sup>+</sup>,K<sub>S</sub><sup>0</sup></sub>)**

VALUE	DOCUMENT ID	TECN	COMMENT
<b>1.17±0.18±0.11</b>	LEES 12w	BABR	e <sup>+</sup> e <sup>-</sup> → T(4S)

**ΔC<sub>T</sub><sup>±</sup>(C<sub>ℓ<sup>-</sup>,K<sub>S</sub><sup>0</sup></sub> - C<sub>ℓ<sup>+</sup>,K<sub>S</sub><sup>0</sup></sub>)**

VALUE	DOCUMENT ID	TECN	COMMENT
<b>0.10±0.14±0.08</b>	LEES 12w	BABR	e <sup>+</sup> e <sup>-</sup> → T(4S)

**ΔC<sub>T</sub><sup>-</sup>(C<sub>ℓ<sup>-</sup>,K<sub>S</sub><sup>0</sup></sub> - C<sub>ℓ<sup>+</sup>,K<sub>S</sub><sup>0</sup></sub>)**

VALUE	DOCUMENT ID	TECN	COMMENT
<b>0.04±0.14±0.08</b>	LEES 12w	BABR	e <sup>+</sup> e <sup>-</sup> → T(4S)

**ΔS<sub>CP</sub><sup>+</sup>(S<sub>ℓ<sup>-</sup>,K<sub>S</sub><sup>0</sup></sub> - S<sub>ℓ<sup>+</sup>,K<sub>S</sub><sup>0</sup></sub>)**

VALUE	DOCUMENT ID	TECN	COMMENT
<b>-1.30±0.11±0.07</b>	LEES 12w	BABR	e <sup>+</sup> e <sup>-</sup> → T(4S)

**ΔS<sub>CP</sub><sup>-</sup>(S<sub>ℓ<sup>-</sup>,K<sub>S</sub><sup>0</sup></sub> - S<sub>ℓ<sup>+</sup>,K<sub>S</sub><sup>0</sup></sub>)**

VALUE	DOCUMENT ID	TECN	COMMENT
<b>1.33±0.12±0.06</b>	LEES 12w	BABR	e <sup>+</sup> e <sup>-</sup> → T(4S)

**ΔC<sub>CP</sub><sup>+</sup>(C<sub>ℓ<sup>-</sup>,K<sub>S</sub><sup>0</sup></sub> - C<sub>ℓ<sup>+</sup>,K<sub>S</sub><sup>0</sup></sub>)**

VALUE	DOCUMENT ID	TECN	COMMENT
<b>0.07±0.09±0.03</b>	LEES 12w	BABR	e <sup>+</sup> e <sup>-</sup> → T(4S)

**ΔC<sub>CP</sub><sup>-</sup>(C<sub>ℓ<sup>-</sup>,K<sub>S</sub><sup>0</sup></sub> - C<sub>ℓ<sup>+</sup>,K<sub>S</sub><sup>0</sup></sub>)**

VALUE	DOCUMENT ID	TECN	COMMENT
<b>0.08±0.10±0.04</b>	LEES 12w	BABR	e <sup>+</sup> e <sup>-</sup> → T(4S)

**ΔS<sub>CPT</sub><sup>±</sup>(S<sub>ℓ<sup>-</sup>,K<sub>S</sub><sup>0</sup></sub> - S<sub>ℓ<sup>+</sup>,K<sub>S</sub><sup>0</sup></sub>)**

VALUE	DOCUMENT ID	TECN	COMMENT
<b>0.16±0.21±0.09</b>	LEES 12w	BABR	e <sup>+</sup> e <sup>-</sup> → T(4S)

# Meson Particle Listings

## $B^0$

### $\Delta S_{CPT} (S^+_{\ell^+, K^0_S} - S^-_{\ell^+, K^0_S})$

VALUE	DOCUMENT ID	TECN	COMMENT
$-0.03 \pm 0.13 \pm 0.06$	LEES	12W	BABR $e^+ e^- \rightarrow \Upsilon(4S)$

### $\Delta C^+_{CPT} (C^-_{\ell^+, K^0_S} - C^+_{\ell^+, K^0_S})$

VALUE	DOCUMENT ID	TECN	COMMENT
$0.14 \pm 0.15 \pm 0.07$	LEES	12W	BABR $e^+ e^- \rightarrow \Upsilon(4S)$

### $\Delta C^-_{CPT} (C^+_{\ell^+, K^0_S} - C^-_{\ell^+, K^0_S})$

VALUE	DOCUMENT ID	TECN	COMMENT
$0.03 \pm 0.12 \pm 0.08$	LEES	12W	BABR $e^+ e^- \rightarrow \Upsilon(4S)$

### $\Delta a_{||}$ CPT parameter in $B^0$ mixing

VALUE ( $10^{-15}$ GeV)	DOCUMENT ID	TECN	COMMENT
$-0.10 \pm 0.82 \pm 0.54$	<sup>1</sup> AAIJ	16E	LHCB $pp$ at 7, 8 TeV

<sup>1</sup> Uses  $B^0 \rightarrow J/\psi K^0_S$  decays.

### $\Delta a_{\perp}$ CPT parameter in $B^0$ mixing

VALUE ( $10^{-13}$ GeV)	DOCUMENT ID	TECN	COMMENT
$-0.20 \pm 0.22 \pm 0.04$	<sup>1</sup> AAIJ	16E	LHCB $pp$ at 7, 8 TeV

<sup>1</sup> Uses  $B^0 \rightarrow J/\psi K^0_S$  decays.

### $\Delta a_{\chi}$ CPT parameter in $B^0$ mixing

VALUE ( $10^{-15}$ GeV)	DOCUMENT ID	TECN	COMMENT
$+1.97 \pm 1.30 \pm 0.29$	<sup>1</sup> AAIJ	16E	LHCB $pp$ at 7, 8 TeV

<sup>1</sup> Uses  $B^0 \rightarrow J/\psi K^0_S$  decays.

### $\Delta a_{\gamma}$ CPT parameter in $B^0$ mixing

VALUE ( $10^{-15}$ GeV)	DOCUMENT ID	TECN	COMMENT
$+0.44 \pm 1.26 \pm 0.29$	<sup>1</sup> AAIJ	16E	LHCB $pp$ at 7, 8 TeV

<sup>1</sup> Uses  $B^0 \rightarrow J/\psi K^0_S$  decays.

### $B^0 \rightarrow D^{*-} \ell^+ \nu_{\ell}$ FORM FACTORS

$R_1$  (form factor ratio  $\sim V/A_1$ )

VALUE	DOCUMENT ID	TECN	COMMENT
<b><math>1.239 \pm 0.029</math> OUR AVERAGE</b>			
$1.229 \pm 0.028 \pm 0.009$	<sup>1</sup> WAHEED	19	BELL $e^+ e^- \rightarrow \Upsilon(4S)$
$1.56 \pm 0.07 \pm 0.15$	AUBERT	09A	BABR $e^+ e^- \rightarrow \Upsilon(4S)$
$1.18 \pm 0.30 \pm 0.12$	DUBOSCQ	96	CLE2 $e^+ e^- \rightarrow \Upsilon(4S)$

••• We do not use the following data for averages, fits, limits, etc. •••

$1.401 \pm 0.034 \pm 0.018$	<sup>1</sup> DUNGEL	10	BELL Repl. by WAHEED 19
$1.429 \pm 0.061 \pm 0.044$	AUBERT	08R	BABR Repl. by AUBERT 09A
$1.396 \pm 0.060 \pm 0.044$	AUBERT,B	06Z	BABR Repl. by AUBERT 08R

<sup>1</sup> Uses fully reconstructed  $D^{*-} \ell^+ \nu$  events ( $\ell = e$  or  $\mu$ ).

$R_2$  (form factor ratio  $\sim A_2/A_1$ )

VALUE	DOCUMENT ID	TECN	COMMENT
<b><math>0.84 \pm 0.04</math> OUR AVERAGE</b>			Error includes scale factor of 1.8.
$0.852 \pm 0.021 \pm 0.006$	<sup>1</sup> WAHEED	19	BELL $e^+ e^- \rightarrow \Upsilon(4S)$
$0.66 \pm 0.05 \pm 0.09$	AUBERT	09A	BABR $e^+ e^- \rightarrow \Upsilon(4S)$
$0.71 \pm 0.22 \pm 0.07$	DUBOSCQ	96	CLE2 $e^+ e^- \rightarrow \Upsilon(4S)$

••• We do not use the following data for averages, fits, limits, etc. •••

$0.864 \pm 0.024 \pm 0.008$	<sup>1</sup> DUNGEL	10	BELL Repl. by WAHEED 19
$0.827 \pm 0.038 \pm 0.022$	AUBERT	08R	BABR Repl. by AUBERT 09A
$0.885 \pm 0.040 \pm 0.026$	AUBERT,B	06Z	BABR Repl. by AUBERT 08R

<sup>1</sup> Uses fully reconstructed  $D^{*-} \ell^+ \nu$  events ( $\ell = e$  or  $\mu$ ).

$\rho^2_{A_1}$  (form factor slope)

VALUE	DOCUMENT ID	TECN	COMMENT
<b><math>1.12 \pm 0.04</math> OUR AVERAGE</b>			Error includes scale factor of 1.5.
$1.106 \pm 0.031 \pm 0.007$	<sup>1</sup> WAHEED	19	BELL $e^+ e^- \rightarrow \Upsilon(4S)$
$1.22 \pm 0.02 \pm 0.07$	AUBERT	09A	BABR $e^+ e^- \rightarrow \Upsilon(4S)$
$0.91 \pm 0.15 \pm 0.06$	DUBOSCQ	96	CLE2 $e^+ e^- \rightarrow \Upsilon(4S)$

••• We do not use the following data for averages, fits, limits, etc. •••

$1.214 \pm 0.034 \pm 0.009$	<sup>1</sup> DUNGEL	10	BELL Repl. by WAHEED 19
$1.191 \pm 0.048 \pm 0.028$	AUBERT	08R	BABR Repl. by AUBERT 09A
$1.145 \pm 0.059 \pm 0.046$	AUBERT,B	06Z	BABR Repl. by AUBERT 08R

<sup>1</sup> Uses fully reconstructed  $D^{*-} \ell^+ \nu$  events ( $\ell = e$  or  $\mu$ ).

### PARTIAL BRANCHING FRACTIONS IN $B^0 \rightarrow K^{(*)0} \ell^+ \ell^-$

#### $B(B^0 \rightarrow K^{*0} e^+ e^-) (0.0009 < q^2 < 1.0 \text{ GeV}^2/c^4)$

VALUE (units $10^{-7}$ )	DOCUMENT ID	TECN	COMMENT
<b><math>3.1^{+0.9+0.2}_{-0.8-0.3} \pm 0.2</math></b>	<sup>1</sup> AAIJ	13U	LHCB $pp$ at 7 TeV

<sup>1</sup> The last uncertainty is due to uncertainties of  $B(B^0 \rightarrow J/\psi K^{*0})$  and  $B(J/\psi \rightarrow e^+ e^-)$  branching fraction measurements.

#### $B(B^0 \rightarrow K^{*0} \ell^+ \ell^-) (0.1 < q^2 < 2.0 \text{ GeV}^2/c^4)$

VALUE (units $10^{-7}$ )	DOCUMENT ID	TECN	COMMENT
<b><math>1.24^{+0.23}_{-0.27}</math> OUR AVERAGE</b>			Error includes scale factor of 1.6.
$1.14 \pm 0.11^{+0.11}_{-0.15}$	AAIJ	13Y	LHCB $pp$ at 7 TeV, $K^{*0} \mu^+ \mu^-$
$1.80 \pm 0.36 \pm 0.11$	AALTONEN	11AI	CDF $p\bar{p}$ at 1.96 TeV

••• We do not use the following data for averages, fits, limits, etc. •••

$0.48^{+0.14}_{-0.12} \pm 0.04$	<sup>1</sup> CHATRCHYAN	13BL	CMS $pp$ at 7 TeV
$1.16 \pm 0.23 \pm 0.11$	AAIJ	12U	LHCB Repl. by AAIJ 13Y

<sup>1</sup> CHATRCHYAN 13BL uses, for this bin,  $1.0 < q^2 < 2.0 \text{ GeV}^2/c^4$ .

#### $B(B^0 \rightarrow K^{*0} \ell^+ \ell^-) (2.0 < q^2 < 4.3 \text{ GeV}^2/c^4)$

VALUE (units $10^{-7}$ )	DOCUMENT ID	TECN	COMMENT
<b><math>0.76 \pm 0.07</math> OUR AVERAGE</b>			
$0.759 \pm 0.115 \pm 0.046$	KHACHATRY..	16D	CMS $pp$ at 8 TeV
$0.69 \pm 0.07 \pm 0.09$	AAIJ	13Y	LHCB $pp$ at 7 TeV, $K^{*0} \mu^+ \mu^-$
$0.87 \pm 0.16 \pm 0.07$	CHATRCHYAN	13BL	CMS $pp$ at 7 TeV
$0.84 \pm 0.28 \pm 0.06$	AALTONEN	11AI	CDF $p\bar{p}$ at 1.96 TeV

••• We do not use the following data for averages, fits, limits, etc. •••

$0.78 \pm 0.21 \pm 0.05$	AAIJ	12U	LHCB Repl. by AAIJ 13Y
--------------------------	------	-----	------------------------

#### $B(B^0 \rightarrow K^{*0} \ell^+ \ell^-) (4.3 < q^2 < 8.68 \text{ GeV}^2/c^4)$

VALUE (units $10^{-7}$ )	DOCUMENT ID	TECN	COMMENT
<b><math>1.87 \pm 0.21</math> OUR AVERAGE</b>			
$2.15 \pm 0.18^{+0.22}_{-0.28}$	AAIJ	13Y	LHCB $pp$ at 7 TeV, $K^{*0} \mu^+ \mu^-$
$1.62 \pm 0.31 \pm 0.18$	CHATRCHYAN	13BL	CMS $pp$ at 7 TeV
$1.73 \pm 0.43 \pm 0.15$	AALTONEN	11AI	CDF $p\bar{p}$ at 1.96 TeV

••• We do not use the following data for averages, fits, limits, etc. •••

$3.02 \pm 0.35 \pm 0.22$	AAIJ	12U	LHCB Repl. by AAIJ 13Y
--------------------------	------	-----	------------------------

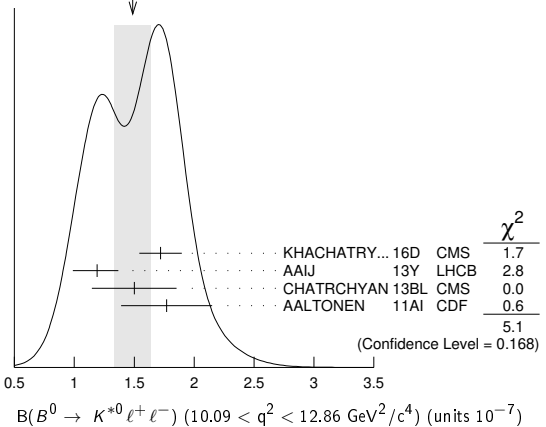
#### $B(B^0 \rightarrow K^{*0} \ell^+ \ell^-) (10.09 < q^2 < 12.86 \text{ GeV}^2/c^4)$

VALUE (units $10^{-7}$ )	DOCUMENT ID	TECN	COMMENT
<b><math>1.49 \pm 0.15</math> OUR AVERAGE</b>			Error includes scale factor of 1.3. See the ideogram below.
$1.72 \pm 0.11 \pm 0.14$	KHACHATRY..	16D	CMS $pp$ at 8 TeV
$1.19 \pm 0.11^{+0.14}_{-0.17}$	AAIJ	13Y	LHCB $pp$ at 7 TeV, $K^{*0} \mu^+ \mu^-$
$1.50 \pm 0.25 \pm 0.25$	CHATRCHYAN	13BL	CMS $pp$ at 7 TeV
$1.77 \pm 0.36 \pm 0.12$	AALTONEN	11AI	CDF $p\bar{p}$ at 1.96 TeV

••• We do not use the following data for averages, fits, limits, etc. •••

$1.52 \pm 0.25 \pm 0.19$	AAIJ	12U	LHCB Repl. by AAIJ 13Y
--------------------------	------	-----	------------------------

WEIGHTED AVERAGE  
1.49±0.15 (Error scaled by 1.3)



#### $B(B^0 \rightarrow K^{*0} \ell^+ \ell^-) (14.18 < q^2 < 16.0 \text{ GeV}^2/c^4)$

VALUE (units $10^{-7}$ )	DOCUMENT ID	TECN	COMMENT
<b><math>1.09 \pm 0.10</math> OUR AVERAGE</b>			Error includes scale factor of 1.1.
$1.22 \pm 0.11 \pm 0.09$	KHACHATRY..	16D	CMS $pp$ at 8 TeV
$1.02 \pm 0.11^{+0.11}_{-0.15}$	AAIJ	13Y	LHCB $pp$ at 7 TeV, $K^{*0} \mu^+ \mu^-$
$0.84^{+0.16}_{-0.15} \pm 0.09$	CHATRCHYAN	13BL	CMS $pp$ at 7 TeV
$1.34 \pm 0.26 \pm 0.08$	AALTONEN	11AI	CDF $p\bar{p}$ at 1.96 TeV

••• We do not use the following data for averages, fits, limits, etc. •••

$1.15 \pm 0.20 \pm 0.09$	AAIJ	12U	LHCB Repl. by AAIJ 13Y
--------------------------	------	-----	------------------------

See key on page 999

## Meson Particle Listings

 $B^0$  $B(B^0 \rightarrow K^{*0} \ell^+ \ell^-) (16.0 < q^2 < 19.0 \text{ GeV}^2/c^4)$ 

VALUE (units $10^{-7}$ )	DOCUMENT ID	TECN	COMMENT
<b>1.27 ± 0.09 OUR AVERAGE</b>			
1.26 ± 0.09 ± 0.09	KHACHATRY...16D	CMS	$pp$ at 8 TeV
1.23 ± 0.12 <sup>+0.15</sup> <sub>-0.18</sub>	AAIJ	13Y LHCb	$pp$ at 7 TeV, $K^{*0} \mu^+ \mu^-$
1.56 ± 0.18 ± 0.15	CHATRCHYAN13BL	CMS	$pp$ at 7 TeV
0.97 ± 0.26 ± 0.07	AALTONEN	11AI CDF	$p\bar{p}$ at 1.96 TeV
• • • We do not use the following data for averages, fits, limits, etc. • • •			
1.50 ± 0.24 ± 0.15	AAIJ	12U LHCb	Repl. by AAIJ 13Y

 $B(B^0 \rightarrow K^*(892)^0 \ell^+ \ell^-) (15.0 < q^2 < 19.0 \text{ GeV}^2/c^4)$ 

VALUE (units $10^{-7}$ )	DOCUMENT ID	TECN	COMMENT
<b>1.744<sup>+0.072</sup><sub>-0.076</sub> ± 0.123</b>	AAIJ	17Q LHCb	$pp$ at 7, 8 TeV
• • • We do not use the following data for averages, fits, limits, etc. • • •			
1.95 <sup>+0.08</sup> <sub>-0.09</sub> ± 0.13	AAIJ	16Ao LHCb	Repl. by AAIJ 17Q

 $B(B^0 \rightarrow K^{*0} \ell^+ \ell^-) (1.0 < q^2 < 6.0 \text{ GeV}^2/c^4)$ 

VALUE (units $10^{-7}$ )	DOCUMENT ID	TECN	COMMENT
<b>1.73 ± 0.11 OUR AVERAGE</b>			
1.68 ± 0.083 ± 0.12	<sup>1</sup> AAIJ	17Q LHCb	$pp$ at 7, 8 TeV
1.90 ± 0.20	KHACHATRY...16D	CMS	$pp$ at 7, 8 TeV
1.42 ± 0.41 ± 0.12	AALTONEN	11AI CDF	$p\bar{p}$ at 1.96 TeV
• • • We do not use the following data for averages, fits, limits, etc. • • •			
1.92 <sup>+0.10</sup> <sub>-0.09</sub> ± 0.14	AAIJ	16Ao LHCb	Repl. by AAIJ 17Q
1.70 ± 0.15 <sup>+0.20</sup> <sub>-0.25</sub>	AAIJ	13Y LHCb	Repl. by AAIJ 16Ao
2.20 ± 0.30 ± 0.20	CHATRCHYAN13BL	CMS	Repl. by KHACHATRYAN 16D
2.10 ± 0.30 ± 0.15	AAIJ	12U LHCb	Repl. by AAIJ 13Y
<sup>1</sup> AAIJ 17Q result is determined for the range $1.1 < q^2 < 6.0 \text{ GeV}^2/c^2$ .			

 $B(B^0 \rightarrow K^{*0} \ell^+ \ell^-) (0.0 < q^2 < 4.3 \text{ GeV}^2/c^4)$ 

VALUE (units $10^{-7}$ )	DOCUMENT ID	TECN	COMMENT
<b>2.60 ± 0.45 ± 0.17</b>	AALTONEN	11AI CDF	$p\bar{p}$ at 1.96 TeV

 $B(B^0 \rightarrow K^{*0} \mu^+ \mu^-) / B(B^0 \rightarrow K^{*0} e^+ e^-) (0.045 < q^2 < 1.1 \text{ GeV}^2/c^4)$ 

VALUE	DOCUMENT ID	TECN	COMMENT
<b>0.66<sup>+0.11</sup><sub>-0.07</sub> ± 0.03</b>	AAIJ	17W LHCb	$pp$ at 7, 8 TeV

 $B(B^0 \rightarrow K^{*0} \mu^+ \mu^-) / B(B^0 \rightarrow K^{*0} e^+ e^-) (1.1 < q^2 < 6.0 \text{ GeV}^2/c^4)$ 

VALUE	DOCUMENT ID	TECN	COMMENT
<b>0.69<sup>+0.11</sup><sub>-0.07</sub> ± 0.05</b>	AAIJ	17W LHCb	$pp$ at 7, 8 TeV

 $B(B^0 \rightarrow K^0 \ell^+ \ell^-) (q^2 < 2.0 \text{ GeV}^2/c^4)$ 

VALUE (units $10^{-7}$ )	DOCUMENT ID	TECN	COMMENT
<b>0.24<sup>+0.22</sup><sub>-0.20</sub> OUR AVERAGE</b>			
0.21 <sup>+0.27</sup> <sub>-0.23</sub>	AAIJ	12AH LHCb	$pp$ at 7 TeV
0.31 ± 0.37 ± 0.02	AALTONEN	11AI CDF	$p\bar{p}$ at 1.96 TeV

 $B(B^0 \rightarrow K^0 \ell^+ \ell^-) (2.0 < q^2 < 4.3 \text{ GeV}^2/c^4)$ 

VALUE (units $10^{-7}$ )	DOCUMENT ID	TECN	COMMENT
<b>0.24<sup>+0.35</sup><sub>-0.30</sub> OUR AVERAGE</b>			Error includes scale factor of 1.6.
0.07 <sup>+0.25</sup> <sub>-0.21</sub>	AAIJ	12AH LHCb	$pp$ at 7 TeV
0.93 ± 0.49 ± 0.07	AALTONEN	11AI CDF	$p\bar{p}$ at 1.96 TeV

 $B(B^0 \rightarrow K^0 \ell^+ \ell^-) (4.3 < q^2 < 8.68 \text{ GeV}^2/c^4)$ 

VALUE (units $10^{-7}$ )	DOCUMENT ID	TECN	COMMENT
<b>1.08 ± 0.27 OUR AVERAGE</b>			
1.23 ± 0.31	AAIJ	12AH LHCb	$pp$ at 7 TeV
0.66 ± 0.51 ± 0.05	AALTONEN	11AI CDF	$p\bar{p}$ at 1.96 TeV

 $B(B^0 \rightarrow K^0 \ell^+ \ell^-) (10.09 < q^2 < 12.86 \text{ GeV}^2/c^4)$ 

VALUE (units $10^{-7}$ )	DOCUMENT ID	TECN	COMMENT
<b>0.27 ± 0.27 OUR AVERAGE</b>			Error includes scale factor of 1.8.
0.50 <sup>+0.22</sup> <sub>-0.19</sub>	AAIJ	12AH LHCb	$pp$ at 7 TeV
-0.03 ± 0.22 ± 0.01	AALTONEN	11AI CDF	$p\bar{p}$ at 1.96 TeV

 $B(B^0 \rightarrow K^0 \ell^+ \ell^-) (14.18 < q^2 < 16.0 \text{ GeV}^2/c^4)$ 

VALUE (units $10^{-7}$ )	DOCUMENT ID	TECN	COMMENT
<b>0.29<sup>+0.21</sup><sub>-0.15</sub> OUR AVERAGE</b>			Error includes scale factor of 1.8.
0.20 <sup>+0.13</sup> <sub>-0.09</sub>	AAIJ	12AH LHCb	$pp$ at 7 TeV
0.73 ± 0.26 ± 0.06	AALTONEN	11AI CDF	$p\bar{p}$ at 1.96 TeV

 $B(B^0 \rightarrow K^0 \ell^+ \ell^-) (q^2 > 16.0 \text{ GeV}^2/c^4)$ 

VALUE (units $10^{-7}$ )	DOCUMENT ID	TECN	COMMENT
<b>0.31<sup>+0.16</sup><sub>-0.12</sub> OUR AVERAGE</b>			
0.35 <sup>+0.21</sup> <sub>-0.14</sub>	AAIJ	12AH LHCb	$pp$ at 7 TeV
0.21 ± 0.18 ± 0.16	AALTONEN	11AI CDF	$p\bar{p}$ at 1.96 TeV

 $B(B^0 \rightarrow K^0 \ell^+ \ell^-) (1.0 < q^2 < 6.0 \text{ GeV}^2/c^4)$ 

VALUE (units $10^{-7}$ )	DOCUMENT ID	TECN	COMMENT
<b>0.92 ± 0.16 OUR AVERAGE</b>			
0.916 <sup>+0.172</sup> <sub>-0.157</sub> ± 0.004	<sup>1</sup> AAIJ	14M LHCb	$pp$ at 7, 8 TeV
0.98 ± 0.61 ± 0.08	AALTONEN	11AI CDF	$p\bar{p}$ at 1.96 TeV
• • • We do not use the following data for averages, fits, limits, etc. • • •			
0.65 <sup>+0.45</sup> <sub>-0.35</sub>	AAIJ	12AH LHCb	Repl. by AAIJ 14M
<sup>1</sup> Uses $B(B^0 \rightarrow J/\psi(1S) K^0) = (0.928 \pm 0.013 \pm 0.037) \times 10^{-3}$ for normalisation and $\mu^+ \mu^-$ as a lepton pair. Measured in $1.1 < q^2 < 6.0 \text{ GeV}^2/c^4$ .			

 $B(B^0 \rightarrow K^0 \ell^+ \ell^-) (0.0 < q^2 < 4.3 \text{ GeV}^2/c^4)$ 

VALUE (units $10^{-7}$ )	DOCUMENT ID	TECN	COMMENT
<b>1.27 ± 0.62 ± 0.10</b>	AALTONEN	11AI CDF	$p\bar{p}$ at 1.96 TeV

 $B(B^0 \rightarrow K^0 \ell^+ \ell^-) (15.0 < q^2 < 22.0 \text{ GeV}^2/c^4)$ 

VALUE (units $10^{-7}$ )	DOCUMENT ID	TECN	COMMENT
<b>0.61<sup>+0.11</sup><sub>-0.11</sub> ± 0.04</b>	<sup>1</sup> AAIJ	14M LHCb	$pp$ at 7, 8 TeV
<sup>1</sup> Uses $B(B^0 \rightarrow J/\psi(1S) K^0) = (0.928 \pm 0.013 \pm 0.037) \times 10^{-3}$ for normalisation and $\mu^+ \mu^-$ as a lepton pair.			

 $B(B^0 \rightarrow K_{0,2}^{*0} (1430)^0 \mu^+ \mu^-) (1.10 < q^2 < 6.00 \text{ GeV}^2/c^4)$ 

VALUE (units $10^{-8}$ )	DOCUMENT ID	TECN	COMMENT
<b>4.02 ± 0.44 ± 0.31</b>	<sup>1,2</sup> AAIJ	16AP LHCb	$pp$ at 7, 8 TeV
<sup>1</sup> Measured the differential branching fraction and angular moments of the decay $B^0 \rightarrow K^+ \pi^- \mu^+ \mu^-$ in the $K^+ \pi^-$ invariant mass range $1330 < m(K^+ \pi^-) < 1530 \text{ MeV}/c^2$ .			
<sup>2</sup> The reported value is converted from the measured $d\mathcal{B}/dq^2 = (0.82 \pm 0.09 \pm 0.063) \times 10^{-8} (\text{GeV}^2/c^4)^{-1}$ by multiplying by the $\Delta q^2 = 4.9 \text{ GeV}^2/c^4$ range.			

 $F_H(B^0 \rightarrow K^0 \mu^+ \mu^-) (1.1 < q^2 < 6.0 \text{ GeV}^2/c^4)$ 

VALUE	DOCUMENT ID	TECN	COMMENT
<b>0.78 ± 0.46 ± 0.09</b>	<sup>1</sup> AAIJ	14o LHCb	$pp$ at 7, 8 TeV
<sup>1</sup> AAIJ 14o reports 68% C.L. interval, which we encode as midpoint with uncertainty as half of the width of interval.			

 $F_H(B^0 \rightarrow K^0 \mu^+ \mu^-) (15.0 < q^2 < 22.0 \text{ GeV}^2/c^4)$ 

VALUE	DOCUMENT ID	TECN	COMMENT
<b>0.34 ± 0.25 ± 0.03</b>	<sup>1</sup> AAIJ	14o LHCb	$pp$ at 7, 8 TeV
<sup>1</sup> AAIJ 14o reports 68% C.L. interval, which we encode as midpoint with uncertainty as half of the width of interval.			

## PRODUCTION ASYMMETRIES

 $A_P(B^0)$ 

VALUE (units $10^{-2}$ )	DOCUMENT ID	TECN	COMMENT
<b>-0.3 ± 0.6 OUR AVERAGE</b>			Error includes scale factor of 1.7. See the ideogram below.
0.44 ± 0.88 ± 0.11	<sup>1</sup> AAIJ	17BF LHCb	$pp$ at 7 TeV
-1.40 ± 0.55 ± 0.10	<sup>1</sup> AAIJ	17BF LHCb	$pp$ at 8 TeV
0.25 ± 0.48 ± 0.05	<sup>2</sup> AABOUD	16G ATLS	$pp$ at 7, 8 TeV
• • • We do not use the following data for averages, fits, limits, etc. • • •			
-0.35 ± 0.76 ± 0.28	<sup>3</sup> AAIJ	14BP LHCb	Repl. by AAIJ 17BF, $pp$ at 7 TeV
<sup>1</sup> AAIJ 17BF uses $B^0 \rightarrow J/\psi K^{*0}$ decays with $B^0$ transverse momenta $p_T$ and rapidities $y$ in the region of $0 < p_T < 30 \text{ GeV}/c$ and $2.1 < y < 4.5$ .			
<sup>2</sup> Based on time-dependent analysis of $B^0 \rightarrow J/\psi K^{*0}$ decay in kinematic range $p_T > 10 \text{ GeV}/c$ and $ \eta  < 2.5$ .			
<sup>3</sup> Based on time-dependent analysis of $B^0 \rightarrow J/\psi K^{*0}$ and $B^0 \rightarrow D^- \pi^+$ in kinematic range $4 < p_T < 30 \text{ GeV}/c$ and $2.5 < \eta < 4.5$ .			









Meson Particle Listings
B0, B±/B0 ADMIXTURE

Table listing meson particles with columns for name, quantum numbers, and references. Includes entries like AUBERT, ARTUSO, BEHRENS, etc.

Table listing meson particles with columns for name, quantum numbers, and references. Includes entries like ABREU, ALBRECHT, AMMAR, etc.

B±/B0 ADMIXTURE

B DECAY MODES

The branching fraction measurements are for an admixture of B mesons at the T(4S). The values quoted assume that B(T(4S) -> B\*B) = 100%.

For inclusive branching fractions, e.g., B -> D± anything, the treatment of multiple D's in the final state must be defined. One possibility would be to count the number of events with one-or-more D's and divide by the total number of B's.

B-bar modes are charge conjugates of the modes below. Reactions indicate the weak decay vertex and do not include mixing.

Table of B decay modes with columns for Mode, Fraction (Gamma\_i/Gamma), and Scale factor/Confidence level. Includes semileptonic and leptonic modes.

Published in B Decays, 2nd Edition, World Scientific, Singapore

## Meson Particle Listings

 $B^\pm/B^0$  ADMIXTURE

$\Gamma_{11}$	$\bar{D}_1(2420)\ell^+\nu_\ell$ anything	( 3.8 ± 1.3 ) × 10 <sup>-3</sup>	S=2.4	$\Gamma_{72}$	$K_4^*(2045)\gamma$	< 1.0	× 10 <sup>-3</sup>	CL=90%
$\Gamma_{12}$	$D\pi\ell^+\nu_\ell$ anything + $D^*\pi\ell^+\nu_\ell$ anything	( 2.6 ± 0.5 ) %	S=1.5	$\Gamma_{73}$	$K\eta'(958)$	( 8.3 ± 1.1 ) × 10 <sup>-5</sup>		
$\Gamma_{13}$	$D\pi\ell^+\nu_\ell$ anything	( 1.5 ± 0.6 ) %		$\Gamma_{74}$	$K^*(892)\eta'(958)$	( 4.1 ± 1.1 ) × 10 <sup>-6</sup>		
$\Gamma_{14}$	$D^*\pi\ell^+\nu_\ell$ anything	( 1.9 ± 0.4 ) %		$\Gamma_{75}$	$K\eta$	< 5.2	× 10 <sup>-6</sup>	CL=90%
$\Gamma_{15}$	$\bar{D}_2^*(2460)\ell^+\nu_\ell$ anything	( 4.4 ± 1.6 ) × 10 <sup>-3</sup>		$\Gamma_{76}$	$K^*(892)\eta$	( 1.8 ± 0.5 ) × 10 <sup>-5</sup>		
$\Gamma_{16}$	$D^*\pi^+\ell^+\nu_\ell$ anything	( 1.00 ± 0.34 ) %		$\Gamma_{77}$	$K\phi\phi$	( 2.3 ± 0.9 ) × 10 <sup>-6</sup>		
$\Gamma_{17}$	$\bar{D}\pi^+\pi^-\ell^+\nu_\ell$	( 1.62 ± 0.32 ) × 10 <sup>-3</sup>		$\Gamma_{78}$	$\bar{b} \rightarrow \bar{s}\gamma$	( 3.49 ± 0.19 ) × 10 <sup>-4</sup>		
$\Gamma_{18}$	$\bar{D}^*\pi^+\pi^-\ell^+\nu_\ell$	( 9.4 ± 3.2 ) × 10 <sup>-4</sup>		$\Gamma_{79}$	$\bar{b} \rightarrow \bar{d}\gamma$	( 9.2 ± 3.0 ) × 10 <sup>-6</sup>		
$\Gamma_{19}$	$D_s^-\ell^+\nu_\ell$ anything	[b] < 7	× 10 <sup>-3</sup> CL=90%	$\Gamma_{80}$	$\bar{b} \rightarrow \bar{s}$ gluon	< 6.8	%	CL=90%
$\Gamma_{20}$	$D_s^-\ell^+\nu_\ell K^+$ anything	[b] < 5	× 10 <sup>-3</sup> CL=90%	$\Gamma_{81}$	$\eta$ anything	( 2.6 ± 0.5 ) × 10 <sup>-4</sup>		
$\Gamma_{21}$	$D_s^-\ell^+\nu_\ell K^0$ anything	[b] < 7	× 10 <sup>-3</sup> CL=90%	$\Gamma_{82}$	$\eta'$ anything	( 4.2 ± 0.9 ) × 10 <sup>-4</sup>		
$\Gamma_{22}$	$X_c\ell^+\nu_\ell$	( 10.65 ± 0.16 ) %		$\Gamma_{83}$	$K^+$ gluon (charmless)	< 1.87	× 10 <sup>-4</sup>	CL=90%
$\Gamma_{23}$	$X_u\ell^+\nu_\ell$	( 2.13 ± 0.30 ) × 10 <sup>-3</sup>		$\Gamma_{84}$	$K^0$ gluon (charmless)	( 1.9 ± 0.7 ) × 10 <sup>-4</sup>		
$\Gamma_{24}$	$K^+\ell^+\nu_\ell$ anything	[b] ( 6.3 ± 0.6 ) %		<b>Light unflavored meson modes</b>				
$\Gamma_{25}$	$K^-\ell^+\nu_\ell$ anything	[b] ( 10 ± 4 ) × 10 <sup>-3</sup>		$\Gamma_{85}$	$\rho\gamma$	( 1.39 ± 0.25 ) × 10 <sup>-6</sup>		S=1.2
$\Gamma_{26}$	$K^0/\bar{K}^0\ell^+\nu_\ell$ anything	[b] ( 4.6 ± 0.5 ) %		$\Gamma_{86}$	$\rho/\omega\gamma$	( 1.30 ± 0.23 ) × 10 <sup>-6</sup>		S=1.2
$\Gamma_{27}$	$\bar{D}^*\tau^+\nu_\tau$	( 9.9 ± 1.2 ) × 10 <sup>-3</sup>		$\Gamma_{87}$	$\pi^\pm$ anything	[f,i] ( 358 ± 7 ) %		
$\Gamma_{28}$	$D^*\tau^+\nu_\tau$	( 1.50 ± 0.08 ) %		$\Gamma_{88}$	$\pi^0$ anything	( 235 ± 11 ) %		
<b>D, D*, or D<sub>s</sub> modes</b>				$\Gamma_{89}$	$\eta$ anything	( 17.6 ± 1.6 ) %		
$\Gamma_{29}$	$D^\pm$ anything	( 23.1 ± 1.2 ) %		$\Gamma_{90}$	$\rho^0$ anything	( 21 ± 5 ) %		
$\Gamma_{30}$	$D^0/\bar{D}^0$ anything	( 61.5 ± 2.9 ) %	S=1.3	$\Gamma_{91}$	$\omega$ anything	< 81	%	CL=90%
$\Gamma_{31}$	$D^*(2010)^\pm$ anything	( 22.5 ± 1.5 ) %		$\Gamma_{92}$	$\phi$ anything	( 3.43 ± 0.12 ) %		
$\Gamma_{32}$	$D^*(2007)^0$ anything	( 26.0 ± 2.7 ) %		$\Gamma_{93}$	$\phi K^*(892)$	< 2.2	× 10 <sup>-5</sup>	CL=90%
$\Gamma_{33}$	$D_s^\pm$ anything	[f] ( 8.3 ± 0.8 ) %		$\Gamma_{94}$	$\bar{b} \rightarrow \bar{d}$ gluon			
$\Gamma_{34}$	$D_s^\pm$ anything	( 6.3 ± 1.0 ) %		$\Gamma_{95}$	$\pi^+$ gluon (charmless)	( 3.7 ± 0.8 ) × 10 <sup>-4</sup>		
$\Gamma_{35}$	$D_s^\pm \bar{D}^*(*)$	( 3.4 ± 0.6 ) %		<b>Baryon modes</b>				
$\Gamma_{36}$	$\bar{D} D_{s0}(2317)$	seen		$\Gamma_{96}$	$\Lambda_c^+ / \bar{\Lambda}_c^-$ anything	( 3.6 ± 0.4 ) %		
$\Gamma_{37}$	$\bar{D} D_{sJ}(2457)$	seen		$\Gamma_{97}$	$\Lambda_c^+$ anything	< 1.3	%	CL=90%
$\Gamma_{38}$	$D^*(*)\bar{D}^*(*)K^0 + D^*(*)\bar{D}^*(*)K^\pm$ [f,g]	( 7.1 ± 2.7 ) %		$\Gamma_{98}$	$\bar{\Lambda}_c^-$ anything	< 7	%	CL=90%
$\Gamma_{39}$	$b \rightarrow c\bar{c}s$	( 22 ± 4 ) %		$\Gamma_{99}$	$\bar{\Lambda}_c^- \ell^+$ anything	< 9	× 10 <sup>-4</sup>	CL=90%
$\Gamma_{40}$	$D_s^*(*)\bar{D}^*(*)$	[f,g] ( 3.9 ± 0.4 ) %		$\Gamma_{100}$	$\bar{\Lambda}_c^- e^+$ anything	< 1.8	× 10 <sup>-3</sup>	CL=90%
$\Gamma_{41}$	$D^*(2010)^\pm$	[f] < 5.9	× 10 <sup>-3</sup> CL=90%	$\Gamma_{101}$	$\bar{\Lambda}_c^- \mu^+$ anything	< 1.4	× 10 <sup>-3</sup>	CL=90%
$\Gamma_{42}$	$D D^*(2010)^\pm + D^* D^\pm$	[f] < 5.5	× 10 <sup>-3</sup> CL=90%	$\Gamma_{102}$	$\bar{\Lambda}_c^- p$ anything	( 2.04 ± 0.33 ) %		
$\Gamma_{43}$	$D D^\pm$	[f] < 3.1	× 10 <sup>-3</sup> CL=90%	$\Gamma_{103}$	$\bar{\Lambda}_c^- p e^+ \nu_e$	< 8	× 10 <sup>-4</sup>	CL=90%
$\Gamma_{44}$	$D_s^*(*)\bar{D}^*(*)X(n\pi^\pm)$	[f,g] ( 9 ± 5 ) %		$\Gamma_{104}$	$\Sigma_c^{--}$ anything	( 3.3 ± 1.7 ) × 10 <sup>-3</sup>		
$\Gamma_{45}$	$D^*(2010)\gamma$	< 1.1	× 10 <sup>-3</sup> CL=90%	$\Gamma_{105}$	$\Sigma_c^-$ anything	< 8	× 10 <sup>-3</sup>	CL=90%
$\Gamma_{46}$	$D_s^+ \pi^-, D_s^{*+} \pi^-, D_s^+ \rho^-, D_s^{*+} \rho^-, D_s^+ \pi^0, D_s^{*+} \pi^0, D_s^+ \eta, D_s^{*+} \eta, D_s^+ \rho^0, D_s^{*+} \rho^0, D_s^+ \omega, D_s^{*+} \omega$	[f] < 4	× 10 <sup>-4</sup> CL=90%	$\Gamma_{106}$	$\Sigma_c^0$ anything	( 3.7 ± 1.7 ) × 10 <sup>-3</sup>		
$\Gamma_{47}$	$D_{s1}(2536)^+$ anything	< 9.5	× 10 <sup>-3</sup> CL=90%	$\Gamma_{107}$	$\Sigma_c^0 N(N = p \text{ or } n)$	< 1.2	× 10 <sup>-3</sup>	CL=90%
<b>Charmonium modes</b>				$\Gamma_{108}$	$\Xi_c^0$ anything, $\Xi_c^0 \rightarrow \Xi^- \pi^+$	( 1.93 ± 0.30 ) × 10 <sup>-4</sup>		S=1.1
$\Gamma_{48}$	$J/\psi(1S)$ anything	( 1.094 ± 0.032 ) %	S=1.1	$\Gamma_{109}$	$\Xi_c^+, \Xi_c^+ \rightarrow \Xi^- \pi^+ \pi^+$	( 4.5 ± 1.3 ) × 10 <sup>-4</sup>		
$\Gamma_{49}$	$J/\psi(1S)$ (direct) anything	( 7.8 ± 0.4 ) × 10 <sup>-3</sup>	S=1.1	$\Gamma_{110}$	$\rho/\bar{\rho}$ anything	[f] ( 8.0 ± 0.4 ) %		
$\Gamma_{50}$	$\psi(2S)$ anything	( 3.07 ± 0.21 ) × 10 <sup>-3</sup>		$\Gamma_{111}$	$\rho/\bar{\rho}$ (direct) anything	[f] ( 5.5 ± 0.5 ) %		
$\Gamma_{51}$	$\chi_{c1}(1P)$ anything	( 3.55 ± 0.27 ) × 10 <sup>-3</sup>	S=1.3	$\Gamma_{112}$	$\bar{p}e^+ \nu_e$ anything	< 5.9	× 10 <sup>-4</sup>	CL=90%
$\Gamma_{52}$	$\chi_{c1}(1P)$ (direct) anything	( 3.08 ± 0.19 ) × 10 <sup>-3</sup>		$\Gamma_{113}$	$\Lambda/\bar{\Lambda}$ anything	[f] ( 4.0 ± 0.5 ) %		
$\Gamma_{53}$	$\chi_{c2}(1P)$ anything	( 10.0 ± 1.7 ) × 10 <sup>-4</sup>	S=1.6	$\Gamma_{114}$	$\Lambda$ anything	seen		
$\Gamma_{54}$	$\chi_{c2}(1P)$ (direct) anything	( 7.5 ± 1.1 ) × 10 <sup>-4</sup>		$\Gamma_{115}$	$\bar{\Lambda}$ anything	seen		
$\Gamma_{55}$	$\eta_c(1S)$ anything	< 9	× 10 <sup>-3</sup> CL=90%	$\Gamma_{116}$	$\Xi^- / \Xi^+$ anything	[f] ( 2.7 ± 0.6 ) × 10 <sup>-3</sup>		
$\Gamma_{56}$	$K\chi_{c1}(3872), \chi_{c1} \rightarrow D^0 \bar{D}^0 \pi^0$	( 1.2 ± 0.4 ) × 10 <sup>-4</sup>		$\Gamma_{117}$	baryons anything	( 6.8 ± 0.6 ) %		
$\Gamma_{57}$	$K\chi_{c1}(3872), \chi_{c1} \rightarrow D^{*0} D^0$	( 8.0 ± 2.2 ) × 10 <sup>-5</sup>		$\Gamma_{118}$	$p\bar{p}$ anything	( 2.47 ± 0.23 ) %		
$\Gamma_{58}$	$KX(3940), X \rightarrow D^{*0} D^0$	< 6.7	× 10 <sup>-5</sup> CL=90%	$\Gamma_{119}$	$\Lambda\bar{\Lambda}/\bar{\Lambda}p$ anything	[f] ( 2.5 ± 0.4 ) %		
$\Gamma_{59}$	$KX(3915), X \rightarrow \omega J/\psi$	[h] ( 7.1 ± 3.4 ) × 10 <sup>-5</sup>		$\Gamma_{120}$	$\Lambda\bar{\Lambda}$ anything	< 5	× 10 <sup>-3</sup>	CL=90%
<b>K or K* modes</b>				<b>Lepton Family number (LF) violating modes or <math>\Delta B = 1</math> weak neutral current (B1) modes</b>				
$\Gamma_{60}$	$K^\pm$ anything	[f] ( 78.9 ± 2.5 ) %		$\Gamma_{121}$	$se^+e^-$	B1 ( 6.7 ± 1.7 ) × 10 <sup>-6</sup>		S=2.0
$\Gamma_{61}$	$K^+$ anything	( 66 ± 5 ) %		$\Gamma_{122}$	$s\mu^+\mu^-$	B1 ( 4.3 ± 1.0 ) × 10 <sup>-6</sup>		
$\Gamma_{62}$	$K^-$ anything	( 13 ± 4 ) %		$\Gamma_{123}$	$s\ell^+\ell^-$	B1 [b] ( 5.8 ± 1.3 ) × 10 <sup>-6</sup>		S=1.8
$\Gamma_{63}$	$K^0/\bar{K}^0$ anything	[f] ( 64 ± 4 ) %		$\Gamma_{124}$	$\pi\ell^+\ell^-$	B1 < 5.9	× 10 <sup>-8</sup>	CL=90%
$\Gamma_{64}$	$K^*(892)^\pm$ anything	( 18 ± 6 ) %		$\Gamma_{125}$	$\pi e^+ e^-$	B1 < 1.10	× 10 <sup>-7</sup>	CL=90%
$\Gamma_{65}$	$K^*(892)^0/\bar{K}^*(892)^0$ anything	[f] ( 14.6 ± 2.6 ) %		$\Gamma_{126}$	$\pi\mu^+\mu^-$	B1 < 5.0	× 10 <sup>-8</sup>	CL=90%
$\Gamma_{66}$	$K^*(892)\gamma$	( 4.2 ± 0.6 ) × 10 <sup>-5</sup>		$\Gamma_{127}$	$Ke^+e^-$	B1 ( 4.4 ± 0.6 ) × 10 <sup>-7</sup>		
$\Gamma_{67}$	$\eta K\gamma$	( 8.5 ± 1.8 ) × 10 <sup>-6</sup>		$\Gamma_{128}$	$K^*(892)e^+e^-$	B1 ( 1.19 ± 0.20 ) × 10 <sup>-6</sup>		S=1.2
$\Gamma_{68}$	$K_1(1400)\gamma$	< 1.27	× 10 <sup>-4</sup> CL=90%	$\Gamma_{129}$	$K\mu^+\mu^-$	B1 ( 4.4 ± 0.4 ) × 10 <sup>-7</sup>		
$\Gamma_{69}$	$K_2^0(1430)\gamma$	( 1.7 ± 0.6 ) × 10 <sup>-5</sup>		$\Gamma_{130}$	$K^*(892)\mu^+\mu^-$	B1 ( 1.06 ± 0.09 ) × 10 <sup>-6</sup>		
$\Gamma_{70}$	$K_2(1770)\gamma$	< 1.2	× 10 <sup>-3</sup> CL=90%	$\Gamma_{131}$	$K\ell^+\ell^-$	B1 ( 4.8 ± 0.4 ) × 10 <sup>-7</sup>		
$\Gamma_{71}$	$K_3^0(1780)\gamma$	< 3.7	× 10 <sup>-5</sup> CL=90%	$\Gamma_{132}$	$K^*(892)\ell^+\ell^-$	B1 ( 1.05 ± 0.10 ) × 10 <sup>-6</sup>		
				$\Gamma_{133}$	$K\nu\bar{\nu}$	B1 < 1.6	× 10 <sup>-5</sup>	CL=90%
				$\Gamma_{134}$	$K^*\nu\bar{\nu}$	B1 < 2.7	× 10 <sup>-5</sup>	CL=90%
				$\Gamma_{135}$	$\pi\nu\bar{\nu}$	B1 < 8	× 10 <sup>-6</sup>	CL=90%
				$\Gamma_{136}$	$\rho\nu\bar{\nu}$	B1 < 2.8	× 10 <sup>-5</sup>	CL=90%
				$\Gamma_{137}$	$se^\pm\mu^\mp$	LF [f] < 2.2	× 10 <sup>-5</sup>	CL=90%

$\Gamma_{138}$	$\pi e^\pm \mu^\mp$	LF	<	9.2	$\times 10^{-8}$	CL=90%
$\Gamma_{139}$	$\rho e^\pm \mu^\mp$	LF	<	3.2	$\times 10^{-6}$	CL=90%
$\Gamma_{140}$	$K e^\pm \mu^\mp$	LF	<	3.8	$\times 10^{-8}$	CL=90%
$\Gamma_{141}$	$K^*(892) e^\pm \mu^\mp$	LF	<	5.1	$\times 10^{-7}$	CL=90%

- [a] These values are model dependent.
- [b] An  $\ell$  indicates an  $e$  or a  $\mu$  mode, not a sum over these modes.
- [c] Here "anything" means at least one particle observed.
- [d] This is a  $B(B^0 \rightarrow D^{*-} \ell^+ \nu_\ell)$  value.
- [e]  $D^{**}$  stands for the sum of the  $D(1^1P_1)$ ,  $D(1^3P_0)$ ,  $D(1^3P_1)$ ,  $D(1^3P_2)$ ,  $D(2^1S_0)$ , and  $D(2^1S_1)$  resonances.
- [f] The value is for the sum of the charge states or particle/antiparticle states indicated.
- [g]  $D^{(*)} \bar{D}^{(*)}$  stands for the sum of  $D^* \bar{D}^*$ ,  $D^* \bar{D}$ ,  $D \bar{D}^*$ , and  $D \bar{D}$ .
- [h]  $X(3915)$  denotes a near-threshold enhancement in the  $\omega J/\psi$  mass spectrum.
- [i] Inclusive branching fractions have a multiplicity definition and can be greater than 100%.

$B^\pm/B^0$  ADMIXTURE BRANCHING RATIOS

$\Gamma(\ell^+ \nu_\ell \text{ anything})/\Gamma_{\text{total}}$   $\Gamma_3/\Gamma$   
 These branching fraction values are model dependent.

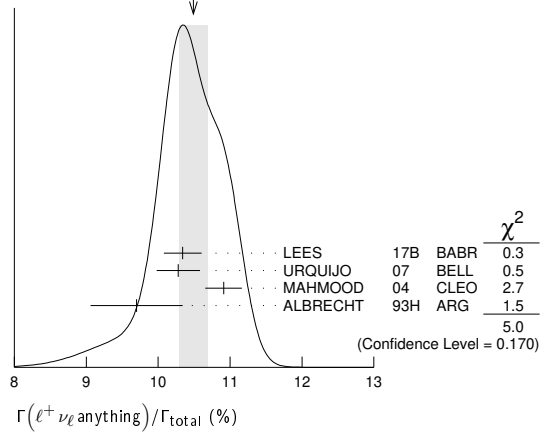
"OUR EVALUATION" assumes lepton universality and is an average using rescaled values of the data listed below. The average and rescaling were performed by the Heavy Flavor Averaging Group (HFLAV) and are described at <https://hflav.web.cern.ch/>. The averaging/rescaling procedure takes into account correlations between the measurements.

VALUE (%)	DOCUMENT ID	TECN	COMMENT
<b>10.86 ± 0.16 OUR EVALUATION</b>			
<b>10.49 ± 0.20 OUR AVERAGE</b>	Error includes scale factor of 1.3. See the ideogram below.		
10.34 ± 0.04 ± 0.26	1 LEES	17B	BABR $e^+ e^- \rightarrow \Upsilon(4S)$
10.28 ± 0.18 ± 0.24	2 URQUIJO	07	BELL $e^+ e^- \rightarrow \Upsilon(4S)$
10.91 ± 0.09 ± 0.24	3 MAHMOOD	04	CLEO $e^+ e^- \rightarrow \Upsilon(4S)$
9.7 ± 0.5 ± 0.4	4 ALBRECHT	93H	ARG $e^+ e^- \rightarrow \Upsilon(4S)$
• • • We do not use the following data for averages, fits, limits, etc. • • •			
9.96 ± 0.19 ± 0.32	5 AUBERT,B	06Y	BABR Repl. by LEES 17B
10.85 ± 0.21 ± 0.36	6 OKABE	05	BELL Repl. by URQUIJO 07
10.83 ± 0.16 ± 0.06	7 AUBERT	04X	BABR Repl. by AUBERT,B 06Y
10.36 ± 0.06 ± 0.23	8 AUBERT,B	04A	BABR $e^+ e^- \rightarrow \Upsilon(4S)$
10.87 ± 0.18 ± 0.30	9 AUBERT	03	BABR Repl. by AUBERT 04X
10.90 ± 0.12 ± 0.49	10 ABE	02Y	BELL Repl. by OKABE 05
10.49 ± 0.17 ± 0.43	11 BARISH	96B	CLE2 Repl. by MAHMOOD 04
10.80 ± 0.20 ± 0.56	12 HENDERSON	92	CLEO $e^+ e^- \rightarrow \Upsilon(4S)$
10.0 ± 0.4 ± 0.3	13 YANAGISAWA	91	CSB2 $e^+ e^- \rightarrow \Upsilon(4S)$
10.3 ± 0.6 ± 0.2	14 ALBRECHT	90H	ARG Direct $e$ at $\Upsilon(4S)$
10.0 ± 0.6 ± 0.2	15 ALBRECHT	90H	ARG Direct $\mu$ at $\Upsilon(4S)$
11.7 ± 0.4 ± 1.0	16 WACHS	89	CBAL Direct $e$ at $\Upsilon(4S)$
12.0 ± 0.7 ± 0.5	CHEN	84	CLEO Direct $e$ at $\Upsilon(4S)$
10.8 ± 0.6 ± 1.0	CHEN	84	CLEO Direct $\mu$ at $\Upsilon(4S)$
11.2 ± 0.9 ± 1.0	LEVYMAN	84	CUSB Direct $e$ at $\Upsilon(4S)$
13.2 ± 0.8 ± 1.4	17 KLOPFEN...	83B	CUSB Direct $e$ at $\Upsilon(4S)$

- 1 LEES 17B measurement is obtained from semileptonic decays to electrons. The result is averaged over  $B^\pm$  and  $B^0$  mesons, assuming lepton universality.
- 2 URQUIJO 07 report a measurement of  $(10.07 \pm 0.18 \pm 0.21)\%$  for the partial branching fraction of  $B \rightarrow e \nu_e X_c$  decay with electron energy above 0.6 GeV. We converted the result to  $B \rightarrow e \nu_e X$  branching fraction.
- 3 Uses charge and angular correlations in  $\Upsilon(4S)$  events with a high-momentum lepton and an additional electron.
- 4 ALBRECHT 93H analysis performed using tagged semileptonic decays of the  $B$ . This technique is almost model independent for the lepton branching ratio.
- 5 The measurements are obtained for charged and neutral  $B$  mesons partial rates of semileptonic decay to electrons with momentum above 0.6 GeV/c in the  $B$  rest frame. The best precision on the ratio is achieved for a momentum threshold of 1.0 GeV:  $B(B^+ \rightarrow e^+ \nu_e X) / B(B^0 \rightarrow e^+ \nu_e X) = 1.074 \pm 0.041 \pm 0.026$ .
- 6 The measurements are obtained for charged and neutral  $B$  mesons partial rates of semileptonic decay to electrons with momentum above 0.6 GeV/c in the  $B$  rest frame, and their ratio of  $B(B^+ \rightarrow e^+ \nu_e X) / B(B^0 \rightarrow e^+ \nu_e X) = 1.08 \pm 0.05 \pm 0.02$ .
- 7 The semileptonic branching ratio,  $|V_{cb}|$  and other heavy-quark parameters are determined from a simultaneous fit to moments of the hadronic-mass and lepton-energy distribution.
- 8 Uses the high-momentum lepton tag method and requires the electron energy above 0.6 GeV.
- 9 Uses the high-momentum lepton tag method. They also report  $|V_{cb}| = 0.0423 \pm 0.0007(\text{exp}) \pm 0.0020(\text{theo.})$ .
- 10 Uses the high-momentum lepton tag method. ABE 02Y also reports  $|V_{cb}| = 0.0408 \pm 0.0010(\text{exp}) \pm 0.0025(\text{theo.})$ . The second error is due to uncertainties of theoretical inputs.
- 11 BARISH 96B analysis performed using tagged semileptonic decays of the  $B$ . This technique is almost model independent for the lepton branching ratio.
- 12 HENDERSON 92 measurement employs  $e$  and  $\mu$ . The systematic error contains 0.004 in quadrature from model dependence. The authors average a variation of the Isgur, Scora,

- Grinstein, and Wise model with that of the Altarelli-Cabibbo-Corbo-Maiani-Martinelli model for semileptonic decays to correct the acceptance.
- 13 YA NAGISAWA 91 also measures an average semileptonic branching ratio at the  $\Upsilon(5S)$  of 9.6–10.5% depending on assumptions about the relative production of different  $B$  meson species.
- 14 ALBRECHT 90H uses the model of ALTARELLI 82 to correct over all lepton momenta.  $0.099 \pm 0.006$  is obtained using ISGUR 89b.
- 15 ALBRECHT 90H uses the model of ALTARELLI 82 to correct over all lepton momenta.  $0.097 \pm 0.006$  is obtained using ISGUR 89b.
- 16 Using data above  $p(e) = 2.4$  GeV, WACHS 89 determine  $\sigma(B \rightarrow e \nu \mu p) / \sigma(B \rightarrow e \nu \text{charm}) < 0.065$  at 90% CL.
- 17 Ratio  $\sigma(b \rightarrow e \nu \mu p) / \sigma(b \rightarrow e \nu \text{charm}) < 0.055$  at CL = 90%.

WEIGHTED AVERAGE  
 10.49 ± 0.20 (Error scaled by 1.3)



$\Gamma(D^- \ell^+ \nu_\ell \text{ anything})/\Gamma(\ell^+ \nu_\ell \text{ anything})$   $\Gamma_4/\Gamma_3$   
 $\ell = e \text{ or } \mu$ .

VALUE	DOCUMENT ID	TECN	COMMENT
<b>0.26 ± 0.07 ± 0.04</b>	1 FULTON	91	CLEO $e^+ e^- \rightarrow \Upsilon(4S)$

1 FULTON 91 uses  $B(D^+ \rightarrow K^- \pi^+ \pi^+) = (9.1 \pm 1.3 \pm 0.4)\%$  as measured by MARK III.

$\Gamma(\bar{D}^0 \ell^+ \nu_\ell \text{ anything})/\Gamma(\ell^+ \nu_\ell \text{ anything})$   $\Gamma_5/\Gamma_3$   
 $\ell = e \text{ or } \mu$ .

VALUE	DOCUMENT ID	TECN	COMMENT
<b>0.67 ± 0.09 ± 0.10</b>	1 FULTON	91	CLEO $e^+ e^- \rightarrow \Upsilon(4S)$

1 FULTON 91 uses  $B(D^0 \rightarrow K^- \pi^+) = (4.2 \pm 0.4 \pm 0.4)\%$  as measured by MARK III.

$\Gamma(\bar{D} \ell^+ \nu_\ell)/\Gamma(\ell^+ \nu_\ell \text{ anything})$   $\Gamma_6/\Gamma_3$

VALUE	DOCUMENT ID	TECN	COMMENT
<b>0.223 ± 0.006 ± 0.009</b>	1 AUBERT	10	BABR $e^+ e^- \rightarrow \Upsilon(4S)$

1 Uses a fully reconstructed  $B$  meson as a tag on the recoil side.

$\Gamma(D^{*-} \ell^+ \nu_\ell \text{ anything})/\Gamma_{\text{total}}$   $\Gamma_7/\Gamma$

VALUE (units $10^{-2}$ )	DOCUMENT ID	TECN	COMMENT
<b>0.67 ± 0.08 ± 0.10</b>	ABDALLAH	04D	DLPH $e^+ e^- \rightarrow Z^0$

• • • We do not use the following data for averages, fits, limits, etc. • • •  
 0.6 ± 0.3 ± 0.1 1 BARISH 95 CLE2  $e^+ e^- \rightarrow \Upsilon(4S)$

1 BARISH 95 use  $B(D^0 \rightarrow K^- \pi^+) = (3.91 \pm 0.08 \pm 0.17)\%$  and  $B(D^{*+} \rightarrow D^0 \pi^+) = (68.1 \pm 1.0 \pm 1.3)\%$ .

$\Gamma(D^{*0} \ell^+ \nu_\ell \text{ anything})/\Gamma_{\text{total}}$   $\Gamma_8/\Gamma$

VALUE (units $10^{-2}$ )	DOCUMENT ID	TECN	COMMENT
0.6 ± 0.6 ± 0.1	1 BARISH	95	CLE2 $e^+ e^- \rightarrow \Upsilon(4S)$

1 BARISH 95 use  $B(D^0 \rightarrow K^- \pi^+) = (3.91 \pm 0.08 \pm 0.17)\%$ ,  $B(D^{*+} \rightarrow D^0 \pi^+) = (68.1 \pm 1.0 \pm 1.3)\%$ ,  $B(D^{*0} \rightarrow D^0 \pi^0) = (63.6 \pm 2.3 \pm 3.3)\%$ .

$\Gamma(D^{**} \ell^+ \nu_\ell)/\Gamma_{\text{total}}$   $\Gamma_{10}/\Gamma$   
 $D^{**}$  stands for the sum of the  $D(1^1P_1)$ ,  $D(1^3P_0)$ ,  $D(1^3P_1)$ ,  $D(1^3P_2)$ ,  $D(2^1S_0)$ , and  $D(2^1S_1)$  resonances.  $\ell = e \text{ or } \mu$ , not sum over  $e$  and  $\mu$  modes.

VALUE	CL%	EVTS	DOCUMENT ID	TECN	COMMENT
<b>0.027 ± 0.005 ± 0.005</b>		63	1 ALBRECHT	93	ARG $e^+ e^- \rightarrow \Upsilon(4S)$

• • • We do not use the following data for averages, fits, limits, etc. • • •  
 < 0.028 95 2 BARISH 95 CLE2  $e^+ e^- \rightarrow \Upsilon(4S)$

- 1 ALBRECHT 93 assumes the GISW model to correct for unseen modes. Using the BHK model, the result becomes  $0.023 \pm 0.006 \pm 0.004$ . Assumes  $B(D^{*+} \rightarrow D^0 \pi^+) = 68.1\%$ ,  $B(D^0 \rightarrow K^- \pi^+) = 3.65\%$ ,  $B(D^0 \rightarrow K^- \pi^+ \pi^- \pi^+) = 7.5\%$ . We have taken their average  $e$  and  $\mu$  value.
- 2 BARISH 95 use  $B(D^0 \rightarrow K^- \pi^+) = (3.91 \pm 0.08 \pm 0.17)\%$ , assume all nonresonant channels are zero, and use GISW model for relative abundances of  $D^{**}$  states.

## Meson Particle Listings

 $B^\pm/B^0$  ADMIXTURE $\Gamma(\bar{D}_1(2420)\ell^+\nu_\ell\text{anything})/\Gamma_{\text{total}}$   $\Gamma_{11}/\Gamma$ 

VALUE	DOCUMENT ID	TECN	COMMENT
<b>0.0038 ± 0.0013 OUR AVERAGE</b>	Error includes scale factor of 2.4.		
0.0033 ± 0.0006	<sup>1</sup> ABAZOV 05o D0		$p\bar{p}$ at 1.96 TeV
0.0074 ± 0.0016	<sup>2</sup> BUSKULIC 97b ALEP		$e^+e^- \rightarrow Z$
• • • We do not use the following data for averages, fits, limits, etc. • • •			
seen	<sup>3</sup> BUSKULIC 95b ALEP		Repl. by BUSKULIC 97b

- <sup>1</sup> Assumes  $B(D_1 \rightarrow D^*\pi) = 1$ ,  $B(D_1 \rightarrow D^*\pi^\pm) = 2/3$ , and  $B(b \rightarrow B) = 0.397$ .  
<sup>2</sup> BUSKULIC 97b assumes  $B(D_1(2420) \rightarrow D^*\pi) = 1$ ,  $B(D_1(2420) \rightarrow D^*\pi^\pm) = 2/3$ , and  $B(b \rightarrow B) = 0.378 \pm 0.022$ .  
<sup>3</sup> BUSKULIC 95b reports  $f_B \times B(B \rightarrow \bar{D}_1(2420)^0\ell^+\nu_\ell\text{anything}) \times B(\bar{D}_1(2420)^0 \rightarrow \bar{D}^*(2010)^-\pi^+) = (2.04 \pm 0.58 \pm 0.34)10^{-3}$ , where  $f_B$  is the production fraction for a single  $B$  charge state.

 $\Gamma(D\pi\ell^+\nu_\ell\text{anything}) + \Gamma(D^*\pi\ell^+\nu_\ell\text{anything})/\Gamma_{\text{total}}$   $\Gamma_{12}/\Gamma$ 

VALUE	DOCUMENT ID	TECN	COMMENT
<b>0.026 ± 0.005 OUR AVERAGE</b>	Error includes scale factor of 1.5.		
0.0340 ± 0.0052 ± 0.0032	<sup>1</sup> ABREU 00r DLPH		$e^+e^- \rightarrow Z$
0.0226 ± 0.0029 ± 0.0033	<sup>2</sup> BUSKULIC 97b ALEP		$e^+e^- \rightarrow Z$

- <sup>1</sup> Assumes no contribution from  $B_s$  and  $b$  baryons. Further assumes contributions from single pion ( $D\pi$  and  $D^*\pi$ ) states only, allowing isospin conservation to relate the relative  $\pi^0$  and  $\pi^\pm$  rates.  
<sup>2</sup> BUSKULIC 97b assumes  $B(b \rightarrow B) = 0.378 \pm 0.022$  and uses isospin invariance by assuming that all observed  $D^0\pi^+$ ,  $D^{*0}\pi^+$ ,  $D^+\pi^-$ , and  $D^{*+}\pi^-$  are from  $D^{**}$  states. A correction has been applied to account for the production of  $B_s^0$  and  $L_b^0$ .

 $\Gamma(D\pi\ell^+\nu_\ell\text{anything})/\Gamma_{\text{total}}$   $\Gamma_{13}/\Gamma$ 

VALUE	DOCUMENT ID	TECN	COMMENT
<b>0.0154 ± 0.0061</b>	ABREU 00r DLPH		$e^+e^- \rightarrow Z$

 $\Gamma(D^*\pi\ell^+\nu_\ell\text{anything})/\Gamma_{\text{total}}$   $\Gamma_{14}/\Gamma$ 

VALUE	DOCUMENT ID	TECN	COMMENT
<b>0.0186 ± 0.0038</b>	ABREU 00r DLPH		$e^+e^- \rightarrow Z$

 $\Gamma(\bar{D}_2^*(2460)\ell^+\nu_\ell\text{anything})/\Gamma_{\text{total}}$   $\Gamma_{15}/\Gamma$ 

VALUE	CL%	DOCUMENT ID	TECN	COMMENT
<b>0.0044 ± 0.0016</b>		<sup>1</sup> ABAZOV 05o D0		$p\bar{p}$ at 1.96 TeV
• • • We do not use the following data for averages, fits, limits, etc. • • •				
<0.0065	95	<sup>2</sup> BUSKULIC 97b ALEP		$e^+e^- \rightarrow Z$
not seen		<sup>3</sup> BUSKULIC 95b ALEP		$e^+e^- \rightarrow Z$

- <sup>1</sup> Assumes  $B(D_2^* \rightarrow D^*\pi^\pm) = 0.30 \pm 0.06$  and  $B(b \rightarrow B) = 0.397$ .  
<sup>2</sup> A revised number based on BUSKULIC 97b which assumes  $B(D_2^*(2460) \rightarrow D^*\pi^\pm) = 0.20$  and  $B(b \rightarrow B) = 0.378 \pm 0.022$ .  
<sup>3</sup> BUSKULIC 95b reports  $f_B \times B(B \rightarrow \bar{D}_2^*(2460)^0\ell^+\nu_\ell\text{anything}) \times B(\bar{D}_2^*(2460)^0 \rightarrow \bar{D}^*(2010)^-\pi^+) \leq 0.81 \times 10^{-3}$  at CL=95%, where  $f_B$  is the production fraction for a single  $B$  charge state.

 $\Gamma(B \rightarrow \bar{D}_2^*(2460)\ell^+\nu_\ell\text{anything}) \times B(D_2^*(2460) \rightarrow D^-\pi^+)$  $\Gamma(B \rightarrow \bar{D}_1(2420)\ell^+\nu_\ell\text{anything}) \times B(\bar{D}_1(2420) \rightarrow D^-\pi^+)$ 

VALUE	DOCUMENT ID	TECN	COMMENT
<b>0.39 ± 0.09 ± 0.12</b>	ABAZOV 05o D0		$p\bar{p}$ at 1.96 TeV

 $\Gamma(D^-\pi^+\ell^+\nu_\ell\text{anything})/\Gamma_{\text{total}}$   $\Gamma_{16}/\Gamma$ 

VALUE (units $10^{-3}$ )	DOCUMENT ID	TECN	COMMENT
<b>10.0 ± 2.7 ± 2.1</b>	<sup>1</sup> BUSKULIC 95b ALEP		$e^+e^- \rightarrow Z$
<sup>1</sup> BUSKULIC 95b reports $f_B \times B(B \rightarrow \bar{D}^*(2010)^-\pi^+\ell^+\nu_\ell\text{anything}) = (3.7 \pm 1.0 \pm 0.7)10^{-3}$ . Above value assumes $f_B = 0.37 \pm 0.03$ .			

 $\Gamma(\bar{D}\pi^+\pi^-\ell^+\nu_\ell)/\Gamma(\bar{D}\ell^+\nu_\ell)$   $\Gamma_{17}/\Gamma_6$ 

VALUE (units $10^{-2}$ )	DOCUMENT ID	TECN	COMMENT
<b>6.7 ± 1.0 ± 0.8</b>	<sup>1</sup> LEES 16 BABR		$e^+e^- \rightarrow \Upsilon(4S)$

- <sup>1</sup> Measurement used electrons and muons as leptons.

 $\Gamma(\bar{D}^*\pi^+\pi^-\ell^+\nu_\ell)/\Gamma(D^*\ell^+\nu_\ell)$   $\Gamma_{18}/\Gamma_9$ 

VALUE (units $10^{-2}$ )	DOCUMENT ID	TECN	COMMENT
<b>1.9 ± 0.5 ± 0.4</b>	<sup>1</sup> LEES 16 BABR		$e^+e^- \rightarrow \Upsilon(4S)$

- <sup>1</sup> Measurement used electrons and muons as leptons.

 $\Gamma(D_s^-\ell^+\nu_\ell\text{anything})/\Gamma_{\text{total}}$   $\Gamma_{19}/\Gamma$ 

VALUE	CL%	DOCUMENT ID	TECN	COMMENT
<b>&lt;7 × 10<sup>-3</sup></b>	90	<sup>1</sup> ALBRECHT 93E ARG		$e^+e^- \rightarrow \Upsilon(4S)$

- <sup>1</sup> ALBRECHT 93E reports  $< 0.012$  from a measurement of  $[\Gamma(B \rightarrow D_s^-\ell^+\nu_\ell\text{anything})/\Gamma_{\text{total}}] \times [B(D_s^+ \rightarrow \phi\pi^+)]$  assuming  $B(D_s^+ \rightarrow \phi\pi^+) = 0.027$ , which we rescale to our best value  $B(D_s^+ \rightarrow \phi\pi^+) = 4.5 \times 10^{-2}$ .

 $\Gamma(D_s^-\ell^+\nu_\ell K^+\text{anything})/\Gamma_{\text{total}}$   $\Gamma_{20}/\Gamma$ 

VALUE	CL%	DOCUMENT ID	TECN	COMMENT
<b>&lt;5 × 10<sup>-3</sup></b>	90	<sup>1</sup> ALBRECHT 93E ARG		$e^+e^- \rightarrow \Upsilon(4S)$

- <sup>1</sup> ALBRECHT 93E reports  $< 0.008$  from a measurement of  $[\Gamma(B \rightarrow D_s^-\ell^+\nu_\ell K^+\text{anything})/\Gamma_{\text{total}}] \times [B(D_s^+ \rightarrow \phi\pi^+)]$  assuming  $B(D_s^+ \rightarrow \phi\pi^+) = 0.027$ , which we rescale to our best value  $B(D_s^+ \rightarrow \phi\pi^+) = 4.5 \times 10^{-2}$ .

 $\Gamma(D_s^-\ell^+\nu_\ell K^0\text{anything})/\Gamma_{\text{total}}$   $\Gamma_{21}/\Gamma$ 

VALUE	CL%	DOCUMENT ID	TECN	COMMENT
<b>&lt;7 × 10<sup>-3</sup></b>	90	<sup>1</sup> ALBRECHT 93E ARG		$e^+e^- \rightarrow \Upsilon(4S)$

- <sup>1</sup> ALBRECHT 93E reports  $< 0.012$  from a measurement of  $[\Gamma(B \rightarrow D_s^-\ell^+\nu_\ell K^0\text{anything})/\Gamma_{\text{total}}] \times [B(D_s^+ \rightarrow \phi\pi^+)]$  assuming  $B(D_s^+ \rightarrow \phi\pi^+) = 0.027$ , which we rescale to our best value  $B(D_s^+ \rightarrow \phi\pi^+) = 4.5 \times 10^{-2}$ .

 $\Gamma(X_c\ell^+\nu_\ell)/\Gamma_{\text{total}}$   $\Gamma_{22}/\Gamma$ 

"OUR EVALUATION" is an average using rescaled values of the data listed below. The average and rescaling were performed by the Heavy Flavor Averaging Group (HFLAV) and are described at <https://hflav.web.cern.ch/>. The averaging/rescaling procedure takes into account correlations between the measurements.

**0.65 ± 0.16 OUR EVALUATION****0.29 ± 0.19 OUR AVERAGE**

VALUE (%)	DOCUMENT ID	TECN	COMMENT
10.18 ± 0.03 ± 0.24	<sup>1</sup> LEES 17b BABR		$e^+e^- \rightarrow \Upsilon(4S)$
10.44 ± 0.19 ± 0.22	<sup>2</sup> URQUIJO 07 BELL		$e^+e^- \rightarrow \Upsilon(4S)$
• • • We do not use the following data for averages, fits, limits, etc. • • •			
10.64 ± 0.17 ± 0.06	<sup>3</sup> AUBERT 10a BABR		Repl. by LEES 17b
10.61 ± 0.16 ± 0.06	<sup>4</sup> AUBERT 04x BABR		Repl. by AUBERT 10a

- <sup>1</sup> The measurement is obtained from semileptonic decays to electrons  $B \rightarrow X_c e \nu$ , and using a theoretical model (GAMBINO 07, GAMBINO 11) to predict the contribution from  $B \rightarrow X_c \mu \nu$ . The result is averaged over  $B^\pm$  and  $B^0$  mesons, assuming lepton universality.  
<sup>2</sup> Measured the independent  $B^+$  and  $B^0$  partial branching fractions with electron energy above 0.4 GeV.  
<sup>3</sup> Obtained from a combined fit to the moments of observed spectra in inclusive  $B \rightarrow X_c \ell^+ \nu_\ell$  decay.  
<sup>4</sup> The semileptonic branching ratio,  $|V_{cb}|$  and other heavy-quark parameters are determined from a simultaneous fit to moments of the hadronic-mass and lepton-energy distribution.

 $\Gamma(X_u\ell^+\nu_\ell)/\Gamma_{\text{total}}$   $\Gamma_{23}/\Gamma$ 

"OUR EVALUATION" is an average using rescaled values of the data listed below. The average and rescaling were performed by the Heavy Flavor Averaging Group (HFLAV) and are described at <https://hflav.web.cern.ch/>. The averaging/rescaling procedure takes into account correlations between the measurements.

**2.13 ± 0.30 OUR EVALUATION****1.665 ± 0.087 ± 0.103**

VALUE (units $10^{-3}$ )	DOCUMENT ID	TECN	COMMENT
1.665 ± 0.087 ± 0.103	<sup>1</sup> LEES 17b BABR		$e^+e^- \rightarrow \Upsilon(4S)$
2.01 ± 0.15 ± 0.25	<sup>2</sup> LEES 12r BABR		$e^+e^- \rightarrow \Upsilon(4S)$
2.53 ± 0.24 ± 0.24	<sup>3</sup> AUBERT,B 05x BABR		$e^+e^- \rightarrow \Upsilon(4S)$
2.80 ± 0.52 ± 0.41	<sup>4</sup> LIMOSANI 05 BELL		$e^+e^- \rightarrow \Upsilon(4S)$
1.77 ± 0.29 ± 0.38	<sup>5</sup> BORNHEIM 02 CLE2		$e^+e^- \rightarrow \Upsilon(4S)$

- • • We do not use the following data for averages, fits, limits, etc. • • •  
<sup>6</sup> URQUIJO 10 BELL  $e^+e^- \rightarrow \Upsilon(4S)$   
<sup>7</sup> AUBERT 08as BABR Repl. by LEES 12r  
<sup>8</sup> AUBERT 06h BABR Repl. by LEES 17b  
<sup>9,10</sup> AUBERT 04i BABR Repl. by AUBERT,B 05x

- <sup>1</sup> Obtained from the partial rate  $\Delta B = (1.554 \pm 0.082 \pm 0.095 \pm 0.086) \times 10^{-3}$  for the electron momentum interval of 0.8–2.7 GeV/c based on GGOU1 method ( $X_c \ell \nu$ ,  $m_c$  constraint fit of SF parameters).

- <sup>2</sup> Measures several partial branching fractions in different phase space regions. The most precise result on the full branching fraction is obtained in the region for lepton momentum in  $B$  rest frame  $p_\ell^* > 1$  GeV/c, where the measured partial branching fraction is  $\Delta B = (1.80 \pm 0.13 \pm 0.15) \times 10^{-3}$ . The acceptance in that region is reported in a private communication by the Authors to be 0.894. The corresponding  $|V_{ub}|$  from the BLPN method is  $(4.28 \pm 0.15 \pm 0.18 \pm 0.19) \times 10^{-3}$ , where the last uncertainty comes from theoretical prediction.

- <sup>3</sup> Determined from the partial rate  $\Delta B = (4.41 \pm 0.42 \pm 0.42) \times 10^{-4}$  measured for electron energy  $> 2$  GeV and hadronic mass squared  $< 3.5$  GeV<sup>2</sup>, and calculated acceptance 0.174 in that region. The  $V_{ub}$  is measured as  $(4.41 \pm 0.30 \pm 0.65 \pm 0.28) \times 10^{-3}$ .

- <sup>4</sup> Uses electrons in the momentum interval 1.9–2.6 GeV/c in the center-of-mass frame. The  $V_{ub}$  is found to be  $(5.08 \pm 0.47 \pm 0.49 \pm 0.48) \times 10^{-3}$ .

- <sup>5</sup> BORNHEIM 02 uses the observed yield of leptons from semileptonic  $B$  decays in the end-point momentum interval 2.2–2.6 GeV/c with recent CLEO-2 data on  $B \rightarrow X_s \gamma$ . The  $V_{ub}$  is found to be  $(4.08 \pm 0.34 \pm 0.53) \times 10^{-3}$ .

- <sup>6</sup> Uses a multivariate analysis method and requires lepton momentum in the  $B$  rest frame,  $p_\ell^{*B} > 1.0$  GeV/c.

- <sup>7</sup> Measures several partial branching fractions in different phase space regions. The most precise result is obtained in the region for hadronic mass  $M_X < 1.55$  GeV/c<sup>2</sup>, and is  $\Delta B = (1.18 \pm 0.09 \pm 0.07) \times 10^{-3}$ . The corresponding  $|V_{ub}|$  from the BLPN method

See key on page 999

Meson Particle Listings  
 $B^{\pm}/B^0$  ADMIXTURE

is  $(4.27 \pm 0.16 \pm 0.13 \pm 0.30) \times 10^{-3}$ , where the last uncertainty comes from the theoretical prediction of the partial rate in the given phase-space region.

<sup>8</sup> Obtained from the partial rate  $\Delta B = (0.572 \pm 0.041 \pm 0.065) \times 10^{-3}$  for the electron momentum interval of 2.0–2.6 GeV/c based on BLNP method.

<sup>9</sup> Used BaBar measurement of Semileptonic branching fraction  $B(B \rightarrow X \ell \nu_{\ell}) = (10.87 \pm 0.18 \pm 0.30)\%$  to convert the ratio of rates to branching fraction.

<sup>10</sup> The third error includes the systematics and theoretical errors summed in quadrature.

$\Gamma(X_u \ell^+ \nu_{\ell})/\Gamma(\ell^+ \nu_{\ell} \text{ anything})$   $\Gamma_{23}/\Gamma_3$   
 $\ell$  denotes e or  $\mu$ , not the sum. These experiments measure this ratio in very limited momentum intervals.

VALUE (units $10^{-2}$ )	CL%	EVTS	DOCUMENT ID	TECN	COMMENT
<b>2.06 ± 0.25 ± 0.42</b>			1 AUBERT	04i BABR	$e^+e^- \rightarrow \Upsilon(4S)$
			2 ALBRECHT	94c ARG	$e^+e^- \rightarrow \Upsilon(4S)$
		107	3 BARTELT	93b CLE2	$e^+e^- \rightarrow \Upsilon(4S)$
		77	4 ALBRECHT	91c ARG	$e^+e^- \rightarrow \Upsilon(4S)$
		41	5 ALBRECHT	90 ARG	$e^+e^- \rightarrow \Upsilon(4S)$
		76	6 FULTON	90 CLEO	$e^+e^- \rightarrow \Upsilon(4S)$
<4.0	90		7 BEHREND	87 CLEO	$e^+e^- \rightarrow \Upsilon(4S)$
<4.0	90		8 CHEN	84 CLEO	Direct e at $\Upsilon(4S)$
<5.5	90		KLOPFEN...	83b CUSB	Direct e at $\Upsilon(4S)$

<sup>1</sup> The third error includes the systematics and theoretical errors summed in quadrature.  
<sup>2</sup> ALBRECHT 94c find  $\Gamma(b \rightarrow c)/\Gamma(b \rightarrow \text{all}) = 0.99 \pm 0.02 \pm 0.04$ .  
<sup>3</sup> BARTELT 93b (CLEO II) measures an excess of  $107 \pm 15 \pm 11$  leptons in the lepton momentum interval 2.3–2.6 GeV/c which is attributed to  $b \rightarrow u \ell \nu_{\ell}$ . This corresponds to a model-dependent partial branching ratio  $\Delta_{ub}$  between  $(1.15 \pm 0.16 \pm 0.15) \times 10^{-4}$ , as evaluated using the KS model (KOERNER 88), and  $(1.54 \pm 0.22 \pm 0.20) \times 10^{-4}$  using the ACCMM model (ARTUSO 93). The corresponding values of  $|V_{ub}/V_{cb}|$  are  $0.056 \pm 0.006$  and  $0.076 \pm 0.008$ , respectively.  
<sup>4</sup> ALBRECHT 91c result supersedes ALBRECHT 90. Two events are fully reconstructed providing evidence for the  $b \rightarrow u$  transition. Using the model of ALTARELLI 82, they obtain  $|V_{ub}/V_{cb}| = 0.11 \pm 0.012$  from 77 leptons in the 2.3–2.6 GeV momentum range.  
<sup>5</sup> ALBRECHT 90 observes  $41 \pm 10$  excess e and  $\mu$  (lepton) events in the momentum interval  $p = 2.3$ – $2.6$  GeV signaling the presence of the  $b \rightarrow u$  transition. The events correspond to a model-dependent measurement of  $|V_{ub}/V_{cb}| = 0.10 \pm 0.01$ .  
<sup>6</sup> FULTON 90 observe  $76 \pm 20$  excess e and  $\mu$  (lepton) events in the momentum interval  $p = 2.4$ – $2.6$  GeV signaling the presence of the  $b \rightarrow u$  transition. The average branching ratio,  $(1.8 \pm 0.4 \pm 0.3) \times 10^{-4}$ , corresponds to a model-dependent measurement of approximately  $|V_{ub}/V_{cb}| = 0.1$  using  $B(b \rightarrow c \ell \nu) = 10.2 \pm 0.2 \pm 0.7\%$ .  
<sup>7</sup> The quoted possible limits range from 0.018 to 0.04 for the ratio, depending on which model or momentum range is chosen. We select the most conservative limit they have calculated. This corresponds to a limit on  $|V_{ub}/V_{cb}| < 0.20$ . While the endpoint technique employed is more robust than their previous results in CHEN 84, these results do not provide a numerical improvement in the limit.

$\Gamma(K^+ \ell^+ \nu_{\ell} \text{ anything})/\Gamma(\ell^+ \nu_{\ell} \text{ anything})$   $\Gamma_{24}/\Gamma_3$   
 $\ell$  denotes e or  $\mu$ , not the sum.

VALUE	DOCUMENT ID	TECN	COMMENT
<b>0.58 ± 0.05 OUR AVERAGE</b>			
$0.594 \pm 0.021 \pm 0.056$	ALBRECHT 94c ARG		$e^+e^- \rightarrow \Upsilon(4S)$
$0.54 \pm 0.07 \pm 0.06$	1 ALAM 87b CLEO		$e^+e^- \rightarrow \Upsilon(4S)$

<sup>1</sup> ALAM 87b measurement relies on lepton-kaon correlations.

$\Gamma(K^- \ell^+ \nu_{\ell} \text{ anything})/\Gamma(\ell^+ \nu_{\ell} \text{ anything})$   $\Gamma_{25}/\Gamma_3$   
 $\ell$  denotes e or  $\mu$ , not the sum.

VALUE	DOCUMENT ID	TECN	COMMENT
<b>0.092 ± 0.035 OUR AVERAGE</b>			
$0.086 \pm 0.011 \pm 0.044$	ALBRECHT 94c ARG		$e^+e^- \rightarrow \Upsilon(4S)$
$0.10 \pm 0.05 \pm 0.02$	1 ALAM 87b CLEO		$e^+e^- \rightarrow \Upsilon(4S)$

<sup>1</sup> ALAM 87b measurement relies on lepton-kaon correlations.

$\Gamma(K^0/\bar{K}^0 \ell^+ \nu_{\ell} \text{ anything})/\Gamma(\ell^+ \nu_{\ell} \text{ anything})$   $\Gamma_{26}/\Gamma_3$   
 $\ell$  denotes e or  $\mu$ , not the sum. Sum over  $K^0$  and  $\bar{K}^0$  states.

VALUE	DOCUMENT ID	TECN	COMMENT
<b>0.42 ± 0.05 OUR AVERAGE</b>			
$0.452 \pm 0.038 \pm 0.056$	1 ALBRECHT 94c ARG		$e^+e^- \rightarrow \Upsilon(4S)$
$0.39 \pm 0.06 \pm 0.04$	2 ALAM 87b CLEO		$e^+e^- \rightarrow \Upsilon(4S)$

<sup>1</sup> ALBRECHT 94c assume a  $K^0/\bar{K}^0$  multiplicity twice that of  $K_S^0$ .

<sup>2</sup> ALAM 87b measurement relies on lepton-kaon correlations.

$\Gamma(\bar{D} \tau^+ \nu_{\tau})/\Gamma(\bar{D} \ell^+ \nu_{\ell})$   $\Gamma_{27}/\Gamma_6$   
 “OUR EVALUATION” is an average using rescaled values of the data listed below. The average and rescaling were performed by the Heavy Flavor Averaging Group (HFLAV) and are described at <https://hflav.web.cern.ch/>. The averaging/rescaling procedure takes into account correlations between the measurements.

VALUE (units $10^{-2}$ )	DOCUMENT ID	TECN	COMMENT
<b>40.7 ± 4.6 OUR EVALUATION</b>			
<b>41.1 ± 5.0 OUR AVERAGE</b>			
$37.5 \pm 6.4 \pm 2.6$	1,2 HUSCHLE 15 BELL		$e^+e^- \rightarrow \Upsilon(4S)$
$44.0 \pm 5.8 \pm 4.2$	1,2 LEES 12d BABR		$e^+e^- \rightarrow \Upsilon(4S)$
	••• We do not use the following data for averages, fits, limits, etc. •••		
$4.16 \pm 11.7 \pm 5.2$	1 AUBERT 08n BABR		Repl. by LEES 12d
	<sup>1</sup> Uses a fully reconstructed B meson as a tag on the recoil side.		
	<sup>2</sup> Uses $\tau^+ \rightarrow e^+ \nu_e \bar{\nu}_{\tau}$ and $\tau^+ \rightarrow \mu^+ \nu_{\mu} \bar{\nu}_{\tau}$ and $e^+$ or $\mu^+$ as $\ell^+$ . Obtained from simultaneous fit to $B^+$ and $B^0$ assuming isospin symmetry.		

$\Gamma(D^* \tau^+ \nu_{\tau})/\Gamma(D^* \ell^+ \nu_{\ell})$   $\Gamma_{28}/\Gamma_9$   
 “OUR EVALUATION” is an average using rescaled values of the data listed below. The average and rescaling were performed by the Heavy Flavor Averaging Group (HFLAV) and are described at <https://hflav.web.cern.ch/>. The averaging/rescaling procedure takes into account correlations between the measurements.

VALUE (units $10^{-2}$ )	DOCUMENT ID	TECN	COMMENT
<b>30.4 ± 1.5 OUR EVALUATION</b>			
<b>30.7 ± 2.1 OUR AVERAGE</b>			
$27.0 \pm 3.5 \pm 2.8$	1 HIROSE 17 BELL		$e^+e^- \rightarrow \Upsilon(4S)$
$29.3 \pm 3.8 \pm 1.5$	2 HUSCHLE 15 BELL		$e^+e^- \rightarrow \Upsilon(4S)$
$33.2 \pm 2.4 \pm 1.8$	2 LEES 12d BABR		$e^+e^- \rightarrow \Upsilon(4S)$
	••• We do not use the following data for averages, fits, limits, etc. •••		
$29.7 \pm 5.6 \pm 1.8$	3 AUBERT 08n BABR		Repl. by LEES 12d
	<sup>1</sup> Uses a fully reconstructed B meson as a tag on the recoil side.		
	<sup>2</sup> Uses $\tau^+ \rightarrow e^+ \nu_e \bar{\nu}_{\tau}$ and $\tau^+ \rightarrow \mu^+ \nu_{\mu} \bar{\nu}_{\tau}$ and $e^+$ or $\mu^+$ as $\ell^+$ . Obtained from simultaneous fit to $B^+$ and $B^0$ assuming isospin symmetry. Uses a fully reconstructed B meson as a tag on the recoil side.		
	<sup>3</sup> Uses a fully reconstructed B meson as a tag on the recoil side. The results are normalized to the $B^+$ decay rate.		

$\langle n_c \rangle$

VALUE	DOCUMENT ID	TECN	COMMENT
<b>1.10 ± 0.05</b>	1 GIBBONS 97b CLE2		$e^+e^- \rightarrow \Upsilon(4S)$
	••• We do not use the following data for averages, fits, limits, etc. •••		
$0.98 \pm 0.16 \pm 0.12$	2 ALAM 87b CLEO		$e^+e^- \rightarrow \Upsilon(4S)$
	<sup>1</sup> GIBBONS 97b from charm counting using $B(D_s^+ \rightarrow \phi \pi) = 0.036 \pm 0.009$ and $B(\Lambda_c^+ \rightarrow p K^- \pi^+) = 0.044 \pm 0.006$ .		
	<sup>2</sup> From the difference between $K^-$ and $K^+$ widths. ALAM 87b measurement relies on lepton-kaon correlations. It does not consider the possibility of $B^+B^-$ mixing. We have thus removed it from the average.		

$\Gamma(D^{\pm} \text{ anything})/\Gamma_{\text{total}}$   $\Gamma_{29}/\Gamma$

VALUE	EVTS	DOCUMENT ID	TECN	COMMENT
<b>0.231 ± 0.012 OUR AVERAGE</b>				
$0.230 \pm 0.012 \pm 0.004$		1 GIBBONS 97b CLE2		$e^+e^- \rightarrow \Upsilon(4S)$
$0.241 \pm 0.037 \pm 0.004$		2 BORTOLETTO92 CLEO		$e^+e^- \rightarrow \Upsilon(4S)$
$0.223 \pm 0.051 \pm 0.004$		3 ALBRECHT 91h ARG		$e^+e^- \rightarrow \Upsilon(4S)$
	••• We do not use the following data for averages, fits, limits, etc. •••			
$0.203 \pm 0.048 \pm 0.003$	20k	4 BORTOLETTO87 CLEO		Sup. by BORTOLETTO 92

<sup>1</sup> GIBBONS 97b reports  $[\Gamma(B \rightarrow D^{\pm} \text{ anything})/\Gamma_{\text{total}}] \times [B(D^+ \rightarrow K^- 2\pi^+)] = 0.0216 \pm 0.0008 \pm 0.00082$  which we divide by our best value  $B(D^+ \rightarrow K^- 2\pi^+) = (9.38 \pm 0.16) \times 10^{-2}$ . Our first error is their experiment’s error and our second error is the systematic error from using our best value.  
<sup>2</sup> BORTOLETTO 92 reports  $[\Gamma(B \rightarrow D^{\pm} \text{ anything})/\Gamma_{\text{total}}] \times [B(D^+ \rightarrow K^- 2\pi^+)] = 0.0226 \pm 0.0030 \pm 0.0018$  which we divide by our best value  $B(D^+ \rightarrow K^- 2\pi^+) = (9.38 \pm 0.16) \times 10^{-2}$ . Our first error is their experiment’s error and our second error is the systematic error from using our best value.  
<sup>3</sup> ALBRECHT 91h reports  $[\Gamma(B \rightarrow D^{\pm} \text{ anything})/\Gamma_{\text{total}}] \times [B(D^+ \rightarrow K^- 2\pi^+)] = 0.0209 \pm 0.0027 \pm 0.0040$  which we divide by our best value  $B(D^+ \rightarrow K^- 2\pi^+) = (9.38 \pm 0.16) \times 10^{-2}$ . Our first error is their experiment’s error and our second error is the systematic error from using our best value.  
<sup>4</sup> BORTOLETTO 87 reports  $[\Gamma(B \rightarrow D^{\pm} \text{ anything})/\Gamma_{\text{total}}] \times [B(D^+ \rightarrow K^- 2\pi^+)] = 0.019 \pm 0.004 \pm 0.002$  which we divide by our best value  $B(D^+ \rightarrow K^- 2\pi^+) = (9.38 \pm 0.16) \times 10^{-2}$ . Our first error is their experiment’s error and our second error is the systematic error from using our best value.

$\Gamma(D^0/\bar{D}^0 \text{ anything})/\Gamma_{\text{total}}$   $\Gamma_{30}/\Gamma$

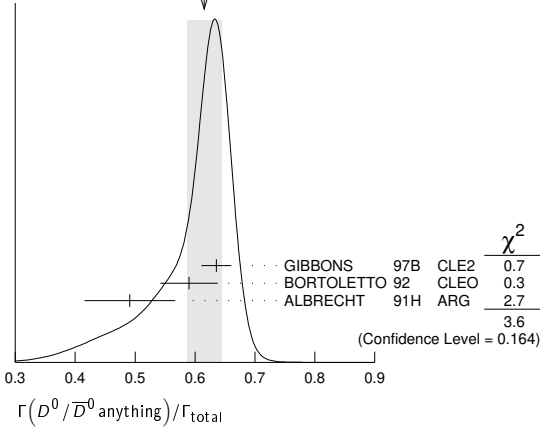
VALUE	EVTS	DOCUMENT ID	TECN	COMMENT
<b>0.615 ± 0.029 OUR AVERAGE</b>				
		Error includes scale factor of 1.3. See the ideogram below.		
$0.635 \pm 0.024 \pm 0.005$		1 GIBBONS 97b CLE2		$e^+e^- \rightarrow \Upsilon(4S)$
$0.590 \pm 0.047 \pm 0.005$		2 BORTOLETTO92 CLEO		$e^+e^- \rightarrow \Upsilon(4S)$
$0.491 \pm 0.074 \pm 0.004$		3 ALBRECHT 91h ARG		$e^+e^- \rightarrow \Upsilon(4S)$
	••• We do not use the following data for averages, fits, limits, etc. •••			
$0.532 \pm 0.065 \pm 0.004$	21k	4 BORTOLETTO87 CLEO		$e^+e^- \rightarrow \Upsilon(4S)$
$0.608 \pm 0.183 \pm 0.005$		5 GREEN 83 CLEO		Repl. by BORTOLETTO 87
	<sup>1</sup> GIBBONS 97b reports $[\Gamma(B \rightarrow D^0/\bar{D}^0 \text{ anything})/\Gamma_{\text{total}}] \times [B(D^0 \rightarrow K^- \pi^+)] = 0.0251 \pm 0.0006 \pm 0.00075$ which we divide by our best value $B(D^0 \rightarrow K^- \pi^+) = (3.950 \pm 0.031) \times 10^{-2}$ . Our first error is their experiment’s error and our second error is the systematic error from using our best value.			
	<sup>2</sup> BORTOLETTO 92 reports $[\Gamma(B \rightarrow D^0/\bar{D}^0 \text{ anything})/\Gamma_{\text{total}}] \times [B(D^0 \rightarrow K^- \pi^+)] = 0.0233 \pm 0.0012 \pm 0.0014$ which we divide by our best value $B(D^0 \rightarrow K^- \pi^+) = (3.950 \pm 0.031) \times 10^{-2}$ . Our first error is their experiment’s error and our second error is the systematic error from using our best value.			
	<sup>3</sup> ALBRECHT 91h reports $[\Gamma(B \rightarrow D^0/\bar{D}^0 \text{ anything})/\Gamma_{\text{total}}] \times [B(D^0 \rightarrow K^- \pi^+)] = 0.0194 \pm 0.0015 \pm 0.0025$ which we divide by our best value $B(D^0 \rightarrow K^- \pi^+) = (3.950 \pm 0.031) \times 10^{-2}$ . Our first error is their experiment’s error and our second error is the systematic error from using our best value.			
	<sup>4</sup> BORTOLETTO 87 reports $[\Gamma(B \rightarrow D^0/\bar{D}^0 \text{ anything})/\Gamma_{\text{total}}] \times [B(D^0 \rightarrow K^- \pi^+)] = 0.0210 \pm 0.0015 \pm 0.0021$ which we divide by our best value $B(D^0 \rightarrow K^- \pi^+) = (3.950 \pm 0.031) \times 10^{-2}$ . Our first error is their experiment’s error and our second error is the systematic error from using our best value.			
	<sup>5</sup> GREEN 83 reports $[\Gamma(B \rightarrow D^0/\bar{D}^0 \text{ anything})/\Gamma_{\text{total}}] \times [B(D^0 \rightarrow K^- \pi^+)] = 0.024 \pm 0.006 \pm 0.004$ which we divide by our best value $B(D^0 \rightarrow K^- \pi^+) = (3.950 \pm 0.031) \times$			

# Meson Particle Listings

## $B^\pm/B^0$ ADMIXTURE

$10^{-2}$ . Our first error is their experiment's error and our second error is the systematic error from using our best value.

WEIGHTED AVERAGE  
0.615±0.029 (Error scaled by 1.3)



### $\Gamma(D^- \ell^+ \nu_\ell \text{ anything})/\Gamma(D^0 \ell^+ \nu_\ell \text{ anything})$ $\Gamma_4/\Gamma_5$

VALUE	DOCUMENT ID	TECN	COMMENT
<b>0.359±0.006±0.009</b>	<sup>1</sup> AAIJ	19AD LHCb	$p\bar{p}$ at 13 TeV

<sup>1</sup> AAIJ 19AD uses  $D^0 \rightarrow K^- \pi^+$  and  $D^+ \rightarrow K^- \pi^+ \pi^+$  modes.

### $\Gamma(D^*(2010)^\pm \text{ anything})/\Gamma_{\text{total}}$ $\Gamma_{31}/\Gamma$

VALUE	EVTS	DOCUMENT ID	TECN	COMMENT
<b>0.225±0.015 OUR AVERAGE</b>				
0.247±0.019±0.01		<sup>1</sup> GIBBONS 97B	CLE2	$e^+e^- \rightarrow \Upsilon(4S)$
0.205±0.019±0.007		<sup>2</sup> ALBRECHT 96D	ARG	$e^+e^- \rightarrow \Upsilon(4S)$
0.230±0.028±0.009		<sup>3</sup> BORTOLETTO 92	CLEO	$e^+e^- \rightarrow \Upsilon(4S)$
0.283±0.053±0.002		<sup>4</sup> ALBRECHT 91H	ARG	Sup. by ALBRECHT 96D
0.22 ± 0.04 $^{+0.07}_{-0.04}$	5200	<sup>5</sup> BORTOLETTO 87	CLEO	$e^+e^- \rightarrow \Upsilon(4S)$
0.27 ± 0.06 $^{+0.08}_{-0.06}$	510	<sup>6</sup> CSORNA 85	CLEO	Repl. by BORTOLETTO 87

<sup>1</sup> GIBBONS 97B reports  $B(B \rightarrow D^*(2010)^+ \text{ anything}) = 0.239 \pm 0.015 \pm 0.014 \pm 0.009$  using CLEO measured  $D$  and  $D^*$  branching fractions. We rescale to our PDG 96 values of  $D$  and  $D^*$  branching ratios. Our first error is their experiment's error and our second error is the systematic error from using our best value.

<sup>2</sup> ALBRECHT 96D reports  $B(B \rightarrow D^*(2010)^+ \text{ anything}) = 0.196 \pm 0.019$  using CLEO measured  $B(D^*(2010)^+ \rightarrow D^0 \pi^+) = 0.681 \pm 0.01 \pm 0.013$ ,  $B(D^0 \rightarrow K^- \pi^+) = 0.0401 \pm 0.0014$ ,  $B(D^0 \rightarrow K^- \pi^+ \pi^+) = 0.081 \pm 0.005$ . We rescale to our PDG 96 values of  $D$  and  $D^*$  branching ratios. Our first error is their experiment's error and our second error is the systematic error from using our best value.

<sup>3</sup> BORTOLETTO 92 reports  $B(B \rightarrow D^*(2010)^+ \text{ anything}) = 0.25 \pm 0.03 \pm 0.04$  using MARK II  $B(D^*(2010)^+ \rightarrow D^0 \pi^+) = 0.57 \pm 0.06$  and  $B(D^0 \rightarrow K^- \pi^+) = 0.042 \pm 0.008$ . We rescale to our PDG 96 values of  $D$  and  $D^*$  branching ratios. Our first error is their experiment's error and our second error is the systematic error from using our best value.

<sup>4</sup> ALBRECHT 91H reports  $0.348 \pm 0.060 \pm 0.035$  from a measurement of  $[\Gamma(B \rightarrow D^*(2010)^\pm \text{ anything})/\Gamma_{\text{total}}] \times [B(D^*(2010)^+ \rightarrow D^0 \pi^+)]$  assuming  $B(D^*(2010)^+ \rightarrow D^0 \pi^+) = 0.55 \pm 0.04$ , which we rescale to our best value  $B(D^*(2010)^+ \rightarrow D^0 \pi^+) = (67.7 \pm 0.5) \times 10^{-2}$ . Our first error is their experiment's error and our second error is the systematic error from using our best value. Uses the PDG 90  $B(D^0 \rightarrow K^- \pi^+) = 0.0371 \pm 0.0025$ .

<sup>5</sup> BORTOLETTO 87 uses old MARK III (BALTRUSAITIS 86E) branching ratios  $B(D^0 \rightarrow K^- \pi^+) = 0.056 \pm 0.004 \pm 0.003$  and also assumes  $B(D^*(2010)^+ \rightarrow D^0 \pi^+) = 0.60^{+0.08}_{-0.15}$ . The product branching ratio for  $B(B \rightarrow D^*(2010)^+) B(D^*(2010)^+ \rightarrow D^0 \pi^+)$  is  $0.13 \pm 0.02 \pm 0.012$ . Superseded by BORTOLETTO 92.

<sup>6</sup>  $V-A$  momentum spectrum used to extrapolate below  $p = 1$  GeV. We correct the value assuming  $B(D^0 \rightarrow K^- \pi^+) = 0.042 \pm 0.006$  and  $B(D^+ \rightarrow D^0 \pi^+) = 0.6^{+0.08}_{-0.15}$ . The product branching fraction is  $B(B \rightarrow D^*(2010)^+) B(D^*(2010)^+ \rightarrow D^0 \pi^+) = (68 \pm 15 \pm 9) \times 10^{-4}$ .

### $\Gamma(D^*(2007)^0 \text{ anything})/\Gamma_{\text{total}}$ $\Gamma_{32}/\Gamma$

VALUE	DOCUMENT ID	TECN	COMMENT
<b>0.260±0.023±0.015</b>	<sup>1</sup> GIBBONS 97B	CLE2	$e^+e^- \rightarrow \Upsilon(4S)$

<sup>1</sup> GIBBONS 97B reports  $B(B \rightarrow D^*(2007)^0 \text{ anything}) = 0.247 \pm 0.012 \pm 0.018 \pm 0.018$  using CLEO measured  $D$  and  $D^*$  branching fractions. We rescale to our PDG 96 values of  $D$  and  $D^*$  branching ratios. Our first error is their experiment's error and our second error is the systematic error from using our best value.

### $\Gamma(D_s^\pm \text{ anything})/\Gamma_{\text{total}}$ $\Gamma_{33}/\Gamma$

VALUE	EVTS	DOCUMENT ID	TECN	COMMENT
<b>0.083±0.008 OUR AVERAGE</b>				
0.089±0.010±0.008		<sup>1</sup> ARTUSO 05B	CLE2	$e^+e^- \rightarrow \Upsilon(5S)$
0.087±0.005±0.008		<sup>2</sup> AUBERT 02G	BABR	$e^+e^- \rightarrow \Upsilon(4S)$
0.065±0.011±0.006		<sup>3</sup> ALBRECHT 92G	ARG	$e^+e^- \rightarrow \Upsilon(4S)$
0.068±0.010±0.006	257	<sup>4</sup> BORTOLETTO 90	CLEO	$e^+e^- \rightarrow \Upsilon(4S)$
0.085±0.022±0.008		<sup>5</sup> HAAS 86	CLEO	$e^+e^- \rightarrow \Upsilon(4S)$
0.094±0.007±0.008		<sup>6</sup> GIBAUT 96	CLE2	Repl. by ARTUSO 05B
0.094±0.024±0.008		<sup>7</sup> ALBRECHT 87H	ARG	$e^+e^- \rightarrow \Upsilon(4S)$

<sup>1</sup> ARTUSO 05B reports  $0.0905 \pm 0.0025 \pm 0.0140$  from a measurement of  $[\Gamma(B \rightarrow D_s^\pm \text{ anything})/\Gamma_{\text{total}}] \times [B(D_s^\pm \rightarrow \phi \pi^\pm)]$  assuming  $B(D_s^\pm \rightarrow \phi \pi^\pm) = (4.4 \pm 0.5) \times 10^{-2}$ , which we rescale to our best value  $B(D_s^\pm \rightarrow \phi \pi^\pm) = (4.5 \pm 0.4) \times 10^{-2}$ . Our first error is their experiment's error and our second error is the systematic error from using our best value.

<sup>2</sup> AUBERT 02G reports  $[\Gamma(B \rightarrow D_s^\pm \text{ anything})/\Gamma_{\text{total}}] \times [B(D_s^\pm \rightarrow \phi \pi^\pm)] = 0.00393 \pm 0.00007 \pm 0.00021$  which we divide by our best value  $B(D_s^\pm \rightarrow \phi \pi^\pm) = (4.5 \pm 0.4) \times 10^{-2}$ . Our first error is their experiment's error and our second error is the systematic error from using our best value.

<sup>3</sup> ALBRECHT 92G reports  $[\Gamma(B \rightarrow D_s^\pm \text{ anything})/\Gamma_{\text{total}}] \times [B(D_s^\pm \rightarrow \phi \pi^\pm)] = 0.00292 \pm 0.00039 \pm 0.00031$  which we divide by our best value  $B(D_s^\pm \rightarrow \phi \pi^\pm) = (4.5 \pm 0.4) \times 10^{-2}$ . Our first error is their experiment's error and our second error is the systematic error from using our best value.

<sup>4</sup> BORTOLETTO 90 reports  $[\Gamma(B \rightarrow D_s^\pm \text{ anything})/\Gamma_{\text{total}}] \times [B(D_s^\pm \rightarrow \phi \pi^\pm)] = 0.00306 \pm 0.00047$  which we divide by our best value  $B(D_s^\pm \rightarrow \phi \pi^\pm) = (4.5 \pm 0.4) \times 10^{-2}$ . Our first error is their experiment's error and our second error is the systematic error from using our best value.

<sup>5</sup> HAAS 86 reports  $[\Gamma(B \rightarrow D_s^\pm \text{ anything})/\Gamma_{\text{total}}] \times [B(D_s^\pm \rightarrow \phi \pi^\pm)] = 0.0038 \pm 0.0010$  which we divide by our best value  $B(D_s^\pm \rightarrow \phi \pi^\pm) = (4.5 \pm 0.4) \times 10^{-2}$ . Our first error is their experiment's error and our second error is the systematic error from using our best value. 64 ± 22% decays are 2-body.

<sup>6</sup> GIBAUT 96 reports  $0.1211 \pm 0.0039 \pm 0.0088$  from a measurement of  $[\Gamma(B \rightarrow D_s^\pm \text{ anything})/\Gamma_{\text{total}}] \times [B(D_s^\pm \rightarrow \phi \pi^\pm)]$  assuming  $B(D_s^\pm \rightarrow \phi \pi^\pm) = 0.035$ , which we rescale to our best value  $B(D_s^\pm \rightarrow \phi \pi^\pm) = (4.5 \pm 0.4) \times 10^{-2}$ . Our first error is their experiment's error and our second error is the systematic error from using our best value.

<sup>7</sup> ALBRECHT 87H reports  $[\Gamma(B \rightarrow D_s^\pm \text{ anything})/\Gamma_{\text{total}}] \times [B(D_s^\pm \rightarrow \phi \pi^\pm)] = 0.0042 \pm 0.0009 \pm 0.0006$  which we divide by our best value  $B(D_s^\pm \rightarrow \phi \pi^\pm) = (4.5 \pm 0.4) \times 10^{-2}$ . Our first error is their experiment's error and our second error is the systematic error from using our best value. 46 ± 16% of  $B \rightarrow D_s X$  decays are 2-body. Superseded by ALBRECHT 92G.

### $\Gamma(D_s^{\pm*} \text{ anything})/\Gamma_{\text{total}}$ $\Gamma_{34}/\Gamma$

VALUE	DOCUMENT ID	TECN	COMMENT
<b>0.063±0.009±0.006</b>	<sup>1</sup> AUBERT 02G	BABR	$e^+e^- \rightarrow \Upsilon(4S)$

<sup>1</sup> AUBERT 02G reports  $[\Gamma(B \rightarrow D_s^{\pm*} \text{ anything})/\Gamma_{\text{total}}] \times [B(D_s^{\pm*} \rightarrow \phi \pi^\pm)] = 0.00284 \pm 0.00029 \pm 0.00025$  which we divide by our best value  $B(D_s^{\pm*} \rightarrow \phi \pi^\pm) = (4.5 \pm 0.4) \times 10^{-2}$ . Our first error is their experiment's error and our second error is the systematic error from using our best value.

### $\Gamma(D_s^{\pm*} \bar{D}^{(*)})/\Gamma(D_s^{\pm*} \text{ anything})$ $\Gamma_{35}/\Gamma_{34}$

VALUE	DOCUMENT ID	TECN	COMMENT
<b>0.533±0.037±0.037</b>	AUBERT	02G	BABR $e^+e^- \rightarrow \Upsilon(4S)$

### $\Gamma(\bar{D}_{S0}(2317))/\Gamma_{\text{total}}$ $\Gamma_{36}/\Gamma$

VALUE	DOCUMENT ID	TECN	COMMENT
seen	<sup>1</sup> KROKOVNY 03B	BELL	$e^+e^- \rightarrow \Upsilon(4S)$

<sup>1</sup> The product branching ratio for  $B(B \rightarrow \bar{D}_{S0}(2317)^+) \times B(D_{S0}(2317)^+ \rightarrow D_s \pi^0)$  is measured to be  $(8.5^{+2.1}_{-1.9} \pm 2.6) \times 10^{-4}$ .

### $\Gamma(\bar{D}_{S0}(2457))/\Gamma_{\text{total}}$ $\Gamma_{37}/\Gamma$

VALUE	DOCUMENT ID	TECN	COMMENT
seen	<sup>1</sup> KROKOVNY 03B	BELL	$e^+e^- \rightarrow \Upsilon(4S)$

<sup>1</sup> The product branching ratio for  $B(B \rightarrow \bar{D}_{S0}(2457)^+) \times B(D_{S0}(2457)^+ \rightarrow D_s^* \pi^0, D_s^* \gamma)$  are measured to be  $(17.8^{+4.5}_{-3.9} \pm 5.3) \times 10^{-4}$  and  $(6.7^{+1.3}_{-1.2} \pm 2.0) \times 10^{-4}$ , respectively.

### $[\Gamma(D^{(*)} \bar{D}^{(*)} K^0) + \Gamma(D^{(*)} \bar{D}^{(*)} K^\pm)]/\Gamma_{\text{total}}$ $\Gamma_{38}/\Gamma$

VALUE	DOCUMENT ID	TECN	COMMENT
<b>0.071±0.025±0.010</b> $^{+0.015}_{-0.009}$	<sup>1</sup> BARATE 98Q	ALEP	$e^+e^- \rightarrow Z$

<sup>1</sup> The systematic error includes the uncertainties due to the charm branching ratios.

### $\Gamma(b \rightarrow c \bar{c} s)/\Gamma_{\text{total}}$ $\Gamma_{39}/\Gamma$

VALUE	DOCUMENT ID	TECN	COMMENT
<b>0.219±0.037</b>	<sup>1</sup> COAN 98	CLE2	$e^+e^- \rightarrow \Upsilon(4S)$

<sup>1</sup> COAN 98 uses  $D-\ell$  correlation.

See key on page 999

Meson Particle Listings
B±/B0 ADMIXTURE

Table with 5 columns: VALUE, DOCUMENT ID, TECN, COMMENT, and Γ40/Γ33. Row 1: 0.469 ± 0.017 OUR AVERAGE. Row 2: 0.464 ± 0.013 ± 0.015. Row 3: 0.56 ± 0.21 ± 0.09 / -0.15 -0.08. Row 4: 0.457 ± 0.019 ± 0.037. Row 5: 0.58 ± 0.07 ± 0.09. Row 6: 0.56 ± 0.10.

1 BARATE 98Q measures B(B → Ds(\*)D(\*)̄) = 0.056 ± 0.021 + 0.009 - 0.019 / -0.015 -0.008 -0.011, where the third error results from the uncertainty on the different D branching ratios and is dominated by the uncertainty on B(Ds+ → φπ+). We divide B(B → Ds(\*)D(\*)̄) by our best value of B(B → Ds anything) = 0.1 ± 0.025.

Table with 5 columns: VALUE, CL%, DOCUMENT ID, TECN, COMMENT, and Γ41/Γ. Row 1: <5.9 x 10^-3, 90, BARATE, 98Q, ALEP, e+e- → Z.

Table with 5 columns: VALUE, CL%, DOCUMENT ID, TECN, COMMENT, and Γ42/Γ. Row 1: <5.5 x 10^-3, 90, BARATE, 98Q, ALEP, e+e- → Z.

Table with 5 columns: VALUE, CL%, DOCUMENT ID, TECN, COMMENT, and Γ43/Γ. Row 1: <3.1 x 10^-3, 90, BARATE, 98Q, ALEP, e+e- → Z.

Table with 5 columns: VALUE, DOCUMENT ID, TECN, COMMENT, and Γ44/Γ. Row 1: 0.094 ± 0.040 + 0.034 / -0.031 -0.024, 1 BARATE, 98Q, ALEP, e+e- → Z.

1 The systematic error includes the uncertainties due to the charm branching ratios.

Table with 5 columns: VALUE, CL%, DOCUMENT ID, TECN, COMMENT, and Γ45/Γ. Row 1: <1.1 x 10^-3, 90, 1 LESIAK, 92, CBAL, e+e- → T(4S).

1 LESIAK 92 set a limit on the inclusive process B(b → sγ) < 2.8 x 10^-3 at 90% CL for the range of masses of 892-2045 MeV, independent of assumptions about s-quark hadronization.

Table with 5 columns: VALUE, CL%, DOCUMENT ID, TECN, COMMENT, and Γ46/Γ. Row 1: <4 x 10^-4, 90, 1 ALEXANDER, 93B, CLE2, e+e- → T(4S).

1 ALEXANDER 93B reports < 4.8 x 10^-4 from a measurement of [Γ(B → Ds+ π-, Ds+ π-, Ds+ ρ-, Ds+ ρ-, Ds+ π0, Ds+ π0, Ds+ η, Ds+ η, Ds+ ρ0, Ds+ ρ0, Ds+ ω, Ds+ ω)/Γtotal] × [B(Ds+ → φπ+)] assuming B(Ds+ → φπ+) = 0.037, which we rescale to our best value B(Ds+ → φπ+) = 4.5 x 10^-2. This branching ratio limit provides a model-dependent upper limit |Vub|/|Vcb| < 0.16 at CL=90%.

Table with 5 columns: VALUE, CL%, DOCUMENT ID, TECN, COMMENT, and Γ47/Γ. Row 1: <0.0095, 90, 1 BISHAI, 98, CLE2, e+e- → T(4S).

1 Assuming factorization, the decay constant fD\_s1+ is at least a factor of 2.5 times smaller than fD\_s+.

Table with 5 columns: VALUE (units 10^-2), EVTS, DOCUMENT ID, TECN, COMMENT, and Γ48/Γ. Row 1: 1.094 ± 0.032 OUR AVERAGE. Row 2: 1.057 ± 0.012 ± 0.040. Row 3: 1.121 ± 0.013 ± 0.042. Row 4: 1.29 ± 0.45 ± 0.01. Row 5: 1.24 ± 0.27 ± 0.01. Row 6: 1.35 ± 0.24 ± 0.01. Row 7: 1.12 ± 0.06 ± 0.01. Row 8: 1.4 ± 0.6 / -0.5. Row 9: 1.1 ± 0.21 ± 0.23.

1 AUBERT 03F also reports the momentum distribution and helicity of J/ψ → e+e- in the T(4S) center-of-mass frame. 2 MASCHMANN 90 reports (1.12 ± 0.33 ± 0.25) x 10^-2 from a measurement of [Γ(B → J/ψ(1S) anything)/Γtotal] × [B(J/ψ(1S) → e+e-)] assuming B(J/ψ(1S) → e+e-) = 0.069 ± 0.009, which we rescale to our best value B(J/ψ(1S) → e+e-) = (5.971 ± 0.032) x 10^-2. Our first error is their experiment's error and our second error is the systematic error from using our best value. 3 ALBRECHT 87D reports (1.07 ± 0.16 ± 0.22) x 10^-2 from a measurement of [Γ(B → J/ψ(1S) anything)/Γtotal] × [B(J/ψ(1S) → e+e-)] assuming B(J/ψ(1S) → e+e-) = 0.069 ± 0.009, which we rescale to our best value B(J/ψ(1S) → e+e-) = (5.971 ± 0.032) x 10^-2. Our first error is their experiment's error and our second error is the systematic error from using our best value. 4 ALAM 86 reports (1.09 ± 0.16 ± 0.21) x 10^-2 from a measurement of [Γ(B → J/ψ(1S) anything)/Γtotal] × [B(J/ψ(1S) → μ+μ-)] assuming B(J/ψ(1S) → μ+μ-) = 0.074 ± 0.012, which we rescale to our best value B(J/ψ(1S) → μ+μ-) = (5.961 ± 0.033) x 10^-2. Our first error is their experiment's error and our second error is the systematic error from using our best value. 5 BALEST 95B reports (1.12 ± 0.04 ± 0.06) x 10^-2 from a measurement of [Γ(B → J/ψ(1S) anything)/Γtotal] × [B(J/ψ(1S) → e+e-)] assuming B(J/ψ(1S) → e+e-) = 0.0599 ± 0.0025, which we rescale to our best value B(J/ψ(1S) → e+e-) = (5.971 ± 0.032) x 10^-2. Our first error is their experiment's error and our second error is the systematic error from using our best value. They measure J/ψ(1S) → e+e- and μ+μ- and use PDG 1994 values for the branching fractions. The rescaling is the same for either mode so we use e+e-. 6 Statistical and systematic errors were added in quadrature. ALBRECHT 85H also report a CL = 90% limit of 0.007 for B → J/ψ(1S) + X where mX < 1 GeV. 7 Dimoun and dielectron events used.

0.032) x 10^-2. Our first error is their experiment's error and our second error is the systematic error from using our best value. ALBRECHT 87D find the branching ratio for J/ψ not from ψ(2S) to be 0.0081 ± 0.0023. 4 ALAM 86 reports (1.09 ± 0.16 ± 0.21) x 10^-2 from a measurement of [Γ(B → J/ψ(1S) anything)/Γtotal] × [B(J/ψ(1S) → μ+μ-)] assuming B(J/ψ(1S) → μ+μ-) = 0.074 ± 0.012, which we rescale to our best value B(J/ψ(1S) → μ+μ-) = (5.961 ± 0.033) x 10^-2. Our first error is their experiment's error and our second error is the systematic error from using our best value. 5 BALEST 95B reports (1.12 ± 0.04 ± 0.06) x 10^-2 from a measurement of [Γ(B → J/ψ(1S) anything)/Γtotal] × [B(J/ψ(1S) → e+e-)] assuming B(J/ψ(1S) → e+e-) = 0.0599 ± 0.0025, which we rescale to our best value B(J/ψ(1S) → e+e-) = (5.971 ± 0.032) x 10^-2. Our first error is their experiment's error and our second error is the systematic error from using our best value. They measure J/ψ(1S) → e+e- and μ+μ- and use PDG 1994 values for the branching fractions. The rescaling is the same for either mode so we use e+e-. 6 Statistical and systematic errors were added in quadrature. ALBRECHT 85H also report a CL = 90% limit of 0.007 for B → J/ψ(1S) + X where mX < 1 GeV. 7 Dimoun and dielectron events used.

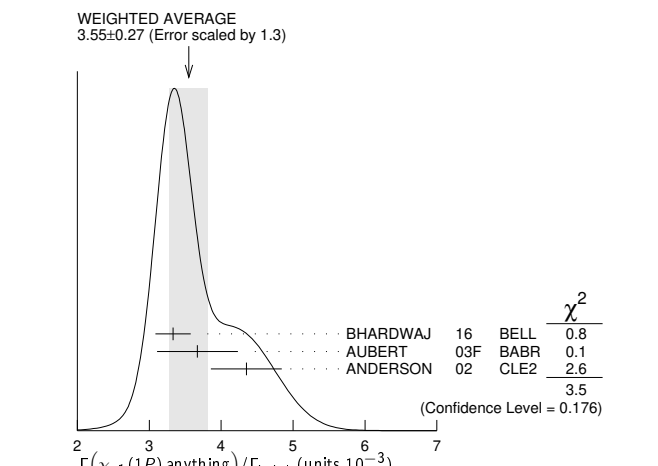
Table with 5 columns: VALUE, DOCUMENT ID, TECN, COMMENT, and Γ49/Γ. Row 1: 0.0078 ± 0.0004 OUR AVERAGE. Row 2: 0.00740 ± 0.00023 ± 0.00043. Row 3: 0.00813 ± 0.00017 ± 0.00037. Row 4: 0.0080 ± 0.0008.

1 AUBERT 03F also reports the helicity of J/ψ → e+e- produced directly in B decay. 2 Also reports the measurement of J/ψ → e+e- polarization produced directly from B decay. 3 BALEST 95B assume PDG 1994 values for sub mode branching ratios. J/ψ(1S) mesons are reconstructed in J/ψ(1S) → e+e- and J/ψ(1S) → μ+μ-. The B → J/ψ(1S) X branching ratio contains J/ψ(1S) mesons directly from B decays and also from feeddown through ψ(2S) → J/ψ(1S), χc1(1P) → J/ψ(1S), or χc2(1P) → J/ψ(1S). Using the measured inclusive rates, BALEST 95B corrects for the feeddown and finds the B → J/ψ(1S) (direct) X branching ratio.

Table with 5 columns: VALUE, EVTS, DOCUMENT ID, TECN, COMMENT, and Γ50/Γ. Row 1: 0.00307 ± 0.00021 OUR AVERAGE. Row 2: 0.00297 ± 0.00020 ± 0.00020. Row 3: 0.00316 ± 0.00014 ± 0.00028. Row 4: 0.0046 ± 0.0017 ± 0.0011. Row 5: 0.0034 ± 0.0004 ± 0.0003.

1 Also reports the measurement of ψ(2S) → e+e- polarization produced directly from B decay. 2 BALEST 95B assume PDG 1994 values for sub mode branching ratios. They find B(B → ψ(2S) X, ψ(2S) → e+e-) = 0.30 ± 0.05 ± 0.04 and B(B → ψ(2S) X, ψ(2S) → J/ψ(1S) π+ π-) = 0.37 ± 0.05 ± 0.05. Weighted average is quoted for B(B → ψ(2S) X).

Table with 5 columns: VALUE (units 10^-3), EVTS, DOCUMENT ID, TECN, COMMENT, and Γ51/Γ. Row 1: 3.55 ± 0.27 OUR AVERAGE. Row 2: 3.33 ± 0.05 ± 0.24. Row 3: 3.67 ± 0.35 ± 0.44. Row 4: 4.35 ± 0.29 ± 0.40. Row 5: 3.63 ± 0.22 ± 0.34. Row 6: 3.30 ± 0.35 ± 0.09. Row 7: 4.0 ± 0.6 ± 0.4. Row 8: 10.5 ± 3.5 ± 2.5.



1 Assumes equal production of B+ and B0 at the T(4S).



# Meson Particle Listings

## $B^\pm/B^0$ ADMIXTURE

<sup>2</sup>ABE 02L uses PDG 01 values for  $B(J/\psi(1S) \rightarrow \ell^+ \ell^-)$  and  $B(\chi_{c1,c2} \rightarrow J/\psi(1S)\gamma)$ .

<sup>3</sup>CHEN 01 reports  $0.00414 \pm 0.00031 \pm 0.00040$  from a measurement of  $[\Gamma(B \rightarrow \chi_{c1}(1P) \text{ anything})/\Gamma_{\text{total}}] \times [B(\chi_{c1}(1P) \rightarrow \gamma J/\psi(1S))]$  assuming  $B(\chi_{c1}(1P) \rightarrow \gamma J/\psi(1S)) = 0.273 \pm 0.016$ , which we rescale to our best value  $B(\chi_{c1}(1P) \rightarrow \gamma J/\psi(1S)) = (34.3 \pm 1.0) \times 10^{-2}$ . Our first error is their experiment's error and our second error is the systematic error from using our best value. Assumes equal production of  $B^+$  and  $B^0$  at the  $T(4S)$ .

<sup>4</sup>BALEST 95B assume  $B(\chi_{c1}(1P) \rightarrow J/\psi(1S)\gamma) = (27.3 \pm 1.6) \times 10^{-2}$ , the PDG 1994 value. Fit to  $\psi$ -photon invariant mass distribution allows for a  $\chi_{c1}(1P)$  and a  $\chi_{c2}(1P)$  component.

<sup>5</sup>ALBRECHT 92E assumes no  $\chi_{c2}(1P)$  production.

### $\Gamma(\chi_{c1}(1P) \text{ (direct) anything})/\Gamma_{\text{total}}$ $\Gamma_{52}/\Gamma$

VALUE (units $10^{-3}$ )	DOCUMENT ID	TECN	COMMENT
<b>3.08 ± 0.19 OUR AVERAGE</b>			
$3.03 \pm 0.05 \pm 0.24$	<sup>1</sup> BHARDWAJ 16	BELL	$e^+ e^- \rightarrow T(4S)$
$3.41 \pm 0.35 \pm 0.42$	AUBERT 03F	BABR	$e^+ e^- \rightarrow T(4S)$
$3.1 \pm 0.4 \pm 0.1$	<sup>2</sup> CHEN 01	CLE2	$e^+ e^- \rightarrow T(4S)$
$3.32 \pm 0.22 \pm 0.34$	<sup>3</sup> ABE 02L	BELL	Repl. by BHARDWAJ 16
$3.7 \pm 0.7$	<sup>4</sup> BALEST 95B	CLE2	Repl. by CHEN 01

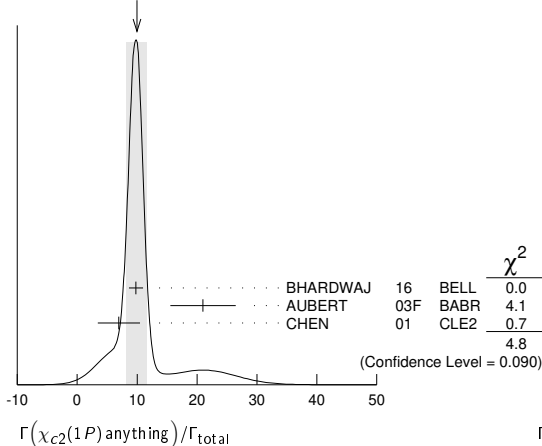
- • • We do not use the following data for averages, fits, limits, etc. • • •
- <sup>1</sup>Assumes equal production of  $B^+$  and  $B^0$  at the  $T(4S)$ .
- <sup>2</sup>CHEN 01 reports  $0.00383 \pm 0.00031 \pm 0.00040$  from a measurement of  $[\Gamma(B \rightarrow \chi_{c1}(1P) \text{ (direct) anything})/\Gamma_{\text{total}}] \times [B(\chi_{c1}(1P) \rightarrow \gamma J/\psi(1S))]$  assuming  $B(\chi_{c1}(1P) \rightarrow \gamma J/\psi(1S)) = 0.273 \pm 0.016$ , which we rescale to our best value  $B(\chi_{c1}(1P) \rightarrow \gamma J/\psi(1S)) = (34.3 \pm 1.0) \times 10^{-2}$ . Our first error is their experiment's error and our second error is the systematic error from using our best value. Assumes equal production of  $B^+$  and  $B^0$  at the  $T(4S)$ .
- <sup>3</sup>ABE 02L uses PDG 01 values for  $B(J/\psi(1S) \rightarrow \ell^+ \ell^-)$  and  $B(\chi_{c1,c2} \rightarrow J/\psi(1S)\gamma)$ .
- <sup>4</sup>BALEST 95B assume PDG 1994 values.  $J/\psi(1S)$  mesons are reconstructed in the  $e^+ e^-$  and  $\mu^+ \mu^-$  modes. The  $B \rightarrow \chi_{c1}(1P)X$  branching ratio contains  $\chi_{c1}(1P)$  mesons directly from  $B$  decays and also from feeddown through  $\psi(2S) \rightarrow \chi_{c1}(1P)\gamma$ . Using the measured inclusive rates, BALEST 95B corrects for the feeddown and finds the  $B \rightarrow \chi_{c1}(1P) \text{ (direct) } X$  branching ratio.

### $\Gamma(\chi_{c2}(1P) \text{ anything})/\Gamma_{\text{total}}$ $\Gamma_{53}/\Gamma$

VALUE (units $10^{-4}$ )	CL%	DOCUMENT ID	TECN	COMMENT
<b>10.0 ± 1.7 OUR AVERAGE</b>				Error includes scale factor of 1.6. See the ideogram below.
$9.8 \pm 0.6 \pm 1.0$		<sup>1</sup> BHARDWAJ 16	BELL	$e^+ e^- \rightarrow T(4S)$
$21.0 \pm 4.5 \pm 3.1$		AUBERT 03F	BABR	$e^+ e^- \rightarrow T(4S)$
$7.0 \pm 3.5 \pm 0.2$		<sup>2</sup> CHEN 01	CLE2	$e^+ e^- \rightarrow T(4S)$
$18.0^{+2.3}_{-2.8} \pm 2.6$		<sup>3</sup> ABE 02L	BELL	Repl. by BHARDWAJ 16
<38	90	<sup>4</sup> BALEST 95B	CLE2	Repl. by CHEN 01

- • • We do not use the following data for averages, fits, limits, etc. • • •
- <sup>1</sup>Assumes equal production of  $B^+$  and  $B^0$  at the  $T(4S)$ .
- <sup>2</sup>CHEN 01 reports  $(9.8 \pm 4.8 \pm 1.5) \times 10^{-4}$  from a measurement of  $[\Gamma(B \rightarrow \chi_{c2}(1P) \text{ anything})/\Gamma_{\text{total}}] \times [B(\chi_{c2}(1P) \rightarrow \gamma J/\psi(1S))]$  assuming  $B(\chi_{c2}(1P) \rightarrow \gamma J/\psi(1S)) = 0.135 \pm 0.011$ , which we rescale to our best value  $B(\chi_{c2}(1P) \rightarrow \gamma J/\psi(1S)) = (19.0 \pm 0.5) \times 10^{-2}$ . Our first error is their experiment's error and our second error is the systematic error from using our best value. Assumes equal production of  $B^+$  and  $B^0$  at the  $T(4S)$ .
- <sup>3</sup>ABE 02L uses PDG 01 values for  $B(J/\psi(1S) \rightarrow \ell^+ \ell^-)$  and  $B(\chi_{c1,c2} \rightarrow J/\psi(1S)\gamma)$ .
- <sup>4</sup>BALEST 95B assume  $B(\chi_{c2}(1P) \rightarrow J/\psi(1S)\gamma) = (13.5 \pm 1.1) \times 10^{-2}$ , the PDG 1994 value.  $J/\psi(1S)$  mesons are reconstructed in the  $e^+ e^-$  and  $\mu^+ \mu^-$  modes, and PDG 1994 branching fractions are used. If interpreted as signal, the  $35 \pm 13$  events correspond to  $B(B \rightarrow \chi_{c2}(1P)X) = (0.25 \pm 0.10 \pm 0.03) \times 10^{-2}$ .

WEIGHTED AVERAGE  
10.0 ± 1.7 (Error scaled by 1.6)



### $\Gamma(\chi_{c2}(1P) \text{ (direct) anything})/\Gamma_{\text{total}}$ $\Gamma_{54}/\Gamma$

VALUE (units $10^{-3}$ )	DOCUMENT ID	TECN	COMMENT
<b>0.75 ± 0.11 OUR AVERAGE</b>			
$0.70 \pm 0.06 \pm 0.10$	<sup>1</sup> BHARDWAJ 16	BELL	$e^+ e^- \rightarrow T(4S)$
$1.90 \pm 0.45 \pm 0.29$	AUBERT 03F	BABR	$e^+ e^- \rightarrow T(4S)$
$1.53^{+0.23}_{-0.28} \pm 0.27$	<sup>2</sup> ABE 02L	BELL	Repl. by BHARDWAJ 16

### $\Gamma(\eta_c(1S) \text{ anything})/\Gamma_{\text{total}}$ $\Gamma_{55}/\Gamma$

VALUE	CL%	DOCUMENT ID	TECN	COMMENT
<b>&lt;0.009</b>		<sup>1</sup> BALEST 95B	CLE2	$e^+ e^- \rightarrow T(4S)$

<sup>1</sup>BALEST 95B assume PDG 1994 values for sub mode branching ratios.  $J/\psi(1S)$  mesons are reconstructed in  $J/\psi(1S) \rightarrow e^+ e^-$  and  $J/\psi(1S) \rightarrow \mu^+ \mu^-$ . Search region  $2960 < m_{\eta_c(1S)} < 3010$  MeV/ $c^2$ .

### $\Gamma(K\chi_{c1}(3872), \chi_{c1} \rightarrow D^0 \bar{D}^0 \pi^0)/\Gamma_{\text{total}}$ $\Gamma_{56}/\Gamma$

VALUE (units $10^{-4}$ )	DOCUMENT ID	TECN	COMMENT
<b>1.22 ± 0.31 ± 0.23</b>	<sup>1</sup> GOKHROO 06	BELL	$e^+ e^- \rightarrow T(4S)$

<sup>1</sup> Measure the near-threshold enhancements in the  $(D^0 \bar{D}^0 \pi^0)$  system at a mass  $3875.2 \pm 0.7^{+0.3}_{-1.6} \pm 0.8$  MeV/ $c^2$ .

### $\Gamma(K\chi_{c1}(3872), \chi_{c1} \rightarrow D^{*0} D^0)/\Gamma_{\text{total}}$ $\Gamma_{57}/\Gamma$

VALUE (units $10^{-4}$ )	DOCUMENT ID	TECN	COMMENT
<b>0.80 ± 0.20 ± 0.10</b>	AUSHEV 10	BELL	$e^+ e^- \rightarrow T(4S)$

### $\Gamma(KX(3940), X \rightarrow D^{*0} D^0)/\Gamma_{\text{total}}$ $\Gamma_{58}/\Gamma$

VALUE (units $10^{-4}$ )	CL%	DOCUMENT ID	TECN	COMMENT
<b>&lt;0.67</b>	90	AUSHEV 10	BELL	$e^+ e^- \rightarrow T(4S)$

### $\Gamma(KX(3915), X \rightarrow \omega J/\psi)/\Gamma_{\text{total}}$ $\Gamma_{59}/\Gamma$

VALUE (units $10^{-5}$ )	DOCUMENT ID	TECN	COMMENT
<b>7.1 ± 1.3 ± 3.1</b>	<sup>1</sup> CHOI 05	BELL	$e^+ e^- \rightarrow T(4S)$

<sup>1</sup>CHOI 05 reports the observation of a near-threshold enhancement in the  $\omega J/\psi$  mass spectrum in exclusive  $B \rightarrow K\omega J/\psi$ . The new state, denoted as  $X(3915)$ , is measured to have a mass of  $3943 \pm 11 \pm 13$  GeV/ $c^2$  and a width  $\Gamma = 87 \pm 22 \pm 26$  MeV.

### $\Gamma(K^\pm \text{ anything})/\Gamma_{\text{total}}$ $\Gamma_{60}/\Gamma$

VALUE	DOCUMENT ID	TECN	COMMENT
<b>0.789 ± 0.025 OUR AVERAGE</b>			
$0.82 \pm 0.01 \pm 0.05$	ALBRECHT 94c	ARG	$e^+ e^- \rightarrow T(4S)$
$0.775 \pm 0.015 \pm 0.025$	<sup>1</sup> ALBRECHT 93i	ARG	$e^+ e^- \rightarrow T(4S)$
$0.85 \pm 0.07 \pm 0.09$	ALAM 87b	CLEO	$e^+ e^- \rightarrow T(4S)$
$0.620 \pm 0.013 \pm 0.038$	<sup>2</sup> ALBRECHT 94c	ARG	$e^+ e^- \rightarrow T(4S)$
$0.66 \pm 0.05 \pm 0.07$	<sup>2</sup> ALAM 87b	CLEO	$e^+ e^- \rightarrow T(4S)$

- • • We do not use the following data for averages, fits, limits, etc. • • •
- <sup>1</sup>ALBRECHT 93i value is not independent of the sum of  $B \rightarrow K^+ \text{ anything}$  and  $B \rightarrow K^- \text{ anything}$  ALBRECHT 94c values.
- <sup>2</sup>Assuming  $T(4S) \rightarrow B\bar{B}$ , a total of  $3.38 \pm 0.34 \pm 0.68$  kaons per  $T(4S)$  decay is found (the second error is systematic). In the context of the standard  $B$ -decay model, this leads to a value for  $(b\text{-quark} \rightarrow c\text{-quark})/(b\text{-quark} \rightarrow \text{all})$  of  $1.09 \pm 0.33 \pm 0.13$ .
- <sup>3</sup>GIANNINI 82 at CESR-CUSB observed  $1.58 \pm 0.35$   $K^0$  per hadronic event much higher than  $0.82 \pm 0.10$  below threshold. Consistent with predominant  $b \rightarrow cX$  decay.

### $\Gamma(K^+ \text{ anything})/\Gamma_{\text{total}}$ $\Gamma_{61}/\Gamma$

VALUE	DOCUMENT ID	TECN	COMMENT
<b>0.66 ± 0.05</b>	<sup>1</sup> ALBRECHT 94c	ARG	$e^+ e^- \rightarrow T(4S)$
$0.620 \pm 0.013 \pm 0.038$	<sup>2</sup> ALBRECHT 94c	ARG	$e^+ e^- \rightarrow T(4S)$
$0.66 \pm 0.05 \pm 0.07$	<sup>2</sup> ALAM 87b	CLEO	$e^+ e^- \rightarrow T(4S)$

<sup>1</sup> Measurement relies on lepton-kaon correlations. It is for the weak decay vertex and does not include mixing of the neutral  $B$  meson. Mixing effects were corrected for by assuming a mixing parameter  $r$  of  $(18.1 \pm 4.3)\%$ .

<sup>2</sup> Measurement relies on lepton-kaon correlations. It includes production through mixing of the neutral  $B$  meson.

### $\Gamma(K^- \text{ anything})/\Gamma_{\text{total}}$ $\Gamma_{62}/\Gamma$

VALUE	DOCUMENT ID	TECN	COMMENT
<b>0.13 ± 0.04</b>	<sup>1</sup> ALBRECHT 94c	ARG	$e^+ e^- \rightarrow T(4S)$
$0.165 \pm 0.011 \pm 0.036$	<sup>2</sup> ALBRECHT 94c	ARG	$e^+ e^- \rightarrow T(4S)$
$0.19 \pm 0.05 \pm 0.02$	<sup>2</sup> ALAM 87b	CLEO	$e^+ e^- \rightarrow T(4S)$

<sup>1</sup> Measurement relies on lepton-kaon correlations. It is for the weak decay vertex and does not include mixing of the neutral  $B$  meson. Mixing effects were corrected for by assuming a mixing parameter  $r$  of  $(18.1 \pm 4.3)\%$ .

<sup>2</sup> Measurement relies on lepton-kaon correlations. It includes production through mixing of the neutral  $B$  meson.

See key on page 999

# Meson Particle Listings

## $B^\pm/B^0$ ADMIXTURE

$\Gamma(K^0/\bar{K}^0 \text{ anything})/\Gamma_{\text{total}}$		$\Gamma_{63}/\Gamma$	
VALUE	DOCUMENT ID	TECN	COMMENT
<b>0.64 ± 0.04 OUR AVERAGE</b>			
0.642 ± 0.010 ± 0.042	<sup>1</sup> ALBRECHT 94C	ARG	$e^+e^- \rightarrow \Upsilon(4S)$
0.63 ± 0.06 ± 0.06	ALAM	87B	CLEO $e^+e^- \rightarrow \Upsilon(4S)$
<sup>1</sup> ALBRECHT 94c assume a $K^0/\bar{K}^0$ multiplicity twice that of $K_S^0$ .			

$\Gamma(K^*(892)^\pm \text{ anything})/\Gamma_{\text{total}}$		$\Gamma_{64}/\Gamma$	
VALUE	DOCUMENT ID	TECN	COMMENT
<b>0.182 ± 0.054 ± 0.024</b>	ALBRECHT 94J	ARG	$e^+e^- \rightarrow \Upsilon(4S)$

$\Gamma(K^*(892)^0/\bar{K}^*(892)^0 \text{ anything})/\Gamma_{\text{total}}$		$\Gamma_{65}/\Gamma$	
VALUE	DOCUMENT ID	TECN	COMMENT
<b>0.146 ± 0.016 ± 0.020</b>	ALBRECHT 94J	ARG	$e^+e^- \rightarrow \Upsilon(4S)$

$\Gamma(K^*(892)\gamma)/\Gamma_{\text{total}}$		$\Gamma_{66}/\Gamma$	
VALUE (units $10^{-5}$ )	CL%	DOCUMENT ID	TECN
<b>4.24 ± 0.54 ± 0.32</b>		<sup>1</sup> COAN 00	CLE2 $e^+e^- \rightarrow \Upsilon(4S)$
• • • We do not use the following data for averages, fits, limits, etc. • • •			
<15.0	90	<sup>2</sup> LESIAK 92	CBAL $e^+e^- \rightarrow \Upsilon(4S)$
<24	90	ALBRECHT 88H	ARG $e^+e^- \rightarrow \Upsilon(4S)$

<sup>1</sup> An average of  $B(B^+ \rightarrow K^*(892)^+\gamma)$  and  $B(B^0 \rightarrow K^*(892)^0\gamma)$  measurements reported in COAN 00 by assuming full correlated systematic errors.  
<sup>2</sup> LESIAK 92 set a limit on the inclusive process  $B(b \rightarrow s\gamma) < 2.8 \times 10^{-3}$  at 90% CL for the range of masses of 892–2045 MeV, independent of assumptions about s-quark hadronization.

$\Gamma(\eta K\gamma)/\Gamma_{\text{total}}$		$\Gamma_{67}/\Gamma$	
VALUE (units $10^{-6}$ )	CL%	DOCUMENT ID	TECN
<b>8.5 ± 1.3<sup>+1.2</sup><sub>-0.9</sub></b>		<sup>1</sup> NISHIDA 05	BELL $e^+e^- \rightarrow \Upsilon(4S)$
<sup>1</sup> $m_{\eta K} < 2.4 \text{ GeV}/c^2$			

$\Gamma(K_1(1400)\gamma)/\Gamma_{\text{total}}$		$\Gamma_{68}/\Gamma$	
VALUE	CL%	DOCUMENT ID	TECN
<b>&lt;12.7 × 10<sup>-5</sup></b>	90	<sup>1</sup> COAN 00	CLE2 $e^+e^- \rightarrow \Upsilon(4S)$
• • • We do not use the following data for averages, fits, limits, etc. • • •			
< 1.6 × 10 <sup>-3</sup>	90	<sup>2</sup> LESIAK 92	CBAL $e^+e^- \rightarrow \Upsilon(4S)$
< 4.1 × 10 <sup>-4</sup>	90	ALBRECHT 88H	ARG $e^+e^- \rightarrow \Upsilon(4S)$

<sup>1</sup> Assumes equal production of  $B^+$  and  $B^0$  at the  $\Upsilon(4S)$ .  
<sup>2</sup> LESIAK 92 set a limit on the inclusive process  $B(b \rightarrow s\gamma) < 2.8 \times 10^{-3}$  at 90% CL for the range of masses of 892–2045 MeV, independent of assumptions about s-quark hadronization.

$\Gamma(K_2^*(1430)\gamma)/\Gamma_{\text{total}}$		$\Gamma_{69}/\Gamma$	
VALUE (units $10^{-5}$ )	CL%	DOCUMENT ID	TECN
<b>1.66 ± 0.59 ± 0.13</b>		<sup>1</sup> COAN 00	CLE2 $e^+e^- \rightarrow \Upsilon(4S)$
• • • We do not use the following data for averages, fits, limits, etc. • • •			
<83	90	ALBRECHT 88H	ARG $e^+e^- \rightarrow \Upsilon(4S)$

<sup>1</sup> COAN 00 obtains a fitted signal yield of  $15.9^{+5.7}_{-5.2}$  events. A search for contamination by  $K^*(1410)$  yielded a rate consistent with 0; the central value assumes no contamination.

$\Gamma(K_2(1770)\gamma)/\Gamma_{\text{total}}$		$\Gamma_{70}/\Gamma$	
VALUE	CL%	DOCUMENT ID	TECN
<b>&lt;1.2 × 10<sup>-3</sup></b>	90	<sup>1</sup> LESIAK 92	CBAL $e^+e^- \rightarrow \Upsilon(4S)$
<sup>1</sup> LESIAK 92 set a limit on the inclusive process $B(b \rightarrow s\gamma) < 2.8 \times 10^{-3}$ at 90% CL for the range of masses of 892–2045 MeV, independent of assumptions about s-quark hadronization.			

$\Gamma(K_3^*(1780)\gamma)/\Gamma_{\text{total}}$		$\Gamma_{71}/\Gamma$	
VALUE	CL%	DOCUMENT ID	TECN
<b>&lt;3.7 × 10<sup>-5</sup></b>	90	<sup>1</sup> NISHIDA 05	BELL $e^+e^- \rightarrow \Upsilon(4S)$
• • • We do not use the following data for averages, fits, limits, etc. • • •			
<3.0 × 10 <sup>-3</sup>	90	ALBRECHT 88H	ARG $e^+e^- \rightarrow \Upsilon(4S)$
<sup>1</sup> Uses $B(K_3^*(1780) \rightarrow \eta K) = 0.11^{+0.05}_{-0.04}$ .			

$\Gamma(K_3^*(2045)\gamma)/\Gamma_{\text{total}}$		$\Gamma_{72}/\Gamma$	
VALUE	CL%	DOCUMENT ID	TECN
<b>&lt;1.0 × 10<sup>-3</sup></b>	90	<sup>1</sup> LESIAK 92	CBAL $e^+e^- \rightarrow \Upsilon(4S)$
<sup>1</sup> LESIAK 92 set a limit on the inclusive process $B(b \rightarrow s\gamma) < 2.8 \times 10^{-3}$ at 90% CL for the range of masses of 892–2045 MeV, independent of assumptions about s-quark hadronization.			

$\Gamma(K\eta(958))/\Gamma_{\text{total}}$		$\Gamma_{73}/\Gamma$	
VALUE	CL%	DOCUMENT ID	TECN
<b>(8.3<sup>+0.9</sup><sub>-0.8</sub> ± 0.7) × 10<sup>-5</sup></b>		<sup>1</sup> RICHICHI 00	CLE2 $e^+e^- \rightarrow \Upsilon(4S)$
<sup>1</sup> Assumes equal production of $B^+$ and $B^0$ at the $\Upsilon(4S)$ .			

$\Gamma(K^*(892)\eta'(958))/\Gamma_{\text{total}}$		$\Gamma_{74}/\Gamma$	
VALUE (units $10^{-6}$ )	CL%	DOCUMENT ID	TECN
<b>4.1 ± 1.0<sub>-0.9</sub> ± 0.5</b>		<sup>1</sup> AUBERT 07E	BABR $e^+e^- \rightarrow \Upsilon(4S)$

• • • We do not use the following data for averages, fits, limits, etc. • • •  
 <22 90 <sup>1</sup> RICHICHI 00 CLE2  $e^+e^- \rightarrow \Upsilon(4S)$   
<sup>1</sup> Assumes equal production of  $B^+$  and  $B^0$  at the  $\Upsilon(4S)$ .

$\Gamma(K\eta)/\Gamma_{\text{total}}$		$\Gamma_{75}/\Gamma$	
VALUE	CL%	DOCUMENT ID	TECN
<b>&lt;5.2 × 10<sup>-6</sup></b>	90	<sup>1</sup> RICHICHI 00	CLE2 $e^+e^- \rightarrow \Upsilon(4S)$
<sup>1</sup> Assumes equal production of $B^+$ and $B^0$ at the $\Upsilon(4S)$ .			

$\Gamma(K^*(892)\eta)/\Gamma_{\text{total}}$		$\Gamma_{76}/\Gamma$	
VALUE	CL%	DOCUMENT ID	TECN
<b>(1.80 ± 0.49 ± 0.18) × 10<sup>-5</sup></b>		<sup>1</sup> RICHICHI 00	CLE2 $e^+e^- \rightarrow \Upsilon(4S)$
<sup>1</sup> Assumes equal production of $B^+$ and $B^0$ at the $\Upsilon(4S)$ .			

$\Gamma(K\phi\phi)/\Gamma_{\text{total}}$		$\Gamma_{77}/\Gamma$	
VALUE (units $10^{-6}$ )	CL%	DOCUMENT ID	TECN
<b>2.3 ± 0.9 ± 0.3</b>		<sup>1</sup> HUANG 03	BELL $e^+e^- \rightarrow \Upsilon(4S)$
<sup>1</sup> Assumes equal production of charged and neutral $B$ meson pairs and isospin symmetry.			

$\Gamma(\bar{b} \rightarrow \bar{s}\gamma)/\Gamma_{\text{total}}$		$\Gamma_{78}/\Gamma$	
VALUE (units $10^{-4}$ )	CL%	DOCUMENT ID	TECN
<b>3.49 ± 0.19 OUR AVERAGE</b>			
3.75 ± 0.18 ± 0.35		<sup>1,2</sup> SAITO 15	BELL $e^+e^- \rightarrow \Upsilon(4S)$
3.52 ± 0.20 ± 0.51		<sup>1,3</sup> LEES 12u	BABR $e^+e^- \rightarrow \Upsilon(4S)$
3.32 ± 0.16 ± 0.31		<sup>1,4</sup> LEES 12v	BABR $e^+e^- \rightarrow \Upsilon(4S)$
3.47 ± 0.15 ± 0.40		<sup>1,5</sup> LIMOSANI 09	BELL $e^+e^- \rightarrow \Upsilon(4S)$
3.90 ± 0.91 ± 0.64		<sup>1,6</sup> AUBERT 08o	BABR $e^+e^- \rightarrow \Upsilon(4S)$
3.29 ± 0.44 ± 0.29		<sup>1,7</sup> CHEN 01c	CLE2 $e^+e^- \rightarrow \Upsilon(4S)$
• • • We do not use the following data for averages, fits, limits, etc. • • •			
2.30 ± 0.08 ± 0.30		<sup>8</sup> DEL-AMO-SA...10M	BABR $e^+e^- \rightarrow \Upsilon(4S)$
4.3 ± 0.3 ± 0.7		<sup>9</sup> AUBERT 09u	BABR Repl. by DEL-AMO-SANCHEZ 10M
3.92 ± 0.31 ± 0.47		<sup>1,10</sup> AUBERT, BE 06b	BABR Repl. by LEES 12v
3.49 ± 0.20 ± 0.59 <sub>-0.46</sub>		<sup>1,11</sup> AUBERT, B 05r	BABR Repl. by LEES 12u
3.50 ± 0.32 ± 0.31		<sup>1,12</sup> KOPPENBURG 04	BELL Repl. by LIMOSANI 09
3.36 ± 0.53 ± 0.65 <sub>-0.68</sub>		<sup>13</sup> ABE 01f	BELL Repl. by SAITO 15
2.32 ± 0.57 ± 0.35		ALAM 95	CLE2 Repl. by CHEN 01c

<sup>1</sup> We extrapolate the measured value to  $E_\gamma > 1.6 \text{ GeV}$  using the method of BUCHMUELLER 06 (average of three theoretical models).  
<sup>2</sup> SAITO 15 measured  $(3.51 \pm 0.17 \pm 0.33) \times 10^{-4}$  using a sum-of-exclusive approach in which 38 of the hadronic final states with  $m_{X_S} < 2.8 \text{ GeV}/c^2$  are reconstructed. The cut of minimum photon energy is  $E_\gamma > 1.9 \text{ GeV}$ .  
<sup>3</sup> Reports  $(3.29 \pm 0.19 \pm 0.48) \times 10^{-4}$  for  $E_\gamma > 1.9 \text{ GeV}$ .  
<sup>4</sup> Reports  $(3.21 \pm 0.15 \pm 0.29 \pm 0.08) \times 10^{-4}$  for  $1.8 < E_\gamma < 2.8 \text{ GeV}$ , where the last systematic uncertainty is for model dependency. Results with other cutoffs are also reported.  
<sup>5</sup> The measurement reported is  $(3.45 \pm 0.15 \pm 0.40) \times 10^{-4}$  for  $E_\gamma > 1.7 \text{ GeV}$ .  
<sup>6</sup> Uses a fully reconstructed  $B$  meson as a tag on the recoil side. The measurement reported is  $(3.66 \pm 0.85 \pm 0.60) \times 10^{-4}$  for  $E_\gamma > 1.9 \text{ GeV}$ .  
<sup>7</sup> The measurement reported is  $(3.21 \pm 0.43^{+0.32}_{-0.29}) \times 10^{-4}$  for  $E_\gamma > 2.0 \text{ GeV}$ .  
<sup>8</sup> Measured using sums of seven exclusive final states  $B \rightarrow X_{d(s)}\gamma$  where  $X_{d(s)}$  is a nonstrange (strange) charmless hadronic system in mass range 0.5–2.0  $\text{GeV}/c^2$ .  
<sup>9</sup> Measured using sums of seven exclusive final states  $B \rightarrow X_{d(s)}\gamma$  where  $X_{d(s)}$  is a nonstrange (strange) charmless hadronic system in mass range 0.6–1.8  $\text{GeV}/c^2$ .  
<sup>10</sup> The measurement reported is  $(3.67 \pm 0.29 \pm 0.45) \times 10^{-4}$  for  $E_\gamma > 1.9 \text{ GeV}$ .  
<sup>11</sup> The measurement reported is  $(3.27 \pm 0.18^{+0.55}_{-0.42}) \times 10^{-4}$  for  $E_\gamma > 1.9 \text{ GeV}$ .  
<sup>12</sup> The measurement reported is  $(3.55 \pm 0.32 \pm 0.32) \times 10^{-4}$  for  $E_\gamma > 1.8 \text{ GeV}$ .  
<sup>13</sup> ABE 01f reports their systematic errors  $(\pm 0.42^{+0.50}_{-0.54}) \times 10^{-4}$ , where the second error is due to the theoretical uncertainty. We combine them in quadrature.

$\Gamma(\bar{b} \rightarrow \bar{d}\gamma)/\Gamma_{\text{total}}$		$\Gamma_{79}/\Gamma$	
VALUE (units $10^{-6}$ )	CL%	DOCUMENT ID	TECN
<b>9.2 ± 2.0 ± 2.3</b>		<sup>1</sup> DEL-AMO-SA...10M	BABR $e^+e^- \rightarrow \Upsilon(4S)$
• • • We do not use the following data for averages, fits, limits, etc. • • •			
14 ± 5 ± 4		<sup>2</sup> AUBERT 09u	BABR Repl. by DEL-AMO-SANCHEZ 10M
<sup>1</sup> Measured using sums of seven exclusive final states $B \rightarrow X_{d(s)}\gamma$ where $X_{d(s)}$ is a nonstrange (strange) charmless hadronic system in mass range 0.5–2.0 $\text{GeV}/c^2$ . <sup>2</sup> Measured using sums of seven exclusive final states $B \rightarrow X_{d(s)}\gamma$ where $X_{d(s)}$ is a nonstrange (strange) charmless hadronic system in mass range 0.6–1.8 $\text{GeV}/c^2$ .			

## Meson Particle Listings

 $B^\pm/B^0$  ADMIXTURE $\Gamma(\bar{b} \rightarrow \bar{s}\gamma)/\Gamma(\bar{b} \rightarrow \bar{s}\gamma)$  $\Gamma_{79}/\Gamma_{78}$ 

VALUE	DOCUMENT ID	TECN	COMMENT
<b>0.040 ± 0.009 ± 0.010</b>	1 DEL-AMO-SA..10M	BABR	$e^+e^- \rightarrow \Upsilon(4S)$
0.033 ± 0.013 ± 0.009	2 AUBERT	09u	Repl. by DEL-AMO-SANCHEZ 10M

1 Measured using sums of seven exclusive final states  $B \rightarrow X_{d(s)}\gamma$  where  $X_{d(s)}$  is a nonstrange (strange) charmless hadronic system in mass range 0.5–2.0 GeV/c<sup>2</sup>.  
 2 Measured using sums of seven exclusive final states  $B \rightarrow X_{d(s)}\gamma$  where  $X_{d(s)}$  is a nonstrange (strange) charmless hadronic system in mass range 0.6–1.8 GeV/c<sup>2</sup>.

 $\Gamma(\bar{b} \rightarrow \bar{s}\text{gluon})/\Gamma_{\text{total}}$  $\Gamma_{80}/\Gamma$ 

VALUE	CL%	EVTS	DOCUMENT ID	TECN	COMMENT
<b>&lt;0.068</b>	90		1 COAN	98	CLE2 $e^+e^- \rightarrow \Upsilon(4S)$
<0.08	2		2 ALBRECHT	95D	ARG $e^+e^- \rightarrow \Upsilon(4S)$

1 COAN 98 uses  $D$ - $\ell$  correlation.  
 2 ALBRECHT 95D use full reconstruction of one  $B$  decay as tag. Two candidate events for charmless  $B$  decay can be interpreted as either  $b \rightarrow \text{sgluon}$  or  $b \rightarrow u$  transition. If interpreted as  $b \rightarrow \text{sgluon}$  they find a branching ratio of  $\sim 0.026$  or the upper limit quoted above. Result is highly model dependent.

 $\Gamma(\eta \text{ anything})/\Gamma_{\text{total}}$  $\Gamma_{81}/\Gamma$ 

VALUE (units $10^{-4}$ )	CL%	DOCUMENT ID	TECN	COMMENT
<b>2.61 ± 0.30 ± 0.44</b>		1 NISHIMURA	10	BELL $e^+e^- \rightarrow \Upsilon(4S)$
1.69 ± 0.29 ± 0.36		2 NISHIMURA	10	BELL $e^+e^- \rightarrow \Upsilon(4S)$
<4.4	90	3 BROWDER	98	CLE2 $e^+e^- \rightarrow \Upsilon(4S)$

1 Uses  $B \rightarrow \eta X_S$  with  $0.4 < m_{X_S} < 2.6$  GeV/c<sup>2</sup>.  
 2 Uses  $B \rightarrow \eta X_S$  with  $1.8 < m_{X_S} < 2.6$  GeV/c<sup>2</sup>.  
 3 BROWDER 98 search for high momentum  $B \rightarrow \eta X_S$  between 2.1 and 2.7 GeV/c.

 $\Gamma(\eta' \text{ anything})/\Gamma_{\text{total}}$  $\Gamma_{82}/\Gamma$ 

VALUE (units $10^{-4}$ )	DOCUMENT ID	TECN	COMMENT
<b>4.2 ± 0.9 OUR AVERAGE</b>			
3.9 ± 0.8 ± 0.9	1 AUBERT,B	04F	BABR $e^+e^- \rightarrow \Upsilon(4S)$
4.6 ± 1.1 ± 0.6	2 BONVICINI	03	CLE2 $e^+e^- \rightarrow \Upsilon(4S)$
6.2 ± 1.6 ± 1.3	3 BROWDER	98	CLE2 $e^+e^- \rightarrow \Upsilon(4S)$

1 AUBERT,B 04F reports branching ratio  $B \rightarrow \eta' X_S$  for high momentum  $\eta'$  between 2.0 and 2.7 GeV/c in the  $\Upsilon(4S)$  center-of-mass frame.  $X_S$  represents a recoil system consisting of a kaon and zero to four pions.  
 2 BONVICINI 03 observed a signal of 61.2 ± 13.9 events in  $B \rightarrow \eta' X_{nc}$  production for high momentum  $\eta'$  between 2.0 and 2.7 GeV/c in the  $\Upsilon(4S)$  center-of-mass frame. The  $X_{nc}$  denotes "charmless" hadronic states recoiling against  $\eta'$ . The second error combines systematic and background subtraction uncertainties in quadrature.  
 3 BROWDER 98 observed a signal of 39.0 ± 11.6 events in high momentum  $B \rightarrow \eta' X_S$  production between 2.0 and 2.7 GeV/c. The branching fraction is based on the interpretation of  $b \rightarrow \text{sg}$ , where the last error includes additional uncertainties due to the color-suppressed  $b \rightarrow \text{backgrounds}$ .

 $\Gamma(K^+ \text{ gluon (charmless)})/\Gamma_{\text{total}}$  $\Gamma_{83}/\Gamma$ 

VALUE (units $10^{-4}$ )	CL%	DOCUMENT ID	TECN	COMMENT
<b>&lt;1.87</b>	90	1 DEL-AMO-SA..11	BABR	$e^+e^- \rightarrow \Upsilon(4S)$

1  $B \rightarrow K^+ X$  with  $m_X < 1.69$  GeV/c<sup>2</sup>.

 $\Gamma(K^0 \text{ gluon (charmless)})/\Gamma_{\text{total}}$  $\Gamma_{84}/\Gamma$ 

VALUE (units $10^{-4}$ )	DOCUMENT ID	TECN	COMMENT
<b>1.95 ± 0.51 ± 0.50</b>	1 DEL-AMO-SA..11	BABR	$e^+e^- \rightarrow \Upsilon(4S)$

1  $B \rightarrow K^0 X$  with  $m_X < 1.69$  GeV/c<sup>2</sup>.

 $\Gamma(\rho\gamma)/\Gamma_{\text{total}}$  $\Gamma_{85}/\Gamma$ 

VALUE (units $10^{-6}$ )	CL%	DOCUMENT ID	TECN	COMMENT
<b>1.39 ± 0.25 OUR AVERAGE</b>				Error includes scale factor of 1.2.
1.73 ± 0.34 ± 0.17		1,2 AUBERT	08BH	BABR $e^+e^- \rightarrow \Upsilon(4S)$
1.21 ± 0.24 ± 0.12		1,2 TANIGUCHI	08	BELL $e^+e^- \rightarrow \Upsilon(4S)$
1.36 ± 0.29 ± 0.10		1,3 AUBERT	07L	BABR Repl. by AUBERT 08BH
< 1.9	90	1,3 AUBERT	04c	BABR Repl. by AUBERT 07L
< 14	90	1,4 COAN	00	CLE2 $e^+e^- \rightarrow \Upsilon(4S)$

1 Assumes equal production of  $B^+$  and  $B^0$  at the  $\Upsilon(4S)$ .  
 2 Assumes  $\Gamma(B \rightarrow \rho\gamma) = \Gamma(B^+ \rightarrow \rho^+\gamma) = 2\Gamma(B^0 \rightarrow \rho^0\gamma)$  and uses lifetime ratio of  $\tau_{B^+}/\tau_{B^0} = 1.071 \pm 0.009$ .  
 3 Assumes  $\Gamma(B \rightarrow \rho\gamma) = \Gamma(B^+ \rightarrow \rho^+\gamma) = 2\Gamma(B^0 \rightarrow \rho^0\gamma)$  and uses lifetime ratio of  $\tau_{B^+}/\tau_{B^0} = 1.083 \pm 0.017$ .  
 4 COAN 00 reports  $B(B \rightarrow \rho\gamma)/B(B \rightarrow K^*(892)\gamma) < 0.32$  at 90%CL and scaled by the central value of  $B(B \rightarrow K^*(892)\gamma) = (4.24 \pm 0.54 \pm 0.32) \times 10^{-5}$ .

 $\Gamma(\rho\gamma)/\Gamma(K^*(892)\gamma)$  $\Gamma_{85}/\Gamma_{66}$ 

VALUE (units $10^{-2}$ )	DOCUMENT ID	TECN	COMMENT
<b>3.02 ± 0.60 ± 0.26</b>	TANIGUCHI	08	BELL $e^+e^- \rightarrow \Upsilon(4S)$

 $\Gamma(\rho/\omega\gamma)/\Gamma_{\text{total}}$  $\Gamma_{86}/\Gamma$ 

VALUE (units $10^{-6}$ )	CL%	DOCUMENT ID	TECN	COMMENT
<b>1.30 ± 0.23 OUR AVERAGE</b>				Error includes scale factor of 1.2.
1.63 ± 0.30 ± 0.16		1,2,3 AUBERT	08BH	BABR $e^+e^- \rightarrow \Upsilon(4S)$
1.14 ± 0.20 ± 0.10		1,3 TANIGUCHI	08	BELL $e^+e^- \rightarrow \Upsilon(4S)$
1.25 ± 0.25 ± 0.09		4 AUBERT	07L	BABR Repl. by AUBERT 08BH
1.32 ± 0.34 ± 0.10		4 MOHAPATRA	06	BELL Repl. by TANIGUCHI 08
0.6 ± 0.3 ± 0.1		4 AUBERT	05	BABR Repl. by AUBERT 07L
< 1.4	90	4 MOHAPATRA	05	BELL $e^+e^- \rightarrow \Upsilon(4S)$

1 Assumes  $\Gamma(B \rightarrow \rho\gamma) = \Gamma(B^+ \rightarrow \rho^+\gamma) = 2\Gamma(B^0 \rightarrow \rho^0\gamma)$  and uses lifetime ratio of  $\tau_{B^+}/\tau_{B^0} = 1.071 \pm 0.009$ .  
 2 Also reports  $|V_{td}/V_{ts}| = 0.233^{+0.025+0.022}_{-0.024-0.021}$ .  
 3 Assumes equal production of  $B^+$  and  $B^0$  at the  $\Upsilon(4S)$ .  
 4 Assumes  $\Gamma(B \rightarrow \rho\gamma) = \Gamma(B^+ \rightarrow \rho^+\gamma) = 2\Gamma(B^0 \rightarrow \rho^0\gamma)$  and uses lifetime ratio of  $\tau_{B^+}/\tau_{B^0} = 1.083 \pm 0.017$ .

 $\Gamma(\rho/\omega\gamma)/\Gamma(K^*(892)\gamma)$  $\Gamma_{86}/\Gamma_{66}$ 

VALUE (units $10^{-2}$ )	CL%	DOCUMENT ID	TECN	COMMENT
<b>2.84 ± 0.50 ± 0.27</b>		1 TANIGUCHI	08	BELL $e^+e^- \rightarrow \Upsilon(4S)$
< 3.5	90	MOHAPATRA	05	BELL Repl. by TANIGUCHI 08

1 Also reports  $|V_{td}/V_{ts}| = 0.195^{+0.020}_{-0.019} \pm 0.015$ .

 $\Gamma(\pi^\pm \text{ anything})/\Gamma_{\text{total}}$  $\Gamma_{87}/\Gamma$ 

VALUE	DOCUMENT ID	TECN	COMMENT
<b>3.95 ± 0.025 ± 0.070</b>	1 ALBRECHT	93i	ARG $e^+e^- \rightarrow \Upsilon(4S)$

1 ALBRECHT 93 excludes  $\pi^\pm$  from  $K_S^0$  and  $\Lambda$  decays. If included, they find  $4.105 \pm 0.025 \pm 0.080$ .

 $\Gamma(\pi^0 \text{ anything})/\Gamma_{\text{total}}$  $\Gamma_{88}/\Gamma$ 

VALUE	DOCUMENT ID	TECN	COMMENT
<b>2.35 ± 0.02 ± 0.11</b>	1 ABE	01j	BELL $e^+e^- \rightarrow \Upsilon(4S)$

1 From fully inclusive  $\pi^0$  yield with no corrections from decays of  $K_S^0$  or other particles.

 $\Gamma(\eta \text{ anything})/\Gamma_{\text{total}}$  $\Gamma_{89}/\Gamma$ 

VALUE	DOCUMENT ID	TECN	COMMENT
<b>0.176 ± 0.011 ± 0.012</b>	KUBOTA	96	CLE2 $e^+e^- \rightarrow \Upsilon(4S)$

 $\Gamma(\rho^0 \text{ anything})/\Gamma_{\text{total}}$  $\Gamma_{90}/\Gamma$ 

VALUE	DOCUMENT ID	TECN	COMMENT
<b>0.208 ± 0.042 ± 0.032</b>	ALBRECHT	94j	ARG $e^+e^- \rightarrow \Upsilon(4S)$

 $\Gamma(\omega \text{ anything})/\Gamma_{\text{total}}$  $\Gamma_{91}/\Gamma$ 

VALUE	CL%	DOCUMENT ID	TECN	COMMENT
<b>&lt;0.81</b>	90	ALBRECHT	94j	ARG $e^+e^- \rightarrow \Upsilon(4S)$

 $\Gamma(\phi \text{ anything})/\Gamma_{\text{total}}$  $\Gamma_{92}/\Gamma$ 

VALUE	DOCUMENT ID	TECN	COMMENT
<b>0.0343 ± 0.0012 OUR AVERAGE</b>			
0.0353 ± 0.0005 ± 0.0030	HUANG	07	CLEO $e^+e^- \rightarrow \Upsilon(4S)$
0.0341 ± 0.0006 ± 0.0012	AUBERT	04s	BABR $e^+e^- \rightarrow \Upsilon(4S)$
0.0390 ± 0.0030 ± 0.0035	ALBRECHT	94j	ARG $e^+e^- \rightarrow \Upsilon(4S)$
0.023 ± 0.006 ± 0.005	BORTOLETTO	086	CLEO $e^+e^- \rightarrow \Upsilon(4S)$

 $\Gamma(\phi K^*(892))/\Gamma_{\text{total}}$  $\Gamma_{93}/\Gamma$ 

VALUE	CL%	DOCUMENT ID	TECN	COMMENT
<b>&lt;2.2 × 10<sup>-5</sup></b>	90	1 BERGFELD	98	CLE2

1 Assumes equal production of  $B^+$  and  $B^0$  at the  $\Upsilon(4S)$ .

 $\Gamma(\pi^+ \text{ gluon (charmless)})/\Gamma_{\text{total}}$  $\Gamma_{95}/\Gamma$ 

VALUE (units $10^{-4}$ )	DOCUMENT ID	TECN	COMMENT
<b>3.72 ± 0.59 ± 0.59</b>	1 DEL-AMO-SA..11	BABR	$e^+e^- \rightarrow \Upsilon(4S)$

1  $B \rightarrow \pi^+ X$  with  $m_X < 1.71$  GeV/c<sup>2</sup>.

# Meson Particle Listings

## $B^\pm/B^0$ ADMIXTURE

### $\Gamma(\Lambda_c^+ / \bar{\Lambda}_c^- \text{ anything}) / \Gamma_{\text{total}}$ $\Gamma_{96} / \Gamma$

VALUE (%)	CL%	DOCUMENT ID	TECN	COMMENT
$3.59 \pm 0.32 \pm 0.19$ $-0.18$		1 AUBERT 07c	BABR	$e^+e^- \rightarrow \Upsilon(4S)$
6.4 ± 0.8 ± 0.8		2 CRAWFORD 92	CLEO	$e^+e^- \rightarrow \Upsilon(4S)$
14 ± 9		3 ALBRECHT 88E	ARG	$e^+e^- \rightarrow \Upsilon(4S)$
<11.2	90	4 ALAM 87	CLEO	$e^+e^- \rightarrow \Upsilon(4S)$

• • • We do not use the following data for averages, fits, limits, etc. • • •

1 AUBERT 07c reports  $0.045 \pm 0.003 \pm 0.012$  from a measurement of  $[\Gamma(B \rightarrow \Lambda_c^+ / \bar{\Lambda}_c^- \text{ anything}) / \Gamma_{\text{total}}] \times [B(\Lambda_c^+ \rightarrow pK^- \pi^+)]$  assuming  $B(\Lambda_c^+ \rightarrow pK^- \pi^+) = (5.0 \pm 1.3) \times 10^{-2}$ , which we rescale to our best value  $B(\Lambda_c^+ \rightarrow pK^- \pi^+) = (6.28 \pm 0.32) \times 10^{-2}$ . Our first error is their experiment's error and our second error is the systematic error from using our best value.

2 CRAWFORD 92 result derived from lepton baryon correlations. Assumes all charmed baryons in  $B^0$  and  $B^\pm$  decay are  $\Lambda_c$ .

3 ALBRECHT 88E measured  $B(B \rightarrow \Lambda_c^+ X) \cdot B(\Lambda_c^+ \rightarrow pK^- \pi^+) = (0.30 \pm 0.12 \pm 0.06)\%$  and used  $B(\Lambda_c^+ \rightarrow pK^- \pi^+) = (2.2 \pm 1.0)\%$  from ABRAMS 80 to obtain above number.

4 Assuming all baryons result from charmed baryons, ALAM 86 conclude the branching fraction is  $7.4 \pm 2.9\%$ . The limit given above is model independent.

### $\Gamma(\Lambda_c^+ \text{ anything}) / \Gamma(\bar{\Lambda}_c^- \text{ anything})$ $\Gamma_{97} / \Gamma_{98}$

VALUE	DOCUMENT ID	TECN	COMMENT
$0.19 \pm 0.13 \pm 0.04$	1 AMMAR 97	CLE2	$e^+e^- \rightarrow \Upsilon(4S)$

1 AMMAR 97 uses a high-momentum lepton tag ( $P_\ell > 1.4 \text{ GeV}/c^2$ ).

### $\Gamma(\bar{\Lambda}_c^- \mu^+ \text{ anything}) / \Gamma(\bar{\Lambda}_c^- \text{ anything})$ $\Gamma_{101} / \Gamma_{98}$

VALUE (units $10^{-2}$ )	DOCUMENT ID	TECN	COMMENT
$-2.0 \pm 2.0 \pm 1.9$	LEES 12	BABR	$e^+e^- \rightarrow \Upsilon(4S)$

### $\Gamma(\bar{\Lambda}_c^- \ell^+ \text{ anything}) / \Gamma(\Lambda_c^+ / \bar{\Lambda}_c^- \text{ anything})$ $\Gamma_{99} / \Gamma_{96}$

VALUE	CL%	DOCUMENT ID	TECN	COMMENT
$<2.5 \times 10^{-2}$	90	1 LEES 12	BABR	$e^+e^- \rightarrow \Upsilon(4S)$

1 LEES 12 quotes also the measurement  $\Gamma(B \rightarrow \bar{\Lambda}_c^- \ell^+ \text{ anything}) / \Gamma(B \rightarrow \Lambda_c^+ / \bar{\Lambda}_c^- \text{ anything}) = (1.2 \pm 0.7 \pm 0.4) \times 10^{-2}$ .

### $\Gamma(\bar{\Lambda}_c^- e^+ \text{ anything}) / \Gamma(\Lambda_c^+ / \bar{\Lambda}_c^- \text{ anything})$ $\Gamma_{100} / \Gamma_{96}$

VALUE	CL%	DOCUMENT ID	TECN	COMMENT
$<0.05$	90	1 BONVICINI 98	CLE2	$e^+e^- \rightarrow \Upsilon(4S)$

1 BONVICINI 98 uses the electron with momentum above 0.6 GeV/c.

### $\Gamma(\bar{\Lambda}_c^- e^+ \text{ anything}) / \Gamma(\bar{\Lambda}_c^- \text{ anything})$ $\Gamma_{100} / \Gamma_{98}$

VALUE (units $10^{-2}$ )	DOCUMENT ID	TECN	COMMENT
$2.5 \pm 1.1 \pm 0.6$	1 LEES 12	BABR	$e^+e^- \rightarrow \Upsilon(4S)$

1 Uses the full reconstruction of the recoiling B in a hadronic decay as a tag.

### $\Gamma(\bar{\Lambda}_c^- \ell^+ \text{ anything}) / \Gamma(\bar{\Lambda}_c^- \text{ anything})$ $\Gamma_{99} / \Gamma_{98}$

VALUE	CL%	DOCUMENT ID	TECN	COMMENT
$<3.5 \times 10^{-2}$	90	1 LEES 12	BABR	$e^+e^- \rightarrow \Upsilon(4S)$

1 LEES 12 quotes also the measurement  $\Gamma(B \rightarrow \bar{\Lambda}_c^- \ell^+ \text{ anything}) / \Gamma(B \rightarrow \bar{\Lambda}_c^- \text{ anything}) = (1.7 \pm 1.0 \pm 0.6) \times 10^{-2}$ .

### $\Gamma(\bar{\Lambda}_c^- p \text{ anything}) / \Gamma(\Lambda_c^+ / \bar{\Lambda}_c^- \text{ anything})$ $\Gamma_{102} / \Gamma_{96}$

VALUE	DOCUMENT ID	TECN	COMMENT
$0.57 \pm 0.05 \pm 0.05$	BONVICINI 98	CLE2	$e^+e^- \rightarrow \Upsilon(4S)$

### $\Gamma(\bar{\Lambda}_c^- p e^+ \nu_e) / \Gamma(\bar{\Lambda}_c^- p \text{ anything})$ $\Gamma_{103} / \Gamma_{102}$

VALUE	CL%	DOCUMENT ID	TECN	COMMENT
$<0.04$	90	1 BONVICINI 98	CLE2	$e^+e^- \rightarrow \Upsilon(4S)$

1 BONVICINI 98 uses the electron with momentum above 0.6 GeV/c.

### $\Gamma(\Sigma_c^{--} \text{ anything}) / \Gamma_{\text{total}}$ $\Gamma_{104} / \Gamma$

VALUE	EVTS	DOCUMENT ID	TECN	COMMENT
$0.0033 \pm 0.0017 \pm 0.0002$	77	1 PROCARIO 94	CLE2	$e^+e^- \rightarrow \Upsilon(4S)$

1 PROCARIO 94 reports  $[\Gamma(B \rightarrow \Sigma_c^{--} \text{ anything}) / \Gamma_{\text{total}}] \times [B(\Lambda_c^+ \rightarrow pK^- \pi^+)] = 0.00021 \pm 0.00008 \pm 0.00007$  which we divide by our best value  $B(\Lambda_c^+ \rightarrow pK^- \pi^+) = (6.28 \pm 0.32) \times 10^{-2}$ . Our first error is their experiment's error and our second error is the systematic error from using our best value.

### $\Gamma(\Sigma_c^- \text{ anything}) / \Gamma_{\text{total}}$ $\Gamma_{105} / \Gamma$

VALUE	CL%	DOCUMENT ID	TECN	COMMENT
$<8 \times 10^{-3}$	90	1 PROCARIO 94	CLE2	$e^+e^- \rightarrow \Upsilon(4S)$

1 PROCARIO 94 reports  $[\Gamma(B \rightarrow \Sigma_c^- \text{ anything}) / \Gamma_{\text{total}}] \times [B(\Lambda_c^+ \rightarrow pK^- \pi^+)] < 0.00048$  which we divide by our best value  $B(\Lambda_c^+ \rightarrow pK^- \pi^+) = 6.28 \times 10^{-2}$ .

### $\Gamma(\Sigma_c^0 \text{ anything}) / \Gamma_{\text{total}}$ $\Gamma_{106} / \Gamma$

VALUE	EVTS	DOCUMENT ID	TECN	COMMENT
$0.0037 \pm 0.0017 \pm 0.0002$	76	1 PROCARIO 94	CLE2	$e^+e^- \rightarrow \Upsilon(4S)$

1 PROCARIO 94 reports  $[\Gamma(B \rightarrow \Sigma_c^0 \text{ anything}) / \Gamma_{\text{total}}] \times [B(\Lambda_c^+ \rightarrow pK^- \pi^+)] = 0.00023 \pm 0.00008 \pm 0.00007$  which we divide by our best value  $B(\Lambda_c^+ \rightarrow pK^- \pi^+) = (6.28 \pm 0.32) \times 10^{-2}$ . Our first error is their experiment's error and our second error is the systematic error from using our best value.

### $\Gamma(\Sigma_c^0 N(N = p \text{ or } n)) / \Gamma_{\text{total}}$ $\Gamma_{107} / \Gamma$

VALUE	CL%	DOCUMENT ID	TECN	COMMENT
$<1.2 \times 10^{-3}$	90	1 PROCARIO 94	CLE2	$e^+e^- \rightarrow \Upsilon(4S)$

1 PROCARIO 94 reports  $< 0.0017$  from a measurement of  $[\Gamma(B \rightarrow \Sigma_c^0 N(N = p \text{ or } n)) / \Gamma_{\text{total}}] \times [B(\Lambda_c^+ \rightarrow pK^- \pi^+)]$  assuming  $B(\Lambda_c^+ \rightarrow pK^- \pi^+) = 0.043$ , which we rescale to our best value  $B(\Lambda_c^+ \rightarrow pK^- \pi^+) = 6.28 \times 10^{-2}$ .

### $\Gamma(\Xi_c^0 \text{ anything}, \Xi_c^0 \rightarrow \Xi^- \pi^+) / \Gamma_{\text{total}}$ $\Gamma_{108} / \Gamma$

VALUE (units $10^{-3}$ )	DOCUMENT ID	TECN	COMMENT
$0.193 \pm 0.030$ OUR AVERAGE	Error includes scale factor of 1.1.		
$0.211 \pm 0.019 \pm 0.025$	1 AUBERT B 05M	BABR	$e^+e^- \rightarrow \Upsilon(4S)$
$0.144 \pm 0.048 \pm 0.021$	2 BARISH 97	CLE2	$e^+e^- \rightarrow \Upsilon(4S)$

1 The yield is obtained by requiring the momentum  $P < 2.15 \text{ GeV}/c$ .  
2 BARISH 97 find  $79 \pm 27 \Xi_c^0$  events.

### $\Gamma(\Xi_c^+ \Xi_c^+ \rightarrow \Xi^- \pi^+ \pi^+) / \Gamma_{\text{total}}$ $\Gamma_{109} / \Gamma$

VALUE (units $10^{-3}$ )	DOCUMENT ID	TECN	COMMENT
$0.453 \pm 0.096 \pm 0.085$ $-0.065$	1 BARISH 97	CLE2	$e^+e^- \rightarrow \Upsilon(4S)$

1 BARISH 97 find  $125 \pm 28 \Xi_c^+$  events.

### $\Gamma(p/\bar{p} \text{ anything}) / \Gamma_{\text{total}}$ $\Gamma_{110} / \Gamma$

Includes p and  $\bar{p}$  from  $\Lambda$  and  $\bar{\Lambda}$  decay.

VALUE	EVTS	DOCUMENT ID	TECN	COMMENT
$0.080 \pm 0.004$ OUR AVERAGE				
$0.080 \pm 0.005 \pm 0.005$		ALBRECHT 93i	ARG	$e^+e^- \rightarrow \Upsilon(4S)$
$0.080 \pm 0.005 \pm 0.003$		CRAWFORD 92	CLEO	$e^+e^- \rightarrow \Upsilon(4S)$
$0.082 \pm 0.005 \pm 0.013$ $-0.010$	2163	1 ALBRECHT 89k	ARG	$e^+e^- \rightarrow \Upsilon(4S)$

• • • We do not use the following data for averages, fits, limits, etc. • • •

>0.021

2 ALAM 83b reported their result as  $> 0.036 \pm 0.006 \pm 0.009$ . Data are consistent with equal yields of p and  $\bar{p}$ . Using assumed yields below cut,  $B(B \rightarrow p + X) = 0.03$  not including protons from  $\Lambda$  decays.

### $\Gamma(p/\bar{p} \text{ (direct) anything}) / \Gamma_{\text{total}}$ $\Gamma_{111} / \Gamma$

VALUE	EVTS	DOCUMENT ID	TECN	COMMENT
$0.055 \pm 0.005$ OUR AVERAGE				
$0.055 \pm 0.005 \pm 0.0035$		ALBRECHT 93i	ARG	$e^+e^- \rightarrow \Upsilon(4S)$
$0.056 \pm 0.006 \pm 0.005$		CRAWFORD 92	CLEO	$e^+e^- \rightarrow \Upsilon(4S)$
$0.055 \pm 0.016$	1220	1 ALBRECHT 89k	ARG	$e^+e^- \rightarrow \Upsilon(4S)$

1 ALBRECHT 89k subtract contribution of  $\Lambda$  decay from the inclusive proton yield.

### $\Gamma(\bar{p} e^+ \nu_e \text{ anything}) / \Gamma_{\text{total}}$ $\Gamma_{112} / \Gamma$

VALUE	CL%	DOCUMENT ID	TECN	COMMENT
$< 5.9 \times 10^{-4}$	90	1 ADAM 03b	CLE2	$e^+e^- \rightarrow \Upsilon(4S)$

• • • We do not use the following data for averages, fits, limits, etc. • • •

VALUE	CL%	DOCUMENT ID	TECN	COMMENT
$<16 \times 10^{-4}$	90	ALBRECHT 90H	ARG	$e^+e^- \rightarrow \Upsilon(4S)$

1 Based on V-A model.

### $\Gamma(\Lambda/\bar{\Lambda} \text{ anything}) / \Gamma_{\text{total}}$ $\Gamma_{113} / \Gamma$

VALUE	EVTS	DOCUMENT ID	TECN	COMMENT
$0.040 \pm 0.005$ OUR AVERAGE				
$0.038 \pm 0.004 \pm 0.006$	2998	CRAWFORD 92	CLEO	$e^+e^- \rightarrow \Upsilon(4S)$
$0.042 \pm 0.005 \pm 0.006$	943	ALBRECHT 89k	ARG	$e^+e^- \rightarrow \Upsilon(4S)$

• • • We do not use the following data for averages, fits, limits, etc. • • •

$0.022 \pm 0.003 \pm 0.0022$

>0.011

1 ACKERSTAFF 97N OPAL  $e^+e^- \rightarrow Z$

2 ALAM 83B CLEO  $e^+e^- \rightarrow \Upsilon(4S)$

1 ACKERSTAFF 97N assumes  $B(b \rightarrow B) = 0.868 \pm 0.041$ , i.e., an admixture of  $B^0, B^\pm$ , and  $B_s$ .

2 ALAM 83b reported their result as  $> 0.022 \pm 0.007 \pm 0.004$ . Values are for  $(B(\Lambda X) + B(\bar{\Lambda} X))/2$ . Data are consistent with equal yields of p and  $\bar{p}$ . Using assumed yields below cut,  $B(B \rightarrow \Lambda X) = 0.03$ .

### $\Gamma(\Lambda \text{ anything}) / \Gamma(\bar{\Lambda} \text{ anything})$ $\Gamma_{114} / \Gamma_{115}$

VALUE	DOCUMENT ID	TECN	COMMENT
$0.43 \pm 0.09 \pm 0.07$	1 AMMAR 97	CLE2	$e^+e^- \rightarrow \Upsilon(4S)$

1 AMMAR 97 uses a high-momentum lepton tag ( $P_\ell > 1.4 \text{ GeV}/c^2$ ).

### $\Gamma(\Xi^- / \Xi^+ \text{ anything}) / \Gamma_{\text{total}}$ $\Gamma_{116} / \Gamma$

VALUE	EVTS	DOCUMENT ID	TECN	COMMENT
$0.0027 \pm 0.0006$ OUR AVERAGE				
$0.0027 \pm 0.0005 \pm 0.0004$	147	CRAWFORD 92	CLEO	$e^+e^- \rightarrow \Upsilon(4S)$
$0.0028 \pm 0.0014$	54	ALBRECHT 89k	ARG	$e^+e^- \rightarrow \Upsilon(4S)$

# Meson Particle Listings

## $B^\pm/B^0$ ADMIXTURE

### $\Gamma(\text{baryons anything})/\Gamma_{\text{total}}$ $\Gamma_{117}/\Gamma$

VALUE	DOCUMENT ID	TECN	COMMENT
<b>0.068 ± 0.005 ± 0.003</b>	<sup>1</sup> ALBRECHT 92a	ARG	$e^+e^- \rightarrow \Upsilon(4S)$
0.076 ± 0.014	<sup>2</sup> ALBRECHT 89k	ARG	$e^+e^- \rightarrow \Upsilon(4S)$

• • • We do not use the following data for averages, fits, limits, etc. • • •

<sup>1</sup> ALBRECHT 92a result is from simultaneous analysis of  $p$  and  $\Lambda$  yields,  $p\bar{p}$  and  $\Lambda\bar{\Lambda}$  correlations, and various lepton-baryon and lepton-baryon-antibaryon correlations. Supersedes ALBRECHT 89k.

<sup>2</sup> ALBRECHT 89k obtain this result by adding their their measurements (5.5 ± 1.6)% for direct protons and (4.2 ± 0.5 ± 0.6)% for inclusive  $\Lambda$  production. They then assume (5.5 ± 1.6)% for neutron production and add it in also. Since each  $B$  decay has two baryons, they divide by 2 to obtain (7.6 ± 1.4)%.

### $\Gamma(p\bar{p} \text{ anything})/\Gamma_{\text{total}}$ $\Gamma_{118}/\Gamma$

VALUE	EVTS	DOCUMENT ID	TECN	COMMENT
<b>0.0247 ± 0.0023 OUR AVERAGE</b>				
0.024 ± 0.001 ± 0.004		CRAWFORD 92	CLEO	$e^+e^- \rightarrow \Upsilon(4S)$
0.025 ± 0.002 ± 0.002	918	ALBRECHT 89k	ARG	$e^+e^- \rightarrow \Upsilon(4S)$

### $\Gamma(p\bar{p} \text{ anything})/\Gamma(p/\bar{p} \text{ anything})$ $\Gamma_{118}/\Gamma_{110}$

VALUE	DOCUMENT ID	TECN	COMMENT
0.30 ± 0.02 ± 0.05	<sup>1</sup> CRAWFORD 92	CLEO	$e^+e^- \rightarrow \Upsilon(4S)$

Includes  $p$  and  $\bar{p}$  from  $\Lambda$  and  $\bar{\Lambda}$  decay.

• • • We do not use the following data for averages, fits, limits, etc. • • •

<sup>1</sup> CRAWFORD 92 value is not independent of their  $\Gamma(p\bar{p} \text{ anything})/\Gamma_{\text{total}}$  value.

### $\Gamma(\Lambda\bar{\Lambda}/\bar{\Lambda}p \text{ anything})/\Gamma_{\text{total}}$ $\Gamma_{119}/\Gamma$

VALUE	EVTS	DOCUMENT ID	TECN	COMMENT
<b>0.025 ± 0.004 OUR AVERAGE</b>				
0.029 ± 0.005 ± 0.005		CRAWFORD 92	CLEO	$e^+e^- \rightarrow \Upsilon(4S)$
0.023 ± 0.004 ± 0.003	165	ALBRECHT 89k	ARG	$e^+e^- \rightarrow \Upsilon(4S)$

Includes  $p$  and  $\bar{p}$  from  $\Lambda$  and  $\bar{\Lambda}$  decay.

### $\Gamma(\Lambda\bar{\Lambda}/\bar{\Lambda}p \text{ anything})/\Gamma(\Lambda/\bar{\Lambda} \text{ anything})$ $\Gamma_{119}/\Gamma_{113}$

VALUE	DOCUMENT ID	TECN	COMMENT
0.76 ± 0.11 ± 0.08	<sup>1</sup> CRAWFORD 92	CLEO	$e^+e^- \rightarrow \Upsilon(4S)$

Includes  $p$  and  $\bar{p}$  from  $\Lambda$  and  $\bar{\Lambda}$  decay.

• • • We do not use the following data for averages, fits, limits, etc. • • •

<sup>1</sup> CRAWFORD 92 value is not independent of their  $[\Gamma(\Lambda\bar{\Lambda} \text{ anything}) + \Gamma(\bar{\Lambda}p \text{ anything})]/\Gamma_{\text{total}}$  value.

### $\Gamma(\Lambda\bar{\Lambda} \text{ anything})/\Gamma_{\text{total}}$ $\Gamma_{120}/\Gamma$

VALUE	CL%	EVTS	DOCUMENT ID	TECN	COMMENT
<b>&lt;0.005</b>	90		CRAWFORD 92	CLEO	$e^+e^- \rightarrow \Upsilon(4S)$
<0.0088	90	12	ALBRECHT 89k	ARG	$e^+e^- \rightarrow \Upsilon(4S)$

• • • We do not use the following data for averages, fits, limits, etc. • • •

### $\Gamma(\Lambda\bar{\Lambda} \text{ anything})/\Gamma(\Lambda/\bar{\Lambda} \text{ anything})$ $\Gamma_{120}/\Gamma_{113}$

VALUE	CL%	DOCUMENT ID	TECN	COMMENT
<0.13	90	<sup>1</sup> CRAWFORD 92	CLEO	$e^+e^- \rightarrow \Upsilon(4S)$

• • • We do not use the following data for averages, fits, limits, etc. • • •

<sup>1</sup> CRAWFORD 92 value is not independent of their  $\Gamma(\Lambda\bar{\Lambda} \text{ anything})/\Gamma_{\text{total}}$  value.

### $\Gamma(s e^+ e^-)/\Gamma_{\text{total}}$ $\Gamma_{121}/\Gamma$

Test for  $\Delta B = 1$  weak neutral current. Allowed by higher-order electroweak interactions.

VALUE (units $10^{-6}$ )	CL%	DOCUMENT ID	TECN	COMMENT
<b>6.7 ± 1.7 OUR AVERAGE</b>				Error includes scale factor of 2.0.
7.69 <sup>+0.82</sup> <sub>-0.77</sub> ± 0.71 <sup>+0.63</sup> <sub>-0.60</sub>		<sup>1</sup> LEES 14d	BABR	$e^+e^- \rightarrow \Upsilon(4S)$
4.04 ± 1.30 <sup>+0.87</sup> <sub>-0.83</sub>		<sup>2</sup> IWASAKI 05	BELL	$e^+e^- \rightarrow \Upsilon(4S)$

• • • We do not use the following data for averages, fits, limits, etc. • • •

6.0 ± 1.7 ± 1.3 <sup>2</sup> AUBERT,B 04i BABR Repl. by LEES 14d

5.0 ± 2.3<sup>+1.3</sup><sub>-1.1</sub> <sup>2</sup> KANEKO 03 BELL Repl. by IWASAKI 05

< 57 90 GLENN 98 CLEO  $e^+e^- \rightarrow \Upsilon(4S)$

<50000 90 BEBEK 81 CLEO  $e^+e^- \rightarrow \Upsilon(4S)$

<sup>1</sup> Measured from sum of exclusive modes through  $K^+$ ,  $K^+\pi^0$ ,  $K^+\pi^-$ ,  $K^+\pi^-\pi^0$ ,  $K^+\pi^-\pi^+$ ,  $K_S^0$ ,  $K_S^0\pi^0$ ,  $K_S^0\pi^+$ ,  $K_S^0\pi^+\pi^0$ , and  $K_S^0\pi^+\pi^-$  corrected for unobserved modes.

<sup>2</sup> Requires  $M_{e^+e^-} > 0.2 \text{ GeV}/c^2$ .

### $\Gamma(s\mu^+\mu^-)/\Gamma_{\text{total}}$ $\Gamma_{122}/\Gamma$

Test for  $\Delta B = 1$  weak neutral current. Allowed by higher-order electroweak interactions.

VALUE (units $10^{-6}$ )	CL%	DOCUMENT ID	TECN	COMMENT
<b>4.3 ± 1.0 OUR AVERAGE</b>				
4.41 <sup>+1.31</sup> <sub>-1.17</sub> ± 0.63 <sup>+0.63</sup> <sub>-0.50</sub>		<sup>1</sup> LEES 14d	BABR	$e^+e^- \rightarrow \Upsilon(4S)$
4.13 ± 1.05 <sup>+0.85</sup> <sub>-0.81</sub>		<sup>2</sup> IWASAKI 05	BELL	$e^+e^- \rightarrow \Upsilon(4S)$

• • • We do not use the following data for averages, fits, limits, etc. • • •

5.0 ± 2.8 ± 1.2	AUBERT,B 04i	BABR	Repl. by LEES 14d
7.9 ± 2.1 <sup>+2.1</sup> <sub>-1.5</sub>	KANEKO 03	BELL	Repl. by IWASAKI 05
< 58	90	GLENN 98	CLEO $e^+e^- \rightarrow \Upsilon(4S)$
<17000	90	CHADWICK 81	CLEO $e^+e^- \rightarrow \Upsilon(4S)$

<sup>1</sup> Measured from sum of exclusive modes through  $K^+$ ,  $K^+\pi^0$ ,  $K^+\pi^-$ ,  $K^+\pi^-\pi^0$ ,  $K^+\pi^-\pi^+$ ,  $K_S^0$ ,  $K_S^0\pi^0$ ,  $K_S^0\pi^+$ ,  $K_S^0\pi^+\pi^0$ , and  $K_S^0\pi^+\pi^-$  corrected for unobserved modes.

<sup>2</sup> Requires  $M_{e^+e^-} > 0.2 \text{ GeV}/c^2$ .

### $[\Gamma(s e^+ e^-) + \Gamma(s\mu^+\mu^-)]/\Gamma_{\text{total}}$ $(\Gamma_{121} + \Gamma_{122})/\Gamma$

Test for  $\Delta B = 1$  weak neutral current. Allowed by higher-order electroweak interactions.

VALUE	CL%	DOCUMENT ID	TECN	COMMENT
<b>&lt;4.2 × 10<sup>-5</sup></b>	90	GLENN 98	CLEO	$e^+e^- \rightarrow \Upsilon(4S)$
<0.0024	90	<sup>1</sup> BEAN 87	CLEO	Repl. by GLENN 98
<0.0062	90	<sup>2</sup> AVERY 90	CLEO	Repl. by BEAN 87

<sup>1</sup> BEAN 87 reports  $[(\mu^+\mu^-) + (e^+e^-)]/2$  and we converted it.

<sup>2</sup> Determine ratio of  $B^+$  to  $B^0$  semileptonic decays to be in the range 0.25–2.9.

### $\Gamma(s\ell^+\ell^-)/\Gamma_{\text{total}}$ $\Gamma_{123}/\Gamma$

Test for  $\Delta B = 1$  weak neutral current.

VALUE (units $10^{-6}$ )	CL%	DOCUMENT ID	TECN	COMMENT
<b>5.8 ± 1.3 OUR AVERAGE</b>				Error includes scale factor of 1.8.
6.73 <sup>+0.70</sup> <sub>-0.64</sub> ± 0.60 <sup>+0.60</sup> <sub>-0.56</sub>		<sup>1</sup> LEES 14d	BABR	$e^+e^- \rightarrow \Upsilon(4S)$
4.11 ± 0.83 <sup>+0.85</sup> <sub>-0.81</sub>		<sup>2</sup> IWASAKI 05	BELL	$e^+e^- \rightarrow \Upsilon(4S)$

• • • We do not use the following data for averages, fits, limits, etc. • • •

5.6 ± 1.5 ± 1.3 <sup>3</sup> AUBERT,B 04i BABR Repl. by LEES 14d

6.1 ± 1.4<sup>+1.4</sup><sub>-1.1</sub> <sup>3</sup> KANEKO 03 BELL Repl. by IWASAKI 05

<sup>1</sup> Measured from sum of exclusive modes through  $K^+$ ,  $K^+\pi^0$ ,  $K^+\pi^-$ ,  $K^+\pi^-\pi^0$ ,  $K^+\pi^-\pi^+$ ,  $K_S^0$ ,  $K_S^0\pi^0$ ,  $K_S^0\pi^+$ ,  $K_S^0\pi^+\pi^0$ , and  $K_S^0\pi^+\pi^-$  corrected for unobserved modes.

<sup>2</sup> Requires  $M_{e^+e^-} > 0.2 \text{ GeV}/c^2$ .

<sup>3</sup> Requires  $M_{e^+e^-} > 0.2 \text{ GeV}/c^2$ .

### $\Gamma(\pi\ell^+\ell^-)/\Gamma_{\text{total}}$ $\Gamma_{124}/\Gamma$

VALUE	CL%	DOCUMENT ID	TECN	COMMENT
<b>&lt;5.9 × 10<sup>-8</sup></b>	90	<sup>1</sup> LEES 13m	BABR	$e^+e^- \rightarrow \Upsilon(4S)$
<6.2 × 10 <sup>-8</sup>	90	<sup>1</sup> WEI 08a	BELL	$e^+e^- \rightarrow \Upsilon(4S)$
<9.1 × 10 <sup>-8</sup>	90	<sup>1</sup> AUBERT 07a	BABR	$e^+e^- \rightarrow \Upsilon(4S)$

• • • We do not use the following data for averages, fits, limits, etc. • • •

<sup>1</sup> Assumes equal production of  $B^+$  and  $B^0$  at the  $\Upsilon(4S)$ .

### $\Gamma(\pi e^+ e^-)/\Gamma_{\text{total}}$ $\Gamma_{125}/\Gamma$

VALUE	CL%	DOCUMENT ID	TECN	COMMENT
<b>&lt;11.0 × 10<sup>-8</sup></b>	90	<sup>1</sup> LEES 13m	BABR	$e^+e^- \rightarrow \Upsilon(4S)$

• • • We do not use the following data for averages, fits, limits, etc. • • •

<sup>1</sup> Assumes equal production of  $B^+$  and  $B^0$  at the  $\Upsilon(4S)$ .

### $\Gamma(\pi\mu^+\mu^-)/\Gamma_{\text{total}}$ $\Gamma_{126}/\Gamma$

VALUE	CL%	DOCUMENT ID	TECN	COMMENT
<b>&lt;5.0 × 10<sup>-8</sup></b>	90	<sup>1</sup> LEES 13m	BABR	$e^+e^- \rightarrow \Upsilon(4S)$

• • • We do not use the following data for averages, fits, limits, etc. • • •

<sup>1</sup> Assumes equal production of  $B^+$  and  $B^0$  at the  $\Upsilon(4S)$ .

### $\Gamma(K e^+ e^-)/\Gamma_{\text{total}}$ $\Gamma_{127}/\Gamma$

Test for  $\Delta B = 1$  weak neutral current. Allowed by higher-order electroweak interactions.

VALUE (units $10^{-7}$ )	CL%	DOCUMENT ID	TECN	COMMENT
<b>4.4 ± 0.6 OUR AVERAGE</b>				
3.9 <sup>+0.9</sup> <sub>-0.8</sub> ± 0.2		<sup>1</sup> AUBERT 09t	BABR	$e^+e^- \rightarrow \Upsilon(4S)$
4.8 <sup>+0.8</sup> <sub>-0.7</sub> ± 0.3		<sup>1</sup> WEI 09a	BELL	$e^+e^- \rightarrow \Upsilon(4S)$

• • • We do not use the following data for averages, fits, limits, etc. • • •

3.3<sup>+0.9</sup><sub>-0.8</sub> ± 0.2 <sup>1</sup> AUBERT,B 06j BABR Repl. by AUBERT 09t

7.4<sup>+1.8</sup><sub>-1.6</sub> ± 0.5 <sup>1</sup> AUBERT 03u BABR Repl. by AUBERT,B 06j

4.8<sup>+1.5</sup><sub>-1.3</sub> ± 0.3 <sup>1,2</sup> ISHIKAWA 03 BELL Repl. by WEI 09a

<13 90 ABE 02 BELL Repl. by ISHIKAWA 03

<sup>1</sup> Assumes equal production of  $B^+$  and  $B^0$  at the  $\Upsilon(4S)$ .

<sup>2</sup> The second error is a total of systematic uncertainties including model dependence.

# Meson Particle Listings

## $B^\pm/B^0$ ADMIXTURE

$\Gamma(K^*(892)e^+e^-)/\Gamma_{\text{total}}$   $\Gamma_{128}/\Gamma$   
 Test for  $\Delta B = 1$  weak neutral current. Allowed by higher-order electroweak interactions.

VALUE (units $10^{-7}$ )	CL%	DOCUMENT ID	TECN	COMMENT
<b>11.9 ± 2.0 OUR AVERAGE</b>		Error includes scale factor of 1.2.		
$9.9^{+2.3}_{-2.1} \pm 0.6$		1 AUBERT	09T BABR	$e^+e^- \rightarrow \Upsilon(4S)$
$13.9^{+2.3}_{-2.0} \pm 1.2$		1 WEI	09A BELL	$e^+e^- \rightarrow \Upsilon(4S)$
• • • We do not use the following data for averages, fits, limits, etc. • • •				
$9.7^{+3.0}_{-2.7} \pm 1.4$		1 AUBERT,B	06J BABR	Repl. by AUBERT 09T
$9.8^{+5.0}_{-4.2} \pm 1.1$		1 AUBERT	03U BABR	Repl. by AUBERT,B 06J
$14.9^{+5.2+1.2}_{-4.6-1.3}$		2 ISHIKAWA	03 BELL	Repl. by WEI 09A
<56	90	ABE	02 BELL	Repl. by ISHIKAWA 03

<sup>1</sup> Assumes equal production of  $B^+$  and  $B^0$  at the  $\Upsilon(4S)$ .  
<sup>2</sup> Assumes equal production of  $B^0$  and  $B^+$  at  $\Upsilon(4S)$ . The second error is a total of systematic uncertainties including model dependence.

$\Gamma(K\mu^+\mu^-)/\Gamma_{\text{total}}$   $\Gamma_{129}/\Gamma$   
 Test for  $\Delta B = 1$  weak neutral current. Allowed by higher-order electroweak interactions.

VALUE (units $10^{-7}$ )	DOCUMENT ID	TECN	COMMENT
<b>4.4 ± 0.4 OUR AVERAGE</b>			
$4.2 \pm 0.4 \pm 0.2$	AALTONEN	11A1 CDF	$p\bar{p}$ at 1.96 TeV
$4.1^{+1.3}_{-1.2} \pm 0.2$	1 AUBERT	09T BABR	$e^+e^- \rightarrow \Upsilon(4S)$
$5.0 \pm 0.6 \pm 0.3$	1 WEI	09A BELL	$e^+e^- \rightarrow \Upsilon(4S)$
• • • We do not use the following data for averages, fits, limits, etc. • • •			
$3.5^{+1.3}_{-1.1} \pm 0.3$	1 AUBERT,B	06J BABR	Repl. by AUBERT 09T
$4.5^{+2.3}_{-1.9} \pm 0.4$	1 AUBERT	03U BABR	Repl. by AUBERT,B 06J
$4.8^{+1.2}_{-1.1} \pm 0.4$	1,2 ISHIKAWA	03 BELL	Repl. by WEI 09A
$9.9^{+4.0+1.3}_{-3.2-1.0}$	ABE	02 BELL	Repl. by ISHIKAWA 03

<sup>1</sup> Assumes equal production of  $B^+$  and  $B^0$  at the  $\Upsilon(4S)$ .  
<sup>2</sup> The second error is a total of systematic uncertainties including model dependence.

$\Gamma(K\mu^+\mu^-)/\Gamma(Ke^+e^-)$   $\Gamma_{129}/\Gamma_{127}$

VALUE	DOCUMENT ID	TECN	COMMENT
<b>1.01 ± 0.15 OUR AVERAGE</b>			
$1.00^{+0.31}_{-0.25} \pm 0.07$	1 LEES	12s BABR	$e^+e^- \rightarrow \Upsilon(4S)$
$0.96^{+0.44}_{-0.34} \pm 0.05$	AUBERT	09T BABR	$e^+e^- \rightarrow \Upsilon(4S)$
$1.03 \pm 0.19 \pm 0.06$	WEI	09A BELL	$e^+e^- \rightarrow \Upsilon(4S)$
• • • We do not use the following data for averages, fits, limits, etc. • • •			
$1.06 \pm 0.48 \pm 0.08$	AUBERT,B	06J BABR	Repl. by AUBERT 09T
<sup>1</sup> Measured in the union of $0.10 < q^2 < 8.12 \text{ GeV}^2/c^4$ and $q^2 > 10.11 \text{ GeV}^2/c^4$ . LEES 12s reports also individual measurements $\Gamma(B \rightarrow K\mu^+\mu^-)/\Gamma(B \rightarrow Ke^+e^-) = 0.74^{+0.40}_{-0.31} \pm 0.06$ for $0.10 < q^2 < 8.12 \text{ GeV}^2/c^4$ and $\Gamma(B \rightarrow K\mu^+\mu^-)/\Gamma(B \rightarrow Ke^+e^-) = 1.43^{+0.65}_{-0.44} \pm 0.12$ for $q^2 > 10.11 \text{ GeV}^2/c^4$ .			

$\Gamma(K^*(892)\mu^+\mu^-)/\Gamma_{\text{total}}$   $\Gamma_{130}/\Gamma$   
 Test for  $\Delta B = 1$  weak neutral current. Allowed by higher-order electroweak interactions.

VALUE (units $10^{-7}$ )	CL%	DOCUMENT ID	TECN	COMMENT
<b>10.6 ± 0.9 OUR AVERAGE</b>				
$10.1 \pm 1.0 \pm 0.5$		AALTONEN	11A1 CDF	$p\bar{p}$ at 1.96 TeV
$13.5^{+3.5}_{-3.3} \pm 1.0$		1 AUBERT	09T BABR	$e^+e^- \rightarrow \Upsilon(4S)$
$11.0^{+1.6}_{-1.4} \pm 0.8$		1 WEI	09A BELL	$e^+e^- \rightarrow \Upsilon(4S)$
• • • We do not use the following data for averages, fits, limits, etc. • • •				
$8.8^{+3.5}_{-3.0} \pm 1.2$		1 AUBERT,B	06J BABR	Repl. by AUBERT 09T
$12.7^{+7.6}_{-6.1} \pm 1.6$		1 AUBERT	03U BABR	Repl. by AUBERT,B 06J
$11.7^{+3.6}_{-3.1} \pm 1.0$		2 ISHIKAWA	03 BELL	Repl. by WEI 09A
<31	90	ABE	02 BELL	Repl. by ISHIKAWA 03

<sup>1</sup> Assumes equal production of  $B^+$  and  $B^0$  at the  $\Upsilon(4S)$ .  
<sup>2</sup> Assumes equal production of  $B^0$  and  $B^+$  at  $\Upsilon(4S)$ . The second error is a total of systematic uncertainties including model dependence.

$\Gamma(K^*(892)\mu^+\mu^-)/\Gamma(K^*(892)e^+e^-)$   $\Gamma_{130}/\Gamma_{128}$

VALUE	DOCUMENT ID	TECN	COMMENT
<b>0.98 ± 0.15 OUR AVERAGE</b>			
$1.13^{+0.34}_{-0.26} \pm 0.10$	1 LEES	12s BABR	$e^+e^- \rightarrow \Upsilon(4S)$
$1.37^{+0.53}_{-0.40} \pm 0.09$	AUBERT	09T BABR	$e^+e^- \rightarrow \Upsilon(4S)$
$0.83 \pm 0.17 \pm 0.08$	WEI	09A BELL	$e^+e^- \rightarrow \Upsilon(4S)$

• • • We do not use the following data for averages, fits, limits, etc. • • •  
 $0.91 \pm 0.45 \pm 0.06$  AUBERT,B 06J BABR Repl. by AUBERT 09T

<sup>1</sup> Measured in the union of  $0.10 < q^2 < 8.12 \text{ GeV}^2/c^4$  and  $q^2 > 10.11 \text{ GeV}^2/c^4$ . LEES 12s reports also individual measurements  $\Gamma(B \rightarrow K^*(892)\mu^+\mu^-)/\Gamma(B \rightarrow K^*(892)e^+e^-) = 1.06^{+0.48}_{-0.33} \pm 0.08$  for  $0.10 < q^2 < 8.12 \text{ GeV}^2/c^4$  and  $\Gamma(B \rightarrow K^*(892)\mu^+\mu^-)/\Gamma(B \rightarrow K^*(892)e^+e^-) = 1.18^{+0.55}_{-0.37} \pm 0.11$  for  $q^2 > 10.11 \text{ GeV}^2/c^4$ .

$\Gamma(K\ell^+\ell^-)/\Gamma_{\text{total}}$   $\Gamma_{131}/\Gamma$   
 Test for  $\Delta B = 1$  weak neutral current. Allowed by higher-order electroweak interactions.

VALUE (units $10^{-7}$ )	CL%	DOCUMENT ID	TECN	COMMENT
<b>4.8 ± 0.4 OUR AVERAGE</b>				
$4.7 \pm 0.6 \pm 0.2$		LEES	12s BABR	$e^+e^- \rightarrow \Upsilon(4S)$
$4.8^{+0.5}_{-0.4} \pm 0.3$		WEI	09A BELL	$e^+e^- \rightarrow \Upsilon(4S)$
• • • We do not use the following data for averages, fits, limits, etc. • • •				
$3.9 \pm 0.7 \pm 0.2$		1 AUBERT	09T BABR	Repl. by LEES 12s
$3.4 \pm 0.7 \pm 0.2$		1 AUBERT,B	06J BABR	Repl. by AUBERT 09T
$6.5^{+1.4}_{-1.3} \pm 0.4$		2 AUBERT	03U BABR	Repl. by AUBERT,B 06J
$4.8^{+1.0}_{-0.9} \pm 0.3$		3 ISHIKAWA	03 BELL	Repl. by WEI 09A
$7.5^{+2.5}_{-2.1} \pm 0.6$		4 ABE	02 BELL	Repl. by ISHIKAWA 03
< 5.1	90	1 AUBERT	02L BABR	$e^+e^- \rightarrow \Upsilon(4S)$
< 17	90	5 ANDERSON	01B CLE2	$e^+e^- \rightarrow \Upsilon(4S)$

<sup>1</sup> Assumes equal production of  $B^+$  and  $B^0$  at the  $\Upsilon(4S)$ .  
<sup>2</sup> Assumes all four  $B \rightarrow K\ell^+\ell^-$  modes having equal partial widths in the fit.  
<sup>3</sup> Assumes equal production rate for charge and neutral  $B$  meson pairs, isospin invariance, lepton universality for  $B \rightarrow K\ell^+\ell^-$ , and  $B(B \rightarrow K^*(892)\mu^+\mu^-) = 1.33$ . The second error is total systematic uncertainties including model dependence.  
<sup>4</sup> Assumes lepton universality.  
<sup>5</sup> The result is for di-lepton masses above 0.5 GeV.

$\Gamma(K^*(892)\ell^+\ell^-)/\Gamma_{\text{total}}$   $\Gamma_{132}/\Gamma$   
 Test for  $\Delta B = 1$  weak neutral current. Allowed by higher-order electroweak interactions.

VALUE (units $10^{-7}$ )	CL%	DOCUMENT ID	TECN	COMMENT
<b>10.5 ± 1.0 OUR AVERAGE</b>				
$10.2^{+1.4}_{-1.3} \pm 0.5$		LEES	12s BABR	$e^+e^- \rightarrow \Upsilon(4S)$
$10.7^{+1.1}_{-1.0} \pm 0.9$		WEI	09A BELL	$e^+e^- \rightarrow \Upsilon(4S)$
• • • We do not use the following data for averages, fits, limits, etc. • • •				
$11.1^{+1.9}_{-1.8} \pm 0.7$		1 AUBERT	09T BABR	Repl. by LEES 12s
$7.8^{+1.9}_{-1.7} \pm 1.1$		1 AUBERT,B	06J BABR	Repl. by AUBERT 09T
$8.8^{+3.3}_{-2.9} \pm 1.0$		2 AUBERT	03U BABR	Repl. by AUBERT,B 06J
$11.5^{+2.6}_{-2.4} \pm 0.8$		3 ISHIKAWA	03 BELL	Repl. by WEI 09A
< 31	90	1,4 AUBERT	02L BABR	Repl. by AUBERT 03U
< 33	90	5 ANDERSON	01B CLE2	$e^+e^- \rightarrow \Upsilon(4S)$

<sup>1</sup> Assumes equal production of  $B^+$  and  $B^0$  at the  $\Upsilon(4S)$ .  
<sup>2</sup> Assumes the partial width ratio of electron and muon modes to be  $\Gamma(B \rightarrow K^*(892)e^+e^-)/\Gamma(B \rightarrow K^*(892)\mu^+\mu^-) = 1.33$ .  
<sup>3</sup> Assumes equal production rate for charge and neutral  $B$  meson pairs, isospin invariance, lepton universality for  $B \rightarrow K\ell^+\ell^-$ , and  $B(B \rightarrow K^*(892)\mu^+\mu^-) = 1.33$ . The second error is total systematic uncertainties including model dependence.  
<sup>4</sup> For averaging  $K^*(892)\mu^+\mu^-$  and  $K^*(892)e^+e^-$  modes, AUBERT 02L assumed  $B(B \rightarrow K^*(892)e^+e^-)/B(B \rightarrow K^*(892)\mu^+\mu^-) = 1.2$ .  
<sup>5</sup> The result is for di-lepton masses above 0.5 GeV.

$\Gamma(K\nu\bar{\nu})/\Gamma_{\text{total}}$   $\Gamma_{133}/\Gamma$   
 Test for  $\Delta B = 1$  weak neutral current.

VALUE	CL%	DOCUMENT ID	TECN	COMMENT
<b>&lt; 1.6 × 10<sup>-5</sup></b>		1 GRYGIER	17 BELL	$e^+e^- \rightarrow \Upsilon(4S)$
< 1.7 × 10 <sup>-5</sup>	90	1,2 LEES	13i BABR	$e^+e^- \rightarrow \Upsilon(4S)$
< 1.4 × 10 <sup>-5</sup>	90	1 DEL-AMO-SA...	10q BABR	Repl. by LEES 13i

<sup>1</sup> Assumes equal production of  $B^+$  and  $B^0$  at the  $\Upsilon(4S)$ .  
<sup>2</sup> Also reported a limit  $< 3.2 \times 10^{-5}$  at 90% CL obtained using a fully reconstructed hadronic  $B$ -tag events.

$\Gamma(K^*\nu\bar{\nu})/\Gamma_{\text{total}}$   $\Gamma_{134}/\Gamma$   
 Test for  $\Delta B = 1$  weak neutral current.

VALUE	CL%	DOCUMENT ID	TECN	COMMENT
<b>&lt; 2.7 × 10<sup>-5</sup></b>		1 GRYGIER	17 BELL	$e^+e^- \rightarrow \Upsilon(4S)$
• • • We do not use the following data for averages, fits, limits, etc. • • •				
< 7.6 × 10 <sup>-5</sup>	90	1,2 LEES	13i BABR	$e^+e^- \rightarrow \Upsilon(4S)$
< 8 × 10 <sup>-5</sup>	90	AUBERT	08bC BABR	Repl. by LEES 13i

<sup>1</sup> Assumes equal production of  $B^+$  and  $B^0$  at the  $\Upsilon(4S)$ .  
<sup>2</sup> Also reported a limit  $< 7.9 \times 10^{-5}$  at 90% CL obtained using a fully reconstructed hadronic  $B$ -tag events.

## Meson Particle Listings

 $B^\pm/B^0$  ADMIXTURE

$\Gamma(\pi\nu\bar{\nu})/\Gamma_{\text{total}}$					$\Gamma_{135}/\Gamma$
VALUE	CL%	DOCUMENT ID	TECN	COMMENT	
$<0.8 \times 10^{-5}$	90	<sup>1</sup> GRYGIER 17	BELL	$e^+e^- \rightarrow \Upsilon(4S)$	
<sup>1</sup> Assumes equal production of $B^+$ and $B^0$ at the $\Upsilon(4S)$ .					

$\Gamma(\rho\nu\bar{\nu})/\Gamma_{\text{total}}$					$\Gamma_{136}/\Gamma$
VALUE	CL%	DOCUMENT ID	TECN	COMMENT	
$<2.8 \times 10^{-5}$	90	<sup>1</sup> GRYGIER 17	BELL	$e^+e^- \rightarrow \Upsilon(4S)$	
<sup>1</sup> Assumes equal production of $B^+$ and $B^0$ at the $\Upsilon(4S)$ .					

$\Gamma(s e^\pm \mu^\mp)/\Gamma_{\text{total}}$					$\Gamma_{137}/\Gamma$
VALUE	CL%	DOCUMENT ID	TECN	COMMENT	
$<2.2 \times 10^{-5}$	90	GLENN 98	CLEO	$e^+e^- \rightarrow \Upsilon(4S)$	
Test of lepton family number conservation. Allowed by higher-order electroweak interactions.					

$\Gamma(\pi e^\pm \mu^\mp)/\Gamma_{\text{total}}$					$\Gamma_{138}/\Gamma$
VALUE	CL%	DOCUMENT ID	TECN	COMMENT	
$<9.2 \times 10^{-8}$	90	<sup>1</sup> AUBERT 07AG	BABR	$e^+e^- \rightarrow \Upsilon(4S)$	
••• We do not use the following data for averages, fits, limits, etc. •••					
$<1.6 \times 10^{-6}$	90	<sup>1</sup> EDWARDS 02B	CLE2	$e^+e^- \rightarrow \Upsilon(4S)$	
<sup>1</sup> Assumes equal production of $B^+$ and $B^0$ at the $\Upsilon(4S)$ .					

$\Gamma(\rho e^\pm \mu^\mp)/\Gamma_{\text{total}}$					$\Gamma_{139}/\Gamma$
VALUE	CL%	DOCUMENT ID	TECN	COMMENT	
$<3.2 \times 10^{-6}$	90	<sup>1</sup> EDWARDS 02B	CLE2	$e^+e^- \rightarrow \Upsilon(4S)$	
<sup>1</sup> Assumes equal production of $B^+$ and $B^0$ at the $\Upsilon(4S)$ .					

$\Gamma(K e^\pm \mu^\mp)/\Gamma_{\text{total}}$					$\Gamma_{140}/\Gamma$
VALUE (units $10^{-7}$ )	CL%	DOCUMENT ID	TECN	COMMENT	
$<0.38$	90	<sup>1</sup> AUBERT,B 06J	BABR	$e^+e^- \rightarrow \Upsilon(4S)$	
••• We do not use the following data for averages, fits, limits, etc. •••					
$<16$	90	<sup>1</sup> EDWARDS 02B	CLE2	$e^+e^- \rightarrow \Upsilon(4S)$	
<sup>1</sup> Assumes equal production of $B^+$ and $B^0$ at the $\Upsilon(4S)$ .					

$\Gamma(K^*(892) e^\pm \mu^\mp)/\Gamma_{\text{total}}$					$\Gamma_{141}/\Gamma$
VALUE (units $10^{-7}$ )	CL%	DOCUMENT ID	TECN	COMMENT	
$<5.1$	90	<sup>1</sup> AUBERT,B 06J	BABR	$e^+e^- \rightarrow \Upsilon(4S)$	
••• We do not use the following data for averages, fits, limits, etc. •••					
$<62$	90	<sup>1</sup> EDWARDS 02B	CLE2	$e^+e^- \rightarrow \Upsilon(4S)$	
<sup>1</sup> Assumes equal production of $B^+$ and $B^0$ at the $\Upsilon(4S)$ .					

## CP VIOLATION

$A_{CP}$  is defined as

$$\frac{B(\bar{B} \rightarrow \bar{f}) - B(B \rightarrow f)}{B(\bar{B} \rightarrow \bar{f}) + B(B \rightarrow f)},$$

the CP-violation charge asymmetry of inclusive  $B^\pm$  and  $B^0$  decay.

$A_{CP}(B \rightarrow K^*(892)\gamma)$				
VALUE	DOCUMENT ID	TECN	COMMENT	
<b><math>-0.003 \pm 0.011</math> OUR AVERAGE</b>				
$-0.004 \pm 0.014 \pm 0.003$	<sup>1</sup> HORIGUCHI 17	BELL	$e^+e^- \rightarrow \Upsilon(4S)$	
$-0.003 \pm 0.017 \pm 0.007$	<sup>2</sup> AUBERT 09A0	BABR	$e^+e^- \rightarrow \Upsilon(4S)$	
$0.08 \pm 0.13 \pm 0.03$	<sup>3</sup> COAN 00	CLE2	$e^+e^- \rightarrow \Upsilon(4S)$	
••• We do not use the following data for averages, fits, limits, etc. •••				
$-0.013 \pm 0.036 \pm 0.010$	<sup>4</sup> AUBERT,BE 04A	BABR	Repl. by AUBERT 09A0	
$-0.015 \pm 0.044 \pm 0.012$	<sup>3</sup> NAKAO 04	BELL	Repl. by HORIGUCHI 17	
$-0.044 \pm 0.076 \pm 0.012$	<sup>5</sup> AUBERT 02c	BABR	Repl. by AUBERT,BE 04A	
<sup>1</sup> Uses $B(\Upsilon(4S) \rightarrow B^+B^-) = (51.4 \pm 0.6)\%$ and $B(\Upsilon(4S) \rightarrow B^0\bar{B}^0) = (48.6 \pm 0.6)\%$ .				
<sup>2</sup> Corresponds to a 90% CL interval $-0.033 < A_{CP} < 0.028$ .				
<sup>3</sup> Assumes equal production of $B^+$ and $B^0$ at the $\Upsilon(4S)$ .				
<sup>4</sup> Corresponds to a 90% CL allowed region, $-0.074 < A_{CP} < 0.049$ .				
<sup>5</sup> A 90% CL range is $-0.170 < A_{CP} < 0.082$ .				

$A_{CP}(B \rightarrow s\gamma)$				
VALUE	DOCUMENT ID	TECN	COMMENT	
<b><math>0.015 \pm 0.011</math> OUR AVERAGE</b>				
$0.0144 \pm 0.0128 \pm 0.0011$	<sup>1</sup> WATANUKI 19	BELL	$e^+e^- \rightarrow \Upsilon(4S)$	
$0.017 \pm 0.019 \pm 0.010$	<sup>2</sup> LEES 14k	BABR	$e^+e^- \rightarrow \Upsilon(4S)$	
••• We do not use the following data for averages, fits, limits, etc. •••				
$-0.011 \pm 0.030 \pm 0.014$	<sup>3</sup> AUBERT 08BJ	BABR	Repl. by LEES 14k	
$0.025 \pm 0.050 \pm 0.015$	<sup>4</sup> AUBERT,B 04E	BABR	Repl. by AUBERT 08BJ	
$0.002 \pm 0.050 \pm 0.030$	<sup>5</sup> NISHIDA 04	BELL	Repl. by WATANUKI 19	
<sup>1</sup> Using a sum-of-exclusive technique with $m_{X_S} < 2.8 \text{ GeV}/c^2$ .				
<sup>2</sup> Measured with 16 exclusively reconstructed $B \rightarrow X_S\gamma$ decays with $0.6 < m_{X_S} < 2.0 \text{ GeV}/c^2$ (ten charged and six neutral self-tagging $B$ modes).				
<sup>3</sup> Uses a sum of exclusively reconstructed $B \rightarrow X_S$ decay modes, with $X_S$ mass between $0.6$ and $2.8 \text{ GeV}/c^2$ .				
<sup>4</sup> Corresponds to $-0.06 < A_{CP} < 0.11$ at 90% CL.				
<sup>5</sup> This measurement is performed inclusively for recoil mass $X_S$ less than $2.1 \text{ GeV}$ , which corresponds to $-0.093 < A_{CP} < 0.096$ at 90% CL.				

$A_{CP}(B \rightarrow (s+d)\gamma)$				
VALUE	DOCUMENT ID	TECN	COMMENT	
<b><math>0.010 \pm 0.031</math> OUR AVERAGE</b>				
$0.022 \pm 0.039 \pm 0.009$	<sup>1</sup> PESANTEZ 15	BELL	$e^+e^- \rightarrow \Upsilon(4S)$	
$0.057 \pm 0.060 \pm 0.018$	LEES 12v	BABR	$e^+e^- \rightarrow \Upsilon(4S)$	
$-0.10 \pm 0.18 \pm 0.05$	<sup>2</sup> AUBERT 08o	BABR	$e^+e^- \rightarrow \Upsilon(4S)$	
$-0.110 \pm 0.115 \pm 0.017$	AUBERT,BE 06B	BABR	$e^+e^- \rightarrow \Upsilon(4S)$	
$-0.079 \pm 0.108 \pm 0.022$	<sup>3</sup> COAN 01	CLE2	$e^+e^- \rightarrow \Upsilon(4S)$	
<sup>1</sup> Assumes equal production of $B^+$ and $B^0$ at the $\Upsilon(4S)$ . Uses an opposite side lepton tag. Requires center-of-mass frame $E_\gamma > 2.1 \text{ GeV}$ .				
<sup>2</sup> Uses a fully reconstructed $B$ meson as a tag on the recoil side. Requires $E_\gamma > 2.2 \text{ GeV}$ .				
<sup>3</sup> Corresponds to $-0.27 < A_{CP} < 0.10$ at 90% CL.				

$A_{CP}(B \rightarrow X_S \ell^+ \ell^-)$				
VALUE	DOCUMENT ID	TECN	COMMENT	
<b><math>0.04 \pm 0.11 \pm 0.01</math></b>	<sup>1</sup> LEES 14D	BABR	$e^+e^- \rightarrow \Upsilon(4S)$	
••• We do not use the following data for averages, fits, limits, etc. •••				
$-0.22 \pm 0.26 \pm 0.02$	<sup>2</sup> AUBERT,B 04i	BABR	Repl. by LEES 14D	
<sup>1</sup> Measured from sum of exclusive modes through $K^+$ , $K^+\pi^0$ , $K^+\pi^-$ , $K^+\pi^-\pi^0$ , $K^+\pi^-\pi^+$ , $K_S^0\pi^+$ , and $K_S^0\pi^+\pi^0$ .				
<sup>2</sup> The final state flavor is determined by the kaon and pion charges where modes with $X_S = K_S^0$ , $K_S^0\pi^0$ or $K_S^0\pi^+\pi^-$ are not used.				

$A_{CP}(B \rightarrow X_S \ell^+ \ell^-) (1.0 < q^2 < 6.0 \text{ GeV}^2/c^4)$				
VALUE	DOCUMENT ID	TECN	COMMENT	
<b><math>-0.06 \pm 0.22 \pm 0.01</math></b>	<sup>1</sup> LEES 14D	BABR	$e^+e^- \rightarrow \Upsilon(4S)$	
<sup>1</sup> Measured from sum of exclusive modes through $K^+$ , $K^+\pi^0$ , $K^+\pi^-$ , $K^+\pi^-\pi^0$ , $K^+\pi^-\pi^+$ , $K_S^0\pi^+$ , and $K_S^0\pi^+\pi^0$ .				

$A_{CP}(B \rightarrow X_S \ell^+ \ell^-) (10.1 < q^2 < 12.9 \text{ or } q^2 > 14.2 \text{ GeV}^2/c^4)$				
VALUE	DOCUMENT ID	TECN	COMMENT	
<b><math>0.19 \pm 0.18</math> <math>-0.17 \pm 0.01</math></b>	<sup>1</sup> LEES 14D	BABR	$e^+e^- \rightarrow \Upsilon(4S)$	
<sup>1</sup> Measured from sum of exclusive modes through $K^+$ , $K^+\pi^0$ , $K^+\pi^-$ , $K^+\pi^-\pi^0$ , $K^+\pi^-\pi^+$ , $K_S^0\pi^+$ , and $K_S^0\pi^+\pi^-$ .				

$A_{CP}(B \rightarrow K^* e^+ e^-)$				
VALUE	DOCUMENT ID	TECN	COMMENT	
<b><math>-0.18 \pm 0.15 \pm 0.01</math></b>	WEI 09A	BELL	$e^+e^- \rightarrow \Upsilon(4S)$	

$A_{CP}(B \rightarrow K^* \mu^+ \mu^-)$				
VALUE	DOCUMENT ID	TECN	COMMENT	
<b><math>-0.03 \pm 0.13 \pm 0.02</math></b>	WEI 09A	BELL	$e^+e^- \rightarrow \Upsilon(4S)$	

$A_{CP}(B \rightarrow K^* \ell^+ \ell^-)$				
VALUE	DOCUMENT ID	TECN	COMMENT	
<b><math>-0.04 \pm 0.07</math> OUR AVERAGE</b>				
$0.03 \pm 0.13 \pm 0.01$	<sup>1</sup> LEES 12s	BABR	$e^+e^- \rightarrow \Upsilon(4S)$	
$+0.01 \pm 0.16 \pm 0.01$	AUBERT 09T	BABR	$e^+e^- \rightarrow \Upsilon(4S)$	
$-0.10 \pm 0.10 \pm 0.01$	WEI 09A	BELL	$e^+e^- \rightarrow \Upsilon(4S)$	
<sup>1</sup> Measured in the union of $0.10 < q^2 < 8.12 \text{ GeV}^2/c^4$ and $q^2 > 10.11 \text{ GeV}^2/c^4$ . LEES 12s reports also individual measurements $A_{CP}(B \rightarrow K^* \ell^+ \ell^-) = -0.13 \pm 0.18 \pm 0.01$ for $0.10 < q^2 < 8.12 \text{ GeV}^2/c^4$ and $A_{CP}(B \rightarrow K^* \ell^+ \ell^-) = 0.16 \pm 0.18 \pm 0.19$ for $q^2 > 10.11 \text{ GeV}^2/c^4$ .				

$A_{CP}(B \rightarrow \eta \text{ anything})$				
VALUE	DOCUMENT ID	TECN	COMMENT	
<b><math>-0.13 \pm 0.04 \pm 0.02</math> <math>-0.03</math></b>	<sup>1</sup> NISHIMURA 10	BELL	$e^+e^- \rightarrow \Upsilon(4S)$	
<sup>1</sup> Uses $B \rightarrow \eta X_S$ with $0.4 < m_{X_S} < 2.6 \text{ GeV}/c^2$ .				

$\Delta A_{CP}(X_S\gamma) = A_{CP}(B^\pm \rightarrow X_S\gamma) - A_{CP}(B^0 \rightarrow X_S\gamma)$				
VALUE	DOCUMENT ID	TECN	COMMENT	
<b><math>0.041 \pm 0.023</math> OUR AVERAGE</b>				
$0.0369 \pm 0.0265 \pm 0.0076$	<sup>1</sup> WATANUKI 19	BELL	$e^+e^- \rightarrow \Upsilon(4S)$	
$0.050 \pm 0.039 \pm 0.015$	<sup>2</sup> LEES 14k	BABR	$e^+e^- \rightarrow \Upsilon(4S)$	
<sup>1</sup> Using a sum-of-exclusive technique with $m_{X_S} < 2.8 \text{ GeV}/c^2$ .				
<sup>2</sup> Measured with 16 exclusively reconstructed $B \rightarrow X_S\gamma$ decays with $0.6 < m_{X_S} < 2.0 \text{ GeV}/c^2$ (ten charged and six neutral self-tagging $B$ modes).				

$\bar{A}_{CP}(B \rightarrow X_S\gamma) = (A_{CP}(B^+ \rightarrow X_S\gamma) + A_{CP}(B^0 \rightarrow X_S\gamma))/2$				
VALUE	DOCUMENT ID	TECN	COMMENT	
<b><math>0.0091 \pm 0.0121 \pm 0.0013</math></b>	<sup>1</sup> WATANUKI 19	BELL	$e^+e^- \rightarrow \Upsilon(4S)$	
<sup>1</sup> Using a sum-of-exclusive technique with $m_{X_S} < 2.8 \text{ GeV}/c^2$ .				

$\Delta A_{CP}(B \rightarrow K^*\gamma) = A_{CP}(B^+ \rightarrow K^{*+}\gamma) - A_{CP}(B^0 \rightarrow K^{*0}\gamma)$				
VALUE	DOCUMENT ID	TECN	COMMENT	
<b><math>0.024 \pm 0.028 \pm 0.005</math></b>	<sup>1</sup> HORIGUCHI 17	BELL	$e^+e^- \rightarrow \Upsilon(4S)$	
<sup>1</sup> Uses $B(\Upsilon(4S) \rightarrow B^+B^-) = (51.4 \pm 0.6)\%$ and $B(\Upsilon(4S) \rightarrow B^0\bar{B}^0) = (48.6 \pm 0.6)\%$ .				

See key on page 999

# Meson Particle Listings

## $B^\pm/B^0$ ADMIXTURE

### $\overline{A}_{CP}(B \rightarrow K^*\gamma) = (A_{CP}(B^+ \rightarrow K^{*+}\gamma) + A_{CP}(B^0 \rightarrow K^{*0}\gamma))/2$

This is the average CP asymmetry.

VALUE	DOCUMENT ID	TECN	COMMENT
$-0.001 \pm 0.014 \pm 0.003$	<sup>1</sup> Horiguchi 17	BELL	$e^+e^- \rightarrow \Upsilon(4S)$

<sup>1</sup> Uses  $B(\Upsilon(4S) \rightarrow B^+B^-) = (51.4 \pm 0.6)\%$  and  $B(\Upsilon(4S) \rightarrow B^0\overline{B}^0) = (48.6 \pm 0.6)\%$ .

### POLARIZATION IN B DECAY

In decays involving two vector mesons, one can distinguish among the states in which meson polarizations are both longitudinal (L) or both are transverse and parallel (||) or perpendicular (⊥) to each other with the parameters  $\Gamma_L/\Gamma$ ,  $\Gamma_{\parallel}/\Gamma$ , and the relative phases  $\phi_{\parallel}$  and  $\phi_{\perp}$ . See the definitions in the note on "Polarization in B Decays" review in the  $B^0$  Particle Listings.

### $F_L(B \rightarrow K^*\ell^+\ell^-) (q^2 > 0.1 \text{ GeV}^2/c^4)$

VALUE	DOCUMENT ID	TECN	COMMENT
$0.63^{+0.18}_{-0.19} \pm 0.05$	<sup>1</sup> Aubert, B	06J	BABR $e^+e^- \rightarrow \Upsilon(4S)$

<sup>1</sup> Results with different  $q^2$  cuts are also reported.

### $F_L(B \rightarrow K^*\ell^+\ell^-) (m_{\ell\ell} < 2.5 \text{ GeV}/c^2)$

VALUE	DOCUMENT ID	TECN	COMMENT
$0.35 \pm 0.16 \pm 0.04$	Aubert	09N	BABR $e^+e^- \rightarrow \Upsilon(4S)$

### $F_L(B \rightarrow K^*\ell^+\ell^-) (m_{\ell\ell} > 3.2 \text{ GeV}/c^2)$

VALUE	DOCUMENT ID	TECN	COMMENT
$0.71^{+0.20}_{-0.22} \pm 0.04$	Aubert	09N	BABR $e^+e^- \rightarrow \Upsilon(4S)$

### $F_L(B \rightarrow K^*\ell^+\ell^-) (0.10 < q^2 < 0.98 \text{ GeV}^2/c^4)$

VALUE	DOCUMENT ID	TECN	COMMENT
$0.263^{+0.045}_{-0.044} \pm 0.017$	AAIJ	16B	LHCB $pp$ at 7, 8 TeV

### $F_L(B \rightarrow K^*\ell^+\ell^-) (1.1 < q^2 < 2.5 \text{ GeV}^2/c^4)$

VALUE	DOCUMENT ID	TECN	COMMENT
$0.660^{+0.083}_{-0.077} \pm 0.022$	AAIJ	16B	LHCB $pp$ at 7, 8 TeV

### $F_L(B \rightarrow K^*\ell^+\ell^-) (0.1 < q^2 < 2.0 \text{ GeV}^2/c^4)$

VALUE	DOCUMENT ID	TECN	COMMENT
$0.34^{+0.08}_{-0.07} \pm 0.019$	<b>OUR AVERAGE</b>		

$0.37^{+0.10}_{-0.09} \pm 0.04$	AAIJ	13Y	LHCB $pp$ at 7 TeV, $K^{*0}\mu^+\mu^-$
$0.30 \pm 0.16 \pm 0.02$	AALTONEN	12I	CDF $p\overline{p}$ at 1.96 TeV
$0.29^{+0.21}_{-0.18} \pm 0.02$	WEI	09A	BELL $e^+e^- \rightarrow \Upsilon(4S)$

• • • We do not use the following data for averages, fits, limits, etc. • • •

$0.60^{+0.00}_{-0.28} \pm 0.19$	<sup>1</sup> Chatrchyan 13BL	CMS	$pp$ at 7 TeV
$0.00^{+0.13}_{-0.06} \pm 0.02$	AAIJ	12U	LHCB Repl. by AAIJ 13Y
$0.53^{+0.32}_{-0.34} \pm 0.07$	AALTONEN	11L	CDF Repl. by AALTONEN 12I

<sup>1</sup> Chatrchyan 13BL uses, for this bin,  $1.0 < q^2 < 2.0 \text{ GeV}^2/c^4$ .

### $F_L(B \rightarrow K^*\ell^+\ell^-) (2.0 < q^2 < 4.3 \text{ GeV}^2/c^4)$

VALUE	DOCUMENT ID	TECN	COMMENT
$0.77 \pm 0.05$	<b>OUR AVERAGE</b>		

$0.876^{+0.109}_{-0.097} \pm 0.017$	<sup>1</sup> AAIJ	16B	LHCB $pp$ at 7, 8 TeV
$0.80 \pm 0.08 \pm 0.06$	Khachatryan...16D	CMS	$pp$ at 8 TeV
$0.74^{+0.10}_{-0.09} \pm 0.02$	AAIJ	13Y	LHCB $pp$ at 7 TeV, $K^{*0}\mu^+\mu^-$
$0.65 \pm 0.17 \pm 0.03$	Chatrchyan 13BL	CMS	$pp$ at 7 TeV
$0.37^{+0.25}_{-0.24} \pm 0.10$	AALTONEN	12I	CDF $p\overline{p}$ at 1.96 TeV
$0.71 \pm 0.24 \pm 0.05$	WEI	09A	BELL $e^+e^- \rightarrow \Upsilon(4S)$
$0.77 \pm 0.15 \pm 0.03$	AAIJ	12U	LHCB Repl. by AAIJ 13Y
$0.40^{+0.32}_{-0.33} \pm 0.08$	AALTONEN	11L	CDF Repl. by AALTONEN 12I

<sup>1</sup> Measured in  $2.5 < q^2 < 4.0 \text{ GeV}^2/c^4$ .

### $F_L(B \rightarrow K^*\ell^+\ell^-) (4.0 < q^2 < 6.0 \text{ GeV}^2/c^4)$

VALUE	DOCUMENT ID	TECN	COMMENT
$0.611^{+0.052}_{-0.053} \pm 0.017$	AAIJ	16B	LHCB $pp$ at 7, 8 TeV

### $F_L(B \rightarrow K^*\ell^+\ell^-) (6.0 < q^2 < 8.0 \text{ GeV}^2/c^4)$

VALUE	DOCUMENT ID	TECN	COMMENT
$0.579 \pm 0.046 \pm 0.015$	AAIJ	16B	LHCB $pp$ at 7, 8 TeV

### $F_L(B \rightarrow K^*\ell^+\ell^-) (4.3 < q^2 < 8.6 \text{ GeV}^2/c^4)$

VALUE	DOCUMENT ID	TECN	COMMENT
$0.64 \pm 0.06$	<b>OUR AVERAGE</b>		
$0.57 \pm 0.07 \pm 0.03$	AAIJ	13Y	LHCB $pp$ at 7 TeV, $K^{*0}\mu^+\mu^-$
$0.81^{+0.13}_{-0.12} \pm 0.05$	Chatrchyan 13BL	CMS	$pp$ at 7 TeV
$0.68^{+0.15}_{-0.17} \pm 0.09$	AALTONEN	12I	CDF $p\overline{p}$ at 1.96 TeV
$0.64^{+0.23}_{-0.24} \pm 0.07$	WEI	09A	BELL $e^+e^- \rightarrow \Upsilon(4S)$
• • • We do not use the following data for averages, fits, limits, etc. • • •			
$0.60^{+0.06}_{-0.07} \pm 0.01$	AAIJ	12U	LHCB Repl. by AAIJ 13Y
$0.82^{+0.19}_{-0.23} \pm 0.07$	AALTONEN	11L	CDF Repl. by AALTONEN 12I

### $F_L(B \rightarrow K^*\ell^+\ell^-) (10.09 < q^2 < 12.86 \text{ GeV}^2/c^4)$

VALUE	DOCUMENT ID	TECN	COMMENT
$0.448 \pm 0.033$	<b>OUR AVERAGE</b>		
$0.493^{+0.049}_{-0.047} \pm 0.013$	<sup>1</sup> AAIJ	16B	LHCB $pp$ at 7, 8 TeV
$0.39 \pm 0.05 \pm 0.04$	Khachatryan...16D	CMS	$pp$ at 8 TeV
$0.48^{+0.08}_{-0.09} \pm 0.03$	AAIJ	13Y	LHCB $pp$ at 7 TeV, $K^{*0}\mu^+\mu^-$
$0.45^{+0.10}_{-0.11} \pm 0.04$	Chatrchyan 13BL	CMS	$pp$ at 7 TeV
$0.47 \pm 0.14 \pm 0.03$	AALTONEN	12I	CDF $p\overline{p}$ at 1.96 TeV
$0.17^{+0.17}_{-0.15} \pm 0.03$	WEI	09A	BELL $e^+e^- \rightarrow \Upsilon(4S)$
• • • We do not use the following data for averages, fits, limits, etc. • • •			
$0.41 \pm 0.11 \pm 0.03$	AAIJ	12U	LHCB Repl. by AAIJ 13Y
$0.31^{+0.19}_{-0.18} \pm 0.02$	AALTONEN	11L	CDF Repl. by AALTONEN 12I

<sup>1</sup> Measured in  $11.0 < q^2 < 12.5 \text{ GeV}^2/c^4$ .

### $F_L(B \rightarrow K^*\ell^+\ell^-) (15.0 < q^2 < 17.0 \text{ GeV}^2/c^4)$

VALUE	DOCUMENT ID	TECN	COMMENT
$0.349 \pm 0.039 \pm 0.009$	AAIJ	16B	LHCB $pp$ at 7, 8 TeV

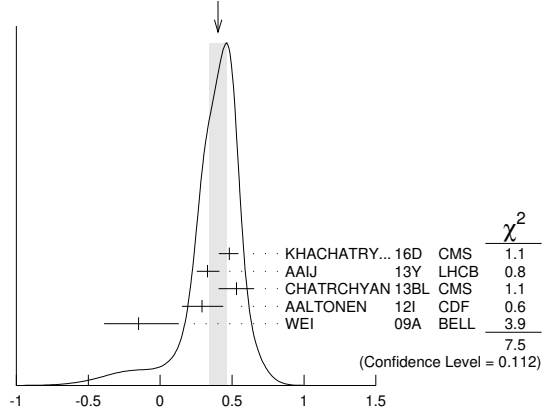
### $F_L(B \rightarrow K^*\ell^+\ell^-) (17.0 < q^2 < 19.0 \text{ GeV}^2/c^4)$

VALUE	DOCUMENT ID	TECN	COMMENT
$0.354^{+0.049}_{-0.048} \pm 0.025$	AAIJ	16B	LHCB $pp$ at 7, 8 TeV

### $F_L(B \rightarrow K^*\ell^+\ell^-) (14.18 < q^2 < 16.0 \text{ GeV}^2/c^4)$

VALUE	DOCUMENT ID	TECN	COMMENT
$0.40 \pm 0.06$	<b>OUR AVERAGE</b>		
Error includes scale factor of 1.4. See the ideogram below.			
$0.48^{+0.05}_{-0.06} \pm 0.04$	Khachatryan...16D	CMS	$pp$ at 8 TeV
$0.33^{+0.08+0.02}_{-0.07-0.03}$	AAIJ	13Y	LHCB $pp$ at 7 TeV, $K^{*0}\mu^+\mu^-$
$0.53 \pm 0.12 \pm 0.03$	Chatrchyan 13BL	CMS	$pp$ at 7 TeV
$0.29^{+0.14}_{-0.13} \pm 0.05$	AALTONEN	12I	CDF $p\overline{p}$ at 1.96 TeV
$-0.15^{+0.27}_{-0.23} \pm 0.07$	WEI	09A	BELL $e^+e^- \rightarrow \Upsilon(4S)$
• • • We do not use the following data for averages, fits, limits, etc. • • •			
$0.37 \pm 0.09 \pm 0.05$	AAIJ	12U	LHCB Repl. by AAIJ 13Y
$0.55^{+0.17}_{-0.18} \pm 0.02$	AALTONEN	11L	CDF Repl. by AALTONEN 12I

WEIGHTED AVERAGE  
0.40±0.06 (Error scaled by 1.4)



$F_L(B \rightarrow K^*\ell^+\ell^-) (14.18 < q^2 < 16.0 \text{ GeV}^2/c^4)$



## Meson Particle Listings

 $B^\pm/B^0$  ADMIXTURE $F_L(B \rightarrow K^* \ell^+ \ell^-)$  ( $16.0 < q^2 < 19.0 \text{ GeV}^2/c^4$ )

VALUE	DOCUMENT ID	TECN	COMMENT
<b>0.353 ± 0.024 OUR AVERAGE</b>			
0.344 <sup>+0.028</sup> <sub>-0.030</sub> ± 0.008	<sup>1</sup> AAIJ	16B LHCb	$pp$ at 7, 8 TeV
0.38 <sup>+0.05</sup> <sub>-0.06</sub> ± 0.04	KHACHATRYAN16D	CMS	$pp$ at 8 TeV
0.38 <sup>+0.09</sup> <sub>-0.07</sub> ± 0.03	AAIJ	13Y LHCb	$pp$ at 7 TeV, $K^*0 \mu^+ \mu^-$
0.44 ± 0.07 ± 0.03	CHATRCHYAN13BL	CMS	$pp$ at 7 TeV
0.20 <sup>+0.19</sup> <sub>-0.17</sub> ± 0.05	AALTONEN	12i CDF	$p\bar{p}$ at 1.96 TeV
0.12 <sup>+0.15</sup> <sub>-0.13</sub> ± 0.02	WEI	09A BELL	$e^+ e^- \rightarrow \Upsilon(4S)$
••• We do not use the following data for averages, fits, limits, etc. •••			
0.26 <sup>+0.10</sup> <sub>-0.08</sub> ± 0.03	AAIJ	12u LHCb	Repl. by AAIJ 13Y
0.09 <sup>+0.18</sup> <sub>-0.14</sub> ± 0.03	AALTONEN	11L CDF	Repl. by AALTONEN 12i

<sup>1</sup> Measured in  $15.0 < q^2 < 19.0 \text{ GeV}^2/c^4$ .

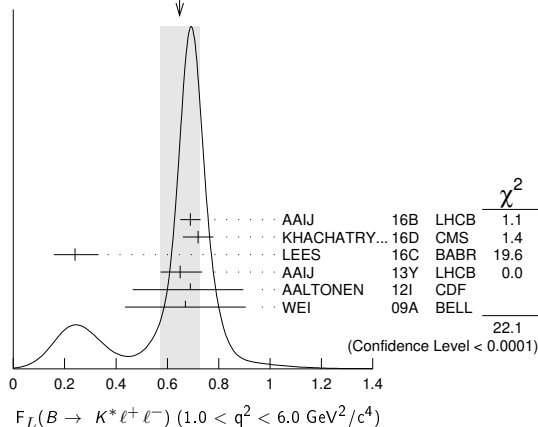
 $F_L(B \rightarrow K^* \ell^+ \ell^-)$  ( $1.0 < q^2 < 6.0 \text{ GeV}^2/c^4$ )

VALUE	DOCUMENT ID	TECN	COMMENT
<b>0.65 ± 0.08 OUR AVERAGE</b>			Error includes scale factor of 2.7. See the ideogram below.
0.690 <sup>+0.035</sup> <sub>-0.036</sub> ± 0.017	<sup>1</sup> AAIJ	16B LHCb	$pp$ at 7, 8 TeV
0.72 ± 0.06	KHACHATRYAN16D	CMS	$pp$ at 7, 8 TeV
0.24 <sup>+0.09</sup> <sub>-0.08</sub> ± 0.02	<sup>2</sup> LEES	16C BABR	$e^+ e^- \rightarrow \Upsilon(4S)$
0.65 <sup>+0.08</sup> <sub>-0.07</sub> ± 0.03	AAIJ	13Y LHCb	$pp$ at 7 TeV, $K^*0 \mu^+ \mu^-$
0.69 <sup>+0.19</sup> <sub>-0.21</sub> ± 0.08	AALTONEN	12i CDF	$p\bar{p}$ at 1.96 TeV
0.67 ± 0.23 ± 0.05	WEI	09A BELL	$e^+ e^- \rightarrow \Upsilon(4S)$
••• We do not use the following data for averages, fits, limits, etc. •••			
0.68 ± 0.10 ± 0.02	CHATRCHYAN13BL	CMS	Repl. by KHACHATRYAN 16D
0.55 ± 0.10 ± 0.03	AAIJ	12u LHCb	Repl. by AAIJ 13Y
0.50 <sup>+0.27</sup> <sub>-0.30</sub> ± 0.03	AALTONEN	11L CDF	Repl. by AALTONEN 12i

<sup>1</sup> Measured in  $1.1 < q^2 < 6.0 \text{ GeV}^2/c^4$ .

<sup>2</sup> Measured by combining  $B^0$  and  $B^+$  with  $e$  and  $\mu$  as leptons. Results are also provided separately for  $B^0$  and  $B^+$ .

WEIGHTED AVERAGE  
0.65 ± 0.08 (Error scaled by 2.7)

 $F_L(B \rightarrow K^* \ell^+ \ell^-)$  ( $0.0 < q^2 < 4.3 \text{ GeV}^2/c^4$ )

VALUE	DOCUMENT ID	TECN	COMMENT
<b>0.33<sup>+0.14</sup><sub>-0.13</sub> ± 0.03</b>	AALTONEN	12i CDF	$p\bar{p}$ at 1.96 TeV
••• We do not use the following data for averages, fits, limits, etc. •••			
0.47 <sup>+0.23</sup> <sub>-0.24</sub> ± 0.03	AALTONEN	11L CDF	Repl. by AALTONEN 12i

 $P_\tau(B \rightarrow D^* \tau^+ \nu_\tau)$ 

Measures difference in decay widths with positive and negative  $\tau^+$  helicities normalized to the sum of those decay widths.

VALUE	DOCUMENT ID	TECN	COMMENT
<b>-0.38 ± 0.51<sup>+0.21</sup><sub>-0.16</sub></b>	<sup>1</sup> HIROSE	17 BELL	$e^+ e^- \rightarrow \Upsilon(4S)$

<sup>1</sup> Uses a fully reconstructed  $B$  meson as a tag on the recoil side.

PARTIAL BRANCHING FRACTIONS IN  $B \rightarrow K^*(\ell^+ \ell^-)$  $B(B \rightarrow K^* \ell^+ \ell^-)$  ( $q^2 < 2.0 \text{ GeV}^2/c^4$ )

VALUE (units $10^{-7}$ )	DOCUMENT ID	TECN	COMMENT
<b>1.68 ± 0.23 OUR AVERAGE</b>			
1.89 <sup>+0.52</sup> <sub>-0.46</sub> ± 0.06	<sup>1</sup> LEES	12s BABR	$e^+ e^- \rightarrow \Upsilon(4S)$
1.73 ± 0.33 ± 0.10	AALTONEN	11A CDF	$p\bar{p}$ at 1.96 TeV
1.46 <sup>+0.40</sup> <sub>-0.35</sub> ± 0.11	WEI	09A BELL	$e^+ e^- \rightarrow \Upsilon(4S)$
••• We do not use the following data for averages, fits, limits, etc. •••			
0.98 ± 0.40 ± 0.09	AALTONEN	11L CDF	Repl. by AALTONEN 11A1

<sup>1</sup> The value reported here from LEES 12s refers to  $0.1 < q^2 < 2.0 \text{ GeV}^2/c^2$ .

 $B(B \rightarrow K^* \ell^+ \ell^-)$  ( $2.0 < q^2 < 4.3 \text{ GeV}^2/c^4$ )

VALUE (units $10^{-7}$ )	DOCUMENT ID	TECN	COMMENT
<b>0.87 ± 0.17 OUR AVERAGE</b>			
0.95 <sup>+0.35</sup> <sub>-0.30</sub> ± 0.04	LEES	12s BABR	$e^+ e^- \rightarrow \Upsilon(4S)$
0.82 ± 0.26 ± 0.06	AALTONEN	11A CDF	$p\bar{p}$ at 1.96 TeV
0.86 <sup>+0.31</sup> <sub>-0.27</sub> ± 0.07	WEI	09A BELL	$e^+ e^- \rightarrow \Upsilon(4S)$
••• We do not use the following data for averages, fits, limits, etc. •••			
1.00 ± 0.38 ± 0.09	AALTONEN	11L CDF	Repl. by AALTONEN 11A1

 $B(B \rightarrow K^* \ell^+ \ell^-)$  ( $4.3 < q^2 < 8.68 \text{ GeV}^2/c^4$ )

VALUE (units $10^{-7}$ )	DOCUMENT ID	TECN	COMMENT
<b>1.67 ± 0.29 OUR AVERAGE</b>			
1.82 <sup>+0.56</sup> <sub>-0.52</sub> ± 0.09	<sup>1</sup> LEES	12s BABR	$e^+ e^- \rightarrow \Upsilon(4S)$
1.72 ± 0.41 ± 0.14	AALTONEN	11A CDF	$p\bar{p}$ at 1.96 TeV
1.37 <sup>+0.47</sup> <sub>-0.42</sub> ± 0.39	WEI	09A BELL	$e^+ e^- \rightarrow \Upsilon(4S)$
••• We do not use the following data for averages, fits, limits, etc. •••			
1.69 ± 0.57 ± 0.15	AALTONEN	11L CDF	Repl. by AALTONEN 11A1

<sup>1</sup> The value reported here from LEES 12s refers to  $4.3 < q^2 < 8.12 \text{ GeV}^2/c^2$ .

 $B(B \rightarrow K^* \ell^+ \ell^-)$  ( $10.09 < q^2 < 12.86 \text{ GeV}^2/c^4$ )

VALUE (units $10^{-7}$ )	DOCUMENT ID	TECN	COMMENT
<b>1.93 ± 0.25 OUR AVERAGE</b>			
1.86 <sup>+0.52</sup> <sub>-0.48</sub> ± 0.10	<sup>1</sup> LEES	12s BABR	$e^+ e^- \rightarrow \Upsilon(4S)$
1.77 ± 0.34 ± 0.11	AALTONEN	11A CDF	$p\bar{p}$ at 1.96 TeV
2.24 <sup>+0.44</sup> <sub>-0.40</sub> ± 0.19	WEI	09A BELL	$e^+ e^- \rightarrow \Upsilon(4S)$
••• We do not use the following data for averages, fits, limits, etc. •••			
1.97 ± 0.47 ± 0.17	AALTONEN	11L CDF	Repl. by AALTONEN 11A1

<sup>1</sup> The value reported here from LEES 12s refers to  $10.11 < q^2 < 12.89 \text{ GeV}^2/c^2$ .

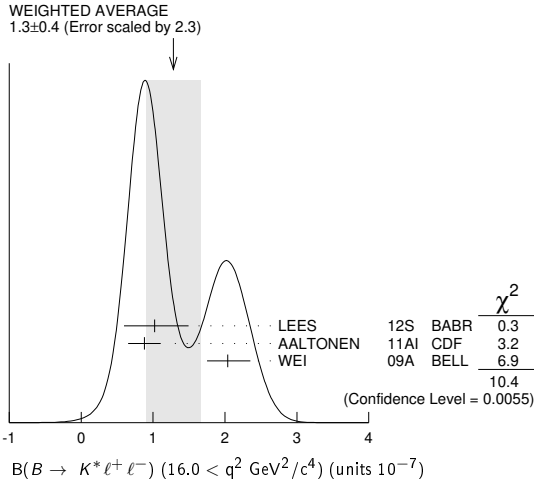
 $B(B \rightarrow K^* \ell^+ \ell^-)$  ( $14.18 < q^2 < 16.0 \text{ GeV}^2/c^4$ )

VALUE (units $10^{-7}$ )	DOCUMENT ID	TECN	COMMENT
<b>1.21 ± 0.17 OUR AVERAGE</b>			
1.46 <sup>+0.41</sup> <sub>-0.36</sub> ± 0.06	<sup>1</sup> LEES	12s BABR	$e^+ e^- \rightarrow \Upsilon(4S)$
1.21 ± 0.24 ± 0.07	AALTONEN	11A CDF	$p\bar{p}$ at 1.96 TeV
1.05 <sup>+0.29</sup> <sub>-0.26</sub> ± 0.08	WEI	09A BELL	$e^+ e^- \rightarrow \Upsilon(4S)$
••• We do not use the following data for averages, fits, limits, etc. •••			
1.51 ± 0.36 ± 0.13	AALTONEN	11L CDF	Repl. by AALTONEN 11A1

<sup>1</sup> The value reported here from LEES 12s refers to  $14.21 < q^2 < 16.0 \text{ GeV}^2/c^2$ .

 $B(B \rightarrow K^* \ell^+ \ell^-)$  ( $16.0 < q^2 \text{ GeV}^2/c^4$ )

VALUE (units $10^{-7}$ )	DOCUMENT ID	TECN	COMMENT
<b>1.3 ± 0.4 OUR AVERAGE</b>			Error includes scale factor of 2.3. See the ideogram below.
1.02 <sup>+0.47</sup> <sub>-0.42</sub> ± 0.06	LEES	12s BABR	$e^+ e^- \rightarrow \Upsilon(4S)$
0.88 ± 0.22 ± 0.05	AALTONEN	11A CDF	$p\bar{p}$ at 1.96 TeV
2.04 <sup>+0.27</sup> <sub>-0.24</sub> ± 0.16	WEI	09A BELL	$e^+ e^- \rightarrow \Upsilon(4S)$
••• We do not use the following data for averages, fits, limits, etc. •••			
1.35 ± 0.37 ± 0.12	AALTONEN	11L CDF	Repl. by AALTONEN 11A1



**$B(B \rightarrow K^* \ell^+ \ell^-)$  ( $1.0 < q^2 < 6.0 \text{ GeV}^2/c^4$ )**

VALUE (units $10^{-7}$ )	DOCUMENT ID	TECN	COMMENT
<b><math>1.64 \pm 0.26</math> OUR AVERAGE</b>	Error includes scale factor of 1.4. See the ideogram below.		
$2.05^{+0.53}_{-0.48} \pm 0.07$	LEES	12s BABR	$e^+ e^- \rightarrow \Upsilon(4S)$
$1.48 \pm 0.39 \pm 0.12$	AALTONEN	11A1 CDF	$p\bar{p}$ at 1.96 TeV
$1.49^{+0.45}_{-0.40} \pm 0.12$	WEI	09A BELL	$e^+ e^- \rightarrow \Upsilon(4S)$
• • • We do not use the following data for averages, fits, limits, etc. • • •			
$1.60 \pm 0.54 \pm 0.14$	AALTONEN	11L CDF	Repl. by AALTONEN 11A1

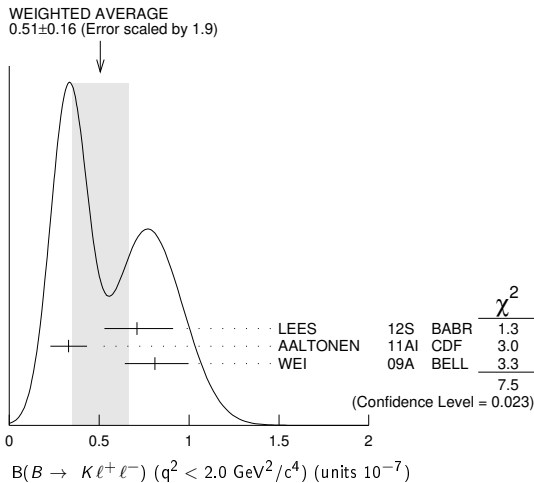
**$B(B \rightarrow K^* \ell^+ \ell^-)$  ( $0.0 < q^2 < 4.3 \text{ GeV}^2/c^4$ )**

VALUE (units $10^{-7}$ )	DOCUMENT ID	TECN	COMMENT
<b><math>2.53 \pm 0.43 \pm 0.15</math></b>	AALTONEN	11A1 CDF	$p\bar{p}$ at 1.96 TeV
• • • We do not use the following data for averages, fits, limits, etc. • • •			
$1.98 \pm 0.55 \pm 0.18$	AALTONEN	11L CDF	Repl. by AALTONEN 11A1

**$B(B \rightarrow K \ell^+ \ell^-)$  ( $q^2 < 2.0 \text{ GeV}^2/c^4$ )**

VALUE (units $10^{-7}$ )	DOCUMENT ID	TECN	COMMENT
<b><math>0.51 \pm 0.16</math> OUR AVERAGE</b>	Error includes scale factor of 1.9. See the ideogram below.		
$0.71^{+0.20}_{-0.18} \pm 0.02$	<sup>1</sup> LEES	12s BABR	$e^+ e^- \rightarrow \Upsilon(4S)$
$0.33 \pm 0.10 \pm 0.02$	AALTONEN	11A1 CDF	$p\bar{p}$ at 1.96 TeV
$0.81^{+0.18}_{-0.16} \pm 0.05$	WEI	09A BELL	$e^+ e^- \rightarrow \Upsilon(4S)$
• • • We do not use the following data for averages, fits, limits, etc. • • •			
$0.38 \pm 0.16 \pm 0.03$	AALTONEN	11L CDF	Repl. by AALTONEN 11A1

<sup>1</sup> The value reported here from LEES 12s refers to  $0.1 < q^2 < 2.0 \text{ GeV}^2/c^2$ .



**$B(B \rightarrow K \ell^+ \ell^-)$  ( $2.0 < q^2 < 4.3 \text{ GeV}^2/c^4$ )**

VALUE (units $10^{-7}$ )	DOCUMENT ID	TECN	COMMENT
<b><math>0.57^{+0.10}_{-0.09}</math> OUR AVERAGE</b>	Error includes scale factor of 1.2.		
$0.49^{+0.15}_{-0.13} \pm 0.01$	LEES	12s BABR	$e^+ e^- \rightarrow \Upsilon(4S)$
$0.77 \pm 0.14 \pm 0.05$	AALTONEN	11A1 CDF	$p\bar{p}$ at 1.96 TeV
$0.46^{+0.14}_{-0.12} \pm 0.03$	WEI	09A BELL	$e^+ e^- \rightarrow \Upsilon(4S)$
• • • We do not use the following data for averages, fits, limits, etc. • • •			
$0.58 \pm 0.19 \pm 0.04$	AALTONEN	11L CDF	Repl. by AALTONEN 11A1

**$B(B \rightarrow K \ell^+ \ell^-)$  ( $4.3 < q^2 < 8.68 \text{ GeV}^2/c^4$ )**

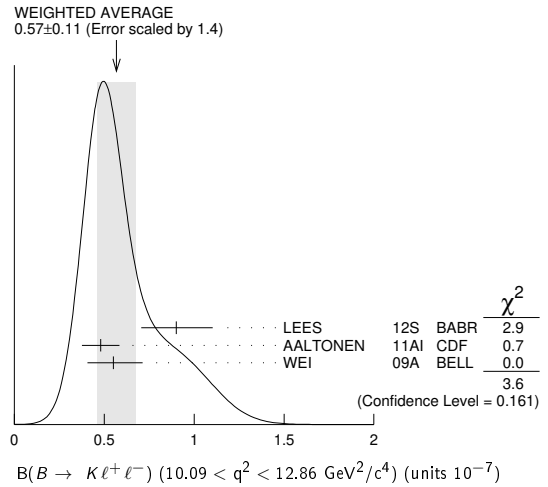
VALUE (units $10^{-7}$ )	DOCUMENT ID	TECN	COMMENT
<b><math>1.00 \pm 0.11</math> OUR AVERAGE</b>	Error includes scale factor of 1.4. See the ideogram below.		
$0.94^{+0.20}_{-0.19} \pm 0.02$	<sup>1</sup> LEES	12s BABR	$e^+ e^- \rightarrow \Upsilon(4S)$
$1.05 \pm 0.17 \pm 0.07$	AALTONEN	11A1 CDF	$p\bar{p}$ at 1.96 TeV
$1.00^{+0.19}_{-0.18} \pm 0.06$	WEI	09A BELL	$e^+ e^- \rightarrow \Upsilon(4S)$
• • • We do not use the following data for averages, fits, limits, etc. • • •			
$0.93 \pm 0.25 \pm 0.06$	AALTONEN	11L CDF	Repl. by AALTONEN 11A1

<sup>1</sup> The value reported here from LEES 12s refers to  $4.3 < q^2 < 8.12 \text{ GeV}^2/c^2$ .

**$B(B \rightarrow K \ell^+ \ell^-)$  ( $10.09 < q^2 < 12.86 \text{ GeV}^2/c^4$ )**

VALUE (units $10^{-7}$ )	DOCUMENT ID	TECN	COMMENT
<b><math>0.57 \pm 0.11</math> OUR AVERAGE</b>	Error includes scale factor of 1.4. See the ideogram below.		
$0.90^{+0.20}_{-0.19} \pm 0.04$	<sup>1</sup> LEES	12s BABR	$e^+ e^- \rightarrow \Upsilon(4S)$
$0.48 \pm 0.10 \pm 0.03$	AALTONEN	11A1 CDF	$p\bar{p}$ at 1.96 TeV
$0.55^{+0.16}_{-0.14} \pm 0.03$	WEI	09A BELL	$e^+ e^- \rightarrow \Upsilon(4S)$
• • • We do not use the following data for averages, fits, limits, etc. • • •			
$0.72 \pm 0.17 \pm 0.05$	AALTONEN	11L CDF	Repl. by AALTONEN 11A1

<sup>1</sup> The value reported here from LEES 12s refers to  $10.11 < q^2 < 12.89 \text{ GeV}^2/c^2$ .



**$B(B \rightarrow K \ell^+ \ell^-)$  ( $14.18 < q^2 < 16.0 \text{ GeV}^2/c^4$ )**

VALUE (units $10^{-7}$ )	DOCUMENT ID	TECN	COMMENT
<b><math>0.49 \pm 0.07</math> OUR AVERAGE</b>	Error includes scale factor of 2.1. See the ideogram below.		
$0.49^{+0.15}_{-0.14} \pm 0.02$	<sup>1</sup> LEES	12s BABR	$e^+ e^- \rightarrow \Upsilon(4S)$
$0.52 \pm 0.09 \pm 0.03$	AALTONEN	11A1 CDF	$p\bar{p}$ at 1.96 TeV
$0.38^{+0.19}_{-0.12} \pm 0.02$	WEI	09A BELL	$e^+ e^- \rightarrow \Upsilon(4S)$
• • • We do not use the following data for averages, fits, limits, etc. • • •			
$0.38 \pm 0.12 \pm 0.03$	AALTONEN	11L CDF	Repl. by AALTONEN 11A1

<sup>1</sup> The value reported here from LEES 12s refers to  $14.21 < q^2 < 16.0 \text{ GeV}^2/c^2$ .

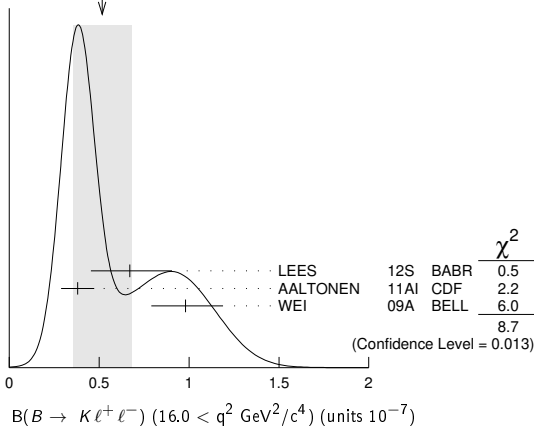
**$B(B \rightarrow K \ell^+ \ell^-)$  ( $16.0 < q^2 < 2.0 \text{ GeV}^2/c^4$ )**

VALUE (units $10^{-7}$ )	DOCUMENT ID	TECN	COMMENT
<b><math>0.52 \pm 0.16</math> OUR AVERAGE</b>	Error includes scale factor of 2.1. See the ideogram below.		
$0.67^{+0.23}_{-0.21} \pm 0.05$	LEES	12s BABR	$e^+ e^- \rightarrow \Upsilon(4S)$
$0.38 \pm 0.09 \pm 0.02$	AALTONEN	11A1 CDF	$p\bar{p}$ at 1.96 TeV
$0.98^{+0.20}_{-0.18} \pm 0.06$	WEI	09A BELL	$e^+ e^- \rightarrow \Upsilon(4S)$
• • • We do not use the following data for averages, fits, limits, etc. • • •			
$0.35 \pm 0.13 \pm 0.02$	AALTONEN	11L CDF	Repl. by AALTONEN 11A1

# Meson Particle Listings

## $B^\pm/B^0$ ADMIXTURE

WEIGHTED AVERAGE  
0.52±0.16 (Error scaled by 2.1)



### $B(B \rightarrow K \ell^+ \ell^-)$ ( $1.0 < q^2 < 6.0 \text{ GeV}^2/c^4$ )

VALUE (units $10^{-7}$ )	DOCUMENT ID	TECN	COMMENT
<b>1.33±0.13 OUR AVERAGE</b>			
1.36 $^{+0.27}_{-0.24}$ ±0.03	LEES	12s BABR	$e^+e^- \rightarrow \Upsilon(4S)$
1.29±0.18±0.08	AALTONEN	11AI CDF	$p\bar{p}$ at 1.96 TeV
1.36 $^{+0.23}_{-0.21}$ ±0.08	WEI	09A BELL	$e^+e^- \rightarrow \Upsilon(4S)$
••• We do not use the following data for averages, fits, limits, etc. •••			
1.01±0.26±0.07	AALTONEN	11L CDF	Repl. by AALTONEN 11AI

### $B(B \rightarrow K \ell^+ \ell^-)$ ( $0.0 < q^2 < 4.3 \text{ GeV}^2/c^4$ )

VALUE (units $10^{-7}$ )	DOCUMENT ID	TECN	COMMENT
<b>1.07±0.17±0.07</b>	AALTONEN	11AI CDF	$p\bar{p}$ at 1.96 TeV
••• We do not use the following data for averages, fits, limits, etc. •••			
0.96±0.25±0.06	AALTONEN	11L CDF	Repl. by AALTONEN 11AI

### $B(B \rightarrow X_s \ell^+ \ell^-)$ ( $1.0 < q^2 < 6.0 \text{ GeV}^2/c^4$ )

VALUE (units $10^{-6}$ )	DOCUMENT ID	TECN	COMMENT
<b>1.60<math>^{+0.41+0.25}_{-0.39-0.22}</math></b>	<sup>1</sup> LEES	14D BABR	$e^+e^- \rightarrow \Upsilon(4S)$
<sup>1</sup> Measured from sum of exclusive modes through $K^+$ , $K^+\pi^0$ , $K^+\pi^-$ , $K^+\pi^-\pi^0$ , $K^+\pi^-\pi^+$ , $K_S^0$ , $K_S^0\pi^0$ , $K_S^0\pi^+$ , $K_S^0\pi^+\pi^0$ , and $K_S^0\pi^+\pi^-$ corrected for unobserved modes.			

### $B(B \rightarrow X_s e^+ e^-)$ ( $1.0 < q^2 < 6.0 \text{ GeV}^2/c^4$ )

VALUE (units $10^{-6}$ )	DOCUMENT ID	TECN	COMMENT
<b>1.93<math>^{+0.47+0.28}_{-0.45-0.24}</math></b>	<sup>1</sup> LEES	14D BABR	$e^+e^- \rightarrow \Upsilon(4S)$
<sup>1</sup> Measured from sum of exclusive modes through $K^+$ , $K^+\pi^0$ , $K^+\pi^-$ , $K^+\pi^-\pi^0$ , $K^+\pi^-\pi^+$ , $K_S^0$ , $K_S^0\pi^0$ , $K_S^0\pi^+$ , $K_S^0\pi^+\pi^0$ , and $K_S^0\pi^+\pi^-$ corrected for unobserved modes.			

### $B(B \rightarrow X_s \mu^+ \mu^-)$ ( $1.0 < q^2 < 6.0 \text{ GeV}^2/c^4$ )

VALUE (units $10^{-6}$ )	DOCUMENT ID	TECN	COMMENT
<b>0.66<math>^{+0.82+0.31}_{-0.76-0.25}</math></b>	<sup>1</sup> LEES	14D BABR	$e^+e^- \rightarrow \Upsilon(4S)$
<sup>1</sup> Measured from sum of exclusive modes through $K^+$ , $K^+\pi^0$ , $K^+\pi^-$ , $K^+\pi^-\pi^0$ , $K^+\pi^-\pi^+$ , $K_S^0$ , $K_S^0\pi^0$ , $K_S^0\pi^+$ , $K_S^0\pi^+\pi^0$ , and $K_S^0\pi^+\pi^-$ corrected for unobserved modes.			

### $B(B \rightarrow X_s \ell^+ \ell^-)$ ( $14.2 < q^2 < 17.0 \text{ GeV}^2/c^4$ )

VALUE (units $10^{-6}$ )	DOCUMENT ID	TECN	COMMENT
<b>0.57<math>^{+0.16+0.03}_{-0.15-0.02}</math></b>	<sup>1</sup> LEES	14D BABR	$e^+e^- \rightarrow \Upsilon(4S)$
<sup>1</sup> Measured from sum of exclusive modes through $K^+$ , $K^+\pi^0$ , $K^+\pi^-$ , $K^+\pi^-\pi^0$ , $K^+\pi^-\pi^+$ , $K_S^0$ , $K_S^0\pi^0$ , $K_S^0\pi^+$ , $K_S^0\pi^+\pi^0$ , and $K_S^0\pi^+\pi^-$ corrected for unobserved modes.			

### $B(B \rightarrow X_s e^+ e^-)$ ( $14.2 < q^2 < 17.0 \text{ GeV}^2/c^4$ )

VALUE (units $10^{-6}$ )	DOCUMENT ID	TECN	COMMENT
<b>0.56<math>^{+0.19+0.03}_{-0.18-0.03}</math></b>	<sup>1</sup> LEES	14D BABR	$e^+e^- \rightarrow \Upsilon(4S)$
<sup>1</sup> Measured from sum of exclusive modes through $K^+$ , $K^+\pi^0$ , $K^+\pi^-$ , $K^+\pi^-\pi^0$ , $K^+\pi^-\pi^+$ , $K_S^0$ , $K_S^0\pi^0$ , $K_S^0\pi^+$ , $K_S^0\pi^+\pi^0$ , and $K_S^0\pi^+\pi^-$ corrected for unobserved modes.			

### $B(B \rightarrow X_s \mu^+ \mu^-)$ ( $14.2 < q^2 < 17.0 \text{ GeV}^2/c^4$ )

VALUE (units $10^{-6}$ )	DOCUMENT ID	TECN	COMMENT
<b>0.60<math>^{+0.31+0.05}_{-0.29-0.04}</math></b>	<sup>1</sup> LEES	14D BABR	$e^+e^- \rightarrow \Upsilon(4S)$
<sup>1</sup> Measured from sum of exclusive modes through $K^+$ , $K^+\pi^0$ , $K^+\pi^-$ , $K^+\pi^-\pi^0$ , $K^+\pi^-\pi^+$ , $K_S^0$ , $K_S^0\pi^0$ , $K_S^0\pi^+$ , $K_S^0\pi^+\pi^0$ , and $K_S^0\pi^+\pi^-$ corrected for unobserved modes.			

### LEPTON (HADRON) FORWARD-BACKWARD ASYMMETRY IN $B \rightarrow K^{(*)} \ell^+ \ell^-$ ( $B \rightarrow K/\pi h^+ h^-$ ) DECAY

The forward-backward angular asymmetry of the lepton pair in  $B \rightarrow K^{(*)} \ell^+ \ell^-$  ( $B \rightarrow K/\pi h^+ h^-$ ) decay is defined as

$$A_{FB}(s) = \frac{N(\cos\theta > 0) - N(\cos\theta < 0)}{N(\cos\theta > 0) + N(\cos\theta < 0)}$$

where  $s=q^2/m_B^2$ , and  $\theta$  is the angle of the  $\ell^-$  ( $h^-$ ) with respect to the flight direction of the  $B$  meson, measured in the dilepton (dihadron) rest frame. In addition, the fraction of longitudinal polarization  $F_L$  of the  $K^*$  and  $F_S$ , the relative contribution from scalar and pseudoscalar penguin amplitudes in  $B \rightarrow K \ell^+ \ell^-$ , can be measured from the angular distribution of its decay products.

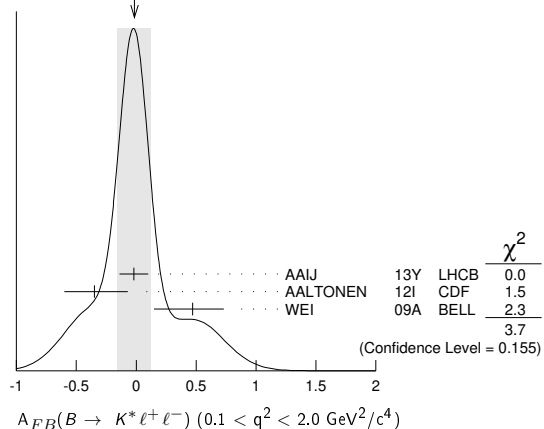
### $A_{FB}(B \rightarrow K^* \ell^+ \ell^-)$ ( $q^2 > 0.1 \text{ GeV}^2/c^4$ )

VALUE	CL%	DOCUMENT ID	TECN	COMMENT
<b>0.50±0.15±0.02</b>		<sup>1</sup> ISHIKAWA	06 BELL	$e^+e^- \rightarrow \Upsilon(4S)$
••• We do not use the following data for averages, fits, limits, etc. •••				
>0.55	95	<sup>2</sup> AUBERT,B	06J BABR	$e^+e^- \rightarrow \Upsilon(4S)$
<sup>1</sup> Using an unbinned max. likelihood fits to the $M_{bc}$ distribution in five $q^2$ bins for $\cos\theta > 0$ and $\cos\theta < 0$ .				
<sup>2</sup> Results with different $q^2$ cuts are also reported.				

### $A_{FB}(B \rightarrow K^* \ell^+ \ell^-)$ ( $0.1 < q^2 < 2.0 \text{ GeV}^2/c^4$ )

VALUE	DOCUMENT ID	TECN	COMMENT
<b>-0.01±0.14 OUR AVERAGE</b>	Error includes scale factor of 1.4. See the ideogram below.		
-0.02±0.12±0.01	AAIJ	13Y LHCb	$p\bar{p}$ at 7 TeV, $K^*0 \mu^+ \mu^-$
-0.35 $^{+0.26}_{-0.23}$ ±0.10	AALTONEN	12I CDF	$p\bar{p}$ at 1.96 TeV
0.47 $^{+0.26}_{-0.32}$ ±0.03	WEI	09A BELL	$e^+e^- \rightarrow \Upsilon(4S)$
••• We do not use the following data for averages, fits, limits, etc. •••			
-0.29 $^{+0.37}_{-0.00}$ ±0.18	<sup>1</sup> CHATRCHYAN	13BL CMS	$p\bar{p}$ at 7 TeV
-0.15±0.20±0.06	AAIJ	12U LHCb	Repl. by AAIJ 13Y
0.13 $^{+1.65}_{-0.75}$ ±0.25	AALTONEN	11L CDF	Repl. by AALTONEN 12I
<sup>1</sup> CHATRCHYAN 13BL uses, for this bin, $1.0 < q^2 < 2.0 \text{ GeV}^2/c^4$ .			

WEIGHTED AVERAGE  
-0.01±0.14 (Error scaled by 1.4)



### $A_{FB}(B \rightarrow K^* \ell^+ \ell^-)$ ( $m_{\ell\ell} < 2.5 \text{ GeV}/c^2$ )

VALUE	DOCUMENT ID	TECN	COMMENT
<b>0.24<math>^{+0.18}_{-0.23}</math>±0.05</b>	AUBERT	09N BABR	$e^+e^- \rightarrow \Upsilon(4S)$

### $A_{FB}(B \rightarrow K^* \ell^+ \ell^-)$ ( $m_{\ell\ell} > 3.2 \text{ GeV}/c^2$ )

VALUE	DOCUMENT ID	TECN	COMMENT
<b>0.76<math>^{+0.52}_{-0.32}</math>±0.07</b>	AUBERT	09N BABR	$e^+e^- \rightarrow \Upsilon(4S)$

### $A_{FB}(B \rightarrow K^* \ell^+ \ell^-)$ ( $0.10 < q^2 < 0.98 \text{ GeV}^2/c^4$ )

VALUE	DOCUMENT ID	TECN	COMMENT
<b>-0.003<math>^{+0.059}_{-0.057}</math>±0.009</b>	AAIJ	16B LHCb	$p\bar{p}$ at 7, 8 TeV

# Meson Particle Listings

## $B^\pm/B^0$ ADMIXTURE

### $A_{FB}(B \rightarrow K^* \ell^+ \ell^-)$ ( $1.1 < q^2 < 2.5 \text{ GeV}^2/c^4$ )

VALUE	DOCUMENT ID	TECN	COMMENT
$-0.191 \pm 0.068 \pm 0.012$	AAIJ	16b LHCb	$pp$ at 7, 8 TeV

### $A_{FB}(B \rightarrow K^* \ell^+ \ell^-)$ ( $2.0 < q^2 < 4.3 \text{ GeV}^2/c^4$ )

VALUE	DOCUMENT ID	TECN	COMMENT
<b><math>-0.14 \pm 0.05</math> OUR AVERAGE</b>			
$-0.118 \pm 0.082 \pm 0.007$	<sup>1</sup> AAIJ	16b LHCb	$pp$ at 7, 8 TeV
$-0.12 \pm 0.15 \pm 0.05$	KHACHATRY...16D	CMS	$pp$ at 8 TeV
$-0.20 \pm 0.08 \pm 0.01$	AAIJ	13Y LHCb	$pp$ at 7 TeV, $K^{*0} \mu^+ \mu^-$
$-0.07 \pm 0.20 \pm 0.02$	CHATRCHYAN13BL	CMS	$pp$ at 7 TeV
$0.29 \pm 0.32 \pm 0.15$	AALTONEN	12i CDF	$p\bar{p}$ at 1.96 TeV
$0.11 \pm 0.31 \pm 0.07$	WEI	09A BELL	$e^+e^- \rightarrow \Upsilon(4S)$
••• We do not use the following data for averages, fits, limits, etc. •••			
$0.05 \pm 0.16 \pm 0.04$	AAIJ	12u LHCb	Repl. by AAIJ 13Y
$0.19 \pm 0.40 \pm 0.14$	AALTONEN	11L CDF	Repl. by AALTONEN 12i

<sup>1</sup> Measured in  $2.5 < q^2 < 4.0 \text{ GeV}^2/c^4$ .

### $A_{FB}(B \rightarrow K^* \ell^+ \ell^-)$ ( $0.0 < q^2 < 4.3 \text{ GeV}^2/c^4$ )

VALUE	DOCUMENT ID	TECN	COMMENT
<b><math>-0.08 \pm 0.21 \pm 0.05</math></b>	AALTONEN	12i CDF	$p\bar{p}$ at 1.96 TeV
••• We do not use the following data for averages, fits, limits, etc. •••			
$0.21 \pm 0.31 \pm 0.05$	AALTONEN	11L CDF	Repl. by AALTONEN 12i

### $A_{FB}(B \rightarrow K^* \ell^+ \ell^-)$ ( $4.0 < q^2 < 6.0 \text{ GeV}^2/c^4$ )

VALUE	DOCUMENT ID	TECN	COMMENT
<b><math>0.025 \pm 0.051 \pm 0.004</math></b>	AAIJ	16b LHCb	$pp$ at 7, 8 TeV

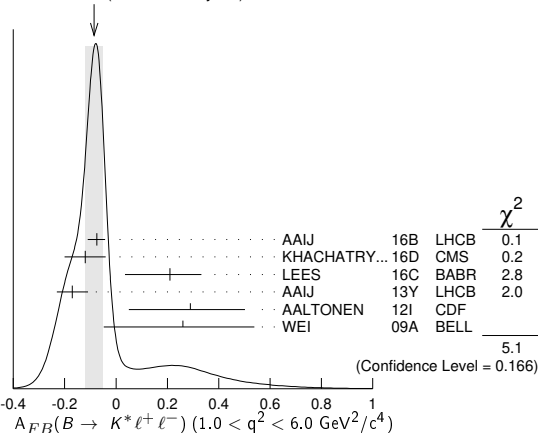
### $A_{FB}(B \rightarrow K^* \ell^+ \ell^-)$ ( $6.0 < q^2 < 8.0 \text{ GeV}^2/c^4$ )

VALUE	DOCUMENT ID	TECN	COMMENT
<b><math>0.152 \pm 0.041 \pm 0.008</math></b>	AAIJ	16b LHCb	$pp$ at 7, 8 TeV

### $A_{FB}(B \rightarrow K^* \ell^+ \ell^-)$ ( $1.0 < q^2 < 6.0 \text{ GeV}^2/c^4$ )

VALUE	DOCUMENT ID	TECN	COMMENT
<b><math>-0.085 \pm 0.035</math> OUR AVERAGE</b>			Error includes scale factor of 1.3. See the ideogram below.
$-0.075 \pm 0.032 \pm 0.007$	<sup>1</sup> AAIJ	16b LHCb	$pp$ at 7, 8 TeV
$-0.12 \pm 0.08$	KHACHATRY...16D	CMS	$pp$ at 7, 8 TeV
$0.21 \pm 0.10 \pm 0.07$	<sup>2</sup> LEES	16c BABR	$e^+e^- \rightarrow \Upsilon(4S)$
$-0.17 \pm 0.06 \pm 0.01$	AAIJ	13Y LHCb	$pp$ at 7 TeV, $K^{*0} \mu^+ \mu^-$
$0.29 \pm 0.20 \pm 0.07$	AALTONEN	12i CDF	$p\bar{p}$ at 1.96 TeV
$0.26 \pm 0.27 \pm 0.07$	WEI	09A BELL	$e^+e^- \rightarrow \Upsilon(4S)$
••• We do not use the following data for averages, fits, limits, etc. •••			
$0.55 \pm 0.43$	<sup>3</sup> SATO	16 BELL	$e^+e^- \rightarrow \Upsilon(4S)$
$-0.07 \pm 0.12 \pm 0.01$	CHATRCHYAN13BL	CMS	Repl. by KHACHATRYAN 16D
$-0.06 \pm 0.13 \pm 0.07$	AAIJ	12u LHCb	Repl. by AAIJ 13Y
$0.43 \pm 0.36 \pm 0.06$	AALTONEN	11L CDF	Repl. by AALTONEN 12i

WEIGHTED AVERAGE  
 $-0.085 \pm 0.035$  (Error scaled by 1.3)



<sup>1</sup> Measured in  $1.1 < q^2 < 6.0 \text{ GeV}^2/c^4$ .

<sup>2</sup> Measured by combining  $B^0$  and  $B^+$  with  $e$  and  $\mu$  as leptons. Results are also provided separately for  $B^0$  and  $B^+$ .

<sup>3</sup> Uses  $K^* \rightarrow K^- \pi^+$ ,  $K^- \pi^0$ ,  $K_S^0 \pi^-$  in the range  $M(K\pi) < 1.1 \text{ GeV}/c^2$ . Uncertainty is statistical only.

### $A_{FB}(B \rightarrow K^* \ell^+ \ell^-)$ ( $4.3 < q^2 < 8.6 \text{ GeV}^2/c^4$ )

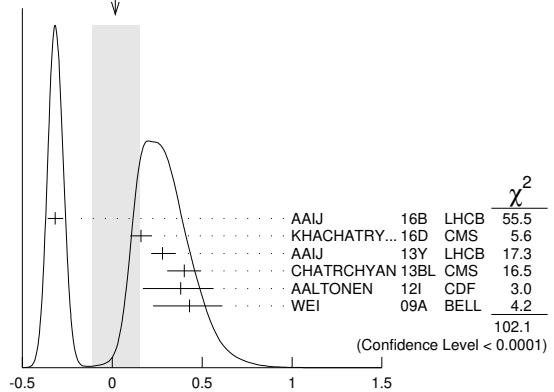
VALUE	DOCUMENT ID	TECN	COMMENT
<b><math>0.13 \pm 0.06 \pm 0.05</math> OUR AVERAGE</b>			Error includes scale factor of 1.1.
$0.16 \pm 0.06 \pm 0.01$	AAIJ	13Y LHCb	$pp$ at 7 TeV, $K^{*0} \mu^+ \mu^-$
$-0.01 \pm 0.11 \pm 0.03$	CHATRCHYAN13BL	CMS	$pp$ at 7 TeV
$0.01 \pm 0.20 \pm 0.09$	AALTONEN	12i CDF	$p\bar{p}$ at 1.96 TeV
$0.45 \pm 0.15 \pm 0.15$	WEI	09A BELL	$e^+e^- \rightarrow \Upsilon(4S)$
••• We do not use the following data for averages, fits, limits, etc. •••			
$0.27 \pm 0.06 \pm 0.02$	AAIJ	12u LHCb	Repl. by AAIJ 13Y
$-0.06 \pm 0.30 \pm 0.05$	AALTONEN	11L CDF	Repl. by AALTONEN 12i

### $A_{FB}(B \rightarrow K^* \ell^+ \ell^-)$ ( $10.09 < q^2 < 12.86 \text{ GeV}^2/c^4$ )

VALUE	DOCUMENT ID	TECN	COMMENT
<b><math>0.02 \pm 0.13</math> OUR AVERAGE</b>			Error includes scale factor of 4.5. See the ideogram below.
$-0.318 \pm 0.044 \pm 0.009$	<sup>1</sup> AAIJ	16b LHCb	$pp$ at 7, 8 TeV
$0.16 \pm 0.06 \pm 0.01$	KHACHATRY...16D	CMS	$pp$ at 8 TeV
$0.28 \pm 0.07 \pm 0.02$	AAIJ	13Y LHCb	$pp$ at 7 TeV, $K^{*0} \mu^+ \mu^-$
$0.40 \pm 0.08 \pm 0.05$	CHATRCHYAN13BL	CMS	$pp$ at 7 TeV
$0.38 \pm 0.16 \pm 0.09$	AALTONEN	12i CDF	$p\bar{p}$ at 1.96 TeV
$0.43 \pm 0.18 \pm 0.03$	WEI	09A BELL	$e^+e^- \rightarrow \Upsilon(4S)$
••• We do not use the following data for averages, fits, limits, etc. •••			
$0.27 \pm 0.11 \pm 0.02$	AAIJ	12u LHCb	Repl. by AAIJ 13Y
$0.66 \pm 0.23 \pm 0.07$	AALTONEN	11L CDF	Repl. by AALTONEN 12i

<sup>1</sup> Measured in  $11.0 < q^2 < 12.5 \text{ GeV}^2/c^4$ .

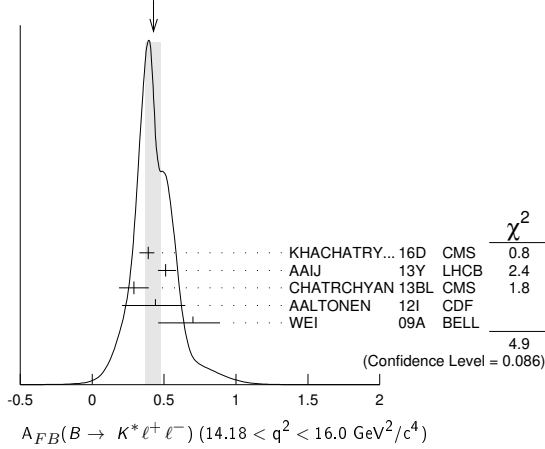
WEIGHTED AVERAGE  
 $0.02 \pm 0.13$  (Error scaled by 4.5)



### $A_{FB}(B \rightarrow K^* \ell^+ \ell^-)$ ( $14.18 < q^2 < 16.0 \text{ GeV}^2/c^4$ )

VALUE	DOCUMENT ID	TECN	COMMENT
<b><math>0.43 \pm 0.05 \pm 0.06</math> OUR AVERAGE</b>			Error includes scale factor of 1.6. See the ideogram below.
$0.39 \pm 0.04 \pm 0.06$	KHACHATRY...16D	CMS	$pp$ at 8 TeV
$0.51 \pm 0.07 \pm 0.02$	AAIJ	13Y LHCb	$pp$ at 7 TeV, $K^{*0} \mu^+ \mu^-$
$0.29 \pm 0.09 \pm 0.05$	CHATRCHYAN13BL	CMS	$pp$ at 7 TeV
$0.44 \pm 0.18 \pm 0.10$	AALTONEN	12i CDF	$p\bar{p}$ at 1.96 TeV
$0.70 \pm 0.16 \pm 0.10$	WEI	09A BELL	$e^+e^- \rightarrow \Upsilon(4S)$
••• We do not use the following data for averages, fits, limits, etc. •••			
$0.47 \pm 0.06 \pm 0.03$	AAIJ	12u LHCb	Repl. by AAIJ 13Y
$0.42 \pm 0.16 \pm 0.09$	AALTONEN	11L CDF	Repl. by AALTONEN 12i

## Meson Particle Listings

 $B^\pm/B^0$  ADMIXTUREWEIGHTED AVERAGE  
0.43±0.05-0.06 (Error scaled by 1.6) $A_{FB}(B \rightarrow K^* \ell^+ \ell^-)$  (15.0 <  $q^2$  < 17.0  $\text{GeV}^2/c^4$ )

VALUE	DOCUMENT ID	TECN	COMMENT
$0.411^{+0.41}_{-0.037} \pm 0.008$	AAIJ	16B	LHCB $pp$ at 7, 8 TeV

 $A_{FB}(B \rightarrow K^* \ell^+ \ell^-)$  (17.0 <  $q^2$  < 19.0  $\text{GeV}^2/c^4$ )

VALUE	DOCUMENT ID	TECN	COMMENT
$0.305^{+0.049}_{-0.048} \pm 0.013$	AAIJ	16B	LHCB $pp$ at 7, 8 TeV

 $A_{FB}(B \rightarrow K^* \ell^+ \ell^-)$  (16.0 <  $q^2$  < 19.0  $\text{GeV}^2/c^4$ )

VALUE	DOCUMENT ID	TECN	COMMENT
$0.367 \pm 0.024$ OUR AVERAGE	Error includes scale factor of 1.1.		
$0.355 \pm 0.027 \pm 0.009$	1 AAIJ	16B	LHCB $pp$ at 7, 8 TeV
$0.35 \pm 0.07 \pm 0.01$	KHACHATRYAN 16D CMS $pp$ at 8 TeV		
$0.30 \pm 0.08^{+0.01}_{-0.02}$	AAIJ	13Y	LHCB $pp$ at 7 TeV, $K^*0 \mu^+ \mu^-$
$0.41 \pm 0.05 \pm 0.03$	CHATRCHYAN 13BL CMS $pp$ at 7 TeV		
$0.65^{+0.17}_{-0.18} \pm 0.16$	AALTONEN	12I	CDF $p\bar{p}$ at 1.96 TeV
$0.66^{+0.11}_{-0.16} \pm 0.04$	WEI	09A	BELL $e^+ e^- \rightarrow \Upsilon(4S)$
••• We do not use the following data for averages, fits, limits, etc. •••			
$0.16^{+0.11}_{-0.13} \pm 0.06$	AAIJ	12U	LHCB Repl. by AAIJ 13Y
$0.70^{+0.16}_{-0.25} \pm 0.10$	AALTONEN	11L	CDF Repl. by AALTONEN 12I

<sup>1</sup> Measured in  $15.0 < q^2 < 19.0 \text{ GeV}^2/c^4$ . $A_{FB}(B \rightarrow K \ell^+ \ell^-)$  ( $q^2 > 0.1 \text{ GeV}^2/c^4$ )

VALUE	DOCUMENT ID	TECN	COMMENT
$0.11 \pm 0.12$ OUR AVERAGE			
$0.15^{+0.21}_{-0.23} \pm 0.08$	1 AUBERT,B	06J	BABR $e^+ e^- \rightarrow \Upsilon(4S)$
$0.10 \pm 0.14 \pm 0.01$	2 ISHIKAWA	06	BELL $e^+ e^- \rightarrow \Upsilon(4S)$

<sup>1</sup> Results with different  $q^2$  cuts are also reported.<sup>2</sup> Using an unbinned max. likelihood fits to the  $M_{bc}$  distribution in five  $q^2$  bins for  $\cos \theta > 0$  and  $\cos \theta < 0$ . $A_{FB}(B \rightarrow K \ell^+ \ell^-)$  ( $q^2 < 2.0 \text{ GeV}^2/c^4$ )

VALUE	DOCUMENT ID	TECN	COMMENT
$0.00^{+0.06}_{-0.05}$ OUR AVERAGE			
$0.00^{+0.06+0.03}_{-0.05-0.01}$	AAIJ	13H	LHCB $pp$ at 7 TeV
$0.13^{+0.42}_{-0.43} \pm 0.07$	AALTONEN	12I	CDF $p\bar{p}$ at 1.96 TeV
$0.06^{+0.32}_{-0.35} \pm 0.02$	WEI	09A	BELL $e^+ e^- \rightarrow \Upsilon(4S)$
••• We do not use the following data for averages, fits, limits, etc. •••			
$-0.15^{+0.46}_{-0.39} \pm 0.08$	AALTONEN	11L	CDF Repl. by AALTONEN 12I

 $A_{FB}(B \rightarrow K \ell^+ \ell^-)$  (2.0 <  $q^2$  < 4.3  $\text{GeV}^2/c^4$ )

VALUE	DOCUMENT ID	TECN	COMMENT
$0.09^{+0.10}_{-0.07}$ OUR AVERAGE	Error includes scale factor of 1.4.		
$0.07^{+0.08+0.02}_{-0.05-0.01}$	AAIJ	13H	LHCB $pp$ at 7 TeV
$0.32^{+0.15}_{-0.16} \pm 0.05$	AALTONEN	12I	CDF $p\bar{p}$ at 1.96 TeV
$-0.43^{+0.38}_{-0.40} \pm 0.09$	WEI	09A	BELL $e^+ e^- \rightarrow \Upsilon(4S)$
••• We do not use the following data for averages, fits, limits, etc. •••			
$0.72^{+0.40}_{-0.35} \pm 0.07$	AALTONEN	11L	CDF Repl. by AALTONEN 12I

 $A_{FB}(B \rightarrow K \ell^+ \ell^-)$  (0.0 <  $q^2$  < 4.3  $\text{GeV}^2/c^4$ )

VALUE	DOCUMENT ID	TECN	COMMENT
$0.31 \pm 0.16 \pm 0.04$	AALTONEN	12I	CDF $p\bar{p}$ at 1.96 TeV
••• We do not use the following data for averages, fits, limits, etc. •••			
$0.36^{+0.24}_{-0.26} \pm 0.06$	AALTONEN	11L	CDF Repl. by AALTONEN 12I

 $A_{FB}(B \rightarrow K \ell^+ \ell^-)$  (1.0 <  $q^2$  < 6.0  $\text{GeV}^2/c^4$ )

VALUE	DOCUMENT ID	TECN	COMMENT
$0.034^{+0.040}_{-0.029}$ OUR AVERAGE			
$0.02^{+0.05+0.02}_{-0.03-0.01}$	AAIJ	13H	LHCB $pp$ at 7 TeV
$0.13 \pm 0.09 \pm 0.02$	AALTONEN	12I	CDF $p\bar{p}$ at 1.96 TeV
$-0.04^{+0.13}_{-0.16} \pm 0.05$	WEI	09A	BELL $e^+ e^- \rightarrow \Upsilon(4S)$
••• We do not use the following data for averages, fits, limits, etc. •••			
$0.00 \pm 0.13$	1 SATO	16	BELL $e^+ e^- \rightarrow \Upsilon(4S)$
$0.08^{+0.27}_{-0.22} \pm 0.07$	AALTONEN	11L	CDF Repl. by AALTONEN 12I

<sup>1</sup> Statistical uncertainty only. $A_{FB}(B \rightarrow K \ell^+ \ell^-)$  (4.3 <  $q^2$  < 8.6  $\text{GeV}^2/c^4$ )

VALUE	DOCUMENT ID	TECN	COMMENT
$-0.04^{+0.04}_{-0.05}$ OUR AVERAGE			
$-0.02^{+0.03}_{-0.05} \pm 0.03$	AAIJ	13H	LHCB $pp$ at 7 TeV
$0.01^{+0.13}_{-0.10} \pm 0.01$	AALTONEN	12I	CDF $p\bar{p}$ at 1.96 TeV
$-0.20^{+0.12}_{-0.14} \pm 0.03$	WEI	09A	BELL $e^+ e^- \rightarrow \Upsilon(4S)$
••• We do not use the following data for averages, fits, limits, etc. •••			
$-0.20^{+0.17}_{-0.28} \pm 0.03$	AALTONEN	11L	CDF Repl. by AALTONEN 12I

 $A_{FB}(B \rightarrow K \ell^+ \ell^-)$  (10.09 <  $q^2$  < 12.86  $\text{GeV}^2/c^4$ )

VALUE	DOCUMENT ID	TECN	COMMENT
$-0.05 \pm 0.06$ OUR AVERAGE			
$-0.03 \pm 0.07 \pm 0.01$	AAIJ	13H	LHCB $pp$ at 7 TeV
$-0.03^{+0.11}_{-0.10} \pm 0.04$	AALTONEN	12I	CDF $p\bar{p}$ at 1.96 TeV
$-0.21^{+0.17}_{-0.15} \pm 0.06$	WEI	09A	BELL $e^+ e^- \rightarrow \Upsilon(4S)$
••• We do not use the following data for averages, fits, limits, etc. •••			
$-0.10^{+0.17}_{-0.15} \pm 0.07$	AALTONEN	11L	CDF Repl. by AALTONEN 12I

 $A_{FB}(B \rightarrow K \ell^+ \ell^-)$  (14.18 <  $q^2$  < 16.0  $\text{GeV}^2/c^4$ )

VALUE	DOCUMENT ID	TECN	COMMENT
$-0.02^{+0.07}_{-0.05}$ OUR AVERAGE			
$-0.01^{+0.12}_{-0.06} \pm 0.01$	AAIJ	13H	LHCB $pp$ at 7 TeV
$-0.05^{+0.09}_{-0.11} \pm 0.03$	AALTONEN	12I	CDF $p\bar{p}$ at 1.96 TeV
$0.04^{+0.32}_{-0.26} \pm 0.05$	WEI	09A	BELL $e^+ e^- \rightarrow \Upsilon(4S)$
••• We do not use the following data for averages, fits, limits, etc. •••			
$0.03^{+0.49}_{-0.16} \pm 0.04$	AALTONEN	11L	CDF Repl. by AALTONEN 12I

 $A_{FB}(B \rightarrow K \ell^+ \ell^-)$  (16.0 <  $q^2$  < 18.0  $\text{GeV}^2/c^4$ )

VALUE	DOCUMENT ID	TECN	COMMENT
$-0.09^{+0.07+0.02}_{-0.09-0.01}$	AAIJ	13H	LHCB $pp$ at 7 TeV

 $A_{FB}(B \rightarrow K \ell^+ \ell^-)$  (18.0 <  $q^2$  < 22.0  $\text{GeV}^2/c^4$ )

VALUE	DOCUMENT ID	TECN	COMMENT
$0.02 \pm 0.11 \pm 0.01$	AAIJ	13H	LHCB $pp$ at 7 TeV

 $A_{FB}(B \rightarrow K \ell^+ \ell^-)$  ( $q^2 > 16.0 \text{ GeV}^2/c^4$ )

VALUE	DOCUMENT ID	TECN	COMMENT
$0.04^{+0.09}_{-0.07}$ OUR AVERAGE			
$0.09^{+0.17}_{-0.13} \pm 0.03$	AALTONEN	12I	CDF $p\bar{p}$ at 1.96 TeV
$0.02^{+0.11}_{-0.08} \pm 0.02$	WEI	09A	BELL $e^+ e^- \rightarrow \Upsilon(4S)$
••• We do not use the following data for averages, fits, limits, etc. •••			
$0.07^{+0.30}_{-0.23} \pm 0.02$	AALTONEN	11L	CDF Repl. by AALTONEN 12I

 $A_{FB}(B \rightarrow X_s \ell^+ \ell^-)$  (1.0 <  $q^2$  < 6.0  $\text{GeV}^2/c^4$ )

VALUE	DOCUMENT ID	TECN	COMMENT
$0.74 \pm 0.54$	1 SATO	16	BELL $e^+ e^- \rightarrow \Upsilon(4S)$
••• We do not use the following data for averages, fits, limits, etc. •••			
<sup>1</sup> Uses the sum of 10 exclusive $X_S$ modes in the range $M(X_S) > 1.1 \text{ GeV}/c^2$ . Uncertainty is statistical only.			

See key on page 999

# Meson Particle Listings

## $B^\pm/B^0$ ADMIXTURE

 **$F_S(B \rightarrow K\ell^+\ell^-)$  ( $q^2 > 0.1 \text{ GeV}^2/c^4$ )**

VALUE	DOCUMENT ID	TECN	COMMENT
$0.81^{+0.58}_{-0.61} \pm 0.46$	<sup>1</sup> AUBERT,B	06J	BABR $e^+e^- \rightarrow \Upsilon(4S)$

<sup>1</sup> Results with different  $q^2$  cuts are also reported. **$A_{FB}(B \rightarrow K\rho\bar{\rho})$  ( $m_{\rho\bar{\rho}} < 2.85 \text{ GeV}/c^2$ )**

VALUE	DOCUMENT ID	TECN	COMMENT
$0.495 \pm 0.012 \pm 0.007$	<sup>1</sup> AAIJ	14AF	LHCB $pp$ at 7, 8 TeV

<sup>1</sup> Measured in  $B^+ \rightarrow K^+\rho\bar{\rho}$  decays. **$A_{FB}(B \rightarrow \pi\rho\bar{\rho})$  ( $m_{\rho\bar{\rho}} < 2.85 \text{ GeV}/c^2$ )**

VALUE	DOCUMENT ID	TECN	COMMENT
$-0.409 \pm 0.033 \pm 0.006$	<sup>1</sup> AAIJ	14AF	LHCB $pp$ at 7, 8 TeV

<sup>1</sup> Measured in  $B^+ \rightarrow \pi^+\rho\bar{\rho}$  decays.**ISOSPIN ASYMMETRY** $\Delta_{0-}$  is defined as

$$\frac{\Gamma(\bar{B}^0 \rightarrow f_{\pi^0}) - \Gamma(B^- \rightarrow f_{\pi^0})}{\Gamma(\bar{B}^0 \rightarrow f_{\pi^0}) + \Gamma(B^- \rightarrow f_{\pi^0})},$$

the isospin asymmetry of inclusive neutral and charged B decay.

 **$\Delta_{0-}(B \rightarrow X_S \gamma)$** 

VALUE	DOCUMENT ID	TECN	COMMENT
<b><math>-0.005 \pm 0.020</math> OUR AVERAGE</b>			
$-0.0048 \pm 0.0149 \pm 0.0150$	<sup>1</sup> WATANUKI	19	BELL $e^+e^- \rightarrow \Upsilon(4S)$
$-0.006 \pm 0.058 \pm 0.026$	AUBERT,B	05R	BABR $e^+e^- \rightarrow \Upsilon(4S)$

<sup>1</sup> Using a sum-of-exclusive technique with  $m_{X_S} < 2.8 \text{ GeV}/c^2$ . **$\Delta_{0-}(B \rightarrow X_S d\gamma)$** 

VALUE	DOCUMENT ID	TECN	COMMENT
<b><math>-0.06 \pm 0.15 \pm 0.07</math></b>	<sup>1</sup> AUBERT	08o	BABR $e^+e^- \rightarrow \Upsilon(4S)$

<sup>1</sup> Uses a fully reconstructed B meson as a tag on the recoil side. The result is for  $E_\gamma > 2.2 \text{ GeV}$ . **$\Delta_{0+}(B \rightarrow K^*(892)\gamma)$**  $\Delta_{0+}$  describes the isospin asymmetry between  $\Gamma(B^0 \rightarrow K^*(892)^0\gamma)$  and  $\Gamma(B^+ \rightarrow K^*(892)^+\gamma)$ .

VALUE	DOCUMENT ID	TECN	COMMENT
<b><math>0.063 \pm 0.017</math> OUR AVERAGE</b>			
$0.062 \pm 0.015 \pm 0.013$	<sup>1</sup> HORIGUCHI	17	BELL $e^+e^- \rightarrow \Upsilon(4S)$
$0.066 \pm 0.021 \pm 0.022$	<sup>2</sup> AUBERT	09A0	BABR $e^+e^- \rightarrow \Upsilon(4S)$
$0.050 \pm 0.045 \pm 0.037$	<sup>3</sup> AUBERT,BE	04A	BABR Repl. by AUBERT 09A0
$0.012 \pm 0.044 \pm 0.026$	NAKAO	04	BELL Repl. by HORIGUCHI 17

<sup>1</sup> Uses  $B(\Upsilon(4S) \rightarrow B^+B^-) = (51.4 \pm 0.6)\%$  and  $B(\Upsilon(4S) \rightarrow B^0\bar{B}^0) = (48.6 \pm 0.6)\%$ .  
<sup>2</sup> Uses the production ratio of charged and neutral B from  $\Upsilon(4S)$  decays and the lifetime ratio  $\tau_{B^+}/\tau_{B^0} = 1.071 \pm 0.009$ . The 90% CL interval is  $0.017 < \Delta_{0+} < 0.116$ .  
<sup>3</sup> Uses the production ratio of charged and neutral B from  $\Upsilon(4S)$  decays  $R^{+/0} = 1.006 \pm 0.048$  and the lifetime ratio of  $\tau_{B^+}/\tau_{B^0} = 1.083 \pm 0.017$ . The 90% CL interval is  $-0.046 < \Delta_{0+} < 0.146$ .

 **$\Delta_{\rho\gamma} = \Gamma(B^+ \rightarrow \rho^+\gamma) / (2 \cdot \Gamma(B^0 \rightarrow \rho^0\gamma)) - 1$** 

VALUE	DOCUMENT ID	TECN	COMMENT
<b><math>-0.46 \pm 0.17</math> OUR AVERAGE</b>			
$-0.43^{+0.25}_{-0.23} \pm 0.10$	AUBERT	08BH	BABR $e^+e^- \rightarrow \Upsilon(4S)$
$-0.48^{+0.21}_{-0.19} \pm 0.08$	TANIGUCHI	08	BELL $e^+e^- \rightarrow \Upsilon(4S)$

 **$\Delta_{0-}(B \rightarrow K\ell^+\ell^-)$** 

VALUE	DOCUMENT ID	TECN	COMMENT
<b><math>-0.13 \pm 0.06</math> OUR AVERAGE</b>	Error includes scale factor of 1.1.		
$-0.10^{+0.08}_{-0.09} \pm 0.02$	<sup>1</sup> AAIJ	14M	LHCB $pp$ at 7, 8 TeV
$-0.09^{+0.08}_{-0.08} \pm 0.02$	<sup>2</sup> AAIJ	14M	LHCB $pp$ at 7, 8 TeV
$-0.58^{+0.29}_{-0.37} \pm 0.02$	<sup>3</sup> LEES	12s	BABR $e^+e^- \rightarrow \Upsilon(4S)$
$-0.31^{+0.17}_{-0.14} \pm 0.08$	<sup>4</sup> WEI	09A	BELL $e^+e^- \rightarrow \Upsilon(4S)$
$-0.35^{+0.23}_{-0.27}$	<sup>5</sup> AAIJ	12AH	LHCB Repl. by AAIJ 14M
$-1.43^{+0.56}_{-0.85} \pm 0.05$	<sup>6,7</sup> AUBERT	09T	BABR Repl. by LEES 12s

<sup>1</sup> For  $1.1 < q^2 < 6.0 \text{ GeV}^2/c^4$  using  $\mu^+\mu^-$  as a lepton pair and assuming isospin symmetry for the  $B \rightarrow J/\psi(1S)K$ . Measurements in other  $q^2$  bins are also reported.  
<sup>2</sup> For  $15.0 < q^2 < 19.0 \text{ GeV}^2/c^4$  using  $\mu^+\mu^-$  as a lepton pair and assuming isospin symmetry for the  $B \rightarrow J/\psi(1S)K$ . Measurements in other  $q^2$  bins are also reported.  
<sup>3</sup> For  $0.10 < q^2 < 8.12 \text{ GeV}^2/c^4$ . Measurements in other  $q^2$  bins are also reported.  
<sup>4</sup> For  $q^2 < 8.68 \text{ GeV}^2/c^4$ .  
<sup>5</sup> For  $1 < q^2 < 6 \text{ GeV}^2/c^4$ .  
<sup>6</sup> For  $0.1 < m_{\ell^+\ell^-}^2 < 7.02 \text{ GeV}^2/c^4$ .  
<sup>7</sup> Assumes equal production of  $B^+$  and  $B^0$  at the  $\Upsilon(4S)$ .

 **$\Delta_{0-}(B(B \rightarrow K^*\ell^+\ell^-))$** 

VALUE	DOCUMENT ID	TECN	COMMENT
<b><math>-0.03^{+0.08}_{-0.07}</math> OUR AVERAGE</b>	Error includes scale factor of 1.2.		
$0.00^{+0.12}_{-0.10} \pm 0.02$	<sup>1</sup> AAIJ	14M	LHCB $pp$ at 7, 8 TeV
$0.06^{+0.10}_{-0.09} \pm 0.02$	<sup>2</sup> AAIJ	14M	LHCB $pp$ at 7, 8 TeV
$-0.25^{+0.20}_{-0.17} \pm 0.03$	<sup>3</sup> LEES	12s	BABR $e^+e^- \rightarrow \Upsilon(4S)$
$-0.29 \pm 0.16 \pm 0.09$	<sup>4</sup> WEI	09A	BELL $e^+e^- \rightarrow \Upsilon(4S)$
$-0.15 \pm 0.16$	<sup>5</sup> AAIJ	12AH	LHCB Repl. by AAIJ 14M
$-0.56^{+0.17}_{-0.15} \pm 0.03$	<sup>6,7</sup> AUBERT	09T	BABR Repl. by LEES 12s

<sup>1</sup> For  $1.1 < q^2 < 6.0 \text{ GeV}^2/c^4$  using  $\mu^+\mu^-$  as a lepton pair and assuming isospin symmetry for the  $B(B \rightarrow J/\psi(1S)K^*(892))$ . Measurements in other  $q^2$  bins are also reported.  
<sup>2</sup> For  $15.0 < q^2 < 22.0 \text{ GeV}^2/c^4$  using  $\mu^+\mu^-$  as a lepton pair and assuming isospin symmetry for the  $B(B \rightarrow J/\psi(1S)K^*(892))$ . Measurements in other  $q^2$  bins are also reported.  
<sup>3</sup> For  $0.10 < q^2 < 8.12 \text{ GeV}^2/c^4$ . Measurements in other  $q^2$  bins are also reported.  
<sup>4</sup> For  $q^2 < 8.68 \text{ GeV}^2/c^4$ .  
<sup>5</sup> For  $1 < q^2 < 6 \text{ GeV}^2/c^4$ .  
<sup>6</sup> For  $0.1 < m_{\ell^+\ell^-}^2 < 7.02 \text{ GeV}^2/c^4$ .  
<sup>7</sup> Assumes equal production of  $B^+$  and  $B^0$  at the  $\Upsilon(4S)$ .

 **$\Delta_{0-}(B(B \rightarrow K^*(*)\ell^+\ell^-))$** 

VALUE	DOCUMENT ID	TECN	COMMENT
<b><math>-0.45 \pm 0.17</math> OUR AVERAGE</b>	Error includes scale factor of 1.7.		
$-0.64^{+0.15}_{-0.14} \pm 0.03$	<sup>1,2</sup> AUBERT	09T	BABR $e^+e^- \rightarrow \Upsilon(4S)$
$-0.30^{+0.12}_{-0.11} \pm 0.08$	<sup>3</sup> WEI	09A	BELL $e^+e^- \rightarrow \Upsilon(4S)$

<sup>1</sup> For  $0.1 < m_{\ell^+\ell^-}^2 < 7.02 \text{ GeV}^2/c^4$ .  
<sup>2</sup> Assumes equal production of  $B^+$  and  $B^0$  at the  $\Upsilon(4S)$ .  
<sup>3</sup> For  $q^2 < 8.68 \text{ GeV}^2/c^2$ .

 **$B \rightarrow X_c \ell \nu$  HADRONIC MASS MOMENTS** **$\langle M_X^2 - \overline{M}_D^2 \rangle$  (First Moments)**

VALUE ( $\text{GeV}^2$ )	DOCUMENT ID	TECN	COMMENT
<b><math>0.36 \pm 0.08</math> OUR AVERAGE</b>	Error includes scale factor of 1.8.		
$0.467 \pm 0.038 \pm 0.068$	<sup>1</sup> ACOSTA	05F	CDF $p\bar{p}$ at 1.96 TeV
$0.293 \pm 0.012 \pm 0.058$	<sup>2</sup> CSORNA	04	CLE2 $e^+e^- \rightarrow \Upsilon(4S)$
$0.251 \pm 0.023 \pm 0.062$	<sup>3</sup> CRONIN-HEN..01B	CLE2	$e^+e^- \rightarrow \Upsilon(4S)$

<sup>1</sup> Moments are measured with a minimum lepton momentum of  $0.7 \text{ GeV}/c$  in the B rest frame;  
<sup>2</sup> Uses minimum lepton energy of  $1.5 \text{ GeV}$  and also reports moments with  $E_\ell > 1.0 \text{ GeV}$ .  
<sup>3</sup> The leptons are required to have  $P_\ell > 1.5 \text{ GeV}/c$ .

 **$\langle M_X^2 \rangle$  (First Moments)**

VALUE ( $\text{GeV}^2$ )	DOCUMENT ID	TECN	COMMENT
<b><math>4.156 \pm 0.029</math> OUR AVERAGE</b>			
$4.144 \pm 0.028 \pm 0.022$	<sup>1</sup> SCHWANDA	07	BELL $e^+e^- \rightarrow \Upsilon(4S)$
$4.18 \pm 0.04 \pm 0.03$	<sup>1</sup> AUBERT,B	04	BABR $e^+e^- \rightarrow \Upsilon(4S)$

<sup>1</sup> The leptons are required to have  $E_\ell > 1.5 \text{ GeV}/c$ . **$\langle (M_X^2 - \overline{M}_X^2)^2 \rangle$  (Second Moments)**

VALUE ( $\text{GeV}^4$ )	DOCUMENT ID	TECN	COMMENT
<b><math>0.55 \pm 0.08</math> OUR AVERAGE</b>			
$0.515 \pm 0.061 \pm 0.064$	<sup>1</sup> SCHWANDA	07	BELL $e^+e^- \rightarrow \Upsilon(4S)$
$0.629 \pm 0.031 \pm 0.143$	<sup>2</sup> CSORNA	04	CLE2 $e^+e^- \rightarrow \Upsilon(4S)$
$1.05 \pm 0.26 \pm 0.13$	<sup>3</sup> ACOSTA	05F	CDF $p\bar{p}$ at 1.96 TeV
$0.576 \pm 0.048 \pm 0.168$	<sup>1</sup> CRONIN-HEN..01B	CLE2	$e^+e^- \rightarrow \Upsilon(4S)$

<sup>1</sup> The leptons are required to have  $E_\ell > 1.5 \text{ GeV}/c$ .  
<sup>2</sup> Uses minimum lepton energy of  $1.5 \text{ GeV}$  and also reports moments with  $E_\ell > 1.0 \text{ GeV}$ .  
<sup>3</sup> Moments are measured with a minimum lepton momentum of  $0.7 \text{ GeV}/c$  in the B rest frame;

 **$\langle (M_X^2 - \overline{M}_D^2)^2 \rangle$  (Second Moments)**

VALUE ( $\text{GeV}^4$ )	DOCUMENT ID	TECN	COMMENT
<b><math>0.639 \pm 0.056 \pm 0.178</math></b>	<sup>1</sup> CRONIN-HEN..01B	CLE2	$e^+e^- \rightarrow \Upsilon(4S)$

<sup>1</sup> The leptons are required to have  $E_\ell > 1.5 \text{ GeV}/c$ . **$B \rightarrow X_c \ell \nu$  LEPTON MOMENTUM MOMENTS** **$R_0$  ( $\Gamma_{E_\ell > 1.7 \text{ GeV}} / \Gamma_{E_\ell > 1.5 \text{ GeV}}$ )**

VALUE	DOCUMENT ID	TECN	COMMENT
<b><math>0.6187 \pm 0.0014 \pm 0.0016</math></b>	<sup>1</sup> MAHMOOD	03	CLE2 $e^+e^- \rightarrow \Upsilon(4S)$

<sup>1</sup> The leptons are required to have  $E_\ell > 1.5 \text{ GeV}$  in the B rest frame.







# Meson Particle Listings

## $B^\pm/B^0/B_s^0/b$ -baryon ADMIXTURE

- <sup>18</sup>BUSKULIC 92F uses the lepton impact parameter distribution for data from the 1991 run.
- <sup>19</sup>BUSKULIC 92c use  $J/\psi(1S)$  tags to measure the average  $b$  lifetime. This is comparable to other methods only if the  $J/\psi(1S)$  branching fractions of the different  $b$ -flavored hadrons are in the same ratio.
- <sup>20</sup>Using  $Z \rightarrow e^+X$  or  $\mu^+X$ , ADEVA 91H determined the average lifetime for an admixture of  $B$  hadrons from the impact parameter distribution of the lepton.
- <sup>21</sup>Using  $Z \rightarrow J/\psi(1S)X$ ,  $J/\psi(1S) \rightarrow \ell^+\ell^-$ , ALEXANDER 91G determined the average lifetime for an admixture of  $B$  hadrons from the decay point of the  $J/\psi(1S)$ .
- <sup>22</sup>Using  $Z \rightarrow eX$  or  $\mu X$ , DECAMP 91c determines the average lifetime for an admixture of  $B$  hadrons from the signed impact parameter distribution of the lepton.
- <sup>23</sup>HAGEMANN 90 uses electrons and muons in an impact parameter analysis.
- <sup>24</sup>LYONS 90 combine the results of the  $B$  lifetime measurements of ONG 89, BRAUNSCHWEIG 89B, KLEM 88, and ASH 87, and JADE data by private communication. They use statistical techniques which include variation of the error with the mean life, and possible correlations between the systematic errors. This result is not independent of the measured results used in our average.
- <sup>25</sup>We have combined an overall scale error of 15% in quadrature with the systematic error of  $\pm 0.7$  to obtain  $\pm 2.1$  systematic error.
- <sup>26</sup>Statistical and systematic errors were combined by BROM 87.

$$\text{cor}(B_s^0, B^\pm=B^0) = -0.633$$

$$\text{cor}(b\text{-baryon}, B^\pm=B^0) = -0.813.$$

The notation for production fractions varies in the literature ( $f_B, d_{B^0}, f(b \rightarrow \bar{B}^0), \text{Br}(b \rightarrow \bar{B}^0)$ ). We use our own branching fraction notation here,  $\text{B}(\bar{b} \rightarrow B^0)$ .

Note these production fractions are  $b$ -hadronization fractions, not the conventional branching fractions of  $b$ -quark to a  $B$ -hadron, which may have considerable dependence on the initial and final state kinematic and production environment.

$\Gamma_1$	$B^+$	( 40.8 $\pm$ 0.7 ) %
$\Gamma_2$	$B^0$	( 40.8 $\pm$ 0.7 ) %
$\Gamma_3$	$B_s^0$	( 10.0 $\pm$ 0.8 ) %
$\Gamma_4$	$B_c^+$	
$\Gamma_5$	$b$ -baryon	( 8.4 $\pm$ 1.1 ) %

### CHARGED $b$ -HADRON ADMIXTURE MEAN LIFE

VALUE ( $10^{-12}$ s)	DOCUMENT ID	TECN	COMMENT
<b>1.72 <math>\pm</math> 0.08 <math>\pm</math> 0.06</b>	<sup>1</sup> ADAM	95	DLPH $e^+e^- \rightarrow Z$

<sup>1</sup> ADAM 95 data analyzed using vertex-charge technique to tag  $b$ -hadron charge.

### NEUTRAL $b$ -HADRON ADMIXTURE MEAN LIFE

VALUE ( $10^{-12}$ s)	DOCUMENT ID	TECN	COMMENT
<b>1.58 <math>\pm</math> 0.11 <math>\pm</math> 0.09</b>	<sup>1</sup> ADAM	95	DLPH $e^+e^- \rightarrow Z$

<sup>1</sup> ADAM 95 data analyzed using vertex-charge technique to tag  $b$ -hadron charge.

### MEAN LIFE RATIO $\tau_{\text{charged } b\text{-hadron}}/\tau_{\text{neutral } b\text{-hadron}}$

VALUE	DOCUMENT ID	TECN	COMMENT
<b>1.09 <math>\pm</math> 0.11 <math>\pm</math> 0.08</b> <b>-0.10 <math>\pm</math> 0.08</b>	<sup>1</sup> ADAM	95	DLPH $e^+e^- \rightarrow Z$

<sup>1</sup> ADAM 95 data analyzed using vertex-charge technique to tag  $b$ -hadron charge.

$$|\Delta\tau_b|/\tau_{b,\bar{b}}$$

$\tau_{b,\bar{b}}$  and  $|\Delta\tau_b|$  are the mean life average and difference between  $b$  and  $\bar{b}$  hadrons.

VALUE	DOCUMENT ID	TECN	COMMENT
<b>-0.001 <math>\pm</math> 0.012 <math>\pm</math> 0.008</b>	<sup>1</sup> ABBIENDI	99j	OPAL $e^+e^- \rightarrow Z$

<sup>1</sup> Data analyzed using both the jet charge and the charge of secondary vertex in the opposite hemisphere.

### $\bar{b}$ PRODUCTION FRACTIONS AND DECAY MODES

The branching fraction measurements are for an admixture of  $B$  mesons and baryons at energies above the  $T(4S)$ . Only the highest energy results (LHC, LEP, Tevatron,  $S\bar{p}\bar{S}$ ) are used in the branching fraction averages. In the following, we assume that the production fractions are the same at the LHC, LEP, and at the Tevatron.

For inclusive branching fractions, e.g.,  $B \rightarrow D^\pm$  anything, the values usually are multiplicities, not branching fractions. They can be greater than one.

The modes below are listed for a  $\bar{b}$  initial state.  $b$  modes are their charge conjugates. Reactions indicate the weak decay vertex and do not include mixing.

Mode	Fraction ( $\Gamma_j/\Gamma$ )	Scale factor/ Confidence level
------	--------------------------------	-----------------------------------

### PRODUCTION FRACTIONS

The production fractions for weakly decaying  $b$ -hadrons at high energy have been calculated from the best values of mean lives, mixing parameters, and branching fractions in this edition by the Heavy Flavor Averaging Group (HFLAV) as described in the note " $B^0\text{-}\bar{B}^0$  Mixing" in the  $B^0$  Particle Listings. We no longer provide world averages of the  $b$ -hadron production fractions, where results from LEP, Tevatron and LHC are averaged together; indeed the available data (from CDF and LHCb) shows that the fractions depend on the kinematics (in particular the  $p_T$ ) of the produced  $b$  hadron. Hence we would like to list the fractions in  $Z$  decays instead, which are well-defined physics observables. The production fractions in  $p\bar{p}$  collisions at the Tevatron are also listed at the end of the section. Values assume

$$\text{B}(\bar{b} \rightarrow B^+) = \text{B}(\bar{b} \rightarrow B^0)$$

$$\text{B}(\bar{b} \rightarrow B^+) + \text{B}(\bar{b} \rightarrow B^0) + \text{B}(\bar{b} \rightarrow B_s^0) + \text{B}(b \rightarrow b\text{-baryon}) = 100\%.$$

The correlation coefficients between production fractions are also reported:  
 $\text{cor}(B_s^0, b\text{-baryon}) = 0.064$

### DECAY MODES

#### Semileptonic and leptonic modes

$\Gamma_6$	$\nu$ anything	( 23.1 $\pm$ 1.5 ) %	
$\Gamma_7$	$\ell^+ \nu_\ell$ anything	[a] ( 10.69 $\pm$ 0.22 ) %	
$\Gamma_8$	$e^+ \nu_e$ anything	( 10.86 $\pm$ 0.35 ) %	
$\Gamma_9$	$\mu^+ \nu_\mu$ anything	( 10.95 $\pm$ 0.29 / 0.25 ) %	
$\Gamma_{10}$	$D^- \ell^+ \nu_\ell$ anything	[a] ( 2.2 $\pm$ 0.4 ) %	S=1.9
$\Gamma_{11}$	$D^- \pi^+ \ell^+ \nu_\ell$ anything	( 4.9 $\pm$ 1.9 ) $\times 10^{-3}$	
$\Gamma_{12}$	$D^- \pi^- \ell^+ \nu_\ell$ anything	( 2.6 $\pm$ 1.6 ) $\times 10^{-3}$	
$\Gamma_{13}$	$\bar{D}^0 \ell^+ \nu_\ell$ anything	[a] ( 6.79 $\pm$ 0.34 ) %	
$\Gamma_{14}$	$\bar{D}^0 \pi^- \ell^+ \nu_\ell$ anything	( 1.07 $\pm$ 0.27 ) %	
$\Gamma_{15}$	$\bar{D}^0 \pi^+ \ell^+ \nu_\ell$ anything	( 2.3 $\pm$ 1.6 ) $\times 10^{-3}$	
$\Gamma_{16}$	$D^{*-} \ell^+ \nu_\ell$ anything	[a] ( 2.75 $\pm$ 0.19 ) %	
$\Gamma_{17}$	$D^{*-} \pi^- \ell^+ \nu_\ell$ anything	( 6 $\pm$ 7 ) $\times 10^{-4}$	
$\Gamma_{18}$	$D^{*-} \pi^+ \ell^+ \nu_\ell$ anything	( 4.8 $\pm$ 1.0 ) $\times 10^{-3}$	
$\Gamma_{19}$	$\bar{D}_j^0 \ell^+ \nu_\ell$ anything $\times$ $\text{B}(\bar{D}_j^0 \rightarrow D^{*+} \pi^-)$	[a,b] ( 2.6 $\pm$ 0.9 ) $\times 10^{-3}$	
$\Gamma_{20}$	$D_j^- \ell^+ \nu_\ell$ anything $\times$ $\text{B}(D_j^- \rightarrow D^0 \pi^-)$	[a,b] ( 7.0 $\pm$ 2.3 ) $\times 10^{-3}$	
$\Gamma_{21}$	$\bar{D}_2^*(2460)^0 \ell^+ \nu_\ell$ anything $\times \text{B}(\bar{D}_2^*(2460)^0 \rightarrow$ $D^{*-} \pi^+)$	< 1.4 $\times 10^{-3}$	CL=90%
$\Gamma_{22}$	$D_2^*(2460)^- \ell^+ \nu_\ell$ anything $\times \text{B}(D_2^*(2460)^- \rightarrow$ $D^0 \pi^-)$	( 4.2 $\pm$ 1.5 / 1.8 ) $\times 10^{-3}$	
$\Gamma_{23}$	$\bar{D}_2^*(2460)^0 \ell^+ \nu_\ell$ anything $\times \text{B}(\bar{D}_2^*(2460)^0 \rightarrow$ $D^- \pi^+)$	( 1.6 $\pm$ 0.8 ) $\times 10^{-3}$	
$\Gamma_{24}$	charmless $\ell \bar{\nu}_\ell$	[a] ( 1.7 $\pm$ 0.5 ) $\times 10^{-3}$	
$\Gamma_{25}$	$\tau^+ \nu_\tau$ anything	( 2.41 $\pm$ 0.23 ) %	
$\Gamma_{26}$	$D^{*-} \tau \nu_\tau$ anything	( 9 $\pm$ 4 ) $\times 10^{-3}$	
$\Gamma_{27}$	$\bar{c} \rightarrow \ell^- \bar{\nu}_\ell$ anything	[a] ( 8.02 $\pm$ 0.19 ) %	
$\Gamma_{28}$	$c \rightarrow \ell^+ \nu$ anything	( 1.6 $\pm$ 0.4 / 0.5 ) %	

#### Charmed meson and baryon modes

$\Gamma_{29}$	$\bar{D}^0$ anything	( 58.7 $\pm$ 2.8 ) %	
$\Gamma_{30}$	$D^0 D_s^\pm$ anything	[c] ( 9.1 $\pm$ 4.0 / 2.8 ) %	
$\Gamma_{31}$	$D^\mp D_s^\pm$ anything	[c] ( 4.0 $\pm$ 2.3 / 1.8 ) %	
$\Gamma_{32}$	$\bar{D}^0 D^0$ anything	[c] ( 5.1 $\pm$ 2.0 / 1.8 ) %	
$\Gamma_{33}$	$D^0 D^\pm$ anything	[c] ( 2.7 $\pm$ 1.8 / 1.6 ) %	
$\Gamma_{34}$	$D^\pm D^\mp$ anything	[c] < 9 $\times 10^{-3}$	CL=90%
$\Gamma_{35}$	$D^0$ anything		
$\Gamma_{36}$	$D^+$ anything		
$\Gamma_{37}$	$D^-$ anything	( 22.7 $\pm$ 1.6 ) %	
$\Gamma_{38}$	$D^*(2010)^+$ anything	( 17.3 $\pm$ 2.0 ) %	
$\Gamma_{39}$	$D_1(2420)^0$ anything	( 5.0 $\pm$ 1.5 ) %	
$\Gamma_{40}$	$D^*(2010)^\mp D_s^\pm$ anything	[c] ( 3.3 $\pm$ 1.6 / 1.3 ) %	
$\Gamma_{41}$	$D^0 D^*(2010)^\pm$ anything	[c] ( 3.0 $\pm$ 1.1 / 0.9 ) %	
$\Gamma_{42}$	$D^*(2010)^\pm D^\mp$ anything	[c] ( 2.5 $\pm$ 1.2 / 1.0 ) %	
$\Gamma_{43}$	$D^*(2010)^\pm D^*(2010)^\mp$ anything	[c] ( 1.2 $\pm$ 0.4 ) %	
$\Gamma_{44}$	$\bar{D} D$ anything	( 10 $\pm$ 11 / -10 ) %	

See key on page 999

# Meson Particle Listings

## $B^\pm/B^0/B_s^0/b$ -baryon ADMIXTURE

$\Gamma_{45}$	$D_2^*(2460)^0$ anything	( 4.7 ± 2.7 ) %
$\Gamma_{46}$	$D_s^-$ anything	( 14.7 ± 2.1 ) %
$\Gamma_{47}$	$D_s^+$ anything	( 10.1 ± 3.1 ) %
$\Gamma_{48}$	$\Lambda_c^+$ anything	( 7.7 ± 1.1 ) %
$\Gamma_{49}$	$\bar{c}/c$ anything	[d] (116.2 ± 3.2 ) %

### Charmonium modes

$\Gamma_{50}$	$J/\psi(1S)$ anything	( 1.16 ± 0.10 ) %
$\Gamma_{51}$	$\psi(2S)$ anything	( 2.86 ± 0.28 ) × 10 <sup>-3</sup>
$\Gamma_{52}$	$\chi_{c0}(1P)$ anything	( 1.5 ± 0.6 ) %
$\Gamma_{53}$	$\chi_{c1}(1P)$ anything	( 1.4 ± 0.4 ) %
$\Gamma_{54}$	$\chi_{c2}(1P)$ anything	( 6.2 ± 2.9 ) × 10 <sup>-3</sup>
$\Gamma_{55}$	$\chi_c(2P)$ anything, $\chi_c \rightarrow \phi\phi$	< 2.8 × 10 <sup>-7</sup> CL=95%
$\Gamma_{56}$	$\eta_c(1S)$ anything	( 4.5 ± 1.9 ) %
$\Gamma_{57}$	$\eta_c(2S)$ anything, $\eta_c \rightarrow \phi\phi$	( 3.2 ± 1.7 ) × 10 <sup>-6</sup>
$\Gamma_{58}$	$\chi_{c1}(3872)$ anything, $\chi_{c1} \rightarrow \phi\phi$	< 4.5 × 10 <sup>-7</sup> CL=95%
$\Gamma_{59}$	$X(3915)$ anything, $X \rightarrow \phi\phi$	< 3.1 × 10 <sup>-7</sup> CL=95%

### K or K\* modes

$\Gamma_{60}$	$\bar{S}\gamma$	( 3.1 ± 1.1 ) × 10 <sup>-4</sup>
$\Gamma_{61}$	$\bar{S}\bar{D}\nu$	B1 < 6.4 × 10 <sup>-4</sup> CL=90%
$\Gamma_{62}$	$K^\pm$ anything	( 74 ± 6 ) %
$\Gamma_{63}$	$K_S^0$ anything	( 29.0 ± 2.9 ) %

### Pion modes

$\Gamma_{64}$	$\pi^\pm$ anything	( 397 ± 21 ) %
$\Gamma_{65}$	$\pi^0$ anything	[d] ( 278 ± 60 ) %
$\Gamma_{66}$	$\phi$ anything	( 2.82 ± 0.23 ) %

### Baryon modes

$\Gamma_{67}$	$p/\bar{p}$ anything	( 13.1 ± 1.1 ) %
$\Gamma_{68}$	$\Lambda/\bar{\Lambda}$ anything	( 5.9 ± 0.6 ) %
$\Gamma_{69}$	$b$ -baryon anything	( 10.2 ± 2.8 ) %
$\Gamma_{70}$	$\bar{\Lambda}_b^0$ anything	
$\Gamma_{71}$	$\bar{\Xi}_b^+$ anything	

### Other modes

$\Gamma_{72}$	charged anything	[d] ( 497 ± 7 ) %
$\Gamma_{73}$	hadron <sup>+</sup> hadron <sup>-</sup>	( 1.7 + 1.0 / - 0.7 ) × 10 <sup>-5</sup>
$\Gamma_{74}$	charmless	( 7 ± 21 ) × 10 <sup>-3</sup>

### $\Delta B = 1$ weak neutral current (B1) modes

$\Gamma_{75}$	$e^+ e^-$ anything	
$\Gamma_{76}$	$\mu^+ \mu^-$ anything	B1 < 3.2 × 10 <sup>-4</sup> CL=90%
$\Gamma_{77}$	$\nu\bar{\nu}$ anything	

- [a] An  $\ell$  indicates an  $e$  or a  $\mu$  mode, not a sum over these modes.
- [b]  $D_j$  represents an unresolved mixture of pseudoscalar and tensor  $D^{**}$  ( $P$ -wave) states.
- [c] The value is for the sum of the charge states or particle/antiparticle states indicated.
- [d] Inclusive branching fractions have a multiplicity definition and can be greater than 100%.

## $B^\pm/B^0/B_s^0/b$ -baryon ADMIXTURE BRANCHING RATIOS

$\Gamma(B^+)/\Gamma_{total}$   $\Gamma_1/\Gamma$   
 "OUR EVALUATION" is an average from Z decay obtained by the Heavy Flavor Averaging Group (HFLAV) as described at <https://hflav.web.cern.ch/>.

VALUE	DOCUMENT ID	TECN	COMMENT
<b>0.408 ± 0.007 OUR EVALUATION</b>			
<b>0.4099 ± 0.0082 ± 0.0111</b>	1 ABDALLAH 03k DLPH		$e^+ e^- \rightarrow Z$

1 The analysis is based on a neural network, to estimate the charge of the weakly-decaying  $b$ -hadron by distinguishing its decay products from particles produced at the primary vertex.

VALUE	DOCUMENT ID	TECN	COMMENT
<b>1.054 ± 0.018 +0.052 / -0.074</b>	AALTONEN 08N CDF		$p\bar{p}$ at 1.96 TeV

$\Gamma(B_s^0)/[\Gamma(B^+) + \Gamma(B^0)]$   $\Gamma_3/(\Gamma_1 + \Gamma_2)$   
 "OUR EVALUATION" is an average from Z decay obtained by the Heavy Flavor Averaging Group (HFLAV) as described at <https://hflav.web.cern.ch/>.

VALUE	DOCUMENT ID	TECN	COMMENT
<b>0.1230 ± 0.0115 OUR EVALUATION</b>			
0.122 ± 0.006	1 AAIJ	19AD LHCb	$pp$ at 13 TeV
0.134 ± 0.004 +0.011 / -0.010	2 AAIJ	12J LHCb	$pp$ at 7 TeV
0.1265 ± 0.0085 ± 0.0131	3 AAIJ	11F LHCb	$pp$ at 7 TeV
0.128 +0.011 / -0.010 ± 0.011	4 AALTONEN	08N CDF	$p\bar{p}$ at 1.96 TeV
0.213 ± 0.068	5 AFFOLDER	00E CDF	$p\bar{p}$ at 1.8 TeV
0.21 ± 0.036 +0.038 / -0.030	6 ABE	99P CDF	$p\bar{p}$ at 1.8 TeV

- 1 AAIJ 19AD measured the average value using  $b$ -hadron semileptonic decays and assuming isospin symmetry for  $b$ -hadron  $p_T$  of 4 and 25 GeV and  $\eta$  of 2 and 5.
- 2 AAIJ 12J measured this value using  $b$ -hadron semileptonic decays and assuming isospin symmetry.
- 3 AAIJ 11F measured  $f_s/f_d = 0.253 \pm 0.017 \pm 0.017 \pm 0.020$ , where the errors are statistical, systematic, and theoretical. We divide their value by 2. Our second error combines systematic and theoretical uncertainties.
- 4 AALTONEN 08N reports  $[\Gamma(\bar{b} \rightarrow B_s^0)/[\Gamma(\bar{b} \rightarrow B^+) + \Gamma(\bar{b} \rightarrow B^0)]] \times [B(D_s^+ \rightarrow \phi\pi^+)] = (5.76 \pm 0.18 +0.45 / -0.42) \times 10^{-3}$  which we divide by our best value  $B(D_s^+ \rightarrow \phi\pi^+) = (4.5 \pm 0.4) \times 10^{-2}$ . Our first error is their experiment's error and our second error is the systematic error from using our best value.
- 5 AFFOLDER 00E uses several electron-charm final states in  $b \rightarrow ce^-X$ .
- 6 ABE 99P uses the numbers of  $K^*(892)^0$ ,  $K^*(892)^+$ , and  $\phi(1020)$  events produced in association with the double semileptonic decays  $b \rightarrow c\mu^-X$  with  $c \rightarrow s\mu^+X$ .

$\Gamma(B_s^0)/\Gamma(B^0)$   $\Gamma_3/\Gamma_2$   
 "OUR EVALUATION" has been provided by the Heavy Flavor Averaging Group (HFLAV, <https://hflav.web.cern.ch/>).

VALUE	DOCUMENT ID	TECN	COMMENT
<b>0.246 ± 0.023 OUR EVALUATION</b>			
<b>0.239 ± 0.016 OUR AVERAGE</b>			
0.240 ± 0.004 ± 0.020	1 AAD	15CMATLS	$pp$ at 7 TeV
0.238 ± 0.004 ± 0.015 ± 0.021	2 AAIJ	13P LHCb	$pp$ at 7 TeV

- 1 The measurement is derived from the observed  $B_s^0 \rightarrow J/\psi\phi$  and  $B_d^0 \rightarrow J/\psi K^{*0}$  yields and a recent theory prediction of  $B(B_s^0 \rightarrow J/\psi\phi)/B(B_d^0 \rightarrow J/\psi K^{*0})$ . The second uncertainty combines in quadrature systematic and theoretical uncertainties.
- 2 AAIJ 13P studies also separately the  $p_T(B)$  and  $\eta(B)$  dependency of  $\Gamma(\bar{b} \rightarrow B_s^0)/\Gamma(\bar{b} \rightarrow B^0)$ , finding  $f_s/f_d(p_T) = (0.256 \pm 0.020) + (-2.0 \pm 0.6) 10^{-3} / \text{GeV}/c (p_T - \langle p_T \rangle)$  and  $f_s/f_d(\eta) = (0.256 \pm 0.020) + (0.005 \pm 0.006) (\eta - \langle \eta \rangle)$ , where  $\langle p_T \rangle = 10.4 \text{ GeV}/c$  and  $\langle \eta \rangle = 3.28$ .

$\Gamma(B_c^+)/[\Gamma(B^+) + \Gamma(B^0)]$   $\Gamma_4/(\Gamma_1 + \Gamma_2)$   
 "OUR EVALUATION" is an average from Z decay obtained by the Heavy Flavor Averaging Group (HFLAV) as described at <https://hflav.web.cern.ch/>.

VALUE (units 10 <sup>-3</sup> )	DOCUMENT ID	TECN	COMMENT
<b>3.7 ± 0.6 OUR AVERAGE</b>			
3.63 ± 0.08 ± 0.87	1 AAIJ	19A LHCb	$pp$ at 7 TeV
3.78 ± 0.04 ± 0.90	1 AAIJ	19A LHCb	$pp$ at 13 TeV

1 Measured using  $B_c^+$  semileptonic decays.

$\Gamma(b\text{-baryon})/[\Gamma(B^+) + \Gamma(B^0)]$   $\Gamma_5/(\Gamma_1 + \Gamma_2)$   
 "OUR EVALUATION" is an average from Z decay obtained by the Heavy Flavor Averaging Group (HFLAV) as described at <https://hflav.web.cern.ch/>.

VALUE	DOCUMENT ID	TECN	COMMENT
<b>0.103 ± 0.015 OUR EVALUATION</b>			
0.259 ± 0.018	1 AAIJ	19AD LHCb	$pp$ at 13 TeV
0.305 ± 0.010 ± 0.081	2 AAIJ	12J LHCb	$pp$ at 7 TeV
0.31 ± 0.11 +0.12 / -0.08	3 AALTONEN	09E CDF	$p\bar{p}$ at 1.8 TeV
0.22 +0.08 / -0.07 ± 0.01	4 AALTONEN	08N CDF	$p\bar{p}$ at 1.96 TeV
0.118 ± 0.042	3,5 AFFOLDER	00E CDF	$p\bar{p}$ at 1.8 TeV

- 1 AAIJ 19AD measured the average value for  $\Lambda_b^0$  using semileptonic decays and assuming isospin symmetry for  $b$ -hadron  $p_T$  of 4 and 25 GeV and  $\eta$  of 2 and 5.
- 2 AAIJ 12J measured the ratio to be  $(0.404 \pm 0.017 \pm 0.027 \pm 0.105) \times [1 - (0.031 \pm 0.004 \pm 0.003) \times P_T]$  using  $b$ -hadron semileptonic decays where the  $P_T$  is the momentum of charmed hadron-muon pair in GeV/c. We quote their weighted average value where the second error combines systematic and the error on  $B(\Lambda_c^+ \rightarrow pK^- \pi^+)$ .
- 3 AALTONEN 09E errata to the measurement reported in AFFOLDER 00E using the  $p_T$  spectra from fully reconstructed  $B^0$  and  $\Lambda_b$  decays.
- 4 AALTONEN 08N reports  $[\Gamma(\bar{b} \rightarrow b\text{-baryon})/[\Gamma(\bar{b} \rightarrow B^+) + \Gamma(\bar{b} \rightarrow B^0)]] \times [B(\Lambda_c^+ \rightarrow pK^- \pi^+)] = (14.1 \pm 0.6 +5.3 / -4.4) \times 10^{-3}$  which we divide by our best value  $B(\Lambda_c^+ \rightarrow pK^- \pi^+) = (6.28 \pm 0.32) \times 10^{-2}$ . Our first error is their experiment's error and our second error is the systematic error from using our best value.
- 5 AFFOLDER 00E uses several electron-charm final states in  $b \rightarrow ce^-X$ .

# Meson Particle Listings

## $B^\pm/B^0/B_s^0$ -baryon ADMIXTURE

$\Gamma(\nu \text{ anything})/\Gamma_{\text{total}}$	$\Gamma_6/\Gamma$
VALUE	DOCUMENT ID TECN COMMENT

<b>0.2308 ± 0.0077 ± 0.0124</b>	1,2 ACCIARRI 96c L3 $e^+e^- \rightarrow Z$
<sup>1</sup> ACCIARRI 96c assumes relative $b$ semileptonic decay rates $\epsilon:\mu:\tau$ of 1:1:0.25. Based on missing-energy spectrum. <sup>2</sup> Assumes Standard Model value for $R_B$ .	

$\Gamma(\ell^+ \nu_\ell \text{ anything})/\Gamma_{\text{total}}$	$\Gamma_7/\Gamma$
VALUE	DOCUMENT ID TECN COMMENT

<b>0.1069 ± 0.0022 OUR EVALUATION</b>	
<b>0.1064 ± 0.0016 OUR AVERAGE</b>	
0.1070 ± 0.0010 ± 0.0035	<sup>1</sup> HEISTER 02G ALEP $e^+e^- \rightarrow Z$
0.1070 ± 0.0008 ± 0.0037 - 0.0049	<sup>2</sup> ABREU 01L DLPH $e^+e^- \rightarrow Z$
0.1083 ± 0.0010 ± 0.0028 - 0.0024	<sup>3</sup> ABBIENDI 00E OPAL $e^+e^- \rightarrow Z$
0.1016 ± 0.0013 ± 0.0030	<sup>4</sup> ACCIARRI 00 L3 $e^+e^- \rightarrow Z$
0.1085 ± 0.0012 ± 0.0047	<sup>5,6</sup> ACCIARRI 96c L3 $e^+e^- \rightarrow Z$
• • • We do not use the following data for averages, fits, limits, etc. • • •	
0.1106 ± 0.0039 ± 0.0022	<sup>7</sup> ABREU 95D DLPH $e^+e^- \rightarrow Z$
0.114 ± 0.003 ± 0.004	<sup>8</sup> BUSKULIC 94G ALEP $e^+e^- \rightarrow Z$
0.100 ± 0.007 ± 0.007	<sup>9</sup> ABREU 93c DLPH $e^+e^- \rightarrow Z$
0.105 ± 0.006 ± 0.005	<sup>10</sup> AKERS 93B OPAL Repl. by ABBI- ENDI 00E

- Uses the combination of lepton transverse momentum spectrum and the correlation between the charge of the lepton and opposite jet charge. The first error is statistic and the second error is the total systematic error including the modeling.
- The experimental systematic and model uncertainties are combined in quadrature.
- ABBIENDI 00E result is determined by comparing the distribution of several kinematic variables of leptonic events in a lifetime tagged  $Z \rightarrow b\bar{b}$  sample using artificial neural network techniques. The first error is statistic; the second error is the total systematic error.
- ACCIARRI 00 result obtained from a combined fit of  $R_D = \Gamma(Z \rightarrow b\bar{b})/\Gamma(Z \rightarrow \text{hadrons})$  and  $B(b \rightarrow \ell\nu X)$ , using double-tagging method.
- ACCIARRI 96c result obtained by a fit to the single lepton spectrum.
- Assumes Standard Model value for  $R_B$ .
- ABREU 95D give systematic errors  $\pm 0.0019$  (model) and  $0.0012$  ( $R_c$ ). We combine these in quadrature.
- BUSKULIC 94G uses  $e$  and  $\mu$  events. This value is from a global fit to the lepton  $p$  and  $p_T$  (relative to jet) spectra which also determines the  $b$  and  $c$  production fractions, the fragmentation functions, and the forward-backward asymmetries. This branching ratio depends primarily on the ratio of dileptons to single leptons at high  $p_T$ , but the lower  $p_T$  portion of the lepton spectrum is included in the global fit to reduce the model dependence. The model dependence is  $\pm 0.0026$  and is included in the systematic error.
- ABREU 93c event count includes  $e\bar{e}$  events. Combining  $e\bar{e}$ ,  $\mu\mu$ , and  $e\mu$  events, they obtain  $0.100 \pm 0.007 \pm 0.007$ .
- AKERS 93B analysis performed using single and dilepton events.

$\Gamma(e^+ \nu_e \text{ anything})/\Gamma_{\text{total}}$	$\Gamma_8/\Gamma$
VALUE	DOCUMENT ID TECN COMMENT

<b>0.1086 ± 0.0035 OUR AVERAGE</b>	
0.1078 ± 0.0008 ± 0.0050 - 0.0046	<sup>1</sup> ABBIENDI 00E OPAL $e^+e^- \rightarrow Z$
0.1089 ± 0.0020 ± 0.0051	<sup>2,3</sup> ACCIARRI 96c L3 $e^+e^- \rightarrow Z$
0.107 ± 0.015 ± 0.007	<sup>4</sup> ABREU 93c DLPH $e^+e^- \rightarrow Z$
0.138 ± 0.032 ± 0.008	<sup>5</sup> ADEVA 91c L3 $e^+e^- \rightarrow Z$
• • • We do not use the following data for averages, fits, limits, etc. • • •	
0.086 ± 0.027 ± 0.008	<sup>6</sup> ABE 93E VNS $E_{\text{cm}}^{ee} = 58$ GeV
0.109 ± 0.014 ± 0.0055 - 0.013	<sup>7</sup> AKERS 93B OPAL Repl. by ABBI- ENDI 00E
0.111 ± 0.028 ± 0.026	BEHREND 90D CELL $E_{\text{cm}}^{ee} = 43$ GeV
0.150 ± 0.011 ± 0.022	BEHREND 90D CELL $E_{\text{cm}}^{ee} = 35$ GeV
0.112 ± 0.009 ± 0.011	ONG 88 MRK2 $E_{\text{cm}}^{ee} = 29$ GeV
0.149 ± 0.022 ± 0.019	PAL 86 DLCO $E_{\text{cm}}^{ee} = 29$ GeV
0.110 ± 0.018 ± 0.010	AIHARA 85 TPC $E_{\text{cm}}^{ee} = 29$ GeV
0.111 ± 0.034 ± 0.040	ALTHOFF 84J TASS $E_{\text{cm}}^{ee} = 34.6$ GeV
0.146 ± 0.028	KOOP 84 DLCO Repl. by PAL 86
0.116 ± 0.021 ± 0.017	NELSON 83 MRK2 $E_{\text{cm}}^{ee} = 29$ GeV

- ABBIENDI 00E result is determined by comparing the distribution of several kinematic variables of leptonic events in a lifetime tagged  $Z \rightarrow b\bar{b}$  sample using artificial neural network techniques. The first error is statistic; the second error is the total systematic error.
- ACCIARRI 96c result obtained by a fit to the single lepton spectrum.
- Assumes Standard Model value for  $R_B$ .
- ABREU 93c event count includes  $e\bar{e}$  events. Combining  $e\bar{e}$ ,  $\mu\mu$ , and  $e\mu$  events, they obtain  $0.100 \pm 0.007 \pm 0.007$ .
- ADEVA 91c measure the average  $B(b \rightarrow eX)$  branching ratio using single and double tagged  $b$  enhanced  $Z$  events. Combining  $e$  and  $\mu$  results, they obtain  $0.113 \pm 0.010 \pm 0.006$ . Constraining the initial number of  $b$  quarks by the Standard Model prediction ( $378 \pm 3$  MeV) for the decay of the  $Z$  into  $b\bar{b}$ , the electron result gives  $0.112 \pm 0.004 \pm 0.008$ . They obtain  $0.119 \pm 0.003 \pm 0.006$  when  $e$  and  $\mu$  results are combined. Used to measure the  $b\bar{b}$  width itself, this electron result gives  $370 \pm 12 \pm 24$  MeV and combined with the muon result gives  $385 \pm 7 \pm 22$  MeV.
- ABE 93E experiment also measures forward-backward asymmetries and fragmentation functions for  $b$  and  $c$ .
- AKERS 93B analysis performed using single and dilepton events.

$\Gamma(\mu^+ \nu_\mu \text{ anything})/\Gamma_{\text{total}}$	$\Gamma_9/\Gamma$
VALUE	EVTs DOCUMENT ID TECN COMMENT

<b>0.1095 ± 0.0029 ± 0.0025 OUR AVERAGE</b>	
0.1096 ± 0.0008 ± 0.0034 - 0.0027	<sup>1</sup> ABBIENDI 00E OPAL $e^+e^- \rightarrow Z$
0.1082 ± 0.0015 ± 0.0059	<sup>2,3</sup> ACCIARRI 96c L3 $e^+e^- \rightarrow Z$
0.110 ± 0.012 ± 0.007	<sup>4</sup> ABREU 93c DLPH $e^+e^- \rightarrow Z$
0.113 ± 0.012 ± 0.006	<sup>5</sup> ADEVA 91c L3 $e^+e^- \rightarrow Z$
• • • We do not use the following data for averages, fits, limits, etc. • • •	
0.122 ± 0.006 ± 0.007	<sup>3</sup> UENO 96 AMY $e^+e^-$ at 57.9 GeV
0.101 ± 0.010 ± 0.0055 - 0.009	<sup>6</sup> AKERS 93B OPAL Repl. by ABBI- ENDI 00E
0.104 ± 0.023 ± 0.016	BEHREND 90D CELL $E_{\text{cm}}^{ee} = 43$ GeV
0.148 ± 0.010 ± 0.016	BEHREND 90D CELL $E_{\text{cm}}^{ee} = 35$ GeV
0.118 ± 0.012 ± 0.010	ONG 88 MRK2 $E_{\text{cm}}^{ee} = 29$ GeV
0.117 ± 0.016 ± 0.015	BARTEL 87 JADE $E_{\text{cm}}^{ee} = 34.6$ GeV
0.114 ± 0.018 ± 0.025	BARTEL 85J JADE Repl. by BARTEL 87
0.117 ± 0.028 ± 0.010	ALTHOFF 84G TASS $E_{\text{cm}}^{ee} = 34.5$ GeV
0.105 ± 0.015 ± 0.013	ADEVA 83B MRKJ $E_{\text{cm}}^{ee} = 33\text{--}38.5$ GeV
0.155 ± 0.054 ± 0.029	FERNANDEZ 83D MAC $E_{\text{cm}}^{ee} = 29$ GeV

- ABBIENDI 00E result is determined by comparing the distribution of several kinematic variables of leptonic events in a lifetime tagged  $Z \rightarrow b\bar{b}$  sample using artificial neural network techniques. The first error is statistic; the second error is the total systematic error.
- ACCIARRI 96c result obtained by a fit to the single lepton spectrum.
- Assumes Standard Model value for  $R_B$ .
- ABREU 93c event count includes  $\mu\mu$  events. Combining  $e\bar{e}$ ,  $\mu\mu$ , and  $e\mu$  events, they obtain  $0.100 \pm 0.007 \pm 0.007$ .
- ADEVA 91c measure the average  $B(b \rightarrow eX)$  branching ratio using single and double tagged  $b$  enhanced  $Z$  events. Combining  $e$  and  $\mu$  results, they obtain  $0.113 \pm 0.010 \pm 0.006$ . Constraining the initial number of  $b$  quarks by the Standard Model prediction ( $378 \pm 3$  MeV) for the decay of the  $Z$  into  $b\bar{b}$ , the muon result gives  $0.123 \pm 0.003 \pm 0.006$ . They obtain  $0.119 \pm 0.003 \pm 0.006$  when  $e$  and  $\mu$  results are combined. Used to measure the  $b\bar{b}$  width itself, this muon result gives  $394 \pm 9 \pm 22$  MeV and combined with the electron result gives  $385 \pm 7 \pm 22$  MeV.
- AKERS 93B analysis performed using single and dilepton events.

$\Gamma(D^- \ell^+ \nu_\ell \text{ anything})/\Gamma_{\text{total}}$	$\Gamma_{10}/\Gamma$
VALUE	DOCUMENT ID TECN COMMENT

<b>0.022 ± 0.004 OUR AVERAGE</b>	Error includes scale factor of 1.9.
0.0272 ± 0.0028 ± 0.0018	<sup>1</sup> ABREU 00R DLPH $e^+e^- \rightarrow Z$
0.0194 ± 0.0025 ± 0.0003	<sup>2</sup> AKERS 95Q OPAL $e^+e^- \rightarrow Z$

- ABREU 00R reports their experiment's uncertainties  $\pm 0.0019 \pm 0.0016 \pm 0.0018$ , where the first error is statistical, the second is systematic, and the third is the uncertainty due to the  $D$  branching fraction. We combine first two in quadrature.
- AKERS 95Q reports  $[\Gamma(\bar{b} \rightarrow D^- \ell^+ \nu_\ell \text{ anything})/\Gamma_{\text{total}}] \times [B(D^+ \rightarrow K^- 2\pi^+)] = (1.82 \pm 0.20 \pm 0.12) \times 10^{-3}$  which we divide by our best value  $B(D^+ \rightarrow K^- 2\pi^+) = (9.38 \pm 0.16) \times 10^{-2}$ . Our first error is their experiment's error and our second error is the systematic error from using our best value.

$\Gamma(D^- \pi^+ \ell^+ \nu_\ell \text{ anything})/\Gamma_{\text{total}}$	$\Gamma_{11}/\Gamma$
VALUE	DOCUMENT ID TECN COMMENT

<b>0.0049 ± 0.0018 ± 0.0007</b>	ABREU 00R DLPH $e^+e^- \rightarrow Z$
---------------------------------	---------------------------------------

$\Gamma(D^- \pi^- \ell^+ \nu_\ell \text{ anything})/\Gamma_{\text{total}}$	$\Gamma_{12}/\Gamma$
VALUE	DOCUMENT ID TECN COMMENT

<b>0.0026 ± 0.0015 ± 0.0004</b>	ABREU 00R DLPH $e^+e^- \rightarrow Z$
---------------------------------	---------------------------------------

$\Gamma(D^0 \ell^+ \nu_\ell \text{ anything})/\Gamma_{\text{total}}$	$\Gamma_{13}/\Gamma$
VALUE	DOCUMENT ID TECN COMMENT

<b>0.0679 ± 0.0034 OUR AVERAGE</b>	
0.0704 ± 0.0040 ± 0.0017	<sup>1</sup> ABREU 00R DLPH $e^+e^- \rightarrow Z$
0.0638 ± 0.0056 ± 0.0005	<sup>2</sup> AKERS 95Q OPAL $e^+e^- \rightarrow Z$

- ABREU 00R reports their experiment's uncertainties  $\pm 0.0034 \pm 0.0036 \pm 0.0017$ , where the first error is statistical, the second is systematic, and the third is the uncertainty due to the  $D$  branching fraction. We combine first two in quadrature.
- AKERS 95Q reports  $[\Gamma(\bar{b} \rightarrow D^0 \ell^+ \nu_\ell \text{ anything})/\Gamma_{\text{total}}] \times [B(D^0 \rightarrow K^- \pi^+)] = (2.52 \pm 0.14 \pm 0.17) \times 10^{-3}$  which we divide by our best value  $B(D^0 \rightarrow K^- \pi^+) = (3.950 \pm 0.031) \times 10^{-2}$ . Our first error is their experiment's error and our second error is the systematic error from using our best value.

$\Gamma(D^0 \pi^- \ell^+ \nu_\ell \text{ anything})/\Gamma_{\text{total}}$	$\Gamma_{14}/\Gamma$
VALUE	DOCUMENT ID TECN COMMENT

<b>0.0107 ± 0.0025 ± 0.0011</b>	ABREU 00R DLPH $e^+e^- \rightarrow Z$
---------------------------------	---------------------------------------

$\Gamma(D^0 \pi^+ \ell^+ \nu_\ell \text{ anything})/\Gamma_{\text{total}}$	$\Gamma_{15}/\Gamma$
VALUE	DOCUMENT ID TECN COMMENT

<b>0.0023 ± 0.0015 ± 0.0004</b>	ABREU 00R DLPH $e^+e^- \rightarrow Z$
---------------------------------	---------------------------------------

Meson Particle Listings
B±/B0/Bs0/b-baryon ADMIXTURE

Gamma(D\*- l+ nu\_e anything)/Gamma\_total
Gamma\_16/Gamma
VALUE DOCUMENT ID TECN COMMENT
0.0275 +/- 0.0019 OUR AVERAGE
0.0275 +/- 0.0021 +/- 0.0009 1 ABREU 00R DLPH e+ e- -> Z
0.0276 +/- 0.0027 +/- 0.0011 2 AKERS 95Q OPAL e+ e- -> Z

1 ABREU 00R reports their experiment's uncertainties +/- 0.0017 +/- 0.0013 +/- 0.0009, where the first error is statistical, the second is systematic, and the third is the uncertainty due to the D branching fraction. We combine first two in quadrature.
2 AKERS 95Q reports [B(D-bar -> D\* l+ nu\_e X) x B(D\*+ -> D0 pi+) x B(D0 -> K- pi+)] = ((7.53 +/- 0.47 +/- 0.56) x 10^-4) and uses B(D\*+ -> D0 pi+) = 0.681 +/- 0.013 and B(D0 -> K- pi+) = 0.0401 +/- 0.0014 to obtain the above result. The first error is the experiments error and the second error is the systematic error from the D\*+ and D0 branching ratios.

Gamma(D\*- pi- l+ nu\_e anything)/Gamma\_total
Gamma\_17/Gamma
VALUE DOCUMENT ID TECN COMMENT
0.0006 +/- 0.0007 +/- 0.0002 ABREU 00R DLPH e+ e- -> Z

Gamma(D\*- pi+ l+ nu\_e anything)/Gamma\_total
Gamma\_18/Gamma
VALUE DOCUMENT ID TECN COMMENT
0.0048 +/- 0.0009 +/- 0.0005 ABREU 00R DLPH e+ e- -> Z

Gamma(Dj l+ nu\_e anything x B(Dj -> D\*+ pi-))/Gamma\_total
Gamma\_19/Gamma
Dj represents an unresolved mixture of pseudoscalar and tensor D\*\* (P-wave) states.
VALUE (units 10^-3) DOCUMENT ID TECN COMMENT
2.64 +/- 0.79 +/- 0.39 ABBIENDI 03M OPAL e+ e- -> Z
6.1 +/- 1.3 +/- 1.3 AKERS 95Q OPAL Repl. by ABBIENDI 03M

Gamma(Dj- l+ nu\_e anything x B(Dj- -> D0 pi-))/Gamma\_total
Gamma\_20/Gamma
Dj represents an unresolved mixture of pseudoscalar and tensor D\*\* (P-wave) states.
VALUE (units 10^-3) DOCUMENT ID TECN COMMENT
7.0 +/- 1.9 +/- 1.2 AKERS 95Q OPAL e+ e- -> Z

Gamma(Ds2(2460)0 l+ nu\_e anything x B(Ds2(2460)0 -> D\*+ pi-))/Gamma\_total
Gamma\_21/Gamma
VALUE (units 10^-3) CL% DOCUMENT ID TECN COMMENT
<1.4 90 ABBIENDI 03M OPAL e+ e- -> Z

Gamma(Ds2(2460)- l+ nu\_e anything x B(Ds2(2460)- -> D0 pi-))/Gamma\_total
Gamma\_22/Gamma
VALUE (units 10^-3) DOCUMENT ID TECN COMMENT
4.2 +/- 1.3 +/- 0.7 AKERS 95Q OPAL e+ e- -> Z

Gamma(Ds2(2460)0 l+ nu\_e anything x B(Ds2(2460)0 -> D- pi+))/Gamma\_total
Gamma\_23/Gamma
VALUE (units 10^-3) DOCUMENT ID TECN COMMENT
1.6 +/- 0.7 +/- 0.3 AKERS 95Q OPAL e+ e- -> Z

Gamma(charmless l nu\_e)/Gamma\_total
Gamma\_24/Gamma
"OUR EVALUATION" is an average of the data listed below performed by the LEP Heavy Flavour Steering Group. The averaging procedure takes into account correlations between the measurements.

Gamma(charmless l nu\_e)/Gamma\_total
Gamma\_24/Gamma
OUR EVALUATION
OUR AVERAGE
0.00171 +/- 0.00052 OUR EVALUATION
0.0017 +/- 0.0004 OUR AVERAGE
0.00163 +/- 0.00053 +/- 0.00055 +/- 0.00062 1 ABBIENDI 01R OPAL e+ e- -> Z
0.00157 +/- 0.00035 +/- 0.00055 2 ABREU 00D DLPH e+ e- -> Z
0.00173 +/- 0.00055 +/- 0.00055 3 BARATE 99G ALEP e+ e- -> Z
0.0033 +/- 0.0010 +/- 0.0017 4 ACCIARRI 98K L3 e+ e- -> Z

1 Obtained from the best fit of the MC simulated events to the data based on the b -> Xu l nu neutral network output distributions.
2 ABREU 00D result obtained from a fit to the numbers of decays in b -> u enriched and depleted samples and their lepton spectra, and assuming |Vcb| = 0.0384 +/- 0.0033 and tau\_b = 1.564 +/- 0.014 ps.
3 Uses lifetime tagged b b-bar sample.
4 ACCIARRI 98K assumes R\_b = 0.2174 +/- 0.0009 at Z decay.

Gamma(tau+ nu\_tau anything)/Gamma\_total
Gamma\_25/Gamma
VALUE (units 10^-2) EVTS DOCUMENT ID TECN COMMENT
2.41 +/- 0.23 OUR AVERAGE
2.78 +/- 0.18 +/- 0.51 1 ABBIENDI 01Q OPAL e+ e- -> Z
2.43 +/- 0.20 +/- 0.25 2 BARATE 01E ALEP e+ e- -> Z
2.19 +/- 0.24 +/- 0.39 3 ABREU 00C DLPH e+ e- -> Z
1.7 +/- 0.5 +/- 1.1 4,5 ACCIARRI 96C L3 e+ e- -> Z
2.4 +/- 0.7 +/- 0.8 1032 6 ACCIARRI 94C L3 e+ e- -> Z
2.75 +/- 0.30 +/- 0.37 405 7 BUSKULIC 95 ALEP Repl. by BARATE 01E
4.08 +/- 0.76 +/- 0.62 BUSKULIC 93B ALEP Repl. by BUSKULIC 95

1 ABBIENDI 01Q uses a missing energy technique.
2 The energy-flow and b-tagging algorithms were used.
3 Uses the missing energy in Z -> b b-bar decays without identifying leptons.
4 ACCIARRI 96C result obtained from missing energy spectrum.
5 Assumes Standard Model value for R\_b.
6 This is a direct result using tagged b b-bar events at the Z, but species are not separated.
7 BUSKULIC 95 uses missing-energy technique.

Gamma(D\*- tau nu\_tau anything)/Gamma\_total
Gamma\_26/Gamma
VALUE DOCUMENT ID TECN COMMENT
(0.88 +/- 0.31 +/- 0.28) x 10^-2 1 BARATE 01E ALEP e+ e- -> Z
1 The energy-flow and b-tagging algorithms were used.

Gamma(D-bar -> tau -> l- nu\_l anything)/Gamma\_total
Gamma\_27/Gamma
"OUR EVALUATION" is an average of the data listed below, excluding all asymmetry measurements, performed by the LEP Electroweak Working Group as described in the "Note on the Z boson" in the Z Particle Listings.

Gamma(D-bar -> tau -> l- nu\_l anything)/Gamma\_total
Gamma\_27/Gamma
OUR EVALUATION
OUR AVERAGE
0.0818 +/- 0.0015 +/- 0.0024 +/- 0.0026 1 HEISTER 02G ALEP e+ e- -> Z
0.0798 +/- 0.0022 +/- 0.0025 +/- 0.0029 2 ABREU 01L DLPH e+ e- -> Z
0.0840 +/- 0.0016 +/- 0.0039 +/- 0.0036 3 ABBIENDI 00E OPAL e+ e- -> Z
0.0770 +/- 0.0097 +/- 0.0046 4 ABREU 95D DLPH e+ e- -> Z
0.082 +/- 0.003 +/- 0.012 5 BUSKULIC 94G ALEP e+ e- -> Z
0.077 +/- 0.004 +/- 0.007 6 AKERS 93B OPAL Repl. by ABBI- ENDI 00E

1 Uses the combination of lepton transverse momentum spectrum and the correlation between the charge of the lepton and opposite jet charge. The first error is statistic and the second error is the total systematic error including the modeling.
2 The experimental systematic and model uncertainties are combined in quadrature.
3 ABBIENDI 00E result is determined by comparing the distribution of several kinematic variables of leptonic events in a lifetime tagged Z -> b b-bar sample using artificial neural network techniques. The first error is statistic; the second error is the total systematic error.
4 ABREU 95D give systematic errors +/- 0.0033 (model) and 0.0032 (R\_c). We combine these in quadrature. This result is from the same global fit as their Gamma(D-bar -> l+ nu\_l X) data.
5 BUSKULIC 94G uses e and mu events. This value is from the same global fit as their Gamma(D-bar -> l+ nu\_l anything)/Gamma\_total data.
6 AKERS 93B analysis performed using single and dilepton events.

Gamma(c -> l+ nu anything)/Gamma\_total
Gamma\_28/Gamma
VALUE DOCUMENT ID TECN COMMENT
0.0161 +/- 0.0020 +/- 0.0034 +/- 0.0047 1 ABREU 01L DLPH e+ e- -> Z
1 The experimental systematic and model uncertainties are combined in quadrature.

Gamma(D0 anything)/Gamma\_total
Gamma\_29/Gamma
VALUE DOCUMENT ID TECN COMMENT
0.587 +/- 0.028 +/- 0.005 1 BUSKULIC 96V ALEP e+ e- -> Z

1 BUSKULIC 96V reports 0.605 +/- 0.024 +/- 0.016 from a measurement of [Gamma(D-bar -> D0 anything)/Gamma\_total] x [B(D0 -> K- pi+)] assuming B(D0 -> K- pi+) = 0.0383, which we rescale to our best value B(D0 -> K- pi+) = (3.950 +/- 0.031) x 10^-2. Our first error is their experiment's error and our second error is the systematic error from using our best value.

Gamma(D0 Ds+ anything)/Gamma\_total
Gamma\_30/Gamma
VALUE DOCUMENT ID TECN COMMENT
0.091 +/- 0.020 +/- 0.034 +/- 0.018 +/- 0.022 1 BARATE 98Q ALEP e+ e- -> Z

1 The systematic error includes the uncertainties due to the charm branching ratios.

Gamma(D- Ds+ anything)/Gamma\_total
Gamma\_31/Gamma
VALUE DOCUMENT ID TECN COMMENT
0.040 +/- 0.017 +/- 0.016 +/- 0.014 +/- 0.011 1 BARATE 98Q ALEP e+ e- -> Z

1 The systematic error includes the uncertainties due to the charm branching ratios.

[Gamma(D0 Ds+ anything) + Gamma(D- Ds+ anything)]/Gamma\_total
Gamma\_30+Gamma\_31/Gamma
VALUE DOCUMENT ID TECN COMMENT
0.131 +/- 0.026 +/- 0.048 +/- 0.022 +/- 0.031 1 BARATE 98Q ALEP e+ e- -> Z

1 The systematic error includes the uncertainties due to the charm branching ratios.

Gamma(D0 D0 anything)/Gamma\_total
Gamma\_32/Gamma
VALUE DOCUMENT ID TECN COMMENT
0.051 +/- 0.016 +/- 0.012 +/- 0.014 +/- 0.011 1 BARATE 98Q ALEP e+ e- -> Z

1 The systematic error includes the uncertainties due to the charm branching ratios.

Gamma(D0 D+ anything)/Gamma\_total
Gamma\_33/Gamma
VALUE DOCUMENT ID TECN COMMENT
0.027 +/- 0.015 +/- 0.010 +/- 0.013 +/- 0.009 1 BARATE 98Q ALEP e+ e- -> Z

1 The systematic error includes the uncertainties due to the charm branching ratios.

[Gamma(D0 D0 anything) + Gamma(D0 D+ anything)]/Gamma\_total
Gamma\_32+Gamma\_33/Gamma
VALUE DOCUMENT ID TECN COMMENT
0.078 +/- 0.020 +/- 0.018 +/- 0.018 +/- 0.016 1 BARATE 98Q ALEP e+ e- -> Z

1 The systematic error includes the uncertainties due to the charm branching ratios.

## Meson Particle Listings

 $B^\pm/B^0/B_s^0/b$ -baryon ADMIXTURE

$\Gamma(D^\pm D^\mp \text{ anything})/\Gamma_{\text{total}}$		$\Gamma_{34}/\Gamma$		
VALUE	CL%	DOCUMENT ID	TECN	COMMENT
$<0.009$	90	BARATE	98Q	ALEP $e^+e^- \rightarrow Z$

$[\Gamma(D^0 \text{ anything}) + \Gamma(D^+ \text{ anything})]/\Gamma_{\text{total}}$		$(\Gamma_{35} + \Gamma_{36})/\Gamma$		
VALUE	CL%	DOCUMENT ID	TECN	COMMENT
$0.093 \pm 0.017 \pm 0.014$		1 ABDALLAH	03E	DLPH $e^+e^- \rightarrow Z$

<sup>1</sup>The second error is the total of systematic uncertainties including the branching fractions used in the measurement.

$\Gamma(D^- \text{ anything})/\Gamma_{\text{total}}$		$\Gamma_{37}/\Gamma$		
VALUE	CL%	DOCUMENT ID	TECN	COMMENT
$0.227 \pm 0.016 \pm 0.004$		1 BUSKULIC	96Y	ALEP $e^+e^- \rightarrow Z$

<sup>1</sup>BUSKULIC 96Y reports  $0.234 \pm 0.013 \pm 0.010$  from a measurement of  $[\Gamma(\bar{D}^- \rightarrow D^- \text{ anything})/\Gamma_{\text{total}}] \times [B(D^+ \rightarrow K^- 2\pi^+)]$  assuming  $B(D^+ \rightarrow K^- 2\pi^+) = 0.091$ , which we rescale to our best value  $B(D^+ \rightarrow K^- 2\pi^+) = (9.38 \pm 0.16) \times 10^{-2}$ . Our first error is their experiment's error and our second error is the systematic error from using our best value.

$\Gamma(D^*(2010)^+ \text{ anything})/\Gamma_{\text{total}}$		$\Gamma_{38}/\Gamma$		
VALUE	CL%	DOCUMENT ID	TECN	COMMENT
$0.173 \pm 0.016 \pm 0.012$		1 ACKERSTAFF	98E	OPAL $e^+e^- \rightarrow Z$

<sup>1</sup>Uses lepton tags to select  $Z \rightarrow b\bar{b}$  events.

$\Gamma(D_1(2420)^0 \text{ anything})/\Gamma_{\text{total}}$		$\Gamma_{39}/\Gamma$		
VALUE	CL%	DOCUMENT ID	TECN	COMMENT
$0.050 \pm 0.014 \pm 0.006$		1 ACKERSTAFF	97W	OPAL $e^+e^- \rightarrow Z$

<sup>1</sup>ACKERSTAFF 97W assumes  $B(D_1^*(2460)^0 \rightarrow D^{*+}\pi^-) = 0.21 \pm 0.04$  and  $\Gamma_{b\bar{b}}/\Gamma_{\text{hadrons}} = 0.216$  at  $Z$  decay.

$\Gamma(D^*(2010)^{\pm} D_s^{\pm} \text{ anything})/\Gamma_{\text{total}}$		$\Gamma_{40}/\Gamma$		
VALUE	CL%	DOCUMENT ID	TECN	COMMENT
$0.033 \pm 0.010 \pm 0.012$ $-0.009 - 0.009$		1 BARATE	98Q	ALEP $e^+e^- \rightarrow Z$

<sup>1</sup>The systematic error includes the uncertainties due to the charm branching ratios.

$\Gamma(D^0 D^*(2010)^{\pm} \text{ anything})/\Gamma_{\text{total}}$		$\Gamma_{41}/\Gamma$		
VALUE	CL%	DOCUMENT ID	TECN	COMMENT
$0.030 \pm 0.009 \pm 0.007$ $-0.008 - 0.005$		1 BARATE	98Q	ALEP $e^+e^- \rightarrow Z$

<sup>1</sup>The systematic error includes the uncertainties due to the charm branching ratios.

$\Gamma(D^*(2010)^{\pm} D^\mp \text{ anything})/\Gamma_{\text{total}}$		$\Gamma_{42}/\Gamma$		
VALUE	CL%	DOCUMENT ID	TECN	COMMENT
$0.025 \pm 0.010 \pm 0.006$ $-0.009 - 0.005$		1 BARATE	98Q	ALEP $e^+e^- \rightarrow Z$

<sup>1</sup>The systematic error includes the uncertainties due to the charm branching ratios.

$\Gamma(D^*(2010)^{\pm} D^*(2010)^{\mp} \text{ anything})/\Gamma_{\text{total}}$		$\Gamma_{43}/\Gamma$		
VALUE	CL%	DOCUMENT ID	TECN	COMMENT
$0.012 \pm 0.004$ $-0.003 \pm 0.002$		1 BARATE	98Q	ALEP $e^+e^- \rightarrow Z$

<sup>1</sup>The systematic error includes the uncertainties due to the charm branching ratios.

$\Gamma(\bar{D} D \text{ anything})/\Gamma_{\text{total}}$		$\Gamma_{44}/\Gamma$		
VALUE	CL%	DOCUMENT ID	TECN	COMMENT
$0.10 \pm 0.032 \pm 0.107$ $-0.095$		1 ABBIENDI	04I	OPAL $e^+e^- \rightarrow Z$

<sup>1</sup>Measurement performed using an inclusive identification of  $B$  mesons and the  $D$  candidates.

$\Gamma(D_s^*(2460)^0 \text{ anything})/\Gamma_{\text{total}}$		$\Gamma_{45}/\Gamma$		
VALUE	CL%	DOCUMENT ID	TECN	COMMENT
$0.047 \pm 0.024 \pm 0.013$		1 ACKERSTAFF	97W	OPAL $e^+e^- \rightarrow Z$

<sup>1</sup>ACKERSTAFF 97W assumes  $B(D_s^*(2460)^0 \rightarrow D^{*+}\pi^-) = 0.21 \pm 0.04$  and  $\Gamma_{b\bar{b}}/\Gamma_{\text{hadrons}} = 0.216$  at  $Z$  decay.

$\Gamma(D_s^- \text{ anything})/\Gamma_{\text{total}}$		$\Gamma_{46}/\Gamma$		
VALUE	CL%	DOCUMENT ID	TECN	COMMENT
$0.147 \pm 0.017 \pm 0.013$		1 BUSKULIC	96Y	ALEP $e^+e^- \rightarrow Z$

<sup>1</sup>BUSKULIC 96Y reports  $0.183 \pm 0.019 \pm 0.009$  from a measurement of  $[\Gamma(\bar{D}^- \rightarrow D_s^- \text{ anything})/\Gamma_{\text{total}}] \times [B(D_s^+ \rightarrow \phi\pi^+)]$  assuming  $B(D_s^+ \rightarrow \phi\pi^+) = 0.036$ , which we rescale to our best value  $B(D_s^+ \rightarrow \phi\pi^+) = (4.5 \pm 0.4) \times 10^{-2}$ . Our first error is their experiment's error and our second error is the systematic error from using our best value.

$\Gamma(D_s^+ \text{ anything})/\Gamma_{\text{total}}$		$\Gamma_{47}/\Gamma$		
VALUE	CL%	DOCUMENT ID	TECN	COMMENT
$0.101 \pm 0.010 \pm 0.029$		1 ABDALLAH	03E	DLPH $e^+e^- \rightarrow Z$

<sup>1</sup>The second error is the total of systematic uncertainties including the branching fractions used in the measurement.

$\Gamma(b \rightarrow \Lambda_c^+ \text{ anything})/\Gamma_{\text{total}}$		$\Gamma_{48}/\Gamma$		
VALUE	CL%	DOCUMENT ID	TECN	COMMENT
$0.077 \pm 0.011 \pm 0.004$		1 BUSKULIC	96Y	ALEP $e^+e^- \rightarrow Z$

<sup>1</sup>BUSKULIC 96Y reports  $0.110 \pm 0.014 \pm 0.006$  from a measurement of  $[\Gamma(b \rightarrow \Lambda_c^+ \text{ anything})/\Gamma_{\text{total}}] \times [B(\Lambda_c^+ \rightarrow pK^- \pi^+)]$  assuming  $B(\Lambda_c^+ \rightarrow pK^- \pi^+) = 0.044$ , which we rescale to our best value  $B(\Lambda_c^+ \rightarrow pK^- \pi^+) = (6.28 \pm 0.32) \times 10^{-2}$ . Our first error is their experiment's error and our second error is the systematic error from using our best value.

$\Gamma(\tau/c \text{ anything})/\Gamma_{\text{total}}$		$\Gamma_{49}/\Gamma$		
VALUE	CL%	DOCUMENT ID	TECN	COMMENT
<b>1.162 ± 0.032 OUR AVERAGE</b>				
$1.12 \pm 0.11$ $-0.10$		1 ABBIENDI	04I	OPAL $e^+e^- \rightarrow Z$
$1.166 \pm 0.031 \pm 0.080$		2 ABREU	00	DLPH $e^+e^- \rightarrow Z$
$1.147 \pm 0.041$		3 ABREU	98D	DLPH $e^+e^- \rightarrow Z$
$1.230 \pm 0.036 \pm 0.065$		4 BUSKULIC	96Y	ALEP $e^+e^- \rightarrow Z$

<sup>1</sup>Measurement performed using an inclusive identification of  $B$  mesons and the  $D$  candidates.

<sup>2</sup>Evaluated via summation of exclusive and inclusive channels.

<sup>3</sup>ABREU 98D results are extracted from a fit to the  $b$ -tagging probability distribution based on the impact parameter.

<sup>4</sup>BUSKULIC 96Y assumes PDG 96 production fractions for  $B^0, B^+, B_s, b$  baryons, and PDG 96 branching ratios for charm decays. This is sum of their inclusive  $\bar{D}^0, D^-, \bar{D}_s, \Lambda_c$  branching ratios, corrected to include inclusive  $\Xi_c$  and charmonium.

$\Gamma(J/\psi(1S) \text{ anything})/\Gamma_{\text{total}}$		$\Gamma_{50}/\Gamma$			
VALUE (units $10^{-2}$ )	CL%	EVTS	DOCUMENT ID	TECN	COMMENT
<b>1.16 ± 0.10 OUR AVERAGE</b>					
$1.12 \pm 0.12 \pm 0.10$			1 ABREU	94P	DLPH $e^+e^- \rightarrow Z$
$1.16 \pm 0.16 \pm 0.14$		121	2 ADRIANI	93J	L3 $e^+e^- \rightarrow Z$
$1.21 \pm 0.13 \pm 0.08$			BUSKULIC	92G	ALEP $e^+e^- \rightarrow Z$

<sup>1</sup>ABREU 94P is an inclusive measurement from  $b$  decays at the  $Z$ . Uses  $J/\psi(1S) \rightarrow e^+e^-$  and  $\mu^+\mu^-$  channels. Assumes  $\Gamma(Z \rightarrow b\bar{b})/\Gamma_{\text{hadron}} = 0.22$ .

<sup>2</sup>ADRIANI 93J is an inclusive measurement from  $b$  decays at the  $Z$ . Uses  $J/\psi(1S) \rightarrow \mu^+\mu^-$  and  $J/\psi(1S) \rightarrow e^+e^-$  channels.

<sup>3</sup>ADRIANI 92 measurement is an inclusive result for  $B(Z \rightarrow J/\psi(1S)X) = (4.1 \pm 0.7 \pm 0.3) \times 10^{-3}$  which is used to extract the  $b$ -hadron contribution to  $J/\psi(1S)$  production.

<sup>4</sup>We do not use the following data for averages, fits, limits, etc.   
<sup>1</sup>ABREU 94P is an inclusive measurement from  $b$  decays at the  $Z$ . Uses  $J/\psi(1S) \rightarrow e^+e^-$  and  $\mu^+\mu^-$  channels. Assumes  $\Gamma(Z \rightarrow b\bar{b})/\Gamma_{\text{hadron}} = 0.22$ .  
<sup>2</sup>ADRIANI 93J is an inclusive measurement from  $b$  decays at the  $Z$ . Uses  $J/\psi(1S) \rightarrow \mu^+\mu^-$  and  $J/\psi(1S) \rightarrow e^+e^-$  channels.  
<sup>3</sup>ADRIANI 92 measurement is an inclusive result for  $B(Z \rightarrow J/\psi(1S)X) = (4.1 \pm 0.7 \pm 0.3) \times 10^{-3}$  which is used to extract the  $b$ -hadron contribution to  $J/\psi(1S)$  production.

$\Gamma(\psi(2S) \text{ anything})/\Gamma_{\text{total}}$		$\Gamma_{51}/\Gamma$		
VALUE	CL%	DOCUMENT ID	TECN	COMMENT
$0.0048 \pm 0.0022 \pm 0.0010$		1 ABREU	94P	DLPH $e^+e^- \rightarrow Z$

<sup>1</sup>ABREU 94P is an inclusive measurement from  $b$  decays at the  $Z$ . Uses  $\psi(2S) \rightarrow J/\psi(1S)\pi^+\pi^-, J/\psi(1S) \rightarrow \mu^+\mu^-$  channels. Assumes  $\Gamma(Z \rightarrow b\bar{b})/\Gamma_{\text{hadron}} = 0.22$ .

$\Gamma(\psi(2S) \text{ anything})/\Gamma(J/\psi(1S) \text{ anything})$		$\Gamma_{51}/\Gamma_{50}$		
VALUE	CL%	DOCUMENT ID	TECN	COMMENT
<b>0.245 ± 0.013 OUR AVERAGE</b>				
$0.240 \pm 0.015 \pm 0.005$		1,2 AAJJ	12BD LHCB	$pp$ at 7 TeV
$0.257 \pm 0.015 \pm 0.019$		3,4	CHATRCHYAN 12AK CMS	$pp$ at 7 TeV

<sup>1</sup>AAJJ 12BD reports  $0.235 \pm 0.005 \pm 0.015$  from a measurement of  $[\Gamma(\bar{D}^- \rightarrow \psi(2S) \text{ anything})/\Gamma(\bar{D}^- \rightarrow J/\psi(1S) \text{ anything})] \times [B(J/\psi(1S) \rightarrow \mu^+\mu^-)] / [B(\psi(2S) \rightarrow e^+e^-)]$  assuming  $B(J/\psi(1S) \rightarrow \mu^+\mu^-) = (5.93 \pm 0.06) \times 10^{-2}$ ,  $B(\psi(2S) \rightarrow e^+e^-) = (7.72 \pm 0.17) \times 10^{-3}$ , which we rescale to our best values  $B(J/\psi(1S) \rightarrow \mu^+\mu^-) = (5.961 \pm 0.033) \times 10^{-2}$ ,  $B(\psi(2S) \rightarrow e^+e^-) = (7.93 \pm 0.17) \times 10^{-3}$ . Our first error is their experiment's error and our second error is the systematic error from using our best values.

<sup>2</sup>Assumes lepton universality imposing  $B(\psi(2S) \rightarrow \mu^+\mu^-) = B(\psi(2S) \rightarrow e^+e^-)$ .  
<sup>3</sup>CHATRCHYAN 12AK really reports  $\Gamma_{51}/\Gamma = (3.08 \pm 0.12 \pm 0.13 \pm 0.42) \times 10^{-3}$  assuming PDG 10 value of  $\Gamma_{50}/\Gamma = (1.16 \pm 0.10) \times 10^{-2}$  which we present as a ratio of  $\Gamma_{51}/\Gamma_{50} = (26.5 \pm 1.0 \pm 1.1 \pm 2.8) \times 10^{-2}$ .

<sup>4</sup>CHATRCHYAN 12AK reports  $(26.5 \pm 1.0 \pm 1.1 \pm 2.8) \times 10^{-2}$  from a measurement of  $[\Gamma(\bar{D}^- \rightarrow \psi(2S) \text{ anything})/\Gamma(\bar{D}^- \rightarrow J/\psi(1S) \text{ anything})] \times [B(\psi(2S) \rightarrow \mu^+\mu^-)] / [B(J/\psi(1S) \rightarrow \mu^+\mu^-)]$  assuming  $B(\psi(2S) \rightarrow \mu^+\mu^-) = (7.7 \pm 0.8) \times 10^{-3}$ ,  $B(J/\psi(1S) \rightarrow \mu^+\mu^-) = (5.93 \pm 0.06) \times 10^{-2}$ , which we rescale to our best values  $B(\psi(2S) \rightarrow \mu^+\mu^-) = (8.0 \pm 0.6) \times 10^{-3}$ ,  $B(J/\psi(1S) \rightarrow \mu^+\mu^-) = (5.961 \pm 0.033) \times 10^{-2}$ . Our first error is their experiment's error and our second error is the systematic error from using our best values.

$\Gamma(\chi_{c0}(1P) \text{ anything})/\Gamma(\eta_c(1S) \text{ anything})$		$\Gamma_{52}/\Gamma_{56}$		
VALUE	CL%	DOCUMENT ID	TECN	COMMENT
<b>0.33 ± 0.06 ± 0.05</b>		1 AAJJ	17BB LHCB	$pp$ at 7, 8 TeV

<sup>1</sup>AAJJ 17BB reports  $[\Gamma(\bar{D}^- \rightarrow \chi_{c0}(1P) \text{ anything})/\Gamma(\bar{D}^- \rightarrow \eta_c(1S) \text{ anything})] / [B(\eta_c(1S) \rightarrow \phi\phi)] \times [B(\chi_{c0}(1P) \rightarrow \phi\phi)] = 0.147 \pm 0.023 \pm 0.011$  which we multiply or divide by our best values  $B(\eta_c(1S) \rightarrow \phi\phi) = (1.77 \pm 0.19) \times 10^{-3}$ ,  $B(\chi_{c0}(1P) \rightarrow \phi\phi) = (8.0 \pm 0.7) \times 10^{-4}$ . Our first error is their experiment's error and our second error is the systematic error from using our best values.

$\Gamma(\chi_{c1}(1P)\text{ anything})/\Gamma_{\text{total}}$					$\Gamma_{53}/\Gamma$
VALUE	EVTS	DOCUMENT ID	TECN	COMMENT	

**0.014 ± 0.004 OUR AVERAGE**

0.0112 ± 0.0057 ± 0.0003  
 0.019 ± 0.007 ± 0.001 19

<sup>1</sup> ABREU 94P reports 0.014 ± 0.006 ± 0.004 from a measurement of  $[\Gamma(\bar{b} \rightarrow \chi_{c1}(1P)\text{ anything})/\Gamma_{\text{total}}] \times [B(\chi_{c1}(1P) \rightarrow \gamma J/\psi(1S))] / [B(\chi_{c1}(1P) \rightarrow \gamma J/\psi(1S))] = 0.273 \pm 0.016$ , which we rescale to our best value  $B(\chi_{c1}(1P) \rightarrow \gamma J/\psi(1S)) = (34.3 \pm 1.0) \times 10^{-2}$ . Our first error is their experiment's error and our second error is the systematic error from using our best value. Assumes no  $\chi_{c2}(1P)$  and  $\Gamma(Z \rightarrow b\bar{b})/\Gamma_{\text{hadron}} = 0.22$ .

<sup>2</sup> ADRIANI 93J reports 0.024 ± 0.009 ± 0.002 from a measurement of  $[\Gamma(\bar{b} \rightarrow \chi_{c1}(1P)\text{ anything})/\Gamma_{\text{total}}] \times [B(\chi_{c1}(1P) \rightarrow \gamma J/\psi(1S))] / [B(\chi_{c1}(1P) \rightarrow \gamma J/\psi(1S))] = 0.273 \pm 0.016$ , which we rescale to our best value  $B(\chi_{c1}(1P) \rightarrow \gamma J/\psi(1S)) = (34.3 \pm 1.0) \times 10^{-2}$ . Our first error is their experiment's error and our second error is the systematic error from using our best value.

$\Gamma(\chi_{c1}(1P)\text{ anything})/\Gamma(J/\psi(1S)\text{ anything})$					$\Gamma_{53}/\Gamma_{50}$
VALUE	EVTS	DOCUMENT ID	TECN	COMMENT	

**• • • We do not use the following data for averages, fits, limits, etc. • • •**

1.92 ± 0.82 121 <sup>1</sup> ADRIANI 93J L3  $e^+e^- \rightarrow Z$

<sup>1</sup> ADRIANI 93J is a ratio of inclusive measurements from  $b$  decays at the Z using only the  $J/\psi(1S) \rightarrow \mu^+\mu^-$  channel since some systematics cancel.

$\Gamma(\chi_{c1}(1P)\text{ anything})/\Gamma(\chi_{c0}(1P)\text{ anything})$					$\Gamma_{53}/\Gamma_{52}$
VALUE	DOCUMENT ID	TECN	COMMENT		

**0.96 ± 0.21 ± 0.15**

<sup>1</sup> AAJ 17Bb reports  $[\Gamma(\bar{b} \rightarrow \chi_{c1}(1P)\text{ anything})/\Gamma(\bar{b} \rightarrow \chi_{c0}(1P)\text{ anything})] / [B(\chi_{c0}(1P) \rightarrow \phi\phi)] \times [B(\chi_{c1}(1P) \rightarrow \phi\phi)] = 0.50 \pm 0.11 \pm 0.01$  which we multiply or divide by our best values  $B(\chi_{c0}(1P) \rightarrow \phi\phi) = (8.0 \pm 0.7) \times 10^{-4}$ ,  $B(\chi_{c1}(1P) \rightarrow \phi\phi) = (4.2 \pm 0.5) \times 10^{-4}$ . Our first error is their experiment's error and our second error is the systematic error from using our best values.

$\Gamma(\chi_{c1}(1P)\text{ anything})/\Gamma(\eta_c(1S)\text{ anything})$					$\Gamma_{53}/\Gamma_{56}$
VALUE	DOCUMENT ID	TECN	COMMENT		

**0.31 ± 0.07 ± 0.05**

<sup>1</sup> AAJ 17Bb reports  $[\Gamma(\bar{b} \rightarrow \chi_{c1}(1P)\text{ anything})/\Gamma(\bar{b} \rightarrow \eta_c(1S)\text{ anything})] / [B(\eta_c(1S) \rightarrow \phi\phi)] \times [B(\chi_{c1}(1P) \rightarrow \phi\phi)] = 0.073 \pm 0.016 \pm 0.006$  which we multiply or divide by our best values  $B(\eta_c(1S) \rightarrow \phi\phi) = (1.77 \pm 0.19) \times 10^{-3}$ ,  $B(\chi_{c1}(1P) \rightarrow \phi\phi) = (4.2 \pm 0.5) \times 10^{-4}$ . Our first error is their experiment's error and our second error is the systematic error from using our best values.

$\Gamma(\chi_{c2}(1P)\text{ anything})/\Gamma(\chi_{c0}(1P)\text{ anything})$					$\Gamma_{54}/\Gamma_{52}$
VALUE	DOCUMENT ID	TECN	COMMENT		

**0.42 ± 0.08 ± 0.05**

<sup>1</sup> AAJ 17Bb reports  $[\Gamma(\bar{b} \rightarrow \chi_{c2}(1P)\text{ anything})/\Gamma(\bar{b} \rightarrow \chi_{c0}(1P)\text{ anything})] / [B(\chi_{c0}(1P) \rightarrow \phi\phi)] \times [B(\chi_{c2}(1P) \rightarrow \phi\phi)] = 0.56 \pm 0.10 \pm 0.01$  which we multiply or divide by our best values  $B(\chi_{c0}(1P) \rightarrow \phi\phi) = (8.0 \pm 0.7) \times 10^{-4}$ ,  $B(\chi_{c2}(1P) \rightarrow \phi\phi) = (1.06 \pm 0.09) \times 10^{-3}$ . Our first error is their experiment's error and our second error is the systematic error from using our best values.

$\Gamma(\chi_{c2}(1P)\text{ anything})/\Gamma(\eta_c(1S)\text{ anything})$					$\Gamma_{54}/\Gamma_{56}$
VALUE	DOCUMENT ID	TECN	COMMENT		

**0.135 ± 0.023 ± 0.018**

<sup>1</sup> AAJ 17Bb reports  $[\Gamma(\bar{b} \rightarrow \chi_{c2}(1P)\text{ anything})/\Gamma(\bar{b} \rightarrow \eta_c(1S)\text{ anything})] / [B(\eta_c(1S) \rightarrow \phi\phi)] \times [B(\chi_{c2}(1P) \rightarrow \phi\phi)] = 0.081 \pm 0.013 \pm 0.005$  which we multiply or divide by our best values  $B(\eta_c(1S) \rightarrow \phi\phi) = (1.77 \pm 0.19) \times 10^{-3}$ ,  $B(\chi_{c2}(1P) \rightarrow \phi\phi) = (1.06 \pm 0.09) \times 10^{-3}$ . Our first error is their experiment's error and our second error is the systematic error from using our best values.

$\Gamma(\chi_{c2}(2P)\text{ anything, } \chi_{c2} \rightarrow \phi\phi)/\Gamma_{\text{total}}$					$\Gamma_{55}/\Gamma$
VALUE	CL%	DOCUMENT ID	TECN	COMMENT	

**< 2.8 × 10<sup>-7</sup>** 95 AAJ 17Bb LHCb  $pp$  at 7, 8 TeV

$\Gamma(\eta_c(2S)\text{ anything, } \eta_c \rightarrow \phi\phi)/\Gamma(\eta_c(1S)\text{ anything})$					$\Gamma_{57}/\Gamma_{56}$
VALUE (units 10 <sup>-5</sup> )	DOCUMENT ID	TECN	COMMENT		

**7.1 ± 2.1 ± 0.8**

<sup>1</sup> AAJ 17Bb reports  $[\Gamma(\bar{b} \rightarrow \eta_c(2S)\text{ anything, } \eta_c \rightarrow \phi\phi)/\Gamma(\bar{b} \rightarrow \eta_c(1S)\text{ anything})] / [B(\eta_c(1S) \rightarrow \phi\phi)] = 0.040 \pm 0.011 \pm 0.004$  which we multiply by our best value  $B(\eta_c(1S) \rightarrow \phi\phi) = (1.77 \pm 0.19) \times 10^{-3}$ . Our first error is their experiment's error and our second error is the systematic error from using our best value.

$\Gamma(\chi_{c1}(3872)\text{ anything, } \chi_{c1} \rightarrow \phi\phi)/\Gamma_{\text{total}}$					$\Gamma_{58}/\Gamma$
VALUE	CL%	DOCUMENT ID	TECN	COMMENT	

**< 4.5 × 10<sup>-7</sup>** 95 AAJ 17Bb LHCb  $pp$  at 7, 8 TeV

$\Gamma(X(3915)\text{ anything, } X \rightarrow \phi\phi)/\Gamma_{\text{total}}$					$\Gamma_{59}/\Gamma$
VALUE	CL%	DOCUMENT ID	TECN	COMMENT	

**< 3.1 × 10<sup>-7</sup>** 95 AAJ 17Bb LHCb  $pp$  at 7, 8 TeV

$\Gamma(\bar{\Sigma}\gamma)/\Gamma_{\text{total}}$					$\Gamma_{60}/\Gamma$
VALUE (units 10 <sup>-4</sup> )	CL%	DOCUMENT ID	TECN	COMMENT	

**3.11 ± 0.80 ± 0.72**

<sup>1</sup> BARATE 98i ALEP  $e^+e^- \rightarrow Z$

**• • • We do not use the following data for averages, fits, limits, etc. • • •**

< 5.4 90 <sup>2</sup> ADAM 96d DLPH  $e^+e^- \rightarrow Z$   
 < 2.1 90 <sup>3</sup> ADRIANI 93L L3  $e^+e^- \rightarrow Z$

<sup>1</sup> BARATE 98i uses lifetime tagged  $Z \rightarrow b\bar{b}$  sample.  
<sup>2</sup> ADAM 96d assumes  $f_{B^0} = f_{B^-} = 0.39$  and  $f_{B_s} = 0.12$ .  
<sup>3</sup> ADRIANI 93L result is for  $\bar{b} \rightarrow \bar{\Sigma}\gamma$  is performed inclusively.

$\Gamma(\bar{\Sigma}\nu)/\Gamma_{\text{total}}$					$\Gamma_{61}/\Gamma$
VALUE	CL%	DOCUMENT ID	TECN	COMMENT	

**< 6.4 × 10<sup>-4</sup>** 90 <sup>1</sup> BARATE 01E ALEP  $e^+e^- \rightarrow Z$

<sup>1</sup> The energy-flow and  $b$ -tagging algorithms were used.

$\Gamma(K^\pm\text{ anything})/\Gamma_{\text{total}}$					$\Gamma_{62}/\Gamma$
VALUE	DOCUMENT ID	TECN	COMMENT		

**0.74 ± 0.06 OUR AVERAGE**

0.72 ± 0.02 ± 0.06 BARATE 98v ALEP  $e^+e^- \rightarrow Z$   
 0.88 ± 0.05 ± 0.18 ABREU 95c DLPH  $e^+e^- \rightarrow Z$

$\Gamma(K_S^0\text{ anything})/\Gamma_{\text{total}}$					$\Gamma_{63}/\Gamma$
VALUE	DOCUMENT ID	TECN	COMMENT		

**0.290 ± 0.011 ± 0.027** ABREU 95c DLPH  $e^+e^- \rightarrow Z$

$\Gamma(\pi^\pm\text{ anything})/\Gamma_{\text{total}}$					$\Gamma_{64}/\Gamma$
VALUE	DOCUMENT ID	TECN	COMMENT		

**3.97 ± 0.02 ± 0.21** BARATE 98v ALEP  $e^+e^- \rightarrow Z$

$\Gamma(\pi^0\text{ anything})/\Gamma_{\text{total}}$					$\Gamma_{65}/\Gamma$
VALUE	DOCUMENT ID	TECN	COMMENT		

**2.78 ± 0.15 ± 0.60** <sup>1</sup> ADAM 96 DLPH  $e^+e^- \rightarrow Z$

<sup>1</sup> ADAM 96 measurement obtained from a fit to the rapidity distribution of  $\pi^0$ 's in  $Z \rightarrow b\bar{b}$  events.

$\Gamma(\phi\text{ anything})/\Gamma_{\text{total}}$					$\Gamma_{66}/\Gamma$
VALUE	DOCUMENT ID	TECN	COMMENT		

**0.0282 ± 0.0013 ± 0.0019** ABBIENDI 00z OPAL  $e^+e^- \rightarrow Z$

$\Gamma(p/\bar{p}\text{ anything})/\Gamma_{\text{total}}$					$\Gamma_{67}/\Gamma$
VALUE	DOCUMENT ID	TECN	COMMENT		

**0.131 ± 0.011 OUR AVERAGE**

0.131 ± 0.004 ± 0.011 BARATE 98v ALEP  $e^+e^- \rightarrow Z$   
 0.141 ± 0.018 ± 0.056 ABREU 95c DLPH  $e^+e^- \rightarrow Z$

$\Gamma(\Lambda/\bar{\Lambda}\text{ anything})/\Gamma_{\text{total}}$					$\Gamma_{68}/\Gamma$
VALUE	DOCUMENT ID	TECN	COMMENT		

**0.059 ± 0.006 OUR AVERAGE**

0.0587 ± 0.0046 ± 0.0048 ACKERSTAFF 97N OPAL  $e^+e^- \rightarrow Z$   
 0.059 ± 0.007 ± 0.009 ABREU 95c DLPH  $e^+e^- \rightarrow Z$

$\Gamma(b\text{-baryon anything})/\Gamma_{\text{total}}$					$\Gamma_{69}/\Gamma$
VALUE	DOCUMENT ID	TECN	COMMENT		

**0.102 ± 0.007 ± 0.027** <sup>1</sup> BARATE 98v ALEP  $e^+e^- \rightarrow Z$

<sup>1</sup> BARATE 98v assumes  $B(B_S \rightarrow pX) = 8 \pm 4\%$  and  $B(b\text{-baryon} \rightarrow pX) = 58 \pm 6\%$ .

$\Gamma(\Xi_b^\pm\text{ anything})/\Gamma(\bar{\Lambda}_b^0\text{ anything})$					$\Gamma_{71}/\Gamma_{70}$
VALUE (units 10 <sup>-2</sup> )	DOCUMENT ID	TECN	COMMENT		

**7.3 ± 1.7 OUR AVERAGE**

6.7 ± 0.5 ± 2.1 <sup>1</sup> AAJ 19Ab LHCb  $pp$  at 7 and 8 TeV  
 8.2 ± 0.7 ± 2.6 <sup>1</sup> AAJ 19Ab LHCb  $pp$  at 13 TeV

<sup>1</sup> Measured from  $R = [B(\bar{b} \rightarrow \Xi_b^\pm) \times B(\Xi_b \rightarrow J/\psi \Xi^\pm)] / [B(\bar{b} \rightarrow \bar{\Lambda}_b^0) \times B(\bar{\Lambda}_b^0 \rightarrow J/\psi \bar{\Lambda}^0)]$  and assumes  $\Gamma_{\Xi_b^\pm \rightarrow J/\psi \Xi^\pm} / \Gamma_{\bar{\Lambda}_b^0 \rightarrow J/\psi \bar{\Lambda}^0} = 3/2$  related through SU(3) flavor symmetry.

$\Gamma(\text{charged anything})/\Gamma_{\text{total}}$					$\Gamma_{72}/\Gamma$
VALUE	DOCUMENT ID	TECN	COMMENT		

**4.97 ± 0.03 ± 0.06** <sup>1</sup> ABREU 98h DLPH  $e^+e^- \rightarrow Z$

**• • • We do not use the following data for averages, fits, limits, etc. • • •**

5.84 ± 0.04 ± 0.38 ABREU 95c DLPH Repl. by ABREU 98h

<sup>1</sup> ABREU 98h measurement excludes the contribution from  $K^0$  and  $\Lambda$  decay.

$\Gamma(\text{hadron}^+\text{ hadron}^-)/\Gamma_{\text{total}}$					$\Gamma_{73}/\Gamma$
VALUE (units 10 <sup>-5</sup> )	DOCUMENT ID	TECN	COMMENT		

**1.7 ± 1.0 ± 0.7 ± 0.2** <sup>1,2</sup> BUSKULIC 96v ALEP  $e^+e^- \rightarrow Z$

<sup>1</sup> BUSKULIC 96v assumes PDG 96 production fractions for  $B^0, B^+, B_s, b$  baryons.  
<sup>2</sup> Average branching fraction of weakly decaying  $B$  hadrons into two long-lived charged hadrons, weighted by their production cross section and lifetimes.

# Meson Particle Listings

## $B^\pm/B^0/B_s^0/b$ -baryon ADMIXTURE

### $\Gamma(\text{charmless})/\Gamma_{\text{total}}$

VALUE	DOCUMENT ID	TECN	COMMENT	$\Gamma_{74}/\Gamma$
<b>0.007 ± 0.021</b>	1 ABREU	98D	DLPH $e^+e^- \rightarrow Z$	

<sup>1</sup> ABREU 98D results are extracted from a fit to the  $b$ -tagging probability distribution based on the impact parameter. The expected hidden charm contribution of  $0.026 \pm 0.004$  has been subtracted.

### $\Gamma(\mu^+\mu^- \text{ anything})/\Gamma_{\text{total}}$

VALUE	CL%	DOCUMENT ID	TECN	COMMENT	$\Gamma_{76}/\Gamma$
<b>&lt; 3.2 × 10<sup>-4</sup></b>	90	ABBOTT	98B	D0 $p\bar{p}$ 1.8 TeV	
• • • We do not use the following data for averages, fits, limits, etc. • • •					
< 5.0 × 10 <sup>-5</sup>	90	1 ALBAJAR	91c	UA1 $E_{\text{cm}}^{\mu\mu} = 630$ GeV	
< 0.02	95	ALTHOFF	84G	TASS $E_{\text{cm}}^{\mu\mu} = 34.5$ GeV	
< 0.007	95	ADEVA	83	MRKJ $E_{\text{cm}}^{\mu\mu} = 30\text{--}38$ GeV	
< 0.007	95	BARTEL	83B	JADE $E_{\text{cm}}^{\mu\mu} = 33\text{--}37$ GeV	

<sup>1</sup> Both ABBOTT 98B and GLENN 98 claim that the efficiency quoted in ALBAJAR 91c was overestimated by a large factor.

### $[\Gamma(e^+e^- \text{ anything}) + \Gamma(\mu^+\mu^- \text{ anything})]/\Gamma_{\text{total}}$

VALUE	CL%	DOCUMENT ID	TECN	COMMENT	$(\Gamma_{75} + \Gamma_{76})/\Gamma$
<b>&lt; 0.008</b>	90	MATTEUZZI	83	MRK2 $E_{\text{cm}}^{\mu\mu} = 29$ GeV	

### $\Gamma(\nu \bar{\nu} \text{ anything})/\Gamma_{\text{total}}$

VALUE	DOCUMENT ID	TECN	COMMENT	$\Gamma_{77}/\Gamma$
<b>&lt; 3.9 × 10<sup>-4</sup></b>	1 GROSSMAN	96	RVUE $e^+e^- \rightarrow Z$	

<sup>1</sup> GROSSMAN 96 limit is derived from the ALEPH BUSKULIC 95 limit  $B(B^+ \rightarrow \tau^+ \nu_\tau) < 1.8 \times 10^{-3}$  at CL=90% using conservative simplifying assumptions.

### $\chi_b$ AT HIGH ENERGY

For a discussion of  $B\text{--}\bar{B}$  mixing, see the note on “ $B^0\text{--}\bar{B}^0$  Mixing” in the  $B^0$  Particle Listings.

$\chi_b$  is the average  $B\text{--}\bar{B}$  mixing parameter at high-energy  $\chi_b = f'_d \chi_d + f'_s \chi_s$  where  $f'_d$  and  $f'_s$  are the fractions of  $B^0$  and  $B_s^0$  hadrons in an unbiased sample of semileptonic  $b$ -hadron decays.

“OUR EVALUATION” is an average using rescaled values of the data listed below. The average and rescaling were performed by the Heavy Flavor Averaging Group (HFLAV) and are described at <https://hflav.web.cern.ch/>. The averaging/rescaling procedure takes into account correlations between the measurements.

VALUE	EVTS	DOCUMENT ID	TECN	COMMENT
<b>0.1284 ± 0.0069 OUR EVALUATION</b>				
<b>0.129 ± 0.004 OUR AVERAGE</b>				
0.132 ± 0.001 ± 0.024		1 ABAZOV	06s	D0 $p\bar{p}$ at 1.96 TeV
0.152 ± 0.007 ± 0.011		2 ACOSTA	04A	CDF $p\bar{p}$ at 1.8 TeV
0.1312 ± 0.0049 ± 0.0042		3 ABBIENDI	03P	OPAL $e^+e^- \rightarrow Z$
0.127 ± 0.013 ± 0.006		4 ABREU	01L	DLPH $e^+e^- \rightarrow Z$
0.1192 ± 0.0068 ± 0.0051		5 ACCIARRI	99D	L3 $e^+e^- \rightarrow Z$
0.121 ± 0.016 ± 0.006		6 ABREU	94J	DLPH $e^+e^- \rightarrow Z$
0.114 ± 0.014 ± 0.008		7 BUSKULIC	94G	ALEP $e^+e^- \rightarrow Z$
0.129 ± 0.022		8 BUSKULIC	92B	ALEP $e^+e^- \rightarrow Z$
0.176 ± 0.031 ± 0.032	1112	9 ABE	91G	CDF $p\bar{p}$ 1.8 TeV
0.148 ± 0.029 ± 0.017		10 ALBAJAR	91D	UA1 $p\bar{p}$ 630 GeV
• • • We do not use the following data for averages, fits, limits, etc. • • •				
0.131 ± 0.020 ± 0.016		11 ABE	97I	CDF Repl. by ACOSTA 04A
0.1107 ± 0.0062 ± 0.0055		12 ALEXANDER	96	OPAL Rep. by ABBIENDI 03P
0.136 ± 0.037 ± 0.040		13 UENO	96	AMY $e^+e^-$ at 57.9 GeV
0.144 ± 0.014 ± 0.017		14 ABREU	94F	DLPH Sup. by ABREU 94J
0.131 ± 0.014		15 ABREU	94J	DLPH $e^+e^- \rightarrow Z$
0.123 ± 0.012 ± 0.008		ACCIARRI	94D	L3 Repl. by ACCIARRI 99D
0.157 ± 0.020 ± 0.032		16 ALBAJAR	94	UA1 $\sqrt{s} = 630$ GeV
0.121 ± 0.044 ± 0.017	1665	17 ABREU	93C	DLPH Sup. by ABREU 94J
0.143 ± 0.022 ± 0.007		18 AKERS	93B	OPAL Sup. by ALEXANDER 96
0.145 ± 0.041 ± 0.018		19 ACTON	92C	OPAL $e^+e^- \rightarrow Z$
0.121 ± 0.017 ± 0.006		20 ADEVA	92C	L3 Sup. by ACCIARRI 94D
0.132 ± 0.22 ± 0.015	823	21 DECAMP	91	ALEP $e^+e^- \rightarrow Z$
0.178 ± 0.049 ± 0.020		22 ADEVA	90P	L3 $e^+e^- \rightarrow Z$
0.17 ± 0.15 ± 0.08		23,24 WEIR	90	MRK2 $e^+e^-$ 29 GeV
0.21 ± 0.29 ± 0.15		23 BAND	88	MAC $E_{\text{cm}}^{\mu\mu} = 29$ GeV
> 0.02 at 90% CL		23 BAND	88	MAC $E_{\text{cm}}^{\mu\mu} = 29$ GeV
0.121 ± 0.047		23,25 ALBAJAR	87C	UA1 Repl. by ALBAJAR 91D
< 0.12 at 90% CL		23,26 SCHAAD	85	MRK2 $E_{\text{cm}}^{\mu\mu} = 29$ GeV

<sup>1</sup> Uses the dimuon charge asymmetry. Averaged over the mix of  $b$ -flavored hadrons.

- <sup>2</sup> Measurement performed using events containing a dimuon or an  $e/\mu$  pair.
- <sup>3</sup> The average  $B$  mixing parameter is determined simultaneously with  $b$  and  $c$  forward-backward asymmetries in the fit.
- <sup>4</sup> The experimental systematic and model uncertainties are combined in quadrature.
- <sup>5</sup> ACCIARRI 99D uses maximum-likelihood fits to extract  $\chi_b$  as well as the  $A_{FB}^b$  in  $Z \rightarrow b\bar{b}$  events containing prompt leptons.
- <sup>6</sup> This ABREU 94J result is from 5182  $\ell\ell$  and 279  $\ell\ell$  events. The systematic error includes 0.004 for model dependence.
- <sup>7</sup> BUSKULIC 94G data analyzed using  $ee$ ,  $e\mu$ , and  $\mu\mu$  events.
- <sup>8</sup> BUSKULIC 92B uses a jet charge technique combined with electrons and muons.
- <sup>9</sup> ABE 91G measurement of  $\chi$  is done with  $e\mu$  and  $ee$  events.
- <sup>10</sup> ALBAJAR 91D measurement of  $\chi$  is done with dimuons.
- <sup>11</sup> Uses di-muon events.
- <sup>12</sup> ALEXANDER 96 uses a maximum likelihood fit to simultaneously extract  $\chi$  as well as the forward-backward asymmetries in  $e^+e^- \rightarrow Z \rightarrow b\bar{b}$  and  $c\bar{c}$ .
- <sup>13</sup> UENO 96 extracted  $\chi$  from the energy dependence of the forward-backward asymmetry.
- <sup>14</sup> ABREU 94F uses the average electric charge sum of the jets recoiling against a  $b$ -quark jet tagged by a high  $p_T$  muon. The result is for  $\bar{\chi} = f_d \chi_d + 0.9 f_s \chi_s$ .
- <sup>15</sup> This ABREU 94J result combines  $\ell\ell$ ,  $\ell\ell$ , and jet-charge  $\ell$  (ABREU 94F) analyses. It is for  $\bar{\chi} = f_d \chi_d + 0.96 f_s \chi_s$ .
- <sup>16</sup> ALBAJAR 94 uses dimuon events. Not independent of ALBAJAR 91D.
- <sup>17</sup> ABREU 93C data analyzed using  $ee$ ,  $e\mu$ , and  $\mu\mu$  events.
- <sup>18</sup> AKERS 93B analysis performed using dilepton events.
- <sup>19</sup> ACTON 92C uses electrons and muons. Superseded by AKERS 93B.
- <sup>20</sup> ADEVA 92C uses electrons and muons.
- <sup>21</sup> DECAMP 91 done with opposite and like-sign dileptons. Superseded by BUSKULIC 92B.
- <sup>22</sup> ADEVA 90P measurement uses  $ee$ ,  $\mu\mu$ , and  $e\mu$  events from 118k events at the Z. Superseded by ADEVA 92C.
- <sup>23</sup> These experiments are not in the average because the combination of  $B_s$  and  $B_d$  mesons which they see could differ from those at higher energy.
- <sup>24</sup> The WEIR 90 measurement supersedes the limit obtained in SCHAAD 85. The 90% CL are 0.06 and 0.38.
- <sup>25</sup> ALBAJAR 87C measured  $\chi = (\bar{B}^0 \rightarrow B^0 \rightarrow \mu^+ X)$  divided by the average production weighted semileptonic branching fraction for  $B$  hadrons at 546 and 630 GeV.
- <sup>26</sup> Limit is average probability for hadron containing  $B$  quark to produce a positive lepton.

### CP VIOLATION PARAMETERS in semileptonic $b$ -hadron decays.

#### $\text{Re}(\epsilon_b) / (1 + |\epsilon_b|^2)$

CP impurity in semileptonic  $b$ -hadron decays.

VALUE (units 10 <sup>-3</sup> )	DOCUMENT ID	TECN	COMMENT
• • • We do not use the following data for averages, fits, limits, etc. • • •			
-6.2 ± 5.2 ± 4.7	1 AABOUD	17E	ATLS $p\bar{p}$ at 8 TeV
-1.24 ± 0.38 ± 0.18	2 ABAZOV	14	D0 $p\bar{p}$ at 1.96 TeV
-1.97 ± 0.43 ± 0.23	3 ABAZOV	11U	D0 Repl. by ABAZOV 14
-2.39 ± 0.63 ± 0.37	4 ABAZOV	10H	D0 Repl. by ABAZOV 11U

<sup>1</sup> AABOUD 17E reports a measurement of charge asymmetry of  $A_{SL}^b = (-25 \pm 21 \pm 19) \times 10^{-3}$  in lepton + jets  $t\bar{t}$  events in which a  $b$ -hadron decays semileptonically to a soft muon.

<sup>2</sup> ABAZOV 14 reports a measurement of like-sign dimuon charge asymmetry of  $A_{SL}^b = (-4.96 \pm 1.53 \pm 0.72) \times 10^{-3}$  in semileptonic  $b$ -hadron decays.

<sup>3</sup> ABAZOV 11U reports a measurement of like-sign dimuon charge asymmetry of  $A_{SL}^b = (-7.87 \pm 1.72 \pm 0.93) \times 10^{-3}$  in semileptonic  $b$ -hadron decays.

<sup>4</sup> ABAZOV 10H reports a measurement of like-sign dimuon charge asymmetry of  $A_{SL}^b = (-9.57 \pm 2.51 \pm 1.46) \times 10^{-3}$  in semileptonic  $b$ -hadron decays. Using the measured production ratio of  $B_d^0$  and  $B_s^0$ , and the asymmetry of  $B_d^0, A_{SL}^d = (-4.7 \pm 4.6) \times 10^{-3}$  measured from  $B$ -factories, they obtain the asymmetry for  $B_s^0$  as  $A_{SL}^s = (-14.6 \pm 7.5) \times 10^{-3}$ .

### B-HADRON PRODUCTION FRACTIONS IN $p\bar{p}$ COLLISIONS AT Tevatron

The production fractions for  $b$ -hadrons in  $p\bar{p}$  collisions at the Tevatron have been calculated from the best values of mean lifetimes, mixing parameters, and branching fractions in this edition by the Heavy Flavor Averaging Group (HFLAV) (see <https://hflav.web.cern.ch/>).

The values reported below assume:

$$f(\bar{b} \rightarrow B^+) = f(\bar{b} \rightarrow B^0)$$

$$f(\bar{b} \rightarrow B^+) + f(\bar{b} \rightarrow B^0) + f(\bar{b} \rightarrow B_s^0) + f(b \rightarrow b\text{-baryon}) = 1$$

The values are:

$$f(\bar{b} \rightarrow B^+) = f(\bar{b} \rightarrow B^0) = 0.344 \pm 0.021$$

$$f(\bar{b} \rightarrow B_s^0) = 0.115 \pm 0.013$$

$$f(b \rightarrow b\text{-baryon}) = 0.198 \pm 0.046$$

$$f(\bar{b} \rightarrow B_s^0) / f(\bar{b} \rightarrow B_d^0) = 0.334 \pm 0.041$$

and their correlation coefficients are:

$$\text{cor}(B_s^0, b\text{-baryon}) = -0.429$$

$$\text{cor}(B_s^0, B^+ = B^0) = +0.159$$

$$\text{cor}(b\text{-baryon}, B^+ = B^0) = -0.960$$

as obtained with the Tevatron average of time-integrated mixing parameter

$$\bar{\chi} = 0.147 \pm 0.011.$$





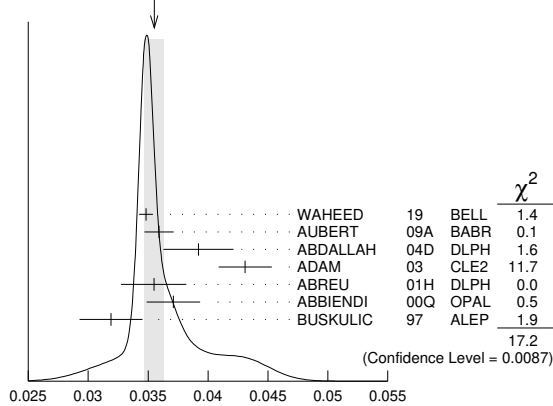
# Meson Particle Listings

## $V_{cb}$ and $V_{ub}$ CKM Matrix Elements, $B^*$

0.0431 ± 0.0013 ± 0.0018	14 BRIERE	02 CLE2	$e^+e^- \rightarrow \Upsilon(4S)$
0.0328 ± 0.0019 ± 0.0022	ACKERSTAFF	97G OPAL	Repl. by ABBIENDI 00q
0.0350 ± 0.0019 ± 0.0023	15 ABREU	96P DLPH	Repl. by ABREU 01H
0.0351 ± 0.0019 ± 0.0020	16 BARISH	95 CLE2	Repl. by ADAM 03
0.0314 ± 0.0023 ± 0.0025	BUSKULIC	95N ALEP	Repl. by BUSKULIC 97

- Uses fully reconstructed  $D^{*+} \ell^+ \nu$  events ( $\ell = e$  or  $\mu$ ) and  $\eta_{EW} = 1.0066$ .
- Obtained from a global fit to  $B \rightarrow D^{(*)} \ell \nu \ell$  events, with reconstructed  $D^0 \ell$  and  $D^+ \ell$  final states and  $\rho^2 = 1.22 \pm 0.02 \pm 0.07$ .
- Measurement using fully reconstructed  $D^*$  sample with a  $\rho^2 = 1.32 \pm 0.15 \pm 0.33$ .
- Average of the  $B^0 \rightarrow D^{*}(2010)^- \ell^+ \nu$  and  $B^+ \rightarrow \bar{D}^{*}(2007)^+ \ell^+ \nu$  modes with  $\rho^2 = 1.61 \pm 0.09 \pm 0.21$  and  $f_{\pm} = 0.521 \pm 0.012$ .
- ABREU 01H measured using about 5000 partial reconstructed  $D^*$  sample with a  $\rho^2 = 1.34 \pm 0.14^{+0.24}_{-0.22}$ .
- ABBIENDI 00q: measured using both inclusively and exclusively reconstructed  $D^{*\pm}$  samples with a  $\rho^2 = 1.21 \pm 0.12 \pm 0.20$ . The statistical and systematic correlations between  $|V_{cb}| \times F(1)$  and  $\rho^2$  are 0.90 and 0.54 respectively.
- BUSKULIC 97: measured using exclusively reconstructed  $D^{*\pm}$  with a  $a^2 = 0.31 \pm 0.17 \pm 0.08$ . The statistical correlation is 0.92.
- Uses fully reconstructed  $D^{*+} \ell^+ \nu$  events ( $\ell = e$  or  $\mu$ ).
- Measured using the dependence of  $B^- \rightarrow D^{*0} e^- \bar{\nu}_e$  decay differential rate and the form factor description by CAPRINI 98 with  $\rho^2 = 1.16 \pm 0.06 \pm 0.08$ .
- Measured using fully reconstructed  $D^*$  sample and a simultaneous fit to the Caprini-Lellouch-Neubert form factor parameters:  $\rho^2 = 1.191 \pm 0.048 \pm 0.028$ ,  $R_1(1) = 1.429 \pm 0.061 \pm 0.044$ , and  $R_2(1) = 0.827 \pm 0.038 \pm 0.022$ .
- Measurement using fully reconstructed  $D^*$  sample with a  $\rho^2 = 1.29 \pm 0.03 \pm 0.27$ .
- Combines with previous partial reconstructed  $D^*$  measurement with a  $\rho^2 = 1.39 \pm 0.10 \pm 0.33$ .
- Measured using exclusive  $B^0 \rightarrow D^{*}(892)^- e^+ \nu$  decays with  $\rho^2 = 1.35 \pm 0.17 \pm 0.19$  and a correlation of 0.91.
- BRIERE 02 result is based on the same analysis and data sample reported in ADAM 03.
- ABREU 96p: measured using both inclusively and exclusively reconstructed  $D^{*\pm}$  samples.
- BARISH 95: measured using both exclusive reconstructed  $B^0 \rightarrow D^{*-} \ell^+ \nu$  and  $B^+ \rightarrow D^{*0} \ell^+ \nu$  samples. They report their experiment's uncertainties  $\pm 0.0019 \pm 0.0018 \pm 0.0008$ , where the first error is statistical, the second is systematic, and the third is the uncertainty in the lifetimes. We combine the last two in quadrature.

WEIGHTED AVERAGE  
0.0355 ± 0.0008 (Error scaled by 1.7)



$|V_{cb}| \times F(1)$  (from  $B^0 \rightarrow D^{*-} \ell^+ \nu$ )

### $|V_{cb}| \times G(1)$ (from $B \rightarrow D^- \ell^+ \nu$ )

VALUE	DOCUMENT ID	TECN	COMMENT
<b>0.04157 ± 0.00100 OUR EVALUATION</b>	with $\rho^2 = 1.128 \pm 0.033$ and a correlation of 0.751. The fitted $\chi^2$ is 4.7 for 8 degrees of freedom.		
<b>0.0422 ± 0.0010 OUR AVERAGE</b>			
0.04229 ± 0.00137	1 GLATTAUER	16 BELL	$e^+e^- \rightarrow \Upsilon(4S)$
0.0423 ± 0.0019 ± 0.0014	2 AUBERT	10 BABR	$e^+e^- \rightarrow \Upsilon(4S)$
0.0431 ± 0.0008 ± 0.0023	3 AUBERT	09A BABR	$e^+e^- \rightarrow \Upsilon(4S)$
0.0416 ± 0.0047 ± 0.0037	4 BARTELT	99 CLE2	$e^+e^- \rightarrow \Upsilon(4S)$
0.0278 ± 0.0068 ± 0.0065	5 BUSKULIC	97 ALEP	$e^+e^- \rightarrow Z$
••• We do not use the following data for averages, fits, limits, etc. •••			
0.0411 ± 0.0044 ± 0.0052	6 ABE	02E BELL	Repl. by GLATTAUER 16
0.0337 ± 0.0044 ± 0.0072 ± 0.0049	7 ATHANAS	97 CLE2	Repl. by BARTELT 99

- Obtained from a fit to the combined partially reconstructed  $B \rightarrow \bar{D} \ell \nu \ell$  sample while tagged by the other fully reconstructed  $B$  meson in the event. Also reports fitted  $\rho^2 = 1.09 \pm 0.05$ .
- Obtained from a fit to the combined  $B \rightarrow \bar{D} \ell^+ \nu \ell$  sample in which a hadronic decay of the second  $B$  meson is fully reconstructed and  $\rho^2 = 1.20 \pm 0.09 \pm 0.04$ .
- Obtained from a global fit to  $B \rightarrow D^{(*)} \ell \nu \ell$  events, with reconstructed  $D^0 \ell$  and  $D^+ \ell$  final states and  $\rho^2 = 1.20 \pm 0.04 \pm 0.07$ .
- BARTELT 99: measured using both exclusive reconstructed  $B^0 \rightarrow D^- \ell^+ \nu$  and  $B^+ \rightarrow D^0 \ell^+ \nu$  samples.
- BUSKULIC 97: measured using exclusively reconstructed  $D^\pm$  with a  $a^2 = -0.05 \pm 0.53 \pm 0.38$ . The statistical correlation is 0.99.

- Using the missing energy and momentum to extract kinematic information about the undetected neutrino in the  $B^0 \rightarrow D^- \ell^+ \nu$  decay.
- ATHANAS 97: measured using both exclusive reconstructed  $B^0 \rightarrow D^- \ell^+ \nu$  and  $B^+ \rightarrow D^0 \ell^+ \nu$  samples with a  $\rho^2 = 0.59 \pm 0.22 \pm 0.12^{+0.59}_{-0}$ . They report their experiment's uncertainties  $\pm 0.0044 \pm 0.0048^{+0.0053}_{-0.0012}$ , where the first error is statistical, the second is systematic, and the third is the uncertainty due to the form factor model variations. We combine the last two in quadrature.

### $V_{ub}$ MEASUREMENTS

For the discussion of  $V_{ub}$  measurements, which is not repeated here, see the review on "Determination of  $|V_{cb}|$  and  $|V_{ub}|$ ."

The CKM matrix element  $|V_{ub}|$  can be determined by studying the rate of the charmless semileptonic decay  $b \rightarrow u \ell \nu$ . The relevant branching ratio measurements based on exclusive and inclusive decays can be found in the  $B$  Listings, and are not repeated here.

### $V_{cb}$ and $V_{ub}$ CKM Matrix Elements REFERENCES

WAHEED	19 PR D100 052007	E. Waheed <i>et al.</i>	(BELLE Collab.)
GLATTAUER	16 PR D93 032006	R. Glattauer <i>et al.</i>	(BELLE Collab.)
AUBERT	10 PRL 104 011802	B. Aubert <i>et al.</i>	(BABAR Collab.)
DUNDEL	10 PR D82 112007	W. Dungenl <i>et al.</i>	(BELLE Collab.)
AUBERT	09A PR D79 012002	B. Aubert <i>et al.</i>	(BABAR Collab.)
AUBERT	08AT PRL 100 231803	B. Aubert <i>et al.</i>	(BABAR Collab.)
AUBERT	08R PR D77 032002	B. Aubert <i>et al.</i>	(BABAR Collab.)
AUBERT	05E PR D71 051502	B. Aubert <i>et al.</i>	(BABAR Collab.)
ABDALLAH	04D EPJ C33 213	J. Abdallah <i>et al.</i>	(DELPHI Collab.)
ADAM	03 PR D67 032001	N.E. Adam <i>et al.</i>	(CLEO Collab.)
ABE	02E PL B526 258	K. Abe <i>et al.</i>	(BELLE Collab.)
ABE	02F PL B526 247	K. Abe <i>et al.</i>	(BELLE Collab.)
BRIERE	02 PRL 89 081803	R. Briere <i>et al.</i>	(CLEO Collab.)
ABREU	01H PL B510 55	P. Abreu <i>et al.</i>	(DELPHI Collab.)
ABBIENDI	00Q PL B482 15	G. Abbiendi <i>et al.</i>	(OPAL Collab.)
BARTELT	99 PRL 82 3746	J. Bartelt <i>et al.</i>	(CLEO Collab.)
CAPRINI	98 NP B530 153	I. Caprini, L. Lellouch, M. Neubert	(BCIP, CERN)
ACKERSTAFF	97G PL B395 128	K. Ackerstaff <i>et al.</i>	(OPAL Collab.)
ATHANAS	97 PRL 79 2208	M. Athanas <i>et al.</i>	(CLEO Collab.)
BUSKULIC	97 PL B395 373	D. Buskulic <i>et al.</i>	(ALEPH Collab.)
ABREU	96P ZPHY C71 539	P. Abreu <i>et al.</i>	(DELPHI Collab.)
BARISH	95 PR D51 1014	B.C. Barish <i>et al.</i>	(CLEO Collab.)
BUSKULIC	95N PL B359 236	D. Buskulic <i>et al.</i>	(ALEPH Collab.)

### $B^*$

$$I(J^P) = \frac{1}{2}(1^-)$$

$I, J, P$  need confirmation.

Quantum numbers shown are quark-model predictions.

### $B^*$ MASS

From mass difference below and the average of our  $B$  masses ( $m_{B^\pm} + m_{B^0}$ )/2.

VALUE (MeV)	DOCUMENT ID
<b>5324.70 ± 0.21 OUR FIT</b>	

### $m_{B^*} - m_B$

VALUE (MeV)	EVTS	DOCUMENT ID	TECN	COMMENT
<b>45.21 ± 0.21 OUR FIT</b>				
<b>45.42 ± 0.26 OUR AVERAGE</b>				Includes data from the datablock that follows this one.
46.2 ± 0.3 ± 0.8		1 ACKERSTAFF 97M OPAL		$e^+e^- \rightarrow Z$
45.3 ± 0.35 ± 0.87	4227	1 BUSKULIC 96D ALEP		$E_{cm}^{ee} = 88-94$ GeV
45.5 ± 0.3 ± 0.8		1 ABREU 95R DLPH		$E_{cm}^{ee} = 88-94$ GeV
46.3 ± 1.9	1378	1 ACCIARRI 95B L3		$E_{cm}^{ee} = 88-94$ GeV
46.4 ± 0.3 ± 0.8		2 AKERIB 91 CLE2		$e^+e^- \rightarrow \gamma X$
45.6 ± 0.8		2 WU 91 CSB2		$e^+e^- \rightarrow \gamma X, \gamma \ell X$
45.4 ± 1.0		3 LEE-FRANZINI 90 CSB2		$e^+e^- \rightarrow \Upsilon(5S)$
••• We do not use the following data for averages, fits, limits, etc. •••				
52 ± 2 ± 4	1400	4 HAN 85 CUSB		$e^+e^- \rightarrow \gamma e X$

- $u, d, s$  flavor averaged.
- These papers report  $E_\gamma$  in the  $B^*$  center of mass. The  $m_{B^*} - m_B$  is 0.2 MeV higher.  $E_{cm} = 10.61-10.7$  GeV. Admixture of  $B^0$  and  $B^+$  mesons, but not  $B_s$ .
- LEE-FRANZINI 90 value is for an admixture of  $B^0$  and  $B^+$ . They measure  $46.7 \pm 0.4 \pm 0.2$  MeV for an admixture of  $B^0, B^+,$  and  $B_s$ , and use the shape of the photon line to separate the above value.
- HAN 85 is for  $E_{cm} = 10.6-11.2$  GeV, giving an admixture of  $B^0, B^+,$  and  $B_s$ .

### $m_{B^{*+}} - m_{B^+}$

VALUE (MeV)	DOCUMENT ID	TECN	COMMENT
The data in this block is included in the average printed for a previous datablock.			

VALUE (MeV)	CL%	DOCUMENT ID	TECN	COMMENT
<b>45.37 ± 0.21 OUR FIT</b>				
<b>45.01 ± 0.30 ± 0.23</b>		5 AAIJ 130 LHCB		$pp$ at 7 TeV
5 Obtained the mass difference between $B^{*+} K^-$ and $B^+ K^-$ from $B_{s2}^*(5840)^0$ decay.				

### $|(m_{B^{*+}} - m_{B^+}) - (m_{B^0} - m_{B^+})|$

VALUE (MeV)	CL%	DOCUMENT ID	TECN	COMMENT
<b>&lt;6</b>	95	ABREU 95R DLPH		$E_{cm}^{ee} = 88-94$ GeV

See key on page 999

Meson Particle Listings

$B^*, B_1(5721)^+, B_1(5721)^0, B_J^*(5732)$

**$B^*$  DECAY MODES**

Mode	Fraction ( $\Gamma_i/\Gamma$ )
$\Gamma_1 B \gamma$	seen

**$B^*$  REFERENCES**

AAIJ	13O	PRL 110 151803	R. Aaij <i>et al.</i>	(LHCb Collab.)
ACKERSTAFF	97M	ZPHY C74 413	K. Ackerstaff <i>et al.</i>	(OPAL Collab.)
BUSKULIC	96D	ZPHY C69 393	D. Buskulic <i>et al.</i>	(ALEPH Collab.)
ABREU	95R	ZPHY C68 353	P. Abreu <i>et al.</i>	(DELPHI Collab.)
ACCIARRI	95B	PL B345 589	M. Acciarri <i>et al.</i>	(L3 Collab.)
AKERIB	91	PRL 67 1692	D.S. Akerib <i>et al.</i>	(CLEO Collab.)
WU	91	PL B273 177	Q.W. Wu <i>et al.</i>	(CUSB II Collab.)
LEE-FRANZINI	90	PRL 65 2947	J. Lee-Franzini <i>et al.</i>	(CUSB II Collab.)
HAN	85	PRL 55 36	K. Han <i>et al.</i>	(COLU, LSU, MPIM, STON)

$B_1(5721)^+$

$I(J^P) = \frac{1}{2}(1^+)$   
I, J, P need confirmation.

Quantum numbers shown are quark-model predictions.

**$B_1(5721)^+$  MASS**

OUR FIT uses  $m_{B^*0}$  and  $m_{B_1^+} - m_{B^*0}$  to determine  $m_{B_1(5721)^+}$ .

VALUE (MeV)	DOCUMENT ID
<b>5725.9 ± 2.5 ± 2.7 OUR FIT</b>	

**$m_{B_1^+} - m_{B^*0}$**

VALUE (MeV)	EVTS	DOCUMENT ID	TECN	COMMENT
<b>401.2 ± 2.4 ± 2.7 OUR FIT</b>				
<b>401.2 ± 2.4 ± 2.7 OUR AVERAGE</b>				
400.5 ± 1.8 ± 3.1	8K	<sup>1</sup> AAIJ	15AB LHCB	$p\bar{p}$ at 7, 8 TeV
402 ± 3 ± 1		<sup>2</sup> AALTONEN	14i CDF	$p\bar{p}$ at 1.96 TeV

<sup>1</sup> AAIJ 15AB reports  $[m_{B_1^+} - m_{B^*0}] - (m_{B^*0} - m_{B^0}) - m_{\pi^+} = 260.9 \pm 1.8 \pm 3.1$  MeV which we adjust by the  $\pi^+$  mass and assume  $(m_{B^*0} - m_{B^0}) = (m_{B^{*+}} - m_{B^+}) = 45.01 \pm 0.30 \pm 0.23$  MeV. The masses inside the square brackets were measured for each candidate event.

<sup>2</sup> AALTONEN 14i reports  $m_{B_1(5721)^+} - m_{B^*0} - m_{\pi^+} = 262 \pm 3^{+1}_{-3}$  MeV which we adjusted by the  $\pi^+$  mass.

**$B_1(5721)^+$  WIDTH**

VALUE (MeV)	EVTS	DOCUMENT ID	TECN	COMMENT
<b>31 ± 6 OUR AVERAGE</b>				Error includes scale factor of 1.1.
29.1 ± 3.6 ± 4.3	8K	AAIJ	15AB LHCB	$p\bar{p}$ at 7, 8 TeV
49 ± 12 ± 13		AALTONEN	14i CDF	$p\bar{p}$ at 1.96 TeV

**$B_1(5721)^+$  DECAY MODES**

Mode	Fraction ( $\Gamma_i/\Gamma$ )
$\Gamma_1 B^*0 \pi^+$	seen

**$B_1(5721)^+$  BRANCHING RATIOS**

$\Gamma(B^*0 \pi^+)/\Gamma_{total}$	EVTS	DOCUMENT ID	TECN	COMMENT	$\Gamma_1/\Gamma$
seen	8K	AAIJ	15AB LHCB	$p\bar{p}$ at 7, 8 TeV	
seen		AALTONEN	14i CDF	$p\bar{p}$ at 1.96 TeV	

**$B_1(5721)^+$  REFERENCES**

AAIJ	15AB	JHEP 1504 024	R. Aaij <i>et al.</i>	(LHCb Collab.)
AALTONEN	14i	PR D90 012013	T. Aaltonen <i>et al.</i>	(CDF Collab.)

$B_1(5721)^0$

$I(J^P) = \frac{1}{2}(1^+)$   
I, J, P need confirmation.

Quantum numbers shown are quark-model predictions.

**$B_1(5721)^0$  MASS**

OUR FIT uses mass differences measurements listed below to determine the mass  $m_{B_1(5721)^0}$ .

VALUE (MeV)	DOCUMENT ID
<b>5726.1 ± 1.3 OUR FIT</b>	Error includes scale factor of 1.2.

**$m_{B_1^0} - m_{B^+}$**

VALUE (MeV)	DOCUMENT ID	TECN	COMMENT
<b>446.7 ± 1.3 OUR FIT</b>	Error includes scale factor of 1.2.		
<b>441.5 ± 2.4 ± 1.3</b>	<sup>1</sup> ABAZOV	07T D0	$p\bar{p}$ at 1.96 TeV
• • • We do not use the following data for averages, fits, limits, etc. • • •			
446.2 ± 1.9 ± 1.0	<sup>1</sup> AALTONEN	09D CDF	Repl. by AALTONEN 14i
-2.1 -1.2			
<sup>1</sup> Observed in $B_1^0 \rightarrow B^*+ \pi^-$ .			

**$m_{B_1^0} - m_{B^{*+}}$**

VALUE (MeV)	EVTS	DOCUMENT ID	TECN	COMMENT
<b>401.4 ± 1.2 OUR FIT</b>				Error includes scale factor of 1.2.
<b>402.8 ± 1.1 OUR AVERAGE</b>				
403.4 ± 0.7 ± 1.5	35K	<sup>1</sup> AAIJ	15AB LHCB	$p\bar{p}$ at 7, 8 TeV
402.3 ± 0.9 ± 1.1		<sup>2</sup> AALTONEN	14i CDF	$p\bar{p}$ at 1.96 TeV
-1.2				
<sup>1</sup> AAIJ 15AB reports $[m_{B_1^0} - m_{B^+}] - (m_{B^{*+}} - m_{B^+}) - m_{\pi^-} = 263.9 \pm 0.7 \pm 1.4$ MeV which we adjust by the $\pi^-$ mass and $(m_{B^{*+}} - m_{B^+}) = 45.01 \pm 0.30 \pm 0.23$ MeV. The masses inside the square brackets were measured for each candidate event.				
<sup>2</sup> AALTONEN 14i reports $m_{B_1(5721)^0} - m_{B^{*+}} - m_{\pi^-} = 262.7 \pm 0.9^{+1.1}_{-1.2}$ MeV which we adjusted by the $\pi^-$ mass.				

**$B_1(5721)^0$  WIDTH**

VALUE (MeV)	EVTS	DOCUMENT ID	TECN	COMMENT
<b>27.5 ± 3.4 OUR AVERAGE</b>				Error includes scale factor of 1.1.
30.1 ± 1.5 ± 3.5	35k	AAIJ	15AB LHCB	$p\bar{p}$ at 7, 8 TeV
23 ± 3 ± 4		AALTONEN	14i CDF	$p\bar{p}$ at 1.96 TeV

**$B_1(5721)^0$  DECAY MODES**

Mode	Fraction ( $\Gamma_i/\Gamma$ )
$\Gamma_1 B^{*+} \pi^-$	seen

**$B_1(5721)^0$  BRANCHING RATIOS**

$\Gamma(B^{*+} \pi^-)/\Gamma_{total}$	EVTS	DOCUMENT ID	TECN	COMMENT	$\Gamma_1/\Gamma$
seen	35K	AAIJ	15AB LHCB	$p\bar{p}$ at 7, 8 TeV	
seen		AALTONEN	09D CDF	$p\bar{p}$ at 1.96 TeV	
seen		<sup>1</sup> ABAZOV	07T D0	$p\bar{p}$ at 1.96 TeV	
<sup>1</sup> Observed in $B_1^0 \rightarrow B^*+ \pi^-$ with $B^*+ \rightarrow B^+ \gamma$ and $B^+ \rightarrow J/\psi \pi^+$ .					

**$B_1(5721)^0$  REFERENCES**

AAIJ	15AB	JHEP 1504 024	R. Aaij <i>et al.</i>	(LHCb Collab.)
AALTONEN	14i	PR D90 012013	T. Aaltonen <i>et al.</i>	(CDF Collab.)
AALTONEN	09D	PRL 102 102003	T. Aaltonen <i>et al.</i>	(CDF Collab.)
ABAZOV	07T	PRL 99 172001	V.M. Abazov <i>et al.</i>	(D0 Collab.)

$B_J^*(5732)$

$I(J^P) = ?(??)$   
I, J, P need confirmation.

OMITTED FROM SUMMARY TABLE  
also known as  $B^{**}$

Quantum numbers shown are quark-model predictions. Signal can be interpreted as stemming from several narrow and broad resonances.

**$B_J^*(5732)$  MASS**

VALUE (MeV)	EVTS	DOCUMENT ID	TECN	COMMENT
<b>5698 ± 8 OUR AVERAGE</b>				Error includes scale factor of 1.2.
5710 ± 20		<sup>1</sup> AFFOLDER	01F CDF	$p\bar{p}$ at 1.8 TeV
5695 ± 17		<sup>2</sup> BARATE	98L ALEP	$e^+ e^- \rightarrow Z$
-19				
5704 ± 4 ± 10	1944	<sup>3</sup> BUSKULIC	96D ALEP	$E_{cm}^{ee} = 88-94$ GeV
5732 ± 5 ± 20	2157	ABREU	95B DLPH	$E_{cm}^{ee} = 88-94$ GeV
5681 ± 11	1738	AKERS	95E OPAL	$E_{cm}^{ee} = 88-94$ GeV

# Meson Particle Listings

## $B_J^*(5732), B_2^*(5747)^+, B_2^*(5747)^0$

- • • We do not use the following data for averages, fits, limits, etc. • • •
- 5713 ± 2 <sup>4</sup> ACCIARRI 99N L3  $e^+e^- \rightarrow Z$
- <sup>1</sup> AFFOLDER 01F uses the reconstructed  $B$  meson through semileptonic decay channels. The fraction of light  $B$  mesons that are produced at  $L=1$   $B^{**}$  states is measured to be  $0.28 \pm 0.06 \pm 0.03$ .
- <sup>2</sup> BARATE 98L uses fully reconstructed  $B$  mesons to search for  $B^{**}$  production in the  $B\pi^\pm$  system. In the framework of heavy quark symmetry (HQs), they also measured the mass of  $B_2^*$  to be  $5739^{+8+6}_{-11-4}$  MeV/ $c^2$  and the relative production rate of  $B(b \rightarrow B_2^* \rightarrow B^*(*)\pi)/B(b \rightarrow B_{u,d}) = (31 \pm 9^{+6}_{-5})\%$ .
- <sup>3</sup> Using  $m_{B\pi} - m_B = 424 \pm 4 \pm 10$  MeV.
- <sup>4</sup> ACCIARRI 99N uses inclusive reconstructed  $B$  mesons to search for  $B^{**}$  production in the  $B^*(*)\pi^\pm$  system. In the framework of HQET, they measured the mass of  $B_1^*$  and  $B_2^*$  to be  $5670 \pm 10 \pm 13$  MeV and  $5768 \pm 5 \pm 6$  with the  $B(b \rightarrow B^{**}) = (32 \pm 3 \pm 6) \times 10^{-2}$ . They also reported the evidence for the existence of an excited  $B$ -meson state or mixture of states in the region 5.9–6.0 GeV.

### $B_J^*(5732)$ WIDTH

VALUE (MeV)	EVTS	DOCUMENT ID	TECN	COMMENT
<b>128 ± 16 OUR AVERAGE</b>				
145 ± 28	2157	ABREU	95B DLPH	$E_{cm}^{ec} = 88-94$ GeV
116 ± 24	1738	AKERS	95E OPAL	$E_{cm}^{ec} = 88-94$ GeV

### $B_J^*(5732)$ DECAY MODES

Mode	Fraction ( $\Gamma_i/\Gamma$ )
$\Gamma_1$ $B^*\pi + B\pi$	seen
$\Gamma_2$ $B^*\pi(X)$	[a] (85 ± 29) %

[a] X refers to decay modes with or without additional accompanying decay particles.

### $B_J^*(5732)$ BRANCHING RATIOS

X refers to decay modes with or without additional accompanying decay particles.

$\Gamma(B^*\pi(X))/\Gamma_{total}$	DOCUMENT ID	TECN	COMMENT	$\Gamma_2/\Gamma$
<b>0.85 <math>\pm</math> 0.26 <math>\pm</math> 0.12</b>	ABBIENDI	02E OPAL	$e^+e^- \rightarrow Z$	

### $B_J^*(5732)$ REFERENCES

ABBIENDI 02E EPJ C23 437	G. Abbiendi et al.	(OPAL Collab.)
AFFOLDER 01F PR D64 072002	T. Affolder et al.	(CDF Collab.)
ACCIARRI 99N PL B465 323	M. Acciari et al.	(L3 Collab.)
BARATE 98L PL B425 215	R. Barate et al.	(ALEPH Collab.)
BUSKULIC 96D ZPHY C69 393	D. Buskulic et al.	(ALEPH Collab.)
ABREU 95B PL B345 590	P. Abreu et al.	(DELPHI Collab.)
AKERS 95E ZPHY C66 19	R. Akers et al.	(OPAL Collab.)

$B_2^*(5747)^+$

 $I(J^P) = \frac{1}{2}(2^+)$   
 $I, J, P$  need confirmation.  
 Quantum numbers shown are quark-model predictions.

### $B_2^*(5747)^+$ MASS

OUR FIT uses  $m_{B_0}$  and  $m_{B_2^{*+}} - m_{B_0}$  to determine  $m_{B_2^*(5747)^+}$ .

VALUE (MeV)	DOCUMENT ID
<b>5737.2 ± 0.7 OUR FIT</b>	

### $m_{B_2^{*+}} - m_{B_0}$

VALUE (MeV)	EVTS	DOCUMENT ID	TECN	COMMENT
<b>457.5 ± 0.7 OUR FIT</b>				
<b>457.5 ± 0.7 OUR AVERAGE</b>				
457.62 ± 0.72 ± 0.40	4K	<sup>1</sup> AAIJ	15AB LHCB	$p\bar{p}$ at 7, 8 TeV
457.3 ± 1.3 $\pm$ 0.3 $\pm$ 0.9		<sup>2</sup> AALTONEN	14i CDF	$p\bar{p}$ at 1.96 TeV

- <sup>1</sup> AAIJ 15AB reports  $[m_{B_2^{*+}} - m_{B_0}] - m_{\pi^+} = 318.1 \pm 0.7 \pm 0.4$  MeV which we adjust by the  $\pi^+$  mass. The masses inside the square brackets were measured for each candidate event.
- <sup>2</sup> AALTONEN 14i reports  $m_{B_2^*(5747)^+} - m_{B_0} - m_{\pi^+} = 317.7 \pm 1.2^{+0.3}_{-0.9}$  MeV which we adjusted by the  $\pi^+$  mass.

### $B_2^*(5747)^+$ WIDTH

VALUE (MeV)	EVTS	DOCUMENT ID	TECN	COMMENT
<b>20 ± 5 OUR AVERAGE</b>				Error includes scale factor of 2.2.
23.6 ± 2.0 ± 2.1	4K	AAIJ	15AB LHCB	$p\bar{p}$ at 7, 8 TeV
11 $\pm$ 4 $\pm$ 3 $\pm$ 4		AALTONEN	14i CDF	$p\bar{p}$ at 1.96 TeV

### $B_2^*(5747)^+$ DECAY MODES

Mode	Fraction ( $\Gamma_i/\Gamma$ )
$\Gamma_1$ $B^0\pi^+$	seen
$\Gamma_2$ $B^{*0}\pi^+$	seen

### $B_2^*(5747)^+$ BRANCHING RATIOS

$\Gamma(B^0\pi^+)/\Gamma_{total}$	DOCUMENT ID	TECN	COMMENT	$\Gamma_1/\Gamma$
seen	AAIJ	15AB LHCB	$p\bar{p}$ at 7, 8 TeV	
seen	AALTONEN	14i CDF	$p\bar{p}$ at 1.96 TeV	

$\Gamma(B^{*0}\pi^+)/\Gamma_{total}$	DOCUMENT ID	TECN	COMMENT	$\Gamma_2/\Gamma$
seen	AAIJ	15AB LHCB	$p\bar{p}$ at 7, 8 TeV	

$\Gamma(B^{*0}\pi^+)/\Gamma(B^0\pi^+)$	DOCUMENT ID	TECN	COMMENT	$\Gamma_2/\Gamma_1$
<b>1.0 ± 0.5 ± 0.8</b>	AAIJ	15AB LHCB	$p\bar{p}$ at 7, 8 TeV	

### $B_2^*(5747)^+$ REFERENCES

AAIJ 15AB JHEP 1504 024	R. Aaij et al.	(LHCb Collab.)
AALTONEN 14i PR D90 012013	T. Aaltonen et al.	(CDF Collab.)

$B_2^*(5747)^0$

$I(J^P) = \frac{1}{2}(2^+)$   
 $I, J, P$  need confirmation.

Quantum numbers shown are quark-model predictions.

### $B_2^*(5747)^0$ MASS

OUR FIT uses  $m_{B^{*+}}, m_{B_1^0} - m_{B^{*+}}$ , and  $m_{B_2^0} - m_{B_1^0}$  to determine  $m_{B_2^*(5747)^0}$ . The  $-0.659$  correlation between statistical uncertainties of  $m_{B_1^0} - m_{B^{*+}}$  and  $m_{B_2^0} - m_{B_1^0}$  measurements reported by ABAAZOV 07r is taken into account.

VALUE (MeV)	DOCUMENT ID
<b>5739.5 ± 0.7 OUR FIT</b>	Error includes scale factor of 1.4.

### $m_{B_2^0} - m_{B_1^0}$

VALUE (MeV)	DOCUMENT ID	TECN	COMMENT
<b>13.4 ± 1.4 OUR FIT</b>	Error includes scale factor of 1.3.		
<b>16.2 ± 3.1 ± 0.9</b>	<sup>1</sup> ABAAZOV 07r D0		$p\bar{p}$ at 1.96 TeV
14.9 $\pm$ 2.2 $\pm$ 1.2 $\pm$ 2.5 $\pm$ 1.4	<sup>1</sup> AALTONEN 09D CDF		Repl. by AALTONEN 14i

- • • We do not use the following data for averages, fits, limits, etc. • • •
- <sup>1</sup> Observed in  $B_2^0 \rightarrow B^{*+}\pi^-$  and  $B_2^0 \rightarrow B^+\pi^-$ .

### $m_{B_2^0} - m_{B^+}$

VALUE (MeV)	EVTS	DOCUMENT ID	TECN	COMMENT
<b>460.2 ± 0.6 OUR FIT</b>				Error includes scale factor of 1.4.
<b>459.9 ± 0.8 OUR AVERAGE</b>				Error includes scale factor of 1.8.
460.18 ± 0.37 ± 0.33	17K	<sup>1</sup> AAIJ	15AB LHCB	$p\bar{p}$ at 7, 8 TeV
457.5 ± 1.2 $\pm$ 0.8 $\pm$ 0.9		<sup>2</sup> AALTONEN	14i CDF	$p\bar{p}$ at 1.96 TeV

- <sup>1</sup> AAIJ 15AB reports  $[m_{B_2^0} - m_{B^+}] - m_{\pi^-} = 320.6 \pm 0.4 \pm 0.3$  MeV which we adjust by the  $\pi^-$  mass. The masses inside the square brackets were measured for each candidate event.
- <sup>2</sup> AALTONEN 14i reports  $m_{B_2^*(5747)^0} - m_{B^+} - m_{\pi^-} = 317.9 \pm 1.2^{+0.8}_{-0.9}$  MeV which we adjusted by the  $\pi^-$  mass.

### $B_2^*(5747)^0$ WIDTH

VALUE (MeV)	EVTS	DOCUMENT ID	TECN	COMMENT
<b>24.2 ± 1.7 OUR AVERAGE</b>				
24.5 ± 1.0 ± 1.5	17K	AAIJ	15AB LHCB	$p\bar{p}$ at 7, 8 TeV
22 $\pm$ 3 $\pm$ 4		AALTONEN	14i CDF	$p\bar{p}$ at 1.96 TeV
• • • We do not use the following data for averages, fits, limits, etc. • • •				
22.7 $\pm$ 3.8 $\pm$ 3.2 $\pm$ 3.2 $\pm$ 10.2		AALTONEN	09D CDF	Repl. by AALTONEN 14i

### $B_2^*(5747)^0$ DECAY MODES

Mode	Fraction ( $\Gamma_i/\Gamma$ )
$\Gamma_1$ $B^+\pi^-$	seen
$\Gamma_2$ $B^{*+}\pi^-$	seen

See key on page 999

Meson Particle Listings

$B_2^*(5747)^0, B_J(5840)^+, B_J(5840)^0$

$B_2^*(5747)^0$  BRANCHING RATIOS

$\Gamma(B^+\pi^-)/\Gamma_{total}$					$\Gamma_1/\Gamma$
VALUE	EVTs	DOCUMENT ID	TECN	COMMENT	
seen	17K	AAIJ	15AB LHCB	$pp$ at 7, 8 TeV	
seen		AALTONEN	09D CDF	$p\bar{p}$ at 1.96 TeV	
seen		ABAZOV	07T D0	$p\bar{p}$ at 1.96 TeV	

$\Gamma(B^{*+}\pi^-)/\Gamma_{total}$					$\Gamma_2/\Gamma$
VALUE	EVTs	DOCUMENT ID	TECN	COMMENT	
seen	17K	AAIJ	15AB LHCB	$pp$ at 7, 8 TeV	
seen		AALTONEN	09D CDF	$p\bar{p}$ at 1.96 TeV	
seen		ABAZOV	07T D0	$p\bar{p}$ at 1.96 TeV	

$\Gamma(B^{*+}\pi^-)/\Gamma(B^+\pi^-)$					$\Gamma_2/\Gamma_1$
VALUE	EVTs	DOCUMENT ID	TECN	COMMENT	
<b>0.82 ± 0.28 OUR AVERAGE</b>					
0.71 ± 0.14 ± 0.30	17K	AAIJ	15AB LHCB	$pp$ at 7, 8 TeV	
1.10 ± 0.42 ± 0.31		<sup>1</sup> ABAZOV	07T D0	$p\bar{p}$ at 1.96 TeV	

<sup>1</sup> Converted from measured ratio of  $R = B(B_2^{*0} \rightarrow B^{*+}\pi^-) / B(B_2^{*0} \rightarrow B^{(*)+}\pi^-) = 0.475 \pm 0.095 \pm 0.069$ .

$B_2^*(5747)^0$  REFERENCES

AAIJ	15AB JHEP 1504 024	R. Aaij et al.	(LHCb Collab.)
AALTONEN	14I PR D90 012013	T. Aaltonen et al.	(CDF Collab.)
AALTONEN	09D PRL 102 102003	T. Aaltonen et al.	(CDF Collab.)
ABAZOV	07T PRL 99 172001	V.M. Abazov et al.	(D0 Collab.)

$B_J(5840)^+$

$I(J^P) = \frac{1}{2}(??)$   
I, J, P need confirmation.

OMITTED FROM SUMMARY TABLE  
Quantum numbers shown are quark-model predictions.

$B_J(5840)^+$  MASS

OUR FIT uses  $m_{B^0}$  and  $m_{B_J(5840)^+} - m_{B^0}$  to determine  $m_{B_J(5840)^+}$ .

VALUE (MeV)	DOCUMENT ID
<b>5851 ± 19 OUR FIT</b>	

$m_{B_J(5840)^+} - m_{B^0}$

VALUE (MeV)	EVTs	DOCUMENT ID	TECN	COMMENT
<b>571 ± 19 OUR FIT</b>				
<b>571 ± 13 ± 14</b>	7k	<sup>1</sup> AAIJ	15AB LHCB	$pp$ at 7, 8 TeV
• • • We do not use the following data for averages, fits, limits, etc. • • •				
595 ± 26 ± 14	7k	<sup>2</sup> AAIJ	15AB LHCB	$pp$ at 7, 8 TeV

<sup>1</sup> AAIJ 15AB reports  $[m_{B_J^+} - m_{B^0}] - m_{\pi^+} = 431 \pm 13 \pm 14$  MeV which we adjust by the  $\pi^+$  mass. The masses inside the square brackets were measured for each candidate event. The result assumes  $P = (-1)^J$  and uses two relativistic Breit-Wigner functions in the fit for mass difference.

<sup>2</sup> AAIJ 15AB reports  $[m_{B_J^+} - m_{B^0}] - m_{\pi^+} = 455 \pm 26 \pm 14$  MeV which we adjust by the  $\pi^+$  mass. The masses inside the square brackets were measured for each candidate event. The result assumes  $P = (-1)^J$  and uses three relativistic Breit-Wigner functions in the fit for mass difference.

$m_{B_J(5840)^+} - m_{B^+}$

VALUE (MeV)	EVTs	DOCUMENT ID	TECN	COMMENT
• • • We do not use the following data for averages, fits, limits, etc. • • •				
565 ± 15 ± 14	7k	<sup>1</sup> AAIJ	15AB LHCB	$pp$ at 7, 8 TeV

<sup>1</sup> AAIJ 15AB reports  $[m_{B_J^+} - m_{B^0}] - (m_{B^{*+}} - m_{B^+}) - m_{\pi^+} = 425 \pm 15 \pm 14$  MeV which we adjust by the  $\pi^+$  mass. The masses inside the square brackets were measured for each candidate event. The result assumes  $P = (-1)^J, (m_{B^0} - m_{B^+}) = (m_{B^{*+}} - m_{B^+}) = 45.01 \pm 0.30 \pm 0.23$  MeV, and uses three relativistic Breit-Wigner functions in the fit for mass difference.

$B_J(5840)^+$  WIDTH

VALUE (MeV)	EVTs	DOCUMENT ID	TECN	COMMENT
<b>224 ± 24 ± 80</b>	7k	<sup>1</sup> AAIJ	15AB LHCB	$pp$ at 7, 8 TeV
• • • We do not use the following data for averages, fits, limits, etc. • • •				
215 ± 27 ± 80	7k	<sup>2</sup> AAIJ	15AB LHCB	$pp$ at 7, 8 TeV
229 ± 27 ± 80	7k	<sup>3</sup> AAIJ	15AB LHCB	$pp$ at 7, 8 TeV

<sup>1</sup> Assuming  $P = (-1)^J$  and using two relativistic Breit-Wigner functions in the fit for mass difference.  
<sup>2</sup> Assuming  $P = (-1)^J$  and using three relativistic Breit-Wigner functions in the fit for mass difference.  
<sup>3</sup> Assuming  $P = (-1)^J$  and using three relativistic Breit-Wigner functions in the fit for mass difference.

$B_J(5840)^+$  DECAY MODES

Mode	Fraction ( $\Gamma_i/\Gamma$ )
$\Gamma_1$ $B^{*0}\pi^+$	seen
$\Gamma_2$ $B^0\pi^+$	possibly seen

$B_J(5840)^+$  BRANCHING RATIOS

$\Gamma(B^{*0}\pi^+)/\Gamma_{total}$					$\Gamma_1/\Gamma$
VALUE	EVTs	DOCUMENT ID	TECN	COMMENT	
seen	7k	AAIJ	15AB LHCB	$pp$ at 7, 8 TeV	

$\Gamma(B^0\pi^+)/\Gamma_{total}$					$\Gamma_2/\Gamma$
VALUE	EVTs	DOCUMENT ID	TECN	COMMENT	
possibly seen	7k	<sup>1</sup> AAIJ	15AB LHCB	$pp$ at 7, 8 TeV	

<sup>1</sup> A  $B\pi$  decay is forbidden from a  $P = -(-1)^J$  parent, whereas  $B^*\pi$  is allowed.

$B_J(5840)^+$  REFERENCES

AAIJ	15AB JHEP 1504 024	R. Aaij et al.	(LHCb Collab.)
------	--------------------	----------------	----------------

$B_J(5840)^0$

$I(J^P) = \frac{1}{2}(??)$   
I, J, P need confirmation.

OMITTED FROM SUMMARY TABLE  
Quantum numbers shown are quark-model predictions.

$B_J(5840)^0$  MASS

OUR FIT uses  $m_{B^+}$  and  $m_{B_J(5840)^0} - m_{B^+}$  to determine  $m_{B_J(5840)^0}$ .

VALUE (MeV)	DOCUMENT ID
<b>5863 ± 9 OUR FIT</b>	

$m_{B_J(5840)^0} - m_{B^+}$

VALUE (MeV)	EVTs	DOCUMENT ID	TECN	COMMENT
<b>584 ± 9 OUR FIT</b>				
<b>584 ± 5 ± 7</b>	12k	<sup>1</sup> AAIJ	15AB LHCB	$pp$ at 7, 8 TeV
• • • We do not use the following data for averages, fits, limits, etc. • • •				
610 ± 22 ± 7	12k	<sup>2</sup> AAIJ	15AB LHCB	$pp$ at 7, 8 TeV

<sup>1</sup> AAIJ 15AB reports  $[m_{B_J^0} - m_{B^+}] - m_{\pi^-} = 444 \pm 5 \pm 7$  MeV which we adjust by

the  $\pi^-$  mass. The masses inside the square brackets were measured for each candidate event. The result assumes  $P = (-1)^J$  and uses two relativistic Breit-Wigner functions in the fit for mass difference.

<sup>2</sup> AAIJ 15AB reports  $[m_{B_J^0} - m_{B^+}] - m_{\pi^-} = 471 \pm 22 \pm 7$  MeV which we adjust by

the  $\pi^-$  mass. The masses inside the square brackets were measured for each candidate event. The result assumes  $P = (-1)^J$  and uses three relativistic Breit-Wigner functions in the fit for mass difference.

$m_{B_J(5840)^0} - m_{B^{*+}}$

VALUE (MeV)	EVTs	DOCUMENT ID	TECN	COMMENT
• • • We do not use the following data for averages, fits, limits, etc. • • •				
584 ± 5 ± 7	12k	<sup>1</sup> AAIJ	15AB LHCB	$pp$ at 7, 8 TeV

<sup>1</sup> AAIJ 15AB reports  $[m_{B_J^0} - m_{B^+}] - (m_{B^{*+}} - m_{B^+}) - m_{\pi^-} = 444 \pm 5 \pm 7$  MeV

which we adjust by the  $\pi^-$  mass. The masses inside the square brackets were measured for each candidate event. The result assumes  $P = -(-1)^J, (m_{B^0} - m_{B^+}) = 45.01 \pm 0.30 \pm 0.23$  MeV, and uses three relativistic Breit-Wigner functions in the fit for mass difference.

$B_J(5840)^0$  WIDTH

VALUE (MeV)	EVTs	DOCUMENT ID	TECN	COMMENT
<b>127 ± 17 ± 34</b>	12k	<sup>1</sup> AAIJ	15AB LHCB	$pp$ at 7, 8 TeV
• • • We do not use the following data for averages, fits, limits, etc. • • •				
107 ± 20 ± 34	12k	<sup>2</sup> AAIJ	15AB LHCB	$pp$ at 7, 8 TeV
119 ± 17 ± 34	12k	<sup>3</sup> AAIJ	15AB LHCB	$pp$ at 7, 8 TeV

<sup>1</sup> Assuming  $P = (-1)^J$  and using two relativistic Breit-Wigner functions in the fit for mass difference.

<sup>2</sup> Assuming  $P = (-1)^J$  and using three relativistic Breit-Wigner functions in the fit for mass difference.

<sup>3</sup> Assuming  $P = -(-1)^J$  and using three relativistic Breit-Wigner functions in the fit for mass difference.

$B_J(5840)^0$  DECAY MODES

Mode	Fraction ( $\Gamma_i/\Gamma$ )
$\Gamma_1$ $B^{*+}\pi^-$	seen
$\Gamma_2$ $B^+\pi^-$	possibly seen

## Meson Particle Listings

 $B_J(5840)^0, B_J(5970)^+, B_J(5970)^0$  $B_J(5840)^0$  BRANCHING RATIOS

$\Gamma(B^{*+}\pi^-)/\Gamma_{\text{total}}$					$\Gamma_1/\Gamma$
VALUE	EVTS	DOCUMENT ID	TECN	COMMENT	
seen	12k	AAIJ	15AB LHCb	$p\bar{p}$ at 7, 8 TeV	

$\Gamma(B^+\pi^-)/\Gamma_{\text{total}}$					$\Gamma_2/\Gamma$
VALUE	EVTS	DOCUMENT ID	TECN	COMMENT	
possibly seen		<sup>1</sup> AAIJ	15AB LHCb	$p\bar{p}$ at 7, 8 TeV	

<sup>1</sup> A  $B\pi$  decay is forbidden from a  $P = -(-1)^J$  parent, whereas  $B^*\pi$  is allowed.

 $B_J(5840)^0$  REFERENCES

AAIJ 15AB JHEP 1504 024 R. Aaij *et al.* (LHCb Collab.)

$B_J(5970)^+$	$I(J^P) = \frac{1}{2}(??)$
	$I, J, P$ need confirmation.
Quantum numbers shown are quark-model predictions.	

 $B_J(5970)^+$  MASS

OUR FIT uses  $m_{B^0}$  and  $m_{B_J(5970)^+} - m_{B^0}$  to determine  $m_{B_J(5970)^+}$ .

VALUE (MeV)	DOCUMENT ID
<b>5964 ± 5 OUR FIT</b>	

 $m_{B_J(5970)^+} - m_{B^0}$ 

VALUE (MeV)	EVTS	DOCUMENT ID	TECN	COMMENT
<b>685 ± 5 OUR FIT</b>				
<b>685 ± 5 OUR AVERAGE</b>				
685.3 ± 4.1 ± 2.5	2K	<sup>1</sup> AAIJ	15AB LHCb	$p\bar{p}$ at 7, 8 TeV
681 ± 5 ± 12	1.4k	<sup>2</sup> AALTONEN	14i CDF	$p\bar{p}$ at 1.96 TeV

• • • We do not use the following data for averages, fits, limits, etc. • • •

686.8 ± 4.5 ± 2.5 2K <sup>3</sup>AAIJ 15AB LHCb  $p\bar{p}$  at 7, 8 TeV

<sup>1</sup>AAIJ 15AB reports  $[m_{B_J^+} - m_{B^0}] - m_{\pi^+} = 545.8 \pm 4.1 \pm 2.5$  MeV which we adjust by

the  $\pi^+$  mass. The masses inside the square brackets were measured for each candidate event. The result assumes  $P = (-1)^J$  and uses two relativistic Breit-Wigner functions in the fit for mass difference.

<sup>2</sup>AALTONEN 14i reports  $m_{B_J(5970)^+} - m_{B^0} - m_{\pi^+} = 541 \pm 5 \pm 12$  MeV which we adjust by the  $\pi^+$  mass.

<sup>3</sup>AAIJ 15AB reports  $[m_{B_J^+} - m_{B^0}] - m_{\pi^+} = 547 \pm 5 \pm 3$  MeV which we adjust by

the  $\pi^+$  mass. The masses inside the square brackets were measured for each candidate event. The result assumes  $P = (-1)^J$  and uses three relativistic Breit-Wigner functions in the fit for mass difference.

 $m_{B_J(5970)^+} - m_{B^{*0}}$ 

VALUE (MeV)	EVTS	DOCUMENT ID	TECN	COMMENT
• • • We do not use the following data for averages, fits, limits, etc. • • •				
686.0 ± 4.0 ± 2.5	2k	<sup>1</sup> AAIJ	15AB LHCb	$p\bar{p}$ at 7, 8 TeV

<sup>1</sup>AAIJ 15AB reports  $[m_{B_J^+} - m_{B^0}] - (m_{B^{*+}} - m_{B^+}) - m_{\pi^+} = 547 \pm 4 \pm 3$  MeV which

we adjust by the  $\pi^+$  mass. The masses inside the square brackets were measured for each candidate event. The result assumes  $P = -(-1)^J$ ,  $(m_{B^{*0}} - m_{B^0}) = (m_{B^{*+}} - m_{B^+}) = 45.01 \pm 0.30 \pm 0.23$  MeV, and uses three relativistic Breit-Wigner functions in the fit for mass difference.

 $B_J(5970)^+$  WIDTH

VALUE (MeV)	EVTS	DOCUMENT ID	TECN	COMMENT
<b>62 ± 20 OUR AVERAGE</b>				
63 ± 15 ± 17	2K	<sup>1</sup> AAIJ	15AB LHCb	$p\bar{p}$ at 7, 8 TeV
60 ± 30 ± 40	1.4k	AALTONEN	14i CDF	$p\bar{p}$ at 1.96 TeV

• • • We do not use the following data for averages, fits, limits, etc. • • •

61 ± 14 ± 17 2K <sup>2</sup>AAIJ 15AB LHCb  $p\bar{p}$  at 7, 8 TeV

61 ± 15 ± 17 2K <sup>3</sup>AAIJ 15AB LHCb  $p\bar{p}$  at 7, 8 TeV

<sup>1</sup> Assuming  $P = (-1)^J$  and using two relativistic Breit-Wigner functions in the fit for mass difference.

<sup>2</sup> Assuming  $P = (-1)^J$  and using three relativistic Breit-Wigner functions in the fit for mass difference.

<sup>3</sup> Assuming  $P = -(-1)^J$  and using three relativistic Breit-Wigner functions in the fit for mass difference.

 $B_J(5970)^+$  DECAY MODES

Mode	Fraction ( $\Gamma_i/\Gamma$ )
$\Gamma_1$ $B^0\pi^+$	possibly seen
$\Gamma_2$ $B^{*0}\pi^+$	seen

 $B_J(5970)^+$  BRANCHING RATIOS

$\Gamma(B^0\pi^+)/\Gamma_{\text{total}}$					$\Gamma_1/\Gamma$
VALUE	EVTS	DOCUMENT ID	TECN	COMMENT	
possibly seen	2K	<sup>1</sup> AAIJ	15AB LHCb	$p\bar{p}$ at 7, 8 TeV	
possibly seen	1.4k	AALTONEN	14i CDF	$p\bar{p}$ at 1.96 TeV	

<sup>1</sup> A  $B\pi$  decay is forbidden from a  $P = -(-1)^J$  parent, whereas  $B^*\pi$  is allowed.

$\Gamma(B^{*0}\pi^+)/\Gamma_{\text{total}}$					$\Gamma_2/\Gamma$
VALUE	EVTS	DOCUMENT ID	TECN	COMMENT	
seen	2k	AAIJ	15AB LHCb	$p\bar{p}$ at 7, 8 TeV	
seen	1.4k	AALTONEN	14i CDF	$p\bar{p}$ at 1.96 TeV	

 $B_J(5970)^+$  REFERENCES

AAIJ 15AB JHEP 1504 024 R. Aaij *et al.* (LHCb Collab.)  
AALTONEN 14i PR D90 012013 T. Aaltonen *et al.* (CDF Collab.)

$B_J(5970)^0$	$I(J^P) = \frac{1}{2}(??)$
	$I, J, P$ need confirmation.
Quantum numbers shown are quark-model predictions.	

 $B_J(5970)^0$  MASS

OUR FIT uses  $m_{B^+}$  and  $m_{B_J(5970)^0} - m_{B^+}$  to determine  $m_{B_J(5970)^0}$ .

VALUE (MeV)	DOCUMENT ID
<b>5971 ± 5 OUR FIT</b>	

 $m_{B_J(5970)^0} - m_{B^+}$ 

VALUE (MeV)	EVTS	DOCUMENT ID	TECN	COMMENT
<b>691 ± 5 OUR FIT</b>				
<b>691 ± 5 OUR AVERAGE</b>				
689.9 ± 2.9 ± 5.1	10K	<sup>1</sup> AAIJ	15AB LHCb	$p\bar{p}$ at 7, 8 TeV
698 ± 5 ± 12	2.6k	<sup>2</sup> AALTONEN	14i CDF	$p\bar{p}$ at 1.96 TeV

• • • We do not use the following data for averages, fits, limits, etc. • • •

714.3 ± 6.4 ± 5.1 10K <sup>3</sup>AAIJ 15AB LHCb  $p\bar{p}$  at 7, 8 TeV

<sup>1</sup>AAIJ 15AB reports  $[m_{B_J^0} - m_{B^+}] - m_{\pi^-} = 550.4 \pm 2.9 \pm 5.1$  MeV which we adjust by

the  $\pi^-$  mass. The masses inside the square brackets were measured for each candidate event. The result assumes  $P = (-1)^J$  and uses two relativistic Breit-Wigner functions in the fit for mass difference.

<sup>2</sup>AALTONEN 14i reports  $m_{B_J(5970)^0} - m_{B^+} - m_{\pi^-} = 558 \pm 5 \pm 12$  MeV which we adjust by the  $\pi^-$  mass.

<sup>3</sup>AAIJ 15AB reports  $[m_{B_J^0} - m_{B^+}] - m_{\pi^-} = 575 \pm 6 \pm 5$  MeV which we adjust by

the  $\pi^-$  mass. The masses inside the square brackets were measured for each candidate event. The result assumes  $P = (-1)^J$  and uses three relativistic Breit-Wigner functions in the fit for mass difference.

 $m_{B_J(5970)^0} - m_{B^{*+}}$ 

VALUE (MeV)	EVTS	DOCUMENT ID	TECN	COMMENT
• • • We do not use the following data for averages, fits, limits, etc. • • •				
691.6 ± 3.7 ± 5.1	10k	<sup>1</sup> AAIJ	15AB LHCb	$p\bar{p}$ at 7, 8 TeV

<sup>1</sup>AAIJ 15AB reports  $[m_{B_J^0} - m_{B^+}] - (m_{B^{*+}} - m_{B^+}) - m_{\pi^-} = 552 \pm 4 \pm 5$  MeV

which we adjust by the  $\pi^-$  mass. The masses inside the square brackets were measured for each candidate event. The result assumes  $P = -(-1)^J$ ,  $(m_{B^{*+}} - m_{B^+}) = 45.01 \pm 0.30 \pm 0.23$  MeV, and uses three relativistic Breit-Wigner functions in the fit for mass difference.

 $B_J(5970)^0$  WIDTH

VALUE (MeV)	EVTS	DOCUMENT ID	TECN	COMMENT
<b>81 ± 12 OUR AVERAGE</b>				
82 ± 8 ± 9	10K	<sup>1</sup> AAIJ	15AB LHCb	$p\bar{p}$ at 7, 8 TeV
70 ± 30 ± 30	2.6k	AALTONEN	14i CDF	$p\bar{p}$ at 1.96 TeV

• • • We do not use the following data for averages, fits, limits, etc. • • •

56 ± 7 ± 9 10K <sup>2</sup>AAIJ 15AB LHCb  $p\bar{p}$  at 7, 8 TeV

82 ± 10 ± 9 10K <sup>3</sup>AAIJ 15AB LHCb  $p\bar{p}$  at 7, 8 TeV

<sup>1</sup> Assuming  $P = (-1)^J$  and using two relativistic Breit-Wigner functions in the fit for mass difference.

<sup>2</sup> Assuming  $P = (-1)^J$  and using three relativistic Breit-Wigner functions in the fit for mass difference.

<sup>3</sup> Assuming  $P = -(-1)^J$  and using three relativistic Breit-Wigner functions in the fit for mass difference.

 $B_J(5970)^0$  DECAY MODES

Mode	Fraction ( $\Gamma_i/\Gamma$ )
$\Gamma_1$ $B^+\pi^-$	possibly seen
$\Gamma_2$ $B^{*+}\pi^-$	seen

See key on page 999

## Meson Particle Listings

 $B_J(5970)^0$  $B_J(5970)^0$  BRANCHING RATIOS $B_J(5970)^0$  REFERENCES

$\Gamma(B^+\pi^-)/\Gamma_{\text{total}}$					$\Gamma_1/\Gamma$
VALUE	EVTs	DOCUMENT ID	TECN	COMMENT	
possibly seen	10K	<sup>1</sup> AAIJ	15AB LHCb	$pp$ at 7, 8 TeV	
possibly seen	2.6k	AALTONEN	14i CDF	$p\bar{p}$ at 1.96 TeV	

<sup>1</sup> A  $B\pi$  decay is forbidden from a  $P = -(-1)^J$  parent, whereas  $B^*\pi$  is allowed.

$\Gamma(B^{*+}\pi^-)/\Gamma_{\text{total}}$					$\Gamma_2/\Gamma$
VALUE	EVTs	DOCUMENT ID	TECN	COMMENT	
seen	10K	AAIJ	15AB LHCb	$pp$ at 7, 8 TeV	
seen	2.6k	AALTONEN	14i CDF	$p\bar{p}$ at 1.96 TeV	

AAIJ	15AB	JHEP 1504 024	R. Aaij et al.	(LHCb Collab.)
AALTONEN	14i	PR D90 012013	T. Aaltonen et al.	(CDF Collab.)

# Meson Particle Listings

$B_s^0$

## BOTTOM, STRANGE MESONS

### $(B = \pm 1, S = \mp 1)$

$B_s^0 = s\bar{b}, \bar{B}_s^0 = \bar{s}b$ , similarly for  $B_s^{*\prime}s$

$B_s^0$

$$I(J^P) = 0(0^-)$$

$I, J, P$  need confirmation. Quantum numbers shown are quark-model predictions.

### $B_s^0$ MASS

VALUE (MeV)	EVTS	DOCUMENT ID	TECN	COMMENT
<b>5366.88 ± 0.14 OUR FIT</b>				
<b>5366.84 ± 0.15 OUR AVERAGE</b>				
5366.85 ± 0.19 ± 0.13		1 AAIJ	19U	LHCB $pp$ at 7, 8, 13 TeV
5366.83 ± 0.25 ± 0.27		2 AAIJ	18AC	LHCB $pp$ at 7, 8, 13 TeV
5367.08 ± 0.38 ± 0.15	128	3 AAIJ	16U	LHCB $pp$ at 7, 8 TeV
5366.90 ± 0.28 ± 0.23		4 AAIJ	12E	LHCB $pp$ at 7 TeV
5364.4 ± 1.3 ± 0.7		LOUVOT	09	BELL $e^+e^- \rightarrow \Upsilon(5S)$
5366.01 ± 0.73 ± 0.33		5 ACOSTA	06	CDF $p\bar{p}$ at 1.96 TeV
5369.9 ± 2.3 ± 1.3	32	6 ABE	96B	CDF $p\bar{p}$ at 1.8 TeV
5374 ± 16 ± 2	3	7 ABREU	94D	DLPH $e^+e^- \rightarrow Z$
5359 ± 19 ± 7	1	8 AKERS	94J	OPAL $e^+e^- \rightarrow Z$
5368.6 ± 5.6 ± 1.5	2	9 BUSKULIC	93G	ALEP $e^+e^- \rightarrow Z$
• • • We do not use the following data for averages, fits, limits, etc. • • •				
5370 ± 1 ± 3		10 DRUTSKOY	07A	BELL Repl. by LOUVOT 09
5370 ± 40	6	11 AKERS	94J	OPAL $e^+e^- \rightarrow Z$
5383.3 ± 4.5 ± 5.0	14	12 ABE	93F	CDF Repl. by ABE 96B

- 1 Uses  $B_s^0 \rightarrow J/\psi p\bar{p}$  decays.
- 2 Uses  $B_s \rightarrow \chi_{c1} K^+ K^-$  mode.
- 3 Uses  $J/\psi \rightarrow \mu^+ \mu^-, \phi \rightarrow K^+ K^-$  decays, and observes 128 ± 13 events of  $B_s^0 \rightarrow J/\psi \phi \phi$ .
- 4 Uses  $B_s^0 \rightarrow J/\psi \phi$  fully reconstructed decays.
- 5 Uses exclusively reconstructed final states containing a  $J/\psi \rightarrow \mu^+ \mu^-$  decays.
- 6 From the decay  $B_s \rightarrow J/\psi(1S) \phi$ .
- 7 From the decay  $B_s \rightarrow D_s^- \pi^+$ .

$$m_{B_s^0} - m_B$$

$m_B$  is the average of our  $B$  masses  $(m_{B^\pm} + m_{B^0})/2$ .

VALUE (MeV)	CL%	DOCUMENT ID	TECN	COMMENT
<b>87.38 ± 0.16 OUR FIT</b>				
<b>87.42 ± 0.24 OUR AVERAGE</b>				
87.60 ± 0.44 ± 0.09		1 AAIJ	15U	LHCB $pp$ at 7, 8 TeV
87.42 ± 0.30 ± 0.09		2 AAIJ	12E	LHCB $pp$ at 7 TeV
86.64 ± 0.80 ± 0.08		3 ACOSTA	06	CDF $p\bar{p}$ at 1.96 TeV
• • • We use the following data for averages but not for fits. • • •				
89.7 ± 2.7 ± 1.2		4 ABE	96B	CDF $p\bar{p}$ at 1.8 TeV
• • • We do not use the following data for averages, fits, limits, etc. • • •				
80 to 130	68	5 LEE-FRANZINI	90	CSB2 $e^+e^- \rightarrow \Upsilon(5S)$

- 1 The reported result is  $m_{B_s^0} - m_{B^0} = 87.45 \pm 0.44 \pm 0.09$  MeV. We convert it to the mass difference with respect to the average of  $(m_{B^\pm} + m_{B^0})/2$ . Uses the mode  $B_s^0 \rightarrow \psi(2S) K^- \pi^+$ .
- 2 The reported result is  $m_{B_s^0} - m_{B^+} = 87.52 \pm 0.30 \pm 0.12$  MeV. We convert it to the mass difference with respect to the average of  $(m_{B^\pm} + m_{B^0})/2$ .
- 3 The reported result is  $m_{B_s^0} - m_{B^0} = 86.38 \pm 0.90 \pm 0.06$  MeV. We convert it to the mass difference with respect to the average of  $(m_{B^\pm} + m_{B^0})/2$ .

$$m_{B_s^0 H} - m_{B_s^0 L}$$

See the  $B_s^0 \bar{B}_s^0$  MIXING section near the end of these  $B_s^0$  Listings.

### $B_s^0$ MEAN LIFE

"OUR EVALUATION" is provided by the Heavy Flavor Averaging Group (HFLAV, <https://hflav.web.cern.ch/>). It is derived from the average of  $\Gamma_{B_s^0}$ .

VALUE ( $10^{-12}$ s)	EVTS	DOCUMENT ID	TECN	COMMENT
<b>1.515 ± 0.004 OUR EVALUATION</b>				
• • • We do not use the following data for averages, fits, limits, etc. • • •				
1.518 ± 0.041 ± 0.027		1 AALTONEN	11AP	CDF $p\bar{p}$ at 1.96 TeV

1.398 ± 0.044 ± 0.028 -0.025		2 ABAZOV	06V	D0 $p\bar{p}$ at 1.96 TeV
1.42 ± 0.14 ± 0.03 -0.13		3 ABREU	00Y	DLPH $e^+e^- \rightarrow Z$
1.53 ± 0.16 ± 0.07 -0.15		4 ABREU,P	00G	DLPH $e^+e^- \rightarrow Z$
1.36 ± 0.09 ± 0.06 -0.05		5 ABE	99D	CDF $p\bar{p}$ at 1.8 TeV
1.72 ± 0.20 ± 0.18 -0.19 -0.17		6 ACKERSTAFF	98F	OPAL $e^+e^- \rightarrow Z$
1.50 ± 0.16 ± 0.04 -0.15		5 ACKERSTAFF	98G	OPAL $e^+e^- \rightarrow Z$
1.47 ± 0.14 ± 0.08		4 BARATE	98C	ALEP $e^+e^- \rightarrow Z$
1.51 ± 0.11		7 BARATE	98C	ALEP $e^+e^- \rightarrow Z$
1.56 ± 0.29 ± 0.08 -0.26 -0.07		5 ABREU	96F	DLPH Repl. by ABREU 00Y
1.65 ± 0.34 ± 0.12 -0.31		4 ABREU	96F	DLPH Repl. by ABREU 00Y
1.76 ± 0.20 ± 0.15 -0.10		8 ABREU	96F	DLPH Repl. by ABREU 00Y
1.60 ± 0.26 ± 0.13 -0.15		9 ABREU	96F	DLPH Repl. by ABREU,P 00G
1.67 ± 0.14		10 ABREU	96F	DLPH $e^+e^- \rightarrow Z$
1.61 ± 0.30 ± 0.18 -0.29 -0.16	90	4 BUSKULIC	96E	ALEP Repl. by BARATE 98C
1.54 ± 0.14 ± 0.04 -0.13		5 BUSKULIC	96M	ALEP $e^+e^- \rightarrow Z$
1.42 ± 0.27 ± 0.11 -0.23	76	5 ABE	95R	CDF Repl. by ABE 99D
1.74 ± 1.08 ± 0.07 -0.69	8	11 ABE	95R	CDF Sup. by ABE 96N
1.54 ± 0.25 ± 0.06 -0.21	79	5 AKERS	95G	OPAL Repl. by ACKERSTAFF 98G
1.59 ± 0.17 ± 0.03 -0.15	134	5 BUSKULIC	95O	ALEP Sup. by BUSKULIC 96M
0.96 ± 0.37	41	12 ABREU	94E	DLPH Sup. by ABREU 96F
1.92 ± 0.45 ± 0.04 -0.35	31	5 BUSKULIC	94C	ALEP Sup. by BUSKULIC 95O
1.13 ± 0.35 ± 0.09 -0.26	22	5 ACTON	93H	OPAL Sup. by AKERS 95G

- 1 AALTONEN 11AP combines the fully reconstructed  $B_s^0 \rightarrow D_s^- \pi^+$  decays and partially reconstructed  $B_s^0 \rightarrow D_s^- X$  decays.
- 2 Measured using  $D_s \mu^+$  vertices.
- 3 Uses  $D_s^- \ell^+$ , and  $\phi \ell^+$  vertices.
- 4 Measured using  $D_s$  hadron vertices.
- 5 Measured using  $D_s^- \ell^+$  vertices.
- 6 ACKERSTAFF 98F use fully reconstructed  $D_s^- \rightarrow \phi \pi^-$  and  $D_s^- \rightarrow K^*0 K^-$  in the inclusive  $B_s^0$  decay.
- 7 Combined results from  $D_s^- \ell^+$  and  $D_s$  hadron.
- 8 Measured using  $\phi \ell$  vertices.
- 9 Measured using inclusive  $D_s$  vertices.
- 10 Combined result for the four ABREU 96F methods.
- 11 Exclusive reconstruction of  $B_s \rightarrow \psi \phi$ .
- 12 ABREU 94E uses the flight-distance distribution of  $D_s$  vertices,  $\phi$ -lepton vertices, and  $D_s \mu$  vertices.

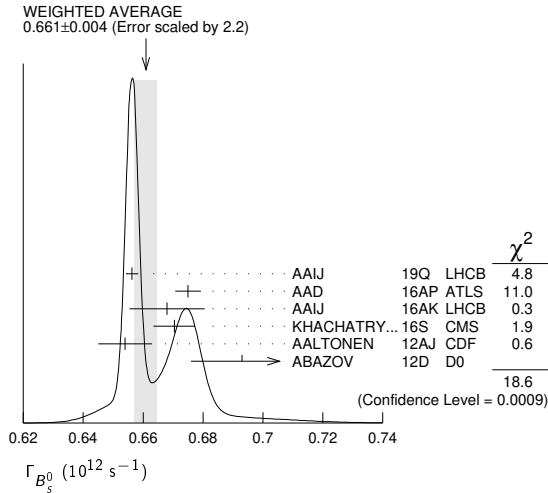
### $\Gamma_{B_s^0}$

"OUR EVALUATION" is an average performed by the Heavy Flavor Averaging Group (HFLAV, <https://hflav.web.cern.ch/>) as described in our "Review on  $B-\bar{B}$  Mixing" in the  $B^0$  section of these Listings. It includes the measurements of  $\Gamma_{B^0}$  and  $\Delta \Gamma_{B^0}$  listed in this section, as well as constraints from effective lifetimes with pure  $CP$  modes and flavor-specific modes.

VALUE ( $10^{12}$ s $^{-1}$ )	DOCUMENT ID	TECN	COMMENT
<b>0.6600 ± 0.0016 OUR EVALUATION</b>			
<b>0.661 ± 0.004 OUR AVERAGE</b>			Error includes scale factor of 2.2. See the ideogram below.
0.6563 ± 0.0021	1 AAIJ	19Q	LHCB $pp$ at 7, 8, 13 TeV
0.675 ± 0.003 ± 0.003	2 AAD	16AP	ATLS $pp$ at 7, 8 TeV
0.668 ± 0.011 ± 0.006	3 AAIJ	16AK	LHCB $pp$ at 7, 8 TeV
0.6704 ± 0.0043 ± 0.0055	2 KHACHATRY...	16S	CMS $pp$ at 8 TeV
0.654 ± 0.008 ± 0.004	2 AALTONEN	12AJ	CDF $p\bar{p}$ at 1.96 TeV
0.693 ± 0.018 -0.017	2 ABAZOV	12D	D0 $p\bar{p}$ at 1.96 TeV
• • • We do not use the following data for averages, fits, limits, etc. • • •			
0.650 ± 0.006 ± 0.004	1 AAIJ	17V	LHCB Repl. by AAIJ 19Q
0.6603 ± 0.0027 ± 0.0015	4 AAIJ	15I	LHCB Repl. by AAIJ 19Q
0.677 ± 0.007 ± 0.004	2 AAD	14U	ATLS Repl. by AAD 16AP
0.661 ± 0.004 ± 0.006	5 AAIJ	13AR	LHCB Repl. by AAIJ 15I
0.677 ± 0.007 ± 0.004	2 AAD	12CV	ATLS Repl. by AAD 14U
0.657 ± 0.009 ± 0.008	2 AAIJ	12D	LHCB Repl. by AAIJ 13AR
0.654 ± 0.011 ± 0.005	2.6 AALTONEN	12D	CDF Repl. by AALTONEN 12AJ
0.672 ± 0.027 ± 0.013	2 ABAZOV	09E	D0 Repl. by ABAZOV 08AM
0.658 ± 0.017 ± 0.009	2.7 AALTONEN	08J	CDF Repl. by AALTONEN 12D
0.658 ± 0.022 ± 0.004	2 ABAZOV	08AMD	D0 Repl. by ABAZOV 12D
0.658 ± 0.035 ± 0.0130 -0.004	2.7 ABAZOV	07	D0 Repl. by ABAZOV 09E
0.714 ± 0.007 ± 0.010 -0.008	2.7 ACOSTA	05	CDF Repl. by AALTONEN 08J

- 1 Measured using time-dependent angular analysis of  $B_S^0 \rightarrow J/\psi K^+ K^-$  in the region  $m(KK) > 1.05$  GeV.
- 2 Measured using a time-dependent angular analysis of  $B_S^0 \rightarrow J/\psi \phi$  decays.
- 3 Measured using a time-dependent angular analysis of  $B_S^0 \rightarrow \psi(2S) \phi$  decays.
- 4 Measured using a time-dependent angular analysis of  $B_S^0 \rightarrow J/\psi K^+ K^-$  decays.
- 5 Measured using a combined time-dependent angular analysis of  $B_S^0 \rightarrow J/\psi K^+ K^-$  and  $B_S^0 \rightarrow J/\psi \pi^+ \pi^-$  decays.
- 6 Assuming CPV phase  $\phi_S = -0.04$ .
- 7 Assuming CPV phase  $\phi_S = 0$ .

- 7 Uses the time-dependent angular analysis of  $B_S^0 \rightarrow J/\psi \phi$  decays and assuming CP-violating angle  $\beta_S(B^0 \rightarrow J/\psi \phi) = 0.02$ .
- 8 Measured the angular and lifetime parameters for the time-dependent angular untagged decays  $B_d^0 \rightarrow J/\psi K^{*0}$  and  $B_S^0 \rightarrow J/\psi \phi$ .
- 9 Measured using the time-dependent angular analysis of  $B_S^0 \rightarrow J/\psi \phi$  decays and assuming CP-violating phase  $\phi_S = 0$ .
- 10 Obtains 90% CL interval  $-0.06 < \Delta\Gamma_S < 0.30$ .
- 11 ABAZOV 07 reports  $0.17 \pm 0.09 \pm 0.02$  with CP-violating phase  $\phi_S$  as a free parameter.
- 12 Combines  $D^0$  measurements of time-dependent angular distributions in  $B_S^0 \rightarrow J/\psi \phi$  and charge asymmetry in semileptonic decays. There is a 4-fold ambiguity in the solution.



$\Delta\Gamma_{B_S^0}$

"OUR EVALUATION" is an average performed by the Heavy Flavor Averaging Group (HFLAV, <https://hflav.web.cern.ch/>) as described in our "Review on  $B-\bar{B}$  Mixing" in the  $B^0$  section of these Listings. It includes the measurements of  $\Gamma_{B_S^0}$  and  $\Delta\Gamma_{B_S^0}$  listed in this section, as well as constraints from effective lifetimes with pure CP modes and flavor-specific modes.

VALUE ( $10^{12} \text{ s}^{-1}$ )	DOCUMENT ID	TECN	COMMENT
<b>0.085 ± 0.004 OUR EVALUATION</b>			
<b>0.081 ± 0.006 OUR AVERAGE</b>			
0.077 ± 0.008 ± 0.003	1 AAIJ	19Q LHCb	$pp$ at 13 TeV
0.066 ± 0.018 ± 0.010	2 AAIJ	17V LHCb	$pp$ at 7, 8 TeV
0.085 ± 0.011 ± 0.007	3 AAD	16AP ATLS	$pp$ at 7, 8 TeV
0.066 ± 0.041 ± 0.007	4 AAIJ	16AK LHCb	$pp$ at 7, 8 TeV
0.095 ± 0.013 ± 0.007	3 KHACHATRY...	16S CMS	$pp$ at 8 TeV
0.068 ± 0.026 ± 0.009	3 AALTONEN	12AJ CDF	$p\bar{p}$ at 1.96 TeV
0.163 ± 0.065 ± 0.064	3,5 ABAZOV	12D D0	$p\bar{p}$ at 1.96 TeV
• • • We do not use the following data for averages, fits, limits, etc. • • •			
0.0805 ± 0.0091 ± 0.0032	1 AAIJ	15I LHCb	Repl. by AAIJ 19Q
0.053 ± 0.021 ± 0.010	3 AAD	14U ATLS	Repl. by AAD 16AP
0.106 ± 0.011 ± 0.007	6 AAIJ	13AR LHCb	Repl. by AAIJ 15I
0.053 ± 0.021 ± 0.010	3 AAD	12CV ATLS	Repl. by AAD 14U
0.123 ± 0.029 ± 0.011	3 AAIJ	12D LHCb	Repl. by AAIJ 13AR
0.075 ± 0.035 ± 0.006	7 AALTONEN	12D CDF	Repl. by AALTONEN 12AJ
0.085 ± 0.072 ± 0.001	8 ABAZOV	09E D0	Repl. by ABAZOV 08AM
0.076 ± 0.059 ± 0.006	9 AALTONEN	08J CDF	Repl. by AALTONEN 12D
0.19 ± 0.07 ± 0.02 ± 0.01	3,10 ABAZOV	08AMD0	Repl. by ABAZOV 12D
0.12 ± 0.08 ± 0.10 ± 0.02	9,11 ABAZOV	07 D0	Repl. by ABAZOV 07N
0.13 ± 0.09	12 ABAZOV	07N D0	Repl. by ABAZOV 09E
0.47 ± 0.19 ± 0.24 ± 0.01	9 ACOSTA	05 CDF	Repl. by AALTONEN 08J

- 1 Measured using time-dependent angular analysis of  $B_S^0 \rightarrow J/\psi K^+ K^-$  decays.
- 2 Measured using time-dependent angular analysis of  $B_S^0 \rightarrow J/\psi K^+ K^-$  in the region  $m(KK) > 1.05$  GeV.
- 3 Measured using the time-dependent angular analysis of  $B_S^0 \rightarrow J/\psi \phi$  decays.
- 4 Measured using time-dependent angular analysis of  $B_S^0 \rightarrow \psi(2S) \phi$  decays.
- 5 The error includes both statistical and systematic uncertainties.
- 6 AAIJ 13AR result comes from a combined fit to  $B_S^0 \rightarrow J/\psi K^+ K^-$  and  $B_S^0 \rightarrow J/\psi \pi^+ \pi^-$  data sets. Also reports  $\Delta\Gamma_S = 0.100 \pm 0.016 \pm 0.003 \text{ ps}^{-1}$  from a fit to  $B_S^0 \rightarrow J/\psi K^+ K^-$  decays.

$\Delta\Gamma_{B_S^0}/\Gamma_{B_S^0}$

$\Gamma_{B_S^0}$  and  $\Delta\Gamma_{B_S^0}$  are the decay rate average and difference between two  $B_S^0$  CP eigenstates (light – heavy).

"OUR EVALUATION" is provided by the Heavy Flavor Averaging Group (HFLAV, <https://hflav.web.cern.ch/>). It is derived from the averages of  $\Gamma_{B_S^0}$  and  $\Delta\Gamma_{B_S^0}$  (and their correlation).

VALUE	CL%	DOCUMENT ID	TECN	COMMENT
<b>0.129 ± 0.006 OUR EVALUATION</b>				
• • • We do not use the following data for averages, fits, limits, etc. • • •				
0.090 ± 0.009 ± 0.023		1 ESEN	13 BELL	$e^+ e^- \rightarrow \Upsilon(5S)$
		2 AAIJ	12D LHCb	$pp$ at 7 TeV
		3 AALTONEN	12D CDF	$p\bar{p}$ at 1.96 TeV
		4 ABAZOV	12D D0	$p\bar{p}$ at 1.96 TeV
0.147 + 0.036 + 0.042 - 0.030 - 0.041		1 ESEN	10 BELL	$e^+ e^- \rightarrow \Upsilon(5S)$
0.072 ± 0.021 ± 0.022		5 ABAZOV	09I D0	$p\bar{p}$ at 1.96 TeV
> 0.012	95	5 AALTONEN	08F CDF	$p\bar{p}$ at 1.96 TeV
0.116 + 0.09 - 0.10 ± 0.010		6 AALTONEN	08J CDF	Repl. by AALTONEN 12D
0.079 + 0.038 + 0.031 - 0.035 - 0.030		5 ABAZOV	07Y D0	Repl. by ABAZOV 09I
0.24 + 0.28 + 0.03 - 0.38 - 0.04		6,7 ABAZOV	05W D0	Repl. by ABAZOV 08AM
0.65 + 0.25 - 0.33 ± 0.01		6 ACOSTA	05 CDF	Repl. by AALTONEN 08J
< 0.46	95	8 ABREU	00Y DLPH	$e^+ e^- \rightarrow Z$
< 0.69	95	9 ABREU,P	00G DLPH	$e^+ e^- \rightarrow Z$
0.25 + 0.21 - 0.14		10 BARATE	00K ALEP	$e^+ e^- \rightarrow Z$
< 0.83	95	11 ABE	99D CDF	$p\bar{p}$ at 1.8 TeV
< 0.67	95	12 ACCIARRI	98S L3	$e^+ e^- \rightarrow Z$

- 1 Assumes CP violation is negligible.
- 2 Measured using the time-dependent angular analysis of  $B_S^0 \rightarrow J/\psi \phi$  decays.
- 3 Uses the time-dependent angular analysis of  $B_S^0 \rightarrow J/\psi \phi$  decays and assuming CP-violating angle  $\beta_S(B^0 \rightarrow J/\psi \phi) = 0.02$ .
- 4 Measured using fully reconstructed  $B_S \rightarrow J/\psi \phi$  decays.
- 5 Assumes  $2 \text{B}(B_S^0 \rightarrow D_S^{(*)} D_S^{(*)}) \simeq \Delta\Gamma_{B_S^0}^{CP} / \Gamma_S$ .
- 6 Measured using the time-dependent angular analysis of  $B_S^0 \rightarrow J/\psi \phi$  decays.
- 7 Uses  $|A_0|^2 - |A_{||}|^2 = 0.355 \pm 0.066$  from ACOSTA 05.
- 8 Uses  $D_S^- \ell^+$ , and  $\phi \ell^+$  vertices.
- 9 Measured using  $D_S$  hadron vertices.
- 10 Uses  $\phi \phi$  correlations from  $B_S^0 \rightarrow D_S^{(*)+} D_S^{(*)-}$ .
- 11 ABE 99D assumes  $\tau_{B_S^0} = 1.55 \pm 0.05$  ps.
- 12 ACCIARRI 98S assumes  $\tau_{B_S^0} = 1.49 \pm 0.06$  ps and PDG 98 values of  $b$  production fraction.

$B_{SH}^0$  MEAN LIFE

$B_{SH}^0$  is the heavy mass state of two  $B_S^0$  CP eigenstates.

"OUR EVALUATION" is provided by the Heavy Flavor Averaging Group (HFLAV, <https://hflav.web.cern.ch/>). It is derived from the averages of  $\Gamma_{B_S^0}$  and  $\Delta\Gamma_{B_S^0}$  (and their correlation).

VALUE ( $10^{-12} \text{ s}$ )	DOCUMENT ID	TECN	COMMENT
<b>1.620 ± 0.007 OUR EVALUATION</b>			
• • • We do not use the following data for averages, fits, limits, etc. • • •			
1.677 ± 0.034 ± 0.011	1 SIRU NYAN	18BY CMS	$pp$ at 8 TeV
2.04 ± 0.44 ± 0.05	2 AAIJ	17AI LHCb	$pp$ at 7, 8, 13 TeV
1.70 ± 0.14 ± 0.05	3 ABAZOV	16C D0	$p\bar{p}$ at 1.96 TeV
1.75 ± 0.12 ± 0.07	4 AAIJ	13AB LHCb	$pp$ at 7 TeV
1.652 ± 0.024 ± 0.024	5 AAIJ	13AR LHCb	$pp$ at 7 TeV
1.700 ± 0.040 ± 0.026	6 AAIJ	12AN LHCb	$pp$ at 7 TeV
	7 AALTONEN	12D CDF	$p\bar{p}$ at 1.96 TeV
	6 AALTONEN	11AB CDF	$p\bar{p}$ at 1.96 TeV
1.70 + 0.12 - 0.11 ± 0.03	8,9 AALTONEN	08J CDF	Repl. by AALTONEN 12D
1.613 + 0.123 - 0.113			
1.58 + 0.39 + 0.01 - 0.42 - 0.02	9 ABAZOV	05W D0	Repl. by ABAZOV 08AM
2.07 + 0.58 - 0.46 ± 0.03	9 ACOSTA	05 CDF	Repl. by AALTONEN 08J



# Meson Particle Listings

## $B_S^0$

- Measured using  $B_S^0 \rightarrow J/\psi \pi^+ \pi^-$  decays with  $0.9240 < m(\pi\pi) < 1.0204$  GeV, which is dominated by the  $f_0(980)$  resonance, making it a  $CP$ -odd state.
- Measured using  $B_S \rightarrow \mu^+ \mu^-$  decays which, in the Standard Model, correspond to  $B_{SH}^0$  decays. Assumes  $-2 \operatorname{Re}(\lambda)/(1 + |\lambda|^2) = 1$ .
- Measured using  $J/\psi \pi^+ \pi^-$  mode with  $0.880 < m(\pi\pi) < 1.080$  GeV/ $c^2$ , which is mostly  $J/\psi f(0)(980)$  mode, a pure  $CP$ -odd final state.
- Measured using a pure  $CP$ -odd final state  $J/\psi K_S^0$  with the assumption that contributions from penguin diagrams are small.
- Measured using  $B_S \rightarrow J/\psi \pi^+ \pi^-$  decays which, in the limit of  $\phi_S = 0$  and  $|\lambda| = 1$ , correspond to  $B_{SH}^0$  decays.
- Measured using a pure  $CP$ -odd final state  $J/\psi f_0(980)$ .
- Uses the time-dependent angular analysis of  $B_S^0 \rightarrow J/\psi \phi$  decays assuming  $CP$ -violating angle  $\beta_S(B^0 \rightarrow J/\psi \phi) = 0.02$ .
- Obtained from  $\Delta\Gamma_S$  and  $\Gamma_S$  fit with a correlation of 0.6.
- Measured using the time-dependent angular analysis of  $B_S^0 \rightarrow J/\psi \phi$  decays.

### $B_{sL}^0$ MEAN LIFE

$B_{sL}^0$  is the light mass state of two  $B_S^0$   $CP$  eigenstates.

"OUR EVALUATION" is provided by the Heavy Flavor Averaging Group (HFLAV, <https://hflav.web.cern.ch/>). It is derived from the averages of  $\Gamma_{B_S^0}$  and  $\Delta\Gamma_{B_S^0}$  (and their correlation).

VALUE ( $10^{-12}$ s)	DOCUMENT ID	TECN	COMMENT
-----------------------	-------------	------	---------

#### 1.423 ± 0.005 OUR EVALUATION

• • • We do not use the following data for averages, fits, limits, etc. • • •			
1.40 ± 0.02	1	SIRUNYAN	18BY CMS $pp$ at 8 TeV
1.479 ± 0.034 ± 0.011	2	AAIJ	16AL LHCb $pp$ at 7, 8 TeV
1.379 ± 0.026 ± 0.017	3	AAIJ	14F LHCb $pp$ at 7, 8 TeV
1.407 ± 0.016 ± 0.007	4	AAIJ	14R LHCb $pp$ at 7 TeV
1.440 ± 0.096 ± 0.009	4	AAIJ	12 LHCb Repl. by AAIJ 14R
1.455 ± 0.046 ± 0.006	4	AAIJ	12R LHCb Repl. by AAIJ 14R
	5	AALTONEN	12D CDF $p\bar{p}$ at 1.96 TeV
1.437 <sup>+0.054</sup> <sub>-0.047</sub>	6,7	AALTONEN	08J CDF Repl. by AALTONEN 12D
1.24 <sup>+0.14</sup> <sub>-0.11</sub> <sup>+0.01</sup> <sub>-0.02</sub>	7	ABAZOV	05W D0 Repl. by ABAZOV 08AM
1.05 <sup>+0.16</sup> <sub>-0.13</sub> ± 0.02	7	ACOSTA	05 CDF Repl. by AALTONEN 08J
1.27 ± 0.33 ± 0.08	8	BARATE	00K ALEP $e^+e^- \rightarrow Z$

- Measured using results in SIRUNYAN 18BY for the heavy  $B_S^0$  lifetime obtained from  $B_S^0 \rightarrow J/\psi \pi^+ \pi^-$  decays and the average effective  $B_S^0 \rightarrow J/\psi \phi$  lifetime, and magnitude squared of the  $CP$ -odd amplitude  $|A_{\perp}|^2 = 0.250 \pm 0.006$ . The uncertainty includes all statistical and systematic contributions.
- Measured using  $B_S^0 \rightarrow J/\psi \eta$  decays.
- Measured using  $B_S^0 \rightarrow D_S^- D_S^+$ . The effective lifetime is translated into a decay width of  $\Gamma_L = 0.725 \pm 0.014 \pm 0.009$  ps<sup>-1</sup>.
- Measured using  $B_S^0 \rightarrow K^+ K^-$  decays. There may still be CPV in the decay.
- Uses the time-dependent angular analysis of  $B_S^0 \rightarrow J/\psi \phi$  decays and assuming  $CP$ -violating angle  $\beta_S(B^0 \rightarrow J/\psi \phi) = 0.02$ .
- Obtained from  $\Delta\Gamma_S$  and  $\Gamma_S$  fit with a correlation of 0.6.
- Measured using the time-dependent angular analysis of  $B_S^0 \rightarrow J/\psi \phi$  decays.
- Uses  $\phi$  correlations from  $B_S^0 \rightarrow D_S^{(*)+} D_S^{(*)-}$ .

### $B_S^0$ MEAN LIFE (Flavor specific)

VALUE ( $10^{-12}$ s)	DOCUMENT ID	TECN	COMMENT
-----------------------	-------------	------	---------

#### 1.527 ± 0.011 OUR EVALUATION

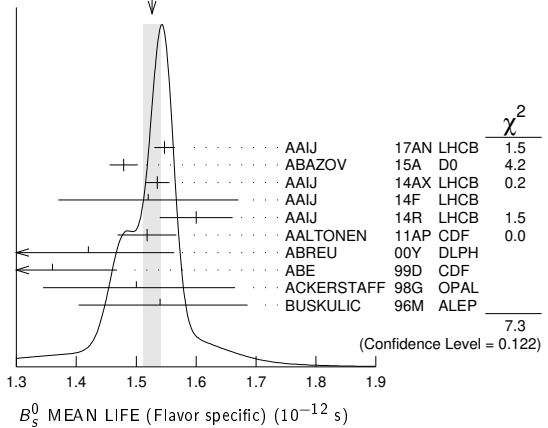
1.526 ± 0.015 OUR AVERAGE Error includes scale factor of 1.3. See the ideogram below.			
1.547 ± 0.013 ± 0.011	1	AAIJ	17AN LHCb $pp$ at 7, 8 TeV
1.479 ± 0.010 ± 0.021	2	ABAZOV	15A D0 $p\bar{p}$ at 1.96 TeV
1.535 ± 0.015 ± 0.014	3	AAIJ	14AX LHCb $pp$ at 7 TeV
1.52 ± 0.15 ± 0.01	4	AAIJ	14F LHCb $pp$ at 7, 8 TeV
1.60 ± 0.06 ± 0.01	5	AAIJ	14R LHCb $pp$ at 7 TeV
1.518 ± 0.041 ± 0.027	6	AALTONEN	11AP CDF $p\bar{p}$ at 1.96 TeV
1.42 <sup>+0.14</sup> <sub>-0.13</sub> ± 0.03	7	ABREU	00Y DLPH $e^+e^- \rightarrow Z$
1.36 ± 0.09 <sup>+0.06</sup> <sub>-0.05</sub>	8	ABE	99D CDF $p\bar{p}$ at 1.8 TeV
1.50 <sup>+0.16</sup> <sub>-0.15</sub> ± 0.04	8	ACKERSTAFF	98G OPAL $e^+e^- \rightarrow Z$
1.54 <sup>+0.14</sup> <sub>-0.13</sub> ± 0.04	8	BUSKULIC	96M ALEP $e^+e^- \rightarrow Z$

- • • We do not use the following data for averages, fits, limits, etc. • • •
- |   |   |        |                            |
|---|---|--------|----------------------------|
| 1.398 ± 0.044 <sup>+0.028</sup> <sub>-0.025</sub> | 9 | ABAZOV | 06V D0 Repl. by ABAZOV 15A |
|---|---|--------|----------------------------|

- AAIJ 17AN value was measured using  $B_S^0 \rightarrow D_S^{(*)-} \mu^+ \nu_\mu$  decays relative to  $B^0 \rightarrow D^{(*)-} \mu^+ \nu_\mu$  decays.
- Measured using  $B_S^0 \rightarrow D_S^- \mu^+ \nu_\mu X$  decays.
- Measured using the  $B_S^0 \rightarrow D_S^- \pi^+$  decays.
- Measured using  $B_S^0 \rightarrow D^+ D_S^-$ .

- Measured using  $B_S^0 \rightarrow \pi^+ K^-$  decays.
- AALTONEN 11AP combines the fully reconstructed  $B_S^0 \rightarrow D_S^- \pi^+$  decays and partially reconstructed  $B_S^0 \rightarrow D_S X$  decays.
- Uses  $D_S^- \ell^+$ , and  $\phi \ell^+$  vertices.
- Measured using  $D_S^- \ell^+$  vertices.
- Measured using  $D_S^- \mu^+$  vertices.

WEIGHTED AVERAGE  
1.526 ± 0.015 (Error scaled by 1.3)



### $B_S^0$ MEAN LIFE ( $B_S \rightarrow J/\psi \phi$ )

VALUE ( $10^{-12}$ s)	DOCUMENT ID	TECN	COMMENT
-----------------------	-------------	------	---------

#### 1.480 ± 0.007 OUR EVALUATION

1.480 ± 0.007 OUR AVERAGE			
1.481 ± 0.007 ± 0.005	1	SIRUNYAN	18BY CMS $pp$ at 8 TeV
1.480 ± 0.011 ± 0.005	1	AAIJ	14E LHCb $pp$ at 7 TeV
1.444 <sup>+0.098</sup> <sub>-0.090</sub> ± 0.020	1	ABAZOV	05B D0 $p\bar{p}$ at 1.96 TeV
1.34 <sup>+0.23</sup> <sub>-0.19</sub> ± 0.05	2	ABE	98B CDF $p\bar{p}$ at 1.8 TeV
1.39 <sup>+0.13</sup> <sub>-0.16</sub> <sup>+0.01</sup> <sub>-0.02</sub>	2	ABAZOV	05W D0 $p\bar{p}$ at 1.96 TeV
1.34 <sup>+0.23</sup> <sub>-0.19</sub> ± 0.05	3	ABE	96N CDF Repl. by ABE 98B

- • • We do not use the following data for averages, fits, limits, etc. • • •
- Measured using fully reconstructed  $B_S \rightarrow J/\psi \phi$  decays.
  - Measured using the time-dependent angular analysis of  $B_S^0 \rightarrow J/\psi \phi$  decays.
  - ABE 96N uses 58 ± 12 exclusive  $B_S \rightarrow J/\psi \phi$  events.

### $\tau_{B_S^0}/\tau_{B^0}$ MEAN LIFE RATIO

$\tau_{B_S^0}/\tau_{B^0}$  (direct measurements)

VALUE	DOCUMENT ID	TECN	COMMENT
-------	-------------	------	---------

#### 0.980 ± 0.006 ± 0.003

0.980 ± 0.006 ± 0.003	1	SIRUNYAN	18BY CMS $pp$ at 8 TeV
-----------------------	---	----------	------------------------

- 1 Measured using  $B_S^0 \rightarrow J/\psi \phi(1020)$  and  $B^0 \rightarrow J/\psi K^*(892)^0$  decays.
- | VALUE ( $10^{12}$ s <sup>-1</sup> ) | DOCUMENT ID | TECN | COMMENT                 |
|-------------------------------------|-------------|------|-------------------------|
| -0.0041 ± 0.0024 ± 0.0015           | 1           | AAIJ | 19Q LHCb $pp$ at 13 TeV |
- 1 Measured using time-dependent angular analysis of  $B_S^0 \rightarrow J/\psi K^+ K^-$  decays.

### $\Gamma_{B_{SH}^0} - \Gamma_{B^0}$

VALUE ( $10^{12}$ s <sup>-1</sup> )	DOCUMENT ID	TECN	COMMENT
-------------------------------------	-------------	------	---------

#### -0.05 ± 0.004 ± 0.004

-0.05 ± 0.004 ± 0.004	1	AAIJ	19AF LHCb $pp$ at 7, 8, 13 TeV
-----------------------	---	------	--------------------------------

- 1 Measured in  $B_S^0 \rightarrow J/\psi \pi^+ \pi^-$  decays.

### $B_S^0$ DECAY MODES

These branching fractions all scale with  $B(\bar{B} \rightarrow B_S^0)$ .

The branching fraction  $B(B_S^0 \rightarrow D_S^- \ell^+ \nu_\ell \text{ anything})$  is not a pure measurement since the measured product branching fraction  $B(\bar{B} \rightarrow B_S^0) \times B(B_S^0 \rightarrow D_S^- \ell^+ \nu_\ell \text{ anything})$  was used to determine  $B(\bar{B} \rightarrow B_S^0)$ , as described in the note on " $B^0$ - $\bar{B}^0$  Mixing"

For inclusive branching fractions, e.g.,  $B \rightarrow D^\pm \text{ anything}$ , the values usually are multiplicities, not branching fractions. They can be greater than one.

Mode	Fraction ( $\Gamma_i/\Gamma$ )	Scale factor/ Confidence level			
$\Gamma_1 D_s^-$ anything	(93 ± 25) %		$\Gamma_{60} J/\psi(1S) f_2(1270), f_2 \rightarrow$	$(1.1 \pm 0.4) \times 10^{-6}$	
$\Gamma_2 \ell \nu_\ell X$	(9.6 ± 0.8) %		$\Gamma_{61} J/\psi(1S) f_2(1270)_0, f_2 \rightarrow$	$(7.5 \pm 1.8) \times 10^{-7}$	
$\Gamma_3 e^+ \nu X^-$	(9.1 ± 0.8) %		$\Gamma_{62} J/\psi(1S) f_2(1270)_\parallel, f_2 \rightarrow$	$(1.09 \pm 0.34) \times 10^{-6}$	
$\Gamma_4 \mu^+ \nu X^-$	(10.2 ± 1.0) %		$\Gamma_{63} J/\psi(1S) f_2(1270)_\perp, f_2 \rightarrow$	$(1.3 \pm 0.8) \times 10^{-6}$	
$\Gamma_5 D_s^- \ell^+ \nu_\ell$ anything	[a] (8.1 ± 1.3) %		$\Gamma_{64} J/\psi(1S) f_0(1370), f_0 \rightarrow$	$(4.5 \pm_{-4.0}^{+0.7}) \times 10^{-5}$	
$\Gamma_6 D_s^{*-} \ell^+ \nu_\ell$ anything	(5.4 ± 1.1) %		$\Gamma_{65} J/\psi(1S) f_0(1500), f_0 \rightarrow$	$(2.11 \pm_{-0.29}^{+0.40}) \times 10^{-5}$	
$\Gamma_7 D_{s1}(2536)^- \mu^+ \nu_\mu, D_{s1}^- \rightarrow$ $D^{*-} K_S^0$	(2.7 ± 0.7) × 10 <sup>-3</sup>		$\Gamma_{66} J/\psi(1S) f_2'(1525)_0, f_2' \rightarrow$	$(1.07 \pm 0.24) \times 10^{-6}$	
$\Gamma_8 D_{s1}(2536)^- X \mu^+ \nu, D_{s1}^- \rightarrow$ $\bar{D}^0 K^+$	(4.4 ± 1.3) × 10 <sup>-3</sup>		$\Gamma_{67} J/\psi(1S) f_2'(1525)_\parallel, f_2' \rightarrow$	$(1.3 \pm_{-0.9}^{+2.7}) \times 10^{-7}$	
$\Gamma_9 D_{s2}(2573)^- X \mu^+ \nu, D_{s2}^- \rightarrow$ $\bar{D}^0 K^+$	(2.7 ± 1.0) × 10 <sup>-3</sup>		$\Gamma_{68} J/\psi(1S) f_2'(1525)_\perp, f_2' \rightarrow$	$(5 \pm 4) \times 10^{-7}$	
$\Gamma_{10} D_s^- \pi^+$	(3.00 ± 0.23) × 10 <sup>-3</sup>		$\Gamma_{69} J/\psi(1S) f_0(1790), f_0 \rightarrow$	$(5.0 \pm_{-1.1}^{+11.0}) \times 10^{-6}$	
$\Gamma_{11} D_s^- \rho^+$	(6.9 ± 1.4) × 10 <sup>-3</sup>		$\Gamma_{70} J/\psi(1S) \pi^+ \pi^-$ (nonresonant)	$(1.8 \pm_{-0.4}^{+1.1}) \times 10^{-5}$	
$\Gamma_{12} D_s^- \pi^+ \pi^+ \pi^-$	(6.1 ± 1.0) × 10 <sup>-3</sup>		$\Gamma_{71} J/\psi(1S) \bar{K}^0 \pi^+ \pi^-$	$< 4.4 \times 10^{-5}$	CL=90%
$\Gamma_{13} D_{s1}(2536)^- \pi^+, D_{s1}^- \rightarrow$ $D_s^- \pi^+ \pi^-$	(2.5 ± 0.8) × 10 <sup>-5</sup>		$\Gamma_{72} J/\psi(1S) K^+ K^-$	$(7.9 \pm 0.7) \times 10^{-4}$	
$\Gamma_{14} D_s^{\mp} K^\pm$	(2.27 ± 0.19) × 10 <sup>-4</sup>		$\Gamma_{73} J/\psi(1S) K^0 K^- \pi^+ + c.c.$	$(9.2 \pm 1.3) \times 10^{-4}$	
$\Gamma_{15} D_s^- K^+ \pi^+ \pi^-$	(3.2 ± 0.6) × 10 <sup>-4</sup>		$\Gamma_{74} J/\psi(1S) \bar{K}^0 K^+ K^-$	$< 1.2 \times 10^{-5}$	CL=90%
$\Gamma_{16} D_s^+ D_s^-$	(4.4 ± 0.5) × 10 <sup>-3</sup>		$\Gamma_{75} J/\psi(1S) f_2'(1525)$	$(2.6 \pm 0.6) \times 10^{-4}$	
$\Gamma_{17} D_s^- D^+$	(2.8 ± 0.5) × 10 <sup>-4</sup>		$\Gamma_{76} J/\psi(1S) \rho \bar{\rho}$	$(3.6 \pm 0.4) \times 10^{-6}$	
$\Gamma_{18} D^+ D^-$	(2.2 ± 0.6) × 10 <sup>-4</sup>		$\Gamma_{77} J/\psi(1S) \gamma$	$< 7.3 \times 10^{-6}$	CL=90%
$\Gamma_{19} D^0 \bar{D}^0$	(1.9 ± 0.5) × 10 <sup>-4</sup>		$\Gamma_{78} J/\psi(1S) \pi^+ \pi^- \pi^+ \pi^-$	$(7.8 \pm 1.0) \times 10^{-5}$	
$\Gamma_{20} D_s^{*-} \pi^+$	(2.0 ± 0.5) × 10 <sup>-3</sup>		$\Gamma_{79} J/\psi(1S) f_1(1285)$	$(7.2 \pm 1.4) \times 10^{-5}$	
$\Gamma_{21} D_s^{\mp} K^\pm$	(1.33 ± 0.35) × 10 <sup>-4</sup>		$\Gamma_{80} \psi(2S) \eta$	$(3.3 \pm 0.9) \times 10^{-4}$	
$\Gamma_{22} D_s^{\mp} \rho^+$	(9.6 ± 2.1) × 10 <sup>-3</sup>		$\Gamma_{81} \psi(2S) \eta'$	$(1.29 \pm 0.35) \times 10^{-4}$	
$\Gamma_{23} D_s^{*+} D_s^- + D_s^{*-} D_s^+$	(1.39 ± 0.17) %		$\Gamma_{82} \psi(2S) \pi^+ \pi^-$	$(7.1 \pm 1.3) \times 10^{-5}$	
$\Gamma_{24} D_s^{*+} D_s^{*-}$	(1.44 ± 0.21) %	S=1.1	$\Gamma_{83} \psi(2S) \phi$	$(5.4 \pm 0.6) \times 10^{-4}$	
$\Gamma_{25} D_s^{(*)+} D_s^{*-}$	(4.5 ± 1.4) %		$\Gamma_{84} \psi(2S) K^- \pi^+$	$(3.1 \pm 0.4) \times 10^{-5}$	
$\Gamma_{26} \bar{D}^{*0} \bar{K}^0$	(2.8 ± 1.1) × 10 <sup>-4</sup>		$\Gamma_{85} \psi(2S) \bar{K}^*(892)^0$	$(3.3 \pm 0.5) \times 10^{-5}$	
$\Gamma_{27} \bar{D}^0 \bar{K}^0$	(4.3 ± 0.9) × 10 <sup>-4</sup>		$\Gamma_{86} \chi_{c1} \phi$	$(2.04 \pm 0.30) \times 10^{-4}$	
$\Gamma_{28} \bar{D}^0 K^- \pi^+$	(1.04 ± 0.13) × 10 <sup>-3</sup>		$\Gamma_{87} \chi_{c1} K^+ K^-$		
$\Gamma_{29} \bar{D}^0 \bar{K}^*(892)^0$	(4.4 ± 0.6) × 10 <sup>-4</sup>		$\Gamma_{88} \chi_{c2} K^+ K^-$		
$\Gamma_{30} \bar{D}^0 \bar{K}^*(1410)$	(3.9 ± 3.5) × 10 <sup>-4</sup>		$\Gamma_{89} \pi^+ \pi^-$	$(7.0 \pm 1.0) \times 10^{-7}$	
$\Gamma_{31} \bar{D}^0 \bar{K}_0^*(1430)$	(3.0 ± 0.7) × 10 <sup>-4</sup>		$\Gamma_{90} \pi^0 \pi^0$	$< 2.1 \times 10^{-4}$	CL=90%
$\Gamma_{32} \bar{D}^0 \bar{K}_2^*(1430)$	(1.1 ± 0.4) × 10 <sup>-4</sup>		$\Gamma_{91} \eta \pi^0$	$< 1.0 \times 10^{-3}$	CL=90%
$\Gamma_{33} \bar{D}^0 \bar{K}^*(1680)$	$< 7.8 \times 10^{-5}$	CL=90%	$\Gamma_{92} \eta \eta$	$< 1.5 \times 10^{-3}$	CL=90%
$\Gamma_{34} \bar{D}^0 \bar{K}_0^*(1950)$	$< 1.1 \times 10^{-4}$	CL=90%	$\Gamma_{93} \rho^0 \rho^0$	$< 3.20 \times 10^{-4}$	CL=90%
$\Gamma_{35} \bar{D}^0 \bar{K}_2^*(1780)$	$< 2.6 \times 10^{-5}$	CL=90%	$\Gamma_{94} \eta' \eta'$	$(3.3 \pm 0.7) \times 10^{-5}$	
$\Gamma_{36} \bar{D}^0 \bar{K}_4^*(2045)$	$< 3.1 \times 10^{-5}$	CL=90%	$\Gamma_{95} \eta' \phi$	$< 8.2 \times 10^{-7}$	CL=90%
$\Gamma_{37} \bar{D}^0 K^- \pi^+$ (non-resonant)	(2.1 ± 0.8) × 10 <sup>-4</sup>		$\Gamma_{96} \phi f_0(980), f_0(980) \rightarrow \pi^+ \pi^-$	$(1.12 \pm 0.21) \times 10^{-6}$	
$\Gamma_{38} D_{s2}^*(2573)^- \pi^+, D_{s2}^* \rightarrow$ $\bar{D}^0 K^-$	(2.6 ± 0.4) × 10 <sup>-4</sup>		$\Gamma_{97} \phi f_2(1270), f_2(1270) \rightarrow$ $\pi^+ \pi^-$	$(6.1 \pm_{-1.5}^{+1.8}) \times 10^{-7}$	
$\Gamma_{39} D_{s1}^*(2700)^- \pi^+, D_{s1}^* \rightarrow$ $\bar{D}^0 K^-$	(1.6 ± 0.8) × 10 <sup>-5</sup>		$\Gamma_{98} \phi \rho^0$	$(2.7 \pm 0.8) \times 10^{-7}$	
$\Gamma_{40} D_{s1}^*(2860)^- \pi^+, D_{s1}^* \rightarrow$ $\bar{D}^0 K^-$	(5 ± 4) × 10 <sup>-5</sup>		$\Gamma_{99} \phi \pi^+ \pi^-$	$(3.5 \pm 0.5) \times 10^{-6}$	
$\Gamma_{41} D_{s3}^*(2860)^- \pi^+, D_{s3}^* \rightarrow$ $\bar{D}^0 K^-$	(2.2 ± 0.6) × 10 <sup>-5</sup>		$\Gamma_{100} \phi \phi$	$(1.87 \pm 0.15) \times 10^{-5}$	
$\Gamma_{42} \bar{D}^0 K^+ K^-$	(5.5 ± 0.8) × 10 <sup>-5</sup>		$\Gamma_{101} \phi \phi \phi$	$(2.2 \pm 0.7) \times 10^{-6}$	
$\Gamma_{43} \bar{D}^0 f_0(980)$	$< 3.1 \times 10^{-6}$	CL=90%	$\Gamma_{102} \pi^+ K^-$	$(5.8 \pm 0.7) \times 10^{-6}$	
$\Gamma_{44} \bar{D}^0 \phi$	(3.0 ± 0.5) × 10 <sup>-5</sup>		$\Gamma_{103} K^+ K^-$	$(2.66 \pm 0.22) \times 10^{-5}$	
$\Gamma_{45} \bar{D}^{*0} \phi$	(3.7 ± 0.6) × 10 <sup>-5</sup>		$\Gamma_{104} K^0 \bar{K}^0$	$(2.0 \pm 0.6) \times 10^{-5}$	
$\Gamma_{46} D^{*\mp} \pi^\pm$	$< 6.1 \times 10^{-6}$	CL=90%	$\Gamma_{105} K^0 \pi^+ \pi^-$	$(9.5 \pm 2.1) \times 10^{-6}$	
$\Gamma_{47} \eta_c \phi$	(5.0 ± 0.9) × 10 <sup>-4</sup>		$\Gamma_{106} K^0 K^\pm \pi^\mp$	$(8.4 \pm 0.9) \times 10^{-5}$	
$\Gamma_{48} \eta_c \pi^+ \pi^-$	(1.8 ± 0.7) × 10 <sup>-4</sup>		$\Gamma_{107} K^*(892)^- \pi^+$	$(2.9 \pm 1.1) \times 10^{-6}$	
$\Gamma_{49} J/\psi(1S) \phi$	(1.08 ± 0.08) × 10 <sup>-3</sup>		$\Gamma_{108} K^*(892)^\pm K^\mp$	$(1.9 \pm 0.5) \times 10^{-5}$	
$\Gamma_{50} J/\psi(1S) \phi \phi$	$(1.24 \pm_{-0.19}^{+0.17}) \times 10^{-5}$		$\Gamma_{109} K_0^*(1430)^\pm K^\mp$	$(3.1 \pm 2.5) \times 10^{-5}$	
$\Gamma_{51} J/\psi(1S) \pi^0$	$< 1.2 \times 10^{-3}$	CL=90%	$\Gamma_{110} K_2^*(1430)^\pm K^\mp$	$(1.0 \pm 1.7) \times 10^{-5}$	
$\Gamma_{52} J/\psi(1S) \eta$	(4.0 ± 0.7) × 10 <sup>-4</sup>	S=1.4	$\Gamma_{111} K^*(892)^0 \bar{K}^0 + c.c.$	$(2.0 \pm 0.6) \times 10^{-5}$	
$\Gamma_{53} J/\psi(1S) K_S^0$	(1.88 ± 0.15) × 10 <sup>-5</sup>		$\Gamma_{112} K_0^*(1430) \bar{K}^0 + c.c.$	$(3.3 \pm 1.0) \times 10^{-5}$	
$\Gamma_{54} J/\psi(1S) \bar{K}^*(892)^0$	(4.1 ± 0.4) × 10 <sup>-5</sup>		$\Gamma_{113} K_2^*(1430)^0 \bar{K}^0 + c.c.$	$(1.7 \pm 2.2) \times 10^{-5}$	
$\Gamma_{55} J/\psi(1S) \eta'$	(3.3 ± 0.4) × 10 <sup>-4</sup>		$\Gamma_{114} K_0^0 \bar{K}^*(892)^0 + c.c.$	$(1.6 \pm 0.4) \times 10^{-5}$	
$\Gamma_{56} J/\psi(1S) \pi^+ \pi^-$	(2.09 ± 0.23) × 10 <sup>-4</sup>	S=1.3	$\Gamma_{115} K^0 K^+ K^-$	$(1.3 \pm 0.6) \times 10^{-6}$	
$\Gamma_{57} J/\psi(1S) f_0(500), f_0 \rightarrow$ $\pi^+ \pi^-$	$< 4 \times 10^{-6}$	CL=90%	$\Gamma_{116} \bar{K}^*(892)^0 \rho^0$	$< 7.67 \times 10^{-4}$	CL=90%
$\Gamma_{58} J/\psi(1S) \rho, \rho \rightarrow \pi^+ \pi^-$	$< 4 \times 10^{-6}$	CL=90%	$\Gamma_{117} \bar{K}^*(892)^0 K^*(892)^0$	$(1.11 \pm 0.27) \times 10^{-5}$	
$\Gamma_{59} J/\psi(1S) f_0(980), f_0 \rightarrow$ $\pi^+ \pi^-$	(1.28 ± 0.18) × 10 <sup>-4</sup>	S=1.7	$\Gamma_{118} K^*(892)^0 \bar{K}_2^*(1430)^0$		
			$\Gamma_{119} K_2^*(1430)^0 \bar{K}^*(892)^0$		
			$\Gamma_{120} K_2^*(1430)^0 \bar{K}_2^*(1430)^0$		
			$\Gamma_{121} \phi K^*(892)^0$	$(1.14 \pm 0.30) \times 10^{-6}$	
			$\Gamma_{122} \rho \bar{\rho}$	$< 1.5 \times 10^{-8}$	CL=90%

## Meson Particle Listings

 $B_s^0$ 

$\Gamma_{123}$	$p\bar{p}K^+K^-$		$(4.5 \pm 0.5) \times 10^{-6}$	
$\Gamma_{124}$	$p\bar{p}K^+\pi^-$		$(1.39 \pm 0.26) \times 10^{-6}$	
$\Gamma_{125}$	$p\bar{p}\pi^+\pi^-$		$(4.3 \pm 2.0) \times 10^{-7}$	
$\Gamma_{126}$	$p\bar{p}K^- + c.c.$		$(5.5 \pm 1.0) \times 10^{-6}$	
$\Gamma_{127}$	$\Lambda_c^- \Lambda\pi^+$		$(3.6 \pm 1.6) \times 10^{-4}$	
$\Gamma_{128}$	$\Lambda_c^- \Lambda_c^+$		$< 8.0 \times 10^{-5}$	CL=95%

Lepton Family number (LF) violating modes or  $\Delta B = 1$  weak neutral current (B1) modes

$\Gamma_{129}$	$\gamma\gamma$	B1	$< 3.1 \times 10^{-6}$	CL=90%
$\Gamma_{130}$	$\phi\gamma$	B1	$(3.4 \pm 0.4) \times 10^{-5}$	
$\Gamma_{131}$	$\mu^+\mu^-$	B1	$(3.0 \pm 0.4) \times 10^{-9}$	
$\Gamma_{132}$	$e^+e^-$	B1	$< 2.8 \times 10^{-7}$	CL=90%
$\Gamma_{133}$	$\tau^+\tau^-$	B1	$< 6.8 \times 10^{-3}$	CL=95%
$\Gamma_{134}$	$\mu^+\mu^-\mu^+\mu^-$	B1	$< 2.5 \times 10^{-9}$	CL=95%
$\Gamma_{135}$	$SP, S \rightarrow \mu^+\mu^-, P \rightarrow \mu^+\mu^-$	B1	$[b] < 2.2 \times 10^{-9}$	CL=95%
$\Gamma_{136}$	$\phi(1020)\mu^+\mu^-$	B1	$(8.2 \pm 1.2) \times 10^{-7}$	
$\Gamma_{137}$	$K^*(892)^0\mu^+\mu^-$		$(2.9 \pm 1.1) \times 10^{-8}$	
$\Gamma_{138}$	$\pi^+\pi^-\mu^+\mu^-$	B1	$(8.4 \pm 1.7) \times 10^{-8}$	
$\Gamma_{139}$	$\phi\nu\bar{\nu}$	B1	$< 5.4 \times 10^{-3}$	CL=90%
$\Gamma_{140}$	$e^\pm\mu^\mp$	LF	$[c] < 5.4 \times 10^{-9}$	CL=90%
$\Gamma_{141}$	$\mu^\pm\tau^\mp$		$< 4.2 \times 10^{-5}$	CL=95%

- [a] Not a pure measurement. See note at head of  $B_s^0$  Decay Modes.  
 [b] Here  $S$  and  $P$  are the hypothetical scalar and pseudoscalar particles with masses of 2.5 GeV/ $c^2$  and 214.3 MeV/ $c^2$ , respectively.  
 [c] The value is for the sum of the charge states or particle/antiparticle states indicated.

## CONSTRAINED FIT INFORMATION

An overall fit to 12 branching ratios uses 20 measurements and one constraint to determine 8 parameters. The overall fit has a  $\chi^2 = 26.7$  for 13 degrees of freedom.

The following *off-diagonal* array elements are the correlation coefficients  $\langle \delta x_i \delta x_j \rangle / (\delta x_i \delta x_j)$ , in percent, from the fit to the branching fractions,  $x_i \equiv \Gamma_i / \Gamma_{\text{total}}$ . The fit constrains the  $x_i$  whose labels appear in this array to sum to one.

$x_{12}$	28					
$x_{14}$	92	26				
$x_{49}$	0	0	0			
$x_{56}$	0	0	0	72		
$x_{59}$	0	0	0	57	67	
$x_{100}$	0	0	0	29	21	17
	$x_{10}$	$x_{12}$	$x_{14}$	$x_{49}$	$x_{56}$	$x_{59}$

 $B_s^0$  BRANCHING RATIOS $\Gamma(D_s^- \text{ anything}) / \Gamma_{\text{total}}$   $\Gamma_1 / \Gamma$ 

VALUE	EVTS	DOCUMENT ID	TECN	COMMENT
<b>0.93 ± 0.25 OUR AVERAGE</b>				
0.91 ± 0.18 ± 0.41		<sup>1</sup> DRUTSKOY 07	BELL	$e^+e^- \rightarrow \Upsilon(4S)$
0.81 ± 0.24 ± 0.22	90	<sup>2</sup> BUSKULIC 96E	ALEP	$e^+e^- \rightarrow Z$
1.56 ± 0.58 ± 0.44	147	<sup>3</sup> ACTON 92N	OPAL	$e^+e^- \rightarrow Z$

<sup>1</sup> The extraction of this result takes into account the correlation between the measurements of  $B(\Upsilon(5S) \rightarrow D_s X)$  and  $B(\Upsilon(5S) \rightarrow D^0 X)$ .

<sup>2</sup> BUSKULIC 96E separate  $c\bar{c}$  and  $b\bar{b}$  sources of  $D_s^+$  mesons using a lifetime tag, subtract generic  $\bar{B} \rightarrow W^+ \rightarrow D_s^+ \text{ anything}$  events, and obtain  $B(\bar{B} \rightarrow B_s^0) \times B(B_s^0 \rightarrow D_s^- \text{ anything}) = 0.088 \pm 0.020 \pm 0.020$  assuming  $B(D_s \rightarrow \phi\pi) = (3.5 \pm 0.4) \times 10^{-2}$  and PDG 1994 values for the relative partial widths to other  $D_s$  channels. We evaluate using our current values  $B(\bar{B} \rightarrow B_s^0) = 0.107 \pm 0.014$  and  $B(D_s \rightarrow \phi\pi) = 0.036 \pm 0.009$ . Our first error is their experiment's and our second error is that due to  $B(\bar{B} \rightarrow B_s^0)$  and  $B(D_s \rightarrow \phi\pi)$ .

<sup>3</sup> ACTON 92N assume that excess of  $147 \pm 48 D_s^0$  events over that expected from  $B^0, B^+,$  and  $c\bar{c}$  is all from  $B_s^0$  decay. The product branching fraction is measured to be  $B(\bar{B} \rightarrow B_s^0)B(B_s^0 \rightarrow D_s^- \text{ anything}) \times B(D_s^- \rightarrow \phi\pi^-) = (5.9 \pm 1.9 \pm 1.1) \times 10^{-3}$ . We evaluate using our current values  $B(\bar{B} \rightarrow B_s^0) = 0.107 \pm 0.014$  and  $B(D_s \rightarrow \phi\pi) = 0.036 \pm 0.009$ . Our first error is their experiment's and our second error is that due to  $B(\bar{B} \rightarrow B_s^0)$  and  $B(D_s \rightarrow \phi\pi)$ .

 $\Gamma(\ell\nu_e X) / \Gamma_{\text{total}}$   $\Gamma_2 / \Gamma$ 

VALUE (units $10^{-2}$ )	DOCUMENT ID	TECN	COMMENT
<b>9.6 ± 0.8 OUR AVERAGE</b>			
9.6 ± 0.4 ± 0.7	<sup>1</sup> OSWALD 13	BELL	$e^+e^- \rightarrow \Upsilon(5S)$
9.5 <sup>+2.5+1.1</sup> <sub>-2.0-1.9</sub>	<sup>2</sup> LEES 12A	BABR	$e^+e^-$

<sup>1</sup> The measurement corresponds to the average of the electron and muon branching fractions.

<sup>2</sup> The measurement corresponds to a branching fraction where the lepton originates from bottom decay and is the average between the electron and muon branching fractions. LEES 12A uses the correlation of the production of  $\phi$  mesons in association with a lepton in  $e^+e^-$  data taken at center-of-mass energies between 10.54 and 11.2 GeV.

 $\Gamma(e^+ \nu X^-) / \Gamma_{\text{total}}$   $\Gamma_3 / \Gamma$ 

VALUE (units $10^{-2}$ )	DOCUMENT ID	TECN	COMMENT
<b>9.1 ± 0.5 ± 0.6</b>			
	OSWALD 13	BELL	$e^+e^- \rightarrow \Upsilon(5S)$

 $\Gamma(\mu^+ \nu X^-) / \Gamma_{\text{total}}$   $\Gamma_4 / \Gamma$ 

VALUE (units $10^{-2}$ )	DOCUMENT ID	TECN	COMMENT
<b>10.2 ± 0.6 ± 0.8</b>			
	OSWALD 13	BELL	$e^+e^- \rightarrow \Upsilon(5S)$

 $\Gamma(D_s^- \ell^+ \nu_\ell \text{ anything}) / \Gamma_{\text{total}}$   $\Gamma_5 / \Gamma$ 

The values and averages in this section serve only to show what values result if one assumes our  $B(\bar{B} \rightarrow B_s^0)$ . They cannot be thought of as measurements since the underlying product branching fractions were also used to determine  $B(\bar{B} \rightarrow B_s^0)$  as described in the note on "Production and Decay of b-Flavored Hadrons."

VALUE (units $10^{-2}$ )	EVTS	DOCUMENT ID	TECN	COMMENT
<b>8.1 ± 1.3 OUR AVERAGE</b>				
8.2 ± 0.2 ± 1.5		<sup>1</sup> OSWALD 15	BELL	$e^+e^- \rightarrow \Upsilon(5S)$
7.6 ± 1.2 ± 2.1	134	<sup>2</sup> BUSKULIC 95O	ALEP	$e^+e^- \rightarrow Z$
10.7 ± 4.3 ± 2.9		<sup>3</sup> ABREU 92M	DLPH	$e^+e^- \rightarrow Z$
10.3 ± 3.6 ± 2.8	18	<sup>4</sup> ACTON 92N	OPAL	$e^+e^- \rightarrow Z$
13 ± 4 ± 4	27	<sup>5</sup> BUSKULIC 92E	ALEP	$e^+e^- \rightarrow Z$

••• We do not use the following data for averages, fits, limits, etc. •••

<sup>1</sup> Obtains  $B_s \rightarrow D_s X e \nu$ , and  $D_s X \mu \nu$  separately, then combines them by assuming systematic uncertainties are fully correlated, except for the one on lepton identification. The third uncertainty adds in quadrature systematic uncertainties from external sources (number of  $B_s$  events, and  $D_s^{(*)}$  branching fractions). OSWALD 15 also measures the cross-section  $\sigma(e^+e^- \rightarrow B_s^{(*)} \bar{B}_s^{(*)}) = 53.8 \pm 1.4 \pm 5.3$  pb at  $\sqrt{s} = 10.86$  GeV.

<sup>2</sup> BUSKULIC 95O use  $D_s \ell$  correlations. The measured product branching ratio is  $B(\bar{B} \rightarrow B_s) \times B(B_s \rightarrow D_s^- \ell^+ \nu_\ell \text{ anything}) = (0.82 \pm 0.09_{-0.13}^{+0.13})\%$  assuming  $B(D_s \rightarrow \phi\pi) = (3.5 \pm 0.4) \times 10^{-2}$  and PDG 1994 values for the relative partial widths to the six other  $D_s$  channels used in this analysis. Combined with results from  $\Upsilon(4S)$  experiments this can be used to extract  $B(\bar{B} \rightarrow B_s) = (11.0 \pm 1.2_{-2.6}^{+2.5})\%$ . We evaluate using our current values  $B(\bar{B} \rightarrow B_s^0) = 0.107 \pm 0.014$  and  $B(D_s \rightarrow \phi\pi) = 0.036 \pm 0.009$ . Our first error is their experiment's and our second error is that due to  $B(\bar{B} \rightarrow B_s^0)$  and  $B(D_s \rightarrow \phi\pi)$ .

<sup>3</sup> ABREU 92M measured muons only and obtained product branching ratio  $B(Z \rightarrow b\bar{b}) \times B(\bar{B} \rightarrow B_s) \times B(B_s \rightarrow D_s \mu^+ \nu_\mu \text{ anything}) \times B(D_s \rightarrow \phi\pi) = (18 \pm 8) \times 10^{-5}$ . We evaluate using our current values  $B(\bar{B} \rightarrow B_s^0) = 0.107 \pm 0.014$  and  $B(D_s \rightarrow \phi\pi) = 0.036 \pm 0.009$ . Our first error is their experiment's and our second error is that due to  $B(\bar{B} \rightarrow B_s^0)$  and  $B(D_s \rightarrow \phi\pi)$ . We use  $B(Z \rightarrow b\bar{b}) = 2B(Z \rightarrow b\bar{b}) = 2 \times (0.2212 \pm 0.0019)$ .

<sup>4</sup> ACTON 92N is measured using  $D_s \rightarrow \phi\pi^+$  and  $K^*(892)^0 K^+$  events. The product branching fraction measured is measured to be  $B(\bar{B} \rightarrow B_s^0)B(B_s^0 \rightarrow D_s^- \ell^+ \nu_\ell \text{ anything}) \times B(D_s^- \rightarrow \phi\pi^-) = (3.9 \pm 1.1 \pm 0.8) \times 10^{-4}$ . We evaluate using our current values  $B(\bar{B} \rightarrow B_s^0) = 0.107 \pm 0.014$  and  $B(D_s \rightarrow \phi\pi) = 0.036 \pm 0.009$ . Our first error is their experiment's and our second error is that due to  $B(\bar{B} \rightarrow B_s^0)$  and  $B(D_s \rightarrow \phi\pi)$ .

<sup>5</sup> BUSKULIC 92E is measured using  $D_s \rightarrow \phi\pi^+$  and  $K^*(892)^0 K^+$  events. They use  $2.7 \pm 0.7\%$  for the  $\phi\pi^+$  branching fraction. The average product branching fraction is measured to be  $B(\bar{B} \rightarrow B_s^0)B(B_s^0 \rightarrow D_s^- \ell^+ \nu_\ell \text{ anything}) = 0.020 \pm 0.0055_{-0.006}^{+0.005}$ . We evaluate using our current values  $B(\bar{B} \rightarrow B_s^0) = 0.107 \pm 0.014$  and  $B(D_s \rightarrow \phi\pi) = 0.036 \pm 0.009$ . Our first error is their experiment's and our second error is that due to  $B(\bar{B} \rightarrow B_s^0)$  and  $B(D_s \rightarrow \phi\pi)$ . Superseded by BUSKULIC 95O.

 $\Gamma(D_s^- \ell^+ \nu_\ell \text{ anything}) / \Gamma_{\text{total}}$   $\Gamma_6 / \Gamma$ 

VALUE (units $10^{-2}$ )	DOCUMENT ID	TECN	COMMENT
<b>5.4 ± 0.4 ± 1.0</b>			
	<sup>1</sup> OSWALD 15	BELL	$e^+e^- \rightarrow \Upsilon(5S)$

<sup>1</sup> Obtains  $B_s \rightarrow D_s^* X e \nu$ , and  $D_s^* X \mu \nu$  separately, then combines them by assuming systematic uncertainties are fully correlated, except for the one on lepton identification. The third uncertainty adds in quadrature systematic uncertainties from external sources (number of  $B_s$  events, and  $D_s^{(*)}$  branching fractions). OSWALD 15 also measures the cross-section  $\sigma(e^+e^- \rightarrow B_s^{(*)} \bar{B}_s^{(*)}) = 53.8 \pm 1.4 \pm 5.3$  pb at  $\sqrt{s} = 10.86$  GeV.

$\Gamma(D_{s1}(2536)^- \mu^+ \nu_\mu, D_{s1}^- \rightarrow D^{*-} K_S^0)/\Gamma_{total}$	$\Gamma_7/\Gamma$		
VALUE (units $10^{-3}$ )	DOCUMENT ID	TECN	COMMENT
<b>2.7 ± 0.7 ± 0.2</b>	<sup>1</sup> ABAZOV	09G	D0 $p\bar{p}$ at 1.96 TeV

<sup>1</sup> ABAZOV 09G reports  $[\Gamma(B_s^0 \rightarrow D_{s1}(2536)^- \mu^+ \nu_\mu, D_{s1}^- \rightarrow D^{*-} K_S^0)/\Gamma_{total}] \times [B(\bar{b} \rightarrow B_s^0)] = (2.66 \pm 0.52 \pm 0.45) \times 10^{-4}$  which we divide by our best value  $B(\bar{b} \rightarrow B_s^0) = (10.0 \pm 0.8) \times 10^{-2}$ . Our first error is their experiment's error and our second error is the systematic error from using our best value.

$\Gamma(D_{s1}(2536)^- X \mu^+ \nu, D_{s1}^- \rightarrow \bar{D}^0 K^+)/\Gamma(D_s^- \ell^+ \nu_\ell \text{ anything})$	$\Gamma_8/\Gamma_5$		
VALUE (units $10^{-2}$ )	DOCUMENT ID	TECN	COMMENT
<b>5.4 ± 1.2 ± 0.5</b>	AAIJ	11A	LHCB $pp$ at 7 TeV

$\Gamma(D_{s2}(2573)^- X \mu^+ \nu, D_{s2}^- \rightarrow \bar{D}^0 K^+)/\Gamma(D_s^- \ell^+ \nu_\ell \text{ anything})$	$\Gamma_9/\Gamma_5$		
VALUE (units $10^{-2}$ )	DOCUMENT ID	TECN	COMMENT
<b>3.3 ± 1.0 ± 0.4</b>	AAIJ	11A	LHCB $pp$ at 7 TeV

$\Gamma(D_{s1}(2536)^- X \mu^+ \nu, D_{s1}^- \rightarrow \bar{D}^0 K^+)/\Gamma(D_{s2}(2573)^- X \mu^+ \nu, D_{s2}^- \rightarrow \bar{D}^0 K^+)$	$\Gamma_8/\Gamma_9$		
VALUE	DOCUMENT ID	TECN	COMMENT
$0.61 \pm 0.14 \pm 0.05$	<sup>1</sup> AAIJ	11A	LHCB $pp$ at 7 TeV
<sup>1</sup> Not independent of other AAIJ 11A measurements.			

$\Gamma(D_s^- \pi^+)/\Gamma_{total}$	$\Gamma_{10}/\Gamma$			
VALUE (units $10^{-3}$ )	EVTS	DOCUMENT ID	TECN	COMMENT
<b>3.00 ± 0.23 OUR FIT</b>				
<b>2.99 ± 0.24 OUR AVERAGE</b>				
$2.95 \pm 0.05 \pm 0.25$		<sup>1</sup> AAIJ	12AG	LHCB $pp$ at 7 TeV
$3.6 \pm 0.5 \pm 0.5$		<sup>2</sup> LOUVOT	09	BELL $e^+e^- \rightarrow \Upsilon(5S)$
$2.8 \pm 0.6 \pm 0.1$		<sup>3</sup> ABULENCIA	07c	CDF $p\bar{p}$ at 1.96 TeV
• • • We do not use the following data for averages, fits, limits, etc. • • •				
$6.8 \pm 2.2 \pm 1.6$		DRUTSKOY	07A	BELL Repl. by LOUVOT 09
$3.3 \pm 1.1 \pm 0.2$		<sup>4</sup> ABULENCIA	06j	CDF Repl. by ABULENCIA 07c
<130 seen	6	<sup>5</sup> AKERS	94j	OPAL $e^+e^- \rightarrow Z$
	1	BUSKULIC	93G	ALEP $e^+e^- \rightarrow Z$

<sup>1</sup> AAIJ 12AG reports  $(2.95 \pm 0.05 \pm 0.17 \pm 0.18) \times 10^{-3}$  where the last uncertainty comes from the semileptonic  $f_S/f_d$  measurement. We combined the systematics in quadrature.

<sup>2</sup> LOUVOT 09 reports  $(3.67 \pm 0.35 \pm 0.65) \times 10^{-3}$  from a measurement of  $[\Gamma(B_s^0 \rightarrow D_s^- \pi^+)/\Gamma_{total}] \times [B(\Upsilon(10860) \rightarrow B_s^{(*)} \bar{B}_s^{(*)})]$  assuming  $B(\Upsilon(10860) \rightarrow B_s^{(*)} \bar{B}_s^{(*)}) = (19.5 \pm 2.6) \times 10^{-2}$ , which we rescale to our best value  $B(\Upsilon(10860) \rightarrow B_s^{(*)} \bar{B}_s^{(*)}) = (20.1 \pm 3.1) \times 10^{-2}$ . Our first error is their experiment's error and our second error is the systematic error from using our best value.

<sup>3</sup> ABULENCIA 07c reports  $[\Gamma(B_s^0 \rightarrow D_s^- \pi^+)/\Gamma_{total}] / [B(B^0 \rightarrow D^- \pi^+)] = 1.13 \pm 0.08 \pm 0.23$  which we multiply by our best value  $B(B^0 \rightarrow D^- \pi^+) = (2.52 \pm 0.13) \times 10^{-3}$ . Our first error is their experiment's error and our second error is the systematic error from using our best value.

<sup>4</sup> ABULENCIA 06j reports  $[\Gamma(B_s^0 \rightarrow D_s^- \pi^+)/\Gamma_{total}] / [B(B^0 \rightarrow D^- \pi^+)] = 1.32 \pm 0.18 \pm 0.38$  which we multiply by our best value  $B(B^0 \rightarrow D^- \pi^+) = (2.52 \pm 0.13) \times 10^{-3}$ . Our first error is their experiment's error and our second error is the systematic error from using our best value.

<sup>5</sup> AKERS 94j sees  $\leq 6$  events and measures the limit on the product branching fraction  $f(\bar{b} \rightarrow B_s^0) \cdot B(B_s^0 \rightarrow D_s^- \pi^+) < 1.3\%$  at CL = 90%. We divide by our current value  $B(\bar{b} \rightarrow B_s^0) = 0.105$ .

$\Gamma(D_s^- \rho^+)/\Gamma(D_s^- \pi^+)$	$\Gamma_{11}/\Gamma_{10}$		
VALUE	DOCUMENT ID	TECN	COMMENT
<b>2.3 ± 0.4 ± 0.2</b>	LOUVOT	10	BELL $e^+e^- \rightarrow \Upsilon(5S)$

$\Gamma(D_s^- \pi^+ \pi^+ \pi^-)/\Gamma_{total}$	$\Gamma_{12}/\Gamma$		
VALUE (units $10^{-3}$ )	DOCUMENT ID	TECN	COMMENT
<b>6.1 ± 1.0 OUR FIT</b>			
<b>6.3 ± 1.5 ± 0.7</b>	<sup>1</sup> ABULENCIA	07c	CDF $p\bar{p}$ at 1.96 TeV

<sup>1</sup> ABULENCIA 07c reports  $[\Gamma(B_s^0 \rightarrow D_s^- \pi^+ \pi^+ \pi^-)/\Gamma_{total}] / [B(B^0 \rightarrow D^- \pi^+ \pi^+ \pi^-)] = 1.05 \pm 0.10 \pm 0.22$  which we multiply by our best value  $B(B^0 \rightarrow D^- \pi^+ \pi^+ \pi^-) = (6.0 \pm 0.7) \times 10^{-3}$ . Our first error is their experiment's error and our second error is the systematic error from using our best value.

$\Gamma(D_s^- \pi^+ \pi^+ \pi^-)/\Gamma(D_s^- \pi^+)$	$\Gamma_{12}/\Gamma_{10}$		
VALUE	DOCUMENT ID	TECN	COMMENT
<b>2.05 ± 0.34 OUR FIT</b>			
<b>2.01 ± 0.37 ± 0.20</b>	AAIJ	11E	LHCB $pp$ at 7 TeV

$\Gamma(D_{s1}(2536)^- \pi^+, D_{s1}^- \rightarrow D_s^- \pi^+ \pi^-)/\Gamma(D_s^- \pi^+ \pi^+ \pi^-)$	$\Gamma_{13}/\Gamma_{12}$		
VALUE (units $10^{-3}$ )	DOCUMENT ID	TECN	COMMENT
<b>4.0 ± 1.0 ± 0.4</b>	AAIJ	12AX	LHCB $pp$ at 7 TeV

$\Gamma(D_s^- K^+)/\Gamma_{total}$	$\Gamma_{14}/\Gamma$		
VALUE (units $10^{-4}$ )	DOCUMENT ID	TECN	COMMENT
<b>2.27 ± 0.19 OUR FIT</b>			
<b>2.3 <math>^{+1.2}_{-1.0} \pm 0.4</math></b>	<sup>1</sup> LOUVOT	09	BELL $e^+e^- \rightarrow \Upsilon(5S)$

<sup>1</sup> LOUVOT 09 reports  $(2.4 \pm 1.2 \pm 0.4) \times 10^{-4}$  from a measurement of  $[\Gamma(B_s^0 \rightarrow D_s^- K^+)/\Gamma_{total}] \times [B(\Upsilon(10860) \rightarrow B_s^{(*)} \bar{B}_s^{(*)})]$  assuming  $B(\Upsilon(10860) \rightarrow B_s^{(*)} \bar{B}_s^{(*)}) = (19.5 \pm 2.6) \times 10^{-2}$ , which we rescale to our best value  $B(\Upsilon(10860) \rightarrow B_s^{(*)} \bar{B}_s^{(*)}) = (20.1 \pm 3.1) \times 10^{-2}$ . Our first error is their experiment's error and our second error is the systematic error from using our best value.

$\Gamma(D_s^- K^+)/\Gamma(D_s^- \pi^+)$	$\Gamma_{14}/\Gamma_{10}$		
VALUE (units $10^{-2}$ )	DOCUMENT ID	TECN	COMMENT
<b>7.55 ± 0.24 OUR FIT</b>			
<b>7.55 ± 0.24 OUR AVERAGE</b>			
$7.52 \pm 0.15 \pm 0.19$	AAIJ	15AC	LHCB $pp$ at 7, 8 TeV
$9.7 \pm 1.8 \pm 0.9$	AALTONEN	09AQ	CDF $p\bar{p}$ at 1.96 TeV
• • • We do not use the following data for averages, fits, limits, etc. • • •			
$6.46 \pm 0.43 \pm 0.25$	AAIJ	12AG	LHCB Repl. by AAIJ 15AC

$\Gamma(D_s^- K^+ \pi^+ \pi^-)/\Gamma(D_s^- \pi^+ \pi^+ \pi^-)$	$\Gamma_{15}/\Gamma_{12}$		
VALUE (units $10^{-2}$ )	DOCUMENT ID	TECN	COMMENT
<b>5.2 ± 0.5 ± 0.3</b>	AAIJ	12AX	LHCB $pp$ at 7 TeV

$\Gamma(D_s^+ D_s^-)/\Gamma_{total}$	$\Gamma_{16}/\Gamma$			
VALUE (units $10^{-3}$ )	CL%	DOCUMENT ID	TECN	COMMENT
<b>4.4 ± 0.5 OUR AVERAGE</b>				
$4.0 \pm 0.2 \pm 0.5$		<sup>1</sup> AAIJ	13AP	LHCB $pp$ at 7 TeV
$5.8 \pm 1.1$		<sup>2</sup> ESEN	13	BELL $e^+e^- \rightarrow \Upsilon(5S)$
$0.9 \pm 1.3$		<sup>3</sup> AALTONEN	12c	CDF $p\bar{p}$ at 1.96 TeV
$5.4 \pm 0.8 \pm 0.8$		• • • We do not use the following data for averages, fits, limits, etc. • • •		
$10.3 \pm 3.9 \pm 2.6$		<sup>4</sup> ESEN	10	BELL Repl. by ESEN 13
$-3.2 \pm 2.5$		<sup>5</sup> AALTONEN	08F	CDF Repl. by AALTONEN 12c
$10.4 \pm 3.5 \pm 1.1$		DRUTSKOY	07A	BELL Repl. by ESEN 10
<67	90			

<sup>1</sup> Uses  $B(B^0 \rightarrow D^- D_s^+) = (7.2 \pm 0.8) \times 10^{-3}$ .

<sup>2</sup> Uses  $\Upsilon(5S) \rightarrow B_s^* \bar{B}_s^*$  decays assuming  $B(\Upsilon(5S) \rightarrow B_s^* \bar{B}_s^*) = (17.1 \pm 3.0)\%$  and  $\Gamma(\Upsilon(5S) \rightarrow B_s^* \bar{B}_s^*) / \Gamma(\Upsilon(5S) \rightarrow B_s^{(*)} \bar{B}_s^{(*)}) = (87.0 \pm 1.7)\%$ .

<sup>3</sup> AALTONEN 12c reports  $(f_S/f_d) (B(B_s^0 \rightarrow D_s^+ D_s^-) / B(B^0 \rightarrow D^- D_s^+)) = 0.183 \pm 0.021 \pm 0.017$ . We multiply this result by our best value of  $B(B^0 \rightarrow D^- D_s^+) = (7.2 \pm 0.8) \times 10^{-3}$  and divide by our best value of  $f_S/f_d$ , where  $1/2 f_S/f_d = 0.1230 \pm 0.0115$ . Our first quoted uncertainty is the combined experiment's uncertainty and our second is the systematic uncertainty from using our best values.

<sup>4</sup> Uses  $\Upsilon(10860) \rightarrow B_s^* \bar{B}_s^*$  assuming  $B(\Upsilon(10860) \rightarrow B_s^{(*)} \bar{B}_s^{(*)}) = (19.3 \pm 2.9)\%$  and  $\Gamma(\Upsilon(10860) \rightarrow B_s^* \bar{B}_s^*) / \Gamma(\Upsilon(10860) \rightarrow B_s^{(*)} \bar{B}_s^{(*)}) = (90.1 \pm 4.0)\%$ .

<sup>5</sup> AALTONEN 08F reports  $[\Gamma(B_s^0 \rightarrow D_s^+ D_s^-)/\Gamma_{total}] / [B(B^0 \rightarrow D^- D_s^+)] = 1.44 \pm 0.48$  which we multiply by our best value  $B(B^0 \rightarrow D^- D_s^+) = (7.2 \pm 0.8) \times 10^{-3}$ . Our first error is their experiment's error and our second error is the systematic error from using our best value.

$\Gamma(D_s^- D^+)/\Gamma_{total}$	$\Gamma_{17}/\Gamma$		
VALUE (units $10^{-4}$ )	DOCUMENT ID	TECN	COMMENT
<b>2.8 ± 0.4 ± 0.3</b>	<sup>1</sup> AAIJ	14AA	LHCB $pp$ at 7 TeV
• • • We do not use the following data for averages, fits, limits, etc. • • •			
$3.6 \pm 0.6 \pm 0.5$	<sup>2</sup> AAIJ	13AP	LHCB Repl. by AAIJ 14AA

<sup>1</sup> AAIJ 14AA reports  $[\Gamma(B_s^0 \rightarrow D_s^- D^+)/\Gamma_{total}] / [B(B^0 \rightarrow D^- D_s^+)] = 0.038 \pm 0.004 \pm 0.003$  which we multiply by our best value  $B(B^0 \rightarrow D^- D_s^+) = (7.2 \pm 0.8) \times 10^{-3}$ . Our first error is their experiment's error and our second error is the systematic error from using our best value.

<sup>2</sup> Uses  $B(B^0 \rightarrow D^- D_s^+) = (7.2 \pm 0.8) \times 10^{-3}$ .

$\Gamma(D^+ D^-)/\Gamma_{total}$	$\Gamma_{18}/\Gamma$		
VALUE (units $10^{-4}$ )	DOCUMENT ID	TECN	COMMENT
<b>2.2 ± 0.4 ± 0.4</b>	<sup>1</sup> AAIJ	13AP	LHCB $pp$ at 7 TeV
• • • We do not use the following data for averages, fits, limits, etc. • • •			
$2.1 \pm 0.3 \pm 0.4$	<sup>1</sup> Uses $B(B^0 \rightarrow D^- D^+) = (2.11 \pm 0.31) \times 10^{-4}$ and $B(B^+ \rightarrow \bar{D}^0 D_s^+) = (10.1 \pm 1.7) \times 10^{-3}$ .		

$\Gamma(D^0 \bar{D}^0)/\Gamma_{total}$	$\Gamma_{19}/\Gamma$		
VALUE (units $10^{-4}$ )	DOCUMENT ID	TECN	COMMENT
<b>1.9 ± 0.3 ± 0.4</b>	<sup>1</sup> AAIJ	13AP	LHCB $pp$ at 7 TeV
• • • We do not use the following data for averages, fits, limits, etc. • • •			
$1.9 \pm 0.3 \pm 0.4$	<sup>1</sup> Uses $B(B^0 \rightarrow D^- D^+) = (2.11 \pm 0.31) \times 10^{-4}$ and $B(B^+ \rightarrow \bar{D}^0 D_s^+) = (10.1 \pm 1.7) \times 10^{-3}$ .		

$\Gamma(D_s^{*-} \pi^+)/\Gamma(D_s^- \pi^+)$	$\Gamma_{20}/\Gamma_{10}$		
VALUE	DOCUMENT ID	TECN	COMMENT
<b>0.65 <math>^{+0.15}_{-0.13} \pm 0.07</math></b>	LOUVOT	10	BELL $e^+e^- \rightarrow \Upsilon(5S)$

## Meson Particle Listings

 $B_S^0$  $\Gamma(D_S^{*\mp} K^\pm)/\Gamma(D_S^{*-} \pi^+)$   $\Gamma_{21}/\Gamma_{20}$ 

VALUE	DOCUMENT ID	TECN	COMMENT
$0.068 \pm 0.005 \pm 0.003$ $-0.002$	AAIJ	15AD	LHCB $pp$ at 7, 8 TeV

 $\Gamma(D_S^{*-} \rho^+)/\Gamma(D_S^- \pi^+)$   $\Gamma_{22}/\Gamma_{10}$ 

VALUE	DOCUMENT ID	TECN	COMMENT
$3.2 \pm 0.6 \pm 0.3$	LOUVOT	10	BELL $e^+ e^- \rightarrow \Upsilon(5S)$

 $\Gamma(D_S^{*-} \rho^+)/\Gamma(D_S^- \rho^+)$   $\Gamma_{22}/\Gamma_{11}$ 

VALUE	DOCUMENT ID	TECN	COMMENT
$1.4 \pm 0.3 \pm 0.1$	LOUVOT	10	BELL $e^+ e^- \rightarrow \Upsilon(5S)$

• • • We do not use the following data for averages, fits, limits, etc. • • •

1 LOUVOT 10 BELL  $e^+ e^- \rightarrow \Upsilon(5S)$   
 † Not independent of other LOUVOT 10 measurements.

 $[\Gamma(D_S^{*+} D_S^-) + \Gamma(D_S^{*-} D_S^+)]/\Gamma_{\text{total}}$   $\Gamma_{23}/\Gamma$ 

VALUE (units $10^{-3}$ )	CL%	DOCUMENT ID	TECN	COMMENT
<b>13.9 ± 1.7 OUR AVERAGE</b>				
13.6 ± 1.0 ± 1.4		1 AAIJ	16P	LHCB $pp$ at 7 TeV
17.6 ± 2.3 ± 4.0		2 ESEN	13	BELL $e^+ e^- \rightarrow \Upsilon(5S)$
12.5 ± 1.7 ± 1.8		3 AALTONEN	12c	CDF $p\bar{p}$ at 1.96 TeV

• • • We do not use the following data for averages, fits, limits, etc. • • •

27.5 ± 8.3 ± 6.9  
 $-7.1$   
 <121 90 DRUTSKOY 07A BELL Repl. by ESEN 10

1 AAIJ 16P reports  $[\Gamma(B_S^0 \rightarrow D_S^{*+} D_S^-) + \Gamma(D_S^{*-} D_S^+)]/\Gamma_{\text{total}} / [B(B^0 \rightarrow D^- D_S^+)] = 1.88 \pm 0.08 \pm 0.12$  which we multiply by our best value  $B(B^0 \rightarrow D^- D_S^+) = (7.2 \pm 0.8) \times 10^{-3}$ . Our first error is their experiment's error and our second error is the systematic error from using our best value.

2 Use  $\Upsilon(5S) \rightarrow B_S^* \bar{B}_S^*$  decays assuming  $B(\Upsilon(5S) \rightarrow B_S^* \bar{B}_S^*) = (17.1 \pm 3.0)\%$  and  $\Gamma(\Upsilon(5S) \rightarrow B_S^* \bar{B}_S^*) / \Gamma(\Upsilon(5S) \rightarrow B_S^{(*)} \bar{B}_S^{(*)}) = (87.0 \pm 1.7)\%$ .

3 AALTONEN 12c reports  $(f_S/f_d) (B(B_S^0 \rightarrow D_S^{*+} D_S^- + D_S^{*-} D_S^+) / B(B^0 \rightarrow D^- D_S^+)) = 0.424 \pm 0.046 \pm 0.035$ . We multiply this result by our best value of  $B(B^0 \rightarrow D^- D_S^+) = (7.2 \pm 0.8) \times 10^{-3}$  and divide by our best value of  $f_S/f_d$ , where  $1/2 f_S/f_d = 0.1230 \pm 0.0115$ . Our first quoted uncertainty is the combined experiment's uncertainty and our second is the systematic uncertainty from using our best values.

4 Uses  $\Upsilon(10860) \rightarrow B_S^* \bar{B}_S^*$  assuming  $B(\Upsilon(10860) \rightarrow B_S^{(*)} \bar{B}_S^{(*)}) = (19.3 \pm 2.9)\%$  and  $\Gamma(\Upsilon(10860) \rightarrow B_S^* \bar{B}_S^*) / \Gamma(\Upsilon(10860) \rightarrow B_S^{(*)} \bar{B}_S^{(*)}) = (90.1 \pm 3.8)_{-4.0}^{\%}$ .

 $\Gamma(D_S^{*+} D_S^{*-})/\Gamma_{\text{total}}$   $\Gamma_{24}/\Gamma$ 

VALUE (units $10^{-3}$ )	CL%	DOCUMENT ID	TECN	COMMENT
<b>14.4 ± 2.1 OUR AVERAGE</b>				
12.7 ± 1.3 ± 1.4		1 AAIJ	16P	LHCB $pp$ at 7 TeV
19.8 ± 3.3 ± 5.2 $-3.1 - 5.0$		2 ESEN	13	BELL $e^+ e^- \rightarrow \Upsilon(5S)$
19.2 ± 2.9 ± 2.7		3 AALTONEN	12c	CDF $p\bar{p}$ at 1.96 TeV

• • • We do not use the following data for averages, fits, limits, etc. • • •

30.8 ± 12.2 ± 8.5  
 $-10.4 - 8.6$   
 <257 90 DRUTSKOY 07A BELL Repl. by ESEN 10

1 AAIJ 16P reports  $[\Gamma(B_S^0 \rightarrow D_S^{*+} D_S^{*-})/\Gamma_{\text{total}}] / [B(B^0 \rightarrow D^- D_S^+)] = 1.76 \pm 0.11 \pm 0.14$  which we multiply by our best value  $B(B^0 \rightarrow D^- D_S^+) = (7.2 \pm 0.8) \times 10^{-3}$ . Our first error is their experiment's error and our second error is the systematic error from using our best value.

2 Use  $\Upsilon(5S) \rightarrow B_S^* \bar{B}_S^*$  decays assuming  $B(\Upsilon(5S) \rightarrow B_S^* \bar{B}_S^*) = (17.1 \pm 3.0)\%$  and  $\Gamma(\Upsilon(5S) \rightarrow B_S^* \bar{B}_S^*) / \Gamma(\Upsilon(5S) \rightarrow B_S^{(*)} \bar{B}_S^{(*)}) = (87.0 \pm 1.7)\%$ .

3 AALTONEN 12c reports  $(f_S/f_d) (B(B_S^0 \rightarrow D_S^{*+} D_S^{*-}) / B(B^0 \rightarrow D^- D_S^+)) = 0.654 \pm 0.072 \pm 0.065$ . We multiply this result by our best value of  $B(B^0 \rightarrow D^- D_S^+) = (7.2 \pm 0.8) \times 10^{-3}$  and divide by our best value of  $f_S/f_d$ , where  $1/2 f_S/f_d = 0.1230 \pm 0.0115$ . Our first quoted uncertainty is the combined experiment's uncertainty and our second is the systematic uncertainty from using our best values.

4 Uses  $\Upsilon(10860) \rightarrow B_S^* \bar{B}_S^*$  assuming  $B(\Upsilon(10860) \rightarrow B_S^{(*)} \bar{B}_S^{(*)}) = (19.3 \pm 2.9)\%$  and  $\Gamma(\Upsilon(10860) \rightarrow B_S^* \bar{B}_S^*) / \Gamma(\Upsilon(10860) \rightarrow B_S^{(*)} \bar{B}_S^{(*)}) = (90.1 \pm 3.8)_{-4.0}^{\%}$ .

 $\Gamma(D_S^{*+} D_S^{*-})/\Gamma_{\text{total}}$   $\Gamma_{25}/\Gamma$ 

"OUR EVALUATION" is an average using rescaled values of the data listed below. The average and rescaling were performed by the Heavy Flavor Averaging Group (HFLAV, <https://hflav.web.cern.ch/>) and are described at <https://hflav.web.cern.ch/>. The averaging/rescaling procedure takes into account correlations between the measurements.

VALUE (%)	CL%	DOCUMENT ID	TECN	COMMENT
<b>4.5 ± 1.4 OUR EVALUATION</b>				
<b>3.4 ± 0.4 OUR AVERAGE</b>				
3.07 ± 0.22 ± 0.33		1 AAIJ	16P	LHCB $pp$ at 7 TeV
4.32 ± 0.42 ± 1.04 $-0.39 - 1.03$		2 ESEN	13	BELL $e^+ e^- \rightarrow \Upsilon(5S)$
3.7 ± 0.4 ± 0.5		3 AALTONEN	12c	CDF $p\bar{p}$ at 1.96 TeV
3.5 ± 1.0 ± 1.1		4 ABAZOV	09I	D0 $p\bar{p}$ at 1.96 TeV
14 ± 6 ± 3		5,6 BARATE	00K	ALEP $e^+ e^- \rightarrow Z$

• • • We do not use the following data for averages, fits, limits, etc. • • •

6.85 ± 1.53 ± 1.79  
 $-1.30 - 1.80$  7,8 ESEN 10 BELL Repl. by ESEN 13  
 3.9 ± 1.9 ± 1.6  
 $-1.7 - 1.5$  4 ABAZOV 07Y D0 Repl. by ABAZOV 09I  
 <0.218 90 BARATE 98Q ALEP  $e^+ e^- \rightarrow Z$

1 AAIJ 16P reports  $[\Gamma(B_S^0 \rightarrow D_S^{*+} D_S^{*-})/\Gamma_{\text{total}}] / [B(B^0 \rightarrow D^- D_S^+)] = 4.24 \pm 0.14 \pm 0.27$  which we multiply by our best value  $B(B^0 \rightarrow D^- D_S^+) = (7.2 \pm 0.8) \times 10^{-3}$ . Our first error is their experiment's error and our second error is the systematic error from using our best value.

2 Use  $\Upsilon(5S) \rightarrow B_S^* \bar{B}_S^*$  decays assuming  $B(\Upsilon(5S) \rightarrow B_S^* \bar{B}_S^*) = (17.1 \pm 3.0)\%$  and  $\Gamma(\Upsilon(5S) \rightarrow B_S^* \bar{B}_S^*) / \Gamma(\Upsilon(5S) \rightarrow B_S^{(*)} \bar{B}_S^{(*)}) = (87.0 \pm 1.7)\%$ .

3 AALTONEN 12c reports  $(f_S/f_d) (B(B_S^0 \rightarrow D_S^{*+} D_S^{*-}) / B(B^0 \rightarrow D^- D_S^+)) = 1.261 \pm 0.095 \pm 0.112$ . We multiply this result by our best value of  $B(B^0 \rightarrow D^- D_S^+) = (7.2 \pm 0.8) \times 10^{-3}$  and divide by our best value of  $f_S/f_d$ , where  $1/2 f_S/f_d = 0.1230 \pm 0.0115$ . Our first quoted uncertainty is the combined experiment's uncertainty and our second is the systematic uncertainty from using our best values.

4 Uses the final states where  $D_S^+ \rightarrow \phi \pi^+$  and  $D_S^- \rightarrow \phi \mu^- \bar{\nu}_\mu$ .

5 Reports  $B(B_S^0 \text{ (short)} \rightarrow D_S^{*+} D_S^{*-}) = (0.23 \pm 0.10 \pm 0.05) \cdot [0.17/B(D_S \rightarrow \phi \chi)]^2$  assuming  $B(B^0 \rightarrow B_S^0 \text{ (short)}) = 50\%$ . We use our best value of  $B(D_S \rightarrow \phi \chi) = 15.7 \pm 1.0\%$  to obtain the quoted result.

6 Uses  $\phi\phi$  correlations from  $B_S^0 \text{ (short)} \rightarrow D_S^{*+} D_S^{*-}$ .

7 Sum of exclusive  $B_S \rightarrow D_S^+ D_S^-$ ,  $B_S \rightarrow D_S^{*+} D_S^{*-}$  and  $B_S \rightarrow D_S^{*+} D_S^{*-}$ .

8 Uses  $\Upsilon(10860) \rightarrow B_S^* \bar{B}_S^*$  assuming  $B(\Upsilon(10860) \rightarrow B_S^{(*)} \bar{B}_S^{(*)}) = (19.3 \pm 2.9)\%$  and  $\Gamma(\Upsilon(10860) \rightarrow B_S^* \bar{B}_S^*) / \Gamma(\Upsilon(10860) \rightarrow B_S^{(*)} \bar{B}_S^{(*)}) = (90.1 \pm 3.8)_{-4.0}^{\%}$ .

 $\Gamma(\bar{D}^0 \bar{K}^0)/\Gamma_{\text{total}}$   $\Gamma_{26}/\Gamma$ 

VALUE (units $10^{-4}$ )	DOCUMENT ID	TECN	COMMENT
<b>2.8 ± 1.0 ± 0.5</b>	1 AAIJ	16c	LHCB $pp$ at 7, 8 TeV

1 Measured and normalized to the  $B_S^0 \rightarrow \bar{D}^0 \bar{K}_S^0$  decay with  $f_S/f_d = 0.259 \pm 0.015$ . Signal significance is 4.4 standard deviations.

 $\Gamma(\bar{D}^0 \bar{K}^0)/\Gamma_{\text{total}}$   $\Gamma_{27}/\Gamma$ 

VALUE (units $10^{-4}$ )	DOCUMENT ID	TECN	COMMENT
<b>4.3 ± 0.5 ± 0.7</b>	1 AAIJ	16c	LHCB $pp$ at 7, 8 TeV

1 Measured and normalized to the  $B^0 \rightarrow \bar{D}^0 \bar{K}_S^0$  decay with  $f_S/f_d = 0.259 \pm 0.015$ .

 $\Gamma(\bar{D}^0 K^- \pi^+)/\Gamma_{\text{total}}$   $\Gamma_{28}/\Gamma$ 

VALUE (units $10^{-4}$ )	DOCUMENT ID	TECN	COMMENT
<b>10.4 ± 1.1 ± 0.5</b>	1 AAIJ	13AQ	LHCB $pp$ at 7 TeV

1 AAIJ 13AQ reports  $[\Gamma(B_S^0 \rightarrow \bar{D}^0 K^- \pi^+)/\Gamma_{\text{total}}] / [B(B^0 \rightarrow \bar{D}^0 \pi^+ \pi^-)] = 1.18 \pm 0.05 \pm 0.12$  which we multiply by our best value  $B(B^0 \rightarrow \bar{D}^0 \pi^+ \pi^-) = (8.8 \pm 0.5) \times 10^{-4}$ . Our first error is their experiment's error and our second error is the systematic error from using our best value.

 $\Gamma(\bar{D}^0 \bar{K}^*(892)^0)/\Gamma_{\text{total}}$   $\Gamma_{29}/\Gamma$ 

VALUE (units $10^{-4}$ )	DOCUMENT ID	TECN	COMMENT
<b>4.4 ± 0.6 OUR AVERAGE</b>			
4.29 ± 0.09 ± 0.65	1 AAIJ	14BH	LHCB $pp$ at 7, 8 TeV
4.7 ± 1.2 ± 0.3	2 AAIJ	11D	LHCB $pp$ at 7 TeV

• • • We do not use the following data for averages, fits, limits, etc. • • •

3.5 ± 0.4 ± 0.4 3 AAIJ 13BX LHCB Repl. by AAIJ 14BH  
 1 Uses Dalitz plot analysis of  $B^0 \rightarrow \bar{D}^0 K^- \pi^+$  decays.  
 2 AAIJ 11D reports  $[\Gamma(B_S^0 \rightarrow \bar{D}^0 \bar{K}^*(892)^0)/\Gamma_{\text{total}}] / [B(B^0 \rightarrow \bar{D}^0 \rho^0)] = 1.48 \pm 0.34 \pm 0.19$  which we multiply by our best value  $B(B^0 \rightarrow \bar{D}^0 \rho^0) = (3.21 \pm 0.21) \times 10^{-4}$ . Our first error is their experiment's error and our second error is the systematic error from using our best value.

3 AAIJ 13BX reports  $[\Gamma(B_S^0 \rightarrow \bar{D}^0 \bar{K}^*(892)^0)/\Gamma_{\text{total}}] / [B(B^0 \rightarrow \bar{D}^0 K^*(892)^0)] = 7.8 \pm 0.7 \pm 0.3 \pm 0.6$  which we multiply by our best value  $B(B^0 \rightarrow \bar{D}^0 K^*(892)^0) = (4.5 \pm 0.6) \times 10^{-6}$ . Our first error is their experiment's error and our second error is the systematic error from using our best value.

 $\Gamma(\bar{D}^0 \bar{K}^*(1410))/\Gamma_{\text{total}}$   $\Gamma_{30}/\Gamma$ 

VALUE (units $10^{-5}$ )	DOCUMENT ID	TECN	COMMENT
<b>38.6 ± 11.4 ± 33.3</b>	1 AAIJ	14BH	LHCB $pp$ at 7, 8 TeV

1 Uses Dalitz plot analysis of  $B_S^0 \rightarrow \bar{D}^0 K^- \pi^+$  decays.

 $\Gamma(\bar{D}^0 \bar{K}_0^*(1430))/\Gamma_{\text{total}}$   $\Gamma_{31}/\Gamma$ 

VALUE (units $10^{-5}$ )	DOCUMENT ID	TECN	COMMENT
<b>30.0 ± 2.4 ± 6.8</b>	1 AAIJ	14BH	LHCB $pp$ at 7, 8 TeV

1 Uses Dalitz plot analysis of  $B_S^0 \rightarrow \bar{D}^0 K^- \pi^+$  decays. Corresponds to the resonant  $K_0^*(1430)$  part of LASS parametrization.

 $\Gamma(\bar{D}^0 \bar{K}_2^*(1430))/\Gamma_{\text{total}}$   $\Gamma_{32}/\Gamma$ 

VALUE (units $10^{-5}$ )	DOCUMENT ID	TECN	COMMENT
<b>11.1 ± 1.8 ± 3.8</b>	1 AAIJ	14BH	LHCB $pp$ at 7, 8 TeV

1 Uses Dalitz plot analysis of  $B_S^0 \rightarrow \bar{D}^0 K^- \pi^+$  decays.

$\Gamma(\overline{D}^0 \overline{K}^*(1680))/\Gamma_{\text{total}}$					$\Gamma_{33}/\Gamma$
VALUE (units $10^{-5}$ )	CL%	DOCUMENT ID	TECN	COMMENT	
<7.8	90	<sup>1</sup> AAIJ	14BH LHCb	$pp$ at 7, 8 TeV	

<sup>1</sup> Uses Dalitz plot analysis of  $B_s^0 \rightarrow \overline{D}^0 K^- \pi^+$  decays.

$\Gamma(\overline{D}^0 \overline{K}_0^*(1950))/\Gamma_{\text{total}}$					$\Gamma_{34}/\Gamma$
VALUE (units $10^{-5}$ )	CL%	DOCUMENT ID	TECN	COMMENT	
<11	90	<sup>1</sup> AAIJ	14BH LHCb	$pp$ at 7, 8 TeV	

<sup>1</sup> Uses Dalitz plot analysis of  $B_s^0 \rightarrow \overline{D}^0 K^- \pi^+$  decays.

$\Gamma(\overline{D}^0 \overline{K}_3^*(1780))/\Gamma_{\text{total}}$					$\Gamma_{35}/\Gamma$
VALUE (units $10^{-5}$ )	CL%	DOCUMENT ID	TECN	COMMENT	
<2.6	90	<sup>1</sup> AAIJ	14BH LHCb	$pp$ at 7, 8 TeV	

<sup>1</sup> Uses Dalitz plot analysis of  $B_s^0 \rightarrow \overline{D}^0 K^- \pi^+$  decays.

$\Gamma(\overline{D}^0 \overline{K}_4^*(2045))/\Gamma_{\text{total}}$					$\Gamma_{36}/\Gamma$
VALUE (units $10^{-5}$ )	CL%	DOCUMENT ID	TECN	COMMENT	
<3.1	90	<sup>1</sup> AAIJ	14BH LHCb	$pp$ at 7, 8 TeV	

<sup>1</sup> Uses Dalitz plot analysis of  $B_s^0 \rightarrow \overline{D}^0 K^- \pi^+$  decays.

$\Gamma(\overline{D}^0 K^- \pi^+ (\text{non-resonant}))/\Gamma_{\text{total}}$					$\Gamma_{37}/\Gamma$
VALUE (units $10^{-5}$ )	CL%	DOCUMENT ID	TECN	COMMENT	
$20.6 \pm 3.8 \pm 7.3$		<sup>1</sup> AAIJ	14BH LHCb	$pp$ at 7, 8 TeV	

<sup>1</sup> Uses Dalitz plot analysis of  $B_s^0 \rightarrow \overline{D}^0 K^- \pi^+$  decays. Corresponds to the non-resonant part of the LASS parametrization.

$\Gamma(D_{s2}^*(2573)^- \pi^+, D_{s2}^* \rightarrow \overline{D}^0 K^-)/\Gamma_{\text{total}}$					$\Gamma_{38}/\Gamma$
VALUE (units $10^{-5}$ )	CL%	DOCUMENT ID	TECN	COMMENT	
$25.7 \pm 0.7 \pm 4.0$		<sup>1</sup> AAIJ	14BH LHCb	$pp$ at 7, 8 TeV	

<sup>1</sup> Uses Dalitz plot analysis of  $B_s^0 \rightarrow \overline{D}^0 K^- \pi^+$  decays.

$\Gamma(D_{s1}^*(2700)^- \pi^+, D_{s1}^* \rightarrow \overline{D}^0 K^-)/\Gamma_{\text{total}}$					$\Gamma_{39}/\Gamma$
VALUE (units $10^{-5}$ )	CL%	DOCUMENT ID	TECN	COMMENT	
$1.6 \pm 0.4 \pm 0.7$		<sup>1</sup> AAIJ	14BH LHCb	$pp$ at 7, 8 TeV	

<sup>1</sup> Uses Dalitz plot analysis of  $B_s^0 \rightarrow \overline{D}^0 K^- \pi^+$  decays.

$\Gamma(D_{s1}^*(2860)^- \pi^+, D_{s1}^* \rightarrow \overline{D}^0 K^-)/\Gamma_{\text{total}}$					$\Gamma_{40}/\Gamma$
VALUE (units $10^{-5}$ )	CL%	DOCUMENT ID	TECN	COMMENT	
$5.0 \pm 1.2 \pm 3.4$		<sup>1</sup> AAIJ	14BH LHCb	$pp$ at 7, 8 TeV	

<sup>1</sup> Uses Dalitz plot analysis of  $B_s^0 \rightarrow \overline{D}^0 K^- \pi^+$  decays.

$\Gamma(D_{s3}^*(2860)^- \pi^+, D_{s3}^* \rightarrow \overline{D}^0 K^-)/\Gamma_{\text{total}}$					$\Gamma_{41}/\Gamma$
VALUE (units $10^{-5}$ )	CL%	DOCUMENT ID	TECN	COMMENT	
$2.2 \pm 0.1 \pm 0.6$		<sup>1</sup> AAIJ	14BH LHCb	$pp$ at 7, 8 TeV	

<sup>1</sup> Uses Dalitz plot analysis of  $B_s^0 \rightarrow \overline{D}^0 K^- \pi^+$  decays.

$\Gamma(\overline{D}^0 K^+ K^-)/\Gamma_{\text{total}}$					$\Gamma_{42}/\Gamma$
VALUE (units $10^{-5}$ )	CL%	DOCUMENT ID	TECN	COMMENT	
$5.5 \pm 0.7 \pm 0.5$		<sup>1</sup> AAIJ	18AZ LHCb	$pp$ at 7, 8 TeV	

• • • We do not use the following data for averages, fits, limits, etc. • • •  
 $5.3 \pm 2.0 \pm 0.5$  <sup>2,3</sup> AAIJ 12AMLHCb Repl. by AAIJ 18AZ

<sup>1</sup> AAIJ 18AZ reports  $[\Gamma(B_s^0 \rightarrow \overline{D}^0 K^+ K^-)/\Gamma_{\text{total}}] / [B(B^0 \rightarrow \overline{D}^0 K^+ K^-)] = 0.930 \pm 0.089 \pm 0.069$  which we multiply by our best value  $B(B^0 \rightarrow \overline{D}^0 K^+ K^-) = (5.9 \pm 0.5) \times 10^{-5}$ . Our first error is their experiment's error and our second error is the systematic error from using our best value.

<sup>2</sup> AAIJ 12AM reports  $[\Gamma(B_s^0 \rightarrow \overline{D}^0 K^+ K^-)/\Gamma_{\text{total}}] / [B(B^0 \rightarrow \overline{D}^0 K^+ K^-)] = 0.90 \pm 0.27 \pm 0.20$  which we multiply by our best value  $B(B^0 \rightarrow \overline{D}^0 K^+ K^-) = (5.9 \pm 0.5) \times 10^{-5}$ . Our first error is their experiment's error and our second error is the systematic error from using our best value.

<sup>3</sup> Uses  $B(b \rightarrow B_s^0)/B(b \rightarrow B^0) = 0.267_{-0.020}^{+0.023}$  measured by the same authors.

$\Gamma(\overline{D}^0 f_0(980))/\Gamma_{\text{total}}$					$\Gamma_{43}/\Gamma$
VALUE	CL%	DOCUMENT ID	TECN	COMMENT	
< $3.1 \times 10^{-6}$	90	AAIJ	15AG LHCb	$pp$ at 7, 8 TeV	

$\Gamma(\overline{D}^0 \phi)/\Gamma(\overline{D}^0 \overline{K}^*(892)^0)$					$\Gamma_{44}/\Gamma_{29}$
VALUE	CL%	DOCUMENT ID	TECN	COMMENT	
$0.069 \pm 0.013 \pm 0.007$		AAIJ	13BX LHCb	Repl. by AAIJ 18AY	

$\Gamma(\overline{D}^0 \phi)/\Gamma_{\text{total}}$					$\Gamma_{44}/\Gamma$
VALUE (units $10^{-5}$ )	CL%	DOCUMENT ID	TECN	COMMENT	
$3.0 \pm 0.4 \pm 0.2$		<sup>1</sup> AAIJ	18AY LHCb	$pp$ at 7 and 8 TeV	

<sup>1</sup> AAIJ 18AY reports  $[\Gamma(B_s^0 \rightarrow \overline{D}^0 \phi)/\Gamma_{\text{total}}] / [B(B^0 \rightarrow \overline{D}^0 \pi^+ \pi^-)] = (3.4 \pm 0.4 \pm 0.3) \times 10^{-2}$  which we multiply by our best value  $B(B^0 \rightarrow \overline{D}^0 \pi^+ \pi^-) = (8.8 \pm 0.5) \times 10^{-4}$ . Our first error is their experiment's error and our second error is the systematic error from using our best value.

$\Gamma(\overline{D}^{*0} \phi)/\Gamma_{\text{total}}$					$\Gamma_{45}/\Gamma$
VALUE (units $10^{-5}$ )	CL%	DOCUMENT ID	TECN	COMMENT	
$3.7 \pm 0.6 \pm 0.2$		<sup>1</sup> AAIJ	18AY LHCb	$pp$ at 7 and 8 TeV	

<sup>1</sup> AAIJ 18AY reports  $[\Gamma(B_s^0 \rightarrow \overline{D}^{*0} \phi)/\Gamma_{\text{total}}] / [B(B^0 \rightarrow \overline{D}^0 \pi^+ \pi^-)] = (4.2 \pm 0.5 \pm 0.4) \times 10^{-2}$  which we multiply by our best value  $B(B^0 \rightarrow \overline{D}^0 \pi^+ \pi^-) = (8.8 \pm 0.5) \times 10^{-4}$ . Our first error is their experiment's error and our second error is the systematic error from using our best value.

$\Gamma(D^{*+} \pi^-)/\Gamma_{\text{total}}$					$\Gamma_{46}/\Gamma$
VALUE	CL%	DOCUMENT ID	TECN	COMMENT	
< $6.1 \times 10^{-6}$	90	<sup>1</sup> AAIJ	13AL LHCb	$pp$ at 7 TeV	

<sup>1</sup> Uses  $f_s/f_d = 0.256 \pm 0.020$  and  $B(B^0 \rightarrow D^{*+} \pi^-) = (2.76 \pm 0.13) \times 10^{-3}$ .

$\Gamma(\eta_c \phi)/\Gamma_{\text{total}}$					$\Gamma_{47}/\Gamma$
VALUE (units $10^{-4}$ )	CL%	DOCUMENT ID	TECN	COMMENT	
$5.01 \pm 0.53 \pm 0.68$		<sup>1</sup> AAIJ	17U LHCb	$pp$ at 7, 8 TeV	

<sup>1</sup> The last uncertainty includes the limited knowledge of the external branching fractions where the  $\eta_c$  is reconstructed in the  $p\overline{p}, K^+ K^- \pi^+ \pi^-, \pi^+ \pi^- \pi^+ \pi^-$ , and  $K^+ K^- K^+ K^-$  decays and  $\phi(1020) \rightarrow K^+ K^-$ .

$\Gamma(\eta_c \pi^+ \pi^-)/\Gamma_{\text{total}}$					$\Gamma_{48}/\Gamma$
VALUE (units $10^{-4}$ )	CL%	DOCUMENT ID	TECN	COMMENT	
$1.76 \pm 0.59 \pm 0.31$		<sup>1</sup> AAIJ	17U LHCb	$pp$ at 7, 8 TeV	

<sup>1</sup> The last uncertainty includes the limited knowledge of the external branching fractions where the  $\eta_c$  is reconstructed in the  $p\overline{p}, K^+ K^- \pi^+ \pi^-, \pi^+ \pi^- \pi^+ \pi^-$ , and  $K^+ K^- K^+ K^-$  decays. The significance of the signal, including systematic uncertainties, is 4.6 standard deviations.

$\Gamma(J/\psi(1S) \phi)/\Gamma_{\text{total}}$					$\Gamma_{49}/\Gamma$
VALUE (units $10^{-3}$ )	CL%	DOCUMENT ID	TECN	COMMENT	
$1.08 \pm 0.08$		OUR FIT			
$1.10 \pm 0.09$		OUR AVERAGE			

<sup>1</sup> AAIJ 13AN LHCb  $pp$  at 7 TeV  
<sup>2</sup> THORNE 13 BELL  $e^+ e^- \rightarrow \Upsilon(5S)$   
<sup>3</sup> ABE 96Q CDF  $p\overline{p}$

• • • We do not use the following data for averages, fits, limits, etc. • • •  
 <6 <sup>1</sup> AKERS 94J OPAL  $e^+ e^- \rightarrow Z$   
 seen 14 <sup>5</sup> ABE 93F CDF  $p\overline{p}$  at 1.8 TeV  
 seen 1 <sup>6</sup> ACTON 92N OPAL Sup. by AKERS 94J

<sup>1</sup> Uses  $f_s/f_d = 0.256 \pm 0.020$  and  $B(B^+ \rightarrow J/\psi K^+) = (10.18 \pm 0.42) \times 10^{-4}$ .

<sup>2</sup> Uses  $f_s = (17.2 \pm 3.0)\%$  as the fraction of  $\Upsilon(5S)$  decaying to  $B_s^{(*)} \overline{B}_s^{(*)}$ .

<sup>3</sup> ABE 96Q reports  $[\Gamma(B_s^0 \rightarrow J/\psi(1S) \phi)/\Gamma_{\text{total}}] \times [\Gamma(\overline{B} \rightarrow B_s^0)/\Gamma(\overline{B} \rightarrow B^+) + \Gamma(\overline{B} \rightarrow B^0)] = (0.185 \pm 0.055 \pm 0.020) \times 10^{-3}$  which we divide by our best value  $\Gamma(\overline{B} \rightarrow B_s^0)/[\Gamma(\overline{B} \rightarrow B^+) + \Gamma(\overline{B} \rightarrow B^0)] = 0.1230 \pm 0.0115$ . Our first error is their experiment's error and our second error is the systematic error from using our best value.

<sup>4</sup> AKERS 94J sees one event and measures the limit on the product branching fraction  $f(\overline{B} \rightarrow B_s^0) \cdot B(B_s^0 \rightarrow J/\psi(1S) \phi) < 7 \times 10^{-4}$  at CL = 90%. We divide by  $B(\overline{B} \rightarrow B_s^0) = 0.112$ .

<sup>5</sup> ABE 93F measured using  $J/\psi(1S) \rightarrow \mu^+ \mu^-$  and  $\phi \rightarrow K^+ K^-$ .

<sup>6</sup> In ACTON 92N a limit on the product branching fraction is measured to be  $f(\overline{B} \rightarrow B_s^0) \cdot B(B_s^0 \rightarrow J/\psi(1S) \phi) \leq 0.22 \times 10^{-2}$ .

$\Gamma(J/\psi(1S) \phi \phi)/\Gamma(J/\psi(1S) \phi)$					$\Gamma_{50}/\Gamma_{49}$
VALUE (units $10^{-2}$ )	CL%	DOCUMENT ID	TECN	COMMENT	
$1.15 \pm 0.12 \pm 0.05$		128	<sup>1</sup> AAIJ	16U LHCb $pp$ at 7, 8 TeV	

<sup>1</sup> Uses  $J/\psi \rightarrow \mu^+ \mu^-$ ,  $\phi \rightarrow K^+ K^-$  decays, and observes  $128 \pm 13$  events of  $B_s^0 \rightarrow J/\psi \phi \phi$ .

$\Gamma(J/\psi(1S) \pi^0)/\Gamma_{\text{total}}$					$\Gamma_{51}/\Gamma$
VALUE	CL%	DOCUMENT ID	TECN	COMMENT	
< $1.2 \times 10^{-3}$	90	<sup>1</sup> ACCIARRI	97c L3		

<sup>1</sup> ACCIARRI 97c assumes  $B^0$  production fraction  $(39.5 \pm 4.0\%)$  and  $B_s$   $(12.0 \pm 3.0\%)$ .

$\Gamma(J/\psi(1S) \eta)/\Gamma_{\text{total}}$					$\Gamma_{52}/\Gamma$
VALUE (units $10^{-4}$ )	CL%	DOCUMENT ID	TECN	COMMENT	
$4.0 \pm 0.7$		OUR AVERAGE		Error includes scale factor of 1.4.	

$3.6_{-0.6}^{+0.5+0.3}$  <sup>1</sup> AAIJ 13A LHCb  $pp$  at 7 TeV  
 $5.10 \pm 0.50_{-0.83}^{+1.17}$  <sup>2</sup> LI 12 BELL  $e^+ e^- \rightarrow \Upsilon(4S)$

• • • We do not use the following data for averages, fits, limits, etc. • • •  
 <38 90 <sup>3</sup> ACCIARRI 97c L3

<sup>1</sup> AAIJ 13A reports  $[\Gamma(B_s^0 \rightarrow J/\psi(1S) \eta)/\Gamma_{\text{total}}] / [B(B^0 \rightarrow J/\psi(1S) \rho^0)] = 14.0 \pm 1.2_{-1.5}^{+1.1+1.1}$  which we multiply by our best value  $B(B^0 \rightarrow J/\psi(1S) \rho^0) = (2.55_{-0.16}^{+0.18}) \times 10^{-5}$ . Our first error is their experiment's error and our second error is the systematic error from using our best value.

<sup>2</sup> Observed for the first time with significances over  $10 \sigma$ . The second error are total systematic uncertainties including the error on  $N(B_s^{(*)} \overline{B}_s^{(*)})$ .

<sup>3</sup> ACCIARRI 97c assumes  $B^0$  production fraction  $(39.5 \pm 4.0\%)$  and  $B_s$   $(12.0 \pm 3.0\%)$ .

## Meson Particle Listings

 $B_S^0$ 

$\Gamma(J/\psi(1S)K_S^0)/\Gamma_{total}$	DOCUMENT ID	TECN	COMMENT	$\Gamma_{53}/\Gamma$
<b>1.88±0.15 OUR AVERAGE</b>				
1.87±0.14±0.06	1 AAIJ	15AL LHCB	$p\bar{p}$ at 7, 8 TeV	
1.9 ±0.4 ±0.2	2 AALTONEN	11A CDF	$p\bar{p}$ at 1.96 TeV	
• • • We do not use the following data for averages, fits, limits, etc. • • •				
1.98±0.16±0.20	3 AAIJ	13AB LHCB	Repl. by AAIJ 15AL	
1.98±0.25±0.20	4 AAIJ	12O LHCB	Repl. by AAIJ 13AB	

- <sup>1</sup> AAIJ 15AL reports  $[\Gamma(B_S^0 \rightarrow J/\psi(1S)K_S^0)/\Gamma_{total}] / [B(B^0 \rightarrow J/\psi(1S)K_S^0)] = (4.31 \pm 0.17 \pm 0.12 \pm 0.25) \times 10^{-2}$  which we multiply by our best value  $B(B^0 \rightarrow J/\psi(1S)K_S^0) = (4.34 \pm 0.15) \times 10^{-4}$ . Our first error is their experiment's error and our second error is the systematic error from using our best value.
- <sup>2</sup> AALTONEN 11A reports  $[\Gamma(B_S^0 \rightarrow J/\psi(1S)K_S^0)/\Gamma_{total}] \times [B(\bar{B} \rightarrow B_S^0)] / [B(\bar{B} \rightarrow B^0)] / [B(B^0 \rightarrow J/\psi(1S)K_S^0)] = (1.09 \pm 0.19 \pm 0.11) \times 10^{-2}$  which we multiply or divide by our best values  $B(\bar{B} \rightarrow B_S^0) = (10.0 \pm 0.8) \times 10^{-2}$ ,  $B(\bar{B} \rightarrow B^0) = (40.8 \pm 0.7) \times 10^{-2}$ ,  $B(B^0 \rightarrow J/\psi(1S)K_S^0) = 1/2 \times B(B^0 \rightarrow J/\psi(1S)K^0) = 1/2 \times (8.68 \pm 0.30) \times 10^{-4}$ . Our first error is their experiment's error and our second error is the systematic error from using our best values.
- <sup>3</sup> AAIJ 13AB reports  $(1.97 \pm 0.14 \pm 0.07 \pm 0.15 \pm 0.08) \times 10^{-5}$  from a measurement of  $[\Gamma(B_S^0 \rightarrow J/\psi(1S)K_S^0)/\Gamma_{total}] / [B(B^0 \rightarrow J/\psi(1S)K^0)] \times [\Gamma(\bar{B} \rightarrow B_S^0)/\Gamma(\bar{B} \rightarrow B^0)]$  assuming  $B(B^0 \rightarrow J/\psi(1S)K^0) = (8.98 \pm 0.35) \times 10^{-4}$ ,  $\Gamma(\bar{B} \rightarrow B_S^0)/\Gamma(\bar{B} \rightarrow B^0) = 0.256 \pm 0.020$ , which we rescale to our best values  $B(B^0 \rightarrow J/\psi(1S)K^0) = (8.68 \pm 0.30) \times 10^{-4}$ ,  $\Gamma(\bar{B} \rightarrow B_S^0)/\Gamma(\bar{B} \rightarrow B^0) = 0.246 \pm 0.023$ . Our first error is their experiment's error and our second error is the systematic error from using our best values.
- <sup>4</sup> AAIJ 12O reports  $(1.83 \pm 0.21 \pm 0.10 \pm 0.14 \pm 0.07) \times 10^{-5}$  from a measurement of  $[\Gamma(B_S^0 \rightarrow J/\psi(1S)K_S^0)/\Gamma_{total}] / [B(B^0 \rightarrow J/\psi(1S)K^0)] \times [\Gamma(\bar{B} \rightarrow B_S^0)/\Gamma(\bar{B} \rightarrow B^0)]$  assuming  $B(B^0 \rightarrow J/\psi(1S)K^0) = (8.71 \pm 0.32) \times 10^{-4}$ ,  $\Gamma(\bar{B} \rightarrow B_S^0)/\Gamma(\bar{B} \rightarrow B^0) = 0.267^{+0.021}_{-0.02}$ , which we rescale to our best values  $B(B^0 \rightarrow J/\psi(1S)K^0) = (8.68 \pm 0.30) \times 10^{-4}$ ,  $\Gamma(\bar{B} \rightarrow B_S^0)/\Gamma(\bar{B} \rightarrow B^0) = 0.246 \pm 0.023$ . Our first error is their experiment's error and our second error is the systematic error from using our best values.

$\Gamma(J/\psi(1S)\bar{K}^*(892)^0)/\Gamma_{total}$	DOCUMENT ID	TECN	COMMENT	$\Gamma_{54}/\Gamma$
<b>4.14±0.18±0.35</b>				
• • • We do not use the following data for averages, fits, limits, etc. • • •				
4.4 $^{+0.5}_{-0.4}$ ±0.8	2 AAIJ	12AP LHCB	Repl. by AAIJ 15AV	
9 ±4 ±1	3 AALTONEN	11A CDF	$p\bar{p}$ at 1.96 TeV	

- <sup>1</sup> AAIJ 15AV result combines two measurements with different normalizing modes of  $B^0 \rightarrow J/\psi K^*(892)^0$  and  $B_S^0 \rightarrow J/\psi\phi$ .
- <sup>2</sup> AAIJ 12AP reports  $B(B_S^0 \rightarrow J/\psi(1S)\bar{K}^*(892)^0)/B(B^0 \rightarrow J/\psi(1S)K^*(892)^0) = (3.43^{+0.34}_{-0.36} \pm 0.50) \times 10^{-2}$  and  $B(B^0 \rightarrow J/\psi(1S)K^*(892)^0) = (1.29 \pm 0.05 \pm 0.13) \times 10^{-3}$  after correcting for the contribution from  $K\pi$  S-wave beneath the  $K^*$  peak.
- <sup>3</sup> AALTONEN 11A reports  $[\Gamma(B_S^0 \rightarrow J/\psi(1S)\bar{K}^*(892)^0)/\Gamma_{total}] \times [B(\bar{B} \rightarrow B_S^0)] / [B(\bar{B} \rightarrow B^0)] / [B(B^0 \rightarrow J/\psi(1S)K^*(892)^0)] = 0.0168 \pm 0.0024 \pm 0.0068$  which we multiply or divide by our best values  $B(\bar{B} \rightarrow B_S^0) = (10.0 \pm 0.8) \times 10^{-2}$ ,  $B(\bar{B} \rightarrow B^0) = (40.8 \pm 0.7) \times 10^{-2}$ ,  $B(B^0 \rightarrow J/\psi(1S)K^*(892)^0) = (1.27 \pm 0.05) \times 10^{-3}$ . Our first error is their experiment's error and our second error is the systematic error from using our best values.

$\Gamma(J/\psi(1S)\eta)/\Gamma_{total}$	DOCUMENT ID	TECN	COMMENT	$\Gamma_{55}/\Gamma$
<b>3.3 ±0.4 OUR AVERAGE</b>				
3.2 $^{+0.4}_{-0.5}$ ±0.2	1 AAIJ	13A LHCB	$p\bar{p}$ at 7 TeV	
3.71±0.61±0.85 -0.60	2 LI	12 BELL	$e^+e^- \rightarrow \Upsilon(4S)$	

- <sup>1</sup> AAIJ 13A reports  $[\Gamma(B_S^0 \rightarrow J/\psi(1S)\eta)/\Gamma_{total}] / [B(B^0 \rightarrow J/\psi(1S)\rho^0)] = 12.7 \pm 1.1^{+0.5+1.0}_{-1.3-0.9}$  which we multiply by our best value  $B(B^0 \rightarrow J/\psi(1S)\rho^0) = (2.55^{+0.18}_{-0.16}) \times 10^{-5}$ . Our first error is their experiment's error and our second error is the systematic error from using our best value.
- <sup>2</sup> Observed for the first time with significances over  $10\sigma$ . The second error are total systematic uncertainties including the error on  $N(B_S^{(*)}\bar{B}_S^{(*)})$ .

$\Gamma(J/\psi(1S)\eta')/\Gamma(J/\psi(1S)\eta)$	DOCUMENT ID	TECN	COMMENT	$\Gamma_{55}/\Gamma_{52}$
<b>0.87 ±0.06 OUR AVERAGE</b>				
0.902±0.072±0.045	1 AAIJ	15D LHCB	$p\bar{p}$ at 7, 8 TeV	
0.90 ±0.09 $^{+0.06}_{-0.02}$	2 AAIJ	13A LHCB	$p\bar{p}$ at 7 TeV	
0.73 ±0.14 ±0.02	2 LI	12 BELL	$e^+e^- \rightarrow \Upsilon(4S)$	

- <sup>1</sup> Uses  $J/\psi \rightarrow \mu^+\mu^-$ ,  $\eta' \rightarrow \rho^0\gamma$ , and  $\eta' \rightarrow \eta\pi^+\pi^-$  decays.
- <sup>2</sup> Strongly correlated with measurements of  $\Gamma(J/\psi(1S)\eta)/\Gamma$  and  $\Gamma(J/\psi(1S)\eta')/\Gamma$  reported in the same reference.

$\Gamma(J/\psi(1S)\pi^+\pi^-)/\Gamma(J/\psi(1S)\phi)$	DOCUMENT ID	TECN	COMMENT	$\Gamma_{56}/\Gamma_{49}$
<b>19.4±1.5 OUR FIT</b>				
19.9±0.7±0.2	1 AAIJ	12AO LHCB	$p\bar{p}$ at 7 TeV	

- Error includes scale factor of 2.2.
- <sup>1</sup> AAIJ 12AO reports  $(19.79 \pm 0.47 \pm 0.52) \times 10^{-2}$  from a measurement of  $[\Gamma(B_S^0 \rightarrow J/\psi(1S)\pi^+\pi^-)/\Gamma(B_S^0 \rightarrow J/\psi(1S)\phi)] / [B(\phi(1020) \rightarrow K^+K^-)]$  assuming  $B(\phi(1020) \rightarrow K^+K^-) = (48.9 \pm 0.5) \times 10^{-2}$ , which we rescale to our best value  $B(\phi(1020) \rightarrow K^+K^-) = (49.2 \pm 0.5) \times 10^{-2}$ . Our first error is their experiment's error and our second error is the systematic error from using our best value.

$\Gamma(J/\psi(1S)f_0(980), f_0 \rightarrow \pi^+\pi^-)/\Gamma_{total}$	DOCUMENT ID	TECN	COMMENT	$\Gamma_{59}/\Gamma$
<b>1.28±0.18 OUR FIT</b>				
1.16 $^{+0.31}_{-0.19}$ $^{+0.30}_{-0.25}$	1 LI	11 BELL	$e^+e^- \rightarrow \Upsilon(5S)$	

- The second error includes both the detector systematic and the uncertainty in the number of produced  $\Upsilon(5S) \rightarrow B_S^{(*)}\bar{B}_S^{(*)}$  pairs.

$\Gamma(J/\psi(1S)f_0(500), f_0 \rightarrow \pi^+\pi^-)/\Gamma(J/\psi(1S)f_0(980), f_0 \rightarrow \pi^+\pi^-)$	DOCUMENT ID	TECN	COMMENT	$\Gamma_{57}/\Gamma_{59}$
<b>&lt;0.034</b>				
<0.034	1 AAIJ	14BR LHCB	$p\bar{p}$ at 7, 8 TeV	

- <sup>1</sup> Reported first of two solutions using the full Dalitz analysis.

$\Gamma(J/\psi(1S)\rho, \rho \rightarrow \pi^+\pi^-)/\Gamma(J/\psi(1S)\pi^+\pi^-)$	DOCUMENT ID	TECN	COMMENT	$\Gamma_{58}/\Gamma_{56}$
<b>&lt;0.017</b>				
<0.017	1 AAIJ	14BR LHCB	$p\bar{p}$ at 7, 8 TeV	

- <sup>1</sup> Reported first of two solutions using the full Dalitz analysis.

$\Gamma(J/\psi(1S)f_0(980), f_0 \rightarrow \pi^+\pi^-)/\Gamma(J/\psi(1S)\pi^+\pi^-)$	DOCUMENT ID	TECN	COMMENT	$\Gamma_{59}/\Gamma_{56}$
<b>0.61 <math>^{+0.06}_{-0.07}</math> OUR FIT</b>				
0.703±0.015 $^{+0.004}_{-0.051}$	1 AAIJ	14BR LHCB	$p\bar{p}$ at 7, 8 TeV	

- <sup>1</sup> Reported first of two solutions using the full Dalitz analysis.

$\Gamma(J/\psi(1S)f_2(1270)_0, f_2 \rightarrow \pi^+\pi^-)/\Gamma(J/\psi(1S)\pi^+\pi^-)$	DOCUMENT ID	TECN	COMMENT	$\Gamma_{61}/\Gamma_{56}$
<b>0.36±0.07±0.03</b>				
0.36±0.07±0.03	1 AAIJ	14BR LHCB	$p\bar{p}$ at 7, 8 TeV	

- <sup>1</sup> Reported first of two solutions using the full Dalitz analysis.

$\Gamma(J/\psi(1S)f_2(1270)_\parallel, f_2 \rightarrow \pi^+\pi^-)/\Gamma(J/\psi(1S)\pi^+\pi^-)$	DOCUMENT ID	TECN	COMMENT	$\Gamma_{62}/\Gamma_{56}$
<b>0.52±0.15 <math>^{+0.05}_{-0.02}</math></b>				
0.52±0.15 $^{+0.05}_{-0.02}$	1 AAIJ	14BR LHCB	$p\bar{p}$ at 7, 8 TeV	

- <sup>1</sup> Reported first of two solutions using the full Dalitz analysis.

$\Gamma(J/\psi(1S)f_2(1270)_\perp, f_2 \rightarrow \pi^+\pi^-)/\Gamma(J/\psi(1S)\pi^+\pi^-)$	DOCUMENT ID	TECN	COMMENT	$\Gamma_{63}/\Gamma_{56}$
<b>0.63±0.34 <math>^{+0.16}_{-0.08}</math></b>				
0.63±0.34 $^{+0.16}_{-0.08}$	1 AAIJ	14BR LHCB	$p\bar{p}$ at 7, 8 TeV	

- <sup>1</sup> Reported first of two solutions using the full Dalitz analysis.

$\Gamma(J/\psi(1S)f_0(1500), f_0 \rightarrow \pi^+\pi^-)/\Gamma(J/\psi(1S)\pi^+\pi^-)$	DOCUMENT ID	TECN	COMMENT	$\Gamma_{65}/\Gamma_{56}$
<b>0.101±0.008 <math>^{+0.011}_{-0.003}</math></b>				
0.101±0.008 $^{+0.011}_{-0.003}$	1 AAIJ	14BR LHCB	$p\bar{p}$ at 7, 8 TeV	

- <sup>1</sup> Reported first of two solutions using the full Dalitz analysis.

$\Gamma(J/\psi(1S)f_2'(1525)_0, f_2' \rightarrow \pi^+\pi^-)/\Gamma(J/\psi(1S)\pi^+\pi^-)$	DOCUMENT ID	TECN	COMMENT	$\Gamma_{66}/\Gamma_{56}$
<b>0.51±0.09 <math>^{+0.05}_{-0.04}</math></b>				
0.51±0.09 $^{+0.05}_{-0.04}$	1 AAIJ	14BR LHCB	$p\bar{p}$ at 7, 8 TeV	

- <sup>1</sup> Reported first of two solutions using the full Dalitz analysis.

$\Gamma(J/\psi(1S)f_2'(1525)_\parallel, f_2' \rightarrow \pi^+\pi^-)/\Gamma(J/\psi(1S)\pi^+\pi^-)$	DOCUMENT ID	TECN	COMMENT	$\Gamma_{67}/\Gamma_{56}$
<b>0.06 <math>^{+0.13}_{-0.04}</math> ±0.01</b>				
0.06 $^{+0.13}_{-0.04}$ ±0.01	1 AAIJ	14BR LHCB	$p\bar{p}$ at 7, 8 TeV	

- <sup>1</sup> Reported first of two solutions using the full Dalitz analysis.

$\Gamma(J/\psi(1S)f_2'(1525)_\perp, f_2' \rightarrow \pi^+\pi^-)/\Gamma(J/\psi(1S)\pi^+\pi^-)$	DOCUMENT ID	TECN	COMMENT	$\Gamma_{68}/\Gamma_{56}$
<b>0.26±0.18 <math>^{+0.06}_{-0.04}</math></b>				
0.26±0.18 $^{+0.06}_{-0.04}$	1 AAIJ	14BR LHCB	$p\bar{p}$ at 7, 8 TeV	

- <sup>1</sup> Reported first of two solutions using the full Dalitz analysis.

$\Gamma(J/\psi(1S)f_0(1790), f_0 \rightarrow \pi^+\pi^-)/\Gamma(J/\psi(1S)\pi^+\pi^-)$	DOCUMENT ID	TECN	COMMENT	$\Gamma_{69}/\Gamma_{56}$
<b>0.024±0.004 <math>^{+0.050}_{-0.002}</math></b>				
0.024±0.004 $^{+0.050}_{-0.002}$	1 AAIJ	14BR LHCB	$p\bar{p}$ at 7, 8 TeV	

- <sup>1</sup> Reported first of two solutions using the full Dalitz analysis.

$\Gamma(J/\psi(1S) f_0(980), f_0 \rightarrow \pi^+ \pi^-) / \Gamma(J/\psi(1S) \phi)$   $\Gamma_{59} / \Gamma_{49}$

VALUE	DOCUMENT ID	TECN	COMMENT
-------	-------------	------	---------

**0.119<sup>+0.013</sup><sub>-0.014</sub> OUR FIT** Error includes scale factor of 2.4.

**0.111<sup>+0.020</sup><sub>-0.018</sub> OUR AVERAGE** Error includes scale factor of 2.5. See the ideogram below.

0.069 ± 0.012 ± 0.001	1 KHACHATRYAN	16Q CMS	pp at 7 TeV
0.140 ± 0.026 <sub>-0.013</sub> ± 0.002	2,3 AAIJ	12A0 LHCB	pp at 7 TeV
0.135 ± 0.036 ± 0.001	4 ABAZOV	12C D0	p $\bar{p}$ at 1.96 TeV
0.126 ± 0.012 ± 0.001	5 AALTONEN	11AB CDF	p $\bar{p}$ at 1.96 TeV

• • • We do not use the following data for averages, fits, limits, etc. • • •

0.124 ± 0.026<sub>-0.023</sub> ± 0.001  $\Gamma_{59} / \Gamma_{49}$

1 KHACHATRYAN 16Q reports  $[\Gamma(B_s^0 \rightarrow J/\psi(1S) f_0(980), f_0 \rightarrow \pi^+ \pi^-) / \Gamma(B_s^0 \rightarrow J/\psi(1S) \phi)] / [B(\phi(1020) \rightarrow K^+ K^-)] = 0.140 \pm 0.008 \pm 0.023$  which we multiply by our best value  $B(\phi(1020) \rightarrow K^+ K^-) = (49.2 \pm 0.5) \times 10^{-2}$ . Our first error is their experiment's error and our second error is the systematic error from using our best value.

2 AAIJ 12A0 reports  $(13.9 \pm 0.6 + 2.5_{-1.2}) \times 10^{-2}$  from a measurement of  $[\Gamma(B_s^0 \rightarrow J/\psi(1S) f_0(980), f_0 \rightarrow \pi^+ \pi^-) / \Gamma(B_s^0 \rightarrow J/\psi(1S) \phi)] / [B(\phi(1020) \rightarrow K^+ K^-)]$  assuming  $B(\phi(1020) \rightarrow K^+ K^-) = (48.9 \pm 0.5) \times 10^{-2}$ , which we rescale to our best value  $B(\phi(1020) \rightarrow K^+ K^-) = (49.2 \pm 0.5) \times 10^{-2}$ . Our first error is their experiment's error and our second error is the systematic error from using our best value.

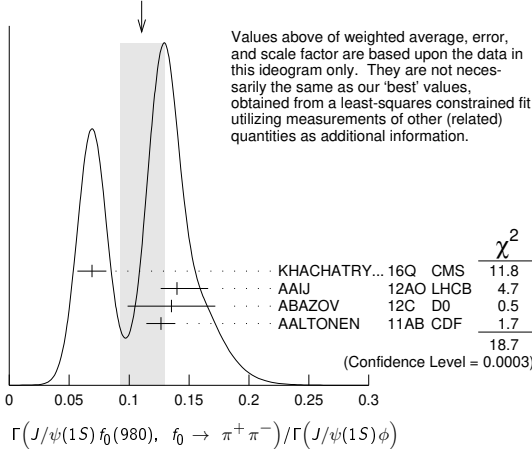
3 Measured in Dalitz plot like analysis of  $B_s \rightarrow J/\psi \pi^+ \pi^-$  decays.

4 ABAZOV 12C reports  $[\Gamma(B_s^0 \rightarrow J/\psi(1S) f_0(980), f_0 \rightarrow \pi^+ \pi^-) / \Gamma(B_s^0 \rightarrow J/\psi(1S) \phi)] / [B(\phi(1020) \rightarrow K^+ K^-)] = 0.275 \pm 0.041 \pm 0.061$  which we multiply by our best value  $B(\phi(1020) \rightarrow K^+ K^-) = (49.2 \pm 0.5) \times 10^{-2}$ . Our first error is their experiment's error and our second error is the systematic error from using our best value.

5 AALTONEN 11AB reports  $[\Gamma(B_s^0 \rightarrow J/\psi(1S) f_0(980), f_0 \rightarrow \pi^+ \pi^-) / \Gamma(B_s^0 \rightarrow J/\psi(1S) \phi)] / [B(\phi(1020) \rightarrow K^+ K^-)] = 0.257 \pm 0.020 \pm 0.014$  which we multiply by our best value  $B(\phi(1020) \rightarrow K^+ K^-) = (49.2 \pm 0.5) \times 10^{-2}$ . Our first error is their experiment's error and our second error is the systematic error from using our best value.

6 AAIJ 11 reports  $[\Gamma(B_s^0 \rightarrow J/\psi(1S) f_0(980), f_0 \rightarrow \pi^+ \pi^-) / \Gamma(B_s^0 \rightarrow J/\psi(1S) \phi)] / [B(\phi(1020) \rightarrow K^+ K^-)] = 0.252 \pm 0.046 + 0.027_{-0.032 - 0.033}$  which we multiply by our best value  $B(\phi(1020) \rightarrow K^+ K^-) = (49.2 \pm 0.5) \times 10^{-2}$ . Our first error is their experiment's error and our second error is the systematic error from using our best value.

WEIGHTED AVERAGE  
0.111±0.020-0.018 (Error scaled by 2.5)



$\Gamma(J/\psi(1S) f_0(1370), f_0 \rightarrow \pi^+ \pi^-) / \Gamma_{total}$   $\Gamma_{64} / \Gamma$

VALUE (units 10 <sup>-4</sup> )	DOCUMENT ID	TECN	COMMENT
---------------------------------	-------------	------	---------

• • • We do not use the following data for averages, fits, limits, etc. • • •

0.34<sup>+0.11+0.085</sup><sub>-0.14-0.054</sub>  $\Gamma_{64} / \Gamma$

1 The second error includes both the detector systematic and the uncertainty in the number of produced  $Y(5S) \rightarrow B_s^{(*)} \bar{B}_s^{(*)}$  pairs.

$\Gamma(J/\psi(1S) f_0(1370), f_0 \rightarrow \pi^+ \pi^-) / \Gamma(J/\psi(1S) \phi)$   $\Gamma_{64} / \Gamma_{49}$

VALUE (units 10 <sup>-2</sup> )	DOCUMENT ID	TECN	COMMENT
---------------------------------	-------------	------	---------

**4.22<sup>+0.55</sup><sub>-3.76</sub> ± 0.05**  $\Gamma_{64} / \Gamma_{49}$

1 AAIJ 12A0 reports  $(4.19 \pm 0.53 + 0.12_{-3.7}) \times 10^{-2}$  from a measurement of  $[\Gamma(B_s^0 \rightarrow J/\psi(1S) f_0(1370), f_0 \rightarrow \pi^+ \pi^-) / \Gamma(B_s^0 \rightarrow J/\psi(1S) \phi)] / [B(\phi(1020) \rightarrow K^+ K^-)]$  assuming  $B(\phi(1020) \rightarrow K^+ K^-) = (48.9 \pm 0.5) \times 10^{-2}$ , which we rescale to our best value  $B(\phi(1020) \rightarrow K^+ K^-) = (49.2 \pm 0.5) \times 10^{-2}$ . Our first error is their experiment's error and our second error is the systematic error from using our best value.

2 Measured in Dalitz plot like analysis of  $B_s \rightarrow J/\psi \pi^+ \pi^-$  decays.

$\Gamma(J/\psi(1S) f_2(1270), f_2 \rightarrow \pi^+ \pi^-) / \Gamma(J/\psi(1S) \phi)$   $\Gamma_{60} / \Gamma_{49}$

VALUE (units 10 <sup>-4</sup> )	DOCUMENT ID	TECN	COMMENT
---------------------------------	-------------	------	---------

**9.9 ± 3.4<sub>-3.6</sub> ± 0.1**  $\Gamma_{60} / \Gamma_{49}$

1 AAIJ 12A0 reports  $(0.098 \pm 0.033 + 0.006_{-0.015}) \times 10^{-2}$  from a measurement of  $[\Gamma(B_s^0 \rightarrow J/\psi(1S) f_2(1270), f_2 \rightarrow \pi^+ \pi^-) / \Gamma(B_s^0 \rightarrow J/\psi(1S) \phi)] / [B(\phi(1020) \rightarrow K^+ K^-)]$  assuming  $B(\phi(1020) \rightarrow K^+ K^-) = (48.9 \pm 0.5) \times 10^{-2}$ , which we rescale to our best value  $B(\phi(1020) \rightarrow K^+ K^-) = (49.2 \pm 0.5) \times 10^{-2}$ . Our first error is their experiment's error and our second error is the systematic error from using our best value.

2 Measured in Dalitz plot like analysis of  $B_s \rightarrow J/\psi \pi^+ \pi^-$  decays for the  $f_2$  helicity state  $\lambda = 0$ .

$\Gamma(J/\psi(1S) \pi^+ \pi^- (\text{nonresonant})) / \Gamma(J/\psi(1S) \phi)$   $\Gamma_{70} / \Gamma_{49}$

VALUE (units 10 <sup>-2</sup> )	DOCUMENT ID	TECN	COMMENT
---------------------------------	-------------	------	---------

**1.67<sup>+1.02</sup><sub>-0.32</sub> ± 0.02**  $\Gamma_{70} / \Gamma_{49}$

1 AAIJ 12A0 reports  $(1.66 \pm 0.31 + 0.96_{-0.08}) \times 10^{-2}$  from a measurement of  $[\Gamma(B_s^0 \rightarrow J/\psi(1S) \pi^+ \pi^- (\text{nonresonant})) / \Gamma(B_s^0 \rightarrow J/\psi(1S) \phi)] / [B(\phi(1020) \rightarrow K^+ K^-)]$  assuming  $B(\phi(1020) \rightarrow K^+ K^-) = (48.9 \pm 0.5) \times 10^{-2}$ , which we rescale to our best value  $B(\phi(1020) \rightarrow K^+ K^-) = (49.2 \pm 0.5) \times 10^{-2}$ . Our first error is their experiment's error and our second error is the systematic error from using our best value.

2 Measured in Dalitz plot like analysis of  $B_s \rightarrow J/\psi \pi^+ \pi^-$  decays.

$\Gamma(J/\psi(1S) \bar{K}^0 \pi^+ \pi^-) / \Gamma_{total}$   $\Gamma_{71} / \Gamma$

VALUE	CL%	DOCUMENT ID	TECN	COMMENT
-------	-----	-------------	------	---------

**<4.4 × 10<sup>-5</sup>**  $\Gamma_{71} / \Gamma$

1 Measured with  $B(B_s^0 \rightarrow J/\psi K_S^0 \pi^+ \pi^-) / B(B^0 \rightarrow J/\psi K_S^0 \pi^+ \pi^-)$  using PDG 12 values for the involved branching fractions.

$\Gamma(J/\psi(1S) K^+ K^-) / \Gamma_{total}$   $\Gamma_{72} / \Gamma$

VALUE (units 10 <sup>-4</sup> )	DOCUMENT ID	TECN	COMMENT
---------------------------------	-------------	------	---------

**7.9 ± 0.7 OUR AVERAGE**  $\Gamma_{72} / \Gamma$

7.70 ± 0.08 ± 0.72  $\Gamma_{72} / \Gamma$

10.1 ± 0.9 ± 2.1  $\Gamma_{72} / \Gamma$

1 Uses  $f_s / f_d = 0.256 \pm 0.020$  and  $B(B^+ \rightarrow J/\psi K^+) = (10.18 \pm 0.42) \times 10^{-4}$ .

2 Uses  $f_s = (17.2 \pm 3.0)\%$  as the fraction of  $\Upsilon(5S)$  decaying to  $B_s^{(*)} \bar{B}_s^{(*)}$ .

$\Gamma(J/\psi(1S) K^0 K^- \pi^+ + \text{c.c.}) / \Gamma_{total}$   $\Gamma_{73} / \Gamma$

VALUE (units 10 <sup>-4</sup> )	DOCUMENT ID	TECN	COMMENT
---------------------------------	-------------	------	---------

**9.2 ± 1.0 ± 0.9**  $\Gamma_{73} / \Gamma$

1 AAIJ 14L reports  $[\Gamma(B_s^0 \rightarrow J/\psi(1S) K^0 K^- \pi^+ + \text{c.c.}) / \Gamma_{total}] / [B(B^0 \rightarrow J/\psi(1S) K^0 \pi^+ \pi^-)] = 2.12 \pm 0.15 \pm 0.18$  which we multiply by our best value  $B(B^0 \rightarrow J/\psi(1S) K^0 \pi^+ \pi^-) = (4.3 \pm 0.4) \times 10^{-4}$ . Our first error is their experiment's error and our second error is the systematic error from using our best value. This is an observation of  $B_s^0 \rightarrow J/\psi K_S^0 K^\pm \pi^\mp$  with more than 10 standard deviations.

$\Gamma(J/\psi(1S) \bar{K}^0 K^+ K^-) / \Gamma_{total}$   $\Gamma_{74} / \Gamma$

VALUE	CL%	DOCUMENT ID	TECN	COMMENT
-------	-----	-------------	------	---------

**<12 × 10<sup>-6</sup>**  $\Gamma_{74} / \Gamma$

1 Measured with  $B(B_s^0 \rightarrow J/\psi K_S^0 K^+ K^-) / B(B^0 \rightarrow J/\psi K_S^0 \pi^+ \pi^-)$  using PDG 12 values for the involved branching fractions.

$\Gamma(J/\psi(1S) f_2'(1525)) / \Gamma(J/\psi(1S) \phi)$   $\Gamma_{75} / \Gamma_{49}$

VALUE (units 10 <sup>-2</sup> )	DOCUMENT ID	TECN	COMMENT
---------------------------------	-------------	------	---------

**21 ± 4 OUR AVERAGE**  $\Gamma_{75} / \Gamma_{49}$

21.5 ± 4.9 ± 2.6  $\Gamma_{75} / \Gamma_{49}$

21 ± 7 ± 1  $\Gamma_{75} / \Gamma_{49}$

• • • We do not use the following data for averages, fits, limits, etc. • • •

27 ± 4 ± 1  $\Gamma_{75} / \Gamma_{49}$

1 Uses  $B(f_2'(1525) \rightarrow K^+ K^-) = (44.4 \pm 1.1)\%$ .

2 ABAZOV 12AF reports  $[\Gamma(B_s^0 \rightarrow J/\psi(1S) f_2'(1525)) / \Gamma(B_s^0 \rightarrow J/\psi(1S) \phi)] \times B(f_2'(1525) \rightarrow K^+ K^-) / B(\phi(1020) \rightarrow K^+ K^-) = 0.19 \pm 0.05 \pm 0.04$  which we divide and multiply by our best values  $B(f_2'(1525) \rightarrow K^+ K^-) = \frac{1}{2} (87.6 \pm 2.2) \times 10^{-2}$ ,  $B(\phi(1020) \rightarrow K^+ K^-) = (49.2 \pm 0.5) \times 10^{-2}$ . Our first error is their experiment's error and our second error is the systematic error from using our best values.

3 ABAZOV 12AF fits the invariant masses of the  $K^+ K^-$  pair in the range  $1.35 < M(K^+ K^-) < 2$  GeV.

4 AAIJ 12S reports  $[(26.4 \pm 2.7 \pm 2.4) \times 10^{-2}]$  from a measurement of  $[\Gamma(B_s^0 \rightarrow J/\psi(1S) f_2'(1525)) / \Gamma(B_s^0 \rightarrow J/\psi(1S) \phi)] \times B(f_2'(1525) \rightarrow K^+ K^-) / B(\phi(1020) \rightarrow K^+ K^-)$  assuming  $B(f_2'(1525) \rightarrow K^+ K^-) = (44.4 \pm 1.1) \times 10^{-2}$ ,  $B(\phi(1020) \rightarrow K^+ K^-) = (48.9 \pm 0.5) \times 10^{-2}$ , which we rescale to our best values  $B(f_2'(1525) \rightarrow K^+ K^-) = \frac{1}{2} (87.6 \pm 2.2) \times 10^{-2}$ ,  $B(\phi(1020) \rightarrow K^+ K^-) = (49.2 \pm 0.5) \times 10^{-2}$ . Our first error is their experiment's error and our second error is the systematic error from using our best values.

$\Gamma(J/\psi(1S) f_2'(1525)) / \Gamma_{total}$   $\Gamma_{75} / \Gamma$

VALUE (units 10 <sup>-4</sup> )	DOCUMENT ID	TECN	COMMENT
---------------------------------	-------------	------	---------

**2.61 ± 0.20 ± 0.56<sub>-0.50</sub>**  $\Gamma_{75} / \Gamma$

1 Uses  $f_s / f_d = 0.256 \pm 0.020$  and  $B(B^+ \rightarrow J/\psi K^+) = (10.18 \pm 0.42) \times 10^{-4}$ .





See key on page 999

Meson Particle Listings

$B_S^0$

$\Gamma(\eta'\eta')/\Gamma_{total}$   $\Gamma_{94}/\Gamma$

VALUE (units $10^{-5}$ )	CL%	DOCUMENT ID	TECN	COMMENT
<b>3.3 ± 0.7 ± 0.1</b>		1 AAIJ	15o LHCb	$pp$ at 7, 8 TeV

<sup>1</sup> AAIJ 15o reports  $[\Gamma(B_S^0 \rightarrow \eta'\eta')/\Gamma_{total}] / [B(B^+ \rightarrow \eta'K^+)] = 0.47 \pm 0.09 \pm 0.04$  which we multiply by our best value  $B(B^+ \rightarrow \eta'K^+) = (7.04 \pm 0.25) \times 10^{-5}$ . Our first error is their experiment's error and our second error is the systematic error from using our best value.

$\Gamma(\eta'\phi)/\Gamma_{total}$   $\Gamma_{95}/\Gamma$

VALUE	CL%	DOCUMENT ID	TECN	COMMENT
<b>&lt;0.82 × 10<sup>-6</sup></b>	90	1 AAIJ	17BA LHCb	$pp$ at 7, 8 TeV

<sup>1</sup> Corresponds to the 95% CL upper limit  $1.01 \times 10^{-6}$ . Uses the normalization mode  $B^+ \rightarrow \eta'K^+$  with branching fraction  $(70.6 \pm 2.5) \times 10^{-6}$  and the ratio of hadronisation fractions  $f_s/f_d = 0.259 \pm 0.015$ , which is assumed equal to  $f_s/f_u$ .

$\Gamma(\phi\pi^+\pi^-)/\Gamma_{total}$   $\Gamma_{99}/\Gamma$

VALUE (units $10^{-6}$ )	CL%	DOCUMENT ID	TECN	COMMENT
<b>3.48 ± 0.23 ± 0.39</b>		1 AAIJ	17A LHCb	$pp$ at 7, 8 TeV

<sup>1</sup> Inclusive decays in mass range  $400 < m(\pi^+\pi^-) < 1600$  MeV/c<sup>2</sup>.

$\Gamma(\phi\rho^0)/\Gamma_{total}$   $\Gamma_{98}/\Gamma$

VALUE (units $10^{-7}$ )	CL%	DOCUMENT ID	TECN	COMMENT
<b>2.7 ± 0.7 ± 0.3</b>		1 AAIJ	17A LHCb	$pp$ at 7, 8 TeV

• • • We do not use the following data for averages, fits, limits, etc. • • •  
 <6170 90 <sup>2</sup> ABE 00c SLD  $e^+e^- \rightarrow Z$   
<sup>1</sup> Signal evidence is 4 standard deviations.  
<sup>2</sup> ABE 00c assumes  $B(Z \rightarrow b\bar{b}) = (21.7 \pm 0.1)\%$  and the  $B$  fractions  $f_{B^0} = f_{B^+} = (39.7 \pm 1.8 \pm 2.2)\%$  and  $f_{B_S} = (10.5 \pm 1.8 \pm 2.2)\%$ .

$\Gamma(\phi f_0(980), f_0(980) \rightarrow \pi^+\pi^-)/\Gamma_{total}$   $\Gamma_{96}/\Gamma$

VALUE (units $10^{-6}$ )	CL%	DOCUMENT ID	TECN	COMMENT
<b>1.12 ± 0.16 ± 0.14</b>		1 AAIJ	17A LHCb	$pp$ at 7, 8 TeV

<sup>1</sup> Signal is observed with 8 standard deviations significance.

$\Gamma(\phi f_2(1270), f_2(1270) \rightarrow \pi^+\pi^-)/\Gamma_{total}$   $\Gamma_{97}/\Gamma$

VALUE (units $10^{-6}$ )	CL%	DOCUMENT ID	TECN	COMMENT
<b>0.61 ± 0.13 ± 0.13 ± 0.08</b>		1 AAIJ	17A LHCb	$pp$ at 7, 8 TeV

<sup>1</sup> Signal is observed with 5 standard deviations significance.

$\Gamma(\phi\phi)/\Gamma_{total}$   $\Gamma_{100}/\Gamma$

VALUE (units $10^{-6}$ )	CL%	DOCUMENT ID	TECN	COMMENT
<b>18.7 ± 1.5 OUR FIT</b> <b>18.5 ± 1.4 ± 1.0</b>		1 AAIJ	15AS LHCb	$pp$ at 7, 8 TeV

• • • We do not use the following data for averages, fits, limits, etc. • • •  
 14 <sup>+</sup><sub>-5</sub> ± 6 <sup>2</sup> ACOSTA 05J CDF Repl. by AALTONEN 11AN  
 <1183 90 <sup>3</sup> ABE 00c SLD  $e^+e^- \rightarrow Z$   
<sup>1</sup> AAIJ 15AS reports  $[\Gamma(B_S^0 \rightarrow \phi\phi)/\Gamma_{total}] / [B(B^0 \rightarrow K^*(892)^0\phi)] = 1.84 \pm 0.05 \pm 0.13$  which we multiply by our best value  $B(B^0 \rightarrow K^*(892)^0\phi) = (1.00 \pm 0.05) \times 10^{-5}$ . Our first error is their experiment's error and our second error is the systematic error from using our best value.  
<sup>2</sup> Uses  $B(B^0 \rightarrow J/\psi\phi) = (1.38 \pm 0.49) \times 10^{-3}$  and production cross-section ratio of  $\sigma(B_S)/\sigma(B^0) = 0.26 \pm 0.04$ .  
<sup>3</sup> ABE 00c assumes  $B(Z \rightarrow b\bar{b}) = (21.7 \pm 0.1)\%$  and the  $B$  fractions  $f_{B^0} = f_{B^+} = (39.7 \pm 1.8 \pm 2.2)\%$  and  $f_{B_S} = (10.5 \pm 1.8 \pm 2.2)\%$ .

$\Gamma(\phi\phi)/\Gamma(J/\psi(1S)\phi)$   $\Gamma_{100}/\Gamma_{49}$

VALUE (units $10^{-2}$ )	CL%	DOCUMENT ID	TECN	COMMENT
<b>1.73 ± 0.16 OUR FIT</b> <b>1.78 ± 0.14 ± 0.20</b>		AALTONEN	11AN CDF	$p\bar{p}$ at 1.96 TeV

$\Gamma(\phi\phi\phi)/\Gamma(\phi\phi)$   $\Gamma_{101}/\Gamma_{100}$

VALUE	CL%	DOCUMENT ID	TECN	COMMENT
<b>0.117 ± 0.030 ± 0.015</b>		AAIJ	17Bb LHCb	$pp$ at 7, 8 TeV

$\Gamma(\pi^+K^-)/\Gamma_{total}$   $\Gamma_{102}/\Gamma$

VALUE (units $10^{-6}$ )	CL%	DOCUMENT ID	TECN	COMMENT
<b>5.8 ± 0.7 OUR AVERAGE</b>				
5.9 ± 0.7 ± 0.6		1 AAIJ	12AR LHCb	$pp$ at 7 TeV
5.7 ± 1.0 ± 0.5		2 AALTONEN	09c CDF	$p\bar{p}$ at 1.96 TeV

• • • We do not use the following data for averages, fits, limits, etc. • • •  
 < 26 90 <sup>3</sup> PENG 10 BELL  $e^+e^- \rightarrow \Upsilon(5S)$   
 < 5.6 90 <sup>4</sup> ABULENCIA,A 06D CDF Repl. by AALTONEN 09c  
 <261 90 <sup>5</sup> ABE 00c SLD  $e^+e^- \rightarrow Z$   
 <210 90 <sup>6</sup> BUSKULIC 96v ALEP  $e^+e^- \rightarrow Z$   
 <260 90 <sup>7</sup> AKERS 94L OPAL  $e^+e^- \rightarrow Z$   
<sup>1</sup> AAIJ 12AR reports  $[\Gamma(B_S^0 \rightarrow \pi^+K^-)/\Gamma_{total}] / [B(B^0 \rightarrow K^+\pi^-)] \times [\Gamma(\bar{b} \rightarrow B_S^0)/\Gamma(\bar{b} \rightarrow B^0)] = 0.074 \pm 0.006 \pm 0.006$  which we multiply or divide by our best values  $B(B^0 \rightarrow K^+\pi^-) = (1.96 \pm 0.05) \times 10^{-5}$ ,  $\Gamma(\bar{b} \rightarrow B_S^0)/\Gamma(\bar{b} \rightarrow B^0) = 0.246 \pm 0.023$ .

Our first error is their experiment's error and our second error is the systematic error from using our best values.  
<sup>2</sup> AALTONEN 09c reports  $[\Gamma(B_S^0 \rightarrow \pi^+K^-)/\Gamma_{total}] / [B(B^0 \rightarrow K^+\pi^-)] \times [B(\bar{b} \rightarrow B_S^0)] / [B(\bar{b} \rightarrow B^0)] = 0.071 \pm 0.010 \pm 0.007$  which we multiply or divide by our best values  $B(B^0 \rightarrow K^+\pi^-) = (1.96 \pm 0.05) \times 10^{-5}$ ,  $B(\bar{b} \rightarrow B_S^0) = (10.0 \pm 0.8) \times 10^{-2}$ ,  $B(\bar{b} \rightarrow B^0) = (40.8 \pm 0.7) \times 10^{-2}$ . Our first error is their experiment's error and our second error is the systematic error from using our best values.  
<sup>3</sup> Uses  $\Upsilon(10860) \rightarrow B_S^* \bar{B}_S^*$  and assumes  $B(\Upsilon(10860) \rightarrow B_S^{(*)} \bar{B}_S^{(*)}) = (19.3 \pm 2.9)\%$  and  $\Gamma(\Upsilon(10860) \rightarrow B_S^* \bar{B}_S^*) / \Gamma(\Upsilon(10860) \rightarrow B_S^{(*)} \bar{B}_S^{(*)}) = (90.1 \pm 3.8 \pm 4.0)\%$ .  
<sup>4</sup> ABULENCIA,A 06D obtains this from  $(f_s/f_d) (B(B_S \rightarrow \pi^+K^-) / B(B^0 \rightarrow K^+\pi^-)) < 0.08$  at 90% CL, assuming  $f_s/f_d = 0.260 \pm 0.039$  and  $B(B^0 \rightarrow K^+\pi^-) = (18.9 \pm 0.7) \times 10^{-6}$ .  
<sup>5</sup> ABE 00c assumes  $B(Z \rightarrow b\bar{b}) = (21.7 \pm 0.1)\%$  and the  $B$  fractions  $f_{B^0} = f_{B^+} = (39.7 \pm 1.8 \pm 2.2)\%$  and  $f_{B_S} = (10.5 \pm 1.8 \pm 2.2)\%$ .  
<sup>6</sup> BUSKULIC 96v assumes PDG 96 production fractions for  $B^0, B^+, B_S, b$  baryons.  
<sup>7</sup> Assumes  $B(Z \rightarrow b\bar{b}) = 0.217$  and  $B_d^0(B_S^0)$  fraction 39.5% (12%).

$\Gamma(K^+K^-)/\Gamma_{total}$   $\Gamma_{103}/\Gamma$

VALUE (units $10^{-6}$ )	CL%	DOCUMENT ID	TECN	COMMENT
<b>26.6 ± 2.2 OUR AVERAGE</b>				
25.2 ± 1.7 ± 2.4		1 AAIJ	12AR LHCb	$pp$ at 7 TeV
27.6 ± 2.3 ± 2.7		2 AALTONEN	11N CDF	$p\bar{p}$ at 1.96 TeV

38 <sup>+</sup><sub>-9</sub> ± 7 <sup>3</sup> PENG 10 BELL  $e^+e^- \rightarrow \Upsilon(5S)$   
 • • • We do not use the following data for averages, fits, limits, etc. • • •  
 <310 90 DRUTSKOY 07A BELL  $e^+e^- \rightarrow \Upsilon(5S)$   
 33 ± 6 ± 7 <sup>4</sup> ABULENCIA,A 06D CDF Repl. by AALTONEN 11N  
 <283 90 <sup>5</sup> ABE 00c SLD  $e^+e^- \rightarrow Z$   
 < 59 90 <sup>6</sup> BUSKULIC 96v ALEP  $e^+e^- \rightarrow Z$   
 <140 90 <sup>7</sup> AKERS 94L OPAL  $e^+e^- \rightarrow Z$

<sup>1</sup> AAIJ 12AR reports  $[\Gamma(B_S^0 \rightarrow K^+K^-)/\Gamma_{total}] / [B(B^0 \rightarrow K^+\pi^-)] \times [\Gamma(\bar{b} \rightarrow B_S^0)/\Gamma(\bar{b} \rightarrow B^0)] = 0.316 \pm 0.009 \pm 0.019$  which we multiply or divide by our best values  $B(B^0 \rightarrow K^+\pi^-) = (1.96 \pm 0.05) \times 10^{-5}$ ,  $\Gamma(\bar{b} \rightarrow B_S^0)/\Gamma(\bar{b} \rightarrow B^0) = 0.246 \pm 0.023$ . Our first error is their experiment's error and our second error is the systematic error from using our best values.  
<sup>2</sup> AALTONEN 11N reports  $(f_s/f_d) (B(B_S^0 \rightarrow K^+K^-) / B(B^0 \rightarrow K^+\pi^-)) = 0.347 \pm 0.020 \pm 0.021$ . We multiply this result by our best value of  $B(B^0 \rightarrow K^+\pi^-) = (1.96 \pm 0.05) \times 10^{-5}$  and divide by our best value of  $f_s/f_d$ , where  $1/2 f_s/f_d = 0.1230 \pm 0.0115$ . Our first uncertainty is their combined experiment's uncertainty and our second is the systematic uncertainty from using our best values.  
<sup>3</sup> Uses  $\Upsilon(10860) \rightarrow B_S^* \bar{B}_S^*$  and assumes  $B(\Upsilon(10860) \rightarrow B_S^{(*)} \bar{B}_S^{(*)}) = (19.3 \pm 2.9)\%$  and  $\Gamma(\Upsilon(10860) \rightarrow B_S^* \bar{B}_S^*) / \Gamma(\Upsilon(10860) \rightarrow B_S^{(*)} \bar{B}_S^{(*)}) = (90.1 \pm 3.8 \pm 4.0)\%$ .  
<sup>4</sup> ABULENCIA,A 06D obtains this from  $(f_s/f_d) (B(B_S \rightarrow K^+K^-) / B(B^0 \rightarrow K^+\pi^-)) = 0.46 \pm 0.08 \pm 0.07$ , assuming  $f_s/f_d = 0.260 \pm 0.039$  and  $B(B^0 \rightarrow K^+\pi^-) = (18.9 \pm 0.7) \times 10^{-6}$ .  
<sup>5</sup> ABE 00c assumes  $B(Z \rightarrow b\bar{b}) = (21.7 \pm 0.1)\%$  and the  $B$  fractions  $f_{B^0} = f_{B^+} = (39.7 \pm 1.8 \pm 2.2)\%$  and  $f_{B_S} = (10.5 \pm 1.8 \pm 2.2)\%$ .  
<sup>6</sup> BUSKULIC 96v assumes PDG 96 production fractions for  $B^0, B^+, B_S, b$  baryons.  
<sup>7</sup> Assumes  $B(Z \rightarrow b\bar{b}) = 0.217$  and  $B_d^0(B_S^0)$  fraction 39.5% (12%).

$\Gamma(K^0\bar{K}^0)/\Gamma_{total}$   $\Gamma_{104}/\Gamma$

VALUE (units $10^{-5}$ )	CL%	DOCUMENT ID	TECN	COMMENT
<b>1.96 ± 0.58 ± 0.51 ± 0.10 ± 0.20</b>		1 PAL	16 BELL	$e^+e^- \rightarrow \Upsilon(5S)$

• • • We do not use the following data for averages, fits, limits, etc. • • •  
 <6.6 90 <sup>2</sup> PENG 10 BELL Repl. by PAL 16  
<sup>1</sup> Observed in  $B_S^0 \rightarrow K_S^0 K_S^0$  with significance of 5.1  $\sigma$ . The last uncertainty is due to the uncertainty of the total number of  $B_S^0 \bar{B}_S^0$  pairs.  
<sup>2</sup> Uses  $\Upsilon(10860) \rightarrow B_S^* \bar{B}_S^*$  and assumes  $B(\Upsilon(10860) \rightarrow B_S^{(*)} \bar{B}_S^{(*)}) = (19.3 \pm 2.9)\%$  and  $\Gamma(\Upsilon(10860) \rightarrow B_S^* \bar{B}_S^*) / \Gamma(\Upsilon(10860) \rightarrow B_S^{(*)} \bar{B}_S^{(*)}) = (90.1 \pm 3.8 \pm 4.0)\%$ .

$\Gamma(K^0\pi^+\pi^-)/\Gamma_{total}$   $\Gamma_{105}/\Gamma$

VALUE (units $10^{-6}$ )	CL%	DOCUMENT ID	TECN	COMMENT
<b>9.5 ± 2.1 ± 0.3</b>		1,2 AAIJ	17BP LHCb	$pp$ at 7, 8 TeV

• • • We do not use the following data for averages, fits, limits, etc. • • •  
 14 ± 4 ± 1 <sup>3</sup> AAIJ 13BP LHCb Repl. by AAIJ 17BP  
<sup>1</sup> AAIJ 17BP reports  $[\Gamma(B_S^0 \rightarrow K^0\pi^+\pi^-)/\Gamma_{total}] / [B(B^0 \rightarrow K^0\pi^+\pi^-)] = 0.191 \pm 0.027 \pm 0.033$  which we multiply by our best value  $B(B^0 \rightarrow K^0\pi^+\pi^-) = (4.97 \pm 0.18) \times 10^{-5}$ . Our first error is their experiment's error and our second error is the systematic error from using our best value.  
<sup>2</sup> Used  $f_s/f_d = 0.259 \pm 0.015$ .  
<sup>3</sup> AAIJ 13BP reports  $[\Gamma(B_S^0 \rightarrow K^0\pi^+\pi^-)/\Gamma_{total}] / [B(B^0 \rightarrow K^0\pi^+\pi^-)] = 0.29 \pm 0.06 \pm 0.04$  which we multiply by our best value  $B(B^0 \rightarrow K^0\pi^+\pi^-) = (4.97 \pm 0.18) \times 10^{-5}$ . Our first error is their experiment's error and our second error is the systematic error from using our best value.

## Meson Particle Listings

 $B_S^0$  $\Gamma(K^*(892)^-\pi^+)/\Gamma_{\text{total}}$   $\Gamma_{107}/\Gamma$ 

VALUE (units $10^{-6}$ )	DOCUMENT ID	TECN	COMMENT
<b><math>2.9 \pm 1.0 \pm 0.2</math></b>	1,2 AAIJ	14BMLHCB	$pp$ at 7 TeV

- <sup>1</sup> AAIJ 14BML reports  $[\Gamma(B_S^0 \rightarrow K^*(892)^-\pi^+)/\Gamma_{\text{total}}] / [B(B^0 \rightarrow K^*(892)^+\pi^-)] = 0.39 \pm 0.13 \pm 0.05$  which we multiply by our best value  $B(B^0 \rightarrow K^*(892)^+\pi^-) = (7.5 \pm 0.4) \times 10^{-6}$ . Our first error is their experiment's error and our second error is the systematic error from using our best value.
- <sup>2</sup> Uses  $f_s/f_d = 0.259 \pm 0.015$ .

 $\Gamma(K^0 K^\pm \pi^\mp)/\Gamma_{\text{total}}$   $\Gamma_{106}/\Gamma$ 

VALUE (units $10^{-5}$ )	DOCUMENT ID	TECN	COMMENT
<b><math>8.4 \pm 0.8 \pm 0.3</math></b>	1,2 AAIJ	17BP LHCBC	$pp$ at 7, 8 TeV

- We do not use the following data for averages, fits, limits, etc. •••
- $7.4 \pm 0.9 \pm 0.3$  <sup>3</sup> AAIJ 13BP LHCBC Repl. by AAIJ 17BP
- <sup>1</sup> AAIJ 17BP reports  $[\Gamma(B_S^0 \rightarrow K^0 K^\pm \pi^\mp)/\Gamma_{\text{total}}] / [B(B^0 \rightarrow K^0 \pi^+ \pi^-)] = 1.70 \pm 0.07 \pm 0.15$  which we multiply by our best value  $B(B^0 \rightarrow K^0 \pi^+ \pi^-) = (4.97 \pm 0.18) \times 10^{-5}$ . Our first error is their experiment's error and our second error is the systematic error from using our best value.
- <sup>2</sup> Used  $f_s/f_d = 0.259 \pm 0.015$ .
- <sup>3</sup> AAIJ 13BP reports  $[\Gamma(B_S^0 \rightarrow K^0 K^\pm \pi^\mp)/\Gamma_{\text{total}}] / [B(B^0 \rightarrow K^0 \pi^+ \pi^-)] = 1.48 \pm 0.12 \pm 0.14$  which we multiply by our best value  $B(B^0 \rightarrow K^0 \pi^+ \pi^-) = (4.97 \pm 0.18) \times 10^{-5}$ . Our first error is their experiment's error and our second error is the systematic error from using our best value.

 $\Gamma(K^*(892)^\pm K^\mp)/\Gamma_{\text{total}}$   $\Gamma_{108}/\Gamma$ 

VALUE (units $10^{-5}$ )	DOCUMENT ID	TECN	COMMENT
<b><math>1.86 \pm 0.12 \pm 0.45</math></b>	1,2 AAIJ	19K LHCBC	$pp$ at 7, 8 TeV

- We do not use the following data for averages, fits, limits, etc. •••
- $1.12 \pm 0.21 \pm \frac{0.07}{0.06}$  <sup>3,4</sup> AAIJ 14BMLHCB Repl. by AAIJ 19K
- <sup>1</sup> AAIJ 19K reports  $(18.6 \pm 1.2 \pm 0.8 \pm 4.0 \pm 2.0) \times 10^{-6}$  as the measured value. We have combined in quadrature all systematic uncertainties into a single one.
- <sup>2</sup> Measured in Dalitz plot analysis of  $B_S^0 \rightarrow K_S^0 K^\pm \pi^\mp$  decays.
- <sup>3</sup> AAIJ 14BML reports  $[\Gamma(B_S^0 \rightarrow K^*(892)^\pm K^\mp)/\Gamma_{\text{total}}] / [B(B^0 \rightarrow K^*(892)^+\pi^-)] = 1.49 \pm 0.22 \pm 0.18$  which we multiply by our best value  $B(B^0 \rightarrow K^*(892)^+\pi^-) = (7.5 \pm 0.4) \times 10^{-6}$ . Our first error is their experiment's error and our second error is the systematic error from using our best value.
- <sup>4</sup> Uses  $f_s/f_d = 0.259 \pm 0.015$ .

 $\Gamma(K_S^0(1430)^\pm K^\mp)/\Gamma_{\text{total}}$   $\Gamma_{109}/\Gamma$ 

VALUE (units $10^{-5}$ )	DOCUMENT ID	TECN	COMMENT
<b><math>3.13 \pm 0.23 \pm 2.53</math></b>	1,2 AAIJ	19K LHCBC	$pp$ at 7, 8 TeV

- <sup>1</sup> AAIJ 19K reports  $(31.3 \pm 2.3 \pm 0.7 \pm 25.1 \pm 3.3) \times 10^{-6}$  as the measured value. We have combined in quadrature all systematic uncertainties into a single one.
- <sup>2</sup> Measured in Dalitz plot analysis of  $B_S^0 \rightarrow K_S^0 K^\pm \pi^\mp$  decays.

 $\Gamma(K_S^0(1430)^\pm K^\mp)/\Gamma_{\text{total}}$   $\Gamma_{110}/\Gamma$ 

VALUE (units $10^{-5}$ )	DOCUMENT ID	TECN	COMMENT
<b><math>1.03 \pm 0.25 \pm 1.64</math></b>	1,2 AAIJ	19K LHCBC	$pp$ at 7, 8 TeV

- <sup>1</sup> AAIJ 19K reports  $(10.3 \pm 2.5 \pm 1.1 \pm 16.3 \pm 1.1) \times 10^{-6}$  as the measured value. We have combined in quadrature all systematic uncertainties into a single one.
- <sup>2</sup> Measured in Dalitz plot analysis of  $B_S^0 \rightarrow K_S^0 K^\pm \pi^\mp$  decays.

 $\Gamma(K^*(892)^0 \bar{K}^0 + c.c.)/\Gamma_{\text{total}}$   $\Gamma_{111}/\Gamma$ 

VALUE (units $10^{-5}$ )	DOCUMENT ID	TECN	COMMENT
<b><math>1.98 \pm 0.28 \pm 0.50</math></b>	1,2 AAIJ	19K LHCBC	$pp$ at 7, 8 TeV

- <sup>1</sup> AAIJ 19K reports  $(19.8 \pm 2.8 \pm 1.2 \pm 4.4 \pm 2.1) \times 10^{-6}$  as the measured value. We have combined in quadrature all systematic uncertainties into a single one.
- <sup>2</sup> Measured in Dalitz plot analysis of  $B_S^0 \rightarrow K_S^0 K^\pm \pi^\mp$  decays.

 $\Gamma(K_S^0(1430) \bar{K}^0 + c.c.)/\Gamma_{\text{total}}$   $\Gamma_{112}/\Gamma$ 

VALUE (units $10^{-5}$ )	DOCUMENT ID	TECN	COMMENT
<b><math>3.30 \pm 0.25 \pm 0.98</math></b>	1,2 AAIJ	19K LHCBC	$pp$ at 7, 8 TeV

- <sup>1</sup> AAIJ 19K reports  $(33.0 \pm 2.5 \pm 0.9 \pm 9.1 \pm 3.5) \times 10^{-6}$  as the measured value. We have combined in quadrature all systematic uncertainties into a single one.
- <sup>2</sup> Measured in Dalitz plot analysis of  $B_S^0 \rightarrow K_S^0 K^\pm \pi^\mp$  decays.

 $\Gamma(K_S^0(1430) \bar{K}^0 + c.c.)/\Gamma_{\text{total}}$   $\Gamma_{113}/\Gamma$ 

VALUE (units $10^{-5}$ )	DOCUMENT ID	TECN	COMMENT
<b><math>1.68 \pm 0.45 \pm 2.13</math></b>	1,2 AAIJ	19K LHCBC	$pp$ at 7, 8 TeV

- <sup>1</sup> AAIJ 19K reports  $(16.8 \pm 4.5 \pm 1.7 \pm 21.2 \pm 1.8) \times 10^{-6}$  as the measured value. We have combined in quadrature all systematic uncertainties into a single one.
- <sup>2</sup> Measured in Dalitz plot analysis of  $B_S^0 \rightarrow K_S^0 K^\pm \pi^\mp$  decays.

 $\Gamma(K_S^0 \bar{K}^*(892)^0 + c.c.)/\Gamma_{\text{total}}$   $\Gamma_{114}/\Gamma$ 

VALUE (units $10^{-6}$ )	DOCUMENT ID	TECN	COMMENT
<b><math>16.4 \pm 3.4 \pm 2.3</math></b>	<sup>1</sup> AAIJ	16 LHCBC	$pp$ at 7 TeV

- <sup>1</sup> Measured relative to  $B^0 \rightarrow K_S^0 \pi^+ \pi^-$  using the value of  $B(B^0 \rightarrow K^0 \pi^+ \pi^-) = (4.96 \pm 0.2) \times 10^{-5}$ .

 $\Gamma(K^0 K^+ K^-)/\Gamma_{\text{total}}$   $\Gamma_{115}/\Gamma$ 

VALUE (units $10^{-7}$ )	CL%	DOCUMENT ID	TECN	COMMENT
<b><math>12.9 \pm 6.5 \pm 0.5</math></b>		1,2,3 AAIJ	17BP LHCBC	$pp$ at 7, 8 TeV

- We do not use the following data for averages, fits, limits, etc. •••
- <34 90 <sup>4</sup> AAIJ 13BP LHCBC Repl. by AAIJ 17BP
- <sup>1</sup> AAIJ 17BP reports  $[\Gamma(B_S^0 \rightarrow K^0 K^+ K^-)/\Gamma_{\text{total}}] / [B(B^0 \rightarrow K^0 \pi^+ \pi^-)] = 0.026 \pm 0.011 \pm 0.007$  which we multiply by our best value  $B(B^0 \rightarrow K^0 \pi^+ \pi^-) = (4.97 \pm 0.18) \times 10^{-5}$ . Our first error is their experiment's error and our second error is the systematic error from using our best value.
- <sup>2</sup> AAIJ 17BP also set the limit range  $4-25 \times 10^{-7}$  at 90% CL using the world average value  $B(B^0 \rightarrow K^0 \pi^+ \pi^-) = (4.96 \pm 0.20) \times 10^{-5}$ .
- <sup>3</sup> Used  $f_s/f_d = 0.259 \pm 0.015$ .
- <sup>4</sup> AAIJ 13BP reports  $[\Gamma(B_S^0 \rightarrow K^0 K^+ K^-)/\Gamma_{\text{total}}] / [B(B^0 \rightarrow K^0 \pi^+ \pi^-)] < 0.068$  which we multiply by our best value  $B(B^0 \rightarrow K^0 \pi^+ \pi^-) = 4.97 \times 10^{-5}$ .

 $\Gamma(\bar{K}^*(892)^0 \rho^0)/\Gamma_{\text{total}}$   $\Gamma_{116}/\Gamma$ 

VALUE	CL%	DOCUMENT ID	TECN	COMMENT
<b><math>&lt; 7.67 \times 10^{-4}</math></b>	90	<sup>1</sup> ABE	00c SLD	$e^+e^- \rightarrow Z$

- <sup>1</sup> ABE 00c assumes  $B(Z \rightarrow b\bar{b}) = (21.7 \pm 0.1)\%$  and the  $B$  fractions  $f_{B^0} = f_{B^+} = (39.7 \pm 1.8, 2.2)\%$  and  $f_{B_S} = (10.5 \pm 1.8, 2.2)\%$ .

 $\Gamma(\bar{K}^*(892)^0 K^*(892)^0)/\Gamma_{\text{total}}$   $\Gamma_{117}/\Gamma$ 

VALUE (units $10^{-5}$ )	CL%	DOCUMENT ID	TECN	COMMENT
<b><math>1.11 \pm 0.26 \pm 0.06</math></b>		<sup>1</sup> AAIJ	15AF LHCBC	$pp$ at 7 TeV

- We do not use the following data for averages, fits, limits, etc. •••
- $2.81 \pm 0.46 \pm 0.56$  <sup>2</sup> AAIJ 12F LHCBC Repl. by AAIJ 15AF
- <168.1 90 <sup>3</sup> ABE 00c SLD  $e^+e^- \rightarrow Z$
- <sup>1</sup> AAIJ 15AF reports  $[\Gamma(B_S^0 \rightarrow \bar{K}^*(892)^0 K^*(892)^0)/\Gamma_{\text{total}}] / [B(B^0 \rightarrow K^*(892)^0 \phi)] = 1.11 \pm 0.22 \pm 0.12 \pm 0.06$  which we multiply by our best value  $B(B^0 \rightarrow K^*(892)^0 \phi) = (1.00 \pm 0.05) \times 10^{-5}$ . Our first error is their experiment's error and our second error is the systematic error from using our best value.
- <sup>2</sup> Uses  $B^0 \rightarrow J/\psi K^{*0}$  for normalization and assumes  $B(B^0 \rightarrow J/\psi K^{*0}) B(J/\psi \rightarrow \mu^+ \mu^-) B(K^{*0} \rightarrow K^+ \pi^-) = (1.33 \pm 0.06) \times 10^{-3}$  and  $f_s/f_d = 0.253 \pm 0.031$ . The second quoted error is total uncertainty including the error of 0.34 on  $f_s/f_d$ .
- <sup>3</sup> ABE 00c assumes  $B(Z \rightarrow b\bar{b}) = (21.7 \pm 0.1)\%$  and the  $B$  fractions  $f_{B^0} = f_{B^+} = (39.7 \pm 1.8, 2.2)\%$  and  $f_{B_S} = (10.5 \pm 1.8, 2.2)\%$ .

 $\Gamma(\phi K^*(892)^0)/\Gamma_{\text{total}}$   $\Gamma_{121}/\Gamma$ 

VALUE (units $10^{-6}$ )	CL%	DOCUMENT ID	TECN	COMMENT
<b><math>1.14 \pm 0.29 \pm 0.06</math></b>		<sup>1</sup> AAIJ	13BW LHCBC	$pp$ at 7 TeV

- We do not use the following data for averages, fits, limits, etc. •••
- <1013 90 <sup>2</sup> ABE 00c SLD  $e^+e^- \rightarrow Z$
- <sup>1</sup> AAIJ 13BW reports  $[\Gamma(B_S^0 \rightarrow \phi K^*(892)^0)/\Gamma_{\text{total}}] / [B(B^0 \rightarrow K^*(892)^0 \phi)] = 0.113 \pm 0.024 \pm 0.016$  which we multiply by our best value  $B(B^0 \rightarrow K^*(892)^0 \phi) = (1.00 \pm 0.05) \times 10^{-5}$ . Our first error is their experiment's error and our second error is the systematic error from using our best value.
- <sup>2</sup> ABE 00c assumes  $B(Z \rightarrow b\bar{b}) = (21.7 \pm 0.1)\%$  and the  $B$  fractions  $f_{B^0} = f_{B^+} = (39.7 \pm 1.8, 2.2)\%$  and  $f_{B_S} = (10.5 \pm 1.8, 2.2)\%$ .

 $\Gamma(p\bar{p})/\Gamma_{\text{total}}$   $\Gamma_{122}/\Gamma$ 

VALUE (units $10^{-8}$ )	CL%	DOCUMENT ID	TECN	COMMENT
<b><math>&lt; 1.5</math></b>	90	<sup>1</sup> AAIJ	17Bj LHCBC	$pp$ at 7 and 8 TeV

- We do not use the following data for averages, fits, limits, etc. •••
- $2.84 + 2.03 + 0.85$   
 $-1.68 - 0.18$  <sup>2</sup> AAIJ 13Bq LHCBC Repl. by AAIJ 17Bj
- <5900 90 <sup>3</sup> BUSKULIC 96v ALEP  $e^+e^- \rightarrow Z$
- <sup>1</sup> Uses normalization mode  $B(B^0 \rightarrow K^+ \pi^-) = (19.6 \pm 0.5) \times 10^{-6}$  and  $B$  production ratio  $f(\bar{b} \rightarrow B_S^0)/f(\bar{b} \rightarrow B_d^0) = 0.259 \pm 0.015$ .
- <sup>2</sup> Uses normalization mode  $B(B^0 \rightarrow K^+ \pi^-) = (19.55 \pm 0.54) \times 10^{-6}$  and  $B$  production ratio  $f(\bar{b} \rightarrow B_S^0)/f(\bar{b} \rightarrow B_d^0) = 0.256 \pm 0.020$ .
- <sup>3</sup> BUSKULIC 96v assumes PDG 96 production fractions for  $B^0, B^+, B_S, b$  baryons.

 $\Gamma(p\bar{p} K^+ K^-)/\Gamma_{\text{total}}$   $\Gamma_{123}/\Gamma$ 

VALUE (units $10^{-6}$ )	DOCUMENT ID	TECN	COMMENT
<b><math>4.5 \pm 0.4 \pm 0.2</math></b>	1,2 AAIJ	17Bd LHCBC	$pp$ at 7, 8 TeV

- <sup>1</sup> AAIJ 17Bd reports  $[\Gamma(B_S^0 \rightarrow p\bar{p} K^+ K^-)/\Gamma_{\text{total}}] / [B(B^0 \rightarrow J/\psi(1S) K^*(892)^0)] / [B(J/\psi(1S) \rightarrow p\bar{p})] / [B(K^*(892) \rightarrow (K \pi)^\pm)] = 1.67 \pm 0.12 \pm 0.11$  which we multiply by our best values  $B(B^0 \rightarrow J/\psi(1S) K^*(892)^0) = (1.27 \pm 0.05) \times 10^{-3}$ ,  $B(J/\psi(1S) \rightarrow p\bar{p}) = (2.121 \pm 0.029) \times 10^{-3}$ ,  $B(K^*(892) \rightarrow (K \pi)^\pm) = (99.901 \pm 0.009) \times 10^{-2}$ . Our first error is their experiment's error and our second error is the systematic error from using our best values. Reported value assumes  $f_s/f_d = 0.259 \pm 0.015$ .
- <sup>2</sup> The branching ratio is given for  $m_{p\bar{p}} < 2.85$  GeV.

$\Gamma(p\bar{p}K^+\pi^-)/\Gamma_{total}$   $\Gamma_{124}/\Gamma$

Table with 4 columns: VALUE (units 10^-7), DOCUMENT ID, TECN, COMMENT. Row 1: 13.9 ± 2.5 ± 0.5, 1.2 AAIJ, 17BD LHCB, pp at 7, 8 TeV

1 AAIJ 17BD reports [ $\Gamma(B_s^0 \to p\bar{p}K^+\pi^-)/\Gamma_{total}$ ] / [ $B(B^0 \to J/\psi(1S)K^*(892)^0$ ] / [ $B(J/\psi(1S) \to p\bar{p})$ ] / [ $B(K^*(892) \to (K\pi)^\pm)$ ] =  $0.52 \pm 0.08 \pm 0.05$  which we multiply by our best values  $B(B^0 \to J/\psi(1S)K^*(892)^0) = (1.27 \pm 0.05) \times 10^{-3}$ ,  $B(J/\psi(1S) \to p\bar{p}) = (2.121 \pm 0.029) \times 10^{-3}$ ,  $B(K^*(892) \to (K\pi)^\pm) = (99.901 \pm 0.009) \times 10^{-2}$ . Our first error is their experiment's error and our second error is the systematic error from using our best values. Reported value assumes  $f_s/f_d = 0.259 \pm 0.015$ .

2 The branching ratio is given for  $m_{p\bar{p}} < 2.85$  GeV.

$\Gamma(p\bar{p}K^+\pi^-)/\Gamma(p\bar{p}K^+K^-)$   $\Gamma_{124}/\Gamma_{123}$

Table with 4 columns: VALUE, DOCUMENT ID, TECN, COMMENT. Row 1: 0.31 ± 0.05 ± 0.02, 1.2 AAIJ, 17BD LHCB, pp at 7, 8 TeV

1 Reports  $B(B_s^0 \to p\bar{p}K^+\pi^-) / B(B^0 \to p\bar{p}K^+\pi^-) = 0.22 \pm 0.04 \pm 0.02 \pm 0.01$ , where the third error is due to  $f_s/f_d$ .

2 The ratio is given for  $m_{p\bar{p}} < 2.85$  GeV and assuming  $f_s/f_d = 0.259 \pm 0.015$ .

$\Gamma(p\bar{p}\pi^+\pi^-)/\Gamma_{total}$   $\Gamma_{125}/\Gamma$

Table with 4 columns: VALUE (units 10^-7), DOCUMENT ID, TECN, COMMENT. Row 1: 4.3 ± 2.0 ± 0.2, 1.2 AAIJ, 17BD LHCB, pp at 7, 8 TeV

1 AAIJ 17BD reports [ $\Gamma(B_s^0 \to p\bar{p}\pi^+\pi^-)/\Gamma_{total}$ ] / [ $B(B^0 \to J/\psi(1S)K^*(892)^0$ ] / [ $B(J/\psi(1S) \to p\bar{p})$ ] / [ $B(K^*(892) \to (K\pi)^\pm)$ ] =  $0.16 \pm 0.07 \pm 0.02$  which we multiply by our best values  $B(B^0 \to J/\psi(1S)K^*(892)^0) = (1.27 \pm 0.05) \times 10^{-3}$ ,  $B(J/\psi(1S) \to p\bar{p}) = (2.121 \pm 0.029) \times 10^{-3}$ ,  $B(K^*(892) \to (K\pi)^\pm) = (99.901 \pm 0.009) \times 10^{-2}$ . Our first error is their experiment's error and our second error is the systematic error from using our best values. Reported value assumes  $f_s/f_d = 0.259 \pm 0.015$ .

2 The branching ratio is given for  $m_{p\bar{p}} < 2.85$  GeV.

$\Gamma(p\bar{p}K^- + c.c.)/\Gamma_{total}$   $\Gamma_{126}/\Gamma$

Table with 4 columns: VALUE (units 10^-6), DOCUMENT ID, TECN, COMMENT. Row 1: 5.5 ± 0.6 ± 0.8, 1.2 AAIJ, 17AL LHCB, pp at 7, 8 TeV

1 AAIJ 17AL reports  $(5.46 \pm 0.61 \pm 0.82) \times 10^{-6}$  from a measurement of [ $\Gamma(B_s^0 \to p\bar{p}K^- + c.c.)/\Gamma_{total}$ ] / [ $B(B^0 \to p\bar{p}\pi^-)$ ] assuming  $B(B^0 \to p\bar{p}\pi^-) = (3.14 \pm 0.29) \times 10^{-6}$ .

2 AAIJ 17AL value represents the sum of  $B_s^0 \to p\bar{p}K^-$  and  $B_s^0 \to p\bar{p}K^+$  and assumes the fraction  $f_s/f_d = 0.259 \pm 0.015$ .

$\Gamma(\Lambda_c^- \Lambda \pi^+)/\Gamma_{total}$   $\Gamma_{127}/\Gamma$

Table with 4 columns: VALUE (units 10^-4), DOCUMENT ID, TECN, COMMENT. Row 1: 3.6 ± 1.1 ± 1.2, 1 SOLOVIEVA, 13 BELL, e+e- -> T(4S)

1 The second error is the total systematic uncertainty including the  $\Lambda_c$  absolute branching fractions and the normalization number of  $B_s$  events.

$\Gamma(\Lambda_c^- \Lambda_c^+)/\Gamma_{total}$   $\Gamma_{128}/\Gamma$

Table with 4 columns: VALUE, CL%, DOCUMENT ID, TECN, COMMENT. Row 1: < 8.0 x 10^-5, 95, 1 AAIJ, 14AA LHCB, pp at 7 TeV

1 Uses  $B(\bar{B}^0 \to D^+ D_s^-) = (7.2 \pm 0.8) \times 10^{-3}$ .

$\Gamma(\gamma)/\Gamma_{total}$   $\Gamma_{129}/\Gamma$

Table with 4 columns: VALUE (units 10^-6), CL%, DOCUMENT ID, TECN, COMMENT. Row 1: < 3.1, 90, 1 DUTTA, 15 BELL, e+e- -> T(5S)

1 Assumes the fraction of  $B_s^{(*)}\bar{B}_s^{(*)}$  in  $b\bar{b}$  events is  $f_s = (17.2 \pm 3.0)\%$ .  
2 Assumes  $\Upsilon(5S) \to B_s^* \bar{B}_s^* = (19.5 \pm 3.0)\%$ .  
3 ACCIARRI 95i assumes  $f_{B^0} = 39.5 \pm 4.0$  and  $f_{B_s} = (12.0 \pm 3.0)\%$ .

$\Gamma(\phi\gamma)/\Gamma_{total}$   $\Gamma_{130}/\Gamma$

Table with 4 columns: VALUE (units 10^-6), CL%, DOCUMENT ID, TECN, COMMENT. Row 1: 34 ± 4 OUR AVERAGE

1 Assumes the fraction of  $B_s^{(*)}\bar{B}_s^{(*)}$  in  $b\bar{b}$  events is  $f_s = (17.2 \pm 3.0)\%$ . The systematic uncertainty from  $f_s$  is  $0.6 \times 10^{-5}$ .  
2 AAIJ 13 reports [ $\Gamma(B_s^0 \to \phi\gamma)/\Gamma_{total}$ ] / [ $B(B^0 \to K^*(892)^0\gamma)$ ] =  $0.81 \pm 0.04 \pm 0.07$  which we multiply by our best value  $B(B^0 \to K^*(892)^0\gamma) = (4.18 \pm 0.25) \times 10^{-5}$ . Our first error is their experiment's error and our second error is the systematic error from using our best value.

3 Measures  $B(B^0 \to K^{*0}\gamma)/B(B_s \to \phi\gamma) = 1.12 \pm 0.08(stat) +0.06(sys) +0.09(f_s/f_d)$  and uses current world-average value of  $B(B^0 \to K^{*0}\gamma) = (4.33 \pm 0.15) \times 10^{-5}$ .

4 Assumes  $\Upsilon(5S) \to B_s^* \bar{B}_s^* = (19.5 \pm 3.0)\%$ .

5 ADAM 96d assumes  $f_{B^0} = f_{B^-} = 0.39$  and  $f_{B_s} = 0.12$ .

$\Gamma(\mu^+\mu^-)/\Gamma_{total}$   $\Gamma_{131}/\Gamma$

Table with 4 columns: VALUE (units 10^-3), CL%, DOCUMENT ID, TECN, COMMENT. Row 1: 3.0 ± 0.4 OUR AVERAGE

Table with 4 columns: VALUE, CL%, DOCUMENT ID, TECN, COMMENT. Rows 1-16 listing various experiments and their results.

• • • We do not use the following data for averages, fits, limits, etc. • • •

1 Uses normalization mode  $B(B^+ \to J/\psi K^+) = (1.010 \pm 0.029) \times 10^{-3}$  and  $B$  production ratio  $f(b \to B_s^0)/f(b \to B^0) = 0.256 \pm 0.013$ .  
2 Uses normalization mode  $B(B^+ \to J/\psi K^+) = (10.22 \pm 0.35) \times 10^{-4}$  and  $B$  production ratio  $f(\bar{b} \to B_s^0)/f(\bar{b} \to B_d^0) = 0.28 \pm 0.04$ .  
3 Uses  $B$  production ratio  $f(\bar{b} \to B_s^0)/f(\bar{b} \to B_d^0) = 0.256 \pm 0.020$  and  $B(B^+ \to J/\psi K^+ \to \mu^+ \mu^- K^+) = (6.0 \pm 0.2) \times 10^{-5}$  for normalization.  
4 This value corresponds to an upper limit of  $< 3.0 \times 10^{-9}$  at 95% C.L. It uses  $f_s/f_d = 0.24 \pm 0.02$ .  
5 Determined from the joint fit to CMS and LHCb data. Uncertainty includes both statistical and systematic component.  
6 Uses  $B$  production ratio  $f(\bar{b} \to B_s^0)/f(\bar{b} \to B_d^0) = 0.256 \pm 0.020$  and two normalization modes:  $B(B^+ \to J/\psi K^+ \to \mu^+ \mu^- K^+) = (6.01 \pm 0.21) \times 10^{-5}$  and  $B(B^0 \to K^+ \pi^-) = (1.94 \pm 0.06) \times 10^{-5}$ .  
7 Uses  $B$  production ratio  $f(\bar{b} \to B_s^0)/f(\bar{b} \to B_d^0) = 0.259 \pm 0.015$  and normalization modes  $B^+ \to J/\psi K^+ \to \mu^+ \mu^- K^+$  and  $B^0 \to K^+ \pi^-$ .  
8 Uses normalization mode  $B(B^+ \to J/\psi K^+ \to \mu^+ \mu^- K^+) = (6.01 \pm 0.21) \times 10^{-5}$  and  $B$  production ratio  $f(\bar{b} \to B_s^0)/f(\bar{b} \to B_d^0) = 0.263 \pm 0.017$ .  
9 Uses  $B$  production ratio  $f(\bar{b} \to B^+)/f(\bar{b} \to B_s^0) = 3.75 \pm 0.29$  and  $B(B^+ \to J/\psi K^+ \to \mu^+ \mu^- K^+) = (6.0 \pm 0.2) \times 10^{-5}$ .  
10 Uses  $B$  production ratio  $f(\bar{b} \to B_s^0)/f(\bar{b} \to B_d^0) = 0.267 \pm 0.021$  and three normalization modes  $B(B^+ \to J/\psi K^+ \to \mu^+ \mu^- K^+) = (6.01 \pm 0.21) \times 10^{-5}$ ,  $B(B^0 \to K^+ \pi^-) = (1.94 \pm 0.06) \times 10^{-5}$ , and  $B(B_s^0 \to J/\psi\phi \to \mu^+ \mu^- K^+ K^-) = (3.4 \pm 0.9) \times 10^{-5}$ .  
11 Uses  $B$  production ratio  $f(\bar{b} \to B_s^0)/f(\bar{b} \to B_d^0) = 0.267 \pm 0.021$  and three normalization modes of  $B^+ \to J/\psi K^+$ ,  $B^0 \to K^+ \pi^-$ , and  $B_s^0 \to J/\psi\phi$ .  
12 Uses  $f_s/f_d = 0.267 \pm 0.021$  and  $B(B^+ \to J/\psi K^+ \to \mu^+ \mu^- K^+) = (6.0 \pm 0.2) \times 10^{-5}$ .  
13 Uses  $B$  production ratio  $f(\bar{b} \to B^+)/f(\bar{b} \to B_s^0) = 3.71 \pm 0.47$  and three normalization modes.  
14 Uses  $B$  production ratio  $f(\bar{b} \to B^+)/f(\bar{b} \to B_s^0) = 3.55 \pm 0.47$  and  $B(B^+ \to J/\psi K^+ \to \mu^+ \mu^- K^+) = (6.01 \pm 0.21) \times 10^{-5}$ .  
15 Uses  $B$  production ratio  $f(\bar{b} \to B^+)/f(\bar{b} \to B_s^0) = 3.55 \pm 0.42$  and  $B(B^+ \to J/\psi K^+ \to \mu^+ \mu^- K^+) = (6.0 \pm 0.2) \times 10^{-5}$ .  
16 Uses  $B$  production ratio  $f(\bar{b} \to B^+)/f(\bar{b} \to B_s^0) = 3.86 \pm 0.59$ , and the number of  $B^+ \to J/\psi K^+$  decays.

$\Gamma(e^+e^-)/\Gamma_{total}$   $\Gamma_{132}/\Gamma$

Table with 4 columns: VALUE, CL%, DOCUMENT ID, TECN, COMMENT. Row 1: < 2.8 x 10^-7, 90, AALTONEN 09P CDF, p\bar{p} at 1.96 TeV

• • • We do not use the following data for averages, fits, limits, etc. • • •

1 ACCIARRI 97B assume PDG 96 production fractions for  $B^+$ ,  $B^0$ ,  $B_s$ , and  $\Lambda_b$ .

$\Gamma(\tau^+\tau^-)/\Gamma_{total}$   $\Gamma_{133}/\Gamma$

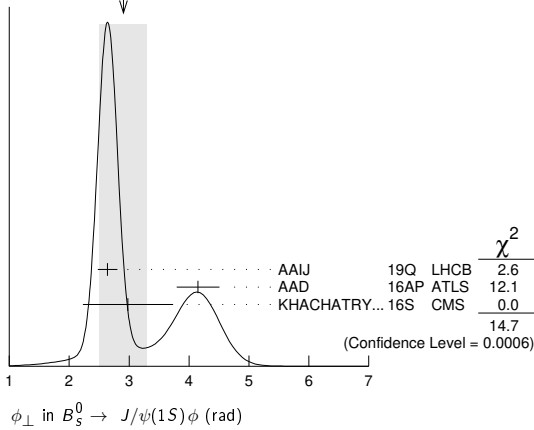
Table with 4 columns: VALUE, CL%, DOCUMENT ID, TECN, COMMENT. Row 1: < 6.8 x 10^-3, 95, 1 AAIJ, 17AJ LHCB, pp at 7, 8 TeV

1 Assuming no contribution from  $B^0 \to \tau^+ \tau^-$ .



$\phi_\perp$  in  $B_s^0 \rightarrow J/\psi(1S)\phi$ 

VALUE (rad)	DOCUMENT ID	TECN	COMMENT
<b>2.9 ± 0.4 OUR AVERAGE</b>	Error includes scale factor of 2.7. See the ideogram below.		
2.64 ± 0.13 ± 0.10	AAIJ	19Q LHCb	pp at 13 TeV
4.15 ± 0.32 ± 0.16	<sup>1</sup> AAD	16AP ATLAS	pp at 7, 8 TeV
2.98 ± 0.36 ± 0.66	KHACHATRY...16S	CMS	pp at 8 TeV
• • • We do not use the following data for averages, fits, limits, etc. • • •			
3.08 <sup>+0.14</sup> <sub>-0.15</sub> ± 0.06	AAIJ	15i LHCb	Repl. by AAIJ 19Q
3.89 ± 0.47 ± 0.11	<sup>1</sup> AAD	14U ATLAS	Repl. by AAD 16AP
<sup>1</sup> Measured using a tagged, time-dependent angular analysis of $B_s^0 \rightarrow J/\psi\phi$ decays.			

WEIGHTED AVERAGE  
2.9 ± 0.4 (Error scaled by 2.7) $\Gamma_\perp/\Gamma$  in  $B_s^0 \rightarrow \psi(2S)\phi$ 

VALUE	DOCUMENT ID	TECN	COMMENT
<b>0.264 ± 0.024 ± 0.002</b>	<sup>1</sup> AAIJ	16AK LHCb	pp at 7, 8 TeV
<sup>1</sup> Measured using time-dependent angular analysis of $B_s^0 \rightarrow \psi(2S)\phi$ decays.			

 $\phi_\parallel$  in  $B_s^0 \rightarrow \psi(2S)\phi$ 

VALUE (rad)	DOCUMENT ID	TECN	COMMENT
<b>3.67 ± 0.13 ± 0.03</b>	<sup>1</sup> AAIJ	16AK LHCb	pp at 7, 8 TeV
<sup>1</sup> Measured using time-dependent angular analysis of $B_s^0 \rightarrow \psi(2S)\phi$ decays.			

 $\phi_\perp$  in  $B_s^0 \rightarrow \psi(2S)\phi$ 

VALUE (rad)	DOCUMENT ID	TECN	COMMENT
<b>3.29 ± 0.43 ± 0.04</b>	<sup>1</sup> AAIJ	16AK LHCb	pp at 7, 8 TeV
<sup>1</sup> Measured using time-dependent angular analysis of $B_s^0 \rightarrow \psi(2S)\phi$ decays.			

 $\Gamma_L/\Gamma$  for  $B_s^0 \rightarrow J/\psi(1S)\bar{K}^*(892)^0$ Longitudinal polarization fraction, equals to  $f_L$  using notation of "Polarization in B decays" review.

VALUE	DOCUMENT ID	TECN	COMMENT
<b>0.497 ± 0.025 ± 0.025</b>	AAIJ	15AV LHCb	pp at 7, 8 TeV
• • • We do not use the following data for averages, fits, limits, etc. • • •			
0.50 ± 0.08 ± 0.02	<sup>1</sup> AAIJ	12AP LHCb	Repl. by AAIJ 15AV
<sup>1</sup> The non-resonant $K\pi$ background contributions are subtracted. Also reports an S-wave amplitude $ A_S ^2 = 0.07^{+0.15}_{-0.07}$ .			

 $\Gamma_\parallel/\Gamma$  for  $B_s^0 \rightarrow J/\psi(1S)\bar{K}^*(892)^0$ Parallel polarization fraction, equals to  $1 - f_L - f_\perp$  using notation of "Polarization in B decays" review.

VALUE	DOCUMENT ID	TECN	COMMENT
<b>0.179 ± 0.027 ± 0.013</b>	AAIJ	15AV LHCb	pp at 7, 8 TeV
• • • We do not use the following data for averages, fits, limits, etc. • • •			
0.19 <sup>+0.10</sup> <sub>-0.08</sub> ± 0.02	<sup>1</sup> AAIJ	12AP LHCb	Repl. by AAIJ 15AV
<sup>1</sup> The non-resonant $K\pi$ background contributions are subtracted. Also reports an S-wave amplitude $ A_S ^2 = 0.07^{+0.15}_{-0.07}$ .			

 $\Gamma_\parallel/\Gamma$  of  $K^*(892)^0$  in  $B_s^0 \rightarrow \psi(2S)\bar{K}^*(892)^0$ 

VALUE	DOCUMENT ID	TECN	COMMENT
<b>0.524 ± 0.056 ± 0.029</b>	AAIJ	15U LHCb	pp at 7, 8 TeV

 $\Gamma_L/\Gamma$  in  $B_s^0 \rightarrow \phi\phi$ 

VALUE	DOCUMENT ID	TECN	COMMENT
<b>0.378 ± 0.013 OUR AVERAGE</b>			
0.381 ± 0.007 ± 0.012	AAIJ	19AP LHCb	pp at 7, 8 and 13 TeV
0.348 ± 0.041 ± 0.021	AALTONEN	11AN CDF	$p\bar{p}$ at 1.96 TeV
• • • We do not use the following data for averages, fits, limits, etc. • • •			
0.364 ± 0.012 ± 0.009	AAIJ	14AE LHCb	Repl. by AAIJ 19AP
0.365 ± 0.022 ± 0.012	AAIJ	12P LHCb	Repl. by AAIJ 14AE

 $\Gamma_\perp/\Gamma$  in  $B_s^0 \rightarrow \phi\phi$ 

VALUE	DOCUMENT ID	TECN	COMMENT
<b>0.292 ± 0.009 OUR AVERAGE</b>			
0.290 ± 0.008 ± 0.005	<sup>1</sup> AAIJ	19AP LHCb	pp at 7, 8 and 13 TeV
0.365 ± 0.044 ± 0.027	AALTONEN	11AN CDF	$p\bar{p}$ at 1.96 TeV
• • • We do not use the following data for averages, fits, limits, etc. • • •			
0.305 ± 0.013 ± 0.005	AAIJ	14AE LHCb	Repl. by AAIJ 19AP
0.291 ± 0.024 ± 0.010	AAIJ	12P LHCb	Repl. by AAIJ 14AE

<sup>1</sup> Note: in the summary of AAIJ 19AP the systematic uncertainty is 0.007. We take the systematic uncertainty as given in Table 5 in the paper. $\phi_\parallel$  in  $B_s^0 \rightarrow \phi\phi$ 

VALUE (rad)	DOCUMENT ID	TECN	COMMENT
<b>2.56 ± 0.06 OUR AVERAGE</b>			
2.559 ± 0.045 ± 0.033	AAIJ	19AP LHCb	pp at 7, 8 and 13 TeV
2.71 <sup>+0.31</sup> <sub>-0.36</sub> ± 0.22	<sup>1</sup> AALTONEN	11AN CDF	$p\bar{p}$ at 1.96 TeV
• • • We do not use the following data for averages, fits, limits, etc. • • •			
2.54 ± 0.07 ± 0.09	<sup>2</sup> AAIJ	14AE LHCb	Repl. by AAIJ 19AP
2.57 ± 0.15 ± 0.06	<sup>3</sup> AAIJ	12P LHCb	Repl. by AAIJ 14AE

<sup>1</sup> AALTONEN 11AN quotes  $\cos\phi_\parallel = -0.91^{+0.15}_{-0.13} \pm 0.09$  which we convert to  $\phi_\parallel$  taking the smaller solution.<sup>2</sup> AAIJ 14AE reports measurement of  $\phi_\perp$  and  $\phi_\perp - \phi_\parallel$ , which we convert into  $\phi_\parallel$ . Statistical uncertainty includes correlation between measured parameters, while systematic uncertainties are assumed uncorrelated.<sup>3</sup> AAIJ 12P quotes  $\cos\phi_\parallel = -0.844 \pm 0.068 \pm 0.029$  which we convert to  $\phi_\parallel$ , taking the smaller solution. $\phi_\perp$  in  $B_s^0 \rightarrow \phi\phi$ 

VALUE (rad)	DOCUMENT ID	TECN	COMMENT
<b>2.818 ± 0.178 ± 0.073</b>	AAIJ	19AP LHCb	pp at 7, 8 and 13 TeV
• • • We do not use the following data for averages, fits, limits, etc. • • •			
2.67 ± 0.23 ± 0.07	AAIJ	14AE LHCb	Repl. by AAIJ 19AP

 $\Gamma_L/\Gamma$  in  $B_s^0 \rightarrow K^{*0}\bar{K}^{*0}$ 

VALUE	DOCUMENT ID	TECN	COMMENT
<b>0.240 ± 0.031 ± 0.025</b>	<sup>1</sup> AAIJ	19L LHCb	pp at 7 and 8 TeV
• • • We do not use the following data for averages, fits, limits, etc. • • •			
0.208 ± 0.032 ± 0.046	<sup>2</sup> AAIJ	18S LHCb	Repl. by AAIJ 19L
0.201 ± 0.057 ± 0.040	<sup>3</sup> AAIJ	15AF LHCb	Repl. by AAIJ 18S
0.31 ± 0.12 ± 0.04	AAIJ	12F LHCb	Repl. by AAIJ 15AF

<sup>1</sup> Untagged and time-integrated analysis within 150 MeV of the  $K^{*0}$  mass.<sup>2</sup> Measured in angular analysis, which takes into account S-, P- and D-wave contributions.<sup>3</sup> Measured in angular analysis, which takes into account S-wave contributions. $\Gamma_\perp/\Gamma$  in  $B_s^0 \rightarrow K^{*0}\bar{K}^{*0}$ 

VALUE	DOCUMENT ID	TECN	COMMENT
<b>0.38 ± 0.11 ± 0.04</b>	AAIJ	12F LHCb	pp at 7 TeV

 $\Gamma_\parallel/\Gamma$  in  $B_s^0 \rightarrow K^*(892)^0\bar{K}^*(892)^0$ 

VALUE	DOCUMENT ID	TECN	COMMENT
<b>0.297 ± 0.029 ± 0.042</b>	<sup>1</sup> AAIJ	18S LHCb	pp at 7, 8 TeV
• • • We do not use the following data for averages, fits, limits, etc. • • •			
0.215 ± 0.046 ± 0.015	AAIJ	15AF LHCb	Repl. by AAIJ 18S
<sup>1</sup> Measured in angular analysis, which takes into account S-, P- and D-wave contributions.			

 $\Phi_\parallel$  in  $B_s^0 \rightarrow K^*(892)^0\bar{K}^*(892)^0$ 

VALUE	DOCUMENT ID	TECN	COMMENT
<b>2.40 ± 0.11 ± 0.33</b>	<sup>1</sup> AAIJ	18S LHCb	pp at 7, 8 TeV
• • • We do not use the following data for averages, fits, limits, etc. • • •			
5.31 ± 0.24 ± 0.14	AAIJ	15AF LHCb	Repl. by AAIJ 18S
<sup>1</sup> Measured in angular analysis, which takes into account S-, P- and D-wave contributions.			

 $\Phi_\perp$  in  $B_s^0 \rightarrow K^*(892)^0\bar{K}^*(892)^0$ 

VALUE (rad)	DOCUMENT ID	TECN	COMMENT
<b>2.62 ± 0.26 ± 0.64</b>	<sup>1</sup> AAIJ	18S LHCb	pp at 7, 8 TeV
<sup>1</sup> Measured in angular analysis, which takes into account S-, P- and D-wave contributions.			

 $\Gamma_L/\Gamma$  in  $B_s^0 \rightarrow \phi\bar{K}^{*0}$ 

VALUE	DOCUMENT ID	TECN	COMMENT
<b>0.51 ± 0.15 ± 0.07</b>	AAIJ	13BW LHCb	pp at 7 TeV

# Meson Particle Listings

$B_s^0$

$\Gamma_{\parallel}/\Gamma$  in  $B_s^0 \rightarrow \phi \bar{K}^{*0}$

VALUE	DOCUMENT ID	TECN	COMMENT
$0.21 \pm 0.11 \pm 0.02$	AAIJ	13BW LHCB	$p\bar{p}$ at 7 TeV

$\phi_{\parallel}$  in  $B_s^0 \rightarrow \phi \bar{K}^{*0}$

VALUE (rad)	DOCUMENT ID	TECN	COMMENT
$1.75 \pm 0.53 \pm 0.29$	<sup>1</sup> AAIJ	13BW LHCB	$p\bar{p}$ at 7 TeV

<sup>1</sup> Measures  $\cos(\phi_{\parallel}) = -0.18 \pm 0.52 \pm 0.29$ , which we convert to  $\phi_{\parallel}$  by taking the smaller solution.

$\Gamma_L/\Gamma$  in  $B_s^0 \rightarrow \bar{D}^{*0} \phi$

VALUE	DOCUMENT ID	TECN	COMMENT
$0.73 \pm 0.15 \pm 0.04$	AAIJ	18AY LHCB	$p\bar{p}$ at 7 and 8 TeV

$\Gamma_L/\Gamma$  in  $B_s^0 \rightarrow K^*(892)^0 \bar{K}_2^*(1430)^0$

VALUE	DOCUMENT ID	TECN	COMMENT
$0.911 \pm 0.020 \pm 0.165$	<sup>1</sup> AAIJ	18S LHCB	$p\bar{p}$ at 7, 8 TeV

<sup>1</sup> Measured in angular analysis, which takes into account S-, P- and D-wave. contributions.

$\Gamma_{\parallel}/\Gamma$  in  $B_s^0 \rightarrow K^*(892)^0 \bar{K}_2^*(1430)^0$

VALUE	DOCUMENT ID	TECN	COMMENT
$0.012 \pm 0.008 \pm 0.053$	<sup>1</sup> AAIJ	18S LHCB	$p\bar{p}$ at 7, 8 TeV

<sup>1</sup> Measured in angular analysis, which takes into account S-, P- and D-wave. contributions.

$\Gamma_L/\Gamma$  in  $B_s^0 \rightarrow K_2^*(1430)^0 \bar{K}^*(892)^0$

VALUE	DOCUMENT ID	TECN	COMMENT
$0.62 \pm 0.16 \pm 0.25$	<sup>1</sup> AAIJ	18S LHCB	$p\bar{p}$ at 7, 8 TeV

<sup>1</sup> Measured in angular analysis, which takes into account S-, P- and D-wave. contributions.

$\Gamma_{\parallel}/\Gamma$  in  $B_s^0 \rightarrow K_2^*(1430)^0 \bar{K}^*(892)^0$

VALUE	DOCUMENT ID	TECN	COMMENT
$0.24 \pm 0.10 \pm 0.14$	<sup>1</sup> AAIJ	18S LHCB	$p\bar{p}$ at 7, 8 TeV

<sup>1</sup> Measured in angular analysis, which takes into account S-, P- and D-wave. contributions.

$\Gamma_L/\Gamma$  in  $B_s^0 \rightarrow K_2^*(1430)^0 \bar{K}_2^*(1430)^0$

VALUE	DOCUMENT ID	TECN	COMMENT
$0.25 \pm 0.14 \pm 0.18$	<sup>1</sup> AAIJ	18S LHCB	$p\bar{p}$ at 7, 8 TeV

<sup>1</sup> Measured in angular analysis, which takes into account S-, P- and D-wave. contributions.

$\Gamma_{\parallel 1}/\Gamma$  in  $B_s^0 \rightarrow K_2^*(1430)^0 \bar{K}_2^*(1430)^0$

VALUE	DOCUMENT ID	TECN	COMMENT
$0.17 \pm 0.11 \pm 0.14$	<sup>1</sup> AAIJ	18S LHCB	$p\bar{p}$ at 7, 8 TeV

<sup>1</sup> Measured in angular analysis, which takes into account S-, P- and D-wave. contributions.

$\Gamma_{\parallel 1}/\Gamma$  in  $B_s^0 \rightarrow K_2^*(1430)^0 \bar{K}_2^*(1430)^0$

VALUE	DOCUMENT ID	TECN	COMMENT
$0.30 \pm 0.18 \pm 0.21$	<sup>1</sup> AAIJ	18S LHCB	$p\bar{p}$ at 7, 8 TeV

<sup>1</sup> Measured in angular analysis, which takes into account S-, P- and D-wave. contributions.

$\Gamma_{\parallel 2}/\Gamma$  in  $B_s^0 \rightarrow K_2^*(1430)^0 \bar{K}_2^*(1430)^0$

VALUE	DOCUMENT ID	TECN	COMMENT
$0.015 \pm 0.033 \pm 0.107$	<sup>1</sup> AAIJ	18S LHCB	$p\bar{p}$ at 7, 8 TeV

<sup>1</sup> Measured in angular analysis, which takes into account S-, P- and D-wave. contributions.

$F_L(B_s^0 \rightarrow \phi \mu^+ \mu^-)$  ( $0.10 < q^2 < 2.00 \text{ GeV}^2/c^4$ )

VALUE	DOCUMENT ID	TECN	COMMENT
$0.20^{+0.08}_{-0.09} \pm 0.02$	AAIJ	15AQ LHCB	$p\bar{p}$ at 7, 8 TeV

••• We do not use the following data for averages, fits, limits, etc. •••

$0.37^{+0.19}_{-0.17} \pm 0.07$	AAIJ	13X LHCB	Repl. by AAIJ 15AQ
---------------------------------	------	----------	--------------------

$F_L(B_s^0 \rightarrow \phi \mu^+ \mu^-)$  ( $2.00 < q^2 < 5.0 \text{ GeV}^2/c^4$ )

VALUE	DOCUMENT ID	TECN	COMMENT
$0.68^{+0.16}_{-0.13} \pm 0.03$	AAIJ	15AQ LHCB	$p\bar{p}$ at 7, 8 TeV

••• We do not use the following data for averages, fits, limits, etc. •••

$0.53^{+0.25}_{-0.23} \pm 0.10$	<sup>1</sup> AAIJ	13X LHCB	Repl. by AAIJ 15AQ
---------------------------------	-------------------	----------	--------------------

<sup>1</sup> Measured in  $2.0 < q^2 < 4.3 \text{ GeV}^2/c^4$ .

$F_L(B_s^0 \rightarrow \phi \mu^+ \mu^-)$  ( $5.0 < q^2 < 8.0 \text{ GeV}^2/c^4$ )

VALUE	DOCUMENT ID	TECN	COMMENT
$0.54^{+0.10}_{-0.09} \pm 0.02$	AAIJ	15AQ LHCB	$p\bar{p}$ at 7, 8 TeV

••• We do not use the following data for averages, fits, limits, etc. •••

$0.81^{+0.11}_{-0.13} \pm 0.05$	<sup>1</sup> AAIJ	13X LHCB	Repl. by AAIJ 15AQ
---------------------------------	-------------------	----------	--------------------

<sup>1</sup> Measured in  $4.3 < q^2 < 8.68 \text{ GeV}^2/c^4$ .

$F_L(B_s^0 \rightarrow \phi \mu^+ \mu^-)$  ( $11.0 < q^2 < 12.5 \text{ GeV}^2/c^4$ )

VALUE	DOCUMENT ID	TECN	COMMENT
$0.29 \pm 0.11 \pm 0.04$	AAIJ	15AQ LHCB	$p\bar{p}$ at 7, 8 TeV

••• We do not use the following data for averages, fits, limits, etc. •••

$0.33^{+0.14}_{-0.12} \pm 0.06$	<sup>1</sup> AAIJ	13X LHCB	Repl. by AAIJ 15AQ
---------------------------------	-------------------	----------	--------------------

<sup>1</sup> Measured in  $10.09 < q^2 < 12.90 \text{ GeV}^2/c^4$ .

$F_L(B_s^0 \rightarrow \phi \mu^+ \mu^-)$  ( $15.0 < q^2 < 17.0 \text{ GeV}^2/c^4$ )

VALUE	DOCUMENT ID	TECN	COMMENT
$0.23^{+0.09}_{-0.08} \pm 0.02$	AAIJ	15AQ LHCB	$p\bar{p}$ at 7, 8 TeV

••• We do not use the following data for averages, fits, limits, etc. •••

$0.34^{+0.18}_{-0.17} \pm 0.07$	<sup>1</sup> AAIJ	13X LHCB	Repl. by AAIJ 15AQ
---------------------------------	-------------------	----------	--------------------

<sup>1</sup> Measured in  $14.18 < q^2 < 16 \text{ GeV}^2/c^4$ .

$F_L(B_s^0 \rightarrow \phi \mu^+ \mu^-)$  ( $17.0 < q^2 < 19.0 \text{ GeV}^2/c^4$ )

VALUE	DOCUMENT ID	TECN	COMMENT
$0.40^{+0.13}_{-0.15} \pm 0.02$	AAIJ	15AQ LHCB	$p\bar{p}$ at 7, 8 TeV

••• We do not use the following data for averages, fits, limits, etc. •••

$0.16^{+0.17}_{-0.10} \pm 0.07$	<sup>1</sup> AAIJ	13X LHCB	Repl. by AAIJ 15AQ
---------------------------------	-------------------	----------	--------------------

<sup>1</sup> Measured in  $16.0 < q^2 < 19.0 \text{ GeV}^2/c^4$ .

$F_L(B_s^0 \rightarrow \phi \mu^+ \mu^-)$  ( $1.00 < q^2 < 6.00 \text{ GeV}^2/c^4$ )

VALUE	DOCUMENT ID	TECN	COMMENT
$0.63^{+0.09}_{-0.09} \pm 0.03$	AAIJ	15AQ LHCB	$p\bar{p}$ at 7, 8 TeV

••• We do not use the following data for averages, fits, limits, etc. •••

$0.56^{+0.17}_{-0.16} \pm 0.09$	AAIJ	13X LHCB	Repl. by AAIJ 15AQ
---------------------------------	------	----------	--------------------

## $B_s^0$ - $\bar{B}_s^0$ MIXING

For a discussion of  $B_s^0$ - $\bar{B}_s^0$  mixing see the note on “ $B^0$ - $\bar{B}^0$  Mixing” in the  $B^0$  Particle Listings above.

$\chi_S$  is a measure of the time-integrated  $B_s^0$ - $\bar{B}_s^0$  mixing probability that produced  $B_s^0$  ( $\bar{B}_s^0$ ) decays as a  $\bar{B}_s^0$  ( $B_s^0$ ). Mixing violates  $\Delta B \neq 2$  rule.

$$\chi_S = \frac{x_S^2}{2(1+x_S^2)}$$

$$x_S = \frac{\Delta m_{B_S^0}}{\Gamma_{B_S^0}} = (m_{B_{S,H}^0} - m_{B_{S,L}^0}) \tau_{B_S^0}$$

where H, L stand for heavy and light states of two  $B_s^0$  CP eigenstates and  $\tau_{B_S^0} = \frac{1}{0.5(\Gamma_{B_{S,H}^0} + \Gamma_{B_{S,L}^0})}$ .

## $\Delta m_{B_S^0} = m_{B_{S,H}^0} - m_{B_{S,L}^0}$

$\Delta m_{B_S^0}$  is a measure of  $2\pi$  times the  $B_s^0$ - $\bar{B}_s^0$  oscillation frequency in time-dependent mixing experiments.

“OUR EVALUATION” is provided by the Heavy Flavor Averaging Group (HFLAV, <https://hflav.web.cern.ch/>) by taking into account correlations between measurements.

VALUE ( $10^{12} \tau_s^{-1}$ )	CL%	DOCUMENT ID	TECN	COMMENT
<b>17.749 ± 0.020 OUR EVALUATION</b>				
<b>17.756 ± 0.021 OUR AVERAGE</b>				
$17.703 \pm 0.059 \pm 0.018$		<sup>1</sup> AAIJ	19Q LHCB	$p\bar{p}$ at 13 TeV
$17.768 \pm 0.023 \pm 0.006$		<sup>2</sup> AAIJ	13BI LHCB	$p\bar{p}$ at 7 TeV
$17.93 \pm 0.22 \pm 0.15$		<sup>3</sup> AAIJ	13CF LHCB	$p\bar{p}$ at 7 TeV
$17.63 \pm 0.11 \pm 0.02$		<sup>4</sup> AAIJ	12I LHCB	$p\bar{p}$ at 7 TeV
$17.77 \pm 0.10 \pm 0.07$		<sup>5</sup> ABULENCIA,A	06G CDF	$p\bar{p}$ at 1.96 TeV
••• We do not use the following data for averages, fits, limits, etc. •••				
$17.711^{+0.055}_{-0.057} \pm 0.011$		<sup>1</sup> AAIJ	15I LHCB	Repl. by AAIJ 19Q
$17-21$	90	<sup>6</sup> ABAZOV	06B D0	$p\bar{p}$ at 1.96 TeV
$17.31^{+0.33}_{-0.18} \pm 0.07$		<sup>7</sup> ABULENCIA	06Q CDF	Repl. by ABULENCIA,A 06G
$> 8.0$	95	<sup>8</sup> ABDALLAH	04J DLPH	$e^+e^- \rightarrow Z^0$
$> 4.9$	95	<sup>9</sup> ABDALLAH	04J DLPH	$e^+e^- \rightarrow Z^0$
$> 8.5$	95	<sup>10</sup> ABDALLAH	04J DLPH	$e^+e^- \rightarrow Z^0$
$> 5.0$	95	<sup>11</sup> ABDALLAH	03B DLPH	$e^+e^- \rightarrow Z$
$> 10.3$	95	<sup>12</sup> ABE	03 SLD	$e^+e^- \rightarrow Z$
$> 10.9$	95	<sup>13</sup> HEISTER	03E ALEP	$e^+e^- \rightarrow Z$
$> 5.3$	95	<sup>14</sup> ABE	02V SLD	$e^+e^- \rightarrow Z$
$> 1.0$	95	<sup>15</sup> ABBIENDI	01D OPAL	$e^+e^- \rightarrow Z$
$> 7.4$	95	<sup>16</sup> ABREU	00Y DLPH	Repl. by ABDALLAH 04J
$> 4.0$	95	<sup>17</sup> ABREU,P	00G DLPH	$e^+e^- \rightarrow Z$

> 5.2	95	18	ABBIENDI	99S	OPAL	$e^+ e^- \rightarrow Z$
< 96	95	19	ABE	99D	CDF	$p\bar{p}$ at 1.8 TeV
> 5.8	95	20	ABE	99J	CDF	$p\bar{p}$ at 1.8 TeV
> 9.6	95	21	BARATE	99J	ALEP	$e^+ e^- \rightarrow Z$
> 7.9	95	22	BARATE	98C	ALEP	Repl. by BARATE 99J
> 3.1	95	23	ACKERSTAFF	97U	OPAL	Repl. by ABBIENDI 99S
> 2.2	95	24	ACKERSTAFF	97V	OPAL	Repl. by ABBIENDI 99S
> 6.5	95	25	ADAM	97	DLPH	Repl. by ABREU 00Y
> 6.6	95	26	BUSKULIC	96M	ALEP	Repl. by BARATE 98C
> 2.2	95	24	AKERS	95J	OPAL	Sup. by ACKERSTAFF 97V
> 5.7	95	27	BUSKULIC	95J	ALEP	$e^+ e^- \rightarrow Z$
> 1.8	95	24	BUSKULIC	94B	ALEP	$e^+ e^- \rightarrow Z$

- Measured using time-dependent angular analysis of  $B_s^0 \rightarrow J/\psi K^+ K^-$  decays.
- Measured using  $B_s^0 \rightarrow D_s^- \pi^+$  decays.
- Measured using  $B_s^0 \rightarrow D_s^- \mu^+ \nu_\mu X$  decays.
- Measured using  $B_s^0 \rightarrow D_s^- \pi^+$  and  $D_s^- \pi^+ \pi^- \pi^+$  decays.
- Significance of oscillation signal is  $5.4 \sigma$ . Also reports  $|V_{td} / V_{ts}| = 0.2060 \pm 0.0007 + 0.0081 - 0.0060$ .
- A likelihood scan over the oscillation frequency,  $\Delta m_s$ , gives a most probable value of  $19 \text{ ps}^{-1}$  and a range of  $17 < \Delta m_s < 21 \text{ (ps}^{-1}\text{)}$  at 90% C.L. assuming Gaussian uncertainties. Also excludes  $\Delta m_s < 14.8 \text{ ps}^{-1}$  at 95% C.L.
- Significance of oscillation signal is 0.2%. Also reported the value  $|V_{td} / V_{ts}| = 0.208 + 0.001 + 0.008 - 0.002 - 0.006$ .
- Uses leptons emitted with large momentum transverse to a jet and improved techniques for vertexing and flavor-tagging.
- Updates of  $D_s$ -lepton analysis.
- Combined results from all Delphi analyses.
- Events with a high transverse momentum lepton were removed and an inclusively reconstructed vertex was required.
- ABE 03 uses the novel "charge dipole" technique to reconstruct separate secondary and tertiary vertices originating from the  $B \rightarrow D$  decay chain. The analysis excludes  $\Delta m_s < 4.9 \text{ ps}^{-1}$  and  $7.9 < \Delta m_s < 10.3 \text{ ps}^{-1}$ .
- Three analyses based on complementary event selections: (1) fully-reconstructed hadronic decays; (2) semileptonic decays with  $D_s$  exclusively reconstructed; (3) inclusive semileptonic decays.
- ABE 02v uses exclusively reconstructed  $D_s^-$  mesons and excludes  $\Delta m_s < 1.4 \text{ ps}^{-1}$  and  $2.4 < \Delta m_s < 5.3 \text{ ps}^{-1}$  at 95% C.L.
- Uses fully or partially reconstructed  $D_s \ell$  vertices and a mixing tag as a flavor tagging.
- Replaced by ABDALLAH 04A. Uses  $D_s^- \ell^+$ , and  $\phi \ell^+$  vertices, and a multi-variable discriminant as a flavor tagging.
- Uses inclusive  $D_s$  vertices and fully reconstructed  $B_s$  decays and a multi-variable discriminant as a flavor tagging.
- Uses  $\ell$ - $Q_{\text{hem}}$  and  $\ell$ - $\ell$ .
- ABE 99D assumes  $\tau_{B_s^0} = 1.55 \pm 0.05 \text{ ps}$  and  $\Delta\Gamma/\Delta m = (5.6 \pm 2.6) \times 10^{-3}$ .
- ABE 99J uses  $\phi$   $\ell$ - $\ell$  correlation.
- BARATE 99J uses combination of an inclusive lepton and  $D_s^-$ -based analyses.
- BARATE 98C combines results from  $D_s h$ - $\ell/Q_{\text{hem}}$ ,  $D_s h$ - $K$  in the same side,  $D_s \ell$ - $\ell/Q_{\text{hem}}$  and  $D_s \ell$ - $K$  in the same side.
- Uses  $\ell$ - $Q_{\text{hem}}$ .
- Uses  $\ell$ - $\ell$ .
- ADAM 97 combines results from  $D_s \ell$ - $Q_{\text{hem}}$ ,  $\ell$ - $Q_{\text{hem}}$ , and  $\ell$ - $\ell$ .
- BUSKULIC 96M uses  $D_s$  lepton correlations and lepton, kaon, and jet charge tags.
- BUSKULIC 95J uses  $\ell$ - $Q_{\text{hem}}$ . They find  $\Delta m_s > 5.6$  [ $> 6.1$ ] for  $r_s = 10\%$  [12%]. We interpolate to our central value  $r_s = 10.5\%$ .

$x_s = \frac{\Delta m_{B_s^0}}{\Gamma_{B_s^0}}$   
 This is derived by the Heavy Flavor Averaging Group (HFLAV, <https://hflav.web.cern.ch/>) from the results on  $\Delta m_{B_s^0}$  and "OUR EVALUATION" of the  $B_s^0$  mean lifetime.

VALUE DOCUMENT ID  
**26.89 ± 0.07 OUR EVALUATION**

$X_s$   
 This is a  $B_s^0 \bar{B}_s^0$  integrated mixing parameter derived from  $x_s$  above and OUR EVALUATION of  $\Delta\Gamma_{B_s^0}/\Gamma_{B_s^0}$ .

VALUE DOCUMENT ID  
**0.49931 ± 0.00004 OUR EVALUATION**

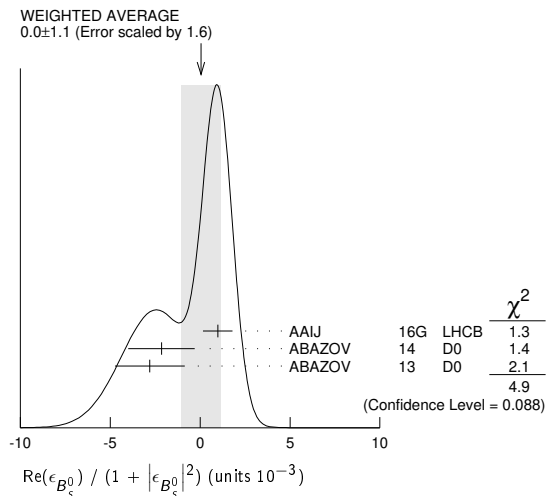
**CP VIOLATION PARAMETERS in  $B_s^0$**

$\text{Re}(\epsilon_{B_s^0}) / (1 + |\epsilon_{B_s^0}|^2)$   
 CP impurity in  $B_s^0$  system.

"OUR EVALUATION" is an average obtained by the Heavy Flavor Averaging Group (HFLAV, <https://hflav.web.cern.ch/>) and described at <https://hflav.web.cern.ch/>. It is the result of a fit to  $B_d$  and  $B_s$  CP asymmetries, which includes the  $B_s$  measurements listed below and the  $B_d$  measurements listed in the  $B_d$  section, and takes into account correlations between those measurements.

VALUE (units $10^{-3}$ )	DOCUMENT ID	TECN	COMMENT
<b>-0.15 ± 0.70 OUR EVALUATION</b>			
<b>0.0 ± 1.1 OUR AVERAGE</b>	Error includes scale factor of 1.6. See the ideogram below.		
0.98 ± 0.65 ± 0.5	1	AAIJ	16G LHCb $pp$ at 7, 8 TeV
-2.15 ± 1.85	2	ABAZOV	14 D0 $p\bar{p}$ at 1.96 TeV
-2.8 ± 1.9 ± 0.4	3	ABAZOV	13 D0 $p\bar{p}$ at 1.96 TeV

- We do not use the following data for averages, fits, limits, etc.
- 0.15 ± 1.25 ± 0.90      4 AAIJ      14D LHCb      Repl. by AAIJ 16G
- 4.5 ± 2.7      5 ABAZOV      11U D0      Repl. by ABAZOV 14
- 0.4 ± 2.3 ± 0.4      6 ABAZOV      10E D0      Repl. by ABAZOV 13
- 3.6 ± 1.9      7 ABAZOV      10H D0      Repl. by ABAZOV 11U
- 6.1 ± 4.8 ± 0.9      8 ABAZOV      07A D0      Repl. by ABAZOV 10E
- 1 AAIJ 16G reports a measurement of time-integrated flavor-specific asymmetry in  $B_s^0 \rightarrow \mu^+ D_s^- X$  decays,  $A_{SL}^s = (0.39 \pm 0.26 \pm 0.20)\%$ , which is approximately equal to  $4 \times \text{Re}(\epsilon_{B_s^0}) / (1 + |\epsilon_{B_s^0}|^2)$ .
- 2 ABAZOV 14 uses the dimuon charge asymmetry with different impact parameters from which it reports  $A_{SL}^s = (-0.86 \pm 0.74) \times 10^{-2}$ .
- 3 ABAZOV 13 reports a measurement of time-integrated flavor-specific asymmetry in mixed semileptonic  $B_s^0 \rightarrow \mu^+ D_s^- X$  decays  $A_{SL}^s = (-1.12 \pm 0.74 \pm 0.17)\%$  which is approximately equal to  $4 \times \text{Re}(\epsilon_{B_s^0}) / (1 + |\epsilon_{B_s^0}|^2)$ .
- 4 AAIJ 14D reports a measurement of time-integrated flavor-specific asymmetry in  $B_s^0 \rightarrow \mu^+ D_s^- X$  decays,  $A_{SL}^s = (-0.06 \pm 0.50 \pm 0.36)\%$ , which is approximately equal to  $4 \times \text{Re}(\epsilon_{B_s^0}) / (1 + |\epsilon_{B_s^0}|^2)$ .
- 5 ABAZOV 11U uses the dimuon charge asymmetry with different impact parameters from which it reports  $A_{SL}^s = (-18.1 \pm 10.6) \times 10^{-3}$ .
- 6 ABAZOV 10E reports a measurement of flavor-specific asymmetry in  $B_{(s)}^0 \rightarrow \mu^+ D_{(s)}^{*-} X$  decays with a decay-time analysis including initial-state flavor tagging,  $A_{SL}^s = (-1.7 \pm 9.1 - 1.4) \times 10^{-3}$  which is approximately equal to  $4 \times \text{Re}(\epsilon_{B_s^0}) / (1 + |\epsilon_{B_s^0}|^2)$ .
- 7 ABAZOV 10H reports a measurement of like-sign dimuon charge asymmetry of  $A_{SL}^s = (-9.57 \pm 2.51 \pm 1.46) \times 10^{-3}$  in semileptonic  $b$ -hadron decays. Using the measured production ratio of  $B_d^0$  and  $B_s^0$ , and the asymmetry of  $B_d^0$   $A_{SL}^s = (-4.7 \pm 4.6) \times 10^{-3}$  measured from  $B$ -factories, they obtain the asymmetry for  $B_s^0$ .
- 8 The first direct measurement of the time integrated flavor untagged charge asymmetry in semileptonic  $B_s^0$  decays is reported as  $2 \times A_{SL}^s(\text{untagged}) = A_{SL}^s = (2.45 \pm 1.93 \pm 0.35) \times 10^{-2}$ .



$C_{KK}(B_s^0 \rightarrow K^+ K^-)$   
 VALUE DOCUMENT ID TECN COMMENT  
**0.14 ± 0.11 ± 0.03**      AAIJ      13B0 LHCb       $pp$  at 7 TeV

$S_{KK}(B_s^0 \rightarrow K^+ K^-)$   
 VALUE DOCUMENT ID TECN COMMENT  
**0.30 ± 0.12 ± 0.04**      AAIJ      13B0 LHCb       $pp$  at 7 TeV

$r_B(B_s^0 \rightarrow D_s^{\mp} K^{\pm})$   
 $r_B$  and  $\phi_B$  are the amplitude ratio and relative strong phase between the amplitudes of  $A(B_s^0 \rightarrow D_s^+ K^-)$  and  $A(B_s^0 \rightarrow D_s^- K^+)$ ,

VALUE DOCUMENT ID TECN COMMENT  
**0.37 ± 0.10 - 0.09**      1 AAIJ      18U LHCb       $pp$  at 7, 8 TeV

- We do not use the following data for averages, fits, limits, etc.
- 0.53 ± 0.17 - 0.16      2 AAIJ      14BF LHCb      Repl. by AAIJ 18U

- Measured in  $B_s^0 \rightarrow D_s^{\mp} K^{\pm}$  decays, constraining  $-2\beta_s$  by the measurement of  $\phi_s = -0.030 \pm 0.033$  from HFLAV.
- Measured in  $B_s^0 \rightarrow D_s^{\mp} K^{\pm}$  decays, constraining  $-2\beta_s$  by the measurement of  $\phi_s = 0.01 \pm 0.07 \pm 0.0$  from AAIJ 13AR. At 68% CL.



## Meson Particle Listings

 $B_S^0$  $\delta_B(B_S^0 \rightarrow D_S^\pm K^\mp)$ 

VALUE (°)	DOCUMENT ID	TECN	COMMENT
<b>358<sup>+13</sup><sub>-14</sub></b>	1 AAIJ	18U LHCb	$pp$ at 7, 8 TeV
• • • We do not use the following data for averages, fits, limits, etc. • • •			
$3^{+19}$ $-20$	2 AAIJ	14BF LHCb	Repl. by AAIJ 18U

<sup>1</sup> Measured in  $B_S^0 \rightarrow D_S^\mp K^\pm$  decays, constraining  $-2\beta_S$  by the measurement of  $\phi_S = 0.030 \pm 0.033$  from HFLAV. The value is modulo  $180^\circ$ .

<sup>2</sup> Measured in  $B_S^0 \rightarrow D_S^\mp K^\pm$  decays, constraining  $-2\beta_S$  by the measurement of  $\phi_S = 0.01 \pm 0.07 \pm 0.0$  from AAIJ 13AR. The value is modulo  $180^\circ$  at 68% CL.

CP Violation phase  $\beta_S$ 

$-2\beta_S$  is the weak phase difference between  $B_S^0$  mixing amplitude and the  $B_S^0 \rightarrow J/\psi\phi$  decay amplitude driven by the  $b \rightarrow c\bar{c}s$  transition (such as  $B_S \rightarrow J/\psi\phi, J/\psi K^+ K^-, J/\psi\pi^+\pi^-,$  and  $D_S^+ D_S^-$ ). The Standard Model value of  $\beta_S$  is  $\arg(-\frac{V_{ts}V_{tb}}{V_{cs}V_{cb}})$  if penguin contributions are neglected.

“OUR EVALUATION” is an average using rescaled values of the data listed below. The average and rescaling were performed by the Heavy Flavor Averaging Group (HFLAV, <https://hflav.web.cern.ch/>) and are described at <https://hflav.web.cern.ch/>. The averaging/scaling procedure takes into account correlation between the measurements.

VALUE ( $10^{-2}$ rad)	DOCUMENT ID	TECN	COMMENT
<b>2.55 ± 1.15 OUR EVALUATION</b>			
<b>2.6 ± 1.4 OUR AVERAGE</b>			
- 0.1 ± 2.2 ± 0.6	1 AAIJ	19AF LHCb	$pp$ at 7, 8, 13 TeV
4.15 ± 2.05 ± 0.30	2 AAIJ	19Q LHCb	$pp$ at 13 TeV
11.9 ± 10.7 ± 3.4	3 AAIJ	17V LHCb	$pp$ at 7, 8 TeV
4.5 ± 3.9 ± 2.1	4 AAD	16AP ATLS	$pp$ at 7, 8 TeV
-11.5 <sup>+14</sup> <sub>-14.5</sub> ± 1	5 AAIJ	16AK LHCb	$pp$ at 7, 8 TeV
3.75 ± 4.85 ± 1.55	6 KHACHATRYAN...16s	CMS	$pp$ at 8 TeV
- 1 ± 9 ± 1	7 AAIJ	14AY LHCb	$pp$ at 7, 8 TeV
	8 AALTONEN	12AJ CDF	$p\bar{p}$ at 1.96 TeV
28 <sup>+18</sup> <sub>-19</sub>	9 ABZOV	12D D0	$p\bar{p}$ at 1.96 TeV
• • • We do not use the following data for averages, fits, limits, etc. • • •			
3.7 ± 5.8 ± 1.4	10,11 AAIJ	19AP LHCb	$pp$ at 7, 8, 13 TeV
5.0 ± 6.5 ± 7.0	12 AAIJ	18s LHCb	$pp$ at 7, 8 TeV
2.9 ± 2.5 ± 0.3	13 AAIJ	15i LHCb	Repl. by AAIJ 19Q
6 <sup>+8</sup> <sub>-7</sub>	14,15 AAIJ	15K LHCb	$pp$ at 7, 8 TeV
- 6 ± 13 ± 3	16 AAD	14U ATLS	Repl. by AAD 16AP
8.5 ± 7.5 ± 1.5	17 AAIJ	14AE LHCb	Repl. by AAIJ 19AP
- 3.5 ± 3.4 ± 0.4	18 AAIJ	14s LHCb	Repl. by AAIJ 19AF
- 0.5 ± 3.5 ± 0.5	19 AAIJ	13AR LHCb	Repl. by AAIJ 15i
	20 AAIJ	13AY LHCb	$pp$ at 7 TeV
-11.0 ± 20.5 ± 5.0	21 AAD	12CV ATLS	Repl. by AAD 14U
22 ± 22 ± 1	22 AAIJ	12B LHCb	Repl. by AAIJ 12Q
- 8 ± 9 ± 3	23 AAIJ	12D LHCb	Repl. by AAIJ 13AR
0.95 <sup>+8.70+0.15</sup> <sub>-8.65-0.20</sub>	24 AAIJ	12Q LHCb	Repl. by AAIJ 13AR
	25 AALTONEN	12D CDF	Repl. by AALTONEN 12AJ
	26 AALTONEN	08G CDF	Repl. by AALTONEN 12D
28 <sup>+12</sup> <sub>-15</sub> ± 4 <sup>+1</sup> <sub>-1</sub>	9,27 ABZOV	08AMD0	Repl. by ABZOV 12D
39.5 ± 28.0 ± 7.0	28,29 ABZOV	07 D0	Repl. by ABZOV 07N
35 <sup>+20</sup> <sub>-24</sub>	29,30 ABZOV	07N D0	Repl. by ABZOV 08AM

<sup>1</sup> AAIJ 19AF reports  $\phi_S = -2\beta_S = 0.002 \pm 0.044 \pm 0.012$  rad. and  $|\lambda| = 0.949 \pm 0.036 \pm 0.019$ , when direct CP violation is allowed. Measured using a time-dependent fit to  $B_S^0 \rightarrow J/\psi\pi^+\pi^-$  decays, which is sensitive to  $\phi_S(s\bar{s}s)$ , not  $\phi_S(c\bar{c}s)$ .

<sup>2</sup> AAIJ 19Q reports  $\phi_S = -2\beta_S = -0.083 \pm 0.041 \pm 0.006$  rad. that was measured using a time-dependent angular analysis of  $B_S^0 \rightarrow J/\psi K^+ K^-$  decays.

<sup>3</sup> Measured using time-dependent angular analysis of  $B_S^0 \rightarrow J/\psi K^+ K^-$  in the region  $m(KK) > 1.05$  GeV.

<sup>4</sup> AAD 16AP reports  $\phi_S = -2\beta_S = -0.090 \pm 0.078 \pm 0.041$  rad. that was measured using a time-dependent angular analysis of  $B_S^0 \rightarrow J/\psi\phi$  decays.

<sup>5</sup> AAIJ 16AK reports  $\phi_S = -2\beta_S = 0.23^{+0.29}_{-0.28} \pm 0.02$  rad. that was measured using a time-dependent angular analysis of  $B_S^0 \rightarrow \psi(2S)\phi$  decays.

<sup>6</sup> KHACHATRYAN 16s reports  $\phi_S = -2\beta_S = -0.075 \pm 0.097 \pm 0.031$  rad. that was measured using a time-dependent angular analysis of  $B_S^0 \rightarrow J/\psi\phi$  decays.

<sup>7</sup> AAIJ 14AY reports  $\phi_S = -2\beta_S = 0.02 \pm 0.17 \pm 0.02$  rad. in a time-dependent fit to  $B_S^0 \rightarrow D_S^+ D_S^-$ , while allowing CP violation in decay.

<sup>8</sup> AALTONEN 12AJ reports  $-\pi/2 < \beta_S < -1.51$  or  $-0.06 < \beta_S < 0.30$ , or  $1.26 < \beta_S < \pi/2$  rad. at 68% CL. Measured using the time-dependent angular analysis of  $B_S^0 \rightarrow J/\psi\phi$  decays.

<sup>9</sup> ABZOV 12D reports  $\phi_S = -2\beta_S = -0.55^{+0.38}_{-0.36}$  rad. that was measured using a time-dependent angular analysis of  $B_S^0 \rightarrow J/\psi\phi$  decays. A single error includes both statistical and systematic uncertainties.

<sup>10</sup> AAIJ 19AP reports  $\phi_S^{S\bar{S}} = -0.073 \pm 0.115 \pm 0.027$  rad and  $|\lambda| = 0.99 \pm 0.05 \pm 0.01$ . Measured using a time-dependent fit to  $B_S^0 \rightarrow \phi\phi$  decays, assuming independence of the helicity of the  $\phi\phi$  decay.

<sup>11</sup> AAIJ 19AP reports also polarisation-dependent results assuming that the longitudinal weak phase is CP-conserving and that there is no direct CP violation, giving  $\phi_{S||} = 0.014 \pm 0.055 \pm 0.011$  rad and  $\phi_{S\perp} = 0.044 \pm 0.059 \pm 0.019$  rad.

<sup>12</sup> AAIJ 18s reports  $\phi_S = -2\beta_S = -0.10 \pm 0.13 \pm 0.14$  rad measured in  $B_S^0 \rightarrow (K^+\pi^-)(K^-\pi^+)$  in the region  $0.75 < m(K^\pm\pi^\mp) < 1.6$  GeV. This is a  $b \rightarrow d\bar{d}s$  transition with a decay amplitude phase different from that of  $b \rightarrow c\bar{c}s$  transition.

<sup>13</sup> AAIJ 15i reports  $\phi_S = -2\beta_S = -0.058 \pm 0.049 \pm 0.006$  rad. that was measured using a time-dependent angular analysis of  $B_S^0 \rightarrow J/\psi K^+ K^-$  decays. It also combines this result with that of AAIJ 14s and quotes  $\phi_S = -2\beta_S = -0.010 \pm 0.039$  rad.

<sup>14</sup> AAIJ 15K reports  $-2\beta_S = -0.12^{+0.14}_{-0.16}$  rad. The value was obtained by measuring time-dependent CP asymmetry in  $B_S^0 \rightarrow K^+ K^-$  and using a U-spin relation between  $B_S^0 \rightarrow K^+ K^-$  and  $B^0 \rightarrow \pi^+ \pi^-$ .

<sup>15</sup> Results are also presented using additional inputs on  $B^0 \rightarrow \pi^0\pi^0$  and  $B^+ \rightarrow \pi^+\pi^0$  decays from other experiments and isospin symmetry assumptions. The dependence of the results on the maximum allowed amount of U-spin breaking up to 50% is also included.

<sup>16</sup> AAD 14U reports  $\phi_S = -2\beta_S = 0.12 \pm 0.25 \pm 0.05$  rad. that was measured using a time-dependent angular analysis of  $B_S^0 \rightarrow J/\psi\phi$  decays.

<sup>17</sup> AAIJ 14AE value measured in  $B_S^0 \rightarrow \phi\phi$  decays. This is a  $b \rightarrow s\bar{s}s$  transition with a decay amplitude phase different from that of  $b \rightarrow c\bar{c}s$  transition. Also reports  $\phi_S = -0.17 \pm 0.15 \pm 0.03$  rad.

<sup>18</sup> AAIJ 14s reports  $\phi_S = -2\beta_S = 0.070 \pm 0.068 \pm 0.008$  rad. and  $|\lambda| = 0.89 \pm 0.05 \pm 0.01$ , when direct CP violation is allowed. Measured using a time-dependent fit to  $B_S^0 \rightarrow J/\psi\pi^+\pi^-$  decays.

<sup>19</sup> AAIJ 13AR reports  $\phi_S = -2\beta_S = 0.01 \pm 0.07 \pm 0.01$  rad. obtained from combined fit to  $B_S^0 \rightarrow J/\psi K^+ K^-$  and  $B_S^0 \rightarrow J/\psi\pi^+\pi^-$  data sets. Also reports separate results of  $\phi_S = 0.07 \pm 0.09 \pm 0.01$  rad. from  $B_S^0 \rightarrow J/\psi K^+ K^-$  decays and  $\phi_S = -0.14^{+0.17}_{-0.16} \pm 0.01$  rad. from  $B_S^0 \rightarrow J/\psi\pi^+\pi^-$  decays.

<sup>20</sup> AAIJ 13AY uses  $B_S^0 \rightarrow \phi\phi$  mode, and reports the 68% CL interval of  $\phi_S = -2\beta_S$  as  $[-2.46, -0.76]$  rad.

<sup>21</sup> AAD 12CV reports  $\phi_S = -2\beta_S = 0.22 \pm 0.41 \pm 0.10$  rad. that was measured using a time-dependent angular analysis of  $B_S^0 \rightarrow J/\psi\phi$  decays.

<sup>22</sup> Reports  $\phi_S = -2\beta_S = -0.44 \pm 0.44 \pm 0.02$  rad. that was measured using a time-dependent fit to  $B_S^0 \rightarrow J/\psi\eta(980)$  decays.

<sup>23</sup> Reports  $\phi_S = -2\beta_S = 0.15 \pm 0.18 \pm 0.06$  rad. that was measured using a time-dependent angular analysis of  $B_S^0 \rightarrow J/\psi\phi$  decays.

<sup>24</sup> Reports  $\phi_S = -2\beta_S = -0.019^{+0.173+0.004}_{-0.174-0.003}$  rad. which was measured using a time-dependent fit to  $B_S^0 \rightarrow J/\psi\pi^+\pi^-$  decays, with the  $\pi^+\pi^-$  mass within 775–1550 MeV. Searches for, but finds no evidence, for direct CP violation in  $B_S^0 \rightarrow J/\psi\pi\pi$  decays.

<sup>25</sup> Reports  $0.02 < \phi_S < 0.52$  or  $1.08 < \phi_S < 1.55$  rad. at 68% C.L. confidence regions in the two-dimensional space of  $\phi_S$  and  $\Delta\Gamma_{B_S^0}$  from  $B_S^0 \rightarrow J/\psi\phi$  decays.

<sup>26</sup> Reports  $0.32 < 2\beta_S < 2.82$  rad. at 68% C.L. and confidence regions in the two-dimensional space of  $2\beta_S$  and  $\Delta\Gamma$  from the first measurement of  $B_S^0 \rightarrow J/\psi\phi$  decays using flavor tagging. The probability of a deviation from SM prediction as large as the level of observed data is 15%.

<sup>27</sup> Reports  $\phi_S = -2\beta_S$  and obtains 90% CL interval  $-0.03 < \beta_S < 0.60$  rad.

<sup>28</sup> The first direct measurement of the CP-violating mixing phase is reported from the time-dependent analysis of flavor untagged  $B_S^0 \rightarrow J/\psi\phi$  decays.

<sup>29</sup> Reports  $\phi_S$  which equals to  $-2\beta_S$ .

<sup>30</sup> Combines D0 collaboration measurements of time-dependent angular distributions in  $B_S^0 \rightarrow J/\psi\phi$  and charge asymmetry in semileptonic decays. There is a 4-fold ambiguity in the solution.

 $|\lambda|(B_S^0 \rightarrow J/\psi(1S)\phi)$ 

VALUE	DOCUMENT ID	TECN	COMMENT
<b>1.012 ± 0.016 ± 0.006</b>	AAIJ	19Q LHCb	$pp$ at 13 TeV
• • • We do not use the following data for averages, fits, limits, etc. • • •			
0.964 ± 0.019 ± 0.007	AAIJ	15i LHCb	Repl. by AAIJ 19Q

 $|\lambda|$ 

VALUE	DOCUMENT ID	TECN	COMMENT
<b>0.999 ± 0.017 OUR AVERAGE</b>			
0.99 ± 0.05 ± 0.01	1 AAIJ	19AP LHCb	$pp$ at 7, 8, 13 TeV
1.035 ± 0.034 ± 0.089	2 AAIJ	18s LHCb	$pp$ at 7, 8 TeV
0.994 ± 0.018 ± 0.006	3 AAIJ	17V LHCb	$pp$ at 7, 8 TeV
1.045 <sup>+0.069</sup> <sub>-0.050</sub> ± 0.007	4 AAIJ	16AK LHCb	$pp$ at 7, 8 TeV
0.91 <sup>+0.18</sup> <sub>-0.15</sub> ± 0.02	5 AAIJ	14AY LHCb	$pp$ at 7, 8 TeV
• • • We do not use the following data for averages, fits, limits, etc. • • •			
0.949 ± 0.036 ± 0.019	6 AAIJ	19AF LHCb	$pp$ at 7, 8, 13 TeV
1.04 ± 0.07 ± 0.03	7 AAIJ	14AE LHCb	Repl. by AAIJ 19AP

<sup>1</sup> Measured in  $B_S^0 \rightarrow \phi\phi$  decays.

<sup>2</sup> Measured in  $B_S^0 \rightarrow (K^+\pi^-)(K^-\pi^+)$  in the region  $0.75 < m(K^\pm\pi^\mp) < 1.6$  GeV.

<sup>3</sup> Measured using time-dependent angular analysis of  $B_S^0 \rightarrow J/\psi K^+ K^-$  in the region  $m(KK) > 1.05$  GeV.

<sup>4</sup> Measured using time-dependent angular analysis of  $B_S^0 \rightarrow \psi(2S)\phi$  decays.

<sup>5</sup> Measured in  $B_S^0 \rightarrow D_S^+ D_S^-$  decays.

<sup>6</sup> Measured using time-dependent analysis of  $B_S^0 \rightarrow J/\psi\pi^+\pi^-$  decays.

<sup>7</sup> Measured in  $B_S^0 \rightarrow \phi\phi$  decays.

**A, CP violation parameter**

$$A = -2 \operatorname{Re}(\lambda) / (1 + |\lambda|^2)$$

VALUE	DOCUMENT ID	TECN	COMMENT
<b>-0.75 ± 0.12 OUR AVERAGE</b>			
-0.79 ± 0.07 ± 0.10	<sup>1</sup> AAIJ	18o LHCb	pp at 7, 8 TeV
0.49 <sup>+0.77</sup> <sub>-0.65</sub> ± 0.06	<sup>2</sup> AAIJ	15AL LHCb	pp at 7, 8 TeV
<sup>1</sup> Measured in $B_s^0 \rightarrow K^+ K^-$ decays.			
<sup>2</sup> Measured in $B_s^0 \rightarrow J/\psi K_S^0$ decays.			

**C, CP violation parameter**

$$C = (1 - |\lambda|^2) / (1 + |\lambda|^2)$$

VALUE	DOCUMENT ID	TECN	COMMENT
<b>0.19 ± 0.06 OUR AVERAGE</b>			
0.20 ± 0.06 ± 0.02	<sup>1</sup> AAIJ	18o LHCb	pp at 7, 8 TeV
-0.28 ± 0.41 ± 0.08	<sup>2</sup> AAIJ	15AL LHCb	pp at 7, 8 TeV
<sup>1</sup> Measured in $B_s^0 \rightarrow K^+ K^-$ decays.			
<sup>2</sup> Measured in $B_s^0 \rightarrow J/\psi K_S^0$ decays.			

**S, CP violation parameter**

$$S = -2 \operatorname{Im}(\lambda) / (1 + |\lambda|^2)$$

VALUE	DOCUMENT ID	TECN	COMMENT
<b>0.17 ± 0.06 OUR AVERAGE</b>			
0.18 ± 0.06 ± 0.02	<sup>1</sup> AAIJ	18o LHCb	pp at 7, 8 TeV
-0.08 ± 0.40 ± 0.08	<sup>2</sup> AAIJ	15AL LHCb	pp at 7, 8 TeV
<sup>1</sup> Measured in $B_s^0 \rightarrow K^+ K^-$ decays.			
<sup>2</sup> Measured in $B_s^0 \rightarrow J/\psi K_S^0$ decays.			

**$A_{CP}^L(B_s \rightarrow J/\psi \bar{K}^*(892)^0)$**

VALUE	DOCUMENT ID	TECN	COMMENT
<b>-0.048 ± 0.057 ± 0.020</b>	AAIJ	15AV LHCb	pp at 7, 8 TeV

**$A_{CP}^{\parallel}(B_s \rightarrow J/\psi \bar{K}^*(892)^0)$**

VALUE	DOCUMENT ID	TECN	COMMENT
<b>0.171 ± 0.152 ± 0.028</b>	AAIJ	15AV LHCb	pp at 7, 8 TeV

**$A_{CP}^{\perp}(B_s \rightarrow J/\psi \bar{K}^*(892)^0)$**

VALUE	DOCUMENT ID	TECN	COMMENT
<b>-0.049 ± 0.096 ± 0.025</b>	AAIJ	15AV LHCb	pp at 7, 8 TeV

**$A_{CP}(B_s \rightarrow \pi^+ K^-)$**

$A_{CP}$  is defined as

$$\frac{B(\bar{B}_s^0 \rightarrow f) - B(B_s^0 \rightarrow \bar{f})}{B(\bar{B}_s^0 \rightarrow f) + B(B_s^0 \rightarrow \bar{f})}$$

the CP-violation asymmetry of exclusive  $B_s^0$  and  $\bar{B}_s^0$  decay.

VALUE	DOCUMENT ID	TECN	COMMENT
<b>0.221 ± 0.015 OUR AVERAGE</b>			
0.213 ± 0.015 ± 0.007	AAIJ	18o LHCb	pp at 7, 8 TeV
0.22 ± 0.07 ± 0.02	AALTONEN	14P CDF	p $\bar{p}$ at 1.96 TeV
0.27 ± 0.04 ± 0.01	AAIJ	13AX LHCb	pp at 7 TeV
••• We do not use the following data for averages, fits, limits, etc. •••			
0.27 ± 0.08 ± 0.02	AAIJ	12V LHCb	Repl. by AAIJ 13AX
0.39 ± 0.15 ± 0.08	AALTONEN	11N CDF	Repl. by AALTONEN 14P

**$A_{CP}(B_s^0 \rightarrow [K^+ K^-]_D \bar{K}^*(892)^0)$**

VALUE	DOCUMENT ID	TECN	COMMENT
<b>-0.04 ± 0.07 ± 0.02</b>	AAIJ	14BN LHCb	pp at 7, 8 TeV
••• We do not use the following data for averages, fits, limits, etc. •••			
0.04 ± 0.16 ± 0.01	AAIJ	13L LHCb	Repl. by AAIJ 14BN

**$A_{CP}(B_s^0 \rightarrow [\pi^+ K^-]_D K^*(892)^0)$**

VALUE	DOCUMENT ID	TECN	COMMENT
<b>-0.01 ± 0.03 ± 0.02</b>	AAIJ	14BN LHCb	pp at 7, 8 TeV

**$A_{CP}(B_s^0 \rightarrow [\pi^+ \pi^-]_D K^*(892)^0)$**

VALUE	DOCUMENT ID	TECN	COMMENT
<b>0.06 ± 0.13 ± 0.02</b>	AAIJ	14BN LHCb	pp at 7, 8 TeV

**$S(B_s^0 \rightarrow \phi\gamma)$**

VALUE	DOCUMENT ID	TECN	COMMENT
<b>0.43 ± 0.30 ± 0.11</b>	<sup>1</sup> AAIJ	19AE LHCb	pp at 7, 8 TeV
<sup>1</sup> Measured in flavor tagged time dependent analysis.			

**$C(B_s^0 \rightarrow \phi\gamma)$**

VALUE	DOCUMENT ID	TECN	COMMENT
<b>0.11 ± 0.29 ± 0.11</b>	<sup>1</sup> AAIJ	19AE LHCb	pp at 7, 8 TeV
<sup>1</sup> Measured in flavor tagged time dependent analysis.			

**$A^\Delta(B_s \rightarrow \phi\gamma)$**

$A^\Delta(B_s \rightarrow \phi\gamma)$  is the multiplicative coefficient of the  $\sinh(\Delta\Gamma/2)$  term in the  $B_s \rightarrow \phi\gamma$  decay rate time dependence.

VALUE	DOCUMENT ID	TECN	COMMENT
<b>-0.67 ± 0.37 ± 0.41 ± 0.17</b>	<sup>1</sup> AAIJ	19AE LHCb	pp at 7, 8 TeV
••• We do not use the following data for averages, fits, limits, etc. •••			
-0.98 ± 0.46 ± 0.23 -0.52 - 0.20	<sup>2</sup> AAIJ	17B LHCb	Repl. by AAIJ 19AE
<sup>1</sup> Measured in flavor tagged time dependent analysis, using tagged and un-tagged events. This result updates AAIJ 17B with better selection efficiency and other analysis improvements.			
<sup>2</sup> Measured in time dependent analysis without initial flavor tagging.			

**CPT VIOLATION PARAMETERS**

In the  $B_s^0$  mixing, propagating mass eigenstates can be written as

$$\begin{aligned} |B_{sL}\rangle &\propto p \sqrt{1-\xi} |B_s^0\rangle + q \sqrt{1+\xi} |\bar{B}_s^0\rangle \\ |B_{sH}\rangle &\propto p \sqrt{1+\xi} |B_s^0\rangle - q \sqrt{1-\xi} |\bar{B}_s^0\rangle \end{aligned}$$

where parameter  $\xi$  controls CPT violation. If  $\xi$  is zero, then CPT is conserved. The parameter  $\xi$  can be written as

$$\xi = \frac{2(M_{11}-M_{22})-i(\Gamma_{11}-\Gamma_{22})}{-2\Delta m_s+i\Delta\Gamma_s} \approx \frac{-2\beta^\mu \Delta a_\mu}{2\Delta m_s-i\Delta\Gamma_s}$$

where  $M_{ii}$ ,  $\Gamma_{ii}$ ,  $\Delta m_s$ , and  $\Delta\Gamma_s$  are parameters of Hamiltonian governing  $B_s$  oscillations,  $\beta^\mu$  is the  $B_s^0$  meson velocity and  $\Delta a_\mu$  characterizes Lorentz-invariance violation.

**$\Delta a_\perp$**

VALUE (10 <sup>-12</sup> GeV)	CL%	DOCUMENT ID	TECN	COMMENT
<b>-0.47 ± 0.39 ± 0.08</b>		<sup>1</sup> AAIJ	16E LHCb	pp at 7, 8 TeV
< 1.2	95	<sup>2</sup> ABAZOV	15L D0	p $\bar{p}$ at 1.96 TeV
<sup>1</sup> Uses $B_s^0 \rightarrow J/\psi K^+ K^-$ decays.				
<sup>2</sup> Measured in semileptonic $B_s^0 \rightarrow D_s^- \mu^+ X$ decays. Also extracts limit on time and longitudinal components ( $-0.8 < \Delta a_T - 0.396 \Delta a_Z < 3.9$ ) 10 <sup>-13</sup> GeV.				

**$\Delta a_\parallel$**

VALUE (10 <sup>-14</sup> GeV)	DOCUMENT ID	TECN	COMMENT
<b>-0.89 ± 1.41 ± 0.36</b>	<sup>1</sup> AAIJ	16E LHCb	pp at 7, 8 TeV
<sup>1</sup> Uses $B_s^0 \rightarrow J/\psi K^+ K^-$ decays.			

**$\Delta a_X$**

VALUE (10 <sup>-14</sup> GeV)	DOCUMENT ID	TECN	COMMENT
<b>+1.01 ± 2.08 ± 0.71</b>	<sup>1</sup> AAIJ	16E LHCb	pp at 7, 8 TeV
<sup>1</sup> Uses $B_s^0 \rightarrow J/\psi K^+ K^-$ decays.			

**$\Delta a_Y$**

VALUE (10 <sup>-14</sup> GeV)	DOCUMENT ID	TECN	COMMENT
<b>-3.83 ± 2.09 ± 0.71</b>	<sup>1</sup> AAIJ	16E LHCb	pp at 7, 8 TeV
<sup>1</sup> Uses $B_s^0 \rightarrow J/\psi K^+ K^-$ decays.			

**Re( $\xi$ )**

VALUE	DOCUMENT ID	TECN	COMMENT
<b>-0.022 ± 0.033 ± 0.003</b>	<sup>1</sup> AAIJ	16E LHCb	pp at 7, 8 TeV
<sup>1</sup> Uses $B_s^0 \rightarrow J/\psi K^+ K^-$ decays.			

**Im( $\xi$ )**

VALUE	DOCUMENT ID	TECN	COMMENT
<b>0.004 ± 0.011 ± 0.002</b>	<sup>1</sup> AAIJ	16E LHCb	pp at 7, 8 TeV
<sup>1</sup> Uses $B_s^0 \rightarrow J/\psi K^+ K^-$ decays.			

**PARTIAL BRANCHING FRACTIONS IN  $B_s \rightarrow \phi \ell^+ \ell^-$**

**$B(B_s \rightarrow \phi \ell^+ \ell^-)$  (0.1 < q<sup>2</sup> < 2.0 GeV<sup>2</sup>/c<sup>4</sup>)**

VALUE (units 10 <sup>-7</sup> )	DOCUMENT ID	TECN	COMMENT
<b>1.14 ± 0.16 OUR AVERAGE</b>			
1.11 <sup>+0.14</sup> <sub>-0.13</sub> ± 0.09	<sup>1</sup> AAIJ	15AQ LHCb	pp at 7, 8 TeV
2.78 ± 0.95 ± 0.89	AALTONEN	11AI CDF	p $\bar{p}$ at 1.96 TeV
••• We do not use the following data for averages, fits, limits, etc. •••			
0.897 <sup>+0.207</sup> <sub>-0.186</sub> ± 0.097	<sup>1</sup> AAIJ	13X LHCb	Repl. by AAIJ 15AQ
<sup>1</sup> Measured in $B_s^0 \rightarrow \phi \mu^+ \mu^-$ decays.			

**$B(B_s \rightarrow \phi \ell^+ \ell^-)$  (2.0 < q<sup>2</sup> < 5.0 GeV<sup>2</sup>/c<sup>4</sup>)**

VALUE (units 10 <sup>-7</sup> )	DOCUMENT ID	TECN	COMMENT
<b>0.77 ± 0.12 ± 0.06</b>	<sup>1</sup> AAIJ	15AQ LHCb	pp at 7, 8 TeV
••• We do not use the following data for averages, fits, limits, etc. •••			
0.529 <sup>+0.182</sup> <sub>-0.159</sub> ± 0.057	<sup>1,2</sup> AAIJ	13X LHCb	Repl. by AAIJ 15AQ
0.58 ± 0.55 ± 0.19	<sup>2</sup> AALTONEN	11AI CDF	p $\bar{p}$ at 1.96 TeV
<sup>1</sup> Measured in $B_s^0 \rightarrow \phi \mu^+ \mu^-$ decays.			
<sup>2</sup> Measured in 2 < q <sup>2</sup> < 4.3 GeV <sup>2</sup> /c <sup>4</sup> .			

# Meson Particle Listings

## $B_s^0$

### $B(B_s \to \phi \ell^+ \ell^-)$ ( $5.0 < q^2 < 8.0 \text{ GeV}^2/c^4$ )

VALUE (units $10^{-7}$ )	DOCUMENT ID	TECN	COMMENT
<b><math>0.96 \pm 0.13 \pm 0.08</math></b>	<sup>1</sup> AAIJ	15AQ LHCb	$pp$ at 7, 8 TeV
••• We do not use the following data for averages, fits, limits, etc. •••			
$1.38^{+0.25}_{-0.23} \pm 0.14$	<sup>1,2</sup> AAIJ	13X LHCb	Repl. by AAIJ 15AQ
$1.34 \pm 0.83 \pm 0.43$	<sup>2</sup> AALTONEN	11AI CDF	$p\bar{p}$ at 1.96 TeV
<sup>1</sup> Measured in $B_s^0 \to \phi \mu^+ \mu^-$ decays.			
<sup>2</sup> Measured in $4.3 < q^2 < 8.68 \text{ GeV}^2/c^4$ .			

### $B(B_s \to \phi \ell^+ \ell^-)$ ( $11.0 < q^2 < 12.5 \text{ GeV}^2/c^4$ )

VALUE (units $10^{-7}$ )	DOCUMENT ID	TECN	COMMENT
<b><math>0.71 \pm 0.10 \pm 0.06</math></b>	<sup>1</sup> AAIJ	15AQ LHCb	$pp$ at 7, 8 TeV
••• We do not use the following data for averages, fits, limits, etc. •••			
$1.18^{+0.22}_{-0.21} \pm 0.14$	<sup>1,2</sup> AAIJ	13X LHCb	Repl. by AAIJ 15AQ
$2.98 \pm 0.95 \pm 0.95$	<sup>2</sup> AALTONEN	11AI CDF	$p\bar{p}$ at 1.96 TeV
<sup>1</sup> Measured in $B_s^0 \to \phi \mu^+ \mu^-$ decays.			
<sup>2</sup> Measured in $10.9 < q^2 < 12.86 \text{ GeV}^2/c^4$ .			

### $B(B_s \to \phi \ell^+ \ell^-)$ ( $15.0 < q^2 < 17.0 \text{ GeV}^2/c^4$ )

VALUE (units $10^{-7}$ )	DOCUMENT ID	TECN	COMMENT
<b><math>0.90 \pm 0.11 \pm 0.07</math></b>	<sup>1</sup> AAIJ	15AQ LHCb	$pp$ at 7, 8 TeV
••• We do not use the following data for averages, fits, limits, etc. •••			
$0.760^{+0.189}_{-0.169} \pm 0.087$	<sup>1,2</sup> AAIJ	13X LHCb	Repl. by AAIJ 15AQ
$1.86 \pm 0.66 \pm 0.59$	<sup>2</sup> AALTONEN	11AI CDF	$p\bar{p}$ at 1.96 TeV
<sup>1</sup> Measured in $B_s^0 \to \phi \mu^+ \mu^-$ decays.			
<sup>2</sup> Measured in $14.18 < q^2 < 16 \text{ GeV}^2/c^4$ .			

### $B(B_s \to \phi \ell^+ \ell^-)$ ( $17.0 < q^2 < 19.0 \text{ GeV}^2/c^4$ )

VALUE (units $10^{-7}$ )	DOCUMENT ID	TECN	COMMENT
<b><math>0.79 \pm 0.11 \pm 0.07</math></b>	<sup>1</sup> AAIJ	15AQ LHCb	$pp$ at 7, 8 TeV
••• We do not use the following data for averages, fits, limits, etc. •••			
$1.06^{+0.23}_{-0.21} \pm 0.12$	<sup>1,2</sup> AAIJ	13X LHCb	Repl. by AAIJ 15AQ
$2.32 \pm 0.76 \pm 0.74$	<sup>2</sup> AALTONEN	11AI CDF	$p\bar{p}$ at 1.96 TeV
<sup>1</sup> Measured in $B_s^0 \to \phi \mu^+ \mu^-$ decays.			
<sup>2</sup> Measured in $16 < q^2 < 19 \text{ GeV}^2/c^4$ .			

### $B(B_s \to \phi \ell^+ \ell^-)$ ( $1.0 < q^2 < 6.0 \text{ GeV}^2/c^4$ )

VALUE (units $10^{-7}$ )	DOCUMENT ID	TECN	COMMENT
<b><math>1.28 \pm 0.18</math> OUR AVERAGE</b>			
$1.29 \pm 0.16 \pm 0.10$	<sup>1</sup> AAIJ	15AQ LHCb	$pp$ at 7, 8 TeV
$1.14 \pm 0.79 \pm 0.36$	AALTONEN	11AI CDF	$p\bar{p}$ at 1.96 TeV
••• We do not use the following data for averages, fits, limits, etc. •••			
$1.14^{+0.25}_{-0.23} \pm 0.13$	<sup>1</sup> AAIJ	13X LHCb	Repl. by AAIJ 15AQ
<sup>1</sup> Measured in $B_s^0 \to \phi \mu^+ \mu^-$ decays.			

### $B(B_s \to \phi \ell^+ \ell^-)$ ( $0.0 < q^2 < 4.3 \text{ GeV}^2/c^4$ )

VALUE (units $10^{-7}$ )	DOCUMENT ID	TECN	COMMENT
<b><math>3.30 \pm 1.09 \pm 1.05</math></b>	AALTONEN	11AI CDF	$p\bar{p}$ at 1.96 TeV

## PRODUCTION ASYMMETRIES

### $A_P(B_s^0)$

$$A_P(B_s^0) = [\sigma(\bar{B}_s^0) - \sigma(B_s^0)] / [\sigma(\bar{B}_s^0) + \sigma(B_s^0)]$$

VALUE (units $10^{-2}$ )	DOCUMENT ID	TECN	COMMENT
<b><math>1.2 \pm 1.6</math> OUR AVERAGE</b>			
$-0.65 \pm 2.88 \pm 0.59$	<sup>1</sup> AAIJ	17Bf LHCb	$pp$ at 7 TeV
$1.98 \pm 1.90 \pm 0.59$	<sup>1</sup> AAIJ	17Bf LHCb	$pp$ at 8 TeV
••• We do not use the following data for averages, fits, limits, etc. •••			
$1.09 \pm 2.61 \pm 0.66$	<sup>2</sup> AAIJ	14Bf LHCb	Repl. by AAIJ 17Bf, $pp$ at 7 TeV
<sup>1</sup> Based on time-dependent analysis of $B_s^0 \rightarrow D_s^- \pi^+$ in kinematic range $2 < p_T < 30 \text{ GeV}/c$ and $2.1 < \eta < 4.5$ .			
<sup>2</sup> Based on time-dependent analysis of $B_s^0 \rightarrow D_s^- \pi^+$ in kinematic range $4 < p_T < 30 \text{ GeV}/c$ and $2.5 < \eta < 4.5$ .			

## $B_s^0$ REFERENCES

AABOUD 19L JHEP 1904 098 (ATLAS Collab.)  
 AAIJ 194E PRL 123 081802 (LHCb Collab.)  
 AAIJ 194F PL B797 134789 (LHCb Collab.)  
 AAIJ 194K PRL 123 211801 (LHCb Collab.)  
 AAIJ 194P JHEP 1912 155 (LHCb Collab.)  
 AAIJ 194Q JHEP 1906 114 (LHCb Collab.)  
 AAIJ 194R JHEP 1907 032 (LHCb Collab.)  
 AAIJ 194S EPJ C79 706 (LHCb Collab.)  
 AAIJ 194T PRL 122 191804 (LHCb Collab.)  
 AAIJ 18AB JHEP 1807 020 (LHCb Collab.)  
 AAIJ 18AC JHEP 1808 191 (LHCb Collab.)  
 AAIJ 18AD PR D98 071103 (LHCb Collab.)  
 AAIJ 18AE PR D98 072006 (LHCb Collab.)  
 AAIJ 18AF PR D98 032004 (LHCb Collab.)  
 AAIJ 18B JHEP 1803 140 (LHCb Collab.)  
 AAIJ 18C JHEP 1803 078 (LHCb Collab.)  
 AAIJ 18D JHEP 1803 059 (LHCb Collab.)

SIRUNYAN 18BY EPJ C78 457 (CMS Collab.)  
 AAIJ 17A PR D95 012006 (LHCb Collab.)  
 AAIJ 17AI PRL 118 191801 (LHCb Collab.)  
 AAIJ 17AJ PRL 118 251802 (LHCb Collab.)  
 AAIJ 17AL PRL 119 041802 (LHCb Collab.)  
 AAIJ 17AM PRL 119 101801 (LHCb Collab.)  
 AAIJ 17B PRL 118 021801 (LHCb Collab.)  
 AAIJ 17BA JHEP 1705 158 (LHCb Collab.)  
 AAIJ 17BB EPJ C77 809 (LHCb Collab.)  
 AAIJ 17BD PR D96 051103 (LHCb Collab.)  
 AAIJ 17BF PL B774 139 (LHCb Collab.)  
 AAIJ 17BJ PRL 119 232001 (LHCb Collab.)  
 AAIJ 17BP JHEP 1711 027 (LHCb Collab.)  
 AAIJ 17G PRL 118 081801 (LHCb Collab.)  
 AAIJ 17N JHEP 1703 001 (LHCb Collab.)  
 AAIJ 17U JHEP 1707 021 (LHCb Collab.)  
 AAIJ 17V JHEP 1708 037 (LHCb Collab.)  
 AABOUD 16L EPJ C76 513 (ATLAS Collab.)  
 AAD 16AP JHEP 1608 147 (ATLAS Collab.)  
 AAIJ 16 JHEP 1601 012 (LHCb Collab.)  
 AAIJ 16AK PL B762 253 (LHCb Collab.)  
 AAIJ 16AL PL B762 484 (LHCb Collab.)  
 AAIJ 16C PRL 116 161802 (LHCb Collab.)  
 AAIJ 16E PRL 116 241601 (LHCb Collab.)  
 AAIJ 16G PRL 117 061803 (LHCb Collab.)  
 AAIJ 16P PR D93 092008 (LHCb Collab.)  
 AAIJ 16U JHEP 1603 040 (LHCb Collab.)  
 ABZOV 16C PR D94 012001 (DO Collab.)  
 KHACHATRYAN... 16Q PL B756 84 (CMS Collab.)  
 KHACHATRYAN... 16S PL B757 97 (CMS Collab.)  
 PAL 16 PRL 116 161801 (LHCb Collab.)  
 AAIJ 15AC JHEP 1505 019 (LHCb Collab.)  
 AAIJ 15AD JHEP 1506 130 (LHCb Collab.)  
 AAIJ 15AF JHEP 1507 166 (LHCb Collab.)  
 AAIJ 15AG JHEP 1508 005 (LHCb Collab.)  
 AAIJ 15AL JHEP 1506 131 (LHCb Collab.)  
 AAIJ 15AQ JHEP 1509 179 (LHCb Collab.)  
 AAIJ 15AS JHEP 1510 053 (LHCb Collab.)  
 AAIJ 15AV JHEP 1511 082 (LHCb Collab.)  
 AAIJ 15BB PR D92 112002 (LHCb Collab.)  
 AAIJ 15D JHEP 1501 024 (LHCb Collab.)  
 AAIJ 15I PRL 114 041801 (LHCb Collab.)  
 AAIJ 15K PL B741 1 (LHCb Collab.)  
 AAIJ 15O PRL 115 051801 (LHCb Collab.)  
 AAIJ 15P PL B743 46 (LHCb Collab.)  
 AAIJ 15U PL B747 484 (LHCb Collab.)  
 ABZOV 15A PRL 114 062001 (DO Collab.)  
 ABZOV 15L PRL 115 161601 (DO Collab.)  
 DUTTA 15 PR D91 011101 (DO Collab.)  
 KHACHATRYAN... 15BE NAT 522 68 (CMS and LHCb Collab.)  
 OSWALD 15 PR D92 072013 (BELLE Collab.)  
 AAD 14U PR D90 052007 (ATLAS Collab.)  
 AAIJ 14AA PRL 112 202001 (LHCb Collab.)  
 AAIJ 14AE PR D90 052011 (LHCb Collab.)  
 AAIJ 14AX PRL 113 172001 (LHCb Collab.)  
 AAIJ 14AY PRL 113 211801 (LHCb Collab.)  
 AAIJ 14BF JHEP 1411 060 (LHCb Collab.)  
 AAIJ 14BH PR D90 072003 (LHCb Collab.)  
 AAIJ 14BM NJP 16 123001 (LHCb Collab.)  
 AAIJ 14BN PR D90 112002 (LHCb Collab.)  
 AAIJ 14BP PL B739 218 (LHCb Collab.)  
 AAIJ 14BR PR D89 092006 (LHCb Collab.)  
 AAIJ 14D PL B728 607 (LHCb Collab.)  
 AAIJ 14E JHEP 1404 114 (LHCb Collab.)  
 AAIJ 14F PRL 112 111802 (LHCb Collab.)  
 AAIJ 14L JHEP 1407 140 (LHCb Collab.)  
 AAIJ 14R PL B736 446 (LHCb Collab.)  
 AAIJ 14S PL B736 186 (LHCb Collab.)  
 AAIJ 14Y PRL 112 091802 (LHCb Collab.)  
 AALTONEN 14P PRL 113 242001 (CDF Collab.)  
 ABZOV 14 PR D89 012002 (DO Collab.)  
 PDG 14 CP C38 070001 (PDG Collab.)  
 AAIJ 13 NP B867 1 (LHCb Collab.)  
 AAIJ 13A NP B867 547 (LHCb Collab.)  
 AAIJ 13AA NP B871 403 (LHCb Collab.)  
 AAIJ 13AB NP B873 275 (LHCb Collab.)  
 AAIJ 13AC NP B874 663 (LHCb Collab.)  
 AAIJ 13AL PR D87 071101 (LHCb Collab.)  
 AAIJ 13AN PR D87 072004 (LHCb Collab.)  
 AAIJ 13AP PR D87 092007 (LHCb Collab.)  
 AAIJ 13AQ PR D87 112009 (LHCb Collab.)  
 AAIJ 13AR PR D87 112010 (LHCb Collab.)  
 AAIJ 13AW PRL 110 211801 (LHCb Collab.)  
 AAIJ 13AX PRL 110 221601 (LHCb Collab.)  
 AAIJ 13AY PRL 110 241802 (LHCb Collab.)  
 AAIJ 13B PRL 110 021801 (LHCb Collab.)  
 AAIJ 13BA PRL 111 101805 (LHCb Collab.)  
 AAIJ 13BI NJP 15 052021 (LHCb Collab.)  
 AAIJ 13BM PRL 111 141801 (LHCb Collab.)  
 AAIJ 13BO JHEP 1310 183 (LHCb Collab.)  
 AAIJ 13BP JHEP 1310 143 (LHCb Collab.)  
 AAIJ 13BQ JHEP 1310 005 (LHCb Collab.)  
 AAIJ 13BW JHEP 1311 092 (LHCb Collab.)  
 AAIJ 13BX PL B727 403 (LHCb Collab.)  
 AAIJ 13CF EPJ C73 2655 (LHCb Collab.)  
 AAIJ 13X JHEP 1303 067 (LHCb Collab.)  
 AAIJ 13Y JHEP 1307 084 (LHCb Collab.)  
 AAIJ 13Z JHEP 1309 006 (LHCb Collab.)  
 AALTONEN 13F PR D87 072003 (CDF Collab.)  
 ABZOV 13 PRL 110 011801 (DO Collab.)  
 ABZOV 13C PR D87 072006 (DO Collab.)  
 CHATRCHYAN 13AW PRL 111 101804 (CMS Collab.)  
 ESEN 13 PR D87 031101 (BELLE Collab.)  
 OSWALD 13 PR D87 072008 (BELLE Collab.)  
 Also PR D90 119901 (errata.) (BELLE Collab.)  
 SOLOVIEVA 13 PL B726 206 (BELLE Collab.)  
 THORNE 13 PR D88 114006 (ATLAS Collab.)  
 AAD 12AE PL B713 387 (G. Aad et al.)  
 AAD 12CV JHEP 1212 072 (ATLAS Collab.)  
 AAIJ 12 PL B707 349 (LHCb Collab.)  
 AAIJ 12A PL B708 55 (LHCb Collab.)  
 AAIJ 12AE PR D85 112013 (LHCb Collab.)  
 AAIJ 12AG JHEP 1206 115 (LHCb Collab.)  
 AAIJ 12AM PRL 109 131801 (LHCb Collab.)  
 AAIJ 12AN PRL 109 152002 (LHCb Collab.)  
 AAIJ 12AO PR D86 052006 (LHCb Collab.)  
 AAIJ 12AP PR D86 071102 (LHCb Collab.)  
 AAIJ 12AR JHEP 1210 037 (LHCb Collab.)  
 AAIJ 12AX PR D86 112005 (LHCb Collab.)  
 AAIJ 12B PL B707 497 (LHCb Collab.)  
 AAIJ 12D PRL 108 101803 (LHCb Collab.)  
 AAIJ 12E PL B708 241 (LHCb Collab.)

B<sup>0</sup><sub>s</sub>, B<sup>\*</sup><sub>s</sub>

Table listing meson particles and their properties. Columns include particle name, quantum numbers (J<sup>PC</sup>), production experiments, and references. Examples: AAUJ 12F PL B709 50, AAUJ 12I PL B709 177, AAUJ 12L EPJ C72 2118, etc.

Table listing meson particles and their properties (continued). Columns include particle name, quantum numbers (J<sup>PC</sup>), production experiments, and references. Examples: ABE 95Z PRL 75 3068, ACCIARRI 95H PL B363 127, ACCIARRI 95I PL B363 137, etc.

Table listing meson particles and their properties (continued). Columns include particle name, quantum numbers (J<sup>PC</sup>), production experiments, and references. Examples: F. Abe et al. (CDF Collab.), M. Acciaroni et al. (L3 Collab.), M. Acciaroni et al. (L3 Collab.), etc.

B<sup>\*</sup><sub>s</sub>

I(J<sup>P</sup>) = 0(1<sup>-</sup>)

I, J, P need confirmation. Quantum numbers shown are quark-model predictions.

B<sup>\*</sup><sub>s</sub> MASS

From mass difference below and the B<sup>0</sup><sub>s</sub> mass.

Table with columns: VALUE (MeV), DOCUMENT ID, TECN, COMMENT

5415.4<sup>+1.8</sup><sub>-1.5</sub> OUR FIT Error includes scale factor of 2.9.

5415.8±1.5 OUR AVERAGE Error includes scale factor of 2.6.

Table with columns: VALUE, DOCUMENT ID, TECN, COMMENT. Includes entries like 5416.4±0.4±0.5 LOUVOT 09 BELL e<sup>+</sup>e<sup>-</sup> → T(5S).

• • • We do not use the following data for averages, fits, limits, etc. • • •

Table with columns: VALUE, DOCUMENT ID, TECN, COMMENT. Includes entries like 5418 ±1 ±3 DRUTSKOY 07A BELL Repl. by LOUVOT 09.

1 Utilized the beam constrained invariant mass peak positions for B\* and B<sup>\*</sup><sub>s</sub> to extract the measurement.

2 Uses 14 candidates consistent with B<sub>s</sub> decays into final states with a J/ψ and a D<sub>s</sub><sup>(\*)-</sup>.

m<sub>B<sup>\*</sup><sub>s</sub></sub> - m<sub>B<sub>s</sub></sub>

Table with columns: VALUE (MeV), DOCUMENT ID, TECN, COMMENT

46.6<sup>+1.8</sup><sub>-1.5</sub> OUR FIT Error includes scale factor of 2.9.

46.1±1.5 OUR AVERAGE

Table with columns: VALUE, DOCUMENT ID, TECN, COMMENT. Includes entries like 45.7±1.7±0.7 AQUINES 06 CLEO e<sup>+</sup>e<sup>-</sup> → T(5S).

• • • We do not use the following data for averages, fits, limits, etc. • • •

48 ±1 ±3 5 BONVICINI 06 CLEO Repl. by AQUINES 06

3 Utilized the beam constrained invariant mass peak positions for B\* and B<sup>\*</sup><sub>s</sub> to extract the measurement.

4 LEE-FRANZINI 90 measure 46.7 ± 0.4 ± 0.2 MeV for an admixture of B<sup>0</sup>, B<sup>+</sup>, and B<sub>s</sub>. They use the shape of the photon line to separate the above value for B<sub>s</sub>.

5 Uses 14 candidates consistent with B<sub>s</sub> decays into final states with a J/ψ and a D<sub>s</sub><sup>(\*)-</sup>.

|(m<sub>B<sup>\*</sup><sub>s</sub></sub> - m<sub>B<sub>s</sub></sub>) - (m<sub>B<sup>\*</sup><sub>s</sub></sub> - m<sub>B</sub>)|

Table with columns: VALUE (MeV), CL%, DOCUMENT ID, TECN, COMMENT

<6 95 ABREU 95R DLPH E<sub>cm</sub><sup>pe</sup> = 88-94 GeV

B<sup>\*</sup><sub>s</sub> DECAY MODES

Table with columns: Mode, Fraction (Γ<sub>j</sub>/Γ)

Γ<sub>1</sub> B<sub>s</sub> γ seen

B<sup>\*</sup><sub>s</sub> REFERENCES

Table listing references for B<sup>\*</sup><sub>s</sub>. Columns include author names, journal names, volumes, and page numbers. Examples: LOUVOT 09 PRL 102 021801, DRUTSKOY 07A PR D76 012002, AQUINES 06 PRL 96 152001, etc.

Downloaded from https://academic.oup.com/ptep/article/2020/8/083C01/5891211 by guest on 12 November 2020

## Meson Particle Listings

 $B_s^*$ ,  $X(5568)^\pm$ ,  $B_{s1}(5830)^0$  $X(5568)^\pm$ 

$I(J^P) = ?(??)$

OMITTED FROM SUMMARY TABLE

Seen as a peak in the  $B_s \pi^\pm$  mass spectrum with a significance of more than  $3\sigma$  by ABAZOV 16E and ABAZOV 18A in inclusive  $p\bar{p}$  collisions at 1.96 TeV. Not seen by AAIJ 16AI, AABOUD 18L, AALTONEN 18A, and SIRUNYAN 18J. Needs confirmation.

 $X(5568)^\pm$  MASS

VALUE (MeV)	EVTS	DOCUMENT ID	TECN	COMMENT
$5566.9^{+3.2+0.6}_{-3.1-1.2}$	278	<sup>1</sup> ABAZOV	18A D0	$p\bar{p} \rightarrow B_s^0 \pi^\pm X$
$5567.8 \pm 2.9^{+0.9}_{-1.9}$	133	<sup>2</sup> ABAZOV	16E D0	$p\bar{p} \rightarrow B_s^0 \pi^\pm X$

- • • We do not use the following data for averages, fits, limits, etc. • • •
- <sup>1</sup> From the combined analysis of  $B_s^0 \rightarrow J/\psi \phi$  and  $B_s^0 \rightarrow D_s^\pm \mu^\mp X$  decays.
- <sup>2</sup> Assumes  $X(5568)^\pm \rightarrow B_s \pi^\pm$  decay. If  $X(5568)^\pm \rightarrow B_s^* \pi^\pm$  decay is assumed, the mass shifts upward by 49 MeV.

 $X(5568)^\pm$  WIDTH

VALUE (MeV)	EVTS	DOCUMENT ID	TECN	COMMENT
$18.6^{+7.9+3.5}_{-6.1-3.8}$	278	<sup>1</sup> ABAZOV	18A D0	$p\bar{p} \rightarrow B_s \pi^\pm X$
$21.9 \pm 6.4^{+5.0}_{-2.5}$	133	ABAZOV	16E D0	$p\bar{p} \rightarrow B_s \pi^\pm X$

- • • We do not use the following data for averages, fits, limits, etc. • • •
- <sup>1</sup> From the combined analysis of  $B_s^0 \rightarrow J/\psi \phi$  and  $B_s^0 \rightarrow D_s^\pm \mu^\mp X$  decays.

 $X(5568)^\pm$  DECAY MODES

Mode	Fraction ( $\Gamma_i/\Gamma$ )
$\Gamma_1 B_s \pi^\pm$	seen

 $\Gamma(B_s \pi^\pm)/\Gamma_{\text{total}}$ 

VALUE	EVTS	DOCUMENT ID	TECN	COMMENT	$\Gamma_1/\Gamma$
seen	145	<sup>1</sup> ABAZOV	18A D0	$p\bar{p} \rightarrow B_s^0 \pi^\pm X$	
seen	133	<sup>2</sup> ABAZOV	16E D0	$p\bar{p} \rightarrow B_s^0 \pi^\pm X$	
not seen		<sup>3</sup> AABOUD	18L ATLS	$p\bar{p} \rightarrow B_s^0 \pi^\pm X$	
not seen		<sup>4</sup> AALTONEN	18A CDF	$p\bar{p} \rightarrow B_s^0 \pi^\pm X$	
not seen		<sup>5</sup> SIRUNYAN	18J CMS	$p\bar{p} \rightarrow B_s^0 \pi^\pm X$	
not seen		<sup>6</sup> AAIJ	16AI LHCB	$p\bar{p} \rightarrow B_s^0 \pi^\pm X$	

- • • We do not use the following data for averages, fits, limits, etc. • • •
- <sup>1</sup> With  $B_s$  mesons reconstructed in decays to  $D_s^\pm \mu^\mp X$ .
- <sup>2</sup> Seen in  $p\bar{p}$  collisions at 1.96 TeV at a rate of  $(8.6 \pm 1.9 \pm 1.4)\%$  relative to inclusive  $B_s$  production in the kinematic region  $10 < p_T(B_s) < 30$  GeV/c, with  $B_s$  mesons reconstructed in decays to  $J/\psi \phi$ . An alternative possibility,  $X(5568)^\pm \rightarrow B_s^* \pi^\pm$  with a missing  $\gamma$ , could not be ruled out.
- <sup>3</sup> Not seen in  $24.4 \text{ fb}^{-1}$  of  $p\bar{p}$  collision data at  $\sqrt{s} = 7$  and 8 TeV with  $B_s$  mesons reconstructed in decays to  $J/\psi \phi$ . An upper limit on the production rate times branching fraction for  $X(5568)^\pm \rightarrow B_s \pi^\pm$  relative to inclusive  $B_s$  production is less than 1.5% at  $p_T(B_s) > 10$  GeV/c and less than 1.6% at  $p_T(B_s) > 15$  GeV/c at 95% CL.
- <sup>4</sup> Not seen in  $9.6 \text{ fb}^{-1}$  of  $p\bar{p}$  collision data at  $\sqrt{s} = 1.96$  TeV with  $B_s$  mesons reconstructed in decays to  $J/\psi \phi$ . An upper limit on the production rate times branching fraction for  $X(5568)^\pm \rightarrow B_s \pi^\pm$  relative to inclusive  $B_s$  production is less than 6.7% at 95% CL.
- <sup>5</sup> Not seen in  $19.7 \text{ fb}^{-1}$  of  $p\bar{p}$  collisions data at  $\sqrt{s} = 8$  TeV with  $B_s$  mesons reconstructed in decays to  $J/\psi \phi$ . An upper limit on the production rate times branching fraction for  $X(5568)^\pm \rightarrow B_s \pi^\pm$  relative to inclusive  $B_s$  production is less than 1.1% at  $p_T(B_s) > 10$  GeV/c and less than 1.0% at  $p_T(B_s) > 15$  GeV/c at 95% CL.
- <sup>6</sup> Not seen in  $3 \text{ fb}^{-1}$  of  $p\bar{p}$  collision data at  $\sqrt{s} = 7$  and 8 TeV in a scan over the  $X(5568)$  mass and width, with  $B_s$  mesons reconstructed in decays to  $D_s^\pm \pi^\mp$  or  $J/\psi \phi$ . An upper limit on the production rate times branching fraction for  $X(5568)^\pm \rightarrow B_s \pi^\pm$  relative to inclusive  $B_s$  production is less than 2.1% at  $p_T(B_s) > 10$  GeV/c at 90% CL.

 $X(5568)^\pm$  REFERENCES

AABOUD	18L	PRL 120 202007	M. Aaboud et al.	(ATLAS Collab.)
AALTONEN	18A	PRL 120 202006	T. Aaltonen et al.	(CDF Collab.)
ABAZOV	18A	PR D97 092004	V.M. Abazov et al.	(D0 Collab.)
SIRUNYAN	18J	PRL 120 202005	A.M. Sirunyan et al.	(CMS Collab.)
AAIJ	16AI	PRL 117 152003	R. Aaij et al.	(LHCb Collab.)
ABAZOV	16E	PRL 117 022003	V.M. Abazov et al.	(D0 Collab.)

 $B_{s1}(5830)^0$ 

$I(J^P) = 0(1^+)$   
 $I, J, P$  need confirmation.

Quantum numbers shown are quark-model predictions.

 $B_{s1}(5830)^0$  MASS

VALUE (MeV)	DOCUMENT ID	TECN	COMMENT
<b>5828.70 ± 0.20 OUR FIT</b>			
<b>5828.65 ± 0.24 OUR AVERAGE</b>			
$5828.78 \pm 0.09 \pm 0.29$	SIRUNYAN	18DF CMS	$pp$ at 8 TeV
$5828.40 \pm 0.04 \pm 0.41$	<sup>1</sup> AAIJ	13o LHCB	$pp$ at 7 TeV
$5829.4 \pm 0.7$	<sup>2</sup> AALTONEN	08K CDF	Repl. by AALTONEN 14I

- • • We do not use the following data for averages, fits, limits, etc. • • •
- <sup>1</sup> Uses  $B_{s1}(5830)^0 \rightarrow B^{*+} K^-$  decay.
- <sup>2</sup> Uses two-body decays into  $K^-$  and  $B^+$  mesons reconstructed as  $B^+ \rightarrow J/\psi K^+$ ,  $J/\psi \rightarrow \mu^+ \mu^-$  or  $B^+ \rightarrow \bar{D}^0 \pi^+$ ,  $\bar{D}^0 \rightarrow K^+ \pi^-$ .

 $m_{B_{s1}^0} - m_{B^{*+}}$ 

VALUE (MeV)	DOCUMENT ID	TECN	COMMENT
<b>504.00 ± 0.17 OUR FIT</b>			
<b>504.03 ± 0.12 ± 0.15</b>			
$504.41 \pm 0.21 \pm 0.14$	<sup>1</sup> AALTONEN	14I CDF	$p\bar{p}$ at 1.96 TeV
$504.41 \pm 0.21 \pm 0.14$	<sup>2</sup> AALTONEN	08K CDF	Repl. by AALTONEN 14I

- • • We do not use the following data for averages, fits, limits, etc. • • •
- <sup>1</sup> AALTONEN 14I reports  $m_{B_{s1}(5830)^0} - m_{B^{*+}} - m_{K^-} = 10.35 \pm 0.12 \pm 0.15$  MeV which we adjusted by the  $K^-$  mass.
- <sup>2</sup> Uses two-body decays into  $K^-$  and  $B^+$  mesons reconstructed as  $B^+ \rightarrow J/\psi K^+$ ,  $J/\psi \rightarrow \mu^+ \mu^-$  or  $B^+ \rightarrow \bar{D}^0 \pi^+$ ,  $\bar{D}^0 \rightarrow K^+ \pi^-$ .

 $B_{s1}(5830)^0$  WIDTH

VALUE (MeV)	DOCUMENT ID	TECN	COMMENT
<b>0.5 ± 0.3 ± 0.3</b>	AALTONEN	14I CDF	$p\bar{p}$ at 1.96 TeV

 $B_{s1}(5830)^0$  DECAY MODES

Mode	Fraction ( $\Gamma_i/\Gamma$ )
$\Gamma_1 B^{*+} K^-$	seen
$\Gamma_2 B^{*0} K_S^0$	

 $B_{s1}(5830)^0$  BRANCHING RATIOS

$\Gamma(B^{*+} K^-)/\Gamma_{\text{total}}$	$\Gamma_1/\Gamma$
seen	

$\Gamma(B^{*0} K_S^0)/\Gamma(B^{*+} K^-)$	$\Gamma_2/\Gamma_1$
<b>0.49 ± 0.12 ± 0.07</b>	

- • • We do not use the following data for averages, fits, limits, etc. • • •
- <sup>1</sup> With the branching fractions  $B(B^{*+} \rightarrow J/\psi K^+) = (1.026 \pm 0.031) \times 10^{-3}$  and  $B(B^0 \rightarrow J/\psi K^{*0}) = (1.28 \pm 0.05) \times 10^{-3}$ .

 $B_{s1}(5830)^0$  REFERENCES

SIRUNYAN	18DF	EPJ C78 939	A.M. Sirunyan et al.	(CMS Collab.)
AALTONEN	14I	PR D90 012013	T. Aaltonen et al.	(CDF Collab.)
AAIJ	13O	PRL 110 151803	R. Aaij et al.	(LHCb Collab.)
AALTONEN	08K	PRL 100 082001	T. Aaltonen et al.	(CDF Collab.)

See key on page 999

Meson Particle Listings

$B_{s2}^*(5840)^0, B_{sJ}^*(5850)$

**$B_{s2}^*(5840)^0$**   $I(J^P) = 0(2^+)$   
*I, J, P need confirmation.*  
 Quantum numbers shown are quark-model predictions.

$B_{s2}^*(5840)^0$  MASS

VALUE (MeV)	DOCUMENT ID	TECN	COMMENT
<b>5839.86 ± 0.12 OUR FIT</b>			
<b>5839.92 ± 0.14 OUR AVERAGE</b>			
5839.86 ± 0.09 ± 0.17	SIRUNYAN	18DF CMS	<i>pp</i> at 8 TeV
5839.99 ± 0.05 ± 0.20	AAIJ	13o LHCB	<i>pp</i> at 7 TeV
5839.6 ± 1.1 ± 0.7	<sup>1</sup> ABAZOV	08E D0	<i>p</i> $\bar{p}$ at 1.96 TeV
• • • We do not use the following data for averages, fits, limits, etc. • • •			
5839.7 ± 0.7	<sup>2</sup> AALTONEN	08K CDF	Repl. by AALTONEN 14i
<sup>1</sup> Observed in $B_{s2}^{*0} \rightarrow B^+ K^-$ . Measured production rate of $B_{s2}^{*0}$ relative to $B^+$ to be $(1.15 \pm 0.23 \pm 0.13)\%$ .			
<sup>2</sup> Uses two-body decays into $K^-$ and $B^+$ mesons reconstructed as $B^+ \rightarrow J/\psi K^+$ , $J/\psi \rightarrow \mu^+ \mu^-$ or $B^+ \rightarrow \bar{D}^0 \pi^+$ , $\bar{D}^0 \rightarrow K^+ \pi^-$ .			

$m_{B_{s2}^{*0}} - m_{B_{s1}^0}$

VALUE (MeV)	DOCUMENT ID	TECN	COMMENT
• • • We do not use the following data for averages, fits, limits, etc. • • •			
10.5 ± 0.6	<sup>1</sup> AALTONEN	08K CDF	Repl. by AALTONEN 14i
<sup>1</sup> Uses two-body decays into $K^-$ and $B^+$ mesons reconstructed as $B^+ \rightarrow J/\psi K^+$ , $J/\psi \rightarrow \mu^+ \mu^-$ or $B^+ \rightarrow \bar{D}^0 \pi^+$ , $\bar{D}^0 \rightarrow K^+ \pi^-$ .			

$m_{B_{s2}^{*0}} - m_{B^+}$

VALUE (MeV)	DOCUMENT ID	TECN	COMMENT
<b>560.52 ± 0.14 OUR FIT</b>			
<b>560.41 ± 0.13 ± 0.14</b>	<sup>1</sup> AALTONEN	14i CDF	<i>p</i> $\bar{p}$ at 1.96 TeV
<sup>1</sup> AALTONEN 14i reports $m_{B_{s2}^*(5840)^0} - m_{B^+} - m_{K^-} = 66.73 \pm 0.13 \pm 0.14$ MeV which we adjusted by the $K^-$ mass.			

$B_{s2}^*(5840)^0$  WIDTH

VALUE (MeV)	DOCUMENT ID	TECN	COMMENT
<b>1.49 ± 0.27 OUR AVERAGE</b>			
1.52 ± 0.34 ± 0.30	SIRUNYAN	18DF CMS	<i>pp</i> at 8 TeV
1.4 ± 0.4 ± 0.2	AALTONEN	14i CDF	<i>p</i> $\bar{p}$ at 1.96 TeV
1.56 ± 0.13 ± 0.47	<sup>1</sup> AAIJ	13o LHCB	<i>pp</i> at 7 TeV
<sup>1</sup> Uses $B_{s2}^*(5840)^0 \rightarrow B^{*+} K^-$ decays.			

$B_{s2}^*(5840)^0$  DECAY MODES

Mode	Fraction ( $\Gamma_j/\Gamma$ )
$\Gamma_1$ $B^+ K^-$	<b>DEFINED AS 1</b>
$\Gamma_2$ $B^{*+} K^-$	0.093 ± 0.018
$\Gamma_3$ $B^0 K_S^0$	0.43 ± 0.11
$\Gamma_4$ $B^{*0} K_S^0$	0.04 ± 0.04

$B_{s2}^*(5840)^0$  BRANCHING RATIOS

$\Gamma(B^+ K^-)/\Gamma_{total}$	DOCUMENT ID	TECN	COMMENT	$\Gamma_1/\Gamma$
seen	AALTONEN	08K CDF	<i>p</i> $\bar{p}$ at 1.96 TeV	
seen	<sup>1</sup> ABAZOV	08E D0	<i>p</i> $\bar{p}$ at 1.96 TeV	
<sup>1</sup> Measured production rate of $B_{s2}^{*0}$ relative to $B^+$ to be $(1.15 \pm 0.23 \pm 0.13)\%$ .				
$\Gamma(B^{*+} K^-)/\Gamma(B^+ K^-)$	DOCUMENT ID	TECN	COMMENT	$\Gamma_2/\Gamma_1$
<b>0.093 ± 0.013 ± 0.012</b>	AAIJ	13o LHCB	<i>pp</i> at 7 TeV	
$\Gamma(B^{*0} K_S^0)/\Gamma(B^0 K_S^0)$	DOCUMENT ID	TECN	COMMENT	$\Gamma_4/\Gamma_3$
<b>0.093 ± 0.086 ± 0.014</b>	<sup>1</sup> SIRUNYAN	18DF CMS	<i>pp</i> at 8 TeV	
<sup>1</sup> With the branching fraction $B(B^0 \rightarrow J/\psi K^{*0}) = (1.28 \pm 0.05) \times 10^{-3}$ .				
$\Gamma(B^0 K_S^0)/\Gamma(B^+ K^-)$	DOCUMENT ID	TECN	COMMENT	$\Gamma_3/\Gamma_1$
<b>0.432 ± 0.077 ± 0.078</b>	<sup>1</sup> SIRUNYAN	18DF CMS	<i>pp</i> at 8 TeV	
<sup>1</sup> With the branching fractions $B(B^+ \rightarrow J/\psi K^+) = (1.026 \pm 0.031) \times 10^{-3}$ and $B(B^0 \rightarrow J/\psi K^{*0}) = (1.28 \pm 0.05) \times 10^{-3}$ .				
$\Gamma(B^{*+} K^-)/\Gamma(B^+ K^-)$	DOCUMENT ID	TECN	COMMENT	$\Gamma_2/\Gamma_1$
<b>0.081 ± 0.021 ± 0.015</b>	<sup>1</sup> SIRUNYAN	18DF CMS	<i>pp</i> at 8 TeV	
<sup>1</sup> With the branching fraction $B(B^+ \rightarrow J/\psi K^+) = (1.026 \pm 0.031) \times 10^{-3}$ .				

$B_{s2}^*(5840)^0$  REFERENCES

SIRUNYAN	18DF EPJ C78 939	A.M. Sirunyan et al.	(CMS Collab.)
AALTONEN	14i PR D90 012013	T. Aaltonen et al.	(CDF Collab.)
AAIJ	13O PRL 110 151803	R. Aaij et al.	(LHCb Collab.)
AALTONEN	08K PRL 100 082001	T. Aaltonen et al.	(CDF Collab.)
ABAZOV	08E PRL 100 082002	V.M. Abazov et al.	(D0 Collab.)

**$B_{sJ}^*(5850)$**

$I(J^P) = ?(??)$   
*I, J, P need confirmation.*

OMITTED FROM SUMMARY TABLE  
 Signal can be interpreted as coming from  $\bar{b}s$  states. Needs confirmation.

$B_{sJ}^*(5850)$  MASS

VALUE (MeV)	EVTS	DOCUMENT ID	TECN	COMMENT
<b>5853 ± 15</b>	141	AKERS	95E OPAL	$E_{cm}^{Ee} = 88-94$ GeV

$B_{sJ}^*(5850)$  WIDTH

VALUE (MeV)	EVTS	DOCUMENT ID	TECN	COMMENT
<b>47 ± 22</b>	141	AKERS	95E OPAL	$E_{cm}^{Ee} = 88-94$ GeV

$B_{sJ}^*(5850)$  REFERENCES

AKERS	95E ZPHY C66 19	R. Akers et al.	(OPAL Collab.)
-------	-----------------	-----------------	----------------

# Meson Particle Listings

$B_c^+$

## BOTTOM, CHARMED MESONS

### ( $B = C = \pm 1$ )

$B_c^+ = c\bar{b}, B_c^- = \bar{c}b$ , similarly for  $B_c^{*}$ 's

$B_c^+$

$I(J^P) = 0(0^-)$   
*I, J, P* need confirmation.

Quantum numbers shown are quark-model predictions.

### $B_c^+$ MASS

VALUE (MeV)	DOCUMENT ID	TECN	COMMENT
<b>6274.9 ± 0.8 OUR AVERAGE</b>			
6274.28 ± 1.40 ± 0.32	1 AAIJ	17L LHCB	$pp$ at 7, 8 TeV
6274.0 ± 1.8 ± 0.4	2 AAIJ	14Aq LHCB	$pp$ at 7, 8 TeV
6276.28 ± 1.44 ± 0.36	3 AAIJ	13As LHCB	$pp$ at 7, 8 TeV
6273.7 ± 1.3 ± 1.6	4 AAIJ	12Av LHCB	$pp$ at 7 TeV
6275.6 ± 2.9 ± 2.5	5 AALTONEN	08M CDF	$p\bar{p}$ at 1.96 TeV
6300 ± 14 ± 5	5 ABAZOV	08T D0	$p\bar{p}$ at 1.96 TeV
6400 ± 390 ± 130	6 ABE	98M CDF	$p\bar{p}$ at 1.8 TeV
6285.7 ± 5.3 ± 1.2	5 ABULENCIA	06c CDF	Repl. by AALTONEN 08M
6320 ± 60	7 ACKERSTAFF	98o OPAL	$e^+e^- \rightarrow Z$

- • • We do not use the following data for averages, fits, limits, etc. • • •
- 1 Measured using  $B_c^+ \rightarrow J/\psi D^0 K^+$  decays.
- 2 Uses  $B_c^+ \rightarrow J/\psi p \bar{p} \pi^+$  decays.
- 3 AAIJ 13As uses the  $B_c^+ \rightarrow J/\psi D_s^+$ .
- 4 AAIJ 12Av uses the  $B_c^+ \rightarrow J/\psi \pi^+$  mode and also measures the mass difference  $M(B_c^+) - M(B^+) = 994.6 \pm 1.3 \pm 0.6$  MeV/ $c^2$ .
- 5 Measured using a fully reconstructed decay mode of  $B_c \rightarrow J/\psi \pi$ .
- 6 ABE 98M observed  $20.4^{+6.2}_{-5.5}$  events in the  $B_c^+ \rightarrow J/\psi(1S) \ell \nu_\ell$  with a significance of  $> 4.8$  standard deviations. The mass value is estimated from  $m(J/\psi(1S) \ell)$ .
- 7 ACKERSTAFF 98o observed 2 candidate events in the  $B_c^+ \rightarrow J/\psi(1S) \pi^+$  channel with an estimated background of  $0.63 \pm 0.20$  events.

### $B_c^+$ MEAN LIFE

"OUR EVALUATION" is an average using rescaled values of the data listed below. The average and rescaling were performed by the Heavy Flavor Averaging Group (HFLAV) and are described at <https://hflav.web.cern.ch/>. The averaging/rescaling procedure takes into account correlations between the measurements.

VALUE ( $10^{-12}$ s)	DOCUMENT ID	TECN	COMMENT
<b>0.510 ± 0.009 OUR EVALUATION</b>			
<b>0.510 ± 0.009 OUR AVERAGE</b>			
0.541 ± 0.026 ± 0.014	1 SIRUNYAN	18BY CMS	$pp$ at 8 TeV
0.5134 ± 0.0110 ± 0.0057	2,3 AAIJ	15G LHCB	$pp$ at 7, 8 TeV
0.509 ± 0.008 ± 0.012	4 AAIJ	14G LHCB	$pp$ at 8 TeV
0.452 ± 0.048 ± 0.027	3 AALTONEN	13 CDF	$p\bar{p}$ at 1.96 TeV
0.448 ± 0.038 ± 0.036 ± 0.032	5 ABAZOV	09H D0	$p\bar{p}$ at 1.96 TeV
0.463 ± 0.073 ± 0.065 ± 0.036	5 ABULENCIA	06o CDF	$p\bar{p}$ at 1.96 TeV
0.46 ± 0.18 ± 0.16 ± 0.03	5 ABE	98M CDF	$p\bar{p}$ 1.8 TeV

- 1 The lifetime is measured using the decays  $B_c^+ \rightarrow J/\psi \pi^+$  and  $B^+ \rightarrow J/\psi K^+$ .
- 2 Also measures the width difference  $\Delta\Gamma = \Gamma_{B_c^+} - \Gamma_{B^+} = 4.46 \pm 0.14 \pm 0.07$   $\text{mm}^{-1}c$ .
- 3 Uses fully reconstructed  $B_c^+ \rightarrow J/\psi \pi^+$  decays.
- 4 Measured using  $B_c^+ \rightarrow J/\psi \mu^+ \nu_\mu X$  decays.
- 5 The lifetime is measured from the  $J/\psi e$  decay vertices.

### $B_c^+$ DECAY MODES × $B(\bar{b} \rightarrow B_c)$

$B_c^-$  modes are charge conjugates of the modes below.

Mode	Fraction ( $\Gamma_i/\Gamma$ )	Confidence level
The following quantities are not pure branching ratios; rather the fraction $\Gamma_i/\Gamma \times B(\bar{b} \rightarrow B_c)$ .		
$\Gamma_1$ $J/\psi(1S) \ell^+ \nu_\ell$ anything	$(8.1 \pm 1.2) \times 10^{-5}$	
$\Gamma_2$ $J/\psi(1S) \mu^+ \nu_\mu$		
$\Gamma_3$ $J/\psi(1S) \tau^+ \nu_\tau$		
$\Gamma_4$ $J/\psi(1S) \pi^+$	seen	
$\Gamma_5$ $J/\psi(1S) K^+$	seen	
$\Gamma_6$ $J/\psi(1S) \pi^+ \pi^+ \pi^-$	seen	
$\Gamma_7$ $J/\psi(1S) a_1(1260)$	$< 1.2 \times 10^{-3}$	90%

$\Gamma_8$ $J/\psi(1S) K^+ K^- \pi^+$	seen	
$\Gamma_9$ $J/\psi(1S) \pi^+ \pi^+ \pi^+ \pi^- \pi^-$	seen	
$\Gamma_{10}$ $\psi(2S) \pi^+$	seen	
$\Gamma_{11}$ $J/\psi(1S) D^0 K^+$	seen	
$\Gamma_{12}$ $J/\psi(1S) D^*(2007)^0 K^+$	seen	
$\Gamma_{13}$ $J/\psi(1S) D^*(2010)^+ K^{*0}$	seen	
$\Gamma_{14}$ $J/\psi(1S) D^+ K^{*0}$	seen	
$\Gamma_{15}$ $J/\psi(1S) D_s^+$	seen	
$\Gamma_{16}$ $J/\psi(1S) D_s^{*+}$	seen	
$\Gamma_{17}$ $J/\psi(1S) \rho \bar{p} \pi^+$	seen	
$\Gamma_{18}$ $\chi_c^0 \pi^+$	$(2.4^{+0.9}_{-0.8}) \times 10^{-5}$	
$\Gamma_{19}$ $p \bar{p} \pi^+$	not seen	
$\Gamma_{20}$ $D^0 K^+$	$(3.8^{+1.2}_{-1.1}) \times 10^{-7}$	
$\Gamma_{21}$ $D^0 \pi^+$	$< 1.6 \times 10^{-7}$	95%
$\Gamma_{22}$ $D^{*0} \pi^+$	$< 4 \times 10^{-7}$	95%
$\Gamma_{23}$ $D^{*0} K^+$	$< 4 \times 10^{-7}$	95%
$\Gamma_{24}$ $D_s^+ \bar{D}^0$	$< 1.4 \times 10^{-7}$	90%
$\Gamma_{25}$ $D_s^+ D^0$	$< 6 \times 10^{-8}$	90%
$\Gamma_{26}$ $D^+ \bar{D}^0$	$< 3.0 \times 10^{-6}$	90%
$\Gamma_{27}$ $D^+ D^0$	$< 1.9 \times 10^{-6}$	90%
$\Gamma_{28}$ $D_s^{*+} \bar{D}^0$		
$\Gamma_{29}$ $D_s^+ \bar{D}^*(2007)^0$		
$\Gamma_{30}$ $D_s^{*+} D^0$		
$\Gamma_{31}$ $D_s^+ D^*(2007)^0$		
$\Gamma_{32}$ $D^*(2010)^+ \bar{D}^0$	$< 6.2 \times 10^{-3}$	90%
$\Gamma_{33}$ $D^*(2010)^+ \bar{D}^0, D^{*+} \rightarrow D^+ \pi^0 / \gamma$		
$\Gamma_{34}$ $D^+ \bar{D}^*(2007)^0$		
$\Gamma_{35}$ $D^*(2010)^+ D^0, D^{*+} \rightarrow D^+ \pi^0 / \gamma$		
$\Gamma_{36}$ $D^+ D^*(2007)^0$		
$\Gamma_{37}$ $D_s^{*+} \bar{D}^*(2007)^0$	$< 1.7 \times 10^{-6}$	90%
$\Gamma_{38}$ $D_s^{*+} D^*(2007)^0$	$< 3.1 \times 10^{-6}$	90%
$\Gamma_{39}$ $D^*(2010)^+ \bar{D}^*(2007)^0$	$< 1.0 \times 10^{-4}$	90%
$\Gamma_{40}$ $D^*(2010)^+ D^*(2007)^0$	$< 2.0 \times 10^{-5}$	90%
$\Gamma_{41}$ $D^+ K^{*0}$	$< 0.20 \times 10^{-6}$	90%
$\Gamma_{42}$ $D^+ \bar{K}^{*0}$	$< 0.16 \times 10^{-6}$	90%
$\Gamma_{43}$ $D_s^+ K^{*0}$	$< 0.28 \times 10^{-6}$	90%
$\Gamma_{44}$ $D_s^+ \bar{K}^{*0}$	$< 0.4 \times 10^{-6}$	90%
$\Gamma_{45}$ $D_s^+ \phi$	$< 0.32 \times 10^{-6}$	90%
$\Gamma_{46}$ $K^+ K^0$	$< 4.6 \times 10^{-7}$	90%
$\Gamma_{47}$ $B_s^0 \pi^+ / B(\bar{b} \rightarrow B_s)$	$(2.37^{+0.37}_{-0.35}) \times 10^{-3}$	

### $B_c^+$ BRANCHING RATIOS

VALUE (units $10^{-5}$ )	CL%	DOCUMENT ID	TECN	COMMENT	$\Gamma_1/\Gamma \times B$
<b>8.1 ± 1.2 OUR AVERAGE</b>		Error includes scale factor of 1.3.			
$8.7 \pm 1.0 \pm 0.3$	1,2	AALTONEN	16A CDF	$p\bar{p}$ at 1.96 TeV	
$5.2^{+2.4}_{-2.1}$	3	ABE	98M CDF	$p\bar{p}$ 1.8 TeV	

- • • We do not use the following data for averages, fits, limits, etc. • • •
- $< 16$  90 4 ACKERSTAFF 98o OPAL  $e^+e^- \rightarrow Z$
- $< 19$  90 5 ABREU 97E DLPH  $e^+e^- \rightarrow Z$
- $< 12$  90 6 BARATE 97H ALEP  $e^+e^- \rightarrow Z$
- 1 AALTONEN 16A reports  $[\Gamma(B_c^+ \rightarrow J/\psi(1S) \ell^+ \nu_\ell \text{ anything})/\Gamma_{\text{total}} \times B(\bar{b} \rightarrow B_c)] / [B(\bar{b} \rightarrow B^+)] / [B(B^+ \rightarrow J/\psi(1S) K^+)] = 0.211 \pm 0.012^{+0.021}_{-0.020}$  which we multiply by our best values  $B(\bar{b} \rightarrow B^+) = (40.8 \pm 0.7) \times 10^{-2}$ ,  $B(B^+ \rightarrow J/\psi(1S) K^+) = (1.006 \pm 0.027) \times 10^{-3}$ . Our first error is their experiment's error and our second error is the systematic error from using our best values.
- 2 AALTONEN 16A also measures the cross-section  $\sigma(B_c) \times B(B_c \rightarrow J/\psi \mu \nu_\mu) = 0.60 \pm 0.09$  nb and estimates the total cross-section  $\sigma(B_c)$  to be in the range  $25 \pm 4$  to  $52 \pm 8$  nb for  $p_T(B_c) > 6$  GeV/ $c$  and  $|y(B_c)| < 1$ .
- 3 ABE 98M result is derived from the measurement of  $[\sigma(B_c) \times B(B_c \rightarrow J/\psi(1S) \ell \nu_\ell)] / [\sigma(B^+) \times B(B^+ \rightarrow J/\psi(1S) K^+)] = 0.132^{+0.041}_{-0.037}(\text{stat}) \pm 0.031(\text{sys})^{+0.032}_{-0.020}(\text{lifetime})$  by using PDG 98 values of  $B(b \rightarrow B^+)$  and  $B(B^+ \rightarrow J/\psi(1S) K^+)$ .
- 4 ACKERSTAFF 98o reports  $B(Z \rightarrow B_c X)/B(Z \rightarrow qq) \times B(B_c \rightarrow J/\psi(1S) \ell \nu_\ell) < 6.95 \times 10^{-5}$  at 90%CL. We rescale to our PDG 98 values of  $B(Z \rightarrow b\bar{b})$ .
- 5 ABREU 97E value listed is for an assumed  $\tau_{B_c} = 0.4$  ps and improves to  $1.6 \times 10^{-4}$  for  $\tau_{B_c} = 1.4$  ps.
- 6 BARATE 97H reports  $B(Z \rightarrow B_c X)/B(Z \rightarrow qq) \times B(B_c \rightarrow J/\psi(1S) \ell \nu_\ell) < 5.2 \times 10^{-5}$  at 90%CL. We rescale to our PDG 96 values of  $B(Z \rightarrow b\bar{b})$ . A  $B_c^+ \rightarrow J/\psi(1S) \mu^+ \nu_\mu$  candidate event is found, compared to all the known background sources  $2 \times 10^{-3}$ , which gives  $m_{B_c} = 5.96^{+0.25}_{-0.19}$  GeV and  $\tau_{B_c} = 1.77 \pm 0.17$  ps.

See key on page 999

Meson Particle Listings

$B_c^+$

$\Gamma(J/\psi(1S)\tau^+\nu_\tau)/\Gamma(J/\psi(1S)\mu^+\nu_\mu)$				$\Gamma_3/\Gamma_2$
VALUE	DOCUMENT ID	TECN	COMMENT	
<b>0.71 ± 0.17 ± 0.18</b>	<sup>1</sup> AAIJ	18c	LHCB <i>pp</i> at 7, 8 TeV	
<sup>1</sup> AAIJ 18c uses $\tau^+ \rightarrow \mu^+ \nu_\mu \bar{\nu}_\tau$ mode to obtain the ratio value.				

$\Gamma(J/\psi(1S)\pi^+)/\Gamma_{total} \times B(\bar{B} \rightarrow B_c)$				$\Gamma_4/\Gamma \times B$
VALUE	CL%	DOCUMENT ID	TECN	COMMENT
seen		<sup>1</sup> AAIJ	15M	LHCB <i>pp</i> at 8 TeV
seen		<sup>2</sup> KHACHATRY...15AA	CMS	<i>pp</i> at 7 TeV
seen		AALTONEN	13	CDF $p\bar{p}$ at 1.96 TeV
seen		<sup>3</sup> AAIJ	12AV	LHCB <i>pp</i> at 7 TeV
seen		AALTONEN	08M	CDF $p\bar{p}$ at 1.96 TeV
seen		ABAZOV	08T	D0 $p\bar{p}$ at 1.96 TeV
• • • We do not use the following data for averages, fits, limits, etc. • • •				
<2.4 × 10 <sup>-4</sup>	90	<sup>4</sup> ACKERSTAFF	98o	OPAL $e^+e^- \rightarrow Z$
<3.4 × 10 <sup>-4</sup>	90	<sup>5</sup> ABREU	97E	DLPH $e^+e^- \rightarrow Z$
<8.2 × 10 <sup>-5</sup>	90	<sup>6</sup> BARATE	97H	ALEP $e^+e^- \rightarrow Z$
<2.0 × 10 <sup>-5</sup>	95	<sup>7</sup> ABE	96R	CDF $p\bar{p}$ 1.8 TeV

<sup>1</sup> AAIJ 15M reports a measurement of  $B(B_c^+ \rightarrow J/\psi\pi^+)/B(B^+ \rightarrow J/\psi K^+) \cdot f_c/f_u = (0.683 \pm 0.018 \pm 0.009)\%$  at  $p_T(B) < 20$  GeV and  $2.0 < y(B) < 4.5$ .

<sup>2</sup> KHACHATRYAN 15AA reports a measurement of  $B(B_c^+ \rightarrow J/\psi\pi^+)/B(B^+ \rightarrow J/\psi K^+) \cdot f_c/f_u = (0.48 \pm 0.05 \pm 0.03 \pm 0.05)\%$ , at  $p_T > 15$  GeV and  $|\eta(B)| < 1.6$ .

<sup>3</sup> AAIJ 12AV reports a measurement of  $B(B_c^+ \rightarrow J/\psi\pi^+)/B(B^+ \rightarrow J/\psi K^+) \cdot f_c/f_u = (0.68 \pm 0.10 \pm 0.03 \pm 0.05)\%$  at  $p_T(B) > 4$  GeV and  $2.5 < \eta(B) < 4.5$ .

<sup>4</sup> ACKERSTAFF 98o reports  $B(Z \rightarrow B_c X)/B(Z \rightarrow qq) \times B(B_c \rightarrow J/\psi(1S)\pi^+) < 1.06 \times 10^{-4}$  at 90%CL. We rescale to our PDG 98 values of  $B(Z \rightarrow b\bar{b})$ .

<sup>5</sup> ABREU 97E value listed is for an assumed  $\tau_{B_c} = 0.4$  ps and improves to  $2.7 \times 10^{-4}$  for  $\tau_{B_c} = 1.4$  ps.

<sup>6</sup> BARATE 97H reports  $B(Z \rightarrow B_c X)/B(Z \rightarrow qq) \times B(B_c \rightarrow J/\psi(1S)\pi) < 3.6 \times 10^{-5}$  at 90%CL. We rescale to our PDG 96 values of  $B(Z \rightarrow b\bar{b})$ .

<sup>7</sup> ABE 96R reports  $B(b \rightarrow B_c X)/B(b \rightarrow B^+ X) \times B(B_c^+ \rightarrow J/\psi(1S)\pi^+)/B(B^+ \rightarrow J/\psi(1S)K^+) < 0.053$  at 95%CL for  $\tau_{B_c} = 0.8$  ps. It changes from 0.15 to 0.04 for  $0.17 \text{ ps} < \tau_{B_c} < 1.6$  ps. We rescale to our PDG 96 values of  $B(b \rightarrow B^+) = 0.378 \pm 0.022$  and  $B(B^+ \rightarrow J/\psi(1S)K^+) = 0.00101 \pm 0.00014$ .

$\Gamma(J/\psi(1S)\pi^+)/\Gamma(J/\psi(1S)\mu^+\nu_\mu)$				$\Gamma_4/\Gamma_2$
VALUE (units 10 <sup>-2</sup> )	DOCUMENT ID	TECN	COMMENT	
<b>4.69 ± 0.28 ± 0.46</b>	<sup>1</sup> AAIJ	14W	LHCB <i>pp</i> at 7 TeV	
<sup>1</sup> AAIJ 14W reports also a measurement $B(B_c^+ \rightarrow J/\psi\pi^+)/B(B_c^+ \rightarrow J/\psi\mu^+\nu_\mu) = 0.271 \pm 0.016 \pm 0.016$ in the region $m_{J/\psi\mu^+} > 5.3$ GeV.				

$\Gamma(J/\psi(1S)K^+)/\Gamma(J/\psi(1S)\pi^+)$				$\Gamma_5/\Gamma_4$
VALUE	EVTs	DOCUMENT ID	TECN	COMMENT
<b>0.079 ± 0.007 ± 0.003</b>		AAIJ	16AF	LHCB <i>pp</i> at 7, 8 TeV
• • • We do not use the following data for averages, fits, limits, etc. • • •				
0.069 ± 0.019 ± 0.005	50	AAIJ	13BY	LHCB Repl. by AAIJ 16AF

$\Gamma(J/\psi(1S)\pi^+\pi^+\pi^-)/\Gamma_{total} \times B(\bar{B} \rightarrow B_c)$				$\Gamma_6/\Gamma \times B$
VALUE	CL%	DOCUMENT ID	TECN	COMMENT
seen		AAIJ	12Y	LHCB <i>pp</i> at 7 TeV
• • • We do not use the following data for averages, fits, limits, etc. • • •				
<5.7 × 10 <sup>-4</sup>	90	<sup>1</sup> ABREU	97E	DLPH $e^+e^- \rightarrow Z$
<sup>1</sup> ABREU 97E value listed is independent of 0.4 ps $< \tau_{B_c} < 1.4$ ps.				

$\Gamma(J/\psi(1S)\pi^+\pi^+\pi^-)/\Gamma(J/\psi(1S)\pi^+)$				$\Gamma_6/\Gamma_4$
VALUE	DOCUMENT ID	TECN	COMMENT	
<b>2.4 ± 0.4 OUR AVERAGE</b>				
2.55 ± 0.80 ± 0.33 <sup>+0.04</sup> <sub>-0.01</sub>	KHACHATRY...15AA	CMS	<i>pp</i> at 7 TeV	
2.41 ± 0.30 ± 0.33	AAIJ	12Y	LHCB <i>pp</i> at 7 TeV	

$\Gamma(J/\psi(1S)a_1(1260))/\Gamma_{total} \times B(\bar{B} \rightarrow B_c)$				$\Gamma_7/\Gamma \times B$
VALUE	CL%	DOCUMENT ID	TECN	COMMENT
<b>&lt;1.2 × 10<sup>-3</sup></b>		<sup>1</sup> ACKERSTAFF	98o	OPAL $e^+e^- \rightarrow Z$
<sup>1</sup> ACKERSTAFF 98o reports $B(Z \rightarrow B_c X)/B(Z \rightarrow qq) \times B(B_c \rightarrow J/\psi(1S)a_1(1260)) < 5.29 \times 10^{-4}$ at 90%CL. We rescale to our PDG 98 values of $B(Z \rightarrow b\bar{b})$ .				

$\Gamma(J/\psi(1S)K^+K^-\pi^+)/\Gamma_{total} \times B(\bar{B} \rightarrow B_c)$				$\Gamma_8/\Gamma \times B$
VALUE	DOCUMENT ID	TECN	COMMENT	
seen	<sup>1</sup> AAIJ	13CA	LHCB <i>pp</i> at 7, 8 TeV	
<sup>1</sup> A signal yield of 78 ± 14 decays is reported with a significance of 6.2 standard deviations using an integrated luminosity of 3 fb <sup>-1</sup> data.				

$\Gamma(J/\psi(1S)K^+K^-\pi^+)/\Gamma(J/\psi(1S)\pi^+)$				$\Gamma_8/\Gamma_4$
VALUE	DOCUMENT ID	TECN	COMMENT	
<b>0.53 ± 0.10 ± 0.05</b>	<sup>1</sup> AAIJ	13CA	LHCB <i>pp</i> at 7, 8 TeV	
<sup>1</sup> A signal yield of 78 ± 14 decays is reported with a significance of 6.2 standard deviations using an integrated luminosity of 3 fb <sup>-1</sup> data.				

$\Gamma(J/\psi(1S)\pi^+\pi^+\pi^-\pi^-)/\Gamma(J/\psi(1S)\pi^+)$				$\Gamma_9/\Gamma_4$
VALUE	DOCUMENT ID	TECN	COMMENT	
<b>1.74 ± 0.44 ± 0.24</b>	<sup>1</sup> AAIJ	14P	LHCB <i>pp</i> at 7, 8 TeV	
<sup>1</sup> A signal yield of 32 ± 8 decays is reported with a significance of 4.5 standard deviations.				

$\Gamma(\psi(2S)\pi^+)/\Gamma(J/\psi(1S)\pi^+)$				$\Gamma_{10}/\Gamma_4$
VALUE	DOCUMENT ID	TECN	COMMENT	
<b>0.268 ± 0.032 ± 0.007 ± 0.006</b>	<sup>1</sup> AAIJ	15AY	LHCB <i>pp</i> at 7, 8 TeV	
• • • We do not use the following data for averages, fits, limits, etc. • • •				
0.250 ± 0.068 ± 0.014 ± 0.006	<sup>1</sup> AAIJ	13AM	LHCB Repl. by AAIJ 15AY	
<sup>1</sup> The last uncertainty is due to the uncertainty of the $B(\psi(2S) \rightarrow \mu^+\mu^-)/B(J/\psi \rightarrow \mu^+\mu^-)$ ratio measurement.				

$\Gamma(J/\psi(1S)D^0K^+)/\Gamma(J/\psi(1S)\pi^+)$				$\Gamma_{11}/\Gamma_4$
VALUE	DOCUMENT ID	TECN	COMMENT	
<b>0.432 ± 0.136 ± 0.028</b>	AAIJ	17L	LHCB <i>pp</i> at 7, 8 TeV	

$\Gamma(J/\psi(1S)D^*(2007)^0K^+)/\Gamma(J/\psi(1S)D^0K^+)$				$\Gamma_{12}/\Gamma_{11}$
VALUE	DOCUMENT ID	TECN	COMMENT	
<b>5.1 ± 1.8 ± 0.4</b>	AAIJ	17L	LHCB <i>pp</i> at 7, 8 TeV	

$\Gamma(J/\psi(1S)D^*(2010)^+K^{*0})/\Gamma(J/\psi(1S)D^0K^+)$				$\Gamma_{13}/\Gamma_{11}$
VALUE	DOCUMENT ID	TECN	COMMENT	
<b>2.10 ± 1.08 ± 0.34</b>	AAIJ	17L	LHCB <i>pp</i> at 7, 8 TeV	

$\Gamma(J/\psi(1S)D^+K^{*0})/\Gamma(J/\psi(1S)D^0K^+)$				$\Gamma_{14}/\Gamma_{11}$
VALUE	DOCUMENT ID	TECN	COMMENT	
<b>0.63 ± 0.39 ± 0.08</b>	AAIJ	17L	LHCB <i>pp</i> at 7, 8 TeV	

$\Gamma(J/\psi(1S)D_s^+)/\Gamma(J/\psi(1S)\pi^+)$				$\Gamma_{15}/\Gamma_4$
VALUE	DOCUMENT ID	TECN	COMMENT	
<b>3.1 ± 0.5 OUR AVERAGE</b>				
3.8 ± 1.1 ± 0.4	AAD	16H	ATLS <i>pp</i> at 7, 8 TeV	
2.90 ± 0.57 ± 0.24	AAIJ	13As	LHCB <i>pp</i> at 7, 8 TeV	

$\Gamma(J/\psi(1S)D_s^{*+})/\Gamma(J/\psi(1S)\pi^+)$				$\Gamma_{16}/\Gamma_4$
VALUE	DOCUMENT ID	TECN	COMMENT	
<b>10.4 ± 3.1 ± 1.6</b>	AAD	16H	ATLS <i>pp</i> at 7, 8 TeV	

$\Gamma(J/\psi(1S)D_s^{*+})/\Gamma(J/\psi(1S)D_s^+)$				$\Gamma_{16}/\Gamma_{15}$
VALUE	DOCUMENT ID	TECN	COMMENT	
<b>2.5 ± 0.5 OUR AVERAGE</b>				
2.8 <sup>+1.2</sup> <sub>-0.8</sub> ± 0.3	AAD	16H	ATLS <i>pp</i> at 7, 8 TeV	
2.37 ± 0.56 ± 0.10	AAIJ	13As	LHCB <i>pp</i> at 7, 8 TeV	

$\Gamma(J/\psi(1S)p\bar{p}\pi^+)/\Gamma(J/\psi(1S)\pi^+)$				$\Gamma_{17}/\Gamma_4$
VALUE	DOCUMENT ID	TECN	COMMENT	
<b>0.143 ± 0.041</b> <b>-0.036</b>	AAIJ	14AQ	LHCB <i>pp</i> at 7, 8 TeV	

$\Gamma(\chi_c^0\pi^+)/\Gamma_{total}$				$\Gamma_{18}/\Gamma$
VALUE (units 10 <sup>-6</sup> )	DOCUMENT ID	TECN	COMMENT	
<b>24.0<sup>+8.6</sup><sub>-7.6</sub> ± 0.4</b>	<sup>1,2</sup> AAIJ	16AT	LHCB <i>pp</i> at 7 and 8 TeV	
<sup>1</sup> AAIJ 16AT reports $[\Gamma(B_c^+ \rightarrow \chi_c^0\pi^+)/\Gamma_{total}] \times [\Gamma(\bar{B} \rightarrow B^+)/\Gamma_{total}] = (9.8 \pm 3.4 \pm 0.8) \times 10^{-6}$ which we divide by our best value $\Gamma(\bar{B} \rightarrow B^+)/\Gamma_{total} = 0.408 \pm 0.007$ . Our first error is their experiment's error and our second error is the systematic error from using our best value.				
<sup>2</sup> The significance of the observed signal is 4.0 standard deviations.				

$\Gamma(p\bar{p}\pi^+)/\Gamma_{total}$				$\Gamma_{19}/\Gamma$
VALUE	DOCUMENT ID	TECN	COMMENT	
<b>not seen</b>	<sup>1</sup> AAIJ	16K	LHCB <i>pp</i> at 7, 8 TeV	
<sup>1</sup> Measures the ratio $(f_c/f_u) \times B(B_c^+ \rightarrow p\bar{p}\pi^+) < 3.6 \times 10^{-8}$ at 95% CL, in the region $m(p\bar{p}) < 2.85$ GeV/c <sup>2</sup> , where $f_c$ ( $f_u$ ) represents the fragmentation fraction of the b-quark into the $B_c^+$ ( $B_u^+$ ) meson.				

$\Gamma(D^0K^+)/\Gamma_{total} \times B(\bar{B} \rightarrow B_c)$				$\Gamma_{20}/\Gamma \times B$
VALUE (units 10 <sup>-7</sup> )	DOCUMENT ID	TECN	COMMENT	
<b>3.8 ± 1.2 ± 0.1</b>	<sup>1</sup> AAIJ	17AG	LHCB <i>pp</i> at 7, 8 TeV	
<sup>1</sup> AAIJ 17AG reports $[\Gamma(B_c^+ \rightarrow D^0K^+)/\Gamma_{total} \times B(\bar{B} \rightarrow B_c)] / [B(\bar{B} \rightarrow B^+)] = (9.3 \pm 2.8 \pm 0.6) \times 10^{-7}$ which we multiply by our best value $B(\bar{B} \rightarrow B^+) = (40.8 \pm 0.7) \times 10^{-2}$ . Our first error is their experiment's error and our second error is the systematic error from using our best value.				

$\Gamma(D^0\pi^+)/\Gamma_{total} \times B(\bar{B} \rightarrow B_c)$				$\Gamma_{21}/\Gamma \times B$
VALUE	CL%	DOCUMENT ID	TECN	COMMENT
<b>&lt;1.6 × 10<sup>-7</sup></b>	95	<sup>1</sup> AAIJ	17AG	LHCB <i>pp</i> at 7, 8 TeV
<sup>1</sup> AAIJ 17AG reports $[\Gamma(B_c^+ \rightarrow D^0\pi^+)/\Gamma_{total} \times B(\bar{B} \rightarrow B_c)] / [B(\bar{B} \rightarrow B^+)] < 3.9 \times 10^{-7}$ which we multiply by our best value $B(\bar{B} \rightarrow B^+) = 40.8 \times 10^{-2}$ .				



## Meson Particle Listings

 $B_C^+$ 

$\Gamma(D^{*0}\pi^+)/\Gamma_{\text{total}} \times B(\bar{B} \rightarrow B_c)$					$\Gamma_{22}/\Gamma \times B$
VALUE	CL%	DOCUMENT ID	TECN	COMMENT	

$<4 \times 10^{-7}$  95 1 AAIJ 17AG LHCB *pp* at 7, 8 TeV  
 1 AAIJ 17AG reports  $[\Gamma(B_C^+ \rightarrow D^{*0}\pi^+)/\Gamma_{\text{total}} \times B(\bar{B} \rightarrow B_c)] / [B(\bar{B} \rightarrow B^+)] < 1.1 \times 10^{-6}$  which we multiply by our best value  $B(\bar{B} \rightarrow B^+) = 40.8 \times 10^{-2}$ .

$\Gamma(D^{*0}K^+)/\Gamma_{\text{total}} \times B(\bar{B} \rightarrow B_c)$					$\Gamma_{23}/\Gamma \times B$
VALUE	CL%	DOCUMENT ID	TECN	COMMENT	

$<4 \times 10^{-7}$  95 1 AAIJ 17AG LHCB *pp* at 7, 8 TeV  
 1 AAIJ 17AG reports  $[\Gamma(B_C^+ \rightarrow D^{*0}K^+)/\Gamma_{\text{total}} \times B(\bar{B} \rightarrow B_c)] / [B(\bar{B} \rightarrow B^+)] < 1.1 \times 10^{-6}$  which we multiply by our best value  $B(\bar{B} \rightarrow B^+) = 40.8 \times 10^{-2}$ .

$\Gamma(D_s^+ \bar{D}^0)/\Gamma_{\text{total}} \times B(\bar{B} \rightarrow B_c)$					$\Gamma_{24}/\Gamma \times B$
VALUE	CL%	DOCUMENT ID	TECN	COMMENT	

$<1.4 \times 10^{-7}$  90 1 AAIJ 18P LHCB *pp* at 7, 8 TeV  
 1 AAIJ 18P reports  $[\Gamma(B_C^+ \rightarrow D_s^+ \bar{D}^0)/\Gamma_{\text{total}} \times B(\bar{B} \rightarrow B_c)] / [B(\bar{B} \rightarrow B^+)] / [B(B^+ \rightarrow \bar{D}^0 D^+)] < 0.9 \times 10^{-3}$  which we multiply by our best values  $B(\bar{B} \rightarrow B^+) = 40.8 \times 10^{-2}$ ,  $B(B^+ \rightarrow \bar{D}^0 D^+) = 3.8 \times 10^{-4}$ .

$\Gamma(D_s^+ D^0)/\Gamma_{\text{total}} \times B(\bar{B} \rightarrow B_c)$					$\Gamma_{25}/\Gamma \times B$
VALUE	CL%	DOCUMENT ID	TECN	COMMENT	

$<6 \times 10^{-8}$  90 1 AAIJ 18P LHCB *pp* at 7, 8 TeV  
 1 AAIJ 18P reports  $[\Gamma(B_C^+ \rightarrow D_s^+ D^0)/\Gamma_{\text{total}} \times B(\bar{B} \rightarrow B_c)] / [B(\bar{B} \rightarrow B^+)] / [B(B^+ \rightarrow \bar{D}^0 D^+)] < 3.7 \times 10^{-4}$  which we multiply by our best values  $B(\bar{B} \rightarrow B^+) = 40.8 \times 10^{-2}$ ,  $B(B^+ \rightarrow \bar{D}^0 D^+) = 3.8 \times 10^{-4}$ .

$\Gamma(D^+ \bar{D}^0)/\Gamma_{\text{total}} \times B(\bar{B} \rightarrow B_c)$					$\Gamma_{26}/\Gamma \times B$
VALUE	CL%	DOCUMENT ID	TECN	COMMENT	

$<3.0 \times 10^{-6}$  90 1 AAIJ 18P LHCB *pp* at 7, 8 TeV  
 1 AAIJ 18P reports  $[\Gamma(B_C^+ \rightarrow D^+ \bar{D}^0)/\Gamma_{\text{total}} \times B(\bar{B} \rightarrow B_c)] / [B(\bar{B} \rightarrow B^+)] / [B(B^+ \rightarrow \bar{D}^0 D^+)] < 1.9 \times 10^{-2}$  which we multiply by our best values  $B(\bar{B} \rightarrow B^+) = 40.8 \times 10^{-2}$ ,  $B(B^+ \rightarrow \bar{D}^0 D^+) = 3.8 \times 10^{-4}$ .

$\Gamma(D^+ D^0)/\Gamma_{\text{total}} \times B(\bar{B} \rightarrow B_c)$					$\Gamma_{27}/\Gamma \times B$
VALUE	CL%	DOCUMENT ID	TECN	COMMENT	

$<1.9 \times 10^{-6}$  90 1 AAIJ 18P LHCB *pp* at 7, 8 TeV  
 1 AAIJ 18P reports  $[\Gamma(B_C^+ \rightarrow D^+ D^0)/\Gamma_{\text{total}} \times B(\bar{B} \rightarrow B_c)] / [B(\bar{B} \rightarrow B^+)] / [B(B^+ \rightarrow \bar{D}^0 D^+)] < 1.2 \times 10^{-2}$  which we multiply by our best values  $B(\bar{B} \rightarrow B^+) = 40.8 \times 10^{-2}$ ,  $B(B^+ \rightarrow \bar{D}^0 D^+) = 3.8 \times 10^{-4}$ .

$[\Gamma(D_s^+ \bar{D}^0) + \Gamma(D_s^+ \bar{D}^*(2007)^0)]/\Gamma_{\text{total}} \times B(\bar{B} \rightarrow B_c)$					$(\Gamma_{28} + \Gamma_{29})/\Gamma \times B$
VALUE	CL%	DOCUMENT ID	TECN	COMMENT	

$<4 \times 10^{-7}$  90 1 AAIJ 18P LHCB *pp* at 7, 8 TeV  
 1 AAIJ 18P reports  $[\Gamma(B_C^+ \rightarrow D_s^+ \bar{D}^0) + \Gamma(B_C^+ \rightarrow D_s^+ \bar{D}^*(2007)^0)]/\Gamma_{\text{total}} \times B(\bar{B} \rightarrow B_c) / [B(\bar{B} \rightarrow B^+)] / [B(B^+ \rightarrow \bar{D}^0 D^+)] < 2.8 \times 10^{-3}$  which we multiply by our best values  $B(\bar{B} \rightarrow B^+) = 40.8 \times 10^{-2}$ ,  $B(B^+ \rightarrow \bar{D}^0 D^+) = 3.8 \times 10^{-4}$ .

$[\Gamma(D_s^+ D^0) + \Gamma(D_s^+ D^*(2007)^0)]/\Gamma_{\text{total}} \times B(\bar{B} \rightarrow B_c)$					$(\Gamma_{30} + \Gamma_{31})/\Gamma \times B$
VALUE	CL%	DOCUMENT ID	TECN	COMMENT	

$<5 \times 10^{-7}$  90 1 AAIJ 18P LHCB *pp* at 7, 8 TeV  
 1 AAIJ 18P reports  $[\Gamma(B_C^+ \rightarrow D_s^+ D^0) + \Gamma(B_C^+ \rightarrow D_s^+ D^*(2007)^0)]/\Gamma_{\text{total}} \times B(\bar{B} \rightarrow B_c) / [B(\bar{B} \rightarrow B^+)] / [B(B^+ \rightarrow \bar{D}^0 D^+)] < 3.0 \times 10^{-3}$  which we multiply by our best values  $B(\bar{B} \rightarrow B^+) = 40.8 \times 10^{-2}$ ,  $B(B^+ \rightarrow \bar{D}^0 D^+) = 3.8 \times 10^{-4}$ .

$\Gamma(D^*(2010)^+ \bar{D}^0)/\Gamma_{\text{total}} \times B(\bar{B} \rightarrow B_c)$					$\Gamma_{32}/\Gamma \times B$
VALUE	CL%	DOCUMENT ID	TECN	COMMENT	

$<6.2 \times 10^{-3}$  90 1 BARATE 98Q ALEP  $e^+e^- \rightarrow Z$   
 1 BARATE 98Q reports  $B(Z \rightarrow B_c X) \times B(B_c \rightarrow D^*(2010)^+ \bar{D}^0) < 1.9 \times 10^{-3}$  at 90%CL. We rescale to our PDG 98 values of  $B(Z \rightarrow b\bar{b})$ .

$[\Gamma(D^*(2010)^+ \bar{D}^0, D^{*+} \rightarrow D^+ \pi^0/\gamma) + \Gamma(D^+ \bar{D}^*(2007)^0)]/\Gamma_{\text{total}} \times B(\bar{B} \rightarrow B_c)$					$(\Gamma_{33} + \Gamma_{34})/\Gamma \times B$
VALUE	CL%	DOCUMENT ID	TECN	COMMENT	

$<9 \times 10^{-6}$  90 1 AAIJ 18P LHCB *pp* at 7, 8 TeV  
 1 AAIJ 18P reports  $[\Gamma(B_C^+ \rightarrow D^*(2010)^+ \bar{D}^0, D^{*+} \rightarrow D^+ \pi^0/\gamma) + \Gamma(B_C^+ \rightarrow D^+ \bar{D}^*(2007)^0)]/\Gamma_{\text{total}} \times B(\bar{B} \rightarrow B_c) / [B(\bar{B} \rightarrow B^+)] / [B(B^+ \rightarrow \bar{D}^0 D^+)] < 5.5 \times 10^{-2}$  which we multiply by our best values  $B(\bar{B} \rightarrow B^+) = 40.8 \times 10^{-2}$ ,  $B(B^+ \rightarrow \bar{D}^0 D^+) = 3.8 \times 10^{-4}$ .

$[\Gamma(D^*(2010)^+ D^0, D^{*+} \rightarrow D^+ \pi^0/\gamma) + \Gamma(D^+ D^*(2007)^0)]/\Gamma_{\text{total}} \times B(\bar{B} \rightarrow B_c)$					$(\Gamma_{35} + \Gamma_{36})/\Gamma \times B$
VALUE	CL%	DOCUMENT ID	TECN	COMMENT	

$<3.4 \times 10^{-6}$  90 1 AAIJ 18P LHCB *pp* at 7, 8 TeV

1 AAIJ 18P reports  $[\Gamma(B_C^+ \rightarrow D^*(2010)^+ D^0, D^{*+} \rightarrow D^+ \pi^0/\gamma) + \Gamma(B_C^+ \rightarrow D^+ D^*(2007)^0)]/\Gamma_{\text{total}} \times B(\bar{B} \rightarrow B_c) / [B(\bar{B} \rightarrow B^+)] / [B(B^+ \rightarrow \bar{D}^0 D^+)] < 2.2 \times 10^{-2}$  which we multiply by our best values  $B(\bar{B} \rightarrow B^+) = 40.8 \times 10^{-2}$ ,  $B(B^+ \rightarrow \bar{D}^0 D^+) = 3.8 \times 10^{-4}$ .

$\Gamma(D_s^+ \bar{D}^*(2007)^0)/\Gamma_{\text{total}} \times B(\bar{B} \rightarrow B_c)$					$\Gamma_{37}/\Gamma \times B$
VALUE	CL%	DOCUMENT ID	TECN	COMMENT	

$<1.7 \times 10^{-6}$  90 1 AAIJ 18P LHCB *pp* at 7, 8 TeV  
 1 AAIJ 18P reports  $[\Gamma(B_C^+ \rightarrow D_s^+ \bar{D}^*(2007)^0)/\Gamma_{\text{total}} \times B(\bar{B} \rightarrow B_c)] / [B(\bar{B} \rightarrow B^+)] / [B(B^+ \rightarrow \bar{D}^0 D^+)] < 1.1 \times 10^{-2}$  which we multiply by our best values  $B(\bar{B} \rightarrow B^+) = 40.8 \times 10^{-2}$ ,  $B(B^+ \rightarrow \bar{D}^0 D^+) = 3.8 \times 10^{-4}$ .

$\Gamma(D_s^+ D^*(2007)^0)/\Gamma_{\text{total}} \times B(\bar{B} \rightarrow B_c)$					$\Gamma_{38}/\Gamma \times B$
VALUE	CL%	DOCUMENT ID	TECN	COMMENT	

$<3.1 \times 10^{-6}$  90 1 AAIJ 18P LHCB *pp* at 7, 8 TeV  
 1 AAIJ 18P reports  $[\Gamma(B_C^+ \rightarrow D_s^+ D^*(2007)^0)/\Gamma_{\text{total}} \times B(\bar{B} \rightarrow B_c)] / [B(\bar{B} \rightarrow B^+)] / [B(B^+ \rightarrow \bar{D}^0 D^+)] < 2.0 \times 10^{-2}$  which we multiply by our best values  $B(\bar{B} \rightarrow B^+) = 40.8 \times 10^{-2}$ ,  $B(B^+ \rightarrow \bar{D}^0 D^+) = 3.8 \times 10^{-4}$ .

$\Gamma(D^*(2010)^+ \bar{D}^*(2007)^0)/\Gamma_{\text{total}} \times B(\bar{B} \rightarrow B_c)$					$\Gamma_{39}/\Gamma \times B$
VALUE	CL%	DOCUMENT ID	TECN	COMMENT	

$<1.0 \times 10^{-4}$  90 1 AAIJ 18P LHCB *pp* at 7, 8 TeV  
 1 AAIJ 18P reports  $[\Gamma(B_C^+ \rightarrow D^*(2010)^+ \bar{D}^*(2007)^0)/\Gamma_{\text{total}} \times B(\bar{B} \rightarrow B_c)] / [B(\bar{B} \rightarrow B^+)] / [B(B^+ \rightarrow \bar{D}^0 D^+)] < 6.5 \times 10^{-1}$  which we multiply by our best values  $B(\bar{B} \rightarrow B^+) = 40.8 \times 10^{-2}$ ,  $B(B^+ \rightarrow \bar{D}^0 D^+) = 3.8 \times 10^{-4}$ .

$\Gamma(D^*(2010)^+ D^*(2007)^0)/\Gamma_{\text{total}} \times B(\bar{B} \rightarrow B_c)$					$\Gamma_{40}/\Gamma \times B$
VALUE	CL%	DOCUMENT ID	TECN	COMMENT	

$<2.0 \times 10^{-5}$  90 1 AAIJ 18P LHCB *pp* at 7, 8 TeV  
 1 AAIJ 18P reports  $[\Gamma(B_C^+ \rightarrow D^*(2010)^+ D^*(2007)^0)/\Gamma_{\text{total}} \times B(\bar{B} \rightarrow B_c)] / [B(\bar{B} \rightarrow B^+)] / [B(B^+ \rightarrow \bar{D}^0 D^+)] < 1.3 \times 10^{-1}$  which we multiply by our best values  $B(\bar{B} \rightarrow B^+) = 40.8 \times 10^{-2}$ ,  $B(B^+ \rightarrow \bar{D}^0 D^+) = 3.8 \times 10^{-4}$ .

$\Gamma(D^+ K^*)/\Gamma_{\text{total}} \times B(\bar{B} \rightarrow B_c)$					$\Gamma_{41}/\Gamma \times B$
VALUE	CL%	DOCUMENT ID	TECN	COMMENT	

$<2.0 \times 10^{-7}$  90 1 AAIJ 13R LHCB *pp* at 7 TeV  
 1 AAIJ 13R reports  $[\Gamma(B_C^+ \rightarrow D^+ K^*)/\Gamma_{\text{total}} \times B(\bar{B} \rightarrow B_c)] / [B(\bar{B} \rightarrow B^+)] < 0.5 \times 10^{-6}$  which we multiply by our best value  $B(\bar{B} \rightarrow B^+) = 40.8 \times 10^{-2}$ .

$\Gamma(D^+ \bar{K}^*)/\Gamma_{\text{total}} \times B(\bar{B} \rightarrow B_c)$					$\Gamma_{42}/\Gamma \times B$
VALUE	CL%	DOCUMENT ID	TECN	COMMENT	

$<1.6 \times 10^{-7}$  90 1 AAIJ 13R LHCB *pp* at 7 TeV  
 1 AAIJ 13R reports  $[\Gamma(B_C^+ \rightarrow D^+ \bar{K}^*)/\Gamma_{\text{total}} \times B(\bar{B} \rightarrow B_c)] / [B(\bar{B} \rightarrow B^+)] < 0.4 \times 10^{-6}$  which we multiply by our best value  $B(\bar{B} \rightarrow B^+) = 40.8 \times 10^{-2}$ .

$\Gamma(D_s^+ K^*)/\Gamma_{\text{total}} \times B(\bar{B} \rightarrow B_c)$					$\Gamma_{43}/\Gamma \times B$
VALUE	CL%	DOCUMENT ID	TECN	COMMENT	

$<2.9 \times 10^{-7}$  90 1 AAIJ 13R LHCB *pp* at 7 TeV  
 1 AAIJ 13R reports  $[\Gamma(B_C^+ \rightarrow D_s^+ K^*)/\Gamma_{\text{total}} \times B(\bar{B} \rightarrow B_c)] / [B(\bar{B} \rightarrow B^+)] < 0.7 \times 10^{-6}$  which we multiply by our best value  $B(\bar{B} \rightarrow B^+) = 40.8 \times 10^{-2}$ .

$\Gamma(D_s^+ \bar{K}^*)/\Gamma_{\text{total}} \times B(\bar{B} \rightarrow B_c)$					$\Gamma_{44}/\Gamma \times B$
VALUE	CL%	DOCUMENT ID	TECN	COMMENT	

$<4 \times 10^{-7}$  90 1 AAIJ 13R LHCB *pp* at 7 TeV  
 1 AAIJ 13R reports  $[\Gamma(B_C^+ \rightarrow D_s^+ \bar{K}^*)/\Gamma_{\text{total}} \times B(\bar{B} \rightarrow B_c)] / [B(\bar{B} \rightarrow B^+)] < 1.1 \times 10^{-6}$  which we multiply by our best value  $B(\bar{B} \rightarrow B^+) = 40.8 \times 10^{-2}$ .

$\Gamma(D_s^+ \phi)/\Gamma_{\text{total}} \times B(\bar{B} \rightarrow B_c)$					$\Gamma_{45}/\Gamma \times B$
VALUE	CL%	DOCUMENT ID	TECN	COMMENT	

$<3.3 \times 10^{-7}$  90 1 AAIJ 13R LHCB *pp* at 7 TeV  
 1 AAIJ 13R reports  $[\Gamma(B_C^+ \rightarrow D_s^+ \phi)/\Gamma_{\text{total}} \times B(\bar{B} \rightarrow B_c)] / [B(\bar{B} \rightarrow B^+)] < 0.8 \times 10^{-6}$  which we multiply by our best value  $B(\bar{B} \rightarrow B^+) = 40.8 \times 10^{-2}$ .

$\Gamma(K^+ K^0)/\Gamma_{\text{total}} \times B(\bar{B} \rightarrow B_c)$					$\Gamma_{46}/\Gamma \times B$
VALUE	CL%	DOCUMENT ID	TECN	COMMENT	

$<4.6 \times 10^{-7}$  90 1 AAIJ 13Bs LHCB *pp* at 7 TeV  
 1 Derived from  $\Gamma(K^+ K^0)/\Gamma \times B(\bar{B} \rightarrow B_c) / (B(B^+ \rightarrow K^0 \pi^+) B(\bar{B} \rightarrow B^+)) < 5.8\%$  at 90% CL using normalization mode  $B(B^+ \rightarrow K^0 \pi^+) = (23.97 \pm 0.53 \pm 0.71) \times 10^{-6}$  and assuming a  $B$  production ratio  $f(\bar{B} \rightarrow B^+) = 0.33$ .

$\Gamma(B_s^+ \pi^+)/B(\bar{B} \rightarrow B_s) \times B(\bar{B} \rightarrow B_c)$					$\Gamma_{47}/\Gamma \times B$
VALUE (units $10^{-3}$ )	CL%	DOCUMENT ID	TECN	COMMENT	

$2.37 \pm 0.31 \pm 0.11 \text{ }^{+0.17}_{-0.13}$  1 AAIJ 13Bu LHCB *pp* at 7, 8 TeV

1 The last uncertainty is due to the uncertainty of the  $B_C^+$  lifetime measurement.

**POLARIZATION IN  $B_c^+$  DECAY**

In decays involving two vector mesons, one can distinguish among the states in which meson polarizations are both longitudinal ( $L$ ) or both are transverse and parallel ( $\parallel$ ) or perpendicular ( $\perp$ ) to each other with the parameters  $\Gamma_L/\Gamma$ ,  $\Gamma_\perp/\Gamma$ , and the relative phases  $\phi_\parallel$  and  $\phi_\perp$ . See the definitions in the note on "Polarization in  $B$  Decays" review in the  $B^0$  Particle Listings.

**$\Gamma_L/\Gamma$  in  $B_c^+ \rightarrow J/\psi D_s^{*+}$**

VALUE	DOCUMENT ID	TECN	COMMENT
<b><math>0.54 \pm 0.15</math> OUR AVERAGE</b>			
$0.62 \pm 0.24$	<sup>1</sup> AAD	16H ATLS	$pp$ at 7, 8 TeV
$0.48 \pm 0.20$	<sup>2</sup> AAIJ	13As LHCb	$pp$ at 7, 8 TeV

<sup>1</sup> AAD 16H measures  $1 - \Gamma_\perp/\Gamma = 0.38 \pm 0.24$ .  
<sup>2</sup> AAIJ 13As measures  $1 - \Gamma_\perp/\Gamma = 0.52 \pm 0.20$ .

**$A_P(B_c^+)$**

$$A_P(B_c^+) = [\sigma(B_c^-) - \sigma(B_c^+)] / [\sigma(B_c^-) + \sigma(B_c^+)]$$

VALUE (units $10^{-2}$ )	DOCUMENT ID	TECN	COMMENT
<b><math>-1.0 \pm 1.0</math> OUR AVERAGE</b>			
$-2.5 \pm 2.1 \pm 0.5$	<sup>1</sup> AAIJ	19Al LHCb	$pp$ at 7 TeV
$-0.5 \pm 1.1 \pm 0.4$	<sup>1</sup> AAIJ	19Al LHCb	$pp$ at 13 TeV

<sup>1</sup> Measured using  $B_c^+$  semileptonic decays.

**$B_c^+$  REFERENCES**

AAIJ	19Al	PR D100 112006	R. Aaij et al.	(LHCb Collab.)
AAIJ	18C	PRL 120 121801	R. Aaij et al.	(LHCb Collab.)
AAIJ	18P	NP B930 563	R. Aaij et al.	(CMS Collab.)
SIRUNYAN	18BY	EPJ C78 457	A.M. Sirunyan et al.	(CMS Collab.)
AAIJ	17AG	PRL 118 111803	R. Aaij et al.	(LHCb Collab.)
AAIJ	17L	PR D95 032005	R. Aaij et al.	(LHCb Collab.)
AAD	16H	EPJ C76 4	G. Aad et al.	(ATLAS Collab.)
AAIJ	16AF	JHEP 1609 153	R. Aaij et al.	(LHCb Collab.)
AAIJ	16AT	PR D94 091102	R. Aaij et al.	(LHCb Collab.)
AAIJ	16K	PL B759 313	R. Aaij et al.	(LHCb Collab.)
AALTONEN	16A	PR D93 052001	T. Aaltonen et al.	(CDF Collab.)
AAIJ	15AY	PR D92 072007	R. Aaij et al.	(LHCb Collab.)
AAIJ	15G	PL B742 29	R. Aaij et al.	(LHCb Collab.)
AAIJ	15M	PRL 114 132001	R. Aaij et al.	(LHCb Collab.)
KHACHATRYAN	15AA	JHEP 1501 063	V. Khachatryan et al.	(CMS Collab.)
AAIJ	14AQ	PRL 113 152003	R. Aaij et al.	(LHCb Collab.)
AAIJ	14G	EPJ C74 2839	R. Aaij et al.	(LHCb Collab.)
AAIJ	14P	JHEP 1405 148	R. Aaij et al.	(LHCb Collab.)
AAIJ	14W	PR D90 032009	R. Aaij et al.	(LHCb Collab.)
AAIJ	13AM	PR D87 071103	R. Aaij et al.	(LHCb Collab.)
AAIJ	13AS	PR D87 112012	R. Aaij et al.	(LHCb Collab.)
Also		PR D89 019901 (errat.)	R. Aaij et al.	(LHCb Collab.)
AAIJ	13BS	PL B726 646	R. Aaij et al.	(LHCb Collab.)
AAIJ	13BU	PRL 111 181801	R. Aaij et al.	(LHCb Collab.)
AAIJ	13BY	JHEP 1309 075	R. Aaij et al.	(LHCb Collab.)
AAIJ	13CA	JHEP 1311 094	R. Aaij et al.	(LHCb Collab.)
AAIJ	13R	JHEP 1302 043	R. Aaij et al.	(LHCb Collab.)
AALTONEN	13	PR D87 011101	T. Aaltonen et al.	(CDF Collab.)
AAIJ	12AV	PRL 109 232001	R. Aaij et al.	(LHCb Collab.)
AAIJ	12Y	PRL 108 251802	R. Aaij et al.	(LHCb Collab.)
ABAZOV	09H	PRL 102 092001	V.M. Abazov et al.	(DO Collab.)
AALTONEN	08M	PRL 100 182002	T. Aaltonen et al.	(CDF Collab.)
ABAZOV	08T	PRL 101 012001	V.M. Abazov et al.	(DO Collab.)
ABULENCIA	06C	PRL 96 082002	A. Abulencia et al.	(CDF Collab.)
ABULENCIA	06O	PRL 97 012002	A. Abulencia et al.	(CDF Collab.)
ABE	98M	PRL 81 2432	F. Abe et al.	(CDF Collab.)
Also		PR D58 112004	F. Abe et al.	(CDF Collab.)
ACKERSTAFF	98O	PL B420 157	K. Ackerstaff et al.	(OPAL Collab.)
BARATE	98Q	EPJ C4 387	R. Barate et al.	(ALEPH Collab.)
PDG	98	EPJ C3 1	C. Caso et al.	(PDG Collab.)
ABREU	97E	PL B398 207	P. Abreu et al.	(DELPHI Collab.)
BARATE	97H	PL B402 213	R. Barate et al.	(ALEPH Collab.)
ABE	96R	PRL 77 5176	F. Abe et al.	(CDF Collab.)
PDG	96	PR D54 1	R. M. Barnett et al.	(PDG Collab.)

**$B_c(2S)^\pm$**

$$I(J^P) = 0(0^-)$$

OMITTED FROM SUMMARY TABLE

Quantum numbers neither measured nor confirmed.

**$B_c(2S)^\pm$  MASS**

VALUE (MeV)	EVTS	DOCUMENT ID	TECN	COMMENT
<b><math>6871.6 \pm 1.1</math> OUR AVERAGE</b>				
$6872.1 \pm 1.3 \pm 0.8$	24	<sup>1,2</sup> AAIJ	19Y LHCb	$pp$ at 7, 8, 13 TeV
$6871.0 \pm 1.4 \pm 0.8$	51	<sup>3,4</sup> SIRUNYAN	19M CMS	$pp$ at 13 TeV
• • • We do not use the following data for averages, fits, limits, etc. • • •				
not seen		<sup>5</sup> AAIJ	18AL LHCb	$pp$ at 8 TeV
$6842 \pm 4 \pm 5$	57	<sup>6,7</sup> AAD	14AQ ATLS	$pp$ at 7, 8 TeV

<sup>1</sup> AAIJ 19Y observed  $B_c(2S)^+$  in the decay mode  $B_c(2S)^+ \rightarrow B_c^+ \pi^+ \pi^-$  ( $B_c^+ \rightarrow J/\psi \pi^+$ ) with 2.2 (3.2) global (local) standard deviations significance.  
<sup>2</sup> AAIJ 19Y reports mass difference measurement of  $M(B_c(2S)^+) - M(B_c^+) = 597.2 \pm 1.3 \pm 0.1$  MeV. We have adjusted this measurement with our best value of  $M(B_c^+) = 6274.9 \pm 0.8$  MeV. The first uncertainty of the  $M(B_c(2S)^+)$  value is a total of uncertainties reported by the experiment and the second one comes from our best value of  $M(B_c^+)$ .  
<sup>3</sup> SIRUNYAN 19M observed  $B_c(2S)^+$  in the decay mode  $B_c(2S)^+ \rightarrow B_c^+ \pi^+ \pi^-$  ( $B_c^+ \rightarrow J/\psi \pi^+$ ) with 6.5 standard deviations significance.  
<sup>4</sup> SIRUNYAN 19M reports mass difference measurement of  $M(B_c(2S)^+) - M(B_c^+) = 596.1 \pm 1.2 \pm 0.8$  MeV. We have adjusted this measurement with our best value of  $M(B_c^+) = 6274.9 \pm 0.8$  MeV. The first uncertainty of the  $M(B_c(2S)^+)$  value is a total of uncertainties reported by the experiment and the second one comes from our best value of  $M(B_c^+)$ .  
<sup>5</sup> AAIJ 18AL reports an upper limit on the ratio of production cross sections for  $[\sigma(B_c(2S)^+)/\sigma(B_c^+)] \cdot B(B_c(2S)^+ \rightarrow B_c^+ \pi^+ \pi^-) < 0.04-0.09$  at 95% CL for the mass value reported by AAD 14AQ.  
<sup>6</sup> Observed in the decay mode  $B_c(2S)^+ \rightarrow B_c^+ \pi^+ \pi^-$  ( $B_c^+ \rightarrow J/\psi \pi^+$ ) with 5.2 standard deviations significance.  
<sup>7</sup> Might be the  $B_c^*(2S)$ .

**$B_c(2S)^\pm$  DECAY MODES**

Mode	Fraction ( $\Gamma_i/\Gamma$ )
$\Gamma_1 B_c^+ \pi^+ \pi^-$	seen

**$B_c(2S)^\pm$  BRANCHING RATIOS**

$\Gamma(B_c^+ \pi^+ \pi^-)/\Gamma_{total}$	$\Gamma_1/\Gamma$			
VALUE	EVTS	DOCUMENT ID	TECN	COMMENT
seen	57	<sup>1</sup> AAD	14AQ ATLS	$pp$ at 7, 8 TeV
• • • We do not use the following data for averages, fits, limits, etc. • • •				
not seen		<sup>2</sup> AAIJ	18AL LHCb	$pp$ at 8 TeV

<sup>1</sup> Observed with 5.2 standard deviations significance.  
<sup>2</sup> AAIJ 18AL reports an upper limit on the ratio of production cross sections for  $[\sigma(B_c(2S)^+)/\sigma(B_c^+)] \cdot B(B_c(2S)^+ \rightarrow B_c^+ \pi^+ \pi^-) < 0.04-0.09$  at 95% CL for the mass value reported by AAD 14AQ.

**$B_c(2S)^\pm$  REFERENCES**

AAIJ	19Y	PRL 122 232001	R. Aaij et al.	(LHCb Collab.)
SIRUNYAN	19M	PRL 122 132001	A.M. Sirunyan et al.	(CMS Collab.)
AAIJ	18AL	JHEP 1801 138	R. Aaij et al.	(LHCb Collab.)
AAD	14AQ	PRL 113 212004	G. Aad et al.	(ATLAS Collab.)

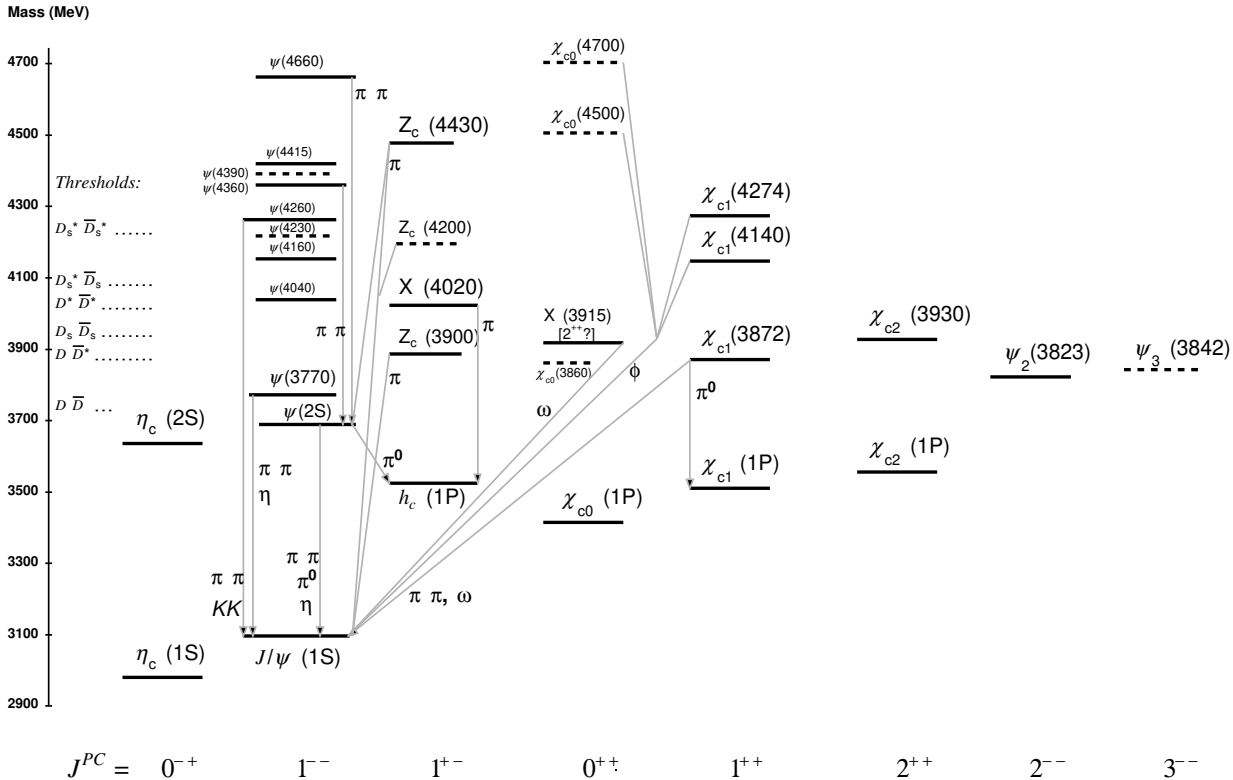
See the related review(s):

Spectroscopy of Mesons Containing Two Heavy Quarks

# Meson Particle Listings

## Charmonium, $\eta_c(1S)$

### $c\bar{c}$ MESONS (including possibly non- $q\bar{q}$ states)



The level scheme of meson states containing a minimal quark content of  $c\bar{c}$ . The name of a state is determined by its quantum numbers  $I^G J^{PC}$  (see the review “Naming Scheme for Hadrons”). States with unestablished quantum numbers are called  $X$  and are drawn according to our best estimate of their likely  $J^{PC}$ . States included in the Summary Tables are shown with solid lines; selected states not in the Summary Tables, but with assigned quantum numbers, are shown with dotted lines. The arrows indicate the most dominant hadronic transitions. Single photon transitions, including  $\psi(nS) \rightarrow \gamma\eta_c(mS)$ ,  $\psi(nS) \rightarrow \gamma\chi_{cJ}(1P)$ , and  $\chi_{cJ}(1P) \rightarrow \gamma J/\psi$ , are omitted for clarity. For orientation, the location of the thresholds related to a pair of ground state open charm mesons is indicated in the figure.

$\eta_c(1S)$		$J^G(J^{PC}) = 0^+(0^{-+})$		
$\eta_c(1S)$ MASS				
VALUE (MeV)	EVTS	DOCUMENT ID	TECN	COMMENT
<b>2983.9 ± 0.5</b>	<b>OUR AVERAGE</b>	Error includes scale factor of 1.3. See the ideogram below.		
2985.9 ± 0.7 ± 2.1	1705	ABL IKIM	19AV BES3	$J/\psi \rightarrow \gamma\omega\omega$
2984.6 ± 0.7 ± 2.2	2673	XU	18 BELL	$e^+e^- \rightarrow K^+K^-\pi^+\pi^-$
2986.7 ± 0.5 ± 0.9	11K	1 AAIJ	17AD LHCB	$pp \rightarrow B^+X \rightarrow p\bar{p}K^+X$
2982.8 ± 1.0 ± 0.5	6.4k	2 AAIJ	17BB LHCB	$pp \rightarrow b\bar{b}X \rightarrow 2(K^+K^-)X$
2982.2 ± 1.5 ± 0.1	2.0k	3 AAIJ	15BI LHCB	$pp \rightarrow \eta_c(1S)X$
2983.5 ± 1.4 ± 1.6 ± 3.6		4 ANASHIN	14 KEDR	$J/\psi \rightarrow \gamma\eta_c$
2979.8 ± 0.8 ± 3.5	4.5k	5,6 LEES	14E BABR	$\gamma\gamma \rightarrow K^+K^-\pi^0$
2984.1 ± 1.1 ± 2.1	900	5,6,7 LEES	14E BABR	$\gamma\gamma \rightarrow K^+K^-\eta$
2984.3 ± 0.6 ± 0.6		8,9 ABLIKIM	12F BES3	$\psi(2S) \rightarrow \gamma\eta_c$
2984.49 ± 1.16 ± 0.52	832	5 ABLIKIM	12N BES3	$\psi(2S) \rightarrow \pi^0\gamma$ hadrons
2982.7 ± 1.8 ± 2.2	486	ZHANG	12A BELL	$e^+e^- \rightarrow K^+K^-\pi^+\pi^-$
2984.5 ± 0.8 ± 3.1	11k	DEL-AMO-SA...11M	BABR	$\gamma\gamma \rightarrow K^+K^-\pi^+\pi^-$
2985.4 ± 1.5 ± 0.5 ± 2.0	920	9 VINOKUROVA	11 BELL	$B^\pm \rightarrow K^\pm(K_S^0 K^\pm\pi^\mp)$

2982.2 ± 0.4 ± 1.6	14k	10 LEES	10 BABR	10.6 $e^+e^- \rightarrow K_S^0 K^\pm\pi^\mp$
2985.8 ± 1.5 ± 3.1	0.9k	AUBERT	08AB BABR	$B \rightarrow \eta_c(1S) K^*(*) \rightarrow K\bar{K}\pi K^*(*)$
2986.1 ± 1.0 ± 2.5	7.5k	UEHARA	08 BELL	$\gamma\gamma \rightarrow \eta_c \rightarrow$ hadrons
2970 ± 5 ± 6	5.01	11 ABE	07 BELL	$e^+e^- \rightarrow J/\psi(c\bar{c})$
2971 ± 3 ± 1	1.95	WU	06 BELL	$B^+ \rightarrow p\bar{p}K^+$
2974 ± 7 ± 1	20	WU	06 BELL	$B^+ \rightarrow \Lambda\bar{\Lambda}K^+$
2981.8 ± 1.3 ± 1.5	5.92	ASNER	04 CLEO	$\gamma\gamma \rightarrow \eta_c \rightarrow K_S^0 K^\pm\pi^\mp$
2984.1 ± 2.1 ± 1.0	190	12 AMBROGIANI	03 E835	$\bar{p}p \rightarrow \eta_c \rightarrow \gamma\gamma$
● ● ● We do not use the following data for averages, fits, limits, etc. ● ● ●				
2982.5 ± 0.4 ± 1.4	12k	13 DEL-AMO-SA...11M	BABR	$\gamma\gamma \rightarrow K_S^0 K^\pm\pi^\mp$
2982.2 ± 0.6		14 MITCHELL	09 CLEO	$e^+e^- \rightarrow \gamma X$
2982 ± 5	270	15 AUBERT	06E BABR	$B^\pm \rightarrow K^\pm X_{c2}$
2982.5 ± 1.1 ± 0.9	2.5k	16 AUBERT	04D BABR	$\gamma\gamma \rightarrow \eta_c(1S) \rightarrow K\bar{K}\pi$
2977.5 ± 1.0 ± 1.2		14,17 BAI	03 BES	$J/\psi \rightarrow \gamma\eta_c$
2979.6 ± 2.3 ± 1.6	180	18 FANG	03 BELL	$B \rightarrow \eta_c K$
2976.3 ± 2.3 ± 1.2		14,19 BAI	00F BES	$J/\psi, \psi(2S) \rightarrow \gamma\eta_c$
2976.6 ± 2.9 ± 1.3	140	14,20 BAI	00F BES	$J/\psi \rightarrow \gamma\eta_c$
2980.4 ± 2.3 ± 0.6		21 BRANDENB...	00B CLE2	$\gamma\gamma \rightarrow \eta_c \rightarrow K^\pm K_S^0\pi^\mp$
2975.8 ± 3.9 ± 1.2		20 BAI	99B BES	Sup. by BAI 00F
2999 ± 8	25	ABREU	98o DLPH	$e^+e^- \rightarrow e^+e^-$ hadrons

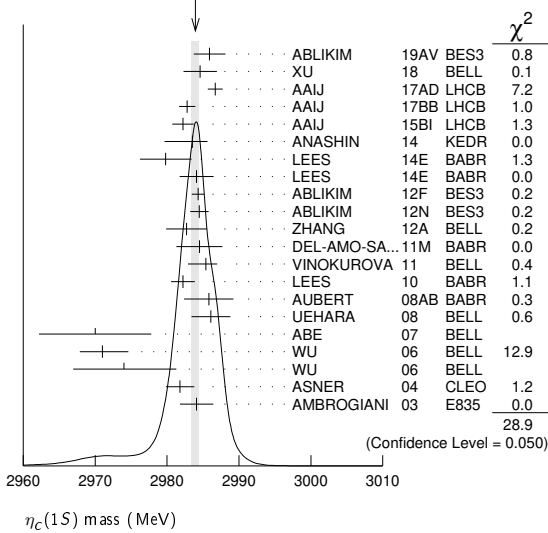
2988.3 ± 3.3		ARMSTRONG 95F	E760	$\bar{p}p \rightarrow \gamma\gamma$
2974.4 ± 1.9	14,22	BISELLO	91 DM2	$J/\psi \rightarrow \eta_c\gamma$
2969 ± 4 ± 4	80 14	BAI	90B MRK3	$J/\psi \rightarrow \gamma K^+ K^- K^+ K^-$
2956 ± 12 ± 12	14	BAI	90B MRK3	$J/\psi \rightarrow \gamma K^+ K^- K_S^0 K_L^0$
2982.6 ± 2.7	12	BAGLIN	87B SPEC	$\bar{p}p \rightarrow \gamma\gamma$
2980.2 ± 1.6	14,22	BALTRUSAIT..86	MRK3	$J/\psi \rightarrow \eta_c\gamma$
2984 ± 2.3 ± 4.0	14	GAISER	86 CBAL	$J/\psi \rightarrow \gamma X, \psi(2S) \rightarrow \gamma X$
2976 ± 8	14,23	BALTRUSAIT..86	MRK3	$J/\psi \rightarrow 2\phi\gamma$
2982 ± 8	18 24	HIMEL	80B MRK2	$e^+e^- \rightarrow \dots$
2980 ± 9	24	PARTRIDGE	80B CBAL	$e^+e^- \rightarrow \dots$

31.4 ± 3.5 ± 2.0	6.4k	<sup>1</sup> AAIJ	17BB LHCB	$pp \rightarrow b\bar{b}X \rightarrow 2(K^+K^-)X$
27.2 ± 3.1 <sup>+5.4</sup> <sub>-2.6</sub>		<sup>2</sup> ANASHIN	14 KEDR	$J/\psi \rightarrow \gamma\eta_c$
25.2 ± 2.6 ± 2.4	4.5k	<sup>3,4</sup> LEES	14E BABR	$\gamma\gamma \rightarrow K^+K^-\pi^0$
34.8 ± 3.1 ± 4.0	900	<sup>3,4,5</sup> LEES	14E BABR	$\gamma\gamma \rightarrow K^+K^-\eta$
32.0 ± 1.2 ± 1.0		<sup>6,7</sup> ABLIKIM	12F BES3	$\psi(2S) \rightarrow \gamma\eta_c$
36.4 ± 3.2 ± 1.7	832	<sup>3</sup> ABLIKIM	12N BES3	$\psi(2S) \rightarrow \pi^0\gamma$ hadrons
37.8 ± 5.8 <sup>+3.1</sup> <sub>-5.3</sub>	486	ZHANG	12A BELL	$e^+e^- \rightarrow e^+e^-\eta'/\pi^+\pi^-$
36.2 ± 2.8 ± 3.0	11k	DEL-AMO-SA...11M	BABR	$\gamma\gamma \rightarrow K^+K^-\pi^+\pi^-$
35.1 ± 3.1 <sup>+1.0</sup> <sub>-1.6</sub>	920	<sup>7</sup> VINOKUROVA	11 BELL	$B^\pm \rightarrow K^\pm(K_S^0 K^\pm\pi^\mp)$
31.7 ± 1.2 ± 0.8	14k	<sup>8</sup> LEES	10 BABR	$10.6 e^+e^- \rightarrow e^+e^-K_S^0 K^\pm\pi^\mp$

- <sup>1</sup>AAIJ 17AD report  $m_{J/\psi} - m_{\eta_c(1S)} = 110.2 \pm 0.5 \pm 0.9$  MeV. We use the current value  $m_{J/\psi} = 3096.900 \pm 0.006$  MeV to obtain the quoted mass.
- <sup>2</sup>From a fit of the  $\phi\phi$  invariant mass with the mass and width of  $\eta_c(1S)$  as free parameters.
- <sup>3</sup>AAIJ 15BI reports  $m_{J/\psi} - m_{\eta_c(1S)} = 114.7 \pm 1.5 \pm 0.1$  MeV from a sample of  $\eta_c(1S)$  and  $J/\psi$  produced in  $b$ -hadron decays. We have used current value of  $m_{J/\psi} = 3096.900 \pm 0.006$  MeV to arrive at the quoted  $m_{\eta_c(1S)}$  result.
- <sup>4</sup>Taking into account an asymmetric photon lineshape.
- <sup>5</sup>With floating width.
- <sup>6</sup>Ignoring possible interference with the non-resonant  $0^-$  amplitude.
- <sup>7</sup>Using both,  $\eta \rightarrow \gamma\gamma$  and  $\eta \rightarrow \pi^+\pi^-\pi^0$  decays.
- <sup>8</sup>From a simultaneous fit to six decay modes of the  $\eta_c$ .
- <sup>9</sup>Accounts for interference with non-resonant continuum.
- <sup>10</sup>Taking into account interference with the non-resonant  $J^P = 0^-$  amplitude.
- <sup>11</sup>From a fit of the  $J/\psi$  recoil mass spectrum. Supersedes ABE,K 02 and ABE 04g.
- <sup>12</sup>Using mass of  $\psi(2S) = 3686.00$  MeV.
- <sup>13</sup>Not independent from the measurements reported by LEES 10.
- <sup>14</sup>MITCHELL 09 observes a significant asymmetry in the lineshapes of  $\psi(2S) \rightarrow \gamma\eta_c$  and  $J/\psi \rightarrow \gamma\eta_c$  transitions. If ignored, this asymmetry could lead to significant bias whenever the mass and width are measured in  $\psi(2S)$  or  $J/\psi$  radiative decays.
- <sup>15</sup>From the fit of the kaon momentum spectrum. Systematic errors not evaluated.
- <sup>16</sup>Superseded by LEES 10.
- <sup>17</sup>From a simultaneous fit of five decay modes of the  $\eta_c$ .
- <sup>18</sup>Superseded by VINOKUROVA 11.
- <sup>19</sup>Weighted average of the  $\psi(2S)$  and  $J/\psi(1S)$  samples. Using an  $\eta_c$  width of 13.2 MeV.
- <sup>20</sup>Average of several decay modes. Using an  $\eta_c$  width of 13.2 MeV.
- <sup>21</sup>Superseded by ASNER 04.
- <sup>22</sup>Average of several decay modes.
- <sup>23</sup> $\eta_c \rightarrow \phi\phi$ .
- <sup>24</sup>Mass adjusted by us to correspond to  $J/\psi(1S)$  mass = 3097 MeV.

- |   |      |               |           |  |
|---|------|---------------|-----------|--|
| 36.3 ± 3.7 <sup>+4.4</sup> <sub>-3.6</sub>  | 0.9k | AUBERT        | 08AB BABR | $B \rightarrow \eta_c(1S) K^{(*)} \rightarrow K\bar{K}\pi K^{(*)}$ |
| 28.1 ± 3.2 ± 2.2                            | 7.5k | UEHARA        | 08 BELL   | $\gamma\gamma \rightarrow \eta_c \rightarrow$ hadrons              |
| 48 ± 8 ± 5                                  | 195  | WU            | 06 BELL   | $B^+ \rightarrow \rho\bar{p}K^+$                                   |
| 40 ± 19 ± 5                                 | 20   | WU            | 06 BELL   | $B^+ \rightarrow \Lambda\bar{\Lambda}K^+$                          |
| 24.8 ± 3.4 ± 3.5                            | 592  | ASNER         | 04 CLEO   | $\gamma\gamma \rightarrow \eta_c \rightarrow K_S^0 K^\pm\pi^\mp$   |
| 20.4 ± 7.7 <sup>+2.0</sup> <sub>-6.7</sub>  | 190  | AMBROGIANI    | 03 E835   | $\bar{p}p \rightarrow \eta_c \rightarrow \gamma\gamma$             |
| 23.9 ± 12.6 <sup>+7.1</sup> <sub>-7.1</sub> |      | ARMSTRONG 95F | E760      | $\bar{p}p \rightarrow \gamma\gamma$                                |
- We do not use the following data for averages, fits, limits, etc. •••
- |   |      |                               |          |   |
|---|------|-------------------------------|----------|---|
| 32.1 ± 1.1 ± 1.3                            | 12k  | <sup>9</sup> DEL-AMO-SA...11M | BABR     | $\gamma\gamma \rightarrow K_S^0 K^\pm\pi^\mp$                             |
| 34.3 ± 2.3 ± 0.9                            | 2.5k | <sup>10</sup> AUBERT          | 04D BABR | $\gamma\gamma \rightarrow \eta_c(1S) \rightarrow K\bar{K}\pi$             |
| 17.0 ± 3.7 ± 7.4                            |      | <sup>11</sup> BAI             | 03 BES   | $J/\psi \rightarrow \gamma\eta_c$   |
| 29 ± 8 ± 6                                  | 180  | <sup>12</sup> FANG            | 03 BELL  | $B \rightarrow \eta_c K$  |
| 11.0 ± 8.1 ± 4.1                            |      | <sup>13</sup> BAI             | 00F BES  | $J/\psi \rightarrow \gamma\eta_c$ and $\psi(2S) \rightarrow \gamma\eta_c$ |
| 27.0 ± 5.8 ± 1.4                            |      | <sup>14</sup> BRANDENB...     | 00B CLE2 | $\gamma\gamma \rightarrow \eta_c \rightarrow K^\pm K_S^0\pi^\mp$          |
| 7.0 ± 7.5 <sup>+7.0</sup> <sub>-7.0</sub>   | 12   | BAGLIN                        | 87B SPEC | $\bar{p}p \rightarrow \gamma\gamma$                                       |
| 10.1 ± 33.0 <sup>+8.2</sup> <sub>-8.2</sub> | 23   | <sup>15</sup> BALTRUSAIT..86  | MRK3     | $J/\psi \rightarrow \gamma\rho\bar{\rho}$                                 |
| 11.5 ± 4.5                                  |      | GAISER                        | 86 CBAL  | $J/\psi \rightarrow \gamma X, \psi(2S) \rightarrow \gamma X$              |
| < 40 90% CL                                 | 18   | HIMEL                         | 80B MRK2 | $e^+e^- \rightarrow \dots$  |
| < 20 90% CL                                 |      | PARTRIDGE                     | 80B CBAL | $e^+e^- \rightarrow \dots$  |
- <sup>1</sup>From a fit of the  $\phi\phi$  invariant mass with the mass and width of  $\eta_c(1S)$  as free parameters.
  - <sup>2</sup>Taking into account an asymmetric photon lineshape.
  - <sup>3</sup>With floating mass.
  - <sup>4</sup>Ignoring possible interference with the non-resonant  $0^-$  amplitude.
  - <sup>5</sup>Using both,  $\eta \rightarrow \gamma\gamma$  and  $\eta \rightarrow \pi^+\pi^-\pi^0$  decays.
  - <sup>6</sup>From a simultaneous fit to six decay modes of the  $\eta_c$ .
  - <sup>7</sup>Accounts for interference with non-resonant continuum.
  - <sup>8</sup>Taking into account interference with the non-resonant  $J^P = 0^-$  amplitude.
  - <sup>9</sup>Not independent from the measurements reported by LEES 10.
  - <sup>10</sup>Superseded by LEES 10.
  - <sup>11</sup>From a simultaneous fit of five decay modes of the  $\eta_c$ .
  - <sup>12</sup>Superseded by VINOKUROVA 11.
  - <sup>13</sup>From a fit to the 4-prong invariant mass in  $\psi(2S) \rightarrow \gamma\eta_c$  and  $J/\psi(1S) \rightarrow \gamma\eta_c$  decays.
  - <sup>14</sup>Superseded by ASNER 04.
  - <sup>15</sup>Positive and negative errors correspond to 90% confidence level.

WEIGHTED AVERAGE  
2983.9±0.5 (Error scaled by 1.3)



$\eta_c(1S)$  WIDTH

VALUE (MeV)	EVTS	DOCUMENT ID	TECN	COMMENT
<b>32.0 ± 0.7 OUR FIT</b>				
<b>32.1 ± 0.8 OUR AVERAGE</b>				Error includes scale factor of 1.1.
33.8 ± 1.6 ± 4.1	1705	ABLIKIM 19AV	BES3	$J/\psi \rightarrow \gamma\omega\omega$
30.8 ± 2.3 ± 2.9	2673	XU 18	BELL	$e^+e^- \rightarrow e^+e^-\eta'/\pi^+\pi^-$
34.0 ± 1.9 ± 1.3	11K	AAIJ 17AD	LHCB	$pp \rightarrow B^+X \rightarrow p\bar{p}K^+X$

$\eta_c(1S)$  DECAY MODES

Mode	Fraction ( $\Gamma_i/\Gamma$ )	Confidence level
<b>Decays involving hadronic resonances</b>		
$\Gamma_1$ $\eta'(958)\pi\pi$	( 4.1 ± 1.7 ) %	
$\Gamma_2$ $\rho\rho$	( 1.8 ± 0.5 ) %	
$\Gamma_3$ $K^*(892)^0 K^-\pi^+ + c.c.$	( 2.0 ± 0.7 ) %	
$\Gamma_4$ $K^*(892)^0 \bar{K}^*(892)$	( 7.0 ± 1.3 ) × 10 <sup>-3</sup>	
$\Gamma_5$ $K^*(892)^0 \bar{K}^*(892)^0 \pi^+\pi^-$	( 1.1 ± 0.5 ) %	
$\Gamma_6$ $\phi K^+ K^-$	( 2.9 ± 1.4 ) × 10 <sup>-3</sup>	
$\Gamma_7$ $\phi\phi$	( 1.77 ± 0.19 ) × 10 <sup>-3</sup>	
$\Gamma_8$ $\phi 2(\pi^+\pi^-)$	< 4 × 10 <sup>-3</sup>	90%
$\Gamma_9$ $a_0(980)\pi$	< 2 %	90%
$\Gamma_{10}$ $a_2(1320)\pi$	< 2 %	90%
$\Gamma_{11}$ $K^*(892)\bar{K} + c.c.$	< 1.28 %	90%
$\Gamma_{12}$ $f_2(1270)\eta$	< 1.1 %	90%
$\Gamma_{13}$ $\omega\omega$	( 2.9 ± 0.8 ) × 10 <sup>-3</sup>	
$\Gamma_{14}$ $\omega\phi$	< 2.5 × 10 <sup>-4</sup>	90%
$\Gamma_{15}$ $f_2(1270)f_2(1270)$	( 9.8 ± 2.5 ) × 10 <sup>-3</sup>	
$\Gamma_{16}$ $f_2(1270)f_2'(1525)$	( 9.7 ± 3.2 ) × 10 <sup>-3</sup>	
$\Gamma_{17}$ $f_0(980)\eta$	seen	
$\Gamma_{18}$ $f_0(1500)\eta$	seen	
$\Gamma_{19}$ $f_0(2200)\eta$	seen	

# Meson Particle Listings

## $\eta_c(1S)$

$\Gamma_{20}$	$a_0(980)\pi$	seen
$\Gamma_{21}$	$a_0(1320)\pi$	seen
$\Gamma_{22}$	$a_0(1450)\pi$	seen
$\Gamma_{23}$	$a_0(1950)\pi$	seen
$\Gamma_{24}$	$K_0^*(1430)\bar{K}$	seen
$\Gamma_{25}$	$K_2^*(1430)\bar{K}$	seen
$\Gamma_{26}$	$K_0^*(1950)\bar{K}$	seen

### Decays into stable hadrons

$\Gamma_{27}$	$K\bar{K}\pi$	( 7.3 ± 0.4 ) %	
$\Gamma_{28}$	$K\bar{K}\eta$	( 1.36 ± 0.15 ) %	
$\Gamma_{29}$	$\eta\pi^+\pi^-$	( 1.7 ± 0.5 ) %	
$\Gamma_{30}$	$\eta 2(\pi^+\pi^-)$	( 4.4 ± 1.3 ) %	
$\Gamma_{31}$	$K^+K^-\pi^+\pi^-$	( 6.9 ± 1.0 ) × 10 <sup>-3</sup>	
$\Gamma_{32}$	$K^+K^-\pi^+\pi^-\pi^0$	( 3.5 ± 0.6 ) %	
$\Gamma_{33}$	$K^0K^-\pi^+\pi^-\pi^0 + c.c.$	( 5.6 ± 1.5 ) %	
$\Gamma_{34}$	$K^+K^-2(\pi^+\pi^-)$	( 7.5 ± 2.4 ) × 10 <sup>-3</sup>	
$\Gamma_{35}$	$2(K^+K^-)$	( 1.46 ± 0.30 ) × 10 <sup>-3</sup>	
$\Gamma_{36}$	$\pi^+\pi^-\pi^0$	< 5 × 10 <sup>-4</sup>	90%
$\Gamma_{37}$	$\pi^+\pi^-\pi^0\pi^0$	( 4.7 ± 1.0 ) %	
$\Gamma_{38}$	$2(\pi^+\pi^-)$	( 9.7 ± 1.2 ) × 10 <sup>-3</sup>	
$\Gamma_{39}$	$2(\pi^+\pi^-\pi^0)$	( 16.1 ± 2.0 ) %	
$\Gamma_{40}$	$3(\pi^+\pi^-)$	( 1.8 ± 0.4 ) %	
$\Gamma_{41}$	$\rho\bar{\rho}$	( 1.45 ± 0.14 ) × 10 <sup>-3</sup>	
$\Gamma_{42}$	$\rho\bar{\rho}\pi^0$	( 3.6 ± 1.3 ) × 10 <sup>-3</sup>	
$\Gamma_{43}$	$\Lambda\bar{\Lambda}$	( 1.07 ± 0.24 ) × 10 <sup>-3</sup>	
$\Gamma_{44}$	$K^+\bar{p}\Lambda + c.c.$	( 2.6 ± 0.4 ) × 10 <sup>-3</sup>	
$\Gamma_{45}$	$\bar{\Lambda}(1520)\Lambda + c.c.$	( 3.1 ± 1.4 ) × 10 <sup>-3</sup>	
$\Gamma_{46}$	$\Sigma^+\Sigma^-$	( 2.1 ± 0.6 ) × 10 <sup>-3</sup>	
$\Gamma_{47}$	$\Xi^-\Xi^+$	( 9.0 ± 2.6 ) × 10 <sup>-4</sup>	
$\Gamma_{48}$	$\pi^+\pi^-\rho\bar{\rho}$	( 5.3 ± 1.8 ) × 10 <sup>-3</sup>	

### Radiative decays

$\Gamma_{49}$	$\gamma\gamma$	( 1.58 ± 0.11 ) × 10 <sup>-4</sup>
---------------	----------------	------------------------------------

### Charge conjugation (C), Parity (P), Lepton family number (LF) violating modes

$\Gamma_{50}$	$\pi^+\pi^-$	$P, CP < 1.1$	× 10 <sup>-4</sup>	90%
$\Gamma_{51}$	$\pi^0\pi^0$	$P, CP < 4$	× 10 <sup>-5</sup>	90%
$\Gamma_{52}$	$K^+K^-$	$P, CP < 6$	× 10 <sup>-4</sup>	90%
$\Gamma_{53}$	$K_S^0K_S^0$	$P, CP < 3.1$	× 10 <sup>-4</sup>	90%

### CONSTRAINED FIT INFORMATION

An overall fit to the total width, 8 combinations of partial widths obtained from integrated cross section, and 19 branching ratios uses 93 measurements and one constraint to determine 13 parameters. The overall fit has a  $\chi^2 = 121.6$  for 81 degrees of freedom.

The following *off-diagonal* array elements are the correlation coefficients  $\langle \delta p_i \delta p_j \rangle / (\delta p_i \delta p_j)$ , in percent, from the fit to parameters  $p_i$ , including the branching fractions,  $x_i \equiv \Gamma_i / \Gamma_{total}$ . The fit constrains the  $x_i$  whose labels appear in this array to sum to one.

$x_7$	15									
$x_{15}$	3	5								
$x_{27}$	17	33	6							
$x_{28}$	7	15	3	45						
$x_{31}$	9	17	3	19	9					
$x_{35}$	7	12	2	20	9	8				
$x_{38}$	11	21	4	24	11	13	9			
$x_{41}$	10	19	3	25	11	11	9	14		
$x_{43}$	2	4	1	6	3	3	2	3	23	
$x_{49}$	-26	-49	-9	-56	-25	-30	-22	-37	-36	-8
$\Gamma$	-1	-2	0	-3	-1	-2	-1	-2	6	1
	$x_4$	$x_7$	$x_{15}$	$x_{27}$	$x_{28}$	$x_{31}$	$x_{35}$	$x_{38}$	$x_{41}$	$x_{43}$
$\Gamma$	-29									
	$x_{49}$									

Mode	Rate (MeV)	
$\Gamma_4$	$K^*(892)\bar{K}^*(892)$	0.22 ± 0.04
$\Gamma_7$	$\phi\phi$	0.057 ± 0.006
$\Gamma_{15}$	$f_2(1270)f_2(1270)$	0.31 ± 0.08
$\Gamma_{27}$	$K\bar{K}\pi$	2.33 ± 0.13
$\Gamma_{28}$	$K\bar{K}\eta$	0.43 ± 0.05

$\Gamma_{31}$	$K^+K^-\pi^+\pi^-$	0.220 ± 0.034
$\Gamma_{35}$	$2(K^+K^-)$	0.047 ± 0.010
$\Gamma_{38}$	$2(\pi^+\pi^-)$	0.31 ± 0.04
$\Gamma_{41}$	$\rho\bar{\rho}$	0.046 ± 0.005
$\Gamma_{43}$	$\Lambda\bar{\Lambda}$	0.034 ± 0.008
$\Gamma_{49}$	$\gamma\gamma$	0.00506 ± 0.00034

### $\eta_c(1S)$ PARTIAL WIDTHS

$\Gamma(\gamma\gamma)$	VALUE (keV)	EVTS	DOCUMENT ID	TECN	COMMENT	$\Gamma_{49}$
<b>5.06 ± 0.34 OUR FIT</b>						
• • • We do not use the following data for averages, fits, limits, etc. • • •						
5.8 ± 1.1		486	<sup>1</sup> ZHANG	12A	BELL $e^+e^- \rightarrow e^+e^-\eta'/\pi^+\pi^-$	
5.2 ± 1.2		273 ± 43	<sup>2,3</sup> AUBERT	06E	BABR $B^{\pm} \rightarrow K^{\pm}X_c\bar{c}$	
5.5 ± 1.2 ± 1.8		57 ± 33	<sup>4</sup> KUO	05	BELL $\gamma\gamma \rightarrow \rho\bar{\rho}$	
7.4 ± 0.4 ± 2.3			<sup>5</sup> ASNER	04	CLEO $\gamma\gamma \rightarrow \eta_c \rightarrow K_S^0 K^{\pm}\pi^{\mp}$	
13.9 ± 2.0 ± 3.0		41	<sup>6</sup> ABDALLAH	03J	DLPH $\gamma\gamma \rightarrow \eta_c$	
3.8 ± 1.1 + 1.9 - 1.0 - 1.0		190	<sup>7</sup> AMBROGIANI	03	E835 $\bar{p}p \rightarrow \eta_c \rightarrow \gamma\gamma$	
7.6 ± 0.8 ± 2.3			<sup>5,8</sup> BRANDENB...	00B	CLE2 $\gamma\gamma \rightarrow \eta_c \rightarrow K^{\pm}K_S^0\pi^{\mp}$	
6.9 ± 1.7 ± 2.1		76	<sup>9</sup> ACCIARRI	99T	L3 $e^+e^- \rightarrow e^+e^-\eta_c$	
27 ± 16 ± 10		5	<sup>5</sup> SHIRAI	98	AMY $58 e^+e^-$	
6.7 ± 2.4 ± 2.3			<sup>4</sup> ARMSTRONG	95F	E760 $\bar{p}p \rightarrow \gamma\gamma$	
11.3 ± 4.2			<sup>10</sup> ALBRECHT	94H	ARG $e^+e^- \rightarrow e^+e^-\eta_c$	
8.0 ± 2.3 ± 2.4		17	<sup>11</sup> ADRIANI	93N	L3 $e^+e^- \rightarrow e^+e^-\eta_c$	
5.9 ± 2.1 ± 1.9			<sup>7</sup> CHEN	90B	CLEO $e^+e^- \rightarrow e^+e^-\eta_c$	
6.4 ± 5.0 - 3.4			<sup>12</sup> AIHARA	88D	TPC $e^+e^- \rightarrow e^+e^-X$	
4.3 ± 3.4 ± 2.4			<sup>4</sup> BAGLIN	87B	SPEC $\bar{p}p \rightarrow \gamma\gamma$	
28 ± 15			<sup>5,13</sup> BERGER	86	PLUT $\gamma\gamma \rightarrow K\bar{K}\pi$	

- Assuming there is no interference with the non-resonant background.
- Calculated by us using  $\Gamma(\eta_c \rightarrow K\bar{K}\pi) \times \Gamma(\eta_c \rightarrow \gamma\gamma) / \Gamma = 0.44 \pm 0.05$  keV from PDG 06 and  $B(\eta_c \rightarrow K\bar{K}\pi) = (8.5 \pm 1.8)\%$  from AUBERT 06E.
- Systematic errors not evaluated.
- Normalized to  $B(\eta_c \rightarrow \rho\bar{\rho}) = (1.3 \pm 0.4) \times 10^{-3}$ .
- Normalized to  $B(\eta_c \rightarrow K^{\pm}K_S^0\pi^{\mp})$ .
- Average of  $K_S^0 K^{\pm}\pi^{\mp}$ ,  $\pi^+\pi^-K^+K^-$ , and  $2(K^+K^-)$  decay modes.
- Normalized to the sum of  $B(\eta_c \rightarrow K^{\pm}K_S^0\pi^{\mp})$ ,  $B(\eta_c \rightarrow K^+K^-\pi^+\pi^-)$ , and  $B(\eta_c \rightarrow 2\pi^+2\pi^-)$ .
- Superseded by ASNER 04.
- Normalized to the sum of 9 branching ratios.
- Normalized to the sum of  $B(\eta_c \rightarrow K^{\pm}K_S^0\pi^{\mp})$ ,  $B(\eta_c \rightarrow \phi\phi)$ ,  $B(\eta_c \rightarrow K^+K^-\pi^+\pi^-)$ , and  $B(\eta_c \rightarrow 2\pi^+2\pi^-)$ .
- Superseded by ACCIARRI 99T.
- Normalized to the sum of  $B(\eta_c \rightarrow K^{\pm}K_S^0\pi^{\mp})$ ,  $B(\eta_c \rightarrow 2K^+2K^-)$ ,  $B(\eta_c \rightarrow K^+K^-\pi^+\pi^-)$ , and  $B(\eta_c \rightarrow 2\pi^+2\pi^-)$ .
- Re-evaluated by AIHARA 88D.

### $\eta_c(1S) \Gamma(i)\Gamma(\gamma\gamma)/\Gamma(total)$

$\Gamma(\eta'(958)\pi\pi) \times \Gamma(\gamma\gamma)/\Gamma_{total}$	VALUE (eV)	EVTS	DOCUMENT ID	TECN	COMMENT	$\Gamma_1\Gamma_{49}/\Gamma$
<b>98.1 ± 3.9 ± 11.7</b>		2673	XU	18	BELL $e^+e^- \rightarrow e^+e^-\eta'/\pi^+\pi^-$	
• • • We do not use the following data for averages, fits, limits, etc. • • •						
75.8 ± 6.3 ± 8.4		486	<sup>1</sup> ZHANG	12A	BELL $e^+e^- \rightarrow e^+e^-\eta'/\pi^+\pi^-$	
<sup>1</sup> Superseded by XU 18.						

$\Gamma(\rho\rho) \times \Gamma(\gamma\gamma)/\Gamma_{total}$	VALUE (eV)	CL%	EVTS	DOCUMENT ID	TECN	COMMENT	$\Gamma_2\Gamma_{49}/\Gamma$
<b>36 ± 6 OUR FIT</b>							
<b>32.4 ± 4.2 ± 5.8</b>			882 ± 115	UEHARA	08	BELL $\gamma\gamma \rightarrow \pi^+\pi^-K^+K^-$	
• • • We do not use the following data for averages, fits, limits, etc. • • •							
< 39		90	< 1556	UEHARA	08	BELL $\gamma\gamma \rightarrow 2(\pi^+\pi^-)$	

$\Gamma(K^*(892)\bar{K}^*(892)) \times \Gamma(\gamma\gamma)/\Gamma_{total}$	VALUE (eV)	EVTS	DOCUMENT ID	TECN	COMMENT	$\Gamma_4\Gamma_{49}/\Gamma$
<b>36 ± 6 OUR FIT</b>						
<b>32.4 ± 4.2 ± 5.8</b>		882 ± 115	UEHARA	08	BELL $\gamma\gamma \rightarrow \pi^+\pi^-K^+K^-$	

$\Gamma(\phi\phi) \times \Gamma(\gamma\gamma)/\Gamma_{total}$	VALUE (eV)	EVTS	DOCUMENT ID	TECN	COMMENT	$\Gamma_7\Gamma_{49}/\Gamma$
<b>9.0 ± 0.8 OUR FIT</b>						
<b>7.5 ± 0.66 ± 0.62</b>		386 ± 31	<sup>1</sup> LIU	12B	BELL $\gamma\gamma \rightarrow 2(K^+K^-)$	
• • • We do not use the following data for averages, fits, limits, etc. • • •						
6.8 ± 1.2 ± 1.3		132 ± 23	UEHARA	08	BELL $\gamma\gamma \rightarrow 2(K^+K^-)$	
<sup>1</sup> Supersedes UEHARA 08. Using $B(\phi \rightarrow K^+K^-) = (48.9 \pm 0.5)\%$ .						

$\Gamma(\omega) \times \Gamma(\gamma\gamma)/\Gamma_{total}$		$\Gamma_{13}\Gamma_{49}/\Gamma$		
VALUE (eV)	EVTS	DOCUMENT ID	TECN	COMMENT
$8.67 \pm 2.86 \pm 0.96$	$85 \pm 29$	<sup>1</sup> LIU	12B BELL	$\gamma\gamma \rightarrow 2(\pi^+ \pi^- \pi^0)$
<sup>1</sup> Using $B(\omega \rightarrow \pi^+ \pi^- \pi^0) = (89.2 \pm 0.7)\%$ .				

$\Gamma(\omega\phi) \times \Gamma(\gamma\gamma)/\Gamma_{total}$		$\Gamma_{14}\Gamma_{49}/\Gamma$		
VALUE (eV)	CL%	DOCUMENT ID	TECN	COMMENT
••• We do not use the following data for averages, fits, limits, etc. •••				
<0.49	90	<sup>1</sup> LIU	12B BELL	$\gamma\gamma \rightarrow K^+ K^- \pi^+ \pi^- \pi^0$
<sup>1</sup> Using $B(\phi \rightarrow K^+ K^-) = (48.9 \pm 0.5)\%$ and $B(\omega \rightarrow \pi^+ \pi^- \pi^0) = (89.2 \pm 0.7)\%$ .				

$\Gamma(f_2(1270) f_2'(1270)) \times \Gamma(\gamma\gamma)/\Gamma_{total}$		$\Gamma_{15}\Gamma_{49}/\Gamma$		
VALUE (eV)	EVTS	DOCUMENT ID	TECN	COMMENT
<b>50 ± 13 OUR FIT</b>				
$69 \pm 17 \pm 12$	$3182 \pm 766$	UEHARA	08 BELL	$\gamma\gamma \rightarrow 2(\pi^+ \pi^-)$

$\Gamma(f_2(1270) f_2'(1525)) \times \Gamma(\gamma\gamma)/\Gamma_{total}$		$\Gamma_{16}\Gamma_{49}/\Gamma$		
VALUE (eV)	EVTS	DOCUMENT ID	TECN	COMMENT
$49 \pm 9 \pm 13$	$1128 \pm 206$	UEHARA	08 BELL	$\gamma\gamma \rightarrow \pi^+ \pi^- K^+ K^-$

$\Gamma(K\bar{K}\pi) \times \Gamma(\gamma\gamma)/\Gamma_{total}$		$\Gamma_{27}\Gamma_{49}/\Gamma$		
VALUE (keV)	CL% EVTS	DOCUMENT ID	TECN	COMMENT
<b>0.369 ± 0.020 OUR FIT</b>				
<b>0.407 ± 0.027 OUR AVERAGE</b> Error includes scale factor of 1.2.				
$0.374 \pm 0.009 \pm 0.031$	14k	<sup>1</sup> LEES	10 BABR	$10.6 e^+ e^- \rightarrow e^+ e^- K_S^0 K_{S\pi}^{\pm\mp}$
$0.407 \pm 0.022 \pm 0.028$		<sup>2,3</sup> ASNER	04 CLEO	$\gamma\gamma \rightarrow \eta_C \rightarrow K_S^0 K_{S\pi}^{\pm\mp}$
$0.60 \pm 0.12 \pm 0.09$	41	<sup>3,4</sup> ABDALLAH	03J DLPH	$\gamma\gamma \rightarrow K_S^0 K_{S\pi}^{\pm\mp}$
$1.47 \pm 0.87 \pm 0.27$		<sup>3</sup> SHIRAI	98 AMY	$\gamma\gamma \rightarrow \eta_C \rightarrow K_{S\pi}^{\pm\mp}$
$0.84 \pm 0.21$		<sup>3</sup> ALBRECHT	94H ARG	$\gamma\gamma \rightarrow K_{S\pi}^{\pm\mp}$
$0.60 \pm 0.23 \pm 0.20$		<sup>3</sup> CHEN	90B CLEO	$\gamma\gamma \rightarrow \eta_C K_{S\pi}^{\pm\mp}$
$1.06 \pm 0.41 \pm 0.27$	11	<sup>3</sup> BRAUNSCH...	89 TASS	$\gamma\gamma \rightarrow K\bar{K}\pi$
$1.5 \pm 0.60 \pm 0.3$	7	<sup>3</sup> BERGER	86 PLUT	$\gamma\gamma \rightarrow K\bar{K}\pi$

••• We do not use the following data for averages, fits, limits, etc. •••

$0.386 \pm 0.008 \pm 0.021$  12k <sup>5</sup> DEL-AMO-SA...11M BABR  $\gamma\gamma \rightarrow K_S^0 K_{S\pi}^{\pm\mp}$

$0.418 \pm 0.044 \pm 0.022$  <sup>3,6</sup> BRANDENB... 00B CLE2  $\gamma\gamma \rightarrow \eta_C \rightarrow K_{S\pi}^{\pm\mp}$

<0.63 95 <sup>3</sup> BEHREND 89 CELL  $\gamma\gamma \rightarrow K_S^0 K_{S\pi}^{\pm\mp}$

<4.4 95 ALTHOFF 85B TASS  $\gamma\gamma \rightarrow K\bar{K}\pi$

<sup>1</sup> From the corrected and unfolded mass spectrum.

<sup>2</sup> Calculated by us from the value reported in ASNER 04 that assumes  $B(\eta_C \rightarrow K\bar{K}\pi) = 5.5 \pm 1.7\%$ .

<sup>3</sup> We have multiplied  $K_{S\pi}^{\pm\mp}$  measurement by 3 to obtain  $K\bar{K}\pi$ .

<sup>4</sup> Calculated by us from the value reported in ABDALLAH 03J, which uses  $B(\eta_C \rightarrow K_S^0 K_{S\pi}^{\pm\mp}) = (1.5 \pm 0.4)\%$ .

<sup>5</sup> Not independent from the measurements reported by LEES 10.

<sup>6</sup> Superseded by ASNER 04.

$\Gamma(K^+ K^- \pi^+ \pi^-) \times \Gamma(\gamma\gamma)/\Gamma_{total}$		$\Gamma_{31}\Gamma_{49}/\Gamma$		
VALUE (eV)	EVTS	DOCUMENT ID	TECN	COMMENT
<b>35 ± 5 OUR FIT</b>				
<b>27 ± 6 OUR AVERAGE</b>				
$25.7 \pm 3.2 \pm 4.9$	$2019 \pm 248$	UEHARA	08 BELL	$\gamma\gamma \rightarrow \pi^+ \pi^- K^+ K^-$
$280 \pm 100 \pm 60$	42	<sup>1</sup> ABDALLAH	03J DLPH	$\gamma\gamma \rightarrow \pi^+ \pi^- K^+ K^-$
$170 \pm 80 \pm 20$	$13.9 \pm 6.6$	ALBRECHT	94H ARG	$\gamma\gamma \rightarrow \pi^+ \pi^- K^+ K^-$
<sup>1</sup> Calculated by us from the value reported in ABDALLAH 03J, which uses $B(\eta_C \rightarrow \pi^+ \pi^- K^+ K^-) = (2.0 \pm 0.7)\%$ .				

$\Gamma(K^+ K^- \pi^+ \pi^- \pi^0) \times \Gamma(\gamma\gamma)/\Gamma_{total}$		$\Gamma_{32}\Gamma_{49}/\Gamma$		
VALUE (keV)	EVTS	DOCUMENT ID	TECN	COMMENT
••• We do not use the following data for averages, fits, limits, etc. •••				
$0.190 \pm 0.006 \pm 0.028$	11k	<sup>1</sup> DEL-AMO-SA...11M BABR	$\gamma\gamma \rightarrow K^+ K^- \pi^+ \pi^- \pi^0$	
<sup>1</sup> Not independent from other measurements reported in DEL-AMO-SANCHEZ 11M.				

$\Gamma(2(K^+ K^-)) \times \Gamma(\gamma\gamma)/\Gamma_{total}$		$\Gamma_{35}\Gamma_{49}/\Gamma$		
VALUE (eV)	EVTS	DOCUMENT ID	TECN	COMMENT
<b>7.4 ± 1.5 OUR FIT</b>				
<b>5.8 ± 1.9 OUR AVERAGE</b>				
$5.6 \pm 1.1 \pm 1.6$	$216 \pm 42$	UEHARA	08 BELL	$\gamma\gamma \rightarrow 2(K^+ K^-)$
$350 \pm 90 \pm 60$	46	<sup>1</sup> ABDALLAH	03J DLPH	$\gamma\gamma \rightarrow 2(K^+ K^-)$
$231 \pm 90 \pm 23$	$9.1 \pm 3.3$	<sup>2</sup> ALBRECHT	94H ARG	$\gamma\gamma \rightarrow 2(K^+ K^-)$
<sup>1</sup> Calculated by us from the value reported in ABDALLAH 03J, which uses $B(\eta_C \rightarrow 2(K^+ K^-)) = (2.1 \pm 1.2)\%$ .				
<sup>2</sup> Includes all topological modes except $\eta_C \rightarrow \phi\phi$ .				

$\Gamma(2(\pi^+ \pi^-)) \times \Gamma(\gamma\gamma)/\Gamma_{total}$		$\Gamma_{38}\Gamma_{49}/\Gamma$		
VALUE (eV)	EVTS	DOCUMENT ID	TECN	COMMENT
<b>49 ± 6 OUR FIT</b>				
<b>42 ± 6 OUR AVERAGE</b>				
$40.7 \pm 3.7 \pm 5.3$	$5381 \pm 492$	UEHARA	08 BELL	$\gamma\gamma \rightarrow 2(\pi^+ \pi^-)$
$180 \pm 70 \pm 20$	$21.4 \pm 8.6$	ALBRECHT	94H ARG	$\gamma\gamma \rightarrow 2(\pi^+ \pi^-)$

$\Gamma(\rho\bar{\rho}) \times \Gamma(\gamma\gamma)/\Gamma_{total}$		$\Gamma_{41}\Gamma_{49}/\Gamma$		
VALUE (eV)	EVTS	DOCUMENT ID	TECN	COMMENT
<b>7.4 ± 0.7 OUR FIT</b>				
<b>7.20 ± 1.53 ± 0.67 ± 0.75</b> 157 ± 33 <sup>1</sup> KUO 05 BELL $\gamma\gamma \rightarrow \rho\bar{\rho}$				

••• We do not use the following data for averages, fits, limits, etc. •••

$4.6 \pm 1.3 \pm 0.4$  190 <sup>1</sup> AMBROGIANI 03 E835  $\bar{p}p \rightarrow \gamma\gamma$

$8.1 \pm 2.9 \pm 2.0$  <sup>1</sup> ARMSTRONG 95F E760  $\bar{p}p \rightarrow \gamma\gamma$

<sup>1</sup> Not independent from the  $\Gamma_{\gamma\gamma}$  reported by the same experiment.

$\Gamma(K_S^0 K_S^0) \times \Gamma(\gamma\gamma)/\Gamma_{total}$		$\Gamma_{53}\Gamma_{49}/\Gamma$		
VALUE (eV)	CL%	DOCUMENT ID	TECN	COMMENT
<b>&lt;1.6</b> 90 <sup>1</sup> UEHARA 13 BELL $\gamma\gamma \rightarrow K_S^0 K_S^0$				
••• We do not use the following data for averages, fits, limits, etc. •••				
<0.29	90	<sup>2</sup> UEHARA	13 BELL	$\gamma\gamma \rightarrow K_S^0 K_S^0$

<sup>1</sup> Taking into account interference with the non-resonant continuum.

<sup>2</sup> Neglecting interference with the non-resonant continuum.

$\eta_c(1S)$  BRANCHING RATIOS

HADRONIC DECAYS

$\Gamma(\eta'(958) \pi\pi)/\Gamma_{total}$		$\Gamma_1/\Gamma$		
VALUE	EVTS	DOCUMENT ID	TECN	COMMENT
<b>0.041 ± 0.017</b> 14 <sup>1</sup> BALTRUSAIT...86 MRK3 $J/\psi \rightarrow \eta_C \gamma$				
<sup>1</sup> The quoted branching ratios use $B(J/\psi(1S) \rightarrow \gamma\eta_c(1S)) = 0.0127 \pm 0.0036$ .				

$\Gamma(\rho\rho)/\Gamma_{total}$		$\Gamma_2/\Gamma$		
VALUE (units $10^{-3}$ )	CL% EVTS	DOCUMENT ID	TECN	COMMENT
<b>18 ± 5 OUR AVERAGE</b>				
$12.6 \pm 3.8 \pm 5.1$	72	<sup>1</sup> ABLIKIM	05L BES2	$J/\psi \rightarrow \pi^+ \pi^- \pi^+ \pi^-$
$26.0 \pm 2.4 \pm 8.8$	113	<sup>1</sup> BISELLO	91 DM2	$J/\psi \rightarrow \gamma\rho^0\rho^0$
$23.6 \pm 10.6 \pm 8.2$	32	<sup>1</sup> BISELLO	91 DM2	$J/\psi \rightarrow \gamma\rho^+\rho^-$
••• We do not use the following data for averages, fits, limits, etc. •••				
<14	90	<sup>1</sup> BALTRUSAIT...86 MRK3	$J/\psi \rightarrow \eta_C \gamma$	

<sup>1</sup> The quoted branching ratios use  $B(J/\psi(1S) \rightarrow \gamma\eta_c(1S)) = 0.0127 \pm 0.0036$ . Where relevant, the error in this branching ratio is treated as a common systematic in computing averages.

$\Gamma(K^*(892)^0 K^- \pi^+ + c.c.)/\Gamma_{total}$		$\Gamma_3/\Gamma$		
VALUE	EVTS	DOCUMENT ID	TECN	COMMENT
<b>0.02 ± 0.007</b> 63 <sup>1,2</sup> BALTRUSAIT...86 MRK3 $J/\psi \rightarrow \eta_C \gamma$				
<sup>1</sup> BALTRUSAIT'S 86 has an error according to Partridge.				
<sup>2</sup> The quoted branching ratios use $B(J/\psi(1S) \rightarrow \gamma\eta_c(1S)) = 0.0127 \pm 0.0036$ .				

$\Gamma(K^*(892) \bar{K}^*(892))/\Gamma_{total}$		$\Gamma_4/\Gamma$		
VALUE (units $10^{-4}$ )	EVTS	DOCUMENT ID	TECN	COMMENT
<b>70 ± 13 OUR FIT</b>				
<b>91 ± 26 OUR AVERAGE</b>				
$108 \pm 25 \pm 44$	60	<sup>1</sup> ABLIKIM	05L BES2	$J/\psi \rightarrow K^+ K^- \pi^+ \pi^- \gamma$
$82 \pm 28 \pm 27$	14	<sup>1</sup> BISELLO	91 DM2	$e^+ e^- \rightarrow \gamma K^+ K^- \pi^+ \pi^-$
$90 \pm 50$	9	<sup>1</sup> BALTRUSAIT...86 MRK3	$J/\psi \rightarrow \eta_C \gamma$	

<sup>1</sup> The quoted branching ratios use  $B(J/\psi(1S) \rightarrow \gamma\eta_c(1S)) = 0.0127 \pm 0.0036$ . Where relevant, the error in this branching ratio is treated as a common systematic in computing averages.

$\Gamma(K^*(892)^0 \bar{K}^*(892)^0 \pi^+ \pi^-)/\Gamma_{total}$		$\Gamma_5/\Gamma$		
VALUE (units $10^{-4}$ )	EVTS	DOCUMENT ID	TECN	COMMENT
<b>113 ± 47 ± 24</b> 45 <sup>1</sup> ABLIKIM 06A BES2 $J/\psi \rightarrow K^{*0} \bar{K}^{*0} \pi^+ \pi^- \gamma$				
ABLIKIM 06A reports $[\Gamma(\eta_c(1S) \rightarrow K^*(892)^0 \bar{K}^*(892)^0 \pi^+ \pi^-)/\Gamma_{total}] \times [B(J/\psi(1S) \rightarrow \gamma\eta_c(1S))] = (1.91 \pm 0.64 \pm 0.48) \times 10^{-4}$ which we divide by our best value $B(J/\psi(1S) \rightarrow \gamma\eta_c(1S)) = (1.7 \pm 0.4) \times 10^{-2}$ . Our first error is their experiment's error and our second error is the systematic error from using our best value.				

$\Gamma(\phi K^+ K^-)/\Gamma_{total}$		$\Gamma_6/\Gamma$		
VALUE (units $10^{-3}$ )	EVTS	DOCUMENT ID	TECN	COMMENT
<b>2.9 ± 0.9 ± 1.1</b> 14.1 ± 4.4 ± 3.7 <sup>1</sup> HUANG 03 BELL $B^+ \rightarrow (\phi K^+ K^-) K^+$				
<sup>1</sup> Using $B(B^+ \rightarrow \eta_C K^+) = (1.25 \pm 0.12 \pm 0.10) \times 10^{-3}$ from FANG 03 and $B(\eta_C \rightarrow K\bar{K}\pi) = (5.5 \pm 1.7) \times 10^{-2}$ .				

## Meson Particle Listings

 $\eta_c(1S)$  $\Gamma(\phi\phi)/\Gamma_{total}$   $\Gamma_7/\Gamma$ 

VALUE (units $10^{-4}$ )	EVTS	DOCUMENT ID	TECN	COMMENT
<b>17.7 ± 1.9 OUR FIT</b>				
<b>28 ± 4 OUR AVERAGE</b>				
26 $\pm \frac{4}{8} \pm 5$	1.2K	<sup>1</sup> ABLIKIM	17P BES3	$J/\psi \rightarrow K^+ K^- K^+ K^- \gamma$
25.3 ± 5.1 ± 9.1	72	<sup>2</sup> ABLIKIM	05L BES2	$J/\psi \rightarrow K^+ K^- K^+ K^- \gamma$
26 ± 9	357	<sup>2</sup> BAI	04 BES	$J/\psi \rightarrow \gamma K^+ K^- K^+ K^-$
31 ± 7 ± 10	19	<sup>2</sup> BISELLO	91 DM2	$J/\psi \rightarrow \gamma K^+ K^- K^+ K^-$
30 $\pm \frac{18}{-12} \pm 10$	5	<sup>2</sup> BISELLO	91 DM2	$J/\psi \rightarrow \gamma K^+ K^- K_S^0 K_L^0$
74 ± 18 ± 24	80	<sup>2</sup> BAI	90B MRK3	$J/\psi \rightarrow \gamma K^+ K^- K^+ K^-$
67 ± 21 ± 24		<sup>2</sup> BAI	90B MRK3	$J/\psi \rightarrow \gamma K^+ K^- K_S^0 K_L^0$

• • • We do not use the following data for averages, fits, limits, etc. • • •

<sup>1</sup> ABLIKIM 17P reports  $[\Gamma(\eta_c(1S) \rightarrow \phi\phi)/\Gamma_{total}] \times [B(J/\psi(1S) \rightarrow \gamma\eta_c(1S))] = (4.3 \pm 0.5 \pm 0.5) \times 10^{-5}$  which we divide by our best value  $B(J/\psi(1S) \rightarrow \gamma\eta_c(1S)) = (1.7 \pm 0.4) \times 10^{-2}$ . Our first error is their experiment's error and our second error is the systematic error from using our best value.

<sup>2</sup> The quoted branching ratios use  $B(J/\psi(1S) \rightarrow \gamma\eta_c(1S)) = 0.0127 \pm 0.0036$ . Where relevant, the error in this branching ratio is treated as a common systematic in computing averages.

<sup>3</sup> Using  $B(B^+ \rightarrow \eta_c K^+) = (1.25 \pm 0.12 \pm \frac{0.10}{-0.12}) \times 10^{-3}$  from FANG 03 and  $B(\eta_c \rightarrow K\bar{K}\pi) = (5.5 \pm 1.7) \times 10^{-2}$ .

 $\Gamma(\phi\phi)/\Gamma(K\bar{K}\pi)$   $\Gamma_7/\Gamma_{27}$ 

VALUE	EVTS	DOCUMENT ID	TECN	COMMENT
<b>0.0243 ± 0.0025 OUR FIT</b>				
<b>0.044 <math>\pm \frac{0.012}{-0.010}</math> OUR AVERAGE</b>				
0.055 ± 0.014 ± 0.005		AUBERT,B	04B BABR	$B^\pm \rightarrow K^\pm \eta_c$
0.032 $\pm \frac{0.014}{-0.010} \pm 0.009$	7	<sup>1</sup> HUANG	03 BELL	$B^\pm \rightarrow K^\pm \phi$

<sup>1</sup> Using  $B(B^+ \rightarrow \eta_c K^+) = (1.25 \pm 0.12 \pm \frac{0.10}{-0.12}) \times 10^{-3}$  from FANG 03 and  $B(\eta_c \rightarrow K\bar{K}\pi) = (5.5 \pm 1.7) \times 10^{-2}$ .

 $\Gamma(\phi\phi)/\Gamma(p\bar{p})$   $\Gamma_7/\Gamma_{41}$ 

VALUE	EVTS	DOCUMENT ID	TECN	COMMENT
<b>1.79 ± 0.14 ± 0.32</b>	6.4k	<sup>1</sup> AAIJ	17Bb LHCB	$pp \rightarrow b\bar{b} X \rightarrow 2(K^+ K^-) X$

<sup>1</sup> Using inputs from AAIJ 15As and AAIJ 15B1 and  $\Gamma(b \rightarrow J/\psi(1S) \text{ anything})/\Gamma_{total} = (1.16 \pm 0.10)\%$  and  $\Gamma(J/\psi(1S) \rightarrow p\bar{p})/\Gamma_{total} = (2.120 \pm 0.029) \times 10^{-3}$  from PDG 16.

 $\Gamma(\phi_2(\pi^+ \pi^-))/\Gamma_{total}$   $\Gamma_8/\Gamma$ 

VALUE (units $10^{-4}$ )	CL%	DOCUMENT ID	TECN	COMMENT
<b>&lt; 40</b>	90	<sup>1</sup> ABLIKIM	06A BES2	$J/\psi \rightarrow \phi_2(\pi^+ \pi^-) \gamma$

<sup>1</sup> ABLIKIM 06A reports  $[\Gamma(\eta_c(1S) \rightarrow \phi_2(\pi^+ \pi^-))/\Gamma_{total}] \times [B(J/\psi(1S) \rightarrow \gamma\eta_c(1S))] < 0.603 \times 10^{-4}$  which we divide by our best value  $B(J/\psi(1S) \rightarrow \gamma\eta_c(1S)) = 1.7 \times 10^{-2}$ .

 $\Gamma(a_0(980)\pi)/\Gamma_{total}$   $\Gamma_9/\Gamma$ 

VALUE	CL%	DOCUMENT ID	TECN	COMMENT
<b>&lt; 0.02</b>	90	<sup>1,2</sup> BALTRUSAIT..86	MRK3	$J/\psi \rightarrow \eta_c \gamma$

<sup>1</sup> The quoted branching ratios use  $B(J/\psi(1S) \rightarrow \gamma\eta_c(1S)) = 0.0127 \pm 0.0036$ .

<sup>2</sup> We are assuming  $B(a_0(980) \rightarrow \eta\pi) > 0.5$ .

 $\Gamma(a_2(1320)\pi)/\Gamma_{total}$   $\Gamma_{10}/\Gamma$ 

VALUE	CL%	DOCUMENT ID	TECN	COMMENT
<b>&lt; 0.02</b>	90	<sup>1</sup> BALTRUSAIT..86	MRK3	$J/\psi \rightarrow \eta_c \gamma$

<sup>1</sup> The quoted branching ratios use  $B(J/\psi(1S) \rightarrow \gamma\eta_c(1S)) = 0.0127 \pm 0.0036$ .

 $\Gamma(K^*(892)\bar{K} + c.c.)/\Gamma_{total}$   $\Gamma_{11}/\Gamma$ 

VALUE	CL%	DOCUMENT ID	TECN	COMMENT
<b>&lt; 0.0128</b>	90	<sup>1</sup> BISELLO	91 DM2	$J/\psi \rightarrow \gamma K_S^0 K^\pm \pi^\mp$
< 0.0132	90	<sup>1</sup> BISELLO	91 DM2	$J/\psi \rightarrow \gamma K^+ K^- \pi^0$

<sup>1</sup> The quoted branching ratios use  $B(J/\psi(1S) \rightarrow \gamma\eta_c(1S)) = 0.0127 \pm 0.0036$ .

 $\Gamma(f_2(1270)\eta)/\Gamma_{total}$   $\Gamma_{12}/\Gamma$ 

VALUE	CL%	DOCUMENT ID	TECN	COMMENT
<b>&lt; 0.011</b>	90	<sup>1</sup> BALTRUSAIT..86	MRK3	$J/\psi \rightarrow \eta_c \gamma$

<sup>1</sup> The quoted branching ratios use  $B(J/\psi(1S) \rightarrow \gamma\eta_c(1S)) = 0.0127 \pm 0.0036$ .

 $\Gamma(\omega\omega)/\Gamma_{total}$   $\Gamma_{13}/\Gamma$ 

VALUE (units $10^{-3}$ )	CL%	EVTS	DOCUMENT ID	TECN	COMMENT
<b>2.9 ± 0.5 ± 0.6</b>		1705	<sup>1</sup> ABLIKIM	19AP BES3	$J/\psi \rightarrow \gamma\omega\omega$
< 6.3	90		<sup>2</sup> ABLIKIM	05L BES2	$J/\psi \rightarrow 2(\pi^+ \pi^- \pi^0) \gamma$
< 6.3	90		<sup>2</sup> BISELLO	91 DM2	$J/\psi \rightarrow \gamma\omega\omega$
< 3.1	90		<sup>2</sup> BALTRUSAIT..86	MRK3	$J/\psi \rightarrow \eta_c \gamma$

<sup>1</sup> ABLIKIM 19AP reports  $[\Gamma(\eta_c(1S) \rightarrow \omega\omega)/\Gamma_{total}] \times [B(J/\psi(1S) \rightarrow \gamma\eta_c(1S))] = (4.90 \pm 0.17 \pm 0.77) \times 10^{-3}$  which we divide by our best value  $B(J/\psi(1S) \rightarrow \gamma\eta_c(1S)) = (1.7 \pm 0.4) \times 10^{-2}$ . Our first error is their experiment's error and our second error is the systematic error from using our best value.

<sup>2</sup> The quoted branching ratios use  $B(J/\psi(1S) \rightarrow \gamma\eta_c(1S)) = 0.0127 \pm 0.0036$ . Where relevant, the error in this branching ratio is treated as a common systematic in computing averages.

 $\Gamma(\omega\phi)/\Gamma_{total}$   $\Gamma_{14}/\Gamma$ 

VALUE	CL%	DOCUMENT ID	TECN	COMMENT
<b>&lt; 2.5 × 10<sup>-4</sup></b>	90	<sup>1</sup> ABLIKIM	17P BES3	$J/\psi \rightarrow \pi^+ \pi^- \pi^0 K^+ K^- \gamma$
< 17 × 10 <sup>-4</sup>	90	<sup>2</sup> ABLIKIM	05L BES2	$J/\psi \rightarrow \pi^+ \pi^- \pi^0 K^+ K^- \gamma$

<sup>1</sup> Using  $B(J/\psi \rightarrow \gamma\eta_c) = 0.017 \pm 0.004$ .

<sup>2</sup> The quoted branching ratios use  $B(J/\psi(1S) \rightarrow \gamma\eta_c(1S)) = 0.0127 \pm 0.0036$ .

 $\Gamma(f_2(1270)f_2(1270))/\Gamma_{total}$   $\Gamma_{15}/\Gamma$ 

VALUE (units $10^{-2}$ )	EVTS	DOCUMENT ID	TECN	COMMENT
<b>0.98 ± 0.25 OUR FIT</b>				
<b>0.77 <math>\pm \frac{0.25}{-0.30} \pm 0.17</math></b>	91.2 ± 19.8	<sup>1</sup> ABLIKIM	04M BES	$J/\psi \rightarrow \gamma 2\pi^+ 2\pi^-$

<sup>1</sup> ABLIKIM 04M reports  $[\Gamma(\eta_c(1S) \rightarrow f_2(1270)f_2(1270))/\Gamma_{total}] \times [B(J/\psi(1S) \rightarrow \gamma\eta_c(1S))] = (1.3 \pm 0.3 \pm \frac{0.3}{-0.4}) \times 10^{-4}$  which we divide by our best value  $B(J/\psi(1S) \rightarrow \gamma\eta_c(1S)) = (1.7 \pm 0.4) \times 10^{-2}$ . Our first error is their experiment's error and our second error is the systematic error from using our best value.

 $\Gamma(f_0(980)\eta)/\Gamma_{total}$   $\Gamma_{17}/\Gamma$ 

VALUE	DOCUMENT ID	TECN	COMMENT
seen	LEES	14E BABR	Dalitz anal. of $\eta_c \rightarrow K^+ K^- \eta$

 $\Gamma(f_0(1500)\eta)/\Gamma_{total}$   $\Gamma_{18}/\Gamma$ 

VALUE	DOCUMENT ID	TECN	COMMENT
seen	LEES	14E BABR	Dalitz anal. of $\eta_c \rightarrow K^+ K^- \eta$

 $\Gamma(f_0(2200)\eta)/\Gamma_{total}$   $\Gamma_{19}/\Gamma$ 

VALUE	DOCUMENT ID	TECN	COMMENT
seen	LEES	14E BABR	Dalitz anal. of $\eta_c \rightarrow K^+ K^- \eta$

 $\Gamma(a_0(980)\pi)/\Gamma_{total}$   $\Gamma_{20}/\Gamma$ 

VALUE	DOCUMENT ID	TECN	COMMENT
seen	LEES	14E BABR	Dalitz anal. of $\eta_c \rightarrow K^+ K^- \pi^0$

 $\Gamma(a_0(1320)\pi)/\Gamma_{total}$   $\Gamma_{21}/\Gamma$ 

VALUE	DOCUMENT ID	TECN	COMMENT
seen	LEES	14E BABR	Dalitz anal. of $\eta_c \rightarrow K^+ K^- \pi^0$

 $\Gamma(a_0(1450)\pi)/\Gamma_{total}$   $\Gamma_{22}/\Gamma$ 

VALUE	DOCUMENT ID	TECN	COMMENT
seen	LEES	14E BABR	Dalitz anal. of $\eta_c \rightarrow K^+ K^- \pi^0$

 $\Gamma(a_0(1950)\pi)/\Gamma_{total}$   $\Gamma_{23}/\Gamma$ 

VALUE	EVTS	DOCUMENT ID	TECN	COMMENT
seen	12k	<sup>1</sup> LEES	16A BABR	$\gamma\gamma \rightarrow \eta_c(1S) \rightarrow K\bar{K}\pi$

<sup>1</sup> From a model-independent partial wave analysis.

 $\Gamma(K_0^*(1430)\bar{K})/\Gamma_{total}$   $\Gamma_{24}/\Gamma$ 

VALUE	EVTS	DOCUMENT ID	TECN	COMMENT
seen	12k	<sup>1</sup> LEES	16A BABR	$\gamma\gamma \rightarrow \eta_c(1S) \rightarrow K\bar{K}\pi$
seen		LEES	14E BABR	Dalitz anal. of $\eta_c \rightarrow K^+ K^- \eta/\pi^0$

<sup>1</sup> From a model-independent partial wave analysis.

 $\Gamma(K_2^*(1430)\bar{K})/\Gamma_{total}$   $\Gamma_{25}/\Gamma$ 

VALUE	DOCUMENT ID	TECN	COMMENT
seen	LEES	14E BABR	Dalitz anal. of $\eta_c \rightarrow K^+ K^- \pi^0$

 $\Gamma(K_0^*(1950)\bar{K})/\Gamma_{total}$   $\Gamma_{26}/\Gamma$ 

VALUE	EVTS	DOCUMENT ID	TECN	COMMENT
seen	12K	<sup>1</sup> LEES	16A BABR	$\gamma\gamma \rightarrow \eta_c(1S) \rightarrow K\bar{K}\pi$
seen		LEES	14E BABR	Dalitz anal. of $\eta_c \rightarrow K^+ K^- \eta/\pi^0$

<sup>1</sup> From a Dalitz plot analysis using an isobar model.

 $\Gamma(K\bar{K}\pi)/\Gamma_{total}$   $\Gamma_{27}/\Gamma$ 

VALUE (units $10^{-2}$ )	EVTS	DOCUMENT ID	TECN	COMMENT
<b>7.3 ± 0.4 OUR FIT</b>				
<b>6.9 ± 0.4 OUR AVERAGE</b>				
6.9 ± 0.7 ± 0.6	146	<sup>1</sup> ABLIKIM	19AP BES3	$h_c \rightarrow \gamma\eta_c$
7.8 ± 0.6 ± 0.6	267	<sup>2</sup> ABLIKIM	19AP BES3	$h_c \rightarrow \gamma\eta_c$
6.3 ± 1.3 ± 0.6	55	<sup>3,4</sup> ABLIKIM	12N BES3	$\psi(2S) \rightarrow \pi^0 \gamma K^+ K^- \pi^0$
7.9 ± 1.4 ± 0.7	107	<sup>5,6</sup> ABLIKIM	12N BES3	$\psi(2S) \rightarrow \pi^0 \gamma K_S^0 K^\mp \pi^\pm$
8.5 ± 1.8		<sup>7</sup> AUBERT	06E BABR	$B^\pm \rightarrow K^\pm X_{c\bar{c}}$
5.1 ± 2.1	0.6k	<sup>8</sup> BAI	04 BES	$J/\psi \rightarrow \gamma K^\pm \pi^\mp K_S^0$
6.90 ± 1.42 ± 1.32	33	<sup>8</sup> BISELLO	91 DM2	$J/\psi \rightarrow \gamma K^+ K^- \pi^0$
5.43 ± 0.94 ± 0.94	68	<sup>8</sup> BISELLO	91 DM2	$J/\psi \rightarrow \gamma K^\pm \pi^\mp K_S^0$
4.8 ± 1.7	95	<sup>8,9</sup> BALTRUSAIT..86	MRK3	$J/\psi \rightarrow \eta_c \gamma$
16.1 $\pm \frac{9.2}{-7.3}$		<sup>10,11</sup> HIMEL	80B MRK2	$\psi(2S) \rightarrow \eta_c \gamma$

- We do not use the following data for averages, fits, limits, etc. •••
- < 10.7 90% CL <sup>8,12</sup> PARTRIDGE 80B CBAL  $J/\psi \rightarrow \eta_c \gamma$
- <sup>1</sup> ABLIKIM 19AP quotes  $B(\eta_c \rightarrow K^+ K^- \pi^0) = (1.15 \pm 0.12 \pm 0.10) \times 10^{-2}$  which we multiply by 6 to account for isospin symmetry.
- <sup>2</sup> ABLIKIM 19AP quotes  $B(\eta_c \rightarrow K_S^0 K^\pm \pi^\mp) = (2.60 \pm 0.21 \pm 0.20) \times 10^{-2}$  which we multiply by 3 to account for isospin symmetry.
- <sup>3</sup> ABLIKIM 12N quotes  $B(\psi(2S) \rightarrow \pi^0 h_c) \cdot B(h_c \rightarrow \gamma \eta_c) \cdot B(\eta_c \rightarrow K^+ K^- \pi^0) = (4.54 \pm 0.76 \pm 0.48) \times 10^{-6}$  which we multiply by 6 to account for isospin symmetry.
- <sup>4</sup> ABLIKIM 12N reports  $[\Gamma(\eta_c(1S) \rightarrow K \bar{K} \pi)/\Gamma_{\text{total}}] \times [\Gamma(h_c(1P) \rightarrow \gamma \eta_c(1S))/\Gamma_{\text{total}} \times \Gamma(\psi(2S) \rightarrow \pi^0 h_c(1P))/\Gamma_{\text{total}}] = (27.24 \pm 4.56 \pm 2.88) \times 10^{-6}$  which we divide by our best value  $\Gamma(h_c(1P) \rightarrow \gamma \eta_c(1S))/\Gamma_{\text{total}} \times \Gamma(\psi(2S) \rightarrow \pi^0 h_c(1P))/\Gamma_{\text{total}} = (4.3 \pm 0.4) \times 10^{-4}$ . Our first error is their experiment's error and our second error is the systematic error from using our best value.
- <sup>5</sup> ABLIKIM 12N quotes  $B(\psi(2S) \rightarrow \pi^0 h_c) \cdot B(h_c \rightarrow \gamma \eta_c) \cdot B(\eta_c \rightarrow K_S^0 K^\pm \pi^\mp) = (11.35 \pm 1.25 \pm 1.50) \times 10^{-6}$  which we multiply by 3 to account for isospin symmetry.
- <sup>6</sup> ABLIKIM 12N reports  $[\Gamma(\eta_c(1S) \rightarrow K \bar{K} \pi)/\Gamma_{\text{total}}] \times [\Gamma(h_c(1P) \rightarrow \gamma \eta_c(1S))/\Gamma_{\text{total}} \times \Gamma(\psi(2S) \rightarrow \pi^0 h_c(1P))/\Gamma_{\text{total}}] = (34.05 \pm 3.75 \pm 4.50) \times 10^{-6}$  which we divide by our best value  $\Gamma(h_c(1P) \rightarrow \gamma \eta_c(1S))/\Gamma_{\text{total}} \times \Gamma(\psi(2S) \rightarrow \pi^0 h_c(1P))/\Gamma_{\text{total}} = (4.3 \pm 0.4) \times 10^{-4}$ . Our first error is their experiment's error and our second error is the systematic error from using our best value.
- <sup>7</sup> Determined from the ratio of  $B(B^\pm \rightarrow K^\pm \eta_c) B(\eta_c \rightarrow K \bar{K} \pi) = (7.4 \pm 0.5 \pm 0.7) \times 10^{-5}$  reported in AUBERT, B 04B and  $B(B^\pm \rightarrow K^\pm \eta_c) = (8.7 \pm 1.5) \times 10^{-3}$  reported in AUBERT 06E.
- <sup>8</sup> The quoted branching ratios use  $B(J/\psi(1S) \rightarrow \gamma \eta_c(1S)) = 0.0127 \pm 0.0036$ . Where relevant, the error in this branching ratio is treated as a common systematic in computing averages.
- <sup>9</sup> Average from  $K^+ K^- \pi^0$  and  $K^\pm K_S^0 \pi^\mp$  decay channels.
- <sup>10</sup>  $K^\pm K_S^0 \pi^\mp$  corrected to  $K \bar{K} \pi$  by factor 3. KS, MR.
- <sup>11</sup> Estimated using  $B(\psi(2S) \rightarrow \gamma \eta_c(1S)) = 0.0028 \pm 0.0006$ .
- <sup>12</sup>  $K^+ K^- \pi^0$  corrected to  $K \bar{K} \pi$  by factor 6. KS, MR

**$\Gamma(\phi K^+ K^-)/\Gamma(K \bar{K} \pi)$   $\Gamma_6/\Gamma_{27}$**

VALUE	EVTS	DOCUMENT ID	TECN	COMMENT
<b><math>0.052 \pm 0.016 \pm 0.014</math></b>	7	<sup>1</sup> HUANG 03	BELL	$B^\pm \rightarrow K^\pm \phi$

<sup>1</sup> Using  $B(B^+ \rightarrow \eta_c K^+) = (1.25 \pm 0.12 \pm 0.10) \times 10^{-3}$  from FANG 03 and  $B(\eta_c \rightarrow K \bar{K} \pi) = (5.5 \pm 1.7) \times 10^{-2}$ .

**$\Gamma(K \bar{K} \eta)/\Gamma_{\text{total}}$   $\Gamma_{28}/\Gamma$**

VALUE (units $10^{-2}$ )	CL%	EVTS	DOCUMENT ID	TECN	COMMENT
<b><math>1.36 \pm 0.15</math> OUR FIT</b>					
<b><math>1.0 \pm 0.5</math></b>	<b><math>\pm 0.2</math></b>	7	<sup>1,2</sup> ABLIKIM 12N	BES3	$\psi(2S) \rightarrow \pi^0 \gamma \eta K^+ K^-$

- We do not use the following data for averages, fits, limits, etc. •••
- < 3.1 90 <sup>3</sup> BALTRUSAIT...86 MRK3  $J/\psi \rightarrow \eta_c \gamma$

<sup>1</sup> ABLIKIM 12N quotes  $B(\psi(2S) \rightarrow \pi^0 h_c) \cdot B(h_c \rightarrow \gamma \eta_c) \cdot B(\eta_c \rightarrow K^+ K^- \eta) = (2.11 \pm 1.01 \pm 0.32) \times 10^{-6}$  which we multiply by 2 to account for isospin symmetry.

<sup>2</sup> ABLIKIM 12N reports  $[\Gamma(\eta_c(1S) \rightarrow K \bar{K} \eta)/\Gamma_{\text{total}}] \times [B(\psi(2S) \rightarrow \pi^0 h_c(1P))] \times [B(h_c(1P) \rightarrow \gamma \eta_c(1S))] = (4.22 \pm 2.02 \pm 0.64) \times 10^{-6}$  which we divide by our best values  $B(\psi(2S) \rightarrow \pi^0 h_c(1P)) = (8.6 \pm 1.3) \times 10^{-4}$ ,  $B(h_c(1P) \rightarrow \gamma \eta_c(1S)) = (51 \pm 6) \times 10^{-2}$ . Our first error is their experiment's error and our second error is the systematic error from using our best values.

<sup>3</sup> The quoted branching ratios use  $B(J/\psi(1S) \rightarrow \gamma \eta_c(1S)) = 0.0127 \pm 0.0036$ .

**$\Gamma(K \bar{K} \eta)/\Gamma(K \bar{K} \pi)$   $\Gamma_{28}/\Gamma_{27}$**

VALUE	EVTS	DOCUMENT ID	TECN	COMMENT
<b><math>0.186 \pm 0.018</math> OUR FIT</b>				
<b><math>0.190 \pm 0.008 \pm 0.017</math></b>	5.4k	<sup>1</sup> LEES 14E	BABR	$\gamma \gamma \rightarrow K^+ K^- \eta/\pi^0$

<sup>1</sup> LEES 14E reports  $B(\eta_c(1S) \rightarrow K^+ K^- \eta)/B(\eta_c(1S) \rightarrow K^+ K^- \pi^0) = 0.571 \pm 0.025 \pm 0.051$ , which we divide by 3 to account for isospin symmetry. It uses both  $\eta \rightarrow \gamma \gamma$  and  $\eta \rightarrow \pi^+ \pi^- \pi^0$  decays.

**$\Gamma(\eta \pi^+ \pi^-)/\Gamma_{\text{total}}$   $\Gamma_{29}/\Gamma$**

VALUE (units $10^{-2}$ )	EVTS	DOCUMENT ID	TECN	COMMENT
<b><math>1.7 \pm 0.4 \pm 0.1</math></b>	33	<sup>1</sup> ABLIKIM 12N	BES3	$\psi(2S) \rightarrow \pi^0 \gamma \eta \pi^+ \pi^-$

- We do not use the following data for averages, fits, limits, etc. •••
- 5.4 ± 2.0 <sup>2</sup> BALTRUSAIT...86 MRK3  $J/\psi \rightarrow \eta_c \gamma$
- 3.7 ± 1.3 ± 2.0 <sup>3</sup> PARTRIDGE 80B CBAL  $J/\psi \rightarrow \eta \pi^+ \pi^- \gamma$

<sup>1</sup> ABLIKIM 12N reports  $[\Gamma(\eta_c(1S) \rightarrow \eta \pi^+ \pi^-)/\Gamma_{\text{total}}] \times [\Gamma(h_c(1P) \rightarrow \gamma \eta_c(1S))/\Gamma_{\text{total}} \times \Gamma(\psi(2S) \rightarrow \pi^0 h_c(1P))/\Gamma_{\text{total}}] = (7.22 \pm 1.47 \pm 1.11) \times 10^{-6}$  which we divide by our best value  $\Gamma(h_c(1P) \rightarrow \gamma \eta_c(1S))/\Gamma_{\text{total}} \times \Gamma(\psi(2S) \rightarrow \pi^0 h_c(1P))/\Gamma_{\text{total}} = (4.3 \pm 0.4) \times 10^{-4}$ . Our first error is their experiment's error and our second error is the systematic error from using our best value.

<sup>2</sup> The quoted branching ratios use  $B(J/\psi(1S) \rightarrow \gamma \eta_c(1S)) = 0.0127 \pm 0.0036$ . Where relevant, the error in this branching ratio is treated as a common systematic in computing averages.

**$\Gamma(\eta 2(\pi^+ \pi^-))/\Gamma_{\text{total}}$   $\Gamma_{30}/\Gamma$**

VALUE (units $10^{-2}$ )	EVTS	DOCUMENT ID	TECN	COMMENT
<b><math>4.4 \pm 1.2 \pm 0.4</math></b>	39	<sup>1</sup> ABLIKIM 12N	BES3	$\psi(2S) \rightarrow \pi^0 \gamma \eta 2(\pi^+ \pi^-)$

<sup>1</sup> ABLIKIM 12N reports  $[\Gamma(\eta_c(1S) \rightarrow \eta 2(\pi^+ \pi^-))/\Gamma_{\text{total}}] \times [\Gamma(h_c(1P) \rightarrow \gamma \eta_c(1S))/\Gamma_{\text{total}} \times \Gamma(\psi(2S) \rightarrow \pi^0 h_c(1P))/\Gamma_{\text{total}}] = (19.17 \pm 3.77 \pm 3.72) \times 10^{-6}$  which we divide by our best value  $\Gamma(h_c(1P) \rightarrow \gamma \eta_c(1S))/\Gamma_{\text{total}} \times \Gamma(\psi(2S) \rightarrow \pi^0 h_c(1P))/\Gamma_{\text{total}} = (4.3 \pm 0.4) \times 10^{-4}$ . Our first error is their experiment's error and our second error is the systematic error from using our best value.

**$\Gamma(K^+ K^- \pi^+ \pi^-)/\Gamma_{\text{total}}$   $\Gamma_{31}/\Gamma$**

VALUE (units $10^{-3}$ )	EVTS	DOCUMENT ID	TECN	COMMENT
<b><math>6.9 \pm 1.0</math> OUR FIT</b>				
<b><math>11.2 \pm 1.9</math> OUR AVERAGE</b>				
$9.7 \pm 2.2 \pm 0.9$	38	<sup>1</sup> ABLIKIM 12N	BES3	$\psi(2S) \rightarrow \pi^0 \gamma K^+ K^- \pi^+ \pi^-$
$12 \pm 4$	0.4k	<sup>2</sup> BAI 04	BES	$J/\psi \rightarrow \gamma K^+ K^- \pi^+ \pi^-$
$21 \pm 7$	110	<sup>2</sup> BALTRUSAIT...86	MRK3	$J/\psi \rightarrow \eta_c \gamma$
$14 \pm 2.9$		<sup>3</sup> HIMEL	.80B	MRK2 $\psi(2S) \rightarrow \eta_c \gamma$

<sup>1</sup> ABLIKIM 12N reports  $[\Gamma(\eta_c(1S) \rightarrow K^+ K^- \pi^+ \pi^-)/\Gamma_{\text{total}}] \times [\Gamma(h_c(1P) \rightarrow \gamma \eta_c(1S))/\Gamma_{\text{total}} \times \Gamma(\psi(2S) \rightarrow \pi^0 h_c(1P))/\Gamma_{\text{total}}] = (4.16 \pm 0.76 \pm 0.59) \times 10^{-6}$  which we divide by our best value  $\Gamma(h_c(1P) \rightarrow \gamma \eta_c(1S))/\Gamma_{\text{total}} \times \Gamma(\psi(2S) \rightarrow \pi^0 h_c(1P))/\Gamma_{\text{total}} = (4.3 \pm 0.4) \times 10^{-4}$ . Our first error is their experiment's error and our second error is the systematic error from using our best value.

<sup>2</sup> The quoted branching ratios use  $B(J/\psi(1S) \rightarrow \gamma \eta_c(1S)) = 0.0127 \pm 0.0036$ . Where relevant, the error in this branching ratio is treated as a common systematic in computing averages.

<sup>3</sup> Estimated using  $B(\psi(2S) \rightarrow \gamma \eta_c(1S)) = 0.0028 \pm 0.0006$ .

**$\Gamma(K^+ K^- \pi^+ \pi^- \pi^0)/\Gamma(K \bar{K} \pi)$   $\Gamma_{32}/\Gamma_{27}$**

VALUE	EVTS	DOCUMENT ID	TECN	COMMENT
<b><math>0.477 \pm 0.017 \pm 0.070</math></b>	11k	<sup>1</sup> DEL-AMO-SA...11M	BABR	$\gamma \gamma \rightarrow K^+ K^- \pi^+ \pi^- \pi^0$

<sup>1</sup> We have multiplied the value of  $\Gamma(K^+ K^- \pi^+ \pi^- \pi^0)/\Gamma(K_S^0 K^\pm \pi^\mp)$  reported in DEL-AMO-SANCHEZ 11M by a factor 1/3 to obtain  $\Gamma(K^+ K^- \pi^+ \pi^- \pi^0)/\Gamma(K \bar{K} \pi)$ . Not independent from other measurements reported in DEL-AMO-SANCHEZ 11M.

**$\Gamma(K^0 K^- \pi^+ \pi^- \pi^+ + c.c.)/\Gamma_{\text{total}}$   $\Gamma_{33}/\Gamma$**

VALUE (units $10^{-2}$ )	EVTS	DOCUMENT ID	TECN	COMMENT
<b><math>5.6 \pm 1.4 \pm 0.5</math></b>	43	<sup>1,2</sup> ABLIKIM 12N	BES3	$\psi(2S) \rightarrow \pi^0 \gamma K_S^0 K^\mp \pi^\mp 2\pi^\pm$

<sup>1</sup> ABLIKIM 12N quotes  $B(\psi(2S) \rightarrow \pi^0 h_c) \cdot B(h_c \rightarrow \gamma \eta_c) \cdot B(\eta_c \rightarrow K_S^0 K^- \pi^+ 2\pi^+) = (12.01 \pm 2.22 \pm 2.04) \times 10^{-6}$  which we multiply by 2 to take c.c. into account.

<sup>2</sup> ABLIKIM 12N reports  $[\Gamma(\eta_c(1S) \rightarrow K^0 K^- \pi^+ \pi^- \pi^+ + c.c.)/\Gamma_{\text{total}}] \times [\Gamma(h_c(1P) \rightarrow \gamma \eta_c(1S))/\Gamma_{\text{total}} \times \Gamma(\psi(2S) \rightarrow \pi^0 h_c(1P))/\Gamma_{\text{total}}] = (24.02 \pm 4.44 \pm 4.08) \times 10^{-6}$  which we divide by our best value  $\Gamma(h_c(1P) \rightarrow \gamma \eta_c(1S))/\Gamma_{\text{total}} \times \Gamma(\psi(2S) \rightarrow \pi^0 h_c(1P))/\Gamma_{\text{total}} = (4.3 \pm 0.4) \times 10^{-4}$ . Our first error is their experiment's error and our second error is the systematic error from using our best value.

**$\Gamma(K^+ K^- 2(\pi^+ \pi^-))/\Gamma_{\text{total}}$   $\Gamma_{34}/\Gamma$**

VALUE (units $10^{-3}$ )	EVTS	DOCUMENT ID	TECN	COMMENT
<b><math>7.5 \pm 2.4</math> OUR AVERAGE</b>				
$8 \pm 4 \pm 1$	10	<sup>1</sup> ABLIKIM 12N	BES3	$\psi(2S) \rightarrow \pi^0 \gamma K^+ K^- 2(\pi^+ \pi^-)$
$7.2 \pm 2.4 \pm 1.5$	100	<sup>2</sup> ABLIKIM 06A	BES2	$J/\psi \rightarrow K^+ K^- 2(\pi^+ \pi^-) \gamma$

<sup>1</sup> ABLIKIM 12N reports  $[\Gamma(\eta_c(1S) \rightarrow K^+ K^- 2(\pi^+ \pi^-))/\Gamma_{\text{total}}] \times [\Gamma(h_c(1P) \rightarrow \gamma \eta_c(1S))/\Gamma_{\text{total}} \times \Gamma(\psi(2S) \rightarrow \pi^0 h_c(1P))/\Gamma_{\text{total}}] = (3.60 \pm 1.71 \pm 0.64) \times 10^{-6}$  which we divide by our best value  $\Gamma(h_c(1P) \rightarrow \gamma \eta_c(1S))/\Gamma_{\text{total}} \times \Gamma(\psi(2S) \rightarrow \pi^0 h_c(1P))/\Gamma_{\text{total}} = (4.3 \pm 0.4) \times 10^{-4}$ . Our first error is their experiment's error and our second error is the systematic error from using our best value.

<sup>2</sup> ABLIKIM 06A reports  $[\Gamma(\eta_c(1S) \rightarrow K^+ K^- 2(\pi^+ \pi^-))/\Gamma_{\text{total}}] \times [B(J/\psi(1S) \rightarrow \gamma \eta_c(1S))] = (1.21 \pm 0.32 \pm 0.24) \times 10^{-4}$  which we divide by our best value  $B(J/\psi(1S) \rightarrow \gamma \eta_c(1S)) = (1.7 \pm 0.4) \times 10^{-2}$ . Our first error is their experiment's error and our second error is the systematic error from using our best value.

**$\Gamma(2(K^+ K^-))/\Gamma_{\text{total}}$   $\Gamma_{35}/\Gamma$**

VALUE (units $10^{-3}$ )	EVTS	DOCUMENT ID	TECN	COMMENT
<b><math>1.46 \pm 0.30</math> OUR FIT</b>				
<b><math>2.2 \pm 0.9 \pm 0.2</math></b>	7	<sup>1</sup> ABLIKIM 12N	BES3	$\psi(2S) \rightarrow \pi^0 \gamma 2(K^+ K^-)$

- We do not use the following data for averages, fits, limits, etc. •••
- $1.4 \pm 0.5 \pm 0.6$   $14.5 \pm 4.6 \pm 3.0$  <sup>2</sup> HUANG 03 BELL  $B^+ \rightarrow 2(K^+ K^-) K^+$

$21 \pm 10 \pm 6$  <sup>3</sup> ALBRECHT 94H ARG  $\gamma \gamma \rightarrow K^+ K^- K^+ K^-$

<sup>1</sup> ABLIKIM 12N reports  $[\Gamma(\eta_c(1S) \rightarrow 2(K^+ K^-))/\Gamma_{\text{total}}] \times [\Gamma(h_c(1P) \rightarrow \gamma \eta_c(1S))/\Gamma_{\text{total}} \times \Gamma(\psi(2S) \rightarrow \pi^0 h_c(1P))/\Gamma_{\text{total}}] = (0.94 \pm 0.37 \pm 0.14) \times 10^{-6}$  which we divide by our best value  $\Gamma(h_c(1P) \rightarrow \gamma \eta_c(1S))/\Gamma_{\text{total}} \times \Gamma(\psi(2S) \rightarrow \pi^0 h_c(1P))/\Gamma_{\text{total}} = (4.3 \pm 0.4) \times 10^{-4}$ . Our first error is their experiment's error and our second error is the systematic error from using our best value.

<sup>2</sup> Using  $B(B^+ \rightarrow \eta_c K^+) = (1.25 \pm 0.12 \pm 0.10) \times 10^{-3}$  from FANG 03 and  $B(\eta_c \rightarrow K \bar{K} \pi) = (5.5 \pm 1.7) \times 10^{-2}$ .

<sup>3</sup> Normalized to the sum of  $B(\eta_c \rightarrow K^\pm K_S^0 \pi^\mp)$ ,  $B(\eta_c \rightarrow \phi \phi)$ ,  $B(\eta_c \rightarrow K^+ K^- \pi^+ \pi^-)$ , and  $B(\eta_c \rightarrow 2\pi^+ 2\pi^-)$ .

**$\Gamma(2(K^+ K^-))/\Gamma(K \bar{K} \pi)$   $\Gamma_{35}/\Gamma_{27}$**

VALUE	EVTS	DOCUMENT ID	TECN	COMMENT
<b><math>0.020 \pm 0.004</math> OUR FIT</b>				
<b><math>0.024 \pm 0.007</math> OUR AVERAGE</b>				
$0.023 \pm 0.007 \pm 0.006$		AUBERT, B 04B	BABR	$B^\pm \rightarrow K^\pm \eta_c$
$0.026 \pm 0.009 \pm 0.007$	15	<sup>1</sup> HUANG 03	BELL	$B^\pm \rightarrow K^\pm (2K^+ 2K^-)$

<sup>1</sup> Using  $B(B^+ \rightarrow \eta_c K^+) = (1.25 \pm 0.12 \pm 0.10) \times 10^{-3}$  from FANG 03 and  $B(\eta_c \rightarrow K \bar{K} \pi) = (5.5 \pm 1.7) \times 10^{-2}$ .



## Meson Particle Listings

 $\eta_c(1S)$ 

$\Gamma(\pi^+\pi^-\pi^0)/\Gamma_{\text{total}}$		$\Gamma_{36}/\Gamma$	
VALUE	CL%	DOCUMENT ID	TECN COMMENT

**$<5 \times 10^{-4}$**  90 1 ABLIKIM 17AJ BES3  $\psi(2S) \rightarrow \gamma\pi^+\pi^-\pi^0$   
 1 ABLIKIM 17AJ reports  $[\Gamma(\eta_c(1S) \rightarrow \pi^+\pi^-\pi^0)/\Gamma_{\text{total}}] \times [B(\psi(2S) \rightarrow \gamma\eta_c(1S))]$   
 $< 1.6 \times 10^{-6}$  which we divide by our best value  $B(\psi(2S) \rightarrow \gamma\eta_c(1S)) = 3.4 \times 10^{-3}$ .

$\Gamma(\pi^+\pi^-\pi^0\pi^0)/\Gamma_{\text{total}}$		$\Gamma_{37}/\Gamma$	
VALUE (units $10^{-2}$ )	EVTS	DOCUMENT ID	TECN COMMENT

**$4.7 \pm 0.9 \pm 0.4$**  118 1 ABLIKIM 12N BES3  $\psi(2S) \rightarrow \pi^0\gamma\pi^+\pi^-\pi^0$   
 1 ABLIKIM 12N reports  $[\Gamma(\eta_c(1S) \rightarrow \pi^+\pi^-\pi^0\pi^0)/\Gamma_{\text{total}}] \times [\Gamma(h_c(1P) \rightarrow \gamma\eta_c(1S))/\Gamma_{\text{total}} \times \Gamma(\psi(2S) \rightarrow \pi^0 h_c(1P))/\Gamma_{\text{total}}] = (20.31 \pm 2.20 \pm 3.33) \times 10^{-6}$  which we divide by our best value  $\Gamma(h_c(1P) \rightarrow \gamma\eta_c(1S))/\Gamma_{\text{total}} \times \Gamma(\psi(2S) \rightarrow \pi^0 h_c(1P))/\Gamma_{\text{total}} = (4.3 \pm 0.4) \times 10^{-4}$ . Our first error is their experiment's error and our second error is the systematic error from using our best value.

$\Gamma(2(\pi^+\pi^-))/\Gamma_{\text{total}}$		$\Gamma_{38}/\Gamma$	
VALUE (units $10^{-2}$ )	EVTS	DOCUMENT ID	TECN COMMENT

**$0.97 \pm 0.12$  OUR FIT**  
 **$1.35 \pm 0.21$  OUR AVERAGE**

1.74  $\pm$  0.32  $\pm$  0.15 100 1 ABLIKIM 12N BES3  $\psi(2S) \rightarrow \pi^0\gamma 2(\pi^+\pi^-)$   
 1.0  $\pm$  0.5 542  $\pm$  75 2 BAI 04 BES  $J/\psi \rightarrow \gamma 2(\pi^+\pi^-)$   
 1.05  $\pm$  0.17  $\pm$  0.34 137 2 BISELLO 91 DM2  $J/\psi \rightarrow \gamma 2\pi^+ 2\pi^-$   
 1.3  $\pm$  0.6 25 2 BALTRUSAIT..86 MRK3  $J/\psi \rightarrow \eta_c\gamma$   
 2.0  $\pm$  1.5 3 HIMEL 80B MRK2  $\psi(2S) \rightarrow \eta_c\gamma$

1 ABLIKIM 12N reports  $[\Gamma(\eta_c(1S) \rightarrow 2(\pi^+\pi^-))/\Gamma_{\text{total}}] \times [\Gamma(h_c(1P) \rightarrow \gamma\eta_c(1S))/\Gamma_{\text{total}} \times \Gamma(\psi(2S) \rightarrow \pi^0 h_c(1P))/\Gamma_{\text{total}}] = (7.51 \pm 0.85 \pm 1.11) \times 10^{-6}$  which we divide by our best value  $\Gamma(h_c(1P) \rightarrow \gamma\eta_c(1S))/\Gamma_{\text{total}} \times \Gamma(\psi(2S) \rightarrow \pi^0 h_c(1P))/\Gamma_{\text{total}} = (4.3 \pm 0.4) \times 10^{-4}$ . Our first error is their experiment's error and our second error is the systematic error from using our best value.

2 The quoted branching ratios use  $B(J/\psi(1S) \rightarrow \gamma\eta_c(1S)) = 0.0127 \pm 0.0036$ . Where relevant, the error in this branching ratio is treated as a common systematic in computing averages.

3 Estimated using  $B(\psi(2S) \rightarrow \gamma\eta_c(1S)) = 0.0028 \pm 0.0006$ .

$\Gamma(2(\pi^+\pi^-\pi^0))/\Gamma_{\text{total}}$		$\Gamma_{39}/\Gamma$	
VALUE (units $10^{-2}$ )	EVTS	DOCUMENT ID	TECN COMMENT

**$16.1 \pm 2.0$  OUR AVERAGE**  
 15.3  $\pm$  1.8  $\pm$  1.8 333 ABLIKIM 19AP BES3  $h_c \rightarrow \gamma\eta_c$   
 17.4  $\pm$  2.9  $\pm$  1.5 175 1 ABLIKIM 12N BES3  $\psi(2S) \rightarrow \pi^0\gamma 2(\pi^+\pi^-\pi^0)$

1 ABLIKIM 12N reports  $[\Gamma(\eta_c(1S) \rightarrow 2(\pi^+\pi^-\pi^0))/\Gamma_{\text{total}}] \times [\Gamma(h_c(1P) \rightarrow \gamma\eta_c(1S))/\Gamma_{\text{total}} \times \Gamma(\psi(2S) \rightarrow \pi^0 h_c(1P))/\Gamma_{\text{total}}] = (75.13 \pm 7.42 \pm 9.99) \times 10^{-6}$  which we divide by our best value  $\Gamma(h_c(1P) \rightarrow \gamma\eta_c(1S))/\Gamma_{\text{total}} \times \Gamma(\psi(2S) \rightarrow \pi^0 h_c(1P))/\Gamma_{\text{total}} = (4.3 \pm 0.4) \times 10^{-4}$ . Our first error is their experiment's error and our second error is the systematic error from using our best value.

$\Gamma(3(\pi^+\pi^-))/\Gamma_{\text{total}}$		$\Gamma_{40}/\Gamma$	
VALUE (units $10^{-3}$ )	EVTS	DOCUMENT ID	TECN COMMENT

**$18 \pm 4$  OUR AVERAGE**  
 20  $\pm$  5  $\pm$  2 51 1 ABLIKIM 12N BES3  $\psi(2S) \rightarrow \pi^0\gamma 3(\pi^+\pi^-)$   
 15.4  $\pm$  3.4  $\pm$  3.3 479 2 ABLIKIM 06A BES2  $J/\psi \rightarrow 3(\pi^+\pi^-)\gamma$

1 ABLIKIM 12N reports  $[\Gamma(\eta_c(1S) \rightarrow 3(\pi^+\pi^-))/\Gamma_{\text{total}}] \times [\Gamma(h_c(1P) \rightarrow \gamma\eta_c(1S))/\Gamma_{\text{total}} \times \Gamma(\psi(2S) \rightarrow \pi^0 h_c(1P))/\Gamma_{\text{total}}] = (8.82 \pm 1.57 \pm 1.59) \times 10^{-6}$  which we divide by our best value  $\Gamma(h_c(1P) \rightarrow \gamma\eta_c(1S))/\Gamma_{\text{total}} \times \Gamma(\psi(2S) \rightarrow \pi^0 h_c(1P))/\Gamma_{\text{total}} = (4.3 \pm 0.4) \times 10^{-4}$ . Our first error is their experiment's error and our second error is the systematic error from using our best value.

2 ABLIKIM 06A reports  $[\Gamma(\eta_c(1S) \rightarrow 3(\pi^+\pi^-))/\Gamma_{\text{total}}] \times [B(J/\psi(1S) \rightarrow \gamma\eta_c(1S))] = (2.59 \pm 0.32 \pm 0.47) \times 10^{-4}$  which we divide by our best value  $B(J/\psi(1S) \rightarrow \gamma\eta_c(1S)) = (1.7 \pm 0.4) \times 10^{-2}$ . Our first error is their experiment's error and our second error is the systematic error from using our best value.

$\Gamma(\rho\bar{\rho})/\Gamma_{\text{total}}$		$\Gamma_{41}/\Gamma$	
VALUE (units $10^{-4}$ )	EVTS	DOCUMENT ID	TECN COMMENT

**$14.5 \pm 1.4$  OUR FIT**  
 **$12.7 \pm 2.0$  OUR AVERAGE**

12.0  $\pm$  2.6  $\pm$  1.5 34 ABLIKIM 19APBES3  $h_c \rightarrow \gamma\eta_c$   
 15  $\pm$  5  $\pm$  1 15 1 ABLIKIM 12N BES3  $\psi(2S) \rightarrow \pi^0\gamma\rho\bar{\rho}$   
 15  $\pm$  6 213  $\pm$  33 2 BAI 04 BES  $J/\psi \rightarrow \gamma\rho\bar{\rho}$   
 10  $\pm$  3  $\pm$  4 18 2 BISELLO 91 DM2  $J/\psi \rightarrow \gamma\rho\bar{\rho}$   
 11  $\pm$  6 23 2 BALTRUSAIT..86 MRK3  $J/\psi \rightarrow \eta_c\gamma$   
 29  $\pm$  29 3 HIMEL 80B MRK2  $\psi(2S) \rightarrow \eta_c\gamma$   
 -15

• • • We do not use the following data for averages, fits, limits, etc. • • •

13.4  $\pm$  1.9  $\pm$  1.1 195 4 WU 06 BELL  $B^+ \rightarrow \rho\bar{\rho}K^+$

1 ABLIKIM 12N reports  $[\Gamma(\eta_c(1S) \rightarrow \rho\bar{\rho})/\Gamma_{\text{total}}] \times [\Gamma(h_c(1P) \rightarrow \gamma\eta_c(1S))/\Gamma_{\text{total}} \times \Gamma(\psi(2S) \rightarrow \pi^0 h_c(1P))/\Gamma_{\text{total}}] = (0.65 \pm 0.19 \pm 0.10) \times 10^{-6}$  which we divide by our best value  $\Gamma(h_c(1P) \rightarrow \gamma\eta_c(1S))/\Gamma_{\text{total}} \times \Gamma(\psi(2S) \rightarrow \pi^0 h_c(1P))/\Gamma_{\text{total}} = (4.3 \pm 0.4) \times 10^{-4}$ . Our first error is their experiment's error and our second error is the systematic error from using our best value.

2 The quoted branching ratios use  $B(J/\psi(1S) \rightarrow \gamma\eta_c(1S)) = 0.0127 \pm 0.0036$ . Where relevant, the error in this branching ratio is treated as a common systematic in computing averages.

<sup>3</sup> Estimated using  $B(\psi(2S) \rightarrow \gamma\eta_c(1S)) = 0.0028 \pm 0.0006$ .

<sup>4</sup> WU 06 reports  $[\Gamma(\eta_c(1S) \rightarrow \rho\bar{\rho})/\Gamma_{\text{total}}] \times [B(B^+ \rightarrow \eta_c K^+)] = (1.42 \pm 0.11 \pm 0.16) \times 10^{-6}$  which we divide by our best value  $B(B^+ \rightarrow \eta_c K^+) = (1.06 \pm 0.09) \times 10^{-3}$ . Our first error is their experiment's error and our second error is the systematic error from using our best value.

$\Gamma(\rho\bar{\rho})/\Gamma(K\bar{K}\pi)$		$\Gamma_{41}/\Gamma_{27}$	
VALUE	EVTS	DOCUMENT ID	TECN COMMENT

**$0.0199 \pm 0.0019$  OUR FIT**  
 **$0.021 \pm 0.002 \pm 0.004$**  195 1 WU 06 BELL  $B^\pm \rightarrow K^\pm\rho\bar{\rho}$

1 Using  $B(B^+ \rightarrow \eta_c K^+) = (1.25 \pm 0.12 \pm 0.10) \times 10^{-3}$  from FANG 03 and  $B(\eta_c \rightarrow K\bar{K}\pi) = (5.5 \pm 1.7) \times 10^{-2}$ .

$\Gamma(\rho\bar{\rho})/\Gamma_{\text{total}} \times \Gamma(\phi\phi)/\Gamma_{\text{total}}$		$\Gamma_{41}/\Gamma \times \Gamma_7/\Gamma$	
VALUE (units $10^{-5}$ )	EVTS	DOCUMENT ID	TECN COMMENT

**$0.26 \pm 0.04$  OUR FIT**  
 **$4.0 \pm 3.5$**  BAGLIN 89 SPEC  $\bar{p}p \rightarrow K^+K^-K^+K^-$   
 **$-3.2$**

$\Gamma(\rho\bar{\rho}\pi^0)/\Gamma_{\text{total}}$		$\Gamma_{42}/\Gamma$	
VALUE (units $10^{-2}$ )	EVTS	DOCUMENT ID	TECN COMMENT

**$0.36 \pm 0.13 \pm 0.03$**  14 1 ABLIKIM 12N BES3  $\psi(2S) \rightarrow \pi^0\gamma\rho\bar{\rho}\pi^0$

1 ABLIKIM 12N reports  $[\Gamma(\eta_c(1S) \rightarrow \rho\bar{\rho}\pi^0)/\Gamma_{\text{total}}] \times [\Gamma(h_c(1P) \rightarrow \gamma\eta_c(1S))/\Gamma_{\text{total}} \times \Gamma(\psi(2S) \rightarrow \pi^0 h_c(1P))/\Gamma_{\text{total}}] = (1.53 \pm 0.49 \pm 0.23) \times 10^{-6}$  which we divide by our best value  $\Gamma(h_c(1P) \rightarrow \gamma\eta_c(1S))/\Gamma_{\text{total}} \times \Gamma(\psi(2S) \rightarrow \pi^0 h_c(1P))/\Gamma_{\text{total}} = (4.3 \pm 0.4) \times 10^{-4}$ . Our first error is their experiment's error and our second error is the systematic error from using our best value.

$\Gamma(\Lambda\bar{\Lambda})/\Gamma_{\text{total}}$		$\Gamma_{43}/\Gamma$	
VALUE (units $10^{-4}$ )	CL% EVTS	DOCUMENT ID	TECN COMMENT

**$10.7 \pm 2.4$  OUR FIT**  
 **$11.8 \pm 2.3 \pm 2.5$**  1 ABLIKIM 12B BES3

• • • We do not use the following data for averages, fits, limits, etc. • • •

8.9  $\pm$  2.5  $\pm$  0.7 20 2 WU 06 BELL  $B^+ \rightarrow \Lambda\bar{\Lambda}K^+$   
 $<20$  90 3 BISELLO 91 DM2  $e^+e^- \rightarrow \gamma\Lambda\bar{\Lambda}$

1 ABLIKIM 12B reports  $[\Gamma(\eta_c(1S) \rightarrow \Lambda\bar{\Lambda})/\Gamma_{\text{total}}] \times [B(J/\psi(1S) \rightarrow \gamma\eta_c(1S))] = (0.198 \pm 0.021 \pm 0.032) \times 10^{-4}$  which we divide by our best value  $B(J/\psi(1S) \rightarrow \gamma\eta_c(1S)) = (1.7 \pm 0.4) \times 10^{-2}$ . Our first error is their experiment's error and our second error is the systematic error from using our best value.

2 WU 06 reports  $[\Gamma(\eta_c(1S) \rightarrow \Lambda\bar{\Lambda})/\Gamma_{\text{total}}] \times [B(B^+ \rightarrow \eta_c K^+)] = (0.95 \pm 0.25 \pm 0.08) \times 10^{-6}$  which we divide by our best value  $B(B^+ \rightarrow \eta_c K^+) = (1.06 \pm 0.09) \times 10^{-3}$ . Our first error is their experiment's error and our second error is the systematic error from using our best value.

3 The quoted branching ratios use  $B(J/\psi(1S) \rightarrow \gamma\eta_c(1S)) = 0.0127 \pm 0.0036$ .

$\Gamma(\Lambda\bar{\Lambda})/\Gamma(\rho\bar{\rho})$		$\Gamma_{43}/\Gamma_{41}$	
VALUE	EVTS	DOCUMENT ID	TECN COMMENT

**$0.73 \pm 0.16$  OUR FIT**  
 **$0.67 \pm 0.19 \pm 0.12$**  1 WU 06 BELL  $B^+ \rightarrow \rho\bar{\rho}K^+, \Lambda\bar{\Lambda}K^+$

1 Not independent from other  $\eta_c \rightarrow \Lambda\bar{\Lambda}, \rho\bar{\rho}$  branching ratios reported by WU 06.

$\Gamma(K^+\bar{p}\Lambda + \text{c.c.})/\Gamma_{\text{total}}$		$\Gamma_{44}/\Gamma$	
VALUE (units $10^{-3}$ )	EVTS	DOCUMENT ID	TECN COMMENT

**$2.56 \pm 0.35$**  157 1 LU 19 BELL  $B^+ \rightarrow \bar{p}\Lambda K^+ K^+$   
 **$-0.33 \pm 0.21$**

1 LU 19 reports  $(2.83 \pm 0.36 \pm 0.35) \times 10^{-3}$  from a measurement of  $[\Gamma(\eta_c(1S) \rightarrow K^+\bar{p}\Lambda + \text{c.c.})/\Gamma_{\text{total}}] \times [B(B^+ \rightarrow \eta_c K^+)]$  assuming  $B(B^+ \rightarrow \eta_c K^+) = (9.6 \pm 1.1) \times 10^{-4}$ , which we rescale to our best value  $B(B^+ \rightarrow \eta_c K^+) = (1.06 \pm 0.09) \times 10^{-3}$ . Our first error is their experiment's error and our second error is the systematic error from using our best value.

$\Gamma(\bar{\Lambda}(1520)\Lambda + \text{c.c.})/\Gamma_{\text{total}}$		$\Gamma_{45}/\Gamma$	
VALUE (units $10^{-3}$ )	EVTS	DOCUMENT ID	TECN COMMENT

**$3.1 \pm 1.4 \pm 0.3$**  43 1 LU 19 BELL  $B^+ \rightarrow \bar{p}\Lambda K^+ K^+$

1 LU 19 reports  $(3.48 \pm 1.48 \pm 0.46) \times 10^{-3}$  from a measurement of  $[\Gamma(\eta_c(1S) \rightarrow \bar{\Lambda}(1520)\Lambda + \text{c.c.})/\Gamma_{\text{total}}] \times [B(B^+ \rightarrow \eta_c K^+)]$  assuming  $B(B^+ \rightarrow \eta_c K^+) = (9.6 \pm 1.1) \times 10^{-4}$ , which we rescale to our best value  $B(B^+ \rightarrow \eta_c K^+) = (1.06 \pm 0.09) \times 10^{-3}$ . Our first error is their experiment's error and our second error is the systematic error from using our best value.

$\Gamma(\Sigma^+\Sigma^-)/\Gamma_{\text{total}}$		$\Gamma_{46}/\Gamma$	
VALUE (units $10^{-3}$ )	EVTS	DOCUMENT ID	TECN COMMENT

**$2.1 \pm 0.3 \pm 0.5$**  112 1 ABLIKIM 13C BES3  $J/\psi \rightarrow \gamma\rho\bar{\rho}\pi^0\pi^0$

1 ABLIKIM 13C reports  $[\Gamma(\eta_c(1S) \rightarrow \Sigma^+\Sigma^-)/\Gamma_{\text{total}}] \times [B(J/\psi(1S) \rightarrow \gamma\eta_c(1S))] = (3.60 \pm 0.48 \pm 0.31) \times 10^{-5}$  which we divide by our best value  $B(J/\psi(1S) \rightarrow \gamma\eta_c(1S)) = (1.7 \pm 0.4) \times 10^{-2}$ . Our first error is their experiment's error and our second error is the systematic error from using our best value.

See key on page 999

Meson Particle Listings
ηc(1S)

Table with 5 columns: VALUE (units 10^-3), EVTS, DOCUMENT ID, TECN, COMMENT. Row 1: 0.90 ± 0.18 ± 0.19, 78, 1 ABLIKIM 13c BES3 J/ψ → γΛΛπ+π-

Table with 5 columns: VALUE (units 10^-3), CL%, EVTS, DOCUMENT ID, TECN, COMMENT. Row 1: 5.3 ± 1.7 ± 0.5, 19, 1 ABLIKIM 12N BES3 ψ(2S) → π0 γ p p-bar π+ π-

RADIATIVE DECAYS

Table with 5 columns: VALUE (units 10^-4), CL%, EVTS, DOCUMENT ID, TECN, COMMENT. Row 1: 1.56 ± 0.11 OUR FIT, 1.9 +0.7 -0.6 OUR AVERAGE

1 ABLIKIM 13i reports [Γ(ηc(1S) → γγ)/Γtotal] × [B(J/ψ(1S) → γηc(1S))] = (4.5 ± 1.2 ± 0.4) × 10^-6 which we divide by our best value B(J/ψ(1S) → γηc(1S)) = (1.7 ± 0.6) × 10^-2.

Table with 5 columns: VALUE (units 10^-3), EVTS, DOCUMENT ID, TECN, COMMENT. Row 1: 2.17 ± 0.23 OUR FIT, 3.2 +1.3 +0.8 -1.0 -0.6, 13, 1 WICHT 08 BELL B± → K± γγ

Table with 5 columns: VALUE (units 10^-6), EVTS, DOCUMENT ID, TECN, COMMENT. Row 1: 0.230 ± 0.022 OUR FIT, 0.26 ± 0.05 OUR AVERAGE, Error includes scale factor of 1.4.

Charge conjugation (C), Parity (P), Lepton family number (LF) violating modes

Table with 5 columns: VALUE (units 10^-5), CL%, DOCUMENT ID, TECN, COMMENT. Row 1: <11, 90, 1 ABLIKIM 11G BES3 J/ψ → γπ+π-

Table with 5 columns: VALUE (units 10^-9), CL%, DOCUMENT ID, TECN, COMMENT. Row 1: <4, 90, 1 ABLIKIM 11G BES3 J/ψ → γπ0 π0

Table with 5 columns: VALUE (units 10^-9), CL%, DOCUMENT ID, TECN, COMMENT. Row 1: <60, 90, 1 ABLIKIM 06B BES2 J/ψ → K+K-γ

Table with 5 columns: VALUE (units 10^-5), CL%, DOCUMENT ID, TECN, COMMENT. Row 1: <31, 90, 1 ABLIKIM 06B BES2 J/ψ → K\_S^0 K\_S^0 γ

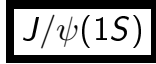
1 ABLIKIM 06B reports [Γ(ηc(1S) → K\_S^0 K\_S^0)/Γtotal] × [B(J/ψ(1S) → γηc(1S))] < 0.53 × 10^-5 which we divide by our best value B(J/ψ(1S) → γηc(1S)) = 1.7 × 10^-2.

ηc(1S) REFERENCES

ABLIKIM 19AP PR D100 012003 M. Ablikim et al. (BESIII Collab.)
ABLIKIM 19AV PR D100 052012 M. Ablikim et al. (BESIII Collab.)
LU 19 PR D99 032003 P.-C. Lu et al. (BELLE Collab.)

# Meson Particle Listings

## $J/\psi(1S)$



$$I^G(J^{PC}) = 0^-(1^{--})$$

### $J/\psi(1S)$ MASS

VALUE (MeV)	EVTs	DOCUMENT ID	TECN	COMMENT
<b>3096.900 ± 0.006 OUR AVERAGE</b>				
3096.900 ± 0.002 ± 0.006		1 ANASHIN 15	KEDR	$e^+e^- \rightarrow$ hadrons
3096.89 ± 0.09	502	2 ARTAMONOV 00	OLYA	$e^+e^- \rightarrow$ hadrons
3096.91 ± 0.03 ± 0.01		3 ARMSTRONG 93B	E760	$\bar{p}p \rightarrow e^+e^-$
3096.95 ± 0.1 ± 0.3	193	BAGLIN 87	SPEC	$\bar{p}p \rightarrow e^+e^-X$
••• We do not use the following data for averages, fits, limits, etc. •••				
3096.66 ± 0.19 ± 0.02	6.1k	4 AAIJ 15B1	LHCB	$pp \rightarrow J/\psi X$
3096.917 ± 0.010 ± 0.007		AULCHENKO 03	KEDR	$e^+e^- \rightarrow$ hadrons
3097.5 ± 0.3		GRIBUSHIN 96	FMP5	$515 \pi^-Be \rightarrow 2\mu X$
3098.4 ± 2.0	38k	LEMOIGNE 82	GOLI	$185 \pi^-Be \rightarrow \gamma \mu^+ \mu^- A$
3096.93 ± 0.09	502	5 ZHOLENTZ 80	REDE	$e^+e^-$
3097.0 ± 1		6 BRANDELIK 79c	DASP	$e^+e^-$

1 Supersedes AULCHENKO 03.  
 2 Reanalysis of ZHOLENTZ 80 using new electron mass (COHEN 87) and radiative corrections (KURAEV 85).  
 3 Mass central value and systematic error recalculated by us according to Eq. (16) in ARMSTRONG 93B, using the value for the  $\psi(2S)$  mass from AULCHENKO 03.  
 4 From a sample of  $\eta_c(1S)$  and  $J/\psi$  produced in  $b$ -hadron decays. Systematic uncertainties not estimated.  
 5 Superseded by ARTAMONOV 00.  
 6 From a simultaneous fit to  $e^+e^-$ ,  $\mu^+\mu^-$  and hadronic channels assuming  $\Gamma(e^+e^-) = \Gamma(\mu^+\mu^-)$ .

### $J/\psi(1S)$ WIDTH

VALUE (keV)	EVTs	DOCUMENT ID	TECN	COMMENT
<b>92.9 ± 2.8 OUR AVERAGE</b>				Error includes scale factor of 1.1.
96.1 ± 3.2	13k	1 ADAMS 06A	CLEO	$e^+e^- \rightarrow \mu^+\mu^-\gamma$
84.4 ± 8.9		BAI 95B	BES	$e^+e^-$
91 ± 11 ± 6		2 ARMSTRONG 93B	E760	$\bar{p}p \rightarrow e^+e^-$
85.5 ± 6.1 ± 5.8		3 HSUEH 92	RVUE	See $\Upsilon$ mini-review
••• We do not use the following data for averages, fits, limits, etc. •••				
92.94 ± 1.83		4 ANASHIN 18A	KEDR	$e^+e^-$
94.1 ± 2.7		5 ANASHIN 10	KEDR	$3.097 e^+e^- \rightarrow e^+e^-$ , $\mu^+\mu^-$
93.7 ± 3.5	7.8k	1 AUBERT 04	BABR	$e^+e^- \rightarrow \mu^+\mu^-\gamma$

1 Calculated by us from the reported values of  $\Gamma(e^+e^-) \times B(\mu^+\mu^-)$  using  $B(e^+e^-) = (5.94 \pm 0.06)\%$  and  $B(\mu^+\mu^-) = (5.93 \pm 0.06)\%$ .  
 2 The initial-state radiation correction reevaluated by ANDREOTTI 07 in its Ref. [4].  
 3 Using data from COFFMAN 92, BALDINI-CELIO 75, BOYARSKI 75, ESPOSITO 75B, BRANDELIK 79c.  
 4 Using  $\Gamma(e^+e^-)$  from ANASHIN 18A and  $B(J/\psi(1S) \rightarrow e^+e^-) = (5.971 \pm 0.032)\%$  from PDG 16.  
 5 Assuming  $\Gamma(e^+e^-) = \Gamma(\mu^+\mu^-)$  and using  $\Gamma(e^+e^-)/\Gamma_{\text{total}} = (5.94 \pm 0.06)\%$ .

### $J/\psi(1S)$ DECAY MODES

Mode	Fraction ( $\Gamma_i/\Gamma$ )	Scale factor/ Confidence level
$\Gamma_1$ hadrons	(87.7 ± 0.5) %	
$\Gamma_2$ virtual $\gamma \rightarrow$ hadrons	(13.50 ± 0.30) %	
$\Gamma_3$ $ggg$	(64.1 ± 1.0) %	
$\Gamma_4$ $\gamma gg$	(8.8 ± 1.1) %	
$\Gamma_5$ $e^+e^-$	(5.971 ± 0.032) %	
$\Gamma_6$ $e^+e^-\gamma$	[a] (8.8 ± 1.4) × 10 <sup>-3</sup>	
$\Gamma_7$ $\mu^+\mu^-$	(5.961 ± 0.033) %	
<b>Decays involving hadronic resonances</b>		
$\Gamma_8$ $\rho\pi$	(1.69 ± 0.15) %	S=2.4
$\Gamma_9$ $\rho^0\pi^0$	(5.6 ± 0.7) × 10 <sup>-3</sup>	
$\Gamma_{10}$ $\rho(770)^\mp K^\pm K_S^0$	(1.9 ± 0.4) × 10 <sup>-3</sup>	
$\Gamma_{11}$ $\rho(1450)\pi$		
$\Gamma_{12}$ $\rho(1450)\pi \rightarrow \pi^+\pi^-\pi^0$	(2.3 ± 0.7) × 10 <sup>-3</sup>	
$\Gamma_{13}$ $\rho(1450)^\pm \pi^\mp \rightarrow K_S^0 K^\pm \pi^\mp$	(3.5 ± 0.6) × 10 <sup>-4</sup>	
$\Gamma_{14}$ $\rho(1450)^0 \pi^0 \rightarrow K^+K^-\pi^0$	(2.7 ± 0.6) × 10 <sup>-4</sup>	
$\Gamma_{15}$ $\rho(1450)\eta'(958) \rightarrow \pi^+\pi^-\eta'(958)$	(3.3 ± 0.7) × 10 <sup>-6</sup>	
$\Gamma_{16}$ $\rho(1700)\pi$		
$\Gamma_{17}$ $\rho(1700)\pi \rightarrow \pi^+\pi^-\pi^0$	(1.7 ± 1.1) × 10 <sup>-4</sup>	
$\Gamma_{18}$ $\rho(2150)\pi$		
$\Gamma_{19}$ $\rho(2150)\pi \rightarrow \pi^+\pi^-\pi^0$	(8 ± 40) × 10 <sup>-6</sup>	
$\Gamma_{20}$ $\rho_3(1690)\pi \rightarrow \pi^+\pi^-\pi^0$		
$\Gamma_{21}$ $a_2(1320)\rho$	(1.09 ± 0.22) %	
$\Gamma_{22}$ $\omega\pi^+\pi^+\pi^-\pi^-$	(8.5 ± 3.4) × 10 <sup>-3</sup>	

$\Gamma_{23}$ $\omega\pi^+\pi^-\pi^0$	(4.0 ± 0.7) × 10 <sup>-3</sup>	
$\Gamma_{24}$ $\omega\pi^+\pi^-$	(7.2 ± 1.0) × 10 <sup>-3</sup>	
$\Gamma_{25}$ $\omega f_2(1270)$	(4.3 ± 0.6) × 10 <sup>-3</sup>	
$\Gamma_{26}$ $K^*(892)^0 \bar{K}^*(892)^0$	(2.3 ± 0.6) × 10 <sup>-4</sup>	
$\Gamma_{27}$ $K^*(892)^\pm K^*(892)^\mp$	(1.00 ± 0.22 ± 0.40) × 10 <sup>-3</sup>	
$\Gamma_{28}$ $K^*(892)^\pm K^*(700)^\mp$	(1.1 ± 1.0 ± 0.6) × 10 <sup>-3</sup>	
$\Gamma_{29}$ $K_S^0 \pi^- K^*(892)^+ + \text{c.c.}$	(2.0 ± 0.5) × 10 <sup>-3</sup>	
$\Gamma_{30}$ $K_S^0 \pi^- K^*(892)^+ + \text{c.c.} \rightarrow K_S^0 K_S^0 \pi^+ \pi^-$	(6.7 ± 2.2) × 10 <sup>-4</sup>	
$\Gamma_{31}$ $K_S^0 K^*(892)^0 \rightarrow \gamma K_S^0 K_S^0$	(6.3 ± 0.6 ± 0.5) × 10 <sup>-6</sup>	
$\Gamma_{32}$ $K_2^*(1430)^+ K^- + \text{c.c.} \rightarrow K^+ K^- \pi^0$	(2.69 ± 0.25 ± 0.19) × 10 <sup>-4</sup>	
$\Gamma_{33}$ $K_2^*(1980)^+ K^- + \text{c.c.} \rightarrow K^+ K^- \pi^0$	(1.10 ± 0.60 ± 0.14) × 10 <sup>-5</sup>	
$\Gamma_{34}$ $K_4^*(2045)^+ K^- + \text{c.c.} \rightarrow K^+ K^- \pi^0$	(6.2 ± 2.9 ± 1.6) × 10 <sup>-6</sup>	
$\Gamma_{35}$ $\eta K^*(892)^0 \bar{K}^*(892)^0$	(1.15 ± 0.26) × 10 <sup>-3</sup>	
$\Gamma_{36}$ $\eta' K^* K^\mp$	(1.48 ± 0.13) × 10 <sup>-3</sup>	
$\Gamma_{37}$ $\eta' K^* \bar{K}^0 + \text{c.c.}$	(1.66 ± 0.21) × 10 <sup>-3</sup>	
$\Gamma_{38}$ $\eta' h_1(1415) \rightarrow \eta' K^* \bar{K}^0 + \text{c.c.}$	(2.16 ± 0.31) × 10 <sup>-4</sup>	
$\Gamma_{39}$ $\eta' h_1(1415) \rightarrow \eta' K^* K^\mp$	(1.51 ± 0.23) × 10 <sup>-4</sup>	
$\Gamma_{40}$ $K^*(1410) \bar{K} + \text{c.c.}$		
$\Gamma_{41}$ $K^*(1410) \bar{K} + \text{c.c.} \rightarrow K^\pm K^\mp \pi^0$	(7 ± 4) × 10 <sup>-5</sup>	
$\Gamma_{42}$ $K^*(1410) \bar{K} + \text{c.c.} \rightarrow K_S^0 K^\pm \pi^\mp$	(8 ± 6) × 10 <sup>-5</sup>	
$\Gamma_{43}$ $K_2^*(1430) \bar{K} + \text{c.c.}$		
$\Gamma_{44}$ $K_2^*(1430) \bar{K} + \text{c.c.} \rightarrow K^\pm K^\mp \pi^0$	(1.0 ± 0.5) × 10 <sup>-4</sup>	
$\Gamma_{45}$ $K_2^*(1430) \bar{K} + \text{c.c.} \rightarrow K_S^0 K^\pm \pi^\mp$	(4.0 ± 1.0) × 10 <sup>-4</sup>	
$\Gamma_{46}$ $K^*(892)^0 \bar{K}_2^*(1430)^0 + \text{c.c.}$	(4.66 ± 0.31) × 10 <sup>-3</sup>	
$\Gamma_{47}$ $K^*(892)^+ K_2^*(1430)^- + \text{c.c.}$	(3.4 ± 2.9) × 10 <sup>-3</sup>	
$\Gamma_{48}$ $K^*(892)^+ K_2^*(1430)^- + \text{c.c.} \rightarrow K^*(892)^+ K_S^0 \pi^- + \text{c.c.}$	(4 ± 4) × 10 <sup>-4</sup>	
$\Gamma_{49}$ $K^*(892)^0 \bar{K}_2^*(1770)^0 + \text{c.c.} \rightarrow K^*(892)^0 K^- \pi^+ + \text{c.c.}$	(6.9 ± 0.9) × 10 <sup>-4</sup>	
$\Gamma_{50}$ $\omega K^*(892) \bar{K} + \text{c.c.}$	(6.1 ± 0.9) × 10 <sup>-3</sup>	
$\Gamma_{51}$ $\bar{K} K^*(892) + \text{c.c.}$		
$\Gamma_{52}$ $\bar{K} K^*(892) + \text{c.c.} \rightarrow K_S^0 K^\pm \pi^\mp$	(5.0 ± 0.5) × 10 <sup>-3</sup>	
$\Gamma_{53}$ $K^+ K^*(892)^- + \text{c.c.}$	(6.0 ± 0.8 ± 1.0) × 10 <sup>-3</sup>	S=2.9
$\Gamma_{54}$ $K^+ K^*(892)^- + \text{c.c.} \rightarrow K^+ K^- \pi^0$	(2.69 ± 0.13 ± 0.20) × 10 <sup>-3</sup>	
$\Gamma_{55}$ $K^+ K^*(892)^- + \text{c.c.} \rightarrow K^0 K^\pm \pi^\mp + \text{c.c.}$	(3.0 ± 0.4) × 10 <sup>-3</sup>	
$\Gamma_{56}$ $K^0 \bar{K}^*(892)^0 + \text{c.c.}$	(4.2 ± 0.4) × 10 <sup>-3</sup>	
$\Gamma_{57}$ $K^0 \bar{K}^*(892)^0 + \text{c.c.} \rightarrow K^0 K^\pm \pi^\mp + \text{c.c.}$	(3.2 ± 0.4) × 10 <sup>-3</sup>	
$\Gamma_{58}$ $K_1(1400)^\pm K^\mp$	(3.8 ± 1.4) × 10 <sup>-3</sup>	
$\Gamma_{59}$ $\bar{K}^*(892)^0 K^+ \pi^- + \text{c.c.}$	(7.7 ± 1.6) × 10 <sup>-3</sup>	
$\Gamma_{60}$ $K^*(892)^\pm K^\mp \pi^0$	(4.1 ± 1.3) × 10 <sup>-3</sup>	
$\Gamma_{61}$ $K^*(892)^0 K_S^0 \pi^0$	(6 ± 4) × 10 <sup>-4</sup>	
$\Gamma_{62}$ $\omega\pi^0\pi^0$	(3.4 ± 0.8) × 10 <sup>-3</sup>	
$\Gamma_{63}$ $\omega\pi^0\eta$	(3.4 ± 1.7) × 10 <sup>-4</sup>	
$\Gamma_{64}$ $b_1(1235)^\pm \pi^\mp$	[b] (3.0 ± 0.5) × 10 <sup>-3</sup>	
$\Gamma_{65}$ $\omega K^\pm K_S^0 \pi^\mp$	[b] (3.4 ± 0.5) × 10 <sup>-3</sup>	
$\Gamma_{66}$ $b_1(1235)^0 \pi^0$	(2.3 ± 0.6) × 10 <sup>-3</sup>	
$\Gamma_{67}$ $\eta K^\pm K_S^0 \pi^\mp$	[b] (2.2 ± 0.4) × 10 <sup>-3</sup>	
$\Gamma_{68}$ $\phi K^*(892) \bar{K} + \text{c.c.}$	(2.18 ± 0.23) × 10 <sup>-3</sup>	
$\Gamma_{69}$ $\omega K \bar{K}$	(1.9 ± 0.4) × 10 <sup>-3</sup>	
$\Gamma_{70}$ $\omega f_0(1710) \rightarrow \omega K \bar{K}$	(4.8 ± 1.1) × 10 <sup>-4</sup>	
$\Gamma_{71}$ $\phi 2(\pi^+\pi^-)$	(1.60 ± 0.32) × 10 <sup>-3</sup>	
$\Gamma_{72}$ $\Delta(1232)^{++} \bar{p}\pi^-$	(1.6 ± 0.5) × 10 <sup>-3</sup>	
$\Gamma_{73}$ $\omega\eta$	(1.74 ± 0.20) × 10 <sup>-3</sup>	S=1.6
$\Gamma_{74}$ $\omega\eta' \pi^+ \pi^-$	(1.12 ± 0.13) × 10 <sup>-3</sup>	
$\Gamma_{75}$ $\phi K \bar{K}$	(1.77 ± 0.16) × 10 <sup>-3</sup>	S=1.3
$\Gamma_{76}$ $\phi K_S^0 K_S^0$	(5.9 ± 1.5) × 10 <sup>-4</sup>	
$\Gamma_{77}$ $\phi f_0(1710) \rightarrow \phi K \bar{K}$	(3.6 ± 0.6) × 10 <sup>-4</sup>	
$\Gamma_{78}$ $\phi K^+ K^-$	(8.3 ± 1.2) × 10 <sup>-4</sup>	
$\Gamma_{79}$ $\phi f_2(1270)$	(3.2 ± 0.6) × 10 <sup>-4</sup>	





Γ(μ<sup>+</sup>μ<sup>-</sup>) Γ<sub>7</sub>

Table with columns: VALUE (keV), DOCUMENT ID, TECN, COMMENT. Includes entries for BAI, BOYARSKI, ESPOSITO, BES, MRK1, FRAM.

Γ(γγ) Γ<sub>303</sub>

Table with columns: VALUE (eV), CL%, DOCUMENT ID, TECN, COMMENT. Includes entry for BRANDELIK.

J/ψ(1S) Γ(i)Γ(e<sup>+</sup>e<sup>-</sup>)/Γ(total)

This combination of a partial width with the partial width into e<sup>+</sup>e<sup>-</sup> and with the total width is obtained from the integrated cross section into channel i in the e<sup>+</sup>e<sup>-</sup> annihilation.

Γ(hadrons) × Γ(e<sup>+</sup>e<sup>-</sup>)/Γ<sub>total</sub> Γ<sub>1</sub>Γ<sub>5</sub>/Γ

Table with columns: VALUE (keV), DOCUMENT ID, TECN, COMMENT. Includes entries for ANASHIN, BALDINI..., ESPOSITO, KEDR, FRAG, FRAM.

1 From the cross sections of e<sup>+</sup>e<sup>-</sup> → e<sup>+</sup>e<sup>-</sup> and e<sup>+</sup>e<sup>-</sup> → hadrons near the J/ψ(1S) peak. 2 Data redundant with branching ratios or partial widths above.

Γ(e<sup>+</sup>e<sup>-</sup>) × Γ(e<sup>+</sup>e<sup>-</sup>)/Γ<sub>total</sub> Γ<sub>5</sub>Γ<sub>5</sub>/Γ

Table with columns: VALUE (eV), DOCUMENT ID, TECN, COMMENT. Includes entries for ANASHIN, BRANDELIK, BALDINI..., ESPOSITO, FORD.

1 From the cross sections of e<sup>+</sup>e<sup>-</sup> → e<sup>+</sup>e<sup>-</sup> and e<sup>+</sup>e<sup>-</sup> → hadrons near the J/ψ(1S) peak. 2 Data redundant with branching ratios or partial widths above.

Γ(μ<sup>+</sup>μ<sup>-</sup>) × Γ(e<sup>+</sup>e<sup>-</sup>)/Γ<sub>total</sub> Γ<sub>7</sub>Γ<sub>5</sub>/Γ

Table with columns: VALUE (eV), EVTS, DOCUMENT ID, TECN, COMMENT. Includes entries for ABLIKIM, ANASHIN, ADAMS, AUBERT, DASP, ESPOSITO.

1 Data redundant with branching ratios or partial widths above.

Γ(ρ(770)<sup>±</sup>K<sup>±</sup>K<sub>S</sub><sup>0</sup>) × Γ(e<sup>+</sup>e<sup>-</sup>)/Γ<sub>total</sub> Γ<sub>10</sub>Γ<sub>5</sub>/Γ

Table with columns: VALUE (eV), EVTS, DOCUMENT ID, TECN, COMMENT. Includes entry for LEES.

Γ(ωπ<sup>+</sup>π<sup>-</sup>π<sup>0</sup>) × Γ(e<sup>+</sup>e<sup>-</sup>)/Γ<sub>total</sub> Γ<sub>23</sub>Γ<sub>5</sub>/Γ

Table with columns: VALUE (10<sup>-2</sup> keV), EVTS, DOCUMENT ID, TECN, COMMENT. Includes entry for AUBERT.

Γ(ωπ<sup>+</sup>π<sup>-</sup>) × Γ(e<sup>+</sup>e<sup>-</sup>)/Γ<sub>total</sub> Γ<sub>24</sub>Γ<sub>5</sub>/Γ

Table with columns: VALUE (eV), EVTS, DOCUMENT ID, TECN, COMMENT. Includes entry for AUBERT.

1 AUBERT 07AU reports [Γ(J/ψ(1S) → ωπ<sup>+</sup>π<sup>-</sup>) × Γ(J/ψ(1S) → e<sup>+</sup>e<sup>-</sup>)/Γ<sub>total</sub>] × [B(ω(782) → π<sup>+</sup>π<sup>-</sup>π<sup>0</sup>)] = 47.8 ± 3.1 ± 3.2 eV which we divide by our best value B(ω(782) → π<sup>+</sup>π<sup>-</sup>π<sup>0</sup>) = (89.3 ± 0.6) × 10<sup>-2</sup>. Our first error is their experiment's error and our second error is the systematic error from using our best value.

Γ(ωπ<sup>0</sup>π<sup>0</sup>) × Γ(e<sup>+</sup>e<sup>-</sup>)/Γ<sub>total</sub> Γ<sub>62</sub>Γ<sub>5</sub>/Γ

Table with columns: VALUE (eV), EVTS, DOCUMENT ID, TECN, COMMENT. Includes entry for LEES.

1 LEES 18E reports [Γ(J/ψ(1S) → ωπ<sup>0</sup>π<sup>0</sup>) × Γ(J/ψ(1S) → e<sup>+</sup>e<sup>-</sup>)/Γ<sub>total</sub>] × [B(ω(782) → π<sup>+</sup>π<sup>-</sup>π<sup>0</sup>)] = 24.8 ± 1.8 ± 2.5 eV which we divide by our best value B(ω(782) → π<sup>+</sup>π<sup>-</sup>π<sup>0</sup>) = (89.3 ± 0.6) × 10<sup>-2</sup>. Our first error is their experiment's error and our second error is the systematic error from using our best value.

Γ(K\*(892)<sup>0</sup>K\*(892)<sup>0</sup>) × Γ(e<sup>+</sup>e<sup>-</sup>)/Γ<sub>total</sub> Γ<sub>26</sub>Γ<sub>5</sub>/Γ

Table with columns: VALUE (eV), EVTS, DOCUMENT ID, TECN, COMMENT. Includes entry for LEES.

• • • We do not use the following data for averages, fits, limits, etc. • • •

Table with columns: VALUE, EVTS, DOCUMENT ID, TECN, COMMENT. Includes entry for AUBERT.

Γ(K\*(892)<sup>±</sup>K\*(892)<sup>∓</sup>) × Γ(e<sup>+</sup>e<sup>-</sup>)/Γ<sub>total</sub> Γ<sub>27</sub>Γ<sub>5</sub>/Γ

Table with columns: VALUE (eV), EVTS, DOCUMENT ID, TECN, COMMENT. Includes entry for LEES.

1 Dividing by (1/4)<sup>2</sup> to take twice into account B(K\*(892) → K<sub>S</sub><sup>0</sup>π) = 1/4.

Γ(K<sub>S</sub><sup>0</sup>π<sup>-</sup>K\*(892)<sup>+</sup>+ c.c.) × Γ(e<sup>+</sup>e<sup>-</sup>)/Γ<sub>total</sub> Γ<sub>29</sub>Γ<sub>5</sub>/Γ

Table with columns: VALUE (eV), EVTS, DOCUMENT ID, TECN, COMMENT. Includes entries for LEES, BABR.

1 Dividing by 1/2 to take into account B(K\*(892)<sup>±</sup> → K<sup>±</sup>π<sup>∓</sup>) = 1/2. 2 Dividing by 1/4 to take into account B(K\*(892) → K<sub>S</sub><sup>0</sup>π) = 1/4.

Γ(K<sub>S</sub><sup>0</sup>π<sup>-</sup>K\*(892)<sup>+</sup>+ c.c. → K<sub>S</sub><sup>0</sup>K<sub>S</sub><sup>0</sup>π<sup>+</sup>π<sup>-</sup>) × Γ(e<sup>+</sup>e<sup>-</sup>)/Γ<sub>total</sub> Γ<sub>30</sub>Γ<sub>5</sub>/Γ

Table with columns: VALUE (eV), EVTS, DOCUMENT ID, TECN, COMMENT. Includes entry for LEES.

Γ(K\*(892)<sup>0</sup>K<sub>2</sub><sup>\*(1430)</sup><sup>0</sup>+ c.c.) × Γ(e<sup>+</sup>e<sup>-</sup>)/Γ<sub>total</sub> Γ<sub>46</sub>Γ<sub>5</sub>/Γ

Table with columns: VALUE (eV), EVTS, DOCUMENT ID, TECN, COMMENT. Includes entries for LEES, BABR.

• • • We do not use the following data for averages, fits, limits, etc. • • • 1 LEES 12F reports [Γ(J/ψ(1S) → K\*(892)<sup>0</sup>K<sub>2</sub><sup>\*(1430)</sup><sup>0</sup>+ c.c.) × Γ(J/ψ(1S) → e<sup>+</sup>e<sup>-</sup>)/Γ<sub>total</sub>] × [B(K<sub>2</sub><sup>\*(1430)</sup> → Kπ)] = 12.89 ± 0.54 ± 0.41 eV which we divide by our best value B(K<sub>2</sub><sup>\*(1430)</sup> → Kπ) = (49.9 ± 1.2) × 10<sup>-2</sup>. Our first error is their experiment's error and our second error is the systematic error from using our best value. 2 Dividing by 2/3 to take into account that B(K\*(892)<sup>0</sup> → K<sup>+</sup>π<sup>-</sup>) = 2/3 B(K\*(892)<sup>0</sup> → Kπ). 3 The K<sub>2</sub><sup>\*(1430)</sup> cannot be distinguished from the K<sub>0</sub><sup>\*</sup>(1430). 4 Superseded by LEES 12F. AUBERT 07AK reports [Γ(J/ψ(1S) → K\*(892)<sup>0</sup>K<sub>2</sub><sup>\*(1430)</sup><sup>0</sup>+ c.c.) × Γ(J/ψ(1S) → e<sup>+</sup>e<sup>-</sup>)/Γ<sub>total</sub>] × [B(K<sub>2</sub><sup>\*(1430)</sup> → Kπ)] = 16.4 ± 1.1 ± 1.4 eV which we divide by our best value B(K<sub>2</sub><sup>\*(1430)</sup> → Kπ) = (49.9 ± 1.2) × 10<sup>-2</sup>. Our first error is their experiment's error and our second error is the systematic error from using our best value.

Γ(K\*(892)<sup>+</sup>K<sub>2</sub><sup>\*(1430)</sup><sup>-</sup>+ c.c.) × Γ(e<sup>+</sup>e<sup>-</sup>)/Γ<sub>total</sub> Γ<sub>47</sub>Γ<sub>5</sub>/Γ

Table with columns: VALUE (eV), EVTS, DOCUMENT ID, TECN, COMMENT. Includes entry for LEES.

1 Dividing by (1/4)<sup>2</sup> to take into account B(K\*(892) → K<sub>S</sub><sup>0</sup>π) = 1/4 and B(K\*(1430) → K<sub>S</sub><sup>0</sup>π) = 1/4 B(K\*(1430) → Kπ). 2 LEES 14H reports [Γ(J/ψ(1S) → K\*(892)<sup>+</sup>K<sub>2</sub><sup>\*(1430)</sup><sup>-</sup>+ c.c.) × Γ(J/ψ(1S) → e<sup>+</sup>e<sup>-</sup>)/Γ<sub>total</sub>] × [B(K<sub>2</sub><sup>\*(1430)</sup> → Kπ)] = 9.28 ± 8.0 ± 0.32 eV which we divide by our best value B(K<sub>2</sub><sup>\*(1430)</sup> → Kπ) = (49.9 ± 1.2) × 10<sup>-2</sup>. Our first error is their experiment's error and our second error is the systematic error from using our best value.

Γ(K\*(892)<sup>+</sup>K<sub>2</sub><sup>\*(1430)</sup><sup>-</sup>+ c.c. → K\*(892)<sup>0</sup>K<sub>S</sub><sup>0</sup>π<sup>+</sup>+ c.c.) × Γ(e<sup>+</sup>e<sup>-</sup>)/Γ<sub>total</sub> Γ<sub>48</sub>Γ<sub>5</sub>/Γ

Table with columns: VALUE (eV), EVTS, DOCUMENT ID, TECN, COMMENT. Includes entry for LEES.

1 Dividing by 1/4 to take into account B(K\*(892) → K<sub>S</sub><sup>0</sup>π) = 1/4.

Γ(K\*(892)<sup>0</sup>K<sub>2</sub><sup>\*(1770)</sup><sup>0</sup>+ c.c. → K\*(892)<sup>0</sup>K<sup>-</sup>π<sup>+</sup>+ c.c.) × Γ(e<sup>+</sup>e<sup>-</sup>)/Γ<sub>total</sub> Γ<sub>49</sub>Γ<sub>5</sub>/Γ

Table with columns: VALUE (eV), EVTS, DOCUMENT ID, TECN, COMMENT. Includes entry for AUBERT.

1 Dividing by 2/3 to take into account that B(K\*(892)<sup>0</sup> → K<sup>+</sup>π<sup>-</sup>) = 2/3.

Γ(K<sup>+</sup>K\*(892)<sup>-</sup>+ c.c.) × Γ(e<sup>+</sup>e<sup>-</sup>)/Γ<sub>total</sub> Γ<sub>53</sub>Γ<sub>5</sub>/Γ

Table with columns: VALUE (eV), DOCUMENT ID, TECN, COMMENT. Includes entry for AUBERT.

1 LEES 18E reports [Γ(J/ψ(1S) → ωπ<sup>0</sup>π<sup>0</sup>) × Γ(J/ψ(1S) → e<sup>+</sup>e<sup>-</sup>)/Γ<sub>total</sub>] × [B(ω(782) → π<sup>+</sup>π<sup>-</sup>π<sup>0</sup>)] = 24.8 ± 1.8 ± 2.5 eV which we divide by our best value B(ω(782) → π<sup>+</sup>π<sup>-</sup>π<sup>0</sup>) = (89.3 ± 0.6) × 10<sup>-2</sup>. Our first error is their experiment's error and our second error is the systematic error from using our best value.

Γ(K<sup>+</sup>K\*(892)<sup>-</sup>+ c.c. → K<sup>+</sup>K<sup>-</sup>π<sup>0</sup>) × Γ(e<sup>+</sup>e<sup>-</sup>)/Γ<sub>total</sub> Γ<sub>54</sub>Γ<sub>5</sub>/Γ

Table with columns: VALUE (eV), EVTS, DOCUMENT ID, TECN, COMMENT. Includes entry for AUBERT.

Γ(K<sup>+</sup>K\*(892)<sup>-</sup>+ c.c. → K<sup>+</sup>K<sup>-</sup>π<sup>0</sup>)/Γ<sub>total</sub> Γ<sub>54</sub>/Γ

Table with columns: VALUE (units 10<sup>-3</sup>), EVTS, DOCUMENT ID, TECN, COMMENT. Includes entry for ABLIKIM.



••• We do not use the following data for averages, fits, limits, etc. •••  
3.13±0.88±0.03 23 2 AUBERT,BE 06D BABR 10.6 e+e- -> K+K-pi0-pi0-gamma

1 LEES 12F reports [Gamma(J/psi(1S) -> phi-pi0-pi0) x Gamma(J/psi(1S) -> e+e-)/Gamma\_total] x [B(phi(1020) -> K+K-)] = 1.36 ± 0.27 ± 0.07 eV which we divide by our best value B(phi(1020) -> K+K-) = (49.2 ± 0.5) x 10^-2. Our first error is their experiment's error and our second error is the systematic error from using our best value.  
2 Superseded by LEES 12F. AUBERT,BE 06D reports [Gamma(J/psi(1S) -> phi-pi0-pi0) x Gamma(J/psi(1S) -> e+e-)/Gamma\_total] x [B(phi(1020) -> K+K-)] = 1.54 ± 0.40 ± 0.16 eV which we divide by our best value B(phi(1020) -> K+K-) = (49.2 ± 0.5) x 10^-2. Our first error is their experiment's error and our second error is the systematic error from using our best value.

Gamma(phi eta) x Gamma(e+e-)/Gamma\_total G89 G5/G  
VALUE (eV) EVTS DOCUMENT ID TECN COMMENT  
6.1 ± 2.7 ± 0.4 6 1 AUBERT 07AU BABR 10.6 e+e- -> phi eta gamma  
1 AUBERT 07AU quotes Gamma\_e+e-^J/psi . B(J/psi -> phi eta) . B(phi -> K+K-) . B(eta -> 3pi) = 0.84 ± 0.37 ± 0.05 eV.

Gamma(phi\_0(980) -> phi pi pi-) x Gamma(e+e-)/Gamma\_total G97 G5/G  
VALUE (eV) EVTS DOCUMENT ID TECN COMMENT  
1.44 ± 0.19 OUR AVERAGE  
1.40 ± 0.25 ± 0.02 57 ± 9 1 LEES 12F BABR 10.6 e+e- -> pi+ pi- K+ K- gamma  
1.48 ± 0.27 ± 0.09 60 ± 11 2 SHEN 09 BELL 10.6 e+e- -> K+ K- pi+ pi- gamma  
••• We do not use the following data for averages, fits, limits, etc. •••

1.02 ± 0.24 ± 0.01 20 ± 5 3 AUBERT 07AK BABR 10.6 e+e- -> pi+ pi- K+ K- gamma  
1 LEES 12F reports [Gamma(J/psi(1S) -> phi\_0(980) -> phi pi pi-) x Gamma(J/psi(1S) -> e+e-)/Gamma\_total] x [B(phi(1020) -> K+K-)] = 0.69 ± 0.11 ± 0.05 eV which we divide by our best value B(phi(1020) -> K+K-) = (49.2 ± 0.5) x 10^-2. Our first error is their experiment's error and our second error is the systematic error from using our best value.  
2 Multiplied by 2/3 to take into account the phi pi pi- mode only. Using B(phi -> K+K-) = (49.2 ± 0.6)%.  
3 Superseded by LEES 12F. AUBERT 07AK reports [Gamma(J/psi(1S) -> phi\_0(980) -> phi pi pi-) x Gamma(J/psi(1S) -> e+e-)/Gamma\_total] x [B(phi(1020) -> K+K-)] = 0.50 ± 0.11 ± 0.04 eV which we divide by our best value B(phi(1020) -> K+K-) = (49.2 ± 0.5) x 10^-2. Our first error is their experiment's error and our second error is the systematic error from using our best value.

Gamma(phi\_0(980) -> phi pi pi^0) x Gamma(e+e-)/Gamma\_total G98 G5/G  
VALUE (eV) EVTS DOCUMENT ID TECN COMMENT  
0.98 ± 0.26 ± 0.01 16 ± 4 1 LEES 12F BABR 10.6 e+e- -> pi^0 pi^0 K+ K- gamma  
••• We do not use the following data for averages, fits, limits, etc. •••

0.95 ± 0.40 ± 0.01 7.0 ± 2.8 2 AUBERT 07AK BABR 10.6 e+e- -> pi^0 pi^0 K+ K- gamma  
1 LEES 12F reports [Gamma(J/psi(1S) -> phi\_0(980) -> phi pi pi^0) x Gamma(J/psi(1S) -> e+e-)/Gamma\_total] x [B(phi(1020) -> K+K-)] = 0.48 ± 0.12 ± 0.05 eV which we divide by our best value B(phi(1020) -> K+K-) = (49.2 ± 0.5) x 10^-2. Our first error is their experiment's error and our second error is the systematic error from using our best value.  
2 Superseded by LEES 12F. AUBERT 07AK reports [Gamma(J/psi(1S) -> phi\_0(980) -> phi pi pi^0) x Gamma(J/psi(1S) -> e+e-)/Gamma\_total] x [B(phi(1020) -> K+K-)] = 0.47 ± 0.19 ± 0.05 eV which we divide by our best value B(phi(1020) -> K+K-) = (49.2 ± 0.5) x 10^-2. Our first error is their experiment's error and our second error is the systematic error from using our best value.

Gamma(eta pi pi-) x Gamma(e+e-)/Gamma\_total G109 G5/G  
VALUE (eV) EVTS DOCUMENT ID TECN COMMENT  
2.3 ± 0.4 OUR AVERAGE  
2.34 ± 0.43 ± 0.16 49 LEES 18 BABR e+e- -> eta pi+ pi- gamma  
2.23 ± 0.97 ± 0.03 9 1 AUBERT 07AU BABR 10.6 e+e- -> eta pi+ pi- gamma

1 AUBERT 07AU reports [Gamma(J/psi(1S) -> eta pi pi-) x Gamma(J/psi(1S) -> e+e-)/Gamma\_total] x [B(eta -> pi+ pi- pi^0)] = 0.51 ± 0.22 ± 0.03 eV which we divide by our best value B(eta -> pi+ pi- pi^0) = (22.92 ± 0.28) x 10^-2. Our first error is their experiment's error and our second error is the systematic error from using our best value.

Gamma(K\_S^0 pi- K\_2^\*(1430)+ + c.c.) x Gamma(e+e-)/Gamma\_total G118 G5/G  
VALUE (eV) EVTS DOCUMENT ID TECN COMMENT  
20.1 ± 9.8 ± 0.5 35 1,2 LEES 14H BABR e+e- -> pi+ pi- K\_S^0 K\_S^0 gamma

1 Dividing by 1/4 to take into account B(K\*(1430) -> K\_S^0 pi) = 1/4 B(K\*(1430) -> K pi).  
2 LEES 14H reports [Gamma(J/psi(1S) -> K\_S^0 pi- K\_2^\*(1430)+ + c.c.) x Gamma(J/psi(1S) -> e+e-)/Gamma\_total] x [B(K\_2^\*(1430) -> K pi)] = 10.0 ± 4.8 ± 0.8 eV which we divide by our best value B(K\_2^\*(1430) -> K pi) = (49.9 ± 1.2) x 10^-2. Our first error is their experiment's error and our second error is the systematic error from using our best value.

Gamma(2(pi+ pi-) pi^0) x Gamma(e+e-)/Gamma\_total G139 G5/G  
VALUE (eV) EVTS DOCUMENT ID TECN COMMENT  
303 ± 5 ± 18 4990 AUBERT 07AU BABR 10.6 e+e- -> 2(pi+ pi-) pi^0 gamma

Gamma(pi+ pi- pi^0) x Gamma(e+e-)/Gamma\_total G141 G5/G  
VALUE (keV) EVTS DOCUMENT ID TECN COMMENT  
0.122 ± 0.005 ± 0.008 AUBERT,B 04N BABR 10.6 e+e- -> pi+ pi- pi^0 gamma

Gamma(pi+ pi- pi^0 pi^0) x Gamma(e+e-)/Gamma\_total G142 G5/G  
VALUE (eV) EVTS DOCUMENT ID TECN COMMENT  
150.0 ± 4.0 ± 15.0 2.3k LEES 18E BABR 10.6 e+e- -> pi+ pi- 3 pi^0 gamma

Gamma(rho+ pi- pi^0 pi^0) x Gamma(e+e-)/Gamma\_total G143 G5/G  
VALUE (eV) EVTS DOCUMENT ID TECN COMMENT  
78.0 ± 9.0 ± 8.0 1.2k LEES 18E BABR 10.6 e+e- -> pi+ pi- 3 pi^0 gamma

Gamma(rho+ rho- pi^0) x Gamma(e+e-)/Gamma\_total G144 G5/G  
VALUE (eV) EVTS DOCUMENT ID TECN COMMENT  
33.0 ± 5.0 ± 3.3 529 LEES 18E BABR 10.6 e+e- -> pi+ pi- 3 pi^0 gamma

Gamma(pi+ pi- pi^0 K+ K-) x Gamma(e+e-)/Gamma\_total G145 G5/G  
VALUE (eV) EVTS DOCUMENT ID TECN COMMENT  
107.0 ± 4.3 ± 6.4 768 AUBERT 07AU BABR 10.6 e+e- -> K+ K- pi+ pi- pi^0 gamma

Gamma(pi+ pi- K+ K-) x Gamma(e+e-)/Gamma\_total G147 G5/G  
VALUE (eV) EVTS DOCUMENT ID TECN COMMENT  
37.94 ± 0.81 ± 1.10 3.1k LEES 12F BABR 10.6 e+e- -> pi+ pi- K+ K- gamma

••• We do not use the following data for averages, fits, limits, etc. •••  
36.3 ± 1.3 ± 2.1 1.5k 1 AUBERT 07AK BABR 10.6 e+e- -> pi+ pi- K+ K- gamma  
33.6 ± 2.7 ± 2.7 233 2 AUBERT 05D BABR 10.6 e+e- -> K+ K- pi+ pi- gamma  
1 Superseded by LEES 12F.  
2 Superseded by AUBERT 07AK.

Gamma(pi+ pi- K\_S^0 K\_L^0) x Gamma(e+e-)/Gamma\_total G148 G5/G  
VALUE (eV) EVTS DOCUMENT ID TECN COMMENT  
20.8 ± 2.3 ± 2.1 248 LEES 14H BABR e+e- -> pi+ pi- K\_S^0 K\_L^0 gamma

Gamma(pi+ pi- K\_S^0 K\_S^0) x Gamma(e+e-)/Gamma\_total G149 G5/G  
VALUE (eV) EVTS DOCUMENT ID TECN COMMENT  
9.3 ± 0.9 ± 0.5 133 LEES 14H BABR e+e- -> pi+ pi- K\_S^0 K\_S^0 gamma

Gamma(pi+ pi^0 K+ K\_S^0) x Gamma(e+e-)/Gamma\_total G150 G5/G  
VALUE (eV) EVTS DOCUMENT ID TECN COMMENT  
31.7 ± 1.9 ± 1.8 393 LEES 17D BABR e+e- -> K\_S^0 K+ pi+ pi^0 gamma

Gamma(K+ K- K\_S^0 K\_S^0) x Gamma(e+e-)/Gamma\_total G151 G5/G  
VALUE (eV) EVTS DOCUMENT ID TECN COMMENT  
2.3 ± 0.4 ± 0.1 29 LEES 14H BABR e+e- -> K\_S^0 K\_S^0 K+ K- gamma

Gamma(pi+ pi- K+ K- eta) x Gamma(e+e-)/Gamma\_total G152 G5/G  
VALUE (eV) EVTS DOCUMENT ID TECN COMMENT  
25.9 ± 3.9 ± 0.1 73 1 AUBERT 07AU BABR 10.6 e+e- -> K+ K- pi+ pi- eta gamma

1 AUBERT 07AU reports [Gamma(J/psi(1S) -> pi+ pi- K+ K- eta) x Gamma(J/psi(1S) -> e+e-)/Gamma\_total] x [B(eta -> 2 gamma)] = 10.2 ± 1.3 ± 0.8 eV which we divide by our best value B(eta -> 2 gamma) = (39.41 ± 0.20) x 10^-2. Our first error is their experiment's error and our second error is the systematic error from using our best value.

Gamma(pi^0 pi^0 K+ K-) x Gamma(e+e-)/Gamma\_total G153 G5/G  
VALUE (eV) EVTS DOCUMENT ID TECN COMMENT  
11.75 ± 0.81 ± 0.90 388 LEES 12F BABR 10.6 e+e- -> pi^0 pi^0 K+ K- gamma

••• We do not use the following data for averages, fits, limits, etc. •••  
13.6 ± 1.1 ± 1.3 203 1 AUBERT 07AK BABR 10.6 e+e- -> pi^0 pi^0 K+ K- gamma  
1 Superseded by LEES 12F.

Gamma(pi^0 pi^0 K\_S^0 K\_L^0) x Gamma(e+e-)/Gamma\_total G154 G5/G  
VALUE (eV) EVTS DOCUMENT ID TECN COMMENT  
10.3 ± 2.3 ± 0.5 47 LEES 17A BABR e+e- -> K\_S^0 K\_L^0 pi^0 pi^0 gamma

Gamma(K\_S^0 K\_L^0 pi^0) x Gamma(e+e-)/Gamma\_total G158 G5/G  
VALUE (eV) EVTS DOCUMENT ID TECN COMMENT  
11.4 ± 1.3 ± 0.6 182 LEES 17A BABR e+e- -> K\_S^0 K\_L^0 pi^0 gamma

Gamma(K\*(892)^0 K^0 + c.c. -> K\_S^0 K\_L^0 pi^0) x Gamma(e+e-)/Gamma\_total G159 G5/G  
VALUE (eV) EVTS DOCUMENT ID TECN COMMENT  
6.7 ± 0.9 ± 0.4 106 LEES 17A BABR e+e- -> K\_S^0 K\_L^0 pi^0 gamma

Gamma(K\_2^\*(1430)^0 K^0 + c.c. -> K\_S^0 K\_L^0 pi^0) x Gamma(e+e-)/Gamma\_total G160 G5/G  
VALUE (eV) EVTS DOCUMENT ID TECN COMMENT  
2.4 ± 0.7 ± 0.1 37 LEES 17A BABR e+e- -> K\_S^0 K\_L^0 pi^0 gamma

Gamma(K\_S^0 K\_L^0 eta) x Gamma(e+e-)/Gamma\_total G161 G5/G  
VALUE (eV) EVTS DOCUMENT ID TECN COMMENT  
8.0 ± 1.8 ± 0.4 45 LEES 17A BABR e+e- -> K\_S^0 K\_L^0 eta gamma

Gamma(2(pi+ pi-)) x Gamma(e+e-)/Gamma\_total G162 G5/G  
VALUE (eV) EVTS DOCUMENT ID TECN COMMENT  
20.4 ± 0.9 ± 0.4 LEES 12E BABR 10.6 e+e- -> 2 pi+ 2 pi- gamma



# Meson Particle Listings

## $J/\psi(1S)$

••• We do not use the following data for averages, fits, limits, etc. •••

19.5 ± 1.4 ± 1.3	270	<sup>1</sup> AUBERT	05D	BABR	10.6 e <sup>+</sup> e <sup>-</sup> → 2(π <sup>+</sup> π <sup>-</sup> )γ
<sup>1</sup> Superseded by LEES 12E.					

### $\Gamma(3(\pi^+\pi^-)) \times \Gamma(e^+e^-)/\Gamma_{total}$ $\Gamma_{163}\Gamma_5/\Gamma$

VALUE (10 <sup>-2</sup> keV)	EVTS	DOCUMENT ID	TECN	COMMENT
<b>2.37 ± 0.16 ± 0.14</b>	496	AUBERT	06D	BABR 10.6 e <sup>+</sup> e <sup>-</sup> → 3(π <sup>+</sup> π <sup>-</sup> )γ

### $\Gamma(2(\pi^+\pi^-\pi^0)) \times \Gamma(e^+e^-)/\Gamma_{total}$ $\Gamma_{164}\Gamma_5/\Gamma$

VALUE (10 <sup>-2</sup> keV)	EVTS	DOCUMENT ID	TECN	COMMENT
<b>8.9 ± 0.5 ± 1.0</b>	761	AUBERT	06D	BABR 10.6 e <sup>+</sup> e <sup>-</sup> → 2(π <sup>+</sup> π <sup>-</sup> π <sup>0</sup> )γ

### $\Gamma(2(\pi^+\pi^-)\eta) \times \Gamma(e^+e^-)/\Gamma_{total}$ $\Gamma_{165}\Gamma_5/\Gamma$

VALUE (eV)	EVTS	DOCUMENT ID	TECN	COMMENT
<b>13.1 ± 2.4 ± 0.1</b>	85	<sup>1</sup> AUBERT	07AU	BABR 10.6 e <sup>+</sup> e <sup>-</sup> → 2(π <sup>+</sup> π <sup>-</sup> )ηγ

<sup>1</sup> AUBERT 07AU reports [ $\Gamma(J/\psi(1S) \rightarrow 2(\pi^+\pi^-)\eta) \times \Gamma(J/\psi(1S) \rightarrow e^+e^-)/\Gamma_{total}] \times [B(\eta \rightarrow 2\gamma)] = 5.16 \pm 0.85 \pm 0.39$  eV which we divide by our best value  $B(\eta \rightarrow 2\gamma) = (39.41 \pm 0.20) \times 10^{-2}$ . Our first error is their experiment's error and our second error is the systematic error from using our best value.

### $\Gamma(\pi^+\pi^-\pi^0\eta) \times \Gamma(e^+e^-)/\Gamma_{total}$ $\Gamma_{167}\Gamma_5/\Gamma$

VALUE (eV)	EVTS	DOCUMENT ID	TECN	COMMENT
<b>12.8 ± 1.8 ± 2.0</b>	203	LEES	18E	BABR 10.6 e <sup>+</sup> e <sup>-</sup> → π <sup>+</sup> π <sup>-</sup> π <sup>0</sup> ηγ

### $\Gamma(\omega\pi^0\eta) \times \Gamma(e^+e^-)/\Gamma_{total}$ $\Gamma_{63}\Gamma_5/\Gamma$

VALUE (eV)	EVTS	DOCUMENT ID	TECN	COMMENT
<b>1.90 ± 0.96 ± 0.01</b>	27	<sup>1</sup> LEES	18E	BABR 10.6 e <sup>+</sup> e <sup>-</sup> → π <sup>+</sup> π <sup>-</sup> π <sup>0</sup> ηγ

<sup>1</sup> LEES 18E reports [ $\Gamma(J/\psi(1S) \rightarrow \omega\pi^0\eta) \times \Gamma(J/\psi(1S) \rightarrow e^+e^-)/\Gamma_{total}] \times [B(\omega(782) \rightarrow \pi^+\pi^-\pi^0)] = 1.7 \pm 0.8 \pm 0.3$  eV which we divide by our best value  $B(\omega(782) \rightarrow \pi^+\pi^-\pi^0) = (89.3 \pm 0.6) \times 10^{-2}$ . Our first error is their experiment's error and our second error is the systematic error from using our best value.

### $\Gamma(\rho^+\pi^-\pi^0\eta) \times \Gamma(e^+e^-)/\Gamma_{total}$ $\Gamma_{168}\Gamma_5/\Gamma$

VALUE (eV)	EVTS	DOCUMENT ID	TECN	COMMENT
<b>10.5 ± 4.1 ± 1.6</b>	168	LEES	18E	BABR 10.6 e <sup>+</sup> e <sup>-</sup> → π <sup>+</sup> π <sup>-</sup> π <sup>0</sup> ηγ

### $\Gamma(\rho\bar{\rho}) \times \Gamma(e^+e^-)/\Gamma_{total}$ $\Gamma_{169}\Gamma_5/\Gamma$

VALUE (eV)	EVTS	DOCUMENT ID	TECN	COMMENT
<b>11.9 ± 0.6 OUR AVERAGE</b>	Error includes scale factor of 1.8. See the ideogram below.			

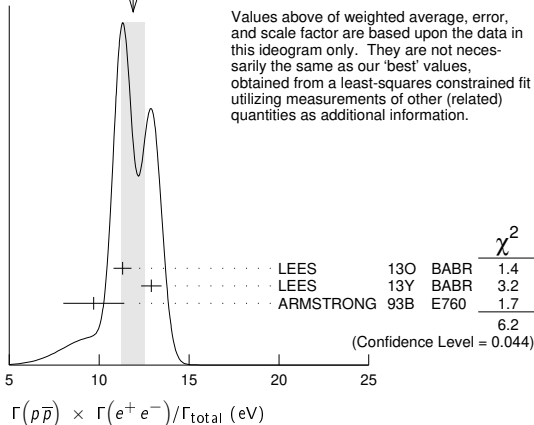
11.3 ± 0.4 ± 0.3	821	<sup>1</sup> LEES	13O	BABR e <sup>+</sup> e <sup>-</sup> → ρ <sup>+</sup> ρ <sup>-</sup> γ
12.9 ± 0.4 ± 0.4	918	<sup>2</sup> LEES	13Y	BABR e <sup>+</sup> e <sup>-</sup> → ρ <sup>+</sup> ρ <sup>-</sup> γ
9.7 ± 1.7		<sup>3</sup> ARMSTRONG	93B	E760 $\bar{p}p \rightarrow e^+e^-$

••• We do not use the following data for averages, fits, limits, etc. •••

12.0 ± 0.6 ± 0.5	438	<sup>4</sup> AUBERT	06B	BABR e <sup>+</sup> e <sup>-</sup> → ρ <sup>+</sup> ρ <sup>-</sup> γ
------------------	-----	---------------------	-----	--

- <sup>1</sup>ISR photon reconstructed in the detector
- <sup>2</sup>ISR photon undetected
- <sup>3</sup>Using  $\Gamma_{total} = 85.5_{-5.8}^{+6.1}$  MeV.
- <sup>4</sup>Superseded by LEES 13O

WEIGHTED AVERAGE  
11.9 ± 0.6 (Error scaled by 1.8)



Values above of weighted average, error, and scale factor are based upon the data in this ideogram only. They are not necessarily the same as our 'best' values, obtained from a least-squares constrained fit utilizing measurements of other (related) quantities as additional information.

### $\Gamma(\Sigma^0\bar{\Sigma}^0) \times \Gamma(e^+e^-)/\Gamma_{total}$ $\Gamma_{182}\Gamma_5/\Gamma$

VALUE (eV)	DOCUMENT ID	TECN	COMMENT
<b>6.4 ± 1.2 ± 0.6</b>	AUBERT	07Bd	BABR 10.6 e <sup>+</sup> e <sup>-</sup> → Σ <sup>0</sup> $\bar{\Sigma}^0$ γ

### $\Gamma(2(\pi^+\pi^-)K^+K^-) \times \Gamma(e^+e^-)/\Gamma_{total}$ $\Gamma_{183}\Gamma_5/\Gamma$

VALUE (10 <sup>-2</sup> keV)	EVTS	DOCUMENT ID	TECN	COMMENT
<b>2.75 ± 0.23 ± 0.17</b>	205	AUBERT	06D	BABR 10.6 e <sup>+</sup> e <sup>-</sup> → K <sup>+</sup> K <sup>-</sup> 2(π <sup>+</sup> π <sup>-</sup> )γ

### $\Gamma(\Lambda\bar{\Lambda}) \times \Gamma(e^+e^-)/\Gamma_{total}$ $\Gamma_{189}\Gamma_5/\Gamma$

VALUE (eV)	DOCUMENT ID	TECN	COMMENT
<b>10.7 ± 0.9 ± 0.7</b>	AUBERT	07Bd	BABR 10.6 e <sup>+</sup> e <sup>-</sup> → Λ $\bar{\Lambda}$ γ

### $\Gamma(2(K^+K^-)) \times \Gamma(e^+e^-)/\Gamma_{total}$ $\Gamma_{192}\Gamma_5/\Gamma$

VALUE (eV)	EVTS	DOCUMENT ID	TECN	COMMENT
<b>4.00 ± 0.33 ± 0.29</b>	287 ± 24	LEES	12F	BABR 10.6 e <sup>+</sup> e <sup>-</sup> → 2(K <sup>+</sup> K <sup>-</sup> )γ

••• We do not use the following data for averages, fits, limits, etc. •••

4.11 ± 0.39 ± 0.30	156 ± 15	<sup>1</sup> AUBERT	07AK	BABR 10.6 e <sup>+</sup> e <sup>-</sup> → 2(K <sup>+</sup> K <sup>-</sup> )γ
4.0 ± 0.7 ± 0.6	38	<sup>2</sup> AUBERT	05D	BABR 10.6 e <sup>+</sup> e <sup>-</sup> → 2(K <sup>+</sup> K <sup>-</sup> )γ

- <sup>1</sup> Superseded by LEES 12F.
- <sup>2</sup> Superseded by AUBERT 07AK.

### $\Gamma(K^+K^-) \times \Gamma(e^+e^-)/\Gamma_{total}$ $\Gamma_{194}\Gamma_5/\Gamma$

VALUE (eV)	EVTS	DOCUMENT ID	TECN	COMMENT
<b>1.78 ± 0.11 ± 0.05</b>	462	<sup>1</sup> LEES	15J	BABR e <sup>+</sup> e <sup>-</sup> → K <sup>+</sup> K <sup>-</sup> γ

1.94 ± 0.11 ± 0.05	462	<sup>2</sup> LEES	15J	BABR e <sup>+</sup> e <sup>-</sup> → K <sup>+</sup> K <sup>-</sup> γ
--------------------	-----	-------------------	-----	--

1.42 ± 0.23 ± 0.08	51	<sup>3</sup> LEES	13Q	BABR e <sup>+</sup> e <sup>-</sup> → K <sup>+</sup> K <sup>-</sup> γ
--------------------	----	-------------------	-----	--

- <sup>1</sup> sin φ > 0.
- <sup>2</sup> sin φ < 0.
- <sup>3</sup> Interference with non-resonant K<sup>+</sup>K<sup>-</sup> production not taken into account.

## J/ψ(1S) BRANCHING RATIOS

For the first four branching ratios, see also the partial widths, and (partial widths) × Γ(e<sup>+</sup>e<sup>-</sup>)/Γ<sub>total</sub> above.

### $\Gamma(\text{hadrons})/\Gamma_{total}$ $\Gamma_1/\Gamma$

VALUE	DOCUMENT ID	TECN	COMMENT
<b>0.877 ± 0.005 OUR AVERAGE</b>			
0.878 ± 0.005	BAI	95B	BES e <sup>+</sup> e <sup>-</sup>
0.86 ± 0.02	BOYARSKI	75	MRK1 e <sup>+</sup> e <sup>-</sup>

### $\Gamma(\text{virtual}\gamma \rightarrow \text{hadrons})/\Gamma_{total}$ $\Gamma_2/\Gamma$

VALUE	DOCUMENT ID	TECN	COMMENT
<b>0.135 ± 0.003</b>	<sup>1,2</sup> SETH	04	RVUE e <sup>+</sup> e <sup>-</sup>
0.17 ± 0.02	<sup>1</sup> BOYARSKI	75	MRK1 e <sup>+</sup> e <sup>-</sup>

- We do not use the following data for averages, fits, limits, etc. •••
- <sup>1</sup>Included in Γ(hadrons)/Γ<sub>total</sub>.
- <sup>2</sup>Using  $B(J/\psi \rightarrow \ell^+\ell^-) = (5.90 \pm 0.09)\%$  from RPP-2002 and  $R = 2.28 \pm 0.04$  determined by a fit to data from BAI 00 and BAI 02c.

### $\Gamma(g\bar{g})/\Gamma_{total}$ $\Gamma_3/\Gamma$

VALUE (units 10 <sup>-2</sup> )	EVTS	DOCUMENT ID	TECN	COMMENT
<b>64.1 ± 1.0</b>	6 M	<sup>1</sup> BESSON	08	CLEO ψ(2S) → π <sup>+</sup> π <sup>-</sup> + hadrons

<sup>1</sup> Calculated using the value  $\Gamma(\gamma g\bar{g})/\Gamma(g\bar{g}) = 0.137 \pm 0.001 \pm 0.016 \pm 0.004$  from BESSON 08 and the PDG 08 values of  $B(\ell^+\ell^-)$ ,  $B(\text{virtual}\gamma \rightarrow \text{hadrons})$ , and  $B(\gamma\eta_c)$ . The statistical error is negligible and the systematic error is partially correlated with that of  $\Gamma(\gamma g\bar{g})/\Gamma_{total}$  measurement of BESSON 08.

### $\Gamma(\gamma g\bar{g})/\Gamma_{total}$ $\Gamma_4/\Gamma$

VALUE (units 10 <sup>-2</sup> )	EVTS	DOCUMENT ID	TECN	COMMENT
<b>8.79 ± 1.05</b>	200 k	<sup>1</sup> BESSON	08	CLEO ψ(2S) → π <sup>+</sup> π <sup>-</sup> γ + hadrons

<sup>1</sup> Calculated using the value  $\Gamma(\gamma g\bar{g})/\Gamma(g\bar{g}) = 0.137 \pm 0.001 \pm 0.016 \pm 0.004$  from BESSON 08 and the value of  $\Gamma(g\bar{g})/\Gamma_{total}$ . The statistical error is negligible and the systematic error is partially correlated with that of  $\Gamma(g\bar{g})/\Gamma_{total}$  measurement of BESSON 08.

### $\Gamma(\gamma g\bar{g})/\Gamma(g\bar{g})$ $\Gamma_4/\Gamma_3$

VALUE (units 10 <sup>-2</sup> )	EVTS	DOCUMENT ID	TECN	COMMENT
<b>13.7 ± 0.1 ± 0.7</b>	6 M	BESSON	08	CLEO ψ(2S) → π <sup>+</sup> π <sup>-</sup> J/ψ

### $\Gamma(e^+e^-)/\Gamma_{total}$ $\Gamma_5/\Gamma$

VALUE (units 10 <sup>-2</sup> )	EVTS	DOCUMENT ID	TECN	COMMENT
<b>5.971 ± 0.032 OUR AVERAGE</b>				
5.983 ± 0.007 ± 0.037	720k	ABLIKIM	13R	BES3 ψ(2S) → J/ψπ <sup>+</sup> π <sup>-</sup>
5.945 ± 0.067 ± 0.042	15k	LI	05c	CLEO ψ(2S) → J/ψπ <sup>+</sup> π <sup>-</sup>
5.90 ± 0.05 ± 0.10		BAI	98D	BES ψ(2S) → J/ψπ <sup>+</sup> π <sup>-</sup>
6.09 ± 0.33		BAI	95B	BES e <sup>+</sup> e <sup>-</sup>
5.92 ± 0.15 ± 0.20		COFFMAN	92	MRK3 ψ(2S) → J/ψπ <sup>+</sup> π <sup>-</sup>
6.9 ± 0.9		BOYARSKI	75	MRK1 e <sup>+</sup> e <sup>-</sup>

### $\Gamma(e^+e^-\gamma)/\Gamma_{total}$ $\Gamma_6/\Gamma$

VALUE (units 10 <sup>-3</sup> )	DOCUMENT ID	TECN	COMMENT
<b>8.8 ± 1.3 ± 0.4</b>	<sup>1</sup> ARMSTRONG	96	E760 $\bar{p}p \rightarrow e^+e^-\gamma$

- <sup>1</sup> For  $E_\gamma > 100$  MeV.

$\Gamma(\mu^+\mu^-)/\Gamma_{total}$					$\Gamma_7/\Gamma$
VALUE (units $10^{-2}$ )	EVTS	DOCUMENT ID	TECN	COMMENT	
<b>5.961 ± 0.033 OUR AVERAGE</b>					
5.973 ± 0.007 ± 0.038	770k	ABLIKIM	13R	BES3 $\psi(2S) \rightarrow J/\psi \pi^+ \pi^-$	
5.960 ± 0.065 ± 0.050	17k	LI	05c	CLEO $\psi(2S) \rightarrow J/\psi \pi^+ \pi^-$	
5.84 ± 0.06 ± 0.10		BAI	98D	BES $\psi(2S) \rightarrow J/\psi \pi^+ \pi^-$	
6.08 ± 0.33		BAI	95B	BES $e^+ e^-$	
5.90 ± 0.15 ± 0.19		COFFMAN	92	MRK3 $\psi(2S) \rightarrow J/\psi \pi^+ \pi^-$	
6.9 ± 0.9		BOYARSKI	75	MRK1 $e^+ e^-$	

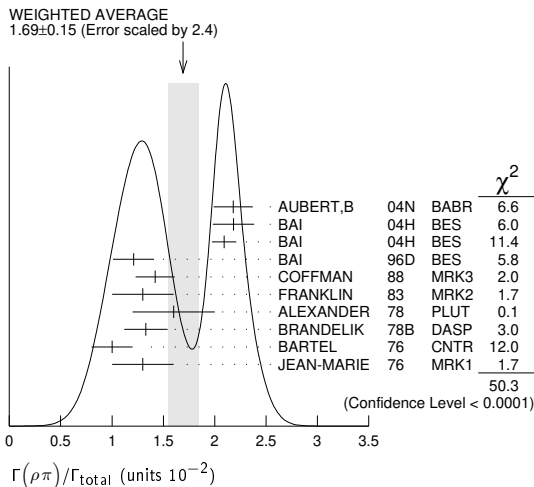
$\Gamma(e^+e^-)/\Gamma(\mu^+\mu^-)$					$\Gamma_5/\Gamma_7$
VALUE	DOCUMENT ID	TECN	COMMENT		
<b>1.0016 ± 0.0031 OUR AVERAGE</b>					
1.0022 ± 0.0044 ± 0.0048	<sup>1</sup> AULCHENKO	14	KEDR	3.097 $e^+ e^- \rightarrow e^+ e^- \mu^+ \mu^-$	
1.0017 ± 0.0017 ± 0.0033	<sup>2</sup> ABLIKIM	13R	BES3	$\psi(2S) \rightarrow J/\psi \pi^+ \pi^-$	
1.002 ± 0.021 ± 0.013	<sup>3</sup> ANASHIN	10	KEDR	3.097 $e^+ e^- \rightarrow e^+ e^- \mu^+ \mu^-$	
0.997 ± 0.012 ± 0.006	LI	05c	CLEO	$\psi(2S) \rightarrow J/\psi \pi^+ \pi^-$	
• • • We do not use the following data for averages, fits, limits, etc. • • •					
1.011 ± 0.013 ± 0.016	BAI	98D	BES	$\psi(2S) \rightarrow J/\psi \pi^+ \pi^-$	
1.00 ± 0.07	BAI	95B	BES	$e^+ e^-$	
1.00 ± 0.05	BOYARSKI	75	MRK1	$e^+ e^-$	
0.91 ± 0.15	ESPOSITO	75B	FRAM	$e^+ e^-$	
0.93 ± 0.10	FORD	75	SPEC	$e^+ e^-$	

<sup>1</sup> From 235.3k  $J/\psi \rightarrow e^+ e^-$  and 156.6k  $J/\psi \rightarrow \mu^+ \mu^-$  observed events.  
<sup>2</sup> Not independent of the corresponding measurements of  $\Gamma(e^+e^-)/\Gamma_{total}$  and  $\Gamma(\mu^+\mu^-)/\Gamma_{total}$ .  
<sup>3</sup> Not independent of the corresponding measurements of  $\Gamma(e^+e^-) \times \Gamma(e^+e^-)/\Gamma_{total}$  and  $\Gamma(\mu^+\mu^-) \times \Gamma(e^+e^-)/\Gamma_{total}$ .

**HADRONIC DECAYS**

$\Gamma(\rho\pi)/\Gamma_{total}$					$\Gamma_8/\Gamma$
VALUE (units $10^{-2}$ )	EVTS	DOCUMENT ID	TECN	COMMENT	
<b>1.69 ± 0.15 OUR AVERAGE</b>					
2.18 ± 0.19		<sup>1,2</sup> AUBERT,B	04N	BABR 10.6 $e^+ e^- \rightarrow \pi^+ \pi^- \pi^0 \gamma$	
2.184 ± 0.005 ± 0.201	220k	<sup>2,3</sup> BAI	04H	BES $e^+ e^- \rightarrow J/\psi \rightarrow \pi^+ \pi^- \pi^0$	
2.091 ± 0.021 ± 0.116		<sup>2,4</sup> BAI	04H	BES $\psi(2S) \rightarrow \pi^+ \pi^- J/\psi$	
1.21 ± 0.20		BAI	96D	BES $e^+ e^- \rightarrow \rho\pi$	
1.42 ± 0.01 ± 0.19		COFFMAN	88	MRK3 $e^+ e^-$	
1.3 ± 0.3	150	FRANKLIN	83	MRK2 $e^+ e^-$	
1.6 ± 0.4	183	ALEXANDER	78	PLUT $e^+ e^-$	
1.33 ± 0.21		BRANDELIK	78B	DASP $e^+ e^-$	
1.0 ± 0.2	543	BARTEL	76	CNTR $e^+ e^-$	
1.3 ± 0.3	153	JEAN-MARIE	76	MRK1 $e^+ e^-$	

<sup>1</sup> From the ratio of  $\Gamma(e^+e^-) B(\pi^+ \pi^- \pi^0)$  and  $\Gamma(e^+e^-) B(\mu^+ \mu^-)$  (AUBERT 04).  
<sup>2</sup> Not independent of their  $B(\pi^+ \pi^- \pi^0)$ .  
<sup>3</sup> From  $J/\psi \rightarrow \pi^+ \pi^- \pi^0$  events directly.  
<sup>4</sup> Obtained comparing the rates for  $\pi^+ \pi^- \pi^0$  and  $\mu^+ \mu^-$ , using  $J/\psi$  events produced via  $\psi(2S) \rightarrow \pi^+ \pi^- J/\psi$  and with  $B(J/\psi \rightarrow \mu^+ \mu^-) = 5.88 \pm 0.10\%$ .



$\Gamma(\rho\pi)/\Gamma(\pi^+\pi^-\pi^0)$					$\Gamma_8/\Gamma_{141}$
VALUE	EVTS	DOCUMENT ID	TECN	COMMENT	
<b>1.142 ± 0.011 ± 0.026</b>	20K	<sup>1</sup> LEES	17c	BABR $J/\psi \rightarrow \pi^+ \pi^- \pi^0$	
1.331 ± 0.033	20K	<sup>2</sup> LEES	17c	BABR $J/\psi \rightarrow \pi^+ \pi^- \pi^0$	

<sup>1</sup> From a Dalitz plot analysis in an isobar model.  
<sup>2</sup> From a Dalitz plot analysis in a Veneziano model.

$\Gamma(\rho^0\pi^0)/\Gamma(\rho\pi)$					$\Gamma_9/\Gamma_8$
VALUE	DOCUMENT ID	TECN	COMMENT		
<b>0.328 ± 0.005 ± 0.027</b>	COFFMAN	88	MRK3	$e^+ e^-$	
• • • We do not use the following data for averages, fits, limits, etc. • • •					
0.35 ± 0.08	ALEXANDER	78	PLUT	$e^+ e^-$	
0.32 ± 0.08	BRANDELIK	78B	DASP	$e^+ e^-$	
0.39 ± 0.11	BARTEL	76	CNTR	$e^+ e^-$	
0.37 ± 0.09	JEAN-MARIE	76	MRK1	$e^+ e^-$	

$\Gamma(\rho(1450)\pi \rightarrow \pi^+\pi^-\pi^0)/\Gamma(\pi^+\pi^-\pi^0)$					$\Gamma_{12}/\Gamma_{141}$
VALUE (%)	EVTS	DOCUMENT ID	TECN	COMMENT	
<b>10.9 ± 1.7 ± 2.7</b>	20K	<sup>1</sup> LEES	17c	BABR $J/\psi \rightarrow \pi^+ \pi^- \pi^0$	
• • • We do not use the following data for averages, fits, limits, etc. • • •					
0.80 ± 0.27	20K	<sup>2</sup> LEES	17c	BABR $J/\psi \rightarrow \pi^+ \pi^- \pi^0$	

<sup>1</sup> From a Dalitz plot analysis in an isobar model.  
<sup>2</sup> From a Dalitz plot analysis in a Veneziano model.

$\Gamma(\rho(1450)\pi \rightarrow K^+K^-\pi^0)/\Gamma(K^+K^-\pi^0)$					$\Gamma_{13}/\Gamma_{157}$
VALUE (%)	EVTS	DOCUMENT ID	TECN	COMMENT	
<b>6.3 ± 0.8 ± 0.6</b>	4K	<sup>1</sup> LEES	17c	BABR $J/\psi \rightarrow K^+ K^- \pi^0$	

<sup>1</sup> From a Dalitz plot analysis in an isobar model.

$\Gamma(\rho(1450)\pi^0 \rightarrow K^+K^-\pi^0)/\Gamma(K^+K^-\pi^0)$					$\Gamma_{14}/\Gamma_{156}$
VALUE (%)	EVTS	DOCUMENT ID	TECN	COMMENT	
<b>9.3 ± 2.0 ± 0.6</b>	2K	<sup>1</sup> LEES	17c	BABR $J/\psi \rightarrow K^+ K^- \pi^0$	

<sup>1</sup> From a Dalitz plot analysis in an isobar model.

$\Gamma(\rho(1450)\eta(958) \rightarrow \pi^+\pi^-\eta(958))/\Gamma_{total}$					$\Gamma_{15}/\Gamma$
VALUE (units $10^{-6}$ )	EVTS	DOCUMENT ID	TECN	COMMENT	
<b>3.28 ± 0.55 ± 0.44</b>	119	<sup>1</sup> ABLIKIM	17AK	BES3 $J/\psi \rightarrow \pi^+ \pi^- \eta'$	

<sup>1</sup> From a partial wave analysis of the decay  $J/\psi \rightarrow \pi^+ \pi^- \eta'$ .

$\Gamma(\rho(1700)\pi \rightarrow \pi^+\pi^-\pi^0)/\Gamma(\pi^+\pi^-\pi^0)$					$\Gamma_{17}/\Gamma_{141}$
VALUE (units $10^{-3}$ )	EVTS	DOCUMENT ID	TECN	COMMENT	
<b>8 ± 2 ± 5</b>	20K	<sup>1</sup> LEES	17c	BABR $J/\psi \rightarrow \pi^+ \pi^- \pi^0$	
• • • We do not use the following data for averages, fits, limits, etc. • • •					
22 ± 6	20K	<sup>2</sup> LEES	17c	BABR $J/\psi \rightarrow \pi^+ \pi^- \pi^0$	

<sup>1</sup> From a Dalitz plot analysis in an isobar model.  
<sup>2</sup> From a Dalitz plot analysis in a Veneziano model.

$\Gamma(\rho(2150)\pi \rightarrow \pi^+\pi^-\pi^0)/\Gamma(\pi^+\pi^-\pi^0)$					$\Gamma_{19}/\Gamma_{141}$
VALUE (units $10^{-4}$ )	EVTS	DOCUMENT ID	TECN	COMMENT	
<b>4 ± 1 ± 20</b>	20K	<sup>1</sup> LEES	17c	BABR $J/\psi \rightarrow \pi^+ \pi^- \pi^0$	
• • • We do not use the following data for averages, fits, limits, etc. • • •					
600 ± 250	20K	<sup>2</sup> LEES	17c	BABR $J/\psi \rightarrow \pi^+ \pi^- \pi^0$	

<sup>1</sup> From a Dalitz plot analysis in an isobar model.  
<sup>2</sup> From a Dalitz plot analysis in a Veneziano model.

$\Gamma(\rho_3(1690)\pi \rightarrow \pi^+\pi^-\pi^0)/\Gamma(\pi^+\pi^-\pi^0)$					$\Gamma_{20}/\Gamma_{141}$
VALUE (units $10^{-3}$ )	EVTS	DOCUMENT ID	TECN	COMMENT	
<b>4.0 ± 0.8</b>	20K	<sup>1</sup> LEES	17c	BABR $J/\psi \rightarrow \pi^+ \pi^- \pi^0$	

<sup>1</sup> From a Dalitz plot analysis in a Veneziano model.

$\Gamma(\rho_2(1320)\rho)/\Gamma_{total}$					$\Gamma_{21}/\Gamma$
VALUE (units $10^{-3}$ )	EVTS	DOCUMENT ID	TECN	COMMENT	
<b>10.9 ± 2.2 OUR AVERAGE</b>					
11.7 ± 0.7 ± 2.5	7584	AUGUSTIN	89	DM2 $J/\psi \rightarrow \rho^0 \rho^\pm \pi^\mp$	
8.4 ± 4.5	36	VANNUCCI	77	MRK1 $e^+ e^- \rightarrow 2(\pi^+ \pi^-) \pi^0$	

$\Gamma(\omega\pi^+\pi^-\pi^0)/\Gamma_{total}$					$\Gamma_{22}/\Gamma$
VALUE (units $10^{-4}$ )	EVTS	DOCUMENT ID	TECN	COMMENT	
<b>85 ± 34</b>	140	VANNUCCI	77	MRK1 $e^+ e^- \rightarrow 3(\pi^+ \pi^-) \pi^0$	

$\Gamma(\omega\pi^+\pi^-)/\Gamma_{total}$					$\Gamma_{24}/\Gamma$
VALUE (units $10^{-3}$ )	EVTS	DOCUMENT ID	TECN	COMMENT	
<b>7.2 ± 1.0 OUR AVERAGE</b>					
7.0 ± 1.6	18058	AUGUSTIN	89	DM2 $J/\psi \rightarrow 2(\pi^+ \pi^-) \pi^0$	
7.8 ± 1.6	215	BURMESTER	77D	PLUT $e^+ e^-$	
6.8 ± 1.9	348	VANNUCCI	77	MRK1 $e^+ e^- \rightarrow 2(\pi^+ \pi^-) \pi^0$	

$\Gamma(\omega\eta'\pi^+\pi^-)/\Gamma_{total}$					$\Gamma_{74}/\Gamma$
VALUE (units $10^{-3}$ )	EVTS	DOCUMENT ID	TECN	COMMENT	
<b>1.12 ± 0.02 ± 0.13</b>	14k	<sup>1</sup> ABLIKIM	19AC	BES3 $J/\psi \rightarrow \omega \eta' \pi^+ \pi^-$	

<sup>1</sup> Using the decays  $\omega \rightarrow \pi^+ \pi^- \pi^0$  and  $\eta' \rightarrow \eta \pi^+ \pi^-$ .

# Meson Particle Listings

## $J/\psi(1S)$

### $\Gamma(\omega f_2(1270))/\Gamma_{total}$ $\Gamma_{25}/\Gamma$

VALUE (units $10^{-3}$ )	EVTS	DOCUMENT ID	TECN	COMMENT
<b>4.3 ± 0.6 OUR AVERAGE</b>				
4.3 ± 0.2 ± 0.6	5860	AUGUSTIN 89	DM2	$e^+ e^-$
4.0 ± 1.6	70	BURMESTER 77D	PLUT	$e^+ e^-$
• • • We do not use the following data for averages, fits, limits, etc. • • •				
1.9 ± 0.8	81	VANNUCCI 77	MRK1	$e^+ e^- \rightarrow 2(\pi^+ \pi^-) \pi^0$

### $\Gamma(K^*(892)^0 \bar{K}^*(892)^0)/\Gamma_{total}$ $\Gamma_{26}/\Gamma$

VALUE (units $10^{-4}$ )	CL%	DOCUMENT ID	TECN	COMMENT
• • • We do not use the following data for averages, fits, limits, etc. • • •				
<5	90	VANNUCCI 77	MRK1	$e^+ e^- \rightarrow \pi^+ \pi^- K^+ K^-$

### $\Gamma(K^*(892)^\pm K^*(892)^\mp)/\Gamma_{total}$ $\Gamma_{27}/\Gamma$

VALUE (units $10^{-3}$ )	EVTS	DOCUMENT ID	TECN	COMMENT
<b>1.00 ± 0.19 ± 0.11 ± 0.32</b>	323	ABLIKIM 10E	BES2	$J/\psi \rightarrow K^\pm K_S^0 \pi^\mp \pi^0$

### $\Gamma(K^*(892)^\pm K^*(700)^\mp)/\Gamma_{total}$ $\Gamma_{28}/\Gamma$

VALUE (units $10^{-3}$ )	EVTS	DOCUMENT ID	TECN	COMMENT
<b>1.09 ± 0.18 ± 0.94 ± 0.54</b>	655	ABLIKIM 10E	BES2	$J/\psi \rightarrow K^\pm K_S^0 \pi^\mp \pi^0$

### $\Gamma(\eta K^*(892)^0 \bar{K}^*(892)^0)/\Gamma_{total}$ $\Gamma_{35}/\Gamma$

VALUE (units $10^{-3}$ )	EVTS	DOCUMENT ID	TECN	COMMENT
<b>1.15 ± 0.13 ± 0.22</b>	209	ABLIKIM 10C	BES2	$J/\psi \rightarrow \eta K^+ \pi^- K^- \pi^+$

### $\Gamma(K^*(1410) \bar{K} + c.c. \rightarrow K^\pm K^\mp \pi^0)/\Gamma(K^+ K^- \pi^0)$ $\Gamma_{41}/\Gamma_{156}$

VALUE (%)	EVTS	DOCUMENT ID	TECN	COMMENT
<b>2.3 ± 1.1 ± 0.7</b>	2K	<sup>1</sup> LEES 17C	BABR	$J/\psi \rightarrow K^+ K^- \pi^0$
<sup>1</sup> From a Dalitz plot analysis in an isobar model.				

### $\Gamma(K^*(1410) \bar{K} + c.c. \rightarrow K_S^0 K^\pm \pi^\mp)/\Gamma(K_S^0 K^\pm \pi^\mp)$ $\Gamma_{42}/\Gamma_{157}$

VALUE (%)	EVTS	DOCUMENT ID	TECN	COMMENT
<b>1.5 ± 0.5 ± 0.9</b>	4K	<sup>1</sup> LEES 17C	BABR	$J/\psi \rightarrow K_S^0 K^\pm \pi^\mp$
<sup>1</sup> From a Dalitz plot analysis in an isobar model.				

### $\Gamma(K_S^0(1430) \bar{K} + c.c. \rightarrow K^\pm K^\mp \pi^0)/\Gamma(K^+ K^- \pi^0)$ $\Gamma_{44}/\Gamma_{156}$

VALUE (%)	EVTS	DOCUMENT ID	TECN	COMMENT
<b>3.5 ± 1.3 ± 0.9</b>	2K	<sup>1</sup> LEES 17C	BABR	$J/\psi \rightarrow K^+ K^- \pi^0$
<sup>1</sup> From a Dalitz plot analysis in an isobar model.				

### $\Gamma(K_S^0(1430) \bar{K} + c.c. \rightarrow K_S^0 K^\pm \pi^\mp)/\Gamma(K_S^0 K^\pm \pi^\mp)$ $\Gamma_{45}/\Gamma_{157}$

VALUE (%)	EVTS	DOCUMENT ID	TECN	COMMENT
<b>7.1 ± 1.3 ± 1.2</b>	4K	<sup>1</sup> LEES 17C	BABR	$J/\psi \rightarrow K_S^0 K^\pm \pi^\mp$
<sup>1</sup> From a Dalitz plot analysis in an isobar model.				

### $\Gamma(K^*(892)^0 \bar{K}_S^0(1430)^0 + c.c.)/\Gamma_{total}$ $\Gamma_{46}/\Gamma$

VALUE (units $10^{-3}$ )	EVTS	DOCUMENT ID	TECN	COMMENT
• • • We do not use the following data for averages, fits, limits, etc. • • •				
6.7 ± 2.6	40	VANNUCCI 77	MRK1	$e^+ e^- \rightarrow \pi^+ \pi^- K^+ K^-$

### $\Gamma(\omega K^*(892) \bar{K} + c.c.)/\Gamma_{total}$ $\Gamma_{50}/\Gamma$

VALUE (units $10^{-4}$ )	EVTS	DOCUMENT ID	TECN	COMMENT
<b>61 ± 9 OUR AVERAGE</b>				
62.0 ± 6.8 ± 10.6	899 ± 98	ABLIKIM 08E	BES2	$J/\psi \rightarrow \omega K_S^0 K^\pm \pi^\mp$
65.3 ± 10.2 ± 13.5	176 ± 28	ABLIKIM 08E	BES2	$J/\psi \rightarrow \omega K^+ K^- \pi^0$
53 ± 14 ± 14	530 ± 140	BECKER 87	MRK3	$e^+ e^- \rightarrow \text{hadrons}$

### $\Gamma(\bar{K} K^*(892) + c.c. \rightarrow K_S^0 K^\pm \pi^\mp)/\Gamma(K_S^0 K^\pm \pi^\mp)$ $\Gamma_{52}/\Gamma_{157}$

VALUE (%)	EVTS	DOCUMENT ID	TECN	COMMENT
<b>90.5 ± 0.9 ± 3.8</b>	4K	<sup>1</sup> LEES 17C	BABR	$J/\psi \rightarrow K_S^0 K^\pm \pi^\mp$
<sup>1</sup> From a Dalitz plot analysis in an isobar model.				

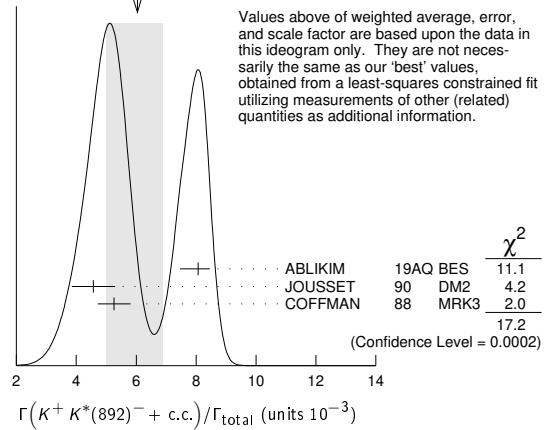
### $\Gamma(K^+ K^*(892)^- + c.c.)/\Gamma_{total}$ $\Gamma_{53}/\Gamma$

VALUE (units $10^{-3}$ )	EVTS	DOCUMENT ID	TECN	COMMENT
<b>6.0 ± 0.8 ± 1.0 OUR AVERAGE</b>				Error includes scale factor of 2.9. See the ideogram below.
8.07 ± 0.04 ± 0.38 ± 0.61	183k	ABLIKIM 19AQ	BES	$J/\psi \rightarrow K^+ K^- \pi^0$
4.57 ± 0.17 ± 0.70	2285	JOUSSET 90	DM2	$J/\psi \rightarrow \text{hadrons}$
5.26 ± 0.13 ± 0.53		COFFMAN 88	MRK3	$J/\psi \rightarrow K^\pm K_S^0 \pi^\mp, K^+ K^- \pi^0$

• • • We do not use the following data for averages, fits, limits, etc. • • •

2.6 ± 0.6	24	FRANKLIN 83	MRK2	$J/\psi \rightarrow K^+ K^- \pi^0$
3.2 ± 0.6	48	VANNUCCI 77	MRK1	$J/\psi \rightarrow K^\pm K_S^0 \pi^\mp$
4.1 ± 1.2	39	BRAUNSCH... 76	DASP	$J/\psi \rightarrow K^\pm X$

WEIGHTED AVERAGE  
6.0±0.8-1.0 (Error scaled by 2.9)



### $\Gamma(K^+ K^*(892)^- + c.c. \rightarrow K^+ K^- \pi^0)/\Gamma(K^+ K^- \pi^0)$ $\Gamma_{54}/\Gamma_{156}$

VALUE (%)	EVTS	DOCUMENT ID	TECN	COMMENT
<b>92.4 ± 1.5 ± 3.4</b>	2K	<sup>1</sup> LEES 17C	BABR	$J/\psi \rightarrow K^+ K^- \pi^0$
<sup>1</sup> From a Dalitz plot analysis in an isobar model.				

### $\Gamma(K^0 \bar{K}^*(892)^0 + c.c.)/\Gamma_{total}$ $\Gamma_{56}/\Gamma$

VALUE (units $10^{-3}$ )	EVTS	DOCUMENT ID	TECN	COMMENT
<b>4.2 ± 0.4 OUR AVERAGE</b>				
3.96 ± 0.15 ± 0.60	1192	JOUSSET 90	DM2	$J/\psi \rightarrow \text{hadrons}$
4.33 ± 0.12 ± 0.45		COFFMAN 88	MRK3	$J/\psi \rightarrow K^\pm K_S^0 \pi^\mp$
• • • We do not use the following data for averages, fits, limits, etc. • • •				
2.7 ± 0.6	45	VANNUCCI 77	MRK1	$J/\psi \rightarrow K^\pm K_S^0 \pi^\mp$

### $\Gamma(K_1(1400)^\pm K^\mp)/\Gamma_{total}$ $\Gamma_{58}/\Gamma$

VALUE (units $10^{-3}$ )	DOCUMENT ID	TECN	COMMENT
<b>3.8 ± 0.8 ± 1.2</b>	<sup>1</sup> BAI 99C	BES	$e^+ e^-$
<sup>1</sup> Assuming $B(K_1(1400) \rightarrow K^* \pi) = 0.94 \pm 0.06$			

### $\Gamma(\bar{K}^*(892)^0 K^+ \pi^- + c.c.)/\Gamma_{total}$ $\Gamma_{59}/\Gamma$

VALUE	DOCUMENT ID	TECN	COMMENT
• • • We do not use the following data for averages, fits, limits, etc. • • •			
seen	<sup>1</sup> ABLIKIM 06C	BES2	$J/\psi \rightarrow \bar{K}^*(892)^0 K^+ \pi^-$
<sup>1</sup> A $K_0^*(700)$ is observed by ABLIKIM 06C in the $K^+ \pi^-$ mass spectrum of the $\bar{K}^*(892)^0 K^+ \pi^-$ final state against the $\bar{K}^*(892)$ . A corresponding branching fraction of the $J/\psi(1S)$ is not presented.			

### $\Gamma(\omega \pi^0 \pi^0)/\Gamma_{total}$ $\Gamma_{62}/\Gamma$

VALUE (units $10^{-3}$ )	EVTS	DOCUMENT ID	TECN	COMMENT
<b>3.4 ± 0.3 ± 0.7</b>	509	AUGUSTIN 89	DM2	$J/\psi \rightarrow \pi^+ \pi^- 3\pi^0$

### $\Gamma(b_1(1235)^\pm \pi^\mp)/\Gamma_{total}$ $\Gamma_{64}/\Gamma$

VALUE (units $10^{-4}$ )	EVTS	DOCUMENT ID	TECN	COMMENT
<b>30 ± 5 OUR AVERAGE</b>				
31 ± 6	4600	AUGUSTIN 89	DM2	$J/\psi \rightarrow 2(\pi^+ \pi^-) \pi^0$
29 ± 7	87	BURMESTER 77D	PLUT	$e^+ e^-$

### $\Gamma(\omega K^\pm K_S^0 \pi^\mp)/\Gamma_{total}$ $\Gamma_{65}/\Gamma$

VALUE (units $10^{-4}$ )	EVTS	DOCUMENT ID	TECN	COMMENT
<b>34 ± 5 OUR AVERAGE</b>				
37.7 ± 0.8 ± 5.8	1972 ± 41	ABLIKIM 08E	BES2	$e^+ e^- \rightarrow J/\psi$
29.5 ± 1.4 ± 7.0	879 ± 41	BECKER 87	MRK3	$e^+ e^- \rightarrow \text{hadrons}$

### $\Gamma(b_1(1235)^0 \pi^0)/\Gamma_{total}$ $\Gamma_{66}/\Gamma$

VALUE (units $10^{-4}$ )	EVTS	DOCUMENT ID	TECN	COMMENT
<b>23 ± 3 ± 5</b>	229	AUGUSTIN 89	DM2	$e^+ e^-$

### $\Gamma(\eta K^\pm K_S^0 \pi^\mp)/\Gamma_{total}$ $\Gamma_{67}/\Gamma$

VALUE (units $10^{-4}$ )	EVTS	DOCUMENT ID	TECN	COMMENT
<b>21.8 ± 2.2 ± 3.4</b>	232 ± 23	ABLIKIM 08E	BES2	$e^+ e^- \rightarrow J/\psi$

### $\Gamma(\eta' K^{*0} \bar{K}^0 + c.c.)/\Gamma_{total}$ $\Gamma_{37}/\Gamma$

VALUE (units $10^{-3}$ )	DOCUMENT ID	TECN	COMMENT
<b>1.66 ± 0.03 ± 0.21</b>	<sup>1</sup> ABLIKIM 18AB	BES3	$J/\psi \rightarrow \eta' K^* \bar{K}$
<sup>1</sup> From $\eta' K_S^0 K^\pm \pi^\mp$ .			

$\Gamma(\eta' K^* \pm K^\mp)/\Gamma_{total}$   $\Gamma_{36}/\Gamma$

VALUE (units $10^{-3}$ )	DOCUMENT ID	TECN	COMMENT
<b>1.48 ± 0.13 OUR AVERAGE</b>			
1.50 ± 0.02 ± 0.19	<sup>1</sup> ABLIKIM	18AB BES3	$J/\psi \rightarrow \eta' K^* \bar{K}$
1.47 ± 0.03 ± 0.17	<sup>2</sup> ABLIKIM	18AB BES3	$J/\psi \rightarrow \eta' K^* \bar{K}$

<sup>1</sup> From  $\eta' K^+ K^- \pi^0$ .  
<sup>2</sup> From  $\eta' K_S^0 K^\pm \pi^\mp$ .

$\Gamma(\eta' h_1(1415) \rightarrow \eta' K^* \pm K^\mp)/\Gamma_{total}$   $\Gamma_{39}/\Gamma$

VALUE (units $10^{-4}$ )	EVTS	DOCUMENT ID	TECN	COMMENT
<b>1.51 ± 0.09 ± 0.21</b>	1.0k	<sup>1</sup> ABLIKIM	18AB BES3	$J/\psi \rightarrow \eta' h_1 \rightarrow \eta' K^* \bar{K}$

<sup>1</sup> From  $\eta' K^+ K^- \pi^0$ .

$\Gamma(\eta' h_1(1415) \rightarrow \eta' K^* \bar{K} + c.c.)/\Gamma_{total}$   $\Gamma_{38}/\Gamma$

VALUE (units $10^{-4}$ )	EVTS	DOCUMENT ID	TECN	COMMENT
<b>2.16 ± 0.12 ± 0.29</b>	1.1k	<sup>1</sup> ABLIKIM	18AB BES3	$J/\psi \rightarrow \eta' h_1 \rightarrow \eta' K^* \bar{K}$

<sup>1</sup> From  $\eta' K_S^0 K^\pm \pi^\mp$ .

$\Gamma(\phi K^*(892) \bar{K} + c.c.)/\Gamma_{total}$   $\Gamma_{68}/\Gamma$

VALUE (units $10^{-4}$ )	EVTS	DOCUMENT ID	TECN	COMMENT
<b>21.8 ± 2.3 OUR AVERAGE</b>				
20.8 ± 2.7 ± 3.9	195 ± 25	ABLIKIM	08E BES2	$J/\psi \rightarrow \phi K_S^0 K^\pm \pi^\mp$
29.6 ± 3.7 ± 4.7	238 ± 30	ABLIKIM	08E BES2	$J/\psi \rightarrow \phi K^+ K^- \pi^0$
20.7 ± 2.4 ± 3.0		FALVARD	88 DM2	$J/\psi \rightarrow$ hadrons
20 ± 3 ± 3	155 ± 20	BECKER	87 MRK3	$e^+ e^- \rightarrow$ hadrons

$\Gamma(\omega K \bar{K})/\Gamma_{total}$   $\Gamma_{69}/\Gamma$

VALUE (units $10^{-4}$ )	EVTS	DOCUMENT ID	TECN	COMMENT
<b>19 ± 4 OUR AVERAGE</b>				
19.8 ± 2.1 ± 3.9		<sup>1</sup> FALVARD	88 DM2	$J/\psi \rightarrow$ hadrons
16 ± 10	22	FELDMAN	77 MRK1	$e^+ e^-$

<sup>1</sup> Addition of  $\omega K^+ K^-$  and  $\omega K^0 \bar{K}^0$  branching ratios.

$\Gamma(\omega f_0(1710) \rightarrow \omega K \bar{K})/\Gamma_{total}$   $\Gamma_{70}/\Gamma$

VALUE (units $10^{-4}$ )	DOCUMENT ID	TECN	COMMENT
<b>4.8 ± 1.1 ± 0.3</b>	<sup>1,2</sup> FALVARD	88 DM2	$J/\psi \rightarrow$ hadrons

<sup>1</sup> Includes unknown branching fraction  $f_0(1710) \rightarrow K \bar{K}$ .  
<sup>2</sup> Addition of  $f_0(1710) \rightarrow K^+ K^-$  and  $f_0(1710) \rightarrow K^0 \bar{K}^0$  branching ratios.

$\Gamma(\phi 2(\pi^+ \pi^-))/\Gamma_{total}$   $\Gamma_{71}/\Gamma$

VALUE (units $10^{-4}$ )	DOCUMENT ID	TECN	COMMENT
<b>16.0 ± 1.0 ± 3.0</b>	FALVARD	88 DM2	$J/\psi \rightarrow$ hadrons

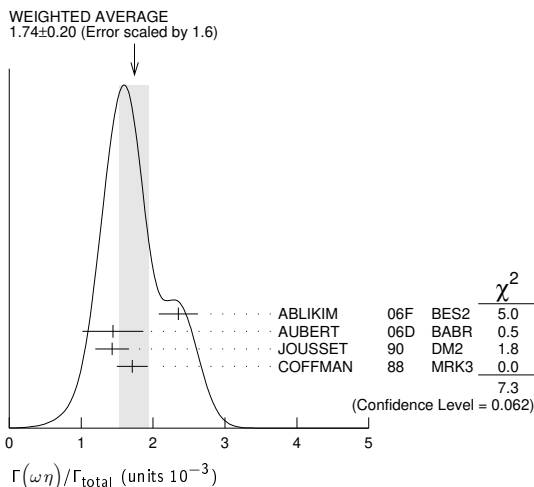
$\Gamma(\Delta(1232)^{++} \bar{p} \pi^-)/\Gamma_{total}$   $\Gamma_{72}/\Gamma$

VALUE (units $10^{-3}$ )	EVTS	DOCUMENT ID	TECN	COMMENT
<b>1.58 ± 0.23 ± 0.40</b>	332	EATON	84 MRK2	$e^+ e^-$

$\Gamma(\omega \eta)/\Gamma_{total}$   $\Gamma_{73}/\Gamma$

VALUE (units $10^{-3}$ )	EVTS	DOCUMENT ID	TECN	COMMENT
<b>1.74 ± 0.20 OUR AVERAGE</b>				Error includes scale factor of 1.6. See the ideogram below.
2.352 ± 0.273	5k	<sup>1</sup> ABLIKIM	06F BES2	$J/\psi \rightarrow \omega \eta$
1.44 ± 0.40 ± 0.14	13	<sup>2</sup> AUBERT	06D BABR	10.6 $e^+ e^- \rightarrow \omega \eta \gamma$
1.43 ± 0.10 ± 0.21	378	JOUSSET	90 DM2	$J/\psi \rightarrow$ hadrons
1.71 ± 0.08 ± 0.20		COFFMAN	88 MRK3	$e^+ e^- \rightarrow 3\pi \eta$

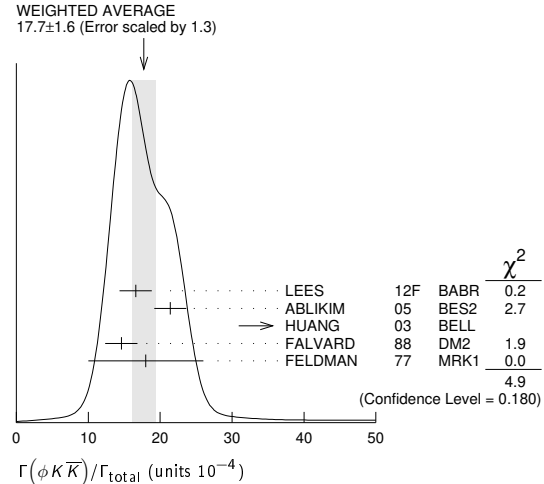
<sup>1</sup> Using  $B(\eta \rightarrow 2\gamma) = (39.43 \pm 0.26)\%$ ,  $B(\eta \rightarrow \pi^+ \pi^- \pi^0) = 22.6 \pm 0.4\%$ ,  $B(\eta \rightarrow \pi^+ \pi^- \gamma) = 4.68 \pm 0.11\%$ , and  $B(\omega \rightarrow \pi^+ \pi^- \pi^0) = (89.1 \pm 0.7)\%$ .  
<sup>2</sup> Using  $\Gamma(J/\psi \rightarrow e^+ e^-) = 5.52 \pm 0.14 \pm 0.04$  keV.



$\Gamma(\phi K \bar{K})/\Gamma_{total}$   $\Gamma_{75}/\Gamma$

VALUE (units $10^{-4}$ )	EVTS	DOCUMENT ID	TECN	COMMENT
<b>17.7 ± 1.6 OUR AVERAGE</b>				Error includes scale factor of 1.3. See the ideogram below.
16.6 ± 1.9 ± 1.2	163 ± 19	LEES	12F BABR	10.6 $e^+ e^- \rightarrow 2(K^+ K^-) \gamma$
21.4 ± 0.4 ± 2.2		ABLIKIM	05 BES2	$J/\psi \rightarrow \phi \pi^+ \pi^-$
48 <sup>+20</sup> <sub>-16</sub> ± 6	9.0 <sup>+3.7</sup> <sub>-3.0</sub>	<sup>1,2</sup> HUANG	03 BELL	$B^+ \rightarrow (\phi K^+ K^-) K^+$
14.6 ± 0.8 ± 2.1		<sup>3</sup> FALVARD	88 DM2	$J/\psi \rightarrow$ hadrons
18 ± 8	14	FELDMAN	77 MRK1	$e^+ e^-$

<sup>1</sup> We have multiplied  $K^+ K^-$  measurement by 2 to obtain  $K \bar{K}$ .  
<sup>2</sup> Using  $B(B^+ \rightarrow J/\psi K^+) = (1.01 \pm 0.05) \times 10^{-3}$ .  
<sup>3</sup> Addition of  $\phi K^+ K^-$  and  $\phi K^0 \bar{K}^0$  branching ratios.



$\Gamma(\phi f_0(1710) \rightarrow \phi K \bar{K})/\Gamma_{total}$   $\Gamma_{77}/\Gamma$

VALUE (units $10^{-4}$ )	DOCUMENT ID	TECN	COMMENT
<b>3.6 ± 0.2 ± 0.6</b>	<sup>1,2</sup> FALVARD	88 DM2	$J/\psi \rightarrow$ hadrons

<sup>1</sup> Including interference with  $f_2'(1525)$ .  
<sup>2</sup> Includes unknown branching fraction  $f_0(1710) \rightarrow K \bar{K}$ .

$\Gamma(\phi f_2(1270))/\Gamma_{total}$   $\Gamma_{79}/\Gamma$

VALUE (units $10^{-3}$ )	CL%	DOCUMENT ID	TECN	COMMENT
• • • We do not use the following data for averages, fits, limits, etc. • • •				
< 0.45	90	FALVARD	88 DM2	$J/\psi \rightarrow$ hadrons
< 0.37	90	VANNUCCI	77 MRK1	$e^+ e^- \rightarrow \pi^+ \pi^- K^+ K^-$

$\Gamma(\Delta(1232)^{++} \bar{\Delta}(1232)^{--})/\Gamma_{total}$   $\Gamma_{80}/\Gamma$

VALUE (units $10^{-3}$ )	EVTS	DOCUMENT ID	TECN	COMMENT
<b>1.10 ± 0.09 ± 0.28</b>	233	EATON	84 MRK2	$e^+ e^-$

$\Gamma(\Sigma(1385)^- \bar{\Sigma}(1385)^+ (\text{or c.c.}))/\Gamma_{total}$   $\Gamma_{81}/\Gamma$

VALUE (units $10^{-3}$ )	EVTS	DOCUMENT ID	TECN	COMMENT
<b>1.16 ± 0.05 OUR AVERAGE</b>				
1.096 ± 0.012 ± 0.071	43k	ABLIKIM	16L BES3	$J/\psi \rightarrow \Sigma(1385)^- \bar{\Sigma}(1385)^+$
1.258 ± 0.014 ± 0.078	53k	ABLIKIM	16L BES3	$J/\psi \rightarrow \Sigma(1385)^+ \bar{\Sigma}(1385)^-$
1.23 ± 0.07 ± 0.30	0.8k	ABLIKIM	12P BES2	$J/\psi \rightarrow \Sigma(1385)^- \bar{\Sigma}(1385)^+$
1.50 ± 0.08 ± 0.38	1k	ABLIKIM	12P BES2	$J/\psi \rightarrow \Sigma(1385)^+ \bar{\Sigma}(1385)^-$
1.00 ± 0.04 ± 0.21	0.6k	HENRRARD	87 DM2	$e^+ e^- \rightarrow \Sigma^{*-}$
1.19 ± 0.04 ± 0.25	0.7k	HENRRARD	87 DM2	$e^+ e^- \rightarrow \Sigma^{*+}$
0.86 ± 0.18 ± 0.22	56	EATON	84 MRK2	$e^+ e^- \rightarrow \Sigma^{*-}$
1.03 ± 0.24 ± 0.25	68	EATON	84 MRK2	$e^+ e^- \rightarrow \Sigma^{*+}$

$\Gamma(\Sigma(1385)^0 \bar{\Sigma}(1385)^0)/\Gamma_{total}$   $\Gamma_{82}/\Gamma$

VALUE (units $10^{-3}$ )	EVTS	DOCUMENT ID	TECN	COMMENT
<b>1.071 ± 0.009 ± 0.082</b>	103k	ABLIKIM	17E BES3	$e^+ e^- \rightarrow J/\psi \rightarrow$ hadrons

$\Gamma(\phi f_2'(1525))/\Gamma_{total}$   $\Gamma_{84}/\Gamma$

VALUE (units $10^{-4}$ )	EVTS	DOCUMENT ID	TECN	COMMENT
<b>8 ± 4 OUR AVERAGE</b>				Error includes scale factor of 2.7.
12.3 ± 0.6 ± 2.0		<sup>1,2</sup> FALVARD	88 DM2	$J/\psi \rightarrow$ hadrons
4.8 ± 1.8	46	<sup>1</sup> GIDAL	81 MRK2	$J/\psi \rightarrow K^+ K^- K^+ K^-$

<sup>1</sup> Re-evaluated using  $B(f_2'(1525) \rightarrow K \bar{K}) = 0.713$ .  
<sup>2</sup> Including interference with  $f_0(1710)$ .

## Meson Particle Listings

 $J/\psi(1S)$  $\Gamma(\phi\pi^+\pi^-)/\Gamma_{\text{total}}$   $\Gamma_{85}/\Gamma$ 

VALUE (units $10^{-3}$ )	EVTS	DOCUMENT ID	TECN	COMMENT
<b><math>0.94 \pm 0.15</math></b>	<b>OUR AVERAGE</b>	Error includes scale factor of 1.7.		
$1.09 \pm 0.02 \pm 0.13$		ABLIKIM	05 BES2	$J/\psi \rightarrow \phi\pi^+\pi^-$
$0.78 \pm 0.03 \pm 0.12$		FALVARD	88 DM2	$J/\psi \rightarrow$ hadrons
$2.1 \pm 0.9$	23	FELDMAN	77 MRK1	$e^+e^-$

 $\Gamma(\phi K^\pm K_S^0 \pi^\mp)/\Gamma_{\text{total}}$   $\Gamma_{87}/\Gamma$ 

VALUE (units $10^{-4}$ )	EVTS	DOCUMENT ID	TECN	COMMENT
<b><math>7.2 \pm 0.8</math></b>	<b>OUR AVERAGE</b>			
$7.4 \pm 0.6 \pm 1.4$	227 $\pm$ 19	ABLIKIM	08E BES2	$e^+e^- \rightarrow J/\psi$
$7.4 \pm 0.9 \pm 1.1$		FALVARD	88 DM2	$J/\psi \rightarrow$ hadrons
$7 \pm 0.6 \pm 1.0$	163 $\pm$ 15	BECKER	87 MRK3	$e^+e^- \rightarrow$ hadrons

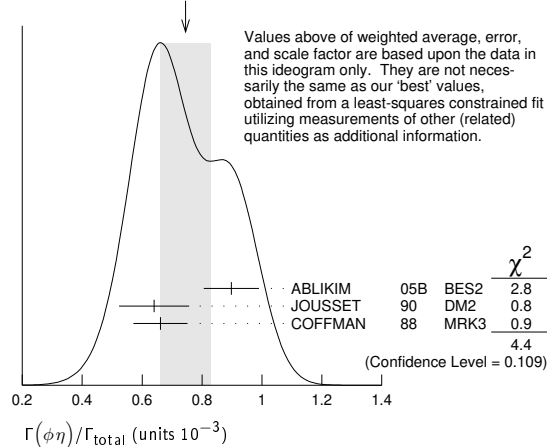
 $\Gamma(\omega f_1(1420))/\Gamma_{\text{total}}$   $\Gamma_{88}/\Gamma$ 

VALUE (units $10^{-4}$ )	EVTS	DOCUMENT ID	TECN	COMMENT
<b><math>6.8 \pm 1.9</math></b>	<b><math>111 \pm 31</math></b>	<b>OUR AVERAGE</b>		
$6.8 \pm 1.6 \pm 1.7$	$111 \pm 26$			
		BECKER	87 MRK3	$e^+e^- \rightarrow$ hadrons

 $\Gamma(\phi\eta)/\Gamma_{\text{total}}$   $\Gamma_{89}/\Gamma$ 

VALUE (units $10^{-3}$ )	EVTS	DOCUMENT ID	TECN	COMMENT
<b><math>0.74 \pm 0.08</math></b>	<b>OUR AVERAGE</b>	Error includes scale factor of 1.5. See the ideogram below.		
$0.898 \pm 0.024 \pm 0.089$		ABLIKIM	05B BES2	$e^+e^- \rightarrow J/\psi \rightarrow$ hadr
$0.64 \pm 0.04 \pm 0.11$	346	JOUSSET	90 DM2	$J/\psi \rightarrow$ hadrons
$0.661 \pm 0.045 \pm 0.078$		COFFMAN	88 MRK3	$e^+e^- \rightarrow K^+K^-\eta$

WEIGHTED AVERAGE  
0.74 $\pm$ 0.08 (Error scaled by 1.5)

 $\Gamma(\phi\eta\eta')/\Gamma_{\text{total}}$   $\Gamma_{99}/\Gamma$ 

VALUE (units $10^{-4}$ )	EVTS	DOCUMENT ID	TECN	COMMENT
<b><math>2.32 \pm 0.06 \pm 0.16</math></b>	2.2k	<b>OUR AVERAGE</b>		
		1 ABLIKIM	19AN BES3	$e^+e^- \rightarrow J/\psi \rightarrow$ hadrons

<sup>1</sup> Including contributions from intermediate resonances. Evidence for an intermediate resonance at  $M \approx 2$  GeV and  $\Gamma \approx 150$  MeV decaying to  $\phi\eta'$  with  $J^P = 1^+$  or  $J^P = 1^-$ , and  $B(J/\psi \rightarrow \eta X) \times B(X \rightarrow \phi\eta') \approx 10^{-4}$ .

 $\Gamma(\Xi^0 \Xi^0)/\Gamma_{\text{total}}$   $\Gamma_{90}/\Gamma$ 

VALUE (units $10^{-3}$ )	EVTS	DOCUMENT ID	TECN	COMMENT
<b><math>1.17 \pm 0.04</math></b>	<b>OUR AVERAGE</b>			
$1.165 \pm 0.004 \pm 0.043$	135K			
		ABLIKIM	17E BES3	$e^+e^- \rightarrow J/\psi \rightarrow$ hadrons
$1.20 \pm 0.12 \pm 0.21$	206	ABLIKIM	08o BES2	$e^+e^- \rightarrow J/\psi$

 $\Gamma(\Xi(1530)^-\Xi^+ + \text{c.c.})/\Gamma_{\text{total}}$   $\Gamma_{91}/\Gamma$ 

VALUE (units $10^{-3}$ )	EVTS	DOCUMENT ID	TECN	COMMENT
<b><math>0.318 \pm 0.008</math></b>	<b>OUR AVERAGE</b>			
$0.317 \pm 0.002 \pm 0.008$	70k			
		ABLIKIM	20 BES3	$e^+e^- \rightarrow J/\psi$
$0.59 \pm 0.09 \pm 0.12$	75	HENRARD	87 DM2	$e^+e^-$

 $\Gamma(\rho K^- \Sigma(1385)^0)/\Gamma_{\text{total}}$   $\Gamma_{92}/\Gamma$ 

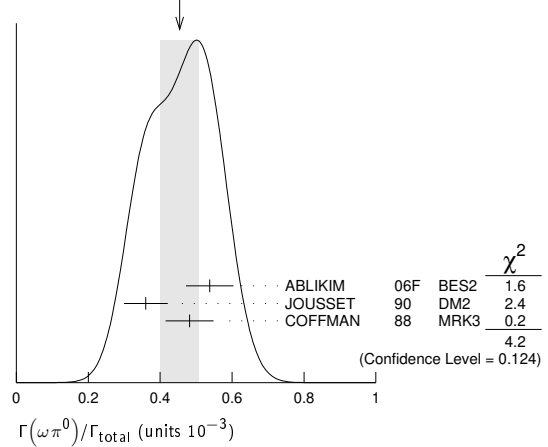
VALUE (units $10^{-3}$ )	EVTS	DOCUMENT ID	TECN	COMMENT
<b><math>0.51 \pm 0.26 \pm 0.18</math></b>	89			
		EATON	84 MRK2	$e^+e^-$

 $\Gamma(\omega\pi^0)/\Gamma_{\text{total}}$   $\Gamma_{93}/\Gamma$ 

VALUE (units $10^{-3}$ )	EVTS	DOCUMENT ID	TECN	COMMENT
<b><math>0.45 \pm 0.05</math></b>	<b>OUR AVERAGE</b>	Error includes scale factor of 1.4. See the ideogram below.		
$0.538 \pm 0.012 \pm 0.065$	2090			
		1 ABLIKIM	06F BES2	$J/\psi \rightarrow \omega\pi^0$
$0.360 \pm 0.028 \pm 0.054$	222	JOUSSET	90 DM2	$J/\psi \rightarrow$ hadrons
$0.482 \pm 0.019 \pm 0.064$		COFFMAN	88 MRK3	$e^+e^- \rightarrow \pi^0\pi^+\pi^-\pi^0$

<sup>1</sup> Using  $B(\omega \rightarrow \pi^+\pi^-\pi^0) = (89.1 \pm 0.7)\%$ .

WEIGHTED AVERAGE  
0.45 $\pm$ 0.05 (Error scaled by 1.4)

 $\Gamma(\omega\pi^0 \rightarrow \pi^+\pi^-\pi^0)/\Gamma(\pi^+\pi^-\pi^0)$   $\Gamma_{94}/\Gamma_{141}$ 

VALUE (units $10^{-4}$ )	EVTS	DOCUMENT ID	TECN	COMMENT
<b><math>8 \pm 3 \pm 2</math></b>	20K	<b>OUR AVERAGE</b>		
		1 LEES	17c BABR	$J/\psi \rightarrow \pi^+\pi^-\pi^0$

<sup>1</sup> From a Dalitz plot analysis in an isobar model and significance  $4.9\sigma$ .

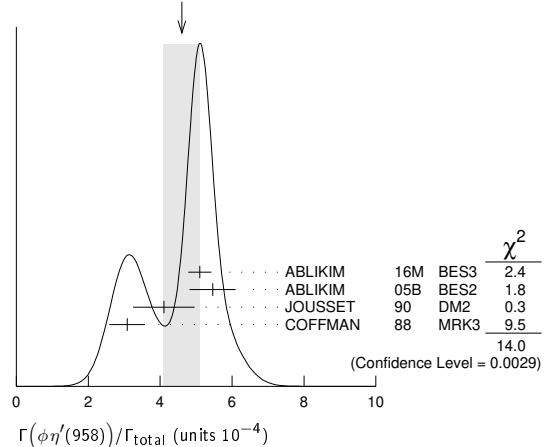
 $\Gamma(\phi\eta'(958))/\Gamma_{\text{total}}$   $\Gamma_{95}/\Gamma$ 

VALUE (units $10^{-4}$ )	CL% EVTS	DOCUMENT ID	TECN	COMMENT
<b><math>4.6 \pm 0.5</math></b>	<b>OUR AVERAGE</b>	Error includes scale factor of 2.2. See the ideogram below.		
$5.10 \pm 0.03 \pm 0.32$	31k	ABLIKIM	16M BES3	$e^+e^- \rightarrow J/\psi \rightarrow$ hadrons
$5.46 \pm 0.31 \pm 0.56$		ABLIKIM	05B BES2	$e^+e^- \rightarrow J/\psi \rightarrow$ hadrons
$4.1 \pm 0.3 \pm 0.8$	167	JOUSSET	90 DM2	$J/\psi \rightarrow$ hadrons
$3.08 \pm 0.34 \pm 0.36$		COFFMAN	88 MRK3	$e^+e^- \rightarrow K^+K^-\eta'$

••• We do not use the following data for averages, fits, limits, etc. •••

< 13      90      VANNUCCI    77    MRK1     $e^+e^-$

WEIGHTED AVERAGE  
4.6 $\pm$ 0.5 (Error scaled by 2.2)

 $\Gamma(\phi f_0(980))/\Gamma_{\text{total}}$   $\Gamma_{96}/\Gamma$ 

VALUE (units $10^{-4}$ )	EVTS	DOCUMENT ID	TECN	COMMENT
<b><math>3.2 \pm 0.9</math></b>	<b>OUR AVERAGE</b>	Error includes scale factor of 1.9.		
$4.6 \pm 0.4 \pm 0.8$		1 FALVARD	88 DM2	$J/\psi \rightarrow$ hadrons
$2.6 \pm 0.6$	50	1 GIDAL	81 MRK2	$J/\psi \rightarrow K^+K^-K^+K^-$

<sup>1</sup> Assuming  $B(f_0(980) \rightarrow \pi\pi) = 0.78$ .

 $\Gamma(\phi\pi^0 f_0(980) \rightarrow \phi\pi^0\pi^+\pi^-)/\Gamma_{\text{total}}$   $\Gamma_{100}/\Gamma$ 

VALUE (units $10^{-6}$ )	EVTS	DOCUMENT ID	TECN	COMMENT
<b><math>4.50 \pm 0.80 \pm 0.61</math></b>	355			
		ABLIKIM	15P BES3	$J/\psi \rightarrow K^+K^-3\pi$

 $\Gamma(\phi\pi^0 f_0(980) \rightarrow \phi\pi^0\rho^0\pi^0)/\Gamma_{\text{total}}$   $\Gamma_{101}/\Gamma$ 

VALUE (units $10^{-6}$ )	EVTS	DOCUMENT ID	TECN	COMMENT
<b><math>1.67 \pm 0.50 \pm 0.24</math></b>	70			
		ABLIKIM	15P BES3	$J/\psi \rightarrow K^+K^-3\pi$

 $\Gamma(\eta\phi f_0(980) \rightarrow \eta\phi\pi^+\pi^-)/\Gamma_{\text{total}}$   $\Gamma_{102}/\Gamma$ 

VALUE (units $10^{-4}$ )	EVTS	DOCUMENT ID	TECN	COMMENT
<b><math>3.23 \pm 0.75 \pm 0.73</math></b>	52			
		ABLIKIM	08F BES	$J/\psi \rightarrow \eta\phi f_0(980)$

See key on page 999

Meson Particle Listings

J/ψ(1S)

Γ(φa0(980)0 → φηπ0)/Γtotal Γ103/Γ

Table with columns: VALUE (units 10^-6), DOCUMENT ID, TECN, COMMENT. Row 1: 4.37±1.35, ABLIKIM 18D BES3 J/ψ → φηπ0. Row 2: 5.0 ± 2.7 ± 2.5, ABLIKIM 11D BES3 J/ψ → φηπ0.

Assuming constructive interference between a0(980) - f0(980) mixing and electromagnetic decay. Destructive interference gives a value of (4.93 ± 1.77) × 10^-6 for this branching fraction. Assuming a0(980) - f0(980) mixing and isospin breaking via γ\* and K\* K loops.

Γ(Ξ(1530)0Ξ0)/Γtotal Γ104/Γ

Table with columns: VALUE (units 10^-3), EVTS, DOCUMENT ID, TECN, COMMENT. Row 1: 0.32±0.12±0.07, 24 ± 9, HENRRARD 87 DM2 e+ e-

Γ(Σ(1385)-Σ+(or c.c.))/Γtotal Γ105/Γ

Table with columns: VALUE (units 10^-3), EVTS, DOCUMENT ID, TECN, COMMENT. Row 1: 0.31±0.05 OUR AVERAGE. Rows 2-5: 0.30±0.03±0.07, 0.34±0.04±0.07, 0.29±0.11±0.10, 0.31±0.11±0.11 with various document IDs and comments.

Γ(φf1(1285))/Γtotal Γ106/Γ

Table with columns: VALUE (units 10^-4), EVTS, DOCUMENT ID, TECN, COMMENT. Row 1: 2.6±0.5 OUR AVERAGE. Rows 2-4: 3.4±1.8±1.5, 3.2±0.6±0.4, 2.1±0.5±0.4 with various document IDs and comments.

ABLIKIM 15H reports [Γ(J/ψ(1S) → φf1(1285))/Γtotal] × [B(f1(1285) → ηπ+π-)] = (1.20 ± 0.6 ± 0.14) × 10^-4 which we divide by our best value B(f1(1285) → ηπ+π-) = (35 ± 15) × 10^-2. Our first error is their experiment's error and our second error is the systematic error from using our best value. We attribute to the f1(1285) the signal observed in the π+π-η invariant mass distribution at 1297 MeV.

Γ(φf1(1285) → φπ0 f0(980) → φπ0π+π-)/Γtotal Γ107/Γ

Table with columns: VALUE (units 10^-7), EVTS, DOCUMENT ID, TECN, COMMENT. Row 1: 9.3E±2.31±1.54, 78, ABLIKIM 15P BES3 J/ψ → K+ K- 3π

Γ(φf1(1285) → φπ0 f0(980) → φπ0π0π0)/Γtotal Γ108/Γ

Table with columns: VALUE (units 10^-7), EVTS, DOCUMENT ID, TECN, COMMENT. Row 1: 2.0E±1.63±1.47, 9, ABLIKIM 15P BES3 J/ψ → K+ K- 3π

Γ(ηπ+π-)/Γtotal Γ109/Γ

Table with columns: VALUE (units 10^-4), EVTS, DOCUMENT ID, TECN, COMMENT. Row 1: 3.7E±0.6E, 471, ABLIKIM 19Q BES3 e+ e- → J/ψ → ηπ+π-

From an energy scan of e+ e- → J/ψ → ηπ+π- assuming PDG 16 values for Γ(e+ e-), Γ(μ+ μ-), and Γ(total).

Γ(ηρ)/Γtotal Γ110/Γ

Table with columns: VALUE (units 10^-3), EVTS, DOCUMENT ID, TECN, COMMENT. Row 1: 0.193±0.023 OUR AVERAGE. Rows 2-3: 0.194±0.017±0.029, 0.193±0.013±0.029 with various document IDs and comments.

Γ(ωη'(958))/Γtotal Γ111/Γ

Table with columns: VALUE (units 10^-4), EVTS, DOCUMENT ID, TECN, COMMENT. Row 1: 1.89±0.18 OUR AVERAGE. Rows 2-4: 2.08±0.30±0.14, 2.26±0.43, 1.8 ±1.0 ±0.8, 1.66±0.17±0.19 with various document IDs and comments.

From a partial wave analysis of the decay J/ψ → π+ π- η'. Using B(η' → π+ π- η) = (44.3 ± 1.5)%, B(η' → π+ π- γ) = 29.5 ± 1.0%, B(η → 2γ) = 39.43 ± 0.26%, and B(ω → π+ π- π0) = (89.1 ± 0.7)%.

Γ(ω f0(980))/Γtotal Γ112/Γ

Table with columns: VALUE (units 10^-4), DOCUMENT ID, TECN, COMMENT. Row 1: 1.41±0.27±0.47, AUGUSTIN 89 DM2 J/ψ → 2(π+ π-) π0

Assuming B(f0(980) → ππ) = 0.78.

Γ(ρη'(958))/Γtotal Γ113/Γ

Table with columns: VALUE (units 10^-5), EVTS, DOCUMENT ID, TECN, COMMENT. Row 1: 8.1 ± 0.8 OUR AVERAGE. Rows 2-4: 7.90±0.19±0.49, 8.3 ± 3.0 ± 1.2, 11.4 ± 1.4 ± 1.6 with various document IDs and comments.

From a partial wave analysis of the decay J/ψ → π+ π- η'.

Γ(a2(1320)± π∓)/Γtotal Γ114/Γ

Table with columns: VALUE, CL%, DOCUMENT ID, TECN, COMMENT. Row 1: <43 × 10^-4, 90, BRAUNSCH... 76 DASP e+ e-

Γ(KK\*2(1430) + c.c.)/Γtotal Γ115/Γ

Table with columns: VALUE, CL%, DOCUMENT ID, TECN, COMMENT. Row 1: <40 × 10^-4, 90, VANNUCCI 77 MRK1 e+ e- → K0 K\*0. Row 2: <66 × 10^-4, 90, BRAUNSCH... 76 DASP e+ e- → K± K\*∓.

Γ(K1(1270)± K∓)/Γtotal Γ116/Γ

Table with columns: VALUE, CL%, DOCUMENT ID, TECN, COMMENT. Row 1: <3.0 × 10^-3, 90, BAI 99c BES e+ e-. Row 2: Assuming B(K1(1270) → Kρ) = 0.42 ± 0.06.

Γ(K1(1270) K0 → γ K0 K0)/Γtotal Γ117/Γ

Table with columns: VALUE (units 10^-7), DOCUMENT ID, TECN, COMMENT. Row 1: 8.54 ± 1.07 ± 2.35 ± 1.20 - 2.13, ABLIKIM 18AA BES3 J/ψ → γ K0 K0

Γ(K2(1430)0 K2(1430)0)/Γtotal Γ119/Γ

Table with columns: VALUE, CL%, DOCUMENT ID, TECN, COMMENT. Row 1: <29 × 10^-4, 90, VANNUCCI 77 MRK1 e+ e- → π+ π- K+ K-

Γ(φπ0)/Γtotal Γ120/Γ

The two different fit values of ABLIKIM 15K below have the same statistical significance of 6.4 σ and cannot be distinguished at this moment.

Table with columns: VALUE (units 10^-6), CL%, EVTS, DOCUMENT ID, TECN, COMMENT. Row 1: 2.94 ± 0.16 ± 0.16, 0.8k, ABLIKIM 15K BES3 e+ e- → J/ψ → K+ K- γγ. Row 2: 0.124±0.033±0.030, 35 ± 9, ABLIKIM 15K BES3 e+ e- → J/ψ → K+ K- γγ.

We do not use the following data for averages, fits, limits, etc. 3 ABLIKIM 05B BES2 e+ e- → J/ψ → φγγ. COFFMAN 88 MRK3 e+ e- → K+ K- π0.

Corresponding to one of the two fit solutions with δ = (-95.9 ± 1.5)° for the phase angle between the resonant J/ψ → φπ0 and non-φ J/ψ → K+ K- π0 contributions. Corresponding to one of the two fit solutions with δ = (-152.1 ± 7.7)° for the phase angle between the resonant J/ψ → φπ0 and non-φ J/ψ → K+ K- π0 contributions. Superseded by ABLIKIM 15K.

Γ(φη(1405) → φηπ+ π-)/Γtotal Γ121/Γ

Table with columns: VALUE (units 10^-5), CL%, EVTS, DOCUMENT ID, TECN, COMMENT. Row 1: 2.01±0.5E±0.82, 172, ABLIKIM 15H BES3 e+ e- → J/ψ → φηπ+ π-

We do not use the following data for averages, fits, limits, etc. 2 FALVARD 88 DM2 J/ψ → hadrons. With 3.6 σ significance. Includes unknown branching fraction η(1405) → ηππ.

Γ(ωf2(1525))/Γtotal Γ122/Γ

Table with columns: VALUE, CL%, DOCUMENT ID, TECN, COMMENT. Row 1: <2.2 × 10^-4, 90, VANNUCCI 77 MRK1 e+ e- → π+ π- π0 K+ K-. Row 2: <2.8 × 10^-4, 90, FALVARD 88 DM2 J/ψ → hadrons.

Re-evaluated assuming B(f2(1525) → K K) = 0.713.

Γ(ωX(1835) → ωρρ)/Γtotal Γ123/Γ

Table with columns: VALUE, CL%, DOCUMENT ID, TECN, COMMENT. Row 1: <3.9 × 10^-6, 95, ABLIKIM 13P BES3 J/ψ → γπ0 ρρ

Γ(ωX(1835), X → η'π+ π-)/Γtotal Γ124/Γ

Table with columns: VALUE, DOCUMENT ID, TECN, COMMENT. Row 1: <6.2 × 10^-5, ABLIKIM 19Ac BES3 J/ψ → ωη'π+ π-

Using the decays ω → π+ π- π0 and η' → ηπ+ π-.

Γ(φX(1835) → φρρ)/Γtotal Γ125/Γ

Table with columns: VALUE, CL%, DOCUMENT ID, TECN, COMMENT. Row 1: <2.1 × 10^-7, 90, ABLIKIM 16K BES3 J/ψ → ρρ K0 K0, ρρ K+ K-

Upper limit applies to any ρρ mass enhancement near threshold.

Γ(φX(1835) → φηπ+ π-)/Γtotal Γ126/Γ

Table with columns: VALUE, CL%, DOCUMENT ID, TECN, COMMENT. Row 1: <2.8 × 10^-4, 90, ABLIKIM 15H BES3 e+ e- → J/ψ → φηπ+ π-

Γ(φX(1870) → φηπ+ π-)/Γtotal Γ127/Γ

Table with columns: VALUE, CL%, DOCUMENT ID, TECN, COMMENT. Row 1: <6.13 × 10^-5, 90, ABLIKIM 15H BES3 e+ e- → J/ψ → φηπ+ π-

Downloaded from https://academic.oup.com/ptep/article/2020/8/083C01/5891211 by guest on 12 November 2020

# Meson Particle Listings

## $J/\psi(1S)$

$\Gamma(\eta\phi(2170) \rightarrow \eta\phi f_0(980) \rightarrow \eta\phi\pi^+\pi^-)/\Gamma_{total}$					$\Gamma_{128}/\Gamma$
VALUE (units $10^{-4}$ )	EVTS	DOCUMENT ID	TECN	COMMENT	
<b><math>1.20 \pm 0.14 \pm 0.37</math></b>	471	ABLIKIM	15H BES3	$e^+e^- \rightarrow J/\psi \rightarrow \phi\eta\pi^+\pi^-$	

$\Gamma(\eta\phi(2170) \rightarrow \eta K^*(892)^0 \bar{K}^*(892)^0)/\Gamma_{total}$					$\Gamma_{129}/\Gamma$
VALUE	CL%	DOCUMENT ID	TECN	COMMENT	
<b><math>&lt;2.52 \times 10^{-4}</math></b>	90	ABLIKIM	10c BES2	$J/\psi \rightarrow \eta K^+\pi^- K^-\pi^+$	

$\Gamma(\Sigma(1385)^0 \bar{\Lambda} + c.c.)/\Gamma_{total}$					$\Gamma_{130}/\Gamma$
VALUE	CL%	DOCUMENT ID	TECN	COMMENT	
<b><math>&lt;0.82 \times 10^{-5}</math></b>	90	ABLIKIM	13F BES3	$J/\psi \rightarrow \rho\bar{p}\pi^+\pi^-\gamma\gamma$	
••• We do not use the following data for averages, fits, limits, etc. •••					
$<0.2 \times 10^{-3}$	90	HENRRARD	87 DM2	$e^+e^-$	

$\Gamma(\Delta(1232)^+ \bar{p})/\Gamma_{total}$					$\Gamma_{131}/\Gamma$
VALUE	CL%	DOCUMENT ID	TECN	COMMENT	
<b><math>&lt;0.1 \times 10^{-3}</math></b>	90	HENRRARD	87 DM2	$e^+e^-$	

$\Gamma(\Lambda(1520)\bar{\Lambda} + c.c. \rightarrow \gamma\Lambda\bar{\Lambda})/\Gamma_{total}$					$\Gamma_{132}/\Gamma$
VALUE	CL%	DOCUMENT ID	TECN	COMMENT	
<b><math>&lt;4.1 \times 10^{-6}</math></b>	90	ABLIKIM	12B BES3	$J/\psi \rightarrow \Lambda\bar{\Lambda}\gamma$	

$\Gamma(\bar{\Lambda}(1520)\Lambda + c.c.)/\Gamma_{total}$					$\Gamma_{133}/\Gamma$
VALUE	CL%	DOCUMENT ID	TECN	COMMENT	
<b><math>&lt;1.80 \times 10^{-3}</math></b>	90	LU	19 BELL	$B^+ \rightarrow \bar{p}\Lambda K^+ K^+$	

$\Gamma(\Theta(1540)\bar{\Theta}(1540) \rightarrow K_S^0 p K^-\bar{n} + c.c.)/\Gamma_{total}$					$\Gamma_{134}/\Gamma$
VALUE	CL%	DOCUMENT ID	TECN	COMMENT	
<b><math>&lt;1.1 \times 10^{-5}</math></b>	90	BAI	04G BES2	$e^+e^-$	

$\Gamma(\Theta(1540)K^-\bar{n} \rightarrow K_S^0 p K^-\bar{n})/\Gamma_{total}$					$\Gamma_{135}/\Gamma$
VALUE	CL%	DOCUMENT ID	TECN	COMMENT	
<b><math>&lt;2.1 \times 10^{-5}</math></b>	90	BAI	04G BES2	$e^+e^-$	

$\Gamma(\Theta(1540)K_S^0\bar{p} \rightarrow K_S^0\bar{p}K^+n)/\Gamma_{total}$					$\Gamma_{136}/\Gamma$
VALUE	CL%	DOCUMENT ID	TECN	COMMENT	
<b><math>&lt;1.6 \times 10^{-5}</math></b>	90	BAI	04G BES2	$e^+e^-$	

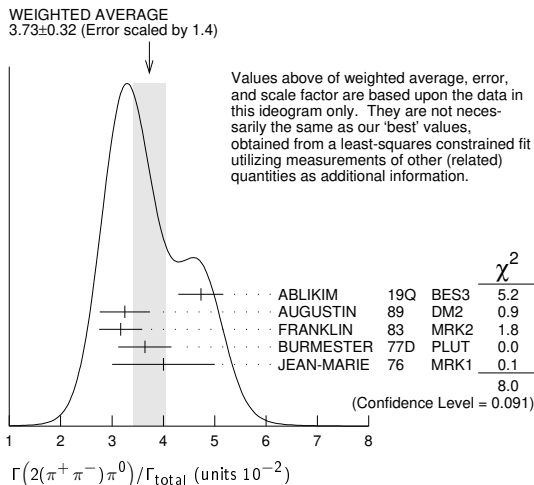
$\Gamma(\bar{\Theta}(1540)K^+n \rightarrow K_S^0\bar{p}K^+n)/\Gamma_{total}$					$\Gamma_{137}/\Gamma$
VALUE	CL%	DOCUMENT ID	TECN	COMMENT	
<b><math>&lt;5.6 \times 10^{-5}</math></b>	90	BAI	04G BES2	$e^+e^-$	

$\Gamma(\bar{\Theta}(1540)K_S^0p \rightarrow K_S^0pK^-\bar{n})/\Gamma_{total}$					$\Gamma_{138}/\Gamma$
VALUE	CL%	DOCUMENT ID	TECN	COMMENT	
<b><math>&lt;1.1 \times 10^{-5}</math></b>	90	BAI	04G BES2	$e^+e^-$	

STABLE HADRONS

$\Gamma(2(\pi^+\pi^-\pi^0))/\Gamma_{total}$					$\Gamma_{139}/\Gamma$
VALUE (units $10^{-2}$ )	EVTS	DOCUMENT ID	TECN	COMMENT	
<b><math>3.73 \pm 0.32</math> OUR AVERAGE</b>		Error includes scale factor of 1.4. See the ideogram below.			
$4.73 \pm 0.44$	228K	1 ABLIKIM	19Q BES3	$J/\psi \rightarrow 2(\pi^+\pi^-\pi^0)$	
$3.25 \pm 0.49$	46055	AUGUSTIN	89 DM2	$J/\psi \rightarrow 2(\pi^+\pi^-\pi^0)$	
$3.17 \pm 0.42$	147	FRANKLIN	83 MRK2	$e^+e^- \rightarrow$ hadrons	
$3.64 \pm 0.52$	1500	BURMESTER	77D PLUT	$e^+e^-$	
$4 \pm 1$	675	JEAN-MARIE	76 MRK1	$e^+e^-$	

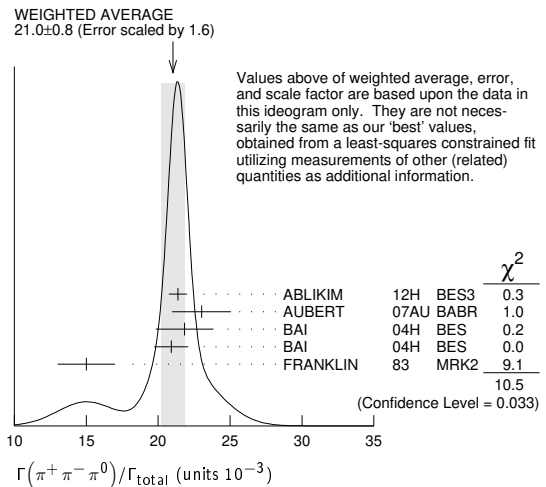
<sup>1</sup> From an energy scan of  $e^+e^- \rightarrow J/\psi \rightarrow 2(\pi^+\pi^-\pi^0)$ , assuming PDG 16 values for  $\Gamma(e^+e^-)$ ,  $\Gamma(\mu^+\mu^-)$ , and  $\Gamma(total)$ , and for a phase difference between strong and electromagnetic amplitudes of  $(84.9 \pm 3.6)^\circ$ . An alternative solution is  $(4.85 \pm 0.45)^\circ$  with a phase of  $(-84.7 \pm 3.1)^\circ$ .



$\Gamma(3(\pi^+\pi^-\pi^0))/\Gamma_{total}$					$\Gamma_{140}/\Gamma$
VALUE	EVTS	DOCUMENT ID	TECN	COMMENT	
<b><math>0.029 \pm 0.006</math> OUR AVERAGE</b>					
$0.028 \pm 0.009$	11	FRANKLIN	83 MRK2	$e^+e^- \rightarrow$ hadrons	
$0.029 \pm 0.007$	181	JEAN-MARIE	76 MRK1	$e^+e^-$	

$\Gamma(\pi^+\pi^-\pi^0)/\Gamma_{total}$					$\Gamma_{141}/\Gamma$
VALUE (units $10^{-3}$ )	EVTS	DOCUMENT ID	TECN	COMMENT	
<b><math>21.0 \pm 0.8</math> OUR AVERAGE</b>		Error includes scale factor of 1.6. See the ideogram below.			
$21.37 \pm 0.04 \pm 0.64$	1.8M	1,2 ABLIKIM	12H BES3	$e^+e^- \rightarrow J/\psi$	
$23.0 \pm 2.0 \pm 0.4$	256	3 AUBERT	07AU BABR	$10.6 e^+e^- \rightarrow J/\psi\pi^+\pi^-\gamma$	
$21.84 \pm 0.05 \pm 2.01$	220k	1,4 BAI	04H BES	$e^+e^-$	
$20.91 \pm 0.21 \pm 1.16$		4,5 BAI	04H BES	$e^+e^-$	
$15 \pm 2$	168	FRANKLIN	83 MRK2	$e^+e^-$	

<sup>1</sup> From  $J/\psi \rightarrow \pi^+\pi^-\pi^0$  events directly.  
<sup>2</sup> The quoted systematic error includes a contribution of 1.23% (added in quadrature) from the uncertainty on the number of  $J/\psi$  events.  
<sup>3</sup> AUBERT 07AU reports  $[\Gamma(J/\psi(1S) \rightarrow \pi^+\pi^-\pi^0)/\Gamma_{total}] \times [\Gamma(\psi(2S) \rightarrow J/\psi(1S)\pi^+\pi^-) \times \Gamma(\psi(2S) \rightarrow e^+e^-)]/\Gamma_{total} = (18.6 \pm 1.2 \pm 1.1) \times 10^{-3}$  keV which we divide by our best value  $\Gamma(\psi(2S) \rightarrow J/\psi(1S)\pi^+\pi^-) \times \Gamma(\psi(2S) \rightarrow e^+e^-)/\Gamma_{total} = 0.808 \pm 0.013$  keV. Our first error is their experiment's error and our second error is the systematic error from using our best value.  
<sup>4</sup> Mostly  $\rho\pi$ , see also  $\rho\pi$  subsection.  
<sup>5</sup> Obtained comparing the rates for  $\pi^+\pi^-\pi^0$  and  $\mu^+\mu^-$ , using  $J/\psi$  events produced via  $\psi(2S) \rightarrow \pi^+\pi^-J/\psi$  and with  $B(J/\psi \rightarrow \mu^+\mu^-) = 5.88 \pm 0.10\%$ .



$\Gamma(\pi^+\pi^-\pi^0 K^+K^-)/\Gamma_{total}$					$\Gamma_{145}/\Gamma$
VALUE (units $10^{-2}$ )	EVTS	DOCUMENT ID	TECN	COMMENT	
<b><math>1.2 \pm 0.3</math></b>	309	VANNUCCI	77 MRK1	$e^+e^-$	

$\Gamma(4(\pi^+\pi^-\pi^0))/\Gamma_{total}$					$\Gamma_{146}/\Gamma$
VALUE (units $10^{-4}$ )	EVTS	DOCUMENT ID	TECN	COMMENT	
<b><math>90 \pm 30</math></b>	13	JEAN-MARIE	76 MRK1	$e^+e^-$	

$\Gamma(\pi^+\pi^-K^+K^-)/\Gamma_{total}$					$\Gamma_{147}/\Gamma$
VALUE (units $10^{-3}$ )	EVTS	DOCUMENT ID	TECN	COMMENT	
$7.2 \pm 2.3$	205	VANNUCCI	77 MRK1	$e^+e^-$	

$\Gamma(K\bar{K}\pi)/\Gamma_{total}$					$\Gamma_{155}/\Gamma$
VALUE (units $10^{-4}$ )	EVTS	DOCUMENT ID	TECN	COMMENT	
<b><math>61 \pm 10</math> OUR AVERAGE</b>					
$55.2 \pm 12.0$	25	FRANKLIN	83 MRK2	$e^+e^- \rightarrow K^+K^-\pi^0$	
$78.0 \pm 21.0$	126	VANNUCCI	77 MRK1	$e^+e^- \rightarrow K_S^0 K^\pm\pi^\mp$	

$\Gamma(K^+K^-\pi^0)/\Gamma_{total}$					$\Gamma_{156}/\Gamma$
VALUE (units $10^{-3}$ )	EVTS	DOCUMENT ID	TECN	COMMENT	
<b><math>2.88 \pm 0.01 \pm 0.12</math></b>	183k	ABLIKIM	19AQ BES	$J/\psi \rightarrow K^+K^-\pi^0$	

$\Gamma(K^+K^-\pi^0)/\Gamma(\pi^+\pi^-\pi^0)$					$\Gamma_{156}/\Gamma_{141}$
VALUE (%)	EVTS	DOCUMENT ID	TECN	COMMENT	
<b><math>12.0 \pm 0.3 \pm 0.9</math></b>	23K	LEES	17c BABR	$J/\psi \rightarrow h^+h^-\pi^0$	

$\Gamma(K_S^0 K^\pm\pi^\mp)/\Gamma(\pi^+\pi^-\pi^0)$					$\Gamma_{157}/\Gamma_{141}$
VALUE (%)	EVTS	DOCUMENT ID	TECN	COMMENT	
<b><math>26.5 \pm 0.5 \pm 2.1</math></b>	24K	LEES	17c BABR	$J/\psi \rightarrow h^0 h^+ h^-$	

$\Gamma(2(\pi^+\pi^-))/\Gamma_{total}$   $\Gamma_{162}/\Gamma$

VALUE (units $10^{-3}$ )	EVTS	DOCUMENT ID	TECN	COMMENT
<b>3.57±0.30 OUR AVERAGE</b>				
3.53±0.12±0.29	1107	<sup>1</sup> ABLIKIM	05H BES2	$e^+e^- \rightarrow \psi(2S) \rightarrow J/\psi \pi^+\pi^-$ , $J/\psi \rightarrow 2(\pi^+\pi^-)$
4.0 ±1.0	76	JEAN-MARIE	76 MRK1	$e^+e^-$

<sup>1</sup> Computed using  $B(J/\psi \rightarrow \mu^+\mu^-) = 0.0588 \pm 0.0010$ .

$\Gamma(3(\pi^+\pi^-))/\Gamma_{total}$   $\Gamma_{163}/\Gamma$

VALUE (units $10^{-4}$ )	EVTS	DOCUMENT ID	TECN	COMMENT
<b>40±20</b>	32	JEAN-MARIE	76 MRK1	$e^+e^-$

• • • We do not use the following data for averages, fits, limits, etc. • • •

$\Gamma(2(\pi^+\pi^-\eta))/\Gamma_{total}$   $\Gamma_{165}/\Gamma$

VALUE (units $10^{-3}$ )	EVTS	DOCUMENT ID	TECN	COMMENT
<b>2.26±0.08±0.27</b>	4.8k	ABLIKIM	05c BES2	$e^+e^- \rightarrow 2(\pi^+\pi^-\eta)$

$\Gamma(3(\pi^+\pi^-\eta))/\Gamma_{total}$   $\Gamma_{166}/\Gamma$

VALUE (units $10^{-4}$ )	EVTS	DOCUMENT ID	TECN	COMMENT
<b>7.24±0.96±1.11</b>	616	ABLIKIM	05c BES2	$e^+e^- \rightarrow 3(\pi^+\pi^-\eta)$

$\Gamma(p\bar{p})/\Gamma_{total}$   $\Gamma_{169}/\Gamma$

VALUE (units $10^{-3}$ )	EVTS	DOCUMENT ID	TECN	COMMENT
<b>2.121±0.029 OUR AVERAGE</b>				
2.112±0.004±0.031	314k	ABLIKIM	12c BES3	$e^+e^-$
2.20 ±0.16 ±0.06	317	<sup>1</sup> WU	06 BELL	$B^+ \rightarrow p\bar{p}K^+$
2.26 ±0.01 ±0.14	63316	BAI	04E BES2	$e^+e^- \rightarrow J/\psi$
1.97 ±0.22	99	BALDINI	98 FENI	$e^+e^-$
1.91 ±0.04 ±0.30		PALLIN	87 DM2	$e^+e^-$
2.16 ±0.07 ±0.15	1420	EATON	84 MRK2	$e^+e^-$
2.5 ±0.4	133	BRANDELIK	79c DASP	$e^+e^-$
2.0 ±0.5		BESCH	78 BONA	$e^+e^-$
2.2 ±0.2	331	<sup>2</sup> PERUZZI	78 MRK1	$e^+e^-$
2.0 ±0.3	48	ANTONELLI	93 SPEC	$e^+e^-$

• • • We do not use the following data for averages, fits, limits, etc. • • •

<sup>1</sup> WU 06 reports  $[\Gamma(J/\psi(1S) \rightarrow p\bar{p})/\Gamma_{total}] \times [B(B^+ \rightarrow J/\psi(1S)K^+)] = (2.21 \pm 0.13 \pm 0.10) \times 10^{-6}$  which we divide by our best value  $B(B^+ \rightarrow J/\psi(1S)K^+) = (1.006 \pm 0.027) \times 10^{-3}$ . Our first error is their experiment's error and our second error is the systematic error from using our best value.

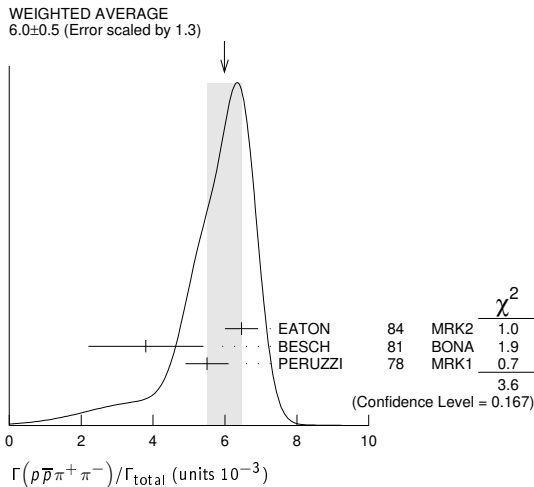
<sup>2</sup> Assuming angular distribution  $(1+\cos^2\theta)$ .

$\Gamma(p\bar{p}\pi^0)/\Gamma_{total}$   $\Gamma_{170}/\Gamma$

VALUE (units $10^{-3}$ )	EVTS	DOCUMENT ID	TECN	COMMENT
<b>1.19±0.08 OUR AVERAGE</b>				Error includes scale factor of 1.1.
1.33±0.02±0.11	11k	ABLIKIM	09B BES2	$e^+e^-$
1.13±0.09±0.09	685	EATON	84 MRK2	$e^+e^-$
1.4 ±0.4		BRANDELIK	79c DASP	$e^+e^-$
1.00±0.15	109	PERUZZI	78 MRK1	$e^+e^-$

$\Gamma(p\bar{p}\pi^+\pi^-)/\Gamma_{total}$   $\Gamma_{171}/\Gamma$

VALUE (units $10^{-3}$ )	EVTS	DOCUMENT ID	TECN	COMMENT
<b>6.0 ±0.5 OUR AVERAGE</b>				Error includes scale factor of 1.3. See the ideogram below.
6.46±0.17±0.43	1435	EATON	84 MRK2	$e^+e^-$
3.8 ±1.6	48	BESCH	81 BONA	$e^+e^-$
5.5 ±0.6	533	PERUZZI	78 MRK1	$e^+e^-$



$\Gamma(p\bar{p}\pi^+\pi^-\pi^0)/\Gamma_{total}$   $\Gamma_{172}/\Gamma$

Including  $p\bar{p}\pi^+\pi^-\gamma$  and excluding  $\omega, \eta, \eta'$

VALUE (units $10^{-3}$ )	EVTS	DOCUMENT ID	TECN	COMMENT
<b>2.3 ±0.9 OUR AVERAGE</b>				Error includes scale factor of 1.9.
3.36±0.65±0.28	364	EATON	84 MRK2	$e^+e^-$
1.6 ±0.6	39	PERUZZI	78 MRK1	$e^+e^-$

$\Gamma(p\bar{p}\eta)/\Gamma_{total}$   $\Gamma_{173}/\Gamma$

VALUE (units $10^{-3}$ )	EVTS	DOCUMENT ID	TECN	COMMENT
<b>2.00±0.12 OUR AVERAGE</b>				
1.91±0.02±0.17	13k	<sup>1</sup> ABLIKIM	09 BES2	$e^+e^-$
2.03±0.13±0.15	826	EATON	84 MRK2	$e^+e^-$
2.5 ±1.2		BRANDELIK	79c DASP	$e^+e^-$
2.3 ±0.4	197	PERUZZI	78 MRK1	$e^+e^-$

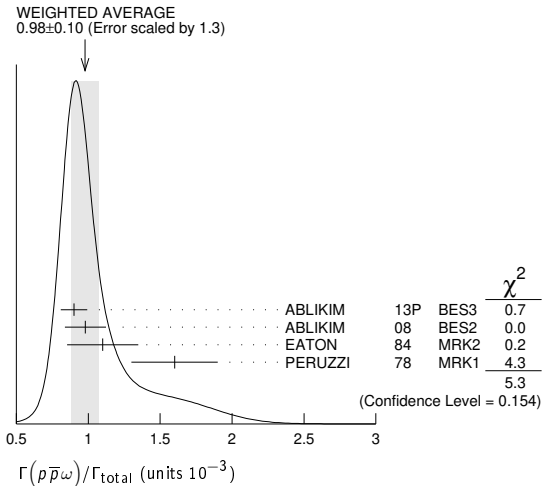
<sup>1</sup> From the combination of  $p\bar{p}\eta' \rightarrow p\bar{p}\pi^+\pi^-\eta$  and  $p\bar{p}\eta' \rightarrow p\bar{p}\pi^+\pi^-\gamma$  channels.

$\Gamma(p\bar{p}\rho)/\Gamma_{total}$   $\Gamma_{174}/\Gamma$

VALUE	CL%	DOCUMENT ID	TECN	COMMENT
<b>&lt;0.31 × 10<sup>-3</sup></b>	90	EATON	84 MRK2	$e^+e^- \rightarrow \text{hadrons}$

$\Gamma(p\bar{p}\omega)/\Gamma_{total}$   $\Gamma_{175}/\Gamma$

VALUE (units $10^{-3}$ )	EVTS	DOCUMENT ID	TECN	COMMENT
<b>0.98±0.10 OUR AVERAGE</b>				Error includes scale factor of 1.3. See the ideogram below.
0.90±0.02±0.09	2670	ABLIKIM	13P BES3	$e^+e^-$
0.98±0.03±0.14	2449	ABLIKIM	08 BES2	$e^+e^-$
1.10±0.17±0.18	486	EATON	84 MRK2	$e^+e^-$
1.6 ±0.3	77	PERUZZI	78 MRK1	$e^+e^-$



$\Gamma(p\bar{p}\eta'(958))/\Gamma_{total}$   $\Gamma_{176}/\Gamma$

VALUE (units $10^{-3}$ )	EVTS	DOCUMENT ID	TECN	COMMENT
<b>0.129±0.014 OUR AVERAGE</b>				Error includes scale factor of 2.0.
0.126±0.002±0.007	16K	<sup>1</sup> ABLIKIM	19N BES3	$e^+e^-$
0.200±0.023±0.028	265 ± 31	<sup>2</sup> ABLIKIM	09 BES2	$e^+e^-$
0.68 ±0.23 ±0.17	19	EATON	84 MRK2	$e^+e^-$
1.8 ±0.6	19	PERUZZI	78 MRK1	$e^+e^-$

<sup>1</sup> From the combination of  $p\bar{p}\eta' \rightarrow p\bar{p}\pi^+\pi^-\eta$  and  $p\bar{p}\eta' \rightarrow p\bar{p}\pi^+\pi^-\gamma$  channels.

<sup>2</sup> From the combination of  $p\bar{p}\eta' \rightarrow p\bar{p}\pi^+\pi^-\eta$  and  $p\bar{p}\eta' \rightarrow p\bar{p}\gamma\rho^0$  channels.

$\Gamma(p\bar{p}a_0(980) \rightarrow p\bar{p}\pi^0\eta)/\Gamma_{total}$   $\Gamma_{177}/\Gamma$

VALUE (units $10^{-3}$ )	DOCUMENT ID	TECN	COMMENT
<b>6.8±1.2±1.3</b>	ABLIKIM	14N BES3	$e^+e^- \rightarrow J/\psi$

$\Gamma(p\bar{p}\phi)/\Gamma_{total}$   $\Gamma_{178}/\Gamma$

VALUE (units $10^{-4}$ )	EVTS	DOCUMENT ID	TECN	COMMENT
<b>0.519±0.033 OUR AVERAGE</b>				
0.523±0.006±0.033	14K	ABLIKIM	16k BES3	$J/\psi \rightarrow p\bar{p}K_S^0 K_L^0$ , $p\bar{p}K^+ K^-$
0.45 ±0.13 ±0.07		FALVARD	88 DM2	$J/\psi \rightarrow \text{hadrons}$

$\Gamma(n\bar{n})/\Gamma_{total}$   $\Gamma_{179}/\Gamma$

VALUE (units $10^{-3}$ )	EVTS	DOCUMENT ID	TECN	COMMENT
<b>2.09±0.16 OUR AVERAGE</b>				
2.07±0.01±0.17	36k	ABLIKIM	12c BES3	$e^+e^-$
2.31±0.49	79	BALDINI	98 FENI	$e^+e^-$
1.8 ±0.9		BESCH	78 BONA	$e^+e^-$
1.90±0.55	40	ANTONELLI	93 SPEC	$e^+e^-$

• • • We do not use the following data for averages, fits, limits, etc. • • •



# Meson Particle Listings

## $J/\psi(1S)$

$\Gamma(n\bar{n}\pi^+\pi^-)/\Gamma_{total}$		$\Gamma_{180}/\Gamma$		
VALUE (units $10^{-3}$ )	EVTS	DOCUMENT ID	TECN	COMMENT
<b><math>3.8 \pm 3.6</math></b>	5	BESCH	81	BONA $e^+e^-$

$\Gamma(\Sigma^+\bar{\Sigma}^-)/\Gamma_{total}$		$\Gamma_{181}/\Gamma$		
VALUE (units $10^{-3}$ )	EVTS	DOCUMENT ID	TECN	COMMENT
<b><math>1.50 \pm 0.10 \pm 0.22</math></b>	399	ABLIKIM	080	BES2 $e^+e^- \rightarrow J/\psi$

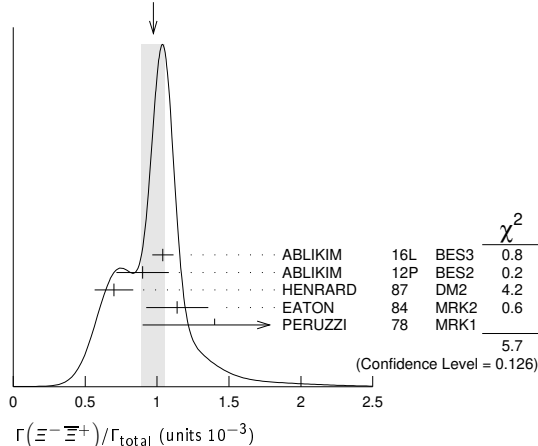
$\Gamma(\Sigma^0\bar{\Sigma}^0)/\Gamma_{total}$		$\Gamma_{182}/\Gamma$		
VALUE (units $10^{-3}$ )	EVTS	DOCUMENT ID	TECN	COMMENT
<b><math>1.172 \pm 0.032</math> OUR AVERAGE</b>		Error includes scale factor of 1.4.		
1.164 $\pm 0.004 \pm 0.023$	111k	ABLIKIM	17L	BES3 $J/\psi \rightarrow \Sigma^0\bar{\Sigma}^0$
1.33 $\pm 0.04 \pm 0.11$	1.7k	ABLIKIM	06	BES2 $J/\psi \rightarrow \Sigma^0\bar{\Sigma}^0$
1.06 $\pm 0.04 \pm 0.23$	884	PALLIN	87	DM2 $e^+e^- \rightarrow \Sigma^0\bar{\Sigma}^0$
1.58 $\pm 0.16 \pm 0.25$	90	EATON	84	MRK2 $e^+e^- \rightarrow \Sigma^0\bar{\Sigma}^0$
1.3 $\pm 0.4$	52	PERUZZI	78	MRK1 $e^+e^- \rightarrow \Sigma^0\bar{\Sigma}^0$
• • • We do not use the following data for averages, fits, limits, etc. • • •				
2.4 $\pm 2.6$	3	BESCH	81	BONA $e^+e^- \rightarrow \Sigma^+\bar{\Sigma}^-$

$\Gamma(2(\pi^+\pi^-)K^+K^-)/\Gamma_{total}$		$\Gamma_{183}/\Gamma$		
VALUE (units $10^{-4}$ )	EVTS	DOCUMENT ID	TECN	COMMENT
<b><math>31 \pm 13</math></b>	30	VANNUCCI	77	MRK1 $e^+e^-$

$\Gamma(\rho\pi\pi^-)/\Gamma_{total}$		$\Gamma_{184}/\Gamma$		
VALUE (units $10^{-3}$ )	EVTS	DOCUMENT ID	TECN	COMMENT
<b><math>2.12 \pm 0.09</math> OUR AVERAGE</b>				
2.36 $\pm 0.02 \pm 0.21$	59k	ABLIKIM	06k	BES2 $J/\psi \rightarrow \rho\pi\pi^-$
2.47 $\pm 0.02 \pm 0.24$	55k	ABLIKIM	06k	BES2 $J/\psi \rightarrow \bar{\rho}\pi^+\pi^-$
2.02 $\pm 0.07 \pm 0.16$	1288	EATON	84	MRK2 $e^+e^- \rightarrow \rho\pi^-$
1.93 $\pm 0.07 \pm 0.16$	1191	EATON	84	MRK2 $e^+e^- \rightarrow \bar{\rho}\pi^+$
1.7 $\pm 0.7$	32	BESCH	81	BONA $e^+e^- \rightarrow \rho\pi^-$
1.6 $\pm 1.2$	5	BESCH	81	BONA $e^+e^- \rightarrow \bar{\rho}\pi^+$
2.16 $\pm 0.29$	194	PERUZZI	78	MRK1 $e^+e^- \rightarrow \rho\pi^-$
2.04 $\pm 0.27$	204	PERUZZI	78	MRK1 $e^+e^- \rightarrow \bar{\rho}\pi^+$

$\Gamma(\Xi^-\bar{\Xi}^+)/\Gamma_{total}$		$\Gamma_{188}/\Gamma$		
VALUE (units $10^{-3}$ )	EVTS	DOCUMENT ID	TECN	COMMENT
<b><math>0.97 \pm 0.08</math> OUR AVERAGE</b>		Error includes scale factor of 1.4. See the ideogram below.		
1.040 $\pm 0.006 \pm 0.074$	43k	ABLIKIM	16L	BES3 $J/\psi \rightarrow \Xi^-\bar{\Xi}^+$
0.90 $\pm 0.03 \pm 0.18$	961	ABLIKIM	12P	BES2 $J/\psi \rightarrow \Xi^-\bar{\Xi}^+$
0.70 $\pm 0.06 \pm 0.12$	132	HENRRARD	87	DM2 $e^+e^- \rightarrow \Xi^-\bar{\Xi}^+$
1.14 $\pm 0.08 \pm 0.20$	194	EATON	84	MRK2 $e^+e^- \rightarrow \Xi^-\bar{\Xi}^+$
1.4 $\pm 0.5$	51	PERUZZI	78	MRK1 $e^+e^- \rightarrow \Xi^-\bar{\Xi}^+$

WEIGHTED AVERAGE  
0.97 $\pm$ 0.08 (Error scaled by 1.4)

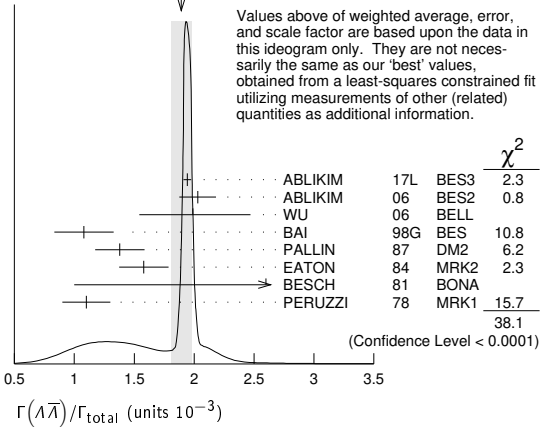


$\Gamma(\Lambda\bar{\Lambda})/\Gamma_{total}$		$\Gamma_{189}/\Gamma$		
VALUE (units $10^{-3}$ )	EVTS	DOCUMENT ID	TECN	COMMENT
<b><math>1.89 \pm 0.09</math> OUR AVERAGE</b>		Error includes scale factor of 2.8. See the ideogram below.		
1.943 $\pm 0.003 \pm 0.033$	441k	ABLIKIM	17L	BES3 $e^+e^-$
2.03 $\pm 0.03 \pm 0.15$	8887	ABLIKIM	06	BES2 $J/\psi \rightarrow \Lambda\bar{\Lambda}$
2.0 $^{+0.5}_{-0.4} \pm 0.1$	46	<sup>1</sup> WU	06	BELL $B^+ \rightarrow \Lambda\bar{\Lambda}K^+$
1.08 $\pm 0.06 \pm 0.24$	631	BAI	98G	BES $e^+e^-$
1.38 $\pm 0.05 \pm 0.20$	1847	PALLIN	87	DM2 $e^+e^-$
1.58 $\pm 0.08 \pm 0.19$	365	EATON	84	MRK2 $e^+e^-$
2.6 $\pm 1.6$	5	BESCH	81	BONA $e^+e^-$
1.1 $\pm 0.2$	196	PERUZZI	78	MRK1 $e^+e^-$

<sup>1</sup>WU 06 reports  $[\Gamma(J/\psi(1S) \rightarrow \Lambda\bar{\Lambda})/\Gamma_{total}] \times [B(B^+ \rightarrow J/\psi(1S)K^+)] = (2.00^{+0.34}_{-0.29} \pm 0.34) \times 10^{-6}$  which we divide by our best value  $B(B^+ \rightarrow J/\psi(1S)K^+) =$

$= (1.006 \pm 0.027) \times 10^{-3}$ . Our first error is their experiment's error and our second error is the systematic error from using our best value.

WEIGHTED AVERAGE  
1.89 $\pm$ 0.09 (Error scaled by 2.8)



$\Gamma(\Lambda\Sigma^-\pi^+ \text{ (or c.c.)})/\Gamma_{total}$		$\Gamma_{190}/\Gamma$		
VALUE (units $10^{-3}$ )	EVTS	DOCUMENT ID	TECN	COMMENT
<b><math>0.83 \pm 0.07</math> OUR AVERAGE</b>		Error includes scale factor of 1.2.		
0.770 $\pm 0.051 \pm 0.083$	335	<sup>1</sup> ABLIKIM	07H	BES2 $e^+e^- \rightarrow \Lambda\Sigma^-\pi^-$
0.747 $\pm 0.056 \pm 0.076$	254	<sup>1</sup> ABLIKIM	07H	BES2 $e^+e^- \rightarrow \Lambda\Sigma^-\pi^+$
0.90 $\pm 0.06 \pm 0.16$	225 $\pm 15$	HENRRARD	87	DM2 $e^+e^- \rightarrow \Lambda\Sigma^+\pi^-$
1.11 $\pm 0.06 \pm 0.20$	342 $\pm 18$	HENRRARD	87	DM2 $e^+e^- \rightarrow \Lambda\Sigma^-\pi^+$
1.53 $\pm 0.17 \pm 0.38$	135	EATON	84	MRK2 $e^+e^- \rightarrow \Lambda\Sigma^+\pi^-$
1.38 $\pm 0.21 \pm 0.35$	118	EATON	84	MRK2 $e^+e^- \rightarrow \Lambda\Sigma^-\pi^+$

<sup>1</sup> Using  $B(\Lambda \rightarrow \pi^-p) = 63.9\%$  and  $B(\Sigma^+ \rightarrow \pi^0p) = 51.6\%$ .

$\Gamma(\rho K^-\bar{\Lambda} + \text{c.c.})/\Gamma_{total}$		$\Gamma_{191}/\Gamma$		
VALUE (units $10^{-3}$ )	EVTS	DOCUMENT ID	TECN	COMMENT
<b><math>0.87 \pm 0.11</math> OUR AVERAGE</b>				
0.85 $^{+0.17}_{-0.15} \pm 0.02$	45	<sup>1</sup> LU	19	BELL $B^+ \rightarrow \bar{\rho}\Lambda K^+ K^+$
0.89 $\pm 0.07 \pm 0.14$	307	EATON	84	MRK2 $e^+e^-$

<sup>1</sup>LU 19 reports  $(8.32^{+1.63}_{-1.45} \pm 0.49) \times 10^{-4}$  from a measurement of  $[\Gamma(J/\psi(1S) \rightarrow \rho K^-\bar{\Lambda} + \text{c.c.})/\Gamma_{total}] \times [B(B^+ \rightarrow J/\psi(1S)K^+)]$  assuming  $B(B^+ \rightarrow J/\psi(1S)K^+) = (1.026 \pm 0.031) \times 10^{-3}$ , which we rescale to our best value  $B(B^+ \rightarrow J/\psi(1S)K^+) = (1.006 \pm 0.027) \times 10^{-3}$ . Our first error is their experiment's error and our second error is the systematic error from using our best value.

$\Gamma(2(K^+K^-))/\Gamma_{total}$		$\Gamma_{192}/\Gamma$		
VALUE (units $10^{-3}$ )	EVTS	DOCUMENT ID	TECN	COMMENT
• • • We do not use the following data for averages, fits, limits, etc. • • •				
1.4 $^{+0.5}_{-0.4} \pm 0.2$	11.0 $^{+4.3}_{-3.5}$	<sup>1</sup> HUANG	03	BELL $B^+ \rightarrow 2(K^+K^-)K^+$
0.7 $\pm 0.3$		VANNUCCI	77	MRK1 $e^+e^-$

<sup>1</sup> Using  $B(B^+ \rightarrow J/\psi K^+) = (1.01 \pm 0.05) \times 10^{-3}$ .

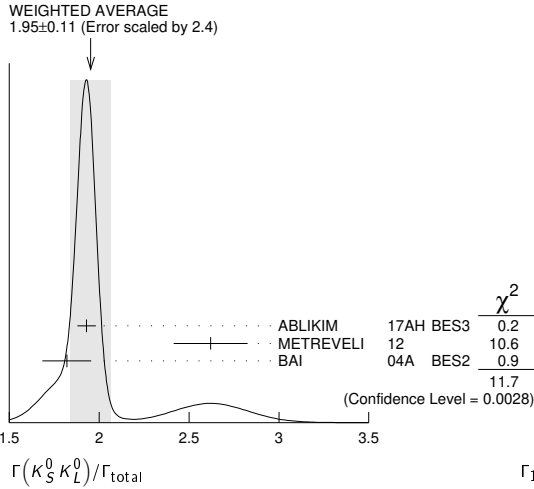
$\Gamma(\rho K^-\Sigma^0)/\Gamma_{total}$		$\Gamma_{193}/\Gamma$		
VALUE (units $10^{-3}$ )	EVTS	DOCUMENT ID	TECN	COMMENT
<b><math>0.29 \pm 0.06 \pm 0.05</math></b>	90	EATON	84	MRK2 $e^+e^-$

$\Gamma(K^+K^-)/\Gamma_{total}$		$\Gamma_{194}/\Gamma$		
VALUE (units $10^{-4}$ )	EVTS	DOCUMENT ID	TECN	COMMENT
<b><math>2.86 \pm 0.09 \pm 0.19</math></b>	1k	<sup>1</sup> METREVELLI	12	$\psi(2S) \rightarrow \pi^+\pi^-K^+K^-$
• • • We do not use the following data for averages, fits, limits, etc. • • •				
2.39 $\pm 0.24 \pm 0.22$	107	<sup>2</sup> BALTRUSAIT...85D	MRK3	$e^+e^-$
2.2 $\pm 0.9$	6	<sup>2</sup> BRANDELIK	79c	DASP $e^+e^-$

<sup>1</sup> Obtained by analyzing CLEO-c data but not authored by the CLEO Collaboration.  
<sup>2</sup> Interference with non-resonant  $K^+K^-$  production not taken into account.

$\Gamma(K_S^0 K_L^0)/\Gamma_{total}$		$\Gamma_{195}/\Gamma$		
VALUE (units $10^{-4}$ )	EVTS	DOCUMENT ID	TECN	COMMENT
<b><math>1.95 \pm 0.11</math> OUR AVERAGE</b>		Error includes scale factor of 2.4. See the ideogram below.		
1.93 $\pm 0.01 \pm 0.05$	110K	ABLIKIM	17AH	BES3 $J/\psi \rightarrow K_S^0 K_L^0 \rightarrow \pi^+\pi^-X$
2.62 $\pm 0.15 \pm 0.14$	0.3k	<sup>1</sup> METREVELLI	12	$\psi(2S) \rightarrow \pi^+\pi^-K_S^0 K_L^0$
1.82 $\pm 0.04 \pm 0.13$	2.1k	<sup>2</sup> BAI	04A	BES2 $J/\psi \rightarrow K_S^0 K_L^0 \rightarrow \pi^+\pi^-X$
• • • We do not use the following data for averages, fits, limits, etc. • • •				
1.18 $\pm 0.12 \pm 0.18$		JOUSSET	90	DM2 $J/\psi \rightarrow \text{hadrons}$
1.01 $\pm 0.16 \pm 0.09$	74	BALTRUSAIT...85D	MRK3	$e^+e^-$

<sup>1</sup> Obtained by analyzing CLEO-c data but not authored by the CLEO Collaboration.  
<sup>2</sup> Using  $B(K_S^0 \rightarrow \pi^+\pi^-) = 0.6868 \pm 0.0027$ .



RADIATIVE DECAYS

$\Gamma(3\gamma)/\Gamma_{total}$	CL%	EVTS	DOCUMENT ID	TECN	COMMENT	$\Gamma_{203}/\Gamma$
<b>11.6 ± 2.2 OUR AVERAGE</b>						
11.3 ± 1.8 ± 2.0	113 ± 18		ABLIKIM	13I BES3	$\psi(2S) \rightarrow \pi^+ \pi^- J/\psi$	
12 ± 3 ± 2	24.2 <sup>+7.2</sup> <sub>-6.0</sub>		ADAMS	08 CLEO	$\psi(2S) \rightarrow \pi^+ \pi^- J/\psi$	
• • • We do not use the following data for averages, fits, limits, etc. • • •						
<55	90		PARTRIDGE	80 CBAL	$e^+ e^-$	
$\Gamma(4\gamma)/\Gamma_{total}$	CL%	EVTS	DOCUMENT ID	TECN	COMMENT	$\Gamma_{204}/\Gamma$
<b>&lt;9 × 10<sup>-6</sup></b>	90		ADAMS	08 CLEO	$\psi(2S) \rightarrow \pi^+ \pi^- J/\psi$	
$\Gamma(5\gamma)/\Gamma_{total}$	CL%	EVTS	DOCUMENT ID	TECN	COMMENT	$\Gamma_{205}/\Gamma$
<b>&lt;15 × 10<sup>-6</sup></b>	90		ADAMS	08 CLEO	$\psi(2S) \rightarrow \pi^+ \pi^- J/\psi$	
$\Gamma(\gamma\pi^0\pi^0)/\Gamma_{total}$	CL%	EVTS	DOCUMENT ID	TECN	COMMENT	$\Gamma_{206}/\Gamma$
<b>1.15 ± 0.05</b>			<sup>1</sup> ABLIKIM	15AE BES3	$J/\psi \rightarrow \gamma\pi^0\pi^0$	
<sup>1</sup> The uncertainty is systematic as statistical is negligible.						
$\Gamma(\gamma\eta\pi^0)/\Gamma_{total}$	CL%	EVTS	DOCUMENT ID	TECN	COMMENT	$\Gamma_{207}/\Gamma$
<b>21.4 ± 1.8 ± 2.5</b>	596		ABLIKIM	16P BES3	$J/\psi \rightarrow 5\gamma$	
$\Gamma(\gamma a_0(980)^0 \rightarrow \gamma\eta\pi^0)/\Gamma_{total}$	CL%	EVTS	DOCUMENT ID	TECN	COMMENT	$\Gamma_{208}/\Gamma$
<b>&lt;2.5 × 10<sup>-6</sup></b>	95		ABLIKIM	16P BES3	$J/\psi \rightarrow 5\gamma$	
$\Gamma(\gamma a_2(1320)^0 \rightarrow \gamma\eta\pi^0)/\Gamma_{total}$	CL%	EVTS	DOCUMENT ID	TECN	COMMENT	$\Gamma_{209}/\Gamma$
<b>&lt;6.6 × 10<sup>-6</sup></b>	95		ABLIKIM	16P BES3	$J/\psi \rightarrow 5\gamma$	
$\Gamma(\gamma K_S^0 K_S^0)/\Gamma_{total}$	CL%	EVTS	DOCUMENT ID	TECN	COMMENT	$\Gamma_{210}/\Gamma$
<b>8.1 ± 0.4</b>			ABLIKIM	18AA BES3	$J/\psi \rightarrow \gamma K_S^0 K_S^0$	
$\Gamma(\gamma\eta_c(1S))/\Gamma_{total}$	CL%	EVTS	DOCUMENT ID	TECN	COMMENT	$\Gamma_{211}/\Gamma$
<b>1.7 ± 0.4 OUR AVERAGE</b>					Error includes scale factor of 1.5.	
2.00 ± 0.31 ± 0.02			<sup>1</sup> MITCHELL	09 CLEO	$e^+ e^- \rightarrow \gamma X$	
1.27 ± 0.36			GAISER	86 CBAL	$J/\psi \rightarrow \gamma X$	
• • • We do not use the following data for averages, fits, limits, etc. • • •						
seen			ANASHIN	14 KEDR	$J/\psi \rightarrow \gamma\eta_c$	
0.79 ± 0.20	273 ± 43		<sup>2</sup> AUBERT	06E BABR	$B^\pm \rightarrow K^\pm X_c \bar{c}$	
seen	16		BALTRUSAITIS...	84 MRK3	$J/\psi \rightarrow 2\phi\gamma$	
<sup>1</sup> MITCHELL 09 reports $(1.98 \pm 0.09 \pm 0.30) \times 10^{-2}$ from a measurement of $[\Gamma(J/\psi(1S) \rightarrow \gamma\eta_c(1S))/\Gamma_{total}] \times [B(\psi(2S) \rightarrow J/\psi(1S)\pi^+\pi^-)]$ assuming $B(\psi(2S) \rightarrow J/\psi(1S)\pi^+\pi^-) = (35.04 \pm 0.07 \pm 0.77) \times 10^{-2}$ , which we rescale to our best value $B(\psi(2S) \rightarrow J/\psi(1S)\pi^+\pi^-) = (34.68 \pm 0.30) \times 10^{-2}$ . Our first error is their experiment's error and our second error is the systematic error from using our best value.						
<sup>2</sup> Calculated by the authors using an average of $B(J/\psi \rightarrow \gamma\eta_c) \times B(\eta_c \rightarrow K\bar{K}\pi)$ from BALTRUSAITIS 86, BISELLO 91, BAI 04 and $B(\eta_c \rightarrow K\bar{K}\pi) = (8.5 \pm 1.8)\%$ from AUBERT 06E.						
$\Gamma(\gamma\eta_c(1S) \rightarrow 3\gamma)/\Gamma_{total}$	CL%	EVTS	DOCUMENT ID	TECN	COMMENT	$\Gamma_{212}/\Gamma$
<b>3.8 ± 1.3 OUR AVERAGE</b>					Error includes scale factor of 1.1.	
4.5 ± 1.2 ± 0.6	33 ± 9		ABLIKIM	13I BES3	$\psi(2S) \rightarrow \pi^+ \pi^- J/\psi$	
1.2 ± 2.7 <sub>-1.1</sub> ± 0.3	1.2 <sup>+2.8</sup> <sub>-1.1</sub>		ADAMS	08 CLEO	$\psi(2S) \rightarrow \pi^+ \pi^- J/\psi$	
$\Gamma(\gamma\pi^+\pi^-\pi^0)/\Gamma_{total}$	CL%	EVTS	DOCUMENT ID	TECN	COMMENT	$\Gamma_{213}/\Gamma$
<b>8.3 ± 0.2 ± 3.1</b>			<sup>1</sup> BALTRUSAITIS...	86B MRK3	$J/\psi \rightarrow 4\pi\gamma$	
<sup>1</sup> $4\pi$ mass less than 2.0 GeV.						
$\Gamma(\gamma\eta\pi\pi)/\Gamma_{total}$	CL%	EVTS	DOCUMENT ID	TECN	COMMENT	$\Gamma_{214}/\Gamma$
<b>6.1 ± 1.0 OUR AVERAGE</b>						
5.85 ± 0.3 ± 1.05			<sup>1</sup> EDWARDS	83B CBAL	$J/\psi \rightarrow \eta\pi^+\pi^-$	
7.8 ± 1.2 ± 2.4			<sup>1</sup> EDWARDS	83B CBAL	$J/\psi \rightarrow \eta 2\pi^0$	
<sup>1</sup> Broad enhancement at 1700 MeV.						
$\Gamma(\gamma\eta_2(1870) \rightarrow \gamma\eta\pi^+\pi^-)/\Gamma_{total}$	CL%	EVTS	DOCUMENT ID	TECN	COMMENT	$\Gamma_{215}/\Gamma$
<b>6.2 ± 2.2 ± 0.9</b>			BAI	99 BES	$J/\psi \rightarrow \gamma\eta\pi^+\pi^-$	

$\Gamma(K_S^0 K_L^0)/\Gamma_{total}$	CL%	EVTS	DOCUMENT ID	TECN	COMMENT	$\Gamma_{195}/\Gamma$
<b>16.2 ± 1.7 OUR AVERAGE</b>						
15.7 ± 0.80 ± 1.54	454		<sup>1</sup> ABLIKIM	13F BES3	$J/\psi \rightarrow p\bar{p}\pi^+\pi^-\gamma\gamma$	
26.2 ± 6.0 ± 4.4	44		<sup>2</sup> ABLIKIM	07H BES2	$e^+ e^- \rightarrow \psi(2S)$	
<sup>1</sup> Using $B(\Lambda \rightarrow \pi^- p) = 63.9\%$ and $B(\eta \rightarrow \gamma\gamma) = 39.31\%$ .						
<sup>2</sup> Using $B(\Lambda \rightarrow \pi^- p) = 63.9\%$ and $B(\eta \rightarrow \gamma\gamma) = 39.4\%$ .						

$\Gamma(\Lambda\bar{\Lambda}\pi^+\pi^-)/\Gamma_{total}$	CL%	EVTS	DOCUMENT ID	TECN	COMMENT	$\Gamma_{196}/\Gamma$
<b>4.30 ± 0.13 ± 0.99</b>	2.4k		ABLIKIM	12P BES2	$J/\psi$	

$\Gamma(\Lambda\bar{\Lambda}\eta)/\Gamma_{total}$	CL%	EVTS	DOCUMENT ID	TECN	COMMENT	$\Gamma_{197}/\Gamma$
<b>16.2 ± 1.7 OUR AVERAGE</b>						
15.7 ± 0.80 ± 1.54	454		<sup>1</sup> ABLIKIM	13F BES3	$J/\psi \rightarrow p\bar{p}\pi^+\pi^-\gamma\gamma$	
26.2 ± 6.0 ± 4.4	44		<sup>2</sup> ABLIKIM	07H BES2	$e^+ e^- \rightarrow \psi(2S)$	
<sup>1</sup> Using $B(\Lambda \rightarrow \pi^- p) = 63.9\%$ and $B(\eta \rightarrow \gamma\gamma) = 39.31\%$ .						
<sup>2</sup> Using $B(\Lambda \rightarrow \pi^- p) = 63.9\%$ and $B(\eta \rightarrow \gamma\gamma) = 39.4\%$ .						

$\Gamma(\Lambda\bar{\Lambda}\pi^0 + c.c.)/\Gamma_{total}$	CL%	EVTS	DOCUMENT ID	TECN	COMMENT	$\Gamma_{198}/\Gamma$
<b>3.78 ± 0.27 ± 0.30</b>	323		<sup>1</sup> ABLIKIM	13F BES3	$J/\psi \rightarrow p\bar{p}\pi^+\pi^-\gamma\gamma$	
• • • We do not use the following data for averages, fits, limits, etc. • • •						
< 6.4	90		<sup>2</sup> ABLIKIM	07H BES2	$e^+ e^- \rightarrow \psi(2S)$	
23 ± 7 ± 8	11		BAI	98G BES	$e^+ e^-$	
22 ± 5 ± 5	19		HENRRARD	87 DM2	$e^+ e^-$	
<sup>1</sup> Using $B(\Lambda \rightarrow \pi^- p) = 63.9\%$ and $B(\pi^0 \rightarrow \gamma\gamma) = 98.8\%$ .						
<sup>2</sup> Using $B(\Lambda \rightarrow \pi^- p) = 63.9\%$ .						

$\Gamma(\Lambda\bar{\Lambda}\eta + c.c.)/\Gamma_{total}$	CL%	EVTS	DOCUMENT ID	TECN	COMMENT	$\Gamma_{199}/\Gamma$
<b>6.46 ± 0.20 ± 1.07</b>	1058		<sup>1</sup> ABLIKIM	08C BES2	$e^+ e^- \rightarrow J/\psi$	
<sup>1</sup> Using $B(\bar{\Lambda} \rightarrow \bar{p}\pi^+) = 63.9\%$ and $B(K_S^0 \rightarrow \pi^+\pi^-) = 69.2\%$ .						

$\Gamma(\pi^+\pi^-)/\Gamma_{total}$	CL%	EVTS	DOCUMENT ID	TECN	COMMENT	$\Gamma_{200}/\Gamma$
<b>1.47 ± 0.14 OUR AVERAGE</b>						
1.47 ± 0.13 ± 0.13	140		<sup>1</sup> METREVELI	12	$\psi(2S) \rightarrow 2(\pi^+\pi^-)$	
1.58 ± 0.20 ± 0.15	84		BALTRUSAITIS...	85D MRK3	$e^+ e^-$	
1.0 ± 0.5	5		BRA NDELIK	78B DASP	$e^+ e^-$	
1.6 ± 1.6	1		VANNUCCI	77 MRK1	$e^+ e^-$	
<sup>1</sup> Obtained by analyzing CLEO-c data but not authored by the CLEO Collaboration.						

$\Gamma(\Lambda\bar{\Lambda}\Sigma + c.c.)/\Gamma_{total}$	CL%	EVTS	DOCUMENT ID	TECN	COMMENT	$\Gamma_{201}/\Gamma$
<b>2.83 ± 0.23 OUR AVERAGE</b>						
2.74 ± 0.24 ± 0.22	234 ± 21		<sup>1</sup> ABLIKIM	12B BES3	$J/\psi \rightarrow \Lambda\bar{\Sigma}^0$	
2.92 ± 0.22 ± 0.24	308 ± 24		<sup>2</sup> ABLIKIM	12B BES3	$J/\psi \rightarrow \bar{\Lambda}\Sigma^0$	
• • • We do not use the following data for averages, fits, limits, etc. • • •						
<18			<sup>2</sup> HENRRARD	87 DM2	$J/\psi \rightarrow \bar{\Lambda}\Sigma^0$	
<15	90		PERUZZI	78 MRK1	$e^+ e^- \rightarrow \Lambda X$	
<sup>1</sup> ABLIKIM 12B quotes $B(J/\psi \rightarrow \Lambda\bar{\Sigma}^0)$ which we multiply by 2.						
<sup>2</sup> ABLIKIM 12B and HENRRARD 87 quote results for $B(J/\psi \rightarrow \bar{\Lambda}\Sigma^0)$ which we multiply by 2.						

$\Gamma(K_S^0 K_S^0)/\Gamma_{total}$	CL%	EVTS	DOCUMENT ID	TECN	COMMENT	$\Gamma_{202}/\Gamma$
<b>&lt;1.4 × 10<sup>-8</sup></b>	95		<sup>1</sup> ABLIKIM	17AH BES3	$J/\psi \rightarrow K_S^0 K_S^0 \rightarrow \pi^+\pi^-\pi^+\pi^-$	
• • • We do not use the following data for averages, fits, limits, etc. • • •						
<1 × 10 <sup>-6</sup>	95		<sup>1</sup> BAI	04D BES	$e^+ e^-$	
<5.2 × 10 <sup>-6</sup>	90		<sup>1</sup> BALTRUSAITIS...	85C MRK3	$e^+ e^-$	
<sup>1</sup> Forbidden by CP.						

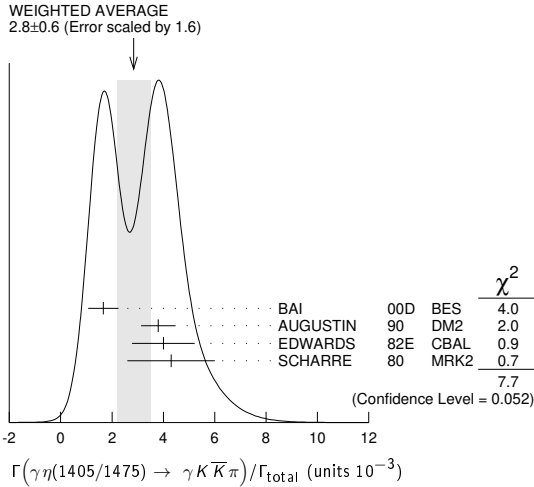
# Meson Particle Listings

## $J/\psi(1S)$

### $\Gamma(\gamma\eta(1405/1475) \rightarrow \gamma K \bar{K} \pi) / \Gamma_{\text{total}}$ $\Gamma_{216} / \Gamma$

VALUE (units $10^{-3}$ )	DOCUMENT ID	TECN	COMMENT
<b><math>2.8 \pm 0.6</math> OUR AVERAGE</b>	Error includes scale factor of 1.6. See the ideogram below.		
$1.66 \pm 0.1 \pm 0.58$	1,2 BAI	00D	BES $J/\psi \rightarrow \gamma K^\pm K_S^0 \pi^\mp$
$3.8 \pm 0.3 \pm 0.6$	3 AUGUSTIN	90	DM2 $J/\psi \rightarrow \gamma K \bar{K} \pi$
$4.0 \pm 0.7 \pm 1.0$	3 EDWARDS	82E	CBAL $J/\psi \rightarrow K^+ K^- \pi^0 \gamma$
$4.3 \pm 1.7$	3,4 SCHARRE	80	MRK2 $e^+ e^-$
• • • We do not use the following data for averages, fits, limits, etc. • • •			
$1.78 \pm 0.21 \pm 0.33$	3,5,6 AUGUSTIN	92	DM2 $J/\psi \rightarrow \gamma K \bar{K} \pi$
$0.83 \pm 0.13 \pm 0.18$	3,7,8 AUGUSTIN	92	DM2 $J/\psi \rightarrow \gamma K \bar{K} \pi$
$0.66 \pm 0.17 \pm 0.24$ $-0.16 - 0.15$	3,6,9 BAI	90C	MRK3 $J/\psi \rightarrow \gamma K_S^0 K^\pm \pi^\mp$
$1.03 \pm 0.21 \pm 0.26$ $-0.18 - 0.19$	3,8,10 BAI	90C	MRK3 $J/\psi \rightarrow \gamma K_S^0 K^\pm \pi^\mp$

- Interference with the  $J/\psi(1S)$  radiative transition to the broad  $K \bar{K} \pi$  pseudoscalar state around 1800 is  $(0.15 \pm 0.01 \pm 0.05) \times 10^{-3}$ .
- Interference with  $J/\psi \rightarrow \gamma f_1(1420)$  is  $(-0.03 \pm 0.01 \pm 0.01) \times 10^{-3}$ .
- Includes unknown branching fraction  $\eta(1405) \rightarrow K \bar{K} \pi$ .
- Corrected for spin-zero hypothesis for  $\eta(1405)$ .
- From fit to the  $a_0(980) \pi^0 \pi^+$  partial wave.
- $a_0(980) \pi$  mode.
- From fit to the  $K^*(892) K^0 \pi^+$  partial wave.
- $K^* K$  mode.
- From  $a_0(980) \pi$  final state.
- From  $K^*(890) K$  final state.



### $\Gamma(\gamma\eta(1405/1475) \rightarrow \gamma\gamma\rho^0) / \Gamma_{\text{total}}$ $\Gamma_{217} / \Gamma$

VALUE (units $10^{-4}$ )	DOCUMENT ID	TECN	COMMENT
<b><math>0.78 \pm 0.20</math> OUR AVERAGE</b>	Error includes scale factor of 1.8.		
$1.07 \pm 0.17 \pm 0.11$	1 BAI	04J	BES2 $J/\psi \rightarrow \gamma\gamma\pi^+\pi^-$
$0.64 \pm 0.12 \pm 0.07$	1 COFFMAN	90	MRK3 $J/\psi \rightarrow \gamma\gamma\pi^+\pi^-$

1 Includes unknown branching fraction  $\eta(1405) \rightarrow \gamma\rho^0$ .

### $\Gamma(\gamma\eta(1405/1475) \rightarrow \gamma\eta\pi^+\pi^-) / \Gamma_{\text{total}}$ $\Gamma_{218} / \Gamma$

VALUE (units $10^{-4}$ )	EVTS	DOCUMENT ID	TECN	COMMENT
<b><math>3.0 \pm 0.5</math> OUR AVERAGE</b>				
$2.6 \pm 0.7 \pm 0.4$		BAI	99	BES $J/\psi \rightarrow \gamma\eta\pi^+\pi^-$
$3.38 \pm 0.33 \pm 0.64$		1 BOLTON	92B	MRK3 $J/\psi \rightarrow \gamma\eta\pi^+\pi^-$
• • • We do not use the following data for averages, fits, limits, etc. • • •				
$7.0 \pm 0.6 \pm 1.1$	261	2 AUGUSTIN	90	DM2 $J/\psi \rightarrow \gamma\eta\pi^+\pi^-$
1 Via $a_0(980) \pi$ .				
2 Includes unknown branching fraction to $\eta\pi^+\pi^-$ .				

### $\Gamma(\gamma\eta(1405/1475) \rightarrow \gamma\gamma\phi) / \Gamma_{\text{total}}$ $\Gamma_{219} / \Gamma$

VALUE (units $10^{-6}$ )	CL%	EVTS	DOCUMENT ID	TECN	COMMENT
<b>&lt;82</b>	95		BAI	04J	BES2 $J/\psi \rightarrow \gamma\gamma K^+ K^-$
• • • We do not use the following data for averages, fits, limits, etc. • • •					
$7.03 \pm 0.92 \pm 0.91$	1.3k		1 ABLIKIM	18I	BES3 $J/\psi \rightarrow \gamma\gamma\phi(1020)$
$10.36 \pm 1.51 \pm 1.54$	1.9k		2 ABLIKIM	18I	BES3 $J/\psi \rightarrow \gamma\gamma\phi(1020)$
1 Constructive interference between the $X(1835)$ and $\eta(1405)/\eta(1475)$ is assumed in a fit to the $\gamma\phi$ invariant mass.					
2 Destructive interference between the $X(1835)$ and $\eta(1405)/\eta(1475)$ is assumed in a fit to the $\gamma\phi$ invariant mass.					

### $\Gamma(\gamma\eta(1405) \rightarrow \gamma\gamma\gamma) / \Gamma_{\text{total}}$ $\Gamma_{220} / \Gamma$

VALUE	CL%	DOCUMENT ID	TECN	COMMENT
<b>&lt;2.63 <math>\times 10^{-6}</math></b>	90	ABLIKIM	180	BES3 $\psi(2S) \rightarrow \pi^+\pi^-\gamma\gamma\gamma$

### $\Gamma(\gamma\eta(1475) \rightarrow \gamma\gamma\gamma) / \Gamma_{\text{total}}$ $\Gamma_{221} / \Gamma$

VALUE	CL%	DOCUMENT ID	TECN	COMMENT
<b>&lt;1.86 <math>\times 10^{-6}</math></b>	90	ABLIKIM	180	BES3 $\psi(2S) \rightarrow \pi^+\pi^-\gamma\gamma\gamma$

### $\Gamma(\gamma\rho\rho) / \Gamma_{\text{total}}$ $\Gamma_{222} / \Gamma$

VALUE (units $10^{-3}$ )	CL%	DOCUMENT ID	TECN	COMMENT
<b><math>4.5 \pm 0.8</math> OUR AVERAGE</b>				
$4.7 \pm 0.3 \pm 0.9$		1 BALTRUSAIT...86B	MRK3	$J/\psi \rightarrow 4\pi\gamma$
$3.75 \pm 1.05 \pm 1.20$		2 BURKE	82	MRK2 $J/\psi \rightarrow 4\pi\gamma$
• • • We do not use the following data for averages, fits, limits, etc. • • •				
<0.09	90	3 BISELLO	89B	$J/\psi \rightarrow 4\pi\gamma$
1 $4\pi$ mass less than 2.0 GeV.				
2 $4\pi$ mass less than 2.0 GeV. We have multiplied $2\rho^0$ measurement by 3 to obtain $2\rho$ .				
3 $4\pi$ mass in the range 2.0-25 GeV.				

### $\Gamma(\gamma\rho\omega) / \Gamma_{\text{total}}$ $\Gamma_{223} / \Gamma$

VALUE	CL%	DOCUMENT ID	TECN	COMMENT
<b>&lt;5.4 <math>\times 10^{-4}</math></b>	90	ABLIKIM	08A	BES2 $e^+e^- \rightarrow J/\psi$

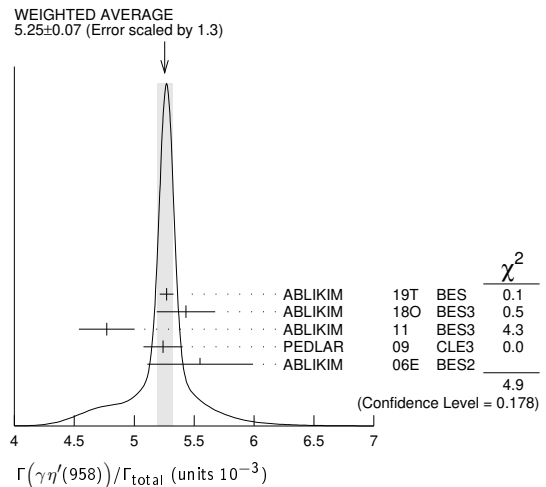
### $\Gamma(\gamma\rho\phi) / \Gamma_{\text{total}}$ $\Gamma_{224} / \Gamma$

VALUE	CL%	DOCUMENT ID	TECN	COMMENT
<b>&lt;8.8 <math>\times 10^{-5}</math></b>	90	ABLIKIM	08A	BES2 $e^+e^- \rightarrow J/\psi$

### $\Gamma(\gamma\eta'(958)) / \Gamma_{\text{total}}$ $\Gamma_{225} / \Gamma$

VALUE (units $10^{-3}$ )	EVTS	DOCUMENT ID	TECN	COMMENT
<b><math>5.25 \pm 0.07</math> OUR AVERAGE</b>	Error includes scale factor of 1.3. See the ideogram below.			
$5.27 \pm 0.03 \pm 0.05$	36k	ABLIKIM	19T	BES $J/\psi \rightarrow \gamma\eta'$
$5.43 \pm 0.23 \pm 0.09$	5.0k	1 ABLIKIM	180	BES3 $\psi(2S) \rightarrow \pi^+\pi^-\gamma\gamma\gamma$
$4.77 \pm 0.22 \pm 0.06$		2 ABLIKIM	11	BES3 $J/\psi \rightarrow \eta'\gamma$
$5.24 \pm 0.12 \pm 0.11$		PEDLAR	09	CLE3 $J/\psi \rightarrow \eta'\gamma$
$5.55 \pm 0.44$	35k	ABLIKIM	06E	BES2 $J/\psi \rightarrow \eta'\gamma$
• • • We do not use the following data for averages, fits, limits, etc. • • •				
$4.50 \pm 0.14 \pm 0.53$		BOLTON	92B	MRK3 $J/\psi \rightarrow \gamma\pi^+\pi^-\eta, \eta \rightarrow \gamma\gamma$
$4.30 \pm 0.31 \pm 0.71$		BOLTON	92B	MRK3 $J/\psi \rightarrow \gamma\pi^+\pi^-\eta, \eta \rightarrow \pi^+\pi^-\pi^0$
$4.04 \pm 0.16 \pm 0.85$	622	AUGUSTIN	90	DM2 $J/\psi \rightarrow \gamma\eta\pi^+\pi^-$
$4.39 \pm 0.09 \pm 0.66$	2420	AUGUSTIN	90	DM2 $J/\psi \rightarrow \gamma\gamma\pi^+\pi^-$
$4.1 \pm 0.3 \pm 0.6$		BLOOM	83	CBAL $e^+e^- \rightarrow 3\gamma + \text{hadrons}$
$2.9 \pm 1.1$	6	BRANDELIK	79C	DASP $e^+e^- \rightarrow 3\gamma$
$2.4 \pm 0.7$	57	BARTEL	76	CNTR $e^+e^- \rightarrow 2\gamma\rho$

- ABLIKIM 180 reports  $[\Gamma(J/\psi(1S) \rightarrow \gamma\eta'(958)) / \Gamma_{\text{total}}] \times [B(\eta'(958) \rightarrow \gamma\gamma)] = (1.26 \pm 0.02 \pm 0.05) \times 10^{-4}$  from a measurement of  $[\Gamma(J/\psi(1S) \rightarrow \gamma\eta'(958)) / \Gamma_{\text{total}}] \times [B(\eta'(958) \rightarrow \gamma\gamma)] \times [B(\psi(2S) \rightarrow J/\psi(1S)\pi^+\pi^-)]$  assuming  $B(\psi(2S) \rightarrow J/\psi(1S)\pi^+\pi^-) = (34.49 \pm 0.30) \times 10^{-2}$ , which we rescale to our best values  $B(\eta'(958) \rightarrow \gamma\gamma) = (2.307 \pm 0.033) \times 10^{-2}$ ,  $B(\psi(2S) \rightarrow J/\psi(1S)\pi^+\pi^-) = (34.68 \pm 0.30) \times 10^{-2}$ . Our first error is their experiment's error and our second error is the systematic error from using our best values.
- ABLIKIM 11 reports  $(4.84 \pm 0.03 \pm 0.24) \times 10^{-3}$  from a measurement of  $[\Gamma(J/\psi(1S) \rightarrow \gamma\eta'(958)) / \Gamma_{\text{total}}] / [B(\eta'(958) \rightarrow \pi^+\pi^-\eta)] / [B(\eta \rightarrow 2\gamma)]$  assuming  $B(\eta(958) \rightarrow \pi^+\pi^-\eta) = (43.2 \pm 0.7) \times 10^{-2}$ ,  $B(\eta \rightarrow 2\gamma) = (39.31 \pm 0.20) \times 10^{-2}$ , which we rescale to our best values  $B(\eta'(958) \rightarrow \pi^+\pi^-\eta) = (42.5 \pm 0.5) \times 10^{-2}$ ,  $B(\eta \rightarrow 2\gamma) = (39.41 \pm 0.20) \times 10^{-2}$ . Our first error is their experiment's error and our second error is the systematic error from using our best values.



See key on page 999

# Meson Particle Listings

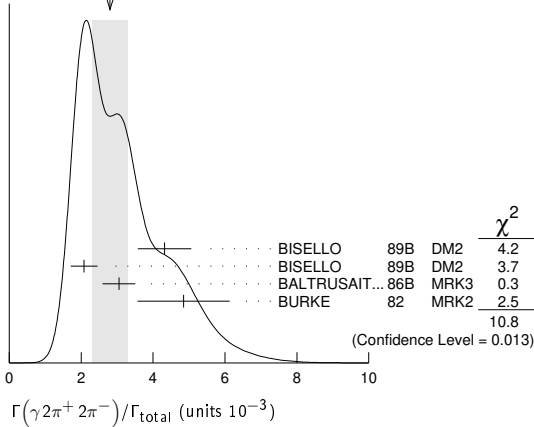
## $J/\psi(1S)$

### $\Gamma(\gamma 2\pi^+ 2\pi^-)/\Gamma_{total}$ $\Gamma_{226}/\Gamma$

VALUE (units $10^{-3}$ )	DOCUMENT ID	TECN	COMMENT
<b>2.8 ± 0.5 OUR AVERAGE</b>	Error includes scale factor of 1.9. See the ideogram below.		
4.32 ± 0.14 ± 0.73	1 BISELLO	89B DM2	$J/\psi \rightarrow 4\pi\gamma$
2.08 ± 0.13 ± 0.35	2 BISELLO	89B DM2	$J/\psi \rightarrow 4\pi\gamma$
3.05 ± 0.08 ± 0.45	2 BALTRUSAIT...86B	MRK3	$J/\psi \rightarrow 4\pi\gamma$
4.85 ± 0.45 ± 1.20	3 BURKE	82 MRK2	$e^+e^-$

- <sup>1</sup>  $4\pi$  mass less than 3.0 GeV.
- <sup>2</sup>  $4\pi$  mass less than 2.0 GeV.
- <sup>3</sup>  $4\pi$  mass less than 2.5 GeV.

WEIGHTED AVERAGE  
2.8±0.5 (Error scaled by 1.9)



### $\Gamma(\gamma f_2(1270) f_2(1270))/\Gamma_{total}$ $\Gamma_{227}/\Gamma$

VALUE (units $10^{-4}$ )	EVTS	DOCUMENT ID	TECN	COMMENT
<b>9.5 ± 0.7 ± 1.6</b>	646 ± 45	ABLIKIM	04M BES	$J/\psi \rightarrow \gamma 2\pi^+ 2\pi^-$

### $\Gamma(\gamma f_2(1270) f_2(1270) \text{ (non resonant)})/\Gamma_{total}$ $\Gamma_{228}/\Gamma$

VALUE (units $10^{-4}$ )	DOCUMENT ID	TECN	COMMENT
<b>8.2 ± 0.8 ± 1.7</b>	1 ABLIKIM	04M BES	$J/\psi \rightarrow \gamma 2\pi^+ 2\pi^-$

<sup>1</sup> Subtracting contribution from intermediate  $\eta_c(1S)$  decays.

### $\Gamma(\gamma K^+ K^- \pi^+ \pi^-)/\Gamma_{total}$ $\Gamma_{229}/\Gamma$

VALUE (units $10^{-3}$ )	EVTS	DOCUMENT ID	TECN	COMMENT
<b>2.1 ± 0.1 ± 0.6</b>	1516	BAI	00B BES	$J/\psi \rightarrow \gamma K^+ K^0 \pi^+ \pi^-$

### $\Gamma(\gamma f_4(2050))/\Gamma_{total}$ $\Gamma_{230}/\Gamma$

VALUE (units $10^{-3}$ )	DOCUMENT ID	TECN	COMMENT
<b>2.7 ± 0.5 ± 0.5</b>	1 BALTRUSAIT...87	MRK3	$J/\psi \rightarrow \gamma \pi^+ \pi^-$

<sup>1</sup> Assuming branching fraction  $f_4(2050) \rightarrow \pi\pi/\text{total} = 0.167$ .

### $\Gamma(\gamma\omega)/\Gamma_{total}$ $\Gamma_{231}/\Gamma$

VALUE (units $10^{-3}$ )	EVTS	DOCUMENT ID	TECN	COMMENT
<b>1.61 ± 0.33 OUR AVERAGE</b>				
6.0 ± 4.8 ± 1.8		ABLIKIM	08A BES2	$J/\psi \rightarrow \gamma\omega\pi^+\pi^-$
1.41 ± 0.2 ± 0.42	120 ± 17	BISELLO	87 SPEC	$e^+e^-$ , hadrons $\gamma$
1.76 ± 0.09 ± 0.45		BALTRUSAIT...85c	MRK3	$e^+e^- \rightarrow$ hadrons $\gamma$

### $\Gamma(\gamma\eta(1405/1475) \rightarrow \gamma\rho^0\rho^0)/\Gamma_{total}$ $\Gamma_{232}/\Gamma$

VALUE (units $10^{-3}$ )	DOCUMENT ID	TECN	COMMENT
<b>1.7 ± 0.4 OUR AVERAGE</b>	Error includes scale factor of 1.3.		
2.1 ± 0.4	BUGG	95 MRK3	$J/\psi \rightarrow \gamma\pi^+\pi^-\pi^+\pi^-$
1.36 ± 0.38	1,2 BISELLO	89B DM2	$J/\psi \rightarrow 4\pi\gamma$

- <sup>1</sup> Estimated by us from various fits.
- <sup>2</sup> Includes unknown branching fraction to  $\rho^0\rho^0$ .

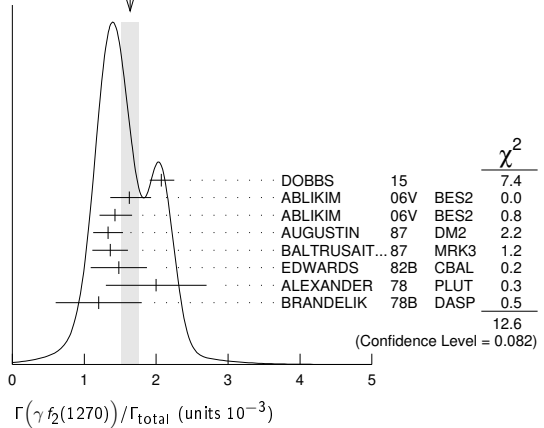
### $\Gamma(\gamma f_2(1270))/\Gamma_{total}$ $\Gamma_{233}/\Gamma$

VALUE (units $10^{-3}$ )	EVTS	DOCUMENT ID	TECN	COMMENT
<b>1.64 ± 0.12 OUR AVERAGE</b>	Error includes scale factor of 1.3. See the ideogram below.			
2.07 ± 0.16 ± 0.02 ± 0.07	2.4k	1,2 DOBBS	15	$J/\psi \rightarrow \gamma\pi\pi$
1.63 ± 0.26 ± 0.02 ± 0.06		3 ABLIKIM	06v BES2	$e^+e^- \rightarrow J/\psi \rightarrow \gamma\pi^+\pi^-$
1.42 ± 0.21 ± 0.01 ± 0.05		4 ABLIKIM	06v BES2	$e^+e^- \rightarrow J/\psi \rightarrow \gamma\pi^0\pi^0$
1.33 ± 0.05 ± 0.20		5 AUGUSTIN	87 DM2	$J/\psi \rightarrow \gamma\pi^+\pi^-$
1.36 ± 0.09 ± 0.23		5 BALTRUSAIT...87	MRK3	$J/\psi \rightarrow \gamma\pi^+\pi^-$
1.48 ± 0.25 ± 0.30	178	EDWARDS	82B CBAL	$e^+e^- \rightarrow 2\pi^0\gamma$
2.0 ± 0.7	35	ALEXANDER	78 PLUT	$e^+e^-$
1.2 ± 0.6	30	6 BRANDELIK	78B DASP	$e^+e^- \rightarrow \pi^+\pi^-\gamma$

<sup>1</sup> Using CLEO-c data but not authored by the CLEO Collaboration.

- <sup>2</sup> DOBBS 15 reports  $[\Gamma(J/\psi(1S) \rightarrow \gamma f_2(1270))/\Gamma_{total}] \times [B(f_2(1270) \rightarrow \pi\pi)] = (1.744 \pm 0.052 \pm 0.122) \times 10^{-3}$  which we divide by our best value  $B(f_2(1270) \rightarrow \pi\pi) = (84.2^{+2.9}_{-0.9}) \times 10^{-2}$ . Our first error is their experiment's error and our second error is the systematic error from using our best value.
- <sup>3</sup> ABLIKIM 06v reports  $[\Gamma(J/\psi(1S) \rightarrow \gamma f_2(1270))/\Gamma_{total}] \times [B(f_2(1270) \rightarrow \pi\pi)] = (1.371 \pm 0.010 \pm 0.222) \times 10^{-3}$  which we divide by our best value  $B(f_2(1270) \rightarrow \pi\pi) = (84.2^{+2.9}_{-0.9}) \times 10^{-2}$ . Our first error is their experiment's error and our second error is the systematic error from using our best value.
- <sup>4</sup> ABLIKIM 06v reports  $[\Gamma(J/\psi(1S) \rightarrow \gamma f_2(1270))/\Gamma_{total}] \times [B(f_2(1270) \rightarrow \pi\pi)] = (1.200 \pm 0.027 \pm 0.174) \times 10^{-3}$  which we divide by our best value  $B(f_2(1270) \rightarrow \pi\pi) = (84.2^{+2.9}_{-0.9}) \times 10^{-2}$ . Our first error is their experiment's error and our second error is the systematic error from using our best value.
- <sup>5</sup> Estimated using  $B(f_2(1270) \rightarrow \pi\pi) = 0.843 \pm 0.012$ . The errors do not contain the uncertainty in the  $f_2(1270)$  decay.
- <sup>6</sup> Restated by us to take account of spread of E1, M2, E3 transitions.

WEIGHTED AVERAGE  
1.64±0.12 (Error scaled by 1.3)



### $\Gamma(\gamma f_2(1270) \rightarrow \gamma K_S^0 K_S^0)/\Gamma_{total}$ $\Gamma_{234}/\Gamma$

VALUE (units $10^{-5}$ )	DOCUMENT ID	TECN	COMMENT
<b>2.58 ± 0.08 ± 0.59 ± 0.09 ± 0.20</b>	ABLIKIM	18AA BES3	$J/\psi \rightarrow \gamma K_S^0 K_S^0$

### $\Gamma(\gamma f_0(1370) \rightarrow \gamma K\bar{K})/\Gamma_{total}$ $\Gamma_{235}/\Gamma$

VALUE (units $10^{-4}$ )	EVTS	DOCUMENT ID	COMMENT
<b>4.19 ± 0.73 ± 1.34</b>	478	1 DOBBS	15 $J/\psi \rightarrow \gamma K\bar{K}$

<sup>1</sup> Using CLEO-c data but not authored by the CLEO Collaboration.

### $\Gamma(\gamma f_0(1370) \rightarrow \gamma K_S^0 K_S^0)/\Gamma_{total}$ $\Gamma_{236}/\Gamma$

VALUE (units $10^{-5}$ )	DOCUMENT ID	TECN	COMMENT
<b>1.07 ± 0.08 ± 0.36 ± 0.07 ± 0.34</b>	ABLIKIM	18AA BES3	$J/\psi \rightarrow \gamma K_S^0 K_S^0$

### $\Gamma(\gamma f_0(1500) \rightarrow \gamma K_S^0 K_S^0)/\Gamma_{total}$ $\Gamma_{237}/\Gamma$

VALUE (units $10^{-5}$ )	DOCUMENT ID	TECN	COMMENT
<b>1.59 ± 0.16 ± 0.18 ± 0.06</b>	ABLIKIM	18AA BES3	$J/\psi \rightarrow \gamma K_S^0 K_S^0$

### $\Gamma(\gamma f_0(1710) \rightarrow \gamma K\bar{K})/\Gamma_{total}$ $\Gamma_{238}/\Gamma$

VALUE (units $10^{-4}$ )	CL%	EVTS	DOCUMENT ID	TECN	COMMENT
<b>9.5 ± 1.0 ± 0.5 OUR AVERAGE</b>	Error includes scale factor of 1.5. See the ideogram below.				
8.00 ± 0.12 ± 1.24 ± 0.08 ± 0.40			1 ABLIKIM	18AA BES3	$J/\psi \rightarrow \gamma K_S^0 K_S^0$
11.76 ± 0.54 ± 0.94	1.2k		2 DOBBS	15	$J/\psi \rightarrow \gamma K\bar{K}$
9.62 ± 0.29 ± 1.86			3 BAI	03G BES	$J/\psi \rightarrow \gamma K\bar{K}$
5.0 ± 0.8 ± 1.8 ± 0.4			1,4 BAI	96C BES	$J/\psi \rightarrow \gamma K^+ K^-$
9.2 ± 1.4 ± 1.4			1 AUGUSTIN	88 DM2	$J/\psi \rightarrow \gamma K^+ K^-$
10.4 ± 1.2 ± 1.6			1 AUGUSTIN	88 DM2	$J/\psi \rightarrow \gamma K_S^0 K_S^0$
9.6 ± 1.2 ± 1.8			1 BALTRUSAIT...87	MRK3	$J/\psi \rightarrow \gamma K^+ K^-$
1.6 ± 0.2 ± 0.6 ± 0.2			1,5 BAI	96C BES	$J/\psi \rightarrow \gamma K^+ K^-$
< 1.8 ± 0.4 ± 0.3	90		6 BISELLO	89B	$J/\psi \rightarrow 4\pi\gamma$
3.8 ± 1.6			7 BALTRUSAIT...87	MRK3	$J/\psi \rightarrow \gamma\pi^+\pi^-$
			8 EDWARDS	82D CBAL	$e^+e^- \rightarrow \eta\eta\gamma$

- • • We do not use the following data for averages, fits, limits, etc. • • •
- <sup>1</sup> Includes unknown branching fraction to  $K^+K^-$  or  $K_S^0 K_S^0$ . We have multiplied  $K^+K^-$  measurement by 2, and  $K_S^0 K_S^0$  by 4 to obtain  $K\bar{K}$  result.
- <sup>2</sup> Using CLEO-c data but not authored by the CLEO Collaboration.

# Meson Particle Listings

## $J/\psi(1S)$

<sup>3</sup>Includes unknown branching ratio to  $K^+K^-$  or  $K_S^0 K_S^0$ .

<sup>4</sup>Assuming  $J^P = 2^+$  for  $f_0(1710)$ .

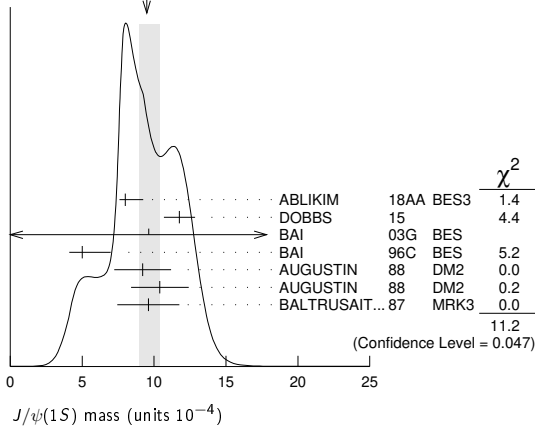
<sup>5</sup>Assuming  $J^P = 0^+$  for  $f_0(1710)$ .

<sup>6</sup>Includes unknown branching fraction to  $\rho^0 \rho^0$ .

<sup>7</sup>Includes unknown branching fraction to  $\pi^+ \pi^-$ .

<sup>8</sup>Includes unknown branching fraction to  $\eta \eta$ .

WEIGHTED AVERAGE  
9.5+1.0-0.5 (Error scaled by 1.5)



### $\Gamma(\gamma f_0(1710) \rightarrow \gamma \pi \pi) / \Gamma_{\text{total}}$ $\Gamma_{239} / \Gamma$

VALUE (units $10^{-4}$ )	EVTS	DOCUMENT ID	TECN	COMMENT	$\chi^2$
<b>3.8 ± 0.5 OUR AVERAGE</b>					
3.72 ± 0.30 ± 0.43	483	<sup>1</sup> DOBBS	15	$J/\psi \rightarrow \gamma \pi \pi$	1.4
3.96 ± 0.06 ± 1.12		<sup>2</sup> ABLIKIM	06v BES2	$e^+ e^- \rightarrow J/\psi \rightarrow \gamma \pi^+ \pi^-$	4.4
3.99 ± 0.15 ± 2.64		<sup>2</sup> ABLIKIM	06v BES2	$e^+ e^- \rightarrow J/\psi \rightarrow \gamma \pi^0 \pi^0$	5.2
• • • We do not use the following data for averages, fits, limits, etc. • • •					
2.5 ± 1.6 ± 0.8		BAI	98h BES	$J/\psi \rightarrow \gamma \pi^0 \pi^0$	11.2

<sup>1</sup>Using CLEO-c data but not authored by the CLEO Collaboration.  
<sup>2</sup>Including unknown branching fraction to  $\pi \pi$ .

### $\Gamma(\gamma f_0(1710) \rightarrow \gamma \omega \omega) / \Gamma_{\text{total}}$ $\Gamma_{240} / \Gamma$

VALUE (units $10^{-3}$ )	EVTS	DOCUMENT ID	TECN	COMMENT
<b>0.31 ± 0.06 ± 0.08</b>	180	ABLIKIM	06h BES	$J/\psi \rightarrow \gamma \omega \omega$

### $\Gamma(\gamma f_0(1710) \rightarrow \gamma \eta \eta) / \Gamma_{\text{total}}$ $\Gamma_{241} / \Gamma$

VALUE (units $10^{-4}$ )	EVTS	DOCUMENT ID	TECN	COMMENT
<b>2.35<sup>+0.13+1.24</sup><sub>-0.11-0.74</sub></b>	5.5k	<sup>1</sup> ABLIKIM	13n BES3	$J/\psi \rightarrow \gamma \eta \eta$

<sup>1</sup>From partial wave analysis including all possible combinations of  $0^{++}$ ,  $2^{++}$ , and  $4^{++}$  resonances.

### $\Gamma(\gamma \eta) / \Gamma_{\text{total}}$ $\Gamma_{242} / \Gamma$

VALUE (units $10^{-3}$ )	EVTS	DOCUMENT ID	TECN	COMMENT
<b>1.108 ± 0.027 OUR AVERAGE</b>				
1.12 ± 0.05 ± 0.01	18.6k	<sup>1</sup> ABLIKIM	18o BES3	$\psi(2S) \rightarrow \pi^+ \pi^- \gamma \gamma \gamma$
1.101 ± 0.029 ± 0.022		PEDLAR	09 CLE3	$J/\psi \rightarrow \gamma \eta \gamma$
1.123 ± 0.089	11k	ABLIKIM	06E BES2	$J/\psi \rightarrow \gamma \eta \gamma$
• • • We do not use the following data for averages, fits, limits, etc. • • •				
0.88 ± 0.08 ± 0.11		BLOOM	83 CBAL	$e^+ e^-$
0.82 ± 0.10		BRANDELIK	79c DASP	$e^+ e^-$
1.3 ± 0.4	21	BARTEL	77 CNTR	$e^+ e^-$

<sup>1</sup>ABLIKIM 18o reports  $[\Gamma(J/\psi(1S) \rightarrow \gamma \eta) / \Gamma_{\text{total}}] \times [B(\eta \rightarrow 2\gamma)] = (4.42 \pm 0.04 \pm 0.18) \times 10^{-4}$  from a measurement of  $[\Gamma(J/\psi(1S) \rightarrow \gamma \eta) / \Gamma_{\text{total}}] \times [B(\eta \rightarrow 2\gamma)] \times [B(\psi(2S) \rightarrow J/\psi(1S) \pi^+ \pi^-)]$  assuming  $B(\psi(2S) \rightarrow J/\psi(1S) \pi^+ \pi^-) = (34.49 \pm 0.30) \times 10^{-2}$ , which we rescale to our best values  $B(\eta \rightarrow 2\gamma) = (39.41 \pm 0.20) \times 10^{-2}$ ,  $B(\psi(2S) \rightarrow J/\psi(1S) \pi^+ \pi^-) = (34.68 \pm 0.30) \times 10^{-2}$ . Our first error is their experiment's error and our second error is the systematic error from using our best values.

### $\Gamma(\gamma f_1(1420) \rightarrow \gamma K \bar{K} \pi) / \Gamma_{\text{total}}$ $\Gamma_{243} / \Gamma$

VALUE (units $10^{-3}$ )	DOCUMENT ID	TECN	COMMENT
<b>0.79 ± 0.13 OUR AVERAGE</b>			
0.68 ± 0.04 ± 0.24	BAI	00D BES	$J/\psi \rightarrow \gamma K^\pm K_S^0 \pi^\mp$
0.76 ± 0.15 ± 0.21	<sup>1,2</sup> AUGUSTIN	92 DM2	$J/\psi \rightarrow \gamma K \bar{K} \pi$
0.87 ± 0.14 <sup>+0.14</sup> <sub>-0.11</sub>	<sup>1</sup> BAI	90c MRK3	$J/\psi \rightarrow \gamma K_S^0 K^\pm \pi^\mp$

<sup>1</sup>Included unknown branching fraction  $f_1(1420) \rightarrow K \bar{K} \pi$ .  
<sup>2</sup>From fit to the  $K^*(892) K 1^{++}$  partial wave.

### $\Gamma(\gamma f_1(1285)) / \Gamma_{\text{total}}$ $\Gamma_{244} / \Gamma$

VALUE (units $10^{-3}$ )	DOCUMENT ID	TECN	COMMENT
<b>0.61 ± 0.08 OUR AVERAGE</b>			
0.69 ± 0.16 ± 0.20	<sup>1</sup> BAI	04J BES2	$J/\psi \rightarrow \gamma \gamma \rho^0$
0.61 ± 0.04 ± 0.21	<sup>2</sup> BAI	00D BES	$J/\psi \rightarrow \gamma K^\pm K_S^0 \pi^\mp$
0.45 ± 0.09 ± 0.17	<sup>3</sup> BAI	99 BES	$J/\psi \rightarrow \gamma \eta \pi^+ \pi^-$
0.625 ± 0.063 ± 0.103	<sup>4</sup> BOLTON	92 MRK3	$J/\psi \rightarrow \gamma f_1(1285)$
0.70 ± 0.08 ± 0.16	<sup>5</sup> BOLTON	92B MRK3	$J/\psi \rightarrow \gamma \eta \pi^+ \pi^-$

<sup>1</sup>Assuming  $B(f_1(1285) \rightarrow \rho^0 \gamma) = 0.055 \pm 0.013$ .  
<sup>2</sup>Assuming  $\Gamma(f_1(1285) \rightarrow K \bar{K} \pi) / \Gamma_{\text{total}} = 0.090 \pm 0.004$ .  
<sup>3</sup>Assuming  $\Gamma(f_1(1285) \rightarrow \eta \pi \pi) / \Gamma_{\text{total}} = 0.5 \pm 0.18$ .  
<sup>4</sup>Obtained summing the sequential decay channels  
 $B(J/\psi \rightarrow \gamma f_1(1285), f_1(1285) \rightarrow \pi \pi \pi \pi) = (1.44 \pm 0.39 \pm 0.27) \times 10^{-4}$ ;  
 $B(J/\psi \rightarrow \gamma f_1(1285), f_1(1285) \rightarrow a_0(980) \pi, a_0(980) \rightarrow \eta \pi) = (3.90 \pm 0.42 \pm 0.87) \times 10^{-4}$ ;  
 $B(J/\psi \rightarrow \gamma f_1(1285), f_1(1285) \rightarrow a_0(980) \pi, a_0(980) \rightarrow K \bar{K}) = (0.66 \pm 0.26 \pm 0.29) \times 10^{-4}$ ;  
 $B(J/\psi \rightarrow \gamma f_1(1285), f_1(1285) \rightarrow \gamma \rho^0) = (0.25 \pm 0.07 \pm 0.03) \times 10^{-4}$ .  
<sup>5</sup>Using  $B(f_1(1285) \rightarrow a_0(980) \pi) = 0.37$ , and including unknown branching ratio for  $a_0(980) \rightarrow \eta \pi$ .

### $\Gamma(\gamma f_1(1510) \rightarrow \gamma \eta \pi^+ \pi^-) / \Gamma_{\text{total}}$ $\Gamma_{245} / \Gamma$

VALUE (units $10^{-4}$ )	DOCUMENT ID	TECN	COMMENT
<b>4.5 ± 1.0 ± 0.7</b>	BAI	99 BES	$J/\psi \rightarrow \gamma \eta \pi^+ \pi^-$

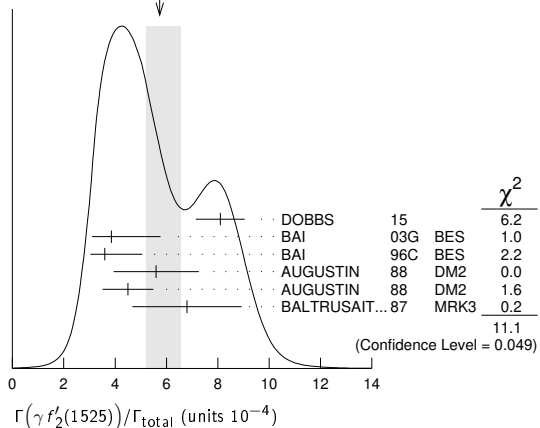
### $\Gamma(\gamma f'_2(1525)) / \Gamma_{\text{total}}$ $\Gamma_{246} / \Gamma$

VALUE (units $10^{-4}$ )	CL%	EVTS	DOCUMENT ID	TECN	COMMENT
<b>5.7<sup>+0.8</sup><sub>-0.5</sub> OUR AVERAGE</b>					Error includes scale factor of 1.5. See the ideogram below.

8.1 ± 0.9 ± 0.2	750	<sup>1,2</sup> DOBBS	15	$J/\psi \rightarrow \gamma K \bar{K}$	
3.85 ± 0.17 <sup>+1.91</sup> <sub>-0.73</sub>		<sup>3</sup> BAI	03G BES	$J/\psi \rightarrow \gamma K \bar{K}$	
3.6 ± 0.4 <sup>+1.4</sup> <sub>-0.4</sub>		<sup>3</sup> BAI	96c BES	$J/\psi \rightarrow \gamma K^+ K^-$	
5.6 ± 1.4 ± 0.9		<sup>3</sup> AUGUSTIN	88 DM2	$J/\psi \rightarrow \gamma K^+ K^-$	
4.5 ± 0.4 ± 0.9		<sup>3</sup> AUGUSTIN	88 DM2	$J/\psi \rightarrow \gamma K_S^0 K_S^0$	
6.8 ± 1.6 ± 1.4		<sup>3</sup> BALTRUSAIT...87	MRK3	$J/\psi \rightarrow \gamma K^+ K^-$	
• • • We do not use the following data for averages, fits, limits, etc. • • •					
<3.4	90	4	BRANDELIK	79c DASP	$e^+ e^- \rightarrow \pi^+ \pi^- \gamma$
<2.3	90	3	ALEXANDER	78 PLUT	$e^+ e^- \rightarrow K^+ K^- \gamma$

<sup>1</sup>Using CLEO-c data but not authored by the CLEO Collaboration.  
<sup>2</sup>DOBBS 15 reports  $[\Gamma(J/\psi(1S) \rightarrow \gamma f'_2(1525)) / \Gamma_{\text{total}}] \times [B(f'_2(1525) \rightarrow K \bar{K})] = (7.09 \pm 0.46 \pm 0.67) \times 10^{-4}$  which we divide by our best value  $B(f'_2(1525) \rightarrow K \bar{K}) = (87.6 \pm 2.2) \times 10^{-2}$ . Our first error is their experiment's error and our second error is the systematic error from using our best value.  
<sup>3</sup>Using  $B(f'_2(1525) \rightarrow K \bar{K}) = 0.888$ .  
<sup>4</sup>Assuming isotropic production and decay of the  $f'_2(1525)$  and isospin.

WEIGHTED AVERAGE  
5.7+0.8-0.5 (Error scaled by 1.5)



### $\Gamma(\gamma f'_2(1525) \rightarrow \gamma K_S^0 K_S^0) / \Gamma_{\text{total}}$ $\Gamma_{247} / \Gamma$

VALUE (units $10^{-5}$ )	DOCUMENT ID	TECN	COMMENT
<b>7.99<sup>+0.03+0.69</sup><sub>-0.04-0.50</sub></b>	ABLIKIM	18AA BES3	$J/\psi \rightarrow \gamma K_S^0 K_S^0$

### $\Gamma(\gamma f'_2(1525) \rightarrow \gamma \eta \eta) / \Gamma_{\text{total}}$ $\Gamma_{248} / \Gamma$

VALUE (units $10^{-5}$ )	EVTS	DOCUMENT ID	TECN	COMMENT
<b>3.42<sup>+0.43+1.37</sup><sub>-0.51-1.30</sub></b>	5.5k	<sup>1</sup> ABLIKIM	13n BES3	$J/\psi \rightarrow \gamma \eta \eta$

<sup>1</sup>From partial wave analysis including all possible combinations of  $0^{++}$ ,  $2^{++}$ , and  $4^{++}$  resonances.

See key on page 999

Meson Particle Listings

$J/\psi(1S)$

$\Gamma(\gamma f_2(1640) \rightarrow \gamma\omega\phi)/\Gamma_{total}$					$\Gamma_{249}/\Gamma$
VALUE (units $10^{-3}$ )	EVTS	DOCUMENT ID	TECN	COMMENT	
$0.28 \pm 0.05 \pm 0.17$	141	ABLIKIM	06H	BES	$J/\psi \rightarrow \gamma\omega\phi$

$\Gamma(\gamma f_2(1910) \rightarrow \gamma\omega\phi)/\Gamma_{total}$					$\Gamma_{250}/\Gamma$
VALUE (units $10^{-3}$ )	EVTS	DOCUMENT ID	TECN	COMMENT	
$0.20 \pm 0.04 \pm 0.13$	151	ABLIKIM	06H	BES	$J/\psi \rightarrow \gamma\omega\phi$

$\Gamma(\gamma f_0(1750) \rightarrow \gamma K_S^0 K_S^0)/\Gamma_{total}$					$\Gamma_{251}/\Gamma$
VALUE (units $10^{-5}$ )	EVTS	DOCUMENT ID	TECN	COMMENT	
$1.11 \pm 0.06 \pm 0.19$ $-0.32$		ABLIKIM	18AA	BES3	$J/\psi \rightarrow \gamma K_S^0 K_S^0$

$\Gamma(\gamma f_0(1800) \rightarrow \gamma\omega\phi)/\Gamma_{total}$					$\Gamma_{252}/\Gamma$
VALUE (units $10^{-4}$ )	EVTS	DOCUMENT ID	TECN	COMMENT	
<b><math>2.5 \pm 0.6</math> OUR AVERAGE</b>					
$2.00 \pm 0.08 \pm 1.38$ $-1.64$	1.3k	ABLIKIM	13J	BES3	$J/\psi \rightarrow \gamma\omega\phi$
$2.61 \pm 0.27 \pm 0.65$	95	ABLIKIM	06J	BES2	$J/\psi \rightarrow \gamma\omega\phi$

$\Gamma(\gamma f_2(1810) \rightarrow \gamma\eta\eta)/\Gamma_{total}$					$\Gamma_{253}/\Gamma$
VALUE (units $10^{-5}$ )	EVTS	DOCUMENT ID	TECN	COMMENT	
$5.40 \pm 0.60 \pm 3.42$ $-0.67 - 2.35$	5.5k	<sup>1</sup> ABLIKIM	13N	BES3	$J/\psi \rightarrow \gamma\eta\eta$

<sup>1</sup> From partial wave analysis including all possible combinations of  $0^{++}$ ,  $2^{++}$ , and  $4^{++}$  resonances.

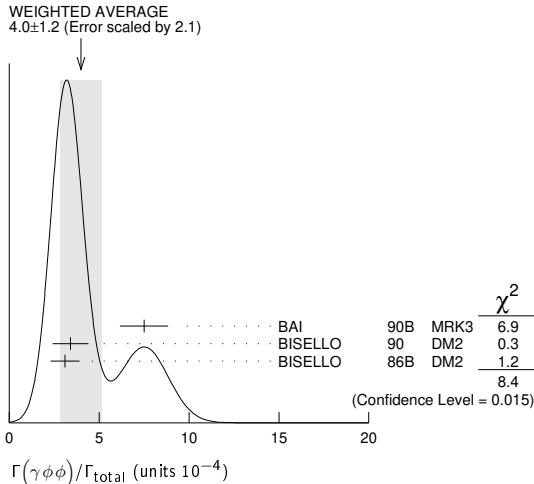
$\Gamma(\gamma f_2(1950) \rightarrow \gamma K^*(892) \bar{K}^*(892))/\Gamma_{total}$					$\Gamma_{254}/\Gamma$
VALUE (units $10^{-3}$ )	EVTS	DOCUMENT ID	TECN	COMMENT	
$0.7 \pm 0.1 \pm 0.2$		BAI	00B	BES	$J/\psi \rightarrow \gamma K^+ K^0 \pi^+ \pi^-$

$\Gamma(\gamma K^*(892) \bar{K}^*(892))/\Gamma_{total}$					$\Gamma_{255}/\Gamma$
VALUE (units $10^{-3}$ )	EVTS	DOCUMENT ID	TECN	COMMENT	
$4.0 \pm 0.3 \pm 1.3$	320	<sup>1</sup> BAI	00B	BES	$J/\psi \rightarrow \gamma K^+ K^0 \pi^+ \pi^-$

<sup>1</sup> Summed over all charges.

$\Gamma(\gamma\phi\phi)/\Gamma_{total}$					$\Gamma_{256}/\Gamma$
VALUE (units $10^{-4}$ )	EVTS	DOCUMENT ID	TECN	COMMENT	
<b><math>4.0 \pm 1.2</math> OUR AVERAGE</b>					Error includes scale factor of 2.1. See the ideogram below.
$7.5 \pm 0.6 \pm 1.2$	168	BAI	90B	MRK3	$J/\psi \rightarrow \gamma 4K$
$3.4 \pm 0.8 \pm 0.6$	$33 \pm 7$	<sup>1</sup> BISELLO	90	DM2	$J/\psi \rightarrow \gamma K^+ K^- K_S^0 K_L^0$
$3.1 \pm 0.7 \pm 0.4$		<sup>1</sup> BISELLO	86B	DM2	$J/\psi \rightarrow \gamma K^+ K^- K^+ K^-$

<sup>1</sup>  $\phi$  mass less than 2.9 GeV,  $\eta_C$  excluded.



$\Gamma(\gamma\rho\bar{\rho})/\Gamma_{total}$					$\Gamma_{257}/\Gamma$
VALUE (units $10^{-3}$ )	CL%	EVTS	DOCUMENT ID	TECN	COMMENT
$0.38 \pm 0.07 \pm 0.07$		49	EATON	84	MRK2 $e^+e^-$
••• We do not use the following data for averages, fits, limits, etc. •••					
$<0.11$		90	PERUZZI	78	MRK1 $e^+e^-$

$\Gamma(\gamma\eta(2225))/\Gamma_{total}$					$\Gamma_{258}/\Gamma$
VALUE (units $10^{-4}$ )	EVTS	DOCUMENT ID	TECN	COMMENT	
<b><math>3.14 \pm 0.50</math> OUR AVERAGE</b>					
$2.40 \pm 0.10 \pm 2.47$ $-0.18$		<sup>1,2</sup> ABLIKIM	16N	BES3	$J/\psi \rightarrow \gamma K^+ K^- K^+ K^-$
$4.4 \pm 0.4 \pm 0.8$	196	<sup>2</sup> ABLIKIM	08i	BES	$J/\psi \rightarrow \gamma K^+ K^- K_S^0 K_L^0$
$3.3 \pm 0.8 \pm 0.5$		<sup>2</sup> BAI	90b	MRK3	$J/\psi \rightarrow \gamma K^+ K^- K^+ K^-$

$2.7 \pm 0.6 \pm 0.6$		<sup>2</sup> BAI	90b	MRK3	$J/\psi \rightarrow \gamma K^+ K^- K_S^0 K_L^0$
$2.4 \pm 1.5$ $-1.0$		<sup>3,4</sup> BISELLO	89b	DM2	$J/\psi \rightarrow 4\pi\gamma$

<sup>1</sup> From a partial wave analysis of  $J/\psi \rightarrow \gamma\phi\phi$  that also finds significant signals for  $\eta(2100)$ ,  $0^{-+}$  phase space,  $f_0(2100)$ ,  $f_2(2010)$ ,  $f_2(2300)$ ,  $f_2(2340)$ , and a previously unseen  $0^{-+}$  state  $X(2500)$  ( $M = 2470 \pm 15 \pm 101$  MeV,  $\Gamma = 230 \pm 64 \pm 56$  MeV).

<sup>2</sup> Includes unknown branching fraction to  $\phi\phi$ .

<sup>3</sup> Estimated by us from various fits.

<sup>4</sup> Includes unknown branching fraction to  $\rho^0\rho^0$ .

$\Gamma(\gamma\eta(1760) \rightarrow \gamma\rho^0\rho^0)/\Gamma_{total}$					$\Gamma_{259}/\Gamma$
VALUE (units $10^{-3}$ )	EVTS	DOCUMENT ID	TECN	COMMENT	
$0.13 \pm 0.09$		<sup>1,2</sup> BISELLO	89b	DM2	$J/\psi \rightarrow 4\pi\gamma$

<sup>1</sup> Estimated by us from various fits.

<sup>2</sup> Includes unknown branching fraction to  $\rho^0\rho^0$ .

$\Gamma(\gamma\eta(1760) \rightarrow \gamma\omega\omega)/\Gamma_{total}$					$\Gamma_{260}/\Gamma$
VALUE (units $10^{-3}$ )	EVTS	DOCUMENT ID	TECN	COMMENT	
$1.98 \pm 0.08 \pm 0.32$	1045	ABLIKIM	06H	BES	$J/\psi \rightarrow \gamma\omega\omega$

$\Gamma(\gamma\eta(1760) \rightarrow \gamma\gamma\gamma)/\Gamma_{total}$					$\Gamma_{261}/\Gamma$
VALUE	CL%	DOCUMENT ID	TECN	COMMENT	
$<4.80 \times 10^{-6}$	90	ABLIKIM	18o	BES3	$\psi(2S) \rightarrow \pi^+ \pi^- \gamma\gamma\gamma$

$\Gamma(\gamma X(1835) \rightarrow \gamma\pi^+ \pi^- \eta')/\Gamma_{total}$					$\Gamma_{262}/\Gamma$
VALUE (units $10^{-4}$ )	EVTS	DOCUMENT ID	TECN	COMMENT	
$2.77 \pm 0.34$ $-0.40$ OUR AVERAGE					Error includes scale factor of 1.1.

$3.93 \pm 0.38 \pm 0.31$   
 $-0.84$  <sup>1</sup>ABLIKIM 16j BES3  $J/\psi \rightarrow \gamma\pi^+ \pi^- \eta'$

$2.87 \pm 0.09 \pm 0.49$   
 $-0.52$  <sup>2</sup>ABLIKIM 11c BES3  $J/\psi \rightarrow \gamma\pi^+ \pi^- \eta'$

$2.2 \pm 0.4 \pm 0.4$  264 ABLIKIM 05R BES2  $J/\psi \rightarrow \gamma\pi^+ \pi^- \eta'$

<sup>1</sup> From a fit of the measured  $\pi^+ \pi^- \eta'$  lineshape that accounts for the abrupt distortion observed at the  $p\bar{p}$  threshold with a Flatté formula in addition to known backgrounds and contributors, as well as an *ad hoc* Breit-Wigner ( $M \approx 1919$  MeV;  $\Gamma \approx 51$  MeV) that is required for a good fit. Another explanation for the distortion provided by ABLIKIM 16j is that a second resonance near 1870 MeV interferes with the  $X(1835)$ ; fits to this possibility yield product branching fraction values compatible with that shown within the respective systematic uncertainties.

<sup>2</sup> From a fit of the  $\pi^+ \pi^- \eta'$  mass distribution to a combination of  $\gamma f_1(1510)$ ,  $\gamma X(1835)$ , and two unconfirmed states  $\gamma X(2120)$ , and  $\gamma X(2370)$ , for  $M(p\bar{p}) < 2.8$  GeV, and accounting for backgrounds from non- $\eta'$  events and  $J/\psi \rightarrow \pi^0 \pi^+ \pi^- \eta'$ .

$\Gamma(\gamma X(1835) \rightarrow \gamma\rho\bar{\rho})/\Gamma_{total}$					$\Gamma_{263}/\Gamma$
VALUE (units $10^{-4}$ )	EVTS	DOCUMENT ID	TECN	COMMENT	
$0.77 \pm 0.15$ $-0.09$ OUR AVERAGE					
$0.90 \pm 0.04 \pm 0.27$ $-0.11 - 0.55$		<sup>1</sup> ABLIKIM	12D	BES3	$J/\psi \rightarrow \gamma\rho\bar{\rho}$
$1.14 \pm 0.43 \pm 0.42$ $-0.30 - 0.26$	231	<sup>2</sup> ALEXANDER	10	CLEO	$J/\psi \rightarrow \gamma\rho\bar{\rho}$
$0.70 \pm 0.04 \pm 0.19$ $-0.08$		BAI	03F	BES2	$J/\psi \rightarrow \gamma\rho\bar{\rho}$

<sup>1</sup> From the fit including final state interaction effects in isospin 0 S-wave according to SIBIRTSSEV 05A.

<sup>2</sup> From a fit of the  $p\bar{p}$  mass distribution to a combination of  $\gamma X(1835)$ ,  $\gamma R$  with  $M(R) = 2100$  MeV and  $\Gamma(R) = 160$  MeV, and  $\gamma\rho\bar{\rho}$  phase space, for  $M(p\bar{p}) < 2.85$  GeV.

$\Gamma(\gamma X(1835) \rightarrow \gamma K_S^0 K_S^0 \eta)/\Gamma_{total}$					$\Gamma_{264}/\Gamma$
VALUE (units $10^{-5}$ )	EVTS	DOCUMENT ID	TECN	COMMENT	
$3.31 \pm 0.33 \pm 1.96$ $-0.30 - 1.29$		ABLIKIM	15T	BES3	$J/\psi \rightarrow \gamma K_S^0 K_S^0 \eta$

$\Gamma(\gamma X(1835) \rightarrow \gamma\gamma\phi(1020))/\Gamma_{total}$					$\Gamma_{265}/\Gamma$
VALUE (units $10^{-6}$ )	EVTS	DOCUMENT ID	TECN	COMMENT	
••• We do not use the following data for averages, fits, limits, etc. •••					
$1.77 \pm 0.35 \pm 0.25$	305	<sup>1</sup> ABLIKIM	18i	BES3	$J/\psi \rightarrow \gamma\gamma\phi(1020)$
$8.09 \pm 1.99 \pm 1.36$	1.3k	<sup>2</sup> ABLIKIM	18i	BES3	$J/\psi \rightarrow \gamma\gamma\phi(1020)$

<sup>1</sup> Constructive interference between the  $X(1835)$  and  $\eta(1405)/\eta(1475)$  is assumed in a fit to the  $\gamma\phi$  invariant mass.

<sup>2</sup> Destructive interference between the  $X(1835)$  and  $\eta(1405)/\eta(1475)$  is assumed in a fit to the  $\gamma\phi$  invariant mass.

$\Gamma(\gamma X(1835) \rightarrow \gamma\gamma\gamma)/\Gamma_{total}$					$\Gamma_{266}/\Gamma$
VALUE	CL%	DOCUMENT ID	TECN	COMMENT	
$<3.56 \times 10^{-6}$	90	ABLIKIM	18o	BES3	$\psi(2S) \rightarrow \pi^+ \pi^- \gamma\gamma\gamma$

$\Gamma(\gamma X(1840) \rightarrow \gamma 3(\pi^+ \pi^-))/\Gamma_{total}$					$\Gamma_{267}/\Gamma$
VALUE (units $10^{-5}$ )	EVTS	DOCUMENT ID	TECN	COMMENT	
$2.44 \pm 0.36 \pm 0.60$ $-0.74$	0.6k	ABLIKIM	13U	BES3	$J/\psi \rightarrow \gamma 3(\pi^+ \pi^-)$

Meson Particle Listings

J/ψ(1S)

Γ(γ(KK̄π)[P<sup>PC</sup> = 0<sup>-+</sup>])/Γ<sub>total</sub> Γ<sub>268</sub>/Γ

Table with 4 columns: VALUE (units 10^-3), DOCUMENT ID, TECN, COMMENT. Row 1: 0.7 ± 0.4 OUR AVERAGE Error includes scale factor of 2.1. Row 2: 0.58 ± 0.03 ± 0.20 1 BAI 00D BES J/ψ → γK± K\_S^0 π∓. Row 3: 2.1 ± 0.1 ± 0.7 2 BAI 00D BES J/ψ → γK± K\_S^0 π∓.

1 For a broad structure around 1800 MeV.
2 For a broad structure around 2040 MeV.

Γ(γπ^0)/Γ<sub>total</sub> Γ<sub>269</sub>/Γ

Table with 4 columns: VALUE (units 10^-5), DOCUMENT ID, TECN, COMMENT. Row 1: 3.56 ± 0.17 OUR AVERAGE. Row 2: 3.59 ± 0.20 ± 0.03 1.6k 1 ABLIKIM 18o BES3 ψ(2S) → π+ π- γγγ. Row 3: 3.63 ± 0.36 ± 0.13 PEDLAR 09 CLE3 J/ψ → π^0 γ. Row 4: 3.13 ± 0.65 / -0.47 586 ABLIKIM 06E BES2 J/ψ → π^0 γ.

• • • We do not use the following data for averages, fits, limits, etc.
3.6 ± 1.1 ± 0.7 BLOOM 83 CBAL e+ e-
7.3 ± 4.7 10 BRANDELIK 79c DASP e+ e-
1 ABLIKIM 18o reports [Γ(J/ψ(1S) → γπ^0)/Γ<sub>total</sub>] × [B(π^0 → 2γ)] = (3.57 ± 0.12 ± 0.16) × 10^-5 from a measurement of [Γ(J/ψ(1S) → γπ^0)/Γ<sub>total</sub>] × [B(π^0 → 2γ)] × [B(ψ(2S) → J/ψ(1S)π+ π-)] assuming B(ψ(2S) → J/ψ(1S)π+ π-) = (34.49 ± 0.30) × 10^-2, which we rescale to our best values B(π^0 → 2γ) = (98.823 ± 0.034) × 10^-2, B(ψ(2S) → J/ψ(1S)π+ π-) = (34.68 ± 0.30) × 10^-2. Our first error is their experiment's error and our second error is the systematic error from using our best values.

Γ(γρ̄ππ+ π-)/Γ<sub>total</sub> Γ<sub>270</sub>/Γ

Table with 4 columns: VALUE, CL%, DOCUMENT ID, TECN, COMMENT. Row 1: <0.79 × 10^-3 90 EATON 84 MRK2 e+ e-

Γ(γĀ)/Γ<sub>total</sub> Γ<sub>271</sub>/Γ

Table with 4 columns: VALUE, CL%, DOCUMENT ID, TECN, COMMENT. Row 1: <0.13 × 10^-3 90 HENRRARD 87 DM2 e+ e-
• • • We do not use the following data for averages, fits, limits, etc.
<0.16 × 10^-3 90 BAI 98G BES e+ e-

Γ(γf\_0(2100) → γηη)/Γ<sub>total</sub> Γ<sub>272</sub>/Γ

Table with 4 columns: VALUE (units 10^-4), EVTS, DOCUMENT ID, TECN, COMMENT. Row 1: 1.13 ± 0.09 ± 0.64 / -0.10 - 0.28 5.5k 1 ABLIKIM 13N BES3 J/ψ → γηη

1 From partial wave analysis including all possible combinations of 0++, 2++, and 4++ resonances.

Γ(γf\_0(2100) → γππ)/Γ<sub>total</sub> Γ<sub>273</sub>/Γ

Table with 4 columns: VALUE (units 10^-4), EVTS, DOCUMENT ID, COMMENT. Row 1: 6.24 ± 0.48 ± 0.87 744 1 DOBBS 15 J/ψ → γππ

1 Using CLEO-c data but not authored by the CLEO Collaboration.

Γ(γf\_0(2200))/Γ<sub>total</sub> Γ<sub>274</sub>/Γ

Table with 4 columns: VALUE (units 10^-4), DOCUMENT ID, TECN, COMMENT. Row 1: • • • We do not use the following data for averages, fits, limits, etc.
1.5 1 AUGUSTIN 88 DM2 J/ψ → γK\_S^0 K\_S^0

• • • We do not use the following data for averages, fits, limits, etc.
1.5 1 AUGUSTIN 88 DM2 J/ψ → γK\_S^0 K\_S^0
1 Includes unknown branching fraction to K\_S^0 K\_S^0.

Γ(γf\_0(2200) → γK̄K)/Γ<sub>total</sub> Γ<sub>275</sub>/Γ

Table with 4 columns: VALUE (units 10^-4), EVTS, DOCUMENT ID, COMMENT. Row 1: 5.86 ± 0.49 ± 1.20 490 1 DOBBS 15 J/ψ → γK̄K

1 Using CLEO-c data but not authored by the CLEO Collaboration.

Γ(γf\_0(2200) → γK\_S^0 K\_S^0)/Γ<sub>total</sub> Γ<sub>276</sub>/Γ

Table with 4 columns: VALUE (units 10^-4), DOCUMENT ID, TECN, COMMENT. Row 1: 2.72 ± 0.08 ± 0.17 / -0.06 - 0.47 ABLIKIM 18AA BES3 J/ψ → γK\_S^0 K\_S^0

Γ(γf\_J(2220))/Γ<sub>total</sub> Γ<sub>277</sub>/Γ

Table with 4 columns: VALUE (units 10^-5), CL%, EVTS, DOCUMENT ID, TECN, COMMENT. Row 1: • • • We do not use the following data for averages, fits, limits, etc.
>300 1 BAI 96B BES e+ e- → γρ̄p, K̄K̄
>250 99.9 2 HASAN 96 SPEC p̄p → π+ π-
< 2.3 95 3 AUGUSTIN 88 DM2 J/ψ → γK+ K-
< 1.6 95 3 AUGUSTIN 88 DM2 J/ψ → γK\_S^0 K\_S^0
12.4 + 6.4 / -5.2 ± 2.8 23 3 BALTRUSAIT..86D MRK3 J/ψ → γK\_S^0 K\_S^0
8.4 + 3.4 / -2.8 ± 1.6 93 3 BALTRUSAIT..86D MRK3 J/ψ → γK+ K-

1 Using BARNES 93.
2 Using BAI 96b.
3 Includes unknown branching fraction to K+ K- or K\_S^0 K\_S^0.

Γ(γf\_J(2220) → γππ)/Γ<sub>total</sub> Γ<sub>278</sub>/Γ

Table with 4 columns: VALUE (units 10^-5), CL%, DOCUMENT ID, TECN, COMMENT. Row 1: < 3.9 90 1,2 DOBBS 15 J/ψ → γππ
• • • We do not use the following data for averages, fits, limits, etc.
14 ± 8 ± 4 BAI 98H BES J/ψ → γπ^0 π^0
8.4 ± 2.6 ± 3.0 BAI 96B BES e+ e- → J/ψ → γπ+ π-

1 Using CLEO-c data but not authored by the CLEO Collaboration.
2 For Γ = 20/50 MeV, the 90% CL upper limits for π+ π- and π^0 π^0 are 2.6/5.2 × 10^-5 and 1.3/1.9 × 10^-5, respectively.

Γ(γf\_J(2220) → γK̄K)/Γ<sub>total</sub> Γ<sub>279</sub>/Γ

Table with 4 columns: VALUE (units 10^-5), CL%, DOCUMENT ID, TECN, COMMENT. Row 1: < 4.1 90 1,2 DOBBS 15 J/ψ → γK̄K
• • • We do not use the following data for averages, fits, limits, etc.
< 3.6 3 DEL-AMO-SA...10o BABR e+ e- → J/ψ → γK+ K-
< 2.9 3 DEL-AMO-SA...10o BABR e+ e- → J/ψ → γK\_S^0 K\_S^0
6.6 ± 2.9 ± 2.4 BAI 96B BES e+ e- → J/ψ → γK+ K-
10.8 ± 4.0 ± 3.2 BAI 96B BES e+ e- → J/ψ → γK\_S^0 K\_S^0

1 Using CLEO-c data but not authored by the CLEO Collaboration.
2 For Γ = 20/50 MeV, the 90% CL upper limits for K+ K- and K\_S^0 K\_S^0 are 1.7/3.1 × 10^-5 and 1.2/2.0 × 10^-5, respectively.
3 For spin 2 and helicity 0; other combinations lead to more stringent upper limits.

Γ(γf\_J(2220) → γρ̄p̄)/Γ<sub>total</sub> Γ<sub>280</sub>/Γ

Table with 4 columns: VALUE (units 10^-5), DOCUMENT ID, TECN, COMMENT. Row 1: 1.5 ± 0.6 ± 0.5 BAI 96B BES e+ e- → J/ψ → γρ̄p̄

Γ(γf\_0(2330) → γK\_S^0 K\_S^0)/Γ<sub>total</sub> Γ<sub>281</sub>/Γ

Table with 4 columns: VALUE (units 10^-5), DOCUMENT ID, TECN, COMMENT. Row 1: 4.95 ± 0.21 ± 0.66 / -0.72 ABLIKIM 18AA BES3 J/ψ → γK\_S^0 K\_S^0

Γ(γf\_2(2340) → γηη)/Γ<sub>total</sub> Γ<sub>282</sub>/Γ

Table with 4 columns: VALUE (units 10^-5), EVTS, DOCUMENT ID, TECN, COMMENT. Row 1: 5.60 + 0.62 + 2.37 / -0.65 - 2.07 5.5k 1 ABLIKIM 13N BES3 J/ψ → γηη

1 From partial wave analysis including all possible combinations of 0++, 2++, and 4++ resonances.

Γ(γf\_2(2340) → γK\_S^0 K\_S^0)/Γ<sub>total</sub> Γ<sub>283</sub>/Γ

Table with 4 columns: VALUE (units 10^-5), DOCUMENT ID, TECN, COMMENT. Row 1: 5.54 + 0.34 + 3.82 / -0.40 - 1.49 ABLIKIM 18AA BES3 J/ψ → γK\_S^0 K\_S^0

Γ(γf\_0(1500) → γππ)/Γ<sub>total</sub> Γ<sub>284</sub>/Γ

Table with 4 columns: VALUE (units 10^-4), EVTS, DOCUMENT ID, TECN, COMMENT. Row 1: 1.09 ± 0.24 OUR AVERAGE
1.21 ± 0.29 ± 0.24 174 1 DOBBS 15 J/ψ → γππ
1.00 ± 0.03 ± 0.45 2 ABLIKIM 06v BES2 e+ e- → J/ψ → γπ+ π-
1.02 ± 0.09 ± 0.45 2 ABLIKIM 06v BES2 e+ e- → J/ψ → γπ^0 π^0
• • • We do not use the following data for averages, fits, limits, etc.
5.7 ± 0.8 3,4 BUGG 95 MRK3 J/ψ → γπ+ π- π+ π-

1 Using CLEO-c data but not authored by the CLEO Collaboration.
2 Including unknown branching fraction to π.
3 Including unknown branching ratio for f\_0(1500) → π+ π- π+ π-.
4 Assuming that f\_0(1500) decays only to two S-wave dipions.

Γ(γf\_0(1500) → γηη)/Γ<sub>total</sub> Γ<sub>285</sub>/Γ

Table with 4 columns: VALUE (units 10^-5), EVTS, DOCUMENT ID, TECN, COMMENT. Row 1: 1.65 + 0.26 + 0.51 / -0.31 - 1.40 5.5k 1 ABLIKIM 13N BES3 J/ψ → γηη

1 From partial wave analysis including all possible combinations of 0++, 2++, and 4++ resonances.

Γ(γA → γinvisible)/Γ<sub>total</sub> (narrow state A with m\_A < 960 MeV) Γ<sub>286</sub>/Γ

Table with 4 columns: VALUE, CL%, DOCUMENT ID, TECN, COMMENT. Row 1: < 6.3 × 10^-6 90 1 INSLER 10 CLEO e+ e- → π+ π- J/ψ
1 The limit varies with mass m\_A of a narrow state A and is 4.3 × 10^-6 for m\_A = 0 MeV, reaches its largest value of 6.3 × 10^-6 at m\_A = 500 MeV, and is 3.6 × 10^-6 at m\_A = 960 MeV.

Γ(γA^0 → γμ+ μ-)/Γ<sub>total</sub> (narrow state A^0 with 0.2 GeV < m\_A^0 < 3 GeV) Γ<sub>287</sub>/Γ

Table with 4 columns: VALUE, CL%, DOCUMENT ID, TECN, COMMENT. Row 1: < 0.5 × 10^-5 90 1 ABLIKIM 16E BES3 J/ψ → γμ+ μ-
• • • We do not use the following data for averages, fits, limits, etc.
< 2.1 × 10^-5 90 2 ABLIKIM 12 BES3 J/ψ → γμ+ μ-

1 For a narrow scalar or pseudoscalar, A^0, with a mass in the range 0.212-3 GeV. The measured 90% CL limit as a function of m\_A^0 is in the range (2.8-495.3) × 10^-8.
2 For a narrow scalar or pseudoscalar, A^0, with a mass in the range 0.21-3.00 GeV. The measured 90% CL limit as a function of m\_A^0 ranges from 4 × 10^-7 to 2.1 × 10^-5.

DALITZ DECAYS

Table with 5 columns: VALUE (units 10^-7), EVTS, DOCUMENT ID, TECN, COMMENT. Row 1: Γ(π0 e+ e-)/Γtotal, 7.56 ± 1.32 ± 0.50, 39, ABLIKIM 141, BES3, J/ψ → π0 e+ e-

Table with 5 columns: VALUE (units 10^-5), EVTS, DOCUMENT ID, TECN, COMMENT. Row 1: Γ(η e+ e-)/Γtotal, 1.43 ± 0.04 ± 0.06, 2.47k, 1,2 ABLIKIM 19A, BES3, J/ψ → η e+ e-

Table with 5 columns: VALUE (units 10^-5), EVTS, DOCUMENT ID, TECN, COMMENT. Row 1: Γ(η'(958) e+ e-)/Γtotal, 1.16 ± 0.07 ± 0.06, 320, 1 ABLIKIM 141, BES3, J/ψ → η' e+ e-

Table with 5 columns: VALUE (units 10^-5), EVTS, DOCUMENT ID, TECN, COMMENT. Row 1: Γ(η'(958) U → η'(958) e+ e-)/Γtotal, 6.59 ± 0.07 ± 0.17, 8.9k, 1 ABLIKIM 19H, BES3, J/ψ → η'(958) e+ e-

Table with 5 columns: VALUE (units 10^-7), CL%, DOCUMENT ID, TECN, COMMENT. Row 1: Γ(η U → η e+ e-)/Γtotal, <9.11 × 10^-7, 90, 1 ABLIKIM 19A, BES3, J/ψ → η e+ e-

Table with 5 columns: VALUE (units 10^-7), CL%, DOCUMENT ID, TECN, COMMENT. Row 1: Γ(η'(958) U → η'(958) e+ e-)/Γtotal, <2.0 × 10^-7, 90, 1 ABLIKIM 19H, BES3, J/ψ → η'(958) e+ e-

Table with 5 columns: VALUE (units 10^-7), CL%, DOCUMENT ID, TECN, COMMENT. Row 1: Γ(φ e+ e-)/Γtotal, <1.2, 90, 1 ABLIKIM 19AB, BES3, J/ψ → φ e+ e-

WEAK DECAYS

Table with 5 columns: VALUE (units 10^-5), CL%, DOCUMENT ID, TECN, COMMENT. Row 1: Γ(D- e+ νe + c.c.)/Γtotal, <1.2 × 10^-5, 90, ABLIKIM 06M, BES2, e+ e- → J/ψ

Table with 5 columns: VALUE (units 10^-8), CL%, DOCUMENT ID, TECN, COMMENT. Row 1: Γ(D0 e+ e- + c.c.)/Γtotal, <8.5 × 10^-8, 90, 1 ABLIKIM 17AF, BES3, e+ e- → J/ψ

Table with 5 columns: VALUE (units 10^-6), CL%, DOCUMENT ID, TECN, COMMENT. Row 1: Γ(Ds- e+ νe + c.c.)/Γtotal, <1.3 × 10^-6, 90, ABLIKIM 14R, BES3, e+ e- → J/ψ

Table with 5 columns: VALUE (units 10^-5), CL%, DOCUMENT ID, TECN, COMMENT. Row 1: Γ(Ds- π+ + c.c.)/Γtotal, <3.6 × 10^-5, 90, 1 ABLIKIM 06M, BES2, e+ e- → J/ψ

Table with 5 columns: VALUE (units 10^-6), CL%, DOCUMENT ID, TECN, COMMENT. Row 1: Γ(Ds- π+ + c.c.)/Γtotal, <1.8 × 10^-6, 90, ABLIKIM 14R, BES3, e+ e- → J/ψ

Table with 5 columns: VALUE (units 10^-5), CL%, DOCUMENT ID, TECN, COMMENT. Row 1: Γ(D- π+ + c.c.)/Γtotal, <7.5 × 10^-5, 90, ABLIKIM 08J, BES2, e+ e- → J/ψ

Table with 5 columns: VALUE (units 10^-4), CL%, DOCUMENT ID, TECN, COMMENT. Row 1: Γ(D0 K0 + c.c.)/Γtotal, <1.7 × 10^-4, 90, ABLIKIM 08J, BES2, e+ e- → J/ψ

Table with 5 columns: VALUE (units 10^-6), CL%, DOCUMENT ID, TECN, COMMENT. Row 1: Γ(D0 K\*0 + c.c.)/Γtotal, <2.5 × 10^-6, 90, ABLIKIM 14K, BES3, e+ e- → J/ψ

Table with 5 columns: VALUE (units 10^-4), CL%, DOCUMENT ID, TECN, COMMENT. Row 1: Γ(Ds- π+ + c.c.)/Γtotal, <1.3 × 10^-4, 90, ABLIKIM 08J, BES2, e+ e- → J/ψ

Table with 5 columns: VALUE (units 10^-5), CL%, DOCUMENT ID, TECN, COMMENT. Row 1: Γ(Ds- ρ+ + c.c.)/Γtotal, <1.3 × 10^-5, 90, ABLIKIM 14K, BES3, e+ e- → J/ψ

CHARGE CONJUGATION (C), PARITY (P), LEPTON FAMILY NUMBER (LF) VIOLATING MODES

Table with 5 columns: VALUE (units 10^-7), CL%, DOCUMENT ID, TECN, COMMENT. Row 1: Γ(γγ)/Γtotal, <2.7 × 10^-7, 90, ABLIKIM 14Q, BES3, ψ(2S) → π+ π- J/ψ

Table with 5 columns: VALUE (units 10^-5), CL%, DOCUMENT ID, TECN, COMMENT. Row 1: Γ(γγ)/Γtotal, <0.5 × 10^-5, 90, ADAMS 08, CLEO, ψ(2S) → π+ π- J/ψ

Table with 5 columns: VALUE (units 10^-6), CL%, DOCUMENT ID, TECN, COMMENT. Row 1: Γ(γφ)/Γtotal, <1.4 × 10^-6, 90, ABLIKIM 14Q, BES3, ψ(2S) → π+ π- J/ψ

Table with 5 columns: VALUE (units 10^-7), CL%, DOCUMENT ID, TECN, COMMENT. Row 1: Γ(e± μ∓)/Γtotal, <1.6 × 10^-7, 90, ABLIKIM 13L, BES3, e+ e- → J/ψ

Table with 5 columns: VALUE (units 10^-6), CL%, DOCUMENT ID, TECN, COMMENT. Row 1: Γ(e± τ∓)/Γtotal, <8.3 × 10^-6, 90, ABLIKIM 04, BES, e+ e- → J/ψ

Table with 5 columns: VALUE (units 10^-8), CL%, DOCUMENT ID, TECN, COMMENT. Row 1: Γ(Ac e- + c.c.)/Γtotal, <6.9 × 10^-8, 90, ABLIKIM 19AF, BES3, e+ e- → J/ψ → p K- π+ e- (+ c.c.)

Table with 5 columns: VALUE (units 10^-6), CL%, DOCUMENT ID, TECN, COMMENT. Row 1: Γ(μ± τ∓)/Γtotal, <2.0 × 10^-6, 90, ABLIKIM 04, BES, e+ e- → J/ψ

OTHER DECAYS

Table with 5 columns: VALUE (units 10^-2), CL%, DOCUMENT ID, TECN, COMMENT. Row 1: Γ(invisible)/Γ(e+ e-), <6.6 × 10^-2, 90, LEES 13I, BABR, B → K(\*) J/ψ

Table with 5 columns: VALUE (units 10^-2), CL%, DOCUMENT ID, TECN, COMMENT. Row 1: Γ(invisible)/Γ(μ+ μ-), <1.2 × 10^-2, 90, ABLIKIM 08G, BES2, ψ(2S) → π+ π- J/ψ

J/ψ(1S) REFERENCES

ABLIKIM 20 PR D101 012004 M. Ablikim et al. (BESIII Collab.)
ABLIKIM 19A PR D99 012006 M. Ablikim et al. (BESIII Collab.)
ABLIKIM 19AB PR D99 052010 M. Ablikim et al. (BESIII Collab.)
ABLIKIM 19AC PR D99 071101 M. Ablikim et al. (BESIII Collab.)
ABLIKIM 19AF PR D99 072006 M. Ablikim et al. (BESIII Collab.)
ABLIKIM 19AN PR D99 112008 M. Ablikim et al. (BESIII Collab.)
ABLIKIM 19AQ PR D100 032004 M. Ablikim et al. (BESIII Collab.)
ABLIKIM 19H PR D99 012013 M. Ablikim et al. (BESIII Collab.)
ABLIKIM 19N PR D99 032006 M. Ablikim et al. (BESIII Collab.)
ABLIKIM 19Q PL B791 375 M. Ablikim et al. (BESIII Collab.)
ABLIKIM 19T PRL 122 142002 M. Ablikim et al. (BESIII Collab.)
LU 19 PR D99 032003 P.-C. Lu et al. (BELLE Collab.)
ABLIKIM 18AA PR D98 072003 M. Ablikim et al. (BESIII Collab.)
ABLIKIM 18AB PR D98 072005 M. Ablikim et al. (BESIII Collab.)
ABLIKIM 18D PRL 121 022001 M. Ablikim et al. (BESIII Collab.)
ABLIKIM 18I PR D97 051101 M. Ablikim et al. (BESIII Collab.)
ABLIKIM 18O PR D97 072014 M. Ablikim et al. (BESIII Collab.)
ANASHIN 18A JHEP 1805 119 V.V. Anashin et al. (KEDR Collab.)
LEES 18 PR D97 052007 J.P. Lees et al. (BABAR Collab.)
LEES 18E PR D98 112015 J.P. Lees et al. (BABAR Collab.)
ABLIKIM 17AF PR D96 111101 M. Ablikim et al. (BESIII Collab.)
ABLIKIM 17AH PR D96 112001 M. Ablikim et al. (BESIII Collab.)
ABLIKIM 17AK PR D96 112012 M. Ablikim et al. (BESIII Collab.)
ABLIKIM 17E PL B770 217 M. Ablikim et al. (BESIII Collab.)
ABLIKIM 17L PR D95 052003 M. Ablikim et al. (BESIII Collab.)
LEES 17A PR D95 052001 J.P. Lees et al. (BABAR Collab.)
LEES 17C PR D95 072007 J.P. Lees et al. (BABAR Collab.)
LEES 17D PR D95 092005 J.P. Lees et al. (BABAR Collab.)
ABLIKIM 16E PR D93 052005 M. Ablikim et al. (BESIII Collab.)
ABLIKIM 16J PRL 117 042002 M. Ablikim et al. (BESIII Collab.)
ABLIKIM 16K PR D93 052010 M. Ablikim et al. (BESIII Collab.)
ABLIKIM 16L PR D93 072003 M. Ablikim et al. (BESIII Collab.)
ABLIKIM 16M PR D93 072008 M. Ablikim et al. (BESIII Collab.)
ABLIKIM 16N PR D93 112011 M. Ablikim et al. (BESIII Collab.)
ABLIKIM 16P PR D94 072005 M. Ablikim et al. (BESIII Collab.)
ABLIKIM 16Q PL B761 98 M. Ablikim et al. (BESIII Collab.)
PDG 16 CP C40 100011 C. Patrignani et al. (PDG Collab.)

Downloaded from https://academic.oup.com/ptep/article/2020/8/083C01/5891211 by guest on 12 November 2020





# Meson Particle Listings

## Branching Ratios of $\psi$ 's and $\chi$ 's, $\chi_{c0}(1P)$

the required branching ratios. However, the values are frequently taken from the *Review of Particle Physics* (RPP), which in turn uses the branching ratio reported by the experiment in the following edition, giving rise either to correlations or to plain vicious circles, as discussed in more detail in earlier editions of this review [1,2].

The way to avoid these dependencies and correlations is to extract the branching ratios through a fit that uses the truly measured combinations of branching fractions and partial widths. This fit, in fact, should involve decays from the four concerned particles,  $\psi(2S)$ ,  $\chi_{c0}$ ,  $\chi_{c1}$ , and  $\chi_{c2}$ , and occasionally some combinations of branching ratios of more than one of them. This is what is done since the 2002 edition [3].

The PDG policy is to quote the results of the collaborations in a manner as close as possible to what appears in their original publications. However, in order to avoid the problems mentioned above, we had in some cases to work out the values originally measured, using the number of events and detection efficiencies given by the collaborations, or rescaling back the published results. The information was sometimes spread over several articles, and some articles referred to papers still unpublished, which in turn contained the relevant numbers in footnotes.

Even though the experimental collaborations are entitled to extract whatever branching ratios they consider appropriate by using other published results, we would like to encourage them to also quote explicitly in their articles the actual quantities measured, so that they can be used directly in averages and fits of different experimental determinations.

To inform the reader how we computed some of the values used in this edition of RPP, we use footnotes to indicate the branching ratios actually given by the experiments and the quantities they use to derive them from the true combination of branching ratios actually measured.

None of the branching ratios of the  $\chi_{c0,1,2}$  are measured independently of the  $\psi(2S)$  radiative decays. We tried to identify those branching ratios which can be correlated in a non-trivial way, and although we cannot preclude the existence of other cases, we are confident that the most relevant correlations have already been removed. Nevertheless, correlations in the errors of different quantities measured by the same experiment have not been taken into account.

### Fit information

This is an overall fit to 4 total widths, 1 partial width, 26 combinations of partial widths, 24 branching ratios, and 108 combinations of branching ratios. Of the latter 62 involve decays of more than one particle.

The overall fit uses 248 measurements to determine 49 parameters and has a  $\chi^2$  of 378.1 for 199 degrees of freedom.

The relatively high  $\chi^2$  of the fit, 1.9 per d.o.f., can be traced back to a few specific discrepancies in the data. No scaling factors to fit uncertainties have been applied.

In the listing we provide the inter-particle correlation coefficients  $\langle \delta x_i \delta x_j \rangle / (\delta x_i \cdot \delta x_j)$ , in percent, from the fit to the corresponding parameter  $x_i$ .

### References

1. Y.F. Gu and X.H. Li, Phys. Lett. **B449**, 361 (1999).
2. C. Patrignani, Phys. Rev. **D64**, 034017 (2001).
3. Particle Data Group, K.Hagiwara *et al.*, Phys. Rev. **D68**, 010001 (2002).

## $\chi_{c0}(1P)$

$$I^G(J^{PC}) = 0^+(0^{++})$$

### $\chi_{c0}(1P)$ MASS

VALUE (MeV)	EVTs	DOCUMENT ID	TECN	COMMENT
<b>3414.71 ± 0.30 OUR AVERAGE</b>				
3413.0 ± 1.9 ± 0.6	933	1 AAIJ	17B8 LHCB	$p p \rightarrow b \bar{b} X \rightarrow 2(K+K^-)X$
3414.2 ± 0.5 ± 2.3	5.4k	UEHARA	08 BELL	$\gamma\gamma \rightarrow \chi_{c0} \rightarrow \text{hadrons}$
3406 ± 7 ± 6	230	2 ABE	07 BELL	$e^+e^- \rightarrow J/\psi(c\bar{c})$
3414.21 ± 0.39 ± 0.27		ABLIKIM	05G BES2	$\psi(2S) \rightarrow \gamma\chi_{c0}$
3414.7 ± 0.7 ± 0.6	± 0.2	3 ANDREOTTI	03 E835	$\bar{p}p \rightarrow \chi_{c0} \rightarrow \pi^0\pi^0$
3415.5 ± 0.4 ± 0.4	392	4 BAGNASCO	02 E835	$\bar{p}p \rightarrow \chi_{c0} \rightarrow J/\psi\gamma$
3417.4 ± 1.8 ± 1.9	± 0.2	3 AMBROGIANI	99B E835	$\bar{p}p \rightarrow e^+e^-\gamma$
3414.1 ± 0.6 ± 0.8		BAI	99B BES	$\psi(2S) \rightarrow \gamma X$
3417.8 ± 0.4 ± 4		3 GAISER	86 CBAL	$\psi(2S) \rightarrow \gamma X$
3416 ± 3 ± 4		5 TANENBAUM	78 MRK1	$e^+e^-$
••• We do not use the following data for averages, fits, limits, etc. •••				
3414.6 ± 1.1	266	UEHARA	13 BELL	$\gamma\gamma \rightarrow K_S^0 K_S^0$
3416.5 ± 3.0		EISENSTEIN	01 CLE2	$e^+e^- \rightarrow e^+e^-\chi_{c0}$
3422 ± 10		5 BARTEL	78B CNTR	$e^+e^- \rightarrow J/\psi 2\gamma$
3415 ± 9		5 BIDDICK	77 CNTR	$e^+e^- \rightarrow \gamma X$

<sup>1</sup> From a fit of the  $\phi\phi$  invariant mass with the width of  $\chi_{c0}(1P)$  fixed to the PDG 16 value.  
<sup>2</sup> From a fit of the  $J/\psi$  recoil mass spectrum. Supersedes ABE,K 02 and ABE 04G.  
<sup>3</sup> Using mass of  $\psi(2S) = 3686.0$  MeV.  
<sup>4</sup> Recalculated by ANDREOTTI 05A, using the value of  $\psi(2S)$  mass from AULCHENKO 03.  
<sup>5</sup> Mass value shifted by us by amount appropriate for  $\psi(2S)$  mass = 3686 MeV and  $J/\psi(1S)$  mass = 3097 MeV.

### $\chi_{c0}(1P)$ WIDTH

VALUE (MeV)	EVTs	DOCUMENT ID	TECN	COMMENT
<b>10.8 ± 0.6 OUR FIT</b>				
<b>10.5 ± 0.8 OUR AVERAGE</b>	Error includes scale factor of 1.1.			
10.6 ± 1.9 ± 2.6	5.4k	UEHARA	08 BELL	$\gamma\gamma \rightarrow \chi_{c0} \rightarrow \text{hadrons}$
12.6 <sup>+1.5+0.9</sup> <sub>-1.6-1.1</sub>		ABLIKIM	05G BES2	$\psi(2S) \rightarrow \gamma\chi_{c0}$
8.6 <sup>+1.7±0.1</sup> <sub>-1.3</sub>		ANDREOTTI	03 E835	$\bar{p}p \rightarrow \chi_{c0} \rightarrow \pi^0\pi^0$
9.7 ± 1.0	392	1 BAGNASCO	02 E835	$\bar{p}p \rightarrow \chi_{c0} \rightarrow J/\psi\gamma$
16.6 <sup>+5.2±0.1</sup> <sub>-3.7</sub>		AMBROGIANI	99B E835	$\bar{p}p \rightarrow e^+e^-\gamma$
14.3 ± 2.0 ± 3.0		BAI	98I BES	$\psi(2S) \rightarrow \gamma\pi^+\pi^-$
13.5 ± 3.3 ± 4.2		GAISER	86 CBAL	$\psi(2S) \rightarrow \gamma X, \gamma\pi^0\pi^0$
••• We do not use the following data for averages, fits, limits, etc. •••				
13.2 ± 2.1	266	UEHARA	13 BELL	$\gamma\gamma \rightarrow K_S^0 K_S^0$

<sup>1</sup> Recalculated by ANDREOTTI 05A.

### $\chi_{c0}(1P)$ DECAY MODES

Mode	Fraction ( $\Gamma_i/\Gamma$ )	Scale factor/ Confidence level
<b>Hadronic decays</b>		
$\Gamma_1$ $2(\pi^+\pi^-)$	(2.34 ± 0.18) %	
$\Gamma_2$ $\rho^0\pi^+\pi^-$	(9.1 ± 2.9) × 10 <sup>-3</sup>	
$\Gamma_3$ $\rho^0\rho^0$		
$\Gamma_4$ $f_0(980)f_0(980)$	(6.6 ± 2.1) × 10 <sup>-4</sup>	
$\Gamma_5$ $\pi^+\pi^-\pi^0\pi^0$	(3.3 ± 0.4) %	
$\Gamma_6$ $\rho^+\pi^-\pi^0 + c.c.$	(2.9 ± 0.4) %	
$\Gamma_7$ $4\pi^0$	(3.3 ± 0.4) × 10 <sup>-3</sup>	
$\Gamma_8$ $\pi^+\pi^-K^+K^-$	(1.81 ± 0.14) %	
$\Gamma_9$ $K_0^*(1430)^0 \bar{K}_0^*(1430)^0 \rightarrow \pi^+\pi^-K^+K^-$	(9.8 <sup>+4.0</sup> <sub>-2.8</sub> ) × 10 <sup>-4</sup>	



$\Gamma(\rho^0 \rho^0) \times \Gamma(\gamma\gamma)/\Gamma_{total}$		$\Gamma_3 \Gamma_{93}/\Gamma$	
VALUE (eV)	CL% EVTS	DOCUMENT ID	TECN COMMENT

••• We do not use the following data for averages, fits, limits, etc. •••

<12	90 <252	UEHARA	08 BELL $\gamma\gamma \rightarrow \chi_{c0} \rightarrow 2(\pi^+\pi^-)$
-----	---------	--------	--

$\Gamma(\pi^+\pi^- K^+ K^-) \times \Gamma(\gamma\gamma)/\Gamma_{total}$		$\Gamma_8 \Gamma_{93}/\Gamma$	
VALUE (eV)	CL% EVTS	DOCUMENT ID	TECN COMMENT

**40.0 ± 3.5 OUR FIT**  
**38.8 ± 3.7 ± 4.7** 1.7k UEHARA 08 BELL  $\gamma\gamma \rightarrow \chi_{c0} \rightarrow K^+ K^- \pi^+ \pi^-$

$\Gamma(K^+ K^- \pi^+ \pi^- \pi^0) \times \Gamma(\gamma\gamma)/\Gamma_{total}$		$\Gamma_{21} \Gamma_{93}/\Gamma$	
VALUE (eV)	CL% EVTS	DOCUMENT ID	TECN COMMENT

**26 ± 4 ± 4** 1094 DEL-AMO-SA...11M BABR  $\gamma\gamma \rightarrow K^+ K^- \pi^+ \pi^- \pi^0$

$\Gamma(K^+ \bar{K}^*(892)^0 \pi^- + c.c.) \times \Gamma(\gamma\gamma)/\Gamma_{total}$		$\Gamma_{30} \Gamma_{93}/\Gamma$	
VALUE (eV)	CL% EVTS	DOCUMENT ID	TECN COMMENT

**16 ± 4 OUR FIT**  
**16.7 ± 6.1 ± 3.0** 495 ± 182 UEHARA 08 BELL  $\gamma\gamma \rightarrow \chi_{c0} \rightarrow K^+ K^- \pi^+ \pi^-$

$\Gamma(K^*(892)^0 \bar{K}^*(892)^0) \times \Gamma(\gamma\gamma)/\Gamma_{total}$		$\Gamma_{31} \Gamma_{93}/\Gamma$	
VALUE (eV)	CL% EVTS	DOCUMENT ID	TECN COMMENT

••• We do not use the following data for averages, fits, limits, etc. •••

<6	90 <148	UEHARA	08 BELL $\gamma\gamma \rightarrow \chi_{c0} \rightarrow K^+ K^- \pi^+ \pi^-$
----	---------	--------	--

$\Gamma(\pi\pi) \times \Gamma(\gamma\gamma)/\Gamma_{total}$		$\Gamma_{32} \Gamma_{93}/\Gamma$	
VALUE (eV)	CL% EVTS	DOCUMENT ID	TECN COMMENT

**18.8 ± 1.3 OUR FIT**  
**23 ± 5 OUR AVERAGE**

29.7<sup>+17.4</sup><sub>-12.0</sub> ± 4.8 103<sup>+60</sup><sub>-42</sub> 1 UEHARA 09 BELL 10.6  $e^+e^- \rightarrow e^+e^- \pi^0 \pi^0$   
 22.7 ± 3.2 ± 3.5 129 ± 18 2 NAKAZAWA 05 BELL 10.6  $e^+e^- \rightarrow e^+e^- \pi^+ \pi^-$

1 We multiplied the measurement by 3 to convert from  $\pi^0 \pi^0$  to  $\pi\pi$ . Interference with the continuum included.  
 2 We have multiplied  $\pi^+\pi^-$  measurement by 3/2 to obtain  $\pi\pi$ .

$\Gamma(\eta\eta) \times \Gamma(\gamma\gamma)/\Gamma_{total}$		$\Gamma_{36} \Gamma_{93}/\Gamma$	
VALUE (eV)	CL% EVTS	DOCUMENT ID	TECN COMMENT

**9.4 ± 2.3 ± 1.2** 22 1 UEHARA 10A BELL 10.6  $e^+e^- \rightarrow e^+e^- \eta\eta$

1 Interference with the continuum not included.

$\Gamma(\omega\omega) \times \Gamma(\gamma\gamma)/\Gamma_{total}$		$\Gamma_{39} \Gamma_{93}/\Gamma$	
VALUE (eV)	CL% EVTS	DOCUMENT ID	TECN COMMENT

••• We do not use the following data for averages, fits, limits, etc. •••

<3.9	90	1 LIU	12B BELL $\gamma\gamma \rightarrow 2(\pi^+\pi^-\pi^0)$
------	----	-------	--

1 Using  $B(\omega \rightarrow \pi^+\pi^-\pi^0) = (89.2 \pm 0.7)\%$ .

$\Gamma(\omega\phi) \times \Gamma(\gamma\gamma)/\Gamma_{total}$		$\Gamma_{40} \Gamma_{93}/\Gamma$	
VALUE (eV)	CL% EVTS	DOCUMENT ID	TECN COMMENT

••• We do not use the following data for averages, fits, limits, etc. •••

<0.34	90	1 LIU	12B BELL $\gamma\gamma \rightarrow K^+ K^- \pi^+ \pi^- \pi^0$
-------	----	-------	---

1 Using  $B(\phi \rightarrow K^+ K^-) = (48.9 \pm 0.5)\%$  and  $B(\omega \rightarrow \pi^+\pi^-\pi^0) = (89.2 \pm 0.7)\%$ .

$\Gamma(K^+ K^-) \times \Gamma(\gamma\gamma)/\Gamma_{total}$		$\Gamma_{42} \Gamma_{93}/\Gamma$	
VALUE (eV)	CL% EVTS	DOCUMENT ID	TECN COMMENT

**13.4 ± 1.0 OUR FIT**  
**14.3 ± 1.6 ± 2.3** 153 ± 17 NAKAZAWA 05 BELL 10.6  $e^+e^- \rightarrow e^+e^- K^+ K^-$

$\Gamma(K_S^0 K_S^0) \times \Gamma(\gamma\gamma)/\Gamma_{total}$		$\Gamma_{43} \Gamma_{93}/\Gamma$	
VALUE (eV)	CL% EVTS	DOCUMENT ID	TECN COMMENT

**7.0 ± 0.5 OUR FIT**  
**8.7 ± 1.7 ± 0.9** 266 1 UEHARA 13 BELL  $\gamma\gamma \rightarrow K_S^0 K_S^0$

••• We do not use the following data for averages, fits, limits, etc. •••

7.00 ± 0.65 ± 0.71	134 ± 12	CHEN	07B BELL $e^+e^- \rightarrow e^+e^- \chi_{c0}$
--------------------	----------	------	--

1 Supersedes CHEN 07B.

$\Gamma(K^+ K^- K^+ K^-) \times \Gamma(\gamma\gamma)/\Gamma_{total}$		$\Gamma_{51} \Gamma_{93}/\Gamma$	
VALUE (eV)	CL% EVTS	DOCUMENT ID	TECN COMMENT

**6.2 ± 0.7 OUR FIT**  
**7.9 ± 1.3 ± 1.1** 215 ± 36 UEHARA 08 BELL  $\gamma\gamma \rightarrow \chi_{c0} \rightarrow 2(K^+ K^-)$

$\Gamma(\phi\phi) \times \Gamma(\gamma\gamma)/\Gamma_{total}$		$\Gamma_{56} \Gamma_{93}/\Gamma$	
VALUE (eV)	CL% EVTS	DOCUMENT ID	TECN COMMENT

**1.76 ± 0.18 OUR FIT**  
**1.72 ± 0.33 ± 0.14** 56 ± 11 1 LIU 12B BELL  $\gamma\gamma \rightarrow 2(K^+ K^-)$

••• We do not use the following data for averages, fits, limits, etc. •••

2.3 ± 0.9 ± 0.4	23.6 ± 9.6	UEHARA	08 BELL $\gamma\gamma \rightarrow \chi_{c0} \rightarrow 2(K^+ K^-)$
-----------------	------------	--------	---

1 Supersedes UEHARA 08. Using  $B(\phi \rightarrow K^+ K^-) = (48.9 \pm 0.5)\%$ .

$\chi_{c0}(1P)$  BRANCHING RATIOS

HADRONIC DECAYS

$\Gamma(2(\pi^+\pi^-))/\Gamma_{total}$		$\Gamma_1/\Gamma$	
VALUE	DOCUMENT ID		

**0.0234 ± 0.0018 OUR FIT**

$\Gamma(\rho^0 \pi^+ \pi^-)/\Gamma(2(\pi^+\pi^-))$		$\Gamma_2/\Gamma_1$	
VALUE	DOCUMENT ID	TECN	COMMENT

**0.39 ± 0.12 OUR FIT**  
**0.39 ± 0.12** TANENBAUM 78 MRK1  $\psi(2S) \rightarrow \gamma\chi_{c0}$

$\Gamma(\rho^0 \pi^+ \pi^-)/\Gamma_{total}$		$\Gamma_2/\Gamma$	
VALUE	DOCUMENT ID		

**0.0091 ± 0.0029 OUR FIT**

$\Gamma(f_0(980) f_0(980))/\Gamma_{total}$		$\Gamma_4/\Gamma$	
VALUE (units 10 <sup>-4</sup> )	EVTS	DOCUMENT ID	TECN COMMENT

**6.6 ± 2.1 ± 0.1** 36 ± 9 1 ABLIKIM 04G BES  $\psi(2S) \rightarrow \gamma\pi^+\pi^-$

1 ABLIKIM 04G reports  $[\Gamma(\chi_{c0}(1P) \rightarrow f_0(980) f_0(980))/\Gamma_{total}] \times [B(\psi(2S) \rightarrow \gamma\chi_{c0}(1P))]$  =  $(6.5 \pm 1.6 \pm 1.3) \times 10^{-5}$  which we divide by our best value  $B(\psi(2S) \rightarrow \gamma\chi_{c0}(1P)) = (9.79 \pm 0.20) \times 10^{-2}$ . Our first error is their experiment's error and our second error is the systematic error from using our best value.

$\Gamma(\pi^+\pi^-\pi^0\pi^0)/\Gamma_{total}$		$\Gamma_5/\Gamma$	
VALUE (%)	EVTS	DOCUMENT ID	TECN COMMENT

**3.3 ± 0.4 ± 0.1** 1751.4 1 HE 08B CLEO  $e^+e^- \rightarrow \gamma h^+ h^- h^0 h^0$

1 HE 08B reports  $3.54 \pm 0.10 \pm 0.43 \pm 0.18\%$  from a measurement of  $[\Gamma(\chi_{c0}(1P) \rightarrow \pi^+\pi^-\pi^0\pi^0)/\Gamma_{total}] \times [B(\psi(2S) \rightarrow \gamma\chi_{c0}(1P))]$  assuming  $B(\psi(2S) \rightarrow \gamma\chi_{c0}(1P)) = (9.22 \pm 0.11 \pm 0.46) \times 10^{-2}$ , which we rescale to our best value  $B(\psi(2S) \rightarrow \gamma\chi_{c0}(1P)) = (9.79 \pm 0.20) \times 10^{-2}$ . Our first error is their experiment's error and our second error is the systematic error from using our best value.

$\Gamma(\rho^+\pi^-\pi^0 + c.c.)/\Gamma_{total}$		$\Gamma_6/\Gamma$	
VALUE (%)	EVTS	DOCUMENT ID	TECN COMMENT

**2.9 ± 0.4 ± 0.1** 1358.5 1,2 HE 08B CLEO  $e^+e^- \rightarrow \gamma h^+ h^- h^0 h^0$

1 HE 08B reports  $3.04 \pm 0.18 \pm 0.42 \pm 0.16\%$  from a measurement of  $[\Gamma(\chi_{c0}(1P) \rightarrow \rho^+\pi^-\pi^0 + c.c.)/\Gamma_{total}] \times [B(\psi(2S) \rightarrow \gamma\chi_{c0}(1P))]$  assuming  $B(\psi(2S) \rightarrow \gamma\chi_{c0}(1P)) = (9.22 \pm 0.11 \pm 0.46) \times 10^{-2}$ , which we rescale to our best value  $B(\psi(2S) \rightarrow \gamma\chi_{c0}(1P)) = (9.79 \pm 0.20) \times 10^{-2}$ . Our first error is their experiment's error and our second error is the systematic error from using our best value.

2 Calculated by us. We have added the values from HE 08B for  $\rho^+\pi^-\pi^0$  and  $\rho^-\pi^+\pi^0$  decays assuming uncorrelated statistical and fully correlated systematic uncertainties.

$\Gamma(4\pi^0)/\Gamma_{total}$		$\Gamma_7/\Gamma$	
VALUE (units 10 <sup>-3</sup> )	EVTS	DOCUMENT ID	TECN COMMENT

**3.3 ± 0.4 ± 0.1** 3296 1 ABLIKIM 11A BES3  $e^+e^- \rightarrow \psi(2S) \rightarrow \gamma\chi_{c0}$

1 ABLIKIM 11A reports  $(3.34 \pm 0.06 \pm 0.44) \times 10^{-3}$  from a measurement of  $[\Gamma(\chi_{c0}(1P) \rightarrow 4\pi^0)/\Gamma_{total}] \times [B(\psi(2S) \rightarrow \gamma\chi_{c0}(1P))]$  assuming  $B(\psi(2S) \rightarrow \gamma\chi_{c0}(1P)) = (9.62 \pm 0.31) \times 10^{-2}$ , which we rescale to our best value  $B(\psi(2S) \rightarrow \gamma\chi_{c0}(1P)) = (9.79 \pm 0.20) \times 10^{-2}$ . Our first error is their experiment's error and our second error is the systematic error from using our best value.

$\Gamma(\pi^+\pi^- K^+ K^-)/\Gamma_{total}$		$\Gamma_8/\Gamma$	
VALUE (units 10 <sup>-3</sup> )	DOCUMENT ID		

**18.1 ± 1.4 OUR FIT**

$\Gamma(K^+ \bar{K}^*(892)^0 \pi^- + c.c.)/\Gamma(\pi^+\pi^- K^+ K^-)$		$\Gamma_{30}/\Gamma_8$	
VALUE	DOCUMENT ID	TECN	COMMENT

**0.41 ± 0.09 OUR FIT**  
**0.41 ± 0.10** TANENBAUM 78 MRK1  $\psi(2S) \rightarrow \gamma\chi_{c0}$

$\Gamma(K_0^*(1430)^0 \bar{K}_0^*(1430)^0 \rightarrow \pi^+\pi^- K^+ K^-)/\Gamma_{total}$		$\Gamma_9/\Gamma$	
VALUE (units 10 <sup>-4</sup> )	EVTS	DOCUMENT ID	TECN COMMENT

**9.8 ± 3.6 ± 0.2** 83 1 ABLIKIM 05q BES2  $\psi(2S) \rightarrow \gamma\pi^+\pi^- K^+ K^-$

1 ABLIKIM 05q reports  $(10.44 \pm 2.37 \pm 1.32 \pm 1.90) \times 10^{-4}$  from a measurement of  $[\Gamma(\chi_{c0}(1P) \rightarrow K_0^*(1430)^0 \bar{K}_0^*(1430)^0 \rightarrow \pi^+\pi^- K^+ K^-)/\Gamma_{total}] \times [B(\psi(2S) \rightarrow \gamma\chi_{c0}(1P))]$  assuming  $B(\psi(2S) \rightarrow \gamma\chi_{c0}(1P)) = (9.22 \pm 0.11 \pm 0.46) \times 10^{-2}$ , which we rescale to our best value  $B(\psi(2S) \rightarrow \gamma\chi_{c0}(1P)) = (9.79 \pm 0.20) \times 10^{-2}$ . Our first error is their experiment's error and our second error is the systematic error from using our best value.

$\Gamma(K_0^*(1430)^0 \bar{K}_2^*(1430)^0 + c.c. \rightarrow \pi^+\pi^- K^+ K^-)/\Gamma_{total}$		$\Gamma_{10}/\Gamma$	
VALUE (units 10 <sup>-4</sup> )	EVTS	DOCUMENT ID	TECN COMMENT

**8.0 ± 2.0 ± 0.2** 62 1 ABLIKIM 05q BES2  $\psi(2S) \rightarrow \gamma\pi^+\pi^- K^+ K^-$

1 ABLIKIM 05q reports  $(8.49 \pm 1.66 \pm 1.32 \pm 1.99) \times 10^{-4}$  from a measurement of  $[\Gamma(\chi_{c0}(1P) \rightarrow K_0^*(1430)^0 \bar{K}_2^*(1430)^0 + c.c. \rightarrow \pi^+\pi^- K^+ K^-)/\Gamma_{total}] \times [B(\psi(2S) \rightarrow \gamma\chi_{c0}(1P))]$  assuming  $B(\psi(2S) \rightarrow \gamma\chi_{c0}(1P)) = (9.22 \pm 0.11 \pm 0.46) \times 10^{-2}$ , which we rescale to our best value  $B(\psi(2S) \rightarrow \gamma\chi_{c0}(1P)) = (9.79 \pm 0.20) \times 10^{-2}$ . Our first error is their experiment's error and our second error is the systematic error from using our best value.

## Meson Particle Listings

 $\chi_{c0}(1P)$  $\Gamma(K_1(1270)^+ K^- + c.c. \rightarrow \pi^+ \pi^- K^+ K^-)/\Gamma_{total}$   $\Gamma_{11}/\Gamma$ 

VALUE (units $10^{-3}$ )	EVTS	DOCUMENT ID	TECN	COMMENT
<b><math>6.3 \pm 1.9 \pm 0.1</math></b>	68	<sup>1</sup> ABLIKIM	05q BES2	$\psi(2S) \rightarrow \gamma \pi^+ \pi^- K^+ K^-$
<sup>1</sup> ABLIKIM 05q reports $(6.66 \pm 1.31 \pm 1.60_{-1.51}) \times 10^{-3}$ from a measurement of $[\Gamma(\chi_{c0}(1P) \rightarrow K_1(1270)^+ K^- + c.c. \rightarrow \pi^+ \pi^- K^+ K^-)/\Gamma_{total}] \times [B(\psi(2S) \rightarrow \gamma \chi_{c0}(1P))]$ assuming $B(\psi(2S) \rightarrow \gamma \chi_{c0}(1P)) = (9.22 \pm 0.11 \pm 0.46) \times 10^{-2}$ , which we rescale to our best value $B(\psi(2S) \rightarrow \gamma \chi_{c0}(1P)) = (9.79 \pm 0.20) \times 10^{-2}$ . Our first error is their experiment's error and our second error is the systematic error from using our best value. The measurement assumes $B(K_1(1270) \rightarrow K \rho(770)) = 42 \pm 6\%$ .				

 $\Gamma(K_1(1400)^+ K^- + c.c. \rightarrow \pi^+ \pi^- K^+ K^-)/\Gamma_{total}$   $\Gamma_{12}/\Gamma$ 

VALUE (units $10^{-3}$ )	CL%	DOCUMENT ID	TECN	COMMENT
<b>&lt;2.7</b>	90	<sup>1</sup> ABLIKIM	05q BES2	$\psi(2S) \rightarrow \gamma \pi^+ \pi^- K^+ K^-$
<sup>1</sup> ABLIKIM 05q reports $< 2.85 \times 10^{-3}$ from a measurement of $[\Gamma(\chi_{c0}(1P) \rightarrow K_1(1400)^+ K^- + c.c. \rightarrow \pi^+ \pi^- K^+ K^-)/\Gamma_{total}] \times [B(\psi(2S) \rightarrow \gamma \chi_{c0}(1P))]$ assuming $B(\psi(2S) \rightarrow \gamma \chi_{c0}(1P)) = (9.22 \pm 0.11 \pm 0.46) \times 10^{-2}$ , which we rescale to our best value $B(\psi(2S) \rightarrow \gamma \chi_{c0}(1P)) = 9.79 \times 10^{-2}$ . The measurement assumes $B(K_1(1400) \rightarrow K^*(892)\pi) = 94 \pm 6\%$ .				

 $\Gamma(f_0(980) f_0(980))/\Gamma_{total}$   $\Gamma_{13}/\Gamma$ 

VALUE (units $10^{-5}$ )	EVTS	DOCUMENT ID	TECN	COMMENT
<b><math>16.2^{+10.4}_{-9.0} \pm 0.3</math></b>	28	<sup>1</sup> ABLIKIM	05q BES2	$\psi(2S) \rightarrow \gamma \pi^+ \pi^- K^+ K^-$
<sup>1</sup> ABLIKIM 05q reports $[\Gamma(\chi_{c0}(1P) \rightarrow f_0(980) f_0(980))/\Gamma_{total}] \times [B(\psi(2S) \rightarrow \gamma \chi_{c0}(1P))]$ $= (1.59 \pm 0.50 \pm 0.89_{-0.72}) \times 10^{-5}$ which we divide by our best value $B(\psi(2S) \rightarrow \gamma \chi_{c0}(1P)) = (9.79 \pm 0.20) \times 10^{-2}$ . Our first error is their experiment's error and our second error is the systematic error from using our best value. One of the $f_0(980)$ mesons is identified via decay to $\pi^+ \pi^-$ while the other via $K^+ K^-$ decay.				

 $\Gamma(f_0(980) f_0(2200))/\Gamma_{total}$   $\Gamma_{14}/\Gamma$ 

VALUE (units $10^{-4}$ )	EVTS	DOCUMENT ID	TECN	COMMENT
<b><math>7.9^{+2.0}_{-2.5} \pm 0.2</math></b>	77	<sup>1</sup> ABLIKIM	05q BES2	$\psi(2S) \rightarrow \gamma \pi^+ \pi^- K^+ K^-$
<sup>1</sup> ABLIKIM 05q reports $(8.42 \pm 1.42 \pm 1.65_{-2.29}) \times 10^{-4}$ from a measurement of $[\Gamma(\chi_{c0}(1P) \rightarrow f_0(980) f_0(2200))/\Gamma_{total}] \times [B(\psi(2S) \rightarrow \gamma \chi_{c0}(1P))]$ assuming $B(\psi(2S) \rightarrow \gamma \chi_{c0}(1P)) = (9.22 \pm 0.11 \pm 0.46) \times 10^{-2}$ , which we rescale to our best value $B(\psi(2S) \rightarrow \gamma \chi_{c0}(1P)) = (9.79 \pm 0.20) \times 10^{-2}$ . Our first error is their experiment's error and our second error is the systematic error from using our best value. The $f_0$ mesons are identified via $f_0(980) \rightarrow \pi^+ \pi^-$ and $f_0(2200) \rightarrow K^+ K^-$ decays.				

 $\Gamma(f_0(1370) f_0(1370))/\Gamma_{total}$   $\Gamma_{15}/\Gamma$ 

VALUE (units $10^{-4}$ )	CL%	DOCUMENT ID	TECN	COMMENT
<b>&lt;2.7</b>	90	<sup>1</sup> ABLIKIM	05q BES2	$\psi(2S) \rightarrow \gamma \pi^+ \pi^- K^+ K^-$
<sup>1</sup> ABLIKIM 05q reports $< 2.9 \times 10^{-4}$ from a measurement of $[\Gamma(\chi_{c0}(1P) \rightarrow f_0(1370) f_0(1370))/\Gamma_{total}] \times [B(\psi(2S) \rightarrow \gamma \chi_{c0}(1P))]$ assuming $B(\psi(2S) \rightarrow \gamma \chi_{c0}(1P)) = (9.22 \pm 0.11 \pm 0.46) \times 10^{-2}$ , which we rescale to our best value $B(\psi(2S) \rightarrow \gamma \chi_{c0}(1P)) = 9.79 \times 10^{-2}$ . One of the $f_0(1370)$ mesons is identified via decay to $\pi^+ \pi^-$ while the other via $K^+ K^-$ decay. Both branching fractions for these $f_0$ decays are implicitly included in the quoted result.				

 $\Gamma(f_0(1370) f_0(1500))/\Gamma_{total}$   $\Gamma_{16}/\Gamma$ 

VALUE (units $10^{-4}$ )	CL%	DOCUMENT ID	TECN	COMMENT
<b>&lt;1.7</b>	90	<sup>1</sup> ABLIKIM	05q BES2	$\psi(2S) \rightarrow \gamma \pi^+ \pi^- K^+ K^-$
<sup>1</sup> ABLIKIM 05q reports $< 1.8 \times 10^{-4}$ from a measurement of $[\Gamma(\chi_{c0}(1P) \rightarrow f_0(1370) f_0(1500))/\Gamma_{total}] \times [B(\psi(2S) \rightarrow \gamma \chi_{c0}(1P))]$ assuming $B(\psi(2S) \rightarrow \gamma \chi_{c0}(1P)) = (9.22 \pm 0.11 \pm 0.46) \times 10^{-2}$ , which we rescale to our best value $B(\psi(2S) \rightarrow \gamma \chi_{c0}(1P)) = (9.79 \pm 0.20) \times 10^{-2}$ . The $f_0$ mesons are identified via $f_0(1370) \rightarrow \pi^+ \pi^-$ and $f_0(1500) \rightarrow K^+ K^-$ decays. Both branching fractions for these $f_0$ decays are implicitly included in the quoted result.				

 $\Gamma(f_0(1370) f_0(1710))/\Gamma_{total}$   $\Gamma_{17}/\Gamma$ 

VALUE (units $10^{-4}$ )	EVTS	DOCUMENT ID	TECN	COMMENT
<b><math>6.7^{+3.5}_{-2.3} \pm 0.1</math></b>	61	<sup>1</sup> ABLIKIM	05q BES2	$\psi(2S) \rightarrow \gamma \pi^+ \pi^- K^+ K^-$
<sup>1</sup> ABLIKIM 05q reports $(7.12 \pm 1.85 \pm 3.28_{-1.68}) \times 10^{-4}$ from a measurement of $[\Gamma(\chi_{c0}(1P) \rightarrow f_0(1370) f_0(1710))/\Gamma_{total}] \times [B(\psi(2S) \rightarrow \gamma \chi_{c0}(1P))]$ assuming $B(\psi(2S) \rightarrow \gamma \chi_{c0}(1P)) = (9.22 \pm 0.11 \pm 0.46) \times 10^{-2}$ , which we rescale to our best value $B(\psi(2S) \rightarrow \gamma \chi_{c0}(1P)) = (9.79 \pm 0.20) \times 10^{-2}$ . Our first error is their experiment's error and our second error is the systematic error from using our best value. The $f_0$ mesons are identified via $f_0(1370) \rightarrow \pi^+ \pi^-$ and $f_0(1710) \rightarrow K^+ K^-$ decays. Both branching fractions for these $f_0$ decays are implicitly included in the quoted result.				

 $\Gamma(f_0(1500) f_0(1370))/\Gamma_{total}$   $\Gamma_{18}/\Gamma$ 

VALUE (units $10^{-4}$ )	CL%	DOCUMENT ID	TECN	COMMENT
<b>&lt;1.3</b>	90	<sup>1</sup> ABLIKIM	05q BES2	$\psi(2S) \rightarrow \gamma \pi^+ \pi^- K^+ K^-$
<sup>1</sup> ABLIKIM 05q reports $< 1.4 \times 10^{-4}$ from a measurement of $[\Gamma(\chi_{c0}(1P) \rightarrow f_0(1500) f_0(1370))/\Gamma_{total}] \times [B(\psi(2S) \rightarrow \gamma \chi_{c0}(1P))]$ assuming $B(\psi(2S) \rightarrow \gamma \chi_{c0}(1P)) = (9.22 \pm 0.11 \pm 0.46) \times 10^{-2}$ , which we rescale to our best value $B(\psi(2S) \rightarrow \gamma \chi_{c0}(1P)) = 9.79 \times 10^{-2}$ . The $f_0$ mesons are identified via $f_0(1500) \rightarrow \pi^+ \pi^-$ and $f_0(1370) \rightarrow K^+ K^-$ decays. Both branching fractions for these $f_0$ decays are implicitly included in the quoted result.				

 $\Gamma(f_0(1500) f_0(1500))/\Gamma_{total}$   $\Gamma_{19}/\Gamma$ 

VALUE (units $10^{-4}$ )	CL%	DOCUMENT ID	TECN	COMMENT
<b>&lt;0.5</b>	90	<sup>1</sup> ABLIKIM	05q BES2	$\psi(2S) \rightarrow \gamma \pi^+ \pi^- K^+ K^-$
<sup>1</sup> ABLIKIM 05q reports $< 0.55 \times 10^{-4}$ from a measurement of $[\Gamma(\chi_{c0}(1P) \rightarrow f_0(1500) f_0(1500))/\Gamma_{total}] \times [B(\psi(2S) \rightarrow \gamma \chi_{c0}(1P))]$ assuming $B(\psi(2S) \rightarrow \gamma \chi_{c0}(1P)) = (9.22 \pm 0.11 \pm 0.46) \times 10^{-2}$ , which we rescale to our best value $B(\psi(2S) \rightarrow \gamma \chi_{c0}(1P)) = 9.79 \times 10^{-2}$ . One of the $f_0(1500)$ is identified via decay to $\pi^+ \pi^-$ while the other via $K^+ K^-$ decay. Both branching fractions for these $f_0$ decays are implicitly included in the quoted result.				

 $\Gamma(f_0(1500) f_0(1710))/\Gamma_{total}$   $\Gamma_{20}/\Gamma$ 

VALUE (units $10^{-4}$ )	CL%	DOCUMENT ID	TECN	COMMENT
<b>&lt;0.7</b>	90	<sup>1</sup> ABLIKIM	05q BES2	$\psi(2S) \rightarrow \gamma \pi^+ \pi^- K^+ K^-$
<sup>1</sup> ABLIKIM 05q reports $< 0.73 \times 10^{-4}$ from a measurement of $[\Gamma(\chi_{c0}(1P) \rightarrow f_0(1500) f_0(1710))/\Gamma_{total}] \times [B(\psi(2S) \rightarrow \gamma \chi_{c0}(1P))]$ assuming $B(\psi(2S) \rightarrow \gamma \chi_{c0}(1P)) = (9.22 \pm 0.11 \pm 0.46) \times 10^{-2}$ , which we rescale to our best value $B(\psi(2S) \rightarrow \gamma \chi_{c0}(1P)) = 9.79 \times 10^{-2}$ . The $f_0$ mesons are identified via $f_0(1500) \rightarrow \pi^+ \pi^-$ and $f_0(1710) \rightarrow K^+ K^-$ decays. Both branching fractions for these $f_0$ decays are implicitly included in the quoted result.				

 $\Gamma(K^+ K^- \pi^+ \pi^- \pi^0)/\Gamma_{total}$   $\Gamma_{21}/\Gamma$ 

VALUE (units $10^{-3}$ )	EVTS	DOCUMENT ID	TECN	COMMENT
<b><math>8.61 \pm 0.13 \pm 0.94</math></b>	9.0k	<sup>1</sup> ABLIKIM	13B BES3	$e^+ e^- \rightarrow \psi(2S) \rightarrow \gamma \chi_{c0}$
<sup>1</sup> Using $1.06 \times 10^8 \psi(2S)$ mesons and $B(\psi(2S) \rightarrow \chi_{c0} \gamma) = (9.68 \pm 0.31)\%$ .				

 $\Gamma(K_S^0 K^\pm \pi^\mp \pi^\pm \pi^-)/\Gamma_{total}$   $\Gamma_{22}/\Gamma$ 

VALUE (units $10^{-3}$ )	EVTS	DOCUMENT ID	TECN	COMMENT
<b><math>4.22 \pm 0.10 \pm 0.43</math></b>	2.7k	<sup>1</sup> ABLIKIM	13B BES3	$e^+ e^- \rightarrow \psi(2S) \rightarrow \gamma \chi_{c0}$
<sup>1</sup> Using $1.06 \times 10^8 \psi(2S)$ mesons and $B(\psi(2S) \rightarrow \chi_{c0} \gamma) = (9.68 \pm 0.31)\%$ .				

 $\Gamma(K^+ K^- \pi^0 \pi^0)/\Gamma_{total}$   $\Gamma_{23}/\Gamma$ 

VALUE (%)	EVTS	DOCUMENT ID	TECN	COMMENT
<b><math>0.56 \pm 0.09 \pm 0.01</math></b>	213.5	<sup>1</sup> HE	08B CLEO	$e^+ e^- \rightarrow \gamma h^+ h^- h^0 h^0$
<sup>1</sup> HE 08B reports $0.59 \pm 0.05 \pm 0.08 \pm 0.03\%$ from a measurement of $[\Gamma(\chi_{c0}(1P) \rightarrow K^+ K^- \pi^0 \pi^0)/\Gamma_{total}] \times [B(\psi(2S) \rightarrow \gamma \chi_{c0}(1P))]$ assuming $B(\psi(2S) \rightarrow \gamma \chi_{c0}(1P)) = (9.22 \pm 0.11 \pm 0.46) \times 10^{-2}$ , which we rescale to our best value $B(\psi(2S) \rightarrow \gamma \chi_{c0}(1P)) = (9.79 \pm 0.20) \times 10^{-2}$ . Our first error is their experiment's error and our second error is the systematic error from using our best value.				

 $\Gamma(K^+ \pi^- \bar{K}^0 \pi^0 + c.c.)/\Gamma_{total}$   $\Gamma_{24}/\Gamma$ 

VALUE (%)	EVTS	DOCUMENT ID	TECN	COMMENT
<b><math>2.49 \pm 0.33 \pm 0.05</math></b>	401.7	<sup>1</sup> HE	08B CLEO	$e^+ e^- \rightarrow \gamma h^+ h^- h^0 h^0$
<sup>1</sup> HE 08B reports $2.64 \pm 0.15 \pm 0.31 \pm 0.14\%$ from a measurement of $[\Gamma(\chi_{c0}(1P) \rightarrow K^+ \pi^- \bar{K}^0 \pi^0 + c.c.)/\Gamma_{total}] \times [B(\psi(2S) \rightarrow \gamma \chi_{c0}(1P))]$ assuming $B(\psi(2S) \rightarrow \gamma \chi_{c0}(1P)) = (9.22 \pm 0.11 \pm 0.46) \times 10^{-2}$ , which we rescale to our best value $B(\psi(2S) \rightarrow \gamma \chi_{c0}(1P)) = (9.79 \pm 0.20) \times 10^{-2}$ . Our first error is their experiment's error and our second error is the systematic error from using our best value.				

 $\Gamma(\rho^+ K^- K^0 + c.c.)/\Gamma_{total}$   $\Gamma_{25}/\Gamma$ 

VALUE (%)	EVTS	DOCUMENT ID	TECN	COMMENT
<b><math>1.21 \pm 0.21 \pm 0.02</math></b>	179.7	<sup>1</sup> HE	08B CLEO	$e^+ e^- \rightarrow \gamma h^+ h^- h^0 h^0$
<sup>1</sup> HE 08B reports $1.28 \pm 0.16 \pm 0.15 \pm 0.07\%$ from a measurement of $[\Gamma(\chi_{c0}(1P) \rightarrow \rho^+ K^- K^0 + c.c.)/\Gamma_{total}] \times [B(\psi(2S) \rightarrow \gamma \chi_{c0}(1P))]$ assuming $B(\psi(2S) \rightarrow \gamma \chi_{c0}(1P)) = (9.22 \pm 0.11 \pm 0.46) \times 10^{-2}$ , which we rescale to our best value $B(\psi(2S) \rightarrow \gamma \chi_{c0}(1P)) = (9.79 \pm 0.20) \times 10^{-2}$ . Our first error is their experiment's error and our second error is the systematic error from using our best value.				

 $\Gamma(K^*(892)^- K^+ \pi^0 \rightarrow K^+ \pi^- \bar{K}^0 \pi^0 + c.c.)/\Gamma_{total}$   $\Gamma_{26}/\Gamma$ 

VALUE (%)	EVTS	DOCUMENT ID	TECN	COMMENT
<b><math>0.46 \pm 0.12 \pm 0.01</math></b>	64.1	<sup>1</sup> HE	08B CLEO	$e^+ e^- \rightarrow \gamma h^+ h^- h^0 h^0$
<sup>1</sup> HE 08B reports $0.49 \pm 0.10 \pm 0.07 \pm 0.03\%$ from a measurement of $[\Gamma(\chi_{c0}(1P) \rightarrow K^*(892)^- K^+ \pi^0 \rightarrow K^+ \pi^- \bar{K}^0 \pi^0 + c.c.)/\Gamma_{total}] \times [B(\psi(2S) \rightarrow \gamma \chi_{c0}(1P))]$ assuming $B(\psi(2S) \rightarrow \gamma \chi_{c0}(1P)) = (9.22 \pm 0.11 \pm 0.46) \times 10^{-2}$ , which we rescale to our best value $B(\psi(2S) \rightarrow \gamma \chi_{c0}(1P)) = (9.79 \pm 0.20) \times 10^{-2}$ . Our first error is their experiment's error and our second error is the systematic error from using our best value.				

 $\Gamma(K_S^0 K_S^0 \pi^+ \pi^-)/\Gamma_{total}$   $\Gamma_{27}/\Gamma$ 

VALUE (units $10^{-3}$ )	EVTS	DOCUMENT ID	TECN	COMMENT
<b><math>5.7 \pm 1.0 \pm 0.1</math></b>	152 $\pm$ 14	<sup>1</sup> ABLIKIM	05o BES2	$\psi(2S) \rightarrow \gamma \chi_{c0}$
<sup>1</sup> ABLIKIM 05o reports $[\Gamma(\chi_{c0}(1P) \rightarrow K_S^0 K_S^0 \pi^+ \pi^-)/\Gamma_{total}] \times [B(\psi(2S) \rightarrow \gamma \chi_{c0}(1P))]$ $= (0.558 \pm 0.051 \pm 0.089) \times 10^{-3}$ which we divide by our best value $B(\psi(2S) \rightarrow \gamma \chi_{c0}(1P)) = (9.79 \pm 0.20) \times 10^{-2}$ . Our first error is their experiment's error and our second error is the systematic error from using our best value.				

$\Gamma(K^+ K^- \eta \pi^0)/\Gamma_{total}$		$\Gamma_{28}/\Gamma$	
VALUE (%)	EVTS	DOCUMENT ID	TECN COMMENT
<b>0.30 ± 0.07 ± 0.01</b>	56.4	<sup>1</sup> HE	08B CLEO $e^+e^- \rightarrow \gamma h^+ h^- h^0 h^0$

<sup>1</sup> HE 08B reports  $0.32 \pm 0.05 \pm 0.05 \pm 0.02$  % from a measurement of  $[\Gamma(\chi_{c0}(1P) \rightarrow K^+ K^- \eta \pi^0)/\Gamma_{total}] \times [B(\psi(2S) \rightarrow \gamma \chi_{c0}(1P))]$  assuming  $B(\psi(2S) \rightarrow \gamma \chi_{c0}(1P)) = (9.22 \pm 0.11 \pm 0.46) \times 10^{-2}$ , which we rescale to our best value  $B(\psi(2S) \rightarrow \gamma \chi_{c0}(1P)) = (9.79 \pm 0.20) \times 10^{-2}$ . Our first error is their experiment's error and our second error is the systematic error from using our best value.

$\Gamma(3(\pi^+ \pi^-))/\Gamma_{total}$		$\Gamma_{29}/\Gamma$	
VALUE (units $10^{-3}$ )	DOCUMENT ID	TECN	COMMENT
<b>12.0 ± 1.8 OUR EVALUATION</b>	Treating systematic error as correlated.		
<b>12.0 ± 1.7 OUR AVERAGE</b>			
11.7 ± 1.0 ± 1.9	<sup>1</sup> BAI	99B BES	$\psi(2S) \rightarrow \gamma \chi_{c0}$
12.5 ± 2.9 ± 0.5	<sup>1</sup> TANENBAUM	78 MRK1	$\psi(2S) \rightarrow \gamma \chi_{c0}$

<sup>1</sup> Rescaled by us using  $B(\psi(2S) \rightarrow \gamma \chi_{c0}) = (9.4 \pm 0.4)$  % and  $B(\psi(2S) \rightarrow J/\psi(1S) \pi^+ \pi^-) = (32.6 \pm 0.5)$  %.

$\Gamma(K^+ \bar{K}^*(892)^0 \pi^- + c.c.)/\Gamma_{total}$		$\Gamma_{30}/\Gamma$	
VALUE	DOCUMENT ID	TECN	COMMENT
<b>0.0075 ± 0.0016 OUR FIT</b>			

$\Gamma(K^*(892)^0 \bar{K}^*(892)^0)/\Gamma_{total}$		$\Gamma_{31}/\Gamma$	
VALUE (units $10^{-3}$ )	EVTS	DOCUMENT ID	TECN COMMENT
<b>1.72 ± 0.60 ± 0.54 ± 0.04</b>	64	<sup>1</sup> ABLIKIM	05Q BES2 $\psi(2S) \rightarrow \gamma \pi^+ \pi^- K^+ K^-$

• • • We do not use the following data for averages, fits, limits, etc. • • •

1.56 ± 0.40 ± 0.03 30 ± 6 <sup>2,3</sup> ABLIKIM 04H BES Repl. by ABLIKIM 05Q

<sup>1</sup> ABLIKIM 05Q reports  $[\Gamma(\chi_{c0}(1P) \rightarrow K^*(892)^0 \bar{K}^*(892)^0)/\Gamma_{total}] \times [B(\psi(2S) \rightarrow \gamma \chi_{c0}(1P))] = (0.168 \pm 0.035 \pm 0.047 \pm 0.040) \times 10^{-3}$  which we divide by our best value  $B(\psi(2S) \rightarrow \gamma \chi_{c0}(1P)) = (9.79 \pm 0.20) \times 10^{-2}$ . Our first error is their experiment's error and our second error is the systematic error from using our best value.

<sup>2</sup> Assumes  $B(K^*(892)^0 \rightarrow K^- \pi^+) = 2/3$ .

<sup>3</sup> ABLIKIM 04H reports  $[\Gamma(\chi_{c0}(1P) \rightarrow K^*(892)^0 \bar{K}^*(892)^0)/\Gamma_{total}] \times [B(\psi(2S) \rightarrow \gamma \chi_{c0}(1P))] = (1.53 \pm 0.29 \pm 0.26) \times 10^{-4}$  which we divide by our best value  $B(\psi(2S) \rightarrow \gamma \chi_{c0}(1P)) = (9.79 \pm 0.20) \times 10^{-2}$ . Our first error is their experiment's error and our second error is the systematic error from using our best value.

$\Gamma(\pi \pi)/\Gamma_{total}$		$\Gamma_{32}/\Gamma$	
VALUE (units $10^{-3}$ )	DOCUMENT ID	TECN	COMMENT
<b>8.51 ± 0.33 OUR FIT</b>			

$\Gamma(\pi^0 \eta_c)/\Gamma_{total}$		$\Gamma_{35}/\Gamma$	
VALUE	CL%	DOCUMENT ID	TECN COMMENT
<b>&lt; 1.6 × 10<sup>-3</sup></b>		<sup>1</sup> ABLIKIM	15N BES3 $\psi(2S) e^+ e^- \rightarrow \gamma \pi^0 \eta_c$

<sup>1</sup> Using  $B(\eta_c \rightarrow K_S^0 K^\pm \pi^\mp) \times B(K_S^0 \rightarrow \pi^+ \pi^-) \times B(\pi^0 \rightarrow \gamma \gamma) = (1.66 \pm 0.11) \times 10^{-2}$ .

$\Gamma(\eta \eta)/\Gamma_{total}$		$\Gamma_{36}/\Gamma$	
VALUE (units $10^{-3}$ )	DOCUMENT ID	TECN	COMMENT
<b>3.01 ± 0.19 OUR FIT</b>			

$\Gamma(\eta \eta)/\Gamma(\pi \pi)$		$\Gamma_{36}/\Gamma_{32}$	
VALUE	DOCUMENT ID	TECN	COMMENT
<b>0.353 ± 0.025 OUR FIT</b>			

• • • We do not use the following data for averages, fits, limits, etc. • • •

0.26 ± 0.09 +0.03 -0.02 <sup>1</sup> ANDREOTTI 05C E835  $\bar{p}p \rightarrow 2$  mesons

0.24 ± 0.10 ± 0.08 <sup>1</sup> BAI 03C BES  $\psi(2S) \rightarrow 5\gamma$

<sup>1</sup> We have multiplied  $\pi^0 \pi^0$  measurement by 3 to obtain  $\pi \pi$ .

$\Gamma(\eta \eta')/\Gamma_{total}$		$\Gamma_{37}/\Gamma$	
VALUE (units $10^{-5}$ )	CL%	EVTS	DOCUMENT ID
<b>9.1 ± 1.1 ± 0.2</b>		85	<sup>1</sup> ABLIKIM 17A1 BES3 $\psi(2S) \rightarrow \gamma \eta' \eta$

• • • We do not use the following data for averages, fits, limits, etc. • • •

<24 90 35 ± 13 <sup>2</sup> ASNER 09 CLEO  $\psi(2S) \rightarrow \gamma \eta' \eta$

<50 90 <sup>3</sup> ADAMS 07 CLEO  $\psi(2S) \rightarrow \gamma \chi_{c0}$

<sup>1</sup> ABLIKIM 17A1 reports  $(8.92 \pm 0.84 \pm 0.65) \times 10^{-5}$  from a measurement of  $[\Gamma(\chi_{c0}(1P) \rightarrow \eta \eta')/\Gamma_{total}] \times [B(\psi(2S) \rightarrow \gamma \chi_{c0}(1P))]$  assuming  $B(\psi(2S) \rightarrow \gamma \chi_{c0}(1P)) = (9.99 \pm 0.27) \times 10^{-2}$ , which we rescale to our best value  $B(\psi(2S) \rightarrow \gamma \chi_{c0}(1P)) = (9.79 \pm 0.20) \times 10^{-2}$ . Our first error is their experiment's error and our second error is the systematic error from using our best value.

<sup>2</sup> ASNER 09 reports  $< 0.25 \times 10^{-3}$  from a measurement of  $[\Gamma(\chi_{c0}(1P) \rightarrow \eta \eta')/\Gamma_{total}] \times [B(\psi(2S) \rightarrow \gamma \chi_{c0}(1P))]$  assuming  $B(\psi(2S) \rightarrow \gamma \chi_{c0}(1P)) = (9.22 \pm 0.11 \pm 0.46) \times 10^{-2}$ , which we rescale to our best value  $B(\psi(2S) \rightarrow \gamma \chi_{c0}(1P)) = 9.79 \times 10^{-2}$ .

<sup>3</sup> Superseded by ASNER 09. ADAMS 07 reports  $< 0.5 \times 10^{-3}$  from a measurement of  $[\Gamma(\chi_{c0}(1P) \rightarrow \eta \eta')/\Gamma_{total}] \times [B(\psi(2S) \rightarrow \gamma \chi_{c0}(1P))]$  assuming  $B(\psi(2S) \rightarrow \gamma \chi_{c0}(1P)) = (9.22 \pm 0.11 \pm 0.46) \times 10^{-2}$ , which we rescale to our best value  $B(\psi(2S) \rightarrow \gamma \chi_{c0}(1P)) = 9.79 \times 10^{-2}$ .

$\Gamma(\eta' \eta')/\Gamma_{total}$		$\Gamma_{38}/\Gamma$	
VALUE (units $10^{-3}$ )	EVTS	DOCUMENT ID	TECN COMMENT
<b>2.17 ± 0.12 OUR AVERAGE</b>			

2.23 ± 0.13 ± 0.05 2.5k <sup>1</sup> ABLIKIM 17A1 BES3  $\psi(2S) \rightarrow \gamma \eta' \eta'$

2.00 ± 0.21 ± 0.04 0.4k <sup>2</sup> ASNER 09 CLEO  $\psi(2S) \rightarrow \gamma \eta' \eta'$

• • • We do not use the following data for averages, fits, limits, etc. • • •

1.60 ± 0.41 ± 0.03 23 <sup>3</sup> ADAMS 07 CLEO  $\psi(2S) \rightarrow \gamma \chi_{c0}$

<sup>1</sup> ABLIKIM 17A1 reports  $(2.19 \pm 0.03 \pm 0.14) \times 10^{-3}$  from a measurement of  $[\Gamma(\chi_{c0}(1P) \rightarrow \eta' \eta')/\Gamma_{total}] \times [B(\psi(2S) \rightarrow \gamma \chi_{c0}(1P))]$  assuming  $B(\psi(2S) \rightarrow \gamma \chi_{c0}(1P)) = (9.99 \pm 0.27) \times 10^{-2}$ , which we rescale to our best value  $B(\psi(2S) \rightarrow \gamma \chi_{c0}(1P)) = (9.79 \pm 0.20) \times 10^{-2}$ . Our first error is their experiment's error and our second error is the systematic error from using our best value.

<sup>2</sup> ASNER 09 reports  $(2.12 \pm 0.13 \pm 0.21) \times 10^{-3}$  from a measurement of  $[\Gamma(\chi_{c0}(1P) \rightarrow \eta' \eta')/\Gamma_{total}] \times [B(\psi(2S) \rightarrow \gamma \chi_{c0}(1P))]$  assuming  $B(\psi(2S) \rightarrow \gamma \chi_{c0}(1P)) = (9.22 \pm 0.11 \pm 0.46) \times 10^{-2}$ , which we rescale to our best value  $B(\psi(2S) \rightarrow \gamma \chi_{c0}(1P)) = (9.79 \pm 0.20) \times 10^{-2}$ . Our first error is their experiment's error and our second error is the systematic error from using our best value.

<sup>3</sup> Superseded by ASNER 09. ADAMS 07 reports  $(1.7 \pm 0.4 \pm 0.2) \times 10^{-3}$  from a measurement of  $[\Gamma(\chi_{c0}(1P) \rightarrow \eta' \eta')/\Gamma_{total}] \times [B(\psi(2S) \rightarrow \gamma \chi_{c0}(1P))]$  assuming  $B(\psi(2S) \rightarrow \gamma \chi_{c0}(1P)) = 0.0922 \pm 0.0011 \pm 0.0046$ , which we rescale to our best value  $B(\psi(2S) \rightarrow \gamma \chi_{c0}(1P)) = (9.79 \pm 0.20) \times 10^{-2}$ . Our first error is their experiment's error and our second error is the systematic error from using our best value.

$\Gamma(\omega \omega)/\Gamma_{total}$		$\Gamma_{39}/\Gamma$	
VALUE (units $10^{-3}$ )	EVTS	DOCUMENT ID	TECN COMMENT
<b>0.97 ± 0.11 OUR AVERAGE</b>			

0.93 ± 0.11 ± 0.02 991 <sup>1</sup> ABLIKIM 11K BES3  $\psi(2S) \rightarrow \gamma$  hadrons

2.16 ± 0.66 ± 0.04 38.1 ± 9.6 <sup>2</sup> ABLIKIM 05N BES2  $\psi(2S) \rightarrow \gamma \chi_{c0} \rightarrow \gamma 6\pi$

<sup>1</sup> ABLIKIM 11K reports  $(0.95 \pm 0.03 \pm 0.11) \times 10^{-3}$  from a measurement of  $[\Gamma(\chi_{c0}(1P) \rightarrow \omega \omega)/\Gamma_{total}] \times [B(\psi(2S) \rightarrow \gamma \chi_{c0}(1P))]$  assuming  $B(\psi(2S) \rightarrow \gamma \chi_{c0}(1P)) = (9.62 \pm 0.31) \times 10^{-2}$ , which we rescale to our best value  $B(\psi(2S) \rightarrow \gamma \chi_{c0}(1P)) = (9.79 \pm 0.20) \times 10^{-2}$ . Our first error is their experiment's error and our second error is the systematic error from using our best value.

<sup>2</sup> ABLIKIM 05N reports  $[\Gamma(\chi_{c0}(1P) \rightarrow \omega \omega)/\Gamma_{total}] \times [B(\psi(2S) \rightarrow \gamma \chi_{c0}(1P))] = (0.212 \pm 0.053 \pm 0.037) \times 10^{-3}$  which we divide by our best value  $B(\psi(2S) \rightarrow \gamma \chi_{c0}(1P)) = (9.79 \pm 0.20) \times 10^{-2}$ . Our first error is their experiment's error and our second error is the systematic error from using our best value.

$\Gamma(\omega \phi)/\Gamma_{total}$		$\Gamma_{40}/\Gamma$	
VALUE (units $10^{-4}$ )	EVTS	DOCUMENT ID	TECN COMMENT
<b>1.41 ± 0.13 ± 0.03</b>	486	<sup>1</sup> ABLIKIM 19J	BES3 $\psi(2S) \rightarrow \gamma$ hadrons

• • • We do not use the following data for averages, fits, limits, etc. • • •

1.18 ± 0.22 ± 0.02 76 <sup>2,3</sup> ABLIKIM 11K BES3  $\psi(2S) \rightarrow \gamma$  hadrons

<sup>1</sup> ABLIKIM 19J reports  $[\Gamma(\chi_{c0}(1P) \rightarrow \omega \phi)/\Gamma_{total}] \times [B(\psi(2S) \rightarrow \gamma \chi_{c0}(1P))] = (13.83 \pm 0.70 \pm 1.01) \times 10^{-6}$  which we divide by our best value  $B(\psi(2S) \rightarrow \gamma \chi_{c0}(1P)) = (9.79 \pm 0.20) \times 10^{-2}$ . Our first error is their experiment's error and our second error is the systematic error from using our best value.

<sup>2</sup> ABLIKIM 11K reports  $(1.2 \pm 0.1 \pm 0.2) \times 10^{-4}$  from a measurement of  $[\Gamma(\chi_{c0}(1P) \rightarrow \omega \phi)/\Gamma_{total}] \times [B(\psi(2S) \rightarrow \gamma \chi_{c0}(1P))]$  assuming  $B(\psi(2S) \rightarrow \gamma \chi_{c0}(1P)) = (9.62 \pm 0.31) \times 10^{-2}$ , which we rescale to our best value  $B(\psi(2S) \rightarrow \gamma \chi_{c0}(1P)) = (9.79 \pm 0.20) \times 10^{-2}$ . Our first error is their experiment's error and our second error is the systematic error from using our best value.

<sup>3</sup> Superseded by ABLIKIM 19J.

$\Gamma(\omega K^+ K^-)/\Gamma_{total}$		$\Gamma_{41}/\Gamma$	
VALUE (units $10^{-3}$ )	EVTS	DOCUMENT ID	TECN COMMENT
<b>1.94 ± 0.06 ± 0.20</b>	1.4k	<sup>1</sup> ABLIKIM 13B	BES3 $e^+e^- \rightarrow \psi(2S) \rightarrow \gamma \chi_{c0}$

<sup>1</sup> Using  $1.06 \times 10^8$   $\psi(2S)$  mesons and  $B(\psi(2S) \rightarrow \chi_{c0} \gamma) = (9.68 \pm 0.31)$  %.

$\Gamma(K^+ K^-)/\Gamma_{total}$		$\Gamma_{42}/\Gamma$	
VALUE (units $10^{-3}$ )	DOCUMENT ID	TECN	COMMENT
<b>6.05 ± 0.31 OUR FIT</b>			

$\Gamma(K_S^0 K_S^0)/\Gamma_{total}$		$\Gamma_{43}/\Gamma$	
VALUE (units $10^{-3}$ )	DOCUMENT ID	TECN	COMMENT
<b>3.16 ± 0.17 OUR FIT</b>			

$\Gamma(K_S^0 K_S^0)/\Gamma(\pi \pi)$		$\Gamma_{43}/\Gamma_{32}$	
VALUE	DOCUMENT ID	TECN	COMMENT
<b>0.371 ± 0.023 OUR FIT</b>			

• • • We do not use the following data for averages, fits, limits, etc. • • •

0.31 ± 0.05 ± 0.05 <sup>1,2</sup> CHEN 07B BELL  $e^+e^- \rightarrow e^+e^- \chi_{c0}$

<sup>1</sup> Using  $\Gamma(\pi \pi) \times \Gamma(\gamma \gamma)/\Gamma_{total}$  from the  $\pi^+ \pi^-$  measurement of NAKAZAWA 05 rescaled by 3/2 to convert to  $\pi \pi$ .

<sup>2</sup> Not independent from other measurements.

$\Gamma(K_S^0 K_S^0)/\Gamma(K^+ K^-)$		$\Gamma_{43}/\Gamma_{42}$	
VALUE	DOCUMENT ID	TECN	COMMENT
<b>0.52 ± 0.04 OUR FIT</b>			

• • • We do not use the following data for averages, fits, limits, etc. • • •

0.49 ± 0.07 ± 0.08 <sup>1,2</sup> CHEN 07B BELL  $e^+e^- \rightarrow e^+e^- \chi_{c0}$

<sup>1</sup> Using  $\Gamma(K^+ K^-) \times \Gamma(\gamma \gamma)/\Gamma_{total}$  from NAKAZAWA 05.

<sup>2</sup> Not independent from other measurements.

## Meson Particle Listings

 $\chi_{c0}(1P)$ 

$\Gamma(\pi^+\pi^-\eta)/\Gamma_{\text{total}}$	CL%	DOCUMENT ID	TECN	COMMENT	$\Gamma_{44}/\Gamma$
--	-----	-------------	------	---------	----------------------

**<0.20** 90 <sup>1</sup>ATHAR 07 CLEO  $\psi(2S) \rightarrow \gamma h^+ h^- h^0$

• • • We do not use the following data for averages, fits, limits, etc. • • •

<1.0 90 <sup>2</sup>ABLIKIM 06R BES2  $\psi(2S) \rightarrow \gamma\chi_{c0}$

<sup>1</sup>ATHAR 07 reports  $< 0.21 \times 10^{-3}$  from a measurement of  $[\Gamma(\chi_{c0}(1P) \rightarrow \pi^+\pi^-\eta)/\Gamma_{\text{total}}] \times [B(\psi(2S) \rightarrow \gamma\chi_{c0}(1P))]$  assuming  $B(\psi(2S) \rightarrow \gamma\chi_{c0}(1P)) = (9.22 \pm 0.11 \pm 0.46) \times 10^{-2}$ , which we rescale to our best value  $B(\psi(2S) \rightarrow \gamma\chi_{c0}(1P)) = 9.79 \times 10^{-2}$ .

<sup>2</sup>ABLIKIM 06R reports  $< 1.1 \times 10^{-3}$  from a measurement of  $[\Gamma(\chi_{c0}(1P) \rightarrow \pi^+\pi^-\eta)/\Gamma_{\text{total}}] \times [B(\psi(2S) \rightarrow \gamma\chi_{c0}(1P))]$  assuming  $B(\psi(2S) \rightarrow \gamma\chi_{c0}(1P)) = (9.2 \pm 0.4) \times 10^{-2}$ , which we rescale to our best value  $B(\psi(2S) \rightarrow \gamma\chi_{c0}(1P)) = 9.79 \times 10^{-2}$ .

$\Gamma(\pi^+\pi^-\eta')/\Gamma_{\text{total}}$	CL%	DOCUMENT ID	TECN	COMMENT	$\Gamma_{45}/\Gamma$
---	-----	-------------	------	---------	----------------------

**<0.4** 90 <sup>1</sup>ATHAR 07 CLEO  $\psi(2S) \rightarrow \gamma h^+ h^- h^0$

<sup>1</sup>ATHAR 07 reports  $< 0.38 \times 10^{-3}$  from a measurement of  $[\Gamma(\chi_{c0}(1P) \rightarrow \pi^+\pi^-\eta')/\Gamma_{\text{total}}] \times [B(\psi(2S) \rightarrow \gamma\chi_{c0}(1P))]$  assuming  $B(\psi(2S) \rightarrow \gamma\chi_{c0}(1P)) = (9.22 \pm 0.11 \pm 0.46) \times 10^{-2}$ , which we rescale to our best value  $B(\psi(2S) \rightarrow \gamma\chi_{c0}(1P)) = 9.79 \times 10^{-2}$ .

$\Gamma(\bar{K}^0 K^+ \pi^- + \text{c.c.})/\Gamma_{\text{total}}$	CL%	DOCUMENT ID	TECN	COMMENT	$\Gamma_{46}/\Gamma$
---	-----	-------------	------	---------	----------------------

**<0.09** 90 <sup>1</sup>ATHAR 07 CLEO  $\psi(2S) \rightarrow \gamma h^+ h^- h^0$

• • • We do not use the following data for averages, fits, limits, etc. • • •

<0.7 90 <sup>2,3</sup>ABLIKIM 06R BES2  $\psi(2S) \rightarrow \gamma\chi_{c0}$

<0.7 90 <sup>3,4</sup>BAI 99B BES  $\psi(2S) \rightarrow \gamma\chi_{c0}$

<sup>1</sup>ATHAR 07 reports  $< 0.10 \times 10^{-3}$  from a measurement of  $[\Gamma(\chi_{c0}(1P) \rightarrow \bar{K}^0 K^+ \pi^- + \text{c.c.})/\Gamma_{\text{total}}] \times [B(\psi(2S) \rightarrow \gamma\chi_{c0}(1P))]$  assuming  $B(\psi(2S) \rightarrow \gamma\chi_{c0}(1P)) = (9.22 \pm 0.11 \pm 0.46) \times 10^{-2}$ , which we rescale to our best value  $B(\psi(2S) \rightarrow \gamma\chi_{c0}(1P)) = 9.79 \times 10^{-2}$ .

<sup>2</sup>ABLIKIM 06R reports  $< 0.70 \times 10^{-3}$  from a measurement of  $[\Gamma(\chi_{c0}(1P) \rightarrow \bar{K}^0 K^+ \pi^- + \text{c.c.})/\Gamma_{\text{total}}] \times [B(\psi(2S) \rightarrow \gamma\chi_{c0}(1P))]$  assuming  $B(\psi(2S) \rightarrow \gamma\chi_{c0}(1P)) = (9.2 \pm 0.4) \times 10^{-2}$ , which we rescale to our best value  $B(\psi(2S) \rightarrow \gamma\chi_{c0}(1P)) = 9.79 \times 10^{-2}$ .

<sup>3</sup>We have multiplied the  $K_S^0 K^+ \pi^-$  measurement by a factor of 2 to convert to  $K^0 K^+ \pi^-$ .

<sup>4</sup>Rescaled by us using  $B(\psi(2S) \rightarrow \gamma\chi_{c0}) = (9.4 \pm 0.4)\%$  and  $B(\psi(2S) \rightarrow J/\psi(1S) \pi^+ \pi^-) = (32.6 \pm 0.5)\%$ .

$\Gamma(K^+ K^- \pi^0)/\Gamma_{\text{total}}$	CL%	DOCUMENT ID	TECN	COMMENT	$\Gamma_{47}/\Gamma$
---	-----	-------------	------	---------	----------------------

**<0.06** 90 <sup>1</sup>ATHAR 07 CLEO  $\psi(2S) \rightarrow \gamma h^+ h^- h^0$

<sup>1</sup>ATHAR 07 reports  $< 0.06 \times 10^{-3}$  from a measurement of  $[\Gamma(\chi_{c0}(1P) \rightarrow K^+ K^- \pi^0)/\Gamma_{\text{total}}] \times [B(\psi(2S) \rightarrow \gamma\chi_{c0}(1P))]$  assuming  $B(\psi(2S) \rightarrow \gamma\chi_{c0}(1P)) = (9.22 \pm 0.11 \pm 0.46) \times 10^{-2}$ , which we rescale to our best value  $B(\psi(2S) \rightarrow \gamma\chi_{c0}(1P)) = 9.79 \times 10^{-2}$ .

$\Gamma(K^+ K^- \eta)/\Gamma_{\text{total}}$	CL%	DOCUMENT ID	TECN	COMMENT	$\Gamma_{48}/\Gamma$
--	-----	-------------	------	---------	----------------------

**<0.23** 90 <sup>1</sup>ATHAR 07 CLEO  $\psi(2S) \rightarrow \gamma h^+ h^- h^0$

<sup>1</sup>ATHAR 07 reports  $< 0.24 \times 10^{-3}$  from a measurement of  $[\Gamma(\chi_{c0}(1P) \rightarrow K^+ K^- \eta)/\Gamma_{\text{total}}] \times [B(\psi(2S) \rightarrow \gamma\chi_{c0}(1P))]$  assuming  $B(\psi(2S) \rightarrow \gamma\chi_{c0}(1P)) = (9.22 \pm 0.11 \pm 0.46) \times 10^{-2}$ , which we rescale to our best value  $B(\psi(2S) \rightarrow \gamma\chi_{c0}(1P)) = 9.79 \times 10^{-2}$ .

$\Gamma(K^+ K^- K_S^0 K_S^0)/\Gamma_{\text{total}}$	CL%	DOCUMENT ID	TECN	COMMENT	$\Gamma_{49}/\Gamma$
---	-----	-------------	------	---------	----------------------

**1.41 ± 0.47 ± 0.03** 16.8 ± 4.8 <sup>1</sup>ABLIKIM 05o BES2  $\psi(2S) \rightarrow \gamma\chi_{c0}$

<sup>1</sup>ABLIKIM 05o reports  $[\Gamma(\chi_{c0}(1P) \rightarrow K^+ K^- K_S^0 K_S^0)/\Gamma_{\text{total}}] \times [B(\psi(2S) \rightarrow \gamma\chi_{c0}(1P))]$  =  $(0.138 \pm 0.039 \pm 0.025) \times 10^{-3}$  which we divide by our best value  $B(\psi(2S) \rightarrow \gamma\chi_{c0}(1P)) = (9.79 \pm 0.20) \times 10^{-2}$ . Our first error is their experiment's error and our second error is the systematic error from using our best value.

$\Gamma(K_S^0 K_S^0 K_S^0 K_S^0)/\Gamma_{\text{total}}$	CL%	DOCUMENT ID	TECN	COMMENT	$\Gamma_{50}/\Gamma$
---	-----	-------------	------	---------	----------------------

**5.8 ± 0.5 ± 0.1** 319 <sup>1</sup>ABLIKIM 19AA BES3  $\psi(2S) \rightarrow \gamma 4K_S^0$

<sup>1</sup>Using  $B(K_S^0 \rightarrow \pi^+ \pi^-) = (69.20 \pm 0.05)\%$ . ABLIKIM 19AA reports  $[\Gamma(\chi_{c0}(1P) \rightarrow K_S^0 K_S^0 K_S^0 K_S^0)/\Gamma_{\text{total}}] \times [B(\psi(2S) \rightarrow \gamma\chi_{c0}(1P))]$  =  $(5.64 \pm 0.33 \pm 0.37) \times 10^{-5}$  which we divide by our best value  $B(\psi(2S) \rightarrow \gamma\chi_{c0}(1P)) = (9.79 \pm 0.20) \times 10^{-2}$ . Our first error is their experiment's error and our second error is the systematic error from using our best value.

$\Gamma(K^+ K^- K^+ K^-)/\Gamma_{\text{total}}$	CL%	DOCUMENT ID	TECN	COMMENT	$\Gamma_{51}/\Gamma$
---	-----	-------------	------	---------	----------------------

**2.82 ± 0.29 OUR FIT**

$\Gamma(K^+ K^- \phi)/\Gamma_{\text{total}}$	CL%	DOCUMENT ID	TECN	COMMENT	$\Gamma_{52}/\Gamma$
--	-----	-------------	------	---------	----------------------

**0.97 ± 0.25 ± 0.02** 38 <sup>1</sup>ABLIKIM 06T BES2  $\psi(2S) \rightarrow \gamma 2K^+ 2K^-$

<sup>1</sup>ABLIKIM 06T reports  $(1.03 \pm 0.22 \pm 0.15) \times 10^{-3}$  from a measurement of  $[\Gamma(\chi_{c0}(1P) \rightarrow K^+ K^- \phi)/\Gamma_{\text{total}}] \times [B(\psi(2S) \rightarrow \gamma\chi_{c0}(1P))]$  assuming  $B(\psi(2S) \rightarrow \gamma\chi_{c0}(1P)) = (9.2 \pm 0.4) \times 10^{-2}$ , which we rescale to our best value  $B(\psi(2S) \rightarrow \gamma\chi_{c0}(1P)) = (9.79 \pm 0.20) \times 10^{-2}$ . Our first error is their experiment's error and our second error is the systematic error from using our best value.

$\Gamma(\bar{K}^0 K^+ \pi^- \phi + \text{c.c.})/\Gamma_{\text{total}}$	CL%	DOCUMENT ID	TECN	COMMENT	$\Gamma_{53}/\Gamma$
--	-----	-------------	------	---------	----------------------

**3.68 ± 0.30 ± 0.50** ABLIKIM 15M BES3  $\psi(2S) \rightarrow \gamma\chi_{c0}$

$\Gamma(K^+ K^- \pi^0 \phi)/\Gamma_{\text{total}}$	CL%	DOCUMENT ID	TECN	COMMENT	$\Gamma_{54}/\Gamma$
--	-----	-------------	------	---------	----------------------

**1.90 ± 0.14 ± 0.32** ABLIKIM 15M BES3  $\psi(2S) \rightarrow \gamma\chi_{c0}$

$\Gamma(\phi \pi^+ \pi^- \pi^0)/\Gamma_{\text{total}}$	CL%	DOCUMENT ID	TECN	COMMENT	$\Gamma_{55}/\Gamma$
--	-----	-------------	------	---------	----------------------

**1.18 ± 0.07 ± 0.13** 538 <sup>1</sup>ABLIKIM 13B BES3  $e^+ e^- \rightarrow \psi(2S) \rightarrow \gamma\chi_{c0}$

<sup>1</sup>Using  $1.06 \times 10^8 \psi(2S)$  mesons and  $B(\psi(2S) \rightarrow \chi_{c0} \gamma) = (9.68 \pm 0.31)\%$ .

$\Gamma(\phi \phi)/\Gamma_{\text{total}}$	CL%	DOCUMENT ID	TECN	COMMENT	$\Gamma_{56}/\Gamma$
---	-----	-------------	------	---------	----------------------

**0.80 ± 0.07 OUR FIT**

$\Gamma(\phi \phi \eta)/\Gamma_{\text{total}}$	CL%	DOCUMENT ID	TECN	COMMENT	$\Gamma_{57}/\Gamma$
--	-----	-------------	------	---------	----------------------

**8.4 ± 0.7 ± 0.6** 186.6 <sup>1</sup>ABLIKIM 20B BES3  $\psi(2S) \rightarrow \gamma \phi \phi \eta$

<sup>1</sup>ABLIKIM 20B reports  $(8.41 \pm 0.74 \pm 0.62) \times 10^{-4}$  from a measurement of  $[\Gamma(\chi_{c0}(1P) \rightarrow \phi \phi \eta)/\Gamma_{\text{total}}] \times [B(\psi(2S) \rightarrow \gamma\chi_{c0}(1P))]$  assuming  $B(\psi(2S) \rightarrow \gamma\chi_{c0}(1P)) = (9.79 \pm 0.20) \times 10^{-2}$ .

$\Gamma(\rho \bar{\rho})/\Gamma_{\text{total}}$	CL%	DOCUMENT ID	TECN	COMMENT	$\Gamma_{58}/\Gamma$
---	-----	-------------	------	---------	----------------------

**2.21 ± 0.08 OUR FIT**

$\Gamma(\rho \bar{\rho} \pi^0)/\Gamma_{\text{total}}$	CL%	DOCUMENT ID	TECN	COMMENT	$\Gamma_{59}/\Gamma$
---	-----	-------------	------	---------	----------------------

**0.70 ± 0.07 OUR AVERAGE** Error includes scale factor of 1.3.

0.73 ± 0.06 ± 0.01 <sup>1</sup>ONYISI 10 CLE3  $\psi(2S) \rightarrow \gamma \rho \bar{\rho} X$

0.56 ± 0.12 ± 0.01 <sup>2</sup>ATHAR 07 CLEO  $\psi(2S) \rightarrow \gamma h^+ h^- h^0$

<sup>1</sup>ONYISI 10 reports  $(7.76 \pm 0.37 \pm 0.51 \pm 0.39) \times 10^{-4}$  from a measurement of  $[\Gamma(\chi_{c0}(1P) \rightarrow \rho \bar{\rho} \pi^0)/\Gamma_{\text{total}}] \times [B(\psi(2S) \rightarrow \gamma\chi_{c0}(1P))]$  assuming  $B(\psi(2S) \rightarrow \gamma\chi_{c0}(1P)) = (9.22 \pm 0.11 \pm 0.46) \times 10^{-2}$ , which we rescale to our best value  $B(\psi(2S) \rightarrow \gamma\chi_{c0}(1P)) = (9.79 \pm 0.20) \times 10^{-2}$ . Our first error is their experiment's error and our second error is the systematic error from using our best value.

<sup>2</sup>ATHAR 07 reports  $(0.59 \pm 0.10 \pm 0.08) \times 10^{-3}$  from a measurement of  $[\Gamma(\chi_{c0}(1P) \rightarrow \rho \bar{\rho} \pi^0)/\Gamma_{\text{total}}] \times [B(\psi(2S) \rightarrow \gamma\chi_{c0}(1P))]$  assuming  $B(\psi(2S) \rightarrow \gamma\chi_{c0}(1P)) = (9.22 \pm 0.11 \pm 0.46) \times 10^{-2}$ , which we rescale to our best value  $B(\psi(2S) \rightarrow \gamma\chi_{c0}(1P)) = (9.79 \pm 0.20) \times 10^{-2}$ . Our first error is their experiment's error and our second error is the systematic error from using our best value.

$\Gamma(\rho \bar{\rho} \eta)/\Gamma_{\text{total}}$	CL%	DOCUMENT ID	TECN	COMMENT	$\Gamma_{60}/\Gamma$
--	-----	-------------	------	---------	----------------------

**0.35 ± 0.04 OUR AVERAGE**

0.35 ± 0.04 ± 0.01 <sup>1</sup>ONYISI 10 CLE3  $\psi(2S) \rightarrow \gamma \rho \bar{\rho} X$

0.37 ± 0.11 ± 0.01 <sup>2</sup>ATHAR 07 CLEO  $\psi(2S) \rightarrow \gamma h^+ h^- h^0$

<sup>1</sup>ONYISI 10 reports  $(3.73 \pm 0.38 \pm 0.28 \pm 0.19) \times 10^{-4}$  from a measurement of  $[\Gamma(\chi_{c0}(1P) \rightarrow \rho \bar{\rho} \eta)/\Gamma_{\text{total}}] \times [B(\psi(2S) \rightarrow \gamma\chi_{c0}(1P))]$  assuming  $B(\psi(2S) \rightarrow \gamma\chi_{c0}(1P)) = (9.22 \pm 0.11 \pm 0.46) \times 10^{-2}$ , which we rescale to our best value  $B(\psi(2S) \rightarrow \gamma\chi_{c0}(1P)) = (9.79 \pm 0.20) \times 10^{-2}$ . Our first error is their experiment's error and our second error is the systematic error from using our best value.

<sup>2</sup>ATHAR 07 reports  $(0.39 \pm 0.11 \pm 0.04) \times 10^{-3}$  from a measurement of  $[\Gamma(\chi_{c0}(1P) \rightarrow \rho \bar{\rho} \eta)/\Gamma_{\text{total}}] \times [B(\psi(2S) \rightarrow \gamma\chi_{c0}(1P))]$  assuming  $B(\psi(2S) \rightarrow \gamma\chi_{c0}(1P)) = (9.22 \pm 0.11 \pm 0.46) \times 10^{-2}$ , which we rescale to our best value  $B(\psi(2S) \rightarrow \gamma\chi_{c0}(1P)) = (9.79 \pm 0.20) \times 10^{-2}$ . Our first error is their experiment's error and our second error is the systematic error from using our best value.

$\Gamma(\rho \bar{\rho} \omega)/\Gamma_{\text{total}}$	CL%	DOCUMENT ID	TECN	COMMENT	$\Gamma_{61}/\Gamma$
--	-----	-------------	------	---------	----------------------

**0.52 ± 0.06 ± 0.01** <sup>1</sup>ONYISI 10 CLE3  $\psi(2S) \rightarrow \gamma \rho \bar{\rho} X$

<sup>1</sup>ONYISI 10 reports  $(5.57 \pm 0.48 \pm 0.42 \pm 0.14) \times 10^{-4}$  from a measurement of  $[\Gamma(\chi_{c0}(1P) \rightarrow \rho \bar{\rho} \omega)/\Gamma_{\text{total}}] \times [B(\psi(2S) \rightarrow \gamma\chi_{c0}(1P))]$  assuming  $B(\psi(2S) \rightarrow \gamma\chi_{c0}(1P)) = (9.22 \pm 0.11 \pm 0.46) \times 10^{-2}$ , which we rescale to our best value  $B(\psi(2S) \rightarrow \gamma\chi_{c0}(1P)) = (9.79 \pm 0.20) \times 10^{-2}$ . Our first error is their experiment's error and our second error is the systematic error from using our best value.

$\Gamma(\rho\bar{p}\phi)/\Gamma_{\text{total}}$		$\Gamma_{62}/\Gamma$	
VALUE (units $10^{-5}$ )	EVTS	DOCUMENT ID	TECN COMMENT

**6.0 ± 1.4 ± 0.1** 42 ± 8 <sup>1</sup> ABLIKIM 11F BES3  $\psi(2S) \rightarrow \gamma\rho\bar{p}K^+K^-$   
<sup>1</sup> ABLIKIM 11F reports  $(6.12 \pm 1.18 \pm 0.86) \times 10^{-5}$  from a measurement of  $[\Gamma(\chi_{c0}(1P) \rightarrow \rho\bar{p}\phi)/\Gamma_{\text{total}}] \times [B(\psi(2S) \rightarrow \gamma\chi_{c0}(1P))]$  assuming  $B(\psi(2S) \rightarrow \gamma\chi_{c0}(1P)) = (9.62 \pm 0.31) \times 10^{-2}$ , which we rescale to our best value  $B(\psi(2S) \rightarrow \gamma\chi_{c0}(1P)) = (9.79 \pm 0.20) \times 10^{-2}$ . Our first error is their experiment's error and our second error is the systematic error from using our best value.

$\Gamma(\rho\bar{p}\pi^+\pi^-)/\Gamma_{\text{total}}$		$\Gamma_{63}/\Gamma$	
VALUE (units $10^{-3}$ )	EVTS	DOCUMENT ID	TECN COMMENT

**2.1 ± 0.7 OUR EVALUATION** Error includes scale factor of 1.4. Treating systematic error as correlated.  
**2.1 ± 1.0 OUR AVERAGE** Error includes scale factor of 2.0.  
 1.57 ± 0.21 ± 0.53 <sup>1</sup> BAI 99B BES  $\psi(2S) \rightarrow \gamma\chi_{c0}$   
 4.20 ± 1.15 ± 0.18 <sup>1</sup> TANENBAUM 78 MRK1  $\psi(2S) \rightarrow \gamma\chi_{c0}$   
<sup>1</sup> Rescaled by us using  $B(\psi(2S) \rightarrow \gamma\chi_{c0}) = (9.4 \pm 0.4)\%$  and  $B(\psi(2S) \rightarrow J/\psi(1S)\pi^+\pi^-) = (32.6 \pm 0.5)\%$ .

$\Gamma(\rho\bar{p}\pi^0\pi^0)/\Gamma_{\text{total}}$		$\Gamma_{64}/\Gamma$	
VALUE (%)	EVTS	DOCUMENT ID	TECN COMMENT

**0.104 ± 0.028 ± 0.002** 39.5 <sup>1</sup> HE 08B CLEO  $e^+e^- \rightarrow \gamma h^+h^-h^0h^0$   
<sup>1</sup> HE 08B reports  $0.11 \pm 0.02 \pm 0.02 \pm 0.01\%$  from a measurement of  $[\Gamma(\chi_{c0}(1P) \rightarrow \rho\bar{p}\pi^0\pi^0)/\Gamma_{\text{total}}] \times [B(\psi(2S) \rightarrow \gamma\chi_{c0}(1P))]$  assuming  $B(\psi(2S) \rightarrow \gamma\chi_{c0}(1P)) = (9.22 \pm 0.11 \pm 0.46) \times 10^{-2}$ , which we rescale to our best value  $B(\psi(2S) \rightarrow \gamma\chi_{c0}(1P)) = (9.79 \pm 0.20) \times 10^{-2}$ . Our first error is their experiment's error and our second error is the systematic error from using our best value.

$\Gamma(\rho\bar{p}K^+K^- \text{ (non-resonant)})/\Gamma_{\text{total}}$		$\Gamma_{65}/\Gamma$	
VALUE (units $10^{-4}$ )	EVTS	DOCUMENT ID	TECN COMMENT

**1.22 ± 0.26 ± 0.02** 48 ± 8 <sup>1</sup> ABLIKIM 11F BES3  $\psi(2S) \rightarrow \gamma\rho\bar{p}K^+K^-$   
<sup>1</sup> ABLIKIM 11F reports  $(1.24 \pm 0.20 \pm 0.18) \times 10^{-4}$  from a measurement of  $[\Gamma(\chi_{c0}(1P) \rightarrow \rho\bar{p}K^+K^- \text{ (non-resonant)})/\Gamma_{\text{total}}] \times [B(\psi(2S) \rightarrow \gamma\chi_{c0}(1P))]$  assuming  $B(\psi(2S) \rightarrow \gamma\chi_{c0}(1P)) = (9.62 \pm 0.31) \times 10^{-2}$ , which we rescale to our best value  $B(\psi(2S) \rightarrow \gamma\chi_{c0}(1P)) = (9.79 \pm 0.20) \times 10^{-2}$ . Our first error is their experiment's error and our second error is the systematic error from using our best value.

$\Gamma(\rho\bar{p}K_S^0K_S^0)/\Gamma_{\text{total}}$		$\Gamma_{66}/\Gamma$	
VALUE (units $10^{-4}$ )	CL%	DOCUMENT ID	TECN COMMENT

**< 8.8** 90 <sup>1</sup> ABLIKIM 06D BES2  $\psi(2S) \rightarrow \chi_{c0}\gamma$   
<sup>1</sup> Using  $B(\psi(2S) \rightarrow \chi_{c0}\gamma) = (9.2 \pm 0.5)\%$

$\Gamma(\rho\bar{p}\pi^-)/\Gamma_{\text{total}}$		$\Gamma_{67}/\Gamma$	
VALUE (units $10^{-4}$ )	EVTS	DOCUMENT ID	TECN COMMENT

**12.7 ± 1.1 OUR AVERAGE**  
 12.9 ± 1.1 ± 0.3 5150 <sup>1</sup> ABLIKIM 12J BES3  $\psi(2S) \rightarrow \gamma\rho\bar{p}\pi^-$   
 11.2 ± 3.1 ± 0.2 <sup>2</sup> ABLIKIM 06I BES2  $\psi(2S) \rightarrow \gamma\rho\pi^-X$   
<sup>1</sup> ABLIKIM 12J reports  $[\Gamma(\chi_{c0}(1P) \rightarrow \rho\bar{p}\pi^-)/\Gamma_{\text{total}}] \times [B(\psi(2S) \rightarrow \gamma\chi_{c0}(1P))] = (1.26 \pm 0.02 \pm 0.11) \times 10^{-4}$  which we divide by our best value  $B(\psi(2S) \rightarrow \gamma\chi_{c0}(1P)) = (9.79 \pm 0.20) \times 10^{-2}$ . Our first error is their experiment's error and our second error is the systematic error from using our best value.  
<sup>2</sup> ABLIKIM 06I reports  $[\Gamma(\chi_{c0}(1P) \rightarrow \rho\bar{p}\pi^-)/\Gamma_{\text{total}}] \times [B(\psi(2S) \rightarrow \gamma\chi_{c0}(1P))] = (1.10 \pm 0.24 \pm 0.18) \times 10^{-4}$  which we divide by our best value  $B(\psi(2S) \rightarrow \gamma\chi_{c0}(1P)) = (9.79 \pm 0.20) \times 10^{-2}$ . Our first error is their experiment's error and our second error is the systematic error from using our best value.

$\Gamma(\bar{p}n\pi^+)/\Gamma_{\text{total}}$		$\Gamma_{68}/\Gamma$	
VALUE (units $10^{-4}$ )	EVTS	DOCUMENT ID	TECN COMMENT

**13.7 ± 1.2 ± 0.3** 5808 <sup>1</sup> ABLIKIM 12J BES3  $\psi(2S) \rightarrow \gamma\bar{p}n\pi^+$   
<sup>1</sup> ABLIKIM 12J reports  $[\Gamma(\chi_{c0}(1P) \rightarrow \bar{p}n\pi^+)/\Gamma_{\text{total}}] \times [B(\psi(2S) \rightarrow \gamma\chi_{c0}(1P))] = (1.34 \pm 0.03 \pm 0.11) \times 10^{-4}$  which we divide by our best value  $B(\psi(2S) \rightarrow \gamma\chi_{c0}(1P)) = (9.79 \pm 0.20) \times 10^{-2}$ . Our first error is their experiment's error and our second error is the systematic error from using our best value.

$\Gamma(\rho\bar{p}\pi^-\pi^0)/\Gamma_{\text{total}}$		$\Gamma_{69}/\Gamma$	
VALUE (units $10^{-4}$ )	EVTS	DOCUMENT ID	TECN COMMENT

**23.4 ± 2.0 ± 0.5** 2480 <sup>1</sup> ABLIKIM 12J BES3  $\psi(2S) \rightarrow \gamma\rho\bar{p}\pi^-\pi^0$   
<sup>1</sup> ABLIKIM 12J reports  $[\Gamma(\chi_{c0}(1P) \rightarrow \rho\bar{p}\pi^-\pi^0)/\Gamma_{\text{total}}] \times [B(\psi(2S) \rightarrow \gamma\chi_{c0}(1P))] = (2.29 \pm 0.08 \pm 0.18) \times 10^{-4}$  which we divide by our best value  $B(\psi(2S) \rightarrow \gamma\chi_{c0}(1P)) = (9.79 \pm 0.20) \times 10^{-2}$ . Our first error is their experiment's error and our second error is the systematic error from using our best value.

$\Gamma(\bar{p}n\pi^+\pi^0)/\Gamma_{\text{total}}$		$\Gamma_{70}/\Gamma$	
VALUE (units $10^{-4}$ )	EVTS	DOCUMENT ID	TECN COMMENT

**22.1 ± 1.8 ± 0.5** 2757 <sup>1</sup> ABLIKIM 12J BES3  $\psi(2S) \rightarrow \gamma\bar{p}n\pi^+\pi^0$   
<sup>1</sup> ABLIKIM 12J reports  $[\Gamma(\chi_{c0}(1P) \rightarrow \bar{p}n\pi^+\pi^0)/\Gamma_{\text{total}}] \times [B(\psi(2S) \rightarrow \gamma\chi_{c0}(1P))] = (2.16 \pm 0.07 \pm 0.16) \times 10^{-4}$  which we divide by our best value  $B(\psi(2S) \rightarrow \gamma\chi_{c0}(1P)) = (9.79 \pm 0.20) \times 10^{-2}$ . Our first error is their experiment's error and our second error is the systematic error from using our best value.

$\Gamma(\Lambda\bar{\Lambda})/\Gamma_{\text{total}}$		$\Gamma_{71}/\Gamma$	
VALUE (units $10^{-4}$ )	DOCUMENT ID	TECN COMMENT	

**3.27 ± 0.24 OUR FIT**

$\Gamma(\Lambda\bar{\Lambda}\pi^+\pi^-)/\Gamma_{\text{total}}$		$\Gamma_{72}/\Gamma$	
VALUE (units $10^{-5}$ )	CL%	EVTS	DOCUMENT ID TECN COMMENT

**118 ± 12 ± 2** 426 <sup>1</sup> ABLIKIM 12I BES3  $\psi(2S) \rightarrow \gamma\Lambda\bar{\Lambda}\pi^+\pi^-$   
 ••• We do not use the following data for averages, fits, limits, etc. •••  
 < 400 90 <sup>2</sup> ABLIKIM 06D BES2  $\psi(2S) \rightarrow \chi_{c0}\gamma$   
<sup>1</sup> ABLIKIM 12I reports  $(119.0 \pm 6.4 \pm 11.4) \times 10^{-5}$  from a measurement of  $[\Gamma(\chi_{c0}(1P) \rightarrow \Lambda\bar{\Lambda}\pi^+\pi^-)/\Gamma_{\text{total}}] \times [B(\psi(2S) \rightarrow \gamma\chi_{c0}(1P))]$  assuming  $B(\psi(2S) \rightarrow \gamma\chi_{c0}(1P)) = (9.68 \pm 0.31) \times 10^{-2}$ , which we rescale to our best value  $B(\psi(2S) \rightarrow \gamma\chi_{c0}(1P)) = (9.79 \pm 0.20) \times 10^{-2}$ . Our first error is their experiment's error and our second error is the systematic error from using our best value.  
<sup>2</sup> Using  $B(\psi(2S) \rightarrow \chi_{c0}\gamma) = (9.2 \pm 0.5)\%$

$\Gamma(\Lambda\bar{\Lambda}\pi^+\pi^- \text{ (non-resonant)})/\Gamma_{\text{total}}$		$\Gamma_{73}/\Gamma$	
VALUE (units $10^{-5}$ )	CL%	DOCUMENT ID	TECN COMMENT

**< 50** 90 <sup>1</sup> ABLIKIM 12I BES3  $\psi(2S) \rightarrow \gamma\Lambda\bar{\Lambda}\pi^+\pi^-$   
<sup>1</sup> ABLIKIM 12I reports  $< 54 \times 10^{-5}$  from a measurement of  $[\Gamma(\chi_{c0}(1P) \rightarrow \Lambda\bar{\Lambda}\pi^+\pi^- \text{ (non-resonant)})/\Gamma_{\text{total}}] \times [B(\psi(2S) \rightarrow \gamma\chi_{c0}(1P))]$  assuming  $B(\psi(2S) \rightarrow \gamma\chi_{c0}(1P)) = (9.68 \pm 0.31) \times 10^{-2}$ , which we rescale to our best value  $B(\psi(2S) \rightarrow \gamma\chi_{c0}(1P)) = (9.79 \pm 0.20) \times 10^{-2}$ .

$\Gamma(\Sigma(1385)^+\bar{\Lambda}\pi^- + \text{c.c.})/\Gamma_{\text{total}}$		$\Gamma_{74}/\Gamma$	
VALUE (units $10^{-5}$ )	CL%	DOCUMENT ID	TECN COMMENT

**< 50** 90 <sup>1</sup> ABLIKIM 12I BES3  $\psi(2S) \rightarrow \gamma\Sigma(1385)^+\bar{\Lambda}\pi^-$   
<sup>1</sup> ABLIKIM 12I reports  $< 55 \times 10^{-5}$  from a measurement of  $[\Gamma(\chi_{c0}(1P) \rightarrow \Sigma(1385)^+\bar{\Lambda}\pi^- + \text{c.c.})/\Gamma_{\text{total}}] \times [B(\psi(2S) \rightarrow \gamma\chi_{c0}(1P))]$  assuming  $B(\psi(2S) \rightarrow \gamma\chi_{c0}(1P)) = (9.68 \pm 0.31) \times 10^{-2}$ , which we rescale to our best value  $B(\psi(2S) \rightarrow \gamma\chi_{c0}(1P)) = 9.79 \times 10^{-2}$ .

$\Gamma(\Sigma(1385)^-\bar{\Lambda}\pi^+ + \text{c.c.})/\Gamma_{\text{total}}$		$\Gamma_{75}/\Gamma$	
VALUE (units $10^{-5}$ )	CL%	DOCUMENT ID	TECN COMMENT

**< 50** 90 <sup>1</sup> ABLIKIM 12I BES3  $\psi(2S) \rightarrow \gamma\Sigma(1385)^-\bar{\Lambda}\pi^+$   
<sup>1</sup> ABLIKIM 12I reports  $< 50 \times 10^{-5}$  from a measurement of  $[\Gamma(\chi_{c0}(1P) \rightarrow \Sigma(1385)^-\bar{\Lambda}\pi^+ + \text{c.c.})/\Gamma_{\text{total}}] \times [B(\psi(2S) \rightarrow \gamma\chi_{c0}(1P))]$  assuming  $B(\psi(2S) \rightarrow \gamma\chi_{c0}(1P)) = (9.68 \pm 0.31) \times 10^{-2}$ , which we rescale to our best value  $B(\psi(2S) \rightarrow \gamma\chi_{c0}(1P)) = 9.79 \times 10^{-2}$ .

$\Gamma(K^+\bar{p}\Lambda + \text{c.c.})/\Gamma_{\text{total}}$		$\Gamma_{76}/\Gamma$	
VALUE (units $10^{-3}$ )	EVTS	DOCUMENT ID	TECN COMMENT

**1.25 ± 0.12 OUR AVERAGE** Error includes scale factor of 1.3.  
 1.30 ± 0.09 ± 0.03 9k <sup>1,2</sup> ABLIKIM 13D BES3  $\psi(2S) \rightarrow \gamma\Lambda\bar{p}K^+$   
 1.01 ± 0.19 ± 0.02 <sup>3</sup> ATHAR 07 CLEO  $\psi(2S) \rightarrow \gamma h^+h^-h^0$   
<sup>1</sup> ABLIKIM 13D reports  $(1.32 \pm 0.03 \pm 0.10) \times 10^{-3}$  from a measurement of  $[\Gamma(\chi_{c0}(1P) \rightarrow K^+\bar{p}\Lambda + \text{c.c.})/\Gamma_{\text{total}}] \times [B(\psi(2S) \rightarrow \gamma\chi_{c0}(1P))]$  assuming  $B(\psi(2S) \rightarrow \gamma\chi_{c0}(1P)) = (9.68 \pm 0.31) \times 10^{-2}$ , which we rescale to our best value  $B(\psi(2S) \rightarrow \gamma\chi_{c0}(1P)) = (9.79 \pm 0.20) \times 10^{-2}$ . Our first error is their experiment's error and our second error is the systematic error from using our best value.  
<sup>2</sup> Using  $B(\Lambda \rightarrow p\pi^-) = 63.9\%$ .  
<sup>3</sup> ATHAR 07 reports  $(1.07 \pm 0.17 \pm 0.12) \times 10^{-3}$  from a measurement of  $[\Gamma(\chi_{c0}(1P) \rightarrow K^+\bar{p}\Lambda + \text{c.c.})/\Gamma_{\text{total}}] \times [B(\psi(2S) \rightarrow \gamma\chi_{c0}(1P))]$  assuming  $B(\psi(2S) \rightarrow \gamma\chi_{c0}(1P)) = (9.22 \pm 0.11 \pm 0.46) \times 10^{-2}$ , which we rescale to our best value  $B(\psi(2S) \rightarrow \gamma\chi_{c0}(1P)) = (9.79 \pm 0.20) \times 10^{-2}$ . Our first error is their experiment's error and our second error is the systematic error from using our best value.

$\Gamma(K^*(892)^+\bar{p}\Lambda + \text{c.c.})/\Gamma_{\text{total}}$		$\Gamma_{77}/\Gamma$	
VALUE (units $10^{-4}$ )	EVTS	DOCUMENT ID	TECN COMMENT

**4.8 ± 0.9 ± 0.1** 254 <sup>1</sup> ABLIKIM 19AU BES3  $\psi(2S) \rightarrow \gamma K^{*+}\bar{p}\Lambda$   
<sup>1</sup> ABLIKIM 19AU reports  $[\Gamma(\chi_{c0}(1P) \rightarrow K^*(892)^+\bar{p}\Lambda + \text{c.c.})/\Gamma_{\text{total}}] \times [B(\psi(2S) \rightarrow \gamma\chi_{c0}(1P))] = (4.7 \pm 0.7 \pm 0.5) \times 10^{-5}$  which we divide by our best value  $B(\psi(2S) \rightarrow \gamma\chi_{c0}(1P)) = (9.79 \pm 0.20) \times 10^{-2}$ . Our first error is their experiment's error and our second error is the systematic error from using our best value.

$\Gamma(K^+\bar{p}\Lambda(1520) + \text{c.c.})/\Gamma_{\text{total}}$		$\Gamma_{78}/\Gamma$	
VALUE (units $10^{-4}$ )	EVTS	DOCUMENT ID	TECN COMMENT

**2.9 ± 0.7 ± 0.1** 62 ± 12 <sup>1</sup> ABLIKIM 11F BES3  $\psi(2S) \rightarrow \gamma\rho\bar{p}K^+K^-$   
<sup>1</sup> ABLIKIM 11F reports  $(3.00 \pm 0.58 \pm 0.50) \times 10^{-4}$  from a measurement of  $[\Gamma(\chi_{c0}(1P) \rightarrow K^+\bar{p}\Lambda(1520) + \text{c.c.})/\Gamma_{\text{total}}] \times [B(\psi(2S) \rightarrow \gamma\chi_{c0}(1P))]$  assuming  $B(\psi(2S) \rightarrow \gamma\chi_{c0}(1P)) = (9.62 \pm 0.31) \times 10^{-2}$ , which we rescale to our best value  $B(\psi(2S) \rightarrow \gamma\chi_{c0}(1P)) = (9.79 \pm 0.20) \times 10^{-2}$ . Our first error is their experiment's error and our second error is the systematic error from using our best value.



## Meson Particle Listings

 $\chi_{c0}(1P)$  $\Gamma(\Lambda(1520)\bar{\Lambda}(1520))/\Gamma_{\text{total}}$   $\Gamma_{79}/\Gamma$ 

VALUE (units $10^{-4}$ )	EVTs	DOCUMENT ID	TECN	COMMENT
<b>3.1 ± 1.2 ± 0.1</b>	28 ± 10	<sup>1</sup> ABLIKIM	11F BES3	$\psi(2S) \rightarrow \gamma p \bar{p} K^+ K^-$
<sup>1</sup> ABLIKIM 11F reports $(3.18 \pm 1.11 \pm 0.53) \times 10^{-4}$ from a measurement of $[\Gamma(\chi_{c0}(1P) \rightarrow \Lambda(1520)\bar{\Lambda}(1520))/\Gamma_{\text{total}}] \times [B(\psi(2S) \rightarrow \gamma \chi_{c0}(1P))]$ assuming $B(\psi(2S) \rightarrow \gamma \chi_{c0}(1P)) = (9.62 \pm 0.31) \times 10^{-2}$ , which we rescale to our best value $B(\psi(2S) \rightarrow \gamma \chi_{c0}(1P)) = (9.79 \pm 0.20) \times 10^{-2}$ . Our first error is their experiment's error and our second error is the systematic error from using our best value.				

 $\Gamma(\Sigma^0 \bar{\Sigma}^0)/\Gamma_{\text{total}}$   $\Gamma_{80}/\Gamma$ 

VALUE (units $10^{-4}$ )	EVTs	DOCUMENT ID	TECN	COMMENT
<b>4.68 ± 0.32 OUR AVERAGE</b>				
4.82 ± 0.34 ± 0.10	1046	<sup>1</sup> ABLIKIM	18V BES3	$\psi(2S) \rightarrow \gamma \Sigma^0 \bar{\Sigma}^0$
4.2 ± 0.7 ± 0.1	78 ± 10	<sup>2</sup> NAIK	08 CLEO	$\psi(2S) \rightarrow \gamma \Sigma^0 \bar{\Sigma}^0$
• • • We do not use the following data for averages, fits, limits, etc. • • •				
4.7 ± 0.5 ± 0.1	243	<sup>3,4</sup> ABLIKIM	13H BES3	$\psi(2S) \rightarrow \gamma \Sigma^0 \bar{\Sigma}^0$
<sup>1</sup> ABLIKIM 18V reports $[\Gamma(\chi_{c0}(1P) \rightarrow \Sigma^0 \bar{\Sigma}^0)/\Gamma_{\text{total}}] \times [B(\psi(2S) \rightarrow \gamma \chi_{c0}(1P))] = (4.72 \pm 0.18 \pm 0.28) \times 10^{-5}$ which we divide by our best value $B(\psi(2S) \rightarrow \gamma \chi_{c0}(1P)) = (9.79 \pm 0.20) \times 10^{-2}$ . Our first error is their experiment's error and our second error is the systematic error from using our best value.				
<sup>2</sup> NAIK 08 reports $(4.41 \pm 0.56 \pm 0.47) \times 10^{-4}$ from a measurement of $[\Gamma(\chi_{c0}(1P) \rightarrow \Sigma^0 \bar{\Sigma}^0)/\Gamma_{\text{total}}] \times [B(\psi(2S) \rightarrow \gamma \chi_{c0}(1P))]$ assuming $B(\psi(2S) \rightarrow \gamma \chi_{c0}(1P)) = (9.22 \pm 0.11 \pm 0.46) \times 10^{-2}$ , which we rescale to our best value $B(\psi(2S) \rightarrow \gamma \chi_{c0}(1P)) = (9.79 \pm 0.20) \times 10^{-2}$ . Our first error is their experiment's error and our second error is the systematic error from using our best value.				
<sup>3</sup> ABLIKIM 13H reports $(4.78 \pm 0.34 \pm 0.39) \times 10^{-4}$ from a measurement of $[\Gamma(\chi_{c0}(1P) \rightarrow \Sigma^0 \bar{\Sigma}^0)/\Gamma_{\text{total}}] \times [B(\psi(2S) \rightarrow \gamma \chi_{c0}(1P))]$ assuming $B(\psi(2S) \rightarrow \gamma \chi_{c0}(1P)) = (9.62 \pm 0.31) \times 10^{-2}$ , which we rescale to our best value $B(\psi(2S) \rightarrow \gamma \chi_{c0}(1P)) = (9.79 \pm 0.20) \times 10^{-2}$ . Our first error is their experiment's error and our second error is the systematic error from using our best value.				
<sup>4</sup> Superseded by ABLIKIM 18V				

 $\Gamma(\Sigma^+ \bar{\Sigma}^-)/\Gamma_{\text{total}}$   $\Gamma_{82}/\Gamma$ 

VALUE (units $10^{-4}$ )	EVTs	DOCUMENT ID	TECN	COMMENT
<b>4.6 ± 0.8 OUR AVERAGE</b>	Error includes scale factor of 2.6.			
5.10 ± 0.35 ± 0.10	747	<sup>1</sup> ABLIKIM	18V BES3	$\psi(2S) \rightarrow \gamma \Sigma^+ \bar{\Sigma}^-$
3.1 ± 0.7 ± 0.1	39 ± 7	<sup>2</sup> NAIK	08 CLEO	$\psi(2S) \rightarrow \gamma \Sigma^+ \bar{\Sigma}^-$
• • • We do not use the following data for averages, fits, limits, etc. • • •				
4.5 ± 0.5 ± 0.1	148	<sup>3,4</sup> ABLIKIM	13H BES3	$\psi(2S) \rightarrow \gamma \Sigma^+ \bar{\Sigma}^-$
<sup>1</sup> ABLIKIM 18V reports $[\Gamma(\chi_{c0}(1P) \rightarrow \Sigma^+ \bar{\Sigma}^-)/\Gamma_{\text{total}}] \times [B(\psi(2S) \rightarrow \gamma \chi_{c0}(1P))] = (4.99 \pm 0.24 \pm 0.24) \times 10^{-5}$ which we divide by our best value $B(\psi(2S) \rightarrow \gamma \chi_{c0}(1P)) = (9.79 \pm 0.20) \times 10^{-2}$ . Our first error is their experiment's error and our second error is the systematic error from using our best value.				
<sup>2</sup> NAIK 08 reports $(3.25 \pm 0.57 \pm 0.43) \times 10^{-4}$ from a measurement of $[\Gamma(\chi_{c0}(1P) \rightarrow \Sigma^+ \bar{\Sigma}^-)/\Gamma_{\text{total}}] \times [B(\psi(2S) \rightarrow \gamma \chi_{c0}(1P))]$ assuming $B(\psi(2S) \rightarrow \gamma \chi_{c0}(1P)) = (9.22 \pm 0.11 \pm 0.46) \times 10^{-2}$ , which we rescale to our best value $B(\psi(2S) \rightarrow \gamma \chi_{c0}(1P)) = (9.79 \pm 0.20) \times 10^{-2}$ . Our first error is their experiment's error and our second error is the systematic error from using our best value.				
<sup>3</sup> ABLIKIM 13H reports $(4.54 \pm 0.42 \pm 0.30) \times 10^{-4}$ from a measurement of $[\Gamma(\chi_{c0}(1P) \rightarrow \Sigma^+ \bar{\Sigma}^-)/\Gamma_{\text{total}}] \times [B(\psi(2S) \rightarrow \gamma \chi_{c0}(1P))]$ assuming $B(\psi(2S) \rightarrow \gamma \chi_{c0}(1P)) = (9.62 \pm 0.31) \times 10^{-2}$ , which we rescale to our best value $B(\psi(2S) \rightarrow \gamma \chi_{c0}(1P)) = (9.79 \pm 0.20) \times 10^{-2}$ . Our first error is their experiment's error and our second error is the systematic error from using our best value.				
<sup>4</sup> Superseded by ABLIKIM 18V				

 $\Gamma(\Sigma(1385)^+ \bar{\Sigma}(1385)^-)/\Gamma_{\text{total}}$   $\Gamma_{83}/\Gamma$ 

VALUE (units $10^{-5}$ )	EVTs	DOCUMENT ID	TECN	COMMENT
<b>16.2 ± 5.8 ± 0.3</b>	27	<sup>1</sup> ABLIKIM	12I BES3	$\psi(2S) \rightarrow \gamma \Lambda \bar{\Lambda} \pi^+ \pi^-$
<sup>1</sup> ABLIKIM 12I reports $(16.4 \pm 5.7 \pm 1.6) \times 10^{-5}$ from a measurement of $[\Gamma(\chi_{c0}(1P) \rightarrow \Sigma(1385)^+ \bar{\Sigma}(1385)^-)/\Gamma_{\text{total}}] \times [B(\psi(2S) \rightarrow \gamma \chi_{c0}(1P))]$ assuming $B(\psi(2S) \rightarrow \gamma \chi_{c0}(1P)) = (9.68 \pm 0.31) \times 10^{-2}$ , which we rescale to our best value $B(\psi(2S) \rightarrow \gamma \chi_{c0}(1P)) = (9.79 \pm 0.20) \times 10^{-2}$ . Our first error is their experiment's error and our second error is the systematic error from using our best value.				

 $\Gamma(\Sigma(1385)^- \bar{\Sigma}(1385)^+)/\Gamma_{\text{total}}$   $\Gamma_{84}/\Gamma$ 

VALUE (units $10^{-5}$ )	EVTs	DOCUMENT ID	TECN	COMMENT
<b>23.2 ± 6.5 ± 0.5</b>	33	<sup>1</sup> ABLIKIM	12I BES3	$\psi(2S) \rightarrow \gamma \Lambda \bar{\Lambda} \pi^+ \pi^-$
<sup>1</sup> ABLIKIM 12I reports $(23.5 \pm 6.2 \pm 2.3) \times 10^{-5}$ from a measurement of $[\Gamma(\chi_{c0}(1P) \rightarrow \Sigma(1385)^- \bar{\Sigma}(1385)^+)/\Gamma_{\text{total}}] \times [B(\psi(2S) \rightarrow \gamma \chi_{c0}(1P))]$ assuming $B(\psi(2S) \rightarrow \gamma \chi_{c0}(1P)) = (9.68 \pm 0.31) \times 10^{-2}$ , which we rescale to our best value $B(\psi(2S) \rightarrow \gamma \chi_{c0}(1P)) = (9.79 \pm 0.20) \times 10^{-2}$ . Our first error is their experiment's error and our second error is the systematic error from using our best value.				

 $\Gamma(K^- \Lambda \bar{\Xi}^+ + \text{c.c.})/\Gamma_{\text{total}}$   $\Gamma_{85}/\Gamma$ 

VALUE (units $10^{-4}$ )	EVTs	DOCUMENT ID	TECN	COMMENT
<b>1.94 ± 0.35 ± 0.04</b>	57	<sup>1</sup> ABLIKIM	15I BES3	$\psi(2S) \rightarrow \gamma K^- \Lambda \bar{\Xi}^+ + \text{c.c.}$
<sup>1</sup> ABLIKIM 15I reports $[\Gamma(\chi_{c0}(1P) \rightarrow K^- \Lambda \bar{\Xi}^+ + \text{c.c.})/\Gamma_{\text{total}}] \times [B(\psi(2S) \rightarrow \gamma \chi_{c0}(1P))] = (1.90 \pm 0.30 \pm 0.16) \times 10^{-5}$ which we divide by our best value $B(\psi(2S) \rightarrow \gamma \chi_{c0}(1P)) = (9.79 \pm 0.20) \times 10^{-2}$ . Our first error is their experiment's error and our second error is the systematic error from using our best value.				

 $\Gamma(\Xi^0 \bar{\Xi}^0)/\Gamma_{\text{total}}$   $\Gamma_{86}/\Gamma$ 

VALUE (units $10^{-4}$ )	EVTs	DOCUMENT ID	TECN	COMMENT
<b>3.1 ± 0.8 ± 0.1</b>	23.3 ± 4.9	<sup>1</sup> NAIK	08 CLEO	$\psi(2S) \rightarrow \gamma \Xi^0 \bar{\Xi}^0$
<sup>1</sup> NAIK 08 reports $(3.34 \pm 0.70 \pm 0.48) \times 10^{-4}$ from a measurement of $[\Gamma(\chi_{c0}(1P) \rightarrow \Xi^0 \bar{\Xi}^0)/\Gamma_{\text{total}}] \times [B(\psi(2S) \rightarrow \gamma \chi_{c0}(1P))]$ assuming $B(\psi(2S) \rightarrow \gamma \chi_{c0}(1P)) = (9.22 \pm 0.11 \pm 0.46) \times 10^{-2}$ , which we rescale to our best value $B(\psi(2S) \rightarrow \gamma \chi_{c0}(1P)) = (9.79 \pm 0.20) \times 10^{-2}$ . Our first error is their experiment's error and our second error is the systematic error from using our best value.				

 $\Gamma(\Xi^- \bar{\Xi}^+)/\Gamma_{\text{total}}$   $\Gamma_{87}/\Gamma$ 

VALUE (units $10^{-4}$ )	CL%	EVTs	DOCUMENT ID	TECN	COMMENT
<b>4.8 ± 0.7 ± 0.1</b>		95 ± 11	<sup>1</sup> NAIK	08 CLEO	$\psi(2S) \rightarrow \gamma \Xi^- \bar{\Xi}^+$
• • • We do not use the following data for averages, fits, limits, etc. • • •					
< 10.3		90	<sup>2</sup> ABLIKIM	06D BES2	$\psi(2S) \rightarrow \chi_{c0} \gamma$
<sup>1</sup> NAIK 08 reports $(5.14 \pm 0.60 \pm 0.47) \times 10^{-4}$ from a measurement of $[\Gamma(\chi_{c0}(1P) \rightarrow \Xi^- \bar{\Xi}^+)/\Gamma_{\text{total}}] \times [B(\psi(2S) \rightarrow \gamma \chi_{c0}(1P))]$ assuming $B(\psi(2S) \rightarrow \gamma \chi_{c0}(1P)) = (9.22 \pm 0.11 \pm 0.46) \times 10^{-2}$ , which we rescale to our best value $B(\psi(2S) \rightarrow \gamma \chi_{c0}(1P)) = (9.79 \pm 0.20) \times 10^{-2}$ . Our first error is their experiment's error and our second error is the systematic error from using our best value.					
<sup>2</sup> Using $B(\psi(2S) \rightarrow \chi_{c0} \gamma) = (9.2 \pm 0.5)\%$					

 $\Gamma(\eta_c \pi^+ \pi^-)/\Gamma_{\text{total}}$   $\Gamma_{88}/\Gamma$ 

VALUE	CL%	DOCUMENT ID	TECN	COMMENT
<b>&lt; 7 × 10<sup>-4</sup></b>	90	<sup>1,2</sup> ABLIKIM	13B BES3	$e^+ e^- \rightarrow \psi(2S) \rightarrow \gamma \chi_{c0}$
• • • We do not use the following data for averages, fits, limits, etc. • • •				
< 41 × 10 <sup>-4</sup>	90	<sup>1,3</sup> ABLIKIM	13B BES3	$e^+ e^- \rightarrow \psi(2S) \rightarrow \gamma \chi_{c0}$
<sup>1</sup> Using $1.06 \times 10^8 \psi(2S)$ mesons and $B(\psi(2S) \rightarrow \chi_{c0} \gamma) = (9.68 \pm 0.31)\%$ .				
<sup>2</sup> From the $\eta_c \rightarrow K_S^0 K^\pm \pi^\mp$ decays.				
<sup>3</sup> From the $\eta_c \rightarrow K^+ K^- \pi^0$ decays.				

 $\Gamma(\rho \bar{\rho})/\Gamma_{\text{total}} \times \Gamma(\pi \pi)/\Gamma_{\text{total}}$   $\Gamma_{58}/\Gamma \times \Gamma_{32}/\Gamma$ 

VALUE (units $10^{-7}$ )	DOCUMENT ID	TECN	COMMENT
<b>18.8 ± 1.0 OUR FIT</b>			
<b>15.3 ± 2.4 ± 0.8</b>	<sup>1</sup> ANDREOTTI	03 E835	$\bar{p} p \rightarrow \chi_{c0} \rightarrow \pi^0 \pi^0$
<sup>1</sup> We have multiplied $B(\rho \bar{\rho}) \cdot B(\pi^0 \pi^0)$ measurement by 3 to obtain $B(\rho \bar{\rho}) \cdot B(\pi \pi)$ .			

 $\Gamma(\rho \bar{\rho})/\Gamma_{\text{total}} \times \Gamma(\pi^0 \eta)/\Gamma_{\text{total}}$   $\Gamma_{58}/\Gamma \times \Gamma_{33}/\Gamma$ 

VALUE (units $10^{-7}$ )	DOCUMENT ID	TECN	COMMENT
<b>&lt; 0.4</b>	ANDREOTTI	05c E835	$\bar{p} p \rightarrow \pi^0 \eta$

 $\Gamma(\rho \bar{\rho})/\Gamma_{\text{total}} \times \Gamma(\pi^0 \eta')/\Gamma_{\text{total}}$   $\Gamma_{58}/\Gamma \times \Gamma_{34}/\Gamma$ 

VALUE (units $10^{-7}$ )	DOCUMENT ID	TECN	COMMENT
<b>&lt; 2.5</b>	ANDREOTTI	05c E835	$\bar{p} p \rightarrow \pi^0 \eta'$

 $\Gamma(\rho \bar{\rho})/\Gamma_{\text{total}} \times \Gamma(\eta \eta)/\Gamma_{\text{total}}$   $\Gamma_{58}/\Gamma \times \Gamma_{36}/\Gamma$ 

VALUE (units $10^{-7}$ )	DOCUMENT ID	TECN	COMMENT
<b>6.7 ± 0.5 OUR FIT</b>			
<b>4.0 ± 1.2 ± 0.5</b>	ANDREOTTI	05c E835	$\bar{p} p \rightarrow \eta \eta$

 $\Gamma(\rho \bar{\rho})/\Gamma_{\text{total}} \times \Gamma(\eta \eta')/\Gamma_{\text{total}}$   $\Gamma_{58}/\Gamma \times \Gamma_{37}/\Gamma$ 

VALUE (units $10^{-6}$ )	DOCUMENT ID	TECN	COMMENT
<b>2.1<sup>+2.3</sup><sub>-1.5</sub></b>	ANDREOTTI	05c E835	$\bar{p} p \rightarrow \pi^0 \eta$

## RADIATIVE DECAYS

 $\Gamma(\gamma J/\psi(1S))/\Gamma_{\text{total}}$   $\Gamma_{89}/\Gamma$ 

VALUE (units $10^{-2}$ )	EVTs	DOCUMENT ID	TECN	COMMENT
<b>1.40 ± 0.05 OUR FIT</b>				
0.25 ± 0.16 ± 2.15	12k	<sup>1</sup> ABLIKIM	17U BES3	$e^+ e^- \rightarrow \gamma X$
2.0 ± 0.2 ± 0.2		<sup>2</sup> ADAM	05A CLEO	$e^+ e^- \rightarrow \psi(2S) \rightarrow \gamma \chi_{c0}$
<sup>1</sup> Not independent from $B(\psi(2S) \rightarrow \gamma \chi_{c0}(1P))$ and the product $B(\psi(2S) \rightarrow \gamma \chi_{c0}(1P)) \times B(\chi_{c0}(1P) \rightarrow \gamma J/\psi(1S))$ also measured in ABLIKIM 17U.				
<sup>2</sup> Uses $B(\psi(2S) \rightarrow \gamma \chi_{c0}) \rightarrow \gamma J/\psi$ from ADAM 05A and $B(\psi(2S) \rightarrow \gamma \chi_{c0})$ from ATHAR 04.				

 $\Gamma(\gamma \rho^0)/\Gamma_{\text{total}}$   $\Gamma_{90}/\Gamma$ 

VALUE (units $10^{-6}$ )	CL%	EVTs	DOCUMENT ID	TECN	COMMENT	
<b>&lt; 9</b>	90	1.2 ± 4.5	<sup>1</sup> BENNETT	08A CLEO	$\psi(2S) \rightarrow \gamma \gamma \rho^0$	
• • • We do not use the following data for averages, fits, limits, etc. • • •						
< 10		90	6 ± 12	<sup>2</sup> ABLIKIM	11E BES3	$\psi(2S) \rightarrow \gamma \gamma \rho^0$
<sup>1</sup> BENNETT 08A reports $< 9.6 \times 10^{-6}$ from a measurement of $[\Gamma(\chi_{c0}(1P) \rightarrow \gamma \rho^0)/\Gamma_{\text{total}}] \times [B(\psi(2S) \rightarrow \gamma \chi_{c0}(1P))]$ assuming $B(\psi(2S) \rightarrow \gamma \chi_{c0}(1P)) = (9.2 \pm 0.4) \times 10^{-2}$ , which we rescale to our best value $B(\psi(2S) \rightarrow \gamma \chi_{c0}(1P)) = 9.79 \times 10^{-2}$ .						
<sup>2</sup> ABLIKIM 11E reports $< 10.5 \times 10^{-6}$ from a measurement of $[\Gamma(\chi_{c0}(1P) \rightarrow \gamma \rho^0)/\Gamma_{\text{total}}] \times [B(\psi(2S) \rightarrow \gamma \chi_{c0}(1P))]$ assuming $B(\psi(2S) \rightarrow \gamma \chi_{c0}(1P)) = (9.62 \pm 0.31) \times 10^{-2}$ , which we rescale to our best value $B(\psi(2S) \rightarrow \gamma \chi_{c0}(1P)) = 9.79 \times 10^{-2}$ .						

$\Gamma(\gamma\omega)/\Gamma_{total}$   $\Gamma_{91}/\Gamma$

VALUE (units 10 <sup>-6</sup> )	CL%	EVTS	DOCUMENT ID	TECN	COMMENT
< 8	90	0.0 ± 2.8	<sup>1</sup> BENNETT 08A	CLEO	$\psi(2S) \rightarrow \gamma\gamma\omega$
••• We do not use the following data for averages, fits, limits, etc. •••					
<13	90	5 ± 11	<sup>2</sup> ABLIKIM 11E	BES3	$\psi(2S) \rightarrow \gamma\gamma\omega$
<sup>1</sup> BENNETT 08A reports < 8.8 × 10 <sup>-6</sup> from a measurement of $[\Gamma(\chi_{c0}(1P) \rightarrow \gamma\omega)/\Gamma_{total}] \times [B(\psi(2S) \rightarrow \gamma\chi_{c0}(1P))]$ assuming $B(\psi(2S) \rightarrow \gamma\chi_{c0}(1P)) = (9.2 \pm 0.4) \times 10^{-2}$ , which we rescale to our best value $B(\psi(2S) \rightarrow \gamma\chi_{c0}(1P)) = 9.79 \times 10^{-2}$ . <sup>2</sup> ABLIKIM 11E reports < 12.9 × 10 <sup>-6</sup> from a measurement of $[\Gamma(\chi_{c0}(1P) \rightarrow \gamma\omega)/\Gamma_{total}] \times [B(\psi(2S) \rightarrow \gamma\chi_{c0}(1P))]$ assuming $B(\psi(2S) \rightarrow \gamma\chi_{c0}(1P)) = (9.62 \pm 0.31) \times 10^{-2}$ , which we rescale to our best value $B(\psi(2S) \rightarrow \gamma\chi_{c0}(1P)) = 9.79 \times 10^{-2}$ .					

$\Gamma(\gamma\phi)/\Gamma_{total}$   $\Gamma_{92}/\Gamma$

VALUE (units 10 <sup>-6</sup> )	CL%	EVTS	DOCUMENT ID	TECN	COMMENT
< 6	90	0.1 ± 1.6	<sup>1</sup> BENNETT 08A	CLEO	$\psi(2S) \rightarrow \gamma\gamma\phi$
••• We do not use the following data for averages, fits, limits, etc. •••					
<16	90	15 ± 7	<sup>2</sup> ABLIKIM 11E	BES3	$\psi(2S) \rightarrow \gamma\gamma\phi$
<sup>1</sup> BENNETT 08A reports < 6.4 × 10 <sup>-6</sup> from a measurement of $[\Gamma(\chi_{c0}(1P) \rightarrow \gamma\phi)/\Gamma_{total}] \times [B(\psi(2S) \rightarrow \gamma\chi_{c0}(1P))]$ assuming $B(\psi(2S) \rightarrow \gamma\chi_{c0}(1P)) = (9.2 \pm 0.4) \times 10^{-2}$ , which we rescale to our best value $B(\psi(2S) \rightarrow \gamma\chi_{c0}(1P)) = 9.79 \times 10^{-2}$ . <sup>2</sup> ABLIKIM 11E reports < 16.2 × 10 <sup>-6</sup> from a measurement of $[\Gamma(\chi_{c0}(1P) \rightarrow \gamma\phi)/\Gamma_{total}] \times [B(\psi(2S) \rightarrow \gamma\chi_{c0}(1P))]$ assuming $B(\psi(2S) \rightarrow \gamma\chi_{c0}(1P)) = (9.62 \pm 0.31) \times 10^{-2}$ , which we rescale to our best value $B(\psi(2S) \rightarrow \gamma\chi_{c0}(1P)) = 9.79 \times 10^{-2}$ .					

$\Gamma(\gamma\gamma)/\Gamma_{total}$   $\Gamma_{93}/\Gamma$

VALUE (units 10 <sup>-4</sup> )	CL%	DOCUMENT ID	TECN	COMMENT
<b>2.04 ± 0.09 OUR FIT</b>				
••• We do not use the following data for averages, fits, limits, etc. •••				
<7	90	<sup>1</sup> WICHT 08	BELL	$B^{\pm} \rightarrow K^{\pm}\gamma\gamma$
<sup>1</sup> WICHT 08 reports $[\Gamma(\chi_{c0}(1P) \rightarrow \gamma\gamma)/\Gamma_{total}] \times [B(B^{\pm} \rightarrow \chi_{c0} K^{\pm})] < 0.11 \times 10^{-6}$ which we divide by our best value $B(B^{\pm} \rightarrow \chi_{c0} K^{\pm}) = 1.50 \times 10^{-4}$ .				

$\Gamma(e^+e^-J/\psi(1S))/\Gamma_{total}$   $\Gamma_{94}/\Gamma$

VALUE (units 10 <sup>-4</sup> )	EVTS	DOCUMENT ID	TECN	COMMENT
1.54 ± 0.33 ± 0.03	56	<sup>1,2</sup> ABLIKIM 17I	BES3	$\psi(2S) \rightarrow \gamma e^+e^-J/\psi$
<sup>1</sup> ABLIKIM 17I reports $(1.51 \pm 0.30 \pm 0.13) \times 10^{-4}$ from a measurement of $[\Gamma(\chi_{c0}(1P) \rightarrow e^+e^-J/\psi(1S))/\Gamma_{total}] \times [B(\psi(2S) \rightarrow \gamma\chi_{c0}(1P))]$ assuming $B(\psi(2S) \rightarrow \gamma\chi_{c0}(1P)) = (9.99 \pm 0.27) \times 10^{-2}$ , which we rescale to our best value $B(\psi(2S) \rightarrow \gamma\chi_{c0}(1P)) = (9.79 \pm 0.20) \times 10^{-2}$ . Our first error is their experiment's error and our second error is the systematic error from using our best value. <sup>2</sup> Not independent from other measurements reported by ABLIKIM 17I				

$\Gamma(e^+e^-J/\psi(1S))/\Gamma(\gamma J/\psi(1S))$   $\Gamma_{94}/\Gamma_{89}$

VALUE (units 10 <sup>-3</sup> )	EVTS	DOCUMENT ID	TECN	COMMENT
<b>9.5 ± 1.9 ± 0.7</b>	56	<sup>1</sup> ABLIKIM 17I	BES3	$\psi(2S) \rightarrow e^+e^-J/\psi$
<sup>1</sup> Uses $B(\psi(2S) \rightarrow \gamma\chi_{c0}(1P)) \times B(\chi_{c0}(1P) \rightarrow \gamma J/\psi(1S)) = (15.8 \pm 0.3 \pm 0.6) \times 10^{-4}$ from ABLIKIM 17N and accounts for common systematic errors.				

$\Gamma(\mu^+\mu^-J/\psi(1S))/\Gamma(e^+e^-J/\psi(1S))$   $\Gamma_{95}/\Gamma_{94}$

VALUE	CL%	EVTS	DOCUMENT ID	TECN	COMMENT
<0.14	90	<9.5	ABLIKIM 19Z	BES3	$\psi(2S) \rightarrow \gamma\chi_c \rightarrow \gamma(\mu^+\mu^-J/\psi)$

$\Gamma(\gamma\gamma)/\Gamma(\gamma J/\psi(1S))$   $\Gamma_{93}/\Gamma_{89}$

VALUE (units 10 <sup>-2</sup> )	DOCUMENT ID	TECN	COMMENT
<b>1.45 ± 0.08 OUR FIT</b>			
<b>2.0 ± 0.4 OUR AVERAGE</b>			
2.2 ± 0.4 ± 0.1 ± 0.2	<sup>1</sup> ANDREOTTI 04	E835	$p\bar{p} \rightarrow \chi_{c0} \rightarrow \gamma\gamma$
1.45 ± 0.74	<sup>2</sup> AMBROGIANI 00B	E835	$p\bar{p} \rightarrow \chi_{c2} \rightarrow \gamma\gamma, \gamma J/\psi$
<sup>1</sup> The values of $B(p\bar{p})B(\gamma\gamma)$ and $B(\gamma\gamma)B(\gamma J/\psi)$ measured by ANDREOTTI 04 are not independent. The latter is used in the fit because of smaller systematics. <sup>2</sup> Calculated by us using $B(J/\psi(1S) \rightarrow e^+e^-) = 0.0593 \pm 0.0010$ .			

$\Gamma(p\bar{p})/\Gamma_{total} \times \Gamma(\gamma J/\psi(1S))/\Gamma_{total}$   $\Gamma_{58}/\Gamma \times \Gamma_{89}/\Gamma$

VALUE (units 10 <sup>-7</sup> )	EVTS	DOCUMENT ID	TECN	COMMENT
<b>31.1 ± 1.5 OUR FIT</b>				
<b>28.2 ± 2.1 OUR AVERAGE</b>				
28.0 ± 1.9 ± 1.3	392	<sup>1,2,3</sup> BAGNASCO 02	E835	$p\bar{p} \rightarrow \chi_{c0} \rightarrow J/\psi\gamma$
29.3 ± 5.7 ± 1.5	89	<sup>1,2</sup> AMBROGIANI 99B		$p\bar{p} \rightarrow \chi_{c0} \rightarrow J/\psi\gamma$
<sup>1</sup> Values in $(\Gamma(p\bar{p}) \times \Gamma(\gamma J/\psi(1S))/\Gamma_{total})$ and $(\Gamma(p\bar{p})/\Gamma_{total} \times \Gamma(\gamma J/\psi(1S))/\Gamma_{total})$ are not independent. The latter is used in the fit since it is less correlated to the total width. <sup>2</sup> Calculated by us using $B(J/\psi(1S) \rightarrow e^+e^-) = 0.0593 \pm 0.0010$ . <sup>3</sup> Recalculated by ANDREOTTI 05A.				

$\Gamma(p\bar{p})/\Gamma_{total} \times \Gamma(\gamma\gamma)/\Gamma_{total}$   $\Gamma_{58}/\Gamma \times \Gamma_{93}/\Gamma$

VALUE (units 10 <sup>-8</sup> )	DOCUMENT ID	TECN	COMMENT
<b>4.52 ± 0.27 OUR FIT</b>			
••• We do not use the following data for averages, fits, limits, etc. •••			
6.52 ± 1.18 ± 0.48 ± 0.72	<sup>1</sup> ANDREOTTI 04	E835	$p\bar{p} \rightarrow \chi_{c0} \rightarrow \gamma\gamma$
<sup>1</sup> The values of $B(p\bar{p})B(\gamma\gamma)$ and $B(\gamma\gamma)B(\gamma J/\psi)$ measured by ANDREOTTI 04 are not independent. The latter is used in the fit because of smaller systematics.			

$\chi_{c0}(1P)$  CROSS-PARTICLE BRANCHING RATIOS

$\Gamma(\chi_{c0}(1P) \rightarrow p\bar{p})/\Gamma_{total} \times \Gamma(\psi(2S) \rightarrow \gamma\chi_{c0}(1P))/\Gamma_{total}$

VALUE (units 10 <sup>-6</sup> )	EVTS	DOCUMENT ID	TECN	COMMENT
<b>21.7 ± 0.9 OUR FIT</b>				
<b>23.7 ± 1.0 OUR AVERAGE</b>				
23.7 ± 0.8 ± 0.9	1222	ABLIKIM 13V	BES3	$\psi(2S) \rightarrow \gamma p\bar{p}$
23.7 ± 1.4 ± 1.4	383 ± 22	<sup>1</sup> NAIK 08	CLEO	$\psi(2S) \rightarrow \gamma p\bar{p}$
23.6 ± 3.7 ± 3.4	89.5 ± 14	BAI	04F	BES $\psi(2S) \rightarrow \gamma\chi_{c0}(1P) \rightarrow \gamma p\bar{p}$

<sup>1</sup> Calculated by us. NAIK 08 reports  $B(\chi_{c0} \rightarrow p\bar{p}) = (25.7 \pm 1.5 \pm 1.5 \pm 1.3) \times 10^{-5}$  using  $B(\psi(2S) \rightarrow \gamma\chi_{c0}) = (9.22 \pm 0.11 \pm 0.46)\%$ .

$\Gamma(\chi_{c0}(1P) \rightarrow p\bar{p})/\Gamma_{total} \times \Gamma(\psi(2S) \rightarrow \gamma\chi_{c0}(1P))/\Gamma(\psi(2S) \rightarrow J/\psi(1S)\pi^+\pi^-)$

VALUE (units 10 <sup>-5</sup> )	DOCUMENT ID	TECN	COMMENT
<b>6.25 ± 0.26 OUR FIT</b>			
<b>4.6 ± 1.9</b>	<sup>1</sup> BAI	98I	BES $\psi(2S) \rightarrow \gamma\chi_{c0} \rightarrow \gamma p\bar{p}$

<sup>1</sup> Calculated by us. The value for  $B(\chi_{c0} \rightarrow p\bar{p})$  reported in BAI 98I is derived using  $B(\psi(2S) \rightarrow \gamma\chi_{c0}) = (9.3 \pm 0.8)\%$  and  $B(\psi(2S) \rightarrow J/\psi(1S)\pi^+\pi^-) = (32.4 \pm 2.6)\%$  [BAI 98d].

$\Gamma(\chi_{c0}(1P) \rightarrow \Lambda\bar{\Lambda})/\Gamma_{total} \times \Gamma(\psi(2S) \rightarrow \gamma\chi_{c0}(1P))/\Gamma_{total}$

VALUE (units 10 <sup>-6</sup> )	EVTS	DOCUMENT ID	TECN	COMMENT
<b>32.0 ± 2.3 OUR FIT</b>				
<b>31.7 ± 2.3 OUR AVERAGE</b>				
32.0 ± 1.9 ± 2.2	369	<sup>1</sup> ABLIKIM 13H	BES3	$\psi(2S) \rightarrow \gamma\Lambda\bar{\Lambda}$
31.2 ± 3.3 ± 2.0	131 ± 12	<sup>2</sup> NAIK 08	CLEO	$\psi(2S) \rightarrow \gamma\Lambda\bar{\Lambda}$

<sup>1</sup> Calculated by us. ABLIKIM 13H reports  $B(\chi_{c0} \rightarrow \Lambda\bar{\Lambda}) = (33.3 \pm 2.0 \pm 2.6) \times 10^{-5}$  from a measurement of  $B(\chi_{c0} \rightarrow \Lambda\bar{\Lambda}) \times B(\psi(2S) \rightarrow \gamma\chi_{c0})$  assuming  $B(\psi(2S) \rightarrow \gamma\chi_{c0}) = (9.62 \pm 0.31)\%$ .

<sup>2</sup> Calculated by us. NAIK 08 reports  $B(\chi_{c0} \rightarrow \Lambda\bar{\Lambda}) = (33.8 \pm 3.6 \pm 2.2 \pm 1.7) \times 10^{-5}$  using  $B(\psi(2S) \rightarrow \gamma\chi_{c0}) = (9.22 \pm 0.11 \pm 0.46)\%$ .

$\Gamma(\chi_{c0}(1P) \rightarrow \Lambda\bar{\Lambda})/\Gamma_{total} \times \Gamma(\psi(2S) \rightarrow \gamma\chi_{c0}(1P))/\Gamma(\psi(2S) \rightarrow J/\psi(1S)\pi^+\pi^-)$

VALUE (units 10 <sup>-5</sup> )	EVTS	DOCUMENT ID	TECN	COMMENT
<b>9.2 ± 0.7 OUR FIT</b>				
<b>13.0 ± 3.6 ± 2.5</b>	15.2 ± 4.2 ± 4.0	<sup>1</sup> BAI	03E	BES $\psi(2S) \rightarrow \gamma\Lambda\bar{\Lambda}$

<sup>1</sup> BAI 03E reports  $[B(\chi_{c0} \rightarrow \Lambda\bar{\Lambda})B(\psi(2S) \rightarrow \gamma\chi_{c0})/B(\psi(2S) \rightarrow J/\psi\pi^+\pi^-)] \times [B^2(\Lambda \rightarrow \pi^-\rho)/B(J/\psi \rightarrow p\bar{p})] = (2.45^{+0.68}_{-0.65} \pm 0.46)\%$ . We calculate from this measurement the presented value using  $B(\Lambda \rightarrow \pi^-\rho) = (63.9 \pm 0.5)\%$  and  $B(J/\psi \rightarrow p\bar{p}) = (2.17 \pm 0.07) \times 10^{-3}$ .

$\Gamma(\chi_{c0}(1P) \rightarrow \gamma J/\psi(1S))/\Gamma_{total} \times \Gamma(\psi(2S) \rightarrow \gamma\chi_{c0}(1P))/\Gamma_{total}$

VALUE (units 10 <sup>-2</sup> )	EVTS	DOCUMENT ID	TECN	COMMENT
<b>0.138 ± 0.005 OUR FIT</b>				
<b>0.147 ± 0.029 OUR AVERAGE</b>				
0.158 ± 0.003 ± 0.006	4.8k	<sup>1</sup> ABLIKIM 17N	BES3	$\psi(2S) \rightarrow \gamma\gamma J/\psi$
0.024 ± 0.015 ± 0.205	12k	ABLIKIM 17U	BES3	$e^+e^- \rightarrow \gamma X$
0.069 ± 0.018		<sup>2</sup> OREGLIA 82	CBAL	$\psi(2S) \rightarrow \gamma\chi_{c0}$
0.4 ± 0.3		<sup>3</sup> BRANDELIC 79B	DASP	$\psi(2S) \rightarrow \gamma\chi_{c0}$
0.16 ± 0.11		<sup>3</sup> BARTEL 78B	CNTR	$\psi(2S) \rightarrow \gamma\chi_{c0}$
3.3 ± 1.7		<sup>4</sup> BIDDICK 77	CNTR	$e^+e^- \rightarrow \gamma X$
••• We do not use the following data for averages, fits, limits, etc. •••				
0.151 ± 0.003 ± 0.010	4.3k	<sup>5</sup> ABLIKIM 12O	BES3	$\psi(2S) \rightarrow \gamma\chi_{c0}$
0.125 ± 0.007 ± 0.013	560	<sup>6</sup> MENDEZ 08	CLEO	$\psi(2S) \rightarrow \gamma\chi_{c0}$
0.18 ± 0.01 ± 0.02	172	<sup>7</sup> ADAM 05A	CLEO	Repl. by MENDEZ 08

<sup>1</sup> Uses  $B(J/\psi \rightarrow e^+e^-) = (5.971 \pm 0.032)\%$  and  $B(J/\psi \rightarrow \mu^+\mu^-) = (5.961 \pm 0.033)\%$ .  
<sup>2</sup> Recalculated by us using  $B(J/\psi(1S) \rightarrow \ell^+\ell^-) = 0.1181 \pm 0.0020$ .  
<sup>3</sup> Recalculated by us using  $B(J/\psi(1S) \rightarrow \mu^+\mu^-) = 0.0588 \pm 0.0010$ .  
<sup>4</sup> Assumes isotropic gamma distribution.  
<sup>5</sup> Superseded by ABLIKIM 17N.  
<sup>6</sup> Not independent from other measurements of MENDEZ 08.  
<sup>7</sup> Not independent from other values reported by ADAM 05A.

## Meson Particle Listings

 $\chi_{c0}(1P)$ 

$$\Gamma(\chi_{c0}(1P) \rightarrow \gamma J/\psi(1S))/\Gamma_{\text{total}} \times \Gamma(\psi(2S) \rightarrow \gamma \chi_{c0}(1P))/\Gamma(\psi(2S) \rightarrow J/\psi(1S) \text{ anything})$$

$$\frac{\Gamma_{89}/\Gamma \times \Gamma_{153}^{\psi(2S)} / \Gamma_9^{\psi(2S)}}{0.343\Gamma_{154}^{\psi(2S)} + 0.190\Gamma_{155}^{\psi(2S)}}$$

VALUE (units  $10^{-2}$ ) EVTS DOCUMENT ID TECN COMMENT  
**0.224±0.009 OUR FIT**

• • • We do not use the following data for averages, fits, limits, etc. • • •

0.201±0.011±0.021 560 <sup>1</sup> MENDEZ 08 CLEO  $\psi(2S) \rightarrow \gamma \chi_{c0}$   
 0.31 ± 0.02 ± 0.03 172 ADAM 05A CLEO Repl. by MENDEZ 08

<sup>1</sup> Not independent from other measurements of MENDEZ 08.

$$\Gamma(\chi_{c0}(1P) \rightarrow \gamma J/\psi(1S))/\Gamma_{\text{total}} \times \Gamma(\psi(2S) \rightarrow \gamma \chi_{c0}(1P))/\Gamma(\psi(2S) \rightarrow J/\psi(1S) \pi^+ \pi^-)$$

$$\frac{\Gamma_{89}/\Gamma \times \Gamma_{153}^{\psi(2S)} / \Gamma_{11}^{\psi(2S)}}{\Gamma_{11}^{\psi(2S)}}$$

VALUE (units  $10^{-2}$ ) EVTS DOCUMENT ID TECN COMMENT  
**0.397±0.015 OUR FIT**  
**0.358±0.020±0.037**

• • • We do not use the following data for averages, fits, limits, etc. • • •

0.55 ± 0.04 ± 0.06 172 <sup>1</sup> ADAM 05A CLEO Repl. by MENDEZ 08

<sup>1</sup> Not independent from other values reported by ADAM 05A.

$$\Gamma(\chi_{c0}(1P) \rightarrow \gamma \gamma)/\Gamma_{\text{total}} \times \Gamma(\psi(2S) \rightarrow \gamma \chi_{c0}(1P))/\Gamma_{\text{total}}$$

$$\frac{\Gamma_{93}/\Gamma \times \Gamma_{153}^{\psi(2S)} / \Gamma_{\psi(2S)}}{\Gamma_{\psi(2S)}}$$

VALUE (units  $10^{-5}$ ) EVTS DOCUMENT ID TECN COMMENT  
**2.00±0.08 OUR FIT**  
**1.95±0.09 OUR AVERAGE**

1.93±0.08±0.05 3.5k ABLIKIM 17Ae BES3  $\psi(2S) \rightarrow \gamma \chi_{c0} \rightarrow 3\gamma$   
 2.17±0.32±0.10 0.2k ECKLUND 08A CLEO  $\psi(2S) \rightarrow \gamma \chi_{c0} \rightarrow 3\gamma$   
 3.7 ± 1.8 ± 1.0 LEE 85 CBAL  $\psi(2S) \rightarrow \gamma \chi_{c0}$

• • • We do not use the following data for averages, fits, limits, etc. • • •

2.17±0.17±0.12 0.8k <sup>1</sup> ABLIKIM 12A BES3  $\psi(2S) \rightarrow \gamma \chi_{c0} \rightarrow 3\gamma$

<sup>1</sup> Superseded by ABLIKIM 17Ae.

$$\Gamma(\chi_{c0}(1P) \rightarrow \pi \pi)/\Gamma_{\text{total}} \times \Gamma(\psi(2S) \rightarrow \gamma \chi_{c0}(1P))/\Gamma_{\text{total}}$$

$$\frac{\Gamma_{32}/\Gamma \times \Gamma_{153}^{\psi(2S)} / \Gamma_{\psi(2S)}}{\Gamma_{\psi(2S)}}$$

VALUE (units  $10^{-4}$ ) EVTS DOCUMENT ID TECN COMMENT  
**8.34±0.29 OUR FIT**  
**8.80±0.34 OUR AVERAGE**

9.11±0.08±0.65 17k <sup>1</sup> ABLIKIM 10A BES3  $e^+e^- \rightarrow \psi(2S) \rightarrow \gamma \chi_{c0}$   
 8.81±0.11±0.43 8.9k <sup>2</sup> ASNER 09 CLEO  $\psi(2S) \rightarrow \gamma \pi^+ \pi^-$   
 8.13±0.19±0.89 2.8k <sup>3</sup> ASNER 09 CLEO  $\psi(2S) \rightarrow \gamma \pi^0 \pi^0$

<sup>1</sup> Calculated by us. ABLIKIM 10A reports  $B(\chi_{c0} \rightarrow \pi^0 \pi^0) = (3.23 \pm 0.03 \pm 0.23 \pm 0.14) \times 10^{-3}$  using  $B(\psi(2S) \rightarrow \gamma \chi_{c0}) = (9.4 \pm 0.4)\%$ . We have multiplied the  $\pi^0 \pi^0$  measurement by 3 to obtain  $\pi \pi$ .

<sup>2</sup> Calculated by us. ASNER 09 reports  $B(\chi_{c0} \rightarrow \pi^+ \pi^-) = (6.37 \pm 0.08 \pm 0.31 \pm 0.32) \times 10^{-3}$  using  $B(\psi(2S) \rightarrow \gamma \chi_{c0}) = (9.22 \pm 0.11 \pm 0.46)\%$ . We have multiplied the  $\pi^+ \pi^-$  measurement by 3/2 to obtain  $\pi \pi$ .

<sup>3</sup> Calculated by us. ASNER 09 reports  $B(\chi_{c0} \rightarrow \pi^0 \pi^0) = (2.94 \pm 0.07 \pm 0.32 \pm 0.15) \times 10^{-3}$  using  $B(\psi(2S) \rightarrow \gamma \chi_{c0}) = (9.22 \pm 0.11 \pm 0.46)\%$ . We have multiplied the  $\pi^0 \pi^0$  measurement by 3 to obtain  $\pi \pi$ .

$$\Gamma(\chi_{c0}(1P) \rightarrow \pi \pi)/\Gamma_{\text{total}} \times \Gamma(\psi(2S) \rightarrow \gamma \chi_{c0}(1P))/\Gamma(\psi(2S) \rightarrow J/\psi(1S) \pi^+ \pi^-)$$

$$\frac{\Gamma_{32}/\Gamma \times \Gamma_{153}^{\psi(2S)} / \Gamma_{11}^{\psi(2S)}}{\Gamma_{11}^{\psi(2S)}}$$

VALUE (units  $10^{-4}$ ) EVTS DOCUMENT ID TECN COMMENT  
**24.0±0.8 OUR FIT**  
**20.7±1.7 OUR AVERAGE**

23.9±2.7±4.1 97 ± 11 <sup>1</sup> BAI 03c BES  $\psi(2S) \rightarrow \gamma \chi_{c0} \rightarrow \gamma \pi^0 \pi^0$   
 20.2±1.1±1.5 720 ± 32 <sup>2</sup> BAI 98i BES  $\psi(2S) \rightarrow \gamma \chi_{c0} \rightarrow \gamma \pi^+ \pi^-$

<sup>1</sup> We have multiplied  $\pi^0 \pi^0$  measurement by 3 to obtain  $\pi \pi$ .

<sup>2</sup> Calculated by us. The value for  $B(\chi_{c0} \rightarrow \pi^+ \pi^-)$  reported in BAI 98i is derived using  $B(\psi' \rightarrow \gamma \chi_{c0}) = (9.3 \pm 0.8)\%$  and  $B(\psi' \rightarrow J/\psi \pi^+ \pi^-) = (32.4 \pm 2.6)\%$  [BAI 98d]. We have multiplied  $\pi^+ \pi^-$  measurement by 3/2 to obtain  $\pi \pi$ .

$$\Gamma(\chi_{c0}(1P) \rightarrow \eta \eta)/\Gamma_{\text{total}} \times \Gamma(\psi(2S) \rightarrow \gamma \chi_{c0}(1P))/\Gamma_{\text{total}}$$

$$\frac{\Gamma_{36}/\Gamma \times \Gamma_{153}^{\psi(2S)} / \Gamma_{\psi(2S)}}{\Gamma_{\psi(2S)}}$$

VALUE (units  $10^{-4}$ ) EVTS DOCUMENT ID TECN COMMENT  
**2.95±0.18 OUR FIT**  
**3.12±0.19 OUR AVERAGE**

3.23±0.09±0.23 2132 <sup>1</sup> ABLIKIM 10A BES3  $e^+e^- \rightarrow \psi(2S) \rightarrow \gamma \chi_{c0}$   
 2.93±0.12±0.29 0.9k <sup>2</sup> ASNER 09 CLEO  $\psi(2S) \rightarrow \gamma \eta \eta$

• • • We do not use the following data for averages, fits, limits, etc. • • •

2.86±0.46±0.37 48 <sup>3</sup> ADAMS 07 CLEO  $\psi(2S) \rightarrow \gamma \chi_{c0}$

<sup>1</sup> Calculated by us. ABLIKIM 10A reports  $B(\chi_{c0} \rightarrow \eta \eta) = (3.44 \pm 0.10 \pm 0.24 \pm 0.13) \times 10^{-3}$  using  $B(\psi(2S) \rightarrow \gamma \chi_{c0}) = (9.4 \pm 0.4)\%$ .

<sup>2</sup> Calculated by us. ASNER 09 reports  $B(\chi_{c0} \rightarrow \eta \eta) = (3.18 \pm 0.13 \pm 0.31 \pm 0.16) \times 10^{-3}$  using  $B(\psi(2S) \rightarrow \gamma \chi_{c0}) = (9.22 \pm 0.11 \pm 0.46)\%$ .

<sup>3</sup> Superseded by ASNER 09. Calculated by us. The value of  $B(\chi_{c0}(1P) \rightarrow \eta \eta)$  reported by ADAMS 07 was derived using  $B(\psi(2S) \rightarrow \gamma \chi_{c0}(1P)) = (9.22 \pm 0.11 \pm 0.46)\%$  (ATHAR 04).

$$\Gamma(\chi_{c0}(1P) \rightarrow \eta \eta)/\Gamma_{\text{total}} \times \Gamma(\psi(2S) \rightarrow \gamma \chi_{c0}(1P))/\Gamma(\psi(2S) \rightarrow J/\psi(1S) \pi^+ \pi^-)$$

$$\frac{\Gamma_{36}/\Gamma \times \Gamma_{153}^{\psi(2S)} / \Gamma_{11}^{\psi(2S)}}{\Gamma_{11}^{\psi(2S)}}$$

VALUE (units  $10^{-3}$ ) DOCUMENT ID TECN COMMENT  
**0.85 ± 0.05 OUR FIT**  
**0.578±0.241±0.158**

BAI 03c BES  $\psi(2S) \rightarrow \gamma \eta \eta$

$$\Gamma(\chi_{c0}(1P) \rightarrow K^+ K^-)/\Gamma_{\text{total}} \times \Gamma(\psi(2S) \rightarrow \gamma \chi_{c0}(1P))/\Gamma_{\text{total}}$$

$$\frac{\Gamma_{42}/\Gamma \times \Gamma_{153}^{\psi(2S)} / \Gamma_{\psi(2S)}}{\Gamma_{\psi(2S)}}$$

VALUE (units  $10^{-4}$ ) EVTS DOCUMENT ID TECN COMMENT  
**5.92±0.28 OUR FIT**  
**5.97±0.07±0.32**

8.1k <sup>1</sup> ASNER 09 CLEO  $\psi(2S) \rightarrow \gamma K^+ K^-$

<sup>1</sup> Calculated by us. ASNER 09 reports  $B(\chi_{c0} \rightarrow K^+ K^-) = (6.47 \pm 0.08 \pm 0.35 \pm 0.32) \times 10^{-3}$  using  $B(\psi(2S) \rightarrow \gamma \chi_{c0}) = (9.22 \pm 0.11 \pm 0.46)\%$ .

$$\Gamma(\chi_{c0}(1P) \rightarrow K^+ K^-)/\Gamma_{\text{total}} \times \Gamma(\psi(2S) \rightarrow \gamma \chi_{c0}(1P))/\Gamma(\psi(2S) \rightarrow J/\psi(1S) \pi^+ \pi^-)$$

$$\frac{\Gamma_{42}/\Gamma \times \Gamma_{153}^{\psi(2S)} / \Gamma_{11}^{\psi(2S)}}{\Gamma_{11}^{\psi(2S)}}$$

VALUE (units  $10^{-3}$ ) EVTS DOCUMENT ID TECN COMMENT  
**1.71±0.08 OUR FIT**  
**1.63±0.10±0.15**

774 ± 38 <sup>1</sup> BAI 98i BES  $\psi(2S) \rightarrow \gamma K^+ K^-$

<sup>1</sup> Calculated by us. The value for  $B(\chi_{c0} \rightarrow K^+ K^-)$  reported by BAI 98i is derived using  $B(\psi(2S) \rightarrow \gamma \chi_{c0}) = (9.3 \pm 0.8)\%$  and  $B(\psi(2S) \rightarrow J/\psi \pi^+ \pi^-) = (32.4 \pm 2.6)\%$  [BAI 98d].

$$\Gamma(\chi_{c0}(1P) \rightarrow K_S^0 K_S^0)/\Gamma_{\text{total}} \times \Gamma(\psi(2S) \rightarrow \gamma \chi_{c0}(1P))/\Gamma_{\text{total}}$$

$$\frac{\Gamma_{43}/\Gamma \times \Gamma_{153}^{\psi(2S)} / \Gamma_{\psi(2S)}}{\Gamma_{\psi(2S)}}$$

VALUE (units  $10^{-4}$ ) EVTS DOCUMENT ID TECN COMMENT  
**3.10±0.16 OUR FIT**  
**3.18±0.17 OUR AVERAGE**

3.22±0.07±0.17 2.1k <sup>1</sup> ASNER 09 CLEO  $\psi(2S) \rightarrow \gamma K_S^0 K_S^0$   
 3.02±0.19±0.33 322 ABLIKIM 05o BES2  $\psi(2S) \rightarrow \gamma K_S^0 K_S^0$

<sup>1</sup> Calculated by us. ASNER 09 reports  $B(\chi_{c0} \rightarrow K_S^0 K_S^0) = (3.49 \pm 0.08 \pm 0.18 \pm 0.17) \times 10^{-3}$  using  $B(\psi(2S) \rightarrow \gamma \chi_{c0}) = (9.22 \pm 0.11 \pm 0.46)\%$ .

$$\Gamma(\chi_{c0}(1P) \rightarrow K_S^0 K_S^0)/\Gamma_{\text{total}} \times \Gamma(\psi(2S) \rightarrow \gamma \chi_{c0}(1P))/\Gamma(\psi(2S) \rightarrow J/\psi(1S) \pi^+ \pi^-)$$

$$\frac{\Gamma_{43}/\Gamma \times \Gamma_{153}^{\psi(2S)} / \Gamma_{11}^{\psi(2S)}}{\Gamma_{11}^{\psi(2S)}}$$

VALUE (units  $10^{-4}$ ) EVTS DOCUMENT ID TECN COMMENT  
**8.9±0.5 OUR FIT**  
**5.6±0.8±1.3**

<sup>1</sup> BAI 99b BES  $\psi(2S) \rightarrow \gamma K_S^0 K_S^0$

<sup>1</sup> Calculated by us. The value of  $B(\chi_{c0} \rightarrow K_S^0 K_S^0)$  reported by BAI 99b was derived using  $B(\psi(2S) \rightarrow \gamma \chi_{c0}(1P)) = (9.3 \pm 0.8)\%$  and  $B(\psi(2S) \rightarrow J/\psi \pi^+ \pi^-) = (32.4 \pm 2.6)\%$  [BAI 98d].

$$\Gamma(\chi_{c0}(1P) \rightarrow 2(\pi^+ \pi^-))/\Gamma_{\text{total}} \times \Gamma(\psi(2S) \rightarrow \gamma \chi_{c0}(1P))/\Gamma(\psi(2S) \rightarrow J/\psi(1S) \pi^+ \pi^-)$$

$$\frac{\Gamma_{11}/\Gamma \times \Gamma_{153}^{\psi(2S)} / \Gamma_{11}^{\psi(2S)}}{\Gamma_{11}^{\psi(2S)}}$$

VALUE (units  $10^{-3}$ ) DOCUMENT ID TECN COMMENT  
**6.6±0.5 OUR FIT**  
**6.9±2.4 OUR AVERAGE**

Error includes scale factor of 3.8.

4.4±0.1±0.9 <sup>1</sup> BAI 99b BES  $\psi(2S) \rightarrow \gamma \chi_{c0}$   
 9.3±0.9 <sup>2</sup> TANENBAUM 78 MRK1  $\psi(2S) \rightarrow \gamma \chi_{c0}$

<sup>1</sup> Calculated by us. The value for  $B(\chi_{c0} \rightarrow 2\pi^+ 2\pi^-)$  reported in BAI 99b is derived using  $B(\psi(2S) \rightarrow \gamma \chi_{c0}) = (9.3 \pm 0.8)\%$  and  $B(\psi(2S) \rightarrow J/\psi(1S) \pi^+ \pi^-) = (32.4 \pm 2.6)\%$  [BAI 98d].

<sup>2</sup> The value  $B(\psi(1S) \rightarrow \gamma \chi_{c0}) \times B(\chi_{c0} \rightarrow 2\pi^+ 2\pi^-)$  reported in TANENBAUM 78 is derived using  $B(\psi(2S) \rightarrow J/\psi(1S) \pi^+ \pi^-) \times B(J/\psi(1S) \rightarrow \ell^+ \ell^-) = (4.6 \pm 0.7)\%$ . Calculated by us using  $B(J/\psi(1S) \rightarrow \ell^+ \ell^-) = 0.1181 \pm 0.0020$ .

$$\Gamma(\chi_{c0}(1P) \rightarrow \pi^+ \pi^- K^+ K^-)/\Gamma_{\text{total}} \times \Gamma(\psi(2S) \rightarrow \gamma \chi_{c0}(1P))/\Gamma_{\text{total}}$$

$$\frac{\Gamma_8/\Gamma \times \Gamma_{153}^{\psi(2S)} / \Gamma_{\psi(2S)}}{\Gamma_{\psi(2S)}}$$

VALUE (units  $10^{-3}$ ) DOCUMENT ID TECN COMMENT  
**1.78±0.14 OUR FIT**  
**1.64±0.05±0.2**

ABLIKIM 05q BES2  $\psi(2S) \rightarrow \gamma \chi_{c0}$

$$\Gamma(\chi_{c0}(1P) \rightarrow \pi^+ \pi^- K^+ K^-)/\Gamma_{\text{total}} \times \Gamma(\psi(2S) \rightarrow \gamma \chi_{c0}(1P))/\Gamma(\psi(2S) \rightarrow J/\psi(1S) \pi^+ \pi^-)$$

$$\frac{\Gamma_8/\Gamma \times \Gamma_{153}^{\psi(2S)} / \Gamma_{11}^{\psi(2S)}}{\Gamma_{11}^{\psi(2S)}}$$

VALUE (units  $10^{-3}$ ) DOCUMENT ID TECN COMMENT  
**5.1 ± 0.4 OUR FIT**  
**5.8 ± 1.6 OUR AVERAGE**

Error includes scale factor of 2.3.

4.22±0.20±0.97 BAI 99b BES  $\psi(2S) \rightarrow \gamma \chi_{c0}$   
 7.4 ± 1.0 <sup>1</sup> TANENBAUM 78 MRK1  $\psi(2S) \rightarrow \gamma \chi_{c0}$

<sup>1</sup> The reported value is derived using  $B(\psi(2S) \rightarrow \pi^+ \pi^- J/\psi) \times B(J/\psi \rightarrow \ell^+ \ell^-) = (4.6 \pm 0.7)\%$ . Calculated by us using  $B(J/\psi \rightarrow \ell^+ \ell^-) = 0.1181 \pm 0.0020$ .

$$\Gamma(\chi_{c0}(1P) \rightarrow K^+ K^- K^+ K^-)/\Gamma_{\text{total}} \times \Gamma(\psi(2S) \rightarrow \gamma \chi_{c0}(1P))/\Gamma_{\text{total}}$$

$$\frac{\Gamma_{51}/\Gamma \times \Gamma_{153}^{\psi(2S)} / \Gamma_{\psi(2S)}}{\Gamma_{\psi(2S)}}$$

VALUE (units  $10^{-4}$ ) EVTS DOCUMENT ID TECN COMMENT  
**2.76±0.28 OUR FIT**  
**3.20±0.11±0.41**

278 <sup>1</sup> ABLIKIM 06t BES2  $\psi(2S) \rightarrow \gamma 2K^+ 2K^-$

<sup>1</sup> Calculated by us. The value of  $B(\chi_{c0} \rightarrow 2K^+ 2K^-)$  reported by ABLIKIM 06t was derived using  $B(\psi(2S) \rightarrow \gamma \chi_{c0}(1P)) = (9.2 \pm 0.4)\%$ .

See key on page 999

Meson Particle Listings

$\chi_{c0}(1P), \chi_{c1}(1P)$

$\Gamma(\chi_{c0}(1P) \to K^+ K^- K^+ K^-) / \Gamma_{total} \times \Gamma(\psi(2S) \to \gamma \chi_{c0}(1P)) / \Gamma(\psi(2S) \to J/\psi(1S) \pi^+ \pi^-)$

Table with 4 columns: VALUE (units 10^-4), DOCUMENT ID, TECN, COMMENT. Includes rows for 8.0 ± 0.8 OUR FIT and 6.1 ± 0.8 ± 0.9.

$\Gamma(\chi_{c0}(1P) \to \phi\phi) / \Gamma_{total} \times \Gamma(\psi(2S) \to \gamma \chi_{c0}(1P)) / \Gamma_{total}$

Table with 4 columns: VALUE (units 10^-4), EVTS, DOCUMENT ID, TECN, COMMENT. Includes rows for 0.78 ± 0.07 OUR FIT and 0.78 ± 0.08 OUR AVERAGE.

1 Calculated by us. The value of  $B(\chi_{c0} \to 2K^+ 2K^-)$  reported by BAI 99b was derived using  $B(\psi(2S) \to \gamma \chi_{c0}(1P)) = (9.3 \pm 0.8)\%$  and  $B(\psi(2S) \to J/\psi \pi^+ \pi^-) = (32.4 \pm 2.6)\%$  [BAI 98d].

$\Gamma(\chi_{c0}(1P) \to \phi\phi) / \Gamma_{total} \times \Gamma(\psi(2S) \to \gamma \chi_{c0}(1P)) / \Gamma(\psi(2S) \to J/\psi(1S) \pi^+ \pi^-)$

Table with 4 columns: VALUE (units 10^-4), DOCUMENT ID, TECN, COMMENT. Includes rows for 2.25 ± 0.21 OUR FIT and 2.6 ± 1.0 ± 1.1.

1 Calculated by us. The value of  $B(\chi_{c0} \to \phi\phi)$  reported by BAI 99b was derived using  $B(\psi(2S) \to \gamma \chi_{c0}(1P)) = (9.3 \pm 0.8)\%$  and  $B(\psi(2S) \to J/\psi \pi^+ \pi^-) = (32.4 \pm 2.6)\%$  [BAI 98d].

$\Gamma(\chi_{c0}(1P) \to \Sigma^+ \bar{p} K_S^0 + c.c.) / \Gamma_{total} \times \Gamma(\psi(2S) \to \gamma \chi_{c0}(1P)) / \Gamma_{total}$

Table with 4 columns: VALUE (units 10^-5), EVTS, DOCUMENT ID, TECN, COMMENT. Includes rows for 3.45 ± 0.17 ± 0.19.

$\chi_{c0}(1P)$  REFERENCES

List of references for  $\chi_{c0}(1P)$  from ABLIKIM, ANDREOTTI, etc. Includes document IDs, TECN codes, and comments.

Table listing various meson decays and associated literature references (e.g., NP B717 34, PR D72 112002, etc.).

$\chi_{c1}(1P)$   $I^G(J^{PC}) = 0^+(1^+ +)$  See the Review on " $\psi(2S)$  and  $\chi_c$  branching ratios" before the  $\chi_{c0}(1P)$  Listings.

$\chi_{c1}(1P)$  MASS

Table with 5 columns: VALUE (MeV), EVTS, DOCUMENT ID, TECN, COMMENT. Includes rows for 3510.67 ± 0.05 OUR AVERAGE and various experimental values.

••• We do not use the following data for averages, fits, limits, etc. •••
1 From a fit of the  $\phi\phi$  invariant mass with the width of  $\chi_{c1}(1P)$  fixed to the PDG 16 value.
2 AAIJ 17B1 reports also  $m(\chi_{c2}) - m(\chi_{c1}) = 45.39 \pm 0.07 \pm 0.03$  MeV.
3 Recalculated by ANDREOTTI 05A, using the value of  $\psi(2S)$  mass from AULCHENKO 03.
4 Using mass of  $\psi(2S) = 3686.0$  MeV.
5  $J/\psi(1S)$  mass constrained to 3097 MeV.
6 Mass value shifted by us by amount appropriate for  $\psi(2S)$  mass = 3686 MeV and  $J/\psi(1S)$  mass = 3097 MeV.
7 From a simultaneous fit to radiative and hadronic decay channels.

$\chi_{c1}(1P)$  WIDTH

Table with 5 columns: VALUE (MeV), CL%, EVTS, DOCUMENT ID, TECN, COMMENT. Includes rows for 0.84 ± 0.04 OUR FIT and 0.88 ± 0.05 OUR AVERAGE.

$\chi_{c1}(1P)$  DECAY MODES

Table with 3 columns: Mode, Fraction ( $\Gamma_i/\Gamma$ ), Scale factor/Confidence level. Includes rows for Hadronic decays like  $3(\pi^+ \pi^-)$  and  $2(\pi^+ \pi^0 \pi^0)$ .

Downloaded from https://academic.oup.com/ptep/article/2020/8/083C01/5891211 by guest on 12 November 2020

# Meson Particle Listings

## $\chi_{c1}(1P)$

$\Gamma_4$	$\rho^+ \pi^- \pi^0 + c.c.$	$(1.45 \pm 0.24) \%$	
$\Gamma_5$	$\rho^0 \pi^+ \pi^-$	$(3.9 \pm 3.5) \times 10^{-3}$	
$\Gamma_6$	$4\pi^0$	$(5.4 \pm 0.8) \times 10^{-4}$	
$\Gamma_7$	$\pi^+ \pi^- K^+ K^-$	$(4.5 \pm 1.0) \times 10^{-3}$	
$\Gamma_8$	$K^+ K^- \pi^0 \pi^0$	$(1.12 \pm 0.27) \times 10^{-3}$	
$\Gamma_9$	$K^+ K^- \pi^+ \pi^- \pi^0$	$(1.15 \pm 0.13) \%$	
$\Gamma_{10}$	$K_S^0 K_S^+ \pi^+ \pi^- \pi^0$	$(7.5 \pm 0.8) \times 10^{-3}$	
$\Gamma_{11}$	$K^+ \pi^- \bar{K}^0 \pi^0 + c.c.$	$(8.6 \pm 1.4) \times 10^{-3}$	
$\Gamma_{12}$	$\rho^- K^+ \bar{K}^0 + c.c.$	$(5.0 \pm 1.2) \times 10^{-3}$	
$\Gamma_{13}$	$K^*(892)^0 \bar{K}^0 \pi^0 \rightarrow K^+ \pi^- \bar{K}^0 \pi^0 + c.c.$	$(2.3 \pm 0.6) \times 10^{-3}$	
$\Gamma_{14}$	$K^+ K^- \eta \pi^0$	$(1.12 \pm 0.34) \times 10^{-3}$	
$\Gamma_{15}$	$\pi^+ \pi^- K_S^0 K_S^0$	$(6.9 \pm 2.9) \times 10^{-4}$	
$\Gamma_{16}$	$K^+ K^- \eta$	$(3.2 \pm 1.0) \times 10^{-4}$	
$\Gamma_{17}$	$\bar{K}^0 K^+ \pi^- + c.c.$	$(7.0 \pm 0.6) \times 10^{-3}$	
$\Gamma_{18}$	$K^*(892)^0 \bar{K}^0 + c.c.$	$(10 \pm 4) \times 10^{-4}$	
$\Gamma_{19}$	$K^*(892)^+ K^- + c.c.$	$(1.4 \pm 0.6) \times 10^{-3}$	
$\Gamma_{20}$	$K_J^*(1430)^0 \bar{K}^0 + c.c. \rightarrow K_S^0 K^+ \pi^- + c.c.$	$< 8 \times 10^{-4}$	CL=90%
$\Gamma_{21}$	$K_J^*(1430)^+ K^- + c.c. \rightarrow K_S^0 K^+ \pi^- + c.c.$	$< 2.1 \times 10^{-3}$	CL=90%
$\Gamma_{22}$	$K^+ K^- \pi^0$	$(1.81 \pm 0.24) \times 10^{-3}$	
$\Gamma_{23}$	$\eta \pi^+ \pi^-$	$(4.62 \pm 0.23) \times 10^{-3}$	
$\Gamma_{24}$	$a_0(980)^+ \pi^- + c.c. \rightarrow \eta \pi^+ \pi^-$	$(3.2 \pm 0.4) \times 10^{-3}$	S=2.2
$\Gamma_{25}$	$a_2(1320)^+ \pi^- + c.c. \rightarrow \eta \pi^+ \pi^-$	$(1.76 \pm 0.24) \times 10^{-4}$	
$\Gamma_{26}$	$a_2(1700)^+ \pi^- + c.c. \rightarrow \eta \pi^+ \pi^-$	$(4.6 \pm 0.7) \times 10^{-5}$	
$\Gamma_{27}$	$f_2(1270) \eta \rightarrow \eta \pi^+ \pi^-$	$(3.5 \pm 0.6) \times 10^{-4}$	
$\Gamma_{28}$	$f_4(2050) \eta \rightarrow \eta \pi^+ \pi^-$	$(2.5 \pm 0.9) \times 10^{-5}$	
$\Gamma_{29}$	$\pi_1(1400)^+ \pi^- + c.c. \rightarrow \eta \pi^+ \pi^-$	$< 5 \times 10^{-5}$	CL=90%
$\Gamma_{30}$	$\pi_1(1600)^+ \pi^- + c.c. \rightarrow \eta \pi^+ \pi^-$	$< 1.5 \times 10^{-5}$	CL=90%
$\Gamma_{31}$	$\pi_1(2015)^+ \pi^- + c.c. \rightarrow \eta \pi^+ \pi^-$	$< 8 \times 10^{-6}$	CL=90%
$\Gamma_{32}$	$f_2(1270) \eta$	$(6.7 \pm 1.1) \times 10^{-4}$	
$\Gamma_{33}$	$\pi^+ \pi^- \eta'$	$(2.2 \pm 0.4) \times 10^{-3}$	
$\Gamma_{34}$	$K^+ K^- \eta'(958)$	$(8.8 \pm 0.9) \times 10^{-4}$	
$\Gamma_{35}$	$K_0^*(1430)^+ K^- + c.c.$	$(6.4 \pm 2.2) \times 10^{-4}$	
$\Gamma_{36}$	$f_0(980) \eta'(958)$	$(1.6 \pm 1.4) \times 10^{-4}$	
$\Gamma_{37}$	$f_0(1710) \eta'(958)$	$(7 \pm 7) \times 10^{-5}$	
$\Gamma_{38}$	$f_2'(1525) \eta'(958)$	$(9 \pm 6) \times 10^{-5}$	
$\Gamma_{39}$	$\pi^0 f_0(980) \rightarrow \pi^0 \pi^+ \pi^-$	$(3.5 \pm 0.9) \times 10^{-7}$	
$\Gamma_{40}$	$K^+ \bar{K}^*(892)^0 \pi^- + c.c.$	$(3.2 \pm 2.1) \times 10^{-3}$	
$\Gamma_{41}$	$K^*(892)^0 \bar{K}^*(892)^0$	$(1.4 \pm 0.4) \times 10^{-3}$	
$\Gamma_{42}$	$K^+ K^- K_S^0 K_S^0$	$< 4 \times 10^{-4}$	CL=90%
$\Gamma_{43}$	$K_S^0 K_S^0 K_S^0 K_S^0$	$(3.5 \pm 1.0) \times 10^{-5}$	
$\Gamma_{44}$	$K^+ K^- K^+ K^-$	$(5.4 \pm 1.1) \times 10^{-4}$	
$\Gamma_{45}$	$K^+ K^- \phi$	$(4.1 \pm 1.5) \times 10^{-4}$	
$\Gamma_{46}$	$\bar{K}^0 K^+ \pi^- \phi + c.c.$	$(3.3 \pm 0.5) \times 10^{-3}$	
$\Gamma_{47}$	$K^+ K^- \pi^0 \phi$	$(1.62 \pm 0.30) \times 10^{-3}$	
$\Gamma_{48}$	$\phi \pi^+ \pi^- \pi^0$	$(7.5 \pm 1.0) \times 10^{-4}$	
$\Gamma_{49}$	$\omega \omega$	$(5.7 \pm 0.7) \times 10^{-4}$	
$\Gamma_{50}$	$\omega K^+ K^-$	$(7.8 \pm 0.9) \times 10^{-4}$	
$\Gamma_{51}$	$\omega \phi$	$(2.7 \pm 0.4) \times 10^{-5}$	
$\Gamma_{52}$	$\phi \phi$	$(4.2 \pm 0.5) \times 10^{-4}$	
$\Gamma_{53}$	$\phi \phi \eta$	$(3.0 \pm 0.5) \times 10^{-4}$	
$\Gamma_{54}$	$\rho \bar{\rho}$	$(7.60 \pm 0.34) \times 10^{-5}$	
$\Gamma_{55}$	$\rho \bar{\rho} \pi^0$	$(1.55 \pm 0.18) \times 10^{-4}$	
$\Gamma_{56}$	$\rho \bar{\rho} \eta$	$(1.45 \pm 0.25) \times 10^{-4}$	
$\Gamma_{57}$	$\rho \bar{\rho} \omega$	$(2.12 \pm 0.31) \times 10^{-4}$	
$\Gamma_{58}$	$\rho \bar{\rho} \phi$	$< 1.7 \times 10^{-5}$	CL=90%
$\Gamma_{59}$	$\rho \bar{\rho} \pi^+ \pi^-$	$(5.0 \pm 1.9) \times 10^{-4}$	
$\Gamma_{60}$	$\rho \bar{\rho} \pi^0 \pi^0$	$< 5 \times 10^{-4}$	CL=90%
$\Gamma_{61}$	$\rho \bar{\rho} K^+ K^-$ (non-resonant)	$(1.27 \pm 0.22) \times 10^{-4}$	
$\Gamma_{62}$	$\rho \bar{\rho} K_S^0 K_S^0$	$< 4.5 \times 10^{-4}$	CL=90%
$\Gamma_{63}$	$\rho \bar{\rho} \pi^-$	$(3.8 \pm 0.5) \times 10^{-4}$	
$\Gamma_{64}$	$\rho \bar{\rho} \pi^+$	$(3.9 \pm 0.5) \times 10^{-4}$	
$\Gamma_{65}$	$\rho \bar{\rho} \pi^- \pi^0$	$(1.03 \pm 0.12) \times 10^{-3}$	
$\Gamma_{66}$	$\rho \bar{\rho} \pi^+ \pi^0$	$(1.01 \pm 0.12) \times 10^{-3}$	
$\Gamma_{67}$	$\Lambda \bar{\Lambda}$	$(1.14 \pm 0.11) \times 10^{-4}$	
$\Gamma_{68}$	$\Lambda \bar{\Lambda} \pi^+ \pi^-$	$(2.9 \pm 0.5) \times 10^{-4}$	
$\Gamma_{69}$	$\Lambda \bar{\Lambda} \pi^+ \pi^-$ (non-resonant)	$(2.5 \pm 0.6) \times 10^{-4}$	
$\Gamma_{70}$	$\Sigma(1385)^+ \bar{\Lambda} \pi^- + c.c.$	$< 1.3 \times 10^{-4}$	CL=90%
$\Gamma_{71}$	$\Sigma(1385)^- \bar{\Lambda} \pi^+ + c.c.$	$< 1.3 \times 10^{-4}$	CL=90%
$\Gamma_{72}$	$K^+ \bar{p} \Lambda + c.c.$	$(4.2 \pm 0.4) \times 10^{-4}$	S=1.2
$\Gamma_{73}$	$K^*(892)^+ \bar{p} \Lambda + c.c.$	$(4.9 \pm 0.7) \times 10^{-4}$	

$\Gamma_{74}$	$K^+ \bar{p} \Lambda(1520) + c.c.$	$(1.7 \pm 0.4) \times 10^{-4}$	
$\Gamma_{75}$	$\Lambda(1520) \bar{\Lambda}(1520)$	$< 9 \times 10^{-5}$	CL=90%
$\Gamma_{76}$	$\Sigma^0 \bar{\Sigma}^0$	$(4.2 \pm 0.6) \times 10^{-5}$	
$\Gamma_{77}$	$\Sigma^+ \bar{p} K_S^0 + c.c.$	$(1.53 \pm 0.12) \times 10^{-4}$	
$\Gamma_{78}$	$\Sigma^+ \bar{\Sigma}^-$	$(3.6 \pm 0.7) \times 10^{-5}$	
$\Gamma_{79}$	$\Sigma(1385)^+ \bar{\Sigma}(1385)^-$	$< 9 \times 10^{-5}$	CL=90%
$\Gamma_{80}$	$\Sigma(1385)^- \bar{\Sigma}(1385)^+$	$< 5 \times 10^{-5}$	CL=90%
$\Gamma_{81}$	$K^- \Lambda \bar{\Xi}^+ + c.c.$	$(1.35 \pm 0.24) \times 10^{-4}$	
$\Gamma_{82}$	$\Xi^0 \Xi^0$	$< 6 \times 10^{-5}$	CL=90%
$\Gamma_{83}$	$\Xi^- \Xi^+$	$(8.0 \pm 2.1) \times 10^{-5}$	
$\Gamma_{84}$	$\pi^+ \pi^- + K^+ K^-$	$< 2.1 \times 10^{-3}$	
$\Gamma_{85}$	$K_S^0 K_S^0$	$< 6 \times 10^{-5}$	CL=90%
$\Gamma_{86}$	$\eta_c \pi^+ \pi^-$	$< 3.2 \times 10^{-3}$	CL=90%

### Radiative decays

$\Gamma_{87}$	$\gamma J/\psi(1S)$	$(34.3 \pm 1.0) \%$	
$\Gamma_{88}$	$\gamma \rho^0$	$(2.16 \pm 0.17) \times 10^{-4}$	
$\Gamma_{89}$	$\gamma \omega$	$(6.8 \pm 0.8) \times 10^{-5}$	
$\Gamma_{90}$	$\gamma \phi$	$(2.4 \pm 0.5) \times 10^{-5}$	
$\Gamma_{91}$	$\gamma \gamma$	$< 6.3 \times 10^{-6}$	CL=90%
$\Gamma_{92}$	$e^+ e^- J/\psi(1S)$	$(3.46 \pm 0.22) \times 10^{-3}$	
$\Gamma_{93}$	$\mu^+ \mu^- J/\psi(1S)$	$(2.33 \pm 0.29) \times 10^{-4}$	

### CONSTRAINED FIT INFORMATION

A multiparticle fit to  $\chi_{c1}(1P)$ ,  $\chi_{c0}(1P)$ ,  $\chi_{c2}(1P)$ , and  $\psi(2S)$  with 4 total widths, a partial width, 25 combinations of partial widths obtained from integrated cross section, and 84 branching ratios uses 248 measurements to determine 49 parameters. The overall fit has a  $\chi^2 = 378.1$  for 199 degrees of freedom.

The following *off-diagonal* array elements are the correlation coefficients  $\langle \delta p_i \delta p_j \rangle / (\delta p_i \delta p_j)$ , in percent, from the fit to parameters  $p_i$ , including the branching fractions,  $x_i \equiv \Gamma_i / \Gamma_{total}$ .

$x_{44}$	3				
$x_{54}$	4	2			
$x_{67}$	7	3	4		
$x_{87}$	23	9	2	20	
$\Gamma$	-12	-5	-63	-10	-41
	$x_{17}$	$x_{44}$	$x_{54}$	$x_{67}$	$x_{87}$

### $\chi_{c1}(1P)$ PARTIAL WIDTHS

$\chi_{c1}(1P) \Gamma(i) \Gamma(\gamma J/\psi(1S)) / \Gamma_{total}$				$\Gamma_{54} \Gamma_{87} / \Gamma$
$\Gamma(\rho \bar{\rho}) \times \Gamma(\gamma J/\psi(1S)) / \Gamma_{total}$	VALUE (eV)	DOCUMENT ID	TECN	COMMENT
<b>21.9 ± 0.8 OUR FIT</b>				
<b>21.4 ± 0.9 OUR AVERAGE</b>				
21.5 ± 0.5 ± 0.8		<sup>1</sup> ANDREOTTI 05A	E835	$\rho \bar{\rho} \rightarrow e^+ e^- \gamma$
21.4 ± 1.5 ± 2.2		<sup>1,2</sup> ARMSTRONG 92	E760	$\bar{p} p \rightarrow e^+ e^- \gamma$
19.9 <sup>+4.4</sup> <sub>-4.0</sub>		<sup>1</sup> BAGLIN	86B SPEC	$\bar{p} p \rightarrow e^+ e^- X$
<sup>1</sup> Calculated by us using $B(J/\psi(1S) \rightarrow e^+ e^-) = 0.0593 \pm 0.0010$ .				
<sup>2</sup> Recalculated by ANDREOTTI 05A.				

### $\chi_{c1}(1P)$ BRANCHING RATIOS

#### HADRONIC DECAYS

$\Gamma(3(\pi^+ \pi^-)) / \Gamma_{total}$				$\Gamma_1 / \Gamma$
VALUE (units $10^{-3}$ )	DOCUMENT ID	TECN	COMMENT	
<b>5.8 ± 1.4 OUR EVALUATION</b>	Error includes scale factor of 1.2. Treating systematic error as correlated.			
<b>5.8 ± 1.1 OUR AVERAGE</b>				
5.4 ± 0.7 ± 0.9	<sup>1</sup> BAI	99B	BES	$\psi(2S) \rightarrow \gamma \chi_{c1}$
16.0 ± 5.9 ± 0.8	<sup>1</sup> TANENBAUM 78	MRK1	$\psi(2S) \rightarrow \gamma \chi_{c1}$	
<sup>1</sup> Rescaled by us using $B(\psi(2S) \rightarrow \gamma \chi_{c1}) = (8.8 \pm 0.4)\%$ and $B(\psi(2S) \rightarrow J/\psi(1S) \pi^+ \pi^-) = (32.6 \pm 0.5)\%$ .				
$\Gamma(2(\pi^+ \pi^-)) / \Gamma_{total}$				$\Gamma_2 / \Gamma$
VALUE (units $10^{-3}$ )	DOCUMENT ID	TECN	COMMENT	
<b>7.6 ± 2.6 OUR EVALUATION</b>	Treating systematic error as correlated.			
<b>8 ± 4 OUR AVERAGE</b>	Error includes scale factor of 1.5.			
4.6 ± 2.1 ± 2.6	<sup>1</sup> BAI	99B	BES	$\psi(2S) \rightarrow \gamma \chi_{c1}$
12.5 ± 4.2 ± 0.6	<sup>1</sup> TANENBAUM 78	MRK1	$\psi(2S) \rightarrow \gamma \chi_{c1}$	
<sup>1</sup> Rescaled by us using $B(\psi(2S) \rightarrow \gamma \chi_{c1}) = (8.8 \pm 0.4)\%$ and $B(\psi(2S) \rightarrow J/\psi(1S) \pi^+ \pi^-) = (32.6 \pm 0.5)\%$ .				

$\Gamma(\pi^+\pi^-\pi^0\pi^0)/\Gamma_{total}$					$\Gamma_3/\Gamma$
VALUE (%)	EVTS	DOCUMENT ID	TECN	COMMENT	

**1.19±0.15±0.03** 604.7 <sup>1</sup>HE 08B CLEO  $e^+e^- \rightarrow \gamma h^+h^-h^0h^0$   
<sup>1</sup>HE 08B reports  $1.28 \pm 0.06 \pm 0.15 \pm 0.08$  % from a measurement of  $[\Gamma(\chi_{c1}(1P) \rightarrow \pi^+\pi^-\pi^0\pi^0)/\Gamma_{total}] \times [B(\psi(2S) \rightarrow \gamma\chi_{c1}(1P))]$  assuming  $B(\psi(2S) \rightarrow \gamma\chi_{c1}(1P)) = (9.07 \pm 0.11 \pm 0.54) \times 10^{-2}$ , which we rescale to our best value  $B(\psi(2S) \rightarrow \gamma\chi_{c1}(1P)) = (9.75 \pm 0.24) \times 10^{-2}$ . Our first error is their experiment's error and our second error is the systematic error from using our best value.

$\Gamma(\rho^+\pi^-\pi^0 + c.c.)/\Gamma_{total}$					$\Gamma_4/\Gamma$
VALUE (%)	EVTS	DOCUMENT ID	TECN	COMMENT	

**1.45±0.24±0.04** 712.3 <sup>1,2</sup>HE 08B CLEO  $e^+e^- \rightarrow \gamma h^+h^-h^0h^0$   
<sup>1</sup>HE 08B reports  $1.56 \pm 0.13 \pm 0.22 \pm 0.10$  % from a measurement of  $[\Gamma(\chi_{c1}(1P) \rightarrow \rho^+\pi^-\pi^0 + c.c.)/\Gamma_{total}] \times [B(\psi(2S) \rightarrow \gamma\chi_{c1}(1P))]$  assuming  $B(\psi(2S) \rightarrow \gamma\chi_{c1}(1P)) = (9.07 \pm 0.11 \pm 0.54) \times 10^{-2}$ , which we rescale to our best value  $B(\psi(2S) \rightarrow \gamma\chi_{c1}(1P)) = (9.75 \pm 0.24) \times 10^{-2}$ . Our first error is their experiment's error and our second error is the systematic error from using our best value.  
<sup>2</sup>Calculated by us. We have added the values from HE 08B for  $\rho^+\pi^-\pi^0$  and  $\rho^-\pi^+\pi^0$  decays assuming uncorrelated statistical and fully correlated systematic uncertainties.

$\Gamma(\rho^0\pi^+\pi^-)/\Gamma_{total}$					$\Gamma_5/\Gamma$
VALUE (units $10^{-3}$ )	EVTS	DOCUMENT ID	TECN	COMMENT	

**3.9±3.5** <sup>1</sup>TANENBAUM 78 MRK1  $\psi(2S) \rightarrow \gamma\chi_{c1}$   
<sup>1</sup>Estimated using  $B(\psi(2S) \rightarrow \gamma\chi_{c1}(1P)) = 0.087$ . The errors do not contain the uncertainty in the  $\psi(2S)$  decay.

$\Gamma(4\pi^0)/\Gamma_{total}$					$\Gamma_6/\Gamma$
VALUE (units $10^{-4}$ )	EVTS	DOCUMENT ID	TECN	COMMENT	

**5.4±0.8±0.1** 608 <sup>1</sup>ABLIKIM 11A BES3  $e^+e^- \rightarrow \psi(2S) \rightarrow \gamma\chi_{c1}$   
<sup>1</sup>ABLIKIM 11A reports  $(0.57 \pm 0.03 \pm 0.08) \times 10^{-3}$  from a measurement of  $[\Gamma(\chi_{c1}(1P) \rightarrow 4\pi^0)/\Gamma_{total}] \times [B(\psi(2S) \rightarrow \gamma\chi_{c1}(1P))]$  assuming  $B(\psi(2S) \rightarrow \gamma\chi_{c1}(1P)) = (9.2 \pm 0.4) \times 10^{-2}$ , which we rescale to our best value  $B(\psi(2S) \rightarrow \gamma\chi_{c1}(1P)) = (9.75 \pm 0.24) \times 10^{-2}$ . Our first error is their experiment's error and our second error is the systematic error from using our best value.

$\Gamma(\pi^+\pi^-K^+K^-)/\Gamma_{total}$					$\Gamma_7/\Gamma$
VALUE (units $10^{-3}$ )	EVTS	DOCUMENT ID	TECN	COMMENT	

**4.5±1.0 OUR EVALUATION** Treating systematic error as correlated.  
**4.5±0.9 OUR AVERAGE**  
 4.2±0.4±0.9 <sup>1</sup>BAI 99B BES  $\psi(2S) \rightarrow \gamma\chi_{c1}$   
 7.3±3.0±0.4 <sup>1</sup>TANENBAUM 78 MRK1  $\psi(2S) \rightarrow \gamma\chi_{c1}$   
<sup>1</sup>Rescaled by us using  $B(\psi(2S) \rightarrow \gamma\chi_{c1}) = (8.8 \pm 0.4)\%$  and  $B(\psi(2S) \rightarrow J/\psi(1S)\pi^+\pi^-) = (32.6 \pm 0.5)\%$ .

$\Gamma(K^+K^-\pi^0\pi^0)/\Gamma_{total}$					$\Gamma_8/\Gamma$
VALUE (units $10^{-3}$ )	EVTS	DOCUMENT ID	TECN	COMMENT	

**1.12±0.27±0.03** 45.1 <sup>1</sup>HE 08B CLEO  $e^+e^- \rightarrow \gamma h^+h^-h^0h^0$   
<sup>1</sup>HE 08B reports  $(0.12 \pm 0.02 \pm 0.02 \pm 0.01) \times 10^{-2}$  from a measurement of  $[\Gamma(\chi_{c1}(1P) \rightarrow K^+K^-\pi^0\pi^0)/\Gamma_{total}] \times [B(\psi(2S) \rightarrow \gamma\chi_{c1}(1P))]$  assuming  $B(\psi(2S) \rightarrow \gamma\chi_{c1}(1P)) = (9.07 \pm 0.11 \pm 0.54) \times 10^{-2}$ , which we rescale to our best value  $B(\psi(2S) \rightarrow \gamma\chi_{c1}(1P)) = (9.75 \pm 0.24) \times 10^{-2}$ . Our first error is their experiment's error and our second error is the systematic error from using our best value.

$\Gamma(K^+K^-\pi^+\pi^-)/\Gamma_{total}$					$\Gamma_9/\Gamma$
VALUE (units $10^{-3}$ )	EVTS	DOCUMENT ID	TECN	COMMENT	

**11.46±0.12±1.29** 12k <sup>1</sup>ABLIKIM 13B BES3  $e^+e^- \rightarrow \psi(2S) \rightarrow \gamma\chi_{c1}$   
<sup>1</sup>Using  $1.06 \times 10^8$   $\psi(2S)$  mesons and  $B(\psi(2S) \rightarrow \chi_{c1}\gamma) = (9.2 \pm 0.4)\%$ .

$\Gamma(K_S^0K^\pm\pi^\mp\pi^\pm)/\Gamma_{total}$					$\Gamma_{10}/\Gamma$
VALUE (units $10^{-3}$ )	EVTS	DOCUMENT ID	TECN	COMMENT	

**7.5±0.11±0.79** 5.1k <sup>1</sup>ABLIKIM 13B BES3  $e^+e^- \rightarrow \psi(2S) \rightarrow \gamma\chi_{c1}$   
<sup>1</sup>Using  $1.06 \times 10^8$   $\psi(2S)$  mesons and  $B(\psi(2S) \rightarrow \chi_{c1}\gamma) = (9.2 \pm 0.4)\%$ .

$\Gamma(K^+\pi^-\bar{K}^0\pi^0 + c.c.)/\Gamma_{total}$					$\Gamma_{11}/\Gamma$
VALUE (%)	EVTS	DOCUMENT ID	TECN	COMMENT	

**0.86±0.13±0.02** 141.3 <sup>1</sup>HE 08B CLEO  $e^+e^- \rightarrow \gamma h^+h^-h^0h^0$   
<sup>1</sup>HE 08B reports  $0.92 \pm 0.09 \pm 0.11 \pm 0.06$  % from a measurement of  $[\Gamma(\chi_{c1}(1P) \rightarrow K^+\pi^-\bar{K}^0\pi^0 + c.c.)/\Gamma_{total}] \times [B(\psi(2S) \rightarrow \gamma\chi_{c1}(1P))]$  assuming  $B(\psi(2S) \rightarrow \gamma\chi_{c1}(1P)) = (9.07 \pm 0.11 \pm 0.54) \times 10^{-2}$ , which we rescale to our best value  $B(\psi(2S) \rightarrow \gamma\chi_{c1}(1P)) = (9.75 \pm 0.24) \times 10^{-2}$ . Our first error is their experiment's error and our second error is the systematic error from using our best value.

$\Gamma(\rho^-K^+\bar{K}^0 + c.c.)/\Gamma_{total}$					$\Gamma_{12}/\Gamma$
VALUE (%)	EVTS	DOCUMENT ID	TECN	COMMENT	

**0.50±0.12±0.01** 141.3 <sup>1</sup>HE 08B CLEO  $e^+e^- \rightarrow \gamma h^+h^-h^0h^0$   
<sup>1</sup>HE 08B reports  $0.54 \pm 0.11 \pm 0.07 \pm 0.03$  % from a measurement of  $[\Gamma(\chi_{c1}(1P) \rightarrow \rho^-K^+\bar{K}^0 + c.c.)/\Gamma_{total}] \times [B(\psi(2S) \rightarrow \gamma\chi_{c1}(1P))]$  assuming  $B(\psi(2S) \rightarrow \gamma\chi_{c1}(1P)) = (9.07 \pm 0.11 \pm 0.54) \times 10^{-2}$ , which we rescale to our best value  $B(\psi(2S) \rightarrow \gamma\chi_{c1}(1P)) = (9.75 \pm 0.24) \times 10^{-2}$ . Our first error is their experiment's error and our second error is the systematic error from using our best value.

$\Gamma(K^*(892)^0\bar{K}^0\pi^0 \rightarrow K^+\pi^-\bar{K}^0\pi^0 + c.c.)/\Gamma_{total}$					$\Gamma_{13}/\Gamma$
VALUE (%)	EVTS	DOCUMENT ID	TECN	COMMENT	

**0.23±0.06±0.01** 141.3 <sup>1</sup>HE 08B CLEO  $e^+e^- \rightarrow \gamma h^+h^-h^0h^0$   
<sup>1</sup>HE 08B reports  $0.25 \pm 0.06 \pm 0.03 \pm 0.02$  % from a measurement of  $[\Gamma(\chi_{c1}(1P) \rightarrow K^*(892)^0\bar{K}^0\pi^0 \rightarrow K^+\pi^-\bar{K}^0\pi^0 + c.c.)/\Gamma_{total}] \times [B(\psi(2S) \rightarrow \gamma\chi_{c1}(1P))]$  assuming  $B(\psi(2S) \rightarrow \gamma\chi_{c1}(1P)) = (9.07 \pm 0.11 \pm 0.54) \times 10^{-2}$ , which we rescale to our best value  $B(\psi(2S) \rightarrow \gamma\chi_{c1}(1P)) = (9.75 \pm 0.24) \times 10^{-2}$ . Our first error is their experiment's error and our second error is the systematic error from using our best value.

$\Gamma(K^+K^-\eta\pi^0)/\Gamma_{total}$					$\Gamma_{14}/\Gamma$
VALUE (%)	EVTS	DOCUMENT ID	TECN	COMMENT	

**0.112±0.034±0.003** 141.3 <sup>1</sup>HE 08B CLEO  $e^+e^- \rightarrow \gamma h^+h^-h^0h^0$   
<sup>1</sup>HE 08B reports  $0.12 \pm 0.03 \pm 0.02 \pm 0.01$  % from a measurement of  $[\Gamma(\chi_{c1}(1P) \rightarrow K^+K^-\eta\pi^0)/\Gamma_{total}] \times [B(\psi(2S) \rightarrow \gamma\chi_{c1}(1P))]$  assuming  $B(\psi(2S) \rightarrow \gamma\chi_{c1}(1P)) = (9.07 \pm 0.11 \pm 0.54) \times 10^{-2}$ , which we rescale to our best value  $B(\psi(2S) \rightarrow \gamma\chi_{c1}(1P)) = (9.75 \pm 0.24) \times 10^{-2}$ . Our first error is their experiment's error and our second error is the systematic error from using our best value.

$\Gamma(\pi^+\pi^-K_S^0K_S^0)/\Gamma_{total}$					$\Gamma_{15}/\Gamma$
VALUE (units $10^{-4}$ )	EVTS	DOCUMENT ID	TECN	COMMENT	

**6.9±2.9±0.2** 19.8±7.7 <sup>1</sup>ABLIKIM 05o BES2  $\psi(2S) \rightarrow \chi_{c1}\gamma$   
<sup>1</sup>ABLIKIM 05o reports  $[\Gamma(\chi_{c1}(1P) \rightarrow \pi^+\pi^-K_S^0K_S^0)/\Gamma_{total}] \times [B(\psi(2S) \rightarrow \gamma\chi_{c1}(1P))]$  =  $(0.67 \pm 0.26 \pm 0.11) \times 10^{-4}$  which we divide by our best value  $B(\psi(2S) \rightarrow \gamma\chi_{c1}(1P)) = (9.75 \pm 0.24) \times 10^{-2}$ . Our first error is their experiment's error and our second error is the systematic error from using our best value.

$\Gamma(K^+K^-\eta)/\Gamma_{total}$					$\Gamma_{16}/\Gamma$
VALUE (units $10^{-4}$ )	EVTS	DOCUMENT ID	TECN	COMMENT	

**3.2±1.0±0.1** <sup>1</sup>ATHAR 07 CLEO  $\psi(2S) \rightarrow \gamma h^+h^-h^0$   
<sup>1</sup>ATHAR 07 reports  $(0.34 \pm 0.10 \pm 0.04) \times 10^{-3}$  from a measurement of  $[\Gamma(\chi_{c1}(1P) \rightarrow K^+K^-\eta)/\Gamma_{total}] \times [B(\psi(2S) \rightarrow \gamma\chi_{c1}(1P))]$  assuming  $B(\psi(2S) \rightarrow \gamma\chi_{c1}(1P)) = 0.0907 \pm 0.0011 \pm 0.0054$ , which we rescale to our best value  $B(\psi(2S) \rightarrow \gamma\chi_{c1}(1P)) = (9.75 \pm 0.24) \times 10^{-2}$ . Our first error is their experiment's error and our second error is the systematic error from using our best value.

$\Gamma(\bar{K}^0K^+\pi^- + c.c.)/\Gamma_{total}$					$\Gamma_{17}/\Gamma$
VALUE (units $10^{-3}$ )	EVTS	DOCUMENT ID	TECN	COMMENT	

**7.0±0.6 OUR FIT**

$\Gamma(K^*(892)^0\bar{K}^0 + c.c.)/\Gamma_{total}$					$\Gamma_{18}/\Gamma$
VALUE (units $10^{-3}$ )	EVTS	DOCUMENT ID	TECN	COMMENT	

**0.98±0.37±0.02** 22 <sup>1</sup>ABLIKIM 06R BES2  $\psi(2S) \rightarrow \gamma\chi_{c1}$   
<sup>1</sup>ABLIKIM 06R reports  $(1.1 \pm 0.4 \pm 0.1) \times 10^{-3}$  from a measurement of  $[\Gamma(\chi_{c1}(1P) \rightarrow K^*(892)^0\bar{K}^0 + c.c.)/\Gamma_{total}] \times [B(\psi(2S) \rightarrow \gamma\chi_{c1}(1P))]$  assuming  $B(\psi(2S) \rightarrow \gamma\chi_{c1}(1P)) = (8.7 \pm 0.4) \times 10^{-2}$ , which we rescale to our best value  $B(\psi(2S) \rightarrow \gamma\chi_{c1}(1P)) = (9.75 \pm 0.24) \times 10^{-2}$ . Our first error is their experiment's error and our second error is the systematic error from using our best value.

$\Gamma(K^*(892)^+K^- + c.c.)/\Gamma_{total}$					$\Gamma_{19}/\Gamma$
VALUE (units $10^{-3}$ )	EVTS	DOCUMENT ID	TECN	COMMENT	

**1.43±0.65±0.03** 27 <sup>1</sup>ABLIKIM 06R BES2  $\psi(2S) \rightarrow \gamma\chi_{c1}$   
<sup>1</sup>ABLIKIM 06R reports  $(1.6 \pm 0.7 \pm 0.2) \times 10^{-3}$  from a measurement of  $[\Gamma(\chi_{c1}(1P) \rightarrow K^*(892)^+K^- + c.c.)/\Gamma_{total}] \times [B(\psi(2S) \rightarrow \gamma\chi_{c1}(1P))]$  assuming  $B(\psi(2S) \rightarrow \gamma\chi_{c1}(1P)) = (8.7 \pm 0.4) \times 10^{-2}$ , which we rescale to our best value  $B(\psi(2S) \rightarrow \gamma\chi_{c1}(1P)) = (9.75 \pm 0.24) \times 10^{-2}$ . Our first error is their experiment's error and our second error is the systematic error from using our best value.

$\Gamma(K_S^*(1430)^0\bar{K}^0 + c.c. \rightarrow K_S^0K^+\pi^- + c.c.)/\Gamma_{total}$					$\Gamma_{20}/\Gamma$
VALUE	CL%	DOCUMENT ID	TECN	COMMENT	

**<8 × 10<sup>-4</sup>** 90 <sup>1</sup>ABLIKIM 06R BES2  $\psi(2S) \rightarrow \gamma\chi_{c1}$   
<sup>1</sup>ABLIKIM 06R reports  $< 0.9 \times 10^{-3}$  from a measurement of  $[\Gamma(\chi_{c1}(1P) \rightarrow K_S^*(1430)^0\bar{K}^0 + c.c. \rightarrow K_S^0K^+\pi^- + c.c.)/\Gamma_{total}] \times [B(\psi(2S) \rightarrow \gamma\chi_{c1}(1P))]$  assuming  $B(\psi(2S) \rightarrow \gamma\chi_{c1}(1P)) = (8.7 \pm 0.4) \times 10^{-2}$ , which we rescale to our best value  $B(\psi(2S) \rightarrow \gamma\chi_{c1}(1P)) = 9.75 \times 10^{-2}$ .

$\Gamma(K_S^*(1430)^+K^- + c.c. \rightarrow K_S^0K^+\pi^- + c.c.)/\Gamma_{total}$					$\Gamma_{21}/\Gamma$
VALUE	CL%	DOCUMENT ID	TECN	COMMENT	

**<2.1 × 10<sup>-3</sup>** 90 <sup>1</sup>ABLIKIM 06R BES2  $\psi(2S) \rightarrow \gamma\chi_{c1}$   
<sup>1</sup>ABLIKIM 06R reports  $< 2.4 \times 10^{-3}$  from a measurement of  $[\Gamma(\chi_{c1}(1P) \rightarrow K_S^*(1430)^+K^- + c.c. \rightarrow K_S^0K^+\pi^- + c.c.)/\Gamma_{total}] \times [B(\psi(2S) \rightarrow \gamma\chi_{c1}(1P))]$  assuming  $B(\psi(2S) \rightarrow \gamma\chi_{c1}(1P)) = (8.7 \pm 0.4) \times 10^{-2}$ , which we rescale to our best value  $B(\psi(2S) \rightarrow \gamma\chi_{c1}(1P)) = 9.75 \times 10^{-2}$ .

$\Gamma(K^+K^-\pi^0)/\Gamma_{total}$					$\Gamma_{22}/\Gamma$
VALUE (units $10^{-3}$ )	EVTS	DOCUMENT ID	TECN	COMMENT	

**1.81±0.24±0.04** <sup>1</sup>ATHAR 07 CLEO  $\psi(2S) \rightarrow \gamma h^+h^-h^0$   
<sup>1</sup>ATHAR 07 reports  $(1.95 \pm 0.16 \pm 0.23) \times 10^{-3}$  from a measurement of  $[\Gamma(\chi_{c1}(1P) \rightarrow K^+K^-\pi^0)/\Gamma_{total}] \times [B(\psi(2S) \rightarrow \gamma\chi_{c1}(1P))]$  assuming  $B(\psi(2S) \rightarrow \gamma\chi_{c1}(1P)) = 0.0907 \pm 0.0011 \pm 0.0054$ , which we rescale to our best value  $B(\psi(2S) \rightarrow \gamma\chi_{c1}(1P)) = (9.75 \pm 0.24) \times 10^{-2}$ . Our first error is their experiment's error and our second error is the systematic error from using our best value.



$\Gamma(\pi^0 f_0(980) \rightarrow \pi^0 \pi^+ \pi^-) / \Gamma_{\text{total}}$		$\Gamma_{39} / \Gamma$	
VALUE (units $10^{-6}$ )	CL%	DOCUMENT ID	TECN COMMENT

**0.35 ± 0.09** ABLIKIM 18D BES3  $\psi(2S) \rightarrow \gamma \pi^0 \pi^+ \pi^-$   
 • • • We do not use the following data for averages, fits, limits, etc. • • •  
 <6 90 1 ABLIKIM 11D BES3  $\psi(2S) \rightarrow \gamma \pi^0 \pi^+ \pi^-$   
 1 ABLIKIM 11D reports  $[\Gamma(\chi_{c1}(1P) \rightarrow \pi^0 f_0(980) \rightarrow \pi^0 \pi^+ \pi^-) / \Gamma_{\text{total}}] \times [B(\psi(2S) \rightarrow \gamma \chi_{c1}(1P))] < 6.0 \times 10^{-7}$  which we divide by our best value  $B(\psi(2S) \rightarrow \gamma \chi_{c1}(1P)) = 9.75 \times 10^{-2}$ .

$\Gamma(K^+ \bar{K}^*(892)^0 \pi^- + \text{c.c.}) / \Gamma_{\text{total}}$		$\Gamma_{40} / \Gamma$	
VALUE (units $10^{-4}$ )	CL%	DOCUMENT ID	TECN COMMENT

**32 ± 21** 1 TANENBAUM 78 MRK1  $\psi(2S) \rightarrow \gamma \chi_{c1}$   
 1 Estimated using  $B(\psi(2S) \rightarrow \gamma \chi_{c1}(1P)) = 0.087$ . The errors do not contain the uncertainty in the  $\psi(2S)$  decay.

$\Gamma(K^*(892)^0 \bar{K}^*(892)^0) / \Gamma_{\text{total}}$		$\Gamma_{41} / \Gamma$	
VALUE (units $10^{-3}$ )	EVTS	DOCUMENT ID	TECN COMMENT

**1.44 ± 0.36 ± 0.03** 28.4 ± 5.5 1,2 ABLIKIM 04H BES  $\psi(2S) \rightarrow \gamma K^+ K^- \pi^+ \pi^-$   
 1 ABLIKIM 04H reports  $[\Gamma(\chi_{c1}(1P) \rightarrow K^*(892)^0 \bar{K}^*(892)^0) / \Gamma_{\text{total}}] \times [B(\psi(2S) \rightarrow \gamma \chi_{c1}(1P))] = (1.40 \pm 0.27 \pm 0.22) \times 10^{-4}$  which we divide by our best value  $B(\psi(2S) \rightarrow \gamma \chi_{c1}(1P)) = (9.75 \pm 0.24) \times 10^{-2}$ . Our first error is their experiment's error and our second error is the systematic error from using our best value.  
 2 Assumes  $B(K^*(892)^0 \rightarrow K^- \pi^+) = 2/3$ .

$\Gamma(K^+ K^- K_S^0 \bar{K}_S^0) / \Gamma_{\text{total}}$		$\Gamma_{42} / \Gamma$	
VALUE	CL%	EVTS	DOCUMENT ID TECN COMMENT

**<4 × 10<sup>-4</sup>** 90 3.2 ± 2.4 1 ABLIKIM 050 BES2  $\psi(2S) \rightarrow \chi_{c1} \gamma$   
 1 ABLIKIM 050 reports  $[\Gamma(\chi_{c1}(1P) \rightarrow K^+ K^- K_S^0 \bar{K}_S^0) / \Gamma_{\text{total}}] \times [B(\psi(2S) \rightarrow \gamma \chi_{c1}(1P))] < 4.2 \times 10^{-5}$  which we divide by our best value  $B(\psi(2S) \rightarrow \gamma \chi_{c1}(1P)) = 9.75 \times 10^{-2}$ .

$\Gamma(K_S^0 \bar{K}_S^0 K_S^0 \bar{K}_S^0) / \Gamma_{\text{total}}$		$\Gamma_{43} / \Gamma$	
VALUE (units $10^{-4}$ )	EVTS	DOCUMENT ID	TECN COMMENT

**0.35 ± 0.10 ± 0.01** 22 1 ABLIKIM 19AA BES3  $\psi(2S) \rightarrow \gamma 4K_S^0$   
 1 Using  $B(K_S^0 \rightarrow \pi^+ \pi^-) = (69.20 \pm 0.05)\%$ . ABLIKIM 19AA reports  $[\Gamma(\chi_{c1}(1P) \rightarrow K_S^0 \bar{K}_S^0 K_S^0 \bar{K}_S^0) / \Gamma_{\text{total}}] \times [B(\psi(2S) \rightarrow \gamma \chi_{c1}(1P))] = (3.4 \pm 0.9 \pm 0.3) \times 10^{-6}$  which we divide by our best value  $B(\psi(2S) \rightarrow \gamma \chi_{c1}(1P)) = (9.75 \pm 0.24) \times 10^{-2}$ . Our first error is their experiment's error and our second error is the systematic error from using our best value.

$\Gamma(K^+ K^- K^+ K^-) / \Gamma_{\text{total}}$		$\Gamma_{44} / \Gamma$	
VALUE (units $10^{-3}$ )	CL%	DOCUMENT ID	TECN COMMENT

**0.54 ± 0.11 OUR FIT**

$\Gamma(K^+ K^- \phi) / \Gamma_{\text{total}}$		$\Gamma_{45} / \Gamma$	
VALUE (units $10^{-3}$ )	EVTS	DOCUMENT ID	TECN COMMENT

**0.41 ± 0.15 ± 0.01** 17 1 ABLIKIM 06T BES2  $\psi(2S) \rightarrow \gamma 2K^+ 2K^-$   
 1 ABLIKIM 06T reports  $(0.46 \pm 0.16 \pm 0.06) \times 10^{-3}$  from a measurement of  $[\Gamma(\chi_{c1}(1P) \rightarrow K^+ K^- \phi) / \Gamma_{\text{total}}] \times [B(\psi(2S) \rightarrow \gamma \chi_{c1}(1P))]$  assuming  $B(\psi(2S) \rightarrow \gamma \chi_{c1}(1P)) = (8.7 \pm 0.4) \times 10^{-2}$ , which we rescale to our best value  $B(\psi(2S) \rightarrow \gamma \chi_{c1}(1P)) = (9.75 \pm 0.24) \times 10^{-2}$ . Our first error is their experiment's error and our second error is the systematic error from using our best value.

$\Gamma(\bar{K}^0 K^+ \pi^- \phi + \text{c.c.}) / \Gamma_{\text{total}}$		$\Gamma_{46} / \Gamma$	
VALUE (units $10^{-3}$ )	CL%	DOCUMENT ID	TECN COMMENT

**3.27 ± 0.28 ± 0.46** ABLIKIM 15M BES3  $\psi(2S) \rightarrow \gamma \chi_{c1}$

$\Gamma(K^+ K^- \pi^0 \phi) / \Gamma_{\text{total}}$		$\Gamma_{47} / \Gamma$	
VALUE (units $10^{-3}$ )	CL%	DOCUMENT ID	TECN COMMENT

**1.62 ± 0.12 ± 0.28** ABLIKIM 15M BES3  $\psi(2S) \rightarrow \gamma \chi_{c1}$

$\Gamma(\phi \pi^+ \pi^- \pi^0) / \Gamma_{\text{total}}$		$\Gamma_{48} / \Gamma$	
VALUE (units $10^{-3}$ )	EVTS	DOCUMENT ID	TECN COMMENT

**0.75 ± 0.06 ± 0.08** 373 1 ABLIKIM 13B BES3  $e^+ e^- \rightarrow \psi(2S) \rightarrow \gamma \chi_{c1}$   
 1 Using  $1.06 \times 10^8 \psi(2S)$  mesons and  $B(\psi(2S) \rightarrow \chi_{c1} \gamma) = (9.2 \pm 0.4)\%$ .

$\Gamma(\omega \gamma) / \Gamma_{\text{total}}$		$\Gamma_{49} / \Gamma$	
VALUE (units $10^{-4}$ )	EVTS	DOCUMENT ID	TECN COMMENT

**5.7 ± 0.7 ± 0.1** 597 1 ABLIKIM 11K BES3  $\psi(2S) \rightarrow \gamma$  hadrons  
 1 ABLIKIM 11K reports  $(6.0 \pm 0.3 \pm 0.7) \times 10^{-4}$  from a measurement of  $[\Gamma(\chi_{c1}(1P) \rightarrow \omega \gamma) / \Gamma_{\text{total}}] \times [B(\psi(2S) \rightarrow \gamma \chi_{c1}(1P))]$  assuming  $B(\psi(2S) \rightarrow \gamma \chi_{c1}(1P)) = (9.2 \pm 0.4) \times 10^{-2}$ , which we rescale to our best value  $B(\psi(2S) \rightarrow \gamma \chi_{c1}(1P)) = (9.75 \pm 0.24) \times 10^{-2}$ . Our first error is their experiment's error and our second error is the systematic error from using our best value.

$\Gamma(\omega K^+ K^-) / \Gamma_{\text{total}}$		$\Gamma_{50} / \Gamma$	
VALUE (units $10^{-3}$ )	EVTS	DOCUMENT ID	TECN COMMENT

**0.75 ± 0.04 ± 0.08** 628 1 ABLIKIM 13B BES3  $e^+ e^- \rightarrow \psi(2S) \rightarrow \gamma \chi_{c1}$   
 1 Using  $1.06 \times 10^8 \psi(2S)$  mesons and  $B(\psi(2S) \rightarrow \chi_{c1} \gamma) = (9.2 \pm 0.4)\%$ .

$\Gamma(\omega \phi) / \Gamma_{\text{total}}$		$\Gamma_{51} / \Gamma$	
VALUE (units $10^{-4}$ )	EVTS	DOCUMENT ID	TECN COMMENT

**0.27 ± 0.04 ± 0.01** 105 1 ABLIKIM 19J BES3  $\psi(2S) \rightarrow \gamma$  hadrons  
 • • • We do not use the following data for averages, fits, limits, etc. • • •  
 0.21 ± 0.06 ± 0.01 15 2,3 ABLIKIM 11K BES3  $\psi(2S) \rightarrow \gamma$  hadrons  
 1 ABLIKIM 19J reports  $[\Gamma(\chi_{c1}(1P) \rightarrow \omega \phi) / \Gamma_{\text{total}}] \times [B(\psi(2S) \rightarrow \gamma \chi_{c1}(1P))] = (2.67 \pm 0.31 \pm 0.27) \times 10^{-6}$  which we divide by our best value  $B(\psi(2S) \rightarrow \gamma \chi_{c1}(1P)) = (9.75 \pm 0.24) \times 10^{-2}$ . Our first error is their experiment's error and our second error is the systematic error from using our best value.  
 2 ABLIKIM 11K reports  $(0.22 \pm 0.06 \pm 0.02) \times 10^{-4}$  from a measurement of  $[\Gamma(\chi_{c1}(1P) \rightarrow \omega \phi) / \Gamma_{\text{total}}] \times [B(\psi(2S) \rightarrow \gamma \chi_{c1}(1P))]$  assuming  $B(\psi(2S) \rightarrow \gamma \chi_{c1}(1P)) = (9.2 \pm 0.4) \times 10^{-2}$ , which we rescale to our best value  $B(\psi(2S) \rightarrow \gamma \chi_{c1}(1P)) = (9.75 \pm 0.24) \times 10^{-2}$ . Our first error is their experiment's error and our second error is the systematic error from using our best value.  
 3 Superseded by ABLIKIM 19J.

$\Gamma(\phi \phi) / \Gamma_{\text{total}}$		$\Gamma_{52} / \Gamma$	
VALUE (units $10^{-4}$ )	EVTS	DOCUMENT ID	TECN COMMENT

**4.2 ± 0.5 ± 0.1** 366 1 ABLIKIM 11K BES3  $\psi(2S) \rightarrow \gamma$  hadrons  
 1 ABLIKIM 11K reports  $(4.4 \pm 0.3 \pm 0.5) \times 10^{-4}$  from a measurement of  $[\Gamma(\chi_{c1}(1P) \rightarrow \phi \phi) / \Gamma_{\text{total}}] \times [B(\psi(2S) \rightarrow \gamma \chi_{c1}(1P))]$  assuming  $B(\psi(2S) \rightarrow \gamma \chi_{c1}(1P)) = (9.2 \pm 0.4) \times 10^{-2}$ , which we rescale to our best value  $B(\psi(2S) \rightarrow \gamma \chi_{c1}(1P)) = (9.75 \pm 0.24) \times 10^{-2}$ . Our first error is their experiment's error and our second error is the systematic error from using our best value.

$\Gamma(\phi \phi \eta) / \Gamma_{\text{total}}$		$\Gamma_{53} / \Gamma$	
VALUE (units $10^{-4}$ )	EVTS	DOCUMENT ID	TECN COMMENT

**3.0 ± 0.4 ± 0.2** 83.6 1 ABLIKIM 20B BES3  $\psi(2S) \rightarrow \gamma \phi \phi \eta$   
 1 ABLIKIM 20B reports  $(2.96 \pm 0.43 \pm 0.22) \times 10^{-4}$  from a measurement of  $[\Gamma(\chi_{c1}(1P) \rightarrow \phi \phi \eta) / \Gamma_{\text{total}}] \times [B(\psi(2S) \rightarrow \gamma \chi_{c1}(1P))]$  assuming  $B(\psi(2S) \rightarrow \gamma \chi_{c1}(1P)) = (9.75 \pm 0.24) \times 10^{-2}$ .

$\Gamma(p \bar{p}) / \Gamma_{\text{total}}$		$\Gamma_{54} / \Gamma$	
VALUE (units $10^{-4}$ )	CL%	DOCUMENT ID	TECN COMMENT

**0.760 ± 0.034 OUR FIT**

$\Gamma(p \bar{p} \pi^0) / \Gamma_{\text{total}}$		$\Gamma_{55} / \Gamma$	
VALUE (units $10^{-3}$ )	CL%	DOCUMENT ID	TECN COMMENT

**0.155 ± 0.018 OUR AVERAGE**  
 0.163 ± 0.019 ± 0.004 1 ONYISI 10 CLE3  $\psi(2S) \rightarrow \gamma p \bar{p} X$   
 0.112 ± 0.047 ± 0.003 2 ATHAR 07 CLEO  $\psi(2S) \rightarrow \gamma h^+ h^- h^0$   
 1 ONYISI 10 reports  $(1.75 \pm 0.16 \pm 0.13 \pm 0.11) \times 10^{-4}$  from a measurement of  $[\Gamma(\chi_{c1}(1P) \rightarrow p \bar{p} \pi^0) / \Gamma_{\text{total}}] \times [B(\psi(2S) \rightarrow \gamma \chi_{c1}(1P))]$  assuming  $B(\psi(2S) \rightarrow \gamma \chi_{c1}(1P)) = (9.07 \pm 0.11 \pm 0.54) \times 10^{-2}$ , which we rescale to our best value  $B(\psi(2S) \rightarrow \gamma \chi_{c1}(1P)) = (9.75 \pm 0.24) \times 10^{-2}$ . Our first error is their experiment's error and our second error is the systematic error from using our best value.  
 2 ATHAR 07 reports  $(1.2 \pm 0.5 \pm 0.1) \times 10^{-4}$  from a measurement of  $[\Gamma(\chi_{c1}(1P) \rightarrow p \bar{p} \pi^0) / \Gamma_{\text{total}}] \times [B(\psi(2S) \rightarrow \gamma \chi_{c1}(1P))]$  assuming  $B(\psi(2S) \rightarrow \gamma \chi_{c1}(1P)) = (9.07 \pm 0.11 \pm 0.54) \times 10^{-2}$ , which we rescale to our best value  $B(\psi(2S) \rightarrow \gamma \chi_{c1}(1P)) = (9.75 \pm 0.24) \times 10^{-2}$ . Our first error is their experiment's error and our second error is the systematic error from using our best value.

$\Gamma(p \bar{p} \eta) / \Gamma_{\text{total}}$		$\Gamma_{56} / \Gamma$	
VALUE (units $10^{-3}$ )	CL%	DOCUMENT ID	TECN COMMENT

**0.145 ± 0.024 ± 0.004** 1 ONYISI 10 CLE3  $\psi(2S) \rightarrow \gamma p \bar{p} X$   
 • • • We do not use the following data for averages, fits, limits, etc. • • •  
 <0.15 90 2 ATHAR 07 CLEO  $\psi(2S) \rightarrow \gamma h^+ h^- h^0$   
 1 ONYISI 10 reports  $(1.56 \pm 0.22 \pm 0.14 \pm 0.10) \times 10^{-4}$  from a measurement of  $[\Gamma(\chi_{c1}(1P) \rightarrow p \bar{p} \eta) / \Gamma_{\text{total}}] \times [B(\psi(2S) \rightarrow \gamma \chi_{c1}(1P))]$  assuming  $B(\psi(2S) \rightarrow \gamma \chi_{c1}(1P)) = (9.07 \pm 0.11 \pm 0.54) \times 10^{-2}$ , which we rescale to our best value  $B(\psi(2S) \rightarrow \gamma \chi_{c1}(1P)) = (9.75 \pm 0.24) \times 10^{-2}$ . Our first error is their experiment's error and our second error is the systematic error from using our best value.  
 2 ATHAR 07 reports  $< 0.16 \times 10^{-3}$  from a measurement of  $[\Gamma(\chi_{c1}(1P) \rightarrow p \bar{p} \eta) / \Gamma_{\text{total}}] \times [B(\psi(2S) \rightarrow \gamma \chi_{c1}(1P))]$  assuming  $B(\psi(2S) \rightarrow \gamma \chi_{c1}(1P)) = (9.07 \pm 0.11 \pm 0.54) \times 10^{-2}$ , which we rescale to our best value  $B(\psi(2S) \rightarrow \gamma \chi_{c1}(1P)) = 9.75 \times 10^{-2}$ .

$\Gamma(p \bar{p} \omega) / \Gamma_{\text{total}}$		$\Gamma_{57} / \Gamma$	
VALUE (units $10^{-3}$ )	CL%	DOCUMENT ID	TECN COMMENT

**0.212 ± 0.030 ± 0.005** 1 ONYISI 10 CLE3  $\psi(2S) \rightarrow \gamma p \bar{p} X$   
 1 ONYISI 10 reports  $(2.28 \pm 0.28 \pm 0.16 \pm 0.14) \times 10^{-4}$  from a measurement of  $[\Gamma(\chi_{c1}(1P) \rightarrow p \bar{p} \omega) / \Gamma_{\text{total}}] \times [B(\psi(2S) \rightarrow \gamma \chi_{c1}(1P))]$  assuming  $B(\psi(2S) \rightarrow \gamma \chi_{c1}(1P)) = (9.07 \pm 0.11 \pm 0.54) \times 10^{-2}$ , which we rescale to our best value  $B(\psi(2S) \rightarrow \gamma \chi_{c1}(1P)) = (9.75 \pm 0.24) \times 10^{-2}$ . Our first error is their experiment's error and our second error is the systematic error from using our best value.

$\Gamma(p \bar{p} \phi) / \Gamma_{\text{total}}$		$\Gamma_{58} / \Gamma$	
VALUE	CL%	DOCUMENT ID	TECN COMMENT

**<1.7 × 10<sup>-5</sup>** 90 1 ABLIKIM 11F BES3  $\psi(2S) \rightarrow \gamma p \bar{p} K^+ K^-$   
 1 ABLIKIM 11F reports  $< 1.82 \times 10^{-5}$  from a measurement of  $[\Gamma(\chi_{c1}(1P) \rightarrow p \bar{p} \phi) / \Gamma_{\text{total}}] \times [B(\psi(2S) \rightarrow \gamma \chi_{c1}(1P))]$  assuming  $B(\psi(2S) \rightarrow \gamma \chi_{c1}(1P)) = (9.2 \pm 0.4) \times 10^{-2}$ , which we rescale to our best value  $B(\psi(2S) \rightarrow \gamma \chi_{c1}(1P)) = 9.75 \times 10^{-2}$ .



## Meson Particle Listings

 $\chi_{c1}(1P)$  $\Gamma(p\bar{p}\pi^+\pi^-)/\Gamma_{\text{total}}$   $\Gamma_{59}/\Gamma$ 

VALUE (units $10^{-3}$ )	CL%	DOCUMENT ID	TECN	COMMENT
<b>0.50±0.19 OUR EVALUATION</b>				Treating systematic error as correlated.
<b>0.50±0.19 OUR AVERAGE</b>				
0.46±0.12±0.15		<sup>1</sup> BAI	99B BES	$\psi(2S) \rightarrow \gamma\chi_{c1}$
1.08±0.77±0.05		<sup>1</sup> TANENBAUM	78 MRK1	$\psi(2S) \rightarrow \gamma\chi_{c1}$
<sup>1</sup> Rescaled by us using $B(\psi(2S) \rightarrow \gamma\chi_{c1}) = (8.8 \pm 0.4)\%$ and $B(\psi(2S) \rightarrow J/\psi(1S)\pi^+\pi^-) = (32.6 \pm 0.5)\%$ .				

 $\Gamma(p\bar{p}\pi^0\pi^0)/\Gamma_{\text{total}}$   $\Gamma_{60}/\Gamma$ 

VALUE	CL%	DOCUMENT ID	TECN	COMMENT
<b>&lt;5 × 10<sup>-4</sup></b>	90	<sup>1</sup> HE	08B CLEO	$e^+e^- \rightarrow \gamma h^+ h^- h^0$
<sup>1</sup> HE 08B reports $< 0.05 \times 10^{-2}$ from a measurement of $[\Gamma(\chi_{c1}(1P) \rightarrow p\bar{p}\pi^0\pi^0)/\Gamma_{\text{total}}] \times [B(\psi(2S) \rightarrow \gamma\chi_{c1}(1P))]$ assuming $B(\psi(2S) \rightarrow \gamma\chi_{c1}(1P)) = (9.07 \pm 0.11 \pm 0.54) \times 10^{-2}$ , which we rescale to our best value $B(\psi(2S) \rightarrow \gamma\chi_{c1}(1P)) = 9.75 \times 10^{-2}$ .				

 $\Gamma(p\bar{p}K^+K^- \text{ (non-resonant)})/\Gamma_{\text{total}}$   $\Gamma_{61}/\Gamma$ 

VALUE (units $10^{-4}$ )	EVTS	DOCUMENT ID	TECN	COMMENT
<b>1.27±0.22±0.03</b>	82 ± 9	<sup>1</sup> ABLIKIM	11F BES3	$\psi(2S) \rightarrow \gamma p\bar{p}K^+K^-$
<sup>1</sup> ABLIKIM 11F reports $(1.35 \pm 0.15 \pm 0.19) \times 10^{-4}$ from a measurement of $[\Gamma(\chi_{c1}(1P) \rightarrow p\bar{p}K^+K^- \text{ (non-resonant)})/\Gamma_{\text{total}}] \times [B(\psi(2S) \rightarrow \gamma\chi_{c1}(1P))]$ assuming $B(\psi(2S) \rightarrow \gamma\chi_{c1}(1P)) = (9.2 \pm 0.4) \times 10^{-2}$ , which we rescale to our best value $B(\psi(2S) \rightarrow \gamma\chi_{c1}(1P)) = (9.75 \pm 0.24) \times 10^{-2}$ . Our first error is their experiment's error and our second error is the systematic error from using our best value.				

 $\Gamma(p\bar{p}K_S^0 K_S^0)/\Gamma_{\text{total}}$   $\Gamma_{62}/\Gamma$ 

VALUE (units $10^{-4}$ )	CL%	DOCUMENT ID	TECN	COMMENT
<b>&lt;4.5</b>	90	<sup>1</sup> ABLIKIM	06D BES2	$\psi(2S) \rightarrow \gamma\chi_{c1}$
<sup>1</sup> Using $B(\psi(2S) \rightarrow \chi_{c1}\gamma) = (9.1 \pm 0.6)\%$ .				

 $\Gamma(p\bar{p}\pi^-)/\Gamma_{\text{total}}$   $\Gamma_{63}/\Gamma$ 

VALUE (units $10^{-4}$ )	EVTS	DOCUMENT ID	TECN	COMMENT
<b>3.8±0.5±0.1</b>	1412	<sup>1</sup> ABLIKIM	12J BES3	$\psi(2S) \rightarrow \gamma p\bar{p}\pi^-$
<sup>1</sup> ABLIKIM 12J reports $[\Gamma(\chi_{c1}(1P) \rightarrow p\bar{p}\pi^-)/\Gamma_{\text{total}}] \times [B(\psi(2S) \rightarrow \gamma\chi_{c1}(1P))] = (0.37 \pm 0.02 \pm 0.04) \times 10^{-4}$ which we divide by our best value $B(\psi(2S) \rightarrow \gamma\chi_{c1}(1P)) = (9.75 \pm 0.24) \times 10^{-2}$ . Our first error is their experiment's error and our second error is the systematic error from using our best value.				

 $\Gamma(\bar{p}n\pi^+)/\Gamma_{\text{total}}$   $\Gamma_{64}/\Gamma$ 

VALUE (units $10^{-4}$ )	EVTS	DOCUMENT ID	TECN	COMMENT
<b>3.9±0.5±0.1</b>	1625	<sup>1</sup> ABLIKIM	12J BES3	$\psi(2S) \rightarrow \gamma \bar{p}n\pi^+$
<sup>1</sup> ABLIKIM 12J reports $[\Gamma(\chi_{c1}(1P) \rightarrow \bar{p}n\pi^+)/\Gamma_{\text{total}}] \times [B(\psi(2S) \rightarrow \gamma\chi_{c1}(1P))] = (0.38 \pm 0.02 \pm 0.04) \times 10^{-4}$ which we divide by our best value $B(\psi(2S) \rightarrow \gamma\chi_{c1}(1P)) = (9.75 \pm 0.24) \times 10^{-2}$ . Our first error is their experiment's error and our second error is the systematic error from using our best value.				

 $\Gamma(p\bar{p}\pi^-\pi^0)/\Gamma_{\text{total}}$   $\Gamma_{65}/\Gamma$ 

VALUE (units $10^{-4}$ )	EVTS	DOCUMENT ID	TECN	COMMENT
<b>10.3±1.1±0.2</b>	1082	<sup>1</sup> ABLIKIM	12J BES3	$\psi(2S) \rightarrow \gamma p\bar{p}\pi^-\pi^0$
<sup>1</sup> ABLIKIM 12J reports $[\Gamma(\chi_{c1}(1P) \rightarrow p\bar{p}\pi^-\pi^0)/\Gamma_{\text{total}}] \times [B(\psi(2S) \rightarrow \gamma\chi_{c1}(1P))] = (1.00 \pm 0.05 \pm 0.10) \times 10^{-4}$ which we divide by our best value $B(\psi(2S) \rightarrow \gamma\chi_{c1}(1P)) = (9.75 \pm 0.24) \times 10^{-2}$ . Our first error is their experiment's error and our second error is the systematic error from using our best value.				

 $\Gamma(\bar{p}n\pi^+\pi^0)/\Gamma_{\text{total}}$   $\Gamma_{66}/\Gamma$ 

VALUE (units $10^{-4}$ )	EVTS	DOCUMENT ID	TECN	COMMENT
<b>10.1±1.1±0.2</b>	1261	<sup>1</sup> ABLIKIM	12J BES3	$\psi(2S) \rightarrow \gamma \bar{p}n\pi^+\pi^0$
<sup>1</sup> ABLIKIM 12J reports $[\Gamma(\chi_{c1}(1P) \rightarrow \bar{p}n\pi^+\pi^0)/\Gamma_{\text{total}}] \times [B(\psi(2S) \rightarrow \gamma\chi_{c1}(1P))] = (0.98 \pm 0.05 \pm 0.10) \times 10^{-4}$ which we divide by our best value $B(\psi(2S) \rightarrow \gamma\chi_{c1}(1P)) = (9.75 \pm 0.24) \times 10^{-2}$ . Our first error is their experiment's error and our second error is the systematic error from using our best value.				

 $\Gamma(\Lambda\bar{\Lambda})/\Gamma_{\text{total}}$   $\Gamma_{67}/\Gamma$ 

VALUE (units $10^{-4}$ )	DOCUMENT ID
<b>1.14±0.11 OUR FIT</b>	

 $\Gamma(\Lambda\bar{\Lambda}\pi^+\pi^-)/\Gamma_{\text{total}}$   $\Gamma_{68}/\Gamma$ 

VALUE (units $10^{-5}$ )	CL%	EVTS	DOCUMENT ID	TECN	COMMENT
<b>29±5±1</b>	105		<sup>1</sup> ABLIKIM	12I BES3	$\psi(2S) \rightarrow \gamma\Lambda\bar{\Lambda}\pi^+\pi^-$
••• We do not use the following data for averages, fits, limits, etc. •••					
<150	90		<sup>2</sup> ABLIKIM	06D BES2	$\psi(2S) \rightarrow \gamma\chi_{c1}$
<sup>1</sup> ABLIKIM 12I reports $(31.1 \pm 3.4 \pm 3.9) \times 10^{-5}$ from a measurement of $[\Gamma(\chi_{c1}(1P) \rightarrow \Lambda\bar{\Lambda}\pi^+\pi^-)/\Gamma_{\text{total}}] \times [B(\psi(2S) \rightarrow \gamma\chi_{c1}(1P))]$ assuming $B(\psi(2S) \rightarrow \gamma\chi_{c1}(1P)) = (9.2 \pm 0.4) \times 10^{-2}$ , which we rescale to our best value $B(\psi(2S) \rightarrow \gamma\chi_{c1}(1P)) = (9.75 \pm 0.24) \times 10^{-2}$ . Our first error is their experiment's error and our second error is the systematic error from using our best value.					
<sup>2</sup> Using $B(\psi(2S) \rightarrow \chi_{c1}\gamma) = (9.1 \pm 0.6)\%$ .					

 $\Gamma(\Lambda\bar{\Lambda}\pi^+\pi^- \text{ (non-resonant)})/\Gamma_{\text{total}}$   $\Gamma_{69}/\Gamma$ 

VALUE (units $10^{-5}$ )	EVTS	DOCUMENT ID	TECN	COMMENT
<b>25±6±1</b>	13	<sup>1</sup> ABLIKIM	12I BES3	$\psi(2S) \rightarrow \gamma\Lambda\bar{\Lambda}\pi^+\pi^-$
<sup>1</sup> ABLIKIM 12I reports $(26.2 \pm 5.5 \pm 3.3) \times 10^{-5}$ from a measurement of $[\Gamma(\chi_{c1}(1P) \rightarrow \Lambda\bar{\Lambda}\pi^+\pi^- \text{ (non-resonant)})/\Gamma_{\text{total}}] \times [B(\psi(2S) \rightarrow \gamma\chi_{c1}(1P))]$ assuming $B(\psi(2S) \rightarrow \gamma\chi_{c1}(1P)) = (9.2 \pm 0.4) \times 10^{-2}$ , which we rescale to our best value $B(\psi(2S) \rightarrow \gamma\chi_{c1}(1P)) = (9.75 \pm 0.24) \times 10^{-2}$ . Our first error is their experiment's error and our second error is the systematic error from using our best value.				

 $\Gamma(\Sigma(1385)^+\bar{\Lambda}\pi^- + \text{c.c.})/\Gamma_{\text{total}}$   $\Gamma_{70}/\Gamma$ 

VALUE	CL%	DOCUMENT ID	TECN	COMMENT
<b>&lt;1.3 × 10<sup>-4</sup></b>	90	<sup>1</sup> ABLIKIM	12I BES3	$\psi(2S) \rightarrow \gamma\Sigma(1385)^+\bar{\Lambda}\pi^-$
<sup>1</sup> ABLIKIM 12I reports $< 14 \times 10^{-5}$ from a measurement of $[\Gamma(\chi_{c1}(1P) \rightarrow \Sigma(1385)^+\bar{\Lambda}\pi^- + \text{c.c.})/\Gamma_{\text{total}}] \times [B(\psi(2S) \rightarrow \gamma\chi_{c1}(1P))]$ assuming $B(\psi(2S) \rightarrow \gamma\chi_{c1}(1P)) = (9.2 \pm 0.4) \times 10^{-2}$ , which we rescale to our best value $B(\psi(2S) \rightarrow \gamma\chi_{c1}(1P)) = 9.75 \times 10^{-2}$ .				

 $\Gamma(\Sigma(1385)^-\bar{\Lambda}\pi^+ + \text{c.c.})/\Gamma_{\text{total}}$   $\Gamma_{71}/\Gamma$ 

VALUE (units $10^{-5}$ )	CL%	DOCUMENT ID	TECN	COMMENT
<b>&lt;13</b>	90	<sup>1</sup> ABLIKIM	12I BES3	$\psi(2S) \rightarrow \gamma\Sigma(1385)^-\bar{\Lambda}\pi^+$
<sup>1</sup> ABLIKIM 12I reports $< 14 \times 10^{-5}$ from a measurement of $[\Gamma(\chi_{c1}(1P) \rightarrow \Sigma(1385)^-\bar{\Lambda}\pi^+ + \text{c.c.})/\Gamma_{\text{total}}] \times [B(\psi(2S) \rightarrow \gamma\chi_{c1}(1P))]$ assuming $B(\psi(2S) \rightarrow \gamma\chi_{c1}(1P)) = (9.2 \pm 0.4) \times 10^{-2}$ , which we rescale to our best value $B(\psi(2S) \rightarrow \gamma\chi_{c1}(1P)) = 9.75 \times 10^{-2}$ .				

 $\Gamma(K^+\bar{p}\Lambda + \text{c.c.})/\Gamma_{\text{total}}$   $\Gamma_{72}/\Gamma$ 

VALUE (units $10^{-4}$ )	EVTS	DOCUMENT ID	TECN	COMMENT
<b>4.2±0.4 OUR AVERAGE</b>				Error includes scale factor of 1.2.
9.0 <sup>+2.7</sup> <sub>-2.3</sub> ±0.6	24	<sup>1</sup> LU	19 BELL	$B^+ \rightarrow \bar{p}\Lambda K^+ K^+$
4.2±0.4±0.1	3k	<sup>2,3</sup> ABLIKIM	13D BES3	$\psi(2S) \rightarrow \gamma\Lambda\bar{p}K^+$
3.1±0.9±0.1		<sup>4</sup> ATHAR	07 CLEO	$\psi(2S) \rightarrow \gamma h^+ h^- h^0$
<sup>1</sup> LU 19 reports $(9.15 \pm 2.63 \pm 0.86) \times 10^{-4}$ from a measurement of $[\Gamma(\chi_{c1}(1P) \rightarrow K^+\bar{p}\Lambda + \text{c.c.})/\Gamma_{\text{total}}] \times [B(B^+ \rightarrow \chi_{c1}(1P)K^+)]$ assuming $B(B^+ \rightarrow \chi_{c1}(1P)K^+) = (4.79 \pm 0.23) \times 10^{-4}$ , which we rescale to our best value $B(B^+ \rightarrow \chi_{c1}(1P)K^+) = (4.85 \pm 0.33) \times 10^{-4}$ . Our first error is their experiment's error and our second error is the systematic error from using our best value.				
<sup>2</sup> ABLIKIM 13D reports $(4.5 \pm 0.2 \pm 0.4) \times 10^{-4}$ from a measurement of $[\Gamma(\chi_{c1}(1P) \rightarrow K^+\bar{p}\Lambda + \text{c.c.})/\Gamma_{\text{total}}] \times [B(\psi(2S) \rightarrow \gamma\chi_{c1}(1P))]$ assuming $B(\psi(2S) \rightarrow \gamma\chi_{c1}(1P)) = (9.2 \pm 0.4) \times 10^{-2}$ , which we rescale to our best value $B(\psi(2S) \rightarrow \gamma\chi_{c1}(1P)) = (9.75 \pm 0.24) \times 10^{-2}$ . Our first error is their experiment's error and our second error is the systematic error from using our best value.				
<sup>3</sup> Using $B(\Lambda \rightarrow p\pi^-) = 63.9\%$ .				
<sup>4</sup> ATHAR 07 reports $(3.3 \pm 0.9 \pm 0.4) \times 10^{-4}$ from a measurement of $[\Gamma(\chi_{c1}(1P) \rightarrow K^+\bar{p}\Lambda + \text{c.c.})/\Gamma_{\text{total}}] \times [B(\psi(2S) \rightarrow \gamma\chi_{c1}(1P))]$ assuming $B(\psi(2S) \rightarrow \gamma\chi_{c1}(1P)) = (9.07 \pm 0.11 \pm 0.54) \times 10^{-2}$ , which we rescale to our best value $B(\psi(2S) \rightarrow \gamma\chi_{c1}(1P)) = (9.75 \pm 0.24) \times 10^{-2}$ . Our first error is their experiment's error and our second error is the systematic error from using our best value.				

 $\Gamma(K^*(892)^+\bar{p}\Lambda + \text{c.c.})/\Gamma_{\text{total}}$   $\Gamma_{73}/\Gamma$ 

VALUE (units $10^{-4}$ )	EVTS	DOCUMENT ID	TECN	COMMENT
<b>4.9±0.7±0.1</b>	328	<sup>1</sup> ABLIKIM	19AU BES3	$\psi(2S) \rightarrow \gamma K^*\bar{p}\Lambda$
<sup>1</sup> ABLIKIM 19AU reports $[\Gamma(\chi_{c1}(1P) \rightarrow K^*(892)^+\bar{p}\Lambda + \text{c.c.})/\Gamma_{\text{total}}] \times [B(\psi(2S) \rightarrow \gamma\chi_{c1}(1P))] = (4.8 \pm 0.5 \pm 0.4) \times 10^{-5}$ which we divide by our best value $B(\psi(2S) \rightarrow \gamma\chi_{c1}(1P)) = (9.75 \pm 0.24) \times 10^{-2}$ . Our first error is their experiment's error and our second error is the systematic error from using our best value.				

 $\Gamma(K^+\bar{p}\Lambda(1520) + \text{c.c.})/\Gamma_{\text{total}}$   $\Gamma_{74}/\Gamma$ 

VALUE (units $10^{-4}$ )	EVTS	DOCUMENT ID	TECN	COMMENT
<b>1.71±0.44±0.04</b>	48 ± 10	<sup>1</sup> ABLIKIM	11F BES3	$\psi(2S) \rightarrow \gamma p\bar{p}K^+K^-$
<sup>1</sup> ABLIKIM 11F reports $(1.81 \pm 0.38 \pm 0.28) \times 10^{-4}$ from a measurement of $[\Gamma(\chi_{c1}(1P) \rightarrow K^+\bar{p}\Lambda(1520) + \text{c.c.})/\Gamma_{\text{total}}] \times [B(\psi(2S) \rightarrow \gamma\chi_{c1}(1P))]$ assuming $B(\psi(2S) \rightarrow \gamma\chi_{c1}(1P)) = (9.2 \pm 0.4) \times 10^{-2}$ , which we rescale to our best value $B(\psi(2S) \rightarrow \gamma\chi_{c1}(1P)) = (9.75 \pm 0.24) \times 10^{-2}$ . Our first error is their experiment's error and our second error is the systematic error from using our best value.				

 $\Gamma(\Lambda(1520)\bar{\Lambda}(1520))/\Gamma_{\text{total}}$   $\Gamma_{75}/\Gamma$ 

VALUE	CL%	DOCUMENT ID	TECN	COMMENT
<b>&lt;9 × 10<sup>-5</sup></b>	90	<sup>1</sup> ABLIKIM	11F BES3	$\psi(2S) \rightarrow \gamma p\bar{p}K^+K^-$
<sup>1</sup> ABLIKIM 11F reports $< 1.00 \times 10^{-4}$ from a measurement of $[\Gamma(\chi_{c1}(1P) \rightarrow \Lambda(1520)\bar{\Lambda}(1520))/\Gamma_{\text{total}}] \times [B(\psi(2S) \rightarrow \gamma\chi_{c1}(1P))]$ assuming $B(\psi(2S) \rightarrow \gamma\chi_{c1}(1P)) = (9.2 \pm 0.4) \times 10^{-2}$ , which we rescale to our best value $B(\psi(2S) \rightarrow \gamma\chi_{c1}(1P)) = 9.75 \times 10^{-2}$ .				

 $\Gamma(\Sigma^0\bar{\Sigma}^0)/\Gamma_{\text{total}}$   $\Gamma_{76}/\Gamma$ 

VALUE (units $10^{-5}$ )	CL%	EVTS	DOCUMENT ID	TECN	COMMENT
<b>4.2±0.6±0.1</b>		103	<sup>1</sup> ABLIKIM	18V BES3	$\psi(2S) \rightarrow \gamma\Sigma^0\bar{\Sigma}^0$



## Meson Particle Listings

 $\chi_{c1}(1P)$ 

$\Gamma(e^+e^- J/\psi(1S))/\Gamma_{\text{total}}$					$\Gamma_{92}/\Gamma$
VALUE (units $10^{-3}$ )	EVTS	DOCUMENT ID	TECN	COMMENT	

• • • We do not use the following data for averages, fits, limits, etc. • • •

$3.65 \pm 0.23 \pm 0.09$  1.9k <sup>1,2</sup> ABLIKIM 17I BES3  $\psi(2S) \rightarrow \gamma e^+e^- J/\psi$

<sup>1</sup> ABLIKIM 17I reports  $(3.73 \pm 0.09 \pm 0.25) \times 10^{-3}$  from a measurement of  $[\Gamma(\chi_{c1}(1P) \rightarrow e^+e^- J/\psi(1S))/\Gamma_{\text{total}}] \times [B(\psi(2S) \rightarrow \gamma \chi_{c1}(1P))]$  assuming  $B(\psi(2S) \rightarrow \gamma \chi_{c1}(1P)) = (9.55 \pm 0.31) \times 10^{-2}$ , which we rescale to our best value  $B(\psi(2S) \rightarrow \gamma \chi_{c1}(1P)) = (9.75 \pm 0.24) \times 10^{-2}$ . Our first error is their experiment's error and our second error is the systematic error from using our best value.

<sup>2</sup> Not independent from other measurements reported by ABLIKIM 17I

$\Gamma(e^+e^- J/\psi(1S))/\Gamma(\gamma J/\psi(1S))$					$\Gamma_{92}/\Gamma_{87}$
VALUE (units $10^{-3}$ )	EVTS	DOCUMENT ID	TECN	COMMENT	

$10.1 \pm 0.3 \pm 0.5$  1.9k <sup>1</sup> ABLIKIM 17I BES3  $\psi(2S) \rightarrow e^+e^- \gamma J/\psi$

<sup>1</sup> Uses  $B(\psi(2S) \rightarrow \gamma \chi_{c1}(1P)) \times B(\chi_{c1}(1P) \rightarrow \gamma J/\psi(1S)) = (351.8 \pm 1.0 \pm 12.0) \times 10^{-4}$  from ABLIKIM 17N and accounts for common systematic errors.

$\Gamma(\mu^+\mu^- J/\psi(1S))/\Gamma(e^+e^- J/\psi(1S))$					$\Gamma_{93}/\Gamma_{92}$
VALUE (units $10^{-2}$ )	EVTS	DOCUMENT ID	TECN	COMMENT	

$6.73 \pm 0.51 \pm 0.50$  222 ABLIKIM 19Z BES3  $\psi(2S) \rightarrow \gamma \chi_{c1} \rightarrow \gamma(\mu^+\mu^- J/\psi)$

 $\chi_{c1}(1P)$  CROSS-PARTICLE BRANCHING RATIOS

$\Gamma(\chi_{c1}(1P) \rightarrow p\bar{p})/\Gamma_{\text{total}} \times \Gamma(\psi(2S) \rightarrow \gamma \chi_{c1}(1P))/\Gamma(\psi(2S) \rightarrow \gamma J/\psi(1S) \pi^+ \pi^-)$					$\Gamma_{54}/\Gamma \times \Gamma_{154}^{\psi(2S)}/\Gamma_{11}^{\psi(2S)}$
VALUE (units $10^{-5}$ )	DOCUMENT ID	TECN	COMMENT		

$2.14 \pm 0.10$  OUR FIT

$1.1 \pm 1.0$  <sup>1</sup> BAI 98I BES  $\psi(2S) \rightarrow \gamma \chi_{c1} \rightarrow \gamma p\bar{p}$

<sup>1</sup> Calculated by us. The value for  $B(\chi_{c1} \rightarrow p\bar{p})$  reported in BAI 98I is derived using  $B(\psi(2S) \rightarrow \gamma \chi_{c1}) = (8.7 \pm 0.8)\%$  and  $B(\psi(2S) \rightarrow J/\psi(1S) \pi^+ \pi^-) = (32.4 \pm 2.6)\%$  [BAI 98b].

$\Gamma(\chi_{c1}(1P) \rightarrow \Lambda\bar{\Lambda})/\Gamma_{\text{total}} \times \Gamma(\psi(2S) \rightarrow \gamma \chi_{c1}(1P))/\Gamma_{\text{total}}$					$\Gamma_{67}/\Gamma \times \Gamma_{154}^{\psi(2S)}/\Gamma_{11}^{\psi(2S)}$
VALUE (units $10^{-6}$ )	EVTS	DOCUMENT ID	TECN	COMMENT	

$11.1 \pm 1.1$  OUR FIT

$10.9 \pm 1.1$  OUR AVERAGE

$11.2 \pm 1.0 \pm 0.9$  136 <sup>1</sup> ABLIKIM 13H BES3  $\psi(2S) \rightarrow \gamma \Lambda\bar{\Lambda}$

$10.5 \pm 1.6 \pm 0.6$  46  $\pm$  7 <sup>2</sup> NAIK 08 CLEO  $\psi(2S) \rightarrow \gamma \Lambda\bar{\Lambda}$

<sup>1</sup> Calculated by us. ABLIKIM 13H reports  $B(\chi_{c1} \rightarrow \Lambda\bar{\Lambda}) = (12.2 \pm 1.1 \pm 1.1) \times 10^{-5}$  from a measurement of  $B(\chi_{c1} \rightarrow \Lambda\bar{\Lambda}) \times B(\psi(2S) \rightarrow \gamma \chi_{c1})$  assuming  $B(\psi(2S) \rightarrow \gamma \chi_{c1}) = (9.2 \pm 0.4)\%$ .

<sup>2</sup> Calculated by us. NAIK 08 reports  $B(\chi_{c1} \rightarrow \Lambda\bar{\Lambda}) = (11.6 \pm 1.8 \pm 0.7 \pm 0.7) \times 10^{-5}$  using  $B(\psi(2S) \rightarrow \gamma \chi_{c1}) = (9.07 \pm 0.11 \pm 0.54)\%$ .

$\Gamma(\chi_{c1}(1P) \rightarrow \Lambda\bar{\Lambda})/\Gamma_{\text{total}} \times \Gamma(\psi(2S) \rightarrow \gamma \chi_{c1}(1P))/\Gamma(\psi(2S) \rightarrow J/\psi(1S) \pi^+ \pi^-)$					$\Gamma_{67}/\Gamma \times \Gamma_{154}^{\psi(2S)}/\Gamma_{11}^{\psi(2S)}$
VALUE (units $10^{-5}$ )	EVTS	DOCUMENT ID	TECN	COMMENT	

$3.20 \pm 0.30$  OUR FIT

$7.1 \pm 2.8 \pm 1.3$  9.0  $\pm$  3.5  $\pm$  3.1 <sup>1</sup> BAI 03E BES  $\psi(2S) \rightarrow \gamma \Lambda\bar{\Lambda}$

<sup>1</sup> BAI 03E reports  $[B(\chi_{c1} \rightarrow \Lambda\bar{\Lambda}) B(\psi(2S) \rightarrow \gamma \chi_{c1}) / B(\psi(2S) \rightarrow J/\psi \pi^+ \pi^-)] \times [B^2(\Lambda \rightarrow \pi^- p) / B(J/\psi \rightarrow p\bar{p})] = (1.33 \pm 0.52 \pm 0.25)\%$ . We calculate from this measurement the presented value using  $B(\Lambda \rightarrow \pi^- p) = (63.9 \pm 0.5)\%$  and  $B(J/\psi \rightarrow p\bar{p}) = (2.17 \pm 0.07) \times 10^{-3}$ .

$\Gamma(\chi_{c1}(1P) \rightarrow \gamma J/\psi(1S))/\Gamma_{\text{total}} \times \Gamma(\psi(2S) \rightarrow \gamma \chi_{c1}(1P))/\Gamma_{\text{total}}$					$\Gamma_{87}/\Gamma \times \Gamma_{154}^{\psi(2S)}/\Gamma_{11}^{\psi(2S)}$
VALUE (units $10^{-2}$ )	EVTS	DOCUMENT ID	TECN	COMMENT	

$3.34 \pm 0.06$  OUR FIT

$3.24 \pm 0.16$  OUR AVERAGE

3.518  $\pm$  0.010  $\pm$  0.120 143k <sup>1</sup> ABLIKIM 17N BES3  $\psi(2S) \rightarrow \gamma \gamma J/\psi$

3.442  $\pm$  0.010  $\pm$  0.132 1.9M ABLIKIM 17U BES3  $e^+e^- \rightarrow \gamma X$

2.81  $\pm$  0.05  $\pm$  0.23 13k BAI 04I BES2  $\psi(2S) \rightarrow J/\psi \gamma \gamma$

2.56  $\pm$  0.12  $\pm$  0.20 GAISER 86 CBAL  $\psi(2S) \rightarrow \gamma X$

2.78  $\pm$  0.30 <sup>2</sup> OREGLIA 82 CBAL  $\psi(2S) \rightarrow \gamma \chi_{c1}$

2.2  $\pm$  0.5 <sup>3</sup> BRANDELIK 79B DASP  $\psi(2S) \rightarrow \gamma \chi_{c1}$

2.9  $\pm$  0.5 <sup>3</sup> BARTEL 78B CNTR  $\psi(2S) \rightarrow \gamma \chi_{c1}$

5.0  $\pm$  1.5 <sup>4</sup> BIDDICK 77 CNTR  $e^+e^- \rightarrow \gamma X$

2.8  $\pm$  0.9 <sup>2</sup> WHITAKER 76 MRK1  $e^+e^-$

• • • We do not use the following data for averages, fits, limits, etc. • • •

3.377  $\pm$  0.009  $\pm$  0.183 142k <sup>5</sup> ABLIKIM 12O BES3  $\psi(2S) \rightarrow \gamma \chi_{c1}$

3.56  $\pm$  0.03  $\pm$  0.12 24.9k <sup>6</sup> MENDEZ 08 CLEO  $\psi(2S) \rightarrow \gamma \chi_{c1}$

3.44  $\pm$  0.06  $\pm$  0.13 3.7k <sup>7</sup> ADAM 05A CLEO Repl. by MENDEZ 08

<sup>1</sup> Uses  $B(J/\psi \rightarrow e^+e^-) = (5.971 \pm 0.032)\%$  and  $B(J/\psi \rightarrow \mu^+\mu^-) = (5.961 \pm 0.033)\%$ .

<sup>2</sup> Recalculated by us using  $B(J/\psi(1S) \rightarrow \ell^+\ell^-) = 0.1181 \pm 0.0020$ .

<sup>3</sup> Recalculated by us using  $B(J/\psi(1S) \rightarrow \mu^+\mu^-) = 0.0588 \pm 0.0010$ .

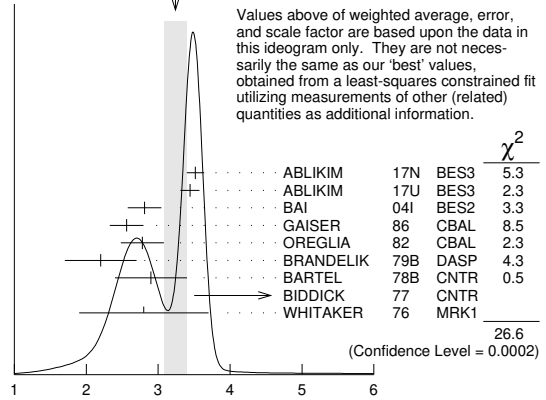
<sup>4</sup> Assumes isotropic gamma distribution.

<sup>5</sup> Superseded by ABLIKIM 17N.

<sup>6</sup> Not independent from other measurements of MENDEZ 08.

<sup>7</sup> Not independent from other values reported by ADAM 05A.

WEIGHTED AVERAGE  
3.24  $\pm$  0.16 (Error scaled by 2.1)



$\Gamma(\chi_{c1}(1P) \rightarrow \gamma J/\psi(1S))/\Gamma_{\text{total}} \times \Gamma(\psi(2S) \rightarrow \gamma \chi_{c1}(1P))/\Gamma_{\text{total}}$  (units  $10^{-2}$ )

$\Gamma(\chi_{c1}(1P) \rightarrow \gamma J/\psi(1S))/\Gamma_{\text{total}} \times \Gamma(\psi(2S) \rightarrow \gamma \chi_{c1}(1P))/\Gamma(\psi(2S) \rightarrow J/\psi(1S) \text{ anything})$					$\Gamma_{87}/\Gamma \times \Gamma_{154}^{\psi(2S)}/\Gamma_{9}^{\psi(2S)}$
VALUE (units $10^{-2}$ )	EVTS	DOCUMENT ID	TECN	COMMENT	

$9.63 \pm 0.17$  OUR FIT

$10.15 \pm 0.28$  OUR AVERAGE

$5.70 \pm 0.04 \pm 0.15$  24.9k <sup>1</sup> MENDEZ 08 CLEO  $\psi(2S) \rightarrow \gamma \chi_{c1}$

$5.77 \pm 0.10 \pm 0.12$  3.7k ADAM 05A CLEO Repl. by MENDEZ 08

<sup>1</sup> Not independent from other measurements of MENDEZ 08.

$\Gamma(\chi_{c1}(1P) \rightarrow \gamma J/\psi(1S))/\Gamma_{\text{total}} \times \Gamma(\psi(2S) \rightarrow \gamma \chi_{c1}(1P))/\Gamma(\psi(2S) \rightarrow J/\psi(1S) \pi^+ \pi^-)$					$\Gamma_{87}/\Gamma \times \Gamma_{154}^{\psi(2S)}/\Gamma_{11}^{\psi(2S)}$
VALUE (units $10^{-2}$ )	EVTS	DOCUMENT ID	TECN	COMMENT	

$9.63 \pm 0.17$  OUR FIT

$10.15 \pm 0.28$  OUR AVERAGE

$10.17 \pm 0.07 \pm 0.27$  24.9k MENDEZ 08 CLEO  $\psi(2S) \rightarrow \gamma \chi_{c1}$

$12.6 \pm 0.3 \pm 3.8$  3k <sup>1</sup> ABLIKIM 04B BES  $\psi(2S) \rightarrow J/\psi X$

$8.5 \pm 2.1$  <sup>2</sup> HIMEL 80 MRK2  $\psi(2S) \rightarrow \gamma \chi_{c1}$

• • • We do not use the following data for averages, fits, limits, etc. • • •

$10.24 \pm 0.17 \pm 0.23$  3.7k <sup>3</sup> ADAM 05A CLEO Repl. by MENDEZ 08

<sup>1</sup> From a fit to the  $J/\psi$  recoil mass spectra.

<sup>2</sup> The value for  $B(\psi(2S) \rightarrow \gamma \chi_{c1}) \times B(\chi_{c1} \rightarrow \gamma J/\psi(1S))$  quoted in HIMEL 80 is derived using  $B(\psi(2S) \rightarrow J/\psi(1S) \pi^+ \pi^-) = (33 \pm 3)\%$  and  $B(J/\psi(1S) \rightarrow \ell^+ \ell^-) = 0.138 \pm 0.018$ . Calculated by us using  $B(J/\psi(1S) \rightarrow \ell^+ \ell^-) = 0.1181 \pm 0.0020$ .

<sup>3</sup> Not independent from other values reported by ADAM 05A.

$\Gamma(\chi_{c1}(1P) \rightarrow \bar{K}^0 K^+ \pi^- + \text{c.c.})/\Gamma_{\text{total}} \times \Gamma(\psi(2S) \rightarrow \gamma \chi_{c1}(1P))/\Gamma_{\text{total}}$					$\Gamma_{17}/\Gamma \times \Gamma_{154}^{\psi(2S)}/\Gamma_{11}^{\psi(2S)}$
VALUE (units $10^{-4}$ )	DOCUMENT ID	TECN	COMMENT		

$6.8 \pm 0.5$  OUR FIT

$7.2 \pm 0.6$  OUR AVERAGE

$7.3 \pm 0.5 \pm 0.5$  <sup>1</sup> ATHAR 07 CLEO  $\psi(2S) \rightarrow \gamma K_S^0 K^+ \pi^-$

$7.0 \pm 0.5 \pm 0.9$  <sup>2</sup> ABLIKIM 06R BES2  $\psi(2S) \rightarrow \gamma \chi_{c1}$

<sup>1</sup> Calculated by us. The value of  $B(\chi_{c1} \rightarrow K^0 K^+ \pi^- + \text{c.c.})$  reported by ATHAR 07 was derived using  $B(\psi(2S) \rightarrow \gamma \chi_{c1}(1P)) = (9.07 \pm 0.11 \pm 0.54)\%$ .

<sup>2</sup> Calculated by us. ABLIKIM 06R reports  $B(\chi_{c1} \rightarrow K_S^0 K^+ \pi^-) = (4.0 \pm 0.3 \pm 0.5) \times 10^{-3}$ . We use  $B(\psi(2S) \rightarrow \gamma \chi_{c1}) = (8.7 \pm 0.4) \times 10^{-2}$ .

$\Gamma(\chi_{c1}(1P) \rightarrow \bar{K}^0 K^+ \pi^- + \text{c.c.})/\Gamma_{\text{total}} \times \Gamma(\psi(2S) \rightarrow \gamma \chi_{c1}(1P))/\Gamma(\psi(2S) \rightarrow J/\psi(1S) \pi^+ \pi^-)$					$\Gamma_{17}/\Gamma \times \Gamma_{154}^{\psi(2S)}/\Gamma_{11}^{\psi(2S)}$
VALUE (units $10^{-4}$ )	DOCUMENT ID	TECN	COMMENT		

$19.6 \pm 1.6$  OUR FIT

$13.2 \pm 2.4 \pm 3.2$  <sup>1</sup> BAI 99B BES  $\psi(2S) \rightarrow \gamma K_S^0 K^+ \pi^-$

<sup>1</sup> Calculated by us. The value of  $B(\chi_{c1} \rightarrow K_S^0 K^+ \pi^-)$  reported by BAI 99B was derived using  $B(\psi(2S) \rightarrow \gamma \chi_{c1}(1P)) = (8.7 \pm 0.8)\%$  and  $B(\psi(2S) \rightarrow J/\psi \pi^+ \pi^-) = (32.4 \pm 2.6)\%$  [BAI 98d].

$$\Gamma(\chi_{c1}(1P) \rightarrow K^+ K^- K^+ K^-) / \Gamma_{\text{total}} \times \Gamma(\psi(2S) \rightarrow \gamma \chi_{c1}(1P)) / \Gamma_{\text{total}}$$

$$\Gamma_{44} / \Gamma \times \Gamma_{154}^{\psi(2S)} / \Gamma_{11}^{\psi(2S)}$$

VALUE (units $10^{-4}$ )	EVTS	DOCUMENT ID	TECN	COMMENT
<b>0.53 ± 0.11 OUR FIT</b>				
0.61 ± 0.11 ± 0.08	54	<sup>1</sup> ABLIKIM	06T BES2	$\psi(2S) \rightarrow \gamma K^+ K^+ K^- K^-$

<sup>1</sup> Calculated by us. The value of  $B(\chi_{c1} \rightarrow 2K^+ 2K^-)$  reported by ABLIKIM 06T was derived using  $B(\psi(2S) \rightarrow \gamma \chi_{c1}(1P)) = (8.7 \pm 0.8)\%$ .

$$\Gamma(\chi_{c1}(1P) \rightarrow K^+ K^- K^+ K^-) / \Gamma_{\text{total}} \times \Gamma(\psi(2S) \rightarrow \gamma \chi_{c1}(1P)) / \Gamma_{\text{total}}$$

$$\Gamma(\psi(2S) \rightarrow J/\psi(1S) \pi^+ \pi^-)$$

$$\Gamma_{44} / \Gamma \times \Gamma_{154}^{\psi(2S)} / \Gamma_{11}^{\psi(2S)}$$

VALUE (units $10^{-4}$ )	EVTS	DOCUMENT ID	TECN	COMMENT
<b>1.52 ± 0.31 OUR FIT</b>				
1.73 ± 0.40 ± 0.29		<sup>1</sup> BAI	99B BES	$\psi(2S) \rightarrow \gamma K^+ K^+ K^- K^-$

<sup>1</sup> Calculated by us. The value of  $B(\chi_{c1} \rightarrow 2K^+ 2K^-)$  reported by BAI 99B was derived using  $B(\psi(2S) \rightarrow \gamma \chi_{c1}(1P)) = (8.7 \pm 0.8)\%$  and  $B(\psi(2S) \rightarrow J/\psi \pi^+ \pi^-) = (32.4 \pm 2.6)\%$  [BAI 98D].

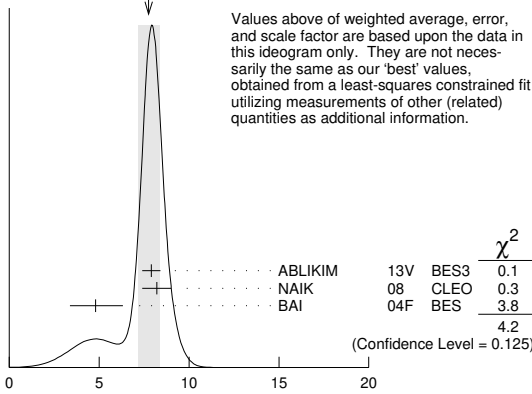
$$\Gamma(\chi_{c1}(1P) \rightarrow p\bar{p}) / \Gamma_{\text{total}} \times \Gamma(\psi(2S) \rightarrow \gamma \chi_{c1}(1P)) / \Gamma_{\text{total}}$$

$$\Gamma_{54} / \Gamma \times \Gamma_{154}^{\psi(2S)} / \Gamma_{11}^{\psi(2S)}$$

VALUE (units $10^{-6}$ )	EVTS	DOCUMENT ID	TECN	COMMENT
<b>7.41 ± 0.35 OUR FIT</b>				
7.8 ± 0.6 OUR AVERAGE				Error includes scale factor of 1.4. See the ideogram below.
7.9 ± 0.4 ± 0.3	453	ABLIKIM	13V BES3	$\psi(2S) \rightarrow \gamma p\bar{p}$
8.2 ± 0.7 ± 0.4	141 ± 13	<sup>1</sup> NAIK	08 CLEO	$\psi(2S) \rightarrow \gamma p\bar{p}$
4.8 +1.4 ± 0.6	18.2 +5.5 -4.9	BAI	04F BES	$\psi(2S) \rightarrow \gamma \chi_{c1}(1P) \rightarrow \gamma p\bar{p}$

<sup>1</sup> Calculated by us. NAIK 08 reports  $B(\chi_{c1} \rightarrow p\bar{p}) = (9.0 \pm 0.8 \pm 0.4 \pm 0.5) \times 10^{-5}$  using  $B(\psi(2S) \rightarrow \gamma \chi_{c1}(1P)) = (9.07 \pm 0.11 \pm 0.54)\%$ .

WEIGHTED AVERAGE  
7.8 ± 0.6 (Error scaled by 1.4)



$$\Gamma(\chi_{c1}(1P) \rightarrow p\bar{p}) / \Gamma_{\text{total}} \times \Gamma(\psi(2S) \rightarrow \gamma \chi_{c1}(1P)) / \Gamma_{\text{total}} \text{ (units } 10^{-6}\text{)}$$

$$\Gamma(\chi_{c1}(1P) \rightarrow \Sigma^+ \bar{p} K_S^0 + \text{c.c.}) / \Gamma_{\text{total}} \times \Gamma(\psi(2S) \rightarrow \gamma \chi_{c1}(1P)) / \Gamma_{\text{total}}$$

$$\Gamma_{77} / \Gamma \times \Gamma_{154}^{\psi(2S)} / \Gamma_{11}^{\psi(2S)}$$

VALUE (units $10^{-5}$ )	EVTS	DOCUMENT ID	TECN	COMMENT
<b>1.49 ± 0.09 ± 0.07</b>	258	<sup>1</sup> ABLIKIM	19BB BES3	$\psi(2S) \rightarrow \gamma \Sigma^+ \bar{p} K_S^0 + \text{c.c.}$

<sup>1</sup> Calculated by us. ABLIKIM 19BB reports  $B(\chi_{c1} \rightarrow \Sigma^+ \bar{p} K_S^0 + \text{c.c.}) = (1.53 \pm 0.10 \pm 0.08) \times 10^{-4}$  using  $B(\psi(2S) \rightarrow \gamma \chi_{c1}(1P)) = (9.75 \pm 0.24)\%$  and other branching fractions from PDG 18.

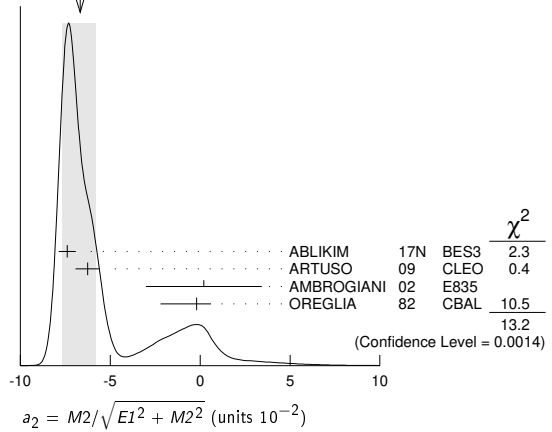
**MULTIPOLE AMPLITUDES IN  $\chi_{c1}(1P) \rightarrow \gamma J/\psi(1S)$**

$a_2 = M_2 / \sqrt{E_1^2 + M_2^2}$  Magnetic quadrupole fractional transition amplitude

VALUE (units $10^{-2}$ )	EVTS	DOCUMENT ID	TECN	COMMENT
<b>-6.7 ± 0.9 OUR AVERAGE</b>				Error includes scale factor of 2.6. See the ideogram below.
-7.40 ± 0.33 ± 0.34	164k	<sup>1</sup> ABLIKIM	17N BES3	$\psi(2S) \rightarrow \gamma \gamma \ell^+ \ell^-$
-6.26 ± 0.63 ± 0.24	39k	ARTUSO	09 CLEO	$\psi(2S) \rightarrow \gamma \gamma \ell^+ \ell^-$
0.2 ± 3.2 ± 0.4	2090	AMBROGIANI	02 E835	$p\bar{p} \rightarrow \chi_{c1} \rightarrow J/\psi \gamma$
-0.2 +0.8 -2.0	921	OREGLIA	82 CBAL	$\psi(2S) \rightarrow \chi_{c1} \gamma \rightarrow J/\psi \gamma \gamma$

<sup>1</sup> Correlated with  $b_2$  with correlation coefficient  $\rho_{a_2 b_2} = 0.133$ .

WEIGHTED AVERAGE  
-6.7 ± 0.9 (Error scaled by 2.6)



**MULTIPOLE AMPLITUDES IN  $\psi(2S) \rightarrow \gamma \chi_{c1}(1S)$  RADIATIVE DECAY**

$b_2 = M_2 / \sqrt{E_1^2 + M_2^2}$  Magnetic quadrupole fractional transition amplitude

VALUE (units $10^{-2}$ )	EVTS	DOCUMENT ID	TECN	COMMENT
<b>2.5 ± 0.4 OUR AVERAGE</b>				
2.29 ± 0.39 ± 0.27	164k	<sup>1</sup> ABLIKIM	17N BES3	$\psi(2S) \rightarrow \gamma \gamma \ell^+ \ell^-$
2.76 ± 0.73 ± 0.23	39k	ARTUSO	09 CLEO	$\psi(2S) \rightarrow \gamma \gamma \ell^+ \ell^-$
7.7 +5.0 -4.5	921	OREGLIA	82 CBAL	$\psi(2S) \rightarrow \gamma \gamma \ell^+ \ell^-$

<sup>1</sup> Correlated with  $a_2$  with correlation coefficient  $\rho_{a_2 b_2} = 0.133$ .

**MULTIPOLE AMPLITUDE RATIOS IN RADIATIVE DECAYS  
 $\psi(2S) \rightarrow \gamma \chi_{c1}(1S)$  and  $\chi_{c1} \rightarrow \gamma J/\psi(1S)$**

$a_2/b_2$  Magnetic quadrupole transition amplitude ratio

VALUE	EVTS	DOCUMENT ID	TECN	COMMENT
<b>-2.27 +0.57 -0.99</b>	39k	<sup>1</sup> ARTUSO	09 CLEO	$\psi(2S) \rightarrow \gamma \gamma \ell^+ \ell^-$

<sup>1</sup> Statistical and systematic errors combined. Not independent of  $a_2(\chi_{c1})$  and  $b_2(\chi_{c1})$  values from ARTUSO 09.

**$\chi_{c1}(1P)$  REFERENCES**

ABLIKIM	20B	PR D101 012012	M. Ablikim et al.	(BESIII Collab.)
ABLIKIM	19AA	PR D99 052008	M. Ablikim et al.	(BESIII Collab.)
ABLIKIM	19AU	PR D100 052010	M. Ablikim et al.	(BESIII Collab.)
ABLIKIM	19BB	PR D100 092006	M. Ablikim et al.	(BESIII Collab.)
ABLIKIM	19J	PR D99 012015	M. Ablikim et al.	(BESIII Collab.)
ABLIKIM	19Z	PR D99 051101	M. Ablikim et al.	(BESIII Collab.)
LU	19	PR D99 032003	P.-C. Lu et al.	(BELLE Collab.)
ABLIKIM	18D	PRL 121 022001	M. Ablikim et al.	(BESIII Collab.)
ABLIKIM	18V	PR D97 052011	M. Ablikim et al.	(BESIII Collab.)
PDG	18	PR D98 030001	M. Tanabashi et al.	(PDG Collab.)
AAIJ	17BB	EPL C77 609	R. Aaij et al.	(LHCb Collab.)
AAIJ	17BI	PRL 119 221801	R. Aaij et al.	(LHCb Collab.)
ABLIKIM	17AE	PR D96 092007	M. Ablikim et al.	(BESIII Collab.)
ABLIKIM	17I	PRL 118 221802	M. Ablikim et al.	(BESIII Collab.)
ABLIKIM	17K	PR D95 032002	M. Ablikim et al.	(BESIII Collab.)
ABLIKIM	17N	PR D95 072004	M. Ablikim et al.	(BESIII Collab.)
ABLIKIM	17U	PR D96 032001	M. Ablikim et al.	(BESIII Collab.)
PDG	16	CP C40 100001	C. Patrignani et al.	(PDG Collab.)
ABLIKIM	15I	PR D91 092006	M. Ablikim et al.	(BESIII Collab.)
ABLIKIM	15M	PR D91 112008	M. Ablikim et al.	(BESIII Collab.)
ABLIKIM	14J	PR D89 074030	M. Ablikim et al.	(BESIII Collab.)
ABLIKIM	13B	PR D87 012002	M. Ablikim et al.	(BESIII Collab.)
ABLIKIM	13D	PR D87 012007	M. Ablikim et al.	(BESIII Collab.)
ABLIKIM	13H	PR D87 032007	M. Ablikim et al.	(BESIII Collab.)
ABLIKIM	13V	PR D88 112001	M. Ablikim et al.	(BESIII Collab.)
ABLIKIM	12I	PR D86 052004	M. Ablikim et al.	(BESIII Collab.)
ABLIKIM	12J	PR D86 052011	M. Ablikim et al.	(BESIII Collab.)
ABLIKIM	12O	PRL 109 172002	M. Ablikim et al.	(BESIII Collab.)
ABLIKIM	11A	PR D83 012006	M. Ablikim et al.	(BESIII Collab.)
ABLIKIM	11E	PR D83 032003	M. Ablikim et al.	(BESIII Collab.)
ABLIKIM	11D	PR D83 112005	M. Ablikim et al.	(BESIII Collab.)
ABLIKIM	11F	PR D83 112009	M. Ablikim et al.	(BESIII Collab.)
ABLIKIM	11K	PRL 107 092001	M. Ablikim et al.	(BESIII Collab.)
ONYISI	10	PR D82 011103	F.U.E. Onyisi et al.	(CLEO Collab.)
ARTUSO	09	PR D80 112003	M. Artuso et al.	(CLEO Collab.)
BENNETT	08A	PRL 101 151801	J.V. Bennett et al.	(CLEO Collab.)
ECKLUND	08A	PR D78 091501	K.M. Ecklund et al.	(CLEO Collab.)
HE	08B	PR D78 092004	Q. He et al.	(CLEO Collab.)
MENDEZ	08	PR D78 011102	H. Mendez et al.	(CLEO Collab.)
NAIK	08	PR D78 031101	P. Naik et al.	(CLEO Collab.)
ATHAR	07	PR D75 032002	S.B. Athar et al.	(CLEO Collab.)
ABLIKIM	06D	PR D73 052006	M. Ablikim et al.	(BES Collab.)
ABLIKIM	06R	PR D74 072001	M. Ablikim et al.	(BES Collab.)
ABLIKIM	06T	PL B642 197	M. Ablikim et al.	(BES Collab.)
ABLIKIM	05G	PR D71 092002	M. Ablikim et al.	(BES Collab.)
ABLIKIM	05O	PL B630 21	M. Ablikim et al.	(BES Collab.)
ADAM	05A	PRL 94 232002	N.E. Adam et al.	(CLEO Collab.)
ANDREOTTI	05A	NP B717 34	M. Andreotti et al.	(FNAL E835 Collab.)
ABLIKIM	04B	PR D70 012003	M. Ablikim et al.	(BES Collab.)
ABLIKIM	04H	PR D70 092003	M. Ablikim et al.	(BES Collab.)
ATHAR	04	PR D70 112002	S.B. Athar et al.	(CLEO Collab.)
BAI	04F	PR D69 092001	J.Z. Bai et al.	(BES Collab.)

# Meson Particle Listings

## $\chi_{c1}(1P), h_c(1P)$

BAI	041	PR D70 012006	J.Z. Bai <i>et al.</i>	(BES Collab.)
AULCHENKO	03	PL B573 63	V.M. Aulchenko <i>et al.</i>	(KEDR Collab.)
BAI	03E	PR D67 112001	J.Z. Bai <i>et al.</i>	(BES Collab.)
AMBROGIANI	02	PR D65 052002	M. Ambrogiani <i>et al.</i>	(FNAL E835 Collab.)
BAI	99B	PR D60 072001	J.Z. Bai <i>et al.</i>	(BES Collab.)
BAI	98D	PR D58 092006	J.Z. Bai <i>et al.</i>	(BES Collab.)
BAI	98I	PRL 81 3091	J.Z. Bai <i>et al.</i>	(BES Collab.)
ARMSTRONG	92	NP B373 35	T.A. Armstrong <i>et al.</i>	(FNAL, FERR, GENO+)
		PRL 69 1468	T.A. Armstrong <i>et al.</i>	(FNAL, FERR, GENO+)
BAGLIN	86B	PL B172 455	C. Baglin	(LAPP, CERN, GENO, LYON, OSLO+)
GAISER	86	PR D34 711	J. Gaiser <i>et al.</i>	(Crystal Ball Collab.)
LEM OIGNE	82	PL 113B 509	Y. Lemoigne <i>et al.</i>	(SACL, LOIC, SHMP+)
OREGLIA	82	PR D25 2259	M.J. Oreglia <i>et al.</i>	(SLAC, CIT, HARV+)
		Private Comm.	M.J. Oreglia	(EFI)
HIMEL	80	PRL 44 920	T. Himel <i>et al.</i>	(LBL, SLAC)
		Private Comm.	C. Trilling	(LBL, UCB)
BRANDELIK	79B	NP B160 426	R. Brandelik <i>et al.</i>	(DASP Collab.)
BARTEL	78B	PL 79B 492	W. Bartel <i>et al.</i>	(DESY, HEIDP)
TANENBAUM	78	PR D17 1731	W.M. Tanenbaum <i>et al.</i>	(SLAC, LBL)
		Private Comm.	C. Trilling	(LBL, UCB)
BIDDICK	77	PRL 38 1324	C.J. Biddick <i>et al.</i>	(UCSD, UMD, PAVI+)
FELDMAN	77	PRPL 33C 285	G.J. Feldman, M.L. Perl	(LBL, SLAC)
YAMADA	77	Hamburg Conf. 69	S. Yamada	(DASP Collab.)
WHITAKER	76	PRL 37 1596	J.S. Whitaker <i>et al.</i>	(SLAC, LBL)
TANENBAUM	75	PRL 35 1323	W.M. Tanenbaum <i>et al.</i>	(LBL, SLAC)

**$h_c(1P)$**

$$I^G(J^{PC}) = 0^-(1^{+-})$$

Quantum numbers are quark model prediction,  $C = -$  established by  $\eta_c \gamma$  decay.

### $h_c(1P)$ MASS

VALUE (MeV)	EVTS	DOCUMENT ID	TECN	COMMENT
<b><math>3525.38 \pm 0.11</math></b>	<b>OUR AVERAGE</b>			
$3525.31 \pm 0.11 \pm 0.14$	832	<sup>1</sup> ABLIKIM	12N BES3	$\psi(2S) \rightarrow \pi^0 \gamma$ hadrons
$3525.40 \pm 0.13 \pm 0.18$	3679	ABLIKIM	10B BES3	$\psi(2S) \rightarrow \pi^0 \gamma \eta_c$
$3525.20 \pm 0.18 \pm 0.12$	1282	<sup>2</sup> DOBBS	08A CLEO	$\psi(2S) \rightarrow \pi^0 \gamma \eta_c$
$3525.8 \pm 0.2 \pm 0.2$	13	ANDREOTTI	05B E835	$\bar{p}p \rightarrow \eta_c \gamma$
$3525.6 \pm 0.5$	$92^{+23}_{-22}$	ADAMS	09 CLEO	$\psi(2S) \rightarrow 2(\pi^+ \pi^- \pi^0)$
$3524.4 \pm 0.6 \pm 0.4$	$168 \pm 40$	<sup>3</sup> ROSNER	05 CLEO	$\psi(2S) \rightarrow \pi^0 \eta_c \gamma$
$3527 \pm 8$	42	ANTONIAZZI	94 E705	$300 \pi^\pm, pLi \rightarrow J/\psi \pi^0 X$
$3526.28 \pm 0.18 \pm 0.19$	59	<sup>4</sup> ARMSTRONG	92D E760	$\bar{p}p \rightarrow J/\psi \pi^0$
$3525.4 \pm 0.8 \pm 0.4$	5	BAGLIN	86 SPEC	$\bar{p}p \rightarrow J/\psi X$

<sup>1</sup> With floating width.  
<sup>2</sup> Combination of exclusive and inclusive analyses for the reaction  $\psi(2S) \rightarrow \pi^0 h_c \rightarrow \pi^0 \eta_c \gamma$ . This result is the average of DOBBS 08A and ROSNER 05.  
<sup>3</sup> Superseded by DOBBS 08A.  
<sup>4</sup> Mass central value and systematic error recalculated by us according to Eq. (16) in ARMSTRONG 93B, using the value for the  $\psi(2S)$  mass from AULCHENKO 03.

### $h_c(1P)$ WIDTH

VALUE (MeV)	CL%	EVTS	DOCUMENT ID	TECN	COMMENT
<b><math>0.70 \pm 0.28 \pm 0.22</math></b>		832	<sup>1</sup> ABLIKIM	12N BES3	$\psi(2S) \rightarrow \pi^0 \gamma$ hadrons
$< 1.44$	90	3679	<sup>2</sup> ABLIKIM	10B BES3	$\psi(2S) \rightarrow \pi^0 \gamma \eta_c$
$< 1$		13	ANDREOTTI	05B E835	$\bar{p}p \rightarrow \eta_c \gamma$
$< 1.1$	90	59	ARMSTRONG	92D E760	$\bar{p}p \rightarrow J/\psi \pi^0$

<sup>1</sup> With floating mass.  
<sup>2</sup> The central value is  $\Gamma = 0.73 \pm 0.45 \pm 0.28$  MeV.

### $h_c(1P)$ DECAY MODES

Mode	Fraction ( $\Gamma_i/\Gamma$ )	Confidence level
$\Gamma_1$	$J/\psi(1S) \pi^0$	
$\Gamma_2$	$J/\psi(1S) \pi \pi$	not seen
$\Gamma_3$	$J/\psi(1S) \pi^+ \pi^-$	
$\Gamma_4$	$\rho \bar{\rho}$	$< 2.3 \times 10^{-3}$ 90%
$\Gamma_5$	$\rho \bar{\rho} \pi^+ \pi^-$	$< 1.5 \times 10^{-4}$ 90%
$\Gamma_6$	$\rho \bar{\rho} \pi^+ \pi^-$	$(2.9 \pm 0.6) \times 10^{-3}$
$\Gamma_7$	$\pi^+ \pi^- \pi^0$	$(1.6 \pm 0.5) \times 10^{-3}$
$\Gamma_8$	$2\pi^+ 2\pi^- \pi^0$	$(8.1 \pm 1.8) \times 10^{-3}$
$\Gamma_9$	$3\pi^+ 3\pi^- \pi^0$	$< 9 \times 10^{-3}$ 90%
$\Gamma_9$	$K^+ K^- \pi^+ \pi^-$	$< 6 \times 10^{-4}$ 90%

### Radiative decays

$\Gamma_{10}$	$\gamma \eta$	$(4.7 \pm 2.1) \times 10^{-4}$
$\Gamma_{11}$	$\gamma \eta'(958)$	$(1.5 \pm 0.4) \times 10^{-3}$
$\Gamma_{12}$	$\gamma \eta_c(1S)$	$(51 \pm 6) \%$

### $h_c(1P)$ PARTIAL WIDTHS

#### $h_c(1P) \Gamma(i)\Gamma(\bar{p}p)/\Gamma(\text{total})$

$\Gamma(\gamma \eta_c(1S)) \times \Gamma(\bar{p}p)/\Gamma(\text{total})$	$\Gamma_{12}\Gamma_4/\Gamma$			
VALUE (eV)	EVTS	DOCUMENT ID	TECN	COMMENT
$12.0 \pm 4.5$	13	<sup>1</sup> ANDREOTTI	05B E835	$\bar{p}p \rightarrow \eta_c \gamma$

<sup>1</sup> Assuming  $\Gamma = 1$  MeV.

### $h_c(1P)$ BRANCHING RATIOS

$\Gamma(J/\psi(1S) \pi \pi)/\Gamma(J/\psi(1S) \pi^0)$	$\Gamma_2/\Gamma_1$			
VALUE	CL%	DOCUMENT ID	TECN	COMMENT
<b><math>&lt; 0.18</math></b>	90	ARMSTRONG	92D E760	$\bar{p}p \rightarrow J/\psi \pi^0$

$\Gamma(J/\psi(1S) \pi^+ \pi^-)/\Gamma(\text{total})$	$\Gamma_3/\Gamma$			
VALUE	CL%	DOCUMENT ID	TECN	COMMENT
$< 2.3 \times 10^{-3}$	90	<sup>1</sup> ABLIKIM	18M BES3	$\psi(2S) \rightarrow \pi^0 \pi^+ \pi^- J/\psi$

<sup>1</sup> ABLIKIM 18M reports  $[\Gamma(h_c(1P) \rightarrow J/\psi(1S) \pi^+ \pi^-)/\Gamma(\text{total})] \times [B(\psi(2S) \rightarrow \pi^0 h_c(1P))]$   $< 2.0 \times 10^{-6}$  which we divide by our best value  $B(\psi(2S) \rightarrow \pi^0 h_c(1P)) = 8.6 \times 10^{-4}$ .

$\Gamma(\pi^+ \pi^- \pi^0)/\Gamma(\text{total})$	$\Gamma_6/\Gamma$				
VALUE (units $10^{-3}$ )	CL%	EVTS	DOCUMENT ID	TECN	COMMENT
<b><math>1.6 \pm 0.5 \pm 0.2</math></b>	101		<sup>1</sup> ABLIKIM	19AG BES3	$\psi(2S) \rightarrow \pi^0 h_c(1P)$

**•••** We do not use the following data for averages, fits, limits, etc. **••••**  
 $< 2.2$  90 <sup>2</sup> ADAMS 09 CLEO  $\psi(2S) \rightarrow \pi^0 \gamma \eta_c$   
<sup>1</sup> ABLIKIM 19AG reports  $[\Gamma(h_c(1P) \rightarrow \pi^+ \pi^- \pi^0)/\Gamma(\text{total})] \times [B(\psi(2S) \rightarrow \pi^0 h_c(1P))]$   $= (1.38 \pm 0.35 \pm 0.17) \times 10^{-6}$  which we divide by our best value  $B(\psi(2S) \rightarrow \pi^0 h_c(1P)) = (8.6 \pm 1.3) \times 10^{-4}$ . Our first error is their experiment's error and our second error is the systematic error from using our best value.  
<sup>2</sup> ADAMS 09 reports  $[\Gamma(h_c(1P) \rightarrow \pi^+ \pi^- \pi^0)/\Gamma(\text{total})] \times [B(\psi(2S) \rightarrow \pi^0 h_c(1P))]$   $< 0.19 \times 10^{-5}$  which we divide by our best value  $B(\psi(2S) \rightarrow \pi^0 h_c(1P)) = 8.6 \times 10^{-4}$ .

$\Gamma(2\pi^+ 2\pi^- \pi^0)/\Gamma(\text{total})$	$\Gamma_7/\Gamma$				
VALUE (units $10^{-2}$ )	CL%	EVTS	DOCUMENT ID	TECN	COMMENT
<b><math>0.81 \pm 0.18</math></b>	OUR AVERAGE				
$0.74 \pm 0.14 \pm 0.11$	254		<sup>1</sup> ABLIKIM	19AG BES3	$\psi(2S) \rightarrow \pi^0 h_c(1P)$
$2.2^{+0.8}_{-0.6} \pm 0.3$	92		<sup>2</sup> ADAMS	09 CLEO	$\psi(2S) \rightarrow \pi^0 \gamma \eta_c$

<sup>1</sup> ABLIKIM 19AG reports  $[\Gamma(h_c(1P) \rightarrow 2\pi^+ 2\pi^- \pi^0)/\Gamma(\text{total})] \times [B(\psi(2S) \rightarrow \pi^0 h_c(1P))]$   $= (6.40 \pm 0.81 \pm 0.87) \times 10^{-6}$  which we divide by our best value  $B(\psi(2S) \rightarrow \pi^0 h_c(1P)) = (8.6 \pm 1.3) \times 10^{-4}$ . Our first error is their experiment's error and our second error is the systematic error from using our best value.  
<sup>2</sup> ADAMS 09 reports  $[\Gamma(h_c(1P) \rightarrow 2\pi^+ 2\pi^- \pi^0)/\Gamma(\text{total})] \times [B(\psi(2S) \rightarrow \pi^0 h_c(1P))]$   $= (1.88^{+0.48+0.47}_{-0.45-0.36}) \times 10^{-5}$  which we divide by our best value  $B(\psi(2S) \rightarrow \pi^0 h_c(1P)) = (8.6 \pm 1.3) \times 10^{-4}$ . Our first error is their experiment's error and our second error is the systematic error from using our best value.

$\Gamma(3\pi^+ 3\pi^- \pi^0)/\Gamma(\text{total})$	$\Gamma_8/\Gamma$			
VALUE	CL%	DOCUMENT ID	TECN	COMMENT
<b><math>&lt; 9 \times 10^{-3}</math></b>	90	<sup>1</sup> ABLIKIM	19AG BES3	$\psi(2S) \rightarrow \pi^0 h_c(1P)$

**•••** We do not use the following data for averages, fits, limits, etc. **••••**  
 $< 0.029$  90 <sup>2</sup> ADAMS 09 CLEO  $\psi(2S) \rightarrow \pi^0 \gamma \eta_c$   
<sup>1</sup> ABLIKIM 19AG reports  $[\Gamma(h_c(1P) \rightarrow 3\pi^+ 3\pi^- \pi^0)/\Gamma(\text{total})] \times [B(\psi(2S) \rightarrow \pi^0 h_c(1P))]$   $< 7.5 \times 10^{-6}$  which we divide by our best value  $B(\psi(2S) \rightarrow \pi^0 h_c(1P)) = 8.6 \times 10^{-4}$ .  
<sup>2</sup> ADAMS 09 reports  $[\Gamma(h_c(1P) \rightarrow 3\pi^+ 3\pi^- \pi^0)/\Gamma(\text{total})] \times [B(\psi(2S) \rightarrow \pi^0 h_c(1P))]$   $< 2.5 \times 10^{-5}$  which we divide by our best value  $B(\psi(2S) \rightarrow \pi^0 h_c(1P)) = 8.6 \times 10^{-4}$ .

$\Gamma(\rho \bar{\rho} \pi^+ \pi^-)/\Gamma(\text{total})$	$\Gamma_5/\Gamma$			
VALUE (units $10^{-3}$ )	EVTS	DOCUMENT ID	TECN	COMMENT
<b><math>2.9 \pm 0.5 \pm 0.4</math></b>	230	<sup>1</sup> ABLIKIM	19AG BES3	$\psi(2S) \rightarrow \pi^0 h_c(1P)$

<sup>1</sup> ABLIKIM 19AG reports  $[\Gamma(h_c(1P) \rightarrow \rho \bar{\rho} \pi^+ \pi^-)/\Gamma(\text{total})] \times [B(\psi(2S) \rightarrow \pi^0 h_c(1P))]$   $= (2.49 \pm 0.27 \pm 0.28) \times 10^{-6}$  which we divide by our best value  $B(\psi(2S) \rightarrow \pi^0 h_c(1P)) = (8.6 \pm 1.3) \times 10^{-4}$ . Our first error is their experiment's error and our second error is the systematic error from using our best value.

$\Gamma(K^+ K^- \pi^+ \pi^-)/\Gamma(\text{total})$	$\Gamma_9/\Gamma$			
VALUE	CL%	DOCUMENT ID	TECN	COMMENT
<b><math>&lt; 6 \times 10^{-4}</math></b>	90	<sup>1</sup> ABLIKIM	19AG BES3	$\psi(2S) \rightarrow \pi^0 h_c(1P)$

<sup>1</sup> ABLIKIM 19AG reports  $[\Gamma(h_c(1P) \rightarrow K^+ K^- \pi^+ \pi^-)/\Gamma(\text{total})] \times [B(\psi(2S) \rightarrow \pi^0 h_c(1P))]$   $< 0.5 \times 10^{-6}$  which we divide by our best value  $B(\psi(2S) \rightarrow \pi^0 h_c(1P)) = 8.6 \times 10^{-4}$ .

h<sub>c</sub>(1P), χ<sub>c2</sub>(1P)

RADIATIVE DECAYS

Table with 5 columns: Γ(γη)/Γ<sub>total</sub>, VALUE (units 10<sup>-4</sup>), EVTS, DOCUMENT ID, TECN, COMMENT. Includes entry for ABLIKIM 16i BES3 ψ(2S) → π<sup>0</sup>γη.

Table with 5 columns: Γ(γη'(958))/Γ<sub>total</sub>, VALUE (units 10<sup>-3</sup>), EVTS, DOCUMENT ID, TECN, COMMENT. Includes entry for ABLIKIM 16i BES3 ψ(2S) → π<sup>0</sup>γη'(958).

Table with 5 columns: Γ(γη<sub>c</sub>(1S))/Γ<sub>total</sub>, VALUE (units 10<sup>-2</sup>), EVTS, DOCUMENT ID, TECN, COMMENT. Includes entries for ABLIKIM 10B BES3 and DOBBS 08A CLEO.

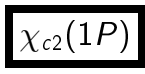
CROSS-PARTICLE BRANCHING RATIOS

Table with 5 columns: Γ(h<sub>c</sub>(1P) → pρ)/Γ<sub>total</sub> × Γ(ψ(2S) → π<sup>0</sup>h<sub>c</sub>(1P))/Γ<sub>total</sub>, VALUE, CL%, DOCUMENT ID, TECN, COMMENT. Includes entry for ABLIKIM 13v BES3.

Table with 5 columns: Γ(h<sub>c</sub>(1P) → γη<sub>c</sub>(1S))/Γ<sub>total</sub> × Γ(ψ(2S) → π<sup>0</sup>h<sub>c</sub>(1P))/Γ<sub>total</sub>, VALUE (units 10<sup>-4</sup>), EVTS, DOCUMENT ID, TECN, COMMENT. Includes entries for ABLIKIM 10B BES3 and DOBBS 08A CLEO.

h<sub>c</sub>(1P) REFERENCES

Table with 4 columns: AUTHOR, YEAR, PUBLICATION, REFERENCE. Lists various experimental papers for h<sub>c</sub>(1P).



I<sup>G</sup>(J<sup>PC</sup>) = 0<sup>+</sup>(2<sup>++</sup>)

See the Review on “ψ(2S) and χ<sub>c</sub> branching ratios” before the χ<sub>c0</sub>(1P) Listings.

χ<sub>c2</sub>(1P) MASS

Table with 5 columns: VALUE (MeV), EVTS, DOCUMENT ID, TECN, COMMENT. Includes entries for AAIJ 17Bb LHCb and UEHARA 08 BELL.

Table with 5 columns: VALUE, EVTS, DOCUMENT ID, TECN, COMMENT. Includes entries for GAISER 86 CBAL and LEMOIGNE 82 GOLI.

1 From a fit of the φφ invariant mass with the width of χ<sub>c2</sub>(1P) fixed to the PDG 16 value.
2 AAIJ 17Bb reports also m(χ<sub>c2</sub>) - m(χ<sub>c1</sub>) = 45.39 ± 0.07 ± 0.03 MeV.
3 Recalculated by ANDREOTTI 05A, using the value of ψ(2S) mass from AULCHENKO 03.
4 Using mass of ψ(2S) = 3686.0 MeV.
5 J/ψ(1S) mass constrained to 3097 MeV.
6 Assuming ψ(2S) mass = 3686 MeV and J/ψ(1S) mass = 3097 MeV.
7 Mass value shifted by us by amount appropriate for ψ(2S) mass = 3686 MeV and J/ψ(1S) mass = 3097 MeV.
8 From a simultaneous fit to radiative and hadronic decay channels.

χ<sub>c2</sub>(1P) WIDTH

Table with 5 columns: VALUE (MeV), EVTS, DOCUMENT ID, TECN, COMMENT. Includes entries for AAIJ 17Bi LHCb and ANDREOTTI 05A E835.

χ<sub>c2</sub>(1P) DECAY MODES

Table with 3 columns: Mode, Fraction (Γ<sub>i</sub>/Γ), Confidence level. Lists various decay modes for χ<sub>c2</sub>(1P) such as 2(π<sup>+</sup>π<sup>-</sup>), ρρ, π<sup>+</sup>π<sup>-</sup>π<sup>0</sup>, etc.

Downloaded from https://academic.oup.com/ptep/article/2020/8/083C01/5891211 by guest on 12 November 2020



Meson Particle Listings

$\chi_{c2}(1P)$

Table with columns: VALUE (eV), EVTS, DOCUMENT ID, TECN, COMMENT. Row for  $\Gamma(K^+ K^- \pi^+ \pi^-) \times \Gamma(\gamma\gamma)/\Gamma_{total}$  with value 4.7 ± 0.5 OUR FIT.

Table with columns: VALUE (eV), EVTS, DOCUMENT ID, TECN, COMMENT. Row for  $\Gamma(K^+ K^- \pi^+ \pi^- \pi^0) \times \Gamma(\gamma\gamma)/\Gamma_{total}$  with value 6.5 ± 0.9 ± 1.5.

Table with columns: VALUE (eV), EVTS, DOCUMENT ID, TECN, COMMENT. Row for  $\Gamma(K^*(892)^0 \bar{K}^*(892)^0) \times \Gamma(\gamma\gamma)/\Gamma_{total}$  with value 1.26 ± 0.24 OUR FIT.

Table with columns: VALUE (eV), EVTS, DOCUMENT ID, TECN, COMMENT. Row for  $\Gamma(\phi\phi) \times \Gamma(\gamma\gamma)/\Gamma_{total}$  with value 0.60 ± 0.05 OUR FIT.

• • • We do not use the following data for averages, fits, limits, etc. • • •
0.58 ± 0.18 ± 0.16 26.5 ± 8.1 UEHARA 08 BELL  $\gamma\gamma \rightarrow \chi_{c2} \rightarrow 2(K^+ K^-)$ 
1 Supersedes UEHARA 08. Using  $B(\phi \rightarrow K^+ K^-) = (48.9 \pm 0.5)\%$ .

Table with columns: VALUE (eV), CL%, DOCUMENT ID, TECN, COMMENT. Row for  $\Gamma(\omega\omega) \times \Gamma(\gamma\gamma)/\Gamma_{total}$  with value <0.64.

• • • We do not use the following data for averages, fits, limits, etc. • • •
<0.64 90 1 LIU 12B BELL  $\gamma\gamma \rightarrow 2(\pi^+ \pi^- \pi^0)$ 
1 Using  $B(\omega \rightarrow \pi^+ \pi^- \pi^0) = (89.2 \pm 0.7)\%$ .

Table with columns: VALUE (eV), CL%, DOCUMENT ID, TECN, COMMENT. Row for  $\Gamma(\omega\phi) \times \Gamma(\gamma\gamma)/\Gamma_{total}$  with value <0.04.

• • • We do not use the following data for averages, fits, limits, etc. • • •
<0.04 90 1 LIU 12B BELL  $\gamma\gamma \rightarrow K^+ K^- \pi^+ \pi^- \pi^0$ 
1 Using  $B(\phi \rightarrow K^+ K^-) = (48.9 \pm 0.5)\%$  and  $B(\omega \rightarrow \pi^+ \pi^- \pi^0) = (89.2 \pm 0.7)\%$ .

Table with columns: VALUE (eV), EVTS, DOCUMENT ID, TECN, COMMENT. Row for  $\Gamma(\pi\pi) \times \Gamma(\gamma\gamma)/\Gamma_{total}$  with value 1.25 ± 0.07 OUR FIT.

1.18 ± 0.25 OUR AVERAGE
1.44 ± 0.54 ± 0.47 34 ± 13 1 UEHARA 09 BELL 10.6 e+ e- -> e+ e- pi0 pi0
1.14 ± 0.21 ± 0.17 54 ± 10 2 NAKAZAWA 05 BELL 10.6 e+ e- -> e+ e- pi+ pi-
1 We multiplied the measurement by 3 to convert from pi0 pi0 to pi pi. Interference with the continuum included.
2 We have multiplied pi+ pi- measurement by 3/2 to obtain pi pi.

Table with columns: VALUE (eV), EVTS, DOCUMENT ID, TECN, COMMENT. Row for  $\Gamma(\rho^0 \pi^+ \pi^-) \times \Gamma(\gamma\gamma)/\Gamma_{total}$  with value 2.1 ± 0.9 OUR FIT.

3.2 ± 1.9 ± 0.5 986 ± 578 UEHARA 08 BELL  $\gamma\gamma \rightarrow \chi_{c2} \rightarrow 2(\pi^+ \pi^-)$

Table with columns: VALUE (eV), EVTS, DOCUMENT ID, TECN, COMMENT. Row for  $\Gamma(\eta\eta) \times \Gamma(\gamma\gamma)/\Gamma_{total}$  with value 0.53 ± 0.22 ± 0.09.

1 Interference with the continuum not included.

Table with columns: VALUE (eV), EVTS, DOCUMENT ID, TECN, COMMENT. Row for  $\Gamma(K^+ K^-) \times \Gamma(\gamma\gamma)/\Gamma_{total}$  with value 0.56 ± 0.04 OUR FIT.

0.44 ± 0.11 ± 0.07 33 ± 8 NAKAZAWA 05 BELL 10.6 e+ e- -> e+ e- K+ K-

Table with columns: VALUE (eV), EVTS, DOCUMENT ID, TECN, COMMENT. Row for  $\Gamma(K_S^0 \bar{K}_S^0) \times \Gamma(\gamma\gamma)/\Gamma_{total}$  with value 0.294 ± 0.025 OUR FIT.

0.27 ± 0.07 ± 0.03 53 1 UEHARA 13 BELL  $\gamma\gamma \rightarrow K_S^0 \bar{K}_S^0$ 
• • • We do not use the following data for averages, fits, limits, etc. • • •
0.31 ± 0.05 ± 0.03 38 ± 7 CHEN 07B BELL e+ e- -> e+ e- chi\_c2
1 Supersedes CHEN 07B.

Table with columns: VALUE (eV), EVTS, DOCUMENT ID, TECN, COMMENT. Row for  $\Gamma(\bar{K}^0 K^+ \pi^- + c.c.) \times \Gamma(\gamma\gamma)/\Gamma_{total}$  with value 0.72 ± 0.11 OUR FIT.

1.20 ± 0.33 ± 0.13 126 1 DEL-AMO-SA...11M BABR  $\gamma\gamma \rightarrow K_S^0 K^\pm \pi^\mp$ 
1 We have multiplied  $\bar{K} K \pi$  by 2/3 to obtain  $\bar{K}^0 K^+ \pi^- + c.c.$

Table with columns: VALUE (eV), EVTS, DOCUMENT ID, TECN, COMMENT. Row for  $\Gamma(K^+ K^- K^+ K^-) \times \Gamma(\gamma\gamma)/\Gamma_{total}$  with value 0.93 ± 0.11 OUR FIT.

1.10 ± 0.21 ± 0.15 126 ± 24 UEHARA 08 BELL  $\gamma\gamma \rightarrow \chi_{c2} \rightarrow 2(K^+ K^-)$

Table with columns: VALUE (eV), CL%, DOCUMENT ID, TECN, COMMENT. Row for  $\Gamma(\eta_c(1S) \pi^+ \pi^-) \times \Gamma(\gamma\gamma)/\Gamma_{total}$  with value <15.7.

chi\_c2(1P) BRANCHING RATIOS

HADRONIC DECAYS

Table with columns: VALUE, DOCUMENT ID. Row for  $\Gamma(2(\pi^+ \pi^-))/\Gamma_{total}$  with value 0.0102 ± 0.0009 OUR FIT.

Table with columns: VALUE, DOCUMENT ID, TECN, COMMENT. Row for  $\Gamma(\rho^0 \pi^+ \pi^-)/\Gamma(2(\pi^+ \pi^-))$  with value 0.36 ± 0.15 OUR FIT.

Table with columns: VALUE (%), EVTS, DOCUMENT ID, TECN, COMMENT. Row for  $\Gamma(\pi^+ \pi^- \pi^0 \pi^0)/\Gamma_{total}$  with value 1.83 ± 0.23 ± 0.04.

1 HE 08B reports 1.87 ± 0.07 ± 0.22 ± 0.13 % from a measurement of  $[\Gamma(\chi_{c2}(1P) \rightarrow \pi^+ \pi^- \pi^0 \pi^0)/\Gamma_{total}] \times [B(\psi(2S) \rightarrow \gamma \chi_{c2}(1P))]$  assuming  $B(\psi(2S) \rightarrow \gamma \chi_{c2}(1P)) = (9.33 \pm 0.14 \pm 0.61) \times 10^{-2}$ , which we rescale to our best value  $B(\psi(2S) \rightarrow \gamma \chi_{c2}(1P)) = (9.52 \pm 0.20) \times 10^{-2}$ . Our first error is their experiment's error and our second error is the systematic error from using our best value.

Table with columns: VALUE (%), EVTS, DOCUMENT ID, TECN, COMMENT. Row for  $\Gamma(\rho^+ \pi^- \pi^0 + c.c.)/\Gamma_{total}$  with value 2.19 ± 0.34 ± 0.05.

1 HE 08B reports 2.23 ± 0.11 ± 0.32 ± 0.16 % from a measurement of  $[\Gamma(\chi_{c2}(1P) \rightarrow \rho^+ \pi^- \pi^0 + c.c.)/\Gamma_{total}] \times [B(\psi(2S) \rightarrow \gamma \chi_{c2}(1P))]$  assuming  $B(\psi(2S) \rightarrow \gamma \chi_{c2}(1P)) = (9.33 \pm 0.14 \pm 0.61) \times 10^{-2}$ , which we rescale to our best value  $B(\psi(2S) \rightarrow \gamma \chi_{c2}(1P)) = (9.52 \pm 0.20) \times 10^{-2}$ . Our first error is their experiment's error and our second error is the systematic error from using our best value.
2 Calculated by us. We have added the values from HE 08B for  $\rho^+ \pi^- \pi^0$  and  $\rho^- \pi^+ \pi^0$  decays assuming uncorrelated statistical and fully correlated systematic uncertainties.

Table with columns: VALUE (units 10^-3), EVTS, DOCUMENT ID, TECN, COMMENT. Row for  $\Gamma(4\pi^0)/\Gamma_{total}$  with value 1.11 ± 0.15 ± 0.02.

1 ABLIKIM 11A reports  $(1.21 \pm 0.05 \pm 0.16) \times 10^{-3}$  from a measurement of  $[\Gamma(\chi_{c2}(1P) \rightarrow 4\pi^0)/\Gamma_{total}] \times [B(\psi(2S) \rightarrow \gamma \chi_{c2}(1P))]$  assuming  $B(\psi(2S) \rightarrow \gamma \chi_{c2}(1P)) = (8.74 \pm 0.35) \times 10^{-2}$ , which we rescale to our best value  $B(\psi(2S) \rightarrow \gamma \chi_{c2}(1P)) = (9.52 \pm 0.20) \times 10^{-2}$ . Our first error is their experiment's error and our second error is the systematic error from using our best value.

Table with columns: VALUE (%), EVTS, DOCUMENT ID, TECN, COMMENT. Row for  $\Gamma(K^+ K^- \pi^0 \pi^0)/\Gamma_{total}$  with value 0.206 ± 0.040 ± 0.004.

1 HE 08B reports 0.21 ± 0.03 ± 0.03 ± 0.01 % from a measurement of  $[\Gamma(\chi_{c2}(1P) \rightarrow K^+ K^- \pi^0 \pi^0)/\Gamma_{total}] \times [B(\psi(2S) \rightarrow \gamma \chi_{c2}(1P))]$  assuming  $B(\psi(2S) \rightarrow \gamma \chi_{c2}(1P)) = (9.33 \pm 0.14 \pm 0.61) \times 10^{-2}$ , which we rescale to our best value  $B(\psi(2S) \rightarrow \gamma \chi_{c2}(1P)) = (9.52 \pm 0.20) \times 10^{-2}$ . Our first error is their experiment's error and our second error is the systematic error from using our best value.

Table with columns: VALUE (%), EVTS, DOCUMENT ID, TECN, COMMENT. Row for  $\Gamma(K^+ \pi^- \bar{K}^0 \pi^0 + c.c.)/\Gamma_{total}$  with value 1.38 ± 0.19 ± 0.03.

1 HE 08B reports 1.41 ± 0.11 ± 0.16 ± 0.10 % from a measurement of  $[\Gamma(\chi_{c2}(1P) \rightarrow K^+ \pi^- \bar{K}^0 \pi^0 + c.c.)/\Gamma_{total}] \times [B(\psi(2S) \rightarrow \gamma \chi_{c2}(1P))]$  assuming  $B(\psi(2S) \rightarrow \gamma \chi_{c2}(1P)) = (9.33 \pm 0.14 \pm 0.61) \times 10^{-2}$ , which we rescale to our best value  $B(\psi(2S) \rightarrow \gamma \chi_{c2}(1P)) = (9.52 \pm 0.20) \times 10^{-2}$ . Our first error is their experiment's error and our second error is the systematic error from using our best value.

Table with columns: VALUE (%), EVTS, DOCUMENT ID, TECN, COMMENT. Row for  $\Gamma(\rho^- K^+ \bar{K}^0 + c.c.)/\Gamma_{total}$  with value 0.41 ± 0.12 ± 0.01.

1 HE 08B reports 0.42 ± 0.11 ± 0.06 ± 0.03 % from a measurement of  $[\Gamma(\chi_{c2}(1P) \rightarrow \rho^- K^+ \bar{K}^0 + c.c.)/\Gamma_{total}] \times [B(\psi(2S) \rightarrow \gamma \chi_{c2}(1P))]$  assuming  $B(\psi(2S) \rightarrow \gamma \chi_{c2}(1P)) = (9.33 \pm 0.14 \pm 0.61) \times 10^{-2}$ , which we rescale to our best value  $B(\psi(2S) \rightarrow \gamma \chi_{c2}(1P)) = (9.52 \pm 0.20) \times 10^{-2}$ . Our first error is their experiment's error and our second error is the systematic error from using our best value.

Table with columns: VALUE (%), EVTS, DOCUMENT ID, TECN, COMMENT. Row for  $\Gamma(K^*(892)^0 K^- \pi^+ \rightarrow K^- \pi^+ K^0 \pi^0 + c.c.)/\Gamma_{total}$  with value 0.29 ± 0.08 ± 0.01.

1 HE 08B reports 0.30 ± 0.07 ± 0.04 ± 0.02 % from a measurement of  $[\Gamma(\chi_{c2}(1P) \rightarrow K^*(892)^0 K^- \pi^+ \rightarrow K^- \pi^+ K^0 \pi^0 + c.c.)/\Gamma_{total}] \times [B(\psi(2S) \rightarrow \gamma \chi_{c2}(1P))]$  assuming  $B(\psi(2S) \rightarrow \gamma \chi_{c2}(1P)) = (9.33 \pm 0.14 \pm 0.61) \times 10^{-2}$ , which we rescale to our best value  $B(\psi(2S) \rightarrow \gamma \chi_{c2}(1P)) = (9.52 \pm 0.20) \times 10^{-2}$ . Our first error is their experiment's error and our second error is the systematic error from using our best value.

Downloaded from https://academic.oup.com/ptep/article/2020/8/083C01/5891211 by guest on 12 November 2020



## Meson Particle Listings

 $\chi_{c2}(1P)$ 

$\Gamma(K^*(892)^0 \bar{K}^0 \pi^0 \rightarrow K^+ \pi^- \bar{K}^0 \pi^0 + \text{c.c.})/\Gamma_{\text{total}}$					$\Gamma_{10}/\Gamma$
VALUE (%)	EVTS	DOCUMENT ID	TECN	COMMENT	
<b>0.38 ± 0.09 ± 0.01</b>	63.0	<sup>1</sup> HE	08B CLEO	$e^+ e^- \rightarrow \gamma h^+ h^- h^0 h^0$	

<sup>1</sup> HE 08B reports  $0.39 \pm 0.07 \pm 0.05 \pm 0.03$  % from a measurement of  $[\Gamma(\chi_{c2}(1P) \rightarrow K^*(892)^0 \bar{K}^0 \pi^0 \rightarrow K^+ \pi^- \bar{K}^0 \pi^0 + \text{c.c.})/\Gamma_{\text{total}}] \times [B(\psi(2S) \rightarrow \gamma \chi_{c2}(1P))]$  assuming  $B(\psi(2S) \rightarrow \gamma \chi_{c2}(1P)) = (9.33 \pm 0.14 \pm 0.61) \times 10^{-2}$ , which we rescale to our best value  $B(\psi(2S) \rightarrow \gamma \chi_{c2}(1P)) = (9.52 \pm 0.20) \times 10^{-2}$ . Our first error is their experiment's error and our second error is the systematic error from using our best value.

$\Gamma(K^*(892)^- K^+ \pi^0 \rightarrow K^+ \pi^- \bar{K}^0 \pi^0 + \text{c.c.})/\Gamma_{\text{total}}$					$\Gamma_{11}/\Gamma$
VALUE (%)	EVTS	DOCUMENT ID	TECN	COMMENT	
<b>0.37 ± 0.08 ± 0.01</b>	51.1	<sup>1</sup> HE	08B CLEO	$e^+ e^- \rightarrow \gamma h^+ h^- h^0 h^0$	

<sup>1</sup> HE 08B reports  $0.38 \pm 0.07 \pm 0.04 \pm 0.03$  % from a measurement of  $[\Gamma(\chi_{c2}(1P) \rightarrow K^*(892)^- K^+ \pi^0 \rightarrow K^+ \pi^- \bar{K}^0 \pi^0 + \text{c.c.})/\Gamma_{\text{total}}] \times [B(\psi(2S) \rightarrow \gamma \chi_{c2}(1P))]$  assuming  $B(\psi(2S) \rightarrow \gamma \chi_{c2}(1P)) = (9.33 \pm 0.14 \pm 0.61) \times 10^{-2}$ , which we rescale to our best value  $B(\psi(2S) \rightarrow \gamma \chi_{c2}(1P)) = (9.52 \pm 0.20) \times 10^{-2}$ . Our first error is their experiment's error and our second error is the systematic error from using our best value.

$\Gamma(K^*(892)^+ \bar{K}^0 \pi^- \rightarrow K^+ \pi^- \bar{K}^0 \pi^0 + \text{c.c.})/\Gamma_{\text{total}}$					$\Gamma_{12}/\Gamma$
VALUE (%)	EVTS	DOCUMENT ID	TECN	COMMENT	
<b>0.29 ± 0.08 ± 0.01</b>	39.3	<sup>1</sup> HE	08B CLEO	$e^+ e^- \rightarrow \gamma h^+ h^- h^0 h^0$	

<sup>1</sup> HE 08B reports  $0.30 \pm 0.07 \pm 0.04 \pm 0.02$  % from a measurement of  $[\Gamma(\chi_{c2}(1P) \rightarrow K^*(892)^+ \bar{K}^0 \pi^- \rightarrow K^+ \pi^- \bar{K}^0 \pi^0 + \text{c.c.})/\Gamma_{\text{total}}] \times [B(\psi(2S) \rightarrow \gamma \chi_{c2}(1P))]$  assuming  $B(\psi(2S) \rightarrow \gamma \chi_{c2}(1P)) = (9.33 \pm 0.14 \pm 0.61) \times 10^{-2}$ , which we rescale to our best value  $B(\psi(2S) \rightarrow \gamma \chi_{c2}(1P)) = (9.52 \pm 0.20) \times 10^{-2}$ . Our first error is their experiment's error and our second error is the systematic error from using our best value.

$\Gamma(K^+ K^- \eta \pi^0)/\Gamma_{\text{total}}$					$\Gamma_{13}/\Gamma$
VALUE (%)	EVTS	DOCUMENT ID	TECN	COMMENT	
<b>0.127 ± 0.044 ± 0.003</b>	22.9	<sup>1</sup> HE	08B CLEO	$e^+ e^- \rightarrow \gamma h^+ h^- h^0 h^0$	

<sup>1</sup> HE 08B reports  $0.13 \pm 0.04 \pm 0.02 \pm 0.01$  % from a measurement of  $[\Gamma(\chi_{c2}(1P) \rightarrow K^+ K^- \eta \pi^0)/\Gamma_{\text{total}}] \times [B(\psi(2S) \rightarrow \gamma \chi_{c2}(1P))]$  assuming  $B(\psi(2S) \rightarrow \gamma \chi_{c2}(1P)) = (9.33 \pm 0.14 \pm 0.61) \times 10^{-2}$ , which we rescale to our best value  $B(\psi(2S) \rightarrow \gamma \chi_{c2}(1P)) = (9.52 \pm 0.20) \times 10^{-2}$ . Our first error is their experiment's error and our second error is the systematic error from using our best value.

$\Gamma(K^+ K^- \pi^+ \pi^-)/\Gamma_{\text{total}}$					$\Gamma_{14}/\Gamma$
VALUE (units $10^{-3}$ )	DOCUMENT ID	TECN	COMMENT		
<b>8.4 ± 0.9 OUR FIT</b>					

$\Gamma(K^+ K^- \pi^+ \pi^- \pi^0)/\Gamma_{\text{total}}$					$\Gamma_{15}/\Gamma$
VALUE (units $10^{-3}$ )	EVTS	DOCUMENT ID	TECN	COMMENT	
<b>11.69 ± 0.13 ± 1.31</b>	11k	<sup>1</sup> ABLIKIM	13B BES3	$e^+ e^- \rightarrow \psi(2S) \rightarrow \gamma \chi_{c2}$	

<sup>1</sup> Using  $1.06 \times 10^8$   $\psi(2S)$  mesons and  $B(\psi(2S) \rightarrow \chi_{c2} \gamma) = (8.72 \pm 0.34)$  %.

$\Gamma(K_S^0 K^\pm \pi^\mp \pi^+ \pi^-)/\Gamma_{\text{total}}$					$\Gamma_{16}/\Gamma$
VALUE (units $10^{-3}$ )	EVTS	DOCUMENT ID	TECN	COMMENT	
<b>7.30 ± 0.11 ± 0.75</b>	4.5k	<sup>1</sup> ABLIKIM	13B BES3	$e^+ e^- \rightarrow \psi(2S) \rightarrow \gamma \chi_{c2}$	

<sup>1</sup> Using  $1.06 \times 10^8$   $\psi(2S)$  mesons and  $B(\psi(2S) \rightarrow \chi_{c2} \gamma) = (8.72 \pm 0.34)$  %.

$\Gamma(K^+ \bar{K}^*(892)^0 \pi^- + \text{c.c.})/\Gamma(K^+ K^- \pi^+ \pi^-)$				$\Gamma_{17}/\Gamma_{14}$
VALUE	DOCUMENT ID	TECN	COMMENT	
<b>0.25 ± 0.13 OUR FIT</b>				
<b>0.25 ± 0.13</b>	TANENBAUM 78	MRK1	$\psi(2S) \rightarrow \gamma \chi_{c2}$	

$\Gamma(K^+ \bar{K}^*(892)^0 \pi^- + \text{c.c.})/\Gamma_{\text{total}}$				$\Gamma_{17}/\Gamma$
VALUE (units $10^{-4}$ )	DOCUMENT ID	TECN	COMMENT	
<b>21 ± 11 OUR FIT</b>				

$\Gamma(K^*(892)^0 \bar{K}^*(892)^0)/\Gamma_{\text{total}}$					$\Gamma_{18}/\Gamma$
VALUE (units $10^{-3}$ )	DOCUMENT ID	TECN	COMMENT		
<b>2.3 ± 0.4 OUR FIT</b>					

$\Gamma(3(\pi^+ \pi^-))/\Gamma_{\text{total}}$					$\Gamma_{19}/\Gamma$
VALUE (units $10^{-3}$ )	DOCUMENT ID	TECN	COMMENT		
<b>8.6 ± 1.8 OUR EVALUATION</b>	Treating systematic error as correlated.				
<b>8.6 ± 1.8 OUR AVERAGE</b>					

<sup>1</sup> Rescaled by us using  $B(\psi(2S) \rightarrow \gamma \chi_{c2}) = (8.3 \pm 0.4)$  % and  $B(\psi(2S) \rightarrow J/\psi(1S) \pi^+ \pi^-) = (32.6 \pm 0.5)$  %. Multiplied by a factor of 2 to convert from  $K_S^0 K^+ \pi^-$  to  $K^0 K^+ \pi^-$  decay.

$\Gamma(\phi\phi)/\Gamma_{\text{total}}$					$\Gamma_{20}/\Gamma$
VALUE (units $10^{-3}$ )	DOCUMENT ID	TECN	COMMENT		
<b>1.06 ± 0.09 OUR FIT</b>					

$\Gamma(\phi\phi\eta)/\Gamma_{\text{total}}$					$\Gamma_{21}/\Gamma$
VALUE (units $10^{-4}$ )	EVTS	DOCUMENT ID	TECN	COMMENT	
<b>5.3 ± 0.5 ± 0.4</b>	143.6	<sup>1</sup> ABLIKIM	20B BES3	$\psi(2S) \rightarrow \gamma \phi\phi\eta$	

<sup>1</sup> ABLIKIM 20B reports  $(5.33 \pm 0.52 \pm 0.39) \times 10^{-4}$  from a measurement of  $[\Gamma(\chi_{c2}(1P) \rightarrow \phi\phi\eta)/\Gamma_{\text{total}}] \times [B(\psi(2S) \rightarrow \gamma \chi_{c2}(1P))]$  assuming  $B(\psi(2S) \rightarrow \gamma \chi_{c2}(1P)) = (9.52 \pm 0.20) \times 10^{-2}$ .

$\Gamma(\omega\omega)/\Gamma_{\text{total}}$					$\Gamma_{22}/\Gamma$
VALUE (units $10^{-3}$ )	EVTS	DOCUMENT ID	TECN	COMMENT	
<b>0.84 ± 0.10 OUR AVERAGE</b>					
0.82 ± 0.10 ± 0.02	762	<sup>1</sup> ABLIKIM	11K BES3	$\psi(2S) \rightarrow \gamma$ hadrons	
1.73 ± 0.57 ± 0.04	27.7 ± 7.4	<sup>2</sup> ABLIKIM	05N BES2	$\psi(2S) \rightarrow \gamma \chi_{c2} \rightarrow \gamma 6\pi$	

<sup>1</sup> ABLIKIM 11K reports  $(8.9 \pm 0.3 \pm 1.1) \times 10^{-4}$  from a measurement of  $[\Gamma(\chi_{c2}(1P) \rightarrow \omega\omega)/\Gamma_{\text{total}}] \times [B(\psi(2S) \rightarrow \gamma \chi_{c2}(1P))]$  assuming  $B(\psi(2S) \rightarrow \gamma \chi_{c2}(1P)) = (8.74 \pm 0.35) \times 10^{-2}$ , which we rescale to our best value  $B(\psi(2S) \rightarrow \gamma \chi_{c2}(1P)) = (9.52 \pm 0.20) \times 10^{-2}$ . Our first error is their experiment's error and our second error is the systematic error from using our best value.

<sup>2</sup> ABLIKIM 05N reports  $[\Gamma(\chi_{c2}(1P) \rightarrow \omega\omega)/\Gamma_{\text{total}}] \times [B(\psi(2S) \rightarrow \gamma \chi_{c2}(1P))]$  =  $(0.165 \pm 0.044 \pm 0.032) \times 10^{-3}$  which we divide by our best value  $B(\psi(2S) \rightarrow \gamma \chi_{c2}(1P)) = (9.52 \pm 0.20) \times 10^{-2}$ . Our first error is their experiment's error and our second error is the systematic error from using our best value.

$\Gamma(\omega K^+ K^-)/\Gamma_{\text{total}}$					$\Gamma_{23}/\Gamma$
VALUE (units $10^{-3}$ )	EVTS	DOCUMENT ID	TECN	COMMENT	
<b>0.73 ± 0.04 ± 0.08</b>	512	<sup>1</sup> ABLIKIM	13B BES3	$e^+ e^- \rightarrow \psi(2S) \rightarrow \gamma \chi_{c2}$	

<sup>1</sup> Using  $1.06 \times 10^8$   $\psi(2S)$  mesons and  $B(\psi(2S) \rightarrow \chi_{c2} \gamma) = (8.72 \pm 0.34)$  %.

$\Gamma(\omega\phi)/\Gamma_{\text{total}}$					$\Gamma_{24}/\Gamma$
VALUE (units $10^{-6}$ )	CL%	EVTS	DOCUMENT ID	TECN	COMMENT
<b>9.6 ± 2.7 ± 0.2</b>	33		<sup>1</sup> ABLIKIM	19J BES3	$\psi(2S) \rightarrow \gamma$ hadrons
<18	90		<sup>2,3</sup> ABLIKIM	11K BES3	$\psi(2S) \rightarrow \gamma$ hadrons

• • • We do not use the following data for averages, fits, limits, etc. • • •

<sup>1</sup> ABLIKIM 19J reports  $[\Gamma(\chi_{c2}(1P) \rightarrow \omega\phi)/\Gamma_{\text{total}}] \times [B(\psi(2S) \rightarrow \gamma \chi_{c2}(1P))]$  =  $(0.91 \pm 0.23 \pm 0.12) \times 10^{-6}$  which we divide by our best value  $B(\psi(2S) \rightarrow \gamma \chi_{c2}(1P)) = (9.52 \pm 0.20) \times 10^{-2}$ . Our first error is their experiment's error and our second error is the systematic error from using our best value.

<sup>2</sup> ABLIKIM 11K reports  $< 2 \times 10^{-5}$  from a measurement of  $[\Gamma(\chi_{c2}(1P) \rightarrow \omega\phi)/\Gamma_{\text{total}}] \times [B(\psi(2S) \rightarrow \gamma \chi_{c2}(1P))]$  assuming  $B(\psi(2S) \rightarrow \gamma \chi_{c2}(1P)) = (8.74 \pm 0.35) \times 10^{-2}$ , which we rescale to our best value  $B(\psi(2S) \rightarrow \gamma \chi_{c2}(1P)) = 9.52 \times 10^{-2}$ .

<sup>3</sup> Superseded by ABLIKIM 19J.

$\Gamma(\pi\pi)/\Gamma_{\text{total}}$					$\Gamma_{25}/\Gamma$
VALUE (units $10^{-3}$ )	DOCUMENT ID	TECN	COMMENT		
<b>2.23 ± 0.09 OUR FIT</b>					

$\Gamma(\rho^0 \pi^+ \pi^-)/\Gamma_{\text{total}}$					$\Gamma_{26}/\Gamma$
VALUE (units $10^{-4}$ )	DOCUMENT ID	TECN	COMMENT		
<b>37 ± 16 OUR FIT</b>					

$\Gamma(\pi^+ \pi^- \pi^0 (\text{non-resonant}))/\Gamma_{\text{total}}$					$\Gamma_{27}/\Gamma$
VALUE (units $10^{-5}$ )	EVTS	DOCUMENT ID	TECN	COMMENT	
<b>2.01 ± 0.42 ± 0.04</b>	64	<sup>1</sup> ABLIKIM	17AG BES3	$\psi(2S) \rightarrow \gamma \pi^+ \pi^- \pi^0$	

<sup>1</sup> ABLIKIM 17AG reports  $(2.1 \pm 0.4 \pm 0.2) \times 10^{-5}$  from a measurement of  $[\Gamma(\chi_{c2}(1P) \rightarrow \pi^+ \pi^- \pi^0 (\text{non-resonant}))/\Gamma_{\text{total}}] \times [B(\psi(2S) \rightarrow \gamma \chi_{c2}(1P))]$  assuming  $B(\psi(2S) \rightarrow \gamma \chi_{c2}(1P)) = (9.11 \pm 0.31) \times 10^{-2}$ , which we rescale to our best value  $B(\psi(2S) \rightarrow \gamma \chi_{c2}(1P)) = (9.52 \pm 0.20) \times 10^{-2}$ . Our first error is their experiment's error and our second error is the systematic error from using our best value.

$\Gamma(\rho(770)^\pm \pi^\mp)/\Gamma_{\text{total}}$					$\Gamma_{28}/\Gamma$
VALUE (units $10^{-5}$ )	EVTS	DOCUMENT ID	TECN	COMMENT	
<b>0.61 ± 0.38 ± 0.01</b>	15	<sup>1</sup> ABLIKIM	17AG BES3	$\psi(2S) \rightarrow \gamma \pi^+ \pi^- \pi^0$	

<sup>1</sup> ABLIKIM 17AG reports  $(0.64 \pm 0.39 \pm 0.07) \times 10^{-5}$  from a measurement of  $[\Gamma(\chi_{c2}(1P) \rightarrow \rho(770)^\pm \pi^\mp)/\Gamma_{\text{total}}] \times [B(\psi(2S) \rightarrow \gamma \chi_{c2}(1P))]$  assuming  $B(\psi(2S) \rightarrow \gamma \chi_{c2}(1P)) = (9.11 \pm 0.31) \times 10^{-2}$ , which we rescale to our best value  $B(\psi(2S) \rightarrow \gamma \chi_{c2}(1P)) = (9.52 \pm 0.20) \times 10^{-2}$ . Our first error is their experiment's error and our second error is the systematic error from using our best value.

$\Gamma(\pi^+ \pi^- \eta)/\Gamma_{\text{total}}$					$\Gamma_{29}/\Gamma$
VALUE (units $10^{-3}$ )	CL%	DOCUMENT ID	TECN	COMMENT	
<b>0.48 ± 0.13 ± 0.01</b>		<sup>1</sup> ATHAR	07 CLEO	$\psi(2S) \rightarrow \gamma h^+ h^- h^0$	
<1.4	90	<sup>2</sup> ABLIKIM	06R BES2	$\psi(2S) \rightarrow \gamma \chi_{c2}$	

• • • We do not use the following data for averages, fits, limits, etc. • • •

<sup>1</sup> ATHAR 07 reports  $(0.49 \pm 0.12 \pm 0.06) \times 10^{-3}$  from a measurement of  $[\Gamma(\chi_{c2}(1P) \rightarrow \pi^+ \pi^- \eta)/\Gamma_{\text{total}}] \times [B(\psi(2S) \rightarrow \gamma \chi_{c2}(1P))]$  assuming  $B(\psi(2S) \rightarrow \gamma \chi_{c2}(1P)) = (9.33 \pm 0.14 \pm 0.61) \times 10^{-2}$ , which we rescale to our best value  $B(\psi(2S) \rightarrow \gamma \chi_{c2}(1P)) = (9.52 \pm 0.20) \times 10^{-2}$ . Our first error is their experiment's error and our second error is the systematic error from using our best value.

<sup>2</sup> ABLIKIM 06R reports  $< 1.7 \times 10^{-3}$  from a measurement of  $[\Gamma(\chi_{c2}(1P) \rightarrow \pi^+ \pi^- \eta)/\Gamma_{\text{total}}] \times [B(\psi(2S) \rightarrow \gamma \chi_{c2}(1P))]$  assuming  $B(\psi(2S) \rightarrow \gamma \chi_{c2}(1P)) = (8.1 \pm 0.4) \times 10^{-2}$ , which we rescale to our best value  $B(\psi(2S) \rightarrow \gamma \chi_{c2}(1P)) = 9.52 \times 10^{-2}$ .

See key on page 999

Meson Particle Listings

$\chi_{c2}(1P)$

$\Gamma(\pi^+\pi^-\eta')/\Gamma_{total}$	$\Gamma_{30}/\Gamma$		
VALUE (units $10^{-3}$ )	DOCUMENT ID	TECN	COMMENT
<b>0.50±0.18±0.01</b>	<sup>1</sup> ATHAR	07	CLEO $\psi(2S) \rightarrow \gamma h^+ h^- h^0$

<sup>1</sup>ATHAR 07 reports  $(0.51 \pm 0.18 \pm 0.06) \times 10^{-3}$  from a measurement of  $[\Gamma(\chi_{c2}(1P) \rightarrow \pi^+\pi^-\eta')/\Gamma_{total}] \times [B(\psi(2S) \rightarrow \gamma\chi_{c2}(1P))]$  assuming  $B(\psi(2S) \rightarrow \gamma\chi_{c2}(1P)) = (9.33 \pm 0.14 \pm 0.61) \times 10^{-2}$ , which we rescale to our best value  $B(\psi(2S) \rightarrow \gamma\chi_{c2}(1P)) = (9.52 \pm 0.20) \times 10^{-2}$ . Our first error is their experiment's error and our second error is the systematic error from using our best value.

$\Gamma(\eta\eta)/\Gamma_{total}$	$\Gamma_{31}/\Gamma$		
VALUE (units $10^{-4}$ )	DOCUMENT ID	TECN	COMMENT
<b>5.4±0.4 OUR FIT</b>			

$\Gamma(K^+K^-)/\Gamma_{total}$	$\Gamma_{32}/\Gamma$		
VALUE (units $10^{-3}$ )	DOCUMENT ID	TECN	COMMENT
<b>1.01±0.06 OUR FIT</b>			

$\Gamma(K_S^0 K_S^0)/\Gamma_{total}$	$\Gamma_{33}/\Gamma$		
VALUE (units $10^{-3}$ )	DOCUMENT ID	TECN	COMMENT
<b>0.52±0.04 OUR FIT</b>			

$\Gamma(K_S^0 K_S^0)/\Gamma(\pi\pi)$	$\Gamma_{33}/\Gamma_{25}$		
VALUE	DOCUMENT ID	TECN	COMMENT
<b>0.235±0.019 OUR FIT</b>			

• • • We do not use the following data for averages, fits, limits, etc. • • •  
 0.27 ± 0.07 ± 0.04 <sup>1,2</sup> CHEN 07B BELL  $e^+e^- \rightarrow e^+e^-\chi_{c2}$   
<sup>1</sup>Using  $\Gamma(\pi\pi) \times \Gamma(\gamma\gamma)/\Gamma_{total}$  from the  $\pi^+\pi^-$  measurement of NAKAZAWA 05 rescaled by 2 to convert to  $\pi\pi$ .  
<sup>2</sup>Not independent from other measurements.

$\Gamma(K_S^0 K_S^0)/\Gamma(K^+K^-)$	$\Gamma_{33}/\Gamma_{32}$		
VALUE	DOCUMENT ID	TECN	COMMENT
<b>0.52±0.05 OUR FIT</b>			

• • • We do not use the following data for averages, fits, limits, etc. • • •  
 0.70±0.21±0.12 <sup>1,2</sup> CHEN 07B BELL  $e^+e^- \rightarrow e^+e^-\chi_{c2}$   
<sup>1</sup>Using  $\Gamma(K^+K^-) \times \Gamma(\gamma\gamma)/\Gamma_{total}$  from NAKAZAWA 05.  
<sup>2</sup>Not independent from other measurements.

$\Gamma(K^*(892^\pm K^\mp)/\Gamma_{total}$	$\Gamma_{34}/\Gamma$		
VALUE (units $10^{-4}$ )	DOCUMENT ID	TECN	COMMENT
<b>1.44±0.21±0.03</b>	<sup>1</sup> ABLIKIM	17AG BES3	$\psi(2S) \rightarrow \gamma K \bar{K} \pi$

• • • We do not use the following data for averages, fits, limits, etc. • • •  
 1.72±0.26±0.04 <sup>2</sup> ABLIKIM 17AG BES3  $\psi(2S) \rightarrow \gamma K^+ K^- \pi^0$   
 1.34±0.27±0.03 <sup>3</sup> ABLIKIM 17AG BES3  $\psi(2S) \rightarrow \gamma K_S^0 K^\pm \pi^\mp$

<sup>1</sup>ABLIKIM 17AG reports  $(1.5 \pm 0.1 \pm 0.2) \times 10^{-4}$  from a measurement of  $[\Gamma(\chi_{c2}(1P) \rightarrow K^*(892^\pm K^\mp)/\Gamma_{total}) \times [B(\psi(2S) \rightarrow \gamma\chi_{c2}(1P))]]$  assuming  $B(\psi(2S) \rightarrow \gamma\chi_{c2}(1P)) = (9.11 \pm 0.31) \times 10^{-2}$ , which we rescale to our best value  $B(\psi(2S) \rightarrow \gamma\chi_{c2}(1P)) = (9.52 \pm 0.20) \times 10^{-2}$ . Our first error is their experiment's error and our second error is the systematic error from using our best value.  
<sup>2</sup>ABLIKIM 17AG reports  $(1.8 \pm 0.2 \pm 0.2) \times 10^{-4}$  from a measurement of  $[\Gamma(\chi_{c2}(1P) \rightarrow K^*(892^\pm K^\mp)/\Gamma_{total}) \times [B(\psi(2S) \rightarrow \gamma\chi_{c2}(1P))]]$  assuming  $B(\psi(2S) \rightarrow \gamma\chi_{c2}(1P)) = (9.11 \pm 0.31) \times 10^{-2}$ , which we rescale to our best value  $B(\psi(2S) \rightarrow \gamma\chi_{c2}(1P)) = (9.52 \pm 0.20) \times 10^{-2}$ . Our first error is their experiment's error and our second error is the systematic error from using our best value.  
<sup>3</sup>ABLIKIM 17AG reports  $(1.4 \pm 0.2 \pm 0.2) \times 10^{-4}$  from a measurement of  $[\Gamma(\chi_{c2}(1P) \rightarrow K^*(892^\pm K^\mp)/\Gamma_{total}) \times [B(\psi(2S) \rightarrow \gamma\chi_{c2}(1P))]]$  assuming  $B(\psi(2S) \rightarrow \gamma\chi_{c2}(1P)) = (9.11 \pm 0.31) \times 10^{-2}$ , which we rescale to our best value  $B(\psi(2S) \rightarrow \gamma\chi_{c2}(1P)) = (9.52 \pm 0.20) \times 10^{-2}$ . Our first error is their experiment's error and our second error is the systematic error from using our best value.

$\Gamma(K^*(892^0 \bar{K}^0 + c.c.)/\Gamma_{total}$	$\Gamma_{35}/\Gamma$		
VALUE (units $10^{-4}$ )	DOCUMENT ID	TECN	COMMENT
<b>1.24±0.27±0.03</b>	<sup>1</sup> ABLIKIM	17AG BES3	$\psi(2S) \rightarrow \gamma K_S^0 K^\pm \pi^\mp$

<sup>1</sup>ABLIKIM 17AG reports  $(1.3 \pm 0.2 \pm 0.2) \times 10^{-4}$  from a measurement of  $[\Gamma(\chi_{c2}(1P) \rightarrow K^*(892^0 \bar{K}^0 + c.c.)/\Gamma_{total}) \times [B(\psi(2S) \rightarrow \gamma\chi_{c2}(1P))]]$  assuming  $B(\psi(2S) \rightarrow \gamma\chi_{c2}(1P)) = (9.11 \pm 0.31) \times 10^{-2}$ , which we rescale to our best value  $B(\psi(2S) \rightarrow \gamma\chi_{c2}(1P)) = (9.52 \pm 0.20) \times 10^{-2}$ . Our first error is their experiment's error and our second error is the systematic error from using our best value.

$\Gamma(K_2^*(1430^\pm K^\mp)/\Gamma_{total}$	$\Gamma_{36}/\Gamma$		
VALUE (units $10^{-4}$ )	DOCUMENT ID	TECN	COMMENT
<b>14.8±1.2±0.3</b>	<sup>1</sup> ABLIKIM	17AG BES3	$\psi(2S) \rightarrow \gamma K \bar{K} \pi$

• • • We do not use the following data for averages, fits, limits, etc. • • •  
 17.4±1.6±0.4 <sup>2</sup> ABLIKIM 17AG BES3  $\psi(2S) \rightarrow \gamma K^+ K^- \pi^0$   
 13.0±1.5±0.3 <sup>3</sup> ABLIKIM 17AG BES3  $\psi(2S) \rightarrow \gamma K_S^0 K^\pm \pi^\mp$   
<sup>1</sup>ABLIKIM 17AG reports  $(15.5 \pm 0.6 \pm 1.2) \times 10^{-4}$  from a measurement of  $[\Gamma(\chi_{c2}(1P) \rightarrow K_2^*(1430^\pm K^\mp)/\Gamma_{total}) \times [B(\psi(2S) \rightarrow \gamma\chi_{c2}(1P))]]$  assuming  $B(\psi(2S) \rightarrow \gamma\chi_{c2}(1P)) = (9.11 \pm 0.31) \times 10^{-2}$ , which we rescale to our best value  $B(\psi(2S) \rightarrow \gamma\chi_{c2}(1P)) = (9.52 \pm 0.20) \times 10^{-2}$ . Our first error is their experiment's error and our second error is the systematic error from using our best value.

<sup>2</sup>ABLIKIM 17AG reports  $(18.2 \pm 0.8 \pm 1.6) \times 10^{-4}$  from a measurement of  $[\Gamma(\chi_{c2}(1P) \rightarrow K_2^*(1430^\pm K^\mp)/\Gamma_{total}) \times [B(\psi(2S) \rightarrow \gamma\chi_{c2}(1P))]]$  assuming  $B(\psi(2S) \rightarrow \gamma\chi_{c2}(1P)) = (9.11 \pm 0.31) \times 10^{-2}$ , which we rescale to our best value  $B(\psi(2S) \rightarrow \gamma\chi_{c2}(1P)) = (9.52 \pm 0.20) \times 10^{-2}$ . Our first error is their experiment's error and our second error is the systematic error from using our best value.

<sup>3</sup>ABLIKIM 17AG reports  $(13.6 \pm 0.8 \pm 1.4) \times 10^{-4}$  from a measurement of  $[\Gamma(\chi_{c2}(1P) \rightarrow K_2^*(1430^\pm K^\mp)/\Gamma_{total}) \times [B(\psi(2S) \rightarrow \gamma\chi_{c2}(1P))]]$  assuming  $B(\psi(2S) \rightarrow \gamma\chi_{c2}(1P)) = (9.11 \pm 0.31) \times 10^{-2}$ , which we rescale to our best value  $B(\psi(2S) \rightarrow \gamma\chi_{c2}(1P)) = (9.52 \pm 0.20) \times 10^{-2}$ . Our first error is their experiment's error and our second error is the systematic error from using our best value.

$\Gamma(K_2^*(1430^0 \bar{K}^0 + c.c.)/\Gamma_{total}$	$\Gamma_{37}/\Gamma$		
VALUE (units $10^{-4}$ )	DOCUMENT ID	TECN	COMMENT
<b>12.4±1.7±0.3</b>	<sup>1</sup> ABLIKIM	17AG BES3	$\psi(2S) \rightarrow \gamma K_S^0 K^\pm \pi^\mp$

<sup>1</sup>ABLIKIM 17AG reports  $(13.0 \pm 1.0 \pm 1.5) \times 10^{-4}$  from a measurement of  $[\Gamma(\chi_{c2}(1P) \rightarrow K_2^*(1430^0 \bar{K}^0 + c.c.)/\Gamma_{total}) \times [B(\psi(2S) \rightarrow \gamma\chi_{c2}(1P))]]$  assuming  $B(\psi(2S) \rightarrow \gamma\chi_{c2}(1P)) = (9.11 \pm 0.31) \times 10^{-2}$ , which we rescale to our best value  $B(\psi(2S) \rightarrow \gamma\chi_{c2}(1P)) = (9.52 \pm 0.20) \times 10^{-2}$ . Our first error is their experiment's error and our second error is the systematic error from using our best value.

$\Gamma(K_3^*(1780^\pm K^\mp)/\Gamma_{total}$	$\Gamma_{38}/\Gamma$		
VALUE (units $10^{-4}$ )	DOCUMENT ID	TECN	COMMENT
<b>5.2±0.8±0.1</b>	<sup>1</sup> ABLIKIM	17AG BES3	$\psi(2S) \rightarrow \gamma K \bar{K} \pi$

• • • We do not use the following data for averages, fits, limits, etc. • • •  
 5.1±1.0±0.1 <sup>2</sup> ABLIKIM 17AG BES3  $\psi(2S) \rightarrow \gamma K^+ K^- \pi^0$   
 5.6±1.8±0.1 <sup>3</sup> ABLIKIM 17AG BES3  $\psi(2S) \rightarrow \gamma K_S^0 K^\pm \pi^\mp$

<sup>1</sup>ABLIKIM 17AG reports  $(5.4 \pm 0.5 \pm 0.7) \times 10^{-4}$  from a measurement of  $[\Gamma(\chi_{c2}(1P) \rightarrow K_3^*(1780^\pm K^\mp)/\Gamma_{total}) \times [B(\psi(2S) \rightarrow \gamma\chi_{c2}(1P))]]$  assuming  $B(\psi(2S) \rightarrow \gamma\chi_{c2}(1P)) = (9.11 \pm 0.31) \times 10^{-2}$ , which we rescale to our best value  $B(\psi(2S) \rightarrow \gamma\chi_{c2}(1P)) = (9.52 \pm 0.20) \times 10^{-2}$ . Our first error is their experiment's error and our second error is the systematic error from using our best value.

<sup>2</sup>ABLIKIM 17AG reports  $(5.3 \pm 0.5 \pm 0.9) \times 10^{-4}$  from a measurement of  $[\Gamma(\chi_{c2}(1P) \rightarrow K_3^*(1780^\pm K^\mp)/\Gamma_{total}) \times [B(\psi(2S) \rightarrow \gamma\chi_{c2}(1P))]]$  assuming  $B(\psi(2S) \rightarrow \gamma\chi_{c2}(1P)) = (9.11 \pm 0.31) \times 10^{-2}$ , which we rescale to our best value  $B(\psi(2S) \rightarrow \gamma\chi_{c2}(1P)) = (9.52 \pm 0.20) \times 10^{-2}$ . Our first error is their experiment's error and our second error is the systematic error from using our best value.

<sup>3</sup>ABLIKIM 17AG reports  $(5.9 \pm 1.1 \pm 1.5) \times 10^{-4}$  from a measurement of  $[\Gamma(\chi_{c2}(1P) \rightarrow K_3^*(1780^\pm K^\mp)/\Gamma_{total}) \times [B(\psi(2S) \rightarrow \gamma\chi_{c2}(1P))]]$  assuming  $B(\psi(2S) \rightarrow \gamma\chi_{c2}(1P)) = (9.11 \pm 0.31) \times 10^{-2}$ , which we rescale to our best value  $B(\psi(2S) \rightarrow \gamma\chi_{c2}(1P)) = (9.52 \pm 0.20) \times 10^{-2}$ . Our first error is their experiment's error and our second error is the systematic error from using our best value.

$\Gamma(K_3^*(1780^0 \bar{K}^0 + c.c.)/\Gamma_{total}$	$\Gamma_{39}/\Gamma$		
VALUE (units $10^{-4}$ )	DOCUMENT ID	TECN	COMMENT
<b>5.6±2.1±0.1</b>	<sup>1</sup> ABLIKIM	17AG BES3	$\psi(2S) \rightarrow \gamma K_S^0 K^\pm \pi^\mp$

<sup>1</sup>ABLIKIM 17AG reports  $(5.9 \pm 1.6 \pm 1.5) \times 10^{-4}$  from a measurement of  $[\Gamma(\chi_{c2}(1P) \rightarrow K_3^*(1780^0 \bar{K}^0 + c.c.)/\Gamma_{total}) \times [B(\psi(2S) \rightarrow \gamma\chi_{c2}(1P))]]$  assuming  $B(\psi(2S) \rightarrow \gamma\chi_{c2}(1P)) = (9.11 \pm 0.31) \times 10^{-2}$ , which we rescale to our best value  $B(\psi(2S) \rightarrow \gamma\chi_{c2}(1P)) = (9.52 \pm 0.20) \times 10^{-2}$ . Our first error is their experiment's error and our second error is the systematic error from using our best value.

$\Gamma(a_2(1320^0 \pi^0)/\Gamma_{total}$	$\Gamma_{40}/\Gamma$		
VALUE (units $10^{-4}$ )	DOCUMENT ID	TECN	COMMENT
<b>12.9±3.4±0.3</b>	<sup>1</sup> ABLIKIM	17AG BES3	$\psi(2S) \rightarrow \gamma K^+ K^- \pi^0$

<sup>1</sup>ABLIKIM 17AG reports  $(13.5 \pm 1.6 \pm 3.2) \times 10^{-4}$  from a measurement of  $[\Gamma(\chi_{c2}(1P) \rightarrow a_2(1320^0 \pi^0)/\Gamma_{total}) \times [B(\psi(2S) \rightarrow \gamma\chi_{c2}(1P))]]$  assuming  $B(\psi(2S) \rightarrow \gamma\chi_{c2}(1P)) = (9.11 \pm 0.31) \times 10^{-2}$ , which we rescale to our best value  $B(\psi(2S) \rightarrow \gamma\chi_{c2}(1P)) = (9.52 \pm 0.20) \times 10^{-2}$ . Our first error is their experiment's error and our second error is the systematic error from using our best value.

$\Gamma(a_2(1320^\pm \pi^\mp)/\Gamma_{total}$	$\Gamma_{41}/\Gamma$		
VALUE (units $10^{-4}$ )	DOCUMENT ID	TECN	COMMENT
<b>17.6±6.1±0.4</b>	<sup>1</sup> ABLIKIM	17AG BES3	$\psi(2S) \rightarrow \gamma K_S^0 K^\pm \pi^\mp$

<sup>1</sup>ABLIKIM 17AG reports  $(18.4 \pm 3.3 \pm 5.5) \times 10^{-4}$  from a measurement of  $[\Gamma(\chi_{c2}(1P) \rightarrow a_2(1320^\pm \pi^\mp)/\Gamma_{total}) \times [B(\psi(2S) \rightarrow \gamma\chi_{c2}(1P))]]$  assuming  $B(\psi(2S) \rightarrow \gamma\chi_{c2}(1P)) = (9.11 \pm 0.31) \times 10^{-2}$ , which we rescale to our best value  $B(\psi(2S) \rightarrow \gamma\chi_{c2}(1P)) = (9.52 \pm 0.20) \times 10^{-2}$ . Our first error is their experiment's error and our second error is the systematic error from using our best value.

$\Gamma(K^+ K^- \pi^0)/\Gamma_{total}$	$\Gamma_{43}/\Gamma$		
VALUE (units $10^{-3}$ )	DOCUMENT ID	TECN	COMMENT
<b>0.30±0.08±0.01</b>	<sup>1</sup> ATHAR	07	CLEO $\psi(2S) \rightarrow \gamma h^+ h^- h^0$

<sup>1</sup>ATHAR 07 reports  $(0.31 \pm 0.07 \pm 0.04) \times 10^{-3}$  from a measurement of  $[\Gamma(\chi_{c2}(1P) \rightarrow K^+ K^- \pi^0)/\Gamma_{total}] \times [B(\psi(2S) \rightarrow \gamma\chi_{c2}(1P))]$  assuming  $B(\psi(2S) \rightarrow \gamma\chi_{c2}(1P)) = (9.33 \pm 0.14 \pm 0.61) \times 10^{-2}$ , which we rescale to our best value  $B(\psi(2S) \rightarrow \gamma\chi_{c2}(1P)) = (9.52 \pm 0.20) \times 10^{-2}$ . Our first error is their experiment's error and our second error is the systematic error from using our best value.

## Meson Particle Listings

 $\chi_{c2}(1P)$ 

$\Gamma(K^+ K^- \eta)/\Gamma_{\text{total}}$		$\Gamma_{44}/\Gamma$	
VALUE (units $10^{-3}$ )	CL%	DOCUMENT ID	TECN COMMENT

**<0.32** 90 <sup>1</sup>ATHAR 07 CLEO  $\psi(2S) \rightarrow \gamma h^+ h^- h^0$   
<sup>1</sup>ATHAR 07 reports  $< 0.33 \times 10^{-3}$  from a measurement of  $[\Gamma(\chi_{c2}(1P) \rightarrow K^+ K^- \eta)/\Gamma_{\text{total}}] \times [B(\psi(2S) \rightarrow \gamma \chi_{c2}(1P))]$  assuming  $B(\psi(2S) \rightarrow \gamma \chi_{c2}(1P)) = (9.33 \pm 0.14 \pm 0.61) \times 10^{-2}$ , which we rescale to our best value  $B(\psi(2S) \rightarrow \gamma \chi_{c2}(1P)) = 9.52 \times 10^{-2}$ .

$\Gamma(K^+ K^- \eta'(958))/\Gamma_{\text{total}}$		$\Gamma_{45}/\Gamma$	
VALUE (units $10^{-4}$ )	EVTS	DOCUMENT ID	TECN COMMENT

**1.94 ± 0.34** 107 <sup>1</sup>ABLIKIM 14J BES3  $\psi(2S) \rightarrow \gamma K^+ K^- \eta'(958)$   
<sup>1</sup>Derived using  $B(\psi(2S) \rightarrow \gamma \chi_{c2}) = (8.72 \pm 0.34)\%$ . Uncertainty includes both statistical and systematic contributions combined in quadrature.

$\Gamma(\eta\eta')/\Gamma_{\text{total}}$		$\Gamma_{46}/\Gamma$	
VALUE (units $10^{-5}$ )	CL%	EVTS	DOCUMENT ID TECN COMMENT

**2.17 ± 0.47 ± 0.05** 20 <sup>1</sup>ABLIKIM 17AI BES3  $\psi(2S) \rightarrow \gamma \eta' \eta$   
 • • • We do not use the following data for averages, fits, limits, etc. • • •  
 < 6 90 3.3 ± 8.0 <sup>2</sup>ASNER 09 CLEO  $\psi(2S) \rightarrow \gamma \eta \eta'$   
 < 23 90 <sup>3</sup>ADAMS 07 CLEO  $\psi(2S) \rightarrow \gamma \chi_{c2}$

<sup>1</sup>ABLIKIM 17AI reports  $(2.27 \pm 0.43 \pm 0.25) \times 10^{-5}$  from a measurement of  $[\Gamma(\chi_{c2}(1P) \rightarrow \eta\eta')/\Gamma_{\text{total}}] \times [B(\psi(2S) \rightarrow \gamma \chi_{c2}(1P))]$  assuming  $B(\psi(2S) \rightarrow \gamma \chi_{c2}(1P)) = (9.11 \pm 0.31) \times 10^{-2}$ , which we rescale to our best value  $B(\psi(2S) \rightarrow \gamma \chi_{c2}(1P)) = (9.52 \pm 0.20) \times 10^{-2}$ . Our first error is their experiment's error and our second error is the systematic error from using our best value.  
<sup>2</sup>ASNER 09 reports  $< 0.6 \times 10^{-4}$  from a measurement of  $[\Gamma(\chi_{c2}(1P) \rightarrow \eta\eta')/\Gamma_{\text{total}}] \times [B(\psi(2S) \rightarrow \gamma \chi_{c2}(1P))]$  assuming  $B(\psi(2S) \rightarrow \gamma \chi_{c2}(1P)) = (9.33 \pm 0.14 \pm 0.61) \times 10^{-2}$ , which we rescale to our best value  $B(\psi(2S) \rightarrow \gamma \chi_{c2}(1P)) = 9.52 \times 10^{-2}$ .  
<sup>3</sup>Superseded by ASNER 09. ADAMS 07 reports  $< 2.3 \times 10^{-4}$  from a measurement of  $[\Gamma(\chi_{c2}(1P) \rightarrow \eta\eta')/\Gamma_{\text{total}}] \times [B(\psi(2S) \rightarrow \gamma \chi_{c2}(1P))]$  assuming  $B(\psi(2S) \rightarrow \gamma \chi_{c2}(1P)) = 0.0933 \pm 0.0014 \pm 0.0061$ , which we rescale to our best value  $B(\psi(2S) \rightarrow \gamma \chi_{c2}(1P)) = 9.52 \times 10^{-2}$ .

$\Gamma(\eta'\eta')/\Gamma_{\text{total}}$		$\Gamma_{47}/\Gamma$	
VALUE (units $10^{-5}$ )	CL%	EVTS	DOCUMENT ID TECN COMMENT

**4.4 ± 0.6 ± 0.1** 60 <sup>1</sup>ABLIKIM 17AI BES3  $\psi(2S) \rightarrow \gamma \eta' \eta'$   
 • • • We do not use the following data for averages, fits, limits, etc. • • •  
 < 10 90 12 ± 7 <sup>2</sup>ASNER 09 CLEO  $\psi(2S) \rightarrow \gamma \eta' \eta'$   
 < 30 90 <sup>3</sup>ADAMS 07 CLEO  $\psi(2S) \rightarrow \gamma \chi_{c2}$

<sup>1</sup>ABLIKIM 17AI reports  $(4.76 \pm 0.56 \pm 0.38) \times 10^{-5}$  from a measurement of  $[\Gamma(\chi_{c2}(1P) \rightarrow \eta'\eta')/\Gamma_{\text{total}}] \times [B(\psi(2S) \rightarrow \gamma \chi_{c2}(1P))]$  assuming  $B(\psi(2S) \rightarrow \gamma \chi_{c2}(1P)) = (9.11 \pm 0.31) \times 10^{-2}$ , which we rescale to our best value  $B(\psi(2S) \rightarrow \gamma \chi_{c2}(1P)) = (9.52 \pm 0.20) \times 10^{-2}$ . Our first error is their experiment's error and our second error is the systematic error from using our best value.  
<sup>2</sup>ASNER 09 reports  $< 1.0 \times 10^{-4}$  from a measurement of  $[\Gamma(\chi_{c2}(1P) \rightarrow \eta'\eta')/\Gamma_{\text{total}}] \times [B(\psi(2S) \rightarrow \gamma \chi_{c2}(1P))]$  assuming  $B(\psi(2S) \rightarrow \gamma \chi_{c2}(1P)) = (9.33 \pm 0.14 \pm 0.61) \times 10^{-2}$ , which we rescale to our best value  $B(\psi(2S) \rightarrow \gamma \chi_{c2}(1P)) = 9.52 \times 10^{-2}$ .  
<sup>3</sup>Superseded by ASNER 09. ADAMS 07 reports  $< 3.1 \times 10^{-4}$  from a measurement of  $[\Gamma(\chi_{c2}(1P) \rightarrow \eta'\eta')/\Gamma_{\text{total}}] \times [B(\psi(2S) \rightarrow \gamma \chi_{c2}(1P))]$  assuming  $B(\psi(2S) \rightarrow \gamma \chi_{c2}(1P)) = 0.0933 \pm 0.0014 \pm 0.0061$ , which we rescale to our best value  $B(\psi(2S) \rightarrow \gamma \chi_{c2}(1P)) = 9.52 \times 10^{-2}$ .

$\Gamma(\pi^+ \pi^- K_S^0 K_S^0)/\Gamma_{\text{total}}$		$\Gamma_{48}/\Gamma$	
VALUE (units $10^{-3}$ )	EVTS	DOCUMENT ID	TECN COMMENT

**2.17 ± 0.54 ± 0.05** 57 ± 11 <sup>1</sup>ABLIKIM 05O BES2  $\psi(2S) \rightarrow \gamma \chi_{c2}$   
<sup>1</sup>ABLIKIM 05O reports  $[\Gamma(\chi_{c2}(1P) \rightarrow \pi^+ \pi^- K_S^0 K_S^0)/\Gamma_{\text{total}}] \times [B(\psi(2S) \rightarrow \gamma \chi_{c2}(1P))] = (0.207 \pm 0.039 \pm 0.033) \times 10^{-3}$  which we divide by our best value  $B(\psi(2S) \rightarrow \gamma \chi_{c2}(1P)) = (9.52 \pm 0.20) \times 10^{-2}$ . Our first error is their experiment's error and our second error is the systematic error from using our best value.

$\Gamma(K^+ K^- K_S^0 K_S^0)/\Gamma_{\text{total}}$		$\Gamma_{49}/\Gamma$	
VALUE (units $10^{-4}$ )	CL%	EVTS	DOCUMENT ID TECN COMMENT

**<4** 90 2.3 ± 2.2 <sup>1</sup>ABLIKIM 05O BES2  $e^+ e^- \rightarrow \chi_{c2} \gamma$   
<sup>1</sup>ABLIKIM 05O reports  $[\Gamma(\chi_{c2}(1P) \rightarrow K^+ K^- K_S^0 K_S^0)/\Gamma_{\text{total}}] \times [B(\psi(2S) \rightarrow \gamma \chi_{c2}(1P))] < 3.5 \times 10^{-5}$  which we divide by our best value  $B(\psi(2S) \rightarrow \gamma \chi_{c2}(1P)) = 9.52 \times 10^{-2}$ .

$\Gamma(K_S^0 K_S^0 K_S^0 K_S^0)/\Gamma_{\text{total}}$		$\Gamma_{50}/\Gamma$	
VALUE (units $10^{-4}$ )	EVTS	DOCUMENT ID	TECN COMMENT

**1.13 ± 0.18 ± 0.02** 68 <sup>1</sup>ABLIKIM 19AA BES3  $\psi(2S) \rightarrow \gamma 4K_S^0$   
<sup>1</sup>Using  $B(K_S^0 \rightarrow \pi^+ \pi^-) = (69.20 \pm 0.05)\%$ . ABLIKIM 19AA reports  $[\Gamma(\chi_{c2}(1P) \rightarrow K_S^0 K_S^0 K_S^0 K_S^0)/\Gamma_{\text{total}}] \times [B(\psi(2S) \rightarrow \gamma \chi_{c2}(1P))] = (10.8 \pm 1.5 \pm 0.8) \times 10^{-6}$  which we divide by our best value  $B(\psi(2S) \rightarrow \gamma \chi_{c2}(1P)) = (9.52 \pm 0.20) \times 10^{-2}$ . Our first error is their experiment's error and our second error is the systematic error from using our best value..

$\Gamma(K^+ K^- K^+ K^-)/\Gamma_{\text{total}}$		$\Gamma_{51}/\Gamma$	
VALUE (units $10^{-3}$ )		DOCUMENT ID	

**1.65 ± 0.20 OUR FIT**

$\Gamma(K^+ K^- \phi)/\Gamma_{\text{total}}$		$\Gamma_{52}/\Gamma$	
VALUE (units $10^{-3}$ )	EVTS	DOCUMENT ID	TECN COMMENT

**1.42 ± 0.29 ± 0.03** 52 <sup>1</sup>ABLIKIM 06T BES2  $\psi(2S) \rightarrow \gamma 2K^+ 2K^-$   
<sup>1</sup>ABLIKIM 06T reports  $(1.67 \pm 0.26 \pm 0.24) \times 10^{-3}$  from a measurement of  $[\Gamma(\chi_{c2}(1P) \rightarrow K^+ K^- \phi)/\Gamma_{\text{total}}] \times [B(\psi(2S) \rightarrow \gamma \chi_{c2}(1P))]$  assuming  $B(\psi(2S) \rightarrow \gamma \chi_{c2}(1P)) = (8.1 \pm 0.4) \times 10^{-2}$ , which we rescale to our best value  $B(\psi(2S) \rightarrow \gamma \chi_{c2}(1P)) = (9.52 \pm 0.20) \times 10^{-2}$ . Our first error is their experiment's error and our second error is the systematic error from using our best value.

$\Gamma(K^0 K^+ \pi^- \phi + \text{c.c.})/\Gamma_{\text{total}}$		$\Gamma_{53}/\Gamma$	
VALUE (units $10^{-3}$ )		DOCUMENT ID	TECN COMMENT

**4.83 ± 0.32 ± 0.66** ABLIKIM 15M BES3  $\psi(2S) \rightarrow \gamma \chi_{c2}$

$\Gamma(K^+ K^- \pi^0 \phi)/\Gamma_{\text{total}}$		$\Gamma_{54}/\Gamma$	
VALUE (units $10^{-3}$ )		DOCUMENT ID	TECN COMMENT

**2.74 ± 0.16 ± 0.44** ABLIKIM 15M BES3  $\psi(2S) \rightarrow \gamma \chi_{c2}$

$\Gamma(\phi \pi^+ \pi^- \pi^0)/\Gamma_{\text{total}}$		$\Gamma_{55}/\Gamma$	
VALUE (units $10^{-3}$ )	EVTS	DOCUMENT ID	TECN COMMENT

**0.93 ± 0.06 ± 0.10** 408 <sup>1</sup>ABLIKIM 13B BES3  $e^+ e^- \rightarrow \psi(2S) \rightarrow \gamma \chi_{c2}$   
<sup>1</sup>Using  $1.06 \times 10^8 \psi(2S)$  mesons and  $B(\psi(2S) \rightarrow \chi_{c2} \gamma) = (8.72 \pm 0.34)\%$ .

$\Gamma(p\bar{p})/\Gamma_{\text{total}}$		$\Gamma_{56}/\Gamma$	
VALUE (units $10^{-4}$ )		DOCUMENT ID	

**0.733 ± 0.033 OUR FIT**

$\Gamma(p\bar{p}\pi^0)/\Gamma_{\text{total}}$		$\Gamma_{57}/\Gamma$	
VALUE (units $10^{-3}$ )		DOCUMENT ID	TECN COMMENT

**0.47 ± 0.04 OUR AVERAGE**  
 0.47 ± 0.04 ± 0.01 <sup>1</sup>ONYISI 10 CLE3  $\psi(2S) \rightarrow \gamma p\bar{p}\pi^0$   
 0.43 ± 0.09 ± 0.01 <sup>2</sup>ATHAR 07 CLEO  $\psi(2S) \rightarrow \gamma h^+ h^- h^0$

<sup>1</sup>ONYISI 10 reports  $(4.83 \pm 0.25 \pm 0.35 \pm 0.31) \times 10^{-4}$  from a measurement of  $[\Gamma(\chi_{c2}(1P) \rightarrow p\bar{p}\pi^0)/\Gamma_{\text{total}}] \times [B(\psi(2S) \rightarrow \gamma \chi_{c2}(1P))]$  assuming  $B(\psi(2S) \rightarrow \gamma \chi_{c2}(1P)) = (9.33 \pm 0.14 \pm 0.61) \times 10^{-2}$ , which we rescale to our best value  $B(\psi(2S) \rightarrow \gamma \chi_{c2}(1P)) = (9.52 \pm 0.20) \times 10^{-2}$ . Our first error is their experiment's error and our second error is the systematic error from using our best value.  
<sup>2</sup>ATHAR 07 reports  $(0.44 \pm 0.08 \pm 0.05) \times 10^{-3}$  from a measurement of  $[\Gamma(\chi_{c2}(1P) \rightarrow p\bar{p}\pi^0)/\Gamma_{\text{total}}] \times [B(\psi(2S) \rightarrow \gamma \chi_{c2}(1P))]$  assuming  $B(\psi(2S) \rightarrow \gamma \chi_{c2}(1P)) = (9.33 \pm 0.14 \pm 0.61) \times 10^{-2}$ , which we rescale to our best value  $B(\psi(2S) \rightarrow \gamma \chi_{c2}(1P)) = (9.52 \pm 0.20) \times 10^{-2}$ . Our first error is their experiment's error and our second error is the systematic error from using our best value.

$\Gamma(p\bar{p}\eta)/\Gamma_{\text{total}}$		$\Gamma_{58}/\Gamma$	
VALUE (units $10^{-3}$ )		DOCUMENT ID	TECN COMMENT

**0.174 ± 0.025 OUR AVERAGE**  
 0.172 ± 0.026 ± 0.004 <sup>1</sup>ONYISI 10 CLE3  $\psi(2S) \rightarrow \gamma p\bar{p}\eta$   
 0.186 ± 0.070 ± 0.004 <sup>2</sup>ATHAR 07 CLEO  $\psi(2S) \rightarrow \gamma h^+ h^- h^0$

<sup>1</sup>ONYISI 10 reports  $(1.76 \pm 0.23 \pm 0.14 \pm 0.11) \times 10^{-4}$  from a measurement of  $[\Gamma(\chi_{c2}(1P) \rightarrow p\bar{p}\eta)/\Gamma_{\text{total}}] \times [B(\psi(2S) \rightarrow \gamma \chi_{c2}(1P))]$  assuming  $B(\psi(2S) \rightarrow \gamma \chi_{c2}(1P)) = (9.33 \pm 0.14 \pm 0.61) \times 10^{-2}$ , which we rescale to our best value  $B(\psi(2S) \rightarrow \gamma \chi_{c2}(1P)) = (9.52 \pm 0.20) \times 10^{-2}$ . Our first error is their experiment's error and our second error is the systematic error from using our best value.  
<sup>2</sup>ATHAR 07 reports  $(0.19 \pm 0.07 \pm 0.02) \times 10^{-3}$  from a measurement of  $[\Gamma(\chi_{c2}(1P) \rightarrow p\bar{p}\eta)/\Gamma_{\text{total}}] \times [B(\psi(2S) \rightarrow \gamma \chi_{c2}(1P))]$  assuming  $B(\psi(2S) \rightarrow \gamma \chi_{c2}(1P)) = (9.33 \pm 0.14 \pm 0.61) \times 10^{-2}$ , which we rescale to our best value  $B(\psi(2S) \rightarrow \gamma \chi_{c2}(1P)) = (9.52 \pm 0.20) \times 10^{-2}$ . Our first error is their experiment's error and our second error is the systematic error from using our best value.

$\Gamma(p\bar{p}\omega)/\Gamma_{\text{total}}$		$\Gamma_{59}/\Gamma$	
VALUE (units $10^{-3}$ )		DOCUMENT ID	TECN COMMENT

**0.36 ± 0.04 ± 0.01** <sup>1</sup>ONYISI 10 CLE3  $\psi(2S) \rightarrow \gamma p\bar{p}\omega$   
<sup>1</sup>ONYISI 10 reports  $(3.68 \pm 0.35 \pm 0.26 \pm 0.24) \times 10^{-4}$  from a measurement of  $[\Gamma(\chi_{c2}(1P) \rightarrow p\bar{p}\omega)/\Gamma_{\text{total}}] \times [B(\psi(2S) \rightarrow \gamma \chi_{c2}(1P))]$  assuming  $B(\psi(2S) \rightarrow \gamma \chi_{c2}(1P)) = (9.33 \pm 0.14 \pm 0.61) \times 10^{-2}$ , which we rescale to our best value  $B(\psi(2S) \rightarrow \gamma \chi_{c2}(1P)) = (9.52 \pm 0.20) \times 10^{-2}$ . Our first error is their experiment's error and our second error is the systematic error from using our best value.

$\Gamma(p\bar{p}\phi)/\Gamma_{\text{total}}$		$\Gamma_{60}/\Gamma$	
VALUE (units $10^{-3}$ )	EVTS	DOCUMENT ID	TECN COMMENT

**2.8 ± 0.9 ± 0.1** 24 ± 7 <sup>1</sup>ABLIKIM 11F BES3  $\psi(2S) \rightarrow \gamma p\bar{p}K^+ K^-$   
<sup>1</sup>ABLIKIM 11F reports  $(3.04 \pm 0.85 \pm 0.43) \times 10^{-5}$  from a measurement of  $[\Gamma(\chi_{c2}(1P) \rightarrow p\bar{p}\phi)/\Gamma_{\text{total}}] \times [B(\psi(2S) \rightarrow \gamma \chi_{c2}(1P))]$  assuming  $B(\psi(2S) \rightarrow \gamma \chi_{c2}(1P)) = (8.74 \pm 0.35) \times 10^{-2}$ , which we rescale to our best value  $B(\psi(2S) \rightarrow \gamma \chi_{c2}(1P)) = (9.52 \pm 0.20) \times 10^{-2}$ . Our first error is their experiment's error and our second error is the systematic error from using our best value.

$\Gamma(p\bar{p}\pi^+\pi^-)/\Gamma_{total}$   $\Gamma_{61}/\Gamma$

VALUE (units $10^{-3}$ )	DOCUMENT ID	TECN	COMMENT
<b>1.32 ± 0.34 OUR EVALUATION</b>	Treating systematic error as correlated.		
<b>1.3 ± 0.4 OUR AVERAGE</b>	Error includes scale factor of 1.3.		
1.17 ± 0.19 ± 0.30	<sup>1</sup> BAI	99B BES	$\psi(2S) \rightarrow \gamma\chi_{c2}$
2.64 ± 1.03 ± 0.14	<sup>1</sup> TANENBAUM	78 MRK1	$\psi(2S) \rightarrow \gamma\chi_{c2}$

<sup>1</sup>Rescaled by us using  $B(\psi(2S) \rightarrow \gamma\chi_{c2}) = (8.3 \pm 0.4)\%$  and  $B(\psi(2S) \rightarrow J/\psi(1S)\pi^+\pi^-) = (32.6 \pm 0.5)\%$ . Multiplied by a factor of 2 to convert from  $K_S^0 K^+\pi^-$  to  $K^0 K^+\pi^-$  decay.

$\Gamma(p\bar{p}\pi^0\pi^0)/\Gamma_{total}$   $\Gamma_{62}/\Gamma$

VALUE (%)	EVTS	DOCUMENT ID	TECN	COMMENT
<b>0.078 ± 0.023 ± 0.002</b>	29.2	<sup>1</sup> HE	08B CLEO	$e^+e^- \rightarrow \gamma h^+ h^- h^0 h^0$

<sup>1</sup>HE 08B reports  $0.08 \pm 0.02 \pm 0.01 \pm 0.01\%$  from a measurement of  $[\Gamma(\chi_{c2}(1P) \rightarrow p\bar{p}\pi^0\pi^0)/\Gamma_{total}] \times [B(\psi(2S) \rightarrow \gamma\chi_{c2}(1P))]$  assuming  $B(\psi(2S) \rightarrow \gamma\chi_{c2}(1P)) = (9.33 \pm 0.14 \pm 0.61) \times 10^{-2}$ , which we rescale to our best value  $B(\psi(2S) \rightarrow \gamma\chi_{c2}(1P)) = (9.52 \pm 0.20) \times 10^{-2}$ . Our first error is their experiment's error and our second error is the systematic error from using our best value.

$\Gamma(p\bar{p}K^+K^- \text{ (non-resonant)})/\Gamma_{total}$   $\Gamma_{63}/\Gamma$

VALUE (units $10^{-4}$ )	EVTS	DOCUMENT ID	TECN	COMMENT
<b>1.91 ± 0.32 ± 0.04</b>	131 ± 12	<sup>1</sup> ABLIKIM	11F BES3	$\psi(2S) \rightarrow \gamma p\bar{p}K^+K^-$

<sup>1</sup>ABLIKIM 11F reports  $(2.08 \pm 0.19 \pm 0.30) \times 10^{-4}$  from a measurement of  $[\Gamma(\chi_{c2}(1P) \rightarrow p\bar{p}K^+K^- \text{ (non-resonant)})/\Gamma_{total}] \times [B(\psi(2S) \rightarrow \gamma\chi_{c2}(1P))]$  assuming  $B(\psi(2S) \rightarrow \gamma\chi_{c2}(1P)) = (8.74 \pm 0.35) \times 10^{-2}$ , which we rescale to our best value  $B(\psi(2S) \rightarrow \gamma\chi_{c2}(1P)) = (9.52 \pm 0.20) \times 10^{-2}$ . Our first error is their experiment's error and our second error is the systematic error from using our best value.

$\Gamma(p\bar{p}K_S^0 K_S^0)/\Gamma_{total}$   $\Gamma_{64}/\Gamma$

VALUE (units $10^{-4}$ )	CL%	DOCUMENT ID	TECN	COMMENT
<b>&lt;7.9</b>	90	<sup>1</sup> ABLIKIM	06D BES2	$\psi(2S) \rightarrow \chi_{c2}\gamma$

<sup>1</sup>Using  $B(\psi(2S) \rightarrow \chi_{c2}\gamma) = (9.3 \pm 0.6)\%$ .

$\Gamma(p\bar{p}\pi^-)/\Gamma_{total}$   $\Gamma_{65}/\Gamma$

VALUE (units $10^{-4}$ )	EVTS	DOCUMENT ID	TECN	COMMENT
<b>8.5 ± 0.9 OUR AVERAGE</b>				
8.4 ± 1.0 ± 0.2	3309	<sup>1</sup> ABLIKIM	12J BES3	$\psi(2S) \rightarrow \gamma p\bar{p}\pi^-$
10.2 ± 3.4 ± 0.2		<sup>2</sup> ABLIKIM	06I BES2	$\psi(2S) \rightarrow \gamma p\pi^- X$

<sup>1</sup>ABLIKIM 12J reports  $[\Gamma(\chi_{c2}(1P) \rightarrow p\bar{p}\pi^-)/\Gamma_{total}] \times [B(\psi(2S) \rightarrow \gamma\chi_{c2}(1P))] = (0.80 \pm 0.02 \pm 0.09) \times 10^{-4}$  which we divide by our best value  $B(\psi(2S) \rightarrow \gamma\chi_{c2}(1P)) = (9.52 \pm 0.20) \times 10^{-2}$ . Our first error is their experiment's error and our second error is the systematic error from using our best value.

<sup>2</sup>ABLIKIM 06I reports  $[\Gamma(\chi_{c2}(1P) \rightarrow p\bar{p}\pi^-)/\Gamma_{total}] \times [B(\psi(2S) \rightarrow \gamma\chi_{c2}(1P))] = (0.97 \pm 0.20 \pm 0.26) \times 10^{-4}$  which we divide by our best value  $B(\psi(2S) \rightarrow \gamma\chi_{c2}(1P)) = (9.52 \pm 0.20) \times 10^{-2}$ . Our first error is their experiment's error and our second error is the systematic error from using our best value.

$\Gamma(p\bar{p}n\pi^+)/\Gamma_{total}$   $\Gamma_{66}/\Gamma$

VALUE (units $10^{-4}$ )	EVTS	DOCUMENT ID	TECN	COMMENT
<b>8.9 ± 0.8 ± 0.2</b>	3732	<sup>1</sup> ABLIKIM	12J BES3	$\psi(2S) \rightarrow \gamma p\bar{p}n\pi^+$

<sup>1</sup>ABLIKIM 12J reports  $[\Gamma(\chi_{c2}(1P) \rightarrow p\bar{p}n\pi^+)/\Gamma_{total}] \times [B(\psi(2S) \rightarrow \gamma\chi_{c2}(1P))] = (0.85 \pm 0.02 \pm 0.07) \times 10^{-4}$  which we divide by our best value  $B(\psi(2S) \rightarrow \gamma\chi_{c2}(1P)) = (9.52 \pm 0.20) \times 10^{-2}$ . Our first error is their experiment's error and our second error is the systematic error from using our best value.

$\Gamma(p\bar{p}\pi^-\pi^0)/\Gamma_{total}$   $\Gamma_{67}/\Gamma$

VALUE (units $10^{-4}$ )	EVTS	DOCUMENT ID	TECN	COMMENT
<b>21.7 ± 1.7 ± 0.5</b>	2128	<sup>1</sup> ABLIKIM	12J BES3	$\psi(2S) \rightarrow \gamma p\bar{p}\pi^-\pi^0$

<sup>1</sup>ABLIKIM 12J reports  $[\Gamma(\chi_{c2}(1P) \rightarrow p\bar{p}\pi^-\pi^0)/\Gamma_{total}] \times [B(\psi(2S) \rightarrow \gamma\chi_{c2}(1P))] = (2.07 \pm 0.06 \pm 0.15) \times 10^{-4}$  which we divide by our best value  $B(\psi(2S) \rightarrow \gamma\chi_{c2}(1P)) = (9.52 \pm 0.20) \times 10^{-2}$ . Our first error is their experiment's error and our second error is the systematic error from using our best value.

$\Gamma(p\bar{p}n\pi^+\pi^0)/\Gamma_{total}$   $\Gamma_{68}/\Gamma$

VALUE (units $10^{-4}$ )	EVTS	DOCUMENT ID	TECN	COMMENT
<b>21.1 ± 1.8 ± 0.4</b>	2352	<sup>1</sup> ABLIKIM	12J BES3	$\psi(2S) \rightarrow \gamma p\bar{p}n\pi^+\pi^0$

<sup>1</sup>ABLIKIM 12J reports  $[\Gamma(\chi_{c2}(1P) \rightarrow p\bar{p}n\pi^+\pi^0)/\Gamma_{total}] \times [B(\psi(2S) \rightarrow \gamma\chi_{c2}(1P))] = (2.01 \pm 0.06 \pm 0.16) \times 10^{-4}$  which we divide by our best value  $B(\psi(2S) \rightarrow \gamma\chi_{c2}(1P)) = (9.52 \pm 0.20) \times 10^{-2}$ . Our first error is their experiment's error and our second error is the systematic error from using our best value.

$\Gamma(\Lambda\bar{\Lambda})/\Gamma_{total}$   $\Gamma_{69}/\Gamma$

VALUE (units $10^{-4}$ )	DOCUMENT ID
<b>1.84 ± 0.15 OUR FIT</b>	

$\Gamma(\Lambda\bar{\Lambda}\pi^+\pi^-)/\Gamma_{total}$   $\Gamma_{70}/\Gamma$

VALUE (units $10^{-5}$ )	CL%	EVTS	DOCUMENT ID	TECN	COMMENT
<b>125 ± 15 ± 3</b>		371	<sup>1</sup> ABLIKIM	12I BES3	$\psi(2S) \rightarrow \gamma\Lambda\bar{\Lambda}\pi^+\pi^-$

• • • We do not use the following data for averages, fits, limits, etc. • • •

<350 90 <sup>2</sup>ABLIKIM 06D BES2  $\psi(2S) \rightarrow \chi_{c2}\gamma$   
<sup>1</sup>ABLIKIM 12I reports  $(137.0 \pm 7.6 \pm 15.7) \times 10^{-5}$  from a measurement of  $[\Gamma(\chi_{c2}(1P) \rightarrow \Lambda\bar{\Lambda}\pi^+\pi^-)/\Gamma_{total}] \times [B(\psi(2S) \rightarrow \gamma\chi_{c2}(1P))]$  assuming  $B(\psi(2S) \rightarrow \gamma\chi_{c2}(1P)) = (8.72 \pm 0.34) \times 10^{-2}$ , which we rescale to our best value  $B(\psi(2S) \rightarrow \gamma\chi_{c2}(1P)) = (9.52 \pm 0.20) \times 10^{-2}$ . Our first error is their experiment's error and our second error is the systematic error from using our best value.  
<sup>2</sup>Using  $B(\psi(2S) \rightarrow \chi_{c2}\gamma) = (9.3 \pm 0.6)\%$ .

$\Gamma(\Lambda\bar{\Lambda}\pi^+\pi^- \text{ (non-resonant)})/\Gamma_{total}$   $\Gamma_{71}/\Gamma$

VALUE (units $10^{-5}$ )	EVTS	DOCUMENT ID	TECN	COMMENT
<b>66 ± 15 ± 1</b>	36	<sup>1</sup> ABLIKIM	12I BES3	$\psi(2S) \rightarrow \gamma\Lambda\bar{\Lambda}\pi^+\pi^-$

<sup>1</sup>ABLIKIM 12I reports  $(71.8 \pm 14.5 \pm 8.2) \times 10^{-5}$  from a measurement of  $[\Gamma(\chi_{c2}(1P) \rightarrow \Lambda\bar{\Lambda}\pi^+\pi^- \text{ (non-resonant)})/\Gamma_{total}] \times [B(\psi(2S) \rightarrow \gamma\chi_{c2}(1P))]$  assuming  $B(\psi(2S) \rightarrow \gamma\chi_{c2}(1P)) = (8.72 \pm 0.34) \times 10^{-2}$ , which we rescale to our best value  $B(\psi(2S) \rightarrow \gamma\chi_{c2}(1P)) = (9.52 \pm 0.20) \times 10^{-2}$ . Our first error is their experiment's error and our second error is the systematic error from using our best value.

$\Gamma(\Sigma(1385)^+\bar{\Lambda}\pi^- + c.c.)/\Gamma_{total}$   $\Gamma_{72}/\Gamma$

VALUE (units $10^{-5}$ )	CL%	DOCUMENT ID	TECN	COMMENT
<b>&lt;40</b>	90	<sup>1</sup> ABLIKIM	12I BES3	$\psi(2S) \rightarrow \gamma\Sigma(1385)^+\bar{\Lambda}\pi^-$

<sup>1</sup>ABLIKIM 12I reports  $< 42 \times 10^{-5}$  from a measurement of  $[\Gamma(\chi_{c2}(1P) \rightarrow \Sigma(1385)^+\bar{\Lambda}\pi^- + c.c.)/\Gamma_{total}] \times [B(\psi(2S) \rightarrow \gamma\chi_{c2}(1P))]$  assuming  $B(\psi(2S) \rightarrow \gamma\chi_{c2}(1P)) = (8.72 \pm 0.34) \times 10^{-2}$ , which we rescale to our best value  $B(\psi(2S) \rightarrow \gamma\chi_{c2}(1P)) = 9.52 \times 10^{-2}$ .

$\Gamma(\Sigma(1385)^-\bar{\Lambda}\pi^+ + c.c.)/\Gamma_{total}$   $\Gamma_{73}/\Gamma$

VALUE (units $10^{-5}$ )	CL%	DOCUMENT ID	TECN	COMMENT
<b>&lt;60</b>	90	<sup>1</sup> ABLIKIM	12I BES3	$\psi(2S) \rightarrow \gamma\Sigma(1385)^-\bar{\Lambda}\pi^+$

<sup>1</sup>ABLIKIM 12I reports  $< 61 \times 10^{-5}$  from a measurement of  $[\Gamma(\chi_{c2}(1P) \rightarrow \Sigma(1385)^-\bar{\Lambda}\pi^+ + c.c.)/\Gamma_{total}] \times [B(\psi(2S) \rightarrow \gamma\chi_{c2}(1P))]$  assuming  $B(\psi(2S) \rightarrow \gamma\chi_{c2}(1P)) = (8.72 \pm 0.34) \times 10^{-2}$ , which we rescale to our best value  $B(\psi(2S) \rightarrow \gamma\chi_{c2}(1P)) = 9.52 \times 10^{-2}$ .

$\Gamma(K^+\bar{p}\Lambda + c.c.)/\Gamma_{total}$   $\Gamma_{74}/\Gamma$

VALUE (units $10^{-4}$ )	EVTS	DOCUMENT ID	TECN	COMMENT
<b>7.8 ± 0.5 OUR AVERAGE</b>				
7.7 ± 0.5 ± 0.2	5k	<sup>1,2</sup> ABLIKIM	13D BES3	$\psi(2S) \rightarrow \gamma\Lambda\bar{p}K^+$
8.3 ± 1.6 ± 0.2		<sup>3</sup> ATHAR	07 CLEO	$\psi(2S) \rightarrow \gamma h^+ h^- h^0$

<sup>1</sup>ABLIKIM 13D reports  $(8.4 \pm 0.3 \pm 0.6) \times 10^{-4}$  from a measurement of  $[\Gamma(\chi_{c2}(1P) \rightarrow K^+\bar{p}\Lambda + c.c.)/\Gamma_{total}] \times [B(\psi(2S) \rightarrow \gamma\chi_{c2}(1P))]$  assuming  $B(\psi(2S) \rightarrow \gamma\chi_{c2}(1P)) = (8.72 \pm 0.34) \times 10^{-2}$ , which we rescale to our best value  $B(\psi(2S) \rightarrow \gamma\chi_{c2}(1P)) = (9.52 \pm 0.20) \times 10^{-2}$ . Our first error is their experiment's error and our second error is the systematic error from using our best value.  
<sup>2</sup>Using  $B(\Lambda \rightarrow p\pi^-) = 63.9\%$ .  
<sup>3</sup>ATHAR 07 reports  $(8.5 \pm 1.4 \pm 1.0) \times 10^{-4}$  from a measurement of  $[\Gamma(\chi_{c2}(1P) \rightarrow K^+\bar{p}\Lambda + c.c.)/\Gamma_{total}] \times [B(\psi(2S) \rightarrow \gamma\chi_{c2}(1P))]$  assuming  $B(\psi(2S) \rightarrow \gamma\chi_{c2}(1P)) = (9.33 \pm 0.14 \pm 0.61) \times 10^{-2}$ , which we rescale to our best value  $B(\psi(2S) \rightarrow \gamma\chi_{c2}(1P)) = (9.52 \pm 0.20) \times 10^{-2}$ . Our first error is their experiment's error and our second error is the systematic error from using our best value.

$\Gamma(K^*(892)^+\bar{p}\Lambda + c.c.)/\Gamma_{total}$   $\Gamma_{75}/\Gamma$

VALUE (units $10^{-4}$ )	EVTS	DOCUMENT ID	TECN	COMMENT
<b>8.2 ± 1.1 ± 0.2</b>	476	<sup>1</sup> ABLIKIM	19AU BES3	$\psi(2S) \rightarrow \gamma K^*\bar{p}\Lambda$

<sup>1</sup>ABLIKIM 19AU reports  $[\Gamma(\chi_{c2}(1P) \rightarrow K^*(892)^+\bar{p}\Lambda + c.c.)/\Gamma_{total}] \times [B(\psi(2S) \rightarrow \gamma\chi_{c2}(1P))] = (7.8 \pm 0.9 \pm 0.6) \times 10^{-5}$  which we divide by our best value  $B(\psi(2S) \rightarrow \gamma\chi_{c2}(1P)) = (9.52 \pm 0.20) \times 10^{-2}$ . Our first error is their experiment's error and our second error is the systematic error from using our best value.

$\Gamma(K^+\bar{p}\Lambda(1520) + c.c.)/\Gamma_{total}$   $\Gamma_{76}/\Gamma$

VALUE (units $10^{-4}$ )	EVTS	DOCUMENT ID	TECN	COMMENT
<b>2.8 ± 0.7 ± 0.1</b>	79 ± 13	<sup>1</sup> ABLIKIM	11F BES3	$\psi(2S) \rightarrow \gamma p\bar{p}K^+K^-$

<sup>1</sup>ABLIKIM 11F reports  $(3.06 \pm 0.50 \pm 0.54) \times 10^{-4}$  from a measurement of  $[\Gamma(\chi_{c2}(1P) \rightarrow K^+\bar{p}\Lambda(1520) + c.c.)/\Gamma_{total}] \times [B(\psi(2S) \rightarrow \gamma\chi_{c2}(1P))]$  assuming  $B(\psi(2S) \rightarrow \gamma\chi_{c2}(1P)) = (8.74 \pm 0.35) \times 10^{-2}$ , which we rescale to our best value  $B(\psi(2S) \rightarrow \gamma\chi_{c2}(1P)) = (9.52 \pm 0.20) \times 10^{-2}$ . Our first error is their experiment's error and our second error is the systematic error from using our best value.

$\Gamma(\Lambda(1520)\bar{\Lambda}(1520))/\Gamma_{total}$   $\Gamma_{77}/\Gamma$

VALUE (units $10^{-4}$ )	EVTS	DOCUMENT ID	TECN	COMMENT
<b>4.6 ± 1.4 ± 0.1</b>	29 ± 7	<sup>1</sup> ABLIKIM	11F BES3	$\psi(2S) \rightarrow \gamma p\bar{p}K^+K^-$

<sup>1</sup>ABLIKIM 11F reports  $(5.05 \pm 1.29 \pm 0.93) \times 10^{-4}$  from a measurement of  $[\Gamma(\chi_{c2}(1P) \rightarrow \Lambda(1520)\bar{\Lambda}(1520))/\Gamma_{total}] \times [B(\psi(2S) \rightarrow \gamma\chi_{c2}(1P))]$  assuming  $B(\psi(2S) \rightarrow \gamma\chi_{c2}(1P)) = (8.74 \pm 0.35) \times 10^{-2}$ , which we rescale to our best value  $B(\psi(2S) \rightarrow \gamma\chi_{c2}(1P)) = (9.52 \pm 0.20) \times 10^{-2}$ . Our first error is their experiment's error and our second error is the systematic error from using our best value.



$\Gamma(e^+e^-J/\psi(1S))/\Gamma_{total}$   $\Gamma_{94}/\Gamma$   

VALUE (units $10^{-3}$ )	EVTS	DOCUMENT ID	TECN	COMMENT
--------------------------	------	-------------	------	---------

••• We do not use the following data for averages, fits, limits, etc. •••

2.37±0.15±0.05 1.3k 1,2 ABLIKIM 17i BES3  $\psi(2S) \rightarrow \gamma e^+e^-J/\psi$

<sup>1</sup> ABLIKIM 17i reports  $(2.48 \pm 0.08 \pm 0.16) \times 10^{-3}$  from a measurement of  $[\Gamma(\chi_{c2}(1P) \rightarrow e^+e^-J/\psi(1S))/\Gamma_{total}] \times [B(\psi(2S) \rightarrow \gamma\chi_{c2}(1P))]$  assuming  $B(\psi(2S) \rightarrow \gamma\chi_{c2}(1P)) = (9.11 \pm 0.31) \times 10^{-2}$ , which we rescale to our best value  $B(\psi(2S) \rightarrow \gamma\chi_{c2}(1P)) = (9.52 \pm 0.20) \times 10^{-2}$ . Our first error is their experiment's error and our second error is the systematic error from using our best value.

<sup>2</sup> Not independent from other measurements reported by ABLIKIM 17i

$\Gamma(e^+e^-J/\psi(1S))/\Gamma(\gamma J/\psi(1S))$   $\Gamma_{94}/\Gamma_{99}$   

VALUE (units $10^{-3}$ )	EVTS	DOCUMENT ID	TECN	COMMENT
--------------------------	------	-------------	------	---------

11.3±0.4±0.5 1.3k <sup>1</sup> ABLIKIM 17i BES3  $\psi(2S) \rightarrow e^+e^-J/\psi$

<sup>1</sup> Uses  $B(\psi(2S) \rightarrow \gamma\chi_{c2}(1P)) \times B(\chi_{c2}(1P) \rightarrow \gamma J/\psi(1S)) = (199.6 \pm 0.8 \pm 7.0) \times 10^{-4}$  from ABLIKIM 17i and accounts for common systematic errors.

$\Gamma(\mu^+\mu^-J/\psi(1S))/\Gamma(e^+e^-J/\psi(1S))$   $\Gamma_{95}/\Gamma_{94}$   

VALUE (units $10^{-2}$ )	EVTS	DOCUMENT ID	TECN	COMMENT
--------------------------	------	-------------	------	---------

9.40±0.79±1.15 219 ABLIKIM 19z BES3  $\psi(2S) \rightarrow \gamma\chi_{c2} \rightarrow \gamma(\mu^+\mu^-J/\psi)$

$\Gamma(\gamma\gamma)/\Gamma(\gamma J/\psi(1S))$   $\Gamma_{93}/\Gamma_{89}$   

VALUE (units $10^{-3}$ )	DOCUMENT ID	TECN	COMMENT
--------------------------	-------------	------	---------

1.50±0.05 OUR FIT  
0.99±0.18 <sup>1</sup> AMBROGIANI 00b E835  $\bar{p}p \rightarrow \chi_{c2} \rightarrow \gamma\gamma, \gamma J/\psi$

<sup>1</sup> Calculated by us using  $B(J/\psi(1S) \rightarrow e^+e^-) = 0.0593 \pm 0.0010$ .

$\Gamma(\gamma\gamma)/\Gamma_{total} \times \Gamma(p\bar{p})/\Gamma_{total}$   $\Gamma_{93}/\Gamma \times \Gamma_{56}/\Gamma$   

VALUE (units $10^{-8}$ )	DOCUMENT ID	TECN	COMMENT
--------------------------	-------------	------	---------

2.09±0.13 OUR FIT  
1.7 ± 0.4 OUR AVERAGE

1.60±0.42 ARMSTRONG 93 E760  $\bar{p}p \rightarrow \gamma\gamma X$   
9.9 ± 4.5 BAGLIN 87b SPEC  $\bar{p}p \rightarrow \gamma\gamma X$

$\chi_{c2}(1P)$  CROSS-PARTICLE BRANCHING RATIOS

$\Gamma(\chi_{c2}(1P) \rightarrow K^+K^-\pi^+\pi^-)/\Gamma_{total} \times \Gamma(\psi(2S) \rightarrow \gamma\chi_{c2}(1P))/\Gamma(\psi(2S) \rightarrow J/\psi(1S)\pi^+\pi^-)$   $\Gamma_{14}/\Gamma \times \Gamma_{155}^{\psi(2S)}/\Gamma_{11}^{\psi(2S)}$

VALUE (units $10^{-3}$ )	DOCUMENT ID	TECN	COMMENT
--------------------------	-------------	------	---------

2.31±0.26 OUR FIT  
2.5 ± 0.9 OUR AVERAGE Error includes scale factor of 2.3.

1.90±0.14±0.44 BAI 99b BES  $\psi(2S) \rightarrow \gamma\chi_{c2}$   
3.8 ± 0.67 <sup>1</sup> TANENBAUM 78 MRK1  $\psi(2S) \rightarrow \gamma\chi_{c2}$

<sup>1</sup> The reported value is derived using  $B(\psi(2S) \rightarrow \pi^+\pi^-J/\psi) \times B(J/\psi \rightarrow \ell^+\ell^-) = (4.6 \pm 0.7)\%$ . Calculated by us using  $B(J/\psi \rightarrow \ell^+\ell^-) = 0.1181 \pm 0.0020$ .

$\Gamma(\chi_{c2}(1P) \rightarrow K^*(892)^0\bar{K}^*(892)^0)/\Gamma_{total} \times \Gamma(\psi(2S) \rightarrow \gamma\chi_{c2}(1P))/\Gamma_{total}$   $\Gamma_{18}/\Gamma \times \Gamma_{155}^{\psi(2S)}/\Gamma_{155}^{\psi(2S)}$

VALUE (units $10^{-4}$ )	DOCUMENT ID	TECN	COMMENT
--------------------------	-------------	------	---------

2.1 ± 0.4 OUR FIT  
3.11±0.36±0.48 ABLIKIM 04h BES2  $\psi(2S) \rightarrow \gamma\chi_{c2}$

$\Gamma(\chi_{c2}(1P) \rightarrow p\bar{p})/\Gamma_{total} \times \Gamma(\psi(2S) \rightarrow \gamma\chi_{c2}(1P))/\Gamma(\psi(2S) \rightarrow J/\psi(1S)\pi^+\pi^-)$   $\Gamma_{56}/\Gamma \times \Gamma_{155}^{\psi(2S)}/\Gamma_{11}^{\psi(2S)}$

VALUE (units $10^{-5}$ )	DOCUMENT ID	TECN	COMMENT
--------------------------	-------------	------	---------

2.01±0.09 OUR FIT  
1.4 ± 1.1 <sup>1</sup> BAI 98i BES  $\psi(2S) \rightarrow \gamma\chi_{c2} \rightarrow \gamma\bar{p}p$

<sup>1</sup> Calculated by us. The value for  $B(\chi_{c2} \rightarrow p\bar{p})$  reported in BAI 98i is derived using  $B(\psi(2S) \rightarrow \gamma\chi_{c2}) = (7.8 \pm 0.8)\%$  and  $B(\psi(2S) \rightarrow J/\psi(1S)\pi^+\pi^-) = (32.4 \pm 2.6)\%$  [BAI 98d].

$\Gamma(\chi_{c2}(1P) \rightarrow p\bar{p})/\Gamma_{total} \times \Gamma(\psi(2S) \rightarrow \gamma\chi_{c2}(1P))/\Gamma_{total}$   $\Gamma_{56}/\Gamma \times \Gamma_{155}^{\psi(2S)}/\Gamma_{155}^{\psi(2S)}$

VALUE (units $10^{-6}$ )	EVTS	DOCUMENT ID	TECN	COMMENT
--------------------------	------	-------------	------	---------

6.98±0.32 OUR FIT  
7.1 ± 0.5 OUR AVERAGE Error includes scale factor of 1.2.

7.3 ± 0.4 ± 0.3 405 ABLIKIM 13v BES3  $\psi(2S) \rightarrow \gamma p\bar{p}$   
7.2 ± 0.7 ± 0.4 121 ± 12 <sup>1</sup> NAIK 08 CLEO  $\psi(2S) \rightarrow \gamma p\bar{p}$   
4.4 +1.6 ± 0.6 14.3 +5.2 -1.4 BAI 04f BES  $\psi(2S) \rightarrow \gamma\chi_{c2}(1P) \rightarrow \gamma\bar{p}p$

<sup>1</sup> Calculated by us. NAIK 08 reports  $B(\chi_{c2} \rightarrow p\bar{p}) = (7.7 \pm 0.8 \pm 0.4 \pm 0.5) \times 10^{-5}$  using  $B(\psi(2S) \rightarrow \gamma\chi_{c2}) = (9.33 \pm 0.14 \pm 0.61)\%$ .

$\Gamma(\chi_{c2}(1P) \rightarrow \Lambda\bar{\Lambda})/\Gamma_{total} \times \Gamma(\psi(2S) \rightarrow \gamma\chi_{c2}(1P))/\Gamma_{total}$   $\Gamma_{69}/\Gamma \times \Gamma_{155}^{\psi(2S)}/\Gamma_{155}^{\psi(2S)}$

VALUE (units $10^{-6}$ )	EVTS	DOCUMENT ID	TECN	COMMENT
--------------------------	------	-------------	------	---------

17.5±1.3 OUR FIT  
17.4±1.4 OUR AVERAGE

18.2±1.4±0.9 207 <sup>1</sup> ABLIKIM 13h BES3  $\psi(2S) \rightarrow \gamma\Lambda\bar{\Lambda}$   
15.9±2.1±1.0 71 ± 9 <sup>2</sup> NAIK 08 CLEO  $\psi(2S) \rightarrow \gamma\Lambda\bar{\Lambda}$

<sup>1</sup> Calculated by us. ABLIKIM 13h reports  $B(\chi_{c2} \rightarrow \Lambda\bar{\Lambda}) = (20.8 \pm 1.6 \pm 2.3) \times 10^{-5}$  from a measurement of  $B(\chi_{c2} \rightarrow \Lambda\bar{\Lambda}) \times B(\psi(2S) \rightarrow \gamma\chi_{c2})$  assuming  $B(\psi(2S) \rightarrow \gamma\chi_{c2}) = (8.74 \pm 0.35)\%$ .

<sup>2</sup> Calculated by us. NAIK 08 reports  $B(\chi_{c2} \rightarrow \Lambda\bar{\Lambda}) = (17.0 \pm 2.2 \pm 1.1 \pm 1.1) \times 10^{-5}$  using  $B(\psi(2S) \rightarrow \gamma\chi_{c2}) = (9.33 \pm 0.14 \pm 0.61)\%$ .

$\Gamma(\chi_{c2}(1P) \rightarrow \Lambda\bar{\Lambda})/\Gamma_{total} \times \Gamma(\psi(2S) \rightarrow \gamma\chi_{c2}(1P))/\Gamma(\psi(2S) \rightarrow J/\psi(1S)\pi^+\pi^-)$   $\Gamma_{69}/\Gamma \times \Gamma_{155}^{\psi(2S)}/\Gamma_{11}^{\psi(2S)}$

VALUE (units $10^{-5}$ )	EVTS	DOCUMENT ID	TECN	COMMENT
--------------------------	------	-------------	------	---------

5.1±0.4 OUR FIT  
7.1+3.1 -2.9±1.3 8.3+3.7 -3.4 <sup>1</sup> BAI 03E BES  $\psi(2S) \rightarrow \gamma\Lambda\bar{\Lambda}$

<sup>1</sup> BAI 03E reports  $[B(\chi_{c2} \rightarrow \Lambda\bar{\Lambda})B(\psi(2S) \rightarrow \gamma\chi_{c2})/B(\psi(2S) \rightarrow J/\psi\pi^+\pi^-)] \times [B^2(\Lambda \rightarrow \pi^-\rho)/B(J/\psi \rightarrow \rho\bar{\rho})] = (1.33 +0.59 -0.55 \pm 0.25)\%$ . We calculate from this measurement the presented value using  $B(\Lambda \rightarrow \pi^-\rho) = (63.9 \pm 0.5)\%$  and  $B(J/\psi \rightarrow \rho\bar{\rho}) = (2.17 \pm 0.07) \times 10^{-3}$ .

$\Gamma(\chi_{c2}(1P) \rightarrow \pi\pi)/\Gamma_{total} \times \Gamma(\psi(2S) \rightarrow \gamma\chi_{c2}(1P))/\Gamma_{total}$   $\Gamma_{25}/\Gamma \times \Gamma_{155}^{\psi(2S)}/\Gamma_{155}^{\psi(2S)}$

VALUE (units $10^{-4}$ )	EVTS	DOCUMENT ID	TECN	COMMENT
--------------------------	------	-------------	------	---------

2.12±0.08 OUR FIT  
2.17±0.09 OUR AVERAGE

2.19±0.05±0.15 4.5k <sup>1</sup> ABLIKIM 10A BES3  $e^+e^- \rightarrow \psi(2S) \rightarrow \gamma\chi_{c2}$   
2.23±0.06±0.10 2.5k <sup>2</sup> ASNER 09 CLEO  $\psi(2S) \rightarrow \gamma\pi^+\pi^-$   
1.90±0.08±0.20 0.8k <sup>3</sup> ASNER 09 CLEO  $\psi(2S) \rightarrow \gamma\pi^0\pi^0$

<sup>1</sup> Calculated by us. ABLIKIM 10A reports  $B(\chi_{c2} \rightarrow \pi^0\pi^0) = (0.88 \pm 0.02 \pm 0.06 \pm 0.04) \times 10^{-3}$  using  $B(\psi(2S) \rightarrow \gamma\chi_{c2}) = (8.3 \pm 0.4)\%$ . We have multiplied the  $\pi^0\pi^0$  measurement by 3 to obtain  $\pi\pi$ .

<sup>2</sup> Calculated by us. ASNER 09 reports  $B(\chi_{c2} \rightarrow \pi^+\pi^-) = (1.59 \pm 0.04 \pm 0.07 \pm 0.10) \times 10^{-3}$  using  $B(\psi(2S) \rightarrow \gamma\chi_{c2}) = (9.33 \pm 0.14 \pm 0.61)\%$ . We have multiplied the  $\pi^+\pi^-$  measurement by 3/2 to obtain  $\pi\pi$ .

<sup>3</sup> Calculated by us. ASNER 09 reports  $B(\chi_{c2} \rightarrow \pi^0\pi^0) = (0.68 \pm 0.03 \pm 0.07 \pm 0.04) \times 10^{-3}$  using  $B(\psi(2S) \rightarrow \gamma\chi_{c2}) = (9.33 \pm 0.14 \pm 0.61)\%$ . We have multiplied the  $\pi^0\pi^0$  measurement by 3 to obtain  $\pi\pi$ .

$\Gamma(\chi_{c2}(1P) \rightarrow \pi\pi)/\Gamma_{total} \times \Gamma(\psi(2S) \rightarrow \gamma\chi_{c2}(1P))/\Gamma(\psi(2S) \rightarrow J/\psi(1S)\pi^+\pi^-)$   $\Gamma_{25}/\Gamma \times \Gamma_{155}^{\psi(2S)}/\Gamma_{11}^{\psi(2S)}$

VALUE (units $10^{-3}$ )	EVTS	DOCUMENT ID	TECN	COMMENT
--------------------------	------	-------------	------	---------

0.612±0.023 OUR FIT  
0.54 ± 0.06 OUR AVERAGE

0.66 ± 0.18 ± 0.37 21 ± 6 <sup>1</sup> BAI 03c BES  $\psi(2S) \rightarrow \gamma\pi^0\pi^0$   
0.54 ± 0.05 ± 0.04 185 ± 16 <sup>2</sup> BAI 98i BES  $\psi(2S) \rightarrow \gamma\pi^+\pi^-$

<sup>1</sup> We have multiplied  $\pi^0\pi^0$  measurement by 3 to obtain  $\pi\pi$ .

<sup>2</sup> Calculated by us. The value for  $B(\chi_{c2} \rightarrow \pi^+\pi^-)$  reported by BAI 98i is derived using  $B(\psi(2S) \rightarrow \gamma\chi_{c2}) = (7.8 \pm 0.8)\%$  and  $B(\psi(2S) \rightarrow J/\psi\pi^+\pi^-) = (32.4 \pm 2.6)\%$  [BAI 98d]. We have multiplied  $\pi^+\pi^-$  measurement by 3/2 to obtain  $\pi\pi$ .

$\Gamma(\chi_{c2}(1P) \rightarrow \eta\eta)/\Gamma_{total} \times \Gamma(\psi(2S) \rightarrow \gamma\chi_{c2}(1P))/\Gamma_{total}$   $\Gamma_{31}/\Gamma \times \Gamma_{155}^{\psi(2S)}/\Gamma_{155}^{\psi(2S)}$

VALUE (units $10^{-4}$ )	CL%	EVTS	DOCUMENT ID	TECN	COMMENT
--------------------------	-----	------	-------------	------	---------

0.52±0.04 OUR FIT  
0.52±0.04 OUR AVERAGE

0.54±0.03±0.04 386 <sup>1</sup> ABLIKIM 10A BES3  $e^+e^- \rightarrow \psi(2S) \rightarrow \gamma\chi_{c2}$   
0.47±0.05±0.05 156 ASNER 09 CLEO  $\psi(2S) \rightarrow \gamma\eta\eta$   
••• We do not use the following data for averages, fits, limits, etc. •••  
< 0.44 90 <sup>2</sup> ADAMS 07 CLEO  $\psi(2S) \rightarrow \gamma\chi_{c2}$   
< 3 90 BAI 03c BES  $\psi(2S) \rightarrow \gamma\eta\eta \rightarrow 5\gamma$   
0.62±0.31±0.19 LEE 85 CBAL  $\psi(2S) \rightarrow \text{photons}$

<sup>1</sup> Calculated by us. ABLIKIM 10A reports  $B(\chi_{c2} \rightarrow \eta\eta) = (0.65 \pm 0.04 \pm 0.05 \pm 0.03) \times 10^{-3}$  using  $B(\psi(2S) \rightarrow \gamma\chi_{c2}) = (8.3 \pm 0.4)\%$ .

<sup>2</sup> Superseded by ASNER 09.

$\Gamma(\chi_{c2}(1P) \rightarrow K^+K^-)/\Gamma_{total} \times \Gamma(\psi(2S) \rightarrow \gamma\chi_{c2}(1P))/\Gamma_{total}$   $\Gamma_{32}/\Gamma \times \Gamma_{155}^{\psi(2S)}/\Gamma_{155}^{\psi(2S)}$

VALUE (units $10^{-5}$ )	EVTS	DOCUMENT ID	TECN	COMMENT
--------------------------	------	-------------	------	---------

9.6±0.6 OUR FIT  
10.5±0.3±0.6 1.6k <sup>1</sup> ASNER 09 CLEO  $\psi(2S) \rightarrow \gamma K^+K^-$

<sup>1</sup> Calculated by us. ASNER 09 reports  $B(\chi_{c2} \rightarrow K^+K^-) = (1.13 \pm 0.03 \pm 0.06 \pm 0.07) \times 10^{-3}$  using  $B(\psi(2S) \rightarrow \gamma\chi_{c2}) = (9.33 \pm 0.14 \pm 0.61)\%$ .

Meson Particle Listings

$\chi_{c2}(1P)$

$$\Gamma(\chi_{c2}(1P) \rightarrow K^+ K^-) / \Gamma_{\text{total}} \times \Gamma(\psi(2S) \rightarrow \gamma \chi_{c2}(1P)) / \Gamma(\psi(2S) \rightarrow J/\psi(1S) \pi^+ \pi^-) / \Gamma_{\text{total}} \times \Gamma(\psi(2S) \rightarrow \gamma \chi_{c2}(1P)) / \Gamma(\psi(2S) \rightarrow J/\psi(1S) \pi^+ \pi^-)$$

VALUE (units $10^{-3}$ )	EVTS	DOCUMENT ID	TECN	COMMENT
<b>0.276 ± 0.017 OUR FIT</b>				
0.190 ± 0.034 ± 0.019	115 ± 13	<sup>1</sup> BAI	98i	BES $\psi(2S) \rightarrow \gamma K^+ K^-$

<sup>1</sup> Calculated by us. The value for  $B(\chi_{c2} \rightarrow K^+ K^-)$  reported by BAI 98i is derived using  $B(\psi(2S) \rightarrow \gamma \chi_{c2}) = (7.8 \pm 0.8)\%$  and  $B(\psi(2S) \rightarrow J/\psi \pi^+ \pi^-) = (32.4 \pm 2.6)\%$  [BAI 98b].

$$\Gamma(\chi_{c2}(1P) \rightarrow K_S^0 K_S^0) / \Gamma_{\text{total}} \times \Gamma(\psi(2S) \rightarrow \gamma \chi_{c2}(1P)) / \Gamma_{\text{total}} \times \Gamma(\psi(2S) \rightarrow \gamma \chi_{c2}(1P)) / \Gamma(\psi(2S) \rightarrow J/\psi(1S) \pi^+ \pi^-)$$

VALUE (units $10^{-5}$ )	EVTS	DOCUMENT ID	TECN	COMMENT
<b>5.0 ± 0.4 OUR FIT</b>				
<b>5.0 ± 0.4 OUR AVERAGE</b>				
4.9 ± 0.3 ± 0.3	373 ± 20	<sup>1</sup> ASNER	09	CLEO $\psi(2S) \rightarrow \gamma K_S^0 K_S^0$
5.72 ± 0.76 ± 0.63	65	ABLIKIM	05o	BES2 $\psi(2S) \rightarrow \gamma K_S^0 K_S^0$

<sup>1</sup> Calculated by us. ASNER 09 reports  $B(\chi_{c2} \rightarrow K_S^0 K_S^0) = (0.53 \pm 0.03 \pm 0.03 \pm 0.03) \times 10^{-3}$  using  $B(\psi(2S) \rightarrow \gamma \chi_{c2}) = (9.33 \pm 0.14 \pm 0.61)\%$ .

$$\Gamma(\chi_{c2}(1P) \rightarrow K_S^0 K_S^0) / \Gamma_{\text{total}} \times \Gamma(\psi(2S) \rightarrow \gamma \chi_{c2}(1P)) / \Gamma_{\text{total}} \times \Gamma(\psi(2S) \rightarrow \gamma \chi_{c2}(1P)) / \Gamma(\psi(2S) \rightarrow J/\psi(1S) \pi^+ \pi^-)$$

VALUE (units $10^{-5}$ )	DOCUMENT ID	TECN	COMMENT
<b>14.4 ± 1.1 OUR FIT</b>			
<b>14.7 ± 1.1 ± 3.3</b>	<sup>1</sup> BAI	99b	BES $\psi(2S) \rightarrow \gamma K_S^0 K_S^0$

<sup>1</sup> Calculated by us. The value of  $B(\chi_{c2} \rightarrow K_S^0 K_S^0)$  reported by BAI 99b was derived using  $B(\psi(2S) \rightarrow \gamma \chi_{c2}(1P)) = (7.8 \pm 0.8)\%$  and  $B(\psi(2S) \rightarrow J/\psi \pi^+ \pi^-) = (32.4 \pm 2.6)\%$  [BAI 98b].

$$\Gamma(\chi_{c2}(1P) \rightarrow \bar{K}^0 K^+ \pi^- + c.c.) / \Gamma_{\text{total}} \times \Gamma(\psi(2S) \rightarrow \gamma \chi_{c2}(1P)) / \Gamma_{\text{total}} \times \Gamma(\psi(2S) \rightarrow \gamma \chi_{c2}(1P)) / \Gamma(\psi(2S) \rightarrow J/\psi(1S) \pi^+ \pi^-)$$

VALUE (units $10^{-4}$ )	EVTS	DOCUMENT ID	TECN	COMMENT
<b>1.22 ± 0.17 OUR FIT</b>				
<b>1.15 ± 0.18 OUR AVERAGE</b>				
1.21 ± 0.19 ± 0.09	37	<sup>1</sup> ATHAR	07	CLEO $\psi(2S) \rightarrow \gamma K_S^0 K^{\pm} \pi^{\mp}$
0.97 ± 0.32 ± 0.13	28	<sup>2</sup> ABLIKIM	06R	BES2 $\psi(2S) \rightarrow \gamma K_S^0 K^{\pm} \pi^{\mp}$

<sup>1</sup> Calculated by us. ATHAR 07 reports  $B(\chi_{c2} \rightarrow \bar{K}^0 K^+ \pi^- + c.c.) = (1.3 \pm 0.2 \pm 0.1 \pm 0.1) \times 10^{-3}$  using  $B(\psi(2S) \rightarrow \gamma \chi_{c2}) = (9.33 \pm 0.14 \pm 0.61)\%$ .  
<sup>2</sup> Calculated by us. ABLIKIM 06R reports  $B(\chi_{c2} \rightarrow K_S^0 K^{\pm} \pi^{\mp}) = (0.6 \pm 0.2 \pm 0.1) \times 10^{-3}$  using  $B(\psi(2S) \rightarrow \gamma \chi_{c2}) = (8.1 \pm 0.6)\%$ . We have multiplied by 2 to obtain  $\bar{K}^0 K^+ \pi^- + c.c.$  from  $K_S^0 K^{\pm} \pi^{\mp}$ .

$$\Gamma(\chi_{c2}(1P) \rightarrow 2(\pi^+ \pi^-)) / \Gamma_{\text{total}} \times \Gamma(\psi(2S) \rightarrow \gamma \chi_{c2}(1P)) / \Gamma_{\text{total}} \times \Gamma(\psi(2S) \rightarrow \gamma \chi_{c2}(1P)) / \Gamma(\psi(2S) \rightarrow J/\psi(1S) \pi^+ \pi^-)$$

VALUE (units $10^{-3}$ )	DOCUMENT ID	TECN	COMMENT
<b>2.79 ± 0.26 OUR FIT</b>			
<b>3.1 ± 1.0 OUR AVERAGE</b>			Error includes scale factor of 2.5.
2.3 ± 0.1 ± 0.5	<sup>1</sup> BAI	99b	BES $\psi(2S) \rightarrow \gamma \chi_{c2}$
4.3 ± 0.6	<sup>2</sup> TANENBAUM	78	MRK1 $\psi(2S) \rightarrow \gamma \chi_{c2}$

<sup>1</sup> Calculated by us. The value for  $B(\chi_{c2} \rightarrow 2\pi^+ 2\pi^-)$  reported in BAI 99b is derived using  $B(\psi(2S) \rightarrow \gamma \chi_{c2}) = (7.8 \pm 0.8)\%$  and  $B(\psi(2S) \rightarrow J/\psi(1S) \pi^+ \pi^-) = (32.4 \pm 2.6)\%$  [BAI 98b].  
<sup>2</sup> The value for  $B(\psi(2S) \rightarrow \gamma \chi_{c2}) \times B(\chi_{c2} \rightarrow 2\pi^+ \pi^-)$  reported in TANENBAUM 78 is derived using  $B(\psi(2S) \rightarrow J/\psi(1S) \pi^+ \pi^-) \times B(J/\psi(1S) \ell^+ \ell^-) = (4.6 \pm 0.7)\%$ . Calculated by us using  $B(J/\psi(1S) \rightarrow \ell^+ \ell^-) = 0.1181 \pm 0.0020$ .

$$\Gamma(\chi_{c2}(1P) \rightarrow K^+ K^- K^+ K^-) / \Gamma_{\text{total}} \times \Gamma(\psi(2S) \rightarrow \gamma \chi_{c2}(1P)) / \Gamma_{\text{total}} \times \Gamma(\psi(2S) \rightarrow \gamma \chi_{c2}(1P)) / \Gamma(\psi(2S) \rightarrow J/\psi(1S) \pi^+ \pi^-)$$

VALUE (units $10^{-4}$ )	EVTS	DOCUMENT ID	TECN	COMMENT
<b>1.57 ± 0.19 OUR FIT</b>				
<b>1.76 ± 0.16 ± 0.24</b>	160	<sup>1</sup> ABLIKIM	06T	BES2 $\psi(2S) \rightarrow \gamma 2K^+ 2K^-$

<sup>1</sup> Calculated by us. The value of  $B(\chi_{c2} \rightarrow 2K^+ 2K^-)$  reported by ABLIKIM 06T was derived using  $B(\psi(2S) \rightarrow \gamma \chi_{c2}(1P)) = (8.1 \pm 0.4)\%$ .

$$\Gamma(\chi_{c2}(1P) \rightarrow K^+ K^- K^+ K^-) / \Gamma_{\text{total}} \times \Gamma(\psi(2S) \rightarrow \gamma \chi_{c2}(1P)) / \Gamma_{\text{total}} \times \Gamma(\psi(2S) \rightarrow \gamma \chi_{c2}(1P)) / \Gamma(\psi(2S) \rightarrow J/\psi(1S) \pi^+ \pi^-)$$

VALUE (units $10^{-4}$ )	EVTS	DOCUMENT ID	TECN	COMMENT
<b>4.5 ± 0.5 OUR FIT</b>				
<b>3.6 ± 0.6 ± 0.6</b>		<sup>1</sup> BAI	99b	BES $\psi(2S) \rightarrow \gamma 2K^+ 2K^-$

<sup>1</sup> Calculated by us. The value of  $B(\chi_{c2} \rightarrow 2K^+ 2K^-)$  reported by BAI 99b was derived using  $B(\psi(2S) \rightarrow \gamma \chi_{c2}(1P)) = (7.8 \pm 0.8)\%$  and  $B(\psi(2S) \rightarrow J/\psi \pi^+ \pi^-) = (32.4 \pm 2.6)\%$  [BAI 98b].

$$\Gamma(\chi_{c2}(1P) \rightarrow \phi \phi) / \Gamma_{\text{total}} \times \Gamma(\psi(2S) \rightarrow \gamma \chi_{c2}(1P)) / \Gamma_{\text{total}} \times \Gamma(\psi(2S) \rightarrow \gamma \chi_{c2}(1P)) / \Gamma(\psi(2S) \rightarrow J/\psi(1S) \pi^+ \pi^-)$$

VALUE (units $10^{-4}$ )	EVTS	DOCUMENT ID	TECN	COMMENT
<b>1.01 ± 0.08 OUR FIT</b>				
<b>0.98 ± 0.13 OUR AVERAGE</b>				Error includes scale factor of 1.3.
0.94 ± 0.03 ± 0.10	849	<sup>1</sup> ABLIKIM	11k	BES3 $\psi(2S) \rightarrow \gamma$ hadrons
1.38 ± 0.24 ± 0.23	41	<sup>2</sup> ABLIKIM	06T	BES2 $\psi(2S) \rightarrow \gamma 2K^+ 2K^-$

<sup>1</sup> Calculated by us. The value of  $B(\chi_{c2} \rightarrow \phi \phi)$  reported by ABLIKIM 11k was derived using  $B(\psi(2S) \rightarrow \gamma \chi_{c2}(1P)) = (8.74 \pm 0.35)\%$ .  
<sup>2</sup> Calculated by us. The value of  $B(\chi_{c2} \rightarrow \phi \phi)$  reported by ABLIKIM 06T was derived using  $B(\psi(2S) \rightarrow \gamma \chi_{c2}(1P)) = (8.1 \pm 0.4)\%$ .

$$\Gamma(\chi_{c2}(1P) \rightarrow \phi \phi) / \Gamma_{\text{total}} \times \Gamma(\psi(2S) \rightarrow \gamma \chi_{c2}(1P)) / \Gamma_{\text{total}} \times \Gamma(\psi(2S) \rightarrow \gamma \chi_{c2}(1P)) / \Gamma(\psi(2S) \rightarrow J/\psi(1S) \pi^+ \pi^-)$$

VALUE (units $10^{-4}$ )	DOCUMENT ID	TECN	COMMENT
<b>2.92 ± 0.24 OUR FIT</b>			
<b>4.8 ± 1.3 ± 1.3</b>	<sup>1</sup> BAI	99b	BES $\psi(2S) \rightarrow \gamma 2K^+ 2K^-$

<sup>1</sup> Calculated by us. The value of  $B(\chi_{c2} \rightarrow \phi \phi)$  reported by BAI 99b was derived using  $B(\psi(2S) \rightarrow \gamma \chi_{c2}(1P)) = (7.8 \pm 0.8)\%$  and  $B(\psi(2S) \rightarrow J/\psi \pi^+ \pi^-) = (32.4 \pm 2.6)\%$  [BAI 98b].

$$\Gamma(\chi_{c2}(1P) \rightarrow \Sigma^+ \bar{p} K_S^0 + c.c.) / \Gamma_{\text{total}} \times \Gamma(\psi(2S) \rightarrow \gamma \chi_{c2}(1P)) / \Gamma_{\text{total}} \times \Gamma(\psi(2S) \rightarrow \gamma \chi_{c2}(1P)) / \Gamma(\psi(2S) \rightarrow J/\psi(1S) \pi^+ \pi^-)$$

VALUE (units $10^{-6}$ )	EVTS	DOCUMENT ID	TECN	COMMENT
<b>7.85 ± 0.77 ± 0.44</b>	129	<sup>1</sup> ABLIKIM	19bb	BES3 $\psi(2S) \rightarrow \gamma \Sigma^+ \bar{p} K_S^0 + c.c.$

<sup>1</sup> Calculated by us. ABLIKIM 19bb reports  $B(\chi_{c2} \rightarrow \Sigma^+ \bar{p} K_S^0 + c.c.) = (8.25 \pm 0.83 \pm 0.49) \times 10^{-5}$  using  $B(\psi(2S) \rightarrow \gamma \chi_{c2}) = (9.52 \pm 0.20)\%$  and other branching fractions from PDG 18.

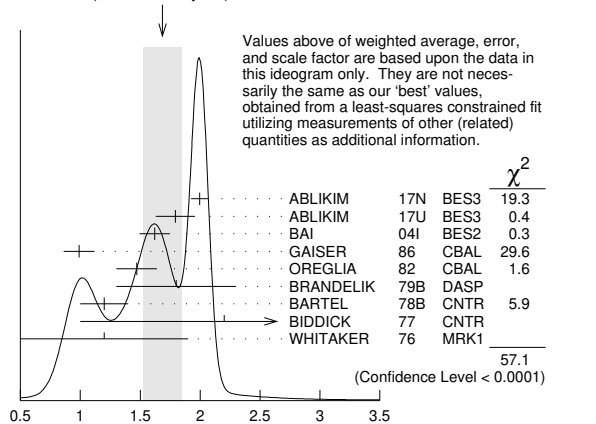
$$\Gamma(\chi_{c2}(1P) \rightarrow \gamma J/\psi(1S)) / \Gamma_{\text{total}} \times \Gamma(\psi(2S) \rightarrow \gamma \chi_{c2}(1P)) / \Gamma_{\text{total}} \times \Gamma(\psi(2S) \rightarrow \gamma \chi_{c2}(1P)) / \Gamma(\psi(2S) \rightarrow J/\psi(1S) \pi^+ \pi^-)$$

VALUE (units $10^{-2}$ )	EVTS	DOCUMENT ID	TECN	COMMENT
<b>1.81 ± 0.04 OUR FIT</b>				
<b>1.69 ± 0.16 OUR AVERAGE</b>				Error includes scale factor of 3.4. See the ideogram below.
1.996 ± 0.008 ± 0.070	81k	<sup>1</sup> ABLIKIM	17n	BES3 $\psi(2S) \rightarrow \gamma \gamma J/\psi$
1.793 ± 0.008 ± 0.163	1.0M	ABLIKIM	17u	BES3 $e^+ e^- \rightarrow \gamma X$
1.62 ± 0.04 ± 0.12	5.8k	BAI	04i	BES2 $\psi(2S) \rightarrow J/\psi \gamma \gamma$
0.99 ± 0.10 ± 0.08		GAISER	86	CBAL $\psi(2S) \rightarrow \gamma X$
1.47 ± 0.17		<sup>2</sup> OREGLIA	82	CBAL $\psi(2S) \rightarrow \gamma \chi_{c2}$
1.8 ± 0.5		<sup>3</sup> BRANDELIC	79b	DASP $\psi(2S) \rightarrow \gamma \chi_{c2}$
1.2 ± 0.2		<sup>3</sup> BARTEL	78b	CNTR $\psi(2S) \rightarrow \gamma \chi_{c2}$
2.2 ± 1.2		<sup>4</sup> BIDDICK	77	CNTR $e^+ e^- \rightarrow \gamma X$
1.2 ± 0.7		<sup>2</sup> WHITAKER	76	MRK1 $e^+ e^-$

• • • We do not use the following data for averages, fits, limits, etc. • • •  
 1.874 ± 0.007 ± 0.102 76k <sup>5</sup> ABLIKIM 12o BES3  $\psi(2S) \rightarrow \gamma \chi_{c2}$   
 1.95 ± 0.02 ± 0.07 12.4k <sup>6</sup> MENDEZ 08 CLEO  $\psi(2S) \rightarrow \gamma \chi_{c2}$   
 1.85 ± 0.04 ± 0.07 1.9k <sup>7</sup> ADAM 05a CLEO Repl. by MENDEZ 08

<sup>1</sup> Uses  $B(J/\psi \rightarrow e^+ e^-) = (5.971 \pm 0.032)\%$  and  $B(J/\psi \rightarrow \mu^+ \mu^-) = (5.961 \pm 0.033)\%$ .  
<sup>2</sup> Recalculated by us using  $B(J/\psi(1S) \rightarrow \ell^+ \ell^-) = 0.1181 \pm 0.0020$ .  
<sup>3</sup> Recalculated by us using  $B(J/\psi(1S) \rightarrow \mu^+ \mu^-) = 0.0588 \pm 0.0010$ .  
<sup>4</sup> Assumes isotropic gamma distribution.  
<sup>5</sup> Superseded by ABLIKIM 17n.  
<sup>6</sup> Not independent from other measurements of MENDEZ 08.  
<sup>7</sup> Not independent from other values reported by ADAM 05a.

WEIGHTED AVERAGE  
 1.69 ± 0.16 (Error scaled by 3.4)



$\Gamma(\chi_{c2}(1P) \rightarrow \gamma J/\psi(1S)) / \Gamma_{\text{total}} \times \Gamma(\psi(2S) \rightarrow \gamma \chi_{c2}(1P)) / \Gamma_{\text{total}}$  (units  $10^{-2}$ )

$$\Gamma(\chi_{c2}(1P) \rightarrow \gamma J/\psi(1S))/\Gamma_{\text{total}} \times \Gamma(\psi(2S) \rightarrow \gamma \chi_{c2}(1P))/\Gamma(\psi(2S) \rightarrow J/\psi(1S) \text{ anything})$$

$$\frac{\Gamma_{89}/\Gamma \times \Gamma_{155}^{\psi(2S)}/\Gamma_9^{\psi(2S)}}{\Gamma_{155}^{\psi(2S)}/\Gamma_9^{\psi(2S)} + \Gamma_{155}^{\psi(2S)}/\Gamma_{11}^{\psi(2S)} + \Gamma_{12}^{\psi(2S)} + \Gamma_{13}^{\psi(2S)} + 0.343\Gamma_{154}^{\psi(2S)} + 0.190\Gamma_{155}^{\psi(2S)}}$$

VALUE (units $10^{-2}$ )	EVTS	DOCUMENT ID	TECN	COMMENT
<b>2.95±0.06 OUR FIT</b>				
• • • We do not use the following data for averages, fits, limits, etc. • • •				
3.12±0.03±0.09	12.4k	<sup>1</sup> MENDEZ	08 CLEO	$\psi(2S) \rightarrow \gamma \chi_{c2}$
3.11±0.07±0.07	1.9k	ADAM	05A CLEO	Repl. by MENDEZ 08
<sup>1</sup> Not independent from other measurements of MENDEZ 08.				

$$\Gamma(\chi_{c2}(1P) \rightarrow \gamma J/\psi(1S))/\Gamma_{\text{total}} \times \Gamma(\psi(2S) \rightarrow \gamma \chi_{c2}(1P))/\Gamma(\psi(2S) \rightarrow J/\psi(1S) \pi^+ \pi^-)$$

$$\frac{\Gamma_{89}/\Gamma \times \Gamma_{155}^{\psi(2S)}/\Gamma_{11}^{\psi(2S)}}{\Gamma_{155}^{\psi(2S)}/\Gamma_{11}^{\psi(2S)}}$$

VALUE (units $10^{-2}$ )	EVTS	DOCUMENT ID	TECN	COMMENT
<b>5.22±0.11 OUR FIT</b>				
<b>5.53±0.17 OUR AVERAGE</b>				
5.56±0.05±0.16	12.4k	MENDEZ	08 CLEO	$\psi(2S) \rightarrow \gamma \chi_{c2}$
6.0 ± 2.8	1.3k	<sup>1</sup> ABLIKIM	04B BES	$\psi(2S) \rightarrow J/\psi X$
3.9 ± 1.2		<sup>2</sup> HIMEL	80 MRK2	$\psi(2S) \rightarrow \gamma \chi_{c2}$
• • • We do not use the following data for averages, fits, limits, etc. • • •				
5.52±0.13±0.13	1.9k	<sup>3</sup> ADAM	05A CLEO	Repl. by MENDEZ 08
<sup>1</sup> From a fit to the $J/\psi$ recoil mass spectra.				
<sup>2</sup> The value for $B(\psi(2S) \rightarrow \gamma \chi_{c2}) \times B(\chi_{c2} \rightarrow \gamma J/\psi(1S))$ reported in HIMEL 80 is derived using $B(\psi(2S) \rightarrow J/\psi(1S) \pi^+ \pi^-) = (33 \pm 3)\%$ and $B(J/\psi(1S) \rightarrow \ell^+ \ell^-) = 0.138 \pm 0.018$ . Calculated by us using $B(J/\psi(1S) \rightarrow \ell^+ \ell^-) = (0.1181 \pm 0.0020)$ .				
<sup>3</sup> Not independent from other values reported by ADAM 05A.				

$$\Gamma(\chi_{c2}(1P) \rightarrow \gamma \gamma)/\Gamma_{\text{total}} \times \Gamma(\psi(2S) \rightarrow \gamma \chi_{c2}(1P))/\Gamma_{\text{total}}$$

$$\frac{\Gamma_{93}/\Gamma \times \Gamma_{155}^{\psi(2S)}/\Gamma_{155}^{\psi(2S)}}{\Gamma_{155}^{\psi(2S)}/\Gamma_{155}^{\psi(2S)}}$$

VALUE (units $10^{-5}$ )	EVTS	DOCUMENT ID	TECN	COMMENT
<b>2.71±0.08 OUR FIT</b>				
<b>2.82±0.10 OUR AVERAGE</b>				
2.83±0.08±0.06	5k	<sup>1</sup> ABLIKIM	17AE BES3	$\psi(2S) \rightarrow \gamma \chi_{c2} \rightarrow 3\gamma$
2.68±0.28±0.15	0.3k	ECKLUND	08A CLEO	$\psi(2S) \rightarrow \gamma \chi_{c2} \rightarrow 3\gamma$
7.0 ± 2.1 ± 2.0		LEE	85 CBAL	$\psi(2S) \rightarrow \gamma \chi_{c2}$
• • • We do not use the following data for averages, fits, limits, etc. • • •				
2.81±0.17±0.15	1.1k	<sup>2</sup> ABLIKIM	12A BES3	$\psi(2S) \rightarrow \gamma \chi_{c2} \rightarrow 3\gamma$
<sup>1</sup> ABLIKIM 17AE measures the ratio of two-photon partial widths for the helicity $\lambda = 0$ and helicity $\lambda = 2$ components to be $f_{0/2} = \Gamma_{\gamma\gamma}^{\lambda=0} / \Gamma_{\gamma\gamma}^{\lambda=2} = 0.000 \pm 0.006 \pm 0.012$ .				
<sup>2</sup> ABLIKIM 12A measures the ratio of two-photon partial widths for the helicity $\lambda = 0$ and helicity $\lambda = 2$ components to be $f_{0/2} = \Gamma_{\gamma\gamma}^{\lambda=0} / \Gamma_{\gamma\gamma}^{\lambda=2} = 0.00 \pm 0.02 \pm 0.02$ . Superseded by ABLIKIM 17AE.				

$$\Gamma(\chi_{c2}(1P) \rightarrow \gamma \gamma)/\Gamma(\chi_{c0}(1P) \rightarrow \gamma \gamma)$$

$$\frac{\Gamma_{93}/\Gamma_{93}^{\chi_{c0}(1P)}}{\Gamma_{93}^{\chi_{c0}(1P)}}$$

VALUE	EVTS	DOCUMENT ID	TECN	COMMENT
<b>0.292±0.028 OUR AVERAGE</b>				
0.295±0.014±0.028	8k	<sup>1</sup> ABLIKIM	17AE BES3	$\psi(2S) \rightarrow \gamma \chi_{cJ} \rightarrow 3\gamma$
0.278±0.050±0.036	0.5k	<sup>1</sup> ECKLUND	08A CLEO	$\psi(2S) \rightarrow \gamma \chi_{cJ} \rightarrow 3\gamma$
• • • We do not use the following data for averages, fits, limits, etc. • • •				
0.271±0.029±0.030	1.9k	<sup>1,2</sup> ABLIKIM	12A BES3	$\psi(2S) \rightarrow \gamma \chi_{cJ} \rightarrow 3\gamma$
<sup>1</sup> Not independent from the values of $\Gamma(\chi_{c0}, \chi_{c2})$ and $B(\psi(2S) \rightarrow \chi_{c0}, \chi_{c2})$ .				
<sup>2</sup> Superseded by ABLIKIM 17AE.				

**MULTIPOLE AMPLITUDES IN  $\chi_{c2}(1P) \rightarrow \gamma J/\psi(1S)$  RADIATIVE DECAY**

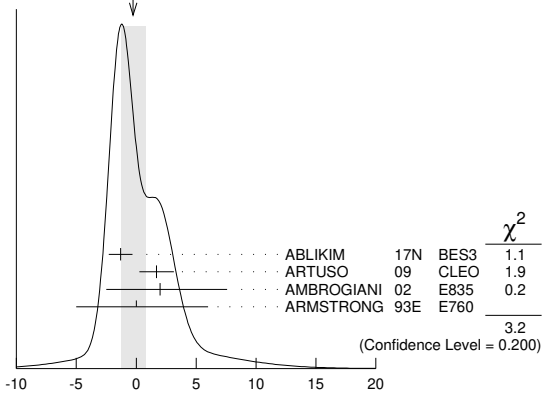
$a_2 = M_2/\sqrt{E_1^2 + M_2^2 + E_3^2}$  Magnetic quadrupole fractional transition amplitude

VALUE (units $10^{-2}$ )	EVTS	DOCUMENT ID	TECN	COMMENT
<b>-11.0± 1.0 OUR AVERAGE</b>				
-12.0± 1.3±0.4	89k	<sup>1</sup> ABLIKIM	17N BES3	$\psi(2S) \rightarrow \gamma \gamma \ell^+ \ell^-$
- 9.3± 1.6±0.3	19.8k	<sup>2</sup> ARTUSO	09 CLEO	$\psi(2S) \rightarrow \gamma \gamma \ell^+ \ell^-$
- 9.3 <sup>+3.9</sup> <sub>-4.1</sub> ±0.6	5.9k	<sup>3</sup> AMBROGIANI	02 E835	$p\bar{p} \rightarrow \chi_{c2} \rightarrow J/\psi \gamma$
-14 ± 6	1.9k	<sup>3</sup> ARMSTRONG	93E E760	$p\bar{p} \rightarrow \chi_{c2} \rightarrow J/\psi \gamma$
-33.3 <sup>+11.6</sup> <sub>-29.2</sub>	441	<sup>3</sup> OREGLIA	82 CBAL	$\psi(2S) \rightarrow \chi_{c1} \gamma \rightarrow J/\psi \gamma \gamma$
• • • We do not use the following data for averages, fits, limits, etc. • • •				
- 7.9± 1.9±0.3	19.8k	<sup>4</sup> ARTUSO	09 CLEO	$\psi(2S) \rightarrow \gamma \gamma \ell^+ \ell^-$
<sup>1</sup> Correlated with $a_3, b_2,$ and $b_3$ with correlation coefficients $\rho_{a_2 a_3} = 0.733, \rho_{a_2 b_2} = -0.605,$ and $\rho_{a_2 b_3} = -0.095$ .				
<sup>2</sup> From a fit with floating $M_2$ amplitudes $a_2$ and $b_2,$ and fixed $E_3$ amplitudes $a_3=b_3=0$ .				
<sup>3</sup> Assuming $a_3=0$ .				
<sup>4</sup> From a fit with floating $M_2$ and $E_3$ amplitudes $a_2, b_2,$ and $a_3,$ and $b_3$ .				

$a_3 = E_3/\sqrt{E_1^2 + M_2^2 + E_3^2}$  Electric octupole fractional transition amplitude

VALUE (units $10^{-2}$ )	EVTS	DOCUMENT ID	TECN	COMMENT
<b>-0.3±1.0 OUR AVERAGE</b>				Error includes scale factor of 1.3. See the ideogram below.
-1.3±0.9±0.4	89k	<sup>1</sup> ABLIKIM	17N BES3	$\psi(2S) \rightarrow \gamma \gamma \ell^+ \ell^-$
1.7±1.4±0.3	19.8k	<sup>2</sup> ARTUSO	09 CLEO	$\psi(2S) \rightarrow \gamma \gamma \ell^+ \ell^-$
2.0 <sup>+5.5</sup> <sub>-4.4</sub> ±0.9	5908	AMBROGIANI	02 E835	$p\bar{p} \rightarrow \chi_{c2} \rightarrow J/\psi \gamma$
0 ± 6	1904	ARMSTRONG	93E E760	$p\bar{p} \rightarrow \chi_{c2} \rightarrow J/\psi \gamma$
<sup>1</sup> Correlated with $a_2, b_2,$ and $b_3$ with correlation coefficients $\rho_{a_2 a_3} = 0.733, \rho_{a_3 b_2} = -0.422,$ and $\rho_{a_3 b_3} = -0.024$ .				
<sup>2</sup> From a fit with floating $M_2$ and $E_3$ amplitudes $a_2, b_2,$ and $a_3,$ and $b_3$ .				

WEIGHTED AVERAGE  
-0.3±1.0 (Error scaled by 1.3)



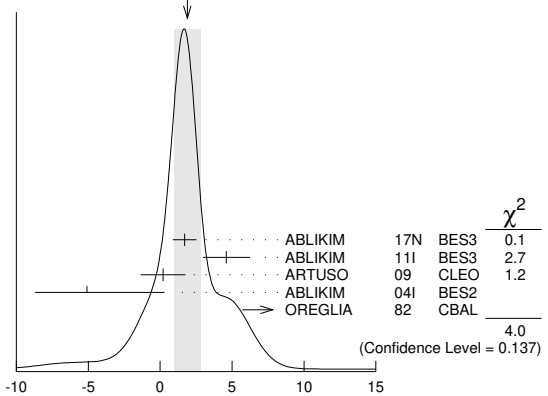
$a_3 = E_3/\sqrt{E_1^2 + M_2^2 + E_3^2}$  Electric octupole fractional transition amplitude (units  $10^{-2}$ )

**MULTIPOLE AMPLITUDES IN  $\psi(2S) \rightarrow \gamma \chi_{c2}(1P)$  RADIATIVE DECAY**

$b_2 = M_2/\sqrt{E_1^2 + M_2^2 + E_3^2}$  Magnetic quadrupole fractional transition amplitude

VALUE (units $10^{-2}$ )	EVTS	DOCUMENT ID	TECN	COMMENT
<b>1.9±0.9 OUR AVERAGE</b>				Error includes scale factor of 1.4. See the ideogram below.
1.7±0.8±0.2	89k	<sup>1</sup> ABLIKIM	17N BES3	$\psi(2S) \rightarrow \gamma \gamma \ell^+ \ell^-$
4.6±1.0±1.3	13.8k	<sup>2</sup> ABLIKIM	11I BES3	$\psi(2S) \rightarrow \gamma \pi^+ \pi^-, \gamma K^+ K^-$
0.2±1.5±0.4	19.8k	<sup>3</sup> ARTUSO	09 CLEO	$\psi(2S) \rightarrow \gamma \gamma \ell^+ \ell^-$
- 5.1 <sup>+5.4</sup> <sub>-3.6</sub>	721	<sup>2</sup> ABLIKIM	04I BES2	$\psi(2S) \rightarrow \gamma \pi^+ \pi^-, \gamma K^+ K^-$
13.2 <sup>+9.8</sup> <sub>-7.5</sub>	441	<sup>4</sup> OREGLIA	82 CBAL	$\psi(2S) \rightarrow \gamma \gamma \ell^+ \ell^-$
• • • We do not use the following data for averages, fits, limits, etc. • • •				
1.0±1.3±0.3	19.8k	<sup>4</sup> ARTUSO	09 CLEO	$\psi(2S) \rightarrow \gamma \gamma \ell^+ \ell^-$
<sup>1</sup> Correlated with $a_2, a_3,$ and $b_3$ with correlation coefficients $\rho_{a_2 b_2} = -0.605, \rho_{a_3 b_2} = -0.422,$ and $\rho_{b_2 b_3} = 0.384$ .				
<sup>2</sup> From a fit with floating $M_2$ and $E_3$ amplitudes $b_2$ and $b_3$ .				
<sup>3</sup> From a fit with floating $M_2$ and $E_3$ amplitudes $a_2, b_2,$ and $a_3,$ and $b_3$ .				
<sup>4</sup> From a fit with floating $M_2$ amplitudes $a_2$ and $b_2,$ and fixed $E_3$ amplitudes $a_3=b_3=0$ .				

WEIGHTED AVERAGE  
1.9±0.9 (Error scaled by 1.4)



$b_2 = M_2/\sqrt{E_1^2 + M_2^2 + E_3^2}$  Magnetic quadrupole fractional transition amplitude (units  $10^{-2}$ )





<55	90	39 ± 11	<sup>18</sup> CHOI	02	BELL	$B \rightarrow K K_S K^- \pi^+$
<8.0	95		<sup>19</sup> EDWARDS	82c	CBAL	$e^+ e^- \rightarrow \gamma X$

<sup>13</sup> From a simultaneous fit to  $K_S^0 K^\pm \pi^\mp$  and  $K^+ K^- \pi^0$  decay modes.  
<sup>14</sup> Ignoring possible interference with continuum.  
<sup>15</sup> Accounts for interference with non-resonant continuum.  
<sup>16</sup> From the fit of the kaon momentum spectrum. Systematic errors not evaluated.  
<sup>17</sup> Superseded by DEL-AMO-SANCHEZ 11M.  
<sup>18</sup> For a mass value of 3654 ± 6 MeV. Superseded by VINOKUROVA 11.  
<sup>19</sup> For a mass value of 3594 ± 5 MeV

$\eta_c(2S)$  DECAY MODES

Mode	Fraction ( $\Gamma_i/\Gamma$ )	Confidence level
$\Gamma_1$ hadrons	not seen	
$\Gamma_2$ $K \bar{K} \pi$	( 1.9 ± 1.2 ) %	
$\Gamma_3$ $K \bar{K} \eta$	( 5 ± 4 ) × 10 <sup>-3</sup>	
$\Gamma_4$ $2\pi^+ 2\pi^-$	not seen	
$\Gamma_5$ $\rho^0 \rho^0$	not seen	
$\Gamma_6$ $3\pi^+ 3\pi^-$	not seen	
$\Gamma_7$ $K^+ K^- \pi^+ \pi^-$	not seen	
$\Gamma_8$ $K^{*0} \bar{K}^{*0}$	not seen	
$\Gamma_9$ $K^+ K^- \pi^+ \pi^- \pi^0$	( 1.4 ± 1.0 ) %	
$\Gamma_{10}$ $K^+ K^- 2\pi^+ 2\pi^-$	not seen	
$\Gamma_{11}$ $K_S^0 K^- 2\pi^+ \pi^- + c.c.$	seen	
$\Gamma_{12}$ $2K^+ 2K^-$	not seen	
$\Gamma_{13}$ $\phi\phi$	not seen	
$\Gamma_{14}$ $p\bar{p}$	seen	
$\Gamma_{15}$ $p\bar{p} \pi^+ \pi^-$	seen	
$\Gamma_{16}$ $\gamma\gamma$	( 1.9 ± 1.3 ) × 10 <sup>-4</sup>	
$\Gamma_{17}$ $\gamma J/\psi(1S)$	< 1.4 %	90%
$\Gamma_{18}$ $\pi^+ \pi^- \eta$	not seen	
$\Gamma_{19}$ $\pi^+ \pi^- \eta'$	not seen	
$\Gamma_{20}$ $\pi^+ \pi^- \eta_c(1S)$	< 25 %	90%

$\eta_c(2S)$  PARTIAL WIDTHS

$\Gamma(\gamma\gamma)$	VALUE (keV)	EVTS	DOCUMENT ID	TECN	COMMENT	$\Gamma_{16}$
	0.44 ± 0.14	106	20 XU	18	BELL $e^+ e^- \rightarrow e^+ e^- \eta' / \pi^+ \pi^-$	
	1.3 ± 0.6		21 ASNER	04	CLEO $\gamma\gamma \rightarrow \eta_c \rightarrow K_S^0 K^\pm \pi^\mp$	

<sup>20</sup> Assuming that the branching fraction into  $\eta' \pi^+ \pi^-$  is the same as for  $\eta_c(1S)$ .  
<sup>21</sup> They measure  $\Gamma(\eta_c(2S) \gamma\gamma) B(\eta_c(2S) \rightarrow K \bar{K} \pi) = (0.18 \pm 0.05 \pm 0.02) \Gamma(\eta_c(1S) \gamma\gamma) B(\eta_c(1S) \rightarrow K \bar{K} \pi)$ . The value for  $\Gamma(\eta_c(2S) \rightarrow \gamma\gamma)$  is derived assuming that the branching fractions for  $\eta_c(2S)$  and  $\eta_c(1S)$  decays to  $K_S K \pi$  are equal and using  $\Gamma(\eta_c(1S) \rightarrow \gamma\gamma) = 7.4 \pm 0.4 \pm 2.3$  keV.

$\Gamma(\gamma\gamma) \times \Gamma(\pi^+ \pi^- \eta')/\Gamma_{total}$	VALUE (eV)	EVTS	DOCUMENT ID	TECN	COMMENT	$\Gamma_{16} \Gamma_{19}/\Gamma$
	5.6 <sup>+1.2</sup> ± 1.1 <sup>-1.1</sup>	106	XU	18	BELL $e^+ e^- \rightarrow e^+ e^- \eta' / \pi^+ \pi^-$	

$\eta_c(2S)$   $\Gamma(i)\Gamma(\gamma\gamma)/\Gamma(total)$

$\Gamma(2\pi^+ 2\pi^-) \times \Gamma(\gamma\gamma)/\Gamma_{total}$	VALUE (eV)	CL%	DOCUMENT ID	TECN	COMMENT	$\Gamma_4 \Gamma_{16}/\Gamma$
	<6.5	90	UEHARA	08	BELL $\gamma\gamma \rightarrow \eta_c(2S) \rightarrow 2(\pi^+ \pi^-)$	

$\Gamma(K \bar{K} \pi) \times \Gamma(\gamma\gamma)/\Gamma_{total}$	VALUE (eV)	EVTS	DOCUMENT ID	TECN	COMMENT	$\Gamma_2 \Gamma_{16}/\Gamma$
	41 ± 4 ± 6	624	22 DEL-AMO-SA..11M	BABR	$\gamma\gamma \rightarrow K_S^0 K^\pm \pi^\mp$	

<sup>22</sup> Not independent from other measurements reported in DEL-AMO-SANCHEZ 11M.

$\Gamma(K^+ K^- \pi^+ \pi^-) \times \Gamma(\gamma\gamma)/\Gamma_{total}$	VALUE (eV)	CL%	DOCUMENT ID	TECN	COMMENT	$\Gamma_7 \Gamma_{16}/\Gamma$
	<5.0	90	UEHARA	08	BELL $\gamma\gamma \rightarrow \eta_c(2S) \rightarrow K^+ K^- \pi^+ \pi^-$	

$\Gamma(K^+ K^- \pi^+ \pi^- \pi^0) \times \Gamma(\gamma\gamma)/\Gamma_{total}$	VALUE (eV)	EVTS	DOCUMENT ID	TECN	COMMENT	$\Gamma_9 \Gamma_{16}/\Gamma$
	30 ± 6 ± 5	1201	23 DEL-AMO-SA..11M	BABR	$\gamma\gamma \rightarrow K^+ K^- \pi^+ \pi^- \pi^0$	

<sup>23</sup> Not independent from other measurements reported in DEL-AMO-SANCHEZ 11M.

$\Gamma(2K^+ 2K^-) \times \Gamma(\gamma\gamma)/\Gamma_{total}$	VALUE (eV)	CL%	DOCUMENT ID	TECN	COMMENT	$\Gamma_{12} \Gamma_{16}/\Gamma$
	<2.9	90	UEHARA	08	BELL $\gamma\gamma \rightarrow \eta_c(2S) \rightarrow 2(K^+ K^-)$	

$\Gamma(\pi^+ \pi^- \eta_c(1S)) \times \Gamma(\gamma\gamma)/\Gamma_{total}$	VALUE (eV)	CL%	DOCUMENT ID	TECN	COMMENT	$\Gamma_{20} \Gamma_{16}/\Gamma$
	<133	90	LEES	12AE	BABR $e^+ e^- \rightarrow e^+ e^- \pi^+ \pi^- \eta_c$	

$\eta_c(2S)$   $\Gamma(i)\Gamma(\gamma\gamma)/\Gamma^2(total)$

$\Gamma(p\bar{p})/\Gamma_{total} \times \Gamma(\gamma\gamma)/\Gamma_{total}$	VALUE (units 10 <sup>-8</sup> )	CL%	DOCUMENT ID	TECN	COMMENT	$\Gamma_{14}/\Gamma \times \Gamma_{16}/\Gamma$
	< 5.6	90 <sup>24,25,26</sup>	AMBROGIANI 01	E835	$p\bar{p} \rightarrow \gamma\gamma$	
• • • We do not use the following data for averages, fits, limits, etc. • • •						
	< 8.0	90 <sup>24,25,27</sup>	AMBROGIANI 01	E835	$p\bar{p} \rightarrow \gamma\gamma$	
	<12.0	90	25,27	AMBROGIANI 01	E835	$p\bar{p} \rightarrow \gamma\gamma$

<sup>24</sup> Including the measurements of ARMSTRONG 95F in the AMBROGIANI 01 analysis.  
<sup>25</sup> For a total width  $\Gamma=5$  MeV.  
<sup>26</sup> For the resonance mass region 3589–3599 MeV/c<sup>2</sup>.  
<sup>27</sup> For the resonance mass region 3575–3660 MeV/c<sup>2</sup>.

$\eta_c(2S)$  BRANCHING RATIOS

$\Gamma(hadrons)/\Gamma_{total}$	VALUE	DOCUMENT ID	TECN	COMMENT	$\Gamma_1/\Gamma$
	not seen	ABREU	980	DLPH $e^+ e^- \rightarrow e^+ e^- + hadrons$	
• • • We do not use the following data for averages, fits, limits, etc. • • •					
	seen	28	EDWARDS	82c	CBAL $e^+ e^- \rightarrow \gamma X$

<sup>28</sup> For a mass value of 3594 ± 5 MeV

$\Gamma(K \bar{K} \pi)/\Gamma_{total}$	VALUE (units 10 <sup>-2</sup> )	EVTS	DOCUMENT ID	TECN	COMMENT	$\Gamma_2/\Gamma$
	1.9 ± 0.4 ± 1.1	59 ± 12	29	AUBERT	08AB	BABR $B \rightarrow \eta_c(2S) K \rightarrow K \bar{K} \pi$
• • • We do not use the following data for averages, fits, limits, etc. • • •						
	seen	127 ± 18	ABLIKIM	13k	BES3 $\psi(2S) \rightarrow \gamma K \bar{K} \pi$	
	seen	39 ± 11	30	CHOI	02	BELL $B \rightarrow K K_S K^- \pi^+$

<sup>29</sup> Derived from a measurement of  $[B(B^+ \rightarrow \eta_c(2S) K^+) \times B(\eta_c(2S) \rightarrow K \bar{K} \pi)] / [B(B^+ \rightarrow \eta_c K^+) \times B(\eta_c \rightarrow K \bar{K} \pi)] = (9.6^{+2.0}_{-1.9} \pm 2.5)\%$  and using  $B(B^+ \rightarrow \eta_c(2S) K^+) = (3.4 \pm 1.8) \times 10^{-4}$ , and  $[B(B^+ \rightarrow \eta_c K^+) \times B(\eta_c \rightarrow K \bar{K} \pi)] = (6.88 \pm 0.77^{+0.55}_{-0.66}) \times 10^{-5}$ .  
<sup>30</sup> For a mass value of 3654 ± 6 MeV

$\Gamma(K \bar{K} \eta)/\Gamma(K \bar{K} \pi)$	VALUE (units 10 <sup>-2</sup> )	EVTS	DOCUMENT ID	TECN	COMMENT	$\Gamma_3/\Gamma_2$
	27.3 ± 7.0 ± 9.0	225	31	LEES	14E	BABR $\gamma\gamma \rightarrow K^+ K^- \gamma\gamma$

<sup>31</sup> LEES 14E reports  $B(\eta_c(2S) \rightarrow K^+ K^- \eta)/B(\eta_c(2S) \rightarrow K^+ K^- \pi^0) = 0.82 \pm 0.21 \pm 0.27$ , which we divide by 3 to account for isospin symmetry.

$\Gamma(2\pi^+ 2\pi^-)/\Gamma_{total}$	VALUE	DOCUMENT ID	TECN	COMMENT	$\Gamma_4/\Gamma$
	not seen	UEHARA	08	BELL $\gamma\gamma \rightarrow \eta_c(2S)$	

$\Gamma(\rho^0 \rho^0)/\Gamma_{total}$	VALUE	DOCUMENT ID	TECN	COMMENT	$\Gamma_5/\Gamma$
	not seen	ABLIKIM	11H	BES3 $\psi(2S) \rightarrow \gamma 2\pi^+ 2\pi^-$	

$\Gamma(K^+ K^- \pi^+ \pi^-)/\Gamma_{total}$	VALUE	DOCUMENT ID	TECN	COMMENT	$\Gamma_7/\Gamma$
	not seen	UEHARA	08	BELL $\gamma\gamma \rightarrow \eta_c(2S)$	

$\Gamma(K^+ K^- \pi^+ \pi^- \pi^0)/\Gamma(K \bar{K} \pi)$	VALUE	EVTS	DOCUMENT ID	TECN	COMMENT	$\Gamma_9/\Gamma_2$
	0.73 ± 0.17 ± 0.17	1201	32	DEL-AMO-SA..11M	BABR $\gamma\gamma \rightarrow K^+ K^- \pi^+ \pi^- \pi^0$	

<sup>32</sup> We have multiplied the value of  $\Gamma(K^+ K^- \pi^+ \pi^- \pi^0)/\Gamma(K_S^0 K^\pm \pi^\mp)$  reported in DEL-AMO-SANCHEZ 11M by a factor 1/3 to obtain  $\Gamma(K^+ K^- \pi^+ \pi^- \pi^0)/\Gamma(K \bar{K} \pi)$ . Not independent from other measurements reported in DEL-AMO-SANCHEZ 11M.

$\Gamma(K^{*0} \bar{K}^{*0})/\Gamma_{total}$	VALUE	DOCUMENT ID	TECN	COMMENT	$\Gamma_8/\Gamma$
	not seen	ABLIKIM	11H	BES3 $\psi(2S) \rightarrow \gamma K^+ K^- \pi^+ \pi^-$	

$\Gamma(K_S^0 K^- 2\pi^+ \pi^- + c.c.)/\Gamma_{total}$	VALUE	EVTS	DOCUMENT ID	TECN	COMMENT	$\Gamma_{11}/\Gamma$
	seen	57 ± 17	ABLIKIM	13k	BES3 $\psi(2S) \rightarrow \gamma K_S^0 K^\pm \pi^\mp \pi^\pm \pi^-$	

$\Gamma(2K^+ 2K^-)/\Gamma_{total}$	VALUE	DOCUMENT ID	TECN	COMMENT	$\Gamma_{12}/\Gamma$
	not seen	UEHARA	08	BELL $\gamma\gamma \rightarrow \eta_c(2S)$	

$\Gamma(\phi\phi)/\Gamma_{total}$	VALUE	DOCUMENT ID	TECN	COMMENT	$\Gamma_{13}/\Gamma$
	not seen	ABLIKIM	11H	BES3 $\psi(2S) \rightarrow \gamma K^+ K^- K^+ K^-$	

# Meson Particle Listings

## $\eta_c(2S)$

$\Gamma(p\bar{p})/\Gamma_{total}$					$\Gamma_{14}/\Gamma$
VALUE	CL%	DOCUMENT ID	TECN	COMMENT	
seen	106	33 AAIJ	17AD LHCB	$p\bar{p} \rightarrow B^+ X \rightarrow p\bar{p}K^+ X$	
33 AAIJ 17AD report a 6.4 standard deviation signal, with $B(B^+ \rightarrow \eta_c(2S)K^+ \rightarrow p\bar{p}K^+)/B(B^+ \rightarrow J/\psi K^+ \rightarrow p\bar{p}K^+) = (1.58 \pm 0.33 \pm 0.09) \times 10^{-2}$ .					

$\Gamma(p\bar{p}\pi^+\pi^-)/\Gamma_{total}$					$\Gamma_{15}/\Gamma$
VALUE	CL%	DOCUMENT ID	TECN	COMMENT	
seen	110	34 CHILIKIN	19 BELL	$e^+e^- \rightarrow \Upsilon(4S)$	
34 CHILIKIN 19 reports signals in $B^+ \rightarrow \eta_c(2S)K^+$ and $B^0 \rightarrow \eta_c(2S)K_S^0$ with 12.3 and 5.9 standard deviations, respectively.					

$\Gamma(\gamma\gamma)/\Gamma_{total}$					$\Gamma_{16}/\Gamma$
VALUE	CL%	DOCUMENT ID	TECN	COMMENT	
• • • We do not use the following data for averages, fits, limits, etc. • • •					
$<4 \times 10^{-4}$	90	35 WICHT	08 BELL	$B^\pm \rightarrow K^\pm \gamma\gamma$	
not seen			AMBROGIANI 01	$\bar{p}p \rightarrow \gamma\gamma$	
$<0.01$	90	LEE	85 CBAL	$\psi' \rightarrow$ photons	
35 WICHT 08 reports $[\Gamma(\eta_c(2S) \rightarrow \gamma\gamma)/\Gamma_{total}] \times [B(B^+ \rightarrow \eta_c(2S)K^+)] < 0.18 \times 10^{-6}$ which we divide by our best value $B(B^+ \rightarrow \eta_c(2S)K^+) = 4.4 \times 10^{-4}$ .					

$\Gamma(\pi^+\pi^-\eta_c(1S))/\Gamma(K\bar{K}\pi)$					$\Gamma_{20}/\Gamma_2$
VALUE	CL%	DOCUMENT ID	TECN	COMMENT	
$<3.33$	90	36 LEES	12AE BABR	$e^+e^- \rightarrow e^+e^-\pi^+\pi^-\eta_c$	
36 We divided the reported limit by 3 to take into account isospin relations.					

### $\eta_c(2S)$ CROSS-PARTICLE BRANCHING RATIOS

$\Gamma(\eta_c(2S) \rightarrow K\bar{K}\eta)/\Gamma_{total} \times \Gamma(\psi(2S) \rightarrow \gamma\eta_c(2S))/\Gamma_{total}$					$\Gamma_3/\Gamma \times \Gamma_{157}^{\psi(2S)}/\Gamma_{\psi(2S)}$
VALUE	CL%	DOCUMENT ID	TECN	COMMENT	
• • • We do not use the following data for averages, fits, limits, etc. • • •					
$<11.8 \times 10^{-6}$	90	37 CRONIN-HEN..10	CLEO	$\psi(2S) \rightarrow \gamma K^+ K^- \eta$	
37 CRONIN-HENNESSY 10 reports a limit of $< 5.9 \times 10^{-6}$ for the decay $\eta_c(2S) \rightarrow K^+ K^- \eta$ which we multiply by 2 account for isospin symmetry. It assumes $\Gamma(\eta_c(2S)) = 14$ MeV. It also gives the analytic dependence of limits on width.					

$\Gamma(\eta_c(2S) \rightarrow 2\pi^+ 2\pi^-)/\Gamma_{total} \times \Gamma(\psi(2S) \rightarrow \gamma\eta_c(2S))/\Gamma_{total}$					$\Gamma_4/\Gamma \times \Gamma_{157}^{\psi(2S)}/\Gamma_{\psi(2S)}$
VALUE	CL%	DOCUMENT ID	TECN	COMMENT	
$<14.6 \times 10^{-6}$	90	38 CRONIN-HEN..10	CLEO	$\psi(2S) \rightarrow \gamma 2\pi^+ 2\pi^-$	
38 Assuming $\Gamma(\eta_c(2S)) = 14$ MeV. CRONIN-HENNESSY 10 gives the analytic dependence of limits on width.					

$\Gamma(\eta_c(2S) \rightarrow \rho^0 \rho^0)/\Gamma_{total} \times \Gamma(\psi(2S) \rightarrow \gamma\eta_c(2S))/\Gamma_{total}$					$\Gamma_5/\Gamma \times \Gamma_{157}^{\psi(2S)}/\Gamma_{\psi(2S)}$
VALUE	CL%	DOCUMENT ID	TECN	COMMENT	
$<12.7 \times 10^{-7}$	90	ABLIKIM	11H BES3	$\psi(2S) \rightarrow \gamma 2\pi^+ 2\pi^-$	

$\Gamma(\eta_c(2S) \rightarrow 3\pi^+ 3\pi^-)/\Gamma_{total} \times \Gamma(\psi(2S) \rightarrow \gamma\eta_c(2S))/\Gamma_{total}$					$\Gamma_6/\Gamma \times \Gamma_{157}^{\psi(2S)}/\Gamma_{\psi(2S)}$
VALUE	CL%	DOCUMENT ID	TECN	COMMENT	
$<13.2 \times 10^{-6}$	90	39 CRONIN-HEN..10	CLEO	$\psi(2S) \rightarrow \gamma 3\pi^+ 3\pi^-$	
39 Assuming $\Gamma(\eta_c(2S)) = 14$ MeV. CRONIN-HENNESSY 10 gives the analytic dependence of limits on width.					

$\Gamma(\eta_c(2S) \rightarrow K^+ K^- \pi^+ \pi^-)/\Gamma_{total} \times \Gamma(\psi(2S) \rightarrow \gamma\eta_c(2S))/\Gamma_{total}$					$\Gamma_7/\Gamma \times \Gamma_{157}^{\psi(2S)}/\Gamma_{\psi(2S)}$
VALUE	CL%	DOCUMENT ID	TECN	COMMENT	
$<9.6 \times 10^{-6}$	90	40 CRONIN-HEN..10	CLEO	$\psi(2S) \rightarrow \gamma K^+ K^- \pi^+ \pi^-$	
40 Assuming $\Gamma(\eta_c(2S)) = 14$ MeV. CRONIN-HENNESSY 10 gives the analytic dependence of limits on width.					

$\Gamma(\eta_c(2S) \rightarrow K^{*0} \bar{K}^{*0})/\Gamma_{total} \times \Gamma(\psi(2S) \rightarrow \gamma\eta_c(2S))/\Gamma_{total}$					$\Gamma_8/\Gamma \times \Gamma_{157}^{\psi(2S)}/\Gamma_{\psi(2S)}$
VALUE	CL%	DOCUMENT ID	TECN	COMMENT	
$<19.6 \times 10^{-7}$	90	ABLIKIM	11H BES3	$\psi(2S) \rightarrow \gamma K^+ K^- \pi^+ \pi^-$	

$\Gamma(\eta_c(2S) \rightarrow K^+ K^- \pi^+ \pi^- \pi^0)/\Gamma_{total} \times \Gamma(\psi(2S) \rightarrow \gamma\eta_c(2S))/\Gamma_{total}$					$\Gamma_9/\Gamma \times \Gamma_{157}^{\psi(2S)}/\Gamma_{\psi(2S)}$
VALUE	CL%	DOCUMENT ID	TECN	COMMENT	
$<43.0 \times 10^{-6}$	90	41 CRONIN-HEN..10	CLEO	$\psi(2S) \rightarrow \gamma K^+ K^- \pi^+ \pi^- \pi^0$	

41 Assuming  $\Gamma(\eta_c(2S)) = 14$  MeV. CRONIN-HENNESSY 10 gives the analytic dependence of limits on width.

$\Gamma(\eta_c(2S) \rightarrow K^+ K^- 2\pi^+ 2\pi^-)/\Gamma_{total} \times \Gamma(\psi(2S) \rightarrow \gamma\eta_c(2S))/\Gamma_{total}$					$\Gamma_{10}/\Gamma \times \Gamma_{157}^{\psi(2S)}/\Gamma_{\psi(2S)}$
VALUE	CL%	DOCUMENT ID	TECN	COMMENT	
$<9.7 \times 10^{-6}$	90	42 CRONIN-HEN..10	CLEO	$\psi(2S) \rightarrow \gamma K^+ K^- 2\pi^+ 2\pi^-$	
42 Assuming $\Gamma(\eta_c(2S)) = 14$ MeV. CRONIN-HENNESSY 10 gives the analytic dependence of limits on width.					

$\Gamma(\eta_c(2S) \rightarrow K_S^0 K^- 2\pi^+ \pi^- + c.c.)/\Gamma_{total} \times \Gamma(\psi(2S) \rightarrow \gamma\eta_c(2S))/\Gamma_{total}$					$\Gamma_{11}/\Gamma \times \Gamma_{157}^{\psi(2S)}/\Gamma_{\psi(2S)}$
VALUE (units $10^{-6}$ )	CL%	DOCUMENT ID	TECN	COMMENT	
$7.03 \pm 2.10 \pm 0.7$	60	ABLIKIM	13k BES3	$\psi(2S) \rightarrow \gamma K_S^0 K^- 2\pi^+ \pi^- + c.c.$	

• • • We do not use the following data for averages, fits, limits, etc. • • •  
 $< 15.2$  90 43 CRONIN-HEN..10 CLEO  $\psi(2S) \rightarrow \gamma K_S^0 K^- 2\pi^+ \pi^- + c.c.$   
43 Assuming  $\Gamma(\eta_c(2S)) = 14$  MeV. CRONIN-HENNESSY 10 gives the analytic dependence of limits on width.

$\Gamma(\eta_c(2S) \rightarrow \phi\phi)/\Gamma_{total} \times \Gamma(\psi(2S) \rightarrow \gamma\eta_c(2S))/\Gamma_{total}$					$\Gamma_{13}/\Gamma \times \Gamma_{157}^{\psi(2S)}/\Gamma_{\psi(2S)}$
VALUE	CL%	DOCUMENT ID	TECN	COMMENT	
$<7.8 \times 10^{-7}$	90	ABLIKIM	11H BES3	$\psi(2S) \rightarrow \gamma K^+ K^- K^+ K^-$	

$\Gamma(\eta_c(2S) \rightarrow \rho\bar{\rho})/\Gamma_{total} \times \Gamma(\psi(2S) \rightarrow \gamma\eta_c(2S))/\Gamma_{total}$					$\Gamma_{14}/\Gamma \times \Gamma_{157}^{\psi(2S)}/\Gamma_{\psi(2S)}$
VALUE	CL%	DOCUMENT ID	TECN	COMMENT	
$<1.4 \times 10^{-6}$	90	ABLIKIM	13v BES3	$\psi(2S) \rightarrow \gamma \rho\bar{\rho}$	

$\Gamma(\eta_c(2S) \rightarrow \gamma J/\psi(1S))/\Gamma_{total} \times \Gamma(\psi(2S) \rightarrow \gamma\eta_c(2S))/\Gamma_{total}$					$\Gamma_{17}/\Gamma \times \Gamma_{157}^{\psi(2S)}/\Gamma_{\psi(2S)}$
VALUE	CL%	DOCUMENT ID	TECN	COMMENT	
$<9.7 \times 10^{-6}$	90	33	44 ABLIKIM	17N BES3 $\psi(2S) \rightarrow \gamma\gamma J/\psi$	
44 Uses $B(J/\psi \rightarrow e^+e^-) = (5.971 \pm 0.032)\%$ and $B(J/\psi \rightarrow \mu^+\mu^-) = (5.961 \pm 0.033)\%$ .					

$\Gamma(\eta_c(2S) \rightarrow \pi^+ \pi^- \eta)/\Gamma_{total} \times \Gamma(\psi(2S) \rightarrow \gamma\eta_c(2S))/\Gamma_{total}$					$\Gamma_{18}/\Gamma \times \Gamma_{157}^{\psi(2S)}/\Gamma_{\psi(2S)}$
VALUE	CL%	DOCUMENT ID	TECN	COMMENT	
$<4.3 \times 10^{-6}$	90	45 CRONIN-HEN..10	CLEO	$\psi(2S) \rightarrow \gamma \pi^+ \pi^- \eta$	
45 Assuming $\Gamma(\eta_c(2S)) = 14$ MeV. CRONIN-HENNESSY 10 gives the analytic dependence of limits on width.					

$\Gamma(\eta_c(2S) \rightarrow \pi^+ \pi^- \eta')/\Gamma_{total} \times \Gamma(\psi(2S) \rightarrow \gamma\eta_c(2S))/\Gamma_{total}$					$\Gamma_{19}/\Gamma \times \Gamma_{157}^{\psi(2S)}/\Gamma_{\psi(2S)}$
VALUE	CL%	DOCUMENT ID	TECN	COMMENT	
$<14.2 \times 10^{-6}$	90	46 CRONIN-HEN..10	CLEO	$\psi(2S) \rightarrow \gamma \pi^+ \pi^- \eta'$	
46 Assuming $\Gamma(\eta_c(2S)) = 14$ MeV. CRONIN-HENNESSY 10 gives the analytic dependence of limits on width.					

$\Gamma(\eta_c(2S) \rightarrow \pi^+ \pi^- \eta_c(1S))/\Gamma_{total} \times \Gamma(\psi(2S) \rightarrow \gamma\eta_c(2S))/\Gamma_{total}$					$\Gamma_{20}/\Gamma \times \Gamma_{157}^{\psi(2S)}/\Gamma_{\psi(2S)}$
VALUE	CL%	DOCUMENT ID	TECN	COMMENT	
$<1.7 \times 10^{-4}$	90	47 CRONIN-HEN..10	CLEO	$\psi(2S) \rightarrow \gamma \pi^+ \pi^- \eta_c(1S)$	
47 Assuming $\Gamma(\eta_c(2S)) = 14$ MeV. CRONIN-HENNESSY 10 gives the analytic dependence of limits on width.					

### $\eta_c(2S)$ REFERENCES

CHILIKIN	19	PR D100 012001	K. Chilikin et al.	(BELLE Collab.)
XU	18	PR D98 072001	Q.N. Xu et al.	(BELLE Collab.)
AAIJ	17AD	PL B769 305	R. Aaij et al.	(LHCb Collab.)
AAIJ	17BB	EPJ C77 609	R. Aaij et al.	(LHCb Collab.)
ABLIKIM	17N	PR D95 072004	M. Ablikim et al.	(BESIII Collab.)
PDC	16	CP C40 100001	C. Patrignani et al.	(PDG Collab.)
LEES	14E	PR D89 112004	J.P. Lees et al.	(BABAR Collab.)
ABLIKIM	13K	PR D87 052005	M. Ablikim et al.	(BESIII Collab.)
ABLIKIM	13V	PR D88 112001	M. Ablikim et al.	(BESIII Collab.)
ABLIKIM	12G	PRL 109 042003	M. Ablikim et al.	(BESIII Collab.)
LEES	12AE	PR D86 092005	J.P. Lees et al.	(BABAR Collab.)
ABLIKIM	11H	PR D84 091102	M. Ablikim et al.	(BESIII Collab.)
DEL-AMO-SA...	11M	PR D84 012004	P. del Amo Sanchez et al.	(BABAR Collab.)
VINOKUROVA	11	PL B706 139	A. Vinokurova et al.	(BELLE Collab.)
CRONIN-HEN..10	10	PR D81 052002	D. Cronin-Hennessey et al.	(CLEO Collab.)
AUBERT	08AB	PR D78 012006	B. Aubert et al.	(BABAR Collab.)
UEHARA	08	EPJ C53 1	S. Uehara et al.	(BELLE Collab.)
WICHT	08	PL B662 323	J. Wicht et al.	(BELLE Collab.)
ABE	07	PRL 98 082001	K. Abe et al.	(BELLE Collab.)
AUBERT	06E	PRL 96 052002	B. Aubert et al.	(BABAR Collab.)
AUBERT	05C	PR D72 031101	B. Aubert et al.	(BABAR Collab.)
ABE	04G	PR D70 071102	K. Abe et al.	(BELLE Collab.)
ASNER	04	PRL 92 142001	D.M. Asner et al.	(BESIII Collab.)
AUBERT	04D	PRL 92 142002	B. Aubert et al.	(BABAR Collab.)
ABE,K	02	PRL 89 142001	K. Abe et al.	(BELLE Collab.)
CHOI	02	PRL 89 102001	S.-K. Choi et al.	(BELLE Collab.)
AMBROGIANI	01	PR D64 052003	M. Ambrogiani et al.	(FNAL E835 Collab.)
ABREU	98O	PL B44 1479	P. Abreu et al.	(DELPHI Collab.)
ARMSTRONG	95F	PR D52 4839	T.A. Armstrong et al.	(FNAL, FERR, GENO+)
LEE	85	SLAC 282	R.A. Lee	(SLAC)
EDWARDS	82C	PRL 48 70	C. Edwards et al.	(CIT, HARV, PRIN+)

$\psi(2S)$

$$I^G(J^{PC}) = 0^-(1^{--})$$

See the Review on " $\psi(2S)$  and  $\chi_c$  branching ratios" before the  $\chi_{c0}(1P)$  Listings.

$\psi(2S)$  MASS

OUR FIT includes measurements of  $m_{\psi(2S)}$ ,  $m_{\psi(3770)}$ , and  $m_{\psi(3770)} - m_{\psi(2S)}$ .

VALUE (MeV)	EVTS	DOCUMENT ID	TECN	COMMENT
<b>3686.10 ± 0.06 OUR FIT</b>				Error includes scale factor of 5.9.
<b>3686.097 ± 0.010 OUR AVERAGE</b>				
3686.099 ± 0.004 ± 0.009		<sup>1</sup> ANASHIN 15	KEDR	$e^+e^- \rightarrow$ hadrons
3686.12 ± 0.06 ± 0.10	4k	AAIJ 12H	LHCB	$pp \rightarrow J/\psi \pi^+ \pi^- X$
3685.95 ± 0.10	413	<sup>2</sup> ARTAMONOV 00	OLYA	$e^+e^- \rightarrow$ hadrons
3685.98 ± 0.09 ± 0.04		<sup>3</sup> ARMSTRONG 93B	E760	$\bar{p}p \rightarrow e^+e^-$
3686.114 ± 0.007 <sup>+0.011</sup> <sub>-0.016</sub>		<sup>4</sup> ANASHIN 12	KEDR	$e^+e^- \rightarrow$ hadrons
3686.111 ± 0.025 ± 0.009		AULCHENKO 03	KEDR	$e^+e^- \rightarrow$ hadrons
3686.00 ± 0.10	413	<sup>5</sup> ZHOLENTZ 80	OLYA	$e^+e^-$

- <sup>1</sup> Supersedes AULCHENKO 03 and ANASHIN 12.
- <sup>2</sup> Reanalysis of ZHOLENTZ 80 using new electron mass (COHEN 87) and radiative corrections (KURAEV 85).
- <sup>3</sup> Mass central value and systematic error recalculated by us according to Eq. (16) in ARMSTRONG 93B, using the value for the  $J/\psi(1S)$  mass from AULCHENKO 03.
- <sup>4</sup> From the scans in 2004 and 2006. ANASHIN 12 reports the value  $3686.114 \pm 0.007 \pm 0.011 \pm 0.002$  MeV, where the third uncertainty is due to assumptions on the interference between the resonance and hadronic continuum. We combined the two systematic uncertainties.
- <sup>5</sup> Superseded by ARTAMONOV 00.

$m_{\psi(2S)} - m_{J/\psi(1S)}$

VALUE (MeV)	DOCUMENT ID	TECN	COMMENT
<b>589.188 ± 0.028 OUR AVERAGE</b>			
589.194 ± 0.027 ± 0.011	<sup>1</sup> AULCHENKO 03	KEDR	$e^+e^- \rightarrow$ hadrons
589.7 ± 1.2	LEMOIGNE 82	GOLI	$185 \pi^- Be \rightarrow \gamma \mu^+ \mu^- A$
589.07 ± 0.13	<sup>1</sup> ZHOLENTZ 80	OLYA	$e^+e^-$
588.7 ± 0.8	LUTH 75	MRK1	
588 ± 1	<sup>2</sup> BAI 98E	BES	$e^+e^-$

- <sup>1</sup> Redundant with data in mass above.
- <sup>2</sup> Systematic errors not evaluated.

$\psi(2S)$  WIDTH

VALUE (keV)	EVTS	DOCUMENT ID	TECN	COMMENT
<b>294 ± 8 OUR FIT</b>				
<b>286 ± 16 OUR AVERAGE</b>				
358 ± 8 ± 4		ABLIIKIM 08B	BES2	$e^+e^- \rightarrow$ hadrons
290 ± 25 ± 4	2.7k	ANDREOTTI 07	E835	$p\bar{p} \rightarrow e^+e^-, J/\psi X$
331 ± 5 ± 2		ABLIIKIM 06L	BES2	$e^+e^- \rightarrow$ hadrons
264 ± 27		<sup>1</sup> BAI 02B	BES2	$e^+e^-$
287 ± 37 ± 16		<sup>2</sup> ARMSTRONG 93B	E760	$\bar{p}p \rightarrow e^+e^-$

- <sup>1</sup> From a simultaneous fit to the hadronic and  $\mu^+ \mu^-$  cross section, assuming  $\Gamma = \Gamma_h + \Gamma_e + \Gamma_\mu + \Gamma_\tau$  and lepton universality. Does not include vacuum polarization correction.
- <sup>2</sup> The initial-state radiation correction reevaluated by ANDREOTTI 07 in its Ref. [4].

$\psi(2S)$  DECAY MODES

Mode	Fraction ( $\Gamma_i/\Gamma$ )	Scale factor/ Confidence level
$\Gamma_1$ hadrons	(97.85 ± 0.13) %	
$\Gamma_2$ virtual $\gamma \rightarrow$ hadrons	(1.73 ± 0.14) %	S=1.5
$\Gamma_3$ $ggg$	(10.6 ± 1.6) %	
$\Gamma_4$ $\gamma gg$	(1.03 ± 0.29) %	
$\Gamma_5$ light hadrons	(15.4 ± 1.5) %	
$\Gamma_6$ $e^+e^-$	(7.93 ± 0.17) × 10 <sup>-3</sup>	
$\Gamma_7$ $\mu^+ \mu^-$	(8.0 ± 0.6) × 10 <sup>-3</sup>	
$\Gamma_8$ $\tau^+ \tau^-$	(3.1 ± 0.4) × 10 <sup>-3</sup>	

Decays into  $J/\psi(1S)$  and anything

$\Gamma_9$ $J/\psi(1S)$ anything	(61.4 ± 0.6) %
$\Gamma_{10}$ $J/\psi(1S)$ neutrals	(25.38 ± 0.32) %
$\Gamma_{11}$ $J/\psi(1S) \pi^+ \pi^-$	(34.68 ± 0.30) %
$\Gamma_{12}$ $J/\psi(1S) \pi^0 \pi^0$	(18.24 ± 0.31) %
$\Gamma_{13}$ $J/\psi(1S) \eta$	(3.37 ± 0.05) %
$\Gamma_{14}$ $J/\psi(1S) \pi^0$	(1.268 ± 0.032) × 10 <sup>-3</sup>

Hadronic decays

$\Gamma_{15}$ $\pi^0 h_c(1P)$	(8.6 ± 1.3) × 10 <sup>-4</sup>	
$\Gamma_{16}$ $3(\pi^+ \pi^-) \pi^0$	(3.5 ± 1.6) × 10 <sup>-3</sup>	
$\Gamma_{17}$ $2(\pi^+ \pi^-) \pi^0$	(2.9 ± 1.0) × 10 <sup>-3</sup>	S=4.7
$\Gamma_{18}$ $\rho \partial_2(1320)$	(2.6 ± 0.9) × 10 <sup>-4</sup>	
$\Gamma_{19}$ $\pi^+ \pi^- \pi^0 \pi^0 \pi^0$	(5.3 ± 0.9) × 10 <sup>-3</sup>	
$\Gamma_{20}$ $\rho^\pm \pi^\mp \pi^0 \pi^0$	< 2.7 × 10 <sup>-3</sup>	CL=90%
$\Gamma_{21}$ $p\bar{p}$	(2.94 ± 0.08) × 10 <sup>-4</sup>	
$\Gamma_{22}$ $n\bar{n}$	(3.06 ± 0.15) × 10 <sup>-4</sup>	
$\Gamma_{23}$ $\Delta^{++} \bar{\Delta}^{--}$	(1.28 ± 0.35) × 10 <sup>-4</sup>	
$\Gamma_{24}$ $\Lambda \bar{\Lambda} \pi^0$	< 2.9 × 10 <sup>-6</sup>	CL=90%
$\Gamma_{25}$ $\Lambda \bar{\Lambda} \eta$	(2.5 ± 0.4) × 10 <sup>-5</sup>	
$\Gamma_{26}$ $\Lambda \bar{p} K^+$	(1.00 ± 0.14) × 10 <sup>-4</sup>	
$\Gamma_{27}$ $K^*(892)^+ \bar{p} \Lambda + c.c.$	(6.3 ± 0.7) × 10 <sup>-5</sup>	
$\Gamma_{28}$ $\Lambda \bar{p} K^+ \pi^+ \pi^-$	(1.8 ± 0.4) × 10 <sup>-4</sup>	
$\Gamma_{29}$ $\Lambda \bar{\Lambda} \pi^+ \pi^-$	(2.8 ± 0.6) × 10 <sup>-4</sup>	
$\Gamma_{30}$ $\Lambda \bar{\Lambda}$	(3.81 ± 0.13) × 10 <sup>-4</sup>	S=1.4
$\Gamma_{31}$ $\Lambda \bar{\Sigma}^+ \pi^- + c.c.$	(1.40 ± 0.13) × 10 <sup>-4</sup>	
$\Gamma_{32}$ $\Lambda \bar{\Sigma}^- \pi^+ + c.c.$	(1.54 ± 0.14) × 10 <sup>-4</sup>	
$\Gamma_{33}$ $\Lambda \bar{\Sigma}^0$	(1.23 ± 0.24) × 10 <sup>-5</sup>	
$\Gamma_{34}$ $\Sigma^0 \bar{p} K^+ + c.c.$	(1.67 ± 0.18) × 10 <sup>-5</sup>	
$\Gamma_{35}$ $\Sigma^+ \bar{\Sigma}^-$	(2.32 ± 0.12) × 10 <sup>-4</sup>	
$\Gamma_{36}$ $\Sigma^0 \bar{\Sigma}^0$	(2.35 ± 0.09) × 10 <sup>-4</sup>	S=1.1
$\Gamma_{37}$ $\Sigma(1385)^+ \bar{\Sigma}(1385)^-$	(8.5 ± 0.7) × 10 <sup>-5</sup>	
$\Gamma_{38}$ $\Sigma(1385)^- \bar{\Sigma}(1385)^+$	(8.5 ± 0.8) × 10 <sup>-5</sup>	
$\Gamma_{39}$ $\Sigma(1385)^0 \bar{\Sigma}(1385)^0$	(6.9 ± 0.7) × 10 <sup>-5</sup>	
$\Gamma_{40}$ $\Xi^- \bar{\Xi}^+$	(2.87 ± 0.11) × 10 <sup>-4</sup>	S=1.1
$\Gamma_{41}$ $\Xi^0 \bar{\Xi}^0$	(2.3 ± 0.4) × 10 <sup>-4</sup>	S=4.2
$\Gamma_{42}$ $\Xi(1530)^0 \bar{\Xi}(1530)^0$	(5.2 ± 3.2 <sub>-1.2</sub> ) × 10 <sup>-5</sup>	
$\Gamma_{43}$ $K^- \Lambda \bar{\Xi}^+ + c.c.$	(3.9 ± 0.4) × 10 <sup>-5</sup>	
$\Gamma_{44}$ $\Xi(1530)^- \bar{\Xi}(1530)^+$	(1.15 ± 0.07) × 10 <sup>-4</sup>	
$\Gamma_{45}$ $\Xi(1530)^- \bar{\Xi}^+$	(7.0 ± 1.2) × 10 <sup>-6</sup>	
$\Gamma_{46}$ $\Xi(1690)^- \bar{\Xi}^+ \rightarrow K^- \Lambda \bar{\Xi}^+ + c.c.$	(5.2 ± 1.6) × 10 <sup>-6</sup>	
$\Gamma_{47}$ $\Xi(1820)^- \bar{\Xi}^+ \rightarrow K^- \Lambda \bar{\Xi}^+ + c.c.$	(1.20 ± 0.32) × 10 <sup>-5</sup>	
$\Gamma_{48}$ $K^- \Sigma^0 \bar{\Xi}^+ + c.c.$	(3.7 ± 0.4) × 10 <sup>-5</sup>	
$\Gamma_{49}$ $\Omega^- \bar{\Omega}^+$	(5.2 ± 0.4) × 10 <sup>-5</sup>	
$\Gamma_{50}$ $\pi^0 p\bar{p}$	(1.53 ± 0.07) × 10 <sup>-4</sup>	
$\Gamma_{51}$ $N(940) \bar{p} + c.c. \rightarrow \pi^0 p\bar{p}$	(6.4 ± 1.8 <sub>-1.3</sub> ) × 10 <sup>-5</sup>	
$\Gamma_{52}$ $N(1440) \bar{p} + c.c. \rightarrow \pi^0 p\bar{p}$	(7.3 ± 1.7 <sub>-1.5</sub> ) × 10 <sup>-5</sup>	S=2.5
$\Gamma_{53}$ $N(1520) \bar{p} + c.c. \rightarrow \pi^0 p\bar{p}$	(6.4 ± 2.3 <sub>-1.8</sub> ) × 10 <sup>-6</sup>	
$\Gamma_{54}$ $N(1535) \bar{p} + c.c. \rightarrow \pi^0 p\bar{p}$	(2.5 ± 1.0) × 10 <sup>-5</sup>	
$\Gamma_{55}$ $N(1650) \bar{p} + c.c. \rightarrow \pi^0 p\bar{p}$	(3.8 ± 1.4 <sub>-1.7</sub> ) × 10 <sup>-5</sup>	
$\Gamma_{56}$ $N(1720) \bar{p} + c.c. \rightarrow \pi^0 p\bar{p}$	(1.79 ± 0.26 <sub>-0.70</sub> ) × 10 <sup>-5</sup>	
$\Gamma_{57}$ $N(2300) \bar{p} + c.c. \rightarrow \pi^0 p\bar{p}$	(2.6 ± 1.2 <sub>-0.7</sub> ) × 10 <sup>-5</sup>	
$\Gamma_{58}$ $N(2570) \bar{p} + c.c. \rightarrow \pi^0 p\bar{p}$	(2.13 ± 0.40 <sub>-0.31</sub> ) × 10 <sup>-5</sup>	
$\Gamma_{59}$ $\pi^0 f_0(2100) \rightarrow \pi^0 p\bar{p}$	(1.1 ± 0.4) × 10 <sup>-5</sup>	
$\Gamma_{60}$ $\eta p\bar{p}$	(6.0 ± 0.4) × 10 <sup>-5</sup>	
$\Gamma_{61}$ $\eta f_0(2100) \rightarrow \eta p\bar{p}$	(1.2 ± 0.4) × 10 <sup>-5</sup>	
$\Gamma_{62}$ $N(1535) \bar{p} \rightarrow \eta p\bar{p}$	(4.4 ± 0.7) × 10 <sup>-5</sup>	
$\Gamma_{63}$ $\omega p\bar{p}$	(6.9 ± 2.1) × 10 <sup>-5</sup>	
$\Gamma_{64}$ $\eta' p\bar{p}$	(1.10 ± 0.13) × 10 <sup>-5</sup>	
$\Gamma_{65}$ $\phi p\bar{p}$	(6.1 ± 0.6) × 10 <sup>-6</sup>	
$\Gamma_{66}$ $\phi X(1835) \rightarrow \phi p\bar{p}$	< 1.82 × 10 <sup>-7</sup>	CL=90%
$\Gamma_{67}$ $\pi^+ \pi^- p\bar{p}$	(6.0 ± 0.4) × 10 <sup>-4</sup>	
$\Gamma_{68}$ $p\bar{p} \pi^-$ or c.c.	(2.48 ± 0.17) × 10 <sup>-4</sup>	
$\Gamma_{69}$ $p\bar{p} \pi^- \pi^0$	(3.2 ± 0.7) × 10 <sup>-4</sup>	
$\Gamma_{70}$ $2(\pi^+ \pi^- \pi^0)$	(4.8 ± 1.5) × 10 <sup>-3</sup>	
$\Gamma_{71}$ $\eta \pi^+ \pi^-$	< 1.6 × 10 <sup>-4</sup>	CL=90%
$\Gamma_{72}$ $\eta \pi^+ \pi^- \pi^0$	(9.5 ± 1.7) × 10 <sup>-4</sup>	
$\Gamma_{73}$ $2(\pi^+ \pi^-) \eta$	(1.2 ± 0.6) × 10 <sup>-3</sup>	
$\Gamma_{74}$ $\pi^+ \pi^- \pi^0 \pi^0 \eta$	< 4 × 10 <sup>-4</sup>	CL=90%
$\Gamma_{75}$ $\eta' \pi^+ \pi^- \pi^0$	(4.5 ± 2.1) × 10 <sup>-4</sup>	
$\Gamma_{76}$ $\omega \pi^+ \pi^-$	(7.3 ± 1.2) × 10 <sup>-4</sup>	S=2.1
$\Gamma_{77}$ $b_1^\pm \pi^\mp$	(4.0 ± 0.6) × 10 <sup>-4</sup>	S=1.1
$\Gamma_{78}$ $b_1^0 \pi^0$	(2.4 ± 0.6) × 10 <sup>-4</sup>	
$\Gamma_{79}$ $\omega f_2(1270)$	(2.2 ± 0.4) × 10 <sup>-4</sup>	
$\Gamma_{80}$ $\omega \pi^0 \pi^0$	(1.11 ± 0.35) × 10 <sup>-3</sup>	
$\Gamma_{81}$ $\pi^0 \pi^0 K^+ K^-$	(2.6 ± 1.3) × 10 <sup>-4</sup>	
$\Gamma_{82}$ $\pi^+ \pi^- K^+ K^-$	(7.3 ± 0.5) × 10 <sup>-4</sup>	

## Meson Particle Listings

 $\psi(2S)$ 

$\Gamma_{83}$	$\pi^0 \pi^0 K_S^0 K_L^0$	$(1.3 \pm 0.6) \times 10^{-3}$	
$\Gamma_{84}$	$\rho^0 K^+ K^-$	$(2.2 \pm 0.4) \times 10^{-4}$	
$\Gamma_{85}$	$K^*(892)^0 \bar{K}_2^*(1430)^0$	$(1.9 \pm 0.5) \times 10^{-4}$	
$\Gamma_{86}$	$K^+ K^- \pi^+ \pi^- \eta$	$(1.3 \pm 0.7) \times 10^{-3}$	
$\Gamma_{87}$	$K^+ K^- 2(\pi^+ \pi^-) \pi^0$	$(1.00 \pm 0.31) \times 10^{-3}$	
$\Gamma_{88}$	$K^+ K^- 2(\pi^+ \pi^-)$	$(1.9 \pm 0.9) \times 10^{-3}$	
$\Gamma_{89}$	$K_1(1270)^\pm K^\mp$	$(1.00 \pm 0.28) \times 10^{-3}$	
$\Gamma_{90}$	$K_S^0 K_S^0 \pi^+ \pi^-$	$(2.2 \pm 0.4) \times 10^{-4}$	
$\Gamma_{91}$	$\rho^0 p \bar{p}$	$(5.0 \pm 2.2) \times 10^{-5}$	
$\Gamma_{92}$	$K^+ \bar{K}^*(892)^0 \pi^- + c.c.$	$(6.7 \pm 2.5) \times 10^{-4}$	
$\Gamma_{93}$	$2(\pi^+ \pi^-)$	$(2.4 \pm 0.6) \times 10^{-4}$	S=2.2
$\Gamma_{94}$	$\rho^0 \pi^+ \pi^-$	$(2.2 \pm 0.6) \times 10^{-4}$	S=1.4
$\Gamma_{95}$	$K^+ K^- \pi^+ \pi^- \pi^0$	$(1.26 \pm 0.09) \times 10^{-3}$	
$\Gamma_{96}$	$\omega f_0(1710) \rightarrow \omega K^+ K^-$	$(5.9 \pm 2.2) \times 10^{-5}$	
$\Gamma_{97}$	$K^*(892)^0 K^- \pi^+ \pi^0 + c.c.$	$(8.6 \pm 2.2) \times 10^{-4}$	
$\Gamma_{98}$	$K^*(892)^+ K^- \pi^+ \pi^- + c.c.$	$(9.6 \pm 2.8) \times 10^{-4}$	
$\Gamma_{99}$	$K^*(892)^+ K^- \rho^0 + c.c.$	$(7.3 \pm 2.6) \times 10^{-4}$	
$\Gamma_{100}$	$K^*(892)^0 K^- \rho^+ + c.c.$	$(6.1 \pm 1.8) \times 10^{-4}$	
$\Gamma_{101}$	$\eta K^+ K^-$ , no $\eta \phi$	$(3.1 \pm 0.4) \times 10^{-5}$	
$\Gamma_{102}$	$\omega K^+ K^-$	$(1.62 \pm 0.11) \times 10^{-4}$	S=1.1
$\Gamma_{103}$	$\omega K^*(892)^+ K^- + c.c.$	$(2.07 \pm 0.26) \times 10^{-4}$	
$\Gamma_{104}$	$\omega K_2^*(1430)^+ K^- + c.c.$	$(6.1 \pm 1.2) \times 10^{-5}$	
$\Gamma_{105}$	$\omega \bar{K}^*(892)^0 K^0$	$(1.68 \pm 0.30) \times 10^{-4}$	
$\Gamma_{106}$	$\omega \bar{K}_2^*(1430)^0 K^0$	$(5.8 \pm 2.2) \times 10^{-5}$	
$\Gamma_{107}$	$\omega X(1440) \rightarrow \omega K_S^0 K^- \pi^+ + c.c.$	$(1.6 \pm 0.4) \times 10^{-5}$	
$\Gamma_{108}$	$\omega X(1440) \rightarrow \omega K^+ K^- \pi^0$	$(1.09 \pm 0.26) \times 10^{-5}$	
$\Gamma_{109}$	$\omega f_1(1285) \rightarrow \omega K_S^0 K^- \pi^+ + c.c.$	$(3.0 \pm 1.0) \times 10^{-6}$	
$\Gamma_{110}$	$\omega f_1(1285) \rightarrow \omega K^+ K^- \pi^0$	$(1.2 \pm 0.7) \times 10^{-6}$	
$\Gamma_{111}$	$3(\pi^+ \pi^-)$	$(3.5 \pm 2.0) \times 10^{-4}$	S=2.8
$\Gamma_{112}$	$p \bar{p} \pi^+ \pi^- \pi^0$	$(7.3 \pm 0.7) \times 10^{-4}$	
$\Gamma_{113}$	$K^+ K^-$	$(7.5 \pm 0.5) \times 10^{-5}$	
$\Gamma_{114}$	$K_S^0 K_L^0$	$(5.34 \pm 0.33) \times 10^{-5}$	
$\Gamma_{115}$	$\pi^+ \pi^- \pi^0$	$(2.01 \pm 0.17) \times 10^{-4}$	S=1.7
$\Gamma_{116}$	$\rho(2150) \pi \rightarrow \pi^+ \pi^- \pi^0$	$(1.9 \pm 1.2) \times 10^{-4}$	
$\Gamma_{117}$	$\rho(770) \pi \rightarrow \pi^+ \pi^- \pi^0$	$(3.2 \pm 1.2) \times 10^{-5}$	S=1.8
$\Gamma_{118}$	$\pi^+ \pi^-$	$(7.8 \pm 2.6) \times 10^{-6}$	
$\Gamma_{119}$	$K_1(1400)^\pm K^\mp$	$< 3.1 \times 10^{-4}$	CL=90%
$\Gamma_{120}$	$K_2^*(1430)^\pm K^\mp$	$(7.1 \pm 0.9) \times 10^{-5}$	
$\Gamma_{121}$	$K^+ K^- \pi^0$	$(4.07 \pm 0.31) \times 10^{-5}$	
$\Gamma_{122}$	$K_S^0 K_L^0 \pi^0$	$< 3.0 \times 10^{-4}$	CL=90%
$\Gamma_{123}$	$K_S^0 K_L^0 \eta$	$(1.3 \pm 0.5) \times 10^{-3}$	
$\Gamma_{124}$	$K^+ K^*(892)^- + c.c.$	$(2.9 \pm 0.4) \times 10^{-5}$	S=1.2
$\Gamma_{125}$	$K^*(892)^0 \bar{K}^0 + c.c.$	$(1.09 \pm 0.20) \times 10^{-4}$	
$\Gamma_{126}$	$\phi \pi^+ \pi^-$	$(1.18 \pm 0.26) \times 10^{-4}$	S=1.5
$\Gamma_{127}$	$\phi f_0(980) \rightarrow \pi^+ \pi^-$	$(7.5 \pm 3.3) \times 10^{-5}$	S=1.6
$\Gamma_{128}$	$2(K^+ K^-)$	$(6.3 \pm 1.3) \times 10^{-5}$	
$\Gamma_{129}$	$\phi K^+ K^-$	$(7.0 \pm 1.6) \times 10^{-5}$	
$\Gamma_{130}$	$2(K^+ K^-) \pi^0$	$(1.10 \pm 0.28) \times 10^{-4}$	
$\Gamma_{131}$	$\phi \eta$	$(3.10 \pm 0.31) \times 10^{-5}$	
$\Gamma_{132}$	$\eta \phi(2170)$ , $\phi(2170) \rightarrow \phi f_0(980)$ , $f_0 \rightarrow \pi^+ \pi^-$	$< 2.2 \times 10^{-6}$	CL=90%
$\Gamma_{133}$	$\phi \eta'$	$(1.54 \pm 0.20) \times 10^{-5}$	
$\Gamma_{134}$	$\phi f_1(1285)$	$(3.0 \pm 1.3) \times 10^{-5}$	
$\Gamma_{135}$	$\phi \eta(1405) \rightarrow \phi \pi^+ \pi^- \eta$	$(8.5 \pm 1.7) \times 10^{-6}$	
$\Gamma_{136}$	$\omega \eta'$	$(3.2 \pm 2.5) \times 10^{-5}$	
$\Gamma_{137}$	$\omega \pi^0$	$(2.1 \pm 0.6) \times 10^{-5}$	
$\Gamma_{138}$	$\rho \eta'$	$(1.9 \pm 1.7) \times 10^{-5}$	
$\Gamma_{139}$	$\rho \eta$	$(2.2 \pm 0.6) \times 10^{-5}$	S=1.1
$\Gamma_{140}$	$\omega \eta$	$< 1.1 \times 10^{-5}$	CL=90%
$\Gamma_{141}$	$\phi \pi^0$	$< 4 \times 10^{-7}$	CL=90%
$\Gamma_{142}$	$\eta_c \pi^+ \pi^- \pi^0$	$< 1.0 \times 10^{-3}$	CL=90%
$\Gamma_{143}$	$p \bar{p} K^+ K^-$	$(2.7 \pm 0.7) \times 10^{-5}$	
$\Gamma_{144}$	$\bar{\Lambda} n K_S^0 + c.c.$	$(8.1 \pm 1.8) \times 10^{-5}$	
$\Gamma_{145}$	$\phi f_2'(1525)$	$(4.4 \pm 1.6) \times 10^{-5}$	
$\Gamma_{146}$	$\Theta(1540) \bar{\Theta}(1540) \rightarrow K_S^0 p K^- \bar{n} + c.c.$	$< 8.8 \times 10^{-6}$	CL=90%
$\Gamma_{147}$	$\Theta(1540) K^- \bar{n} \rightarrow K_S^0 p K^- \bar{n}$	$< 1.0 \times 10^{-5}$	CL=90%
$\Gamma_{148}$	$\Theta(1540) K_S^0 \bar{p} \rightarrow K_S^0 \bar{p} K^+ n$	$< 7.0 \times 10^{-6}$	CL=90%
$\Gamma_{149}$	$\bar{\Theta}(1540) K^+ n \rightarrow K_S^0 \bar{p} K^+ n$	$< 2.6 \times 10^{-5}$	CL=90%

$\Gamma_{150}$	$\bar{\Theta}(1540) K_S^0 p \rightarrow K_S^0 p K^- \bar{n}$	$< 6.0 \times 10^{-6}$	CL=90%
$\Gamma_{151}$	$K_S^0 K_S^0$	$< 4.6 \times 10^{-6}$	
$\Gamma_{152}$	$\Lambda_c^+ \bar{p} e^+ e^- + c.c.$	$< 1.7 \times 10^{-6}$	CL=90%

## Radiative decays

$\Gamma_{153}$	$\gamma \chi_{c0}(1P)$	$(9.79 \pm 0.20) \%$	
$\Gamma_{154}$	$\gamma \chi_{c1}(1P)$	$(9.75 \pm 0.24) \%$	
$\Gamma_{155}$	$\gamma \chi_{c2}(1P)$	$(9.52 \pm 0.20) \%$	
$\Gamma_{156}$	$\gamma \eta_c(1S)$	$(3.4 \pm 0.5) \times 10^{-3}$	S=1.3
$\Gamma_{157}$	$\gamma \eta_c'(2S)$	$(7 \pm 5) \times 10^{-4}$	
$\Gamma_{158}$	$\gamma \pi^0$	$(1.04 \pm 0.22) \times 10^{-6}$	S=1.4
$\Gamma_{159}$	$\gamma \eta'(958)$	$(1.24 \pm 0.04) \times 10^{-4}$	
$\Gamma_{160}$	$\gamma f_2(1270)$	$(2.73 \pm 0.29) \times 10^{-4}$	S=1.8
$\Gamma_{161}$	$\gamma f_0(1370) \rightarrow \gamma K \bar{K}$	$(3.1 \pm 1.7) \times 10^{-5}$	
$\Gamma_{162}$	$\gamma f_0(1500)$	$(9.3 \pm 1.9) \times 10^{-5}$	
$\Gamma_{163}$	$\gamma f_2'(1525)$	$(3.3 \pm 0.8) \times 10^{-5}$	
$\Gamma_{164}$	$\gamma f_0(1710)$		
$\Gamma_{165}$	$\gamma f_0(1710) \rightarrow \gamma \pi \pi$	$(3.5 \pm 0.6) \times 10^{-5}$	
$\Gamma_{166}$	$\gamma f_0(1710) \rightarrow \gamma K \bar{K}$	$(6.6 \pm 0.7) \times 10^{-5}$	
$\Gamma_{167}$	$\gamma f_0(2100) \rightarrow \gamma \pi \pi$	$(4.8 \pm 1.0) \times 10^{-6}$	
$\Gamma_{168}$	$\gamma f_0(2200) \rightarrow \gamma K \bar{K}$	$(3.2 \pm 1.0) \times 10^{-6}$	
$\Gamma_{169}$	$\gamma f_j(2220) \rightarrow \gamma \pi \pi$	$< 5.8 \times 10^{-6}$	CL=90%
$\Gamma_{170}$	$\gamma f_j(2220) \rightarrow \gamma K \bar{K}$	$< 9.5 \times 10^{-6}$	CL=90%
$\Gamma_{171}$	$\gamma \gamma$	$< 1.5 \times 10^{-4}$	CL=90%
$\Gamma_{172}$	$\gamma \eta$	$(9.2 \pm 1.8) \times 10^{-7}$	
$\Gamma_{173}$	$\gamma \eta \pi^+ \pi^-$	$(8.7 \pm 2.1) \times 10^{-4}$	
$\Gamma_{174}$	$\gamma \eta(1405)$		
$\Gamma_{175}$	$\gamma \eta(1405) \rightarrow \gamma K \bar{K} \pi$	$< 9 \times 10^{-5}$	CL=90%
$\Gamma_{176}$	$\gamma \eta(1405) \rightarrow \eta \pi^+ \pi^-$	$(3.6 \pm 2.5) \times 10^{-5}$	
$\Gamma_{177}$	$\gamma \eta(1405) \rightarrow \gamma f_0(980) \pi^0 \rightarrow \gamma \pi^+ \pi^- \pi^0$	$< 5.0 \times 10^{-7}$	CL=90%
$\Gamma_{178}$	$\gamma \eta(1475)$		
$\Gamma_{179}$	$\gamma \eta(1475) \rightarrow K \bar{K} \pi$	$< 1.4 \times 10^{-4}$	CL=90%
$\Gamma_{180}$	$\gamma \eta(1475) \rightarrow \eta \pi^+ \pi^-$	$< 8.8 \times 10^{-5}$	CL=90%
$\Gamma_{181}$	$\gamma 2(\pi^+ \pi^-)$	$(4.0 \pm 0.6) \times 10^{-4}$	
$\Gamma_{182}$	$\gamma K^{*0} K^+ \pi^- + c.c.$	$(3.7 \pm 0.9) \times 10^{-4}$	
$\Gamma_{183}$	$\gamma K^{*0} \bar{K}^{*0}$	$(2.4 \pm 0.7) \times 10^{-4}$	
$\Gamma_{184}$	$\gamma K_S^0 K^+ \pi^- + c.c.$	$(2.6 \pm 0.5) \times 10^{-4}$	
$\Gamma_{185}$	$\gamma K^+ K^- \pi^+ \pi^-$	$(1.9 \pm 0.5) \times 10^{-4}$	
$\Gamma_{186}$	$\gamma p \bar{p}$	$(3.9 \pm 0.5) \times 10^{-5}$	S=2.0
$\Gamma_{187}$	$\gamma f_2(1950) \rightarrow \gamma p \bar{p}$	$(1.20 \pm 0.22) \times 10^{-5}$	
$\Gamma_{188}$	$\gamma f_2(2150) \rightarrow \gamma p \bar{p}$	$(7.2 \pm 1.8) \times 10^{-6}$	
$\Gamma_{189}$	$\gamma X(1835) \rightarrow \gamma p \bar{p}$	$(4.6 \pm 1.8) \times 10^{-6}$	
$\Gamma_{190}$	$\gamma X \rightarrow \gamma p \bar{p}$	$[a] < 2 \times 10^{-6}$	CL=90%
$\Gamma_{191}$	$\gamma \pi^+ \pi^- p \bar{p}$	$(2.8 \pm 1.4) \times 10^{-5}$	
$\Gamma_{192}$	$\gamma 2(\pi^+ \pi^-) K^+ K^-$	$< 2.2 \times 10^{-4}$	CL=90%
$\Gamma_{193}$	$\gamma 3(\pi^+ \pi^-)$	$< 1.7 \times 10^{-4}$	CL=90%
$\Gamma_{194}$	$\gamma K^+ K^- K^+ K^-$	$< 4 \times 10^{-5}$	CL=90%
$\Gamma_{195}$	$\gamma \gamma J/\psi$	$(3.1 \pm 1.0) \times 10^{-4}$	
$\Gamma_{196}$	$e^+ e^- \eta'$	$(1.90 \pm 0.26) \times 10^{-6}$	
$\Gamma_{197}$	$e^+ e^- \chi_{c0}(1P)$	$(1.06 \pm 0.24) \times 10^{-3}$	
$\Gamma_{198}$	$e^+ e^- \chi_{c1}(1P)$	$(8.5 \pm 0.6) \times 10^{-4}$	
$\Gamma_{199}$	$e^+ e^- \chi_{c2}(1P)$	$(7.0 \pm 0.8) \times 10^{-4}$	

## Weak decays

$\Gamma_{200}$	$D^0 e^+ e^- + c.c.$	$< 1.4 \times 10^{-7}$	CL=90%
----------------	----------------------	------------------------	--------

## Other decays

$\Gamma_{201}$	invisible	$< 1.6 \%$	CL=90%
----------------	-----------	------------	--------

[a] For a narrow resonance in the range  $2.2 < M(X) < 2.8$  GeV.

## CONSTRAINED FIT INFORMATION

A multiparticle fit to  $\chi_{c1}(1P)$ ,  $\chi_{c0}(1P)$ ,  $\chi_{c2}(1P)$ , and  $\psi(2S)$  with 4 total widths, a partial width, 25 combinations of partial widths obtained from integrated cross section, and 84 branching ratios uses 248 measurements to determine 49 parameters. The overall fit has a  $\chi^2 = 378.1$  for 199 degrees of freedom.

The following off-diagonal array elements are the correlation coefficients  $\langle \delta p_i \delta p_j \rangle / (\delta p_i \delta p_j)$ , in percent, from the fit to parameters  $p_i$ , including the branching fractions,  $x_i \equiv \Gamma_i / \Gamma_{\text{total}}$ .

$x_7$	3									
$x_8$	1	0								
$x_{11}$	29	11	2							
$x_{12}$	28	6	1	48						
$x_{13}$	13	4	1	36	15					
$x_{21}$	0	0	0	4	3	2				
$x_{153}$	1	0	0	2	1	1	0			
$x_{154}$	1	0	0	2	1	1	0	0		
$x_{155}$	1	0	0	3	1	1	0	0	0	
$\Gamma$	-81	-4	-1	-38	-34	-16	-7	-1	-1	-1
	$x_6$	$x_7$	$x_8$	$x_{11}$	$x_{12}$	$x_{13}$	$x_{21}$	$x_{153}$	$x_{154}$	$x_{155}$

$\psi(2S)$  PARTIAL WIDTHS

$\Gamma(\text{hadrons})$

VALUE (keV)	DOCUMENT ID	TECN	COMMENT
258±26	BAI	02B	BES2 $e^+e^-$
224±56	LUTH	75	MRK1 $e^+e^-$

$\Gamma(e^+e^-)$

VALUE (keV)	DOCUMENT ID	TECN	COMMENT
<b>2.33 ± 0.04 OUR FIT</b>			
<b>2.29 ± 0.06 OUR AVERAGE</b>			
2.23 ± 0.10 ± 0.02	<sup>1</sup> ABLIKIM	15v	BES3 $4.0\text{--}4.4 e^+e^- \rightarrow \pi^+\pi^- J/\psi$
2.338±0.037±0.096	ABLIKIM	08B	BES2 $e^+e^- \rightarrow \text{hadrons}$
2.330±0.036±0.110	ABLIKIM	06L	BES2 $e^+e^- \rightarrow \text{hadrons}$
2.44 ± 0.21	<sup>2</sup> BAI	02B	BES2 $e^+e^-$
2.14 ± 0.21	ALEXANDER	89	RVUE See $\Upsilon$ mini-review
2.279±0.015±0.042	<sup>3</sup> ANASHIN	18	KEDR $e^+e^-$
2.282±0.015±0.042	<sup>4</sup> ANASHIN	18	KEDR $e^+e^-$
2.0 ± 0.3	BRANDELIK	79c	DASP $e^+e^-$
2.1 ± 0.3	<sup>5</sup> LUTH	75	MRK1 $e^+e^-$

<sup>1</sup>ABLIKIM 15v reports  $2.213 \pm 0.018 \pm 0.099$  keV from a measurement of  $[\Gamma(\psi(2S) \rightarrow e^+e^-)] \times [B(\psi(2S) \rightarrow J/\psi(1S)\pi^+\pi^-)]$  assuming  $B(\psi(2S) \rightarrow J/\psi(1S)\pi^+\pi^-) = (34.95 \pm 0.45) \times 10^{-2}$ , which we rescale to our best value  $B(\psi(2S) \rightarrow J/\psi(1S)\pi^+\pi^-) = (34.68 \pm 0.30) \times 10^{-2}$ . Our first error is their experiment's error and our second error is the systematic error from using our best value.

<sup>2</sup>From a simultaneous fit to  $e^+e^-$ ,  $\mu^+\mu^-$ , and hadronic channel, assuming  $\Gamma_e = \Gamma_\mu = \Gamma_\tau/0.38847$ .

<sup>3</sup>Combining  $\Gamma_{e^+e^-} \cdot B(\mu^+\mu^-)$  from ANASHIN 18 with  $\Gamma_{e^+e^-} \cdot B(\text{hadrons})$  from ANASHIN 12 and assuming lepton universality.

<sup>4</sup>From the sum of  $\Gamma_{e^+e^-} \cdot B(\text{hadrons})$  from ANASHIN 12,  $\Gamma_{e^+e^-} \cdot B(e^+e^-)$  and  $\Gamma_{e^+e^-} \cdot B(\mu^+\mu^-)$  from ANASHIN 18, and  $\Gamma_{e^+e^-} \cdot B(\tau^+\tau^-)$  from ANASHIN 07.

<sup>5</sup>From a simultaneous fit to  $e^+e^-$ ,  $\mu^+\mu^-$ , and hadronic channels assuming  $\Gamma(e^+e^-) = \Gamma(\mu^+\mu^-)$ .

$\Gamma(\gamma\gamma)$

VALUE (eV)	CL%	DOCUMENT ID	TECN	COMMENT
<b>&lt;43</b>	90	BRANDELIK	79c	DASP $e^+e^-$

$\psi(2S) \Gamma(i)\Gamma(e^+e^-)/\Gamma(\text{total})$

This combination of a partial width with the partial width into  $e^+e^-$  and with the total width is obtained from the integrated cross section into channel(i) in the  $e^+e^-$  annihilation. We list only data that have not been used to determine the partial width  $\Gamma(i)$  or the branching ratio  $\Gamma(i)/\text{total}$ .

$\Gamma(\text{hadrons}) \times \Gamma(e^+e^-)/\Gamma_{\text{total}}$

VALUE (keV)	DOCUMENT ID	TECN	COMMENT
<b>2.233±0.015±0.042</b>	<sup>1</sup> ANASHIN	12	KEDR $e^+e^- \rightarrow \text{hadrons}$
2.2 ± 0.4	ABRAMS	75	MRK1 $e^+e^-$

<sup>1</sup>ANASHIN 12 reports the value  $2.233 \pm 0.015 \pm 0.037 \pm 0.020$  keV, where the third uncertainty is due to assumptions on the interference between the resonance and hadronic continuum. We combined the two systematic uncertainties.

$\Gamma(e^+e^-) \times \Gamma(e^+e^-)/\Gamma_{\text{total}}$

VALUE (eV)	DOCUMENT ID	TECN	COMMENT
<b>21.2±0.7±1.2</b>	<sup>1</sup> ANASHIN	18	KEDR $e^+e^-$

<sup>1</sup>From the average of nine scans of the  $\psi(2S)$ .

$\Gamma(\mu^+\mu^-) \times \Gamma(e^+e^-)/\Gamma_{\text{total}}$

VALUE (eV)	DOCUMENT ID	TECN	COMMENT
<b>19.3±0.3±0.5</b>	<sup>1</sup> ANASHIN	18	KEDR $\psi(2S) \rightarrow \mu^+\mu^-$

<sup>1</sup>From the average of nine scans of the  $\psi(2S)$ .

$\Gamma(\tau^+\tau^-) \times \Gamma(e^+e^-)/\Gamma_{\text{total}}$

VALUE (eV)	EVTs	DOCUMENT ID	TECN	COMMENT
<b>9.0±2.6</b>	79	<sup>1</sup> ANASHIN	07	KEDR $e^+e^- \rightarrow \psi(2S) \rightarrow \tau^+\tau^-$

<sup>1</sup>Using  $\psi(2S)$  total width of  $337 \pm 13$  keV. Systematic errors not evaluated.

$\Gamma(J/\psi(1S)\pi^+\pi^-) \times \Gamma(e^+e^-)/\Gamma_{\text{total}}$

VALUE (keV)	EVTs	DOCUMENT ID	TECN	COMMENT
<b>0.808±0.013 OUR FIT</b>				
<b>0.837±0.025 OUR AVERAGE</b>				Error includes scale factor of 1.3. See the ideogram below.
0.837±0.028±0.005		<sup>1</sup> LEES	12E	BABR $10.6 e^+e^- \rightarrow 2\pi^+2\pi^-\gamma$
0.852±0.010±0.026	19.5k	ADAM	06	CLEO $3.773 e^+e^- \rightarrow \gamma\psi(2S)$
0.68 ± 0.09		<sup>2</sup> BAI	98E	BES $e^+e^-$
0.88 ± 0.08 ± 0.03	256	<sup>3</sup> AUBERT	07AU	BABR $10.6 e^+e^- \rightarrow J/\psi\pi^+\pi^-\gamma$
0.755±0.048±0.004	544	<sup>4</sup> AUBERT	05D	BABR $10.6 e^+e^- \rightarrow \pi^+\pi^-\mu^+\mu^-\gamma$

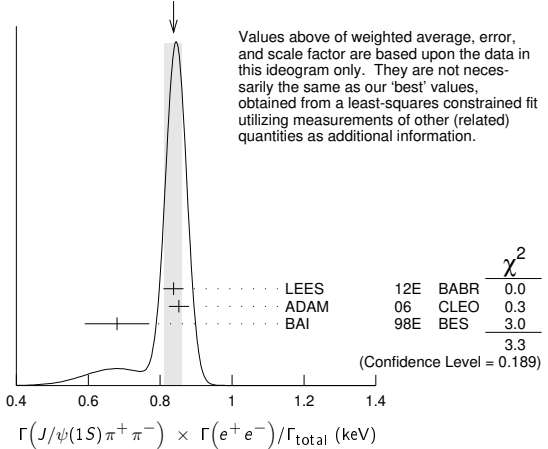
<sup>1</sup>LEES 12E reports  $[\Gamma(\psi(2S) \rightarrow J/\psi(1S)\pi^+\pi^-) \times \Gamma(\psi(2S) \rightarrow e^+e^-)/\Gamma_{\text{total}}] \times [B(J/\psi(1S) \rightarrow \mu^+\mu^-)] = (49.9 \pm 1.3 \pm 1.0) \times 10^{-3}$  keV which we divide by our best value  $B(J/\psi(1S) \rightarrow \mu^+\mu^-) = (5.961 \pm 0.033) \times 10^{-2}$ . Our first error is their experiment's error and our second error is the systematic error from using our best value.

<sup>2</sup>The value of  $\Gamma(e^+e^-)$  quoted in BAI 98E is derived using  $B(\psi(2S) \rightarrow J/\psi(1S)\pi^+\pi^-) = (32.4 \pm 2.6) \times 10^{-2}$  and  $B(J/\psi(1S) \rightarrow \ell^+\ell^-) = 0.1203 \pm 0.0038$ . Recalculated by us using  $B(J/\psi(1S) \rightarrow \ell^+\ell^-) = 0.1181 \pm 0.0020$ .

<sup>3</sup>AUBERT 07AU reports  $[\Gamma(\psi(2S) \rightarrow J/\psi(1S)\pi^+\pi^-) \times \Gamma(\psi(2S) \rightarrow e^+e^-)/\Gamma_{\text{total}}] \times [B(J/\psi(1S) \rightarrow \pi^+\pi^-\pi^0)] = 0.0186 \pm 0.0012 \pm 0.0011$  keV which we divide by our best value  $B(J/\psi(1S) \rightarrow \pi^+\pi^-\pi^0) = (2.10 \pm 0.08) \times 10^{-2}$ . Our first error is their experiment's error and our second error is the systematic error from using our best value.

<sup>4</sup>AUBERT 05D reports  $[\Gamma(\psi(2S) \rightarrow J/\psi(1S)\pi^+\pi^-) \times \Gamma(\psi(2S) \rightarrow e^+e^-)/\Gamma_{\text{total}}] \times [B(J/\psi(1S) \rightarrow \mu^+\mu^-)] = 0.0450 \pm 0.0018 \pm 0.0022$  keV which we divide by our best value  $B(J/\psi(1S) \rightarrow \mu^+\mu^-) = (5.961 \pm 0.033) \times 10^{-2}$ . Our first error is their experiment's error and our second error is the systematic error from using our best value. Superseded by LEES 12E.

WEIGHTED AVERAGE  
0.837±0.025 (Error scaled by 1.3)



$\Gamma(J/\psi(1S)\pi^0\pi^0) \times \Gamma(e^+e^-)/\Gamma_{\text{total}}$

VALUE (keV)	EVTs	DOCUMENT ID	TECN	COMMENT
<b>0.425±0.009 OUR FIT</b>				
<b>0.411±0.008±0.018</b>	3.6k	ADAM	06	CLEO $3.773 e^+e^- \rightarrow \gamma\psi(2S)$
0.48 ± 0.09 ± 0.02	142	<sup>1</sup> LEES	18E	BABR $10.6 e^+e^- \rightarrow J/\psi\pi^0\pi^0\gamma$

<sup>1</sup>LEES 18E reports  $[\Gamma(\psi(2S) \rightarrow J/\psi(1S)\pi^0\pi^0) \times \Gamma(\psi(2S) \rightarrow e^+e^-)/\Gamma_{\text{total}}] \times [B(J/\psi(1S) \rightarrow \pi^+\pi^-\pi^0)] = 0.0101 \pm 0.0015 \pm 0.0011$  keV which we divide by our best value  $B(J/\psi(1S) \rightarrow \pi^+\pi^-\pi^0) = (2.10 \pm 0.08) \times 10^{-2}$ . Our first error is their experiment's error and our second error is the systematic error from using our best value.

$\Gamma(J/\psi(1S)\eta) \times \Gamma(e^+e^-)/\Gamma_{\text{total}}$

VALUE (eV)	EVTs	DOCUMENT ID	TECN	COMMENT
<b>78.6± 1.6 OUR FIT</b>				
<b>87 ± 9 OUR AVERAGE</b>				
83 ± 25 ± 5	14	<sup>1</sup> AUBERT	07AU	BABR $10.6 e^+e^- \rightarrow J/\psi\pi^+\pi^-\pi^0\gamma$
88 ± 6 ± 7	291 ± 24	ADAM	06	CLEO $3.773 e^+e^- \rightarrow \gamma\psi(2S)$
		<sup>1</sup> AUBERT	07AU	quotes $\Gamma_{ee}^{\psi(2S)} \cdot B(\psi(2S) \rightarrow J/\psi\eta) \cdot B(J/\psi \rightarrow \mu^+\mu^-) \cdot B(\eta \rightarrow \pi^+\pi^-\pi^0) = 1.11 \pm 0.33 \pm 0.07$ eV.

$\Gamma(J/\psi(1S)\pi^0) \times \Gamma(e^+e^-)/\Gamma_{\text{total}}$

VALUE (eV)	CL%	EVTs	DOCUMENT ID	TECN	COMMENT
<b>&lt;8</b>	90	<37	ADAM	06	CLEO $3.773 e^+e^- \rightarrow \gamma\psi(2S)$

## Meson Particle Listings

 $\psi(2S)$  $\Gamma(p\bar{p}) \times \Gamma(e^+e^-)/\Gamma_{\text{total}}$   $\Gamma_{21}\Gamma_6/\Gamma$ 

VALUE (eV)	EVTS	DOCUMENT ID	TECN	COMMENT
<b>0.686 ± 0.019 OUR FIT</b>				
<b>0.63 ± 0.05 OUR AVERAGE</b>				Error includes scale factor of 1.2.
0.67 ± 0.12 ± 0.02	43	<sup>1</sup> LEES	130 BABR	$e^+e^- \rightarrow p\bar{p}\gamma$
0.74 ± 0.07 ± 0.04	142	<sup>2</sup> LEES	13Y BABR	$e^+e^- \rightarrow p\bar{p}\gamma$
0.579 ± 0.038 ± 0.036	2.7k	ANDREOTTI 07	E835	$p\bar{p} \rightarrow e^+e^-, J/\psi X$
• • • We do not use the following data for averages, fits, limits, etc. • • •				
0.70 ± 0.17 ± 0.03	22	<sup>3</sup> AUBERT	06B BABR	$e^+e^- \rightarrow p\bar{p}\gamma$

- <sup>1</sup>ISR photon reconstructed in the detector  
<sup>2</sup>ISR photon undetected  
<sup>3</sup>Superseded by LEES 130

VALUE (eV)	EVTS	DOCUMENT ID	TECN	COMMENT
<b>1.5 ± 0.4 ± 0.1</b>		AUBERT	07BD	BABR 10.6 $e^+e^- \rightarrow \Lambda\bar{\Lambda}\gamma$

VALUE (eV)	EVTS	DOCUMENT ID	TECN	COMMENT
<b>11.2 ± 3.3 ± 1.3</b>	43	AUBERT	06D	BABR 10.6 $e^+e^- \rightarrow 2(\pi^+\pi^-\pi^0)\gamma$

VALUE (eV)	EVTS	DOCUMENT ID	TECN	COMMENT
<b>0.60 ± 0.31 ± 0.03</b>	17	LEES	12F	BABR 10.6 $e^+e^- \rightarrow \pi^0\pi^0 K^+K^-\gamma$

VALUE (eV)	EVTS	DOCUMENT ID	TECN	COMMENT
<b>4.4 ± 2.1 ± 0.3</b>	26	AUBERT	06D	BABR 10.6 $e^+e^- \rightarrow K^+K^-\pi^+\pi^-\gamma$

VALUE (eV)	EVTS	DOCUMENT ID	TECN	COMMENT
<b>1.92 ± 0.30 ± 0.06</b>	133	LEES	12F	BABR 10.6 $e^+e^- \rightarrow \pi^+\pi^-K^+K^-\gamma$
• • • We do not use the following data for averages, fits, limits, etc. • • •				
2.56 ± 0.42 ± 0.16	85	<sup>1</sup> AUBERT	07AK	BABR 10.6 $e^+e^- \rightarrow \pi^+\pi^-K^+K^-\gamma$
<sup>1</sup> Superseded by LEES 12F.				

VALUE (eV)	EVTS	DOCUMENT ID	TECN	COMMENT
<b>2.92 ± 1.27 ± 0.15</b>	14	LEES	17A	BABR $e^+e^- \rightarrow K_S^0 K_L^0 \pi^0 \pi^0 \gamma$

VALUE (eV)	CL%	EVTS	DOCUMENT ID	TECN	COMMENT
<b>&lt;0.7</b>	90	8	LEES	17A	BABR $e^+e^- \rightarrow K_S^0 K_L^0 \pi^0 \gamma$

VALUE (eV)	EVTS	DOCUMENT ID	TECN	COMMENT
<b>3.14 ± 1.08 ± 0.16</b>	16	LEES	17A	BABR $e^+e^- \rightarrow K_S^0 K_L^0 \eta \gamma$

VALUE (eV)	EVTS	DOCUMENT ID	TECN	COMMENT
<b>0.345 ± 0.128 ± 0.004</b>	12	<sup>1</sup> LEES	12F	BABR 10.6 $e^+e^- \rightarrow \pi^+\pi^-K^+K^-\gamma$

- • • We do not use the following data for averages, fits, limits, etc. • • •  
0.345 ± 0.168 ± 0.004 6 ± 3 <sup>2</sup> AUBERT 07AK BABR 10.6  $e^+e^- \rightarrow \pi^+\pi^-K^+K^-\gamma$

- <sup>1</sup> LEES 12F reports  $[\Gamma(\psi(2S) \rightarrow \phi_0(980) \rightarrow \pi^+\pi^-) \times \Gamma(\psi(2S) \rightarrow e^+e^-)/\Gamma_{\text{total}}] \times [B(\phi(1020) \rightarrow K^+K^-)] = 0.17 \pm 0.06 \pm 0.02$  eV which we divide by our best value  $B(\phi(1020) \rightarrow K^+K^-) = (49.2 \pm 0.5) \times 10^{-2}$ . Our first error is their experiment's error and our second error is the systematic error from using our best value.  
<sup>2</sup> Superseded by LEES 12F. AUBERT 07AK reports  $[\Gamma(\psi(2S) \rightarrow \phi_0(980) \rightarrow \pi^+\pi^-) \times \Gamma(\psi(2S) \rightarrow e^+e^-)/\Gamma_{\text{total}}] \times [B(\phi(1020) \rightarrow K^+K^-)] = 0.17 \pm 0.08 \pm 0.02$  eV which we divide by our best value  $B(\phi(1020) \rightarrow K^+K^-) = (49.2 \pm 0.5) \times 10^{-2}$ . Our first error is their experiment's error and our second error is the systematic error from using our best value.

VALUE (eV)	EVTS	DOCUMENT ID	TECN	COMMENT
<b>0.22 ± 0.10 ± 0.02</b>	13	LEES	12F	BABR 10.6 $e^+e^- \rightarrow K^+K^-\pi^+\pi^-\gamma$

VALUE (eV)	EVTS	DOCUMENT ID	TECN	COMMENT
<b>0.55 ± 0.19 ± 0.01</b>	19	<sup>1</sup> LEES	12F	BABR 10.6 $e^+e^- \rightarrow K^+K^-\pi^+\pi^-\gamma$
• • • We do not use the following data for averages, fits, limits, etc. • • •				
0.57 ± 0.23 ± 0.01	10	<sup>2</sup> AUBERT, BE	06D	BABR 10.6 $e^+e^- \rightarrow K^+K^-\pi^+\pi^-\gamma$

- <sup>1</sup> LEES 12F reports  $[\Gamma(\psi(2S) \rightarrow \phi\pi^+\pi^-) \times \Gamma(\psi(2S) \rightarrow e^+e^-)/\Gamma_{\text{total}}] \times [B(\phi(1020) \rightarrow K^+K^-)] = 0.27 \pm 0.09 \pm 0.02$  eV which we divide by our best value  $B(\phi(1020) \rightarrow K^+K^-) = (49.2 \pm 0.5) \times 10^{-2}$ . Our first error is their experiment's error and our second error is the systematic error from using our best value.  
<sup>2</sup> Superseded by LEES 12F. AUBERT, BE 06D reports  $[\Gamma(\psi(2S) \rightarrow \phi\pi^+\pi^-) \times \Gamma(\psi(2S) \rightarrow e^+e^-)/\Gamma_{\text{total}}] \times [B(\phi(1020) \rightarrow K^+K^-)] = 0.28 \pm 0.11 \pm 0.02$  eV which we divide by our best value  $B(\phi(1020) \rightarrow K^+K^-) = (49.2 \pm 0.5) \times 10^{-2}$ . Our first error is their experiment's error and our second error is the systematic error from using our best value.

VALUE (eV)	EVTS	DOCUMENT ID	TECN	COMMENT
<b>29.7 ± 2.2 ± 1.8</b>	410	AUBERT	07AU	BABR 10.6 $e^+e^- \rightarrow 2(\pi^+\pi^-)\pi^0\gamma$

VALUE (eV)	EVTS	DOCUMENT ID	TECN	COMMENT
<b>12.4 ± 1.8 ± 1.2</b>	177	LEES	18E	BABR 10.6 $e^+e^- \rightarrow \pi^+\pi^-\pi^0\gamma$

VALUE (eV)	CL%	DOCUMENT ID	TECN	COMMENT
<b>&lt;6.2</b>	90	LEES	18E	BABR 10.6 $e^+e^- \rightarrow \pi^+\pi^-\pi^0\gamma$

VALUE (eV)	EVTS	DOCUMENT ID	TECN	COMMENT
<b>3.01 ± 0.84 ± 0.02</b>	37	<sup>1</sup> AUBERT	07AU	BABR 10.6 $e^+e^- \rightarrow \omega\pi^+\pi^-\gamma$

- <sup>1</sup> AUBERT 07AU reports  $[\Gamma(\psi(2S) \rightarrow \omega\pi^+\pi^-) \times \Gamma(\psi(2S) \rightarrow e^+e^-)/\Gamma_{\text{total}}] \times [B(\omega(782) \rightarrow \pi^+\pi^-\pi^0)] = 2.69 \pm 0.73 \pm 0.16$  eV which we divide by our best value  $B(\omega(782) \rightarrow \pi^+\pi^-\pi^0) = (89.3 \pm 0.6) \times 10^{-2}$ . Our first error is their experiment's error and our second error is the systematic error from using our best value.

VALUE (eV)	EVTS	DOCUMENT ID	TECN	COMMENT
<b>2.58 ± 0.82 ± 0.02</b>	33	<sup>1</sup> LEES	18E	BABR 10.6 $e^+e^- \rightarrow \pi^+\pi^-\pi^0\gamma$

- <sup>1</sup> LEES 18E reports  $[\Gamma(\psi(2S) \rightarrow \omega\pi^0\pi^0) \times \Gamma(\psi(2S) \rightarrow e^+e^-)/\Gamma_{\text{total}}] \times [B(\omega(782) \rightarrow \pi^+\pi^-\pi^0)] = 2.3 \pm 0.7 \pm 0.2$  eV which we divide by our best value  $B(\omega(782) \rightarrow \pi^+\pi^-\pi^0) = (89.3 \pm 0.6) \times 10^{-2}$ . Our first error is their experiment's error and our second error is the systematic error from using our best value.

VALUE (eV)	EVTS	DOCUMENT ID	TECN	COMMENT
<b>2.87 ± 1.41 ± 0.01</b>	16	<sup>1</sup> AUBERT	07AU	BABR 10.6 $e^+e^- \rightarrow 2(\pi^+\pi^-)\eta\gamma$

- <sup>1</sup> AUBERT 07AU reports  $[\Gamma(\psi(2S) \rightarrow 2(\pi^+\pi^-)\eta) \times \Gamma(\psi(2S) \rightarrow e^+e^-)/\Gamma_{\text{total}}] \times [B(\eta \rightarrow 2\gamma)] = 1.13 \pm 0.55 \pm 0.08$  eV which we divide by our best value  $B(\eta \rightarrow 2\gamma) = (39.41 \pm 0.20) \times 10^{-2}$ . Our first error is their experiment's error and our second error is the systematic error from using our best value.

VALUE (eV)	CL%	DOCUMENT ID	TECN	COMMENT
<b>&lt;0.85</b>	90	LEES	18E	BABR 10.6 $e^+e^- \rightarrow \pi^+\pi^-\pi^0\pi^0\eta\gamma$

VALUE (eV)	EVTS	DOCUMENT ID	TECN	COMMENT
<b>4.4 ± 1.3 ± 0.3</b>	32	AUBERT	07AU	BABR 10.6 $e^+e^- \rightarrow K^+K^-\pi^+\pi^-\pi^0\gamma$

VALUE (eV)	EVTS	DOCUMENT ID	TECN	COMMENT
<b>3.04 ± 1.79 ± 0.02</b>	7	<sup>1</sup> AUBERT	07AU	BABR 10.6 $e^+e^- \rightarrow K^+K^-\pi^+\pi^-\eta\gamma$

- <sup>1</sup> AUBERT 07AU reports  $[\Gamma(\psi(2S) \rightarrow K^+K^-\pi^+\pi^-\eta) \times \Gamma(\psi(2S) \rightarrow e^+e^-)/\Gamma_{\text{total}}] \times [B(\eta \rightarrow 2\gamma)] = 1.2 \pm 0.7 \pm 0.1$  eV which we divide by our best value  $B(\eta \rightarrow 2\gamma) = (39.41 \pm 0.20) \times 10^{-2}$ . Our first error is their experiment's error and our second error is the systematic error from using our best value.

VALUE (eV)	EVTS	DOCUMENT ID	TECN	COMMENT
0.147 ± 0.035 ± 0.005	66	<sup>1</sup> LEES	15J	BABR $e^+e^- \rightarrow K^+K^-\gamma$
0.197 ± 0.035 ± 0.005	66	<sup>2</sup> LEES	15J	BABR $e^+e^- \rightarrow K^+K^-\gamma$
0.35 ± 0.14 ± 0.03	11	<sup>3</sup> LEES	13Q	BABR $e^+e^- \rightarrow K^+K^-\gamma$

- <sup>1</sup>  $\sin\phi > 0$ .  
<sup>2</sup>  $\sin\phi < 0$ .

- <sup>3</sup> Interference with non-resonant  $K^+K^-$  production not taken into account.

 $\psi(2S)$  BRANCHING RATIOS

VALUE	DOCUMENT ID	TECN	COMMENT
<b>0.9785 ± 0.0013 OUR AVERAGE</b>			
0.9779 ± 0.0015	<sup>1</sup> BAI	02B	BES2 $e^+e^-$
0.981 ± 0.003	<sup>1</sup> LUTH	75	MRK1 $e^+e^-$

- <sup>1</sup> Includes cascade decay into  $J/\psi(1S)$ .

VALUE	DOCUMENT ID	TECN	COMMENT
<b>0.0173 ± 0.0014 OUR AVERAGE</b>			Error includes scale factor of 1.5.
0.0166 ± 0.0010	<sup>1,2</sup> SETH	04	RVUE $e^+e^-$
0.0199 ± 0.0019	<sup>1</sup> BAI	02B	BES2 $e^+e^-$
• • • We do not use the following data for averages, fits, limits, etc. • • •			
0.029 ± 0.004	<sup>1</sup> LUTH	75	MRK1 $e^+e^-$

- <sup>1</sup> Included in  $\Gamma(\text{hadrons})/\Gamma_{\text{total}}$ .

- <sup>2</sup> Using  $B(\psi(2S) \rightarrow \ell^+\ell^-) = (0.73 \pm 0.04)\%$  from RPP-2002 and  $R = 2.28 \pm 0.04$  determined by a fit to data from BAI 00 and BAI 02c.

$\Gamma(ggg)/\Gamma_{total}$   $\Gamma_3/\Gamma$

VALUE (units $10^{-2}$ )	EVTS	DOCUMENT ID	TECN	COMMENT
<b>10.58 ± 1.62</b>	2.9 M	<sup>1</sup> LIBBY 09	CLEO	$\psi(2S) \rightarrow$ hadrons

<sup>1</sup> Calculated using  $\Gamma(\gamma gg)/\Gamma(ggg) = 0.097 \pm 0.026 \pm 0.016$  from LIBBY 09,  $B(\psi(2S) \rightarrow X J/\psi)$  relative and absolute branching fractions from MENDEZ 08,  $B(\psi(2S) \rightarrow \gamma \eta_c)$  from MITCHELL 09, and  $B(\psi(2S) \rightarrow$  virtual  $\gamma \rightarrow$  hadrons),  $B(\psi(2S) \rightarrow \gamma \chi_{cJ})$ , and  $B(\psi(2S) \rightarrow \ell^+ \ell^-)$  from PDG 08. The statistical error is negligible and the systematic error is largely uncorrelated with that of  $\Gamma(\gamma gg)/\Gamma_{total}$  LIBBY 09 measurement.

$\Gamma(\gamma gg)/\Gamma_{total}$   $\Gamma_4/\Gamma$

VALUE (units $10^{-2}$ )	EVTS	DOCUMENT ID	TECN	COMMENT
<b>1.025 ± 0.288</b>	200 k	<sup>1</sup> LIBBY 09	CLEO	$\psi(2S) \rightarrow \gamma +$ hadrons

<sup>1</sup> Calculated using  $\Gamma(\gamma gg)/\Gamma(ggg) = 0.097 \pm 0.026 \pm 0.016$  from LIBBY 09. The statistical error is negligible and the systematic error is largely uncorrelated with that of  $\Gamma(ggg)/\Gamma_{total}$  LIBBY 09 measurement.

$\Gamma(\gamma gg)/\Gamma(ggg)$   $\Gamma_4/\Gamma_3$

VALUE (units $10^{-2}$ )	EVTS	DOCUMENT ID	TECN	COMMENT
<b>9.7 ± 2.6 ± 1.6</b>	2.9 M	LIBBY 09	CLEO	$\psi(2S) \rightarrow (\gamma +)$ hadrons

$\Gamma(\text{light hadrons})/\Gamma_{total}$   $\Gamma_5/\Gamma$

VALUE	DOCUMENT ID	TECN	COMMENT
<b>0.154 ± 0.015</b>	<sup>1</sup> MENDEZ 08	CLEO	$e^+ e^- \rightarrow \psi(2S)$
• • • We do not use the following data for averages, fits, limits, etc. • • •			
0.169 ± 0.026	<sup>2</sup> ADAM 05A	CLEO	$e^+ e^- \rightarrow \psi(2S)$

<sup>1</sup> Uses  $B(\psi(2S) \rightarrow J/\psi X)$  from MENDEZ 08 and other branching fractions from PDG 07.  
<sup>2</sup> Uses  $B(J/\psi X)$  from ADAM 05A,  $B(\chi_{cJ} \gamma)$ ,  $B(\eta_c \gamma)$  from ATHAR 04 and  $B(\ell^+ \ell^-)$  from PDG 04. Superseded by MENDEZ 08.

$\Gamma(e^+ e^-)/\Gamma_{total}$   $\Gamma_6/\Gamma$

VALUE (units $10^{-4}$ )	DOCUMENT ID	TECN	COMMENT
<b>79.3 ± 1.7 OUR FIT</b>			
• • • We do not use the following data for averages, fits, limits, etc. • • •			
88 ± 13	<sup>1</sup> FELDMAN 77	RVUE	$e^+ e^-$

<sup>1</sup> From an overall fit assuming equal partial widths for  $e^+ e^-$  and  $\mu^+ \mu^-$ . For a measurement of the ratio see the entry  $\Gamma(\mu^+ \mu^-)/\Gamma(e^+ e^-)$  below. Includes LUTH 75, HILGER 75, BURMESTER 77.

$\Gamma(\mu^+ \mu^-)/\Gamma_{total}$   $\Gamma_7/\Gamma$

VALUE (units $10^{-4}$ )	DOCUMENT ID	TECN	COMMENT
<b>80 ± 6 OUR FIT</b>			

$\Gamma(\mu^+ \mu^-)/\Gamma(e^+ e^-)$   $\Gamma_7/\Gamma_6$

VALUE	DOCUMENT ID	TECN	COMMENT
<b>1.00 ± 0.08 OUR FIT</b>			
• • • We do not use the following data for averages, fits, limits, etc. • • •			
0.89 ± 0.16	BOYARSKI 75c	MRK1	$e^+ e^-$

$\Gamma(\tau^+ \tau^-)/\Gamma_{total}$   $\Gamma_8/\Gamma$

VALUE (units $10^{-4}$ )	DOCUMENT ID	TECN	COMMENT
<b>31 ± 4 OUR FIT</b>			
<b>30.8 ± 2.1 ± 3.8</b>	<sup>1</sup> ABLIKIM 06w	BES	$e^+ e^- \rightarrow \psi(2S)$

<sup>1</sup> Computed using PDG 02 value of  $B(\psi(2S) \rightarrow$  hadrons) = 0.9810 ± 0.0030 to estimate the total number of  $\psi(2S)$  events.

DECAYS INTO  $J/\psi(1S)$  AND ANYTHING

$\Gamma(J/\psi(1S) \text{ anything})/\Gamma_{total}$   $\Gamma_9/\Gamma$

VALUE	EVTS	DOCUMENT ID	TECN	COMMENT
<b>0.614 ± 0.006 OUR FIT</b>				
<b>0.55 ± 0.07 OUR AVERAGE</b>				
0.51 ± 0.12		BRANDELIK 79c	DASP	$e^+ e^- \rightarrow \mu^+ \mu^- X$
0.57 ± 0.08		ABRAMS 75b	MRK1	$e^+ e^- \rightarrow \mu^+ \mu^- X$
• • • We do not use the following data for averages, fits, limits, etc. • • •				
0.6254 ± 0.0016 ± 0.0155	1.1M	<sup>1</sup> MENDEZ 08	CLEO	$\psi(2S) \rightarrow \ell^+ \ell^- X$
0.5950 ± 0.0015 ± 0.0190	151k	ADAM 05A	CLEO	Repl. by MENDEZ 08

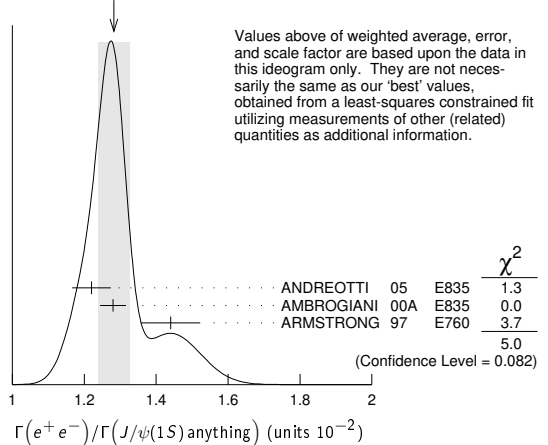
<sup>1</sup> Not independent from other measurements of MENDEZ 08.

$\Gamma(e^+ e^-)/\Gamma(J/\psi(1S) \text{ anything})$   
 $\Gamma_6/\Gamma_9 = \Gamma_6/(\Gamma_{11} + \Gamma_{12} + \Gamma_{13} + 0.343\Gamma_{154} + 0.190\Gamma_{155})$

VALUE (units $10^{-2}$ )	EVTS	DOCUMENT ID	TECN	COMMENT
<b>1.291 ± 0.026 OUR FIT</b>				
<b>1.28 ± 0.04 OUR AVERAGE</b>				Error includes scale factor of 1.6. See the ideogram below.
1.22 ± 0.02 ± 0.05	5097 ± 73	<sup>1</sup> ANDREOTTI 05	E835	$\rho \bar{p} \rightarrow \psi(2S) \rightarrow e^+ e^-$
1.28 ± 0.03 ± 0.02		<sup>1</sup> AMBROGIANI 00A	E835	$\rho \bar{p} \rightarrow \psi(2S)$
1.44 ± 0.08 ± 0.02		<sup>1</sup> ARMSTRONG 97	E760	$\bar{p} p \rightarrow \psi(2S)$

<sup>1</sup> Using  $B(J/\psi(1S) \rightarrow e^+ e^-) = 0.0593 \pm 0.0010$ .

WEIGHTED AVERAGE  
 1.28 ± 0.04 (Error scaled by 1.6)



Values above of weighted average, error, and scale factor are based upon the data in this ideogram only. They are not necessarily the same as our 'best' values, obtained from a least-squares constrained fit utilizing measurements of other (related) quantities as additional information.

$\Gamma(\mu^+ \mu^-)/\Gamma(J/\psi(1S) \text{ anything})$   
 $\Gamma_7/\Gamma_9 = \Gamma_7/(\Gamma_{11} + \Gamma_{12} + \Gamma_{13} + 0.343\Gamma_{154} + 0.190\Gamma_{155})$

VALUE	DOCUMENT ID	TECN	COMMENT
<b>0.0130 ± 0.0010 OUR FIT</b>			
<b>0.014 ± 0.003</b>	HILGER 75	SPEC	$e^+ e^-$

$\Gamma(J/\psi(1S) \text{ neutrals})/\Gamma_{total}$   $\Gamma_{10}/\Gamma$

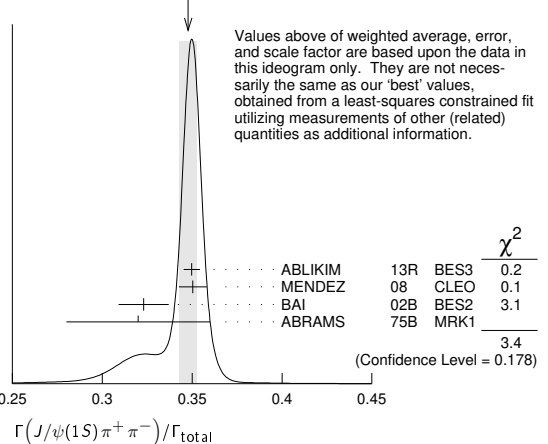
VALUE	DOCUMENT ID	TECN	COMMENT
<b>0.2538 ± 0.0032 OUR FIT</b>			

$\Gamma(J/\psi(1S) \pi^+ \pi^-)/\Gamma_{total}$   $\Gamma_{11}/\Gamma$

VALUE	EVTS	DOCUMENT ID	TECN	COMMENT
<b>0.3468 ± 0.0030 OUR FIT</b>				
<b>0.348 ± 0.005 OUR AVERAGE</b>				Error includes scale factor of 1.3. See the ideogram below.
0.3498 ± 0.0002 ± 0.0045	20M	ABLIKIM 13R	BES3	$\psi(2S) \rightarrow J/\psi \pi^+ \pi^-$
0.3504 ± 0.0007 ± 0.0077	565k	MENDEZ 08	CLEO	$\psi(2S) \rightarrow \ell^+ \ell^- \pi^+ \pi^-$
0.323 ± 0.014		BAI 02b	BES2	$e^+ e^-$
0.32 ± 0.04		ABRAMS 75b	MRK1	$e^+ e^- \rightarrow J/\psi \pi^+ \pi^-$
• • • We do not use the following data for averages, fits, limits, etc. • • •				
0.3354 ± 0.0014 ± 0.0110	60k	<sup>1</sup> ADAM 05A	CLEO	Repl. by MENDEZ 08

<sup>1</sup> Not independent from other values reported by ADAM 05A.

WEIGHTED AVERAGE  
 0.348 ± 0.005 (Error scaled by 1.3)



Values above of weighted average, error, and scale factor are based upon the data in this ideogram only. They are not necessarily the same as our 'best' values, obtained from a least-squares constrained fit utilizing measurements of other (related) quantities as additional information.

$\Gamma(e^+ e^-)/\Gamma(J/\psi(1S) \pi^+ \pi^-)$   $\Gamma_6/\Gamma_{11}$

VALUE	DOCUMENT ID	TECN	COMMENT
<b>0.0229 ± 0.0005 OUR FIT</b>			
<b>0.0252 ± 0.0028 ± 0.0011</b>	<sup>1</sup> AUBERT 02b	BABR	$e^+ e^-$

<sup>1</sup> Using  $B(J/\psi(1S) \rightarrow e^+ e^-) = 0.0593 \pm 0.0010$ .

$\Gamma(\mu^+ \mu^-)/\Gamma(J/\psi(1S) \pi^+ \pi^-)$   $\Gamma_7/\Gamma_{11}$

VALUE	DOCUMENT ID	TECN	COMMENT
<b>0.0230 ± 0.0017 OUR FIT</b>			
<b>0.0228 ± 0.0018 OUR AVERAGE</b>			
0.0230 ± 0.0020 ± 0.0012	<sup>1</sup> AAJ 16y	LHCb	$\Lambda_b^0 \rightarrow \psi(2S) X$
0.0216 ± 0.0026 ± 0.0014	<sup>2</sup> AUBERT 02b	BABR	$e^+ e^-$
0.0327 ± 0.0077 ± 0.0072	<sup>2</sup> GRIBUSHIN 96	FMP5	515 $\pi^- Be \rightarrow 2\mu X$

<sup>1</sup> Using  $B(J/\psi(1S) \rightarrow \mu^+ \mu^-) = (5.961 \pm 0.033) \times 10^{-2}$ .  
<sup>2</sup> Using  $B(J/\psi(1S) \rightarrow \mu^+ \mu^-) = (5.88 \pm 0.10) \times 10^{-2}$ .



## Meson Particle Listings

 $\psi(2S)$  $\Gamma(\tau^+\tau^-)/\Gamma(J/\psi(1S)\pi^+\pi^-)$   $\Gamma_8/\Gamma_{11}$ 

VALUE (units $10^{-3}$ )	DOCUMENT ID	TECN	COMMENT
<b>8.8 ± 1.1 OUR FIT</b>			
<b>8.73 ± 1.39 ± 1.57</b>	BAI	02	BES $e^+e^-$

 $\Gamma(J/\psi(1S)\pi^+\pi^-)/\Gamma(J/\psi(1S)\text{anything})$   $\Gamma_{11}/\Gamma_9$ 

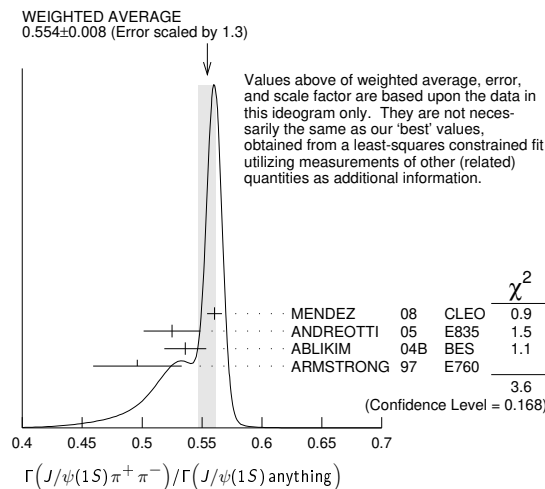
VALUE	EVTs	DOCUMENT ID	TECN	COMMENT
<b>0.5645 ± 0.0026 OUR FIT</b>				
<b>0.554 ± 0.008 OUR AVERAGE</b>				Error includes scale factor of 1.3. See the ideogram below.

0.5604 ± 0.0009 ± 0.0062	565k	MENDEZ	08	CLEO $\psi(2S) \rightarrow \ell^+\ell^-\pi^+\pi^-$
0.525 ± 0.009 ± 0.022	4k	ANDREOTTI	05	E835 $\psi(2S) \rightarrow J/\psi X$
0.536 ± 0.007 ± 0.016	20k	<sup>1,2</sup> ABLIKIM	04B	BES $\psi(2S) \rightarrow J/\psi X$
0.496 ± 0.037		ARMSTRONG	97	E760 $\bar{p}p \rightarrow \psi(2S)$

• • • We do not use the following data for averages, fits, limits, etc. • • •  
 0.5637 ± 0.0027 ± 0.0046 60k ADAM 05A CLEO Repl. by MENDEZ 08

<sup>1</sup> From a fit to the  $J/\psi$  recoil mass spectra.

<sup>2</sup> ABLIKIM 04B quotes  $B(\psi(2S) \rightarrow J/\psi X) / B(\psi(2S) \rightarrow J/\psi\pi^+\pi^-)$ .

 $\Gamma(J/\psi(1S)\text{neutrals})/\Gamma(J/\psi(1S)\pi^+\pi^-)$   $\Gamma_{10}/\Gamma_{11} = (0.9761\Gamma_{12} + 0.719\Gamma_{13} + 0.343\Gamma_{154} + 0.190\Gamma_{155})/\Gamma_{11}$ 

VALUE	DOCUMENT ID	TECN	COMMENT
<b>0.732 ± 0.008 OUR FIT</b>			
<b>0.73 ± 0.09</b>	TANENBAUM 76	MRK1	$e^+e^-$

 $\Gamma(J/\psi(1S)\pi^0\pi^0)/\Gamma_{\text{total}}$   $\Gamma_{12}/\Gamma$ 

VALUE	EVTs	DOCUMENT ID	TECN	COMMENT
<b>0.1824 ± 0.0031 OUR FIT</b>				

• • • We do not use the following data for averages, fits, limits, etc. • • •  
 0.1769 ± 0.0008 ± 0.0053 61k <sup>1</sup> MENDEZ 08 CLEO  $\psi(2S) \rightarrow \ell^+\ell^-2\pi^0$   
 0.1652 ± 0.0014 ± 0.0058 13.4k <sup>2</sup> ADAM 05A CLEO Repl. by MENDEZ 08

<sup>1</sup> Not independent from other measurements of MENDEZ 08.

<sup>2</sup> Not independent from other values reported by ADAM 05A.

 $\Gamma(J/\psi(1S)\pi^0\pi^0)/\Gamma(J/\psi(1S)\text{anything})$   $\Gamma_{12}/\Gamma_9$ 

VALUE	EVTs	DOCUMENT ID	TECN	COMMENT
<b>0.2968 ± 0.0031 OUR FIT</b>				
<b>0.320 ± 0.012 OUR AVERAGE</b>				

0.300 ± 0.008 ± 0.022	1655 ± 44	ANDREOTTI 05	E835	$\psi(2S) \rightarrow J/\psi X$
0.328 ± 0.013 ± 0.008		AMBROGIANI 00A	E835	$p\bar{p} \rightarrow \psi(2S)$
0.323 ± 0.033		ARMSTRONG 97	E760	$\bar{p}p \rightarrow \psi(2S)$

• • • We do not use the following data for averages, fits, limits, etc. • • •

0.2829 ± 0.0012 ± 0.0056	61k	MENDEZ 08	CLEO	$\psi(2S) \rightarrow \ell^+\ell^-2\pi^0$
0.2776 ± 0.0025 ± 0.0043	13.4k	ADAM 05A	CLEO	Repl. by MENDEZ 08

 $\Gamma(J/\psi(1S)\pi^0\pi^0)/\Gamma(J/\psi(1S)\pi^+\pi^-)$   $\Gamma_{12}/\Gamma_{11}$ 

VALUE	EVTs	DOCUMENT ID	TECN	COMMENT
<b>0.526 ± 0.008 OUR FIT</b>				
<b>0.513 ± 0.022 OUR AVERAGE</b>				Error includes scale factor of 2.2.

0.5047 ± 0.0022 ± 0.0102	61k	MENDEZ 08	CLEO	$\psi(2S) \rightarrow \ell^+\ell^-2\pi^0$
0.570 ± 0.009 ± 0.026	14k	<sup>1</sup> ABLIKIM	04B	BES $\psi(2S) \rightarrow J/\psi X$

• • • We do not use the following data for averages, fits, limits, etc. • • •

0.4924 ± 0.0047 ± 0.0086	73k	<sup>2,3</sup> ADAM	05A	CLEO Repl. by MENDEZ 08
0.571 ± 0.018 ± 0.044		<sup>4</sup> ANDREOTTI 05	E835	$\psi(2S) \rightarrow J/\psi X$
0.53 ± 0.06		TANENBAUM 76	MRK1	$e^+e^-$
0.64 ± 0.15		<sup>5</sup> HILGER	75	SPEC $e^+e^-$

<sup>1</sup> From a fit to the  $J/\psi$  recoil mass spectra.

<sup>2</sup> Not independent from other values reported by ADAM 05A.

<sup>3</sup> Using 13,217  $J/\psi\pi^0\pi^0$  and 60,010  $J/\psi\pi^+\pi^-$  events.

<sup>4</sup> Not independent from other values reported by ANDREOTTI 05.

<sup>5</sup> Ignoring the  $J/\psi(1S)\eta$  and  $J/\psi(1S)\gamma\gamma$  decays.

 $\Gamma(J/\psi(1S)\eta)/\Gamma_{\text{total}}$   $\Gamma_{13}/\Gamma$ 

VALUE (units $10^{-3}$ )	EVTs	DOCUMENT ID	TECN	COMMENT
<b>33.9 ± 0.5 OUR FIT</b>				
<b>32.9 ± 1.7 OUR AVERAGE</b>				Error includes scale factor of 2.1. See the ideogram below.

33.75 ± 0.17 ± 0.86	68.2k	ABLIKIM	12M	BES3 $e^+e^- \rightarrow \ell^+\ell^-2\gamma$
29.8 ± 0.9 ± 2.3	5.7k	BAI	04I	BES2 $\psi(2S) \rightarrow J/\psi\gamma\gamma$
25.5 ± 2.9	386	<sup>1</sup> OREGLIA	80	CBAL $e^+e^- \rightarrow J/\psi 2\gamma$
45 ± 12	17	<sup>2</sup> BRANDELIK	79B	DASP $e^+e^- \rightarrow J/\psi 2\gamma$
42 ± 6	164	<sup>2</sup> BARTEL	78B	CNTR $e^+e^-$

• • • We do not use the following data for averages, fits, limits, etc. • • •

34.3 ± 0.4 ± 0.9 18.4k <sup>3</sup> MENDEZ 08 CLEO  $\psi(2S) \rightarrow \ell^+\ell^-\eta$

32.5 ± 0.6 ± 1.1 2.8k <sup>4</sup> ADAM 05A CLEO Repl. by MENDEZ 08

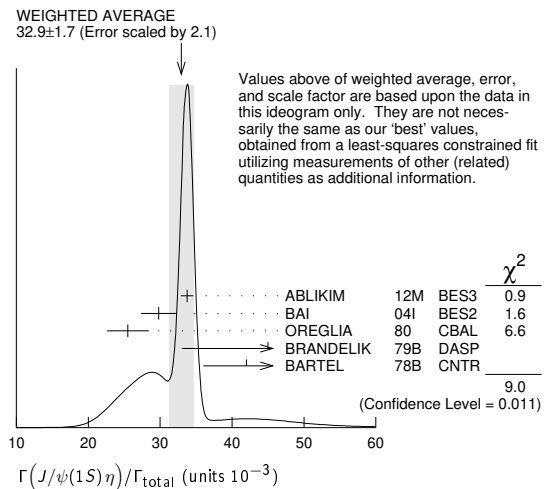
43 ± 8 44 TANENBAUM 76 MRK1  $e^+e^-$

<sup>1</sup> Recalculated by us using  $B(J/\psi(1S) \rightarrow \ell^+\ell^-) = 0.1181 \pm 0.0020$ .

<sup>2</sup> Recalculated by us using  $B(J/\psi(1S) \rightarrow \mu^+\mu^-) = 0.0588 \pm 0.0010$ .

<sup>3</sup> Not independent from other measurements of MENDEZ 08.

<sup>4</sup> Not independent from other values reported by ADAM 05A.

 $\Gamma(J/\psi(1S)\eta)/\Gamma(J/\psi(1S)\text{anything})$   $\Gamma_{13}/\Gamma_9$ 

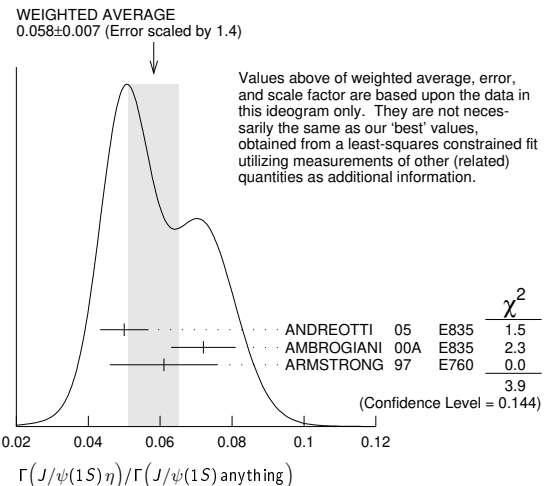
VALUE	EVTs	DOCUMENT ID	TECN	COMMENT
<b>0.0549 ± 0.0008 OUR FIT</b>				
<b>0.058 ± 0.007 OUR AVERAGE</b>				Error includes scale factor of 1.4. See the ideogram below.

0.050 ± 0.006 ± 0.003	298 ± 20	ANDREOTTI 05	E835	$\psi(2S) \rightarrow J/\psi X$
0.072 ± 0.009		AMBROGIANI 00A	E835	$p\bar{p} \rightarrow \psi(2S)$
0.061 ± 0.015		ARMSTRONG 97	E760	$\bar{p}p \rightarrow \psi(2S)$

• • • We do not use the following data for averages, fits, limits, etc. • • •

0.0549 ± 0.0006 ± 0.0009	18.4k	<sup>1</sup> MENDEZ 08	CLEO	$\psi(2S) \rightarrow \ell^+\ell^-\eta$
0.0546 ± 0.0010 ± 0.0007	2.8k	ADAM 05A	CLEO	Repl. by MENDEZ 08

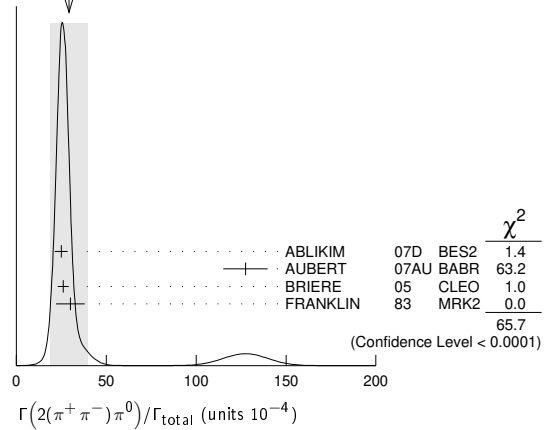
<sup>1</sup> Not independent from other measurements of MENDEZ 08.



$\Gamma(J/\psi(1S)\eta)/\Gamma(J/\psi(1S)\pi^+\pi^-)$   $\Gamma_{13}/\Gamma_{11}$

VALUE	EVTs	DOCUMENT ID	TECN	COMMENT
<b>0.0972 ± 0.0014 OUR FIT</b>				
<b>0.0979 ± 0.0018 OUR AVERAGE</b>				
0.0979 ± 0.0010 ± 0.0015	18.4k	MENDEZ	08	CLEO $\psi(2S) \rightarrow \ell^+\ell^-\eta$
0.098 ± 0.005 ± 0.010	2k	<sup>1</sup> ABLIKIM	04b	BES $\psi(2S) \rightarrow J/\psi X$
0.091 ± 0.021		<sup>2</sup> HIMEL	80	MRK2 $e^+e^- \rightarrow \psi(2S)X$
• • • We do not use the following data for averages, fits, limits, etc. • • •				
0.0968 ± 0.0019 ± 0.0013	2.8k	<sup>3</sup> ADAM	05A	CLEO Repl. by MENDEZ 08
0.095 ± 0.007 ± 0.007		<sup>4</sup> ANDREOTTI	05	E835 $\psi(2S) \rightarrow J/\psi X$
<sup>1</sup> From a fit to the $J/\psi$ recoil mass spectra.				
<sup>2</sup> The value for $B(\psi(2S) \rightarrow J/\psi(1S)\eta)$ reported in HIMEL 80 is derived using $B(\psi(2S) \rightarrow J/\psi(1S)\pi^+\pi^-) = (33 \pm 3)\%$ and $B(J/\psi(1S) \rightarrow \ell^+\ell^-) = 0.138 \pm 0.018$ . Calculated by us using $B(J/\psi(1S) \rightarrow \ell^+\ell^-) = (0.1181 \pm 0.0020)$ .				
<sup>3</sup> Not independent from other values reported by ADAM 05A.				
<sup>4</sup> Not independent from other values reported by ANDREOTTI 05.				

WEIGHTED AVERAGE  
 $29 \pm 10$  (Error scaled by 4.7)



$\Gamma(J/\psi(1S)\pi^0)/\Gamma_{total}$   $\Gamma_{14}/\Gamma$

VALUE (units $10^{-4}$ )	EVTs	DOCUMENT ID	TECN	COMMENT
<b>12.68 ± 0.32 OUR AVERAGE</b>				
12.6 ± 0.2 ± 0.3	4.1k	ABLIKIM	12M	BES3 $e^+e^- \rightarrow \ell^+\ell^-2\gamma$
13.3 ± 0.8 ± 0.3	530	MENDEZ	08	CLEO $\psi(2S) \rightarrow \ell^+\ell^-2\gamma$
14.3 ± 1.4 ± 1.2	280	BAI	04i	BES2 $\psi(2S) \rightarrow J/\psi\gamma\gamma$
14 ± 6	7	HIMEL	80	MRK2 $e^+e^-$
9 ± 2 ± 1	23	<sup>1</sup> OREGLIA	80	CBAL $\psi(2S) \rightarrow J/\psi 2\gamma$
• • • We do not use the following data for averages, fits, limits, etc. • • •				
13 ± 1 ± 1	88	ADAM	05A	CLEO Repl. by MENDEZ 08
<sup>1</sup> Recalculated by us using $B(J/\psi(1S) \rightarrow \ell^+\ell^-) = 0.1181 \pm 0.0020$ .				

$\Gamma(\rho_{22}(1320))/\Gamma_{total}$   $\Gamma_{18}/\Gamma$

VALUE (units $10^{-4}$ )	CL%	EVTs	DOCUMENT ID	TECN	COMMENT
<b>2.55 ± 0.73 ± 0.47</b>		112 ± 31	BAI	04c	BES2 $\psi(2S) \rightarrow 2(\pi^+\pi^-)\pi^0$
• • • We do not use the following data for averages, fits, limits, etc. • • •					
< 2.3		90	BAI	98J	BES $e^+e^-$

$\Gamma(J/\psi(1S)\pi^0)/\Gamma(J/\psi(1S)\text{ anything})$   
 $\Gamma_{14}/\Gamma_9 = \Gamma_{14}/(\Gamma_{11} + \Gamma_{12} + \Gamma_{13} + 0.343\Gamma_{154} + 0.190\Gamma_{155})$

VALUE (units $10^{-2}$ )	EVTs	DOCUMENT ID	TECN	COMMENT
• • • We do not use the following data for averages, fits, limits, etc. • • •				
0.213 ± 0.012 ± 0.003	527	<sup>1</sup> MENDEZ	08	CLEO $e^+e^- \rightarrow J/\psi\gamma\gamma$
0.22 ± 0.02 ± 0.01		<sup>2</sup> ADAM	05A	CLEO $e^+e^- \rightarrow \psi(2S) \rightarrow J/\psi\gamma\gamma$
<sup>1</sup> Not independent from other values reported by MENDEZ 08. Supersedes ADAM 05A.				
<sup>2</sup> Not independent from other values reported by ADAM 05A.				

$\Gamma(\rho\bar{\rho})/\Gamma_{total}$   $\Gamma_{21}/\Gamma$

VALUE (units $10^{-4}$ )	EVTs	DOCUMENT ID	TECN	COMMENT
<b>2.94 ± 0.08 OUR FIT</b>				
<b>3.02 ± 0.08 OUR AVERAGE</b>				
3.05 ± 0.02 ± 0.12	19k	ABLIKIM	18T	BES3 $e^+e^- \rightarrow \psi(2S) \rightarrow \rho\bar{\rho}$
3.08 ± 0.05 ± 0.18	4.5k	<sup>1</sup> DOBBS	14	$e^+e^- \rightarrow \psi(2S) \rightarrow \rho\bar{\rho}$
3.36 ± 0.09 ± 0.25	1.6k	ABLIKIM	07c	BES $e^+e^- \rightarrow \psi(2S) \rightarrow \rho\bar{\rho}$
2.87 ± 0.12 ± 0.15	557	PEDLAR	05	CLEO $e^+e^- \rightarrow \psi(2S) \rightarrow \rho\bar{\rho}$
1.4 ± 0.8	4	BRANDELIK	79c	DASP $e^+e^- \rightarrow \psi(2S) \rightarrow \rho\bar{\rho}$
2.3 ± 0.7		FELDMAN	77	MRK1 $e^+e^- \rightarrow \psi(2S) \rightarrow \rho\bar{\rho}$
<sup>1</sup> Using CLEO-c data but not authored by the CLEO Collaboration.				

$\Gamma(J/\psi(1S)\pi^0)/\Gamma(J/\psi(1S)\pi^+\pi^-)$   $\Gamma_{14}/\Gamma_{11}$

VALUE (units $10^{-2}$ )	EVTs	DOCUMENT ID	TECN	COMMENT
• • • We do not use the following data for averages, fits, limits, etc. • • •				
0.380 ± 0.022 ± 0.005	527	<sup>1</sup> MENDEZ	08	CLEO $e^+e^- \rightarrow J/\psi\gamma\gamma$
0.39 ± 0.04 ± 0.01		<sup>2</sup> ADAM	05A	CLEO $e^+e^- \rightarrow \psi(2S) \rightarrow J/\psi\gamma\gamma$
<sup>1</sup> Not independent from other values reported by MENDEZ 08. Supersedes ADAM 05A.				
<sup>2</sup> Not independent from other values reported by ADAM 05A.				

$\Gamma(\rho\bar{\rho})/\Gamma(J/\psi(1S)\pi^+\pi^-)$   $\Gamma_{21}/\Gamma_{11}$

VALUE (units $10^{-4}$ )	DOCUMENT ID	TECN	COMMENT
<b>8.49 ± 0.23 OUR FIT</b>			
<b>6.98 ± 0.49 ± 0.97</b>	BAI	01	BES $e^+e^- \rightarrow \psi(2S) \rightarrow \rho\bar{\rho}$

HADRONIC DECAYS

$\Gamma(\pi^0 h_c(1P))/\Gamma_{total}$   $\Gamma_{15}/\Gamma$

VALUE (units $10^{-4}$ )	EVTs	DOCUMENT ID	TECN	COMMENT
<b>8.6 ± 1.3 OUR AVERAGE</b>				
9.0 ± 1.5 ± 1.3	3k	<sup>1</sup> GE	11	CLEO $\psi(2S) \rightarrow \pi^0$ anything
8.4 ± 1.3 ± 1.0	11k	ABLIKIM	10b	BES3 $\psi(2S) \rightarrow \pi^0 h_c$
• • • We do not use the following data for averages, fits, limits, etc. • • •				
seen	92 ± 23	ADAMS	09	CLEO $\psi(2S) \rightarrow 2\pi^+ 2\pi^- 2\pi^0$
seen	1282	DOBBS	08A	CLEO $\psi(2S) \rightarrow \pi^0 \eta_c \gamma$
seen	168 ± 40	ROSNER	05	CLEO $\psi(2S) \rightarrow \pi^0 \eta_c \gamma$
<sup>1</sup> Assuming a width $\Gamma(h_c(1P)) = 0.86 \text{ MeV} \equiv \Gamma_0$ , a measured dependence of the central value of $B = (7.6 \pm 1.4 \times \Gamma(h_c(1P))/\Gamma_0) \times 10^{-4}$ , and with a systematic error that accounts for the width variation range 0.43–1.29 MeV.				

$\Gamma(n\bar{n})/\Gamma_{total}$   $\Gamma_{22}/\Gamma$

VALUE (units $10^{-4}$ )	EVTs	DOCUMENT ID	TECN	COMMENT
<b>3.06 ± 0.06 ± 0.14</b>	6k	ABLIKIM	18T	BES3 $e^+e^- \rightarrow \psi(2S) \rightarrow n\bar{n}$

$\Gamma(\Delta^{++}\bar{\Delta}^{--})/\Gamma_{total}$   $\Gamma_{23}/\Gamma$

VALUE (units $10^{-5}$ )	EVTs	DOCUMENT ID	TECN	COMMENT
<b>12.8 ± 1.0 ± 3.4</b>	157	<sup>1</sup> BAI	01	BES $e^+e^- \rightarrow \psi(2S) \rightarrow$ hadrons
<sup>1</sup> Estimated using $B(\psi(2S) \rightarrow J/\psi\pi^+\pi^-) = 0.310 \pm 0.028$ .				

$\Gamma(3(\pi^+\pi^-)\pi^0)/\Gamma_{total}$   $\Gamma_{16}/\Gamma$

VALUE (units $10^{-4}$ )	EVTs	DOCUMENT ID	TECN	COMMENT
<b>35 ± 16</b>	6	FRANKLIN	83	MRK2 $e^+e^- \rightarrow$ hadrons

$\Gamma(\Lambda\bar{\Lambda}\pi^0)/\Gamma_{total}$   $\Gamma_{24}/\Gamma$

VALUE (units $10^{-5}$ )	CL%	EVTs	DOCUMENT ID	TECN	COMMENT
<b>&lt; 0.29</b>	90	<sup>1</sup> ABLIKIM	13F	BES3 $\psi(2S) \rightarrow p\bar{p}\pi^+\pi^-\gamma\gamma$	
• • • We do not use the following data for averages, fits, limits, etc. • • •					
< 12	90	<sup>2</sup> ABLIKIM	07H	BES2 $e^+e^- \rightarrow \psi(2S)$	
<sup>1</sup> Using $B(\Lambda \rightarrow \pi^- p) = 63.9\%$ and $B(\pi^0 \rightarrow \gamma\gamma) = 98.8\%$ .					
<sup>2</sup> Using $B(\Lambda \rightarrow \pi^- p) = 63.9\%$ and $B(\eta \rightarrow \gamma\gamma) = 39.4\%$ .					

$\Gamma(2(\pi^+\pi^-)\pi^0)/\Gamma_{total}$   $\Gamma_{17}/\Gamma$

VALUE (units $10^{-4}$ )	EVTs	DOCUMENT ID	TECN	COMMENT
<b>29 ± 10 OUR AVERAGE</b>				
Error includes scale factor of 4.7. See the ideogram below.				
24.9 ± 0.7 ± 3.6	2173	ABLIKIM	07d	BES2 $e^+e^- \rightarrow \psi(2S)$
127 ± 12 ± 2	410	<sup>1</sup> AUBERT	07AU	BABR 10.6 $e^+e^- \rightarrow 2(\pi^+\pi^-)\pi^0\gamma$
26.1 ± 0.7 ± 3.0	1703	BRIERE	05	CLEO $e^+e^- \rightarrow \psi(2S) \rightarrow 2(\pi^+\pi^-)\pi^0$
30 ± 8	42	FRANKLIN	83	MRK2 $e^+e^-$
<sup>1</sup> AUBERT 07AU reports $[\Gamma(\psi(2S) \rightarrow 2(\pi^+\pi^-)\pi^0)/\Gamma_{total}] \times [\Gamma(\psi(2S) \rightarrow e^+e^-)] = (297 \pm 22 \pm 18) \times 10^{-4} \text{ keV}$ which we divide by our best value $\Gamma(\psi(2S) \rightarrow e^+e^-) = 2.33 \pm 0.04 \text{ keV}$ . Our first error is their experiment's error and our second error is the systematic error from using our best value.				

$\Gamma(\Lambda\bar{\Lambda}\eta)/\Gamma_{total}$   $\Gamma_{25}/\Gamma$

VALUE (units $10^{-5}$ )	CL%	EVTs	DOCUMENT ID	TECN	COMMENT
<b>2.46 ± 0.34 ± 0.19</b>	60	<sup>1</sup> ABLIKIM	13F	BES3 $\psi(2S) \rightarrow p\bar{p}\pi^+\pi^-\gamma\gamma$	
• • • We do not use the following data for averages, fits, limits, etc. • • •					
< 4.9	90	<sup>2</sup> ABLIKIM	07H	BES2 $e^+e^- \rightarrow \psi(2S)$	
<sup>1</sup> Using $B(\Lambda \rightarrow \pi^- p) = 63.9\%$ and $B(\eta \rightarrow \gamma\gamma) = 39.31\%$ .					
<sup>2</sup> Using $B(\Lambda \rightarrow \pi^- p) = 63.9\%$ .					

$\Gamma(\Lambda\bar{\Lambda}K^+)/\Gamma_{total}$   $\Gamma_{26}/\Gamma$

VALUE (units $10^{-4}$ )	EVTs	DOCUMENT ID	TECN	COMMENT
<b>1.0 ± 0.1 ± 0.1</b>	74.0	BRIERE	05	CLEO $e^+e^- \rightarrow \psi(2S) \rightarrow p\bar{p}K^+\pi^-$

$\Gamma(K^*(892)^+\bar{p}\Lambda + \text{c.c.})/\Gamma_{total}$   $\Gamma_{27}/\Gamma$

VALUE (units $10^{-5}$ )	EVTs	DOCUMENT ID	TECN	COMMENT
<b>6.3 ± 0.5 ± 0.5</b>	1011	ABLIKIM	19AU	BES3 $e^+e^- \rightarrow \psi(2S)$

# Meson Particle Listings

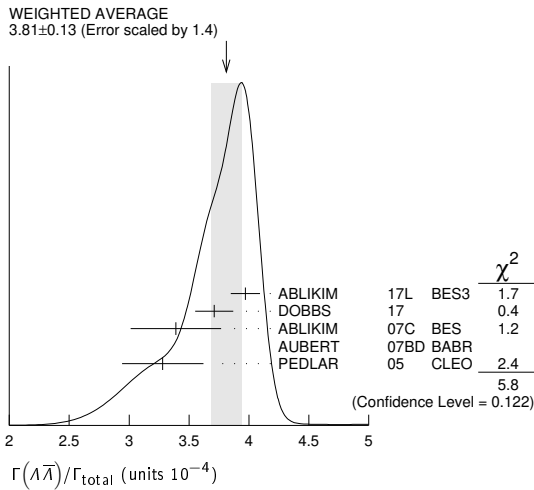
## $\psi(2S)$

$\Gamma(\Lambda\bar{p}K^+\pi^+\pi^-)/\Gamma_{total}$				$\Gamma_{28}/\Gamma$
VALUE (units $10^{-4}$ )	EVTS	DOCUMENT ID	TECN	COMMENT
<b>1.8 ± 0.3 ± 0.3</b>	45.8	BRIERE	05	CLEO $e^+e^- \rightarrow \psi(2S) \rightarrow p\bar{p}K^+\pi^+\pi^-$

$\Gamma(\Lambda\bar{\Lambda}\pi^+\pi^-)/\Gamma_{total}$				$\Gamma_{29}/\Gamma$
VALUE (units $10^{-4}$ )	EVTS	DOCUMENT ID	TECN	COMMENT
<b>2.8 ± 0.4 ± 0.5</b>	73.4	BRIERE	05	CLEO $e^+e^- \rightarrow \psi(2S) \rightarrow p\bar{p}2(\pi^+\pi^-)$

$\Gamma(\Lambda\bar{\Lambda})/\Gamma_{total}$				$\Gamma_{30}/\Gamma$
VALUE (units $10^{-4}$ )	CL% EVTS	DOCUMENT ID	TECN	COMMENT
<b>3.81 ± 0.13 OUR AVERAGE</b>		Error includes scale factor of 1.4. See the ideogram below.		
3.97 ± 0.02 ± 0.12	31k	ABLIKIM	17L	BES3 $e^+e^- \rightarrow \Lambda\bar{\Lambda}$
3.71 ± 0.05 ± 0.15	6.5k	<sup>1</sup> DOBBS	17	$e^+e^- \rightarrow \Lambda\bar{\Lambda}$
3.39 ± 0.20 ± 0.32	337	ABLIKIM	07c	BES $e^+e^- \rightarrow \psi(2S) \rightarrow$ hadrons
6.4 ± 1.8 ± 0.1		<sup>2</sup> AUBERT	07BD	BABR 10.6 $e^+e^- \rightarrow \Lambda\bar{\Lambda}\gamma$
3.28 ± 0.23 ± 0.25	208	PEDLAR	05	CLEO $e^+e^- \rightarrow \psi(2S) \rightarrow$ hadrons
• • • We do not use the following data for averages, fits, limits, etc. • • •				
3.75 ± 0.09 ± 0.23	1.9k	<sup>1,3</sup> DOBBS	14	$e^+e^- \rightarrow \Lambda\bar{\Lambda}$
1.81 ± 0.20 ± 0.27	80	<sup>4</sup> BAI	01	BES $e^+e^- \rightarrow \psi(2S) \rightarrow$ hadrons
< 4	90	FELDMAN	77	MRK1 $e^+e^- \rightarrow \psi(2S) \rightarrow$ hadrons

- Using CLEO-c data but not authored by the CLEO Collaboration.
- AUBERT 07BD reports  $[\Gamma(\psi(2S) \rightarrow \Lambda\bar{\Lambda})/\Gamma_{total}] \times [\Gamma(\psi(2S) \rightarrow e^+e^-)] = (15 \pm 4 \pm 1) \times 10^{-4}$  keV, which we divide by our best value  $\Gamma(\psi(2S) \rightarrow e^+e^-) = 2.33 \pm 0.04$  keV. Our first error is their experiment's error and our second error is the systematic error from using our best value.
- Superseded by DOBBS 17.
- Estimated using  $B(\psi(2S) \rightarrow J/\psi\pi^+\pi^-) = 0.310 \pm 0.028$ .



$\Gamma(\Lambda\Sigma^+\pi^- + c.c.)/\Gamma_{total}$				$\Gamma_{31}/\Gamma$
VALUE (units $10^{-4}$ )	EVTS	DOCUMENT ID	TECN	COMMENT
<b>1.40 ± 0.03 ± 0.13</b>	2.8k	ABLIKIM	13W	BES3 $\psi(2S) \rightarrow$ hadrons

$\Gamma(\Lambda\Sigma^-\pi^+ + c.c.)/\Gamma_{total}$				$\Gamma_{32}/\Gamma$
VALUE (units $10^{-4}$ )	EVTS	DOCUMENT ID	TECN	COMMENT
<b>1.54 ± 0.04 ± 0.13</b>	2.8k	ABLIKIM	13W	BES3 $\psi(2S) \rightarrow$ hadrons

$\Gamma(\Lambda\Sigma^0)/\Gamma_{total}$				$\Gamma_{33}/\Gamma$
VALUE (units $10^{-5}$ )	EVTS	DOCUMENT ID	COMMENT	
<b>1.23 ± 0.23 ± 0.08</b>	30	<sup>1</sup> DOBBS	17	$e^+e^- \rightarrow \psi(2S) \rightarrow$ hadrons

<sup>1</sup> Using CLEO-c data but not authored by the CLEO Collaboration.

$\Gamma(\Sigma^0\bar{p}K^+ + c.c.)/\Gamma_{total}$				$\Gamma_{34}/\Gamma$
VALUE (units $10^{-5}$ )	EVTS	DOCUMENT ID	TECN	COMMENT
<b>1.67 ± 0.13 ± 0.12</b>	276	<sup>1</sup> ABLIKIM	13D	BES3 $\psi(2S) \rightarrow \gamma\Lambda\bar{p}K^+$

<sup>1</sup> Using  $B(\Lambda \rightarrow p\pi^-) = 63.9\%$ , and  $B(\Sigma^0 \rightarrow \Lambda\gamma) = 100\%$ .

$\Gamma(\Sigma^+\bar{\Sigma}^-)/\Gamma_{total}$				$\Gamma_{35}/\Gamma$
VALUE (units $10^{-4}$ )	CL% EVTS	DOCUMENT ID	TECN	COMMENT
<b>2.32 ± 0.12 OUR AVERAGE</b>		Error includes scale factor of 1.4. See the ideogram below.		
2.31 ± 0.06 ± 0.10	1.9k	<sup>1</sup> DOBBS	17	$e^+e^- \rightarrow \psi(2S) \rightarrow$ hadrons
2.57 ± 0.44 ± 0.68	35	PEDLAR	05	CLEO $e^+e^- \rightarrow \psi(2S) \rightarrow$ hadrons
• • • We do not use the following data for averages, fits, limits, etc. • • •				
2.51 ± 0.15 ± 0.16	281	<sup>1,2</sup> DOBBS	14	$e^+e^- \rightarrow \psi(2S) \rightarrow$ hadrons

<sup>1</sup> Using CLEO-c data but not authored by the CLEO Collaboration.  
<sup>2</sup> Superseded by DOBBS 17.

$\Gamma(\Sigma^0\bar{\Sigma}^0)/\Gamma_{total}$				$\Gamma_{36}/\Gamma$
VALUE (units $10^{-4}$ )	EVTS	DOCUMENT ID	TECN	COMMENT
<b>2.35 ± 0.09 OUR AVERAGE</b>		Error includes scale factor of 1.1.		
2.44 ± 0.03 ± 0.11	7k	ABLIKIM	17L	BES3 $e^+e^- \rightarrow \psi(2S) \rightarrow$ hadrons
2.22 ± 0.05 ± 0.11	2.6k	<sup>1</sup> DOBBS	17	$e^+e^- \rightarrow \psi(2S) \rightarrow$ hadrons
2.35 ± 0.36 ± 0.32	59	ABLIKIM	07c	BES $e^+e^- \rightarrow \psi(2S) \rightarrow$ hadrons
2.63 ± 0.35 ± 0.21	58	PEDLAR	05	CLEO $e^+e^- \rightarrow \psi(2S) \rightarrow$ hadrons
• • • We do not use the following data for averages, fits, limits, etc. • • •				
2.25 ± 0.11 ± 0.16	439	<sup>1,2</sup> DOBBS	14	$e^+e^- \rightarrow \psi(2S) \rightarrow$ hadrons
1.2 ± 0.4 ± 0.4	8	<sup>3</sup> BAI	01	BES $e^+e^- \rightarrow \psi(2S) \rightarrow$ hadrons

<sup>1</sup> Using CLEO-c data but not authored by the CLEO Collaboration.  
<sup>2</sup> Superseded by DOBBS 17.  
<sup>3</sup> Estimated using  $B(\psi(2S) \rightarrow J/\psi\pi^+\pi^-) = 0.310 \pm 0.028$ .

$\Gamma(\Sigma(1385)^+\bar{\Sigma}(1385)^-)/\Gamma_{total}$				$\Gamma_{37}/\Gamma$
VALUE (units $10^{-5}$ )	EVTS	DOCUMENT ID	TECN	COMMENT
<b>8.5 ± 0.7 OUR AVERAGE</b>		Error includes scale factor of 1.1.		
8.4 ± 0.5 ± 0.5	1.5k	ABLIKIM	16L	BES3 $\psi(2S) \rightarrow \Sigma(1385)^+\bar{\Sigma}(1385)^-$
11 ± 3 ± 3	14	<sup>1</sup> BAI	01	BES $e^+e^- \rightarrow \psi(2S) \rightarrow$ hadrons

<sup>1</sup> Estimated using  $B(\psi(2S) \rightarrow J/\psi\pi^+\pi^-) = 0.310 \pm 0.028$ .

$\Gamma(\Sigma(1385)^-\bar{\Sigma}(1385)^+)/\Gamma_{total}$				$\Gamma_{38}/\Gamma$
VALUE (units $10^{-5}$ )	EVTS	DOCUMENT ID	TECN	COMMENT
<b>8.5 ± 0.6 ± 0.6</b>	1.4k	ABLIKIM	16L	BES3 $\psi(2S) \rightarrow \Sigma(1385)^-\bar{\Sigma}(1385)^+$

$\Gamma(\Sigma(1385)^0\bar{\Sigma}(1385)^0)/\Gamma_{total}$				$\Gamma_{39}/\Gamma$
VALUE (units $10^{-4}$ )	EVTS	DOCUMENT ID	TECN	COMMENT
<b>0.69 ± 0.05 ± 0.05</b>	2.2k	ABLIKIM	17E	BES3 $e^+e^- \rightarrow \psi(2S) \rightarrow$ hadrons

$\Gamma(\Xi^-\bar{\Xi}^+)/\Gamma_{total}$				$\Gamma_{40}/\Gamma$
VALUE (units $10^{-4}$ )	CL% EVTS	DOCUMENT ID	TECN	COMMENT
<b>2.87 ± 0.11 OUR AVERAGE</b>		Error includes scale factor of 1.1.		
3.03 ± 0.05 ± 0.14	3.6k	<sup>1</sup> DOBBS	17	$e^+e^- \rightarrow \psi(2S) \rightarrow$ hadrons
2.78 ± 0.05 ± 0.14	5k	ABLIKIM	16L	BES3 $\psi(2S) \rightarrow \Xi^-\bar{\Xi}^+$
3.03 ± 0.40 ± 0.32	67	ABLIKIM	07c	BES $e^+e^- \rightarrow \psi(2S) \rightarrow$ hadrons
2.38 ± 0.30 ± 0.21	63	PEDLAR	05	CLEO $e^+e^- \rightarrow \psi(2S) \rightarrow$ hadrons
• • • We do not use the following data for averages, fits, limits, etc. • • •				
2.66 ± 0.12 ± 0.20	548	<sup>1,2</sup> DOBBS	14	$e^+e^- \rightarrow \psi(2S) \rightarrow$ hadrons
0.94 ± 0.27 ± 0.15	12	<sup>3</sup> BAI	01	BES $e^+e^- \rightarrow \psi(2S) \rightarrow$ hadrons
< 2	90	FELDMAN	77	MRK1 $e^+e^- \rightarrow \psi(2S) \rightarrow$ hadrons

<sup>1</sup> Using CLEO-c data but not authored by the CLEO Collaboration.  
<sup>2</sup> Superseded by DOBBS 17.  
<sup>3</sup> Estimated using  $B(\psi(2S) \rightarrow J/\psi\pi^+\pi^-) = 0.310 \pm 0.028$ .

$\Gamma(\Xi^0\bar{\Xi}^0)/\Gamma_{total}$				$\Gamma_{41}/\Gamma$
VALUE (units $10^{-4}$ )	EVTS	DOCUMENT ID	TECN	COMMENT
<b>2.3 ± 0.4 OUR AVERAGE</b>		Error includes scale factor of 4.2.		
2.73 ± 0.03 ± 0.13	11k	ABLIKIM	17E	BES3 $e^+e^- \rightarrow \psi(2S) \rightarrow$ hadrons
1.97 ± 0.06 ± 0.11	1.2k	<sup>1</sup> DOBBS	17	$e^+e^- \rightarrow \psi(2S) \rightarrow$ hadrons
2.75 ± 0.64 ± 0.61	19	PEDLAR	05	CLEO $e^+e^- \rightarrow \psi(2S) \rightarrow$ hadrons
• • • We do not use the following data for averages, fits, limits, etc. • • •				
2.02 ± 0.19 ± 0.15	112	<sup>1,2</sup> DOBBS	14	$e^+e^- \rightarrow \psi(2S) \rightarrow$ hadrons

<sup>1</sup> Using CLEO-c data but not authored by the CLEO Collaboration.  
<sup>2</sup> Superseded by DOBBS 17.

$\Gamma(\Xi(1530)^0\bar{\Xi}(1530)^0)/\Gamma_{total}$				$\Gamma_{42}/\Gamma$
VALUE (units $10^{-5}$ )	CL% EVTS	DOCUMENT ID	TECN	COMMENT
<b>5.2 ± 0.3 ± 3.2 ± 1.2</b>	527	<sup>1</sup> ABLIKIM	13S	BES3 $\psi(2S) \rightarrow \eta\rho\bar{p}$
• • • We do not use the following data for averages, fits, limits, etc. • • •				
< 32	90	PEDLAR	05	CLEO $e^+e^- \rightarrow \psi(2S) \rightarrow$ hadrons
< 8.1	90	<sup>2</sup> BAI	01	BES $e^+e^- \rightarrow \psi(2S) \rightarrow$ hadrons

<sup>1</sup> With  $N(1535)$  decaying to  $p\eta$ .  
<sup>2</sup> Estimated using  $B(\psi(2S) \rightarrow J/\psi\pi^+\pi^-) = 0.310 \pm 0.028$ .

$\Gamma(\Xi(1530)^-\bar{\Xi}(1530)^+)/\Gamma_{total}$				$\Gamma_{44}/\Gamma$
VALUE (units $10^{-5}$ )	EVTS	DOCUMENT ID	TECN	COMMENT
<b>11.45 ± 0.40 ± 0.59</b>	5k	ABLIKIM	19AT	BES3 $e^+e^- \rightarrow \psi(2S) \rightarrow$ hadrons

$\Gamma(\Xi(1530)^-\bar{\Xi}^+)/\Gamma_{total}$				$\Gamma_{45}/\Gamma$
VALUE (units $10^{-6}$ )	EVTS	DOCUMENT ID	TECN	COMMENT
<b>7.0 ± 1.1 ± 0.4</b>	399	ABLIKIM	19AT	BES3 $e^+e^- \rightarrow \psi(2S) \rightarrow$ hadrons

$\Gamma(K^-\Lambda\bar{\Xi}^+ + c.c.)/\Gamma_{total}$				$\Gamma_{43}/\Gamma$
VALUE (units $10^{-5}$ )	EVTS	DOCUMENT ID	TECN	COMMENT
<b>3.86 ± 0.27 ± 0.32</b>	236	ABLIKIM	15I	BES3 $e^+e^- \rightarrow \psi(2S) \rightarrow K^-\Lambda\bar{\Xi}^+ + c.c.$



# Meson Particle Listings

## $\psi(2S)$

$\Gamma(\rho^0 \pi^+ \pi^- \pi^0)/\Gamma_{total}$			$\Gamma_{69}/\Gamma$		
VALUE (units $10^{-4}$ )	EVTS	DOCUMENT ID	TECN	COMMENT	
<b><math>3.18 \pm 0.50 \pm 0.50</math></b>	135 ± 21	ABLIKIM	06i	BES2	$e^+e^- \rightarrow \rho \pi^- \pi^0 \chi$

$\Gamma(\eta \pi^+ \pi^-)/\Gamma_{total}$			$\Gamma_{71}/\Gamma$		
VALUE (units $10^{-4}$ )	CL%	DOCUMENT ID	TECN	COMMENT	
<b>&lt;1.6</b>	90	BRIERE	05	CLEO	$e^+e^- \rightarrow \psi(2S) \rightarrow 2(\pi^+ \pi^-) \pi^0$

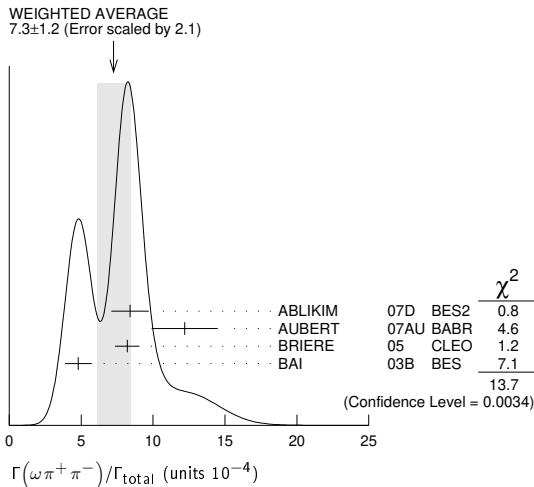
$\Gamma(\eta \pi^+ \pi^- \pi^0)/\Gamma_{total}$			$\Gamma_{72}/\Gamma$		
VALUE (units $10^{-4}$ )	EVTS	DOCUMENT ID	TECN	COMMENT	
<b><math>9.5 \pm 0.7 \pm 1.5</math></b>		<sup>1</sup> BRIERE	05	CLEO	$e^+e^- \rightarrow \psi(2S) \rightarrow \text{hadr}$
• • • We do not use the following data for averages, fits, limits, etc. • • •					
$10.3 \pm 0.8 \pm 1.4$	201.7	<sup>2</sup> BRIERE	05	CLEO	$e^+e^- \rightarrow \psi(2S) \rightarrow \eta 3\pi(\eta \rightarrow \gamma\gamma)$
$8.1 \pm 1.4 \pm 1.6$	50.0	<sup>2</sup> BRIERE	05	CLEO	$e^+e^- \rightarrow \psi(2S) \rightarrow \eta 3\pi(\eta \rightarrow 3\pi)$

<sup>1</sup> Average of  $\eta \rightarrow \gamma\gamma$  and  $\eta \rightarrow 3\pi$ .  
<sup>2</sup> Not independent from other values reported by BRIERE 05.

$\Gamma(2(\pi^+ \pi^-)\eta)/\Gamma_{total}$			$\Gamma_{73}/\Gamma$		
VALUE (units $10^{-3}$ )	EVTS	DOCUMENT ID	TECN	COMMENT	
<b><math>1.2 \pm 0.6 \pm 0.1</math></b>	16	<sup>1</sup> AUBERT	07AU	BABR	$10.6 e^+e^- \rightarrow 2(\pi^+ \pi^-)\eta\gamma$
<sup>1</sup> AUBERT 07AU quotes $\Gamma_{ee}^{\psi(2S)} \cdot B(\psi(2S) \rightarrow 2(\pi^+ \pi^-)\eta) \cdot B(\eta \rightarrow \gamma\gamma) = 1.2 \pm 0.7 \pm 0.1 \text{ eV}$ .					

$\Gamma(\eta' \pi^+ \pi^- \pi^0)/\Gamma_{total}$			$\Gamma_{75}/\Gamma$		
VALUE (units $10^{-4}$ )	EVTS	DOCUMENT ID	TECN	COMMENT	
<b><math>4.5 \pm 1.6 \pm 1.3</math></b>	12.8	BRIERE	05	CLEO	$e^+e^- \rightarrow \psi(2S) \rightarrow \text{hadr}$

$\Gamma(\omega \pi^+ \pi^-)/\Gamma_{total}$			$\Gamma_{76}/\Gamma$		
VALUE (units $10^{-4}$ )	EVTS	DOCUMENT ID	TECN	COMMENT	
<b><math>7.3 \pm 1.2</math> OUR AVERAGE</b>		Error includes scale factor of 2.1. See the ideogram below.			
$8.4 \pm 0.5 \pm 1.2$	386	ABLIKIM	07D	BES2	$e^+e^- \rightarrow \psi(2S)$
$12.2 \pm 2.2 \pm 0.7$	37	<sup>1</sup> AUBERT	07AU	BABR	$10.6 e^+e^- \rightarrow \omega \pi^+ \pi^- \gamma$
$8.2 \pm 0.5 \pm 0.7$	391	BRIERE	05	CLEO	$e^+e^- \rightarrow \psi(2S) \rightarrow 2(\pi^+ \pi^-) \pi^0$
$4.8 \pm 0.6 \pm 0.7$	100 ± 22	<sup>2</sup> BAI	03B	BES	$\psi(2S) \rightarrow 2(\pi^+ \pi^-) \pi^0$
<sup>1</sup> AUBERT 07AU quotes $\Gamma_{ee}^{\psi(2S)} \cdot B(\psi(2S) \rightarrow \omega \pi^+ \pi^-) \cdot B(\omega \rightarrow 3\pi) = 2.69 \pm 0.73 \pm 0.16 \text{ eV}$ .					
<sup>2</sup> Normalized to $B(\psi(2S) \rightarrow J/\psi \pi^+ \pi^-) = 0.305 \pm 0.016$ .					



$\Gamma(b_1^\pm \pi^\mp)/\Gamma_{total}$			$\Gamma_{77}/\Gamma$		
VALUE (units $10^{-4}$ )	EVTS	DOCUMENT ID	TECN	COMMENT	
<b><math>4.0 \pm 0.6</math> OUR AVERAGE</b>		Error includes scale factor of 1.1.			
$5.1 \pm 0.6 \pm 0.8$	202	ABLIKIM	07D	BES2	$e^+e^- \rightarrow \psi(2S)$
$4.18^{+0.43}_{-0.42} \pm 0.92$	170	ADAM	05	CLEO	$e^+e^- \rightarrow \psi(2S)$
$3.2 \pm 0.6 \pm 0.5$	61 ± 11	<sup>1,2</sup> BAI	03B	BES	$\psi(2S) \rightarrow 2(\pi^+ \pi^-) \pi^0$
• • • We do not use the following data for averages, fits, limits, etc. • • •					
$5.2 \pm 0.8 \pm 1.0$		<sup>1</sup> BAI	99c	BES	Repl. by BAI 03B
<sup>1</sup> Assuming $B(b_1 \rightarrow \omega \pi) = 1$ .					
<sup>2</sup> Normalized to $B(\psi(2S) \rightarrow J/\psi \pi^+ \pi^-) = 0.305 \pm 0.016$ .					

$\Gamma(b_1^0 \pi^0)/\Gamma_{total}$			$\Gamma_{78}/\Gamma$		
VALUE (units $10^{-4}$ )	EVTS	DOCUMENT ID	TECN	COMMENT	
<b><math>2.35^{+0.47}_{-0.42} \pm 0.40</math></b>	45	ADAM	05	CLEO	$e^+e^- \rightarrow \psi(2S)$

$\Gamma(\omega f_2(1270))/\Gamma_{total}$			$\Gamma_{79}/\Gamma$			
VALUE (units $10^{-4}$ )	CL%	EVTS	DOCUMENT ID	TECN	COMMENT	
<b><math>2.2 \pm 0.4</math> OUR AVERAGE</b>						
$2.3 \pm 0.5 \pm 0.4$		57	ABLIKIM	07D	BES2	$e^+e^- \rightarrow \psi(2S)$
$2.05 \pm 0.41 \pm 0.38$		62 ± 12	BAI	04c	BES2	$\psi(2S) \rightarrow 2(\pi^+ \pi^-) \pi^0$
• • • We do not use the following data for averages, fits, limits, etc. • • •						
<1.5	90		<sup>1</sup> BAI	03B	BES	$\psi(2S) \rightarrow 2(\pi^+ \pi^-) \pi^0$
<1.7	90		BAI	98J	BES	Repl. by BAI 03B

<sup>1</sup> Normalized to  $B(\psi(2S) \rightarrow J/\psi \pi^+ \pi^-) = 0.305 \pm 0.016$ .

$\Gamma(\pi^+ \pi^- K^+ K^-)/\Gamma_{total}$			$\Gamma_{82}/\Gamma$		
VALUE (units $10^{-4}$ )	EVTS	DOCUMENT ID	TECN	COMMENT	
<b><math>7.3 \pm 0.5</math> OUR AVERAGE</b>					
$8.1 \pm 1.3 \pm 0.3$	133	LEES	12F	BABR	$10.6 e^+e^- \rightarrow \pi^+ \pi^- K^+ K^- \gamma$
$7.1 \pm 0.3 \pm 0.4$	817.2	BRIERE	05	CLEO	$e^+e^- \rightarrow \psi(2S) \rightarrow K^+ K^- \pi^+ \pi^-$
$16 \pm 4$		<sup>1</sup> TANENBAUM	78	MRK1	$e^+e^-$
• • • We do not use the following data for averages, fits, limits, etc. • • •					
$11.0 \pm 1.9 \pm 0.2$	85	<sup>2</sup> AUBERT	07AK	BABR	$10.6 e^+e^- \rightarrow \pi^+ \pi^- K^+ K^- \gamma$

<sup>1</sup> Assuming entirely strong decay.  
<sup>2</sup> Superseded by LEES 12F. AUBERT 07AK reports  $[\Gamma(\psi(2S) \rightarrow \pi^+ \pi^- K^+ K^-)/\Gamma_{total}] \times [\Gamma(\psi(2S) \rightarrow e^+e^-)] = (2.56 \pm 0.42 \pm 0.16) \times 10^{-3} \text{ keV}$  which we divide by our best value  $\Gamma(\psi(2S) \rightarrow e^+e^-) = 2.33 \pm 0.04 \text{ keV}$ . Our first error is their experiment's error and our second error is the systematic error from using our best value.

$\Gamma(\rho^0 K^+ K^-)/\Gamma_{total}$			$\Gamma_{84}/\Gamma$		
VALUE (units $10^{-4}$ )	EVTS	DOCUMENT ID	TECN	COMMENT	
<b><math>2.2 \pm 0.2 \pm 0.4</math></b>	223.8	BRIERE	05	CLEO	$e^+e^- \rightarrow \psi(2S) \rightarrow K^+ K^- \pi^+ \pi^-$

$\Gamma(K^*(892)^0 \bar{K}_S^0(1430)^0)/\Gamma_{total}$			$\Gamma_{85}/\Gamma$			
VALUE (units $10^{-4}$ )	CL%	EVTS	DOCUMENT ID	TECN	COMMENT	
<b><math>1.86 \pm 0.32 \pm 0.43</math></b>		93 ± 16	BAI	04c	$\psi(2S) \rightarrow K^+ K^- \pi^+ \pi^-$	
• • • We do not use the following data for averages, fits, limits, etc. • • •						
<1.2	90		BAI	98J	BES	$e^+e^-$

$\Gamma(K^+ K^- \pi^+ \pi^- \eta)/\Gamma_{total}$			$\Gamma_{86}/\Gamma$		
VALUE (units $10^{-3}$ )	EVTS	DOCUMENT ID	TECN	COMMENT	
<b><math>1.3 \pm 0.7 \pm 0.1</math></b>	7	<sup>1</sup> AUBERT	07AU	BABR	$10.6 e^+e^- \rightarrow K^+ K^- \pi^+ \pi^- \eta\gamma$
<sup>1</sup> AUBERT 07AU quotes $\Gamma_{ee}^{\psi(2S)} \cdot B(\psi(2S) \rightarrow 2(\pi^+ \pi^-)\eta) \cdot B(\eta \rightarrow \gamma\gamma) = 1.2 \pm 0.7 \pm 0.1 \text{ eV}$ .					

$\Gamma(K^+ K^- 2(\pi^+ \pi^-) \pi^0)/\Gamma_{total}$			$\Gamma_{87}/\Gamma$		
VALUE (units $10^{-4}$ )	EVTS	DOCUMENT ID	TECN	COMMENT	
<b><math>10.0 \pm 2.5 \pm 1.8</math></b>	65	ABLIKIM	07D	BES2	$e^+e^- \rightarrow \psi(2S)$

$\Gamma(K_1(1270)^\pm K^\mp)/\Gamma_{total}$			$\Gamma_{89}/\Gamma$		
VALUE (units $10^{-4}$ )	EVTS	DOCUMENT ID	TECN	COMMENT	
<b><math>10.0 \pm 1.8 \pm 2.1</math></b>		<sup>1</sup> BAI	99c	BES	$e^+e^-$
<sup>1</sup> Assuming $B(K_1(1270) \rightarrow K \rho) = 0.42 \pm 0.06$					

$\Gamma(K_S^0 K_S^0 \pi^+ \pi^-)/\Gamma_{total}$			$\Gamma_{90}/\Gamma$		
VALUE (units $10^{-4}$ )	EVTS	DOCUMENT ID	TECN	COMMENT	
<b><math>2.20 \pm 0.25 \pm 0.37</math></b>	83 ± 9	ABLIKIM	05o	BES2	$e^+e^- \rightarrow \psi(2S)$

$\Gamma(\rho^0 p \bar{p})/\Gamma_{total}$			$\Gamma_{91}/\Gamma$		
VALUE (units $10^{-4}$ )	EVTS	DOCUMENT ID	TECN	COMMENT	
<b><math>0.5 \pm 0.1 \pm 0.2</math></b>	61.1	BRIERE	05	CLEO	$e^+e^- \rightarrow \psi(2S) \rightarrow p \bar{p} \pi^+ \pi^-$

$\Gamma(K^+ \bar{K}^*(892)^0 \pi^- + c.c.)/\Gamma_{total}$			$\Gamma_{92}/\Gamma$		
VALUE (units $10^{-4}$ )	EVTS	DOCUMENT ID	TECN	COMMENT	
<b><math>6.7 \pm 2.5</math></b>		TANENBAUM	78	MRK1	$e^+e^-$

$\Gamma(2(\pi^+ \pi^-))/\Gamma_{total}$			$\Gamma_{93}/\Gamma$		
VALUE (units $10^{-4}$ )	EVTS	DOCUMENT ID	TECN	COMMENT	
<b><math>2.4 \pm 0.6</math> OUR AVERAGE</b>		Error includes scale factor of 2.2.			
$2.2 \pm 0.2 \pm 0.2$	308	BRIERE	05	CLEO	$e^+e^- \rightarrow \psi(2S) \rightarrow 2(\pi^+ \pi^-)$
$4.5 \pm 1.0$		TANENBAUM	78	MRK1	$e^+e^-$

$\Gamma(\rho^0 \pi^+ \pi^-)/\Gamma_{total}$			$\Gamma_{94}/\Gamma$		
VALUE (units $10^{-4}$ )	EVTS	DOCUMENT ID	TECN	COMMENT	
<b><math>2.2 \pm 0.6</math> OUR AVERAGE</b>		Error includes scale factor of 1.4.			
$2.0 \pm 0.2 \pm 0.4$	285.5	BRIERE	05	CLEO	$e^+e^- \rightarrow \psi(2S) \rightarrow 2(\pi^+ \pi^-)$
$4.2 \pm 1.5$		TANENBAUM	78	MRK1	$e^+e^-$

See key on page 999

## Meson Particle Listings

 $\psi(2S)$  $\Gamma(K^+ K^- \pi^+ \pi^- \pi^0)/\Gamma_{\text{total}}$   $\Gamma_{95}/\Gamma$ 

VALUE (units $10^{-4}$ )	EVTS	DOCUMENT ID	TECN	COMMENT
<b>12.6 ± 0.9 OUR AVERAGE</b>				
18.9 ± 5.7 ± 0.3	32	<sup>1</sup> AUBERT	07AU BABR	10.6 $e^+ e^- \rightarrow K^+ K^- \pi^+ \pi^- \pi^0 \gamma$
11.7 ± 1.0 ± 1.5	597	ABLIKIM	06G BES2	$\psi(2S) \rightarrow K^+ K^- \pi^+ \pi^- \pi^0$
12.7 ± 0.5 ± 1.0	711.6	BRIERE	05 CLEO	$e^+ e^- \rightarrow \psi(2S) \rightarrow K^+ K^- \pi^+ \pi^- \pi^0$

<sup>1</sup>AUBERT 07AU reports  $[\Gamma(\psi(2S) \rightarrow K^+ K^- \pi^+ \pi^- \pi^0)/\Gamma_{\text{total}}] \times [\Gamma(\psi(2S) \rightarrow e^+ e^-)] = (44 \pm 13 \pm 3) \times 10^{-4}$  keV which we divide by our best value  $\Gamma(\psi(2S) \rightarrow e^+ e^-) = 2.33 \pm 0.04$  keV. Our first error is their experiment's error and our second error is the systematic error from using our best value.

 $\Gamma(\omega f_0(1710) \rightarrow \omega K^+ K^-)/\Gamma_{\text{total}}$   $\Gamma_{96}/\Gamma$ 

VALUE (units $10^{-5}$ )	EVTS	DOCUMENT ID	TECN	COMMENT
<b>5.9 ± 2.0 ± 0.9</b>	19	ABLIKIM	06G BES2	$\psi(2S) \rightarrow K^+ K^- \pi^+ \pi^- \pi^0$

 $\Gamma(K^*(892)^0 K^- \pi^+ \pi^0 + \text{c.c.})/\Gamma_{\text{total}}$   $\Gamma_{97}/\Gamma$ 

VALUE (units $10^{-4}$ )	EVTS	DOCUMENT ID	TECN	COMMENT
<b>8.6 ± 1.3 ± 1.8</b>	238	ABLIKIM	06G BES2	$\psi(2S) \rightarrow K^+ K^- \pi^+ \pi^- \pi^0$

 $\Gamma(K^*(892)^+ K^- \pi^+ \pi^- + \text{c.c.})/\Gamma_{\text{total}}$   $\Gamma_{98}/\Gamma$ 

VALUE (units $10^{-4}$ )	EVTS	DOCUMENT ID	TECN	COMMENT
<b>9.6 ± 2.2 ± 1.7</b>	133	ABLIKIM	06G BES2	$\psi(2S) \rightarrow K^+ K^- \pi^+ \pi^- \pi^0$

 $\Gamma(K^*(892)^+ K^- \rho^0 + \text{c.c.})/\Gamma_{\text{total}}$   $\Gamma_{99}/\Gamma$ 

VALUE (units $10^{-4}$ )	EVTS	DOCUMENT ID	TECN	COMMENT
<b>7.3 ± 2.2 ± 1.4</b>	78	ABLIKIM	06G BES2	$\psi(2S) \rightarrow K^+ K^- \pi^+ \pi^- \pi^0$

 $\Gamma(K^*(892)^0 K^- \rho^+ + \text{c.c.})/\Gamma_{\text{total}}$   $\Gamma_{100}/\Gamma$ 

VALUE (units $10^{-4}$ )	EVTS	DOCUMENT ID	TECN	COMMENT
<b>6.1 ± 1.3 ± 1.2</b>	125	ABLIKIM	06G BES2	$\psi(2S) \rightarrow K^+ K^- \pi^+ \pi^- \pi^0$

 $\Gamma(\eta K^+ K^-, \text{no } \eta\phi)/\Gamma_{\text{total}}$   $\Gamma_{101}/\Gamma$ 

VALUE (units $10^{-5}$ )	CL%	EVTS	DOCUMENT ID	TECN	COMMENT
<b>3.08 ± 0.29 ± 0.25</b>	0.3k		<sup>1</sup> ABLIKIM	12L BES3	$\psi(2S) \rightarrow K^+ K^- \gamma \gamma$
<13	90		BRIERE	05 CLEO	$e^+ e^- \rightarrow \psi(2S) \rightarrow K^+ K^- \pi^+ \pi^- \pi^0$

• • • We do not use the following data for averages, fits, limits, etc. • • •

<sup>1</sup>Excluding  $\eta\phi$ .

 $\Gamma(\omega K^+ K^-)/\Gamma_{\text{total}}$   $\Gamma_{102}/\Gamma$ 

VALUE (units $10^{-4}$ )	EVTS	DOCUMENT ID	TECN	COMMENT
<b>1.62 ± 0.11 OUR AVERAGE</b>				Error includes scale factor of 1.1.
1.56 ± 0.04 ± 0.11	2.8k	ABLIKIM	14G BES3	$\psi(2S) \rightarrow K^+ K^- \pi^+ \pi^- \pi^0$
2.38 ± 0.37 ± 0.29	78	ABLIKIM	06G BES2	$\psi(2S) \rightarrow K^+ K^- \pi^+ \pi^- \pi^0$
1.9 ± 0.3 ± 0.3	76.8	BRIERE	05 CLEO	$e^+ e^- \rightarrow \psi(2S) \rightarrow K^+ K^- \pi^+ \pi^- \pi^0$
1.5 ± 0.3 ± 0.2	23	<sup>1</sup> BAI	03B BES	$\psi(2S) \rightarrow K^+ K^- \pi^+ \pi^- \pi^0$

<sup>1</sup>Normalized to  $B(\psi(2S) \rightarrow J/\psi \pi^+ \pi^-) = 0.305 \pm 0.016$ .

 $\Gamma(\omega K^*(892)^+ K^- + \text{c.c.})/\Gamma_{\text{total}}$   $\Gamma_{103}/\Gamma$ 

VALUE (units $10^{-5}$ )	EVTS	DOCUMENT ID	TECN	COMMENT
<b>20.7 ± 2.6 OUR AVERAGE</b>				
18.9 ± 2.9 ± 2.2	396	ABLIKIM	13M BES3	$\psi(2S) \rightarrow \omega K_S^0 K^- \pi^+$
22.6 ± 3.0 ± 2.4	535	ABLIKIM	13M BES3	$\psi(2S) \rightarrow \omega K^+ K^- \pi^0$

 $\Gamma(\omega K_S^0(1430)^+ K^- + \text{c.c.})/\Gamma_{\text{total}}$   $\Gamma_{104}/\Gamma$ 

VALUE (units $10^{-5}$ )	EVTS	DOCUMENT ID	TECN	COMMENT
<b>6.1 ± 1.2 OUR AVERAGE</b>				
6.39 ± 1.50 ± 0.78	128	ABLIKIM	13M BES3	$\psi(2S) \rightarrow \omega K_S^0 K^- \pi^+$
5.86 ± 1.61 ± 0.83	143	ABLIKIM	13M BES3	$\psi(2S) \rightarrow \omega K^+ K^- \pi^0$

 $\Gamma(\omega \bar{K}^*(892)^0 K^0)/\Gamma_{\text{total}}$   $\Gamma_{105}/\Gamma$ 

VALUE (units $10^{-5}$ )	EVTS	DOCUMENT ID	TECN	COMMENT
<b>16.8 ± 2.5 ± 1.6</b>	356	ABLIKIM	13M BES3	$\psi(2S) \rightarrow \omega K_S^0 K^- \pi^+$

 $\Gamma(\omega \bar{K}_2^*(1430)^0 K^0)/\Gamma_{\text{total}}$   $\Gamma_{106}/\Gamma$ 

VALUE (units $10^{-5}$ )	EVTS	DOCUMENT ID	TECN	COMMENT
<b>5.82 ± 2.08 ± 0.72</b>	116	ABLIKIM	13M BES3	$\psi(2S) \rightarrow \omega K_S^0 K^- \pi^+$

 $\Gamma(\omega X(1440) \rightarrow \omega K_S^0 K^- \pi^+ + \text{c.c.})/\Gamma_{\text{total}}$   $\Gamma_{107}/\Gamma$ 

VALUE (units $10^{-5}$ )	EVTS	DOCUMENT ID	TECN	COMMENT
<b>1.60 ± 0.27 ± 0.24</b>	109	<sup>1</sup> ABLIKIM	13M BES3	$\psi(2S) \rightarrow \omega K_S^0 K^- \pi^+$

<sup>1</sup>X(1440) compatible with  $\eta(1405)$  and  $\eta(1475)$ . A  $f_1(1420)$  is also possible.

 $\Gamma(\omega X(1440) \rightarrow \omega K^+ K^- \pi^0)/\Gamma_{\text{total}}$   $\Gamma_{108}/\Gamma$ 

VALUE (units $10^{-5}$ )	EVTS	DOCUMENT ID	TECN	COMMENT
<b>1.09 ± 0.20 ± 0.16</b>	82	<sup>1</sup> ABLIKIM	13M BES3	$\psi(2S) \rightarrow \omega K^+ K^- \pi^0$

<sup>1</sup>X(1440) compatible with  $\eta(1405)$  and  $\eta(1475)$ . A  $f_1(1420)$  is also possible.

 $\Gamma(\omega f_1(1285) \rightarrow \omega K_S^0 K^- \pi^+ + \text{c.c.})/\Gamma_{\text{total}}$   $\Gamma_{109}/\Gamma$ 

VALUE (units $10^{-5}$ )	EVTS	DOCUMENT ID	TECN	COMMENT
<b>0.302 ± 0.098 ± 0.027</b>	22	<sup>1</sup> ABLIKIM	13M BES3	$\psi(2S) \rightarrow \omega K_S^0 K^- \pi^+$

<sup>1</sup>Statistical significance 4.5  $\sigma$ . This measurement is equivalent to a limit of  $< 0.478 \times 10^{-5}$  at 90% C.L.

 $\Gamma(\omega f_1(1285) \rightarrow \omega K^+ K^- \pi^0)/\Gamma_{\text{total}}$   $\Gamma_{110}/\Gamma$ 

VALUE (units $10^{-5}$ )	EVTS	DOCUMENT ID	TECN	COMMENT
<b>0.125 ± 0.070 ± 0.013</b>	10	<sup>1</sup> ABLIKIM	13M BES3	$\psi(2S) \rightarrow \omega K^+ K^- \pi^0$

<sup>1</sup>Statistical significance 3.2  $\sigma$ . This measurement is equivalent to a limit of  $< 0.221 \times 10^{-5}$  at 90% C.L.

 $\Gamma(3(\pi^+ \pi^-))/\Gamma_{\text{total}}$   $\Gamma_{111}/\Gamma$ 

VALUE (units $10^{-4}$ )	EVTS	DOCUMENT ID	TECN	COMMENT
<b>3.5 ± 2.0 OUR AVERAGE</b>				Error includes scale factor of 2.8.
5.45 ± 0.42 ± 0.87	671	ABLIKIM	05H BES2	$e^+ e^- \rightarrow \psi(2S) \rightarrow 3(\pi^+ \pi^-)$
1.5 ± 1.0		<sup>1</sup> TANENBAUM	78 MRK1	$e^+ e^-$

<sup>1</sup>Assuming entirely strong decay.

 $\Gamma(\rho \bar{\rho} \pi^+ \pi^- \pi^0)/\Gamma_{\text{total}}$   $\Gamma_{112}/\Gamma$ 

VALUE (units $10^{-4}$ )	EVTS	DOCUMENT ID	TECN	COMMENT
<b>7.3 ± 0.4 ± 0.6</b>	434.9	BRIERE	05 CLEO	$e^+ e^- \rightarrow \psi(2S) \rightarrow \rho \bar{\rho} \pi^+ \pi^- \pi^0$

 $\Gamma(K^+ K^-)/\Gamma_{\text{total}}$   $\Gamma_{113}/\Gamma$ 

VALUE (units $10^{-5}$ )	CL%	EVTS	DOCUMENT ID	TECN	COMMENT
<b>7.48 ± 0.23 ± 0.39</b>	1.3k		<sup>1</sup> METREVELI	12	$\psi(2S) \rightarrow K^+ K^-$
6.2 ± 1.5 ± 0.2	66	<sup>2,3</sup> LEES	15J BABR		$e^+ e^- \rightarrow K^+ K^- \gamma$
8.3 ± 1.5 ± 0.2	66	<sup>3,4</sup> LEES	15J BABR		$e^+ e^- \rightarrow K^+ K^- \gamma$
6.3 ± 0.6 ± 0.3		<sup>5</sup> DOBBS	06A CLEO		$e^+ e^-$
10 ± 7		<sup>5</sup> BRANDELIC	79C DASP		$e^+ e^-$
< 5	90		FELDMAN	77 MRK1	$e^+ e^-$

• • • We do not use the following data for averages, fits, limits, etc. • • •

<sup>1</sup>Obtained by analyzing CLEO-c data but not authored by the CLEO Collaboration.

<sup>2</sup> $\sin\phi > 0$ .

<sup>3</sup>Using  $\Gamma(\psi(2S) \rightarrow e^+ e^-) = (2.37 \pm 0.04)$  keV.

<sup>4</sup> $\sin\phi < 0$ .

<sup>5</sup>Interference with non-resonant  $K^+ K^-$  production not taken into account.

 $\Gamma(K_S^0 K_L^0)/\Gamma_{\text{total}}$   $\Gamma_{114}/\Gamma$ 

VALUE (units $10^{-5}$ )	EVTS	DOCUMENT ID	TECN	COMMENT
<b>5.34 ± 0.33 OUR AVERAGE</b>				
5.28 ± 0.25 ± 0.34	478 ± 23	<sup>1</sup> METREVELI	12	$\psi(2S) \rightarrow K_S^0 K_L^0$
5.8 ± 0.8 ± 0.4		DOBBS	06A CLEO	$e^+ e^-$
5.24 ± 0.47 ± 0.48	156 ± 14	<sup>2</sup> BAI	04B BES2	$\psi(2S) \rightarrow K_S^0 K_L^0 \rightarrow \pi^+ \pi^- X$

<sup>1</sup>Obtained by analyzing CLEO-c data but not authored by the CLEO Collaboration.

<sup>2</sup>Using  $B(K_S^0 \rightarrow \pi^+ \pi^-) = 0.6860 \pm 0.0027$ .

 $\Gamma(\pi^+ \pi^- \pi^0)/\Gamma_{\text{total}}$   $\Gamma_{115}/\Gamma$ 

VALUE (units $10^{-4}$ )	EVTS	DOCUMENT ID	TECN	COMMENT
<b>2.01 ± 0.17 OUR AVERAGE</b>				Error includes scale factor of 1.7. See the ideogram below.
2.14 ± 0.03 ± 0.12 ± 0.11	7k	<sup>1</sup> ABLIKIM	12H BES3	$e^+ e^- \rightarrow \psi(2S)$
1.81 ± 0.18 ± 0.19	260 ± 19	<sup>2</sup> ABLIKIM	05J BES2	$e^+ e^- \rightarrow \psi(2S)$
1.88 ± 0.16 ± 0.28 ± 0.15	194	ADAM	05 CLEO	$e^+ e^- \rightarrow \psi(2S)$
0.85 ± 0.46	4	FRANKLIN	83 MRK2	$e^+ e^- \rightarrow \text{hadrons}$

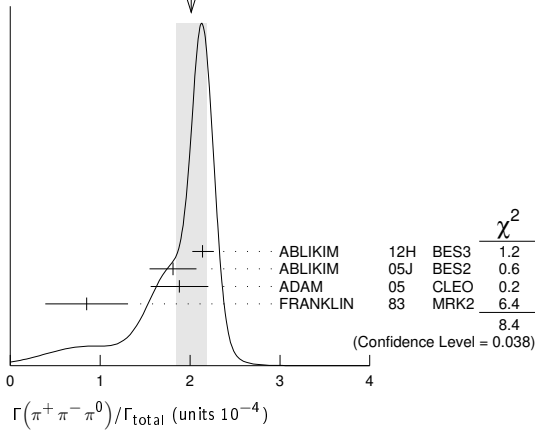
<sup>1</sup>From  $\psi(2S) \rightarrow \pi^+ \pi^- \pi^0$  events directly. The quoted systematic error includes a contribution of 4% (added in quadrature) from the uncertainty on the number of  $\psi(2S)$  events.

<sup>2</sup>From a PW analysis of  $\psi(2S) \rightarrow \pi^+ \pi^- \pi^0$ .

# Meson Particle Listings

## $\psi(2S)$

WEIGHTED AVERAGE  
2.01±0.17 (Error scaled by 1.7)



### $\Gamma(\rho(2150)\pi \rightarrow \pi^+\pi^-\pi^0)/\Gamma_{total}$ $\Gamma_{116}/\Gamma$

VALUE (units $10^{-4}$ )	DOCUMENT ID	TECN	COMMENT
<b>1.94 ± 0.25 ± 1.15</b> -0.34	<sup>1</sup> ABLIKIM	05J BES2	$\psi(2S) \rightarrow \rho(2150)\pi \rightarrow \pi^+\pi^-\pi^0$

<sup>1</sup> From a PW analysis of  $\psi(2S) \rightarrow \pi^+\pi^-\pi^0$ .

### $\Gamma(\rho(770)\pi \rightarrow \pi^+\pi^-\pi^0)/\Gamma_{total}$ $\Gamma_{117}/\Gamma$

VALUE (units $10^{-4}$ )	CL%	EVTS	DOCUMENT ID	TECN	COMMENT
<b>0.32 ± 0.12</b> OUR AVERAGE			Error includes scale factor of 1.8.		
0.51 ± 0.07 ± 0.11			<sup>1</sup> ABLIKIM	05J BES2	$\psi(2S) \rightarrow \rho(770)\pi \rightarrow \pi^+\pi^-\pi^0$
0.24 ± 0.08 ± 0.02		22	ADAM	05 CLEO	$e^+e^- \rightarrow \psi(2S)$

• • • We do not use the following data for averages, fits, limits, etc. • • •

<0.83	90	1	FRANKLIN	83 MRK2	$e^+e^-$
<10	90		BARTEL	76 CNTR	$e^+e^-$
<10	90		<sup>2</sup> ABRAMS	75 MRK1	$e^+e^-$

<sup>1</sup> From a PW analysis of  $\psi(2S) \rightarrow \pi^+\pi^-\pi^0$ .  
<sup>2</sup> Final state  $\rho^0\pi^0$ .

### $\Gamma(\pi^+\pi^-)/\Gamma_{total}$ $\Gamma_{118}/\Gamma$

VALUE (units $10^{-5}$ )	CL%	EVTS	DOCUMENT ID	TECN	COMMENT
<b>0.78 ± 0.26</b> OUR AVERAGE					
0.76 ± 0.25 ± 0.06		30	<sup>1</sup> METREVELI	12	$\psi(2S) \rightarrow \pi^+\pi^-$
8 ± 5			BRANDELIK	79c DASP	$e^+e^-$

• • • We do not use the following data for averages, fits, limits, etc. • • •

<2.1	90		DOBBS	06A CLEO	$e^+e^- \rightarrow \psi(2S)$
<5	90		FELDMAN	77 MRK1	$e^+e^-$

<sup>1</sup> Obtained by analyzing CLEO-c data but not authored by the CLEO Collaboration. Using  $\psi(3770) \rightarrow \pi^+\pi^-$  for continuum subtraction.

### $\Gamma(K_1(1400)^\pm K^\mp)/\Gamma_{total}$ $\Gamma_{119}/\Gamma$

VALUE (units $10^{-4}$ )	CL%	DOCUMENT ID	TECN	COMMENT
<b>&lt;3.1</b>	90	<sup>1</sup> BAI	99c BES	$e^+e^-$

<sup>1</sup> Assuming  $B(K_1(1400) \rightarrow K^*\pi) = 0.94 \pm 0.06$

### $\Gamma(K_2^*(1430)^\pm K^\mp)/\Gamma_{total}$ $\Gamma_{120}/\Gamma$

VALUE (units $10^{-5}$ )	EVTS	DOCUMENT ID	TECN	COMMENT
<b>7.12 ± 0.62 ± 1.13</b> -0.61	251 ± 22	ABLIKIM	12L BES3	$e^+e^- \rightarrow \psi(2S)$

### $\Gamma(K^+K^-\pi^0)/\Gamma_{total}$ $\Gamma_{121}/\Gamma$

VALUE (units $10^{-5}$ )	CL%	EVTS	DOCUMENT ID	TECN	COMMENT
<b>4.07 ± 0.16 ± 0.26</b>		0.9k	ABLIKIM	12L BES3	$e^+e^- \rightarrow \psi(2S)$

• • • We do not use the following data for averages, fits, limits, etc. • • •

<8.9	90	1	FRANKLIN	83 MRK2	$e^+e^- \rightarrow \text{hadrons}$
------	----	---	----------	---------	-------------------------------------

### $\Gamma(K^+K^*(892)^- + c.c.)/\Gamma_{total}$ $\Gamma_{124}/\Gamma$

VALUE (units $10^{-5}$ )	CL%	EVTS	DOCUMENT ID	TECN	COMMENT
<b>2.9 ± 0.4</b> OUR AVERAGE			Error includes scale factor of 1.2.		
3.18 ± 0.30 ± 0.26 -0.31		0.2k	ABLIKIM	12L BES3	$e^+e^- \rightarrow \psi(2S)$
2.9 ± 1.3 -1.7 ± 0.4		9.6 ± 4.2	ABLIKIM	05i BES2	$e^+e^- \rightarrow \psi(2S)$
1.3 ± 1.0 -0.7 ± 0.3		7	ADAM	05 CLEO	$e^+e^- \rightarrow \psi(2S)$

• • • We do not use the following data for averages, fits, limits, etc. • • •

<5.4	90		FRANKLIN	83 MRK2	$e^+e^- \rightarrow \text{hadrons}$
------	----	--	----------	---------	-------------------------------------

### $\Gamma(K^*(892)^0\bar{K}^0 + c.c.)/\Gamma_{total}$ $\Gamma_{125}/\Gamma$

VALUE (units $10^{-5}$ )	EVTS	DOCUMENT ID	TECN	COMMENT
<b>10.9 ± 2.0</b> OUR AVERAGE				
13.3 ± 2.4 -2.8 ± 1.7	65.6 ± 9.0	ABLIKIM	05i BES2	$e^+e^- \rightarrow \psi(2S)$
9.2 ± 2.7 -2.2 ± 0.9	25	ADAM	05 CLEO	$e^+e^- \rightarrow \psi(2S)$

### $\Gamma(K^+K^*(892)^- + c.c.)/\Gamma(K^*(892)^0\bar{K}^0 + c.c.)$ $\Gamma_{124}/\Gamma_{125}$

VALUE	DOCUMENT ID	TECN	COMMENT
<b>0.16 ± 0.06</b> OUR AVERAGE			
0.22 ± 0.10 -0.14	ABLIKIM	05i BES2	$e^+e^- \rightarrow \psi(2S)$
0.14 ± 0.08 -0.06	ADAM	05 CLEO	$e^+e^- \rightarrow \psi(2S)$

### $\Gamma(\phi\pi^+\pi^-)/\Gamma_{total}$ $\Gamma_{126}/\Gamma$

VALUE (units $10^{-4}$ )	EVTS	DOCUMENT ID	TECN	COMMENT
<b>1.18 ± 0.26</b> OUR AVERAGE		Error includes scale factor of 1.5. See the ideogram below.		
2.3 ± 0.8 ± 0.1	19 ± 6	LEES	12F BABR	10.6 $e^+e^- \rightarrow \pi^+\pi^-K^+K^-\gamma$
0.9 ± 0.2 ± 0.1	47.6	BRIERE	05 CLEO	$e^+e^- \rightarrow \psi(2S) \rightarrow \pi^+\pi^-K^+K^-\gamma$
1.5 ± 0.2 ± 0.2	51.5 ± 8.3	<sup>1</sup> BAI	03B BES	$\psi(2S) \rightarrow K^+K^-\pi^+\pi^-$

• • • We do not use the following data for averages, fits, limits, etc. • • •

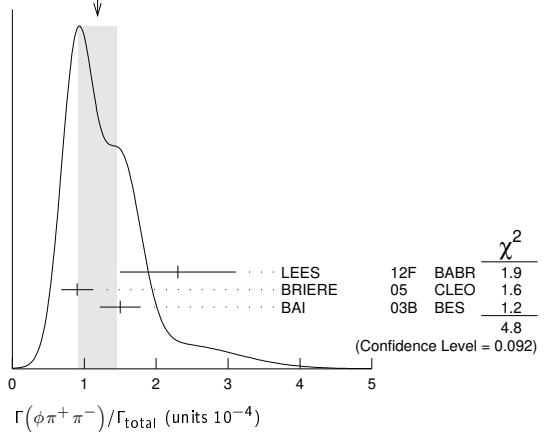
2.45 ± 0.96 ± 0.04	10 ± 4	<sup>2,3</sup> AUBERT	07AK BABR	10.6 $e^+e^- \rightarrow \pi^+\pi^-K^+K^-\gamma$
--------------------	--------	-----------------------	-----------	--

<sup>1</sup> Normalized to  $B(\psi(2S) \rightarrow J/\psi\pi^+\pi^-) = 0.305 \pm 0.016$ .

<sup>2</sup> Superseded by LEES 12F. AUBERT 07AK reports  $[\Gamma(\psi(2S) \rightarrow \phi\pi^+\pi^-)/\Gamma_{total}] \times [\Gamma(\psi(2S) \rightarrow e^+e^-)] = (0.57 \pm 0.22 \pm 0.04) \times 10^{-3}$  keV which we divide by our best value  $\Gamma(\psi(2S) \rightarrow e^+e^-) = 2.33 \pm 0.04$  keV. Our first error is their experiment's error and our second error is the systematic error from using our best value.

<sup>3</sup> Using  $B(\phi \rightarrow K^+K^-) = (49.3 \pm 0.6)\%$ .

WEIGHTED AVERAGE  
1.18±0.26 (Error scaled by 1.5)



### $\Gamma(\phi f_0(980) \rightarrow \pi^+\pi^-)/\Gamma_{total}$ $\Gamma_{127}/\Gamma$

VALUE (units $10^{-4}$ )	EVTS	DOCUMENT ID	TECN	COMMENT
<b>0.75 ± 0.33</b> OUR AVERAGE		Error includes scale factor of 1.6.		
1.5 ± 0.5 ± 0.1	12 ± 4	LEES	12F BABR	10.6 $e^+e^- \rightarrow \pi^+\pi^-K^+K^-\gamma$
0.6 ± 0.2 ± 0.1	18.4 ± 6.4	<sup>1</sup> BAI	03B BES	$\psi(2S) \rightarrow K^+K^-\pi^+\pi^-$

• • • We do not use the following data for averages, fits, limits, etc. • • •

1.46 ± 0.71 ± 0.02	6 ± 3	<sup>2,3</sup> AUBERT	07AK BABR	10.6 $e^+e^- \rightarrow \pi^+\pi^-K^+K^-\gamma$
--------------------	-------	-----------------------	-----------	--

<sup>1</sup> Normalized to  $B(\psi(2S) \rightarrow J/\psi\pi^+\pi^-) = 0.305 \pm 0.016$ .

<sup>2</sup> Superseded by LEES 12F. AUBERT 07AK reports  $[\Gamma(\psi(2S) \rightarrow \phi f_0(980) \rightarrow \pi^+\pi^-)/\Gamma_{total}] \times [\Gamma(\psi(2S) \rightarrow e^+e^-)] = (0.34 \pm 0.16 \pm 0.04) \times 10^{-3}$  keV which we divide by our best value  $\Gamma(\psi(2S) \rightarrow e^+e^-) = 2.33 \pm 0.04$  keV. Our first error is their experiment's error and our second error is the systematic error from using our best value.

<sup>3</sup> Using  $B(\phi \rightarrow K^+K^-) = (49.3 \pm 0.6)\%$ .

### $\Gamma(2(K^+K^-))/\Gamma_{total}$ $\Gamma_{128}/\Gamma$

VALUE (units $10^{-4}$ )	EVTS	DOCUMENT ID	TECN	COMMENT
<b>0.63 ± 0.13</b> OUR AVERAGE				
0.9 ± 0.4 ± 0.1	13	LEES	12F BABR	10.6 $e^+e^- \rightarrow 2(K^+K^-)\gamma$
0.6 ± 0.1 ± 0.1	59.2	BRIERE	05 CLEO	$e^+e^- \rightarrow \psi(2S) \rightarrow 2(K^+K^-)$

$\Gamma(\phi K^+ K^-)/\Gamma_{total}$   $\Gamma_{129}/\Gamma$

VALUE (units $10^{-4}$ )	EVTS	DOCUMENT ID	TECN	COMMENT
<b>0.70 ± 0.16 OUR AVERAGE</b>				
0.8 ± 0.2 ± 0.1	36.8	BRIERE	05 CLEO	$e^+ e^- \rightarrow \psi(2S) \rightarrow 2(K^+ K^-)$

0.6 ± 0.2 ± 0.1 16.1 ± 5.0 <sup>1</sup>BAL 03B BES  $\psi(2S) \rightarrow 2(K^+ K^-)$

<sup>1</sup> Normalized to  $B(\psi(2S) \rightarrow J/\psi \pi^+ \pi^-) = 0.305 \pm 0.016$ .

$\Gamma(2(K^+ K^-)\pi^0)/\Gamma_{total}$   $\Gamma_{130}/\Gamma$

VALUE (units $10^{-4}$ )	EVTS	DOCUMENT ID	TECN	COMMENT
<b>1.1 ± 0.2 ± 0.2</b>	44.7	BRIERE	05 CLEO	$e^+ e^- \rightarrow \psi(2S) \rightarrow 2(K^+ K^-)\pi^0$

$\Gamma(\phi\eta)/\Gamma_{total}$   $\Gamma_{131}/\Gamma$

VALUE (units $10^{-5}$ )	EVTS	DOCUMENT ID	TECN	COMMENT
<b>3.10 ± 0.31 OUR AVERAGE</b>				
3.14 ± 0.23 ± 0.23	0.2k	ABLIKIM	12L BES3	$e^+ e^- \rightarrow \psi(2S)$
2.0 <sup>+1.5</sup> <sub>-1.1</sub> ± 0.4	6	ADAM	05 CLEO	$e^+ e^- \rightarrow \psi(2S)$
3.3 ± 1.1 ± 0.5	17	ABLIKIM	04k BES	$e^+ e^- \rightarrow \psi(2S)$

$\Gamma(\eta\phi(2170), \phi(2170) \rightarrow \phi f_0(980), f_0 \rightarrow \pi^+ \pi^-)/\Gamma_{total}$   $\Gamma_{132}/\Gamma$

VALUE	CL%	DOCUMENT ID	TECN	COMMENT
<b>&lt;2.2 × 10<sup>-6</sup></b>	90	ABLIKIM	19i BES3	$e^+ e^- \rightarrow \eta\phi f_0(980)$

$\Gamma(\phi\eta')/\Gamma_{total}$   $\Gamma_{133}/\Gamma$

VALUE (units $10^{-5}$ )	EVTS	DOCUMENT ID	TECN	COMMENT
<b>1.54 ± 0.20 OUR AVERAGE</b>				
1.51 ± 0.16 ± 0.12	201	ABLIKIM	19BA BES3	$e^+ e^- \rightarrow \psi(2S)$
3.1 ± 1.4 ± 0.7	8	<sup>1</sup> ABLIKIM	04k BES	$e^+ e^- \rightarrow \psi(2S)$

<sup>1</sup> Calculated combining  $\eta' \rightarrow \gamma\rho$  and  $\eta\pi^+\pi^-$  channels.

$\Gamma(\omega\eta')/\Gamma_{total}$   $\Gamma_{136}/\Gamma$

VALUE (units $10^{-5}$ )	EVTS	DOCUMENT ID	TECN	COMMENT
<b>3.2 <sup>+2.4</sup> <sub>-2.0</sub> ± 0.7</b>	4	<sup>1</sup> ABLIKIM	04k BES	$e^+ e^- \rightarrow \psi(2S)$

<sup>1</sup> Calculated combining  $\eta' \rightarrow \gamma\rho$  and  $\eta\pi^+\pi^-$  channels.

$\Gamma(\omega\pi^0)/\Gamma_{total}$   $\Gamma_{137}/\Gamma$

VALUE (units $10^{-5}$ )	EVTS	DOCUMENT ID	TECN	COMMENT
<b>2.1 ± 0.6 OUR AVERAGE</b>				
2.5 <sup>+1.2</sup> <sub>-1.0</sub> ± 0.2	14	ADAM	05 CLEO	$e^+ e^- \rightarrow \psi(2S)$
1.87 <sup>+0.68</sup> <sub>-0.62</sub> ± 0.28	14	ABLIKIM	04L BES	$e^+ e^- \rightarrow \psi(2S)$

$\Gamma(\rho\eta')/\Gamma_{total}$   $\Gamma_{138}/\Gamma$

VALUE (units $10^{-5}$ )	EVTS	DOCUMENT ID	TECN	COMMENT
<b>1.87 <sup>+1.64</sup> <sub>-1.11</sub> ± 0.33</b>	2	ABLIKIM	04L BES	$e^+ e^- \rightarrow \psi(2S)$

• • • We do not use the following data for averages, fits, limits, etc. • • •

1.02 ± 0.11 ± 0.24	143	<sup>1</sup> ABLIKIM	17AK BES3	$e^+ e^- \rightarrow \psi(2S)$
0.569 ± 0.128 ± 0.236	80	<sup>2</sup> ABLIKIM	17AK BES3	$e^+ e^- \rightarrow \psi(2S)$

<sup>1</sup> Destructive-interference solution of a partial wave analysis of the decay  $\psi(2S) \rightarrow \pi^+ \pi^- \eta'$ .

<sup>2</sup> Constructive-interference solution of a partial wave analysis of the decay  $\psi(2S) \rightarrow \pi^+ \pi^- \eta'$ .

$\Gamma(\rho\eta)/\Gamma_{total}$   $\Gamma_{139}/\Gamma$

VALUE (units $10^{-5}$ )	EVTS	DOCUMENT ID	TECN	COMMENT
<b>2.2 ± 0.6 OUR AVERAGE</b>	Error includes scale factor of 1.1.			
3.0 <sup>+1.1</sup> <sub>-0.9</sub> ± 0.2	18	ADAM	05 CLEO	$e^+ e^- \rightarrow \psi(2S)$
1.78 <sup>+0.67</sup> <sub>-0.62</sub> ± 0.17	13	ABLIKIM	04L BES	$e^+ e^- \rightarrow \psi(2S)$

$\Gamma(\omega\eta)/\Gamma_{total}$   $\Gamma_{140}/\Gamma$

VALUE (units $10^{-5}$ )	CL%	DOCUMENT ID	TECN	COMMENT
<b>&lt;1.1</b>	90	ADAM	05 CLEO	$e^+ e^- \rightarrow \psi(2S)$

• • • We do not use the following data for averages, fits, limits, etc. • • •

<3.1	90	ABLIKIM	04k BES	$e^+ e^- \rightarrow \psi(2S)$
------	----	---------	---------	--------------------------------

$\Gamma(\phi\pi^0)/\Gamma_{total}$   $\Gamma_{141}/\Gamma$

VALUE (units $10^{-5}$ )	CL%	DOCUMENT ID	TECN	COMMENT
<b>&lt;0.04</b>	90	ABLIKIM	12L BES3	$e^+ e^- \rightarrow \psi(2S)$

• • • We do not use the following data for averages, fits, limits, etc. • • •

<0.7	90	ADAM	05 CLEO	$e^+ e^- \rightarrow \psi(2S)$
<0.4	90	ABLIKIM	04k BES	$e^+ e^- \rightarrow \psi(2S)$

$\Gamma(\eta_c \pi^+ \pi^- \pi^0)/\Gamma_{total}$   $\Gamma_{142}/\Gamma$

VALUE (units $10^{-3}$ )	CL%	DOCUMENT ID	TECN	COMMENT
<b>&lt;1.0</b>	90	PEDLAR	07 CLEO	$e^+ e^- \rightarrow \psi(2S)$

$\Gamma(\rho\bar{\rho}K^+K^-)/\Gamma_{total}$   $\Gamma_{143}/\Gamma$

VALUE (units $10^{-5}$ )	EVTS	DOCUMENT ID	TECN	COMMENT
<b>2.7 ± 0.6 ± 0.4</b>	30.1	BRIERE	05 CLEO	$e^+ e^- \rightarrow \psi(2S) \rightarrow \rho\bar{\rho}K^+K^-$

$\Gamma(\bar{A}nK_S^0 + c.c.)/\Gamma_{total}$   $\Gamma_{144}/\Gamma$

VALUE (units $10^{-4}$ )	EVTS	DOCUMENT ID	TECN	COMMENT
<b>0.81 ± 0.11 ± 0.14</b>	50	<sup>1</sup> ABLIKIM	08c BES2	$e^+ e^- \rightarrow J/\psi$

<sup>1</sup> Using  $B(\bar{A} \rightarrow \bar{p}\pi^+) = 63.9\%$  and  $B(K_S^0 \rightarrow \pi^+\pi^-) = 69.2\%$ .

$\Gamma(\phi f_2'(1525))/\Gamma_{total}$   $\Gamma_{145}/\Gamma$

VALUE (units $10^{-4}$ )	CL%	EVTS	DOCUMENT ID	TECN	COMMENT
<b>0.44 ± 0.12 ± 0.11</b>		20 ± 6	BAI	04c	$\psi(2S) \rightarrow 2(K^+ K^-)$
• • •					We do not use the following data for averages, fits, limits, etc. • • •
<0.45	90		BAI	98J BES	$e^+ e^- \rightarrow 2(K^+ K^-)$

$\Gamma(\phi f_1(1285))/\Gamma_{total}$   $\Gamma_{134}/\Gamma$

VALUE (units $10^{-3}$ )	EVTS	DOCUMENT ID	TECN	COMMENT
<b>3.0 ± 0.4 ± 1.3</b>	234	<sup>1</sup> ABLIKIM	19BA BES3	$e^+ e^- \rightarrow \psi(2S)$

<sup>1</sup> ABLIKIM 19BA reports  $[\Gamma(\psi(2S) \rightarrow \phi f_1(1285))/\Gamma_{total}] \times [B(f_1(1285) \rightarrow \eta\pi^+\pi^-)] = (1.03 \pm 0.10 \pm 0.09) \times 10^{-5}$  which we divide by our best value  $B(f_1(1285) \rightarrow \eta\pi^+\pi^-) = (35 \pm 15) \times 10^{-2}$ . Our first error is their experiment's error and our second error is the systematic error from using our best value.

$\Gamma(\phi\eta(1405) \rightarrow \phi\pi^+\pi^-\eta)/\Gamma_{total}$   $\Gamma_{135}/\Gamma$

VALUE (units $10^{-6}$ )	EVTS	DOCUMENT ID	TECN	COMMENT
<b>8.46 ± 1.37 ± 0.92</b>	195	ABLIKIM	19BA BES3	$e^+ e^- \rightarrow \psi(2S)$

$\Gamma(\Theta(1540)\bar{\Theta}(1540) \rightarrow K_S^0 \rho K^- \pi^+ + c.c.)/\Gamma_{total}$   $\Gamma_{146}/\Gamma$

VALUE (units $10^{-5}$ )	CL%	DOCUMENT ID	TECN	COMMENT
<b>&lt;0.88</b>	90	BAI	04G BES2	$e^+ e^-$

$\Gamma(\Theta(1540)K^- \pi^+ \rightarrow K_S^0 \rho K^- \pi)/\Gamma_{total}$   $\Gamma_{147}/\Gamma$

VALUE (units $10^{-5}$ )	CL%	DOCUMENT ID	TECN	COMMENT
<b>&lt;1.0</b>	90	BAI	04G BES2	$e^+ e^-$

$\Gamma(\Theta(1540)K_S^0 \bar{p} \rightarrow K_S^0 \bar{p} K^+ n)/\Gamma_{total}$   $\Gamma_{148}/\Gamma$

VALUE (units $10^{-5}$ )	CL%	DOCUMENT ID	TECN	COMMENT
<b>&lt;0.70</b>	90	BAI	04G BES2	$e^+ e^-$

$\Gamma(\bar{\Theta}(1540)K^+ n \rightarrow K_S^0 \bar{p} K^+ n)/\Gamma_{total}$   $\Gamma_{149}/\Gamma$

VALUE (units $10^{-5}$ )	CL%	DOCUMENT ID	TECN	COMMENT
<b>&lt;2.6</b>	90	BAI	04G BES2	$e^+ e^-$

$\Gamma(\bar{\Theta}(1540)K_S^0 \rho \rightarrow K_S^0 \rho K^- \bar{n})/\Gamma_{total}$   $\Gamma_{150}/\Gamma$

VALUE (units $10^{-5}$ )	CL%	DOCUMENT ID	TECN	COMMENT
<b>&lt;0.60</b>	90	BAI	04G BES2	$e^+ e^-$

$\Gamma(K_S^0 K_S^0)/\Gamma_{total}$   $\Gamma_{151}/\Gamma$

VALUE (units $10^{-4}$ )	DOCUMENT ID	TECN	COMMENT
<b>&lt;0.046</b>	<sup>1</sup> BAI	04D BES	$e^+ e^-$

<sup>1</sup> Forbidden by CP.

$\Gamma(A_c^+ \bar{p} e^+ + c.c.)/\Gamma_{total}$   $\Gamma_{152}/\Gamma$

VALUE	CL%	EVTS	DOCUMENT ID	TECN	COMMENT
<b>&lt;1.7 × 10<sup>-6</sup></b>	90	450M	ABLIKIM	18q BES3	$e^+ e^- \rightarrow \psi(2S)$

**RADIATIVE DECAYS**

$\Gamma(\gamma\chi_{c0}(1P))/\Gamma_{total}$   $\Gamma_{153}/\Gamma$

VALUE (units $10^{-2}$ )	EVTS	DOCUMENT ID	TECN	COMMENT
<b>9.79 ± 0.20 OUR FIT</b>				
<b>9.33 ± 0.26 OUR AVERAGE</b>				
9.389 ± 0.014 ± 0.332	4.7M	ABLIKIM	17U BES3	$e^+ e^- \rightarrow \gamma X$
9.22 ± 0.11 ± 0.46	72k	ATHAR	04 CLEO	$e^+ e^- \rightarrow \gamma X$
9.9 ± 0.5 ± 0.8		<sup>1</sup> GAISER	86 CBAL	$e^+ e^- \rightarrow \gamma X$
7.2 ± 2.3		<sup>1</sup> BIDDICK	77 CNTR	$e^+ e^- \rightarrow \gamma X$
7.5 ± 2.6		<sup>1</sup> WHITAKER	76 MRK1	$e^+ e^-$

<sup>1</sup> Angular distribution  $(1+\cos^2\theta)$  assumed.

$\Gamma(\gamma\chi_{c1}(1P))/\Gamma_{total}$   $\Gamma_{154}/\Gamma$

VALUE (units $10^{-2}$ )	EVTS	DOCUMENT ID	TECN	COMMENT
<b>9.75 ± 0.24 OUR FIT</b>				
<b>9.54 ± 0.29 OUR AVERAGE</b>				
9.905 ± 0.011 ± 0.353	5.0M	ABLIKIM	17U BES3	$e^+ e^- \rightarrow \gamma X$
9.07 ± 0.11 ± 0.54	76k	ATHAR	04 CLEO	$e^+ e^- \rightarrow \gamma X$
9.0 ± 0.5 ± 0.7		<sup>1</sup> GAISER	86 CBAL	$e^+ e^- \rightarrow \gamma X$
7.1 ± 1.9		<sup>2</sup> BIDDICK	77 CNTR	$e^+ e^- \rightarrow \gamma X$

<sup>1</sup> Angular distribution  $(1-0.189\cos^2\theta)$  assumed.

<sup>2</sup> Valid for isotropic distribution of the photon.



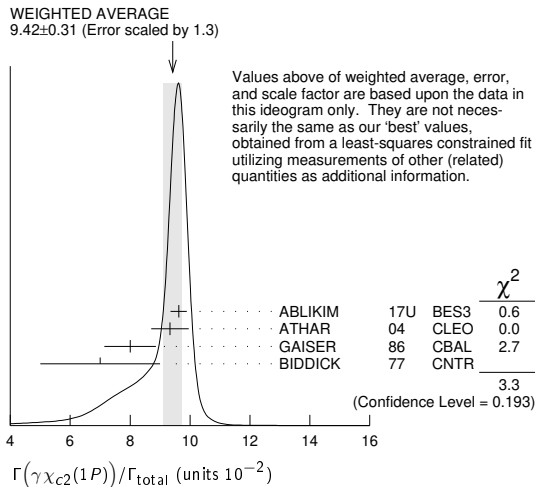
# Meson Particle Listings

## $\psi(2S)$

$\Gamma(\gamma\chi_{c2}(1P))/\Gamma_{total}$

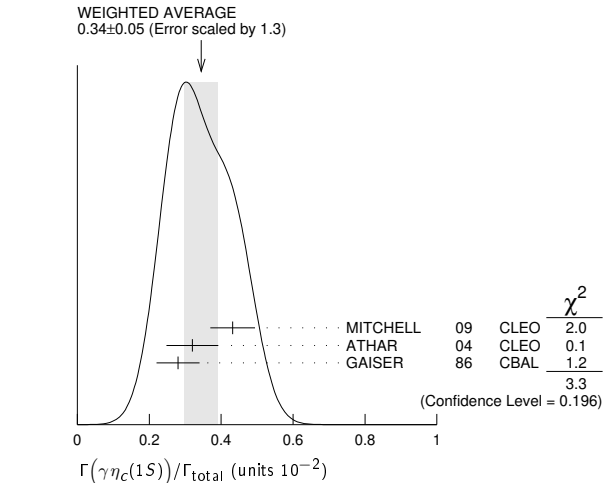
VALUE (units $10^{-2}$ )	EVTS	DOCUMENT ID	TECN	COMMENT
<b>9.52 ± 0.20 OUR FIT</b>				
<b>9.42 ± 0.31 OUR AVERAGE</b>				Error includes scale factor of 1.3. See the ideogram below.
9.621 ± 0.013 ± 0.272	4.2M	ABLIKIM	17U	BES3 $e^+e^- \rightarrow \gamma X$
9.33 ± 0.14 ± 0.61	79k	ATHAR	04	CLEO $e^+e^- \rightarrow \gamma X$
8.0 ± 0.5 ± 0.7		<sup>1</sup> GAISER	86	CBAL $e^+e^- \rightarrow \gamma X$
7.0 ± 2.0		<sup>2</sup> BIDDICK	77	CNTR $e^+e^- \rightarrow \gamma X$

<sup>1</sup> Angular distribution  $(1-0.052 \cos^2\theta)$  assumed.  
<sup>2</sup> Valid for isotropic distribution of the photon.



$[\Gamma(\gamma\chi_{c0}(1P)) + \Gamma(\gamma\chi_{c1}(1P)) + \Gamma(\gamma\chi_{c2}(1P))]/\Gamma_{total}$  ( $\Gamma_{153} + \Gamma_{154} + \Gamma_{155}$ )/ $\Gamma$

VALUE	DOCUMENT ID	TECN	COMMENT
<b>7 ± 2 ± 4</b>			
< 8	90	<sup>2</sup> CRONIN-HENNESSY 10	CLEO $\psi(2S) \rightarrow \gamma K \bar{K} \pi$
< 20	90	ATHAR	04 CLEO $e^+e^- \rightarrow \gamma X$
20-130	95	EDWARDS	82c CBAL $e^+e^- \rightarrow \gamma X$



$\Gamma(\gamma\eta_c(2S))/\Gamma_{total}$   $\Gamma_{157}/\Gamma$

VALUE (units $10^{-4}$ )	CL%	DOCUMENT ID	TECN	COMMENT
<b>7 ± 2 ± 4</b>		<sup>1</sup> ABLIKIM	12G	BES3 $\psi(2S) \rightarrow \gamma K^0 K \pi, K \bar{K} \pi^0$
< 8	90	<sup>2</sup> CRONIN-HENNESSY 10	CLEO	$\psi(2S) \rightarrow \gamma K \bar{K} \pi$
< 20	90	ATHAR	04	CLEO $e^+e^- \rightarrow \gamma X$
20-130	95	EDWARDS	82c	CBAL $e^+e^- \rightarrow \gamma X$

<sup>1</sup> ABLIKIM 12G reports  $[\Gamma(\psi(2S) \rightarrow \gamma\eta_c(2S))/\Gamma_{total}] \times [B(\eta_c(2S) \rightarrow K \bar{K} \pi)] = (1.30 \pm 0.20 \pm 0.30) \times 10^{-5}$  which we divide by our best value  $B(\eta_c(2S) \rightarrow K \bar{K} \pi) = (1.9 \pm 1.2) \times 10^{-2}$ . Our first error is their experiment's error and our second error is the systematic error from using our best value.  
<sup>2</sup> CRONIN-HENNESSY 10 reports  $[\Gamma(\psi(2S) \rightarrow \gamma\eta_c(2S))/\Gamma_{total}] \times [B(\eta_c(2S) \rightarrow K \bar{K} \pi)] < 14.5 \times 10^{-6}$  which we divide by our best value  $B(\eta_c(2S) \rightarrow K \bar{K} \pi) = 1.9 \times 10^{-2}$ . This measurement assumes  $\Gamma(\eta_c(2S)) = 14$  MeV. CRONIN-HENNESSY 10 gives the analytic dependence of limits on width.

$\Gamma(\gamma\pi^0)/\Gamma_{total}$   $\Gamma_{158}/\Gamma$

VALUE (units $10^{-6}$ )	CL%	EVTS	DOCUMENT ID	TECN	COMMENT
<b>1.04 ± 0.22 OUR AVERAGE</b>					Error includes scale factor of 1.4.
0.95 ± 0.16 ± 0.05		423	ABLIKIM	17X	BES3 $\psi(2S) \rightarrow \gamma \pi^0$
1.58 ± 0.40 ± 0.13		37	ABLIKIM	10F	BES3 $\psi(2S) \rightarrow \gamma \pi^0$
< 5	90		PEDLAR	09	CLE3 $\psi(2S) \rightarrow \gamma X$
< 5400	95		<sup>1</sup> LIBERMAN	75	SPEC $e^+e^-$
< $1 \times 10^4$	90		WIJK	75	DASP $e^+e^-$

<sup>1</sup> Restated by us using  $B(\psi(2S) \rightarrow \mu^+ \mu^-) = 0.0077$ .

$\Gamma(\gamma\eta'(958))/\Gamma_{total}$   $\Gamma_{159}/\Gamma$

VALUE (units $10^{-4}$ )	CL%	EVTS	DOCUMENT ID	TECN	COMMENT
<b>1.24 ± 0.04 OUR AVERAGE</b>					
1.251 ± 0.022 ± 0.062		56K	ABLIKIM	17X	BES3 $\psi(2S) \rightarrow \gamma \pi^+ \pi^- \eta, \gamma \pi^0 \pi^0 \eta$
1.26 ± 0.03 ± 0.08		2226	<sup>1</sup> ABLIKIM	10F	BES3 $\psi(2S) \rightarrow 3\gamma \pi^+ \pi^-, 2\gamma \pi^+ \pi^-$
1.19 ± 0.08 ± 0.03			PEDLAR	09	CLE3 $\psi(2S) \rightarrow \gamma X$
1.24 ± 0.27 ± 0.15		23	ABLIKIM	06R	BES2 $e^+e^- \rightarrow \psi(2S)$
1.54 ± 0.31 ± 0.20		~ 43	BAI	98F	BES $\psi(2S) \rightarrow \pi^+ \pi^- 2\gamma, \pi^+ \pi^- 3\gamma$

<sup>1</sup> Restated by us using  $B(\psi(2S) \rightarrow \mu^+ \mu^-) = 0.0077$ .

<sup>1</sup> Combining the results from  $\eta' \rightarrow \pi^+ \pi^- \eta$  and  $\eta' \rightarrow \pi^+ \pi^- \gamma$  decay modes.  
<sup>2</sup> Restated by us using total decay width 228 keV.  
<sup>3</sup> The value is normalized to the branching ratio for  $\Gamma(J/\psi(1S)\eta)/\Gamma_{total}$ .

$\Gamma(\gamma f_2(1270))/\Gamma_{total}$   $\Gamma_{160}/\Gamma$

VALUE (units $10^{-4}$ )	EVTS	DOCUMENT ID	TECN	COMMENT
<b>2.73 ± 0.29 OUR AVERAGE</b>				Error includes scale factor of 1.8.
2.84 ± 0.15 ± 0.03	1.9k	<sup>1,2</sup> DOBBS	15	$\psi(2S) \rightarrow \gamma \pi \pi$
2.12 ± 0.19 ± 0.32		<sup>3,4</sup> BAI	03c	BES $\psi(2S) \rightarrow \gamma \pi \pi$
2.08 ± 0.19 ± 0.33	200.6 ± 18.8	<sup>3</sup> BAI	03c	BES $\psi(2S) \rightarrow \gamma \pi^+ \pi^-$
2.90 ± 1.08 ± 1.07	29.9 ± 11.1	<sup>3</sup> BAI	03c	BES $\psi(2S) \rightarrow \gamma \pi^0 \pi^0$

<sup>1</sup> Using CLEO-c data but not authorized by the CLEO Collaboration.  
<sup>2</sup> DOBBS 15 reports  $[\Gamma(\psi(2S) \rightarrow \gamma f_2(1270))/\Gamma_{total}] \times [B(f_2(1270) \rightarrow \pi \pi)] = (2.39 \pm 0.09 \pm 0.09) \times 10^{-4}$  which we divide by our best value  $B(f_2(1270) \rightarrow \pi \pi) = (84.2 \pm 2.9 \pm 0.9) \times 10^{-2}$ . Our first error is their experiment's error and our second error is the systematic error from using our best value.  
<sup>3</sup> Normalized to  $B(\psi(2S) \rightarrow J/\psi \pi^+ \pi^-) = 0.305 \pm 0.016$ .  
<sup>4</sup> Combining the results from  $\pi^+ \pi^-$  and  $\pi^0 \pi^0$  decay modes.

$\Gamma(\gamma f_0(1370) \rightarrow \gamma K \bar{K})/\Gamma_{\text{total}}$   $\Gamma_{161}/\Gamma$ 

VALUE (units $10^{-5}$ )	EVTS	DOCUMENT ID	TECN	COMMENT
<b><math>3.1 \pm 1.0 \pm 1.4</math></b>	175	<sup>1</sup> DOBBS	15	$\psi(2S) \rightarrow \gamma K \bar{K}$

<sup>1</sup> Using CLEO-c data but not authored by the CLEO Collaboration.

 $\Gamma(\gamma f_0(1500))/\Gamma_{\text{total}}$   $\Gamma_{162}/\Gamma$ 

VALUE (units $10^{-5}$ )	EVTS	DOCUMENT ID	TECN	COMMENT
<b><math>9.3 \pm 1.8 \pm 0.6</math></b>	274	<sup>1,2</sup> DOBBS	15	$\psi(2S) \rightarrow \gamma \pi \pi$

<sup>1</sup> DOBBS 15 reports  $[\Gamma(\psi(2S) \rightarrow \gamma f_0(1500))/\Gamma_{\text{total}}] \times [B(f_0(1500) \rightarrow \pi\pi)] = (3.2 \pm 0.6 \pm 0.2) \times 10^{-5}$  which we divide by our best value  $B(f_0(1500) \rightarrow \pi\pi) = (34.5 \pm 2.2) \times 10^{-2}$ . Our first error is their experiment's error and our second error is the systematic error from using our best value.  
<sup>2</sup> Using CLEO-c data but not authored by the CLEO Collaboration.

 $\Gamma(\gamma f'_2(1525))/\Gamma_{\text{total}}$   $\Gamma_{163}/\Gamma$ 

VALUE (units $10^{-5}$ )	EVTS	DOCUMENT ID	TECN	COMMENT
<b><math>3.3 \pm 0.8 \pm 0.1</math></b>	136	<sup>1,2</sup> DOBBS	15	$\psi(2S) \rightarrow \gamma K \bar{K}$

<sup>1</sup> DOBBS 15 reports  $[\Gamma(\psi(2S) \rightarrow \gamma f'_2(1525))/\Gamma_{\text{total}}] \times [B(f'_2(1525) \rightarrow K \bar{K})] = (2.9 \pm 0.6 \pm 0.3) \times 10^{-5}$  which we divide by our best value  $B(f'_2(1525) \rightarrow K \bar{K}) = (87.6 \pm 2.2) \times 10^{-2}$ . Our first error is their experiment's error and our second error is the systematic error from using our best value.  
<sup>2</sup> Using CLEO-c data but not authored by the CLEO Collaboration.

 $\Gamma(\gamma f_0(1710) \rightarrow \gamma \pi \pi)/\Gamma_{\text{total}}$   $\Gamma_{165}/\Gamma$ 

VALUE (units $10^{-5}$ )	EVTS	DOCUMENT ID	TECN	COMMENT
<b><math>3.5 \pm 0.6</math> OUR AVERAGE</b>				
$3.6 \pm 0.4 \pm 0.5$	290	<sup>1</sup> DOBBS	15	$\psi(2S) \rightarrow \gamma \pi \pi$
$3.01 \pm 0.41 \pm 1.24$	$35.6 \pm 4.8$	<sup>2</sup> BAI	03c BES	$\psi(2S) \rightarrow \gamma \pi^+ \pi^-$

<sup>1</sup> Using CLEO-c data but not authored by the CLEO Collaboration.  
<sup>2</sup> Normalized to  $B(\psi(2S) \rightarrow J/\psi \pi^+ \pi^-) = 0.305 \pm 0.016$ .

 $\Gamma(\gamma f_0(1710) \rightarrow \gamma K \bar{K})/\Gamma_{\text{total}}$   $\Gamma_{166}/\Gamma$ 

VALUE (units $10^{-5}$ )	CL%	EVTS	DOCUMENT ID	TECN	COMMENT
<b><math>6.6 \pm 0.7</math> OUR AVERAGE</b>					
$6.7 \pm 0.6 \pm 0.6$		375	<sup>1</sup> DOBBS	15	$\psi(2S) \rightarrow \gamma K \bar{K}$
$6.04 \pm 0.90 \pm 1.32$		$39.6 \pm 5.9$	<sup>2,3</sup> BAI	03c BES	$\psi(2S) \rightarrow \gamma K^+ K^-$

**• • •** We do not use the following data for averages, fits, limits, etc. **• • •**  
< 15.6      90     $6.8 \pm 3.1$     <sup>2,3</sup> BAI    03c BES     $\psi(2S) \rightarrow \gamma K_S^0 K_S^0$   
<sup>1</sup> Using CLEO-c data but not authored by the CLEO Collaboration.  
<sup>2</sup> Includes unknown branching fractions to  $K^+ K^-$  or  $K_S^0 K_S^0$ . We have multiplied the  $K^+ K^-$  result by a factor of 2 and the  $K_S^0 K_S^0$  result by a factor of 4 to obtain the  $K \bar{K}$  result.  
<sup>3</sup> Normalized to  $B(\psi(2S) \rightarrow J/\psi \pi^+ \pi^-) = 0.305 \pm 0.016$ .

 $\Gamma(\gamma f_0(2100) \rightarrow \gamma \pi \pi)/\Gamma_{\text{total}}$   $\Gamma_{167}/\Gamma$ 

VALUE (units $10^{-6}$ )	EVTS	DOCUMENT ID	TECN	COMMENT
<b><math>4.8 \pm 0.5 \pm 0.9</math></b>	373	<sup>1</sup> DOBBS	15	$\psi(2S) \rightarrow \gamma \pi \pi$

<sup>1</sup> Using CLEO-c data but not authored by the CLEO Collaboration.

 $\Gamma(\gamma f_0(2200) \rightarrow \gamma K \bar{K})/\Gamma_{\text{total}}$   $\Gamma_{168}/\Gamma$ 

VALUE (units $10^{-6}$ )	EVTS	DOCUMENT ID	TECN	COMMENT
<b><math>3.2 \pm 0.6 \pm 0.8</math></b>	207	<sup>1</sup> DOBBS	15	$\psi(2S) \rightarrow \gamma K \bar{K}$

<sup>1</sup> Using CLEO-c data but not authored by the CLEO Collaboration.

 $\Gamma(\gamma f_2(2220) \rightarrow \gamma \pi \pi)/\Gamma_{\text{total}}$   $\Gamma_{169}/\Gamma$ 

VALUE	CL%	EVTS	DOCUMENT ID	TECN	COMMENT
<b><math>&lt; 5.8 \times 10^{-6}</math></b>	90	<sup>1,2</sup> DOBBS	15	$\psi(2S) \rightarrow \gamma \pi \pi$	

<sup>1</sup> Using CLEO-c data but not authored by the CLEO Collaboration.  
<sup>2</sup> For  $\Gamma = 20/50$  MeV, the 90% CL upper limits for  $\pi^+ \pi^-$  and  $\pi^0 \pi^0$  are  $3.2/4.3 \times 10^{-6}$  and  $2.6/4.0 \times 10^{-6}$ , respectively.

 $\Gamma(\gamma f_2(2220) \rightarrow \gamma K \bar{K})/\Gamma_{\text{total}}$   $\Gamma_{170}/\Gamma$ 

VALUE	CL%	EVTS	DOCUMENT ID	TECN	COMMENT
<b><math>&lt; 9.5 \times 10^{-6}</math></b>	90	<sup>1,2</sup> DOBBS	15	$\psi(2S) \rightarrow \gamma K \bar{K}$	

<sup>1</sup> Using CLEO-c data but not authored by the CLEO Collaboration.  
<sup>2</sup> For  $\Gamma = 20/50$  MeV, the 90% CL upper limits for  $K^+ K^-$  and  $K_S^0 K_S^0$  are  $2.1/4.3 \times 10^{-6}$  and  $3.7/5.5 \times 10^{-6}$ , respectively.

 $\Gamma(\gamma)/\Gamma_{\text{total}}$   $\Gamma_{172}/\Gamma$ 

VALUE (units $10^{-6}$ )	CL%	EVTS	DOCUMENT ID	TECN	COMMENT
<b><math>0.92 \pm 0.18</math> OUR AVERAGE</b>					
$0.85 \pm 0.18 \pm 0.04$		382	<sup>1</sup> ABLIKIM	17x BES3	$\psi(2S) \rightarrow \gamma \pi^+ \pi^- \pi^0$ , $\gamma 3\pi^0$
$1.38 \pm 0.48 \pm 0.09$		13	<sup>1</sup> ABLIKIM	10F BES3	$\psi(2S) \rightarrow \gamma \pi^+ \pi^- \pi^0$ , $\gamma 3\pi^0$

**• • •** We do not use the following data for averages, fits, limits, etc. **• • •**  
< 2      90      PEDLAR    09    CLE3     $\psi(2S) \rightarrow \gamma X$   
< 90      90      BAI          98F    BES     $\psi(2S) \rightarrow \pi^+ \pi^- 3\gamma$   
< 200    90      YAMADA    77    DASP     $e^+ e^- \rightarrow 3\gamma$   
<sup>1</sup> Combining the results from  $\eta \rightarrow \pi^+ \pi^- \pi^0$  and  $\eta \rightarrow 3\pi^0$  decay modes.

 $\Gamma(\gamma \eta \pi^+ \pi^-)/\Gamma_{\text{total}}$   $\Gamma_{173}/\Gamma$ 

VALUE (units $10^{-4}$ )	EVTS	DOCUMENT ID	TECN	COMMENT
<b><math>8.71 \pm 1.25 \pm 1.64</math></b>	418	ABLIKIM	06R BES2	$\psi(2S) \rightarrow \gamma \eta \pi^+ \pi^-$

 $\Gamma(\gamma \eta(1405) \rightarrow \gamma K \bar{K} \pi)/\Gamma_{\text{total}}$   $\Gamma_{175}/\Gamma$ 

VALUE (units $10^{-4}$ )	CL%	DOCUMENT ID	TECN	COMMENT
<b>&lt; 0.9</b>	90	ABLIKIM	06R BES2	$\psi(2S) \rightarrow \gamma K_S^0 K^+ \pi^- + \text{c.c.}$

**• • •** We do not use the following data for averages, fits, limits, etc. **• • •**  
< 1.3      90      ABLIKIM    06R BES2     $\psi(2S) \rightarrow \gamma K^+ K^- \pi^0$   
< 1.2      90      <sup>1</sup> SCHARRE    80    MRK1     $e^+ e^-$   
<sup>1</sup> Includes unknown branching fraction  $\eta(1405) \rightarrow K \bar{K} \pi$ .

 $\Gamma(\gamma \eta(1405) \rightarrow \eta \pi^+ \pi^-)/\Gamma_{\text{total}}$   $\Gamma_{176}/\Gamma$ 

VALUE (units $10^{-4}$ )	EVTS	DOCUMENT ID	TECN	COMMENT
<b><math>0.36 \pm 0.25 \pm 0.05</math></b>	10	ABLIKIM	06R BES2	$\psi(2S) \rightarrow \gamma \eta \pi^+ \pi^-$

 $\Gamma(\gamma \eta(1405) \rightarrow \gamma f_0(980) \pi^0 \rightarrow \gamma \pi^+ \pi^- \pi^0)/\Gamma_{\text{total}}$   $\Gamma_{177}/\Gamma$ 

VALUE	CL%	DOCUMENT ID	TECN	COMMENT
<b><math>&lt; 5.0 \times 10^{-7}</math></b>	90	ABLIKIM	17AJ BES3	$\psi(2S) \rightarrow \gamma \pi^+ \pi^- \pi^0$

 $\Gamma(\gamma \eta(1475) \rightarrow K \bar{K} \pi)/\Gamma_{\text{total}}$   $\Gamma_{179}/\Gamma$ 

VALUE (units $10^{-4}$ )	CL%	DOCUMENT ID	TECN	COMMENT
<b>&lt; 1.4</b>	90	ABLIKIM	06R BES2	$\psi(2S) \rightarrow \gamma K^+ K^- \pi^0$

**• • •** We do not use the following data for averages, fits, limits, etc. **• • •**  
< 1.5      90      ABLIKIM    06R BES2     $\psi(2S) \rightarrow \gamma K_S^0 K^+ \pi^- + \text{c.c.}$

 $\Gamma(\gamma \eta(1475) \rightarrow \eta \pi^+ \pi^-)/\Gamma_{\text{total}}$   $\Gamma_{180}/\Gamma$ 

VALUE (units $10^{-4}$ )	CL%	DOCUMENT ID	TECN	COMMENT
<b>&lt; 0.88</b>	90	ABLIKIM	06R BES2	$\psi(2S) \rightarrow \gamma \eta \pi^+ \pi^-$

 $\Gamma(\gamma 2(\pi^+ \pi^-))/\Gamma_{\text{total}}$   $\Gamma_{181}/\Gamma$ 

VALUE (units $10^{-5}$ )	EVTS	DOCUMENT ID	TECN	COMMENT
<b><math>39.6 \pm 2.8 \pm 5.0</math></b>	583	ABLIKIM	07D BES2	$e^+ e^- \rightarrow \psi(2S)$

 $\Gamma(\gamma K^{*0} K^+ \pi^- + \text{c.c.})/\Gamma_{\text{total}}$   $\Gamma_{182}/\Gamma$ 

VALUE (units $10^{-5}$ )	EVTS	DOCUMENT ID	TECN	COMMENT
<b><math>37.0 \pm 6.1 \pm 7.2</math></b>	237	ABLIKIM	07D BES2	$e^+ e^- \rightarrow \psi(2S)$

 $\Gamma(\gamma K^{*0} \bar{K}^{*0})/\Gamma_{\text{total}}$   $\Gamma_{183}/\Gamma$ 

VALUE (units $10^{-5}$ )	EVTS	DOCUMENT ID	TECN	COMMENT
<b><math>24.0 \pm 4.5 \pm 5.0</math></b>	41	ABLIKIM	07D BES2	$e^+ e^- \rightarrow \psi(2S)$

 $\Gamma(\gamma K_S^0 K^+ \pi^- + \text{c.c.})/\Gamma_{\text{total}}$   $\Gamma_{184}/\Gamma$ 

VALUE (units $10^{-5}$ )	EVTS	DOCUMENT ID	TECN	COMMENT
<b><math>25.6 \pm 3.6 \pm 3.6</math></b>	115	ABLIKIM	07D BES2	$e^+ e^- \rightarrow \psi(2S)$

 $\Gamma(\gamma K^+ K^- \pi^+ \pi^-)/\Gamma_{\text{total}}$   $\Gamma_{185}/\Gamma$ 

VALUE (units $10^{-5}$ )	EVTS	DOCUMENT ID	TECN	COMMENT
<b><math>19.1 \pm 2.7 \pm 4.3</math></b>	132	ABLIKIM	07D BES2	$e^+ e^- \rightarrow \psi(2S)$

 $\Gamma(\gamma \rho \bar{\rho})/\Gamma_{\text{total}}$   $\Gamma_{186}/\Gamma$ 

VALUE (units $10^{-5}$ )	EVTS	DOCUMENT ID	TECN	COMMENT
<b><math>3.9 \pm 0.5</math> OUR AVERAGE</b>				Error includes scale factor of 2.0.
$4.18 \pm 0.26 \pm 0.18$	348	<sup>1</sup> ALEXANDER	10 CLEO	$\psi(2S) \rightarrow \gamma \rho \bar{\rho}$
$2.9 \pm 0.4 \pm 0.4$	142	ABLIKIM	07D BES2	$e^+ e^- \rightarrow \psi(2S)$

<sup>1</sup> From a fit of the  $\rho \bar{\rho}$  mass distribution to a combination of  $\gamma f_2(1950)$ ,  $\gamma f_2(2150)$ , and  $\gamma \rho \bar{\rho}$  phase space, for  $M(\rho \bar{\rho}) < 2.85$  GeV, and accounting for backgrounds from  $\psi(2S) \rightarrow \pi^0 \rho \bar{\rho}$  and continuum.

 $\Gamma(\gamma f_2(1950) \rightarrow \gamma \rho \bar{\rho})/\Gamma_{\text{total}}$   $\Gamma_{187}/\Gamma$ 

VALUE (units $10^{-5}$ )	EVTS	DOCUMENT ID	TECN	COMMENT
<b><math>1.2 \pm 0.2 \pm 0.1</math></b>	111	<sup>1</sup> ALEXANDER	10 CLEO	$\psi(2S) \rightarrow \gamma \rho \bar{\rho}$

<sup>1</sup> From a fit of the  $\rho \bar{\rho}$  mass distribution to a combination of  $\gamma f_2(1950)$ ,  $\gamma f_2(2150)$ , and  $\gamma \rho \bar{\rho}$  phase space, for  $M(\rho \bar{\rho}) < 2.85$  GeV, and accounting for backgrounds from  $\psi(2S) \rightarrow \pi^0 \rho \bar{\rho}$  and continuum.

 $\Gamma(\gamma f_2(2150) \rightarrow \gamma \rho \bar{\rho})/\Gamma_{\text{total}}$   $\Gamma_{188}/\Gamma$ 

VALUE (units $10^{-5}$ )	EVTS	DOCUMENT ID	TECN	COMMENT
<b><math>0.72 \pm 0.18 \pm 0.03</math></b>	73	<sup>1</sup> ALEXANDER	10 CLEO	$\psi(2S) \rightarrow \gamma \rho \bar{\rho}$

<sup>1</sup> From a fit of the  $\rho \bar{\rho}$  mass distribution to a combination of  $\gamma f_2(1950)$ ,  $\gamma f_2(2150)$ , and  $\gamma \rho \bar{\rho}$  phase space, for  $M(\rho \bar{\rho}) < 2.85$  GeV, and accounting for backgrounds from  $\psi(2S) \rightarrow \pi^0 \rho \bar{\rho}$  and continuum.

 $\Gamma(\gamma X(1835) \rightarrow \gamma \rho \bar{\rho})/\Gamma_{\text{total}}$   $\Gamma_{189}/\Gamma$ 

VALUE (units $10^{-6}$ )	CL%	DOCUMENT ID	TECN	COMMENT
<b><math>4.57 \pm 0.36 \pm 4.26</math></b>		ABLIKIM	12D BES3	$J/\psi \rightarrow \gamma \rho \bar{\rho}$

**• • •** We do not use the following data for averages, fits, limits, etc. **• • •**  
< 1.6      90      ALEXANDER    10    CLEO     $\psi(2S) \rightarrow \gamma \rho \bar{\rho}$   
< 5.4      90      ABLIKIM      07D    BES     $\psi(2S) \rightarrow \gamma \rho \bar{\rho}$

# Meson Particle Listings

## $\psi(2S)$

**$\Gamma(\gamma X \rightarrow \gamma p \bar{p})/\Gamma_{\text{total}}$**   $\Gamma_{190}/\Gamma$   
For a narrow resonance in the range  $2.2 < M(X) < 2.8$  GeV.

VALUE (units $10^{-6}$ )	CL%	DOCUMENT ID	TECN	COMMENT
<b>&lt;2</b>	90	ALEXANDER 10	CLEO	$\psi(2S) \rightarrow \gamma p \bar{p}$

**$\Gamma(\gamma \pi^+ \pi^- p \bar{p})/\Gamma_{\text{total}}$**   $\Gamma_{191}/\Gamma$

VALUE (units $10^{-5}$ )	EVTS	DOCUMENT ID	TECN	COMMENT
<b><math>2.8 \pm 1.2 \pm 0.7</math></b>	17	ABLIKIM 07D	BES2	$e^+ e^- \rightarrow \psi(2S)$

**$\Gamma(\gamma 2(\pi^+ \pi^-) K^+ K^-)/\Gamma_{\text{total}}$**   $\Gamma_{192}/\Gamma$

VALUE (units $10^{-5}$ )	CL%	DOCUMENT ID	TECN	COMMENT
<b>&lt;22</b>	90	ABLIKIM 07D	BES2	$e^+ e^- \rightarrow \psi(2S)$

**$\Gamma(\gamma 3(\pi^+ \pi^-))/\Gamma_{\text{total}}$**   $\Gamma_{193}/\Gamma$

VALUE (units $10^{-5}$ )	CL%	DOCUMENT ID	TECN	COMMENT
<b>&lt;17</b>	90	ABLIKIM 07D	BES2	$e^+ e^- \rightarrow \psi(2S)$

**$\Gamma(\gamma K^+ K^- K^+ K^-)/\Gamma_{\text{total}}$**   $\Gamma_{194}/\Gamma$

VALUE (units $10^{-5}$ )	CL%	DOCUMENT ID	TECN	COMMENT
<b>&lt;4</b>	90	ABLIKIM 07D	BES2	$e^+ e^- \rightarrow \psi(2S)$

**$\Gamma(\gamma \gamma J/\psi)/\Gamma_{\text{total}}$**   $\Gamma_{195}/\Gamma$

VALUE (units $10^{-4}$ )	EVTS	DOCUMENT ID	TECN	COMMENT
<b><math>3.1 \pm 0.6 \pm 1.0</math></b>	1.1k	ABLIKIM 12o	BES3	$e^+ e^- \rightarrow \psi(2S)$

• • • We do not use the following data for averages, fits, limits, etc. • • •  
 $3.2 \pm 0.6$  1.1k 1 ABLIKIM 17N BES3  $\psi(2S) \rightarrow \gamma \gamma J/\psi$   
<sup>1</sup> Uses  $B(J/\psi \rightarrow e^+ e^-) = (5.971 \pm 0.032)\%$  and  $B(J/\psi \rightarrow \mu^+ \mu^-) = (5.961 \pm 0.033)\%$ . No systematic error estimation.

**$\Gamma(e^+ e^- \eta')/\Gamma_{\text{total}}$**   $\Gamma_{196}/\Gamma$

VALUE (units $10^{-6}$ )	EVTS	DOCUMENT ID	TECN	COMMENT
<b><math>1.90 \pm 0.26</math> OUR AVERAGE</b>				
$1.99 \pm 0.33 \pm 0.12$	57	ABLIKIM 18z	BES3	$\psi(2S) \rightarrow \eta' e^+ e^-$ , $\eta' \rightarrow \gamma \pi^+ \pi^-$
$1.79 \pm 0.38 \pm 0.11$	20	ABLIKIM 18z	BES3	$\psi(2S) \rightarrow \eta' e^+ e^-$ , $\eta' \rightarrow \eta \pi^+ \pi^-$

**$\Gamma(e^+ e^- \chi_{c0}(1P))/\Gamma_{\text{total}}$**   $\Gamma_{197}/\Gamma$

VALUE (units $10^{-4}$ )	EVTS	DOCUMENT ID	TECN	COMMENT
<b><math>10.6 \pm 2.4 \pm 0.4</math></b>	48	1 ABLIKIM 17i	BES3	$\psi(2S) \rightarrow e^+ e^- \gamma J/\psi$

<sup>1</sup> ABLIKIM 17i reports  $(11.7 \pm 2.5 \pm 1.0) \times 10^{-4}$  from a measurement of  $[\Gamma(\psi(2S) \rightarrow e^+ e^- \chi_{c0}(1P))/\Gamma_{\text{total}}] \times [B(\chi_{c0}(1P) \rightarrow \gamma J/\psi(1S))]$  assuming  $B(\chi_{c0}(1P) \rightarrow \gamma J/\psi(1S)) = (1.27 \pm 0.06) \times 10^{-2}$ , which we rescale to our best value  $B(\chi_{c0}(1P) \rightarrow \gamma J/\psi(1S)) = (1.40 \pm 0.05) \times 10^{-2}$ . Our first error is their experiment's error and our second error is the systematic error from using our best value.

**$\Gamma(e^+ e^- \chi_{c1}(1P))/\Gamma_{\text{total}}$**   $\Gamma_{198}/\Gamma$

VALUE (units $10^{-4}$ )	EVTS	DOCUMENT ID	TECN	COMMENT
<b><math>8.5 \pm 0.6 \pm 0.2</math></b>	873	1 ABLIKIM 17i	BES3	$\psi(2S) \rightarrow e^+ e^- \gamma J/\psi$

<sup>1</sup> ABLIKIM 17i reports  $(8.6 \pm 0.3 \pm 0.6) \times 10^{-4}$  from a measurement of  $[\Gamma(\psi(2S) \rightarrow e^+ e^- \chi_{c1}(1P))/\Gamma_{\text{total}}] \times [B(\chi_{c1}(1P) \rightarrow \gamma J/\psi(1S))]$  assuming  $B(\chi_{c1}(1P) \rightarrow \gamma J/\psi(1S)) = (33.9 \pm 1.2) \times 10^{-2}$ , which we rescale to our best value  $B(\chi_{c1}(1P) \rightarrow \gamma J/\psi(1S)) = (34.3 \pm 1.0) \times 10^{-2}$ . Our first error is their experiment's error and our second error is the systematic error from using our best value.

**$\Gamma(e^+ e^- \chi_{c2}(1P))/\Gamma_{\text{total}}$**   $\Gamma_{199}/\Gamma$

VALUE (units $10^{-4}$ )	EVTS	DOCUMENT ID	TECN	COMMENT
<b><math>7.0 \pm 0.7 \pm 0.2</math></b>	227	1 ABLIKIM 17i	BES3	$\psi(2S) \rightarrow e^+ e^- \gamma J/\psi$

<sup>1</sup> ABLIKIM 17i reports  $(6.9 \pm 0.5 \pm 0.6) \times 10^{-4}$  from a measurement of  $[\Gamma(\psi(2S) \rightarrow e^+ e^- \chi_{c2}(1P))/\Gamma_{\text{total}}] \times [B(\chi_{c2}(1P) \rightarrow \gamma J/\psi(1S))]$  assuming  $B(\chi_{c2}(1P) \rightarrow \gamma J/\psi(1S)) = (19.2 \pm 0.7) \times 10^{-2}$ , which we rescale to our best value  $B(\chi_{c2}(1P) \rightarrow \gamma J/\psi(1S)) = (19.0 \pm 0.5) \times 10^{-2}$ . Our first error is their experiment's error and our second error is the systematic error from using our best value.

**$\Gamma(e^+ e^- \chi_{c0}(1P))/\Gamma(\gamma \chi_{c0}(1P))$**   $\Gamma_{197}/\Gamma_{153}$

VALUE (units $10^{-3}$ )	EVTS	DOCUMENT ID	TECN	COMMENT
<b><math>9.4 \pm 1.9 \pm 0.6</math></b>	48	1 ABLIKIM 17i	BES3	$\psi(2S) \rightarrow e^+ e^- \gamma J/\psi$

<sup>1</sup> Uses  $B(\psi(2S) \rightarrow \gamma \chi_{c0}(1P)) \times B(\chi_{c0}(1P) \rightarrow \gamma J/\psi(1S)) = (15.8 \pm 0.3 \pm 0.6) \times 10^{-4}$  from ABLIKIM 17N and accounts for common systematic errors.

**$\Gamma(e^+ e^- \chi_{c1}(1P))/\Gamma(\gamma \chi_{c1}(1P))$**   $\Gamma_{198}/\Gamma_{154}$

VALUE (units $10^{-3}$ )	EVTS	DOCUMENT ID	TECN	COMMENT
<b><math>8.3 \pm 0.3 \pm 0.4</math></b>	873	1 ABLIKIM 17i	BES3	$\psi(2S) \rightarrow e^+ e^- \gamma J/\psi$

<sup>1</sup> Uses  $B(\psi(2S) \rightarrow \gamma \chi_{c1}(1P)) \times B(\chi_{c1}(1P) \rightarrow \gamma J/\psi(1S)) = (351.8 \pm 1.0 \pm 12.0) \times 10^{-4}$  from ABLIKIM 17N and accounts for common systematic errors.

**$\Gamma(e^+ e^- \chi_{c2}(1P))/\Gamma(\gamma \chi_{c2}(1P))$**   $\Gamma_{199}/\Gamma_{155}$

VALUE (units $10^{-3}$ )	EVTS	DOCUMENT ID	TECN	COMMENT
<b><math>6.6 \pm 0.5 \pm 0.4</math></b>	227	1 ABLIKIM 17i	BES3	$\psi(2S) \rightarrow e^+ e^- \gamma J/\psi$

<sup>1</sup> Uses  $B(\psi(2S) \rightarrow \gamma \chi_{c2}(1P)) \times B(\chi_{c2}(1P) \rightarrow \gamma J/\psi(1S)) = (199.6 \pm 0.8 \pm 7.0) \times 10^{-4}$  from ABLIKIM 17N and accounts for common systematic errors.

### WEAK DECAYS

**$\Gamma(D^0 e^+ e^- + c.c.)/\Gamma_{\text{total}}$**   $\Gamma_{200}/\Gamma$

VALUE	CL%	DOCUMENT ID	TECN	COMMENT
<b>&lt;1.4 <math>\times 10^{-7}</math></b>	90	1 ABLIKIM 17AF	BES3	$e^+ e^- \rightarrow \psi(2S)$

<sup>1</sup> Using  $D^0$  decays to  $K^- \pi^+$ ,  $K^- \pi^+ \pi^0$ , and  $K^- \pi^+ \pi^+ \pi^-$ .

### OTHER DECAYS

**$\Gamma(\text{invisible})/\Gamma(e^+ e^-)$**   $\Gamma_{201}/\Gamma_6$

VALUE	CL%	DOCUMENT ID	TECN	COMMENT
<b>&lt;2.0</b>	90	LEES 13i	BABR	$B \rightarrow K^{(*)} \psi(2S)$

### $\psi(2S)$ CROSS-PARTICLE BRANCHING RATIOS

For measurements involving  $B(\psi(2S) \rightarrow \gamma \chi_{cJ}(1P)) \times B(\chi_{cJ}(1P) \rightarrow X)$  see the corresponding entries in the  $\chi_{cJ}(1P)$  sections.

### MULTIPOLE AMPLITUDE RATIOS IN RADIATIVE DECAYS $\psi(2S) \rightarrow \gamma \chi_{cJ}(1P)$ and $\chi_{cJ} \rightarrow \gamma J/\psi(1S)$

**$a_2(\chi_{c1})/a_2(\chi_{c2})$  Magnetic quadrupole transition amplitude ratio**

VALUE (units $10^{-2}$ )	EVTS	DOCUMENT ID	TECN	COMMENT
<b><math>63 \pm 7</math> OUR AVERAGE</b>				
$61.7 \pm 8.3$	253k	1 ABLIKIM 17N	BES3	$\psi(2S) \rightarrow \gamma \gamma \ell^+ \ell^-$
$67^{+19}_{-13}$	59k	2 ARTUSO 09	CLEO	$\psi(2S) \rightarrow \gamma \gamma \ell^+ \ell^-$

<sup>1</sup> Statistical and systematic errors combined.  
<sup>2</sup> Statistical and systematic errors combined. Using values from fits with floating  $M2$  amplitudes  $a_2(\chi_{c1})$ ,  $a_2(\chi_{c2})$ ,  $b_2(\chi_{c1})$ ,  $b_2(\chi_{c2})$  and fixed  $E3$  amplitudes of  $a_3(\chi_{c2}) = b_3(\chi_{c2}) = 0$ . Not independent of values for  $a_2(\chi_{c1}(1P))$  and  $a_2(\chi_{c2}(1P))$  from ARTUSO 09.

**$b_2(\chi_{c2})/b_2(\chi_{c1})$  Magnetic quadrupole transition amplitude ratio**

VALUE (units $10^{-2}$ )	EVTS	DOCUMENT ID	TECN	COMMENT
<b><math>60 \pm 31</math> OUR AVERAGE</b>				
$74 \pm 40$	253k	1 ABLIKIM 17N	BES3	$\psi(2S) \rightarrow \gamma \gamma \ell^+ \ell^-$
$37^{+53}_{-47}$	59k	2 ARTUSO 09	CLEO	$\psi(2S) \rightarrow \gamma \gamma \ell^+ \ell^-$

<sup>1</sup> Statistical and systematic errors combined. Derived from the reported measurement of  $b_2(\chi_{c1})/b_2(\chi_{c2}) = 1.35 \pm 0.72$ .  
<sup>2</sup> Statistical and systematic errors combined. Using values from fits with floating  $M2$  amplitudes  $a_3(\chi_{c1})$ ,  $a_3(\chi_{c2})$ ,  $b_2(\chi_{c1})$ ,  $b_2(\chi_{c2})$  and fixed  $E3$  amplitudes of  $a_3(\chi_{c2}) = b_3(\chi_{c2}) = 0$ . Not independent of values for  $b_2(\chi_{c1}(1P))$  and  $b_2(\chi_{c2}(1P))$  from ARTUSO 09.

### $\psi(2S)$ REFERENCES

ABLIKIM	19A0	PR D99 112010	M. Ablikim et al.	(BESIII Collab.)
ABLIKIM	19AT	PR D100 051101	M. Ablikim et al.	(BESIII Collab.)
ABLIKIM	19AU	PR D100 052010	M. Ablikim et al.	(BESIII Collab.)
ABLIKIM	19BA	PR D100 092003	M. Ablikim et al.	(BESIII Collab.)
ABLIKIM	19I	PR D99 012014	M. Ablikim et al.	(BESIII Collab.)
ABLIKIM	19N	PR D99 032006	M. Ablikim et al.	(BESIII Collab.)
ABLIKIM	18Q	PR D97 091102	M. Ablikim et al.	(BESIII Collab.)
ABLIKIM	18T	PR D98 032006	M. Ablikim et al.	(BESIII Collab.)
ABLIKIM	18Z	PL B783 452	M. Ablikim et al.	(BESIII Collab.)
ANASHIN	18	PL B781 174	V.V. Anashin et al.	(KEDR Collab.)
LEES	18E	PR D98 112015	J.P. Lees et al.	(BABAR Collab.)
ABLIKIM	17AF	PR D96 111101	M. Ablikim et al.	(BESIII Collab.)
ABLIKIM	17AJ	PR D96 112008	M. Ablikim et al.	(BESIII Collab.)
ABLIKIM	17AK	PR D96 112012	M. Ablikim et al.	(BESIII Collab.)
ABLIKIM	17E	PL B770 217	M. Ablikim et al.	(BESIII Collab.)
ABLIKIM	17I	PRL 118 221802	M. Ablikim et al.	(BESIII Collab.)
ABLIKIM	17L	PR D95 052003	M. Ablikim et al.	(BESIII Collab.)
ABLIKIM	17N	PR D95 072004	M. Ablikim et al.	(BESIII Collab.)
ABLIKIM	17U	PR D96 032001	M. Ablikim et al.	(BESIII Collab.)
ABLIKIM	17X	PR D96 052003	M. Ablikim et al.	(BESIII Collab.)
DOBBS	17	PR D96 092004	S. Dobbs et al.	(NWES, WAYN)
LEES	17A	PR D95 052001	J.P. Lees et al.	(BABAR Collab.)
ABLIKIM	16Y	JHEP 1605 132	R. Aaij et al.	(LHCb Collab.)
ABLIKIM	16L	PR D93 072003	M. Ablikim et al.	(BESIII Collab.)
ABLIKIM	15I	PR D91 092006	M. Ablikim et al.	(BESIII Collab.)
ABLIKIM	15V	PL B749 414	M. Ablikim et al.	(BESIII Collab.)
ANASHIN	15	PL B749 50	V.V. Anashin et al.	(KEDR Collab.)
DOBBS	15	PR D91 052006	S. Dobbs et al.	(NWES)
LEES	15J	PR D92 072008	J.P. Lees et al.	(BABAR Collab.)
ABLIKIM	14G	PR D89 112006	M. Ablikim et al.	(BESIII Collab.)
DOBBS	14	PL B739 90	S. Dobbs et al.	(NWES, WAYN)
ABLIKIM	13A	PRL 110 022001	M. Ablikim et al.	(BESIII Collab.)
ABLIKIM	13D	PR D87 012007	M. Ablikim et al.	(BESIII Collab.)
ABLIKIM	13F	PR D87 052007	M. Ablikim et al.	(BESIII Collab.)
ABLIKIM	13M	PR D87 092006	M. Ablikim et al.	(BESIII Collab.)
ABLIKIM	13R	PR D88 032007	M. Ablikim et al.	(BESIII Collab.)
ABLIKIM	13S	PR D88 032010	M. Ablikim et al.	(BESIII Collab.)
ABLIKIM	13W	PR D88 112007	M. Ablikim et al.	(BESIII Collab.)
LEES	13I	PR D87 112005	J.P. Lees et al.	(BABAR Collab.)
LEES	13O	PR D87 092005	J.P. Lees et al.	(BABAR Collab.)
LEES	13Q	PR D88 032013	J.P. Lees et al.	(BABAR Collab.)
LEES	13Y	PR D88 072009	J.P. Lees et al.	(BABAR Collab.)
AAIJ	12D	EPJ C72 1972	R. Aaij et al.	(LHCb Collab.)
ABLIKIM	12D	PRL 108 112003	M. Ablikim et al.	(BESIII Collab.)
ABLIKIM	12G	PRL 109 042003	M. Ablikim et al.	(BESIII Collab.)

See key on page 999

Meson Particle Listings

$\psi(2S), \psi(3770)$

Table listing various meson particles and their properties, including columns for particle name, mass, width, and experimental references. Includes entries like ABLIKIM, METREVELI, ANASHIN, LEES, etc.

$\psi(3770)$

$I^G(J^{PC}) = 0^-(1^{--})$

$\psi(3770)$  MASS (MeV)

OUR FIT includes measurements of  $m_{\psi(2S)}$ ,  $m_{\psi(3770)}$ , and  $m_{\psi(3770)} - m_{\psi(2S)}$ .

Table with columns: VALUE (MeV), EVTS, DOCUMENT ID, TECN, COMMENT. Includes entries like 3773.7 ± 0.4 OUR FIT, 3778.1 ± 0.7 ± 0.6, 3779.2 ± 1.8 + 0.6 - 1.7 - 0.8, etc.

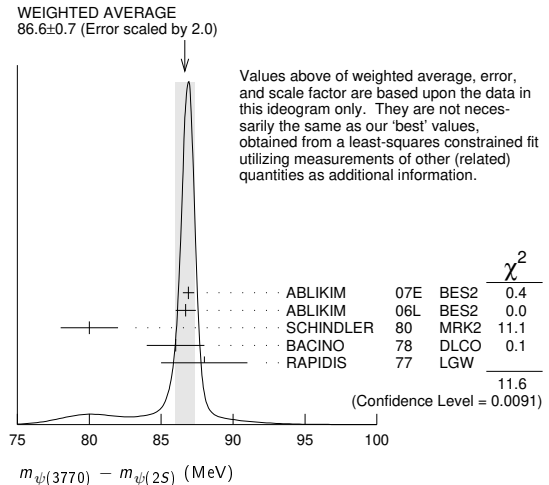
- 1 Measured in prompt hadroproduction.
2 Taking into account interference between the resonant and non-resonant D-D-bar production.
3 From the joint analysis of the data on the D-D-bar and inclusive hadronic cross sections in the psi(3770) region from BaBar, Belle, BES-II, CLEO and KEDR.
4 Reanalysis of data presented in BAI 02c. From a global fit over the center-of-mass energy region 3.7-5.0 GeV covering the psi(3770), psi(4040), psi(4160), and psi(4415) resonances. Phase angle fixed in the fit to delta = 0 degrees.
5 Interference between the resonant and non-resonant D-D-bar production not taken into account.

$m_{\psi(3770)} - m_{\psi(2S)}$

OUR FIT includes measurements of  $m_{\psi(2S)}$ ,  $m_{\psi(3770)}$ , and  $m_{\psi(3770)} - m_{\psi(2S)}$ .

Table with columns: VALUE (MeV), DOCUMENT ID, TECN, COMMENT. Includes entries like 86.6 ± 0.4 OUR FIT, 86.6 ± 0.7 OUR AVERAGE, 86.9 ± 0.4, 86.7 ± 0.7, 80 ± 2, 86 ± 2, 88 ± 3.

- 1 BES-II psi(2S) mass subtracted (see ABLIKIM 06L).
2 SPEAR psi(2S) mass subtracted (see SCHINDLER 80).



$\psi(3770)$  WIDTH

Table with columns: VALUE (MeV), EVTS, DOCUMENT ID, TECN, COMMENT. Includes entries like 27.2 ± 1.0 OUR FIT, 27.5 ± 0.9 OUR AVERAGE, 24.9 ± 4.6 + 0.5 - 4.0 - 1.1, 30.4 ± 8.5, 27 ± 10 ± 5, 28.5 ± 1.2 ± 0.2, 23.5 ± 3.7 ± 0.9, 26.9 ± 2.4 ± 0.3, 24 ± 5, 24 ± 5, 28 ± 5.

• • • We do not use the following data for averages, fits, limits, etc. • • •

## Meson Particle Listings

 $\psi(3770)$ 25.8 ± 1.3      4 SHAMOV    17 RVUE     $e^+e^- \rightarrow D\bar{D}$ , hadrons<sup>1</sup> Taking into account interference between the resonant and non-resonant  $D\bar{D}$  production.<sup>2</sup> Reanalysis of data presented in BAI 02C. From a global fit over the center-of-mass energy region 3.7–5.0 GeV covering the  $\psi(3770)$ ,  $\psi(4040)$ ,  $\psi(4160)$ , and  $\psi(4415)$  resonances. Phase angle fixed in the fit to  $\delta = 0^\circ$ .<sup>3</sup> Interference between the resonant and non-resonant  $D\bar{D}$  production not taken into account.<sup>4</sup> From the joint analysis of the data on the  $D\bar{D}$  and inclusive hadronic cross sections in the  $\psi(3770)$  region from BaBar, Belle, BES-II, CLEO and KEDR. **$\psi(3770)$  DECAY MODES**

In addition to the dominant decay mode to  $D\bar{D}$ ,  $\psi(3770)$  was found to decay into the final states containing the  $J/\psi$  (BAI 05, ADAM 06). ADAMS 06 and HUANG 06a searched for various decay modes with light hadrons and found a statistically significant signal for the decay to  $\phi\eta$  only (ADAMS 06).

Mode	Fraction ( $\Gamma_i/\Gamma$ )	Scale factor/ Confidence level
$\Gamma_1$ $D\bar{D}$	(93 $\frac{+8}{-9}$ ) %	S=2.0
$\Gamma_2$ $D^0\bar{D}^0$	(52 $\frac{+4}{-5}$ ) %	S=2.0
$\Gamma_3$ $D^+D^-$	(41 ± 4) %	S=2.0
$\Gamma_4$ $J/\psi\pi^+\pi^-$	(1.93 ± 0.28) × 10 <sup>-3</sup>	
$\Gamma_5$ $J/\psi\pi^0\pi^0$	(8.0 ± 3.0) × 10 <sup>-4</sup>	
$\Gamma_6$ $J/\psi\eta$	(9 ± 4) × 10 <sup>-4</sup>	
$\Gamma_7$ $J/\psi\pi^0$	< 2.8 × 10 <sup>-4</sup>	CL=90%
$\Gamma_8$ $e^+e^-$	(9.6 ± 0.7) × 10 <sup>-6</sup>	S=1.3

**Decays to light hadrons**

$\Gamma_9$ $b_1(1235)\pi$	< 1.4 × 10 <sup>-5</sup>	CL=90%
$\Gamma_{10}$ $\phi\eta'$	< 7 × 10 <sup>-4</sup>	CL=90%
$\Gamma_{11}$ $\omega\eta'$	< 4 × 10 <sup>-4</sup>	CL=90%
$\Gamma_{12}$ $\rho^0\eta'$	< 6 × 10 <sup>-4</sup>	CL=90%
$\Gamma_{13}$ $\phi\eta$	(3.1 ± 0.7) × 10 <sup>-4</sup>	
$\Gamma_{14}$ $\omega\eta$	< 1.4 × 10 <sup>-5</sup>	CL=90%
$\Gamma_{15}$ $\rho^0\eta$	< 5 × 10 <sup>-4</sup>	CL=90%
$\Gamma_{16}$ $\phi\pi^0$	< 3 × 10 <sup>-5</sup>	CL=90%
$\Gamma_{17}$ $\omega\pi^0$	< 6 × 10 <sup>-4</sup>	CL=90%
$\Gamma_{18}$ $\pi^+\pi^-\pi^0$	< 5 × 10 <sup>-6</sup>	CL=90%
$\Gamma_{19}$ $\rho\pi$	< 5 × 10 <sup>-6</sup>	CL=90%
$\Gamma_{20}$ $K^+K^-$		
$\Gamma_{21}$ $K^*(892)^+K^- + c.c.$	< 1.4 × 10 <sup>-5</sup>	CL=90%
$\Gamma_{22}$ $K^*(892)^0\bar{K}^0 + c.c.$	< 1.2 × 10 <sup>-3</sup>	CL=90%
$\Gamma_{23}$ $K_S^0 K_L^0$	< 1.2 × 10 <sup>-5</sup>	CL=90%
$\Gamma_{24}$ $2(\pi^+\pi^-)$	< 1.12 × 10 <sup>-3</sup>	CL=90%
$\Gamma_{25}$ $2(\pi^+\pi^-)\pi^0$	< 1.06 × 10 <sup>-3</sup>	CL=90%
$\Gamma_{26}$ $2(\pi^+\pi^-\pi^0)$	< 5.85 %	CL=90%
$\Gamma_{27}$ $\omega\pi^+\pi^-$	< 6.0 × 10 <sup>-4</sup>	CL=90%
$\Gamma_{28}$ $3(\pi^+\pi^-)$	< 9.1 × 10 <sup>-3</sup>	CL=90%
$\Gamma_{29}$ $3(\pi^+\pi^-)\pi^0$	< 1.37 %	CL=90%
$\Gamma_{30}$ $3(\pi^+\pi^-)2\pi^0$	< 11.74 %	CL=90%
$\Gamma_{31}$ $\eta\pi^+\pi^-$	< 1.24 × 10 <sup>-3</sup>	CL=90%
$\Gamma_{32}$ $\pi^+\pi^-2\pi^0$	< 8.9 × 10 <sup>-3</sup>	CL=90%
$\Gamma_{33}$ $\rho^0\pi^+\pi^-$	< 6.9 × 10 <sup>-3</sup>	CL=90%
$\Gamma_{34}$ $\eta3\pi$	< 1.34 × 10 <sup>-3</sup>	CL=90%
$\Gamma_{35}$ $\eta2(\pi^+\pi^-)$	< 2.43 %	CL=90%
$\Gamma_{36}$ $\eta\rho^0\pi^+\pi^-$	< 1.45 %	CL=90%
$\Gamma_{37}$ $\eta'3\pi$	< 2.44 × 10 <sup>-3</sup>	CL=90%
$\Gamma_{38}$ $K^+K^-\pi^+\pi^-$	< 9.0 × 10 <sup>-4</sup>	CL=90%
$\Gamma_{39}$ $\phi\pi^+\pi^-$	< 4.1 × 10 <sup>-4</sup>	CL=90%
$\Gamma_{40}$ $K^+K^-2\pi^0$	< 4.2 × 10 <sup>-3</sup>	CL=90%
$\Gamma_{41}$ $4(\pi^+\pi^-)$	< 1.67 %	CL=90%
$\Gamma_{42}$ $4(\pi^+\pi^-)\pi^0$	< 3.06 %	CL=90%
$\Gamma_{43}$ $\phi f_0(980)$	< 4.5 × 10 <sup>-4</sup>	CL=90%
$\Gamma_{44}$ $K^+K^-\pi^+\pi^-\pi^0$	< 2.36 × 10 <sup>-3</sup>	CL=90%
$\Gamma_{45}$ $K^+K^-\rho^0\pi^0$	< 8 × 10 <sup>-4</sup>	CL=90%
$\Gamma_{46}$ $K^+K^-\rho^+\pi^-$	< 1.46 %	CL=90%
$\Gamma_{47}$ $\omega K^+K^-$	< 3.4 × 10 <sup>-4</sup>	CL=90%
$\Gamma_{48}$ $\phi\pi^+\pi^-\pi^0$	< 3.8 × 10 <sup>-3</sup>	CL=90%
$\Gamma_{49}$ $K^{*0}K^-\pi^+\pi^0 + c.c.$	< 1.62 %	CL=90%
$\Gamma_{50}$ $K^{*+}K^-\pi^+\pi^- + c.c.$	< 3.23 %	CL=90%
$\Gamma_{51}$ $K^+K^-\pi^+\pi^-2\pi^0$	< 2.67 %	CL=90%
$\Gamma_{52}$ $K^+K^-2(\pi^+\pi^-)$	< 1.03 %	CL=90%
$\Gamma_{53}$ $K^+K^-2(\pi^+\pi^-)\pi^0$	< 3.60 %	CL=90%
$\Gamma_{54}$ $\eta K^+K^-$	< 4.1 × 10 <sup>-4</sup>	CL=90%
$\Gamma_{55}$ $\eta K^+K^-\pi^+\pi^-$	< 1.24 %	CL=90%
$\Gamma_{56}$ $\rho^0 K^+K^-$	< 5.0 × 10 <sup>-3</sup>	CL=90%

$\Gamma_{57}$ $2(K^+K^-)$	< 6.0 × 10 <sup>-4</sup>	CL=90%
$\Gamma_{58}$ $\phi K^+K^-$	< 7.5 × 10 <sup>-4</sup>	CL=90%
$\Gamma_{59}$ $2(K^+K^-)\pi^0$	< 2.9 × 10 <sup>-4</sup>	CL=90%
$\Gamma_{60}$ $2(K^+K^-)\pi^+\pi^-$	< 3.2 × 10 <sup>-3</sup>	CL=90%
$\Gamma_{61}$ $K_S^0 K^- \pi^+$	< 3.2 × 10 <sup>-3</sup>	CL=90%
$\Gamma_{62}$ $K_S^0 K^- \pi^+ \pi^0$	< 1.33 %	CL=90%
$\Gamma_{63}$ $K_S^0 K^- \rho^+$	< 6.6 × 10 <sup>-3</sup>	CL=90%
$\Gamma_{64}$ $K_S^0 K^- 2\pi^+\pi^-$	< 8.7 × 10 <sup>-3</sup>	CL=90%
$\Gamma_{65}$ $K_S^0 K^- \pi^+ \rho^0$	< 1.6 %	CL=90%
$\Gamma_{66}$ $K_S^0 K^- \pi^+ \eta$	< 1.3 %	CL=90%
$\Gamma_{67}$ $K_S^0 K^- 2\pi^+\pi^-\pi^0$	< 4.18 %	CL=90%
$\Gamma_{68}$ $K_S^0 K^- 2\pi^+\pi^-\eta$	< 4.8 %	CL=90%
$\Gamma_{69}$ $K_S^0 K^- \pi^+ 2(\pi^+\pi^-)$	< 1.22 %	CL=90%
$\Gamma_{70}$ $K_S^0 K^- \pi^+ 2\pi^0$	< 2.65 %	CL=90%
$\Gamma_{71}$ $K_S^0 K^- K^+ K^- \pi^+$	< 4.9 × 10 <sup>-3</sup>	CL=90%
$\Gamma_{72}$ $K_S^0 K^- K^+ K^- \pi^+ \pi^0$	< 3.0 %	CL=90%
$\Gamma_{73}$ $K_S^0 K^- K^+ K^- \pi^+ \eta$	< 2.2 %	CL=90%
$\Gamma_{74}$ $K^{*0} K^- \pi^+ + c.c.$	< 9.7 × 10 <sup>-3</sup>	CL=90%
$\Gamma_{75}$ $\rho\bar{\rho}$		
$\Gamma_{76}$ $\rho\bar{\rho}\pi^0$	< 4 × 10 <sup>-5</sup>	CL=90%
$\Gamma_{77}$ $\rho\bar{\rho}\pi^+\pi^-$	< 5.8 × 10 <sup>-4</sup>	CL=90%
$\Gamma_{78}$ $\Lambda\bar{\Lambda}$	< 1.2 × 10 <sup>-4</sup>	CL=90%
$\Gamma_{79}$ $\rho\bar{\rho}\pi^+\pi^-\pi^0$	< 1.85 × 10 <sup>-3</sup>	CL=90%
$\Gamma_{80}$ $\omega\rho\bar{\rho}$	< 2.9 × 10 <sup>-4</sup>	CL=90%
$\Gamma_{81}$ $\Lambda\bar{\Lambda}\pi^0$	< 7 × 10 <sup>-5</sup>	CL=90%
$\Gamma_{82}$ $\rho\bar{\rho}2(\pi^+\pi^-)$	< 2.6 × 10 <sup>-3</sup>	CL=90%
$\Gamma_{83}$ $\eta\rho\bar{\rho}$	< 5.4 × 10 <sup>-4</sup>	CL=90%
$\Gamma_{84}$ $\eta\rho\bar{\rho}\pi^+\pi^-$	< 3.3 × 10 <sup>-3</sup>	CL=90%
$\Gamma_{85}$ $\rho^0\rho\bar{\rho}$	< 1.7 × 10 <sup>-3</sup>	CL=90%
$\Gamma_{86}$ $\rho\bar{\rho}K^+K^-$	< 3.2 × 10 <sup>-4</sup>	CL=90%
$\Gamma_{87}$ $\eta\rho\bar{\rho}K^+K^-$	< 6.9 × 10 <sup>-3</sup>	CL=90%
$\Gamma_{88}$ $\pi^0\rho\bar{\rho}K^+K^-$	< 1.2 × 10 <sup>-3</sup>	CL=90%
$\Gamma_{89}$ $\phi\rho\bar{\rho}$	< 1.3 × 10 <sup>-4</sup>	CL=90%
$\Gamma_{90}$ $\Lambda\bar{\Lambda}\pi^+\pi^-$	< 2.5 × 10 <sup>-4</sup>	CL=90%
$\Gamma_{91}$ $\Lambda\bar{\rho}K^+$	< 2.8 × 10 <sup>-4</sup>	CL=90%
$\Gamma_{92}$ $\Lambda\bar{\rho}K^+\pi^+\pi^-$	< 6.3 × 10 <sup>-4</sup>	CL=90%
$\Gamma_{93}$ $\Lambda\bar{\Lambda}\eta$	< 1.9 × 10 <sup>-4</sup>	CL=90%
$\Gamma_{94}$ $\Sigma^+\Sigma^-$	< 1.0 × 10 <sup>-4</sup>	CL=90%
$\Gamma_{95}$ $\Sigma^0\Sigma^0$	< 4 × 10 <sup>-5</sup>	CL=90%
$\Gamma_{96}$ $\Xi^+\Xi^-$	< 1.5 × 10 <sup>-4</sup>	CL=90%
$\Gamma_{97}$ $\Xi^0\Xi^0$	< 1.4 × 10 <sup>-4</sup>	CL=90%

**Radiative decays**

$\Gamma_{98}$ $\gamma\chi_{c2}$	< 6.4 × 10 <sup>-4</sup>	CL=90%
$\Gamma_{99}$ $\gamma\chi_{c1}$	(2.49 ± 0.23) × 10 <sup>-3</sup>	
$\Gamma_{100}$ $\gamma\chi_{c0}$	(6.9 ± 0.6) × 10 <sup>-3</sup>	
$\Gamma_{101}$ $\gamma\eta_c$	< 7 × 10 <sup>-4</sup>	CL=90%
$\Gamma_{102}$ $\gamma\eta_c(2S)$	< 9 × 10 <sup>-4</sup>	CL=90%
$\Gamma_{103}$ $\gamma\eta'$	< 1.8 × 10 <sup>-4</sup>	CL=90%
$\Gamma_{104}$ $\gamma\eta$	< 1.5 × 10 <sup>-4</sup>	CL=90%
$\Gamma_{105}$ $\gamma\pi^0$	< 2 × 10 <sup>-4</sup>	CL=90%

**CONSTRAINED FIT INFORMATION**

An overall fit to the total width, a partial width, and 3 branching ratios uses 23 measurements and one constraint to determine 5 parameters. The overall fit has a  $\chi^2 = 20.1$  for 19 degrees of freedom.

The following *off-diagonal* array elements are the correlation coefficients  $\langle \delta p_i \delta p_j \rangle / (\delta p_i \delta p_j)$ , in percent, from the fit to parameters  $p_i$ , including the branching fractions,  $x_i \equiv \Gamma_i/\Gamma_{\text{total}}$ . The fit constrains the  $x_i$  whose labels appear in this array to sum to one.

$x_3$	99		
$x_8$	0	0	
$\Gamma$	0	0	-44
	$x_2$	$x_3$	$x_8$

Mode	Rate (MeV)	Scale factor
$\Gamma_2$ $D^0\bar{D}^0$	14.0 ± 1.4	1.8
$\Gamma_3$ $D^+D^-$	11.2 ± 1.1	1.7
$\Gamma_8$ $e^+e^-$	(2.62 ± 0.18) × 10 <sup>-4</sup>	1.4

$\psi(3770)$  PARTIAL WIDTHS

$\Gamma(e^+e^-)$					$\Gamma_8$
VALUE (keV)	EVTS	DOCUMENT ID	TECN	COMMENT	
<b>0.262 ± 0.018 OUR FIT</b>	Error	includes scale factor of 1.4.			$\Gamma_8$
<b>0.256 ± 0.016 OUR AVERAGE</b>	Error	includes scale factor of 1.2.			
0.154 + 0.079 + 0.021 - 0.058 - 0.027		1,2 ANASHIN	12A KEDR	$e^+e^- \rightarrow D\bar{D}$	
0.22 ± 0.05		3,4 ABLIKIM	08D BES2	$e^+e^- \rightarrow$ hadrons	
0.277 ± 0.011 ± 0.013		4 ABLIKIM	07E BES2	$e^+e^- \rightarrow$ hadrons	
0.203 ± 0.003 + 0.041 - 0.027	1.4M	4,5 BESSON	06 CLEO	$e^+e^- \rightarrow$ hadrons	
0.276 ± 0.050		4 SCHINDLER	80 MRK2	$e^+e^-$	
0.18 ± 0.06		4 BACINO	78 DLCO	$e^+e^-$	
••• We do not use the following data for averages, fits, limits, etc. •••					
0.196 ± 0.018		6 SHAMOV	17 RVUE	$e^+e^- \rightarrow D\bar{D}$ , hadrons	
0.414 + 0.072 + 0.093 - 0.080 - 0.028		2,7 ANASHIN	12A KEDR	$e^+e^- \rightarrow D\bar{D}$	
0.37 ± 0.09		8 RAPIDIS	77 LGW	$e^+e^-$	

1 Solution I of the two solutions.  
 2 Taking into account interference between the resonant and non-resonant  $D\bar{D}$  production.  
 3 Reanalysis of data presented in BAI 02C. From a global fit over the center-of-mass energy region 3.7–5.0 GeV covering the  $\psi(3770)$ ,  $\psi(4040)$ ,  $\psi(4160)$ , and  $\psi(4415)$  resonances. Phase angle fixed in the fit to  $\delta = 0^\circ$ .  
 4 Interference between the resonant and non-resonant  $D\bar{D}$  production not taken into account.  
 5 BESSON 06 (as corrected in BESSON 10) measure  $\sigma(e^+e^- \rightarrow \psi(3770) \rightarrow$  hadrons) =  $6.36 \pm 0.08 + 0.41 - 0.30$  nb at  $\sqrt{s} = 3773 \pm 1$  MeV, and obtain  $\Gamma_{ee}$  from the Born-level cross section calculated using  $\psi(3770)$  mass and width from our 2004 edition, PDG 04.  
 6 From the joint analysis of the data on the  $D\bar{D}$  and inclusive hadronic cross sections in the  $\psi(3770)$  region from BaBar, Belle, BES-II, CLEO and KEDR.  
 7 Solution II of the two solutions.  
 8 See also  $\Gamma(e^+e^-)/\Gamma_{total}$  below.

$\psi(3770)$  BRANCHING RATIOS

$\Gamma(D\bar{D})/\Gamma_{total}$					$\Gamma_1/\Gamma = (\Gamma_2 + \Gamma_3)/\Gamma$
VALUE	EVTS	DOCUMENT ID	TECN	COMMENT	
<b>0.93 ± 0.08 - 0.09 OUR FIT</b>	Error	includes scale factor of 2.0.			$\Gamma_1/\Gamma = (\Gamma_2 + \Gamma_3)/\Gamma$
<b>0.93 ± 0.08 - 0.09 OUR AVERAGE</b>	Error	includes scale factor of 2.1.			
0.849 ± 0.056 ± 0.018		1 ABLIKIM	08B BES2	$e^+e^- \rightarrow$ non- $D\bar{D}$	
1.033 ± 0.014 + 0.048 - 0.066	1.427M	2 BESSON	06 CLEO	$e^+e^- \rightarrow$ hadrons	
••• We do not use the following data for averages, fits, limits, etc. •••					
0.836 ± 0.049		3 SHAMOV	17 RVUE	$e^+e^- \rightarrow D\bar{D}$ , hadrons	
0.866 ± 0.050 ± 0.036		4,5 ABLIKIM	07K BES2	$e^+e^- \rightarrow$ non- $D\bar{D}$	
0.836 ± 0.073 ± 0.042		5 ABLIKIM	06L BES2	$e^+e^- \rightarrow D\bar{D}$	
0.855 ± 0.017 ± 0.058		5,6 ABLIKIM	06N BES2	$e^+e^- \rightarrow D\bar{D}$	

1 Neglecting interference.  
 2 Obtained by comparing a measurement of the total cross section (corrected in BESSON 10) with that of  $D\bar{D}$  reported by CLEO in DOBBS 07.  
 3 From the joint analysis of the data on the  $D\bar{D}$  and inclusive hadronic cross sections in the  $\psi(3770)$  region from BaBar, Belle, BES-II, CLEO and KEDR.  
 4 Using  $\sigma_{obs} = 7.07 \pm 0.58$  nb and neglecting interference.  
 5 Not independent of ABLIKIM 08B.  
 6 From a measurement of  $\sigma(e^+e^- \rightarrow D\bar{D})$  at  $\sqrt{s} = 3773$  MeV, using the  $\psi(3770)$  resonance parameters measured by ABLIKIM 06L.

$\Gamma(D^0\bar{D}^0)/\Gamma_{total}$					$\Gamma_2/\Gamma$
VALUE	EVTS	DOCUMENT ID	TECN	COMMENT	
<b>0.52 ± 0.04 - 0.05 OUR FIT</b>	Error	includes scale factor of 2.0.			$\Gamma_2/\Gamma$
••• We do not use the following data for averages, fits, limits, etc. •••					
0.467 ± 0.047 ± 0.023		ABLIKIM	06L BES2	$e^+e^- \rightarrow D^0\bar{D}^0$	
0.499 ± 0.013 ± 0.038		1 ABLIKIM	06N BES2	$e^+e^- \rightarrow D^0\bar{D}^0$	

1 From a measurement of  $\sigma(e^+e^- \rightarrow D\bar{D})$  at  $\sqrt{s} = 3773$  MeV, using the  $\psi(3770)$  resonance parameters measured by ABLIKIM 06L.

$\Gamma(D^+D^-)/\Gamma_{total}$					$\Gamma_3/\Gamma$
VALUE	EVTS	DOCUMENT ID	TECN	COMMENT	
<b>0.41 ± 0.04 OUR FIT</b>	Error	includes scale factor of 2.0.			$\Gamma_3/\Gamma$
••• We do not use the following data for averages, fits, limits, etc. •••					
0.369 ± 0.037 ± 0.028		ABLIKIM	06L BES2	$e^+e^- \rightarrow D^+D^-$	
0.357 ± 0.011 ± 0.034		1 ABLIKIM	06N BES2	$e^+e^- \rightarrow D^+D^-$	

1 From a measurement of  $\sigma(e^+e^- \rightarrow D\bar{D})$  at  $\sqrt{s} = 3773$  MeV, using the  $\psi(3770)$  resonance parameters measured by ABLIKIM 06L.

$\Gamma(D^0\bar{D}^0)/\Gamma(D^+D^-)$					$\Gamma_2/\Gamma_3$
VALUE	EVTS	DOCUMENT ID	TECN	COMMENT	
<b>1.253 ± 0.016 OUR FIT</b>					$\Gamma_2/\Gamma_3$
<b>1.253 ± 0.016 OUR AVERAGE</b>					
1.252 ± 0.009 ± 0.013	5.3M	BONVICINI	14 CLEO	$e^+e^- \rightarrow D\bar{D}$	
1.39 ± 0.31 ± 0.12		PAKHOVA	08 BELL	$10.6 e^+e^- \rightarrow D\bar{D}\gamma$	
1.78 ± 0.33 ± 0.24		AUBERT	07BE BABR	$e^+e^- \rightarrow D\bar{D}\gamma$	
1.27 ± 0.12 ± 0.08		ABLIKIM	06L BES2	$e^+e^- \rightarrow D\bar{D}$	
2.43 ± 1.50 ± 0.43	34	1 CHISTOV	04 BELL	$B^+ \rightarrow \psi(3770) K^+$	

••• We do not use the following data for averages, fits, limits, etc. •••

1.258 ± 0.016 ± 0.014      2 DOBBS      07 CLEO       $e^+e^- \rightarrow D\bar{D}$

1 See ADLER 88c for older measurements of this quantity.

2 Superseded by BONVICINI 14.

$\Gamma(J/\psi\pi^+\pi^-)/\Gamma_{total}$					$\Gamma_4/\Gamma$
VALUE (units 10 <sup>-3</sup> )	EVTS	DOCUMENT ID	TECN	COMMENT	
<b>1.93 ± 0.28 OUR AVERAGE</b>					$\Gamma_4/\Gamma$
1.89 ± 0.20 ± 0.20	231 ± 33	ADAM	06 CLEO	$e^+e^- \rightarrow \psi(3770)$	
3.4 ± 1.4 ± 0.9	17.8 ± 4.8	BAI	05 BES2	$e^+e^- \rightarrow \psi(3770)$	

$\Gamma(J/\psi\pi^0\pi^0)/\Gamma_{total}$					$\Gamma_5/\Gamma$
VALUE (units 10 <sup>-2</sup> )	EVTS	DOCUMENT ID	TECN	COMMENT	
<b>0.080 ± 0.025 ± 0.016</b>	39 ± 14	ADAM	06 CLEO	$e^+e^- \rightarrow \psi(3770)$	

$\Gamma(J/\psi\eta)/\Gamma_{total}$					$\Gamma_6/\Gamma$
VALUE (units 10 <sup>-5</sup> )	EVTS	DOCUMENT ID	TECN	COMMENT	
<b>87 ± 33 ± 22</b>	22 ± 10	ADAM	06 CLEO	$e^+e^- \rightarrow \psi(3770)$	

$\Gamma(J/\psi\pi^0)/\Gamma_{total}$					$\Gamma_7/\Gamma$
VALUE (units 10 <sup>-5</sup> )	CL%	EVTS	DOCUMENT ID	TECN	
<b>&lt;28</b>	90	<10	ADAM	06 CLEO	$e^+e^- \rightarrow \psi(3770)$

$\Gamma(e^+e^-)/\Gamma_{total}$					$\Gamma_8/\Gamma$
VALUE (units 10 <sup>-5</sup> )	EVTS	DOCUMENT ID	TECN	COMMENT	
<b>0.96 ± 0.07 OUR FIT</b>	Error	includes scale factor of 1.3.			$\Gamma_8/\Gamma$
<b>1.3 ± 0.2</b>		RAPIDIS	77 LGW	$e^+e^-$	

DECAYS TO LIGHT HADRONS

$\Gamma(b_1(1235)\pi)/\Gamma_{total}$					$\Gamma_9/\Gamma$
VALUE (units 10 <sup>-5</sup> )	CL%	DOCUMENT ID	TECN	COMMENT	
<b>&lt;1.4</b>	90	1 ADAMS	06 CLEO	$e^+e^- \rightarrow \psi(3770)$	

1 Comparing cross sections at  $\sqrt{s} = 3.773$  GeV and  $\sqrt{s} = 3.671$  GeV, neglecting interference, and using  $\sigma(\psi(3770) \rightarrow D\bar{D}) = 6.39 \pm 0.20$  nb.

$\Gamma(\phi\eta)/\Gamma_{total}$					$\Gamma_{10}/\Gamma$
VALUE (units 10 <sup>-4</sup> )	CL%	DOCUMENT ID	TECN	COMMENT	
<b>&lt;7</b>	90	1 ADAMS	06 CLEO	$e^+e^- \rightarrow \psi(3770)$	

1 Comparing cross sections at  $\sqrt{s} = 3.773$  GeV and  $\sqrt{s} = 3.671$  GeV, neglecting interference, and using  $\sigma(\psi(3770) \rightarrow D\bar{D}) = 6.39 \pm 0.20$  nb.

$\Gamma(\omega\eta)/\Gamma_{total}$					$\Gamma_{11}/\Gamma$
VALUE (units 10 <sup>-4</sup> )	CL%	DOCUMENT ID	TECN	COMMENT	
<b>&lt;4</b>	90	1 ADAMS	06 CLEO	$e^+e^- \rightarrow \psi(3770)$	

1 Comparing cross sections at  $\sqrt{s} = 3.773$  GeV and  $\sqrt{s} = 3.671$  GeV, neglecting interference, and using  $\sigma(\psi(3770) \rightarrow D\bar{D}) = 6.39 \pm 0.20$  nb.

$\Gamma(\rho^0\eta)/\Gamma_{total}$					$\Gamma_{12}/\Gamma$
VALUE (units 10 <sup>-4</sup> )	CL%	DOCUMENT ID	TECN	COMMENT	
<b>&lt;6</b>	90	1 ADAMS	06 CLEO	$e^+e^- \rightarrow \psi(3770)$	

1 Comparing cross sections at  $\sqrt{s} = 3.773$  GeV and  $\sqrt{s} = 3.671$  GeV, neglecting interference, and using  $\sigma(\psi(3770) \rightarrow D\bar{D}) = 6.39 \pm 0.20$  nb.

$\Gamma(\phi\eta)/\Gamma_{total}$					$\Gamma_{13}/\Gamma$
VALUE (units 10 <sup>-4</sup> )	CL%	DOCUMENT ID	TECN	COMMENT	
<b>3.1 ± 0.6 ± 0.3</b>		1 ADAMS	06 CLEO	$3.773 e^+e^- \rightarrow \phi\eta$	

••• We do not use the following data for averages, fits, limits, etc. •••

<19      90      2 ABLIKIM      07B BES2       $e^+e^- \rightarrow \psi(3770)$

1 Comparing cross sections at  $\sqrt{s} = 3.773$  GeV and  $\sqrt{s} = 3.671$  GeV, neglecting interference, and using  $\sigma(\psi(3770) \rightarrow D\bar{D}) = 6.39 \pm 0.20$  nb.  
 2 Assuming that interference effects between resonance and continuum can be neglected and using  $\sigma_{obs}(e^+e^- \rightarrow \psi(3770)) = 7.15 \pm 0.38$  nb.

$\Gamma(\omega\eta)/\Gamma_{total}$					$\Gamma_{14}/\Gamma$
VALUE (units 10 <sup>-5</sup> )	CL%	DOCUMENT ID	TECN	COMMENT	
<b>&lt;1.4</b>	90	1 ADAMS	06 CLEO	$e^+e^- \rightarrow \psi(3770)$	

1 Comparing cross sections at  $\sqrt{s} = 3.773$  GeV and  $\sqrt{s} = 3.671$  GeV, neglecting interference, and using  $\sigma(\psi(3770) \rightarrow D\bar{D}) = 6.39 \pm 0.20$  nb.

$\Gamma(\rho^0\eta)/\Gamma_{total}$					$\Gamma_{15}/\Gamma$
VALUE (units 10 <sup>-4</sup> )	CL%	DOCUMENT ID	TECN	COMMENT	
<b>&lt;5</b>	90	1 ADAMS	06 CLEO	$e^+e^- \rightarrow \psi(3770)$	

1 Comparing cross sections at  $\sqrt{s} = 3.773$  GeV and  $\sqrt{s} = 3.671$  GeV, neglecting interference, and using  $\sigma(\psi(3770) \rightarrow D\bar{D}) = 6.39 \pm 0.20$  nb.

$\Gamma(\phi\pi^0)/\Gamma_{total}$					$\Gamma_{16}/\Gamma$
VALUE (units 10 <sup>-5</sup> )	CL%	DOCUMENT ID	TECN	COMMENT	
<b>&lt;3</b>	90	1 ADAMS	06 CLEO	$e^+e^- \rightarrow \psi(3770)$	

## Meson Particle Listings

 $\psi(3770)$ 

••• We do not use the following data for averages, fits, limits, etc. •••

<50 90 2 ABLIKIM 07B BES2  $e^+e^- \rightarrow \psi(3770)$

<sup>1</sup> Comparing cross sections at  $\sqrt{s} = 3.773$  GeV and  $\sqrt{s} = 3.671$  GeV, neglecting interference, and using  $\sigma(\psi(3770) \rightarrow D\bar{D}) = 6.39 \pm 0.20$  nb.

<sup>2</sup> Assuming that interference effects between resonance and continuum can be neglected and using  $\sigma^{obs}(e^+e^- \rightarrow \psi(3770)) = 7.15 \pm 0.38$  nb.

$\Gamma(\omega\pi^0)/\Gamma_{total}$   $\Gamma_{17}/\Gamma$

VALUE (units $10^{-4}$ )	CL%	DOCUMENT ID	TECN	COMMENT
<6	90	1 ADAMS 06	CLEO	$e^+e^- \rightarrow \psi(3770)$

<sup>1</sup> Comparing cross sections at  $\sqrt{s} = 3.773$  GeV and  $\sqrt{s} = 3.671$  GeV, neglecting interference, and using  $\sigma(\psi(3770) \rightarrow D\bar{D}) = 6.39 \pm 0.20$  nb.

$\Gamma(\pi^+\pi^-\pi^0)/\Gamma_{total}$   $\Gamma_{18}/\Gamma$

VALUE (units $10^{-6}$ )	CL%	DOCUMENT ID	TECN	COMMENT
<5	90	1,2 ADAMS 06	CLEO	$e^+e^- \rightarrow \psi(3770)$

<sup>1</sup> Data suggest possible destructive interference with continuum.

<sup>2</sup> Comparing cross sections at  $\sqrt{s} = 3.773$  GeV and  $\sqrt{s} = 3.671$  GeV, neglecting interference, and using  $\sigma(\psi(3770) \rightarrow D\bar{D}) = 6.39 \pm 0.20$  nb.

$\Gamma(\rho\pi)/\Gamma_{total}$   $\Gamma_{19}/\Gamma$

VALUE (units $10^{-6}$ )	CL%	DOCUMENT ID	TECN	COMMENT
<5	90	1,2 ADAMS 06	CLEO	$e^+e^- \rightarrow \psi(3770)$

<sup>1</sup> Comparing cross sections at  $\sqrt{s} = 3.773$  GeV and  $\sqrt{s} = 3.671$  GeV, neglecting interference, and using  $\sigma(\psi(3770) \rightarrow D\bar{D}) = 6.39 \pm 0.20$  nb.

<sup>2</sup> Data suggest possible destructive interference with continuum.

$\Gamma(K^+K^-)/\Gamma_{total}$   $\Gamma_{20}/\Gamma$

VALUE	DOCUMENT ID	TECN	COMMENT
$\sim 10^{-5}$	1 DRUZHININ 15	RVUE	$e^+e^- \rightarrow \psi(3770)$

<sup>1</sup> DRUZHININ 15 uses BABAR and CLEO data taking into account interference of the processes  $e^+e^- \rightarrow K^+K^-$  and  $e^+e^- \rightarrow K_S^0 K_L^0$ .

$\Gamma(K^*(892)^+K^- + c.c.)/\Gamma_{total}$   $\Gamma_{21}/\Gamma$

VALUE (units $10^{-5}$ )	CL%	DOCUMENT ID	TECN	COMMENT
<1.4	90	1 ADAMS 06	CLEO	$e^+e^- \rightarrow \psi(3770)$

<sup>1</sup> Comparing cross sections at  $\sqrt{s} = 3.773$  GeV and  $\sqrt{s} = 3.671$  GeV, neglecting interference, and using  $\sigma(\psi(3770) \rightarrow D\bar{D}) = 6.39 \pm 0.20$  nb.

$\Gamma(K^*(892)^0\bar{K}^0 + c.c.)/\Gamma_{total}$   $\Gamma_{22}/\Gamma$

VALUE (units $10^{-3}$ )	CL%	DOCUMENT ID	TECN	COMMENT
<1.2	90	1 ADAMS 06	CLEO	$e^+e^- \rightarrow \psi(3770)$

<sup>1</sup> Comparing cross sections at  $\sqrt{s} = 3.773$  GeV and  $\sqrt{s} = 3.671$  GeV, neglecting interference, and using  $\sigma(\psi(3770) \rightarrow D\bar{D}) = 6.39 \pm 0.20$  nb.

$\Gamma(K_S^0 K_L^0)/\Gamma_{total}$   $\Gamma_{23}/\Gamma$

VALUE (units $10^{-5}$ )	CL%	DOCUMENT ID	TECN	COMMENT
< 1.2	90	1 CRONIN-HEN..06	CLEO	$e^+e^- \rightarrow \psi(3770)$

••• We do not use the following data for averages, fits, limits, etc. •••

<21 90 2 ABLIKIM 04F BES  $e^+e^- \rightarrow \psi(3770)$

<sup>1</sup> Using  $\sigma(e^+e^- \rightarrow \psi(3770) \rightarrow \text{hadrons}) = (6.38 \pm 0.08_{-0.30}^{+0.41})$  nb from BESSON 06 and  $B(K_S^0 \rightarrow \pi^+\pi^-) = 0.6895 \pm 0.0014$ .

<sup>2</sup> Using  $B(K_S^0 \rightarrow \pi^+\pi^-) = 0.6860 \pm 0.0027$ .

$\Gamma(2(\pi^+\pi^-))/\Gamma_{total}$   $\Gamma_{24}/\Gamma$

VALUE (units $10^{-4}$ )	CL%	DOCUMENT ID	TECN	COMMENT
<11.2	90	1 HUANG 06A	CLEO	$e^+e^- \rightarrow \psi(3770)$

••• We do not use the following data for averages, fits, limits, etc. •••

<48 90 2 ABLIKIM 07B BES2  $e^+e^- \rightarrow \psi(3770)$

<sup>1</sup> Using  $\sigma_{tot}(e^+e^- \rightarrow \psi(3770)) = 7.9 \pm 0.6$  nb at the resonance.

<sup>2</sup> Assuming that interference effects between resonance and continuum can be neglected and using  $\sigma^{obs}(e^+e^- \rightarrow \psi(3770)) = 7.15 \pm 0.38$  nb.

$\Gamma(2(\pi^+\pi^-\pi^0))/\Gamma_{total}$   $\Gamma_{25}/\Gamma$

VALUE (units $10^{-4}$ )	CL%	DOCUMENT ID	TECN	COMMENT
<10.6	90	1 HUANG 06A	CLEO	$e^+e^- \rightarrow \psi(3770)$

••• We do not use the following data for averages, fits, limits, etc. •••

<62 90 2 ABLIKIM 07B BES2  $e^+e^- \rightarrow \psi(3770)$

<sup>1</sup> Using  $\sigma_{tot}(e^+e^- \rightarrow \psi(3770)) = 7.9 \pm 0.6$  nb at the resonance.

<sup>2</sup> Assuming that interference effects between resonance and continuum can be neglected and using  $\sigma^{obs}(e^+e^- \rightarrow \psi(3770)) = 7.15 \pm 0.38$  nb.

$\Gamma(2(\pi^+\pi^-\pi^0))/\Gamma_{total}$   $\Gamma_{26}/\Gamma$

VALUE (units $10^{-3}$ )	CL%	EVTS	DOCUMENT ID	TECN	COMMENT
<58.5	90	305	ABLIKIM 08N	BES2	$e^+e^- \rightarrow \psi(3770)$

$\Gamma(\omega\pi^+\pi^-)/\Gamma_{total}$   $\Gamma_{27}/\Gamma$

VALUE (units $10^{-4}$ )	CL%	DOCUMENT ID	TECN	COMMENT
< 6.0	90	1 HUANG 06A	CLEO	$e^+e^- \rightarrow \psi(3770)$

••• We do not use the following data for averages, fits, limits, etc. •••

<55 90 2 ABLIKIM 07I BES2  $3.77 e^+e^-$

<sup>1</sup> Using  $\sigma_{tot}(e^+e^- \rightarrow \psi(3770)) = 7.9 \pm 0.6$  nb at the resonance.

<sup>2</sup> Assuming that interference effects between resonance and continuum can be neglected and using  $\sigma^{obs}(e^+e^- \rightarrow \psi(3770)) = 7.15 \pm 0.38$  nb.

$\Gamma(3(\pi^+\pi^-))/\Gamma_{total}$   $\Gamma_{28}/\Gamma$

VALUE (units $10^{-4}$ )	CL%	DOCUMENT ID	TECN	COMMENT
<91	90	1 ABLIKIM 07B	BES2	$e^+e^- \rightarrow \psi(3770)$

<sup>1</sup> Assuming that interference effects between resonance and continuum can be neglected and using  $\sigma^{obs}(e^+e^- \rightarrow \psi(3770)) = 7.15 \pm 0.38$  nb.

$\Gamma(3(\pi^+\pi^-\pi^0))/\Gamma_{total}$   $\Gamma_{29}/\Gamma$

VALUE (units $10^{-4}$ )	CL%	DOCUMENT ID	TECN	COMMENT
<137	90	1 ABLIKIM 07B	BES2	$e^+e^- \rightarrow \psi(3770)$

<sup>1</sup> Assuming that interference effects between resonance and continuum can be neglected and using  $\sigma^{obs}(e^+e^- \rightarrow \psi(3770)) = 7.15 \pm 0.38$  nb.

$\Gamma(3(\pi^+\pi^-)2\pi^0)/\Gamma_{total}$   $\Gamma_{30}/\Gamma$

VALUE (units $10^{-3}$ )	CL%	EVTS	DOCUMENT ID	TECN	COMMENT
<117.4	90	59	ABLIKIM 08N	BES2	$e^+e^- \rightarrow \psi(3770)$

$\Gamma(\eta\pi^+\pi^-)/\Gamma_{total}$   $\Gamma_{31}/\Gamma$

VALUE (units $10^{-3}$ )	CL%	DOCUMENT ID	TECN	COMMENT
<1.24	90	1 HUANG 06A	CLEO	$e^+e^- \rightarrow \psi(3770)$

••• We do not use the following data for averages, fits, limits, etc. •••

<2.3 90 2 ABLIKIM 10D BES2  $e^+e^- \rightarrow \psi(3770)$

<sup>1</sup> Using  $\sigma_{tot}(e^+e^- \rightarrow \psi(3770)) = 7.9 \pm 0.6$  nb at the resonance.

<sup>2</sup> Assuming that interference effects between resonance and continuum can be neglected and using  $\sigma^{obs}(e^+e^- \rightarrow \psi(3770)) = 7.15 \pm 0.38$  nb.

$\Gamma(\pi^+\pi^-2\pi^0)/\Gamma_{total}$   $\Gamma_{32}/\Gamma$

VALUE (units $10^{-3}$ )	CL%	EVTS	DOCUMENT ID	TECN	COMMENT
<8.9	90	218	ABLIKIM 08N	BES2	$e^+e^- \rightarrow \psi(3770)$

$\Gamma(\rho^0\pi^+\pi^-)/\Gamma_{total}$   $\Gamma_{33}/\Gamma$

VALUE (units $10^{-3}$ )	CL%	DOCUMENT ID	TECN	COMMENT
<6.9	90	1 ABLIKIM 07F	BES2	$e^+e^- \rightarrow \psi(3770)$

<sup>1</sup> Assuming that interference effects between resonance and continuum can be neglected and using  $\sigma^{obs}(e^+e^- \rightarrow \psi(3770)) = 7.15 \pm 0.38$  nb.

$\Gamma(\eta3\pi)/\Gamma_{total}$   $\Gamma_{34}/\Gamma$

VALUE (units $10^{-4}$ )	CL%	DOCUMENT ID	TECN	COMMENT
<13.4	90	1 HUANG 06A	CLEO	$e^+e^- \rightarrow \psi(3770)$

<sup>1</sup> Using  $\sigma_{tot}(e^+e^- \rightarrow \psi(3770)) = 7.9 \pm 0.6$  nb at the resonance.

$\Gamma(\eta2(\pi^+\pi^-))/\Gamma_{total}$   $\Gamma_{35}/\Gamma$

VALUE (units $10^{-4}$ )	CL%	DOCUMENT ID	TECN	COMMENT
<243	90	1 ABLIKIM 07B	BES2	$e^+e^- \rightarrow \psi(3770)$

<sup>1</sup> Assuming that interference effects between resonance and continuum can be neglected and using  $\sigma^{obs}(e^+e^- \rightarrow \psi(3770)) = 7.15 \pm 0.38$  nb.

$\Gamma(\eta\rho^0\pi^+\pi^-)/\Gamma_{total}$   $\Gamma_{36}/\Gamma$

VALUE (units $10^{-2}$ )	CL%	DOCUMENT ID	TECN	COMMENT
<1.45	90	1 ABLIKIM 10D	BES2	$e^+e^- \rightarrow \psi(3770)$

<sup>1</sup> Assuming that interference effects between resonance and continuum can be neglected and using  $\sigma^{obs}(e^+e^- \rightarrow \psi(3770)) = 7.15 \pm 0.38$  nb.

$\Gamma(\eta'3\pi)/\Gamma_{total}$   $\Gamma_{37}/\Gamma$

VALUE (units $10^{-4}$ )	CL%	DOCUMENT ID	TECN	COMMENT
<24.4	90	1 HUANG 06A	CLEO	$e^+e^- \rightarrow \psi(3770)$

<sup>1</sup> Using  $\sigma_{tot}(e^+e^- \rightarrow \psi(3770)) = 7.9 \pm 0.6$  nb at the resonance.

$\Gamma(K^+K^-\pi^+\pi^-)/\Gamma_{total}$   $\Gamma_{38}/\Gamma$

VALUE (units $10^{-4}$ )	CL%	DOCUMENT ID	TECN	COMMENT
< 9.0	90	1 HUANG 06A	CLEO	$e^+e^- \rightarrow \psi(3770)$

••• We do not use the following data for averages, fits, limits, etc. •••

<48 90 2 ABLIKIM 07B BES2  $e^+e^- \rightarrow \psi(3770)$

<sup>1</sup> Using  $\sigma_{tot}(e^+e^- \rightarrow \psi(3770)) = 7.9 \pm 0.6$  nb at the resonance.

<sup>2</sup> Assuming that interference effects between resonance and continuum can be neglected and using  $\sigma^{obs}(e^+e^- \rightarrow \psi(3770)) = 7.15 \pm 0.38$  nb.

$\Gamma(\phi\pi^+\pi^-)/\Gamma_{total}$   $\Gamma_{39}/\Gamma$

VALUE (units $10^{-4}$ )	CL%	DOCUMENT ID	TECN	COMMENT
< 4.1	90	<sup>1</sup> HUANG 06A	CLEO	$e^+e^- \rightarrow \psi(3770)$

• • • We do not use the following data for averages, fits, limits, etc. • • •  
 <16 90 <sup>2</sup> ABLIKIM 07B BES2  $e^+e^- \rightarrow \psi(3770)$   
<sup>1</sup> Using  $\sigma_{tot}(e^+e^- \rightarrow \psi(3770)) = 7.9 \pm 0.6$  nb at the resonance.  
<sup>2</sup> Assuming that interference effects between resonance and continuum can be neglected and using  $\sigma^{obs}(e^+e^- \rightarrow \psi(3770)) = 7.15 \pm 0.38$  nb.

$\Gamma(K^+K^-2\pi^0)/\Gamma_{total}$   $\Gamma_{40}/\Gamma$

VALUE (units $10^{-3}$ )	CL%	EVTS	DOCUMENT ID	TECN	COMMENT
<4.2	90	14	ABLIKIM 08N	BES2	$e^+e^- \rightarrow \psi(3770)$

$\Gamma(4(\pi^+\pi^-))/\Gamma_{total}$   $\Gamma_{41}/\Gamma$

VALUE (units $10^{-3}$ )	CL%	DOCUMENT ID	TECN	COMMENT
<16.7	90	<sup>1</sup> ABLIKIM 07F	BES2	$e^+e^- \rightarrow \psi(3770)$

<sup>1</sup> Assuming that interference effects between resonance and continuum can be neglected and using  $\sigma^{obs}(e^+e^- \rightarrow \psi(3770)) = 7.15 \pm 0.38$  nb.

$\Gamma(4(\pi^+\pi^-\pi^0))/\Gamma_{total}$   $\Gamma_{42}/\Gamma$

VALUE (units $10^{-3}$ )	CL%	DOCUMENT ID	TECN	COMMENT
<30.6	90	<sup>1</sup> ABLIKIM 07F	BES2	$e^+e^- \rightarrow \psi(3770)$

<sup>1</sup> Assuming that interference effects between resonance and continuum can be neglected and using  $\sigma^{obs}(e^+e^- \rightarrow \psi(3770)) = 7.15 \pm 0.38$  nb.

$\Gamma(\phi f_0(980))/\Gamma_{total}$   $\Gamma_{43}/\Gamma$

VALUE (units $10^{-4}$ )	CL%	DOCUMENT ID	TECN	COMMENT
<4.5	90	<sup>1</sup> HUANG 06A	CLEO	$e^+e^- \rightarrow \psi(3770)$

<sup>1</sup> Using  $\sigma_{tot}(e^+e^- \rightarrow \psi(3770)) = 7.9 \pm 0.6$  nb at the resonance.

$\Gamma(K^+K^-\pi^+\pi^-\pi^0)/\Gamma_{total}$   $\Gamma_{44}/\Gamma$

VALUE (units $10^{-4}$ )	CL%	DOCUMENT ID	TECN	COMMENT
< 23.6	90	<sup>1</sup> HUANG 06A	CLEO	$e^+e^- \rightarrow \psi(3770)$

• • • We do not use the following data for averages, fits, limits, etc. • • •  
 <111 90 <sup>2</sup> ABLIKIM 07B BES2  $e^+e^- \rightarrow \psi(3770)$   
<sup>1</sup> Using  $\sigma_{tot}(e^+e^- \rightarrow \psi(3770)) = 7.9 \pm 0.6$  nb at the resonance.  
<sup>2</sup> Assuming that interference effects between resonance and continuum can be neglected and using  $\sigma^{obs}(e^+e^- \rightarrow \psi(3770)) = 7.15 \pm 0.38$  nb.

$\Gamma(K^+K^-\rho^0\pi^0)/\Gamma_{total}$   $\Gamma_{45}/\Gamma$

VALUE (units $10^{-4}$ )	CL%	DOCUMENT ID	TECN	COMMENT
<8	90	<sup>1</sup> ABLIKIM 07I	BES2	$3.77 e^+e^-$

<sup>1</sup> Assuming that interference effects between resonance and continuum can be neglected and using  $\sigma^{obs}(e^+e^- \rightarrow \psi(3770)) = 7.15 \pm 0.38$  nb.

$\Gamma(K^+K^-\rho^+\pi^-)/\Gamma_{total}$   $\Gamma_{46}/\Gamma$

VALUE (units $10^{-4}$ )	CL%	DOCUMENT ID	TECN	COMMENT
<146	90	<sup>1</sup> ABLIKIM 07I	BES2	$3.77 e^+e^-$

<sup>1</sup> Assuming that interference effects between resonance and continuum can be neglected and using  $\sigma^{obs}(e^+e^- \rightarrow \psi(3770)) = 7.15 \pm 0.38$  nb.

$\Gamma(\omega K^+K^-)/\Gamma_{total}$   $\Gamma_{47}/\Gamma$

VALUE (units $10^{-4}$ )	CL%	DOCUMENT ID	TECN	COMMENT
< 3.4	90	<sup>1</sup> HUANG 06A	CLEO	$e^+e^- \rightarrow \psi(3770)$

• • • We do not use the following data for averages, fits, limits, etc. • • •  
 <66 90 <sup>2</sup> ABLIKIM 07I BES2  $3.77 e^+e^-$   
<sup>1</sup> Using  $\sigma_{tot}(e^+e^- \rightarrow \psi(3770)) = 7.9 \pm 0.6$  nb at the resonance.  
<sup>2</sup> Assuming that interference effects between resonance and continuum can be neglected and using  $\sigma^{obs}(e^+e^- \rightarrow \psi(3770)) = 7.15 \pm 0.38$  nb.

$\Gamma(\phi\pi^+\pi^-\pi^0)/\Gamma_{total}$   $\Gamma_{48}/\Gamma$

VALUE (units $10^{-4}$ )	CL%	DOCUMENT ID	TECN	COMMENT
<38	90	<sup>1</sup> ABLIKIM 07I	BES2	$3.77 e^+e^-$

<sup>1</sup> Assuming that interference effects between resonance and continuum can be neglected and using  $\sigma^{obs}(e^+e^- \rightarrow \psi(3770)) = 7.15 \pm 0.38$  nb.

$\Gamma(K^{*0}K^-\pi^+\pi^0 + c.c.)/\Gamma_{total}$   $\Gamma_{49}/\Gamma$

VALUE (units $10^{-4}$ )	CL%	DOCUMENT ID	TECN	COMMENT
<162	90	<sup>1</sup> ABLIKIM 07I	BES2	$3.77 e^+e^-$

<sup>1</sup> Assuming that interference effects between resonance and continuum can be neglected and using  $\sigma^{obs}(e^+e^- \rightarrow \psi(3770)) = 7.15 \pm 0.38$  nb.

$\Gamma(K^{*+}K^-\pi^+\pi^- + c.c.)/\Gamma_{total}$   $\Gamma_{50}/\Gamma$

VALUE (units $10^{-4}$ )	CL%	DOCUMENT ID	TECN	COMMENT
<323	90	<sup>1</sup> ABLIKIM 07I	BES2	$3.77 e^+e^-$

<sup>1</sup> Assuming that interference effects between resonance and continuum can be neglected and using  $\sigma^{obs}(e^+e^- \rightarrow \psi(3770)) = 7.15 \pm 0.38$  nb.

$\Gamma(K^+K^-\pi^+\pi^-2\pi^0)/\Gamma_{total}$   $\Gamma_{51}/\Gamma$

VALUE (units $10^{-3}$ )	CL%	EVTS	DOCUMENT ID	TECN	COMMENT
<26.7	90	24	ABLIKIM 08N	BES2	$e^+e^- \rightarrow \psi(3770)$

$\Gamma(K^+K^-2(\pi^+\pi^-))/\Gamma_{total}$   $\Gamma_{52}/\Gamma$

VALUE (units $10^{-3}$ )	CL%	DOCUMENT ID	TECN	COMMENT
<10.3	90	<sup>1</sup> ABLIKIM 07F	BES2	$e^+e^- \rightarrow \psi(3770)$

<sup>1</sup> Assuming that interference effects between resonance and continuum can be neglected and using  $\sigma^{obs}(e^+e^- \rightarrow \psi(3770)) = 7.15 \pm 0.38$  nb.

$\Gamma(K^+K^-2(\pi^+\pi^-\pi^0))/\Gamma_{total}$   $\Gamma_{53}/\Gamma$

VALUE (units $10^{-3}$ )	CL%	DOCUMENT ID	TECN	COMMENT
<36.0	90	<sup>1</sup> ABLIKIM 07F	BES2	$e^+e^- \rightarrow \psi(3770)$

<sup>1</sup> Assuming that interference effects between resonance and continuum can be neglected and using  $\sigma^{obs}(e^+e^- \rightarrow \psi(3770)) = 7.15 \pm 0.38$  nb.

$\Gamma(\eta K^+K^-)/\Gamma_{total}$   $\Gamma_{54}/\Gamma$

VALUE (units $10^{-4}$ )	CL%	DOCUMENT ID	TECN	COMMENT
< 4.1	90	<sup>1</sup> HUANG 06A	CLEO	$e^+e^- \rightarrow \psi(3770)$

• • • We do not use the following data for averages, fits, limits, etc. • • •  
 <31 90 <sup>2</sup> ABLIKIM 10D BES2  $e^+e^- \rightarrow \psi(3770)$   
<sup>1</sup> Using  $\sigma_{tot}(e^+e^- \rightarrow \psi(3770)) = 7.9 \pm 0.6$  nb at the resonance.  
<sup>2</sup> Assuming that interference effects between resonance and continuum can be neglected and using  $\sigma^{obs}(e^+e^- \rightarrow \psi(3770)) = 7.15 \pm 0.38$  nb.

$\Gamma(\eta K^+K^-\pi^+\pi^-)/\Gamma_{total}$   $\Gamma_{55}/\Gamma$

VALUE (units $10^{-2}$ )	CL%	DOCUMENT ID	TECN	COMMENT
<1.24	90	<sup>1</sup> ABLIKIM 10D	BES2	$e^+e^- \rightarrow \psi(3770)$

<sup>1</sup> Assuming that interference effects between resonance and continuum can be neglected and using  $\sigma^{obs}(e^+e^- \rightarrow \psi(3770)) = 7.15 \pm 0.38$  nb.

$\Gamma(\rho^0 K^+K^-)/\Gamma_{total}$   $\Gamma_{56}/\Gamma$

VALUE (units $10^{-3}$ )	CL%	DOCUMENT ID	TECN	COMMENT
<5.0	90	<sup>1</sup> ABLIKIM 07F	BES2	$e^+e^- \rightarrow \psi(3770)$

<sup>1</sup> Assuming that interference effects between resonance and continuum can be neglected and using  $\sigma^{obs}(e^+e^- \rightarrow \psi(3770)) = 7.15 \pm 0.38$  nb.

$\Gamma(2(K^+K^-))/\Gamma_{total}$   $\Gamma_{57}/\Gamma$

VALUE (units $10^{-4}$ )	CL%	DOCUMENT ID	TECN	COMMENT
< 6.0	90	<sup>1</sup> HUANG 06A	CLEO	$e^+e^- \rightarrow \psi(3770)$

• • • We do not use the following data for averages, fits, limits, etc. • • •  
 <17 90 <sup>2</sup> ABLIKIM 07B BES2  $e^+e^- \rightarrow \psi(3770)$   
<sup>1</sup> Using  $\sigma_{tot}(e^+e^- \rightarrow \psi(3770)) = 7.9 \pm 0.6$  nb at the resonance.  
<sup>2</sup> Assuming that interference effects between resonance and continuum can be neglected and using  $\sigma^{obs}(e^+e^- \rightarrow \psi(3770)) = 7.15 \pm 0.38$  nb.

$\Gamma(\phi K^+K^-)/\Gamma_{total}$   $\Gamma_{58}/\Gamma$

VALUE (units $10^{-4}$ )	CL%	DOCUMENT ID	TECN	COMMENT
< 7.5	90	<sup>1</sup> HUANG 06A	CLEO	$e^+e^- \rightarrow \psi(3770)$

• • • We do not use the following data for averages, fits, limits, etc. • • •  
 <24 90 <sup>2</sup> ABLIKIM 07B BES2  $e^+e^- \rightarrow \psi(3770)$   
<sup>1</sup> Using  $\sigma_{tot}(e^+e^- \rightarrow \psi(3770)) = 7.9 \pm 0.6$  nb at the resonance.  
<sup>2</sup> Assuming that interference effects between resonance and continuum can be neglected and using  $\sigma^{obs}(e^+e^- \rightarrow \psi(3770)) = 7.15 \pm 0.38$  nb.

$\Gamma(2(K^+K^-)\pi^0)/\Gamma_{total}$   $\Gamma_{59}/\Gamma$

VALUE (units $10^{-4}$ )	CL%	DOCUMENT ID	TECN	COMMENT
< 2.9	90	<sup>1</sup> HUANG 06A	CLEO	$e^+e^- \rightarrow \psi(3770)$

• • • We do not use the following data for averages, fits, limits, etc. • • •  
 <46 90 <sup>2</sup> ABLIKIM 07B BES2  $e^+e^- \rightarrow \psi(3770)$   
<sup>1</sup> Using  $\sigma_{tot}(e^+e^- \rightarrow \psi(3770)) = 7.9 \pm 0.6$  nb at the resonance.  
<sup>2</sup> Assuming that interference effects between resonance and continuum can be neglected and using  $\sigma^{obs}(e^+e^- \rightarrow \psi(3770)) = 7.15 \pm 0.38$  nb.

$\Gamma(2(K^+K^-)\pi^+\pi^-)/\Gamma_{total}$   $\Gamma_{60}/\Gamma$

VALUE (units $10^{-3}$ )	CL%	DOCUMENT ID	TECN	COMMENT
<3.2	90	<sup>1</sup> ABLIKIM 07F	BES2	$e^+e^- \rightarrow \psi(3770)$

<sup>1</sup> Assuming that interference effects between resonance and continuum can be neglected and using  $\sigma^{obs}(e^+e^- \rightarrow \psi(3770)) = 7.15 \pm 0.38$  nb.

$\Gamma(K_S^0 K^-\pi^+)/\Gamma_{total}$   $\Gamma_{61}/\Gamma$

VALUE (units $10^{-3}$ )	CL%	EVTS	DOCUMENT ID	TECN	COMMENT
<3.2	90	18	ABLIKIM 08M	BES2	$e^+e^- \rightarrow \psi(3770)$

$\Gamma(K_S^0 K^-\pi^+\pi^0)/\Gamma_{total}$   $\Gamma_{62}/\Gamma$

VALUE (units $10^{-3}$ )	CL%	EVTS	DOCUMENT ID	TECN	COMMENT
<13.3	90	40	ABLIKIM 08M	BES2	$e^+e^- \rightarrow \psi(3770)$



## Meson Particle Listings

 $\psi(3770)$ 

$\Gamma(K_S^0 K^- \rho^+)/\Gamma_{\text{total}}$	$\Gamma_{63}/\Gamma$
VALUE (units $10^{-3}$ ) CL% <b>&lt;6.6</b> 90	DOCUMENT ID TECN COMMENT ABLIKIM 09c BES2 $e^+ e^- \rightarrow \psi(3770)$

$\Gamma(K_S^0 K^- 2\pi^+ \pi^-)/\Gamma_{\text{total}}$	$\Gamma_{64}/\Gamma$
VALUE (units $10^{-3}$ ) CL% EVTS <b>&lt;8.7</b> 90 39	DOCUMENT ID TECN COMMENT ABLIKIM 08M BES2 $e^+ e^- \rightarrow \psi(3770)$

$\Gamma(K_S^0 K^- \pi^+ \rho^0)/\Gamma_{\text{total}}$	$\Gamma_{65}/\Gamma$
VALUE (units $10^{-2}$ ) CL% <b>&lt;1.6</b> 90	DOCUMENT ID TECN COMMENT ABLIKIM 09c BES2 $e^+ e^- \rightarrow \psi(3770)$

$\Gamma(K_S^0 K^- \pi^+ \eta)/\Gamma_{\text{total}}$	$\Gamma_{66}/\Gamma$
VALUE (units $10^{-2}$ ) CL% <b>&lt;1.3</b> 90	DOCUMENT ID TECN COMMENT ABLIKIM 09c BES2 $e^+ e^- \rightarrow \psi(3770)$

$\Gamma(K_S^0 K^- 2\pi^+ \pi^- \pi^0)/\Gamma_{\text{total}}$	$\Gamma_{67}/\Gamma$
VALUE (units $10^{-3}$ ) CL% EVTS <b>&lt;41.8</b> 90 23	DOCUMENT ID TECN COMMENT ABLIKIM 08M BES2 $e^+ e^- \rightarrow \psi(3770)$

$\Gamma(K_S^0 K^- 2\pi^+ \pi^- \eta)/\Gamma_{\text{total}}$	$\Gamma_{68}/\Gamma$
VALUE (units $10^{-2}$ ) CL% <b>&lt;4.8</b> 90	DOCUMENT ID TECN COMMENT ABLIKIM 09c BES2 $e^+ e^- \rightarrow \psi(3770)$

$\Gamma(K_S^0 K^- \pi^+ 2(\pi^+ \pi^-))/\Gamma_{\text{total}}$	$\Gamma_{69}/\Gamma$
VALUE (units $10^{-3}$ ) CL% EVTS <b>&lt;12.2</b> 90 4	DOCUMENT ID TECN COMMENT ABLIKIM 08M BES2 $e^+ e^- \rightarrow \psi(3770)$

$\Gamma(K_S^0 K^- \pi^+ 2\pi^0)/\Gamma_{\text{total}}$	$\Gamma_{70}/\Gamma$
VALUE (units $10^{-3}$ ) CL% EVTS <b>&lt;26.5</b> 90 17	DOCUMENT ID TECN COMMENT ABLIKIM 08M BES2 $e^+ e^- \rightarrow \psi(3770)$

$\Gamma(K_S^0 K^- K^+ K^- \pi^+)/\Gamma_{\text{total}}$	$\Gamma_{71}/\Gamma$
VALUE (units $10^{-3}$ ) CL% <b>&lt;4.9</b> 90	DOCUMENT ID TECN COMMENT ABLIKIM 09c BES2 $e^+ e^- \rightarrow \psi(3770)$

$\Gamma(K_S^0 K^- K^+ K^- \pi^+ \pi^0)/\Gamma_{\text{total}}$	$\Gamma_{72}/\Gamma$
VALUE (units $10^{-2}$ ) CL% <b>&lt;3.0</b> 90	DOCUMENT ID TECN COMMENT ABLIKIM 09c BES2 $e^+ e^- \rightarrow \psi(3770)$

$\Gamma(K_S^0 K^- K^+ K^- \pi^+ \eta)/\Gamma_{\text{total}}$	$\Gamma_{73}/\Gamma$
VALUE (units $10^{-2}$ ) CL% <b>&lt;2.2</b> 90	DOCUMENT ID TECN COMMENT ABLIKIM 09c BES2 $e^+ e^- \rightarrow \psi(3770)$

$\Gamma(K^*0 K^- \pi^+ + \text{c.c.})/\Gamma_{\text{total}}$	$\Gamma_{74}/\Gamma$
VALUE (units $10^{-3}$ ) CL% <b>&lt;9.7</b> 90	DOCUMENT ID TECN COMMENT 1 ABLIKIM 07F BES2 $e^+ e^- \rightarrow \psi(3770)$

<sup>1</sup> Assuming that interference effects between resonance and continuum can be neglected and using  $\sigma_{\text{obs}}(e^+ e^- \rightarrow \psi(3770)) = 7.15 \pm 0.38$  nb.

$\Gamma(\rho\bar{\rho})/\Gamma_{\text{total}}$	$\Gamma_{75}/\Gamma$
VALUE (units $10^{-6}$ ) EVTS <b>•••</b> We do not use the following data for averages, fits, limits, etc. •••	DOCUMENT ID TECN COMMENT

not seen	1 AAIJ 17AD LHCb $p\bar{p} \rightarrow B^+ X \rightarrow \rho\bar{\rho} K^+ X$
$7.1^{+8.6}_{-2.9}$ 684	2 ABLIKIM 14L BES3 $e^+ e^- \rightarrow \psi(3770)$
$310 \pm 30$ 684	3 ABLIKIM 14L BES3 $e^+ e^- \rightarrow \psi(3770)$

<sup>1</sup> AAIJ 17AD reports  $B(B^+ \rightarrow \psi(3770) K^+ \rightarrow \rho\bar{\rho} K^+)/B(B^+ \rightarrow J/\psi K^+ \rightarrow \rho\bar{\rho} K^+) < 0.09$  (0.10) at 90% (95%) CL.

<sup>2</sup> Solution I of two equivalent solutions in a fit with a resonance interfering with continuum.

<sup>3</sup> Solution II of two equivalent solutions in a fit with a resonance interfering with continuum.

$\Gamma(\rho\bar{\rho}\pi^0)/\Gamma_{\text{total}}$	$\Gamma_{76}/\Gamma$
VALUE (units $10^{-4}$ ) CL% <b>&lt; 0.4</b> 90	DOCUMENT ID TECN COMMENT 1,2 ABLIKIM 14o BES3 $e^+ e^- \rightarrow \psi(3770)$

<b>•••</b> We do not use the following data for averages, fits, limits, etc. •••	
$59^{+3}_{-2} \pm 5$	1,3 ABLIKIM 14o BES3 $e^+ e^- \rightarrow \psi(3770)$
<12	4 ABLIKIM 07B BES2 $e^+ e^- \rightarrow \psi(3770)$

<sup>1</sup> Calculated by the authors using  $\sigma(e^+ e^- \rightarrow \psi(3770) \rightarrow \text{hadrons}) = 6.36 \pm 0.08^{+0.41}_{-0.30}$  nb from BESSON 10.

<sup>2</sup> Solution I of two equivalent solutions in a fit with a resonance interfering with continuum.

<sup>3</sup> Solution II of two equivalent solutions in a fit with a resonance interfering with continuum.

<sup>4</sup> Assuming that interference effects between resonance and continuum can be neglected and using  $\sigma_{\text{obs}}(e^+ e^- \rightarrow \psi(3770)) = 7.15 \pm 0.38$  nb.

$\Gamma(\rho\bar{\rho}\pi^+ \pi^-)/\Gamma_{\text{total}}$	$\Gamma_{77}/\Gamma$
VALUE (units $10^{-4}$ ) CL% <b>&lt; 5.8</b> 90	DOCUMENT ID TECN COMMENT 1 HUANG 06A CLEO $e^+ e^- \rightarrow \psi(3770)$

**•••** We do not use the following data for averages, fits, limits, etc. •••

<16 90 2 ABLIKIM 07B BES2  $e^+ e^- \rightarrow \psi(3770)$

<sup>1</sup> Using  $\sigma_{\text{tot}}(e^+ e^- \rightarrow \psi(3770)) = 7.9 \pm 0.6$  nb at the resonance.

<sup>2</sup> Assuming that interference effects between resonance and continuum can be neglected and using  $\sigma_{\text{obs}}(e^+ e^- \rightarrow \psi(3770)) = 7.15 \pm 0.38$  nb.

$\Gamma(\Lambda\bar{\Lambda})/\Gamma_{\text{total}}$	$\Gamma_{78}/\Gamma$
VALUE (units $10^{-4}$ ) CL% <b>&lt;1.2</b> 90	DOCUMENT ID TECN COMMENT 1 HUANG 06A CLEO $e^+ e^- \rightarrow \psi(3770)$

**•••** We do not use the following data for averages, fits, limits, etc. •••

<4 90 2 ABLIKIM 07F BES2  $e^+ e^- \rightarrow \psi(3770)$

<sup>1</sup> Using  $\sigma_{\text{tot}}(e^+ e^- \rightarrow \psi(3770)) = 7.9 \pm 0.6$  nb at the resonance.

<sup>2</sup> Assuming that interference effects between resonance and continuum can be neglected and using  $\sigma_{\text{obs}}(e^+ e^- \rightarrow \psi(3770)) = 7.15 \pm 0.38$  nb.

$\Gamma(\rho\bar{\rho}\pi^+ \pi^- \pi^0)/\Gamma_{\text{total}}$	$\Gamma_{79}/\Gamma$
VALUE (units $10^{-4}$ ) CL% <b>&lt;18.5</b> 90	DOCUMENT ID TECN COMMENT 1 HUANG 06A CLEO $e^+ e^- \rightarrow \psi(3770)$

**•••** We do not use the following data for averages, fits, limits, etc. •••

<73 90 2 ABLIKIM 07B BES2  $e^+ e^- \rightarrow \psi(3770)$

<sup>1</sup> Using  $\sigma_{\text{tot}}(e^+ e^- \rightarrow \psi(3770)) = 7.9 \pm 0.6$  nb at the resonance.

<sup>2</sup> Assuming that interference effects between resonance and continuum can be neglected and using  $\sigma_{\text{obs}}(e^+ e^- \rightarrow \psi(3770)) = 7.15 \pm 0.38$  nb.

$\Gamma(\omega\rho\bar{\rho})/\Gamma_{\text{total}}$	$\Gamma_{80}/\Gamma$
VALUE (units $10^{-4}$ ) CL% <b>&lt; 2.9</b> 90	DOCUMENT ID TECN COMMENT 1 HUANG 06A CLEO $e^+ e^- \rightarrow \psi(3770)$

**•••** We do not use the following data for averages, fits, limits, etc. •••

<30 90 2 ABLIKIM 07i BES2  $3.77 e^+ e^-$

<sup>1</sup> Using  $\sigma_{\text{tot}}(e^+ e^- \rightarrow \psi(3770)) = 7.9 \pm 0.6$  nb at the resonance.

<sup>2</sup> Using  $\sigma_{\text{obs}} = 7.15 \pm 0.27 \pm 0.27$  nb and neglecting interference.

$\Gamma(\Lambda\bar{\Lambda}\pi^0)/\Gamma_{\text{total}}$	$\Gamma_{81}/\Gamma$
VALUE (units $10^{-4}$ ) CL% <b>&lt; 0.7</b> 90	DOCUMENT ID TECN COMMENT 1 ABLIKIM 13Q BES3 $e^+ e^- \rightarrow \psi(3770)$

**•••** We do not use the following data for averages, fits, limits, etc. •••

<12 90 2 ABLIKIM 07i BES2  $3.77 e^+ e^-$

<sup>1</sup> Assuming that interference effects between resonance and continuum can be neglected.

<sup>2</sup> Assuming that interference effects between resonance and continuum can be neglected and using  $\sigma_{\text{obs}}(e^+ e^- \rightarrow \psi(3770)) = 7.15 \pm 0.38$  nb.

$\Gamma(\rho\bar{\rho}2(\pi^+ \pi^-))/\Gamma_{\text{total}}$	$\Gamma_{82}/\Gamma$
VALUE (units $10^{-3}$ ) CL% <b>&lt;2.6</b> 90	DOCUMENT ID TECN COMMENT 1 ABLIKIM 07F BES2 $e^+ e^- \rightarrow \psi(3770)$

<sup>1</sup> Assuming that interference effects between resonance and continuum can be neglected and using  $\sigma_{\text{obs}}(e^+ e^- \rightarrow \psi(3770)) = 7.15 \pm 0.38$  nb.

$\Gamma(\eta\rho\bar{\rho})/\Gamma_{\text{total}}$	$\Gamma_{83}/\Gamma$
VALUE (units $10^{-4}$ ) CL% <b>&lt; 5.4</b> 90	DOCUMENT ID TECN COMMENT 1 HUANG 06A CLEO $e^+ e^- \rightarrow \psi(3770)$

**•••** We do not use the following data for averages, fits, limits, etc. •••

<11 90 2 ABLIKIM 10D BES2  $e^+ e^- \rightarrow \psi(3770)$

<sup>1</sup> Using  $\sigma_{\text{tot}}(e^+ e^- \rightarrow \psi(3770)) = 7.9 \pm 0.6$  nb at the resonance.

<sup>2</sup> Assuming that interference effects between resonance and continuum can be neglected and using  $\sigma_{\text{obs}}(e^+ e^- \rightarrow \psi(3770)) = 7.15 \pm 0.38$  nb.

$\Gamma(\eta\rho\bar{\rho}\pi^+ \pi^-)/\Gamma_{\text{total}}$	$\Gamma_{84}/\Gamma$
VALUE (units $10^{-3}$ ) CL% <b>&lt;3.3</b> 90	DOCUMENT ID TECN COMMENT 1 ABLIKIM 10D BES2 $e^+ e^- \rightarrow \psi(3770)$

<sup>1</sup> Assuming that interference effects between resonance and continuum can be neglected and using  $\sigma_{\text{obs}}(e^+ e^- \rightarrow \psi(3770)) = 7.15 \pm 0.38$  nb.

$\Gamma(\rho^0\rho\bar{\rho})/\Gamma_{\text{total}}$	$\Gamma_{85}/\Gamma$
VALUE (units $10^{-3}$ ) CL% <b>&lt;1.7</b> 90	DOCUMENT ID TECN COMMENT 1 ABLIKIM 07F BES2 $e^+ e^- \rightarrow \psi(3770)$

<sup>1</sup> Assuming that interference effects between resonance and continuum can be neglected and using  $\sigma_{\text{obs}}(e^+ e^- \rightarrow \psi(3770)) = 7.15 \pm 0.38$  nb.

$\Gamma(\rho\bar{\rho}K^+ K^-)/\Gamma_{\text{total}}$	$\Gamma_{86}/\Gamma$
VALUE (units $10^{-4}$ ) CL% <b>&lt; 3.2</b> 90	DOCUMENT ID TECN COMMENT 1 HUANG 06A CLEO $e^+ e^- \rightarrow \psi(3770)$

**•••** We do not use the following data for averages, fits, limits, etc. •••

<11 90 2 ABLIKIM 07B BES2  $e^+ e^- \rightarrow \psi(3770)$

<sup>1</sup> Using  $\sigma_{\text{tot}}(e^+ e^- \rightarrow \psi(3770)) = 7.9 \pm 0.6$  nb at the resonance.

<sup>2</sup> Assuming that interference effects between resonance and continuum can be neglected and using  $\sigma_{\text{obs}}(e^+ e^- \rightarrow \psi(3770)) = 7.15 \pm 0.38$  nb.

$\Gamma(\eta\rho\bar{p}K^+K^-)/\Gamma_{total}$   $\Gamma_{87}/\Gamma$

VALUE (units $10^{-3}$ )	CL%	DOCUMENT ID	TECN	COMMENT
<6.9	90	1 ABLIKIM 10D	BES2	$e^+e^- \rightarrow \psi(3770)$

<sup>1</sup> Assuming that interference effects between resonance and continuum can be neglected and using  $\sigma^{obs}(e^+e^- \rightarrow \psi(3770)) = 7.15 \pm 0.38$  nb.

$\Gamma(\pi^0\rho\bar{p}K^+K^-)/\Gamma_{total}$   $\Gamma_{88}/\Gamma$

VALUE (units $10^{-3}$ )	CL%	DOCUMENT ID	TECN	COMMENT
<1.2	90	1 ABLIKIM 10D	BES2	$e^+e^- \rightarrow \psi(3770)$

<sup>1</sup> Assuming that interference effects between resonance and continuum can be neglected and using  $\sigma^{obs}(e^+e^- \rightarrow \psi(3770)) = 7.15 \pm 0.38$  nb.

$\Gamma(\phi\rho\bar{p})/\Gamma_{total}$   $\Gamma_{89}/\Gamma$

VALUE (units $10^{-4}$ )	CL%	DOCUMENT ID	TECN	COMMENT
<1.3	90	1 HUANG 06A	CLEO	$e^+e^- \rightarrow \psi(3770)$

••• We do not use the following data for averages, fits, limits, etc. •••

<sup>1</sup> Using  $\sigma_{tot}(e^+e^- \rightarrow \psi(3770)) = 7.9 \pm 0.6$  nb at the resonance.  
<sup>2</sup> Assuming that interference effects between resonance and continuum can be neglected and using  $\sigma^{obs}(e^+e^- \rightarrow \psi(3770)) = 7.15 \pm 0.38$  nb.

$\Gamma(\Lambda\bar{\Lambda}\pi^+\pi^-)/\Gamma_{total}$   $\Gamma_{90}/\Gamma$

VALUE (units $10^{-4}$ )	CL%	DOCUMENT ID	TECN	COMMENT
< 2.5	90	1 HUANG 06A	CLEO	$e^+e^- \rightarrow \psi(3770)$
< 4.7	90	2 ABLIKIM 13Q	BES3	$e^+e^- \rightarrow \psi(3770)$
<39	90	3 ABLIKIM 07F	BES2	$e^+e^- \rightarrow \psi(3770)$

<sup>1</sup> Using  $\sigma_{tot}(e^+e^- \rightarrow \psi(3770)) = 7.9 \pm 0.6$  nb at the resonance.  
<sup>2</sup> Assuming that interference effects between resonance and continuum can be neglected.  
<sup>3</sup> Assuming that interference effects between resonance and continuum can be neglected and using  $\sigma^{obs}(e^+e^- \rightarrow \psi(3770)) = 7.15 \pm 0.38$  nb.

$\Gamma(\Lambda\bar{p}K^+)/\Gamma_{total}$   $\Gamma_{91}/\Gamma$

VALUE (units $10^{-4}$ )	CL%	DOCUMENT ID	TECN	COMMENT
<2.8	90	1 HUANG 06A	CLEO	$e^+e^- \rightarrow \psi(3770)$

<sup>1</sup> Using  $\sigma_{tot}(e^+e^- \rightarrow \psi(3770)) = 7.9 \pm 0.6$  nb at the resonance.

$\Gamma(\Lambda\bar{p}K^+\pi^+\pi^-)/\Gamma_{total}$   $\Gamma_{92}/\Gamma$

VALUE (units $10^{-4}$ )	CL%	DOCUMENT ID	TECN	COMMENT
<6.3	90	1 HUANG 06A	CLEO	$e^+e^- \rightarrow \psi(3770)$

<sup>1</sup> Using  $\sigma_{tot}(e^+e^- \rightarrow \psi(3770)) = 7.9 \pm 0.6$  nb at the resonance.

$\Gamma(\Lambda\bar{\Lambda}\eta)/\Gamma_{total}$   $\Gamma_{93}/\Gamma$

VALUE (units $10^{-4}$ )	CL%	DOCUMENT ID	TECN	COMMENT
<1.9	90	1 ABLIKIM 13Q	BES3	$e^+e^- \rightarrow \psi(3770)$

<sup>1</sup> Assuming that interference effects between resonance and continuum can be neglected.

$\Gamma(\Sigma^+\bar{\Sigma}^-)/\Gamma_{total}$   $\Gamma_{94}/\Gamma$

VALUE (units $10^{-4}$ )	CL%	DOCUMENT ID	TECN	COMMENT
<1.0	90	1 ABLIKIM 13Q	BES3	$e^+e^- \rightarrow \psi(3770)$

<sup>1</sup> Assuming that interference effects between resonance and continuum can be neglected.

$\Gamma(\Sigma^0\bar{\Sigma}^0)/\Gamma_{total}$   $\Gamma_{95}/\Gamma$

VALUE (units $10^{-4}$ )	CL%	DOCUMENT ID	TECN	COMMENT
<0.4	90	1 ABLIKIM 13Q	BES3	$e^+e^- \rightarrow \psi(3770)$

<sup>1</sup> Assuming that interference effects between resonance and continuum can be neglected.

$\Gamma(\Xi^+\bar{\Xi}^-)/\Gamma_{total}$   $\Gamma_{96}/\Gamma$

VALUE (units $10^{-4}$ )	CL%	DOCUMENT ID	TECN	COMMENT
<1.5	90	1 ABLIKIM 13Q	BES3	$e^+e^- \rightarrow \psi(3770)$

<sup>1</sup> Assuming that interference effects between resonance and continuum can be neglected.

$\Gamma(\Xi^0\bar{\Xi}^0)/\Gamma_{total}$   $\Gamma_{97}/\Gamma$

VALUE (units $10^{-4}$ )	CL%	DOCUMENT ID	TECN	COMMENT
<1.4	90	1 ABLIKIM 13Q	BES3	$e^+e^- \rightarrow \psi(3770)$

<sup>1</sup> Assuming that interference effects between resonance and continuum can be neglected.

————— RADIATIVE DECAYS —————

$\Gamma(\gamma\chi_{c2})/\Gamma_{total}$   $\Gamma_{98}/\Gamma$

VALUE (units $10^{-3}$ )	CL%	DOCUMENT ID	TECN	COMMENT
<0.64	90	1 ABLIKIM 15J	BES3	$e^+e^- \rightarrow \psi(3770) \rightarrow \gamma\gamma J/\psi$

••• We do not use the following data for averages, fits, limits, etc. •••

<sup>1</sup> This limit is equivalent to  $(0.25 \pm 0.21 \pm 0.18) \times 10^{-3}$  branching fraction value.  
<sup>2</sup> Uses  $B(\psi(2S) \rightarrow \gamma\chi_{c2}) = 9.22 \pm 0.11 \pm 0.46\%$  from ATHAR 04,  $\psi(2S)$  mass and width from PDG 04, and  $\Gamma_{ee}(\psi(2S)) = 2.54 \pm 0.03 \pm 0.11$  keV from ADAM 06.  
<sup>3</sup> Using  $\Gamma_{ee}(\psi(2S)) = (2.54 \pm 0.03 \pm 0.11)$  keV from ADAM 06 and taking  $\sigma(e^+e^- \rightarrow D\bar{D})$  from HE 05 for  $\sigma(e^+e^- \rightarrow \psi(3770))$ .

$\Gamma(\gamma\chi_{c1})/\Gamma_{total}$   $\Gamma_{99}/\Gamma$

VALUE (units $10^{-3}$ )	EVTS	DOCUMENT ID	TECN	COMMENT
<b>2.49 ± 0.23 OUR AVERAGE</b>				
1.98 ± 0.78 ± 0.05	202	1 ABLIKIM 16B	BES3	$e^+e^- \rightarrow \psi(3770) \rightarrow \gamma + \text{hadrons}$
2.48 ± 0.15 ± 0.23	0.6k	ABLIKIM 15J	BES3	$e^+e^- \rightarrow \psi(3770) \rightarrow \gamma\gamma J/\psi$
2.4 ± 0.8 ± 0.2		2 ABLIKIM 14H	BES3	$e^+e^- \rightarrow \psi(3770) \rightarrow K_S^0 K^\pm \pi^\mp$
2.9 ± 0.5 ± 0.4		3 BRIERE 06	CLEO	$e^+e^- \rightarrow \psi(3770) \rightarrow \gamma + \text{hadrons}, \gamma\gamma J/\psi$
3.9 ± 1.4 ± 0.6	54	4 BRIERE 06	CLEO	$e^+e^- \rightarrow \psi(3770) \rightarrow \gamma + \text{hadrons}$
2.8 ± 0.5 ± 0.4	53	5 COAN 06A	CLEO	$e^+e^- \rightarrow \psi(3770) \rightarrow \gamma\gamma J/\psi$

••• We do not use the following data for averages, fits, limits, etc. •••

<sup>1</sup> ABLIKIM 16B reports  $(1.94 \pm 0.42 \pm 0.64) \times 10^{-3}$  from a measurement of  $[\Gamma(\psi(3770) \rightarrow \gamma\chi_{c1})/\Gamma_{total}] / [B(\psi(2S) \rightarrow \gamma\chi_{c1}(1P))]$  assuming  $B(\psi(2S) \rightarrow \gamma\chi_{c1}(1P)) = (9.55 \pm 0.31) \times 10^{-2}$ , which we rescale to our best value  $B(\psi(2S) \rightarrow \gamma\chi_{c1}(1P)) = (9.75 \pm 0.24) \times 10^{-2}$ . Our first error is their experiment's error and our second error is the systematic error from using our best value.

<sup>2</sup> ABLIKIM 14H reports  $[\Gamma(\psi(3770) \rightarrow \gamma\chi_{c1})/\Gamma_{total}] \times [B(\chi_{c1}(1P) \rightarrow K_S^0 K^\pm \pi^\mp)] = (8.51 \pm 2.39 \pm 1.42) \times 10^{-6}$  which we divide by our best value  $B(\chi_{c1}(1P) \rightarrow K_S^0 K^\pm \pi^\mp) = 0.00349 \pm 0.00029$ . Our first error is their experiment's error and our second error is the systematic error from using our best value. We have calculated the best value of  $B(\chi_{c1}(1P) \rightarrow K_S^0 K^\pm \pi^\mp)$  as  $1/2$  of  $B(\chi_{c1}(1P) \rightarrow \bar{K}^0 K^+ \pi^- + c.c.) = (7.0 \pm 0.6) \times 10^{-3}$ .

<sup>3</sup> Averages the two measurements from COAN 06A and BRIERE 06.

<sup>4</sup> Uses  $B(\psi(2S) \rightarrow \gamma\chi_{c1}) = 9.07 \pm 0.11 \pm 0.54\%$  from ATHAR 04,  $\psi(2S)$  mass and width from PDG 04, and  $\Gamma_{ee}(\psi(2S)) = 2.54 \pm 0.03 \pm 0.11$  keV from ADAM 06.

<sup>5</sup> Using  $\Gamma_{ee}(\psi(2S)) = (2.54 \pm 0.03 \pm 0.11)$  keV from ADAM 06 and taking  $\sigma(e^+e^- \rightarrow D\bar{D})$  from HE 05 for  $\sigma(e^+e^- \rightarrow \psi(3770))$ .

$\Gamma(\gamma\chi_{c1})/\Gamma(J/\psi\pi^+\pi^-)$   $\Gamma_{99}/\Gamma_4$

VALUE	EVTS	DOCUMENT ID	TECN	COMMENT
<b>1.49 ± 0.31 ± 0.26</b>	53 ± 10	1 COAN 06A	CLEO	$e^+e^- \rightarrow \psi(3770) \rightarrow \gamma\gamma J/\psi$

<sup>1</sup> Using  $B(\psi(3770) \rightarrow J/\psi\pi^+\pi^-) = (1.89 \pm 0.20 \pm 0.20) \times 10^{-3}$  from ADAM 06.

$\Gamma(\gamma\chi_{c0})/\Gamma_{total}$   $\Gamma_{100}/\Gamma$

VALUE (units $10^{-3}$ )	CL%	EVTS	DOCUMENT ID	TECN	COMMENT
<b>6.9 ± 0.6 OUR AVERAGE</b>					
6.7 ± 0.7 ± 0.1		2.2K	1 ABLIKIM 16B	BES3	$e^+e^- \rightarrow \psi(3770) \rightarrow \gamma + \text{hadrons}$
7.3 ± 0.7 ± 0.6		274	BRIERE 06	CLEO	$e^+e^- \rightarrow \psi(3770) \rightarrow \gamma + \text{hadrons}$
< 44	90		2 COAN 06A	CLEO	$e^+e^- \rightarrow \psi(3770) \rightarrow \gamma\gamma J/\psi$

••• We do not use the following data for averages, fits, limits, etc. •••

<sup>1</sup> ABLIKIM 16B reports  $(6.88 \pm 0.28 \pm 0.67) \times 10^{-3}$  from a measurement of  $[\Gamma(\psi(3770) \rightarrow \gamma\chi_{c0})/\Gamma_{total}] / [B(\psi(2S) \rightarrow \gamma\chi_{c0}(1P))]$  assuming  $B(\psi(2S) \rightarrow \gamma\chi_{c0}(1P)) = (9.99 \pm 0.27) \times 10^{-2}$ , which we rescale to our best value  $B(\psi(2S) \rightarrow \gamma\chi_{c0}(1P)) = (9.79 \pm 0.20) \times 10^{-2}$ . Our first error is their experiment's error and our second error is the systematic error from using our best value.

<sup>2</sup> Using  $\Gamma_{ee}(\psi(2S)) = (2.54 \pm 0.03 \pm 0.11)$  keV from ADAM 06 and taking  $\sigma(e^+e^- \rightarrow D\bar{D})$  from HE 05 for  $\sigma(e^+e^- \rightarrow \psi(3770))$ .

$\Gamma(\gamma\chi_{c0})/\Gamma(\gamma\chi_{c2})$   $\Gamma_{100}/\Gamma_{98}$

VALUE	CL%	DOCUMENT ID	TECN	COMMENT
>8	90	1 BRIERE 06	CLEO	$e^+e^- \rightarrow \psi(3770)$

<sup>1</sup> Not independent of other results in BRIERE 06.

$\Gamma(\gamma\chi_{c0})/\Gamma(\gamma\chi_{c1})$   $\Gamma_{100}/\Gamma_{99}$

VALUE	DOCUMENT ID	TECN	COMMENT
2.5 ± 0.6	1 BRIERE 06	CLEO	$e^+e^- \rightarrow \psi(3770)$

••• We do not use the following data for averages, fits, limits, etc. •••

<sup>1</sup> Not independent of other results in BRIERE 06.

$\Gamma(\gamma\eta_c)/\Gamma_{total}$   $\Gamma_{101}/\Gamma$

VALUE	CL%	DOCUMENT ID	TECN
<7 × 10 <sup>-4</sup>	90	1 ABLIKIM 14H	BES3

<sup>1</sup> ABLIKIM 14H reports  $[\Gamma(\psi(3770) \rightarrow \gamma\eta_c)/\Gamma_{total}] \times [B(\eta_c(1S) \rightarrow K_S^0 K^\pm \pi^\mp)] < 16 \times 10^{-6}$  which we divide by our best value  $B(\eta_c(1S) \rightarrow K_S^0 K^\pm \pi^\mp) = 2.43 \times 10^{-2}$ . We have calculated the best value of  $B(\eta_c(1S) \rightarrow K_S^0 K^\pm \pi^\mp)$  as  $1/3$  of  $B(\eta_c(1S) \rightarrow K\bar{K}\pi) = 7.3 \times 10^{-2}$ .



See key on page 999

Meson Particle Listings

$\psi_3(3842)$ ,  $\chi_{c0}(3860)$ ,  $\chi_{c1}(3872)$

$\psi_3(3842)$  BRANCHING RATIOS

$\Gamma(D^+ D^-)/\Gamma_{total}$	DOCUMENT ID	TECN	COMMENT	$\Gamma_1/\Gamma$
seen	AAIJ	19M LHCb	$pp \rightarrow D\bar{D} + \text{anything}$	

$\Gamma(D^0 \bar{D}^0)/\Gamma_{total}$	DOCUMENT ID	TECN	COMMENT	$\Gamma_2/\Gamma$
seen	AAIJ	19M LHCb	$pp \rightarrow D\bar{D} + \text{anything}$	

$\psi_3(3842)$  REFERENCES

AAIJ 19M JHEP 1907 035 R. Aaij et al. (LHCb Collab.)

$\chi_{c0}(3860) \quad I^G(J^{PC}) = 0^+(0^{++})$

OMITTED FROM SUMMARY TABLE  
 The assignment  $J^P = 0^+$  is preferred over  $2^+$  by 2.5 sigma.  
 Observed by CHILIKIN 17 using full amplitude analysis of the process  $e^+ e^- \rightarrow J/\psi D\bar{D}$ , where  $D = D^0, D^+$ .

$\chi_{c0}(3860)$  MASS

VALUE (MeV)	DOCUMENT ID	TECN	COMMENT
$3862^{+26+40}_{-32-13}$	CHILIKIN	17 BELL	$e^+ e^- \rightarrow J/\psi D\bar{D}$

$\chi_{c0}(3860)$  WIDTH

VALUE (MeV)	DOCUMENT ID	TECN	COMMENT
$201^{+154+88}_{-67-82}$	CHILIKIN	17 BELL	$e^+ e^- \rightarrow J/\psi D\bar{D}$

$\chi_{c0}(3860)$  DECAY MODES

Mode	Fraction ( $\Gamma_i/\Gamma$ )
$\Gamma_1 \quad D^0 \bar{D}^0$	seen
$\Gamma_2 \quad D^+ D^-$	seen

$\chi_{c0}(3860)$  BRANCHING RATIOS

$\Gamma(D^0 \bar{D}^0)/\Gamma_{total}$	DOCUMENT ID	TECN	COMMENT	$\Gamma_1/\Gamma$
seen	CHILIKIN	17 BELL	$e^+ e^- \rightarrow J/\psi D^0 \bar{D}^0$	

$\Gamma(D^+ D^-)/\Gamma_{total}$	DOCUMENT ID	TECN	COMMENT	$\Gamma_2/\Gamma$
seen	CHILIKIN	17 BELL	$e^+ e^- \rightarrow J/\psi D^+ D^-$	

$\chi_{c0}(3860)$  REFERENCES

CHILIKIN 17 PR D95 112003 K. Chilikin et al. (BELLE Collab.) JPC

$\chi_{c1}(3872) \quad I^G(J^{PC}) = 0^+(1^{++})$

also known as  $X(3872)$   
 This state shows properties different from a conventional  $q\bar{q}$  state. A candidate for an exotic structure. See the review on non- $q\bar{q}$  states.

First observed by CHOI 03 in  $B \rightarrow K\pi^+\pi^- J/\psi(1S)$  decays as a narrow peak in the invariant mass distribution of the  $\pi^+\pi^- J/\psi(1S)$  final state. Isovector hypothesis excluded by AUBERT 05B and CHOI 11.

AAIJ 13Q perform a full five-dimensional amplitude analysis of the angular correlations between the decay products in  $B^+ \rightarrow \chi_{c1}(3872) K^+$  decays, where  $\chi_{c1}(3872) \rightarrow J/\psi\pi^+\pi^-$  and  $J/\psi \rightarrow \mu^+\mu^-$ , which unambiguously gives the  $J^{PC} = 1^{++}$  assignment under the assumption that the  $\pi^+\pi^-$  and  $J/\psi$  are in an S-wave. AAIJ 15AO extend this analysis with more data to limit D-wave contributions to  $< 4\%$  at 95% CL.

See the review on "Spectroscopy of Mesons Containing Two Heavy Quarks."

$\chi_{c1}(3872)$  MASS FROM  $J/\psi X$  MODE

VALUE (MeV)	EVTS	DOCUMENT ID	TECN	COMMENT
<b><math>3871.69 \pm 0.17</math></b> OUR AVERAGE				
$3871.9 \pm 0.7 \pm 0.2$	$20 \pm 5$	ABLIKIM 14	BES3	$e^+ e^- \rightarrow J/\psi\pi^+\pi^-\gamma$
$3871.95 \pm 0.48 \pm 0.12$	0.6k	AAIJ 12H	LHCb	$pp \rightarrow J/\psi\pi^+\pi^- X$
$3871.85 \pm 0.27 \pm 0.19$	$\sim 170$	<sup>1</sup> CHOI 11	BELL	$B \rightarrow K\pi^+\pi^- J/\psi$
$3873^{+1.8}_{-1.6} \pm 1.3$	$27 \pm 8$	<sup>2</sup> DEL-AMO-SA.10B	BABR	$B \rightarrow \omega J/\psi K$
$3871.61 \pm 0.16 \pm 0.19$	6k	<sup>2,3</sup> AALTONEN 09AU	CDF2	$p\bar{p} \rightarrow J/\psi\pi^+\pi^- X$
$3871.4 \pm 0.6 \pm 0.1$	93.4	AUBERT 08Y	BABR	$B^+ \rightarrow K^+ J/\psi\pi^+\pi^-$
$3868.7 \pm 1.5 \pm 0.4$	9.4	AUBERT 08Y	BABR	$B^0 \rightarrow K_S^0 J/\psi\pi^+\pi^-$
$3871.8 \pm 3.1 \pm 3.0$	522	<sup>2,4</sup> ABAZOV 04F	D0	$p\bar{p} \rightarrow J/\psi\pi^+\pi^- X$
••• We do not use the following data for averages, fits, limits, etc. •••				
$3873.3 \pm 1.1 \pm 1.0$	45	<sup>5</sup> ABLIKIM 19V	BES	$e^+ e^- \rightarrow \gamma\omega J/\psi$
$3860.0 \pm 10.4$	13.6	<sup>2,6</sup> AGHASYAN 18A	COMP	$\gamma^* N \rightarrow X\pi^\pm N'$
$3868.6 \pm 1.2 \pm 0.2$	8	<sup>7</sup> AUBERT 06	BABR	$B^0 \rightarrow K_S^0 J/\psi\pi^+\pi^-$
$3871.3 \pm 0.6 \pm 0.1$	61	<sup>7</sup> AUBERT 06	BABR	$B^- \rightarrow K^- J/\psi\pi^+\pi^-$
$3873.4 \pm 1.4$	25	<sup>8</sup> AUBERT 05R	BABR	$B^+ \rightarrow K^+ J/\psi\pi^+\pi^-$
$3871.3 \pm 0.7 \pm 0.4$	730	<sup>2,9</sup> ACOSTA 04	CDF2	$p\bar{p} \rightarrow J/\psi\pi^+\pi^- X$
$3872.0 \pm 0.6 \pm 0.5$	36	<sup>10</sup> CHOI 03	BELL	$B \rightarrow K\pi^+\pi^- J/\psi$
$3836 \pm 13$	58	<sup>2,11</sup> ANTONIAZZI 94	E705	$300 \pi^\pm Li \rightarrow J/\psi\pi^+\pi^- X$

- The mass difference for the  $\chi_{c1}(3872)$  produced in  $B^+$  and  $B^0$  decays is  $(-0.71 \pm 0.96 \pm 0.19)$  MeV.
- Width consistent with detector resolution.
- A possible equal mixture of two states with a mass difference greater than 3.6 MeV/c<sup>2</sup> is excluded at 95% CL.
- Calculated from the corresponding  $m_{\chi_{c1}(3872)} - m_{J/\psi}$  using  $m_{J/\psi} = 3096.916$  MeV.
- Fit with fixed width and including two resonances, X(3915) and X(3960).
- Could be a different state.
- Calculated from the corresponding  $m_{\chi_{c1}(3872)} - m_{\psi(2S)}$  using  $m_{\psi(2S)} = 3686.093$  MeV. Superseded by AUBERT 08Y.
- Calculated from the corresponding  $m_{\chi_{c1}(3872)} - m_{\psi(2S)}$  using  $m_{\psi(2S)} = 3685.96$  MeV. Superseded by AUBERT 06.
- Superseded by AALTONEN 09AU.
- Superseded by CHOI 11.
- A lower mass value can be due to an incorrect momentum scale for soft pions.

$\chi_{c1}(3872)$  MASS FROM  $\bar{D}^{*0} D^0$  MODE

VALUE (MeV)	EVTS	DOCUMENT ID	TECN	COMMENT
$3872.9^{+0.6+0.4}_{-0.4-0.5}$	50	<sup>1,2</sup> AUSHEV 10	BELL	$B \rightarrow \bar{D}^{*0} D^0 K$
$3875.1^{+0.7+0.5}_{-0.5-0.5}$	$33 \pm 6$	<sup>2</sup> AUBERT 08B	BABR	$B \rightarrow \bar{D}^{*0} D^0 K$
$3875.2 \pm 0.7^{+0.9}_{-1.8}$	$24 \pm 6$	<sup>2,3</sup> GOKHROO 06	BELL	$B \rightarrow D^0 \bar{D}^0 \pi^0 K$

- Calculated from the measured  $m_{\chi_{c1}(3872)} - m_{D^{*0}} - m_{D^0} = 1.1^{+0.6+0.1}_{-0.4-0.3}$  MeV.
- Experiments report  $D^{*0} \bar{D}^0$  invariant mass above  $D^{*0} \bar{D}^0$  threshold because  $D^{*0}$  decay products are kinematically constrained to the  $D^{*0}$  mass, even though the  $D^{*0}$  may decay off-shell.
- Superseded by AUSHEV 10.

$m_{\chi_{c1}(3872)} - m_{J/\psi}$

VALUE (MeV)	EVTS	DOCUMENT ID	TECN	COMMENT
<b><math>774.9 \pm 3.1 \pm 3.0</math></b>	522	ABAZOV 04F	D0	$p\bar{p} \rightarrow J/\psi\pi^+\pi^- X$

$m_{\chi_{c1}(3872)} - m_{\psi(2S)}$

VALUE (MeV)	EVTS	DOCUMENT ID	TECN	COMMENT
$187.4 \pm 1.4$	25	<sup>1</sup> AUBERT 05R	BABR	$B^+ \rightarrow K^+ J/\psi\pi^+\pi^-$

<sup>1</sup> Superseded by AUBERT 06.

$\chi_{c1}(3872)$  WIDTH

VALUE (MeV)	CL%	EVTS	DOCUMENT ID	TECN	COMMENT
<b><math>&lt; 1.2</math></b>	90		CHOI 11	BELL	$B \rightarrow K\pi^+\pi^- J/\psi$
••• We do not use the following data for averages, fits, limits, etc. •••					
$< 2.4$	90		ABLIKIM 14	BES3	$e^+ e^- \rightarrow J/\psi\pi^+\pi^- \gamma$
$< 3.3$	90		AUBERT 08Y	BABR	$B^+ \rightarrow K^+ J/\psi\pi^+\pi^-$
$< 4.1$	90	69	AUBERT 06	BABR	$B \rightarrow K\pi^+\pi^- J/\psi$
$< 2.3$	90	36	<sup>1</sup> CHOI 03	BELL	$B \rightarrow K\pi^+\pi^- J/\psi$

- <sup>1</sup> Superseded by CHOI 11.

# Meson Particle Listings

## $\chi_{c1}(3872)$

### $\chi_{c1}(3872)$ WIDTH FROM $\bar{D}^{*0} D^0$ MODE

VALUE (MeV)	EVTS	DOCUMENT ID	TECN	COMMENT
$3.9^{+2.8+0.2}_{-1.4-1.1}$	50	<sup>1</sup> AUSHEV	10	BELL $B \rightarrow \bar{D}^{*0} D^0 K$
$3.0^{+1.9}_{-1.4} \pm 0.9$	33 ± 6	AUBERT	08B	BABR $B \rightarrow \bar{D}^{*0} D^0 K$

<sup>1</sup>With a measured value of  $B(B \rightarrow \chi_{c1}(3872) K) \times B(\chi_{c1}(3872) \rightarrow D^{*0} \bar{D}^0) = (0.80 \pm 0.20 \pm 0.10) \times 10^{-4}$ , assumed to be equal for both charged and neutral modes.

### $\chi_{c1}(3872)$ DECAY MODES

Mode	Fraction ( $\Gamma_i/\Gamma$ )
$\Gamma_1$ $e^+ e^-$	
$\Gamma_2$ $\pi^+ \pi^- J/\psi(1S)$	> 3.2 %
$\Gamma_3$ $\rho^0 J/\psi(1S)$	
$\Gamma_4$ $\omega J/\psi(1S)$	> 2.3 %
$\Gamma_5$ $D^0 \bar{D}^0 \pi^0$	>40 %
$\Gamma_6$ $\bar{D}^{*0} D^0$	>30 %
$\Gamma_7$ $\gamma \gamma$	
$\Gamma_8$ $D^0 \bar{D}^0$	
$\Gamma_9$ $D^+ D^-$	
$\Gamma_{10}$ $\gamma \chi_{c1}$	
$\Gamma_{11}$ $\gamma \chi_{c2}$	
$\Gamma_{12}$ $\pi^0 \chi_{c2}$	
$\Gamma_{13}$ $\pi^0 \chi_{c1}$	> 2.8 %
$\Gamma_{14}$ $\pi^0 \chi_{c0}$	
$\Gamma_{15}$ $\gamma J/\psi$	> 7 × 10 <sup>-3</sup>
$\Gamma_{16}$ $\gamma \psi(2S)$	> 4 %
$\Gamma_{17}$ $\pi^+ \pi^- \eta_c(1S)$	not seen
$\Gamma_{18}$ $\pi^+ \pi^- \chi_{c1}$	not seen
$\Gamma_{19}$ $p \bar{p}$	not seen

### C-violating decays

$\Gamma_{20}$   $\eta J/\psi$

### $\chi_{c1}(3872)$ PARTIAL WIDTHS

$\Gamma(e^+ e^-)$					$\Gamma_1$
VALUE (eV)	CL%	DOCUMENT ID	TECN	COMMENT	
••• We do not use the following data for averages, fits, limits, etc. •••					
< 4.3	90	<sup>1</sup> ABLIKIM	15V	BES3	4.0–4.4 $e^+ e^- \rightarrow \pi^+ \pi^- J/\psi$
< 280	90	<sup>2</sup> YUAN	04	RVUE	$e^+ e^- \rightarrow \pi^+ \pi^- J/\psi$

<sup>1</sup>ABLIKIM 15V reports this limit from the measurement of  $\Gamma(\chi_{c1}(3872) \rightarrow \pi^+ \pi^- J/\psi(1S)) \times \Gamma(\chi_{c1}(3872) \rightarrow e^+ e^-) / \Gamma < 0.13$  eV using  $\Gamma(\chi_{c1}(3872) \rightarrow \pi^+ \pi^- J/\psi(1S)) / \Gamma = 3\%$ .

<sup>2</sup>Using BAI 98E data on  $e^+ e^- \rightarrow \pi^+ \pi^- \ell^+ \ell^-$ . Assuming that  $\Gamma(\pi^+ \pi^- J/\psi)$  of  $\chi_{c1}(3872)$  is the same as that of  $\psi(2S)$  (85.4 keV).

### $\chi_{c1}(3872)$ $\Gamma(i)\Gamma(e^+ e^-) / \Gamma(\text{total})$

$\Gamma(\pi^+ \pi^- J/\psi(1S)) \times \Gamma(e^+ e^-) / \Gamma(\text{total})$					$\Gamma_2 \Gamma_1 / \Gamma$
VALUE (eV)	CL%	DOCUMENT ID	TECN	COMMENT	
< 0.13	90	ABLIKIM	15V	BES3	4.0–4.4 $e^+ e^- \rightarrow \pi^+ \pi^- J/\psi$
••• We do not use the following data for averages, fits, limits, etc. •••					
< 6.2	90	<sup>1,2</sup> AUBERT	05D	BABR	10.6 $e^+ e^- \rightarrow K^+ K^- \pi^+ \pi^- \gamma$
< 8.3	90	<sup>2</sup> DOBBS	05	CLE3	$e^+ e^- \rightarrow \pi^+ \pi^- J/\psi$
< 10	90	<sup>3</sup> YUAN	04	RVUE	$e^+ e^- \rightarrow \pi^+ \pi^- J/\psi$

<sup>1</sup>Using  $B(\chi_{c1}(3872) \rightarrow J/\psi \pi^+ \pi^-) \cdot B(J/\psi \rightarrow \mu^+ \mu^-) \cdot \Gamma(\chi_{c1}(3872) \rightarrow e^+ e^-) < 0.37$  eV from AUBERT 05D and  $B(J/\psi \rightarrow \mu^+ \mu^-) = 0.0588 \pm 0.0010$  from the PDG 04.

<sup>2</sup>Assuming  $\chi_{c1}(3872)$  has  $J^{PC} = 1^{--}$ .

<sup>3</sup>Using BAI 98E data on  $e^+ e^- \rightarrow \pi^+ \pi^- \ell^+ \ell^-$ . From theoretical calculation of the production cross section and using  $B(J/\psi \rightarrow \mu^+ \mu^-) = (5.88 \pm 0.10)\%$ .

### $\chi_{c1}(3872)$ $\Gamma(i)\Gamma(\gamma\gamma) / \Gamma(\text{total})$

$\Gamma(\pi^+ \pi^- J/\psi(1S)) \times \Gamma(\gamma\gamma) / \Gamma(\text{total})$					$\Gamma_2 \Gamma_7 / \Gamma$
VALUE (eV)	CL%	DOCUMENT ID	TECN	COMMENT	
••• We do not use the following data for averages, fits, limits, etc. •••					
< 12.9	90	<sup>1</sup> DOBBS	05	CLE3	$e^+ e^- \rightarrow \pi^+ \pi^- J/\psi \gamma$

<sup>1</sup>Assuming  $\chi_{c1}(3872)$  has positive C parity and spin 0.

$\Gamma(\omega J/\psi(1S)) \times \Gamma(\gamma\gamma) / \Gamma(\text{total})$					$\Gamma_4 \Gamma_7 / \Gamma$
VALUE (eV)	CL%	DOCUMENT ID	TECN	COMMENT	
••• We do not use the following data for averages, fits, limits, etc. •••					
< 1.7	90	<sup>1</sup> LEES	12AD	BABR	$e^+ e^- \rightarrow e^+ e^- \omega J/\psi$

<sup>1</sup>Assuming  $\chi_{c1}(3872)$  has spin 2.

$\Gamma(\pi^+ \pi^- \eta_c(1S)) \times \Gamma(\gamma\gamma) / \Gamma(\text{total})$					$\Gamma_{17} \Gamma_7 / \Gamma$
VALUE (eV)	CL%	DOCUMENT ID	TECN	COMMENT	
< 11.1	90	LEES	12AE	BABR	$e^+ e^- \rightarrow e^+ e^- \pi^+ \pi^- \eta_c$

### $\chi_{c1}(3872)$ BRANCHING RATIOS

$\Gamma(\pi^+ \pi^- J/\psi(1S)) / \Gamma(\text{total})$					$\Gamma_2 / \Gamma$
VALUE	EVTS	DOCUMENT ID	TECN	COMMENT	
> 0.032	93 ± 17	<sup>1</sup> AUBERT	08Y	BABR	$B \rightarrow \chi_{c1}(3872) K$
••• We do not use the following data for averages, fits, limits, etc. •••					
seen	151	<sup>2</sup> BALA	15	BELL	$B \rightarrow \chi_{c1}(3872) K \pi$
> 0.05	30	<sup>3</sup> AUBERT	05R	BABR	$B^+ \rightarrow K^+ \pi^+ \pi^- J/\psi$
> 0.05	36 ± 7	<sup>4</sup> CHOI	03	BELL	$B^+ \rightarrow K^+ \pi^+ \pi^- J/\psi$

<sup>1</sup>AUBERT 08Y reports  $[\Gamma(\chi_{c1}(3872) \rightarrow \pi^+ \pi^- J/\psi(1S)) / \Gamma(\text{total})] \times [B(B^+ \rightarrow \chi_{c1}(3872) K^+)] = (8.4 \pm 1.5 \pm 0.7) \times 10^{-6}$  which we divide by our best value  $B(B^+ \rightarrow \chi_{c1}(3872) K^+) < 2.6 \times 10^{-4}$ .

<sup>2</sup>BALA 15 reports  $B(\chi_{c1}(3872) \rightarrow \pi^+ \pi^- J/\psi) \times B(B^0 \rightarrow \chi_{c1}(3872) K^+ \pi^-) = (7.9 \pm 1.3 \pm 0.4) \times 10^{-6}$  and  $B(\chi_{c1}(3872) \rightarrow \pi^+ \pi^- J/\psi) \times B(B^+ \rightarrow \chi_{c1}(3872) K^0 \pi^+) = (10.6 \pm 3.0 \pm 0.9) \times 10^{-6}$ .

<sup>3</sup>Superseded by AUBERT 08Y. AUBERT 05R reports  $[\Gamma(\chi_{c1}(3872) \rightarrow \pi^+ \pi^- J/\psi(1S)) / \Gamma(\text{total})] \times [B(B^+ \rightarrow \chi_{c1}(3872) K^+)] = (1.28 \pm 0.41) \times 10^{-5}$  which we divide by our best value  $B(B^+ \rightarrow \chi_{c1}(3872) K^+) < 2.6 \times 10^{-4}$ .

<sup>4</sup>CHOI 03 reports  $[\Gamma(\chi_{c1}(3872) \rightarrow \pi^+ \pi^- J/\psi(1S)) / \Gamma(\text{total})] \times [B(B^+ \rightarrow \chi_{c1}(3872) K^+)] / [B(B^+ \rightarrow \psi(2S) K^+)] / [B(\psi(2S) \rightarrow J/\psi(1S) \pi^+ \pi^-)] = 0.063 \pm 0.012 \pm 0.007$  which we multiply or divide by our best values  $B(B^+ \rightarrow \chi_{c1}(3872) K^+) < 2.6 \times 10^{-4}$ ,  $B(B^+ \rightarrow \psi(2S) K^+) = (6.19 \pm 0.22) \times 10^{-4}$ ,  $B(\psi(2S) \rightarrow J/\psi(1S) \pi^+ \pi^-) = (34.68 \pm 0.30) \times 10^{-2}$ .

$\Gamma(\omega J/\psi(1S)) / \Gamma(\text{total})$					$\Gamma_4 / \Gamma$
VALUE	EVTS	DOCUMENT ID	TECN	COMMENT	
> 0.023	21 ± 7	<sup>1</sup> DEL-AMO-SA...	10B	BABR	$B^+ \rightarrow \omega J/\psi K^+$

<sup>1</sup>DEL-AMO-SANCHEZ 10B reports  $[\Gamma(\chi_{c1}(3872) \rightarrow \omega J/\psi(1S)) / \Gamma(\text{total})] \times [B(B^+ \rightarrow \chi_{c1}(3872) K^+)] = (6 \pm 2 \pm 1) \times 10^{-6}$  which we divide by our best value  $B(B^+ \rightarrow \chi_{c1}(3872) K^+) < 2.6 \times 10^{-4}$ . DEL-AMO-SANCHEZ 10B also reports  $B(B^0 \rightarrow \chi_{c1}(3872) K^0) \times B(\chi_{c1}(3872) \rightarrow J/\psi \omega) = (6 \pm 3 \pm 1) \times 10^{-6}$ .

$\Gamma(\omega J/\psi(1S)) / \Gamma(\pi^+ \pi^- J/\psi(1S))$					$\Gamma_4 / \Gamma_2$
VALUE	DOCUMENT ID	TECN	COMMENT		
<b>1.1 ± 0.4 OUR AVERAGE</b>	Error includes scale factor of 1.7.				

$1.6^{+0.4}_{-0.3} \pm 0.2$	<sup>1</sup> ABLIKIM	19V	BES	$e^+ e^- \rightarrow \gamma \omega J/\psi$
$0.8 \pm 0.3$	<sup>2</sup> DEL-AMO-SA...	10B	BABR	$B \rightarrow \omega J/\psi K$

<sup>1</sup>Fit with fixed width and including two resonances, X(3915) and X(3960).

<sup>2</sup>Statistical and systematic errors added in quadrature. Uses the values of  $B(B \rightarrow \chi_{c1}(3872) K) \times B(\chi_{c1}(3872) \rightarrow J/\psi \pi^+ \pi^-)$  reported in AUBERT 08Y, taking into account the common systematics.

$\Gamma(D^0 \bar{D}^0 \pi^0) / \Gamma(\text{total})$					$\Gamma_5 / \Gamma$
VALUE	EVTS	DOCUMENT ID	TECN	COMMENT	
> 0.4	17 ± 5	<sup>1</sup> GOKHROO	06	BELL	$B^+ \rightarrow D^0 \bar{D}^0 \pi^0 K^+$

<sup>1</sup>GOKHROO 06 reports  $[\Gamma(\chi_{c1}(3872) \rightarrow D^0 \bar{D}^0 \pi^0) / \Gamma(\text{total})] \times [B(B^+ \rightarrow \chi_{c1}(3872) K^+)] = (1.02 \pm 0.31^{+0.21}_{-0.29}) \times 10^{-4}$  which we divide by our best value  $B(B^+ \rightarrow \chi_{c1}(3872) K^+) < 2.6 \times 10^{-4}$ .

$\Gamma(D^0 \bar{D}^0 \pi^0) / \Gamma(\pi^+ \pi^- J/\psi(1S))$					$\Gamma_5 / \Gamma_2$
VALUE	DOCUMENT ID	TECN	COMMENT		
seen	<sup>1</sup> GOKHROO	06	BELL	$B \rightarrow D^0 \bar{D}^0 \pi^0 K$	

••• We do not use the following data for averages, fits, limits, etc. •••

seen

AUSHEV	10	BELL	$B \rightarrow D^0 \bar{D}^0 \pi^0 K$
--------	----	------	---------------------------------------

<sup>1</sup>May not necessarily be the same state as that observed in the  $J/\psi \pi^+ \pi^-$  mode. Supersedes CHISTOV 04.

$\Gamma(\bar{D}^{*0} D^0) / \Gamma(\text{total})$					$\Gamma_6 / \Gamma$
VALUE	EVTS	DOCUMENT ID	TECN	COMMENT	
> 0.30	$41 \pm \frac{9}{8}$	<sup>1</sup> AUSHEV	10	BELL	$B^+ \rightarrow D^{*0} \bar{D}^0 K^+$

••• We do not use the following data for averages, fits, limits, etc. •••

> 0.6	27 ± 6	<sup>2</sup> AUBERT	08B	BABR	$B^+ \rightarrow \bar{D}^{*0} D^0 K^+$
-------	--------	---------------------	-----	------	--

<sup>1</sup>AUSHEV 10 reports  $[\Gamma(\chi_{c1}(3872) \rightarrow \bar{D}^{*0} D^0) / \Gamma(\text{total})] \times [B(B^+ \rightarrow \chi_{c1}(3872) K^+)] = (0.77 \pm 0.16 \pm 0.10) \times 10^{-4}$  which we divide by our best value  $B(B^+ \rightarrow \chi_{c1}(3872) K^+) < 2.6 \times 10^{-4}$ .

<sup>2</sup>AUBERT 08B reports  $[\Gamma(\chi_{c1}(3872) \rightarrow \bar{D}^{*0} D^0) / \Gamma(\text{total})] \times [B(B^+ \rightarrow \chi_{c1}(3872) K^+)] = (1.67 \pm 0.36 \pm 0.47) \times 10^{-4}$  which we divide by our best value  $B(B^+ \rightarrow \chi_{c1}(3872) K^+) < 2.6 \times 10^{-4}$ .

$\Gamma(D^0 \bar{D}^0) / \Gamma(\pi^+ \pi^- J/\psi(1S))$					$\Gamma_8 / \Gamma_2$
VALUE	DOCUMENT ID	TECN	COMMENT		
not seen	CHISTOV	04	BELL	$B \rightarrow K D^0 \bar{D}^0$	

••• We do not use the following data for averages, fits, limits, etc. •••

See key on page 999

Meson Particle Listings

$\chi_{c1}(3872), Z_c(3900)$

$\Gamma(D^+ D^-)/\Gamma(\pi^+ \pi^- J/\psi(1S))$   $\Gamma_9/\Gamma_2$

Table with columns: VALUE, DOCUMENT ID, TECN, COMMENT. Includes entry for CHISTOV 04 BELL B to KD+D-

$\Gamma(\gamma \chi_{c1})/\Gamma(\pi^+ \pi^- J/\psi(1S))$   $\Gamma_{10}/\Gamma_2$

Table with columns: VALUE, CL%, DOCUMENT ID, TECN, COMMENT. Includes entries for BHARDWAJ 13 BELL and CHOI 03 BELL.

$\Gamma(\gamma \chi_{c2})/\Gamma(\pi^+ \pi^- J/\psi(1S))$   $\Gamma_{11}/\Gamma_2$

Table with columns: VALUE, DOCUMENT ID, TECN, COMMENT. Includes entry for BHARDWAJ 13 BELL.

$\Gamma(\gamma J/\psi)/\Gamma_{total}$   $\Gamma_{15}/\Gamma$

Table with columns: VALUE, EVTS, DOCUMENT ID, TECN, COMMENT. Includes entries for BHARDWAJ 11 BELL, AUBERT 09B BABR, and AUBERT, BE 06M BABR.

$\Gamma(\gamma \psi(2S))/\Gamma_{total}$   $\Gamma_{16}/\Gamma$

Table with columns: VALUE, EVTS, DOCUMENT ID, TECN, COMMENT. Includes entries for AAIJ 14AH LHCb and AUBERT 09B BABR.

$\Gamma(\gamma \psi(2S))/\Gamma(\gamma J/\psi)$   $\Gamma_{16}/\Gamma_{15}$

Table with columns: VALUE, CL%, EVTS, DOCUMENT ID, TECN, COMMENT. Includes entry for AAIJ 14AH LHCb.

$\Gamma(\pi^+ \pi^- \chi_{c1})/\Gamma_{total}$   $\Gamma_{18}/\Gamma$

Table with columns: VALUE, DOCUMENT ID, TECN, COMMENT. Includes entry for BHARDWAJ 16 BELL.

$\Gamma(p\bar{p})/\Gamma_{total}$   $\Gamma_{19}/\Gamma$

Table with columns: VALUE, DOCUMENT ID, TECN, COMMENT. Includes entry for AAIJ 17AD LHCb.

$\Gamma(p\bar{p})/\Gamma(\pi^+ \pi^- J/\psi(1S))$   $\Gamma_{19}/\Gamma_2$

Table with columns: VALUE, CL%, DOCUMENT ID, TECN, COMMENT. Includes entry for AAIJ 13s reports.

$\Gamma(\pi^0 \chi_{c0})/\Gamma(\pi^+ \pi^- J/\psi(1S))$   $\Gamma_{14}/\Gamma_2$

Table with columns: VALUE, CL%, DOCUMENT ID, TECN, COMMENT. Includes entry for ABLIKIM 19U BES3.

$\Gamma(\pi^0 \chi_{c1})/\Gamma(\pi^+ \pi^- J/\psi(1S))$   $\Gamma_{13}/\Gamma_2$

Table with columns: VALUE (units 10^-2), CL%, EVTS, DOCUMENT ID, TECN, COMMENT. Includes entries for ABLIKIM 19U BES3 and BHARDWAJ 19 BELL.

$\Gamma(\pi^0 \chi_{c2})/\Gamma(\pi^+ \pi^- J/\psi(1S))$   $\Gamma_{12}/\Gamma_2$

Table with columns: VALUE, CL%, DOCUMENT ID, TECN, COMMENT. Includes entry for ABLIKIM 19U BES3.

C-violating decays

$\Gamma(\eta J/\psi)/\Gamma(\pi^+ \pi^- J/\psi(1S))$   $\Gamma_{20}/\Gamma_2$

Table with columns: VALUE, CL%, DOCUMENT ID, TECN, COMMENT. Includes entries for IWASHITA 14 BELL and AUBERT 04Y BABR.

$\chi_{c1}(3872)$  REFERENCES

List of references for  $\chi_{c1}(3872)$  from various experiments including ABLIKIM, BHARDWAJ, AGHASYAN, AAIJ, BELL, and others.

$Z_c(3900)$

$I^G(J^{PC}) = 1^+(1^+ -)$

was  $X(3900)$

Properties incompatible with a  $q\bar{q}$  structure (exotic state). See the review on non- $q\bar{q}$  states.

Charged  $Z_c(3900)$  seen as a peak in the invariant mass distribution of the  $J/\psi\pi^\pm$  system by BES III (ABLIKIM 13T) in  $e^+e^- \rightarrow \pi^+\pi^- J/\psi$  at c.m. energy of 4.26 GeV and by radiative return from  $e^+e^-$  collisions at  $\sqrt{s}$  from 9.46 to 10.86 GeV at Belle (LIU 13B).

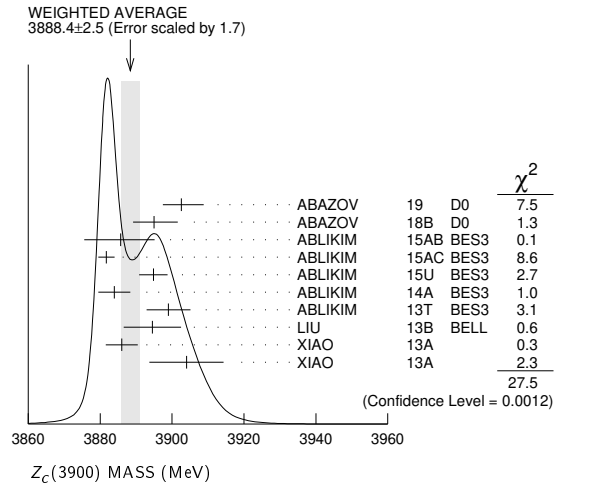
# Meson Particle Listings

## Z<sub>c</sub>(3900)

### Z<sub>c</sub>(3900) MASS

VALUE (MeV)	EVTS	DOCUMENT ID	TECN	CHG	COMMENT
<b>3888.4 ± 2.5 OUR AVERAGE</b> Error includes scale factor of 1.7. See the ideogram below.					
3902.6 <sup>+5.2</sup> <sub>-5.0</sub> ± 3.3 ± 1.4		1 ABAZOV	19 D0		1.96 TeV $p\bar{p} \rightarrow J/\psi\pi^+\pi^-X$
3895.0 ± 5.2 <sup>+4.0</sup> <sub>-2.7</sub>	502	2 ABAZOV	18B D0		1.96 TeV $p\bar{p} \rightarrow J/\psi\pi^+\pi^-X$
3885.7 <sup>+4.3</sup> <sub>-5.7</sub> ± 8.4		3 ABLIKIM	15AB BES3	0	$e^+e^- \rightarrow \pi^0(D\bar{D}^*)^0$
3881.7 ± 1.6 ± 1.6	1.2k	3 ABLIKIM	15AC BES3	±	$e^+e^- \rightarrow \pi^\pm(D\bar{D}^*)^\mp$
3894.8 ± 2.3 ± 3.2	356	3 ABLIKIM	15U BES3	0	$e^+e^- \rightarrow \pi^0\pi^0 J/\psi$
3883.9 ± 1.5 ± 4.2	1.2k	3 ABLIKIM	14A BES3	±	$e^+e^- \rightarrow \pi^\pm(D\bar{D}^*)^\mp$
3899.0 ± 3.6 ± 4.9	307	3 ABLIKIM	13T BES3	±	$e^+e^- \rightarrow \pi^+\pi^- J/\psi$
3894.5 ± 6.6 ± 4.5	159	3 LIU	13B BELL	±	$e^+e^- \rightarrow \gamma\pi^+\pi^- J/\psi$
3886 ± 4 ± 2	81	3,4 XIAO	13A	±	4.17 $e^+e^- \rightarrow \pi^+\pi^- J/\psi$
3904 ± 9 ± 5	25	3,4 XIAO	13A	0	4.17 $e^+e^- \rightarrow \pi^0\pi^0 J/\psi$

- • • We do not use the following data for averages, fits, limits, etc. • • •
- 3881.2 ± 4.2 ± 52.7 6k 5 ABLIKIM 17J BES3 ±  $e^+e^- \rightarrow \pi^+\pi^- J/\psi$
- <sup>1</sup> Measured in weak decays of *b*-flavored hadrons (nonprompt).
- <sup>2</sup> The signal of the Z<sub>c</sub>(3900) is correlated with a parent  $J/\psi\pi^+\pi^-$  system in the invariant mass range 4.2–4.7 GeV.
- <sup>3</sup> Neglecting interference between the Z<sub>c</sub>(3900) and non-resonant continuum.
- <sup>4</sup> For  $M^2(\pi^+\pi^-) < 0.65 \text{ GeV}^2$ . Obtained by analyzing CLEO-c data but not authored by the CLEO Collaboration.
- <sup>5</sup> Pole mass obtained from a fit to a Flatte-like formula.



### Z<sub>c</sub>(3900) WIDTH

VALUE (MeV)	EVTS	DOCUMENT ID	TECN	CHG	COMMENT
<b>28.3 ± 2.5 OUR AVERAGE</b>					
32 <sup>+28</sup> <sub>-21</sub> ± 26 <sup>+26</sup> <sub>-7</sub>		1 ABAZOV	19 D0		1.96 TeV $p\bar{p} \rightarrow \pi^+\pi^- J/\psi X$ (non-prompt)
51.8 ± 4.6 ± 36.0	6 k	2 ABLIKIM	17J BES3	±	$e^+e^- \rightarrow \pi^+\pi^- J/\psi$
35 <sup>+11</sup> <sub>-12</sub> ± 15		3 ABLIKIM	15AB BES3	0	$e^+e^- \rightarrow \pi^0(D\bar{D}^*)^0$
26.6 ± 2.0 ± 2.1	1248	3 ABLIKIM	15AC BES3	±	$e^+e^- \rightarrow \pi^\pm(D\bar{D}^*)^\mp$
29.6 ± 8.2 ± 8.2	356	3 ABLIKIM	15U BES3	0	$e^+e^- \rightarrow \pi^0\pi^0 J/\psi$
24.8 ± 3.3 ± 11.0	1212	3 ABLIKIM	14A BES3	±	$e^+e^- \rightarrow \pi^\pm(D\bar{D}^*)^\mp$
46 ± 10 ± 20	307	3 ABLIKIM	13T BES3	±	$e^+e^- \rightarrow \pi^+\pi^- J/\psi$
63 ± 24 ± 26	159	3 LIU	13B BELL	±	$e^+e^- \rightarrow \gamma\pi^+\pi^- J/\psi$
37 ± 4 ± 8	81	3,4 XIAO	13A	±	4.17 $e^+e^- \rightarrow \pi^+\pi^- J/\psi$

- <sup>1</sup> Measured in weak decays of *b*-flavored hadrons (nonprompt).
- <sup>2</sup> Pole width obtained from a fit to a Flatte-like formula.
- <sup>3</sup> Neglecting interference between the Z<sub>c</sub>(3900) and non-resonant continuum.
- <sup>4</sup> For  $M^2(\pi^+\pi^-) < 0.65 \text{ GeV}^2$ . Obtained by analyzing CLEO-c data but not authored by the CLEO Collaboration.

### Z<sub>c</sub>(3900) DECAY MODES

Mode	Fraction (Γ <sub>i</sub> /Γ)
Γ <sub>1</sub> $J/\psi\pi$	seen
Γ <sub>2</sub> $h_c\pi^\pm$	not seen
Γ <sub>3</sub> $\eta_c\pi^+\pi^-$	not seen
Γ <sub>4</sub> $\eta_c(1S)\rho(770)^\pm$	
Γ <sub>5</sub> $(D\bar{D}^*)^\pm$	seen

Γ <sub>6</sub> $D^0 D^{*-} + \text{c.c.}$	seen
Γ <sub>7</sub> $D^- D^{*0} + \text{c.c.}$	seen
Γ <sub>8</sub> $\omega\pi^\pm$	not seen
Γ <sub>9</sub> $J/\psi\eta$	not seen
Γ <sub>10</sub> $D^+ D^{*-} + \text{c.c.}$	seen
Γ <sub>11</sub> $D^0 \bar{D}^{*0} + \text{c.c.}$	seen

### Z<sub>c</sub>(3900) BRANCHING RATIOS

Γ(J/ψπ)/Γ <sub>total</sub>	VALUE	CL%	EVTS	DOCUMENT ID	TECN	CHG	COMMENT	Γ <sub>1</sub> /Γ
seen			356	ABLIKIM	15U BES3	0	$e^+e^- \rightarrow \pi^0\pi^0 J/\psi$	
seen			307	ABLIKIM	13T BES3	±	$e^+e^- \rightarrow \pi^+\pi^- J/\psi$	
seen			25	1 XIAO	13A	0	4.17 $e^+e^- \rightarrow \pi^0\pi^0 J/\psi$	
not seen				2 ABAZOV	19 D0		1.96 TeV $p\bar{p} \rightarrow \pi^+\pi^- J/\psi X$ (prompt)	
not seen			90	3 ADOLPH	15D COMP	±	$\gamma N \rightarrow Z_c(3900)^\pm N$	

- • • We do not use the following data for averages, fits, limits, etc. • • •
- <sup>1</sup> Obtained by analyzing CLEO-c data but not authored by the CLEO Collaboration.
- <sup>2</sup> Upper limit for the prompt production is set:  $N_{\text{prompt}}/N_{\text{nonprompt}} < 0.70$ , CL = 95%.
- <sup>3</sup> ADOLPH 15D measure  $B(Z_c(3900)^\pm \rightarrow J/\psi\pi^\pm) \sigma(\gamma N \rightarrow Z_c(3900)^\pm N) / \sigma(\gamma N \rightarrow J/\psi N) < 3.7 \times 10^{-3}$  at 90% CL.

Γ(h <sub>c</sub> π <sup>±</sup> )/Γ <sub>total</sub>	VALUE	DOCUMENT ID	TECN	CHG	COMMENT	Γ <sub>2</sub> /Γ
not seen		ABLIKIM	13X BES3	±	$e^+e^- \rightarrow h_c\pi^+\pi^-$	

Γ(η <sub>c</sub> π <sup>+</sup> π <sup>-</sup> )/Γ <sub>total</sub>	VALUE	DOCUMENT ID	TECN	CHG	COMMENT	Γ <sub>3</sub> /Γ
not seen		1 VINOKUROVA	15 BELL	0	$B^+ \rightarrow K^+ \eta_c \pi^+ \pi^-$	
		1 VINOKUROVA	15	reports $B(B^+ \rightarrow K^+ Z_c(3900)^0) \times B(X \rightarrow \eta_c \pi^+ \pi^-) < 4.7 \times 10^{-5}$ at 90% CL.		

Γ((D $\bar{D}^*$ ) <sup>±</sup> )/Γ(J/ψπ)	VALUE	DOCUMENT ID	TECN	CHG	COMMENT	Γ <sub>5</sub> /Γ <sub>1</sub>
<b>6.2 ± 1.1 ± 2.7</b>		1 ABLIKIM	14A BES3	±	$e^+e^- \rightarrow \pi^\pm(D\bar{D}^*)^\mp$	
		<sup>1</sup> Assuming the same origin of the $(D\bar{D}^*)^\pm$ and $\pi^\pm J/\psi$ decay modes.				

Γ(D <sup>0</sup> D <sup>*-</sup> + c.c.)/Γ <sub>total</sub>	VALUE	DOCUMENT ID	TECN	CHG	COMMENT	Γ <sub>6</sub> /Γ
seen		ABLIKIM	15AC BES3	±	$e^+e^- \rightarrow \pi^+ D^0 D^{*-} + \text{c.c.}$	
seen		ABLIKIM	14A BES3	±	$e^+e^- \rightarrow \pi^+ D^0 D^{*-} + \text{c.c.}$	

Γ(D <sup>-</sup> D <sup>*0</sup> + c.c.)/Γ <sub>total</sub>	VALUE	DOCUMENT ID	TECN	CHG	COMMENT	Γ <sub>7</sub> /Γ
seen		ABLIKIM	15AC BES3	±	$e^+e^- \rightarrow \pi^+ D^- D^{*0} + \text{c.c.}$	
seen		ABLIKIM	14A BES3	±	$e^+e^- \rightarrow \pi^+ D^- D^{*0} + \text{c.c.}$	

Γ(ωπ <sup>±</sup> )/Γ <sub>total</sub>	VALUE	DOCUMENT ID	TECN	CHG	COMMENT	Γ <sub>8</sub> /Γ
not seen		ABLIKIM	15R BES3	±	$e^+e^- \rightarrow \omega\pi^+\pi^-$	

Γ(J/ψη)/Γ <sub>total</sub>	VALUE	DOCUMENT ID	TECN	CHG	COMMENT	Γ <sub>9</sub> /Γ
not seen		ABLIKIM	15Q BES3	0	4.0–4.6 $e^+e^- \rightarrow J/\psi\eta\pi^0$	

Γ(J/ψη)/Γ(J/ψπ)	VALUE	CL%	DOCUMENT ID	TECN	CHG	COMMENT	Γ <sub>9</sub> /Γ <sub>1</sub>
<0.15		90	ABLIKIM	15Q BES3	0	4.226 $e^+e^- \rightarrow J/\psi\eta\pi^0$	
<0.65		90	ABLIKIM	15Q BES3	0	4.257 $e^+e^- \rightarrow J/\psi\eta\pi^0$	
• • • We do not use the following data for averages, fits, limits, etc. • • •							

Γ(η <sub>c</sub> (1S)ρ(770) <sup>±</sup> )/Γ(J/ψπ)	VALUE	EVTS	DOCUMENT ID	TECN	COMMENT	Γ <sub>4</sub> /Γ <sub>1</sub>	
<b>2.3 ± 0.8</b>		332	1 ABLIKIM	19bC BES3	$e^+e^- \rightarrow \pi^+\pi^-\pi^0\eta_c(1S)$		
			<sup>1</sup> Using $e^+e^- \rightarrow \pi^\mp(Z_c(3900)^\pm \rightarrow J/\psi\pi^\pm)$ cross section at 4.23 and 4.26 GeV from ABLIKIM 17I.				

Γ(D <sup>+</sup> D <sup>*-</sup> + c.c.)/Γ <sub>total</sub>	VALUE	DOCUMENT ID	TECN	CHG	COMMENT	Γ <sub>10</sub> /Γ
seen		ABLIKIM	15AB BES3	0	$e^+e^- \rightarrow \pi^0(D\bar{D}^*)^0$	

Γ(D <sup>0</sup> $\bar{D}^{*0}$ + c.c.)/Γ <sub>total</sub>	VALUE	DOCUMENT ID	TECN	CHG	COMMENT	Γ <sub>11</sub> /Γ
seen		ABLIKIM	15AB BES3	0	$e^+e^- \rightarrow \pi^0(D\bar{D}^*)^0$	

Γ(D <sup>+</sup> D <sup>*-</sup> + c.c.)/Γ(D <sup>0</sup> $\bar{D}^{*0}$ + c.c.)	VALUE	DOCUMENT ID	TECN	CHG	COMMENT	Γ <sub>10</sub> /Γ <sub>11</sub>
<b>0.96 ± 0.18 ± 0.12</b>		ABLIKIM	15AB BES3	0	$e^+e^- \rightarrow \pi^0(D\bar{D}^*)^0$	

# Meson Particle Listings

## $Z_c(3900)$ , $X(3915)$ , $\chi_{c2}(3930)$

### $Z_c(3900)$ REFERENCES

Author	Year	Pub	Collab
ABAZOV	19	PR D100 012005	V.M. Abazov et al. (DO Collab.)
ABLIKIM	19BC	PR D100 111102	M. Ablikim et al. (BESIII Collab.)
ABAZOV	18B	PR D98 052010	V.M. Abazov et al. (DO Collab.)
ABLIKIM	17J	PRL 119 072001	M. Ablikim et al. (BESIII Collab.)
ABLIKIM	15AB	PRL 115 222002	M. Ablikim et al. (BESIII Collab.)
ABLIKIM	15AC	PR D92 092006	M. Ablikim et al. (BESIII Collab.) JP
ABLIKIM	15Q	PR D92 012008	M. Ablikim et al. (BESIII Collab.)
ABLIKIM	15R	PR D92 032009	M. Ablikim et al. (BESIII Collab.)
ABLIKIM	15U	PRL 115 112003	M. Ablikim et al. (BESIII Collab.)
ADOLPH	15D	PL B742 330	C. Adolph et al. (COMPASS Collab.)
VINOKUROVA	15	JHEP 1506 132	A. Vinokurova et al. (BELLE Collab.)
Also		JHEP 1702 088 (errata.)	A. Vinokurova et al. (BELLE Collab.)
ABLIKIM	14A	PRL 112 022001	M. Ablikim et al. (BESIII Collab.) JP
ABLIKIM	13T	PRL 110 252001	M. Ablikim et al. (BESIII Collab.)
ABLIKIM	13X	PRL 111 242001	M. Ablikim et al. (BESIII Collab.)
LIU	13B	PRL 110 252002	Z.Q. Liu et al. (BELLE Collab.)
XIAO	13A	PL B727 366	T. Xiao et al. (NWES)

$\Gamma(\pi^+\pi^-\eta_c(1S)) \times \Gamma(\gamma\gamma)/\Gamma_{total}$					$\Gamma_3/\Gamma$
VALUE (eV)	CL%	DOCUMENT ID	TECN	COMMENT	
<16	90	LEES	12AE BABR	$e^+e^- \rightarrow e^+e^-\pi^+\pi^-\eta_c$	

$\Gamma(K\bar{K}) \times \Gamma(\gamma\gamma)/\Gamma_{total}$					$\Gamma_6/\Gamma$
VALUE (eV)	CL%	DOCUMENT ID	TECN	COMMENT	
<1.96	90	UEHARA	13 BELL	$\gamma\gamma \rightarrow K_S^0 K_S^0$	

### $X(3915)$ BRANCHING RATIOS

$\Gamma(\omega J/\psi)/\Gamma_{total}$				$\Gamma_1/\Gamma$
VALUE	DOCUMENT ID	TECN	COMMENT	
seen	7 DEL-AMO-SA...10B	BABR	$B \rightarrow \omega J/\psi K$	
seen	8 CHOI	05 BELL	$B \rightarrow \omega J/\psi K$	

7 DEL-AMO-SANCHEZ 10B reports  $B(B^\pm \rightarrow X(3915) K^\pm) \times B(X(3915) \rightarrow J/\psi\omega) = (3.0^{+0.7+0.5}_{-0.6-0.3}) \times 10^{-5}$  and  $B(B^0 \rightarrow X(3915) K^0) \times B(X(3915) \rightarrow J/\psi\omega) = (2.1 \pm 0.9 \pm 0.3) \times 10^{-5}$ .  
 8 CHOI 05 reports  $B(B \rightarrow X(3915) K) \times B(X(3915) \rightarrow J/\psi\omega) = (7.1 \pm 1.3 \pm 3.1) \times 10^{-5}$ .

$\Gamma(\omega J/\psi)/\Gamma(D^{*0} D^0)$					$\Gamma_1/\Gamma_2$
VALUE	CL%	DOCUMENT ID	TECN	COMMENT	
>0.71	90	9 AUSHEV	10 BELL	$B \rightarrow D^{*0} D^0 K$	

9 By combining the upper limit  $B(B \rightarrow X(3915) K) \times B(X(3915) \rightarrow D^{*0} D^0) < 0.67 \times 10^{-4}$  from AUSHEV 10 with the average of CHOI 05 and AUBERT 08w measurements  $B(B \rightarrow X(3915) K) \times B(X(3915) \rightarrow \omega J/\psi) = (0.51 \pm 0.11) \times 10^{-4}$ .

$\Gamma(\eta_c\eta)/\Gamma_{total}$					$\Gamma_4/\Gamma$
VALUE	DOCUMENT ID	TECN	COMMENT		
not seen	10 VINOKUROVA 15	BELL	$B^+ \rightarrow K^+ \eta_c \eta$		
	10 VINOKUROVA 15	reports	$B(B^+ \rightarrow K^+ X(3915)^0) \times B(X \rightarrow \eta_c \eta) < 3.3 \times 10^{-5}$ at 90% CL.		

10 VINOKUROVA 15 reports  $B(B^+ \rightarrow K^+ X(3915)^0) \times B(X \rightarrow \eta_c \eta) < 3.3 \times 10^{-5}$  at 90% CL.

$\Gamma(\eta_c\pi^0)/\Gamma_{total}$					$\Gamma_5/\Gamma$
VALUE	DOCUMENT ID	TECN	COMMENT		
not seen	11 VINOKUROVA 15	BELL	$B^+ \rightarrow K^+ \eta_c \pi^0$		
	11 VINOKUROVA 15	reports	$B(B^+ \rightarrow K^+ X(3915)^0) \times B(X \rightarrow \eta_c \pi^0) < 1.8 \times 10^{-5}$ at 90% CL.		

11 VINOKUROVA 15 reports  $B(B^+ \rightarrow K^+ X(3915)^0) \times B(X \rightarrow \eta_c \pi^0) < 1.8 \times 10^{-5}$  at 90% CL.

$\Gamma(\gamma\gamma)/\Gamma_{total}$					$\Gamma_7/\Gamma$
VALUE	EVTs	DOCUMENT ID	TECN	COMMENT	
seen	59 ± 10	LEES	12AD BABR	$e^+e^- \rightarrow e^+e^-\omega J/\psi$	
seen		UEHARA	10 BELL	$10.6 e^+e^- \rightarrow e^+e^-\omega J/\psi$	

$\Gamma(\pi^0 \chi_{c1})/\Gamma_{total}$					$\Gamma_8/\Gamma$
VALUE	EVTs	DOCUMENT ID	TECN	COMMENT	
not seen	42 ± 14	12 BHARDWAJ 19	BELL	$B^\pm \rightarrow \chi_{c1} \pi^0 K^\pm$	
		12 BHARDWAJ 19	reports	$B(B^+ \rightarrow K^+ X(3915)) \times B(X(3915) \rightarrow \chi_{c1} \pi^0) < 3.8 \times 10^{-5}$ at 90% CL. A signal significance 2.3 standard deviations.	

12 BHARDWAJ 19 reports  $B(B^+ \rightarrow K^+ X(3915)) \times B(X(3915) \rightarrow \chi_{c1} \pi^0) < 3.8 \times 10^{-5}$  at 90% CL. A signal significance 2.3 standard deviations.

### $X(3915)$ REFERENCES

Author	Year	Pub	Collab
ABLIKIM	19V	PRL 122 232002	M. Ablikim et al. (BESIII Collab.)
BHARDWAJ	19	PR D99 111101	V. Bhardwaj et al. (BELLE Collab.)
VINOKUROVA	15	JHEP 1506 132	A. Vinokurova et al. (BELLE Collab.)
Also		JHEP 1702 088 (errata.)	A. Vinokurova et al. (BELLE Collab.)
ZHOU	15C	PRL 115 022001	Z.-Y. Zhou, Z. Xiao, H.-Q. Zhou (BEIJT, NANJ)
UEHARA	13	PTEP 2013 123C01	S. Uehara et al. (BELLE Collab.)
LEES	12AD	PR D86 072002	J.P. Lees et al. (BABAR Collab.)
LEES	12AE	PR D86 092005	J.P. Lees et al. (BABAR Collab.)
AUSHEV	10	PR D81 031103	T. Aushev et al. (BELLE Collab.)
DEL-AMO-SA...10B	PR D82 011101	P. del Amo Sanchez et al. (BABAR Collab.)	
UEHARA	10	PRL 104 092001	S. Uehara et al. (BELLE Collab.)
AUBERT	08W	PRL 101 082001	B. Aubert et al. (BABAR Collab.)
CHOI	05	PRL 94 182002	S.-K. Choi et al. (BELLE Collab.)

$\chi_{c2}(3930)$		$J^{PC}$
		$0^+(2^{++})$

### $\chi_{c2}(3930)$ MASS

VALUE (MeV)	EVTs	DOCUMENT ID	TECN	COMMENT
<b>3922.2 ± 1.0 OUR AVERAGE</b>		Error includes scale factor of 1.6.		
3921.9 ± 0.6 ± 0.2		1 AAIJ	19M LHCb	$pp \rightarrow D\bar{D} + \text{anything}$
3926.7 ± 2.7 ± 1.1	76 ± 17	AUBERT	10G BABR	$10.6 e^+e^- \rightarrow e^+e^- D\bar{D}$
3929 ± 5 ± 2	64	UEHARA	06 BELL	$10.6 e^+e^- \rightarrow e^+e^- D\bar{D}$

1 Measured in prompt hadroproduction.

**$X(3915)$**   $J^{PC} = 0^+(0 \text{ or } 2^{++})$   
 was  $\chi_{c0}(3915)$   
 The experimental analysis prefers  $J^{PC} = 0^{++}$ . However, a re-analysis presented in ZHOU 15C shows that if helicity-2 dominance assumption is abandoned and a sizable helicity-0 component is allowed, a  $J^{PC} = 2^{++}$  assignment is possible.

### $X(3915)$ MASS

VALUE (MeV)	EVTs	DOCUMENT ID	TECN	COMMENT
<b>3918.4 ± 1.9 OUR AVERAGE</b>		Error includes scale factor of 1.1.		
3919.4 ± 2.2 ± 1.6	59 ± 10	LEES	12AD BABR	$e^+e^- \rightarrow e^+e^-\omega J/\psi$
3919.1 ± 3.8 ± 2.0		DEL-AMO-SA...10B	BABR	$B \rightarrow \omega J/\psi K$
3915 ± 3 ± 2	49 ± 15	UEHARA	10 BELL	$10.6 e^+e^- \rightarrow e^+e^-\omega J/\psi$
3943 ± 11 ± 13	58 ± 11	1 CHOI	05 BELL	$B \rightarrow \omega J/\psi K$
3926.4 ± 2.2 ± 1.2		2 ABLIKIM	19v BES	$e^+e^- \rightarrow \gamma\omega J/\psi$
3914.6 ± 3.8 ± 2.0		1 AUBERT	08w BABR	Superseded by DEL-AMO-SANCHEZ 10B

1  $\omega J/\psi$  threshold enhancement fitted as an S-wave Breit-Wigner resonance.  
 2 Could also be  $X(3940)$ . Significance  $3.1\sigma$ . Fit with additional resonance at  $3963.7 \pm 5.7$  MeV, significance  $3.4\sigma$ .

### $X(3915)$ WIDTH

VALUE (MeV)	EVTs	DOCUMENT ID	TECN	COMMENT
<b>20 ± 5 OUR AVERAGE</b>		Error includes scale factor of 1.1.		
13 ± 6 ± 3	59	LEES	12AD BABR	$e^+e^- \rightarrow e^+e^-\omega J/\psi$
31 ± 10 ± 5		DEL-AMO-SA...10B	BABR	$B \rightarrow \omega J/\psi K$
17 ± 10 ± 3	49	UEHARA	10 BELL	$10.6 e^+e^- \rightarrow e^+e^-\omega J/\psi$
87 ± 22 ± 26	58	3 CHOI	05 BELL	$B \rightarrow \omega J/\psi K$
3.8 ± 7.5 ± 2.6		4 ABLIKIM	19v BES	$e^+e^- \rightarrow \gamma\omega J/\psi$
34 ± 12 ± 5		3 AUBERT	08w BABR	Superseded by DEL-AMO-SANCHEZ 10B

3  $\omega J/\psi$  threshold enhancement fitted as an S-wave Breit-Wigner resonance.  
 4 Could also be  $X(3940)$ . Significance  $3.1\sigma$ . Fit with additional resonance at  $3963.7 \pm 5.7$  MeV, significance  $3.4\sigma$ .

### $X(3915)$ DECAY MODES

Mode	Fraction ( $\Gamma_i/\Gamma$ )
$\Gamma_1$ $\omega J/\psi$	seen
$\Gamma_2$ $D^{*0} D^0$	
$\Gamma_3$ $\pi^+\pi^-\eta_c(1S)$	not seen
$\Gamma_4$ $\eta_c\eta$	not seen
$\Gamma_5$ $\eta_c\pi^0$	not seen
$\Gamma_6$ $K\bar{K}$	not seen
$\Gamma_7$ $\gamma\gamma$	seen
$\Gamma_8$ $\pi^0\chi_{c1}$	

### $X(3915)$ $\Gamma(\eta)\Gamma(\gamma\gamma)/\Gamma_{total}$

$\Gamma(\omega J/\psi) \times \Gamma(\gamma\gamma)/\Gamma_{total}$					$\Gamma_1\Gamma_7/\Gamma$
VALUE (eV)	EVTs	DOCUMENT ID	TECN	COMMENT	
<b>54 ± 9 OUR AVERAGE</b>					
52 ± 10 ± 3	59 ± 10	5 LEES	12AD BABR	$e^+e^- \rightarrow e^+e^-\omega J/\psi$	
61 ± 17 ± 8	49 ± 15	5 UEHARA	10 BELL	$10.6 e^+e^- \rightarrow e^+e^-\omega J/\psi$	
18 ± 5 ± 2	49 ± 15	6 UEHARA	10 BELL	$10.6 e^+e^- \rightarrow e^+e^-\omega J/\psi$	

5 For  $J^P = 0^+$ .  
 6 For  $J^P = 2^+$ , helicity-2.



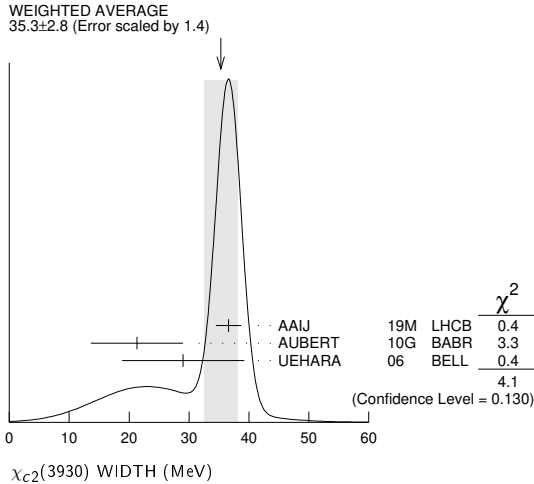
# Meson Particle Listings

## $\chi_{c2}(3930)$ , $X(3940)$

### $\chi_{c2}(3930)$ WIDTH

VALUE (MeV)	EVTS	DOCUMENT ID	TECN	COMMENT
<b>35.3 ± 2.8 OUR AVERAGE</b>		Error includes scale factor of 1.4. See the ideogram below.		
36.6 ± 1.9 ± 0.9		<sup>2</sup> AAIJ	19M LHCb	$pp \rightarrow D\bar{D} + \text{anything}$
21.3 ± 6.8 ± 3.6	76 ± 17	AUBERT	10G BABR	10.6 $e^+e^- \rightarrow e^+e^- D\bar{D}$
29 ± 10 ± 2	64	UEHARA	06 BELL	10.6 $e^+e^- \rightarrow e^+e^- D\bar{D}$

<sup>2</sup> Measured in prompt hadroproduction.



### $\chi_{c2}(3930)$ DECAY MODES

Mode	Fraction ( $\Gamma_i/\Gamma$ )
$\Gamma_1$ $\gamma\gamma$	seen
$\Gamma_2$ $K\bar{K}\pi$	
$\Gamma_3$ $K^+K^-\pi^+\pi^-\pi^0$	
$\Gamma_4$ $D\bar{D}$	seen
$\Gamma_5$ $D^+D^-$	seen
$\Gamma_6$ $D^0\bar{D}^0$	seen
$\Gamma_7$ $\pi^+\pi^-\eta_c(1S)$	not seen
$\Gamma_8$ $K\bar{K}$	not seen

### $\chi_{c2}(3930)$ PARTIAL WIDTHS

#### $\chi_{c2}(3930)$ $\Gamma(i)\Gamma(\gamma\gamma)/\Gamma(\text{total})$

VALUE (eV)	CL%	DOCUMENT ID	TECN	COMMENT	$\Gamma_2\Gamma_1/\Gamma$
<b>&lt;2.1</b>	90	DEL-AMO-SA..11M	BABR	$\gamma\gamma \rightarrow K_S^0 K^\pm \pi^\mp$	

VALUE (eV)	CL%	DOCUMENT ID	TECN	COMMENT	$\Gamma_3\Gamma_1/\Gamma$
<b>&lt;3.4</b>	90	DEL-AMO-SA..11M	BABR	$\gamma\gamma \rightarrow K^+K^-\pi^+\pi^-\pi^0$	

VALUE (keV)	EVTS	DOCUMENT ID	TECN	COMMENT	$\Gamma_4\Gamma_1/\Gamma$
<b>0.21 ± 0.04 OUR AVERAGE</b>					
0.24 ± 0.05 ± 0.04	76 ± 17	AUBERT	10G BABR	10.6 $e^+e^- \rightarrow e^+e^- D\bar{D}$	
0.18 ± 0.05 ± 0.03	64	<sup>3</sup> UEHARA	06 BELL	10.6 $e^+e^- \rightarrow e^+e^- D\bar{D}$	

<sup>3</sup> Assuming  $B(D^+D^-) = 0.89 B(D^0\bar{D}^0)$ .

VALUE (eV)	CL%	DOCUMENT ID	TECN	COMMENT	$\Gamma_7\Gamma_1/\Gamma$
<b>&lt;18</b>	90	LEES	12AE BABR	$e^+e^- \rightarrow e^+e^-\pi^+\pi^-\eta_c$	

VALUE (eV)	CL%	DOCUMENT ID	TECN	COMMENT	$\Gamma_8\Gamma_1/\Gamma$
<b>&lt;0.256</b>	90	UEHARA	13 BELL	$\gamma\gamma \rightarrow K_S^0 K_S^0$	

### $\chi_{c2}(3930)$ BRANCHING RATIOS

VALUE	EVTS	DOCUMENT ID	TECN	COMMENT	$\Gamma_5/\Gamma_6$
<b>0.74 ± 0.43 ± 0.16</b>	64	UEHARA	06 BELL	10.6 $e^+e^- \rightarrow e^+e^- D\bar{D}$	

### $\chi_{c2}(3930)$ REFERENCES

AAIJ	19M	JHEP 1907 035	R. Aaij et al.	(LHCb Collab.)
UEHARA	13	PTEP 2013 123C01	S. Uehara et al.	(BELLE Collab.)
LEES	12AE	PR D86 092005	J.P. Lees et al.	(BABAR Collab.)
DEL-AMO-SA...	11M	PR D84 012004	P. del Amo Sanchez et al.	(BABAR Collab.)
AUBERT	10G	PR D81 092003	B. Aubert et al.	(BABAR Collab.)
UEHARA	06	PRL 96 082003	S. Uehara et al.	(BELLE Collab.)

## $X(3940)$

$$J^G(J^{PC}) = ?^?(?^{??})$$

OMITTED FROM SUMMARY TABLE

Reported by ABE 07, observed in  $e^+e^- \rightarrow J/\psi X$ .

### $X(3940)$ MASS

VALUE (MeV)	EVTS	DOCUMENT ID	TECN	COMMENT
<b>3942<sup>+2</sup><sub>-6</sub></b>	52	PAKHOLOV	08 BELL	$e^+e^- \rightarrow J/\psi X$
• • • We do not use the following data for averages, fits, limits, etc. • • •				
3943 ± 6 ± 6	25	<sup>1</sup> ABE	07 BELL	$e^+e^- \rightarrow J/\psi X$
3936 ± 14	266	<sup>2</sup> ABE	07 BELL	$e^+e^- \rightarrow J/\psi(c\bar{c})$

<sup>1</sup> From a fit to  $D^{*+}D^-$  and  $D^{*0}\bar{D}^0$  events.  
<sup>2</sup> From the inclusive fit. Not independent of the exclusive measurement by ABE 07.

### $X(3940)$ WIDTH

VALUE (MeV)	CL%	EVTS	DOCUMENT ID	TECN	COMMENT
<b>37<sup>+26</sup><sub>-15</sub> ± 8</b>		52	PAKHOLOV	08 BELL	$e^+e^- \rightarrow J/\psi X$
• • • We do not use the following data for averages, fits, limits, etc. • • •					
<52	90	25	ABE	07 BELL	$e^+e^- \rightarrow J/\psi X$

### $X(3940)$ DECAY MODES

Mode	Fraction ( $\Gamma_i/\Gamma$ )
$\Gamma_1$ $D\bar{D}^* + c.c.$	seen
$\Gamma_2$ $D\bar{D}$	not seen
$\Gamma_3$ $J/\psi\omega$	not seen

### $X(3940)$ BRANCHING RATIOS

VALUE	CL%	EVTS	DOCUMENT ID	TECN	COMMENT	$\Gamma_1/\Gamma$
• • • We do not use the following data for averages, fits, limits, etc. • • •						
>0.45	90	25	<sup>1,2</sup> ABE	07 BELL	$e^+e^- \rightarrow J/\psi X$	

<sup>1</sup> For  $X(3940)$  decaying to final states with more than two tracks.  
<sup>2</sup> PAKHOLOV 08 finds that the inclusive peak near 3940 MeV/c<sup>2</sup> may consist of several states.

VALUE	CL%	DOCUMENT ID	TECN	COMMENT	$\Gamma_2/\Gamma$
• • • We do not use the following data for averages, fits, limits, etc. • • •					
<0.41	90	<sup>1,2</sup> ABE	07 BELL	$e^+e^- \rightarrow J/\psi X$	

<sup>1</sup> For  $X(3940)$  decaying to final states with more than two tracks.  
<sup>2</sup> PAKHOLOV 08 finds that the inclusive peak near 3940 MeV/c<sup>2</sup> may consist of several states.

VALUE	CL%	DOCUMENT ID	TECN	COMMENT	$\Gamma_3/\Gamma$
• • • We do not use the following data for averages, fits, limits, etc. • • •					
<0.26	90	<sup>1,2</sup> ABE	07 BELL	$e^+e^- \rightarrow J/\psi X$	

<sup>1</sup> For  $X(3940)$  decaying to final states with more than two tracks.  
<sup>2</sup> PAKHOLOV 08 finds that the inclusive peak near 3940 MeV/c<sup>2</sup> may consist of several states.

### $X(3940)$ REFERENCES

PAKHOLOV	08	PRL 100 202001	P. Pakhlov et al.	(BELLE Collab.)
ABE	07	PRL 98 082001	K. Abe et al.	(BELLE Collab.)

See key on page 999

# Meson Particle Listings

## $X(4020)^\pm, \psi(4040)$

### $X(4020)^\pm$

$$I^G(J^{PC}) = 1^+(?^{?^-})$$

Properties incompatible with a  $q\bar{q}$  structure (exotic state). See the review on non- $q\bar{q}$  states.

Charged  $X(4020)$  seen by ABLIKIM 13X from  $e^+e^- \rightarrow \pi^+\pi^-h_c(1P)$  at c.m. energy from 3.90 to 4.42 GeV as a peak in the invariant mass distribution of the  $\pi^\pm h_c(1P)$  system, and by ABLIKIM 14B from  $e^+e^- \rightarrow (D^*\bar{D}^*)^\pm\pi^\mp$  events in  $(D^*\bar{D}^*)^\pm$  mass. A neutral  $X(4020)$  seen by ABLIKIM 14P at three c.m. energies in the same range in  $e^+e^- \rightarrow \pi^0\pi^0 h_c(1P)$  as a peak in the larger of the two masses recoiling against a  $\pi^0$ . ABLIKIM 15AA observes a  $5.9\sigma$  signal in  $(D^*\bar{D}^*)^0$  in  $e^+e^- \rightarrow (D^*\bar{D}^*)^0\pi^0$  events using collisions at two c.m. energies. Production rates and mass values support grouping neutral and charged  $X(4020)$  together as manifestations of a single  $l = 1$  particle.

#### $X(4020)^\pm$ MASS

VALUE (MeV)	EVTS	DOCUMENT ID	TECN	CHG	COMMENT
<b>4024.1 ± 1.9 OUR AVERAGE</b>					
4025.5 <sup>+2.0</sup> <sub>-4.7</sub> ± 3.1	116	<sup>1</sup> ABLIKIM 15AA	BES3	0	$e^+e^- \rightarrow (D^*\bar{D}^*)^0\pi^0$
4026.3 ± 2.6 ± 3.7	401	<sup>1</sup> ABLIKIM 14B	BES3	±	$e^+e^- \rightarrow (D^*\bar{D}^*)^\pm\pi^\mp$
4023.9 ± 2.2 ± 3.8	61	<sup>1,2</sup> ABLIKIM 14P	BES3	0	$e^+e^- \rightarrow \pi^0\pi^0 h_c$
4022.9 ± 0.8 ± 2.7	253	<sup>1</sup> ABLIKIM 13X	BES3	±	$e^+e^- \rightarrow \pi^+\pi^- h_c$

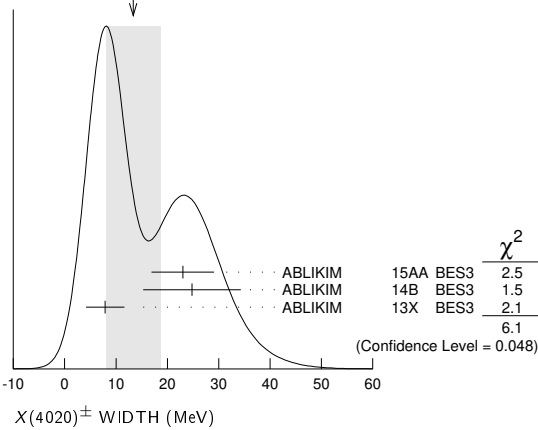
<sup>1</sup> Neglecting interference between the  $X(4020)$  and non-resonant continuum.  
<sup>2</sup> Assuming  $J^P = 1^+$  and width of  $7.9 \pm 2.6$  MeV.

#### $X(4020)^\pm$ WIDTH

VALUE (MeV)	EVTS	DOCUMENT ID	TECN	CHG	COMMENT
<b>13 ± 5 OUR AVERAGE</b>					Error includes scale factor of 1.7. See the ideogram below.
23.0 ± 6.0 ± 1.0	116	<sup>1</sup> ABLIKIM 15AA	BES3	0	$e^+e^- \rightarrow (D^*\bar{D}^*)^0\pi^0$
24.8 ± 5.6 ± 7.7	401	<sup>1</sup> ABLIKIM 14B	BES3	±	$e^+e^- \rightarrow (D^*\bar{D}^*)^\pm\pi^\mp$
7.9 ± 2.7 ± 2.6	253	<sup>1</sup> ABLIKIM 13X	BES3	±	$e^+e^- \rightarrow \pi^+\pi^- h_c$

<sup>1</sup> Neglecting interference between the  $X(4020)$  and non-resonant continuum.

WEIGHTED AVERAGE  
13±5 (Error scaled by 1.7)



#### $X(4020)^\pm$ DECAY MODES

Mode	Fraction ( $\Gamma_i/\Gamma$ )
$\Gamma_1$ $h_c(1P)\pi$	seen
$\Gamma_2$ $D^*\bar{D}^*$	seen
$\Gamma_3$ $D\bar{D}^* + c.c.$	not seen
$\Gamma_4$ $\eta_c\pi^+\pi^-$	not seen
$\Gamma_5$ $\eta_c(1S)\rho(770)^\pm$	
$\Gamma_6$ $J/\psi(1S)\pi^\pm$	not seen

#### $X(4020)^\pm$ BRANCHING RATIOS

$\Gamma(h_c(1P)\pi)/\Gamma_{total}$	VALUE	EVTS	DOCUMENT ID	TECN	CHG	COMMENT
seen	61		ABLIKIM 14P	BES3	0	$e^+e^- \rightarrow \pi^0\pi^0 h_c$
seen	253		ABLIKIM 13X	BES3	±	$e^+e^- \rightarrow \pi^+\pi^- h_c$

#### $\Gamma(D^*\bar{D}^*)/\Gamma_{total}$

VALUE	EVTS	DOCUMENT ID	TECN	CHG	COMMENT
seen	116	<sup>1</sup> ABLIKIM 15AA	BES3	0	$e^+e^- \rightarrow (D^*\bar{D}^*)^0\pi^0$
seen	401	<sup>1</sup> ABLIKIM 14B	BES3	±	$e^+e^- \rightarrow (D^*\bar{D}^*)^\pm\pi^\mp$

<sup>1</sup> Neglecting interference between the  $X(4020)$  and non-resonant continuum.

#### $\Gamma(D\bar{D}^* + c.c.)/\Gamma_{total}$

VALUE	DOCUMENT ID	TECN	CHG	COMMENT
not seen	ABLIKIM 15AC	BES3	±	$e^+e^- \rightarrow \pi^\pm(D\bar{D}^*)^\mp$

#### $\Gamma(\eta_c\pi^+\pi^-)/\Gamma_{total}$

VALUE	DOCUMENT ID	TECN	COMMENT
not seen	<sup>1</sup> VINOKUROVA 15	BELL	$B^+ \rightarrow K^+\eta_c\pi^+\pi^-$

<sup>1</sup> VINOKUROVA 15 reports  $B(B^+ \rightarrow K^+X(4020)^0) \times B(X(4020)^0 \rightarrow \eta_c\pi^+\pi^-) < 1.6 \times 10^{-5}$  at 90% CL.

#### $\Gamma(\eta_c(1S)\rho(770)^\pm)/\Gamma(h_c(1P)\pi)$

VALUE	CL%	DOCUMENT ID	TECN	COMMENT
<1.2	90	<sup>1</sup> ABLIKIM 19Bc	BES3	$e^+e^- \rightarrow \pi^+\pi^-\pi^0\eta_c(1S)$

<sup>1</sup> Using  $e^+e^- \rightarrow \pi^\mp(Z_c(4020)^\pm \rightarrow h_c(1P)\pi^\pm)$  cross section at 4.23, 4.26 and 4.36 GeV from ABLIKIM 13X.

#### $\Gamma(J/\psi(1S)\pi^\pm)/\Gamma_{total}$

VALUE	DOCUMENT ID	TECN	COMMENT
not seen	<sup>1</sup> ABLIKIM 17J	BES3	$e^+e^- \rightarrow \pi^+\pi^-J/\psi$

<sup>1</sup> From Partial Wave Analysis assuming  $J^P = 1^+$ .

#### $X(4020)^\pm$ REFERENCES

ABLIKIM 19BC	PR D100 111102	M. Ablikim <i>et al.</i>	(BESIII Collab.)
ABLIKIM 17J	PRL 119 072001	M. Ablikim <i>et al.</i>	(BESIII Collab.)
ABLIKIM 15AA	PRL 115 182002	M. Ablikim <i>et al.</i>	(BESIII Collab.)
ABLIKIM 15AC	PR D92 092006	M. Ablikim <i>et al.</i>	(BESIII Collab.)
VINOKUROVA 15	JHEP 1506 132	A. Vinokurova <i>et al.</i>	(BELLE Collab.)
Also	JHEP 1702 088 (err.)	A. Vinokurova <i>et al.</i>	(BELLE Collab.)
ABLIKIM 14B	PRL 112 132001	M. Ablikim <i>et al.</i>	(BESIII Collab.)
ABLIKIM 14P	PRL 113 212002	M. Ablikim <i>et al.</i>	(BESIII Collab.)
ABLIKIM 13X	PRL 111 242001	M. Ablikim <i>et al.</i>	(BESIII Collab.)

### $\psi(4040)$

$$I^G(J^{PC}) = 0^-(1^{-}-)$$

#### $\psi(4040)$ MASS

VALUE (MeV)	DOCUMENT ID	TECN	COMMENT
<b>4039 ± 1 OUR ESTIMATE</b>			
<b>4039.6 ± 4.3</b>	<sup>1</sup> ABLIKIM 08D	BES2	$e^+e^- \rightarrow$ hadrons
4034 ± 6	<sup>2</sup> MO 10	RVUE	$e^+e^- \rightarrow$ hadrons
4037 ± 2	<sup>3</sup> SETH 05A	RVUE	$e^+e^- \rightarrow$ hadrons
4040 ± 1	<sup>4</sup> SETH 05A	RVUE	$e^+e^- \rightarrow$ hadrons
4040 ± 10	BRANDELIK 78c	DASP	$e^+e^-$

<sup>1</sup> Reanalysis of data presented in BAI 02c. From a global fit over the center-of-mass energy region 3.7–5.0 GeV covering the  $\psi(3770)$ ,  $\psi(4040)$ ,  $\psi(4160)$ , and  $\psi(4415)$  resonances. Phase angle fixed in the fit to  $\delta = (130 \pm 46)^\circ$ .  
<sup>2</sup> Reanalysis of data presented in BAI 00 and BAI 02c. From a global fit over the center-of-mass energy 3.8–4.8 GeV covering the  $\psi(4040)$ ,  $\psi(4160)$  and  $\psi(4415)$  resonances and including interference effects.  
<sup>3</sup> From a fit to Crystal Ball (OSTERHELD 86) data.  
<sup>4</sup> From a fit to BES (BAI 02c) data.

#### $\psi(4040)$ WIDTH

VALUE (MeV)	DOCUMENT ID	TECN	COMMENT
<b>80 ± 10 OUR ESTIMATE</b>			
<b>84.5 ± 12.3</b>	<sup>5</sup> ABLIKIM 08D	BES2	$e^+e^- \rightarrow$ hadrons
87 ± 11	<sup>6</sup> MO 10	RVUE	$e^+e^- \rightarrow$ hadrons
85 ± 10	<sup>7</sup> SETH 05A	RVUE	$e^+e^- \rightarrow$ hadrons
89 ± 6	<sup>8</sup> SETH 05A	RVUE	$e^+e^- \rightarrow$ hadrons
52 ± 10	BRANDELIK 78c	DASP	$e^+e^-$

<sup>5</sup> Reanalysis of data presented in BAI 02c. From a global fit over the center-of-mass energy region 3.7–5.0 GeV covering the  $\psi(3770)$ ,  $\psi(4040)$ ,  $\psi(4160)$ , and  $\psi(4415)$  resonances. Phase angle fixed in the fit to  $\delta = (130 \pm 46)^\circ$ .  
<sup>6</sup> Reanalysis of data presented in BAI 00 and BAI 02c. From a global fit over the center-of-mass energy 3.8–4.8 GeV covering the  $\psi(4040)$ ,  $\psi(4160)$  and  $\psi(4415)$  resonances and including interference effects.  
<sup>7</sup> From a fit to Crystal Ball (OSTERHELD 86) data.  
<sup>8</sup> From a fit to BES (BAI 02c) data.

# Meson Particle Listings

## $\psi(4040)$

### $\psi(4040)$ DECAY MODES

Due to the complexity of the  $c\bar{c}$  threshold region, in this listing, "seen" ("not seen") means that a cross section for the mode in question has been measured at effective  $\sqrt{s}$  near this particle's central mass value, more (less) than  $2\sigma$  above zero, without regard to any peaking behavior in  $\sqrt{s}$  or absence thereof. See mode listing(s) for details and references.

Mode	Fraction ( $\Gamma_i/\Gamma$ )	Confidence level
$\Gamma_1$ $e^+e^-$	$(1.07 \pm 0.16) \times 10^{-5}$	
$\Gamma_2$ $D\bar{D}$	seen	
$\Gamma_3$ $D^0\bar{D}^0$	seen	
$\Gamma_4$ $D^+D^-$	seen	
$\Gamma_5$ $D^*\bar{D}^+$ + c.c.	seen	
$\Gamma_6$ $D^*(2007)^0\bar{D}^0$ + c.c.	seen	
$\Gamma_7$ $D^*(2010)^+D^-$ + c.c.	seen	
$\Gamma_8$ $D^*\bar{D}^*$	seen	
$\Gamma_9$ $D^*(2007)^0\bar{D}^*(2007)^0$	seen	
$\Gamma_{10}$ $D^*(2010)^+D^*(2010)^-$	seen	
$\Gamma_{11}$ $D\bar{D}\pi$ (excl. $D^*\bar{D}$ )		
$\Gamma_{12}$ $D^0D^-\pi^+$ + c.c. (excl. $D^*(2007)^0\bar{D}^0$ + c.c., $D^*(2010)^+D^-$ + c.c.)	not seen	
$\Gamma_{13}$ $D\bar{D}^*\pi$ (excl. $D^*\bar{D}^*$ )	not seen	
$\Gamma_{14}$ $D^0\bar{D}^*\pi^+$ + c.c. (excl. $D^*(2010)^+D^*(2010)^-$ )	seen	
$\Gamma_{15}$ $D_s^+D_s^-$	seen	
$\Gamma_{16}$ $J/\psi(1S)$ hadrons		
$\Gamma_{17}$ $J/\psi\pi^+\pi^-$	$< 4 \times 10^{-3}$	90%
$\Gamma_{18}$ $J/\psi\pi^0\pi^0$	$< 2 \times 10^{-3}$	90%
$\Gamma_{19}$ $J/\psi\eta$	$(5.2 \pm 0.7) \times 10^{-3}$	
$\Gamma_{20}$ $J/\psi\pi^0$	$< 2.8 \times 10^{-4}$	90%
$\Gamma_{21}$ $J/\psi\pi^+\pi^-\pi^0$	$< 2 \times 10^{-3}$	90%
$\Gamma_{22}$ $\chi_{c1}\gamma$	$< 3.4 \times 10^{-3}$	90%
$\Gamma_{23}$ $\chi_{c2}\gamma$	$< 5 \times 10^{-3}$	90%
$\Gamma_{24}$ $\chi_{c1}\pi^+\pi^-\pi^0$	$< 1.1\%$	90%
$\Gamma_{25}$ $\chi_{c2}\pi^+\pi^-\pi^0$	$< 3.2\%$	90%
$\Gamma_{26}$ $h_c(1P)\pi^+\pi^-$	$< 3 \times 10^{-3}$	90%
$\Gamma_{27}$ $\phi\pi^+\pi^-$	$< 3 \times 10^{-3}$	90%
$\Gamma_{28}$ $\Lambda\bar{\Lambda}\pi^+\pi^-$	$< 2.9 \times 10^{-4}$	90%
$\Gamma_{29}$ $\Lambda\bar{\Lambda}\pi^0$	$< 9 \times 10^{-5}$	90%
$\Gamma_{30}$ $\Lambda\bar{\Lambda}\eta$	$< 3.0 \times 10^{-4}$	90%
$\Gamma_{31}$ $\Sigma^+\Sigma^-$	$< 1.3 \times 10^{-4}$	90%
$\Gamma_{32}$ $\Sigma^0\bar{\Sigma}^0$	$< 7 \times 10^{-5}$	90%
$\Gamma_{33}$ $\Xi^+\Xi^-$	$< 1.6 \times 10^{-4}$	90%
$\Gamma_{34}$ $\Xi^0\bar{\Xi}^0$	$< 1.8 \times 10^{-4}$	90%
$\Gamma_{35}$ $\mu^+\mu^-$		

### $\psi(4040)$ PARTIAL WIDTHS

$\Gamma(e^+e^-)$	$\Gamma_1$
VALUE (keV)	DOCUMENT ID TECN COMMENT
<b><math>0.86 \pm 0.07</math> OUR ESTIMATE</b>	
<b><math>0.83 \pm 0.20</math></b>	<sup>9</sup> ABLIKIM 08D BES2 $e^+e^- \rightarrow$ hadrons
$0.6$ to $1.4$	<sup>10</sup> MO 10 RVUE $e^+e^- \rightarrow$ hadrons
$0.88 \pm 0.11$	<sup>11</sup> SETH 05A RVUE $e^+e^- \rightarrow$ hadrons
$0.91 \pm 0.13$	<sup>12</sup> SETH 05A RVUE $e^+e^- \rightarrow$ hadrons
$0.75 \pm 0.15$	BRANDELIK 78c DASP $e^+e^-$

<sup>9</sup> Reanalysis of data presented in BAI 02c. From a global fit over the center-of-mass energy region 3.7–5.0 GeV covering the  $\psi(3770)$ ,  $\psi(4040)$ ,  $\psi(4160)$ , and  $\psi(4415)$  resonances. Phase angle fixed in the fit to  $\delta = (130 \pm 46)^\circ$ .

<sup>10</sup> Reanalysis of data presented in BAI 00 and BAI 02c. From a global fit over the center-of-mass energy 3.8–4.8 GeV covering the  $\psi(4040)$ ,  $\psi(4160)$  and  $\psi(4415)$  resonances and including interference effects. Four sets of solutions are obtained with the same fit quality, mass and total width, but with different  $e^+e^-$  partial widths. We quote only the range of values.

<sup>11</sup> From a fit to Crystal Ball (OSTERHELD 86) data.

<sup>12</sup> From a fit to BES (BAI 02c) data.

### $\psi(4040)$ $\Gamma(i) \times \Gamma(e^+e^-)/\Gamma(\text{total})$

$\Gamma(\chi_{c1}\gamma) \times \Gamma(e^+e^-)/\Gamma_{\text{total}}$	$\Gamma_{22}\Gamma_1/\Gamma$
VALUE (eV) CL%	DOCUMENT ID TECN COMMENT
<b><math>&lt; 2.9</math></b>	<sup>13</sup> HAN 15 BELL $10.58 e^+e^- \rightarrow \chi_{c1}\gamma$

<sup>13</sup> Using  $B(\eta \rightarrow \gamma\gamma) = (39.41 \pm 0.21)\%$ .

$\Gamma(\chi_{c2}\gamma) \times \Gamma(e^+e^-)/\Gamma_{\text{total}}$	$\Gamma_{23}\Gamma_1/\Gamma$
VALUE (eV) CL%	DOCUMENT ID TECN COMMENT
<b><math>&lt; 4.6</math></b>	<sup>14</sup> HAN 15 BELL $10.58 e^+e^- \rightarrow \chi_{c2}\gamma$

<sup>14</sup> Using  $B(\eta \rightarrow \gamma\gamma) = (39.41 \pm 0.21)\%$ .

### $\psi(4040)$ $\Gamma(i) \times \Gamma(e^+e^-)/\Gamma^2(\text{total})$

$\Gamma(J/\psi\eta)/\Gamma_{\text{total}} \times \Gamma(e^+e^-)/\Gamma_{\text{total}}$	$\Gamma_{19}/\Gamma \times \Gamma_1/\Gamma$
VALUE (units $10^{-8}$ )	DOCUMENT ID TECN COMMENT
$5.1 \pm 1.4 \pm 1.5$	<sup>15</sup> WANG 13B BELL $e^+e^- \rightarrow J/\psi\eta\gamma$
$12.8 \pm 2.1 \pm 1.9$	<sup>16</sup> WANG 13B BELL $e^+e^- \rightarrow J/\psi\eta\gamma$

$\bullet \bullet \bullet$  We do not use the following data for averages, fits, limits, etc.  $\bullet \bullet \bullet$

<sup>15</sup> Solution I of two equivalent solutions in a fit using two interfering resonances. Mass and width fixed at 4039 MeV and 80 MeV, respectively.

<sup>16</sup> Solution II of two equivalent solutions in a fit using two interfering resonances. Mass and width fixed at 4039 MeV and 80 MeV, respectively.

### $\psi(4040)$ BRANCHING RATIOS

$\Gamma(e^+e^-)/\Gamma_{\text{total}}$	$\Gamma_1/\Gamma$
VALUE (units $10^{-5}$ )	DOCUMENT ID TECN COMMENT
$\sim 1.0$	FELDMAN 77 MRK1 $e^+e^-$

$\Gamma(D^0\bar{D}^0)/\Gamma_{\text{total}}$	$\Gamma_3/\Gamma$
VALUE	DOCUMENT ID TECN COMMENT
seen	AUBERT 09M BABR $e^+e^- \rightarrow D^0\bar{D}^0\gamma$
seen	CRONIN-HEN..09 CLEO $e^+e^- \rightarrow D^0\bar{D}^0$
seen	PAKHLOVA 08 BELL $e^+e^- \rightarrow D^0\bar{D}^0\gamma$

$\Gamma(D^+D^-)/\Gamma_{\text{total}}$	$\Gamma_4/\Gamma$
VALUE	DOCUMENT ID TECN COMMENT
seen	AUBERT 09M BABR $e^+e^- \rightarrow D^+D^-\gamma$
seen	CRONIN-HEN..09 CLEO $e^+e^- \rightarrow D^+D^-$
seen	PAKHLOVA 08 BELL $e^+e^- \rightarrow D^+D^-\gamma$

$\Gamma(D\bar{D})/\Gamma(D^*\bar{D} + \text{c.c.})$	$\Gamma_2/\Gamma_5$
VALUE	DOCUMENT ID TECN COMMENT
<b><math>0.24 \pm 0.05 \pm 0.12</math></b>	AUBERT 09M BABR $e^+e^- \rightarrow \gamma D^{(*)}\bar{D}$

$\Gamma(D^0\bar{D}^0)/\Gamma(D^*(2007)^0\bar{D}^0 + \text{c.c.})$	$\Gamma_3/\Gamma_6$
VALUE	DOCUMENT ID TECN COMMENT
<b><math>0.05 \pm 0.03</math></b>	<sup>17</sup> GOLDHABER 77 MRK1 $e^+e^-$

<sup>17</sup> Phase-space factor ( $p^3$ ) explicitly removed.

$\Gamma(D^*(2007)^0\bar{D}^0 + \text{c.c.})/\Gamma_{\text{total}}$	$\Gamma_6/\Gamma$
VALUE	DOCUMENT ID TECN COMMENT
seen	AUBERT 09M BABR $e^+e^- \rightarrow D^{*0}\bar{D}^0\gamma$
seen	CRONIN-HEN..09 CLEO $e^+e^- \rightarrow D^{*0}\bar{D}^0$

$\Gamma(D^*(2010)^+D^- + \text{c.c.})/\Gamma_{\text{total}}$	$\Gamma_7/\Gamma$
VALUE	DOCUMENT ID TECN COMMENT
seen	<sup>18</sup> ZHUKOVA 18 BELL $e^+e^- \rightarrow D^{*+}D^-\gamma$
seen	AUBERT 09M BABR $e^+e^- \rightarrow D^{*+}D^-\gamma$
seen	CRONIN-HEN..09 CLEO $e^+e^- \rightarrow D^{*+}D^-$

$\bullet \bullet \bullet$  We do not use the following data for averages, fits, limits, etc.  $\bullet \bullet \bullet$

seen PAKHLOVA 07 BELL  $e^+e^- \rightarrow D^{*+}D^-\gamma$

<sup>18</sup> Supersedes PAKHLOVA 07.

$\Gamma(D^*(2010)^+D^- + \text{c.c.})/\Gamma(D^*(2007)^0\bar{D}^0 + \text{c.c.})$	$\Gamma_7/\Gamma_6$
VALUE	DOCUMENT ID TECN COMMENT
<b><math>0.95 \pm 0.09 \pm 0.10</math></b>	AUBERT 09M BABR $e^+e^- \rightarrow \gamma D^*\bar{D}$

$\Gamma(D^*\bar{D}^*)/\Gamma(D^*\bar{D} + \text{c.c.})$	$\Gamma_8/\Gamma_5$
VALUE	DOCUMENT ID TECN COMMENT
<b><math>0.18 \pm 0.14 \pm 0.03</math></b>	AUBERT 09M BABR $e^+e^- \rightarrow \gamma D^{(*)}\bar{D}^{(*)}$

$\Gamma(D^*(2007)^0\bar{D}^*(2007)^0)/\Gamma_{\text{total}}$	$\Gamma_9/\Gamma$
VALUE	DOCUMENT ID TECN COMMENT
seen	AUBERT 09M BABR $e^+e^- \rightarrow D^{*0}\bar{D}^{*0}\gamma$
seen	CRONIN-HEN..09 CLEO $e^+e^- \rightarrow D^{*0}\bar{D}^{*0}$

$\Gamma(D^*(2007)^0\bar{D}^*(2007)^0)/\Gamma(D^*(2007)^0\bar{D}^0 + \text{c.c.})$	$\Gamma_9/\Gamma_6$
VALUE	DOCUMENT ID TECN COMMENT
<b><math>32.0 \pm 12.0</math></b>	<sup>19</sup> GOLDHABER 77 MRK1 $e^+e^-$

<sup>19</sup> Phase-space factor ( $p^3$ ) explicitly removed.

See key on page 999

Meson Particle Listings

$\psi(4040), X(4050)^\pm$

Table with 5 columns: VALUE, DOCUMENT ID, TECN, COMMENT, and  $\Gamma_{10}/\Gamma_{total}$ . Row 1: seen, 20 ZHUKOVA 18 BELL  $e^+e^- \rightarrow D^{*+}D^{*-}\gamma$ . Row 2: seen, AUBERT 09M BABR  $e^+e^- \rightarrow D^{*+}D^{*-}\gamma$ . Row 3: seen, CRONIN-HEN..09 CLEO  $e^+e^- \rightarrow D^{*+}D^{*-}$ . Row 4:  $\bullet \bullet \bullet$  We do not use the following data for averages, fits, limits, etc.  $\bullet \bullet \bullet$ . Row 5: seen, PAKHLOVA 07 BELL  $e^+e^- \rightarrow D^{*+}D^{*-}\gamma$ . Row 6: <sup>20</sup> Supersedes PAKHLOVA 07.

Table with 5 columns: VALUE, DOCUMENT ID, TECN, COMMENT, and  $\Gamma_{12}/\Gamma_{total}$ . Row 1: not seen, PAKHLOVA 08A BELL  $e^+e^- \rightarrow D^0 D^- \pi^+ \gamma$ .

Table with 5 columns: VALUE, DOCUMENT ID, TECN, COMMENT, and  $\Gamma_{13}/\Gamma_{total}$ . Row 1: not seen, CRONIN-HEN..09 CLEO  $e^+e^- \rightarrow D \bar{D}^* \pi$ .

Table with 5 columns: VALUE, DOCUMENT ID, TECN, COMMENT, and  $\Gamma_{14}/\Gamma_{total}$ . Row 1: seen, PAKHLOVA 09 BELL  $e^+e^- \rightarrow D^0 D^{*-} \pi^+ \gamma$ .

Table with 5 columns: VALUE, DOCUMENT ID, TECN, COMMENT, and  $\Gamma_{15}/\Gamma_{total}$ . Row 1: seen, PAKHLOVA 11 BELL  $e^+e^- \rightarrow D_s^+ D_s^- \gamma$ . Row 2: seen, DEL-AMO-SA..10N BABR  $e^+e^- \rightarrow D_s^+ D_s^- \gamma$ . Row 3: seen, CRONIN-HEN..09 CLEO  $e^+e^- \rightarrow D_s^+ D_s^-$ .

Table with 5 columns: VALUE, DOCUMENT ID, TECN, COMMENT, and  $\Gamma_{17}/\Gamma_{total}$ . Row 1:  $\Gamma(J/\psi \pi^+ \pi^-)/\Gamma_{total}$ . Row 2: VALUE (units  $10^{-3}$ ), CL%, DOCUMENT ID, TECN, COMMENT. Row 3: <4, 90, COAN 06 CLEO 3.97-4.06  $e^+e^- \rightarrow$  hadrons.

Table with 5 columns: VALUE, DOCUMENT ID, TECN, COMMENT, and  $\Gamma_{18}/\Gamma_{total}$ . Row 1:  $\Gamma(J/\psi \pi^0 \pi^0)/\Gamma_{total}$ . Row 2: VALUE (units  $10^{-3}$ ), CL%, DOCUMENT ID, TECN, COMMENT. Row 3: <2, 90, COAN 06 CLEO 3.97-4.06  $e^+e^- \rightarrow$  hadrons.

Table with 5 columns: VALUE, DOCUMENT ID, TECN, COMMENT, and  $\Gamma_{19}/\Gamma_{total}$ . Row 1:  $\Gamma(J/\psi \eta)/\Gamma_{total}$ . Row 2: VALUE (units  $10^{-3}$ ), CL%, DOCUMENT ID, TECN, COMMENT. Row 3:  $5.2 \pm 0.5 \pm 0.5$ , 21 ABLIKIM 12K BES3  $e^+e^- \rightarrow \ell^+ \ell^- 2\gamma$ . Row 4:  $\bullet \bullet \bullet$  We do not use the following data for averages, fits, limits, etc.  $\bullet \bullet \bullet$ . Row 5: <7, 90, COAN 06 CLEO 3.97-4.06  $e^+e^- \rightarrow$  hadrons. Row 6: <sup>21</sup> ABLIKIM 12K measure  $\sigma(e^+e^- \rightarrow J/\psi \eta) = 32.1 \pm 2.8 \pm 1.3$  pb. They assume the  $\eta J/\psi$  fully originates from  $\psi(4040)$  decays.

Table with 5 columns: VALUE, DOCUMENT ID, TECN, COMMENT, and  $\Gamma_{20}/\Gamma_{total}$ . Row 1:  $\Gamma(J/\psi \pi^0)/\Gamma_{total}$ . Row 2: VALUE (units  $10^{-3}$ ), CL%, DOCUMENT ID, TECN, COMMENT. Row 3: <0.28, 90, 22 ABLIKIM 12K BES3  $e^+e^- \rightarrow \ell^+ \ell^- 2\gamma$ . Row 4:  $\bullet \bullet \bullet$  We do not use the following data for averages, fits, limits, etc.  $\bullet \bullet \bullet$ . Row 5: <2, 90, COAN 06 CLEO 3.97-4.06  $e^+e^- \rightarrow$  hadrons. Row 6: <sup>22</sup> ABLIKIM 12K measure  $\sigma(e^+e^- \rightarrow J/\psi \pi^0) < 1.6$  pb. They assume the  $\eta J/\psi$  fully originates from  $\psi(4040)$  decays.

Table with 5 columns: VALUE, DOCUMENT ID, TECN, COMMENT, and  $\Gamma_{21}/\Gamma_{total}$ . Row 1:  $\Gamma(J/\psi \pi^+ \pi^- \pi^0)/\Gamma_{total}$ . Row 2: VALUE (units  $10^{-3}$ ), CL%, DOCUMENT ID, TECN, COMMENT. Row 3: <2, 90, COAN 06 CLEO 3.97-4.06  $e^+e^- \rightarrow$  hadrons.

Table with 5 columns: VALUE, DOCUMENT ID, TECN, COMMENT, and  $\Gamma_{22}/\Gamma_{total}$ . Row 1:  $\Gamma(\chi_{c1} \gamma)/\Gamma_{total}$ . Row 2: VALUE (units  $10^{-3}$ ), CL%, DOCUMENT ID, TECN, COMMENT. Row 3:  $\bullet \bullet \bullet$  We do not use the following data for averages, fits, limits, etc.  $\bullet \bullet \bullet$ . Row 4: <11, 90, COAN 06 CLEO 3.97-4.06  $e^+e^- \rightarrow$  hadrons.

Table with 5 columns: VALUE, DOCUMENT ID, TECN, COMMENT, and  $\Gamma_{23}/\Gamma_{total}$ . Row 1:  $\Gamma(\chi_{c2} \gamma)/\Gamma_{total}$ . Row 2: VALUE (units  $10^{-3}$ ), CL%, DOCUMENT ID, TECN, COMMENT. Row 3:  $\bullet \bullet \bullet$  We do not use the following data for averages, fits, limits, etc.  $\bullet \bullet \bullet$ . Row 4: <17, 90, COAN 06 CLEO 3.97-4.06  $e^+e^- \rightarrow$  hadrons.

Table with 5 columns: VALUE, DOCUMENT ID, TECN, COMMENT, and  $\Gamma_{24}/\Gamma_{total}$ . Row 1:  $\Gamma(\chi_{c1} \pi^+ \pi^- \pi^0)/\Gamma_{total}$ . Row 2: VALUE (units  $10^{-3}$ ), CL%, DOCUMENT ID, TECN, COMMENT. Row 3: <11, 90, COAN 06 CLEO 3.97-4.06  $e^+e^- \rightarrow$  hadrons.

Table with 5 columns: VALUE, DOCUMENT ID, TECN, COMMENT, and  $\Gamma_{25}/\Gamma_{total}$ . Row 1:  $\Gamma(\chi_{c2} \pi^+ \pi^- \pi^0)/\Gamma_{total}$ . Row 2: VALUE (units  $10^{-3}$ ), CL%, DOCUMENT ID, TECN, COMMENT. Row 3: <32, 90, COAN 06 CLEO 3.97-4.06  $e^+e^- \rightarrow$  hadrons.

Table with 5 columns: VALUE, DOCUMENT ID, TECN, COMMENT, and  $\Gamma_{26}/\Gamma_{total}$ . Row 1:  $\Gamma(h_c(1P) \pi^+ \pi^-)/\Gamma_{total}$ . Row 2: VALUE (units  $10^{-3}$ ), CL%, DOCUMENT ID, TECN, COMMENT. Row 3: <3, 90, 23 PEDLAR 11 CLEO  $e^+e^- \rightarrow h_c(1P) \pi^+ \pi^-$ . Row 4: <sup>23</sup> From several values of  $\sqrt{s}$  near the peak of the  $\psi(4040)$ , PEDLAR 11 measures  $\sigma(e^+e^- \rightarrow h_c(1P) \pi^+ \pi^-) = 1.0 \pm 8.0 \pm 5.4 \pm 0.2$  pb, where the errors are statistical, systematic, and due to uncertainty in  $B(\psi(2S) \rightarrow \pi^0 h_c(1P))$ , respectively.

Table with 5 columns: VALUE, CL%, DOCUMENT ID, TECN, COMMENT, and  $\Gamma_{27}/\Gamma_{total}$ . Row 1:  $\Gamma(\phi \pi^+ \pi^-)/\Gamma_{total}$ . Row 2: VALUE (units  $10^{-3}$ ), CL%, DOCUMENT ID, TECN, COMMENT. Row 3: <3, 90, COAN 06 CLEO 3.97-4.06  $e^+e^- \rightarrow$  hadrons.

Table with 5 columns: VALUE, CL%, DOCUMENT ID, TECN, COMMENT, and  $\Gamma_{28}/\Gamma_{total}$ . Row 1:  $\Gamma(\Lambda \bar{\Lambda} \pi^+ \pi^-)/\Gamma_{total}$ . Row 2: VALUE (units  $10^{-4}$ ), CL%, DOCUMENT ID, TECN, COMMENT. Row 3: <2.9, 90, 24 ABLIKIM 13Q BES3  $e^+e^- \rightarrow \psi(4040)$ . Row 4: <sup>24</sup> Assuming that interference effects between resonance and continuum can be neglected.

Table with 5 columns: VALUE, CL%, DOCUMENT ID, TECN, COMMENT, and  $\Gamma_{29}/\Gamma_{total}$ . Row 1:  $\Gamma(\Lambda \bar{\Lambda} \pi^0)/\Gamma_{total}$ . Row 2: VALUE (units  $10^{-4}$ ), CL%, DOCUMENT ID, TECN, COMMENT. Row 3: <0.9, 90, 25 ABLIKIM 13Q BES3  $e^+e^- \rightarrow \psi(4040)$ . Row 4: <sup>25</sup> Assuming that interference effects between resonance and continuum can be neglected.

Table with 5 columns: VALUE, CL%, DOCUMENT ID, TECN, COMMENT, and  $\Gamma_{30}/\Gamma_{total}$ . Row 1:  $\Gamma(\Lambda \bar{\Lambda} \eta)/\Gamma_{total}$ . Row 2: VALUE (units  $10^{-4}$ ), CL%, DOCUMENT ID, TECN, COMMENT. Row 3: <3.0, 90, 26 ABLIKIM 13Q BES3  $e^+e^- \rightarrow \psi(4040)$ . Row 4: <sup>26</sup> Assuming that interference effects between resonance and continuum can be neglected.

Table with 5 columns: VALUE, CL%, DOCUMENT ID, TECN, COMMENT, and  $\Gamma_{31}/\Gamma_{total}$ . Row 1:  $\Gamma(\Sigma^+ \bar{\Sigma}^-)/\Gamma_{total}$ . Row 2: VALUE (units  $10^{-4}$ ), CL%, DOCUMENT ID, TECN, COMMENT. Row 3: <1.3, 90, 27 ABLIKIM 13Q BES3  $e^+e^- \rightarrow \psi(4040)$ . Row 4: <sup>27</sup> Assuming that interference effects between resonance and continuum can be neglected.

Table with 5 columns: VALUE, CL%, DOCUMENT ID, TECN, COMMENT, and  $\Gamma_{32}/\Gamma_{total}$ . Row 1:  $\Gamma(\Sigma^0 \bar{\Sigma}^0)/\Gamma_{total}$ . Row 2: VALUE (units  $10^{-4}$ ), CL%, DOCUMENT ID, TECN, COMMENT. Row 3: <0.7, 90, 28 ABLIKIM 13Q BES3  $e^+e^- \rightarrow \psi(4040)$ . Row 4: <sup>28</sup> Assuming that interference effects between resonance and continuum can be neglected.

Table with 5 columns: VALUE, CL%, DOCUMENT ID, TECN, COMMENT, and  $\Gamma_{33}/\Gamma_{total}$ . Row 1:  $\Gamma(\Xi^+ \bar{\Xi}^-)/\Gamma_{total}$ . Row 2: VALUE (units  $10^{-4}$ ), CL%, DOCUMENT ID, TECN, COMMENT. Row 3: <1.6, 90, 29 ABLIKIM 13Q BES3  $e^+e^- \rightarrow \psi(4040)$ . Row 4: <sup>29</sup> Assuming that interference effects between resonance and continuum can be neglected.

Table with 5 columns: VALUE, CL%, DOCUMENT ID, TECN, COMMENT, and  $\Gamma_{34}/\Gamma_{total}$ . Row 1:  $\Gamma(\Xi^0 \bar{\Xi}^0)/\Gamma_{total}$ . Row 2: VALUE (units  $10^{-4}$ ), CL%, DOCUMENT ID, TECN, COMMENT. Row 3: <1.8, 90, 30 ABLIKIM 13Q BES3  $e^+e^- \rightarrow \psi(4040)$ . Row 4: <sup>30</sup> Assuming that interference effects between resonance and continuum can be neglected.

$\psi(4040)$  REFERENCES

ZHUKOVA 18 PR D97 012002 V. Zhukova et al. (BELLE Collab.)
HAN 15 PR D92 012011 Y.L. Han et al. (BELLE Collab.)
ABLIKIM 13Q PR D87 112011 Ablikim M. et al. (BESIII Collab.)
WANG 13B PR D87 051101 X.L. Wang et al. (BELLE Collab.)
ABLIKIM 12K PR D86 071101 M. Ablikim et al. (BESIII Collab.)
PAKHLOVA 11 PR D83 011101 G. Pakhlova et al. (BELLE Collab.)
PEDLAR 11 PRL 107 041803 T. Pedlar et al. (CLEO Collab.)
DEL-AMO-SA...10N PR D82 052004 P. del Amo Sanchez et al. (BABAR Collab.)
MO 10 PR D52 077501 X.H. Mo, C.Z. Yuan, P. Wang (BHEP)
AUBERT 09M PR D79 022001 B. Aubert et al. (BABAR Collab.)
CRONIN-HEN...09 PR D80 072001 D. Cronin-Hennessy et al. (CLEO Collab.)
PAKHLOVA 09 PR D80 091101 G. Pakhlova et al. (BELLE Collab.)
ABLIKIM 08D PL B660 315 M. Ablikim et al. (BES Collab.)
PAKHLOVA 08 PR D77 011103 G. Pakhlova et al. (BELLE Collab.)
PAKHLOVA 08A PRL 100 062001 G. Pakhlova et al. (BELLE Collab.)
PAKHLOVA 07 PRL 98 092001 G. Pakhlova et al. (BELLE Collab.)
COAN 06 PRL 96 162003 T.E. Coan et al. (CLEO Collab.)
SETH 05A PR D72 017501 K.K. Seth (BES Collab.)
BAI 02C PRL 88 101802 J.Z. Bai et al. (BES Collab.)
BAI 00 PRL 84 594 J.Z. Bai et al. (BES Collab.)
OSTERHELD 86 SLAC-PUB-4160 A. Osterheld et al. (SLAC Crystal Ball Collab.)
BRANDELIK 78C PL 76B 361 R. Brandelik et al. (DASP Collab.)
Also ZPHY C1 233 R. Brandelik et al. (DASP Collab.)
FELDMAN 77 PRPL 33C 285 G.J. Feldman, M.L. Perl (LBL, SLAC)
GOLDBABER 77 PL 69B 503 G. Goldhaber et al. (Mark I Collab.)

$X(4050)^\pm$

$I^G(J^{PC}) = 1^-(?^?+)$ 
I, G, C need confirmation.

OMITTED FROM SUMMARY TABLE

Properties incompatible with a  $q\bar{q}$  structure (exotic state). See the review on non- $q\bar{q}$  states.

Observed by MIZUK 08 in the  $\pi^+ \chi_{c1}(1P)$  invariant mass distribution in  $\bar{B}^0 \rightarrow K^- \pi^+ \chi_{c1}(1P)$  decays. Not seen by LEES 12B in this same mode after accounting for  $K \pi$  resonant mass and angular structure.

$X(4050)^\pm$  MASS

Table with 5 columns: VALUE (MeV), DOCUMENT ID, TECN, COMMENT. Row 1:  $4051 \pm 14 \pm 20$ , 1 MIZUK 08 BELL  $\bar{B}^0 \rightarrow K^- \pi^+ \chi_{c1}(1P)$ .

<sup>1</sup> From a Dalitz plot analysis with two Breit-Wigner amplitudes.

## Meson Particle Listings

 $X(4050)^\pm$ ,  $X(4055)^\pm$ ,  $X(4100)^\pm$  $X(4050)^\pm$  WIDTH

VALUE (MeV)	DOCUMENT ID	TECN	COMMENT
$82^{+21+47}_{-17-22}$	<sup>1</sup> MIZUK	08 BELL	$\overline{B}^0 \rightarrow K^- \pi^+ \chi_{c1}(1P)$

<sup>1</sup> From a Dalitz plot analysis with two Breit-Wigner amplitudes.

 $X(4050)^\pm$  DECAY MODES

Mode	Fraction ( $\Gamma_i/\Gamma$ )
$\Gamma_1$ $\pi^+ \chi_{c1}(1P)$	seen
$\Gamma_2$ $\pi^\pm \psi(3770)$	not seen

 $X(4050)^\pm$  BRANCHING RATIOS

$\Gamma(\pi^+ \chi_{c1}(1P))/\Gamma_{\text{total}}$	VALUE	DOCUMENT ID	TECN	COMMENT	$\Gamma_1/\Gamma$
seen		<sup>1</sup> MIZUK	08 BELL	$\overline{B}^0 \rightarrow K^- \pi^+ \chi_{c1}(1P)$	
not seen		<sup>2</sup> LEES	12b BABR	$B \rightarrow K \pi \chi_{c1}(1P)$	

<sup>1</sup> With a product branching fraction measurement of  $B(\overline{B}^0 \rightarrow K^- X(4050)^+) \times B(X(4050)^+ \rightarrow \pi^+ \chi_{c1}(1P)) = (3.0^{+1.5+3.7}_{-0.8-1.6}) \times 10^{-5}$ .

<sup>2</sup> With a product branching fraction limit of  $B(\overline{B}^0 \rightarrow X(4050)^+ K^-) \times B(X(4050)^+ \rightarrow \chi_{c1} \pi^+) < 1.8 \times 10^{-5}$  at 90% CL.

$\Gamma(\pi^\pm \psi(3770))/\Gamma_{\text{total}}$	VALUE	DOCUMENT ID	TECN	COMMENT	$\Gamma_2/\Gamma$
not seen		<sup>1</sup> ABLIKIM	19AR BES3	$e^+ e^- \rightarrow \pi^+ \pi^- D \overline{D}$	

<sup>1</sup> From a measurement of  $\sigma(e^+ e^- \rightarrow \pi^+ \pi^- D \overline{D})$  between  $\sqrt{s} = 4.08$  and 4.6 GeV.

 $X(4050)^\pm$  REFERENCES

ABLIKIM	19AR	PR D100 032005	M. Ablikim <i>et al.</i>	(BESIII Collab.)
LEES	12b	PR D85 052003	J.P. Lees <i>et al.</i>	(BABAR Collab.)
MIZUK	08	PR D78 072004	R. Mizuk <i>et al.</i>	(BELLE Collab.)

 $X(4055)^\pm$ 

$$J^G(J^{PC}) = 1^+(?^2-)$$

$I, G, C$  need confirmation.

## OMITTED FROM SUMMARY TABLE

Properties incompatible with a  $q\overline{q}$  structure (exotic state). See the review on non- $q\overline{q}$  states.

Needs confirmation. Seen by WANG 15A in the  $\psi(2S)\pi^+$  invariant mass distribution in  $\psi(4360) \rightarrow \psi(2S)\pi^+\pi^-$  decay.

 $X(4055)^\pm$  MASS

VALUE (MeV)	DOCUMENT ID	TECN	COMMENT
$4054 \pm 3 \pm 1$	<sup>1</sup> WANG	15A BELL	$10.58 e^+ e^- \rightarrow \gamma \pi^+ \pi^- \psi(2S)$
$4039.3 \pm 6.0$	<sup>2</sup> ABLIKIM	18k BES3	$e^+ e^- \rightarrow \pi^0 \pi^0 \psi(2S)$
$4032.1 \pm 2.4$	<sup>3</sup> ABLIKIM	17v BES3	$e^+ e^- \rightarrow \pi^+ \pi^- \psi(2S)$

- <sup>1</sup> Statistical significance of 3.5  $\sigma$ .
- <sup>2</sup> Statistical error only, with significance of 5.9  $\sigma$  (from a fit with a 19% CL). Identified as the same structure observed in ABLIKIM 17v in  $e^+ e^- \rightarrow \pi^+ \pi^- \psi(2S)$  decays.
- <sup>3</sup> Statistical error only, with significance of 9.2  $\sigma$ . From an unbinned maximum likelihood fit of the  $\pi^+ \pi^- \psi(2S)$  Dalitz plot from data collected at  $\sqrt{s} = 4.416$  GeV for a  $J^C = 1^+$  state. The fit does not match the detailed structure of the data, having a C.L. of only 8%.

 $X(4055)^\pm$  WIDTH

VALUE (MeV)	DOCUMENT ID	TECN	COMMENT
$45 \pm 11 \pm 6$	<sup>1</sup> WANG	15A BELL	$10.58 e^+ e^- \rightarrow \gamma \pi^+ \pi^- \psi(2S)$
$31.9 \pm 14.8$	<sup>2</sup> ABLIKIM	18k BES3	$e^+ e^- \rightarrow \pi^0 \pi^0 \psi(2S)$
$26.1 \pm 5.3$	<sup>3</sup> ABLIKIM	17v BES3	$e^+ e^- \rightarrow \pi^+ \pi^- \psi(2S)$

- <sup>1</sup> Statistical significance of 3.5  $\sigma$ .
- <sup>2</sup> Statistical error only, with significance of 5.9  $\sigma$  (from a fit with a 19% CL). Identified as the same structure observed in ABLIKIM 17v in  $e^+ e^- \rightarrow \pi^+ \pi^- \psi(2S)$  decays.
- <sup>3</sup> Statistical error only, with significance of 9.2  $\sigma$ . From an unbinned maximum likelihood fit of the  $\pi^+ \pi^- \psi(2S)$  Dalitz plot from data collected at  $\sqrt{s} = 4.416$  GeV for a  $J^C = 1^+$  state. The fit does not match the detailed structure of the data, having a C.L. of only 8%.

 $X(4055)^\pm$  DECAY MODES

Mode	Fraction ( $\Gamma_i/\Gamma$ )
$\Gamma_1$ $\pi^+ \psi(2S)$	seen
$\Gamma_2$ $\pi^\pm \psi(3770)$	not seen

 $X(4055)^\pm$  BRANCHING RATIOS

$\Gamma(\pi^+ \psi(2S))/\Gamma_{\text{total}}$	VALUE	DOCUMENT ID	TECN	COMMENT	$\Gamma_1/\Gamma$
seen		<sup>1</sup> WANG	15A BELL	$10.58 e^+ e^- \rightarrow \gamma \pi^+ \pi^- \psi(2S)$	

<sup>1</sup> Statistical significance of 3.5  $\sigma$ .

$\Gamma(\pi^\pm \psi(3770))/\Gamma_{\text{total}}$	VALUE	DOCUMENT ID	TECN	COMMENT	$\Gamma_2/\Gamma$
not seen		<sup>1</sup> ABLIKIM	19AR BES3	$e^+ e^- \rightarrow \pi^+ \pi^- D \overline{D}$	

<sup>1</sup> From a measurement of  $\sigma(e^+ e^- \rightarrow \pi^+ \pi^- D \overline{D})$  between  $\sqrt{s} = 4.08$  and 4.6 GeV.

 $X(4055)^\pm$  REFERENCES

ABLIKIM	19AR	PR D100 032005	M. Ablikim <i>et al.</i>	(BESIII Collab.)
ABLIKIM	18k	PR D97 052001	M. Ablikim <i>et al.</i>	(BESIII Collab.)
ABLIKIM	17v	PR D96 032004	M. Ablikim <i>et al.</i>	(BESIII Collab.)
Also		PR D99 019903 (errata.)	M. Ablikim <i>et al.</i>	(BESIII Collab.)
WANG	15A	PR D91 112007	X.L. Wang <i>et al.</i>	(BELLE Collab.)

 $X(4100)^\pm$ 

$$J^G(J^{PC}) = 1^-(???)$$

## OMITTED FROM SUMMARY TABLE

Properties incompatible with a  $q\overline{q}$  structure (exotic state). See the review on non- $q\overline{q}$  states.

Reported by AAIJ 18AN in the  $\eta_c(1S)\pi^-$  invariant mass distribution in  $B^0 \rightarrow \eta_c(1S)K^+\pi^-$  decays with a significance of 3.4 $\sigma$ .  $J^P = 0^+$  or  $1^-$  assignment consistent with data.

 $X(4100)^\pm$  MASS

VALUE (MeV)	DOCUMENT ID	TECN	COMMENT
$4096 \pm 20^{+18}_{-22}$	AAIJ	18AN LHCB	$B^0 \rightarrow \eta_c(1S)K^+\pi^-$

 $X(4100)^\pm$  WIDTH

VALUE (MeV)	DOCUMENT ID	TECN	COMMENT
$152 \pm 5 \pm 60_{-35}$	AAIJ	18AN LHCB	$B^0 \rightarrow \eta_c(1S)K^+\pi^-$

 $X(4100)^\pm$  DECAY MODES

Mode	Fraction ( $\Gamma_i/\Gamma$ )
$\Gamma_1$ $\eta_c(1S)\pi^-$	seen
$\Gamma_2$ $\pi^\pm \psi(3770)$	not seen

 $X(4100)^\pm$  BRANCHING RATIOS

$\Gamma(\eta_c(1S)\pi^-)/\Gamma_{\text{total}}$	VALUE	DOCUMENT ID	TECN	COMMENT	$\Gamma_1/\Gamma$
seen		<sup>1</sup> AAIJ	18AN LHCB	$B^0 \rightarrow \eta_c(1S)K^+\pi^-$	

<sup>1</sup> AAIJ 18AN quotes a fit fraction for  $B^0 \rightarrow X(4100)^- K^+ \rightarrow \eta_c(1S)\pi^- K^+$  of  $(3.3 \pm 1.1^{+1.2}_{-1.1})\%$  from an amplitude analysis.

$\Gamma(\pi^\pm \psi(3770))/\Gamma_{\text{total}}$	VALUE	DOCUMENT ID	TECN	COMMENT	$\Gamma_2/\Gamma$
not seen		<sup>1</sup> ABLIKIM	19AR BES3	$e^+ e^- \rightarrow \pi^+ \pi^- D \overline{D}$	

<sup>1</sup> From a measurement of  $\sigma(e^+ e^- \rightarrow \pi^+ \pi^- D \overline{D})$  between  $\sqrt{s} = 4.08$  and 4.6 GeV.

 $X(4100)^\pm$  REFERENCES

ABLIKIM	19AR	PR D100 032005	M. Ablikim <i>et al.</i>	(BESIII Collab.)
AAIJ	18AN	EPJ C78 1019	R. Aaij <i>et al.</i>	(LHCB Collab.)

See key on page 999

Meson Particle Listings

$\chi_{c1}(4140), \psi(4160)$

**$\chi_{c1}(4140)$**

$I^G(J^{PC}) = 0^+(1^{++})$

was  $X(4140)$

This state shows properties different from a conventional  $q\bar{q}$  state. A candidate for an exotic structure. See the review on non- $q\bar{q}$  states.

Seen by AALTONEN 09AH, ABAZOV 14A, CHATRCHYAN 14M, AAIJ 17C in  $B^+ \rightarrow \chi_{c1} K^+$ ,  $\chi_{c1} \rightarrow J/\psi\phi$ , and by ABAZOV 15M separately in both prompt (4.7  $\sigma$ ) and non-prompt (5.6  $\sigma$ ) production in  $p\bar{p} \rightarrow J/\psi\phi + \text{anything}$ . Not seen by SHEN 10 in  $\gamma\gamma \rightarrow J/\psi\phi$  and ABLIKIM 15 in  $e^+e^- \rightarrow \gamma J/\psi\phi$  at  $\sqrt{s} = 4.23, 4.26, 4.36$  GeV.

**$\chi_{c1}(4140)$  MASS**

VALUE (MeV)	EVTs	DOCUMENT ID	TECN	COMMENT
<b>4146.8 ± 2.4 OUR AVERAGE</b>		Error includes scale factor of 1.1.		
4146.5 ± 4.5 <sup>+4.6</sup> <sub>-2.8</sub>	4289	<sup>1</sup> AAIJ	17c LHCb	$B^+ \rightarrow J/\psi\phi K^+$
4143.4 ± 2.9 <sup>+2.9</sup> <sub>-3.0</sub> ± 0.6	19	<sup>2</sup> AALTONEN	17 CDF	$B^+ \rightarrow J/\psi\phi K^+$
4152.5 ± 1.7 <sup>+6.2</sup> <sub>-5.4</sub>	616	<sup>3</sup> ABAZOV	15M D0	$p\bar{p} \rightarrow J/\psi\phi + \text{anything}$
4159.0 ± 4.3 ± 6.6	52	<sup>4</sup> ABAZOV	14A D0	$B^+ \rightarrow J/\psi\phi K^+$
4148.0 ± 2.4 ± 6.3	0.3k	<sup>5</sup> CHATRCHYAN 14M	CMS	$B^+ \rightarrow J/\psi\phi K^+$
• • • We do not use the following data for averages, fits, limits, etc. • • •				
4143.0 ± 2.9 ± 1.2	14	<sup>6,7</sup> AALTONEN	09AH CDF	$B^+ \rightarrow J/\psi\phi K^+$

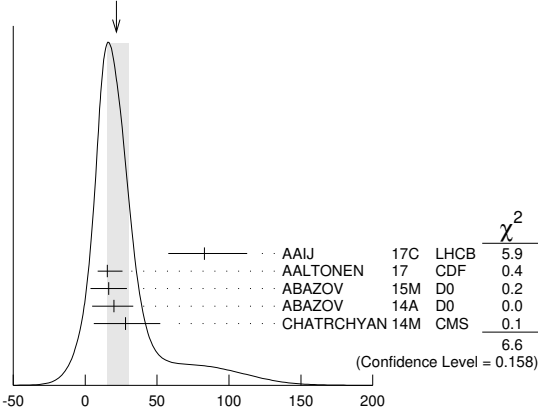
- <sup>1</sup> From an amplitude analysis of the decay  $B^+ \rightarrow J/\psi\phi K^+$  with a significance of 8.4  $\sigma$ .
- <sup>2</sup> Statistical significance of more than 5  $\sigma$ .
- <sup>3</sup> Statistical significance of more than 6  $\sigma$ .
- <sup>4</sup> Statistical significance of 3.1  $\sigma$ .
- <sup>5</sup> From a fit assuming an S-wave relativistic Breit-Wigner shape above a three-body phase-space non-resonant component with statistical significance of more than 5  $\sigma$ .
- <sup>6</sup> Statistical significance of 3.8  $\sigma$ .
- <sup>7</sup> Superseded by AALTONEN 17.

**$\chi_{c1}(4140)$  WIDTH**

VALUE (MeV)	EVTs	DOCUMENT ID	TECN	COMMENT
<b>22 ± 8 OUR AVERAGE</b>		Error includes scale factor of 1.3. See the ideogram below.		
83 ± 21 ± 21 <sup>+8</sup> <sub>-14</sub>	4289	<sup>1</sup> AAIJ	17c LHCb	$B^+ \rightarrow J/\psi\phi K^+$
15.3 ± 10.4 ± 6.1 ± 2.5	19	<sup>2</sup> AALTONEN	17 CDF	$B^+ \rightarrow J/\psi\phi K^+$
16.3 ± 5.6 ± 11.4	616	<sup>3</sup> ABAZOV	15M D0	$p\bar{p} \rightarrow J/\psi\phi + \text{anything}$
20 ± 13 ± 3 <sup>+3</sup> <sub>-8</sub>	52	<sup>4</sup> ABAZOV	14A D0	$B^+ \rightarrow J/\psi\phi K^+$
28 ± 15 ± 11 ± 19	0.3k	<sup>5</sup> CHATRCHYAN 14M	CMS	$B^+ \rightarrow J/\psi\phi K^+$
• • • We do not use the following data for averages, fits, limits, etc. • • •				
11.7 ± 8.3 ± 5.0 ± 3.7	14	<sup>6,7</sup> AALTONEN	09AH CDF	$B^+ \rightarrow J/\psi\phi K^+$

- <sup>1</sup> From an amplitude analysis of the decay  $B^+ \rightarrow J/\psi\phi K^+$  with a significance of 8.4  $\sigma$ .
- <sup>2</sup> Statistical significance of more than 5  $\sigma$ .
- <sup>3</sup> Statistical significance of more than 6  $\sigma$ .
- <sup>4</sup> Statistical significance of 3.1  $\sigma$ .
- <sup>5</sup> From a fit assuming an S-wave relativistic Breit-Wigner shape above a three-body phase-space non-resonant component with statistical significance of more than 5  $\sigma$ .
- <sup>6</sup> Statistical significance of 3.8  $\sigma$ .
- <sup>7</sup> Superseded by AALTONEN 17.

WEIGHTED AVERAGE  
22±8.7 (Error scaled by 1.3)



**$\chi_{c1}(4140)$  DECAY MODES**

Mode	Fraction ( $\Gamma_i/\Gamma$ )
$\Gamma_1$ $J/\psi\phi$	seen
$\Gamma_2$ $\gamma\gamma$	not seen

**$\chi_{c1}(4140)$   $\Gamma(i)\Gamma(\gamma\gamma)/\Gamma(\text{total})$**

VALUE (eV)	CL%	DOCUMENT ID	TECN	COMMENT	$\Gamma_2\Gamma_1/\Gamma$
<b>&lt;41</b>	90	<sup>1</sup> SHEN	10 BELL	10.6 $e^+e^- \rightarrow e^+e^- J/\psi\phi$	
• • • We do not use the following data for averages, fits, limits, etc. • • •					
< 6	90	<sup>2</sup> SHEN	10 BELL	10.6 $e^+e^- \rightarrow e^+e^- J/\psi\phi$	

- <sup>1</sup> For  $J^P = 0^+$ .
- <sup>2</sup> For  $J^P = 2^+$ .

**$\chi_{c1}(4140)$  BRANCHING RATIOS**

$\Gamma(J/\psi\phi)/\Gamma_{\text{total}}$	EVTs	DOCUMENT ID	TECN	COMMENT	$\Gamma_1/\Gamma$
seen	4289	<sup>1</sup> AAIJ	17c LHCb	$B^+ \rightarrow J/\psi\phi K^+$	
seen	616	<sup>2</sup> ABAZOV	15M D0	$p\bar{p} \rightarrow J/\psi\phi + \text{anything}$	
seen	52	<sup>3</sup> ABAZOV	14A D0	$B^+ \rightarrow J/\psi\phi K^+$	
seen	0.3k	<sup>4</sup> CHATRCHYAN 14M	CMS	$B^+ \rightarrow J/\psi\phi K^+$	
seen	14	<sup>5</sup> AALTONEN	09AH CDF	$B^+ \rightarrow J/\psi\phi K^+$	
• • • We do not use the following data for averages, fits, limits, etc. • • •					
not seen		<sup>6</sup> ABLIKIM	15 BES3	$e^+e^- \rightarrow \gamma\phi J/\psi$	
not seen		<sup>7</sup> AAIJ	12AA LHCb	$p\bar{p} \rightarrow B^+ X$ at 7 TeV	

- <sup>1</sup> From an amplitude analysis of the decay  $B^+ \rightarrow J/\psi\phi K^+$  with a significance of 8.4  $\sigma$ .
- <sup>2</sup> Statistical significance of more than 6  $\sigma$ .
- <sup>3</sup> ABAZOV 14A reports  $B(B^+ \rightarrow \chi_{c1}(4140) K^+ \rightarrow J/\psi\phi K^+)/B(B^+ \rightarrow J/\psi\phi K^+) = (19 \pm 7 \pm 4)\%$  with 3.1  $\sigma$  significance.
- <sup>4</sup> From a fit assuming an S-wave relativistic Breit-Wigner shape above a three-body phase-space non-resonant component with statistical significance of more than 5  $\sigma$ .
- <sup>5</sup> Statistical significance of 3.8  $\sigma$ .
- <sup>6</sup> Reported  $\sigma(e^+e^- \rightarrow \gamma\chi_{c1}(4140)) \cdot B(\chi_{c1}(4140) \rightarrow J/\psi\phi) < 0.35, 0.28,$  and  $0.33$  pb at 4.23, 4.26, and 4.36 GeV, respectively, at 90% CL.
- <sup>7</sup> Reported  $B(B^+ \rightarrow \chi_{c1}(4140) K^+) \cdot B(\chi_{c1}(4140) \rightarrow J/\psi\phi)/B(B^+ \rightarrow J/\psi\phi K^+) < 0.07$  at 90% CL.

$\Gamma(\gamma\gamma)/\Gamma_{\text{total}}$	DOCUMENT ID	TECN	COMMENT	$\Gamma_2/\Gamma$
not seen	SHEN	10 BELL	10.6 $e^+e^- \rightarrow e^+e^- J/\psi\phi$	

**$\chi_{c1}(4140)$  REFERENCES**

AAIJ 17C PRL 118 022003	R. Aaij et al.	(LHCb Collab.) JP
Also PR D95 012002	R. Aaij et al.	(LHCb Collab.)
AALTONEN 17 MPL A32 1750139	T. Aaltonen et al.	(CDF Collab.)
ABAZOV 15M PRL 115 232001	V.M. Abazov et al.	(D0 Collab.)
ABLIKIM 15 PR D91 032002	M. Ablikim et al.	(BESIII Collab.)
ABAZOV 14A PR D89 012004	V.M. Abazov et al.	(D0 Collab.)
CHATRCHYAN 14M PL B734 261	S. Chatrchyan et al.	(CMS Collab.)
AAIJ 12AA PR D85 091103	R. Aaij et al.	(LHCb Collab.)
SHEN 10 PRL 104 112004	C.P. Shen et al.	(BELLE Collab.)
AALTONEN 09AH PRL 102 242002	T. Aaltonen et al.	(CDF Collab.)

**$\psi(4160)$**

$I^G(J^{PC}) = 0^-(1^{--})$

**$\psi(4160)$  MASS**

VALUE (MeV)	DOCUMENT ID	TECN	COMMENT
<b>4191 ± 5 OUR AVERAGE</b>			
4191 ± 9	AAIJ	13Bc LHCb	$B^+ \rightarrow K^+ \mu^+ \mu^-$
4191.7 ± 6.5	<sup>1</sup> ABLIKIM	08B BES2	$e^+e^- \rightarrow \text{hadrons}$
• • • We do not use the following data for averages, fits, limits, etc. • • •			
4193 ± 7	<sup>2</sup> MO	10 RVUE	$e^+e^- \rightarrow \text{hadrons}$
4151 ± 4	<sup>3</sup> SETH	05A RVUE	$e^+e^- \rightarrow \text{hadrons}$
4155 ± 5	<sup>4</sup> SETH	05A RVUE	$e^+e^- \rightarrow \text{hadrons}$
4159 ± 20	BRANDELIK	78c DASP	$e^+e^-$

- <sup>1</sup> Reanalysis of data presented in BAI 02c. From a global fit over the center-of-mass energy region 3.7–5.0 GeV covering the  $\psi(3770), \psi(4040), \psi(4160),$  and  $\psi(4415)$  resonances. Phase angle fixed in the fit to  $\delta = (293 \pm 57)^\circ$ .
- <sup>2</sup> Reanalysis of data presented in BAI 00 and BAI 02c. From a global fit over the center-of-mass energy 3.8–4.8 GeV covering the  $\psi(4040), \psi(4160)$  and  $\psi(4415)$  resonances and including interference effects.
- <sup>3</sup> From a fit to Crystal Ball (OSTERHELD 86) data.
- <sup>4</sup> From a fit to BES (BAI 02c) data.

# Meson Particle Listings

## $\psi(4160)$

### $\psi(4160)$ WIDTH

VALUE (MeV)	DOCUMENT ID	TECN	COMMENT
<b>70 ±10 OUR AVERAGE</b>			
65 +22 -16	AAIJ	13Bc LHCb	$B^+ \rightarrow K^+ \mu^+ \mu^-$
71.8 ±12.3	<sup>1</sup> ABLIKIM	08D BES2	$e^+ e^- \rightarrow \text{hadrons}$
• • • We do not use the following data for averages, fits, limits, etc. • • •			
79 ±14	<sup>2</sup> MO	10 RVUE	$e^+ e^- \rightarrow \text{hadrons}$
107 ±10	<sup>3</sup> SETH	05A RVUE	$e^+ e^- \rightarrow \text{hadrons}$
107 ±16	<sup>4</sup> SETH	05A RVUE	$e^+ e^- \rightarrow \text{hadrons}$
78 ±20	BRANDELIK	78c DASP	$e^+ e^-$

<sup>1</sup> Reanalysis of data presented in BAI 02c. From a global fit over the center-of-mass energy region 3.7–5.0 GeV covering the  $\psi(3770)$ ,  $\psi(4040)$ ,  $\psi(4160)$ , and  $\psi(4415)$  resonances. Phase angle fixed in the fit to  $\delta = (293 \pm 57)^\circ$ .

<sup>2</sup> Reanalysis of data presented in BAI 00 and BAI 02c. From a global fit over the center-of-mass energy 3.8–4.8 GeV covering the  $\psi(4040)$ ,  $\psi(4160)$  and  $\psi(4415)$  resonances and including interference effects.

<sup>3</sup> From a fit to Crystal Ball (OSTERHELD 86) data.

<sup>4</sup> From a fit to BES (BAI 02c) data.

### $\psi(4160)$ DECAY MODES

Due to the complexity of the  $c\bar{c}$  threshold region, in this listing, “seen” (“not seen”) means that a cross section for the mode in question has been measured at effective  $\sqrt{s}$  near this particle’s central mass value, more (less) than  $2\sigma$  above zero, without regard to any peaking behavior in  $\sqrt{s}$  or absence thereof. See mode listing(s) for details and references.

Mode	Fraction ( $\Gamma_i/\Gamma$ )	Confidence level
$\Gamma_1$ $e^+ e^-$	$(6.9 \pm 3.3) \times 10^{-6}$	
$\Gamma_2$ $\mu^+ \mu^-$	seen	
$\Gamma_3$ $D\bar{D}$	seen	
$\Gamma_4$ $D^0 \bar{D}^0$	seen	
$\Gamma_5$ $D^+ D^-$	seen	
$\Gamma_6$ $D^* \bar{D}^+ + c.c.$	seen	
$\Gamma_7$ $D^*(2007)^0 \bar{D}^0 + c.c.$	seen	
$\Gamma_8$ $D^*(2010)^+ D^- + c.c.$	seen	
$\Gamma_9$ $D^* \bar{D}^*$	seen	
$\Gamma_{10}$ $D^*(2007)^0 \bar{D}^*(2007)^0$	seen	
$\Gamma_{11}$ $D^*(2010)^+ D^*(2010)^-$	seen	
$\Gamma_{12}$ $D^0 D^- \pi^+ + c.c.$ (excl. $D^*(2007)^0 \bar{D}^0 + c.c., D^*(2010)^+ D^- + c.c.$ )	not seen	
$\Gamma_{13}$ $D\bar{D}^* \pi + c.c.$ (excl. $D^* \bar{D}^*$ )	seen	
$\Gamma_{14}$ $D^0 D^* \pi^+ + c.c.$ (excl. $D^*(2010)^+ D^*(2010)^-$ )	not seen	
$\Gamma_{15}$ $D_s^+ D_s^-$	not seen	
$\Gamma_{16}$ $D_s^+ D_s^- + c.c.$	seen	
$\Gamma_{17}$ $J/\psi \pi^+ \pi^-$	$< 3 \times 10^{-3}$	90%
$\Gamma_{18}$ $J/\psi \pi^0 \pi^0$	$< 3 \times 10^{-3}$	90%
$\Gamma_{19}$ $J/\psi K^+ K^-$	$< 2 \times 10^{-3}$	90%
$\Gamma_{20}$ $J/\psi \eta$	$< 8 \times 10^{-3}$	90%
$\Gamma_{21}$ $J/\psi \pi^0$	$< 1 \times 10^{-3}$	90%
$\Gamma_{22}$ $J/\psi \eta'$	$< 5 \times 10^{-3}$	90%
$\Gamma_{23}$ $J/\psi \pi^+ \pi^- \pi^0$	$< 1 \times 10^{-3}$	90%
$\Gamma_{24}$ $\psi(2S) \pi^+ \pi^-$	$< 4 \times 10^{-3}$	90%
$\Gamma_{25}$ $\chi_{c1} \gamma$	$< 5 \times 10^{-3}$	90%
$\Gamma_{26}$ $\chi_{c2} \gamma$	$< 1.3 \%$	90%
$\Gamma_{27}$ $\chi_{c1} \pi^+ \pi^- \pi^0$	$< 2 \times 10^{-3}$	90%
$\Gamma_{28}$ $\chi_{c2} \pi^+ \pi^- \pi^0$	$< 8 \times 10^{-3}$	90%
$\Gamma_{29}$ $h_c(1P) \pi^+ \pi^-$	$< 5 \times 10^{-3}$	90%
$\Gamma_{30}$ $h_c(1P) \pi^0 \pi^0$	$< 2 \times 10^{-3}$	90%
$\Gamma_{31}$ $h_c(1P) \eta$	$< 2 \times 10^{-3}$	90%
$\Gamma_{32}$ $h_c(1P) \pi^0$	$< 4 \times 10^{-4}$	90%
$\Gamma_{33}$ $\phi \pi^+ \pi^-$	$< 2 \times 10^{-3}$	90%
$\Gamma_{34}$ $\gamma \chi_{c1}(3872) \rightarrow \gamma J/\psi \pi^+ \pi^-$	$< 6.8 \times 10^{-5}$	90%
$\Gamma_{35}$ $\gamma X(3915) \rightarrow \gamma J/\psi \pi^+ \pi^-$	$< 1.36 \times 10^{-4}$	90%
$\Gamma_{36}$ $\gamma X(3930) \rightarrow \gamma J/\psi \pi^+ \pi^-$	$< 1.18 \times 10^{-4}$	90%
$\Gamma_{37}$ $\gamma X(3940) \rightarrow \gamma J/\psi \pi^+ \pi^-$	$< 1.47 \times 10^{-4}$	90%
$\Gamma_{38}$ $\gamma \chi_{c1}(3872) \rightarrow \gamma \gamma J/\psi$	$< 1.05 \times 10^{-4}$	90%
$\Gamma_{39}$ $\gamma X(3915) \rightarrow \gamma \gamma J/\psi$	$< 1.26 \times 10^{-4}$	90%
$\Gamma_{40}$ $\gamma X(3930) \rightarrow \gamma \gamma J/\psi$	$< 8.8 \times 10^{-5}$	90%
$\Gamma_{41}$ $\gamma X(3940) \rightarrow \gamma \gamma J/\psi$	$< 1.79 \times 10^{-4}$	90%
$\Gamma_{42}$ $K^+ K^-$		
$\Gamma_{43}$ $K_S^0 K^\pm \pi^\mp$		

### $\psi(4160)$ PARTIAL WIDTHS

$\Gamma(e^+ e^-)$	DOCUMENT ID	TECN	COMMENT	$\Gamma_1$
<b>0.48 ± 0.22</b>	<sup>1</sup> ABLIKIM	08D BES2	$e^+ e^- \rightarrow \text{hadrons}$	
• • • We do not use the following data for averages, fits, limits, etc. • • •				
0.4 to 1.1	<sup>2</sup> MO	10 RVUE	$e^+ e^- \rightarrow \text{hadrons}$	
0.83 ± 0.08	<sup>3</sup> SETH	05A RVUE	$e^+ e^- \rightarrow \text{hadrons}$	
0.84 ± 0.13	<sup>4</sup> SETH	05A RVUE	$e^+ e^- \rightarrow \text{hadrons}$	
0.77 ± 0.23	BRANDELIK	78c DASP	$e^+ e^-$	

<sup>1</sup> Reanalysis of data presented in BAI 02c. From a global fit over the center-of-mass energy region 3.7–5.0 GeV covering the  $\psi(3770)$ ,  $\psi(4040)$ ,  $\psi(4160)$ , and  $\psi(4415)$  resonances. Phase angle fixed in the fit to  $\delta = (293 \pm 57)^\circ$ .

<sup>2</sup> Reanalysis of data presented in BAI 00 and BAI 02c. From a global fit over the center-of-mass energy 3.8–4.8 GeV covering the  $\psi(4040)$ ,  $\psi(4160)$  and  $\psi(4415)$  resonances and including interference effects. Four sets of solutions are obtained with the same fit quality, mass and total width, but with different  $e^+ e^-$  partial widths. We quote only the range of values.

<sup>3</sup> From a fit to Crystal Ball (OSTERHELD 86) data.

<sup>4</sup> From a fit to BES (BAI 02c) data.

### $\psi(4160)$ $\Gamma(i) \times \Gamma(e^+ e^-) / \Gamma(\text{total})$

$\Gamma(J/\psi \eta) \times \Gamma(e^+ e^-) / \Gamma(\text{total})$	VALUE (eV)	EVTS	DOCUMENT ID	TECN	COMMENT	$\Gamma_{22} \Gamma_1 / \Gamma$
• • • We do not use the following data for averages, fits, limits, etc. • • •						
	0.17 ± 0.04	86	<sup>1,2</sup> ABLIKIM	20A BES3	$e^+ e^- \rightarrow \eta' J/\psi$	
	1.07 ± 0.09	86	<sup>1,3</sup> ABLIKIM	20A BES3	$e^+ e^- \rightarrow \eta' J/\psi$	

<sup>1</sup> Based on a fit to  $\sigma(e^+ e^- \rightarrow \eta' J/\psi)$  from  $\sqrt{s} = 4.18$  to 4.60 GeV assuming interfering  $\psi(4160)$  and  $\psi(4260)$  contributions. At  $\sqrt{s} = 4.18$  GeV,  $\sigma(e^+ e^- \rightarrow \eta' J/\psi) = 2.4 \pm 0.3 \pm 0.2$  pb.

<sup>2</sup> Solution I of the fit, corresponding to a phase of  $-0.03 \pm 0.44$  rad.

<sup>3</sup> Solution II of the fit, corresponding to a phase of  $2.54 \pm 0.04$  rad.

$\Gamma(\chi_{c1} \gamma) \times \Gamma(e^+ e^-) / \Gamma(\text{total})$	VALUE (eV)	CL%	DOCUMENT ID	TECN	COMMENT	$\Gamma_{25} \Gamma_1 / \Gamma$
<b>&lt; 2.2</b>	90		<sup>1</sup> HAN	15 BELL	$10.58 e^+ e^- \rightarrow \chi_{c1} \gamma$	

<sup>1</sup> Using  $B(\eta \rightarrow \gamma \gamma) = (39.41 \pm 0.21)\%$ .

$\Gamma(\chi_{c2} \gamma) \times \Gamma(e^+ e^-) / \Gamma(\text{total})$	VALUE (eV)	CL%	DOCUMENT ID	TECN	COMMENT	$\Gamma_{26} \Gamma_1 / \Gamma$
• • • We do not use the following data for averages, fits, limits, etc. • • •						
	< 6.1	90	<sup>1</sup> HAN	15 BELL	$10.58 e^+ e^- \rightarrow \chi_{c2} \gamma$	

<sup>1</sup> Using  $B(\eta \rightarrow \gamma \gamma) = (39.41 \pm 0.21)\%$ .

$\Gamma(K_S^0 K^\pm \pi^\mp) \times \Gamma(e^+ e^-) / \Gamma(\text{total})$	VALUE (eV)	DOCUMENT ID	TECN	COMMENT	$\Gamma_{43} \Gamma_1 / \Gamma$
• • • We do not use the following data for averages, fits, limits, etc. • • •					
	$2.71 \pm 0.13 \pm 0.12$	<sup>1</sup> ABLIKIM	19A BES3	$e^+ e^- \rightarrow K_S^0 K^\pm \pi^\mp$	
	$0.0095 \pm 0.0088 \pm 0.0004$	<sup>2</sup> ABLIKIM	19A BES3	$e^+ e^- \rightarrow K_S^0 K^\pm \pi^\mp$	

<sup>1</sup> Solution I of the fit including the  $\psi(4160)$  with mass  $4191 \pm 5$  MeV and width  $70 \pm 10$  MeV from PDG 16 and the  $\psi(4230)$  with mass  $4219.6 \pm 3.3 \pm 5.1$  MeV and width  $56.0 \pm 3.6 \pm 6.9$  MeV from GAO 17.

<sup>2</sup> Solution II of the fit including the  $\psi(4160)$  with mass  $4191 \pm 5$  MeV and width  $70 \pm 10$  MeV from PDG 16 and the  $\psi(4230)$  with mass  $4219.6 \pm 3.3 \pm 5.1$  MeV and width  $56.0 \pm 3.6 \pm 6.9$  MeV from GAO 17.

### $\psi(4160)$ $\Gamma(i) \times \Gamma(e^+ e^-) / \Gamma^2(\text{total})$

$\Gamma(J/\psi \eta) / \Gamma(\text{total}) \times \Gamma(e^+ e^-) / \Gamma(\text{total})$	VALUE (units $10^{-8}$ )	DOCUMENT ID	TECN	COMMENT	$\Gamma_{20} / \Gamma \times \Gamma_1 / \Gamma$
• • • We do not use the following data for averages, fits, limits, etc. • • •					
	$2.8 \pm 0.9 \pm 0.9$	<sup>1</sup> WANG	13B BELL	$e^+ e^- \rightarrow J/\psi \eta \gamma$	
	$12.8 \pm 1.7 \pm 2.0$	<sup>2</sup> WANG	13B BELL	$e^+ e^- \rightarrow J/\psi \eta \gamma$	

<sup>1</sup> Solution I of two equivalent solutions in a fit using two interfering resonances. Mass and width fixed at 4153 MeV and 103 MeV, respectively.

<sup>2</sup> Solution II of two equivalent solutions in a fit using two interfering resonances. Mass and width fixed at 4153 MeV and 103 MeV, respectively.

### $\psi(4160)$ BRANCHING RATIOS

$\Gamma(\mu^+ \mu^-) / \Gamma(\text{total})$	DOCUMENT ID	TECN	COMMENT	$\Gamma_2 / \Gamma$
seen	<sup>1</sup> AAIJ	13Bc LHCb	$B^+ \rightarrow K^+ \mu^+ \mu^-$	

<sup>1</sup> AAIJ 13Bc report  $B(B^+ \rightarrow K^+ \psi(4160)) B(\psi(4160) \rightarrow \mu^+ \mu^-) = (3.5^{+0.9}_{-0.8}) \times 10^{-9}$ .

$\Gamma(D\bar{D}) / \Gamma(D^* \bar{D}^*)$	DOCUMENT ID	TECN	COMMENT	$\Gamma_3 / \Gamma_9$
<b>0.02 ± 0.03 ± 0.02</b>	AUBERT	09M BABR	$e^+ e^- \rightarrow \gamma D^*(*) \bar{D}^*(*)$	

$\Gamma(D^0\bar{D}^0)/\Gamma_{\text{total}}$ 

VALUE	DOCUMENT ID	TECN	COMMENT	$\Gamma_4/\Gamma$
seen	CRONIN-HEN..09	CLEO	$e^+e^- \rightarrow D^0\bar{D}^0$	
seen	PAKHLOVA 08	BELL	$e^+e^- \rightarrow D^0\bar{D}^0\gamma$	
• • • We do not use the following data for averages, fits, limits, etc. • • •				
not seen	AUBERT 09M	BABR	$e^+e^- \rightarrow D^0\bar{D}^0\gamma$	

 $\Gamma(D^+D^-)/\Gamma_{\text{total}}$ 

VALUE	DOCUMENT ID	TECN	COMMENT	$\Gamma_5/\Gamma$
seen	CRONIN-HEN..09	CLEO	$e^+e^- \rightarrow D^+D^-$	
seen	PAKHLOVA 08	BELL	$e^+e^- \rightarrow D^+D^-\gamma$	
• • • We do not use the following data for averages, fits, limits, etc. • • •				
not seen	AUBERT 09M	BABR	$e^+e^- \rightarrow D^+D^-\gamma$	

 $\Gamma(D^*(2007)^0\bar{D}^0 + \text{c.c.})/\Gamma_{\text{total}}$ 

VALUE	DOCUMENT ID	TECN	COMMENT	$\Gamma_7/\Gamma$
seen	AUBERT 09M	BABR	$e^+e^- \rightarrow D^{*0}\bar{D}^0\gamma$	
seen	CRONIN-HEN..09	CLEO	$e^+e^- \rightarrow D^{*0}\bar{D}^0$	

 $\Gamma(D^*(2010)^+D^- + \text{c.c.})/\Gamma_{\text{total}}$ 

VALUE	DOCUMENT ID	TECN	COMMENT	$\Gamma_8/\Gamma$
seen	1 ZHUKOVA 18	BELL	$e^+e^- \rightarrow D^{*+}D^-\gamma$	
seen	AUBERT 09M	BABR	$e^+e^- \rightarrow D^{*+}D^-\gamma$	
seen	CRONIN-HEN..09	CLEO	$e^+e^- \rightarrow D^{*+}D^-$	
• • • We do not use the following data for averages, fits, limits, etc. • • •				
seen	PAKHLOVA 07	BELL	$e^+e^- \rightarrow D^{*+}D^-\gamma$	
<sup>1</sup> Supersedes PAKHLOVA 07.				

 $\Gamma(D^*\bar{D} + \text{c.c.})/\Gamma(D^*\bar{D}^*)$ 

VALUE	DOCUMENT ID	TECN	COMMENT	$\Gamma_6/\Gamma_9$
$0.34 \pm 0.14 \pm 0.05$	AUBERT 09M	BABR	$e^+e^- \rightarrow \gamma D^{*+}\bar{D}^{*-}$	

 $\Gamma(D^*(2007)^0\bar{D}^*(2007)^0)/\Gamma_{\text{total}}$ 

VALUE	DOCUMENT ID	TECN	COMMENT	$\Gamma_{10}/\Gamma$
seen	AUBERT 09M	BABR	$e^+e^- \rightarrow D^{*0}\bar{D}^{*0}\gamma$	
seen	CRONIN-HEN..09	CLEO	$e^+e^- \rightarrow D^{*0}\bar{D}^{*0}$	

 $\Gamma(D^*(2010)^+D^*(2010)^-)/\Gamma_{\text{total}}$ 

VALUE	DOCUMENT ID	TECN	COMMENT	$\Gamma_{11}/\Gamma$
seen	1 ZHUKOVA 18	BELL	$e^+e^- \rightarrow D^{*+}D^{*-}\gamma$	
seen	AUBERT 09M	BABR	$e^+e^- \rightarrow D^{*+}D^{*-}\gamma$	
seen	CRONIN-HEN..09	CLEO	$e^+e^- \rightarrow D^{*+}D^{*-}$	
• • • We do not use the following data for averages, fits, limits, etc. • • •				
seen	PAKHLOVA 07	BELL	$e^+e^- \rightarrow D^{*+}D^{*-}\gamma$	
<sup>1</sup> Supersedes PAKHLOVA 07.				

 $\Gamma(D^0D^-\pi^+ + \text{c.c. (excl. } D^*(2007)^0\bar{D}^0 + \text{c.c., } D^*(2010)^+D^-\text{ + c.c.})/\Gamma_{\text{total}}$ 

VALUE	DOCUMENT ID	TECN	COMMENT	$\Gamma_{12}/\Gamma$
not seen	PAKHLOVA 08A	BELL	$e^+e^- \rightarrow D^0D^-\pi^+\gamma$	

 $\Gamma(D\bar{D}^*\pi + \text{c.c. (excl. } D^*\bar{D}^*)/\Gamma_{\text{total}}$ 

VALUE	DOCUMENT ID	TECN	COMMENT	$\Gamma_{13}/\Gamma$
seen	CRONIN-HEN..09	CLEO	$e^+e^- \rightarrow D\bar{D}^*\pi$	

 $\Gamma(D^0D^{*-}\pi^+ + \text{c.c. (excl. } D^*(2010)^+D^*(2010)^-)/\Gamma_{\text{total}}$ 

VALUE	DOCUMENT ID	TECN	COMMENT	$\Gamma_{14}/\Gamma$
not seen	PAKHLOVA 09	BELL	$e^+e^- \rightarrow D^0D^{*-}\pi^+\gamma$	

 $\Gamma(D_s^+D_s^-)/\Gamma_{\text{total}}$ 

VALUE	DOCUMENT ID	TECN	COMMENT	$\Gamma_{15}/\Gamma$
not seen	PAKHLOVA 11	BELL	$e^+e^- \rightarrow D_s^+D_s^-\gamma$	
not seen	DEL-AMO-SA..10N	BABR	$e^+e^- \rightarrow D_s^+D_s^-\gamma$	
not seen	CRONIN-HEN..09	CLEO	$e^+e^- \rightarrow D_s^+D_s^-$	

 $\Gamma(D_s^+D_s^- + \text{c.c.})/\Gamma_{\text{total}}$ 

VALUE	DOCUMENT ID	TECN	COMMENT	$\Gamma_{16}/\Gamma$
seen	PAKHLOVA 11	BELL	$e^+e^- \rightarrow D_s^+D_s^-\gamma$	
seen	DEL-AMO-SA..10N	BABR	$e^+e^- \rightarrow D_s^+D_s^-\gamma$	
seen	CRONIN-HEN..09	CLEO	$e^+e^- \rightarrow D_s^+D_s^-$	

 $\Gamma(J/\psi\pi^+\pi^-)/\Gamma_{\text{total}}$ 

VALUE (units $10^{-3}$ )	CL%	DOCUMENT ID	TECN	COMMENT	$\Gamma_{17}/\Gamma$
<3	90	COAN 06	CLEO	4.12–4.2 $e^+e^- \rightarrow$ hadrons	

 $\Gamma(J/\psi\pi^0\pi^0)/\Gamma_{\text{total}}$ 

VALUE (units $10^{-3}$ )	CL%	DOCUMENT ID	TECN	COMMENT	$\Gamma_{18}/\Gamma$
<3	90	COAN 06	CLEO	4.12–4.2 $e^+e^- \rightarrow$ hadrons	

 $\Gamma(J/\psi K^+ K^-)/\Gamma_{\text{total}}$ 

VALUE (units $10^{-3}$ )	CL%	DOCUMENT ID	TECN	COMMENT	$\Gamma_{19}/\Gamma$
<2	90	COAN 06	CLEO	4.12–4.2 $e^+e^- \rightarrow$ hadrons	

 $\Gamma(J/\psi\eta)/\Gamma_{\text{total}}$ 

VALUE (units $10^{-3}$ )	CL%	DOCUMENT ID	TECN	COMMENT	$\Gamma_{20}/\Gamma$
<8	90	COAN 06	CLEO	4.12–4.2 $e^+e^- \rightarrow$ hadrons	
• • • We do not use the following data for averages, fits, limits, etc. • • •					
possibly seen		1 ABLIKIM 15L	BES3	$e^+e^- \rightarrow J/\psi\eta$	
seen		WANG 13B	BELL	$e^+e^- \rightarrow J/\psi\eta\gamma$	
<sup>1</sup> An enhancement around 4.2 GeV is observed.					

 $\Gamma(J/\psi\pi^0)/\Gamma_{\text{total}}$ 

VALUE (units $10^{-3}$ )	CL%	DOCUMENT ID	TECN	COMMENT	$\Gamma_{21}/\Gamma$
<1	90	COAN 06	CLEO	4.12–4.2 $e^+e^- \rightarrow$ hadrons	

 $\Gamma(J/\psi\eta)/\Gamma_{\text{total}}$ 

VALUE (units $10^{-3}$ )	CL%	DOCUMENT ID	TECN	COMMENT	$\Gamma_{22}/\Gamma$
<5	90	COAN 06	CLEO	4.12–4.2 $e^+e^- \rightarrow$ hadrons	

 $\Gamma(J/\psi\pi^+\pi^-\pi^0)/\Gamma_{\text{total}}$ 

VALUE (units $10^{-3}$ )	CL%	DOCUMENT ID	TECN	COMMENT	$\Gamma_{23}/\Gamma$
<1	90	COAN 06	CLEO	4.12–4.2 $e^+e^- \rightarrow$ hadrons	

 $\Gamma(\psi(2S)\pi^+\pi^-)/\Gamma_{\text{total}}$ 

VALUE (units $10^{-3}$ )	CL%	DOCUMENT ID	TECN	COMMENT	$\Gamma_{24}/\Gamma$
<4	90	COAN 06	CLEO	4.12–4.2 $e^+e^- \rightarrow$ hadrons	

 $\Gamma(\chi_{c1}\gamma)/\Gamma_{\text{total}}$ 

VALUE (units $10^{-3}$ )	CL%	DOCUMENT ID	TECN	COMMENT	$\Gamma_{25}/\Gamma$
<7	90	COAN 06	CLEO	4.12–4.2 $e^+e^- \rightarrow$ hadrons	
• • • We do not use the following data for averages, fits, limits, etc. • • •					

 $\Gamma(\chi_{c2}\gamma)/\Gamma_{\text{total}}$ 

VALUE (units $10^{-3}$ )	CL%	DOCUMENT ID	TECN	COMMENT	$\Gamma_{26}/\Gamma$
<13	90	COAN 06	CLEO	4.12–4.2 $e^+e^- \rightarrow$ hadrons	

 $\Gamma(\chi_{c1}\pi^+\pi^-\pi^0)/\Gamma_{\text{total}}$ 

VALUE (units $10^{-3}$ )	CL%	DOCUMENT ID	TECN	COMMENT	$\Gamma_{27}/\Gamma$
<2	90	COAN 06	CLEO	4.12–4.2 $e^+e^- \rightarrow$ hadrons	

 $\Gamma(\chi_{c2}\pi^+\pi^-\pi^0)/\Gamma_{\text{total}}$ 

VALUE (units $10^{-3}$ )	CL%	DOCUMENT ID	TECN	COMMENT	$\Gamma_{28}/\Gamma$
<8	90	COAN 06	CLEO	4.12–4.2 $e^+e^- \rightarrow$ hadrons	

 $\Gamma(h_c(1P)\pi^+\pi^-)/\Gamma_{\text{total}}$ 

VALUE (units $10^{-3}$ )	CL%	DOCUMENT ID	TECN	COMMENT	$\Gamma_{29}/\Gamma$
<5	90	1 PEDLAR 11	CLEO	$e^+e^- \rightarrow h_c(1P)\pi^+\pi^-$	
<sup>1</sup> At $\sqrt{s} = 4170$ MeV, PEDLAR 11 measures $\sigma(e^+e^- \rightarrow h_c(1P)\pi^+\pi^-) = 15.6 \pm 2.3 \pm 1.9 \pm 3.0$ pb, where the errors are statistical, systematic, and due to uncertainty in $B(\psi(2S) \rightarrow \pi^0 h_c(1P))$ , respectively.					

 $\Gamma(h_c(1P)\pi^0\pi^0)/\Gamma_{\text{total}}$ 

VALUE (units $10^{-3}$ )	CL%	DOCUMENT ID	TECN	COMMENT	$\Gamma_{30}/\Gamma$
<2	90	1 PEDLAR 11	CLEO	$e^+e^- \rightarrow h_c(1P)\pi^0\pi^0$	
<sup>1</sup> At $\sqrt{s} = 4170$ MeV, PEDLAR 11 measures $\sigma(e^+e^- \rightarrow h_c(1P)\pi^0\pi^0) = 3.0 \pm 3.3 \pm 1.1 \pm 0.6$ pb, where the errors are statistical, systematic, and due to uncertainty in $B(\psi(2S) \rightarrow \pi^0 h_c(1P))$ , respectively.					

 $\Gamma(h_c(1P)\eta)/\Gamma_{\text{total}}$ 

VALUE (units $10^{-3}$ )	CL%	EVTS	DOCUMENT ID	TECN	COMMENT	$\Gamma_{31}/\Gamma$
<2	90		1 PEDLAR 11	CLEO	$e^+e^- \rightarrow h_c(1P)\eta$	
• • • We do not use the following data for averages, fits, limits, etc. • • •						
possibly seen		41	2 ABLIKIM 17R	BES3	$e^+e^- \rightarrow h_c(1P)\eta$	
<sup>1</sup> At $\sqrt{s} = 4170$ MeV, PEDLAR 11 measures $\sigma(e^+e^- \rightarrow h_c(1P)\eta) = 4.7 \pm 1.7 \pm 1.0 \pm 0.9$ pb, where the errors are statistical, systematic, and due to uncertainty in $B(\psi(2S) \rightarrow \pi^0 h_c(1P))$ , respectively.						
<sup>2</sup> An enhancement around 4.2 GeV is observed.						

 $\Gamma(h_c(1P)\pi^0)/\Gamma_{\text{total}}$ 

VALUE (units $10^{-3}$ )	CL%	DOCUMENT ID	TECN	COMMENT	$\Gamma_{32}/\Gamma$
<0.4	90	1 PEDLAR 11	CLEO	$e^+e^- \rightarrow h_c(1P)\pi^0$	
<sup>1</sup> At $\sqrt{s} = 4170$ MeV, PEDLAR 11 measures $\sigma(e^+e^- \rightarrow h_c(1P)\pi^0) = -0.7 \pm 1.8 \pm 0.7 \pm 0.1$ pb, where the errors are statistical, systematic, and due to uncertainty in $B(\psi(2S) \rightarrow \pi^0 h_c(1P))$ , respectively.					

 $\Gamma(\phi\pi^+\pi^-)/\Gamma_{\text{total}}$ 

VALUE (units $10^{-3}$ )	CL%	DOCUMENT ID	TECN	COMMENT	$\Gamma_{33}/\Gamma$
<2	90	COAN 06	CLEO	4.12–4.2 $e^+e^- \rightarrow$ hadrons	



## Meson Particle Listings

 $\psi(4160)$ ,  $X(4160)$ ,  $Z_c(4200)$ ,  $\psi(4230)$ 

$\Gamma(\gamma\chi_{c1}(3872) \rightarrow \gamma J/\psi\pi^+\pi^-)/\Gamma_{\text{total}}$				$\Gamma_{34}/\Gamma$
VALUE	CL%	DOCUMENT ID	COMMENT	

$<0.68 \times 10^{-4}$  90 1 XIAO 13  $\psi(4160) \rightarrow \gamma J/\psi\pi^+\pi^-$   
<sup>1</sup> Obtained by analyzing CLEO data but not authored by the CLEO Collaboration.

$\Gamma(\gamma X(3915) \rightarrow \gamma J/\psi\pi^+\pi^-)/\Gamma_{\text{total}}$				$\Gamma_{35}/\Gamma$
VALUE	CL%	DOCUMENT ID	COMMENT	

$<1.36 \times 10^{-4}$  90 1 XIAO 13  $\psi(4160) \rightarrow \gamma J/\psi\pi^+\pi^-$   
<sup>1</sup> Obtained by analyzing CLEO data but not authored by the CLEO Collaboration.

$\Gamma(\gamma X(3930) \rightarrow \gamma J/\psi\pi^+\pi^-)/\Gamma_{\text{total}}$				$\Gamma_{36}/\Gamma$
VALUE	CL%	DOCUMENT ID	COMMENT	

$<1.18 \times 10^{-4}$  90 1 XIAO 13  $\psi(4160) \rightarrow \gamma J/\psi\pi^+\pi^-$   
<sup>1</sup> Obtained by analyzing CLEO data but not authored by the CLEO Collaboration.

$\Gamma(\gamma X(3940) \rightarrow \gamma J/\psi\pi^+\pi^-)/\Gamma_{\text{total}}$				$\Gamma_{37}/\Gamma$
VALUE	CL%	DOCUMENT ID	COMMENT	

$<1.47 \times 10^{-4}$  90 1 XIAO 13  $\psi(4160) \rightarrow \gamma J/\psi\pi^+\pi^-$   
<sup>1</sup> Obtained by analyzing CLEO data but not authored by the CLEO Collaboration.

$\Gamma(\gamma\chi_{c1}(3872) \rightarrow \gamma\gamma J/\psi)/\Gamma_{\text{total}}$				$\Gamma_{38}/\Gamma$
VALUE	CL%	DOCUMENT ID	COMMENT	

$<1.05 \times 10^{-4}$  90 1 XIAO 13  $\psi(4160) \rightarrow \gamma\gamma J/\psi$   
<sup>1</sup> Obtained by analyzing CLEO data but not authored by the CLEO Collaboration.

$\Gamma(\gamma X(3915) \rightarrow \gamma\gamma J/\psi)/\Gamma_{\text{total}}$				$\Gamma_{39}/\Gamma$
VALUE	CL%	DOCUMENT ID	COMMENT	

$<1.26 \times 10^{-4}$  90 1 XIAO 13  $\psi(4160) \rightarrow \gamma\gamma J/\psi$   
<sup>1</sup> Obtained by analyzing CLEO data but not authored by the CLEO Collaboration.

$\Gamma(\gamma X(3930) \rightarrow \gamma\gamma J/\psi)/\Gamma_{\text{total}}$				$\Gamma_{40}/\Gamma$
VALUE	CL%	DOCUMENT ID	COMMENT	

$<0.88 \times 10^{-4}$  90 1 XIAO 13  $\psi(4160) \rightarrow \gamma\gamma J/\psi$   
<sup>1</sup> Obtained by analyzing CLEO data but not authored by the CLEO Collaboration.

$\Gamma(\gamma X(3940) \rightarrow \gamma\gamma J/\psi)/\Gamma_{\text{total}}$				$\Gamma_{41}/\Gamma$
VALUE	CL%	DOCUMENT ID	COMMENT	

$<1.79 \times 10^{-4}$  90 1 XIAO 13  $\psi(4160) \rightarrow \gamma\gamma J/\psi$   
<sup>1</sup> Obtained by analyzing CLEO data but not authored by the CLEO Collaboration.

$\Gamma(K^+K^-)/\Gamma_{\text{total}}$				$\Gamma_{42}/\Gamma$
VALUE	CL%	DOCUMENT ID	TECN COMMENT	

• • • We do not use the following data for averages, fits, limits, etc. • • •  
 $<2 \times 10^{-5}$  90 1 DRUZHININ 15 RVUE  $e^+e^- \rightarrow \psi(3770)$

<sup>1</sup> DRUZHININ 15 uses BABAR and CLEO data takitaking into account interference of the processes  $e^+e^- \rightarrow K^+K^-$  and  $e^+e^- \rightarrow K_S^0 K_L^0$ .

 $\psi(4160)$  REFERENCES

ABLIKIM	20A	PR D101 012008	M. Ablikim et al.	(BESIII Collab.)
ABLIKIM	19AE	PR D99 072005	M. Ablikim et al.	(BESIII Collab.)
ZHUKOVA	18	PR D97 012002	V. Zhukova et al.	(BELLE Collab.)
ABLIKIM	17R	PR D96 012001	M. Ablikim et al.	(BESIII Collab.)
GAO	17	PR D95 092007	X.Y. Gao, C.P. Shen, C.Z. Yuan	(PDG Collab.)
PDG	16	CP C40 100001	C. Patrignani et al.	(BESIII Collab.)
ABLIKIM	15L	PR D91 112005	M. Ablikim et al.	(NOVO)
DRUZHININ	15	PR D92 054024	V.P. Druzhinin	(BESIII Collab.)
HAN	15	PR D92 012011	Y.L. Han et al.	(BELLE Collab.)
AAIJ	13BC	PRL 111 112003	R. Aaij et al.	(LHCb Collab.)
WANG	13B	PR D87 051101	X.L. Wang et al.	(BELLE Collab.)
XIAO	13	PR D87 057501	T. Xiao et al.	(NWES, WAYN)
PAKHOVA	11	PR D83 011101	G. Pakhlova et al.	(BELLE Collab.)
PEDLAR	11	PRL 107 041803	T. Pedlar et al.	(CLEO Collab.)
DEL-AMO-SA..	10N	PR D82 052004	P. del Amo Sanchez et al.	(BABAR Collab.)
MO	10	PR D82 077501	X.H. Mo, C.Z. Yuan, P. Wang	(BHEP)
AUBERT	09M	PR D79 092001	B. Aubert et al.	(BABAR Collab.)
CRONIN-HEN..	09	PR D80 072001	D. Cronin-Hennessy et al.	(CLEO Collab.)
PAKHOVA	09	PR D80 091101	G. Pakhlova et al.	(BELLE Collab.)
ABLIKIM	08D	PL B660 315	M. Ablikim et al.	(BES Collab.)
PAKHOVA	08	PR D77 011103	G. Pakhlova et al.	(BELLE Collab.)
PAKHOVA	08A	PRL 100 062001	G. Pakhlova et al.	(BELLE Collab.)
PAKHOVA	07	PRL 98 092001	G. Pakhlova et al.	(BELLE Collab.)
COAN	06	PRL 96 162003	T.E. Coan et al.	(CLEO Collab.)
SETH	05A	PR D72 017501	K.K. Seth	(CLEO Collab.)
BAI	02C	PRL 88 101802	J.Z. Bai et al.	(BES Collab.)
BAI	00	PRL 84 594	J.Z. Bai et al.	(BES Collab.)
OSTERHELD	86	SLAC-PUB-4160	A. Osterheld et al.	(SLAC Crystal Ball Collab.)
BRANDELIC	78C	PL 76B 361	R. Brandelik et al.	(DASP Collab.)

 $X(4160)$ 

$$I^G(J^{PC}) = ?^?(?^?)$$

OMITTED FROM SUMMARY TABLE

Seen by PAKHOVA 08 in  $e^+e^- \rightarrow J/\psi X$ ,  $X \rightarrow D^* \bar{D}^*$

 $X(4160)$  MASS

VALUE (MeV)	EVTS	DOCUMENT ID	TECN	COMMENT
$4156 \pm_{20}^{25} \pm 15$	24	PAKHLOV 08	BELL	$e^+e^- \rightarrow J/\psi X$

 $X(4160)$  WIDTH

VALUE (MeV)	EVTS	DOCUMENT ID	TECN	COMMENT
$139 \pm_{61}^{111} \pm 21$	24	PAKHLOV 08	BELL	$e^+e^- \rightarrow J/\psi X$

 $X(4160)$  DECAY MODES

Mode	Fraction ( $\Gamma_i/\Gamma$ )
$\Gamma_1$ $D \bar{D}$	not seen
$\Gamma_2$ $D^* \bar{D}^*$ + c.c.	not seen
$\Gamma_3$ $D^* \bar{D}^*$	seen

 $X(4160)$  BRANCHING RATIOS

$\Gamma(D \bar{D})/\Gamma(D^* \bar{D}^*)$				$\Gamma_1/\Gamma_3$
VALUE	CL%	DOCUMENT ID	TECN COMMENT	

$<0.09$  90 PAKHOVA 08 BELL  $e^+e^- \rightarrow J/\psi X$

$\Gamma(D^* \bar{D}^* + \text{c.c.})/\Gamma(D^* \bar{D}^*)$				$\Gamma_2/\Gamma_3$
VALUE	CL%	DOCUMENT ID	TECN COMMENT	

$<0.22$  90 PAKHOVA 08 BELL  $e^+e^- \rightarrow J/\psi X$

 $X(4160)$  REFERENCES

PAKHLOV 08 PRL 100 202001 P. Pakhlov et al. (BELLE Collab.)

 $Z_c(4200)$ 

$$I^G(J^{PC}) = 1^+(1^+ -)$$

$I, G, C$  need confirmation.

OMITTED FROM SUMMARY TABLE

was  $X(4200)^\pm$

This state shows properties different from a conventional  $q\bar{q}$  state. A candidate for an exotic structure. See the review on non- $q\bar{q}$  states.

Reported by CHILIKIN 14 in  $J/\psi\pi^+$  at a significance of  $6.2\sigma$ . Assignments of  $0^-, 1^-, 2^-$ , and  $2^+$  excluded at  $6.1\sigma, 7.4\sigma, 4.4\sigma$ , and  $7.0\sigma$  level, respectively. Needs confirmation.

 $Z_c(4200)$  MASS

VALUE (MeV)	DOCUMENT ID	TECN	COMMENT
$4196 \pm_{29}^{31} \pm 17$	CHILIKIN 14	BELL	$\bar{B}^0 \rightarrow J/\psi K^- \pi^+$

 $Z_c(4200)$  WIDTH

VALUE (MeV)	DOCUMENT ID	TECN	COMMENT
$370 \pm_{70}^{70} \pm 132$	CHILIKIN 14	BELL	$\bar{B}^0 \rightarrow J/\psi K^- \pi^+$

 $Z_c(4200)$  DECAY MODES

Mode	Fraction ( $\Gamma_i/\Gamma$ )
$\Gamma_1$ $J/\psi\pi^+$	seen

 $Z_c(4200)$  BRANCHING RATIOS

$\Gamma(J/\psi\pi^+)/\Gamma_{\text{total}}$				$\Gamma_1/\Gamma$
VALUE	DOCUMENT ID	TECN	COMMENT	

seen CHILIKIN 14 BELL  $\bar{B}^0 \rightarrow J/\psi K^- \pi^+$

• • • We do not use the following data for averages, fits, limits, etc. • • •  
 possibly seen <sup>1</sup> AAIJ 19R LHCb  $B^0 \rightarrow K^+ \pi^- J/\psi + \text{c.c.}$

<sup>1</sup> From a model-independent analysis.

 $Z_c(4200)$  REFERENCES

AAIJ 19R PRL 122 152002 R. Aaij et al. (LHCb Collab.)  
 CHILIKIN 14 PR D90 112009 K. Chilikin et al. (BELLE Collab.)

 $\psi(4230)$ 

$$I^G(J^{PC}) = 0^-(1^- -)$$

also known as  $Y(4230)$ ; was  $X(4230)$

The recent measurement of  $e^+e^- \rightarrow J/\psi\pi\pi$  (ABLIKIM 17B) led to a downward shift in the mass of the  $\psi(4260)$ , also known as  $Y(4260)$ , such that a distinction between the  $\psi(4260)$  and  $\psi(4230)$  no longer appears justified. Therefore, starting from this edition, we include the data of ABLIKIM 17B in this node and have listed the  $\psi(4230)$  in the summary tables instead of the  $\psi(4260)$ .

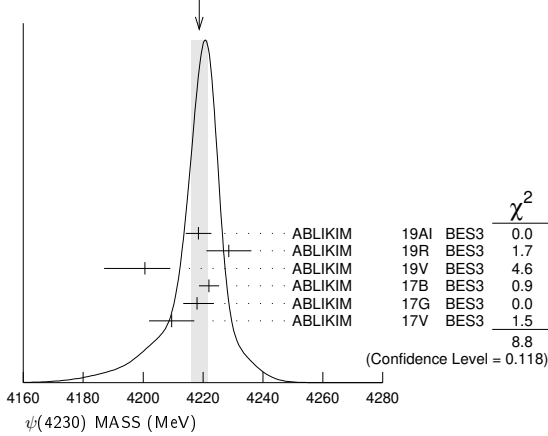
$\psi(4230)$

$\psi(4230)$  MASS

VALUE (MeV)	EVTS	DOCUMENT ID	TECN	COMMENT
<b>4220 ± 15</b>	<b>OUR ESTIMATE</b>			
<b>4218.7 ± 2.8</b>	<b>OUR AVERAGE</b>			Error includes scale factor of 1.3. See the ideogram below.
4218.5 ± 1.6 ± 4.0		<sup>1</sup> ABLIKIM	19A1 BES3	$e^+e^- \rightarrow \omega\chi_{c0}$
4228.6 ± 4.1 ± 6.3		ABLIKIM	19R BES3	$e^+e^- \rightarrow \pi^+D^0D^{*-} + c.c.$
4200.6 + 7.9 - 13.3 ± 3.0		<sup>2</sup> ABLIKIM	19V BES3	$e^+e^- \rightarrow \gamma\chi_{c1}(3872)$
4222.0 ± 3.1 ± 1.4		<sup>3</sup> ABLIKIM	17B BES3	$e^+e^- \rightarrow \pi^+\pi^-J/\psi$
4218 + 5.5 - 4.5 ± 0.9		ABLIKIM	17G BES3	$e^+e^- \rightarrow \pi^+\pi^-h_c$
4209.5 ± 7.4 ± 1.4		<sup>4</sup> ABLIKIM	17V BES3	$e^+e^- \rightarrow \pi^+\pi^-\psi(2S)$
4230 ± 8 ± 6	180	<sup>5</sup> ABLIKIM	15c BES3	$e^+e^- \rightarrow \omega\chi_{c0}$

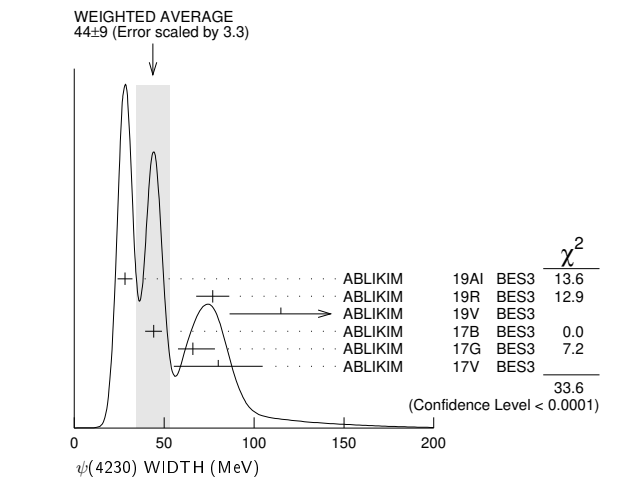
- <sup>1</sup> From a fit of the measured cross section from  $\sqrt{s} = 4.178\text{--}4.278$  GeV. Supersedes ABLIKIM 15c.
- <sup>2</sup> Simultaneous fit to  $\chi_{c1} \rightarrow \omega J/\psi$  and  $\chi_{c1} \rightarrow \pi^+\pi^-J/\psi$ .
- <sup>3</sup> From a three-resonance fit.
- <sup>4</sup> From a fit to the cross section for  $e^+e^- \rightarrow \pi^+\pi^-\psi(2S) \rightarrow 2(\pi^+\pi^-)\ell^+\ell^-$  obtained from 16 center-of-mass energies between 4.008 and 4.600 GeV and comprising 5.1 fb<sup>-1</sup>.
- <sup>5</sup> From a 3-parameter fit of measured cross sections from  $\sqrt{s} = 4.21\text{--}4.42$  GeV to a phase-space modified Breit-Wigner function, using the decays  $\chi_{c0} \rightarrow \pi^+\pi^-$ ,  $\chi_{c0} \rightarrow K^+K^-$ , and  $\omega \rightarrow \pi^+\pi^-\pi^0$ .

WEIGHTED AVERAGE  
4218.7 ± 2.8 (Error scaled by 1.3)



$\psi(4230)$  WIDTH

VALUE (MeV)	EVTS	DOCUMENT ID	TECN	COMMENT
<b>20 to 100</b>	<b>OUR ESTIMATE</b>			
<b>44 ± 9</b>	<b>OUR AVERAGE</b>			Error includes scale factor of 3.3. See the ideogram below.
28.2 ± 3.9 ± 1.6		<sup>1</sup> ABLIKIM	19A1 BES3	$e^+e^- \rightarrow \omega\chi_{c0}$
77.0 ± 6.8 ± 6.3		ABLIKIM	19R BES3	$e^+e^- \rightarrow \pi^+D^0D^{*-} + c.c.$
115 + 38 - 26 ± 12		<sup>2</sup> ABLIKIM	19V BES3	$e^+e^- \rightarrow \gamma\chi_{c1}(3872)$
44.1 ± 4.3 ± 2.0		<sup>3</sup> ABLIKIM	17B BES3	$e^+e^- \rightarrow \pi^+\pi^-J/\psi$
66.0 + 12.3 - 8.3 ± 0.4		ABLIKIM	17G BES3	$e^+e^- \rightarrow \pi^+\pi^-h_c$
80.1 ± 24.6 ± 2.9		<sup>4</sup> ABLIKIM	17V BES3	$e^+e^- \rightarrow \pi^+\pi^-\psi(2S)$
38 ± 12 ± 2	180	<sup>5</sup> ABLIKIM	15c BES3	$e^+e^- \rightarrow \omega\chi_{c0}$



- <sup>1</sup> From a fit of the measured cross section from  $\sqrt{s} = 4.178\text{--}4.278$  GeV. Supersedes ABLIKIM 15c.

- <sup>2</sup> Simultaneous fit to  $\chi_{c1} \rightarrow \omega J/\psi$  and  $\chi_{c1} \rightarrow \pi^+\pi^-J/\psi$ .
- <sup>3</sup> From a three-resonance fit.
- <sup>4</sup> From a fit to the cross section for  $e^+e^- \rightarrow \pi^+\pi^-\psi(2S) \rightarrow 2(\pi^+\pi^-)\ell^+\ell^-$  obtained from 16 center-of-mass energies between 4.008 and 4.600 GeV and comprising 5.1 fb<sup>-1</sup>.
- <sup>5</sup> From a 3-parameter fit of measured cross sections from  $\sqrt{s} = 4.21\text{--}4.42$  GeV to a phase-space modified Breit-Wigner function, using the decays  $\chi_{c0} \rightarrow \pi^+\pi^-$ ,  $\chi_{c0} \rightarrow K^+K^-$ , and  $\omega \rightarrow \pi^+\pi^-\pi^0$ .

$\psi(4230)$  DECAY MODES

Mode	Fraction ( $\Gamma_i/\Gamma$ )
$\Gamma_1$ $e^+e^-$	
$\Gamma_2$ $\omega\chi_{c0}$	seen
$\Gamma_3$ $\pi^+\pi^-h_c$	seen
$\Gamma_4$ $\pi^+\pi^-J/\psi$	seen
$\Gamma_5$ $\pi^+\pi^-\psi(2S)$	seen
$\Gamma_6$ $\pi^+D^0D^{*-} + c.c.$	seen
$\Gamma_7$ $\Xi^-\Xi^+$	
$\Gamma_8$ $\gamma\chi_{c1}(3872)$	seen

$\psi(4230)$   $\Gamma(i)\Gamma(e^+e^-)/\Gamma(\text{total})$

VALUE (eV)	EVTS	DOCUMENT ID	TECN	COMMENT	$\Gamma_2\Gamma_1/\Gamma$
<b>2.5 ± 0.2 ± 0.3</b>		<sup>1</sup> ABLIKIM	19A1 BES3	$e^+e^- \rightarrow \omega\chi_{c0}$	
2.7 ± 0.5 ± 0.4	180	<sup>2</sup> ABLIKIM	15c BES3	$e^+e^- \rightarrow \omega\chi_{c0}$	

- <sup>1</sup> From a fit of the measured cross section from  $\sqrt{s} = 4.178\text{--}4.278$  GeV. Supersedes ABLIKIM 15c.
- <sup>2</sup> From a 3-parameter fit of measured cross sections from  $\sqrt{s} = 4.21\text{--}4.42$  GeV to a phase-space modified Breit-Wigner function, using the decays  $\chi_{c0} \rightarrow \pi^+\pi^-$ ,  $\chi_{c0} \rightarrow K^+K^-$ , and  $\omega \rightarrow \pi^+\pi^-\pi^0$ .

$\Gamma(\pi^+\pi^-\psi(2S)) \times \Gamma(e^+e^-)/\Gamma(\text{total})$

VALUE (eV)	DOCUMENT ID	TECN	COMMENT	$\Gamma_5\Gamma_1/\Gamma$
1.6 ± 1.3	<sup>1</sup> ABLIKIM	19K BES3	$e^+e^- \rightarrow \pi^+\pi^-\psi(2S)$	
1.8 ± 1.4	<sup>2</sup> ABLIKIM	19K BES3	$e^+e^- \rightarrow \pi^+\pi^-\psi(2S)$	

- <sup>1</sup> Solution I of two equivalent solutions in a fit using two interfering resonances.
- <sup>2</sup> Solution II of two equivalent solutions in a fit using two interfering resonances.

$\Gamma(\Xi^-\Xi^+) \times \Gamma(e^+e^-)/\Gamma(\text{total})$

VALUE (eV)	CL%	DOCUMENT ID	TECN	COMMENT	$\Gamma_7\Gamma_1/\Gamma$
<b>&lt; 3.3 × 10<sup>-4</sup></b>	90	ABLIKIM	20c BES3	$e^+e^- \rightarrow \Xi^-\Xi^+$	

$\psi(4230)$  BRANCHING RATIOS

$\Gamma(\omega\chi_{c0})/\Gamma(\text{total})$

VALUE	EVTS	DOCUMENT ID	TECN	COMMENT	$\Gamma_2/\Gamma$
seen	180	<sup>1</sup> ABLIKIM	15c BES3	$e^+e^- \rightarrow \omega\chi_{c0}$	

- <sup>1</sup> From a 3-parameter fit of measured cross sections from  $\sqrt{s} = 4.21\text{--}4.42$  GeV to a phase-space modified Breit-Wigner function, using the decays  $\chi_{c0} \rightarrow \pi^+\pi^-$ ,  $\chi_{c0} \rightarrow K^+K^-$ , and  $\omega \rightarrow \pi^+\pi^-\pi^0$ .

$\Gamma(\pi^+\pi^-h_c)/\Gamma(\text{total})$

VALUE	DOCUMENT ID	TECN	COMMENT	$\Gamma_3/\Gamma$
seen	ABLIKIM	17G BES3	$e^+e^- \rightarrow \pi^+\pi^-h_c$	

$\Gamma(\pi^+\pi^-J/\psi)/\Gamma(\text{total})$

VALUE	DOCUMENT ID	TECN	COMMENT	$\Gamma_4/\Gamma$
seen	ABLIKIM	17B BES3	$e^+e^- \rightarrow \pi^+\pi^-J/\psi$	

$\Gamma(\pi^+\pi^-\psi(2S))/\Gamma(\text{total})$

VALUE	DOCUMENT ID	TECN	COMMENT	$\Gamma_5/\Gamma$
seen	<sup>1</sup> ABLIKIM	17V BES3	$e^+e^- \rightarrow \pi^+\pi^-\psi(2S)$	

- <sup>1</sup> From a fit to the cross section for  $e^+e^- \rightarrow \pi^+\pi^-\psi(2S) \rightarrow 2(\pi^+\pi^-)\ell^+\ell^-$  obtained from 16 center-of-mass energies between 4.008 and 4.600 GeV and comprising 5.1 fb<sup>-1</sup>.

$\Gamma(\pi^+D^0D^{*-} + c.c.)/\Gamma(\text{total})$

VALUE	DOCUMENT ID	TECN	COMMENT	$\Gamma_6/\Gamma$
seen	ABLIKIM	19R BES3	$e^+e^- \rightarrow \pi^+D^0D^{*-} + c.c.$	

$\Gamma(\gamma\chi_{c1}(3872))/\Gamma(\text{total})$

VALUE	DOCUMENT ID	TECN	COMMENT	$\Gamma_8/\Gamma$
seen	ABLIKIM	19V BES3	$e^+e^- \rightarrow \gamma\chi_{c1}(3872)$	

## Meson Particle Listings

 $\psi(4230)$ ,  $R_{c0}(4240)$ ,  $X(4250)^\pm$ ,  $\psi(4260)$  $\psi(4230)$  REFERENCES

ABLIKIM	20C	PRL 124 032002	M. Ablikim <i>et al.</i>	(BESIII Collab.)
ABLIKIM	19AI	PR D99 091103	M. Ablikim <i>et al.</i>	(BESIII Collab.)
ABLIKIM	19K	PR D99 019903 (err.)	M. Ablikim <i>et al.</i>	(BESIII Collab.)
ABLIKIM	19R	PRL 122 102002	M. Ablikim <i>et al.</i>	(BESIII Collab.)
ABLIKIM	19V	PRL 122 232002	M. Ablikim <i>et al.</i>	(BESIII Collab.)
ABLIKIM	17B	PRL 118 092001	M. Ablikim <i>et al.</i>	(BESIII Collab.)
ABLIKIM	17G	PRL 118 092002	M. Ablikim <i>et al.</i>	(BESIII Collab.)
ABLIKIM	17V	PR D96 032004	M. Ablikim <i>et al.</i>	(BESIII Collab.)
Also		PR D99 019903 (err.)	M. Ablikim <i>et al.</i>	(BESIII Collab.)
ABLIKIM	15C	PRL 114 092003	M. Ablikim <i>et al.</i>	(BESIII Collab.)

 **$R_{c0}(4240)$** 

$$I^G(J^{PC}) = 1^+(0^{- -})$$

$I, G, C$  need confirmation.

OMITTED FROM SUMMARY TABLE  
was  $X(4240)^\pm$

Properties incompatible with a  $q\bar{q}$  structure (exotic state). See the review on non- $q\bar{q}$  states.

Spin and parity assignment  $J^P = 0^-$  is favored over  $1^-, 2^-$ , and  $2^+$  by  $8\sigma$  and over  $1^+$  by  $1\sigma$ , according to the four-dimensional amplitude analysis of AAIJ 14AG.

 $R_{c0}(4240)$  MASS

VALUE (MeV)	DOCUMENT ID	TECN	COMMENT
$4239 \pm 18^{+45}_{-10}$	1 AAIJ	14AG LHCB	$B^0 \rightarrow K^+ \pi^- \psi(2S)$

<sup>1</sup> From a 4-dimensional analysis when a second, lower mass resonance is allowed in the  $Z_c(4430)$  fit, with significance  $6\sigma$  including systematic variations.

 $R_{c0}(4240)$  WIDTH

VALUE (MeV)	DOCUMENT ID	TECN	COMMENT
$220 \pm 47^{+108}_{-74}$	1 AAIJ	14AG LHCB	$B^0 \rightarrow K^+ \pi^- \psi(2S)$

<sup>1</sup> From a 4-dimensional analysis when a second, lower mass resonance is allowed in the  $Z_c(4430)$  fit, with significance  $6\sigma$  including systematic variations.

 $R_{c0}(4240)$  DECAY MODES

Mode	Fraction ( $\Gamma_i/\Gamma$ )
$\Gamma_1 \pi^- \psi(2S)$	seen

 $R_{c0}(4240)$  BRANCHING RATIOS

$\Gamma(\pi^- \psi(2S))/\Gamma_{\text{total}}$	$\Gamma_1/\Gamma$
seen	seen

<sup>1</sup> From a 4-dimensional analysis when a second, lower mass resonance is allowed in the  $Z_c(4430)$  fit. No partial branching fraction quoted.

 $R_{c0}(4240)$  REFERENCES

AAIJ	14AG PRL 112 222002	R. Aaij <i>et al.</i>	(LHCb Collab.)
------	---------------------	-----------------------	----------------

 **$X(4250)^\pm$** 

$$I^G(J^{PC}) = 1^-(?^{?+})$$

$I, G, C$  need confirmation.

OMITTED FROM SUMMARY TABLE

Properties incompatible with a  $q\bar{q}$  structure (exotic state). See the review on non- $q\bar{q}$  states.

Observed by MIZUK 08 in the  $\pi^+ \chi_{c1}(1P)$  invariant mass distribution in  $\bar{B}^0 \rightarrow K^- \pi^+ \chi_{c1}(1P)$  decays. Not seen by LEES 12B in this same mode after accounting for  $K\pi$  resonant mass and angular structure.

 $X(4250)^\pm$  MASS

VALUE (MeV)	DOCUMENT ID	TECN	COMMENT
$4248^{+44+180}_{-29-35}$	1 MIZUK	08 BELL	$\bar{B}^0 \rightarrow K^- \pi^+ \chi_{c1}(1P)$

<sup>1</sup> From a Dalitz plot analysis with two Breit-Wigner amplitudes.

 $X(4250)^\pm$  WIDTH

VALUE (MeV)	DOCUMENT ID	TECN	COMMENT
$177^{+54+316}_{-39-61}$	1 MIZUK	08 BELL	$\bar{B}^0 \rightarrow K^- \pi^+ \chi_{c1}(1P)$

<sup>1</sup> From a Dalitz plot analysis with two Breit-Wigner amplitudes.

 $X(4250)^\pm$  DECAY MODES

Mode	Fraction ( $\Gamma_i/\Gamma$ )
$\Gamma_1 \pi^+ \chi_{c1}(1P)$	seen

 $X(4250)^\pm$  BRANCHING RATIOS

$\Gamma(\pi^+ \chi_{c1}(1P))/\Gamma_{\text{total}}$	$\Gamma_1/\Gamma$
---	-------------------

VALUE	DOCUMENT ID	TECN	COMMENT
seen	1 MIZUK	08 BELL	$\bar{B}^0 \rightarrow K^- \pi^+ \chi_{c1}(1P)$

• • • We do not use the following data for averages, fits, limits, etc. • • •

not seen <sup>2</sup> LEES 12B BABR  $B \rightarrow K\pi\chi_{c1}(1P)$

<sup>1</sup> With a product branching fraction measurement of  $B(\bar{B}^0 \rightarrow K^- X(4250)^+) \times B(X(4250)^+ \rightarrow \pi^+ \chi_{c1}(1P)) = (4.0^{+2.3+19.7}_{-0.9-0.5}) \times 10^{-5}$ .

<sup>2</sup> With a product branching fraction limit of  $B(\bar{B}^0 \rightarrow X(4250)^+ K^-) \times B(X(4250)^+ \rightarrow \chi_{c1} \pi^+) < 4.0 \times 10^{-5}$  at 90% CL.

 $X(4250)^\pm$  REFERENCES

LEES	12B PR D85 052003	J.P. Lees <i>et al.</i>	(BABAR Collab.)
MIZUK	08 PR D78 072004	R. Mizuk <i>et al.</i>	(BELLE Collab.)

 **$\psi(4260)$** 

$$I^G(J^{PC}) = 0^-(1^{- -})$$

OMITTED FROM SUMMARY TABLE  
also known as  $Y(4260)$ ; was  $X(4260)$

The state  $\psi(4260)$  received its mass label from a Breit-Wigner (BW) fit to the  $J/\psi\pi\pi$  data listed below. The symmetric BW placed the mass unavoidably into the center of the distribution. The most recent measurement in the 4260 MeV mass range in the same channel (ABLIKIM 17B), however, revealed that the distribution is asymmetric and that the state has a much lower mass consistent with the entry for particle  $\psi(4230)$ . Thus, in this edition we merged the measurement of ABLIKIM 17B with the  $\psi(4230)$  node and labeled the older measurements of this node as not used. For details see the review on "Spectroscopy of mesons containing two heavy quarks."

 $\psi(4260)$  MASS

VALUE (MeV)	EVS	DOCUMENT ID	TECN	COMMENT
$4209.1 \pm 6.8 \pm 7.0$	1	ZHANG	17B RVUE	$e^+e^- \rightarrow \pi^+\pi^-\psi(2S)$
$4223.3 \pm 1.6 \pm 2.5$	2	ZHANG	17c RVUE	$e^+e^- \rightarrow \pi^+\pi^- J/\psi$ or $\psi(2S)$
$4258.6 \pm 8.3 \pm 12.1$	3	LIU	13B BELL	$e^+e^- \rightarrow \gamma\pi^+\pi^- J/\psi$
$4245 \pm 5 \pm 4$	4	LEES	12AC BABR	$10.58 e^+e^- \rightarrow \gamma\pi^+\pi^- J/\psi$
$4247 \pm 12^{+17}_{-32}$	3,5	YUAN	07 BELL	$10.58 e^+e^- \rightarrow \gamma\pi^+\pi^- J/\psi$
$4284^{+17}_{-16} \pm 413.6$	HE	06B CLEO	9.4-10.6	$e^+e^- \rightarrow \gamma\pi^+\pi^- J/\psi$
$4259 \pm 8 \pm 125$	6	AUBERT,B	05i BABR	$10.58 e^+e^- \rightarrow \gamma\pi^+\pi^- J/\psi$

<sup>1</sup> From a three-resonance fit.

<sup>2</sup> From a combined fit of BELLE, BABAR and BES3  $e^+e^- \rightarrow \pi^+\pi^- J/\psi$  and  $e^+e^- \rightarrow \pi^+\pi^-\psi(2S)$  data.

<sup>3</sup> From a two-resonance fit.

<sup>4</sup> From a single-resonance fit. Supersedes AUBERT,B 05i.

<sup>5</sup> Superseded by LIU 13B.

<sup>6</sup> From a single-resonance fit. Two interfering resonances are not excluded. Superseded by LEES 12AC.

 $\psi(4260)$  WIDTH

VALUE (MeV)	EVS	DOCUMENT ID	TECN	COMMENT
$76.6 \pm 14.2 \pm 2.4$	1	ZHANG	17B RVUE	$e^+e^- \rightarrow \pi^+\pi^-\psi(2S)$
$54.2 \pm 2.6 \pm 1.0$	2	ZHANG	17c RVUE	$e^+e^- \rightarrow \pi^+\pi^- J/\psi$ or $\psi(2S)$
$134.1 \pm 16.4 \pm 5.5$	3	LIU	13B BELL	$e^+e^- \rightarrow \gamma\pi^+\pi^- J/\psi$
$114^{+16}_{-15} \pm 7$	4	LEES	12AC BABR	$10.58 e^+e^- \rightarrow \gamma\pi^+\pi^- J/\psi$
$108 \pm 19 \pm 10$	3,5	YUAN	07 BELL	$10.58 e^+e^- \rightarrow \gamma\pi^+\pi^- J/\psi$
$73^{+39}_{-25} \pm 5$	13.6	HE	06B CLEO	9.4-10.6 $e^+e^- \rightarrow \gamma\pi^+\pi^- J/\psi$
$88 \pm 23 \pm 6^{+125}_{-4}$	6	AUBERT,B	05i BABR	$10.58 e^+e^- \rightarrow \gamma\pi^+\pi^- J/\psi$

<sup>1</sup> From a three-resonance fit.

<sup>2</sup> From a combined fit of BELLE, BABAR and BES3  $e^+e^- \rightarrow \pi^+\pi^- J/\psi$  and  $e^+e^- \rightarrow \pi^+\pi^-\psi(2S)$  data.

<sup>3</sup> From a two-resonance fit.

<sup>4</sup> From a single-resonance fit. Supersedes AUBERT,B 05i.

<sup>5</sup> Superseded by LIU 13B.

<sup>6</sup> From a single-resonance fit. Two interfering resonances are not excluded. Superseded by LEES 12AC.

$\psi(4260)$  DECAY MODES

Mode	Fraction ( $\Gamma_i/\Gamma$ )
$\Gamma_1$ $e^+ e^-$	
$\Gamma_2$ $J/\psi \pi^+ \pi^-$	seen
$\Gamma_3$ $J/\psi f_0(980), f_0(980) \rightarrow \pi^+ \pi^-$	seen
$\Gamma_4$ $Z_c(3900)^\pm \pi^\mp, Z_c^\pm \rightarrow J/\psi \pi^\pm$	seen
$\Gamma_5$ $J/\psi \pi^0 \pi^0$	seen
$\Gamma_6$ $J/\psi K^+ K^-$	seen
$\Gamma_7$ $J/\psi K_S^0 K_S^0$	not seen
$\Gamma_8$ $J/\psi \eta$	not seen
$\Gamma_9$ $J/\psi \pi^0$	not seen
$\Gamma_{10}$ $J/\psi \eta'$	not seen
$\Gamma_{11}$ $J/\psi \pi^+ \pi^- \pi^0$	not seen
$\Gamma_{12}$ $J/\psi \eta \pi^0$	not seen
$\Gamma_{13}$ $J/\psi \eta \eta$	not seen
$\Gamma_{14}$ $\psi(2S) \pi^+ \pi^-$	not seen
$\Gamma_{15}$ $\psi(2S) \eta$	not seen
$\Gamma_{16}$ $\chi_{c0} \omega$	not seen
$\Gamma_{17}$ $\chi_{c1} \pi^+ \pi^- \pi^0$	not seen
$\Gamma_{18}$ $\chi_{c2} \pi^+ \pi^- \pi^0$	not seen
$\Gamma_{19}$ $h_c(1P) \pi^+ \pi^-$	not seen
$\Gamma_{20}$ $\phi \pi^+ \pi^-$	not seen
$\Gamma_{21}$ $\phi f_0(980) \rightarrow \phi \pi^+ \pi^-$	not seen
$\Gamma_{22}$ $D \bar{D}$	not seen
$\Gamma_{23}$ $D^0 \bar{D}^0$	not seen
$\Gamma_{24}$ $D^+ D^-$	not seen
$\Gamma_{25}$ $D^* \bar{D} + c.c.$	not seen
$\Gamma_{26}$ $D^*(2007)^0 \bar{D}^0 + c.c.$	not seen
$\Gamma_{27}$ $D^*(2010)^+ D^- + c.c.$	not seen
$\Gamma_{28}$ $D^* \bar{D}^*$	not seen
$\Gamma_{29}$ $D^*(2007)^0 \bar{D}^*(2007)^0$	not seen
$\Gamma_{30}$ $D^*(2010)^+ D^*(2010)^-$	not seen
$\Gamma_{31}$ $D \bar{D} \pi + c.c.$	
$\Gamma_{32}$ $D^0 D^- \pi^+ + c.c. (excl. D^*(2007)^0 \bar{D}^{*0} + c.c., D^*(2010)^+ D^- + c.c.)$	not seen
$\Gamma_{33}$ $D \bar{D}^* \pi + c.c. (excl. D^* \bar{D}^*)$	not seen
$\Gamma_{34}$ $D^0 D^* \pi^+ + c.c. (excl. D^*(2010)^+ D^*(2010)^-)$	not seen
$\Gamma_{35}$ $D^0 D^*(2010)^- \pi^+ + c.c.$	not seen
$\Gamma_{36}$ $D_1(2420) \bar{D} + c.c.$	not seen
$\Gamma_{37}$ $D^* \bar{D}^* \pi$	not seen
$\Gamma_{38}$ $D_s^+ D_s^-$	not seen
$\Gamma_{39}$ $D_s^{*+} D_s^- + c.c.$	not seen
$\Gamma_{40}$ $D_s^{*+} D_s^{*-}$	not seen
$\Gamma_{41}$ $\rho \bar{\rho}$	not seen
$\Gamma_{42}$ $\rho \bar{\rho} \pi^0$	not seen
$\Gamma_{43}$ $\Xi^- \Xi^+$	
$\Gamma_{44}$ $K_S^0 K^\pm \pi^\mp$	not seen
$\Gamma_{45}$ $K_S^0 K^\pm \pi^\mp \pi^0$	
$\Gamma_{46}$ $K_S^0 K^\pm \pi^\mp \eta$	
$\Gamma_{47}$ $K^+ K^- \pi^0$	not seen

Radiative decays

$\Gamma_{48}$ $\eta_c(1S) \gamma$	possibly seen
$\Gamma_{49}$ $\chi_{c1} \gamma$	not seen
$\Gamma_{50}$ $\chi_{c2} \gamma$	not seen
$\Gamma_{51}$ $\chi_{c1}(3872) \gamma$	seen

$\psi(4260) \Gamma(i) \times \Gamma(e^+ e^-)/\Gamma(\text{total})$

$\Gamma(J/\psi \pi^+ \pi^-) \times \Gamma(e^+ e^-)/\Gamma(\text{total})$	$\Gamma_2 \Gamma_1/\Gamma$
VALUE (eV) EVTS DOCUMENT ID TECN COMMENT	
<b>9.2±1.0 OUR AVERAGE</b>	
9.2±0.8±0.7	<sup>1</sup> LEES 12AC BABR 10.58 $e^+ e^- \rightarrow \gamma \pi^+ \pi^- J/\psi$
8.9 <sup>+3.9</sup> <sub>-3.1</sub> ±1.8	8.1 HE 06B CLEO 9.4–10.6 $e^+ e^- \rightarrow \gamma \pi^+ \pi^- J/\psi$
••• We do not use the following data for averages, fits, limits, etc. •••	
6.4±0.8±0.6	<sup>2</sup> LIU 13B BELL $e^+ e^- \rightarrow \gamma \pi^+ \pi^- J/\psi$
20.5±1.4±2.0	<sup>3</sup> LIU 13B BELL $e^+ e^- \rightarrow \gamma \pi^+ \pi^- J/\psi$
6.0±1.2 <sup>+4.7</sup> <sub>-0.5</sub>	2.4 YUAN 07 BELL 10.58 $e^+ e^- \rightarrow \gamma \pi^+ \pi^- J/\psi$
20.6±2.3 <sup>+9.1</sup> <sub>-1.7</sub>	3.4 YUAN 07 BELL 10.58 $e^+ e^- \rightarrow \gamma \pi^+ \pi^- J/\psi$
5.5±1.0 <sup>+9.8</sup> <sub>-0.7</sub>	125 <sup>5</sup> AUBERT,B 05i BABR 10.58 $e^+ e^- \rightarrow \gamma \pi^+ \pi^- J/\psi$

<sup>1</sup> From a single-resonance fit. Supersedes AUBERT,B 05i.

<sup>2</sup> Solution I of two equivalent solutions in a fit using two interfering resonances.

<sup>3</sup> Solution II of two equivalent solutions in a fit using two interfering resonances.

<sup>4</sup> Superseded by LIU 13B.

<sup>5</sup> From a single-resonance fit. Two interfering resonances are not excluded. Superseded by LEES 12Ac.

$\Gamma(J/\psi K^+ K^-) \times \Gamma(e^+ e^-)/\Gamma(\text{total})$   $\Gamma_6 \Gamma_1/\Gamma$

VALUE (eV) CL% DOCUMENT ID TECN COMMENT	
<1.7 90 <sup>1</sup> SHEN 14 BELL 9.4–10.9 $e^+ e^- \rightarrow \gamma K^+ K^- J/\psi$	
••• We do not use the following data for averages, fits, limits, etc. •••	
<1.2 90 <sup>2</sup> YUAN 08 BELL $e^+ e^- \rightarrow \gamma K^+ K^- J/\psi$	

<sup>1</sup> From a fit of the broad  $K^+ K^- J/\psi$  enhancement including a coherent  $\psi(4260)$  amplitude with mass and width from LIU 13B. Supersedes YUAN 08. The shape of the cross section observed by ABLIKIM 18W between 2.2 and 2.3 GeV is incompatible with that of  $e^+ e^- \rightarrow \pi^+ \pi^- J/\psi$  in ABLIKIM 13T and ABLIKIM 17B. They also observe a broad enhancement around 2.5 GeV.

<sup>2</sup> From a fit of the broad  $K^+ K^- J/\psi$  enhancement including a coherent  $\psi(4260)$  amplitude with mass and width from YUAN 07.

$\Gamma(J/\psi K_S^0 K_S^0) \times \Gamma(e^+ e^-)/\Gamma(\text{total})$   $\Gamma_7 \Gamma_1/\Gamma$

VALUE (eV) CL% DOCUMENT ID TECN COMMENT
<0.85 90 <sup>1</sup> SHEN 14 BELL 9.4–10.9 $e^+ e^- \rightarrow \gamma K_S^0 K_S^0 J/\psi$

<sup>1</sup> From a fit of the  $K_S^0 K_S^0 J/\psi$  mass range from 4.4 to 5.5 GeV including a coherent  $\psi(4260)$  amplitude with mass and width from LIU 13B.

$\Gamma(J/\psi \eta) \times \Gamma(e^+ e^-)/\Gamma(\text{total})$   $\Gamma_8 \Gamma_1/\Gamma$

VALUE (eV) CL% DOCUMENT ID TECN COMMENT
<14.2 90 WANG 13B BELL $e^+ e^- \rightarrow J/\psi \eta \eta$

$\Gamma(J/\psi \eta') \times \Gamma(e^+ e^-)/\Gamma(\text{total})$   $\Gamma_{10} \Gamma_1/\Gamma$

VALUE (eV) EVTS DOCUMENT ID TECN COMMENT
0.06±0.03 46 <sup>1,2</sup> ABLIKIM 20A BES3 $e^+ e^- \rightarrow \eta' J/\psi$
1.38±0.11 46 <sup>1,3</sup> ABLIKIM 20A BES3 $e^+ e^- \rightarrow \eta' J/\psi$

<sup>1</sup> Based on a fit to  $\sigma(e^+ e^- \rightarrow \eta' J/\psi)$  from  $\sqrt{s} = 4.18$  to 4.60 GeV assuming interfering  $\psi(4160)$  and  $\psi(4260)$  contributions. At  $\sqrt{s} = 4.23$  GeV,  $\sigma(e^+ e^- \rightarrow \eta' J/\psi) = 3.6 \pm 0.6 \pm 0.3$  pb.

<sup>2</sup> Solution I of the fit, corresponding to a phase of  $-0.03 \pm 0.44$  rad.

<sup>3</sup> Solution II of the fit, corresponding to a phase of  $2.54 \pm 0.04$  rad.

$\Gamma(\psi(2S) \pi^+ \pi^-) \times \Gamma(e^+ e^-)/\Gamma(\text{total})$   $\Gamma_{14} \Gamma_1/\Gamma$

VALUE (eV) CL% DOCUMENT ID TECN COMMENT
<4.3 90 <sup>1</sup> LIU 08H RVUE 10.58 $e^+ e^- \rightarrow \psi(2S) \pi^+ \pi^- \gamma$
7.4 <sup>+2.1</sup> <sub>-1.7</sub> <sup>2</sup> LIU 08H RVUE 10.58 $e^+ e^- \rightarrow \psi(2S) \pi^+ \pi^- \gamma$

<sup>1</sup> For constructive interference with the  $\psi(4360)$  in a combined fit of AUBERT 07s and WANG 07b data with three resonances.

<sup>2</sup> For destructive interference with the  $\psi(4360)$  in a combined fit of AUBERT 07s and WANG 07b data with three resonances.

$\Gamma(\phi \pi^+ \pi^-) \times \Gamma(e^+ e^-)/\Gamma(\text{total})$   $\Gamma_{20} \Gamma_1/\Gamma$

VALUE (eV) CL% DOCUMENT ID TECN COMMENT
<0.4 90 AUBERT,BE 06d BABR 10.6 $e^+ e^- \rightarrow K^+ K^- \pi^+ \pi^- \gamma$

$\Gamma(\phi f_0(980) \rightarrow \phi \pi^+ \pi^-) \times \Gamma(e^+ e^-)/\Gamma(\text{total})$   $\Gamma_{21} \Gamma_1/\Gamma$

VALUE (eV) CL% DOCUMENT ID TECN COMMENT
<0.28 90 <sup>1</sup> AUBERT 07AK BABR 10.6 $e^+ e^- \rightarrow \pi^+ \pi^- K^+ K^- \gamma$

<sup>1</sup> AUBERT 07AK reports  $[\Gamma(\psi(4260) \rightarrow \phi f_0(980) \rightarrow \phi \pi^+ \pi^-) \times \Gamma(\psi(4260) \rightarrow e^+ e^-)/\Gamma(\text{total})] \times [B(\phi(1020) \rightarrow K^+ K^-)] < 0.14$  eV which we divide by our best value  $B(\phi(1020) \rightarrow K^+ K^-) = 49.2 \times 10^{-2}$ .

$\Gamma(\Xi^- \Xi^+) \times \Gamma(e^+ e^-)/\Gamma(\text{total})$   $\Gamma_{43} \Gamma_1/\Gamma$

VALUE (eV) CL% DOCUMENT ID TECN COMMENT
<2.7 × 10 <sup>-4</sup> 90 ABLIKIM 20c BES3 $e^+ e^- \rightarrow \Xi^- \Xi^+$

$\Gamma(K_S^0 K^\pm \pi^\mp) \times \Gamma(e^+ e^-)/\Gamma(\text{total})$   $\Gamma_{44} \Gamma_1/\Gamma$

VALUE (eV) DOCUMENT ID TECN COMMENT			
••• We do not use the following data for averages, fits, limits, etc. •••			
2.04 ± 0.19 ± 0.09	<sup>1</sup> ABLIKIM 19AE BES3 $e^+ e^- \rightarrow K_S^0 K^\pm \pi^\mp$		
0.0027 ± 0.0023 ± 0.0001	<sup>2</sup> ABLIKIM 19AE BES3 $e^+ e^- \rightarrow K_S^0 K^\pm \pi^\mp$		
< 0.5 at 90% CL	AUBERT 08s BABR 10.6 $e^+ e^- \rightarrow K_S^0 K^\pm \pi^\mp \gamma$		

<sup>1</sup> Solution I of the fit including the  $\psi(4160)$  with mass 4191 ± 5 MeV and width 70 ± 10 MeV from PDG 16 and the  $\psi(4230)$  with mass 4219.6 ± 3.3 ± 5.1 MeV and width 56.0 ± 3.6 ± 6.9 MeV from GAO 17.

<sup>2</sup> Solution II of the fit including the  $\psi(4160)$  with mass 4191 ± 5 MeV and width 70 ± 10 MeV from PDG 16 and the  $\psi(4230)$  with mass 4219.6 ± 3.3 ± 5.1 MeV and width 56.0 ± 3.6 ± 6.9 MeV from GAO 17.

## Meson Particle Listings

 $\psi(4260)$ 

$\Gamma(K_S^0 K^\pm \pi^\mp \pi^0) \times \Gamma(e^+ e^-)/\Gamma_{\text{total}}$					$\Gamma_{45}/\Gamma$
VALUE (eV)	CL%	DOCUMENT ID	TECN	COMMENT	
<0.05	90	ABLIKIM	19	BES3 $e^+ e^- \rightarrow K_S^0 K^\pm \pi^\mp \pi^0$	

$\Gamma(K_S^0 K^\pm \pi^\mp \eta) \times \Gamma(e^+ e^-)/\Gamma_{\text{total}}$					$\Gamma_{46}/\Gamma$
VALUE (eV)	CL%	DOCUMENT ID	TECN	COMMENT	
<0.19	90	ABLIKIM	19	BES3 $e^+ e^- \rightarrow K_S^0 K^\pm \pi^\mp \eta$	

$\Gamma(K^+ K^- \pi^0) \times \Gamma(e^+ e^-)/\Gamma_{\text{total}}$					$\Gamma_{47}/\Gamma$
VALUE (eV)	CL%	DOCUMENT ID	TECN	COMMENT	
<0.6	90	AUBERT	08s	BABR $10.6 e^+ e^- \rightarrow K^+ K^- \pi^0 \gamma$	
• • • We do not use the following data for averages, fits, limits, etc. • • •					

$\Gamma(\chi_{c1} \gamma) \times \Gamma(e^+ e^-)/\Gamma_{\text{total}}$					$\Gamma_{49}/\Gamma$
VALUE (eV)	CL%	DOCUMENT ID	TECN	COMMENT	
<1.4	90	<sup>1</sup> HAN	15	BELL $10.58 e^+ e^- \rightarrow \chi_{c1} \gamma$	
<sup>1</sup> Using $B(\eta \rightarrow \gamma\gamma) = (39.41 \pm 0.21)\%$ .					

$\Gamma(\chi_{c2} \gamma) \times \Gamma(e^+ e^-)/\Gamma_{\text{total}}$					$\Gamma_{50}/\Gamma$
VALUE (eV)	CL%	DOCUMENT ID	TECN	COMMENT	
<4.0	90	<sup>1</sup> HAN	15	BELL $10.58 e^+ e^- \rightarrow \chi_{c2} \gamma$	
<sup>1</sup> Using $B(\eta \rightarrow \gamma\gamma) = (39.41 \pm 0.21)\%$ .					

 $\psi(4260)$  BRANCHING RATIOS

$\Gamma(J/\psi f_0(980), f_0(980) \rightarrow \pi^+ \pi^-)/\Gamma(J/\psi \pi^+ \pi^-)$					$\Gamma_3/\Gamma_2$
VALUE	DOCUMENT ID	TECN	COMMENT		
0.17 ± 0.13	<sup>1</sup> LEES	12Ac	BABR	$10.58 e^+ e^- \rightarrow \gamma \pi^+ \pi^- J/\psi$	
<sup>1</sup> Systematic uncertainties not estimated.					

$\Gamma(Z_c(3900)^\pm \pi^\mp, Z_c^\pm \rightarrow J/\psi \pi^\pm)/\Gamma(J/\psi \pi^+ \pi^-)$					$\Gamma_4/\Gamma_2$
VALUE	DOCUMENT ID	TECN	COMMENT		
0.215 ± 0.033 ± 0.075	<sup>1</sup> ABLIKIM	13T	BES3	$e^+ e^- \rightarrow \pi^+ \pi^- J/\psi$	
• • • We do not use the following data for averages, fits, limits, etc. • • •					
0.29 ± 0.08	<sup>2</sup> LIU	13B	BELL	$e^+ e^- \rightarrow \gamma \pi^+ \pi^- J/\psi$	
<sup>1</sup> Assuming that the cross section of $e^+ e^- \rightarrow \pi^+ \pi^- J/\psi$ is fully due to the $\psi(4260)$ .					
<sup>2</sup> Systematic error not evaluated.					

$\Gamma(J/\psi K_S^0 K_S^0)/\Gamma_{\text{total}}$					$\Gamma_7/\Gamma$
VALUE	DOCUMENT ID	TECN	COMMENT		
not seen	SHEN	14	BELL	$9.4-10.9 e^+ e^- \rightarrow \gamma K_S^0 K_S^0 J/\psi$	

$\Gamma(J/\psi \eta \pi^0)/\Gamma_{\text{total}}$					$\Gamma_{12}/\Gamma$
VALUE	DOCUMENT ID	TECN	COMMENT		
not seen	ABLIKIM	15Q	BES3	$4.0-4.6 e^+ e^- \rightarrow J/\psi \eta \pi^0$	

$\Gamma(\psi(2S) \pi^+ \pi^-)/\Gamma(J/\psi \pi^+ \pi^-)$					$\Gamma_{14}/\Gamma_2$
VALUE	DOCUMENT ID	TECN	COMMENT		
(0.11 ± 0.03 ± 0.03) to (0.55 ± 0.18 ± 0.19)	<sup>1</sup> ZHANG	17c	RVUE	$e^+ e^- \rightarrow \pi^+ \pi^- J/\psi$ or $\psi(2S)$	
<sup>1</sup> From a combined fit of BELLE, BABAR and BES3 $e^+ e^- \rightarrow \pi^+ \pi^- J/\psi$ and $e^+ e^- \rightarrow \pi^+ \pi^- \psi(2S)$ data.					

$\Gamma(h_c(1P) \pi^+ \pi^-)/\Gamma(J/\psi \pi^+ \pi^-)$					$\Gamma_{19}/\Gamma_2$
VALUE	CL%	DOCUMENT ID	TECN	COMMENT	
<1.0	90	<sup>1</sup> PEDLAR	11	CLEO $e^+ e^- \rightarrow h_c(1P) \pi^+ \pi^-$	
<sup>1</sup> At $\sqrt{s} = 4260$ MeV, PEDLAR 11 measures $\sigma(e^+ e^- \rightarrow h_c(1P) \pi^+ \pi^-) = 32 \pm 17 \pm 6 \pm 6$ pb, where the errors are statistical, systematic, and due to uncertainty in $B(\psi(2S) \rightarrow \pi^0 h_c(1P))$ , respectively.					

$\Gamma(D\bar{D})/\Gamma(J/\psi \pi^+ \pi^-)$					$\Gamma_{22}/\Gamma_2$
VALUE	CL%	DOCUMENT ID	TECN	COMMENT	
<1.0	90	<sup>1</sup> AUBERT	07B	BABR $e^+ e^- \rightarrow D\bar{D} \gamma$	
• • • We do not use the following data for averages, fits, limits, etc. • • •					
<4.0	90	CRONIN-HEN..09	CLEO	$e^+ e^-$	
<sup>1</sup> Using 4259 ± 10 MeV for the mass and 88 ± 24 MeV for the width of $\psi(4260)$ .					

$\Gamma(D^0 \bar{D}^0)/\Gamma_{\text{total}}$					$\Gamma_{23}/\Gamma$
VALUE	DOCUMENT ID	TECN	COMMENT		
not seen	CRONIN-HEN..09	CLEO	$e^+ e^- \rightarrow D^0 \bar{D}^0$		
• • • We do not use the following data for averages, fits, limits, etc. • • •					
not seen	AUBERT	09M	BABR	$e^+ e^- \rightarrow D^0 \bar{D}^0 \gamma$	
not seen	PAKHLOVA	08	BELL	$e^+ e^- \rightarrow D^0 \bar{D}^0 \gamma$	

$\Gamma(D^+ D^-)/\Gamma_{\text{total}}$					$\Gamma_{24}/\Gamma$
VALUE	DOCUMENT ID	TECN	COMMENT		
not seen	CRONIN-HEN..09	CLEO	$e^+ e^- \rightarrow D^+ D^-$		
• • • We do not use the following data for averages, fits, limits, etc. • • •					
not seen	AUBERT	09M	BABR	$e^+ e^- \rightarrow D^+ D^- \gamma$	
not seen	PAKHLOVA	08	BELL	$e^+ e^- \rightarrow D^+ D^- \gamma$	

$\Gamma(D^* \bar{D} + c.c.)/\Gamma(J/\psi \pi^+ \pi^-)$					$\Gamma_{25}/\Gamma_2$
VALUE	CL%	DOCUMENT ID	TECN	COMMENT	
<34	90	AUBERT	09M	BABR $e^+ e^- \rightarrow \gamma D^* \bar{D}$	
• • • We do not use the following data for averages, fits, limits, etc. • • •					
<45	90	CRONIN-HEN..09	CLEO	$e^+ e^-$	

$\Gamma(D^*(2007)^0 \bar{D}^0 + c.c.)/\Gamma_{\text{total}}$					$\Gamma_{26}/\Gamma$
VALUE	DOCUMENT ID	TECN	COMMENT		
not seen	CRONIN-HEN..09	CLEO	$e^+ e^- \rightarrow D^{*0} \bar{D}^0$		
• • • We do not use the following data for averages, fits, limits, etc. • • •					
not seen	AUBERT	09M	BABR	$e^+ e^- \rightarrow D^{*0} \bar{D}^0 \gamma$	

$\Gamma(D^*(2010)^+ D^- + c.c.)/\Gamma_{\text{total}}$					$\Gamma_{27}/\Gamma$
VALUE	DOCUMENT ID	TECN	COMMENT		
not seen	CRONIN-HEN..09	CLEO	$e^+ e^- \rightarrow D^{*+} D^-$		
not seen	PAKHLOVA	07	BELL	$e^+ e^- \rightarrow D^{*+} D^- \gamma$	
• • • We do not use the following data for averages, fits, limits, etc. • • •					
not seen	AUBERT	09M	BABR	$e^+ e^- \rightarrow D^{*+} D^- \gamma$	

$\Gamma(D^* \bar{D}^*)/\Gamma(J/\psi \pi^+ \pi^-)$					$\Gamma_{28}/\Gamma_2$
VALUE	CL%	DOCUMENT ID	TECN	COMMENT	
<11	90	CRONIN-HEN..09	CLEO	$e^+ e^-$	
• • • We do not use the following data for averages, fits, limits, etc. • • •					
<40	90	AUBERT	09M	BABR $e^+ e^- \rightarrow \gamma D^* \bar{D}^*$	

$\Gamma(D^*(2007)^0 \bar{D}^*(2007)^0)/\Gamma_{\text{total}}$					$\Gamma_{29}/\Gamma$
VALUE	DOCUMENT ID	TECN	COMMENT		
not seen	CRONIN-HEN..09	CLEO	$e^+ e^- \rightarrow D^{*0} \bar{D}^{*0}$		
• • • We do not use the following data for averages, fits, limits, etc. • • •					
not seen	AUBERT	09M	BABR	$e^+ e^- \rightarrow D^{*0} \bar{D}^{*0} \gamma$	

$\Gamma(D^*(2010)^+ D^*(2010)^-)/\Gamma_{\text{total}}$					$\Gamma_{30}/\Gamma$
VALUE	DOCUMENT ID	TECN	COMMENT		
not seen	CRONIN-HEN..09	CLEO	$e^+ e^- \rightarrow D^{*+} D^{*-}$		
not seen	PAKHLOVA	07	BELL	$e^+ e^- \rightarrow D^{*+} D^{*-} \gamma$	
• • • We do not use the following data for averages, fits, limits, etc. • • •					
not seen	AUBERT	09M	BABR	$e^+ e^- \rightarrow D^{*+} D^{*-} \gamma$	

$\Gamma(D^0 D^- \pi^+ + c.c. (\text{excl. } D^*(2007)^0 \bar{D}^{*0} + c.c., D^*(2010)^+ D^- + c.c.))/\Gamma_{\text{total}}$					$\Gamma_{32}/\Gamma$
VALUE	DOCUMENT ID	TECN	COMMENT		
not seen	PAKHLOVA	08A	BELL	$10.6 e^+ e^- \rightarrow D^0 D^- \pi^+ \gamma$	

$\Gamma(D\bar{D}^* \pi + c.c. (\text{excl. } D^* \bar{D}^*))/\Gamma_{\text{total}}$					$\Gamma_{33}/\Gamma$
VALUE	DOCUMENT ID	TECN	COMMENT		
not seen	CRONIN-HEN..09	CLEO	$e^+ e^- \rightarrow D^* \bar{D} \pi$		

$\Gamma(D\bar{D}^* \pi + c.c. (\text{excl. } D^* \bar{D}^*))/\Gamma(J/\psi \pi^+ \pi^-)$					$\Gamma_{33}/\Gamma_2$
VALUE	CL%	DOCUMENT ID	TECN	COMMENT	
<15	90	CRONIN-HEN..09	CLEO	$e^+ e^-$	

$\Gamma(D^0 D^{*-} \pi^+ + c.c. (\text{excl. } D^*(2010)^+ D^*(2010)^-))/\Gamma_{\text{total}}$					$\Gamma_{34}/\Gamma$
VALUE	DOCUMENT ID	TECN	COMMENT		
not seen	PAKHLOVA	09	BELL	$e^+ e^- \rightarrow D^0 D^{*-} \pi^+ \gamma$	

$\Gamma(D^0 D^*(2010)^- \pi^+ + c.c.)/\Gamma(J/\psi \pi^+ \pi^-)$					$\Gamma_{35}/\Gamma_2$
VALUE	CL%	DOCUMENT ID	TECN	COMMENT	
<9	90	PAKHLOVA	09	BELL $e^+ e^- \rightarrow D^0 D^{*-} \pi^+$	

$\Gamma(D^0 D^*(2010)^- \pi^+ + c.c.)/\Gamma_{\text{total}} \times \Gamma(e^+ e^-)/\Gamma_{\text{total}}$					$\Gamma_{35}/\Gamma \times \Gamma_1/\Gamma$
VALUE	CL%	DOCUMENT ID	TECN	COMMENT	
<0.42 × 10 <sup>-6</sup>	90	<sup>1</sup> PAKHLOVA	09	BELL $e^+ e^- \rightarrow D^0 D^{*-} \pi^+$	
<sup>1</sup> Using 4263 <sup>+8</sup> / <sub>-9</sub> MeV for the mass of $\psi(4260)$ .					

$\Gamma(D^* \bar{D}^* \pi)/\Gamma_{\text{total}}$					$\Gamma_{37}/\Gamma$
VALUE	DOCUMENT ID	TECN	COMMENT		
not seen	CRONIN-HEN..09	CLEO	$e^+ e^- \rightarrow D^* \bar{D}^* \pi$		

$\Gamma(D^* \bar{D}^* \pi)/\Gamma(J/\psi \pi^+ \pi^-)$					$\Gamma_{37}/\Gamma_2$
VALUE	CL%	DOCUMENT ID	TECN	COMMENT	
<8.2	90	CRONIN-HEN..09	CLEO	$e^+ e^-$	

$\Gamma(D_1(2420)\bar{D} + c.c.)/\Gamma_{total}$   $\Gamma_{36}/\Gamma$

Table with columns: VALUE, DOCUMENT ID, TECN, COMMENT. Row 1: not seen, 1 ABLIKIM 19AR BES3 e+e- -> pi+pi-D D-bar. Includes a note about the measurement of sigma(e+e- -> D1(2420) D-bar + c.c.) between sqrt(s) = 4.3 and 4.6 GeV.

$\Gamma(D_s^+ D_s^-)/\Gamma_{total}$   $\Gamma_{38}/\Gamma$

Table with columns: VALUE, DOCUMENT ID, TECN, COMMENT. Row 1: not seen, DEL-AMO-SA...10N BABR e+e- -> D\_s^+ D\_s^- gamma. Row 2: not seen, CRONIN-HEN..09 CLEO e+e- -> D\_s^+ D\_s^-.

$\Gamma(D_s^+ D_s^-)/\Gamma(J/\psi\pi^+\pi^-)$   $\Gamma_{38}/\Gamma_2$

Table with columns: VALUE, CL%, DOCUMENT ID, TECN, COMMENT. Row 1: <0.7, 95, DEL-AMO-SA...10N BABR 10.6 e+e-.

$\Gamma(D_s^+ D_s^- + c.c.)/\Gamma_{total}$   $\Gamma_{39}/\Gamma$

Table with columns: VALUE, DOCUMENT ID, TECN, COMMENT. Row 1: not seen, DEL-AMO-SA...10N BABR e+e- -> D\_s^{\*+} D\_s^- gamma. Row 2: not seen, CRONIN-HEN..09 CLEO e+e- -> D\_s^{\*+} D\_s^-.

$\Gamma(D_s^{*+} D_s^- + c.c.)/\Gamma(J/\psi\pi^+\pi^-)$   $\Gamma_{39}/\Gamma_2$

Table with columns: VALUE, CL%, DOCUMENT ID, TECN, COMMENT. Row 1: <0.8, 90, CRONIN-HEN..09 CLEO e+e-.

$\Gamma(D_s^{*+} D_s^{*-})/\Gamma_{total}$   $\Gamma_{40}/\Gamma$

Table with columns: VALUE, DOCUMENT ID, TECN, COMMENT. Row 1: not seen, CRONIN-HEN..09 CLEO e+e- -> D\_s^{\*+} D\_s^{\*-}. Row 2: not seen, PAKHLOVA 11 BELL e+e- -> D\_s^{\*+} D\_s^{\*-} gamma.

$\Gamma(D_s^{*+} D_s^{*-})/\Gamma(J/\psi\pi^+\pi^-)$   $\Gamma_{40}/\Gamma_2$

Table with columns: VALUE, CL%, DOCUMENT ID, TECN, COMMENT. Row 1: <9.5, 90, CRONIN-HEN..09 CLEO e+e-.

$\Gamma(p\bar{p})/\Gamma(J/\psi\pi^+\pi^-)$   $\Gamma_{41}/\Gamma_2$

Table with columns: VALUE, CL%, DOCUMENT ID, TECN, COMMENT. Row 1: <0.13, 90, 1 AUBERT 06B BABR e+e- -> p p-bar gamma. Includes a note about using 4259 +/- 10 MeV for the mass and 88 +/- 24 MeV for the width of psi(4260).

$\Gamma(p\bar{p}\pi^0)/\Gamma(J/\psi\pi^+\pi^-)$   $\Gamma_{42}/\Gamma_2$

Table with columns: VALUE, CL%, DOCUMENT ID, TECN, COMMENT. Row 1: <2 x 10^-4, 90, ABLIKIM 17F BES3 e+e- -> psi(4260) -> hadrons.

Radiative decays

$\Gamma(\eta_c(1S)\gamma)/\Gamma_{total}$   $\Gamma_{48}/\Gamma$

Table with columns: VALUE, DOCUMENT ID, COMMENT. Row 1: possibly seen, 1 ABLIKIM 17W e+e- -> gamma eta\_c(1S). Includes a note about significance ranges from 4.2 sigma to as low as 1.5 sigma for a flat component plus psi(4260) spectrum. Needs confirmation.

$\Gamma(\chi_{c1}(3872)\gamma)/\Gamma_{total}$   $\Gamma_{51}/\Gamma$

Table with columns: VALUE, EVTS, DOCUMENT ID, TECN, COMMENT. Row 1: seen, 20 +/- 5, ABLIKIM 14 BES3 e+e- -> J/psi pi+ pi- gamma.

psi(4260) REFERENCES

Table of references for psi(4260) with columns: AUTHOR, YEAR, JOURNAL, COMMENT. Includes entries for ABLIKIM, GAO, ZHANG, HAN, SHEN, etc.

Table of references for chi\_c1(4274) with columns: AUTHOR, YEAR, JOURNAL, COMMENT. Includes entries for ABLIKIM, LIU, WANG, LEES, PAKHLOVA, PEDLAR, etc.

chi\_c1(4274)  $I^G(J^{PC}) = 0^+(1^{++})$

was X(4274) This state shows properties different from a conventional q q-bar state. A candidate for an exotic structure. See the review on non-q q-bar states.

Seen by AAIJ 17C in B+ -> chi\_c1 K+, chi\_c1 -> J/psi phi using an amplitude analysis of B+ -> J/psi phi K+ with a significance (accounting for systematic uncertainties) of 6.0 sigma.

chi\_c1(4274) MASS

Table with columns: VALUE (MeV), EVTS, DOCUMENT ID, TECN, COMMENT. Row 1: 4274 +/- 8/-6 OUR AVERAGE. Row 2: 4273.3 +/- 8.3 +/- 17.2/-3.6, 4289, 1 AAIJ 17c LHCB B+ -> J/psi phi K+.

1 From an amplitude analysis of the decay B+ -> J/psi phi K+ with a significance of 6.0 sigma. 2 From a fit to the invariant mass spectrum with a significance of 3.1 sigma.

chi\_c1(4274) WIDTH

Table with columns: VALUE (MeV), EVTS, DOCUMENT ID, TECN, COMMENT. Row 1: 49 +/- 12 OUR AVERAGE. Row 2: 56 +/- 11 +/- 8/-11, 4289, 1 AAIJ 17c LHCB B+ -> J/psi phi K+.

1 From an amplitude analysis of the decay B+ -> J/psi phi K+ with a significance of 6.0 sigma. 2 From a fit to the invariant mass spectrum with a significance of 3.1 sigma.

chi\_c1(4274) DECAY MODES

Table with columns: Mode, Fraction (Gamma\_i/Gamma). Row 1: Gamma\_1 J/psi phi, seen.

chi\_c1(4274) BRANCHING RATIOS

Table with columns: Gamma(J/psi phi)/Gamma\_total, EVTS, DOCUMENT ID, TECN, COMMENT, Gamma\_i/Gamma. Row 1: seen, 4289, 1 AAIJ 17c LHCB B+ -> J/psi phi K+.

1 From an amplitude analysis of the decay B+ -> J/psi phi K+ with a significance of 6.0 sigma.

chi\_c1(4274) REFERENCES

Table of references for chi\_c1(4274) with columns: AUTHOR, YEAR, JOURNAL, COMMENT. Includes entries for AAIJ, AALTONEN, etc.

X(4350)  $I^G(J^{PC}) = 0^+(?^{?+})$

OMITTED FROM SUMMARY TABLE Seen by SHEN 10 in the gamma gamma -> J/psi phi. Needs confirmation.

X(4350) MASS

Table with columns: VALUE (MeV), EVTS, DOCUMENT ID, TECN, COMMENT. Row 1: 4350.6 +/- 4.6 +/- 5.1 +/- 0.7, 8.8 +/- 4.2/-3.2, 1 SHEN 10 BELL 10.6 e+e- -> e+e- J/psi phi.

1 Statistical significance of 3.2 sigma.

# Meson Particle Listings

## X(4350), $\psi(4360)$

### X(4350) WIDTH

VALUE (MeV)	EVTs	DOCUMENT ID	TECN	COMMENT
$13^{+18}_{-9} \pm 4$	$8.8^{+4.2}_{-3.2}$	1 SHEN	10 BELL	$10.6 e^+ e^- \rightarrow e^+ e^- J/\psi \phi$

<sup>1</sup> Statistical significance of 3.2  $\sigma$ .

### X(4350) DECAY MODES

Mode	Fraction ( $\Gamma_i/\Gamma$ )
$\Gamma_1$ $J/\psi \phi$	seen
$\Gamma_2$ $\gamma \gamma$	seen

### X(4350) $\Gamma(i)\Gamma(\gamma\gamma)/\Gamma(\text{total})$

VALUE (eV)	EVTs	DOCUMENT ID	TECN	COMMENT	$\Gamma_2\Gamma_1/\Gamma$
$6.7^{+3.2}_{-2.4} \pm 1.1$	$8.8^{+4.2}_{-3.2}$	1 SHEN	10 BELL	$10.6 e^+ e^- \rightarrow e^+ e^- J/\psi \phi$	

• • • We do not use the following data for averages, fits, limits, etc. • • •

$1.5^{+0.7}_{-0.6} \pm 0.3$	$8.8^{+4.2}_{-3.2}$	2 SHEN	10 BELL	$10.6 e^+ e^- \rightarrow e^+ e^- J/\psi \phi$	
-----------------------------	---------------------	--------	---------	--	--

<sup>1</sup> For  $J^P = 0^+$ . Statistical significance of 3.2  $\sigma$ .  
<sup>2</sup> For  $J^P = 2^+$ . Statistical significance of 3.2  $\sigma$ .

### X(4350) BRANCHING RATIOS

$\Gamma(J/\psi\phi)/\Gamma_{\text{total}}$	VALUE	DOCUMENT ID	TECN	COMMENT	$\Gamma_1/\Gamma$
seen		1 SHEN	10 BELL	$10.6 e^+ e^- \rightarrow e^+ e^- J/\psi \phi$	

<sup>1</sup> Statistical significance of 3.2  $\sigma$ .

$\Gamma(\gamma\gamma)/\Gamma_{\text{total}}$	VALUE	DOCUMENT ID	TECN	COMMENT	$\Gamma_2/\Gamma$
seen		1 SHEN	10 BELL	$10.6 e^+ e^- \rightarrow e^+ e^- J/\psi \phi$	

<sup>1</sup> Statistical significance of 3.2  $\sigma$ .

### X(4350) REFERENCES

SHEN 10 PRL 104 112004 C.P. Shen et al. (BELLE Collab.)

$$\psi(4360) \quad I^G(J^{PC}) = 0^-(1^{--})$$

also known as  $Y(4360)$ ; was X(4360)

This state shows properties different from a conventional  $q\bar{q}$  state. A candidate for an exotic structure. See the review on non- $q\bar{q}$  states.

Seen in radiative return from  $e^+ e^-$  collisions at  $\sqrt{s} = 9.54\text{--}10.58$  GeV by AUBERT 07s, WANG 07D, and LEES 14F. See also the review on "Spectroscopy of mesons containing two heavy quarks."

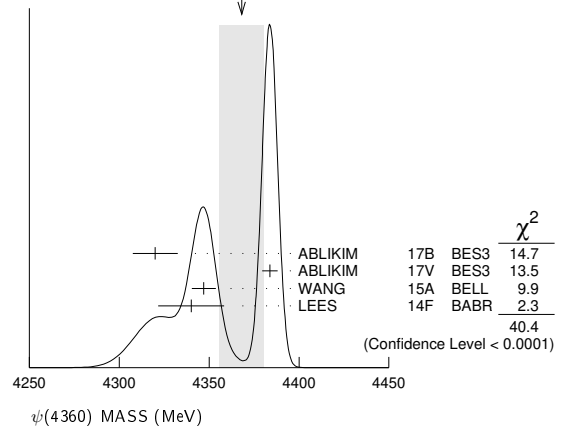
### $\psi(4360)$ MASS

VALUE (MeV)	EVTs	DOCUMENT ID	TECN	COMMENT
<b>4368 <math>\pm</math> 13 OUR AVERAGE</b>				Error includes scale factor of 3.7. See the ideogram below.
$4320.0 \pm 10.4 \pm 7.0$		1 ABLIKIM 17B BES3		$e^+ e^- \rightarrow \pi^+ \pi^- J/\psi$
$4383.8 \pm 4.2 \pm 0.8$		2 ABLIKIM 17V BES3		$e^+ e^- \rightarrow \pi^+ \pi^- \psi(2S)$
$4347 \pm 6 \pm 3$	279	3 WANG 15A BELL		$10.58 e^+ e^- \rightarrow \gamma \pi^+ \pi^- \psi(2S)$
$4340 \pm 16 \pm 9$	37	4 LEES 14F BABR		$10.58 e^+ e^- \rightarrow \gamma \pi^+ \pi^- \psi(2S)$
$4383.7 \pm 2.9 \pm 6.2$		5 ZHANG 17B RVUE		$e^+ e^- \rightarrow \pi^+ \pi^- \psi(2S)$
$4386.4 \pm 2.1 \pm 6.4$		6 ZHANG 17C RVUE		$e^+ e^- \rightarrow \pi^+ \pi^- J/\psi$ or $\psi(2S)$
$4355^{+9}_{-10} \pm 9$	74	7 LIU 08H RVUE		$10.58 e^+ e^- \rightarrow \gamma \pi^+ \pi^- \psi(2S)$
$4324 \pm 24$		8 AUBERT 07s BABR		$10.58 e^+ e^- \rightarrow \gamma \pi^+ \pi^- \psi(2S)$
$4361 \pm 9 \pm 9$	47	4 WANG 07D BELL		$10.58 e^+ e^- \rightarrow \gamma \pi^+ \pi^- \psi(2S)$

• • • We do not use the following data for averages, fits, limits, etc. • • •

<sup>1</sup> From a three-resonance fit.  
<sup>2</sup> From a fit to the cross section for  $e^+ e^- \rightarrow \pi^+ \pi^- \psi(2S) \rightarrow 2(\pi^+ \pi^-) \ell^+ \ell^-$  obtained from 16 center-of-mass energies between 4.008 and 4.600 GeV and comprising 5.1 fb<sup>-1</sup>.  
<sup>3</sup> From a two-resonance fit. Supersedes WANG 07D.  
<sup>4</sup> From a two-resonance fit.  
<sup>5</sup> From a three-resonance fit.  
<sup>6</sup> From a combined fit of BELLE, BABAR and BES3  $e^+ e^- \rightarrow \pi^+ \pi^- J/\psi$  and  $e^+ e^- \rightarrow \pi^+ \pi^- \psi(2S)$  data.  
<sup>7</sup> From a combined fit of AUBERT 07s and WANG 07D data with two resonances.  
<sup>8</sup> From a single-resonance fit. Systematic errors not estimated.

WEIGHTED AVERAGE  
4368 $\pm$ 13 (Error scaled by 3.7)



### $\psi(4360)$ WIDTH

VALUE (MeV)	EVTs	DOCUMENT ID	TECN	COMMENT
<b>96 <math>\pm</math> 7 OUR AVERAGE</b>				
$101.4^{+25.3}_{-19.7} \pm 10.2$		1 ABLIKIM 17B BES3		$e^+ e^- \rightarrow \pi^+ \pi^- J/\psi$
$84.2 \pm 12.5 \pm 2.1$		2 ABLIKIM 17V BES3		$e^+ e^- \rightarrow \pi^+ \pi^- \psi(2S)$
$103 \pm 9 \pm 5$	279	3 WANG 15A BELL		$10.58 e^+ e^- \rightarrow \gamma \pi^+ \pi^- \psi(2S)$
$94 \pm 32 \pm 13$	37	4 LEES 14F BABR		$10.58 e^+ e^- \rightarrow \gamma \pi^+ \pi^- \psi(2S)$
$94.2 \pm 7.3 \pm 2.0$		5 ZHANG 17B RVUE		$e^+ e^- \rightarrow \pi^+ \pi^- \psi(2S)$
$96.0 \pm 6.7 \pm 2.7$		6 ZHANG 17C RVUE		$e^+ e^- \rightarrow \pi^+ \pi^- J/\psi$ or $\psi(2S)$
$103^{+17}_{-15} \pm 11$	74	7 LIU 08H RVUE		$10.58 e^+ e^- \rightarrow \gamma \pi^+ \pi^- \psi(2S)$
$172 \pm 33$		8 AUBERT 07s BABR		$10.58 e^+ e^- \rightarrow \gamma \pi^+ \pi^- \psi(2S)$
$74 \pm 15 \pm 10$	47	4 WANG 07D BELL		$10.58 e^+ e^- \rightarrow \gamma \pi^+ \pi^- \psi(2S)$

• • • We do not use the following data for averages, fits, limits, etc. • • •

<sup>1</sup> From a three-resonance fit.  
<sup>2</sup> From a fit to the cross section for  $e^+ e^- \rightarrow \pi^+ \pi^- \psi(2S) \rightarrow 2(\pi^+ \pi^-) \ell^+ \ell^-$  obtained from 16 center-of-mass energies between 4.008 and 4.600 GeV and comprising 5.1 fb<sup>-1</sup>.  
<sup>3</sup> From a two-resonance fit. Supersedes WANG 07D.  
<sup>4</sup> From a two-resonance fit.  
<sup>5</sup> From a three-resonance fit.  
<sup>6</sup> From a combined fit of BELLE, BABAR and BES3  $e^+ e^- \rightarrow \pi^+ \pi^- J/\psi$  and  $e^+ e^- \rightarrow \pi^+ \pi^- \psi(2S)$  data.  
<sup>7</sup> From a combined fit of AUBERT 07s and WANG 07D data with two resonances.  
<sup>8</sup> From a single-resonance fit. Systematic errors not estimated.

### $\psi(4360)$ DECAY MODES

Mode	Fraction ( $\Gamma_i/\Gamma$ )
$\Gamma_1$ $e^+ e^-$	
$\Gamma_2$ $J/\psi \pi^+ \pi^-$	
$\Gamma_3$ $\psi(2S) \pi^+ \pi^-$	seen
$\Gamma_4$ $\psi_2(3823) \pi^+ \pi^-$	possibly seen
$\Gamma_5$ $J/\psi \eta$	
$\Gamma_6$ $D^0 D^{*-} \pi^+$	
$\Gamma_7$ $D_1(2420) \bar{D}^+ + \text{c.c.}$	possibly seen
$\Gamma_8$ $\chi_{c1} \gamma$	
$\Gamma_9$ $\chi_{c2} \gamma$	

### $\psi(4360)$ $\Gamma(i) \times \Gamma(e^+ e^-)/\Gamma(\text{total})$

$\Gamma(\psi(2S)\pi^+\pi^-) \times \Gamma(e^+ e^-)/\Gamma_{\text{total}}$	VALUE (eV)	EVTs	DOCUMENT ID	TECN	COMMENT	$\Gamma_3\Gamma_1/\Gamma$
	$7.3 \pm 2.8$		1 ABLIKIM 19K BES3		$e^+ e^- \rightarrow \pi^+ \pi^- \psi(2S)$	
	$11.0 \pm 3.8$		2 ABLIKIM 19K BES3		$e^+ e^- \rightarrow \pi^+ \pi^- \psi(2S)$	
	$9.2 \pm 0.6 \pm 0.6$	279	3 WANG 15A BELL		$10.58 e^+ e^- \rightarrow \gamma \pi^+ \pi^- \psi(2S)$	
	$10.9 \pm 0.6 \pm 0.7$	279	4 WANG 15A BELL		$10.58 e^+ e^- \rightarrow \gamma \pi^+ \pi^- \psi(2S)$	
	$6.0 \pm 1.0 \pm 0.5$	37	1 LEES 14F BABR		$10.58 e^+ e^- \rightarrow \gamma \pi^+ \pi^- \psi(2S)$	
	$7.2 \pm 1.0 \pm 0.6$	37	2 LEES 14F BABR		$10.58 e^+ e^- \rightarrow \gamma \pi^+ \pi^- \psi(2S)$	
	$11.1^{+1.3}_{-1.2}$	74	5 LIU 08H RVUE		$10.58 e^+ e^- \rightarrow \gamma \pi^+ \pi^- \psi(2S)$	

• • • We do not use the following data for averages, fits, limits, etc. • • •

See key on page 999

# Meson Particle Listings

## $\psi(4360), \psi(4390), \psi(4415)$

12.3±1.2	74	<sup>6</sup> LIU	08H RVUE	10.58 $e^+e^- \rightarrow \gamma\pi^+\pi^-\psi(2S)$
10.4±1.7±1.5	47	<sup>1</sup> WANG	07D BELL	10.58 $e^+e^- \rightarrow \gamma\pi^+\pi^-\psi(2S)$
11.8±1.8±1.4	47	<sup>2</sup> WANG	07D BELL	10.58 $e^+e^- \rightarrow \gamma\pi^+\pi^-\psi(2S)$

- Solution I of two equivalent solutions in a fit using two interfering resonances.
- Solution II of two equivalent solutions in a fit using two interfering resonances.
- Solution I of two equivalent solutions from a fit using two interfering resonances. Supercedes WANG 07D.
- Solution II of two equivalent solutions from a fit using two interfering resonances. Supercedes WANG 07D.
- Solution I in a combined fit of AUBERT 07s and WANG 07D data with two resonances.
- Solution II in a combined fit of AUBERT 07s and WANG 07D data with two resonances.

$\Gamma(J/\psi\eta) \times \Gamma(e^+e^-)/\Gamma_{total}$		$\Gamma_5\Gamma_1/\Gamma$		
VALUE (eV)	CL%	DOCUMENT ID	TECN	COMMENT

• • • We do not use the following data for averages, fits, limits, etc. • • •  
 <6.8 90 WANG 13B BELL  $e^+e^- \rightarrow J/\psi\eta\gamma$

$\Gamma(\chi_{c1}\gamma) \times \Gamma(e^+e^-)/\Gamma_{total}$		$\Gamma_8\Gamma_1/\Gamma$		
VALUE (eV)	CL%	DOCUMENT ID	TECN	COMMENT

<0.57 90 <sup>1</sup>HAN 15 BELL  $10.58 e^+e^- \rightarrow \chi_{c1}\gamma$   
<sup>1</sup>Using  $B(\eta \rightarrow \gamma\gamma) = (39.41 \pm 0.21)\%$ .

$\Gamma(\chi_{c2}\gamma) \times \Gamma(e^+e^-)/\Gamma_{total}$		$\Gamma_9\Gamma_1/\Gamma$		
VALUE (eV)	CL%	DOCUMENT ID	TECN	COMMENT

<1.9 90 <sup>1</sup>HAN 15 BELL  $10.58 e^+e^- \rightarrow \chi_{c2}\gamma$   
<sup>1</sup>Using  $B(\eta \rightarrow \gamma\gamma) = (39.41 \pm 0.21)\%$ .

### $\psi(4360)$ BRANCHING RATIOS

$\Gamma(D^0 D^{*-} \pi^+)/\Gamma(\psi(2S)\pi^+\pi^-)$		$\Gamma_6/\Gamma_3$		
VALUE	CL%	DOCUMENT ID	TECN	COMMENT

<8 90 PAKHLOVA 09 BELL  $e^+e^- \rightarrow \psi(4360) \rightarrow D^0 D^{*-} \pi^+$

$\Gamma(\psi(2S)\pi^+\pi^-)/\Gamma_{total}$		$\Gamma_3/\Gamma$		
VALUE	DOCUMENT ID	TECN	COMMENT	

seen <sup>1</sup>ABLIKIM 17V BES3  $e^+e^- \rightarrow \pi^+\pi^-\psi(2S)$   
<sup>1</sup>From a fit to the cross section for  $e^+e^- \rightarrow \pi^+\pi^-\psi(2S) \rightarrow 2(\pi^+\pi^-)\ell^+\ell^-$  obtained from 16 center-of-mass energies between 4.008 and 4.600 GeV and comprising 5.1 fb<sup>-1</sup>.

$\Gamma(\psi(2S)\pi^+\pi^-)/\Gamma(J/\psi\pi^+\pi^-)$		$\Gamma_3/\Gamma_2$		
VALUE	DOCUMENT ID	TECN	COMMENT	

• • • We do not use the following data for averages, fits, limits, etc. • • •  
 (0.81 ± 0.12 ± 0.13) to (42 ± 15 ± 15) <sup>1</sup>ZHANG 17C RVUE  $e^+e^- \rightarrow \pi^+\pi^-J/\psi$  or  $\psi(2S)$

<sup>1</sup>From a combined fit of BELLE, BABAR and BES3  $e^+e^- \rightarrow \pi^+\pi^-J/\psi$  and  $e^+e^- \rightarrow \pi^+\pi^-\psi(2S)$  data.

$\Gamma(\psi_2(3823)\pi^+\pi^-)/\Gamma_{total}$		$\Gamma_4/\Gamma$		
VALUE	DOCUMENT ID	TECN	COMMENT	

possibly seen 19 <sup>1</sup>ABLIKIM 15S BES3  $e^+e^- \rightarrow \pi^+\pi^-\chi_{c1}\gamma$   
<sup>1</sup>From a fit of  $e^+e^- \rightarrow \pi^+\pi^-\psi_2(3823), \psi_2(3823) \rightarrow \chi_{c1}\gamma$  cross sections taken at  $\sqrt{s}$  values of 4.23, 4.26, 4.36, 4.42, and 4.60 GeV to the  $\psi(4360)$  line shape.

$\Gamma(D^0 D^{*-} \pi^+)/\Gamma_{total} \times \Gamma(e^+e^-)/\Gamma_{total}$		$\Gamma_6/\Gamma \times \Gamma_1/\Gamma$		
VALUE	CL%	DOCUMENT ID	TECN	COMMENT

<0.72 × 10<sup>-6</sup> 90 <sup>1</sup>PAKHOVA 09 BELL  $e^+e^- \rightarrow \psi(4360) \rightarrow D^0 D^{*-} \pi^+$

<sup>1</sup>Using 4355<sup>+9</sup><sub>-10</sub> ± 9 MeV for the mass of  $\psi(4360)$ .

$\Gamma(D_1(2420)\bar{D} + c.c.)/\Gamma_{total}$		$\Gamma_7/\Gamma$		
VALUE	DOCUMENT ID	TECN	COMMENT	

possibly seen <sup>1</sup>ABLIKIM 19AR BES3  $e^+e^- \rightarrow \pi^+\pi^-D\bar{D}$   
<sup>1</sup>Evidence for  $e^+e^- \rightarrow D_1(2420)\bar{D} + c.c.$  between  $\sqrt{s} = 4.3$  and 4.6 GeV, not necessarily resonant.

### $\psi(4360)$ REFERENCES

ABLIKIM 19AR PR D100 032005	M. Ablikim et al.	(BESIII Collab.)
ABLIKIM 19K PR D99 019903 (errata.)	M. Ablikim et al.	(BESIII Collab.)
ABLIKIM 17B PRL 118 092001	M. Ablikim et al.	(BESIII Collab.)
ABLIKIM 17V PR D96 032004	M. Ablikim et al.	(BESIII Collab.)
Also PR D99 019903 (errata.)	M. Ablikim et al.	(BESIII Collab.)
ZHANG 17B PR D96 054008	J. Zhang, J. Zhang	
ZHANG 17C EPJ C77 727	J. Zhang, L. Yuan	
ABLIKIM 15S PRL 115 011803	M. Ablikim et al.	(BESIII Collab.)
HAN 15 PR D92 012011	Y.L. Han et al.	(BELLE Collab.)
WANG 15A PR D91 112007	X.L. Wang et al.	(BELLE Collab.)
LEES 14F PR D89 111103	J.P. Lees et al.	(BABAR Collab.)
WANG 13B PR D87 051101	X.L. Wang et al.	(BELLE Collab.)
PAKHOVA 09 PR D80 091101	G. Pakhlova et al.	(BELLE Collab.)
LIU 08H PR D78 014032	Z.Q. Liu, X.S. Qin, C.Z. Yuan	
AUBERT 07S PRL 98 212001	B. Aubert et al.	(BABAR Collab.)
WANG 07D PRL 99 142002	X.L. Wang et al.	(BELLE Collab.)

## $\psi(4390)$

$I^G(J^{PC}) = 0^-(1^{--})$   
 I needs confirmation.

OMITTED FROM SUMMARY TABLE  
 was X(4390)

This state shows properties different from a conventional  $q\bar{q}$  state. A candidate for an exotic structure. See the review on non- $q\bar{q}$  states.

### $\psi(4390)$ MASS

VALUE (MeV)	DOCUMENT ID	TECN	COMMENT
-------------	-------------	------	---------

4391.5<sup>+6.3</sup><sub>-6.8</sub> ± 1.0 ABLIKIM 17G BES3  $e^+e^- \rightarrow \pi^+\pi^-h_c$

### $\psi(4390)$ WIDTH

VALUE (MeV)	DOCUMENT ID	TECN	COMMENT
-------------	-------------	------	---------

139.5<sup>+16.2</sup><sub>-20.6</sub> ± 0.6 ABLIKIM 17G BES3  $e^+e^- \rightarrow \pi^+\pi^-h_c$

### $\psi(4390)$ DECAY MODES

Mode	Fraction ( $\Gamma_i/\Gamma$ )
------	--------------------------------

$\Gamma_1$   $\pi^+\pi^-h_c$  seen  
 $\Gamma_2$   $\pi^+\pi^-\psi(3770)$  possibly seen

### $\psi(4390)$ BRANCHING RATIOS

$\Gamma(\pi^+\pi^-h_c)/\Gamma_{total}$		$\Gamma_1/\Gamma$		
VALUE	DOCUMENT ID	TECN	COMMENT	

seen ABLIKIM 17G BES3  $e^+e^- \rightarrow \pi^+\pi^-h_c$

$\Gamma(\pi^+\pi^-\psi(3770))/\Gamma_{total}$		$\Gamma_2/\Gamma$		
VALUE	DOCUMENT ID	TECN	COMMENT	

possibly seen <sup>1</sup>ABLIKIM 19AR BES3  $e^+e^- \rightarrow \pi^+\pi^-D\bar{D}$   
<sup>1</sup>Observe  $e^+e^- \rightarrow \pi^+\pi^-\psi(3770)$  at  $\sqrt{s} = 4.26, 4.36, \text{ and } 4.42$  GeV but cannot establish if continuum or resonant.

### $\psi(4390)$ REFERENCES

ABLIKIM 19AR PR D100 032005	M. Ablikim et al.	(BESIII Collab.)
ABLIKIM 17G PRL 118 092002	M. Ablikim et al.	(BESIII Collab.)

## $\psi(4415)$

$I^G(J^{PC}) = 0^-(1^{--})$

### $\psi(4415)$ MASS

VALUE (MeV)	DOCUMENT ID	TECN	COMMENT
-------------	-------------	------	---------

4421 ± 4 OUR ESTIMATE  
 4415.1 ± 7.9 <sup>1</sup>ABLIKIM 08D BES2  $e^+e^- \rightarrow$  hadrons

• • • We do not use the following data for averages, fits, limits, etc. • • •  
 4412 ± 15 <sup>2</sup>MO 10 RVUE  $e^+e^- \rightarrow$  hadrons  
 4411 ± 7 <sup>3</sup>PAKHOVA 08A BELL  $10.6 e^+e^- \rightarrow D^0 D^- \pi^+ \gamma$   
 4425 ± 6 <sup>4</sup>SETH 05A RVUE  $e^+e^- \rightarrow$  hadrons  
 4429 ± 9 <sup>5</sup>SETH 05A RVUE  $e^+e^- \rightarrow$  hadrons  
 4417 ± 10 BRANDELIC 78C DASP  $e^+e^-$   
 4414 ± 7 SIEGRIST 76 MRK1  $e^+e^-$

- Reanalysis of data presented in BAI 02c. From a global fit over the center-of-mass energy region 3.7–5.0 GeV covering the  $\psi(3770), \psi(4160), \text{ and } \psi(4415)$  resonances. Phase angle fixed in the fit to  $\delta = (234 \pm 88)^\circ$ .
- Reanalysis of data presented in BAI 00 and BAI 02c. From a global fit over the center-of-mass energy 3.8–4.8 GeV covering the  $\psi(4040), \psi(4160)$  and  $\psi(4415)$  resonances and including interference effects.
- Systematic uncertainties not estimated.
- From a fit to Crystal Ball (OSTERHELD 86) data.
- From a fit to BES (BAI 02c) data.

### $\psi(4415)$ WIDTH

VALUE (MeV)	DOCUMENT ID	TECN	COMMENT
-------------	-------------	------	---------

62 ± 20 OUR ESTIMATE  
 71.5 ± 19.0 <sup>6</sup>ABLIKIM 08D BES2  $e^+e^- \rightarrow$  hadrons

• • • We do not use the following data for averages, fits, limits, etc. • • •  
 118 ± 32 <sup>7</sup>MO 10 RVUE  $e^+e^- \rightarrow$  hadrons  
 77 ± 20 <sup>8</sup>PAKHOVA 08A BELL  $10.6 e^+e^- \rightarrow D^0 D^- \pi^+ \gamma$   
 119 ± 16 <sup>9</sup>SETH 05A RVUE  $e^+e^- \rightarrow$  hadrons  
 118 ± 35 <sup>10</sup>SETH 05A RVUE  $e^+e^- \rightarrow$  hadrons  
 66 ± 15 BRANDELIC 78C DASP  $e^+e^-$



# Meson Particle Listings

## $\psi(4415)$

33 ±10 SIEGRIST 76 MRK1  $e^+e^-$

<sup>6</sup> Reanalysis of data presented in BAI 02c. From a global fit over the center-of-mass energy region 3.7–5.0 GeV covering the  $\psi(3770)$ ,  $\psi(4040)$ ,  $\psi(4160)$ , and  $\psi(4415)$  resonances. Phase angle fixed in the fit to  $\delta = (234 \pm 88)^\circ$ .

<sup>7</sup> Reanalysis of data presented in BAI 00 and BAI 02c. From a global fit over the center-of-mass energy 3.8–4.8 GeV covering the  $\psi(4040)$ ,  $\psi(4160)$  and  $\psi(4415)$  resonances and including interference effects.

<sup>8</sup> Systematic uncertainties not estimated.

<sup>9</sup> From a fit to Crystal Ball (OSTERHELD 86) data.

<sup>10</sup> From a fit to BES (BAI 02c) data.

### $\psi(4415)$ DECAY MODES

Due to the complexity of the  $c\bar{c}$  threshold region, in this listing, “seen” (“not seen”) means that a cross section for the mode in question has been measured at effective  $\sqrt{s}$  near this particle’s central mass value, more (less) than  $2\sigma$  above zero, without regard to any peaking behavior in  $\sqrt{s}$  or absence thereof. See mode listing(s) for details and references.

Mode	Fraction ( $\Gamma_i/\Gamma$ )	Confidence level
$\Gamma_1$ $D\bar{D}$	seen	
$\Gamma_2$ $D^0\bar{D}^0$	seen	
$\Gamma_3$ $D^+D^-$	seen	
$\Gamma_4$ $D^*\bar{D} + c.c.$	seen	
$\Gamma_5$ $D^*(2007)^0\bar{D}^0 + c.c.$	seen	
$\Gamma_6$ $D^*(2010)^+D^- + c.c.$	seen	
$\Gamma_7$ $D^*\bar{D}^*$	seen	
$\Gamma_8$ $D^*(2007)^0\bar{D}^*(2007)^0 + c.c.$	seen	
$\Gamma_9$ $D^*(2010)^+D^*(2010)^- + c.c.$	seen	
$\Gamma_{10}$ $D^0D^-\pi^+$ (excl. $D^*(2007)^0\bar{D}^0$ + c.c., $D^*(2010)^+D^- + c.c.$ )	< 2.3 %	90%
$\Gamma_{11}$ $D\bar{D}_2^*(2460) \rightarrow D^0D^-\pi^+ + c.c.$	(10 ± 4) %	
$\Gamma_{12}$ $D^0\bar{D}^*\pi^+ + c.c.$	< 11 %	90%
$\Gamma_{13}$ $D_1(2420)\bar{D} + c.c.$	possibly seen	
$\Gamma_{14}$ $D_s^+D_s^-$	not seen	
$\Gamma_{15}$ $\omega\chi_{c2}$	possibly seen	
$\Gamma_{16}$ $D_s^{*+}D_s^- + c.c.$	seen	
$\Gamma_{17}$ $D_s^+D_s^{*-}$	not seen	
$\Gamma_{18}$ $\psi_2(3823)\pi^+\pi^-$	possibly seen	
$\Gamma_{19}$ $\psi(3770)\pi^+\pi^-$	possibly seen	
$\Gamma_{20}$ $J/\psi\eta$	< 6 × 10 <sup>-3</sup>	90%
$\Gamma_{21}$ $\chi_{c1}\gamma$	< 8 × 10 <sup>-4</sup>	90%
$\Gamma_{22}$ $\chi_{c2}\gamma$	< 4 × 10 <sup>-3</sup>	90%
$\Gamma_{23}$ $e^+e^-$	(9.4 ± 3.2) × 10 <sup>-6</sup>	

### $\psi(4415)$ PARTIAL WIDTHS

$\Gamma(e^+e^-)$	$\Gamma_{23}$
VALUE (keV)	DOCUMENT ID TECN COMMENT
<b>0.58 ± 0.07 OUR ESTIMATE</b>	
<b>0.35 ± 0.12</b>	11 ABLIKIM 08D BES2 $e^+e^- \rightarrow$ hadrons
• • • We do not use the following data for averages, fits, limits, etc. • • •	
0.4 to 0.8	12 MO 10 RVUE $e^+e^- \rightarrow$ hadrons
0.72 ± 0.11	13 SETH 05A RVUE $e^+e^- \rightarrow$ hadrons
0.64 ± 0.23	14 SETH 05A RVUE $e^+e^- \rightarrow$ hadrons
0.49 ± 0.13	BRANDELIK 78C DASP $e^+e^-$
0.44 ± 0.14	SIEGRIST 76 MRK1 $e^+e^-$

<sup>11</sup> Reanalysis of data presented in BAI 00 and BAI 02c. From a global fit over the center-of-mass energy region 3.7–5.0 GeV covering the  $\psi(3770)$ ,  $\psi(4040)$ ,  $\psi(4160)$ , and  $\psi(4415)$  resonances. Phase angle fixed in the fit to  $\delta = (234 \pm 88)^\circ$ .

<sup>12</sup> Reanalysis of data presented in BAI 00 and BAI 02c. From a global fit over the center-of-mass energy 3.8–4.8 GeV covering the  $\psi(4040)$ ,  $\psi(4160)$  and  $\psi(4415)$  resonances and including interference effects. Four sets of solutions are obtained with the same fit quality, mass and total width, but with different  $e^+e^-$  partial widths. We quote only the range of values.

<sup>13</sup> From a fit to Crystal Ball (OSTERHELD 86) data.

<sup>14</sup> From a fit to BES (BAI 02c) data.

### $\psi(4415)$ $\Gamma(i) \times \Gamma(e^+e^-)/\Gamma(\text{total})$

$\Gamma(J/\psi\eta) \times \Gamma(e^+e^-)/\Gamma_{\text{total}}$	$\Gamma_{20}\Gamma_{23}/\Gamma$
VALUE (eV) CL%	DOCUMENT ID TECN COMMENT
<b>&lt;3.6</b>	90 WANG 13B BELL $e^+e^- \rightarrow J/\psi\eta\gamma$

$\Gamma(\chi_{c1}\gamma) \times \Gamma(e^+e^-)/\Gamma_{\text{total}}$	$\Gamma_{21}\Gamma_{23}/\Gamma$
VALUE (eV) CL%	DOCUMENT ID TECN COMMENT
<b>&lt;0.47</b>	90 15 HAN 15 BELL 10.58 $e^+e^- \rightarrow \chi_{c1}\gamma$

<sup>15</sup> Using  $B(\eta \rightarrow \gamma\gamma) = (39.41 \pm 0.21)\%$ .

$\Gamma(\chi_{c2}\gamma) \times \Gamma(e^+e^-)/\Gamma_{\text{total}}$	$\Gamma_{22}\Gamma_{23}/\Gamma$
VALUE (eV) CL%	DOCUMENT ID TECN COMMENT
<b>&lt;2.3</b>	90 16 HAN 15 BELL 10.58 $e^+e^- \rightarrow \chi_{c2}\gamma$

<sup>16</sup> Using  $B(\eta \rightarrow \gamma\gamma) = (39.41 \pm 0.21)\%$ .

### $\psi(4415)$ BRANCHING RATIOS

$\Gamma(D^0\bar{D}^0)/\Gamma_{\text{total}}$	$\Gamma_2/\Gamma$
VALUE	DOCUMENT ID TECN COMMENT
seen	PAKHLOVA 08 BELL $e^+e^- \rightarrow D^0\bar{D}^0\gamma$
• • • We do not use the following data for averages, fits, limits, etc. • • •	
not seen	AUBERT 09M BABR $e^+e^- \rightarrow D^0\bar{D}^0\gamma$

$\Gamma(D^+D^-)/\Gamma_{\text{total}}$	$\Gamma_3/\Gamma$
VALUE	DOCUMENT ID TECN COMMENT
seen	PAKHLOVA 08 BELL $e^+e^- \rightarrow D^+D^-\gamma$
• • • We do not use the following data for averages, fits, limits, etc. • • •	
not seen	AUBERT 09M BABR $e^+e^- \rightarrow D^+D^-\gamma$

$\Gamma(D\bar{D})/\Gamma(D^*\bar{D}^*)$	$\Gamma_1/\Gamma_7$
VALUE	DOCUMENT ID TECN COMMENT
<b>0.14 ± 0.12 ± 0.03</b>	AUBERT 09M BABR $e^+e^- \rightarrow \gamma D^{(*)}\bar{D}^{(*)}$

$\Gamma(D^*(2007)^0\bar{D}^0 + c.c.)/\Gamma_{\text{total}}$	$\Gamma_5/\Gamma$
VALUE	DOCUMENT ID TECN COMMENT
seen	AUBERT 09M BABR $e^+e^- \rightarrow D^{*0}\bar{D}^0\gamma$

$\Gamma(D^*(2010)^+D^- + c.c.)/\Gamma_{\text{total}}$	$\Gamma_6/\Gamma$
VALUE	DOCUMENT ID TECN COMMENT
seen	17 ZHUKOVA 18 BELL $e^+e^- \rightarrow D^{*+}D^-\gamma$
seen	AUBERT 09M BABR $e^+e^- \rightarrow D^{*+}D^-\gamma$
• • • We do not use the following data for averages, fits, limits, etc. • • •	
seen	PAKHLOVA 07 BELL $e^+e^- \rightarrow D^{*+}D^-\gamma$

<sup>17</sup> Supersedes PAKHLOVA 07.

$\Gamma(D^*\bar{D} + c.c.)/\Gamma(D^*\bar{D}^*)$	$\Gamma_4/\Gamma_7$
VALUE	DOCUMENT ID TECN COMMENT
<b>0.17 ± 0.25 ± 0.03</b>	AUBERT 09M BABR $e^+e^- \rightarrow \gamma D^{(*)}\bar{D}^{(*)}$

$\Gamma(D^*(2007)^0\bar{D}^*(2007)^0 + c.c.)/\Gamma_{\text{total}}$	$\Gamma_8/\Gamma$
VALUE	DOCUMENT ID TECN COMMENT
seen	AUBERT 09M BABR $e^+e^- \rightarrow D^{*0}\bar{D}^{*0}\gamma$

$\Gamma(D^*(2010)^+D^*(2010)^- + c.c.)/\Gamma_{\text{total}}$	$\Gamma_9/\Gamma$
VALUE	DOCUMENT ID TECN COMMENT
seen	18 ZHUKOVA 18 BELL $e^+e^- \rightarrow D^{*+}D^{*-}\gamma$
seen	AUBERT 09M BABR $e^+e^- \rightarrow D^{*+}D^{*-}\gamma$
• • • We do not use the following data for averages, fits, limits, etc. • • •	
seen	PAKHLOVA 07 BELL $e^+e^- \rightarrow D^{*+}D^{*-}\gamma$

<sup>18</sup> Supersedes PAKHLOVA 07.

$\Gamma(D\bar{D}_2^*(2460) \rightarrow D^0D^-\pi^+ + c.c.)/\Gamma_{\text{total}}$	$\Gamma_{11}/\Gamma$
VALUE (units 10 <sup>-2</sup> )	DOCUMENT ID TECN COMMENT
<b>10.5 ± 2.4 ± 3.8</b>	19 PAKHLOVA 08A BELL 10.6 $e^+e^- \rightarrow D^0D^-\pi^+\gamma$

<sup>19</sup> Using 4421 ± 4 MeV for the mass and 62 ± 20 MeV for the width of  $\psi(4415)$ .

$\Gamma(D^0D^-\pi^+ \text{ (excl. } D^*(2007)^0\bar{D}^0 + c.c., D^*(2010)^+D^- + c.c.)/\Gamma_{\text{total}}$	$\Gamma_{10}/\Gamma_{11}$
VALUE CL%	DOCUMENT ID TECN COMMENT
<b>&lt;0.22</b>	90 20 PAKHLOVA 08A BELL 10.6 $e^+e^- \rightarrow D^0D^-\pi^+\gamma$

<sup>20</sup> Using 4421 ± 4 MeV for the mass and 62 ± 20 MeV for the width of  $\psi(4415)$ .

$\Gamma(D^0D^{*-}\pi^+ + c.c.)/\Gamma_{\text{total}} \times \Gamma(e^+e^-)/\Gamma_{\text{total}}$	$\Gamma_{12}/\Gamma \times \Gamma_{23}/\Gamma$
VALUE CL%	DOCUMENT ID TECN COMMENT
<b>&lt;0.99 × 10<sup>-6</sup></b>	90 21 PAKHLOVA 09 BELL $e^+e^- \rightarrow D^0D^{*-}\pi^+$

<sup>21</sup> Using 4421 ± 4 MeV for the mass of  $\psi(4415)$ .

$\Gamma(D_1(2420)\bar{D} + c.c.)/\Gamma_{\text{total}}$	$\Gamma_{13}/\Gamma$
VALUE	DOCUMENT ID TECN COMMENT
possibly seen	22 ABLIKIM 19AR BES3 $e^+e^- \rightarrow \pi^+\pi^-\bar{D}\bar{D}$

<sup>22</sup> Evidence for  $e^+e^- \rightarrow D_1(2420)\bar{D} + c.c.$  between  $\sqrt{s} = 4.3$  and 4.6 GeV, not necessarily resonant.

$\Gamma(D_s^+D_s^-)/\Gamma_{\text{total}}$	$\Gamma_{14}/\Gamma$
VALUE	DOCUMENT ID TECN COMMENT
not seen	PAKHLOVA 11 BELL $e^+e^- \rightarrow D_s^+D_s^-\gamma$
not seen	DEL-AMO-SA...10N BABR $e^+e^- \rightarrow D_s^+D_s^-\gamma$

$\Gamma(\omega\chi_{c2})/\Gamma_{\text{total}}$	$\Gamma_{15}/\Gamma$
VALUE	DOCUMENT ID TECN COMMENT
possibly seen	ABLIKIM 16A BES3 $e^+e^- \rightarrow \gamma\pi^+\pi^-\pi^0\ell^+\ell^-$

See key on page 999

Meson Particle Listings

$\psi(4415)$ ,  $Z_c(4430)$ ,  $\chi_{c0}(4500)$

$\Gamma(D_s^{*+} D_s^- + c.c.) / \Gamma_{total}$   $\Gamma_{16} / \Gamma$

VALUE	DOCUMENT ID	TECN	COMMENT
seen	PAKHOVA 11	BELL	$e^+ e^- \rightarrow D_s^{*+} D_s^- \gamma$
seen	DEL-AMO-SA...10N	BABR	$e^+ e^- \rightarrow D_s^{*+} D_s^- \gamma$

$\Gamma(D_s^{*+} D_s^{*-}) / \Gamma_{total}$   $\Gamma_{17} / \Gamma$

VALUE	DOCUMENT ID	TECN	COMMENT
not seen	PAKHOVA 11	BELL	$e^+ e^- \rightarrow D_s^{*+} D_s^{*-} \gamma$
not seen	DEL-AMO-SA...10N	BABR	$e^+ e^- \rightarrow D_s^{*+} D_s^{*-} \gamma$

$\Gamma(\psi(3770) \pi^+ \pi^-) / \Gamma_{total}$   $\Gamma_{19} / \Gamma$

VALUE	DOCUMENT ID	TECN	COMMENT
possibly seen	23 ABLIKIM 19AR	BES3	$e^+ e^- \rightarrow \pi^+ \pi^- D \bar{D}$

<sup>23</sup> Observe  $e^+ e^- \rightarrow \pi^+ \pi^- \psi(3770)$  at  $\sqrt{s} = 4.26, 4.36, \text{ and } 4.42$  GeV but cannot establish if continuum or resonant.

$\Gamma(\psi_2(3823) \pi^+ \pi^-) / \Gamma_{total}$   $\Gamma_{18} / \Gamma$

VALUE	EVTS	DOCUMENT ID	TECN	COMMENT
possibly seen	19	24 ABLIKIM 15s	BES3	$e^+ e^- \rightarrow \pi^+ \pi^- \chi_{c1} \gamma$

<sup>24</sup> From a fit of  $e^+ e^- \rightarrow \pi^+ \pi^- \psi_2(3823)$ ,  $\psi_2(3823) \rightarrow \chi_{c1} \gamma$  cross sections taken at  $\sqrt{s}$  values of 4.23, 4.26, 4.36, 4.42, and 4.60 GeV to the  $\psi(4415)$  line shape.

$\psi(4415)$  REFERENCES

ABLIKIM 19AR	PR D100 032005	M. Ablikim et al.	(BESIII Collab.)
ZHUKOVA 18	PR D97 012002	V. Zhukova et al.	(BELLE Collab.)
ABLIKIM 16A	PR D93 011102	M. Ablikim et al.	(BESIII Collab.)
ABLIKIM 15S	PRL 115 011803	M. Ablikim et al.	(BESIII Collab.)
HAN 15	PR D92 012011	Y.L. Han et al.	(BELLE Collab.)
WANG 13B	PR D87 051101	X.L. Wang et al.	(BELLE Collab.)
PAKHOVA 11	PR D83 011101	G. Pakhlova et al.	(BELLE Collab.)
DEL-AMO-SA...10N	PR D82 052004	P. del Amo Sanchez et al.	(BABAR Collab.)
MO 10	PR D82 077501	X.H. Mo, C.Z. Yuan, P. Wang	(BHEP)
AUBERT 09M	PR D79 092001	B. Aubert et al.	(BABAR Collab.)
PAKHOVA 09	PR D80 091301	G. Pakhlova et al.	(BELLE Collab.)
ABLIKIM 08D	PL B660 315	M. Ablikim et al.	(BES Collab.)
PAKHOVA 08	PR D77 011103	G. Pakhlova et al.	(BELLE Collab.)
PAKHOVA 08A	PRL 100 062001	G. Pakhlova et al.	(BELLE Collab.)
PAKHOVA 07	PRL 98 092001	G. Pakhlova et al.	(BELLE Collab.)
SETH 05A	PR D72 017501	K.K. Seth	(BES Collab.)
BAI 02C	PRL 88 101802	J.Z. Bai et al.	(BES Collab.)
BAI 00	PRL 84 594	J.Z. Bai et al.	(BES Collab.)
OSTERHELD 86	SLAC-PUB-4160	A. Osterheld et al.	(SLAC Crystal Ball Collab.)
BRANDELIK 78C	PL 76B 361	R. Brandelik et al.	(DASP Collab.)
SIEGRIST 76	PRL 36 700	J.L. Siegrist et al.	(LBL, SLAC)

$Z_c(4430)$

$I^G(J^{PC}) = 1^+(1^{+-})$   
 $G, C$  need confirmation.

was  $X(4430)^\pm$   
 Properties incompatible with a  $q\bar{q}$  structure (exotic state). See the review on non- $q\bar{q}$  states.

First seen by CHOI 08 in  $B \rightarrow K\pi^+\psi(2S)$  decays, confirmed by AAIJ 14AG, and confirmed in a model-independent way by AAIJ 15BH. Also seen by CHILIKIN 14 in  $B \rightarrow K^+\pi J/\psi$  decays.  $J^P$  was determined by CHILIKIN 13 and AAIJ 14AG.

$Z_c(4430)$  MASS

VALUE (MeV)	DOCUMENT ID	TECN	COMMENT
<b><math>4478^{+15}_{-18}</math> OUR AVERAGE</b>			
$4475 \pm 7^{+15}_{-25}$	<sup>1</sup> AAIJ 14AG	LHCB	$B^0 \rightarrow K^+\pi^-\psi(2S)$
$4485 \pm 22^{+28}_{-11}$	<sup>1</sup> CHILIKIN 13	BELL	$B^0 \rightarrow K^+\pi^-\psi(2S)$
$4443^{+15}_{-12} \pm 19_{-13}$	<sup>2</sup> MIZUK 09	BELL	$B \rightarrow K\pi^+\psi(2S)$
$4433 \pm 4 \pm 2$	<sup>3</sup> CHOI 08	BELL	$B \rightarrow K\pi^+\psi(2S)$

• • • We do not use the following data for averages, fits, limits, etc. • • •

<sup>1</sup> From a four-dimensional amplitude analysis.  
<sup>2</sup> From a Dalitz plot analysis. Superseded by CHILIKIN 13.  
<sup>3</sup> Superseded by MIZUK 09 and CHILIKIN 13.

$Z_c(4430)$  WIDTH

VALUE (MeV)	DOCUMENT ID	TECN	COMMENT
<b><math>181 \pm 31</math> OUR AVERAGE</b>			
$172 \pm 13^{+37}_{-34}$	<sup>1</sup> AAIJ 14AG	LHCB	$B^0 \rightarrow K^+\pi^-\psi(2S)$
$200^{+41}_{-46} \pm 26_{-35}$	<sup>1</sup> CHILIKIN 13	BELL	$B^0 \rightarrow K^+\pi^-\psi(2S)$
$107^{+86}_{-43} \pm 74_{-56}$	<sup>2</sup> MIZUK 09	BELL	$B \rightarrow K\pi^+\psi(2S)$
$45^{+18}_{-13} \pm 30_{-13}$	<sup>3</sup> CHOI 08	BELL	$B \rightarrow K\pi^+\psi(2S)$

• • • We do not use the following data for averages, fits, limits, etc. • • •

<sup>1</sup> From a four-dimensional amplitude analysis.  
<sup>2</sup> From a Dalitz plot analysis. Superseded by CHILIKIN 13.  
<sup>3</sup> Superseded by MIZUK 09 and CHILIKIN 13.

$Z_c(4430)$  DECAY MODES

Mode	Fraction ( $\Gamma_i/\Gamma$ )
$\Gamma_1 \pi^+ \psi(2S)$	seen
$\Gamma_2 \pi^+ J/\psi$	seen

$Z_c(4430)$  BRANCHING RATIOS

$\Gamma(\pi^+ \psi(2S)) / \Gamma_{total}$   $\Gamma_1 / \Gamma$

VALUE	DOCUMENT ID	TECN	COMMENT
seen	<sup>1</sup> AAIJ 14AG	LHCB	$B^0 \rightarrow K^+\pi^-\psi(2S)$
seen	<sup>2</sup> CHILIKIN 13	BELL	$B^0 \rightarrow K^+\pi^-\psi(2S)$
not seen	<sup>3</sup> AUBERT 09AA	BABR	$B \rightarrow K\pi^+\psi(2S)$
seen	<sup>4</sup> MIZUK 09	BELL	$B \rightarrow K\pi^+\psi(2S)$

• • • We do not use the following data for averages, fits, limits, etc. • • •

<sup>1</sup> From a four-dimensional amplitude analysis. No product of branching fractions quoted.  
<sup>2</sup> From a four-dimensional amplitude analysis. Measured a product of branching fractions  $B(B^0 \rightarrow Z_c(4430)^- K^+) \times B(Z_c(4430)^- \rightarrow \psi(2S) \pi^-) = (6.0^{+1.7+2.5}_{-2.0-1.4}) \times 10^{-5}$ .  
<sup>3</sup> AUBERT 09AA quotes  $B(B^+ \rightarrow \bar{K}^0 Z_c(4430)^+) \times B(Z_c(4430)^+ \rightarrow \pi^+\psi(2S)) < 4.7 \times 10^{-5}$  and  $B(\bar{B}^0 \rightarrow K^- Z_c(4430)^+) \times B(Z_c(4430)^+ \rightarrow \pi^+\psi(2S)) < 3.1 \times 10^{-5}$  at 95% CL.  
<sup>4</sup> Measured a product of branching fractions  $B(\bar{B}^0 \rightarrow K^- Z_c(4430)^+) \times B(Z_c(4430)^+ \rightarrow \pi^+\psi(2S)) = (3.2^{+1.8+5.3}_{-0.9-1.6}) \times 10^{-5}$ . Superseded by CHILIKIN 13.

$\Gamma(\pi^+ J/\psi) / \Gamma_{total}$   $\Gamma_2 / \Gamma$

VALUE	DOCUMENT ID	TECN	COMMENT
seen	<sup>1,2</sup> CHILIKIN 14	BELL	$\bar{B}^0 \rightarrow K^-\pi^+ J/\psi$
not seen	<sup>3</sup> AUBERT 09AA	BABR	$B \rightarrow K\pi^+ J/\psi$

• • • We do not use the following data for averages, fits, limits, etc. • • •

<sup>1</sup> CHILIKIN 14 reports  $B(\bar{B}^0 \rightarrow Z_c(4430)^+ K^-) \times B(Z_c(4430)^+ \rightarrow J/\psi \pi^+) = (5.4^{+4.0+1.1}_{-1.0-0.9}) \times 10^{-6}$ .  
<sup>2</sup> A broad enhancement seen by AAIJ 19R in the decays  $B^0 \rightarrow J/\psi \pi^+ K^-$  at 4600 MeV can be due to an interplay of  $Z_c(4430)$ ,  $Z_c(4200)$  and the fitting polynomials.  
<sup>3</sup> AUBERT 09AA quotes  $B(B^+ \rightarrow \bar{K}^0 Z_c(4430)^+) \times B(Z_c(4430)^+ \rightarrow \pi^+ J/\psi) < 1.5 \times 10^{-5}$  and  $B(\bar{B}^0 \rightarrow K^- Z_c(4430)^+) \times B(Z_c(4430)^+ \rightarrow \pi^+ J/\psi) < 0.4 \times 10^{-5}$  at 95% CL.

$Z_c(4430)$  REFERENCES

AAIJ 19R	PRL 122 152002	R. Aaij et al.	(LHCb Collab.)
AAIJ 15BH	PR D92 112009	R. Aaij et al.	(LHCb Collab.)
AAIJ 14AG	PRL 112 222002	R. Aaij et al.	(LHCb Collab.) JP
CHILIKIN 14	PR D90 112009	K. Chilikin et al.	(BELLE Collab.)
CHILIKIN 13	PR D88 074026	K. Chilikin et al.	(BELLE Collab.) JP
AUBERT 09AA	PR D79 112001	B. Aubert et al.	(BABAR Collab.)
MIZUK 09	PR D80 031104	R. Mizuk et al.	(BELLE Collab.)
CHOI 08	PRL 100 142001	S.-K. Choi et al.	(BELLE Collab.)

$\chi_{c0}(4500)$

$I^G(J^{PC}) = 0^+(0^{++})$

OMITTED FROM SUMMARY TABLE  
 was  $X(4500)$

This state shows properties different from a conventional  $q\bar{q}$  state. A candidate for an exotic structure. See the review on non- $q\bar{q}$  states.  
 Seen by AAIJ 17C in  $B^+ \rightarrow \chi_{c0} K^+$ ,  $\chi_{c0} \rightarrow J/\psi \phi$  using an amplitude analysis of  $B^+ \rightarrow J/\psi \phi K^+$  with a significance (accounting for systematic uncertainties) of 6.1  $\sigma$ .

$\chi_{c0}(4500)$  MASS

VALUE (MeV)	EVTS	DOCUMENT ID	TECN	COMMENT
<b><math>4506 \pm 11^{+12}_{-15}</math></b>	4289	<sup>1</sup> AAIJ 17C	LHCB	$B^+ \rightarrow J/\psi \phi K^+$

<sup>1</sup> From an amplitude analysis of the decay  $B^+ \rightarrow J/\psi \phi K^+$  with a significance of 6.1  $\sigma$ .

$\chi_{c0}(4500)$  WIDTH

VALUE (MeV)	EVTS	DOCUMENT ID	TECN	COMMENT
<b><math>92 \pm 21^{+21}_{-20}</math></b>	4289	<sup>1</sup> AAIJ 17C	LHCB	$B^+ \rightarrow J/\psi \phi K^+$

<sup>1</sup> From an amplitude analysis of the decay  $B^+ \rightarrow J/\psi \phi K^+$  with a significance of 6.1  $\sigma$ .

$\chi_{c0}(4500)$  DECAY MODES

Mode	Fraction ( $\Gamma_i/\Gamma$ )
$\Gamma_1 J/\psi \phi$	seen

# Meson Particle Listings

## $\chi_{c0}(4500), \psi(4660)$

### $\chi_{c0}(4500)$ BRANCHING RATIOS

$\Gamma(J/\psi\phi)/\Gamma_{\text{total}}$	VALUE	EVTS	DOCUMENT ID	TECN	COMMENT	$\Gamma_1/\Gamma$
seen		4289	<sup>1</sup> AAIJ	17c	LHCB $B^+ \rightarrow J/\psi\phi K^+$	

<sup>1</sup> From an amplitude analysis of the decay  $B^+ \rightarrow J/\psi\phi K^+$  with a significance of 6.1  $\sigma$ .

### $\chi_{c0}(4500)$ REFERENCES

AAIJ	17C	PRL 118 022003	R. Aaij <i>et al.</i>	(LHCb Collab.) JP
Also		PR D95 012002	R. Aaij <i>et al.</i>	(LHCb Collab.)

## $\psi(4660)$

$$J^G(J^{PC}) = 0^-(1^{--})$$

also known as  $Y(4660)$ ; was  $X(4660)$

This state shows properties different from a conventional  $q\bar{q}$  state. A candidate for an exotic structure. See the review on non- $q\bar{q}$  states.

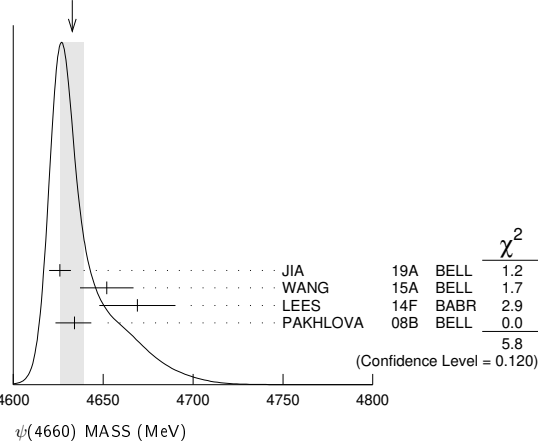
Seen in radiative return from  $e^+e^-$  collisions at  $\sqrt{s} = 9.54\text{--}10.58$  GeV by WANG 07D. Also obtained in a combined fit of WANG 07D, AUBERT 07s, and LEES 14F. See also the review on "Spectroscopy of mesons containing two heavy quarks."

### $\psi(4660)$ MASS

VALUE (MeV)	EVTS	DOCUMENT ID	TECN	COMMENT
<b>4633 ± 7 OUR AVERAGE</b>				Error includes scale factor of 1.4. See the ideogram below.
4625.9 <sup>+6.2</sup> <sub>-6.0</sub> ± 0.4	89	<sup>1</sup> JIA	19A	BELL $e^+e^- \rightarrow \gamma D_s^+ D_{s1}^-(2536)^-$
4652 ± 10 ± 11	279	<sup>2</sup> WANG	15A	BELL 10.58 $e^+e^- \rightarrow \gamma \pi^+ \pi^- \psi(2S)$
4669 ± 21 ± 3	37	<sup>3</sup> LEES	14F	BABR 10.58 $e^+e^- \rightarrow \gamma \pi^+ \pi^- \psi(2S)$
4634 <sup>+8</sup> <sub>-7</sub> ± 5 <sub>8</sub>	142	<sup>4</sup> PAKHLOVA	08B	BELL $e^+e^- \rightarrow \Lambda_c^+ \Lambda_c^-$
4652.5 ± 3.4 ± 1.1		<sup>5</sup> DAI	17	RVUE $e^+e^- \rightarrow \Lambda_c^+ \Lambda_c^-$
4645.2 ± 9.5 ± 6.0		<sup>6</sup> ZHANG	17B	RVUE $e^+e^- \rightarrow \pi^+ \pi^- \psi(2S)$
4646.4 ± 9.7 ± 4.8		<sup>7</sup> ZHANG	17C	RVUE $e^+e^- \rightarrow \pi^+ \pi^- J/\psi$ or $\psi(2S)$
4661 <sup>+9</sup> <sub>-8</sub> ± 6	44	<sup>8</sup> LIU	08H	RVUE 10.58 $e^+e^- \rightarrow \gamma \pi^+ \pi^- \psi(2S)$
4664 ± 11 ± 5	44	WANG	07D	BELL 10.58 $e^+e^- \rightarrow \gamma \pi^+ \pi^- \psi(2S)$

- <sup>1</sup> From a fit of a Breit-Wigner convolved with a Gaussian.
- <sup>2</sup> From a two-resonance fit. Supersedes WANG 07D.
- <sup>3</sup> From a two-resonance fit.
- <sup>4</sup> The  $\pi^+ \pi^- \psi(2S)$  and  $\Lambda_c^+ \Lambda_c^-$  states are not necessarily the same.
- <sup>5</sup> The pole parameters are extracted from the speed plot.
- <sup>6</sup> From a three-resonance fit.
- <sup>7</sup> From a combined fit of BELLE, BABAR and BES3  $e^+e^- \rightarrow \pi^+ \pi^- J/\psi$  and  $e^+e^- \rightarrow \pi^+ \pi^- \psi(2S)$  data.
- <sup>8</sup> From a combined fit of AUBERT 07s and WANG 07D data with two resonances.

WEIGHTED AVERAGE  
4633±7 (Error scaled by 1.4)



### $\psi(4660)$ WIDTH

VALUE (MeV)	EVTS	DOCUMENT ID	TECN	COMMENT
<b>64 ± 9 OUR AVERAGE</b>				
49.8 <sup>+13.9</sup> <sub>-11.5</sub> ± 4.0	89	<sup>1</sup> JIA	19A	BELL $e^+e^- \rightarrow \gamma D_s^+ D_{s1}^-(2536)^-$
68 ± 11 ± 5	279	<sup>2</sup> WANG	15A	BELL 10.58 $e^+e^- \rightarrow \gamma \pi^+ \pi^- \psi(2S)$
104 ± 48 ± 10	37	<sup>3</sup> LEES	14F	BABR 10.58 $e^+e^- \rightarrow \gamma \pi^+ \pi^- \psi(2S)$
92 <sup>+40</sup> <sub>-24</sub> ± 10 <sub>21</sub>	142	<sup>4</sup> PAKHLOVA	08B	BELL $e^+e^- \rightarrow \Lambda_c^+ \Lambda_c^-$

• • • We do not use the following data for averages, fits, limits, etc. • • •

62.6 ± 5.6 ± 4.3		<sup>5</sup> DAI	17	RVUE $e^+e^- \rightarrow \Lambda_c^+ \Lambda_c^-$
113.8 ± 18.1 ± 3.4		<sup>6</sup> ZHANG	17B	RVUE $e^+e^- \rightarrow \pi^+ \pi^- \psi(2S)$
103.5 ± 15.6 ± 4.0		<sup>7</sup> ZHANG	17C	RVUE $e^+e^- \rightarrow \pi^+ \pi^- J/\psi$ or $\psi(2S)$
42 <sup>+17</sup> <sub>-12</sub> ± 6	44	<sup>8</sup> LIU	08H	RVUE 10.58 $e^+e^- \rightarrow \gamma \pi^+ \pi^- \psi(2S)$
48 ± 15 ± 3	44	WANG	07D	BELL 10.58 $e^+e^- \rightarrow \gamma \pi^+ \pi^- \psi(2S)$

- <sup>1</sup> From a fit of a Breit-Wigner convolved with a Gaussian.
- <sup>2</sup> From a two-resonance fit. Supersedes WANG 07D.
- <sup>3</sup> From a two-resonance fit.
- <sup>4</sup> The  $\pi^+ \pi^- \psi(2S)$  and  $\Lambda_c^+ \Lambda_c^-$  states are not necessarily the same.
- <sup>5</sup> The pole parameters are extracted from the speed plot.
- <sup>6</sup> From a three-resonance fit.
- <sup>7</sup> From a combined fit of BELLE, BABAR and BES3  $e^+e^- \rightarrow \pi^+ \pi^- J/\psi$  and  $e^+e^- \rightarrow \pi^+ \pi^- \psi(2S)$  data.
- <sup>8</sup> From a combined fit of AUBERT 07s and WANG 07D data with two resonances.

### $\psi(4660)$ DECAY MODES

Mode	Fraction ( $\Gamma_i/\Gamma$ )
$\Gamma_1$ $e^+e^-$	not seen
$\Gamma_2$ $\psi(2S)\pi^+\pi^-$	seen
$\Gamma_3$ $J/\psi\eta$	not seen
$\Gamma_4$ $D^0 D^{*0}\pi^+$	not seen
$\Gamma_5$ $\chi_{c1}\gamma$	not seen
$\Gamma_6$ $\chi_{c2}\gamma$	not seen
$\Gamma_7$ $\Lambda_c^+ \Lambda_c^-$	seen
$\Gamma_8$ $D_s^+ D_{s1}^-(2536)^-$	seen

### $\psi(4660)$ $\Gamma(i) \times \Gamma(e^+e^-)/\Gamma(\text{total})$

VALUE (eV)	EVTS	DOCUMENT ID	TECN	COMMENT	$\Gamma_2\Gamma_1/\Gamma$
<b>2.0 ± 0.3 ± 0.2</b>	279	<sup>1</sup> WANG	15A	BELL 10.58 $e^+e^- \rightarrow \gamma \pi^+ \pi^- \psi(2S)$	
8.1 ± 1.1 ± 1.0	279	<sup>2</sup> WANG	15A	BELL 10.58 $e^+e^- \rightarrow \gamma \pi^+ \pi^- \psi(2S)$	
2.7 ± 1.3 ± 0.5	37	<sup>3</sup> LEES	14F	BABR 10.58 $e^+e^- \rightarrow \gamma \pi^+ \pi^- \psi(2S)$	
7.5 ± 1.7 ± 0.7	37	<sup>4</sup> LEES	14F	BABR 10.58 $e^+e^- \rightarrow \gamma \pi^+ \pi^- \psi(2S)$	
2.2 <sup>+0.7</sup> <sub>-0.6</sub>	44	<sup>5</sup> LIU	08H	RVUE 10.58 $e^+e^- \rightarrow \gamma \pi^+ \pi^- \psi(2S)$	
5.9 ± 1.6	44	<sup>6</sup> LIU	08H	RVUE 10.58 $e^+e^- \rightarrow \gamma \pi^+ \pi^- \psi(2S)$	
3.0 ± 0.9 ± 0.3	44	<sup>3</sup> WANG	07D	BELL 10.58 $e^+e^- \rightarrow \gamma \pi^+ \pi^- \psi(2S)$	
7.6 ± 1.8 ± 0.8	44	<sup>4</sup> WANG	07D	BELL 10.58 $e^+e^- \rightarrow \gamma \pi^+ \pi^- \psi(2S)$	

- <sup>1</sup> Solution I of two equivalent solutions from a fit using two interfering resonances. Supersedes WANG 07D.
- <sup>2</sup> Solution II of two equivalent solutions from a fit using two interfering resonances. Supersedes WANG 07D.
- <sup>3</sup> Solution I of two equivalent solutions in a fit using two interfering resonances.
- <sup>4</sup> Solution II of two equivalent solutions in a fit using two interfering resonances.
- <sup>5</sup> Solution I in a combined fit of AUBERT 07s and WANG 07D data with two resonances.
- <sup>6</sup> Solution II in a combined fit of AUBERT 07s and WANG 07D data with two resonances.

### $\Gamma(J/\psi\eta) \times \Gamma(e^+e^-)/\Gamma_{\text{total}}$

VALUE (eV)	CL%	DOCUMENT ID	TECN	COMMENT	$\Gamma_3\Gamma_1/\Gamma$
<0.94	90	WANG	13B	BELL $e^+e^- \rightarrow J/\psi\eta\gamma$	

• • • We do not use the following data for averages, fits, limits, etc. • • •

### $\Gamma(\chi_{c1}\gamma) \times \Gamma(e^+e^-)/\Gamma_{\text{total}}$

VALUE (eV)	CL%	DOCUMENT ID	TECN	COMMENT	$\Gamma_5\Gamma_1/\Gamma$
<0.45	90	<sup>1</sup> HAN	15	BELL 10.58 $e^+e^- \rightarrow \chi_{c1}\gamma$	

<sup>1</sup> Using  $B(\eta \rightarrow \gamma\gamma) = (39.41 \pm 0.21)\%$ .

### $\Gamma(\chi_{c2}\gamma) \times \Gamma(e^+e^-)/\Gamma_{\text{total}}$

VALUE (eV)	CL%	DOCUMENT ID	TECN	COMMENT	$\Gamma_6\Gamma_1/\Gamma$
<2.1	90	<sup>1</sup> HAN	15	BELL 10.58 $e^+e^- \rightarrow \chi_{c2}\gamma$	

<sup>1</sup> Using  $B(\eta \rightarrow \gamma\gamma) = (39.41 \pm 0.21)\%$ .

### $\Gamma(D_s^+ D_{s1}^-(2536)^-) \times \Gamma(e^+e^-)/\Gamma_{\text{total}}$

VALUE (eV)	EVTS	DOCUMENT ID	TECN	COMMENT	$\Gamma_8\Gamma_1/\Gamma$
<b>14.3<sup>+2.8</sup><sub>-2.6</sub> ± 1.5</b>	89	<sup>1</sup> JIA	19A	BELL $e^+e^- \rightarrow \gamma D_s^+ D_{s1}^-(2536)^-$	

<sup>1</sup> Using  $D_{s1}^-(2536)^- \rightarrow \bar{D}^{*0} K^-$ .

See key on page 999

Meson Particle Listings

$\psi(4660), \chi_{c0}(4700)$

$\psi(4660)$  BRANCHING RATIOS

$\Gamma(D^0 D^{*-} \pi^+)/\Gamma(\psi(2S)\pi^+\pi^-)$					$\Gamma_4/\Gamma_2$
VALUE	CL%	DOCUMENT ID	TECN	COMMENT	
<10	90	PAKHLOVA 09	BELL	$e^+e^- \rightarrow D^0 D^{*-} \pi^+$	

$\Gamma(D^0 D^{*-} \pi^+)/\Gamma_{total} \times \Gamma(e^+e^-)/\Gamma_{total}$					$\Gamma_4/\Gamma \times \Gamma_1/\Gamma$
VALUE	CL%	DOCUMENT ID	TECN	COMMENT	
<0.37 $\times 10^{-6}$	90	<sup>1</sup> PAKHLOVA 09	BELL	$e^+e^- \rightarrow D^0 D^{*-} \pi^+$	

<sup>1</sup> Using  $4664 \pm 11 \pm 5$  MeV for the mass of  $\psi(4660)$ .

$\Gamma(\Lambda_c^+ \Lambda_c^-)/\Gamma_{total} \times \Gamma(e^+e^-)/\Gamma_{total}$					$\Gamma_7/\Gamma \times \Gamma_1/\Gamma$
VALUE (units $10^{-6}$ )	EVTS	DOCUMENT ID	TECN	COMMENT	
0.68 $\pm 0.16 \pm 0.29$ -0.15 -0.30	142	<sup>1</sup> PAKHLOVA 08B	BELL	$e^+e^- \rightarrow \Lambda_c^+ \Lambda_c^-$	

<sup>1</sup> The  $\pi^+\pi^-\psi(2S)$  and  $\Lambda_c^+ \Lambda_c^-$  states are not necessarily the same.

$\psi(4660)$  REFERENCES

JIA	19A	PR D100 111103	S. Jia <i>et al.</i>	(BELLE Collab.)
DAI	17	PR D96 116001	L.-Y. Dai, J. Haidenbauer, U.-G. Meissner	(JULI+)
ZHANG	17B	PR D96 054008	J. Zhang, J. Zhang	
ZHANG	17C	EPJ C77 727	J. Zhang, L. Yuan	
HAN	15	PR D92 012011	Y.L. Han <i>et al.</i>	(BELLE Collab.)
WANG	15A	PR D91 112007	X.L. Wang <i>et al.</i>	(BELLE Collab.)
LEES	14F	PR D89 111103	J.P. Lees <i>et al.</i>	(BABAR Collab.)
WANG	13B	PR D87 051101	X.L. Wang <i>et al.</i>	(BELLE Collab.)
PAKHLOVA	09	PR D80 091101	G. Pakhlova <i>et al.</i>	(BELLE Collab.)
LIU	08H	PR D78 014032	Z.Q. Liu, X.S. Qin, C.Z. Yuan	
PAKHLOVA	08B	PRL 101 172001	C. Pakhlova <i>et al.</i>	(BELLE Collab.)
AUBERT	07S	PRL 98 212001	B. Aubert <i>et al.</i>	(BABAR Collab.)
WANG	07D	PRL 99 142002	X.L. Wang <i>et al.</i>	(BELLE Collab.)

$\chi_{c0}(4700)$

$$I^G(J^{PC}) = 0^+(0^{++})$$

OMITTED FROM SUMMARY TABLE  
was X(4700)

This state shows properties different from a conventional  $q\bar{q}$  state. A candidate for an exotic structure. See the review on non- $q\bar{q}$  states.

Seen by AAIJ 17C in  $B^+ \rightarrow \chi_{c0} K^+, \chi_{c0} \rightarrow J/\psi \phi$  using an amplitude analysis of  $B^+ \rightarrow J/\psi \phi K^+$  with a significance (accounting for systematic uncertainties) of 5.6  $\sigma$ .

$\chi_{c0}(4700)$  MASS

VALUE (MeV)	EVTS	DOCUMENT ID	TECN	COMMENT
4704 $\pm 10 \pm 14$ -24	4289	<sup>1</sup> AAIJ	17c	LHCB $B^+ \rightarrow J/\psi \phi K^+$

<sup>1</sup> From an amplitude analysis of the decay  $B^+ \rightarrow J/\psi \phi K^+$  with a significance of 5.6  $\sigma$ .

$\chi_{c0}(4700)$  WIDTH

VALUE (MeV)	EVTS	DOCUMENT ID	TECN	COMMENT
120 $\pm 31 \pm 42$ -33	4289	<sup>1</sup> AAIJ	17c	LHCB $B^+ \rightarrow J/\psi \phi K^+$

<sup>1</sup> From an amplitude analysis of the decay  $B^+ \rightarrow J/\psi \phi K^+$  with a significance of 5.6  $\sigma$ .

$\chi_{c0}(4700)$  DECAY MODES

Mode	Fraction ( $\Gamma_i/\Gamma$ )
$\Gamma_1$ $J/\psi \phi$	seen

$\chi_{c0}(4700)$  BRANCHING RATIOS

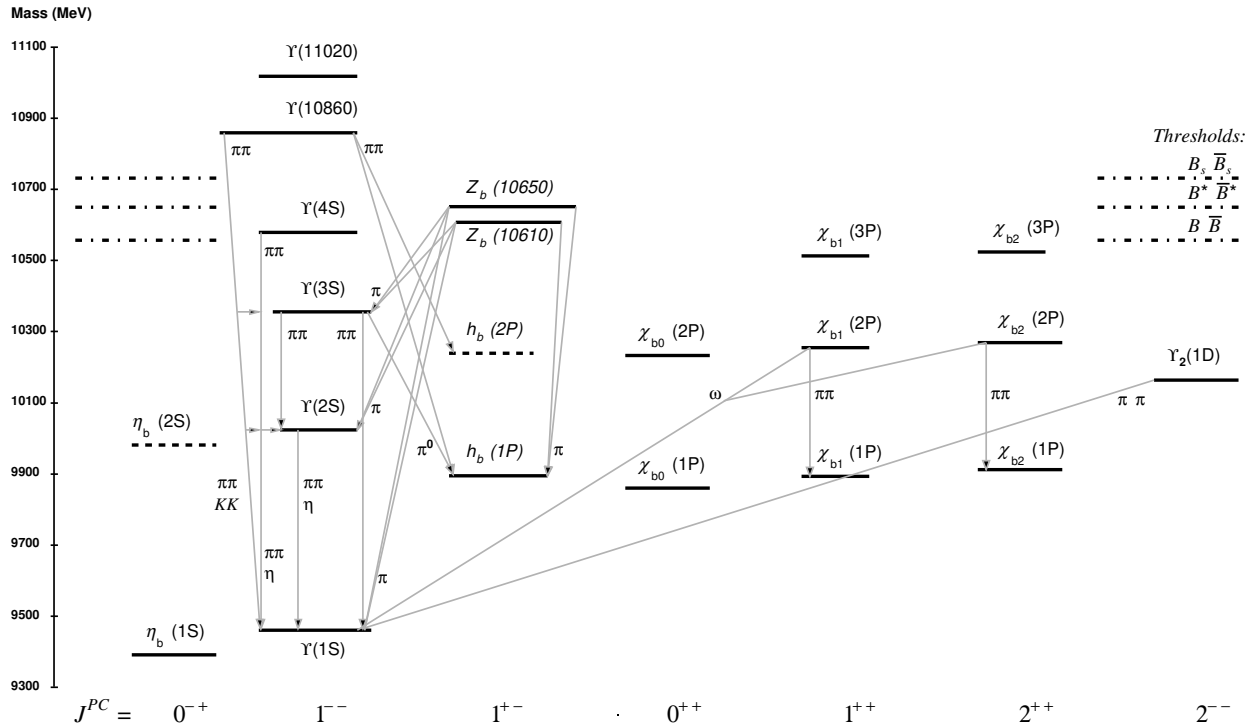
$\Gamma(J/\psi \phi)/\Gamma_{total}$					$\Gamma_1/\Gamma$
VALUE	EVTS	DOCUMENT ID	TECN	COMMENT	
seen	4289	<sup>1</sup> AAIJ	17c	LHCB $B^+ \rightarrow J/\psi \phi K^+$	

<sup>1</sup> From an amplitude analysis of the decay  $B^+ \rightarrow J/\psi \phi K^+$  with a significance of 5.6  $\sigma$ .

$\chi_{c0}(4700)$  REFERENCES

AAIJ	17C	PRL 118 022003	R. Aaij <i>et al.</i>	(LHCb Collab.) JP
Also		PR D95 012002	R. Aaij <i>et al.</i>	(LHCb Collab.)

## $b\bar{b}$ MESONS (including possibly non- $q\bar{q}$ states)



The level scheme of meson states containing a minimal quark content of  $b\bar{b}$ . The name of a state is determined by its quantum numbers  $I^G J^{PC}$  (see the review “Naming Scheme for Hadrons”). States included in the Summary Tables are shown with solid lines; those requiring confirmation are shown with dotted lines. The arrows indicate the most dominant hadronic transitions. Single photon transitions, including  $\Upsilon(nS) \rightarrow \gamma\eta_b(mS)$ ,  $\Upsilon(nS) \rightarrow \gamma\chi_{bJ}(mP)$ , and  $\chi_{bJ}(nP) \rightarrow \gamma\Upsilon(mS)$ , are omitted for clarity. For orientation, the location of the thresholds related to a pair of ground state open bottom mesons is indicated in the figure.

### WIDTH DETERMINATIONS OF THE $\Upsilon$ STATES

As is the case for the  $J/\psi(1S)$  and  $\psi(2S)$ , the full widths of the  $b\bar{b}$  states  $\Upsilon(1S)$ ,  $\Upsilon(2S)$ , and  $\Upsilon(3S)$  are not directly measurable, since they are much narrower than the energy resolution of the  $e^+e^-$  storage rings where these states are produced. The common indirect method to determine  $\Gamma$  starts from

$$\Gamma = \Gamma_{\ell\ell}/B_{\ell\ell}, \quad (1)$$

where  $\Gamma_{\ell\ell}$  is one leptonic partial width and  $B_{\ell\ell}$  is the corresponding branching fraction ( $\ell = e, \mu, \text{ or } \tau$ ). One then assumes  $e-\mu-\tau$  universality and uses

$$\begin{aligned} \Gamma_{\ell\ell} &= \Gamma_{ee} \\ B_{\ell\ell} &= \text{average of } B_{ee}, B_{\mu\mu}, \text{ and } B_{\tau\tau}. \end{aligned} \quad (2)$$

The electronic partial width  $\Gamma_{ee}$  is also not directly measurable at  $e^+e^-$  storage rings, only in the combination  $\Gamma_{ee}\Gamma_{\text{had}}/\Gamma$ , where  $\Gamma_{\text{had}}$  is the hadronic partial width and

$$\Gamma_{\text{had}} + 3\Gamma_{ee} = \Gamma. \quad (3)$$

This combination is obtained experimentally from the energy-integrated hadronic cross section

$$\begin{aligned} \int_{\text{resonance}} \sigma(e^+e^- \rightarrow \Upsilon \rightarrow \text{hadrons})dE \\ = \frac{6\pi^2 \Gamma_{ee}\Gamma_{\text{had}}}{M^2 \Gamma} C_r = \frac{6\pi^2 \Gamma_{ee}^{(0)}\Gamma_{\text{had}}}{M^2 \Gamma} C_r^{(0)}, \end{aligned} \quad (4)$$

where  $M$  is the  $\Upsilon$  mass, and  $C_r$  and  $C_r^{(0)}$  are radiative correction factors.  $C_r$  is used for obtaining  $\Gamma_{ee}$  as defined in Eq. (1), and contains corrections from all orders of QED for describing  $(b\bar{b}) \rightarrow e^+e^-$ . The lowest order QED value  $\Gamma_{ee}^{(0)}$ , relevant for comparison with potential-model calculations, is defined by the lowest order QED graph (Born term) alone, and is about 7% lower than  $\Gamma_{ee}$ .

The Listings give experimental results on  $B_{ee}$ ,  $B_{\mu\mu}$ ,  $B_{\tau\tau}$ , and  $\Gamma_{ee}\Gamma_{\text{had}}/\Gamma$ . The entries of the last quantity have been re-evaluated consistently using the correction procedure of KURAEV 85 [1]. The partial width  $\Gamma_{ee}$  is obtained from the average values for  $\Gamma_{ee}\Gamma_{\text{had}}/\Gamma$  and  $B_{\ell\ell}$  using

$$\Gamma_{ee} = \frac{\Gamma_{ee}\Gamma_{\text{had}}}{\Gamma(1 - 3B_{\ell\ell})}. \quad (5)$$

See key on page 999

# Meson Particle Listings

## Bottomonium, $\eta_b(1S)$

The total width  $\Gamma$  is then obtained from Eq. (1). We do not list  $\Gamma_{ee}$  and  $\Gamma$  values of individual experiments. The  $\Gamma_{ee}$  values in the Meson Summary Table are also those defined in Eq. (1).

### References

- E.A. Kuraev, V.S. Fadin, Sov. J. Nucl. Phys. **41**, 466 (1985).

$\eta_b(1S)$

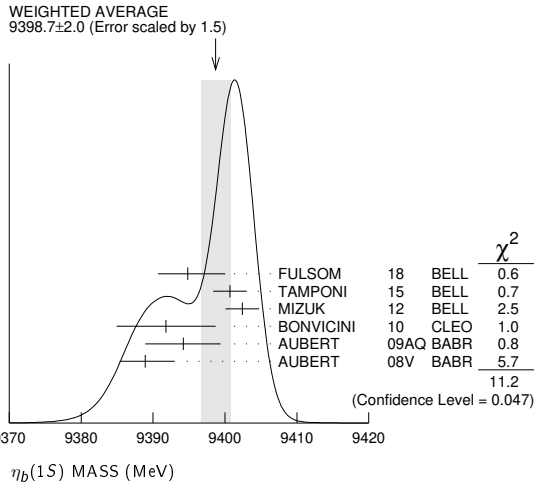
$I^G(J^{PC}) = 0^+(0^{-+})$

Quantum numbers shown are quark-model predictions. Observed in radiative decay of the  $\Upsilon(3S)$ , therefore  $C = +$ .

### $\eta_b(1S)$ MASS

VALUE (MeV)	EVTS	DOCUMENT ID	TECN	COMMENT
<b>9398.7 ± 2.0 OUR AVERAGE</b>				Error includes scale factor of 1.5. See the ideogram below.
9394.8 <sup>+2.7+4.5</sup> <sub>-3.1-2.7</sub>	29K	FULSOM	18 BELL	$\Upsilon(2S) \rightarrow \gamma X$
9400.7 ± 1.7 ± 1.6	33.1k	TAMPONI	15 BELL	$e^+e^- \rightarrow \gamma\eta + \text{hadrons}$
9402.4 ± 1.5 ± 1.8	34k	<sup>1</sup> MIZUK	12 BELL	$e^+e^- \rightarrow \gamma\pi^+\pi^- + \text{hadrons}$
9391.8 ± 6.6 ± 2.0	2.3k	<sup>2</sup> BONVICINI	10 CLEO	$\Upsilon(3S) \rightarrow \gamma X$
9394.2 <sup>+4.8+2.0</sup> <sub>-4.9±2.0</sub>	13k	<sup>2</sup> AUBERT	09AQ BABR	$\Upsilon(2S) \rightarrow \gamma X$
9388.9 <sup>+3.1+2.7</sup> <sub>-2.3±2.7</sub>	19k	<sup>2</sup> AUBERT	08V BABR	$\Upsilon(3S) \rightarrow \gamma X$
9393.2 ± 3.4 ± 2.3	10	<sup>2,3</sup> DOBBS	12	$\Upsilon(2S) \rightarrow \gamma \text{hadrons}$
9300 ± 20 ± 20		HEISTER	02D ALEP	181-209 $e^+e^-$

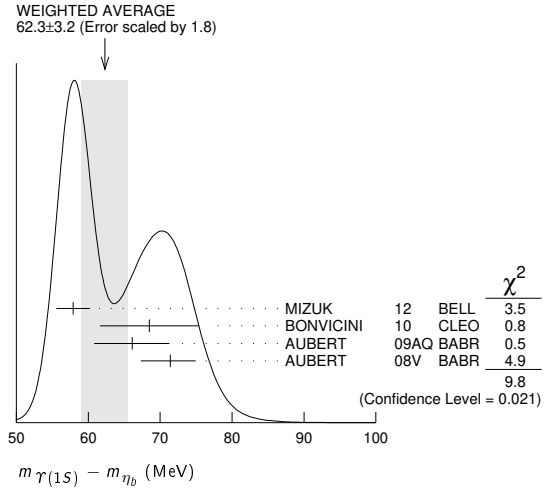
• • • We do not use the following data for averages, fits, limits, etc. • • •  
<sup>1</sup> With floating width. Not independent of the corresponding mass difference measurement.  
<sup>2</sup> Assuming  $\Gamma_{\eta_b(1S)} = 10$  MeV. Not independent of the corresponding  $\gamma$  energy or mass difference measurements.  
<sup>3</sup> Obtained by analyzing CLEO III data but not authored by the CLEO Collaboration.



### $m_{\Upsilon(1S)} - m_{\eta_b}$

VALUE (MeV)	EVTS	DOCUMENT ID	TECN	COMMENT
<b>62.3 ± 3.2 OUR AVERAGE</b>				Error includes scale factor of 1.8. See the ideogram below.
57.9 ± 1.5 ± 1.8	34k	<sup>1</sup> MIZUK	12 BELL	$e^+e^- \rightarrow \gamma\pi^+\pi^- + \text{hadrons}$
68.5 ± 6.6 ± 2.0	2.3 ± 0.5k	<sup>2</sup> BONVICINI	10 CLEO	$\Upsilon(3S) \rightarrow \gamma X$
66.1 <sup>+4.8+2.0</sup> <sub>-4.9±2.0</sub>	13 ± 5k	<sup>2</sup> AUBERT	09AQ BABR	$\Upsilon(2S) \rightarrow \gamma X$
71.4 <sup>+2.3+2.7</sup> <sub>-3.1±2.7</sub>	19 ± 3k	<sup>2</sup> AUBERT	08V BABR	$\Upsilon(3S) \rightarrow \gamma X$
67.1 ± 3.4 ± 2.3	10 <sup>+5</sup> <sub>-4</sub>	<sup>2,3</sup> DOBBS	12	$\Upsilon(2S) \rightarrow \gamma \text{hadrons}$

• • • We do not use the following data for averages, fits, limits, etc. • • •  
<sup>1</sup> With floating width. Not independent of the corresponding mass measurement.  
<sup>2</sup> Assuming  $\Gamma_{\eta_b(1S)} = 10$  MeV. Not independent of the corresponding  $\gamma$  energy or mass measurements.  
<sup>3</sup> Obtained by analyzing CLEO III data but not authored by the CLEO Collaboration.



### $\gamma$ ENERGY IN $\Upsilon(3S)$ DECAY

VALUE (MeV)	EVTS	DOCUMENT ID	TECN	COMMENT
<b>920.6 ± 2.8 OUR AVERAGE</b>				
918.6 ± 6.0 ± 1.9	2.3 ± 0.5k	<sup>1</sup> BONVICINI	10 CLEO	$\Upsilon(3S) \rightarrow \gamma X$
921.2 <sup>+2.1+2.4</sup> <sub>-2.8±2.4</sub>	19 ± 3k	<sup>1</sup> AUBERT	08V BABR	$\Upsilon(3S) \rightarrow \gamma X$

<sup>1</sup> Assuming  $\Gamma_{\eta_b(1S)} = 10$  MeV. Not independent of the corresponding mass or mass difference measurements.

### $\gamma$ ENERGY IN $\Upsilon(2S)$ DECAY

VALUE (MeV)	EVTS	DOCUMENT ID	TECN	COMMENT
<b>609.3 ± 4.6 OUR AVERAGE</b>				
609.3 ± 4.6 ± 1.9	13 ± 5k	<sup>1</sup> AUBERT	09AQ BABR	$\Upsilon(2S) \rightarrow \gamma X$

<sup>1</sup> Assuming  $\Gamma_{\eta_b(1S)} = 10$  MeV. Not independent of the corresponding mass or mass difference measurements.

### $\eta_b(1S)$ WIDTH

VALUE (MeV)	EVTS	DOCUMENT ID	TECN	COMMENT
<b>10<sup>+5</sup><sub>-4</sub> OUR AVERAGE</b>				
8 <sup>+6</sup> <sub>-5</sub> ± 5	33.1k	<sup>1</sup> TAMPONI	15 BELL	$e^+e^- \rightarrow \gamma\eta + \text{hadrons}$
10.8 <sup>+4.0+4.5</sup> <sub>-3.7-2.0</sub>	34k	<sup>1</sup> MIZUK	12 BELL	$e^+e^- \rightarrow \gamma\pi^+\pi^- + \text{hadrons}$

<sup>1</sup> With floating mass.

### $\eta_b(1S)$ DECAY MODES

Mode	Fraction ( $\Gamma_i/\Gamma$ )	Confidence level
$\Gamma_1$ hadrons	seen	
$\Gamma_2$ $3h^+3h^-$	not seen	
$\Gamma_3$ $2h^+2h^-$	not seen	
$\Gamma_4$ $4h^+4h^-$	not seen	
$\Gamma_5$ $\gamma\gamma$	not seen	
$\Gamma_6$ $\mu^+\mu^-$	$< 9 \times 10^{-3}$	90%
$\Gamma_7$ $\tau^+\tau^-$	$< 8\%$	90%

### $\eta_b(1S)$ $\Gamma(i)\Gamma(\gamma\gamma)/\Gamma(\text{total})$

VALUE (eV)	CL%	DOCUMENT ID	TECN	COMMENT
<b><math>\Gamma(3h^+3h^-) \times \Gamma(\gamma\gamma)/\Gamma_{\text{total}}</math></b>				
$\Gamma_2\Gamma_5/\Gamma$				
$< 470$	95	ABDALLAH	06 DLPH	161-209 $e^+e^-$
$< 132$	95	HEISTER	02D ALEP	181-209 $e^+e^-$

VALUE (eV)	CL%	DOCUMENT ID	TECN	COMMENT
<b><math>\Gamma(2h^+2h^-) \times \Gamma(\gamma\gamma)/\Gamma_{\text{total}}</math></b>				
$\Gamma_3\Gamma_5/\Gamma$				
$< 190$	95	ABDALLAH	06 DLPH	161-209 $e^+e^-$
$< 48$	95	HEISTER	02D ALEP	181-209 $e^+e^-$

# Meson Particle Listings

## $\eta_b(1S), \Upsilon(1S)$

$\Gamma(4h^+4h^-) \times \Gamma(\gamma\gamma)/\Gamma_{\text{total}}$					$\Gamma_4\Gamma_5/\Gamma$
VALUE (eV)	CL%	DOCUMENT ID	TECN	COMMENT	
<660	95	ABDALLAH	06	DLPH	161-209 $e^+e^-$

• • • We do not use the following data for averages, fits, limits, etc. • • •

### $\eta_b(1S)$ BRANCHING RATIOS

$\Gamma(\text{hadrons})/\Gamma_{\text{total}}$					$\Gamma_1/\Gamma$
VALUE	EVTS	DOCUMENT ID	TECN	COMMENT	
seen	34k	MIZUK	12	BELL	$e^+e^- \rightarrow \gamma\pi^+\pi^- + \text{hadrons}$

$\Gamma(\mu^+\mu^-)/\Gamma_{\text{total}}$					$\Gamma_6/\Gamma$
VALUE	CL%	DOCUMENT ID	TECN	COMMENT	
$<9 \times 10^{-3}$	90	<sup>1</sup> AUBERT	09Z	BABR	$e^+e^- \rightarrow \Upsilon(2S, 3S) \rightarrow \gamma\eta_b$
<sup>1</sup> Obtained using $B(\Upsilon(2S) \rightarrow \gamma\eta_b) = (4.2^{+1.1}_{-1.0} \pm 0.9) \times 10^{-4}$ and $B(\Upsilon(3S) \rightarrow \gamma\eta_b) = (4.8 \pm 0.5 \pm 0.6) \times 10^{-4}$ . This limit is equivalent to $B(\eta_b \rightarrow \mu^+\mu^-) = (-0.25 \pm 0.51 \pm 0.33)\%$ measurement.					

$\Gamma(\tau^+\tau^-)/\Gamma_{\text{total}}$					$\Gamma_7/\Gamma$
VALUE	CL%	DOCUMENT ID	TECN	COMMENT	
$<8 \times 10^{-2}$	90	AUBERT	09P	BABR	$e^+e^- \rightarrow \gamma\tau^+\tau^-$

### $\eta_b(1S)$ REFERENCES

FULSOM	18	PRL 121 232001	B. G. Fulsom <i>et al.</i>	(BELLE Collab.)
TAMPONI	15	PRL 115 142001	U. Tamponi <i>et al.</i>	(BELLE Collab.)
DOBBS	12	PRL 109 082001	S. Dobbs <i>et al.</i>	
MIZUK	12	PRL 109 232002	R. Mizuk <i>et al.</i>	(BELLE Collab.)
BONVICINI	10	PR D81 031104	G. Bonvicini <i>et al.</i>	(CLEO Collab.)
AUBERT	09AQ	PRL 103 161801	B. Aubert <i>et al.</i>	(BABAR Collab.)
AUBERT	09P	PRL 103 181801	B. Aubert <i>et al.</i>	(BABAR Collab.)
AUBERT	09Z	PRL 103 081803	B. Aubert <i>et al.</i>	(BABAR Collab.)
AUBERT	08V	PRL 101 071801	B. Aubert <i>et al.</i>	(BABAR Collab.)
ABDALLAH	06	PL B634 340	J.M. Abdallah <i>et al.</i>	(DELPHI Collab.)
HEISTER	02D	PL B530 56	A. Heister <i>et al.</i>	(ALEPH Collab.)

## $\Upsilon(1S)$

$$I^G(J^{PC}) = 0^-(1^{--})$$

### $\Upsilon(1S)$ MASS

VALUE (MeV)	DOCUMENT ID	TECN	COMMENT
<b>9460.30 ± 0.26 OUR AVERAGE</b>	Error includes scale factor of 3.3.		
9460.51 ± 0.09 ± 0.05	<sup>1</sup> ARTAMONOV	00	MD1 $e^+e^- \rightarrow \text{hadrons}$
9459.97 ± 0.11 ± 0.07	MACKAY	84	REDE $e^+e^- \rightarrow \text{hadrons}$
9460.60 ± 0.09 ± 0.05	<sup>2,3</sup> BARU	92B	REDE $e^+e^- \rightarrow \text{hadrons}$
9460.59 ± 0.12	BARU	86	REDE $e^+e^- \rightarrow \text{hadrons}$
9460.6 ± 0.4	<sup>3,4</sup> ARTAMONOV	84	REDE $e^+e^- \rightarrow \text{hadrons}$

<sup>1</sup> Reanalysis of BARU 92B and ARTAMONOV 84 using new electron mass (COHEN 87).  
<sup>2</sup> Superseding BARU 86.  
<sup>3</sup> Superseded by ARTAMONOV 00.  
<sup>4</sup> Value includes data of ARTAMONOV 82.

### $\Upsilon(1S)$ WIDTH

VALUE (keV)	DOCUMENT ID
<b>54.02 ± 1.25 OUR EVALUATION</b>	See the Note on "Width Determinations of the $\Upsilon$ States"

### $\Upsilon(1S)$ DECAY MODES

Mode	Fraction ( $\Gamma_i/\Gamma$ )	Scale factor/ Confidence level
$\Gamma_1$ $\tau^+\tau^-$	( 2.60 ± 0.10 ) %	
$\Gamma_2$ $e^+e^-$	( 2.38 ± 0.11 ) %	
$\Gamma_3$ $\mu^+\mu^-$	( 2.48 ± 0.05 ) %	
<b>Hadronic decays</b>		
$\Gamma_4$ $ggg$	(81.7 ± 0.7 ) %	
$\Gamma_5$ $\gamma gg$	( 2.2 ± 0.6 ) %	
$\Gamma_6$ $\eta'(958)$ anything	( 2.94 ± 0.24 ) %	
$\Gamma_7$ $J/\psi(1S)$ anything	( 5.4 ± 0.4 ) × 10 <sup>-4</sup>	S=1.4
$\Gamma_8$ $J/\psi(1S)\eta_c$	< 2.2	× 10 <sup>-6</sup> CL=90%
$\Gamma_9$ $J/\psi(1S)\chi_{c0}$	< 3.4	× 10 <sup>-6</sup> CL=90%
$\Gamma_{10}$ $J/\psi(1S)\chi_{c1}$	( 3.9 ± 1.2 ) × 10 <sup>-6</sup>	
$\Gamma_{11}$ $J/\psi(1S)\chi_{c2}$	< 1.4	× 10 <sup>-6</sup> CL=90%
$\Gamma_{12}$ $J/\psi(1S)\eta_c(2S)$	< 2.2	× 10 <sup>-6</sup> CL=90%
$\Gamma_{13}$ $J/\psi(1S)X(3940)$	< 5.4	× 10 <sup>-6</sup> CL=90%
$\Gamma_{14}$ $J/\psi(1S)X(4160)$	< 5.4	× 10 <sup>-6</sup> CL=90%
$\Gamma_{15}$ $X(4350)$ anything, $X \rightarrow J/\psi(1S)\phi$	< 8.1	× 10 <sup>-6</sup> CL=90%

$\Gamma_{16}$	$Z_c(3900)^\pm$ anything, $Z_c \rightarrow J/\psi(1S)\pi^\pm$	< 1.3	× 10 <sup>-5</sup>	CL=90%
$\Gamma_{17}$	$Z_c(4200)^\pm$ anything, $Z_c \rightarrow J/\psi(1S)\pi^\pm$	< 6.0	× 10 <sup>-5</sup>	CL=90%
$\Gamma_{18}$	$Z_c(4430)^\pm$ anything, $Z_c \rightarrow J/\psi(1S)\pi^\pm$	< 4.9	× 10 <sup>-5</sup>	CL=90%
$\Gamma_{19}$	$X_{cs}^\pm$ anything, $X \rightarrow J/\psi K^\pm$	< 5.7	× 10 <sup>-6</sup>	CL=90%
$\Gamma_{20}$	$\chi_{c1}(3872)$ anything, $\chi_{c1} \rightarrow J/\psi(1S)\pi^+\pi^-$	< 9.5	× 10 <sup>-6</sup>	CL=90%
$\Gamma_{21}$	$\psi(4260)$ anything, $\psi \rightarrow J/\psi(1S)\pi^+\pi^-$	< 3.8	× 10 <sup>-5</sup>	CL=90%
$\Gamma_{22}$	$\psi(4260)$ anything, $\psi \rightarrow J/\psi(1S)K^+K^-$	< 7.5	× 10 <sup>-6</sup>	CL=90%
$\Gamma_{23}$	$\chi_{c1}(4140)$ anything, $\chi_{c1} \rightarrow J/\psi(1S)\phi$	< 5.2	× 10 <sup>-6</sup>	CL=90%
$\Gamma_{24}$	$\chi_{c0}$ anything	< 4	× 10 <sup>-3</sup>	CL=90%
$\Gamma_{25}$	$\chi_{c1}$ anything	( 1.90 ± 0.35 ) × 10 <sup>-4</sup>		
$\Gamma_{26}$	$\chi_{c1}(1P)X_{tetra}$	< 3.78	× 10 <sup>-5</sup>	CL=90%
$\Gamma_{27}$	$\chi_{c2}$ anything	( 2.8 ± 0.8 ) × 10 <sup>-4</sup>		
$\Gamma_{28}$	$\psi(2S)$ anything	( 1.23 ± 0.20 ) × 10 <sup>-4</sup>		
$\Gamma_{29}$	$\psi(2S)\eta_c$	< 3.6	× 10 <sup>-6</sup>	CL=90%
$\Gamma_{30}$	$\psi(2S)\chi_{c0}$	< 6.5	× 10 <sup>-6</sup>	CL=90%
$\Gamma_{31}$	$\psi(2S)\chi_{c1}$	< 4.5	× 10 <sup>-6</sup>	CL=90%
$\Gamma_{32}$	$\psi(2S)\chi_{c2}$	< 2.1	× 10 <sup>-6</sup>	CL=90%
$\Gamma_{33}$	$\psi(2S)\eta_c(2S)$	< 3.2	× 10 <sup>-6</sup>	CL=90%
$\Gamma_{34}$	$\psi(2S)X(3940)$	< 2.9	× 10 <sup>-6</sup>	CL=90%
$\Gamma_{35}$	$\psi(2S)X(4160)$	< 2.9	× 10 <sup>-6</sup>	CL=90%
$\Gamma_{36}$	$\psi(4260)$ anything, $\psi \rightarrow \psi(2S)\pi^+\pi^-$	< 7.9	× 10 <sup>-5</sup>	CL=90%
$\Gamma_{37}$	$\psi(4360)$ anything, $\psi \rightarrow \psi(2S)\pi^+\pi^-$	< 5.2	× 10 <sup>-5</sup>	CL=90%
$\Gamma_{38}$	$\psi(4660)$ anything, $\psi \rightarrow \psi(2S)\pi^+\pi^-$	< 2.2	× 10 <sup>-5</sup>	CL=90%
$\Gamma_{39}$	$X(4050)^\pm$ anything, $X \rightarrow \psi(2S)\pi^\pm$	< 8.8	× 10 <sup>-5</sup>	CL=90%
$\Gamma_{40}$	$Z_c(4430)^\pm$ anything, $Z_c \rightarrow \psi(2S)\pi^\pm$	< 6.7	× 10 <sup>-5</sup>	CL=90%
$\Gamma_{41}$	$Z_c(4200)^+Z_c(4200)^-$	< 2.23	× 10 <sup>-5</sup>	CL=90%
$\Gamma_{42}$	$Z_c(3900)^\pm Z_c(4200)^\mp$	< 8.1	× 10 <sup>-6</sup>	CL=90%
$\Gamma_{43}$	$Z_c(3900)^+Z_c(3900)^-$	< 1.8	× 10 <sup>-6</sup>	CL=90%
$\Gamma_{44}$	$X(4050)^+X(4050)^-$	< 1.58	× 10 <sup>-5</sup>	CL=90%
$\Gamma_{45}$	$X(4250)^+X(4250)^-$	< 2.66	× 10 <sup>-5</sup>	CL=90%
$\Gamma_{46}$	$X(4050)^\pm X(4250)^\mp$	< 4.42	× 10 <sup>-5</sup>	CL=90%
$\Gamma_{47}$	$Z_c(4430)^+Z_c(4430)^-$	< 2.03	× 10 <sup>-5</sup>	CL=90%
$\Gamma_{48}$	$X(4055)^\pm X(4055)^\mp$	< 2.33	× 10 <sup>-5</sup>	CL=90%
$\Gamma_{49}$	$X(4055)^\pm Z_c(4430)^\mp$	< 4.55	× 10 <sup>-5</sup>	CL=90%
$\Gamma_{50}$	$\rho\pi$	< 3.68	× 10 <sup>-6</sup>	CL=90%
$\Gamma_{51}$	$\omega\pi^0$	< 3.90	× 10 <sup>-6</sup>	CL=90%
$\Gamma_{52}$	$\pi^+\pi^-$	< 5	× 10 <sup>-4</sup>	CL=90%
$\Gamma_{53}$	$K^+K^-$	< 5	× 10 <sup>-4</sup>	CL=90%
$\Gamma_{54}$	$\rho\bar{\rho}$	< 5	× 10 <sup>-4</sup>	CL=90%
$\Gamma_{55}$	$\pi^+\pi^-\pi^0$	( 2.1 ± 0.8 ) × 10 <sup>-6</sup>		
$\Gamma_{56}$	$\phi K^+K^-$	( 2.4 ± 0.5 ) × 10 <sup>-6</sup>		
$\Gamma_{57}$	$\omega\pi^+\pi^-$	( 4.5 ± 1.0 ) × 10 <sup>-6</sup>		
$\Gamma_{58}$	$K^*(892)^0 K^- \pi^+ + \text{c.c.}$	( 4.4 ± 0.8 ) × 10 <sup>-6</sup>		
$\Gamma_{59}$	$\phi f'_2(1525)$	< 1.63	× 10 <sup>-6</sup>	CL=90%
$\Gamma_{60}$	$\omega f_2(1270)$	< 1.79	× 10 <sup>-6</sup>	CL=90%
$\Gamma_{61}$	$\rho(770)a_2(1320)$	< 2.24	× 10 <sup>-6</sup>	CL=90%
$\Gamma_{62}$	$K^*(892)^0 \bar{K}_2^*(1430)^0 + \text{c.c.}$	( 3.0 ± 0.8 ) × 10 <sup>-6</sup>		
$\Gamma_{63}$	$K_1(1270)^\pm K^\mp$	< 2.41	× 10 <sup>-6</sup>	CL=90%
$\Gamma_{64}$	$K_1(1400)^\pm K^\mp$	( 1.0 ± 0.4 ) × 10 <sup>-6</sup>		
$\Gamma_{65}$	$b_1(1235)^\pm \pi^\mp$	< 1.25	× 10 <sup>-6</sup>	CL=90%
$\Gamma_{66}$	$\pi^+\pi^-\pi^0$	( 1.28 ± 0.30 ) × 10 <sup>-5</sup>		
$\Gamma_{67}$	$K_S^0 K^+\pi^- + \text{c.c.}$	( 1.6 ± 0.4 ) × 10 <sup>-6</sup>		
$\Gamma_{68}$	$K^*(892)^0 \bar{K}^0 + \text{c.c.}$	( 2.9 ± 0.9 ) × 10 <sup>-6</sup>		
$\Gamma_{69}$	$K^*(892)^- K^+ + \text{c.c.}$	< 1.11	× 10 <sup>-6</sup>	CL=90%
$\Gamma_{70}$	$f_1(1285)$ anything	( 4.6 ± 3.1 ) × 10 <sup>-3</sup>		
$\Gamma_{71}$	$D^*(2010)^\pm$ anything	( 2.52 ± 0.20 ) %		
$\Gamma_{72}$	$f_1(1285)X_{tetra}$	< 6.24	× 10 <sup>-5</sup>	CL=90%
$\Gamma_{73}$	$^2H$ anything	( 2.85 ± 0.25 ) × 10 <sup>-5</sup>		
$\Gamma_{74}$	Sum of 100 exclusive modes	( 1.200 ± 0.017 ) %		
<b>Radiative decays</b>				
$\Gamma_{75}$	$\gamma\pi^+\pi^-$	( 6.3 ± 1.8 ) × 10 <sup>-5</sup>		
$\Gamma_{76}$	$\gamma\pi^0\pi^0$	( 1.7 ± 0.7 ) × 10 <sup>-5</sup>		
$\Gamma_{77}$	$\gamma\pi\pi$ (S-wave)	( 4.6 ± 0.7 ) × 10 <sup>-5</sup>		







See key on page 999

# Meson Particle Listings

## $\Upsilon(1S)$

$\Gamma(Z_c(4430)^\pm \text{ anything}, Z_c \rightarrow \psi(2S)\pi^\pm)/\Gamma_{\text{total}}$					$\Gamma_{40}/\Gamma$
VALUE	CL%	DOCUMENT ID	TECN	COMMENT	
$<6.7 \times 10^{-5}$	90	SHEN	16	BELL $\Upsilon(1S) \rightarrow \psi(2S)\pi^\pm X$	

$\Gamma(Z_c(4200)^+ Z_c(4200)^-)/\Gamma_{\text{total}}$					$\Gamma_{41}/\Gamma$
VALUE	CL%	DOCUMENT ID	TECN	COMMENT	
$<22.3 \times 10^{-6}$	90	<sup>1</sup> JIA	18	BELL $\Upsilon(1S) \rightarrow J/\psi\pi^\pm X$	
<sup>1</sup> Assuming $B(Z_c(4200)^\pm \rightarrow J/\psi\pi^\pm) = 1$ .					

$\Gamma(Z_c(3900)^\pm Z_c(4200)^\mp)/\Gamma_{\text{total}}$					$\Gamma_{42}/\Gamma$
VALUE	CL%	DOCUMENT ID	TECN	COMMENT	
$<8.1 \times 10^{-6}$	90	<sup>1</sup> JIA	18	BELL $\Upsilon(1S) \rightarrow J/\psi\pi^\pm X$	
<sup>1</sup> Assuming $B(Z_c(4200)^\pm \rightarrow J/\psi\pi^\pm) = 1 = B(Z_c(3900)^\pm \rightarrow J/\psi\pi^\pm)$ .					

$\Gamma(Z_c(3900)^+ Z_c(3900)^-)/\Gamma_{\text{total}}$					$\Gamma_{43}/\Gamma$
VALUE	CL%	DOCUMENT ID	TECN	COMMENT	
$<1.8 \times 10^{-6}$	90	<sup>1</sup> JIA	18	BELL $\Upsilon(1S) \rightarrow J/\psi\pi^\pm X$	
<sup>1</sup> Assuming $B(Z_c(3900)^\pm \rightarrow J/\psi\pi^\pm) = 1$					

$\Gamma(X(4050)^+ X(4050)^-)/\Gamma_{\text{total}}$					$\Gamma_{44}/\Gamma$
VALUE	CL%	DOCUMENT ID	TECN	COMMENT	
$<15.8 \times 10^{-6}$	90	<sup>1</sup> JIA	18	BELL $\Upsilon(1S) \rightarrow \chi_{c1}(1P)\pi^\pm X$	
<sup>1</sup> Assuming $B(X(4050)^\pm \rightarrow \chi_{c1}(1P)\pi^\pm) = 1$					

$\Gamma(X(4250)^+ X(4250)^-)/\Gamma_{\text{total}}$					$\Gamma_{45}/\Gamma$
VALUE	CL%	DOCUMENT ID	TECN	COMMENT	
$<26.6 \times 10^{-6}$	90	<sup>1</sup> JIA	18	BELL $\Upsilon(1S) \rightarrow \chi_{c1}(1P)\pi^\pm X$	
<sup>1</sup> Assuming $B(X(4250)^\pm \rightarrow \chi_{c1}(1P)\pi^\pm) = 1$					

$\Gamma(X(4050)^\pm X(4250)^\mp)/\Gamma_{\text{total}}$					$\Gamma_{46}/\Gamma$
VALUE	CL%	DOCUMENT ID	TECN	COMMENT	
$<44.2 \times 10^{-6}$	90	<sup>1</sup> JIA	18	BELL $\Upsilon(1S) \rightarrow \chi_{c1}(1P)\pi^\pm X$	
<sup>1</sup> Assuming $B(X(4050)^\pm \rightarrow \chi_{c1}(1P)\pi^\pm) = 1 = B(X(4250)^\pm \rightarrow \chi_{c1}(1P)\pi^\pm)$					

$\Gamma(Z_c(4430)^+ Z_c(4430)^-)/\Gamma_{\text{total}}$					$\Gamma_{47}/\Gamma$
VALUE	CL%	DOCUMENT ID	TECN	COMMENT	
$<20.3 \times 10^{-6}$	90	<sup>1</sup> JIA	18	BELL $\Upsilon(2S) \rightarrow \psi(2S)\pi^\pm X$	
<sup>1</sup> Assuming $B(Z_c(4430)^\pm \rightarrow \psi(2S)\pi^\pm) = 1$					

$\Gamma(X(4055)^\pm X(4055)^\mp)/\Gamma_{\text{total}}$					$\Gamma_{48}/\Gamma$
VALUE	CL%	DOCUMENT ID	TECN	COMMENT	
$<23.3 \times 10^{-6}$	90	<sup>1</sup> JIA	18	BELL $\Upsilon(1S) \rightarrow \psi(2S)\pi^\pm X$	
<sup>1</sup> Assuming $B(X(4055)^\pm \rightarrow \psi(2S)\pi^\pm) = 1$					

$\Gamma(X(4055)^\pm Z_c(4430)^\mp)/\Gamma_{\text{total}}$					$\Gamma_{49}/\Gamma$
VALUE	CL%	DOCUMENT ID	TECN	COMMENT	
$<45.5 \times 10^{-6}$	90	<sup>1</sup> JIA	18	BELL $\Upsilon(1S) \rightarrow \psi(2S)\pi^\pm X$	
<sup>1</sup> Assuming $B(X(4055)^\pm \rightarrow \psi(2S)\pi^\pm) = 1 = B(Z_c(4430)^\pm \rightarrow \psi(2S)\pi^\pm)$					

$\Gamma(\rho\pi)/\Gamma_{\text{total}}$					$\Gamma_{50}/\Gamma$
VALUE (units $10^{-6}$ )	CL%	DOCUMENT ID	TECN	COMMENT	
$<3.68$	90	SHEN	13	BELL $\Upsilon(1S) \rightarrow \pi^+\pi^-\pi^0$	
••• We do not use the following data for averages, fits, limits, etc. •••					
$<1 \times 10^3$	90	BLINOV	90	MD1 $\Upsilon(1S) \rightarrow \rho^0\pi^0$	
$<2 \times 10^2$	90	FULTON	90B	$\Upsilon(1S) \rightarrow \rho^0\pi^0$	
$<2.1 \times 10^3$	90	NICZYPORUK	83	LENA $\Upsilon(1S) \rightarrow \rho^0\pi^0$	

$\Gamma(\omega\pi^0)/\Gamma_{\text{total}}$					$\Gamma_{51}/\Gamma$
VALUE (units $10^{-6}$ )	CL%	DOCUMENT ID	TECN	COMMENT	
$<3.90$	90	SHEN	13	BELL $\Upsilon(1S) \rightarrow \pi^+\pi^-\pi^0\pi^0$	

$\Gamma(\pi^+\pi^-)/\Gamma_{\text{total}}$					$\Gamma_{52}/\Gamma$
VALUE (units $10^{-4}$ )	CL%	DOCUMENT ID	TECN	COMMENT	
$<5$	90	BARU	92	MD1 $\Upsilon(1S) \rightarrow \pi^+\pi^-$	

$\Gamma(K^+K^-)/\Gamma_{\text{total}}$					$\Gamma_{53}/\Gamma$
VALUE (units $10^{-4}$ )	CL%	DOCUMENT ID	TECN	COMMENT	
$<5$	90	BARU	92	MD1 $\Upsilon(1S) \rightarrow K^+K^-$	

$\Gamma(\rho\bar{\rho})/\Gamma_{\text{total}}$					$\Gamma_{54}/\Gamma$
VALUE (units $10^{-4}$ )	CL%	DOCUMENT ID	TECN	COMMENT	
$<5$	90	<sup>1</sup> BARU	96	MD1 $\Upsilon(1S) \rightarrow \rho\bar{\rho}$	
<sup>1</sup> Supersedes BARU 92 in this node.					

$\Gamma(\pi^+\pi^-\pi^0)/\Gamma_{\text{total}}$					$\Gamma_{55}/\Gamma$
VALUE (units $10^{-6}$ )	CL%	EVTS	DOCUMENT ID	TECN	COMMENT
$2.14 \pm 0.72 \pm 0.34$		$26 \pm 9$	SHEN	13	BELL $\Upsilon(1S) \rightarrow \pi^+\pi^-\pi^0$
••• We do not use the following data for averages, fits, limits, etc. •••					
$<18.4$	90		ANASTASSOV	99	CLE2 $e^+e^- \rightarrow \text{hadrons}$

$\Gamma(\phi K^+ K^-)/\Gamma_{\text{total}}$					$\Gamma_{56}/\Gamma$
VALUE (units $10^{-6}$ )	CL%	EVTS	DOCUMENT ID	TECN	COMMENT
$2.36 \pm 0.37 \pm 0.29$		56	SHEN	12A	BELL $\Upsilon(1S) \rightarrow 2(K^+K^-)$

$\Gamma(\omega\pi^+\pi^-)/\Gamma_{\text{total}}$					$\Gamma_{57}/\Gamma$
VALUE (units $10^{-6}$ )	CL%	EVTS	DOCUMENT ID	TECN	COMMENT
$4.46 \pm 0.67 \pm 0.72$		64	SHEN	12A	BELL $\Upsilon(1S) \rightarrow 2(\pi^+\pi^-)\pi^0$

$\Gamma(K^*(892)^0 K^- \pi^+ + c.c.)/\Gamma_{\text{total}}$					$\Gamma_{58}/\Gamma$
VALUE (units $10^{-6}$ )	CL%	EVTS	DOCUMENT ID	TECN	COMMENT
$4.42 \pm 0.50 \pm 0.58$		173	SHEN	12A	BELL $\Upsilon(1S) \rightarrow K^+K^-\pi^+\pi^-$

$\Gamma(\phi f_2'(1525))/\Gamma_{\text{total}}$					$\Gamma_{59}/\Gamma$
VALUE (units $10^{-6}$ )	CL%	EVTS	DOCUMENT ID	TECN	COMMENT
$<1.63$	90		SHEN	12A	BELL $\Upsilon(1S) \rightarrow 2(K^+K^-)$

$\Gamma(\omega f_2(1270))/\Gamma_{\text{total}}$					$\Gamma_{60}/\Gamma$
VALUE (units $10^{-6}$ )	CL%	EVTS	DOCUMENT ID	TECN	COMMENT
$<1.79$	90		SHEN	12A	BELL $\Upsilon(1S) \rightarrow 2(\pi^+\pi^-)\pi^0$

$\Gamma(\rho(770) a_2(1320))/\Gamma_{\text{total}}$					$\Gamma_{61}/\Gamma$
VALUE (units $10^{-6}$ )	CL%	EVTS	DOCUMENT ID	TECN	COMMENT
$<2.24$	90		SHEN	12A	BELL $\Upsilon(1S) \rightarrow 2(\pi^+\pi^-)\pi^0$

$\Gamma(K^*(892)^0 \bar{K}_2^0(1430)^0 + c.c.)/\Gamma_{\text{total}}$					$\Gamma_{62}/\Gamma$
VALUE (units $10^{-6}$ )	CL%	EVTS	DOCUMENT ID	TECN	COMMENT
$3.02 \pm 0.68 \pm 0.34$		42	SHEN	12A	BELL $\Upsilon(1S) \rightarrow K^+K^-\pi^+\pi^-$

$\Gamma(K_1(1270)^\pm K^\mp)/\Gamma_{\text{total}}$					$\Gamma_{63}/\Gamma$
VALUE (units $10^{-6}$ )	CL%	EVTS	DOCUMENT ID	TECN	COMMENT
$<2.41$	90		SHEN	12A	BELL $\Upsilon(1S) \rightarrow K^+K^-\pi^+\pi^-$

$\Gamma(K_1(1400)^\pm K^\mp)/\Gamma_{\text{total}}$					$\Gamma_{64}/\Gamma$
VALUE (units $10^{-6}$ )	CL%	EVTS	DOCUMENT ID	TECN	COMMENT
$1.02 \pm 0.35 \pm 0.22$		24	SHEN	12A	BELL $\Upsilon(1S) \rightarrow K^+K^-\pi^+\pi^-$

$\Gamma(b_1(1235)^\pm \pi^\mp)/\Gamma_{\text{total}}$					$\Gamma_{65}/\Gamma$
VALUE (units $10^{-6}$ )	CL%	EVTS	DOCUMENT ID	TECN	COMMENT
$<1.25$	90		SHEN	12A	BELL $\Upsilon(1S) \rightarrow 2(\pi^+\pi^-)\pi^0$

$\Gamma(\pi^+\pi^-\pi^0\pi^0)/\Gamma_{\text{total}}$					$\Gamma_{66}/\Gamma$
VALUE (units $10^{-6}$ )	CL%	EVTS	DOCUMENT ID	TECN	COMMENT
$12.8 \pm 2.0 \pm 2.3$		$143 \pm 22$	SHEN	13	BELL $\Upsilon(1S) \rightarrow \pi^+\pi^-\pi^0\pi^0$

$\Gamma(K_S^0 K^+ \pi^- + c.c.)/\Gamma_{\text{total}}$					$\Gamma_{67}/\Gamma$
VALUE (units $10^{-6}$ )	CL%	EVTS	DOCUMENT ID	TECN	COMMENT
$1.59 \pm 0.33 \pm 0.18$		$37 \pm 8$	SHEN	13	BELL $\Upsilon(1S) \rightarrow K_S^0 K^-\pi^+$
••• We do not use the following data for averages, fits, limits, etc. •••					
$<3.4$	90		<sup>1</sup> DOBBS	12A	$\Upsilon(1S) \rightarrow K_S^0 K^-\pi^+$
<sup>1</sup> Obtained by analyzing CLEO III data but not authored by the CLEO Collaboration.					

$\Gamma(K^*(892)^0 \bar{K}^0 + c.c.)/\Gamma_{\text{total}}$					$\Gamma_{68}/\Gamma$
VALUE (units $10^{-6}$ )	CL%	EVTS	DOCUMENT ID	TECN	COMMENT
$2.92 \pm 0.85 \pm 0.37$		$16 \pm 5$	SHEN	13	BELL $\Upsilon(1S) \rightarrow K_S^0 K^-\pi^+$

$\Gamma(K^*(892)^- K^+ + c.c.)/\Gamma_{\text{total}}$					$\Gamma_{69}/\Gamma$
VALUE (units $10^{-6}$ )	CL%	EVTS	DOCUMENT ID	TECN	COMMENT
$<1.11$	90		SHEN	13	BELL $\Upsilon(1S) \rightarrow K_S^0 K^-\pi^+$

$\Gamma(f_1(1285) \text{ anything})/\Gamma_{\text{total}}$					$\Gamma_{70}/\Gamma$
VALUE (units $10^{-3}$ )	CL%	EVTS	DOCUMENT ID	TECN	COMMENT
$4.6 \pm 2.8 \pm 1.3$		3.1k	JIA	17A	BELL $e^+e^- \rightarrow \text{hadrons}$

$\Gamma(D^*(2010)^\pm \text{ anything})/\Gamma_{\text{total}}$					$\Gamma_{71}/\Gamma$
VALUE (units $10^{-3}$ )	CL%	EVTS	DOCUMENT ID	TECN	COMMENT
$25.2 \pm 1.3 \pm 1.5$		$\approx 2k$	<sup>1</sup> AUBERT	10c	BABR $\Upsilon(2S) \rightarrow \pi^+\pi^-\Upsilon(1S)$
••• We do not use the following data for averages, fits, limits, etc. •••					
$<19$	90		<sup>2</sup> ALBRECHT	92J	ARG $e^+e^- \rightarrow D^0\pi^\pm X$
<sup>1</sup> For $x_p > 0.1$ .					
<sup>2</sup> For $x_p > 0.2$ .					

## Meson Particle Listings

 $\Upsilon(1S)$ 

$\Gamma(f_1(1285)X_{tetra})/\Gamma_{total}$	CL%	DOCUMENT ID	TECN	COMMENT	$\Gamma_{72}/\Gamma$
$<62.4 \times 10^{-6}$	90	<sup>1</sup> JIA	17A	BELL $e^+e^- \rightarrow$ hadrons	

<sup>1</sup> For a tetraquark state  $X_{tetra}$ , with mass in the range 1.16–2.46 GeV and width in the range 0–0.3 GeV. Measured 90% CL limits as a function of  $X_{tetra}$  mass and width range from  $4.6 \times 10^{-6}$  to  $62.4 \times 10^{-6}$ .

$\Gamma(2\overline{H} \text{ anything})/\Gamma_{total}$	EVTS	DOCUMENT ID	TECN	COMMENT	$\Gamma_{73}/\Gamma$
<b><math>2.85 \pm 0.25</math> OUR AVERAGE</b>					
$2.81 \pm 0.49^{+0.20}_{-0.24}$		LEES	14G	BABR $e^+e^- \rightarrow 2\overline{H} X$	
$2.86 \pm 0.19 \pm 0.21$	455	ASNER	07	CLEO $e^+e^- \rightarrow 2\overline{H} X$	

$\Gamma(\text{Sum of 100 exclusive modes})/\Gamma_{total}$	CL%	DOCUMENT ID	TECN	COMMENT	$\Gamma_{74}/\Gamma$
<b><math>1.200 \pm 0.017</math></b>		<sup>1,2</sup> DOBBS	12A	$\Upsilon(1S) \rightarrow$ hadrons	

<sup>1</sup> DOBBS 12A presents individual exclusive branching fractions or upper limits for 100 modes of four to ten pions, kaons, or protons.

<sup>2</sup> Obtained by analyzing CLEO III data but not authored by the CLEO Collaboration.

$\Gamma(ggg, \gamma g g \rightarrow \overline{d} \text{ anything})/\Gamma(ggg, \gamma g g \rightarrow \text{anything})$	EVTS	DOCUMENT ID	TECN	COMMENT	$\Gamma_{75}/\Gamma$
<b><math>3.36 \pm 0.23 \pm 0.25</math></b>	455	ASNER	07	CLEO $e^+e^- \rightarrow \overline{d} X$	

$\Gamma(\gamma\pi^+\pi^-)/\Gamma_{total}$	CL%	DOCUMENT ID	TECN	COMMENT	$\Gamma_{75}/\Gamma$
<b><math>6.3 \pm 1.2 \pm 1.3</math></b>		<sup>1</sup> ANASTASSOV	99	CLE2 $e^+e^- \rightarrow$ hadrons	

<sup>1</sup> For  $m_{\pi\pi} > 1$  GeV.

$\Gamma(\gamma\pi^0\pi^0)/\Gamma_{total}$	CL%	DOCUMENT ID	TECN	COMMENT	$\Gamma_{76}/\Gamma$
<b><math>1.7 \pm 0.6 \pm 0.3</math></b>		<sup>1</sup> ANASTASSOV	99	CLE2 $e^+e^- \rightarrow$ hadrons	

<sup>1</sup> For  $m_{\pi\pi} > 1$  GeV.

$\Gamma(\gamma\pi\pi(S\text{-wave}))/\Gamma_{total}$	CL%	DOCUMENT ID	TECN	COMMENT	$\Gamma_{77}/\Gamma$
<b><math>4.63 \pm 0.56 \pm 0.48</math></b>		LEES	18A	BABR $\Upsilon(1S) \rightarrow \gamma\pi^+\pi^-$	

$\Gamma(\gamma\pi^0\eta)/\Gamma_{total}$	CL%	DOCUMENT ID	TECN	COMMENT	$\Gamma_{78}/\Gamma$
<b><math>&lt;2.4</math></b>	90	<sup>1</sup> BESSON	07A	CLEO $e^+e^- \rightarrow \Upsilon(1S)$	

<sup>1</sup> BESSON 07A obtained this limit for  $0.7 < m_{\pi^0\eta} < 3$  GeV.

$\Gamma(\gamma K^+ K^-)/\Gamma_{total}$	CL%	DOCUMENT ID	TECN	COMMENT	$\Gamma_{79}/\Gamma$
$(2 < m_{K^+K^-} < 3 \text{ GeV})$					
<b><math>1.14 \pm 0.08 \pm 0.10</math></b>	90	ATHAR	06	CLE3 $\Upsilon(1S) \rightarrow \gamma K^+ K^-$	

$\Gamma(\gamma\rho\overline{\rho})/\Gamma_{total}$	CL%	DOCUMENT ID	TECN	COMMENT	$\Gamma_{80}/\Gamma$
$(2 < m_{\rho\overline{\rho}} < 3 \text{ GeV})$					
<b><math>&lt;0.6</math></b>	90	ATHAR	06	CLE3 $\Upsilon(1S) \rightarrow \gamma\rho\overline{\rho}$	

$\Gamma(\gamma 2h^+ 2h^-)/\Gamma_{total}$	EVTS	DOCUMENT ID	TECN	COMMENT	$\Gamma_{81}/\Gamma$
<b><math>7.0 \pm 1.1 \pm 1.0</math></b>	80 $\pm$ 12	FULTON	90B	CLEO $e^+e^- \rightarrow$ hadrons	

$\Gamma(\gamma 3h^+ 3h^-)/\Gamma_{total}$	EVTS	DOCUMENT ID	TECN	COMMENT	$\Gamma_{82}/\Gamma$
<b><math>5.4 \pm 1.5 \pm 1.3</math></b>	39 $\pm$ 11	FULTON	90B	CLEO $e^+e^- \rightarrow$ hadrons	

$\Gamma(\gamma 4h^+ 4h^-)/\Gamma_{total}$	EVTS	DOCUMENT ID	TECN	COMMENT	$\Gamma_{83}/\Gamma$
<b><math>7.4 \pm 2.5 \pm 2.5</math></b>	36 $\pm$ 12	FULTON	90B	CLEO $e^+e^- \rightarrow$ hadrons	

$\Gamma(\gamma\pi^+\pi^-K^+K^-)/\Gamma_{total}$	EVTS	DOCUMENT ID	TECN	COMMENT	$\Gamma_{84}/\Gamma$
<b><math>2.9 \pm 0.7 \pm 0.6</math></b>	29 $\pm$ 8	FULTON	90B	CLEO $e^+e^- \rightarrow$ hadrons	

$\Gamma(\gamma 2\pi^+ 2\pi^-)/\Gamma_{total}$	EVTS	DOCUMENT ID	TECN	COMMENT	$\Gamma_{85}/\Gamma$
<b><math>2.5 \pm 0.7 \pm 0.5</math></b>	26 $\pm$ 7	FULTON	90B	CLEO $e^+e^- \rightarrow$ hadrons	

$\Gamma(\gamma 3\pi^+ 3\pi^-)/\Gamma_{total}$	EVTS	DOCUMENT ID	TECN	COMMENT	$\Gamma_{86}/\Gamma$
<b><math>2.5 \pm 0.9 \pm 0.8</math></b>	17 $\pm$ 5	FULTON	90B	CLEO $e^+e^- \rightarrow$ hadrons	

$\Gamma(\gamma 2\pi^+ 2\pi^- K^+ K^-)/\Gamma_{total}$	EVTS	DOCUMENT ID	TECN	COMMENT	$\Gamma_{87}/\Gamma$
<b><math>2.4 \pm 0.9 \pm 0.8</math></b>	18 $\pm$ 7	FULTON	90B	CLEO $e^+e^- \rightarrow$ hadrons	

$\Gamma(\gamma\pi^+\pi^-\rho\overline{\rho})/\Gamma_{total}$	EVTS	DOCUMENT ID	TECN	COMMENT	$\Gamma_{88}/\Gamma$
<b><math>1.5 \pm 0.5 \pm 0.3</math></b>	22 $\pm$ 6	FULTON	90B	CLEO $e^+e^- \rightarrow$ hadrons	

$\Gamma(\gamma 2\pi^+ 2\pi^- \rho\overline{\rho})/\Gamma_{total}$	EVTS	DOCUMENT ID	TECN	COMMENT	$\Gamma_{89}/\Gamma$
<b><math>0.4 \pm 0.4 \pm 0.4</math></b>	7 $\pm$ 6	FULTON	90B	CLEO $e^+e^- \rightarrow$ hadrons	

$\Gamma(\gamma 2K^+ 2K^-)/\Gamma_{total}$	EVTS	DOCUMENT ID	TECN	COMMENT	$\Gamma_{90}/\Gamma$
<b><math>0.2 \pm 0.2</math></b>	2 $\pm$ 2	FULTON	90B	CLEO $e^+e^- \rightarrow$ hadrons	

$\Gamma(\gamma\eta(958))/\Gamma_{total}$	CL%	DOCUMENT ID	TECN	COMMENT	$\Gamma_{91}/\Gamma$
<b><math>&lt; 1.9</math></b>	90	ATHAR	07A	CLEO $\Upsilon(1S) \rightarrow \gamma\eta' \rightarrow \gamma\pi^+\pi^-\eta, \gamma\rho$	
$\bullet \bullet \bullet$ We do not use the following data for averages, fits, limits, etc. $\bullet \bullet \bullet$					
$<16$	90	RICHICHI	01B	CLE2 $\Upsilon(1S) \rightarrow \gamma\eta' \rightarrow \gamma\eta\pi^+\pi^-$	

$\Gamma(\gamma\eta)/\Gamma_{total}$	CL%	DOCUMENT ID	TECN	COMMENT	$\Gamma_{92}/\Gamma$
<b><math>&lt; 1.0</math></b>	90	ATHAR	07A	CLEO $\Upsilon(1S) \rightarrow \gamma\eta \rightarrow \gamma\gamma\gamma, \gamma\pi^+\pi^-\pi^0, \gamma 3\pi^0$	
$\bullet \bullet \bullet$ We do not use the following data for averages, fits, limits, etc. $\bullet \bullet \bullet$					
$<21$	90	MASEK	02	CLEO $\Upsilon(1S) \rightarrow \gamma\eta$	

$\Gamma(\gamma f_0(980))/\Gamma_{total}$	CL%	DOCUMENT ID	TECN	COMMENT	$\Gamma_{93}/\Gamma$
<b><math>&lt;3</math></b>	90	<sup>1</sup> ATHAR	06	CLE3 $\Upsilon(1S) \rightarrow \gamma\pi^+\pi^-$	

<sup>1</sup> Assuming  $B(f_0(980) \rightarrow \pi\pi) = 1$ .

$\Gamma(\gamma f_2'(1525))/\Gamma_{total}$	CL%	EVTS	DOCUMENT ID	TECN	COMMENT	$\Gamma_{94}/\Gamma$
<b><math>2.9 \pm 0.6</math> OUR AVERAGE</b>						
$2.13 \pm 0.28 \pm 0.72$			<sup>1</sup> LEES	18A	BABR $\Upsilon(1S) \rightarrow \gamma K^+ K^-$	
$4.1 \pm 1.4 \pm 0.1$		17	<sup>2</sup> BESSON	11	CLEO $\Upsilon(1S) \rightarrow K_S^0 K_S^0$	
$3.7^{+0.9}_{-0.7} \pm 0.8$			ATHAR	06	CLE3 $\Upsilon(1S) \rightarrow \gamma K^+ K^-$	

$\bullet \bullet \bullet$  We do not use the following data for averages, fits, limits, etc.  $\bullet \bullet \bullet$

$<14$  90 <sup>3</sup> FULTON 90B CLEO  $\Upsilon(1S) \rightarrow \gamma K^+ K^-$

$<19.4$  90 <sup>3</sup> ALBRECHT 89 ARG  $\Upsilon(1S) \rightarrow \gamma K^+ K^-$

<sup>1</sup> Using  $B(f_2'(1525) \rightarrow K\overline{K}) = 0.887 \pm 0.022$  and  $B(K^0\overline{K}^0) = 1/2 B(K\overline{K})$ .

<sup>2</sup> BESSON 11 reports  $(4.0 \pm 1.3 \pm 0.6) \times 10^{-5}$  from a measurement of  $[\Gamma(\Upsilon(1S) \rightarrow \gamma f_2'(1525))/\Gamma_{total}] \times [B(f_2'(1525) \rightarrow K\overline{K})]$  assuming  $B(f_2'(1525) \rightarrow K\overline{K}) = (88.8 \pm 3.1) \times 10^{-2}$ , which we rescale to our best value  $B(f_2'(1525) \rightarrow K\overline{K}) = (87.6 \pm 2.2) \times 10^{-2}$ . Our first error is their experiment's error and our second error is the systematic error from using our best value. The result also assumes  $B(K_S^0 \rightarrow \pi^+\pi^-) = (69.20 \pm 0.05)\%$  and  $B(f_2'(1525) \rightarrow K\overline{K}) = 4 B(f_2'(1525) \rightarrow K_S^0 K_S^0)$ .

<sup>3</sup> Assuming  $B(f_2'(1525) \rightarrow K\overline{K}) = 0.71$ .

$\Gamma(\gamma f_2(1270))/\Gamma_{total}$	CL%	DOCUMENT ID	TECN	COMMENT	$\Gamma_{95}/\Gamma$
<b><math>10.1 \pm 0.6</math> OUR AVERAGE</b>					
$10.15 \pm 0.59^{+0.54}_{-0.43}$		<sup>1</sup> LEES	18A	BABR $\Upsilon(1S) \rightarrow \gamma\pi^+\pi^-$	
$10.5 \pm 1.6^{+1.9}_{-1.8}$		<sup>2</sup> BESSON	07A	CLE3 $\Upsilon(1S) \rightarrow \gamma\pi^0\pi^0$	
$10.2 \pm 0.8 \pm 0.7$		ATHAR	06	CLE3 $\Upsilon(1S) \rightarrow \gamma\pi^+\pi^-$	
$8.1 \pm 2.3^{+2.9}_{-2.7}$		<sup>3</sup> ANASTASSOV	99	CLE2 $e^+e^- \rightarrow$ hadrons	

$\bullet \bullet \bullet$  We do not use the following data for averages, fits, limits, etc.  $\bullet \bullet \bullet$

$<21$  90 <sup>3</sup> FULTON 90B CLEO  $\Upsilon(1S) \rightarrow \gamma\pi^+\pi^-$

$<13$  90 <sup>3</sup> ALBRECHT 89 ARG  $\Upsilon(1S) \rightarrow \gamma\pi^+\pi^-$

$<81$  90 SCHMITT 88 CBAL  $\Upsilon(1S) \rightarrow \gamma X$

<sup>1</sup> Using  $B(f_2(1270) \rightarrow \pi^0\pi^0) = 1/3 B(f_2(1270) \rightarrow \pi\pi)$  and  $B(f_2(1270) \rightarrow \pi\pi) = (84.2^{+2.9}_{-0.9})\%$ .

<sup>2</sup> Using  $B(f_2(1270) \rightarrow \pi^0\pi^0) = B(f_2(1270) \rightarrow \pi\pi)/3$  and  $B(f_2(1270) \rightarrow \pi\pi) = (84.7^{+2.5}_{-1.2})\%$ .

<sup>3</sup> Using  $B(f_2(1270) \rightarrow \pi\pi) = 0.84$ .

$\Gamma(\gamma\eta(1405))/\Gamma_{total}$	CL%	DOCUMENT ID	TECN	COMMENT	$\Gamma_{96}/\Gamma$
<b><math>&lt;8.2</math></b>	90	<sup>1</sup> FULTON	90B	CLEO $\Upsilon(1S) \rightarrow \gamma K^\pm \pi^\mp K_S^0$	

<sup>1</sup> Includes unknown branching ratio of  $\eta(1405) \rightarrow K^\pm \pi^\mp K_S^0$ .

See key on page 999

# Meson Particle Listings

## $\Upsilon(1S)$

$\Gamma(\gamma f_0(1500))/\Gamma_{\text{total}}$   $\Gamma_{97}/\Gamma$

VALUE (units $10^{-5}$ )	CL%	DOCUMENT ID	TECN	COMMENT
<1.5	90	<sup>1</sup> BESSON	07A	CLEO $e^+e^- \rightarrow \Upsilon(1S) \rightarrow \gamma\pi^0\pi^0$
••• We do not use the following data for averages, fits, limits, etc. •••				
<6.1	90	<sup>2</sup> BESSON	07A	CLEO $e^+e^- \rightarrow \Upsilon(1S) \rightarrow \gamma\eta\eta$
<sup>1</sup> Using $B(f_0(1500) \rightarrow \pi^0\pi^0) = B(f_0(1500) \rightarrow \pi\pi)/3$ and $B(f_0(1500) \rightarrow \pi\pi) = (0.349 \pm 0.023)\%$ .				
<sup>2</sup> Calculated by us using $B(f_0(1500) \rightarrow \eta\eta) = (5.1 \pm 0.9)\%$ .				

$\Gamma(\gamma f_0(1500) \rightarrow \gamma K^+ K^-)/\Gamma_{\text{total}}$   $\Gamma_{98}/\Gamma$

VALUE (units $10^{-5}$ )	CL%	DOCUMENT ID	TECN	COMMENT
<b>1.04 ± 0.14 ± 0.33</b>		<sup>1</sup> LEES	18A	BABR $e^+e^- \rightarrow \Upsilon(1S) \rightarrow \gamma K^+ K^-$
<sup>1</sup> LEES 18A quotes $B(\Upsilon(1S) \rightarrow \gamma f_0(1500) \rightarrow \gamma K\bar{K}) = (2.08 \pm 0.27 \pm 0.65) \times 10^{-5}$ assuming $B(K^0\bar{K}^0) = 1/2 B(K\bar{K})$ .				

$\Gamma(\gamma f_0(1710))/\Gamma_{\text{total}}$   $\Gamma_{99}/\Gamma$

VALUE (units $10^{-4}$ )	CL%	DOCUMENT ID	TECN	COMMENT
< 2.6	90	<sup>1</sup> ALBRECHT	89	ARG $\Upsilon(1S) \rightarrow \gamma K^+ K^-$
••• We do not use the following data for averages, fits, limits, etc. •••				
< 6.3	90	<sup>1</sup> FULTON	90B	CLEO $\Upsilon(1S) \rightarrow \gamma K^+ K^-$
<19	90	<sup>1</sup> FULTON	90B	CLEO $\Upsilon(1S) \rightarrow \gamma K_S^0 K_S^0$
< 8	90	<sup>2</sup> ALBRECHT	89	ARG $\Upsilon(1S) \rightarrow \gamma\pi^+\pi^-$
<24	90	<sup>3</sup> SCHMITT	88	CBAL $\Upsilon(1S) \rightarrow \gamma X$
<sup>1</sup> Assuming $B(f_0(1710) \rightarrow K\bar{K}) = 0.38$ .				
<sup>2</sup> Assuming $B(f_0(1710) \rightarrow \pi\pi) = 0.04$ .				
<sup>3</sup> Assuming $B(f_0(1710) \rightarrow \eta\eta) = 0.18$ .				

$\Gamma(\gamma f_0(1710) \rightarrow \gamma K^+ K^-)/\Gamma_{\text{total}}$   $\Gamma_{100}/\Gamma$

VALUE (units $10^{-5}$ )	CL%	DOCUMENT ID	TECN	COMMENT
<b>1.01 ± 0.26 ± 0.18</b>		<sup>1</sup> LEES	18A	BABR $e^+e^- \rightarrow \Upsilon(1S) \rightarrow \gamma K^+ K^-$
••• We do not use the following data for averages, fits, limits, etc. •••				
<0.7	90	ATHAR	06	CLEO $e^+e^- \rightarrow \Upsilon(1S) \rightarrow \gamma K^+ K^-$
<sup>1</sup> LEES 18A quotes $B(\Upsilon(1S) \rightarrow \gamma f_0(1710) \rightarrow \gamma K\bar{K}) = (2.02 \pm 0.51 \pm 0.35) \times 10^{-5}$ assuming $B(K^0\bar{K}^0) = 1/2 B(K\bar{K})$ .				

$\Gamma(\gamma f_0(1710) \rightarrow \gamma\pi^+\pi^-)/\Gamma_{\text{total}}$   $\Gamma_{101}/\Gamma$

VALUE (units $10^{-5}$ )	CL%	DOCUMENT ID	TECN	COMMENT
<b>0.53 ± 0.17 ± 0.11</b>		<sup>1</sup> LEES	18A	BABR $\Upsilon(1S) \rightarrow \gamma\pi^+\pi^-$
<sup>1</sup> LEES 18A quotes $B(\Upsilon(1S) \rightarrow \gamma f_0(1710) \rightarrow \gamma\pi\pi) = (0.79 \pm 0.26 \pm 0.17) \times 10^{-5}$ assuming $B(\pi^0\bar{\pi}^0) = 1/3 B(\pi\pi)$ .				

$\Gamma(\gamma f_0(1710) \rightarrow \gamma\pi^0\pi^0)/\Gamma_{\text{total}}$   $\Gamma_{102}/\Gamma$

VALUE (units $10^{-6}$ )	CL%	DOCUMENT ID	TECN	COMMENT
<1.4	90	BESSON	07A	CLEO $e^+e^- \rightarrow \Upsilon(1S) \rightarrow \gamma\pi^0\pi^0$

$\Gamma(\gamma f_0(1710) \rightarrow \gamma\eta\eta)/\Gamma_{\text{total}}$   $\Gamma_{103}/\Gamma$

VALUE (units $10^{-6}$ )	CL%	DOCUMENT ID	TECN	COMMENT
<1.8	90	BESSON	07A	CLEO $e^+e^- \rightarrow \Upsilon(1S) \rightarrow \gamma\eta\eta$

$\Gamma(\gamma f_4(2050))/\Gamma_{\text{total}}$   $\Gamma_{104}/\Gamma$

VALUE (units $10^{-5}$ )	CL%	DOCUMENT ID	TECN	COMMENT
<5.3	90	<sup>1</sup> ATHAR	06	CLE3 $\Upsilon(1S) \rightarrow \gamma\pi^+\pi^-$
<sup>1</sup> Assuming $B(f_4(2050) \rightarrow \pi\pi) = 0.17$ .				

$\Gamma(\gamma f_0(2200) \rightarrow \gamma K^+ K^-)/\Gamma_{\text{total}}$   $\Gamma_{105}/\Gamma$

VALUE	CL%	DOCUMENT ID	TECN	COMMENT
<0.0002	90	BARU	89	MD1 $\Upsilon(1S) \rightarrow \gamma K^+ K^-$

$\Gamma(\gamma f_J(2220) \rightarrow \gamma K^+ K^-)/\Gamma_{\text{total}}$   $\Gamma_{106}/\Gamma$

VALUE (units $10^{-7}$ )	CL%	DOCUMENT ID	TECN	COMMENT
< 8	90	ATHAR	06	CLE3 $\Upsilon(1S) \rightarrow \gamma K^+ K^-$
••• We do not use the following data for averages, fits, limits, etc. •••				
< 160	90	MASEK	02	CLEO $\Upsilon(1S) \rightarrow \gamma K^+ K^-$
< 150	90	FULTON	90B	CLEO $\Upsilon(1S) \rightarrow \gamma K^+ K^-$
< 290	90	ALBRECHT	89	ARG $\Upsilon(1S) \rightarrow \gamma K^+ K^-$
<2000	90	BARU	89	MD1 $\Upsilon(1S) \rightarrow \gamma K^+ K^-$

$\Gamma(\gamma f_J(2220) \rightarrow \gamma\pi^+\pi^-)/\Gamma_{\text{total}}$   $\Gamma_{107}/\Gamma$

VALUE (units $10^{-7}$ )	CL%	DOCUMENT ID	TECN	COMMENT
< 6	90	ATHAR	06	CLE3 $\Upsilon(1S) \rightarrow \gamma\pi^+\pi^-$
••• We do not use the following data for averages, fits, limits, etc. •••				
<120	90	MASEK	02	CLEO $\Upsilon(1S) \rightarrow \gamma\pi^+\pi^-$

$\Gamma(\gamma f_J(2220) \rightarrow \gamma\rho\bar{\rho})/\Gamma_{\text{total}}$   $\Gamma_{108}/\Gamma$

VALUE (units $10^{-7}$ )	CL%	DOCUMENT ID	TECN	COMMENT
< 11	90	ATHAR	06	CLE3 $\Upsilon(1S) \rightarrow \gamma\rho\bar{\rho}$
••• We do not use the following data for averages, fits, limits, etc. •••				
<160	90	MASEK	02	CLEO $\Upsilon(1S) \rightarrow \gamma\rho\bar{\rho}$

$\Gamma(\gamma\eta(2225) \rightarrow \gamma\phi\phi)/\Gamma_{\text{total}}$   $\Gamma_{109}/\Gamma$

VALUE	CL%	DOCUMENT ID	TECN	COMMENT
<0.003	90	BARU	89	MD1 $\Upsilon(1S) \rightarrow \gamma K^+ K^- K^+ K^-$

$\Gamma(\gamma\eta_c(1S))/\Gamma_{\text{total}}$   $\Gamma_{110}/\Gamma$

VALUE (units $10^{-5}$ )	CL%	DOCUMENT ID	TECN	COMMENT
<5.7	90	SHEN	10A	BELL $\Upsilon(1S) \rightarrow \gamma X$

$\Gamma(\gamma\chi_{c0})/\Gamma_{\text{total}}$   $\Gamma_{111}/\Gamma$

VALUE (units $10^{-4}$ )	CL%	DOCUMENT ID	TECN	COMMENT
<6.5	90	SHEN	10A	BELL $\Upsilon(1S) \rightarrow \gamma X$

$\Gamma(\gamma\chi_{c1})/\Gamma_{\text{total}}$   $\Gamma_{112}/\Gamma$

VALUE (units $10^{-5}$ )	CL%	DOCUMENT ID	TECN	COMMENT
<2.3	90	SHEN	10A	BELL $\Upsilon(1S) \rightarrow \gamma X$

$\Gamma(\gamma\chi_{c2})/\Gamma_{\text{total}}$   $\Gamma_{113}/\Gamma$

VALUE (units $10^{-5}$ )	CL%	DOCUMENT ID	TECN	COMMENT
<7.6	90	SHEN	10A	BELL $\Upsilon(1S) \rightarrow \gamma X$

$\Gamma(\gamma\chi_{c1}(3872) \rightarrow \pi^+\pi^- J/\psi)/\Gamma_{\text{total}}$   $\Gamma_{114}/\Gamma$

VALUE (units $10^{-6}$ )	CL%	DOCUMENT ID	TECN	COMMENT
<1.6	90	SHEN	10A	BELL $\Upsilon(1S) \rightarrow \gamma X$

$\Gamma(\gamma\chi_{c1}(3872) \rightarrow \pi^+\pi^-\pi^0 J/\psi)/\Gamma_{\text{total}}$   $\Gamma_{115}/\Gamma$

VALUE (units $10^{-6}$ )	CL%	DOCUMENT ID	TECN	COMMENT
<2.8	90	SHEN	10A	BELL $\Upsilon(1S) \rightarrow \gamma X$

$\Gamma(\gamma X(3915) \rightarrow \omega J/\psi)/\Gamma_{\text{total}}$   $\Gamma_{116}/\Gamma$

VALUE (units $10^{-6}$ )	CL%	DOCUMENT ID	TECN	COMMENT
<3.0	90	SHEN	10A	BELL $\Upsilon(1S) \rightarrow \gamma X$

$\Gamma(\gamma\chi_{c1}(4140) \rightarrow \phi J/\psi)/\Gamma_{\text{total}}$   $\Gamma_{117}/\Gamma$

VALUE (units $10^{-6}$ )	CL%	DOCUMENT ID	TECN	COMMENT
<2.2	90	SHEN	10A	BELL $\Upsilon(1S) \rightarrow \gamma X$

$\Gamma(\gamma X)/\Gamma_{\text{total}}$   $\Gamma_{118}/\Gamma$

(X = scalar with  $m < 8.0$  GeV)

VALUE (units $10^{-6}$ )	CL%	DOCUMENT ID	TECN	COMMENT
< 4.5	90	<sup>1</sup> DEL-AMO-SA...11J	BABR	$e^+e^- \rightarrow \gamma + X$
••• We do not use the following data for averages, fits, limits, etc. •••				
<30	90	<sup>2</sup> BALEST	95	CLEO $e^+e^- \rightarrow \gamma + X$
<sup>1</sup> For a noninteracting scalar X with mass $m < 8.0$ GeV.				
<sup>2</sup> For a noninteracting pseudoscalar X with mass $< 7.2$ GeV.				

$\Gamma(\gamma X\bar{X}(m_X < 3.1 \text{ GeV}))/\Gamma_{\text{total}}$   $\Gamma_{119}/\Gamma$

( $X\bar{X}$  = vectors with  $m < 3.1$  GeV)

VALUE (units $10^{-3}$ )	CL%	DOCUMENT ID	TECN	COMMENT
<1	90	<sup>1</sup> BALEST	95	CLEO $e^+e^- \rightarrow \gamma + X\bar{X}$
<sup>1</sup> For a noninteracting vector X with mass $< 3.1$ GeV.				

$\Gamma(\gamma X\bar{X}(m_X < 4.5 \text{ GeV}))/\Gamma_{\text{total}}$   $\Gamma_{120}/\Gamma$

X and  $\bar{X}$  = zero spin with  $m < 4.5$  GeV

VALUE (units $10^{-5}$ )	CL%	DOCUMENT ID	TECN	COMMENT
<24	90	<sup>1</sup> DEL-AMO-SA...11J	BABR	$e^+e^- \rightarrow \gamma + X\bar{X}$
<sup>1</sup> For a noninteracting scalar X with mass $m < 4.5$ GeV.				

$\Gamma(\gamma X \rightarrow \gamma + \geq 4 \text{ prongs})/\Gamma_{\text{total}}$   $\Gamma_{121}/\Gamma$

( $1.5 \text{ GeV} < m_X < 5.0 \text{ GeV}$ )

VALUE (units $10^{-4}$ )	CL%	DOCUMENT ID	TECN	COMMENT
<1.78	95	ROSNER	07A	CLEO $e^+e^- \rightarrow \gamma X$

$\Gamma(\gamma a_1^0 \rightarrow \gamma\mu^+\mu^-)/\Gamma_{\text{total}}$   $\Gamma_{122}/\Gamma$

( $201 < M(\mu^+\mu^-) < 3565 \text{ MeV}$ )

VALUE (units $10^{-6}$ )	CL%	DOCUMENT ID	TECN	COMMENT
<9	90	<sup>1</sup> LOVE	08	CLEO $e^+e^- \rightarrow \gamma a_1^0 \rightarrow \gamma\mu^+\mu^-$
••• We do not use the following data for averages, fits, limits, etc. •••				
<9.7	90	<sup>2</sup> LEES	13c	BABR $e^+e^- \rightarrow \gamma a_1^0 \rightarrow \gamma\mu^+\mu^-$
<sup>1</sup> For a narrow scalar or pseudoscalar $a_1^0$ with $201 < M(\mu^+\mu^-) < 3565 \text{ MeV}$ , excluding $J/\psi$ . Measured 90% CL limits as a function of $M(\mu^+\mu^-)$ range from $1-9 \times 10^{-6}$ .				
<sup>2</sup> For a narrow scalar or pseudoscalar $a_1^0$ with mass in the range $212-9200 \text{ MeV}$ , excluding $J/\psi$ and $\psi(2S)$ . Measured 90% CL limits as a function of $m_{a_1^0}$ range from $0.28-9.7 \times 10^{-6}$ .				

$\Gamma(\gamma a_1^0 \rightarrow \gamma\tau^+\tau^-)/\Gamma_{\text{total}}$   $\Gamma_{123}/\Gamma$

( $2m_\tau < M(\tau^+\tau^-) < 9.2 \text{ GeV}$ )

VALUE (units $10^{-6}$ )	CL%	DOCUMENT ID	TECN	COMMENT
<130	90	<sup>1</sup> LEES	13R	BABR $\Upsilon(2S) \rightarrow \gamma\tau^+\tau^-\pi^+\pi^-$



••• We do not use the following data for averages, fits, limits, etc. •••

< 4.6	90	<sup>5</sup> LEES	11J	BABR	$\Upsilon(2S) \rightarrow X\gamma$
< 6	90	WALK	86	CBAL	$\Upsilon(2S) \rightarrow \gamma\gamma\ell^+\ell^-$
<11	90	PAUSS	83	CUSB	$\Upsilon(2S) \rightarrow \gamma\gamma\ell^+\ell^-$

<sup>1</sup> LEES 14M quotes  $\Gamma(\chi_{b0}(1P) \rightarrow \gamma\Upsilon(1S))/\Gamma_{\text{total}} \times \Gamma(\Upsilon(2S) \rightarrow \gamma\chi_{b0}(1P))/\Gamma_{\text{total}}$  =  $(7.75 \pm 0.91) \times 10^{-4}$  combining the results from samples of  $\Upsilon(2S) \rightarrow \gamma\gamma\mu^+\mu^-$  with and without converted photons. Assumes  $B(\Upsilon(1S) \rightarrow \mu^+\mu^-) = (2.48 \pm 0.05)\%$ .

<sup>2</sup> LEES 14M reports  $[\Gamma(\chi_{b0}(1P) \rightarrow \gamma\Upsilon(1S))/\Gamma_{\text{total}}] \times [B(\Upsilon(2S) \rightarrow \gamma\chi_{b0}(1P))] = (7.75 \pm 0.91) \times 10^{-4}$  which we divide by our best value  $B(\Upsilon(2S) \rightarrow \gamma\chi_{b0}(1P)) = (3.8 \pm 0.4) \times 10^{-2}$ . Our first error is their experiment's error and our second error is the systematic error from using our best value.

<sup>3</sup> Assuming  $B(\Upsilon(1S) \rightarrow \ell^+\ell^-) = (2.48 \pm 0.05)\%$ .

<sup>4</sup> KORNICER 11 reports  $[\Gamma(\chi_{b0}(1P) \rightarrow \gamma\Upsilon(1S))/\Gamma_{\text{total}}] \times [B(\Upsilon(2S) \rightarrow \gamma\chi_{b0}(1P))] = (6.59 \pm 0.96 \pm 0.60) \times 10^{-4}$  which we divide by our best value  $B(\Upsilon(2S) \rightarrow \gamma\chi_{b0}(1P)) = (3.8 \pm 0.4) \times 10^{-2}$ . Our first error is their experiment's error and our second error is the systematic error from using our best value.

<sup>5</sup> LEES 11J quotes a central value of  $\Gamma(\chi_{b0}(1P) \rightarrow \gamma\Upsilon(1S))/\Gamma_{\text{total}} \times \Gamma(\Upsilon(2S) \rightarrow \gamma\chi_{b0}(1P))/\Gamma_{\text{total}} = (8.3 \pm 5.6 \pm \frac{3.7}{2.6}) \times 10^{-4}$ .

$\Gamma(D^0 X)/\Gamma_{\text{total}}$					$\Gamma_2/\Gamma$
VALUE (units $10^{-4}$ )	CL%	DOCUMENT ID	TECN	COMMENT	
<10.4 × 10 <sup>-2</sup>	90	<sup>6,7</sup> BRIERE	08	CLEO	$\Upsilon(2S) \rightarrow \gamma D^0 X$

<sup>6</sup> For  $p_{D^0} > 2.5$  GeV/c.

<sup>7</sup> The authors also present their result as  $(5.6 \pm 3.6 \pm 0.5) \times 10^{-2}$ .

$\Gamma(\pi^+\pi^-K^+K^-\pi^0)/\Gamma_{\text{total}}$					$\Gamma_3/\Gamma$
VALUE (units $10^{-4}$ )	CL%	DOCUMENT ID	TECN	COMMENT	
<1.6	90	<sup>8</sup> ASNER	08A	CLEO	$\Upsilon(2S) \rightarrow \gamma\pi^+\pi^-K^+K^-\pi^0$

<sup>8</sup> ASNER 08A reports  $[\Gamma(\chi_{b0}(1P) \rightarrow \pi^+\pi^-K^+K^-\pi^0)/\Gamma_{\text{total}}] \times [B(\Upsilon(2S) \rightarrow \gamma\chi_{b0}(1P))] < 6 \times 10^{-6}$  which we divide by our best value  $B(\Upsilon(2S) \rightarrow \gamma\chi_{b0}(1P)) = 3.8 \times 10^{-2}$ .

$\Gamma(2\pi^+\pi^-K^-K_S^0)/\Gamma_{\text{total}}$					$\Gamma_4/\Gamma$
VALUE (units $10^{-4}$ )	CL%	DOCUMENT ID	TECN	COMMENT	
<0.5	90	<sup>9</sup> ASNER	08A	CLEO	$\Upsilon(2S) \rightarrow \gamma 2\pi^+\pi^-K^-K_S^0$

<sup>9</sup> ASNER 08A reports  $[\Gamma(\chi_{b0}(1P) \rightarrow 2\pi^+\pi^-K^-K_S^0)/\Gamma_{\text{total}}] \times [B(\Upsilon(2S) \rightarrow \gamma\chi_{b0}(1P))] < 2 \times 10^{-6}$  which we divide by our best value  $B(\Upsilon(2S) \rightarrow \gamma\chi_{b0}(1P)) = 3.8 \times 10^{-2}$ .

$\Gamma(2\pi^+\pi^-K^-K_S^0 2\pi^0)/\Gamma_{\text{total}}$					$\Gamma_5/\Gamma$
VALUE (units $10^{-4}$ )	CL%	DOCUMENT ID	TECN	COMMENT	
<5	90	<sup>10</sup> ASNER	08A	CLEO	$\Upsilon(2S) \rightarrow \gamma 2\pi^+\pi^-K^-2\pi^0$

<sup>10</sup> ASNER 08A reports  $[\Gamma(\chi_{b0}(1P) \rightarrow 2\pi^+\pi^-K^-K_S^0 2\pi^0)/\Gamma_{\text{total}}] \times [B(\Upsilon(2S) \rightarrow \gamma\chi_{b0}(1P))] < 18 \times 10^{-6}$  which we divide by our best value  $B(\Upsilon(2S) \rightarrow \gamma\chi_{b0}(1P)) = 3.8 \times 10^{-2}$ .

$\Gamma(2\pi^+2\pi^-2\pi^0)/\Gamma_{\text{total}}$					$\Gamma_6/\Gamma$
VALUE (units $10^{-4}$ )	CL%	DOCUMENT ID	TECN	COMMENT	
<2.1	90	<sup>11</sup> ASNER	08A	CLEO	$\Upsilon(2S) \rightarrow \gamma 2\pi^+2\pi^-2\pi^0$

<sup>11</sup> ASNER 08A reports  $[\Gamma(\chi_{b0}(1P) \rightarrow 2\pi^+2\pi^-2\pi^0)/\Gamma_{\text{total}}] \times [B(\Upsilon(2S) \rightarrow \gamma\chi_{b0}(1P))] < 8 \times 10^{-6}$  which we divide by our best value  $B(\Upsilon(2S) \rightarrow \gamma\chi_{b0}(1P)) = 3.8 \times 10^{-2}$ .

$\Gamma(2\pi^+2\pi^-K^+K^-)/\Gamma_{\text{total}}$					$\Gamma_7/\Gamma$
VALUE (units $10^{-4}$ )	EVTS	DOCUMENT ID	TECN	COMMENT	
1.1 ± 0.6 ± 0.1	7	<sup>12</sup> ASNER	08A	CLEO	$\Upsilon(2S) \rightarrow \gamma 2\pi^+2\pi^-K^+K^-$

<sup>12</sup> ASNER 08A reports  $[\Gamma(\chi_{b0}(1P) \rightarrow 2\pi^+2\pi^-K^+K^-)/\Gamma_{\text{total}}] \times [B(\Upsilon(2S) \rightarrow \gamma\chi_{b0}(1P))] = (4 \pm 2 \pm 1) \times 10^{-6}$  which we divide by our best value  $B(\Upsilon(2S) \rightarrow \gamma\chi_{b0}(1P)) = (3.8 \pm 0.4) \times 10^{-2}$ . Our first error is their experiment's error and our second error is the systematic error from using our best value.

$\Gamma(2\pi^+2\pi^-K^+K^-\pi^0)/\Gamma_{\text{total}}$					$\Gamma_8/\Gamma$
VALUE (units $10^{-4}$ )	CL%	DOCUMENT ID	TECN	COMMENT	
<2.7	90	<sup>13</sup> ASNER	08A	CLEO	$\Upsilon(2S) \rightarrow \gamma 2\pi^+2\pi^-K^+K^-\pi^0$

<sup>13</sup> ASNER 08A reports  $[\Gamma(\chi_{b0}(1P) \rightarrow 2\pi^+2\pi^-K^+K^-\pi^0)/\Gamma_{\text{total}}] \times [B(\Upsilon(2S) \rightarrow \gamma\chi_{b0}(1P))] < 10 \times 10^{-6}$  which we divide by our best value  $B(\Upsilon(2S) \rightarrow \gamma\chi_{b0}(1P)) = 3.8 \times 10^{-2}$ .

$\Gamma(2\pi^+2\pi^-K^+K^-2\pi^0)/\Gamma_{\text{total}}$					$\Gamma_9/\Gamma$
VALUE (units $10^{-4}$ )	CL%	DOCUMENT ID	TECN	COMMENT	
<5	90	<sup>14</sup> ASNER	08A	CLEO	$\Upsilon(2S) \rightarrow \gamma 2\pi^+2\pi^-K^+K^-2\pi^0$

<sup>14</sup> ASNER 08A reports  $[\Gamma(\chi_{b0}(1P) \rightarrow 2\pi^+2\pi^-K^+K^-2\pi^0)/\Gamma_{\text{total}}] \times [B(\Upsilon(2S) \rightarrow \gamma\chi_{b0}(1P))] < 20 \times 10^{-6}$  which we divide by our best value  $B(\Upsilon(2S) \rightarrow \gamma\chi_{b0}(1P)) = 3.8 \times 10^{-2}$ .

$\Gamma(3\pi^+2\pi^-K^-K_S^0\pi^0)/\Gamma_{\text{total}}$					$\Gamma_{10}/\Gamma$
VALUE (units $10^{-4}$ )	CL%	DOCUMENT ID	TECN	COMMENT	
<1.6	90	<sup>15</sup> ASNER	08A	CLEO	$\Upsilon(2S) \rightarrow \gamma 3\pi^+2\pi^-K^-K_S^0\pi^0$

<sup>15</sup> ASNER 08A reports  $[\Gamma(\chi_{b0}(1P) \rightarrow 3\pi^+2\pi^-K^-K_S^0\pi^0)/\Gamma_{\text{total}}] \times [B(\Upsilon(2S) \rightarrow \gamma\chi_{b0}(1P))] < 6 \times 10^{-6}$  which we divide by our best value  $B(\Upsilon(2S) \rightarrow \gamma\chi_{b0}(1P)) = 3.8 \times 10^{-2}$ .

$\Gamma(3\pi^+3\pi^-)/\Gamma_{\text{total}}$					$\Gamma_{11}/\Gamma$
VALUE (units $10^{-4}$ )	CL%	DOCUMENT ID	TECN	COMMENT	
<0.8	90	<sup>16</sup> ASNER	08A	CLEO	$\Upsilon(2S) \rightarrow \gamma 3\pi^+3\pi^-$

<sup>16</sup> ASNER 08A reports  $[\Gamma(\chi_{b0}(1P) \rightarrow 3\pi^+3\pi^-)/\Gamma_{\text{total}}] \times [B(\Upsilon(2S) \rightarrow \gamma\chi_{b0}(1P))] < 3 \times 10^{-6}$  which we divide by our best value  $B(\Upsilon(2S) \rightarrow \gamma\chi_{b0}(1P)) = 3.8 \times 10^{-2}$ .

$\Gamma(3\pi^+3\pi^-2\pi^0)/\Gamma_{\text{total}}$					$\Gamma_{12}/\Gamma$
VALUE (units $10^{-4}$ )	CL%	DOCUMENT ID	TECN	COMMENT	
<6	90	<sup>17</sup> ASNER	08A	CLEO	$\Upsilon(2S) \rightarrow \gamma 3\pi^+3\pi^-2\pi^0$

<sup>17</sup> ASNER 08A reports  $[\Gamma(\chi_{b0}(1P) \rightarrow 3\pi^+3\pi^-2\pi^0)/\Gamma_{\text{total}}] \times [B(\Upsilon(2S) \rightarrow \gamma\chi_{b0}(1P))] < 22 \times 10^{-6}$  which we divide by our best value  $B(\Upsilon(2S) \rightarrow \gamma\chi_{b0}(1P)) = 3.8 \times 10^{-2}$ .

$\Gamma(3\pi^+3\pi^-K^+K^-)/\Gamma_{\text{total}}$					$\Gamma_{13}/\Gamma$
VALUE (units $10^{-4}$ )	EVTS	DOCUMENT ID	TECN	COMMENT	
2.4 ± 1.2 ± 0.2	9	<sup>18</sup> ASNER	08A	CLEO	$\Upsilon(2S) \rightarrow \gamma 3\pi^+3\pi^-K^+K^-$

<sup>18</sup> ASNER 08A reports  $[\Gamma(\chi_{b0}(1P) \rightarrow 3\pi^+3\pi^-K^+K^-)/\Gamma_{\text{total}}] \times [B(\Upsilon(2S) \rightarrow \gamma\chi_{b0}(1P))] = (9 \pm 4 \pm 2) \times 10^{-6}$  which we divide by our best value  $B(\Upsilon(2S) \rightarrow \gamma\chi_{b0}(1P)) = (3.8 \pm 0.4) \times 10^{-2}$ . Our first error is their experiment's error and our second error is the systematic error from using our best value.

$\Gamma(3\pi^+3\pi^-K^+K^-\pi^0)/\Gamma_{\text{total}}$					$\Gamma_{14}/\Gamma$
VALUE (units $10^{-4}$ )	CL%	DOCUMENT ID	TECN	COMMENT	
<10	90	<sup>19</sup> ASNER	08A	CLEO	$\Upsilon(2S) \rightarrow \gamma 3\pi^+3\pi^-K^+K^-\pi^0$

<sup>19</sup> ASNER 08A reports  $[\Gamma(\chi_{b0}(1P) \rightarrow 3\pi^+3\pi^-K^+K^-\pi^0)/\Gamma_{\text{total}}] \times [B(\Upsilon(2S) \rightarrow \gamma\chi_{b0}(1P))] < 37 \times 10^{-6}$  which we divide by our best value  $B(\Upsilon(2S) \rightarrow \gamma\chi_{b0}(1P)) = 3.8 \times 10^{-2}$ .

$\Gamma(4\pi^+4\pi^-)/\Gamma_{\text{total}}$					$\Gamma_{15}/\Gamma$
VALUE (units $10^{-4}$ )	CL%	DOCUMENT ID	TECN	COMMENT	
<0.8	90	<sup>20</sup> ASNER	08A	CLEO	$\Upsilon(2S) \rightarrow \gamma 4\pi^+4\pi^-$

<sup>20</sup> ASNER 08A reports  $[\Gamma(\chi_{b0}(1P) \rightarrow 4\pi^+4\pi^-)/\Gamma_{\text{total}}] \times [B(\Upsilon(2S) \rightarrow \gamma\chi_{b0}(1P))] < 3 \times 10^{-6}$  which we divide by our best value  $B(\Upsilon(2S) \rightarrow \gamma\chi_{b0}(1P)) = 3.8 \times 10^{-2}$ .

$\Gamma(4\pi^+4\pi^-2\pi^0)/\Gamma_{\text{total}}$					$\Gamma_{16}/\Gamma$
VALUE (units $10^{-4}$ )	CL%	DOCUMENT ID	TECN	COMMENT	
<21	90	<sup>21</sup> ASNER	08A	CLEO	$\Upsilon(2S) \rightarrow \gamma 4\pi^+4\pi^-2\pi^0$

<sup>21</sup> ASNER 08A reports  $[\Gamma(\chi_{b0}(1P) \rightarrow 4\pi^+4\pi^-2\pi^0)/\Gamma_{\text{total}}] \times [B(\Upsilon(2S) \rightarrow \gamma\chi_{b0}(1P))] < 77 \times 10^{-6}$  which we divide by our best value  $B(\Upsilon(2S) \rightarrow \gamma\chi_{b0}(1P)) = 3.8 \times 10^{-2}$ .

$\Gamma(J/\psi J/\psi)/\Gamma_{\text{total}}$					$\Gamma_{17}/\Gamma$
VALUE (units $10^{-5}$ )	CL%	DOCUMENT ID	TECN	COMMENT	
<7	90	<sup>22</sup> SHEN	12	BELL	$\Upsilon(2S) \rightarrow \gamma\psi X$

<sup>22</sup> SHEN 12 reports  $< 7.1 \times 10^{-5}$  from a measurement of  $[\Gamma(\chi_{b0}(1P) \rightarrow J/\psi J/\psi)/\Gamma_{\text{total}}] \times [B(\Upsilon(2S) \rightarrow \gamma\chi_{b0}(1P))]$  assuming  $B(\Upsilon(2S) \rightarrow \gamma\chi_{b0}(1P)) = (3.8 \pm 0.4) \times 10^{-2}$ .

$\Gamma(J/\psi\psi(2S))/\Gamma_{\text{total}}$					$\Gamma_{18}/\Gamma$
VALUE (units $10^{-5}$ )	CL%	DOCUMENT ID	TECN	COMMENT	
<12	90	<sup>23</sup> SHEN	12	BELL	$\Upsilon(2S) \rightarrow \gamma\psi X$

<sup>23</sup> SHEN 12 reports  $< 12 \times 10^{-5}$  from a measurement of  $[\Gamma(\chi_{b0}(1P) \rightarrow J/\psi\psi(2S))/\Gamma_{\text{total}}] \times [B(\Upsilon(2S) \rightarrow \gamma\chi_{b0}(1P))]$  assuming  $B(\Upsilon(2S) \rightarrow \gamma\chi_{b0}(1P)) = (3.8 \pm 0.4) \times 10^{-2}$ .

$\Gamma(\psi(2S)\psi(2S))/\Gamma_{\text{total}}$					$\Gamma_{19}/\Gamma$
VALUE (units $10^{-5}$ )	CL%	DOCUMENT ID	TECN	COMMENT	
<3.1	90	<sup>24</sup> SHEN	12	BELL	$\Upsilon(2S) \rightarrow \gamma\psi X$

<sup>24</sup> SHEN 12 reports  $< 3.1 \times 10^{-5}$  from a measurement of  $[\Gamma(\chi_{b0}(1P) \rightarrow \psi(2S)\psi(2S))/\Gamma_{\text{total}}] \times [B(\Upsilon(2S) \rightarrow \gamma\chi_{b0}(1P))]$  assuming  $B(\Upsilon(2S) \rightarrow \gamma\chi_{b0}(1P)) = (3.8 \pm 0.4) \times 10^{-2}$ .

$\Gamma(J/\psi(1S) \text{ anything})/\Gamma_{\text{total}}$					$\Gamma_{20}/\Gamma$
VALUE	CL%	DOCUMENT ID	TECN	COMMENT	
<2.3 × 10 <sup>-3</sup>	90	JIA	17A	BELL	$e^+e^- \rightarrow \text{hadrons}$

$\chi_{b0}(1P)$  CROSS-PARTICLE BRANCHING RATIOS

$\Gamma(\chi_{b0}(1P) \rightarrow \gamma\Upsilon(1S))/\Gamma_{\text{total}} \times \Gamma(\Upsilon(2S) \rightarrow \gamma\chi_{b0}(1P))/\Gamma_{\text{total}}$					$\Gamma_1/\Gamma \times \Gamma_{61}^{(2S)}/\Gamma_{61}^{(2S)}$
VALUE	CL%	DOCUMENT ID	TECN	COMMENT	
<1.7 × 10 <sup>-3</sup>	90	<sup>25</sup> LEES	11J	BABR	$\Upsilon(2S) \rightarrow X\gamma$

<sup>25</sup> LEES 11J quotes a central value of  $\Gamma(\chi_{b0}(1P) \rightarrow \gamma\Upsilon(1S))/\Gamma_{\text{total}} \times \Gamma(\Upsilon(2S) \rightarrow \gamma\chi_{b0}(1P))/\Gamma_{\text{total}} = (8.3 \pm 5.6 \pm \frac{3.7}{2.6}) \times 10^{-4}$  and derives a 90% CL upper limit of  $\Gamma(\gamma\Upsilon(1S))/\Gamma_{\text{total}} < 4.6\%$  using  $B(\Upsilon(2S) \rightarrow \gamma\chi_{b0}(1P)) = (3.8 \pm 0.4)\%$ .

# Meson Particle Listings

## $\chi_{b0}(1P), \chi_{b1}(1P)$

### $B(\chi_{b0}(1P) \rightarrow \gamma T(1S)) \times B(T(2S) \rightarrow \gamma \chi_{b0}(1P)) \times B(T(1S) \rightarrow \ell^+ \ell^-)$

VALUE (units $10^{-5}$ )	EVTS	DOCUMENT ID	TECN	COMMENT
<b>1.67 ± 0.28 OUR AVERAGE</b>				
2.9 <sup>+1.7</sup> <sub>-1.4</sub> ± 0.1 <sup>+0.1</sup> <sub>-0.8</sub>		<sup>26</sup> LEES	14M BABR	$T(2S) \rightarrow \gamma \gamma \mu^+ \mu^-$
1.63 ± 0.24 ± 0.15	87	KORNICER	11 CLEO	$e^+ e^- \rightarrow \gamma \gamma \ell^+ \ell^-$

### $[B(\chi_{b0}(1P) \rightarrow \gamma T(1S)) \times B(T(2S) \rightarrow \gamma \chi_{b0}(1P))] / [B(\chi_{b1}(1P) \rightarrow \gamma T(1S)) \times B(T(2S) \rightarrow \gamma \chi_{b1}(1P))]$

VALUE (%)	DOCUMENT ID	TECN	COMMENT
<b>3.28 ± 0.37</b>			
	<sup>27</sup> LEES	14M BABR	$T(2S) \rightarrow \gamma \gamma \mu^+ \mu^-$

<sup>27</sup> From a sample of  $T(2S) \rightarrow \gamma \gamma \mu^+ \mu^-$  without converted photons.

### $\chi_{b0}(1P)$ REFERENCES

JIA	17A	PR D96 112002	S. Jia et al.	(BELLE Collab.)
LEES	14M	PR D90 112010	J.P. Lees et al.	(BABAR Collab.)
SHEN	12	PR D85 071102	C.P. Shen et al.	(BELLE Collab.)
KORNICER	11	PR D83 054003	M. Kornicer et al.	(CLEO Collab.)
LEES	11J	PR D84 072002	J.P. Lees et al.	(BABAR Collab.)
ASNER	08A	PR D78 091103	D.M. Asner et al.	(CLEO Collab.)
BRIERE	08	PR D78 092007	R.A. Briere et al.	(CLEO Collab.)
ARTUSO	05	PRL 94 032001	M. Artuso et al.	(CLEO Collab.)
EDWARDS	99	PR D59 032003	K.W. Edwards et al.	(CLEO Collab.)
WALK	86	PR D34 2611	W.S. Walk et al.	(Crystal Ball Collab.)
ALBRECHT	85E	PL 160B 331	H. Albrecht et al.	(ARGUS Collab.)
NERNST	85	PRL 54 2195	R. Nernst et al.	(Crystal Ball Collab.)
HAAS	84	PRL 52 799	J. Haas et al.	(CLEO Collab.)
KLOPFEN...	83	PRL 51 160	C. Klopfenstein et al.	(CUSB Collab.)
PAUSS	83	PL 130B 439	F. Pauss et al.	(MPIM, COLU, CORN, LSU+)

## $\chi_{b1}(1P)$

$$J^G(JPC) = 0^+(1^{++})$$

$J$  needs confirmation.

Observed in radiative decay of the  $T(2S)$ , therefore  $C = +$ . Branching ratio requires E1 transition, M1 is strongly disfavored, therefore  $P = +$ .  $J = 1$  from SKWARNICKI 87.

### $\chi_{b1}(1P)$ MASS

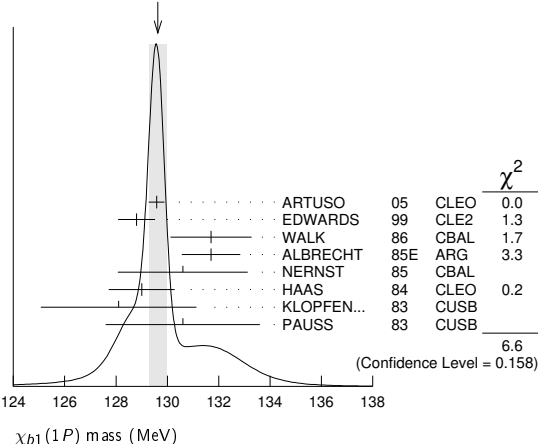
VALUE (MeV)	DOCUMENT ID
<b>9892.78 ± 0.26 ± 0.31 OUR EVALUATION</b>	

From average  $\gamma$  energy below, using  $T(2S)$  mass = 10023.26 ± 0.31 MeV

### $\gamma$ ENERGY IN $T(2S)$ DECAY

VALUE (MeV)	DOCUMENT ID	TECN	COMMENT
<b>129.63 ± 0.33 OUR AVERAGE</b>			
129.58 ± 0.09 ± 0.29	ARTUSO 05	CLEO	$T(2S) \rightarrow \gamma X$
128.8 ± 0.4 ± 0.6	EDWARDS 99	CLE2	$T(2S) \rightarrow \gamma \chi(1P)$
131.7 ± 0.9 ± 1.3	WALK 86	CBAL	$T(2S) \rightarrow \gamma \gamma \ell^+ \ell^-$
131.7 ± 0.3 ± 1.1	ALBRECHT 85E	ARG	$T(2S) \rightarrow \text{conv. } \gamma X$
130.6 ± 0.8 ± 2.4	NERNST 85	CBAL	$T(2S) \rightarrow \gamma X$
129 ± 0.8 ± 1	HAAS 84	CLEO	$T(2S) \rightarrow \text{conv. } \gamma X$
128.1 ± 0.4 ± 3.0	KLOPFEN... 83	CUSB	$T(2S) \rightarrow \gamma X$
130.6 ± 3.0	PAUSS 83	CUSB	$T(2S) \rightarrow \gamma \gamma \ell^+ \ell^-$

WEIGHTED AVERAGE  
129.63 ± 0.33 (Error scaled by 1.3)



### $\chi_{b1}(1P)$ DECAY MODES

Mode	Fraction ( $\Gamma_i/\Gamma$ )	Confidence level
$\Gamma_1 \gamma T(1S)$	(35.2 ± 2.0) %	
$\Gamma_2 D^0 X$	(12.6 ± 2.2) %	
$\Gamma_3 \pi^+ \pi^- K^+ K^- \pi^0$	( 2.0 ± 0.6) × 10 <sup>-4</sup>	
$\Gamma_4 2\pi^+ \pi^- K^- K_S^0$	( 1.3 ± 0.5) × 10 <sup>-4</sup>	
$\Gamma_5 2\pi^+ \pi^- K^- K_S^0 2\pi^0$	< 6 × 10 <sup>-4</sup>	90%
$\Gamma_6 2\pi^+ 2\pi^- 2\pi^0$	( 8.0 ± 2.5) × 10 <sup>-4</sup>	
$\Gamma_7 2\pi^+ 2\pi^- K^+ K^-$	( 1.5 ± 0.5) × 10 <sup>-4</sup>	
$\Gamma_8 2\pi^+ 2\pi^- K^+ K^- \pi^0$	( 3.5 ± 1.2) × 10 <sup>-4</sup>	
$\Gamma_9 2\pi^+ 2\pi^- K^+ K^- 2\pi^0$	( 8.6 ± 3.2) × 10 <sup>-4</sup>	
$\Gamma_{10} 3\pi^+ 2\pi^- K^- K_S^0 \pi^0$	( 9.3 ± 3.3) × 10 <sup>-4</sup>	
$\Gamma_{11} 3\pi^+ 3\pi^-$	( 1.9 ± 0.6) × 10 <sup>-4</sup>	
$\Gamma_{12} 3\pi^+ 3\pi^- 2\pi^0$	( 1.7 ± 0.5) × 10 <sup>-3</sup>	
$\Gamma_{13} 3\pi^+ 3\pi^- K^+ K^-$	( 2.6 ± 0.8) × 10 <sup>-4</sup>	
$\Gamma_{14} 3\pi^+ 3\pi^- K^+ K^- \pi^0$	( 7.5 ± 2.6) × 10 <sup>-4</sup>	
$\Gamma_{15} 4\pi^+ 4\pi^-$	( 2.6 ± 0.9) × 10 <sup>-4</sup>	
$\Gamma_{16} 4\pi^+ 4\pi^- 2\pi^0$	( 1.4 ± 0.6) × 10 <sup>-3</sup>	
$\Gamma_{17} \omega \text{ anything}$	( 4.9 ± 1.4) %	
$\Gamma_{18} \omega X_{tetra}$	< 4.44 × 10 <sup>-4</sup>	90%
$\Gamma_{19} J/\psi J/\psi$	< 2.7 × 10 <sup>-5</sup>	90%
$\Gamma_{20} J/\psi \psi(2S)$	< 1.7 × 10 <sup>-5</sup>	90%
$\Gamma_{21} \psi(2S) \psi(2S)$	< 6 × 10 <sup>-5</sup>	90%
$\Gamma_{22} J/\psi(1S) \text{ anything}$	< 1.1 × 10 <sup>-3</sup>	90%
$\Gamma_{23} J/\psi(1S) X_{tetra}$	< 2.27 × 10 <sup>-4</sup>	90%

### $\chi_{b1}(1P)$ BRANCHING RATIOS

VALUE	EVTS	DOCUMENT ID	TECN	COMMENT	$\Gamma_1/\Gamma$
<b>0.352 ± 0.020 OUR AVERAGE</b>					
0.356 <sup>+0.016</sup> <sub>-0.022</sub> ± 0.019	964k	<sup>1</sup> FULSOM	18 BELL	$T(2S) \rightarrow \gamma X$	
0.364 ± 0.017 ± 0.019		<sup>2,3,4</sup> LEES	14M BABR	$T(2S) \rightarrow \gamma \gamma \mu^+ \mu^-$	
0.331 ± 0.018 ± 0.017	3222	<sup>4,5</sup> KORNICER	11 CLEO	$e^+ e^- \rightarrow \gamma \gamma \ell^+ \ell^-$	
0.350 ± 0.023 ± 0.018	13k	<sup>6</sup> LEES	11J BABR	$T(2S) \rightarrow X \gamma$	
0.34 ± 0.07 ± 0.02	53	<sup>4,7,8</sup> WALK	86 CBAL	$T(2S) \rightarrow \gamma \gamma \ell^+ \ell^-$	
0.47 ± 0.18			83 CUSB	$T(2S) \rightarrow \gamma \gamma \ell^+ \ell^-$	

- FULSOM 18 reports  $[\Gamma(\chi_{b1}(1P) \rightarrow \gamma T(1S))/\Gamma_{total}] \times [B(T(2S) \rightarrow \gamma \chi_{b1}(1P))] = (2.45 \pm 0.02 \pm 0.11) \times 10^{-2}$  which we divide by our best value  $B(T(2S) \rightarrow \gamma \chi_{b1}(1P)) = (6.9 \pm 0.4) \times 10^{-2}$ . Our first error is their experiment's error and our second error is the systematic error from using our best value.
- LEES 14M quotes  $\Gamma(\chi_{b1}(1P) \rightarrow \gamma T(1S))/\Gamma_{total} \times \Gamma(T(2S) \rightarrow \gamma \chi_{b1}(1P))/\Gamma_{total} = (2.51 \pm 0.12) \%$  combining the results from samples of  $T(2S) \rightarrow \gamma \gamma \mu^+ \mu^-$  with and without converted photons.
- LEES 14M reports  $[\Gamma(\chi_{b1}(1P) \rightarrow \gamma T(1S))/\Gamma_{total}] \times [B(T(2S) \rightarrow \gamma \chi_{b1}(1P))] = (2.51 \pm 0.12) \times 10^{-2}$  which we divide by our best value  $B(T(2S) \rightarrow \gamma \chi_{b1}(1P)) = (6.9 \pm 0.4) \times 10^{-2}$ . Our first error is their experiment's error and our second error is the systematic error from using our best value.
- Assuming  $B(T(1S) \rightarrow \mu^+ \mu^-) = (2.48 \pm 0.05) \%$ .
- KORNICER 11 reports  $[\Gamma(\chi_{b1}(1P) \rightarrow \gamma T(1S))/\Gamma_{total}] \times [B(T(2S) \rightarrow \gamma \chi_{b1}(1P))] = (22.8 \pm 0.4 \pm 1.2) \times 10^{-3}$  which we divide by our best value  $B(T(2S) \rightarrow \gamma \chi_{b1}(1P)) = (6.9 \pm 0.4) \times 10^{-2}$ . Our first error is their experiment's error and our second error is the systematic error from using our best value.
- LEES 11J reports  $[\Gamma(\chi_{b1}(1P) \rightarrow \gamma T(1S))/\Gamma_{total}] \times [B(T(2S) \rightarrow \gamma \chi_{b1}(1P))] = (24.1 \pm 0.6 \pm 1.5) \times 10^{-3}$  which we divide by our best value  $B(T(2S) \rightarrow \gamma \chi_{b1}(1P)) = (6.9 \pm 0.4) \times 10^{-2}$ . Our first error is their experiment's error and our second error is the systematic error from using our best value.
- WALK 86 quotes  $B(T(2S) \rightarrow \gamma \chi_{b1}(1P)) \times B(\chi_{b1}(1P) \rightarrow \gamma T(1S)) \times B(T(1S) \rightarrow \ell^+ \ell^-) = (5.8 \pm 0.9 \pm 0.7) \%$ .
- WALK 86 reports  $[\Gamma(\chi_{b1}(1P) \rightarrow \gamma T(1S))/\Gamma_{total}] \times [B(T(2S) \rightarrow \gamma \chi_{b1}(1P))] = (23.4 \pm 3.63 \pm 2.82) \times 10^{-3}$  which we divide by our best value  $B(T(2S) \rightarrow \gamma \chi_{b1}(1P)) = (6.9 \pm 0.4) \times 10^{-2}$ . Our first error is their experiment's error and our second error is the systematic error from using our best value.

VALUE (units $10^{-2}$ )	EVTS	DOCUMENT ID	TECN	COMMENT	$\Gamma_2/\Gamma$
<b>12.6 ± 1.9 ± 1.1</b>					
	2310	<sup>1</sup> BRIERE	08 CLEO	$T(2S) \rightarrow \gamma D^0 X$	

<sup>1</sup> For  $p_{D^0} > 2.5$  GeV/c.

VALUE (units $10^{-4}$ )	EVTS	DOCUMENT ID	TECN	COMMENT	$\Gamma_3/\Gamma$
<b>2.0 ± 0.6 ± 0.1</b>					
	18	<sup>1</sup> ASNER	08A CLEO	$T(2S) \rightarrow \gamma \pi^+ \pi^- K^+ K^- \pi^0$	

- ASNER 08A reports  $[\Gamma(\chi_{b1}(1P) \rightarrow \pi^+ \pi^- K^+ K^- \pi^0)/\Gamma_{total}] \times [B(T(2S) \rightarrow \gamma \chi_{b1}(1P))] = (14 \pm 3 \pm 3) \times 10^{-6}$  which we divide by our best value  $B(T(2S) \rightarrow \gamma \chi_{b1}(1P)) = (6.9 \pm 0.4) \times 10^{-2}$ . Our first error is their experiment's error and our second error is the systematic error from using our best value.

See key on page 999

## Meson Particle Listings

 $\chi_{b1}(1P)$  $\Gamma(2\pi^+\pi^-K^-K_S^0)/\Gamma_{\text{total}}$   $\Gamma_4/\Gamma$ 

VALUE (units $10^{-4}$ )	EVTS	DOCUMENT ID	TECN	COMMENT
<b><math>1.3 \pm 0.5 \pm 0.1</math></b>	11	<sup>1</sup> ASNER	08A CLEO	$\Upsilon(2S) \rightarrow \gamma 2\pi^+\pi^-K^-K_S^0$
<sup>1</sup> ASNER 08A reports $[\Gamma(\chi_{b1}(1P) \rightarrow 2\pi^+\pi^-K^-K_S^0)/\Gamma_{\text{total}}] \times [B(\Upsilon(2S) \rightarrow \gamma\chi_{b1}(1P))]$ = $(9 \pm 3 \pm 2) \times 10^{-6}$ which we divide by our best value $B(\Upsilon(2S) \rightarrow \gamma\chi_{b1}(1P))$ = $(6.9 \pm 0.4) \times 10^{-2}$ . Our first error is their experiment's error and our second error is the systematic error from using our best value.				

 $\Gamma(2\pi^+\pi^-K^-K_S^0 2\pi^0)/\Gamma_{\text{total}}$   $\Gamma_5/\Gamma$ 

VALUE (units $10^{-4}$ )	CL%	DOCUMENT ID	TECN	COMMENT
<b>&lt;6</b>	90	<sup>1</sup> ASNER	08A CLEO	$\Upsilon(2S) \rightarrow \gamma 2\pi^+\pi^-K^-2\pi^0$
<sup>1</sup> ASNER 08A reports $[\Gamma(\chi_{b1}(1P) \rightarrow 2\pi^+\pi^-K^-K_S^0 2\pi^0)/\Gamma_{\text{total}}] \times [B(\Upsilon(2S) \rightarrow \gamma\chi_{b1}(1P))]$ < $42 \times 10^{-6}$ which we divide by our best value $B(\Upsilon(2S) \rightarrow \gamma\chi_{b1}(1P))$ = $6.9 \times 10^{-2}$ .				

 $\Gamma(2\pi^+2\pi^-2\pi^0)/\Gamma_{\text{total}}$   $\Gamma_6/\Gamma$ 

VALUE (units $10^{-4}$ )	EVTS	DOCUMENT ID	TECN	COMMENT
<b><math>8.0 \pm 2.4 \pm 0.4</math></b>	46	<sup>1</sup> ASNER	08A CLEO	$\Upsilon(2S) \rightarrow \gamma 2\pi^+2\pi^-2\pi^0$
<sup>1</sup> ASNER 08A reports $[\Gamma(\chi_{b1}(1P) \rightarrow 2\pi^+2\pi^-2\pi^0)/\Gamma_{\text{total}}] \times [B(\Upsilon(2S) \rightarrow \gamma\chi_{b1}(1P))]$ = $(55 \pm 9 \pm 14) \times 10^{-6}$ which we divide by our best value $B(\Upsilon(2S) \rightarrow \gamma\chi_{b1}(1P))$ = $(6.9 \pm 0.4) \times 10^{-2}$ . Our first error is their experiment's error and our second error is the systematic error from using our best value.				

 $\Gamma(2\pi^+2\pi^-K^+K^-)/\Gamma_{\text{total}}$   $\Gamma_7/\Gamma$ 

VALUE (units $10^{-4}$ )	EVTS	DOCUMENT ID	TECN	COMMENT
<b><math>1.5 \pm 0.5 \pm 0.1</math></b>	18	<sup>1</sup> ASNER	08A CLEO	$\Upsilon(2S) \rightarrow \gamma 2\pi^+2\pi^-K^+K^-$
<sup>1</sup> ASNER 08A reports $[\Gamma(\chi_{b1}(1P) \rightarrow 2\pi^+2\pi^-K^+K^-)/\Gamma_{\text{total}}] \times [B(\Upsilon(2S) \rightarrow \gamma\chi_{b1}(1P))]$ = $(10 \pm 3 \pm 2) \times 10^{-6}$ which we divide by our best value $B(\Upsilon(2S) \rightarrow \gamma\chi_{b1}(1P))$ = $(6.9 \pm 0.4) \times 10^{-2}$ . Our first error is their experiment's error and our second error is the systematic error from using our best value.				

 $\Gamma(2\pi^+2\pi^-K^+K^- \pi^0)/\Gamma_{\text{total}}$   $\Gamma_8/\Gamma$ 

VALUE (units $10^{-4}$ )	EVTS	DOCUMENT ID	TECN	COMMENT
<b><math>3.5 \pm 1.2 \pm 0.2</math></b>	22	<sup>1</sup> ASNER	08A CLEO	$\Upsilon(2S) \rightarrow \gamma 2\pi^+2\pi^-K^+K^- \pi^0$
<sup>1</sup> ASNER 08A reports $[\Gamma(\chi_{b1}(1P) \rightarrow 2\pi^+2\pi^-K^+K^- \pi^0)/\Gamma_{\text{total}}] \times [B(\Upsilon(2S) \rightarrow \gamma\chi_{b1}(1P))]$ = $(24 \pm 6 \pm 6) \times 10^{-6}$ which we divide by our best value $B(\Upsilon(2S) \rightarrow \gamma\chi_{b1}(1P))$ = $(6.9 \pm 0.4) \times 10^{-2}$ . Our first error is their experiment's error and our second error is the systematic error from using our best value.				

 $\Gamma(2\pi^+2\pi^-K^+K^- 2\pi^0)/\Gamma_{\text{total}}$   $\Gamma_9/\Gamma$ 

VALUE (units $10^{-4}$ )	EVTS	DOCUMENT ID	TECN	COMMENT
<b><math>8.6 \pm 3.2 \pm 0.4</math></b>	26	<sup>1</sup> ASNER	08A CLEO	$\Upsilon(2S) \rightarrow \gamma 2\pi^+2\pi^-K^+K^- 2\pi^0$
<sup>1</sup> ASNER 08A reports $[\Gamma(\chi_{b1}(1P) \rightarrow 2\pi^+2\pi^-K^+K^- 2\pi^0)/\Gamma_{\text{total}}] \times [B(\Upsilon(2S) \rightarrow \gamma\chi_{b1}(1P))]$ = $(59 \pm 14 \pm 17) \times 10^{-6}$ which we divide by our best value $B(\Upsilon(2S) \rightarrow \gamma\chi_{b1}(1P))$ = $(6.9 \pm 0.4) \times 10^{-2}$ . Our first error is their experiment's error and our second error is the systematic error from using our best value.				

 $\Gamma(3\pi^+2\pi^-K^-K_S^0 \pi^0)/\Gamma_{\text{total}}$   $\Gamma_{10}/\Gamma$ 

VALUE (units $10^{-4}$ )	EVTS	DOCUMENT ID	TECN	COMMENT
<b><math>9.3 \pm 3.3 \pm 0.5</math></b>	21	<sup>1</sup> ASNER	08A CLEO	$\Upsilon(2S) \rightarrow \gamma 3\pi^+2\pi^-K^-K_S^0 \pi^0$
<sup>1</sup> ASNER 08A reports $[\Gamma(\chi_{b1}(1P) \rightarrow 3\pi^+2\pi^-K^-K_S^0 \pi^0)/\Gamma_{\text{total}}] \times [B(\Upsilon(2S) \rightarrow \gamma\chi_{b1}(1P))]$ = $(64 \pm 16 \pm 16) \times 10^{-6}$ which we divide by our best value $B(\Upsilon(2S) \rightarrow \gamma\chi_{b1}(1P))$ = $(6.9 \pm 0.4) \times 10^{-2}$ . Our first error is their experiment's error and our second error is the systematic error from using our best value.				

 $\Gamma(3\pi^+3\pi^-)/\Gamma_{\text{total}}$   $\Gamma_{11}/\Gamma$ 

VALUE (units $10^{-4}$ )	EVTS	DOCUMENT ID	TECN	COMMENT
<b><math>1.9 \pm 0.6 \pm 0.1</math></b>	25	<sup>1</sup> ASNER	08A CLEO	$\Upsilon(2S) \rightarrow \gamma 3\pi^+3\pi^-$
<sup>1</sup> ASNER 08A reports $[\Gamma(\chi_{b1}(1P) \rightarrow 3\pi^+3\pi^-)/\Gamma_{\text{total}}] \times [B(\Upsilon(2S) \rightarrow \gamma\chi_{b1}(1P))]$ = $(13 \pm 3 \pm 3) \times 10^{-6}$ which we divide by our best value $B(\Upsilon(2S) \rightarrow \gamma\chi_{b1}(1P))$ = $(6.9 \pm 0.4) \times 10^{-2}$ . Our first error is their experiment's error and our second error is the systematic error from using our best value.				

 $\Gamma(3\pi^+3\pi^- 2\pi^0)/\Gamma_{\text{total}}$   $\Gamma_{12}/\Gamma$ 

VALUE (units $10^{-4}$ )	EVTS	DOCUMENT ID	TECN	COMMENT
<b><math>17 \pm 5 \pm 1</math></b>	56	<sup>1</sup> ASNER	08A CLEO	$\Upsilon(2S) \rightarrow \gamma 3\pi^+3\pi^- 2\pi^0$
<sup>1</sup> ASNER 08A reports $[\Gamma(\chi_{b1}(1P) \rightarrow 3\pi^+3\pi^- 2\pi^0)/\Gamma_{\text{total}}] \times [B(\Upsilon(2S) \rightarrow \gamma\chi_{b1}(1P))]$ = $(119 \pm 18 \pm 32) \times 10^{-6}$ which we divide by our best value $B(\Upsilon(2S) \rightarrow \gamma\chi_{b1}(1P))$ = $(6.9 \pm 0.4) \times 10^{-2}$ . Our first error is their experiment's error and our second error is the systematic error from using our best value.				

 $\Gamma(3\pi^+3\pi^-K^+K^-)/\Gamma_{\text{total}}$   $\Gamma_{13}/\Gamma$ 

VALUE (units $10^{-4}$ )	EVTS	DOCUMENT ID	TECN	COMMENT
<b><math>2.6 \pm 0.8 \pm 0.1</math></b>	21	<sup>1</sup> ASNER	08A CLEO	$\Upsilon(2S) \rightarrow \gamma 3\pi^+3\pi^-K^+K^-$
<sup>1</sup> ASNER 08A reports $[\Gamma(\chi_{b1}(1P) \rightarrow 3\pi^+3\pi^-K^+K^-)/\Gamma_{\text{total}}] \times [B(\Upsilon(2S) \rightarrow \gamma\chi_{b1}(1P))]$ = $(18 \pm 4 \pm 4) \times 10^{-6}$ which we divide by our best value $B(\Upsilon(2S) \rightarrow \gamma\chi_{b1}(1P))$ = $(6.9 \pm 0.4) \times 10^{-2}$ . Our first error is their experiment's error and our second error is the systematic error from using our best value.				

 $\Gamma(3\pi^+3\pi^-K^+K^- \pi^0)/\Gamma_{\text{total}}$   $\Gamma_{14}/\Gamma$ 

VALUE (units $10^{-4}$ )	EVTS	DOCUMENT ID	TECN	COMMENT
<b><math>7.5 \pm 2.6 \pm 0.4</math></b>	28	<sup>1</sup> ASNER	08A CLEO	$\Upsilon(2S) \rightarrow \gamma 3\pi^+3\pi^-K^+K^- \pi^0$
<sup>1</sup> ASNER 08A reports $[\Gamma(\chi_{b1}(1P) \rightarrow 3\pi^+3\pi^-K^+K^- \pi^0)/\Gamma_{\text{total}}] \times [B(\Upsilon(2S) \rightarrow \gamma\chi_{b1}(1P))]$ = $(52 \pm 11 \pm 14) \times 10^{-6}$ which we divide by our best value $B(\Upsilon(2S) \rightarrow \gamma\chi_{b1}(1P))$ = $(6.9 \pm 0.4) \times 10^{-2}$ . Our first error is their experiment's error and our second error is the systematic error from using our best value.				

 $\Gamma(4\pi^+4\pi^-)/\Gamma_{\text{total}}$   $\Gamma_{15}/\Gamma$ 

VALUE (units $10^{-4}$ )	EVTS	DOCUMENT ID	TECN	COMMENT
<b><math>2.6 \pm 0.9 \pm 0.1</math></b>	24	<sup>1</sup> ASNER	08A CLEO	$\Upsilon(2S) \rightarrow \gamma 4\pi^+4\pi^-$
<sup>1</sup> ASNER 08A reports $[\Gamma(\chi_{b1}(1P) \rightarrow 4\pi^+4\pi^-)/\Gamma_{\text{total}}] \times [B(\Upsilon(2S) \rightarrow \gamma\chi_{b1}(1P))]$ = $(18 \pm 4 \pm 5) \times 10^{-6}$ which we divide by our best value $B(\Upsilon(2S) \rightarrow \gamma\chi_{b1}(1P))$ = $(6.9 \pm 0.4) \times 10^{-2}$ . Our first error is their experiment's error and our second error is the systematic error from using our best value.				

 $\Gamma(4\pi^+4\pi^- 2\pi^0)/\Gamma_{\text{total}}$   $\Gamma_{16}/\Gamma$ 

VALUE (units $10^{-4}$ )	EVTS	DOCUMENT ID	TECN	COMMENT
<b><math>14 \pm 5 \pm 1</math></b>	26	<sup>1</sup> ASNER	08A CLEO	$\Upsilon(2S) \rightarrow \gamma 4\pi^+4\pi^- 2\pi^0$
<sup>1</sup> ASNER 08A reports $[\Gamma(\chi_{b1}(1P) \rightarrow 4\pi^+4\pi^- 2\pi^0)/\Gamma_{\text{total}}] \times [B(\Upsilon(2S) \rightarrow \gamma\chi_{b1}(1P))]$ = $(96 \pm 24 \pm 29) \times 10^{-6}$ which we divide by our best value $B(\Upsilon(2S) \rightarrow \gamma\chi_{b1}(1P))$ = $(6.9 \pm 0.4) \times 10^{-2}$ . Our first error is their experiment's error and our second error is the systematic error from using our best value.				

 $\Gamma(\omega \text{ anything})/\Gamma_{\text{total}}$   $\Gamma_{17}/\Gamma$ 

VALUE (units $10^{-2}$ )	EVTS	DOCUMENT ID	TECN	COMMENT
<b><math>4.9 \pm 1.3 \pm 0.6</math></b>	51k	JIA	17A BELL	$e^+e^- \rightarrow \text{hadrons}$

 $\Gamma(\omega X_{tetra})/\Gamma_{\text{total}}$   $\Gamma_{18}/\Gamma$ 

VALUE	CL%	DOCUMENT ID	TECN	COMMENT
<b>&lt;44.4</b>	90	<sup>1</sup> JIA	17A BELL	$e^+e^- \rightarrow \text{hadrons}$
<sup>1</sup> For a tetraquark state $X_{tetra}$ , with mass in the range 1.16–2.46 GeV and width in the range 0–0.3 GeV. Measured 90% CL limits as a function of $X_{tetra}$ mass and width range from $3.3 \times 10^{-5}$ to $44.4 \times 10^{-5}$ .				

 $\Gamma(J/\psi J/\psi)/\Gamma_{\text{total}}$   $\Gamma_{19}/\Gamma$ 

VALUE (units $10^{-5}$ )	CL%	DOCUMENT ID	TECN	COMMENT
<b>&lt;2.7</b>	90	<sup>1</sup> SHEN	12 BELL	$\Upsilon(2S) \rightarrow \gamma\psi X$
<sup>1</sup> SHEN 12 reports < $2.7 \times 10^{-5}$ from a measurement of $[\Gamma(\chi_{b1}(1P) \rightarrow J/\psi J/\psi)/\Gamma_{\text{total}}] \times [B(\Upsilon(2S) \rightarrow \gamma\chi_{b1}(1P))]$ assuming $B(\Upsilon(2S) \rightarrow \gamma\chi_{b1}(1P))$ = $(6.9 \pm 0.4) \times 10^{-2}$ .				

 $\Gamma(J/\psi \psi(2S))/\Gamma_{\text{total}}$   $\Gamma_{20}/\Gamma$ 

VALUE (units $10^{-5}$ )	CL%	DOCUMENT ID	TECN	COMMENT
<b>&lt;1.7</b>	90	<sup>1</sup> SHEN	12 BELL	$\Upsilon(2S) \rightarrow \gamma\psi X$
<sup>1</sup> SHEN 12 reports < $1.7 \times 10^{-5}$ from a measurement of $[\Gamma(\chi_{b1}(1P) \rightarrow J/\psi \psi(2S))/\Gamma_{\text{total}}] \times [B(\Upsilon(2S) \rightarrow \gamma\chi_{b1}(1P))]$ assuming $B(\Upsilon(2S) \rightarrow \gamma\chi_{b1}(1P))$ = $(6.9 \pm 0.4) \times 10^{-2}$ .				

 $\Gamma(\psi(2S)\psi(2S))/\Gamma_{\text{total}}$   $\Gamma_{21}/\Gamma$ 

VALUE (units $10^{-5}$ )	CL%	DOCUMENT ID	TECN	COMMENT
<b>&lt;6</b>	90	<sup>1</sup> SHEN	12 BELL	$\Upsilon(2S) \rightarrow \gamma\psi X$
<sup>1</sup> SHEN 12 reports < $6.2 \times 10^{-5}$ from a measurement of $[\Gamma(\chi_{b1}(1P) \rightarrow \psi(2S)\psi(2S))/\Gamma_{\text{total}}] \times [B(\Upsilon(2S) \rightarrow \gamma\chi_{b1}(1P))]$ assuming $B(\Upsilon(2S) \rightarrow \gamma\chi_{b1}(1P))$ = $(6.9 \pm 0.4) \times 10^{-2}$ .				

 $\Gamma(J/\psi(1S) \text{ anything})/\Gamma_{\text{total}}$   $\Gamma_{22}/\Gamma$ 

VALUE	CL%	DOCUMENT ID	TECN	COMMENT
<b>&lt;1.1</b>	90	JIA	17A BELL	$e^+e^- \rightarrow \text{hadrons}$

 $\Gamma(J/\psi(1S) X_{tetra})/\Gamma_{\text{total}}$   $\Gamma_{23}/\Gamma$ 

VALUE	CL%	DOCUMENT ID	TECN	COMMENT
<b>&lt;22.7</b>	90	<sup>1</sup> JIA	17A BELL	$e^+e^- \rightarrow \text{hadrons}$
<sup>1</sup> For a tetraquark state $X_{tetra}$ , with mass in the range 1.16–2.46 GeV and width in the range 0–0.3 GeV. Measured 90% CL limits as a function of $X_{tetra}$ mass and width range from $1.8 \times 10^{-5}$ to $22.7 \times 10^{-5}$ .				

 $\chi_{b1}(1P)$  Cross-Particle Branching Ratios $\Gamma(\chi_{b1}(1P) \rightarrow \gamma \Upsilon(1S))/\Gamma_{\text{total}} \times \Gamma(\Upsilon(2S) \rightarrow \gamma\chi_{b1}(1P))/\Gamma_{\text{total}}$   $\Gamma_{1/\Gamma} \times \Gamma_{59}^{\Upsilon(2S)}/\Gamma \Upsilon(2S)$ 

VALUE (units $10^{-3}$ )	EVTS	DOCUMENT ID	TECN	COMMENT
<b><math>24.1 \pm 0.6 \pm 1.5</math></b>	13k	LEES	11I BABR	$\Upsilon(2S) \rightarrow X\gamma$

 $B(\chi_{b1}(1P) \rightarrow \gamma \Upsilon(1S)) \times B(\Upsilon(2S) \rightarrow \gamma\chi_{b1}(1P)) \times B(\Upsilon(1S) \rightarrow \ell^+\ell^-)$ 

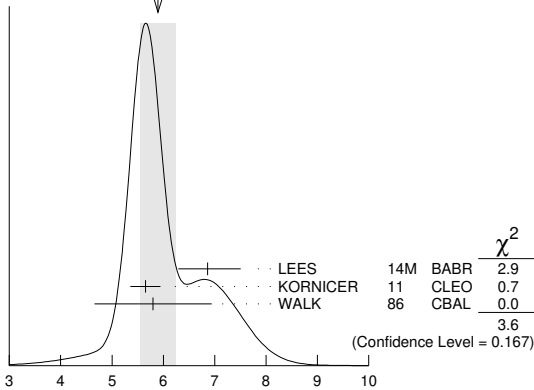
VALUE (units $10^{-4}$ )	EVTS	DOCUMENT ID	TECN	COMMENT
<b><math>5.90 \pm 0.34</math> OUR AVERAGE</b>		Error includes scale factor of 1.3. See the ideogram below.		
$6.86^{+0.47}_{-0.45} \pm 0.35$		<sup>1</sup> LEES	14M BABR	$\Upsilon(2S) \rightarrow \gamma\gamma\mu^+\mu^-$
$5.65 \pm 0.11 \pm 0.27$	3222	KORNICER	11 CLEO	$e^+e^- \rightarrow \gamma\gamma\ell^+\ell^-$
$5.8 \pm 0.9 \pm 0.7$	53	WALK	86 CBAL	$\Upsilon(2S) \rightarrow \gamma\gamma\ell^+\ell^-$
<sup>1</sup> From a sample of $\Upsilon(2S) \rightarrow \gamma\gamma\mu^+\mu^-$ with one converted photon.				



# Meson Particle Listings

## $\chi_{b1}(1P), h_b(1P), \chi_{b2}(1P)$

WEIGHTED AVERAGE  
5.90±0.34 (Error scaled by 1.3)



$$B(\chi_{b1}(1P) \rightarrow \gamma \Upsilon(1S)) \times B(\Upsilon(2S) \rightarrow \gamma \chi_{b1}(1P)) \times B(\Upsilon(1S) \rightarrow \ell^+ \ell^-)$$

(units  $10^{-4}$ )

$$B(\chi_{b1}(1P) \rightarrow \gamma \Upsilon(1S)) \times B(\Upsilon(3S) \rightarrow \gamma \chi_{b1}(1P)) \times B(\Upsilon(1S) \rightarrow \ell^+ \ell^-)$$

VALUE (units $10^{-5}$ )	EVTS	DOCUMENT ID	TECN	COMMENT
<b>1.30±0.34 OUR AVERAGE</b>				

1.16 <sup>+0.78+0.14</sup> <sub>-0.67-0.16</sub>		<sup>1</sup> LEES	14M BABR	$\Upsilon(3S) \rightarrow \gamma \gamma \mu^+ \mu^-$
1.33±0.30±0.23	50	KORNICER	11 CLEO	$e^+ e^- \rightarrow \gamma \gamma \ell^+ \ell^-$

<sup>1</sup> From a sample of  $\Upsilon(3S) \rightarrow \gamma \gamma \mu^+ \mu^-$  with converted photons.

$$B(\chi_{b2}(1P) \rightarrow \rho X + \bar{\rho} X) / B(\chi_{b1}(1P) \rightarrow \rho X + \bar{\rho} X)$$

VALUE	DOCUMENT ID	TECN	COMMENT
<b>1.068±0.010±0.040</b>	BRIERE 07	CLEO	$\Upsilon(2S) \rightarrow \gamma \chi_{bJ}(1P)$

$$B(\chi_{b0}(1P) \rightarrow \rho X + \bar{\rho} X) / B(\chi_{b1}(1P) \rightarrow \rho X + \bar{\rho} X)$$

VALUE	DOCUMENT ID	TECN	COMMENT
<b>1.11±0.15±0.20</b>	BRIERE 07	CLEO	$\Upsilon(2S) \rightarrow \gamma \chi_{bJ}(1P)$

### $\chi_{b1}(1P)$ REFERENCES

Author	Year	Document ID	TECN	COMMENT
FULSOM	18	PRL 121 232001		(BELLE Collab.)
JIA	17A	PR D96 112002		(BELLE Collab.)
LEES	14M	PR D90 112010		(BABAR Collab.)
SHEN	12	PR D85 071102		(BELLE Collab.)
KORNICER	11	PR D83 054003		(CLEO Collab.)
LEES	11J	PR D84 072002		(BABAR Collab.)
ASNER	08A	PR D78 091103		(CLEO Collab.)
BRIERE	08B	PR D78 092007		(CLEO Collab.)
BRIERE	07	PR D76 012005		(CLEO Collab.)
ARTUSO	05	PRL 94 032001		(CLEO Collab.)
EDWARDS	99	PR D59 032003		(CLEO Collab.)
SKWARNICKI	87	PRL 58 972		(Crystal Ball Collab.) <sup>J</sup>
WALK	86	PR D34 2611		(Crystal Ball Collab.)
ALBRECHT	85E	PL 160B 331		(ARGUS Collab.)
NERNST	85	PRL 54 2195		(Crystal Ball Collab.)
HAAS	84	PRL 52 739		(CLEO Collab.)
KLOPFEN...	83	PRL 51 160		(CUSB Collab.)
PAUSS	83	PL 130B 439		(MPIM, COLU, CORN, LSU+)

## $h_b(1P)$

$$I^G(J^{PC}) = 0^-(1^{+-})$$

Quantum numbers are quark model predictions,  $C = -$  established by  $\eta_b \gamma$  decay.

### $h_b(1P)$ MASS

VALUE (MeV)	EVTS	DOCUMENT ID	TECN	COMMENT
<b>9899.3±0.8 OUR AVERAGE</b>				

9899.3±0.4±1.0	112k	TAMPONI	15 BELL	$e^+ e^- \rightarrow \gamma \eta + \text{hadrons}$
9899.1±0.4±1.0	70k	MIZUK	12 BELL	$e^+ e^- \rightarrow \pi^+ \pi^- \text{hadrons}$
9902 ± 4 ± 2	10.8k	LEES	11K BABR	$\Upsilon(3S) \rightarrow \eta_b \gamma \pi^0$

• • • We do not use the following data for averages, fits, limits, etc. • • •

9898.2 <sup>+1.1+1.0</sup> <sub>-1.0-1.1</sub>	50.0k	<sup>1</sup> ADACHI	12 BELL	10.86 $e^+ e^- \rightarrow \pi^+ \pi^- \text{MM}$
--	-------	---------------------	---------	---

<sup>1</sup> Superseded by MIZUK 12.

### $h_b(1P)$ DECAY MODES

Mode	Fraction ( $\Gamma_i/\Gamma$ )
$\Gamma_1$ $\eta_b(1S) \gamma$	(52 <sup>+6</sup> <sub>-5</sub> ) %

### $h_b(1P)$ BRANCHING RATIOS

$\Gamma(\eta_b(1S)\gamma)/\Gamma_{\text{total}}$	VALUE (units $10^{-2}$ )	EVTS	DOCUMENT ID	TECN	COMMENT	$\Gamma_i/\Gamma$
--	--------------------------	------	-------------	------	---------	-------------------

**52<sup>+6</sup><sub>-5</sub> OUR AVERAGE**

56 ± 8 ± 4	33.1k	<sup>1</sup> TAMPONI	15 BELL	$e^+ e^- \rightarrow \gamma \eta + \text{hadrons}$		
49.2±5.7 <sup>+5.6</sup> <sub>-3.3</sub>	24k	MIZUK	12 BELL	$e^+ e^- \rightarrow (\gamma) \pi^+ \pi^- \text{hadrons}$		

• • • We do not use the following data for averages, fits, limits, etc. • • •

seen 10.8k LEES 11K BABR  $\Upsilon(3S) \rightarrow \eta_b \gamma \pi^0$

<sup>1</sup> Using  $B(\eta \rightarrow 2\gamma) = (39.41 \pm 0.20)\%$ .

### $h_b(1P)$ REFERENCES

Author	Year	Document ID	TECN	COMMENT
TAMPONI	15	PRL 115 142001		U. Tamponi et al. (BELLE Collab.)
ADACHI	12	PRL 108 032001		I. Adachi et al. (BELLE Collab.)
MIZUK	12	PRL 109 232002		R. Mizuk et al. (BELLE Collab.)
LEES	11K	PR D84 091101		J.P. Lees et al. (BABAR Collab.)

## $\chi_{b2}(1P)$

$$I^G(J^{PC}) = 0^+(2^{++})$$

$J$  needs confirmation.

Observed in radiative decay of the  $\Upsilon(2S)$ , therefore  $C = +$ . Branching ratio requires E1 transition, M1 is strongly disfavored, therefore  $P = +$ .  $J = 2$  from SKWARNICKI 87.

### $\chi_{b2}(1P)$ MASS

VALUE (MeV)	DOCUMENT ID
<b>9912.21±0.26±0.31 OUR EVALUATION</b>	From average $\gamma$ energy below, using $\Upsilon(2S)$ mass = 10023.26 ± 0.31 MeV

### $m_{\chi_{b2}(1P)} - m_{\chi_{b1}(1P)}$

VALUE (MeV)	DOCUMENT ID	TECN	COMMENT
<b>19.10±0.25 OUR AVERAGE</b>	Error includes scale factor of 1.1.		
19.81±0.65±0.20	<sup>1</sup> AAIJ	14B6 LHCB	$pp \rightarrow \gamma \mu^+ \mu^- X$
19.01±0.24	LEES	14M BABR	$\Upsilon(2S) \rightarrow \gamma \gamma \mu^+ \mu^-$

<sup>1</sup> From the  $\chi_{bJ}(1P) \rightarrow \Upsilon(1S) \gamma$  transition.

### $\gamma$ ENERGY IN $\Upsilon(2S)$ DECAY

VALUE (MeV)	DOCUMENT ID	TECN	COMMENT
<b>110.44±0.29 OUR AVERAGE</b>	Error includes scale factor of 1.1.		
110.58±0.08±0.30	ARTUSO	05 CLEO	$\Upsilon(2S) \rightarrow \gamma X$
110.8 ± 0.3 ± 0.6	EDWARDS	99 CLE2	$\Upsilon(2S) \rightarrow \gamma \chi(1P)$
107.0 ± 1.1 ± 1.3	WALK	86 CBAL	$\Upsilon(2S) \rightarrow \gamma \gamma \ell^+ \ell^-$
110.6 ± 0.3 ± 0.9	ALBRECHT	85E ARG	$\Upsilon(2S) \rightarrow \text{conv. } \gamma X$
110.4 ± 0.8 ± 2.2	NERNST	85 CBAL	$\Upsilon(2S) \rightarrow \gamma X$
109.5 ± 0.7 ± 1.0	HAAS	84 CLEO	$\Upsilon(2S) \rightarrow \text{conv. } \gamma X$
108.2 ± 0.3 ± 2.0	KLOPFEN...	83 CUSB	$\Upsilon(2S) \rightarrow \gamma X$
108.8 ± 4.0	PAUSS	83 CUSB	$\Upsilon(2S) \rightarrow \gamma \gamma \ell^+ \ell^-$

### $\chi_{b2}(1P)$ DECAY MODES

Mode	Fraction ( $\Gamma_i/\Gamma$ )	Confidence level
$\Gamma_1$ $\gamma \Upsilon(1S)$	(18.0±1.0) %	
$\Gamma_2$ $D^0 X$	< 7.9 %	90%
$\Gamma_3$ $\pi^+ \pi^- K^+ K^- \pi^0$	( 8 ± 5 ) × 10 <sup>-5</sup>	
$\Gamma_4$ $2\pi^+ \pi^- K^- K_S^0$	< 1.0 × 10 <sup>-4</sup>	90%
$\Gamma_5$ $2\pi^+ \pi^- K^- K_S^0 2\pi^0$	( 5.3±2.4 ) × 10 <sup>-4</sup>	
$\Gamma_6$ $2\pi^+ 2\pi^- 2\pi^0$	( 3.5±1.4 ) × 10 <sup>-4</sup>	
$\Gamma_7$ $2\pi^+ 2\pi^- K^+ K^-$	( 1.1±0.4 ) × 10 <sup>-4</sup>	
$\Gamma_8$ $2\pi^+ 2\pi^- K^+ K^- \pi^0$	( 2.1±0.9 ) × 10 <sup>-4</sup>	
$\Gamma_9$ $2\pi^+ 2\pi^- K^+ K^- 2\pi^0$	( 3.9±1.8 ) × 10 <sup>-4</sup>	
$\Gamma_{10}$ $3\pi^+ 2\pi^- K^- K_S^0 \pi^0$	< 5 × 10 <sup>-4</sup>	90%
$\Gamma_{11}$ $3\pi^+ 3\pi^-$	( 7.0±3.1 ) × 10 <sup>-5</sup>	
$\Gamma_{12}$ $3\pi^+ 3\pi^- 2\pi^0$	( 1.0±0.4 ) × 10 <sup>-3</sup>	
$\Gamma_{13}$ $3\pi^+ 3\pi^- K^+ K^-$	< 8 × 10 <sup>-5</sup>	90%
$\Gamma_{14}$ $3\pi^+ 3\pi^- K^+ K^- \pi^0$	( 3.6±1.5 ) × 10 <sup>-4</sup>	
$\Gamma_{15}$ $4\pi^+ 4\pi^-$	( 8 ± 4 ) × 10 <sup>-5</sup>	
$\Gamma_{16}$ $4\pi^+ 4\pi^- 2\pi^0$	( 1.8±0.7 ) × 10 <sup>-3</sup>	
$\Gamma_{17}$ $J/\psi J/\psi$	< 4 × 10 <sup>-5</sup>	90%
$\Gamma_{18}$ $J/\psi \psi(2S)$	< 5 × 10 <sup>-5</sup>	90%
$\Gamma_{19}$ $\psi(2S) \psi(2S)$	< 1.6 × 10 <sup>-5</sup>	90%
$\Gamma_{20}$ $J/\psi(1S) \text{anything}$	( 1.5±0.4 ) × 10 <sup>-3</sup>	

See key on page 999

## Meson Particle Listings

 $\chi_{b2}(1P)$  $\chi_{b2}(1P)$  BRANCHING RATIOS

$\Gamma(\gamma \mathcal{T}(1S))/\Gamma_{\text{total}}$					$\Gamma_1/\Gamma$
VALUE	EVTS	DOCUMENT ID	TECN	COMMENT	

**0.180 ± 0.010 OUR AVERAGE**

0.164 <sup>+0.009</sup> <sub>-0.016</sub> ± 0.008	503k	<sup>1</sup> FULSOM	18 BELL	$\mathcal{T}(2S) \rightarrow \gamma X$	
0.185 ± 0.008 ± 0.009	2,3,4	LEES	14M BABR	$\mathcal{T}(2S) \rightarrow \gamma \gamma \mu^+ \mu^-$	
0.186 ± 0.011 ± 0.009	1770	<sup>4,5</sup> KORNICER	11 CLEO	$e^+ e^- \rightarrow \gamma \gamma \ell^+ \ell^-$	
0.194 <sup>+0.014</sup> <sub>-0.017</sub> ± 0.009	8k	<sup>6</sup> LEES	11J BABR	$\mathcal{T}(2S) \rightarrow X \gamma$	
0.25 ± 0.06 ± 0.01	35	<sup>4,7,8</sup> WALK	86 CBAL	$\mathcal{T}(2S) \rightarrow \gamma \gamma \ell^+ \ell^-$	
0.20 ± 0.05		KLOPFEN...	83 CUSB	$\mathcal{T}(2S) \rightarrow \gamma \gamma \ell^+ \ell^-$	

<sup>1</sup> FULSOM 18 reports  $[\Gamma(\chi_{b2}(1P) \rightarrow \gamma \mathcal{T}(1S))/\Gamma_{\text{total}}] \times [B(\mathcal{T}(2S) \rightarrow \gamma \chi_{b2}(1P))] = (1.17 \pm 0.01 \pm 0.09) \times 10^{-2}$  which we divide by our best value  $B(\mathcal{T}(2S) \rightarrow \gamma \chi_{b2}(1P)) = (7.15 \pm 0.35) \times 10^{-2}$ . Our first error is their experiment's error and our second error is the systematic error from using our best value.

<sup>2</sup> LEES 14M quotes  $\Gamma(\chi_{b2}(1P) \rightarrow \gamma \mathcal{T}(1S))/\Gamma_{\text{total}} \times \Gamma(\mathcal{T}(2S) \rightarrow \gamma \chi_{b2}(1P))/\Gamma_{\text{total}} = (1.32 \pm 0.06)\%$  combining the results from samples of  $\mathcal{T}(2S) \rightarrow \gamma \gamma \mu^+ \mu^-$  with and without converted photons.

<sup>3</sup> LEES 14M reports  $[\Gamma(\chi_{b2}(1P) \rightarrow \gamma \mathcal{T}(1S))/\Gamma_{\text{total}}] \times [B(\mathcal{T}(2S) \rightarrow \gamma \chi_{b2}(1P))] = (1.32 \pm 0.06) \times 10^{-2}$  which we divide by our best value  $B(\mathcal{T}(2S) \rightarrow \gamma \chi_{b2}(1P)) = (7.15 \pm 0.35) \times 10^{-2}$ . Our first error is their experiment's error and our second error is the systematic error from using our best value.

<sup>4</sup> Assuming  $B(\mathcal{T}(1S) \rightarrow \mu^+ \mu^-) = (2.48 \pm 0.05)\%$ .

<sup>5</sup> KORNICER 11 reports  $[\Gamma(\chi_{b2}(1P) \rightarrow \gamma \mathcal{T}(1S))/\Gamma_{\text{total}}] \times [B(\mathcal{T}(2S) \rightarrow \gamma \chi_{b2}(1P))] = (1.33 \pm 0.04 \pm 0.07) \times 10^{-2}$  which we divide by our best value  $B(\mathcal{T}(2S) \rightarrow \gamma \chi_{b2}(1P)) = (7.15 \pm 0.35) \times 10^{-2}$ . Our first error is their experiment's error and our second error is the systematic error from using our best value.

<sup>6</sup> LEES 11J reports  $[\Gamma(\chi_{b2}(1P) \rightarrow \gamma \mathcal{T}(1S))/\Gamma_{\text{total}}] \times [B(\mathcal{T}(2S) \rightarrow \gamma \chi_{b2}(1P))] = (13.9 \pm 0.5 \pm 0.9) \times 10^{-3}$  which we divide by our best value  $B(\mathcal{T}(2S) \rightarrow \gamma \chi_{b2}(1P)) = (7.15 \pm 0.35) \times 10^{-2}$ . Our first error is their experiment's error and our second error is the systematic error from using our best value.

<sup>7</sup> WALK 86 quotes  $B(\mathcal{T}(2S) \rightarrow \gamma \chi_{b2}(1P)) \times B(\chi_{b2}(1P) \rightarrow \gamma \mathcal{T}(1S)) \times B(\mathcal{T}(1S) \rightarrow \ell^+ \ell^-) = (4.4 \pm 0.9 \pm 0.5)\%$ .

<sup>8</sup> WALK 86 reports  $[\Gamma(\chi_{b2}(1P) \rightarrow \gamma \mathcal{T}(1S))/\Gamma_{\text{total}}] \times [B(\mathcal{T}(2S) \rightarrow \gamma \chi_{b2}(1P))] = (17.7 \pm 3.6 \pm 2.0) \times 10^{-3}$  which we divide by our best value  $B(\mathcal{T}(2S) \rightarrow \gamma \chi_{b2}(1P)) = (7.15 \pm 0.35) \times 10^{-2}$ . Our first error is their experiment's error and our second error is the systematic error from using our best value.

$\Gamma(D^0 X)/\Gamma_{\text{total}}$					$\Gamma_2/\Gamma$
VALUE	CL%	DOCUMENT ID	TECN	COMMENT	

**<7.9 × 10<sup>-2</sup>**

<sup>1</sup> For  $p_{D^0} > 2.5$  GeV/c.

<sup>2</sup> The authors also present their result as  $(5.4 \pm 1.9 \pm 0.5) \times 10^{-2}$ .

$\Gamma(\pi^+ \pi^- K^+ K^- \pi^0)/\Gamma_{\text{total}}$					$\Gamma_3/\Gamma$
VALUE (units 10 <sup>-4</sup> )	EVTS	DOCUMENT ID	TECN	COMMENT	

**0.84 ± 0.50 ± 0.04**

<sup>1</sup> ASNER 08A reports  $[\Gamma(\chi_{b2}(1P) \rightarrow \pi^+ \pi^- K^+ K^- \pi^0)/\Gamma_{\text{total}}] \times [B(\mathcal{T}(2S) \rightarrow \gamma \chi_{b2}(1P))] = (6 \pm 3 \pm 2) \times 10^{-6}$  which we divide by our best value  $B(\mathcal{T}(2S) \rightarrow \gamma \chi_{b2}(1P)) = (7.15 \pm 0.35) \times 10^{-2}$ . Our first error is their experiment's error and our second error is the systematic error from using our best value.

$\Gamma(2\pi^+ \pi^- K^- K_S^0)/\Gamma_{\text{total}}$					$\Gamma_4/\Gamma$
VALUE (units 10 <sup>-4</sup> )	CL%	DOCUMENT ID	TECN	COMMENT	

**<1.0**

<sup>1</sup> ASNER 08A reports  $[\Gamma(\chi_{b2}(1P) \rightarrow 2\pi^+ \pi^- K^- K_S^0)/\Gamma_{\text{total}}] \times [B(\mathcal{T}(2S) \rightarrow \gamma \chi_{b2}(1P))] < 7 \times 10^{-6}$  which we divide by our best value  $B(\mathcal{T}(2S) \rightarrow \gamma \chi_{b2}(1P)) = 7.15 \times 10^{-2}$ .

$\Gamma(2\pi^+ \pi^- K^- K_S^0 2\pi^0)/\Gamma_{\text{total}}$					$\Gamma_5/\Gamma$
VALUE (units 10 <sup>-4</sup> )	EVTS	DOCUMENT ID	TECN	COMMENT	

**5.3 ± 2.4 ± 0.3**

<sup>1</sup> ASNER 08A reports  $[\Gamma(\chi_{b2}(1P) \rightarrow 2\pi^+ \pi^- K^- K_S^0 2\pi^0)/\Gamma_{\text{total}}] \times [B(\mathcal{T}(2S) \rightarrow \gamma \chi_{b2}(1P))] = (38 \pm 14 \pm 10) \times 10^{-6}$  which we divide by our best value  $B(\mathcal{T}(2S) \rightarrow \gamma \chi_{b2}(1P)) = (7.15 \pm 0.35) \times 10^{-2}$ . Our first error is their experiment's error and our second error is the systematic error from using our best value.

$\Gamma(2\pi^+ 2\pi^- 2\pi^0)/\Gamma_{\text{total}}$					$\Gamma_6/\Gamma$
VALUE (units 10 <sup>-4</sup> )	EVTS	DOCUMENT ID	TECN	COMMENT	

**3.5 ± 1.4 ± 0.2**

<sup>1</sup> ASNER 08A reports  $[\Gamma(\chi_{b2}(1P) \rightarrow 2\pi^+ 2\pi^- 2\pi^0)/\Gamma_{\text{total}}] \times [B(\mathcal{T}(2S) \rightarrow \gamma \chi_{b2}(1P))] = (25 \pm 8 \pm 6) \times 10^{-6}$  which we divide by our best value  $B(\mathcal{T}(2S) \rightarrow \gamma \chi_{b2}(1P)) = (7.15 \pm 0.35) \times 10^{-2}$ . Our first error is their experiment's error and our second error is the systematic error from using our best value.

$\Gamma(2\pi^+ 2\pi^- K^+ K^-)/\Gamma_{\text{total}}$					$\Gamma_7/\Gamma$
VALUE (units 10 <sup>-4</sup> )	EVTS	DOCUMENT ID	TECN	COMMENT	

**1.1 ± 0.4 ± 0.1**

<sup>1</sup> ASNER 08A reports  $[\Gamma(\chi_{b2}(1P) \rightarrow 2\pi^+ 2\pi^- K^+ K^-)/\Gamma_{\text{total}}] \times [B(\mathcal{T}(2S) \rightarrow \gamma \chi_{b2}(1P))] = (8 \pm 2 \pm 2) \times 10^{-6}$  which we divide by our best value  $B(\mathcal{T}(2S) \rightarrow \gamma \chi_{b2}(1P)) = (7.15 \pm 0.35) \times 10^{-2}$ . Our first error is their experiment's error and our second error is the systematic error from using our best value.

$\Gamma(2\pi^+ 2\pi^- K^+ K^- \pi^0)/\Gamma_{\text{total}}$					$\Gamma_8/\Gamma$
VALUE (units 10 <sup>-4</sup> )	EVTS	DOCUMENT ID	TECN	COMMENT	

**2.1 ± 0.9 ± 0.1**

<sup>1</sup> ASNER 08A reports  $[\Gamma(\chi_{b2}(1P) \rightarrow 2\pi^+ 2\pi^- K^+ K^- \pi^0)/\Gamma_{\text{total}}] \times [B(\mathcal{T}(2S) \rightarrow \gamma \chi_{b2}(1P))] = (15 \pm 5 \pm 4) \times 10^{-6}$  which we divide by our best value  $B(\mathcal{T}(2S) \rightarrow \gamma \chi_{b2}(1P)) = (7.15 \pm 0.35) \times 10^{-2}$ . Our first error is their experiment's error and our second error is the systematic error from using our best value.

$\Gamma(2\pi^+ 2\pi^- K^+ K^- 2\pi^0)/\Gamma_{\text{total}}$					$\Gamma_9/\Gamma$
VALUE (units 10 <sup>-4</sup> )	EVTS	DOCUMENT ID	TECN	COMMENT	

**3.9 ± 1.8 ± 0.2**

<sup>1</sup> ASNER 08A reports  $[\Gamma(\chi_{b2}(1P) \rightarrow 2\pi^+ 2\pi^- K^+ K^- 2\pi^0)/\Gamma_{\text{total}}] \times [B(\mathcal{T}(2S) \rightarrow \gamma \chi_{b2}(1P))] = (28 \pm 11 \pm 7) \times 10^{-6}$  which we divide by our best value  $B(\mathcal{T}(2S) \rightarrow \gamma \chi_{b2}(1P)) = (7.15 \pm 0.35) \times 10^{-2}$ . Our first error is their experiment's error and our second error is the systematic error from using our best value.

$\Gamma(3\pi^+ 2\pi^- K^- K_S^0 \pi^0)/\Gamma_{\text{total}}$					$\Gamma_{10}/\Gamma$
VALUE (units 10 <sup>-4</sup> )	CL%	DOCUMENT ID	TECN	COMMENT	

**<5**

<sup>1</sup> ASNER 08A reports  $[\Gamma(\chi_{b2}(1P) \rightarrow 3\pi^+ 2\pi^- K^- K_S^0 \pi^0)/\Gamma_{\text{total}}] \times [B(\mathcal{T}(2S) \rightarrow \gamma \chi_{b2}(1P))] < 36 \times 10^{-6}$  which we divide by our best value  $B(\mathcal{T}(2S) \rightarrow \gamma \chi_{b2}(1P)) = 7.15 \times 10^{-2}$ .

$\Gamma(3\pi^+ 3\pi^-)/\Gamma_{\text{total}}$					$\Gamma_{11}/\Gamma$
VALUE (units 10 <sup>-4</sup> )	EVTS	DOCUMENT ID	TECN	COMMENT	

**0.70 ± 0.31 ± 0.03**

<sup>1</sup> ASNER 08A reports  $[\Gamma(\chi_{b2}(1P) \rightarrow 3\pi^+ 3\pi^-)/\Gamma_{\text{total}}] \times [B(\mathcal{T}(2S) \rightarrow \gamma \chi_{b2}(1P))] = (5 \pm 2 \pm 1) \times 10^{-6}$  which we divide by our best value  $B(\mathcal{T}(2S) \rightarrow \gamma \chi_{b2}(1P)) = (7.15 \pm 0.35) \times 10^{-2}$ . Our first error is their experiment's error and our second error is the systematic error from using our best value.

$\Gamma(3\pi^+ 3\pi^- 2\pi^0)/\Gamma_{\text{total}}$					$\Gamma_{12}/\Gamma$
VALUE (units 10 <sup>-4</sup> )	EVTS	DOCUMENT ID	TECN	COMMENT	

**10.2 ± 3.6 ± 0.5**

<sup>1</sup> ASNER 08A reports  $[\Gamma(\chi_{b2}(1P) \rightarrow 3\pi^+ 3\pi^- 2\pi^0)/\Gamma_{\text{total}}] \times [B(\mathcal{T}(2S) \rightarrow \gamma \chi_{b2}(1P))] = (73 \pm 16 \pm 20) \times 10^{-6}$  which we divide by our best value  $B(\mathcal{T}(2S) \rightarrow \gamma \chi_{b2}(1P)) = (7.15 \pm 0.35) \times 10^{-2}$ . Our first error is their experiment's error and our second error is the systematic error from using our best value.

$\Gamma(3\pi^+ 3\pi^- K^+ K^-)/\Gamma_{\text{total}}$					$\Gamma_{13}/\Gamma$
VALUE (units 10 <sup>-4</sup> )	CL%	DOCUMENT ID	TECN	COMMENT	

**<0.8**

<sup>1</sup> ASNER 08A reports  $[\Gamma(\chi_{b2}(1P) \rightarrow 3\pi^+ 3\pi^- K^+ K^-)/\Gamma_{\text{total}}] \times [B(\mathcal{T}(2S) \rightarrow \gamma \chi_{b2}(1P))] < 6 \times 10^{-6}$  which we divide by our best value  $B(\mathcal{T}(2S) \rightarrow \gamma \chi_{b2}(1P)) = 7.15 \times 10^{-2}$ .

$\Gamma(3\pi^+ 3\pi^- K^+ K^- \pi^0)/\Gamma_{\text{total}}$					$\Gamma_{14}/\Gamma$
VALUE (units 10 <sup>-4</sup> )	EVTS	DOCUMENT ID	TECN	COMMENT	

**3.6 ± 1.5 ± 0.2**

<sup>1</sup> ASNER 08A reports  $[\Gamma(\chi_{b2}(1P) \rightarrow 3\pi^+ 3\pi^- K^+ K^- \pi^0)/\Gamma_{\text{total}}] \times [B(\mathcal{T}(2S) \rightarrow \gamma \chi_{b2}(1P))] = (26 \pm 8 \pm 7) \times 10^{-6}$  which we divide by our best value  $B(\mathcal{T}(2S) \rightarrow \gamma \chi_{b2}(1P)) = (7.15 \pm 0.35) \times 10^{-2}$ . Our first error is their experiment's error and our second error is the systematic error from using our best value.

$\Gamma(4\pi^+ 4\pi^-)/\Gamma_{\text{total}}$					$\Gamma_{15}/\Gamma$
VALUE (units 10 <sup>-4</sup> )	EVTS	DOCUMENT ID	TECN	COMMENT	

**0.84 ± 0.40 ± 0.04**

<sup>1</sup> ASNER 08A reports  $[\Gamma(\chi_{b2}(1P) \rightarrow 4\pi^+ 4\pi^-)/\Gamma_{\text{total}}] \times [B(\mathcal{T}(2S) \rightarrow \gamma \chi_{b2}(1P))] = (6 \pm 2 \pm 2) \times 10^{-6}$  which we divide by our best value  $B(\mathcal{T}(2S) \rightarrow \gamma \chi_{b2}(1P)) = (7.15 \pm 0.35) \times 10^{-2}$ . Our first error is their experiment's error and our second error is the systematic error from using our best value.

$\Gamma(4\pi^+ 4\pi^- 2\pi^0)/\Gamma_{\text{total}}$					$\Gamma_{16}/\Gamma$
VALUE (units 10 <sup>-4</sup> )	EVTS	DOCUMENT ID	TECN	COMMENT	

**18 ± 7 ± 1**

<sup>1</sup> ASNER 08A reports  $[\Gamma(\chi_{b2}(1P) \rightarrow 4\pi^+ 4\pi^- 2\pi^0)/\Gamma_{\text{total}}] \times [B(\mathcal{T}(2S) \rightarrow \gamma \chi_{b2}(1P))] = (132 \pm 31 \pm 40) \times 10^{-6}$  which we divide by our best value  $B(\mathcal{T}(2S) \rightarrow \gamma \chi_{b2}(1P)) = (7.15 \pm 0.35) \times 10^{-2}$ . Our first error is their experiment's error and our second error is the systematic error from using our best value.

# Meson Particle Listings

## $\chi_{b2}(1P), \eta_b(2S), \Upsilon(2S)$

$\Gamma(J/\psi J/\psi)/\Gamma_{total}$		$\Gamma_{17}/\Gamma$	
VALUE (units $10^{-5}$ )	CL%	DOCUMENT ID	TECN COMMENT
<5	90	<sup>1</sup> SHEN 12	BELL $\Upsilon(2S) \rightarrow \gamma\psi X$
<sup>1</sup> SHEN 12 reports $< 4.5 \times 10^{-5}$ from a measurement of $[\Gamma(\chi_{b2}(1P) \rightarrow J/\psi J/\psi)/\Gamma_{total}] \times [B(\Upsilon(2S) \rightarrow \gamma\chi_{b2}(1P))]$ assuming $B(\Upsilon(2S) \rightarrow \gamma\chi_{b2}(1P)) = (7.15 \pm 0.35) \times 10^{-2}$ .			

$\Gamma(J/\psi\psi(2S))/\Gamma_{total}$		$\Gamma_{18}/\Gamma$	
VALUE (units $10^{-5}$ )	CL%	DOCUMENT ID	TECN COMMENT
<5	90	<sup>1</sup> SHEN 12	BELL $\Upsilon(2S) \rightarrow \gamma\psi X$
<sup>1</sup> SHEN 12 reports $< 4.9 \times 10^{-5}$ from a measurement of $[\Gamma(\chi_{b2}(1P) \rightarrow J/\psi\psi(2S))/\Gamma_{total}] \times [B(\Upsilon(2S) \rightarrow \gamma\chi_{b2}(1P))]$ assuming $B(\Upsilon(2S) \rightarrow \gamma\chi_{b2}(1P)) = (7.15 \pm 0.35) \times 10^{-2}$ .			

$\Gamma(\psi(2S)\psi(2S))/\Gamma_{total}$		$\Gamma_{19}/\Gamma$	
VALUE (units $10^{-5}$ )	CL%	DOCUMENT ID	TECN COMMENT
<1.6	90	<sup>1</sup> SHEN 12	BELL $\Upsilon(2S) \rightarrow \gamma\psi X$
<sup>1</sup> SHEN 12 reports $< 1.6 \times 10^{-5}$ from a measurement of $[\Gamma(\chi_{b2}(1P) \rightarrow \psi(2S)\psi(2S))/\Gamma_{total}] \times [B(\Upsilon(2S) \rightarrow \gamma\chi_{b2}(1P))]$ assuming $B(\Upsilon(2S) \rightarrow \gamma\chi_{b2}(1P)) = (7.15 \pm 0.35) \times 10^{-2}$ .			

$\Gamma(J/\psi(1S) \text{ anything})/\Gamma_{total}$		$\Gamma_{20}/\Gamma$	
VALUE (units $10^{-3}$ )	EVTS	DOCUMENT ID	TECN COMMENT
<b>1.50 ± 0.34 ± 0.22</b>	462	JIA	17A BELL $e^+e^- \rightarrow \text{hadrons}$

### $\chi_{b2}(1P)$ Cross-Particle Branching Ratios

$\Gamma(\chi_{b2}(1P) \rightarrow \gamma \Upsilon(1S))/\Gamma_{total} \times \Gamma(\Upsilon(2S) \rightarrow \gamma\chi_{b2}(1P))/\Gamma_{total}$		$\Gamma_1/\Gamma \times \Gamma_{60}^{\Upsilon(2S)}/\Gamma \Upsilon(2S)$	
VALUE (units $10^{-3}$ )	EVTS	DOCUMENT ID	TECN COMMENT
<b>13.9 ± 0.5 ± 0.9</b>	8k	LEES	11J BABR $\Upsilon(2S) \rightarrow X\gamma$

$B(\chi_{b2}(1P) \rightarrow \gamma \Upsilon(1S)) \times B(\Upsilon(2S) \rightarrow \gamma\chi_{b2}(1P)) \times B(\Upsilon(1S) \rightarrow \ell^+\ell^-)$		$\Gamma_{17}/\Gamma$	
VALUE (units $10^{-4}$ )	EVTS	DOCUMENT ID	TECN COMMENT
<b>3.38 ± 0.16 OUR AVERAGE</b>			
$3.63^{+0.36+0.18}_{-0.34-0.19}$		<sup>1</sup> LEES	14M BABR $\Upsilon(2S) \rightarrow \gamma\gamma\mu^+\mu^-$
$3.29 \pm 0.09 \pm 0.16$	1770	KORNICER	11 CLEO $e^+e^- \rightarrow \gamma\gamma\ell^+\ell^-$
$4.4 \pm 0.9 \pm 0.5$	35	WALK	86 CBAL $\Upsilon(2S) \rightarrow \gamma\gamma\ell^+\ell^-$
<sup>1</sup> From a sample of $\Upsilon(2S) \rightarrow \gamma\gamma\mu^+\mu^-$ with converted photons.			

$[B(\chi_{b2}(1P) \rightarrow \gamma \Upsilon(1S)) \times B(\Upsilon(2S) \rightarrow \gamma\chi_{b2}(1P))] / [B(\chi_{b1}(1P) \rightarrow \gamma \Upsilon(1S)) \times B(\Upsilon(2S) \rightarrow \gamma\chi_{b1}(1P))]$		$\Gamma_{17}/\Gamma$	
VALUE (%)	DOCUMENT ID	TECN	COMMENT
<b>55.6 ± 1.6</b>	<sup>1</sup> LEES	14M BABR	$\Upsilon(2S) \rightarrow \gamma\gamma\mu^+\mu^-$
<sup>1</sup> From a sample of $\Upsilon(2S) \rightarrow \gamma\gamma\mu^+\mu^-$ events without converted photons.			

$B(\chi_{b2}(1P) \rightarrow \gamma \Upsilon(1S)) \times B(\Upsilon(3S) \rightarrow \gamma\chi_{b2}(1P)) \times B(\Upsilon(1S) \rightarrow \ell^+\ell^-)$		$\Gamma_{17}/\Gamma$	
VALUE (units $10^{-5}$ )	EVTS	DOCUMENT ID	TECN COMMENT
<b>3.8 ± 0.5 OUR AVERAGE</b>			
$4.68^{+0.99}_{-0.92} \pm 0.37$		<sup>1</sup> LEES	14M BABR $\Upsilon(3S) \rightarrow \gamma\gamma\mu^+\mu^-$
$3.56 \pm 0.40 \pm 0.41$	126	KORNICER	11 CLEO $e^+e^- \rightarrow \gamma\gamma\ell^+\ell^-$
<sup>1</sup> From a sample of $\Upsilon(3S) \rightarrow \gamma\gamma\mu^+\mu^-$ with converted photons.			

### $\chi_{b2}(1P)$ REFERENCES

FULSOM 18	PRL 121 232001	B.G. Fulsom et al.	(BELLE Collab.)
JIA 17A	PR D96 112002	S. Jia et al.	(BELLE Collab.)
AAJ 14BG	JHEP 1410 088	R. Aaij et al.	(LHCb Collab.)
LEES 14M	PR D90 112010	J.P. Lees et al.	(BABAR Collab.)
SHEN 12	PR D85 071102	C.P. Shen et al.	(BELLE Collab.)
KORNICER 11	PR D83 054003	M. Kornicer et al.	(CLEO Collab.)
LEES 11J	PR D84 072002	J.P. Lees et al.	(BABAR Collab.)
ASNER 08A	PR D78 091103	D.M. Asner et al.	(CLEO Collab.)
BRIERE 08	PR D78 092007	R.A. Briere et al.	(CLEO Collab.)
ARTUSO 05	PR 94 032001	M. Artuso et al.	(CLEO Collab.)
EDWARDS 99	PR D59 032003	K.W. Edwards et al.	(CLEO Collab.)
SKWARNICKI 87	PRL 58 972	T. Skwarnicki et al.	(Crystal Ball Collab.)
WALK 86	PR D34 2611	W.S. Walk et al.	(Crystal Ball Collab.)
ALBRECHT 85E	PL 160B 331	H. Albrecht et al.	(ARGUS Collab.)
NERNST 85	PRL 54 2195	R. Nernst et al.	(Crystal Ball Collab.)
HAAS 84	PRL 52 799	J. Haas et al.	(CLEO Collab.)
KLOPFEN... 83	PRL 51 160	C. Klopffenstein et al.	(CUSP Collab.)
PAUSS 83	PL 130B 439	F. Pauss et al.	(MPIM, COLU, CORN, LSU+)

## $\eta_b(2S)$

$$I^G(J^{PC}) = 0^+(0^{-+})$$

OMITTED FROM SUMMARY TABLE  
Quantum numbers shown are quark-model predictions.

### $\eta_b(2S)$ MASS

VALUE (MeV)	EVTS	DOCUMENT ID	TECN	COMMENT
<b>9999.0 ± 3.5 ± 1.9</b>	26k	<sup>1</sup> MIZUK 12	BELL	$e^+e^- \rightarrow \gamma\pi^+\pi^- + \text{hadrons}$

••• We do not use the following data for averages, fits, limits, etc. •••

9974.6 ± 2.3 ± 2.1	11 ± 4	<sup>2,3,4</sup> DOBBS 12	$\Upsilon(2S) \rightarrow \gamma \text{ hadrons}$
--------------------	--------	---------------------------	---

<sup>1</sup> Assuming  $\Gamma_{\eta_b(2S)} = 4.9$  MeV. Not independent of the corresponding mass difference measurement.

<sup>2</sup> SANDILYA 13 (Belle Collab.) search for such a state reconstructed in the same 26 exclusive hadronic final states as DOBBS 12 using a sample of  $(157.8 \pm 3.6) \times 10^6 \Upsilon(2S)$  decays or about 17 times larger and find no evidence for a signal. Their 90% C.L. upper limit on the branching fraction  $B(\Upsilon(2S) \rightarrow \eta_b(2S)\gamma) \times \sum_i B(\eta_b(2S) \rightarrow X_i) < 4.9 \times 10^{-6}$ , summed over the exclusive hadronic final states  $X_i$ , is an order of magnitude smaller than that reported by DOBBS 12.

<sup>3</sup> Obtained by analyzing CLEO III data but not authored by the CLEO Collaboration.

<sup>4</sup> Assuming  $\Gamma_{\eta_b(2S)} = 5$  MeV. Not independent of the corresponding mass difference measurement.

### $m_{\Upsilon(2S)} - m_{\eta_b(2S)}$

VALUE (MeV)	EVTS	DOCUMENT ID	TECN	COMMENT
<b>24.3 ± 3.5 ± 2.8</b>	26k	<sup>5</sup> MIZUK 12	BELL	$e^+e^- \rightarrow \gamma\pi^+\pi^- + \text{hadrons}$

••• We do not use the following data for averages, fits, limits, etc. •••

48.7 ± 2.3 ± 2.1	11 ± 4	<sup>6,7,8</sup> DOBBS 12	$\Upsilon(2S) \rightarrow \gamma \text{ hadrons}$
------------------	--------	---------------------------	---

<sup>5</sup> Assuming  $\Gamma_{\eta_b(2S)} = 4.9$  MeV. Not independent of the corresponding mass measurement.

<sup>6</sup> SANDILYA 13 (Belle Collab.) search for such a state reconstructed in the same 26 exclusive hadronic final states as DOBBS 12 using a sample of  $(157.8 \pm 3.6) \times 10^6 \Upsilon(2S)$  decays or about 17 times larger and find no evidence for a signal. Their 90% C.L. upper limit on the branching fraction  $B(\Upsilon(2S) \rightarrow \eta_b(2S)\gamma) \times \sum_i B(\eta_b(2S) \rightarrow X_i) < 4.9 \times 10^{-6}$ , summed over the exclusive hadronic final states  $X_i$ , is an order of magnitude smaller than that reported by DOBBS 12.

<sup>7</sup> Obtained by analyzing CLEO III data but not authored by the CLEO Collaboration.

<sup>8</sup> Assuming  $\Gamma_{\eta_b(2S)} = 5$  MeV. Not independent of the corresponding mass measurement.

### $\eta_b(2S)$ WIDTH

VALUE (MeV)	CL%	DOCUMENT ID	TECN	COMMENT
<24	90	MIZUK 12	BELL	$e^+e^- \rightarrow \gamma\pi^+\pi^- \text{ hadrons}$

### $\eta_b(2S)$ DECAY MODES

Mode	Fraction ( $\Gamma_i/\Gamma$ )
$\Gamma_1$ hadrons	seen

### $\eta_b(2S)$ BRANCHING RATIOS

$\Gamma(\text{hadrons})/\Gamma_{total}$		$\Gamma_1/\Gamma$	
VALUE	EVTS	DOCUMENT ID	TECN COMMENT
seen	26k	MIZUK 12	BELL $e^+e^- \rightarrow \gamma\pi^+\pi^- \text{ hadrons}$
seen	9,10	DOBBS 12	$\Upsilon(2S) \rightarrow \gamma \text{ hadrons}$

••• We do not use the following data for averages, fits, limits, etc. •••

<sup>9</sup> SANDILYA 13 (Belle Collab.) search for such a state reconstructed in the same 26 exclusive hadronic final states as DOBBS 12 using a sample of  $(157.8 \pm 3.6) \times 10^6 \Upsilon(2S)$  decays or about 17 times larger and find no evidence for a signal. Their 90% C.L. upper limit on the branching fraction  $B(\Upsilon(2S) \rightarrow \eta_b(2S)\gamma) \times \sum_i B(\eta_b(2S) \rightarrow X_i) < 4.9 \times 10^{-6}$ , summed over the exclusive hadronic final states  $X_i$ , is an order of magnitude smaller than that reported by DOBBS 12.

<sup>10</sup> Obtained by analyzing CLEO III data but not authored by the CLEO Collaboration.

### $\eta_b(2S)$ REFERENCES

SANDILYA 13	PRL 111 112001	S. Sandilya et al.	(BELLE Collab.)
DOBBS 12	PRL 109 082001	S. Dobbs et al.	(BELLE Collab.)
MIZUK 12	PRL 109 232002	R. Mizuk et al.	(BELLE Collab.)

## $\Upsilon(2S)$

$$I^G(J^{PC}) = 0^-(1^{--})$$

### $\Upsilon(2S)$ MASS

VALUE (MeV)	DOCUMENT ID	TECN	COMMENT
<b>10023.26 ± 0.31 OUR AVERAGE</b>			
10023.5 ± 0.5	<sup>1</sup> ARTA MONOV 00	MD1	$e^+e^- \rightarrow \text{hadrons}$
10023.1 ± 0.4	BARBER 84	REDE	$e^+e^- \rightarrow \text{hadrons}$

••• We do not use the following data for averages, fits, limits, etc. •••

10023.6 ± 0.5	<sup>2,3</sup> BARU 86B	REDE	$e^+e^- \rightarrow \text{hadrons}$
---------------	-------------------------	------	-------------------------------------

<sup>1</sup> Reanalysis of BARU 86B using new electron mass (COHEN 87).

<sup>2</sup> Reanalysis of ARTAMONOV 84.

<sup>3</sup> Superseded by ARTAMONOV 00.

$m_{\Upsilon(3S)} - m_{\Upsilon(2S)}$

VALUE (MeV)	DOCUMENT ID	TECN	COMMENT
<b>331.50 ± 0.02 ± 0.13</b>	LEES	11c	BABR $e^+e^- \rightarrow \pi^+\pi^-X$

$\Upsilon(2S)$  WIDTH

VALUE (keV)	DOCUMENT ID	COMMENT
<b>31.98 ± 2.63 OUR EVALUATION</b>	See the Note on "Width Determinations of the $\Upsilon$ States"	

$\Upsilon(2S)$  DECAY MODES

Mode	Fraction ( $\Gamma_i/\Gamma$ )	Scale factor / Confidence level
$\Gamma_1$ $\Upsilon(1S)\pi^+\pi^-$	(17.85 ± 0.26) %	
$\Gamma_2$ $\Upsilon(1S)\pi^0\pi^0$	( 8.6 ± 0.4 ) %	
$\Gamma_3$ $\tau^+\tau^-$	( 2.00 ± 0.21 ) %	
$\Gamma_4$ $\mu^+\mu^-$	( 1.93 ± 0.17 ) %	S=2.2
$\Gamma_5$ $e^+e^-$	( 1.91 ± 0.16 ) %	
$\Gamma_6$ $\Upsilon(1S)\pi^0$	< 4 × 10 <sup>-5</sup>	CL=90%
$\Gamma_7$ $\Upsilon(1S)\eta$	( 2.9 ± 0.4 ) × 10 <sup>-4</sup>	S=2.0
$\Gamma_8$ $J/\psi(1S)$ anything	< 6 × 10 <sup>-3</sup>	CL=90%
$\Gamma_9$ $J/\psi(1S)\eta_c$	< 5.4 × 10 <sup>-6</sup>	CL=90%
$\Gamma_{10}$ $J/\psi(1S)\chi_{c0}$	< 3.4 × 10 <sup>-6</sup>	CL=90%
$\Gamma_{11}$ $J/\psi(1S)\chi_{c1}$	< 1.2 × 10 <sup>-6</sup>	CL=90%
$\Gamma_{12}$ $J/\psi(1S)\chi_{c2}$	< 2.0 × 10 <sup>-6</sup>	CL=90%
$\Gamma_{13}$ $J/\psi(1S)\eta_c(2S)$	< 2.5 × 10 <sup>-6</sup>	CL=90%
$\Gamma_{14}$ $J/\psi(1S)X(3940)$	< 2.0 × 10 <sup>-6</sup>	CL=90%
$\Gamma_{15}$ $J/\psi(1S)X(4160)$	< 2.0 × 10 <sup>-6</sup>	CL=90%
$\Gamma_{16}$ $\chi_{c1}$ anything	( 2.2 ± 0.5 ) × 10 <sup>-4</sup>	
$\Gamma_{17}$ $\chi_{c1}(1P)^0 X_{tetra}$	< 3.67 × 10 <sup>-5</sup>	CL=90%
$\Gamma_{18}$ $\chi_{c2}$ anything	( 2.3 ± 0.8 ) × 10 <sup>-4</sup>	
$\Gamma_{19}$ $\psi(2S)\eta_c$	< 5.1 × 10 <sup>-6</sup>	CL=90%
$\Gamma_{20}$ $\psi(2S)\chi_{c0}$	< 4.7 × 10 <sup>-6</sup>	CL=90%
$\Gamma_{21}$ $\psi(2S)\chi_{c1}$	< 2.5 × 10 <sup>-6</sup>	CL=90%
$\Gamma_{22}$ $\psi(2S)\chi_{c2}$	< 1.9 × 10 <sup>-6</sup>	CL=90%
$\Gamma_{23}$ $\psi(2S)\eta_c(2S)$	< 3.3 × 10 <sup>-6</sup>	CL=90%
$\Gamma_{24}$ $\psi(2S)X(3940)$	< 3.9 × 10 <sup>-6</sup>	CL=90%
$\Gamma_{25}$ $\psi(2S)X(4160)$	< 3.9 × 10 <sup>-6</sup>	CL=90%
$\Gamma_{26}$ $Z_c(3900)^+ Z_c(3900)^-$	< 1.0 × 10 <sup>-6</sup>	CL=90%
$\Gamma_{27}$ $Z_c(4200)^+ Z_c(4200)^-$	< 1.67 × 10 <sup>-5</sup>	CL=90%
$\Gamma_{28}$ $Z_c(3900)^{\pm} Z_c(4200)^{\mp}$	< 7.3 × 10 <sup>-6</sup>	CL=90%
$\Gamma_{29}$ $X(4050)^+ X(4050)^-$	< 1.35 × 10 <sup>-5</sup>	CL=90%
$\Gamma_{30}$ $X(4250)^+ X(4250)^-$	< 2.67 × 10 <sup>-5</sup>	CL=90%
$\Gamma_{31}$ $X(4050)^{\pm} X(4250)^{\mp}$	< 2.72 × 10 <sup>-5</sup>	CL=90%
$\Gamma_{32}$ $Z_c(4430)^+ Z_c(4430)^-$	< 2.03 × 10 <sup>-5</sup>	CL=90%
$\Gamma_{33}$ $X(4055)^{\pm} X(4055)^{\mp}$	< 1.11 × 10 <sup>-5</sup>	CL=90%
$\Gamma_{34}$ $X(4055)^{\pm} Z_c(4430)^{\mp}$	< 2.11 × 10 <sup>-5</sup>	CL=90%
$\Gamma_{35}$ ${}^2H$ anything	( 2.78 ± 0.30 / 0.26 ) × 10 <sup>-5</sup>	S=1.2
$\Gamma_{36}$ hadrons	( 94 ± 11 ) %	
$\Gamma_{37}$ $ggg$	( 58.8 ± 1.2 ) %	
$\Gamma_{38}$ $\gamma gg$	( 1.87 ± 0.28 ) %	
$\Gamma_{39}$ $\phi K^+ K^-$	( 1.6 ± 0.4 ) × 10 <sup>-6</sup>	
$\Gamma_{40}$ $\omega\pi^+\pi^-$	< 2.58 × 10 <sup>-6</sup>	CL=90%
$\Gamma_{41}$ $K^*(892)^0 K^- \pi^+ + c.c.$	( 2.3 ± 0.7 ) × 10 <sup>-6</sup>	
$\Gamma_{42}$ $\phi f_2'(1525)$	< 1.33 × 10 <sup>-6</sup>	CL=90%
$\Gamma_{43}$ $\omega f_2'(1270)$	< 5.7 × 10 <sup>-7</sup>	CL=90%
$\Gamma_{44}$ $\rho(770) a_2(1320)$	< 8.8 × 10 <sup>-7</sup>	CL=90%
$\Gamma_{45}$ $K^*(892)^0 K_2^*(1430)^0 + c.c.$	( 1.5 ± 0.6 ) × 10 <sup>-6</sup>	
$\Gamma_{46}$ $K_1(1270)^{\pm} K^{\mp}$	< 3.22 × 10 <sup>-6</sup>	CL=90%
$\Gamma_{47}$ $K_1(1400)^{\pm} K^{\mp}$	< 8.3 × 10 <sup>-7</sup>	CL=90%
$\Gamma_{48}$ $b_1(1235)^{\pm} \pi^{\mp}$	< 4.0 × 10 <sup>-7</sup>	CL=90%
$\Gamma_{49}$ $\rho\pi$	< 1.16 × 10 <sup>-6</sup>	CL=90%
$\Gamma_{50}$ $\pi^+\pi^-\pi^0$	< 8.0 × 10 <sup>-7</sup>	CL=90%
$\Gamma_{51}$ $\omega\pi^0$	< 1.63 × 10 <sup>-6</sup>	CL=90%
$\Gamma_{52}$ $\pi^+\pi^-\pi^0\pi^0$	( 1.30 ± 0.28 ) × 10 <sup>-5</sup>	
$\Gamma_{53}$ $K_S^0 K^+ \pi^- + c.c.$	( 1.14 ± 0.33 ) × 10 <sup>-6</sup>	
$\Gamma_{54}$ $K^*(892)^0 \bar{K}^0 + c.c.$	< 4.22 × 10 <sup>-6</sup>	CL=90%
$\Gamma_{55}$ $K^*(892)^- K^+ + c.c.$	< 1.45 × 10 <sup>-6</sup>	CL=90%
$\Gamma_{56}$ $f_1(1285)$ anything	( 2.2 ± 1.6 ) × 10 <sup>-3</sup>	
$\Gamma_{57}$ $f_1(1285) X_{tetra}$	< 6.47 × 10 <sup>-5</sup>	CL=90%
$\Gamma_{58}$ Sum of 100 exclusive modes	( 2.90 ± 0.30 ) × 10 <sup>-3</sup>	

Radiative decays

$\Gamma_{59}$ $\gamma\chi_{b1}(1P)$	( 6.9 ± 0.4 ) %	
$\Gamma_{60}$ $\gamma\chi_{b2}(1P)$	( 7.15 ± 0.35 ) %	
$\Gamma_{61}$ $\gamma\chi_{b0}(1P)$	( 3.8 ± 0.4 ) %	
$\Gamma_{62}$ $\gamma f_0(1710)$	< 5.9 × 10 <sup>-4</sup>	CL=90%
$\Gamma_{63}$ $\gamma f_2'(1525)$	< 5.3 × 10 <sup>-4</sup>	CL=90%
$\Gamma_{64}$ $\gamma f_2'(1270)$	< 2.41 × 10 <sup>-4</sup>	CL=90%
$\Gamma_{65}$ $\gamma f_3(2220)$		
$\Gamma_{66}$ $\gamma\eta_c(1S)$	< 2.7 × 10 <sup>-5</sup>	CL=90%
$\Gamma_{67}$ $\gamma\chi_{c0}$	< 1.0 × 10 <sup>-4</sup>	CL=90%
$\Gamma_{68}$ $\gamma\chi_{c1}$	< 3.6 × 10 <sup>-6</sup>	CL=90%
$\Gamma_{69}$ $\gamma\chi_{c2}$	< 1.5 × 10 <sup>-5</sup>	CL=90%
$\Gamma_{70}$ $\gamma\chi_{c1}(3872) \rightarrow \pi^+\pi^-J/\psi$	< 8 × 10 <sup>-7</sup>	CL=90%
$\Gamma_{71}$ $\gamma\chi_{c1}(3872) \rightarrow \pi^+\pi^-\pi^0 J/\psi$	< 2.4 × 10 <sup>-6</sup>	CL=90%
$\Gamma_{72}$ $\gamma X(3915) \rightarrow \omega J/\psi$	< 2.8 × 10 <sup>-6</sup>	CL=90%
$\Gamma_{73}$ $\gamma\chi_{c1}(4140) \rightarrow \phi J/\psi$	< 1.2 × 10 <sup>-6</sup>	CL=90%
$\Gamma_{74}$ $\gamma X(4350) \rightarrow \phi J/\psi$	< 1.3 × 10 <sup>-6</sup>	CL=90%
$\Gamma_{75}$ $\gamma\eta_b(1S)$	( 5.5 ± 1.1 / 0.9 ) × 10 <sup>-4</sup>	S=1.2
$\Gamma_{76}$ $\gamma\eta_b(1S) \rightarrow \gamma$ Sum of 26 exclusive modes	< 3.7 × 10 <sup>-6</sup>	CL=90%
$\Gamma_{77}$ $\gamma X_{b\bar{b}} \rightarrow \gamma$ Sum of 26 exclusive modes	< 4.9 × 10 <sup>-6</sup>	CL=90%
$\Gamma_{78}$ $\gamma X \rightarrow \gamma + \geq 4$ prongs	[a] < 1.95 × 10 <sup>-4</sup>	CL=95%
$\Gamma_{79}$ $\gamma A^0 \rightarrow \gamma$ hadrons	< 8 × 10 <sup>-5</sup>	CL=90%
$\Gamma_{80}$ $\gamma a_1^0 \rightarrow \gamma\mu^+\mu^-$	< 8.3 × 10 <sup>-6</sup>	CL=90%

Lepton Family number (LF) violating modes

$\Gamma_{81}$ $e^{\pm}\tau^{\mp}$	LF	< 3.2 × 10 <sup>-6</sup>	CL=90%
$\Gamma_{82}$ $\mu^{\pm}\tau^{\mp}$	LF	< 3.3 × 10 <sup>-6</sup>	CL=90%

[a] 1.5 GeV <  $m_X$  < 5.0 GeV

CONSTRAINED FIT INFORMATION

An overall fit to 3 branching ratios uses 13 measurements and one constraint to determine 3 parameters. The overall fit has a  $\chi^2 = 11.8$  for 11 degrees of freedom.

The following *off-diagonal* array elements are the correlation coefficients  $\langle \delta x_i \delta x_j \rangle / (\delta x_i \delta x_j)$ , in percent, from the fit to the branching fractions,  $x_i \equiv \Gamma_i/\Gamma_{total}$ . The fit constrains the  $x_i$  whose labels appear in this array to sum to one.

$$x_7 \begin{vmatrix} & 2 \\ & x_1 \end{vmatrix}$$

$\Upsilon(2S) \Gamma(i)\Gamma(e^+e^-)/\Gamma(total)$

$\Gamma(\mu^+\mu^-) \times \Gamma(e^+e^-)/\Gamma_{total}$	VALUE (eV)	DOCUMENT ID	TECN	COMMENT	$\Gamma_4\Gamma_5/\Gamma$
<b>6.5 ± 1.5 ± 1.0</b>		KOBEL	92	CBAL $e^+e^- \rightarrow \mu^+\mu^-$	

$\Gamma(\Upsilon(1S)\pi^+\pi^-) \times \Gamma(e^+e^-)/\Gamma_{total}$	VALUE (eV)	EVTS	DOCUMENT ID	TECN	COMMENT	$\Gamma_1\Gamma_5/\Gamma$
<b>105.4 ± 1.0 ± 4.2</b>	11.8K	1	AUBERT	08BP	BABR 10.58 $e^+e^- \rightarrow \gamma\pi^+\pi^-\ell^+\ell^-$	
					<sup>1</sup> Using $B(\Upsilon(1S) \rightarrow e^+e^-) = (2.38 \pm 0.11)\%$ and $B(\Upsilon(1S) \rightarrow \mu^+\mu^-) = (2.48 \pm 0.05)\%$ .	

$\Gamma(hadrons) \times \Gamma(e^+e^-)/\Gamma_{total}$	VALUE (keV)	DOCUMENT ID	TECN	COMMENT	$\Gamma_{36}\Gamma_5/\Gamma$
<b>0.577 ± 0.009 OUR AVERAGE</b>					
0.581 ± 0.004 ± 0.009		1	ROSNER	06	CLEO 10.0 $e^+e^- \rightarrow hadrons$
0.552 ± 0.031 ± 0.017		1	BARU	96	MD1 $e^+e^- \rightarrow hadrons$
0.54 ± 0.04 ± 0.02		1	JAKUBOWSKI	88	CBAL $e^+e^- \rightarrow hadrons$
0.58 ± 0.03 ± 0.04		2	GILES	84B	CLEO $e^+e^- \rightarrow hadrons$
0.60 ± 0.12 ± 0.07		2	ALBRECHT	82	DASP $e^+e^- \rightarrow hadrons$
0.54 ± 0.07 ± 0.09 / -0.05		2	NICZYPORUK	81c	LENA $e^+e^- \rightarrow hadrons$
0.41 ± 0.18		2	BOCK	80	CNTR $e^+e^- \rightarrow hadrons$

<sup>1</sup> Radiative corrections evaluated following KURAEV 85.  
<sup>2</sup> Radiative corrections reevaluated by BUCHMUELLER 88 following KURAEV 85.

$\Upsilon(2S)$  PARTIAL WIDTHS

$\Gamma(e^+e^-)$	VALUE (keV)	DOCUMENT ID
<b>0.612 ± 0.011 OUR EVALUATION</b>		

# Meson Particle Listings

## $\Upsilon(2S)$

### $\Upsilon(2S)$ BRANCHING RATIOS

$\Gamma(\Upsilon(1S)\pi^+\pi^-)/\Gamma_{total}$   $\Gamma_1/\Gamma$   
 Abbreviation MM in the COMMENT field below stands for missing mass.

VALUE (units $10^{-2}$ )	EVTS	DOCUMENT ID	TECN	COMMENT
<b>17.85 ± 0.26 OUR FIT</b>				
<b>17.92 ± 0.26 OUR AVERAGE</b>				
16.8 ± 1.1 ± 1.3	906k	<sup>1</sup> LEES	11C	BABR $e^+e^- \rightarrow \pi^+\pi^- X$
17.80 ± 0.05 ± 0.37	170k	<sup>2</sup> LEES	11L	BABR $\Upsilon(2S) \rightarrow \pi^+\pi^-\mu^+\mu^-$
18.02 ± 0.02 ± 0.61	851k	<sup>3</sup> BHARI	09	CLEO $e^+e^- \rightarrow \pi^+\pi^- MM$
17.22 ± 0.17 ± 0.75	11.8k	<sup>4</sup> AUBERT	08BP	BABR $e^+e^- \rightarrow \gamma\pi^+\pi^-\ell^+\ell^-$
19.2 ± 0.2 ± 1.0	52.6k	<sup>5</sup> ALEXANDER	98	CLE2 $\pi^+\pi^-\ell^+\ell^-, \pi^+\pi^- MM$
18.1 ± 0.5 ± 1.0	11.6k	ALBRECHT	87	ARG $e^+e^- \rightarrow \pi^+\pi^- MM$
16.9 ± 4.0		GELPHMAN	85	CBAL $e^+e^- \rightarrow e^+e^-\pi^+\pi^-$
19.1 ± 1.2 ± 0.6		BESSON	84	CLEO $\pi^+\pi^- MM$
18.9 ± 2.6		FONSECA	84	CUSB $e^+e^- \rightarrow \ell^+\ell^-\pi^+\pi^-$
21 ± 7	7	NICZYPORUK	81B	LENA $e^+e^- \rightarrow \ell^+\ell^-\pi^+\pi^-$

<sup>1</sup> LEES 11c reports  $[\Gamma(\Upsilon(2S) \rightarrow \Upsilon(1S)\pi^+\pi^-)/\Gamma_{total}] \times [B(\Upsilon(3S) \rightarrow \Upsilon(2S)\text{anything})] = (1.78 \pm 0.02 \pm 0.11) \times 10^{-2}$  which we divide by our best value  $B(\Upsilon(3S) \rightarrow \Upsilon(2S)\text{anything}) = (10.6 \pm 0.8) \times 10^{-2}$ . Our first error is their experiment's error and our second error is the systematic error from using our best value.  
<sup>2</sup> Using  $B(\Upsilon(1S) \rightarrow \mu^+\mu^-) = (2.48 \pm 0.05)\%$ .  
<sup>3</sup> A weighted average of the inclusive and exclusive results.  
<sup>4</sup> Using  $B(\Upsilon(2S) \rightarrow e^+e^-) = (1.91 \pm 0.16)\%$ ,  $B(\Upsilon(2S) \rightarrow \mu^+\mu^-) = (1.93 \pm 0.17)\%$  and  $\Gamma_{ee}(\Upsilon(2S)) = 0.612 \pm 0.011$  keV.  
<sup>5</sup> Using  $B(\Upsilon(1S) \rightarrow e^+e^-) = (2.52 \pm 0.17)\%$  and  $B(\Upsilon(1S) \rightarrow \mu^+\mu^-) = (2.48 \pm 0.07)\%$ .

$\Gamma(\Upsilon(1S)\pi^0\pi^0)/\Gamma_{total}$   $\Gamma_2/\Gamma$

VALUE (units $10^{-2}$ )	EVTS	DOCUMENT ID	TECN	COMMENT
<b>8.6 ± 0.4 OUR AVERAGE</b>				
8.43 ± 0.16 ± 0.42	38k	<sup>1</sup> BHARI	09	CLEO $e^+e^- \rightarrow \pi^0\pi^0\ell^+\ell^-$
9.2 ± 0.6 ± 0.8	275	<sup>2</sup> ALEXANDER	98	CLE2 $e^+e^- \rightarrow \pi^0\pi^0\ell^+\ell^-$
9.5 ± 1.9 ± 1.9	25	ALBRECHT	87	ARG $e^+e^- \rightarrow \pi^0\pi^0\ell^+\ell^-$
8.0 ± 1.5		GELPHMAN	85	CBAL $e^+e^- \rightarrow \pi^0\pi^0\ell^+\ell^-$
10.3 ± 2.3		FONSECA	84	CUSB $e^+e^- \rightarrow \pi^0\pi^0\ell^+\ell^-$

<sup>1</sup> Authors assume  $B(\Upsilon(1S) \rightarrow e^+e^-) + B(\Upsilon(1S) \rightarrow \mu^+\mu^-) = 4.96\%$ .  
<sup>2</sup> Using  $B(\Upsilon(1S) \rightarrow e^+e^-) = (2.52 \pm 0.17)\%$  and  $B(\Upsilon(1S) \rightarrow \mu^+\mu^-) = (2.48 \pm 0.07)\%$ .

$\Gamma(\Upsilon(1S)\pi^0\pi^0)/\Gamma(\Upsilon(1S)\pi^+\pi^-)$   $\Gamma_2/\Gamma_1$

VALUE	DOCUMENT ID	TECN	COMMENT
0.462 ± 0.037	<sup>1</sup> BHARI 09	CLEO	$e^+e^- \rightarrow \Upsilon(2S)$

<sup>1</sup> Not independent of other values reported by BHARI 09.

$\Gamma(\tau^+\tau^-)/\Gamma_{total}$   $\Gamma_3/\Gamma$

VALUE (units $10^{-2}$ )	EVTS	DOCUMENT ID	TECN	COMMENT
<b>2.00 ± 0.21 OUR AVERAGE</b>				
2.00 ± 0.12 ± 0.18	22k	<sup>1</sup> BESSON	07	CLEO $e^+e^- \rightarrow \Upsilon(2S) \rightarrow \tau^+\tau^-$
1.7 ± 1.5 ± 0.6		HAAS	84B	CLEO $e^+e^- \rightarrow \tau^+\tau^-$

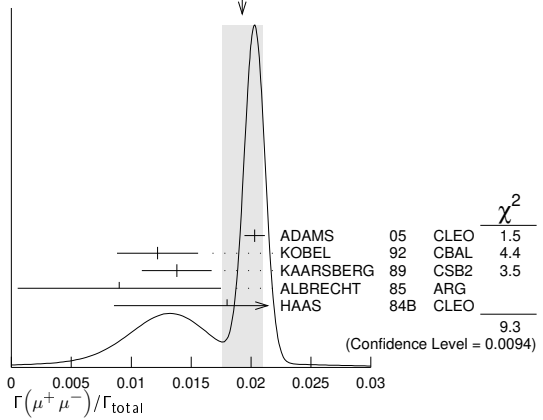
<sup>1</sup> BESSON 07 reports  $[\Gamma(\Upsilon(2S) \rightarrow \tau^+\tau^-)/\Gamma_{total}] / [B(\Upsilon(2S) \rightarrow \mu^+\mu^-)] = 1.04 \pm 0.04 \pm 0.05$  which we multiply by our best value  $B(\Upsilon(2S) \rightarrow \mu^+\mu^-) = (1.93 \pm 0.17) \times 10^{-2}$ . Our first error is their experiment's error and our second error is the systematic error from using our best value.

$\Gamma(\mu^+\mu^-)/\Gamma_{total}$   $\Gamma_4/\Gamma$

VALUE	CL%	EVTS	DOCUMENT ID	TECN	COMMENT
<b>0.0193 ± 0.0017 OUR AVERAGE</b>					Error includes scale factor of 2.2. See the ideogram below.
0.0203 ± 0.0003 ± 0.0008		120k	ADAMS	05	CLEO $e^+e^- \rightarrow \mu^+\mu^-$
0.0122 ± 0.0028 ± 0.0019			<sup>1</sup> KOBEL	92	CBAL $e^+e^- \rightarrow \mu^+\mu^-$
0.0138 ± 0.0025 ± 0.0015			KAARSBERG	89	CSB2 $e^+e^- \rightarrow \mu^+\mu^-$
0.009 ± 0.006 ± 0.006			<sup>2</sup> ALBRECHT	85	ARG $e^+e^- \rightarrow \mu^+\mu^-$
0.018 ± 0.008 ± 0.005			HAAS	84B	CLEO $e^+e^- \rightarrow \mu^+\mu^-$
< 0.038		90	NICZYPORUK	81c	LENA $e^+e^- \rightarrow \mu^+\mu^-$

<sup>1</sup> Taking into account interference between the resonance and continuum.  
<sup>2</sup> Re-evaluated using  $B(\Upsilon(1S) \rightarrow \mu^+\mu^-) = 0.026$ .

WEIGHTED AVERAGE  
 0.0193 ± 0.0017 (Error scaled by 2.2)



$\Gamma(\tau^+\tau^-)/\Gamma(\mu^+\mu^-)$   $\Gamma_3/\Gamma_4$

VALUE	EVTS	DOCUMENT ID	TECN	COMMENT
<b>1.04 ± 0.04 ± 0.05</b>	22k	BESSON	07	CLEO $e^+e^- \rightarrow \Upsilon(2S)$

$\Gamma(\Upsilon(1S)\pi^0)/\Gamma_{total}$   $\Gamma_6/\Gamma$

VALUE (units $10^{-5}$ )	CL%	DOCUMENT ID	TECN	COMMENT
< 4	90	<sup>1</sup> TAMPONI	13	BELL $e^+e^- \rightarrow \Upsilon(1S)\pi^0$
< 18	90	<sup>2</sup> HE	08A	CLEO $e^+e^- \rightarrow \ell^+\ell^-\gamma\gamma$
< 110	90	ALEXANDER	98	CLE2 $e^+e^- \rightarrow \ell^+\ell^-\gamma\gamma$
< 800	90	LURZ	87	CBAL $e^+e^- \rightarrow \ell^+\ell^-\gamma\gamma$

<sup>1</sup> TAMPONI 13 reports  $[\Gamma(\Upsilon(2S) \rightarrow \Upsilon(1S)\pi^0)/\Gamma_{total}] / [B(\Upsilon(2S) \rightarrow \Upsilon(1S)\pi^+\pi^-)] < 2.3 \times 10^{-4}$  which we multiply by our best value  $B(\Upsilon(2S) \rightarrow \Upsilon(1S)\pi^+\pi^-) = 17.85 \times 10^{-2}$ .  
<sup>2</sup> Authors assume  $B(\Upsilon(1S) \rightarrow e^+e^-) + B(\Upsilon(1S) \rightarrow \mu^+\mu^-) = 4.96\%$ .

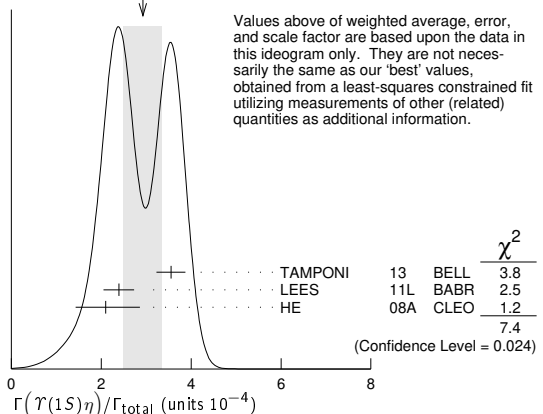
$\Gamma(\Upsilon(1S)\pi^0)/\Gamma(\Upsilon(1S)\pi^+\pi^-)$   $\Gamma_6/\Gamma_1$

VALUE (units $10^{-4}$ )	CL%	DOCUMENT ID	TECN	COMMENT
< 2.3	90	TAMPONI	13	BELL $e^+e^- \rightarrow \Upsilon(1S)\pi^0$

$\Gamma(\Upsilon(1S)\eta)/\Gamma_{total}$   $\Gamma_7/\Gamma$

VALUE (units $10^{-4}$ )	CL%	EVTS	DOCUMENT ID	TECN	COMMENT
<b>2.9 ± 0.4 OUR FIT</b>					Error includes scale factor of 2.0.
<b>2.9 ± 0.4 OUR AVERAGE</b>					Error includes scale factor of 1.9. See the ideogram below.
2.39 ± 0.31 ± 0.14		112	<sup>1</sup> LEES	11L	BABR $\Upsilon(2S) \rightarrow \ell^+\ell^-\eta$
2.1 $^{+0.7}_{-0.6}$ ± 0.3		14	<sup>2</sup> HE	08A	CLEO $e^+e^- \rightarrow \ell^+\ell^-\eta$
3.55 ± 0.32 ± 0.05		241	<sup>3</sup> TAMPONI	13	BELL $e^+e^- \rightarrow \Upsilon(1S)\eta$
< 9	90	<sup>1,4</sup> AUBERT	08BP	BABR $e^+e^- \rightarrow \gamma\pi^+\pi^-\pi^0\ell^+\ell^-$	
< 28	90	ALEXANDER	98	CLE2 $e^+e^- \rightarrow \ell^+\ell^-\eta$	
< 50	90	ALBRECHT	87	ARG $e^+e^- \rightarrow \pi^+\pi^-\ell^+\ell^- MM$	
< 70	90	LURZ	87	CBAL $e^+e^- \rightarrow \ell^+\ell^-(\gamma\gamma, 3\pi^0)$	
< 100	90	BESSON	84	CLEO $e^+e^- \rightarrow \pi^+\pi^-\ell^+\ell^- MM$	
< 20	90	FONSECA	84	CUSB $e^+e^- \rightarrow \ell^+\ell^-(\gamma\gamma, \pi^+\pi^-\pi^0)$	

WEIGHTED AVERAGE  
 2.9 ± 0.4 (Error scaled by 1.9)



<sup>1</sup> Using  $B(\Upsilon(1S) \rightarrow e^+e^-) = (2.38 \pm 0.11)\%$  and  $B(\Upsilon(1S) \rightarrow \mu^+\mu^-) = (2.48 \pm 0.05)\%$ .

<sup>2</sup> Authors assume  $B(\Upsilon(1S) \rightarrow e^+e^-) + B(\Upsilon(1S) \rightarrow \mu^+\mu^-) = 4.96\%$ .

<sup>3</sup> TAMPONI 13 reports  $[\Gamma(\Upsilon(2S) \rightarrow \Upsilon(1S)\eta)/\Gamma_{total}] / [B(\Upsilon(2S) \rightarrow \Upsilon(1S)\pi^+\pi^-)] = (1.99 \pm 0.14 \pm 0.11) \times 10^{-3}$  which we multiply by our best value  $B(\Upsilon(2S) \rightarrow \Upsilon(1S)\pi^+\pi^-) = (17.85 \pm 0.26) \times 10^{-2}$ . Our first error is their experiment's error and our second error is the systematic error from using our best value.

<sup>4</sup> Using  $\Gamma_{ee}(\Upsilon(2S)) = 0.612 \pm 0.011$  keV.

$\Gamma(\Upsilon(1S)\eta)/\Gamma(\Upsilon(1S)\pi^+\pi^-)$   $\Gamma_7/\Gamma_1$

VALUE (units  $10^{-3}$ ) CL% EVTS DOCUMENT ID TECN COMMENT

**1.64 ± 0.25 OUR FIT** Error includes scale factor of 2.0.

**1.99 ± 0.14 ± 0.11** 241 TAMPONI 13 BELL  $e^+e^- \rightarrow \Upsilon(1S)\eta$

• • • We do not use the following data for averages, fits, limits, etc. • • •

1.35 ± 0.17 ± 0.08 <sup>1</sup> LEES 11L BABR  $\Upsilon(2S) \rightarrow (\pi^+\pi^-)(\gamma\gamma)\mu^+\mu^-$

< 5.2 90 <sup>2</sup> AUBERT 08BP BABR  $e^+e^- \rightarrow \gamma\pi^+\pi^-(\pi^0)\ell^+\ell^-$

<sup>1</sup> Not independent of other values reported by LEES 11L.

<sup>2</sup> Not independent of other values reported by AUBERT 08BP.

$\Gamma(\Upsilon(1S)\pi^0)/\Gamma(\Upsilon(1S)\eta)$   $\Gamma_6/\Gamma_7$

VALUE CL% DOCUMENT ID TECN COMMENT

• • • We do not use the following data for averages, fits, limits, etc. • • •

< 0.13 90 TAMPONI 13 BELL  $e^+e^- \rightarrow \Upsilon(1S)\pi^0$

$\Gamma(J/\psi(1S) \text{ anything})/\Gamma_{total}$   $\Gamma_8/\Gamma$

VALUE CL% DOCUMENT ID TECN COMMENT

**< 0.006** 90 MASCHMANN 90 CBAL  $e^+e^- \rightarrow$  hadrons

$\Gamma(J/\psi(1S)\eta_c)/\Gamma_{total}$   $\Gamma_9/\Gamma$

VALUE CL% DOCUMENT ID TECN COMMENT

**< 5.4 × 10<sup>-6</sup>** 90 YANG 14 BELL  $e^+e^- \rightarrow J/\psi X$

$\Gamma(J/\psi(1S)\chi_{c0})/\Gamma_{total}$   $\Gamma_{10}/\Gamma$

VALUE CL% DOCUMENT ID TECN COMMENT

**< 3.4 × 10<sup>-6</sup>** 90 YANG 14 BELL  $e^+e^- \rightarrow J/\psi X$

$\Gamma(J/\psi(1S)\chi_{c1})/\Gamma_{total}$   $\Gamma_{11}/\Gamma$

VALUE CL% DOCUMENT ID TECN COMMENT

**< 1.2 × 10<sup>-6</sup>** 90 YANG 14 BELL  $e^+e^- \rightarrow J/\psi X$

$\Gamma(J/\psi(1S)\chi_{c2})/\Gamma_{total}$   $\Gamma_{12}/\Gamma$

VALUE CL% DOCUMENT ID TECN COMMENT

**< 2.0 × 10<sup>-6</sup>** 90 YANG 14 BELL  $e^+e^- \rightarrow J/\psi X$

$\Gamma(J/\psi(1S)\eta_c(2S))/\Gamma_{total}$   $\Gamma_{13}/\Gamma$

VALUE CL% DOCUMENT ID TECN COMMENT

**< 2.5 × 10<sup>-6</sup>** 90 YANG 14 BELL  $e^+e^- \rightarrow J/\psi X$

$\Gamma(J/\psi(1S)X(3940))/\Gamma_{total}$   $\Gamma_{14}/\Gamma$

VALUE CL% DOCUMENT ID TECN COMMENT

**< 2.0 × 10<sup>-6</sup>** 90 YANG 14 BELL  $e^+e^- \rightarrow J/\psi X$

$\Gamma(J/\psi(1S)X(4160))/\Gamma_{total}$   $\Gamma_{15}/\Gamma$

VALUE CL% DOCUMENT ID TECN COMMENT

**< 2.0 × 10<sup>-6</sup>** 90 YANG 14 BELL  $e^+e^- \rightarrow J/\psi X$

$\Gamma(\chi_{c1} \text{ anything})/\Gamma_{total}$   $\Gamma_{16}/\Gamma$

VALUE (units  $10^{-4}$ ) EVTS DOCUMENT ID TECN COMMENT

**2.24 ± 0.44 ± 0.20** 376 JIA 17 BELL  $\Upsilon(2S) \rightarrow \gamma J/\psi(1S)$

$\Gamma(\chi_{c1}(1P^0)X_{tetra})/\Gamma_{total}$   $\Gamma_{17}/\Gamma$

VALUE CL% DOCUMENT ID TECN COMMENT

**< 36.7 × 10<sup>-6</sup>** 90 <sup>1</sup> JIA 17A BELL  $e^+e^- \rightarrow$  hadrons

<sup>1</sup> For a tetraquark state  $X_{tetra}$ , with mass in the range 1.16–2.46 GeV and width in the range 0–0.3 GeV. Measured 90% CL limits as a function of  $X_{tetra}$  mass and width range from  $4.4 \times 10^{-6}$  to  $36.7 \times 10^{-6}$ .

$\Gamma(\chi_{c2} \text{ anything})/\Gamma_{total}$   $\Gamma_{18}/\Gamma$

VALUE (units  $10^{-4}$ ) DOCUMENT ID TECN COMMENT

**2.28 ± 0.73 ± 0.34** JIA 17 BELL  $\Upsilon(2S) \rightarrow \gamma J/\psi(1S)$

$\Gamma(\psi(2S)\eta_c)/\Gamma_{total}$   $\Gamma_{19}/\Gamma$

VALUE CL% DOCUMENT ID TECN COMMENT

**< 5.1 × 10<sup>-6</sup>** 90 YANG 14 BELL  $e^+e^- \rightarrow \psi(2S)X$

$\Gamma(\psi(2S)\chi_{c0})/\Gamma_{total}$   $\Gamma_{20}/\Gamma$

VALUE CL% DOCUMENT ID TECN COMMENT

**< 4.7 × 10<sup>-6</sup>** 90 YANG 14 BELL  $e^+e^- \rightarrow \psi(2S)X$

$\Gamma(\psi(2S)\chi_{c1})/\Gamma_{total}$   $\Gamma_{21}/\Gamma$

VALUE CL% DOCUMENT ID TECN COMMENT

**< 2.5 × 10<sup>-6</sup>** 90 YANG 14 BELL  $e^+e^- \rightarrow \psi(2S)X$

$\Gamma(\psi(2S)\chi_{c2})/\Gamma_{total}$   $\Gamma_{22}/\Gamma$

VALUE CL% DOCUMENT ID TECN COMMENT

**< 1.9 × 10<sup>-6</sup>** 90 YANG 14 BELL  $e^+e^- \rightarrow \psi(2S)X$

$\Gamma(\psi(2S)\eta_c(2S))/\Gamma_{total}$   $\Gamma_{23}/\Gamma$

VALUE CL% DOCUMENT ID TECN COMMENT

**< 3.3 × 10<sup>-6</sup>** 90 YANG 14 BELL  $e^+e^- \rightarrow \psi(2S)X$

$\Gamma(\psi(2S)X(3940))/\Gamma_{total}$   $\Gamma_{24}/\Gamma$

VALUE CL% DOCUMENT ID TECN COMMENT

**< 3.9 × 10<sup>-6</sup>** 90 YANG 14 BELL  $e^+e^- \rightarrow \psi(2S)X$

$\Gamma(\psi(2S)X(4160))/\Gamma_{total}$   $\Gamma_{25}/\Gamma$

VALUE CL% DOCUMENT ID TECN COMMENT

**< 3.9 × 10<sup>-6</sup>** 90 YANG 14 BELL  $e^+e^- \rightarrow \psi(2S)X$

$\Gamma(Z_c(3900)^+ Z_c(3900)^-)/\Gamma_{total}$   $\Gamma_{26}/\Gamma$

VALUE CL% DOCUMENT ID TECN COMMENT

**< 1.0 × 10<sup>-6</sup>** 90 <sup>1</sup> JIA 18 BELL  $\Upsilon(2S) \rightarrow J/\psi\pi^\pm X$

<sup>1</sup> Assuming  $B(Z_c(3900)^\pm) \rightarrow J/\psi\pi^\pm = 1$ .

$\Gamma(Z_c(4200)^+ Z_c(4200)^-)/\Gamma_{total}$   $\Gamma_{27}/\Gamma$

VALUE CL% DOCUMENT ID TECN COMMENT

**< 16.7 × 10<sup>-6</sup>** 90 <sup>1</sup> JIA 18 BELL  $\Upsilon(1S) \rightarrow J/\psi\pi^\pm X$

<sup>1</sup> Assuming  $B(Z_c(4200)^\pm) \rightarrow J/\psi\pi^\pm = 1$

$\Gamma(Z_c(3900)^\pm Z_c(4200)^\mp)/\Gamma_{total}$   $\Gamma_{28}/\Gamma$

VALUE CL% DOCUMENT ID TECN COMMENT

**< 7.3 × 10<sup>-6</sup>** 90 <sup>1</sup> JIA 18 BELL  $\Upsilon(2S) \rightarrow J/\psi\pi^\pm X$

<sup>1</sup> Assuming  $B(Z_c(4200)^\pm) \rightarrow J/\psi\pi^\pm = 1 = B(Z_c(3900)^\pm) \rightarrow J/\psi\pi^\pm$ .

$\Gamma(X(4050)^+ X(4050)^-)/\Gamma_{total}$   $\Gamma_{29}/\Gamma$

VALUE CL% DOCUMENT ID TECN COMMENT

**< 13.5 × 10<sup>-6</sup>** 90 <sup>1</sup> JIA 18 BELL  $\Upsilon(2S) \rightarrow \chi_{c1}(1P)\pi^\pm X$

<sup>1</sup> Assuming  $B(X(4050)^\pm) \rightarrow \chi_{c1}(1P)\pi^\pm$

$\Gamma(X(4250)^+ X(4250)^-)/\Gamma_{total}$   $\Gamma_{30}/\Gamma$

VALUE CL% DOCUMENT ID TECN COMMENT

**< 26.7 × 10<sup>-6</sup>** 90 <sup>1</sup> JIA 18 BELL  $\Upsilon(2S) \rightarrow \chi_{c1}(1P)\pi^\pm X$

<sup>1</sup> Assuming  $B(X(4250)^\pm) \rightarrow \chi_{c1}(1P)\pi^\pm = 1$

$\Gamma(X(4050)^\pm X(4250)^\mp)/\Gamma_{total}$   $\Gamma_{31}/\Gamma$

VALUE CL% DOCUMENT ID TECN COMMENT

**< 27.2 × 10<sup>-6</sup>** 90 <sup>1</sup> JIA 18 BELL  $\Upsilon(2S) \rightarrow \chi_{c1}(1P)\pi^\pm X$

<sup>1</sup> Assuming  $B(X(4050)^\pm) \rightarrow \chi_{c1}(1P)\pi^\pm = 1 = B(X(4250)^\pm) \rightarrow \chi_{c1}(1P)\pi^\pm$

$\Gamma(Z_c(4430)^+ Z_c(4430)^-)/\Gamma_{total}$   $\Gamma_{32}/\Gamma$

VALUE CL% DOCUMENT ID TECN COMMENT

**< 20.3 × 10<sup>-6</sup>** 90 <sup>1</sup> JIA 18 BELL  $\Upsilon(2S) \rightarrow \psi(2S)\pi^\pm X$

<sup>1</sup> Assuming  $B(Z_c(4430)^\pm) \rightarrow \psi(2P)\pi^\pm = 1$

$\Gamma(X(4055)^\pm X(4055)^\mp)/\Gamma_{total}$   $\Gamma_{33}/\Gamma$

VALUE CL% DOCUMENT ID TECN COMMENT

**< 11.1 × 10<sup>-6</sup>** 90 <sup>1</sup> JIA 18 BELL  $\Upsilon(2S) \rightarrow \psi(2S)\pi^\pm X$

<sup>1</sup> Assuming  $B(X(4055)^\pm) \rightarrow \psi(2S)\pi^\pm = 1$

$\Gamma(X(4055)^\pm Z_c(4430)^\mp)/\Gamma_{total}$   $\Gamma_{34}/\Gamma$

VALUE CL% DOCUMENT ID TECN COMMENT

**< 21.1 × 10<sup>-6</sup>** 90 <sup>1</sup> JIA 18 BELL  $\Upsilon(2S) \rightarrow \psi(2S)\pi^\pm X$

<sup>1</sup> Assuming  $B(X(4055)^\pm) \rightarrow \psi(2S)\pi^\pm = 1 = B(Z_c(4430)^\pm) \rightarrow \psi(2S)\pi^\pm$

$\Gamma(\overline{2}H \text{ anything})/\Gamma_{total}$   $\Gamma_{35}/\Gamma$

VALUE (units  $10^{-5}$ ) EVTS DOCUMENT ID TECN COMMENT

**2.78 <sup>+0.30</sup> -0.26** OUR AVERAGE Error includes scale factor of 1.2.

2.64 ± 0.11 <sup>+0.26</sup> -0.21 LEES 14G BABR  $e^+e^- \rightarrow \overline{2}H X$

3.37 ± 0.50 ± 0.25 58 ASNER 07 CLEO  $e^+e^- \rightarrow \overline{2}H X$

$\Gamma(g g g)/\Gamma_{total}$   $\Gamma_{37}/\Gamma$

VALUE (units  $10^{-2}$ ) EVTS DOCUMENT ID TECN COMMENT

**58.8 ± 1.2** 6M <sup>1</sup> BESSON 06A CLEO  $\Upsilon(2S) \rightarrow$  hadrons

<sup>1</sup> Calculated using the value  $\Gamma(\gamma g g)/\Gamma(g g g) = (3.18 \pm 0.04 \pm 0.22 \pm 0.41)\%$  from BESSON 06A and PDG 08 values of  $B(\pi^+\pi^-\Upsilon(1S)) = (18.1 \pm 0.4)\%$ ,  $B(\pi^0\pi^0\Upsilon(1S)) = (8.6 \pm 0.4)\%$ ,  $B(\mu^+\mu^-\Upsilon(1S)) = (1.93 \pm 0.17)\%$ , and  $R_{hadrons} = 3.51$ . The statistical error is negligible and the systematic error is partially correlated with that of  $\Gamma(\gamma g g)/\Gamma_{total}$  measurement of BESSON 06A.

## Meson Particle Listings

 $\Upsilon(2S)$ 

$\Gamma(\gamma g g)/\Gamma(g g g)$				$\Gamma_{38}/\Gamma_{37}$		
VALUE (units $10^{-2}$ )	EVTS	DOCUMENT ID	TECN	COMMENT		
$3.18 \pm 0.04 \pm 0.47$	6M	BESSON	06A	CLEO	$\Upsilon(2S) \rightarrow (\gamma +) \text{ hadrons}$	
$\Gamma(\phi K^+ K^-)/\Gamma_{\text{total}}$				$\Gamma_{39}/\Gamma$		
VALUE (units $10^{-6}$ )	EVTS	DOCUMENT ID	TECN	COMMENT		
$1.58 \pm 0.33 \pm 0.18$	58	SHEN	12A	BELL	$\Upsilon(1S) \rightarrow 2(K^+ K^-)$	
$\Gamma(\omega \pi^+ \pi^-)/\Gamma_{\text{total}}$				$\Gamma_{40}/\Gamma$		
VALUE (units $10^{-6}$ )	CL%	DOCUMENT ID	TECN	COMMENT		
$<2.58$	90	SHEN	12A	BELL	$\Upsilon(1S) \rightarrow 2(\pi^+ \pi^-) \pi^0$	
$\Gamma(K^*(892)^0 K^- \pi^+ + \text{c.c.})/\Gamma_{\text{total}}$				$\Gamma_{41}/\Gamma$		
VALUE (units $10^{-6}$ )	EVTS	DOCUMENT ID	TECN	COMMENT		
$2.32 \pm 0.40 \pm 0.54$	135	SHEN	12A	BELL	$\Upsilon(1S) \rightarrow K^+ K^- \pi^+ \pi^-$	
$\Gamma(\phi f_2'(1525))/\Gamma_{\text{total}}$				$\Gamma_{42}/\Gamma$		
VALUE (units $10^{-6}$ )	CL%	DOCUMENT ID	TECN	COMMENT		
$<1.33$	90	SHEN	12A	BELL	$\Upsilon(1S) \rightarrow 2(K^+ K^-)$	
$\Gamma(\omega f_2(1270))/\Gamma_{\text{total}}$				$\Gamma_{43}/\Gamma$		
VALUE (units $10^{-6}$ )	CL%	DOCUMENT ID	TECN	COMMENT		
$<0.57$	90	SHEN	12A	BELL	$\Upsilon(1S) \rightarrow 2(\pi^+ \pi^-) \pi^0$	
$\Gamma(\rho(770) \rho_2(1320))/\Gamma_{\text{total}}$				$\Gamma_{44}/\Gamma$		
VALUE (units $10^{-6}$ )	CL%	DOCUMENT ID	TECN	COMMENT		
$<0.88$	90	SHEN	12A	BELL	$\Upsilon(1S) \rightarrow 2(\pi^+ \pi^-) \pi^0$	
$\Gamma(K^*(892)^0 \bar{K}_2^0(1430)^0 + \text{c.c.})/\Gamma_{\text{total}}$				$\Gamma_{45}/\Gamma$		
VALUE (units $10^{-6}$ )	EVTS	DOCUMENT ID	TECN	COMMENT		
$1.53 \pm 0.52 \pm 0.19$	32	SHEN	12A	BELL	$\Upsilon(1S) \rightarrow K^+ K^- \pi^+ \pi^-$	
$\Gamma(K_1(1270)^\pm K^\mp)/\Gamma_{\text{total}}$				$\Gamma_{46}/\Gamma$		
VALUE (units $10^{-6}$ )	CL%	DOCUMENT ID	TECN	COMMENT		
$<3.22$	90	SHEN	12A	BELL	$\Upsilon(1S) \rightarrow K^+ K^- \pi^+ \pi^-$	
$\Gamma(K_1(1400)^\pm K^\mp)/\Gamma_{\text{total}}$				$\Gamma_{47}/\Gamma$		
VALUE (units $10^{-6}$ )	CL%	DOCUMENT ID	TECN	COMMENT		
$<0.83$	90	SHEN	12A	BELL	$\Upsilon(1S) \rightarrow K^+ K^- \pi^+ \pi^-$	
$\Gamma(b_1(1235)^\pm \pi^\mp)/\Gamma_{\text{total}}$				$\Gamma_{48}/\Gamma$		
VALUE (units $10^{-6}$ )	CL%	DOCUMENT ID	TECN	COMMENT		
$<0.40$	90	SHEN	12A	BELL	$\Upsilon(1S) \rightarrow 2(\pi^+ \pi^-) \pi^0$	
$\Gamma(\rho \pi)/\Gamma_{\text{total}}$				$\Gamma_{49}/\Gamma$		
VALUE (units $10^{-6}$ )	CL%	DOCUMENT ID	TECN	COMMENT		
$<1.16$	90	SHEN	13	BELL	$\Upsilon(2S) \rightarrow \pi^+ \pi^- \pi^0$	
$\Gamma(\pi^+ \pi^- \pi^0)/\Gamma_{\text{total}}$				$\Gamma_{50}/\Gamma$		
VALUE (units $10^{-6}$ )	CL%	DOCUMENT ID	TECN	COMMENT		
$<0.80$	90	SHEN	13	BELL	$\Upsilon(2S) \rightarrow \pi^+ \pi^- \pi^0$	
$\Gamma(\omega \pi^0)/\Gamma_{\text{total}}$				$\Gamma_{51}/\Gamma$		
VALUE (units $10^{-6}$ )	CL%	DOCUMENT ID	TECN	COMMENT		
$<1.63$	90	SHEN	13	BELL	$\Upsilon(2S) \rightarrow \pi^+ \pi^- \pi^0 \pi^0$	
$\Gamma(\pi^+ \pi^- \pi^0 \pi^0)/\Gamma_{\text{total}}$				$\Gamma_{52}/\Gamma$		
VALUE (units $10^{-6}$ )	EVTS	DOCUMENT ID	TECN	COMMENT		
$13.0 \pm 1.9 \pm 2.1$	$261 \pm 37$	SHEN	13	BELL	$\Upsilon(2S) \rightarrow \pi^+ \pi^- \pi^0 \pi^0$	
$\Gamma(K_S^0 K^+ \pi^- + \text{c.c.})/\Gamma_{\text{total}}$				$\Gamma_{53}/\Gamma$		
VALUE (units $10^{-6}$ )	CL%	EVTS	DOCUMENT ID	TECN	COMMENT	
$1.14 \pm 0.30 \pm 0.13$		$40 \pm 10$	SHEN	13	BELL	$\Upsilon(2S) \rightarrow K_S^0 K^- \pi^+$
••• We do not use the following data for averages, fits, limits, etc. •••						
$<3.2$	90		<sup>1</sup> DOBBS	12A	$\Upsilon(2S) \rightarrow K_S^0 K^- \pi^+$	
<sup>1</sup> Obtained by analyzing CLEO III data but not authored by the CLEO Collaboration.						
$\Gamma(K^*(892)^0 \bar{K}^0 + \text{c.c.})/\Gamma_{\text{total}}$				$\Gamma_{54}/\Gamma$		
VALUE (units $10^{-6}$ )	CL%	DOCUMENT ID	TECN	COMMENT		
$<4.22$	90	SHEN	13	BELL	$\Upsilon(2S) \rightarrow K_S^0 K^- \pi^+$	
$\Gamma(K^*(892)^- K^+ + \text{c.c.})/\Gamma_{\text{total}}$				$\Gamma_{55}/\Gamma$		
VALUE (units $10^{-6}$ )	CL%	DOCUMENT ID	TECN	COMMENT		
$<1.45$	90	SHEN	13	BELL	$\Upsilon(2S) \rightarrow K_S^0 K^- \pi^+$	
$\Gamma(f_1(1285) \text{ anything})/\Gamma_{\text{total}}$				$\Gamma_{56}/\Gamma$		
VALUE (units $10^{-3}$ )	EVTS	DOCUMENT ID	TECN	COMMENT		
$2.20 \pm 1.50 \pm 0.63$	2.9k	JIA	17A	BELL	$e^+ e^- \rightarrow \text{hadrons}$	
$\Gamma(f_1(1285) X_{tetra})/\Gamma_{\text{total}}$				$\Gamma_{57}/\Gamma$		
VALUE	CL%	DOCUMENT ID	TECN	COMMENT		
$<64.7 \times 10^{-6}$	90	<sup>1</sup> JIA	17A	BELL	$e^+ e^- \rightarrow \text{hadrons}$	
<sup>1</sup> For a tetraquark state $X_{tetra}$ , with mass in the range 1.16–2.46 GeV and width in the range 0–0.3 GeV. Measured 90% CL limits as a function of $X_{tetra}$ mass and width range from $7.8 \times 10^{-6}$ to $64.7 \times 10^{-6}$ .						
$\Gamma(\text{Sum of 100 exclusive modes})/\Gamma_{\text{total}}$				$\Gamma_{58}/\Gamma$		
VALUE (units $10^{-2}$ )	DOCUMENT ID	TECN	COMMENT			
$0.29 \pm 0.03$	<sup>1,2</sup> DOBBS	12A	$\Upsilon(2S) \rightarrow \text{hadrons}$			
<sup>1</sup> DOBBS 12A presents individual exclusive branching fractions or upper limits for 100 modes of four to ten pions, kaons, or protons.						
<sup>2</sup> Obtained by analyzing CLEO III data but not authored by the CLEO Collaboration.						
$\Gamma(\gamma \chi_{b1}(1P))/\Gamma_{\text{total}}$				$\Gamma_{59}/\Gamma$		
VALUE	EVTS	DOCUMENT ID	TECN	COMMENT		
$0.069 \pm 0.004$	OUR AVERAGE					
$0.0693 \pm 0.0012 \pm 0.0041$	407k	ARTUSO	05	CLEO	$e^+ e^- \rightarrow \gamma X$	
$0.069 \pm 0.005 \pm 0.009$		EDWARDS	99	CLE2	$\Upsilon(2S) \rightarrow \gamma \chi(1P)$	
$0.091 \pm 0.018 \pm 0.022$		ALBRECHT	85E	ARG	$e^+ e^- \rightarrow \gamma \text{conv. } X$	
$0.065 \pm 0.007 \pm 0.012$		NERNST	85	CBAL	$e^+ e^- \rightarrow \gamma X$	
$0.080 \pm 0.017 \pm 0.016$		HAAS	84	CLEO	$e^+ e^- \rightarrow \gamma \text{conv. } X$	
$0.059 \pm 0.014$		KLOPFEN...	83	CUSB	$e^+ e^- \rightarrow \gamma X$	
$\Gamma(\gamma \chi_{b2}(1P))/\Gamma_{\text{total}}$				$\Gamma_{60}/\Gamma$		
VALUE	EVTS	DOCUMENT ID	TECN	COMMENT		
$0.0715 \pm 0.0035$	OUR AVERAGE					
$0.0724 \pm 0.0011 \pm 0.0040$	410k	ARTUSO	05	CLEO	$e^+ e^- \rightarrow \gamma X$	
$0.074 \pm 0.005 \pm 0.008$		EDWARDS	99	CLE2	$\Upsilon(2S) \rightarrow \gamma \chi(1P)$	
$0.098 \pm 0.021 \pm 0.024$		ALBRECHT	85E	ARG	$e^+ e^- \rightarrow \gamma \text{conv. } X$	
$0.058 \pm 0.007 \pm 0.010$		NERNST	85	CBAL	$e^+ e^- \rightarrow \gamma X$	
$0.102 \pm 0.018 \pm 0.021$		HAAS	84	CLEO	$e^+ e^- \rightarrow \gamma \text{conv. } X$	
$0.061 \pm 0.014$		KLOPFEN...	83	CUSB	$e^+ e^- \rightarrow \gamma X$	
$\Gamma(\gamma \chi_{b0}(1P))/\Gamma_{\text{total}}$				$\Gamma_{61}/\Gamma$		
VALUE	EVTS	DOCUMENT ID	TECN	COMMENT		
$0.038 \pm 0.004$	OUR AVERAGE					
$0.0375 \pm 0.0012 \pm 0.0047$	198k	ARTUSO	05	CLEO	$e^+ e^- \rightarrow \gamma X$	
$0.034 \pm 0.005 \pm 0.006$		EDWARDS	99	CLE2	$\Upsilon(2S) \rightarrow \gamma \chi(1P)$	
$0.064 \pm 0.014 \pm 0.016$		ALBRECHT	85E	ARG	$e^+ e^- \rightarrow \gamma \text{conv. } X$	
$0.036 \pm 0.008 \pm 0.009$		NERNST	85	CBAL	$e^+ e^- \rightarrow \gamma X$	
$0.044 \pm 0.023 \pm 0.009$		HAAS	84	CLEO	$e^+ e^- \rightarrow \gamma \text{conv. } X$	
••• We do not use the following data for averages, fits, limits, etc. •••						
$0.035 \pm 0.014$		KLOPFEN...	83	CUSB	$e^+ e^- \rightarrow \gamma X$	
$\Gamma(\gamma f_0(1710))/\Gamma_{\text{total}}$				$\Gamma_{62}/\Gamma$		
VALUE (units $10^{-5}$ )	CL%	DOCUMENT ID	TECN	COMMENT		
$<5.9$	90	<sup>1</sup> ALBRECHT	89	ARG	$\Upsilon(2S) \rightarrow \gamma K^+ K^-$	
••• We do not use the following data for averages, fits, limits, etc. •••						
$< 5.9$	90	<sup>2</sup> ALBRECHT	89	ARG	$\Upsilon(2S) \rightarrow \gamma \pi^+ \pi^-$	
<sup>1</sup> Re-evaluated assuming $B(f_0(1710) \rightarrow K^+ K^-) = 0.19$ .						
<sup>2</sup> Includes unknown branching ratio of $f_0(1710) \rightarrow \pi^+ \pi^-$ .						
$\Gamma(\gamma f_2'(1525))/\Gamma_{\text{total}}$				$\Gamma_{63}/\Gamma$		
VALUE (units $10^{-5}$ )	CL%	DOCUMENT ID	TECN	COMMENT		
$<53$	90	<sup>1</sup> ALBRECHT	89	ARG	$\Upsilon(2S) \rightarrow \gamma K^+ K^-$	
<sup>1</sup> Re-evaluated assuming $B(f_2'(1525) \rightarrow K \bar{K}) = 0.71$ .						
$\Gamma(\gamma f_2(1270))/\Gamma_{\text{total}}$				$\Gamma_{64}/\Gamma$		
VALUE (units $10^{-5}$ )	CL%	DOCUMENT ID	TECN	COMMENT		
$<24.1$	90	<sup>1</sup> ALBRECHT	89	ARG	$\Upsilon(2S) \rightarrow \gamma \pi^+ \pi^-$	
<sup>1</sup> Using $B(f_2(1270) \rightarrow \pi \pi) = 0.84$ .						
$\Gamma(\gamma f_J(2220))/\Gamma_{\text{total}}$				$\Gamma_{65}/\Gamma$		
VALUE (units $10^{-5}$ )	CL%	DOCUMENT ID	TECN	COMMENT		
$<6.8$	90	<sup>1</sup> ALBRECHT	89	ARG	$\Upsilon(2S) \rightarrow \gamma K^+ K^-$	
••• We do not use the following data for averages, fits, limits, etc. •••						
<sup>1</sup> Includes unknown branching ratio of $f_J(2220) \rightarrow K^+ K^-$ .						
$\Gamma(\gamma \eta_c(1S))/\Gamma_{\text{total}}$				$\Gamma_{66}/\Gamma$		
VALUE	CL%	DOCUMENT ID	TECN	COMMENT		
$<2.7 \times 10^{-5}$	90	WANG	11B	BELL	$\Upsilon(2S) \rightarrow \gamma X$	
$\Gamma(\gamma \chi_{c0})/\Gamma_{\text{total}}$				$\Gamma_{67}/\Gamma$		
VALUE	CL%	DOCUMENT ID	TECN	COMMENT		
$<1.0 \times 10^{-4}$	90	WANG	11B	BELL	$\Upsilon(2S) \rightarrow \gamma X$	
$\Gamma(\gamma \chi_{c1})/\Gamma_{\text{total}}$				$\Gamma_{68}/\Gamma$		
VALUE	CL%	DOCUMENT ID	TECN	COMMENT		
$<3.6 \times 10^{-6}$	90	WANG	11B	BELL	$\Upsilon(2S) \rightarrow \gamma X$	

See key on page 999

Meson Particle Listings
Gamma(2S), Gamma(1D)

Table with 5 columns: VALUE, CL%, DOCUMENT ID, TECN, COMMENT. Row 1: Gamma(gamma chi c2)/Gamma total <1.5 x 10^-5, 90, WANG, 11B, BELL, T(2S) -> gamma X

Table with 5 columns: VALUE, CL%, DOCUMENT ID, TECN, COMMENT. Row 1: Gamma(gamma chi c1(3872) -> pi+ pi- J/psi)/Gamma total <0.8 x 10^-6, 90, WANG, 11B, BELL, T(2S) -> gamma X

Table with 5 columns: VALUE, CL%, DOCUMENT ID, TECN, COMMENT. Row 1: Gamma(gamma chi c1(3872) -> pi+ pi- pi0 J/psi)/Gamma total <2.4 x 10^-6, 90, WANG, 11B, BELL, T(2S) -> gamma X

Table with 5 columns: VALUE, CL%, DOCUMENT ID, TECN, COMMENT. Row 1: Gamma(gamma X(3915) -> omega J/psi)/Gamma total <2.8 x 10^-6, 90, WANG, 11B, BELL, T(2S) -> gamma X

Table with 5 columns: VALUE, CL%, DOCUMENT ID, TECN, COMMENT. Row 1: Gamma(gamma chi c1(4140) -> phi J/psi)/Gamma total <1.2 x 10^-6, 90, WANG, 11B, BELL, T(2S) -> gamma X

Table with 5 columns: VALUE, CL%, DOCUMENT ID, TECN, COMMENT. Row 1: Gamma(gamma X(4350) -> phi J/psi)/Gamma total <1.3 x 10^-6, 90, WANG, 11B, BELL, T(2S) -> gamma X

Table with 5 columns: VALUE, CL%, EVTS, DOCUMENT ID, TECN, COMMENT. Row 1: Gamma(gamma eta\_b(1S))/Gamma total 5.5 +1.1 -0.9 OUR AVERAGE Error includes scale factor of 1.2.

Table with 5 columns: VALUE, CL%, EVTS, DOCUMENT ID, TECN, COMMENT. Row 1: 6.1 +0.6 -0.7 -0.6, 29k, FULSOM, 18, BELL, T(2S) -> gamma X

Table with 5 columns: VALUE, CL%, EVTS, DOCUMENT ID, TECN, COMMENT. Row 1: 3.9 +/- 1.1 +/- 1.1, 13 +/- 5k, 1 AUBERT, 09AQ, BABR, T(2S) -> gamma X

- We do not use the following data for averages, fits, limits, etc. •••
<21 90 LEES 11J BABR T(2S) -> X gamma
< 8.4 90 1 BONVICINI 10 CLEO T(2S) -> gamma X
< 5.1 90 2 ARTUSO 05 CLEO e+ e- -> gamma X

1 Assuming Gamma eta\_b(1S) = 10 MeV.
2 Superseded by BONVICINI 10.

Table with 5 columns: VALUE, CL%, DOCUMENT ID, TECN, COMMENT. Row 1: Gamma(gamma eta\_b(1S) -> gamma Sum of 26 exclusive modes)/Gamma total <3.7 x 10^-6, SANDILYA, 13, BELL, T(2S) -> gamma hadrons

Table with 5 columns: VALUE, CL%, EVTS, DOCUMENT ID, TECN, COMMENT. Row 1: Gamma(gamma X\_b B -> gamma Sum of 26 exclusive modes)/Gamma total < 4.9, 90, SANDILYA, 13, BELL, T(2S) -> gamma hadrons

- We do not use the following data for averages, fits, limits, etc. •••
46.2 +/- 29.7 +/- 14.2 +/- 10.6, 10, 1 DOBBS, 12, T(2S) -> gamma hadrons

1 Obtained by analyzing CLEO III data but not authored by the CLEO Collaboration.

Table with 5 columns: VALUE, CL%, DOCUMENT ID, TECN, COMMENT. Row 1: Gamma(gamma X -> gamma + >= 4 prongs)/Gamma total (1.5 GeV < m\_X < 5.0 GeV) <1.95, 95, ROSNER, 07A, CLEO, e+ e- -> gamma X

Table with 5 columns: VALUE, CL%, DOCUMENT ID, TECN, COMMENT. Row 1: Gamma(gamma A0 -> gamma hadrons)/Gamma total (0.3 GeV < m\_A0 < 7 GeV) <8 x 10^-5, 90, 1 LEES, 11H, BABR, T(2S) -> gamma hadrons

- 1 For a narrow scalar or pseudoscalar A0, excluding known resonances, with mass in the range 0.3-7 GeV. Measured 90% CL limits as a function of m\_A0 range from 1 x 10^-6 to 8 x 10^-5.

Table with 5 columns: VALUE, CL%, DOCUMENT ID, TECN, COMMENT. Row 1: Gamma(gamma a1^0 -> gamma mu+ mu-)/Gamma total <8.3, 90, 1 AUBERT, 09Z, BABR, e+ e- -> gamma a1^0 -> gamma mu+ mu-

- 1 For a narrow scalar or pseudoscalar a1^0 with mass in the range 212-9300 MeV, excluding J/psi and psi(2S). Measured 90% CL limits as a function of m\_a1^0 range from 0.26-8.3 x 10^-6.

LEPTON FAMILY NUMBER (LF) VIOLATING MODES

Table with 5 columns: VALUE, CL%, DOCUMENT ID, TECN, COMMENT. Row 1: Gamma(e+ tau tau)/Gamma total <3.2, 90, LEES, 10B, BABR, e+ e- -> e+ tau tau

Table with 5 columns: VALUE, CL%, DOCUMENT ID, TECN, COMMENT. Row 1: Gamma(mu+ tau tau)/Gamma total < 3.3, 90, LEES, 10B, BABR, e+ e- -> mu+ tau tau

- We do not use the following data for averages, fits, limits, etc. •••
<14.4 95 LOVE 08A CLEO e+ e- -> mu+ tau tau

T(2S) Cross-Particle Branching Ratios
B(T(2S) -> pi+ pi-) x B(T(3S) -> T(2S)X)
VALUE (units 10^-2) EVTS DOCUMENT ID TECN COMMENT
1.78 +/- 0.02 +/- 0.11 906k LEES 11c BABR e+ e- -> pi+ pi- X

T(2S) REFERENCES
FULSOM 18 PRL 121 232001 B.G. Fulsom et al. (BELLE Collab.)
JIA 18 PR D97 112004 S. Jia et al. (BELLE Collab.)
JIA 17 PR D95 012001 S. Jia et al. (BELLE Collab.)
JIA 17A PR D96 112002 S. Jia et al. (BELLE Collab.)
LEES 14G PR D89 111102 J.P. Lees et al. (BABAR Collab.)
YANG 14 PR D90 112008 S.D. Yang et al. (BELLE Collab.)
SANDILYA 13 PRL 111 112001 S. Sandilya et al. (BELLE Collab.)
SHEN 13 PR D88 011102 C.P. Shen et al. (BELLE Collab.)
TAMPONI 13 PR D87 011104 U. Tamponi et al. (BELLE Collab.)
DOBBS 12 PRL 109 082001 S. Dobbs et al. (BELLE Collab.)
DOBBS 12A PR D86 052003 S. Dobbs et al. (BELLE Collab.)
SHEN 12A PR D86 031102 C.P. Shen et al. (BELLE Collab.)
LEES 11C PR D84 011104 J.P. Lees et al. (BABAR Collab.)
LEES 11H PRL 107 221803 J.P. Lees et al. (BABAR Collab.)
LEES 11J PR D84 072002 J.P. Lees et al. (BABAR Collab.)
LEES 11L PR D84 092003 J.P. Lees et al. (BABAR Collab.)
WANG 11B PR D84 071107 X.L. Wang et al. (BELLE Collab.)
BONVICINI 10 PR D81 031104 G. Bonvicini et al. (CLEO Collab.)
LEES 10B PRL 104 151802 J.P. Lees et al. (CLEO Collab.)
AUBERT 09AQ PRL 103 161801 B. Aubert et al. (BABAR Collab.)
AUBERT 09Z PRL 103 081803 B. Aubert et al. (BABAR Collab.)
BHARI 09Z PR D79 011103 S.R. Bhari et al. (CLEO Collab.)
AUBERT 08BP PR D78 112002 B. Aubert et al. (BABAR Collab.)
HE 08A PRL 101 192001 Q. He et al. (CLEO Collab.)
LOVE 08A PRL 101 201601 W. Love et al. (CLEO Collab.)
PDG 08 PL B667 1 C. Amsler et al. (PDG Collab.)
ASNER 07 PR D75 012009 D.M. Asner et al. (CLEO Collab.)
BESSON 07 PRL 98 052002 D. Besson et al. (CLEO Collab.)
ROSNER 07A PR D76 117102 J.L. Rosner et al. (CLEO Collab.)
BESSON 06A PR D74 012003 D. Besson et al. (CLEO Collab.)
ROSNER 06 PRL 96 092003 J.L. Rosner et al. (CLEO Collab.)
ADAMS 05 PRL 94 012001 G.S. Adams et al. (CLEO Collab.)
ARTUSO 05 PRL 94 032001 M. Artuso et al. (CLEO Collab.)
ARTAMONOV 00 PL B474 427 A.S. Artamonov et al. (CLEO Collab.)
EDWARDS 99 PR D59 032003 K.W. Edwards et al. (CLEO Collab.)
ALEXANDER 98 PR D58 052004 J.P. Alexander et al. (CLEO Collab.)
BARU 96 PRPL 267 71 S.E. Baru et al. (NOVO)
KOBEL 92 ZPHY C53 193 M. Kobel et al. (Crystal Ball Collab.)
MASCHMANN 90 ZPHY C46 555 W.S. Maschmann et al. (Crystal Ball Collab.)
ALBRECHT 89 ZPHY C42 349 H. Albrecht et al. (ARGUS Collab.)
KAARSBERG 89 PRL 62 2077 T.M. Kaarsberg et al. (CUSB Collab.)
BUCHMUELLER 88 HE 4+e- Physics 412 W. Buchmueller, S. Cooper Editors: A. Ali and P. Soeding, World Scientific, Singapore (HANN, DESY, MIT)
JAKUBOWSKI 85 ZPHY C40 49 Z. Jakubowski et al. (Crystal Ball Collab.)
ALBRECHT 87 ZPHY C35 283 H. Albrecht et al. (ARGUS Collab.)
COHEN 87 RMP 59 1121 Z. Cohen, B.N. Taylor (RIS C, NBS)
LURZ 87 ZPHY C36 383 B. Lurz et al. (Crystal Ball Collab.)
BARU 86B ZPHY C32 622 (erratum) S.E. Baru et al. (NOVO)
ALBRECHT 85 ZPHY C28 45 H. Albrecht et al. (ARGUS Collab.)
ALBRECHT 85E PL 160B 331 H. Albrecht et al. (ARGUS Collab.)
GELPHMAN 85 PR D32 2893 D. Gelpman et al. (Crystal Ball Collab.)
KURAEV 85 SJNP 41 466 E.A. Kuraev, V.S. Fadin (NOVO)
Translated from YAF 41 733.
NERNST 85 PRL 54 2195 R. Nernst et al. (Crystal Ball Collab.)
ARTAMONOV 84 PL 137B 272 A.S. Artamonov et al. (NOVO)
BARBER 84 PL 135B 498 D.P. Barber et al. (CLEO Collab.)
BESSON 84 PR D30 1433 D. Besson et al. (CLEO Collab.)
FONSECA 84 NP B242 31 V. Fonseca et al. (CUSB Collab.)
GILES 84B PR D29 1285 R. Giles et al. (CLEO Collab.)
HAAS 84 PRL 52 799 J. Haas et al. (CLEO Collab.)
HAAS 84B PR D30 1996 J. Haas et al. (CLEO Collab.)
KLOPFEN... 83 PRL 51 160 C. Klöpfenstein et al. (CUSB Collab.)
ALBRECHT 82 PL 115B 383 H. Albrecht et al. (DESY, DORT, HEIDH+)
NICZYPORUK 81B PL 100B 95 B. Niczyporuk et al. (LENA Collab.)
NICZYPORUK 81C PL 99B 169 B. Niczyporuk et al. (LENA Collab.)
BOCK 80 ZPHY C6 125 P. Bock et al. (HEIDP, MPIM, DESY, HAMB)

Gamma\_2(1D) I(G(JPC)) = 0^-(2^--)

was Gamma(1D)
First observed by BONVICINI 04 in the decay to gamma gamma T(1S) and confirmed by DEL-AMO-SANCHEZ 10R in the decay to pi+ pi- T(1S).
Data consistent with JP = 2^-. The states with J = 1 and 3 also possibly seen, but need confirmation.

T2(1D) MASS
VALUE (MeV) EVTS DOCUMENT ID TECN COMMENT
10163.7 +/- 1.4 OUR AVERAGE Error includes scale factor of 1.7.
10164.5 +/- 0.8 +/- 0.5 DEL-AMO-SA..10R BABR T(3S) -> gamma gamma pi+ pi- l+ l-
10161.1 +/- 0.6 +/- 1.6 38 BONVICINI 04 CLE3 T(3S) -> 4 gamma l+ l-

T2(1D) DECAY MODES
Mode Fraction (Gamma\_i/Gamma)
Gamma\_1 gamma gamma T(1S) seen
Gamma\_2 gamma chi\_b J(1P) seen
Gamma\_3 eta T(1S) not seen
Gamma\_4 pi+ pi- T(1S) (6.6 +/- 1.6) x 10^-3



# Meson Particle Listings

## $\Upsilon_2(1D), \chi_{b0}(2P)$

### $\Upsilon_2(1D)$ BRANCHING RATIOS

$\Gamma(\eta \Upsilon(1S))/\Gamma(\gamma\gamma \Upsilon(1S))$					$\Gamma_3/\Gamma_1$
VALUE	CL%	DOCUMENT ID	TECN	COMMENT	
<b>&lt;0.25</b>	90	BONVICINI	04	CLE3	$\Upsilon(3S) \rightarrow 4\gamma\ell^+\ell^-$

$\Gamma(\pi^+\pi^-\Upsilon(1S))/\Gamma_{\text{total}}$					$\Gamma_4/\Gamma$
VALUE (units $10^{-2}$ )	CL%	DOCUMENT ID	TECN	COMMENT	
<b><math>0.66^{+0.15}_{-0.14} \pm 0.06</math></b>		<sup>1</sup> DEL-AMO-SA...10R	BABR	$\Upsilon(3S) \rightarrow \gamma\gamma\pi^+\pi^-\ell^+\ell^-$	

<sup>1</sup> Using theoretical predictions for  $B(\chi_{bJ}(2P) \rightarrow \gamma \Upsilon_2(1D))$ .

$\Gamma(\pi^+\pi^-\Upsilon(1S))/\Gamma(\gamma\gamma \Upsilon(1S))$					$\Gamma_4/\Gamma_1$
VALUE	CL%	DOCUMENT ID	TECN	COMMENT	
<b>&lt;1.2</b>	90	<sup>2</sup> BONVICINI	04	CLE3	$\Upsilon(3S) \rightarrow 4\gamma\ell^+\ell^-$

<sup>2</sup> Assuming  $J = 2$ .

### $\Upsilon_2(1D)$ REFERENCES

DEL-AMO-SA...10R	PR D82 111102	P. del Amo Sanchez et al.	(BABAR Collab.)
BONVICINI 04	PR D70 032001	G. Bonvicini et al.	(CLEO Collab.)

## $\chi_{b0}(2P)$

$I^G(J^{PC}) = 0^+(0^{++})$   
 $J$  needs confirmation.

Observed in radiative decay of the  $\Upsilon(3S)$ , therefore  $C = +$ . Branching ratio requires E1 transition, M1 is strongly disfavored, therefore  $P = +$ .

### $\chi_{b0}(2P)$ MASS

VALUE (MeV)	DOCUMENT ID
<b><math>10232.5 \pm 0.4 \pm 0.5</math> OUR EVALUATION</b>	From $\gamma$ energy below, using $\Upsilon(3S)$ mass = $10355.2 \pm 0.5$ MeV

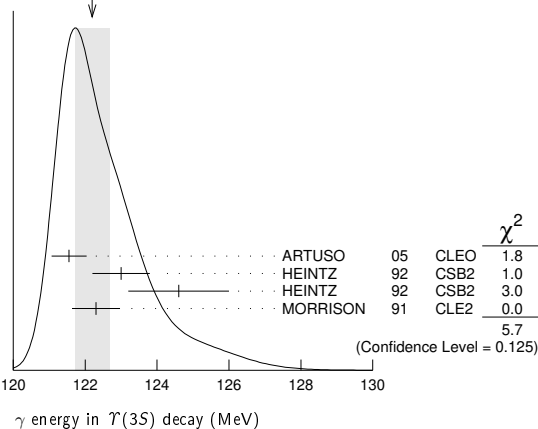
$m_{\chi_{b1}(2P)} - m_{\chi_{b0}(2P)}$				
VALUE (MeV)	DOCUMENT ID	TECN	COMMENT	
<b><math>23.8 \pm 1.7</math></b>	LEES	14M	BABR $\Upsilon(3S) \rightarrow \gamma\gamma\mu^+\mu^-$	

### $\gamma$ ENERGY IN $\Upsilon(3S)$ DECAY

VALUE (MeV)	EVTS	DOCUMENT ID	TECN	COMMENT
<b><math>121.9 \pm 0.4</math> OUR EVALUATION</b>		Treating systematic errors as correlated		
<b><math>122.2 \pm 0.5</math> OUR AVERAGE</b>		Error includes scale factor of 1.4. See the ideogram below.		
$121.55 \pm 0.16 \pm 0.46$		ARTUSO	05	CLEO $\Upsilon(3S) \rightarrow \gamma X$
$123.0 \pm 0.8$	4959	<sup>1</sup> HEINTZ	92	CSB2 $e^+e^- \rightarrow \gamma X$
$124.6 \pm 1.4$	17	<sup>2</sup> HEINTZ	92	CSB2 $e^+e^- \rightarrow \ell^+\ell^-\gamma\gamma$
$122.3 \pm 0.3 \pm 0.6$	9903	MORRISON	91	CLE2 $e^+e^- \rightarrow \gamma X$

<sup>1</sup> A systematic uncertainty on the energy scale of 0.9% not included. Supersedes NARAIN 91.  
<sup>2</sup> A systematic uncertainty on the energy scale of 0.9% not included. Supersedes HEINTZ 91.

WEIGHTED AVERAGE  
 $122.2 \pm 0.5$  (Error scaled by 1.4)



### $\chi_{b0}(2P)$ DECAY MODES

Mode	Fraction ( $\Gamma_i/\Gamma$ )	Confidence level
$\Gamma_1$ $\gamma \Upsilon(2S)$	$(1.38 \pm 0.30)\%$	
$\Gamma_2$ $\gamma \Upsilon(1S)$	$(3.8 \pm 1.7) \times 10^{-3}$	
$\Gamma_3$ $D^0 X$	$< 8.2\%$	90%
$\Gamma_4$ $\pi^+\pi^-K^+K^-\pi^0$	$< 3.4 \times 10^{-5}$	90%
$\Gamma_5$ $2\pi^+\pi^-K^+K^-\pi^0$	$< 5 \times 10^{-5}$	90%
$\Gamma_6$ $2\pi^+\pi^-K^+K^-\pi^0$	$< 2.2 \times 10^{-4}$	90%
$\Gamma_7$ $2\pi^+2\pi^-\pi^0$	$< 2.4 \times 10^{-4}$	90%
$\Gamma_8$ $2\pi^+2\pi^-K^+K^-$	$< 1.5 \times 10^{-4}$	90%
$\Gamma_9$ $2\pi^+2\pi^-K^+K^-\pi^0$	$< 2.2 \times 10^{-4}$	90%
$\Gamma_{10}$ $2\pi^+2\pi^-K^+K^-\pi^0$	$< 1.1 \times 10^{-3}$	90%
$\Gamma_{11}$ $3\pi^+2\pi^-K^+K^-\pi^0$	$< 7 \times 10^{-4}$	90%
$\Gamma_{12}$ $3\pi^+3\pi^-$	$< 7 \times 10^{-5}$	90%
$\Gamma_{13}$ $3\pi^+3\pi^-\pi^0$	$< 1.2 \times 10^{-3}$	90%
$\Gamma_{14}$ $3\pi^+3\pi^-K^+K^-$	$< 1.5 \times 10^{-4}$	90%
$\Gamma_{15}$ $3\pi^+3\pi^-K^+K^-\pi^0$	$< 7 \times 10^{-4}$	90%
$\Gamma_{16}$ $4\pi^+4\pi^-$	$< 1.7 \times 10^{-4}$	90%
$\Gamma_{17}$ $4\pi^+4\pi^-\pi^0$	$< 6 \times 10^{-4}$	90%

### $\chi_{b0}(2P)$ BRANCHING RATIOS

$\Gamma(\gamma \Upsilon(2S))/\Gamma_{\text{total}}$					$\Gamma_1/\Gamma$
VALUE (%)	CL%	DOCUMENT ID	TECN	COMMENT	
<b><math>1.38 \pm 0.30</math> OUR AVERAGE</b>					
$1.31 \pm 0.27^{+0.13}_{-0.12}$		<sup>3,4</sup> LEES	14M	BABR $\Upsilon(3S) \rightarrow \gamma\gamma\mu^+\mu^-$	
$3.6 \pm 1.6 \pm 0.3$		<sup>3,5</sup> HEINTZ	92	CSB2 $e^+e^- \rightarrow \ell^+\ell^-\gamma\gamma$	

••• We do not use the following data for averages, fits, limits, etc. •••

$<2.8$	90	<sup>6</sup> LEES	11J	BABR $\Upsilon(3S) \rightarrow X\gamma$
$<8.9$	90	<sup>7</sup> CRAWFORD	92B	CLE2 $e^+e^- \rightarrow \ell^+\ell^-\gamma\gamma$

<sup>3</sup> Assuming  $B(\Upsilon(2S) \rightarrow \mu^+\mu^-) = (1.93 \pm 0.17)\%$ .  
<sup>4</sup> LEES 14M reports  $[\Gamma(\chi_{b0}(2P) \rightarrow \gamma \Upsilon(2S))/\Gamma_{\text{total}}] \times [B(\Upsilon(3S) \rightarrow \gamma \chi_{b0}(2P))]$  =  $(7.7 \pm 1.6) \times 10^{-4}$  which we divide by our best value  $B(\Upsilon(3S) \rightarrow \gamma \chi_{b0}(2P)) = (5.9 \pm 0.6) \times 10^{-2}$ . Our first error is their experiment's error and our second error is the systematic error from using our best value.  
<sup>5</sup> Recalculated by us. HEINTZ 92 quotes  $B(\Upsilon(3S) \rightarrow \gamma \chi_{b0}(2P)) \times B(\chi_{b0}(2P) \rightarrow \gamma \Upsilon(2S)) = (0.28 \pm 0.12 \pm 0.03)\%$  using  $B(\Upsilon(2S) \rightarrow \mu^+\mu^-) = (1.44 \pm 0.10)\%$ . Supersedes HEINTZ 91.  
<sup>6</sup> LEES 11J quotes a central value of  $\Gamma(\chi_{b0}(2P) \rightarrow \gamma \Upsilon(2S))/\Gamma_{\text{total}} \times \Gamma(\Upsilon(3S) \rightarrow \gamma \chi_{b0}(2P))/\Gamma_{\text{total}} = (-0.3 \pm 0.2^{+0.5}_{-0.4})\%$ .  
<sup>7</sup> Using  $B(\Upsilon(2S) \rightarrow \mu^+\mu^-) = (1.37 \pm 0.26)\%$ ,  $B(\Upsilon(3S) \rightarrow \gamma\gamma \Upsilon(2S)) \times 2 B(\Upsilon(2S) \rightarrow \mu^+\mu^-) < 1.19 \times 10^{-4}$ , and  $B(\Upsilon(3S) \rightarrow \chi_{b0}(2P)\gamma) = 0.049$ .

$\Gamma(\gamma \Upsilon(1S))/\Gamma_{\text{total}}$					$\Gamma_2/\Gamma$
VALUE (%)	CL%	DOCUMENT ID	TECN	COMMENT	
<b><math>0.38 \pm 0.17</math> OUR AVERAGE</b>					
$0.36 \pm 0.17 \pm 0.03$		<sup>8,9,10</sup> LEES	14M	BABR $\Upsilon(3S) \rightarrow \gamma\gamma\mu^+\mu^-$	
$0.9 \pm 0.7 \pm 0.1$		<sup>9,11</sup> HEINTZ	92	CSB2 $e^+e^- \rightarrow \ell^+\ell^-\gamma\gamma$	

••• We do not use the following data for averages, fits, limits, etc. •••

$<1.2$	90	<sup>12</sup> LEES	11J	BABR $\Upsilon(3S) \rightarrow X\gamma$
$<2.5$	90	<sup>13</sup> CRAWFORD	92B	CLE2 $e^+e^- \rightarrow \ell^+\ell^-\gamma\gamma$

<sup>8</sup> LEES 14M quotes  $\Gamma(\chi_{b0}(2P) \rightarrow \gamma \Upsilon(1S))/\Gamma_{\text{total}} \times \Gamma(\Upsilon(3S) \rightarrow \gamma \chi_{b0}(2P))/\Gamma_{\text{total}} = (2.1 \pm 1.0) \times 10^{-4}$  combining the results from  $\Upsilon(3S) \rightarrow \gamma\gamma\mu^+\mu^-$  samples with and without photon conversions.  
<sup>9</sup> Assuming  $B(\Upsilon(1S) \rightarrow \mu^+\mu^-) = (2.48 \pm 0.05)\%$ .  
<sup>10</sup> LEES 14M reports  $[\Gamma(\chi_{b0}(2P) \rightarrow \gamma \Upsilon(1S))/\Gamma_{\text{total}}] \times [B(\Upsilon(3S) \rightarrow \gamma \chi_{b0}(2P))]$  =  $(2.1 \pm 1.0) \times 10^{-4}$  which we divide by our best value  $B(\Upsilon(3S) \rightarrow \gamma \chi_{b0}(2P)) = (5.9 \pm 0.6) \times 10^{-2}$ . Our first error is their experiment's error and our second error is the systematic error from using our best value.  
<sup>11</sup> Recalculated by us. HEINTZ 92 quotes  $B(\Upsilon(3S) \rightarrow \gamma \chi_{b0}(2P)) \times B(\chi_{b0}(2P) \rightarrow \gamma \Upsilon(1S)) = (0.05 \pm 0.04 \pm 0.01)\%$  using  $B(\Upsilon(1S) \rightarrow \mu^+\mu^-) = (2.57 \pm 0.05)\%$ . Supersedes HEINTZ 91.  
<sup>12</sup> LEES 11J quotes a central value of  $\Gamma(\chi_{b0}(2P) \rightarrow \gamma \Upsilon(1S))/\Gamma_{\text{total}} \times \Gamma(\Upsilon(3S) \rightarrow \gamma \chi_{b0}(2P))/\Gamma_{\text{total}} = (3.9 \pm 2.2^{+1.2}_{-0.6}) \times 10^{-4}$ .  
<sup>13</sup> Using  $B(\Upsilon(1S) \rightarrow \mu^+\mu^-) = (2.57 \pm 0.07)\%$ ,  $B(\Upsilon(3S) \rightarrow \gamma\gamma \Upsilon(1S)) \times 2 B(\Upsilon(1S) \rightarrow \mu^+\mu^-) < 0.63 \times 10^{-4}$ , and  $B(\Upsilon(3S) \rightarrow \chi_{b0}(2P)\gamma) = 0.049$ .

$\Gamma(D^0 X)/\Gamma_{\text{total}}$					$\Gamma_3/\Gamma$
VALUE	CL%	DOCUMENT ID	TECN	COMMENT	
<b><math>&lt;8.2 \times 10^{-2}</math></b>	90	<sup>14,15</sup> BRIERE	08	CLEO $\Upsilon(3S) \rightarrow \gamma D^0 X$	

<sup>14</sup> For  $p_{D^0} > 2.5$  GeV/c.  
<sup>15</sup> The authors also present their result as  $(4.1 \pm 3.0 \pm 0.4) \times 10^{-2}$ .

$\Gamma(\pi^+\pi^-K^+K^-\pi^0)/\Gamma_{\text{total}}$					$\Gamma_4/\Gamma$
VALUE (units $10^{-4}$ )	CL%	DOCUMENT ID	TECN	COMMENT	
<b>&lt;0.34</b>	90	<sup>16</sup> ASNER	08A	CLEO $\Upsilon(3S) \rightarrow \gamma\pi^+\pi^-K^+K^-\pi^0$	

<sup>16</sup> ASNER 08A reports  $[\Gamma(\chi_{b0}(2P) \rightarrow \pi^+\pi^-K^+K^-\pi^0)/\Gamma_{\text{total}}] \times [B(\Upsilon(3S) \rightarrow \gamma \chi_{b0}(2P))]$  =  $2 \times 10^{-6}$  which we divide by our best value  $B(\Upsilon(3S) \rightarrow \gamma \chi_{b0}(2P)) = 5.9 \times 10^{-2}$ .

$\Gamma(2\pi^+\pi^-K^-K_S^0)/\Gamma_{\text{total}}$					$\Gamma_5/\Gamma$
VALUE (units $10^{-4}$ )	CL%	DOCUMENT ID	TECN	COMMENT	
<0.5	90	17 ASNER	08A CLEO	$\Upsilon(3S) \rightarrow \gamma 2\pi^+\pi^-K^-K_S^0$	
17 ASNER 08A reports $[\Gamma(\chi_{b0}(2P) \rightarrow 2\pi^+\pi^-K^-K_S^0)/\Gamma_{\text{total}}] \times [B(\Upsilon(3S) \rightarrow \gamma\chi_{b0}(2P))] < 3 \times 10^{-6}$ which we divide by our best value $B(\Upsilon(3S) \rightarrow \gamma\chi_{b0}(2P)) = 5.9 \times 10^{-2}$ .					

$\Gamma(2\pi^+\pi^-K^-K_S^0 2\pi^0)/\Gamma_{\text{total}}$					$\Gamma_6/\Gamma$
VALUE (units $10^{-4}$ )	CL%	DOCUMENT ID	TECN	COMMENT	
<2.2	90	18 ASNER	08A CLEO	$\Upsilon(3S) \rightarrow \gamma 2\pi^+\pi^-K^-2\pi^0$	
18 ASNER 08A reports $[\Gamma(\chi_{b0}(2P) \rightarrow 2\pi^+\pi^-K^-K_S^0 2\pi^0)/\Gamma_{\text{total}}] \times [B(\Upsilon(3S) \rightarrow \gamma\chi_{b0}(2P))] < 13 \times 10^{-6}$ which we divide by our best value $B(\Upsilon(3S) \rightarrow \gamma\chi_{b0}(2P)) = 5.9 \times 10^{-2}$ .					

$\Gamma(2\pi^+2\pi^-2\pi^0)/\Gamma_{\text{total}}$					$\Gamma_7/\Gamma$
VALUE (units $10^{-4}$ )	CL%	DOCUMENT ID	TECN	COMMENT	
<2.4	90	19 ASNER	08A CLEO	$\Upsilon(3S) \rightarrow \gamma 2\pi^+2\pi^-2\pi^0$	
19 ASNER 08A reports $[\Gamma(\chi_{b0}(2P) \rightarrow 2\pi^+2\pi^-2\pi^0)/\Gamma_{\text{total}}] \times [B(\Upsilon(3S) \rightarrow \gamma\chi_{b0}(2P))] < 14 \times 10^{-6}$ which we divide by our best value $B(\Upsilon(3S) \rightarrow \gamma\chi_{b0}(2P)) = 5.9 \times 10^{-2}$ .					

$\Gamma(2\pi^+2\pi^-K^+K^-)/\Gamma_{\text{total}}$					$\Gamma_8/\Gamma$
VALUE (units $10^{-4}$ )	CL%	DOCUMENT ID	TECN	COMMENT	
<1.5	90	20 ASNER	08A CLEO	$\Upsilon(3S) \rightarrow \gamma 2\pi^+2\pi^-K^+K^-$	
20 ASNER 08A reports $[\Gamma(\chi_{b0}(2P) \rightarrow 2\pi^+2\pi^-K^+K^-)/\Gamma_{\text{total}}] \times [B(\Upsilon(3S) \rightarrow \gamma\chi_{b0}(2P))] < 9 \times 10^{-6}$ which we divide by our best value $B(\Upsilon(3S) \rightarrow \gamma\chi_{b0}(2P)) = 5.9 \times 10^{-2}$ .					

$\Gamma(2\pi^+2\pi^-K^+K^-\pi^0)/\Gamma_{\text{total}}$					$\Gamma_9/\Gamma$
VALUE (units $10^{-4}$ )	CL%	DOCUMENT ID	TECN	COMMENT	
<2.2	90	21 ASNER	08A CLEO	$\Upsilon(3S) \rightarrow \gamma 2\pi^+2\pi^-K^+K^-\pi^0$	
21 ASNER 08A reports $[\Gamma(\chi_{b0}(2P) \rightarrow 2\pi^+2\pi^-K^+K^-\pi^0)/\Gamma_{\text{total}}] \times [B(\Upsilon(3S) \rightarrow \gamma\chi_{b0}(2P))] < 13 \times 10^{-6}$ which we divide by our best value $B(\Upsilon(3S) \rightarrow \gamma\chi_{b0}(2P)) = 5.9 \times 10^{-2}$ .					

$\Gamma(2\pi^+2\pi^-K^+K^-2\pi^0)/\Gamma_{\text{total}}$					$\Gamma_{10}/\Gamma$
VALUE (units $10^{-4}$ )	CL%	DOCUMENT ID	TECN	COMMENT	
<1.1	90	22 ASNER	08A CLEO	$\Upsilon(3S) \rightarrow \gamma 2\pi^+2\pi^-K^+K^-2\pi^0$	
22 ASNER 08A reports $[\Gamma(\chi_{b0}(2P) \rightarrow 2\pi^+2\pi^-K^+K^-2\pi^0)/\Gamma_{\text{total}}] \times [B(\Upsilon(3S) \rightarrow \gamma\chi_{b0}(2P))] < 63 \times 10^{-6}$ which we divide by our best value $B(\Upsilon(3S) \rightarrow \gamma\chi_{b0}(2P)) = 5.9 \times 10^{-2}$ .					

$\Gamma(3\pi^+2\pi^-K^-K_S^0\pi^0)/\Gamma_{\text{total}}$					$\Gamma_{11}/\Gamma$
VALUE (units $10^{-4}$ )	CL%	DOCUMENT ID	TECN	COMMENT	
<7	90	23 ASNER	08A CLEO	$\Upsilon(3S) \rightarrow \gamma 3\pi^+2\pi^-K^-K_S^0\pi^0$	
23 ASNER 08A reports $[\Gamma(\chi_{b0}(2P) \rightarrow 3\pi^+2\pi^-K^-K_S^0\pi^0)/\Gamma_{\text{total}}] \times [B(\Upsilon(3S) \rightarrow \gamma\chi_{b0}(2P))] < 39 \times 10^{-6}$ which we divide by our best value $B(\Upsilon(3S) \rightarrow \gamma\chi_{b0}(2P)) = 5.9 \times 10^{-2}$ .					

$\Gamma(3\pi^+3\pi^-)/\Gamma_{\text{total}}$					$\Gamma_{12}/\Gamma$
VALUE (units $10^{-4}$ )	CL%	DOCUMENT ID	TECN	COMMENT	
<0.7	90	24 ASNER	08A CLEO	$\Upsilon(3S) \rightarrow \gamma 3\pi^+3\pi^-$	
24 ASNER 08A reports $[\Gamma(\chi_{b0}(2P) \rightarrow 3\pi^+3\pi^-)/\Gamma_{\text{total}}] \times [B(\Upsilon(3S) \rightarrow \gamma\chi_{b0}(2P))] < 4 \times 10^{-6}$ which we divide by our best value $B(\Upsilon(3S) \rightarrow \gamma\chi_{b0}(2P)) = 5.9 \times 10^{-2}$ .					

$\Gamma(3\pi^+3\pi^-2\pi^0)/\Gamma_{\text{total}}$					$\Gamma_{13}/\Gamma$
VALUE (units $10^{-4}$ )	CL%	DOCUMENT ID	TECN	COMMENT	
<12	90	25 ASNER	08A CLEO	$\Upsilon(3S) \rightarrow \gamma 3\pi^+3\pi^-2\pi^0$	
25 ASNER 08A reports $[\Gamma(\chi_{b0}(2P) \rightarrow 3\pi^+3\pi^-2\pi^0)/\Gamma_{\text{total}}] \times [B(\Upsilon(3S) \rightarrow \gamma\chi_{b0}(2P))] < 72 \times 10^{-6}$ which we divide by our best value $B(\Upsilon(3S) \rightarrow \gamma\chi_{b0}(2P)) = 5.9 \times 10^{-2}$ .					

$\Gamma(3\pi^+3\pi^-K^+K^-)/\Gamma_{\text{total}}$					$\Gamma_{14}/\Gamma$
VALUE (units $10^{-4}$ )	CL%	DOCUMENT ID	TECN	COMMENT	
<1.5	90	26 ASNER	08A CLEO	$\Upsilon(3S) \rightarrow \gamma 3\pi^+3\pi^-K^+K^-$	
26 ASNER 08A reports $[\Gamma(\chi_{b0}(2P) \rightarrow 3\pi^+3\pi^-K^+K^-)/\Gamma_{\text{total}}] \times [B(\Upsilon(3S) \rightarrow \gamma\chi_{b0}(2P))] < 9 \times 10^{-6}$ which we divide by our best value $B(\Upsilon(3S) \rightarrow \gamma\chi_{b0}(2P)) = 5.9 \times 10^{-2}$ .					

$\Gamma(3\pi^+3\pi^-K^+K^-\pi^0)/\Gamma_{\text{total}}$					$\Gamma_{15}/\Gamma$
VALUE (units $10^{-4}$ )	CL%	DOCUMENT ID	TECN	COMMENT	
<7	90	27 ASNER	08A CLEO	$\Upsilon(3S) \rightarrow \gamma 3\pi^+3\pi^-K^+K^-\pi^0$	
27 ASNER 08A reports $[\Gamma(\chi_{b0}(2P) \rightarrow 3\pi^+3\pi^-K^+K^-\pi^0)/\Gamma_{\text{total}}] \times [B(\Upsilon(3S) \rightarrow \gamma\chi_{b0}(2P))] < 43 \times 10^{-6}$ which we divide by our best value $B(\Upsilon(3S) \rightarrow \gamma\chi_{b0}(2P)) = 5.9 \times 10^{-2}$ .					

$\Gamma(4\pi^+4\pi^-)/\Gamma_{\text{total}}$					$\Gamma_{16}/\Gamma$
VALUE (units $10^{-4}$ )	CL%	DOCUMENT ID	TECN	COMMENT	
<1.7	90	28 ASNER	08A CLEO	$\Upsilon(3S) \rightarrow \gamma 4\pi^+4\pi^-$	
28 ASNER 08A reports $[\Gamma(\chi_{b0}(2P) \rightarrow 4\pi^+4\pi^-)/\Gamma_{\text{total}}] \times [B(\Upsilon(3S) \rightarrow \gamma\chi_{b0}(2P))] < 10 \times 10^{-6}$ which we divide by our best value $B(\Upsilon(3S) \rightarrow \gamma\chi_{b0}(2P)) = 5.9 \times 10^{-2}$ .					

$\Gamma(4\pi^+4\pi^-2\pi^0)/\Gamma_{\text{total}}$					$\Gamma_{17}/\Gamma$
VALUE (units $10^{-4}$ )	CL%	DOCUMENT ID	TECN	COMMENT	
<6	90	29 ASNER	08A CLEO	$\Upsilon(3S) \rightarrow \gamma 4\pi^+4\pi^-2\pi^0$	
29 ASNER 08A reports $[\Gamma(\chi_{b0}(2P) \rightarrow 4\pi^+4\pi^-2\pi^0)/\Gamma_{\text{total}}] \times [B(\Upsilon(3S) \rightarrow \gamma\chi_{b0}(2P))] < 38 \times 10^{-6}$ which we divide by our best value $B(\Upsilon(3S) \rightarrow \gamma\chi_{b0}(2P)) = 5.9 \times 10^{-2}$ .					

$\Gamma(\chi_{b0}(2P) \rightarrow \gamma\Upsilon(1S))/\Gamma_{\text{total}} \times \Gamma(\Upsilon(3S) \rightarrow \gamma\chi_{b0}(2P))/\Gamma_{\text{total}}$					$\Gamma_2/\Gamma \times \Gamma_{22}^{(\Upsilon(3S))}/\Gamma\Upsilon(3S)$
VALUE (units $10^{-4}$ )	CL%	DOCUMENT ID	TECN	COMMENT	
<8.2	90	30 LEES	11J BABR	$\Upsilon(3S) \rightarrow X\gamma$	
30 LEES 11J quotes a central value of $\Gamma(\chi_{b0}(2P) \rightarrow \gamma\Upsilon(1S))/\Gamma_{\text{total}} \times \Gamma(\Upsilon(3S) \rightarrow \gamma\chi_{b0}(2P))/\Gamma_{\text{total}} = (3.9 \pm 2.2^{+1.2}_{-0.6}) \times 10^{-4}$ and derives a 90% CL upper limit of $B(\chi_{b0}(2P) \rightarrow \gamma\Upsilon(1S)) < 1.2\%$ using $B(\Upsilon(3S) \rightarrow \gamma\chi_{b0}(2P)) = (5.9 \pm 0.6)\%$ .					

$B(\chi_{b0}(2P) \rightarrow \gamma\Upsilon(1S)) \times B(\Upsilon(3S) \rightarrow \gamma\chi_{b0}(2P)) \times B(\Upsilon(1S) \rightarrow \ell^+\ell^-)$					
VALUE (units $10^{-5}$ )	DOCUMENT ID	TECN	COMMENT		
<b>1.4 ± 0.9 OUR AVERAGE</b>					
$1.7^{+1.5+0.1}_{-1.4-1.2}$	31 LEES	14M BABR	$\Upsilon(3S) \rightarrow \gamma\gamma\mu^+\mu^-$		
$1.3 \pm 1.0 \pm 0.3$	32 HEINTZ	92 CSB2	$\Upsilon(3S) \rightarrow \gamma\gamma\ell^+\ell^-$		
31 From a sample of $\Upsilon(3S) \rightarrow \gamma\gamma\mu^+\mu^-$ with one converted photon.					
32 Calculated by us. HEINTZ 92 quotes $B(\Upsilon(3S) \rightarrow \gamma\chi_{b0}(2P)) \times B(\chi_{b0}(2P) \rightarrow \gamma\Upsilon(1S)) = (0.05 \pm 0.04 \pm 0.01)\%$ using $B(\Upsilon(1S) \rightarrow \mu^+\mu^-) = (2.57 \pm 0.05)\%$ .					

$[B(\chi_{b0}(2P) \rightarrow \gamma\Upsilon(1S)) \times B(\Upsilon(3S) \rightarrow \gamma\chi_{b0}(2P))] / [B(\chi_{b1}(2P) \rightarrow \gamma\Upsilon(1S)) \times B(\Upsilon(3S) \rightarrow \gamma\chi_{b1}(2P))]$					
VALUE (%)	DOCUMENT ID	TECN	COMMENT		
<b>1.71 ± 0.80</b>	33 LEES	14M BABR	$\Upsilon(3S) \rightarrow \gamma\gamma\mu^+\mu^-$		
33 From a sample of $\Upsilon(3S) \rightarrow \gamma\gamma\mu^+\mu^-$ without converted photons.					

$\Gamma(\chi_{b0}(2P) \rightarrow \gamma\Upsilon(2S))/\Gamma_{\text{total}} \times \Gamma(\Upsilon(3S) \rightarrow \gamma\chi_{b0}(2P))/\Gamma_{\text{total}}$					$\Gamma_1/\Gamma \times \Gamma_{22}^{(\Upsilon(3S))}/\Gamma\Upsilon(3S)$
VALUE (units $10^{-3}$ )	CL%	DOCUMENT ID	TECN	COMMENT	
<1.6	90	34 LEES	11J BABR	$\Upsilon(3S) \rightarrow X\gamma$	
34 LEES 11J quotes a central value of $\Gamma(\chi_{b0}(2P) \rightarrow \gamma\Upsilon(2S))/\Gamma_{\text{total}} \times \Gamma(\Upsilon(3S) \rightarrow \gamma\chi_{b0}(2P))/\Gamma_{\text{total}} = (-0.3 \pm 0.2^{+0.3}_{-0.4})\%$ and derives a 90% CL upper limit of $B(\chi_{b0}(2P) \rightarrow \gamma\Upsilon(2S)) < 2.8\%$ using $B(\Upsilon(3S) \rightarrow \gamma\chi_{b0}(2P)) = (5.9 \pm 0.6)\%$ .					

$B(\chi_{b0}(2P) \rightarrow \gamma\Upsilon(2S)) \times B(\Upsilon(3S) \rightarrow \gamma\chi_{b0}(2P)) \times B(\Upsilon(2S) \rightarrow \ell^+\ell^-)$					
VALUE (units $10^{-5}$ )	DOCUMENT ID	TECN	COMMENT		
<b>4.4 ± 1.6 OUR AVERAGE</b>					
$6.6^{+4.9+2.0}_{-4.0-0.3}$	35 LEES	14M BABR	$\Upsilon(3S) \rightarrow \gamma\gamma\mu^+\mu^-$		
$4.0 \pm 1.7 \pm 0.3$	36 HEINTZ	92 CSB2	$\Upsilon(3S) \rightarrow \gamma\gamma\ell^+\ell^-$		
35 From a sample of $\Upsilon(3S) \rightarrow \gamma\gamma\mu^+\mu^-$ with one converted photon.					
36 Calculated by us. HEINTZ 92 quotes $B(\Upsilon(3S) \rightarrow \gamma\chi_{b0}(2P)) \times B(\chi_{b0}(2P) \rightarrow \gamma\Upsilon(2S)) = (0.28 \pm 0.12 \pm 0.03)\%$ using $B(\Upsilon(2S) \rightarrow \mu^+\mu^-) = (1.44 \pm 0.10)\%$ .					

$[B(\chi_{b0}(2P) \rightarrow \gamma\Upsilon(2S)) \times B(\Upsilon(3S) \rightarrow \gamma\chi_{b0}(2P))] / [B(\chi_{b1}(2P) \rightarrow \gamma\Upsilon(2S)) \times B(\Upsilon(3S) \rightarrow \gamma\chi_{b1}(2P))]$					
VALUE (%)	DOCUMENT ID	TECN	COMMENT		
<b>3.31 ± 0.56</b>	37 LEES	14M BABR	$\Upsilon(3S) \rightarrow \gamma\gamma\mu^+\mu^-$		
37 From a sample of $\Upsilon(3S) \rightarrow \gamma\gamma\mu^+\mu^-$ without converted photons.					

$\chi_{b0}(2P)$  REFERENCES

LEES	14M	PR D90 112010	J.P. Lees et al.	(BABAR Collab.)
LEES	11J	PR D84 072002	J.P. Lees et al.	(BABAR Collab.)
ASNER	08A	PR D78 091103	D.M. Asner et al.	(CLEO Collab.)
BRIERE	08	PR D78 092007	R.A. Briere et al.	(CLEO Collab.)
ARTUSO	05	PRL 94 032001	M. Artuso et al.	(CLEO Collab.)
CRAWFORD	92B	PL B294 139	G. Crawford et al.	(CLEO Collab.)
HEINTZ	92	PR D46 1928	U. Heintz et al.	(CUSB II Collab.)
HEINTZ	91	PRL 66 1563	U. Heintz et al.	(CUSB Collab.)
MORRISON	91	PRL 67 1696	R.J. Morrison et al.	(CLEO Collab.)
NARAIN	91	PRL 66 3113	M. Narain et al.	(CUSB Collab.)

$\chi_{b1}(2P)$

$J^C(J^{PC}) = 0^+(1^+ +)$   
 J needs confirmation.

Observed in radiative decay of the  $\Upsilon(3S)$ , therefore  $C = +$ . Branching ratio requires E1 transition, M1 is strongly disfavored, therefore  $P = +$ .

# Meson Particle Listings

## $\chi_{b1}(2P)$

### $\chi_{b1}(2P)$ MASS

VALUE (MeV)	DOCUMENT ID	COMMENT
<b>10295.46 ± 0.22 ± 0.50 OUR EVALUATION</b>		From $\gamma$ energy below, using $\Upsilon(3S)$ mass = 10355.2 ± 0.5 MeV

### $m_{\chi_{b1}(2P)} - m_{\chi_{b0}(2P)}$

VALUE (MeV)	DOCUMENT ID	TECN	COMMENT
<b>23.5 ± 0.7 ± 0.7</b>	<sup>1</sup> HEINTZ	92 CSB2	$e^+e^- \rightarrow \gamma X, \ell^+\ell^-\gamma\gamma$

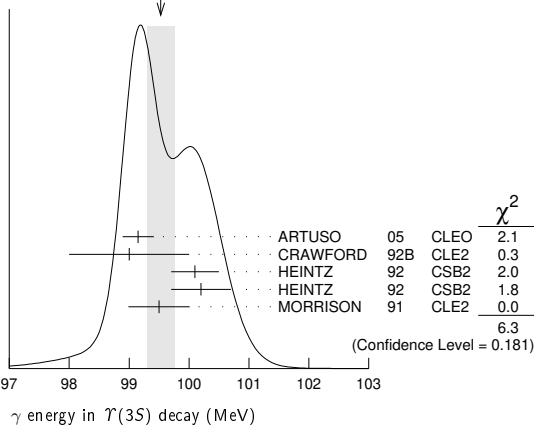
<sup>1</sup> From the average photon energy for inclusive and exclusive events. Supersedes NARAIN 91.

### $\gamma$ ENERGY IN $\Upsilon(3S)$ DECAY

VALUE (MeV)	EVTS	DOCUMENT ID	TECN	COMMENT
<b>99.26 ± 0.22 OUR EVALUATION</b>				Treating systematic errors as correlated
<b>99.53 ± 0.23 OUR AVERAGE</b>				Error includes scale factor of 1.3. See the ideogram below.
99.15 ± 0.07 ± 0.25		ARTUSO 05	CLEO	$\Upsilon(3S) \rightarrow \gamma X$
99 ± 1	169	CRAWFORD 92B	CLE2	$e^+e^- \rightarrow \ell^+\ell^-\gamma\gamma$
100.1 ± 0.4	11147	<sup>2</sup> HEINTZ 92	CSB2	$e^+e^- \rightarrow \gamma X$
100.2 ± 0.5	223	<sup>3</sup> HEINTZ 92	CSB2	$e^+e^- \rightarrow \ell^+\ell^-\gamma\gamma$
99.5 ± 0.1 ± 0.5	25759	MORRISON 91	CLE2	$e^+e^- \rightarrow \gamma X$

<sup>2</sup> A systematic uncertainty on the energy scale of 0.9% not included. Supersedes NARAIN 91.  
<sup>3</sup> A systematic uncertainty on the energy scale of 0.9% not included. Supersedes HEINTZ 91.

WEIGHTED AVERAGE  
99.53 ± 0.23 (Error scaled by 1.3)



### $\chi_{b1}(2P)$ DECAY MODES

Mode	Fraction ( $\Gamma_i/\Gamma$ )
$\Gamma_1$ $\omega \Upsilon(1S)$	(1.63 <sup>+0.40</sup> <sub>-0.34</sub> ) %
$\Gamma_2$ $\gamma \Upsilon(2S)$	(18.1 ± 1.9) %
$\Gamma_3$ $\gamma \Upsilon(1S)$	(9.9 ± 1.0) %
$\Gamma_4$ $\pi\pi \chi_{b1}(1P)$	(9.1 ± 1.3) × 10 <sup>-3</sup>
$\Gamma_5$ $D^0 X$	(8.8 ± 1.7) %
$\Gamma_6$ $\pi^+\pi^-K^+K^-\pi^0$	(3.1 ± 1.0) × 10 <sup>-4</sup>
$\Gamma_7$ $2\pi^+\pi^-K^-K_S^0$	(1.1 ± 0.5) × 10 <sup>-4</sup>
$\Gamma_8$ $2\pi^+\pi^-K^-K_S^0 2\pi^0$	(7.7 ± 3.2) × 10 <sup>-4</sup>
$\Gamma_9$ $2\pi^+2\pi^-2\pi^0$	(5.9 ± 2.0) × 10 <sup>-4</sup>
$\Gamma_{10}$ $2\pi^+2\pi^-K^+K^-$	(10 ± 4) × 10 <sup>-5</sup>
$\Gamma_{11}$ $2\pi^+2\pi^-K^+K^-\pi^0$	(5.5 ± 1.8) × 10 <sup>-4</sup>
$\Gamma_{12}$ $2\pi^+2\pi^-K^+K^-2\pi^0$	(10 ± 4) × 10 <sup>-4</sup>
$\Gamma_{13}$ $3\pi^+2\pi^-K^-K_S^0\pi^0$	(6.7 ± 2.6) × 10 <sup>-4</sup>
$\Gamma_{14}$ $3\pi^+3\pi^-$	(1.2 ± 0.4) × 10 <sup>-4</sup>
$\Gamma_{15}$ $3\pi^+3\pi^-2\pi^0$	(1.2 ± 0.4) × 10 <sup>-3</sup>
$\Gamma_{16}$ $3\pi^+3\pi^-K^+K^-$	(2.0 ± 0.8) × 10 <sup>-4</sup>
$\Gamma_{17}$ $3\pi^+3\pi^-K^+K^-\pi^0$	(6.1 ± 2.2) × 10 <sup>-4</sup>
$\Gamma_{18}$ $4\pi^+4\pi^-$	(1.7 ± 0.6) × 10 <sup>-4</sup>
$\Gamma_{19}$ $4\pi^+4\pi^-2\pi^0$	(1.9 ± 0.7) × 10 <sup>-3</sup>

### $\chi_{b1}(2P)$ BRANCHING RATIOS

$\Gamma(\omega \Upsilon(1S))/\Gamma_{total}$	VALUE (units 10 <sup>-2</sup> )	EVTS	DOCUMENT ID	TECN	COMMENT
<b>1.63 ± 0.35 ± 0.16</b>		32.6 <sup>+6.9</sup> <sub>-6.1</sub>	<sup>4</sup> CRONIN-HEN..04	CLE3	$\Upsilon(3S) \rightarrow \gamma\omega \Upsilon(1S)$

<sup>4</sup> Using  $B(\Upsilon(3S) \rightarrow \gamma\chi_{b1}(2P)) = (11.3 \pm 0.6)\%$  and  $B(\Upsilon(1S) \rightarrow \ell^+\ell^-) = 2 B(\Upsilon(1S) \rightarrow \mu^+\mu^-) = 2(2.48 \pm 0.06)\%$ .

### $\Gamma(\gamma \Upsilon(2S))/\Gamma_{total}$

VALUE	EVTS	DOCUMENT ID	TECN	COMMENT
<b>0.181 ± 0.019 OUR AVERAGE</b>				
0.211 ± 0.017 ± 0.019		<sup>5,6,7</sup> LEES	14M BABR	$\Upsilon(3S) \rightarrow \gamma\gamma\mu^+\mu^-$
0.190 ± 0.018 ± 0.017	4.3k	<sup>8</sup> LEES	11J BABR	$\Upsilon(3S) \rightarrow X\gamma$
0.206 ± 0.035 ± 0.019		<sup>5,9</sup> CRAWFORD	92B CLE2	$e^+e^- \rightarrow \ell^+\ell^-\gamma\gamma$
0.132 ± 0.018 ± 0.012		<sup>5,10</sup> HEINTZ	92 CSB2	$e^+e^- \rightarrow \ell^+\ell^-\gamma\gamma$

<sup>5</sup> Assuming  $B(\Upsilon(2S) \rightarrow \mu^+\mu^-) = (1.93 \pm 0.17)\%$ .  
<sup>6</sup> LEES 14M quotes  $\Gamma(\chi_{b1}(2P) \rightarrow \gamma\Upsilon(2S))/\Gamma_{total} \times \Gamma(\Upsilon(3S) \rightarrow \gamma\chi_{b1}(2P))/\Gamma_{total} = (2.66 \pm 0.22)\%$  combining the results from  $\Upsilon(3S) \rightarrow \gamma\gamma\mu^+\mu^-$  samples with and without photon conversions.  
<sup>7</sup> LEES 14M reports  $[\Gamma(\chi_{b1}(2P) \rightarrow \gamma\Upsilon(2S))/\Gamma_{total}] \times [B(\Upsilon(3S) \rightarrow \gamma\chi_{b1}(2P))] = (2.66 \pm 0.22) \times 10^{-2}$  which we divide by our best value  $B(\Upsilon(3S) \rightarrow \gamma\chi_{b1}(2P)) = (12.6 \pm 1.2) \times 10^{-2}$ . Our first error is their experiment's error and our second error is the systematic error from using our best value.  
<sup>8</sup> LEES 11J reports  $[\Gamma(\chi_{b1}(2P) \rightarrow \gamma\Upsilon(2S))/\Gamma_{total}] \times [B(\Upsilon(3S) \rightarrow \gamma\chi_{b1}(2P))] = (2.4 \pm 0.1 \pm 0.2) \times 10^{-2}$  which we divide by our best value  $B(\Upsilon(3S) \rightarrow \gamma\chi_{b1}(2P)) = (12.6 \pm 1.2) \times 10^{-2}$ . Our first error is their experiment's error and our second error is the systematic error from using our best value.  
<sup>9</sup> CRAWFORD 92B quotes  $B(\Upsilon(3S) \rightarrow \gamma\chi_{b1}(2P)) \times B(\chi_{b1}(2P) \rightarrow \gamma\Upsilon(2S)) \times 2 B(\Upsilon(2S) \rightarrow \ell^+\ell^-) = (10.23 \pm 1.20 \pm 1.26) 10^{-4}$ .  
<sup>10</sup> Recalculated by us. HEINTZ 92 quotes  $B(\Upsilon(3S) \rightarrow \gamma\chi_{b1}(2P)) \times B(\chi_{b1}(2P) \rightarrow \gamma\Upsilon(2S)) = (2.29 \pm 0.23 \pm 0.21) \%$  using  $B(\Upsilon(2S) \rightarrow \mu^+\mu^-) = (1.44 \pm 0.10)\%$ . Supersedes HEINTZ 91.

### $\Gamma(\gamma \Upsilon(1S))/\Gamma_{total}$

VALUE	EVTS	DOCUMENT ID	TECN	COMMENT
<b>0.099 ± 0.010 OUR AVERAGE</b>				
0.107 ± 0.006 ± 0.010	11,12,13	LEES	14M BABR	$\Upsilon(3S) \rightarrow \gamma\gamma\mu^+\mu^-$
0.098 ± 0.005 ± 0.009	15k	<sup>14</sup> LEES	11J BABR	$\Upsilon(3S) \rightarrow X\gamma$
0.103 ± 0.023 ± 0.009		<sup>11,15</sup> CRAWFORD	92B CLE2	$e^+e^- \rightarrow \ell^+\ell^-\gamma\gamma$
0.075 ± 0.010 ± 0.007		<sup>11,16</sup> HEINTZ	92 CSB2	$e^+e^- \rightarrow \ell^+\ell^-\gamma\gamma$

<sup>11</sup> Assuming  $B(\Upsilon(1S) \rightarrow \mu^+\mu^-) = (2.48 \pm 0.05)\%$ .  
<sup>12</sup> LEES 14M quotes  $\Gamma(\chi_{b1}(2P) \rightarrow \gamma\Upsilon(1S))/\Gamma_{total} \times \Gamma(\Upsilon(3S) \rightarrow \gamma\chi_{b1}(2P))/\Gamma_{total} = (13.48 \pm 0.72) \times 10^{-3}$  combining the results from samples of  $\Upsilon(3S) \rightarrow \gamma\gamma\mu^+\mu^-$  with and without converted photons.  
<sup>13</sup> LEES 14M reports  $[\Gamma(\chi_{b1}(2P) \rightarrow \gamma\Upsilon(1S))/\Gamma_{total}] \times [B(\Upsilon(3S) \rightarrow \gamma\chi_{b1}(2P))] = (13.48 \pm 0.72) \times 10^{-3}$  which we divide by our best value  $B(\Upsilon(3S) \rightarrow \gamma\chi_{b1}(2P)) = (12.6 \pm 1.2) \times 10^{-2}$ . Our first error is their experiment's error and our second error is the systematic error from using our best value.  
<sup>14</sup> LEES 11J reports  $[\Gamma(\chi_{b1}(2P) \rightarrow \gamma\Upsilon(1S))/\Gamma_{total}] \times [B(\Upsilon(3S) \rightarrow \gamma\chi_{b1}(2P))] = (12.4 \pm 0.3 \pm 0.6) \times 10^{-3}$  which we divide by our best value  $B(\Upsilon(3S) \rightarrow \gamma\chi_{b1}(2P)) = (12.6 \pm 1.2) \times 10^{-2}$ . Our first error is their experiment's error and our second error is the systematic error from using our best value.  
<sup>15</sup> CRAWFORD 92B quotes  $B(\Upsilon(3S) \rightarrow \gamma\chi_{b1}(2P)) \times B(\chi_{b1}(2P) \rightarrow \gamma\Upsilon(1S)) \times 2 B(\Upsilon(1S) \rightarrow \ell^+\ell^-) = (6.47 \pm 1.12 \pm 0.82) 10^{-4}$ .  
<sup>16</sup> Recalculated by us. HEINTZ 92 quotes  $B(\Upsilon(3S) \rightarrow \gamma\chi_{b1}(2P)) \times B(\chi_{b1}(2P) \rightarrow \gamma\Upsilon(1S)) = (0.91 \pm 0.11 \pm 0.06)\%$  using  $B(\Upsilon(1S) \rightarrow \mu^+\mu^-) = (2.57 \pm 0.05)\%$ . Supersedes HEINTZ 91.

### $\Gamma(\pi\pi\chi_{b1}(1P))/\Gamma_{total}$

VALUE (units 10 <sup>-3</sup> )	EVTS	DOCUMENT ID	TECN	COMMENT
<b>9.1 ± 1.3 OUR AVERAGE</b>				
9.2 ± 1.1 ± 0.8	31k	<sup>17</sup> LEES	11c BABR	$e^+e^- \rightarrow \pi^+\pi^-X$
8.6 ± 2.3 ± 2.1		<sup>18</sup> CAWLFIELD	06 CLE3	$\Upsilon(3S) \rightarrow 2(\gamma\pi\ell)$

<sup>17</sup> LEES 11c measures  $B(\Upsilon(3S) \rightarrow \chi_{b1}(2P)X) \times B(\chi_{b1}(2P) \rightarrow \chi_{b1}(1P)\pi^+\pi^-) = (1.16 \pm 0.07 \pm 0.12) \times 10^{-3}$ . We derive the value assuming  $B(\Upsilon(3S) \rightarrow \chi_{b1}(2P)X) = B(\Upsilon(3S) \rightarrow \chi_{b1}(2P)\gamma) = (12.6 \pm 1.2) \times 10^{-2}$ .  
<sup>18</sup> CAWLFIELD 06 quote  $\Gamma(\chi_b(2P) \rightarrow \pi\pi\chi_b(1P)) = 0.83 \pm 0.22 \pm 0.08 \pm 0.19$  keV assuming l-spin conservation, no D-wave contribution,  $\Gamma(\chi_{b1}(2P)) = 96 \pm 16$  keV, and  $\Gamma(\chi_{b2}(2P)) = 138 \pm 19$  keV.

### $\Gamma(D^0 X)/\Gamma_{total}$

VALUE (units 10 <sup>-2</sup> )	EVTS	DOCUMENT ID	TECN	COMMENT
<b>8.8 ± 1.5 ± 0.8</b>	2243	<sup>19</sup> BRIERE	08 CLEO	$\Upsilon(3S) \rightarrow \gamma D^0 X$

<sup>19</sup> For  $p_{D^0} > 2.5$  GeV/c.

### $\Gamma(\pi^+\pi^-K^+K^-\pi^0)/\Gamma_{total}$

VALUE (units 10 <sup>-4</sup> )	EVTS	DOCUMENT ID	TECN	COMMENT
<b>3.1 ± 1.0 ± 0.3</b>	30	<sup>20</sup> ASNER	08A CLEO	$\Upsilon(3S) \rightarrow \gamma\pi^+\pi^-K^+K^-\pi^0$

<sup>20</sup> ASNER 08A reports  $[\Gamma(\chi_{b1}(2P) \rightarrow \pi^+\pi^-K^+K^-\pi^0)/\Gamma_{total}] \times [B(\Upsilon(3S) \rightarrow \gamma\chi_{b1}(2P))] = (39 \pm 8 \pm 9) \times 10^{-6}$  which we divide by our best value  $B(\Upsilon(3S) \rightarrow \gamma\chi_{b1}(2P)) = (12.6 \pm 1.2) \times 10^{-2}$ . Our first error is their experiment's error and our second error is the systematic error from using our best value.

### $\Gamma(2\pi^+\pi^-K^-K_S^0)/\Gamma_{total}$

VALUE (units 10 <sup>-4</sup> )	EVTS	DOCUMENT ID	TECN	COMMENT
<b>1.1 ± 0.5 ± 0.1</b>	10	<sup>21</sup> ASNER	08A CLEO	$\Upsilon(3S) \rightarrow \gamma 2\pi^+\pi^-K^-K_S^0$

<sup>21</sup> ASNER 08A reports  $[\Gamma(\chi_{b1}(2P) \rightarrow 2\pi^+\pi^-K^-K_S^0)/\Gamma_{total}] \times [B(\Upsilon(3S) \rightarrow \gamma\chi_{b1}(2P))] = (14 \pm 5 \pm 3) \times 10^{-6}$  which we divide by our best value  $B(\Upsilon(3S) \rightarrow \gamma\chi_{b1}(2P)) = (12.6 \pm 1.2) \times 10^{-2}$ . Our first error is their experiment's error and our second error is the systematic error from using our best value.

See key on page 999

Meson Particle Listings

$\chi_{b1}(2P)$

$\Gamma(2\pi^+\pi^-K^-K_S^0 2\pi^0)/\Gamma_{total}$   $\Gamma_8/\Gamma$

VALUE (units $10^{-4}$ )	EVTs	DOCUMENT ID	TECN	COMMENT
<b><math>7.7 \pm 3.1 \pm 0.7</math></b>	15	22 ASNER	08A CLEO	$\Upsilon(3S) \rightarrow \gamma 2\pi^+\pi^-K^-2\pi^0$
22 ASNER 08A reports $[\Gamma(\chi_{b1}(2P) \rightarrow 2\pi^+\pi^-K^-K_S^0 2\pi^0)/\Gamma_{total}] \times [B(\Upsilon(3S) \rightarrow \gamma \chi_{b1}(2P))]$ = $(97 \pm 30 \pm 26) \times 10^{-6}$ which we divide by our best value $B(\Upsilon(3S) \rightarrow \gamma \chi_{b1}(2P)) = (12.6 \pm 1.2) \times 10^{-2}$ . Our first error is their experiment's error and our second error is the systematic error from using our best value.				

$\Gamma(2\pi^+2\pi^-2\pi^0)/\Gamma_{total}$   $\Gamma_9/\Gamma$

VALUE (units $10^{-4}$ )	EVTs	DOCUMENT ID	TECN	COMMENT
<b><math>5.9 \pm 2.0 \pm 0.5</math></b>	36	23 ASNER	08A CLEO	$\Upsilon(3S) \rightarrow \gamma 2\pi^+2\pi^-2\pi^0$
23 ASNER 08A reports $[\Gamma(\chi_{b1}(2P) \rightarrow 2\pi^+2\pi^-2\pi^0)/\Gamma_{total}] \times [B(\Upsilon(3S) \rightarrow \gamma \chi_{b1}(2P))]$ = $(74 \pm 16 \pm 19) \times 10^{-6}$ which we divide by our best value $B(\Upsilon(3S) \rightarrow \gamma \chi_{b1}(2P)) = (12.6 \pm 1.2) \times 10^{-2}$ . Our first error is their experiment's error and our second error is the systematic error from using our best value.				

$\Gamma(2\pi^+2\pi^-K^+K^-)/\Gamma_{total}$   $\Gamma_{10}/\Gamma$

VALUE (units $10^{-4}$ )	EVTs	DOCUMENT ID	TECN	COMMENT
<b><math>1.0 \pm 0.4 \pm 0.1</math></b>	12	24 ASNER	08A CLEO	$\Upsilon(3S) \rightarrow \gamma 2\pi^+2\pi^-K^+K^-$
24 ASNER 08A reports $[\Gamma(\chi_{b1}(2P) \rightarrow 2\pi^+2\pi^-K^+K^-)/\Gamma_{total}] \times [B(\Upsilon(3S) \rightarrow \gamma \chi_{b1}(2P))]$ = $(12 \pm 4 \pm 3) \times 10^{-6}$ which we divide by our best value $B(\Upsilon(3S) \rightarrow \gamma \chi_{b1}(2P)) = (12.6 \pm 1.2) \times 10^{-2}$ . Our first error is their experiment's error and our second error is the systematic error from using our best value.				

$\Gamma(2\pi^+2\pi^-K^+K^-\pi^0)/\Gamma_{total}$   $\Gamma_{11}/\Gamma$

VALUE (units $10^{-4}$ )	EVTs	DOCUMENT ID	TECN	COMMENT
<b><math>5.5 \pm 1.7 \pm 0.5</math></b>	38	25 ASNER	08A CLEO	$\Upsilon(3S) \rightarrow \gamma 2\pi^+2\pi^-K^+K^-\pi^0$
25 ASNER 08A reports $[\Gamma(\chi_{b1}(2P) \rightarrow 2\pi^+2\pi^-K^+K^-\pi^0)/\Gamma_{total}] \times [B(\Upsilon(3S) \rightarrow \gamma \chi_{b1}(2P))]$ = $(69 \pm 13 \pm 17) \times 10^{-6}$ which we divide by our best value $B(\Upsilon(3S) \rightarrow \gamma \chi_{b1}(2P)) = (12.6 \pm 1.2) \times 10^{-2}$ . Our first error is their experiment's error and our second error is the systematic error from using our best value.				

$\Gamma(2\pi^+2\pi^-K^+K^-2\pi^0)/\Gamma_{total}$   $\Gamma_{12}/\Gamma$

VALUE (units $10^{-4}$ )	EVTs	DOCUMENT ID	TECN	COMMENT
<b><math>9.6 \pm 3.5 \pm 0.9</math></b>	27	26 ASNER	08A CLEO	$\Upsilon(3S) \rightarrow \gamma 2\pi^+2\pi^-K^+K^-2\pi^0$
26 ASNER 08A reports $[\Gamma(\chi_{b1}(2P) \rightarrow 2\pi^+2\pi^-K^+K^-2\pi^0)/\Gamma_{total}] \times [B(\Upsilon(3S) \rightarrow \gamma \chi_{b1}(2P))]$ = $(121 \pm 29 \pm 33) \times 10^{-6}$ which we divide by our best value $B(\Upsilon(3S) \rightarrow \gamma \chi_{b1}(2P)) = (12.6 \pm 1.2) \times 10^{-2}$ . Our first error is their experiment's error and our second error is the systematic error from using our best value.				

$\Gamma(3\pi^+2\pi^-K^-K_S^0\pi^0)/\Gamma_{total}$   $\Gamma_{13}/\Gamma$

VALUE (units $10^{-4}$ )	EVTs	DOCUMENT ID	TECN	COMMENT
<b><math>6.7 \pm 2.5 \pm 0.6</math></b>	17	27 ASNER	08A CLEO	$\Upsilon(3S) \rightarrow \gamma 3\pi^+2\pi^-K^-K_S^0\pi^0$
27 ASNER 08A reports $[\Gamma(\chi_{b1}(2P) \rightarrow 3\pi^+2\pi^-K^-K_S^0\pi^0)/\Gamma_{total}] \times [B(\Upsilon(3S) \rightarrow \gamma \chi_{b1}(2P))]$ = $(85 \pm 23 \pm 22) \times 10^{-6}$ which we divide by our best value $B(\Upsilon(3S) \rightarrow \gamma \chi_{b1}(2P)) = (12.6 \pm 1.2) \times 10^{-2}$ . Our first error is their experiment's error and our second error is the systematic error from using our best value.				

$\Gamma(3\pi^+3\pi^-)/\Gamma_{total}$   $\Gamma_{14}/\Gamma$

VALUE (units $10^{-4}$ )	EVTs	DOCUMENT ID	TECN	COMMENT
<b><math>1.2 \pm 0.4 \pm 0.1</math></b>	18	28 ASNER	08A CLEO	$\Upsilon(3S) \rightarrow \gamma 3\pi^+3\pi^-$
28 ASNER 08A reports $[\Gamma(\chi_{b1}(2P) \rightarrow 3\pi^+3\pi^-)/\Gamma_{total}] \times [B(\Upsilon(3S) \rightarrow \gamma \chi_{b1}(2P))]$ = $(15 \pm 4 \pm 3) \times 10^{-6}$ which we divide by our best value $B(\Upsilon(3S) \rightarrow \gamma \chi_{b1}(2P)) = (12.6 \pm 1.2) \times 10^{-2}$ . Our first error is their experiment's error and our second error is the systematic error from using our best value.				

$\Gamma(3\pi^+3\pi^-2\pi^0)/\Gamma_{total}$   $\Gamma_{15}/\Gamma$

VALUE (units $10^{-4}$ )	EVTs	DOCUMENT ID	TECN	COMMENT
<b><math>12 \pm 4 \pm 1</math></b>	44	29 ASNER	08A CLEO	$\Upsilon(3S) \rightarrow \gamma 3\pi^+3\pi^-2\pi^0$
29 ASNER 08A reports $[\Gamma(\chi_{b1}(2P) \rightarrow 3\pi^+3\pi^-2\pi^0)/\Gamma_{total}] \times [B(\Upsilon(3S) \rightarrow \gamma \chi_{b1}(2P))]$ = $(150 \pm 30 \pm 40) \times 10^{-6}$ which we divide by our best value $B(\Upsilon(3S) \rightarrow \gamma \chi_{b1}(2P)) = (12.6 \pm 1.2) \times 10^{-2}$ . Our first error is their experiment's error and our second error is the systematic error from using our best value.				

$\Gamma(3\pi^+3\pi^-K^+K^-)/\Gamma_{total}$   $\Gamma_{16}/\Gamma$

VALUE (units $10^{-4}$ )	EVTs	DOCUMENT ID	TECN	COMMENT
<b><math>2.0 \pm 0.7 \pm 0.2</math></b>	16	30 ASNER	08A CLEO	$\Upsilon(3S) \rightarrow \gamma 3\pi^+3\pi^-K^+K^-$
30 ASNER 08A reports $[\Gamma(\chi_{b1}(2P) \rightarrow 3\pi^+3\pi^-K^+K^-)/\Gamma_{total}] \times [B(\Upsilon(3S) \rightarrow \gamma \chi_{b1}(2P))]$ = $(25 \pm 7 \pm 6) \times 10^{-6}$ which we divide by our best value $B(\Upsilon(3S) \rightarrow \gamma \chi_{b1}(2P)) = (12.6 \pm 1.2) \times 10^{-2}$ . Our first error is their experiment's error and our second error is the systematic error from using our best value.				

$\Gamma(3\pi^+3\pi^-K^+K^-\pi^0)/\Gamma_{total}$   $\Gamma_{17}/\Gamma$

VALUE (units $10^{-4}$ )	EVTs	DOCUMENT ID	TECN	COMMENT
<b><math>6.1 \pm 2.1 \pm 0.6</math></b>	25	31 ASNER	08A CLEO	$\Upsilon(3S) \rightarrow \gamma 3\pi^+3\pi^-K^+K^-\pi^0$
31 ASNER 08A reports $[\Gamma(\chi_{b1}(2P) \rightarrow 3\pi^+3\pi^-K^+K^-\pi^0)/\Gamma_{total}] \times [B(\Upsilon(3S) \rightarrow \gamma \chi_{b1}(2P))]$ = $(77 \pm 17 \pm 21) \times 10^{-6}$ which we divide by our best value $B(\Upsilon(3S) \rightarrow \gamma \chi_{b1}(2P)) = (12.6 \pm 1.2) \times 10^{-2}$ . Our first error is their experiment's error and our second error is the systematic error from using our best value.				

$\Gamma(4\pi^+4\pi^-)/\Gamma_{total}$   $\Gamma_{18}/\Gamma$

VALUE (units $10^{-4}$ )	EVTs	DOCUMENT ID	TECN	COMMENT
<b><math>1.7 \pm 0.6 \pm 0.2</math></b>	16	32 ASNER	08A CLEO	$\Upsilon(3S) \rightarrow \gamma 4\pi^+4\pi^-$
32 ASNER 08A reports $[\Gamma(\chi_{b1}(2P) \rightarrow 4\pi^+4\pi^-)/\Gamma_{total}] \times [B(\Upsilon(3S) \rightarrow \gamma \chi_{b1}(2P))]$ = $(22 \pm 6 \pm 5) \times 10^{-6}$ which we divide by our best value $B(\Upsilon(3S) \rightarrow \gamma \chi_{b1}(2P)) = (12.6 \pm 1.2) \times 10^{-2}$ . Our first error is their experiment's error and our second error is the systematic error from using our best value.				

$\Gamma(4\pi^+4\pi^-2\pi^0)/\Gamma_{total}$   $\Gamma_{19}/\Gamma$

VALUE (units $10^{-4}$ )	EVTs	DOCUMENT ID	TECN	COMMENT
<b><math>19 \pm 7 \pm 2</math></b>	41	33 ASNER	08A CLEO	$\Upsilon(3S) \rightarrow \gamma 4\pi^+4\pi^-2\pi^0$
33 ASNER 08A reports $[\Gamma(\chi_{b1}(2P) \rightarrow 4\pi^+4\pi^-2\pi^0)/\Gamma_{total}] \times [B(\Upsilon(3S) \rightarrow \gamma \chi_{b1}(2P))]$ = $(241 \pm 47 \pm 72) \times 10^{-6}$ which we divide by our best value $B(\Upsilon(3S) \rightarrow \gamma \chi_{b1}(2P)) = (12.6 \pm 1.2) \times 10^{-2}$ . Our first error is their experiment's error and our second error is the systematic error from using our best value.				

$\chi_{b1}(2P)$  Cross-Particle Branching Ratios

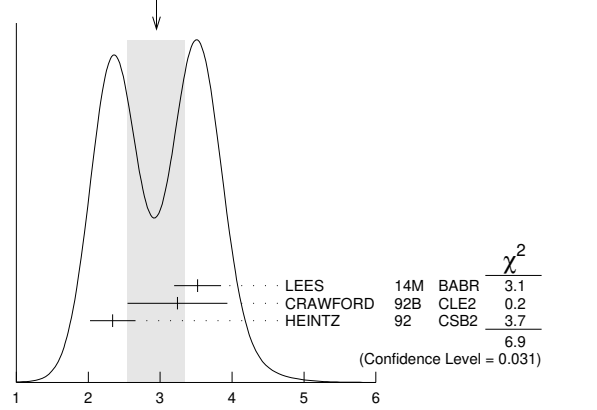
$\Gamma(\chi_{b1}(2P) \rightarrow \gamma \Upsilon(1S))/\Gamma_{total} \times \Gamma(\Upsilon(3S) \rightarrow \gamma \chi_{b1}(2P))/\Gamma_{total}$   
 $\Gamma_3/\Gamma \times \Gamma_{21}^{(3S)}/\Gamma \Upsilon(3S)$

VALUE (units $10^{-3}$ )	EVTs	DOCUMENT ID	TECN	COMMENT
<b><math>12.4 \pm 0.3 \pm 0.6</math></b>	15k	LEES	11J BABR	$\Upsilon(3S) \rightarrow X \gamma$

$B(\chi_{b1}(2P) \rightarrow \gamma \Upsilon(1S)) \times B(\Upsilon(3S) \rightarrow \gamma \chi_{b1}(2P)) \times B(\Upsilon(1S) \rightarrow \ell^+\ell^-)$

VALUE (units $10^{-4}$ )	EVTs	DOCUMENT ID	TECN	COMMENT
<b><math>2.9 \pm 0.4</math> OUR AVERAGE</b>				Error includes scale factor of 1.9. See the ideogram below.
$3.52_{-0.27}^{+0.28+0.17}$		34 LEES	14M BABR	$\Upsilon(3S) \rightarrow \gamma \gamma \mu^+ \mu^-$
$3.24 \pm 0.56 \pm 0.41$	58	35 CRAWFORD	92B CLE2	$\Upsilon(3S) \rightarrow \gamma \gamma \ell^+ \ell^-$
$2.34 \pm 0.28 \pm 0.15$		36 HEINTZ	92 CSB2	$\Upsilon(3S) \rightarrow \gamma \gamma \ell^+ \ell^-$
34 From a sample of $\Upsilon(3S) \rightarrow \gamma \gamma \mu^+ \mu^-$ with one converted photon.				
35 CRAWFORD 92b quotes $2 \times B(\Upsilon(3S) \rightarrow \gamma \chi_{bJ}(2P)) B(\chi_{bJ}(2P) \rightarrow \gamma \Upsilon(nS))$				
$B(\Upsilon(nS) \rightarrow \ell^+ \ell^-)$ .				
36 Calculated by us. HEINTZ 92 quotes $B(\Upsilon(3S) \rightarrow \gamma \chi_{b1}(2P)) \times B(\chi_{b1}(2P) \rightarrow \gamma \Upsilon(1S)) = (0.91 \pm 0.11 \pm 0.06)\%$ using $B(\Upsilon(1S) \rightarrow \mu^+ \mu^-) = (2.57 \pm 0.05)\%$ .				

WEIGHTED AVERAGE  
2.9±0.4 (Error scaled by 1.9)



$B(\chi_{b1}(2P) \rightarrow \gamma \Upsilon(1S)) \times B(\Upsilon(3S) \rightarrow \gamma \chi_{b1}(2P)) \times B(\Upsilon(1S) \rightarrow \ell^+\ell^-)$   
(units  $10^{-4}$ )

$\Gamma(\chi_{b1}(2P) \rightarrow \gamma \Upsilon(2S))/\Gamma_{total} \times \Gamma(\Upsilon(3S) \rightarrow \gamma \chi_{b1}(2P))/\Gamma_{total}$   
 $\Gamma_2/\Gamma \times \Gamma_{21}^{(3S)}/\Gamma \Upsilon(3S)$

VALUE (units $10^{-2}$ )	EVTs	DOCUMENT ID	TECN	COMMENT
<b><math>2.4 \pm 0.1 \pm 0.2</math></b>	4.3k	LEES	11J BABR	$\Upsilon(3S) \rightarrow X \gamma$

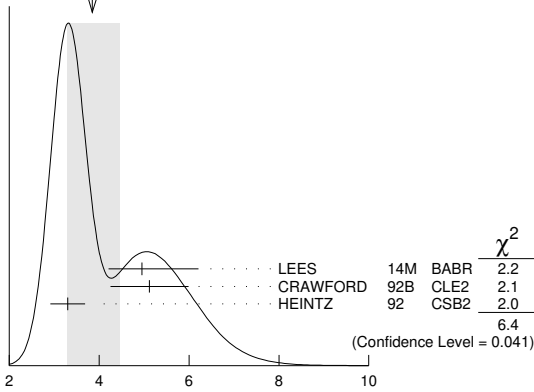
$B(\chi_{b1}(2P) \rightarrow \gamma \Upsilon(2S)) \times B(\Upsilon(3S) \rightarrow \gamma \chi_{b1}(2P)) \times B(\Upsilon(2S) \rightarrow \ell^+\ell^-)$

VALUE (units $10^{-4}$ )	EVTs	DOCUMENT ID	TECN	COMMENT
<b><math>3.8 \pm 0.6</math> OUR AVERAGE</b>				Error includes scale factor of 1.8. See the ideogram below.
$4.95_{-0.70}^{+0.75+1.01}$		37 LEES	14M BABR	$\Upsilon(3S) \rightarrow \gamma \gamma \mu^+ \mu^-$
$5.12 \pm 0.60 \pm 0.63$	111	38 CRAWFORD	92B CLE2	$\Upsilon(3S) \rightarrow \gamma \gamma \ell^+ \ell^-$
$3.30 \pm 0.33 \pm 0.20$		39 HEINTZ	92 CSB2	$\Upsilon(3S) \rightarrow \gamma \gamma \ell^+ \ell^-$
37 From a sample of $\Upsilon(3S) \rightarrow \gamma \gamma \mu^+ \mu^-$ with one converted photon.				
38 CRAWFORD 92b quotes $2 \times B(\Upsilon(3S) \rightarrow \gamma \chi_{bJ}(2P)) B(\chi_{bJ}(2P) \rightarrow \gamma \Upsilon(nS))$				
$B(\Upsilon(nS) \rightarrow \ell^+ \ell^-)$ .				
39 Calculated by us. HEINTZ 92 quotes $B(\Upsilon(3S) \rightarrow \gamma \chi_{b1}(2P)) \times B(\chi_{b1}(2P) \rightarrow \gamma \Upsilon(2S)) = (2.29 \pm 0.23 \pm 0.21)\%$ using $B(\Upsilon(2S) \rightarrow \mu^+ \mu^-) = (1.44 \pm 0.10)\%$ .				

# Meson Particle Listings

## $\chi_{b1}(2P), h_b(2P), \chi_{b2}(2P)$

WEIGHTED AVERAGE  
3.8±0.6 (Error scaled by 1.8)



$$B(\chi_{b1}(2P) \rightarrow \gamma \Upsilon(2S)) \times B(\Upsilon(3S) \rightarrow \gamma \chi_{b1}(2P)) \times B(\Upsilon(2S) \rightarrow \ell^+ \ell^-)$$

(units  $10^{-4}$ )

VALUE (units $10^{-3}$ )	EVTS	DOCUMENT ID	TECN	COMMENT
<b>1.16 ± 0.07 ± 0.12</b>	31k	LEES	11c	BABR $e^+e^- \rightarrow \pi^+\pi^-X$

VALUE	DOCUMENT ID	TECN	COMMENT
<b>1.109 ± 0.007 ± 0.040</b>	BRIERE 07	CLEO	$\Upsilon(3S) \rightarrow \gamma \chi_{b1}(2P)$

VALUE	DOCUMENT ID	TECN	COMMENT
<b>1.082 ± 0.025 ± 0.060</b>	BRIERE 07	CLEO	$\Upsilon(3S) \rightarrow \gamma \chi_{b1}(2P)$

### $\chi_{b1}(2P)$ REFERENCES

LEES 14M	PR D90 112010	J.P. Lees <i>et al.</i>	(BABAR Collab.)
LEES 11C	PR D84 011104	J.P. Lees <i>et al.</i>	(BABAR Collab.)
LEES 11J	PR D84 072002	J.P. Lees <i>et al.</i>	(BABAR Collab.)
ASNER 08A	PR D78 091103	D.M. Asner <i>et al.</i>	(CLEO Collab.)
BRIERE 08	PR D78 092007	R.A. Briere <i>et al.</i>	(CLEO Collab.)
BRIERE 07	PR D76 012005	R.A. Briere <i>et al.</i>	(CLEO Collab.)
CRAWFIELD 06	PR D73 012003	C. Crawford <i>et al.</i>	(CLEO Collab.)
ARTUSO 05	PRL 94 032001	M. Artuso <i>et al.</i>	(CLEO Collab.)
CRONIN-HEN. 04	PRL 92 222002	D. Cronin-Hennessy <i>et al.</i>	(CLEO Collab.)
CRAWFORD 92B	PL B294 139	G. Crawford <i>et al.</i>	(CLEO Collab.)
HEINTZ 92	PR D46 1928	U. Heintz <i>et al.</i>	(CUSB II Collab.)
HEINTZ 91	PRL 66 1563	U. Heintz <i>et al.</i>	(CUSB Collab.)
MORRISON 91	PRL 67 1696	R.J. Morrison <i>et al.</i>	(CLEO Collab.)
NARAIN 91	PRL 66 3113	M. Narain <i>et al.</i>	(CUSB Collab.)

## $h_b(2P)$

$$J^G(J^{PC}) = 0^-(1^{+-})$$

OMITTED FROM SUMMARY TABLE

Quantum numbers are quark model predictions.

### $h_b(2P)$ MASS

VALUE (MeV)	EVTS	DOCUMENT ID	TECN	COMMENT
<b>10259.8 ± 0.5 ± 1.1</b>	90k	MIZUK	12	BELL $e^+e^- \rightarrow \pi^+\pi^-$ hadrons

••• We do not use the following data for averages, fits, limits, etc. •••

10259.8 ± 0.6 <sup>+1.4</sup> <sub>-1.0</sub>	83.9k	<sup>1</sup> ADACHI	12	BELL 10.86 $e^+e^- \rightarrow \pi^+\pi^-$ MM
---	-------	---------------------	----	---

<sup>1</sup> Superseded by MIZUK 12.

### $h_b(2P)$ DECAY MODES

Mode	Fraction ( $\Gamma_i/\Gamma$ )
$\Gamma_1$ hadrons	not seen
$\Gamma_2$ $\eta_b(1S)\gamma$	(22 ± 5) %
$\Gamma_3$ $\eta_b(2S)\gamma$	(48 ± 13) %

### $h_b(2P)$ BRANCHING RATIOS

$\Gamma(\text{hadrons})/\Gamma_{\text{total}}$	$\Gamma_1/\Gamma$
not seen	83.9k

$\Gamma(\eta_b(1S)\gamma)/\Gamma_{\text{total}}$	$\Gamma_2/\Gamma$
<b>22.3 ± 3.8 ± 3.1</b>	10k

$\Gamma(\eta_b(2S)\gamma)/\Gamma_{\text{total}}$	$\Gamma_3/\Gamma$
<b>47.5 ± 10.5 ± 6.8</b> -7.7	26k

### $h_b(2P)$ REFERENCES

ADACHI 12	PRL 108 032001	I. Adachi <i>et al.</i>	(BELLE Collab.)
MIZUK 12	PRL 109 232002	R. Mizuk <i>et al.</i>	(BELLE Collab.)

## $\chi_{b2}(2P)$

$$J^G(J^{PC}) = 0^+(2^{++})$$

J needs confirmation.

Observed in radiative decay of the  $\Upsilon(3S)$ , therefore  $C = +$ . Branching ratio requires E1 transition, M1 is strongly disfavored, therefore  $P = +$ .

### $\chi_{b2}(2P)$ MASS

VALUE (MeV)	DOCUMENT ID
<b>10268.65 ± 0.22 ± 0.50</b> OUR EVALUATION	From $\gamma$ energy below, using $\Upsilon(3S)$ mass = 10355.2 ± 0.5 MeV

### $m_{\chi_{b2}(2P)} - m_{\chi_{b1}(2P)}$

VALUE (MeV)	DOCUMENT ID	TECN	COMMENT
<b>13.10 ± 0.24</b> OUR AVERAGE			
12.3 ± 2.6 ± 0.6	<sup>1</sup> AAIJ	14B6	LHCB $pp \rightarrow \gamma \mu^+ \mu^- X$
13.04 ± 0.26	LEES	14M	BABR $\Upsilon(3S) \rightarrow \gamma \mu^+ \mu^-$
13.5 ± 0.4 ± 0.5	<sup>2</sup> HEINTZ	92	CSB2 $e^+e^- \rightarrow \gamma X, \ell^+ \ell^- \gamma \gamma$

<sup>1</sup> From the  $\chi_{b1}(2P) \rightarrow \Upsilon(1S)\gamma$  transition.

<sup>2</sup> From the average photon energy for inclusive and exclusive events. Supersedes NARAIN 91.

### $\gamma$ ENERGY IN $\Upsilon(3S)$ DECAY

VALUE (MeV)	EVTS	DOCUMENT ID	TECN	COMMENT
<b>86.19 ± 0.22</b> OUR EVALUATION				Treating systematic errors as correlated
<b>86.40 ± 0.18</b> OUR AVERAGE				
86.04 ± 0.06 ± 0.27		ARTUSO 05	CLEO	$\Upsilon(3S) \rightarrow \gamma X$
86 ± 1	101	CRAWFORD 92B	CLE2	$e^+e^- \rightarrow \ell^+ \ell^- \gamma \gamma$
86.7 ± 0.4	10319	<sup>3</sup> HEINTZ 92	CSB2	$e^+e^- \rightarrow \gamma X$
86.9 ± 0.4	157	<sup>4</sup> HEINTZ 92	CSB2	$e^+e^- \rightarrow \ell^+ \ell^- \gamma \gamma$
86.4 ± 0.1 ± 0.4	30741	MORRISON 91	CLE2	$e^+e^- \rightarrow \gamma X$

<sup>3</sup> A systematic uncertainty on the energy scale of 0.9% not included. Supersedes NARAIN 91.

<sup>4</sup> A systematic uncertainty on the energy scale of 0.9% not included. Supersedes HEINTZ 91.

### $\chi_{b2}(2P)$ DECAY MODES

Mode	Fraction ( $\Gamma_i/\Gamma$ )	Confidence level
$\Gamma_1$ $\omega \Upsilon(1S)$	(1.10 <sup>+0.34</sup> <sub>-0.30</sub> ) %	
$\Gamma_2$ $\gamma \Upsilon(2S)$	(8.9 ± 1.2) %	
$\Gamma_3$ $\gamma \Upsilon(1S)$	(6.6 ± 0.8) %	
$\Gamma_4$ $\pi\pi\chi_{b2}(1P)$	(5.1 ± 0.9) × 10 <sup>-3</sup>	
$\Gamma_5$ $D^0 X$	< 2.4 %	90%
$\Gamma_6$ $\pi^+\pi^-K^+K^-\pi^0$	< 1.1 × 10 <sup>-4</sup>	90%
$\Gamma_7$ $2\pi^+\pi^-K^-K_S^0$	< 9 × 10 <sup>-5</sup>	90%
$\Gamma_8$ $2\pi^+\pi^-K^-K_S^0 2\pi^0$	< 7 × 10 <sup>-4</sup>	90%
$\Gamma_9$ $2\pi^+2\pi^-2\pi^0$	(3.9 ± 1.6) × 10 <sup>-4</sup>	
$\Gamma_{10}$ $2\pi^+2\pi^-K^+K^-$	(9 ± 4) × 10 <sup>-5</sup>	
$\Gamma_{11}$ $2\pi^+2\pi^-K^+K^-\pi^0$	(2.4 ± 1.1) × 10 <sup>-4</sup>	
$\Gamma_{12}$ $2\pi^+2\pi^-K^+K^-2\pi^0$	(4.7 ± 2.3) × 10 <sup>-4</sup>	
$\Gamma_{13}$ $3\pi^+2\pi^-K^-K_S^0\pi^0$	< 4 × 10 <sup>-4</sup>	90%
$\Gamma_{14}$ $3\pi^+3\pi^-$	(9 ± 4) × 10 <sup>-5</sup>	
$\Gamma_{15}$ $3\pi^+3\pi^-2\pi^0$	(1.2 ± 0.4) × 10 <sup>-3</sup>	
$\Gamma_{16}$ $3\pi^+3\pi^-K^+K^-$	(1.4 ± 0.7) × 10 <sup>-4</sup>	
$\Gamma_{17}$ $3\pi^+3\pi^-K^+K^-\pi^0$	(4.2 ± 1.7) × 10 <sup>-4</sup>	
$\Gamma_{18}$ $4\pi^+4\pi^-$	(9 ± 5) × 10 <sup>-5</sup>	
$\Gamma_{19}$ $4\pi^+4\pi^-2\pi^0$	(1.3 ± 0.5) × 10 <sup>-3</sup>	

### $\chi_{b2}(2P)$ BRANCHING RATIOS

$\Gamma(\omega \Upsilon(1S))/\Gamma_{\text{total}}$	$\Gamma_1/\Gamma$
<b>1.10 ± 0.32 ± 0.11</b> -0.28 - 0.10	20.1 <sup>+5.8</sup> <sub>-5.1</sub> <sup>5</sup> CRONIN-HEN..04

<sup>5</sup> Using  $B(\Upsilon(3S) \rightarrow \gamma \chi_{b2}(2P)) = (11.4 ± 0.8)\%$  and  $B(\Upsilon(1S) \rightarrow \ell^+ \ell^-) = 2$   
 $B(\Upsilon(1S) \rightarrow \mu^+ \mu^-) = 2(2.48 ± 0.06)\%$ .

See key on page 999

## Meson Particle Listings

 $\chi_{b2}(2P)$  $\Gamma(\gamma T(2S))/\Gamma_{total}$   $\Gamma_2/\Gamma$ 

VALUE	EVTS	DOCUMENT ID	TECN	COMMENT
<b>0.089±0.012 OUR AVERAGE</b>				
0.085±0.010±0.010	6,7,8	LEES	14M	BABR $T(3S) \rightarrow \gamma\gamma\mu^+\mu^-$
0.084±0.011±0.010	2.5k	9 LEES	11J	BABR $T(3S) \rightarrow X\gamma$
0.096±0.022±0.012	7,10	CRAWFORD	92B	CLE2 $e^+e^- \rightarrow \ell^+\ell^-\gamma\gamma$
0.106±0.016±0.013	7,11	HEINTZ	92	CSB2 $e^+e^- \rightarrow \ell^+\ell^-\gamma\gamma$

<sup>6</sup> LEES 14M quotes  $\Gamma(\chi_{b2}(2P) \rightarrow \gamma T(2S))/\Gamma_{total} \times \Gamma(T(3S) \rightarrow \gamma\gamma\mu^+\mu^-)/\Gamma_{total} = (1.12 \pm 0.13)\%$  combining the results from samples of  $T(3S) \rightarrow \gamma\gamma\mu^+\mu^-$  with and without converted photons.

<sup>7</sup> Assuming  $B(T(2S) \rightarrow \mu^+\mu^-) = (1.93 \pm 0.17)\%$ .

<sup>8</sup> LEES 14M reports  $[\Gamma(\chi_{b2}(2P) \rightarrow \gamma T(2S))/\Gamma_{total}] \times [B(T(3S) \rightarrow \gamma\chi_{b2}(2P))] = (1.12 \pm 0.13) \times 10^{-2}$  which we divide by our best value  $B(T(3S) \rightarrow \gamma\chi_{b2}(2P)) = (13.1 \pm 1.6) \times 10^{-2}$ . Our first error is their experiment's error and our second error is the systematic error from using our best value.

<sup>9</sup> LEES 11J reports  $[\Gamma(\chi_{b2}(2P) \rightarrow \gamma T(2S))/\Gamma_{total}] \times [B(T(3S) \rightarrow \gamma\chi_{b2}(2P))] = (1.1 \pm 0.1 \pm 0.1) \times 10^{-2}$  which we divide by our best value  $B(T(3S) \rightarrow \gamma\chi_{b2}(2P)) = (13.1 \pm 1.6) \times 10^{-2}$ . Our first error is their experiment's error and our second error is the systematic error from using our best value.

<sup>10</sup> CRAWFORD 92B quotes  $B(T(3S) \rightarrow \gamma\chi_{b1}(2P)) \times B(\chi_{b2}(2P) \rightarrow \gamma T(2S)) \times 2 B(T(2S) \rightarrow \ell^+\ell^-) = (4.98 \pm 0.94 \pm 0.62) 10^{-4}$ .

<sup>11</sup> Recalculated by us. HEINTZ 92 quotes  $B(T(3S) \rightarrow \gamma\chi_{b2}(2P)) \times B(\chi_{b2}(2P) \rightarrow \gamma T(2S)) = (1.90 \pm 0.23 \pm 0.18) \%$  using  $B(T(2S) \rightarrow \mu^+\mu^-) = (1.44 \pm 0.10)\%$ . Supersedes HEINTZ 91.

 $\Gamma(\gamma T(1S))/\Gamma_{total}$   $\Gamma_3/\Gamma$ 

VALUE	EVTS	DOCUMENT ID	TECN	COMMENT
<b>0.066±0.008 OUR AVERAGE</b>				
0.061±0.004±0.007	12,13,14	LEES	14M	BABR $T(3S) \rightarrow \gamma\gamma\mu^+\mu^-$
0.070±0.004±0.008	11k	15 LEES	11J	BABR $T(3S) \rightarrow X\gamma$
0.077±0.018±0.009	13,16	CRAWFORD	92B	CLE2 $e^+e^- \rightarrow \ell^+\ell^-\gamma\gamma$
0.061±0.009±0.007	13,17	HEINTZ	92	CSB2 $e^+e^- \rightarrow \ell^+\ell^-\gamma\gamma$

<sup>12</sup> LEES 14M quotes  $\Gamma(\chi_{b2}(2P) \rightarrow \gamma T(1S))/\Gamma_{total} \times \Gamma(T(3S) \rightarrow \gamma\gamma\mu^+\mu^-)/\Gamma_{total} = (8.03 \pm 0.50) \times 10^{-3}$  combining the results from samples of  $T(3S) \rightarrow \gamma\gamma\mu^+\mu^-$  with and without converted photons.

<sup>13</sup> Assuming  $B(T(1S) \rightarrow \mu^+\mu^-) = (2.48 \pm 0.05)\%$ .

<sup>14</sup> LEES 14M reports  $[\Gamma(\chi_{b2}(2P) \rightarrow \gamma T(1S))/\Gamma_{total}] \times [B(T(3S) \rightarrow \gamma\chi_{b2}(2P))] = (8.03 \pm 0.50) \times 10^{-3}$  which we divide by our best value  $B(T(3S) \rightarrow \gamma\chi_{b2}(2P)) = (13.1 \pm 1.6) \times 10^{-2}$ . Our first error is their experiment's error and our second error is the systematic error from using our best value.

<sup>15</sup> LEES 11J reports  $[\Gamma(\chi_{b2}(2P) \rightarrow \gamma T(1S))/\Gamma_{total}] \times [B(T(3S) \rightarrow \gamma\chi_{b2}(2P))] = (9.2 \pm 0.3 \pm 0.4) \times 10^{-3}$  which we divide by our best value  $B(T(3S) \rightarrow \gamma\chi_{b2}(2P)) = (13.1 \pm 1.6) \times 10^{-2}$ . Our first error is their experiment's error and our second error is the systematic error from using our best value.

<sup>16</sup> CRAWFORD 92B quotes  $B(T(3S) \rightarrow \gamma\chi_{b2}(2P)) \times B(\chi_{b2}(2P) \rightarrow \gamma T(1S)) \times 2 B(T(1S) \rightarrow \ell^+\ell^-) = (5.03 \pm 0.94 \pm 0.63) 10^{-4}$ .

<sup>17</sup> Recalculated by us. HEINTZ 92 quotes  $B(T(3S) \rightarrow \gamma\chi_{b2}(2P)) \times B(\chi_{b2}(2P) \rightarrow \gamma T(1S)) = (0.77 \pm 0.11 \pm 0.05)\%$  using  $B(T(1S) \rightarrow \mu^+\mu^-) = (2.57 \pm 0.05)\%$ . Supersedes HEINTZ 91.

 $\Gamma(\pi\pi\chi_{b2}(1P))/\Gamma_{total}$   $\Gamma_4/\Gamma$ 

VALUE (units $10^{-3}$ )	EVTS	DOCUMENT ID	TECN	COMMENT
<b>5.1±0.9 OUR AVERAGE</b>				
4.9±0.7±0.6	17k	18 LEES	11C	BABR $e^+e^- \rightarrow \pi^+\pi^-X$
6.0±1.6±1.4		19 CAWFIELD	06	CLE3 $T(3S) \rightarrow 2(\gamma\pi\ell)$

<sup>18</sup>  $(0.64 \pm 0.05 \pm 0.08) \times 10^{-3}$ . We derive the value assuming  $B(T(3S) \rightarrow \chi_{b2}(2P)X) = B(T(3S) \rightarrow \chi_{b2}(2P)\gamma) = (13.1 \pm 1.6) \times 10^{-2}$ .

<sup>19</sup> CAWFIELD 06 quote  $\Gamma(\chi_b(2P) \rightarrow \pi\pi\chi_{b1}(1P)) = 0.83 \pm 0.22 \pm 0.08 \pm 0.19$  keV assuming l-spin conservation, no D-wave contribution,  $\Gamma(\chi_{b1}(2P)) = 96 \pm 16$  keV, and  $\Gamma(\chi_{b2}(2P)) = 138 \pm 19$  keV.

 $\Gamma(D^0 X)/\Gamma_{total}$   $\Gamma_5/\Gamma$ 

VALUE	CL%	DOCUMENT ID	TECN	COMMENT
<b>&lt;2.4 × 10<sup>-2</sup></b>	90	20,21 BRIERE	08	CLEO $T(3S) \rightarrow \gamma D^0 X$

<sup>20</sup> For  $p_{D^0} > 2.5$  GeV/c.

<sup>21</sup> The authors also present their result as  $(0.2 \pm 1.4 \pm 0.1) \times 10^{-2}$ .

 $\Gamma(\pi^+\pi^-K^+K^-\pi^0)/\Gamma_{total}$   $\Gamma_6/\Gamma$ 

VALUE (units $10^{-4}$ )	CL%	DOCUMENT ID	TECN	COMMENT
<b>&lt;1.1</b>	90	22 ASNER	08A	CLEO $T(3S) \rightarrow \gamma\pi^+\pi^-K^+K^-\pi^0$

<sup>22</sup> ASNER 08A reports  $[\Gamma(\chi_{b2}(2P) \rightarrow \pi^+\pi^-K^+K^-\pi^0)/\Gamma_{total}] \times [B(T(3S) \rightarrow \gamma\chi_{b2}(2P))] < 14 \times 10^{-6}$  which we divide by our best value  $B(T(3S) \rightarrow \gamma\chi_{b2}(2P)) = 13.1 \times 10^{-2}$ .

 $\Gamma(2\pi^+\pi^-K^-K_S^0)/\Gamma_{total}$   $\Gamma_7/\Gamma$ 

VALUE (units $10^{-4}$ )	CL%	DOCUMENT ID	TECN	COMMENT
<b>&lt;0.9</b>	90	23 ASNER	08A	CLEO $T(3S) \rightarrow \gamma 2\pi^+\pi^-K^-K_S^0$

<sup>23</sup> ASNER 08A reports  $[\Gamma(\chi_{b2}(2P) \rightarrow 2\pi^+\pi^-K^-K_S^0)/\Gamma_{total}] \times [B(T(3S) \rightarrow \gamma\chi_{b2}(2P))] < 12 \times 10^{-6}$  which we divide by our best value  $B(T(3S) \rightarrow \gamma\chi_{b2}(2P)) = 13.1 \times 10^{-2}$ .

 $\Gamma(2\pi^+\pi^-K^-K_S^0 2\pi^0)/\Gamma_{total}$   $\Gamma_8/\Gamma$ 

VALUE (units $10^{-4}$ )	CL%	DOCUMENT ID	TECN	COMMENT
<b>&lt;7</b>	90	24 ASNER	08A	CLEO $T(3S) \rightarrow \gamma 2\pi^+\pi^-K^-K_S^0 2\pi^0$

<sup>24</sup> ASNER 08A reports  $[\Gamma(\chi_{b2}(2P) \rightarrow 2\pi^+\pi^-K^-K_S^0 2\pi^0)/\Gamma_{total}] \times [B(T(3S) \rightarrow \gamma\chi_{b2}(2P))] < 87 \times 10^{-6}$  which we divide by our best value  $B(T(3S) \rightarrow \gamma\chi_{b2}(2P)) = 13.1 \times 10^{-2}$ .

 $\Gamma(2\pi^+2\pi^-2\pi^0)/\Gamma_{total}$   $\Gamma_9/\Gamma$ 

VALUE (units $10^{-4}$ )	EVTS	DOCUMENT ID	TECN	COMMENT
<b>3.9±1.6±0.5</b>	23	25 ASNER	08A	CLEO $T(3S) \rightarrow \gamma 2\pi^+2\pi^-2\pi^0$

<sup>25</sup> ASNER 08A reports  $[\Gamma(\chi_{b2}(2P) \rightarrow 2\pi^+2\pi^-2\pi^0)/\Gamma_{total}] \times [B(T(3S) \rightarrow \gamma\chi_{b2}(2P))] = (51 \pm 16 \pm 13) \times 10^{-6}$  which we divide by our best value  $B(T(3S) \rightarrow \gamma\chi_{b2}(2P)) = (13.1 \pm 1.6) \times 10^{-2}$ . Our first error is their experiment's error and our second error is the systematic error from using our best value.

 $\Gamma(2\pi^+2\pi^-K^+K^-)/\Gamma_{total}$   $\Gamma_{10}/\Gamma$ 

VALUE (units $10^{-4}$ )	EVTS	DOCUMENT ID	TECN	COMMENT
<b>0.9±0.4±0.1</b>	11	26 ASNER	08A	CLEO $T(3S) \rightarrow \gamma 2\pi^+2\pi^-K^+K^-$

<sup>26</sup> ASNER 08A reports  $[\Gamma(\chi_{b2}(2P) \rightarrow 2\pi^+2\pi^-K^+K^-)/\Gamma_{total}] \times [B(T(3S) \rightarrow \gamma\chi_{b2}(2P))] = (12 \pm 4 \pm 3) \times 10^{-6}$  which we divide by our best value  $B(T(3S) \rightarrow \gamma\chi_{b2}(2P)) = (13.1 \pm 1.6) \times 10^{-2}$ . Our first error is their experiment's error and our second error is the systematic error from using our best value.

 $\Gamma(2\pi^+2\pi^-K^+K^-\pi^0)/\Gamma_{total}$   $\Gamma_{11}/\Gamma$ 

VALUE (units $10^{-4}$ )	EVTS	DOCUMENT ID	TECN	COMMENT
<b>2.4±1.0±0.3</b>	16	27 ASNER	08A	CLEO $T(3S) \rightarrow \gamma 2\pi^+2\pi^-K^+K^-\pi^0$

<sup>27</sup> ASNER 08A reports  $[\Gamma(\chi_{b2}(2P) \rightarrow 2\pi^+2\pi^-K^+K^-\pi^0)/\Gamma_{total}] \times [B(T(3S) \rightarrow \gamma\chi_{b2}(2P))] = (32 \pm 11 \pm 8) \times 10^{-6}$  which we divide by our best value  $B(T(3S) \rightarrow \gamma\chi_{b2}(2P)) = (13.1 \pm 1.6) \times 10^{-2}$ . Our first error is their experiment's error and our second error is the systematic error from using our best value.

 $\Gamma(2\pi^+2\pi^-K^+K^-2\pi^0)/\Gamma_{total}$   $\Gamma_{12}/\Gamma$ 

VALUE (units $10^{-4}$ )	EVTS	DOCUMENT ID	TECN	COMMENT
<b>4.7±2.2±0.6</b>	14	28 ASNER	08A	CLEO $T(3S) \rightarrow \gamma 2\pi^+2\pi^-K^+K^-2\pi^0$

<sup>28</sup> ASNER 08A reports  $[\Gamma(\chi_{b2}(2P) \rightarrow 2\pi^+2\pi^-K^+K^-2\pi^0)/\Gamma_{total}] \times [B(T(3S) \rightarrow \gamma\chi_{b2}(2P))] = (62 \pm 23 \pm 17) \times 10^{-6}$  which we divide by our best value  $B(T(3S) \rightarrow \gamma\chi_{b2}(2P)) = (13.1 \pm 1.6) \times 10^{-2}$ . Our first error is their experiment's error and our second error is the systematic error from using our best value.

 $\Gamma(3\pi^+2\pi^-K^-K_S^0\pi^0)/\Gamma_{total}$   $\Gamma_{13}/\Gamma$ 

VALUE (units $10^{-4}$ )	CL%	DOCUMENT ID	TECN	COMMENT
<b>&lt;4</b>	90	29 ASNER	08A	CLEO $T(3S) \rightarrow \gamma 3\pi^+2\pi^-K^-K_S^0\pi^0$

<sup>29</sup> ASNER 08A reports  $[\Gamma(\chi_{b2}(2P) \rightarrow 3\pi^+2\pi^-K^-K_S^0\pi^0)/\Gamma_{total}] \times [B(T(3S) \rightarrow \gamma\chi_{b2}(2P))] < 58 \times 10^{-6}$  which we divide by our best value  $B(T(3S) \rightarrow \gamma\chi_{b2}(2P)) = 13.1 \times 10^{-2}$ .

 $\Gamma(3\pi^+3\pi^-)/\Gamma_{total}$   $\Gamma_{14}/\Gamma$ 

VALUE (units $10^{-4}$ )	EVTS	DOCUMENT ID	TECN	COMMENT
<b>0.9±0.4±0.1</b>	14	30 ASNER	08A	CLEO $T(3S) \rightarrow \gamma 3\pi^+3\pi^-$

<sup>30</sup> ASNER 08A reports  $[\Gamma(\chi_{b2}(2P) \rightarrow 3\pi^+3\pi^-)/\Gamma_{total}] \times [B(T(3S) \rightarrow \gamma\chi_{b2}(2P))] = (12 \pm 4 \pm 3) \times 10^{-6}$  which we divide by our best value  $B(T(3S) \rightarrow \gamma\chi_{b2}(2P)) = (13.1 \pm 1.6) \times 10^{-2}$ . Our first error is their experiment's error and our second error is the systematic error from using our best value.

 $\Gamma(3\pi^+3\pi^-2\pi^0)/\Gamma_{total}$   $\Gamma_{15}/\Gamma$ 

VALUE (units $10^{-4}$ )	EVTS	DOCUMENT ID	TECN	COMMENT
<b>12±4±1</b>	45	31 ASNER	08A	CLEO $T(3S) \rightarrow \gamma 3\pi^+3\pi^-2\pi^0$

<sup>31</sup> ASNER 08A reports  $[\Gamma(\chi_{b2}(2P) \rightarrow 3\pi^+3\pi^-2\pi^0)/\Gamma_{total}] \times [B(T(3S) \rightarrow \gamma\chi_{b2}(2P))] = (159 \pm 33 \pm 43) \times 10^{-6}$  which we divide by our best value  $B(T(3S) \rightarrow \gamma\chi_{b2}(2P)) = (13.1 \pm 1.6) \times 10^{-2}$ . Our first error is their experiment's error and our second error is the systematic error from using our best value.

 $\Gamma(3\pi^+3\pi^-K^+K^-)/\Gamma_{total}$   $\Gamma_{16}/\Gamma$ 

VALUE (units $10^{-4}$ )	EVTS	DOCUMENT ID	TECN	COMMENT
<b>1.4±0.7±0.2</b>	12	32 ASNER	08A	CLEO $T(3S) \rightarrow \gamma 3\pi^+3\pi^-K^+K^-$

<sup>32</sup> ASNER 08A reports  $[\Gamma(\chi_{b2}(2P) \rightarrow 3\pi^+3\pi^-K^+K^-)/\Gamma_{total}] \times [B(T(3S) \rightarrow \gamma\chi_{b2}(2P))] = (19 \pm 7 \pm 5) \times 10^{-6}$  which we divide by our best value  $B(T(3S) \rightarrow \gamma\chi_{b2}(2P)) = (13.1 \pm 1.6) \times 10^{-2}$ . Our first error is their experiment's error and our second error is the systematic error from using our best value.

 $\Gamma(3\pi^+3\pi^-K^+K^-\pi^0)/\Gamma_{total}$   $\Gamma_{17}/\Gamma$ 

VALUE (units $10^{-4}$ )	EVTS	DOCUMENT ID	TECN	COMMENT
<b>4.2±1.7±0.5</b>	16	33 ASNER	08A	CLEO $T(3S) \rightarrow \gamma 3\pi^+3\pi^-K^+K^-\pi^0$

<sup>33</sup> ASNER 08A reports  $[\Gamma(\chi_{b2}(2P) \rightarrow 3\pi^+3\pi^-K^+K^-\pi^0)/\Gamma_{total}] \times [B(T(3S) \rightarrow \gamma\chi_{b2}(2P))] = (55 \pm 16 \pm 15) \times 10^{-6}$  which we divide by our best value  $B(T(3S) \rightarrow \gamma\chi_{b2}(2P)) = (13.1 \pm 1.6) \times 10^{-2}$ . Our first error is their experiment's error and our second error is the systematic error from using our best value.

# Meson Particle Listings

## $\chi_{b2}(2P), \Upsilon(3S)$

$\Gamma(4\pi^+4\pi^-)/\Gamma_{\text{total}}$				$\Gamma_{18}/\Gamma$
VALUE (units $10^{-4}$ )	EVTS	DOCUMENT ID	TECN	COMMENT

**0.9 ± 0.4 ± 0.1** 9 <sup>34</sup> ASNER 08A CLEO  $\Upsilon(3S) \rightarrow \gamma 4\pi^+ 4\pi^-$   
<sup>34</sup> ASNER 08A reports  $[\Gamma(\chi_{b2}(2P) \rightarrow 4\pi^+ 4\pi^-)/\Gamma_{\text{total}}] \times [B(\Upsilon(3S) \rightarrow \gamma \chi_{b2}(2P))]$   
 $= (12 \pm 5 \pm 3) \times 10^{-6}$  which we divide by our best value  $B(\Upsilon(3S) \rightarrow \gamma \chi_{b2}(2P)) =$   
 $(13.1 \pm 1.6) \times 10^{-2}$ . Our first error is their experiment's error and our second error is  
the systematic error from using our best value.

$\Gamma(4\pi^+4\pi^-2\pi^0)/\Gamma_{\text{total}}$				$\Gamma_{19}/\Gamma$
VALUE (units $10^{-4}$ )	EVTS	DOCUMENT ID	TECN	COMMENT

**13 ± 5 ± 2** 27 <sup>35</sup> ASNER 08A CLEO  $\Upsilon(3S) \rightarrow \gamma 4\pi^+ 4\pi^- 2\pi^0$   
<sup>35</sup> ASNER 08A reports  $[\Gamma(\chi_{b2}(2P) \rightarrow 4\pi^+ 4\pi^- 2\pi^0)/\Gamma_{\text{total}}] \times [B(\Upsilon(3S) \rightarrow \gamma \chi_{b2}(2P))]$   
 $= (165 \pm 46 \pm 50) \times 10^{-6}$  which we divide by our best value  $B(\Upsilon(3S) \rightarrow \gamma \chi_{b2}(2P)) =$   
 $(13.1 \pm 1.6) \times 10^{-2}$ . Our first error is their experiment's error and our second error is  
the systematic error from using our best value.

### $\chi_{b2}(2P)$ Cross-Particle Branching Ratios

$\Gamma(\chi_{b2}(2P) \rightarrow \gamma \Upsilon(1S))/\Gamma_{\text{total}} \times \Gamma(\Upsilon(3S) \rightarrow \gamma \chi_{b2}(2P))/\Gamma_{\text{total}}$				$\Gamma_3/\Gamma \times \Gamma_{20}^{\Upsilon(3S)}/\Gamma \Upsilon(3S)$
VALUE (units $10^{-3}$ )	EVTS	DOCUMENT ID	TECN	COMMENT

**9.2 ± 0.3 ± 0.4** 11k LEES 11J BABR  $\Upsilon(3S) \rightarrow X \gamma$

$\Gamma(\chi_{b2}(2P) \rightarrow \gamma \Upsilon(2S))/\Gamma_{\text{total}} \times \Gamma(\Upsilon(3S) \rightarrow \gamma \chi_{b2}(2P))/\Gamma_{\text{total}}$				$\Gamma_2/\Gamma \times \Gamma_{20}^{\Upsilon(3S)}/\Gamma \Upsilon(3S)$
VALUE (units $10^{-2}$ )	EVTS	DOCUMENT ID	TECN	COMMENT

**1.1 ± 0.1 ± 0.1** 2.5k LEES 11J BABR  $\Upsilon(3S) \rightarrow X \gamma$

$B(\chi_{b2}(2P) \rightarrow \chi_{b2}(1P)\pi^+\pi^-) \times B(\Upsilon(3S) \rightarrow \chi_{b2}(2P)X)$				
VALUE (units $10^{-3}$ )	EVTS	DOCUMENT ID	TECN	COMMENT

**0.6 ± 0.05 ± 0.08** 17k LEES 11c BABR  $e^+e^- \rightarrow \pi^+\pi^-X$

$B(\chi_{b2}(2P) \rightarrow \gamma \Upsilon(1S)) \times B(\Upsilon(3S) \rightarrow \gamma \chi_{b2}(2P)) \times B(\Upsilon(1S) \rightarrow \ell^+\ell^-)$				
VALUE (units $10^{-4}$ )	EVTS	DOCUMENT ID	TECN	COMMENT

**2.02 ± 0.18 OUR AVERAGE**  
1.95<sup>+0.22+0.10</sup><sub>-0.21-0.16</sub> <sup>36</sup> LEES 14M BABR  $\Upsilon(3S) \rightarrow \gamma \gamma \mu^+ \mu^-$   
2.52 ± 0.47 ± 0.32 48 <sup>37</sup> CRAWFORD 92B CLE2  $\Upsilon(3S) \rightarrow \gamma \gamma \ell^+ \ell^-$   
1.98 ± 0.28 ± 0.12 <sup>38</sup> HEINTZ 92 CSB2  $\Upsilon(3S) \rightarrow \gamma \gamma \ell^+ \ell^-$

<sup>36</sup> From a sample of  $\Upsilon(3S) \rightarrow \gamma \gamma \mu^+ \mu^-$  with converted photons.  
<sup>37</sup> CRAWFORD 92B quotes  $2 \times B(\Upsilon(3S) \rightarrow \gamma \chi_{bJ}(2P)) B(\chi_{bJ}(2P) \rightarrow \gamma \Upsilon(nS))$   
 $B(\Upsilon(nS) \rightarrow \ell^+ \ell^-)$ .  
<sup>38</sup> Calculated by us. HEINTZ 92 quotes  $B(\Upsilon(3S) \rightarrow \gamma \chi_{b2}(2P)) \times B(\chi_{b2}(2P) \rightarrow$   
 $\gamma \Upsilon(1S)) = (0.77 \pm 0.11 \pm 0.05)\%$  using  $B(\Upsilon(1S) \rightarrow \mu^+ \mu^-) = (2.57 \pm 0.05)\%$ .

$[B(\chi_{b2}(2P) \rightarrow \gamma \Upsilon(1S)) \times B(\Upsilon(3S) \rightarrow \gamma \chi_{b2}(2P))] / [B(\chi_{b1}(2P) \rightarrow \gamma \Upsilon(1S)) \times B(\Upsilon(3S) \rightarrow \gamma \chi_{b1}(2P))]$			
VALUE (%)	DOCUMENT ID	TECN	COMMENT

**66.6 ± 3.0** <sup>39</sup> LEES 14M BABR  $\Upsilon(3S) \rightarrow \gamma \gamma \mu^+ \mu^-$

<sup>39</sup> From a sample of  $\Upsilon(3S) \rightarrow \gamma \gamma \mu^+ \mu^-$  events without converted photons.

$B(\chi_{b2}(2P) \rightarrow \gamma \Upsilon(2S)) \times B(\Upsilon(3S) \rightarrow \gamma \chi_{b2}(2P)) \times B(\Upsilon(2S) \rightarrow \ell^+\ell^-)$				
VALUE (units $10^{-4}$ )	EVTS	DOCUMENT ID	TECN	COMMENT

**2.74 ± 0.29 OUR AVERAGE**  
3.22<sup>+0.58+0.16</sup><sub>-0.53-0.71</sub> 40 LEES 14M BABR  $\Upsilon(3S) \rightarrow \gamma \gamma \mu^+ \mu^-$   
2.49 ± 0.47 ± 0.31 53 <sup>41</sup> CRAWFORD 92B CLE2  $\Upsilon(3S) \rightarrow \gamma \gamma \ell^+ \ell^-$   
2.74 ± 0.33 ± 0.18 42 HEINTZ 92 CSB2  $\Upsilon(3S) \rightarrow \gamma \gamma \ell^+ \ell^-$

<sup>40</sup> From a sample of  $\Upsilon(3S) \rightarrow \gamma \gamma \mu^+ \mu^-$  with converted photons.  
<sup>41</sup> CRAWFORD 92B quotes  $2 \times B(\Upsilon(3S) \rightarrow \gamma \chi_{bJ}(2P)) B(\chi_{bJ}(2P) \rightarrow \gamma \Upsilon(nS))$   
 $B(\Upsilon(nS) \rightarrow \ell^+ \ell^-)$ .  
<sup>42</sup> Calculated by us. HEINTZ 92 quotes  $B(\Upsilon(3S) \rightarrow \gamma \chi_{b2}(2P)) \times B(\chi_{b2}(2P) \rightarrow$   
 $\gamma \Upsilon(2S)) = (1.90 \pm 0.23 \pm 0.18)\%$  using  $B(\Upsilon(2S) \rightarrow \mu^+ \mu^-) = (1.44 \pm 0.10)\%$ .

$[B(\chi_{b2}(2P) \rightarrow \gamma \Upsilon(2S)) \times B(\Upsilon(3S) \rightarrow \gamma \chi_{b2}(2P))] / [B(\chi_{b1}(2P) \rightarrow \gamma \Upsilon(2S)) \times B(\Upsilon(3S) \rightarrow \gamma \chi_{b1}(2P))]$			
VALUE (%)	DOCUMENT ID	TECN	COMMENT

**46.9 ± 2.0** <sup>43</sup> LEES 14M BABR  $\Upsilon(3S) \rightarrow \gamma \gamma \mu^+ \mu^-$

<sup>43</sup> From a sample of  $\Upsilon(3S) \rightarrow \gamma \gamma \mu^+ \mu^-$  without converted photons.

### $\chi_{b2}(2P)$ REFERENCES

AJLI	14BG	JHEP 1410 088	R. Ajai et al.	(LHCb Collab.)
LEES	14M	PR D90 112010	J.P. Lees et al.	(BABAR Collab.)
LEES	11C	PR D84 011104	J.P. Lees et al.	(BABAR Collab.)
LEES	11J	PR D84 072002	J.P. Lees et al.	(BABAR Collab.)
ASNER	08A	PR D78 091103	D.M. Asner et al.	(CLEO Collab.)
BRIERE	08	PR D78 092007	R.A. Briere et al.	(CLEO Collab.)
CRAWFIELD	06	PR D73 012003	C. Crawford et al.	(CLEO Collab.)
ARTUSO	05	PRL 94 032001	M. Artuso et al.	(CLEO Collab.)
CROMIN-HEN	04	PRL 92 222002	D. Cronin-Hennessy et al.	(CLEO Collab.)
CRAWFORD	92B	PL B294 139	G. Crawford et al.	(CLEO Collab.)
HEINTZ	92	PR D46 1928	U. Heintz et al.	(CUSB II Collab.)
HEINTZ	91	PRL 66 1563	U. Heintz et al.	(CUSB Collab.)
MORRISON	91	PRL 67 1696	R.J. Morrison et al.	(CLEO Collab.)
NARAIN	91	PRL 66 3113	M. Narain et al.	(CUSB Collab.)

## $\Upsilon(3S)$

$$J^{PC} = 0^-(1^{--})$$

### $\Upsilon(3S)$ MASS

VALUE (MeV)	DOCUMENT ID	TECN	COMMENT
-------------	-------------	------	---------

**10355.2 ± 0.5** <sup>1</sup> ARTA MONOV 00 MD1  $e^+e^- \rightarrow$  hadrons  
• • • We do not use the following data for averages, fits, limits, etc. • • •  
10355.3 ± 0.5 <sup>2,3</sup> BARU 86B REDE  $e^+e^- \rightarrow$  hadrons

<sup>1</sup> Reanalysis of BARU 86B using new electron mass (COHEN 87).  
<sup>2</sup> Reanalysis of ARTAMONOV 84.  
<sup>3</sup> Superseded by ARTAMONOV 00.

### $m_{\Upsilon(3S)} - m_{\Upsilon(2S)}$

VALUE (MeV)	DOCUMENT ID	TECN	COMMENT
-------------	-------------	------	---------

**331.50 ± 0.02 ± 0.13** LEES 11c BABR  $e^+e^- \rightarrow \pi^+\pi^-X$

### $\Upsilon(3S)$ WIDTH

VALUE (keV)	DOCUMENT ID
-------------	-------------

**20.32 ± 1.85 OUR EVALUATION** See the Note on "Width Determinations of the  $\Upsilon$  States"

### $\Upsilon(3S)$ DECAY MODES

Mode	Fraction ( $\Gamma_i/\Gamma$ )	Scale factor/ Confidence level
$\Gamma_1$ $\Upsilon(2S)$ anything	(10.6 ± 0.8) %	
$\Gamma_2$ $\Upsilon(2S)\pi^+\pi^-$	(2.82 ± 0.18) %	S=1.6
$\Gamma_3$ $\Upsilon(2S)\pi^0\pi^0$	(1.85 ± 0.14) %	
$\Gamma_4$ $\Upsilon(2S)\gamma\gamma$	(5.0 ± 0.7) %	
$\Gamma_5$ $\Upsilon(2S)\pi^0$	< 5.1	$\times 10^{-4}$ CL=90%
$\Gamma_6$ $\Upsilon(1S)\pi^+\pi^-$	(4.37 ± 0.08) %	
$\Gamma_7$ $\Upsilon(1S)\pi^0\pi^0$	(2.20 ± 0.13) %	
$\Gamma_8$ $\Upsilon(1S)\eta$	< 1	$\times 10^{-4}$ CL=90%
$\Gamma_9$ $\Upsilon(1S)\pi^0$	< 7	$\times 10^{-5}$ CL=90%
$\Gamma_{10}$ $h_b(1P)\pi^0$	< 1.2	$\times 10^{-3}$ CL=90%
$\Gamma_{11}$ $h_b(1P)\pi^0 \rightarrow \gamma h_b(1S)\pi^0$	(4.3 ± 1.4) $\times 10^{-4}$	
$\Gamma_{12}$ $h_b(1P)\pi^+\pi^-$	< 1.2	$\times 10^{-4}$ CL=90%
$\Gamma_{13}$ $\tau^+\tau^-$	(2.29 ± 0.30) %	
$\Gamma_{14}$ $\mu^+\mu^-$	(2.18 ± 0.21) %	S=2.1
$\Gamma_{15}$ $e^+e^-$	(2.18 ± 0.20) %	
$\Gamma_{16}$ hadrons	(93 ± 12) %	
$\Gamma_{17}$ $ggg$	(35.7 ± 2.6) %	
$\Gamma_{18}$ $\gamma gg$	(9.7 ± 1.8) $\times 10^{-3}$	
$\Gamma_{19}$ $^2H$ anything	(2.33 ± 0.33) $\times 10^{-5}$	

### Radiative decays

$\Gamma_{20}$ $\gamma \chi_{b2}(2P)$	(13.1 ± 1.6) %	S=3.4
$\Gamma_{21}$ $\gamma \chi_{b1}(2P)$	(12.6 ± 1.2) %	S=2.4
$\Gamma_{22}$ $\gamma \chi_{b0}(2P)$	(5.9 ± 0.6) %	S=1.4
$\Gamma_{23}$ $\gamma \chi_{b2}(1P)$	(10.0 ± 1.0) $\times 10^{-3}$	S=1.7
$\Gamma_{24}$ $\gamma \chi_{b1}(1P)$	(9 ± 5) $\times 10^{-4}$	S=1.8
$\Gamma_{25}$ $\gamma \chi_{b0}(1P)$	(2.7 ± 0.4) $\times 10^{-3}$	
$\Gamma_{26}$ $\gamma h_b(2S)$	< 6.2	$\times 10^{-4}$ CL=90%
$\Gamma_{27}$ $\gamma h_b(1S)$	(5.1 ± 0.7) $\times 10^{-4}$	
$\Gamma_{28}$ $\gamma A^0 \rightarrow \gamma$ hadrons	< 8	$\times 10^{-5}$ CL=90%
$\Gamma_{29}$ $\gamma X \rightarrow \gamma + \geq 4$ prongs	[a] < 2.2	$\times 10^{-4}$ CL=95%
$\Gamma_{30}$ $\gamma a_1^0 \rightarrow \gamma \mu^+ \mu^-$	< 5.5	$\times 10^{-6}$ CL=90%
$\Gamma_{31}$ $\gamma a_1^0 \rightarrow \gamma \tau^+ \tau^-$	[b] < 1.6	$\times 10^{-4}$ CL=90%

### Lepton Family number (LF) violating modes

$\Gamma_{32}$ $e^\pm \tau^\mp$	LF	< 4.2	$\times 10^{-6}$ CL=90%
$\Gamma_{33}$ $\mu^\pm \tau^\mp$	LF	< 3.1	$\times 10^{-6}$ CL=90%

[a] 1.5 GeV <  $m_X$  < 5.0 GeV

[b] For  $m_{\tau^+\tau^-}$  in the ranges 4.03–9.52 and 9.61–10.10 GeV.

### $\Upsilon(3S)$ $\Gamma(i)\Gamma(e^+e^-)/\Gamma(\text{total})$

VALUE (keV)	DOCUMENT ID	TECN	COMMENT
-------------	-------------	------	---------

**0.414 ± 0.007 OUR AVERAGE**  
0.413 ± 0.004 ± 0.006 ROSNER 06 CLEO 10.4  $e^+e^- \rightarrow$  hadrons  
0.45 ± 0.03 ± 0.03 <sup>4</sup> GILES 84B CLEO  $e^+e^- \rightarrow$  hadrons

<sup>4</sup> Radiative corrections reevaluated by BUCHMUELLER 88 following KURAEV 85.

# Meson Particle Listings

## $\Upsilon(3S)$

$\Gamma(\Upsilon(1S)\pi^+\pi^-) \times \Gamma(e^+e^-)/\Gamma_{\text{total}}$					$\Gamma_6/\Gamma$
VALUE (eV)	EVTS	DOCUMENT ID	TECN	COMMENT	
<b>18.46 ± 0.27 ± 0.77</b>	6.4K	5 AUBERT	08BP BABR	$e^+e^- \rightarrow \gamma\pi^+\pi^-\ell^+\ell^-$	
5 Using $B(\Upsilon(1S) \rightarrow e^+e^-) = (2.38 \pm 0.11)\%$ and $B(\Upsilon(1S) \rightarrow \mu^+\mu^-) = (2.48 \pm 0.05)\%$ .					

### $\Upsilon(3S)$ PARTIAL WIDTHS

$\Gamma(e^+e^-)$		$\Gamma_{15}$
VALUE (keV)	DOCUMENT ID	
<b>0.443 ± 0.008 OUR EVALUATION</b>		

### $\Upsilon(3S)$ BRANCHING RATIOS

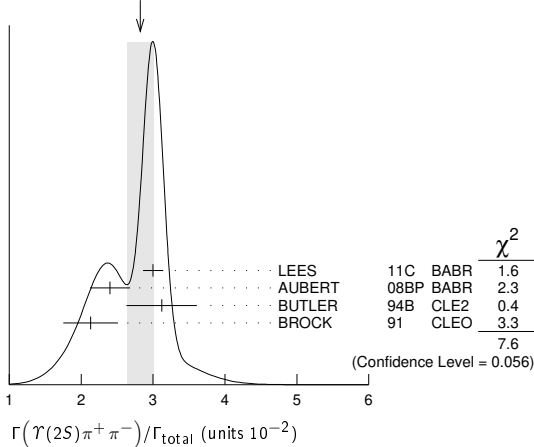
$\Gamma(\Upsilon(2S)\text{anything})/\Gamma_{\text{total}}$					$\Gamma_1/\Gamma$
VALUE	EVTS	DOCUMENT ID	TECN	COMMENT	
<b>0.106 ± 0.008 OUR AVERAGE</b>					
0.1023 ± 0.0105	4625	6,7,8 BUTLER	94B CLE2	$e^+e^- \rightarrow \ell^+\ell^-X$	
0.111 ± 0.012	4891	7,8,9 BROCK	91 CLEO	$e^+e^- \rightarrow \pi^+\pi^-\ell^+\ell^-$	

- 6 Using  $B(\Upsilon(2S) \rightarrow \Upsilon(1S)\gamma\gamma) = (0.038 \pm 0.007)\%$ , and  $B(\Upsilon(2S) \rightarrow \Upsilon(1S)\pi^0\pi^0) = (1/2)B(\Upsilon(2S) \rightarrow \Upsilon(1S)\pi^+\pi^-)$ .
- 7 Using  $B(\Upsilon(1S) \rightarrow \mu^+\mu^-) = (2.48 \pm 0.06)\%$ . With the assumption of  $e\mu$  universality.
- 8 Using  $B(\Upsilon(2S) \rightarrow \Upsilon(1S)\pi^+\pi^-) = (18.5 \pm 0.8)\%$ .
- 9 Using  $B(\Upsilon(2S) \rightarrow \mu^+\mu^-) = (1.31 \pm 0.21)\%$ ,  $B(\Upsilon(2S) \rightarrow \Upsilon(1S)\gamma\gamma) \times 2B(\Upsilon(1S) \rightarrow \mu^+\mu^-) = (0.188 \pm 0.035)\%$ , and  $B(\Upsilon(2S) \rightarrow \Upsilon(1S)\pi^0\pi^0) \times 2B(\Upsilon(1S) \rightarrow \mu^+\mu^-) = (0.436 \pm 0.056)\%$ . With the assumption of  $e\mu$  universality.

$\Gamma(\Upsilon(2S)\pi^+\pi^-)/\Gamma_{\text{total}}$					$\Gamma_2/\Gamma$
VALUE (units $10^{-2}$ )	EVTS	DOCUMENT ID	TECN	COMMENT	
<b>2.82 ± 0.18 OUR AVERAGE</b>					
3.00 ± 0.02 ± 0.14	543k	LEES	11C BABR	$e^+e^- \rightarrow \pi^+\pi^-X$	
2.40 ± 0.10 ± 0.26	800	10 AUBERT	08BP BABR	$e^+e^- \rightarrow \gamma\pi^+\pi^-e^+e^-$	
3.12 ± 0.49	980	11,12 BUTLER	94B CLE2	$e^+e^- \rightarrow \pi^+\pi^-\ell^+\ell^-$	
2.13 ± 0.38	974	13 BROCK	91 CLEO	$e^+e^- \rightarrow \pi^+\pi^-X$ , $\pi^+\pi^-\ell^+\ell^-$	

- • • We do not use the following data for averages, fits, limits, etc. • • •
- 4.82 ± 0.65 ± 0.53 138 13 WU 93 CUSB  $\Upsilon(3S) \rightarrow \pi^+\pi^-\ell^+\ell^-$
- 3.1 ± 2.0 5 5 MAGERAS 82 CUSB  $\Upsilon(3S) \rightarrow \pi^+\pi^-\ell^+\ell^-$
- 10 Using  $B(\Upsilon(1S) \rightarrow e^+e^-) = (2.38 \pm 0.11)\%$ ,  $B(\Upsilon(1S) \rightarrow \mu^+\mu^-) = (2.48 \pm 0.05)\%$ , and  $\Gamma_{ee}(\Upsilon(3S)) = 0.443 \pm 0.008$  keV.
- 11 From the exclusive mode.
- 12 Using  $B(\Upsilon(2S) \rightarrow \Upsilon(1S)\gamma\gamma) = (0.038 \pm 0.007)\%$ , and  $B(\Upsilon(2S) \rightarrow \Upsilon(1S)\pi^0\pi^0) = (1/2)B(\Upsilon(2S) \rightarrow \Upsilon(1S)\pi^+\pi^-)$ .
- 13 Using  $B(\Upsilon(2S) \rightarrow \mu^+\mu^-) = (1.31 \pm 0.21)\%$ ,  $B(\Upsilon(2S) \rightarrow \Upsilon(1S)\gamma\gamma) \times 2B(\Upsilon(1S) \rightarrow \mu^+\mu^-) = (0.188 \pm 0.035)\%$ , and  $B(\Upsilon(2S) \rightarrow \Upsilon(1S)\pi^0\pi^0) \times 2B(\Upsilon(1S) \rightarrow \mu^+\mu^-) = (0.436 \pm 0.056)\%$ . With the assumption of  $e\mu$  universality.

WEIGHTED AVERAGE  
2.82±0.18 (Error scaled by 1.6)



$\Gamma(\Upsilon(2S)\pi^0\pi^0)/\Gamma_{\text{total}}$					$\Gamma_3/\Gamma$
VALUE (units $10^{-2}$ )	EVTS	DOCUMENT ID	TECN	COMMENT	
<b>1.85 ± 0.14 OUR AVERAGE</b>					
1.82 ± 0.09 ± 0.12	4391	14 BHARI	09 CLEO	$e^+e^- \rightarrow \pi^0\pi^0\ell^+\ell^-$	
2.16 ± 0.39		15,16 BUTLER	94B CLE2	$e^+e^- \rightarrow \pi^0\pi^0\ell^+\ell^-$	
1.7 ± 0.5 ± 0.2	10	17 HEINTZ	92 CSB2	$e^+e^- \rightarrow \pi^0\pi^0\ell^+\ell^-$	

- 14 Authors assume  $B(\Upsilon(1S) \rightarrow e^+e^-) + B(\Upsilon(1S) \rightarrow \mu^+\mu^-) = 4.06\%$ .
- 15  $B(\Upsilon(2S) \rightarrow \mu^+\mu^-) = (1.31 \pm 0.21)\%$  and assuming  $e\mu$  universality.
- 16 From the exclusive mode.
- 17  $B(\Upsilon(2S) \rightarrow \mu^+\mu^-) = (1.44 \pm 0.10)\%$  and assuming  $e\mu$  universality. Supersedes HEINTZ 91.

$\Gamma(\Upsilon(2S)\gamma\gamma)/\Gamma_{\text{total}}$				$\Gamma_4/\Gamma$
VALUE	DOCUMENT ID	TECN	COMMENT	
<b>0.0502 ± 0.0069</b>	18 BUTLER	94B CLE2	$e^+e^- \rightarrow \ell^+\ell^-2\gamma$	
18 From the exclusive mode.				

$\Gamma(\Upsilon(2S)\pi^0)/\Gamma_{\text{total}}$				$\Gamma_5/\Gamma$
VALUE (units $10^{-3}$ )	CL%	DOCUMENT ID	TECN	COMMENT
<b>&lt;0.51</b>	90	19 HE	08A CLEO	$e^+e^- \rightarrow \ell^+\ell^-\gamma\gamma$
19 Authors assume $B(\Upsilon(2S) \rightarrow e^+e^-) + B(\Upsilon(1S) \rightarrow \mu^+\mu^-) = 4.06\%$ .				

$\Gamma(\Upsilon(1S)\pi^+\pi^-)/\Gamma_{\text{total}}$					$\Gamma_6/\Gamma$
VALUE (units $10^{-2}$ )	EVTS	DOCUMENT ID	TECN	COMMENT	
<b>4.37 ± 0.08 OUR AVERAGE</b>					
4.32 ± 0.07 ± 0.13	90k	20 LEES	11L BABR	$\Upsilon(3S) \rightarrow \pi^+\pi^-\ell^+\ell^-$	
4.46 ± 0.01 ± 0.13	190k	21 BHARI	09 CLEO	$e^+e^- \rightarrow \pi^+\pi^-MM$	
4.17 ± 0.06 ± 0.19	6.4K	22 AUBERT	08BP BABR	$10.58 e^+e^- \rightarrow \gamma\pi^+\pi^-\ell^+\ell^-$	
4.52 ± 0.35	11830	23 BUTLER	94B CLE2	$e^+e^- \rightarrow \pi^+\pi^-X$ , $\pi^+\pi^-\ell^+\ell^-$	
4.46 ± 0.34 ± 0.50	451	23 WU	93 CUSB	$\Upsilon(3S) \rightarrow \pi^+\pi^-\ell^+\ell^-$	
4.46 ± 0.30	11221	23 BROCK	91 CLEO	$e^+e^- \rightarrow \pi^+\pi^-X$ , $\pi^+\pi^-\ell^+\ell^-$	
• • • We do not use the following data for averages, fits, limits, etc. • • •					
4.9 ± 1.0	22	GREEN	82 CLEO	$\Upsilon(3S) \rightarrow \pi^+\pi^-\ell^+\ell^-$	
3.9 ± 1.3	26	MAGERAS	82 CUSB	$\Upsilon(3S) \rightarrow \pi^+\pi^-\ell^+\ell^-$	

- 20 Using  $B(\Upsilon(1S) \rightarrow e^+e^-) = (2.38 \pm 0.11)\%$  and  $B(\Upsilon(1S) \rightarrow \mu^+\mu^-) = (2.48 \pm 0.05)\%$ .
- 21 A weighted average of the inclusive and exclusive results.
- 22 Using  $B(\Upsilon(2S) \rightarrow e^+e^-) = (1.91 \pm 0.16)\%$ ,  $B(\Upsilon(2S) \rightarrow \mu^+\mu^-) = (1.93 \pm 0.17)\%$ , and  $\Gamma_{ee}(\Upsilon(3S)) = 0.443 \pm 0.008$  keV.
- 23 Using  $B(\Upsilon(1S) \rightarrow \mu^+\mu^-) = (2.48 \pm 0.06)\%$ . With the assumption of  $e\mu$  universality.

$\Gamma(\Upsilon(2S)\pi^+\pi^-)/\Gamma(\Upsilon(1S)\pi^+\pi^-)$					$\Gamma_2/\Gamma_6$
VALUE	EVTS	DOCUMENT ID	TECN	COMMENT	
<b>0.577 ± 0.026 ± 0.060</b>	800	24 AUBERT	08BP BABR	$e^+e^- \rightarrow \gamma\pi^+\pi^-\ell^+\ell^-$	
24 Using $B(\Upsilon(1S) \rightarrow e^+e^-) = (2.38 \pm 0.11)\%$ , $B(\Upsilon(1S) \rightarrow \mu^+\mu^-) = (2.48 \pm 0.05)\%$ , $B(\Upsilon(2S) \rightarrow e^+e^-) = (1.91 \pm 0.16)\%$ , and $B(\Upsilon(2S) \rightarrow \mu^+\mu^-) = (1.93 \pm 0.17)\%$ . Not independent of other values reported by AUBERT 08BP.					

$\Gamma(\Upsilon(1S)\pi^0\pi^0)/\Gamma_{\text{total}}$					$\Gamma_7/\Gamma$
VALUE (units $10^{-2}$ )	EVTS	DOCUMENT ID	TECN	COMMENT	
<b>2.20 ± 0.13 OUR AVERAGE</b>					
2.24 ± 0.09 ± 0.11	6584	25 BHARI	09 CLEO	$e^+e^- \rightarrow \pi^0\pi^0\ell^+\ell^-$	
1.99 ± 0.34	56	26 BUTLER	94B CLE2	$e^+e^- \rightarrow \pi^0\pi^0\ell^+\ell^-$	
2.2 ± 0.4 ± 0.3	33	27 HEINTZ	92 CSB2	$e^+e^- \rightarrow \pi^0\pi^0\ell^+\ell^-$	
25 Authors assume $B(\Upsilon(1S) \rightarrow e^+e^-) + B(\Upsilon(1S) \rightarrow \mu^+\mu^-) = 4.96\%$ .					
26 Using $B(\Upsilon(1S) \rightarrow \mu^+\mu^-) = (2.48 \pm 0.06)\%$ and assuming $e\mu$ universality.					
27 Using $B(\Upsilon(1S) \rightarrow \mu^+\mu^-) = (2.57 \pm 0.07)\%$ and assuming $e\mu$ universality. Supersedes HEINTZ 91.					

$\Gamma(\Upsilon(1S)\pi^0\pi^0)/\Gamma(\Upsilon(1S)\pi^+\pi^-)$				$\Gamma_7/\Gamma_6$
VALUE	DOCUMENT ID	TECN	COMMENT	
<b>0.501 ± 0.043</b>	28 BHARI	09 CLEO	$e^+e^- \rightarrow \Upsilon(3S)$	
28 Not independent of other values reported by BHARI 09.				

$\Gamma(\Upsilon(1S)\eta)/\Gamma_{\text{total}}$					$\Gamma_8/\Gamma$
VALUE (units $10^{-3}$ )	CL%	DOCUMENT ID	TECN	COMMENT	
<b>&lt;0.1</b>	90	29 LEES	11L BABR	$\Upsilon(3S) \rightarrow (\pi^+\pi^-)(\gamma\gamma)\ell^+\ell^-$	
• • • We do not use the following data for averages, fits, limits, etc. • • •					
<0.8	90	29,30 AUBERT	08BP BABR	$e^+e^- \rightarrow \gamma\pi^+\pi^-\pi^0\ell^+\ell^-$	
<0.18	90	31 HE	08A CLEO	$e^+e^- \rightarrow \ell^+\ell^-\eta$	
<2.2	90	BROCK	91 CLEO	$e^+e^- \rightarrow \ell^+\ell^-\eta$	
29 Using $B(\Upsilon(1S) \rightarrow e^+e^-) = (2.38 \pm 0.11)\%$ , $B(\Upsilon(1S) \rightarrow \mu^+\mu^-) = (2.48 \pm 0.05)\%$ .					
30 Using $\Gamma_{ee}(\Upsilon(3S)) = 0.443 \pm 0.008$ keV.					
31 Authors assume $B(\Upsilon(1S) \rightarrow e^+e^-) + B(\Upsilon(1S) \rightarrow \mu^+\mu^-) = 4.96\%$ .					

$\Gamma(\Upsilon(1S)\eta)/\Gamma(\Upsilon(1S)\pi^+\pi^-)$					$\Gamma_8/\Gamma_6$
VALUE (units $10^{-2}$ )	CL%	DOCUMENT ID	TECN	COMMENT	
<b>&lt;0.23</b>	90	32 LEES	11L BABR	$\Upsilon(3S) \rightarrow (\pi^+\pi^-)(\gamma\gamma)\ell^+\ell^-$	
• • • We do not use the following data for averages, fits, limits, etc. • • •					
<1.9	90	33 AUBERT	08BP BABR	$e^+e^- \rightarrow \gamma\pi^+\pi^-(\pi^0)\ell^+\ell^-$	
32 Not independent of other values reported by LEES 11L.					
33 Not independent of other values reported by AUBERT 08BP.					

$\Gamma(\Upsilon(1S)\pi^0)/\Gamma_{\text{total}}$				$\Gamma_9/\Gamma$
VALUE (units $10^{-3}$ )	CL%	DOCUMENT ID	TECN	COMMENT
<b>&lt;0.07</b>	90	34 HE	08A CLEO	$e^+e^- \rightarrow \ell^+\ell^-\gamma\gamma$
34 Authors assume $B(\Upsilon(1S) \rightarrow e^+e^-) + B(\Upsilon(1S) \rightarrow \mu^+\mu^-) = 4.96\%$ .				



# Meson Particle Listings

## $\Upsilon(3S)$

$\Gamma(h_b(1P)\pi^0)/\Gamma_{total}$					$\Gamma_{10}/\Gamma$
VALUE	CL%	DOCUMENT ID	TECN	COMMENT	
$<1.2 \times 10^{-3}$	90	35 GE	11	CLEO $\Upsilon(3S) \rightarrow \pi^0$ anything	
<sup>35</sup> Assuming $M(h_b(1P)) = 9900$ MeV and $\Gamma(h_b(1P)) = 0$ MeV, and allowing $B(h_b(1P) \rightarrow \gamma\eta_b(1S))$ to vary from 0–100%.					

$\Gamma(h_b(1P)\pi^0 \rightarrow \gamma\eta_b(1S)\pi^0)/\Gamma_{total}$					$\Gamma_{11}/\Gamma$
VALUE (units $10^{-4}$ )	DOCUMENT ID	TECN	COMMENT		
$4.3 \pm 1.1 \pm 0.9$	LEES	11k	BABR	$\Upsilon(3S) \rightarrow \eta_b \gamma \pi^0$	

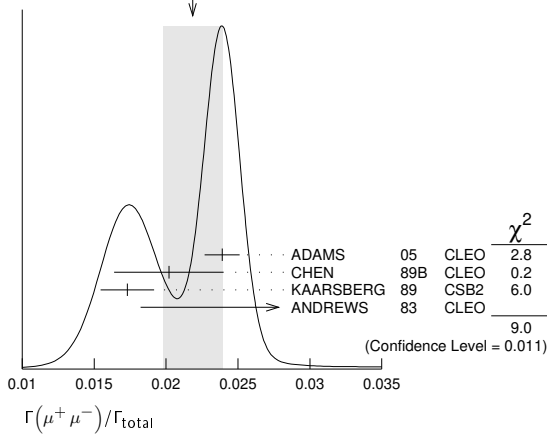
$\Gamma(h_b(1P)\pi^+\pi^-)/\Gamma_{total}$					$\Gamma_{12}/\Gamma$
VALUE (units $10^{-4}$ )	CL%	DOCUMENT ID	TECN	COMMENT	
$< 1.2$	90	36 LEES	11c	BABR $e^+e^- \rightarrow \pi^+\pi^- X$	
••• We do not use the following data for averages, fits, limits, etc. •••					
$<18$		36 BUTLER	94b	CLE2 $e^+e^- \rightarrow \pi^+\pi^- X$	
$<15$		36 BROCK	91	CLEO $e^+e^- \rightarrow \pi^+\pi^- X$	
<sup>36</sup> For $M(h_b(1P)) = 9900$ MeV.					

$\Gamma(\tau^+\tau^-)/\Gamma_{total}$					$\Gamma_{13}/\Gamma$
VALUE (units $10^{-2}$ )	EVTS	DOCUMENT ID	TECN	COMMENT	
$2.29 \pm 0.21 \pm 0.22$	15k	37 BESSON	07	CLEO $e^+e^- \rightarrow \Upsilon(3S) \rightarrow \tau^+\tau^-$	
<sup>37</sup> BESSON 07 reports $[\Gamma(\Upsilon(3S) \rightarrow \tau^+\tau^-)/\Gamma_{total}] / [B(\Upsilon(3S) \rightarrow \mu^+\mu^-)] = 1.05 \pm 0.08 \pm 0.05$ which we multiply by our best value $B(\Upsilon(3S) \rightarrow \mu^+\mu^-) = (2.18 \pm 0.21) \times 10^{-2}$ . Our first error is their experiment's error and our second error is the systematic error from using our best value.					

$\Gamma(\tau^+\tau^-)/\Gamma(\mu^+\mu^-)$					$\Gamma_{13}/\Gamma_{14}$
VALUE	EVTS	DOCUMENT ID	TECN	COMMENT	
$1.05 \pm 0.08 \pm 0.05$	15k	BESSON	07	CLEO $e^+e^- \rightarrow \Upsilon(3S)$	

$\Gamma(\mu^+\mu^-)/\Gamma_{total}$					$\Gamma_{14}/\Gamma$
VALUE	EVTS	DOCUMENT ID	TECN	COMMENT	
$0.0218 \pm 0.0021$ OUR AVERAGE				Error includes scale factor of 2.1. See the ideogram below.	
$0.0239 \pm 0.0007 \pm 0.0010$	81k	ADAMS	05	CLEO $e^+e^- \rightarrow \mu^+\mu^-$	
$0.0202 \pm 0.0019 \pm 0.0033$		CHEN	89b	CLEO $e^+e^- \rightarrow \mu^+\mu^-$	
$0.0173 \pm 0.0015 \pm 0.0011$		KAARSBERG	89	CSB2 $e^+e^- \rightarrow \mu^+\mu^-$	
$0.033 \pm 0.013 \pm 0.007$	1096	ANDREWS	83	CLEO $e^+e^- \rightarrow \mu^+\mu^-$	

WEIGHTED AVERAGE  
0.0218±0.0021 (Error scaled by 2.1)



$\Gamma(gg)/\Gamma_{total}$					$\Gamma_{17}/\Gamma$
VALUE (units $10^{-2}$ )	EVTS	DOCUMENT ID	TECN	COMMENT	
$35.7 \pm 2.6$	3M	38 BESSON	06a	CLEO $\Upsilon(3S) \rightarrow$ hadrons	
<sup>38</sup> Calculated using BESSON 06a value of $\Gamma(\gamma gg)/\Gamma(gg) = (2.72 \pm 0.06 \pm 0.32 \pm 0.37)\%$ and the PDG 08 values of $B(\Upsilon(2S) + \text{anything}) = (10.6 \pm 0.8)\%$ , $B(\pi^+\pi^-\Upsilon(1S)) = (4.40 \pm 0.10)\%$ , $B(\pi^0\pi^0\Upsilon(1S)) = (2.20 \pm 0.13)\%$ , $B(\gamma\chi_{b2}(2P)) = (13.1 \pm 1.6)\%$ , $B(\gamma\chi_{b1}(2P)) = (12.6 \pm 1.2)\%$ , $B(\gamma\chi_{b0}(2P)) = (5.9 \pm 0.6)\%$ , $B(\gamma\chi_{b0}(1P)) = (0.30 \pm 0.11)\%$ , $B(\mu^+\mu^-) = (2.18 \pm 0.21)\%$ , and $R_{\text{hadrons}} = 3.51$ . The statistical error is negligible and the systematic error is partially correlated with $\Gamma(\gamma gg)/\Gamma_{total}$ BESSON 06a value.					

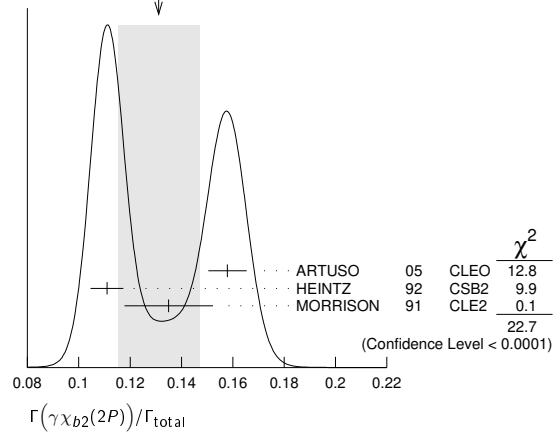
$\Gamma(\gamma gg)/\Gamma_{total}$					$\Gamma_{18}/\Gamma$
VALUE (units $10^{-2}$ )	EVTS	DOCUMENT ID	TECN	COMMENT	
$0.97 \pm 0.18$	60k	39 BESSON	06a	CLEO $\Upsilon(3S) \rightarrow \gamma +$ hadrons	
<sup>39</sup> Calculated using BESSON 06a values of $\Gamma(\gamma gg)/\Gamma(gg) = (2.72 \pm 0.06 \pm 0.32 \pm 0.37)\%$ and $\Gamma(gg)/\Gamma_{total}$ . The statistical error is negligible and the systematic error is partially correlated with $\Gamma(gg)/\Gamma_{total}$ BESSON 06a value.					

$\Gamma(\gamma gg)/\Gamma(ggg)$					$\Gamma_{18}/\Gamma_{17}$
VALUE (units $10^{-2}$ )	EVTS	DOCUMENT ID	TECN	COMMENT	
$2.72 \pm 0.06 \pm 0.49$	3M	BESSON	06a	CLEO $\Upsilon(3S) \rightarrow (\gamma +)$ hadrons	

$\Gamma(2H \text{ anything})/\Gamma_{total}$					$\Gamma_{19}/\Gamma$
VALUE (units $10^{-5}$ )	DOCUMENT ID	TECN	COMMENT		
$2.33 \pm 0.15 \pm 0.31$ $-0.28$	LEES	14g	BABR	$e^+e^- \rightarrow 2H X$	

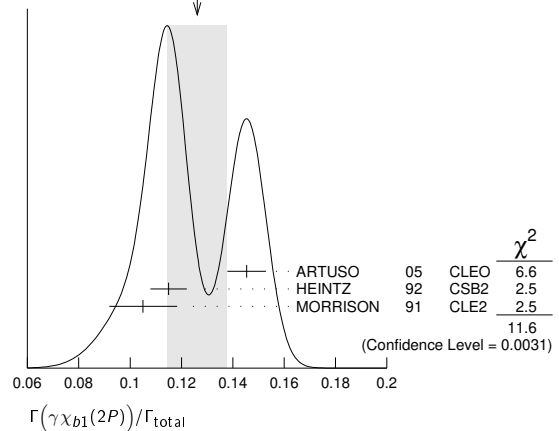
$\Gamma(\gamma\chi_{b2}(2P))/\Gamma_{total}$					$\Gamma_{20}/\Gamma$
VALUE	EVTS	DOCUMENT ID	TECN	COMMENT	
$0.131 \pm 0.016$ OUR AVERAGE				Error includes scale factor of 3.4. See the ideogram below.	
$0.1579 \pm 0.0017 \pm 0.0073$	568k	ARTUSO	05	CLEO $e^+e^- \rightarrow \gamma X$	
$0.111 \pm 0.005 \pm 0.004$	10319	40 HEINTZ	92	CSB2 $e^+e^- \rightarrow \gamma X$	
$0.135 \pm 0.003 \pm 0.017$	30741	MORRISON	91	CLE2 $e^+e^- \rightarrow \gamma X$	
<sup>40</sup> Supersedes NARAIN 91.					

WEIGHTED AVERAGE  
0.131±0.016 (Error scaled by 3.4)



$\Gamma(\gamma\chi_{b1}(2P))/\Gamma_{total}$					$\Gamma_{21}/\Gamma$
VALUE	EVTS	DOCUMENT ID	TECN	COMMENT	
$0.126 \pm 0.012$ OUR AVERAGE				Error includes scale factor of 2.4. See the ideogram below.	
$0.1454 \pm 0.0018 \pm 0.0073$	537k	ARTUSO	05	CLEO $e^+e^- \rightarrow \gamma X$	
$0.115 \pm 0.005 \pm 0.005$	11147	41 HEINTZ	92	CSB2 $e^+e^- \rightarrow \gamma X$	
$0.105 \pm 0.003 \pm 0.013$ $-0.002$	25759	MORRISON	91	CLE2 $e^+e^- \rightarrow \gamma X$	
<sup>41</sup> Supersedes NARAIN 91.					

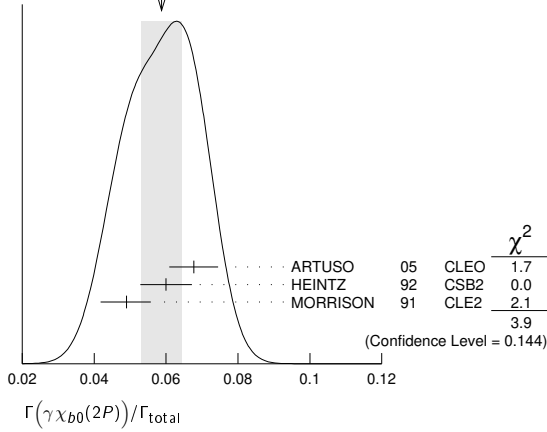
WEIGHTED AVERAGE  
0.126±0.012 (Error scaled by 2.4)



$\Gamma(\gamma\chi_{b0}(2P))/\Gamma_{total}$					$\Gamma_{22}/\Gamma$
VALUE	EVTS	DOCUMENT ID	TECN	COMMENT	
$0.059 \pm 0.006$ OUR AVERAGE				Error includes scale factor of 1.4. See the ideogram below.	
$0.0677 \pm 0.0020 \pm 0.0065$	225k	ARTUSO	05	CLEO $e^+e^- \rightarrow \gamma X$	
$0.060 \pm 0.004 \pm 0.006$	4959	42 HEINTZ	92	CSB2 $e^+e^- \rightarrow \gamma X$	
$0.049 \pm 0.003 \pm 0.006$ $-0.004$	9903	MORRISON	91	CLE2 $e^+e^- \rightarrow \gamma X$	

<sup>42</sup> Supersedes NARAIN 91.

WEIGHTED AVERAGE  
0.059±0.006 (Error scaled by 1.4)



$\Gamma(\chi_{b2}(1P))/\Gamma_{total}$   $\Gamma_{23}/\Gamma$

VALUE (units 10 <sup>-3</sup> )	CL%	EVTS	DOCUMENT ID	TECN	COMMENT
<b>10.0±1.0 OUR AVERAGE</b>			Error includes scale factor of 1.7.		
8.0±1.3±0.4	126	43,44	KORNICER	11	CLEO $e^+e^- \rightarrow \gamma\gamma\ell^+\ell^-$
10.5±0.3 <sup>+0.7</sup> <sub>-0.6</sub>	9.7k		LEES	11J	BABR $\Upsilon(3S) \rightarrow X\gamma$
••• We do not use the following data for averages, fits, limits, etc. •••					
<19	90		45 ASNER	08A	CLEO $\Upsilon(3S) \rightarrow \gamma + \text{hadrons}$ seen
			46 HEINTZ	92	CSB2 $e^+e^- \rightarrow \gamma\gamma\ell^+\ell^-$

<sup>43</sup> Assuming  $B(\Upsilon(1S) \rightarrow \ell^+\ell^-) = (2.48 \pm 0.05)\%$ .  
<sup>44</sup> KORNICER 11 reports  $[\Gamma(\Upsilon(3S) \rightarrow \chi_{b2}(1P))/\Gamma_{total}] \times [B(\chi_{b2}(1P) \rightarrow \gamma\Upsilon(1S))]$  =  $(1.435 \pm 0.162 \pm 0.169) \times 10^{-3}$  which we divide by our best value  $B(\chi_{b2}(1P) \rightarrow \gamma\Upsilon(1S)) = (18.0 \pm 1.0) \times 10^{-2}$ . Our first error is their experiment's error and our second error is the systematic error from using our best value.  
<sup>45</sup> ASNER 08A reports  $[\Gamma(\Upsilon(3S) \rightarrow \chi_{b2}(1P))/\Gamma_{total}] / [B(\Upsilon(2S) \rightarrow \chi_{b2}(1P))]$  <  $27.1 \times 10^{-2}$  which we multiply by our best value  $B(\Upsilon(2S) \rightarrow \chi_{b2}(1P)) = 7.15 \times 10^{-2}$ .  
<sup>46</sup> HEINTZ 92, while unable to distinguish between different  $J$  states, measures  $\sum_J B(\Upsilon(3S) \rightarrow \chi_{bJ}) \times B(\chi_{bJ} \rightarrow \gamma\Upsilon(1S)) = (1.7 \pm 0.4 \pm 0.6) \times 10^{-3}$  for  $J = 0, 1, 2$  using inclusive  $\Upsilon(1S)$  decays and  $(1.2^{+0.4}_{-0.3} \pm 0.09) \times 10^{-3}$  for  $J = 1, 2$  using  $\Upsilon(1S) \rightarrow \ell^+\ell^-$ .

$\Gamma(\chi_{b1}(1P))/\Gamma_{total}$   $\Gamma_{24}/\Gamma$

VALUE (units 10 <sup>-3</sup> )	CL%	EVTS	DOCUMENT ID	TECN	COMMENT
<b>0.9±0.5 OUR AVERAGE</b>			Error includes scale factor of 1.8.		
1.5±0.4±0.1	50	47,48	KORNICER	11	CLEO $e^+e^- \rightarrow \gamma\gamma\ell^+\ell^-$
0.5±0.3 <sup>+0.2</sup> <sub>-0.1</sub>			LEES	11J	BABR $\Upsilon(3S) \rightarrow X\gamma$
••• We do not use the following data for averages, fits, limits, etc. •••					
<1.7	90		49 ASNER	08A	CLEO $\Upsilon(3S) \rightarrow \gamma + \text{hadrons}$ seen
			50 HEINTZ	92	CSB2 $e^+e^- \rightarrow \gamma\gamma\ell^+\ell^-$

<sup>47</sup> Assuming  $B(\Upsilon(1S) \rightarrow \ell^+\ell^-) = (2.48 \pm 0.05)\%$ .  
<sup>48</sup> KORNICER 11 reports  $[\Gamma(\Upsilon(3S) \rightarrow \chi_{b1}(1P))/\Gamma_{total}] \times [B(\chi_{b1}(1P) \rightarrow \gamma\Upsilon(1S))] = (5.38 \pm 1.20 \pm 0.95) \times 10^{-4}$  which we divide by our best value  $B(\chi_{b1}(1P) \rightarrow \gamma\Upsilon(1S)) = (35.2 \pm 2.0) \times 10^{-2}$ . Our first error is their experiment's error and our second error is the systematic error from using our best value.  
<sup>49</sup> ASNER 08A reports  $[\Gamma(\Upsilon(3S) \rightarrow \chi_{b1}(1P))/\Gamma_{total}] / [B(\Upsilon(2S) \rightarrow \chi_{b1}(1P))] < 2.5 \times 10^{-2}$  which we multiply by our best value  $B(\Upsilon(2S) \rightarrow \chi_{b1}(1P)) = 6.9 \times 10^{-2}$ .  
<sup>50</sup> HEINTZ 92, while unable to distinguish between different  $J$  states, measures  $\sum_J B(\Upsilon(3S) \rightarrow \chi_{bJ}) \times B(\chi_{bJ} \rightarrow \gamma\Upsilon(1S)) = (1.7 \pm 0.4 \pm 0.6) \times 10^{-3}$  for  $J = 0, 1, 2$  using inclusive  $\Upsilon(1S)$  decays and  $(1.2^{+0.4}_{-0.3} \pm 0.09) \times 10^{-3}$  for  $J = 1, 2$  using  $\Upsilon(1S) \rightarrow \ell^+\ell^-$ .

$\Gamma(\chi_{b0}(1P))/\Gamma_{total}$   $\Gamma_{25}/\Gamma$

VALUE (units 10 <sup>-2</sup> )	CL%	EVTS	DOCUMENT ID	TECN	COMMENT
<b>0.27±0.04 OUR AVERAGE</b>					
0.27±0.04±0.02	2.3k		LEES	11J	BABR $\Upsilon(3S) \rightarrow X\gamma$
0.30±0.04±0.10	8.7k		ARTUSO	05	CLEO $e^+e^- \rightarrow \gamma X$
••• We do not use the following data for averages, fits, limits, etc. •••					
<0.8	90		51 ASNER	08A	CLEO $\Upsilon(3S) \rightarrow \gamma + \text{hadrons}$

<sup>51</sup> ASNER 08A reports  $[\Gamma(\Upsilon(3S) \rightarrow \chi_{b0}(1P))/\Gamma_{total}] / [B(\Upsilon(2S) \rightarrow \chi_{b0}(1P))] < 21.9 \times 10^{-2}$  which we multiply by our best value  $B(\Upsilon(2S) \rightarrow \chi_{b0}(1P)) = 3.8 \times 10^{-2}$ .

$\Gamma(\gamma\eta_b(2S))/\Gamma_{total}$   $\Gamma_{26}/\Gamma$

VALUE (units 10 <sup>-4</sup> )	CL%	DOCUMENT ID	TECN	COMMENT
<b>&lt; 6.2</b>	90	ARTUSO	05	CLEO $e^+e^- \rightarrow \gamma X$
••• We do not use the following data for averages, fits, limits, etc. •••				
<19	90	LEES	11J	BABR $\Upsilon(3S) \rightarrow X\gamma$

$\Gamma(\gamma\eta_b(1S))/\Gamma_{total}$   $\Gamma_{27}/\Gamma$

VALUE (units 10 <sup>-4</sup> )	CL%	EVTS	DOCUMENT ID	TECN	COMMENT
<b>5.1±0.7 OUR AVERAGE</b>					
7.1±1.8±1.3	2.3±0.5k		52 BONVICINI	10	CLEO $\Upsilon(3S) \rightarrow \gamma X$
4.8±0.5±0.6	19±3k		52 AUBERT	09AQ	BABR $\Upsilon(3S) \rightarrow \gamma X$
••• We do not use the following data for averages, fits, limits, etc. •••					
<8.5	90		LEES	11J	BABR $\Upsilon(3S) \rightarrow X\gamma$
4.8±0.5±1.2	19±3k		52,53 AUBERT	08v	BABR $\Upsilon(3S) \rightarrow \gamma X$
<4.3	90		54 ARTUSO	05	CLEO $e^+e^- \rightarrow \gamma X$
52 Assuming $\Gamma_{\eta_b(1S)} = 10$ MeV. 53 Systematic error re-evaluated by AUBERT 09AQ. 54 Superseded by BONVICINI 10.					

$\Gamma(\gamma A^0 \rightarrow \gamma \text{hadrons})/\Gamma_{total}$   $\Gamma_{28}/\Gamma$   
(0.3 GeV <  $m_{A^0}$  < 7 GeV)

VALUE	CL%	DOCUMENT ID	TECN	COMMENT
<b>&lt; 8 × 10<sup>-5</sup></b>	90	55 LEES	11H	BABR $\Upsilon(3S) \rightarrow \gamma \text{hadrons}$
55 For a narrow scalar or pseudoscalar $A^0$ , excluding known resonances, with mass in the range 0.3–7 GeV. Measured 90% CL limits as a function of $m_{A^0}$ range from $1 \times 10^{-6}$ to $8 \times 10^{-5}$ .				

$\Gamma(\gamma X \rightarrow \gamma + \geq 4 \text{ prongs})/\Gamma_{total}$   $\Gamma_{29}/\Gamma$   
(1.5 GeV <  $m_X$  < 5.0 GeV)

VALUE (units 10 <sup>-4</sup> )	CL%	DOCUMENT ID	TECN	COMMENT
<b>&lt; 2.2</b>	95	ROSNER	07A	CLEO $e^+e^- \rightarrow \gamma X$

$\Gamma(\gamma a_1^0 \rightarrow \gamma \mu^+ \mu^-)/\Gamma_{total}$   $\Gamma_{30}/\Gamma$

VALUE (units 10 <sup>-6</sup> )	CL%	DOCUMENT ID	TECN	COMMENT
<b>&lt; 5.5</b>	90	56 AUBERT	09Z	BABR $e^+e^- \rightarrow \gamma a_1^0 \rightarrow \gamma \mu^+ \mu^-$
56 For a narrow scalar or pseudoscalar $a_1^0$ with mass in the range 212–930 MeV, excluding $J/\psi$ and $\psi(2S)$ . Measured 90% CL limits as a function of $m_{a_1^0}$ range from 0.27–5.5 × 10 <sup>-6</sup> .				

$\Gamma(\gamma a_1^0 \rightarrow \gamma \tau^+ \tau^-)/\Gamma_{total}$   $\Gamma_{31}/\Gamma$

VALUE	CL%	DOCUMENT ID	TECN	COMMENT
<b>&lt; 1.6 × 10<sup>-4</sup></b>	90	57 AUBERT	09P	BABR $e^+e^- \rightarrow \gamma a_1^0 \rightarrow \gamma \tau^+ \tau^-$
57 For a narrow scalar or pseudoscalar $a_1^0$ with $M(\tau^+ \tau^-)$ in the ranges 4.03–9.52 and 9.61–10.10 GeV. Measured 90% CL limits as a function of $M(\tau^+ \tau^-)$ range from $1.5\text{--}16 \times 10^{-5}$ .				

LEPTON FAMILY NUMBER (LF) VIOLATING MODES

$\Gamma(e^\pm \tau^\mp)/\Gamma_{total}$   $\Gamma_{32}/\Gamma$

VALUE (units 10 <sup>-6</sup> )	CL%	DOCUMENT ID	TECN	COMMENT
<b>&lt; 4.2</b>	90	LEES	10B	BABR $e^+e^- \rightarrow e^\pm \tau^\mp$

$\Gamma(\mu^\pm \tau^\mp)/\Gamma_{total}$   $\Gamma_{33}/\Gamma$

VALUE (units 10 <sup>-6</sup> )	CL%	DOCUMENT ID	TECN	COMMENT
<b>&lt; 3.1</b>	90	LEES	10B	BABR $e^+e^- \rightarrow \mu^\pm \tau^\mp$
••• We do not use the following data for averages, fits, limits, etc. •••				
<20.3	95	LOVE	08A	CLEO $e^+e^- \rightarrow \mu^\pm \tau^\mp$

$\Upsilon(3S)$  REFERENCES

LEES	14G	PR D89 111102	J.P. Lees et al.	(BABAR Collab.)
GE	11	PR D84 032008	J.Y. Ge et al.	(CLEO Collab.)
KORNICER	11	PR D83 054003	M. Koricic et al.	(CLEO Collab.)
LEES	11C	PR D84 011104	J.P. Lees et al.	(BABAR Collab.)
LEES	11H	PRL 107 221803	J.P. Lees et al.	(BABAR Collab.)
LEES	11J	PR D84 072002	J.P. Lees et al.	(BABAR Collab.)
LEES	11K	PR D84 091101	J.P. Lees et al.	(BABAR Collab.)
LEES	11L	PR D84 092003	J.P. Lees et al.	(BABAR Collab.)
BONVICINI	10	PR D81 031104	G. Bonvicini et al.	(CLEO Collab.)
LEES	10B	PRL 104 151802	J.P. Lees et al.	(BABAR Collab.)
AUBERT	09AQ	PRL 103 161801	B. Aubert et al.	(BABAR Collab.)
AUBERT	09P	PRL 103 181801	B. Aubert et al.	(BABAR Collab.)
AUBERT	09Z	PRL 103 081803	B. Aubert et al.	(BABAR Collab.)
BHARI	09	PR D79 011103	S.R. Bhari et al.	(CLEO Collab.)
ASNER	08A	PR D78 091103	D.M. Asner et al.	(CLEO Collab.)
AUBERT	08BP	PR D78 112002	B. Aubert et al.	(BABAR Collab.)
AUBERT	08V	PRL 101 071801	B. Aubert et al.	(BABAR Collab.)
HE	08A	PRL 101 192001	Q. He et al.	(CLEO Collab.)
LOVE	08A	PRL 101 201601	W. Love et al.	(CLEO Collab.)
PDG	08	PL B667 1	C. Amisler et al.	(PDG Collab.)
BESSON	07	PRL 98 052002	D. Besson et al.	(CLEO Collab.)
ROSNER	07A	PR D76 117102	J.L. Rosner et al.	(CLEO Collab.)
BESSON	06A	PR D74 012003	D. Besson et al.	(CLEO Collab.)
ROSNER	06	PRL 96 092003	J.L. Rosner et al.	(CLEO Collab.)
ADAMS	05	PRL 94 012001	G.S. Adams et al.	(CLEO Collab.)

# Meson Particle Listings

## $\Upsilon(3S)$ , $\chi_{b1}(3P)$ , $\chi_{b2}(3P)$ , $\Upsilon(4S)$

ARTUSO	05	PRL 94 032001	M. Artuso <i>et al.</i>	(CLEO Collab.)
ARTAMONOV	00	PL B474 427	A.S. Artamonov <i>et al.</i>	
BUTLER	94B	PR D49 40	F. Butler <i>et al.</i>	(CLEO Collab.)
WU	93	PL B301 307	Q.W. Wu <i>et al.</i>	(CUSB Collab.)
HEINTZ	92	PR D46 1928	U. Heintz <i>et al.</i>	(CUSB II Collab.)
BROCK	91	PR D43 1448	I.C. Brock <i>et al.</i>	(CLEO Collab.)
HEINTZ	91	PRL 66 1563	U. Heintz <i>et al.</i>	(CUSB Collab.)
MORRISON	91	PRL 67 1696	R.J. Morrison <i>et al.</i>	(CLEO Collab.)
NARAIN	91	PRL 66 3113	M. Narain <i>et al.</i>	(CUSB Collab.)
CHEN	89B	PR D39 3528	W.Y. Chen <i>et al.</i>	(CLEO Collab.)
KAARSBERG	89	PRL 62 2077	T.M. Kaarsberg <i>et al.</i>	(CUSB Collab.)
BUCHMUELLER...	88	HE $e^+e^-$ Physics 412	W. Buchmueller, S. Cooper	(HANN, DESY, MIT)
Editors: A. Ali and P. Soeding, World Scientific, Singapore				
COHEN	87	RMP 59 1121	E.R. Cohen, B.N. Taylor	(RIS C, NBS)
BARU	86B	ZPHY C32 622 (erratum)	S.E. Baru <i>et al.</i>	(NOVO)
KURAEV	85	SJNP 41 466	E.A. Kurayev, V.S. Fadin	(NOVO)
Translated from YAF 41 733.				
ARTAMONOV	84	PL 137B 272	A.S. Artamonov <i>et al.</i>	(NOVO)
GILES	84B	PR D29 1285	R. Giles <i>et al.</i>	(CLEO Collab.)
ANDREWS	83	PRL 50 807	D.E. Andrews <i>et al.</i>	(CLEO Collab.)
GREEN	82	PRL 49 617	J. Green <i>et al.</i>	(CLEO Collab.)
MAGERAS	82	PL 118B 453	G. Mageras <i>et al.</i>	(COLU, CORN, LSU+)

### $\chi_{b1}(3P)$ REFERENCES

SIRUNYAN	18N	PRL 121 092002	A.M. Sirunyan <i>et al.</i>	(CMS Collab.)
AAIJ	14BG	JHEP 1410 089	R. Aaij <i>et al.</i>	(LHCb Collab.)
AAIJ	14BI	EPJ C74 3092	R. Aaij <i>et al.</i>	(LHCb Collab.)
AAD	12A	PRL 108 152001	G. Aad <i>et al.</i>	(ATLAS Collab.)
ABAZOV	12Q	PR D86 031103	V.M. Abazov <i>et al.</i>	(D0 Collab.)

### $\chi_{b2}(3P)$

$$I^G(J^{PC}) = 0^+(2^{++})$$

Needs confirmation.

Observed in the radiative decay to  $\Upsilon(3S)$ , therefore  $C = +$ .  $J$  needs confirmation.

### $\chi_{b2}(3P)$ MASS

VALUE (MeV)	DOCUMENT ID	TECN	COMMENT
<b>10524.02 ± 0.57 ± 0.53</b>	<sup>1</sup> SIRUNYAN	18N CMS	$pp \rightarrow \gamma \mu^+ \mu^- X$
• • • We do not use the following data for averages, fits, limits, etc. • • •			
10530 ± 5 ± 9	<sup>2</sup> AAD	12A ATLS	$pp \rightarrow \gamma \mu^+ \mu^- X$

<sup>1</sup> Systematic error includes an additional 0.5 MeV for the uncertainty on the  $\Upsilon(3S)$  mass. Also measures  $m_{\chi_{b2}(3P)} - m_{\chi_{b1}(3P)} = 10.60 \pm 0.64 \pm 0.17$  MeV. A total of 372  $\chi_{b1}(3P)$  and  $\chi_{b2}(3P)$  events was observed.

<sup>2</sup> The mass barycenter of the merged lineshapes from the  $J = 1$  and 2 states.

### $\chi_{b2}(3P)$ DECAY MODES

Mode	Fraction ( $\Gamma_i/\Gamma$ )
$\Gamma_1 \Upsilon(3S)\gamma$	seen

### $\chi_{b2}(3P)$ BRANCHING RATIOS

$\Gamma(\Upsilon(3S)\gamma)/\Gamma_{total}$	DOCUMENT ID	TECN	COMMENT	$\Gamma_1/\Gamma$
seen	SIRUNYAN	18N CMS	$pp \rightarrow \gamma \mu^+ \mu^- X$	

### $\chi_{b2}(3P)$ REFERENCES

SIRUNYAN	18N	PRL 121 092002	A.M. Sirunyan <i>et al.</i>	(CMS Collab.)
AAD	12A	PRL 108 152001	G. Aad <i>et al.</i>	(ATLAS Collab.)

### $\Upsilon(4S)$

$$I^G(J^{PC}) = 0^-(1^{--})$$

also known as  $\Upsilon(10580)$

### $\Upsilon(4S)$ MASS

VALUE (MeV)	DOCUMENT ID	TECN	COMMENT
<b>10579.4 ± 1.2 OUR AVERAGE</b>			
10579.3 ± 0.4 ± 1.2	AUBERT	05Q BABR	$e^+e^- \rightarrow$ hadrons
10580.0 ± 3.5	<sup>1</sup> BEBEK	87 CLEO	$e^+e^- \rightarrow$ hadrons
• • • We do not use the following data for averages, fits, limits, etc. • • •			
10577.4 ± 1.0	<sup>2</sup> LOVELOCK	85 CUSB	$e^+e^- \rightarrow$ hadrons

<sup>1</sup> Reanalysis of BESSON 85.

<sup>2</sup> No systematic error given.

### $\Upsilon(4S)$ WIDTH

VALUE (MeV)	DOCUMENT ID	TECN	COMMENT
<b>20.5 ± 2.5 OUR AVERAGE</b>			
20.7 ± 1.6 ± 2.5	AUBERT	05Q BABR	$e^+e^- \rightarrow$ hadrons
20 ± 2 ± 4	BESSON	85 CLEO	$e^+e^- \rightarrow$ hadrons
• • • We do not use the following data for averages, fits, limits, etc. • • •			
25 ± 2.5	LOVELOCK	85 CUSB	$e^+e^- \rightarrow$ hadrons

### $\Upsilon(4S)$ DECAY MODES

Mode	Fraction ( $\Gamma_i/\Gamma$ )	Confidence level
$\Gamma_1 B\bar{B}$	> 96	%
$\Gamma_2 B^+B^-$	(51.4 ± 0.6 )	%
$\Gamma_3 D_s^+ \text{ anything} + c.c.$	(17.8 ± 2.6 )	%
$\Gamma_4 B^0\bar{B}^0$	(48.6 ± 0.6 )	%
$\Gamma_5 J/\psi K_S^0 + (J/\psi, \eta_c) K_S^0$	< 4	$\times 10^{-7}$
$\Gamma_6 \text{non-}B\bar{B}$	< 4	%
$\Gamma_7 e^+e^-$	( 1.57 ± 0.08 )	$\times 10^{-5}$
$\Gamma_8 \rho^+\rho^-$	< 5.7	$\times 10^{-6}$
$\Gamma_9 K^*(892)^0\bar{K}^0$	< 2.0	$\times 10^{-6}$
$\Gamma_{10} J/\psi(1S) \text{ anything}$	< 1.9	$\times 10^{-4}$

### $\chi_{b1}(3P)$

$$I^G(J^{PC}) = 0^+(1^{++})$$

Needs confirmation.

Observed in the radiative decay to  $\Upsilon(1S, 2S, 3S)$ , therefore  $C = +$ .  $J$  needs confirmation.

### $\chi_{b1}(3P)$ MASS

VALUE (MeV)	EVTS	DOCUMENT ID	TECN	COMMENT
<b>10513.42 ± 0.41 ± 0.53</b>		<sup>1</sup> SIRUNYAN	18N CMS	$pp \rightarrow \gamma \mu^+ \mu^- X$
• • • We do not use the following data for averages, fits, limits, etc. • • •				
10515.7 ± 2.2 + 1.5 - 3.9 - 2.1	169	<sup>2</sup> AAIJ	14BG LHCb	$pp \rightarrow \gamma \mu^+ \mu^- X$
10512.1 ± 2.1 ± 0.9	351	<sup>3</sup> AAIJ	14BG LHCb	$pp \rightarrow \gamma \mu^+ \mu^- X$
10511.3 ± 1.7 ± 2.5	182	<sup>4</sup> AAIJ	14BI LHCb	$pp \rightarrow \gamma \mu^+ \mu^- X$
10530 ± 5 ± 9		<sup>5</sup> AAD	12A ATLS	$pp \rightarrow \gamma \mu^+ \mu^- X$
10551 ± 14 ± 17		<sup>5</sup> ABAZOV	12Q D0	$p\bar{p} \rightarrow \gamma \mu^+ \mu^- X$

- <sup>1</sup> Systematic error includes an additional 0.5 MeV for the uncertainty on the  $\Upsilon(3S)$  mass. Also measures  $m_{\chi_{b2}(3P)} - m_{\chi_{b1}(3P)} = 10.60 \pm 0.64 \pm 0.17$  MeV. A total of 372  $\chi_{b1}(3P)$  and  $\chi_{b2}(3P)$  events was observed.
- <sup>2</sup> From  $\chi_{b1}(3P) \rightarrow \Upsilon(1S, 2S)\gamma$  transitions assuming  $m_{\chi_{b2}(3P)} - m_{\chi_{b1}(3P)} = 10.5 \pm 1.5$  MeV and allowing for  $\pm 30\%$  variation in the  $\chi_{b2}(3P)$  production rate relative to that of  $\chi_{b1}(3P)$ .
- <sup>3</sup> The mass of the  $\chi_{b1}(3P)$  state obtained by combining the results of AAIJ 14BG with that of AAIJ 14BI. The first uncertainty is experimental and the second attributable to the unknown mass splitting, assumed to be  $m_{\chi_{b2}(3P)} - m_{\chi_{b1}(3P)} = 10.5 \pm 1.5$  MeV.
- <sup>4</sup> From  $\chi_{b1}(3P) \rightarrow \Upsilon(3S)\gamma$  transition assuming  $m_{\chi_{b2}(3P)} - m_{\chi_{b1}(3P)} = 10.5 \pm 1.5$  MeV.
- <sup>5</sup> The mass barycenter of the merged lineshapes from the  $J = 1$  and 2 states.

### $\chi_{b1}(3P)$ DECAY MODES

Mode	Fraction ( $\Gamma_i/\Gamma$ )
$\Gamma_1 \Upsilon(1S)\gamma$	seen
$\Gamma_2 \Upsilon(2S)\gamma$	seen
$\Gamma_3 \Upsilon(3S)\gamma$	seen

### $\chi_{b1}(3P)$ BRANCHING RATIOS

$\Gamma(\Upsilon(1S)\gamma)/\Gamma_{total}$	DOCUMENT ID	TECN	COMMENT	$\Gamma_1/\Gamma$
seen	169	<sup>1</sup> AAIJ	14BG LHCb	$pp \rightarrow \gamma \mu^+ \mu^- X$
• • • We do not use the following data for averages, fits, limits, etc. • • •				
seen		AAD	12A ATLS	$pp \rightarrow \gamma \mu^+ \mu^- X$
seen		ABAZOV	12Q D0	$p\bar{p} \rightarrow \gamma \mu^+ \mu^- X$

- <sup>1</sup> From  $\chi_{b1}(3P) \rightarrow \Upsilon(1S, 2S)\gamma$  transitions assuming  $m_{\chi_{b2}(3P)} - m_{\chi_{b1}(3P)} = 10.5 \pm 1.5$  MeV and allowing for  $\pm 30\%$  variation in the  $\chi_{b2}(3P)$  production rate relative to that of  $\chi_{b1}(3P)$ .

### $\Gamma(\Upsilon(2S)\gamma)/\Gamma_{total}$

VALUE	EVTS	DOCUMENT ID	TECN	COMMENT	$\Gamma_2/\Gamma$
seen	169	<sup>1</sup> AAIJ	14BG LHCb	$pp \rightarrow \gamma \mu^+ \mu^- X$	
• • • We do not use the following data for averages, fits, limits, etc. • • •					
seen		AAD	12A ATLS	$pp \rightarrow \gamma \mu^+ \mu^- X$	

- <sup>1</sup> From  $\chi_{b1}(3P) \rightarrow \Upsilon(1S, 2S)\gamma$  transitions assuming  $m_{\chi_{b2}(3P)} - m_{\chi_{b1}(3P)} = 10.5 \pm 1.5$  MeV and allowing for  $\pm 30\%$  variation in the  $\chi_{b2}(3P)$  production rate relative to that of  $\chi_{b1}(3P)$ .

### $\Gamma(\Upsilon(3S)\gamma)/\Gamma_{total}$

VALUE	EVTS	DOCUMENT ID	TECN	COMMENT	$\Gamma_3/\Gamma$
seen		SIRUNYAN	18N CMS	$pp \rightarrow \gamma \mu^+ \mu^- X$	
seen	182	AAIJ	14BI LHCb	$pp \rightarrow \gamma \mu^+ \mu^- X$	

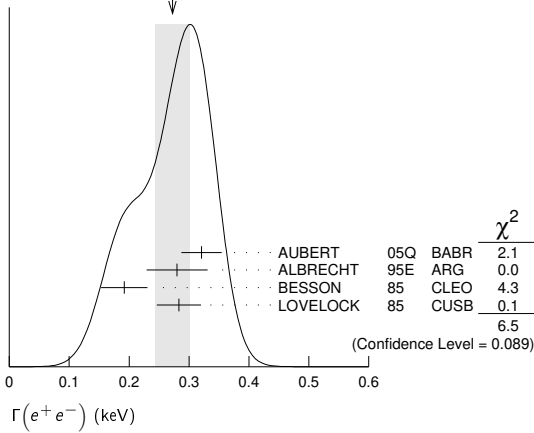
$\Gamma_{11}$	$D^{*+}$ anything + c.c.	< 7.4	%	90%
$\Gamma_{12}$	$\phi$ anything	( 7.1 $\pm$ 0.6 )	%	
$\Gamma_{13}$	$\phi\eta$	< 1.8	$\times 10^{-6}$	90%
$\Gamma_{14}$	$\phi\eta'$	< 4.3	$\times 10^{-6}$	90%
$\Gamma_{15}$	$\rho\eta$	< 1.3	$\times 10^{-6}$	90%
$\Gamma_{16}$	$\rho\eta'$	< 2.5	$\times 10^{-6}$	90%
$\Gamma_{17}$	$\Upsilon(1S)$ anything	< 4	$\times 10^{-3}$	90%
$\Gamma_{18}$	$\Upsilon(1S)\pi^+\pi^-$	( 8.2 $\pm$ 0.4 )	$\times 10^{-5}$	
$\Gamma_{19}$	$\Upsilon(1S)\eta$	( 1.81 $\pm$ 0.18 )	$\times 10^{-4}$	
$\Gamma_{20}$	$\Upsilon(1S)\eta'$	( 3.4 $\pm$ 0.9 )	$\times 10^{-5}$	
$\Gamma_{21}$	$\Upsilon(2S)\pi^+\pi^-$	( 8.2 $\pm$ 0.8 )	$\times 10^{-5}$	
$\Gamma_{22}$	$h_b(1P)\pi^+\pi^-$	not seen		
$\Gamma_{23}$	$h_b(1P)\eta$	( 2.18 $\pm$ 0.21 )	$\times 10^{-3}$	
$\Gamma_{24}$	${}^2H$ anything	< 1.3	$\times 10^{-5}$	90%
<b>Double Radiative Decays</b>				
$\Gamma_{25}$	$\gamma\gamma \Upsilon(D) \rightarrow \gamma\gamma\eta \Upsilon(1S)$	< 2.3	$\times 10^{-5}$	90%

$\Upsilon(4S)$  PARTIAL WIDTHS

$\Gamma(e^+e^-)$				$\Gamma_7$
VALUE (keV)	DOCUMENT ID	TECN	COMMENT	
<b>0.272 <math>\pm</math> 0.029 OUR AVERAGE</b>	Error includes scale factor of 1.5.		See the ideogram below.	
0.321 $\pm$ 0.017 $\pm$ 0.029	AUBERT 05Q	BABR	$e^+e^- \rightarrow$ hadrons	
0.28 $\pm$ 0.05 $\pm$ 0.01	<sup>1</sup> ALBRECHT 95E	ARG	$e^+e^- \rightarrow$ hadrons	
0.192 $\pm$ 0.007 $\pm$ 0.038	BESSION 85	CLEO	$e^+e^- \rightarrow$ hadrons	
0.283 $\pm$ 0.037	LOVELOCK 85	CUSB	$e^+e^- \rightarrow$ hadrons	

<sup>1</sup>Using LEYAOUANC 77 parametrization of  $\Gamma(s)$ .

WEIGHTED AVERAGE  
 0.272  $\pm$  0.029 (Error scaled by 1.5)



$\Upsilon(4S)$  BRANCHING RATIOS

$B\bar{B}$  DECAYS

The ratio of branching fraction to charged and neutral B mesons is often derived assuming isospin invariance in the decays, and relies on the knowledge of the  $B^+/B^0$  lifetime ratio. "OUR EVALUATION" is obtained based on averages of rescaled data listed below. The average and rescaling were performed by the Heavy Flavor Averaging Group (HFLAV) and are described at <https://hflav.web.cern.ch/>. The averaging/rescaling procedure takes into account the common dependence of the measurement on the value of the lifetime ratio.

$\Gamma(B^+B^-)/\Gamma_{total}$				$\Gamma_2/\Gamma$
VALUE	DOCUMENT ID	TECN	COMMENT	
<b>0.514 <math>\pm</math> 0.006 OUR EVALUATION</b>	Assuming $B(\Upsilon(4S) \rightarrow B\bar{B}) = 1$			

$\Gamma(D_s^+ \text{ anything + c.c.})/\Gamma_{total}$				$\Gamma_3/\Gamma$
VALUE	DOCUMENT ID	TECN	COMMENT	
<b>0.178 <math>\pm</math> 0.021 <math>\pm</math> 0.016</b>	<sup>1</sup> ARTUSO 05B	CLE3	$e^+e^- \rightarrow D_s X$	

<sup>1</sup>ARTUSO 05B reports  $[\Gamma(\Upsilon(4S) \rightarrow D_s^+ \text{ anything + c.c.})/\Gamma_{total}] \times [B(D_s^+ \rightarrow \phi\pi^+)] = (8.0 \pm 0.2 \pm 0.9) \times 10^{-3}$  which we divide by our best value  $B(D_s^+ \rightarrow \phi\pi^+) = (4.5 \pm 0.4) \times 10^{-2}$ . Our first error is their experiment's error and our second error is the systematic error from using our best value.

$\Gamma(B^0\bar{B}^0)/\Gamma_{total}$				$\Gamma_4/\Gamma$
---------------------------------------	--	--	--	-------------------

VALUE DOCUMENT ID TECN COMMENT  
**0.486  $\pm$  0.006 OUR EVALUATION** Assuming  $B(\Upsilon(4S) \rightarrow B\bar{B}) = 1$   
 ••• We do not use the following data for averages, fits, limits, etc. •••  
 0.487  $\pm$  0.010  $\pm$  0.008 <sup>1</sup>AUBERT,B 05H BABR  $\Upsilon(4S) \rightarrow \bar{B}B \rightarrow D^*\ell\nu_\ell$   
<sup>1</sup> Direct measurement. This value is averaged with the value extracted from the  $\Gamma(B^+B^-) / \Gamma(B^0\bar{B}^0)$  measurements.

$\Gamma(B^+B^-)/\Gamma(B^0\bar{B}^0)$				$\Gamma_2/\Gamma_4$
---------------------------------------	--	--	--	---------------------

VALUE DOCUMENT ID TECN COMMENT  
**1.058  $\pm$  0.024 OUR EVALUATION**  
 1.006  $\pm$  0.036  $\pm$  0.031 <sup>1</sup>AUBERT 04F BABR  $\Upsilon(4S) \rightarrow B\bar{B} \rightarrow J/\psi K$   
 1.01  $\pm$  0.03  $\pm$  0.09 <sup>1</sup>HASTINGS 03 BELL  $\Upsilon(4S) \rightarrow B\bar{B} \rightarrow$  dileptons  
 1.058  $\pm$  0.084  $\pm$  0.136 <sup>2</sup>ATHAR 02 CLEO  $\Upsilon(4S) \rightarrow B\bar{B} \rightarrow D^*\ell\nu$   
 1.10  $\pm$  0.06  $\pm$  0.05 <sup>3</sup>AUBERT 02 BABR  $\Upsilon(4S) \rightarrow B\bar{B} \rightarrow (c\bar{c})K^*$   
 1.04  $\pm$  0.07  $\pm$  0.04 <sup>4</sup>ALEXANDER 01 CLEO  $\Upsilon(4S) \rightarrow B\bar{B} \rightarrow J/\psi K^*$   
<sup>1</sup>HASTINGS 03 and AUBERT 04F assume  $\tau(B^+) / \tau(B^0) = 1.083 \pm 0.017$ .  
<sup>2</sup>ATHAR 02 assumes  $\tau(B^+) / \tau(B^0) = 1.074 \pm 0.028$ . Supersedes BARISH 95.  
<sup>3</sup>AUBERT 02 assumes  $\tau(B^+) / \tau(B^0) = 1.062 \pm 0.029$ .  
<sup>4</sup>ALEXANDER 01 assumes  $\tau(B^+) / \tau(B^0) = 1.066 \pm 0.024$ .

$[\Gamma(J/\psi K_S^0) + \Gamma(J/\psi, \eta_c) K_S^0]/\Gamma_{total}$				$\Gamma_5/\Gamma$
--	--	--	--	-------------------

Forbidden by CP invariance.  
 VALUE (units  $10^{-7}$ ) CL% DOCUMENT ID TECN COMMENT  
**<4** 90 <sup>1</sup>TAJIMA 07A BELL  $\Upsilon(4S) \rightarrow B^0\bar{B}^0$   
<sup>1</sup>  $\Upsilon(4S)$  with  $CP = +1$  decays to the final state with  $CP = -1$ .

non- $B\bar{B}$  DECAYS

$\Gamma(\text{non-}B\bar{B})/\Gamma_{total}$				$\Gamma_6/\Gamma$
--	--	--	--	-------------------

VALUE CL% DOCUMENT ID TECN COMMENT  
**<0.04** 95 BARISH 96B CLEO  $e^+e^-$

$\Gamma(e^+e^-)/\Gamma_{total}$				$\Gamma_7/\Gamma$
---------------------------------	--	--	--	-------------------

VALUE (units  $10^{-5}$ ) DOCUMENT ID TECN COMMENT  
**1.57  $\pm$  0.08 OUR AVERAGE**  
 1.55  $\pm$  0.04  $\pm$  0.07 AUBERT 05Q BABR  $e^+e^- \rightarrow$  hadrons  
 2.77  $\pm$  0.50  $\pm$  0.49 <sup>1</sup>ALBRECHT 95E ARG  $e^+e^- \rightarrow$  hadrons  
<sup>1</sup>Using LEYAOUANC 77 parametrization of  $\Gamma(s)$ .

$\Gamma(\rho^+\rho^-)/\Gamma_{total}$				$\Gamma_8/\Gamma$
---------------------------------------	--	--	--	-------------------

VALUE CL% DOCUMENT ID TECN COMMENT  
**<5.7  $\times 10^{-6}$**  90 AUBERT 08B BABR  $e^+e^- \rightarrow \pi^+\pi^-\pi^0$

$\Gamma(K^*(892)^0\bar{K}^0)/\Gamma_{total}$				$\Gamma_9/\Gamma$
--	--	--	--	-------------------

VALUE CL% DOCUMENT ID TECN COMMENT  
**<2.0  $\times 10^{-6}$**  90 SHEN 13A BELL  $e^+e^- \rightarrow K^*(892)^0\bar{K}^0$

$\Gamma(J/\psi(1S) \text{ anything})/\Gamma_{total}$				$\Gamma_{10}/\Gamma$
--	--	--	--	----------------------

VALUE (units  $10^{-4}$ ) CL% DOCUMENT ID TECN COMMENT  
**<1.9** 95 <sup>1</sup>ABE 02D BELL  $e^+e^- \rightarrow J/\psi X \rightarrow \ell^+\ell^-X$   
 ••• We do not use the following data for averages, fits, limits, etc. •••  
 <4.7 90 <sup>1</sup>AUBERT 01c BABR  $e^+e^- \rightarrow J/\psi X \rightarrow \ell^+\ell^-X$   
<sup>1</sup>Uses  $B(J/\psi \rightarrow e^+e^-) = 0.0593 \pm 0.0010$  and  $B(J/\psi \rightarrow \mu^+\mu^-) = 0.0588 \pm 0.0010$ .

$\Gamma(D^{*+} \text{ anything + c.c.})/\Gamma_{total}$				$\Gamma_{11}/\Gamma$
---	--	--	--	----------------------

VALUE CL% DOCUMENT ID TECN COMMENT  
**<0.074** 90 <sup>1</sup>ALEXANDER 90c CLEO  $e^+e^-$   
<sup>1</sup>For  $x > 0.473$ .

$\Gamma(\phi \text{ anything})/\Gamma_{total}$				$\Gamma_{12}/\Gamma$
--	--	--	--	----------------------

VALUE (units  $10^{-2}$ ) CL% DOCUMENT ID TECN COMMENT  
**7.1  $\pm$  0.1  $\pm$  0.6** HUANG 07 CLEO  $\Upsilon(4S) \rightarrow \phi X$   
 ••• We do not use the following data for averages, fits, limits, etc. •••  
 <0.23 90 <sup>1</sup>ALEXANDER 90c CLEO  $e^+e^-$   
<sup>1</sup>For  $x > 0.52$ .

$\Gamma(\phi\eta)/\Gamma_{total}$				$\Gamma_{13}/\Gamma$
-----------------------------------	--	--	--	----------------------

VALUE (units  $10^{-6}$ ) CL% DOCUMENT ID TECN COMMENT  
**<1.8** 90 <sup>1</sup>BELOUS 09 BELL  $e^+e^- \rightarrow \phi\eta$   
 ••• We do not use the following data for averages, fits, limits, etc. •••  
 <2.5 90 AUBERT,BE 06F BABR  $e^+e^- \rightarrow \phi\eta$   
<sup>1</sup>Using all intermediate branching fraction values from PDG 08.

$\Gamma(\phi\eta')/\Gamma_{total}$				$\Gamma_{14}/\Gamma$
------------------------------------	--	--	--	----------------------

VALUE (units  $10^{-6}$ ) CL% DOCUMENT ID TECN COMMENT  
**<4.3** 90 <sup>1</sup>BELOUS 09 BELL  $e^+e^- \rightarrow \phi\eta'$   
<sup>1</sup>Using all intermediate branching fraction values from PDG 08.



See key on page 999

Meson Particle Listings

$Z_b(10610)$

10605	$\pm 2 \begin{smallmatrix} +3 \\ -1 \end{smallmatrix}$	<sup>3</sup> BONDAR	12	BELL	$e^+e^- \rightarrow h_b(1P)\pi^+\pi^-$
10599	$\pm 6 \begin{smallmatrix} +5 \\ -4 \end{smallmatrix}$	<sup>3</sup> BONDAR	12	BELL	$e^+e^- \rightarrow h_b(2P)\pi^+\pi^-$

<sup>1</sup> Average of the BONDAR 12 measurements in separate channels.  
<sup>2</sup> Correlated with the corresponding result from BONDAR 12.  
<sup>3</sup> Superseded by the average measurement of BONDAR 12.

$Z_b(10610)^0$  MASS

VALUE (MeV)	DOCUMENT ID	TECN	COMMENT
<b>10609 ± 4 ± 4</b>	<sup>1</sup> KROKOVNY	13	BELL $e^+e^- \rightarrow \gamma(2S)/\gamma(3S)\pi^0\pi^0$

<sup>1</sup> From a simultaneous fit to the KROKOVNY 13 Dalitz analysis of  $e^+e^- \rightarrow \gamma(2S)/\gamma(3S)\pi^0\pi^0$  decays with fixed width  $\Gamma(Z_b(10610)^0) = 18.4$  MeV.

$Z_b(10610)^\pm$  WIDTH

VALUE (MeV)	DOCUMENT ID	TECN	COMMENT
<b>18.4 ± 2.4</b>	<sup>1</sup> BONDAR	12	BELL $e^+e^- \rightarrow$ hadrons
$18.5 \pm 5.3 \begin{smallmatrix} +6.1 \\ -2.3 \end{smallmatrix}$	<sup>2</sup> GARMASH	15	BELL $e^+e^- \rightarrow \gamma(1S)\pi^+\pi^-$
$20.8 \pm 2.5 \begin{smallmatrix} +0.3 \\ -2.1 \end{smallmatrix}$	<sup>2</sup> GARMASH	15	BELL $e^+e^- \rightarrow \gamma(2S)\pi^+\pi^-$
$18.7 \pm 3.4 \begin{smallmatrix} +2.5 \\ -1.3 \end{smallmatrix}$	<sup>2</sup> GARMASH	15	BELL $e^+e^- \rightarrow \gamma(3S)\pi^+\pi^-$
$22.3 \pm 7.7 \begin{smallmatrix} +3.0 \\ -4.0 \end{smallmatrix}$	<sup>3</sup> BONDAR	12	BELL $e^+e^- \rightarrow \gamma(1S)\pi^+\pi^-$
$24.2 \pm 3.1 \begin{smallmatrix} +2.0 \\ -3.0 \end{smallmatrix}$	<sup>3</sup> BONDAR	12	BELL $e^+e^- \rightarrow \gamma(2S)\pi^+\pi^-$
$17.6 \pm 3.0 \pm 3.0$	<sup>3</sup> BONDAR	12	BELL $e^+e^- \rightarrow \gamma(3S)\pi^+\pi^-$
$11.4 \pm 4.5 \begin{smallmatrix} +2.1 \\ -3.9 \end{smallmatrix} \begin{smallmatrix} +1.2 \\ -1.2 \end{smallmatrix}$	<sup>3</sup> BONDAR	12	BELL $e^+e^- \rightarrow h_b(1P)\pi^+\pi^-$
$13 \begin{smallmatrix} +10 \\ -8 \end{smallmatrix} \begin{smallmatrix} +9 \\ -7 \end{smallmatrix}$	<sup>3</sup> BONDAR	12	BELL $e^+e^- \rightarrow h_b(2P)\pi^+\pi^-$

<sup>1</sup> Average of the BONDAR 12 measurements in separate channels.  
<sup>2</sup> Correlated with the corresponding result from BONDAR 12.  
<sup>3</sup> Superseded by the average measurement of BONDAR 12.

$Z_b(10610)$  DECAY MODES

Mode	Fraction ( $\Gamma_i/\Gamma$ )
$\Gamma_1$ $\gamma(1S)\pi^+$	$(5.4 \pm 1.9 \begin{smallmatrix} +1.9 \\ -1.5 \end{smallmatrix}) \times 10^{-3}$
$\Gamma_2$ $\gamma(1S)\pi^0$	not seen
$\Gamma_3$ $\gamma(2S)\pi^+$	$(3.6 \pm 1.1 \begin{smallmatrix} +1.1 \\ -0.8 \end{smallmatrix}) \%$
$\Gamma_4$ $\gamma(2S)\pi^0$	seen
$\Gamma_5$ $\gamma(3S)\pi^+$	$(2.1 \pm 0.8 \begin{smallmatrix} +0.8 \\ -0.6 \end{smallmatrix}) \%$
$\Gamma_6$ $\gamma(3S)\pi^0$	seen
$\Gamma_7$ $h_b(1P)\pi^+$	$(3.5 \pm 1.2 \begin{smallmatrix} +1.2 \\ -0.9 \end{smallmatrix}) \%$
$\Gamma_8$ $h_b(2P)\pi^+$	$(4.7 \pm 1.7 \begin{smallmatrix} +1.7 \\ -1.3 \end{smallmatrix}) \%$
$\Gamma_9$ $B^+\bar{B}^0$	not seen
$\Gamma_{10}$ $B^+\bar{B}^{*0} + B^{*+}\bar{B}^0$	$(85.6 \pm 2.1 \begin{smallmatrix} +2.1 \\ -2.9 \end{smallmatrix}) \%$

$Z_b(10610)$  BRANCHING RATIOS

$\Gamma(\gamma(1S)\pi^+)/\Gamma_{total}$	DOCUMENT ID	TECN	COMMENT	$\Gamma_1/\Gamma$
<b>5.4 ± 1.6 ± 1.1</b> <b>-1.3 - 0.8</b>	<sup>1</sup> GARMASH	16	BELL $e^+e^- \rightarrow \pi^-B^+\bar{B}^{*0}, \pi^-\bar{B}^0B^{*+}$	

• • • We do not use the following data for averages, fits, limits, etc. • • •  
 seen GARMASH 15 BELL  $e^+e^- \rightarrow \gamma(1S)\pi^+\pi^-$   
 seen BONDAR 12 BELL  $e^+e^- \rightarrow \gamma(1S)\pi^+\pi^-$

<sup>1</sup> Assuming the  $Z_b(10610)$  decay width is saturated by the channels  $\pi^+\gamma(1S, 2S, 3S), \pi^+h_b(1P, 2P)$ , and  $B^+\bar{B}^{*0} + \bar{B}^0B^{*+}$ , and using the results from BONDAR 12 and MIZUK 16.

$\Gamma(\gamma(1S)\pi^0)/\Gamma_{total}$	DOCUMENT ID	TECN	COMMENT	$\Gamma_2/\Gamma$
not seen	KROKOVNY	13	BELL $e^+e^- \rightarrow \gamma(1S)\pi^0\pi^0$	

$\Gamma(\gamma(2S)\pi^+)/\Gamma_{total}$	DOCUMENT ID	TECN	COMMENT	$\Gamma_3/\Gamma$
<b>3.62 ± 0.76 ± 0.79</b> <b>-0.59 - 0.53</b>	<sup>1</sup> GARMASH	16	BELL $e^+e^- \rightarrow \pi^-B^+\bar{B}^{*0}, \pi^-\bar{B}^0B^{*+}$	

• • • We do not use the following data for averages, fits, limits, etc. • • •  
 seen GARMASH 15 BELL  $e^+e^- \rightarrow \gamma(2S)\pi^+\pi^-$   
 seen BONDAR 12 BELL  $e^+e^- \rightarrow \gamma(2S)\pi^+\pi^-$

<sup>1</sup> Assuming the  $Z_b(10610)$  decay width is saturated by the channels  $\pi^+\gamma(1S, 2S, 3S), \pi^+h_b(1P, 2P)$ , and  $B^+\bar{B}^{*0} + \bar{B}^0B^{*+}$ , and using the results from BONDAR 12 and MIZUK 16.

$\Gamma(\gamma(2S)\pi^0)/\Gamma_{total}$	DOCUMENT ID	TECN	COMMENT	$\Gamma_4/\Gamma$
seen	<sup>1</sup> KROKOVNY	13	BELL $e^+e^- \rightarrow \gamma(2S)\pi^0\pi^0$	

<sup>1</sup> Combined significance in  $e^+e^- \rightarrow \gamma(2S)/\gamma(3S)\pi^0\pi^0$ , including systematics, of 6.5 $\sigma$ .

$\Gamma(\gamma(3S)\pi^+)/\Gamma_{total}$	DOCUMENT ID	TECN	COMMENT	$\Gamma_5/\Gamma$
<b>2.15 ± 0.55 ± 0.60</b> <b>-0.42 - 0.43</b>	<sup>1</sup> GARMASH	16	BELL $e^+e^- \rightarrow \pi^-B^+\bar{B}^{*0}, \pi^-\bar{B}^0B^{*+}$	

• • • We do not use the following data for averages, fits, limits, etc. • • •  
 seen GARMASH 15 BELL  $e^+e^- \rightarrow \gamma(3S)\pi^+\pi^-$   
 seen BONDAR 12 BELL  $e^+e^- \rightarrow \gamma(3S)\pi^+\pi^-$

<sup>1</sup> Assuming the  $Z_b(10610)$  decay width is saturated by the channels  $\pi^+\gamma(1S, 2S, 3S), \pi^+h_b(1P, 2P)$ , and  $B^+\bar{B}^{*0} + \bar{B}^0B^{*+}$ , and using the results from BONDAR 12 and MIZUK 16.

$\Gamma(\gamma(3S)\pi^0)/\Gamma_{total}$	DOCUMENT ID	TECN	COMMENT	$\Gamma_6/\Gamma$
seen	<sup>1</sup> KROKOVNY	13	BELL $e^+e^- \rightarrow \gamma(3S)\pi^0\pi^0$	

<sup>1</sup> Combined significance in  $e^+e^- \rightarrow \gamma(2S)/\gamma(3S)\pi^0\pi^0$ , including systematics, of 6.5 $\sigma$ .

$\Gamma(h_b(1P)\pi^+)/\Gamma_{total}$	DOCUMENT ID	TECN	COMMENT	$\Gamma_7/\Gamma$
<b>3.45 ± 0.87 ± 0.86</b> <b>-1.00 - 0.89</b>	<sup>1</sup> GARMASH	16	BELL $e^+e^- \rightarrow \pi^-B^+\bar{B}^{*0}, \pi^-\bar{B}^0B^{*+}$	

• • • We do not use the following data for averages, fits, limits, etc. • • •  
 possibly seen <sup>2</sup> MIZUK 16 BELL  $e^+e^- \rightarrow h_b(1P)\pi^+\pi^-$   
 seen <sup>3</sup> BONDAR 12 BELL  $e^+e^- \rightarrow h_b(1P)\pi^+\pi^-$

<sup>1</sup> Assuming the  $Z_b(10610)$  decay width is saturated by the channels  $\pi^+\gamma(1S, 2S, 3S), \pi^+h_b(1P, 2P)$ , and  $B^+\bar{B}^{*0} + \bar{B}^0B^{*+}$ , and using the results from BONDAR 12 and MIZUK 16.  
<sup>2</sup> Using  $e^+e^-$  energies near the  $\gamma(11020)$ .  
<sup>3</sup> Using  $e^+e^-$  energies near the  $\gamma(10860)$ .

$\Gamma(h_b(2P)\pi^+)/\Gamma_{total}$	DOCUMENT ID	TECN	COMMENT	$\Gamma_8/\Gamma$
<b>4.67 ± 1.24 ± 1.18</b> <b>-1.00 - 0.89</b>	<sup>1</sup> GARMASH	16	BELL $e^+e^- \rightarrow \pi^-B^+\bar{B}^{*0}, \pi^-\bar{B}^0B^{*+}$	

• • • We do not use the following data for averages, fits, limits, etc. • • •  
 possibly seen <sup>2</sup> MIZUK 16 BELL  $e^+e^- \rightarrow h_b(2P)\pi^+\pi^-$   
 seen <sup>3</sup> BONDAR 12 BELL  $e^+e^- \rightarrow h_b(2P)\pi^+\pi^-$

<sup>1</sup> Assuming the  $Z_b(10610)$  decay width is saturated by the channels  $\pi^+\gamma(1S, 2S, 3S), \pi^+h_b(1P, 2P)$ , and  $B^+\bar{B}^{*0} + \bar{B}^0B^{*+}$ , and using the results from BONDAR 12 and MIZUK 16.  
<sup>2</sup> Using  $e^+e^-$  energies near the  $\gamma(11020)$ .  
<sup>3</sup> Using  $e^+e^-$  energies near the  $\gamma(10860)$ .

$\Gamma(B^+\bar{B}^0)/\Gamma_{total}$	DOCUMENT ID	TECN	COMMENT	$\Gamma_9/\Gamma$
not seen	GARMASH	16	BELL $e^+e^- \rightarrow \pi^-B^+\bar{B}^0$	

$[\Gamma(B^+\bar{B}^{*0}) + \Gamma(B^{*+}\bar{B}^0)]/\Gamma_{total}$	EVTS	DOCUMENT ID	TECN	COMMENT	$\Gamma_{10}/\Gamma$
<b>85.6 ± 1.5 ± 1.5</b> <b>-2.0 - 2.1</b>	357	<sup>1</sup> GARMASH	16	BELL $e^+e^- \rightarrow \pi^-B^+\bar{B}^{*0}, \pi^-\bar{B}^0B^{*+}$	

<sup>1</sup> Assuming the  $Z_b(10610)$  decay width is saturated by the channels  $\pi^+\gamma(1S, 2S, 3S), \pi^+h_b(1P, 2P)$ , and  $B^+\bar{B}^{*0} + B^{*+}\bar{B}^0$ , and using the results from BONDAR 12 and MIZUK 16. Using the mass and width of the  $Z_b(10610)$  from BONDAR 12.

$[\Gamma(B^+\bar{B}^{*0}) + \Gamma(B^{*+}\bar{B}^0)] / [\Gamma(\gamma(1S)\pi^+) + \Gamma(\gamma(2S)\pi^+) + \Gamma(\gamma(3S)\pi^+) + \Gamma(h_b(1P)\pi^+) + \Gamma(h_b(2P)\pi^+)]$	$\Gamma_{10}/(\Gamma_1 + \Gamma_3 + \Gamma_5 + \Gamma_7 + \Gamma_8)$
<b>5.93 ± 0.99 ± 1.01</b> <b>-0.69 - 0.73</b>	357

• • • We do not use the following data for averages, fits, limits, etc. • • •  
<sup>1</sup> Combined with the results of BONDAR 12 and MIZUK 16. Not independent from  $Z_b(10610)$  branching fractions to  $\pi^+\gamma(1S, 2S, 3S), \pi^+h_b(1P, 2P)$ , and  $B^+\bar{B}^{*0} + \bar{B}^0B^{*+}$ .

$Z_b(10610)$  REFERENCES

GARMASH	16	PRL 116 212001	A. Garmash <i>et al.</i>	(BELLE Collab.)
MIZUK	16	PRL 117 142001	R. Mizuk <i>et al.</i>	(BELLE Collab.)
GARMASH	15	PR D91 072003	A. Garmash <i>et al.</i>	(BELLE Collab.)
KROKOVNY	13	PR D88 052016	P. Krokovny <i>et al.</i>	(BELLE Collab.)
BONDAR	12	PRL 108 122001	A. Bondar <i>et al.</i>	(BELLE Collab.)

## Meson Particle Listings

 $Z_b(10650)$  $Z_b(10650)$ was  $X(10650)^\pm$ 

Properties incompatible with a  $q\bar{q}$  structure (exotic state). See the review on non- $q\bar{q}$  states.

Observed by BONDAR 12 in  $\Upsilon(5S)$  decays to  $\Upsilon(nS)\pi^+\pi^-$  ( $n = 1, 2, 3$ ) and  $h_b(mP)\pi^+\pi^-$  ( $m = 1, 2$ ).  $J^P = 1^+$  is favored from angular analyses.

$$I^G(J^{PC}) = 1^+(1^+-)$$

$I, G, C$  need confirmation.

 $Z_b(10650)$  MASS

VALUE (MeV)	DOCUMENT ID	TECN	COMMENT
$10652.2 \pm 1.5$	<sup>1</sup> BONDAR 12	BELL	$e^+e^- \rightarrow$ hadrons
$10656.7 \pm 5.0^{+1.1}_{-3.1}$	<sup>2</sup> GARMASH 15	BELL	$e^+e^- \rightarrow \Upsilon(1S)\pi^+\pi^-$
$10650.7 \pm 1.5^{+0.5}_{-0.2}$	<sup>2</sup> GARMASH 15	BELL	$e^+e^- \rightarrow \Upsilon(2S)\pi^+\pi^-$
$10651.2 \pm 1.0^{+0.4}_{-0.3}$	<sup>2</sup> GARMASH 15	BELL	$e^+e^- \rightarrow \Upsilon(3S)\pi^+\pi^-$
$10657 \pm 6 \pm 3$	<sup>3</sup> BONDAR 12	BELL	$e^+e^- \rightarrow \Upsilon(1S)\pi^+\pi^-$
$10651 \pm 2 \pm 3$	<sup>3</sup> BONDAR 12	BELL	$e^+e^- \rightarrow \Upsilon(2S)\pi^+\pi^-$
$10652 \pm 1 \pm 2$	<sup>3</sup> BONDAR 12	BELL	$e^+e^- \rightarrow \Upsilon(3S)\pi^+\pi^-$
$10654 \pm 3 \pm 1$	<sup>3</sup> BONDAR 12	BELL	$e^+e^- \rightarrow h_b(1P)\pi^+\pi^-$
$10651 \pm 2 \pm 3$	<sup>3</sup> BONDAR 12	BELL	$e^+e^- \rightarrow h_b(2P)\pi^+\pi^-$

<sup>1</sup> Average of the BONDAR 12 measurements in separate channels.

<sup>2</sup> Correlated with the corresponding result from BONDAR 12.

<sup>3</sup> Superseded by the average measurement of BONDAR 12.

 $Z_b(10650)$  WIDTH

VALUE (MeV)	DOCUMENT ID	TECN	COMMENT
$11.5 \pm 2.2$	<sup>4</sup> BONDAR 12	BELL	$e^+e^- \rightarrow$ hadrons
$12.1^{+11.3+2.7}_{-4.8-0.6}$	<sup>5</sup> GARMASH 15	BELL	$e^+e^- \rightarrow \Upsilon(1S)\pi^+\pi^-$
$14.2 \pm 3.7^{+0.9}_{-0.4}$	<sup>5</sup> GARMASH 15	BELL	$e^+e^- \rightarrow \Upsilon(2S)\pi^+\pi^-$
$9.3 \pm 2.2^{+0.3}_{-0.5}$	<sup>5</sup> GARMASH 15	BELL	$e^+e^- \rightarrow \Upsilon(3S)\pi^+\pi^-$
$16.3 \pm 9.8^{+6.0}_{-2.0}$	<sup>6</sup> BONDAR 12	BELL	$e^+e^- \rightarrow \Upsilon(1S)\pi^+\pi^-$
$13.3 \pm 3.3^{+4.0}_{-3.0}$	<sup>6</sup> BONDAR 12	BELL	$e^+e^- \rightarrow \Upsilon(2S)\pi^+\pi^-$
$8.4 \pm 2.0 \pm 2.0$	<sup>6</sup> BONDAR 12	BELL	$e^+e^- \rightarrow \Upsilon(3S)\pi^+\pi^-$
$20.9^{+5.4+2.1}_{-4.7-5.7}$	<sup>6</sup> BONDAR 12	BELL	$e^+e^- \rightarrow h_b(1P)\pi^+\pi^-$
$19 \pm 7^{+11}_{-7}$	<sup>6</sup> BONDAR 12	BELL	$e^+e^- \rightarrow h_b(2P)\pi^+\pi^-$

<sup>4</sup> Average of the BONDAR 12 measurements in separate channels.

<sup>5</sup> Correlated with the corresponding result from BONDAR 12.

<sup>6</sup> Superseded by the average measurement of BONDAR 12.

 $Z_b(10650)^+$  DECAY MODES

$Z_b(10650)^-$  decay modes are charge conjugates of the modes below.

Mode	Fraction ( $\Gamma_i/\Gamma$ )
$\Gamma_1$ $\Upsilon(1S)\pi^+$	$(1.7^{+0.8}_{-0.6}) \times 10^{-3}$
$\Gamma_2$ $\Upsilon(2S)\pi^+$	$(1.4^{+0.6}_{-0.4})\%$
$\Gamma_3$ $\Upsilon(3S)\pi^+$	$(1.6^{+0.7}_{-0.5})\%$
$\Gamma_4$ $h_b(1P)\pi^+$	$(8.4^{+2.9}_{-2.4})\%$
$\Gamma_5$ $h_b(2P)\pi^+$	$(15 \pm 4)\%$
$\Gamma_6$ $B^+\bar{B}^0$	not seen
$\Gamma_7$ $B^+\bar{B}^{*0} + B^{*+}\bar{B}^0$	not seen
$\Gamma_8$ $B^{*+}\bar{B}^{*0}$	$(74^{+4}_{-6})\%$

 $Z_b(10650)$  BRANCHING RATIOS

$\Gamma(\Upsilon(1S)\pi^+)/\Gamma_{\text{total}}$	DOCUMENT ID	TECN	COMMENT	$\Gamma_1/\Gamma$
$1.7^{+0.7+0.3}_{-0.6-0.2}$	<sup>7</sup> GARMASH 16	BELL	$e^+e^- \rightarrow \pi^-B^{*+}\bar{B}^{*0}$	
••• We do not use the following data for averages, fits, limits, etc. •••				
seen	GARMASH 15	BELL	$e^+e^- \rightarrow \Upsilon(1S)\pi^+\pi^-$	
seen	BONDAR 12	BELL	$e^+e^- \rightarrow \Upsilon(1S)\pi^+\pi^-$	

<sup>7</sup> Assuming the  $Z_b(10650)$  decay width is saturated by the channels  $\pi^+\Upsilon(1S, 2S, 3S)$ ,  $\pi^+h_b(1P, 2P)$ , and  $B^{*+}\bar{B}^{*0}$ , and using the results from BONDAR 12 and MIZUK 16.

 $\Gamma(\Upsilon(2S)\pi^+)/\Gamma_{\text{total}}$ 

VALUE (units $10^{-2}$ )	DOCUMENT ID	TECN	COMMENT	$\Gamma_2/\Gamma$
$1.39^{+0.48+0.34}_{-0.38-0.23}$	<sup>8</sup> GARMASH 16	BELL	$e^+e^- \rightarrow \pi^-B^{*+}\bar{B}^{*0}$	
••• We do not use the following data for averages, fits, limits, etc. •••				
seen	GARMASH 15	BELL	$e^+e^- \rightarrow \Upsilon(2S)\pi^+\pi^-$	
seen	BONDAR 12	BELL	$e^+e^- \rightarrow \Upsilon(2S)\pi^+\pi^-$	

<sup>8</sup> Assuming the  $Z_b(10650)$  decay width is saturated by the channels  $\pi^+\Upsilon(1S, 2S, 3S)$ ,  $\pi^+h_b(1P, 2P)$ , and  $B^{*+}\bar{B}^{*0}$ , and using the results from BONDAR 12 and MIZUK 16.

 $\Gamma(\Upsilon(3S)\pi^+)/\Gamma_{\text{total}}$ 

VALUE (units $10^{-2}$ )	DOCUMENT ID	TECN	COMMENT	$\Gamma_3/\Gamma$
$1.63^{+0.53+0.39}_{-0.42-0.28}$	<sup>9</sup> GARMASH 16	BELL	$e^+e^- \rightarrow \pi^-B^{*+}\bar{B}^{*0}$	
••• We do not use the following data for averages, fits, limits, etc. •••				
seen	GARMASH 15	BELL	$e^+e^- \rightarrow \Upsilon(3S)\pi^+\pi^-$	
seen	BONDAR 12	BELL	$e^+e^- \rightarrow \Upsilon(3S)\pi^+\pi^-$	

<sup>9</sup> Assuming the  $Z_b(10650)$  decay width is saturated by the channels  $\pi^+\Upsilon(1S, 2S, 3S)$ ,  $\pi^+h_b(1P, 2P)$ , and  $B^{*+}\bar{B}^{*0}$ , and using the results from BONDAR 12 and MIZUK 16.

 $\Gamma(h_b(1P)\pi^+)/\Gamma_{\text{total}}$ 

VALUE (units $10^{-2}$ )	DOCUMENT ID	TECN	COMMENT	$\Gamma_4/\Gamma$
$8.41^{+2.43+1.49}_{-2.12-1.06}$	<sup>10</sup> GARMASH 16	BELL	$e^+e^- \rightarrow \pi^-B^{*+}\bar{B}^{*0}$	
••• We do not use the following data for averages, fits, limits, etc. •••				
seen	<sup>11</sup> MIZUK 16	BELL	$e^+e^- \rightarrow h_b(1P)\pi^+\pi^-$	
seen	<sup>12</sup> BONDAR 12	BELL	$e^+e^- \rightarrow h_b(1P)\pi^+\pi^-$	

<sup>10</sup> Assuming the  $Z_b(10650)$  decay width is saturated by the channels  $\pi^+\Upsilon(1S, 2S, 3S)$ ,  $\pi^+h_b(1P, 2P)$ , and  $B^{*+}\bar{B}^{*0}$ , and using the results from BONDAR 12 and MIZUK 16.

<sup>11</sup> Using  $e^+e^-$  energies near the  $\Upsilon(11020)$ .

<sup>12</sup> Using  $e^+e^-$  energies near the  $\Upsilon(10860)$ .

 $\Gamma(h_b(2P)\pi^+)/\Gamma_{\text{total}}$ 

VALUE (units $10^{-2}$ )	DOCUMENT ID	TECN	COMMENT	$\Gamma_5/\Gamma$
$14.7^{+3.2+2.8}_{-2.8-2.3}$	<sup>13</sup> GARMASH 16	BELL	$e^+e^- \rightarrow \pi^-B^{*+}\bar{B}^{*0}$	
••• We do not use the following data for averages, fits, limits, etc. •••				
possibly seen	<sup>14</sup> MIZUK 16	BELL	$e^+e^- \rightarrow h_b(2P)\pi^+\pi^-$	
seen	<sup>15</sup> BONDAR 12	BELL	$e^+e^- \rightarrow h_b(2P)\pi^+\pi^-$	

<sup>13</sup> Assuming the  $Z_b(10650)$  decay width is saturated by the channels  $\pi^+\Upsilon(1S, 2S, 3S)$ ,  $\pi^+h_b(1P, 2P)$ , and  $B^{*+}\bar{B}^{*0}$ , and using the results from BONDAR 12 and MIZUK 16.

<sup>14</sup> Using  $e^+e^-$  energies near the  $\Upsilon(11020)$ .

<sup>15</sup> Using  $e^+e^-$  energies near the  $\Upsilon(10860)$ .

 $\Gamma(B^+\bar{B}^0)/\Gamma_{\text{total}}$ 

VALUE	DOCUMENT ID	TECN	COMMENT	$\Gamma_6/\Gamma$
not seen	GARMASH 16	BELL	$e^+e^- \rightarrow \pi^-B^+\bar{B}^0$	

 $[\Gamma(B^+\bar{B}^{*0}) + \Gamma(B^{*+}\bar{B}^0)]/\Gamma_{\text{total}}$ 

VALUE	DOCUMENT ID	TECN	COMMENT	$\Gamma_7/\Gamma$
not seen	GARMASH 16	BELL	$e^+e^- \rightarrow \pi^-B^+\bar{B}^{*0}, \pi^-\bar{B}^0B^{*+}$	

 $\Gamma(B^{*+}\bar{B}^{*0})/\Gamma_{\text{total}}$ 

VALUE (units $10^{-2}$ )	EVTS	DOCUMENT ID	TECN	COMMENT	$\Gamma_8/\Gamma$
$73.7^{+3.4+2.7}_{-4.4-3.5}$	161	<sup>16</sup> GARMASH 16	BELL	$e^+e^- \rightarrow \pi^-B^{*+}\bar{B}^{*0}$	

<sup>16</sup> Assuming the  $Z_b(10650)$  decay width is saturated by the channels  $\pi^+\Upsilon(1S, 2S, 3S)$ ,  $\pi^+h_b(1P, 2P)$ , and  $B^{*+}\bar{B}^{*0}$ , and using the results from BONDAR 12 and MIZUK 16. Using the mass and width of the  $Z_b(10650)$  from BONDAR 12.

 $\Gamma(B^{*+}\bar{B}^{*0})/[\Gamma(\Upsilon(1S)\pi^+) + \Gamma(\Upsilon(2S)\pi^+) + \Gamma(\Upsilon(3S)\pi^+) + \Gamma(h_b(1P)\pi^+) + \Gamma(h_b(2P)\pi^+)]$ 

VALUE (units $10^{-2}$ )	EVTS	DOCUMENT ID	TECN	COMMENT	$\Gamma_8/(\Gamma_1+\Gamma_2+\Gamma_3+\Gamma_4+\Gamma_5)$
$2.80^{+0.69+0.54}_{-0.40-0.36}$	161	<sup>17</sup> GARMASH 16	BELL	$e^+e^- \rightarrow \pi^-B^{*+}\bar{B}^{*0}$	

••• We do not use the following data for averages, fits, limits, etc. •••

<sup>17</sup> Combined with the results of BONDAR 12 and MIZUK 16. Not independent from  $Z_b(10650)$  branching fractions to  $\pi^+\Upsilon(1S, 2S, 3S)$ ,  $\pi^+h_b(1P, 2P)$ , and  $B^{*+}\bar{B}^{*0}$ .

 $Z_b(10650)$  REFERENCES

GARMASH 16	PRL 116 212001	A. Garmash et al.	(BELLE Collab.)
MIZUK 16	PRL 117 142001	R. Mizuk et al.	(BELLE Collab.)
GARMASH 15	PR D91 072003	A. Garmash et al.	(BELLE Collab.)
BONDAR 12	PRL 108 122001	A. Bondar et al.	(BELLE Collab.)

See key on page 999

# Meson Particle Listings

## $\Upsilon(10753)$ , $\Upsilon(10860)$

### $\Upsilon(10753)$

$$I^G(J^{PC}) = ?^?(1^{--})$$

OMITTED FROM SUMMARY TABLE

A candidate for  $\Upsilon(3D)$  state or an exotic structure.

Seen by MIZUK 19 in  $e^+e^- \rightarrow \Upsilon(nS)\pi^+\pi^-$  ( $n=1,2,3$ ) with a significance of  $5.2\sigma$ .

#### $\Upsilon(10753)$ MASS

VALUE (MeV)	DOCUMENT ID	TECN	COMMENT
<b>10752.7 ± 5.9<sup>+0.7</sup><sub>-1.1</sub></b>	1 MIZUK	19	BELL $e^+e^- \rightarrow \Upsilon(nS)\pi^+\pi^-$

<sup>1</sup> From a simultaneous fit to the  $\Upsilon(nS)\pi^+\pi^-$ ,  $n = 1, 2, 3$ , cross sections at 28 energy points within  $\sqrt{s} = 10.63$ – $11.02$  GeV, including the initial-state radiation at  $\Upsilon(10860)$ .

#### $\Upsilon(10753)$ WIDTH

VALUE (MeV)	DOCUMENT ID	TECN	COMMENT
<b>35.5 ± 17.6 + 3.9<sub>-11.3 - 3.3</sub></b>	1 MIZUK	19	BELL $e^+e^- \rightarrow \Upsilon(nS)\pi^+\pi^-$

<sup>1</sup> From a simultaneous fit to the  $\Upsilon(nS)\pi^+\pi^-$ ,  $n = 1, 2, 3$ , cross sections at 28 energy points within  $\sqrt{s} = 10.63$ – $11.02$  GeV, including the initial-state radiation at  $\Upsilon(10860)$ .

#### $\Upsilon(10753)$ DECAY MODES

Mode
$\Gamma_1 \quad \Upsilon(1S)\pi^+\pi^-$
$\Gamma_2 \quad \Upsilon(2S)\pi^+\pi^-$
$\Gamma_3 \quad \Upsilon(3S)\pi^+\pi^-$
$\Gamma_4 \quad e^+e^-$

#### $\Upsilon(10753)$ $\Gamma(i)\Gamma(e^+e^-)/\Gamma(\text{total})$

$\Gamma(\Upsilon(1S)\pi^+\pi^-) \times \Gamma(e^+e^-)/\Gamma_{\text{total}}$	DOCUMENT ID	TECN	COMMENT	$\Gamma_1\Gamma_4/\Gamma$
<b>0.295 ± 0.175</b>	1,2 MIZUK	19	BELL $e^+e^- \rightarrow \Upsilon(nS)\pi^+\pi^-$	

••• We do not use the following data for averages, fits, limits, etc. •••

<sup>1</sup> From a simultaneous fit to the  $\Upsilon(nS)\pi^+\pi^-$ ,  $n = 1, 2, 3$ , cross sections at 28 energy points within  $\sqrt{s} = 10.63$ – $11.02$  GeV, including the initial-state radiation at  $\Upsilon(10860)$ .

<sup>2</sup> Reported as the range 0.12–0.47 eV obtained from multiple solutions of an amplitude fit within a model composed as a sum of Breit-Wigner functions.

$\Gamma(\Upsilon(2S)\pi^+\pi^-) \times \Gamma(e^+e^-)/\Gamma_{\text{total}}$	DOCUMENT ID	TECN	COMMENT	$\Gamma_2\Gamma_4/\Gamma$
<b>0.875 ± 0.345</b>	1,2 MIZUK	19	BELL $e^+e^- \rightarrow \Upsilon(nS)\pi^+\pi^-$	

••• We do not use the following data for averages, fits, limits, etc. •••

<sup>1</sup> From a simultaneous fit to the  $\Upsilon(nS)\pi^+\pi^-$ ,  $n = 1, 2, 3$ , cross sections at 28 energy points within  $\sqrt{s} = 10.63$ – $11.02$  GeV, including the initial-state radiation at  $\Upsilon(10860)$ .

<sup>2</sup> Reported as the range 0.53–1.22 eV obtained from multiple solutions of an amplitude fit within a model composed as a sum of Breit-Wigner functions.

$\Gamma(\Upsilon(3S)\pi^+\pi^-) \times \Gamma(e^+e^-)/\Gamma_{\text{total}}$	DOCUMENT ID	TECN	COMMENT	$\Gamma_3\Gamma_4/\Gamma$
<b>0.235 ± 0.025</b>	1,2 MIZUK	19	BELL $e^+e^- \rightarrow \Upsilon(nS)\pi^+\pi^-$	

••• We do not use the following data for averages, fits, limits, etc. •••

<sup>1</sup> From a simultaneous fit to the  $\Upsilon(nS)\pi^+\pi^-$ ,  $n = 1, 2, 3$ , cross sections at 28 energy points within  $\sqrt{s} = 10.63$ – $11.02$  GeV, including the initial-state radiation at  $\Upsilon(10860)$ .

<sup>2</sup> Reported as the range 0.21–0.26 eV obtained from multiple solutions of an amplitude fit within a model composed as a sum of Breit-Wigner functions.

#### $\Upsilon(10753)$ REFERENCES

MIZUK	19	JHEP 1910 220	R. Mizuk et al.	(BELLE Collab.)
-------	----	---------------	-----------------	-----------------

### $\Upsilon(10860)$

$$I^G(J^{PC}) = 0^-(1^{--})$$

#### $\Upsilon(10860)$ MASS

VALUE (MeV)	DOCUMENT ID	TECN	COMMENT
<b>10885.2 ± 2.6 OUR AVERAGE</b>			

10885.3 ± 1.5 <sup>+2.2</sup> <sub>-0.9</sub>	1 MIZUK	19	BELL $e^+e^- \rightarrow \Upsilon(nS)\pi^+\pi^-$
10884.7 ± 3.6 + 8.9 <sub>-3.4 - 1.0</sub>	2 MIZUK	16	BELL $e^+e^- \rightarrow h_b(1P, 2P)\pi^+\pi^-$

••• We do not use the following data for averages, fits, limits, etc. •••

10881.8 <sup>+1.0</sup> <sub>-1.1</sub> ± 1.2	3,4 SANTEL	16	BELL $e^+e^- \rightarrow \text{hadrons}$
10891.1 ± 3.2 <sup>+1.2</sup> <sub>-2.0</sub>	5,6 SANTEL	16	BELL $e^+e^- \rightarrow \Upsilon(1S, 2S, 3S)\pi^+\pi^-$
10879 ± 3	7,8 CHEN	10	BELL $e^+e^- \rightarrow \text{hadrons}$
10888.4 ± 2.7 <sup>+1.2</sup> <sub>-2.6</sub>	9 CHEN	10	BELL $e^+e^- \rightarrow \Upsilon(1S, 2S, 3S)\pi^+\pi^-$
10876 ± 2	7 AUBERT	09E	BABR $e^+e^- \rightarrow \text{hadrons}$
10869 ± 2	10 AUBERT	09E	BABR $e^+e^- \rightarrow \text{hadrons}$
10868 ± 6 ± 5	11 BESSON	85	CLEO $e^+e^- \rightarrow \text{hadrons}$
10845 ± 20	12 LOVELOCK	85	CUSB $e^+e^- \rightarrow \text{hadrons}$

<sup>1</sup> From a simultaneous fit to the  $\Upsilon(nS)\pi^+\pi^-$ ,  $n = 1, 2, 3$ , cross sections at 28 energy points within  $\sqrt{s} = 10.6$ – $11.05$  GeV, including the initial-state radiation at  $\Upsilon(10860)$ .

<sup>2</sup> From a simultaneous fit to the  $h_b(nP)\pi^+\pi^-$ ,  $n = 1, 2$  cross sections at 22 energy points within  $\sqrt{s} = 10.77$ – $11.02$  GeV to a pair of interfering Breit-Wigner amplitudes modified by phase space factors, with eight resonance parameters (a mass and width for each of  $\Upsilon(10860)$  and  $\Upsilon(11020)$ , a single relative phase, a single relative amplitude, and two overall normalization factors, one for each  $n$ ). The systematic error estimate is dominated by possible interference with a small nonresonant continuum amplitude.

<sup>3</sup> From a fit to the total hadronic cross sections measured at 60 energy points within  $\sqrt{s} = 10.82$ – $11.05$  GeV to a pair of interfering Breit-Wigner amplitudes and two floating continuum amplitudes with  $1/\sqrt{s}$  dependence, one coherent with the resonances and one incoherent, with six resonance parameters (a mass, width, and an amplitude for each of  $\Upsilon(10860)$  and  $\Upsilon(11020)$ , one relative phase, and one decoherence coefficient).

<sup>4</sup> Not including uncertain and potentially large systematic errors due to assumed continuum amplitude  $1/\sqrt{s}$  dependence and related interference contributions.

<sup>5</sup> From a simultaneous fit to the  $\Upsilon(nS)\pi^+\pi^-$ ,  $n = 1, 2, 3$ , cross sections at 25 energy points within  $\sqrt{s} = 10.6$ – $11.05$  GeV to a pair of interfering Breit-Wigner amplitudes modified by phase space factors, with fourteen resonance parameters (a mass, width, and three amplitudes for each of  $\Upsilon(10860)$  and  $\Upsilon(11020)$ , a single universal relative phase, and three decoherence coefficients, one for each  $n$ ). Continuum contributions were measured (and therefore fixed) to be zero.

<sup>6</sup> Superseded by MIZUK 19.

<sup>7</sup> In a model where a flat non-resonant  $b\bar{b}$ -continuum is incoherently added to a second flat component interfering with two Breit-Wigner resonances. Systematic uncertainties not estimated.

<sup>8</sup> The parameters of the  $\Upsilon(11020)$  are fixed to those in AUBERT 09E.

<sup>9</sup> In a model where a flat nonresonant  $\Upsilon(1S, 2S, 3S)\pi^+\pi^-$  continuum interferes with a single Breit-Wigner resonance.

<sup>10</sup> In a model where a non-resonant  $b\bar{b}$ -continuum represented by a threshold function at  $\sqrt{s} = 2m_B$  is incoherently added to a flat component interfering with two Breit-Wigner resonances. Not independent of other AUBERT 09E results. Systematic uncertainties not estimated.

<sup>11</sup> Assuming four Gaussians with radiative tails and a single step in  $R$ .

<sup>12</sup> In a coupled-channel model with three resonances and a smooth step in  $R$ .

#### $\Upsilon(10860)$ WIDTH

VALUE (MeV)	DOCUMENT ID	TECN	COMMENT
<b>37 ± 4 OUR AVERAGE</b>			
36.6 ± 4.5 + 0.5 <sub>-3.9 - 1.1</sub>	1 MIZUK	19	BELL $e^+e^- \rightarrow \Upsilon(nS)\pi^+\pi^-$
40.6 ± 12.7 + 1.1 <sub>-8.0 - 19.1</sub>	2 MIZUK	16	BELL $e^+e^- \rightarrow h_b(1P, 2P)\pi^+\pi^-$

••• We do not use the following data for averages, fits, limits, etc. •••

3,4 SANTEL 16 BELL  $e^+e^- \rightarrow \text{hadrons}$

5,6 SANTEL 16 BELL  $e^+e^- \rightarrow \Upsilon(1S, 2S, 3S)\pi^+\pi^-$

7,8 CHEN 10 BELL  $e^+e^- \rightarrow \text{hadrons}$

9 CHEN 10 BELL  $e^+e^- \rightarrow \Upsilon(1S, 2S, 3S)\pi^+\pi^-$

7 AUBERT 09E BABR  $e^+e^- \rightarrow \text{hadrons}$

10 AUBERT 09E BABR  $e^+e^- \rightarrow \text{hadrons}$

11 BESSON 85 CLEO  $e^+e^- \rightarrow \text{hadrons}$

12 LOVELOCK 85 CUSB  $e^+e^- \rightarrow \text{hadrons}$

<sup>1</sup> From a simultaneous fit to the  $\Upsilon(nS)\pi^+\pi^-$ ,  $n = 1, 2, 3$ , cross sections at 28 energy points within  $\sqrt{s} = 10.6$ – $11.05$  GeV, including the initial-state radiation at  $\Upsilon(10860)$ .

<sup>2</sup> From a simultaneous fit to the  $h_b(nP)\pi^+\pi^-$ ,  $n = 1, 2$  cross sections at 22 energy points within  $\sqrt{s} = 10.77$ – $11.02$  GeV to a pair of interfering Breit-Wigner amplitudes modified by phase space factors, with eight resonance parameters (a mass and width for each of  $\Upsilon(10860)$  and  $\Upsilon(11020)$ , a single relative phase, a single relative amplitude, and two overall normalization factors, one for each  $n$ ). The systematic error estimate is dominated by possible interference with a small nonresonant continuum amplitude.

<sup>3</sup> From a fit to the total hadronic cross sections measured at 60 energy points within  $\sqrt{s} = 10.82$ – $11.05$  GeV to a pair of interfering Breit-Wigner amplitudes and two floating continuum amplitudes with  $1/\sqrt{s}$  dependence, one coherent with the resonances and one incoherent, with six resonance parameters (a mass, width, and an amplitude for each of  $\Upsilon(10860)$  and  $\Upsilon(11020)$ , one relative phase, and one decoherence coefficient).

<sup>4</sup> Not including uncertain and potentially large systematic errors due to assumed continuum amplitude  $1/\sqrt{s}$  dependence and related interference contributions.

<sup>5</sup> From a simultaneous fit to the  $\Upsilon(nS)\pi^+\pi^-$ ,  $n = 1, 2, 3$ , cross sections at 25 energy points within  $\sqrt{s} = 10.6$ – $11.05$  GeV to a pair of interfering Breit-Wigner amplitudes modified by phase space factors, with fourteen resonance parameters (a mass, width, and three amplitudes for each of  $\Upsilon(10860)$  and  $\Upsilon(11020)$ , a single universal relative phase, and three decoherence coefficients, one for each  $n$ ). Continuum contributions were measured (and therefore fixed) to be zero.

<sup>6</sup> Superseded by MIZUK 19.

<sup>7</sup> In a model where a flat non-resonant  $b\bar{b}$ -continuum is incoherently added to a second flat component interfering with two Breit-Wigner resonances. Systematic uncertainties not estimated.

<sup>8</sup> The parameters of the  $\Upsilon(11020)$  are fixed to those in AUBERT 09E.



## Meson Particle Listings

 $\Upsilon(10860)$ 

<sup>9</sup>In a model where a flat nonresonant  $\Upsilon(1S, 2S, 3S)\pi^+\pi^-$  continuum interferes with a single Breit-Wigner resonance.

<sup>10</sup>In a model where a non-resonant  $b\bar{b}$ -continuum represented by a threshold function at  $\sqrt{s}=2m_B$  is incoherently added to a flat component interfering with two Breit-Wigner resonances. Not independent of other AUBERT 09E results. Systematic uncertainties not estimated.

<sup>11</sup>Assuming four Gaussians with radiative tails and a single step in  $R$ .

<sup>12</sup>In a coupled-channel model with three resonances and a smooth step in  $R$ .

 $\Upsilon(10860)$  DECAY MODES

Mode	Fraction ( $\Gamma_i/\Gamma$ )	Confidence level
$\Gamma_1$ $B\bar{B}X$	( 76.2 $\pm$ 2.7 $\overline{-4.0}$ ) %	
$\Gamma_2$ $B\bar{B}$	( 5.5 $\pm$ 1.0 ) %	
$\Gamma_3$ $B\bar{B}^* + \text{c.c.}$	( 13.7 $\pm$ 1.6 ) %	
$\Gamma_4$ $B^*\bar{B}^*$	( 38.1 $\pm$ 3.4 ) %	
$\Gamma_5$ $B\bar{B}^*\pi$	< 19.7 %	90%
$\Gamma_6$ $B\bar{B}\pi$	( 0.0 $\pm$ 1.2 ) %	
$\Gamma_7$ $B^*\bar{B}\pi + B\bar{B}^*\pi$	( 7.3 $\pm$ 2.3 ) %	
$\Gamma_8$ $B^*B^*\pi$	( 1.0 $\pm$ 1.4 ) %	
$\Gamma_9$ $B\bar{B}\pi\pi$	< 8.9 %	90%
$\Gamma_{10}$ $B_S^{(*)}\bar{B}_S^{(*)}$	( 20.1 $\pm$ 3.1 ) %	
$\Gamma_{11}$ $B_S\bar{B}_S$	( 5 $\pm$ 5 ) $\times 10^{-3}$	
$\Gamma_{12}$ $B_S\bar{B}_S^* + \text{c.c.}$	( 1.35 $\pm$ 0.32 ) %	
$\Gamma_{13}$ $B_S^*\bar{B}_S^*$	( 17.6 $\pm$ 2.7 ) %	
$\Gamma_{14}$ no open-bottom	( 3.8 $\pm$ 5.0 $\overline{-0.5}$ ) %	
$\Gamma_{15}$ $e^+e^-$	( 8.3 $\pm$ 2.1 ) $\times 10^{-6}$	
$\Gamma_{16}$ $K^*(892)^0\bar{K}^0$	< 1.0 $\times 10^{-5}$	90%
$\Gamma_{17}$ $\Upsilon(1S)\pi^+\pi^-$	( 5.3 $\pm$ 0.6 ) $\times 10^{-3}$	
$\Gamma_{18}$ $\Upsilon(2S)\pi^+\pi^-$	( 7.8 $\pm$ 1.3 ) $\times 10^{-3}$	
$\Gamma_{19}$ $\Upsilon(3S)\pi^+\pi^-$	( 4.8 $\pm$ 1.9 $\overline{-1.7}$ ) $\times 10^{-3}$	
$\Gamma_{20}$ $\Upsilon(1S)K^+K^-$	( 6.1 $\pm$ 1.8 ) $\times 10^{-4}$	
$\Gamma_{21}$ $\eta\Upsilon_J(1D)$	( 4.8 $\pm$ 1.1 ) $\times 10^{-3}$	
$\Gamma_{22}$ $h_b(1P)\pi^+\pi^-$	( 3.5 $\pm$ 1.0 $\overline{-1.3}$ ) $\times 10^{-3}$	
$\Gamma_{23}$ $h_b(2P)\pi^+\pi^-$	( 5.7 $\pm$ 1.7 $\overline{-2.1}$ ) $\times 10^{-3}$	
$\Gamma_{24}$ $\chi_{bJ}(1P)\pi^+\pi^-\pi^0$	( 2.5 $\pm$ 2.3 ) $\times 10^{-3}$	
$\Gamma_{25}$ $\chi_{b0}(1P)\pi^+\pi^-\pi^0$	< 6.3 $\times 10^{-3}$	90%
$\Gamma_{26}$ $\chi_{b0}(1P)\omega$	< 3.9 $\times 10^{-3}$	90%
$\Gamma_{27}$ $\chi_{b0}(1P)(\pi^+\pi^-\pi^0)_{\text{non-}\omega}$	< 4.8 $\times 10^{-3}$	90%
$\Gamma_{28}$ $\chi_{b1}(1P)\pi^+\pi^-\pi^0$	( 1.85 $\pm$ 0.33 ) $\times 10^{-3}$	
$\Gamma_{29}$ $\chi_{b1}(1P)\omega$	( 1.57 $\pm$ 0.30 ) $\times 10^{-3}$	
$\Gamma_{30}$ $\chi_{b1}(1P)(\pi^+\pi^-\pi^0)_{\text{non-}\omega}$	( 5.2 $\pm$ 1.9 ) $\times 10^{-4}$	
$\Gamma_{31}$ $\chi_{b2}(1P)\pi^+\pi^-\pi^0$	( 1.17 $\pm$ 0.30 ) $\times 10^{-3}$	
$\Gamma_{32}$ $\chi_{b2}(1P)\omega$	( 6.0 $\pm$ 2.7 ) $\times 10^{-4}$	
$\Gamma_{33}$ $\chi_{b2}(1P)(\pi^+\pi^-\pi^0)_{\text{non-}\omega}$	( 6 $\pm$ 4 ) $\times 10^{-4}$	
$\Gamma_{34}$ $\gamma\chi_b \rightarrow \gamma\Upsilon(1S)\omega$	< 3.8 $\times 10^{-5}$	90%

## Inclusive Decays.

These decay modes are submodes of one or more of the decay modes above.

$\Gamma_{35}$ $\phi$ anything	( 13.8 $\pm$ 2.4 $\overline{-1.7}$ ) %
$\Gamma_{36}$ $D^0$ anything + c.c.	( 108 $\pm$ 8 ) %
$\Gamma_{37}$ $D_s$ anything + c.c.	( 46 $\pm$ 6 ) %
$\Gamma_{38}$ $J/\psi$ anything	( 2.06 $\pm$ 0.21 ) %
$\Gamma_{39}$ $B^0$ anything + c.c.	( 77 $\pm$ 8 ) %
$\Gamma_{40}$ $B^+$ anything + c.c.	( 72 $\pm$ 6 ) %

 $\Upsilon(10860)$  PARTIAL WIDTHS

$\Gamma(e^+e^-)$	$\Gamma_{15}$		
VALUE (keV)	DOCUMENT ID	TECN	COMMENT
<b>0.31 <math>\pm</math> 0.07 OUR AVERAGE</b>	Error	includes scale factor of 1.3.	
0.22 $\pm$ 0.05 $\pm$ 0.07	BESSON	85 CLEO	$e^+e^- \rightarrow$ hadrons
0.365 $\pm$ 0.070	LOVELOCK	85 CUSB	$e^+e^- \rightarrow$ hadrons

$\Gamma(e^+e^-) \times \Gamma(\Upsilon(1S)\pi^+\pi^-)/\Gamma_{\text{total}}$	$\Gamma_{15}\Gamma_{17}/\Gamma$		
VALUE (eV)	DOCUMENT ID	TECN	COMMENT
• • • We do not use the following data for averages, fits, limits, etc. • • •			
1.09 $\pm$ 0.34	<sup>1,2</sup> MIZUK	19 BELL	$e^+e^- \rightarrow \Upsilon(nS)\pi^+\pi^-$

<sup>1</sup>From a simultaneous fit to the  $\Upsilon(nS)\pi^+\pi^-$ ,  $n = 1, 2, 3$ , cross sections at 28 energy points within  $\sqrt{s} = 10.6\text{--}11.05$  GeV, including the initial-state radiation at  $\Upsilon(10860)$ .

<sup>2</sup>Reported as the range 0.75–1.43 eV obtained from multiple solutions of an amplitude fit within a model composed as a sum of Breit-Wigner functions.

$\Gamma(e^+e^-) \times \Gamma(\Upsilon(2S)\pi^+\pi^-)/\Gamma_{\text{total}}$	$\Gamma_{15}\Gamma_{18}/\Gamma$		
VALUE (eV)	DOCUMENT ID	TECN	COMMENT
• • • We do not use the following data for averages, fits, limits, etc. • • •			
2.58 $\pm$ 1.22	<sup>1,2</sup> MIZUK	19 BELL	$e^+e^- \rightarrow \Upsilon(nS)\pi^+\pi^-$

<sup>1</sup>From a simultaneous fit to the  $\Upsilon(nS)\pi^+\pi^-$ ,  $n = 1, 2, 3$ , cross sections at 28 energy points within  $\sqrt{s} = 10.6\text{--}11.05$  GeV, including the initial-state radiation at  $\Upsilon(10860)$ .

<sup>2</sup>Reported as the range 1.35–3.80 eV obtained from multiple solutions of an amplitude fit within a model composed as a sum of Breit-Wigner functions.

$\Gamma(e^+e^-) \times \Gamma(\Upsilon(3S)\pi^+\pi^-)/\Gamma_{\text{total}}$	$\Gamma_{15}\Gamma_{19}/\Gamma$		
VALUE (eV)	DOCUMENT ID	TECN	COMMENT
• • • We do not use the following data for averages, fits, limits, etc. • • •			
0.73 $\pm$ 0.30	<sup>1,2</sup> MIZUK	19 BELL	$e^+e^- \rightarrow \Upsilon(nS)\pi^+\pi^-$

<sup>1</sup>From a simultaneous fit to the  $\Upsilon(nS)\pi^+\pi^-$ ,  $n = 1, 2, 3$ , cross sections at 28 energy points within  $\sqrt{s} = 10.6\text{--}11.05$  GeV, including the initial-state radiation at  $\Upsilon(10860)$ .

<sup>2</sup>Reported as the range 0.43–1.03 eV obtained from multiple solutions of an amplitude fit within a model composed as a sum of Breit-Wigner functions.

 $\Upsilon(10860)$  BRANCHING RATIOS

"OUR EVALUATION" is obtained based on averages of rescaled data listed below. The averages and rescaling were performed by the Heavy Flavor Averaging Group (HFLAV) and are described at <https://hflav.web.cern.ch/>.

$\Gamma(B\bar{B}X)/\Gamma_{\text{total}}$	$\Gamma_1/\Gamma$			
VALUE	EVTS	DOCUMENT ID	TECN	COMMENT
<b>0.762 <math>\pm</math> 0.027 <math>\overline{-0.043}</math> OUR EVALUATION</b>				
<b>0.71 <math>\pm</math> 0.06 OUR AVERAGE</b>				
0.737 $\pm$ 0.032 $\pm$ 0.051	1063	<sup>1</sup> DRUTSKOY	10 BELL	$\Upsilon(5S) \rightarrow B^+X, B^0X$
0.589 $\pm$ 0.100 $\pm$ 0.092		<sup>2</sup> HUANG	07 CLEO	$\Upsilon(5S) \rightarrow$ hadrons

<sup>1</sup>Not independent of DRUTSKOY 10 values for  $\Upsilon(5S) \rightarrow B^{\pm,0}$  anything.

<sup>2</sup>Using measurements or limits from AQUINES 06.

$\Gamma(B\bar{B})/\Gamma_{\text{total}}$	$\Gamma_2/\Gamma$			
VALUE (units $10^{-2}$ )	CL%	DOCUMENT ID	TECN	COMMENT
<b>5.5 <math>\pm</math> 1.0 <math>\overline{-0.9} \pm 0.4</math></b>		<sup>1</sup> DRUTSKOY	10 BELL	$\Upsilon(5S) \rightarrow B^+X, B^0X$

• • • We do not use the following data for averages, fits, limits, etc. • • •

< 13.8 90 <sup>2</sup> HUANG 07 CLEO  $\Upsilon(5S) \rightarrow$  hadrons

<sup>1</sup>Assuming isospin conservation.

<sup>2</sup>Using measurements or limits from AQUINES 06.

$\Gamma(B\bar{B})/\Gamma(B\bar{B}X)$	$\Gamma_2/\Gamma_1$			
VALUE	CL%	DOCUMENT ID	TECN	COMMENT
<b>&lt; 0.22</b>	90	AQUINES	06 CLE3	$\Upsilon(5S) \rightarrow$ hadrons

$\Gamma(B\bar{B}^* + \text{c.c.})/\Gamma_{\text{total}}$	$\Gamma_3/\Gamma$			
VALUE	DOCUMENT ID	TECN	COMMENT	
<b>0.137 <math>\pm</math> 0.016 OUR AVERAGE</b>				
0.137 $\pm$ 0.013 $\pm$ 0.011	<sup>1</sup> DRUTSKOY	10 BELL	$\Upsilon(5S) \rightarrow B^+X, B^0X$	
0.143 $\pm$ 0.053 $\pm$ 0.027	<sup>2</sup> HUANG	07 CLEO	$\Upsilon(5S) \rightarrow$ hadrons	

<sup>1</sup>Assuming isospin conservation.

<sup>2</sup>Using measurements or limits from AQUINES 06.

$\Gamma(B\bar{B}^* + \text{c.c.})/\Gamma(B\bar{B}X)$	$\Gamma_3/\Gamma_1$			
VALUE	EVTS	DOCUMENT ID	TECN	COMMENT
<b>0.24 <math>\pm</math> 0.09 <math>\pm</math> 0.03</b>	10	AQUINES	06 CLE3	$\Upsilon(5S) \rightarrow$ hadrons

$\Gamma(B^*\bar{B}^*)/\Gamma_{\text{total}}$	$\Gamma_4/\Gamma$			
VALUE	DOCUMENT ID	TECN	COMMENT	
<b>0.381 <math>\pm</math> 0.034 OUR AVERAGE</b>				
0.375 $\pm$ 0.021 $\overline{-0.019} \pm 0.030$	<sup>1</sup> DRUTSKOY	10 BELL	$\Upsilon(5S) \rightarrow B^+X, B^0X$	
0.436 $\pm$ 0.083 $\pm$ 0.072	<sup>2</sup> HUANG	07 CLEO	$\Upsilon(5S) \rightarrow$ hadrons	

<sup>1</sup>Assuming isospin conservation.

<sup>2</sup>Using measurements or limits from AQUINES 06.

$\Gamma(B^*\bar{B}^*)/\Gamma(B\bar{B}X)$	$\Gamma_4/\Gamma_1$			
VALUE	EVTS	DOCUMENT ID	TECN	COMMENT
<b>0.74 <math>\pm</math> 0.15 <math>\pm</math> 0.08</b>	31	AQUINES	06 CLE3	$\Upsilon(5S) \rightarrow$ hadrons

$\Gamma(B\bar{B}^*(\pi))/\Gamma_{\text{total}}$	$\Gamma_5/\Gamma$			
VALUE	CL%	DOCUMENT ID	TECN	COMMENT
<b>&lt; 0.197</b>	90	<sup>1</sup> HUANG	07 CLEO	$\Upsilon(5S) \rightarrow$ hadrons

<sup>1</sup>Using measurements or limits from AQUINES 06.

$\Gamma(B\bar{B}^*(\pi))/\Gamma(B\bar{B}X)$	$\Gamma_5/\Gamma_1$			
VALUE	CL%	DOCUMENT ID	TECN	COMMENT
<b>&lt; 0.32</b>	90	AQUINES	06 CLE3	$\Upsilon(5S) \rightarrow$ hadrons

$\Gamma(B\bar{B}\pi)/\Gamma_{\text{total}}$	$\Gamma_6/\Gamma$			
VALUE (units $10^{-2}$ )	EVTS	DOCUMENT ID	TECN	COMMENT
<b>0.0 <math>\pm</math> 1.2 <math>\pm</math> 0.3</b>	0	<sup>1</sup> DRUTSKOY	10 BELL	$\Upsilon(5S) \rightarrow B^{\pm,0}\pi^-X$

<sup>1</sup>Assuming isospin conservation.

# Meson Particle Listings

## $\Upsilon(10860)$

$\Gamma(B^* \bar{B} \pi) + \Gamma(B \bar{B}^* \pi) / \Gamma_{\text{total}}$					$\Gamma_7 / \Gamma$
VALUE (units $10^{-2}$ )	EVTS	DOCUMENT ID	TECN	COMMENT	

**$7.3 \pm 2.3 \pm 0.8$**  38 <sup>1</sup> DRUTSKOY 10 BELL  $\Upsilon(5S) \rightarrow B^{*0} \pi^- X$   
<sup>1</sup> Assuming isospin conservation.

$\Gamma(B^* \bar{B}^* \pi) / \Gamma_{\text{total}}$					$\Gamma_8 / \Gamma$
VALUE (units $10^{-2}$ )	EVTS	DOCUMENT ID	TECN	COMMENT	

**$1.0 \pm 1.4 \pm 0.4$**  5 <sup>1</sup> DRUTSKOY 10 BELL  $\Upsilon(5S) \rightarrow B^{*0} \pi^- X$   
<sup>1</sup> Assuming isospin conservation.

$\Gamma(B \bar{B} \pi \pi) / \Gamma_{\text{total}}$					$\Gamma_9 / \Gamma$
VALUE	CL%	DOCUMENT ID	TECN	COMMENT	

**$<0.089$**  90 <sup>1</sup> HUANG 07 CLEO  $\Upsilon(5S) \rightarrow \text{hadrons}$   
<sup>1</sup> Using measurements or limits from AQUINES 06.

$\Gamma(B \bar{B} \pi \pi) / \Gamma(B \bar{B} X)$					$\Gamma_9 / \Gamma_1$
VALUE	CL%	DOCUMENT ID	TECN	COMMENT	

**$<0.14$**  90 AQUINES 06 CLE3  $\Upsilon(5S) \rightarrow \text{hadrons}$

$\Gamma(B_s^{(*)} \bar{B}_s^{(*)}) / \Gamma_{\text{total}}$					$\Gamma_{10} / \Gamma = (\Gamma_{11} + \Gamma_{12} + \Gamma_{13}) / \Gamma$
VALUE	DOCUMENT ID	TECN	COMMENT		

**$0.201 \pm 0.030$**  OUR EVALUATION  
 **$-0.031$**

**$0.189 \pm 0.027$**  OUR AVERAGE  
 **$-0.021$**

0.172  $\pm$  0.030 <sup>1</sup> ESEN 13 BELL  $\Upsilon(5S) \rightarrow D^0 X, D_s X$

0.21  $\pm$  0.06 <sup>2</sup> HUANG 07 CLEO  $\Upsilon(5S) \rightarrow D_s X$

0.180  $\pm$  0.013  $\pm$  0.032 <sup>3</sup> DRUTSKOY 07 BELL  $\Upsilon(5S) \rightarrow D^0 X, D_s X$

0.160  $\pm$  0.026  $\pm$  0.058 <sup>4</sup> ARTUSO 05B CLEO  $e^+ e^- \rightarrow D_X X$

- • • We do not use the following data for averages, fits, limits, etc. • • •
- <sup>1</sup> Supersedes DRUTSKOY 07.
- <sup>2</sup> Supersedes ARTUSO 05B. Combining inclusive  $\phi, D_s,$  and  $B$  measurements. Using  $B(D_s^+ \rightarrow \phi \pi^+) = 4.4 \pm 0.6\%$  from PDG 06.
- <sup>3</sup> Using  $B(D_s^+ \rightarrow \phi \pi^+) = (4.4 \pm 0.6)\%$  from PDG 06.
- <sup>4</sup> Uses a model-dependent estimate  $B(B_s \rightarrow D_s X) = (92 \pm 11)\%$ .

$\Gamma(B_s^{(*)} \bar{B}_s^{(*)}) / \Gamma(B \bar{B} X)$					$\Gamma_{10} / \Gamma_1$
VALUE	DOCUMENT ID	TECN	COMMENT		

**$0.264 \pm 0.052$**  OUR EVALUATION  
 **$-0.045$**

$\Gamma(B_s^* \bar{B}_s^*) / \Gamma(B_s^{(*)} \bar{B}_s^{(*)})$					$\Gamma_{13} / \Gamma_{10} = \Gamma_{13} / (\Gamma_{11} + \Gamma_{12} + \Gamma_{13})$
VALUE (units $10^{-2}$ )	EVTS	DOCUMENT ID	TECN	COMMENT	

**$87.8 \pm 1.5$**  OUR AVERAGE

87.0  $\pm$  1.7 <sup>1,2</sup> ESEN 13 BELL  $B_s^0 \rightarrow D_s^- \pi^+$

90.5  $\pm$  3.2  $\pm$  0.1 <sup>2,3</sup> LI 12 BELL  $B_s^0 \rightarrow J/\psi \eta(\prime)$

• • • We do not use the following data for averages, fits, limits, etc. • • •

90.1  $\pm$  3.8  $\pm$  0.2 <sup>4</sup> LOUVOT 09 BELL  $10.86 e^+ e^- \rightarrow B_s^{(*)} \bar{B}_s^{(*)}$

93  $\pm$  7  $\pm$  1 <sup>4</sup> DRUTSKOY 07A BELL Superseded by LOUVOT 09

- <sup>1</sup> Supersedes LOUVOT 09.
- <sup>2</sup> With  $N(B_s^{(*)} \bar{B}_s^{(*)}) = (7.11 \pm 1.30) \times 10^6$ .
- <sup>3</sup> The ratios  $N(B_s^* \bar{B}_s^*) / N(B_s^{(*)} \bar{B}_s^{(*)})$  and  $N(B_s^* \bar{B}_s^0) / N(B_s^{(*)} \bar{B}_s^{(*)})$  are measured with a correlation coefficient of  $-0.72$ .
- <sup>4</sup> From a measurement of  $\sigma(e^+ e^- \rightarrow B_s^* \bar{B}_s^*) / \sigma(e^+ e^- \rightarrow B_s^{(*)} \bar{B}_s^{(*)})$  at  $\sqrt{s} = 10.86$  GeV.

$\Gamma(B_s \bar{B}_s) / \Gamma(B_s^{(*)} \bar{B}_s^{(*)})$					$\Gamma_{11} / \Gamma_{10} = \Gamma_{11} / (\Gamma_{11} + \Gamma_{12} + \Gamma_{13})$
VALUE (units $10^{-2}$ )	DOCUMENT ID	TECN	COMMENT		

**$2.6 \pm 2.6$**  LOUVOT 09 BELL  $10.86 e^+ e^- \rightarrow B_s^{(*)} \bar{B}_s^{(*)}$

$\Gamma(B_s \bar{B}_s) / \Gamma(B_s^* \bar{B}_s^*)$					$\Gamma_{11} / \Gamma_{13}$
VALUE	CL%	DOCUMENT ID	TECN	COMMENT	

**$<0.16$**  90 BONVICINI 06 CLE3  $e^+ e^-$

$\Gamma(B_s \bar{B}_s^* + \text{c.c.}) / \Gamma(B_s^{(*)} \bar{B}_s^{(*)})$					$\Gamma_{12} / \Gamma_{10} = \Gamma_{12} / (\Gamma_{11} + \Gamma_{12} + \Gamma_{13})$
VALUE (units $10^{-2}$ )	EVTS	DOCUMENT ID	TECN	COMMENT	

**$6.7 \pm 1.2$**  OUR AVERAGE

7.3  $\pm$  1.5 <sup>1,2</sup> ESEN 13 BELL  $B_s^0 \rightarrow D_s^- \pi^+$

4.9  $\pm$  2.5  $\pm$  0.0 <sup>2,3</sup> LI 12 BELL  $B_s^0 \rightarrow J/\psi \eta(\prime)$

• • • We do not use the following data for averages, fits, limits, etc. • • •

7.3  $\pm$  3.3  $\pm$  0.1 LOUVOT 09 BELL  $10.86 e^+ e^- \rightarrow B_s^{(*)} \bar{B}_s^{(*)}$

- <sup>1</sup> Supersedes LOUVOT 09.
- <sup>2</sup> With  $N(B_s^{(*)} \bar{B}_s^{(*)}) = (7.11 \pm 1.30) \times 10^6$ .
- <sup>3</sup> The ratios  $N(B_s^* \bar{B}_s^*) / N(B_s^{(*)} \bar{B}_s^{(*)})$  and  $N(B_s^* \bar{B}_s^0) / N(B_s^{(*)} \bar{B}_s^{(*)})$  are measured with a correlation coefficient of  $-0.72$ .

$\Gamma(B_s \bar{B}_s^* + \text{c.c.}) / \Gamma(B_s^{(*)} \bar{B}_s^{(*)})$					$\Gamma_{12} / \Gamma_{13}$
VALUE	CL%	DOCUMENT ID	TECN	COMMENT	

**$<0.16$**  90 BONVICINI 06 CLE3  $e^+ e^-$

$\Gamma(\text{no open-bottom}) / \Gamma_{\text{total}}$					$\Gamma_{14} / \Gamma$
VALUE	DOCUMENT ID	TECN	COMMENT		

**$0.038 \pm 0.051$**  OUR EVALUATION  
 **$-0.005$**

$\Gamma(K^*(892)^0 \bar{K}^0) / \Gamma_{\text{total}}$					$\Gamma_{16} / \Gamma$
VALUE	CL%	DOCUMENT ID	TECN	COMMENT	

**$<1.0 \times 10^{-5}$**  90 SHEN 13A BELL  $e^+ e^- \rightarrow K^*(892)^0 \bar{K}^0$

$\Gamma(\eta \mathcal{T}_J(1D)) / \Gamma_{\text{total}}$					$\Gamma_{21} / \Gamma$
VALUE (units $10^{-3}$ )	DOCUMENT ID	TECN	COMMENT		

**$4.82 \pm 0.92 \pm 0.67$**  <sup>1</sup> TAMPONI 18 BELL  $e^+ e^- \rightarrow \Upsilon(5S) \rightarrow \eta X$   
<sup>1</sup> Mainly  $J = 2$ , assumes no continuum contribution under  $\Upsilon(5S)$ .

$\Gamma(\Upsilon(1S) \pi^+ \pi^-) / \Gamma_{\text{total}}$					$\Gamma_{17} / \Gamma$
VALUE (units $10^{-3}$ )	EVTS	DOCUMENT ID	TECN	COMMENT	

**$5.3 \pm 0.3 \pm 0.5$**  325 <sup>1</sup> CHEN 08 BELL  $10.87 e^+ e^- \rightarrow \Upsilon(1S) \pi^+ \pi^-$   
<sup>1</sup> Assuming that the observed events are solely due to the  $\Upsilon(5S)$  resonance.

$\Gamma(\Upsilon(2S) \pi^+ \pi^-) / \Gamma_{\text{total}}$					$\Gamma_{18} / \Gamma$
VALUE (units $10^{-3}$ )	EVTS	DOCUMENT ID	TECN	COMMENT	

**$7.8 \pm 0.6 \pm 1.1$**  186 <sup>1</sup> CHEN 08 BELL  $10.87 e^+ e^- \rightarrow \Upsilon(2S) \pi^+ \pi^-$   
<sup>1</sup> Assuming that the observed events are solely due to the  $\Upsilon(5S)$  resonance.

$\Gamma(\Upsilon(3S) \pi^+ \pi^-) / \Gamma_{\text{total}}$					$\Gamma_{19} / \Gamma$
VALUE (units $10^{-3}$ )	EVTS	DOCUMENT ID	TECN	COMMENT	

**$4.8 \pm 1.8 \pm 0.7$**  10 <sup>1</sup> CHEN 08 BELL  $10.87 e^+ e^- \rightarrow \Upsilon(3S) \pi^+ \pi^-$   
<sup>1</sup> Assuming that the observed events are solely due to the  $\Upsilon(5S)$  resonance.

$\Gamma(\Upsilon(1S) K^+ K^-) / \Gamma_{\text{total}}$					$\Gamma_{20} / \Gamma$
VALUE (units $10^{-4}$ )	EVTS	DOCUMENT ID	TECN	COMMENT	

**$6.1 \pm 1.6 \pm 1.0$**  20 <sup>1</sup> CHEN 08 BELL  $10.87 e^+ e^- \rightarrow \Upsilon(1S) K^+ K^-$   
<sup>1</sup> Assuming that the observed events are solely due to the  $\Upsilon(5S)$  resonance.

$\Gamma(h_b(1P) \pi^+ \pi^-) / \Gamma(\Upsilon(2S) \pi^+ \pi^-)$					$\Gamma_{22} / \Gamma_{18}$
VALUE	DOCUMENT ID	TECN	COMMENT		

**$0.45 \pm 0.08 \pm 0.07$**  ADACHI 12 BELL  $10.86 e^+ e^- \rightarrow \text{hadrons}$

$\Gamma(h_b(2P) \pi^+ \pi^-) / \Gamma(\Upsilon(2S) \pi^+ \pi^-)$					$\Gamma_{23} / \Gamma_{18}$
VALUE	DOCUMENT ID	TECN	COMMENT		

**$0.77 \pm 0.08 \pm 0.22$**  ADACHI 12 BELL  $10.86 e^+ e^- \rightarrow \text{hadrons}$

$\Gamma(h_b(1P) \pi^+ \pi^-) / \Gamma(h_b(2P) \pi^+ \pi^-)$					$\Gamma_{22} / \Gamma_{23}$
VALUE	DOCUMENT ID	TECN	COMMENT		

**$0.616 \pm 0.052 \pm 0.017$**  MIZUK 16 BELL  $e^+ e^- \rightarrow h_b(1P, 2P) \pi^+ \pi^-$

$\Gamma(\chi_{bJ}(1P) \pi^+ \pi^- \pi^0) / \Gamma_{\text{total}}$					$\Gamma_{24} / \Gamma$
VALUE (units $10^{-3}$ )	DOCUMENT ID	TECN	COMMENT		

**$2.5 \pm 0.6 \pm 2.2$**  YIN 18 BELL  $e^+ e^- \rightarrow \text{hadrons}$

$\Gamma(\chi_{b0}(1P) \pi^+ \pi^- \pi^0) / \Gamma_{\text{total}}$					$\Gamma_{25} / \Gamma$
VALUE	CL%	DOCUMENT ID	TECN	COMMENT	

**$<6.3 \times 10^{-3}$**  90 <sup>1</sup> HE 14 BELL  $\Upsilon(5S) \rightarrow \pi^+ \pi^- \pi^0 \gamma \Upsilon(1S)$   
<sup>1</sup> Assuming that all the  $b\bar{b}$  events are from  $\Upsilon(5S)$  resonance decays and using  $\sigma(e^+ e^- \rightarrow b\bar{b}) = 0.340 \pm 0.016$  nb from ESEN 13. Correlated with other results from HE 14.

$\Gamma(\chi_{b0}(1P) \omega) / \Gamma_{\text{total}}$					$\Gamma_{26} / \Gamma$
VALUE	CL%	DOCUMENT ID	TECN	COMMENT	

**$<3.9 \times 10^{-3}$**  90 <sup>1</sup> HE 14 BELL  $\Upsilon(5S) \rightarrow \pi^+ \pi^- \pi^0 \gamma \Upsilon(1S)$   
<sup>1</sup> Assuming that all the  $b\bar{b}$  events are from  $\Upsilon(5S)$  resonance decays and using  $\sigma(e^+ e^- \rightarrow b\bar{b}) = 0.340 \pm 0.016$  nb from ESEN 13. Correlated with other results from HE 14.

$\Gamma(\chi_{b0}(1P) \pi^+ \pi^- \pi^0)_{\text{non-}\omega} / \Gamma_{\text{total}}$					$\Gamma_{27} / \Gamma$
VALUE	CL%	DOCUMENT ID	TECN	COMMENT	

**$<4.8 \times 10^{-3}$**  90 <sup>1</sup> HE 14 BELL  $\Upsilon(5S) \rightarrow \pi^+ \pi^- \pi^0 \gamma \Upsilon(1S)$   
<sup>1</sup> Assuming that all the  $b\bar{b}$  events are from  $\Upsilon(5S)$  resonance decays and using  $\sigma(e^+ e^- \rightarrow b\bar{b}) = 0.340 \pm 0.016$  nb from ESEN 13. Correlated with other results from HE 14.

$\Gamma(\chi_{b1}(1P) \pi^+ \pi^- \pi^0) / \Gamma_{\text{total}}$					$\Gamma_{28} / \Gamma$
VALUE (units $10^{-3}$ )	EVTS	DOCUMENT ID	TECN	COMMENT	

**$1.85 \pm 0.23 \pm 0.23$**  80 <sup>1</sup> HE 14 BELL  $\Upsilon(5S) \rightarrow \pi^+ \pi^- \pi^0 \gamma \Upsilon(1S)$   
<sup>1</sup> Assuming that all the  $b\bar{b}$  events are from  $\Upsilon(5S)$  resonance decays and using  $\sigma(e^+ e^- \rightarrow b\bar{b}) = 0.340 \pm 0.016$  nb from ESEN 13. Correlated with other results from HE 14.

# Meson Particle Listings

## $\Upsilon(10860)$ , $\Upsilon(11020)$

$\Gamma(\chi_{b1}(1P)\omega)/\Gamma_{total}$		$\Gamma_{29}/\Gamma$	
VALUE (units $10^{-3}$ )	EVTS	DOCUMENT ID	TECN COMMENT

**$1.57 \pm 0.22 \pm 0.21$**  60 <sup>1</sup> HE 14 BELL  $\Upsilon(5S) \rightarrow \pi^+ \pi^- \pi^0 \gamma \Upsilon(1S)$   
<sup>1</sup> Assuming that all the  $b\bar{b}$  events are from  $\Upsilon(5S)$  resonance decays and using  $\sigma(e^+e^- \rightarrow b\bar{b}) = 0.340 \pm 0.016$  nb from ESEN 13. Correlated with other results from HE 14.

$\Gamma(\chi_{b1}(1P)(\pi^+ \pi^- \pi^0)_{non-\omega})/\Gamma_{total}$		$\Gamma_{30}/\Gamma$	
VALUE (units $10^{-3}$ )	EVTS	DOCUMENT ID	TECN COMMENT

**$0.52 \pm 0.15 \pm 0.11$**  24 <sup>1</sup> HE 14 BELL  $\Upsilon(5S) \rightarrow \pi^+ \pi^- \pi^0 \gamma \Upsilon(1S)$   
<sup>1</sup> Assuming that all the  $b\bar{b}$  events are from  $\Upsilon(5S)$  resonance decays and using  $\sigma(e^+e^- \rightarrow b\bar{b}) = 0.340 \pm 0.016$  nb from ESEN 13. Correlated with other results from HE 14.

$\Gamma(\chi_{b2}(1P)\pi^+ \pi^- \pi^0)/\Gamma_{total}$		$\Gamma_{31}/\Gamma$	
VALUE (units $10^{-3}$ )	EVTS	DOCUMENT ID	TECN COMMENT

**$1.17 \pm 0.27 \pm 0.14$**  29 <sup>1</sup> HE 14 BELL  $\Upsilon(5S) \rightarrow \pi^+ \pi^- \pi^0 \gamma \Upsilon(1S)$   
<sup>1</sup> Assuming that all the  $b\bar{b}$  events are from  $\Upsilon(5S)$  resonance decays and using  $\sigma(e^+e^- \rightarrow b\bar{b}) = 0.340 \pm 0.016$  nb from ESEN 13. Correlated with other results from HE 14.

$\Gamma(\chi_{b2}(1P)\omega)/\Gamma_{total}$		$\Gamma_{32}/\Gamma$	
VALUE (units $10^{-3}$ )	EVTS	DOCUMENT ID	TECN COMMENT

**$0.60 \pm 0.23 \pm 0.15$**  13 <sup>1</sup> HE 14 BELL  $\Upsilon(5S) \rightarrow \pi^+ \pi^- \pi^0 \gamma \Upsilon(1S)$   
<sup>1</sup> Assuming that all the  $b\bar{b}$  events are from  $\Upsilon(5S)$  resonance decays and using  $\sigma(e^+e^- \rightarrow b\bar{b}) = 0.340 \pm 0.016$  nb from ESEN 13. Correlated with other results from HE 14.

$\Gamma(\chi_{b2}(1P)\omega)/\Gamma(\chi_{b1}(1P)\omega)$		$\Gamma_{32}/\Gamma_{29}$	
VALUE	DOCUMENT ID	TECN	COMMENT

• • • We do not use the following data for averages, fits, limits, etc. • • •  
 $0.38 \pm 0.16 \pm 0.09$  <sup>1</sup> HE 14 BELL  $\Upsilon(5S) \rightarrow \pi^+ \pi^- \pi^0 \gamma \Upsilon(1S)$   
<sup>1</sup> Accounting for correlated systematics.

$\Gamma(\chi_{b2}(1P)(\pi^+ \pi^- \pi^0)_{non-\omega})/\Gamma_{total}$		$\Gamma_{33}/\Gamma$	
VALUE (units $10^{-3}$ )	EVTS	DOCUMENT ID	TECN COMMENT

**$0.61 \pm 0.22 \pm 0.28$**  16 <sup>1</sup> HE 14 BELL  $\Upsilon(5S) \rightarrow \pi^+ \pi^- \pi^0 \gamma \Upsilon(1S)$   
<sup>1</sup> Assuming that all the  $b\bar{b}$  events are from  $\Upsilon(5S)$  resonance decays and using  $\sigma(e^+e^- \rightarrow b\bar{b}) = 0.340 \pm 0.016$  nb from ESEN 13. Correlated with other results from HE 14.

$\Gamma(\chi_{b2}(1P)(\pi^+ \pi^- \pi^0)_{non-\omega})/\Gamma(\chi_{b1}(1P)(\pi^+ \pi^- \pi^0)_{non-\omega})$		$\Gamma_{33}/\Gamma_{30}$	
VALUE	DOCUMENT ID	TECN	COMMENT

• • • We do not use the following data for averages, fits, limits, etc. • • •  
 $1.20 \pm 0.55 \pm 0.65$  <sup>1</sup> HE 14 BELL  $\Upsilon(5S) \rightarrow \pi^+ \pi^- \pi^0 \gamma \Upsilon(1S)$   
<sup>1</sup> Accounting for correlated systematics.

$\Gamma(\gamma X_b \rightarrow \gamma \Upsilon(1S)\omega)/\Gamma_{total}$		$\Gamma_{34}/\Gamma$	
VALUE	CL%	DOCUMENT ID	TECN COMMENT

**$< 3.8 \times 10^{-5}$**  90 <sup>1</sup> HE 14 BELL  $\Upsilon(5S) \rightarrow \pi^+ \pi^- \pi^0 \gamma \Upsilon(1S)$   
<sup>1</sup> Assuming that all the  $b\bar{b}$  events are from  $\Upsilon(5S)$  resonance decays and using  $\sigma(e^+e^- \rightarrow b\bar{b}) = 0.340 \pm 0.016$  nb from ESEN 13. Correlated with other results from HE 14. For a state  $X_b$  with mass between 10.55 GeV/c<sup>2</sup> and 10.65 GeV/c<sup>2</sup>, the obtained 90% upper limit as a function of  $m_{X_b}$  varies from  $2.6 \times 10^{-5}$  to  $3.8 \times 10^{-5}$ .

$\Gamma(\phi \text{ anything})/\Gamma_{total}$		$\Gamma_{35}/\Gamma$	
VALUE	DOCUMENT ID	TECN	COMMENT

**$0.138 \pm 0.007 \pm 0.023$**  HUANG 07 CLEO  $\Upsilon(5S) \rightarrow \phi X$   
 $-0.015$

$\Gamma(D^0 \text{ anything} + \text{c.c.})/\Gamma_{total}$		$\Gamma_{36}/\Gamma$	
VALUE	DOCUMENT ID	TECN	COMMENT

**$1.076 \pm 0.040 \pm 0.068$**  DRUTSKOY 07 BELL  $\Upsilon(5S) \rightarrow D^0 X$

$\Gamma(D_s \text{ anything} + \text{c.c.})/\Gamma_{total}$		$\Gamma_{37}/\Gamma$	
VALUE	DOCUMENT ID	TECN	COMMENT

**$0.46 \pm 0.06$**  OUR AVERAGE  
 $0.472 \pm 0.024 \pm 0.072$  <sup>1</sup> DRUTSKOY 07 BELL  $\Upsilon(5S) \rightarrow D_s X$   
 $0.44 \pm 0.09 \pm 0.04$  <sup>2</sup> ARTUSO 05B CLE3  $e^+e^- \rightarrow D_s X$   
<sup>1</sup> Using  $B(D_s^+ \rightarrow \phi\pi^+) = (4.4 \pm 0.6)\%$  from PDG 06.  
<sup>2</sup> ARTUSO 05B reports  $[\Gamma(\Upsilon(10860) \rightarrow D_s \text{ anything} + \text{c.c.})/\Gamma_{total}] \times [B(D_s^+ \rightarrow \phi\pi^+)] = 0.0198 \pm 0.0019 \pm 0.0038$  which we divide by our best value  $B(D_s^+ \rightarrow \phi\pi^+) = (4.5 \pm 0.4) \times 10^{-2}$ . Our first error is their experiment's error and our second error is the systematic error from using our best value.

$\Gamma(J/\psi \text{ anything})/\Gamma_{total}$		$\Gamma_{38}/\Gamma$	
VALUE (units $10^{-2}$ )	DOCUMENT ID	TECN	COMMENT

**$2.060 \pm 0.160 \pm 0.134$**  DRUTSKOY 07 BELL  $\Upsilon(5S) \rightarrow J/\psi X$

$\Gamma(B^0 \text{ anything} + \text{c.c.})/\Gamma_{total}$		$\Gamma_{39}/\Gamma$	
VALUE	EVTS	DOCUMENT ID	TECN COMMENT

**$0.770 \pm 0.058$**  DRUTSKOY 10 BELL  $\Upsilon(5S) \rightarrow B^0 X$   
 $-0.056 \pm 0.061$  352

$\Gamma(B^+ \text{ anything} + \text{c.c.})/\Gamma_{total}$		$\Gamma_{40}/\Gamma$	
VALUE	EVTS	DOCUMENT ID	TECN COMMENT

**$0.721 \pm 0.039$**  711 DRUTSKOY 10 BELL  $\Upsilon(5S) \rightarrow B^+ X$   
 $-0.038 \pm 0.050$

### $\Upsilon(10860)$ REFERENCES

MIZUK	19	JHEP 1910 220	R. Mizuk et al.	(BELLE Collab.)
TAMPONI	18	EPJ C78 633	U. Tamponi et al.	(BELLE Collab.)
YIN	18	PR D98 091102	J.H. Yin et al.	(BELLE Collab.)
MIZUK	16	PRL 117 142001	R. Mizuk et al.	(BELLE Collab.)
SANTEL	16	PR D93 011101	D. Santel et al.	(BELLE Collab.)
HE	14	PRL 113 142001	X.H. He et al.	(BELLE Collab.)
ESEN	13	PR D87 031101	S. ESEN et al.	(BELLE Collab.)
SHEN	13A	PR D88 052019	C.P. Shen et al.	(BELLE Collab.)
ADACHI	12	PRL 108 032001	I. Adachi et al.	(BELLE Collab.)
LI	12	PRL 108 181808	J. Li et al.	(BELLE Collab.)
CHEN	10	PR D92 091106	K.-F. Chen et al.	(BELLE Collab.)
DRUTSKOY	10	PR D81 112003	A. Drutskoy et al.	(BELLE Collab.)
AUBERT	09E	PRL 102 012001	B. Aubert et al.	(BABAR Collab.)
LOUVOT	09	PRL 102 021801	R. Louvot et al.	(BELLE Collab.)
CHEN	08	PRL 100 112001	K.-F. Chen et al.	(BELLE Collab.)
DRUTSKOY	07	PRL 98 052001	A. Drutskoy et al.	(BELLE Collab.)
DRUTSKOY	07A	PR D76 012002	A. Drutskoy et al.	(BELLE Collab.)
HUANG	07	PR D75 012002	G.S. Huang et al.	(CLEO Collab.)
AQUINES	06	PRL 96 152001	O. Aquines et al.	(CLEO Collab.)
BONVICINI	06	PRL 96 022002	G. Bonvicini et al.	(CLEO Collab.)
PDG	06	JP G33 3	W.-M. Yao et al.	(PDG Collab.)
ARTUSO	05B	PRL 95 261801	M. Artuso et al.	(CLEO Collab.)
BESSION	85	PRL 54 381	D. Besson et al.	(CLEO Collab.)
LOVELOCK	85	PRL 54 377	D.M.J. Lovelock et al.	(CUSB Collab.)

## $\Upsilon(11020)$

$$J^{PC} = 0^{-}(1^{-})^{-}$$

### $\Upsilon(11020)$ MASS

VALUE (MeV)	DOCUMENT ID	TECN	COMMENT
<b><math>11000 \pm 4</math></b> OUR AVERAGE			
$11000.0 \pm 4.0 + 1.0$	<sup>1</sup> MIZUK	19	BELL $e^+e^- \rightarrow \Upsilon(1S, 2S, 3S)\pi^+\pi^-$
$4.5 - 1.3$			
$10999.0 \pm 7.3 + 16.9$	<sup>2</sup> MIZUK	16	BELL $e^+e^- \rightarrow h_b(1P, 2P)\pi^+\pi^-$
$-7.8 - 1.0$			
• • • We do not use the following data for averages, fits, limits, etc. • • •			
$11003.0 \pm 1.1 \pm 0.9$	<sup>3,4</sup> SANTEL	16	BELL $e^+e^- \rightarrow \text{hadrons}$
$1.0 - 1.0$			
$10987.5 \pm 6.4 + 9.1$	<sup>5,6</sup> SANTEL	16	BELL $e^+e^- \rightarrow \Upsilon(1S, 2S, 3S)\pi^+\pi^-$
$2.5 - 2.3$			
$10996 \pm 2$	<sup>7</sup> AUBERT	09E	BABR $e^+e^- \rightarrow \text{hadrons}$
$11019 \pm 5 \pm 7$	BESSION	85	CLEO $e^+e^- \rightarrow \text{hadrons}$
$11020 \pm 30$	LOVELOCK	85	CUSB $e^+e^- \rightarrow \text{hadrons}$

<sup>1</sup> From a simultaneous fit to the  $\Upsilon(nS)\pi^+\pi^-$ ,  $n = 1, 2, 3$ , cross sections at 28 energy points within  $\sqrt{s} = 10.6\text{--}11.05$  GeV, including the initial-state radiation at  $\Upsilon(10860)$ .  
<sup>2</sup> From a simultaneous fit to the  $h_b(nP)\pi^+\pi^-$ ,  $n = 1, 2$  cross sections at 22 energy points within  $\sqrt{s} = 10.77\text{--}11.02$  GeV to a pair of interfering Breit-Wigner amplitudes modified by phase space factors, with eight resonance parameters (a mass and width for each of  $\Upsilon(10860)$  and  $\Upsilon(11020)$ , a single relative phase, a single relative amplitude, and two overall normalization factors, one for each  $n$ ). The systematic error estimate is dominated by possible interference with a small nonresonant continuum amplitude.  
<sup>3</sup> From a fit to the total hadronic cross sections measured at 60 energy points within  $\sqrt{s} = 10.82\text{--}11.05$  GeV to a pair of interfering Breit-Wigner amplitudes and two floating continuum amplitudes with  $1/\sqrt{s}$  dependence, one coherent with the resonances and one incoherent, with six resonance parameters (a mass, width, and an amplitude for each of  $\Upsilon(10860)$  and  $\Upsilon(11020)$ , one relative phase, and one decoherence coefficient).  
<sup>4</sup> Not including uncertain and potentially large systematic errors due to assumed continuum amplitude  $1/\sqrt{s}$  dependence and related interference contributions.  
<sup>5</sup> From a simultaneous fit to the  $\Upsilon(nS)\pi^+\pi^-$ ,  $n = 1, 2, 3$ , cross sections at 25 energy points within  $\sqrt{s} = 10.6\text{--}11.05$  GeV to a pair of interfering Breit-Wigner amplitudes modified by phase space factors, with fourteen resonance parameters (a mass, width, and three amplitudes for each of  $\Upsilon(10860)$  and  $\Upsilon(11020)$ , a single universal relative phase, and three decoherence coefficients, one for each  $n$ ). Continuum contributions were measured (and therefore fixed) to be zero.  
<sup>6</sup> Superseded by MIZUK 19.  
<sup>7</sup> In a model where a flat non-resonant  $b\bar{b}$ -continuum is incoherently added to a second flat component interfering with two Breit-Wigner resonances. Systematic uncertainties not estimated.

### $\Upsilon(11020)$ WIDTH

VALUE (MeV)	DOCUMENT ID	TECN	COMMENT
<b><math>24 \pm 8</math></b> OUR AVERAGE			
$23.8 \pm 8.0 + 0.7$	<sup>1</sup> MIZUK	19	BELL $e^+e^- \rightarrow \Upsilon(nS)\pi^+\pi^-$
$6.8 - 1.8$			
$27 \pm 27 \pm 5$	<sup>2</sup> MIZUK	16	BELL $e^+e^- \rightarrow h_b(1P, 2P)\pi^+\pi^-$
$-11 - 12$			
• • • We do not use the following data for averages, fits, limits, etc. • • •			
$39.3 \pm 1.7 + 1.3$	<sup>3,4</sup> SANTEL	16	BELL $e^+e^- \rightarrow \text{hadrons}$
$1.6 - 2.4$			
$61 \pm 9 \pm 2$	<sup>5,6</sup> SANTEL	16	BELL $e^+e^- \rightarrow \Upsilon(1S, 2S, 3S)\pi^+\pi^-$
$-19 - 20$			
$37 \pm 3$	<sup>7</sup> AUBERT	09E	BABR $e^+e^- \rightarrow \text{hadrons}$
$61 \pm 13 \pm 22$	BESSION	85	CLEO $e^+e^- \rightarrow \text{hadrons}$
$90 \pm 20$	LOVELOCK	85	CUSB $e^+e^- \rightarrow \text{hadrons}$

Meson Particle Listings  
 $\Upsilon(11020)$

- <sup>1</sup> From a simultaneous fit to the  $\Upsilon(nS)\pi^+\pi^-$ ,  $n = 1, 2, 3$ , cross sections at 28 energy points within  $\sqrt{s} = 10.6\text{--}11.05$  GeV, including the initial-state radiation at  $\Upsilon(10860)$ .
- <sup>2</sup> From a simultaneous fit to the  $h_b(nP)\pi^+\pi^-$ ,  $n = 1, 2$  cross sections at 22 energy points within  $\sqrt{s} = 10.77\text{--}11.02$  GeV to a pair of interfering Breit-Wigner amplitudes modified by phase space factors, with eight resonance parameters (a mass and width for each of  $\Upsilon(10860)$  and  $\Upsilon(11020)$ , a single relative phase, a single relative amplitude, and two overall normalization factors, one for each  $n$ ). The systematic error estimate is dominated by possible interference with a small nonresonant continuum amplitude.
- <sup>3</sup> From a fit to the total hadronic cross sections measured at 60 energy points within  $\sqrt{s} = 10.82\text{--}11.05$  GeV to a pair of interfering Breit-Wigner amplitudes and two floating continuum amplitudes with  $1/\sqrt{s}$  dependence, one coherent with the resonances and one incoherent, with six resonance parameters (a mass, width, and an amplitude for each of  $\Upsilon(10860)$  and  $\Upsilon(11020)$ , one relative phase, and one decoherence coefficient).
- <sup>4</sup> Not including uncertain and potentially large systematic errors due to assumed continuum amplitude  $1/\sqrt{s}$  dependence and related interference contributions.
- <sup>5</sup> From a simultaneous fit to the  $\Upsilon(nS)\pi^+\pi^-$ ,  $n = 1, 2, 3$ , cross sections at 25 energy points within  $\sqrt{s} = 10.6\text{--}11.05$  GeV to a pair of interfering Breit-Wigner amplitudes modified by phase space factors, with fourteen resonance parameters (a mass, width, and three amplitudes for each of  $\Upsilon(10860)$  and  $\Upsilon(11020)$ , a single universal relative phase, and three decoherence coefficients, one for each  $n$ ). Continuum contributions were measured (and therefore fixed) to be zero.
- <sup>6</sup> Superseded by MIZUK 19.
- <sup>7</sup> In a model where a flat non-resonant  $b\bar{b}$ -continuum is incoherently added to a second flat component interfering with two Breit-Wigner resonances. Systematic uncertainties not estimated.

$\Upsilon(11020)$  DECAY MODES

Mode	Fraction ( $\Gamma_j/\Gamma$ )
$\Gamma_1$ $e^+e^-$	$(5.4^{+1.9}_{-2.1}) \times 10^{-6}$
$\Gamma_2$ $\Upsilon(1S)\pi^+\pi^-$	
$\Gamma_3$ $\Upsilon(2S)\pi^+\pi^-$	
$\Gamma_4$ $\Upsilon(3S)\pi^+\pi^-$	
$\Gamma_5$ $\chi_{bJ}(1P)\pi^+\pi^-\pi^0$	$(9^{+9}_{-8}) \times 10^{-3}$
$\Gamma_6$ $\chi_{b1}(1P)\pi^+\pi^-\pi^0$	seen
$\Gamma_7$ $\chi_{b2}(1P)\pi^+\pi^-\pi^0$	seen

$\Upsilon(11020)$  PARTIAL WIDTHS

$\Gamma(e^+e^-)$	DOCUMENT ID	TECN	COMMENT	$\Gamma_1$
<b>0.130 ± 0.030 OUR AVERAGE</b>				
0.095 ± 0.03 ± 0.035	BESSION	85	CLEO $e^+e^- \rightarrow$ hadrons	
0.156 ± 0.040	LOVELOCK	85	CUSB $e^+e^- \rightarrow$ hadrons	

$\Gamma(e^+e^-) \times \Gamma(\Upsilon(1S)\pi^+\pi^-)/\Gamma_{\text{total}}$	DOCUMENT ID	TECN	COMMENT	$\Gamma_1\Gamma_2/\Gamma$
0.46 ± 0.08	1,2 MIZUK	19	BELL $e^+e^- \rightarrow \Upsilon(nS)\pi^+\pi^-$	

- <sup>1</sup> From a simultaneous fit to the  $\Upsilon(nS)\pi^+\pi^-$ ,  $n = 1, 2, 3$ , cross sections at 28 energy points within  $\sqrt{s} = 10.6\text{--}11.05$  GeV, including the initial-state radiation at  $\Upsilon(10860)$ .
- <sup>2</sup> Reported as the range 0.38–0.54 eV obtained from multiple solutions of an amplitude fit within a model composed as a sum of Breit-Wigner functions.

$\Gamma(e^+e^-) \times \Gamma(\Upsilon(2S)\pi^+\pi^-)/\Gamma_{\text{total}}$	DOCUMENT ID	TECN	COMMENT	$\Gamma_1\Gamma_3/\Gamma$
0.65 ± 0.52	1,2 MIZUK	19	BELL $e^+e^- \rightarrow \Upsilon(nS)\pi^+\pi^-$	

- <sup>1</sup> From a simultaneous fit to the  $\Upsilon(nS)\pi^+\pi^-$ ,  $n = 1, 2, 3$ , cross sections at 28 energy points within  $\sqrt{s} = 10.6\text{--}11.05$  GeV, including the initial-state radiation at  $\Upsilon(10860)$ .
- <sup>2</sup> Reported as the range 0.13–1.16 eV obtained from multiple solutions of an amplitude fit within a model composed as a sum of Breit-Wigner functions.

$\Gamma(e^+e^-) \times \Gamma(\Upsilon(3S)\pi^+\pi^-)/\Gamma_{\text{total}}$	DOCUMENT ID	TECN	COMMENT	$\Gamma_1\Gamma_4/\Gamma$
0.33 ± 0.16	1,2 MIZUK	19	BELL $e^+e^- \rightarrow \Upsilon(nS)\pi^+\pi^-$	

- <sup>1</sup> From a simultaneous fit to the  $\Upsilon(nS)\pi^+\pi^-$ ,  $n = 1, 2, 3$ , cross sections at 28 energy points within  $\sqrt{s} = 10.6\text{--}11.05$  GeV, including the initial-state radiation at  $\Upsilon(10860)$ .
- <sup>2</sup> Reported as the range 0.17–0.49 eV obtained from multiple solutions of an amplitude fit within a model composed as a sum of Breit-Wigner functions.

$\Gamma(\chi_{bJ}(1P)\pi^+\pi^-\pi^0)/\Gamma_{\text{total}}$	DOCUMENT ID	TECN	COMMENT	$\Gamma_5/\Gamma$
$8.7 \pm 4.3^{+7.6}_{-6.6}$	YIN	18	BELL $e^+e^- \rightarrow$ hadrons	

$\Gamma(\chi_{b1}(1P)\pi^+\pi^-\pi^0)/\Gamma_{\text{total}}$	DOCUMENT ID	TECN	COMMENT	$\Gamma_6/\Gamma$
seen	YIN	18	BELL $e^+e^- \rightarrow$ hadrons	

$\Gamma(\chi_{b2}(1P)\pi^+\pi^-\pi^0)/\Gamma_{\text{total}}$	DOCUMENT ID	TECN	COMMENT	$\Gamma_7/\Gamma$
seen	YIN	18	BELL $e^+e^- \rightarrow$ hadrons	

$\Gamma(\chi_{b2}(1P)\pi^+\pi^-\pi^0)/\Gamma(\chi_{b1}(1P)\pi^+\pi^-\pi^0)$	DOCUMENT ID	TECN	COMMENT	$\Gamma_7/\Gamma_6$
0.4 ± 0.2	YIN	18	BELL $e^+e^- \rightarrow$ hadrons	

$\Upsilon(11020)$  REFERENCES

MIZUK	19	JHEP 1910 220	R. Mizuk <i>et al.</i>	(BELLE Collab.)
YIN	18	PR D98 091102	J.H. Yin <i>et al.</i>	(BELLE Collab.)
MIZUK	16	PRL 117 142001	R. Mizuk <i>et al.</i>	(BELLE Collab.)
SANTELE	16	PR D93 011101	D. Santel <i>et al.</i>	(BELLE Collab.)
AUBERT	09E	PRL 102 012001	B. Aubert <i>et al.</i>	(BABAR Collab.)
BESSION	85	PRL 54 381	D. Besson <i>et al.</i>	(CLEO Collab.)
LOVELOCK	85	PRL 54 377	D.M.J. Lovelock <i>et al.</i>	(CUSB Collab.)



<b><i>N</i> BARYONS (<i>S</i> = 0, <i>I</i> = 1/2)</b>	
<i>p</i> . . . . .	1825
<i>n</i> . . . . .	1834
<i>N</i> resonances . . . . .	1839
<b><math>\Delta</math> BARYONS (<i>S</i> = 0, <i>I</i> = 3/2)</b>	
$\Delta$ resonances . . . . .	1878
<b><math>\Lambda</math> BARYONS (<i>S</i> = -1, <i>I</i> = 0)</b>	
$\Lambda$ . . . . .	1902
$\Lambda$ resonances . . . . .	1905
<b><math>\Sigma</math> BARYONS (<i>S</i> = -1, <i>I</i> = 1)</b>	
$\Sigma^+$ . . . . .	1927
$\Sigma^0$ . . . . .	1929
$\Sigma^-$ . . . . .	1930
$\Sigma$ resonances . . . . .	1932
<b><math>\Xi</math> BARYONS (<i>S</i> = -2, <i>I</i> = 1/2)</b>	
$\Xi^0$ . . . . .	1959
$\Xi^-$ . . . . .	1961
$\Xi$ resonances . . . . .	1964
<b><math>\Omega</math> BARYONS (<i>S</i> = -3, <i>I</i> = 0)</b>	
$\Omega^-$ . . . . .	1971
$\Omega$ resonances . . . . .	1973
<b>CHARMED BARYONS (<i>C</i> = +1)</b>	
$\Lambda_c^+$ . . . . .	1974
$\Lambda_c(2595)^+$ . . . . .	1980
$\Lambda_c(2625)^+$ . . . . .	1981
$\Lambda_c(2765)^+$ . . . . .	1982
$\Lambda_c(2860)^+$ . . . . .	1982
$\Lambda_c(2880)^+$ . . . . .	1982
$\Lambda_c(2940)^+$ . . . . .	1983
$\Sigma_c(2455)$ . . . . .	1983
$\Sigma_c(2520)$ . . . . .	1984
$\Sigma_c(2800)$ . . . . .	1985
$\Xi_c^+$ . . . . .	1985
$\Xi_c^0$ . . . . .	1987
$\Xi_c^+$ . . . . .	1988
$\Xi_c^0$ . . . . .	1989
$\Xi_c(2645)$ . . . . .	1989
$\Xi_c(2790)$ . . . . .	1989
$\Xi_c(2815)$ . . . . .	1990
$\Xi_c(2930)$ . . . . .	1990
$\Xi_c(2970)$ was $\Xi_c(2980)$ . . . . .	1991
$\Xi_c(3055)$ . . . . .	1992
$\Xi_c(3080)$ . . . . .	1992
$\Xi_c(3123)$ . . . . .	1992
$\Omega_c^0$ . . . . .	1993
$\Omega_c(2770)^0$ . . . . .	1994
$\Omega_c(3000)^0$ . . . . .	1994
$\Omega_c(3050)^0$ . . . . .	1994
$\Omega_c(3065)^0$ . . . . .	1994
$\Omega_c(3090)^0$ . . . . .	1995
$\Omega_c(3120)^0$ . . . . .	1995

<b>DOUBLY-CHARMED BARYONS (<i>C</i> = +2)</b>	
$\Xi_{cc}^{++}$ . . . . .	1996
<b>BOTTOM (BEAUTY) BARYONS (<i>B</i> = -1)</b>	
$\Lambda_b^0$ . . . . .	1997
$\Lambda_b(5912)^0$ . . . . .	2005
$\Lambda_b(5920)^0$ . . . . .	2005
$\Lambda_b(6146)^0$ . . . . .	2005
$\Lambda_b(6152)^0$ . . . . .	2005
$\Sigma_b$ . . . . .	2006
$\Sigma_b(6097)^+$ . . . . .	2007
$\Sigma_b(6097)^-$ . . . . .	2007
$\Sigma_b^*$ . . . . .	2006
$\Xi_b^0, \Xi_b^-$ . . . . .	2007
$\Xi_b'(5935)^-$ . . . . .	2009
$\Xi_b(5945)^0$ . . . . .	2010
$\Xi_b(5955)^-$ . . . . .	2010
$\Xi_b(6227)$ . . . . .	2010
$\Omega_b^-$ . . . . .	2011
<i>b</i> -baryon ADMIXTURE ( $\Lambda_b, \Xi_b, \Omega_b$ ) . . . . .	2011
<b>EXOTIC BARYONS</b>	
$P_c(4312)^+$ . . . . .	2014
$P_c(4440)^+$ . . . . .	2014
$P_c(4380)^+$ . . . . .	2014
$P_c(4457)^+$ was $P_c(4450)$ . . . . .	2014

**Notes in the Listings**

$\Sigma(1670)$ region . . . . .	1938
Radiative hyperon decays . . . . .	1960
$\Xi$ resonances . . . . .	1964

**Related Reviews in Volume 1**

79. Baryon decay parameters . . . . .	868
80. <i>N</i> and $\Delta$ resonances (rev.) . . . . .	869
81. Baryon magnetic moments . . . . .	874
82. $\Lambda$ and $\Sigma$ resonances (rev.) . . . . .	875
83. Pole structure of the $\Lambda(1405)$ region (rev.) . . . . .	878
84. Charmed baryons (rev.) . . . . .	879
85. Pentaquarks (rev.) . . . . .	881



# N BARYONS

## (S = 0, I = 1/2)

$p, N^+ = uud; \quad n, N^0 = udd$

$I(J^P) = \frac{1}{2}(\frac{1}{2}^+)$  Status: \* \* \* \*

**p MASS (atomic mass units u)**

The mass is known much more precisely in u (atomic mass units) than in MeV. See the next data block.

VALUE (u)	DOCUMENT ID	TECN	COMMENT
<b>1.00727646662 ± 0.0000000009</b>	<b>OUR AVERAGE</b>	Error	includes scale factor of 3.1.
1.007276466583 ± 0.00000000032	<sup>1</sup> HEISSE	17	SPEC Penning trap
1.007276466879 ± 0.00000000091	MOHR	16	RVUE 2014 CODATA value
• • • We do not use the following data for averages, fits, limits, etc. • • •			
1.007276466812 ± 0.00000000090	MOHR	12	RVUE 2010 CODATA value
1.00727646677 ± 0.00000000010	MOHR	08	RVUE 2006 CODATA value
1.00727646688 ± 0.00000000013	MOHR	05	RVUE 2002 CODATA value
1.00727646688 ± 0.00000000013	MOHR	99	RVUE 1998 CODATA value
1.007276470 ± 0.0000000012	COHEN	87	RVUE 1986 CODATA value

<sup>1</sup> The statistical and systematic errors are 15 and 29 in the last two places of the value. The value disagrees with the MOHR 16 value by over 3 standard deviations.

**p MASS (MeV)**

The mass is known much more precisely in u (atomic mass units) than in MeV. The conversion from u to MeV,  $1 u = 931.494 0054(57) \text{ MeV}/c^2$  (MOHR 16, the 2014 CODATA value), involves the relatively poorly known electronic charge.

VALUE (MeV)	DOCUMENT ID	TECN	COMMENT
<b>938.2720813 ± 0.0000058</b>	MOHR	16	RVUE 2014 CODATA value
• • • We do not use the following data for averages, fits, limits, etc. • • •			
938.272046 ± 0.000021	MOHR	12	RVUE 2010 CODATA value
938.272013 ± 0.000023	MOHR	08	RVUE 2006 CODATA value
938.272029 ± 0.000080	MOHR	05	RVUE 2002 CODATA value
938.271998 ± 0.000038	MOHR	99	RVUE 1998 CODATA value
938.27231 ± 0.00028	COHEN	87	RVUE 1986 CODATA value
938.2796 ± 0.0027	COHEN	73	RVUE 1973 CODATA value

**$|m_p - m_{\bar{p}}|/m_p$**

A test of CPT invariance. Note that the comparison of the  $\bar{p}$  and p charge-to-mass ratio, given in the next data block, is much better determined.

VALUE	CL%	DOCUMENT ID	TECN	COMMENT
<b>&lt;7 × 10<sup>-10</sup></b>	90	<sup>1</sup> HORI	11	SPEC $\bar{p}e^-$ He atom
• • • We do not use the following data for averages, fits, limits, etc. • • •				
<2 × 10 <sup>-9</sup>	90	<sup>1</sup> HORI	06	SPEC $\bar{p}e^-$ He atom
<1.0 × 10 <sup>-8</sup>	90	<sup>1</sup> HORI	03	SPEC $\bar{p}e^-$ <sup>4</sup> He, $\bar{p}e^-$ <sup>3</sup> He
<6 × 10 <sup>-8</sup>	90	<sup>1</sup> HORI	01	SPEC $\bar{p}e^-$ He atom
<5 × 10 <sup>-7</sup>		<sup>2</sup> TORII	99	SPEC $\bar{p}e^-$ He atom

<sup>1</sup> HORI 01, HORI 03, HORI 06, and HORI 11 use the more-precisely-known constraint on the  $\bar{p}$  charge-to-mass ratio of GABRIELSE 99 (see below) to get their results. Their results are not independent of the HORI 01, HORI 03, HORI 06, and HORI 11 values for  $|q_p + q_{\bar{p}}|/e$ , below.

<sup>2</sup> TORII 99 uses the more-precisely-known constraint on the  $\bar{p}$  charge-to-mass ratio of GABRIELSE 95 (see below) to get this result. This is not independent of the TORII 99 value for  $|q_p + q_{\bar{p}}|/e$ , below.

**$\bar{p}/p$  CHARGE-TO-MASS RATIO,  $|\frac{q_{\bar{p}}}{m_{\bar{p}}}|/(\frac{q_p}{m_p})$**

A test of CPT invariance. Listed here are measurements involving the inertial masses. For a discussion of what may be inferred about the ratio of  $\bar{p}$  and p gravitational masses, see ERICSON 90; they obtain an upper bound of  $10^{-6}$ – $10^{-7}$  for violation of the equivalence principle for  $\bar{p}$ 's.

VALUE	DOCUMENT ID	TECN	COMMENT
<b>1.00000000001 ± 0.00000000069</b>	ULMER	15	TRAP Penning trap
• • • We do not use the following data for averages, fits, limits, etc. • • •			
0.99999999991 ± 0.0000000009	GABRIELSE	99	TRAP Penning trap
1.0000000015 ± 0.0000000011	<sup>1</sup> GABRIELSE	95	TRAP Penning trap
1.0000000023 ± 0.0000000042	<sup>2</sup> GABRIELSE	90	TRAP Penning trap

<sup>1</sup> Equation (2) of GABRIELSE 95 should read  $M(\bar{p})/M(p) = 0.999\,999\,9985(11)$  (G. Gabrielse, private communication).

<sup>2</sup> GABRIELSE 90 also measures  $m_{\bar{p}}/m_{e^-} = 1836.152660 \pm 0.000083$  and  $m_p/m_{e^-} = 1836.152680 \pm 0.000088$ . Both are completely consistent with the 1986 CODATA (COHEN 87) value for  $m_p/m_{e^-}$  of  $1836.152701 \pm 0.000037$ .

$(|\frac{q_{\bar{p}}}{m_{\bar{p}}}| - \frac{q_p}{m_p})/\frac{q_p}{m_p}$

A test of CPT invariance. Taken from the  $\bar{p}/p$  charge-to-mass ratio, above.

VALUE	DOCUMENT ID
<b>(0.1 ± 6.9) × 10<sup>-11</sup></b>	<b>OUR EVALUATION</b>

**$|q_p + q_{\bar{p}}|/e$**

A test of CPT invariance. Note that the comparison of the  $\bar{p}$  and p charge-to-mass ratios given above is much better determined. See also a similar test involving the electron.

VALUE	CL%	DOCUMENT ID	TECN	COMMENT
<b>&lt;7 × 10<sup>-10</sup></b>	90	<sup>1</sup> HORI	11	SPEC $\bar{p}e^-$ He atom
• • • We do not use the following data for averages, fits, limits, etc. • • •				
<2 × 10 <sup>-9</sup>	90	<sup>1</sup> HORI	06	SPEC $\bar{p}e^-$ He atom
<1.0 × 10 <sup>-8</sup>	90	<sup>1</sup> HORI	03	SPEC $\bar{p}e^-$ <sup>4</sup> He, $\bar{p}e^-$ <sup>3</sup> He
<6 × 10 <sup>-8</sup>	90	<sup>1</sup> HORI	01	SPEC $\bar{p}e^-$ He atom
<5 × 10 <sup>-7</sup>		<sup>2</sup> TORII	99	SPEC $\bar{p}e^-$ He atom
<2 × 10 <sup>-5</sup>		<sup>3</sup> HUGHES	92	RVUE

<sup>1</sup> HORI 01, HORI 03, HORI 06, and HORI 11 use the more-precisely-known constraint on the  $\bar{p}$  charge-to-mass ratio of GABRIELSE 99 (see above) to get their results. Their results are not independent of the HORI 01, HORI 03, HORI 06, and HORI 11 values for  $|m_p - m_{\bar{p}}|/m_p$ , above.

<sup>2</sup> TORII 99 uses the more-precisely-known constraint on the  $\bar{p}$  charge-to-mass ratio of GABRIELSE 95 (see above) to get this result. This is not independent of the TORII 99 value for  $|m_p - m_{\bar{p}}|/m_p$ , above.

<sup>3</sup> HUGHES 92 uses recent measurements of Rydberg-energy and cyclotron-frequency ratios.

**$|q_p + q_e|/e$**

See BRESSI 11 for a summary of experiments on the neutrality of matter. See also "n CHARGE" in the neutron Listings.

VALUE	DOCUMENT ID	COMMENT
<b>&lt;1 × 10<sup>-21</sup></b>	<sup>1</sup> BRESSI	11 Neutrality of SF <sub>6</sub>
• • • We do not use the following data for averages, fits, limits, etc. • • •		
<3.2 × 10 <sup>-20</sup>	<sup>2</sup> SENGUPTA	00 binary pulsar
<0.8 × 10 <sup>-21</sup>	MARINELLI	84 Magnetic levitation
<1.0 × 10 <sup>-21</sup>	<sup>1</sup> DYLLA	73 Neutrality of SF <sub>6</sub>

<sup>1</sup> BRESSI 11 uses the method of DYLLA 73 but finds serious errors in that experiment that greatly reduce its accuracy. The BRESSI 11 limit assumes that  $n \rightarrow p e^- \nu_e$  conserves charge. Thus the limit applies equally to the charge of the neutron.

<sup>2</sup> SENGUPTA 00 uses the difference between the observed rate of rotational energy loss by the binary pulsar PSR B1913+16 and the rate predicted by general relativity to set this limit. See the paper for assumptions.

**p MAGNETIC MOMENT**

See the "Note on Baryon Magnetic Moments" in the  $\Lambda$  Listings.

VALUE ( $\mu_N$ )	DOCUMENT ID	TECN	COMMENT
<b>2.79284734462 ± 0.00000000082</b>	SCHNEIDER	17	TRAP Double Penning trap
• • • We do not use the following data for averages, fits, limits, etc. • • •			
2.7928473508 ± 0.00000000085	MOHR	16	RVUE 2014 CODATA value
2.792847356 ± 0.0000000023	MOHR	12	RVUE 2010 CODATA value
2.792847356 ± 0.0000000023	MOHR	08	RVUE 2006 CODATA value
2.792847351 ± 0.0000000028	MOHR	05	RVUE 2002 CODATA value
2.792847337 ± 0.0000000029	MOHR	99	RVUE 1998 CODATA value
2.792847386 ± 0.0000000063	COHEN	87	RVUE 1986 CODATA value

**$\bar{p}$  MAGNETIC MOMENT**

A few early results have been omitted.

VALUE ( $\mu_N$ )	DOCUMENT ID	TECN	COMMENT
<b>-2.7928473441 ± 0.00000000042</b>	SMORRA	17	TRAP Hot/cold $\bar{p}$ frequencies, Penning traps
• • • We do not use the following data for averages, fits, limits, etc. • • •			
-2.7928465 ± 0.0000023	NAGAHAMA	17	TRAP Single $\bar{p}$ , Penning trap
-2.792845 ± 0.000012	DISCIACCA	13	TRAP Single $\bar{p}$ , Penning trap
-2.7862 ± 0.0083	PASK	09	CNTR $\bar{p}$ He <sup>+</sup> hyperfine structure
-2.8005 ± 0.0090	KREISSL	88	CNTR $\bar{p}$ <sup>208</sup> Pb 11 → 10 X-ray
-2.817 ± 0.048	ROBERTS	78	CNTR
-2.791 ± 0.021	HU	75	CNTR Exotic atoms



## Baryon Particle Listings

 $\rho$ 

$$(\mu_p + \mu_{\bar{p}}) / \mu_p$$

A test of *CPT* invariance.

VALUE (units $10^{-6}$ )	DOCUMENT ID	TECN	COMMENT
<b>0.002 ± 0.004</b>	SMORRA 17	TRAP	Hot/cold $\bar{p}$ frequencies, Penning traps
0.3 ± 0.8	NAGAHAMA 17	TRAP	Single $\bar{p}$ , Penning trap
0 ± 5	DISCIACCA 13	TRAP	Single $\bar{p}$ , Penning trap

• • • We do not use the following data for averages, fits, limits, etc. • • •

 $\rho$  ELECTRIC DIPOLE MOMENTA nonzero value is forbidden by both *T* invariance and *P* invariance.

VALUE ( $10^{-23}$ e cm)	DOCUMENT ID	TECN	COMMENT
< <b>0.021</b>	1 SAHOO 17		Theory plus $^{199}\text{Hg}$ atom EDM
0.54	1 DMITRIEV 03		Theory plus $^{199}\text{Hg}$ atom EDM
- 3.7 ± 6.3	CHO 89	NMR	TI F molecules
< 400	DZUBA 85	THEO	Uses $^{129}\text{Xe}$ moment
130 ± 200	2 WILKENING 84		
900 ± 1400	3 WILKENING 84		
700 ± 900	HARRISON 69	MBR	Molecular beam

1 SAHOO 17 and DMITRIEV 03 are not direct measurements of the proton electric dipole moment. They use theory to calculate this limit from the limit on the electric dipole moment of the  $^{199}\text{Hg}$  atom.

2 This WILKENING 84 value includes a finite-size effect and a magnetic effect.

3 This WILKENING 84 value is more cautious than the other and excludes the finite-size effect, which relies on uncertain nuclear integrals.

 $\rho$  ELECTRIC POLARIZABILITY  $\alpha_p$ 

For a very complete review of the "polarizability of the nucleon and Compton scattering," see SCHUMACHER 05. His recommended values for the proton are  $\alpha_p = (12.0 \pm 0.6) \times 10^{-4} \text{ fm}^3$  and  $\beta_p = (1.9 \mp 0.6) \times 10^{-4} \text{ fm}^3$ , almost exactly our averages.

VALUE ( $10^{-4} \text{ fm}^3$ )	DOCUMENT ID	TECN	COMMENT
<b>11.2 ± 0.4 OUR AVERAGE</b>			
10.65 ± 0.35 ± 0.36	MCGOVERN 13	RVUE	$\chi\text{EFT} + \text{Compton scattering}$
12.1 ± 1.1 ± 0.5	1 BEANE 03	EF	EFT + $\gamma p$
11.82 ± 0.98 ± 0.52 - 0.98	2 BLANPIED 01	LEGS	$\rho(\vec{\gamma}, \gamma), \rho(\vec{\gamma}, \pi^0), \rho(\vec{\gamma}, \pi^+)$
11.9 ± 0.5 ± 1.3	3 OLMOSDEL... 01	CNTR	$\gamma p$ Compton scattering
12.1 ± 0.8 ± 0.5	4 MACGIBBON 95	RVUE	global average
• • • We do not use the following data for averages, fits, limits, etc. • • •			
11.7 ± 0.8 ± 0.7	5 BARANOV 01	RVUE	Global average
12.5 ± 0.6 ± 0.9	MACGIBBON 95	CNTR	$\gamma p$ Compton scattering
9.8 ± 0.4 ± 1.1	HALLIN 93	CNTR	$\gamma p$ Compton scattering
10.62 ± 1.25 ± 1.07 - 1.19 - 1.03	ZIEGER 92	CNTR	$\gamma p$ Compton scattering
10.9 ± 2.2 ± 1.3	6 FEDERSPIEL 91	CNTR	$\gamma p$ Compton scattering

1 BEANE 03 uses effective field theory and low-energy  $\gamma p$  and  $\gamma d$  Compton-scattering data. It also gets for the isoscalar polarizabilities (see the erratum)  $\alpha_N = (13.0 \pm 1.9 \pm 3.9) \times 10^{-4} \text{ fm}^3$  and  $\beta_N = (-1.8 \pm 1.9 \pm 2.1) \times 10^{-4} \text{ fm}^3$ .

2 BLANPIED 01 gives  $\alpha_p + \beta_p$  and  $\alpha_p - \beta_p$ . The separate  $\alpha_p$  and  $\beta_p$  are provided to us by A. Sandorfi. The first error above is statistics plus systematics; the second is from the model.

3 This OLMOSDELEON 01 result uses the TAPS data alone, and does not use the (re-evaluated) sum-rule constraint that  $\alpha + \beta = (13.8 \pm 0.4) \times 10^{-4} \text{ fm}^3$ . See the paper for a discussion.

4 MACGIBBON 95 combine the results of ZIEGER 92, FEDERSPIEL 91, and their own experiment to get a "global average" in which model errors and systematic errors are treated in a consistent way. See MACGIBBON 95 for a discussion.

5 BARANOV 01 combines the results of 10 experiments from 1958 through 1995 to get a global average that takes into account both systematic and model errors and does not use the theoretical constraint on the sum  $\alpha_p + \beta_p$ .

6 FEDERSPIEL 91 obtains for the (static) electric polarizability  $\alpha_p$ , defined in terms of the induced electric dipole moment by  $\mathbf{D} = 4\pi\epsilon_0\alpha_p\mathbf{E}$ , the value  $(7.0 \pm 2.2 \pm 1.3) \times 10^{-4} \text{ fm}^3$ .

 $\rho$  MAGNETIC POLARIZABILITY  $\beta_p$ 

The electric and magnetic polarizabilities are subject to a dispersion sum-rule constraint  $\bar{\alpha} + \bar{\beta} = (14.2 \pm 0.5) \times 10^{-4} \text{ fm}^3$ . Errors here are anticorrelated with those on  $\bar{\alpha}_p$  due to this constraint.

VALUE ( $10^{-4} \text{ fm}^3$ )	DOCUMENT ID	TECN	COMMENT
<b>2.5 ± 0.4 OUR AVERAGE</b>			Error includes scale factor of 1.2.
3.15 ± 0.35 ± 0.36	MCGOVERN 13	RVUE	$\chi\text{EFT} + \text{Compton scattering}$
3.4 ± 1.1 ± 0.1	1 BEANE 03		EFT + $\gamma p$
1.43 ± 0.98 ± 0.52 - 0.98	2 BLANPIED 01	LEGS	$\rho(\vec{\gamma}, \gamma), \rho(\vec{\gamma}, \pi^0), \rho(\vec{\gamma}, \pi^+)$
1.2 ± 0.7 ± 0.5	3 OLMOSDEL... 01	CNTR	$\gamma p$ Compton scattering
2.1 ± 0.8 ± 0.5	4 MACGIBBON 95	RVUE	global average

• • • We do not use the following data for averages, fits, limits, etc. • • •

2.3 ± 0.9 ± 0.7	5 BARANOV 01	RVUE	Global average
1.7 ± 0.6 ± 0.9	MACGIBBON 95	CNTR	$\gamma p$ Compton scattering
4.4 ± 0.4 ± 1.1	HALLIN 93	CNTR	$\gamma p$ Compton scattering
3.58 ± 1.19 ± 1.03 - 1.25 - 1.07	ZIEGER 92	CNTR	$\gamma p$ Compton scattering
3.3 ± 2.2 ± 1.3	FEDERSPIEL 91	CNTR	$\gamma p$ Compton scattering

1 BEANE 03 uses effective field theory and low-energy  $\gamma p$  and  $\gamma d$  Compton-scattering data. It also gets for the isoscalar polarizabilities (see the erratum)  $\alpha_N = (13.0 \pm 1.9 \pm 3.9) \times 10^{-4} \text{ fm}^3$  and  $\beta_N = (-1.8 \pm 1.9 \pm 2.1) \times 10^{-4} \text{ fm}^3$ .

2 BLANPIED 01 gives  $\alpha_p + \beta_p$  and  $\alpha_p - \beta_p$ . The separate  $\alpha_p$  and  $\beta_p$  are provided to us by A. Sandorfi. The first error above is statistics plus systematics; the second is from the model.

3 This OLMOSDELEON 01 result uses the TAPS data alone, and does not use the (re-evaluated) sum-rule constraint that  $\alpha + \beta = (13.8 \pm 0.4) \times 10^{-4} \text{ fm}^3$ . See the paper for a discussion.

4 MACGIBBON 95 combine the results of ZIEGER 92, FEDERSPIEL 91, and their own experiment to get a "global average" in which model errors and systematic errors are treated in a consistent way. See MACGIBBON 95 for a discussion.

5 BARANOV 01 combines the results of 10 experiments from 1958 through 1995 to get a global average that takes into account both systematic and model errors and does not use the theoretical constraint on the sum  $\alpha_p + \beta_p$ .

 $\rho$  CHARGE RADIUS

This is the rms electric charge radius,  $\sqrt{\langle r_E^2 \rangle}$ .

There are three kinds of measurements of the proton radius: via transitions in atomic hydrogen; via electron scattering off hydrogen; and via muonic hydrogen Lamb shift. Most measurements of the radius of the proton involve electron-proton interactions, the most recent of which is the electron scattering measurement  $r_p = 0.831(14) \text{ fm}$  (XIONG 19), and the atomic-hydrogen value,  $r_p = 0.833(10) \text{ fm}$  (BEZGINOV 19). These agree well with another recent atomic-hydrogen value  $r_p = 0.8335(95) \text{ fm}$  (BEYER 17), and with the best measurement using muonic hydrogen  $r_p = 0.84087(39) \text{ fm}$  (ANTOGNINI 13), that is far more precise.

The MOHR 16 value (2014 CODATA), obtained from the electronic results available at the time, was 0.8751(61) fm. This differs by 5.6 standard deviations from the muonic hydrogen value, leading to the so-called proton charge radius puzzle. See our 2018 edition (Physical Review D98 030001 (2018)) for a further discussion of interpretations of this puzzle. However, reflecting the new electronic measurements, the 2018 CODATA recommended value is 0.8414(19) fm, and the puzzle appears to be resolved.

See our 2014 edition (Chinese Physics C38 070001 (2014)) for values published before 2003.

VALUE (fm)	DOCUMENT ID	TECN	COMMENT
<b>0.8409 ± 0.0004 OUR AVERAGE</b>			
0.833 ± 0.010	1 BEZGINOV 19	LASR	2S-2P transition in H
0.831 ± 0.007 ± 0.012	2 XIONG 19	SPEC	$ep \rightarrow ep$ form factor
0.84087 ± 0.00026 ± 0.00029	ANTOGNINI 13	LASR	$\mu p$ -atom Lamb shift
• • • We do not use the following data for averages, fits, limits, etc. • • •			
0.877 ± 0.013	3 FLEURBAEY 18	LASR	1S-3S transition in H
0.8335 ± 0.0095	4 BEYER 17	LASR	2S-4P transition in H
0.8751 ± 0.0061	MOHR 16	RVUE	2014 CODATA value
0.895 ± 0.014 ± 0.014	5 LEE 15	SPEC	Just 2010 Mainz data
0.916 ± 0.024	LEE 15	SPEC	World data, no Mainz
0.8775 ± 0.0051	MOHR 12	RVUE	2010 CODATA, $ep$ data
0.875 ± 0.008 ± 0.006	ZHAN 11	SPEC	Recoil polarimetry
0.879 ± 0.005 ± 0.006	BERNAUER 10	SPEC	$ep \rightarrow ep$ form factor
0.912 ± 0.009 ± 0.007	BORISYUK 10		reanalyzes old $ep$ data
0.871 ± 0.009 ± 0.003	HILL 10		z-expansion reanalysis
0.84184 ± 0.00036 ± 0.00056	POHL 10	LASR	See ANTOGNINI 13
0.8768 ± 0.0069	MOHR 08	RVUE	2006 CODATA value
0.844 ± 0.008 - 0.004	BELUSHKIN 07		Dispersion analysis
0.897 ± 0.018	BLUNDEN 05		SICK 03 + $2\gamma$ correction
0.8750 ± 0.0068	MOHR 05	RVUE	2002 CODATA value
0.895 ± 0.010 ± 0.013	SICK 03		$ep \rightarrow ep$ reanalysis

1 BEZGINOV 19 measures the  $2S_{1/2}$  to  $2P_{1/2}$  transition frequency in atomic hydrogen using the frequency-offset separated oscillatory field (FOSOF) technique. The result agrees well with the muonic hydrogen Lamb shift value.

2 The XIONG 19 value from  $ep \rightarrow ep$  scattering and supports the muonic hydrogen Lamb shift value.

3 FLEURBAEY 18 measures the 1S-3S transition frequency in hydrogen and in combination with the 1S-2S transition frequency deduces the proton radius and the Rydberg constant.

4 The BEYER 17 result is 3.3 combined standard deviations below the MOHR 16 (2014 CODATA) value. The experiment measures the 2S-4P transition in hydrogen and gets the proton radius and the Rydberg constant.

5 Authors also provide values for combinations of all available data.

**p MAGNETIC RADIUS**

This is the rms magnetic radius,  $\sqrt{\langle r_M^2 \rangle}$ .

VALUE (fm)	DOCUMENT ID	TECN	COMMENT
<b>0.851 ± 0.026</b>	<sup>1</sup> LEE	15	Combination of world and Mainz data
0.87 ± 0.02	EPSTEIN	14	Using $e p, e n, \pi \pi$ data
0.867 ± 0.009 ± 0.018	ZHAN	11	RECOIL polarimetry
0.777 ± 0.013 ± 0.010	BERNAUER	10	SPEC $e p \rightarrow e p$ form factor
0.876 ± 0.010 ± 0.016	BORISYUK	10	Reanalyzes old $e p \rightarrow e p$ data
0.854 ± 0.005	BELUSHKIN	07	Dispersion analysis

• • • We do not use the following data for averages, fits, limits, etc. • • •

<sup>1</sup>In a consistent reanalysis LEE 2015 extract values separately for the Mainz 2010 data only (0.776 ± 0.034 ± 0.017) fm and for the world data without Mainz data (0.914 ± 0.035) fm. The quoted value is a simple combination of the two, which ignores possible discrepancies and unknown correlations and should be considered with caution.

**p MEAN LIFE**

A test of baryon conservation. See the "p Partial Mean Lives" section below for limits for identified final states. The limits here are to "anything" or are for "disappearance" modes of a bound proton (p) or (n). See also the 3ν modes in the "Partial Mean Lives" section. Table 1 of BACK 03 is a nice summary.

LIMIT (years)	PARTICLE	CL%	DOCUMENT ID	TECN	COMMENT
<b>&gt; 3.6 × 10<sup>29</sup></b>	<b>p</b>	90	<sup>1</sup> ANDERSON	19A	SNO+ p → invisible
<b>&gt; 5.8 × 10<sup>29</sup></b>	<b>n</b>	90	<sup>2</sup> ARAKI	06	KLND n → invisible
• • • We do not use the following data for averages, fits, limits, etc. • • •					
> 2.5 × 10 <sup>29</sup>	n	90	<sup>1</sup> ANDERSON	19A	SNO+ n → invisible
> 2.1 × 10 <sup>29</sup>	p	90	<sup>1</sup> AHMED	04	SNO p → invisible
> 1.9 × 10 <sup>29</sup>	n	90	<sup>1</sup> AHMED	04	SNO n → invisible
> 1.8 × 10 <sup>25</sup>	n	90	<sup>3</sup> BACK	03	BORX
> 1.1 × 10 <sup>26</sup>	p	90	<sup>3</sup> BACK	03	BORX
> 3.5 × 10 <sup>28</sup>	p	90	<sup>4</sup> ZDESENKO	03	p → invisible
> 1 × 10 <sup>28</sup>	p	90	<sup>5</sup> AHMAD	02	SNO p → invisible
> 4 × 10 <sup>23</sup>	p	95	<sup>6</sup> TRETAK	01	d → n + ?
> 1.9 × 10 <sup>24</sup>	p	90	<sup>6</sup> BERNABEI	00B	DAMA
> 1.6 × 10 <sup>25</sup>	p, n		<sup>7,8</sup> EVANS	77	
> 3 × 10 <sup>23</sup>	p		<sup>8</sup> DIX	70	CNTR
> 3 × 10 <sup>23</sup>	p, n		<sup>8,9</sup> FLEROV	58	

<sup>1</sup>AHMED 04 and ANDERSON 19A look for γ rays from the de-excitation of a residual <sup>15</sup>O\* or <sup>15</sup>N\* following the disappearance of a neutron or proton in <sup>16</sup>O.  
<sup>2</sup>ARAKI 06 looks for signs of de-excitation of the residual nucleus after disappearance of a neutron from the s shell of <sup>12</sup>C.  
<sup>3</sup>BACK 03 looks for decays of unstable nuclides left after N decays of parent <sup>12</sup>C, <sup>13</sup>C, <sup>16</sup>O nuclei. These are "invisible channel" limits.  
<sup>4</sup>ZDESENKO 03 gets this limit on proton disappearance in deuterium by analyzing SNO data in AHMAD 02.  
<sup>5</sup>AHMAD 02 (see its footnote 7) looks for neutrons left behind after the disappearance of the proton in deuterons.  
<sup>6</sup>BERNABEI 00B looks for the decay of a <sup>128</sup>I nucleus following the disappearance of a proton in the otherwise-stable <sup>129</sup>Xe nucleus.  
<sup>7</sup>EVANS 77 looks for the daughter nuclide <sup>129</sup>Xe from possible <sup>130</sup>Te decays in ancient Te ore samples.  
<sup>8</sup>This mean-life limit has been obtained from a half-life limit by dividing the latter by ln(2) = 0.693.  
<sup>9</sup>FLEROV 58 looks for the spontaneous fission of a <sup>232</sup>Th nucleus after the disappearance of one of its nucleons.

**p̄ MEAN LIFE**

Of the two astrophysical limits here, that of GEER 00D involves considerably more refinements in its modeling. The other limits come from direct observations of stored antiprotons. See also "p̄ Partial Mean Lives" after "p Partial Mean Lives," below, for exclusive-mode limits. The best (lifetime/branching fraction) limit there is 7 × 10<sup>5</sup> years, for p̄ → e<sup>-</sup>γ. We advance only the exclusive-mode limits to our Summary Tables.

LIMIT (years)	CL%	EVTs	DOCUMENT ID	TECN	COMMENT
• • • We do not use the following data for averages, fits, limits, etc. • • •					
> 5.0	90		SELLNER	17	TRAP Penning trap
> 8 × 10 <sup>5</sup>	90		<sup>1</sup> GEER	00D	p̄/p ratio, cosmic rays
> 0.28			GABRIELSE	90	TRAP Penning trap
> 0.08	90	1	BELL	79	CNTR Storage ring
> 1 × 10 <sup>7</sup>			GOLDEN	79	SPEC p̄/p ratio, cosmic rays
> 3.7 × 10 <sup>-3</sup>			BREGMAN	78	CNTR Storage ring

<sup>1</sup>GEER 00D uses agreement between a model of galactic p̄ production and propagation and the observed p̄/p cosmic-ray spectrum to set this limit.

**p DECAY MODES**

See the "Note on Nucleon Decay" in our 1994 edition (Phys. Rev. D50, 1173) for a short review.

The "partial mean life" limits tabulated here are the limits on τ/B<sub>j</sub>, where τ is the total mean life and B<sub>j</sub> is the branching fraction for the mode in question. For N decays, p and n indicate proton and neutron partial lifetimes.

Mode	Partial mean life (10 <sup>30</sup> years)	Confidence level
<b>Antilepton + meson</b>		
τ <sub>1</sub> N → e <sup>+</sup> π	> 5300 (n), > 16000 (p)	90%
τ <sub>2</sub> N → μ <sup>+</sup> π	> 3500 (n), > 7700 (p)	90%
τ <sub>3</sub> N → νπ	> 1100 (n), > 390 (p)	90%
τ <sub>4</sub> p → e <sup>+</sup> η	> 10000	90%
τ <sub>5</sub> p → μ <sup>+</sup> η	> 4700	90%
τ <sub>6</sub> n → νη	> 158	90%
τ <sub>7</sub> N → e <sup>+</sup> ρ	> 217 (n), > 720 (p)	90%
τ <sub>8</sub> N → μ <sup>+</sup> ρ	> 228 (n), > 570 (p)	90%
τ <sub>9</sub> N → νρ	> 19 (n), > 162 (p)	90%
τ <sub>10</sub> p → e <sup>+</sup> ω	> 1600	90%
τ <sub>11</sub> p → μ <sup>+</sup> ω	> 2800	90%
τ <sub>12</sub> n → νω	> 108	90%
τ <sub>13</sub> N → e <sup>+</sup> K	> 17 (n), > 1000 (p)	90%
τ <sub>14</sub> p → e <sup>+</sup> K <sub>S</sub> <sup>0</sup>		
τ <sub>15</sub> p → e <sup>+</sup> K <sub>L</sub> <sup>0</sup>		
τ <sub>16</sub> N → μ <sup>+</sup> K	> 26 (n), > 1600 (p)	90%
τ <sub>17</sub> p → μ <sup>+</sup> K <sub>S</sub> <sup>0</sup>		
τ <sub>18</sub> p → μ <sup>+</sup> K <sub>L</sub> <sup>0</sup>		
τ <sub>19</sub> N → νK	> 86 (n), > 5900 (p)	90%
τ <sub>20</sub> n → νK <sub>S</sub> <sup>0</sup>	> 260	90%
τ <sub>21</sub> p → e <sup>+</sup> K*(892) <sup>0</sup>	> 84	90%
τ <sub>22</sub> N → νK*(892)	> 78 (n), > 51 (p)	90%
<b>Antilepton + mesons</b>		
τ <sub>23</sub> p → e <sup>+</sup> π <sup>+</sup> π <sup>-</sup>	> 82	90%
τ <sub>24</sub> p → e <sup>+</sup> π <sup>0</sup> π <sup>0</sup>	> 147	90%
τ <sub>25</sub> n → e <sup>+</sup> π <sup>-</sup> π <sup>0</sup>	> 52	90%
τ <sub>26</sub> p → μ <sup>+</sup> π <sup>+</sup> π <sup>-</sup>	> 133	90%
τ <sub>27</sub> p → μ <sup>+</sup> π <sup>0</sup> π <sup>0</sup>	> 101	90%
τ <sub>28</sub> n → μ <sup>+</sup> π <sup>-</sup> π <sup>0</sup>	> 74	90%
τ <sub>29</sub> n → e <sup>+</sup> K <sup>0</sup> π <sup>-</sup>	> 18	90%
<b>Lepton + meson</b>		
τ <sub>30</sub> n → e <sup>-</sup> π <sup>+</sup>	> 65	90%
τ <sub>31</sub> n → μ <sup>-</sup> π <sup>+</sup>	> 49	90%
τ <sub>32</sub> n → e <sup>-</sup> ρ <sup>+</sup>	> 62	90%
τ <sub>33</sub> n → μ <sup>-</sup> ρ <sup>+</sup>	> 7	90%
τ <sub>34</sub> n → e <sup>-</sup> K <sup>+</sup>	> 32	90%
τ <sub>35</sub> n → μ <sup>-</sup> K <sup>+</sup>	> 57	90%
<b>Lepton + mesons</b>		
τ <sub>36</sub> p → e <sup>-</sup> π <sup>+</sup> π <sup>+</sup>	> 30	90%
τ <sub>37</sub> n → e <sup>-</sup> π <sup>+</sup> π <sup>0</sup>	> 29	90%
τ <sub>38</sub> p → μ <sup>-</sup> π <sup>+</sup> π <sup>+</sup>	> 17	90%
τ <sub>39</sub> n → μ <sup>-</sup> π <sup>+</sup> π <sup>0</sup>	> 34	90%
τ <sub>40</sub> p → e <sup>-</sup> π <sup>+</sup> K <sup>+</sup>	> 75	90%
τ <sub>41</sub> p → μ <sup>-</sup> π <sup>+</sup> K <sup>+</sup>	> 245	90%
<b>Antilepton + photon(s)</b>		
τ <sub>42</sub> p → e <sup>+</sup> γ	> 670	90%
τ <sub>43</sub> p → μ <sup>+</sup> γ	> 478	90%
τ <sub>44</sub> n → νγ	> 550	90%
τ <sub>45</sub> p → e <sup>+</sup> γγ	> 100	90%
τ <sub>46</sub> n → νγγ	> 219	90%
<b>Antilepton + single massless</b>		
τ <sub>47</sub> p → e <sup>+</sup> X	> 790	90%
τ <sub>48</sub> p → μ <sup>+</sup> X	> 410	90%
<b>Three (or more) leptons</b>		
τ <sub>49</sub> p → e <sup>+</sup> e <sup>+</sup> e <sup>-</sup>	> 793	90%
τ <sub>50</sub> p → e <sup>+</sup> μ <sup>+</sup> μ <sup>-</sup>	> 359	90%
τ <sub>51</sub> p → e <sup>+</sup> νν	> 170	90%
τ <sub>52</sub> n → e <sup>+</sup> e <sup>-</sup> ν	> 257	90%
τ <sub>53</sub> n → μ <sup>+</sup> e <sup>-</sup> ν	> 83	90%
τ <sub>54</sub> n → μ <sup>+</sup> μ <sup>-</sup> ν	> 79	90%
τ <sub>55</sub> p → μ <sup>+</sup> e <sup>+</sup> e <sup>-</sup>	> 529	90%
τ <sub>56</sub> p → μ <sup>+</sup> μ <sup>+</sup> μ <sup>-</sup>	> 675	90%



See key on page 999

Baryon Particle Listings

p

> 200	p	90	5	3.3	HAINES	86	IMB
> 64	p	90	0	<0.8	ARISAKA	85	KAMI
> 64	p (free)	90	5	6.5	BLEWITT	85	IMB
> 200	p	90	5	4.7	BLEWITT	85	IMB
> 1.2	p	90	2		<sup>1</sup> CHERRY	81	HOME

<sup>1</sup>We have converted 2 possible events to 90% CL limit.

**$\tau(p \rightarrow \mu^+ \eta)$**  **75**

LIMIT (10 <sup>30</sup> years)	PARTICLE	CL%	EVTs	BKGD EST	DOCUMENT ID	TECN
>4700	p	90	2	0.85	ABE	17D SKAM
●●● We do not use the following data for averages, fits, limits, etc. ●●●						
>1300	p	90	2	0.49	NISHINO	12 SKAM
> 89	p	90	0	1.6	WALL	00B SOU2
> 126	p	90	3	2.8	MCGREW	99 IMB3
> 26	p	90	1	0.8	BERGER	91 FREJ
> 69	p	90	1	<0.08	HIRATA	89C KAMI
> 1.3	p	90	0	0.7	PHILLIPS	89 HPW
> 34	p	90	1	1.5	SEIDEL	88 IMB
> 46	p	90	7	6	HAINES	86 IMB
> 26	p	90	1	<0.8	ARISAKA	85 KAMI
> 17	p (free)	90	6	6	BLEWITT	85 IMB
> 46	p	90	7	8	BLEWITT	85 IMB

**$\tau(n \rightarrow \nu \rho)$**  **76**

LIMIT (10 <sup>30</sup> years)	PARTICLE	CL%	EVTs	BKGD EST	DOCUMENT ID	TECN
>158	n	90	0	1.2	MCGREW	99 IMB3
●●● We do not use the following data for averages, fits, limits, etc. ●●●						
> 71	n	90	2	3.7	WALL	00B SOU2
> 29	n	90	0	0.9	BERGER	89 FREJ
> 54	n	90	2	0.9	HIRATA	89C KAMI
> 16	n	90	3	2.1	SEIDEL	88 IMB
> 25	n	90	7	6	HAINES	86 IMB
> 30	n	90	0	0.4	KAJITA	86 KAMI
> 18	n	90	4	3	PARK	85 IMB
> 0.6	n	90	2		<sup>1</sup> CHERRY	81 HOME

<sup>1</sup>We have converted 2 possible events to 90% CL limit.

**$\tau(N \rightarrow e^+ \rho)$**  **77**

LIMIT (10 <sup>30</sup> years)	PARTICLE	CL%	EVTs	BKGD EST	DOCUMENT ID	TECN
>720	p	90	2	0.64	ABE	17D SKAM
>217	n	90	4	4.8	MCGREW	99 IMB3
●●● We do not use the following data for averages, fits, limits, etc. ●●●						
> 30	n	90	4	0.87	ABE	17D SKAM
>710	p	90	0	0.35	NISHINO	12 SKAM
> 70	n	90	1	0.38	NISHINO	12 SKAM
> 29	p	90	0	2.2	BERGER	91 FREJ
> 41	n	90	0	1.4	BERGER	91 FREJ
> 75	p	90	2	2.7	HIRATA	89C KAMI
> 58	n	90	0	1.9	HIRATA	89C KAMI
> 38	n	90	2	4.1	SEIDEL	88 IMB
> 1.2	p	90	0		BARTELT	87 SOUD
> 1.5	n	90	0		BARTELT	87 SOUD
> 17	p	90	7	7	HAINES	86 IMB
> 14	n	90	9	4	HAINES	86 IMB
> 12	p	90	0	<1.2	ARISAKA	85 KAMI
> 6	n	90	2	<1	ARISAKA	85 KAMI
> 6.7	p (free)	90	6	6	BLEWITT	85 IMB
> 17	p	90	7	7	BLEWITT	85 IMB
> 12	n	90	4	2	PARK	85 IMB
> 0.6	n	90	1	0.3	<sup>1</sup> BARTELT	83 SOUD
> 0.5	p	90	1	0.3	<sup>2</sup> BARTELT	83 SOUD
> 9.8	p	90	1		<sup>2</sup> KRISHNA...	82 KOLR
> 0.8	p	90	2		<sup>3</sup> CHERRY	81 HOME

<sup>1</sup>Limit based on zero events.  
<sup>2</sup>We have calculated 90% CL limit from 0 confined events.  
<sup>3</sup>We have converted 2 possible events to 90% CL limit.

**$\tau(N \rightarrow \mu^+ \rho)$**  **78**

LIMIT (10 <sup>30</sup> years)	PARTICLE	CL%	EVTs	BKGD EST	DOCUMENT ID	TECN
>570	p	90	1	1.30	ABE	17D SKAM
>228	n	90	3	9.5	MCGREW	99 IMB3
●●● We do not use the following data for averages, fits, limits, etc. ●●●						
> 60	n	90	1	0.96	ABE	17D SKAM
>160	p	90	1	0.42	NISHINO	12 SKAM
> 36	n	90	0	0.29	NISHINO	12 SKAM
> 12	p	90	0	0.5	BERGER	91 FREJ
> 22	n	90	0	1.1	BERGER	91 FREJ
>110	p	90	0	1.7	HIRATA	89C KAMI
> 23	n	90	1	1.8	HIRATA	89C KAMI
> 4.3	p	90	0	0.7	PHILLIPS	89 HPW
> 30	p	90	0	0.5	SEIDEL	88 IMB

> 11	n	90	1	1.1	SEIDEL	88 IMB
> 16	p	90	4	4.5	HAINES	86 IMB
> 7	n	90	6	5	HAINES	86 IMB
> 12	p	90	0	<0.7	ARISAKA	85 KAMI
> 5	n	90	1	<1.2	ARISAKA	85 KAMI
> 5.5	p (free)	90	4	5	BLEWITT	85 IMB
> 16	p	90	4	5	BLEWITT	85 IMB
> 9	n	90	1	2	PARK	85 IMB

**$\tau(N \rightarrow \nu \rho)$**  **79**

LIMIT (10 <sup>30</sup> years)	PARTICLE	CL%	EVTs	BKGD EST	DOCUMENT ID	TECN
>162	p	90	18	21.7	MCGREW	99 IMB3
> 19	n	90	0	0.5	SEIDEL	88 IMB
●●● We do not use the following data for averages, fits, limits, etc. ●●●						
> 9	n	90	4	2.4	BERGER	89 FREJ
> 24	p	90	0	0.9	BERGER	89 FREJ
> 27	p	90	5	1.5	HIRATA	89C KAMI
> 13	n	90	4	3.6	HIRATA	89C KAMI
> 13	p	90	1	1.1	SEIDEL	88 IMB
> 8	p	90	6	5	HAINES	86 IMB
> 2	n	90	15	10	HAINES	86 IMB
> 11	p	90	2	1	KAJITA	86 KAMI
> 4	n	90	2	2	KAJITA	86 KAMI
> 4.1	p (free)	90	6	7	BLEWITT	85 IMB
> 8.4	p	90	6	5	BLEWITT	85 IMB
> 2	n	90	7	3	PARK	85 IMB
> 0.9	p	90	2		<sup>1</sup> CHERRY	81 HOME
> 0.6	n	90	2		<sup>1</sup> CHERRY	81 HOME

<sup>1</sup>We have converted 2 possible events to 90% CL limit.

**$\tau(p \rightarrow e^+ \omega)$**  **710**

LIMIT (10 <sup>30</sup> years)	PARTICLE	CL%	EVTs	BKGD EST	DOCUMENT ID	TECN
>1600	p	90	1	1.35	ABE	17D SKAM
●●● We do not use the following data for averages, fits, limits, etc. ●●●						
> 320	p	90	1	0.53	NISHINO	12 SKAM
> 107	p	90	7	10.8	MCGREW	99 IMB3
> 17	p	90	0	1.1	BERGER	91 FREJ
> 45	p	90	2	1.45	HIRATA	89C KAMI
> 26	p	90	1	1.0	SEIDEL	88 IMB
> 1.5	p	90	0		BARTELT	87 SOUD
> 37	p	90	6	5.3	HAINES	86 IMB
> 25	p	90	1	<1.4	ARISAKA	85 KAMI
> 12	p (free)	90	6	7.5	BLEWITT	85 IMB
> 37	p	90	6	5.7	BLEWITT	85 IMB
> 0.6	p	90	1	0.3	<sup>1</sup> BARTELT	83 SOUD
> 9.8	p	90	1		<sup>2</sup> KRISHNA...	82 KOLR
> 2.8	p	90	2		<sup>3</sup> CHERRY	81 HOME

<sup>1</sup>Limit based on zero events.  
<sup>2</sup>We have calculated 90% CL limit from 0 confined events.  
<sup>3</sup>We have converted 2 possible events to 90% CL limit.

**$\tau(p \rightarrow \mu^+ \omega)$**  **711**

LIMIT (10 <sup>30</sup> years)	PARTICLE	CL%	EVTs	BKGD EST	DOCUMENT ID	TECN
>2800	p	90	0	1.09	ABE	17D SKAM
●●● We do not use the following data for averages, fits, limits, etc. ●●●						
> 780	p	90	0	0.48	NISHINO	12 SKAM
> 117	p	90	11	12.1	MCGREW	99 IMB3
> 11	p	90	0	1.0	BERGER	91 FREJ
> 57	p	90	2	1.9	HIRATA	89C KAMI
> 4.4	p	90	0	0.7	PHILLIPS	89 HPW
> 10	p	90	2	1.3	SEIDEL	88 IMB
> 23	p	90	2	1	HAINES	86 IMB
> 6.5	p (free)	90	9	8.7	BLEWITT	85 IMB
> 23	p	90	8	7	BLEWITT	85 IMB

**$\tau(n \rightarrow \nu \omega)$**  **712**

LIMIT (10 <sup>30</sup> years)	PARTICLE	CL%	EVTs	BKGD EST	DOCUMENT ID	TECN
>108	n	90	12	22.5	MCGREW	99 IMB3
●●● We do not use the following data for averages, fits, limits, etc. ●●●						
> 17	n	90	1	0.7	BERGER	89 FREJ
> 43	n	90	3	2.7	HIRATA	89C KAMI
> 6	n	90	2	1.3	SEIDEL	88 IMB
> 12	n	90	6	6	HAINES	86 IMB
> 18	n	90	2	2	KAJITA	86 KAMI
> 16	n	90	1	2	PARK	85 IMB
> 2.0	n	90	2		<sup>1</sup> CHERRY	81 HOME

<sup>1</sup>We have converted 2 possible events to 90% CL limit.

**$\tau(N \rightarrow e^+ K)$**  **713**

LIMIT (10 <sup>30</sup> years)	PARTICLE	CL%	EVTs	BKGD EST	DOCUMENT ID	TECN
>1000	p	90	6	4.7	KOBAYASHI	05 SKAM
> 17	n	90	35	29.4	MCGREW	99 IMB3



••• We do not use the following data for averages, fits, limits, etc. •••

> 17	p	90	1	2.6	BERGER	91	FREJ
> 3.3	p	90	0	0.7	PHILLIPS	89	HPW

$\tau(p \rightarrow \mu^+ \pi^0 \pi^0)$  **T27**

LIMIT (10 <sup>30</sup> years)	PARTICLE	CL%	EVTs	BKGD EST	DOCUMENT ID	TECN
>101	p	90	3	1.6	MCGREW	99 IMB3
> 33	p	90	1	0.9	BERGER	91 FREJ

••• We do not use the following data for averages, fits, limits, etc. •••

$\tau(n \rightarrow \mu^+ \pi^- \pi^0)$  **T28**

LIMIT (10 <sup>30</sup> years)	PARTICLE	CL%	EVTs	BKGD EST	DOCUMENT ID	TECN
>74	n	90	17	20.8	MCGREW	99 IMB3
>33	n	90	0	1.1	BERGER	91 FREJ

••• We do not use the following data for averages, fits, limits, etc. •••

$\tau(n \rightarrow e^+ K^0 \pi^-)$  **T29**

LIMIT (10 <sup>30</sup> years)	PARTICLE	CL%	EVTs	BKGD EST	DOCUMENT ID	TECN
>18	n	90	1	0.2	BERGER	91 FREJ

Lepton + meson

$\tau(n \rightarrow e^- \pi^+)$  **T30**

LIMIT (10 <sup>30</sup> years)	PARTICLE	CL%	EVTs	BKGD EST	DOCUMENT ID	TECN
>65	n	90	0	1.6	SEIDEL	88 IMB
>55	n	90	0	1.09	BERGER	91B FREJ
>16	n	90	9	7	HAINES	86 IMB
>25	n	90	2	4	PARK	85 IMB

••• We do not use the following data for averages, fits, limits, etc. •••

$\tau(n \rightarrow \mu^- \pi^+)$  **T31**

LIMIT (10 <sup>30</sup> years)	PARTICLE	CL%	EVTs	BKGD EST	DOCUMENT ID	TECN
>49	n	90	0	0.5	SEIDEL	88 IMB
>33	n	90	0	1.40	BERGER	91B FREJ
> 2.7	n	90	0	0.7	PHILLIPS	89 HPW
>25	n	90	7	6	HAINES	86 IMB
>27	n	90	2	3	PARK	85 IMB

••• We do not use the following data for averages, fits, limits, etc. •••

$\tau(n \rightarrow e^- \rho^+)$  **T32**

LIMIT (10 <sup>30</sup> years)	PARTICLE	CL%	EVTs	BKGD EST	DOCUMENT ID	TECN
>62	n	90	2	4.1	SEIDEL	88 IMB
>12	n	90	13	6	HAINES	86 IMB
>12	n	90	5	3	PARK	85 IMB

••• We do not use the following data for averages, fits, limits, etc. •••

$\tau(n \rightarrow \mu^- \rho^+)$  **T33**

LIMIT (10 <sup>30</sup> years)	PARTICLE	CL%	EVTs	BKGD EST	DOCUMENT ID	TECN
>7	n	90	1	1.1	SEIDEL	88 IMB
>2.6	n	90	0	0.7	PHILLIPS	89 HPW
>9	n	90	7	5	HAINES	86 IMB
>9	n	90	2	2	PARK	85 IMB

••• We do not use the following data for averages, fits, limits, etc. •••

$\tau(n \rightarrow e^- K^+)$  **T34**

LIMIT (10 <sup>30</sup> years)	PARTICLE	CL%	EVTs	BKGD EST	DOCUMENT ID	TECN
>32	n	90	3	2.96	BERGER	91B FREJ
> 0.23	n	90	0	0.7	PHILLIPS	89 HPW

••• We do not use the following data for averages, fits, limits, etc. •••

$\tau(n \rightarrow \mu^- K^+)$  **T35**

LIMIT (10 <sup>30</sup> years)	PARTICLE	CL%	EVTs	BKGD EST	DOCUMENT ID	TECN
>57	n	90	0	2.18	BERGER	91B FREJ
> 4.7	n	90	0	0.7	PHILLIPS	89 HPW

••• We do not use the following data for averages, fits, limits, etc. •••

Lepton + mesons

$\tau(p \rightarrow e^- \pi^+ \pi^+)$  **T36**

LIMIT (10 <sup>30</sup> years)	PARTICLE	CL%	EVTs	BKGD EST	DOCUMENT ID	TECN
>30	p	90	1	2.50	BERGER	91B FREJ
> 2.0	p	90	0	0.7	PHILLIPS	89 HPW

••• We do not use the following data for averages, fits, limits, etc. •••

$\tau(n \rightarrow e^- \pi^+ \pi^0)$  **T37**

LIMIT (10 <sup>30</sup> years)	PARTICLE	CL%	EVTs	BKGD EST	DOCUMENT ID	TECN
>29	n	90	1	0.78	BERGER	91B FREJ

$\tau(p \rightarrow \mu^- \pi^+ \pi^+)$  **T38**

LIMIT (10 <sup>30</sup> years)	PARTICLE	CL%	EVTs	BKGD EST	DOCUMENT ID	TECN
>17	p	90	1	1.72	BERGER	91B FREJ
> 7.8	p	90	0	0.7	PHILLIPS	89 HPW

••• We do not use the following data for averages, fits, limits, etc. •••

$\tau(n \rightarrow \mu^- \pi^+ \pi^0)$  **T39**

LIMIT (10 <sup>30</sup> years)	PARTICLE	CL%	EVTs	BKGD EST	DOCUMENT ID	TECN
>34	n	90	0	0.78	BERGER	91B FREJ

$\tau(p \rightarrow e^- \pi^+ K^+)$  **T40**

LIMIT (10 <sup>30</sup> years)	PARTICLE	CL%	EVTs	BKGD EST	DOCUMENT ID	TECN
>75	p	90	81	127.2	MCGREW	99 IMB3
>20	p	90	3	2.50	BERGER	91B FREJ

••• We do not use the following data for averages, fits, limits, etc. •••

$\tau(p \rightarrow \mu^- \pi^+ K^+)$  **T41**

LIMIT (10 <sup>30</sup> years)	PARTICLE	CL%	EVTs	BKGD EST	DOCUMENT ID	TECN
>245	p	90	3	4.0	MCGREW	99 IMB3
> 5	p	90	2	0.78	BERGER	91B FREJ

••• We do not use the following data for averages, fits, limits, etc. •••

Antilepton + photon(s)

$\tau(p \rightarrow e^+ \gamma)$  **T42**

LIMIT (10 <sup>30</sup> years)	PARTICLE	CL%	EVTs	BKGD EST	DOCUMENT ID	TECN
>670	p	90	0	0.1	MCGREW	99 IMB3
>133	p	90	0	0.3	BERGER	91 FREJ
>460	p	90	0	0.6	SEIDEL	88 IMB
>360	p	90	0	0.3	HAINES	86 IMB
> 87	p (free)	90	0	0.2	BLEWITT	85 IMB
>360	p	90	0	0.2	BLEWITT	85 IMB
> 0.1	p	90			1 GURR	67 CNTR

<sup>1</sup> We have converted half-life to 90% CL mean life.

$\tau(p \rightarrow \mu^+ \gamma)$  **T43**

LIMIT (10 <sup>30</sup> years)	PARTICLE	CL%	EVTs	BKGD EST	DOCUMENT ID	TECN
>478	p	90	0	0.1	MCGREW	99 IMB3
>155	p	90	0	0.1	BERGER	91 FREJ
>380	p	90	0	0.5	SEIDEL	88 IMB
> 97	p	90	3	2	HAINES	86 IMB
> 61	p (free)	90	0	0.2	BLEWITT	85 IMB
>280	p	90	0	0.6	BLEWITT	85 IMB
> 0.3	p	90			1 GURR	67 CNTR

<sup>1</sup> We have converted half-life to 90% CL mean life.

$\tau(n \rightarrow \nu \gamma)$  **T44**

LIMIT (10 <sup>30</sup> years)	PARTICLE	CL%	EVTs	BKGD EST	DOCUMENT ID	TECN
>550		90			TAKHISTOV	15 SKAM
> 28	n	90	163	144.7	MCGREW	99 IMB3
> 24	n	90	10	6.86	BERGER	91B FREJ
> 9	n	90	73	60	HAINES	86 IMB
> 11	n	90	28	19	PARK	85 IMB

••• We do not use the following data for averages, fits, limits, etc. •••

$\tau(p \rightarrow e^+ \gamma \gamma)$  **T45**

LIMIT (10 <sup>30</sup> years)	PARTICLE	CL%	EVTs	BKGD EST	DOCUMENT ID	TECN
>100	p	90	1	0.8	BERGER	91 FREJ

$\tau(n \rightarrow \nu \gamma \gamma)$  **T46**

LIMIT (10 <sup>30</sup> years)	PARTICLE	CL%	EVTs	BKGD EST	DOCUMENT ID	TECN
>219	n	90	5	7.5	MCGREW	99 IMB3

Antilepton + single massless

$\tau(p \rightarrow e^+ X)$  **T47**

VALUE (10 <sup>30</sup> years)	CL%	DOCUMENT ID	TECN
>790	90	TAKHISTOV	15 SKAM

# Baryon Particle Listings

$p$

$\tau(p \rightarrow \mu^+ X)$		748	
VALUE ( $10^{30}$ years)	CL%	DOCUMENT ID	TECN
>410	90	TAKHISTOV 15	SKAM

Three (or more) leptons

$\tau(p \rightarrow e^+ e^+ e^-)$		749	
LIMIT ( $10^{30}$ years)	PARTICLE	CL%	EVTs BKGD EST
>793	$p$	90	0 0.5
••• We do not use the following data for averages, fits, limits, etc. •••			
>147	$p$	90	0 0.1
>510	$p$	90	0 0.3
> 89	$p$ (free)	90	0 0.5
>510	$p$	90	0 0.7

$\tau(p \rightarrow e^+ \mu^+ \mu^-)$		750	
LIMIT ( $10^{30}$ years)	PARTICLE	CL%	EVTs BKGD EST
>359	$p$	90	1 0.9
••• We do not use the following data for averages, fits, limits, etc. •••			
> 81	$p$	90	0 0.16
> 5.0	$p$	90	0 0.7

$\tau(p \rightarrow e^+ \nu \nu)$		751	
LIMIT ( $10^{30}$ years)	PARTICLE	CL%	EVTs BKGD EST
>170	$p$	90	1 0.9
••• We do not use the following data for averages, fits, limits, etc. •••			
> 17	$p$	90	152 153.7
> 11	$p$	90	11 6.08

<sup>1</sup> Allowed events at 90% CL are 459.

$\tau(n \rightarrow e^+ e^- \nu)$		752	
LIMIT ( $10^{30}$ years)	PARTICLE	CL%	EVTs BKGD EST
>257	$n$	90	5 7.5
••• We do not use the following data for averages, fits, limits, etc. •••			
> 74	$n$	90	0 < 0.1
> 45	$n$	90	5 5
> 26	$n$	90	4 3

$\tau(n \rightarrow \mu^+ e^- \nu)$		753	
LIMIT ( $10^{30}$ years)	PARTICLE	CL%	EVTs BKGD EST
>83	$n$	90	25 29.4
••• We do not use the following data for averages, fits, limits, etc. •••			
>47	$n$	90	0 < 0.1

$\tau(n \rightarrow \mu^+ \mu^- \nu)$		754	
LIMIT ( $10^{30}$ years)	PARTICLE	CL%	EVTs BKGD EST
>79	$n$	90	100 145
••• We do not use the following data for averages, fits, limits, etc. •••			
>42	$n$	90	0 1.4
> 5.1	$n$	90	0 0.7
>16	$n$	90	14 7
>19	$n$	90	4 7

$\tau(p \rightarrow \mu^+ e^+ e^-)$		755	
LIMIT ( $10^{30}$ years)	PARTICLE	CL%	EVTs BKGD EST
>529	$p$	90	0 1.0
••• We do not use the following data for averages, fits, limits, etc. •••			
> 91	$p$	90	0 $\leq$ 0.1

$\tau(p \rightarrow \mu^+ \mu^+ \mu^-)$		756	
LIMIT ( $10^{30}$ years)	PARTICLE	CL%	EVTs BKGD EST
>675	$p$	90	0 0.3
••• We do not use the following data for averages, fits, limits, etc. •••			
>119	$p$	90	0 0.2
> 10.5	$p$	90	0 0.7
>190	$p$	90	1 0.1
> 44	$p$ (free)	90	1 0.7
>190	$p$	90	1 0.9
> 2.1	$p$	90	1

<sup>1</sup> We have converted 1 possible event to 90% CL limit.

$\tau(p \rightarrow \mu^+ \nu \nu)$		757	
LIMIT ( $10^{30}$ years)	PARTICLE	CL%	EVTs BKGD EST
>220	$p$	90	7 11.23
••• We do not use the following data for averages, fits, limits, etc. •••			
> 21	$p$	90	7 11.23

<sup>1</sup> Allowed events at 90% CL are 286.

$\tau(p \rightarrow e^- \mu^+ \mu^+)$		758	
LIMIT ( $10^{30}$ years)	PARTICLE	CL%	EVTs BKGD EST
>6.0	$p$	90	0 0.7

$\tau(n \rightarrow 3\nu)$		759	
LIMIT ( $10^{30}$ years)	PARTICLE	CL%	EVTs BKGD EST
>0.0049	$n$	90	2 2
••• We do not use the following data for averages, fits, limits, etc. •••			
>0.0023	$n$	90	0
>0.00003	$n$	90	11 6.1
>0.00012	$n$	90	7 11.2
>0.0005	$n$	90	0

See also the "to anything" and "disappearance" limits for bound nucleons in the "p Mean Life" data block just in front of the list of possible  $p$  decay modes. Such modes could of course be to three (or five) neutrinos, and the limits are stronger, but we do not repeat them here.

<sup>1</sup> The SUZUKI 93B limit applies to any of  $\nu_e \nu_e \bar{\nu}_e$ ,  $\nu_\mu \nu_\mu \bar{\nu}_\mu$ , or  $\nu_\tau \nu_\tau \bar{\nu}_\tau$ .

<sup>2</sup> GLICENSTEIN 97 uses Kamioka data and the idea that the disappearance of the neutron's magnetic moment should produce radiation.

<sup>3</sup> The first BERGER 91B limit is for  $n \rightarrow \nu_e \nu_e \bar{\nu}_e$ , the second is for  $n \rightarrow \nu_\mu \nu_\mu \bar{\nu}_\mu$ .

$\tau(n \rightarrow 5\nu)$		760	
LIMIT ( $10^{30}$ years)	PARTICLE	CL%	EVTs BKGD EST
>0.0017	$n$	90	0

See the note on  $\tau(n \rightarrow 3\nu)$  on the previous data block.

<sup>1</sup> GLICENSTEIN 97 uses Kamioka data and the idea that the disappearance of the neutron's magnetic moment should produce radiation.

Inclusive modes

$\tau(N \rightarrow e^+ \text{anything})$		761	
LIMIT ( $10^{30}$ years)	PARTICLE	CL%	EVTs BKGD EST
>0.6	$p, n$	90	0

<sup>1</sup> The electron may be primary or secondary.

$\tau(N \rightarrow \mu^+ \text{anything})$		762	
LIMIT ( $10^{30}$ years)	PARTICLE	CL%	EVTs BKGD EST
>12	$p, n$	90	2
••• We do not use the following data for averages, fits, limits, etc. •••			
> 1.8	$p, n$	90	0
> 6	$p, n$	90	0

<sup>1</sup> We have converted 2 possible events to 90% CL limit.  
<sup>2</sup> The muon may be primary or secondary.

$\tau(N \rightarrow \nu \text{anything})$		763	
LIMIT ( $10^{30}$ years)	PARTICLE	CL%	EVTs BKGD EST
>0.0002	$p, n$	90	0

Anything =  $\pi, \rho, K$ , etc.

$\tau(N \rightarrow e^+ \pi^0 \text{anything})$		764	
LIMIT ( $10^{30}$ years)	PARTICLE	CL%	EVTs BKGD EST
>0.6	$p, n$	90	0

$\tau(N \rightarrow 2 \text{ bodies, } \nu\text{-free})$		765	
LIMIT ( $10^{30}$ years)	PARTICLE	CL%	EVTs BKGD EST
>1.3	$p, n$	90	0

$\Delta B = 2$  dinucleon modes

$\tau(pp \rightarrow \pi^+ \pi^+)$		766	
LIMIT ( $10^{30}$ years)	CL%	EVTs BKGD EST	DOCUMENT ID TECN COMMENT
>72.2	90	2 4.45	GUSTAFSON 15 SKAM per oxygen nucleus
••• We do not use the following data for averages, fits, limits, etc. •••			
> 0.7	90	4 2.34	BERGER 91B FREJ per iron nucleus

$\tau(pn \rightarrow \pi^+ \pi^0)$		767	
LIMIT ( $10^{30}$ years)	CL%	EVTs BKGD EST	DOCUMENT ID TECN COMMENT
>170	90	0 0.31	GUSTAFSON 15 SKAM per oxygen nucleus
••• We do not use the following data for averages, fits, limits, etc. •••			
> 2.0	90	0 0.31	BERGER 91B FREJ per iron nucleus

$\tau(nn \rightarrow \pi^+ \pi^-)$  **768**

LIMIT ( $10^{30}$ years)	CL%	EVTs	BKGD EST	DOCUMENT ID	TECN	COMMENT
>0.7	90	4	2.18	BERGER	91B	FREJ $\tau$ per iron nucleus

$\tau(nn \rightarrow \pi^0 \pi^0)$  **769**

LIMIT ( $10^{30}$ years)	CL%	EVTs	BKGD EST	DOCUMENT ID	TECN	COMMENT
>404	90			GUSTAFSON	15	SKAM per oxygen nucleus
••• We do not use the following data for averages, fits, limits, etc. •••						
> 3.4	90	0	0.78	BERGER	91B	FREJ $\tau$ per iron nucleus

$\tau(pp \rightarrow K^+ K^+)$  **770**

LIMIT ( $10^{30}$ years)	CL%	EVTs	BKGD EST	DOCUMENT ID	TECN	COMMENT
>170	90	0	0.28	LITOS	14	SKAM $\tau$ per oxygen nucleus

$\tau(pp \rightarrow e^+ e^+)$  **771**

LIMIT ( $10^{30}$ years)	CL%	EVTs	BKGD EST	DOCUMENT ID	TECN	COMMENT
>5.8	90	0	<0.1	BERGER	91B	FREJ $\tau$ per iron nucleus

$\tau(pp \rightarrow e^+ \mu^+)$  **772**

LIMIT ( $10^{30}$ years)	CL%	EVTs	BKGD EST	DOCUMENT ID	TECN	COMMENT
>3.6	90	0	<0.1	BERGER	91B	FREJ $\tau$ per iron nucleus

$\tau(pp \rightarrow \mu^+ \mu^+)$  **773**

LIMIT ( $10^{30}$ years)	CL%	EVTs	BKGD EST	DOCUMENT ID	TECN	COMMENT
>1.7	90	0	0.62	BERGER	91B	FREJ $\tau$ per iron nucleus

$\tau(pn \rightarrow e^+ \bar{\nu})$  **774**

LIMIT ( $10^{30}$ years)	CL%	EVTs	BKGD EST	DOCUMENT ID	TECN	COMMENT
>260	90			TAKHISTOV	15	SKAM
••• We do not use the following data for averages, fits, limits, etc. •••						
> 2.8	90	5	9.67	BERGER	91B	FREJ $\tau$ per iron nucleus

$\tau(pn \rightarrow \mu^+ \bar{\nu})$  **775**

LIMIT ( $10^{30}$ years)	CL%	EVTs	BKGD EST	DOCUMENT ID	TECN	COMMENT
>200	90			TAKHISTOV	15	SKAM
••• We do not use the following data for averages, fits, limits, etc. •••						
> 1.6	90	4	4.37	BERGER	91B	FREJ $\tau$ per iron nucleus

$\tau(pn \rightarrow \tau^+ \bar{\nu}_\tau)$  **776**

LIMIT ( $10^{30}$ years)	CL%	EVTs	BKGD EST	DOCUMENT ID	TECN	COMMENT
>29	90			TAKHISTOV	15	SKAM
••• We do not use the following data for averages, fits, limits, etc. •••						
> 1	90			1 BRYMAN	14	CHER
1 BRYMAN 14 uses a MCGREW 99 limit on the $p \rightarrow e^+ \nu \nu$ lifetime to extract this value.						

$\tau(nn \rightarrow \nu_e \bar{\nu}_e)$  **777**

We include "invisible" modes here.

LIMIT ( $10^{30}$ years)	CL%	EVTs	BKGD EST	DOCUMENT ID	TECN	COMMENT
>1.4	90			1 ARAKI	06	KLND $nn \rightarrow$ invisible
••• We do not use the following data for averages, fits, limits, etc. •••						
>0.013	90			2 ANDERSON	19A	SNO+ $nn \rightarrow$ invisible
>0.000042	90			3 TRETAYAK	04	CNTR $nn \rightarrow$ invisible
>0.000049	90			4 BACK	03	BORX $nn \rightarrow$ invisible
>0.000012	90			5 BERNABEI	00B	DAMA $nn \rightarrow$ invisible
>0.000012	90	5	9.7	BERGER	91B	FREJ $\tau$ per iron nucleus

1 ARAKI 06 looks for signs of de-excitation of the residual nucleus after disappearance of two neutrons from the s shell of  $^{12}\text{C}$ .

2 ANDERSON 19A looks for  $\gamma$  rays from the de-excitation of a residual  $^{14}\text{O}^*$  following the disappearance of  $nn$  in  $^{16}\text{O}$ .

3 TRETAYAK 04 uses data from an old Homestake-mine radiochemical experiment on limits for invisible decays of  $^{39}\text{K}$  to  $^{37}\text{Ar}$ .

4 BACK 03 looks for decays of unstable nuclides left after  $NN$  decays of parent  $^{12}\text{C}$ ,  $^{13}\text{C}$ ,  $^{16}\text{O}$  nuclei. These are "invisible channel" limits.

5 BERNABEI 00b looks for the decay of a  $^{127}\text{Te}$  nucleus following the disappearance of an  $nn$  pair in the otherwise-stable  $^{129}\text{Xe}$  nucleus. The limit here applies as well to  $nn \rightarrow \nu_\mu \bar{\nu}_\mu$ ,  $nn \rightarrow \nu_\tau \bar{\nu}_\tau$ , or any "disappearance" mode.

$\tau(nn \rightarrow \nu_\mu \bar{\nu}_\mu)$  **778**

See the preceding data block. "Invisible modes" would include any multi-neutrino mode.

LIMIT ( $10^{30}$ years)	CL%	EVTs	BKGD EST	DOCUMENT ID	TECN	COMMENT
> 1.4 (CL=90%)	OUR LIMIT					
••• We do not use the following data for averages, fits, limits, etc. •••						
>0.000006	90	4	4.4	BERGER	91B	FREJ $\tau$ per iron nucleus

$\tau(pn \rightarrow \text{invisible})$  **779**

This violates charge conservation as well as baryon number conservation.

VALUE ( $10^{30}$ years)	CL%	DOCUMENT ID	TECN
>0.026	90	1 ANDERSON	19A SNO+
>0.000021	90	2 TRETAYAK	04 CNTR

1 ANDERSON 19A looks for  $\gamma$  rays from the de-excitation of a residual  $^{14}\text{N}^*$  following the disappearance of  $pn$  in  $^{16}\text{O}$ .

2 TRETAYAK 04 uses data from an old Homestake-mine radiochemical experiment on limits for invisible decays of  $^{39}\text{K}$  to  $^{37}\text{Ar}$ .

$\tau(pp \rightarrow \text{invisible})$  **780**

This violates charge conservation as well as baryon number conservation.

LIMIT ( $10^{30}$ years)	CL%	EVTs	BKGD EST	DOCUMENT ID	TECN
>0.047	90			1 ANDERSON	19A SNO+
••• We do not use the following data for averages, fits, limits, etc. •••					
>0.000005	90			2 BACK	03 BORX
>0.00000055	90			3 BERNABEI	00B DAMA

1 ANDERSON 19A looks for  $\gamma$  rays from the de-excitation of a residual  $^{14}\text{C}^*$  following the disappearance of  $pp$  in  $^{16}\text{O}$ .

2 BACK 03 looks for decays of unstable nuclides left after  $NN$  decays of parent  $^{12}\text{C}$ ,  $^{13}\text{C}$ ,  $^{16}\text{O}$  nuclei. These are "invisible channel" limits.

3 BERNABEI 00b looks for the decay of a  $^{127}\text{Te}$  nucleus following the disappearance of a  $pp$  pair in the otherwise-stable  $^{129}\text{Xe}$  nucleus.

$\bar{p}$  PARTIAL MEAN LIVES

The "partial mean life" limits tabulated here are the limits on  $\bar{\tau}/B_j$ , where  $\bar{\tau}$  is the total mean life for the antiproton and  $B_j$  is the branching fraction for the mode in question.

$\tau(\bar{p} \rightarrow e^- \gamma)$  **781**

VALUE (years)	CL%	DOCUMENT ID	TECN	COMMENT
> $7 \times 10^5$	90	GEER	00	APEX 8.9 GeV/c $\bar{p}$ beam
••• We do not use the following data for averages, fits, limits, etc. •••				
>1848	95	GEER	94	CALO 8.9 GeV/c $\bar{p}$ beam

$\tau(\bar{p} \rightarrow \mu^- \gamma)$  **782**

VALUE (years)	CL%	DOCUMENT ID	TECN	COMMENT
> $5 \times 10^4$	90	GEER	00	APEX 8.9 GeV/c $\bar{p}$ beam
••• We do not use the following data for averages, fits, limits, etc. •••				
> $5.0 \times 10^4$	90	HU	98B	APEX 8.9 GeV/c $\bar{p}$ beam

$\tau(\bar{p} \rightarrow e^- \pi^0)$  **783**

VALUE (years)	CL%	DOCUMENT ID	TECN	COMMENT
> $4 \times 10^5$	90	GEER	00	APEX 8.9 GeV/c $\bar{p}$ beam
••• We do not use the following data for averages, fits, limits, etc. •••				
>554	95	GEER	94	CALO 8.9 GeV/c $\bar{p}$ beam

$\tau(\bar{p} \rightarrow \mu^- \pi^0)$  **784**

VALUE (years)	CL%	DOCUMENT ID	TECN	COMMENT
> $5 \times 10^4$	90	GEER	00	APEX 8.9 GeV/c $\bar{p}$ beam
••• We do not use the following data for averages, fits, limits, etc. •••				
> $4.8 \times 10^4$	90	HU	98B	APEX 8.9 GeV/c $\bar{p}$ beam

$\tau(\bar{p} \rightarrow e^- \eta)$  **785**

VALUE (years)	CL%	DOCUMENT ID	TECN	COMMENT
> $2 \times 10^4$	90	GEER	00	APEX 8.9 GeV/c $\bar{p}$ beam
••• We do not use the following data for averages, fits, limits, etc. •••				
>171	95	GEER	94	CALO 8.9 GeV/c $\bar{p}$ beam

$\tau(\bar{p} \rightarrow \mu^- \eta)$  **786**

VALUE (years)	CL%	DOCUMENT ID	TECN	COMMENT
> $8 \times 10^3$	90	GEER	00	APEX 8.9 GeV/c $\bar{p}$ beam
••• We do not use the following data for averages, fits, limits, etc. •••				
> $7.9 \times 10^3$	90	HU	98B	APEX 8.9 GeV/c $\bar{p}$ beam

$\tau(\bar{p} \rightarrow e^- K_S^0)$  **787**

VALUE (years)	CL%	DOCUMENT ID	TECN	COMMENT
>900	90	GEER	00	APEX 8.9 GeV/c $\bar{p}$ beam
••• We do not use the following data for averages, fits, limits, etc. •••				
> 29	95	GEER	94	CALO 8.9 GeV/c $\bar{p}$ beam

$\tau(\bar{p} \rightarrow \mu^- K_S^0)$  **788**

VALUE (years)	CL%	DOCUMENT ID	TECN	COMMENT
> $4 \times 10^3$	90	GEER	00	APEX 8.9 GeV/c $\bar{p}$ beam
••• We do not use the following data for averages, fits, limits, etc. •••				
> $4.3 \times 10^3$	90	HU	98B	APEX 8.9 GeV/c $\bar{p}$ beam



# Baryon Particle Listings

$p, n$

$\tau(\bar{p} \rightarrow e^- K_L^0)$ <b>789</b>				
VALUE (years)	CL%	DOCUMENT ID	TECN	COMMENT
$>9 \times 10^3$	90	GEER 00	APEX	8.9 GeV/c $\bar{p}$ beam
••• We do not use the following data for averages, fits, limits, etc. •••				
$>9 \times 10^3$	95	GEER 94	CALO	8.9 GeV/c $\bar{p}$ beam
$\tau(\bar{p} \rightarrow \mu^- K_L^0)$ <b>790</b>				
VALUE (years)	CL%	DOCUMENT ID	TECN	COMMENT
$>7 \times 10^3$	90	GEER 00	APEX	8.9 GeV/c $\bar{p}$ beam
••• We do not use the following data for averages, fits, limits, etc. •••				
$>6.5 \times 10^3$	90	HU 98b	APEX	8.9 GeV/c $\bar{p}$ beam
$\tau(\bar{p} \rightarrow e^- \gamma \gamma)$ <b>791</b>				
VALUE (years)	CL%	DOCUMENT ID	TECN	COMMENT
$>2 \times 10^4$	90	GEER 00	APEX	8.9 GeV/c $\bar{p}$ beam
$\tau(\bar{p} \rightarrow \mu^- \gamma \gamma)$ <b>792</b>				
VALUE (years)	CL%	DOCUMENT ID	TECN	COMMENT
$>2 \times 10^4$	90	GEER 00	APEX	8.9 GeV/c $\bar{p}$ beam
••• We do not use the following data for averages, fits, limits, etc. •••				
$>2.3 \times 10^4$	90	HU 98b	APEX	8.9 GeV/c $\bar{p}$ beam
$\tau(\bar{p} \rightarrow e^- \omega)$ <b>793</b>				
VALUE (years)	CL%	DOCUMENT ID	TECN	COMMENT
$>200$	90	GEER 00	APEX	8.9 GeV/c $\bar{p}$ beam

## p REFERENCES

ANDERSON 19A PR D99 032008  
 BEZGINOV 19 SCI 365 1007  
 XIONG 19 NAT 575 147  
 FLEURBAEY 18 PRL 120 183001  
 PDG 18 PR D98 030001  
 ABE 17 PR D95 012004  
 ABE 17D PR D96 012003  
 BEYER 17 SCI 358 79  
 HEISSE 17 PRL 119 033001  
 NAGAHAMA 17 NATC 8 14084  
 SAHOO 17 PR D95 013002  
 SCHNEIDER 17 SCI 358 1081  
 SELLNER 17 NJP 19 083023  
 SMORRA 17 NAT 550 371  
 MOHR 16 RMP 88 035009  
 ASAKURA 15 PR D92 052006  
 GUSTAFSON 15 PR D91 072009  
 LEE 15 PR D92 013013  
 TAKHISTOV 15 PRL 115 121803  
 ULMER 15 NAT 524 196  
 ABE 14E PRL 113 121802  
 ABE 14G PR D90 072005  
 BRYMAN 14 PL B733 190  
 EPSTEIN 14 PR D90 074027  
 LITOS 14 PRL 112 131803  
 PDG 14 CP C38 070001  
 TAKHISTOV 14 PRL 113 101801  
 ANTONGINI 13 SCI 339 417  
 DIS CIACCA 13 PRL 110 130801  
 MCGOVERN 13 EPJ A49 12  
 MOHR 12 RMP 84 1527  
 NISHINO 12 PR D85 112001  
 REGIS 12 PR D86 012006  
 BRESSI 11 PR AB8 052101  
 HORI 11 NAT 475 484  
 ZHAN 11 PL B705 59  
 BERNAUER 10 PRL 105 242001  
 Also PR C90 015206  
 BORISYUK 10 NP A843 59  
 HILL 10 PR D82 113005  
 POHL 10 NAT 466 213  
 NISHINO 09 PRL 102 141801  
 PASK 09 PL B678 55  
 MOHR 08 RMP 80 633  
 BELUSHKIN 07 PR C75 035202  
 ARAKI 06 PRL 96 101802  
 HORI 06 PRL 96 243401  
 BLUNDEN 05 PR C72 057601  
 KOBAYASHI 05 PR D72 052007  
 MOHR 05 RMP 77 1  
 SCHUMACHER 05 PPNP 55 567  
 AHMAD 04 PRL 92 102004  
 TRETYAK 04 JETPL 79 106  
 Translated from ZETFP 79 136  
 BACK 03 PL B563 23  
 BEANE 03 PL B567 200  
 Also PL B607 320 (err.)  
 DMITRIEV 03 PRL 91 212303  
 HORI 03 PRL 91 123401  
 SICK 03 PL B576 62  
 ZDESENKO 03 PL B553 135  
 AHMAD 02 PRL 89 011301  
 BARANOV 01 PPN 32 376  
 Translated from FCAY 32 699  
 BLANPIED 01 PR C64 025203  
 HORI 01 PRL 87 093401  
 OLMOSDEL... 01 EPJ A10 207  
 TRETYAK 01 PL B505 59  
 BERNABE 00B PL B493 12  
 GEER 00 PRL 84 590  
 Also PR D62 052004  
 Also PRL 85 3546 (err.)  
 GEER 00D APJ 532 648  
 SENGUPTA 00 PL B484 275  
 WALL 00 PR D61 072004  
 WALL 00B PR D62 092003  
 GABRIELSE 99 PRL 82 3198  
 HAYATO 99 PRL 83 1529  
 MCGREW 99 PR D59 052004

MOHR 99 JPCRD 28 1713  
 Also RMP 72 351  
 TORII 99 PR A59 223  
 ALLISON 98 PL B427 217  
 HU 98B PR D58 111101  
 SHIOZAWA 98 PRL 81 3319  
 GLICENSTEIN 97 PL B411 326  
 GABRIELSE 95 PRL 74 3544  
 MACGIBBON 95 PR C52 2097  
 GEER 94 PRL 72 1596  
 HALLIN 93 PR C48 1497  
 SUZUKI 93B PL B311 357  
 HUGHES 92 PRL 69 578  
 ZIEGER 92 PL B278 34  
 Also PL B281 417 (erratum)  
 BERGER 91 ZPHY C50 385  
 BERGER 91B PL B269 227  
 FEDERSPIEL 91 PRL 67 1511  
 BECKER-SZ... 90 PR D42 2374  
 ERICSON 90 EPL 11 295  
 GABRIELSE 90 PRL 65 1317  
 BERGER 89 NP B313 509  
 CHO 89 PRL 63 2559  
 HIRATA 89C PL B220 308  
 PHILLIPS 89 PL B224 348  
 KREISSL 88 ZPHY C37 557  
 SEIDEL 88 PRL 61 2522  
 BARTELT 87 PR D36 1990  
 Also PR D40 1701 (erratum)  
 COHEN 87 RMP 59 1121  
 HAINES 86 PRL 57 1906  
 KAJITA 86 JPSJ 55 711  
 ARIKAKA 85 JPSJ 54 3213  
 BLEWITT 85 PRL 55 2114  
 DZUBA 85 PL 154B 93  
 PARK 85 PRL 54 22  
 BATTISTONI 84 PL 133B 454  
 MARINELLI 84 PL 137B 439  
 WILKENING 84 PR A29 425  
 BARTELT 83 PRL 50 651  
 BATTISTONI 82 PL 118B 461  
 KRISHNA... 82 PL 115B 349  
 ALEKSEEV 81 JETPL 33 651  
 Translated from ZETFP 33 664  
 CHERY 81 PRL 47 1507  
 COWSIK 80 PR D22 2204  
 BELL 79 PL B6B 215  
 GOLDEN 79 PRL 43 1196  
 LEARNED 79 PRL 43 907  
 BREGMAN 78 PL 76B 374  
 ROBERTS 78 PR D17 358  
 EVANS 77 SCI 197 989  
 HU 75 NP A254 403  
 COHEN 73 JPCRD 2 664  
 DYLLA 73 PR A7 1224  
 DIX 70 Thesis Case  
 HARRISON 69 PRL 22 1263  
 GURR 67 PR 158 1321  
 FLEROV 58 DOKL 3 79

P.J. Mohr, B.N. Taylor (NIST)  
 P.J. Mohr, B.N. Taylor (NIST)  
 H.A. Torii et al. (CERN PS-205 Collab.)  
 W.W.M. Allison et al. (Soudan-2 Collab.)  
 M. Hu et al. (FNAL APEX Collab.)  
 M. Shiozawa et al. (Super-Kamiokande Collab.)  
 J.F. Glicenstein (SACL)  
 G. Gabrielse et al. (HARV, MANZ, SEOUL)  
 B.E. MacGibbon et al. (ILL, SASK, INRM)  
 S. Geer et al. (FNAL, UCLA, PSU)  
 E.L. Hallin et al. (SASK, BOST, ILL)  
 Y. Suzuki et al. (Kamiokande Collab.)  
 R.J. Hughes, B.I. Deutch (LANL, AARH)  
 A. Zieger et al. (MPCM)  
 A. Zieger et al. (MPCM)  
 C. Berger et al. (FREJUS Collab.)  
 C. Berger et al. (FREJUS Collab.)  
 F.J. Federspiel et al. (ILL)  
 R.A. Becker-Szendy et al. (IMB-3 Collab.)  
 T.E.O. Ericson, A. Richter (CERN, DARM)  
 G. Gabrielse et al. (HARV, MANZ, WASH+)  
 C. Berger et al. (FREJUS Collab.)  
 D. Cho, K. Sangster, E.A. Hinds (YALE)  
 K.S. Hirata et al. (Kamiokande Collab.)  
 T.J. Phillips et al. (HPW Collab.)  
 A. Kreissl et al. (CERN PS176 Collab.)  
 S. Seidel et al. (IMB Collab.)  
 J.E. Bartelt et al. (Soudan Collab.)  
 J.E. Bartelt et al. (Soudan Collab.)  
 E.R. Cohen, B.N. Taylor (RISC, NBS)  
 T.J. Haines et al. (IMB Collab.)  
 T. Kajita et al. (Kamiokande Collab.)  
 K. Arisaka et al. (Kamiokande Collab.)  
 G.B. Blewitt et al. (IMB Collab.)  
 V.A. Dzuba, V.V. Flambaum, P.G. Silvestrov (NOVO)  
 H.S. Park et al. (IMB Collab.)  
 G. Battistoni et al. (NUSEX Collab.)  
 M. Marinelli, G. Morpurgo (GENO)  
 D.A. Wilkening, N.F. Ramsey, D.J. Larson (HARV+)  
 J.E. Bartelt et al. (MINN, ANL)  
 G. Battistoni et al. (NUSEX Collab.)  
 M.R. Krishnaswamy et al. (TATA, OSK+)  
 E.N. Alekseev et al. (PNPI)

$n$   $I(J^P) = \frac{1}{2}(1^+)$  Status: \* \* \* \*

We have omitted some results that have been superseded by later experiments. See our earlier editions.  
 Anyone interested in the neutron should look at these two review articles: D. Dubbers and M.G. Schmidt, "The neutron and its role in cosmology and particle physics," *Reviews of Modern Physics* **83** 1111 (2011); and F.E. Wietfeldt and G.L. Greene, "The neutron lifetime," *Reviews of Modern Physics* **83** 1173 (2011).

## n MASS (atomic mass units u)

The mass is known much more precisely in u (atomic mass units) than in MeV. See the next data block.

VALUE (u)	DOCUMENT ID	TECN	COMMENT
<b>1.00866491588 ± 0.0000000049</b>	MOHR 16	RVUE	2014 CODATA value
••• We do not use the following data for averages, fits, limits, etc. •••			
1.00866491600 ± 0.0000000043	MOHR 12	RVUE	2010 CODATA value
1.00866491597 ± 0.0000000043	MOHR 08	RVUE	2006 CODATA value
1.00866491560 ± 0.0000000055	MOHR 05	RVUE	2002 CODATA value
1.00866491578 ± 0.0000000055	MOHR 99	RVUE	1998 CODATA value
1.008665904 ± 0.000000014	COHEN 87	RVUE	1986 CODATA value

## n MASS (MeV)

The mass is known much more precisely in u (atomic mass units) than in MeV. The conversion from u to MeV,  $1 u = 931.494 005 4(57) MeV/c^2$  (MOHR 16, the 2014 CODATA value), involves the relatively poorly known electronic charge.

VALUE (MeV)	DOCUMENT ID	TECN	COMMENT
<b>939.5654133 ± 0.0000058</b>	MOHR 16	RVUE	2014 CODATA value
••• We do not use the following data for averages, fits, limits, etc. •••			
939.565379 ± 0.000021	MOHR 12	RVUE	2010 CODATA value
939.565346 ± 0.000023	MOHR 08	RVUE	2006 CODATA value
939.565360 ± 0.000081	MOHR 05	RVUE	2002 CODATA value
939.565331 ± 0.000037	1 KESSLER 99	SPEC	$np \rightarrow d \gamma$
939.565330 ± 0.000038	MOHR 99	RVUE	1998 CODATA value
939.56565 ± 0.00028	2,3 DIFILIPPO 94	TRAP	Penning trap
939.56563 ± 0.00028	COHEN 87	RVUE	1986 CODATA value
939.56564 ± 0.00028	3,4 GREENE 86	SPEC	$np \rightarrow d \gamma$
939.5731 ± 0.0027	3 COHEN 73	RVUE	1973 CODATA value

- <sup>1</sup> We use the 1998 CODATA *u*-to-MeV conversion factor (see the heading above) to get this mass in MeV from the much more precisely measured KESSLER 99 value of  $1.00866491637 \pm 0.0000000082$  u.
- <sup>2</sup> The mass is known much more precisely in *u*:  $m = 1.0086649235 \pm 0.0000000023$  u. We use the 1986 CODATA conversion factor to get the mass in MeV.
- <sup>3</sup> These determinations are not independent of the  $m_n - m_p$  measurements below.
- <sup>4</sup> The mass is known much more precisely in *u*:  $m = 1.008664919 \pm 0.000000014$  u.

**$\bar{n}$  MASS**

VALUE (MeV)	EVTS	DOCUMENT ID	TECN	COMMENT
<b>939.485 ± 0.051</b>	59	<sup>1</sup> CRESTI	86	HBC $\bar{p}p \rightarrow \bar{n}n$

<sup>1</sup> This is a corrected result (see the erratum). The error is statistical. The maximum systematic error is 0.029 MeV.

$(m_n - m_{\bar{n}}) / m_n$

A test of *CPT* invariance. Calculated from the *n* and  $\bar{n}$  masses, above.

VALUE	DOCUMENT ID
<b>(9 ± 6) × 10<sup>-5</sup> OUR EVALUATION</b>	

**$m_n - m_p$**

VALUE (MeV)	DOCUMENT ID	TECN	COMMENT
<b>1.29333205 ± 0.00000051</b>	<sup>1</sup> MOHR	16	RVUE 2014 CODATA value
••• We do not use the following data for averages, fits, limits, etc. •••			
1.29333217 ± 0.00000042	<sup>2</sup> MOHR	12	RVUE 2010 CODATA value
1.29333214 ± 0.00000043	<sup>3</sup> MOHR	08	RVUE 2006 CODATA value
1.2933317 ± 0.00000005	<sup>4</sup> MOHR	05	RVUE 2002 CODATA value
1.2933318 ± 0.00000005	<sup>5</sup> MOHR	99	RVUE 1998 CODATA value
1.2933318 ± 0.00000009	<sup>6</sup> COHEN	87	RVUE 1986 CODATA value
1.2933328 ± 0.00000072	GREENE	86	SPEC $np \rightarrow d\gamma$
1.293429 ± 0.000036	COHEN	73	RVUE 1973 CODATA value

- <sup>1</sup> The 2014 CODATA mass difference in *u* is  $m_n - m_p = 1.00138844900(51) \times 10^{-3}$  u.
- <sup>2</sup> The 2010 CODATA mass difference in *u* is  $m_n - m_p = 1.38844919(45) \times 10^{-3}$  u.
- <sup>3</sup> Calculated by us from the MOHR 08 ratio  $m_n/m_p = 1.00137841918(46)$ . In *u*,  $m_n - m_p = 1.38844920(46) \times 10^{-3}$  u.
- <sup>4</sup> Calculated by us from the MOHR 05 ratio  $m_n/m_p = 1.00137841870 \pm 0.00000000058$ . In *u*,  $m_n - m_p = (1.3884487 \pm 0.00000006) \times 10^{-3}$  u.
- <sup>5</sup> Calculated by us from the MOHR 99 ratio  $m_n/m_p = 1.00137841887 \pm 0.00000000058$ . In *u*,  $m_n - m_p = (1.3884489 \pm 0.00000006) \times 10^{-3}$  u.
- <sup>6</sup> Calculated by us from the COHEN 87 ratio  $m_n/m_p = 1.001378404 \pm 0.000000009$ . In *u*,  $m_n - m_p = 0.001388434 \pm 0.000000009$  u.

***n* MEAN LIFE**

Limits on lifetimes for *bound* neutrons are given in the section “p PARTIAL MEAN LIVES.”

We average seven of the best eight measurements, those made with ultracold neutrons (UCN’s). If we include the one in-beam measurement with a comparable error (YUE 13), we get  $879.6 \pm 0.8$  s, where the scale factor is now 2.0.

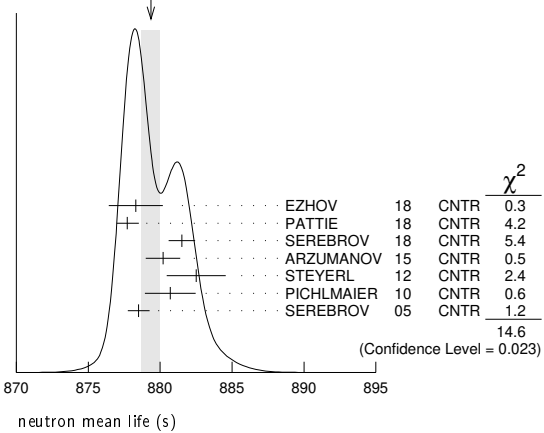
For a recent discussion of the long-standing disagreement between in-beam and UCN results, see CZARNECKI 18 (Physical Review Letters **120** 202002 (2018)). For a full review of all matters concerning the neutron lifetime until about 2010, see WIETFELDT 11, F.E. Wietfeldt and G.L. Greene, “The neutron lifetime,” Reviews of Modern Physics **83** 1173 (2011).

VALUE (s)	DOCUMENT ID	TECN	COMMENT
<b>879.4 ± 0.6 OUR AVERAGE</b>	Error includes scale factor of 1.6. See the ideogram below.		
878.3 ± 1.6 ± 1.0	EZHOV	18	CNTR UCN magneto-gravit. trap
877.7 ± 0.7 ± 0.4	<sup>1</sup> PATTIE	18	CNTR UCN asym. magnetic trap
881.5 ± 0.7 ± 0.6	SEREBROV	18	CNTR UCN gravitational trap
880.2 ± 1.2	<sup>2</sup> ARZUMANOV	15	CNTR UCN double bottle
882.5 ± 1.4 ± 1.5	<sup>3</sup> STEYERL	12	CNTR UCN material bottle
880.7 ± 1.3 ± 1.2	PICHLMAIER	10	CNTR UCN material bottle
878.5 ± 0.7 ± 0.3	SEREBROV	05	CNTR UCN gravitational trap
••• We do not use the following data for averages, fits, limits, etc. •••			
887.7 ± 1.2 ± 1.9	<sup>4</sup> YUE	13	CNTR In-beam <i>n</i> , trapped <i>p</i>
881.6 ± 0.8 ± 1.9	<sup>5</sup> ARZUMANOV	12	CNTR See ARZUMANOV 15
886.3 ± 1.2 ± 3.2	NICO	05	CNTR See YUE 13
886.8 ± 1.2 ± 3.2	DEWEY	03	CNTR See NICO 05
885.4 ± 0.9 ± 0.4	ARZUMANOV	00	CNTR See ARZUMANOV 12
889.2 ± 3.0 ± 3.8	BYRNE	96	CNTR Penning trap
882.6 ± 2.7	<sup>6</sup> MAMPE	93	CNTR UCN material bottle
888.4 ± 3.1 ± 1.1	<sup>7</sup> NESVIZHEV...	92	CNTR UCN material bottle
888.4 ± 2.9	ALFIMENKOV	90	CNTR See NESVIZHEVSKII 92
893.6 ± 3.8 ± 3.7	BYRNE	90	CNTR See BYRNE 96
878 ± 27 ± 14	KOSSAKOW...	89	TPC Pulsed beam

887.6 ± 3.0	MAMPE	89	CNTR See STEYERL 12
877 ± 10	PAUL	89	CNTR Magnetic storage ring
876 ± 10 ± 19	LAST	88	SPEC Pulsed beam
891 ± 9	SPIVAK	88	CNTR Beam
903 ± 13	KOSVINTSEV	86	CNTR UCN material bottle
937 ± 18	<sup>8</sup> BYRNE	80	CNTR
875 ± 95	KOSVINTSEV	80	CNTR
881 ± 8	BONDAREN...	78	CNTR See SPIVAK 88
918 ± 14	CHRISTENSEN72	CNTR	

- <sup>1</sup> PATTIE 18 uses a new technique, with a semi-toroidal magneto-gravitational asymmetric trap and a novel in situ *n*-detector.
- <sup>2</sup> ARZUMANOV 15 is a reanalysis of their 2008–2010 dataset, with improved systematic corrections of ARZUMANOV 00 and ARZUMANOV 12.
- <sup>3</sup> STEYERL 12 is a detailed reanalysis of neutron storage loss corrections to the raw data of MAMPE 89, and it replaces that value.
- <sup>4</sup> YUE 13 differs from NICO 05 in that a different and better method was used to measure the neutron density in the fiducial volume. This shifted the lifetime by +1.4 seconds and reduced the previously largest source of systematic uncertainty by a factor of five.
- <sup>5</sup> ARZUMANOV 12 reanalyzes its systematic corrections in ARZUMANOV 00 and obtains this corrected value.
- <sup>6</sup> IGNATOVICH 95 calls into question some of the corrections and averaging procedures used by MAMPE 93. The response, BONDARENKO 96, denies the validity of the criticisms.
- <sup>7</sup> The NESVIZHEVSKII 92 measurement has been withdrawn by A. Serebrov.
- <sup>8</sup> The BYRNE 80 measurement has been withdrawn (J. Byrne, private communication, 1990).

WEIGHTED AVERAGE  
879.4 ± 0.6 (Error scaled by 1.6)



***n* MAGNETIC MOMENT**

See the “Note on Baryon Magnetic Moments” in the *A* Listings.

VALUE ( $\mu_N$ )	DOCUMENT ID	TECN	COMMENT
<b>-1.91304273 ± 0.00000045</b>	MOHR	16	RVUE 2014 CODATA value
••• We do not use the following data for averages, fits, limits, etc. •••			
-1.91304272 ± 0.00000045	MOHR	12	RVUE 2010 CODATA value
-1.91304273 ± 0.00000045	MOHR	08	RVUE 2006 CODATA value
-1.91304273 ± 0.00000045	MOHR	05	RVUE 2002 CODATA value
-1.91304272 ± 0.00000045	MOHR	99	RVUE 1998 CODATA value
-1.91304275 ± 0.00000045	COHEN	87	RVUE 1986 CODATA value
-1.91304277 ± 0.00000048	<sup>1</sup> GREENE	82	MRS

<sup>1</sup> GREENE 82 measures the moment to be  $(1.04187564 \pm 0.00000026) \times 10^{-3}$  Bohr magnetons. The value above is obtained by multiplying this by  $m_p/m_e = 1836.152701 \pm 0.000037$  (the 1986 CODATA value from COHEN 87).

***n* ELECTRIC DIPOLE MOMENT**

A nonzero value is forbidden by both *T* invariance and *P* invariance. A number of early results have been omitted. See RAMSEY 90, GOLUB 94, and LAMOREAUX 09 for reviews.

The results are upper limits on  $|d_n|$ .

VALUE ( $10^{-25}$ ecm)	CL%	DOCUMENT ID	TECN	COMMENT
<b>&lt; 0.18</b>	90	<sup>1</sup> ABEL	20	MRS UCN
••• We do not use the following data for averages, fits, limits, etc. •••				
< 0.22	95	<sup>2</sup> SAHOO	17	<sup>199</sup> Hg atom EDM + theory
< 0.16	95	GRANER	16	MRS <sup>199</sup> Hg atom EDM + theory
< 0.30	90	<sup>3</sup> PENDLEBURY	15	MRS Superseded by ABEL 20
< 0.55	90	SEREBROV	15	MRS UCN’s, $h\nu = 2\mu_n B \pm 2d_n E$
< 0.55	90	<sup>4</sup> SEREBROV	14	MRS See SEREBROV 15
< 0.29	90	<sup>5</sup> BAKER	06	MRS See PENDLEBURY 15
< 0.63	90	<sup>6</sup> HARRIS	99	MRS $d = (-0.1 \pm 0.36) \times 10^{-25}$

# Baryon Particle Listings

*n*

< 0.97	90	ALTAREV	96	MRS	See SEREBROV 14
< 1.1	95	ALTAREV	92	MRS	See ALTAREV 96
< 1.2	95	SMITH	90	MRS	See HARRIS 99
< 2.6	95	ALTAREV	86	MRS	$d = (-1.4 \pm 0.6) \times 10^{-25}$
0.3 ± 4.8		PENDLEBURY	84	MRS	Ultracold neutrons
< 6	90	ALTAREV	81	MRS	$d = (2.1 \pm 2.4) \times 10^{-25}$
< 16	90	ALTAREV	79	MRS	$d = (4.0 \pm 7.5) \times 10^{-25}$

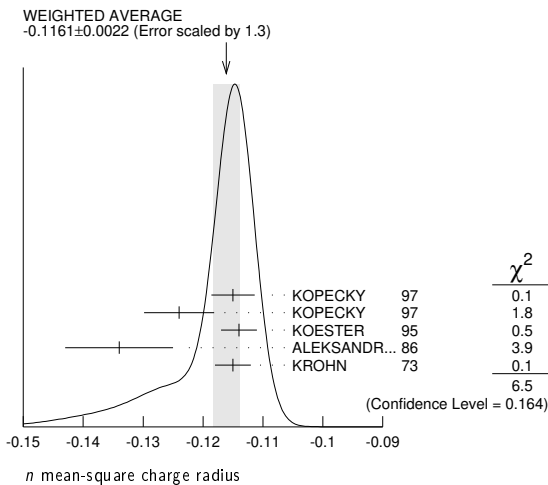
- ABEL 20 reports  $d = (0.0 \pm 1.1 \pm 0.2) \times 10^{-26}$  e cm value corresponding to the listed limit.
- SAHOO 17 develops theory to calculate this limit from the measured limit by GRANER 16 of the  $^{199}\text{Hg}$  atom EDM.
- PENDLEBURY 15 reports  $d = (-0.21 \pm 1.82) \times 10^{-26}$  e cm value corresponding to the listed limit.
- SEREBROV 14 includes the data of ALTAREV 96.
- LAMOREAUX 07 faults BAKER 06 for not including in the estimate of systematic error an effect due to the Earth's rotation. BAKER 07 replies (1) that the effect was included implicitly in the analysis and (2) that further analysis confirms that the BAKER 06 limit is correct as is. See also SILENKO 07.
- This HARRIS 99 result includes the result of SMITH 90. However, the averaging of the results of these two experiments has been criticized by LAMOREAUX 00.

## *n* MEAN-SQUARE CHARGE RADIUS

The mean-square charge radius of the neutron,  $\langle r_n^2 \rangle$ , is related to the neutron-electron scattering length  $b_{ne}$  by  $\langle r_n^2 \rangle = 3(m_e a_0 / m_n) b_{ne}$ , where  $m_e$  and  $m_n$  are the masses of the electron and neutron, and  $a_0$  is the Bohr radius. Numerically,  $\langle r_n^2 \rangle = 86.34 b_{ne}$ , if we use  $a_0$  for a nucleus with infinite mass.

VALUE (fm <sup>2</sup> )	DOCUMENT ID	COMMENT
<b>-0.1161 ± 0.0022 OUR AVERAGE</b>		Error includes scale factor of 1.3. See the ideogram below.
-0.115 ± 0.002 ± 0.003	KOPECKY 97	<i>ne</i> scattering (Pb)
-0.124 ± 0.003 ± 0.005	KOPECKY 97	<i>ne</i> scattering (Bi)
-0.114 ± 0.003	KOESTER 95	<i>ne</i> scattering (Pb, Bi)
-0.134 ± 0.009	ALEKSANDR...86	<i>ne</i> scattering (Bi)
-0.115 ± 0.003	1 KROHN 73	<i>ne</i> scattering (Ne, Ar, Kr, Xe)
• • • We do not use the following data for averages, fits, limits, etc. • • •		
-0.117 ± 0.007 -0.011	BELUSHKIN 07	Dispersion analysis
-0.113 ± 0.003 ± 0.004	KOPECKY 95	<i>ne</i> scattering (Pb)
-0.114 ± 0.003	KOESTER 86	<i>ne</i> scattering (Pb, Bi)
-0.118 ± 0.002	KOESTER 76	<i>ne</i> scattering (Pb)
-0.120 ± 0.002	KOESTER 76	<i>ne</i> scattering (Bi)
-0.116 ± 0.003	KROHN 66	<i>ne</i> scattering (Ne, Ar, Kr, Xe)

<sup>1</sup> This value is as corrected by KOESTER 76.



## *n* MAGNETIC RADIUS

This is the rms magnetic radius,  $\sqrt{\langle r_M^2 \rangle}$ .

VALUE (fm)	DOCUMENT ID	COMMENT
<b>0.864 ± 0.009 -0.008 OUR AVERAGE</b>		
0.89 ± 0.03	EPSTEIN 14	Using <i>ep</i> , <i>en</i> , $\pi\pi$ data
0.862 ± 0.009 -0.008	BELUSHKIN 07	Dispersion analysis

## *n* ELECTRIC POLARIZABILITY $\alpha_n$

Following is the electric polarizability  $\alpha_n$  defined in terms of the induced electric dipole moment by  $\mathbf{D} = 4\pi\epsilon_0\alpha_n\mathbf{E}$ . For a review, see SCHMIED-MAYER 89.

For very complete reviews of the polarizability of the nucleon and Compton scattering, see SCHUMACHER 05 and GRIESSHAMMER 12.

VALUE ( $10^{-4}$ fm <sup>3</sup> )	DOCUMENT ID	TECN	COMMENT
<b>11.8 ± 1.1 OUR AVERAGE</b>			
11.55 ± 1.25 ± 0.8	MYERS 14	CNTR	$\gamma d \rightarrow \gamma d$
12.5 ± 1.8 <sup>+1.6</sup> <sub>-1.3</sub>	1 KOSSERT 03	CNTR	$\gamma d \rightarrow \gamma p n$
12.0 ± 1.5 ± 2.0	SCHMIEDM... 91	CNTR	<i>n</i> Pb transmission
10.7 <sup>+3.3</sup> <sub>-10.7</sub>	ROSE 90b	CNTR	$\gamma d \rightarrow \gamma n p$
• • • We do not use the following data for averages, fits, limits, etc. • • •			
8.8 ± 2.4 ± 3.0	2 LUNDIN 03	CNTR	$\gamma d \rightarrow \gamma d$
13.6	3 KOLB 00	CNTR	$\gamma d \rightarrow \gamma n p$
0.0 ± 5.0	4 KOESTER 95	CNTR	<i>n</i> Pb, <i>n</i> Bi transmission
11.7 <sup>+4.3</sup> <sub>-11.7</sub>	ROSE 90	CNTR	See ROSE 90b
8 ± 10	KOESTER 88	CNTR	<i>n</i> Pb, <i>n</i> Bi transmission
12 ± 10	SCHMIEDM... 88	CNTR	<i>n</i> Pb, <i>n</i> C transmission

- KOSSERT 03 gets  $\alpha_n - \beta_n = (9.8 \pm 3.6 \pm 2.1 \pm 2.2) \times 10^{-4}$  fm<sup>3</sup>, and uses  $\alpha_n + \beta_n = (15.2 \pm 0.5) \times 10^{-4}$  fm<sup>3</sup> from LEVCHUK 00. Thus the errors on  $\alpha_n$  and  $\beta_n$  are anti-correlated.
- LUNDIN 03 measures  $\alpha_N - \beta_N = (6.4 \pm 2.4) \times 10^{-4}$  fm<sup>3</sup> and uses accurate values for  $\alpha_p$  and  $\alpha_p$  and a precise sum-rule result for  $\alpha_n + \beta_n$ . The second error is a model uncertainty, and errors on  $\alpha_n$  and  $\beta_n$  are anticorrelated. The data from this paper are included in the analysis of MYERS 14.
- KOLB 00 obtains this value with a lower limit of  $7.6 \times 10^{-4}$  fm<sup>3</sup> but no upper limit from this experiment alone. Combined with results of ROSE 90, the 1- $\sigma$  range is  $(7.6-14.0) \times 10^{-4}$  fm<sup>3</sup>.
- KOESTER 95 uses natural Pb and the isotopes 208, 207, and 206. See this paper for a discussion of methods used by various groups to extract  $\alpha_n$  from data.

## *n* MAGNETIC POLARIZABILITY $\beta_n$

VALUE ( $10^{-4}$ fm <sup>3</sup> )	DOCUMENT ID	TECN	COMMENT
<b>3.7 ± 1.2 OUR AVERAGE</b>			
3.65 ± 1.25 ± 0.8	MYERS 14	CNTR	$\gamma d \rightarrow \gamma d$
2.7 ± 1.8 <sup>+1.3</sup> <sub>-1.6</sub>	1 KOSSERT 03	CNTR	$\gamma d \rightarrow \gamma p n$
6.5 ± 2.4 ± 3.0	2 LUNDIN 03	CNTR	$\gamma d \rightarrow \gamma d$
• • • We do not use the following data for averages, fits, limits, etc. • • •			
1.6	3 KOLB 00	CNTR	$\gamma d \rightarrow \gamma n p$

- KOSSERT 03 gets  $\alpha_n - \beta_n = (9.8 \pm 3.6 \pm 2.1 \pm 2.2) \times 10^{-4}$  fm<sup>3</sup>, and uses  $\alpha_n + \beta_n = (15.2 \pm 0.5) \times 10^{-4}$  fm<sup>3</sup> from LEVCHUK 00. Thus the errors on  $\alpha_n$  and  $\beta_n$  are anti-correlated.
- LUNDIN 03 measures  $\alpha_N - \beta_N = (6.4 \pm 2.4) \times 10^{-4}$  fm<sup>3</sup> and uses accurate values for  $\alpha_p$  and  $\alpha_p$  and a precise sum-rule result for  $\alpha_n + \beta_n$ . The second error is a model uncertainty, and errors on  $\alpha_n$  and  $\beta_n$  are anticorrelated.
- KOLB 00 obtains this value with an upper limit of  $7.6 \times 10^{-4}$  fm<sup>3</sup> but no lower limit from this experiment alone. Combined with results of ROSE 90, the 1- $\sigma$  range is  $(1.2-7.6) \times 10^{-4}$  fm<sup>3</sup>.

## *n* CHARGE

See also  $|q_p + q_e|/e$  in the proton Listings.

VALUE ( $10^{-21}$ e)	DOCUMENT ID	TECN	COMMENT
<b>-0.2 ± 0.8 OUR AVERAGE</b>			
-0.1 ± 1.1	1 BRESSI 11		Neutrality of SF <sub>6</sub>
-0.4 ± 1.1	2 BAUMANN 88		Cold <i>n</i> deflection
• • • We do not use the following data for averages, fits, limits, etc. • • •			
-15 ± 22	3 GAEHLER 82	CNTR	Cold <i>n</i> deflection

- As a limit, this BRESSI 11 value is  $< 1 \times 10^{-21}$  e.
- The BAUMANN 88 error  $\pm 1.1$  gives the 68% CL limits about the the value -0.4.
- The GAEHLER 82 error  $\pm 22$  gives the 90% CL limits about the the value -15.

## LIMIT ON *n*π OSCILLATIONS

### Mean Time for *n*π Transition in Vacuum

A test of  $\Delta B=2$  baryon number nonconservation. MOHAPATRA 80 and MOHAPATRA 89 discuss the theoretical motivations for looking for *n*π oscillations. DOVER 83 and DOVER 85 give phenomenological analyses. The best limits come from looking for the decay of neutrons bound in nuclei. However, these analyses require model-dependent corrections for nuclear effects. See KABIR 83, DOVER 89, ALBERICO 91, and GAL 00 for discussions. Direct searches for  $n \rightarrow \bar{n}$  transitions using reactor neutrons are cleaner but give somewhat poorer limits. We include limits for both free and bound neutrons in the Summary Table. See MOHAPATRA 09 and PHILLIPS 16 for recent reviews.

VALUE (s)	CL%	DOCUMENT ID	TECN	COMMENT
<b>&gt;2.7 × 10<sup>8</sup></b>	90	ABE	15c	CNTR <i>n</i> bound in oxygen
<b>&gt;8.6 × 10<sup>7</sup></b>	90	BALDO...	94	CNTR Reactor (free) neutrons

See key on page 999

Baryon Particle Listings

n

• • • We do not use the following data for averages, fits, limits, etc. • • •

>1.37 × 10 <sup>8</sup>	90	<sup>1</sup> AHARMIM	17	SNO	n bound in deuteron
>1.3 × 10 <sup>8</sup>	90	CHUNG	02B	SOU2	n bound in iron
>1 × 10 <sup>7</sup>	90	BALDO-...	90	CNTR	See BALDO-CEOLIN 94
>1.2 × 10 <sup>8</sup>	90	BERGER	90	FREJ	n bound in iron
>4.9 × 10 <sup>5</sup>	90	BRESSI	90	CNTR	Reactor neutrons
>4.7 × 10 <sup>5</sup>	90	BRESSI	89	CNTR	See BRESSI 90
>1.2 × 10 <sup>8</sup>	90	TAKITA	86	CNTR	n bound in oxygen
>1 × 10 <sup>6</sup>	90	FIDECARO	85	CNTR	Reactor neutrons
>8.8 × 10 <sup>7</sup>	90	PARK	85B	CNTR	
>3 × 10 <sup>7</sup>		BATTISTONI	84	NUSX	
> 0.27-1.1 × 10 <sup>8</sup>		JONES	84	CNTR	
>2 × 10 <sup>7</sup>		CHERRY	83	CNTR	

<sup>1</sup>The AHARMIM 17 value is an unbounded limit (it does not assume a positive lifetime). The bounded limit is 1.23 × 10<sup>8</sup> sec.

LIMIT ON nn' OSCILLATIONS

Lee and Yang (LEE 56) proposed the existence of mirror world in an attempt to restore global parity symmetry. A possible candidate for dark matter. Limits depend on assumptions about fields B and B'. See the papers for details. See BEREZHIANI 18 for a recent discussion.

VALUE (s)	CL%	DOCUMENT ID	TECN	COMMENT
>448	90	SEREBROV 09A	CNTR	Assumes B' < 100 nT

• • • We do not use the following data for averages, fits, limits, etc. • • •

> 17	95	<sup>1</sup> BEREZHIANI 18	CNTR	UCN, scan of B field
> 12	95	<sup>2</sup> ALTAREV 09A	CNTR	UCN, scan 0 ≤ B ≤ 12.5 μT
>414	90	SEREBROV 08	CNTR	UCN, B field on & off
>103	95	BAN 07	CNTR	UCN, B field on & off

<sup>1</sup>The B field was set to (0.09, 0.12, 0.21) G. Limits on oscillation time are valid for any mirror field B' in (0.08-0.17) G, and for aligned fields B and B'. For larger values of B', the limits are significantly reduced.

<sup>2</sup>Losses of neutrons due to oscillations to mirror neutrons would be maximal when the magnetic fields B and B' in the two worlds were equal. Hence the scan over B by ALTAREV 09A: the limit applies for any B' over the given range. At B' = 0, the limit is 141 s (95% CL).

n DECAY MODES

Mode	Fraction (Γ <sub>i</sub> /Γ)	Confidence level
Γ <sub>1</sub> p e <sup>-</sup> ν <sub>e</sub>	100 %	
Γ <sub>2</sub> p e <sup>-</sup> ν <sub>e</sub> γ	[a] ( 9.2±0.7 ) × 10 <sup>-3</sup>	
Γ <sub>3</sub> hydrogen-atom ν <sub>e</sub>	< 2.7 × 10 <sup>-3</sup>	95%

Charge conservation (Q) violating mode

Γ <sub>4</sub> p ν <sub>e</sub> ν <sub>e</sub>	Q < 8 × 10 <sup>-27</sup>	68%
--	---------------------------	-----

Baryon number violating decay

Γ <sub>5</sub> e <sup>+</sup> e <sup>-</sup> invisible		
--	--	--

[a] This limit is for γ energies between 0.4 and 782 keV.

n BRANCHING RATIOS

Γ(p e <sup>-</sup> ν <sub>e</sub> γ)/Γ <sub>total</sub>	Γ <sub>2</sub> /Γ
9.17 ± 0.24 ± 0.64	

• • • We do not use the following data for averages, fits, limits, etc. • • •

3.09 ± 0.11 ± 0.30	<sup>1</sup> BALES 16	RDK2	Two different set-ups
3.13 ± 0.11 ± 0.33	<sup>2</sup> COOPER 10	CNTR	See BALES 16
<6.9	<sup>3</sup> BECK 02	CNTR	γ, p, e <sup>-</sup> coincidence

<sup>1</sup>BALES 16 gets a branching fraction of (5.82 ± 0.23 ± 0.62) × 10<sup>-3</sup> for a photon energy range 0.4 to 14.0 keV, and with a different detector array, (3.35 ± 0.05 ± 0.15) × 10<sup>-3</sup> for 14.1 to 782 keV. Our result above is the sum; the error on the sum is completely dominated by the error on the lower range.

<sup>2</sup>This COOPER 10 result is for γ energies between 15 and 340 keV.

<sup>3</sup>This BECK 02 limit is for γ energies between 35 and 100 keV.

Γ(hydrogen-atom ν <sub>e</sub> )/Γ <sub>total</sub>	Γ <sub>3</sub> /Γ
<0.27 × 10 <sup>-2</sup>	

• • • We do not use the following data for averages, fits, limits, etc. • • •

<3 × 10 <sup>-2</sup>	95	<sup>1</sup> CZARNECKI 18	Lifetime analysis
	95	<sup>2</sup> GREEN 90	RVUE

<sup>1</sup>CZARNECKI 18 limit from an analysis of experimental discrepancies on the neutron lifetime and axial coupling applies as well to other possible exotic neutron decays.

<sup>2</sup>GREEN 90 infers that τ(hydrogen-atom ν<sub>e</sub>) > 3 × 10<sup>4</sup> s by comparing neutron lifetime measurements made in storage experiments with those made in β-decay experiments. However, the result depends sensitively on the lifetime measurements, and does not of course take into account more recent measurements of same.

Γ(p ν <sub>e</sub> ν <sub>e</sub> )/Γ <sub>total</sub>	Γ <sub>4</sub> /Γ
<8 × 10 <sup>-27</sup>	

Forbidden by charge conservation.

VALUE	CL%	DOCUMENT ID	TECN	COMMENT
<8 × 10 <sup>-27</sup>	68	<sup>1</sup> NORMAN 96	RVUE	<sup>71</sup> Ga → <sup>71</sup> Ge neutrals

• • • We do not use the following data for averages, fits, limits, etc. • • •

<9.7 × 10 <sup>-18</sup>	90	ROY 83	CNTR	<sup>113</sup> Cd → <sup>113m</sup> In neut.
<7.9 × 10 <sup>-21</sup>		VAIDYA 83	CNTR	<sup>87</sup> Rb → <sup>87m</sup> Sr neut.
<9 × 10 <sup>-24</sup>	90	BARABANOV 80	CNTR	<sup>71</sup> Ga → <sup>71</sup> GeX
<3 × 10 <sup>-19</sup>		NORMAN 79	CNTR	<sup>87</sup> Rb → <sup>87m</sup> Sr neut.

<sup>1</sup>NORMAN 96 gets this limit by attributing SAGE and GALLEX counting rates to the charge-nonconserving transition <sup>71</sup>Ga → <sup>71</sup>Ge+neutrals rather than to solar-neutrino reactions.

Γ(e <sup>+</sup> e <sup>-</sup> invisible)/Γ <sub>total</sub>	Γ <sub>5</sub> /Γ
<0.01	

Baryon number violating decay

VALUE	CL%	DOCUMENT ID	TECN	COMMENT
<0.01	90	<sup>1</sup> KLOPF 19	CNTR	re-interpretation of MUND 13
<1 × 10 <sup>-4</sup>	90	<sup>2</sup> SUN 18	SPEC	Ultracold n, polarized

<sup>1</sup>KLOPF 19 value is for baryon number violating decay of neutron to electrons plus an invisible state, χ. The limit is valid for KE(e<sup>+</sup> e<sup>-</sup>) range between 32 keV and 664 keV, strengthening to few × 10<sup>-4</sup> above approximately 100 keV.

<sup>2</sup>SUN 18 value is for baryon number violating decay of neutron to electrons plus an invisible state, χ. The limit is valid for 644 keV > KE(e<sup>+</sup> e<sup>-</sup>) > 100 keV. Assuming this decay χ e e is the only allowed χ decay channel, a 0.01 BR is ruled out for 644 keV > E(e<sup>+</sup> e<sup>-</sup>) > 100 keV at over 5σ.

See the related review(s): Baryon Decay Parameters

n → p e<sup>-</sup> ν<sub>e</sub> DECAY PARAMETERS

See the above "Note on Baryon Decay Parameters." For discussions of recent results, see the references cited at the beginning of the section on the neutron mean life. For discussions of the values of the weak coupling constants g<sub>A</sub> and g<sub>V</sub> obtained using the neutron lifetime and asymmetry parameter A, comparisons with other methods of obtaining these constants, and implications for particle physics and for astrophysics, see DUBBERS 91 and WOOLCOCK 91. For tests of the V-A theory of neutron decay, see EROZOLIMSKII 91B, MOSTOVOI 96, NICO 05, SEVERIJS 06, and ABELE 08.

λ ≡ g<sub>A</sub> / g<sub>V</sub>

VALUE	DOCUMENT ID	TECN	COMMENT
-1.2756 ± 0.0013 OUR AVERAGE			Error includes scale factor of 2.6. See the ideogram below.
-1.27641 ± 0.00045 ± 0.00033	<sup>1</sup> MAERKISCH 19	SPEC	pulsed cold n, polarized
-1.2772 ± 0.0020	<sup>2</sup> BROWN 18	UCNA	Ultracold n, polarized
-1.284 ± 0.014	<sup>3</sup> DARIUS 17	SPEC	Cold n, unpolarized
-1.2748 ± 0.0008 +0.0010 -0.0011	<sup>4</sup> MUND 13	SPEC	Cold n, polarized
-1.275 ± 0.006 ± 0.015	SCHUMANN 08	CNTR	Cold n, polarized
-1.2686 ± 0.0046 ± 0.0007	<sup>5</sup> MOSTOVOI 01	CNTR	A and B × polarizations
-1.266 ± 0.004	LIAUD 97	TPC	Cold n, polarized, A
-1.2594 ± 0.0038	<sup>6</sup> YEROZLIM... 97	CNTR	Cold n, polarized, A
-1.262 ± 0.005	BOPP 86	SPEC	Cold n, polarized, A
-1.2755 ± 0.0030	<sup>7</sup> MENDENHALL13	UCNA	See BROWN 18
-1.27590 ± 0.00239 ± 0.00331 -0.00377	<sup>8</sup> PLASTER 12	UCNA	See MENDENHALL 13
-1.27590 ± 0.00409 -0.00445	LIU 10	UCNA	See PLASTER 12
-1.2739 ± 0.0019	<sup>9</sup> ABELE 02	SPEC	See MUND 13
-1.274 ± 0.003	ABELE 97D	SPEC	Cold n, polarized, A
-1.266 ± 0.004	SCHRECK... 95	TPC	See LIAUD 97
-1.2544 ± 0.0036	EROZOLIM... 91	CNTR	See YEROZOLIMSKY 97
-1.226 ± 0.042	MOSTOVOY 83	RVUE	
-1.261 ± 0.012	EROZOLIM... 79	CNTR	Cold n, polarized, A
-1.259 ± 0.017	STRATOWA 78	CNTR	p recoil spectrum, a
-1.263 ± 0.015	EROZOLIM... 77	CNTR	See EROZOLIMSKII 79
-1.250 ± 0.036	<sup>10</sup> DOBROZE... 75	CNTR	See STRATOWA 78
-1.258 ± 0.015	11 KROHN 75	CNTR	Cold n, polarized, A
-1.263 ± 0.016	12 KROPF 74	RVUE	n decay alone
-1.250 ± 0.009	12 KROPF 74	RVUE	n decay + nuclear ft

<sup>1</sup>MAERKISCH 19 gets A = -0.11985 ± 0.00017 ± 0.00012.

<sup>2</sup>BROWN 18 gets A = -0.12054 ± 0.00044 ± 0.00068 and λ = -1.2783 ± 0.0022. We quote the combined values that include the earlier UCNA measurements (MENDENHALL 13).

<sup>3</sup>DARIUS 17 calculates this value from the measurement of the a parameter (see below).

<sup>4</sup>This MUND 13 value includes earlier PERKEO II measurements (ABELE 02 and ABELE 97D).

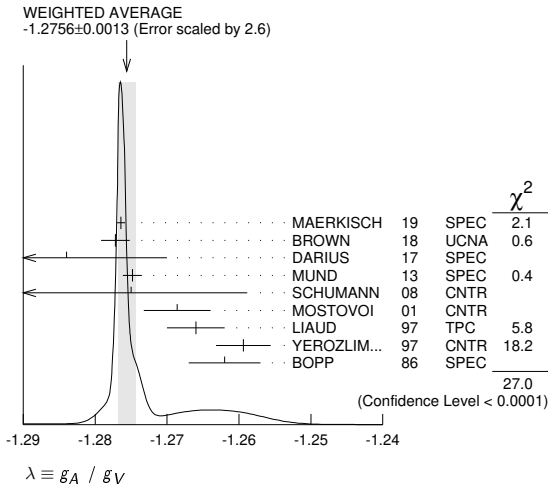
<sup>5</sup>MOSTOVOI 01 measures the two P-odd correlations A and B, or rather SA and SB, where S is the n polarization, in free neutron decay.

<sup>6</sup>YEROZOLIMSKY 97 makes a correction to the EROZOLIMSKII 91 value.

# Baryon Particle Listings

*n*

- <sup>7</sup> MENDENHALL 13 gets  $A = -0.11954 \pm 0.00055 \pm 0.00098$  and  $\lambda = -1.2756 \pm 0.0030$ . We quote the nearly identical values that include the earlier UCNA measurement (PLASTER 12), with a correction to that result.
- <sup>8</sup> This PLASTER 12 value is identical with that given in LIU 10, but the experiment is now described in detail.
- <sup>9</sup> This is the combined result of ABELE 02 and ABELE 97d.
- <sup>10</sup> These experiments measure the absolute value of  $g_A/g_V$  only.
- <sup>11</sup> KROHN 75 includes events of CHRISTENSEN 70.
- <sup>12</sup> KROPP 74 reviews all data through 1972.



## $e^-$ ASYMMETRY PARAMETER A

This is the neutron-spin electron-momentum correlation coefficient. Unless otherwise noted, the values are corrected for radiative effects and weak magnetism. In the Standard Model,  $A$  is related to  $\lambda \equiv g_A/g_V$  by  $A = -2\lambda(\lambda + 1)/(1 + 3\lambda^2)$ ; this assumes that  $g_A$  and  $g_V$  are real.

VALUE	DOCUMENT ID	TECN	COMMENT
<b>-0.11958 ± 0.00021 OUR AVERAGE</b>	Error includes scale factor of 1.2.		
-0.11985 ± 0.00017 ± 0.00012	<sup>1</sup> MAERKISCH 19	SPEC	pulsed cold <i>n</i> , polarized
-0.12015 ± 0.00034 ± 0.00063	<sup>2</sup> BROWN 18	UCNA	Ultracold <i>n</i> , polarized
-0.11926 ± 0.00031 ± 0.00036 ± 0.00042	<sup>3</sup> MUND 13	SPEC	Cold <i>n</i> , polarized
-0.1160 ± 0.0009 ± 0.0012	LIAUD 97	TPC	Cold <i>n</i> , polarized
-0.1135 ± 0.0014	<sup>4</sup> YEROZLIM... 97	CNTR	Cold <i>n</i> , polarized
-0.1146 ± 0.0019	BOPP 86	SPEC	Cold <i>n</i> , polarized
••• We do not use the following data for averages, fits, limits, etc. •••			
-0.11952 ± 0.00110	<sup>5</sup> MENDENHALL 13	UCNA	See BROWN 18
-0.11966 ± 0.00089 ± 0.00123 ± 0.00140	<sup>6</sup> PLASTER 12	UCNA	See MENDENHALL 13
-0.11966 ± 0.00089 ± 0.00123 ± 0.00140	LIU 10	UCNA	See PLASTER 12
-0.1138 ± 0.0046 ± 0.0021	PATTIE 09	SPEC	Ultracold <i>n</i> , polarized
-0.1189 ± 0.0007	<sup>7</sup> ABELE 02	SPEC	See MUND 13
-0.1168 ± 0.0017	<sup>8</sup> MOSTOVOI 01	CNTR	Inferred
-0.1189 ± 0.0012	ABELE 97d	SPEC	Cold <i>n</i> , polarized
-0.1160 ± 0.0009 ± 0.0011	SCHRECK... 95	TPC	See LIAUD 97
-0.1116 ± 0.0014	EROZOLIM... 91	CNTR	See YEROZOLIM-SKY 97
-0.114 ± 0.005	<sup>9</sup> EROZOLIM... 79	CNTR	Cold <i>n</i> , polarized
-0.113 ± 0.006	<sup>9</sup> KROHN 75	CNTR	Cold <i>n</i> , polarized

- <sup>1</sup> MAERKISCH 19 further derive a value for the CKM-element  $|V_{ud}| = 0.97351 \pm 0.00060$ , using  $\tau_n = 879.7(8)$  sec and the relation from CZARNECKI 18.
- <sup>2</sup> BROWN 18 gets  $A = -0.12054 \pm 0.00044 \pm 0.00068$  and  $\lambda = -1.2783 \pm 0.0022$ . We quote the combined values that include the earlier UCNA measurements (MENDENHALL 13).
- <sup>3</sup> This MUND 13 value includes earlier PERKEO II measurements (ABELE 02 and ABELE 97d), with a correction to those results.
- <sup>4</sup> YEROZOLIMSKY 97 makes a correction to the EROZOLIMSKII 91 value.
- <sup>5</sup> MENDENHALL 13 gets  $A = -0.11954 \pm 0.00055 \pm 0.00098$  and  $\lambda = -1.2756 \pm 0.0030$ . We quote the nearly identical values that include the earlier UCNA measurement (PLASTER 12), with a correction to that result.
- <sup>6</sup> This PLASTER 12 value is identical with that given in LIU 10, but the experiment is now described in detail.
- <sup>7</sup> This is the combined result of ABELE 02 and ABELE 97d.
- <sup>8</sup> MOSTOVOI 01 calculates this from its measurement of  $\lambda = g_A/g_V$  above.
- <sup>9</sup> These results are not corrected for radiative effects and weak magnetism, but the corrections are small compared to the errors.

## $\bar{\nu}_e$ ASYMMETRY PARAMETER B

This is the neutron-spin antineutrino-momentum correlation coefficient. In the Standard Model,  $B$  is related to  $\lambda \equiv g_A/g_V$  by  $B = 2\lambda(\lambda - 1)/(1 + 3\lambda^2)$ ; this assumes that  $g_A$  and  $g_V$  are real.

VALUE	DOCUMENT ID	TECN	COMMENT
<b>0.9807 ± 0.0030 OUR AVERAGE</b>			
0.9802 ± 0.0034 ± 0.0036	SCHUMANN 07	CNTR	Cold <i>n</i> , polarized
0.967 ± 0.006 ± 0.010	KREUZ 05	CNTR	Cold <i>n</i> , polarized
0.9801 ± 0.0046	SEREBROV 98	CNTR	Cold <i>n</i> , polarized

0.9894 ± 0.0083	KUZNETSOV 95	CNTR	Cold <i>n</i> , polarized
1.00 ± 0.05	CHRISTENSEN70	CNTR	Cold <i>n</i> , polarized
0.995 ± 0.034	EROZOLIM... 70c	CNTR	Cold <i>n</i> , polarized
••• We do not use the following data for averages, fits, limits, etc. •••			
0.9876 ± 0.0004	<sup>1</sup> MOSTOVOI 01	CNTR	Inferred
	<sup>1</sup> MOSTOVOI 01	calculates this from its measurement of $\lambda = g_A/g_V$ above.	

## PROTON ASYMMETRY PARAMETER C

Describes the correlation between the neutron spin and the proton momentum. In the Standard Model,  $C$  is related to  $\lambda \equiv g_A/g_V$  by  $C = -x_c(A + B) = x_c 4\lambda/(1 + 3\lambda^2)$ , where  $x_c = 0.27484$  is a kinematic factor; this assumes that  $g_A$  and  $g_V$  are real.

VALUE	DOCUMENT ID	TECN	COMMENT
<b>-0.2377 ± 0.0010 ± 0.0024</b>	SCHUMANN 08	CNTR	Cold <i>n</i> , polarized

## $e^- \bar{\nu}_e$ ANGULAR CORRELATION COEFFICIENT a

For a review of past experiments and plans for future measurements of the  $a$  parameter, see WIETFELDT 05. In the Standard Model,  $a$  is related to  $\lambda \equiv g_A/g_V$  by  $a = (1 - \lambda^2)/(1 + 3\lambda^2)$ ; this assumes that  $g_A$  and  $g_V$  are real.

VALUE	DOCUMENT ID	TECN	COMMENT
<b>-0.1059 ± 0.0028 OUR AVERAGE</b>			
-0.1090 ± 0.0030 ± 0.0028	<sup>1</sup> DARIUS 17	SPEC	Cold <i>n</i> , unpolarized
-0.1054 ± 0.0055	BYRNE 02	SPEC	Proton recoil spectrum
-0.1017 ± 0.0051	STRATOWA 78	CNTR	Proton recoil spectrum
-0.091 ± 0.039	GRIGOREV 68	SPEC	Proton recoil spectrum
••• We do not use the following data for averages, fits, limits, etc. •••			
-0.1045 ± 0.0014	<sup>2</sup> MOSTOVOI 01	CNTR	Inferred

- <sup>1</sup> DARIUS 17 exploits a "wishbone" correlation, where the  $p$  time of flight is correlated with the momentum of the electron in delayed coincidence.
- <sup>2</sup> MOSTOVOI 01 calculates this from its measurement of  $\lambda = g_A/g_V$  above.

## $\phi_{AV}$ PHASE OF $g_A$ RELATIVE TO $g_V$

Time reversal invariance requires this to be 0 or 180°. This is related to  $D$  given in the next data block and  $\lambda \equiv g_A/g_V$  by  $\sin(\phi_{AV}) \equiv D(1+3\lambda^2)/2|\lambda|$ ; this assumes that  $g_A$  and  $g_V$  are real.

VALUE (°)	CL%	DOCUMENT ID	TECN	COMMENT
<b>180.017 ± 0.026 OUR AVERAGE</b>				
180.012 ± 0.028	68	CHUPP 12	CNTR	Cold <i>n</i> , polarized > 91%
180.04 ± 0.09		SOLDNER 04	CNTR	Cold <i>n</i> , polarized
180.08 ± 0.13		LISING 00	CNTR	Polarized > 93%
••• We do not use the following data for averages, fits, limits, etc. •••				
180.013 ± 0.028		MUMM 11	CNTR	See CHUPP 12
179.71 ± 0.39		EROZOLIM... 78	CNTR	Cold <i>n</i> , polarized
180.35 ± 0.43		EROZOLIM... 74	CNTR	Cold <i>n</i> , polarized
181.1 ± 1.3		<sup>1</sup> KROPP 74	RVUE	<i>n</i> decay
180.14 ± 0.22		STEINBERG 74	CNTR	Cold <i>n</i> , polarized

- <sup>1</sup> KROPP 74 reviews all data through 1972.

## TRIPLE CORRELATION COEFFICIENT D

These are measurements of the component of  $n$  spin perpendicular to the decay plane in  $\beta$  decay. Should be zero if  $T$  invariance is not violated.

VALUE (units 10 <sup>-4</sup> )	DOCUMENT ID	TECN	COMMENT
<b>-1.2 ± 2.0 OUR AVERAGE</b>			
-0.94 ± 1.89 ± 0.97	CHUPP 12	CNTR	Cold <i>n</i> , polarized > 91%
-2.8 ± 6.4 ± 3.0	SOLDNER 04	CNTR	Cold <i>n</i> , polarized
-6 ± 12 ± 5	LISING 00	CNTR	Polarized > 93%
••• We do not use the following data for averages, fits, limits, etc. •••			
-0.96 ± 1.89 ± 1.01	MUMM 11	CNTR	See CHUPP 12
+22 ± 30	EROZOLIM... 78	CNTR	Cold <i>n</i> , polarized
-27 ± 50	<sup>1</sup> EROZOLIM... 74	CNTR	Cold <i>n</i> , polarized
-11 ± 17	STEINBERG 74	CNTR	Cold <i>n</i> , polarized

- <sup>1</sup> EROZOLIMSKII 78 says asymmetric proton losses and nonuniform beam polarization may give a systematic error up to  $30 \times 10^{-4}$ , thus increasing the EROZOLIMSKII 74 error to  $50 \times 10^{-4}$ . STEINBERG 74 and STEINBERG 76 estimate these systematic errors to be insignificant in their experiment.

## TRIPLE CORRELATION COEFFICIENT R

Another test of time-reversal invariance.  $R$  measures the polarization of the electron in the direction perpendicular to the plane defined by the neutron spin and the electron momentum.  $R = 0$  for  $T$  invariance.

VALUE	DOCUMENT ID	TECN	COMMENT
<b>+0.004 ± 0.012 ± 0.005</b>	<sup>1</sup> KOZELA 12	CNTR	Mott polarimeter
••• We do not use the following data for averages, fits, limits, etc. •••			
+0.008 ± 0.015 ± 0.005	KOZELA 09	CNTR	See KOZELA 12

- <sup>1</sup> KOZELA 12 also measures the polarization of the electron along the direction of the neutron spin. This is nonzero in the Standard Model; the correlation coefficient is  $N = +0.067 \pm 0.011 \pm 0.004$ .

## n REFERENCES

We have omitted some papers that have been superseded by later experiments. See our earlier editions.

ABEL 20	PRL 124 081803	C. Abel et al.	(nEDM Collab.)
KLOPP 19	PRL 122 225003	M. Klopff et al.	(PERKEO II Collab.)
MAERKISCH 19	PRL 122 242501	B. Maerksich et al.	(TUM, ILL, +)
BEREZHIANI 18	EPJ C78 717	Z. Berzhanian et al.	(AQU, INFN, ILLG+)
BROWN 18	PR C97 035505	M.A.-P. Brown et al.	(UCNA Collab.)
CZARNECKI 18	PRL 120 202002	A. Czarnecki, W.J. Marciano, A. Sifflin	(ALB+)

Baryon Particle Listings
n, N's and Δ's, N(1440)

Main table of baryon particle listings with columns for name, mass, and various properties. Includes sub-sections for EROZOLIM..., N(1440) POLE POSITION, and REAL PART.

Downloaded from https://academic.oup.com/ptep/article/2020/8/083C01/5891211 by guest on 12 November 2020

See the related review(s):
N and Δ Resonances

N(1440) 1/2+
i(J^P) = 1/2(1/2+) Status: \*\*\*

Older and obsolete values are listed and referenced in the 2014 edition, Chinese Physics C38 070001 (2014).

N(1440) POLE POSITION

Table with columns: REAL PART, VALUE (MeV), DOCUMENT ID, TECN, COMMENT. Includes rows for 1360 to 1380 (approx 1370) OUR ESTIMATE and 1369 ± 3, 1363 ± 2 ± 2, 1375 ± 30.

## Baryon Particle Listings

 $N(1440)$ 

••• We do not use the following data for averages, fits, limits, etc. •••

VALUE (MeV)	DOCUMENT ID	TECN	COMMENT
1360	HUNT	19	DPWA Multichannel
1355	ROENCHEN	15A	DPWA Multichannel
1386	SHKLYAR	13	DPWA Multichannel
1370 ± 4	ANISOVICH	12A	DPWA Multichannel
1363 ± 11	BATINIC	10	DPWA $\pi N \rightarrow N\pi, N\eta$
1359	ARNDT	06	DPWA $\pi N \rightarrow \pi N, \eta N$
1383	VRANA	00	DPWA Multichannel
1385	HOEHLER	93	SPED $\pi N \rightarrow \pi N$

<sup>1</sup> Fit to the amplitudes of HOEHLER 79.

## -2xIMAGINARY PART

VALUE (MeV)	DOCUMENT ID	TECN	COMMENT
160 to 190 ( $\approx 175$ ) OUR ESTIMATE			

189 ± 5	SOKHOYAN	15A	DPWA Multichannel
180 ± 4 ± 5	<sup>1</sup> SVARC	14	L+P $\pi N \rightarrow \pi N$
180 ± 40	CUTKOSKY	80	IPWA $\pi N \rightarrow \pi N$

••• We do not use the following data for averages, fits, limits, etc. •••

186	HUNT	19	DPWA Multichannel
215	ROENCHEN	15A	DPWA Multichannel
277	SHKLYAR	13	DPWA Multichannel
190 ± 7	ANISOVICH	12A	DPWA Multichannel
151 ± 13	BATINIC	10	DPWA $\pi N \rightarrow N\pi, N\eta$
162	ARNDT	06	DPWA $\pi N \rightarrow \pi N, \eta N$
316	VRANA	00	DPWA Multichannel
164	HOEHLER	93	SPED $\pi N \rightarrow \pi N$

<sup>1</sup> Fit to the amplitudes of HOEHLER 79.

 $N(1440)$  ELASTIC POLE RESIDUEMODULUS  $|r|$ 

VALUE (MeV)	DOCUMENT ID	TECN	COMMENT
46 to 54 ( $\approx 50$ ) OUR ESTIMATE			

49 ± 3	SOKHOYAN	15A	DPWA Multichannel
50 ± 1 ± 2	<sup>1</sup> SVARC	14	L+P $\pi N \rightarrow \pi N$
52 ± 5	CUTKOSKY	80	IPWA $\pi N \rightarrow \pi N$

••• We do not use the following data for averages, fits, limits, etc. •••

62	ROENCHEN	15A	DPWA Multichannel
126	SHKLYAR	13	DPWA Multichannel
48 ± 3	ANISOVICH	12A	DPWA Multichannel
44	BATINIC	10	DPWA $\pi N \rightarrow N\pi, N\eta$
38	ARNDT	06	DPWA $\pi N \rightarrow \pi N, \eta N$
40	HOEHLER	93	SPED $\pi N \rightarrow \pi N$

<sup>1</sup> Fit to the amplitudes of HOEHLER 79.

PHASE  $\theta$ 

VALUE (°)	DOCUMENT ID	TECN	COMMENT
-100 to -80 ( $\approx -90$ ) OUR ESTIMATE			

-82 ± 5	SOKHOYAN	15A	DPWA Multichannel
-88 ± 1 ± 2	<sup>1</sup> SVARC	14	L+P $\pi N \rightarrow \pi N$
-100 ± 35	CUTKOSKY	80	IPWA $\pi N \rightarrow \pi N$

••• We do not use the following data for averages, fits, limits, etc. •••

-98	ROENCHEN	15A	DPWA Multichannel
-60	SHKLYAR	13	DPWA Multichannel
-78 ± 4	ANISOVICH	12A	DPWA Multichannel
-88	BATINIC	10	DPWA $\pi N \rightarrow N\pi, N\eta$
-98	ARNDT	06	DPWA $\pi N \rightarrow \pi N, \eta N$

<sup>1</sup> Fit to the amplitudes of HOEHLER 79.

 $N(1440)$  INELASTIC POLE RESIDUE

The "normalized residue" is the residue divided by  $\Gamma_{pole}/2$ .

Normalized residue in  $N\pi \rightarrow N(1440) \rightarrow N\eta$ 

MODULUS	PHASE (°)	DOCUMENT ID	TECN	COMMENT
0.078	-27	ROENCHEN	15A	DPWA Multichannel

••• We do not use the following data for averages, fits, limits, etc. •••

Normalized residue in  $N\pi \rightarrow N(1440) \rightarrow \Delta\pi, P$ -wave

MODULUS	PHASE (°)	DOCUMENT ID	TECN	COMMENT
0.27 ± 0.02	38 ± 5	SOKHOYAN	15A	DPWA Multichannel

••• We do not use the following data for averages, fits, limits, etc. •••

0.27 ± 0.02	40 ± 5	ANISOVICH	12A	DPWA Multichannel
-------------	--------	-----------	-----	-------------------

Normalized residue in  $N\pi \rightarrow N(1440) \rightarrow \Lambda K$ 

MODULUS	PHASE (°)	DOCUMENT ID	TECN	COMMENT
0.016	145	ROENCHEN	15A	DPWA Multichannel

••• We do not use the following data for averages, fits, limits, etc. •••

0.027	113	ROENCHEN	15A	DPWA Multichannel
-------	-----	----------	-----	-------------------

Normalized residue in  $N\pi \rightarrow N(1440) \rightarrow \Sigma K$ 

MODULUS	PHASE (°)	DOCUMENT ID	TECN	COMMENT
0.027	113	ROENCHEN	15A	DPWA Multichannel

••• We do not use the following data for averages, fits, limits, etc. •••

Normalized residue in  $N\pi \rightarrow N(1440) \rightarrow N(\pi\pi)_{S=0}^{I=0}$ 

MODULUS	PHASE (°)	DOCUMENT ID	TECN	COMMENT
0.21 ± 0.04	-136 ± 4	SOKHOYAN	15A	DPWA Multichannel

••• We do not use the following data for averages, fits, limits, etc. •••

0.21 ± 0.05	-135 ± 7	ANISOVICH	12A	DPWA Multichannel
-------------	----------	-----------	-----	-------------------

 $N(1440)$  BREIT-WIGNER MASS

VALUE (MeV)	DOCUMENT ID	TECN	COMMENT
1410 to 1470 ( $\approx 1440$ ) OUR ESTIMATE			

1417 ± 4	<sup>1</sup> HUNT	19	DPWA Multichannel
1430 ± 10	SOKHOYAN	15A	DPWA Multichannel
1515 ± 15	<sup>1</sup> SHKLYAR	13	DPWA Multichannel
1485.0 ± 1.2	<sup>1</sup> ARNDT	06	DPWA $\pi N \rightarrow \pi N, N\eta$
1440 ± 30	CUTKOSKY	80	IPWA $\pi N \rightarrow \pi N$
1410 ± 12	HOEHLER	79	IPWA $\pi N \rightarrow \pi N$

••• We do not use the following data for averages, fits, limits, etc. •••

1430 ± 8	ANISOVICH	12A	DPWA Multichannel
1412 ± 2	<sup>1</sup> SHRESTHA	12A	DPWA Multichannel
1439 ± 19	BATINIC	10	DPWA $\pi N \rightarrow N\pi, N\eta$
1518 ± 5	PENNER	02C	DPWA Multichannel
1479 ± 80	VRANA	00	DPWA Multichannel

<sup>1</sup> Statistical error only.

 $N(1440)$  BREIT-WIGNER WIDTH

VALUE (MeV)	DOCUMENT ID	TECN	COMMENT
250 to 450 ( $\approx 350$ ) OUR ESTIMATE			

257 ± 11	<sup>1</sup> HUNT	19	DPWA Multichannel
360 ± 30	SOKHOYAN	15A	DPWA Multichannel
605 ± 90	<sup>1</sup> SHKLYAR	13	DPWA Multichannel
284 ± 18	<sup>1</sup> ARNDT	06	DPWA $\pi N \rightarrow \pi N, \eta N$
340 ± 70	CUTKOSKY	80	IPWA $\pi N \rightarrow \pi N$
135 ± 10	HOEHLER	79	IPWA $\pi N \rightarrow \pi N$

••• We do not use the following data for averages, fits, limits, etc. •••

365 ± 35	ANISOVICH	12A	DPWA Multichannel
248 ± 5	<sup>1</sup> SHRESTHA	12A	DPWA Multichannel
437 ± 141	BATINIC	10	DPWA $\pi N \rightarrow N\pi, N\eta$
668 ± 41	PENNER	02C	DPWA Multichannel
490 ± 120	VRANA	00	DPWA Multichannel

<sup>1</sup> Statistical error only.

 $N(1440)$  DECAY MODES

The following branching fractions are our estimates, not fits or averages.

Mode	Fraction ( $\Gamma_i/\Gamma$ )
$\Gamma_1$ $N\pi$	55-75 %
$\Gamma_2$ $N\eta$	<1 %
$\Gamma_3$ $N\pi\pi$	17-50 %
$\Gamma_4$ $\Delta(1232)\pi, P$ -wave	6-27 %
$\Gamma_5$ $N\sigma$	11-23 %
$\Gamma_6$ $p\gamma, \text{helicity}=1/2$	0.035-0.048 %
$\Gamma_7$ $n\gamma, \text{helicity}=1/2$	0.02-0.04 %

 $N(1440)$  BRANCHING RATIOS

$\Gamma(N\pi)/\Gamma_{total}$	$\Gamma_1/\Gamma$
55 to 75 ( $\approx 65$ ) OUR ESTIMATE	

VALUE (%)	DOCUMENT ID	TECN	COMMENT
59 ± 2	<sup>1</sup> HUNT	19	DPWA Multichannel
63 ± 2	SOKHOYAN	15A	DPWA Multichannel
56 ± 2	<sup>1</sup> SHKLYAR	13	DPWA Multichannel
78.7 ± 1.6	<sup>1</sup> ARNDT	06	DPWA $\pi N \rightarrow \pi N, \eta N$
68 ± 4	CUTKOSKY	80	IPWA $\pi N \rightarrow \pi N$
51 ± 5	HOEHLER	79	IPWA $\pi N \rightarrow \pi N$

••• We do not use the following data for averages, fits, limits, etc. •••

62 ± 3	ANISOVICH	12A	DPWA Multichannel
64.8 ± 0.9	<sup>1</sup> SHRESTHA	12A	DPWA Multichannel
62 ± 4	BATINIC	10	DPWA $\pi N \rightarrow N\pi, N\eta$
57 ± 1	PENNER	02C	DPWA Multichannel
72 ± 5	VRANA	00	DPWA Multichannel

<sup>1</sup> Statistical error only.

$\Gamma(N\eta)/\Gamma_{total}$	$\Gamma_2/\Gamma$
0 ± 1	

VALUE (%)	DOCUMENT ID	TECN	COMMENT
0 ± 1	VRANA	00	DPWA Multichannel

••• We do not use the following data for averages, fits, limits, etc. •••

# Baryon Particle Listings

## $N(1440)$ , $N(1520)$

**$\Gamma(\Delta(1232)\pi, P\text{-wave})/\Gamma_{\text{total}}$**

VALUE (%)	DOCUMENT ID	TECN	COMMENT	$\Gamma_4/\Gamma$
<b>6 to 27 (<math>\approx 15</math>) OUR ESTIMATE</b>				
22 $\pm 4$	<sup>1</sup> HUNT	19	DPWA Multichannel	
12 $^{+5}_{-3}$	SHKLYAR	16	DPWA Multichannel	
20 $\pm 7$	SOKHOYAN	15A	DPWA Multichannel	
••• We do not use the following data for averages, fits, limits, etc. •••				
21 $\pm 8$	ANISOVICH	12A	DPWA Multichannel	
6.5 $\pm 0.8$	<sup>1</sup> SHRESTHA	12A	DPWA Multichannel	
16 $\pm 1$	VRANA	00	DPWA Multichannel	

<sup>1</sup> Statistical error only.

**$\Gamma(N\sigma)/\Gamma_{\text{total}}$**

VALUE (%)	DOCUMENT ID	TECN	COMMENT	$\Gamma_5/\Gamma$
16 $\pm 3$	<sup>1</sup> HUNT	19	DPWA Multichannel	
27 $^{+4}_{-9}$	SHKLYAR	16	DPWA Multichannel	
17 $\pm 6$	SOKHOYAN	15A	DPWA Multichannel	
••• We do not use the following data for averages, fits, limits, etc. •••				
17 $\pm 7$	ANISOVICH	12A	DPWA Multichannel	
27 $\pm 1$	<sup>1</sup> SHRESTHA	12A	DPWA Multichannel	
12 $\pm 1$	VRANA	00	DPWA Multichannel	

<sup>1</sup> Statistical error only.

### $N(1440)$ PHOTON DECAY AMPLITUDES AT THE POLE

#### $N(1440) \rightarrow p\gamma$ , helicity-1/2 amplitude $A_{1/2}$

MODULUS ( $\text{GeV}^{-1/2}$ )	PHASE ( $^\circ$ )	DOCUMENT ID	TECN	COMMENT
-0.044 $\pm 0.005$	-40 $\pm 8$	SOKHOYAN	15A	DPWA Multichannel
-0.054 $^{+0.004}_{-0.003}$	5 $^{+2}_{-5}$	ROENCHEN	14	DPWA

••• We do not use the following data for averages, fits, limits, etc. •••

-0.060	-23	ROENCHEN	15A	DPWA Multichannel
--------	-----	----------	-----	-------------------

### $N(1440)$ BREIT-WIGNER PHOTON DECAY AMPLITUDES

#### $N(1440) \rightarrow p\gamma$ , helicity-1/2 amplitude $A_{1/2}$

VALUE ( $\text{GeV}^{-1/2}$ )	DOCUMENT ID	TECN	COMMENT
<b>-0.080 to -0.050 (<math>\approx -0.065</math>) OUR ESTIMATE</b>			
-0.091 $\pm 0.007$	<sup>1</sup> HUNT	19	DPWA Multichannel
-0.061 $\pm 0.006$	SOKHOYAN	15A	DPWA Multichannel
-0.085 $\pm 0.003$	<sup>1</sup> SHKLYAR	13	DPWA Multichannel
-0.056 $\pm 0.001$	<sup>1</sup> WORKMAN	12A	DPWA $\gamma N \rightarrow N\pi$
-0.051 $\pm 0.002$	<sup>1</sup> DUGGER	07	DPWA $\gamma N \rightarrow \pi N$
••• We do not use the following data for averages, fits, limits, etc. •••			
-0.061 $\pm 0.008$	ANISOVICH	12A	DPWA Multichannel
-0.084 $\pm 0.003$	<sup>1</sup> SHRESTHA	12A	DPWA Multichannel
-0.061	DRECHSEL	07	DPWA $\gamma N \rightarrow \pi N$
-0.087	PENNER	02D	DPWA Multichannel

<sup>1</sup> Statistical error only.

#### $N(1440) \rightarrow n\gamma$ , helicity-1/2 amplitude $A_{1/2}$

VALUE ( $\text{GeV}^{-1/2}$ )	DOCUMENT ID	TECN	COMMENT
<b>0.035 to 0.055 (<math>\approx 0.045</math>) OUR ESTIMATE</b>			
0.013 $\pm 0.012$	<sup>1</sup> HUNT	19	DPWA Multichannel
0.043 $\pm 0.012$	ANISOVICH	13B	DPWA Multichannel
0.048 $\pm 0.004$	<sup>1</sup> CHEN	12A	DPWA $\gamma N \rightarrow \pi N$
••• We do not use the following data for averages, fits, limits, etc. •••			
0.040 $\pm 0.005$	<sup>1</sup> SHRESTHA	12A	DPWA Multichannel
0.054	DRECHSEL	07	DPWA $\gamma N \rightarrow \pi N$
0.121	PENNER	02D	DPWA Multichannel

<sup>1</sup> Statistical error only.

### $N(1440)$ REFERENCES

For early references, see Physics Letters **111B** 1 (1982).

HUNT	19	PR C99 055205	B.C. Hunt, D.M. Manley	
SHKLYAR	16	PR C93 045206	V. Shklyar, H. Lenseke, U. Mosel	(GIES)
ROENCHEN	15A	EPJ A51 70	D. Roenchen <i>et al.</i>	
SOKHOYAN	15A	EPJ A51 95	V. Sokhoyan <i>et al.</i>	(CBELSA/TAPS Collab.)
PDG	14	CP C38 070001	K. Olive <i>et al.</i>	(PDG Collab.)
ROENCHEN	14	EPJ A50 101	D. Roenchen <i>et al.</i>	
Also		EPJ A51 63 (errata.)	D. Roenchen <i>et al.</i>	
SVARC	14	PR C89 045205	A. Svarc <i>et al.</i>	(RBI Zagreb, UNI Tuzla)
ANISOVICH	13B	EPJ A49 67	A.V. Anisovich <i>et al.</i>	
SHKLYAR	13	PR C87 015201	V. Shklyar, H. Lenseke, U. Mosel	(GIES)
ANISOVICH	12A	EPJ A48 15	A.V. Anisovich <i>et al.</i>	(BONN, PNPI)
CHEN	12A	PR C86 015206	W. Chen <i>et al.</i>	(DUKE, GWU, MSST, ITEP+)
SHRESTHA	12A	PR C86 055203	M. Shrestha, D.M. Manley	(KSU)
WORKMAN	12A	PR C86 015202	R. Workman <i>et al.</i>	(GWU)
BATINIC	10	PR C82 038203	M. Batinic <i>et al.</i>	(ZAGR)
DRECHSEL	07	EPJ A34 69	D. Drechsel, S.S. Kamalov, L. Tiator	(MAINZ, JINR)
DUGGER	07	PR C76 025211	D. Dugger <i>et al.</i>	(JLab CLAS Collab.)
ARNDT	06	PR C74 045205	R.A. Arndt <i>et al.</i>	(GWU)
PENNER	02C	PR C66 055211	G. Penner, U. Mosel	(GIES)
PENNER	02D	PR C66 055212	G. Penner, U. Mosel	(GIES)

VRANA	00	PRPL 328 181	T.P. Vrana, S.A. Dytman, T.-S.H. Lee	(PITT, ANL)
HOEHLER	93	$\pi N$ Newsletter 9 1	G. Hohlner	(KARL)
CUTKOSKY	80	Toronto Conf. 19	R.E. Cutkosky <i>et al.</i>	(CMU, LBL) IJP
Also		PR D20 2839	R.E. Cutkosky <i>et al.</i>	(CMU, LBL) IJP
HOEHLER	79	PDAT 12-1	G. Hohlner <i>et al.</i>	(KARLT) IJP
Also		Toronto Conf. 3	R. Koch	(KARLT) IJP

## $N(1520) 3/2^-$

$$I(J^P) = \frac{1}{2}(\frac{3}{2}^-) \text{ Status: } ***$$

Older and obsolete values are listed and referenced in the 2014 edition, Chinese Physics **C38** 070001 (2014).

### $N(1520)$ POLE POSITION

#### REAL PART

VALUE (MeV)	DOCUMENT ID	TECN	COMMENT
<b>1505 to 1515 (<math>\approx 1510</math>) OUR ESTIMATE</b>			
1507 $\pm 2$	SOKHOYAN	15A	DPWA Multichannel
1506 $\pm 1 \pm 1$	<sup>1</sup> SVARC	14	L+P $\pi N \rightarrow \pi N$
1510 $\pm 5$	CUTKOSKY	80	IPWA $\pi N \rightarrow \pi N$
••• We do not use the following data for averages, fits, limits, etc. •••			
1500	HUNT	19	DPWA Multichannel
1512	ROENCHEN	15A	DPWA Multichannel
1492	SHKLYAR	13	DPWA Multichannel
1507 $\pm 3$	ANISOVICH	12A	DPWA Multichannel
1506 $\pm 9$	BATINIC	10	DPWA $\pi N \rightarrow N\pi, N\eta$
1515	ARNDT	06	DPWA $\pi N \rightarrow \pi N, \eta N$
1504	VRANA	00	DPWA Multichannel
1510	HOEHLER	93	ARGD $\pi N \rightarrow \pi N$

<sup>1</sup> Fit to the amplitudes of HOEHLER 79.

#### -2xIMAGINARY PART

VALUE (MeV)	DOCUMENT ID	TECN	COMMENT
<b>105 to 120 (<math>\approx 110</math>) OUR ESTIMATE</b>			
111 $\pm 3$	SOKHOYAN	15A	DPWA Multichannel
115 $\pm 2 \pm 1$	<sup>1</sup> SVARC	14	L+P $\pi N \rightarrow \pi N$
114 $\pm 10$	CUTKOSKY	80	IPWA $\pi N \rightarrow \pi N$
••• We do not use the following data for averages, fits, limits, etc. •••			
117	HUNT	19	DPWA Multichannel
89	ROENCHEN	15A	DPWA Multichannel
94	SHKLYAR	13	DPWA Multichannel
111 $\pm 5$	ANISOVICH	12A	DPWA Multichannel
122 $\pm 9$	BATINIC	10	DPWA $\pi N \rightarrow N\pi, N\eta$
113	ARNDT	06	DPWA $\pi N \rightarrow \pi N, \eta N$
112	VRANA	00	DPWA Multichannel
120	HOEHLER	93	ARGD $\pi N \rightarrow \pi N$

<sup>1</sup> Fit to the amplitudes of HOEHLER 79.

### $N(1520)$ ELASTIC POLE RESIDUE

#### MODULUS $|r|$

VALUE (MeV)	DOCUMENT ID	TECN	COMMENT
<b>32 to 38 (<math>\approx 35</math>) OUR ESTIMATE</b>			
36 $\pm 2$	SOKHOYAN	15A	DPWA Multichannel
33 $\pm 1 \pm 1$	<sup>1</sup> SVARC	14	L+P $\pi N \rightarrow \pi N$
35 $\pm 2$	CUTKOSKY	80	IPWA $\pi N \rightarrow \pi N$
••• We do not use the following data for averages, fits, limits, etc. •••			
37	ROENCHEN	15A	DPWA Multichannel
27	SHKLYAR	13	DPWA Multichannel
36 $\pm 3$	ANISOVICH	12A	DPWA Multichannel
35	BATINIC	10	DPWA $\pi N \rightarrow N\pi, N\eta$
38	ARNDT	06	DPWA $\pi N \rightarrow \pi N, \eta N$
32	HOEHLER	93	ARGD $\pi N \rightarrow \pi N$

<sup>1</sup> Fit to the amplitudes of HOEHLER 79.

#### PHASE $\theta$

VALUE ( $^\circ$ )	DOCUMENT ID	TECN	COMMENT
<b>-15 to -5 (<math>\approx -10</math>) OUR ESTIMATE</b>			
-14 $\pm 3$	SOKHOYAN	15A	DPWA Multichannel
-15 $\pm 1 \pm 1$	<sup>1</sup> SVARC	14	L+P $\pi N \rightarrow \pi N$
-12 $\pm 5$	CUTKOSKY	80	IPWA $\pi N \rightarrow \pi N$
••• We do not use the following data for averages, fits, limits, etc. •••			
-6	ROENCHEN	15A	DPWA Multichannel
-35	SHKLYAR	13	DPWA Multichannel
-14 $\pm 3$	ANISOVICH	12A	DPWA Multichannel
-7	BATINIC	10	DPWA $\pi N \rightarrow N\pi, N\eta$
-5	ARNDT	06	DPWA $\pi N \rightarrow \pi N, \eta N$
-8	HOEHLER	93	ARGD $\pi N \rightarrow \pi N$

<sup>1</sup> Fit to the amplitudes of HOEHLER 79.



## Baryon Particle Listings

 $N(1520)$  $N(1520)$  INELASTIC POLE RESIDUE

The "normalized residue" is the residue divided by  $\Gamma_{pole}/2$ .

Normalized residue in  $N\pi \rightarrow N(1520) \rightarrow \Delta\pi, S$ -wave

MODULUS	PHASE ( $^\circ$ )	DOCUMENT ID	TECN	COMMENT
$0.33 \pm 0.04$	$155 \pm 15$	SOKHOYAN 15A	DPWA	Multichannel
•••				We do not use the following data for averages, fits, limits, etc. •••
$0.33 \pm 0.05$	$150 \pm 20$	ANISOVICH 12A	DPWA	Multichannel

Normalized residue in  $N\pi \rightarrow N(1520) \rightarrow \Delta\pi, D$ -wave

MODULUS	PHASE ( $^\circ$ )	DOCUMENT ID	TECN	COMMENT
$0.25 \pm 0.03$	$105 \pm 18$	SOKHOYAN 15A	DPWA	Multichannel
•••				We do not use the following data for averages, fits, limits, etc. •••
$0.25 \pm 0.03$	$100 \pm 20$	ANISOVICH 12A	DPWA	Multichannel

Normalized residue in  $N\pi \rightarrow N(1520) \rightarrow N\eta$ 

MODULUS	PHASE ( $^\circ$ )	DOCUMENT ID	TECN	COMMENT
•••				We do not use the following data for averages, fits, limits, etc. •••
0.026	95	ROENCHEN 15A	DPWA	Multichannel

Normalized residue in  $N\pi \rightarrow N(1520) \rightarrow \Lambda K$ 

MODULUS	PHASE ( $^\circ$ )	DOCUMENT ID	TECN	COMMENT
•••				We do not use the following data for averages, fits, limits, etc. •••
0.069	158	ROENCHEN 15A	DPWA	Multichannel

Normalized residue in  $N\pi \rightarrow N(1520) \rightarrow \Sigma K$ 

MODULUS	PHASE ( $^\circ$ )	DOCUMENT ID	TECN	COMMENT
•••				We do not use the following data for averages, fits, limits, etc. •••
0.049	-41	ROENCHEN 15A	DPWA	Multichannel

Normalized residue in  $N\pi \rightarrow N(1520) \rightarrow N\sigma$ 

MODULUS	PHASE ( $^\circ$ )	DOCUMENT ID	TECN	COMMENT
$0.08 \pm 0.03$	$-45 \pm 25$	SOKHOYAN 15A	DPWA	Multichannel

 $N(1520)$  BREIT-WIGNER MASS

VALUE (MeV)	DOCUMENT ID	TECN	COMMENT
<b>1510 to 1520 (<math>\approx 1515</math>) OUR ESTIMATE</b>			
$1512.0 \pm 1.5$	<sup>1</sup> HUNT 19	DPWA	Multichannel
$1516 \pm 2$	SOKHOYAN 15A	DPWA	Multichannel
$1505 \pm 4$	<sup>1</sup> SHKLYAR 13	DPWA	Multichannel
$1514.5 \pm 0.2$	<sup>1</sup> ARNDT 06	DPWA	$\pi N \rightarrow \pi N, \eta N$
$1525 \pm 10$	CUTKOSKY 80	IPWA	$\pi N \rightarrow \pi N$
$1519 \pm 4$	HOEHLER 79	IPWA	$\pi N \rightarrow \pi N$
•••			We do not use the following data for averages, fits, limits, etc. •••
$1517 \pm 3$	ANISOVICH 12A	DPWA	Multichannel
$1512.6 \pm 0.5$	<sup>1</sup> SHRESTHA 12A	DPWA	Multichannel
$1522 \pm 8$	BATINIC 10	DPWA	$\pi N \rightarrow N\pi, N\eta$
$1509 \pm 1$	PENNER 02c	DPWA	Multichannel
$1518 \pm 3$	VRANA 00	DPWA	Multichannel

<sup>1</sup> Statistical error only.

 $N(1520)$  BREIT-WIGNER WIDTH

VALUE (MeV)	DOCUMENT ID	TECN	COMMENT
<b>100 to 120 (<math>\approx 110</math>) OUR ESTIMATE</b>			
$121 \pm 3$	<sup>1</sup> HUNT 19	DPWA	Multichannel
$113 \pm 4$	SOKHOYAN 15A	DPWA	Multichannel
$100 \pm 2$	<sup>1</sup> SHKLYAR 13	DPWA	Multichannel
$103.6 \pm 0.4$	<sup>1</sup> ARNDT 06	DPWA	$\pi N \rightarrow \pi N, \eta N$
$120 \pm 15$	CUTKOSKY 80	IPWA	$\pi N \rightarrow \pi N$
$114 \pm 7$	HOEHLER 79	IPWA	$\pi N \rightarrow \pi N$
•••			We do not use the following data for averages, fits, limits, etc. •••
$114 \pm 5$	ANISOVICH 12A	DPWA	Multichannel
$117 \pm 1$	<sup>1</sup> SHRESTHA 12A	DPWA	Multichannel
$132 \pm 11$	BATINIC 10	DPWA	$\pi N \rightarrow N\pi, N\eta$
$100 \pm 2$	PENNER 02c	DPWA	Multichannel
$124 \pm 4$	VRANA 00	DPWA	Multichannel

<sup>1</sup> Statistical error only.

 $N(1520)$  DECAY MODES

The following branching fractions are our estimates, not fits or averages.

Mode	Fraction ( $\Gamma_i/\Gamma$ )
$\Gamma_1$ $N\pi$	55–65 %
$\Gamma_2$ $N\eta$	0.07–0.09 %
$\Gamma_3$ $N\pi\pi$	25–35 %
$\Gamma_4$ $\Delta(1232)\pi$	22–34 %
$\Gamma_5$ $\Delta(1232)\pi, S$ -wave	15–23 %
$\Gamma_6$ $\Delta(1232)\pi, D$ -wave	7–11 %

$\Gamma_7$ $N\sigma$	< 2 %
$\Gamma_8$ $p\gamma$	0.31–0.52 %
$\Gamma_9$ $p\gamma, \text{ helicity}=1/2$	0.01–0.02 %
$\Gamma_{10}$ $p\gamma, \text{ helicity}=3/2$	0.30–0.50 %
$\Gamma_{11}$ $n\gamma$	0.30–0.53 %
$\Gamma_{12}$ $n\gamma, \text{ helicity}=1/2$	0.04–0.10 %
$\Gamma_{13}$ $n\gamma, \text{ helicity}=3/2$	0.25–0.45 %

 $N(1520)$  BRANCHING RATIOS

$\Gamma(N\pi)/\Gamma_{total}$	DOCUMENT ID	TECN	COMMENT	$\Gamma_1/\Gamma$
<b>55 to 65 (<math>\approx 60</math>) OUR ESTIMATE</b>				
$58.3 \pm 1.5$	<sup>1</sup> HUNT 19	DPWA	Multichannel	
$61 \pm 2$	SOKHOYAN 15A	DPWA	Multichannel	
$57 \pm 2$	<sup>1</sup> SHKLYAR 13	DPWA	Multichannel	
$63.2 \pm 0.1$	<sup>1</sup> ARNDT 06	DPWA	$\pi N \rightarrow \pi N, \eta N$	
$58 \pm 3$	CUTKOSKY 80	IPWA	$\pi N \rightarrow \pi N$	
$54 \pm 3$	HOEHLER 79	IPWA	$\pi N \rightarrow \pi N$	
•••			We do not use the following data for averages, fits, limits, etc. •••	
$62 \pm 3$	ANISOVICH 12A	DPWA	Multichannel	
$62.7 \pm 0.5$	<sup>1</sup> SHRESTHA 12A	DPWA	Multichannel	
$55 \pm 5$	BATINIC 10	DPWA	$\pi N \rightarrow N\pi, N\eta$	
$56 \pm 1$	PENNER 02c	DPWA	Multichannel	
$63 \pm 2$	VRANA 00	DPWA	Multichannel	

<sup>1</sup> Statistical error only.

$\Gamma(N\eta)/\Gamma_{total}$	DOCUMENT ID	TECN	COMMENT	$\Gamma_2/\Gamma$
<b>0.03 <math>\pm</math> 0.01</b>	<sup>1</sup> HUNT 19	DPWA	Multichannel	
<1	SHKLYAR 13	DPWA	Multichannel	
$0.08 \pm 0.01$	TIATOR 99	DPWA	$\gamma p \rightarrow p\eta$	
•••			We do not use the following data for averages, fits, limits, etc. •••	
$0.1 \pm 0.1$	BATINIC 10	DPWA	$\pi N \rightarrow N\pi, N\eta$	
$0.2 \pm 0.1$	THOMA 08	DPWA	Multichannel	
$0.08 \text{ to } 0.12$	ARNDT 05	DPWA	Multichannel	
$0.23 \pm 0.04$	PENNER 02c	DPWA	Multichannel	
$0 \pm 1$	VRANA 00	DPWA	Multichannel	

<sup>1</sup> Statistical error only.

$\Gamma(\Delta(1232)\pi, S\text{-wave})/\Gamma_{total}$	DOCUMENT ID	TECN	COMMENT	$\Gamma_5/\Gamma$
<b>21 <math>\pm</math> 2</b>	<sup>1</sup> HUNT 19	DPWA	Multichannel	
$19 \pm 4$	SOKHOYAN 15A	DPWA	Multichannel	
•••			We do not use the following data for averages, fits, limits, etc. •••	
$19 \pm 4$	ANISOVICH 12A	DPWA	Multichannel	
$9.3 \pm 0.7$	<sup>1</sup> SHRESTHA 12A	DPWA	Multichannel	
$15 \pm 2$	VRANA 00	DPWA	Multichannel	

<sup>1</sup> Statistical error only.

$\Gamma(\Delta(1232)\pi, D\text{-wave})/\Gamma_{total}$	DOCUMENT ID	TECN	COMMENT	$\Gamma_6/\Gamma$
<b>6 <math>\pm</math> 1</b>	<sup>1</sup> HUNT 19	DPWA	Multichannel	
$9 \pm 2$	SOKHOYAN 15A	DPWA	Multichannel	
•••			We do not use the following data for averages, fits, limits, etc. •••	
$9 \pm 2$	ANISOVICH 12A	DPWA	Multichannel	
$6.3 \pm 0.5$	<sup>1</sup> SHRESTHA 12A	DPWA	Multichannel	
$11 \pm 2$	VRANA 00	DPWA	Multichannel	

<sup>1</sup> Statistical error only.

$\Gamma(N\sigma)/\Gamma_{total}$	DOCUMENT ID	TECN	COMMENT	$\Gamma_7/\Gamma$
<b>&lt;0.7</b>	<sup>1</sup> HUNT 19	DPWA	Multichannel	
<2	SOKHOYAN 15A	DPWA	Multichannel	
•••			We do not use the following data for averages, fits, limits, etc. •••	
<1	<sup>1</sup> SHRESTHA 12A	DPWA	Multichannel	
<4	THOMA 08	DPWA	Multichannel	
$1 \pm 1$	VRANA 00	DPWA	Multichannel	

<sup>1</sup> Statistical error only.

 $N(1520)$  PHOTON DECAY AMPLITUDES AT THE POLE $N(1520) \rightarrow p\gamma, \text{ helicity}=1/2$  amplitude  $A_{1/2}$ 

MODULUS ( $\text{GeV}^{-1/2}$ )	PHASE ( $^\circ$ )	DOCUMENT ID	TECN	COMMENT
$-0.023 \pm 0.004$	$-6 \pm 5$	SOKHOYAN 15A	DPWA	Multichannel
$-0.024^{+0.008}_{-0.003}$	$-17^{+16}_{-6}$	ROENCHEN 14	DPWA	
•••				We do not use the following data for averages, fits, limits, etc. •••
-0.031	-17	ROENCHEN 15A	DPWA	Multichannel

See key on page 999

# Baryon Particle Listings

## $N(1520)$ , $N(1535)$

### $N(1520) \rightarrow p\gamma$ , helicity-3/2 amplitude $A_{3/2}$

MODULUS ( $\text{GeV}^{-1/2}$ )	PHASE ( $^\circ$ )	DOCUMENT ID	TECN	COMMENT
$0.131 \pm 0.006$	$4 \pm 4$	SOKHOYAN 15A	DPWA	Multichannel
$0.117^{+0.006}_{-0.010}$	$26 \pm 2$	ROENCHEN 14	DPWA	
0.075	1.7	ROENCHEN 15A	DPWA	Multichannel

• • • We do not use the following data for averages, fits, limits, etc. • • •

### $N(1520)$ BREIT-WIGNER PHOTON DECAY AMPLITUDES

### $N(1520) \rightarrow p\gamma$ , helicity-1/2 amplitude $A_{1/2}$

VALUE ( $\text{GeV}^{-1/2}$ )	DOCUMENT ID	TECN	COMMENT
<b>-0.030 to -0.015 (<math>\approx -0.025</math>) OUR ESTIMATE</b>			
$-0.034 \pm 0.003$	1 HUNT 19	DPWA	Multichannel
$-0.024 \pm 0.004$	SOKHOYAN 15A	DPWA	Multichannel
$-0.015 \pm 0.001$	1 SHKLYAR 13	DPWA	Multichannel
$-0.019 \pm 0.002$	1 WORKMAN 12A	DPWA	$\gamma N \rightarrow N\pi$
$-0.028 \pm 0.002$	1 DUGGER 07	DPWA	$\gamma N \rightarrow \pi N$
$-0.038 \pm 0.003$	1 AHRENS 02	DPWA	$\gamma N \rightarrow \pi N$
• • • We do not use the following data for averages, fits, limits, etc. • • •			
$-0.022 \pm 0.004$	ANISOVICH 12A	DPWA	Multichannel
$-0.034 \pm 0.001$	1 SHRESTHA 12A	DPWA	Multichannel
$-0.027$	DRECHSEL 07	DPWA	$\gamma N \rightarrow \pi N$
$-0.003$	PENNER 02D	DPWA	Multichannel
$-0.052 \pm 0.010 \pm 0.007$	1 MUKHOPAD... 98		$\gamma p \rightarrow \eta p$
1 Statistical error only.			

### $N(1520) \rightarrow n\gamma$ , helicity-3/2 amplitude $A_{3/2}$

VALUE ( $\text{GeV}^{-1/2}$ )	DOCUMENT ID	TECN	COMMENT
<b>0.135 to 0.145 (<math>\approx 0.140</math>) OUR ESTIMATE</b>			
$0.142 \pm 0.003$	1 HUNT 19	DPWA	Multichannel
$0.130 \pm 0.006$	SOKHOYAN 15A	DPWA	Multichannel
$0.146 \pm 0.001$	1 SHKLYAR 13	DPWA	Multichannel
$0.141 \pm 0.002$	1 WORKMAN 12A	DPWA	$\gamma N \rightarrow N\pi$
$0.143 \pm 0.002$	1 DUGGER 07	DPWA	$\gamma N \rightarrow \pi N$
$0.147 \pm 0.010$	1 AHRENS 02	DPWA	$\gamma N \rightarrow \pi N$
• • • We do not use the following data for averages, fits, limits, etc. • • •			
$0.131 \pm 0.010$	ANISOVICH 12A	DPWA	Multichannel
$0.127 \pm 0.003$	1 SHRESTHA 12A	DPWA	Multichannel
0.161	DRECHSEL 07	DPWA	$\gamma N \rightarrow \pi N$
0.151	PENNER 02D	DPWA	Multichannel
$0.130 \pm 0.020 \pm 0.015$	1 MUKHOPAD... 98		$\gamma p \rightarrow \eta p$
1 Statistical error only.			

### $N(1520) \rightarrow n\gamma$ , helicity-1/2 amplitude $A_{1/2}$

VALUE ( $\text{GeV}^{-1/2}$ )	DOCUMENT ID	TECN	COMMENT
<b>-0.055 to -0.040 (<math>\approx -0.050</math>) OUR ESTIMATE</b>			
$-0.072 \pm 0.003$	1 HUNT 19	DPWA	Multichannel
$-0.049 \pm 0.008$	ANISOVICH 13B	DPWA	Multichannel
$-0.046 \pm 0.006$	1 CHEN 12A	DPWA	$\gamma N \rightarrow \pi N$
• • • We do not use the following data for averages, fits, limits, etc. • • •			
$-0.038 \pm 0.003$	1 SHRESTHA 12A	DPWA	Multichannel
$-0.077$	DRECHSEL 07	DPWA	$\gamma N \rightarrow \pi N$
$-0.084$	PENNER 02D	DPWA	Multichannel
1 Statistical error only.			

### $N(1520) \rightarrow n\gamma$ , helicity-3/2 amplitude $A_{3/2}$

VALUE ( $\text{GeV}^{-1/2}$ )	DOCUMENT ID	TECN	COMMENT
<b>-0.120 to -0.100 (<math>\approx -0.115</math>) OUR ESTIMATE</b>			
$-0.123 \pm 0.006$	1 HUNT 19	DPWA	Multichannel
$-0.113 \pm 0.012$	ANISOVICH 13B	DPWA	Multichannel
$-0.115 \pm 0.005$	1 CHEN 12A	DPWA	$\gamma N \rightarrow \pi N$
• • • We do not use the following data for averages, fits, limits, etc. • • •			
$-0.101 \pm 0.004$	1 SHRESTHA 12A	DPWA	Multichannel
$-0.154$	DRECHSEL 07	DPWA	$\gamma N \rightarrow \pi N$
$-0.159$	PENNER 02D	DPWA	Multichannel
1 Statistical error only.			

### $N(1520)$ REFERENCES

For early references, see Physics Letters **111B** 1 (1982). For very early references, see Reviews of Modern Physics **37** 633 (1965).

HUNT 19	PR C99 055205	B. C. Hunt, D.M. Manley	
ROENCHEN 15A	EPJ A51 70	D. Roenchen et al.	
SOKHOYAN 15A	EPJ A51 95	V. Sokhoyan et al.	(CBELSA/TAPS Collab.)
PDG 14	CP C38 070001	K. Olive et al.	(PDG Collab.)
ROENCHEN 14	EPJ A50 101	D. Roenchen et al.	
Also	EPJ A51 63 (errata.)	D. Roenchen et al.	
SVARC 14	PR C89 045205	A. Svarc et al.	(RBI Zagreb, UNI Tuzla)
ANISOVICH 13B	EPJ A49 67	A.V. Anisovich et al.	
SHKLYAR 13	PR C87 015201	V. Shklyar, H. Lenske, U. Mosel	(GIES)
ANISOVICH 12A	EPJ A48 15	A.V. Anisovich et al.	(BONN, PNPI)
CHEN 12A	PR C86 015206	W. Chen et al.	(DUKE, GWU, MSST, ITEP+)
SHRESTHA 12A	PR C86 055203	M. Shrestha, D.M. Manley	(KSU)
WORKMAN 12A	PR C86 015202	R. Workman et al.	(GWU)
BATINIC 10	PR C82 038203	M. Batinic et al.	(ZAGR)

THOMA 08	PL B659 87	U. Thoma et al.	(CB-ELSA Collab.)
DRECHSEL 07	EPJ A34 69	D. Drechsel, S.S. Kamalov, L. Tiator	(MAINZ, JINR)
DUGGER 07	PR C74 025211	M. Dugger et al.	(JLab CLAS Collab.)
ARNDT 06	PR C74 045205	R.A. Arndt et al.	(GWU)
ARNDT 05	PR C72 045202	R.A. Arndt et al.	(GWU, PNPI)
AHRENS 02C	PRL 88 232002	J. Ahrens et al.	(Mainz MAMI GDH/A2 Collab.)
PENNER 02D	PR C66 055211	G. Penner, U. Mosel	(GIES)
PENNER 02D	PR C66 055212	G. Penner, U. Mosel	(GIES)
VRANA 00	PRPL 320 181	T.P. Vrana, S.A. Dytman, T.-S.H. Lee	(PITT, ANL)
TIATOR 99	PR C60 035210	L. Tiator et al.	
MUKHOPAD... 98	PL B444 7	N. C. Mukhopadhyay, N. Mathur	
HOEHLER 93	$\pi N$ Newsletter 9 1	G. Hoehler	(KARL)
CUTKOSKY 80	Toronto Conf. 19	R.E. Cutkosky et al.	(CMU, LBL) IJP
Also	PR D20 2839	R.E. Cutkosky et al.	(CMU, LBL) IJP
HOEHLER 79	PDAT 12-1	G. Hoehler et al.	(KARLT) IJP
Also	Toronto Conf. 3	R. Koch	(KARLT) IJP

### $N(1535) 1/2^-$

$$I(J^P) = \frac{1}{2}(\frac{1}{2}^-) \text{ Status: } ***$$

Older and obsolete values are listed and referenced in the 2014 edition, Chinese Physics **C38** 070001 (2014).

### $N(1535)$ POLE POSITION

#### REAL PART

VALUE (MeV)	DOCUMENT ID	TECN	COMMENT
<b>1500 to 1520 (<math>\approx 1510</math>) OUR ESTIMATE</b>			
$1500 \pm 4$	SOKHOYAN 15A	DPWA	Multichannel
$1509 \pm 4 \pm 2$	1 SVARC 14	L+P	$\pi N \rightarrow \pi N$
$1510 \pm 50$	CUTKOSKY 80	IPWA	$\pi N \rightarrow \pi N$
• • • We do not use the following data for averages, fits, limits, etc. • • •			
1496	HUNT 19	DPWA	Multichannel
1499	ROENCHEN 15A	DPWA	Multichannel
1490	SHKLYAR 13	DPWA	Multichannel
$1501 \pm 4$	ANISOVICH 12A	DPWA	Multichannel
$1521 \pm 14$	BATINIC 10	DPWA	$\pi N \rightarrow N\pi, N\eta$
1502	ARNDT 06	DPWA	$\pi N \rightarrow \pi N, \eta N$
1525	VRANA 00	DPWA	Multichannel
1487	HOEHLER 93	SPED	$\pi N \rightarrow \pi N$
1 Fit to the amplitudes of HOEHLER 79.			

#### -2xIMAGINARY PART

VALUE (MeV)	DOCUMENT ID	TECN	COMMENT
<b>110 to 150 (<math>\approx 130</math>) OUR ESTIMATE</b>			
$128 \pm 9$	SOKHOYAN 15A	DPWA	Multichannel
$118 \pm 9 \pm 2$	2 SVARC 14	L+P	$\pi N \rightarrow \pi N$
$260 \pm 80$	CUTKOSKY 80	IPWA	$\pi N \rightarrow \pi N$
• • • We do not use the following data for averages, fits, limits, etc. • • •			
119	HUNT 19	DPWA	Multichannel
104	ROENCHEN 15A	DPWA	Multichannel
100	SHKLYAR 13	DPWA	Multichannel
$134 \pm 11$	ANISOVICH 12A	DPWA	Multichannel
$190 \pm 28$	BATINIC 10	DPWA	$\pi N \rightarrow N\pi, N\eta$
95	ARNDT 06	DPWA	$\pi N \rightarrow \pi N, \eta N$
102	VRANA 00	DPWA	Multichannel
2 Fit to the amplitudes of HOEHLER 79.			

### $N(1535)$ ELASTIC POLE RESIDUE

#### MODULUS $|r|$

VALUE (MeV)	DOCUMENT ID	TECN	COMMENT
<b>15 to 35 (<math>\approx 25</math>) OUR ESTIMATE</b>			
$29 \pm 4$	SOKHOYAN 15A	DPWA	Multichannel
$22 \pm 2 \pm 0.4$	3 SVARC 14	L+P	$\pi N \rightarrow \pi N$
$120 \pm 40$	CUTKOSKY 80	IPWA	$\pi N \rightarrow \pi N$
• • • We do not use the following data for averages, fits, limits, etc. • • •			
22	ROENCHEN 15A	DPWA	Multichannel
15	SHKLYAR 13	DPWA	Multichannel
$31 \pm 4$	ANISOVICH 12A	DPWA	Multichannel
68	BATINIC 10	DPWA	$\pi N \rightarrow N\pi, N\eta$
16	ARNDT 06	DPWA	$\pi N \rightarrow \pi N, \eta N$
3 Fit to the amplitudes of HOEHLER 79.			

#### PHASE $\theta$

VALUE ( $^\circ$ )	DOCUMENT ID	TECN	COMMENT
<b>-30 to 0 (<math>\approx -15</math>) OUR ESTIMATE</b>			
$-20 \pm 10$	SOKHOYAN 15A	DPWA	Multichannel
$-5 \pm 5 \pm 3$	4 SVARC 14	L+P	$\pi N \rightarrow \pi N$
$+15 \pm 45$	CUTKOSKY 80	IPWA	$\pi N \rightarrow \pi N$
• • • We do not use the following data for averages, fits, limits, etc. • • •			
-46	ROENCHEN 15A	DPWA	Multichannel
-51	SHKLYAR 13	DPWA	Multichannel
$-29 \pm 5$	ANISOVICH 12A	DPWA	Multichannel
12	BATINIC 10	DPWA	$\pi N \rightarrow N\pi, N\eta$
-16	ARNDT 06	DPWA	$\pi N \rightarrow \pi N, \eta N$
4 Fit to the amplitudes of HOEHLER 79.			

## Baryon Particle Listings

 $N(1535)$  $N(1535)$  INELASTIC POLE RESIDUE

The "normalized residue" is the residue divided by  $\Gamma_{pole}/2$ .

Normalized residue in  $N\pi \rightarrow N(1535) \rightarrow N\eta$ 

MODULUS	PHASE ( $^\circ$ )	DOCUMENT ID	TECN	COMMENT
$0.43 \pm 0.03$	$-76 \pm 5$	ANISOVICH 12A	DPWA	Multichannel
••• We do not use the following data for averages, fits, limits, etc. •••				
0.51	112	ROENCHEN 15A	DPWA	Multichannel

Normalized residue in  $N\pi \rightarrow N(1535) \rightarrow \Lambda K$ 

MODULUS	PHASE ( $^\circ$ )	DOCUMENT ID	TECN	COMMENT
••• We do not use the following data for averages, fits, limits, etc. •••				
0.05	32	ROENCHEN 15A	DPWA	Multichannel

Normalized residue in  $N\pi \rightarrow N(1535) \rightarrow \Sigma K$ 

MODULUS	PHASE ( $^\circ$ )	DOCUMENT ID	TECN	COMMENT
••• We do not use the following data for averages, fits, limits, etc. •••				
0.05	-69	ROENCHEN 15A	DPWA	Multichannel

Normalized residue in  $N\pi \rightarrow N(1535) \rightarrow \Delta\pi, D\text{-wave}$ 

MODULUS	PHASE ( $^\circ$ )	DOCUMENT ID	TECN	COMMENT
••• We do not use the following data for averages, fits, limits, etc. •••				
$0.12 \pm 0.03$	$145 \pm 17$	ANISOVICH 12A	DPWA	Multichannel

Normalized residue in  $N\pi \rightarrow N(1535) \rightarrow N\sigma$ 

MODULUS	PHASE ( $^\circ$ )	DOCUMENT ID	TECN	COMMENT
$0.16 \pm 0.07$	$25 \pm 40$	SOKHOYAN 15A	DPWA	Multichannel

Normalized residue in  $N\pi \rightarrow N(1535) \rightarrow N(1440)\pi$ 

MODULUS	PHASE ( $^\circ$ )	DOCUMENT ID	TECN	COMMENT
$0.21 \pm 0.14$	$-45 \pm 50$	SOKHOYAN 15A	DPWA	Multichannel

 $N(1535)$  BREIT-WIGNER MASS

VALUE (MeV)	DOCUMENT ID	TECN	COMMENT
<b>1515 to 1545 (<math>\approx 1530</math>) OUR ESTIMATE</b>			
$1525 \pm 2$	<sup>5</sup> HUNT 19	DPWA	Multichannel
$1528 \pm 6$	KASHEVAROV 17	DPWA	$\gamma p \rightarrow \eta p, \eta' p$
$1517 \pm 4$	SOKHOYAN 15A	DPWA	Multichannel
$1526 \pm 2$	<sup>5</sup> SHKLYAR 13	DPWA	Multichannel
$1547.0 \pm 0.7$	<sup>5</sup> ARNDT 06	DPWA	$\pi N \rightarrow \pi N, N\eta$
$1550 \pm 40$	CUTKOSKY 80	IPWA	$\pi N \rightarrow \pi N$
$1526 \pm 7$	HOEHLER 79	IPWA	$\pi N \rightarrow \pi N$
••• We do not use the following data for averages, fits, limits, etc. •••			
$1519 \pm 5$	ANISOVICH 12A	DPWA	Multichannel
$1538 \pm 1$	<sup>5</sup> SHRESTHA 12A	DPWA	Multichannel
$1553 \pm 8$	BATINIC 10	DPWA	$\pi N \rightarrow N\pi, N\eta$
$1546.7 \pm 2.2$	ARNDT 04	DPWA	$\pi N \rightarrow \pi N, N\eta$
$1526 \pm 2$	PENNER 02c	DPWA	Multichannel
$1530 \pm 10$	BAI 01B	BES	$J/\psi \rightarrow p\bar{p}\eta$
$1522 \pm 11$	THOMPSON 01	CLAS	$\gamma^* p \rightarrow p\eta$
$1542 \pm 3$	VRANA 00	DPWA	Multichannel
$1532 \pm 5$	ARMSTRONG 99B	DPWA	$\gamma^* p \rightarrow p\eta$

<sup>5</sup> Statistical error only.

 $N(1535)$  BREIT-WIGNER WIDTH

VALUE (MeV)	DOCUMENT ID	TECN	COMMENT
<b>125 to 175 (<math>\approx 150</math>) OUR ESTIMATE</b>			
$147 \pm 5$	<sup>6</sup> HUNT 19	DPWA	Multichannel
$163 \pm 25$	KASHEVAROV 17	DPWA	$\gamma p \rightarrow \eta p, \eta' p$
$120 \pm 10$	SOKHOYAN 15A	DPWA	Multichannel
$131 \pm 12$	<sup>6</sup> SHKLYAR 13	DPWA	Multichannel
$188.4 \pm 3.8$	<sup>6</sup> ARNDT 06	DPWA	$\pi N \rightarrow \pi N, N\eta$
$240 \pm 80$	CUTKOSKY 80	IPWA	$\pi N \rightarrow \pi N$
$120 \pm 20$	HOEHLER 79	IPWA	$\pi N \rightarrow \pi N$
••• We do not use the following data for averages, fits, limits, etc. •••			
$128 \pm 14$	ANISOVICH 12A	DPWA	Multichannel
$141 \pm 4$	<sup>6</sup> SHRESTHA 12A	DPWA	Multichannel
$182 \pm 25$	BATINIC 10	DPWA	$\pi N \rightarrow N\pi, N\eta$
$129 \pm 8$	PENNER 02c	DPWA	Multichannel
$95 \pm 25$	BAI 01B	BES	$J/\psi \rightarrow p\bar{p}\eta$
$143 \pm 18$	THOMPSON 01	CLAS	$\gamma^* p \rightarrow p\eta$
$112 \pm 19$	VRANA 00	DPWA	Multichannel
$154 \pm 20$	ARMSTRONG 99B	DPWA	$\gamma^* p \rightarrow p\eta$

<sup>6</sup> Statistical error only.

 $N(1535)$  DECAY MODES

The following branching fractions are our estimates, not fits or averages.

Mode	Fraction ( $\Gamma_i/\Gamma$ )
$\Gamma_1$ $N\pi$	32-52 %
$\Gamma_2$ $N\eta$	30-55 %
$\Gamma_3$ $N\pi\pi$	3-14 %
$\Gamma_4$ $\Delta(1232)\pi$	
$\Gamma_5$ $\Delta(1232)\pi, D\text{-wave}$	1-4 %
$\Gamma_6$ $N\rho$	
$\Gamma_7$ $N\rho, S=1/2$	
$\Gamma_8$ $N\rho, S=3/2, D\text{-wave}$	
$\Gamma_9$ $N\sigma$	2-10 %
$\Gamma_{10}$ $N(1440)\pi$	5-12 %
$\Gamma_{11}$ $p\gamma, \text{helicity}=1/2$	0.15-0.30 %
$\Gamma_{12}$ $n\gamma, \text{helicity}=1/2$	0.01-0.25 %

 $N(1535)$  BRANCHING RATIOS

$\Gamma(N\pi)/\Gamma_{\text{total}}$	DOCUMENT ID	TECN	COMMENT	$\Gamma_1/\Gamma$
<b>32 to 52 (<math>\approx 42</math>) OUR ESTIMATE</b>				
$42 \pm 2$	<sup>7</sup> HUNT 19	DPWA	Multichannel	
$52 \pm 5$	SOKHOYAN 15A	DPWA	Multichannel	
$35 \pm 3$	<sup>7</sup> SHKLYAR 13	DPWA	Multichannel	
$35.5 \pm 0.2$	<sup>7</sup> ARNDT 06	DPWA	$\pi N \rightarrow \pi N, N\eta$	
$50 \pm 10$	CUTKOSKY 80	IPWA	$\pi N \rightarrow \pi N$	
$38 \pm 4$	HOEHLER 79	IPWA	$\pi N \rightarrow \pi N$	
••• We do not use the following data for averages, fits, limits, etc. •••				
$54 \pm 5$	ANISOVICH 12A	DPWA	Multichannel	
$37 \pm 1$	<sup>7</sup> SHRESTHA 12A	DPWA	Multichannel	
$46 \pm 7$	BATINIC 10	DPWA	$\pi N \rightarrow N\pi, N\eta$	
$36 \pm 1$	PENNER 02c	DPWA	Multichannel	
$35 \pm 8$	VRANA 00	DPWA	Multichannel	

<sup>7</sup> Statistical error only.

$\Gamma(N\eta)/\Gamma_{\text{total}}$	DOCUMENT ID	TECN	COMMENT	$\Gamma_2/\Gamma$
<b>30 to 55 (<math>\approx 42</math>) OUR ESTIMATE</b>				
$43 \pm 3$	<sup>8</sup> HUNT 19	DPWA	Multichannel	
$41 \pm 4$	<sup>9</sup> KASHEVAROV 17	DPWA	$\gamma p \rightarrow \eta p, \eta' p$	
$58 \pm 4$	<sup>8</sup> SHKLYAR 13	DPWA	Multichannel	
$33 \pm 5$	ANISOVICH 12A	DPWA	Multichannel	
$53 \pm 1$	PENNER 02c	DPWA	Multichannel	
$51 \pm 5$	VRANA 00	DPWA	Multichannel	
••• We do not use the following data for averages, fits, limits, etc. •••				
$41 \pm 2$	<sup>8</sup> SHRESTHA 12A	DPWA	Multichannel	
$50 \pm 7$	BATINIC 10	DPWA	$\pi N \rightarrow N\pi, N\eta$	

<sup>8</sup> Statistical error only.

<sup>9</sup> Assuming  $A_{1/2} = 0.115 \text{ GeV}^{-1/2}$ .

$\Gamma(N\eta)/\Gamma(N\pi)$	DOCUMENT ID	TECN	COMMENT	$\Gamma_2/\Gamma_1$
••• We do not use the following data for averages, fits, limits, etc. •••				
$0.95 \pm 0.03$	AZNAURYAN 09	CLAS	$\pi, \eta$ electroproduction	

$\Gamma(\Delta(1232)\pi, D\text{-wave})/\Gamma_{\text{total}}$	DOCUMENT ID	TECN	COMMENT	$\Gamma_5/\Gamma$
<b>30 to 55 (<math>\approx 42</math>) OUR ESTIMATE</b>				
$<1.1$	<sup>10</sup> HUNT 19	DPWA	Multichannel	
$2.5 \pm 1.5$	SOKHOYAN 15A	DPWA	Multichannel	
••• We do not use the following data for averages, fits, limits, etc. •••				
$2.5 \pm 1.5$	ANISOVICH 12A	DPWA	Multichannel	
$1.8 \pm 0.8$	<sup>10</sup> SHRESTHA 12A	DPWA	Multichannel	
$1 \pm 1$	VRANA 00	DPWA	Multichannel	

<sup>10</sup> Statistical error only.

$\Gamma(N\rho, S=1/2)/\Gamma_{\text{total}}$	DOCUMENT ID	TECN	COMMENT	$\Gamma_7/\Gamma$
<b>30 to 55 (<math>\approx 42</math>) OUR ESTIMATE</b>				
$14 \pm 2$	<sup>11</sup> HUNT 19	DPWA	Multichannel	

<sup>11</sup> Statistical error only.

$\Gamma(N\rho, S=3/2, D\text{-wave})/\Gamma_{\text{total}}$	DOCUMENT ID	TECN	COMMENT	$\Gamma_8/\Gamma$
<b>30 to 55 (<math>\approx 42</math>) OUR ESTIMATE</b>				
$<0.3$	<sup>12</sup> HUNT 19	DPWA	Multichannel	

<sup>12</sup> Statistical error only.

**$\Gamma(N\sigma)/\Gamma_{total}$**

VALUE (%)	DOCUMENT ID	TECN	COMMENT
<1	13 HUNT	19 DPWA	Multichannel
6 ± 4	SOKHOYAN	15A DPWA	Multichannel
1.5 ± 0.5	13 SHRESTHA	12A DPWA	Multichannel
2 ± 1	VRANA	00 DPWA	Multichannel

• • • We do not use the following data for averages, fits, limits, etc. • • •

13 Statistical error only.

**$\Gamma(N(1440)\pi)/\Gamma_{total}$**

VALUE (%)	DOCUMENT ID	TECN	COMMENT
< 0.01	14 HUNT	19 DPWA	Multichannel
12 ± 8	SOKHOYAN	15A DPWA	Multichannel
8 ± 2	14 STAROSTIN	03 $\pi^- p \rightarrow n3\pi^0$	
< 1	14 SHRESTHA	12A DPWA	Multichannel
10 ± 9	VRANA	00 DPWA	Multichannel

• • • We do not use the following data for averages, fits, limits, etc. • • •

14 This value is an estimate made using simplest assumptions.

**N(1535) PHOTON DECAY AMPLITUDES AT THE POLE**

**$N(1535) \rightarrow p\gamma$ , helicity-1/2 amplitude  $A_{1/2}$**

MODULUS ( $\text{GeV}^{-1/2}$ )	PHASE ( $^\circ$ )	DOCUMENT ID	TECN	COMMENT
0.093 ± 0.009	8 ± 4	ANISOVICH	17D DPWA	Multichannel
0.050 ± 0.004	-14 ± 10	15 ROENCHEN	14 DPWA	
0.114 ± 0.008	10 ± 5	ANISOVICH	15A DPWA	Multichannel
0.106	5.2	ROENCHEN	15A DPWA	Multichannel
0.114 ± 0.008	10 ± 5	SOKHOYAN	15A DPWA	Multichannel

• • • We do not use the following data for averages, fits, limits, etc. • • •

15 T-Matrix amplitude

**$N(1535) \rightarrow n\gamma$ , helicity-1/2 amplitude  $A_{1/2}$**

MODULUS ( $\text{GeV}^{-1/2}$ )	PHASE ( $^\circ$ )	DOCUMENT ID	TECN	COMMENT
-0.088 ± 0.004	5 ± 4	ANISOVICH	17D DPWA	Multichannel
-0.095 ± 0.006	8 ± 5	ANISOVICH	15A DPWA	Multichannel

• • • We do not use the following data for averages, fits, limits, etc. • • •

**N(1535) BREIT-WIGNER PHOTON DECAY AMPLITUDES**

**$N(1535) \rightarrow p\gamma$ , helicity-1/2 amplitude  $A_{1/2}$**

VALUE ( $\text{GeV}^{-1/2}$ )	DOCUMENT ID	TECN	COMMENT
0.090 to 0.120 ( $\approx 0.105$ ) OUR ESTIMATE	16 HUNT	19 DPWA	Multichannel
0.107 ± 0.003	SOKHOYAN	15A DPWA	Multichannel
0.101 ± 0.007	16 SHKLYAR	13 DPWA	Multichannel
0.091 ± 0.004	16 WORKMAN	12A DPWA	$\gamma N \rightarrow N\pi$
0.128 ± 0.004	16 DUGGER	07 DPWA	$\gamma N \rightarrow \pi N$
0.091 ± 0.002	ANISOVICH	12A DPWA	Multichannel
0.105 ± 0.010	16 SHRESTHA	12A DPWA	Multichannel
0.059 ± 0.003	DRECHSEL	07 DPWA	$\gamma N \rightarrow \pi N$
0.066	PENNER	02D DPWA	Multichannel
0.090			

• • • We do not use the following data for averages, fits, limits, etc. • • •

16 Statistical error only.

**$N(1535) \rightarrow n\gamma$ , helicity-1/2 amplitude  $A_{1/2}$**

VALUE ( $\text{GeV}^{-1/2}$ )	DOCUMENT ID	TECN	COMMENT
-0.095 to -0.055 ( $\approx -0.075$ ) OUR ESTIMATE	17 HUNT	19 DPWA	Multichannel
-0.055 ± 0.006	ANISOVICH	13B DPWA	Multichannel
-0.093 ± 0.011	17 CHEN	12A DPWA	$\gamma N \rightarrow \pi N$
-0.058 ± 0.006	SHRESTHA	12A DPWA	Multichannel
-0.049 ± 0.003	DRECHSEL	07 DPWA	$\gamma N \rightarrow \pi N$
-0.051	PENNER	02D DPWA	Multichannel
-0.024			

• • • We do not use the following data for averages, fits, limits, etc. • • •

17 Statistical error only.

**$N(1535) \rightarrow N\gamma$ , ratio  $A_{1/2}^n/A_{1/2}^p$**

VALUE ( $\text{GeV}^{-1/2}$ )	DOCUMENT ID	TECN	COMMENT
-0.84 ± 0.15	MUKHOPAD... 95B	IPWA	

**N(1535) REFERENCES**

For early references, see Physics Letters **111B 1** (1982).

HUNT	19	PR C99 055205	B.C. Hunt, D.M. Manley
ANISOVICH	17D	PR C95 035211	A.V. Anisovich et al.
KASHEVAROV	17	PRL 118 212001	V.L. Kashevarov et al. (A2/MAMI Collab.)
ANISOVICH	15A	EPJ A51 72	A.V. Anisovich et al.
ROENCHEN	15A	EPJ A51 70	D. Roenchen et al.
SOKHOYAN	15A	EPJ A51 95	V. Sokhoyan et al. (CBELSA/TAPS Collab.)

PDG	14	CP C38 070001	K. Olive et al. (PDG Collab.)
ROENCHEN	14	EPJ A50 101	D. Roenchen et al.
Also		EPJ A51 63 (errat.)	D. Roenchen et al.
SVARC	14	PR C89 045205	A. Svarc et al. (RBI Zagreb, UNI Tuzla)
ANISOVICH	13B	EPJ A49 67	A.V. Anisovich et al.
SHKLYAR	13	PR C87 015201	V. Shklyar, H. Lenske, U. Mosel (GIES)
ANISOVICH	12A	EPJ A48 15	A.V. Anisovich et al. (BONN, PNPI)
CHEN	12A	PR C86 015206	W. Chen et al. (DUKE, GWU, MSST, ITEP+)
SHRESTHA	12A	PR C86 055203	M. Shrestha, D.M. Manley (KSU)
WORKMAN	12A	PR C86 015202	R. Workman et al. (GWU)
BATINIC	10	PR C82 038203	M. Batinic et al. (ZAGR)
AZNAURYAN	09	PR C80 055203	I.G. Aznauryan et al. (JLab CLAS Collab.)
DRECHSEL	07	EPJ A34 69	D. Drechsel, S.S. Kamalov, L. Tiator (MAINZ, JINR)
DUGGER	07	PR C76 025211	M. Dugger et al. (JLab CLAS Collab.)
ARNDT	06	PR C74 045205	R.A. Arndt et al. (GWU)
ARNDT	04	PR C69 035213	R.A. Arndt et al. (GWU, TRIU)
STAROSTIN	03	PR C67 068201	A. Starostin et al. (BNL Crystal Ball Collab.)
PENNER	02C	PR C66 055211	G. Penner, U. Mosel (GIES)
PENNER	02D	PR C66 055212	G. Penner, U. Mosel (GIES)
BAI	01B	PL B510 75	J.Z. Bai et al. (BES Collab.)
THOMPSON	01	PRL 86 1702	R. Thompson et al. (JLab CLAS Collab.)
VRANA	00	PRPL 328 181	T.P. Vrana, S.A. Dytman, T.-S.H. Lee (PIT, ANL)
ARMSTRONG	99B	PR D60 052004	C.S. Armstrong et al.
MUKHOPAD... 95B		PL B364 1	N.C. Mukhopadhyay, J.F. Zhang, M. Benmerrouche
HOEHLER	93	$\pi N$ Newsletter 9 1	G. Hohlner (KARL)
CUTKOSKY	80	Toronto Conf. 19	R.E. Cutkosky et al. (CMU, LBL) IJP
Also		PR D20 2839	R.E. Cutkosky et al. (CMU, LBL) IJP
HOEHLER	79	PDAT 12-1	G. Hohlner et al. (KARLT) IJP
Also		Toronto Conf. 3	R. Koch (KARLT) IJP

**$N(1650) 1/2^-$**   $I(J^P) = \frac{1}{2}(\frac{1}{2}^-)$  Status: \* \* \* \*

Older and obsolete values are listed and referenced in the 2014 edition, Chinese Physics **C38 070001** (2014).

**N(1650) POLE POSITION**

**REAL PART**

VALUE (MeV)	DOCUMENT ID	TECN	COMMENT
<b>1640 to 1670 (<math>\approx 1655</math>) OUR ESTIMATE</b>			
1658 ± 10	ANISOVICH	17A DPWA	Multichannel
1660 ± 5	1 ANISOVICH	17A L+P	$\gamma p, \pi^- p \rightarrow K\Lambda$
1660 ± 3.5 ± 1	2 SVARC	14 L+P	$\pi N \rightarrow \pi N$
1640 ± 20	CUTKOSKY	80 IPWA	$\pi N \rightarrow \pi N$
• • • We do not use the following data for averages, fits, limits, etc. • • •			
1656	HUNT	19 DPWA	Multichannel
1672	ROENCHEN	15A DPWA	Multichannel
1652 ± 7	SOKHOYAN	15A DPWA	Multichannel
1650	SHKLYAR	13 DPWA	Multichannel
1647 ± 6	ANISOVICH	12A DPWA	Multichannel
1646 ± 8	BATINIC	10 DPWA	$\pi N \rightarrow N\pi, N\eta$
1648	ARNDT	06 DPWA	$\pi N \rightarrow \pi N, \eta N$
1663	VRANA	00 DPWA	Multichannel
1670	HOEHLER	93 ARGD	$\pi N \rightarrow \pi N$

1 Statistical error only.  
2 Fit to the amplitudes of HOEHLER 79.

**-2xIMAGINARY PART**

VALUE (MeV)	DOCUMENT ID	TECN	COMMENT
<b>100 to 170 (<math>\approx 135</math>) OUR ESTIMATE</b>			
102 ± 8	ANISOVICH	17A DPWA	Multichannel
59 ± 16	1 ANISOVICH	17A L+P	$\gamma p, \pi^- p \rightarrow K\Lambda$
167 ± 8 ± 2	2 SVARC	14 L+P	$\pi N \rightarrow \pi N$
150 ± 30	CUTKOSKY	80 IPWA	$\pi N \rightarrow \pi N$
• • • We do not use the following data for averages, fits, limits, etc. • • •			
130	HUNT	19 DPWA	Multichannel
137	ROENCHEN	15A DPWA	Multichannel
102 ± 8	SOKHOYAN	15A DPWA	Multichannel
89	SHKLYAR	13 DPWA	Multichannel
103 ± 8	ANISOVICH	12A DPWA	Multichannel
204 ± 17	BATINIC	10 DPWA	$\pi N \rightarrow N\pi, N\eta$
80	ARNDT	06 DPWA	$\pi N \rightarrow \pi N, \eta N$
240	VRANA	00 DPWA	Multichannel
163	HOEHLER	93 ARGD	$\pi N \rightarrow \pi N$

1 Statistical error only.  
2 Fit to the amplitudes of HOEHLER 79.

**N(1650) ELASTIC POLE RESIDUE**

**MODULUS  $|r|$**

VALUE (MeV)	DOCUMENT ID	TECN	COMMENT
<b>25 to 55 (<math>\approx 45</math>) OUR ESTIMATE</b>			
27 ± 6	SOKHOYAN	15A DPWA	Multichannel
47 ± 3 ± 1	1 SVARC	14 L+P	$\pi N \rightarrow \pi N$
60 ± 10	CUTKOSKY	80 IPWA	$\pi N \rightarrow \pi N$
• • • We do not use the following data for averages, fits, limits, etc. • • •			
37	ROENCHEN	15A DPWA	Multichannel
19	SHKLYAR	13 DPWA	Multichannel
24 ± 3	ANISOVICH	12A DPWA	Multichannel
100	BATINIC	10 DPWA	$\pi N \rightarrow N\pi, N\eta$
14	ARNDT	06 DPWA	$\pi N \rightarrow \pi N, \eta N$
39	HOEHLER	93 ARGD	$\pi N \rightarrow \pi N$

1 Fit to the amplitudes of HOEHLER 79.

## Baryon Particle Listings

 $N(1650)$ PHASE  $\theta$ 

VALUE ( $^\circ$ )	DOCUMENT ID	TECN	COMMENT
<b>-80 to -50 (<math>\approx -70</math>) OUR ESTIMATE</b>			
-60 $\pm$ 20	SOKHOYAN 15A	DPWA	Multichannel
-47 $\pm$ 3 $\pm$ 1	<sup>1</sup> SVARC 14	L+P	$\pi N \rightarrow \pi N$
-75 $\pm$ 25	CUTKOSKY 80	IPWA	$\pi N \rightarrow \pi N$
••• We do not use the following data for averages, fits, limits, etc. •••			
-59	ROENCHEN 15A	DPWA	Multichannel
-46	SHKLYAR 13	DPWA	Multichannel
-75 $\pm$ 12	ANISOVICH 12A	DPWA	Multichannel
-65	BATINIC 10	DPWA	$\pi N \rightarrow N\pi, N\eta$
-69	ARNDT 06	DPWA	$\pi N \rightarrow \pi N, \eta N$
-37	HOEHLER 93	ARGD	$\pi N \rightarrow \pi N$

<sup>1</sup> Fit to the amplitudes of HOEHLER 79. $N(1650)$  INELASTIC POLE RESIDUEThe "normalized residue" is the residue divided by  $\Gamma_{pole}/2$ .Normalized residue in  $N\pi \rightarrow N(1650) \rightarrow N\eta$ 

MODULUS	PHASE ( $^\circ$ )	DOCUMENT ID	TECN	COMMENT
0.29 $\pm$ 0.03	134 $\pm$ 10	ANISOVICH 12A	DPWA	Multichannel
••• We do not use the following data for averages, fits, limits, etc. •••				
0.21	48	ROENCHEN 15A	DPWA	Multichannel

Normalized residue in  $N\pi \rightarrow N(1650) \rightarrow \Lambda K$ 

MODULUS	PHASE ( $^\circ$ )	DOCUMENT ID	TECN	COMMENT
0.26 $\pm$ 0.10	110 $\pm$ 20	ANISOVICH 17A	DPWA	Multichannel
0.10 $\pm$ 0.10	95 $\pm$ 33	<sup>1</sup> ANISOVICH 17A	L+P	$\gamma p, \pi^- p \rightarrow \Lambda K$
••• We do not use the following data for averages, fits, limits, etc. •••				
0.20	-54	ROENCHEN 15A	DPWA	Multichannel
0.23 $\pm$ 0.09	85 $\pm$ 9	ANISOVICH 12A	DPWA	Multichannel

<sup>1</sup> Statistical error only.Normalized residue in  $N\pi \rightarrow N(1650) \rightarrow \Sigma K$ 

MODULUS	PHASE ( $^\circ$ )	DOCUMENT ID	TECN	COMMENT
••• We do not use the following data for averages, fits, limits, etc. •••				
0.026	-74	ROENCHEN 15A	DPWA	Multichannel

Normalized residue in  $N\pi \rightarrow N(1650) \rightarrow \Delta\pi, D\text{-wave}$ 

MODULUS	PHASE ( $^\circ$ )	DOCUMENT ID	TECN	COMMENT
0.19 $\pm$ 0.06	-30 $\pm$ 20	SOKHOYAN 15A	DPWA	Multichannel
••• We do not use the following data for averages, fits, limits, etc. •••				
0.23 $\pm$ 0.04	-30 $\pm$ 20	ANISOVICH 12A	DPWA	Multichannel

Normalized residue in  $N\pi \rightarrow N(1650) \rightarrow N\sigma$ 

MODULUS	PHASE ( $^\circ$ )	DOCUMENT ID	TECN	COMMENT
0.20 $\pm$ 0.15	undefined	SOKHOYAN 15A	DPWA	Multichannel

Normalized residue in  $N\pi \rightarrow N(1650) \rightarrow N(1440)\pi$ 

MODULUS	PHASE ( $^\circ$ )	DOCUMENT ID	TECN	COMMENT
0.30 $\pm$ 0.17	undefined	SOKHOYAN 15A	DPWA	Multichannel

 $N(1650)$  BREIT-WIGNER MASS

VALUE (MeV)	DOCUMENT ID	TECN	COMMENT
<b>1635 to 1665 (<math>\approx 1650</math>) OUR ESTIMATE</b>			
1657 $\pm$ 6	GOLOVATCH 19	DPWA	$\gamma p \rightarrow \pi^+ \pi^- p$
1666 $\pm$ 3	<sup>1</sup> HUNT 19	DPWA	Multichannel
1634 $\pm$ 5	KASHEVAROV 17	DPWA	$\gamma p \rightarrow \eta p, \eta' p$
1654 $\pm$ 6	SOKHOYAN 15A	DPWA	Multichannel
1665 $\pm$ 2	<sup>1</sup> SHKLYAR 13	DPWA	Multichannel
1634.7 $\pm$ 1.1	<sup>1</sup> ARNDT 06	DPWA	$\pi N \rightarrow \pi N, \eta N$
1650 $\pm$ 30	CUTKOSKY 80	IPWA	$\pi N \rightarrow \pi N$
1670 $\pm$ 8	HOEHLER 79	IPWA	$\pi N \rightarrow \pi N$
••• We do not use the following data for averages, fits, limits, etc. •••			
1651 $\pm$ 6	ANISOVICH 12A	DPWA	Multichannel
1664 $\pm$ 2	<sup>1</sup> SHRESTHA 12A	DPWA	Multichannel
1652 $\pm$ 9	BATINIC 10	DPWA	$\pi N \rightarrow N\pi, N\eta$
1665 $\pm$ 2	PENNER 02c	DPWA	Multichannel
1647 $\pm$ 20	BAI 01b	BES	$J/\psi \rightarrow p\bar{p}\eta$
1689 $\pm$ 12	VRANA 00	DPWA	Multichannel

<sup>1</sup> Statistical error only. $N(1650)$  BREIT-WIGNER WIDTH

VALUE (MeV)	DOCUMENT ID	TECN	COMMENT
<b>100 to 150 (<math>\approx 125</math>) OUR ESTIMATE</b>			
154 $\pm$ 28	GOLOVATCH 19	DPWA	$\gamma p \rightarrow \pi^+ \pi^- p$
133 $\pm$ 7	<sup>1</sup> HUNT 19	DPWA	Multichannel
128 $\pm$ 16	KASHEVAROV 17	DPWA	$\gamma p \rightarrow \eta p, \eta' p$
102 $\pm$ 8	SOKHOYAN 15A	DPWA	Multichannel
147 $\pm$ 14	<sup>1</sup> SHKLYAR 13	DPWA	Multichannel
115.4 $\pm$ 2.8	<sup>1</sup> ARNDT 06	DPWA	$\pi N \rightarrow \pi N, \eta N$
150 $\pm$ 40	CUTKOSKY 80	IPWA	$\pi N \rightarrow \pi N$
180 $\pm$ 20	HOEHLER 79	IPWA	$\pi N \rightarrow \pi N$

••• We do not use the following data for averages, fits, limits, etc. •••

104 $\pm$ 10	ANISOVICH 12A	DPWA	Multichannel
126 $\pm$ 3	<sup>1</sup> SHRESTHA 12A	DPWA	Multichannel
202 $\pm$ 16	BATINIC 10	DPWA	$\pi N \rightarrow N\pi, N\eta$
138 $\pm$ 7	PENNER 02c	DPWA	Multichannel
145 $\pm$ 80	BAI 01b	BES	$J/\psi \rightarrow p\bar{p}\eta$
202 $\pm$ 40	VRANA 00	DPWA	Multichannel

<sup>1</sup> Statistical error only. $N(1650)$  DECAY MODES

The following branching fractions are our estimates, not fits or averages.

Mode	Fraction ( $\Gamma_i/\Gamma$ )
$\Gamma_1$ $N\pi$	50-70 %
$\Gamma_2$ $N\eta$	15-35 %
$\Gamma_3$ $\Lambda K$	5-15 %
$\Gamma_4$ $N\pi\pi$	8-36 %
$\Gamma_5$ $\Delta(1232)\pi$	
$\Gamma_6$ $\Delta(1232)\pi, D\text{-wave}$	6-18 %
$\Gamma_7$ $N\rho$	
$\Gamma_8$ $N\rho, S=1/2$	
$\Gamma_9$ $N\rho, S=3/2, D\text{-wave}$	
$\Gamma_{10}$ $N\sigma$	2-18 %
$\Gamma_{11}$ $N(1440)\pi$	6-26 %
$\Gamma_{12}$ $p\gamma, \text{helicity}=1/2$	0.04-0.20 %
$\Gamma_{13}$ $n\gamma, \text{helicity}=1/2$	0.003-0.17 %

 $N(1650)$  BRANCHING RATIOS

$\Gamma(N\pi)/\Gamma_{\text{total}}$	VALUE (%)	DOCUMENT ID	TECN	COMMENT	$\Gamma_1/\Gamma$
<b>50 to 70 (<math>\approx 60</math>) OUR ESTIMATE</b>					
	64 $\pm$ 4	<sup>1</sup> HUNT 19	DPWA	Multichannel	
	51 $\pm$ 4	SOKHOYAN 15A	DPWA	Multichannel	
	74 $\pm$ 3	<sup>1</sup> SHKLYAR 13	DPWA	Multichannel	
	65 $\pm$ 10	CUTKOSKY 80	IPWA	$\pi N \rightarrow \pi N$	
	61 $\pm$ 4	HOEHLER 79	IPWA	$\pi N \rightarrow \pi N$	
••• We do not use the following data for averages, fits, limits, etc. •••					
	51 $\pm$ 4	ANISOVICH 12A	DPWA	Multichannel	
	57 $\pm$ 2	<sup>1</sup> SHRESTHA 12A	DPWA	Multichannel	
	79 $\pm$ 6	BATINIC 10	DPWA	$\pi N \rightarrow N\pi, N\eta$	
	100	ARNDT 06	DPWA	$\pi N \rightarrow \pi N, \eta N$	
	65 $\pm$ 4	PENNER 02c	DPWA	Multichannel	
	74 $\pm$ 2	VRANA 00	DPWA	Multichannel	

<sup>1</sup> Statistical error only.

$\Gamma(N\eta)/\Gamma_{\text{total}}$	VALUE (%)	DOCUMENT ID	TECN	COMMENT	$\Gamma_2/\Gamma$
<b>15 to 35 (<math>\approx 25</math>) OUR ESTIMATE</b>					
	0.8 $\pm$ 0.6	<sup>1</sup> HUNT 19	DPWA	Multichannel	
	28 $\pm$ 11	<sup>2</sup> KASHEVAROV 17	DPWA	$\gamma p \rightarrow \eta p, \eta' p$	
	< 3	SHKLYAR 13	DPWA	Multichannel	
	18 $\pm$ 4	ANISOVICH 12A	DPWA	Multichannel	
••• We do not use the following data for averages, fits, limits, etc. •••					
	21 $\pm$ 2	<sup>1</sup> SHRESTHA 12A	DPWA	Multichannel	
	13 $\pm$ 5	BATINIC 10	DPWA	$\pi N \rightarrow N\pi, N\eta$	
	1.0 $\pm$ 0.6	PENNER 02c	DPWA	Multichannel	
	6 $\pm$ 1	VRANA 00	DPWA	Multichannel	

<sup>1</sup> Statistical error only.<sup>2</sup> Assuming  $A_{1/2} = 0.045 \text{ GeV}^{-1/2}$ .

$\Gamma(\Lambda K)/\Gamma_{\text{total}}$	VALUE (%)	DOCUMENT ID	TECN	COMMENT	$\Gamma_3/\Gamma$
<b>5 to 15 (<math>\approx 10</math>) OUR ESTIMATE</b>					
	3.5 $\pm$ 0.2	<sup>1</sup> HUNT 19	DPWA	Multichannel	
	10 $\pm$ 5	ANISOVICH 12A	DPWA	Multichannel	
	4 $\pm$ 1	<sup>1</sup> SHKLYAR 05	DPWA	Multichannel	
••• We do not use the following data for averages, fits, limits, etc. •••					
	8 $\pm$ 1	<sup>1</sup> SHRESTHA 12A	DPWA	Multichannel	
	2.7 $\pm$ 0.4	PENNER 02c	DPWA	Multichannel	

<sup>1</sup> Statistical error only.

$\Gamma(N\pi\pi)/\Gamma_{\text{total}}$	VALUE (%)	DOCUMENT ID	TECN	COMMENT	$\Gamma_4/\Gamma$
<b>0.12 <math>\pm</math> 0.02</b>		GOLOVATCH 19	DPWA	$\gamma p \rightarrow \pi^+ \pi^- p$	

See key on page 999

# Baryon Particle Listings

## $N(1650)$ , $N(1675)$

**$\Gamma(\Delta(1232)\pi, D\text{-wave})/\Gamma_{\text{total}}$**

VALUE (%)	DOCUMENT ID	TECN	COMMENT
< 0.2	<sup>1</sup> HUNT 19	DPWA	Multichannel
12 ± 6	SOKHOYAN 15A	DPWA	Multichannel
••• We do not use the following data for averages, fits, limits, etc. •••			
19 ± 9	ANISOVICH 12A	DPWA	Multichannel
7 ± 2	<sup>1</sup> SHRESTHA 12A	DPWA	Multichannel
2 ± 1	VRANA 00	DPWA	Multichannel

<sup>1</sup> Statistical error only.

**$\Gamma(N\rho, S=1/2)/\Gamma_{\text{total}}$**

VALUE (%)	DOCUMENT ID	TECN	COMMENT
1.8 ± 1.7	<sup>1</sup> HUNT 19	DPWA	Multichannel

<sup>1</sup> Statistical error only.

**$\Gamma(N\rho, S=3/2, D\text{-wave})/\Gamma_{\text{total}}$**

VALUE (%)	DOCUMENT ID	TECN	COMMENT
15 ± 3	<sup>1</sup> HUNT 19	DPWA	Multichannel

<sup>1</sup> Statistical error only.

**$\Gamma(N\sigma)/\Gamma_{\text{total}}$**

VALUE (%)	DOCUMENT ID	TECN	COMMENT
12 ± 4	<sup>1</sup> HUNT 19	DPWA	Multichannel
10 ± 8	SOKHOYAN 15A	DPWA	Multichannel
••• We do not use the following data for averages, fits, limits, etc. •••			
< 1	<sup>1</sup> SHRESTHA 12A	DPWA	Multichannel
1 ± 1	VRANA 00	DPWA	Multichannel

<sup>1</sup> Statistical error only.

**$\Gamma(N(1440)\pi)/\Gamma_{\text{total}}$**

VALUE (%)	DOCUMENT ID	TECN	COMMENT
2 ± 1	<sup>1</sup> HUNT 19	DPWA	Multichannel
16 ± 10	SOKHOYAN 15A	DPWA	Multichannel
••• We do not use the following data for averages, fits, limits, etc. •••			
< 1	<sup>1</sup> SHRESTHA 12A	DPWA	Multichannel
3 ± 1	VRANA 00	DPWA	Multichannel

<sup>1</sup> Statistical error only.

### $N(1650)$ PHOTON DECAY AMPLITUDES AT THE POLE

**$N(1650) \rightarrow p\gamma$ , helicity-1/2 amplitude  $A_{1/2}$**

MODULUS ( $\text{GeV}^{-1/2}$ )	PHASE ( $^\circ$ )	DOCUMENT ID	TECN	COMMENT
0.032 ± 0.006	7 ± 7	ANISOVICH 17D	DPWA	Multichannel
0.023 ± 0.003	6 <sup>+28</sup> <sub>-15</sub>	ROENCHEN 14	DPWA	
••• We do not use the following data for averages, fits, limits, etc. •••				
0.032 ± 0.007	-2 ± 11	ANISOVICH 15A	DPWA	Multichannel
0.059	-14	ROENCHEN 15A	DPWA	Multichannel
0.032 ± 0.006	-2 ± 11	SOKHOYAN 15A	DPWA	Multichannel

**$N(1650) \rightarrow n\gamma$ , helicity-1/2 amplitude  $A_{1/2}$**

MODULUS ( $\text{GeV}^{-1/2}$ )	PHASE ( $^\circ$ )	DOCUMENT ID	TECN	COMMENT
0.016 ± 0.004	-28 ± 10	ANISOVICH 17D	DPWA	Multichannel
••• We do not use the following data for averages, fits, limits, etc. •••				
0.019 ± 0.006	0 ± 15	ANISOVICH 15A	DPWA	Multichannel

### $N(1650)$ BREIT-WIGNER PHOTON DECAY AMPLITUDES

**$N(1650) \rightarrow p\gamma$ , helicity-1/2 amplitude  $A_{1/2}$**

VALUE ( $\text{GeV}^{-1/2}$ )	DOCUMENT ID	TECN	COMMENT
<b>0.035 to 0.055 (<math>\approx 0.045</math>) OUR ESTIMATE</b>			
0.0605 ± 0.0077	GOLOVATCH 19	DPWA	$\gamma\rho \rightarrow \pi^+\pi^-p$
0.048 ± 0.003	<sup>1</sup> HUNT 19	DPWA	Multichannel
0.032 ± 0.006	SOKHOYAN 15A	DPWA	Multichannel
0.063 ± 0.006	<sup>1</sup> SHKLYAR 13	DPWA	Multichannel
0.055 ± 0.030	<sup>1</sup> WORKMAN 12A	DPWA	$\gamma N \rightarrow N\pi$
0.022 ± 0.007	<sup>1</sup> DUGGER 07	DPWA	$\gamma N \rightarrow \pi N$
••• We do not use the following data for averages, fits, limits, etc. •••			
0.033 ± 0.007	ANISOVICH 12A	DPWA	Multichannel
0.030 ± 0.003	<sup>1</sup> SHRESTHA 12A	DPWA	Multichannel
0.033	DRECHSEL 07	DPWA	$\gamma N \rightarrow \pi N$
0.049	PENNER 02D	DPWA	Multichannel

<sup>1</sup> Statistical error only.

**$N(1650) \rightarrow n\gamma$ , helicity-1/2 amplitude  $A_{1/2}$**

VALUE ( $\text{GeV}^{-1/2}$ )	DOCUMENT ID	TECN	COMMENT
<b>-0.040 to 0.030 (<math>\approx -0.010</math>) OUR ESTIMATE</b>			
0.001 ± 0.006	<sup>1</sup> HUNT 19	DPWA	Multichannel
0.025 ± 0.020	ANISOVICH 13B	DPWA	Multichannel
-0.040 ± 0.010	<sup>1</sup> CHEN 12A	DPWA	$\gamma N \rightarrow \pi N$

••• We do not use the following data for averages, fits, limits, etc. •••

0.011 ± 0.002	<sup>1</sup> SHRESTHA 12A	DPWA	Multichannel
0.009	DRECHSEL 07	DPWA	$\gamma N \rightarrow \pi N$
-0.011	PENNER 02D	DPWA	Multichannel

<sup>1</sup> Statistical error only.

### $N(1650)$ REFERENCES

For early references, see Physics Letters **111B** 1 (1982).

GOLOVATCH 19	PL B788 371	E. Golovatch et al.	(CLAS Collab.)
HUNT 19	PR C99 055205	B.C. Hunt, D.M. Manley	
ANISOVICH 17A	PRL 119 062004	A.V. Anisovich et al.	
ANISOVICH 17D	PR C95 035211	A.V. Anisovich et al.	
KASHEVAROV 17	PRL 118 212001	V.L. Kashevarov et al.	(A2/MAMI Collab.)
ANISOVICH 15A	EPJ A51 72	A.V. Anisovich et al.	
ROENCHEN 15A	EPJ A51 70	D. Roenchen et al.	
SOKHOYAN 15A	EPJ A51 95	V. Sokhoyan et al.	(CBELSA/TAPS Collab.)
PDG 14	CP C38 070001	K. Olive et al.	(PDG Collab.)
ROENCHEN 14	EPJ A50 101	D. Roenchen et al.	
Also	EPJ A51 63 (errata.)	D. Roenchen et al.	
SVARC 14	PR C89 045205	A. Svarc et al.	(RBI Zagreb, UNI Tuzla)
ANISOVICH 13B	EPJ A49 67	A.V. Anisovich et al.	
SHKLYAR 13	PR C87 015201	V. Shklyar, H. Lenske, U. Mosel	(GIES)
ANISOVICH 12A	EPJ A48 15	A.V. Anisovich et al.	(BONN, PNPI)
CHEN 12A	PR C86 015206	W. Chen et al.	(DUKE, GWU, MSST, ITEP+)
SHRESTHA 12A	PR C86 055203	M. Shrestha, D.M. Manley	(KSU)
WORKMAN 12A	PR C86 015202	R. Workman et al.	(GWU)
BATINIC 10	PR C82 038203	M. Batinic et al.	(ZAGR)
DRECHSEL 07	EPJ A34 69	D. Drechsel, S.S. Kamalov, L. Tiator	(MAINZ, JINR)
DUGGER 07	PR C76 025211	M. Dugger et al.	(JLab CLAS Collab.)
ARNDT 06	PR C74 045205	R.A. Arndt et al.	(GWU)
SHKLYAR 05	PR C72 015210	V. Shklyar, H. Lenske, U. Mosel	(GIES)
PENNER 02C	PR C66 055211	G. Penner, U. Mosel	(GIES)
PENNER 02D	PR C66 055212	G. Penner, U. Mosel	(GIES)
BAI 01B	PL B510 75	J.Z. Bai et al.	(BES Collab.)
VRANA 00	PRPL 328 181	T.P. Vrana, S.A. Dytman, T.-S.H. Lee	(PITT, ANL)
HOEHLER 93	$\pi N$ Newsletter 9 1	G. Hohlner	(KARL)
CUTKOSKY 80	Toronto Conf. 19	R.E. Cutkosky et al.	(CMU, LBL) IJP
Also	PR D20 2839	R.E. Cutkosky et al.	(CMU, LBL) IJP
HOEHLER 79	PDAT 12-1	G. Hohlner et al.	(KARLT) IJP
Also	Toronto Conf. 3	R. Koch	(KARLT) IJP

## $N(1675) 5/2^-$

$I(J^P) = \frac{1}{2}(\frac{5}{2}^-)$  Status: \*\*\*

Older and obsolete values are listed and referenced in the 2014 edition, Chinese Physics **C38** 070001 (2014).

### $N(1675)$ POLE POSITION

#### REAL PART

VALUE (MeV)	DOCUMENT ID	TECN	COMMENT
<b>1655 to 1665 (<math>\approx 1660</math>) OUR ESTIMATE</b>			
1655 ± 4	SOKHOYAN 15A	DPWA	Multichannel
1654 ± 2	<sup>1</sup> SVARC 14	L+P	$\pi N \rightarrow \pi N$
1660 ± 10	CUTKOSKY 80	IPWA	$\pi N \rightarrow \pi N$
••• We do not use the following data for averages, fits, limits, etc. •••			
1646	HUNT 19	DPWA	Multichannel
1646	ROENCHEN 15A	DPWA	Multichannel
1640	SHKLYAR 13	DPWA	Multichannel
1654 ± 4	ANISOVICH 12A	DPWA	Multichannel
1658 ± 9	BATINIC 10	DPWA	$\pi N \rightarrow N\pi, N\eta$
1657	ARNDT 06	DPWA	$\pi N \rightarrow \pi N, \eta N$
1674	VRANA 00	DPWA	Multichannel
1656	HOEHLER 93	ARGD	$\pi N \rightarrow \pi N$

<sup>1</sup> Fit to the amplitudes of HOEHLER 79.

#### -2xIMAGINARY PART

VALUE (MeV)	DOCUMENT ID	TECN	COMMENT
<b>125 to 150 (<math>\approx 135</math>) OUR ESTIMATE</b>			
147 ± 5	SOKHOYAN 15A	DPWA	Multichannel
125 ± 3 ± 1	<sup>1</sup> SVARC 14	L+P	$\pi N \rightarrow \pi N$
140 ± 10	CUTKOSKY 80	IPWA	$\pi N \rightarrow \pi N$
••• We do not use the following data for averages, fits, limits, etc. •••			
146	HUNT 19	DPWA	Multichannel
125	ROENCHEN 15A	DPWA	Multichannel
108	SHKLYAR 13	DPWA	Multichannel
151 ± 5	ANISOVICH 12A	DPWA	Multichannel
137 ± 7	BATINIC 10	DPWA	$\pi N \rightarrow N\pi, N\eta$
139	ARNDT 06	DPWA	$\pi N \rightarrow \pi N, \eta N$
120	VRANA 00	DPWA	Multichannel
126	HOEHLER 93	ARGD	$\pi N \rightarrow \pi N$

<sup>1</sup> Fit to the amplitudes of HOEHLER 79.

### $N(1675)$ ELASTIC POLE RESIDUE

#### MODULUS $|r|$

VALUE (MeV)	DOCUMENT ID	TECN	COMMENT
<b>23 to 33 (<math>\approx 28</math>) OUR ESTIMATE</b>			
28 ± 1	SOKHOYAN 15A	DPWA	Multichannel
23 ± 1	<sup>1</sup> SVARC 14	L+P	$\pi N \rightarrow \pi N$
31 ± 5	CUTKOSKY 80	IPWA	$\pi N \rightarrow \pi N$

## Baryon Particle Listings

 $N(1675)$ 

••• We do not use the following data for averages, fits, limits, etc. •••

24	ROENCHEN	15A	DPWA	Multichannel
20	SHKLYAR	13	DPWA	Multichannel
28±1	ANISOVICH	12A	DPWA	Multichannel
25	BATINIC	10	DPWA	$\pi N \rightarrow N\pi, N\eta$
27	ARNDT	06	DPWA	$\pi N \rightarrow \pi N, \eta N$
23	HOEHLER	93	ARGD	$\pi N \rightarrow \pi N$

<sup>1</sup> Fit to the amplitudes of HOEHLER 79.

PHASE  $\theta$ 

VALUE (°)	DOCUMENT ID	TECN	COMMENT
-----------	-------------	------	---------

-30 to -20 ( $\approx -25$ ) OUR ESTIMATE

-24 ± 4	SOKHOYAN	15A	DPWA	Multichannel
-25 ± 2	<sup>1</sup> SVARC	14	L+P	$\pi N \rightarrow \pi N$
-30 ± 10	CUTKOSKY	80	IPWA	$\pi N \rightarrow \pi N$

••• We do not use the following data for averages, fits, limits, etc. •••

-22	ROENCHEN	15A	DPWA	Multichannel
-49	SHKLYAR	13	DPWA	Multichannel
-26 ± 4	ANISOVICH	12A	DPWA	Multichannel
-16	BATINIC	10	DPWA	$\pi N \rightarrow N\pi, N\eta$
-21	ARNDT	06	DPWA	$\pi N \rightarrow \pi N, \eta N$
-22	HOEHLER	93	ARGD	$\pi N \rightarrow \pi N$

<sup>1</sup> Fit to the amplitudes of HOEHLER 79.

 $N(1675)$  INELASTIC POLE RESIDUE

The "normalized residue" is the residue divided by  $\Gamma_{pole}/2$ .

Normalized residue in  $N\pi \rightarrow N(1675) \rightarrow \Delta\pi, D\text{-wave}$ 

MODULUS	PHASE (°)	DOCUMENT ID	TECN	COMMENT
---------	-----------	-------------	------	---------

0.33±0.04	90 ± 15	SOKHOYAN	15A	DPWA	Multichannel
-----------	---------	----------	-----	------	--------------

••• We do not use the following data for averages, fits, limits, etc. •••

0.33±0.05	82 ± 10	ANISOVICH	12A	DPWA	Multichannel
-----------	---------	-----------	-----	------	--------------

Normalized residue in  $N\pi \rightarrow N(1675) \rightarrow N\eta$ 

MODULUS	PHASE (°)	DOCUMENT ID	TECN	COMMENT
---------	-----------	-------------	------	---------

••• We do not use the following data for averages, fits, limits, etc. •••

0.044	-43	ROENCHEN	15A	DPWA	Multichannel
-------	-----	----------	-----	------	--------------

Normalized residue in  $N\pi \rightarrow N(1675) \rightarrow \Lambda K$ 

MODULUS	PHASE (°)	DOCUMENT ID	TECN	COMMENT
---------	-----------	-------------	------	---------

••• We do not use the following data for averages, fits, limits, etc. •••

0.001	100	ROENCHEN	15A	DPWA	Multichannel
-------	-----	----------	-----	------	--------------

Normalized residue in  $N\pi \rightarrow N(1675) \rightarrow \Sigma K$ 

MODULUS	PHASE (°)	DOCUMENT ID	TECN	COMMENT
---------	-----------	-------------	------	---------

••• We do not use the following data for averages, fits, limits, etc. •••

0.031	-175	ROENCHEN	15A	DPWA	Multichannel
-------	------	----------	-----	------	--------------

Normalized residue in  $N\pi \rightarrow N(1675) \rightarrow N\sigma$ 

MODULUS	PHASE (°)	DOCUMENT ID	TECN	COMMENT
---------	-----------	-------------	------	---------

••• We do not use the following data for averages, fits, limits, etc. •••

0.15±0.04	132 ± 18	ANISOVICH	12A	DPWA	Multichannel
-----------	----------	-----------	-----	------	--------------

 $N(1675)$  BREIT-WIGNER MASS

VALUE (MeV)	DOCUMENT ID	TECN	COMMENT
-------------	-------------	------	---------

1665 to 1680 ( $\approx 1675$ ) OUR ESTIMATE

1669 ± 2	<sup>1</sup> HUNT	19	DPWA	Multichannel
1663 ± 4	SOKHOYAN	15A	DPWA	Multichannel
1666 ± 2	<sup>1</sup> SHKLYAR	13	DPWA	Multichannel
1674.1 ± 0.2	<sup>1</sup> ARNDT	06	DPWA	$\pi N \rightarrow \pi N, \eta N$
1675 ± 10	CUTKOSKY	80	IPWA	$\pi N \rightarrow \pi N$
1679 ± 8	HOEHLER	79	IPWA	$\pi N \rightarrow \pi N$

••• We do not use the following data for averages, fits, limits, etc. •••

1664 ± 5	ANISOVICH	12A	DPWA	Multichannel
1679 ± 1	<sup>1</sup> SHRESTHA	12A	DPWA	Multichannel
1679 ± 9	BATINIC	10	DPWA	$\pi N \rightarrow N\pi, N\eta$
1685 ± 4	VRANA	00	DPWA	Multichannel

<sup>1</sup> Statistical error only.

 $N(1675)$  BREIT-WIGNER WIDTH

VALUE (MeV)	DOCUMENT ID	TECN	COMMENT
-------------	-------------	------	---------

130 to 160 ( $\approx 145$ ) OUR ESTIMATE

161 ± 8	<sup>1</sup> HUNT	19	DPWA	Multichannel
146 ± 6	SOKHOYAN	15A	DPWA	Multichannel
148 ± 1	<sup>1</sup> SHKLYAR	13	DPWA	Multichannel
146.5 ± 1.0	<sup>1</sup> ARNDT	06	DPWA	$\pi N \rightarrow \pi N, \eta N$
160 ± 20	CUTKOSKY	80	IPWA	$\pi N \rightarrow \pi N$
120 ± 15	HOEHLER	79	IPWA	$\pi N \rightarrow \pi N$

••• We do not use the following data for averages, fits, limits, etc. •••

152 ± 7	ANISOVICH	12A	DPWA	Multichannel
145 ± 4	<sup>1</sup> SHRESTHA	12A	DPWA	Multichannel
152 ± 8	BATINIC	10	DPWA	$\pi N \rightarrow N\pi, N\eta$
131 ± 10	VRANA	00	DPWA	Multichannel

<sup>1</sup> Statistical error only.

 $N(1675)$  DECAY MODES

The following branching fractions are our estimates, not fits or averages.

Mode	Fraction ( $\Gamma_i/\Gamma$ )
$\Gamma_1$ $N\pi$	38-42 %
$\Gamma_2$ $N\eta$	< 1 %
$\Gamma_3$ $\Lambda K$	
$\Gamma_4$ $N\pi\pi$	25-45 %
$\Gamma_5$ $\Delta(1232)\pi$	
$\Gamma_6$ $\Delta(1232)\pi, D\text{-wave}$	23-37 %
$\Gamma_7$ $N\rho$	
$\Gamma_8$ $N\rho, S=1/2$	
$\Gamma_9$ $N\rho, S=3/2, D\text{-wave}$	
$\Gamma_{10}$ $N\sigma$	3-7 %
$\Gamma_{11}$ $p\gamma$	0-0.02 %
$\Gamma_{12}$ $p\gamma, \text{ helicity}=1/2$	0-0.01 %
$\Gamma_{13}$ $p\gamma, \text{ helicity}=3/2$	0-0.01 %
$\Gamma_{14}$ $n\gamma$	0-0.15 %
$\Gamma_{15}$ $n\gamma, \text{ helicity}=1/2$	0-0.05 %
$\Gamma_{16}$ $n\gamma, \text{ helicity}=3/2$	0-0.10 %

 $N(1675)$  BRANCHING RATIOS $\Gamma(N\pi)/\Gamma_{total}$ 

VALUE (%)	DOCUMENT ID	TECN	COMMENT
-----------	-------------	------	---------

38 to 42 ( $\approx 40$ ) OUR ESTIMATE

33 ± 1	<sup>1</sup> HUNT	19	DPWA	Multichannel
41 ± 2	SOKHOYAN	15A	DPWA	Multichannel
41 ± 1	<sup>1</sup> SHKLYAR	13	DPWA	Multichannel
39.3 ± 0.1	<sup>1</sup> ARNDT	06	DPWA	$\pi N \rightarrow \pi N, \eta N$
38 ± 5	CUTKOSKY	80	IPWA	$\pi N \rightarrow \pi N$
38 ± 3	HOEHLER	79	IPWA	$\pi N \rightarrow \pi N$

••• We do not use the following data for averages, fits, limits, etc. •••

40 ± 3	ANISOVICH	12A	DPWA	Multichannel
38.6 ± 0.6	<sup>1</sup> SHRESTHA	12A	DPWA	Multichannel
35 ± 4	BATINIC	10	DPWA	$\pi N \rightarrow N\pi, N\eta$
35 ± 1	VRANA	00	DPWA	Multichannel

<sup>1</sup> Statistical error only.

 $\Gamma(N\eta)/\Gamma_{total}$ 

VALUE (%)	DOCUMENT ID	TECN	COMMENT
-----------	-------------	------	---------

2.0 ± 0.3	<sup>1</sup> HUNT	19	DPWA	Multichannel
-----------	-------------------	----	------	--------------

••• We do not use the following data for averages, fits, limits, etc. •••

< 1	SHKLYAR	13	DPWA	Multichannel
< 1	<sup>1</sup> SHRESTHA	12A	DPWA	Multichannel
0.1 ± 0.1	BATINIC	10	DPWA	$\pi N \rightarrow N\pi, N\eta$
3 ± 3	THOMA	08	DPWA	Multichannel
0 ± 1	VRANA	00	DPWA	Multichannel

<sup>1</sup> Statistical error only.

 $\Gamma(\Lambda K)/\Gamma_{total}$ 

VALUE (%)	DOCUMENT ID	TECN	COMMENT
-----------	-------------	------	---------

< 0.04	<sup>1</sup> HUNT	19	DPWA	Multichannel
--------	-------------------	----	------	--------------

<sup>1</sup> Statistical error only.

 $\Gamma(\Delta(1232)\pi, D\text{-wave})/\Gamma_{total}$ 

VALUE (%)	DOCUMENT ID	TECN	COMMENT
-----------	-------------	------	---------

58.3 ± 0.2	<sup>1</sup> HUNT	19	DPWA	Multichannel
30 ± 7	SOKHOYAN	15A	DPWA	Multichannel

••• We do not use the following data for averages, fits, limits, etc. •••

33 ± 8	ANISOVICH	12A	DPWA	Multichannel
46 ± 1	<sup>1</sup> SHRESTHA	12A	DPWA	Multichannel
63 ± 2	VRANA	00	DPWA	Multichannel

<sup>1</sup> Statistical error only.

 $\Gamma(N\rho, S=1/2)/\Gamma_{total}$ 

VALUE (%)	DOCUMENT ID	TECN	COMMENT
-----------	-------------	------	---------

< 0.2	<sup>1</sup> HUNT	19	DPWA	Multichannel
-------	-------------------	----	------	--------------

<sup>1</sup> Statistical error only.

$\Gamma(N\rho, S=3/2, D\text{-wave})/\Gamma_{\text{total}}$   $\Gamma_9/\Gamma$

VALUE (%)	DOCUMENT ID	TECN	COMMENT
0.4 ± 0.3	<sup>1</sup> HUNT 19	DPWA	Multichannel

<sup>1</sup> Statistical error only.

$\Gamma(N\sigma)/\Gamma_{\text{total}}$   $\Gamma_{10}/\Gamma$

VALUE (%)	DOCUMENT ID	TECN	COMMENT
5 ± 2	SOKHOYAN 15A	DPWA	Multichannel
7 ± 3	ANISOVICH 12A	DPWA	Multichannel

• • • We do not use the following data for averages, fits, limits, etc. • • •

**N(1675) PHOTON DECAY AMPLITUDES AT THE POLE**

**N(1675) → ργ, helicity-1/2 amplitude A<sub>1/2</sub>**

MODULUS (GeV <sup>-1/2</sup> )	PHASE (°)	DOCUMENT ID	TECN	COMMENT
0.022 ± 0.003	-12 ± 7	SOKHOYAN 15A	DPWA	Multichannel
0.022 ± 0.004 -0.007	49 <sup>+5</sup> <sub>-2</sub>	ROENCHEN 14	DPWA	
0.032	36	ROENCHEN 15A	DPWA	Multichannel

• • • We do not use the following data for averages, fits, limits, etc. • • •

**N(1675) → ργ, helicity-3/2 amplitude A<sub>3/2</sub>**

MODULUS (GeV <sup>-1/2</sup> )	PHASE (°)	DOCUMENT ID	TECN	COMMENT
0.028 ± 0.006	-17 ± 6	SOKHOYAN 15A	DPWA	Multichannel
0.036 ± 0.004 -0.005	-30 ± 4	ROENCHEN 14	DPWA	
0.051	-9.3	ROENCHEN 15A	DPWA	Multichannel

• • • We do not use the following data for averages, fits, limits, etc. • • •

**N(1675) BREIT-WIGNER PHOTON DECAY AMPLITUDES**

**N(1675) → ργ, helicity-1/2 amplitude A<sub>1/2</sub>**

VALUE (GeV <sup>-1/2</sup> )	DOCUMENT ID	TECN	COMMENT
<b>0.010 to 0.025 (≈ 0.018) OUR ESTIMATE</b>			
0.026 ± 0.002	<sup>1</sup> HUNT 19	DPWA	Multichannel
0.022 ± 0.003	SOKHOYAN 15A	DPWA	Multichannel
0.009 ± 0.001	<sup>1</sup> SHKLYAR 13	DPWA	Multichannel
0.013 ± 0.001	<sup>1</sup> WORKMAN 12A	DPWA	γN → Nπ
0.018 ± 0.002	<sup>1</sup> DUGGER 07	DPWA	γN → πN
• • • We do not use the following data for averages, fits, limits, etc. • • •			
0.024 ± 0.003	ANISOVICH 12A	DPWA	Multichannel
0.011 ± 0.001	<sup>1</sup> SHRESTHA 12A	DPWA	Multichannel
0.015	DRECHSEL 07	DPWA	γN → πN

<sup>1</sup> Statistical error only.

**N(1675) → ργ, helicity-3/2 amplitude A<sub>3/2</sub>**

VALUE (GeV <sup>-1/2</sup> )	DOCUMENT ID	TECN	COMMENT
<b>0.015 to 0.030 (≈ 0.022) OUR ESTIMATE</b>			
0.005 ± 0.002	<sup>1</sup> HUNT 19	DPWA	Multichannel
0.027 ± 0.006	SOKHOYAN 15A	DPWA	Multichannel
0.021 ± 0.001	<sup>1</sup> SHKLYAR 13	DPWA	Multichannel
0.016 ± 0.001	<sup>1</sup> WORKMAN 12A	DPWA	γN → Nπ
0.021 ± 0.001	<sup>1</sup> DUGGER 07	DPWA	γN → πN
• • • We do not use the following data for averages, fits, limits, etc. • • •			
0.025 ± 0.007	ANISOVICH 12A	DPWA	Multichannel
0.020 ± 0.001	<sup>1</sup> SHRESTHA 12A	DPWA	Multichannel
0.022	DRECHSEL 07	DPWA	γN → πN

<sup>1</sup> Statistical error only.

**N(1675) → nγ, helicity-1/2 amplitude A<sub>1/2</sub>**

VALUE (GeV <sup>-1/2</sup> )	DOCUMENT ID	TECN	COMMENT
<b>-0.065 to -0.055 (≈ -0.060) OUR ESTIMATE</b>			
-0.069 ± 0.005	<sup>1</sup> HUNT 19	DPWA	Multichannel
-0.060 ± 0.007	ANISOVICH 13B	DPWA	Multichannel
-0.058 ± 0.002	<sup>1</sup> CHEN 12A	DPWA	γN → πN
• • • We do not use the following data for averages, fits, limits, etc. • • •			
-0.040 ± 0.004	<sup>1</sup> SHRESTHA 12A	DPWA	Multichannel
-0.062	DRECHSEL 07	DPWA	γN → πN

<sup>1</sup> Statistical error only.

**N(1675) → nγ, helicity-3/2 amplitude A<sub>3/2</sub>**

VALUE (GeV <sup>-1/2</sup> )	DOCUMENT ID	TECN	COMMENT
<b>-0.095 to -0.075 (≈ -0.085) OUR ESTIMATE</b>			
-0.031 ± 0.005	<sup>1</sup> HUNT 19	DPWA	Multichannel
-0.088 ± 0.010	ANISOVICH 13B	DPWA	Multichannel
-0.080 ± 0.005	<sup>1</sup> CHEN 12A	DPWA	γN → πN
• • • We do not use the following data for averages, fits, limits, etc. • • •			
-0.068 ± 0.004	<sup>1</sup> SHRESTHA 12A	DPWA	Multichannel
-0.084	DRECHSEL 07	DPWA	γN → πN

<sup>1</sup> Statistical error only.

**N(1675) REFERENCES**

For early references, see Physics Letters **111B** 1 (1982).

HUNT 19	PR C99 055205	B.C. Hunt, D.M. Manley
ROENCHEN 15A	EPJ A51 70	D. Roenchen <i>et al.</i>
SOKHOYAN 15A	EPJ A51 95	V. Sokhoyan <i>et al.</i> (CBELSA/TAPS Collab.)
PDC 14	CP C38 070001	K. Olive <i>et al.</i> (PDG Collab.)
ROENCHEN 14	EPJ A50 101	D. Roenchen <i>et al.</i>
Also	EPJ A51 63 (errat.)	D. Roenchen <i>et al.</i>
SVARC 14	PR C89 045205	A. Svarc <i>et al.</i> (RBI Zagreb, UNI Tuzla)
ANISOVICH 13B	EPJ A49 67	A.V. Anisovich <i>et al.</i>
SHKLYAR 13	PR C87 015201	V. Shklyar, H. Lenske, U. Mosel (GIES)
ANISOVICH 12A	EPJ A48 15	A.V. Anisovich <i>et al.</i> (BONN, PNPI)
CHEN 12A	PR C86 015206	W. Chen <i>et al.</i> (DUKE, GWU, MSST, ITEP+)
SHRESTHA 12A	PR C86 055203	M. Shrestha, D.M. Manley (KSU)
WORKMAN 12A	PR C86 015202	R. Workman <i>et al.</i> (GWU)
BATINIC 10	PR C82 038203	M. Batinic <i>et al.</i> (ZAGR)
THOMA 08	PL B659 87	U. Thoma <i>et al.</i> (CB-ELSA Collab.)
DRECHSEL 07	EPJ A34 69	D. Drechsel, S.S. Kamalov, L. Tiator (MAINZ, JINR)
DUGGER 07	PR C76 025211	M. Dugger <i>et al.</i> (JLab CLAS Collab.)
ARNDT 06	PR C74 045205	R.A. Arndt <i>et al.</i> (GWU)
VRANA 00	PRPL 328 181	T.P. Vrana, S.A. Dytman, T.-S.H. Lee (PITT, ANL)
HOEHLER 93	πN Newsletter 9 1	G. Hoehler (KARL)
CUTKOSKY 80	Toronto Conf. 19	R.E. Cutkosky <i>et al.</i> (CMU, LBL) IJP
Also	PR D20 2839	R.E. Cutkosky <i>et al.</i> (CMU, LBL) IJP
HOEHLER 79	PDAT 12-1	G. Hoehler <i>et al.</i> (KARLT) IJP
Also	Toronto Conf. 3	R. Koch (KARLT) IJP

**N(1680) 5/2<sup>+</sup>**

$I(J^P) = \frac{1}{2}(5_2^+)$  Status: \*\*\*

Older and obsolete values are listed and referenced in the 2014 edition, Chinese Physics **C38** 070001 (2014).

**N(1680) POLE POSITION**

**REAL PART**

VALUE (MeV)	DOCUMENT ID	TECN	COMMENT
<b>1665 to 1680 (≈ 1675) OUR ESTIMATE</b>			
1678 ± 5	SOKHOYAN 15A	DPWA	Multichannel
1674 ± 2 ± 1	<sup>1</sup> SVARC 14	L+P	πN → πN
1667 ± 5	CUTKOSKY 80	IPWA	πN → πN
• • • We do not use the following data for averages, fits, limits, etc. • • •			
1668	HUNT 19	DPWA	Multichannel
1669	ROENCHEN 15A	DPWA	Multichannel
1660	SHKLYAR 13	DPWA	Multichannel
1676 ± 6	ANISOVICH 12A	DPWA	Multichannel
1666 ± 8	BATINIC 10	DPWA	πN → Nπ, Nη
1674	ARNDT 06	DPWA	πN → πN, ηN
1667	VRANA 00	DPWA	Multichannel
1673	HOEHLER 93	ARGD	πN → πN

<sup>1</sup> Fit to the amplitudes of HOEHLER 79.

**-2×IMAGINARY PART**

VALUE (MeV)	DOCUMENT ID	TECN	COMMENT
<b>110 to 135 (≈ 120) OUR ESTIMATE</b>			
113 ± 4	SOKHOYAN 15A	DPWA	Multichannel
129 ± 3 ± 1	<sup>1</sup> SVARC 14	L+P	πN → πN
110 ± 10	CUTKOSKY 80	IPWA	πN → πN
• • • We do not use the following data for averages, fits, limits, etc. • • •			
118	HUNT 19	DPWA	Multichannel
100	ROENCHEN 15A	DPWA	Multichannel
98	SHKLYAR 13	DPWA	Multichannel
113 ± 4	ANISOVICH 12A	DPWA	Multichannel
135 ± 6	BATINIC 10	DPWA	πN → Nπ, Nη
115	ARNDT 06	DPWA	πN → πN, ηN
122	VRANA 00	DPWA	Multichannel
135	HOEHLER 93	ARGD	πN → πN

<sup>1</sup> Fit to the amplitudes of HOEHLER 79.

**N(1680) ELASTIC POLE RESIDUE**

**MODULUS |r|**

VALUE (MeV)	DOCUMENT ID	TECN	COMMENT
<b>35 to 45 (≈ 40) OUR ESTIMATE</b>			
45 ± 4	SOKHOYAN 15A	DPWA	Multichannel
44 ± 1 ± 1	<sup>1</sup> SVARC 14	L+P	πN → πN
34 ± 2	CUTKOSKY 80	IPWA	πN → πN
• • • We do not use the following data for averages, fits, limits, etc. • • •			
34	ROENCHEN 15A	DPWA	Multichannel
33	SHKLYAR 13	DPWA	Multichannel
43 ± 4	ANISOVICH 12A	DPWA	Multichannel
44	BATINIC 10	DPWA	πN → Nπ, Nη
42	ARNDT 06	DPWA	πN → πN, ηN
44	HOEHLER 93	ARGD	πN → πN

<sup>1</sup> Fit to the amplitudes of HOEHLER 79.



## Baryon Particle Listings

 $N(1680)$ PHASE  $\theta$ 

VALUE ( $^\circ$ )	DOCUMENT ID	TECN	COMMENT
<b>-20 to 10 (<math>\approx -5</math>) OUR ESTIMATE</b>			
5 $\pm$ 10	SOKHOYAN 15A	DPWA	Multichannel
-16 $\pm$ 1 $\pm$ 1	<sup>1</sup> SVARC 14	L+P	$\pi N \rightarrow \pi N$
-25 $\pm$ 5	CUTKOSKY 80	IPWA	$\pi N \rightarrow \pi N$
••• We do not use the following data for averages, fits, limits, etc. •••			
-19	ROENCHEN 15A	DPWA	Multichannel
-32	SHKLYAR 13	DPWA	Multichannel
-2 $\pm$ 10	ANISOVICH 12A	DPWA	Multichannel
-19	BATINIC 10	DPWA	$\pi N \rightarrow N\pi, N\eta$
-4	ARNDT 06	DPWA	$\pi N \rightarrow \pi N, \eta N$
-17	HOEHLER 93	ARGD	$\pi N \rightarrow \pi N$
<sup>1</sup> Fit to the amplitudes of HOEHLER 79.			

 $N(1680)$  INELASTIC POLE RESIDUE

The "normalized residue" is the residue divided by  $\Gamma_{pole}/2$ .

Normalized residue in  $N\pi \rightarrow N(1680) \rightarrow \Delta\pi, P$ -wave

MODULUS	PHASE ( $^\circ$ )	DOCUMENT ID	TECN	COMMENT
0.15 $\pm$ 0.03	-60 $\pm$ 30	SOKHOYAN 15A	DPWA	Multichannel
••• We do not use the following data for averages, fits, limits, etc. •••				
0.15 $\pm$ 0.03	-70 $\pm$ 45	ANISOVICH 12A	DPWA	Multichannel

Normalized residue in  $N\pi \rightarrow N(1680) \rightarrow \Delta\pi, F$ -wave

MODULUS	PHASE ( $^\circ$ )	DOCUMENT ID	TECN	COMMENT
0.23 $\pm$ 0.04	90 $\pm$ 12	SOKHOYAN 15A	DPWA	Multichannel
••• We do not use the following data for averages, fits, limits, etc. •••				
0.23 $\pm$ 0.04	85 $\pm$ 15	ANISOVICH 12A	DPWA	Multichannel

Normalized residue in  $N\pi \rightarrow N(1680) \rightarrow N\eta$ 

MODULUS	PHASE ( $^\circ$ )	DOCUMENT ID	TECN	COMMENT
••• We do not use the following data for averages, fits, limits, etc. •••				
0.027	136	ROENCHEN 15A	DPWA	Multichannel

Normalized residue in  $N\pi \rightarrow N(1680) \rightarrow \Lambda K$ 

MODULUS	PHASE ( $^\circ$ )	DOCUMENT ID	TECN	COMMENT
••• We do not use the following data for averages, fits, limits, etc. •••				
0.001	90	ROENCHEN 15A	DPWA	Multichannel

Normalized residue in  $N\pi \rightarrow N(1680) \rightarrow \Sigma K$ 

MODULUS	PHASE ( $^\circ$ )	DOCUMENT ID	TECN	COMMENT
••• We do not use the following data for averages, fits, limits, etc. •••				
0.004	148	ROENCHEN 15A	DPWA	Multichannel

Normalized residue in  $N\pi \rightarrow N(1680) \rightarrow N(\pi\pi)_{S=0}^{I=0}$ 

MODULUS	PHASE ( $^\circ$ )	DOCUMENT ID	TECN	COMMENT
0.29 $\pm$ 0.06	-45 $\pm$ 15	SOKHOYAN 15A	DPWA	Multichannel
••• We do not use the following data for averages, fits, limits, etc. •••				
0.26 $\pm$ 0.04	-56 $\pm$ 15	ANISOVICH 12A	DPWA	Multichannel

 $N(1680)$  BREIT-WIGNER MASS

VALUE (MeV)	DOCUMENT ID	TECN	COMMENT
<b>1680 to 1690 (<math>\approx 1685</math>) OUR ESTIMATE</b>			
1686 $\pm$ 5	GOLOVATCH 19	DPWA	$\gamma p \rightarrow \pi^+ \pi^- p$
1681.0 $\pm$ 0.1	<sup>1</sup> HUNT 19	DPWA	Multichannel
1690 $\pm$ 5	SOKHOYAN 15A	DPWA	Multichannel
1676 $\pm$ 2	<sup>1</sup> SHKLYAR 13	DPWA	Multichannel
1680.1 $\pm$ 0.2	<sup>1</sup> ARNDT 06	DPWA	$\pi N \rightarrow \pi N, \eta N$
1680 $\pm$ 10	CUTKOSKY 80	IPWA	$\pi N \rightarrow \pi N$
1684 $\pm$ 3	HOEHLER 79	IPWA	$\pi N \rightarrow \pi N$
••• We do not use the following data for averages, fits, limits, etc. •••			
1689 $\pm$ 6	ANISOVICH 12A	DPWA	Multichannel
1682.7 $\pm$ 0.5	<sup>1</sup> SHRESTHA 12A	DPWA	Multichannel
1680 $\pm$ 7	BATINIC 10	DPWA	$\pi N \rightarrow N\pi, N\eta$
1679 $\pm$ 3	VRANA 00	DPWA	Multichannel
<sup>1</sup> Statistical error only.			

 $N(1680)$  BREIT-WIGNER WIDTH

VALUE (MeV)	DOCUMENT ID	TECN	COMMENT
<b>115 to 130 (<math>\approx 120</math>) OUR ESTIMATE</b>			
118 $\pm$ 20	GOLOVATCH 19	DPWA	$\gamma p \rightarrow \pi^+ \pi^- p$
123 $\pm$ 3	<sup>1</sup> HUNT 19	DPWA	Multichannel
119 $\pm$ 4	SOKHOYAN 15A	DPWA	Multichannel
115 $\pm$ 1	<sup>1</sup> SHKLYAR 13	DPWA	Multichannel
128.0 $\pm$ 1.1	<sup>1</sup> ARNDT 06	DPWA	$\pi N \rightarrow \pi N, \eta N$
120 $\pm$ 10	CUTKOSKY 80	IPWA	$\pi N \rightarrow \pi N$
128 $\pm$ 8	HOEHLER 79	IPWA	$\pi N \rightarrow \pi N$

••• We do not use the following data for averages, fits, limits, etc. •••

118 $\pm$ 6	ANISOVICH 12A	DPWA	Multichannel
126 $\pm$ 1	<sup>1</sup> SHRESTHA 12A	DPWA	Multichannel
142 $\pm$ 7	BATINIC 10	DPWA	$\pi N \rightarrow N\pi, N\eta$
128 $\pm$ 9	VRANA 00	DPWA	Multichannel

<sup>1</sup> Statistical error only.

 $N(1680)$  DECAY MODES

The following branching fractions are our estimates, not fits or averages.

Mode	Fraction ( $\Gamma_i/\Gamma$ )
$\Gamma_1$ $N\pi$	60-70 %
$\Gamma_2$ $N\eta$	<1 %
$\Gamma_3$ $\Lambda K$	
$\Gamma_4$ $N\pi\pi$	20-40 %
$\Gamma_5$ $\Delta(1232)\pi$	11-23 %
$\Gamma_6$ $\Delta(1232)\pi, P$ -wave	4-10 %
$\Gamma_7$ $\Delta(1232)\pi, F$ -wave	1-13 %
$\Gamma_8$ $N\rho$	
$\Gamma_9$ $N\rho, S=3/2, P$ -wave	
$\Gamma_{10}$ $N\rho, S=3/2, F$ -wave	
$\Gamma_{11}$ $N\sigma$	9-19 %
$\Gamma_{12}$ $p\gamma$	0.21-0.32 %
$\Gamma_{13}$ $p\gamma, \text{helicity}=1/2$	0.001-0.011 %
$\Gamma_{14}$ $p\gamma, \text{helicity}=3/2$	0.20-0.32 %
$\Gamma_{15}$ $n\gamma$	0.021-0.046 %
$\Gamma_{16}$ $n\gamma, \text{helicity}=1/2$	0.004-0.029 %
$\Gamma_{17}$ $n\gamma, \text{helicity}=3/2$	0.01-0.024 %

 $N(1680)$  BRANCHING RATIOS

$\Gamma(N\pi)/\Gamma_{total}$	VALUE (%)	DOCUMENT ID	TECN	COMMENT	$\Gamma_1/\Gamma$
<b>60 to 70 (<math>\approx 65</math>) OUR ESTIMATE</b>					
68.0 $\pm$ 0.1	<sup>1</sup> HUNT 19	DPWA	Multichannel		
62 $\pm$ 4	SOKHOYAN 15A	DPWA	Multichannel		
68 $\pm$ 1	<sup>1</sup> SHKLYAR 13	DPWA	Multichannel		
70.1 $\pm$ 0.1	<sup>1</sup> ARNDT 06	DPWA	$\pi N \rightarrow \pi N, \eta N$		
62 $\pm$ 5	CUTKOSKY 80	IPWA	$\pi N \rightarrow \pi N$		
65 $\pm$ 2	HOEHLER 79	IPWA	$\pi N \rightarrow \pi N$		
••• We do not use the following data for averages, fits, limits, etc. •••					
64 $\pm$ 5	ANISOVICH 12A	DPWA	Multichannel		
68.0 $\pm$ 0.5	<sup>1</sup> SHRESTHA 12A	DPWA	Multichannel		
67 $\pm$ 3	BATINIC 10	DPWA	$\pi N \rightarrow N\pi, N\eta$		
69 $\pm$ 2	VRANA 00	DPWA	Multichannel		
<sup>1</sup> Statistical error only.					

$\Gamma(N\eta)/\Gamma_{total}$	VALUE (%)	DOCUMENT ID	TECN	COMMENT	$\Gamma_2/\Gamma$
0.09 $\pm$ 0.02	<sup>1</sup> HUNT 19	DPWA	Multichannel		
<1	SHKLYAR 13	DPWA	Multichannel		
0.15 $^{+0.35}_{-0.10}$	TIATOR 99	DPWA	$\gamma p \rightarrow p\eta$		
••• We do not use the following data for averages, fits, limits, etc. •••					
1.0 $\pm$ 0.3	<sup>1</sup> SHRESTHA 12A	DPWA	Multichannel		
0.4 $\pm$ 0.2	BATINIC 10	DPWA	$\pi N \rightarrow N\pi, N\eta$		
<1	THOMA 08	DPWA	Multichannel		
0 $\pm$ 1	VRANA 00	DPWA	Multichannel		
<sup>1</sup> Statistical error only.					

$\Gamma(\Lambda K)/\Gamma_{total}$	VALUE (%)	DOCUMENT ID	TECN	COMMENT	$\Gamma_3/\Gamma$
<b>0.24 <math>\pm</math> 0.04</b>					
	GOLOVATCH 19	DPWA	$\gamma p \rightarrow \pi^+ \pi^- p$		

$\Gamma(\Delta(1232)\pi, P\text{-wave})/\Gamma_{total}$	VALUE (%)	DOCUMENT ID	TECN	COMMENT	$\Gamma_6/\Gamma$
13 $\pm$ 1	<sup>1</sup> HUNT 19	DPWA	Multichannel		
7 $\pm$ 3	SOKHOYAN 15A	DPWA	Multichannel		
••• We do not use the following data for averages, fits, limits, etc. •••					
5 $\pm$ 3	ANISOVICH 12A	DPWA	Multichannel		
10.5 $\pm$ 0.9	<sup>1</sup> SHRESTHA 12A	DPWA	Multichannel		
14 $\pm$ 3	VRANA 00	DPWA	Multichannel		
<sup>1</sup> Statistical error only.					

$\Gamma(\Delta(1232)\pi, F\text{-wave})/\Gamma_{total}$	VALUE (%)	DOCUMENT ID	TECN	COMMENT	$\Gamma_7/\Gamma$
< 0.3	<sup>1</sup> HUNT 19	DPWA	Multichannel		
10 $\pm$ 3	SOKHOYAN 15A	DPWA	Multichannel		

See key on page 999

# Baryon Particle Listings

## $N(1680)$ , $N(1700)$

••• We do not use the following data for averages, fits, limits, etc. •••

10 ± 3	ANISOVICH	12A	DPWA	Multichannel
1.0 ± 0.1	<sup>1</sup> SHRESTHA	12A	DPWA	Multichannel
1 ± 1	VRANA	00	DPWA	Multichannel

<sup>1</sup> Statistical error only.

$\Gamma(N\rho, S=3/2, P\text{-wave})/\Gamma_{\text{total}}$   $\Gamma_9/\Gamma$

VALUE (%)	DOCUMENT ID	TECN	COMMENT
7 ± 1	<sup>1</sup> HUNT	19	DPWA Multichannel

<sup>1</sup> Statistical error only.

$\Gamma(N\rho, S=3/2, F\text{-wave})/\Gamma_{\text{total}}$   $\Gamma_{10}/\Gamma$

VALUE (%)	DOCUMENT ID	TECN	COMMENT
2.4 ± 0.4	<sup>1</sup> HUNT	19	DPWA Multichannel

<sup>1</sup> Statistical error only.

$\Gamma(N\sigma)/\Gamma_{\text{total}}$   $\Gamma_{11}/\Gamma$

VALUE (%)	DOCUMENT ID	TECN	COMMENT
8.7 ± 1.5	<sup>1</sup> HUNT	19	DPWA Multichannel
14 ± 5	SOKHOYAN	15A	DPWA Multichannel

••• We do not use the following data for averages, fits, limits, etc. •••

14 ± 7	ANISOVICH	12A	DPWA	Multichannel
9.4 ± 0.8	<sup>1</sup> SHRESTHA	12A	DPWA	Multichannel
9 ± 1	VRANA	00	DPWA	Multichannel

<sup>1</sup> Statistical error only.

### $N(1680)$ PHOTON DECAY AMPLITUDES AT THE POLE

$N(1680) \rightarrow p\gamma$ , helicity-1/2 amplitude  $A_{1/2}$

MODULUS (GeV <sup>-1/2</sup> )	PHASE (°)	DOCUMENT ID	TECN	COMMENT
-0.013 ± 0.003	-20 ± 17	SOKHOYAN	15A	DPWA Multichannel
-0.013 ± 0.002	-42 <sup>+9</sup> <sub>-18</sub>	ROENCHEN	14	DPWA

••• We do not use the following data for averages, fits, limits, etc. •••

-0.022	-28	ROENCHEN	15A	DPWA Multichannel
--------	-----	----------	-----	-------------------

$N(1680) \rightarrow p\gamma$ , helicity-3/2 amplitude  $A_{3/2}$

MODULUS (GeV <sup>-1/2</sup> )	PHASE (°)	DOCUMENT ID	TECN	COMMENT
0.135 ± 0.005	1 ± 3	SOKHOYAN	15A	DPWA Multichannel
0.126 ± 0.001	-7 <sup>+3</sup> <sub>-2</sub>	ROENCHEN	14	DPWA

••• We do not use the following data for averages, fits, limits, etc. •••

0.102	-11	ROENCHEN	15A	DPWA Multichannel
-------	-----	----------	-----	-------------------

### $N(1680)$ BREIT-WIGNER PHOTON DECAY AMPLITUDES

$N(1680) \rightarrow p\gamma$ , helicity-1/2 amplitude  $A_{1/2}$

VALUE (GeV <sup>-1/2</sup> )	DOCUMENT ID	TECN	COMMENT
<b>-0.018 to -0.005 (≈ -0.010) OUR ESTIMATE</b>			
-0.0278 ± 0.0036	GOLOVATCH	19	DPWA $\gamma p \rightarrow \pi^+ \pi^- p$
-0.026 ± 0.004	<sup>1</sup> HUNT	19	DPWA Multichannel
-0.015 ± 0.002	SOKHOYAN	15A	DPWA Multichannel
0.003 ± 0.001	<sup>1</sup> SHKLYAR	13	DPWA Multichannel
-0.007 ± 0.002	<sup>1</sup> WORKMAN	12A	DPWA $\gamma N \rightarrow N\pi$
-0.017 ± 0.001	<sup>1</sup> DUGGER	07	DPWA $\gamma N \rightarrow \pi N$

••• We do not use the following data for averages, fits, limits, etc. •••

-0.013 ± 0.003	ANISOVICH	12A	DPWA Multichannel
-0.017 ± 0.001	<sup>1</sup> SHRESTHA	12A	DPWA Multichannel
-0.025	DRECHSEL	07	DPWA $\gamma N \rightarrow \pi N$

<sup>1</sup> Statistical error only.

$N(1680) \rightarrow p\gamma$ , helicity-3/2 amplitude  $A_{3/2}$

VALUE (GeV <sup>-1/2</sup> )	DOCUMENT ID	TECN	COMMENT
<b>0.130 to 0.140 (≈ 0.135) OUR ESTIMATE</b>			
0.128 ± 0.011	GOLOVATCH	19	DPWA $\gamma p \rightarrow \pi^+ \pi^- p$
0.112 ± 0.005	<sup>1</sup> HUNT	19	DPWA Multichannel
0.136 ± 0.005	SOKHOYAN	15A	DPWA Multichannel
0.116 ± 0.001	<sup>1</sup> SHKLYAR	13	DPWA Multichannel
0.140 ± 0.002	<sup>1</sup> WORKMAN	12A	DPWA $\gamma N \rightarrow N\pi$
0.134 ± 0.002	<sup>1</sup> DUGGER	07	DPWA $\gamma N \rightarrow \pi N$

••• We do not use the following data for averages, fits, limits, etc. •••

0.135 ± 0.006	ANISOVICH	12A	DPWA Multichannel
0.136 ± 0.001	<sup>1</sup> SHRESTHA	12A	DPWA Multichannel
0.134	DRECHSEL	07	DPWA $\gamma N \rightarrow \pi N$

<sup>1</sup> Statistical error only.

$N(1680) \rightarrow n\gamma$ , helicity-1/2 amplitude  $A_{1/2}$

VALUE (GeV <sup>-1/2</sup> )	DOCUMENT ID	TECN	COMMENT
<b>0.020 to 0.040 (≈ 0.030) OUR ESTIMATE</b>			
0.005 ± 0.004	<sup>1</sup> HUNT	19	DPWA Multichannel
0.034 ± 0.006	ANISOVICH	13B	DPWA Multichannel
0.026 ± 0.004	<sup>1</sup> CHEN	12A	DPWA $\gamma N \rightarrow \pi N$

••• We do not use the following data for averages, fits, limits, etc. •••

0.029 ± 0.002	<sup>1</sup> SHRESTHA	12A	DPWA Multichannel
0.028	DRECHSEL	07	DPWA $\gamma N \rightarrow \pi N$

<sup>1</sup> Statistical error only.

$N(1680) \rightarrow n\gamma$ , helicity-3/2 amplitude  $A_{3/2}$

VALUE (GeV <sup>-1/2</sup> )	DOCUMENT ID	TECN	COMMENT
<b>-0.050 to -0.025 (≈ -0.035) OUR ESTIMATE</b>			
-0.061 ± 0.004	<sup>1</sup> HUNT	19	DPWA Multichannel
-0.044 ± 0.009	ANISOVICH	13B	DPWA Multichannel
-0.029 ± 0.002	<sup>1</sup> CHEN	12A	DPWA $\gamma N \rightarrow \pi N$

••• We do not use the following data for averages, fits, limits, etc. •••

-0.059 ± 0.002	<sup>1</sup> SHRESTHA	12A	DPWA Multichannel
-0.038	DRECHSEL	07	DPWA $\gamma N \rightarrow \pi N$

<sup>1</sup> Statistical error only.

### $N(1680)$ REFERENCES

For early references, see Physics Letters **111B** 1 (1982). For very early references, see Reviews of Modern Physics **37** 633 (1965).

GOLOVATCH	19	PL B788 371	E. Golovatch et al.	(CLAS Collab.)
HUNT	19	PR C99 055205	B.C. Hunt, D.M. Manley	
ROENCHEN	15A	EPJ A51 70	D. Roenchen et al.	
SOKHOYAN	15A	EPJ A51 95	V. Sokhoyan et al.	(CBELSA/TAPS Collab.)
PDG	14	CP C38 070001	K. Olive et al.	(PDG Collab.)
ROENCHEN	14	EPJ A50 101	D. Roenchen et al.	
Also		EPJ A51 63 (errata.)	D. Roenchen et al.	
SVARC	14	PR C89 045205	A. Svarc et al.	(RBI Zagreb, UNI Tuzla)
ANISOVICH	13B	EPJ A49 67	A.V. Anisovich et al.	
SHKLYAR	13	PR C87 015201	V. Shklyar, H. Lenske, U. Mosel	(GIES)
ANISOVICH	12A	EPJ A48 15	A.V. Anisovich et al.	(BONN, PNPI)
CHEN	12A	PR C86 015206	W. Chen et al.	(DUKE, GWU, MSST, ITEP+)
SHRESTHA	12A	PR C86 055203	M. Shrestha, D.M. Manley	(KSU)
WORKMAN	12A	PR C86 015202	R. Workman et al.	(GWU)
BATINIC	10	PR C82 038203	M. Batinic et al.	(ZAGR)
THOMA	08	PL B659 87	U. Thoma et al.	(CB-ELSA Collab.)
DRECHSEL	07	EPJ A34 69	D. Drechsel, S.S. Kamalov, L. Tiator	(MAINZ, JINR)
DUGGER	07	PR C76 025211	M. Dugger et al.	(JLab CLAS Collab.)
ARNDT	06	PR C74 045205	R.A. Arndt et al.	(GWU)
VRANA	00	PRPL 328 181	T.P. Vrana, S.A. Dytman, T.-S.H. Lee	(PITT, ANL)
TIATOR	99	PR C60 035210	L. Tiator et al.	
HOEHLER	93	$\pi N$ Newsletter 9 1	G. Hoehler	(KARL)
CUTKOSKY	80	Toronto Conf. 19	R.E. Cutkosky et al.	(CMU, LBL) IJP
Also		PR D20 2839	R.E. Cutkosky et al.	(CMU, LBL) IJP
HOEHLER	79	PDAT 12-1	G. Hoehler et al.	(KARLT) IJP
Also		Toronto Conf. 3	R. Koch	(KARLT) IJP

## $N(1700)$ 3/2<sup>-</sup>

$$I(J^P) = \frac{1}{2}(\frac{3}{2}^-) \text{ Status: } ** *$$

Older and obsolete values are listed and referenced in the 2014 edition, Chinese Physics **C38** 070001 (2014).

### $N(1700)$ POLE POSITION

**REAL PART**

VALUE (MeV)	DOCUMENT ID	TECN	COMMENT
<b>1650 to 1750 (≈ 1700) OUR ESTIMATE</b>			
1780 ± 35	SOKHOYAN	15A	DPWA Multichannel
1757 ± 4 ± 1	<sup>1</sup> SVARC	14	L+P $\pi N \rightarrow \pi N$
1660 ± 30	CUTKOSKY	80	IPWA $\pi N \rightarrow \pi N$

••• We do not use the following data for averages, fits, limits, etc. •••

1647	HUNT	19	DPWA Multichannel
1770 ± 40	ANISOVICH	12A	DPWA Multichannel
1806 ± 23	BATINIC	10	DPWA $\pi N \rightarrow N\pi, N\eta$
1704	VRANA	00	DPWA Multichannel
1700	HOEHLER	93	SPED $\pi N \rightarrow \pi N$

<sup>1</sup> Fit to the amplitudes of HOEHLER 79.

**-2xIMAGINARY PART**

VALUE (MeV)	DOCUMENT ID	TECN	COMMENT
<b>100 to 300 (≈ 200) OUR ESTIMATE</b>			
420 ± 140	SOKHOYAN	15A	DPWA Multichannel
136 ± 7 ± 4	<sup>1</sup> SVARC	14	L+P $\pi N \rightarrow \pi N$
90 ± 40	CUTKOSKY	80	IPWA $\pi N \rightarrow \pi N$

••• We do not use the following data for averages, fits, limits, etc. •••

79	HUNT	19	DPWA Multichannel
420 ± 180	ANISOVICH	12A	DPWA Multichannel
129 ± 33	BATINIC	10	DPWA $\pi N \rightarrow N\pi, N\eta$
156	VRANA	00	DPWA Multichannel
120	HOEHLER	93	SPED $\pi N \rightarrow \pi N$

<sup>1</sup> Fit to the amplitudes of HOEHLER 79.

## Baryon Particle Listings

 $N(1700)$  $N(1700)$  ELASTIC POLE RESIDUEMODULUS  $|r|$ 

VALUE (MeV)	DOCUMENT ID	TECN	COMMENT
<b>5 to 50 (<math>\approx 10</math>) OUR ESTIMATE</b>			
60 ± 30	SOKHOYAN	15A	DPWA Multichannel
7 ± 1 ± 1	<sup>1</sup> SVARC	14	L+P $\pi N \rightarrow \pi N$
6 ± 3	CUTKOSKY	80	IPWA $\pi N \rightarrow \pi N$
• • • We do not use the following data for averages, fits, limits, etc. • • •			
50 ± 40	ANISOVICH	12A	DPWA Multichannel
7	BATINIC	10	DPWA $\pi N \rightarrow N\pi, N\eta$
5	HOEHLER	93	SPED $\pi N \rightarrow \pi N$

<sup>1</sup> Fit to the amplitudes of HOEHLER 79.PHASE  $\theta$ 

VALUE (°)	DOCUMENT ID	TECN	COMMENT
<b>-120 to 0 (<math>\approx -90</math>) OUR ESTIMATE</b>			
-115 ± 30	SOKHOYAN	15A	DPWA Multichannel
-113 ± 4 ± 2	<sup>1</sup> SVARC	14	L+P $\pi N \rightarrow \pi N$
0 ± 50	CUTKOSKY	80	IPWA $\pi N \rightarrow \pi N$
• • • We do not use the following data for averages, fits, limits, etc. • • •			
-100 ± 40	ANISOVICH	12A	DPWA Multichannel
-34	BATINIC	10	DPWA $\pi N \rightarrow N\pi, N\eta$

<sup>1</sup> Fit to the amplitudes of HOEHLER 79. $N(1700)$  INELASTIC POLE RESIDUEThe "normalized residue" is the residue divided by  $\Gamma_{pole}/2$ .Normalized residue in  $N\pi \rightarrow N(1700) \rightarrow \Delta\pi, S\text{-wave}$ 

MODULUS	PHASE (°)	DOCUMENT ID	TECN	COMMENT
0.33 ± 0.10	-70 ± 25	SOKHOYAN	15A	DPWA Multichannel
• • • We do not use the following data for averages, fits, limits, etc. • • •				
0.34 ± 0.21	-60 ± 40	ANISOVICH	12A	DPWA Multichannel

Normalized residue in  $N\pi \rightarrow N(1700) \rightarrow \Delta\pi, D\text{-wave}$ 

MODULUS	PHASE (°)	DOCUMENT ID	TECN	COMMENT
0.10 ± 0.06	75 ± 30	SOKHOYAN	15A	DPWA Multichannel
• • • We do not use the following data for averages, fits, limits, etc. • • •				
0.08 ± 0.06	90 ± 35	ANISOVICH	12A	DPWA Multichannel

Normalized residue in  $N\pi \rightarrow N(1700) \rightarrow N\sigma$ 

MODULUS	PHASE (°)	DOCUMENT ID	TECN	COMMENT
0.13 ± 0.08	-100 ± 35	SOKHOYAN	15A	DPWA Multichannel

Normalized residue in  $N\pi \rightarrow N(1700) \rightarrow N(1440)\pi$ 

MODULUS	PHASE (°)	DOCUMENT ID	TECN	COMMENT
0.13 ± 0.05	40 ± 35	SOKHOYAN	15A	DPWA Multichannel

Normalized residue in  $N\pi \rightarrow N(1700) \rightarrow N(1520)\pi, P\text{-wave}$ 

MODULUS	PHASE (°)	DOCUMENT ID	TECN	COMMENT
0.07 ± 0.03	160 ± 45	SOKHOYAN	15A	DPWA Multichannel

 $N(1700)$  BREIT-WIGNER MASS

VALUE (MeV)	DOCUMENT ID	TECN	COMMENT
<b>1650 to 1800 (<math>\approx 1720</math>) OUR ESTIMATE</b>			
1653 ± 5	<sup>1</sup> HUNT	19	DPWA Multichannel
1800 ± 35	SOKHOYAN	15A	DPWA Multichannel
1675 ± 25	CUTKOSKY	80	IPWA $\pi N \rightarrow \pi N$
1731 ± 15	HOEHLER	79	IPWA $\pi N \rightarrow \pi N$
• • • We do not use the following data for averages, fits, limits, etc. • • •			
1790 ± 40	ANISOVICH	12A	DPWA Multichannel
1665 ± 3	<sup>1</sup> SHRESTHA	12A	DPWA Multichannel
1817 ± 22	BATINIC	10	DPWA $\pi N \rightarrow N\pi, N\eta$
1736 ± 33	VRANA	00	DPWA Multichannel

<sup>1</sup> Statistical error only. $N(1700)$  BREIT-WIGNER WIDTH

VALUE (MeV)	DOCUMENT ID	TECN	COMMENT
<b>100 to 300 (<math>\approx 200</math>) OUR ESTIMATE</b>			
81 ± 13	<sup>1</sup> HUNT	19	DPWA Multichannel
400 ± 100	SOKHOYAN	15A	DPWA Multichannel
90 ± 40	CUTKOSKY	80	IPWA $\pi N \rightarrow \pi N$
110 ± 30	HOEHLER	79	IPWA $\pi N \rightarrow \pi N$
• • • We do not use the following data for averages, fits, limits, etc. • • •			
390 ± 140	ANISOVICH	12A	DPWA Multichannel
56 ± 8	<sup>1</sup> SHRESTHA	12A	DPWA Multichannel
134 ± 37	BATINIC	10	DPWA $\pi N \rightarrow N\pi, N\eta$
175 ± 133	VRANA	00	DPWA Multichannel

<sup>1</sup> Statistical error only. $N(1700)$  DECAY MODES

The following branching fractions are our estimates, not fits or averages.

Mode	Fraction ( $\Gamma_i/\Gamma$ )
$\Gamma_1$ $N\pi$	7-17 %
$\Gamma_2$ $N\eta$	seen
$\Gamma_3$ $N\omega$	10-34 %
$\Gamma_4$ $\Lambda K$	
$\Gamma_5$ $N\pi\pi$	60-90 %
$\Gamma_6$ $\Delta(1232)\pi$	55-85 %
$\Gamma_7$ $\Delta(1232)\pi, S\text{-wave}$	50-80 %
$\Gamma_8$ $\Delta(1232)\pi, D\text{-wave}$	4-14 %
$\Gamma_9$ $N(1440)\pi$	3-11 %
$\Gamma_{10}$ $N(1520)\pi$	<4 %
$\Gamma_{11}$ $N\rho, S=3/2, S\text{-wave}$	32-44 %
$\Gamma_{12}$ $N\sigma$	2-14 %
$\Gamma_{13}$ $p\gamma$	0.01-0.05 %
$\Gamma_{14}$ $p\gamma, \text{helicity}=1/2$	0.002-0.026 %
$\Gamma_{15}$ $p\gamma, \text{helicity}=3/2$	0.01-0.13 %
$\Gamma_{16}$ $n\gamma$	0.0-0.09 %
$\Gamma_{17}$ $n\gamma, \text{helicity}=1/2$	0.01-0.05 %
$\Gamma_{18}$ $n\gamma, \text{helicity}=3/2$	

 $N(1700)$  BRANCHING RATIOS $\Gamma(N\pi)/\Gamma_{total}$   $\Gamma_1/\Gamma$ 

VALUE (%)	DOCUMENT ID	TECN	COMMENT
<b>7 to 17 (<math>\approx 12</math>) OUR ESTIMATE</b>			
3.7 ± 0.1	<sup>1</sup> HUNT	19	DPWA Multichannel
15 ± 6	SOKHOYAN	15A	DPWA Multichannel
11 ± 5	CUTKOSKY	80	IPWA $\pi N \rightarrow \pi N$
8 ± 3	HOEHLER	79	IPWA $\pi N \rightarrow \pi N$
• • • We do not use the following data for averages, fits, limits, etc. • • •			
12 ± 5	ANISOVICH	12A	DPWA Multichannel
2.8 ± 0.5	<sup>1</sup> SHRESTHA	12A	DPWA Multichannel
9 ± 6	BATINIC	10	DPWA $\pi N \rightarrow N\pi, N\eta$
4 ± 2	VRANA	00	DPWA Multichannel

<sup>1</sup> Statistical error only. $\Gamma(N\eta)/\Gamma_{total}$   $\Gamma_2/\Gamma$ 

VALUE (%)	DOCUMENT ID	TECN	COMMENT
1.1 ± 0.6	<sup>1</sup> HUNT	19	DPWA Multichannel
• • • We do not use the following data for averages, fits, limits, etc. • • •			
14 ± 5	BATINIC	10	DPWA $\pi N \rightarrow N\pi, N\eta$
10 ± 5	THOMA	08	DPWA Multichannel
0 ± 1	VRANA	00	DPWA Multichannel

<sup>1</sup> Statistical error only. $\Gamma(N\omega)/\Gamma_{total}$   $\Gamma_3/\Gamma$ 

VALUE (%)	DOCUMENT ID	TECN	COMMENT
22 ± 12	DENISENKO	16	DPWA Multichannel

 $\Gamma(\Lambda K)/\Gamma_{total}$   $\Gamma_4/\Gamma$ 

VALUE (%)	DOCUMENT ID	TECN	COMMENT
1.3 ± 0.7	<sup>1</sup> HUNT	19	DPWA Multichannel

<sup>1</sup> Statistical error only. $\Gamma(\Delta(1232)\pi, S\text{-wave})/\Gamma_{total}$   $\Gamma_7/\Gamma$ 

VALUE (%)	DOCUMENT ID	TECN	COMMENT
11 ± 8	<sup>1</sup> HUNT	19	DPWA Multichannel
65 ± 15	SOKHOYAN	15A	DPWA Multichannel
• • • We do not use the following data for averages, fits, limits, etc. • • •			
72 ± 23	ANISOVICH	12A	DPWA Multichannel
31 ± 9	<sup>1</sup> SHRESTHA	12A	DPWA Multichannel
11 ± 1	VRANA	00	DPWA Multichannel

<sup>1</sup> Statistical error only. $\Gamma(\Delta(1232)\pi, D\text{-wave})/\Gamma_{total}$   $\Gamma_8/\Gamma$ 

VALUE (%)	DOCUMENT ID	TECN	COMMENT
13 ± 5	<sup>1</sup> HUNT	19	DPWA Multichannel
9 ± 5	SOKHOYAN	15A	DPWA Multichannel
• • • We do not use the following data for averages, fits, limits, etc. • • •			
<10	ANISOVICH	12A	DPWA Multichannel
3 ± 2	<sup>1</sup> SHRESTHA	12A	DPWA Multichannel
79 ± 56	VRANA	00	DPWA Multichannel

<sup>1</sup> Statistical error only. $\Gamma(N(1440)\pi)/\Gamma_{total}$   $\Gamma_9/\Gamma$ 

VALUE (%)	DOCUMENT ID	TECN	COMMENT
7 ± 4	SOKHOYAN	15A	DPWA Multichannel

See key on page 999

# Baryon Particle Listings

## $N(1700)$ , $N(1710)$

$\Gamma(N(1520)\pi)/\Gamma_{total}$	DOCUMENT ID	TECN	COMMENT	$\Gamma_{10}/\Gamma$
VALUE (%)				
<4	SOKHOYAN	15A	DPWA Multichannel	

$\Gamma(N\rho, S=3/2, S\text{-wave})/\Gamma_{total}$	DOCUMENT ID	TECN	COMMENT	$\Gamma_{11}/\Gamma$
VALUE (%)				
$7.5 \pm 3.6$	<sup>1</sup> HUNT	19	DPWA Multichannel	
••• We do not use the following data for averages, fits, limits, etc. •••				
$38 \pm 6$	<sup>1</sup> SHRESTHA	12A	DPWA Multichannel	
$7 \pm 1$	VRANA	00	DPWA Multichannel	
<sup>1</sup> Statistical error only.				

$\Gamma(N\sigma)/\Gamma_{total}$	DOCUMENT ID	TECN	COMMENT	$\Gamma_{12}/\Gamma$
VALUE (%)				
$62 \pm 9$	<sup>1</sup> HUNT	19	DPWA Multichannel	
$8 \pm 6$	SOKHOYAN	15A	DPWA Multichannel	
••• We do not use the following data for averages, fits, limits, etc. •••				
$24 \pm 6$	<sup>1</sup> SHRESTHA	12A	DPWA Multichannel	
$18 \pm 12$	THOMA	08	DPWA Multichannel	
$0 \pm 1$	VRANA	00	DPWA Multichannel	
<sup>1</sup> Statistical error only.				

### $N(1700)$ PHOTON DECAY AMPLITUDES AT THE POLE

$N(1700) \rightarrow \rho\gamma$ , helicity-1/2 amplitude  $A_{1/2}$

MODULUS ( $\text{GeV}^{-1/2}$ )	PHASE ( $^\circ$ )	DOCUMENT ID	TECN	COMMENT
$0.047 \pm 0.016$	$75 \pm 30$	SOKHOYAN	15A	DPWA Multichannel

$N(1700) \rightarrow \rho\gamma$ , helicity-3/2 amplitude  $A_{3/2}$

MODULUS ( $\text{GeV}^{-1/2}$ )	PHASE ( $^\circ$ )	DOCUMENT ID	TECN	COMMENT
$-0.041 \pm 0.014$	$0 \pm 20$	SOKHOYAN	15A	DPWA Multichannel

### $N(1700)$ BREIT-WIGNER PHOTON DECAY AMPLITUDES

$N(1700) \rightarrow \rho\gamma$ , helicity-1/2 amplitude  $A_{1/2}$

VALUE ( $\text{GeV}^{-1/2}$ )	DOCUMENT ID	TECN	COMMENT
$0.032 \pm 0.005$	<sup>1</sup> HUNT	19	DPWA Multichannel
$0.041 \pm 0.017$	ANISOVICH	12A	DPWA Multichannel
••• We do not use the following data for averages, fits, limits, etc. •••			
$0.021 \pm 0.005$	<sup>1</sup> SHRESTHA	12A	DPWA Multichannel
<sup>1</sup> Statistical error only.			

$N(1700) \rightarrow \rho\gamma$ , helicity-3/2 amplitude  $A_{3/2}$

VALUE ( $\text{GeV}^{-1/2}$ )	DOCUMENT ID	TECN	COMMENT
$0.034 \pm 0.006$	<sup>1</sup> HUNT	19	DPWA Multichannel
$-0.037 \pm 0.014$	SOKHOYAN	15A	DPWA Multichannel
••• We do not use the following data for averages, fits, limits, etc. •••			
$-0.034 \pm 0.013$	ANISOVICH	12A	DPWA Multichannel
$0.050 \pm 0.009$	<sup>1</sup> SHRESTHA	12A	DPWA Multichannel
<sup>1</sup> Statistical error only.			

$N(1700) \rightarrow n\gamma$ , helicity-1/2 amplitude  $A_{1/2}$

VALUE ( $\text{GeV}^{-1/2}$ )	DOCUMENT ID	TECN	COMMENT
$0.005 \pm 0.011$	<sup>1</sup> HUNT	19	DPWA Multichannel
$0.025 \pm 0.010$	ANISOVICH	13B	DPWA Multichannel
••• We do not use the following data for averages, fits, limits, etc. •••			
$-0.049 \pm 0.008$	<sup>1</sup> SHRESTHA	12A	DPWA Multichannel
<sup>1</sup> Statistical error only.			

$N(1700) \rightarrow n\gamma$ , helicity-3/2 amplitude  $A_{3/2}$

VALUE ( $\text{GeV}^{-1/2}$ )	DOCUMENT ID	TECN	COMMENT
$-0.094 \pm 0.017$	<sup>1</sup> HUNT	19	DPWA Multichannel
$-0.032 \pm 0.018$	ANISOVICH	13B	DPWA Multichannel
••• We do not use the following data for averages, fits, limits, etc. •••			
$-0.092 \pm 0.014$	<sup>1</sup> SHRESTHA	12A	DPWA Multichannel
<sup>1</sup> Statistical error only.			

### $N(1700)$ REFERENCES

For early references, see Physics Letters **111B** 1 (1982).

HUNT	19	PR C99 055205	B. C. Hunt, D.M. Manley
DENISENKO	16	PL B755 97	I. Denisenko et al.
SOKHOYAN	15A	EPJ A51 95	V. Sokhoyan et al.
PDG	14	CP C38 070001	K. Olive et al. (CBELSA/TAPS Collab.)
SVARC	14	PR C89 045205	A. Svarc et al. (PDG Collab.)
ANISOVICH	13B	EPJ A49 67	A.V. Anisovich et al. (RBI Zagreb, UNI Tuzla)
ANISOVICH	12A	EPJ A48 15	A.V. Anisovich et al. (BONN, PNPI)
SHRESTHA	12A	PR C86 055203	M. Shrestha, D.M. Manley (KSU)
BATINIC	10	PR C82 038203	M. Batinic et al. (ZAGR)
THOMA	08	PL B659 87	U. Thoma et al. (CB-ELSA Collab.)
VRANA	00	PRPL 328 181	T.P. Vrana, S.A. Dytman, T.-S.H. Lee (PITT, ANL)
HOEHLER	93	$\pi$ -N Newsletter 9 1	G. Hohlner (KARL)
CUTKOSKY	80	Toronto Conf. 19	R.E. Cutkosky et al. (CMU, LBL) JUP
Also		PR D20 2839	R.E. Cutkosky et al. (CMU, LBL) JUP
HOEHLER	79	PDAT 12-1	G. Hohlner et al. (KARLT) JUP
Also		Toronto Conf. 3	R. Koch (KARLT) JUP

## $N(1710) 1/2^+$

$$I(J^P) = \frac{1}{2}(\frac{1}{2}^+) \text{ Status: } ****$$

Older and obsolete values are listed and referenced in the 2014 edition, Chinese Physics **C38** 070001 (2014).

### $N(1710)$ POLE POSITION

REAL PART	DOCUMENT ID	TECN	COMMENT
VALUE (MeV)			
<b>1680 to 1720 (<math>\approx 1700</math>) OUR ESTIMATE</b>			
$1690 \pm 15$	ANISOVICH	17A	DPWA Multichannel
$1697 \pm 23$	<sup>1</sup> ANISOVICH	17A	L+P $\gamma p, \pi^- p \rightarrow K A$
$1770 \pm 5 \pm 2$	<sup>2</sup> SVARC	14	L+P $\pi N \rightarrow \pi N$
$1690 \pm 20$	CUTKOSKY	80	IPWA $\pi N \rightarrow \pi N$
••• We do not use the following data for averages, fits, limits, etc. •••			
1615	HUNT	19	DPWA Multichannel
1651	ROENCHEN	15A	DPWA Multichannel
$1690 \pm 15$	SOKHOYAN	15A	DPWA Multichannel
$1690 \pm 15$	GUTZ	14	DPWA Multichannel
1670	SHKLYAR	13	DPWA Multichannel
$1687 \pm 17$	ANISOVICH	12A	DPWA Multichannel
$1711 \pm 15$	<sup>3</sup> BATINIC	10	DPWA $\pi N \rightarrow N\pi, N\eta$
1679	VRANA	00	DPWA Multichannel
1690	HOEHLER	93	SPED $\pi N \rightarrow \pi N$
1698	CUTKOSKY	90	IPWA $\pi N \rightarrow \pi N$

- <sup>1</sup> Statistical error only.
- <sup>2</sup> Fit to the amplitudes of HOEHLER 79.
- <sup>3</sup> BATINIC 10 finds evidence for a second  $P_{11}$  state with all parameters except for the phase of the pole residue very similar to the parameters we give here.

### $-2\times$ IMAGINARY PART

VALUE (MeV)	DOCUMENT ID	TECN	COMMENT
<b>80 to 160 (<math>\approx 120</math>) OUR ESTIMATE</b>			
$155 \pm 25$	ANISOVICH	17A	DPWA Multichannel
$84 \pm 34$	<sup>1</sup> ANISOVICH	17A	L+P $\gamma p, \pi^- p \rightarrow K A$
$98 \pm 8 \pm 5$	<sup>2</sup> SVARC	14	L+P $\pi N \rightarrow \pi N$
$80 \pm 20$	CUTKOSKY	80	IPWA $\pi N \rightarrow \pi N$
••• We do not use the following data for averages, fits, limits, etc. •••			
169	HUNT	19	DPWA Multichannel
121	ROENCHEN	15A	DPWA Multichannel
$170 \pm 20$	SOKHOYAN	15A	DPWA Multichannel
$170 \pm 20$	GUTZ	14	DPWA Multichannel
159	SHKLYAR	13	DPWA Multichannel
$200 \pm 25$	ANISOVICH	12A	DPWA Multichannel
$174 \pm 16$	<sup>3</sup> BATINIC	10	DPWA $\pi N \rightarrow N\pi, N\eta$
132	VRANA	00	DPWA Multichannel
200	HOEHLER	93	SPED $\pi N \rightarrow \pi N$
88	CUTKOSKY	90	IPWA $\pi N \rightarrow \pi N$

- <sup>1</sup> Statistical error only.
- <sup>2</sup> Fit to the amplitudes of HOEHLER 79.
- <sup>3</sup> BATINIC 10 finds evidence for a second  $P_{11}$  state with all parameters except for the phase of the pole residue very similar to the parameters we give here.

### $N(1710)$ ELASTIC POLE RESIDUE

MODULUS $ r $	DOCUMENT ID	TECN	COMMENT
VALUE (MeV)			
<b>4 to 10 (<math>\approx 7</math>) OUR ESTIMATE</b>			
$6 \pm 3$	SOKHOYAN	15A	DPWA Multichannel
$5 \pm 1 \pm 1$	<sup>1</sup> SVARC	14	L+P $\pi N \rightarrow \pi N$
$8 \pm 2$	CUTKOSKY	80	IPWA $\pi N \rightarrow \pi N$
••• We do not use the following data for averages, fits, limits, etc. •••			
3.2	ROENCHEN	15A	DPWA Multichannel
$6 \pm 3$	GUTZ	14	DPWA Multichannel
11	SHKLYAR	13	DPWA Multichannel
$6 \pm 4$	ANISOVICH	12A	DPWA Multichannel
24	<sup>2</sup> BATINIC	10	DPWA $\pi N \rightarrow N\pi, N\eta$
15	HOEHLER	93	SPED $\pi N \rightarrow \pi N$
9	CUTKOSKY	90	IPWA $\pi N \rightarrow \pi N$

- <sup>1</sup> Fit to the amplitudes of HOEHLER 79.
- <sup>2</sup> BATINIC 10 finds evidence for a second  $P_{11}$  state with all parameters except for the phase of the pole residue very similar to the parameters we give here.

### PHASE $\theta$

VALUE ( $^\circ$ )	DOCUMENT ID	TECN	COMMENT
<b>120 to 260 (<math>\approx 190</math>) OUR ESTIMATE</b>			
$130 \pm 35$	SOKHOYAN	15A	DPWA Multichannel
$-104 \pm 7 \pm 3$	<sup>1</sup> SVARC	14	L+P $\pi N \rightarrow \pi N$
$175 \pm 35$	CUTKOSKY	80	IPWA $\pi N \rightarrow \pi N$
••• We do not use the following data for averages, fits, limits, etc. •••			
55	ROENCHEN	15A	DPWA Multichannel
$120 \pm 45$	GUTZ	14	DPWA Multichannel
9	SHKLYAR	13	DPWA Multichannel
$120 \pm 70$	ANISOVICH	12A	DPWA Multichannel
20	<sup>2</sup> BATINIC	10	DPWA $\pi N \rightarrow N\pi, N\eta$
-167	CUTKOSKY	90	IPWA $\pi N \rightarrow \pi N$

## Baryon Particle Listings

 $N(1710)$ <sup>1</sup> Fit to the amplitudes of HOEHLER 79.<sup>2</sup> BATINIC 10 finds evidence for a second  $P_{11}$  state with all parameters except for the phase of the pole residue very similar to the parameters we give here. $N(1710)$  INELASTIC POLE RESIDUEThe "normalized residue" is the residue divided by  $\Gamma_{pole}/2$ .Normalized residue in  $N\pi \rightarrow N(1710) \rightarrow N\eta$ 

MODULUS	PHASE (°)	DOCUMENT ID	TECN	COMMENT
$0.12 \pm 0.04$	$0 \pm 45$	ANISOVICH 12A	DPWA	Multichannel
• • • We do not use the following data for averages, fits, limits, etc. • • •				
0.16	-180	ROENCHEN 15A	DPWA	Multichannel

Normalized residue in  $N\pi \rightarrow N(1710) \rightarrow \Lambda K$ 

MODULUS	PHASE (°)	DOCUMENT ID	TECN	COMMENT
$0.16 \pm 0.05$	$-160 \pm 25$	ANISOVICH 17A	DPWA	Multichannel
$0.12^{+0.24}_{-0.12}$	$-119 \pm 83$	<sup>1</sup> ANISOVICH 17A	L+P	$\gamma\rho, \pi^-p \rightarrow K\Lambda$
• • • We do not use the following data for averages, fits, limits, etc. • • •				
0.12	-32	ROENCHEN 15A	DPWA	Multichannel
$0.17 \pm 0.06$	$-110 \pm 20$	ANISOVICH 12A	DPWA	Multichannel

<sup>1</sup> Statistical error only.Normalized residue in  $N\pi \rightarrow N(1710) \rightarrow \Sigma K$ 

MODULUS	PHASE (°)	DOCUMENT ID	TECN	COMMENT
0.004	-43	ROENCHEN 15A	DPWA	Multichannel

Normalized residue in  $N\pi \rightarrow N(1710) \rightarrow N(1535)\pi$ 

MODULUS	PHASE (°)	DOCUMENT ID	TECN	COMMENT
$0.10 \pm 0.04$	$140 \pm 40$	GUTZ 14	DPWA	Multichannel

 $N(1710)$  BREIT-WIGNER MASS

VALUE (MeV)	DOCUMENT ID	TECN	COMMENT
<b>1680 to 1740 (<math>\approx 1710</math>) OUR ESTIMATE</b>			
$1648 \pm 16$	<sup>1</sup> HUNT 19	DPWA	Multichannel
$1715 \pm 20$	SOKHOYAN 15A	DPWA	Multichannel
$1737 \pm 17$	<sup>1</sup> SHKLYAR 13	DPWA	Multichannel
$1700 \pm 50$	CUTKOSKY 80	IPWA	$\pi N \rightarrow \pi N$
$1723 \pm 9$	HOEHLER 79	IPWA	$\pi N \rightarrow \pi N$
• • • We do not use the following data for averages, fits, limits, etc. • • •			
$1715 \pm 20$	GUTZ 14	DPWA	Multichannel
$1710 \pm 20$	ANISOVICH 12A	DPWA	Multichannel
$1662 \pm 7$	<sup>1</sup> SHRESTHA 12A	DPWA	Multichannel
$1729 \pm 16$	<sup>2</sup> BATINIC 10	DPWA	$\pi N \rightarrow N\pi, N\eta$
$1752 \pm 3$	PENNER 02c	DPWA	Multichannel
$1699 \pm 65$	VRANA 00	DPWA	Multichannel

<sup>1</sup> Statistical error only.<sup>2</sup> BATINIC 10 finds evidence for a second  $P_{11}$  state with all parameters except for the phase of the pole residue very similar to the parameters we give here. $N(1710)$  BREIT-WIGNER WIDTH

VALUE (MeV)	DOCUMENT ID	TECN	COMMENT
<b>80 to 200 (<math>\approx 140</math>) OUR ESTIMATE</b>			
$195 \pm 46$	<sup>1</sup> HUNT 19	DPWA	Multichannel
$175 \pm 15$	SOKHOYAN 15A	DPWA	Multichannel
$368 \pm 120$	<sup>1</sup> SHKLYAR 13	DPWA	Multichannel
$93 \pm 30$	CUTKOSKY 90	IPWA	$\pi N \rightarrow \pi N$
$90 \pm 30$	CUTKOSKY 80	IPWA	$\pi N \rightarrow \pi N$
$120 \pm 15$	HOEHLER 79	IPWA	$\pi N \rightarrow \pi N$
• • • We do not use the following data for averages, fits, limits, etc. • • •			
$175 \pm 15$	GUTZ 14	DPWA	Multichannel
$200 \pm 18$	ANISOVICH 12A	DPWA	Multichannel
$116 \pm 17$	<sup>1</sup> SHRESTHA 12A	DPWA	Multichannel
$180 \pm 17$	<sup>2</sup> BATINIC 10	DPWA	$\pi N \rightarrow N\pi, N\eta$
$386 \pm 59$	PENNER 02c	DPWA	Multichannel
$143 \pm 100$	VRANA 00	DPWA	Multichannel

<sup>1</sup> Statistical error only.<sup>2</sup> BATINIC 10 finds evidence for a second  $P_{11}$  state with all parameters except for the phase of the pole residue very similar to the parameters we give here. $N(1710)$  DECAY MODES

The following branching fractions are our estimates, not fits or averages.

Mode	Fraction ( $\Gamma_i/\Gamma$ )
$\Gamma_1$ $N\pi$	5–20 %
$\Gamma_2$ $N\eta$	10–50 %
$\Gamma_3$ $N\omega$	1–5 %
$\Gamma_4$ $\Lambda K$	5–25 %

$\Gamma_5$ $\Sigma K$	seen
$\Gamma_6$ $N\pi\pi$	seen
$\Gamma_7$ $\Delta(1232)\pi$	
$\Gamma_8$ $\Delta(1232)\pi, P$ -wave	3–9 %
$\Gamma_9$ $N(1535)\pi$	9–21 %
$\Gamma_{10}$ $N\rho$	
$\Gamma_{11}$ $N\rho, S=1/2, P$ -wave	11–23 %
$\Gamma_{12}$ $N\sigma$	
$\Gamma_{13}$ $\rho\gamma, \text{helicity}=1/2$	0.002–0.08 %
$\Gamma_{14}$ $n\gamma, \text{helicity}=1/2$	0.0–0.02 %

 $N(1710)$  BRANCHING RATIOS

$\Gamma(N\pi)/\Gamma_{total}$	VALUE (%)	DOCUMENT ID	TECN	COMMENT	$\Gamma_1/\Gamma$
<b>5 to 20 (<math>\approx 10</math>) OUR ESTIMATE</b>					
$12 \pm 6$		<sup>1</sup> HUNT 19	DPWA	Multichannel	
$5 \pm 3$		SOKHOYAN 15A	DPWA	Multichannel	
$2 \pm 2$		<sup>1</sup> SHKLYAR 13	PWA	Multichannel	
$20 \pm 4$		CUTKOSKY 80	IPWA	$\pi N \rightarrow \pi N$	
$12 \pm 4$		HOEHLER 79	IPWA	$\pi N \rightarrow \pi N$	
• • • We do not use the following data for averages, fits, limits, etc. • • •					
$5 \pm 3$		GUTZ 14	DPWA	Multichannel	
$5 \pm 4$		ANISOVICH 12A	DPWA	Multichannel	
$15 \pm 4$		<sup>1</sup> SHRESTHA 12A	DPWA	Multichannel	
$22 \pm 24$		<sup>2</sup> BATINIC 10	DPWA	$\pi N \rightarrow N\pi, N\eta$	
$14 \pm 8$		PENNER 02c	DPWA	Multichannel	
$27 \pm 13$		VRANA 00	DPWA	Multichannel	

<sup>1</sup> Statistical error only.<sup>2</sup> BATINIC 10 finds evidence for a second  $P_{11}$  state with all parameters except for the phase of the pole residue very similar to the parameters we give here.

$\Gamma(N\eta)/\Gamma_{total}$	VALUE (%)	DOCUMENT ID	TECN	COMMENT	$\Gamma_2/\Gamma$
<b>10 to 50 (<math>\approx 30</math>) OUR ESTIMATE</b>					
$17 \pm 8$		<sup>1</sup> HUNT 19	DPWA	Multichannel	
$45 \pm 4$		<sup>1</sup> SHKLYAR 13	DPWA	Multichannel	
$17 \pm 10$		ANISOVICH 12A	DPWA	Multichannel	
• • • We do not use the following data for averages, fits, limits, etc. • • •					
$11 \pm 7$		<sup>1</sup> SHRESTHA 12A	DPWA	Multichannel	
$6 \pm 8$		<sup>2</sup> BATINIC 10	DPWA	$\pi N \rightarrow N\pi, N\eta$	
$36 \pm 11$		PENNER 02c	DPWA	Multichannel	
$6 \pm 1$		VRANA 00	DPWA	Multichannel	

<sup>1</sup> Statistical error only.<sup>2</sup> BATINIC 10 finds evidence for a second  $P_{11}$  state with all parameters except for the phase of the pole residue very similar to the parameters we give here.

$\Gamma(N\omega)/\Gamma_{total}$	VALUE (%)	DOCUMENT ID	TECN	COMMENT	$\Gamma_3/\Gamma$
<b>1 to 5 (<math>\approx 3</math>) OUR ESTIMATE</b>					
$2 \pm 2$		DENISENKO 16	DPWA	Multichannel	
$3 \pm 2$		<sup>1</sup> SHKLYAR 13	DPWA	Multichannel	
• • • We do not use the following data for averages, fits, limits, etc. • • •					
$13 \pm 2$		PENNER 02c	DPWA	Multichannel	

<sup>1</sup> Statistical error only.

$\Gamma(\Lambda K)/\Gamma_{total}$	VALUE (%)	DOCUMENT ID	TECN	COMMENT	$\Gamma_4/\Gamma$
<b>5 to 25 (<math>\approx 15</math>) OUR ESTIMATE</b>					
$1.8 \pm 1.5$		<sup>1</sup> HUNT 19	DPWA	Multichannel	
$23 \pm 7$		ANISOVICH 12A	DPWA	Multichannel	
$5 \pm 3$		SHKLYAR 05	DPWA	Multichannel	
• • • We do not use the following data for averages, fits, limits, etc. • • •					
$8 \pm 4$		<sup>1</sup> SHRESTHA 12A	DPWA	Multichannel	
$5 \pm 2$		PENNER 02c	DPWA	Multichannel	
$10 \pm 10$		VRANA 00	DPWA	Multichannel	

<sup>1</sup> Statistical error only.

$\Gamma(\Sigma K)/\Gamma_{total}$	VALUE (%)	DOCUMENT ID	TECN	COMMENT	$\Gamma_5/\Gamma$
• • • We do not use the following data for averages, fits, limits, etc. • • •					
$7 \pm 7$		PENNER 02c	DPWA	Multichannel	

$\Gamma(\Delta(1232)\pi, P$ -wave)/ $\Gamma_{total}$	VALUE (%)	DOCUMENT ID	TECN	COMMENT	$\Gamma_8/\Gamma$
$28 \pm 9$		<sup>1</sup> HUNT 19	DPWA	Multichannel	
• • • We do not use the following data for averages, fits, limits, etc. • • •					
$6 \pm 3$		<sup>1</sup> SHRESTHA 12A	DPWA	Multichannel	
$39 \pm 8$		VRANA 00	DPWA	Multichannel	

<sup>1</sup> Statistical error only.

See key on page 999

Baryon Particle Listings
N(1710), N(1720)

Table with 4 columns: VALUE (%), DOCUMENT ID, TECN, COMMENT. Row 1: 15 ± 6, GUTZ, 14, DPWA, Multichannel.

Table with 4 columns: VALUE (%), DOCUMENT ID, TECN, COMMENT. Row 1: 17 ± 9, HUNT, 19, DPWA, Multichannel.

Table with 4 columns: VALUE (%), DOCUMENT ID, TECN, COMMENT. Row 1: 17 ± 6, SHRESTHA, 12A, DPWA, Multichannel.

Table with 4 columns: VALUE (%), DOCUMENT ID, TECN, COMMENT. Row 1: <16, HUNT, 19, DPWA, Multichannel.

N(1710) PHOTON DECAY AMPLITUDES AT THE POLE

Table with 5 columns: MODULUS (GeV^-1/2), PHASE (°), DOCUMENT ID, TECN, COMMENT. Row 1: 0.028 ± 0.009, 103 ± 20, ROENCHEN, 14, DPWA.

N(1710) BREIT-WIGNER PHOTON DECAY AMPLITUDES

Table with 5 columns: VALUE (GeV^-1/2), DOCUMENT ID, TECN, COMMENT. Row 1: 0.014 ± 0.008, HUNT, 19, DPWA, Multichannel.

Table with 5 columns: VALUE (GeV^-1/2), DOCUMENT ID, TECN, COMMENT. Row 1: 0.0053 ± 0.0003, HUNT, 19, DPWA, Multichannel.

N(1710) REFERENCES

For early references, see Physics Letters 111B 1 (1982).

Bibliography table with columns: Author, Year, Reference ID, Author, Year, Reference ID. Includes HUNT 19, ANISOVICH 17A, DENISENKO 16, etc.

N(1720) 3/2+

J(P) = 1/2(3/2+) Status: \*\*\*\*

Older and obsolete values are listed and referenced in the 2014 edition, Chinese Physics C38 070001 (2014).

N(1720) POLE POSITION

Table with 4 columns: VALUE (MeV), DOCUMENT ID, TECN, COMMENT. Section: REAL PART. Row 1: 1660 ± 25, SOKHOYAN, 15A, DPWA, Multichannel.

Table with 4 columns: VALUE (MeV), DOCUMENT ID, TECN, COMMENT. Section: -2xIMAGINARY PART. Row 1: 150 to 400 (≈ 250) OUR ESTIMATE.

N(1720) ELASTIC POLE RESIDUE

Table with 4 columns: VALUE (MeV), DOCUMENT ID, TECN, COMMENT. Section: MODULUS |r|. Row 1: 10 to 25 (≈ 15) OUR ESTIMATE.

Table with 4 columns: VALUE (°), DOCUMENT ID, TECN, COMMENT. Section: PHASE θ. Row 1: -160 to -100 (≈ -130) OUR ESTIMATE.

N(1720) INELASTIC POLE RESIDUE

The "normalized residue" is the residue divided by Γ\_pole/2.

Table with 5 columns: MODULUS, PHASE (°), DOCUMENT ID, TECN, COMMENT. Section: Normalized residue in Nπ → N(1720) → Nη.

Table with 5 columns: MODULUS, PHASE (°), DOCUMENT ID, TECN, COMMENT. Section: Normalized residue in Nπ → N(1720) → ΛK.

## Baryon Particle Listings

 $N(1720)$ Normalized residue in  $N\pi \rightarrow N(1720) \rightarrow \Sigma K$ 

MODULUS	PHASE (°)	DOCUMENT ID	TECN	COMMENT
0.002	79	ROENCHEN 15A	DPWA	Multichannel

Normalized residue in  $N\pi \rightarrow N(1720) \rightarrow \Delta\pi, P\text{-wave}$ 

MODULUS	PHASE (°)	DOCUMENT ID	TECN	COMMENT
0.28±0.09	95±30	SOKHOYAN 15A	DPWA	Multichannel
0.29±0.08	80±40	ANISOVICH 12A	DPWA	Multichannel

Normalized residue in  $N\pi \rightarrow N(1720) \rightarrow \Delta\pi, F\text{-wave}$ 

MODULUS	PHASE (°)	DOCUMENT ID	TECN	COMMENT
0.07±0.05		SOKHOYAN 15A	DPWA	Multichannel
0.03±0.03		ANISOVICH 12A	DPWA	Multichannel

Normalized residue in  $N\pi \rightarrow N(1720) \rightarrow N\sigma$ 

MODULUS	PHASE (°)	DOCUMENT ID	TECN	COMMENT
0.08±0.04	-110±35	SOKHOYAN 15A	DPWA	Multichannel

Normalized residue in  $N\pi \rightarrow N(1720) \rightarrow N(1520)\pi, S\text{-wave}$ 

MODULUS	PHASE (°)	DOCUMENT ID	TECN	COMMENT
0.05±0.04	undefined	SOKHOYAN 15A	DPWA	Multichannel

 $N(1720)$  BREIT-WIGNER MASS

VALUE (MeV)	DOCUMENT ID	TECN	COMMENT
<b>1680 to 1750 (≈ 1720) OUR ESTIMATE</b>			
1745 ± 6	GOLOVATCH 19	DPWA	$\gamma p \rightarrow \pi^+ \pi^- p$
1711 ± 4	<sup>1</sup> HUNT 19	DPWA	Multichannel
1690 ± 30	SOKHOYAN 15A	DPWA	Multichannel
1700 ± 10	<sup>1</sup> SHKLYAR 13	DPWA	Multichannel
1763.8 ± 4.6	ARNDT 06	DPWA	$\pi N \rightarrow \pi N, \eta N$
1700 ± 50	CUTKOSKY 80	IPWA	$\pi N \rightarrow \pi N$
1710 ± 20	HOEHLER 79	IPWA	$\pi N \rightarrow \pi N$
••• We do not use the following data for averages, fits, limits, etc. •••			
1690 + 70 - 35	ANISOVICH 12A	DPWA	Multichannel
1720 ± 5	<sup>1</sup> SHRESTHA 12A	DPWA	Multichannel
1720 ± 18	BATINIC 10	DPWA	$\pi N \rightarrow N\pi, N\eta$
1705 ± 10	PENNER 02c	DPWA	Multichannel
1716 ± 112	VRANA 00	DPWA	Multichannel

<sup>1</sup> Statistical error only. $N(1720)$  BREIT-WIGNER WIDTH

VALUE (MeV)	DOCUMENT ID	TECN	COMMENT
<b>150 to 400 (≈ 250) OUR ESTIMATE</b>			
116 ± 27	GOLOVATCH 19	DPWA	$\gamma p \rightarrow \pi^+ \pi^- p$
229 ± 22	<sup>1</sup> HUNT 19	DPWA	Multichannel
420 ± 80	SOKHOYAN 15A	DPWA	Multichannel
152 ± 2	<sup>1</sup> SHKLYAR 13	DPWA	Multichannel
210 ± 22	ARNDT 06	DPWA	$\pi N \rightarrow \pi N, \eta N$
125 ± 70	CUTKOSKY 80	IPWA	$\pi N \rightarrow \pi N$
190 ± 30	HOEHLER 79	IPWA	$\pi N \rightarrow \pi N$
••• We do not use the following data for averages, fits, limits, etc. •••			
420±100	ANISOVICH 12A	DPWA	Multichannel
200 ± 20	<sup>1</sup> SHRESTHA 12A	DPWA	Multichannel
244 ± 28	BATINIC 10	DPWA	$\pi N \rightarrow N\pi, N\eta$
237 ± 73	PENNER 02c	DPWA	Multichannel
121 ± 39	VRANA 00	DPWA	Multichannel

<sup>1</sup> Statistical error only. $N(1720)$  DECAY MODES

The following branching fractions are our estimates, not fits or averages.

Mode	Fraction ( $\Gamma_j/\Gamma$ )
$\Gamma_1$ $N\pi$	8–14 %
$\Gamma_2$ $N\eta$	1–5 %
$\Gamma_3$ $N\omega$	12–40 %
$\Gamma_4$ $\Lambda K$	4–5 %
$\Gamma_5$ $N\pi\pi$	50–90 %
$\Gamma_6$ $\Delta(1232)\pi$	47–89 %
$\Gamma_7$ $\Delta(1232)\pi, P\text{-wave}$	47–77 %
$\Gamma_8$ $\Delta(1232)\pi, F\text{-wave}$	<12 %
$\Gamma_9$ $N\rho$	
$\Gamma_{10}$ $N\rho, S=1/2, P\text{-wave}$	1–2 %
$\Gamma_{11}$ $N\sigma$	2–14 %

$\Gamma_{12}$ $N(1440)\pi$	<2 %
$\Gamma_{13}$ $N(1520)\pi, S\text{-wave}$	1–5 %
$\Gamma_{14}$ $p\gamma$	0.05–0.25 %
$\Gamma_{15}$ $p\gamma, \text{ helicity}=1/2$	0.05–0.15 %
$\Gamma_{16}$ $p\gamma, \text{ helicity}=3/2$	0.002–0.16 %
$\Gamma_{17}$ $n\gamma$	0.0–0.016 %
$\Gamma_{18}$ $n\gamma, \text{ helicity}=1/2$	0.0–0.01 %
$\Gamma_{19}$ $n\gamma, \text{ helicity}=3/2$	0.0–0.015 %

 $N(1720)$  BRANCHING RATIOS

$\Gamma(N\pi)/\Gamma_{\text{total}}$	DOCUMENT ID	TECN	COMMENT	$\Gamma_1/\Gamma$
<b>8 to 14 (≈ 11) OUR ESTIMATE</b>				
18 ± 2	HUNT 19	DPWA	Multichannel	
11 ± 4	SOKHOYAN 15A	DPWA	Multichannel	
17 ± 2	<sup>1</sup> SHKLYAR 13	DPWA	Multichannel	
9.4±0.5	ARNDT 06	DPWA	$\pi N \rightarrow \pi N, \eta N$	
10 ± 4	CUTKOSKY 80	IPWA	$\pi N \rightarrow \pi N$	
14 ± 3	HOEHLER 79	IPWA	$\pi N \rightarrow \pi N$	
••• We do not use the following data for averages, fits, limits, etc. •••				
10 ± 5	ANISOVICH 12A	DPWA	Multichannel	
13.6±0.6	<sup>1</sup> SHRESTHA 12A	DPWA	Multichannel	
18 ± 3	BATINIC 10	DPWA	$\pi N \rightarrow N\pi, N\eta$	
17 ± 2	PENNER 02c	DPWA	Multichannel	
5 ± 5	VRANA 00	DPWA	Multichannel	

<sup>1</sup> Statistical error only.

$\Gamma(N\eta)/\Gamma_{\text{total}}$	DOCUMENT ID	TECN	COMMENT	$\Gamma_2/\Gamma$
<b>1 to 5 (≈ 3) OUR ESTIMATE</b>				
3.8±0.5	<sup>1</sup> HUNT 19	DPWA	Multichannel	
< 1	SHKLYAR 13	DPWA	Multichannel	
3 ± 2	ANISOVICH 12A	DPWA	Multichannel	
••• We do not use the following data for averages, fits, limits, etc. •••				
< 1	<sup>1</sup> SHRESTHA 12A	DPWA	Multichannel	
0 ± 1	BATINIC 10	DPWA	$\pi N \rightarrow N\pi, N\eta$	
10 ± 7	THOMA 08	DPWA	Multichannel	
0.2±0.2	PENNER 02c	DPWA	Multichannel	
4 ± 1	VRANA 00	DPWA	Multichannel	

<sup>1</sup> Statistical error only.

$\Gamma(N\omega)/\Gamma_{\text{total}}$	DOCUMENT ID	TECN	COMMENT	$\Gamma_3/\Gamma$
26±14	DENISENKO 16	DPWA	Multichannel	

$\Gamma(\Lambda K)/\Gamma_{\text{total}}$	DOCUMENT ID	TECN	COMMENT	$\Gamma_4/\Gamma$
16 ± 3	<sup>1</sup> HUNT 19	DPWA	Multichannel	
4.3±0.4	SHKLYAR 05	DPWA	Multichannel	
••• We do not use the following data for averages, fits, limits, etc. •••				
2.8±0.4	<sup>1</sup> SHRESTHA 12A	DPWA	Multichannel	
12 ± 9	THOMA 08	DPWA	Multichannel	
9 ± 3	PENNER 02c	DPWA	Multichannel	

<sup>1</sup> Statistical error only.

$\Gamma(N\pi\pi)/\Gamma_{\text{total}}$	DOCUMENT ID	TECN	COMMENT	$\Gamma_5/\Gamma$
0.84±0.16	GOLOVATCH 19	DPWA	$\gamma p \rightarrow \pi^+ \pi^- p$	

$\Gamma(\Delta(1232)\pi, P\text{-wave})/\Gamma_{\text{total}}$	DOCUMENT ID	TECN	COMMENT	$\Gamma_7/\Gamma$
62±15	SOKHOYAN 15A	DPWA	Multichannel	
••• We do not use the following data for averages, fits, limits, etc. •••				
75±15	ANISOVICH 12A	DPWA	Multichannel	

$\Gamma(\Delta(1232)\pi, F\text{-wave})/\Gamma_{\text{total}}$	DOCUMENT ID	TECN	COMMENT	$\Gamma_8/\Gamma$
6±6	SOKHOYAN 15A	DPWA	Multichannel	

$\Gamma(N\rho, S=1/2, P\text{-wave})/\Gamma_{\text{total}}$	DOCUMENT ID	TECN	COMMENT	$\Gamma_{10}/\Gamma$
1.4±0.5	<sup>1</sup> SHRESTHA 12A	DPWA	Multichannel	
••• We do not use the following data for averages, fits, limits, etc. •••				
91 ± 1	VRANA 00	DPWA	Multichannel	

<sup>1</sup> Statistical error only.

$\Gamma(N\sigma)/\Gamma_{\text{total}}$	DOCUMENT ID	TECN	COMMENT	$\Gamma_{11}/\Gamma$
8±6	SOKHOYAN 15A	DPWA	Multichannel	

See key on page 999

# Baryon Particle Listings

## $N(1720)$ , $N(1860)$

$\Gamma(N(1440)\pi)/\Gamma_{total}$	DOCUMENT ID	TECN	COMMENT	$\Gamma_{12}/\Gamma$
VALUE (%)				
<2	SOKHOYAN	15A	DPWA Multichannel	

$\Gamma(N(1520)\pi, S\text{-wave})/\Gamma_{total}$	DOCUMENT ID	TECN	COMMENT	$\Gamma_{13}/\Gamma$
VALUE (%)				
3±2	SOKHOYAN	15A	DPWA Multichannel	

### $N(1720)$ PHOTON DECAY AMPLITUDES AT THE POLE

#### $N(1720) \rightarrow p\gamma$ , helicity-1/2 amplitude $A_{1/2}$

MODULUS (GeV <sup>-1/2</sup> )	PHASE (°)	DOCUMENT ID	TECN	COMMENT
0.115 ± 0.045	0 ± 35	SOKHOYAN	15A	DPWA Multichannel
0.051 ± 0.005	57 ± 9	ROENCHEN	14	DPWA
0.051 ± 0.004	57 ± 4	ROENCHEN	14	DPWA

• • • We do not use the following data for averages, fits, limits, etc. • • •

0.039	5.3	ROENCHEN	15A	DPWA Multichannel
-------	-----	----------	-----	-------------------

#### $N(1720) \rightarrow p\gamma$ , helicity-3/2 amplitude $A_{3/2}$

MODULUS (GeV <sup>-1/2</sup> )	PHASE (°)	DOCUMENT ID	TECN	COMMENT
0.140 ± 0.040	65 ± 35	SOKHOYAN	15A	DPWA Multichannel
0.014 + 0.009	102 + 29	ROENCHEN	14	DPWA
0.014 - 0.003	102 - 59	ROENCHEN	14	DPWA

• • • We do not use the following data for averages, fits, limits, etc. • • •

0.032	66	ROENCHEN	15A	DPWA Multichannel
-------	----	----------	-----	-------------------

### $N(1720)$ BREIT-WIGNER PHOTON DECAY AMPLITUDES

#### $N(1720) \rightarrow p\gamma$ , helicity-1/2 amplitude $A_{1/2}$

VALUE (GeV <sup>-1/2</sup> )	DOCUMENT ID	TECN	COMMENT
<b>0.080 to 0.120 (≈ 0.100) OUR ESTIMATE</b>			
0.0809 ± 0.0115	GOLOVATCH	19	DPWA $\gamma p \rightarrow \pi^+ \pi^- p$
0.068 ± 0.004	<sup>1</sup> HUNT	19	DPWA Multichannel
0.115 ± 0.045	SOKHOYAN	15A	DPWA Multichannel
-0.065 ± 0.002	<sup>1</sup> SHKLYAR	13	DPWA Multichannel
0.095 ± 0.002	WORKMAN	12A	DPWA $\gamma N \rightarrow N\pi$
0.110 ± 0.045	ANISOVICH	12A	DPWA Multichannel
0.057 ± 0.003	<sup>1</sup> SHRESTHA	12A	DPWA Multichannel
0.073	DRECHSEL	07	DPWA $\gamma N \rightarrow \pi N$
0.097 ± 0.003	DUGGER	07	DPWA $\gamma N \rightarrow \pi N$
-0.053	PENNER	02D	DPWA Multichannel

<sup>1</sup> Statistical error only.

#### $N(1720) \rightarrow p\gamma$ , helicity-3/2 amplitude $A_{3/2}$

VALUE (GeV <sup>-1/2</sup> )	DOCUMENT ID	TECN	COMMENT
-0.034 ± 0.0076	GOLOVATCH	19	DPWA $\gamma p \rightarrow \pi^+ \pi^- p$
0.028 ± 0.003	<sup>1</sup> HUNT	19	DPWA Multichannel
0.135 ± 0.040	SOKHOYAN	15A	DPWA Multichannel
0.035 ± 0.002	<sup>1</sup> SHKLYAR	13	DPWA Multichannel
-0.048 ± 0.002	WORKMAN	12A	DPWA $\gamma N \rightarrow N\pi$
0.150 ± 0.030	ANISOVICH	12A	DPWA Multichannel
-0.019 ± 0.002	<sup>1</sup> SHRESTHA	12A	DPWA Multichannel
-0.011	DRECHSEL	07	DPWA $\gamma N \rightarrow \pi N$
-0.039 ± 0.003	DUGGER	07	DPWA $\gamma N \rightarrow \pi N$
0.027	PENNER	02D	DPWA Multichannel

<sup>1</sup> Statistical error only.

#### $N(1720) \rightarrow n\gamma$ , helicity-1/2 amplitude $A_{1/2}$

VALUE (GeV <sup>-1/2</sup> )	DOCUMENT ID	TECN	COMMENT
-0.064 ± 0.006	<sup>1</sup> HUNT	19	DPWA Multichannel
-0.080 ± 0.050	ANISOVICH	13B	DPWA Multichannel
0.002 ± 0.001	<sup>1</sup> SHRESTHA	12A	DPWA Multichannel
-0.003	DRECHSEL	07	DPWA $\gamma N \rightarrow \pi N$
-0.004	PENNER	02D	DPWA Multichannel

<sup>1</sup> Statistical error only.

#### $N(1720) \rightarrow n\gamma$ , helicity-3/2 amplitude $A_{3/2}$

VALUE (GeV <sup>-1/2</sup> )	DOCUMENT ID	TECN	COMMENT
-0.004 ± 0.006	<sup>1</sup> HUNT	19	DPWA Multichannel
-0.140 ± 0.065	ANISOVICH	13B	DPWA Multichannel
0.001 ± 0.002	<sup>1</sup> SHRESTHA	12A	DPWA Multichannel
-0.031	DRECHSEL	07	DPWA $\gamma N \rightarrow \pi N$
0.003	PENNER	02D	DPWA Multichannel

<sup>1</sup> Statistical error only.

### $N(1720)$ REFERENCES

For early references, see Physics Letters **111B** 1 (1982).

GOLOVATCH	19	PL B788 371	E. Golovatch <i>et al.</i>	(CLAS Collab.)
HUNT	19	PR C39 055205	B.C. Hunt, D.M. Manley	
DENISEWKO	16	PL B755 97	I. Denisenko <i>et al.</i>	
ROENCHEN	15A	EPJ A51 70	D. Roenchen <i>et al.</i>	
SOKHOYAN	15A	EPJ A51 95	V. Sokhoyan <i>et al.</i>	(CBELSA/TAPS Collab.)
PDG	14	CP C38 070001	K. Olive <i>et al.</i>	(PDG Collab.)
ROENCHEN	14	EPJ A50 101	D. Roenchen <i>et al.</i>	
Also		EPJ A51 63 (errata.)	D. Roenchen <i>et al.</i>	
SVARC	14	PR C89 045205	A. Svarc <i>et al.</i>	(RBI Zagreb, UNI Tuzla)
ANISOVICH	13B	EPJ A49 67	A.V. Anisovich <i>et al.</i>	
SHKLYAR	13	PR C87 015201	V. Shklyar, H. Lenske, U. Mosel	(GIES)
ANISOVICH	12A	EPJ A48 15	A.V. Anisovich <i>et al.</i>	(BONN, PNPI)
SHRESTHA	12A	PR C86 055203	M. Shrestha, D.M. Manley	(KSU)
WORKMAN	12A	PR C86 015202	R. Workman <i>et al.</i>	(GWU)
BATINIC	10	PR C82 038203	M. Batinic <i>et al.</i>	(ZAGR)
THOMA	08	PL B659 87	U. Thoma <i>et al.</i>	(CB-ELSA Collab.)
DRECHSEL	07	EPJ A34 69	D. Drechsel, S.S. Kamalov, L. Tiator	(MAINZ, JINR)
DUGGER	07	PR C76 025211	M. Dugger <i>et al.</i>	(JLab CLAS Collab.)
ARNDT	06	PR C74 045205	R.A. Arndt <i>et al.</i>	(GWU)
SHKLYAR	05	PR C72 015210	V. Shklyar, H. Lenske, U. Mosel	(GIES)
PENNER	02C	PR C66 055211	G. Penner, U. Mosel	(GIES)
PENNER	02D	PR C66 055212	G. Penner, U. Mosel	(GIES)
VRANA	00	PRPL 328 181	T.P. Vrana, S.A. Dytman, T.-S.H. Lee	(PITT, ANL)
HOEHLER	93	$\pi N$ Newsletter 9 1	G. Hoehler	(KARL)
CUTKOSKY	80	Toronto Conf. 19	R.E. Cutkosky <i>et al.</i>	(CMU, LBL) IJP
Also		PR D20 2839	R.E. Cutkosky <i>et al.</i>	(CMU, LBL) IJP
HOEHLER	79	PDAT 12-1	G. Hoehler <i>et al.</i>	(KARLT) IJP
Also		Toronto Conf. 3	R. Koch	(KARLT) IJP

### $N(1860) 5/2^+$

$$I(J^P) = \frac{1}{2}(\frac{5}{2}^+) \text{ Status: } **$$

OMITTED FROM SUMMARY TABLE

Before the 2012 Review, all the evidence for a  $J^P = 5/2^+$  state with a mass above 1800 MeV was filed under a two-star  $N(2000)$ . There is now some evidence from ANISOVICH 12A for two  $5/2^+$  states in this region, so we have split the older data (according to mass) between two two-star  $5/2^+$  states, an  $N(1860)$  and an  $N(2000)$ .

### $N(1860)$ POLE POSITION

#### REAL PART

VALUE (MeV)	DOCUMENT ID	TECN	COMMENT
1834 ± 19 ± 6	<sup>1</sup> SVARC	14	L+P $\pi N \rightarrow \pi N$
1830 + 120	ANISOVICH	12A	DPWA Multichannel
- 60			
1871	HUNT	19	DPWA Multichannel
1807	ARNDT	06	DPWA $\pi N \rightarrow \pi N, \eta N$

<sup>1</sup> Fit to the amplitudes of HOEHLER 79.

#### -2xIMAGINARY PART

VALUE (MeV)	DOCUMENT ID	TECN	COMMENT
122 ± 34 ± 7	<sup>2</sup> SVARC	14	L+P $\pi N \rightarrow \pi N$
250 + 150	ANISOVICH	12A	DPWA Multichannel
- 50			
337	HUNT	19	DPWA Multichannel
109	ARNDT	06	DPWA $\pi N \rightarrow \pi N, \eta N$

<sup>2</sup> Fit to the amplitudes of HOEHLER 79.

### $N(1860)$ ELASTIC POLE RESIDUE

#### MODULUS $|r|$

VALUE (MeV)	DOCUMENT ID	TECN	COMMENT
4 ± 1 ± 1	<sup>3</sup> SVARC	14	L+P $\pi N \rightarrow \pi N$
50 ± 20	ANISOVICH	12A	DPWA Multichannel
60	ARNDT	06	DPWA $\pi N \rightarrow \pi N, \eta N$

<sup>3</sup> Fit to the amplitudes of HOEHLER 79.

#### PHASE $\theta$

VALUE (°)	DOCUMENT ID	TECN	COMMENT
-39 ± 18 ± 9	<sup>4</sup> SVARC	14	L+P $\pi N \rightarrow \pi N$
-80 ± 40	ANISOVICH	12A	DPWA Multichannel
-67	ARNDT	06	DPWA $\pi N \rightarrow \pi N, \eta N$

<sup>4</sup> Fit to the amplitudes of HOEHLER 79.

### $N(1860)$ BREIT-WIGNER MASS

VALUE (MeV)	DOCUMENT ID	TECN	COMMENT
1928 ± 21	<sup>5</sup> HUNT	19	DPWA Multichannel
1860 + 120	ANISOVICH	12A	DPWA Multichannel
- 60			
1882 ± 10	HOEHLER	79	IPWA $\pi N \rightarrow \pi N$
1900 ± 7	<sup>5</sup> SHRESTHA	12A	DPWA Multichannel
1817.7	ARNDT	06	DPWA $\pi N \rightarrow \pi N, \eta N$

• • • We do not use the following data for averages, fits, limits, etc. • • •



# Baryon Particle Listings

## $N(1860)$ , $N(1875)$

<sup>5</sup> Statistical error only.

### $N(1860)$ BREIT-WIGNER WIDTH

VALUE (MeV)	DOCUMENT ID	TECN	COMMENT
376 ± 58	<sup>6</sup> HUNT	19	DPWA Multichannel
270 ± 140 50	ANISOVICH	12A	DPWA Multichannel
95 ± 20	HOEHLER	79	IPWA $\pi N \rightarrow \pi N$
••• We do not use the following data for averages, fits, limits, etc. •••			
219 ± 23	<sup>6</sup> SHRESTHA	12A	DPWA Multichannel
117.6	ARNDT	06	DPWA $\pi N \rightarrow \pi N, \eta N$

<sup>6</sup> Statistical error only.

### $N(1860)$ DECAY MODES

Mode	Fraction ( $\Gamma_i/\Gamma$ )
$\Gamma_1$ $N\pi$	4–20 %
$\Gamma_2$ $N\eta$	2–6 %
$\Gamma_3$ $\Lambda K$	
$\Gamma_4$ $N\pi\pi$	
$\Gamma_5$ $\Delta\pi$	
$\Gamma_6$ $\Delta\pi, P$ -wave	
$\Gamma_7$ $\Delta\pi, F$ -wave	
$\Gamma_8$ $N\rho$	
$\Gamma_9$ $N\rho, S=3/2, P$ -wave	
$\Gamma_{10}$ $N\rho, S=3/2, F$ -wave	
$\Gamma_{11}$ $N\sigma$	35–47 %
$\Gamma_{12}$ $\rho\gamma$	
$\Gamma_{13}$ $\rho\gamma, \text{helicity}=1/2$	seen
$\Gamma_{14}$ $\rho\gamma, \text{helicity}=3/2$	seen
$\Gamma_{15}$ $n\gamma$	0.0017–0.062 %
$\Gamma_{16}$ $n\gamma, \text{helicity}=1/2$	0.0003–0.019 %
$\Gamma_{17}$ $n\gamma, \text{helicity}=3/2$	0.0014–0.043 %

### $N(1860)$ BRANCHING RATIOS

$\Gamma(N\pi)/\Gamma_{\text{total}}$	DOCUMENT ID	TECN	COMMENT	$\Gamma_1/\Gamma$
8.0 ± 0.1	<sup>7</sup> HUNT	19	DPWA Multichannel	
20 ± 6	ANISOVICH	12A	DPWA Multichannel	
4 ± 2	HOEHLER	79	IPWA $\pi N \rightarrow \pi N$	
••• We do not use the following data for averages, fits, limits, etc. •••				
17 ± 1	<sup>7</sup> SHRESTHA	12A	DPWA Multichannel	
12.7	ARNDT	06	DPWA $\pi N \rightarrow \pi N, \eta N$	

<sup>7</sup> Statistical error only.

$\Gamma(N\eta)/\Gamma_{\text{total}}$	DOCUMENT ID	TECN	COMMENT	$\Gamma_2/\Gamma$
0.11 ± 0.09	<sup>8</sup> HUNT	19	DPWA Multichannel	
••• We do not use the following data for averages, fits, limits, etc. •••				
4 ± 2	<sup>8</sup> SHRESTHA	12A	DPWA Multichannel	

<sup>8</sup> Statistical error only.

$\Gamma(\Lambda K)/\Gamma_{\text{total}}$	DOCUMENT ID	TECN	COMMENT	$\Gamma_3/\Gamma$
<0.01	<sup>9</sup> HUNT	19	DPWA Multichannel	

<sup>9</sup> Statistical error only.

$\Gamma(\Delta\pi, P\text{-wave})/\Gamma_{\text{total}}$	DOCUMENT ID	TECN	COMMENT	$\Gamma_6/\Gamma$
10 ± 6	<sup>10</sup> HUNT	19	DPWA Multichannel	

<sup>10</sup> Statistical error only.

$\Gamma(\Delta\pi, F\text{-wave})/\Gamma_{\text{total}}$	DOCUMENT ID	TECN	COMMENT	$\Gamma_7/\Gamma$
27 ± 11	<sup>11</sup> HUNT	19	DPWA Multichannel	

<sup>11</sup> Statistical error only.

$\Gamma(N\rho, S=3/2, P\text{-wave})/\Gamma_{\text{total}}$	DOCUMENT ID	TECN	COMMENT	$\Gamma_9/\Gamma$
<8.5	<sup>12</sup> HUNT	19	DPWA Multichannel	

<sup>12</sup> Statistical error only.

$\Gamma(N\rho, S=3/2, F\text{-wave})/\Gamma_{\text{total}}$	DOCUMENT ID	TECN	COMMENT	$\Gamma_{10}/\Gamma$
<0.1	<sup>13</sup> HUNT	19	DPWA Multichannel	

<sup>13</sup> Statistical error only.

$\Gamma(N\sigma)/\Gamma_{\text{total}}$	DOCUMENT ID	TECN	COMMENT	$\Gamma_{11}/\Gamma$
51 ± 10	<sup>14</sup> HUNT	19	DPWA Multichannel	
••• We do not use the following data for averages, fits, limits, etc. •••				
41 ± 6	<sup>14</sup> SHRESTHA	12A	DPWA Multichannel	

<sup>14</sup> Statistical error only.

### $N(1860)$ BREIT-WIGNER PHOTON DECAY AMPLITUDES

$N(1860) \rightarrow \rho\gamma, \text{helicity-1/2}$ amplitude $A_{1/2}$	DOCUMENT ID	TECN	COMMENT
−0.022 ± 0.020	<sup>15</sup> HUNT	19	DPWA Multichannel
••• We do not use the following data for averages, fits, limits, etc. •••			
−0.017 ± 0.003	<sup>15</sup> SHRESTHA	12A	DPWA Multichannel

<sup>15</sup> Statistical error only.

$N(1860) \rightarrow \rho\gamma, \text{helicity-3/2}$ amplitude $A_{3/2}$	DOCUMENT ID	TECN	COMMENT
−0.032 ± 0.034	<sup>16</sup> HUNT	19	DPWA Multichannel
••• We do not use the following data for averages, fits, limits, etc. •••			
0.029 ± 0.004	<sup>16</sup> SHRESTHA	12A	DPWA Multichannel

<sup>16</sup> Statistical error only.

$N(1860) \rightarrow n\gamma, \text{helicity-1/2}$ amplitude $A_{1/2}$	DOCUMENT ID	TECN	COMMENT
0.021 ± 0.029	<sup>17</sup> HUNT	19	DPWA Multichannel
0.021 ± 0.013	ANISOVICH	13B	DPWA Multichannel
••• We do not use the following data for averages, fits, limits, etc. •••			
0.010 ± 0.005	<sup>17</sup> SHRESTHA	12A	DPWA Multichannel

<sup>17</sup> Statistical error only.

$N(1860) \rightarrow n\gamma, \text{helicity-3/2}$ amplitude $A_{3/2}$	DOCUMENT ID	TECN	COMMENT
0.070 ± 0.035	<sup>18</sup> HUNT	19	DPWA Multichannel
0.034 ± 0.017	ANISOVICH	13B	DPWA Multichannel
••• We do not use the following data for averages, fits, limits, etc. •••			
−0.009 ± 0.005	<sup>18</sup> SHRESTHA	12A	DPWA Multichannel

<sup>18</sup> Statistical error only.

### $N(1860)$ REFERENCES

HUNT	19	PR C99 055205	B.C. Hunt, D.M. Manley	
SVARC	14	PR C89 045205	A. Svarc et al.	(RBI Zagreb, UNI Tuzla)
ANISOVICH	13B	EPJ A49 57	A.V. Anisovich et al.	
ANISOVICH	12A	EPJ A48 15	A.V. Anisovich et al.	(BONN, PNPI)
SHRESTHA	12A	PR C86 055203	M. Shrestha, D.M. Manley	(KSU)
ARNDT	06	PR C74 045205	R.A. Arndt et al.	(GWU)
HOEHLER	79	PDAT 12-1	G. Hohler et al.	(KARLT)

## $N(1875) 3/2^-$

$$I(J^P) = \frac{1}{2}(\frac{3}{2}^-) \text{ Status: } ***$$

Before the 2012 Review, all the evidence for a  $J^P = 3/2^-$  state with a mass above 1800 MeV was filed under a two-star  $N(2080)$ .

There is now evidence from ANISOVICH 12A for two  $3/2^-$  states in this region, so we have split the older data (according to mass) between a three-star  $N(1875)$  and a two-star  $N(2120)$ .

### $N(1875)$ POLE POSITION

REAL PART	DOCUMENT ID	TECN	COMMENT
<b>1850 to 1950 (<math>\approx 1900</math>) OUR ESTIMATE</b>			
1870 ± 20	SOKHOYAN	15A	DPWA Multichannel
1880 ± 100	CUTKOSKY	80	IPWA $\pi N \rightarrow \pi N$ (lower m)
••• We do not use the following data for averages, fits, limits, etc. •••			
1993	HUNT	19	DPWA Multichannel
1810	SHKLYAR	13	DPWA Multichannel
1860 ± 25	ANISOVICH	12A	DPWA Multichannel
1957 ± 49	BATINIC	10	DPWA $\pi N \rightarrow N\pi, N\eta$
1824	VRANA	00	DPWA Multichannel

−2×IMAGINARY PART	DOCUMENT ID	TECN	COMMENT
<b>100 to 220 (<math>\approx 160</math>) OUR ESTIMATE</b>			
200 ± 15	SOKHOYAN	15A	DPWA Multichannel
160 ± 80	CUTKOSKY	80	IPWA $\pi N \rightarrow \pi N$ (lower m)
••• We do not use the following data for averages, fits, limits, etc. •••			
319	HUNT	19	DPWA Multichannel
98	SHKLYAR	13	DPWA Multichannel
200 ± 20	ANISOVICH	12A	DPWA Multichannel
467 ± 106	BATINIC	10	DPWA $\pi N \rightarrow N\pi, N\eta$
614	VRANA	00	DPWA Multichannel

**N(1875) ELASTIC POLE RESIDUE**

**MODULUS |r|**

VALUE (MeV)	DOCUMENT ID	TECN	COMMENT
<b>3 to 12 (≈ 10) OUR ESTIMATE</b>			
3 ± 1.5	SOKHOYAN	15A	DPWA Multichannel
10 ± 5	CUTKOSKY	80	IPWA $\pi N \rightarrow \pi N$ (lower <i>m</i> )
• • • We do not use the following data for averages, fits, limits, etc. • • •			
3	SHKLYAR	13	DPWA Multichannel
2.5 ± 1.0	ANISOVICH	12A	DPWA Multichannel
53	BATINIC	10	DPWA $\pi N \rightarrow N\pi, N\eta$

**PHASE  $\theta$**

VALUE (°)	DOCUMENT ID	TECN	COMMENT
<b>50 to 200 (≈ 100) OUR ESTIMATE</b>			
160 ± 50	SOKHOYAN	15A	DPWA Multichannel
100 ± 80	CUTKOSKY	80	IPWA $\pi N \rightarrow \pi N$ (lower <i>m</i> )
• • • We do not use the following data for averages, fits, limits, etc. • • •			
- 76	SHKLYAR	13	DPWA Multichannel
- 65	BATINIC	10	DPWA $\pi N \rightarrow N\pi, N\eta$

**N(1875) INELASTIC POLE RESIDUE**

The "normalized residue" is the residue divided by  $\Gamma_{pole}/2$ .

**Normalized residue in  $N\pi \rightarrow N(1875) \rightarrow \Lambda K$**

MODULUS	PHASE (°)	DOCUMENT ID	TECN	COMMENT
0.015 ± 0.005		ANISOVICH	12A	DPWA Multichannel

**Normalized residue in  $N\pi \rightarrow N(1875) \rightarrow \Sigma K$**

MODULUS	PHASE (°)	DOCUMENT ID	TECN	COMMENT
0.04 ± 0.02		ANISOVICH	12A	DPWA Multichannel

**Normalized residue in  $N\pi \rightarrow N(1875) \rightarrow N\sigma$**

MODULUS	PHASE (°)	DOCUMENT ID	TECN	COMMENT
0.09 ± 0.03	-175 ± 45	SOKHOYAN	15A	DPWA Multichannel
• • • We do not use the following data for averages, fits, limits, etc. • • •				
0.08 ± 0.03	-170 ± 65	ANISOVICH	12A	DPWA Multichannel

**Normalized residue in  $N\pi \rightarrow N(1875) \rightarrow \Delta(1232)\pi, S\text{-wave}$**

MODULUS	PHASE (°)	DOCUMENT ID	TECN	COMMENT
0.05 ± 0.03	undefined	SOKHOYAN	15A	DPWA Multichannel

**Normalized residue in  $N\pi \rightarrow N(1875) \rightarrow \Delta(1232)\pi, D\text{-wave}$**

MODULUS	PHASE (°)	DOCUMENT ID	TECN	COMMENT
0.04 ± 0.02	undefined	SOKHOYAN	15A	DPWA Multichannel

**Normalized residue in  $N\pi \rightarrow N(1875) \rightarrow N(1440)\pi$**

MODULUS	PHASE (°)	DOCUMENT ID	TECN	COMMENT
0.03 ± 0.02	undefined	SOKHOYAN	15A	DPWA Multichannel

**N(1875) BREIT-WIGNER MASS**

VALUE (MeV)	DOCUMENT ID	TECN	COMMENT
<b>1850 to 1920 (≈ 1875) OUR ESTIMATE</b>			
2005 ± 12	<sup>1</sup> HUNT	19	DPWA Multichannel
1875 ± 20	SOKHOYAN	15A	DPWA Multichannel
1934 ± 10	<sup>1</sup> SHKLYAR	13	DPWA Multichannel
1880 ± 100	CUTKOSKY	80	IPWA $\pi N \rightarrow \pi N$
• • • We do not use the following data for averages, fits, limits, etc. • • •			
1880 ± 20	ANISOVICH	12A	DPWA Multichannel
1951 ± 27	<sup>1</sup> SHRESTHA	12A	DPWA Multichannel
2048 ± 65	BATINIC	10	DPWA $\pi N \rightarrow N\pi, N\eta$
1946 ± 1	PENNER	02c	DPWA Multichannel
1895	MART	00	DPWA $\gamma p \rightarrow \Lambda K^+$
2003 ± 18	VRANA	00	DPWA Multichannel

<sup>1</sup> Statistical error only.

**N(1875) BREIT-WIGNER WIDTH**

VALUE (MeV)	DOCUMENT ID	TECN	COMMENT
<b>120 to 250 (≈ 200) OUR ESTIMATE</b>			
321 ± 21	<sup>1</sup> HUNT	19	DPWA Multichannel
200 ± 25	SOKHOYAN	15A	DPWA Multichannel
857 ± 100	<sup>1</sup> SHKLYAR	13	DPWA Multichannel
180 ± 60	CUTKOSKY	80	IPWA $\pi N \rightarrow \pi N$ (lower <i>m</i> )
• • • We do not use the following data for averages, fits, limits, etc. • • •			
200 ± 25	ANISOVICH	12A	DPWA Multichannel
500 ± 45	<sup>1</sup> SHRESTHA	12A	DPWA Multichannel
529 ± 128	BATINIC	10	DPWA $\pi N \rightarrow N\pi, N\eta$
859 ± 7	PENNER	02c	DPWA Multichannel
372	MART	00	DPWA $\gamma p \rightarrow \Lambda K^+$
1070 ± 858	VRANA	00	DPWA Multichannel

<sup>1</sup> Statistical error only.

**N(1875) DECAY MODES**

Mode	Fraction ( $\Gamma_i/\Gamma$ )
$\Gamma_1$ $N\pi$	3-11 %
$\Gamma_2$ $N\eta$	<1 %
$\Gamma_3$ $N\omega$	15-25 %
$\Gamma_4$ $\Lambda K$	seen
$\Gamma_5$ $\Sigma K$	seen
$\Gamma_6$ $N\pi\pi$	
$\Gamma_7$ $\Delta(1232)\pi$	10-35 %
$\Gamma_8$ $\Delta(1232)\pi, S\text{-wave}$	7-21 %
$\Gamma_9$ $\Delta(1232)\pi, D\text{-wave}$	2-12 %
$\Gamma_{10}$ $N\rho, S=3/2, S\text{-wave}$	seen
$\Gamma_{11}$ $\Lambda K^*(892)$	
$\Gamma_{12}$ $N\sigma$	30-60 %
$\Gamma_{13}$ $N(1440)\pi$	2-8 %
$\Gamma_{14}$ $N(1520)\pi$	<2 %
$\Gamma_{15}$ $p\gamma$	0.001-0.025 %
$\Gamma_{16}$ $p\gamma, \text{helicity}=1/2$	0.001-0.021 %
$\Gamma_{17}$ $p\gamma, \text{helicity}=3/2$	<0.003 %
$\Gamma_{18}$ $n\gamma$	<0.040 %
$\Gamma_{19}$ $n\gamma, \text{helicity}=1/2$	<0.007 %
$\Gamma_{20}$ $n\gamma, \text{helicity}=3/2$	<0.033 %

**N(1875) BRANCHING RATIOS**

$\Gamma(N\pi)/\Gamma_{total}$	VALUE (%)	DOCUMENT ID	TECN	COMMENT	$\Gamma_1/\Gamma$
<b>3 to 11 (≈ 7) OUR ESTIMATE</b>					
	7.5 ± 0.1	<sup>1</sup> HUNT	19	DPWA Multichannel	
	4 ± 2	SOKHOYAN	15A	DPWA Multichannel	
	11 ± 1	<sup>1</sup> SHKLYAR	13	DPWA Multichannel	
	10 ± 4	CUTKOSKY	80	IPWA $\pi N \rightarrow \pi N$ (lower <i>m</i> )	
• • • We do not use the following data for averages, fits, limits, etc. • • •					
	3 ± 2	ANISOVICH	12A	DPWA Multichannel	
	7 ± 2	<sup>1</sup> SHRESTHA	12A	DPWA Multichannel	
	17 ± 7	BATINIC	10	DPWA $\pi N \rightarrow N\pi, N\eta$	
	12 ± 2	PENNER	02c	DPWA Multichannel	
	13 ± 3	VRANA	00	DPWA Multichannel	

<sup>1</sup> Statistical error only.

$\Gamma(N\eta)/\Gamma_{total}$	VALUE (%)	DOCUMENT ID	TECN	COMMENT	$\Gamma_2/\Gamma$
	3.3 ± 0.8	<sup>1</sup> HUNT	19	DPWA Multichannel	
	<1	SHKLYAR	13	DPWA Multichannel	
• • • We do not use the following data for averages, fits, limits, etc. • • •					
	8 ± 3	BATINIC	10	DPWA $\pi N \rightarrow N\pi, N\eta$	
	7 ± 2	PENNER	02c	DPWA Multichannel	
	0 ± 2	VRANA	00	DPWA Multichannel	

<sup>1</sup> Statistical error only.

$\Gamma(N\omega)/\Gamma_{total}$	VALUE (%)	DOCUMENT ID	TECN	COMMENT	$\Gamma_3/\Gamma$
	13 ± 7	DENISENKO	16	DPWA Multichannel	
	20 ± 5	<sup>1</sup> SHKLYAR	13	DPWA Multichannel	
• • • We do not use the following data for averages, fits, limits, etc. • • •					
	21 ± 7	PENNER	02c	DPWA Multichannel	

<sup>1</sup> Statistical error only.

$\Gamma(\Lambda K)/\Gamma_{total}$	VALUE (%)	DOCUMENT ID	TECN	COMMENT	$\Gamma_4/\Gamma$
	1.1 ± 0.4	<sup>1</sup> HUNT	19	DPWA Multichannel	
• • • We do not use the following data for averages, fits, limits, etc. • • •					
	0.2 ± 0.2	PENNER	02c	DPWA Multichannel	

<sup>1</sup> Statistical error only.

$\Gamma(\Sigma K)/\Gamma_{total}$	VALUE (%)	DOCUMENT ID	TECN	COMMENT	$\Gamma_5/\Gamma$
	0.7 ± 0.4	PENNER	02c	DPWA Multichannel	

$\Gamma(\Delta(1232)\pi, S\text{-wave})/\Gamma_{total}$	VALUE (%)	DOCUMENT ID	TECN	COMMENT	$\Gamma_8/\Gamma$
	< 2	<sup>1</sup> HUNT	19	DPWA Multichannel	
	14 ± 7	SOKHOYAN	15A	DPWA Multichannel	
• • • We do not use the following data for averages, fits, limits, etc. • • •					
	87 ± 3	<sup>1</sup> SHRESTHA	12A	DPWA Multichannel	
	40 ± 10	VRANA	00	DPWA Multichannel	

<sup>1</sup> Statistical error only.

## Baryon Particle Listings

 $N(1875)$ ,  $N(1880)$  $\Gamma(\Delta(1232)\pi, D\text{-wave})/\Gamma_{\text{total}}$ 

VALUE (%)	DOCUMENT ID	TECN	COMMENT
$17 \pm 6$	<sup>1</sup> HUNT 19	DPWA	Multichannel
$7 \pm 5$	SOKHOYAN 15A	DPWA	Multichannel
••• We do not use the following data for averages, fits, limits, etc. •••			
$< 6$	<sup>1</sup> SHRESTHA 12A	DPWA	Multichannel
$17 \pm 10$	VRANA 00	DPWA	Multichannel
<sup>1</sup> Statistical error only.			

 $\Gamma_9/\Gamma$  $N(1875) \rightarrow n\gamma$ , helicity-3/2 amplitude  $A_{3/2}$ 

VALUE ( $\text{GeV}^{-1/2}$ )	DOCUMENT ID	TECN	COMMENT
$0.141 \pm 0.022$	<sup>1</sup> HUNT 19	DPWA	Multichannel
$-0.020 \pm 0.015$	ANISOVICH 13B	DPWA	Multichannel
••• We do not use the following data for averages, fits, limits, etc. •••			
$-0.085 \pm 0.031$	<sup>1</sup> SHRESTHA 12A	DPWA	Multichannel
$-0.009$	PENNER 02D	DPWA	Multichannel
<sup>1</sup> Statistical error only.			

 $\Gamma(N\rho, S=3/2, S\text{-wave})/\Gamma_{\text{total}}$ 

VALUE (%)	DOCUMENT ID	TECN	COMMENT
$46 \pm 10$	<sup>1</sup> HUNT 19	DPWA	Multichannel
••• We do not use the following data for averages, fits, limits, etc. •••			
$< 5$	<sup>1</sup> SHRESTHA 12A	DPWA	Multichannel
$6 \pm 6$	VRANA 00	DPWA	Multichannel
<sup>1</sup> Statistical error only.			

 $\Gamma_{10}/\Gamma$ 

## N(1875) REFERENCES

For early references, see Physics Letters **111B** 1 (1982).

HUNT 19	PR C99 055205	B.C. Hunt, D.M. Manley
ANISOVICH 17B	PL B771 142	A.V. Anisovich <i>et al.</i>
DENISENKO 16	PL B755 97	I. Denisenko <i>et al.</i>
SOKHOYAN 15A	EPJ A51 95	V. Sokhoyan <i>et al.</i> (CBELSA/TAPS Collab.)
ANISOVICH 13B	EPJ A49 67	A.V. Anisovich <i>et al.</i>
SHKLYAR 13	PR C87 015201	V. Shklyar, H. Lenske, U. Mosel (GIES)
ANISOVICH 12A	EPJ A48 15	A.V. Anisovich <i>et al.</i> (BONN, PNPI)
SHRESTHA 12A	PR C86 055203	M. Shrestha, D.M. Manley (KSU)
BATINIC 10	PR C82 038203	M. Batinic <i>et al.</i> (ZAGR)
PENNER 02C	PR C66 055211	G. Penner, U. Mosel (GIES)
PENNER 02D	PR C66 055212	G. Penner, U. Mosel (GIES)
MART 00	PR C61 012201	T. Mart, C. Bennhold
VRANA 00	PRPL 328 181	T.P. Vrana, S.A. Dytman, T.-S.H. Lee (PITT, ANL)
CUTKOSKY 80	Toronto Conf. 19	R.E. Cutkosky <i>et al.</i> (CMU, LBL) IJP
Also	PR D20 2839	R.E. Cutkosky <i>et al.</i> (CMU, LBL) IJP

 $\Gamma(\Lambda K^*(892))/\Gamma_{\text{total}}$ 

VALUE	DOCUMENT ID	TECN	COMMENT
$< 0.002$	ANISOVICH 17B	DPWA	Multichannel

 $\Gamma_{11}/\Gamma$  $\Gamma(N\sigma)/\Gamma_{\text{total}}$ 

VALUE (%)	DOCUMENT ID	TECN	COMMENT
$24.3 \pm 8.6$	<sup>1</sup> HUNT 19	DPWA	Multichannel
$45 \pm 15$	SOKHOYAN 15A	DPWA	Multichannel
••• We do not use the following data for averages, fits, limits, etc. •••			
$< 4$	<sup>1</sup> SHRESTHA 12A	DPWA	Multichannel
$24 \pm 24$	VRANA 00	DPWA	Multichannel
<sup>1</sup> Statistical error only.			

 $\Gamma_{12}/\Gamma$  $\Gamma(N(1440)\pi)/\Gamma_{\text{total}}$ 

VALUE (%)	DOCUMENT ID	TECN	COMMENT
$5 \pm 3$	SOKHOYAN 15A	DPWA	Multichannel

 $\Gamma_{13}/\Gamma$  $\Gamma(N(1520)\pi)/\Gamma_{\text{total}}$ 

VALUE (%)	DOCUMENT ID	TECN	COMMENT
$< 2$	SOKHOYAN 15A	DPWA	Multichannel

 $\Gamma_{14}/\Gamma$ 

## N(1875) PHOTON DECAY AMPLITUDES AT THE POLE

 $N(1875) \rightarrow p\gamma$ , helicity-1/2 amplitude  $A_{1/2}$ 

MODULUS ( $\text{GeV}^{-1/2}$ )	PHASE ( $^\circ$ )	DOCUMENT ID	TECN	COMMENT
$0.017 \pm 0.009$	$-110 \pm 40$	SOKHOYAN 15A	DPWA	Multichannel

 $N(1875) \rightarrow p\gamma$ , helicity-3/2 amplitude  $A_{3/2}$ 

MODULUS ( $\text{GeV}^{-1/2}$ )	PHASE ( $^\circ$ )	DOCUMENT ID	TECN	COMMENT
$0.008 \pm 0.004$	$180 \pm 40$	SOKHOYAN 15A	DPWA	Multichannel

## N(1875) BREIT-WIGNER PHOTON DECAY AMPLITUDES

 $N(1875) \rightarrow p\gamma$ , helicity-1/2 amplitude  $A_{1/2}$ 

VALUE ( $\text{GeV}^{-1/2}$ )	DOCUMENT ID	TECN	COMMENT
<b>0.010 to 0.025 (<math>\approx 0.015</math>) OUR ESTIMATE</b>			
$-0.013 \pm 0.008$	<sup>1</sup> HUNT 19	DPWA	Multichannel
$0.011 \pm 0.001$	<sup>1</sup> SHKLYAR 13	DPWA	Multichannel
$0.018 \pm 0.010$	ANISOVICH 12A	DPWA	Multichannel
••• We do not use the following data for averages, fits, limits, etc. •••			
$0.007 \pm 0.008$	<sup>1</sup> SHRESTHA 12A	DPWA	Multichannel
$0.012$	PENNER 02D	DPWA	Multichannel
<sup>1</sup> Statistical error only.			

 $N(1875) \rightarrow p\gamma$ , helicity-3/2 amplitude  $A_{3/2}$ 

VALUE ( $\text{GeV}^{-1/2}$ )	DOCUMENT ID	TECN	COMMENT
<b>-0.010 to 0.025 (<math>\approx -0.005</math>) OUR ESTIMATE</b>			
$-0.093 \pm 0.009$	<sup>1</sup> HUNT 19	DPWA	Multichannel
$-0.007 \pm 0.004$	SOKHOYAN 15A	DPWA	Multichannel
$0.026 \pm 0.001$	<sup>1</sup> SHKLYAR 13	DPWA	Multichannel
••• We do not use the following data for averages, fits, limits, etc. •••			
$-0.009 \pm 0.005$	ANISOVICH 12A	DPWA	Multichannel
$0.043 \pm 0.022$	<sup>1</sup> SHRESTHA 12A	DPWA	Multichannel
$-0.010$	PENNER 02D	DPWA	Multichannel
<sup>1</sup> Statistical error only.			

 $N(1875) \rightarrow n\gamma$ , helicity-1/2 amplitude  $A_{1/2}$ 

VALUE ( $\text{GeV}^{-1/2}$ )	DOCUMENT ID	TECN	COMMENT
$0.050 \pm 0.009$	<sup>1</sup> HUNT 19	DPWA	Multichannel
$0.010 \pm 0.006$	ANISOVICH 13B	DPWA	Multichannel
••• We do not use the following data for averages, fits, limits, etc. •••			
$0.055 \pm 0.021$	<sup>1</sup> SHRESTHA 12A	DPWA	Multichannel
$0.023$	PENNER 02D	DPWA	Multichannel
<sup>1</sup> Statistical error only.			

 $N(1880) 1/2^+$  $I(J^P) = \frac{1}{2}(\frac{1}{2}^+)$  Status: \*\*\*

## N(1880) POLE POSITION

## REAL PART

VALUE (MeV)	DOCUMENT ID	TECN	COMMENT
<b>1820 to 1900 (<math>\approx 1860</math>) OUR ESTIMATE</b>			
$1860 \pm 40$	ANISOVICH 17A	DPWA	Multichannel
••• We do not use the following data for averages, fits, limits, etc. •••			
1880	HUNT 19	DPWA	Multichannel
$1875 \pm 11$	<sup>1</sup> ANISOVICH 17A	L+P	$\gamma p, \pi^- p \rightarrow K\Lambda$
$1870 \pm 40$	SOKHOYAN 15A	DPWA	Multichannel
$1870 \pm 40$	GUTZ 14	DPWA	Multichannel
$1860 \pm 35$	ANISOVICH 12A	DPWA	Multichannel
<sup>1</sup> Statistical error only.			

## -2xIMAGINARY PART

VALUE (MeV)	DOCUMENT ID	TECN	COMMENT
<b>180 to 280 (<math>\approx 230</math>) OUR ESTIMATE</b>			
$230 \pm 50$	ANISOVICH 17A	DPWA	Multichannel
••• We do not use the following data for averages, fits, limits, etc. •••			
429	HUNT 19	DPWA	Multichannel
$33 \pm 9$	<sup>2</sup> ANISOVICH 17A	L+P	$\gamma p, \pi^- p \rightarrow K\Lambda$
$220 \pm 50$	SOKHOYAN 15A	DPWA	Multichannel
$220 \pm 50$	GUTZ 14	DPWA	Multichannel
$250 \pm 70$	ANISOVICH 12A	DPWA	Multichannel
<sup>2</sup> Statistical error only.			

## N(1880) ELASTIC POLE RESIDUE

MODULUS  $|r|$ 

VALUE (MeV)	DOCUMENT ID	TECN	COMMENT
$6 \pm 4$	SOKHOYAN 15A	DPWA	Multichannel
••• We do not use the following data for averages, fits, limits, etc. •••			
$6 \pm 4$	GUTZ 14	DPWA	Multichannel
$6 \pm 4$	ANISOVICH 12A	DPWA	Multichannel

PHASE  $\theta$ 

VALUE ( $^\circ$ )	DOCUMENT ID	TECN	COMMENT
$70 \pm 60$	SOKHOYAN 15A	DPWA	Multichannel
••• We do not use the following data for averages, fits, limits, etc. •••			
$70 \pm 60$	GUTZ 14	DPWA	Multichannel
$80 \pm 65$	ANISOVICH 12A	DPWA	Multichannel

## N(1880) INELASTIC POLE RESIDUE

The "normalized residue" is the residue divided by  $\Gamma_{\text{pole}}/2$ .Normalized residue in  $N\pi \rightarrow N(1880) \rightarrow N\eta$ 

MODULUS	PHASE ( $^\circ$ )	DOCUMENT ID	TECN	COMMENT
$0.11 \pm 0.07$	$-75 \pm 55$	ANISOVICH 12A	DPWA	Multichannel

Normalized residue in  $N\pi \rightarrow N(1880) \rightarrow \Lambda K$ 

MODULUS	PHASE ( $^\circ$ )	DOCUMENT ID	TECN	COMMENT
$0.05 \pm 0.02$	$27 \pm 30$	ANISOVICH 17A	DPWA	$\gamma p, \pi^- p \rightarrow K\Lambda$

See key on page 999

Baryon Particle Listings  
N(1880)

••• We do not use the following data for averages, fits, limits, etc. •••  
 0.3 ± 0.1    82 ± 9    <sup>3</sup> ANISOVICH    17A    L+P     $\gamma p, \pi^- p \rightarrow K \Lambda$   
 0.03 ± 0.02    40 ± 40    ANISOVICH    12A    DPWA    Multichannel  
<sup>3</sup> Statistical error only.

**Normalized residue in  $N\pi \rightarrow N(1880) \rightarrow \Sigma K$**   

MODULUS	PHASE (°)	DOCUMENT ID	TECN	COMMENT
0.11 ± 0.06	95 ± 40	ANISOVICH	12A	DPWA Multichannel

 ••• We do not use the following data for averages, fits, limits, etc. •••

**Normalized residue in  $N\pi \rightarrow N(1880) \rightarrow \Delta\pi, P\text{-wave}$**   

MODULUS	PHASE (°)	DOCUMENT ID	TECN	COMMENT
0.14 ± 0.08	-150 ± 55	SOKHOYAN	15A	DPWA Multichannel

 ••• We do not use the following data for averages, fits, limits, etc. •••  

MODULUS	PHASE (°)	DOCUMENT ID	TECN	COMMENT
0.20 ± 0.08	-150 ± 50	ANISOVICH	12A	DPWA Multichannel

**Normalized residue in  $N\pi \rightarrow N(1880) \rightarrow N(1535)\pi$**   

MODULUS	PHASE (°)	DOCUMENT ID	TECN	COMMENT
0.09 ± 0.05	130 ± 60	GUTZ	14	DPWA Multichannel

**Normalized residue in  $N\pi \rightarrow N(1880) \rightarrow N a_0(980)$**   

MODULUS	PHASE (°)	DOCUMENT ID	TECN	COMMENT
0.04 ± 0.03	40 ± 65	GUTZ	14	DPWA Multichannel

**Normalized residue in  $N\pi \rightarrow N(1880) \rightarrow N\sigma$**   

MODULUS	PHASE (°)	DOCUMENT ID	TECN	COMMENT
0.10 ± 0.05	-140 ± 55	SOKHOYAN	15A	DPWA Multichannel

**N(1880) BREIT-WIGNER MASS**

VALUE (MeV)	DOCUMENT ID	TECN	COMMENT
<b>1830 to 1930 (≈ 1880) OUR ESTIMATE</b>			
1967 ± 20	<sup>4</sup> HUNT	19	DPWA Multichannel
1875 ± 40	SOKHOYAN	15A	DPWA Multichannel
••• We do not use the following data for averages, fits, limits, etc. •••			
1875 ± 40	GUTZ	14	DPWA Multichannel
1870 ± 35	ANISOVICH	12A	DPWA Multichannel
1900 ± 36	<sup>4</sup> SHRESTHA	12A	DPWA Multichannel
<sup>4</sup> Statistical error only.			

**N(1880) BREIT-WIGNER WIDTH**

VALUE (MeV)	DOCUMENT ID	TECN	COMMENT
<b>200 to 400 (≈ 300) OUR ESTIMATE</b>			
500 ± 77	<sup>5</sup> HUNT	19	DPWA Multichannel
230 ± 50	SOKHOYAN	15A	DPWA Multichannel
••• We do not use the following data for averages, fits, limits, etc. •••			
230 ± 50	GUTZ	14	DPWA Multichannel
235 ± 65	ANISOVICH	12A	DPWA Multichannel
485 ± 142	<sup>5</sup> SHRESTHA	12A	DPWA Multichannel
<sup>5</sup> Statistical error only.			

**N(1880) DECAY MODES**

Mode	Fraction ( $\Gamma_i/\Gamma$ )
$\Gamma_1$ $N\pi$	3–9 %
$\Gamma_2$ $N\eta$	5–55 %
$\Gamma_3$ $N\omega$	12–28 %
$\Gamma_4$ $\Lambda K$	12–28 %
$\Gamma_5$ $\Sigma K$	10–24 %
$\Gamma_6$ $N\pi\pi$	30–80 %
$\Gamma_7$ $\Delta(1232)\pi$	18–42 %
$\Gamma_8$ $N\rho, S=1/2$	
$\Gamma_9$ $N\sigma$	10–40 %
$\Gamma_{10}$ $N(1535)\pi$	4–12 %
$\Gamma_{11}$ $N a_0(980)$	1–5 %
$\Gamma_{12}$ $\Lambda K^*(892)$	0.5–1 %
$\Gamma_{13}$ $p\gamma, \text{helicity}=1/2$	seen
$\Gamma_{14}$ $n\gamma, \text{helicity}=1/2$	0.002–0.63 %

**N(1880) BRANCHING RATIOS**

$\Gamma(N\pi)/\Gamma_{\text{total}}$	DOCUMENT ID	TECN	COMMENT	$\Gamma_1/\Gamma$
25 ± 6	<sup>6</sup> HUNT	19	DPWA Multichannel	
6 ± 3	SOKHOYAN	15A	DPWA Multichannel	
••• We do not use the following data for averages, fits, limits, etc. •••				
6 ± 3	GUTZ	14	DPWA Multichannel	
5 ± 3	ANISOVICH	12A	DPWA Multichannel	
15 ± 5	<sup>6</sup> SHRESTHA	12A	DPWA Multichannel	
<sup>6</sup> Statistical error only.				

$\Gamma(N\eta)/\Gamma_{\text{total}}$	DOCUMENT ID	TECN	COMMENT	$\Gamma_2/\Gamma$
2 ± 1	<sup>7</sup> HUNT	19	DPWA Multichannel	
25 $\pm$ 30 20	ANISOVICH	12A	DPWA Multichannel	
••• We do not use the following data for averages, fits, limits, etc. •••				
16 ± 7	<sup>7</sup> SHRESTHA	12A	DPWA Multichannel	
<sup>7</sup> Statistical error only.				

$\Gamma(N\omega)/\Gamma_{\text{total}}$	DOCUMENT ID	TECN	COMMENT	$\Gamma_3/\Gamma$
20 ± 8	DENISENKO	16	DPWA Multichannel	

$\Gamma(\Lambda K)/\Gamma_{\text{total}}$	DOCUMENT ID	TECN	COMMENT	$\Gamma_4/\Gamma$
2 ± 1	<sup>8</sup> HUNT	19	DPWA Multichannel	
2 ± 1	ANISOVICH	12A	DPWA Multichannel	
••• We do not use the following data for averages, fits, limits, etc. •••				
32 ± 10	<sup>8</sup> SHRESTHA	12A	DPWA Multichannel	
<sup>8</sup> Statistical error only.				

$\Gamma(\Sigma K)/\Gamma_{\text{total}}$	DOCUMENT ID	TECN	COMMENT	$\Gamma_5/\Gamma$
17 ± 7	ANISOVICH	12A	DPWA Multichannel	

$\Gamma(\Delta(1232)\pi)/\Gamma_{\text{total}}$	DOCUMENT ID	TECN	COMMENT	$\Gamma_7/\Gamma$
11 ± 6	<sup>9</sup> HUNT	19	DPWA Multichannel	
30 ± 12	SOKHOYAN	15A	DPWA Multichannel	
••• We do not use the following data for averages, fits, limits, etc. •••				
29 ± 12	ANISOVICH	12A	DPWA Multichannel	
< 2	<sup>9</sup> SHRESTHA	12A	DPWA Multichannel	
<sup>9</sup> Statistical error only.				

$\Gamma(N\rho, S=1/2)/\Gamma_{\text{total}}$	DOCUMENT ID	TECN	COMMENT	$\Gamma_8/\Gamma$
32 ± 13	<sup>10</sup> HUNT	19	DPWA Multichannel	
<sup>10</sup> Statistical error only.				

$\Gamma(N\sigma)/\Gamma_{\text{total}}$	DOCUMENT ID	TECN	COMMENT	$\Gamma_9/\Gamma$
< 9	<sup>11</sup> HUNT	19	DPWA Multichannel	
25 ± 15	SOKHOYAN	15A	DPWA Multichannel	
••• We do not use the following data for averages, fits, limits, etc. •••				
8 ± 5	<sup>11</sup> SHRESTHA	12A	DPWA Multichannel	
<sup>11</sup> Statistical error only.				

$\Gamma(N(1535)\pi)/\Gamma_{\text{total}}$	DOCUMENT ID	TECN	COMMENT	$\Gamma_{10}/\Gamma$
8 ± 4	GUTZ	14	DPWA Multichannel	

$\Gamma(N a_0(980))/\Gamma_{\text{total}}$	DOCUMENT ID	TECN	COMMENT	$\Gamma_{11}/\Gamma$
3 ± 2	GUTZ	14	DPWA Multichannel	

$\Gamma(\Lambda K^*(892))/\Gamma_{\text{total}}$	DOCUMENT ID	TECN	COMMENT	$\Gamma_{12}/\Gamma$
0.008 ± 0.003	ANISOVICH	17B	DPWA Multichannel	

**N(1880) BREIT-WIGNER PHOTON DECAY AMPLITUDES**

$N(1880) \rightarrow p\gamma, \text{helicity-1/2}$ amplitude $A_{1/2}$	DOCUMENT ID	TECN	COMMENT
0.119 ± 0.015	<sup>12</sup> HUNT	19	DPWA Multichannel
••• We do not use the following data for averages, fits, limits, etc. •••			
0.021 ± 0.006	<sup>12</sup> SHRESTHA	12A	DPWA Multichannel
<sup>12</sup> Statistical error only.			

$N(1880) \rightarrow n\gamma, \text{helicity-1/2}$ amplitude $A_{1/2}$	DOCUMENT ID	TECN	COMMENT
0.016 ± 0.010	<sup>13</sup> HUNT	19	DPWA Multichannel
-0.060 ± 0.050	ANISOVICH	13B	DPWA Multichannel
0.014 ± 0.007	<sup>13</sup> SHRESTHA	12A	DPWA Multichannel
<sup>13</sup> Statistical error only.			

**N(1880) REFERENCES**

HUNT	19	PR C99 055205	B.C. Hunt, D.M. Manley
ANISOVICH	17A	PRL 119 062004	A.V. Anisovich et al.
ANISOVICH	17B	PL B771 142	A.V. Anisovich et al.
DENISENKO	16	PL B755 97	I. Denisenko et al.

## Baryon Particle Listings

 $N(1880)$ ,  $N(1895)$ 

SOKHOYAN 15A	EPJ A51 95	V. Sokhoyan et al.	(CBELSA/TAPS Collab.)
GUTZ 14	EPJ A50 74	E. Gutz et al.	(CBELSA/TAPS Collab.)
ANISOVICH 13B	EPJ A49 67	A.V. Anisovich et al.	
ANISOVICH 12A	EPJ A48 15	A.V. Anisovich et al.	(BONN, PNPI)
SHRESTHA 12A	PR C86 055203	M. Shrestha, D.M. Manley	(KSU)

 $N(1895) 1/2^-$ 

$$I(J^P) = \frac{1}{2}(\frac{1}{2}^-) \text{ Status: } ***$$

Before our 2012 Review, this state appeared in our Listings as the  $N(2090)$ . Any structure in the  $S_{11}$  wave above 1800 MeV is listed here. A few early results that are now obsolete have been omitted.

 $N(1895)$  POLE POSITION

## REAL PART

VALUE (MeV)	DOCUMENT ID	TECN	COMMENT
<b>1890 to 1930 (<math>\approx 1910</math>) OUR ESTIMATE</b>			
1895 $\pm 15$	ANISOVICH 17A	DPWA	Multichannel
1906 $\pm 17$	<sup>1</sup> ANISOVICH 17A	L+P	$\gamma p, \pi^- p \rightarrow K \Lambda$
1917 $\pm 19 \pm 1$	<sup>2</sup> SVARC 14	L+P	$\pi N \rightarrow \pi N$
••• We do not use the following data for averages, fits, limits, etc. •••			
1956	HUNT 19	DPWA	Multichannel
1907 $\pm 10$	ANISOVICH 17C	DPWA	Multichannel
1907 $\pm 10$	SOKHOYAN 15A	DPWA	Multichannel
1900 $\pm 15$	ANISOVICH 12A	DPWA	Multichannel
1797 $\pm 26$	BATINIC 10	DPWA	$\pi N \rightarrow N\pi, N\eta$
1795	VRANA 00	DPWA	Multichannel
2150 $\pm 70$	CUTKOSKY 80	IPWA	$\pi N \rightarrow \pi N$

<sup>1</sup> Statistical error only.

<sup>2</sup> Fit to the amplitudes of HOEHLER 79.

## -2xIMAGINARY PART

VALUE (MeV)	DOCUMENT ID	TECN	COMMENT
<b>80 to 140 (<math>\approx 110</math>) OUR ESTIMATE</b>			
132 $\pm 30$	ANISOVICH 17A	DPWA	Multichannel
100 $\pm 10$	<sup>1</sup> ANISOVICH 17A	L+P	$\gamma p, \pi^- p \rightarrow K \Lambda$
101 $\pm 36 \pm 1$	<sup>1,2</sup> SVARC 14	L+P	$\pi N \rightarrow \pi N$
••• We do not use the following data for averages, fits, limits, etc. •••			
449	HUNT 19	DPWA	Multichannel
100 $\pm 40$ - 10	ANISOVICH 17C	DPWA	Multichannel
100 $\pm 40$ - 15	SOKHOYAN 15A	DPWA	Multichannel
90 $\pm 30$ - 15	ANISOVICH 12A	DPWA	Multichannel
420 $\pm 45$	BATINIC 10	DPWA	$\pi N \rightarrow N\pi, N\eta$
220	VRANA 00	DPWA	Multichannel
350 $\pm 100$	CUTKOSKY 80	IPWA	$\pi N \rightarrow \pi N$

<sup>1</sup> Statistical error only.

<sup>2</sup> Fit to the amplitudes of HOEHLER 79.

 $N(1895)$  ELASTIC POLE RESIDUEMODULUS  $|r|$ 

VALUE (MeV)	DOCUMENT ID	TECN	COMMENT
<b>1 to 5 (<math>\approx 3</math>) OUR ESTIMATE</b>			
3 $\pm 2$	SOKHOYAN 15A	DPWA	Multichannel
3.1 $\pm 1.4$	<sup>1</sup> SVARC 14	L+P	$\pi N \rightarrow \pi N$
••• We do not use the following data for averages, fits, limits, etc. •••			
1 $\pm 1$	ANISOVICH 12A	DPWA	Multichannel
60	BATINIC 10	DPWA	$\pi N \rightarrow N\pi, N\eta$
40 $\pm 20$	CUTKOSKY 80	IPWA	$\pi N \rightarrow \pi N$
<sup>1</sup> Fit to the amplitudes of HOEHLER 79.			

PHASE  $\theta$ 

VALUE ( $^\circ$ )	DOCUMENT ID	TECN	COMMENT
125 $\pm 45$	SOKHOYAN 15A	DPWA	Multichannel
-107 $\pm 23 \pm 2$	<sup>1</sup> SVARC 14	L+P	$\pi N \rightarrow \pi N$
0 $\pm 90$	CUTKOSKY 80	IPWA	$\pi N \rightarrow \pi N$
••• We do not use the following data for averages, fits, limits, etc. •••			
-164	BATINIC 10	DPWA	$\pi N \rightarrow N\pi, N\eta$
<sup>1</sup> Fit to the amplitudes of HOEHLER 79.			

 $N(1895)$  INELASTIC POLE RESIDUE

The "normalized residue" is the residue divided by  $\Gamma_{pole}/2$ .

Normalized residue in  $N\pi \rightarrow N(1895) \rightarrow \Lambda K$ 

MODULUS	PHASE ( $^\circ$ )	DOCUMENT ID	TECN	COMMENT
0.09 $\pm 0.03$	8 $\pm 30$	ANISOVICH 17A	DPWA	Multichannel
0.06 $\pm 0.02$	87 $\pm 27$	<sup>1</sup> ANISOVICH 17A	L+P	$\gamma p, \pi^- p \rightarrow K \Lambda$
••• We do not use the following data for averages, fits, limits, etc. •••				
0.05 $\pm 0.02$	-90 $\pm 30$	ANISOVICH 12A	DPWA	Multichannel

<sup>1</sup> Statistical error only.

Normalized residue in  $N\pi \rightarrow N(1895) \rightarrow \Sigma K$ 

MODULUS	PHASE ( $^\circ$ )	DOCUMENT ID	TECN	COMMENT
0.06 $\pm 0.02$	40 $\pm 30$	ANISOVICH 12A	DPWA	Multichannel

Normalized residue in  $N\pi \rightarrow N(1895) \rightarrow \Delta(1232)\pi$ 

MODULUS	PHASE ( $^\circ$ )	DOCUMENT ID	TECN	COMMENT
0.05 $\pm 0.025$	-100 $\pm 45$	SOKHOYAN 15A	DPWA	Multichannel

Normalized residue in  $N\pi \rightarrow N(1895) \rightarrow N(1440)\pi$ 

MODULUS	PHASE ( $^\circ$ )	DOCUMENT ID	TECN	COMMENT
0.05 $\pm 0.025$	-100 $\pm 45$	SOKHOYAN 15A	DPWA	Multichannel

 $N(1895)$  BREIT-WIGNER MASS

VALUE (MeV)	DOCUMENT ID	TECN	COMMENT
<b>1870 to 1920 (<math>\approx 1895</math>) OUR ESTIMATE</b>			
2000 $\pm 29$	<sup>1</sup> HUNT 19	DPWA	Multichannel
1890 $\pm 9$ - 23	KASHEVAROV 17	DPWA	$\gamma p \rightarrow \eta p, \eta' p$
1905 $\pm 12$	SOKHOYAN 15A	DPWA	Multichannel
1880 $\pm 20$	HOEHLER 79	IPWA	$\pi N \rightarrow \pi N$
••• We do not use the following data for averages, fits, limits, etc. •••			
1895 $\pm 15$	ANISOVICH 12A	DPWA	Multichannel
1910 $\pm 15$	<sup>1</sup> SHRESTHA 12A	DPWA	Multichannel
1812 $\pm 25$	BATINIC 10	DPWA	$\pi N \rightarrow N\pi, N\eta$
1822 $\pm 43$	VRANA 00	DPWA	Multichannel
2180 $\pm 80$	CUTKOSKY 80	IPWA	$\pi N \rightarrow \pi N$
<sup>1</sup> Statistical error only.			

 $N(1895)$  BREIT-WIGNER WIDTH

VALUE (MeV)	DOCUMENT ID	TECN	COMMENT
<b>80 to 200 (<math>\approx 120</math>) OUR ESTIMATE</b>			
466 $\pm 72$	<sup>1</sup> HUNT 19	DPWA	Multichannel
150 $\pm 57$	KASHEVAROV 17	DPWA	$\gamma p \rightarrow \eta p, \eta' p$
100 $\pm 30$ - 10	SOKHOYAN 15A	DPWA	Multichannel
95 $\pm 30$	HOEHLER 79	IPWA	$\pi N \rightarrow \pi N$
••• We do not use the following data for averages, fits, limits, etc. •••			
90 $\pm 30$ - 15	ANISOVICH 12A	DPWA	Multichannel
502 $\pm 47$	<sup>1</sup> SHRESTHA 12A	DPWA	Multichannel
405 $\pm 40$	BATINIC 10	DPWA	$\pi N \rightarrow N\pi, N\eta$
248 $\pm 185$	VRANA 00	DPWA	Multichannel
350 $\pm 100$	CUTKOSKY 80	IPWA	$\pi N \rightarrow \pi N$
<sup>1</sup> Statistical error only.			

 $N(1895)$  DECAY MODES

Mode	Fraction ( $\Gamma_i/\Gamma$ )
$\Gamma_1$ $N\pi$	2-18 %
$\Gamma_2$ $N\eta$	15-40 %
$\Gamma_3$ $N\eta'$	10-40 %
$\Gamma_4$ $N\omega$	16-40 %
$\Gamma_5$ $\Lambda K$	13-23 %
$\Gamma_6$ $\Sigma K$	6-20 %
$\Gamma_7$ $N\pi\pi$	
$\Gamma_8$ $\Delta(1232)\pi$	
$\Gamma_9$ $\Delta(1232)\pi, D$ -wave	3-11 %
$\Gamma_{10}$ $N\rho$	
$\Gamma_{11}$ $N\rho, S=1/2, S$ -wave	seen
$\Gamma_{12}$ $N\rho, S=3/2, D$ -wave	3-12 %
$\Gamma_{13}$ $\Lambda K^*(892)$	4-9 %
$\Gamma_{14}$ $N\sigma$	seen
$\Gamma_{15}$ $N(1440)\pi$	1-4 %
$\Gamma_{16}$ $p\gamma, \text{ helicity}=1/2$	0.01-0.06 %
$\Gamma_{17}$ $n\gamma, \text{ helicity}=1/2$	0.003-0.05 %

 $N(1895)$  BRANCHING RATIOS

$\Gamma(N\pi)/\Gamma_{total}$	DOCUMENT ID	TECN	COMMENT	$\Gamma_1/\Gamma$
<b>2 to 18 (<math>\approx 10</math>) OUR ESTIMATE</b>				
8 $\pm 4$	<sup>1</sup> HUNT 19	DPWA	Multichannel	
2.5 $\pm 1.5$	SOKHOYAN 15A	DPWA	Multichannel	
9 $\pm 5$	HOEHLER 79	IPWA	$\pi N \rightarrow \pi N$	
••• We do not use the following data for averages, fits, limits, etc. •••				
2 $\pm 1$	ANISOVICH 12A	DPWA	Multichannel	
17 $\pm 2$	<sup>1</sup> SHRESTHA 12A	DPWA	Multichannel	
32 $\pm 6$	BATINIC 10	DPWA	$\pi N \rightarrow N\pi, N\eta$	
17 $\pm 3$	VRANA 00	DPWA	Multichannel	
18 $\pm 8$	CUTKOSKY 80	IPWA	$\pi N \rightarrow \pi N$	
<sup>1</sup> Statistical error only.				

See key on page 999

# Baryon Particle Listings

## $N(1895)$ , $N(1900)$

### $\Gamma(N\eta)/\Gamma_{\text{total}}$ $\Gamma_2/\Gamma$

VALUE (%)	DOCUMENT ID	TECN	COMMENT
<b>15 to 40 (<math>\approx 25</math>) OUR ESTIMATE</b>			
37 ± 9	<sup>1</sup> HUNT 19	DPWA	Multichannel
10 ± 5	ANISOVICH 17c	DPWA	Multichannel
20 ± 6	<sup>2</sup> KASHEVAROV 17	DPWA	$\gamma p \rightarrow \eta p, \eta' p$
• • • We do not use the following data for averages, fits, limits, etc. • • •			
21 ± 6	ANISOVICH 12A	DPWA	Multichannel
40 ± 4	<sup>1</sup> SHRESTHA 12A	DPWA	Multichannel
22 ± 10	BATINIC 10	DPWA	$\pi N \rightarrow \pi\pi, N\eta$
41 ± 4	VRANA 00	DPWA	Multichannel

<sup>1</sup> Statistical error only.  
<sup>2</sup> Assuming  $A_{1/2} = -0.030 \text{ GeV}^{-1/2}$ .

### $\Gamma(N\eta')/\Gamma_{\text{total}}$ $\Gamma_3/\Gamma$

VALUE (%)	DOCUMENT ID	TECN	COMMENT
<b>0.10 to 0.40 (<math>\approx 0.20</math>) OUR ESTIMATE</b>			
0.13 ± 0.05	ANISOVICH 17c	DPWA	Multichannel
0.38 ± 0.20	<sup>1</sup> KASHEVAROV 17	DPWA	$\gamma p \rightarrow \eta p, \eta' p$
• • • We do not use the following data for averages, fits, limits, etc. • • •			
<sup>1</sup> Assuming $A_{1/2} = -0.030 \text{ GeV}^{-1/2}$ .			

### $\Gamma(N\omega)/\Gamma_{\text{total}}$ $\Gamma_4/\Gamma$

VALUE (%)	DOCUMENT ID	TECN	COMMENT
28 ± 12	DENISENKO 16	DPWA	Multichannel

### $\Gamma(\Lambda K)/\Gamma_{\text{total}}$ $\Gamma_5/\Gamma$

VALUE (%)	DOCUMENT ID	TECN	COMMENT
7 ± 4	<sup>1</sup> HUNT 19	DPWA	Multichannel
18 ± 5	ANISOVICH 12A	DPWA	Multichannel
• • • We do not use the following data for averages, fits, limits, etc. • • •			
1.8 ± 0.8	<sup>1</sup> SHRESTHA 12A	DPWA	Multichannel
• • • We do not use the following data for averages, fits, limits, etc. • • •			
<sup>1</sup> Statistical error only.			

### $\Gamma(\Sigma K)/\Gamma_{\text{total}}$ $\Gamma_6/\Gamma$

VALUE (%)	DOCUMENT ID	TECN	COMMENT
13 ± 7	ANISOVICH 12A	DPWA	Multichannel

### $\Gamma(\Delta(1232)\pi, D\text{-wave})/\Gamma_{\text{total}}$ $\Gamma_9/\Gamma$

VALUE (%)	DOCUMENT ID	TECN	COMMENT
<b>&lt;10</b>			
7 ± 4	<sup>1</sup> HUNT 19	DPWA	Multichannel
	SOKHOYAN 15A	DPWA	Multichannel
• • • We do not use the following data for averages, fits, limits, etc. • • •			
7 ± 3	<sup>1</sup> SHRESTHA 12A	DPWA	Multichannel
1 ± 1	VRANA 00	DPWA	Multichannel
• • • We do not use the following data for averages, fits, limits, etc. • • •			
<sup>1</sup> Statistical error only.			

### $\Gamma(N\rho, S=1/2, S\text{-wave})/\Gamma_{\text{total}}$ $\Gamma_{11}/\Gamma$

VALUE (%)	DOCUMENT ID	TECN	COMMENT
<b>&lt;18</b>			
	<sup>1</sup> HUNT 19	DPWA	Multichannel
• • • We do not use the following data for averages, fits, limits, etc. • • •			
< 2	<sup>1</sup> SHRESTHA 12A	DPWA	Multichannel
36 ± 1	VRANA 00	DPWA	Multichannel
• • • We do not use the following data for averages, fits, limits, etc. • • •			
<sup>1</sup> Statistical error only.			

### $\Gamma(N\rho, S=3/2, D\text{-wave})/\Gamma_{\text{total}}$ $\Gamma_{12}/\Gamma$

VALUE (%)	DOCUMENT ID	TECN	COMMENT
23 ± 9	<sup>1</sup> HUNT 19	DPWA	Multichannel
• • • We do not use the following data for averages, fits, limits, etc. • • •			
9 ± 3	<sup>1</sup> SHRESTHA 12A	DPWA	Multichannel
1 ± 1	VRANA 00	DPWA	Multichannel
• • • We do not use the following data for averages, fits, limits, etc. • • •			
<sup>1</sup> Statistical error only.			

### $\Gamma(\Lambda K^*(892))/\Gamma_{\text{total}}$ $\Gamma_{13}/\Gamma$

VALUE (%)	DOCUMENT ID	TECN	COMMENT
0.063 ± 0.025	ANISOVICH 17b	DPWA	Multichannel

### $\Gamma(N\sigma)/\Gamma_{\text{total}}$ $\Gamma_{14}/\Gamma$

VALUE (%)	DOCUMENT ID	TECN	COMMENT
<b>&lt;13</b>			
	<sup>1</sup> HUNT 19	DPWA	Multichannel
• • • We do not use the following data for averages, fits, limits, etc. • • •			
< 2	<sup>1</sup> SHRESTHA 12A	DPWA	Multichannel
2 ± 1	VRANA 00	DPWA	Multichannel
• • • We do not use the following data for averages, fits, limits, etc. • • •			
<sup>1</sup> Statistical error only.			

### $\Gamma(N(1440)\pi)/\Gamma_{\text{total}}$ $\Gamma_{15}/\Gamma$

VALUE (%)	DOCUMENT ID	TECN	COMMENT
7 ± 5	<sup>1</sup> HUNT 19	DPWA	Multichannel
2.5 ± 1.5	SOKHOYAN 15A	DPWA	Multichannel
• • • We do not use the following data for averages, fits, limits, etc. • • •			
24 ± 4	<sup>1</sup> SHRESTHA 12A	DPWA	Multichannel
2 ± 1	VRANA 00	DPWA	Multichannel
• • • We do not use the following data for averages, fits, limits, etc. • • •			
<sup>1</sup> Statistical error only.			

### $N(1895)$ PHOTON DECAY AMPLITUDES AT THE POLE

#### $N(1895) \rightarrow p\gamma$ , helicity-1/2 amplitude $A_{1/2}$

MODULUS ( $\text{GeV}^{-1/2}$ )	PHASE ( $^\circ$ )	DOCUMENT ID	TECN	COMMENT
$-0.015 \pm 0.006$	$-35 \pm 35$	ANISOVICH 17c	DPWA	Multichannel
• • • We do not use the following data for averages, fits, limits, etc. • • •				
$0.015 \pm 0.006$	$145 \pm 35$	SOKHOYAN 15A	DPWA	Multichannel

#### $N(1895)$ BREIT-WIGNER PHOTON DECAY AMPLITUDES

#### $N(1895) \rightarrow p\gamma$ , helicity-1/2 amplitude $A_{1/2}$

VALUE ( $\text{GeV}^{-1/2}$ )	DOCUMENT ID	TECN	COMMENT
$0.017 \pm 0.005$	<sup>1</sup> HUNT 19	DPWA	Multichannel
$-0.016 \pm 0.006$	SOKHOYAN 15A	DPWA	Multichannel
• • • We do not use the following data for averages, fits, limits, etc. • • •			
$0.012 \pm 0.006$	<sup>1</sup> SHRESTHA 12A	DPWA	Multichannel
<sup>1</sup> Statistical error only.			

#### $N(1895) \rightarrow n\gamma$ , helicity-1/2 amplitude $A_{1/2}$

VALUE ( $\text{GeV}^{-1/2}$ )	DOCUMENT ID	TECN	COMMENT
$0.002 \pm 0.013$	<sup>1</sup> HUNT 19	DPWA	Multichannel
$0.013 \pm 0.006$	ANISOVICH 13b	DPWA	Multichannel
• • • We do not use the following data for averages, fits, limits, etc. • • •			
$0.003 \pm 0.007$	<sup>1</sup> SHRESTHA 12A	DPWA	Multichannel
<sup>1</sup> Statistical error only.			

### $N(1895)$ REFERENCES

HUNT 19	PR C99 055205	B.C. Hunt, D.M. Manley
ANISOVICH 17A	PRL 119 062004	A.V. Anisovich et al.
ANISOVICH 17B	PL B771 142	A.V. Anisovich et al.
ANISOVICH 17C	PL B772 247	A.V. Anisovich et al.
KASHEVAROV 17	PRL 118 212001	V.L. Kashevarov et al. (A2/MAMI Collab.)
DENISENKO 16	PL B755 97	I. Denisenko et al.
SOKHOYAN 15A	EPJ A51 95	V. Sokhoyan et al. (CBELSA/TAPS Collab.)
SVARC 14	PR C89 049205	A. Svarc et al. (RBI Zagreb, UNI Tuzla)
ANISOVICH 13B	EPJ A49 67	A.V. Anisovich et al.
ANISOVICH 12A	EPJ A48 15	A.V. Anisovich et al. (BONN, PNPI)
SHRESTHA 12A	PR C86 055203	M. Shrestha, D.M. Manley (KSU)
BATINIC 10	PR C82 038203	M. Batinic et al. (ZAGR)
VRANA 00	PRPL 328 181	T.P. Vrana, S.A. Dytman, T.-S.H. Lee (PITT, ANL)
CUTKOSKY 80	Toronto Conf. 19	R.E. Cutkosky et al. (CMU, LBL) IJP
Also	PR D20 2839	R.E. Cutkosky et al. (CMU, LBL)
HOEHLER 79	PDAT 12-1	G. Hoehler et al. (KARLT) IJP
Also	Toronto Conf. 3	R. Koch (KARLT) IJP

$$N(1900) \ 3/2^+$$

$$I(J^P) = \frac{1}{2}(\frac{3}{2}^+) \text{ Status: } ***$$

### $N(1900)$ POLE POSITION

#### REAL PART

VALUE (MeV)	DOCUMENT ID	TECN	COMMENT
<b>1900 to 1940 (<math>\approx 1920</math>) OUR ESTIMATE</b>			
1945 ± 35	ANISOVICH 17A	DPWA	Multichannel
1928 ± 18 ± 2	<sup>1</sup> SVARC 14	L+P	$\pi N \rightarrow \pi N$
• • • We do not use the following data for averages, fits, limits, etc. • • •			
1856	HUNT 19	DPWA	Multichannel
1912 ± 30	<sup>2</sup> ANISOVICH 17A	L+P	$\gamma p, \pi^- p \rightarrow K\Lambda$
1910 ± 30	SOKHOYAN 15A	DPWA	Multichannel
1910 ± 30	GUTZ 14	DPWA	Multichannel
1910	SHKLYAR 13	DPWA	Multichannel
1900 ± 30	ANISOVICH 12A	DPWA	Multichannel
• • • We do not use the following data for averages, fits, limits, etc. • • •			
<sup>1</sup> Fit to the amplitudes of HOEHLER 79.			
<sup>2</sup> Statistical error only.			

#### -2xIMAGINARY PART

VALUE (MeV)	DOCUMENT ID	TECN	COMMENT
<b>100 to 200 (<math>\approx 150</math>) OUR ESTIMATE</b>			
135 ± $\frac{70}{-30}$	ANISOVICH 17A	DPWA	Multichannel
152 ± 40 ± 9	<sup>1</sup> SVARC 14	L+P	$\pi N \rightarrow \pi N$
• • • We do not use the following data for averages, fits, limits, etc. • • •			
241	HUNT 19	DPWA	Multichannel
166 ± 30	<sup>2</sup> ANISOVICH 17A	L+P	$\gamma p, \pi^- p \rightarrow K\Lambda$
280 ± 50	SOKHOYAN 15A	DPWA	Multichannel
280 ± 50	GUTZ 14	DPWA	Multichannel
173	SHKLYAR 13	DPWA	Multichannel
200 ± $\frac{100}{-60}$	ANISOVICH 12A	DPWA	Multichannel
• • • We do not use the following data for averages, fits, limits, etc. • • •			
<sup>1</sup> Fit to the amplitudes of HOEHLER 79.			
<sup>2</sup> Statistical error only.			



See key on page 999

Baryon Particle Listings  
N(1900), N(1990)

$\Gamma(\Sigma K)/\Gamma_{total}$   $\Gamma_6/\Gamma$

VALUE (%)	DOCUMENT ID	TECN	COMMENT
5 ± 2	ANISOVICH 12A	DPWA	Multichannel
••• We do not use the following data for averages, fits, limits, etc. •••			
1 ± 1	PENNER 02C	DPWA	Multichannel

$\Gamma(\Lambda K^*(892))/\Gamma_{total}$   $\Gamma_{13}/\Gamma$

VALUE	DOCUMENT ID	TECN	COMMENT
<0.002	ANISOVICH 17B	DPWA	Multichannel

$\Gamma(N\rho, S=1/2)/\Gamma_{total}$   $\Gamma_{12}/\Gamma$

VALUE (%)	DOCUMENT ID	TECN	COMMENT
32 ± 7	<sup>1</sup> HUNT 19	DPWA	Multichannel
<sup>1</sup> Statistical error only.			

$\Gamma(N\sigma)/\Gamma_{total}$   $\Gamma_{14}/\Gamma$

VALUE (%)	DOCUMENT ID	TECN	COMMENT
4 ± 3	SOKHOYAN 15A	DPWA	Multichannel

$\Gamma(N(1520)\pi)/\Gamma_{total}$   $\Gamma_{15}/\Gamma$

VALUE (%)	DOCUMENT ID	TECN	COMMENT
15 ± 8	SOKHOYAN 15A	DPWA	Multichannel

$\Gamma(N(1535)\pi)/\Gamma_{total}$   $\Gamma_{16}/\Gamma$

VALUE (%)	DOCUMENT ID	TECN	COMMENT
7 ± 3	GUTZ 14	DPWA	Multichannel

$\Gamma(\Delta(1232)\pi, P\text{-wave})/\Gamma_{total}$   $\Gamma_9/\Gamma$

VALUE (%)	DOCUMENT ID	TECN	COMMENT
17 ± 8	SOKHOYAN 15A	DPWA	Multichannel

$\Gamma(\Delta(1232)\pi, F\text{-wave})/\Gamma_{total}$   $\Gamma_{10}/\Gamma$

VALUE (%)	DOCUMENT ID	TECN	COMMENT
33 ± 12	SOKHOYAN 15A	DPWA	Multichannel

N(1900) PHOTON DECAY AMPLITUDES AT THE POLE

N(1900) → pγ, helicity-1/2 amplitude A<sub>1/2</sub>

MODULUS (GeV <sup>-1/2</sup> )	PHASE (°)	DOCUMENT ID	TECN	COMMENT
0.026 ± 0.014	60 ± 35	SOKHOYAN 15A	DPWA	Multichannel

N(1900) → pγ, helicity-3/2 amplitude A<sub>3/2</sub>

MODULUS (GeV <sup>-1/2</sup> )	PHASE (°)	DOCUMENT ID	TECN	COMMENT
-0.070 ± 0.030	70 ± 50	SOKHOYAN 15A	DPWA	Multichannel

N(1900) BREIT-WIGNER PHOTON DECAY AMPLITUDES

N(1900) → pγ, helicity-1/2 amplitude A<sub>1/2</sub>

VALUE (GeV <sup>-1/2</sup> )	DOCUMENT ID	TECN	COMMENT
0.040 ± 0.004	<sup>1</sup> HUNT 19	DPWA	Multichannel
0.024 ± 0.014	SOKHOYAN 15A	DPWA	Multichannel
-0.008 ± 0.001	<sup>1</sup> SHKLYAR 13	DPWA	Multichannel
••• We do not use the following data for averages, fits, limits, etc. •••			
0.024 ± 0.014	GUTZ 14	DPWA	Multichannel
0.026 ± 0.015	ANISOVICH 12A	DPWA	Multichannel
0.041 ± 0.008	<sup>1</sup> SHRESTHA 12A	DPWA	Multichannel
-0.017	PENNER 02D	DPWA	Multichannel
<sup>1</sup> Statistical error only.			

N(1900) → pγ, helicity-3/2 amplitude A<sub>3/2</sub>

VALUE (GeV <sup>-1/2</sup> )	DOCUMENT ID	TECN	COMMENT
-0.094 ± 0.007	<sup>1</sup> HUNT 19	DPWA	Multichannel
-0.067 ± 0.030	SOKHOYAN 15A	DPWA	Multichannel
< 0.001	SHKLYAR 13	DPWA	Multichannel
••• We do not use the following data for averages, fits, limits, etc. •••			
-0.067 ± 0.030	GUTZ 14	DPWA	Multichannel
-0.065 ± 0.030	ANISOVICH 12A	DPWA	Multichannel
-0.004 ± 0.006	<sup>1</sup> SHRESTHA 12A	DPWA	Multichannel
0.031	PENNER 02D	DPWA	Multichannel
<sup>1</sup> Statistical error only.			

N(1900) → nγ, helicity-1/2 amplitude A<sub>1/2</sub>

VALUE (GeV <sup>-1/2</sup> )	DOCUMENT ID	TECN	COMMENT
0.007 ± 0.014	<sup>1</sup> HUNT 19	DPWA	Multichannel
0.000 ± 0.030	ANISOVICH 13B	DPWA	Multichannel
••• We do not use the following data for averages, fits, limits, etc. •••			
-0.010 ± 0.004	<sup>1</sup> SHRESTHA 12A	DPWA	Multichannel
-0.016	PENNER 02D	DPWA	Multichannel
<sup>1</sup> Statistical error only.			

N(1900) → nγ, helicity-3/2 amplitude A<sub>3/2</sub>

VALUE (GeV <sup>-1/2</sup> )	DOCUMENT ID	TECN	COMMENT
0.007 ± 0.011	<sup>1</sup> HUNT 19	DPWA	Multichannel
-0.060 ± 0.045	ANISOVICH 13B	DPWA	Multichannel
••• We do not use the following data for averages, fits, limits, etc. •••			
-0.011 ± 0.007	<sup>1</sup> SHRESTHA 12A	DPWA	Multichannel
-0.002	PENNER 02D	DPWA	Multichannel
<sup>1</sup> Statistical error only.			

N(1900) REFERENCES

HUNT 19	PR C99 055205	B.C. Hunt, D.M. Manley
ANISOVICH 17A	PRL 119 062004	A.V. Anisovich et al.
ANISOVICH 17B	PL B771 142	A.V. Anisovich et al.
ANISOVICH 17C	PL B772 247	A.V. Anisovich et al.
DENISENKO 16	PL B755 97	I. Denisenko et al.
SOKHOYAN 15A	EPJ A51 95	V. Sokhoyan et al. (CBELSA/TAPS Collab.)
GUTZ 14	EPJ A50 74	E. Gutz et al. (CBELSA/TAPS Collab.)
SVARC 14	PR C89 045205	A. Svarc et al. (RBI Zagreb, UNI Tuzla)
ANISOVICH 13B	EPJ A49 67	A.V. Anisovich et al.
SHKLYAR 13	PR C87 015201	V. Shklyar, H. Lenske, U. Mosel (GIES)
ANISOVICH 12A	EPJ A48 15	A.V. Anisovich et al. (BONN, PNPI)
SHRESTHA 12A	PR C86 055203	M. Shrestha, D.M. Manley (KSU)
NIKONOV 08	PL B662 245	V.A. Nikonov et al. (Bonn, Gatchina)
SHKLYAR 05	PR C72 015210	V. Shklyar, H. Lenske, U. Mosel (GIES)
PENNER 02C	PR C66 055211	G. Penner, U. Mosel (GIES)
PENNER 02D	PR C66 055212	G. Penner, U. Mosel (GIES)
HOEHLER 79	PDAT 12-1	G. Hoehler et al. (KARLT)

$N(1900) 7/2^+$

$I(J^P) = \frac{1}{2}(7^+)$  Status: \*\*

OMITTED FROM SUMMARY TABLE

Older and obsolete values are listed and referenced in the 2014 edition, Chinese Physics C38 070001 (2014).

N(1990) POLE POSITION

REAL PART

VALUE (MeV)	DOCUMENT ID	TECN	COMMENT
2030 ± 65	ANISOVICH 12A	DPWA	Multichannel
1900 ± 30	CUTKOSKY 80	IPWA	π N → π N
••• We do not use the following data for averages, fits, limits, etc. •••			
1913	HUNT 19	DPWA	Multichannel
1738	ROENCHEN 15A	DPWA	Multichannel
2301	VRANA 00	DPWA	Multichannel

-2xIMAGINARY PART

VALUE (MeV)	DOCUMENT ID	TECN	COMMENT
240 ± 60	ANISOVICH 12A	DPWA	Multichannel
260 ± 60	CUTKOSKY 80	IPWA	π N → π N
••• We do not use the following data for averages, fits, limits, etc. •••			
163	HUNT 19	DPWA	Multichannel
188	ROENCHEN 15A	DPWA	Multichannel
202	VRANA 00	DPWA	Multichannel

N(1990) ELASTIC POLE RESIDUE

MODULUS |r|

VALUE (MeV)	DOCUMENT ID	TECN	COMMENT
2 ± 1	ANISOVICH 12A	DPWA	Multichannel
9 ± 3	CUTKOSKY 80	IPWA	π N → π N
••• We do not use the following data for averages, fits, limits, etc. •••			
4.3	ROENCHEN 15A	DPWA	Multichannel

PHASE θ

VALUE (°)	DOCUMENT ID	TECN	COMMENT
125 ± 65	ANISOVICH 12A	DPWA	Multichannel
-60 ± 30	CUTKOSKY 80	IPWA	π N → π N
••• We do not use the following data for averages, fits, limits, etc. •••			
-70	ROENCHEN 15A	DPWA	Multichannel

Δ(1990) INELASTIC POLE RESIDUE

The "normalized residue" is the residue divided by Γ<sub>pole</sub>/2.

Normalized residue in Nπ → N(1990) → Nη

MODULUS	PHASE (°)	DOCUMENT ID	TECN	COMMENT
••• We do not use the following data for averages, fits, limits, etc. •••				
0.013	-82	ROENCHEN 15A	DPWA	Multichannel

Normalized residue in Nπ → N(1990) → ΛK

MODULUS	PHASE (°)	DOCUMENT ID	TECN	COMMENT
••• We do not use the following data for averages, fits, limits, etc. •••				
0.022	-111	ROENCHEN 15A	DPWA	Multichannel



# Baryon Particle Listings

## $N(1990)$ , $N(2000)$

### Normalized residue in $N\pi \rightarrow N(1990) \rightarrow \Sigma K$

MODULUS	PHASE (°)	DOCUMENT ID	TECN	COMMENT
0.005	24	ROENCHEN	15A	DPWA Multichannel

### $N(1990)$ BREIT-WIGNER MASS

VALUE (MeV)	DOCUMENT ID	TECN	COMMENT
<b>1950 to 2100 (≈ 2020) OUR ESTIMATE</b>			
2028 ± 19	<sup>1</sup> HUNT	19	DPWA Multichannel
2060 ± 65	ANISOVICH	12A	DPWA Multichannel
1970 ± 50	CUTKOSKY	80	IPWA $\pi N \rightarrow \pi N$
2005 ± 150	HOEHLER	79	IPWA $\pi N \rightarrow \pi N$
••• We do not use the following data for averages, fits, limits, etc. •••			
1990 ± 45	<sup>1</sup> SHRESTHA	12A	DPWA Multichannel
2311 ± 16	VRANA	00	DPWA Multichannel
<sup>1</sup> Statistical error only.			

### $N(1990)$ BREIT-WIGNER WIDTH

VALUE (MeV)	DOCUMENT ID	TECN	COMMENT
<b>200 to 400 (≈ 300) OUR ESTIMATE</b>			
490 ± 110	<sup>1</sup> HUNT	19	DPWA Multichannel
240 ± 50	ANISOVICH	12A	DPWA Multichannel
350 ± 120	CUTKOSKY	80	IPWA $\pi N \rightarrow \pi N$
350 ± 100	HOEHLER	79	IPWA $\pi N \rightarrow \pi N$
••• We do not use the following data for averages, fits, limits, etc. •••			
203 ± 161	<sup>1</sup> SHRESTHA	12A	DPWA Multichannel
205 ± 72	VRANA	00	DPWA Multichannel
<sup>1</sup> Statistical error only.			

### $N(1990)$ DECAY MODES

Mode	Fraction ( $\Gamma_i/\Gamma$ )
$\Gamma_1$ $N\pi$	2-6 %
$\Gamma_2$ $N\eta$	
$\Gamma_3$ $\Lambda K$	
$\Gamma_4$ $p\gamma$	0.01-0.12 %
$\Gamma_5$ $p\gamma$ , helicity=1/2	0.003-0.042 %
$\Gamma_6$ $p\gamma$ , helicity=3/2	0.009-0.075 %
$\Gamma_7$ $n\gamma$	0.01-0.16 %
$\Gamma_8$ $n\gamma$ , helicity=1/2	0.003-0.066 %
$\Gamma_9$ $n\gamma$ , helicity=3/2	0.003-0.098 %

### $N(1990)$ BRANCHING RATIOS

$\Gamma(N\pi)/\Gamma_{total}$	DOCUMENT ID	TECN	COMMENT	$\Gamma_1/\Gamma$
<b>2 to 6 (≈ 4) OUR ESTIMATE</b>				
1.9 ± 0.4	<sup>1</sup> HUNT	19	DPWA Multichannel	
2 ± 1	ANISOVICH	12A	DPWA Multichannel	
6 ± 2	CUTKOSKY	80	IPWA $\pi N \rightarrow \pi N$	
4 ± 2	HOEHLER	79	IPWA $\pi N \rightarrow \pi N$	
••• We do not use the following data for averages, fits, limits, etc. •••				
2 ± 1	<sup>1</sup> SHRESTHA	12A	DPWA Multichannel	
22 ± 11	VRANA	00	DPWA Multichannel	
<sup>1</sup> Statistical error only.				

$\Gamma(N\eta)/\Gamma_{total}$	DOCUMENT ID	TECN	COMMENT	$\Gamma_2/\Gamma$
1.7 ± 0.9	<sup>1</sup> HUNT	19	DPWA Multichannel	
<sup>1</sup> Statistical error only.				

$\Gamma(\Lambda K)/\Gamma_{total}$	DOCUMENT ID	TECN	COMMENT	$\Gamma_3/\Gamma$
6.0 ± 0.1	<sup>1</sup> HUNT	19	DPWA Multichannel	
<sup>1</sup> Statistical error only.				

### $N(1990)$ PHOTON DECAY AMPLITUDES AT THE POLE

#### $N(1990) \rightarrow p\gamma$ , helicity-1/2 amplitude $A_{1/2}$

MODULUS (GeV <sup>-1/2</sup> )	PHASE (°)	DOCUMENT ID	TECN	COMMENT
0.010 + 0.011 - 0.006	-103 + 108 - 155	ROENCHEN	14	DPWA
••• We do not use the following data for averages, fits, limits, etc. •••				
0.029	67	ROENCHEN	15A	DPWA Multichannel

#### $N(1990) \rightarrow p\gamma$ , helicity-3/2 amplitude $A_{3/2}$

MODULUS (GeV <sup>-1/2</sup> )	PHASE (°)	DOCUMENT ID	TECN	COMMENT
0.053 + 0.023 - 0.028	36 + 17 - 4	ROENCHEN	14	DPWA
••• We do not use the following data for averages, fits, limits, etc. •••				
0.033	39	ROENCHEN	15A	DPWA Multichannel

### $N(1990)$ BREIT-WIGNER PHOTON DECAY AMPLITUDES

#### $N(1990) \rightarrow p\gamma$ , helicity-1/2 amplitude $A_{1/2}$

VALUE (GeV <sup>-1/2</sup> )	DOCUMENT ID	TECN	COMMENT
0.006 ± 0.003	<sup>1</sup> HUNT	19	DPWA Multichannel
0.040 ± 0.012	ANISOVICH	12A	DPWA Multichannel
<sup>1</sup> Statistical error only.			

#### $N(1990) \rightarrow p\gamma$ , helicity-3/2 amplitude $A_{3/2}$

VALUE (GeV <sup>-1/2</sup> )	DOCUMENT ID	TECN	COMMENT
-0.055 ± 0.008	<sup>1</sup> HUNT	19	DPWA Multichannel
0.057 ± 0.012	ANISOVICH	12A	DPWA Multichannel
<sup>1</sup> Statistical error only.			

#### $N(1990) \rightarrow n\gamma$ , helicity-1/2 amplitude $A_{1/2}$

VALUE (GeV <sup>-1/2</sup> )	DOCUMENT ID	TECN	COMMENT
-0.027 ± 0.024	<sup>1</sup> HUNT	19	DPWA Multichannel
-0.045 ± 0.020	ANISOVICH	13B	DPWA Multichannel
<sup>1</sup> Statistical error only.			

#### $N(1990) \rightarrow n\gamma$ , helicity-3/2 amplitude $A_{3/2}$

VALUE (GeV <sup>-1/2</sup> )	DOCUMENT ID	TECN	COMMENT
0.051 ± 0.020	<sup>1</sup> HUNT	19	DPWA Multichannel
-0.052 ± 0.027	ANISOVICH	13B	DPWA Multichannel
<sup>1</sup> Statistical error only.			

### $N(1990)$ REFERENCES

For early references, see Physics Letters **111B** 1 (1982).

HUNT	19	PR C99 055205	B.C. Hunt, D.M. Manley
ROENCHEN	15A	EPJ A51 70	D. Roenchen et al.
PDG	14	CP C38 070001	K. Olive et al. (PDG Collab.)
ROENCHEN	14	EPJ A50 101	D. Roenchen et al.
Also		EPJ A51 63 (errat.)	D. Roenchen et al.
ANISOVICH	13B	EPJ A49 67	A.V. Anisovich et al.
ANISOVICH	12A	EPJ A48 15	A.V. Anisovich et al. (BONN, PNPI)
SHRESTHA	12A	PR C86 055203	M. Shrestha, D.M. Manley (KSU)
VRANA	00	PR L328 181	T.P. Vrana, S.A. Dytman, T.-S.H. Lee (PITT, ANL)
CUTKOSKY	80	Toronto Conf. 19	R.E. Cutkosky et al. (CMU, LBL) IJP
Also		PR D20 2839	R.E. Cutkosky et al. (CMU, LBL) IJP
HOEHLER	79	PDAT 12-1	G. Hoehler et al. (KARLT) IJP
Also		Toronto Conf. 3	R. Koch (KARLT) IJP

**$N(2000) 5/2^+$**

$$I(J^P) = \frac{1}{2} \left( \frac{5}{2}^+ \right) \text{ Status: **}$$

### OMITTED FROM SUMMARY TABLE

Before the 2012 Review, all the evidence for a  $J^P = 5/2^+$  state with a mass above 1800 MeV was filed under a two-star  $N(2000)$ . There is now some evidence from ANISOVICH 12A for two  $5/2^+$  states in this region, so we have split the older data (according to mass) between two two-star  $5/2^+$  states, an  $N(1860)$  and an  $N(2000)$ .

### $N(2000)$ POLE POSITION

#### REAL PART

VALUE (MeV)	DOCUMENT ID	TECN	COMMENT
2030 ± 40	SOKHOYAN	15A	DPWA Multichannel
••• We do not use the following data for averages, fits, limits, etc. •••			
1900	SHKLYAR	13	DPWA Multichannel
2030 ± 110	ANISOVICH	12A	DPWA Multichannel

#### -2xIMAGINARY PART

VALUE (MeV)	DOCUMENT ID	TECN	COMMENT
380 ± 60	SOKHOYAN	15A	DPWA Multichannel
••• We do not use the following data for averages, fits, limits, etc. •••			
123	SHKLYAR	13	DPWA Multichannel
480 ± 100	ANISOVICH	12A	DPWA Multichannel

### $N(2000)$ ELASTIC POLE RESIDUE

#### MODULUS $|r|$

VALUE (MeV)	DOCUMENT ID	TECN	COMMENT
18 ± 8	SOKHOYAN	15A	DPWA Multichannel
••• We do not use the following data for averages, fits, limits, etc. •••			
11	SHKLYAR	13	DPWA Multichannel
35 + 80 - 15	ANISOVICH	12A	DPWA Multichannel

**PHASE  $\theta$**

VALUE (°)	DOCUMENT ID	TECN	COMMENT
-150±40	SOKHOYAN 15A	DPWA	Multichannel
••• We do not use the following data for averages, fits, limits, etc. •••			
-6	SHKLYAR 13	DPWA	Multichannel
-100±40	ANISOVICH 12A	DPWA	Multichannel

**N(2000) INELASTIC POLE RESIDUE**

The "normalized residue" is the residue divided by  $\Gamma_{pole/2}$ .

**Normalized residue in  $N\pi \rightarrow N(2000) \rightarrow \Delta(1232)\pi, P\text{-wave}$**

MODULUS	PHASE (°)	DOCUMENT ID	TECN	COMMENT
0.16±0.06	100 ± 50	SOKHOYAN 15A	DPWA	Multichannel

**Normalized residue in  $N\pi \rightarrow N(2000) \rightarrow \Delta(1232)\pi, F\text{-wave}$**

MODULUS	PHASE (°)	DOCUMENT ID	TECN	COMMENT
0.20±0.10	-20 ± 45	SOKHOYAN 15A	DPWA	Multichannel

**Normalized residue in  $N\pi \rightarrow N(2000) \rightarrow N\sigma$**

MODULUS	PHASE (°)	DOCUMENT ID	TECN	COMMENT
0.12±0.06	80 ± 40	SOKHOYAN 15A	DPWA	Multichannel

**Normalized residue in  $N\pi \rightarrow N(2000) \rightarrow N(1520)\pi, D\text{-wave}$**

MODULUS	PHASE (°)	DOCUMENT ID	TECN	COMMENT
0.17±0.09	-60 ± 35	SOKHOYAN 15A	DPWA	Multichannel

**N(2000) BREIT-WIGNER MASS**

VALUE (MeV)	DOCUMENT ID	TECN	COMMENT
2060 ± 30	SOKHOYAN 15A	DPWA	Multichannel
1946 ± 4	<sup>1</sup> SHKLYAR 13	DPWA	Multichannel
••• We do not use the following data for averages, fits, limits, etc. •••			
2090 ± 120	ANISOVICH 12A	DPWA	Multichannel

<sup>1</sup> Statistical error only.

**N(2000) BREIT-WIGNER WIDTH**

VALUE (MeV)	DOCUMENT ID	TECN	COMMENT
390 ± 55	SOKHOYAN 15A	DPWA	Multichannel
198 ± 2	<sup>2</sup> SHKLYAR 13	DPWA	Multichannel
••• We do not use the following data for averages, fits, limits, etc. •••			
460±100	ANISOVICH 12A	DPWA	Multichannel

<sup>2</sup> Statistical error only.

**N(2000) DECAY MODES**

Mode	Fraction ( $\Gamma_i/\Gamma$ )
$\Gamma_1$ $N\pi$	6-10 %
$\Gamma_2$ $N\eta$	<4 %
$\Gamma_3$ $N\omega$	<2 %
$\Gamma_4$ $N\pi\pi$	35-90 %
$\Gamma_5$ $\Delta(1232)\pi$	30-80 %
$\Gamma_6$ $\Delta(1232)\pi, P\text{-wave}$	12-32 %
$\Gamma_7$ $\Delta(1232)\pi, F\text{-wave}$	19-49 %
$\Gamma_8$ $\Lambda K^*(892)$	(2.2±1.0) %
$\Gamma_9$ $N\sigma$	5-15 %
$\Gamma_{10}$ $N(1520)\pi, D\text{-wave}$	11-31 %
$\Gamma_{11}$ $N(1680)\pi, P\text{-wave}$	17-25 %
$\Gamma_{12}$ $p\gamma$	0.01-0.08 %
$\Gamma_{13}$ $p\gamma, \text{helicity}=1/2$	0.003-0.031 %
$\Gamma_{14}$ $p\gamma, \text{helicity}=3/2$	0.008-0.048 %
$\Gamma_{15}$ $n\gamma$	0.002-0.07 %
$\Gamma_{16}$ $n\gamma, \text{helicity}=1/2$	<0.017 %
$\Gamma_{17}$ $n\gamma, \text{helicity}=3/2$	0.001-0.056 %

**N(2000) BRANCHING RATIOS**

**$\Gamma(N\pi)/\Gamma_{total}$**

VALUE (%)	DOCUMENT ID	TECN	COMMENT
<b>6 to 10 (<math>\approx 8</math>) OUR ESTIMATE</b>			
8±4	SOKHOYAN 15A	DPWA	Multichannel
10±1	<sup>3</sup> SHKLYAR 13	DPWA	Multichannel
••• We do not use the following data for averages, fits, limits, etc. •••			
9±4	ANISOVICH 12A	DPWA	Multichannel

<sup>3</sup> Statistical error only.

**$\Gamma(N\eta)/\Gamma_{total}$**

VALUE (%)	DOCUMENT ID	TECN	COMMENT
2±2	<sup>4</sup> SHKLYAR 13	DPWA	Multichannel

<sup>4</sup> Statistical error only.

**$\Gamma(N\omega)/\Gamma_{total}$**

VALUE (%)	DOCUMENT ID	TECN	COMMENT
18±8	DENISENKO 16	DPWA	Multichannel
1±1	<sup>5</sup> SHKLYAR 13	DPWA	Multichannel

<sup>5</sup> Statistical error only.

**$\Gamma(\Delta(1232)\pi, P\text{-wave})/\Gamma_{total}$**

VALUE (%)	DOCUMENT ID	TECN	COMMENT
22±10	SOKHOYAN 15A	DPWA	Multichannel

**$\Gamma(\Delta(1232)\pi, F\text{-wave})/\Gamma_{total}$**

VALUE (%)	DOCUMENT ID	TECN	COMMENT
34±15	SOKHOYAN 15A	DPWA	Multichannel

**$\Gamma(\Lambda K^*(892))/\Gamma_{total}$**

VALUE (%)	DOCUMENT ID	TECN	COMMENT
0.022±0.010	ANISOVICH 17B	DPWA	Multichannel

**$\Gamma(N\sigma)/\Gamma_{total}$**

VALUE (%)	DOCUMENT ID	TECN	COMMENT
10±5	SOKHOYAN 15A	DPWA	Multichannel

**$\Gamma(N(1520)\pi, D\text{-wave})/\Gamma_{total}$**

VALUE (%)	DOCUMENT ID	TECN	COMMENT
21±10	SOKHOYAN 15A	DPWA	Multichannel

**$\Gamma(N(1680)\pi, P\text{-wave})/\Gamma_{total}$**

VALUE (%)	DOCUMENT ID	TECN	COMMENT
16±9	SOKHOYAN 15A	DPWA	Multichannel

**N(2000) PHOTON DECAY AMPLITUDES AT THE POLE**

**N(2000)  $\rightarrow p\gamma, \text{helicity-1/2}$  amplitude  $A_{1/2}$**

MODULUS (GeV <sup>-1/2</sup> )	PHASE (°)	DOCUMENT ID	TECN	COMMENT
0.033±0.010	15 ± 25	SOKHOYAN 15A	DPWA	Multichannel

**N(2000)  $\rightarrow p\gamma, \text{helicity-3/2}$  amplitude  $A_{3/2}$**

MODULUS (GeV <sup>-1/2</sup> )	PHASE (°)	DOCUMENT ID	TECN	COMMENT
0.045 ± 0.008	-140 ± 25	SOKHOYAN 15A	DPWA	Multichannel

**N(2000) BREIT-WIGNER PHOTON DECAY AMPLITUDES**

**N(2000)  $\rightarrow p\gamma, \text{helicity-1/2}$  amplitude  $A_{1/2}$**

VALUE (GeV <sup>-1/2</sup> )	DOCUMENT ID	TECN	COMMENT
0.031 ± 0.010	SOKHOYAN 15A	DPWA	Multichannel
0.011 ± 0.001	<sup>6</sup> SHKLYAR 13	DPWA	Multichannel

<sup>6</sup> Statistical error only.

**N(2000)  $\rightarrow p\gamma, \text{helicity-3/2}$  amplitude  $A_{3/2}$**

VALUE (GeV <sup>-1/2</sup> )	DOCUMENT ID	TECN	COMMENT
-0.043 ± 0.008	SOKHOYAN 15A	DPWA	Multichannel
0.025 ± 0.001	<sup>7</sup> SHKLYAR 13	DPWA	Multichannel

<sup>7</sup> Statistical error only.

**N(2000)  $\rightarrow n\gamma, \text{helicity-1/2}$  amplitude  $A_{1/2}$**

VALUE (GeV <sup>-1/2</sup> )	DOCUMENT ID	TECN	COMMENT
-0.018 ± 0.012	ANISOVICH 13B	DPWA	Multichannel

**N(2000)  $\rightarrow n\gamma, \text{helicity-3/2}$  amplitude  $A_{3/2}$**

VALUE (GeV <sup>-1/2</sup> )	DOCUMENT ID	TECN	COMMENT
-0.035 ± 0.020	ANISOVICH 13B	DPWA	Multichannel

**N(2000) REFERENCES**

ANISOVICH 17B PL B771 142 A.V. Anisovich et al.  
 DENISENKO 16 PL B755 97 I. Denisenko et al.  
 SOKHOYAN 15A EPJ A51 95 V. Sokhoyan et al. (CBELSA/TAPS Collab.)  
 ANISOVICH 13B EPJ A49 67 A.V. Anisovich et al.  
 SHKLYAR 13 PR C87 015201 V. Shklyar, H. Lenske, U. Mosel (GIES)  
 ANISOVICH 12A EPJ A48 15 A.V. Anisovich et al. (BONN, PNPI)

**N(2040) 3/2<sup>+</sup>**

$J^P = \frac{3}{2}^+$  Status: \*

OMITTED FROM SUMMARY TABLE

**N(2040) MASS**

VALUE (MeV)	DOCUMENT ID	TECN	COMMENT
2040 <sup>+3</sup> <sub>-4</sub> ± 25	ABLIKIM 09B	BES2	$J/\psi \rightarrow p\bar{p}\pi^0$
2068 ± 3 <sup>+15</sup> <sub>-40</sub>	ABLIKIM 06K	BES2	$J/\psi \rightarrow p\bar{n}\pi^-, n\bar{p}\pi^+$
••• We do not use the following data for averages, fits, limits, etc. •••			
2244 ± 30	<sup>1,2</sup> HUNT 19	DPWA	Multichannel

## Baryon Particle Listings

 $N(2040)$ ,  $N(2060)$ <sup>1</sup> Statistical error only.<sup>2</sup> We list here candidates for high-mass  $3/2^+$  states. $N(2040)$  WIDTH

VALUE (MeV)	DOCUMENT ID	TECN	COMMENT
$230 \pm 8 \pm 52$	ABLIKIM 09B	BES2	$J/\psi \rightarrow p\bar{p}\pi^0$
$165 \pm 14 \pm 40$	ABLIKIM 06K	BES2	$J/\psi \rightarrow p\bar{n}\pi^-, n\bar{p}\pi^+$
$530 \pm 89$	<sup>3,4</sup> HUNT 19	DPWA	Multichannel

<sup>3</sup> Statistical error only.<sup>4</sup> We list here candidates for high-mass  $3/2^+$  states. $N(2040)$  REFERENCES

HUNT 19	PR C99 055205	B. C. Hunt, D.M. Manley	
ABLIKIM 09B	PR D80 052004	M. Ablilikim et al.	(BES II Collab.)
ABLIKIM 06K	PRL 97 062001	M. Ablilikim et al.	(BES II Collab.)

 $N(2060) 5/2^-$ 

$$I(J^P) = \frac{1}{2}(\frac{5}{2}^-) \text{ Status: } ***$$

Before our 2012 Review, this state appeared in our Listings as the  $N(2200)$ .

 $N(2060)$  POLE POSITION

## REAL PART

VALUE (MeV)	DOCUMENT ID	TECN	COMMENT
<b>2020 to 2130 (<math>\approx 2070</math>) OUR ESTIMATE</b>			
$2030 \pm 15$	SOKHOYAN 15A	DPWA	Multichannel
$2119 \pm 11 \pm 1$	<sup>1</sup> SVARC 14	L+P	$\pi N \rightarrow \pi N$
$2100 \pm 60$	CUTKOSKY 80	IPWA	$\pi N \rightarrow \pi N$
••• We do not use the following data for averages, fits, limits, etc. •••			
2010	HUNT 19	DPWA	Multichannel
$2040 \pm 15$	ANISOVICH 12A	DPWA	Multichannel
$2144 \pm 31$	BATINIC 10	DPWA	$\pi N \rightarrow N\pi, N\eta$

<sup>1</sup> Fit to the amplitudes of HOEHLER 79. $-2 \times$ IMAGINARY PART

VALUE (MeV)	DOCUMENT ID	TECN	COMMENT
<b>350 to 430 (<math>\approx 400</math>) OUR ESTIMATE</b>			
$400 \pm 35$	SOKHOYAN 15A	DPWA	Multichannel
$370 \pm 20 \pm 5$	<sup>1</sup> SVARC 14	L+P	$\pi N \rightarrow \pi N$
$360 \pm 80$	CUTKOSKY 80	IPWA	$\pi N \rightarrow \pi N$
••• We do not use the following data for averages, fits, limits, etc. •••			
395	HUNT 19	DPWA	Multichannel
$390 \pm 25$	ANISOVICH 12A	DPWA	Multichannel
$438 \pm 13$	BATINIC 10	DPWA	$\pi N \rightarrow N\pi, N\eta$

<sup>1</sup> Fit to the amplitudes of HOEHLER 79. $N(2060)$  ELASTIC POLE RESIDUEMODULUS  $|r|$ 

VALUE (MeV)	DOCUMENT ID	TECN	COMMENT
<b>15 to 30 (<math>\approx 20</math>) OUR ESTIMATE</b>			
$25 \pm 8$	SOKHOYAN 15A	DPWA	Multichannel
$19 \pm 1 \pm 1$	<sup>1</sup> SVARC 14	L+P	$\pi N \rightarrow \pi N$
$20 \pm 10$	CUTKOSKY 80	IPWA	$\pi N \rightarrow \pi N$
••• We do not use the following data for averages, fits, limits, etc. •••			
$19 \pm 5$	ANISOVICH 12A	DPWA	Multichannel
26	BATINIC 10	DPWA	$\pi N \rightarrow N\pi, N\eta$

<sup>1</sup> Fit to the amplitudes of HOEHLER 79.PHASE  $\theta$ 

VALUE ( $^\circ$ )	DOCUMENT ID	TECN	COMMENT
<b><math>-130</math> to <math>-90</math> (<math>\approx -110</math>) OUR ESTIMATE</b>			
$-130 \pm 20$	SOKHOYAN 15A	DPWA	Multichannel
$-94 \pm 5 \pm 1$	<sup>1</sup> SVARC 14	L+P	$\pi N \rightarrow \pi N$
$-90 \pm 50$	CUTKOSKY 80	IPWA	$\pi N \rightarrow \pi N$
••• We do not use the following data for averages, fits, limits, etc. •••			
$-125 \pm 20$	ANISOVICH 12A	DPWA	Multichannel
$-71$	BATINIC 10	DPWA	$\pi N \rightarrow N\pi, N\eta$

<sup>1</sup> Fit to the amplitudes of HOEHLER 79. $N(2060)$  INELASTIC POLE RESIDUE

The "normalized residue" is the residue divided by  $\Gamma_{pole}/2$ .

Normalized residue in  $N\pi \rightarrow N(2060) \rightarrow N\eta$ 

MODULUS	PHASE ( $^\circ$ )	DOCUMENT ID	TECN	COMMENT
$0.05 \pm 0.03$	$40 \pm 25$	ANISOVICH 12A	DPWA	Multichannel

Normalized residue in  $N\pi \rightarrow N(2060) \rightarrow \Lambda K$ 

MODULUS	DOCUMENT ID	TECN	COMMENT
$0.01 \pm 0.005$	ANISOVICH 12A	DPWA	Multichannel

Normalized residue in  $N\pi \rightarrow N(2060) \rightarrow \Sigma K$ 

MODULUS	PHASE ( $^\circ$ )	DOCUMENT ID	TECN	COMMENT
$0.04 \pm 0.02$	$-70 \pm 30$	ANISOVICH 12A	DPWA	Multichannel

Normalized residue in  $N\pi \rightarrow N(2060) \rightarrow \Delta(1232)\pi, D\text{-wave}$ 

MODULUS	PHASE ( $^\circ$ )	DOCUMENT ID	TECN	COMMENT
$0.06 \pm 0.03$	$-90 \pm 40$	SOKHOYAN 15A	DPWA	Multichannel

Normalized residue in  $N\pi \rightarrow N(2060) \rightarrow N\sigma$ 

MODULUS	PHASE ( $^\circ$ )	DOCUMENT ID	TECN	COMMENT
$0.12 \pm 0.06$	$80 \pm 40$	SOKHOYAN 15A	DPWA	Multichannel

Normalized residue in  $N\pi \rightarrow N(2060) \rightarrow N(1440)\pi$ 

MODULUS	PHASE ( $^\circ$ )	DOCUMENT ID	TECN	COMMENT
$0.17 \pm 0.09$	$-60 \pm 35$	SOKHOYAN 15A	DPWA	Multichannel

Normalized residue in  $N\pi \rightarrow N(2060) \rightarrow N(1520)\pi, P\text{-wave}$ 

MODULUS	PHASE ( $^\circ$ )	DOCUMENT ID	TECN	COMMENT
$0.14 \pm 0.06$	$-45 \pm 15$	SOKHOYAN 15A	DPWA	Multichannel

 $N(2060)$  BREIT-WIGNER MASS

VALUE (MeV)	DOCUMENT ID	TECN	COMMENT
<b>2030 to 2200 (<math>\approx 2100</math>) OUR ESTIMATE</b>			
$2111 \pm 17$	<sup>1</sup> HUNT 19	DPWA	Multichannel
$2045 \pm 15$	SOKHOYAN 15A	DPWA	Multichannel
$2180 \pm 80$	CUTKOSKY 80	IPWA	$\pi N \rightarrow \pi N$
$2228 \pm 30$	HOEHLER 79	IPWA	$\pi N \rightarrow \pi N$
••• We do not use the following data for averages, fits, limits, etc. •••			
$2060 \pm 15$	ANISOVICH 12A	DPWA	Multichannel
$2116 \pm 21$	<sup>1</sup> SHRESTHA 12A	DPWA	Multichannel
$2217 \pm 27$	BATINIC 10	DPWA	$\pi N \rightarrow N\pi, N\eta$

<sup>1</sup> Statistical error only. $N(2060)$  BREIT-WIGNER WIDTH

VALUE (MeV)	DOCUMENT ID	TECN	COMMENT
<b>300 to 450 (<math>\approx 400</math>) OUR ESTIMATE</b>			
$499 \pm 70$	<sup>1</sup> HUNT 19	DPWA	Multichannel
$420 \pm 30$	SOKHOYAN 15A	DPWA	Multichannel
$400 \pm 100$	CUTKOSKY 80	IPWA	$\pi N \rightarrow \pi N$
$310 \pm 50$	HOEHLER 79	IPWA	$\pi N \rightarrow \pi N$
••• We do not use the following data for averages, fits, limits, etc. •••			
$375 \pm 25$	ANISOVICH 12A	DPWA	Multichannel
$307 \pm 112$	<sup>1</sup> SHRESTHA 12A	DPWA	Multichannel
$481 \pm 17$	BATINIC 10	DPWA	$\pi N \rightarrow N\pi, N\eta$

<sup>1</sup> Statistical error only. $N(2060)$  DECAY MODES

Mode	Fraction ( $\Gamma_i/\Gamma$ )
$\Gamma_1$ $N\pi$	7–12 %
$\Gamma_2$ $N\eta$	2–6 %
$\Gamma_3$ $N\omega$	1–7 %
$\Gamma_4$ $\Lambda K$	seen
$\Gamma_5$ $\Sigma K$	1–5 %
$\Gamma_6$ $N\pi\pi$	7–19 %
$\Gamma_7$ $\Delta(1232)\pi$	
$\Gamma_8$ $\Delta(1232)\pi, D\text{-wave}$	4–10 %
$\Gamma_9$ $N\rho$	
$\Gamma_{10}$ $N\rho, S=1/2, P\text{-wave}$	seen
$\Gamma_{11}$ $N\rho, S=3/2, D\text{-wave}$	
$\Gamma_{12}$ $\Lambda K^*(892)$	0.3–1.3 %
$\Gamma_{13}$ $N\sigma$	3–9 %
$\Gamma_{14}$ $N(1440)\pi$	4–14 %
$\Gamma_{15}$ $N(1520)\pi, P\text{-wave}$	9–21 %
$\Gamma_{16}$ $N(1680)\pi, S\text{-wave}$	8–22 %
$\Gamma_{17}$ $p\gamma$	0.03–0.19 %
$\Gamma_{18}$ $p\gamma, \text{helicity}=1/2$	0.02–0.08 %
$\Gamma_{19}$ $p\gamma, \text{helicity}=3/2$	0.01–0.10 %
$\Gamma_{20}$ $n\gamma$	0.003–0.07 %
$\Gamma_{21}$ $n\gamma, \text{helicity}=1/2$	0.001–0.02 %
$\Gamma_{22}$ $n\gamma, \text{helicity}=3/2$	0.002–0.05 %

N(2060) BRANCHING RATIOS

$\Gamma(N\pi)/\Gamma_{total}$	DOCUMENT ID	TECN	COMMENT	$\Gamma_1/\Gamma$
VALUE (%)				
<b>7 to 12 (<math>\approx 10</math>) OUR ESTIMATE</b>				
5.3 $\pm$ 1.4	<sup>1</sup> HUNT	19	DPWA	Multichannel
11 $\pm$ 2	SOKHOYAN	15A	DPWA	Multichannel
10 $\pm$ 3	CUTKOSKY	80	IPWA	$\pi N \rightarrow \pi N$
7 $\pm$ 2	HOEHLER	79	IPWA	$\pi N \rightarrow \pi N$
••• We do not use the following data for averages, fits, limits, etc. •••				
8 $\pm$ 2	ANISOVICH	12A	DPWA	Multichannel
9 $\pm$ 2	<sup>1</sup> SHRESTHA	12A	DPWA	Multichannel
13 $\pm$ 4	BATINIC	10	DPWA	$\pi N \rightarrow N\pi, N\eta$

<sup>1</sup> Statistical error only.

$\Gamma(N\eta)/\Gamma_{total}$	DOCUMENT ID	TECN	COMMENT	$\Gamma_2/\Gamma$
VALUE (%)				
30 $\pm$ 8	<sup>1</sup> HUNT	19	DPWA	Multichannel
4 $\pm$ 2	ANISOVICH	12A	DPWA	Multichannel
••• We do not use the following data for averages, fits, limits, etc. •••				
< 1	<sup>1</sup> SHRESTHA	12A	DPWA	Multichannel
0.2 $\pm$ 1.0	BATINIC	10	DPWA	$\pi N \rightarrow N\pi, N\eta$

<sup>1</sup> Statistical error only.

$\Gamma(N\omega)/\Gamma_{total}$	DOCUMENT ID	TECN	COMMENT	$\Gamma_3/\Gamma$
VALUE (%)				
4 $\pm$ 3	DENISENKO	16	DPWA	Multichannel

$\Gamma(\Lambda K)/\Gamma_{total}$	DOCUMENT ID	TECN	COMMENT	$\Gamma_4/\Gamma$
VALUE (%)				
15 $\pm$ 5	<sup>1</sup> HUNT	19	DPWA	Multichannel

<sup>1</sup> Statistical error only.

$\Gamma(\Sigma K)/\Gamma_{total}$	DOCUMENT ID	TECN	COMMENT	$\Gamma_5/\Gamma$
VALUE (%)				
3 $\pm$ 2	ANISOVICH	12A	DPWA	Multichannel

$\Gamma(\Delta(1232)\pi, D\text{-wave})/\Gamma_{total}$	DOCUMENT ID	TECN	COMMENT	$\Gamma_8/\Gamma$
VALUE (%)				
15 $\pm$ 6	<sup>1</sup> HUNT	19	DPWA	Multichannel
7 $\pm$ 3	SOKHOYAN	15A	DPWA	Multichannel
••• We do not use the following data for averages, fits, limits, etc. •••				
40 $\pm$ 13	<sup>1</sup> SHRESTHA	12A	DPWA	Multichannel

<sup>1</sup> Statistical error only.

$\Gamma(N\rho, S=1/2, P\text{-wave})/\Gamma_{total}$	DOCUMENT ID	TECN	COMMENT	$\Gamma_{10}/\Gamma$
VALUE (%)				
<10	<sup>1</sup> HUNT	19	DPWA	Multichannel
••• We do not use the following data for averages, fits, limits, etc. •••				
21 $\pm$ 15	<sup>1</sup> SHRESTHA	12A	DPWA	Multichannel

<sup>1</sup> Statistical error only.

$\Gamma(N\rho, S=3/2, D\text{-wave})/\Gamma_{total}$	DOCUMENT ID	TECN	COMMENT	$\Gamma_{11}/\Gamma$
VALUE (%)				
14 $\pm$ 9	<sup>1</sup> HUNT	19	DPWA	Multichannel

<sup>1</sup> Statistical error only.

$\Gamma(\Lambda K^*(892))/\Gamma_{total}$	DOCUMENT ID	TECN	COMMENT	$\Gamma_{12}/\Gamma$
VALUE				
0.008 $\pm$ 0.005	ANISOVICH	17B	DPWA	Multichannel

$\Gamma(N\sigma)/\Gamma_{total}$	DOCUMENT ID	TECN	COMMENT	$\Gamma_{13}/\Gamma$
VALUE (%)				
6 $\pm$ 3	SOKHOYAN	15A	DPWA	Multichannel

$\Gamma(N(1440)\pi)/\Gamma_{total}$	DOCUMENT ID	TECN	COMMENT	$\Gamma_{14}/\Gamma$
VALUE (%)				
9 $\pm$ 5	SOKHOYAN	15A	DPWA	Multichannel

$\Gamma(N(1520)\pi, P\text{-wave})/\Gamma_{total}$	DOCUMENT ID	TECN	COMMENT	$\Gamma_{15}/\Gamma$
VALUE (%)				
15 $\pm$ 6	SOKHOYAN	15A	DPWA	Multichannel

$\Gamma(N(1680)\pi, S\text{-wave})/\Gamma_{total}$	DOCUMENT ID	TECN	COMMENT	$\Gamma_{16}/\Gamma$
VALUE (%)				
15 $\pm$ 7	SOKHOYAN	15A	DPWA	Multichannel

N(2060) PHOTON DECAY AMPLITUDES AT THE POLE

N(2060)  $\rightarrow p\gamma$ , helicity-1/2 amplitude  $A_{1/2}$

MODULUS (GeV <sup>-1/2</sup> )	PHASE (°)	DOCUMENT ID	TECN	COMMENT
0.064 $\pm$ 0.010	12 $\pm$ 8	SOKHOYAN	15A	DPWA Multichannel

N(2060)  $\rightarrow p\gamma$ , helicity-3/2 amplitude  $A_{3/2}$

MODULUS (GeV <sup>-1/2</sup> )	PHASE (°)	DOCUMENT ID	TECN	COMMENT
0.060 $\pm$ 0.020	13 $\pm$ 10	SOKHOYAN	15A	DPWA Multichannel

N(2060) BREIT-WIGNER PHOTON DECAY AMPLITUDES

N(2060)  $\rightarrow p\gamma$ , helicity-1/2 amplitude  $A_{1/2}$

VALUE (GeV <sup>-1/2</sup> )	DOCUMENT ID	TECN	COMMENT
-0.019 $\pm$ 0.005	<sup>1</sup> HUNT	19	DPWA Multichannel
0.062 $\pm$ 0.010	SOKHOYAN	15A	DPWA Multichannel
••• We do not use the following data for averages, fits, limits, etc. •••			
0.018 $\pm$ 0.004	<sup>1</sup> SHRESTHA	12A	DPWA Multichannel

<sup>1</sup> Statistical error only.

N(2060)  $\rightarrow p\gamma$ , helicity-3/2 amplitude  $A_{3/2}$

VALUE (GeV <sup>-1/2</sup> )	DOCUMENT ID	TECN	COMMENT
0.039 $\pm$ 0.005	<sup>1</sup> HUNT	19	DPWA Multichannel
0.062 $\pm$ 0.020	SOKHOYAN	15A	DPWA Multichannel
••• We do not use the following data for averages, fits, limits, etc. •••			
0.010 $\pm$ 0.004	<sup>1</sup> SHRESTHA	12A	DPWA Multichannel

<sup>1</sup> Statistical error only.

N(2060)  $\rightarrow n\gamma$ , helicity-1/2 amplitude  $A_{1/2}$

VALUE (GeV <sup>-1/2</sup> )	DOCUMENT ID	TECN	COMMENT
0.069 $\pm$ 0.017	<sup>1</sup> HUNT	19	DPWA Multichannel
0.025 $\pm$ 0.011	ANISOVICH	13B	DPWA Multichannel
••• We do not use the following data for averages, fits, limits, etc. •••			
-0.012 $\pm$ 0.017	<sup>1</sup> SHRESTHA	12A	DPWA Multichannel

<sup>1</sup> Statistical error only.

N(2060)  $\rightarrow n\gamma$ , helicity-3/2 amplitude  $A_{3/2}$

VALUE (GeV <sup>-1/2</sup> )	DOCUMENT ID	TECN	COMMENT
-0.023 $\pm$ 0.020	<sup>1</sup> HUNT	19	DPWA Multichannel
-0.037 $\pm$ 0.017	ANISOVICH	13B	DPWA Multichannel
••• We do not use the following data for averages, fits, limits, etc. •••			
-0.023 $\pm$ 0.023	<sup>1</sup> SHRESTHA	12A	DPWA Multichannel

<sup>1</sup> Statistical error only.

N(2060) REFERENCES

HUNT	19	PR C99 055205	B.C. Hunt, D.M. Manley
ANISOVICH	17B	PL B771 142	A.V. Anisovich et al.
DENISENKO	16	PL B755 37	I. Denisenko et al.
SOKHOYAN	15A	EPJ A51 95	V. Sokhoyan et al.
SVARC	14	PR C89 045205	A. Svarc et al. (CBELSA/TAPS Collab.) (RBI Zagreb, UNI Tuzla)
ANISOVICH	13B	EPJ A49 67	A.V. Anisovich et al.
ANISOVICH	12A	EPJ A48 15	A.V. Anisovich et al. (BONN, PNPI)
SHRESTHA	12A	PR C86 055203	M. Shrestha, D.M. Manley (KSU)
BATINIC	10	PR C82 038203	M. Batinic et al. (ZAGR)
CUTKOSKY	80	Toronto Conf. 19	R.E. Cutkosky et al. (CMU, LBL) IJP
Also		PR D20 2839	R.E. Cutkosky et al. (CMU, LBL)
HOEHLER	79	PDAT 12-1	G. Hoehler et al. (KARLT) IJP
Also		Toronto Conf. 3	R. Koch (KARLT) IJP

$N(2100) 1/2^+$

$I(J^P) = \frac{1}{2}(\frac{1}{2}^+)$  Status: \*\*\*

N(2100) POLE POSITION

REAL PART

VALUE (MeV)	DOCUMENT ID	TECN	COMMENT
<b>2050 to 2150 (<math>\approx 2100</math>) OUR ESTIMATE</b>			
2120 $\pm$ 25	SOKHOYAN	15A	DPWA Multichannel
2052 $\pm$ 6 $\pm$ 3	<sup>1</sup> SVARC	14	L+P $\pi N \rightarrow \pi N$
2120 $\pm$ 40	CUTKOSKY	80	IPWA $\pi N \rightarrow \pi N$
••• We do not use the following data for averages, fits, limits, etc. •••			
2217	HUNT	19	DPWA Multichannel
2120 $\pm$ 47	BATINIC	10	DPWA $\pi N \rightarrow N\pi, N\eta$
1810	VRANA	00	DPWA Multichannel

<sup>1</sup> Fit to the amplitudes of HOEHLER 79.

-2xIMAGINARY PART

VALUE (MeV)	DOCUMENT ID	TECN	COMMENT
<b>240 to 340 (<math>\approx 300</math>) OUR ESTIMATE</b>			
290 $\pm$ 30	SOKHOYAN	15A	DPWA Multichannel
337 $\pm$ 10 $\pm$ 4	<sup>1</sup> SVARC	14	L+P $\pi N \rightarrow \pi N$
240 $\pm$ 80	CUTKOSKY	80	IPWA $\pi N \rightarrow \pi N$
••• We do not use the following data for averages, fits, limits, etc. •••			
545	HUNT	19	DPWA Multichannel
346 $\pm$ 80	BATINIC	10	DPWA $\pi N \rightarrow N\pi, N\eta$
622	VRANA	00	DPWA Multichannel

<sup>1</sup> Fit to the amplitudes of HOEHLER 79.

## Baryon Particle Listings

 $N(2100)$  $N(2100)$  ELASTIC POLE RESIDUEMODULUS  $|r|$ 

VALUE (MeV)	DOCUMENT ID	TECN	COMMENT
<b>15 to 30 (<math>\approx 20</math>) OUR ESTIMATE</b>			
23 $\pm$ 5	SOKHOYAN	15A	DPWA Multichannel
30 $\pm$ 1 $\pm$ 1	<sup>1</sup> SVARC	14	L+P $\pi N \rightarrow \pi N$
14 $\pm$ 7	CUTKOSKY	80	IPWA $\pi N \rightarrow \pi N$
••• We do not use the following data for averages, fits, limits, etc. •••			
33	BATINIC	10	DPWA $\pi N \rightarrow N\pi, N\eta$

<sup>1</sup> Fit to the amplitudes of HOEHLER 79.PHASE  $\theta$ 

VALUE (°)	DOCUMENT ID	TECN	COMMENT
<b>-100 to -60 (<math>\approx -80</math>) OUR ESTIMATE</b>			
-70 $\pm$ 25	SOKHOYAN	15A	DPWA Multichannel
-92 $\pm$ 3 $\pm$ 2	<sup>1</sup> SVARC	14	L+P $\pi N \rightarrow \pi N$
35 $\pm$ 25	CUTKOSKY	80	IPWA $\pi N \rightarrow \pi N$
••• We do not use the following data for averages, fits, limits, etc. •••			
-59	BATINIC	10	DPWA $\pi N \rightarrow N\pi, N\eta$

<sup>1</sup> Fit to the amplitudes of HOEHLER 79. $N(2100)$  INELASTIC POLE RESIDUENormalized residue in  $N\pi \rightarrow N(2100) \rightarrow \Delta(1232)\pi$ 

MODULUS	PHASE (°)	DOCUMENT ID	TECN	COMMENT
0.11 $\pm$ 0.05	20 $\pm$ 60	SOKHOYAN	15A	DPWA Multichannel

Normalized residue in  $N\pi \rightarrow N(2100) \rightarrow N\sigma$ 

MODULUS	PHASE (°)	DOCUMENT ID	TECN	COMMENT
0.18 $\pm$ 0.06	125 $\pm$ 25	SOKHOYAN	15A	DPWA Multichannel

Normalized residue in  $N\pi \rightarrow N(2100) \rightarrow N(1535)\pi$ 

MODULUS	PHASE (°)	DOCUMENT ID	TECN	COMMENT
0.22 $\pm$ 0.06	-40 $\pm$ 25	SOKHOYAN	15A	DPWA Multichannel

 $N(2100)$  BREIT-WIGNER MASS

VALUE (MeV)	DOCUMENT ID	TECN	COMMENT
<b>2050 to 2150 (<math>\approx 2100</math>) OUR ESTIMATE</b>			
2221 $\pm$ 92	<sup>1</sup> HUNT	19	DPWA Multichannel
2115 $\pm$ 20	SOKHOYAN	15A	DPWA Multichannel
2125 $\pm$ 75	CUTKOSKY	80	IPWA $\pi N \rightarrow \pi N$
2050 $\pm$ 20	HOEHLER	79	IPWA $\pi N \rightarrow \pi N$
••• We do not use the following data for averages, fits, limits, etc. •••			
2157 $\pm$ 42	BATINIC	10	DPWA $\pi N \rightarrow N\pi, N\eta$
2068 $\pm$ 3 $\pm$ 15	ABLIKIM	06K	BES2 $J/\psi \rightarrow (p\pi^-)\bar{\pi}$
2084 $\pm$ 93	VRANA	00	DPWA Multichannel

<sup>1</sup> Statistical error only. $N(2100)$  BREIT-WIGNER WIDTH

VALUE (MeV)	DOCUMENT ID	TECN	COMMENT
<b>200 to 320 (<math>\approx 260</math>) OUR ESTIMATE</b>			
545 $\pm$ 170	<sup>1</sup> HUNT	19	DPWA Multichannel
290 $\pm$ 20	SOKHOYAN	15A	DPWA Multichannel
260 $\pm$ 100	CUTKOSKY	80	IPWA $\pi N \rightarrow \pi N$
200 $\pm$ 30	HOEHLER	79	IPWA $\pi N \rightarrow \pi N$
••• We do not use the following data for averages, fits, limits, etc. •••			
355 $\pm$ 88	BATINIC	10	DPWA $\pi N \rightarrow N\pi, N\eta$
165 $\pm$ 14 $\pm$ 40	ABLIKIM	06K	BES2 $J/\psi \rightarrow (p\pi^-)\bar{\pi}$
1077 $\pm$ 643	VRANA	00	DPWA Multichannel

<sup>1</sup> Statistical error only. $N(2100)$  DECAY MODES

Mode	Fraction ( $\Gamma_i/\Gamma$ )
$\Gamma_1$ $N\pi$	8-18 %
$\Gamma_2$ $N\eta$	seen
$\Gamma_3$ $N\eta'$	5-11 %
$\Gamma_4$ $N\omega$	10-25 %
$\Gamma_5$ $\Lambda K$	seen
$\Gamma_6$ $N\pi\pi$	20-40 %
$\Gamma_7$ $\Delta(1232)\pi$	
$\Gamma_8$ $\Delta(1232)\pi, P\text{-wave}$	6-14 %
$\Gamma_9$ $N\rho$	
$\Gamma_{10}$ $N\rho, S=1/2, P\text{-wave}$	seen
$\Gamma_{11}$ $\Lambda K^*(892)$	3-11 %
$\Gamma_{12}$ $N\sigma$	14-26 %
$\Gamma_{13}$ $N(1535)\pi$	26-34 %
$\Gamma_{14}$ $N\gamma, \text{helicity}=1/2$	0.001-0.012 %

 $N(2100)$  BRANCHING RATIOS $\Gamma(N\pi)/\Gamma_{\text{total}}$   $\Gamma_1/\Gamma$ 

VALUE (%)	DOCUMENT ID	TECN	COMMENT
<b>8 to 18 (<math>\approx 12</math>) OUR ESTIMATE</b>			
21 $\pm$ 11	<sup>1</sup> HUNT	19	DPWA Multichannel
16 $\pm$ 5	SOKHOYAN	15A	DPWA Multichannel
12 $\pm$ 3	CUTKOSKY	80	IPWA $\pi N \rightarrow \pi N$
10 $\pm$ 4	HOEHLER	79	IPWA $\pi N \rightarrow \pi N$
••• We do not use the following data for averages, fits, limits, etc. •••			
16 $\pm$ 5	BATINIC	10	DPWA $\pi N \rightarrow N\pi, N\eta$
2 $\pm$ 5	VRANA	00	DPWA Multichannel

<sup>1</sup> Statistical error only. $\Gamma(N\eta)/\Gamma_{\text{total}}$   $\Gamma_2/\Gamma$ 

VALUE (%)	DOCUMENT ID	TECN	COMMENT
< 4.7	<sup>1</sup> HUNT	19	DPWA Multichannel
••• We do not use the following data for averages, fits, limits, etc. •••			
83 $\pm$ 5	BATINIC	10	DPWA $\pi N \rightarrow N\pi, N\eta$
61 $\pm$ 61	VRANA	00	DPWA Multichannel

<sup>1</sup> Statistical error only. $\Gamma(N\eta')/\Gamma_{\text{total}}$   $\Gamma_3/\Gamma$ 

VALUE (%)	DOCUMENT ID	TECN	COMMENT
0.08 $\pm$ 0.03	ANISOVICH	17C	DPWA Multichannel

 $\Gamma(N\omega)/\Gamma_{\text{total}}$   $\Gamma_4/\Gamma$ 

VALUE (%)	DOCUMENT ID	TECN	COMMENT
15 $\pm$ 10	DENISENKO	16	DPWA Multichannel

 $\Gamma(\Lambda K)/\Gamma_{\text{total}}$   $\Gamma_5/\Gamma$ 

VALUE (%)	DOCUMENT ID	TECN	COMMENT
< 1.0	<sup>1</sup> HUNT	19	DPWA Multichannel
••• We do not use the following data for averages, fits, limits, etc. •••			
21 $\pm$ 20	VRANA	00	DPWA Multichannel

<sup>1</sup> Statistical error only. $\Gamma(\Delta(1232)\pi, P\text{-wave})/\Gamma_{\text{total}}$   $\Gamma_8/\Gamma$ 

VALUE (%)	DOCUMENT ID	TECN	COMMENT
< 7.5	<sup>1</sup> HUNT	19	DPWA Multichannel
10 $\pm$ 4	SOKHOYAN	15A	DPWA Multichannel
••• We do not use the following data for averages, fits, limits, etc. •••			
2 $\pm$ 1	VRANA	00	DPWA Multichannel

<sup>1</sup> Statistical error only. $\Gamma(N\rho, S=1/2, P\text{-wave})/\Gamma_{\text{total}}$   $\Gamma_{10}/\Gamma$ 

VALUE (%)	DOCUMENT ID	TECN	COMMENT
52 $\pm$ 19	<sup>1</sup> HUNT	19	DPWA Multichannel
••• We do not use the following data for averages, fits, limits, etc. •••			
4 $\pm$ 1	VRANA	00	DPWA Multichannel

<sup>1</sup> Statistical error only. $\Gamma(\Lambda K^*(892))/\Gamma_{\text{total}}$   $\Gamma_{11}/\Gamma$ 

VALUE (%)	DOCUMENT ID	TECN	COMMENT
0.07 $\pm$ 0.04	ANISOVICH	17B	DPWA Multichannel

 $\Gamma(N\sigma)/\Gamma_{\text{total}}$   $\Gamma_{12}/\Gamma$ 

VALUE (%)	DOCUMENT ID	TECN	COMMENT
<35	<sup>1</sup> HUNT	19	DPWA Multichannel
20 $\pm$ 6	SOKHOYAN	15A	DPWA Multichannel
••• We do not use the following data for averages, fits, limits, etc. •••			
10 $\pm$ 1	VRANA	00	DPWA Multichannel

<sup>1</sup> Statistical error only. $\Gamma(N(1535)\pi)/\Gamma_{\text{total}}$   $\Gamma_{13}/\Gamma$ 

VALUE (%)	DOCUMENT ID	TECN	COMMENT
30 $\pm$ 4	SOKHOYAN	15A	DPWA Multichannel

 $N(2100)$  PHOTON DECAY AMPLITUDES AT THE POLE $N(2100) \rightarrow p\gamma, \text{helicity-1/2 amplitude } A_{1/2}$ 

MODULUS ( $\text{GeV}^{-1/2}$ )	PHASE (°)	DOCUMENT ID	TECN	COMMENT
0.011 $\pm$ 0.004	65 $\pm$ 30	SOKHOYAN	15A	DPWA Multichannel

 $N(2100)$  BREIT-WIGNER PHOTON DECAY AMPLITUDES $N(2100) \rightarrow p\gamma, \text{helicity-1/2 amplitude } A_{1/2}$ 

VALUE ( $\text{GeV}^{-1/2}$ )	DOCUMENT ID	TECN	COMMENT
0.032 $\pm$ 0.014	<sup>1</sup> HUNT	19	DPWA Multichannel
0.010 $\pm$ 0.004	SOKHOYAN	15A	DPWA Multichannel

<sup>1</sup> Statistical error only.

See key on page 999

# Baryon Particle Listings

## $N(2100)$ , $N(2120)$

### $N(2100) \rightarrow n\gamma$ , helicity-1/2 amplitude $A_{1/2}$

VALUE (GeV <sup>-1/2</sup> )	DOCUMENT ID	TECN	COMMENT
0.026 ± 0.013	<sup>1</sup> HUNT	19	DPWA Multichannel

<sup>1</sup> Statistical error only.

### $N(2100)$ REFERENCES

HUNT	19	PR C99 055205	B.C. Hunt, D.M. Manley
ANISOVICH	17B	PL B771 142	A.V. Anisovich et al.
ANISOVICH	17C	PL B772 247	A.V. Anisovich et al.
DENISENKO	16	PL B755 97	I. Denisenko et al.
SOKHOYAN	15A	EPJ A51 95	V. Sokhoyan et al. (CBELSA/TAPS Collab.)
SVARC	14	PR C89 045205	A. Svarc et al. (RBI Zagreb, UNI Tuzla)
BATINIC	10	PR C82 038203	M. Batinic et al. (ZAGR)
ABLIKIM	06K	PRL 97 062001	M. Ablikim et al. (BES II Collab.)
VRANA	00	PRPL 328 181	T.P. Vrana, S.A. Dytman, T.-S.H. Lee (PITT, ANL)
CUTKOSKY	80	Toronto Conf. 19	R.E. Cutkosky et al. (CMU, LBL) IJP
Also		PR D20 2839	R.E. Cutkosky et al. (CMU, LBL)
HOEHLER	79	PDAT 12-1	G. Hoehler et al. (KARLT) IJP
Also		Toronto Conf. 3	R. Koch (KARLT) IJP

### $N(2120) 3/2^-$

$$I(J^P) = \frac{1}{2}(3/2^-) \text{ Status: } ***$$

Before the 2012 Review, all the evidence for a  $J^P = 3/2^-$  state with a mass above 1800 MeV was filed under a two-star  $N(2080)$ . There is now evidence from ANISOVICH 12A for two  $3/2^-$  states in this region, so we have split the older data (according to mass) between a three-star  $N(1875)$  and a two-star  $N(2120)$ .

### $N(2120)$ POLE POSITION

#### REAL PART

VALUE (MeV)	DOCUMENT ID	TECN	COMMENT
<b>2050 to 2150 (≈ 2100) OUR ESTIMATE</b>			
2115 ± 40	SOKHOYAN	15A	DPWA Multichannel
2094 ± 7 ± 11	SVARC	14	L+P $\pi N \rightarrow \pi N$
2050 ± 70	CUTKOSKY	80	IPWA $\pi N \rightarrow \pi N$ (higher $m$ )
• • •	We do not use the following data for averages, fits, limits, etc. • • •		
2357	HUNT	19	DPWA Multichannel
2115 ± 40	GUTZ	14	DPWA Multichannel
2110 ± 50	ANISOVICH	12A	DPWA Multichannel

#### -2xIMAGINARY PART

VALUE (MeV)	DOCUMENT ID	TECN	COMMENT
<b>200 to 360 (≈ 280) OUR ESTIMATE</b>			
345 ± 35	SOKHOYAN	15A	DPWA Multichannel
296 ± 15 ± 4	SVARC	14	L+P $\pi N \rightarrow \pi N$
200 ± 80	CUTKOSKY	80	IPWA $\pi N \rightarrow \pi N$ (higher $m$ )
• • •	We do not use the following data for averages, fits, limits, etc. • • •		
503	HUNT	19	DPWA Multichannel
345 ± 35	GUTZ	14	DPWA Multichannel
340 ± 45	ANISOVICH	12A	DPWA Multichannel

### $N(2120)$ ELASTIC POLE RESIDUE

#### MODULUS $|r|$

VALUE (MeV)	DOCUMENT ID	TECN	COMMENT
<b>10 to 30 (≈ 20) OUR ESTIMATE</b>			
11 ± 6	SOKHOYAN	15A	DPWA Multichannel
13 ± 1 ± 1	SVARC	14	L+P $\pi N \rightarrow \pi N$
30 ± 20	CUTKOSKY	80	IPWA $\pi N \rightarrow \pi N$ (higher $m$ )
• • •	We do not use the following data for averages, fits, limits, etc. • • •		
11 ± 6	GUTZ	14	DPWA Multichannel
13 ± 3	ANISOVICH	12A	DPWA Multichannel

#### PHASE $\theta$

VALUE (°)	DOCUMENT ID	TECN	COMMENT
<b>-40 to 20 (≈ -10) OUR ESTIMATE</b>			
-30 ± 20	SOKHOYAN	15A	DPWA Multichannel
-2 ± 4 ± 9	SVARC	14	L+P $\pi N \rightarrow \pi N$
0 ± 100	CUTKOSKY	80	IPWA $\pi N \rightarrow \pi N$ (higher $m$ )
• • •	We do not use the following data for averages, fits, limits, etc. • • •		
-30 ± 20	GUTZ	14	DPWA Multichannel
-20 ± 10	ANISOVICH	12A	DPWA Multichannel

### $N(2120)$ INELASTIC POLE RESIDUE

The "normalized residue" is the residue divided by  $\Gamma_{pole}/2$ .

#### Normalized residue in $N\pi \rightarrow N(2120) \rightarrow \Lambda K$

MODULUS	PHASE (°)	DOCUMENT ID	TECN	COMMENT
0.03 ± 0.01	100 ± 30	ANISOVICH	12A	DPWA Multichannel

#### Normalized residue in $N\pi \rightarrow N(2120) \rightarrow \Sigma K$

MODULUS	PHASE (°)	DOCUMENT ID	TECN	COMMENT
0.02 ± 0.015	-50 ± 40	ANISOVICH	12A	DPWA Multichannel

### Normalized residue in $N\pi \rightarrow N(2120) \rightarrow N(1535)\pi$

MODULUS	PHASE (°)	DOCUMENT ID	TECN	COMMENT
0.15 ± 0.08	-90 ± 40	GUTZ	14	DPWA Multichannel

### Normalized residue in $N\pi \rightarrow N(2120) \rightarrow \Delta(1232)\pi$ , S-wave

MODULUS	PHASE (°)	DOCUMENT ID	TECN	COMMENT
0.25 ± 0.10	undefined	SOKHOYAN	15A	DPWA Multichannel

### Normalized residue in $N\pi \rightarrow N(2120) \rightarrow \Delta(1232)\pi$ , D-wave

MODULUS	PHASE (°)	DOCUMENT ID	TECN	COMMENT
0.15 ± 0.06	-35 ± 30	SOKHOYAN	15A	DPWA Multichannel

### Normalized residue in $N\pi \rightarrow N(2120) \rightarrow N\sigma$

MODULUS	PHASE (°)	DOCUMENT ID	TECN	COMMENT
0.09 ± 0.05	-80 ± 50	SOKHOYAN	15A	DPWA Multichannel

### $N(2120)$ BREIT-WIGNER MASS

VALUE (MeV)	DOCUMENT ID	TECN	COMMENT
<b>2060 to 2160 (≈ 2120) OUR ESTIMATE</b>			
2353 ± 29	<sup>1</sup> HUNT	19	DPWA Multichannel
2120 ± 45	SOKHOYAN	15A	DPWA Multichannel
2060 ± 80	CUTKOSKY	80	IPWA $\pi N \rightarrow \pi N$
2081 ± 20	HOEHLER	79	IPWA $\pi N \rightarrow \pi N$
• • •	We do not use the following data for averages, fits, limits, etc. • • •		
2120 ± 35	GUTZ	14	DPWA Multichannel
2150 ± 60	ANISOVICH	12A	DPWA Multichannel

<sup>1</sup> Statistical error only.

### $N(2120)$ BREIT-WIGNER WIDTH

VALUE (MeV)	DOCUMENT ID	TECN	COMMENT
<b>260 to 360 (≈ 300) OUR ESTIMATE</b>			
503 ± 62	<sup>1</sup> HUNT	19	DPWA Multichannel
340 ± 35	SOKHOYAN	15A	DPWA Multichannel
300 ± 100	CUTKOSKY	80	IPWA $\pi N \rightarrow \pi N$ (higher $m$ )
265 ± 40	HOEHLER	79	IPWA $\pi N \rightarrow \pi N$
• • •	We do not use the following data for averages, fits, limits, etc. • • •		
340 ± 35	GUTZ	14	DPWA Multichannel
330 ± 45	ANISOVICH	12A	DPWA Multichannel

<sup>1</sup> Statistical error only.

### $N(2120)$ DECAY MODES

Mode	Fraction ( $\Gamma_i/\Gamma$ )
$\Gamma_1$ $N\pi$	5-15 %
$\Gamma_2$ $N\eta$	
$\Gamma_3$ $N\eta'$	2-6 %
$\Gamma_4$ $N\omega$	4-20 %
$\Gamma_5$ $\Lambda K$	
$\Gamma_6$ $N\pi\pi$	50-95 %
$\Gamma_7$ $\Delta(1232)\pi$	40-90 %
$\Gamma_8$ $\Delta(1232)\pi$ , S-wave	30-70 %
$\Gamma_9$ $\Delta(1232)\pi$ , D-wave	8-32 %
$\Gamma_{10}$ $N\rho$	
$\Gamma_{11}$ $N\rho$ , S=3/2, S-wave	
$\Gamma_{12}$ $\Lambda K^*(892)$	< 0.2 %
$\Gamma_{13}$ $N\sigma$	7-15 %
$\Gamma_{14}$ $N(1535)\pi$	7-23 %
$\Gamma_{15}$ $p\gamma$	0.16-2.1 %
$\Gamma_{16}$ $p\gamma$ , helicity=1/2	0.07-0.80 %
$\Gamma_{17}$ $p\gamma$ , helicity=3/2	0.09-1.3 %
$\Gamma_{18}$ $n\gamma$	0.04-0.72 %
$\Gamma_{19}$ $n\gamma$ , helicity=1/2	0.04-0.60 %
$\Gamma_{20}$ $n\gamma$ , helicity=3/2	0.001-0.12 %

### $N(2120)$ BRANCHING RATIOS

$\Gamma(N\pi)/\Gamma_{total}$	VALUE (%)	DOCUMENT ID	TECN	COMMENT	$\Gamma_1/\Gamma$
<b>5 to 15 (≈ 10) OUR ESTIMATE</b>					
19 ± 2	<sup>1</sup> HUNT	19	DPWA	Multichannel	
5 ± 3	SOKHOYAN	15A	DPWA	Multichannel	
14 ± 7	CUTKOSKY	80	IPWA	$\pi N \rightarrow \pi N$ (higher $m$ )	
6 ± 2	HOEHLER	79	IPWA	$\pi N \rightarrow \pi N$	
• • •	We do not use the following data for averages, fits, limits, etc. • • •				
5 ± 3	GUTZ	14	DPWA	Multichannel	
6 ± 2	ANISOVICH	12A	DPWA	Multichannel	

<sup>1</sup> Statistical error only.

## Baryon Particle Listings

 $N(2120)$ ,  $N(2190)$  $\Gamma(N\eta)/\Gamma_{\text{total}}$ 

VALUE (%)	DOCUMENT ID	TECN	COMMENT
$3.1 \pm 2.4$	<sup>1</sup> HUNT 19	DPWA	Multichannel

<sup>1</sup> Statistical error only.

 $\Gamma(N\eta')/\Gamma_{\text{total}}$ 

VALUE (%)	DOCUMENT ID	TECN	COMMENT
$0.04 \pm 0.02$	ANISOVICH 17C	DPWA	Multichannel

 $\Gamma(N\omega)/\Gamma_{\text{total}}$ 

VALUE (%)	DOCUMENT ID	TECN	COMMENT
$12 \pm 8$	DENISENKO 16	DPWA	Multichannel

 $\Gamma(\Lambda K)/\Gamma_{\text{total}}$ 

VALUE (%)	DOCUMENT ID	TECN	COMMENT
$8.5 \pm 2.5$	<sup>1</sup> HUNT 19	DPWA	Multichannel

<sup>1</sup> Statistical error only.

 $\Gamma(\Delta(1232)\pi, S\text{-wave})/\Gamma_{\text{total}}$ 

VALUE (%)	DOCUMENT ID	TECN	COMMENT
$25 \pm 11$	<sup>1</sup> HUNT 19	DPWA	Multichannel
$50 \pm 20$	SOKHOYAN 15A	DPWA	Multichannel

<sup>1</sup> Statistical error only.

 $\Gamma(\Delta(1232)\pi, D\text{-wave})/\Gamma_{\text{total}}$ 

VALUE (%)	DOCUMENT ID	TECN	COMMENT
$34 \pm 11$	<sup>1</sup> HUNT 19	DPWA	Multichannel
$20 \pm 12$	SOKHOYAN 15A	DPWA	Multichannel

<sup>1</sup> Statistical error only.

 $\Gamma(N\rho, S=3/2, S\text{-wave})/\Gamma_{\text{total}}$ 

VALUE (%)	DOCUMENT ID	TECN	COMMENT
$< 3$	<sup>1</sup> HUNT 19	DPWA	Multichannel

<sup>1</sup> Statistical error only.

 $\Gamma(\Lambda K^*(892))/\Gamma_{\text{total}}$ 

VALUE (%)	DOCUMENT ID	TECN	COMMENT
$< 0.002$	ANISOVICH 17B	DPWA	Multichannel

 $\Gamma(N\sigma)/\Gamma_{\text{total}}$ 

VALUE (%)	DOCUMENT ID	TECN	COMMENT
$9 \pm 5$	<sup>1</sup> HUNT 19	DPWA	Multichannel
$11 \pm 4$	SOKHOYAN 15A	DPWA	Multichannel

<sup>1</sup> Statistical error only.

 $\Gamma(N(1535)\pi)/\Gamma_{\text{total}}$ 

VALUE (%)	DOCUMENT ID	TECN	COMMENT
$15 \pm 8$	GUTZ 14	DPWA	Multichannel

 **$N(2120)$  PHOTON DECAY AMPLITUDES AT THE POLE** $N(2120) \rightarrow p\gamma$ , helicity-1/2 amplitude  $A_{1/2}$ 

MODULUS ( $\text{GeV}^{-1/2}$ )	PHASE ( $^\circ$ )	DOCUMENT ID	TECN	COMMENT
$0.130 \pm 0.045$	$-40 \pm 25$	SOKHOYAN 15A	DPWA	Multichannel

 $N(2120) \rightarrow p\gamma$ , helicity-3/2 amplitude  $A_{3/2}$ 

MODULUS ( $\text{GeV}^{-1/2}$ )	PHASE ( $^\circ$ )	DOCUMENT ID	TECN	COMMENT
$0.160 \pm 0.060$	$-30 \pm 15$	SOKHOYAN 15A	DPWA	Multichannel

 **$N(2120)$  BREIT-WIGNER PHOTON DECAY AMPLITUDES** $N(2120) \rightarrow p\gamma$ , helicity-1/2 amplitude  $A_{1/2}$ 

VALUE ( $\text{GeV}^{-1/2}$ )	DOCUMENT ID	TECN	COMMENT
$0.047 \pm 0.009$	<sup>1</sup> HUNT 19	DPWA	Multichannel
$0.130 \pm 0.050$	SOKHOYAN 15A	DPWA	Multichannel

• • • We do not use the following data for averages, fits, limits, etc. • • •

$0.130 \pm 0.050$	GUTZ 14	DPWA	Multichannel
-------------------	---------	------	--------------

<sup>1</sup> Statistical error only.

 $N(2120) \rightarrow p\gamma$ , helicity-3/2 amplitude  $A_{3/2}$ 

VALUE ( $\text{GeV}^{-1/2}$ )	DOCUMENT ID	TECN	COMMENT
$0.001 \pm 0.007$	<sup>1</sup> HUNT 19	DPWA	Multichannel
$0.160 \pm 0.065$	SOKHOYAN 15A	DPWA	Multichannel

• • • We do not use the following data for averages, fits, limits, etc. • • •

$0.160 \pm 0.065$	GUTZ 14	DPWA	Multichannel
-------------------	---------	------	--------------

<sup>1</sup> Statistical error only.

 $N(2120) \rightarrow n\gamma$ , helicity-1/2 amplitude  $A_{1/2}$ 

VALUE ( $\text{GeV}^{-1/2}$ )	DOCUMENT ID	TECN	COMMENT
$-0.020 \pm 0.013$	<sup>1</sup> HUNT 19	DPWA	Multichannel
$0.110 \pm 0.045$	ANISOVICH 13B	DPWA	Multichannel

<sup>1</sup> Statistical error only.

 $N(2120) \rightarrow n\gamma$ , helicity-3/2 amplitude  $A_{3/2}$ 

VALUE ( $\text{GeV}^{-1/2}$ )	DOCUMENT ID	TECN	COMMENT
$-0.00 \pm 0.02$	<sup>1</sup> HUNT 19	DPWA	Multichannel
$0.040 \pm 0.030$	ANISOVICH 13B	DPWA	Multichannel

<sup>1</sup> Statistical error only.

 **$N(2120)$  REFERENCES**

HUNT 19	PR C99 055205	B.C. Hunt, D.M. Manley
ANISOVICH 17B	PL B771 142	A.V. Anisovich et al.
ANISOVICH 17C	PL B772 247	A.V. Anisovich et al.
DENISENKO 16	PL B755 97	I. Denisenko et al.
SOKHOYAN 15A	EPJ A51 95	V. Sokhoyan et al. (CBELSA/TAPS Collab.)
GUTZ 14	EPJ A50 74	E. Gutz et al. (CBELSA/TAPS Collab.)
SVARC 14	PR C89 045205	A. Svarc et al. (RBI Zagreb, UNI Tuzla)
ANISOVICH 13B	EPJ A49 67	A.V. Anisovich et al.
ANISOVICH 12A	EPJ A48 15	A.V. Anisovich et al. (BONN, PNPI)
CUTKOSKY 80	Toronto Conf. 19	R.E. Cutkosky et al. (CMU, LBL)
HOEHLER 79	PDAT 12-1	G. Hoehler et al. (KARLT)

 **$N(2190) 7/2^-$** 

$$I(J^P) = \frac{1}{2}(\frac{7}{2}^-) \text{ Status: } ***$$

Older and obsolete values are listed and referenced in the 2014 edition, Chinese Physics C38 070001 (2014).

 **$N(2190)$  POLE POSITION****REAL PART**

VALUE (MeV)	DOCUMENT ID	TECN	COMMENT
-------------	-------------	------	---------

**2050 to 2150 ( $\approx 2100$ ) OUR ESTIMATE**

$2150 \pm 25$	SOKHOYAN 15A	DPWA	Multichannel
$2079 \pm 4 \pm 9$	<sup>1</sup> SVARC 14	L+P	$\pi N \rightarrow \pi N$
$2100 \pm 50$	CUTKOSKY 80	IPWA	$\pi N \rightarrow \pi N$

• • • We do not use the following data for averages, fits, limits, etc. • • •

2162	HUNT 19	DPWA	Multichannel
2074	ROENCHEN 15A	DPWA	Multichannel
$2150 \pm 25$	ANISOVICH 12A	DPWA	Multichannel
$2063 \pm 32$	BATINIC 10	DPWA	$\pi N \rightarrow N\pi, N\eta$
2070	ARNDT 06	DPWA	$\pi N \rightarrow \pi N, \eta N$
2107	VRANA 00	DPWA	Multichannel
2042	HOEHLER 93	SPED	$\pi N \rightarrow \pi N$

<sup>1</sup> Fit to the amplitudes of HOEHLER 79.

**-2xIMAGINARY PART**

VALUE (MeV)	DOCUMENT ID	TECN	COMMENT
-------------	-------------	------	---------

**300 to 500 ( $\approx 400$ ) OUR ESTIMATE**

$325 \pm 25$	SOKHOYAN 15A	DPWA	Multichannel
$509 \pm 7 \pm 16$	<sup>1</sup> SVARC 14	L+P	$\pi N \rightarrow \pi N$
$400 \pm 160$	CUTKOSKY 80	IPWA	$\pi N \rightarrow \pi N$

• • • We do not use the following data for averages, fits, limits, etc. • • •

407	HUNT 19	DPWA	Multichannel
327	ROENCHEN 15A	DPWA	Multichannel
$330 \pm 30$	ANISOVICH 12A	DPWA	Multichannel
$330 \pm 101$	BATINIC 10	DPWA	$\pi N \rightarrow N\pi, N\eta$
520	ARNDT 06	DPWA	$\pi N \rightarrow \pi N, \eta N$
380	VRANA 00	DPWA	Multichannel
482	HOEHLER 93	SPED	$\pi N \rightarrow \pi N$

<sup>1</sup> Fit to the amplitudes of HOEHLER 79.

 **$N(2190)$  ELASTIC POLE RESIDUE****MODULUS  $|r|$** 

VALUE (MeV)	DOCUMENT ID	TECN	COMMENT
-------------	-------------	------	---------

**25 to 70 ( $\approx 50$ ) OUR ESTIMATE**

$30 \pm 4$	SOKHOYAN 15A	DPWA	Multichannel
$54 \pm 1 \pm 3$	<sup>1</sup> SVARC 14	L+P	$\pi N \rightarrow \pi N$
$25 \pm 10$	CUTKOSKY 80	IPWA	$\pi N \rightarrow \pi N$

• • • We do not use the following data for averages, fits, limits, etc. • • •

35	ROENCHEN 15A	DPWA	Multichannel
$30 \pm 5$	ANISOVICH 12A	DPWA	Multichannel
34	BATINIC 10	DPWA	$\pi N \rightarrow N\pi, N\eta$
72	ARNDT 06	DPWA	$\pi N \rightarrow \pi N, \eta N$
45	HOEHLER 93	SPED	$\pi N \rightarrow \pi N$

<sup>1</sup> Fit to the amplitudes of HOEHLER 79.

PHASE  $\theta$ 

VALUE (°)	DOCUMENT ID	TECN	COMMENT
<b>-30 to 30 (<math>\approx 0</math>) OUR ESTIMATE</b>			
28 ± 10	SOKHOYAN 15A	DPWA	Multichannel
-18 ± 1 ± 3	<sup>1</sup> SVARC 14	L+P	$\pi N \rightarrow \pi N$
-30 ± 50	CUTKOSKY 80	IPWA	$\pi N \rightarrow \pi N$
• • • We do not use the following data for averages, fits, limits, etc. • • •			
-40	ROENCHEN 15A	DPWA	Multichannel
30 ± 10	ANISOVICH 12A	DPWA	Multichannel
-19	BATINIC 10	DPWA	$\pi N \rightarrow N\pi, N\eta$
-32	ARNDT 06	DPWA	$\pi N \rightarrow \pi N, \eta N$
<sup>1</sup> Fit to the amplitudes of HOEHLER 79.			

## N(2190) INELASTIC POLE RESIDUE

The "normalized residue" is the residue divided by  $\Gamma_{pole}/2$ .Normalized residue in  $N\pi \rightarrow N(2190) \rightarrow \Lambda K$ 

MODULUS	PHASE (°)	DOCUMENT ID	TECN	COMMENT
0.03 ± 0.01	20 ± 15	ANISOVICH 12A	DPWA	Multichannel
• • • We do not use the following data for averages, fits, limits, etc. • • •				
0.005	-51	ROENCHEN 15A	DPWA	Multichannel

Normalized residue in  $N\pi \rightarrow N(2190) \rightarrow \Sigma K$ 

MODULUS	PHASE (°)	DOCUMENT ID	TECN	COMMENT
• • • We do not use the following data for averages, fits, limits, etc. • • •				
0.013	-69	ROENCHEN 15A	DPWA	Multichannel

Normalized residue in  $N\pi \rightarrow N(2190) \rightarrow N\eta$ 

MODULUS	PHASE (°)	DOCUMENT ID	TECN	COMMENT
• • • We do not use the following data for averages, fits, limits, etc. • • •				
0.016	129	ROENCHEN 15A	DPWA	Multichannel

Normalized residue in  $N\pi \rightarrow N(2190) \rightarrow \Delta(1232)\pi, D\text{-wave}$ 

MODULUS	PHASE (°)	DOCUMENT ID	TECN	COMMENT
0.27 ± 0.04	-165 ± 20	SOKHOYAN 15A	DPWA	Multichannel

Normalized residue in  $N\pi \rightarrow N(2190) \rightarrow N\sigma$ 

MODULUS	PHASE (°)	DOCUMENT ID	TECN	COMMENT
0.13 ± 0.05	50 ± 15	SOKHOYAN 15A	DPWA	Multichannel

## N(2190) BREIT-WIGNER MASS

VALUE (MeV)	DOCUMENT ID	TECN	COMMENT
<b>2140 to 2220 (<math>\approx 2180</math>) OUR ESTIMATE</b>			
2222 ± 15	<sup>1</sup> HUNT 19	DPWA	Multichannel
2205 ± 18	SOKHOYAN 15A	DPWA	Multichannel
2152.4 ± 1.4	<sup>1</sup> ARNDT 06	DPWA	$\pi N \rightarrow \pi N, \eta N$
2200 ± 70	CUTKOSKY 80	IPWA	$\pi N \rightarrow \pi N$
2140 ± 12	HOEHLER 79	IPWA	$\pi N \rightarrow \pi N$
• • • We do not use the following data for averages, fits, limits, etc. • • •			
2180 ± 20	ANISOVICH 12A	DPWA	Multichannel
2150 ± 26	<sup>1</sup> SHRESTHA 12A	DPWA	Multichannel
2125 ± 61	BATINIC 10	DPWA	$\pi N \rightarrow N\pi, N\eta$
2168 ± 18	VRANA 00	DPWA	Multichannel
<sup>1</sup> Statistical error only.			

## N(2190) BREIT-WIGNER WIDTH

VALUE (MeV)	DOCUMENT ID	TECN	COMMENT
<b>300 to 500 (<math>\approx 400</math>) OUR ESTIMATE</b>			
442 ± 40	<sup>1</sup> HUNT 19	DPWA	Multichannel
355 ± 30	SOKHOYAN 15A	DPWA	Multichannel
484 ± 13	<sup>1</sup> ARNDT 06	DPWA	$\pi N \rightarrow \pi N, \eta N$
500 ± 150	CUTKOSKY 80	IPWA	$\pi N \rightarrow \pi N$
390 ± 30	HOEHLER 79	IPWA	$\pi N \rightarrow \pi N$
• • • We do not use the following data for averages, fits, limits, etc. • • •			
335 ± 40	ANISOVICH 12A	DPWA	Multichannel
500 ± 74	<sup>1</sup> SHRESTHA 12A	DPWA	Multichannel
381 ± 160	BATINIC 10	DPWA	$\pi N \rightarrow N\pi, N\eta$
453 ± 101	VRANA 00	DPWA	Multichannel
<sup>1</sup> Statistical error only.			

## N(2190) DECAY MODES

The following branching fractions are our estimates, not fits or averages.

Mode	Fraction ( $\Gamma_i/\Gamma$ )
$\Gamma_1$ $N\pi$	10–20 %
$\Gamma_2$ $N\eta$	1–3 %
$\Gamma_3$ $N\omega$	8–20 %

$\Gamma_4$ $\Lambda K$	
$\Gamma_5$ $N\pi\pi$	
$\Gamma_6$ $\Delta(1232)\pi$	
$\Gamma_7$ $\Delta(1232)\pi, D\text{-wave}$	19–31 %
$\Gamma_8$ $N\rho$	
$\Gamma_9$ $N\rho, S=3/2, D\text{-wave}$	seen
$\Gamma_{10}$ $\Lambda K^*(892)$	0.2–0.8 %
$\Gamma_{11}$ $N\sigma$	3–9 %
$\Gamma_{12}$ $p\gamma$	0.014–0.077 %
$\Gamma_{13}$ $p\gamma, \text{helicity}=1/2$	
$\Gamma_{14}$ $p\gamma, \text{helicity}=3/2$	
$\Gamma_{15}$ $n\gamma$	<0.04 %
$\Gamma_{16}$ $n\gamma, \text{helicity}=1/2$	
$\Gamma_{17}$ $n\gamma, \text{helicity}=3/2$	<0.03 %

## N(2190) BRANCHING RATIOS

$\Gamma(N\pi)/\Gamma_{\text{total}}$	DOCUMENT ID	TECN	COMMENT	$\Gamma_1/\Gamma$
<b>10 to 20 (<math>\approx 15</math>) OUR ESTIMATE</b>				
22.9 ± 0.6	<sup>1</sup> HUNT 19	DPWA	Multichannel	
16 ± 2	SOKHOYAN 15A	DPWA	Multichannel	
23.8 ± 0.1	<sup>1</sup> ARNDT 06	DPWA	$\pi N \rightarrow \pi N, \eta N$	
12 ± 6	CUTKOSKY 80	IPWA	$\pi N \rightarrow \pi N$	
14 ± 2	HOEHLER 79	IPWA	$\pi N \rightarrow \pi N$	
• • • We do not use the following data for averages, fits, limits, etc. • • •				
16 ± 2	ANISOVICH 12A	DPWA	Multichannel	
20 ± 1	<sup>1</sup> SHRESTHA 12A	DPWA	Multichannel	
18 ± 12	BATINIC 10	DPWA	$\pi N \rightarrow N\pi, N\eta$	
20 ± 4	VRANA 00	DPWA	Multichannel	
<sup>1</sup> Statistical error only.				

$\Gamma(N\eta)/\Gamma_{\text{total}}$	DOCUMENT ID	TECN	COMMENT	$\Gamma_2/\Gamma$
<b>10 to 20 (<math>\approx 15</math>) OUR ESTIMATE</b>				
2.7 ± 2.2	<sup>1</sup> HUNT 19	DPWA	Multichannel	
• • • We do not use the following data for averages, fits, limits, etc. • • •				
2 ± 1	<sup>1</sup> SHRESTHA 12A	DPWA	Multichannel	
0.1 ± 0.3	BATINIC 10	DPWA	$\pi N \rightarrow N\pi, N\eta$	
0 ± 1	VRANA 00	DPWA	Multichannel	
<sup>1</sup> Statistical error only.				

$\Gamma(N\omega)/\Gamma_{\text{total}}$	DOCUMENT ID	TECN	COMMENT	$\Gamma_3/\Gamma$
<b>10 to 20 (<math>\approx 15</math>) OUR ESTIMATE</b>				
14 ± 6	DENISENKO 16	DPWA	Multichannel	
• • • We do not use the following data for averages, fits, limits, etc. • • •				
seen	WILLIAMS 09	IPWA	$\gamma p \rightarrow p\omega$	

$\Gamma(\Lambda K)/\Gamma_{\text{total}}$	DOCUMENT ID	TECN	COMMENT	$\Gamma_4/\Gamma$
<b>10 to 20 (<math>\approx 15</math>) OUR ESTIMATE</b>				
0.6 ± 0.1	<sup>1</sup> HUNT 19	DPWA	Multichannel	
0.5 ± 0.3	ANISOVICH 12A	DPWA	Multichannel	
• • • We do not use the following data for averages, fits, limits, etc. • • •				
<1	<sup>1</sup> SHRESTHA 12A	DPWA	Multichannel	
<sup>1</sup> Statistical error only.				

$\Gamma(\Delta(1232)\pi, D\text{-wave})/\Gamma_{\text{total}}$	DOCUMENT ID	TECN	COMMENT	$\Gamma_7/\Gamma$
25 ± 6	SOKHOYAN 15A	DPWA	Multichannel	

$\Gamma(N\rho, S=3/2, D\text{-wave})/\Gamma_{\text{total}}$	DOCUMENT ID	TECN	COMMENT	$\Gamma_9/\Gamma$
<b>10 to 20 (<math>\approx 15</math>) OUR ESTIMATE</b>				
<11	<sup>1</sup> HUNT 19	DPWA	Multichannel	
• • • We do not use the following data for averages, fits, limits, etc. • • •				
29 ± 28	VRANA 00	DPWA	Multichannel	
<sup>1</sup> Statistical error only.				

$\Gamma(\Lambda K^*(892))/\Gamma_{\text{total}}$	DOCUMENT ID	TECN	COMMENT	$\Gamma_{10}/\Gamma$
0.005 ± 0.003	ANISOVICH 17B	DPWA	Multichannel	

$\Gamma(N\sigma)/\Gamma_{\text{total}}$	DOCUMENT ID	TECN	COMMENT	$\Gamma_{11}/\Gamma$
6 ± 3	SOKHOYAN 15A	DPWA	Multichannel	

## N(2190) PHOTON DECAY AMPLITUDES AT THE POLE

N(2190)  $\rightarrow p\gamma, \text{helicity}=1/2$  amplitude  $A_{1/2}$ 

MODULUS ( $\text{GeV}^{-1/2}$ )	PHASE (°)	DOCUMENT ID	TECN	COMMENT
0.068 ± 0.005	-170 ± 12	SOKHOYAN 15A	DPWA	Multichannel
-0.083 ± 0.007	-11 ± 6	ROENCHEN 14	DPWA	
-0.003 ± 0.003	-11 ± 2			
• • • We do not use the following data for averages, fits, limits, etc. • • •				
-0.041	-21	ROENCHEN 15A	DPWA	Multichannel



# Baryon Particle Listings

## $N(2190)$ , $N(2220)$

### $N(2190) \rightarrow p\gamma$ , helicity-3/2 amplitude $A_{3/2}$

MODULUS ( $\text{GeV}^{-1/2}$ )	PHASE ( $^\circ$ )	DOCUMENT ID	TECN	COMMENT
$0.025 \pm 0.010$	$22 \pm 10$	SOKHOYAN 15A	DPWA	Multichannel
$0.095^{+0.013}_{-0.010}$	$-3^{+3}_{-5}$	ROENCHEN 14	DPWA	
0.085	-22	ROENCHEN 15A	DPWA	Multichannel

••• We do not use the following data for averages, fits, limits, etc. •••

### $N(2190)$ BREIT-WIGNER PHOTON DECAY AMPLITUDES

#### $N(2190) \rightarrow p\gamma$ , helicity-1/2 amplitude $A_{1/2}$

VALUE ( $\text{GeV}^{-1/2}$ )	DOCUMENT ID	TECN	COMMENT
$-0.001 \pm 0.002$	<sup>1</sup> HUNT 19	DPWA	Multichannel
$-0.071 \pm 0.006$	SOKHOYAN 15A	DPWA	Multichannel
$-0.065 \pm 0.008$	ANISOVICH 12A	DPWA	Multichannel

••• We do not use the following data for averages, fits, limits, etc. •••

<sup>1</sup> Statistical error only.

#### $N(2190) \rightarrow p\gamma$ , helicity-3/2 amplitude $A_{3/2}$

VALUE ( $\text{GeV}^{-1/2}$ )	DOCUMENT ID	TECN	COMMENT
$0.015 \pm 0.003$	<sup>1</sup> HUNT 19	DPWA	Multichannel
$0.027 \pm 0.010$	SOKHOYAN 15A	DPWA	Multichannel
$0.035 \pm 0.017$	ANISOVICH 12A	DPWA	Multichannel

••• We do not use the following data for averages, fits, limits, etc. •••

<sup>1</sup> Statistical error only.

#### $N(2190) \rightarrow p\gamma$ , ratio of helicity amplitudes $A_{3/2}/A_{1/2}$

VALUE	DOCUMENT ID	TECN	COMMENT
$-0.17 \pm 0.15$	WILLIAMS 09	IPWA	$\gamma p \rightarrow p\omega$

#### $N(2190) \rightarrow n\gamma$ , helicity-1/2 amplitude $A_{1/2}$

VALUE ( $\text{GeV}^{-1/2}$ )	DOCUMENT ID	TECN	COMMENT
$-0.01 \pm 0.02$	<sup>1</sup> HUNT 19	DPWA	Multichannel
$-0.015 \pm 0.013$	ANISOVICH 13B	DPWA	Multichannel

<sup>1</sup> Statistical error only.

#### $N(2190) \rightarrow n\gamma$ , helicity-3/2 amplitude $A_{3/2}$

VALUE ( $\text{GeV}^{-1/2}$ )	DOCUMENT ID	TECN	COMMENT
$-0.023 \pm 0.022$	<sup>1</sup> HUNT 19	DPWA	Multichannel
$-0.034 \pm 0.022$	ANISOVICH 13B	DPWA	Multichannel

<sup>1</sup> Statistical error only.

### $N(2190)$ REFERENCES

For early references, see Physics Letters **111B** 1 (1982).

HUNT 19	PR C99 055205	B. C. Hunt, D.M. Manley
ANISOVICH 17B	PL B771 142	A.V. Anisovich et al.
DENISENKO 16	PL B755 97	I. Denisenko et al.
ROENCHEN 15A	EPJ A51 70	D. Roenchen et al.
SOKHOYAN 15A	EPJ A51 95	V. Sokhoyan et al. (CBELSA/TAPS Collab.)
PDG 14	CP C38 070001	K. Olive et al. (PDG Collab.)
ROENCHEN 14	EPJ A50 101	D. Roenchen et al.
Also	EPJ A51 63 (errata.)	D. Roenchen et al.
SVARC 14	PR C89 045205	A. Svarc et al. (RBI Zagreb, UNI Tuzla)
ANISOVICH 13B	EPJ A49 67	A.V. Anisovich et al.
ANISOVICH 12A	EPJ A48 15	A.V. Anisovich et al. (BONN, PNPI)
SHRESTHA 12A	PR C86 055203	M. Shrestha, D.M. Manley (KSU)
BATINIC 10	PR C82 038203	M. Batinic et al. (ZAGR)
WILLIAMS 09	PR C80 065209	M. Williams et al. (JLab CLAS Collab.)
ARNDT 06	PR C74 045205	R.A. Arndt et al. (GVU)
VRANA 00	PRPL 328 181	T.P. Vrana, S.A. Dytman, T.-S.H. Lee (PITT, ANL)
HOEHLER 93	$\pi N$ Newsletter 9 1	G. Hoehler (KARL)
CUTKOSKY 80	Toronto Conf. 19	R.E. Cutkosky et al. (CMU, LBL) IJP
Also	PR D20 2839	R.E. Cutkosky et al. (CMU, LBL) IJP
HOEHLER 79	PDAT 12-1	G. Hoehler et al. (KARLT) IJP
Also	Toronto Conf. 3	R. Koch (KARLT) IJP

$$N(2220) \ 9/2^+$$

$$I(J^P) = \frac{1}{2}(9/2^+) \text{ Status: } ***$$

Older and obsolete values are listed and referenced in the 2014 edition, Chinese Physics **C38** 070001 (2014).

### $N(2220)$ POLE POSITION

#### REAL PART

VALUE (MeV)	DOCUMENT ID	TECN	COMMENT
<b>2130 to 2200 (<math>\approx 2170</math>) OUR ESTIMATE</b>			
$2127 \pm 3 \pm 24$	<sup>1</sup> SVARC 14	L+P	$\pi N \rightarrow \pi N$
$2150 \pm 35$	ANISOVICH 12A	DPWA	Multichannel
$2160 \pm 80$	CUTKOSKY 80	IPWA	$\pi N \rightarrow \pi N$

••• We do not use the following data for averages, fits, limits, etc. •••

2171	ROENCHEN 15A	DPWA	Multichannel
2199	ARNDT 06	DPWA	$\pi N \rightarrow \pi N, \eta N$
2135	HOEHLER 93	ARGD	$\pi N \rightarrow \pi N$

<sup>1</sup> Fit to the amplitudes of HOEHLER 79.

#### -2xIMAGINARY PART

VALUE (MeV)	DOCUMENT ID	TECN	COMMENT
<b>360 to 480 (<math>\approx 400</math>) OUR ESTIMATE</b>			
$380 \pm 7 \pm 22$	<sup>1</sup> SVARC 14	L+P	$\pi N \rightarrow \pi N$
$440 \pm 40$	ANISOVICH 12A	DPWA	Multichannel
$480 \pm 100$	CUTKOSKY 80	IPWA	$\pi N \rightarrow \pi N$
••• We do not use the following data for averages, fits, limits, etc. •••			
593	ROENCHEN 15A	DPWA	Multichannel
372	ARNDT 06	DPWA	$\pi N \rightarrow \pi N, \eta N$
400	HOEHLER 93	ARGD	$\pi N \rightarrow \pi N$

<sup>1</sup> Fit to the amplitudes of HOEHLER 79.

### $N(2220)$ ELASTIC POLE RESIDUE

#### MODULUS $|r|$

VALUE (MeV)	DOCUMENT ID	TECN	COMMENT
<b>35 to 60 (<math>\approx 45</math>) OUR ESTIMATE</b>			
$38 \pm 1 \pm 5$	<sup>1</sup> SVARC 14	L+P	$\pi N \rightarrow \pi N$
$60 \pm 12$	ANISOVICH 12A	DPWA	Multichannel
$45 \pm 20$	CUTKOSKY 80	IPWA	$\pi N \rightarrow \pi N$
••• We do not use the following data for averages, fits, limits, etc. •••			
62	ROENCHEN 15A	DPWA	Multichannel
33	ARNDT 06	DPWA	$\pi N \rightarrow \pi N, \eta N$
40	HOEHLER 93	ARGD	$\pi N \rightarrow \pi N$

<sup>1</sup> Fit to the amplitudes of HOEHLER 79.

#### PHASE $\theta$

VALUE ( $^\circ$ )	DOCUMENT ID	TECN	COMMENT
<b>-60 to -30 (<math>\approx -50</math>) OUR ESTIMATE</b>			
$-52 \pm 1 \pm 14$	<sup>1</sup> SVARC 14	L+P	$\pi N \rightarrow \pi N$
$-58 \pm 12$	ANISOVICH 12A	DPWA	Multichannel
$-45 \pm 25$	CUTKOSKY 80	IPWA	$\pi N \rightarrow \pi N$
••• We do not use the following data for averages, fits, limits, etc. •••			
-59	ROENCHEN 15A	DPWA	Multichannel
-33	ARNDT 06	DPWA	$\pi N \rightarrow \pi N, \eta N$
-50	HOEHLER 93	ARGD	$\pi N \rightarrow \pi N$

<sup>1</sup> Fit to the amplitudes of HOEHLER 79.

### $N(2220)$ INELASTIC POLE RESIDUE

The "normalized residue" is the residue divided by  $\Gamma_{pole}/2$ .

#### Normalized residue in $N\pi \rightarrow N(2220) \rightarrow N\eta$

MODULUS	PHASE ( $^\circ$ )	DOCUMENT ID	TECN	COMMENT
0.004	-101	ROENCHEN 15A	DPWA	Multichannel

#### Normalized residue in $N\pi \rightarrow N(2220) \rightarrow \Lambda K$

MODULUS	PHASE ( $^\circ$ )	DOCUMENT ID	TECN	COMMENT
0.007	62	ROENCHEN 15A	DPWA	Multichannel

#### Normalized residue in $N\pi \rightarrow N(2220) \rightarrow \Sigma K$

MODULUS	PHASE ( $^\circ$ )	DOCUMENT ID	TECN	COMMENT
0.009	-128	ROENCHEN 15A	DPWA	Multichannel

••• We do not use the following data for averages, fits, limits, etc. •••

### $N(2220)$ BREIT-WIGNER MASS

VALUE (MeV)	DOCUMENT ID	TECN	COMMENT
<b>2200 to 2300 (<math>\approx 2250</math>) OUR ESTIMATE</b>			
$2316.3 \pm 2.9$	<sup>1</sup> ARNDT 06	DPWA	$\pi N \rightarrow \pi N, \eta N$
$2230 \pm 80$	CUTKOSKY 80	IPWA	$\pi N \rightarrow \pi N$
$2205 \pm 10$	HOEHLER 79	IPWA	$\pi N \rightarrow \pi N$

<sup>1</sup> Statistical error only.

### $N(2220)$ BREIT-WIGNER WIDTH

VALUE (MeV)	DOCUMENT ID	TECN	COMMENT
<b>350 to 500 (<math>\approx 400</math>) OUR ESTIMATE</b>			
$633 \pm 17$	<sup>1</sup> ARNDT 06	DPWA	$\pi N \rightarrow \pi N, \eta N$
$500 \pm 150$	CUTKOSKY 80	IPWA	$\pi N \rightarrow \pi N$
$365 \pm 30$	HOEHLER 79	IPWA	$\pi N \rightarrow \pi N$

<sup>1</sup> Statistical error only.

**N(2220) DECAY MODES**

The following branching fractions are our estimates, not fits or averages.

Mode	Fraction ( $\Gamma_i/\Gamma$ )
$\Gamma_1$ $N\pi$	15–30 %

**N(2220) BRANCHING RATIOS**

$\Gamma(N\pi)/\Gamma_{total}$	DOCUMENT ID	TECN	COMMENT	$\Gamma_1/\Gamma$
<b>15 to 30 (≈ 25) OUR ESTIMATE</b>				
24 ± 5	ANISOVICH	12A	DPWA	Multichannel
24.6 ± 0.1	<sup>1</sup> ARNDT	06	DPWA	$\pi N \rightarrow \pi N, \eta N$
15 ± 3	CUTKOSKY	80	IPWA	$\pi N \rightarrow \pi N$
18.0 ± 1.5	HOEHLER	79	IPWA	$\pi N \rightarrow \pi N$

<sup>1</sup> Statistical error only.

**N(2220) PHOTON DECAY AMPLITUDES AT THE POLE**

**N(2220) → pγ, helicity-1/2 amplitude A<sub>1/2</sub>**

MODULUS (GeV <sup>-1/2</sup> )	PHASE (°)	DOCUMENT ID	TECN	COMMENT
-0.233 <sup>+0.084</sup> <sub>-0.044</sub>	-47 <sup>+10</sup> <sub>-6</sub>	ROENCHEN	14	DPWA
0.135	114	ROENCHEN	15A	DPWA Multichannel

• • • We do not use the following data for averages, fits, limits, etc. • • •

**N(2220) → pγ, helicity-3/2 amplitude A<sub>3/2</sub>**

MODULUS (GeV <sup>-1/2</sup> )	PHASE (°)	DOCUMENT ID	TECN	COMMENT
0.162 <sup>+0.041</sup> <sub>-0.038</sub>	-27 <sup>+26</sup> <sub>-13</sub>	ROENCHEN	14	DPWA
0.082	-41	ROENCHEN	15A	DPWA Multichannel

• • • We do not use the following data for averages, fits, limits, etc. • • •

**N(2220) REFERENCES**

For early references, see Physics Letters **111B** 1 (1982).

ROENCHEN 15A	EPJ A51 70	D. Roenchen et al.	
PDG 14	CP C39 070001	K. Olive et al.	(PDG Collab.)
ROENCHEN 14	EPJ A50 101	D. Roenchen et al.	
Also	EPJ A51 63 (errata.)	D. Roenchen et al.	
SVARC 14	PR C89 045205	A. Svarc et al.	(RBI Zagreb, UNI Tuzla)
ANISOVICH 12A	EPJ A48 15	A.V. Anisovich et al.	(BONN, PNPI)
ARNDT 06	PR C74 045205	R.A. Arndt et al.	(GWU)
HOEHLER 93	$\pi N$ Newsletter 9 1	G. Hohlner	(KARL)
CUTKOSKY 80	Toronto Conf. 19	R.E. Cutkosky et al.	(CMU, LBL) IJP
Also	PR D20 2839	R.E. Cutkosky et al.	(CMU, LBL) IJP
HOEHLER 79	PDAT 12-1	G. Hohlner et al.	(KARLT) IJP
Also	Toronto Conf. 3	R. Koch	(KARLT) IJP

**N(2250) 9/2<sup>-</sup>**  $I(J^P) = \frac{1}{2}(9/2^-)$  Status: \* \* \* \*

Older and obsolete values are listed and referenced in the 2014 edition, Chinese Physics **C38** 070001 (2014).

**N(2250) POLE POSITION**

**REAL PART**

VALUE (MeV)	DOCUMENT ID	TECN	COMMENT
<b>2150 to 2250 (≈ 2200) OUR ESTIMATE</b>			
2157 ± 3 ± 14	<sup>1</sup> SVARC	14	L+P $\pi N \rightarrow \pi N$
2195 ± 45	ANISOVICH	12A	DPWA Multichannel
2150 ± 50	CUTKOSKY	80	IPWA $\pi N \rightarrow \pi N$
• • •	We do not use the following data for averages, fits, limits, etc. • • •		
2127	HUNT	19	DPWA Multichannel
2062	ROENCHEN	15A	DPWA Multichannel
2217	ARNDT	06	DPWA $\pi N \rightarrow \pi N, \eta N$
2187	HOEHLER	93	SPED $\pi N \rightarrow \pi N$

<sup>1</sup> Fit to the amplitudes of HOEHLER 79.

**-2xIMAGINARY PART**

VALUE (MeV)	DOCUMENT ID	TECN	COMMENT
<b>350 to 500 (≈ 420) OUR ESTIMATE</b>			
412 ± 7 ± 44	<sup>1</sup> SVARC	14	L+P $\pi N \rightarrow \pi N$
470 ± 50	ANISOVICH	12A	DPWA Multichannel
360 ± 100	CUTKOSKY	80	IPWA $\pi N \rightarrow \pi N$
• • •	We do not use the following data for averages, fits, limits, etc. • • •		
262	HUNT	19	DPWA Multichannel
403	ROENCHEN	15A	DPWA Multichannel
431	ARNDT	06	DPWA $\pi N \rightarrow \pi N, \eta N$
388	HOEHLER	93	SPED $\pi N \rightarrow \pi N$

<sup>1</sup> Fit to the amplitudes of HOEHLER 79.

**N(2250) ELASTIC POLE RESIDUE**

**MODULUS |r|**

VALUE (MeV)	DOCUMENT ID	TECN	COMMENT
<b>20 to 30 (≈ 25) OUR ESTIMATE</b>			
24 ± 1 ± 5	<sup>1</sup> SVARC	14	L+P $\pi N \rightarrow \pi N$
26 ± 5	ANISOVICH	12A	DPWA Multichannel
20 ± 6	CUTKOSKY	80	IPWA $\pi N \rightarrow \pi N$
• • •	We do not use the following data for averages, fits, limits, etc. • • •		
8.2	ROENCHEN	15A	DPWA Multichannel
21	ARNDT	06	DPWA $\pi N \rightarrow \pi N, \eta N$
21	HOEHLER	93	SPED $\pi N \rightarrow \pi N$

<sup>1</sup> Fit to the amplitudes of HOEHLER 79.

**PHASE  $\theta$**

VALUE (°)	DOCUMENT ID	TECN	COMMENT
<b>-60 to -20 (≈ -40) OUR ESTIMATE</b>			
-62 ± 1 ± 11	<sup>1</sup> SVARC	14	L+P $\pi N \rightarrow \pi N$
-38 ± 25	ANISOVICH	12A	DPWA Multichannel
-50 ± 20	CUTKOSKY	80	IPWA $\pi N \rightarrow \pi N$
• • •	We do not use the following data for averages, fits, limits, etc. • • •		
-64	ROENCHEN	15A	DPWA Multichannel
-20	ARNDT	06	DPWA $\pi N \rightarrow \pi N, \eta N$

<sup>1</sup> Fit to the amplitudes of HOEHLER 79.

**N(2250) INELASTIC POLE RESIDUE**

The "normalized residue" is the residue divided by  $\Gamma_{pole}/2$ .

**Normalized residue in  $N\pi \rightarrow N(2250) \rightarrow N\eta$**

MODULUS	PHASE (°)	DOCUMENT ID	TECN	COMMENT
0.017	-89	ROENCHEN	15A	DPWA Multichannel

• • • We do not use the following data for averages, fits, limits, etc. • • •

**Normalized residue in  $N\pi \rightarrow N(2250) \rightarrow \Lambda K$**

MODULUS	PHASE (°)	DOCUMENT ID	TECN	COMMENT
0.006	-101	ROENCHEN	15A	DPWA Multichannel

• • • We do not use the following data for averages, fits, limits, etc. • • •

**Normalized residue in  $N\pi \rightarrow N(2250) \rightarrow \Sigma K$**

MODULUS	PHASE (°)	DOCUMENT ID	TECN	COMMENT
0.002	70	ROENCHEN	15A	DPWA Multichannel

• • • We do not use the following data for averages, fits, limits, etc. • • •

**N(2250) BREIT-WIGNER MASS**

VALUE (MeV)	DOCUMENT ID	TECN	COMMENT
<b>2250 to 2320 (≈ 2280) OUR ESTIMATE</b>			
2200 ± 10	<sup>1</sup> HUNT	19	DPWA Multichannel
2280 ± 40	ANISOVICH	12A	DPWA Multichannel
2302 ± 6	<sup>1</sup> ARNDT	06	DPWA $\pi N \rightarrow \pi N, \eta N$
2250 ± 80	CUTKOSKY	80	IPWA $\pi N \rightarrow \pi N$
2268 ± 15	HOEHLER	79	IPWA $\pi N \rightarrow \pi N$

<sup>1</sup> Statistical error only.

**N(2250) BREIT-WIGNER WIDTH**

VALUE (MeV)	DOCUMENT ID	TECN	COMMENT
<b>300 to 600 (≈ 500) OUR ESTIMATE</b>			
343 ± 51	<sup>1</sup> HUNT	19	DPWA Multichannel
520 ± 50	ANISOVICH	12A	DPWA Multichannel
628 ± 28	<sup>1</sup> ARNDT	06	DPWA $\pi N \rightarrow \pi N, \eta N$
480 ± 120	CUTKOSKY	80	IPWA $\pi N \rightarrow \pi N$
300 ± 40	HOEHLER	79	IPWA $\pi N \rightarrow \pi N$

<sup>1</sup> Statistical error only.

**N(2250) DECAY MODES**

The following branching fractions are our estimates, not fits or averages.

Mode	Fraction ( $\Gamma_i/\Gamma$ )
$\Gamma_1$ $N\pi$	0.05 to 0.15 (≈ 0.10)
$\Gamma_2$ $N\eta$	
$\Gamma_3$ $\Lambda K$	

## Baryon Particle Listings

 $N(2250)$ ,  $N(2300)$ ,  $N(2570)$ ,  $N(2600)$ ,  $N(2700)$  $N(2250)$  BRANCHING RATIOS

$\Gamma(N\pi)/\Gamma_{\text{total}}$	DOCUMENT ID	TECN	COMMENT	$\Gamma_1/\Gamma$
5 to 15 ( $\approx 10$ ) OUR ESTIMATE				

VALUE (%)	DOCUMENT ID	TECN	COMMENT	$\Gamma_1/\Gamma$
8.5 $\pm$ 0.4	<sup>1</sup> HUNT	19	DPWA Multichannel	
12 $\pm$ 4	ANISOVICH	12A	DPWA Multichannel	
8.9 $\pm$ 0.1	<sup>1</sup> ARNDT	06	DPWA $\pi N \rightarrow \pi N, \eta N$	
10 $\pm$ 2	CUTKOSKY	80	IPWA $\pi N \rightarrow \pi N$	
10 $\pm$ 2	HOEHLER	79	IPWA $\pi N \rightarrow \pi N$	

<sup>1</sup> Statistical error only.

$\Gamma(N\eta)/\Gamma_{\text{total}}$	DOCUMENT ID	TECN	COMMENT	$\Gamma_2/\Gamma$
<5	<sup>1</sup> HUNT	19	DPWA Multichannel	

<sup>1</sup> Statistical error only.

$\Gamma(\Lambda K)/\Gamma_{\text{total}}$	DOCUMENT ID	TECN	COMMENT	$\Gamma_3/\Gamma$
2.0 $\pm$ 0.6	<sup>1</sup> HUNT	19	DPWA Multichannel	

<sup>1</sup> Statistical error only. $N(2250)$  PHOTON DECAY AMPLITUDES AT THE POLE $N(2250) \rightarrow p\gamma$ , helicity-1/2 amplitude  $A_{1/2}$ 

MODULUS ( $\text{GeV}^{-1/2}$ )	PHASE ( $^\circ$ )	DOCUMENT ID	TECN	COMMENT
-0.090 $\pm$ 0.025 -0.022	-49 $\pm$ 17 -11	ROENCHEN	14	DPWA
••• We do not use the following data for averages, fits, limits, etc. •••				
0.026	-26	ROENCHEN	15A	DPWA Multichannel

 $N(2250) \rightarrow p\gamma$ , helicity-3/2 amplitude  $A_{3/2}$ 

MODULUS ( $\text{GeV}^{-1/2}$ )	PHASE ( $^\circ$ )	DOCUMENT ID	TECN	COMMENT
0.049 $\pm$ 0.031 -0.019	171 $\pm$ 36 -43	ROENCHEN	14	DPWA
••• We do not use the following data for averages, fits, limits, etc. •••				
0.119	-42	ROENCHEN	15A	DPWA Multichannel

 $N(2250)$  BREIT-WIGNER PHOTON DECAY AMPLITUDES $N(2250) \rightarrow p\gamma$ , helicity-1/2 amplitude  $A_{1/2}$ 

VALUE ( $\text{GeV}^{-1/2}$ )	DOCUMENT ID	TECN	COMMENT
0.0006 $\pm$ 0.0037	<sup>1</sup> HUNT	19	DPWA Multichannel

<sup>1</sup> Statistical error only. $N(2250) \rightarrow p\gamma$ , helicity-3/2 amplitude  $A_{3/2}$ 

VALUE ( $\text{GeV}^{-1/2}$ )	DOCUMENT ID	TECN	COMMENT
0.013 $\pm$ 0.004	<sup>1</sup> HUNT	19	DPWA Multichannel

<sup>1</sup> Statistical error only. $N(2250)$  REFERENCES

HUNT	19	PR C99 055205	B. C. Hunt, D.M. Manley	
ROENCHEN	15A	EPJ A51 70	D. Roenchen et al.	
PDG	14	CP C38 070001	K. Olive et al.	(PDG Collab.)
ROENCHEN	14	EPJ A50 101	D. Roenchen et al.	
Also		EPJ A51 63 (errata.)	D. Roenchen et al.	
SVARC	14	PR C89 045205	A. Svarc et al.	(RBI Zagreb, UNI Tuzla)
ANISOVICH	12A	EPJ A48 15	A.V. Anisovich et al.	(BONN, PNPI)
ARNDT	06	PR C74 045205	R.A. Arndt et al.	(GWU)
HOEHLER	93	$\pi N$ Newsletter 9 1	G. Hoehler	(KARL)
CUTKOSKY	80	Toronto Conf. 19	R.E. Cutkosky et al.	(CMU, LBL) IJP
Also		PR D20 2839	R.E. Cutkosky et al.	(CMU, LBL) IJP
HOEHLER	79	PDAT 12-1	G. Hoehler et al.	(KARL) IJP
Also		Toronto Conf. 3	R. Koch	(KARL) IJP

 $N(2300)$  1/2<sup>+</sup> $I(J^P) = \frac{1}{2}(\frac{1}{2}^+)$  Status: \*\*

OMITTED FROM SUMMARY TABLE

 $N(2300)$  MASS

VALUE (MeV)	DOCUMENT ID	TECN	COMMENT
2300 $\pm$ 40 $\pm$ 109 -30 - 0	ABLIKIM	13A	BES3 $\psi(2S) \rightarrow p\bar{p}\pi^0$

 $N(2300)$  WIDTH

VALUE (MeV)	DOCUMENT ID	TECN	COMMENT
340 $\pm$ 30 $\pm$ 110 58	ABLIKIM	13A	BES3 $\psi(2S) \rightarrow p\bar{p}\pi^0$

 $N(2300)$  REFERENCES

ABLIKIM	13A	PRL 110 022001	M. Ablikim et al.	(BESIII Collab.)
---------	-----	----------------	-------------------	------------------

 $N(2570)$  5/2<sup>-</sup> $I(J^P) = \frac{1}{2}(\frac{5}{2}^-)$  Status: \*\*

OMITTED FROM SUMMARY TABLE

 $N(2570)$  MASS

VALUE (MeV)	DOCUMENT ID	TECN	COMMENT
2570 $\pm$ 19 $\pm$ 34 -10 - 10	ABLIKIM	13A	BES3 $\psi(2S) \rightarrow p\bar{p}\pi^0$

 $N(2570)$  WIDTH

VALUE (MeV)	DOCUMENT ID	TECN	COMMENT
250 $\pm$ 14 $\pm$ 69 -24 - 21	ABLIKIM	13A	BES3 $\psi(2S) \rightarrow p\bar{p}\pi^0$

 $N(2570)$  REFERENCES

ABLIKIM	13A	PRL 110 022001	M. Ablikim et al.	(BESIII Collab.)
---------	-----	----------------	-------------------	------------------

 $N(2600)$  11/2<sup>-</sup> $I(J^P) = \frac{1}{2}(\frac{11}{2}^-)$  Status: \*\*\* $N(2600)$  BREIT-WIGNER MASS

VALUE (MeV)	DOCUMENT ID	TECN	COMMENT
2550 to 2750 ( $\approx 2600$ ) OUR ESTIMATE			
2623 $\pm$ 197	ARNDT	06	DPWA $\pi N \rightarrow \pi N, \eta N$
2577 $\pm$ 50	HOEHLER	79	IPWA $\pi N \rightarrow \pi N$

 $N(2600)$  BREIT-WIGNER WIDTH

VALUE (MeV)	DOCUMENT ID	TECN	COMMENT
500 to 800 ( $\approx 650$ ) OUR ESTIMATE			
1311 $\pm$ 996	ARNDT	06	DPWA $\pi N \rightarrow \pi N, \eta N$
400 $\pm$ 100	HOEHLER	79	IPWA $\pi N \rightarrow \pi N$

 $N(2600)$  DECAY MODES

Mode	Fraction ( $\Gamma_i/\Gamma$ )
$\Gamma_1$ $N\pi$	3-8 %

 $N(2600)$  BRANCHING RATIOS

$\Gamma(N\pi)/\Gamma_{\text{total}}$	DOCUMENT ID	TECN	COMMENT	$\Gamma_1/\Gamma$
3 to 8 ( $\approx 5$ ) OUR ESTIMATE				
5.0 $\pm$ 1.8	ARNDT	06	DPWA $\pi N \rightarrow \pi N, \eta N$	
5 $\pm$ 1	HOEHLER	79	IPWA $\pi N \rightarrow \pi N$	

 $N(2600)$  REFERENCES

ARNDT	06	PR C74 045205	R.A. Arndt et al.	(GWU)
HOEHLER	79	PDAT 12-1	G. Hoehler et al.	(KARL) IJP
Also		Toronto Conf. 3	R. Koch	(KARL) IJP

 $N(2700)$  13/2<sup>+</sup> $I(J^P) = \frac{1}{2}(\frac{13}{2}^+)$  Status: \*\*

OMITTED FROM SUMMARY TABLE

 $N(2700)$  BREIT-WIGNER MASS

VALUE (MeV)	DOCUMENT ID	TECN	COMMENT
2612 $\pm$ 45	HOEHLER	79	IPWA $\pi N \rightarrow \pi N$

 $N(2700)$  BREIT-WIGNER WIDTH

VALUE (MeV)	DOCUMENT ID	TECN	COMMENT
350 $\pm$ 50	HOEHLER	79	IPWA $\pi N \rightarrow \pi N$

 $N(2700)$  DECAY MODES

Mode	Fraction ( $\Gamma_i/\Gamma$ )
$\Gamma_1$ $N\pi$	3-5 %

See key on page 999

Baryon Particle Listings  
 $N(2700)$ ,  $N(\sim 3000)$

**$N(2700)$  BRANCHING RATIOS**

$\Gamma(N\pi)/\Gamma_{\text{total}}$	DOCUMENT ID	TECN	COMMENT	$\Gamma_1/\Gamma$
4±1	HOEHLER	79	IPWA $\pi N \rightarrow \pi N$	

**$N(2700)$  REFERENCES**

HOEHLER	79	PDAT 12-1	G. Hohler <i>et al.</i>	(KARLT) IJP
Also		Toronto Conf. 3	R. Koch	(KARLT) IJP

**$N(\sim 3000)$  Region  
 Partial-Wave Analyses**

OMITTED FROM SUMMARY TABLE

We list here miscellaneous high-mass candidates for isospin-1/2 resonances found in partial-wave analyses.

Our 1982 edition had an  $N(3245)$ , an  $N(3690)$ , and an  $N(3755)$ , each a narrow peak seen in a production experiment. Since nothing has been heard from them since the 1960's, we declare them to be dead. There was also an  $N(3030)$ , deduced from total cross-section and  $180^\circ$  elastic cross-section measurements; it is the KOCH 80  $L_{1,15}$  state below.

**$N(\sim 3000)$  BREIT-WIGNER MASS**

VALUE (MeV)	DOCUMENT ID	TECN	COMMENT
<b><math>\approx 3000</math> OUR ESTIMATE</b>			
2600	KOCH	80	IPWA $\pi N \rightarrow \pi N D_{13}$
3100	KOCH	80	IPWA $\pi N \rightarrow \pi N L_{1,15}$ wave
3500	KOCH	80	IPWA $\pi N \rightarrow \pi N M_{1,17}$ wave
3500 to 4000	KOCH	80	IPWA $\pi N \rightarrow \pi N N_{1,19}$ wave
3500±200	HENDRY	78	MPWA $\pi N \rightarrow \pi N L_{1,15}$ wave
3800±200	HENDRY	78	MPWA $\pi N \rightarrow \pi N M_{1,17}$ wave
4100±200	HENDRY	78	MPWA $\pi N \rightarrow \pi N N_{1,19}$ wave

**$N(\sim 3000)$  BREIT-WIGNER WIDTH**

VALUE (MeV)	DOCUMENT ID	TECN	COMMENT
1300±200	HENDRY	78	MPWA $\pi N \rightarrow \pi N L_{1,15}$ wave
1600±200	HENDRY	78	MPWA $\pi N \rightarrow \pi N M_{1,17}$ wave
1900±300	HENDRY	78	MPWA $\pi N \rightarrow \pi N N_{1,19}$ wave

**$N(\sim 3000)$  DECAY MODES**

Mode
$\Gamma_1 N\pi$

**$N(\sim 3000)$  BRANCHING RATIOS**

$\Gamma(N\pi)/\Gamma_{\text{total}}$	DOCUMENT ID	TECN	COMMENT	$\Gamma_1/\Gamma$
6 ± 2	HENDRY	78	MPWA $\pi N \rightarrow \pi N L_{1,15}$ wave	
4.0±1.5	HENDRY	78	MPWA $\pi N \rightarrow \pi N M_{1,17}$ wave	
3.0±1.5	HENDRY	78	MPWA $\pi N \rightarrow \pi N N_{1,19}$ wave	

**$N(\sim 3000)$  REFERENCES**

KOCH	80	Toronto Conf. 3	R. Koch	(KARLT) IJP
HENDRY	78	PRL 41 222	A.W. Hendry	(IND, LBL) IJP
Also		ANP 136 1	A.W. Hendry	(IND) IJP

## Baryon Particle Listings

 $\Delta(1232)$  **$\Delta$  BARYONS**  
( $S = 0, I = 3/2$ )

$$\Delta^{++} = uuu, \Delta^+ = uud, \Delta^0 = udd, \Delta^- = ddd$$

 **$\Delta(1232) 3/2^+$** 

$$I(J^P) = \frac{3}{2}(\frac{3}{2}^+) \text{ Status: } ****$$

Older and obsolete values are listed and referenced in the 2014 edition, Chinese Physics C38 070001 (2014).

 **$\Delta(1232)$  POLE POSITIONS****REAL PART, MIXED CHARGES**

VALUE (MeV)	DOCUMENT ID	TECN	COMMENT
<b>1209 to 1211 (<math>\approx 1210</math>) OUR ESTIMATE</b>			
1211 $\pm 1 \pm 1$	<sup>1</sup> SVARC 14	L+P	$\pi N \rightarrow \pi N$
1210.5 $\pm 1.0$	ANISOVICH 12A	DPWA	Multichannel
1210 $\pm 1$	CUTKOSKY 80	IPWA	$\pi N \rightarrow \pi N$
••• We do not use the following data for averages, fits, limits, etc. •••			
1212.4	HUNT 19	DPWA	Multichannel
1218	ROENCHEN 15A	DPWA	Multichannel
1211 $\pm 1$	ANISOVICH 10	DPWA	Multichannel
1211	ARNDT 06	DPWA	$\pi N \rightarrow \pi N, \eta N$
1210	ARNDT 04	DPWA	$\pi N \rightarrow \pi N, \eta N$
1209	<sup>2</sup> HOEHLER 93	ARGD	$\pi N \rightarrow \pi N$

<sup>1</sup> Fit to the amplitudes of HOEHLER 79.

<sup>2</sup> See HOEHLER 93 for a detailed discussion of the evidence for and the pole parameters of  $N$  and  $\Delta$  resonances as determined from Argand diagrams of  $\pi N$  elastic partial-wave amplitudes and from plots of the speeds with which the amplitudes traverse the diagrams.

**-2xIMAGINARY PART, MIXED CHARGES**

VALUE (MeV)	DOCUMENT ID	TECN	COMMENT
<b>98 to 102 (<math>\approx 100</math>) OUR ESTIMATE</b>			
98 $\pm 2 \pm 1$	<sup>1</sup> SVARC 14	L+P	$\pi N \rightarrow \pi N$
99 $\pm 2$	ANISOVICH 12A	DPWA	Multichannel
100 $\pm 2$	CUTKOSKY 80	IPWA	$\pi N \rightarrow \pi N$
••• We do not use the following data for averages, fits, limits, etc. •••			
96.8	HUNT 19	DPWA	Multichannel
92	ROENCHEN 15A	DPWA	Multichannel
100 $\pm 2$	ANISOVICH 10	DPWA	Multichannel
99	ARNDT 06	DPWA	$\pi N \rightarrow \pi N, \eta N$
100	ARNDT 04	DPWA	$\pi N \rightarrow \pi N, \eta N$
100	<sup>2</sup> HOEHLER 93	ARGD	$\pi N \rightarrow \pi N$

<sup>1</sup> Fit to the amplitudes of HOEHLER 79.

<sup>2</sup> See HOEHLER 93 for a detailed discussion of the evidence for and the pole parameters of  $N$  and  $\Delta$  resonances as determined from Argand diagrams of  $\pi N$  elastic partial-wave amplitudes and from plots of the speeds with which the amplitudes traverse the diagrams.

**REAL PART,  $\Delta(1232)^{++}$** 

VALUE (MeV)	DOCUMENT ID	COMMENT
••• We do not use the following data for averages, fits, limits, etc. •••		
1212.50 $\pm 0.24$	BERNICHIA 96	Fit to PEDRONI 78

**-2xIMAGINARY PART,  $\Delta(1232)^{++}$** 

VALUE (MeV)	DOCUMENT ID	COMMENT
••• We do not use the following data for averages, fits, limits, etc. •••		
97.37 $\pm 0.42$	BERNICHIA 96	Fit to PEDRONI 78

**REAL PART,  $\Delta(1232)^+$** 

VALUE (MeV)	DOCUMENT ID	TECN	COMMENT
••• We do not use the following data for averages, fits, limits, etc. •••			
1211 $\pm 1$ to 1212 $\pm 1$	HANSTEIN 96	DPWA	$\gamma N \rightarrow \pi N$
1206.9 $\pm 0.9$ to 1210.5 $\pm 1.8$	MIROSHNIC... 79		Fit photoproduction

**-2xIMAGINARY PART,  $\Delta(1232)^+$** 

VALUE (MeV)	DOCUMENT ID	TECN	COMMENT
••• We do not use the following data for averages, fits, limits, etc. •••			
102 $\pm 2$ to 99 $\pm 2$	<sup>1</sup> HANSTEIN 96	DPWA	$\gamma N \rightarrow \pi N$
111.2 $\pm 2.0$ to 116.6 $\pm 2.2$	MIROSHNIC... 79		Fit photoproduction

<sup>1</sup> The second (lower) value of HANSTEIN 96 here goes with the second (higher) value of the real part in the preceding data block.

**REAL PART,  $\Delta(1232)^0$** 

VALUE (MeV)	DOCUMENT ID	COMMENT
••• We do not use the following data for averages, fits, limits, etc. •••		
1213.20 $\pm 0.66$	BERNICHIA 96	Fit to PEDRONI 78

**-2xIMAGINARY PART,  $\Delta(1232)^0$** 

VALUE (MeV)	DOCUMENT ID	COMMENT
••• We do not use the following data for averages, fits, limits, etc. •••		
104.10 $\pm 1.01$	BERNICHIA 96	Fit to PEDRONI 78

 **$\Delta(1232)$  ELASTIC POLE RESIDUES****ABSOLUTE VALUE, MIXED CHARGES**

VALUE (MeV)	DOCUMENT ID	TECN	COMMENT
<b>49 to 52 (<math>\approx 50</math>) OUR ESTIMATE</b>			
50 $\pm 1 \pm 1$	<sup>1</sup> SVARC 14	L+P	$\pi N \rightarrow \pi N$
51.6 $\pm 0.6$	ANISOVICH 12A	DPWA	Multichannel
53 $\pm 2$	CUTKOSKY 80	IPWA	$\pi N \rightarrow \pi N$
••• We do not use the following data for averages, fits, limits, etc. •••			
46	ROENCHEN 15A	DPWA	Multichannel
52	ARNDT 06	DPWA	$\pi N \rightarrow \pi N, \eta N$
53	ARNDT 04	DPWA	$\pi N \rightarrow \pi N, \eta N$
50	HOEHLER 93	ARGD	$\pi N \rightarrow \pi N$

**PHASE, MIXED CHARGES**

VALUE ( $^\circ$ )	DOCUMENT ID	TECN	COMMENT
<b>-48 to -45 (<math>\approx -46</math>) OUR ESTIMATE</b>			
-46 $\pm 1 \pm 1$	<sup>1</sup> SVARC 14	L+P	$\pi N \rightarrow \pi N$
-46 $\pm 1$	ANISOVICH 12A	DPWA	Multichannel
-47 $\pm 1$	CUTKOSKY 80	IPWA	$\pi N \rightarrow \pi N$
••• We do not use the following data for averages, fits, limits, etc. •••			
-36	ROENCHEN 15A	DPWA	Multichannel
-47	ARNDT 06	DPWA	$\pi N \rightarrow \pi N, \eta N$
-47	ARNDT 04	DPWA	$\pi N \rightarrow \pi N, \eta N$
-48	HOEHLER 93	ARGD	$\pi N \rightarrow \pi N$

<sup>1</sup> Fit to the amplitudes of HOEHLER 79.

 **$\Delta(1232)$  BREIT-WIGNER MASSES****MIXED CHARGES**

VALUE (MeV)	DOCUMENT ID	TECN	COMMENT
<b>1230 to 1234 (<math>\approx 1232</math>) OUR ESTIMATE</b>			
1230.8 $\pm 0.4$	<sup>1</sup> HUNT 19	DPWA	Multichannel
1228 $\pm 2$	ANISOVICH 12A	DPWA	Multichannel
1233.4 $\pm 0.4$	<sup>1</sup> ARNDT 06	DPWA	$\pi N \rightarrow \pi N, \eta N$
1232 $\pm 3$	CUTKOSKY 80	IPWA	$\pi N \rightarrow \pi N$
1233 $\pm 2$	HOEHLER 79	IPWA	$\pi N \rightarrow \pi N$
••• We do not use the following data for averages, fits, limits, etc. •••			
1231.1 $\pm 0.2$	<sup>1</sup> SHRESTHA 12A	DPWA	Multichannel
1230 $\pm 2$	ANISOVICH 10	DPWA	Multichannel
1232.9 $\pm 1.2$	ARNDT 04	DPWA	$\pi N \rightarrow \pi N, \eta N$
1228 $\pm 1$	PENNER 02c	DPWA	Multichannel

<sup>1</sup> Statistical error only.

 **$\Delta(1232)^{++}$  MASS**

VALUE (MeV)	DOCUMENT ID	TECN	COMMENT
••• We do not use the following data for averages, fits, limits, etc. •••			
1230.55 $\pm 0.20$	GRIDNEV 06	DPWA	$\pi N \rightarrow \pi N$
1231.88 $\pm 0.29$	BERNICHIA 96		Fit to PEDRONI 78
1230.5 $\pm 0.2$	ABAEV 95	IPWA	$\pi N \rightarrow \pi N$
1230.9 $\pm 0.3$	KOCH 80b	IPWA	$\pi N \rightarrow \pi N$
1231.1 $\pm 0.2$	PEDRONI 78		$\pi N \rightarrow \pi N$ 70-370 MeV

 **$\Delta(1232)^+$  MASS**

VALUE (MeV)	DOCUMENT ID	COMMENT
••• We do not use the following data for averages, fits, limits, etc. •••		
1234.9 $\pm 1.4$	MIROSHNIC... 79	Fit photoproduction

 **$\Delta(1232)^0$  MASS**

VALUE (MeV)	DOCUMENT ID	TECN	COMMENT
••• We do not use the following data for averages, fits, limits, etc. •••			
1231.3 $\pm 0.6$	BREITSCHOP...06	CNTR	Using new CHEX data
1233.40 $\pm 0.22$	GRIDNEV 06	DPWA	$\pi N \rightarrow \pi N$
1234.35 $\pm 0.75$	BERNICHIA 96		Fit to PEDRONI 78
1233.1 $\pm 0.3$	ABAEV 95	IPWA	$\pi N \rightarrow \pi N$
1233.6 $\pm 0.5$	KOCH 80b	IPWA	$\pi N \rightarrow \pi N$
1233.8 $\pm 0.2$	PEDRONI 78		$\pi N \rightarrow \pi N$ 70-370 MeV

 **$m_{\Delta^0} - m_{\Delta^{++}}$** 

VALUE (MeV)	DOCUMENT ID	TECN	COMMENT
••• We do not use the following data for averages, fits, limits, etc. •••			
2.86 $\pm 0.30$	GRIDNEV 06	DPWA	$\pi N \rightarrow \pi N$
2.25 $\pm 0.68$	BERNICHIA 96		Fit to PEDRONI 78
2.6 $\pm 0.4$	ABAEV 95	IPWA	$\pi N \rightarrow \pi N$
2.7 $\pm 0.3$	<sup>1</sup> PEDRONI 78		See the masses

<sup>1</sup> Using  $\pi^\pm d$  as well, PEDRONI 78 determine  $(M^- - M^{++}) + (M^0 - M^+)/3 = 4.6 \pm 0.2$  MeV.

$\Delta(1232)$

$\Delta(1232)$  BREIT-WIGNER WIDTHS

MIXED CHARGES

VALUE (MeV)	DOCUMENT ID	TECN	COMMENT
<b>114 to 120 (<math>\approx 117</math>) OUR ESTIMATE</b>			
110.9 $\pm$ 0.8	<sup>1</sup> HUNT 19	DPWA	Multichannel
110 $\pm$ 3	ANISOVICH 12A	DPWA	Multichannel
118.7 $\pm$ 0.6	<sup>1</sup> ARNDT 06	DPWA	$\pi N \rightarrow \pi N, \eta N$
120 $\pm$ 5	CUTKOSKY 80	IPWA	$\pi N \rightarrow \pi N$
116 $\pm$ 5	HOEHLER 79	IPWA	$\pi N \rightarrow \pi N$
••• We do not use the following data for averages, fits, limits, etc. •••			
113.0 $\pm$ 0.5	<sup>1</sup> SHRESTHA 12A	DPWA	Multichannel
112 $\pm$ 4	ANISOVICH 10	DPWA	Multichannel
118.0 $\pm$ 2.2	ARNDT 04	DPWA	$\pi N \rightarrow \pi N, \eta N$
106 $\pm$ 1	PENNER 02c	DPWA	Multichannel

<sup>1</sup> Statistical error only.

$\Delta(1232)^{++}$  WIDTH

VALUE (MeV)	DOCUMENT ID	TECN	COMMENT
••• We do not use the following data for averages, fits, limits, etc. •••			
112.2 $\pm$ 0.7	GRIDNEV 06	DPWA	$\pi N \rightarrow \pi N$
109.07 $\pm$ 0.48	BERNICH 96		Fit to PEDRONI 78
111.0 $\pm$ 1.0	KOCH 80b	IPWA	$\pi N \rightarrow \pi N$
111.3 $\pm$ 0.5	PEDRONI 78		$\pi N \rightarrow \pi N$ 70–370 MeV

$\Delta(1232)^+$  WIDTH

VALUE (MeV)	DOCUMENT ID	COMMENT
••• We do not use the following data for averages, fits, limits, etc. •••		
131.1 $\pm$ 2.4	MIROSHNIC... 79	Fit photoproduction

$\Delta(1232)^0$  WIDTH

VALUE (MeV)	DOCUMENT ID	TECN	COMMENT
••• We do not use the following data for averages, fits, limits, etc. •••			
112.5 $\pm$ 1.9	BREITSHOP.06	CNTR	Using new CHEX data
116.9 $\pm$ 0.7	GRIDNEV 06	DPWA	$\pi N \rightarrow \pi N$
117.58 $\pm$ 1.16	BERNICH 96		Fit to PEDRONI 78
113.0 $\pm$ 1.5	KOCH 80b	IPWA	$\pi N \rightarrow \pi N$
117.9 $\pm$ 0.9	PEDRONI 78		$\pi N \rightarrow \pi N$ 70–370 MeV

$\Delta^0$ - $\Delta^{++}$  WIDTH DIFFERENCE

VALUE (MeV)	DOCUMENT ID	TECN	COMMENT
••• We do not use the following data for averages, fits, limits, etc. •••			
4.66 $\pm$ 1.0	GRIDNEV 06	DPWA	$\pi N \rightarrow \pi N$
8.45 $\pm$ 1.11	BERNICH 96		Fit to PEDRONI 78
5.1 $\pm$ 1.0	ABAEV 95	IPWA	$\pi N \rightarrow \pi N$
6.6 $\pm$ 1.0	PEDRONI 78		See the widths

$\Delta(1232)$  DECAY MODES

The following branching fractions are our estimates, not fits or averages.

Mode	Fraction ( $\Gamma_j/\Gamma$ )
$\Gamma_1$ $N\pi$	99.4 %
$\Gamma_2$ $N\gamma$	0.55–0.65 %
$\Gamma_3$ $N\gamma$ , helicity=1/2	0.11–0.13 %
$\Gamma_4$ $N\gamma$ , helicity=3/2	0.44–0.52 %
$\Gamma_5$ $pe^+e^-$	(4.2 $\pm$ 0.7) $\times 10^{-5}$

$\Delta(1232)$  BRANCHING RATIOS

$\Gamma(N\pi)/\Gamma_{total}$	DOCUMENT ID	TECN	COMMENT	$\Gamma_1/\Gamma$
<b>0.994 OUR ESTIMATE</b>				
0.9939 $\pm$ 0.0001	<sup>1</sup> HUNT 19	DPWA	Multichannel	
1.00	ARNDT 06	DPWA	$\pi N \rightarrow \pi N, \eta N$	
1.0	CUTKOSKY 80	IPWA	$\pi N \rightarrow \pi N$	
1.0	HOEHLER 79	IPWA	$\pi N \rightarrow \pi N$	
••• We do not use the following data for averages, fits, limits, etc. •••				
0.994	SHRESTHA 12A	DPWA	Multichannel	
1.0	ANISOVICH 10	DPWA	Multichannel	
1.000	ARNDT 04	DPWA	$\pi N \rightarrow \pi N, \eta N$	
1.00	PENNER 02c	DPWA	Multichannel	

<sup>1</sup> Statistical error only.

$\Gamma(pe^+e^-)/\Gamma_{total}$	DOCUMENT ID	COMMENT	$\Gamma_5/\Gamma$
<b>4.19<math>\pm</math>0.34<math>\pm</math>0.62</b>	<sup>1</sup> ADAMCZEV...17		

<sup>1</sup> The systematic uncertainty includes the model dependence.

$\Delta(1232)$  PHOTON DECAY AMPLITUDES AT THE POLE

$\Delta(1232) \rightarrow N\gamma$ , helicity-1/2 amplitude  $A_{1/2}$

MODULUS ( $\text{GeV}^{-1/2}$ )	PHASE ( $^\circ$ )	DOCUMENT ID	TECN	COMMENT
-0.114 <sup>+0.010</sup> <sub>-0.003</sub>	-9 <sup>+4</sup> <sub>-2</sub>	ROENCHEN 14	DPWA	
••• We do not use the following data for averages, fits, limits, etc. •••				
-0.117	-6.6	ROENCHEN 15A	DPWA	Multichannel

$\Delta(1232) \rightarrow N\gamma$ , helicity-3/2 amplitude  $A_{3/2}$

MODULUS ( $\text{GeV}^{-1/2}$ )	PHASE ( $^\circ$ )	DOCUMENT ID	TECN	COMMENT
-0.229 <sup>+0.003</sup> <sub>-0.004</sub>	3 <sup>+0.3</sup> <sub>-0.4</sub>	ROENCHEN 14	DPWA	
••• We do not use the following data for averages, fits, limits, etc. •••				
-0.226	2.8	ROENCHEN 15A	DPWA	Multichannel

$\Delta(1232)$  BREIT-WIGNER PHOTON DECAY AMPLITUDES

Papers on  $\gamma N$  amplitudes predating 1981 may be found in our 2006 edition, Journal of Physics **G33** 1 (2006).

$\Delta(1232) \rightarrow N\gamma$ , helicity-1/2 amplitude  $A_{1/2}$

VALUE ( $\text{GeV}^{-1/2}$ )	DOCUMENT ID	TECN	COMMENT
<b>-0.142 to -0.129 (<math>\approx -0.135</math>) OUR ESTIMATE</b>			
-0.146 $\pm$ 0.002	<sup>1</sup> HUNT 19	DPWA	Multichannel
-0.131 $\pm$ 0.004	ANISOVICH 12A	DPWA	Multichannel
-0.139 $\pm$ 0.002	<sup>1</sup> WORKMAN 12A	DPWA	$\gamma N \rightarrow N\pi$
-0.139 $\pm$ 0.004	<sup>1</sup> DUGGER 07	DPWA	$\gamma N \rightarrow \pi N$
-0.137 $\pm$ 0.005	AHRENS 04A	DPWA	$\tilde{\gamma}\tilde{p} \rightarrow N\pi$
-0.1357 $\pm$ 0.0013 $\pm$ 0.0037	BLANPIED 01	LEGS	$\gamma p \rightarrow p\gamma, p\pi^0, n\pi^+$
-0.131 $\pm$ 0.001	<sup>1</sup> BECK 00	IPWA	$\tilde{\gamma}p \rightarrow p\pi^0, n\pi^+$
-0.140 $\pm$ 0.005	KAMALOV 99	DPWA	$\gamma N \rightarrow \pi N$
-0.1294 $\pm$ 0.0013	HANSTEIN 98	IPWA	$\gamma N \rightarrow \pi N$
-0.1278 $\pm$ 0.0012	DAVIDSON 97	DPWA	$\gamma N \rightarrow \pi N$
••• We do not use the following data for averages, fits, limits, etc. •••			
-0.137 $\pm$ 0.001	<sup>1</sup> SHRESTHA 12A	DPWA	Multichannel
-0.136 $\pm$ 0.005	ANISOVICH 10	DPWA	Multichannel
-0.140	DRECHSEL 07	DPWA	$\gamma N \rightarrow \pi N$
-0.129 $\pm$ 0.001	ARNDT 02	DPWA	$\gamma p \rightarrow N\pi$
-0.128	PENNER 02D	DPWA	Multichannel
-0.1312	HANSTEIN 98	DPWA	$\gamma N \rightarrow \pi N$

<sup>1</sup> Statistical error only.

$\Delta(1232) \rightarrow N\gamma$ , helicity-3/2 amplitude  $A_{3/2}$

VALUE ( $\text{GeV}^{-1/2}$ )	DOCUMENT ID	TECN	COMMENT
<b>-0.262 to -0.248 (<math>\approx -0.255</math>) OUR ESTIMATE</b>			
-0.250 $\pm$ 0.002	<sup>1</sup> HUNT 19	DPWA	Multichannel
-0.254 $\pm$ 0.005	ANISOVICH 12A	DPWA	Multichannel
-0.262 $\pm$ 0.003	WORKMAN 12A	DPWA	$\gamma N \rightarrow N\pi$
-0.258 $\pm$ 0.005	DUGGER 07	DPWA	$\gamma N \rightarrow \pi N$
-0.256 $\pm$ 0.003	AHRENS 04A	DPWA	$\tilde{\gamma}\tilde{p} \rightarrow N\pi$
-0.2669 $\pm$ 0.0016 $\pm$ 0.0078	BLANPIED 01	LEGS	$\gamma p \rightarrow p\gamma, p\pi^0, n\pi^+$
-0.251 $\pm$ 0.001	BECK 00	IPWA	$\tilde{\gamma}p \rightarrow p\pi^0, n\pi^+$
-0.258 $\pm$ 0.006	KAMALOV 99	DPWA	$\gamma N \rightarrow \pi N$
-0.2466 $\pm$ 0.0013	HANSTEIN 98	IPWA	$\gamma N \rightarrow \pi N$
-0.2524 $\pm$ 0.0013	DAVIDSON 97	DPWA	$\gamma N \rightarrow \pi N$
••• We do not use the following data for averages, fits, limits, etc. •••			
-0.251 $\pm$ 0.001	<sup>1</sup> SHRESTHA 12A	DPWA	Multichannel
-0.267 $\pm$ 0.008	ANISOVICH 10	DPWA	Multichannel
-0.265	DRECHSEL 07	DPWA	$\gamma N \rightarrow \pi N$
-0.243 $\pm$ 0.001	ARNDT 02	DPWA	$\gamma p \rightarrow N\pi$
-0.247	PENNER 02D	DPWA	Multichannel
-0.2522	HANSTEIN 98	DPWA	$\gamma N \rightarrow \pi N$

<sup>1</sup> Statistical error only.

$\Delta(1232) \rightarrow N\gamma$ ,  $E_2/M_1$  ratio

VALUE	DOCUMENT ID	TECN	COMMENT
<b>-0.030 to -0.020 (<math>\approx -0.025</math>) OUR ESTIMATE</b>			
-0.0274 $\pm$ 0.0003 $\pm$ 0.0030	AHRENS 04A	DPWA	$\tilde{\gamma}\tilde{p} \rightarrow N\pi$
-0.020 $\pm$ 0.002	ARNDT 02	DPWA	$\gamma p \rightarrow N\pi$
-0.0307 $\pm$ 0.0026 $\pm$ 0.0024	BLANPIED 01	LEGS	$\gamma p \rightarrow p\gamma, p\pi^0, n\pi^+$
-0.016 $\pm$ 0.004 $\pm$ 0.002	GALLER 01	DPWA	$\gamma p \rightarrow \gamma p$
-0.025 $\pm$ 0.001 $\pm$ 0.002	BECK 00	IPWA	$\tilde{\gamma}p \rightarrow p\pi^0, n\pi^+$
-0.0233 $\pm$ 0.0017	HANSTEIN 98	IPWA	$\gamma N \rightarrow \pi N$
-0.015 $\pm$ 0.005	<sup>1</sup> ARNDT 97	IPWA	$\gamma N \rightarrow \pi N$
-0.0319 $\pm$ 0.0024	DAVIDSON 97	DPWA	$\gamma N \rightarrow \pi N$
••• We do not use the following data for averages, fits, limits, etc. •••			
-0.022	DRECHSEL 07	DPWA	$\gamma N \rightarrow \pi N$
-0.026	PENNER 02D	DPWA	Multichannel
-0.0254 $\pm$ 0.0010	HANSTEIN 98	DPWA	$\gamma N \rightarrow \pi N$
-0.025 $\pm$ 0.002 $\pm$ 0.002	BECK 97	IPWA	$\gamma N \rightarrow \pi N$
-0.030 $\pm$ 0.003 $\pm$ 0.002	BLANPIED 97	DPWA	$\gamma N \rightarrow \pi N, \gamma N$

<sup>1</sup> This ARNDT 97 value is very sensitive to the database being fitted. The result is from a fit to the full pion photoproduction database, apart from the BLANPIED 97 cross-section measurements.

Baryon Particle Listings  
 $\Delta(1232), \Delta(1600)$

$\Delta(1232) \rightarrow N\gamma$ , absolute value of  $E_2/M_1$  ratio at pole

VALUE	DOCUMENT ID	TECN	COMMENT
0.065 ± 0.007	ARNDT 97	DPWA	$\gamma N \rightarrow \pi N$
0.058	HANSTEIN 96	DPWA	$\gamma N \rightarrow \pi N$

$\Delta(1232) \rightarrow N\gamma$ , phase of  $E_2/M_1$  ratio at pole

VALUE	DOCUMENT ID	TECN	COMMENT
-122 ± 5	ARNDT 97	DPWA	$\gamma N \rightarrow \pi N$
-127.2	HANSTEIN 96	DPWA	$\gamma N \rightarrow \pi N$

$\Delta(1232)$  MAGNETIC MOMENTS

$\Delta(1232)^{++}$  MAGNETIC MOMENT

The values are extracted from UCLA and SIN data on  $\pi^+ p$  bremsstrahlung using a variety of different theoretical approximations and methods. Our estimate is only a rough guess of the range we expect the moment to lie within.

VALUE ( $\mu_N$ )	DOCUMENT ID	TECN	COMMENT
6.14 ± 0.51	LOPEZCAST... 01	DPWA	$\pi^+ p \rightarrow \pi^+ p \gamma$
4.52 ± 0.50 ± 0.45	BOSSHARD 91		$\pi^+ p \rightarrow \pi^+ p \gamma$ (SIN data)
3.7 to 4.2	LIN 91B		$\pi^+ p \rightarrow \pi^+ p \gamma$ (from UCLA data)
4.6 to 4.9	LIN 91B		$\pi^+ p \rightarrow \pi^+ p \gamma$ (from SIN data)
5.6 to 7.5	WITTMAN 88		$\pi^+ p \rightarrow \pi^+ p \gamma$ (from UCLA data)
6.9 to 9.8	HELLER 87		$\pi^+ p \rightarrow \pi^+ p \gamma$ (from UCLA data)
4.7 to 6.7	NEFKENS 78		$\pi^+ p \rightarrow \pi^+ p \gamma$ (UCLA data)

$\Delta(1232)^+$  MAGNETIC MOMENT

VALUE ( $\mu_N$ )	DOCUMENT ID	COMMENT
2.7 ± 1.0 ± 1.5 ± 3	<sup>1</sup> KOTULLA 02	$\gamma p \rightarrow \rho \pi^0 \gamma'$

<sup>1</sup>The second error is systematic, the third is an estimate of theoretical uncertainties.

$\Delta(1232)$  REFERENCES

For early references, see Physics Letters 111B 1 (1982).

HUNT 19	PR C99 055205	B. C. Hunt, D.M. Manley
ADAMCZEW... 17	PR C95 065205	J. Adamczewski-Musch et al.
ROENCHEN 15A	EPJ A51 70	D. Roenchen et al.
PDG 14	CP 038 070001	K. Olive et al.
ROENCHEN 14	EPJ A50 101	D. Roenchen et al.
Also	EPJ A51 63 (err.)	D. Roenchen et al.
SVARC 14	PR C89 045205	A. Svarc et al.
ANISOVICH 12A	EPJ A48 15	A.V. Anisovich et al.
SHRESTHA 12A	PR C86 055203	M. Shrestha, D.M. Manley
WORKMAN 12A	PR C86 015202	R. Workman et al.
ANISOVICH 10	EPJ A44 203	A.V. Anisovich et al.
DRECHSEL 07	EPJ A34 69	D. Drechsel, S.S. Kamalov, L. Tiator
DUGGER 07	PR C76 025211	M. Dugger et al.
ARNDT 06	PR C74 045205	R.A. Arndt et al.
BREITSCHOP... 06	PL B639 424	J. Breitschopf et al.
GRIDNEV 06	PAN 69 1542	A.B. Gridnev et al.
PDG 06	JP G33 1	W.-M. Yao et al.
AHRENS 04A	EPJ A21 323	J. Ahrens et al.
ARNDT 04	PR C69 035213	R.A. Arndt et al.
ARNDT 02	PR C66 055213	R.A. Arndt et al.
KOTULLA 02	PRL 89 272001	M. Kotulla et al.
PENNER 02C	PR C66 055211	G. Penner, U. Mosel
PENNER 02D	PR C66 055212	G. Penner, U. Mosel
BLANPIED 01	PR C64 025203	G. Blanpied et al.
GALLER 01	PL B503 245	G. Galler et al.
LOPEZCAST... 01	PL B517 339	G. Lopez Castro, A. Mariano
Also	NP A697 440	G. Lopez Castro, A. Mariano
BECK 00	PR C61 035204	R. Beck et al.
KAMALOV 99	PRL 83 4494	S.S. Kamalov, S.N. Yang
HANSTEIN 98	NP A632 561	O. Hanstein, D. Drechsel, L. Tiator
ARNDT 97	PR C56 577	R.A. Arndt, I.I. Strakovsky, R.L. Workman
BECK 97	PRL 79 606	R. Beck et al.
Also	PRL 79 4510	R.L. Beck, H.P. Krahn
Also	PRL 79 4512	R.L. Beck, H.P. Krahn
Also	PRL 79 4515 (erratum)	R.L. Beck et al.
BLANPIED 97	PRL 79 4337	G.S. Blanpied et al.
DAVIDSON 97	PRL 79 4509	R.M. Davidson, N.C.A. Mukhopadhyay
BERNICHIA 96	NP A597 623	A. Bernicha, G. Lopez Castro, J. Pestieau
HANSTEIN 96	PL B385 45	O. Hanstein, D. Drechsel, L. Tiator
ABAEV 95	ZPHY A352 85	V.V. Abaev, S.P. Kruglov
HOEHLER 93	$\pi N$ Newsletter 9 1	G. Hohler
BOSSHARD 91	PR D44 1362	A. Boshard et al.
Also	PRL 64 2619	A. Boshard et al.
LIN 91B	PR C44 1819	D.H. Lin, M.K. Liou, Z.M. Ding
Also	PR C43 R930	D. Lin, M.K. Liou
WITTMAN 88	PR C37 2075	R. Wittman
HELLER 87	PR C35 718	L. Heller et al.
CUTKOSKY 80	Toronto Conf. 19	R.E. Cutkosky et al.
Also	PR D20 2839	R.E. Cutkosky et al.
KOCH 80B	NP A336 331	R. Koch, E. Pietarinen
HOEHLER 79	PDAT 12-1	G. Hohler et al.
Also	Toronto Conf. 3	R. Koch
MIROSHNIC... 79	SJNP 29 94	I.I. Miroshnicenko et al.
Also	Translated from YAF 29 188	I.I. Miroshnicenko et al.
NEFKENS 78	PR D18 3911	B.M.K. Nefkens et al.
PEDRONI 78	NP A300 321	E. Pedroni et al.

$\Delta(1600) 3/2^+$

$I(J^P) = \frac{3}{2}(\frac{3}{2}^+)$  Status: \*\*\*

Older and obsolete values are listed and referenced in the 2014 edition, Chinese Physics C38 070001 (2014).

$\Delta(1600)$  POLE POSITION

REAL PART

VALUE (MeV)	DOCUMENT ID	TECN	COMMENT
<b>1460 to 1560 (<math>\approx</math> 1510) OUR ESTIMATE</b>			
1515 ± 20	SOKHOYAN 15A	DPWA	Multichannel
1469 ± 10 ± 5	<sup>1</sup> SVARC 14	L+P	$\pi N \rightarrow \pi N$
1550 ± 40	CUTKOSKY 80	IPWA	$\pi N \rightarrow \pi N$
••• We do not use the following data for averages, fits, limits, etc. •••			
1619	HUNT 19	DPWA	Multichannel
1552	ROENCHEN 15A	DPWA	Multichannel
1498 ± 25	ANISOVICH 12A	DPWA	Multichannel
1457	ARNDT 06	DPWA	$\pi N \rightarrow \pi N, \eta N$
1599	VRANA 00	DPWA	Multichannel
1550	HOEHLER 93	SPED	$\pi N \rightarrow \pi N$

<sup>1</sup>Fit to the amplitudes of HOEHLER 79.

-2x IMAGINARY PART

VALUE (MeV)	DOCUMENT ID	TECN	COMMENT
<b>200 to 340 (<math>\approx</math> 270) OUR ESTIMATE</b>			
250 ± 30	SOKHOYAN 15A	DPWA	Multichannel
314 ± 18 ± 8	<sup>1</sup> SVARC 14	L+P	$\pi N \rightarrow \pi N$
200 ± 60	CUTKOSKY 80	IPWA	$\pi N \rightarrow \pi N$
••• We do not use the following data for averages, fits, limits, etc. •••			
295	HUNT 19	DPWA	Multichannel
350	ROENCHEN 15A	DPWA	Multichannel
230 ± 50	ANISOVICH 12A	DPWA	Multichannel
400	ARNDT 06	DPWA	$\pi N \rightarrow \pi N, \eta N$
312	VRANA 00	DPWA	Multichannel

<sup>1</sup>Fit to the amplitudes of HOEHLER 79.

$\Delta(1600)$  ELASTIC POLE RESIDUE

MODULUS  $|r|$

VALUE (MeV)	DOCUMENT ID	TECN	COMMENT
<b>10 to 40 (<math>\approx</math> 25) OUR ESTIMATE</b>			
13 ± 3	SOKHOYAN 15A	DPWA	Multichannel
38 ± 2 ± 2	<sup>1</sup> SVARC 14	L+P	$\pi N \rightarrow \pi N$
17 ± 4	CUTKOSKY 80	IPWA	$\pi N \rightarrow \pi N$
••• We do not use the following data for averages, fits, limits, etc. •••			
23	ROENCHEN 15A	DPWA	Multichannel
11 ± 6	ANISOVICH 12A	DPWA	Multichannel
44	ARNDT 06	DPWA	$\pi N \rightarrow \pi N, \eta N$

<sup>1</sup>Fit to the amplitudes of HOEHLER 79.

PHASE  $\theta$

VALUE ( $^\circ$ )	DOCUMENT ID	TECN	COMMENT
<b>150 to 210 (<math>\approx</math> 180) OUR ESTIMATE</b>			
-155 ± 20	SOKHOYAN 15A	DPWA	Multichannel
-173 ± 5 ± 5	<sup>1</sup> SVARC 14	L+P	$\pi N \rightarrow \pi N$
-150 ± 30	CUTKOSKY 80	IPWA	$\pi N \rightarrow \pi N$
••• We do not use the following data for averages, fits, limits, etc. •••			
-155	ROENCHEN 15A	DPWA	Multichannel
-160 ± 33	ANISOVICH 12A	DPWA	Multichannel
+147	ARNDT 06	DPWA	$\pi N \rightarrow \pi N, \eta N$

<sup>1</sup>Fit to the amplitudes of HOEHLER 79.

$\Delta(1600)$  INELASTIC POLE RESIDUE

The "normalized residue" is the residue divided by  $\Gamma_{pole}/2$ .

Normalized residue in  $N\pi \rightarrow \Delta(1600) \rightarrow \Delta\pi, P$ -wave

MODULUS	PHASE ( $^\circ$ )	DOCUMENT ID	TECN	COMMENT
0.15 ± 0.04	30 ± 35	SOKHOYAN 15A	DPWA	Multichannel
••• We do not use the following data for averages, fits, limits, etc. •••				
0.31	31	ROENCHEN 15A	DPWA	Multichannel
0.14 ± 0.10	154 ± 40	ANISOVICH 12A	DPWA	Multichannel

Normalized residue in  $N\pi \rightarrow \Delta(1600) \rightarrow \Delta\pi, F$ -wave

MODULUS	PHASE ( $^\circ$ )	DOCUMENT ID	TECN	COMMENT
0.010 ± 0.005		SOKHOYAN 15A	DPWA	Multichannel
••• We do not use the following data for averages, fits, limits, etc. •••				
0.013	29	ROENCHEN 15A	DPWA	Multichannel
0.010 ± 0.005		ANISOVICH 12A	DPWA	Multichannel

Normalized residue in  $N\pi \rightarrow \Delta(1600) \rightarrow \Sigma K$

MODULUS	PHASE (°)	DOCUMENT ID	TECN	COMMENT
0.13	-5.6	ROENCHEN	15A	DPWA Multichannel

$\Delta(1600)$  BREIT-WIGNER MASS

VALUE (MeV)	DOCUMENT ID	TECN	COMMENT
<b>1500 to 1640 (≈ 1570) OUR ESTIMATE</b>			
1664 ± 16	<sup>1</sup> HUNT	19	DPWA Multichannel
1520 ± 20	SOKHOYAN	15A	DPWA Multichannel
1600 ± 50	CUTKOSKY	80	IPWA $\pi N \rightarrow \pi N$
1522 ± 13	HOEHLER	79	IPWA $\pi N \rightarrow \pi N$
••• We do not use the following data for averages, fits, limits, etc. •••			
1510 ± 20	ANISOVICH	12A	DPWA Multichannel
1626 ± 8	<sup>1</sup> SHRESTHA	12A	DPWA Multichannel
1667 ± 1	PENNER	02C	DPWA Multichannel
1687 ± 44	VRANA	00	DPWA Multichannel

<sup>1</sup> Statistical error only.

$\Delta(1600)$  BREIT-WIGNER WIDTH

VALUE (MeV)	DOCUMENT ID	TECN	COMMENT
<b>200 to 300 (≈ 250) OUR ESTIMATE</b>			
322 ± 46	<sup>1</sup> HUNT	19	DPWA Multichannel
235 ± 30	SOKHOYAN	15A	DPWA Multichannel
300 ± 100	CUTKOSKY	80	IPWA $\pi N \rightarrow \pi N$
220 ± 40	HOEHLER	79	IPWA $\pi N \rightarrow \pi N$
••• We do not use the following data for averages, fits, limits, etc. •••			
220 ± 45	ANISOVICH	12A	DPWA Multichannel
225 ± 18	<sup>1</sup> SHRESTHA	12A	DPWA Multichannel
397 ± 10	PENNER	02C	DPWA Multichannel
493 ± 75	VRANA	00	DPWA Multichannel

<sup>1</sup> Statistical error only.

$\Delta(1600)$  DECAY MODES

The following branching fractions are our estimates, not fits or averages.

Mode	Fraction ( $\Gamma_j/\Gamma$ )
$\Gamma_1$ $N\pi$	8–24 %
$\Gamma_2$ $N\pi\pi$	75–90 %
$\Gamma_3$ $\Delta(1232)\pi$	73–83 %
$\Gamma_4$ $\Delta(1232)\pi, P$ -wave	72–82 %
$\Gamma_5$ $\Delta(1232)\pi, F$ -wave	<2 %
$\Gamma_6$ $N(1440)\pi$	
$\Gamma_7$ $N(1440)\pi, P$ -wave	15–25 %
$\Gamma_8$ $N\gamma$	0.001–0.035 %
$\Gamma_9$ $N\gamma, \text{helicity}=1/2$	0.0–0.02 %
$\Gamma_{10}$ $N\gamma, \text{helicity}=3/2$	0.001–0.015 %

$\Delta(1600)$  BRANCHING RATIOS

$\Gamma(N\pi)/\Gamma_{\text{total}}$	DOCUMENT ID	TECN	COMMENT	$\Gamma_1/\Gamma$
<b>8 to 24 (≈ 16) OUR ESTIMATE</b>				
10.7 ± 1.9	<sup>1</sup> HUNT	19	DPWA Multichannel	
14 ± 4	SOKHOYAN	15A	DPWA Multichannel	
18 ± 4	CUTKOSKY	80	IPWA $\pi N \rightarrow \pi N$	
21 ± 6	HOEHLER	79	IPWA $\pi N \rightarrow \pi N$	
••• We do not use the following data for averages, fits, limits, etc. •••				
12 ± 5	ANISOVICH	12A	DPWA Multichannel	
8 ± 2	<sup>1</sup> SHRESTHA	12A	DPWA Multichannel	
13 ± 1	PENNER	02C	DPWA Multichannel	
28 ± 5	VRANA	00	DPWA Multichannel	

<sup>1</sup> Statistical error only.

$\Gamma(\Delta(1232)\pi, P\text{-wave})/\Gamma_{\text{total}}$

VALUE (%)	DOCUMENT ID	TECN	COMMENT	$\Gamma_4/\Gamma$
64 ± 6	<sup>1</sup> HUNT	19	DPWA Multichannel	
77 ± 5	SOKHOYAN	15A	DPWA Multichannel	
••• We do not use the following data for averages, fits, limits, etc. •••				
78 ± 6	ANISOVICH	12A	DPWA Multichannel	
70 ± 3	<sup>1</sup> SHRESTHA	12A	DPWA Multichannel	
59 ± 10	VRANA	00	DPWA Multichannel	

<sup>1</sup> Statistical error only.

$\Gamma(\Delta(1232)\pi, F\text{-wave})/\Gamma_{\text{total}}$

VALUE (%)	DOCUMENT ID	TECN	COMMENT	$\Gamma_5/\Gamma$
<2	SOKHOYAN	15A	DPWA Multichannel	

$\Gamma(N(1440)\pi)/\Gamma_{\text{total}}$

VALUE (%)	DOCUMENT ID	TECN	COMMENT	$\Gamma_6/\Gamma$
22 ± 5	<sup>1</sup> HUNT	19	DPWA Multichannel	
••• We do not use the following data for averages, fits, limits, etc. •••				
22 ± 3	<sup>1</sup> SHRESTHA	12A	DPWA Multichannel	
13 ± 4	VRANA	00	DPWA Multichannel	

<sup>1</sup> Statistical error only.

$\Delta(1600)$  PHOTON DECAY AMPLITUDES AT THE POLE

$\Delta(1600) \rightarrow N\gamma, \text{helicity-1/2 amplitude } A_{1/2}$

MODULUS ( $\text{GeV}^{-1/2}$ )	PHASE (°)	DOCUMENT ID	TECN	COMMENT
0.053 ± 0.010	130 ± 15	SOKHOYAN	15A	DPWA Multichannel
0.193 <sup>+0.023</sup> <sub>-0.024</sub>	151 <sup>+9</sup> <sub>-15</sub>	ROENCHEN	14	DPWA
••• We do not use the following data for averages, fits, limits, etc. •••				
-0.230	-42	ROENCHEN	15A	DPWA Multichannel

$\Delta(1600) \rightarrow N\gamma, \text{helicity-3/2 amplitude } A_{3/2}$

MODULUS ( $\text{GeV}^{-1/2}$ )	PHASE (°)	DOCUMENT ID	TECN	COMMENT
0.055 ± 0.010	152 ± 15	SOKHOYAN	15A	DPWA Multichannel
-0.254 <sup>+0.085</sup> <sub>-0.086</sub>	110 <sup>+10</sup> <sub>-6</sub>	ROENCHEN	14	DPWA
••• We do not use the following data for averages, fits, limits, etc. •••				
0.332	-71	ROENCHEN	15A	DPWA Multichannel

$\Delta(1600)$  BREIT-WIGNER PHOTON DECAY AMPLITUDES

$\Delta(1600) \rightarrow N\gamma, \text{helicity-1/2 amplitude } A_{1/2}$

VALUE ( $\text{GeV}^{-1/2}$ )	DOCUMENT ID	TECN	COMMENT
<b>-0.060 to -0.030 (≈ -0.045) OUR ESTIMATE</b>			
0.0082 ± 0.0014	<sup>1</sup> HUNT	19	DPWA Multichannel
-0.051 ± 0.010	SOKHOYAN	15A	DPWA Multichannel
-0.018 ± 0.015	<sup>1</sup> ARNDT	96	IPWA $\gamma N \rightarrow \pi N$
••• We do not use the following data for averages, fits, limits, etc. •••			
-0.050 ± 0.009	ANISOVICH	12A	DPWA Multichannel
0.006 ± 0.005	<sup>1</sup> SHRESTHA	12A	DPWA Multichannel
0.0	PENNER	02D	DPWA Multichannel

<sup>1</sup> Statistical error only.

$\Delta(1600) \rightarrow N\gamma, \text{helicity-3/2 amplitude } A_{3/2}$

VALUE ( $\text{GeV}^{-1/2}$ )	DOCUMENT ID	TECN	COMMENT
<b>-0.050 to -0.020 (≈ -0.035) OUR ESTIMATE</b>			
0.048 ± 0.014	<sup>1</sup> HUNT	19	DPWA Multichannel
-0.055 ± 0.010	SOKHOYAN	15A	DPWA Multichannel
-0.025 ± 0.015	<sup>1</sup> ARNDT	96	IPWA $\gamma N \rightarrow \pi N$
••• We do not use the following data for averages, fits, limits, etc. •••			
-0.040 ± 0.012	ANISOVICH	12A	DPWA Multichannel
0.052 ± 0.008	<sup>1</sup> SHRESTHA	12A	DPWA Multichannel
-0.024	PENNER	02D	DPWA Multichannel

<sup>1</sup> Statistical error only.

$\Delta(1600)$  REFERENCES

For early references, see Physics Letters **111B** 1 (1982).

HUNT	19	PR C99 055205	B. C. Hunt, D. M. Manley
ROENCHEN	15A	EPJ A51 70	D. Roenchen <i>et al.</i>
SOKHOYAN	15A	EPJ A51 95	V. Sokhoyan <i>et al.</i> (CBELSA/TAPS Collab.)
PDG	14	CP C38 070001	K. Olive <i>et al.</i> (PDG Collab.)
ROENCHEN	14	EPJ A50 101	D. Roenchen <i>et al.</i>
Also		EPJ A51 63 (errata.)	D. Roenchen <i>et al.</i>
SVARC	14	PR C89 045205	A. Svarc <i>et al.</i> (RBI Zagreb, UNI Tuzla)
ANISOVICH	12A	EPJ A48 15	A. V. Anisovich <i>et al.</i> (BONN, PNPI)
SHRESTHA	12A	PR C86 055203	M. Shrestha, D. M. Manley (KSU)
ARNDT	06	PR C74 045205	R. A. Arndt <i>et al.</i> (GWU)
PENNER	02C	PR C66 055211	G. Penner, U. Mosel (GIES)
PENNER	02D	PR C66 055212	G. Penner, U. Mosel (GIES)
VRANA	00	PRPL 328 181	T. P. Vrana, S. A. Dytman, T.-S. H. Lee (PITT, ANL)
ARNDT	96	PR C53 430	R. A. Arndt, I. I. Strakovsky, R. L. Workman (VPI)
HOEHLER	93	$\pi N$ Newsletter 9 1	G. Hoehler (KARL)
CUTKOSKY	80	Toronto Conf. 19	R. E. Cutkosky <i>et al.</i> (CMU, LBL) IJP
Also		PR D20 2839	R. E. Cutkosky <i>et al.</i> (CMU, LBL) IJP
HOEHLER	79	PDAT 12-1	G. Hoehler <i>et al.</i> (KARL) IJP
Also		Toronto Conf. 3	R. Koch (KARL) IJP

$\Delta(1620) 1/2^-$

$I(J^P) = \frac{3}{2}(\frac{1}{2}^-)$  Status: \*\*\*

Older and obsolete values are listed and referenced in the 2014 edition, Chinese Physics **C38** 070001 (2014).

$\Delta(1620)$  POLE POSITION

REAL PART

VALUE (MeV)	DOCUMENT ID	TECN	COMMENT
<b>1590 to 1610 (≈ 1600) OUR ESTIMATE</b>			
1597 ± 5	SOKHOYAN	15A	DPWA Multichannel
1603 ± 7 ± 2	<sup>1</sup> SVARC	14	L+P $\pi N \rightarrow \pi N$
1600 ± 15	CUTKOSKY	80	IPWA $\pi N \rightarrow \pi N$







# Baryon Particle Listings

## $\Delta(1700)$

### Normalized residue in $N\pi \rightarrow \Delta(1700) \rightarrow N(1520)\pi, P\text{-wave}$

MODULUS	PHASE ( $^\circ$ )	DOCUMENT ID	TECN	COMMENT
$0.10 \pm 0.03$	$-10 \pm 20$	SOKHOYAN 15A	DPWA	Multichannel

### $\Delta(1700)$ BREIT-WIGNER MASS

VALUE (MeV)	DOCUMENT ID	TECN	COMMENT
<b>1690 to 1730 (<math>\approx 1710</math>) OUR ESTIMATE</b>			
$1704 \pm 8$	GOLOVATCH 19	DPWA	$\gamma p \rightarrow \pi^+ \pi^- p$
$1720 \pm 5$	<sup>1</sup> HUNT 19	DPWA	Multichannel
$1715 \pm 20$	SOKHOYAN 15A	DPWA	Multichannel
$1695.0 \pm 1.3$	<sup>1</sup> ARNDT 06	DPWA	$\pi N \rightarrow \pi N, \eta N$
$1710 \pm 30$	CUTKOSKY 80	IPWA	$\pi N \rightarrow \pi N$
$1680 \pm 70$	HOEHLER 79	IPWA	$\pi N \rightarrow \pi N$
••• We do not use the following data for averages, fits, limits, etc. •••			
$1715 \pm 20$	GUTZ 14	DPWA	Multichannel
$1715 \pm 30$	ANISOVICH 12A	DPWA	Multichannel
$1691 \pm 4$	<sup>1</sup> SHRESTHA 12A	DPWA	Multichannel
$1678 \pm 1$	PENNER 02c	DPWA	Multichannel
$1732 \pm 23$	VRANA 00	DPWA	Multichannel
<sup>1</sup> Statistical error only.			

### $\Delta(1700)$ BREIT-WIGNER WIDTH

VALUE (MeV)	DOCUMENT ID	TECN	COMMENT
<b>220 to 380 (<math>\approx 300</math>) OUR ESTIMATE</b>			
$295 \pm 35$	GOLOVATCH 19	DPWA	$\gamma p \rightarrow \pi^+ \pi^- p$
$226 \pm 14$	<sup>1</sup> HUNT 19	DPWA	Multichannel
$300 \pm 25$	SOKHOYAN 15A	DPWA	Multichannel
$375.5 \pm 7.0$	<sup>1</sup> ARNDT 06	DPWA	$\pi N \rightarrow \pi N, \eta N$
$280 \pm 80$	CUTKOSKY 80	IPWA	$\pi N \rightarrow \pi N$
$230 \pm 80$	HOEHLER 79	IPWA	$\pi N \rightarrow \pi N$
••• We do not use the following data for averages, fits, limits, etc. •••			
$300 \pm 25$	GUTZ 14	DPWA	Multichannel
$310 \pm 40$	ANISOVICH 12A	DPWA	Multichannel
$248 \pm 9$	<sup>1</sup> SHRESTHA 12A	DPWA	Multichannel
$606 \pm 15$	PENNER 02c	DPWA	Multichannel
$119 \pm 70$	VRANA 00	DPWA	Multichannel
<sup>1</sup> Statistical error only.			

### $\Delta(1700)$ DECAY MODES

The following branching fractions are our estimates, not fits or averages.

Mode	Fraction ( $\Gamma_i/\Gamma$ )
$\Gamma_1$ $N\pi$	10–20 %
$\Gamma_2$ $N\pi\pi$	10–55 %
$\Gamma_3$ $\Delta(1232)\pi$	10–50 %
$\Gamma_4$ $\Delta(1232)\pi, S\text{-wave}$	5–35 %
$\Gamma_5$ $\Delta(1232)\pi, D\text{-wave}$	4–16 %
$\Gamma_6$ $N\rho$	
$\Gamma_7$ $N\rho, S=3/2, S\text{-wave}$	seen
$\Gamma_8$ $N(1520)\pi, P\text{-wave}$	1–5 %
$\Gamma_9$ $N(1535)\pi$	0.5–1.5 %
$\Gamma_{10}$ $\Delta(1232)\eta$	3–7 %
$\Gamma_{11}$ $N\gamma$	0.22–0.60 %
$\Gamma_{12}$ $N\gamma, \text{helicity}=1/2$	0.12–0.30 %
$\Gamma_{13}$ $N\gamma, \text{helicity}=3/2$	0.10–0.30 %

### $\Delta(1700)$ BRANCHING RATIOS

$\Gamma(N\pi)/\Gamma_{\text{total}}$	DOCUMENT ID	TECN	COMMENT	$\Gamma_1/\Gamma$
<b>10 to 20 OUR ESTIMATE</b>				
$15 \pm 2$	<sup>1</sup> HUNT 19	DPWA	Multichannel	
$22 \pm 4$	SOKHOYAN 15A	DPWA	Multichannel	
$15.6 \pm 0.1$	<sup>1</sup> ARNDT 06	DPWA	$\pi N \rightarrow \pi N, \eta N$	
$12 \pm 3$	CUTKOSKY 80	IPWA	$\pi N \rightarrow \pi N$	
$20 \pm 3$	HOEHLER 79	IPWA	$\pi N \rightarrow \pi N$	
••• We do not use the following data for averages, fits, limits, etc. •••				
$22 \pm 4$	GUTZ 14	DPWA	Multichannel	
$22 \pm 4$	ANISOVICH 12A	DPWA	Multichannel	
$14 \pm 1$	<sup>1</sup> SHRESTHA 12A	DPWA	Multichannel	
$14 \pm 1$	PENNER 02c	DPWA	Multichannel	
$5 \pm 1$	VRANA 00	DPWA	Multichannel	
<sup>1</sup> Statistical error only.				

$\Gamma(N\pi\pi)/\Gamma_{\text{total}}$	DOCUMENT ID	TECN	COMMENT	$\Gamma_2/\Gamma$
$0.89 \pm 0.11$	GOLOVATCH 19	DPWA	$\gamma p \rightarrow \pi^+ \pi^- p$	

### $\Gamma(\Delta(1232)\pi, S\text{-wave})/\Gamma_{\text{total}}$

VALUE (%)	DOCUMENT ID	TECN	COMMENT	$\Gamma_4/\Gamma$
$49 \pm 5$	<sup>1</sup> HUNT 19	DPWA	Multichannel	
$20 \pm 15$	SOKHOYAN 15A	DPWA	Multichannel	
••• We do not use the following data for averages, fits, limits, etc. •••				
$20 \pm 25$	ANISOVICH 12A	DPWA	Multichannel	
$54 \pm 3$	<sup>1</sup> SHRESTHA 12A	DPWA	Multichannel	
$90 \pm 2$	VRANA 00	DPWA	Multichannel	
<sup>1</sup> Statistical error only.				

### $\Gamma(\Delta(1232)\pi, D\text{-wave})/\Gamma_{\text{total}}$

VALUE (%)	DOCUMENT ID	TECN	COMMENT	$\Gamma_5/\Gamma$
$7.6 \pm 0.3$	<sup>1</sup> HUNT 19	DPWA	Multichannel	
$10 \pm 6$	SOKHOYAN 15A	DPWA	Multichannel	
••• We do not use the following data for averages, fits, limits, etc. •••				
$12 \pm 14$	ANISOVICH 12A	DPWA	Multichannel	
$1 \pm 1$	<sup>1</sup> SHRESTHA 12A	DPWA	Multichannel	
$4 \pm 1$	VRANA 00	DPWA	Multichannel	
<sup>1</sup> Statistical error only.				

### $\Gamma(N\rho, S=3/2, S\text{-wave})/\Gamma_{\text{total}}$

VALUE (%)	DOCUMENT ID	TECN	COMMENT	$\Gamma_7/\Gamma$
$27 \pm 5$	<sup>1</sup> HUNT 19	DPWA	Multichannel	
••• We do not use the following data for averages, fits, limits, etc. •••				
$30 \pm 3$	<sup>1</sup> SHRESTHA 12A	DPWA	Multichannel	
$1 \pm 1$	VRANA 00	DPWA	Multichannel	
<sup>1</sup> Statistical error only.				

### $\Gamma(N(1520)\pi, P\text{-wave})/\Gamma_{\text{total}}$

VALUE (%)	DOCUMENT ID	TECN	COMMENT	$\Gamma_8/\Gamma$
$3 \pm 2$	SOKHOYAN 15A	DPWA	Multichannel	

### $\Gamma(N(1535)\pi)/\Gamma_{\text{total}}$

VALUE (%)	DOCUMENT ID	TECN	COMMENT	$\Gamma_9/\Gamma$
$1.0 \pm 0.5$	GUTZ 14	DPWA	Multichannel	
••• We do not use the following data for averages, fits, limits, etc. •••				
$4 \pm 2$	HORN 08A	DPWA	Multichannel	

### $\Gamma(\Delta(1232)\eta)/\Gamma_{\text{total}}$

VALUE (%)	DOCUMENT ID	TECN	COMMENT	$\Gamma_{10}/\Gamma$
$5 \pm 2$	GUTZ 14	DPWA	Multichannel	
••• We do not use the following data for averages, fits, limits, etc. •••				
$5 \pm 2$	ANISOVICH 12A	DPWA	Multichannel	

### $\Gamma(N(1535)\pi)/\Gamma(\Delta(1232)\eta)$

VALUE	DOCUMENT ID	TECN	COMMENT	$\Gamma_9/\Gamma_{10}$
$0.67$	KASHEVAROV 09	CBAL	$\gamma p \rightarrow p \pi^0 \eta$	

### $\Delta(1700)$ PHOTON DECAY AMPLITUDES AT THE POLE

#### $\Delta(1700) \rightarrow N\gamma, \text{helicity-1/2 amplitude } A_{1/2}$

MODULUS ( $\text{GeV}^{-1/2}$ )	PHASE ( $^\circ$ )	DOCUMENT ID	TECN	COMMENT
$0.175 \pm 0.020$	$50 \pm 10$	SOKHOYAN 15A	DPWA	Multichannel
$0.109 \pm 0.010$	$-21 \pm 12$	ROENCHEN 14	DPWA	
••• We do not use the following data for averages, fits, limits, etc. •••				
$0.123$	$1.1$	ROENCHEN 15A	DPWA	Multichannel

#### $\Delta(1700) \rightarrow N\gamma, \text{helicity-3/2 amplitude } A_{3/2}$

MODULUS ( $\text{GeV}^{-1/2}$ )	PHASE ( $^\circ$ )	DOCUMENT ID	TECN	COMMENT
$0.180 \pm 0.020$	$45 \pm 10$	SOKHOYAN 15A	DPWA	Multichannel
$0.111 \pm 0.027$	$12 \pm 9$	ROENCHEN 14	DPWA	
	$-0.006$			
$0.124$	$22$	ROENCHEN 15A	DPWA	Multichannel
••• We do not use the following data for averages, fits, limits, etc. •••				

### $\Delta(1700)$ BREIT-WIGNER PHOTON DECAY AMPLITUDES

#### $\Delta(1700) \rightarrow N\gamma, \text{helicity-1/2 amplitude } A_{1/2}$

VALUE ( $\text{GeV}^{-1/2}$ )	DOCUMENT ID	TECN	COMMENT
<b>0.100 to 0.160 (<math>\approx 0.130</math>) OUR ESTIMATE</b>			
$0.0872 \pm 0.0189$	GOLOVATCH 19	DPWA	$\gamma p \rightarrow \pi^+ \pi^- p$
$0.156 \pm 0.017$	<sup>1</sup> HUNT 19	DPWA	Multichannel
$0.165 \pm 0.020$	SOKHOYAN 15A	DPWA	Multichannel
$0.132 \pm 0.005$	<sup>1</sup> DUGGER 13	DPWA	$\gamma N \rightarrow \pi N$
$0.105 \pm 0.005$	<sup>1</sup> WORKMAN 12A	DPWA	$\gamma N \rightarrow \pi N$

See key on page 999

Baryon Particle Listings
Δ(1700), Δ(1750), Δ(1900)

••• We do not use the following data for averages, fits, limits, etc. •••

Table with columns: VALUE (MeV), DOCUMENT ID, TECN, COMMENT. Rows include GUTZ, ANISOVICH, SHRESTHA, DRECHSEL, DUGGER, PENNER.

1 Statistical error only.

Δ(1700) → Nγ, helicity-3/2 amplitude A3/2

Table with columns: VALUE (GeV^-1/2), DOCUMENT ID, TECN, COMMENT. Rows include GOLOVATCH, HUNT, SOKHOYAN, DUGGER, WORKMAN, GUTZ, ANISOVICH, SHRESTHA, DRECHSEL, DUGGER, PENNER.

1 Statistical error only.

Δ(1700) REFERENCES

For early references, see Physics Letters 111B 1 (1982).

Large reference table with columns: AUTHOR, YEAR, REF ID, TITLE, JOURNAL. Includes references like Golovatch et al., Hunt et al., Roenchen et al., etc.

Δ(1750) 1/2+

I(J^P) = 3/2(1/2+) Status: \*

OMITTED FROM SUMMARY TABLE

Δ(1750) POLE POSITION

Table with columns: REAL PART, VALUE (MeV), DOCUMENT ID, TECN, COMMENT. Rows include ARNDT, VRANA.

-2xIMAGINARY PART

Table with columns: VALUE (MeV), DOCUMENT ID, TECN, COMMENT. Rows include ARNDT, VRANA.

Δ(1750) ELASTIC POLE RESIDUE

Table with columns: MODULUS |r|, VALUE (MeV), DOCUMENT ID, TECN, COMMENT. Rows include ARNDT.

PHASE θ

Table with columns: VALUE (°), DOCUMENT ID, TECN, COMMENT. Row includes ARNDT.

Δ(1750) BREIT-WIGNER MASS

Table with columns: VALUE (MeV), DOCUMENT ID, TECN, COMMENT. Rows include PENNER, VRANA.

Δ(1750) BREIT-WIGNER WIDTH

Table with columns: VALUE (MeV), DOCUMENT ID, TECN, COMMENT. Rows include PENNER, VRANA.

Δ(1750) DECAY MODES

Table with columns: Mode, Fraction (Γi/Γ). Rows include Nπ, Nππ, N(1440)π, ΣK.

Δ(1750) BRANCHING RATIOS

Table with columns: Γ(Nπ)/Γtotal, VALUE (%), DOCUMENT ID, TECN, COMMENT, Γ1/Γ, Γ3/Γ, Γ4/Γ. Rows include PENNER, VRANA.

Δ(1750) BREIT-WIGNER PHOTON DECAY AMPLITUDES

Papers on γN amplitudes predating 1981 may be found in our 2006 edition, Journal of Physics G33 1 (2006).

Δ(1750) → Nγ, helicity-1/2 amplitude A1/2

Table with columns: VALUE (GeV^-1/2), DOCUMENT ID, TECN, COMMENT. Row includes PENNER.

Δ(1750) REFERENCES

Reference table with columns: PDG, ARNDT, PENNER, VRANA, AUTHOR, YEAR, REF ID, TITLE, JOURNAL.

Δ(1900) 1/2-

I(J^P) = 3/2(1/2-) Status: \*\*\*

Older and obsolete values are listed and referenced in the 2014 edition, Chinese Physics C38 070001 (2014).

Δ(1900) POLE POSITION

Table with columns: REAL PART, VALUE (MeV), DOCUMENT ID, TECN, COMMENT. Rows include SOKHOYAN, SVARC, CUTKOSKY, HUNT, GUTZ, ANISOVICH, VRANA, HOEHLER.

1 Fit to the amplitudes of HOEHLER 79.

## Baryon Particle Listings

 $\Delta(1900)$  $-2\times$ IMAGINARY PART

VALUE (MeV)	DOCUMENT ID	TECN	COMMENT
<b>180 to 300 (<math>\approx 240</math>) OUR ESTIMATE</b>			
295 $\pm$ 35	SOKHOYAN 15A	DPWA	Multichannel
187 $\pm$ 5.0 $\pm$ 19	<sup>1</sup> SVARC 14	L+P	$\pi N \rightarrow \pi N$
180 $\pm$ 5.0	CUTKOSKY 80	IPWA	$\pi N \rightarrow \pi N$
• • • We do not use the following data for averages, fits, limits, etc. • • •			
447	HUNT 19	DPWA	Multichannel
295 $\pm$ 35	GUTZ 14	DPWA	Multichannel
300 $\pm$ 45	ANISOVICH 12A	DPWA	Multichannel
58	VRANA 00	DPWA	Multichannel

<sup>1</sup> Fit to the amplitudes of HOEHLER 79.

 $\Delta(1900)$  ELASTIC POLE RESIDUEMODULUS  $|r|$ 

VALUE (MeV)	DOCUMENT ID	TECN	COMMENT
<b>8 to 14 (<math>\approx 11</math>) OUR ESTIMATE</b>			
11 $\pm$ 2	SOKHOYAN 15A	DPWA	Multichannel
11 $\pm$ 4 $\pm$ 2	<sup>1</sup> SVARC 14	L+P	$\pi N \rightarrow \pi N$
10 $\pm$ 3	CUTKOSKY 80	IPWA	$\pi N \rightarrow \pi N$
• • • We do not use the following data for averages, fits, limits, etc. • • •			
11 $\pm$ 2	GUTZ 14	DPWA	Multichannel
10 $\pm$ 3	ANISOVICH 12A	DPWA	Multichannel

<sup>1</sup> Fit to the amplitudes of HOEHLER 79.

PHASE  $\theta$ 

VALUE ( $^\circ$ )	DOCUMENT ID	TECN	COMMENT
-115 $\pm$ 20	SOKHOYAN 15A	DPWA	Multichannel
20 $\pm$ 27 $\pm$ 19	<sup>1</sup> SVARC 14	L+P	$\pi N \rightarrow \pi N$
+ 20 $\pm$ 40	CUTKOSKY 80	IPWA	$\pi N \rightarrow \pi N$
• • • We do not use the following data for averages, fits, limits, etc. • • •			
-115 $\pm$ 20	GUTZ 14	DPWA	Multichannel
-125 $\pm$ 20	ANISOVICH 12A	DPWA	Multichannel

<sup>1</sup> Fit to the amplitudes of HOEHLER 79.

 $\Delta(1900)$  INELASTIC POLE RESIDUE

The "normalized residue" is the residue divided by  $\Gamma_{pole}/2$ .

Normalized residue in  $N\pi \rightarrow \Delta(1900) \rightarrow \Sigma K$ 

MODULUS	PHASE ( $^\circ$ )	DOCUMENT ID	TECN	COMMENT
0.07 $\pm$ 0.02	-50 $\pm$ 30	ANISOVICH 12A	DPWA	Multichannel

Normalized residue in  $N\pi \rightarrow \Delta(1900) \rightarrow \Delta\pi, D$ -wave

MODULUS	PHASE ( $^\circ$ )	DOCUMENT ID	TECN	COMMENT
0.18 $\pm$ 0.10	105 $\pm$ 25	SOKHOYAN 15A	DPWA	Multichannel
• • • We do not use the following data for averages, fits, limits, etc. • • •				
0.12 $^{+0.08}_{-0.05}$	110 $\pm$ 20	ANISOVICH 12A	DPWA	Multichannel

Normalized residue in  $N\pi \rightarrow \Delta(1900) \rightarrow \Delta(1232)\eta$ 

MODULUS	PHASE ( $^\circ$ )	DOCUMENT ID	TECN	COMMENT
0.013 $\pm$ 0.006	undefined	GUTZ 14	DPWA	Multichannel

Normalized residue in  $N\pi \rightarrow \Delta(1900) \rightarrow N(1440)\pi$ 

MODULUS	PHASE ( $^\circ$ )	DOCUMENT ID	TECN	COMMENT
0.11 $\pm$ 0.06	115 $\pm$ 30	SOKHOYAN 15A	DPWA	Multichannel

Normalized residue in  $N\pi \rightarrow \Delta(1900) \rightarrow N(1520)\pi$ 

MODULUS	PHASE ( $^\circ$ )	DOCUMENT ID	TECN	COMMENT
0.06 $\pm$ 0.03	undefined	SOKHOYAN 15A	DPWA	Multichannel

 $\Delta(1900)$  BREIT-WIGNER MASS

VALUE (MeV)	DOCUMENT ID	TECN	COMMENT
<b>1840 to 1920 (<math>\approx 1860</math>) OUR ESTIMATE</b>			
1989 $\pm$ 22	<sup>1</sup> HUNT 19	DPWA	Multichannel
1840 $\pm$ 20	SOKHOYAN 15A	DPWA	Multichannel
1890 $\pm$ 50	CUTKOSKY 80	IPWA	$\pi N \rightarrow \pi N$
1908 $\pm$ 30	HOEHLER 79	IPWA	$\pi N \rightarrow \pi N$
• • • We do not use the following data for averages, fits, limits, etc. • • •			
1840 $\pm$ 20	GUTZ 14	DPWA	Multichannel
1840 $\pm$ 30	ANISOVICH 12A	DPWA	Multichannel
1868 $\pm$ 12	<sup>1</sup> SHRESTHA 12A	DPWA	Multichannel
1802 $\pm$ 87	VRANA 00	DPWA	Multichannel

<sup>1</sup> Statistical error only.

 $\Delta(1900)$  BREIT-WIGNER WIDTH

VALUE (MeV)	DOCUMENT ID	TECN	COMMENT
<b>180 to 320 (<math>\approx 250</math>) OUR ESTIMATE</b>			
457 $\pm$ 60	<sup>1</sup> HUNT 19	DPWA	Multichannel
295 $\pm$ 30	SOKHOYAN 15A	DPWA	Multichannel
170 $\pm$ 50	CUTKOSKY 80	IPWA	$\pi N \rightarrow \pi N$
140 $\pm$ 40	HOEHLER 79	IPWA	$\pi N \rightarrow \pi N$

• • • We do not use the following data for averages, fits, limits, etc. • • •

295 $\pm$ 30	GUTZ 14	DPWA	Multichannel
300 $\pm$ 45	ANISOVICH 12A	DPWA	Multichannel
234 $\pm$ 27	<sup>1</sup> SHRESTHA 12A	DPWA	Multichannel
48 $\pm$ 45	VRANA 00	DPWA	Multichannel

<sup>1</sup> Statistical error only.

 $\Delta(1900)$  DECAY MODES

The following branching fractions are our estimates, not fits or averages.

Mode	Fraction ( $\Gamma_i/\Gamma$ )
$\Gamma_1$ $N\pi$	4–12 %
$\Gamma_2$ $\Sigma K$	seen
$\Gamma_3$ $N\pi\pi$	45–85 %
$\Gamma_4$ $\Delta(1232)\pi$	
$\Gamma_5$ $\Delta(1232)\pi, D$ -wave	30–70 %
$\Gamma_6$ $N\rho$	
$\Gamma_7$ $N\rho, S=1/2, S$ -wave	8–16 %
$\Gamma_8$ $N\rho, S=3/2, D$ -wave	18–28 %
$\Gamma_9$ $N(1440)\pi$	8–32 %
$\Gamma_{10}$ $N(1520)\pi$	2–10 %
$\Gamma_{11}$ $\Delta(1232)\eta$	0–2 %
$\Gamma_{12}$ $N\gamma, \text{ helicity}=1/2$	0.06–0.43 %

 $\Delta(1900)$  BRANCHING RATIOS

$\Gamma(N\pi)/\Gamma_{total}$	DOCUMENT ID	TECN	COMMENT	$\Gamma_1/\Gamma$
<b>4 to 12 (<math>\approx 8</math>) OUR ESTIMATE</b>				
3.7 $\pm$ 0.8	<sup>1</sup> HUNT 19	DPWA	Multichannel	
7 $\pm$ 2	SOKHOYAN 15A	DPWA	Multichannel	
10 $\pm$ 3	CUTKOSKY 80	IPWA	$\pi N \rightarrow \pi N$	
8 $\pm$ 4	HOEHLER 79	IPWA	$\pi N \rightarrow \pi N$	
• • • We do not use the following data for averages, fits, limits, etc. • • •				
7 $\pm$ 2	GUTZ 14	DPWA	Multichannel	
7 $\pm$ 3	ANISOVICH 12A	DPWA	Multichannel	
8 $\pm$ 1	<sup>1</sup> SHRESTHA 12A	DPWA	Multichannel	
33 $\pm$ 10	VRANA 00	DPWA	Multichannel	

<sup>1</sup> Statistical error only.

$\Gamma(\Delta(1232)\pi, D$ -wave)/ $\Gamma_{total}$	DOCUMENT ID	TECN	COMMENT	$\Gamma_5/\Gamma$
<b>4 to 12 (<math>\approx 8</math>) OUR ESTIMATE</b>				
42 $\pm$ 8	<sup>1</sup> HUNT 19	DPWA	Multichannel	
50 $\pm$ 20	SOKHOYAN 15A	DPWA	Multichannel	
• • • We do not use the following data for averages, fits, limits, etc. • • •				
15 $^{+50}_{-10}$	ANISOVICH 12A	DPWA	Multichannel	
56 $\pm$ 6	<sup>1</sup> SHRESTHA 12A	DPWA	Multichannel	
28 $\pm$ 1	VRANA 00	DPWA	Multichannel	

<sup>1</sup> Statistical error only.

$\Gamma(N\rho, S=1/2, S$ -wave)/ $\Gamma_{total}$	DOCUMENT ID	TECN	COMMENT	$\Gamma_7/\Gamma$
<b>4 to 12 (<math>\approx 8</math>) OUR ESTIMATE</b>				
23 $\pm$ 12	<sup>1</sup> HUNT 19	DPWA	Multichannel	
• • • We do not use the following data for averages, fits, limits, etc. • • •				
12 $\pm$ 4	<sup>1</sup> SHRESTHA 12A	DPWA	Multichannel	
30 $\pm$ 2	VRANA 00	DPWA	Multichannel	

<sup>1</sup> Statistical error only.

$\Gamma(N\rho, S=3/2, D$ -wave)/ $\Gamma_{total}$	DOCUMENT ID	TECN	COMMENT	$\Gamma_8/\Gamma$
<b>4 to 12 (<math>\approx 8</math>) OUR ESTIMATE</b>				
18 $\pm$ 7	<sup>1</sup> HUNT 19	DPWA	Multichannel	
• • • We do not use the following data for averages, fits, limits, etc. • • •				
23 $\pm$ 5	<sup>1</sup> SHRESTHA 12A	DPWA	Multichannel	
5 $\pm$ 1	VRANA 00	DPWA	Multichannel	

<sup>1</sup> Statistical error only.

$\Gamma(N(1440)\pi)/\Gamma_{total}$	DOCUMENT ID	TECN	COMMENT	$\Gamma_9/\Gamma$
<b>4 to 12 (<math>\approx 8</math>) OUR ESTIMATE</b>				
12 $\pm$ 9	<sup>1</sup> HUNT 19	DPWA	Multichannel	
20 $\pm$ 12	SOKHOYAN 15A	DPWA	Multichannel	
• • • We do not use the following data for averages, fits, limits, etc. • • •				
< 1	<sup>1</sup> SHRESTHA 12A	DPWA	Multichannel	
4 $\pm$ 1	VRANA 00	DPWA	Multichannel	

<sup>1</sup> Statistical error only.

$\Gamma(N(1520)\pi)/\Gamma_{total}$	DOCUMENT ID	TECN	COMMENT	$\Gamma_{10}/\Gamma$
<b>4 to 12 (<math>\approx 8</math>) OUR ESTIMATE</b>				
6 $\pm$ 4	SOKHOYAN 15A	DPWA	Multichannel	

See key on page 999

Baryon Particle Listings
Δ(1900), Δ(1905)

Table with 4 columns: VALUE (%), DOCUMENT ID, TECN, COMMENT. Row: 1±1, GUTZ, 14, DPWA, Multichannel.

Δ(1900) PHOTON DECAY AMPLITUDES AT THE POLE

Table with 5 columns: MODULUS (GeV^-1/2), PHASE (°), DOCUMENT ID, TECN, COMMENT. Row: 0.064±0.015, 60±20, SOKHOYAN, 15A, DPWA, Multichannel.

Δ(1900) BREIT-WIGNER PHOTON DECAY AMPLITUDES

Table with 4 columns: VALUE (GeV^-1/2), DOCUMENT ID, TECN, COMMENT. Includes a note: 'We do not use the following data for averages, fits, limits, etc.'

Δ(1900) REFERENCES

For early references, see Physics Letters 111B 1 (1982).

Table with 4 columns: AUTHOR, YEAR, DOCUMENT ID, COMMENT. Lists various physics papers related to Δ(1900).

Δ(1905) 5/2+ I(J^P) = 3/2(5/2+) Status: \*\*\*

Older and obsolete values are listed and referenced in the 2014 edition, Chinese Physics C38 070001 (2014).

Δ(1905) POLE POSITION

Table with 4 columns: VALUE (MeV), DOCUMENT ID, TECN, COMMENT. Section: REAL PART. Rows include 1800±6, 1752±3±2, 1830±40, etc.

Table with 4 columns: VALUE (MeV), DOCUMENT ID, TECN, COMMENT. Section: -2xIMAGINARY PART. Rows include 260 to 340 (OUR ESTIMATE), 290±15, 346±6±2, etc.

Δ(1905) ELASTIC POLE RESIDUE

Table with 4 columns: VALUE (MeV), DOCUMENT ID, TECN, COMMENT. Section: MODULUS |r|. Rows include 15 to 25 (OUR ESTIMATE), 19±2, 24±1±1, etc.

Table with 4 columns: VALUE (%), DOCUMENT ID, TECN, COMMENT. Rows include 5.3, 19±2, 20±2, etc.

Table with 4 columns: VALUE (°), DOCUMENT ID, TECN, COMMENT. Section: PHASE θ. Rows include -120 to -30 (OUR ESTIMATE), -45±4, -114±1±2, etc.

Δ(1905) INELASTIC POLE RESIDUE

The "normalized residue" is the residue divided by Γ\_pole/2.

Table with 4 columns: MODULUS, PHASE (°), DOCUMENT ID, TECN, COMMENT. Section: Normalized residue in Nπ → Δ(1905) → Δπ, P-wave. Rows include 0.19±0.07, 10±30, etc.

Table with 4 columns: MODULUS, PHASE (°), DOCUMENT ID, TECN, COMMENT. Section: Normalized residue in Nπ → Δ(1905) → Δπ, F-wave. Rows include 0.0870, 72, etc.

Table with 4 columns: MODULUS, PHASE (°), DOCUMENT ID, TECN, COMMENT. Section: Normalized residue in Nπ → Δ(1905) → ΣK. Rows include 0.001, -155, etc.

Table with 4 columns: MODULUS, PHASE (°), DOCUMENT ID, TECN, COMMENT. Section: Normalized residue in Nπ → Δ(1905) → N(1535)π. Rows include 0.025±0.010, 130±35, etc.

Table with 4 columns: MODULUS, PHASE (°), DOCUMENT ID, TECN, COMMENT. Section: Normalized residue in Nπ → Δ(1905) → Δ(1232)η. Rows include 0.07±0.02, 40±20, etc.

Δ(1905) BREIT-WIGNER MASS

Table with 4 columns: VALUE (MeV), DOCUMENT ID, TECN, COMMENT. Section: 1855 to 1910 (OUR ESTIMATE). Rows include 1883±19, 1866±9, etc.

Δ(1905) BREIT-WIGNER WIDTH

Table with 4 columns: VALUE (MeV), DOCUMENT ID, TECN, COMMENT. Section: 270 to 400 (OUR ESTIMATE). Rows include 327±69, 289±20, etc.

Downloaded from https://academic.oup.com/ptep/article/2020/8/083C01/5891211 by guest on 12 November 2020







## Baryon Particle Listings

 $\Delta(1910)$ ,  $\Delta(1920)$  $\Gamma(\Delta(1232)\eta)/\Gamma_{\text{total}}$ 

VALUE (%)	DOCUMENT ID	TECN	COMMENT
9±4	GUTZ	14	DPWA Multichannel

 $\Gamma_6/\Gamma$  $\Delta(1920)$  ELASTIC POLE RESIDUEMODULUS  $|r|$ 

VALUE (MeV)	DOCUMENT ID	TECN	COMMENT
<b>8 to 24 (<math>\approx 16</math>) OUR ESTIMATE</b>			
16±6	SOKHOYAN	15A	DPWA Multichannel
26±3±2	<sup>1</sup> SVARC	14	L+P $\pi N \rightarrow \pi N$
24±4	CUTKOSKY	80	IPWA $\pi N \rightarrow \pi N$
••• We do not use the following data for averages, fits, limits, etc. •••			
38	ROENCHEN	15A	DPWA Multichannel
16±6	GUTZ	14	DPWA Multichannel
17±8	ANISOVICH	12A	DPWA Multichannel

<sup>1</sup> Fit to the amplitudes of HOEHLER 79.PHASE  $\theta$ 

VALUE (°)	DOCUMENT ID	TECN	COMMENT
<b>-150 to -50 (<math>\approx -100</math>) OUR ESTIMATE</b>			
-50±25	SOKHOYAN	15A	DPWA Multichannel
-130±5±3	<sup>1</sup> SVARC	14	L+P $\pi N \rightarrow \pi N$
-150±30	CUTKOSKY	80	IPWA $\pi N \rightarrow \pi N$
••• We do not use the following data for averages, fits, limits, etc. •••			
146	ROENCHEN	15A	DPWA Multichannel
-50±25	GUTZ	14	DPWA Multichannel
-40±20	ANISOVICH	12A	DPWA Multichannel

<sup>1</sup> Fit to the amplitudes of HOEHLER 79. $\Delta(1920)$  INELASTIC POLE RESIDUEThe "normalized residue" is the residue divided by  $\Gamma_{\text{pole}}/2$ .Normalized residue in  $N\pi \rightarrow \Delta(1920) \rightarrow \Delta\eta$ 

MODULUS	PHASE (°)	DOCUMENT ID	TECN	COMMENT
0.15±0.04	70±20	GUTZ	14	DPWA Multichannel
••• We do not use the following data for averages, fits, limits, etc. •••				
0.17±0.08	70±20	ANISOVICH	12A	DPWA Multichannel

Normalized residue in  $N\pi \rightarrow \Delta(1920) \rightarrow \Sigma K$ 

MODULUS	PHASE (°)	DOCUMENT ID	TECN	COMMENT
0.09±0.03	80±40	ANISOVICH	12A	DPWA Multichannel
••• We do not use the following data for averages, fits, limits, etc. •••				
0.17	-35	ROENCHEN	15A	DPWA Multichannel

Normalized residue in  $N\pi \rightarrow \Delta(1920) \rightarrow \Delta\pi, P\text{-wave}$ 

MODULUS	PHASE (°)	DOCUMENT ID	TECN	COMMENT
0.20±0.08	-105±25	SOKHOYAN	15A	DPWA Multichannel
••• We do not use the following data for averages, fits, limits, etc. •••				
0.069	131	ROENCHEN	15A	DPWA Multichannel
0.20±0.12	-120±30	ANISOVICH	12A	DPWA Multichannel

Normalized residue in  $N\pi \rightarrow \Delta(1920) \rightarrow \Delta\pi, F\text{-wave}$ 

MODULUS	PHASE (°)	DOCUMENT ID	TECN	COMMENT
0.37±0.10	-90±20	SOKHOYAN	15A	DPWA Multichannel
••• We do not use the following data for averages, fits, limits, etc. •••				
0.013	-115	ROENCHEN	15A	DPWA Multichannel
0.28±0.07	-95±35	ANISOVICH	12A	DPWA Multichannel

Normalized residue in  $N\pi \rightarrow \Delta(1920) \rightarrow N(1535)\pi$ 

MODULUS	PHASE (°)	DOCUMENT ID	TECN	COMMENT
0.03±0.02	35±45	GUTZ	14	DPWA Multichannel

Normalized residue in  $N\pi \rightarrow \Delta(1920) \rightarrow N\pi_0(980)$ 

MODULUS	PHASE (°)	DOCUMENT ID	TECN	COMMENT
0.03±0.02	-85±45	GUTZ	14	DPWA Multichannel

Normalized residue in  $N\pi \rightarrow \Delta(1920) \rightarrow N(1440)\pi$ 

MODULUS	PHASE (°)	DOCUMENT ID	TECN	COMMENT
0.04±0.03	undefined	SOKHOYAN	15A	DPWA Multichannel

Normalized residue in  $N\pi \rightarrow \Delta(1920) \rightarrow N(1520)\pi, S\text{-wave}$ 

MODULUS	PHASE (°)	DOCUMENT ID	TECN	COMMENT
0.05±0.05	undefined	SOKHOYAN	15A	DPWA Multichannel

 $\Delta(1920)$  BREIT-WIGNER MASS

VALUE (MeV)	DOCUMENT ID	TECN	COMMENT
<b>1870 to 1970 (<math>\approx 1920</math>) OUR ESTIMATE</b>			
1976±49	HUNT	19	DPWA Multichannel
1880±30	SOKHOYAN	15A	DPWA Multichannel
2146±32	<sup>1</sup> SHRESTHA	12A	DPWA Multichannel
1920±80	CUTKOSKY	80	IPWA $\pi N \rightarrow \pi N$
1868±10	HOEHLER	79	IPWA $\pi N \rightarrow \pi N$

 $\Delta(1910)$  PHOTON DECAY AMPLITUDES AT THE POLE $\Delta(1910) \rightarrow N\gamma$ , helicity-1/2 amplitude  $A_{1/2}$ 

MODULUS ( $\text{GeV}^{-1/2}$ )	PHASE (°)	DOCUMENT ID	TECN	COMMENT
0.027±0.009	-30±60	SOKHOYAN	15A	DPWA Multichannel
-0.246 <sup>+0.024</sup> <sub>-0.047</sub>	159 <sup>+9</sup> <sub>-4</sub>	ROENCHEN	14	DPWA
••• We do not use the following data for averages, fits, limits, etc. •••				
0.321	39	ROENCHEN	15A	DPWA Multichannel

 $\Delta(1910)$  BREIT-WIGNER PHOTON DECAY AMPLITUDES $\Delta(1910) \rightarrow N\gamma$ , helicity-1/2 amplitude  $A_{1/2}$ 

VALUE ( $\text{GeV}^{-1/2}$ )	DOCUMENT ID	TECN	COMMENT
<b>0.010 to 0.030 (<math>\approx 0.020</math>) OUR ESTIMATE</b>			
0.203±0.056	<sup>1</sup> HUNT	19	DPWA Multichannel
0.026±0.008	SOKHOYAN	15A	DPWA Multichannel
-0.002±0.008	<sup>1</sup> ARNDT	96	IPWA $\gamma N \rightarrow \pi N$
••• We do not use the following data for averages, fits, limits, etc. •••			
0.026±0.008	GUTZ	14	DPWA Multichannel
0.022±0.009	ANISOVICH	12A	DPWA Multichannel
0.030±0.002	<sup>1</sup> SHRESTHA	12A	DPWA Multichannel

<sup>1</sup> Statistical error only. $\Delta(1910)$  REFERENCESFor early references, see Physics Letters **111B** 1 (1982).

HUNT	19	PR C99 055205	B. C. Hunt, D.M. Manley
ROENCHEN	15A	EPJ A51 70	D. Roenchen et al.
SOKHOYAN	15A	EPJ A51 95	V. Sokhoyan et al. (CBELSA/TAPS Collab.)
GUTZ	14	EPJ A50 74	E. Gutz et al. (CBELSA/TAPS Collab.)
PDG	14	CP C38 070001	K. Olive et al. (PDG Collab.)
ROENCHEN	14	EPJ A50 101	D. Roenchen et al.
Also		EPJ A51 63 (errat.)	D. Roenchen et al.
SVARC	14	PR C89 045205	A. Svarc et al. (RBI Zagreb, UNI Tuzla)
ANISOVICH	12A	EPJ A48 15	A.V. Anisovich et al. (BONN, PNPI)
SHRESTHA	12A	PR C86 055203	M. Shrestha, D.M. Manley (KSU)
ARNDT	06	PR C74 045205	R.A. Arndt et al. (GWU)
VRANA	00	PRPL 328 181	T.P. Vrana, S.A. Dytman, T.-S.H. Lee (PITT, ANL)
ARNDT	96	PR C53 430	R.A. Arndt, I.I. Strakovsky, R.L. Workman (VPI)
HOEHLER	93	$\pi N$ Newsletter 9 1	G. Hohlner (KARL)
CUTKOSKY	80	Toronto Conf. 19	R.E. Cutkosky et al. (CMU, LBL) IJP
Also		PR D20 2839	R.E. Cutkosky et al. (CMU, LBL) IJP
HOEHLER	79	PDAT 12-1	G. Hohlner et al. (KARL) IJP
Also		Toronto Conf. 3	R. Koch (KARL) IJP

 $\Delta(1920) 3/2^+$ 

$$J(P) = \frac{3}{2}(\frac{3}{2}^+) \text{ Status: } ***$$

Older and obsolete values are listed and referenced in the 2014 edition, Chinese Physics **C38** 070001 (2014). $\Delta(1920)$  POLE POSITION

## REAL PART

VALUE (MeV)	DOCUMENT ID	TECN	COMMENT
<b>1850 to 1950 (<math>\approx 1900</math>) OUR ESTIMATE</b>			
1875±30	SOKHOYAN	15A	DPWA Multichannel
1906±10±2	<sup>1</sup> SVARC	14	L+P $\pi N \rightarrow \pi N$
1900±80	CUTKOSKY	80	IPWA $\pi N \rightarrow \pi N$
••• We do not use the following data for averages, fits, limits, etc. •••			
1910	HUNT	19	DPWA Multichannel
1715	ROENCHEN	15A	DPWA Multichannel
1875±30	GUTZ	14	DPWA Multichannel
1890±30	ANISOVICH	12A	DPWA Multichannel
1880	VRANA	00	DPWA Multichannel
1900	HOEHLER	93	SPED $\pi N \rightarrow \pi N$

<sup>1</sup> Fit to the amplitudes of HOEHLER 79.

## -2xIMAGINARY PART

VALUE (MeV)	DOCUMENT ID	TECN	COMMENT
<b>200 to 400 (<math>\approx 300</math>) OUR ESTIMATE</b>			
300±40	SOKHOYAN	15A	DPWA Multichannel
310±20±11	<sup>1</sup> SVARC	14	L+P $\pi N \rightarrow \pi N$
300±100	CUTKOSKY	80	IPWA $\pi N \rightarrow \pi N$
••• We do not use the following data for averages, fits, limits, etc. •••			
472	HUNT	19	DPWA Multichannel
882	ROENCHEN	15A	DPWA Multichannel
300±40	GUTZ	14	DPWA Multichannel
300±60	ANISOVICH	12A	DPWA Multichannel
120	VRANA	00	DPWA Multichannel

<sup>1</sup> Fit to the amplitudes of HOEHLER 79.

See key on page 999

# Baryon Particle Listings

## $\Delta(1920)$

••• We do not use the following data for averages, fits, limits, etc. •••

1880 ± 30	GUTZ	14	DPWA	Multichannel
1900 ± 30	ANISOVICH	12A	DPWA	Multichannel
2057 ± 1	PENNER	02c	DPWA	Multichannel
1889 ± 100	VRANA	00	DPWA	Multichannel

<sup>1</sup> Statistical error only.

### $\Delta(1920)$ BREIT-WIGNER WIDTH

VALUE (MeV)	DOCUMENT ID	TECN	COMMENT
<b>240 to 360 (≈ 300) OUR ESTIMATE</b>			
509 ± 170	HUNT	19	DPWA Multichannel
300 ± 40	SOKHOYAN	15A	DPWA Multichannel
400 ± 80	<sup>1</sup> SHRESTHA	12A	DPWA Multichannel
300 ± 100	CUTKOSKY	80	IPWA $\pi N \rightarrow \pi N$
220 ± 80	HOEHLER	79	IPWA $\pi N \rightarrow \pi N$
••• We do not use the following data for averages, fits, limits, etc. •••			
300 ± 40	GUTZ	14	DPWA Multichannel
310 ± 60	ANISOVICH	12A	DPWA Multichannel
525 ± 32	PENNER	02c	DPWA Multichannel
123 ± 53	VRANA	00	DPWA Multichannel

<sup>1</sup> Statistical error only.

### $\Delta(1920)$ DECAY MODES

The following branching fractions are our estimates, not fits or averages.

Mode	Fraction ( $\Gamma_i/\Gamma$ )
$\Gamma_1$ $N\pi$	5–20 %
$\Gamma_2$ $\Sigma K$	2–6 %
$\Gamma_3$ $N\pi\pi$	
$\Gamma_4$ $\Delta(1232)\pi$	50–90 %
$\Gamma_5$ $\Delta(1232)\pi, P$ -wave	8–28 %
$\Gamma_6$ $\Delta(1232)\pi, F$ -wave	44–72 %
$\Gamma_7$ $N(1440)\pi, P$ -wave	<4 %
$\Gamma_8$ $N(1520)\pi, S$ -wave	<5 %
$\Gamma_9$ $N(1535)\pi$	<2 %
$\Gamma_{10}$ $N_{a_0}(980)$	seen
$\Gamma_{11}$ $\Delta(1232)\eta$	5–17 %

### $\Delta(1920)$ BRANCHING RATIOS

$\Gamma(N\pi)/\Gamma_{total}$	DOCUMENT ID	TECN	COMMENT	$\Gamma_1/\Gamma$
<b>5 to 20 (≈ 12) OUR ESTIMATE</b>				
10.5 ± 3.0	<sup>1</sup> HUNT	19	DPWA Multichannel	
8 ± 4	SOKHOYAN	15A	DPWA Multichannel	
20 ± 5	CUTKOSKY	80	IPWA $\pi N \rightarrow \pi N$	
14 ± 4	HOEHLER	79	IPWA $\pi N \rightarrow \pi N$	
••• We do not use the following data for averages, fits, limits, etc. •••				
8 ± 4	GUTZ	14	DPWA Multichannel	
8 ± 4	ANISOVICH	12A	DPWA Multichannel	
16 ± 4	<sup>1</sup> SHRESTHA	12A	DPWA Multichannel	
15 ± 1	PENNER	02c	DPWA Multichannel	
5 ± 4	VRANA	00	DPWA Multichannel	

<sup>1</sup> Statistical error only.

$\Gamma(\Sigma K)/\Gamma_{total}$	DOCUMENT ID	TECN	COMMENT	$\Gamma_2/\Gamma$
4 ± 2	ANISOVICH	12A	DPWA Multichannel	
••• We do not use the following data for averages, fits, limits, etc. •••				
2.1 ± 0.3	PENNER	02c	DPWA Multichannel	

$\Gamma(\Delta(1232)\pi, P\text{-wave})/\Gamma_{total}$	DOCUMENT ID	TECN	COMMENT	$\Gamma_5/\Gamma$
VALUE (%)				
< 1.6	<sup>1</sup> HUNT	19	DPWA Multichannel	
18 ± 10	SOKHOYAN	15A	DPWA Multichannel	
••• We do not use the following data for averages, fits, limits, etc. •••				
22 ± 12	ANISOVICH	12A	DPWA Multichannel	
7 ± 5	<sup>1</sup> SHRESTHA	12A	DPWA Multichannel	
41 ± 3	VRANA	00	DPWA Multichannel	

<sup>1</sup> Statistical error only.

$\Gamma(\Delta(1232)\pi, F\text{-wave})/\Gamma_{total}$	DOCUMENT ID	TECN	COMMENT	$\Gamma_6/\Gamma$
VALUE (%)				
58 ± 14	SOKHOYAN	15A	DPWA Multichannel	
••• We do not use the following data for averages, fits, limits, etc. •••				
45 ± 20	ANISOVICH	12A	DPWA Multichannel	

$\Gamma(N(1440)\pi, P\text{-wave})/\Gamma_{total}$	DOCUMENT ID	TECN	COMMENT	$\Gamma_7/\Gamma$
VALUE (%)				
77 ± 9	<sup>1</sup> HUNT	19	DPWA Multichannel	
< 4	SOKHOYAN	15A	DPWA Multichannel	

••• We do not use the following data for averages, fits, limits, etc. •••

$\Gamma(N(1520)\pi, S\text{-wave})/\Gamma_{total}$	DOCUMENT ID	TECN	COMMENT	$\Gamma_8/\Gamma$
VALUE (%)				
< 20	<sup>1</sup> SHRESTHA	12A	DPWA Multichannel	
53 ± 8	VRANA	00	DPWA Multichannel	

<sup>1</sup> Statistical error only.

$\Gamma(N(1535)\pi)/\Gamma_{total}$	DOCUMENT ID	TECN	COMMENT	$\Gamma_9/\Gamma$
VALUE (%)				
< 2	GUTZ	14	DPWA Multichannel	

$\Gamma(N_{a_0}(980))/\Gamma_{total}$	DOCUMENT ID	TECN	COMMENT	$\Gamma_{10}/\Gamma$
VALUE (%)				
4 ± 2	HORN	08A	DPWA Multichannel	

$\Gamma(\Delta(1232)\eta)/\Gamma_{total}$	DOCUMENT ID	TECN	COMMENT	$\Gamma_{11}/\Gamma$
VALUE (%)				
11 ± 6	GUTZ	14	DPWA Multichannel	
••• We do not use the following data for averages, fits, limits, etc. •••				
15 ± 8	ANISOVICH	12A	DPWA Multichannel	

### $\Delta(1920)$ PHOTON DECAY AMPLITUDES AT THE POLE

#### $\Delta(1920) \rightarrow N\gamma$ , helicity-1/2 amplitude $A_{1/2}$

MODULUS ( $\text{GeV}^{-1/2}$ )	PHASE ( $^\circ$ )	DOCUMENT ID	TECN	COMMENT
0.110 ± 0.030	-50 ± 20	SOKHOYAN	15A	DPWA Multichannel
0.190 <sup>+0.050</sup> <sub>-0.022</sub>	-160 <sup>+24</sup> <sub>-11</sub>	ROENCHEN	14	DPWA
••• We do not use the following data for averages, fits, limits, etc. •••				
-0.192	46	ROENCHEN	15A	DPWA Multichannel

#### $\Delta(1920) \rightarrow N\gamma$ , helicity-3/2 amplitude $A_{3/2}$

MODULUS ( $\text{GeV}^{-1/2}$ )	PHASE ( $^\circ$ )	DOCUMENT ID	TECN	COMMENT
-0.100 ± 0.040	0 ± 20	SOKHOYAN	15A	DPWA Multichannel
-0.398 <sup>+0.070</sup> <sub>-0.067</sub>	-110 <sup>+4</sup> <sub>-5</sub>	ROENCHEN	14	DPWA
••• We do not use the following data for averages, fits, limits, etc. •••				
0.522	67	ROENCHEN	15A	DPWA Multichannel

### $\Delta(1920)$ BREIT-WIGNER PHOTON DECAY AMPLITUDES

#### $\Delta(1920) \rightarrow N\gamma$ , helicity-1/2 amplitude $A_{1/2}$

VALUE ( $\text{GeV}^{-1/2}$ )	DOCUMENT ID	TECN	COMMENT
-0.028 ± 0.010	<sup>1</sup> HUNT	19	DPWA Multichannel
0.110 ± 0.030	SOKHOYAN	15A	DPWA Multichannel
••• We do not use the following data for averages, fits, limits, etc. •••			
0.110 ± 0.030	GUTZ	14	DPWA Multichannel
0.130 <sup>+0.030</sup> <sub>-0.060</sub>	ANISOVICH	12A	DPWA Multichannel
0.051 ± 0.010	<sup>1</sup> SHRESTHA	12A	DPWA Multichannel
-0.007	PENNER	02D	DPWA Multichannel

<sup>1</sup> Statistical error only.

#### $\Delta(1920) \rightarrow N\gamma$ , helicity-3/2 amplitude $A_{3/2}$

VALUE ( $\text{GeV}^{-1/2}$ )	DOCUMENT ID	TECN	COMMENT
-0.043 ± 0.014	<sup>1</sup> HUNT	19	DPWA Multichannel
-0.105 ± 0.035	SOKHOYAN	15A	DPWA Multichannel
••• We do not use the following data for averages, fits, limits, etc. •••			
-0.105 ± 0.035	GUTZ	14	DPWA Multichannel
-0.115 <sup>+0.025</sup> <sub>-0.050</sub>	ANISOVICH	12A	DPWA Multichannel
0.017 ± 0.015	<sup>1</sup> SHRESTHA	12A	DPWA Multichannel
-0.001	PENNER	02D	DPWA Multichannel

<sup>1</sup> Statistical error only.

### $\Delta(1920)$ REFERENCES

For early references, see Physics Letters **111B** 1 (1982).

HUNT	19	PR C99 055205	B.C. Hunt, D.M. Manley
ROENCHEN	15A	EPJ A51 70	D. Roenchen <i>et al.</i>
SOKHOYAN	15A	EPJ A51 95	V. Sokhoyan <i>et al.</i>
GUTZ	14	EPJ A50 74	E. Gutz <i>et al.</i>
PDG	14	CP C38 070001	K. Olive <i>et al.</i>

(CBELSA/TAPS Collab.)  
(CBELSA/TAPS Collab.)  
(PDG Collab.)

## Baryon Particle Listings

 $\Delta(1920), \Delta(1930)$ 

ROENCHEN	14	EPJ A50 101	D. Roenchen <i>et al.</i>	
Also		EPJ A51 63 (errat.)	D. Roenchen <i>et al.</i>	
SVARC	14	PR C89 045205	A. Svarc <i>et al.</i>	(RBI Zagreb, UNI Tuzla)
ANISOVICH	12A	EPJ A48 15	A.V. Anisovich <i>et al.</i>	(BOONN, PNPI)
SHRESTHA	12A	PR C86 055203	M. Shrestha, D.M. Manley	(KSU)
HORN	08A	EPJ A38 173	I. Horn <i>et al.</i>	(CB-ELSA Collab.)
Also		PRL 101 202002	I. Horn <i>et al.</i>	(CB-ELSA Collab.)
PENNER	02C	PR C66 055211	G. Penner, U. Mosel	(GIES)
PENNER	02D	PR C66 055212	G. Penner, U. Mosel	(GIES)
VRANA	00	PRPL 320 181	T.P. Vrana, S.A. Dytman, T.-S.H. Lee	(PITT, ANL)
HOEHLER	93	$\pi N$ Newsletter 9 1	G. Hoehler	(KARL)
CUTKOSKY	80	Toronto Conf. 19	R.E. Cutkosky <i>et al.</i>	(CMU, LBL) IJP
Also		PR D20 2839	R.E. Cutkosky <i>et al.</i>	(CMU, LBL) IJP
HOEHLER	79	PDAT 12-1	G. Hoehler <i>et al.</i>	(KARLT) IJP
Also		Toronto Conf. 3	R. Koch	(KARLT) IJP

 $\Delta(1930) 5/2^-$ 

$$I(J^P) = \frac{3}{2}(\frac{5}{2}^-) \text{ Status: } ***$$

Older and obsolete values are listed and referenced in the 2014 edition, Chinese Physics C38 070001 (2014).

 $\Delta(1930)$  POLE POSITION

## REAL PART

VALUE (MeV)	DOCUMENT ID	TECN	COMMENT
<b>1840 to 1920 (<math>\approx 1880</math>) OUR ESTIMATE</b>			
1848 $\pm$ 9 $\pm$ 19	<sup>1</sup> SVARC 14	L+P	$\pi N \rightarrow \pi N$
1890 $\pm$ 50	CUTKOSKY 80	IPWA	$\pi N \rightarrow \pi N$
••• We do not use the following data for averages, fits, limits, etc. •••			
1863	HUNT 19	DPWA	Multichannel
1836	ROENCHEN 15A	DPWA	Multichannel
2001	ARNDT 06	DPWA	$\pi N \rightarrow \pi N, \eta N$
1883	VRANA 00	DPWA	Multichannel
1850	HOEHLER 93	SPED	$\pi N \rightarrow \pi N$

<sup>1</sup> Fit to the amplitudes of HOEHLER 79.

-2*x*IMAGINARY PART

VALUE (MeV)	DOCUMENT ID	TECN	COMMENT
<b>230 to 330 (<math>\approx 280</math>) OUR ESTIMATE</b>			
321 $\pm$ 17 $\pm$ 7	<sup>1</sup> SVARC 14	L+P	$\pi N \rightarrow \pi N$
260 $\pm$ 60	CUTKOSKY 80	IPWA	$\pi N \rightarrow \pi N$
••• We do not use the following data for averages, fits, limits, etc. •••			
260	HUNT 19	DPWA	Multichannel
724	ROENCHEN 15A	DPWA	Multichannel
387	ARNDT 06	DPWA	$\pi N \rightarrow \pi N, \eta N$
250	VRANA 00	DPWA	Multichannel
180	HOEHLER 93	SPED	$\pi N \rightarrow \pi N$

<sup>1</sup> Fit to the amplitudes of HOEHLER 79.

 $\Delta(1930)$  ELASTIC POLE RESIDUEMODULUS  $|r|$ 

VALUE (MeV)	DOCUMENT ID	TECN	COMMENT
<b>8 to 20 (<math>\approx 14</math>) OUR ESTIMATE</b>			
9 $\pm$ 1 $\pm$ 1	<sup>1</sup> SVARC 14	L+P	$\pi N \rightarrow \pi N$
18 $\pm$ 6	CUTKOSKY 80	IPWA	$\pi N \rightarrow \pi N$
••• We do not use the following data for averages, fits, limits, etc. •••			
34	ROENCHEN 15A	DPWA	Multichannel
7	ARNDT 06	DPWA	$\pi N \rightarrow \pi N, \eta N$
20	HOEHLER 93	SPED	$\pi N \rightarrow \pi N$

<sup>1</sup> Fit to the amplitudes of HOEHLER 79.

PHASE  $\theta$ 

VALUE ( $^\circ$ )	DOCUMENT ID	TECN	COMMENT
<b>- 40 to -10 (<math>\approx -30</math>) OUR ESTIMATE</b>			
- 37 $\pm$ 3 $\pm$ 7	<sup>1</sup> SVARC 14	L+P	$\pi N \rightarrow \pi N$
- 20 $\pm$ 40	CUTKOSKY 80	IPWA	$\pi N \rightarrow \pi N$
••• We do not use the following data for averages, fits, limits, etc. •••			
-155	ROENCHEN 15A	DPWA	Multichannel
- 12	ARNDT 06	DPWA	$\pi N \rightarrow \pi N, \eta N$

<sup>1</sup> Fit to the amplitudes of HOEHLER 79.

 $\Delta(1930)$  INELASTIC POLE RESIDUE

The "normalized residue" is the residue divided by  $\Gamma_{pole}/2$ .

Normalized residue in  $N\pi \rightarrow \Delta(1930) \rightarrow \Sigma K$ 

MODULUS	PHASE ( $^\circ$ )	DOCUMENT ID	TECN	COMMENT
••• We do not use the following data for averages, fits, limits, etc. •••				
0.043	- 0.5	ROENCHEN 15A	DPWA	Multichannel

Normalized residue in  $N\pi \rightarrow \Delta(1930) \rightarrow \Delta\pi, D$ -wave

MODULUS	PHASE ( $^\circ$ )	DOCUMENT ID	TECN	COMMENT
••• We do not use the following data for averages, fits, limits, etc. •••				
0.15	30	ROENCHEN 15A	DPWA	Multichannel

Normalized residue in  $N\pi \rightarrow \Delta(1930) \rightarrow \Delta\pi, G$ -wave

MODULUS	PHASE ( $^\circ$ )	DOCUMENT ID	TECN	COMMENT
••• We do not use the following data for averages, fits, limits, etc. •••				
0.009	121	ROENCHEN 15A	DPWA	Multichannel

 $\Delta(1930)$  BREIT-WIGNER MASS

VALUE (MeV)	DOCUMENT ID	TECN	COMMENT
<b>1900 to 2000 (<math>\approx 1950</math>) OUR ESTIMATE</b>			
1988 $\pm$ 32	<sup>1</sup> HUNT 19	DPWA	Multichannel
2233 $\pm$ 53	<sup>1</sup> ARNDT 06	DPWA	$\pi N \rightarrow \pi N, \eta N$
1940 $\pm$ 30	CUTKOSKY 80	IPWA	$\pi N \rightarrow \pi N$
1901 $\pm$ 15	HOEHLER 79	IPWA	$\pi N \rightarrow \pi N$
••• We do not use the following data for averages, fits, limits, etc. •••			
1930 $\pm$ 12	<sup>1</sup> SHRESTHA 12A	DPWA	Multichannel
1932 $\pm$ 100	VRANA 00	DPWA	Multichannel

<sup>1</sup> Statistical error only.

 $\Delta(1930)$  BREIT-WIGNER WIDTH

VALUE (MeV)	DOCUMENT ID	TECN	COMMENT
<b>200 to 400 (<math>\approx 300</math>) OUR ESTIMATE</b>			
500 $\pm$ 160	<sup>1</sup> HUNT 19	DPWA	Multichannel
773 $\pm$ 187	ARNDT 06	DPWA	$\pi N \rightarrow \pi N, \eta N$
320 $\pm$ 60	CUTKOSKY 80	IPWA	$\pi N \rightarrow \pi N$
195 $\pm$ 60	HOEHLER 79	IPWA	$\pi N \rightarrow \pi N$
••• We do not use the following data for averages, fits, limits, etc. •••			
235 $\pm$ 39	<sup>1</sup> SHRESTHA 12A	DPWA	Multichannel
316 $\pm$ 237	VRANA 00	DPWA	Multichannel

<sup>1</sup> Statistical error only.

 $\Delta(1930)$  DECAY MODES

The following branching fractions are our estimates, not fits or averages.

Mode	Fraction ( $\Gamma_i/\Gamma$ )
$\Gamma_1$ $N\pi$	5-15 %
$\Gamma_2$ $N\gamma$	0.0-0.01 %
$\Gamma_3$ $N\gamma$ , helicity=1/2	0.0-0.005 %
$\Gamma_4$ $N\gamma$ , helicity=3/2	0.0-0.004 %

 $\Delta(1930)$  BRANCHING RATIOS

$\Gamma(N\pi)/\Gamma_{total}$	$\Gamma_1/\Gamma$		
<b>VALUE (%)</b>			
<b>5 to 15 (<math>\approx 10</math>) OUR ESTIMATE</b>			
9.5 $\pm$ 0.1	<sup>1</sup> HUNT 19	DPWA	Multichannel
8.1 $\pm$ 1.2	<sup>1</sup> ARNDT 06	DPWA	$\pi N \rightarrow \pi N, \eta N$
14 $\pm$ 4	CUTKOSKY 80	IPWA	$\pi N \rightarrow \pi N$
4 $\pm$ 3	HOEHLER 79	IPWA	$\pi N \rightarrow \pi N$
••• We do not use the following data for averages, fits, limits, etc. •••			
7.9 $\pm$ 0.4	<sup>1</sup> SHRESTHA 12A	DPWA	Multichannel
9 $\pm$ 8	VRANA 00	DPWA	Multichannel

<sup>1</sup> Statistical error only.

 $\Delta(1930)$  PHOTON DECAY AMPLITUDES AT THE POLE $\Delta(1930) \rightarrow N\gamma$ , helicity-1/2 amplitude  $A_{1/2}$ 

MODULUS ( $\text{GeV}^{-1/2}$ )	PHASE ( $^\circ$ )	DOCUMENT ID	TECN	COMMENT
0.130 $\pm$ 0.073 - 0.096	-50 $\pm$ 77 - 26	ROENCHEN 14	DPWA	
••• We do not use the following data for averages, fits, limits, etc. •••				
-0.270	33	ROENCHEN 15A	DPWA	Multichannel

 $\Delta(1930) \rightarrow N\gamma$ , helicity-3/2 amplitude  $A_{3/2}$ 

MODULUS ( $\text{GeV}^{-1/2}$ )	PHASE ( $^\circ$ )	DOCUMENT ID	TECN	COMMENT
-0.056 $\pm$ 0.003 - 0.151	168 $\pm$ 72 - 76	ROENCHEN 14	DPWA	
••• We do not use the following data for averages, fits, limits, etc. •••				
0.153	81	ROENCHEN 15A	DPWA	Multichannel

 $\Delta(1930)$  BREIT-WIGNER PHOTON DECAY AMPLITUDES $\Delta(1930) \rightarrow N\gamma$ , helicity-1/2 amplitude  $A_{1/2}$ 

VALUE ( $\text{GeV}^{-1/2}$ )	DOCUMENT ID	TECN	COMMENT
-0.043 $\pm$ 0.008	<sup>1</sup> HUNT 19	DPWA	Multichannel
-0.007 $\pm$ 0.010	<sup>1</sup> ARNDT 96	IPWA	$\gamma N \rightarrow \pi N$
••• We do not use the following data for averages, fits, limits, etc. •••			
0.011 $\pm$ 0.003	<sup>1</sup> SHRESTHA 12A	DPWA	Multichannel

<sup>1</sup> Statistical error only.

See key on page 999

# Baryon Particle Listings

## $\Delta(1930), \Delta(1940)$

### $\Delta(1930) \rightarrow N\gamma$ , helicity-3/2 amplitude $A_{3/2}$

VALUE (GeV <sup>-1/2</sup> )	DOCUMENT ID	TECN	COMMENT
-0.020 ± 0.017	<sup>1</sup> HUNT 19	DPWA	Multichannel
0.005 ± 0.010	<sup>1</sup> ARNDT 96	IPWA	$\gamma N \rightarrow \pi N$
• • • We do not use the following data for averages, fits, limits, etc. • • •			
0.002 ± 0.002	<sup>1</sup> SHRESTHA 12A	DPWA	Multichannel
<sup>1</sup> Statistical error only.			

### $\Delta(1930)$ REFERENCES

For early references, see Physics Letters **111B** 1 (1982).

HUNT 19	PR C99 055205	B. C. Hunt, D.M. Manley	
ROENCHEN 15A	EPJ A51 70	D. Roenchen et al.	
PDG 14	CP C38 070001	K. Olive et al.	(PDG Collab.)
ROENCHEN 14	EPJ A50 101	D. Roenchen et al.	
Also	EPJ A51 63 (errata.)	D. Roenchen et al.	
SVARC 14	PR C89 045205	A. Svarc et al.	(RBI Zagreb, UNI Tuzla)
SHRESTHA 12A	PR C86 055203	M. Shrestha, D.M. Manley	(KSU)
ARNDT 06	PR C74 045203	R.A. Arndt et al.	(GWU)
VRANA 00	PRPL 328 181	T.P. Vrana, S.A. Dytman, T.-S.H. Lee	(PITT, ANL)
ARNDT 96	PR C53 430	R.A. Arndt, I.I. Strakovsky, R.L. Workman	(VPI)
HOEHLER 93	$\pi N$ Newsletter 9 1	G. Hoehler	(KARL)
CUTKOSKY 80	Toronto Conf. 19	R.E. Cutkosky et al.	(CMU, LBL) IJP
Also	PR D20 2839	R.E. Cutkosky et al.	(CMU, LBL) IJP
HOEHLER 79	PDAT 12-1	G. Hoehler et al.	(KARL) IJP
Also	Toronto Conf. 3	R. Koch	(KARL) IJP

$\Delta(1940) 3/2^-$

 $I(J^P) = \frac{3}{2}(\frac{3}{2}^-)$  Status: \*\*  
 OMITTED FROM SUMMARY TABLE

### $\Delta(1940)$ POLE POSITION

#### REAL PART

VALUE (MeV)	DOCUMENT ID	TECN	COMMENT
<b>1850 to 2050 (≈ 1950) OUR ESTIMATE</b>			
2040 ± 50	SOKHOYAN 15A	DPWA	Multichannel
1878 ± 11 ± 5.5	<sup>1</sup> SVARC 14	L+P	$\pi N \rightarrow \pi N$
1900 ± 100	CUTKOSKY 80	IPWA	$\pi N \rightarrow \pi N$
• • • We do not use the following data for averages, fits, limits, etc. • • •			
2139	HUNT 19	DPWA	Multichannel
2040 ± 50	GUTZ 14	DPWA	Multichannel
1990 ± $\frac{100}{50}$	ANISOVICH 12A	DPWA	Multichannel
<sup>1</sup> Fit to the amplitudes of HOEHLER 79.			

#### -2xIMAGINARY PART

VALUE (MeV)	DOCUMENT ID	TECN	COMMENT
<b>200 to 500 (≈ 350) OUR ESTIMATE</b>			
450 ± 90	SOKHOYAN 15A	DPWA	Multichannel
212 ± 21 ± 6	<sup>1</sup> SVARC 14	L+P	$\pi N \rightarrow \pi N$
200 ± 60	CUTKOSKY 80	IPWA	$\pi N \rightarrow \pi N$
• • • We do not use the following data for averages, fits, limits, etc. • • •			
400	HUNT 19	DPWA	Multichannel
450 ± 90	GUTZ 14	DPWA	Multichannel
450 ± 90	ANISOVICH 12A	DPWA	Multichannel
<sup>1</sup> Fit to the amplitudes of HOEHLER 79.			

### $\Delta(1940)$ ELASTIC POLE RESIDUE

#### MODULUS |r|

VALUE (MeV)	DOCUMENT ID	TECN	COMMENT
<b>4 to 10 (≈ 7) OUR ESTIMATE</b>			
6 ± 3	SOKHOYAN 15A	DPWA	Multichannel
9 ± 1 ± 1	<sup>1</sup> SVARC 14	L+P	$\pi N \rightarrow \pi N$
8 ± 3	CUTKOSKY 80	IPWA	$\pi N \rightarrow \pi N$
• • • We do not use the following data for averages, fits, limits, etc. • • •			
4 ± 3	GUTZ 14	DPWA	Multichannel
4 ± 4	ANISOVICH 12A	DPWA	Multichannel
<sup>1</sup> Fit to the amplitudes of HOEHLER 79.			

#### PHASE $\theta$

VALUE (°)	DOCUMENT ID	TECN	COMMENT
<b>150 to 250 (≈ 200) OUR ESTIMATE</b>			
- 90 ± 35	SOKHOYAN 15A	DPWA	Multichannel
140 ± 7 ± 7	<sup>1</sup> SVARC 14	L+P	$\pi N \rightarrow \pi N$
135 ± 45	CUTKOSKY 80	IPWA	$\pi N \rightarrow \pi N$
• • • We do not use the following data for averages, fits, limits, etc. • • •			
- 50 ± 35	GUTZ 14	DPWA	Multichannel
<sup>1</sup> Fit to the amplitudes of HOEHLER 79.			

### $\Delta(1940)$ INELASTIC POLE RESIDUE

The "normalized residue" is the residue divided by  $\Gamma_{pole}/2$ .

#### Normalized residue in $N\pi \rightarrow \Delta(1940) \rightarrow \Delta(1232)\eta$

MODULUS	PHASE (°)	DOCUMENT ID	TECN	COMMENT
<0.01	undefined	GUTZ 14	DPWA	Multichannel

#### Normalized residue in $N\pi \rightarrow \Delta(1940) \rightarrow N(1535)\pi$

MODULUS	PHASE (°)	DOCUMENT ID	TECN	COMMENT
<0.03	undefined	GUTZ 14	DPWA	Multichannel

#### Normalized residue in $N\pi \rightarrow \Delta(1940) \rightarrow \Delta(1232)\pi$ , S-wave

MODULUS	PHASE (°)	DOCUMENT ID	TECN	COMMENT
0.12 ± 0.06	120 ± 45	SOKHOYAN 15A	DPWA	Multichannel

#### Normalized residue in $N\pi \rightarrow \Delta(1940) \rightarrow \Delta(1232)\pi$ , D-wave

MODULUS	PHASE (°)	DOCUMENT ID	TECN	COMMENT
0.06 ± 0.04	- 80 ± 35	SOKHOYAN 15A	DPWA	Multichannel

### $\Delta(1940)$ BREIT-WIGNER MASS

VALUE (MeV)	DOCUMENT ID	TECN	COMMENT
<b>1940 to 2060 (≈ 2000) OUR ESTIMATE</b>			
2137 ± 13	<sup>1</sup> HUNT 19	DPWA	Multichannel
2050 ± 40	SOKHOYAN 15A	DPWA	Multichannel
1940 ± 100	CUTKOSKY 80	IPWA	$\pi N \rightarrow \pi N$
• • • We do not use the following data for averages, fits, limits, etc. • • •			
2050 ± 40	GUTZ 14	DPWA	Multichannel
1995 ± $\frac{105}{60}$	ANISOVICH 12A	DPWA	Multichannel
<sup>1</sup> Statistical error only.			

### $\Delta(1940)$ BREIT-WIGNER WIDTH

VALUE (MeV)	DOCUMENT ID	TECN	COMMENT
<b>300 to 500 (≈ 400) OUR ESTIMATE</b>			
400 ± 43	<sup>1</sup> HUNT 19	DPWA	Multichannel
450 ± 70	SOKHOYAN 15A	DPWA	Multichannel
200 ± 100	CUTKOSKY 80	IPWA	$\pi N \rightarrow \pi N$
• • • We do not use the following data for averages, fits, limits, etc. • • •			
450 ± 70	GUTZ 14	DPWA	Multichannel
450 ± 100	ANISOVICH 12A	DPWA	Multichannel
<sup>1</sup> Statistical error only.			

### $\Delta(1940)$ DECAY MODES

Mode	Fraction ( $\Gamma_i/\Gamma$ )
$\Gamma_1$ $N\pi$	1-7 %
$\Gamma_2$ $N\pi\pi$	
$\Gamma_3$ $\Delta(1232)\pi$	30-85 %
$\Gamma_4$ $\Delta(1232)\pi$ , S-wave	25-65 %
$\Gamma_5$ $\Delta(1232)\pi$ , D-wave	5-20 %
$\Gamma_6$ $N\rho$	
$\Gamma_7$ $N\rho$ , S=3/2, S-wave	
$\Gamma_8$ $N(1535)\pi$	2-14 %
$\Gamma_9$ $N a_0(980)$	seen
$\Gamma_{10}$ $\Delta(1232)\eta$	4-16 %
$\Gamma_{11}$ $N\gamma$ , helicity=1/2	seen
$\Gamma_{12}$ $N\gamma$ , helicity=3/2	seen

### $\Delta(1940)$ BRANCHING RATIOS

$\Gamma(N\pi)/\Gamma_{total}$	DOCUMENT ID	TECN	COMMENT	$\Gamma_1/\Gamma$
<b>1 to 7 (≈ 4) OUR ESTIMATE</b>				
16 ± 4	<sup>1</sup> HUNT 19	DPWA	Multichannel	
2 ± 1	SOKHOYAN 15A	DPWA	Multichannel	
5 ± 2	CUTKOSKY 80	IPWA	$\pi N \rightarrow \pi N$	
• • • We do not use the following data for averages, fits, limits, etc. • • •				
2 ± 1	GUTZ 14	DPWA	Multichannel	
<sup>1</sup> Statistical error only.				

$\Gamma(\Delta(1232)\pi, S\text{-wave})/\Gamma_{total}$	DOCUMENT ID	TECN	COMMENT	$\Gamma_4/\Gamma$
<b>1 to 7 (≈ 4) OUR ESTIMATE</b>				
< 0.9	<sup>1</sup> HUNT 19	DPWA	Multichannel	
46 ± 20	SOKHOYAN 15A	DPWA	Multichannel	
<sup>1</sup> Statistical error only.				

# Baryon Particle Listings

## $\Delta(1940), \Delta(1950)$

$\Gamma(\Delta(1232)\pi, D\text{-wave})/\Gamma_{\text{total}}$				$\Gamma_5/\Gamma$
VALUE (%)	DOCUMENT ID	TECN	COMMENT	
< 6.3	<sup>1</sup> HUNT	19	DPWA Multichannel	
12 ± 7	SOKHOYAN	15A	DPWA Multichannel	
<sup>1</sup> Statistical error only.				
$\Gamma(N\rho, S=3/2, S\text{-wave})/\Gamma_{\text{total}}$				$\Gamma_7/\Gamma$
VALUE (%)	DOCUMENT ID	TECN	COMMENT	
80 ± 5	<sup>1</sup> HUNT	19	DPWA Multichannel	
<sup>1</sup> Statistical error only.				
$\Gamma(N(1535)\pi)/\Gamma_{\text{total}}$				$\Gamma_8/\Gamma$
VALUE (%)	DOCUMENT ID	TECN	COMMENT	
8 ± 6	GUTZ	14	DPWA Multichannel	
••• We do not use the following data for averages, fits, limits, etc. •••				
2 ± 1	HORN	08A	DPWA Multichannel	
$\Gamma(N\pi_0(980))/\Gamma_{\text{total}}$				$\Gamma_9/\Gamma$
VALUE (%)	DOCUMENT ID	TECN	COMMENT	
••• We do not use the following data for averages, fits, limits, etc. •••				
2 ± 1	HORN	08A	DPWA Multichannel	
$\Gamma(\Delta(1232)\eta)/\Gamma_{\text{total}}$				$\Gamma_{10}/\Gamma$
VALUE (%)	DOCUMENT ID	TECN	COMMENT	
10 ± 6	GUTZ	14	DPWA Multichannel	
••• We do not use the following data for averages, fits, limits, etc. •••				
4 ± 2	HORN	08A	DPWA Multichannel	

### $\Delta(1940)$ PHOTON DECAY AMPLITUDES AT THE POLE

$\Delta(1940) \rightarrow N\gamma, \text{ helicity-1/2 amplitude } A_{1/2}$				
MODULUS ( $\text{GeV}^{-1/2}$ )	PHASE ( $^\circ$ )	DOCUMENT ID	TECN	COMMENT
0.170 $\pm$ $\begin{matrix} +0.120 \\ -0.100 \end{matrix}$	-10 ± 30	SOKHOYAN	15A	DPWA Multichannel
$\Delta(1940) \rightarrow N\gamma, \text{ helicity-3/2 amplitude } A_{3/2}$				
MODULUS ( $\text{GeV}^{-1/2}$ )	PHASE ( $^\circ$ )	DOCUMENT ID	TECN	COMMENT
0.150 ± 0.080	-10 ± 30	SOKHOYAN	15A	DPWA Multichannel

### $\Delta(1940)$ BREIT-WIGNER PHOTON DECAY AMPLITUDES

$\Delta(1940) \rightarrow N\gamma, \text{ helicity-1/2 amplitude } A_{1/2}$				
VALUE ( $\text{GeV}^{-1/2}$ )	DOCUMENT ID	TECN	COMMENT	
0.1614 ± 0.0031	<sup>1</sup> HUNT	19	DPWA Multichannel	
0.170 $\pm$ $\begin{matrix} +0.110 \\ -0.080 \end{matrix}$	SOKHOYAN	15A	DPWA Multichannel	
••• We do not use the following data for averages, fits, limits, etc. •••				
0.170 $\pm$ $\begin{matrix} +0.110 \\ -0.080 \end{matrix}$	GUTZ	14	DPWA Multichannel	
<sup>1</sup> Statistical error only.				
$\Delta(1940) \rightarrow N\gamma, \text{ helicity-3/2 amplitude } A_{3/2}$				
VALUE ( $\text{GeV}^{-1/2}$ )	DOCUMENT ID	TECN	COMMENT	
-0.209 ± 0.023	<sup>1</sup> HUNT	19	DPWA Multichannel	
0.150 ± 0.080	SOKHOYAN	15A	DPWA Multichannel	
••• We do not use the following data for averages, fits, limits, etc. •••				
0.150 ± 0.080	GUTZ	14	DPWA Multichannel	
<sup>1</sup> Statistical error only.				

### $\Delta(1940)$ REFERENCES

HUNT	19	PR C99 055205	B. C. Hunt, D.M. Manley	
SOKHOYAN	15A	EPJ A51 95	V. Sokhoyan et al.	(CBELSA/TAPS Collab.)
GUTZ	14	EPJ A50 74	E. Gutz et al.	(CBELSA/TAPS Collab.)
SVARC	14	PR C89 045205	A. V. Svarc et al.	(RBI Zagreb, UNI Tuzla)
ANISOVICH	12A	EPJ A48 15	A.V. Anisovich et al.	(BONN, PNPI)
HORN	08A	EPJ A38 173	I. Horn et al.	(CB-ELSA Collab.)
		PRL 101 202002	R. E. Cutkosky et al.	(CB-ELSA Collab.)
CUTKOSKY	80	Toronto Conf. 19	R.E. Cutkosky et al.	(CMU, LBL) IJP
		PR D20 2839	R.E. Cutkosky et al.	(CMU, LBL)
HOEHLER	79	PDAT 12-1	G. Hoehler et al.	(KARLT)

## $\Delta(1950) 7/2^+$

$$I(J^P) = \frac{3}{2}(7/2^+) \text{ Status: } ****$$

Older and obsolete values are listed and referenced in the 2014 edition, Chinese Physics C38 070001 (2014).

### $\Delta(1950)$ POLE POSITION

#### REAL PART

VALUE (MeV)	DOCUMENT ID	TECN	COMMENT
1870 to 1890 ( $\approx 1880$ ) OUR ESTIMATE			
1888 ± 4	SOKHOYAN	15A	DPWA Multichannel
1877 ± 2 ± 1	<sup>1</sup> SVARC	14	L+P $\pi N \rightarrow \pi N$
1890 ± 15	CUTKOSKY	80	IPWA $\pi N \rightarrow \pi N$
••• We do not use the following data for averages, fits, limits, etc. •••			
1871	HUNT	19	DPWA Multichannel
1874	ROENCHEN	15A	DPWA Multichannel
1888 ± 4	GUTZ	14	DPWA Multichannel
1890 ± 4	ANISOVICH	12A	DPWA Multichannel
1876	ARNDT	06	DPWA $\pi N \rightarrow \pi N, \eta N$
1910	VRANA	00	DPWA Multichannel
1878	HOEHLER	93	ARGD $\pi N \rightarrow \pi N$
<sup>1</sup> Fit to the amplitudes of HOEHLER 79.			
-2xIMAGINARY PART			
VALUE (MeV)	DOCUMENT ID	TECN	COMMENT
220 to 260 ( $\approx 240$ ) OUR ESTIMATE			
245 ± 8	SOKHOYAN	15A	DPWA Multichannel
223 ± 4 ± 1	<sup>1</sup> SVARC	14	L+P $\pi N \rightarrow \pi N$
260 ± 40	CUTKOSKY	80	IPWA $\pi N \rightarrow \pi N$
••• We do not use the following data for averages, fits, limits, etc. •••			
206	HUNT	19	DPWA Multichannel
239	ROENCHEN	15A	DPWA Multichannel
245 ± 8	GUTZ	14	DPWA Multichannel
243 ± 8	ANISOVICH	12A	DPWA Multichannel
227	ARNDT	06	DPWA $\pi N \rightarrow \pi N, \eta N$
230	VRANA	00	DPWA Multichannel
230	HOEHLER	93	ARGD $\pi N \rightarrow \pi N$
<sup>1</sup> Fit to the amplitudes of HOEHLER 79.			

### $\Delta(1950)$ ELASTIC POLE RESIDUE

MODULUS $ r $				
VALUE (MeV)	DOCUMENT ID	TECN	COMMENT	
44 to 60 ( $\approx 52$ ) OUR ESTIMATE				
58 ± 2	SOKHOYAN	15A	DPWA Multichannel	
44 ± 1	<sup>1</sup> SVARC	14	L+P $\pi N \rightarrow \pi N$	
50 ± 7	CUTKOSKY	80	IPWA $\pi N \rightarrow \pi N$	
••• We do not use the following data for averages, fits, limits, etc. •••				
56	ROENCHEN	15A	DPWA Multichannel	
58 ± 2	GUTZ	14	DPWA Multichannel	
58 ± 2	ANISOVICH	12A	DPWA Multichannel	
53	ARNDT	06	DPWA $\pi N \rightarrow \pi N, \eta N$	
47	HOEHLER	93	ARGD $\pi N \rightarrow \pi N$	
<sup>1</sup> Fit to the amplitudes of HOEHLER 79.				
PHASE $\theta$				
VALUE ( $^\circ$ )	DOCUMENT ID	TECN	COMMENT	
-40 to -24 ( $\approx -32$ ) OUR ESTIMATE				
-24 ± 3	SOKHOYAN	15A	DPWA Multichannel	
-39 ± 1 ± 1	<sup>1</sup> SVARC	14	L+P $\pi N \rightarrow \pi N$	
-33 ± 8	CUTKOSKY	80	IPWA $\pi N \rightarrow \pi N$	
••• We do not use the following data for averages, fits, limits, etc. •••				
-33	ROENCHEN	15A	DPWA Multichannel	
-24 ± 3	GUTZ	14	DPWA Multichannel	
-24 ± 3	ANISOVICH	12A	DPWA Multichannel	
-31	ARNDT	06	DPWA $\pi N \rightarrow \pi N, \eta N$	
-32	HOEHLER	93	ARGD $\pi N \rightarrow \pi N$	
<sup>1</sup> Fit to the amplitudes of HOEHLER 79.				

### $\Delta(1950)$ INELASTIC POLE RESIDUE

The "normalized residue" is the residue divided by  $\Gamma_{\text{pole}}/2$ .

Normalized residue in $N\pi \rightarrow \Delta(1950) \rightarrow \Sigma K$				
MODULUS	PHASE ( $^\circ$ )	DOCUMENT ID	TECN	COMMENT
0.05 ± 0.01	-65 ± 25	ANISOVICH	12A	DPWA Multichannel
••• We do not use the following data for averages, fits, limits, etc. •••				
0.031	-87	ROENCHEN	15A	DPWA Multichannel
Normalized residue in $N\pi \rightarrow \Delta(1950) \rightarrow \Delta\pi, F\text{-wave}$				
MODULUS	PHASE ( $^\circ$ )	DOCUMENT ID	TECN	COMMENT
0.12 ± 0.04	undefined	SOKHOYAN	15A	DPWA Multichannel
••• We do not use the following data for averages, fits, limits, etc. •••				
0.54	131	ROENCHEN	15A	DPWA Multichannel
0.12 ± 0.04	12 ± 10	ANISOVICH	12A	DPWA Multichannel
Normalized residue in $N\pi \rightarrow \Delta(1950) \rightarrow \Delta\pi, H\text{-wave}$				
MODULUS	PHASE ( $^\circ$ )	DOCUMENT ID	TECN	COMMENT
••• We do not use the following data for averages, fits, limits, etc. •••				
0.033	-97	ROENCHEN	15A	DPWA Multichannel

$\Delta(1950)$

**Normalized residue in  $N\pi \rightarrow \Delta(1950) \rightarrow \Delta(1232)\eta$**

MODULUS	PHASE (°)	DOCUMENT ID	TECN	COMMENT
0.035 ± 0.005	90 ± 25	GUTZ	14	DPWA Multichannel

**$\Delta(1950)$  BREIT-WIGNER MASS**

VALUE (MeV)	DOCUMENT ID	TECN	COMMENT
<b>1915 to 1950 (≈ 1930) OUR ESTIMATE</b>			
1943 ± 18	GOLOVATCH	19	DPWA $\gamma p \rightarrow \pi^+ \pi^- p$
1913 ± 4	<sup>1</sup> HUNT	19	DPWA Multichannel
1917 ± 4	ANISOVICH	17	DPWA Multichannel
1921.3 ± 0.2	<sup>1</sup> ARNDT	06	DPWA $\pi N \rightarrow \pi N, \eta N$
1950 ± 15	CUTKOSKY	80	IPWA $\pi N \rightarrow \pi N$
1913 ± 8	HOEHLER	79	IPWA $\pi N \rightarrow \pi N$
• • • We do not use the following data for averages, fits, limits, etc. • • •			
1917 ± 4	SOKHOYAN	15A	DPWA Multichannel
1917 ± 4	GUTZ	14	DPWA Multichannel
1915 ± 6	ANISOVICH	12A	DPWA Multichannel
1918 ± 1	<sup>1</sup> SHRESTHA	12A	DPWA Multichannel
1936 ± 5	VRANA	00	DPWA Multichannel

<sup>1</sup> Statistical error only.

**$\Delta(1950)$  BREIT-WIGNER WIDTH**

VALUE (MeV)	DOCUMENT ID	TECN	COMMENT
<b>235 to 335 (≈ 285) OUR ESTIMATE</b>			
230 ± 88	GOLOVATCH	19	DPWA $\gamma p \rightarrow \pi^+ \pi^- p$
241 ± 10	<sup>1</sup> HUNT	19	DPWA Multichannel
251 ± 8	ANISOVICH	17	DPWA Multichannel
271.1 ± 1.1	<sup>1</sup> ARNDT	06	DPWA $\pi N \rightarrow \pi N, \eta N$
340 ± 5.0	CUTKOSKY	80	IPWA $\pi N \rightarrow \pi N$
224 ± 10	HOEHLER	79	IPWA $\pi N \rightarrow \pi N$
• • • We do not use the following data for averages, fits, limits, etc. • • •			
251 ± 8	SOKHOYAN	15A	DPWA Multichannel
251 ± 8	GUTZ	14	DPWA Multichannel
246 ± 10	ANISOVICH	12A	DPWA Multichannel
259 ± 4	<sup>1</sup> SHRESTHA	12A	DPWA Multichannel
245 ± 12	VRANA	00	DPWA Multichannel

<sup>1</sup> Statistical error only.

**$\Delta(1950)$  DECAY MODES**

The following branching fractions are our estimates, not fits or averages.

Mode	Fraction ( $\Gamma_i/\Gamma$ )
$\Gamma_1$ $N\pi$	35–45 %
$\Gamma_2$ $\Sigma K$	0.3–0.5 %
$\Gamma_3$ $N\pi\pi$	
$\Gamma_4$ $\Delta(1232)\pi, F\text{-wave}$	1–9 %
$\Gamma_5$ $N(1680)\pi, P\text{-wave}$	3–9 %
$\Gamma_6$ $\Delta(1232)\eta$	< 0.6 %

**$\Delta(1950)$  BRANCHING RATIOS**

**$\Gamma(N\pi)/\Gamma_{\text{total}}$**

VALUE (%)	DOCUMENT ID	TECN	COMMENT
<b>35 to 45 (≈ 40) OUR ESTIMATE</b>			
38 ± 2	<sup>1</sup> HUNT	19	DPWA Multichannel
46 ± 2	ANISOVICH	17	DPWA Multichannel
47.1 ± 0.1	<sup>1</sup> ARNDT	06	DPWA $\pi N \rightarrow \pi N, \eta N$
39 ± 4	CUTKOSKY	80	IPWA $\pi N \rightarrow \pi N$
38 ± 2	HOEHLER	79	IPWA $\pi N \rightarrow \pi N$
• • • We do not use the following data for averages, fits, limits, etc. • • •			
0.046 ± 0.002	SOKHOYAN	15A	DPWA Multichannel
46 ± 2	GUTZ	14	DPWA Multichannel
45 ± 2	ANISOVICH	12A	DPWA Multichannel
45.6 ± 0.4	<sup>1</sup> SHRESTHA	12A	DPWA Multichannel
44 ± 1	VRANA	00	DPWA Multichannel

<sup>1</sup> Statistical error only.

**$\Gamma(N\pi\pi)/\Gamma_{\text{total}}$**

VALUE (%)	DOCUMENT ID	TECN	COMMENT
0.57 ± 0.20	GOLOVATCH	19	DPWA $\gamma p \rightarrow \pi^+ \pi^- p$

**$\Gamma(\Sigma K)/\Gamma_{\text{total}}$**

VALUE (%)	DOCUMENT ID	TECN	COMMENT
0.6 ± 0.2	ANISOVICH	17	DPWA Multichannel
• • • We do not use the following data for averages, fits, limits, etc. • • •			
0.4 ± 0.1	ANISOVICH	12A	DPWA Multichannel

**$\Gamma(\Delta(1232)\pi, F\text{-wave})/\Gamma_{\text{total}}$**

VALUE (%)	DOCUMENT ID	TECN	COMMENT
5 ± 3	ANISOVICH	17	DPWA Multichannel
8 ± 1	<sup>1</sup> SHRESTHA	12A	DPWA Multichannel
• • • We do not use the following data for averages, fits, limits, etc. • • •			
5 ± 4	SOKHOYAN	15A	DPWA Multichannel
2.8 ± 1.4	ANISOVICH	12A	DPWA Multichannel
36 ± 1	VRANA	00	DPWA Multichannel

<sup>1</sup> Statistical error only.

**$\Gamma(N(1680)\pi, P\text{-wave})/\Gamma_{\text{total}}$**

VALUE (%)	DOCUMENT ID	TECN	COMMENT
6 ± 3	SOKHOYAN	15A	DPWA Multichannel

**$\Gamma(\Delta(1232)\eta)/\Gamma_{\text{total}}$**

VALUE (%)	DOCUMENT ID	TECN	COMMENT
0.3 ± 0.3	ANISOVICH	17	DPWA Multichannel
• • • We do not use the following data for averages, fits, limits, etc. • • •			
< 1	GUTZ	14	DPWA Multichannel

**$\Delta(1950)$  PHOTON DECAY AMPLITUDES AT THE POLE**

**$\Delta(1950) \rightarrow N\gamma, \text{ helicity-1/2 amplitude } A_{1/2}$**

MODULUS ( $\text{GeV}^{-1/2}$ )	PHASE (°)	DOCUMENT ID	TECN	COMMENT
−0.067 ± 0.004	−10 ± 5	SOKHOYAN	15A	DPWA Multichannel
−0.071 ± 0.004	−14 <sup>+2</sup> <sub>−4</sub>	ROENCHEN	14	DPWA
• • • We do not use the following data for averages, fits, limits, etc. • • •				
−0.068	−19	ROENCHEN	15A	DPWA Multichannel

**$\Delta(1950) \rightarrow N\gamma, \text{ helicity-3/2 amplitude } A_{3/2}$**

MODULUS ( $\text{GeV}^{-1/2}$ )	PHASE (°)	DOCUMENT ID	TECN	COMMENT
−0.095 ± 0.004	−10 ± 5	SOKHOYAN	15A	DPWA Multichannel
−0.089 ± 0.008	−10 <sup>+3</sup> <sub>−1</sub>	ROENCHEN	14	DPWA
• • • We do not use the following data for averages, fits, limits, etc. • • •				
−0.084	−19	ROENCHEN	15A	DPWA Multichannel

**$\Delta(1950)$  BREIT-WIGNER PHOTON DECAY AMPLITUDES**

**$\Delta(1950) \rightarrow N\gamma, \text{ helicity-1/2 amplitude } A_{1/2}$**

VALUE ( $\text{GeV}^{-1/2}$ )	DOCUMENT ID	TECN	COMMENT
<b>−0.075 to −0.065 (≈ −0.070) OUR ESTIMATE</b>			
−0.0698 ± 0.0141	GOLOVATCH	19	DPWA $\gamma p \rightarrow \pi^+ \pi^- p$
−0.047 ± 0.002	<sup>1</sup> HUNT	19	DPWA Multichannel
−0.067 ± 0.005	ANISOVICH	17	DPWA Multichannel
−0.083 ± 0.004	WORKMAN	12A	DPWA $\gamma N \rightarrow N\pi$
• • • We do not use the following data for averages, fits, limits, etc. • • •			
−0.067 ± 0.005	SOKHOYAN	15A	DPWA Multichannel
−0.067 ± 0.005	GUTZ	14	DPWA Multichannel
−0.071 ± 0.004	ANISOVICH	12A	DPWA Multichannel
−0.065 ± 0.001	<sup>1</sup> SHRESTHA	12A	DPWA Multichannel
−0.094	DRECHSEL	07	DPWA $\gamma N \rightarrow \pi N$

<sup>1</sup> Statistical error only.

**$\Delta(1950) \rightarrow N\gamma, \text{ helicity-3/2 amplitude } A_{3/2}$**

VALUE ( $\text{GeV}^{-1/2}$ )	DOCUMENT ID	TECN	COMMENT
<b>−0.100 to −0.080 (≈ −0.090) OUR ESTIMATE</b>			
−0.1181 ± 0.0193	GOLOVATCH	19	DPWA $\gamma p \rightarrow \pi^+ \pi^- p$
−0.074 ± 0.002	<sup>1</sup> HUNT	19	DPWA Multichannel
−0.094 ± 0.004	ANISOVICH	17	DPWA Multichannel
−0.096 ± 0.004	WORKMAN	12A	DPWA $\gamma N \rightarrow N\pi$
• • • We do not use the following data for averages, fits, limits, etc. • • •			
−0.094 ± 0.004	SOKHOYAN	15A	DPWA Multichannel
−0.094 ± 0.004	GUTZ	14	DPWA Multichannel
−0.094 ± 0.005	ANISOVICH	12A	DPWA Multichannel
−0.083 ± 0.001	<sup>1</sup> SHRESTHA	12A	DPWA Multichannel
−0.121	DRECHSEL	07	DPWA $\gamma N \rightarrow \pi N$

<sup>1</sup> Statistical error only.

**$\Delta(1950)$  REFERENCES**

GOLOVATCH	19	PL B788 371	E. Golovatch <i>et al.</i>	(CLAS Collab.)
HUNT	19	PR C99 055205	B.C. Hunt, D.M. Manley	
ANISOVICH	17	PL B766 357	A.V. Anisovich <i>et al.</i>	
ROENCHEN	15A	EPJ A51 70	D. Roenchen <i>et al.</i>	
SOKHOYAN	15A	EPJ A51 95	V. Sokhoyan <i>et al.</i>	(CBELSA/TAPS Collab.)
GUTZ	14	EPJ A50 74	E. Gutz <i>et al.</i>	(CBELSA/TAPS Collab.)
PDG	14	CP C39 070001	K. Olive <i>et al.</i>	(PDG Collab.)
ROENCHEN	14	EPJ A50 101	D. Roenchen <i>et al.</i>	
		Also	EPJ A51 63 (errat.)	
SVARC	14	PR C89 045205	A. Svarc <i>et al.</i>	(RBI Zagreb, UNI Tuzla)

## Baryon Particle Listings

 $\Delta(1950)$ ,  $\Delta(2000)$ ,  $\Delta(2150)$ 

ANISOVICH	12A	EPJ A48 15	A.V. Anisovich et al.	(BONN, PNPI)
SHRESTHA	12A	PR C86 055203	M. Shrestha, D.M. Manley	(KSU)
WORKMAN	12A	PR C86 015202	R. Workman et al.	(GWU)
DRECHSEL	07	EPJ A34 69	D. Drechsel, S.S. Kamalov, L. Tiator	(MAINZ, JINR)
ARNDT	06	PR C74 045205	R.A. Arndt et al.	(GWU)
VRANA	00	PRPL 328 181	T.P. Vrana, S.A. Dytman, T.-S.H. Lee	(PITT, ANL)
HOEHLER	93	$\pi N$ Newsletter 9 1	G. Hohlner	(KARL)
CUTKOSKY	80	Toronto Conf. 19	R.E. Cutkosky et al.	(CMU, LBL) IJP
Also		PR D20 2839	R.E. Cutkosky et al.	(CMU, LBL) IJP
HOEHLER	79	PDAT 12-1	G. Hohlner et al.	(KARLT) IJP
Also		Toronto Conf. 3	R. Koch	(KARLT) IJP

 $\Delta(2000) 5/2^+$  $I(J^P) = \frac{3}{2}(\frac{5}{2}^+)$  Status: \*\*

OMITTED FROM SUMMARY TABLE

 $\Delta(2000)$  POLE POSITION

## REAL PART

VALUE (MeV)	DOCUMENT ID	TECN	COMMENT
$1998 \pm 4 \pm 4$	<sup>1</sup> SVARC 14	L+P	$\pi N \rightarrow \pi N$
1976	SHRESTHA 12A	DPWA	Multichannel
$2150 \pm 100$	CUTKOSKY 80	IPWA	$\pi N \rightarrow \pi N$
••• We do not use the following data for averages, fits, limits, etc. •••			
1697	VRANA 00	DPWA	Multichannel

<sup>1</sup> Fit to the amplitudes of HOEHLER 79.

## -2xIMAGINARY PART

VALUE (MeV)	DOCUMENT ID	TECN	COMMENT
$404 \pm 10 \pm 4$	<sup>1</sup> SVARC 14	L+P	$\pi N \rightarrow \pi N$
$350 \pm 100$	CUTKOSKY 80	IPWA	$\pi N \rightarrow \pi N$
••• We do not use the following data for averages, fits, limits, etc. •••			
488	SHRESTHA 12A	DPWA	Multichannel
112	VRANA 00	DPWA	Multichannel

<sup>1</sup> Fit to the amplitudes of HOEHLER 79. $\Delta(2000)$  ELASTIC POLE RESIDUEMODULUS  $|r|$ 

VALUE (MeV)	DOCUMENT ID	TECN	COMMENT
$34 \pm 1 \pm 1$	<sup>1</sup> SVARC 14	L+P	$\pi N \rightarrow \pi N$
$16 \pm 5$	CUTKOSKY 80	IPWA	$\pi N \rightarrow \pi N$

<sup>1</sup> Fit to the amplitudes of HOEHLER 79.PHASE  $\theta$ 

VALUE (°)	DOCUMENT ID	TECN	COMMENT
$110 \pm 1 \pm 3$	<sup>1</sup> SVARC 14	L+P	$\pi N \rightarrow \pi N$
$150 \pm 90$	CUTKOSKY 80	IPWA	$\pi N \rightarrow \pi N$

<sup>1</sup> Fit to the amplitudes of HOEHLER 79. $\Delta(2000)$  BREIT-WIGNER MASS

VALUE (MeV)	DOCUMENT ID	TECN	COMMENT
$2015 \pm 24$	<sup>1</sup> SHRESTHA 12A	DPWA	Multichannel
$2200 \pm 125$	CUTKOSKY 80	IPWA	$\pi N \rightarrow \pi N$
••• We do not use the following data for averages, fits, limits, etc. •••			
$1724 \pm 61$	VRANA 00	DPWA	Multichannel
$1752 \pm 32$	MANLEY 92	IPWA	$\pi N \rightarrow \pi N$ & $N\pi\pi$

<sup>1</sup> Statistical error only. $\Delta(2000)$  BREIT-WIGNER WIDTH

VALUE (MeV)	DOCUMENT ID	TECN	COMMENT
$500 \pm 52$	<sup>1</sup> SHRESTHA 12A	DPWA	Multichannel
$400 \pm 125$	CUTKOSKY 80	IPWA	$\pi N \rightarrow \pi N$
••• We do not use the following data for averages, fits, limits, etc. •••			
$138 \pm 68$	VRANA 00	DPWA	Multichannel
$251 \pm 93$	MANLEY 92	IPWA	$\pi N \rightarrow \pi N$ & $N\pi\pi$

<sup>1</sup> Statistical error only. $\Delta(2000)$  DECAY MODES

Mode	Fraction ( $\Gamma_i/\Gamma$ )
$\Gamma_1$ $N\pi$	3-11 %
$\Gamma_2$ $N\pi\pi$	
$\Gamma_3$ $\Delta(1232)\pi$ , P-wave	seen
$\Gamma_4$ $\Delta(1232)\pi$ , F-wave	seen
$\Gamma_5$ $N\rho$ , S=3/2, P-wave	seen
$\Gamma_6$ $N\gamma$	
$\Gamma_7$ $N\gamma$ , helicity=1/2	seen
$\Gamma_8$ $N\gamma$ , helicity=3/2	seen

 $\Delta(2000)$  BRANCHING RATIOS

$\Gamma(N\pi)/\Gamma_{total}$	VALUE (%)	DOCUMENT ID	TECN	COMMENT	$\Gamma_1/\Gamma$
$7 \pm 1$		<sup>1</sup> SHRESTHA 12A	DPWA	Multichannel	
$7 \pm 4$		CUTKOSKY 80	IPWA	$\pi N \rightarrow \pi N$	
••• We do not use the following data for averages, fits, limits, etc. •••					
$0 \pm 1$		VRANA 00	DPWA	Multichannel	
$2 \pm 1$		MANLEY 92	IPWA	$\pi N \rightarrow \pi N$ & $N\pi\pi$	

<sup>1</sup> Statistical error only.

$\Gamma(\Delta(1232)\pi, P\text{-wave})/\Gamma_{total}$	VALUE (%)	DOCUMENT ID	TECN	COMMENT	$\Gamma_3/\Gamma$
$3 \pm 3$		<sup>1</sup> SHRESTHA 12A	DPWA	Multichannel	
••• We do not use the following data for averages, fits, limits, etc. •••					
$0 \pm 1$		VRANA 00	DPWA	Multichannel	

<sup>1</sup> Statistical error only.

$\Gamma(\Delta(1232)\pi, F\text{-wave})/\Gamma_{total}$	VALUE (%)	DOCUMENT ID	TECN	COMMENT	$\Gamma_4/\Gamma$
$< 3$		SHRESTHA 12A	DPWA	Multichannel	
••• We do not use the following data for averages, fits, limits, etc. •••					
$40 \pm 1$		VRANA 00	DPWA	Multichannel	

$\Gamma(N\rho, S=3/2, P\text{-wave})/\Gamma_{total}$	VALUE (%)	DOCUMENT ID	TECN	COMMENT	$\Gamma_5/\Gamma$
$90 \pm 3$		<sup>1</sup> SHRESTHA 12A	DPWA	Multichannel	
••• We do not use the following data for averages, fits, limits, etc. •••					
$60 \pm 60$		VRANA 00	DPWA	Multichannel	

<sup>1</sup> Statistical error only. $\Delta(2000)$  BREIT-WIGNER PHOTON DECAY AMPLITUDES $\Delta(2000) \rightarrow p\gamma$ , helicity-1/2 amplitude  $A_{1/2}$ 

VALUE ( $\text{GeV}^{-1/2}$ )	DOCUMENT ID	TECN	COMMENT
$-0.061 \pm 0.018$	<sup>1</sup> SHRESTHA 12A	DPWA	Multichannel

<sup>1</sup> Statistical error only. $\Delta(2000) \rightarrow p\gamma$ , helicity-3/2 amplitude  $A_{3/2}$ 

VALUE ( $\text{GeV}^{-1/2}$ )	DOCUMENT ID	TECN	COMMENT
$0.158 \pm 0.032$	<sup>1</sup> SHRESTHA 12A	DPWA	Multichannel

<sup>1</sup> Statistical error only. $\Delta(2000)$  REFERENCES

SVARC	14	PR C89 045205	A. Svarc et al.	(RBI Zagreb, UNI Tuzla)
SHRESTHA	12A	PR C86 055203	M. Shrestha, D.M. Manley	(KSU)
VRANA	00	PRPL 328 181	T.P. Vrana, S.A. Dytman, T.-S.H. Lee	(PITT, ANL)
MANLEY	92	PR D45 4002	D.M. Manley, E.M. Saleski	(KSA) IJP
Also		PR D30 904	D.M. Manley et al.	(VPI)
CUTKOSKY	80	Toronto Conf. 19	R.E. Cutkosky et al.	(CMU, LBL)
Also		PR D20 2839	R.E. Cutkosky et al.	(CMU, LBL)
HOEHLER	79	PDAT 12-1	G. Hohlner et al.	(KARLT)

 $\Delta(2150) 1/2^-$  $I(J^P) = \frac{3}{2}(\frac{1}{2}^-)$  Status: \*

OMITTED FROM SUMMARY TABLE

 $\Delta(2150)$  POLE POSITION

## REAL PART

VALUE (MeV)	DOCUMENT ID	TECN	COMMENT
$2140 \pm 80$	CUTKOSKY 80	IPWA	$\pi N \rightarrow \pi N$

## -2xIMAGINARY PART

VALUE (MeV)	DOCUMENT ID	TECN	COMMENT
$200 \pm 80$	CUTKOSKY 80	IPWA	$\pi N \rightarrow \pi N$

 $\Delta(2150)$  ELASTIC POLE RESIDUE

MODULUS $ r $	VALUE (MeV)	DOCUMENT ID	TECN	COMMENT
$7 \pm 2$		CUTKOSKY 80	IPWA	$\pi N \rightarrow \pi N$

PHASE  $\theta$ 

VALUE (°)	DOCUMENT ID	TECN	COMMENT
$-60 \pm 90$	CUTKOSKY 80	IPWA	$\pi N \rightarrow \pi N$

$\Delta(2150)$  BREIT-WIGNER MASS

VALUE (MeV)	DOCUMENT ID	TECN	COMMENT
2150 ± 100	CUTKOSKY 80	IPWA	$\pi N \rightarrow \pi N$

$\Delta(2150)$  BREIT-WIGNER WIDTH

VALUE (MeV)	DOCUMENT ID	TECN	COMMENT
200 ± 100	CUTKOSKY 80	IPWA	$\pi N \rightarrow \pi N$

$\Delta(2150)$  DECAY MODES

Mode	Fraction ( $\Gamma_i/\Gamma$ )
$\Gamma_1$ $N\pi$	6-10 %

$\Delta(2150)$  BRANCHING RATIOS

$\Gamma(N\pi)/\Gamma_{total}$	DOCUMENT ID	TECN	COMMENT	$\Gamma_1/\Gamma$
8 ± 2	CUTKOSKY 80	IPWA	$\pi N \rightarrow \pi N$	

$\Delta(2150)$  REFERENCES

CUTKOSKY 80	Toronto Conf. 19	R.E. Cutkosky et al.	(CMU, LBL) IJP
Also	PR D20 2839	R.E. Cutkosky et al.	(CMU, LBL)

$\Delta(2200) 7/2^-$

$$I(J^P) = \frac{3}{2}(\frac{7}{2}^-) \text{ Status: } ***$$

$\Delta(2200)$  POLE POSITION

REAL PART

VALUE (MeV)	DOCUMENT ID	TECN	COMMENT
<b>2050 to 2150 (<math>\approx 2100</math>) OUR ESTIMATE</b>			
2100 ± 50	CUTKOSKY 80	IPWA	$\pi N \rightarrow \pi N$
••• We do not use the following data for averages, fits, limits, etc. •••			
2142	ROENCHEN 15A	DPWA	Multichannel

-2xIMAGINARY PART

VALUE (MeV)	DOCUMENT ID	TECN	COMMENT
<b>260 to 420 (<math>\approx 340</math>) OUR ESTIMATE</b>			
340 ± 80	CUTKOSKY 80	IPWA	$\pi N \rightarrow \pi N$
••• We do not use the following data for averages, fits, limits, etc. •••			
486	ROENCHEN 15A	DPWA	Multichannel

$\Delta(2200)$  ELASTIC POLE RESIDUE

MODULUS  $|r|$

VALUE (MeV)	DOCUMENT ID	TECN	COMMENT
8 ± 3	CUTKOSKY 80	IPWA	$\pi N \rightarrow \pi N$
••• We do not use the following data for averages, fits, limits, etc. •••			
17	ROENCHEN 15A	DPWA	Multichannel

PHASE  $\theta$

VALUE (°)	DOCUMENT ID	TECN	COMMENT
-70 ± 40	CUTKOSKY 80	IPWA	$\pi N \rightarrow \pi N$
••• We do not use the following data for averages, fits, limits, etc. •••			
-56	ROENCHEN 15A	DPWA	Multichannel

$\Delta(2200)$  INELASTIC POLE RESIDUE

The "normalized residue" is the residue divided by  $\Gamma_{pole}/2$ .

Normalized residue in  $N\pi \rightarrow \Delta(2200) \rightarrow \Sigma K$

MODULUS	PHASE (°)	DOCUMENT ID	TECN	COMMENT
••• We do not use the following data for averages, fits, limits, etc. •••				
0.005	-103	ROENCHEN 15A	DPWA	Multichannel

Normalized residue in  $N\pi \rightarrow \Delta(2200) \rightarrow \Delta\pi, D\text{-wave}$

MODULUS	PHASE (°)	DOCUMENT ID	TECN	COMMENT
••• We do not use the following data for averages, fits, limits, etc. •••				
0.23	107	ROENCHEN 15A	DPWA	Multichannel

Normalized residue in  $N\pi \rightarrow \Delta(2200) \rightarrow \Delta\pi, G\text{-wave}$

MODULUS	PHASE (°)	DOCUMENT ID	TECN	COMMENT
••• We do not use the following data for averages, fits, limits, etc. •••				
0.022	-151	ROENCHEN 15A	DPWA	Multichannel

$\Delta(2200)$  BREIT-WIGNER MASS

VALUE (MeV)	DOCUMENT ID	TECN	COMMENT
<b>2150 to 2250 (<math>\approx 2200</math>) OUR ESTIMATE</b>			
2176 ± 40	ANISOVICH 17	DPWA	Multichannel
2200 ± 80	CUTKOSKY 80	IPWA	$\pi N \rightarrow \pi N$
2215 ± 60	HOEHLER 79	IPWA	$\pi N \rightarrow \pi N$

$\Delta(2200)$  BREIT-WIGNER WIDTH

VALUE (MeV)	DOCUMENT ID	TECN	COMMENT
<b>200 to 500 (<math>\approx 350</math>) OUR ESTIMATE</b>			
210 ± 70	ANISOVICH 17	DPWA	Multichannel
450 ± 100	CUTKOSKY 80	IPWA	$\pi N \rightarrow \pi N$
400 ± 100	HOEHLER 79	IPWA	$\pi N \rightarrow \pi N$

$\Delta(2200)$  DECAY MODES

Mode	Fraction ( $\Gamma_i/\Gamma$ )
$\Gamma_1$ $N\pi$	2-8 %
$\Gamma_2$ $\Sigma K$	1-7 %
$\Gamma_3$ $\Delta\pi, D\text{-wave}$	40-100 %
$\Gamma_4$ $\Delta\pi, G\text{-wave}$	5-25 %
$\Gamma_5$ $\Delta\eta, D\text{-wave}$	seen

$\Delta(2200)$  BRANCHING RATIOS

$\Gamma(N\pi)/\Gamma_{total}$	DOCUMENT ID	TECN	COMMENT	$\Gamma_1/\Gamma$
<b>2 to 8 (<math>\approx 5</math>) OUR ESTIMATE</b>				
3.5 ± 1.5	ANISOVICH 17	DPWA	Multichannel	
6 ± 2	CUTKOSKY 80	IPWA	$\pi N \rightarrow \pi N$	
5 ± 2	HOEHLER 79	IPWA	$\pi N \rightarrow \pi N$	

$\Gamma(\Sigma K)/\Gamma_{total}$	DOCUMENT ID	TECN	COMMENT	$\Gamma_2/\Gamma$
0.04 ± 0.03	ANISOVICH 17	DPWA	Multichannel	

$\Gamma(\Delta\pi, D\text{-wave})/\Gamma_{total}$	DOCUMENT ID	TECN	COMMENT	$\Gamma_3/\Gamma$
0.70 ± 0.30	ANISOVICH 17	DPWA	Multichannel	

$\Gamma(\Delta\pi, G\text{-wave})/\Gamma_{total}$	DOCUMENT ID	TECN	COMMENT	$\Gamma_4/\Gamma$
0.15 ± 0.10	ANISOVICH 17	DPWA	Multichannel	

$\Gamma(\Delta\eta, D\text{-wave})/\Gamma_{total}$	DOCUMENT ID	TECN	COMMENT	$\Gamma_5/\Gamma$
~ 0.01	ANISOVICH 17	DPWA	Multichannel	

$\Delta(2200)$  PHOTON DECAY AMPLITUDES AT THE POLE

$\Delta(2200) \rightarrow N\gamma, \text{ helicity-1/2 amplitude } A_{1/2}$

MODULUS ( $\text{GeV}^{-1/2}$ )	PHASE (°)	DOCUMENT ID	TECN	COMMENT
0.107 <sup>+0.011</sup> <sub>-0.020</sub>	-36 ± 5	ROENCHEN 14	DPWA	
••• We do not use the following data for averages, fits, limits, etc. •••				
0.106	-23	ROENCHEN 15A	DPWA	Multichannel

$\Delta(2200) \rightarrow N\gamma, \text{ helicity-3/2 amplitude } A_{3/2}$

MODULUS ( $\text{GeV}^{-1/2}$ )	PHASE (°)	DOCUMENT ID	TECN	COMMENT
-0.131 <sup>+0.024</sup> <sub>-0.009</sub>	113 <sup>+9</sup> <sub>-5</sub>	ROENCHEN 14	DPWA	
••• We do not use the following data for averages, fits, limits, etc. •••				
0.157	-60	ROENCHEN 15A	DPWA	Multichannel

$\Delta(2200)$  REFERENCES

ANISOVICH 17	PL B766 357	A.V. Anisovich et al.	
ROENCHEN 15A	EPJ A51 70	D. Roenchen et al.	
ROENCHEN 14	EPJ A50 101	D. Roenchen et al.	
Also	EPJ A51 63 (errat.)	D. Roenchen et al.	
CUTKOSKY 80	Toronto Conf. 19	R.E. Cutkosky et al.	(CMU, LBL) IJP
Also	PR D20 2839	R.E. Cutkosky et al.	(CMU, LBL) IJP
HOEHLER 79	PDAT 12-1	G. Hoehler et al.	(KARLT) IJP
Also	Toronto Conf. 3	R. Koch	(KARLT) IJP



## Baryon Particle Listings

 $\Delta(2300)$ ,  $\Delta(2350)$ ,  $\Delta(2390)$ 

$$\Delta(2300) \ 9/2^+$$

$$I(J^P) = \frac{3}{2}(\frac{9}{2}^+) \text{ Status: } **$$

OMITTED FROM SUMMARY TABLE

 $\Delta(2300)$  POLE POSITION

## REAL PART

VALUE (MeV)	DOCUMENT ID	TECN	COMMENT
2370 ± 80	CUTKOSKY 80	IPWA	$\pi N \rightarrow \pi N$

## -2xIMAGINARY PART

VALUE (MeV)	DOCUMENT ID	TECN	COMMENT
420 ± 160	CUTKOSKY 80	IPWA	$\pi N \rightarrow \pi N$

 $\Delta(2300)$  ELASTIC POLE RESIDUEMODULUS  $|r|$ 

VALUE (MeV)	DOCUMENT ID	TECN	COMMENT
10 ± 4	CUTKOSKY 80	IPWA	$\pi N \rightarrow \pi N$

PHASE  $\theta$ 

VALUE (°)	DOCUMENT ID	TECN	COMMENT
-20 ± 30	CUTKOSKY 80	IPWA	$\pi N \rightarrow \pi N$

 $\Delta(2300)$  BREIT-WIGNER MASS

VALUE (MeV)	DOCUMENT ID	TECN	COMMENT
2400 ± 125	CUTKOSKY 80	IPWA	$\pi N \rightarrow \pi N$
2217 ± 80	HOEHLER 79	IPWA	$\pi N \rightarrow \pi N$

 $\Delta(2300)$  BREIT-WIGNER WIDTH

VALUE (MeV)	DOCUMENT ID	TECN	COMMENT
425 ± 150	CUTKOSKY 80	IPWA	$\pi N \rightarrow \pi N$
300 ± 100	HOEHLER 79	IPWA	$\pi N \rightarrow \pi N$

 $\Delta(2300)$  DECAY MODES

Mode	Fraction ( $\Gamma_i/\Gamma$ )
$\Gamma_1 \ N \pi$	1-8 %

 $\Delta(2300)$  BRANCHING RATIOS

$\Gamma(N\pi)/\Gamma_{\text{total}}$	DOCUMENT ID	TECN	COMMENT	$\Gamma_1/\Gamma$
6 ± 2	CUTKOSKY 80	IPWA	$\pi N \rightarrow \pi N$	
3 ± 2	HOEHLER 79	IPWA	$\pi N \rightarrow \pi N$	

 $\Delta(2300)$  REFERENCES

CUTKOSKY 80	Toronto Conf. 19	R.E. Cutkosky <i>et al.</i>	(CMU, LBL) IJP
Also	PR D20 2839	R.E. Cutkosky <i>et al.</i>	(CMU, LBL)
HOEHLER 79	PDAT 12-1	G. Hoehler <i>et al.</i>	(KARLT) IJP
Also	Toronto Conf. 3	R. Koch	(KARLT) IJP

$$\Delta(2350) \ 5/2^-$$

$$I(J^P) = \frac{3}{2}(\frac{5}{2}^-) \text{ Status: } *$$

OMITTED FROM SUMMARY TABLE

 $\Delta(2350)$  POLE POSITION

## REAL PART

VALUE (MeV)	DOCUMENT ID	TECN	COMMENT
2400 ± 125	CUTKOSKY 80	IPWA	$\pi N \rightarrow \pi N$

• • • We do not use the following data for averages, fits, limits, etc. • • •

2427	VRANA 00	DPWA	Multichannel
------	----------	------	--------------

## -2xIMAGINARY PART

VALUE (MeV)	DOCUMENT ID	TECN	COMMENT
400 ± 150	CUTKOSKY 80	IPWA	$\pi N \rightarrow \pi N$

• • • We do not use the following data for averages, fits, limits, etc. • • •

458	VRANA 00	DPWA	Multichannel
-----	----------	------	--------------

 $\Delta(2350)$  ELASTIC POLE RESIDUEMODULUS  $|r|$ 

VALUE (MeV)	DOCUMENT ID	TECN	COMMENT
15 ± 8	CUTKOSKY 80	IPWA	$\pi N \rightarrow \pi N$

PHASE  $\theta$ 

VALUE (°)	DOCUMENT ID	TECN	COMMENT
-70 ± 70	CUTKOSKY 80	IPWA	$\pi N \rightarrow \pi N$

 $\Delta(2350)$  BREIT-WIGNER MASS

VALUE (MeV)	DOCUMENT ID	TECN	COMMENT
2400 ± 125	CUTKOSKY 80	IPWA	$\pi N \rightarrow \pi N$
2305 ± 26	HOEHLER 79	IPWA	$\pi N \rightarrow \pi N$

• • • We do not use the following data for averages, fits, limits, etc. • • •

2459 ± 100	VRANA 00	DPWA	Multichannel
------------	----------	------	--------------

 $\Delta(2350)$  BREIT-WIGNER WIDTH

VALUE (MeV)	DOCUMENT ID	TECN	COMMENT
400 ± 150	CUTKOSKY 80	IPWA	$\pi N \rightarrow \pi N$
300 ± 70	HOEHLER 79	IPWA	$\pi N \rightarrow \pi N$

• • • We do not use the following data for averages, fits, limits, etc. • • •

480 ± 360	VRANA 00	DPWA	Multichannel
-----------	----------	------	--------------

 $\Delta(2350)$  DECAY MODES

Mode	Fraction ( $\Gamma_i/\Gamma$ )
$\Gamma_1 \ N \pi$	4-30 %

 $\Delta(2350)$  BRANCHING RATIOS

$\Gamma(N\pi)/\Gamma_{\text{total}}$	DOCUMENT ID	TECN	COMMENT	$\Gamma_1/\Gamma$
20 ± 10	CUTKOSKY 80	IPWA	$\pi N \rightarrow \pi N$	
4 ± 2	HOEHLER 79	IPWA	$\pi N \rightarrow \pi N$	

• • • We do not use the following data for averages, fits, limits, etc. • • •

7 ± 14	VRANA 00	DPWA	Multichannel
--------	----------	------	--------------

 $\Delta(2350)$  REFERENCES

VRANA 00	PRPL 328 181	T.P. Vrana, S.A. Dytman, T.-S.H. Lee	(PITT, ANL)
CUTKOSKY 80	Toronto Conf. 19	R.E. Cutkosky <i>et al.</i>	(CMU, LBL) IJP
Also	PR D20 2839	R.E. Cutkosky <i>et al.</i>	(CMU, LBL)
HOEHLER 79	PDAT 12-1	G. Hoehler <i>et al.</i>	(KARLT) IJP
Also	Toronto Conf. 3	R. Koch	(KARLT) IJP

$$\Delta(2390) \ 7/2^+$$

$$I(J^P) = \frac{3}{2}(\frac{7}{2}^+) \text{ Status: } *$$

OMITTED FROM SUMMARY TABLE

 $\Delta(2390)$  POLE POSITION

## REAL PART

VALUE (MeV)	DOCUMENT ID	TECN	COMMENT
2223 ± 15 ± 19	<sup>1</sup> SVARC 14	L+P	$\pi N \rightarrow \pi N$
2350 ± 100	CUTKOSKY 80	IPWA	$\pi N \rightarrow \pi N$

## -2xIMAGINARY PART

VALUE (MeV)	DOCUMENT ID	TECN	COMMENT
431 ± 26 ± 7	<sup>1</sup> SVARC 14	L+P	$\pi N \rightarrow \pi N$
260 ± 100	CUTKOSKY 80	IPWA	$\pi N \rightarrow \pi N$

 $\Delta(2390)$  ELASTIC POLE RESIDUEMODULUS  $|r|$ 

VALUE (MeV)	DOCUMENT ID	TECN	COMMENT
26 ± 2 ± 1	<sup>1</sup> SVARC 14	L+P	$\pi N \rightarrow \pi N$
12 ± 6	CUTKOSKY 80	IPWA	$\pi N \rightarrow \pi N$

PHASE  $\theta$ 

VALUE (°)	DOCUMENT ID	TECN	COMMENT
-160 ± 5 ± 11	<sup>1</sup> SVARC 14	L+P	$\pi N \rightarrow \pi N$
-90 ± 60	CUTKOSKY 80	IPWA	$\pi N \rightarrow \pi N$

 $\Delta(2390)$  BREIT-WIGNER MASS

VALUE (MeV)	DOCUMENT ID	TECN	COMMENT
2350 ± 100	CUTKOSKY 80	IPWA	$\pi N \rightarrow \pi N$
2425 ± 60	HOEHLER 79	IPWA	$\pi N \rightarrow \pi N$

 $\Delta(2390)$  BREIT-WIGNER WIDTH

VALUE (MeV)	DOCUMENT ID	TECN	COMMENT
300 ± 100	CUTKOSKY 80	IPWA	$\pi N \rightarrow \pi N$
300 ± 80	HOEHLER 79	IPWA	$\pi N \rightarrow \pi N$

See key on page 999

# Baryon Particle Listings

## $\Delta(2390)$ , $\Delta(2400)$ , $\Delta(2420)$

### $\Delta(2390)$ DECAY MODES

Mode	Fraction ( $\Gamma_i/\Gamma$ )
$\Gamma_1$ $N\pi$	3–12 %

### $\Delta(2390)$ BRANCHING RATIOS

$\Gamma(N\pi)/\Gamma_{total}$	DOCUMENT ID	TECN	COMMENT	$\Gamma_1/\Gamma$
8±4	CUTKOSKY 80	IPWA	$\pi N \rightarrow \pi N$	
7±4	HOEHLER 79	IPWA	$\pi N \rightarrow \pi N$	

### $\Delta(2390)$ FOOTNOTES

<sup>1</sup> Fit to the amplitudes of HOEHLER 79.

### $\Delta(2390)$ REFERENCES

SVARC 14	PR C89 045205	A. Svarc et al.	(RBI Zagreb, UNI Tuzla)
CUTKOSKY 80	Toronto Conf. 19	R.E. Cutkosky et al.	(CMU, LBL) IJP
Also	PR D20 2839	R.E. Cutkosky et al.	(CMU, LBL)
HOEHLER 79	PDAT 12-1	G. Hohlner et al.	(KARLT) IJP
Also	Toronto Conf. 3	R. Koch	(KARLT) IJP

## $\Delta(2400)$ $9/2^-$

$$I(J^P) = \frac{3}{2}(\frac{9}{2}^-) \text{ Status: } **$$

OMITTED FROM SUMMARY TABLE

### $\Delta(2400)$ POLE POSITION

#### REAL PART

VALUE (MeV)	DOCUMENT ID	TECN	COMMENT
2260±60	CUTKOSKY 80	IPWA	$\pi N \rightarrow \pi N$
•••	We do not use the following data for averages, fits, limits, etc. •••		
1931	ROENCHEN 15A	DPWA	Multichannel
1983	ARNDT 06	DPWA	$\pi N \rightarrow \pi N, \eta N$

#### -2xIMAGINARY PART

VALUE (MeV)	DOCUMENT ID	TECN	COMMENT
320±160	CUTKOSKY 80	IPWA	$\pi N \rightarrow \pi N$
•••	We do not use the following data for averages, fits, limits, etc. •••		
442	ROENCHEN 15A	DPWA	Multichannel
878	ARNDT 06	DPWA	$\pi N \rightarrow \pi N, \eta N$

### $\Delta(2400)$ ELASTIC POLE RESIDUE

#### MODULUS |r|

VALUE (MeV)	DOCUMENT ID	TECN	COMMENT
8±4	CUTKOSKY 80	IPWA	$\pi N \rightarrow \pi N$
•••	We do not use the following data for averages, fits, limits, etc. •••		
13	ROENCHEN 15A	DPWA	Multichannel
24	ARNDT 06	DPWA	$\pi N \rightarrow \pi N, \eta N$

#### PHASE $\theta$

VALUE (°)	DOCUMENT ID	TECN	COMMENT
-25±15	CUTKOSKY 80	IPWA	$\pi N \rightarrow \pi N$
•••	We do not use the following data for averages, fits, limits, etc. •••		
-96	ROENCHEN 15A	DPWA	Multichannel
-139	ARNDT 06	DPWA	$\pi N \rightarrow \pi N, \eta N$

### $\Delta(2400)$ INELASTIC POLE RESIDUE

The "normalized residue" is the residue divided by  $\Gamma_{pole}/2$ .

#### Normalized residue in $N\pi \rightarrow \Delta(2400) \rightarrow \Sigma K$

MODULUS	PHASE (°)	DOCUMENT ID	TECN	COMMENT
•••	We do not use the following data for averages, fits, limits, etc. •••			
0.009	25	ROENCHEN 15A	DPWA	Multichannel

#### Normalized residue in $N\pi \rightarrow \Delta(2400) \rightarrow \Delta\pi, G\text{-wave}$

MODULUS	PHASE (°)	DOCUMENT ID	TECN	COMMENT
•••	We do not use the following data for averages, fits, limits, etc. •••			
0.18	-110	ROENCHEN 15A	DPWA	Multichannel

#### Normalized residue in $N\pi \rightarrow \Delta(2400) \rightarrow \Delta\pi, I\text{-wave}$

MODULUS	PHASE (°)	DOCUMENT ID	TECN	COMMENT
•••	We do not use the following data for averages, fits, limits, etc. •••			
0.012	-1.0	ROENCHEN 15A	DPWA	Multichannel

### $\Delta(2400)$ BREIT-WIGNER MASS

VALUE (MeV)	DOCUMENT ID	TECN	COMMENT
2643±141	<sup>1</sup> ARNDT 06	DPWA	$\pi N \rightarrow \pi N, \eta N$
2300±100	CUTKOSKY 80	IPWA	$\pi N \rightarrow \pi N$
2468±50	HOEHLER 79	IPWA	$\pi N \rightarrow \pi N$

<sup>1</sup> Statistical error only.

### $\Delta(2400)$ BREIT-WIGNER WIDTH

VALUE (MeV)	DOCUMENT ID	TECN	COMMENT
895±432	<sup>2</sup> ARNDT 06	DPWA	$\pi N \rightarrow \pi N, \eta N$
330±100	CUTKOSKY 80	IPWA	$\pi N \rightarrow \pi N$
480±100	HOEHLER 79	IPWA	$\pi N \rightarrow \pi N$

<sup>2</sup> Statistical error only.

### $\Delta(2400)$ DECAY MODES

Mode	Fraction ( $\Gamma_i/\Gamma$ )
$\Gamma_1$ $N\pi$	3–9 %

### $\Delta(2400)$ BRANCHING RATIOS

$\Gamma(N\pi)/\Gamma_{total}$	DOCUMENT ID	TECN	COMMENT	$\Gamma_1/\Gamma$
6.4±2.2	<sup>3</sup> ARNDT 06	DPWA	$\pi N \rightarrow \pi N, \eta N$	
5 ± 2	CUTKOSKY 80	IPWA	$\pi N \rightarrow \pi N$	
6 ± 3	HOEHLER 79	IPWA	$\pi N \rightarrow \pi N$	

<sup>3</sup> Statistical error only.

### $\Delta(2400)$ PHOTON DECAY AMPLITUDES AT THE POLE

#### $\Delta(2400) \rightarrow N\gamma$ , helicity-1/2 amplitude $A_{1/2}$

MODULUS ( $\text{GeV}^{-1/2}$ )	PHASE (°)	DOCUMENT ID	TECN	COMMENT
-0.128 <sup>+0.046</sup> <sub>-0.012</sub>	118 <sup>+24</sup> <sub>-3</sub>	ROENCHEN 14	DPWA	
•••	We do not use the following data for averages, fits, limits, etc. •••			
-0.034	63	ROENCHEN 15A	DPWA	Multichannel

#### $\Delta(2400) \rightarrow N\gamma$ , helicity-3/2 amplitude $A_{3/2}$

MODULUS ( $\text{GeV}^{-1/2}$ )	PHASE (°)	DOCUMENT ID	TECN	COMMENT
-0.115 <sup>+0.042</sup> <sub>-0.024</sub>	140 <sup>+17</sup> <sub>-28</sub>	ROENCHEN 14	DPWA	
•••	We do not use the following data for averages, fits, limits, etc. •••			
0.054	-75	ROENCHEN 15A	DPWA	Multichannel

### $\Delta(2400)$ REFERENCES

ROENCHEN 15A	EPJ A51 70	D. Roenchen et al.
ROENCHEN 14	EPJ A50 101	D. Roenchen et al.
Also	EPJ A51 63 (errat.)	D. Roenchen et al.
ARNDT 06	PR C74 045205	R.A. Arndt et al.
CUTKOSKY 80	Toronto Conf. 19	R.E. Cutkosky et al.
Also	PR D20 2839	R.E. Cutkosky et al.
HOEHLER 79	PDAT 12-1	G. Hohlner et al.
Also	Toronto Conf. 3	R. Koch

## $\Delta(2420)$ $11/2^+$

$$I(J^P) = \frac{3}{2}(\frac{11}{2}^+) \text{ Status: } ***$$

Older and obsolete values are listed and referenced in the 2014 edition, Chinese Physics C38 070001 (2014).

### $\Delta(2420)$ POLE POSITION

#### REAL PART

VALUE (MeV)	DOCUMENT ID	TECN	COMMENT
<b>2300 to 2500 (<math>\approx 2400</math>) OUR ESTIMATE</b>			
2454 ± 4 ± 11	<sup>1</sup> SVARC 14	L+P	$\pi N \rightarrow \pi N$
2360±100	CUTKOSKY 80	IPWA	$\pi N \rightarrow \pi N$
•••	We do not use the following data for averages, fits, limits, etc. •••		
2529	ARNDT 06	DPWA	$\pi N \rightarrow \pi N, \eta N$
2300	HOEHLER 93	ARGD	$\pi N \rightarrow \pi N$

<sup>1</sup> Fit to the amplitudes of HOEHLER 79.

#### -2xIMAGINARY PART

VALUE (MeV)	DOCUMENT ID	TECN	COMMENT
<b>350 to 550 (<math>\approx 450</math>) OUR ESTIMATE</b>			
462 ± 8 ± 50	<sup>1</sup> SVARC 14	L+P	$\pi N \rightarrow \pi N$
420±100	CUTKOSKY 80	IPWA	$\pi N \rightarrow \pi N$
•••	We do not use the following data for averages, fits, limits, etc. •••		
621	ARNDT 06	DPWA	$\pi N \rightarrow \pi N, \eta N$
620	HOEHLER 93	ARGD	$\pi N \rightarrow \pi N$

<sup>1</sup> Fit to the amplitudes of HOEHLER 79.

## Baryon Particle Listings

 $\Delta(2420)$ ,  $\Delta(2750)$ ,  $\Delta(2950)$ ,  $\Delta(\sim 3000)$  $\Delta(2420)$  ELASTIC POLE RESIDUEMODULUS  $|r|$ 

VALUE (MeV)	DOCUMENT ID	TECN	COMMENT
<b>20 to 40 (<math>\approx 30</math>) OUR ESTIMATE</b>			
$30 \pm 1 \pm 7$	<sup>1</sup> SVARC	14	L+P $\pi N \rightarrow \pi N$
$18 \pm 6$	CUTKOSKY	80	IPWA $\pi N \rightarrow \pi N$
••• We do not use the following data for averages, fits, limits, etc. •••			
33	ARNDT	06	DPWA $\pi N \rightarrow \pi N, \eta N$
39	HOEHLER	93	ARGD $\pi N \rightarrow \pi N$
<sup>1</sup> Fit to the amplitudes of HOEHLER 79.			

PHASE  $\theta$ 

VALUE (°)	DOCUMENT ID	TECN	COMMENT
<b>-60 to 20 (<math>\approx -20</math>) OUR ESTIMATE</b>			
$11 \pm 1 \pm 8$	<sup>1</sup> SVARC	14	L+P $\pi N \rightarrow \pi N$
$-30 \pm 40$	CUTKOSKY	80	IPWA $\pi N \rightarrow \pi N$
••• We do not use the following data for averages, fits, limits, etc. •••			
-45	ARNDT	06	DPWA $\pi N \rightarrow \pi N, \eta N$
-60	HOEHLER	93	ARGD $\pi N \rightarrow \pi N$
<sup>1</sup> Fit to the amplitudes of HOEHLER 79.			

 $\Delta(2420)$  BREIT-WIGNER MASS

VALUE (MeV)	DOCUMENT ID	TECN	COMMENT
<b>2300 to 2600 (<math>\approx 2450</math>) OUR ESTIMATE</b>			
$2633 \pm 29$	<sup>1</sup> ARNDT	06	DPWA $\pi N \rightarrow \pi N, \eta N$
$2400 \pm 125$	CUTKOSKY	80	IPWA $\pi N \rightarrow \pi N$
$2416 \pm 17$	HOEHLER	79	IPWA $\pi N \rightarrow \pi N$
<sup>1</sup> Statistical error only.			

 $\Delta(2420)$  BREIT-WIGNER WIDTH

VALUE (MeV)	DOCUMENT ID	TECN	COMMENT
<b>300 to 700 (<math>\approx 500</math>) OUR ESTIMATE</b>			
$692 \pm 47$	<sup>1</sup> ARNDT	06	DPWA $\pi N \rightarrow \pi N, \eta N$
$450 \pm 150$	CUTKOSKY	80	IPWA $\pi N \rightarrow \pi N$
$340 \pm 28$	HOEHLER	79	IPWA $\pi N \rightarrow \pi N$
<sup>1</sup> Statistical error only.			

 $\Delta(2420)$  DECAY MODES

The following branching fractions are our estimates, not fits or averages.

Mode	Fraction ( $\Gamma_i/\Gamma$ )
$\Gamma_1 \quad N\pi$	5-10 %

 $\Delta(2420)$  BRANCHING RATIOS

$\Gamma(N\pi)/\Gamma_{\text{total}}$	DOCUMENT ID	TECN	COMMENT	$\Gamma_1/\Gamma$
<b>5 to 10 (<math>\approx 8</math>) OUR ESTIMATE</b>				
$8.5 \pm 0.8$	<sup>1</sup> ARNDT	06	DPWA $\pi N \rightarrow \pi N, \eta N$	
$8 \pm 3$	CUTKOSKY	80	IPWA $\pi N \rightarrow \pi N$	
$8.0 \pm 1.5$	HOEHLER	79	IPWA $\pi N \rightarrow \pi N$	
<sup>1</sup> Statistical error only.				

 $\Delta(2420)$  REFERENCES

PDG	14	CP C38 070001	K. Olive <i>et al.</i>	(PDG Collab.)
SVARC	14	PR C89 045205	A. Svarc <i>et al.</i>	(RBI Zagreb, UNI Tuzla)
ARNDT	06	PR C74 045205	R.A. Arndt <i>et al.</i>	(GWU)
HOEHLER	93	$\pi N$ Newsletter 9 1	G. Höhler	(KARL)
CUTKOSKY	80	Toronto Conf. 19	R.E. Cutkosky <i>et al.</i>	(CMU, LBL) IJP
Also		PR D20 2839	R.E. Cutkosky <i>et al.</i>	(CMU, LBL)
HOEHLER	79	PDAT 12-1	G. Höhler <i>et al.</i>	(KARLT) IJP
Also		Toronto Conf. 3	R. Koch	(KARLT) IJP

$$\Delta(2750) 13/2^- \quad I(J^P) = \frac{3}{2}(\frac{13}{2}^-) \text{Status: } **$$

OMITTED FROM SUMMARY TABLE

 $\Delta(2750)$  BREIT-WIGNER MASS

VALUE (MeV)	DOCUMENT ID	TECN	COMMENT
$2794 \pm 80$	HOEHLER	79	IPWA $\pi N \rightarrow \pi N$

 $\Delta(2750)$  BREIT-WIGNER WIDTH

VALUE (MeV)	DOCUMENT ID	TECN	COMMENT
$350 \pm 100$	HOEHLER	79	IPWA $\pi N \rightarrow \pi N$

 $\Delta(2750)$  DECAY MODES

Mode	Fraction ( $\Gamma_i/\Gamma$ )
$\Gamma_1 \quad N\pi$	2-6 %

 $\Delta(2750)$  BRANCHING RATIOS

$\Gamma(N\pi)/\Gamma_{\text{total}}$	DOCUMENT ID	TECN	COMMENT	$\Gamma_1/\Gamma$
$4.0 \pm 1.5$	HOEHLER	79	IPWA $\pi N \rightarrow \pi N$	

 $\Delta(2750)$  REFERENCES

HOEHLER	79	PDAT 12-1	G. Höhler <i>et al.</i>	(KARLT) IJP
Also		Toronto Conf. 3	R. Koch	(KARLT) IJP

$$\Delta(2950) 15/2^+ \quad I(J^P) = \frac{3}{2}(\frac{15}{2}^+) \text{Status: } **$$

OMITTED FROM SUMMARY TABLE

 $\Delta(2950)$  BREIT-WIGNER MASS

VALUE (MeV)	DOCUMENT ID	TECN	COMMENT
$2990 \pm 100$	HOEHLER	79	IPWA $\pi N \rightarrow \pi N$

 $\Delta(2950)$  BREIT-WIGNER WIDTH

VALUE (MeV)	DOCUMENT ID	TECN	COMMENT
$330 \pm 100$	HOEHLER	79	IPWA $\pi N \rightarrow \pi N$

 $\Delta(2950)$  DECAY MODES

Mode	Fraction ( $\Gamma_i/\Gamma$ )
$\Gamma_1 \quad N\pi$	2-6 %

 $\Delta(2950)$  BRANCHING RATIOS

$\Gamma(N\pi)/\Gamma_{\text{total}}$	DOCUMENT ID	TECN	COMMENT	$\Gamma_1/\Gamma$
$4 \pm 2$	HOEHLER	79	IPWA $\pi N \rightarrow \pi N$	

 $\Delta(2950)$  REFERENCES

HOEHLER	79	PDAT 12-1	G. Höhler <i>et al.</i>	(KARLT) IJP
Also		Toronto Conf. 3	R. Koch	(KARLT) IJP

$$\Delta(\sim 3000 \text{ Region})$$

$$\text{Partial-Wave Analyses}$$

OMITTED FROM SUMMARY TABLE

We list here miscellaneous high-mass candidates for isospin-3/2 resonances found in partial-wave analyses.

Our 1982 edition also had a  $\Delta(2850)$  and a  $\Delta(3230)$ . The evidence for them was deduced from total cross-section and  $180^\circ$  elastic cross-section measurements. The  $\Delta(2850)$  has been resolved into the  $\Delta(2750) \mathcal{B}_{3,13}$  and  $\Delta(2950) \mathcal{K}_{3,15}$ . The  $\Delta(3230)$  is perhaps related to the  $\mathcal{K}_{3,13}$  of HENDRY 78 and to the  $\mathcal{L}_{3,17}$  of KOCH 80.

 $\Delta(\sim 3000)$  BREIT-WIGNER MASS

VALUE (MeV)	DOCUMENT ID	TECN	COMMENT
3300	<sup>1</sup> KOCH	80	IPWA $\pi N \rightarrow \pi N \mathcal{L}_{3,17}$ wave
3500	<sup>1</sup> KOCH	80	IPWA $\pi N \rightarrow \pi N \mathcal{M}_{3,19}$ wave
$2850 \pm 150$	HENDRY	78	MPWA $\pi N \rightarrow \pi N \mathcal{I}_{3,11}$ wave
$3200 \pm 200$	HENDRY	78	MPWA $\pi N \rightarrow \pi N \mathcal{K}_{3,13}$ wave
$3300 \pm 200$	HENDRY	78	MPWA $\pi N \rightarrow \pi N \mathcal{L}_{3,17}$ wave
$3700 \pm 200$	HENDRY	78	MPWA $\pi N \rightarrow \pi N \mathcal{M}_{3,19}$ wave
$4100 \pm 300$	HENDRY	78	MPWA $\pi N \rightarrow \pi N \mathcal{N}_{3,21}$ wave

 $\Delta(\sim 3000)$  BREIT-WIGNER WIDTH

VALUE (MeV)	DOCUMENT ID	TECN	COMMENT
$700 \pm 200$	HENDRY	78	MPWA $\pi N \rightarrow \pi N \mathcal{I}_{3,11}$ wave
$1000 \pm 300$	HENDRY	78	MPWA $\pi N \rightarrow \pi N \mathcal{K}_{3,13}$ wave
$1100 \pm 300$	HENDRY	78	MPWA $\pi N \rightarrow \pi N \mathcal{L}_{3,17}$ wave
$1300 \pm 400$	HENDRY	78	MPWA $\pi N \rightarrow \pi N \mathcal{M}_{3,19}$ wave
$1600 \pm 500$	HENDRY	78	MPWA $\pi N \rightarrow \pi N \mathcal{N}_{3,21}$ wave

See key on page 999

## Baryon Particle Listings

 $\Delta(\sim 3000)$  $\Delta(\sim 3000)$  DECAY MODES

Mode	Fraction ( $\Gamma_i/\Gamma$ )
$\Gamma_1$ $N\pi$	seen

 $\Delta(\sim 3000)$  BRANCHING RATIOS

$\Gamma(N\pi)/\Gamma_{\text{total}}$ VALUE (%)	DOCUMENT ID	TECN	COMMENT	$\Gamma_1/\Gamma$
$6\pm 2$	HENDRY	78	MPWA $\pi N \rightarrow \pi N I_{3,11}$ wave	
$5\pm 2$	HENDRY	78	MPWA $\pi N \rightarrow \pi N K_{3,13}$ wave	
$3\pm 1$	HENDRY	78	MPWA $\pi N \rightarrow \pi N L_{3,17}$ wave	
$3\pm 1$	HENDRY	78	MPWA $\pi N \rightarrow \pi N M_{3,19}$ wave	
$2\pm 1$	HENDRY	78	MPWA $\pi N \rightarrow \pi N N_{3,21}$ wave	

 $\Delta(\sim 3000)$  FOOTNOTES

<sup>1</sup> In addition, KOCH 80 reports some evidence for an  $S_{31}$   $\Delta(2700)$  and a  $P_{33}$   $\Delta(2800)$ .

 $\Delta(\sim 3000)$  REFERENCES

KOCH	80	Toronto Conf. 3	R. Koch	(KARLT) IJP
HENDRY	78	PRL 41 222	A.W. Hendry	(IND, LBL) IJP
Also		ANP 136 1	A.W. Hendry	(IND)

# Baryon Particle Listings

$\Lambda$

## $\Lambda$ BARYONS

$(S = -1, I = 0)$

$\Lambda^0 = uds$

$I(J^P) = 0(\frac{1}{2}^+)$  Status: \*\*\*\*

We have omitted some results that have been superseded by later experiments. See our earlier editions.

### $\Lambda$ MASS

The fit uses  $\Lambda$ ,  $\Sigma^+$ ,  $\Sigma^0$ ,  $\Sigma^-$  mass and mass-difference measurements.

VALUE (MeV)	EVTS	DOCUMENT ID	TECN	COMMENT
<b>1115.683 ± 0.006 OUR FIT</b>				
<b>1115.683 ± 0.006 OUR AVERAGE</b>				
1115.678 ± 0.006 ± 0.006	20k	HARTOUNI 94	SPEC	pp 27.5 GeV/c
1115.690 ± 0.008 ± 0.006	18k	<sup>1</sup> HARTOUNI 94	SPEC	pp 27.5 GeV/c
••• We do not use the following data for averages, fits, limits, etc. •••				
1115.59 ± 0.08	935	HYMAN 72	HEBC	
1115.39 ± 0.12	195	MAYEUR 67	EMUL	
1115.6 ± 0.4		LONDON 66	HBC	
1115.65 ± 0.07	488	<sup>2</sup> SCHMIDT 65	HBC	
1115.44 ± 0.12		<sup>3</sup> BHOWMIK 63	RVUE	

<sup>1</sup>We assume CPT invariance: this is the  $\bar{\Lambda}$  mass as measured by HARTOUNI 94. See below for the fractional mass difference, testing CPT.

<sup>2</sup>The SCHMIDT 65 masses have been reevaluated using our April 1973 proton and  $K^\pm$  and  $\pi^\pm$  masses. P. Schmidt, private communication (1974).

<sup>3</sup>The mass has been raised 35 keV to take into account a 46 keV increase in the proton mass and an 11 keV decrease in the  $\pi^\pm$  mass (note added Reviews of Modern Physics **39** 1 (1967)).

$$(m_\Lambda - m_{\bar{\Lambda}}) / m_\Lambda$$

A test of CPT invariance.

VALUE (units $10^{-5}$ )	EVTS	DOCUMENT ID	TECN	COMMENT
<b>-0.1 ± 1.1 OUR AVERAGE</b>				Error includes scale factor of 1.6.
+ 1.3 ± 1.2	31k	<sup>1</sup> RYBICKI 96	NA32	$\pi^-$ Cu, 230 GeV
- 1.08 ± 0.90		HARTOUNI 94	SPEC	pp 27.5 GeV/c
4.5 ± 5.4		CHIEN 66	HBC	6.9 GeV/c $\bar{p}p$
••• We do not use the following data for averages, fits, limits, etc. •••				
-26 ± 13		BADIER 67	HBC	2.4 GeV/c $\bar{p}p$

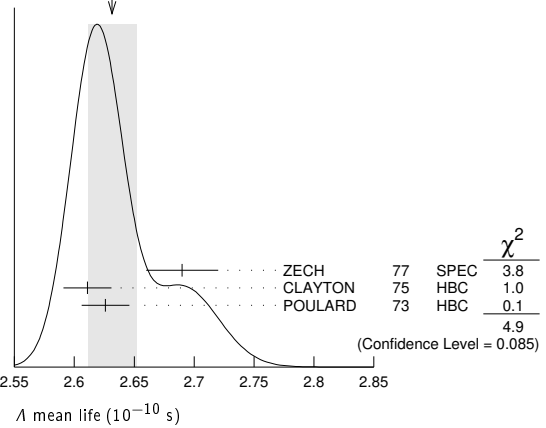
<sup>1</sup>RYBICKI 96 is an analysis of old ACCMOR (NA32) data.

### $\Lambda$ MEAN LIFE

Measurements with an error  $\geq 0.1 \times 10^{-10}$  s have been omitted altogether, and only the latest high-statistics measurements are used for the average.

VALUE ( $10^{-10}$ s)	EVTS	DOCUMENT ID	TECN	COMMENT
<b>2.632 ± 0.020 OUR AVERAGE</b>				Error includes scale factor of 1.6. See the ideogram below.
2.69 ± 0.03	53k	ZECH 77	SPEC	Neutral hyperon beam
2.611 ± 0.020	34k	CLAYTON 75	HBC	0.96-1.4 GeV/c $K^- p$
2.626 ± 0.020	36k	POULARD 73	HBC	0.4-2.3 GeV/c $K^- p$
••• We do not use the following data for averages, fits, limits, etc. •••				
2.69 ± 0.05	6582	ALTHOFF 73B	OSPK	$\pi^+ n \rightarrow \Lambda K^+$
2.54 ± 0.04	4572	BALTAY 71B	HBC	$K^- p$ at rest
2.535 ± 0.035	8342	GRIMM 68	HBC	
2.47 ± 0.08	2600	HEPP 68	HBC	
2.35 ± 0.09	916	BURAN 66	HLBC	
2.452 + 0.056 - 0.054	2213	ENGELMANN 66	HBC	
2.59 ± 0.09	794	HUBBARD 64	HBC	
2.59 ± 0.07	1378	SCHWARTZ 64	HBC	
2.36 ± 0.06	2239	BLOCK 63	HEBC	

WEIGHTED AVERAGE  
2.631 ± 0.020 (Error scaled by 1.6)



$$(\tau_\Lambda - \tau_{\bar{\Lambda}}) / \tau_\Lambda$$

A test of CPT invariance.

VALUE	DOCUMENT ID	TECN	COMMENT
<b>-0.001 ± 0.009 OUR AVERAGE</b>			
-0.0018 ± 0.0066 ± 0.0056	BARNES 96	CNTR	LEAR $\bar{p}p \rightarrow \bar{\Lambda}\Lambda$
0.044 ± 0.085	BADIER 67	HBC	2.4 GeV/c $\bar{p}p$

See the related review(s):  
Baryon Magnetic Moments

### $\Lambda$ MAGNETIC MOMENT

See the "Note on Baryon Magnetic Moments" above. Measurements with an error  $\geq 0.15 \mu_N$  have been omitted.

VALUE ( $\mu_N$ )	EVTS	DOCUMENT ID	TECN	COMMENT
<b>-0.613 ± 0.004 OUR AVERAGE</b>				
-0.606 ± 0.015	200k	COX 81	SPEC	
-0.6138 ± 0.0047	3M	SCHACHIN...	78	SPEC
-0.59 ± 0.07	350k	HELLER 77	SPEC	
-0.57 ± 0.05	1.2M	BUNCE 76	SPEC	
-0.66 ± 0.07	1300	DAHL-JENSEN 71	EMUL	200 kG field

### $\Lambda$ ELECTRIC DIPOLE MOMENT

A nonzero value is forbidden by both T invariance and P invariance.

VALUE ( $10^{-16}$ e-cm)	CL%	DOCUMENT ID	TECN
<b>&lt; 1.5</b>	95	<sup>1</sup> PONDROM 81	SPEC
••• We do not use the following data for averages, fits, limits, etc. •••			
<100	95	<sup>2</sup> BARONI 71	EMUL
<500	95	GIBSON 66	EMUL
<sup>1</sup> PONDROM 81 measures $(-3.0 \pm 7.4) \times 10^{-17}$ e-cm.			
<sup>2</sup> BARONI 71 measures $(-5.9 \pm 2.9) \times 10^{-15}$ e-cm.			

### $\Lambda$ DECAY MODES

Mode	Fraction ( $\Gamma_i/\Gamma$ )	Confidence level
$\Gamma_1$ $p\pi^-$	(63.9 ± 0.5) %	
$\Gamma_2$ $n\pi^0$	(35.8 ± 0.5) %	
$\Gamma_3$ $n\gamma$	(1.75 ± 0.15) × 10 <sup>-3</sup>	
$\Gamma_4$ $p\pi^-\gamma$	[a] (8.4 ± 1.4) × 10 <sup>-4</sup>	
$\Gamma_5$ $p e^- \bar{\nu}_e$	(8.32 ± 0.14) × 10 <sup>-4</sup>	
$\Gamma_6$ $p\mu^- \bar{\nu}_\mu$	(1.57 ± 0.35) × 10 <sup>-4</sup>	

#### Lepton (L) and/or Baryon (B) number violating decay modes

Mode	L, B	Confidence level
$\Gamma_7$ $\pi^+ e^-$	L, B < 6	× 10 <sup>-7</sup> 90%
$\Gamma_8$ $\pi^+ \mu^-$	L, B < 6	× 10 <sup>-7</sup> 90%
$\Gamma_9$ $\pi^- e^+$	L, B < 4	× 10 <sup>-7</sup> 90%
$\Gamma_{10}$ $\pi^- \mu^+$	L, B < 6	× 10 <sup>-7</sup> 90%
$\Gamma_{11}$ $K^+ e^-$	L, B < 2	× 10 <sup>-6</sup> 90%
$\Gamma_{12}$ $K^+ \mu^-$	L, B < 3	× 10 <sup>-6</sup> 90%
$\Gamma_{13}$ $K^- e^+$	L, B < 2	× 10 <sup>-6</sup> 90%
$\Gamma_{14}$ $K^- \mu^+$	L, B < 3	× 10 <sup>-6</sup> 90%
$\Gamma_{15}$ $K_S^0 \nu$	L, B < 2	× 10 <sup>-5</sup> 90%
$\Gamma_{16}$ $\bar{p}\pi^+$	B < 9	× 10 <sup>-7</sup> 90%

[a] See the Listings below for the pion momentum range used in this measurement.

**CONSTRAINED FIT INFORMATION**

An overall fit to 5 branching ratios uses 20 measurements and one constraint to determine 5 parameters. The overall fit has a  $\chi^2 = 10.5$  for 16 degrees of freedom.

The following *off-diagonal* array elements are the correlation coefficients  $\langle \delta x_i \delta x_j \rangle / (\delta x_i \delta x_j)$ , in percent, from the fit to the branching fractions,  $x_i \equiv \Gamma_i / \Gamma_{\text{total}}$ . The fit constrains the  $x_i$  whose labels appear in this array to sum to one.

$x_2$	-100			
$x_3$	-2	-1		
$x_5$	46	-46	-1	
$x_6$	0	0	0	0
	$x_1$	$x_2$	$x_3$	$x_5$

**Λ BRANCHING RATIOS**

$\Gamma(p\pi^-) / \Gamma(N\pi)$				$\Gamma_1 / (\Gamma_1 + \Gamma_2)$	
VALUE	EVTS	DOCUMENT ID	TECN	COMMENT	
<b>0.641 ± 0.005 OUR FIT</b>					
<b>0.640 ± 0.005 OUR AVERAGE</b>					
0.646 ± 0.008	4572	BALTAY	71B	HBC	$K^- p$ at rest
0.635 ± 0.007	6736	DOYLE	69	HBC	$\pi^- p \rightarrow \Lambda K^0$
0.643 ± 0.016	903	HUMPHREY	62	HBC	
0.624 ± 0.030		CRAWFORD	59B	HBC	$\pi^- p \rightarrow \Lambda K^0$

$\Gamma(n\pi^0) / \Gamma(N\pi)$				$\Gamma_2 / (\Gamma_1 + \Gamma_2)$	
VALUE	EVTS	DOCUMENT ID	TECN	COMMENT	
<b>0.359 ± 0.005 OUR FIT</b>					
<b>0.310 ± 0.028 OUR AVERAGE</b>					
0.35 ± 0.05		BROWN	63	HLBC	
0.291 ± 0.034	75	CHRETIEN	63	HLBC	

$\Gamma(n\gamma) / \Gamma_{\text{total}}$				$\Gamma_3 / \Gamma$	
VALUE (units $10^{-3}$ )	EVTS	DOCUMENT ID	TECN	COMMENT	
<b>1.75 ± 0.15 OUR FIT</b>					
<b>1.75 ± 0.15</b>	1816	LARSON	93	SPEC	$K^- p$ at rest
• • • We do not use the following data for averages, fits, limits, etc. • • •					
1.78 ± 0.24 <sup>+0.14</sup> <sub>-0.16</sub>	287	NOBLE	92	SPEC	See LARSON 93

$\Gamma(n\gamma) / \Gamma(n\pi^0)$				$\Gamma_3 / \Gamma_2$	
VALUE (units $10^{-3}$ )	EVTS	DOCUMENT ID	TECN	COMMENT	
• • • We do not use the following data for averages, fits, limits, etc. • • •					
2.86 ± 0.74 ± 0.57	24	BIAGI	86	SPEC	SPS hyperon beam

$\Gamma(p\pi^- \gamma) / \Gamma(p\pi^-)$				$\Gamma_4 / \Gamma_1$	
VALUE (units $10^{-3}$ )	EVTS	DOCUMENT ID	TECN	COMMENT	
<b>1.32 ± 0.22</b>	72	BAGGETT	72c	HBC	$\pi^- < 95$ MeV/c

$\Gamma(p e^- \bar{\nu}_e) / \Gamma(p\pi^-)$				$\Gamma_5 / \Gamma_1$	
VALUE (units $10^{-3}$ )	EVTS	DOCUMENT ID	TECN	COMMENT	
<b>1.301 ± 0.019 OUR FIT</b>					
<b>1.301 ± 0.019 OUR AVERAGE</b>					
1.335 ± 0.056	7111	BOURQUIN	83	SPEC	SPS hyperon beam
1.313 ± 0.024	10k	WISE	80	SPEC	
1.23 ± 0.11	544	LINDQUIST	77	SPEC	$\pi^- p \rightarrow K^0 \Lambda$
1.27 ± 0.07	1089	KATZ	73	HBC	
1.31 ± 0.06	1078	ALTHOFF	71	OSPK	
1.17 ± 0.13	86	1 CANTER	71	HBC	$K^- p$ at rest
1.20 ± 0.12	143	2 MALONEY	69	HBC	
1.17 ± 0.18	120	2 BAGLIN	64	FBC	$K^-$ freon 1.45 GeV/c
1.23 ± 0.20	150	2 ELY	63	FBC	
• • • We do not use the following data for averages, fits, limits, etc. • • •					
1.32 ± 0.15	218	1 LINDQUIST	71	OSPK	See LINDQUIST 77

<sup>1</sup> Changed by us from  $\Gamma(p e^- \bar{\nu}_e) / \Gamma(N\pi)$  assuming the authors used  $\Gamma(\Lambda \rightarrow p\pi^-) / \Gamma(\text{total}) = 2/3$ .  
<sup>2</sup> Changed by us from  $\Gamma(p e^- \bar{\nu}_e) / \Gamma(N\pi)$  because  $\Gamma(p e^- \nu) / \Gamma(p\pi^-)$  is the directly measured quantity.

$\Gamma(p\mu^- \bar{\nu}_\mu) / \Gamma(N\pi)$				$\Gamma_6 / (\Gamma_1 + \Gamma_2)$	
VALUE (units $10^{-4}$ )	EVTS	DOCUMENT ID	TECN	COMMENT	
<b>1.57 ± 0.35 OUR FIT</b>					
<b>1.57 ± 0.35 OUR AVERAGE</b>					
1.4 ± 0.5	14	BAGGETT	72B	HBC	$K^- p$ at rest
2.4 ± 0.8	9	CANTER	71B	HBC	$K^- p$ at rest
1.3 ± 0.7	3	LIND	64	RVUE	
1.5 ± 1.2	2	RONNE	64	FBC	

**Lepton (L) and/or Baryon (B) number violating decay modes**

$\Gamma(\pi^+ e^-) / \Gamma_{\text{total}}$				$\Gamma_7 / \Gamma$	
VALUE	CL%	DOCUMENT ID	TECN	COMMENT	
<b>&lt;6 × 10<sup>-7</sup></b>	90	1 MCCracken	15	CLAS	$\gamma p \rightarrow K^+ \Lambda$
<sup>1</sup> Uses $B(\Lambda \rightarrow p\pi^-) = (63.9 \pm 0.5)\%$ for normalization mode.					

$\Gamma(\pi^+ \mu^-) / \Gamma_{\text{total}}$				$\Gamma_8 / \Gamma$	
VALUE	CL%	DOCUMENT ID	TECN	COMMENT	
<b>&lt;6 × 10<sup>-7</sup></b>	90	1 MCCracken	15	CLAS	$\gamma p \rightarrow K^+ \Lambda$
<sup>1</sup> Uses $B(\Lambda \rightarrow p\pi^-) = (63.9 \pm 0.5)\%$ for normalization mode.					

$\Gamma(\pi^- e^+) / \Gamma_{\text{total}}$				$\Gamma_9 / \Gamma$	
VALUE	CL%	DOCUMENT ID	TECN	COMMENT	
<b>&lt;4 × 10<sup>-7</sup></b>	90	1 MCCracken	15	CLAS	$\gamma p \rightarrow K^+ \Lambda$
<sup>1</sup> Uses $B(\Lambda \rightarrow p\pi^-) = (63.9 \pm 0.5)\%$ for normalization mode.					

$\Gamma(\pi^- \mu^+) / \Gamma_{\text{total}}$				$\Gamma_{10} / \Gamma$	
VALUE	CL%	DOCUMENT ID	TECN	COMMENT	
<b>&lt;6 × 10<sup>-7</sup></b>	90	1 MCCracken	15	CLAS	$\gamma p \rightarrow K^+ \Lambda$
<sup>1</sup> Uses $B(\Lambda \rightarrow p\pi^-) = (63.9 \pm 0.5)\%$ for normalization mode.					

$\Gamma(K^+ e^-) / \Gamma_{\text{total}}$				$\Gamma_{11} / \Gamma$	
VALUE	CL%	DOCUMENT ID	TECN	COMMENT	
<b>&lt;2 × 10<sup>-6</sup></b>	90	1 MCCracken	15	CLAS	$\gamma p \rightarrow K^+ \Lambda$
<sup>1</sup> Uses $B(\Lambda \rightarrow p\pi^-) = (63.9 \pm 0.5)\%$ for normalization mode.					

$\Gamma(K^+ \mu^-) / \Gamma_{\text{total}}$				$\Gamma_{12} / \Gamma$	
VALUE	CL%	DOCUMENT ID	TECN	COMMENT	
<b>&lt;3 × 10<sup>-6</sup></b>	90	1 MCCracken	15	CLAS	$\gamma p \rightarrow K^+ \Lambda$
<sup>1</sup> Uses $B(\Lambda \rightarrow p\pi^-) = (63.9 \pm 0.5)\%$ for normalization mode.					

$\Gamma(K^- e^+) / \Gamma_{\text{total}}$				$\Gamma_{13} / \Gamma$	
VALUE	CL%	DOCUMENT ID	TECN	COMMENT	
<b>&lt;2 × 10<sup>-6</sup></b>	90	1 MCCracken	15	CLAS	$\gamma p \rightarrow K^+ \Lambda$
<sup>1</sup> Uses $B(\Lambda \rightarrow p\pi^-) = (63.9 \pm 0.5)\%$ for normalization mode.					

$\Gamma(K^- \mu^+) / \Gamma_{\text{total}}$				$\Gamma_{14} / \Gamma$	
VALUE	CL%	DOCUMENT ID	TECN	COMMENT	
<b>&lt;3 × 10<sup>-6</sup></b>	90	1 MCCracken	15	CLAS	$\gamma p \rightarrow K^+ \Lambda$
<sup>1</sup> Uses $B(\Lambda \rightarrow p\pi^-) = (63.9 \pm 0.5)\%$ for normalization mode.					

$\Gamma(K_S^0 \nu) / \Gamma_{\text{total}}$				$\Gamma_{15} / \Gamma$	
VALUE	CL%	DOCUMENT ID	TECN	COMMENT	
<b>&lt;2 × 10<sup>-5</sup></b>	90	1 MCCracken	15	CLAS	$\gamma p \rightarrow K^+ \Lambda$
<sup>1</sup> Uses $B(\Lambda \rightarrow p\pi^-) = (63.9 \pm 0.5)\%$ for normalization mode.					

$\Gamma(\bar{p}\pi^+) / \Gamma_{\text{total}}$				$\Gamma_{16} / \Gamma$	
VALUE	CL%	DOCUMENT ID	TECN	COMMENT	
<b>&lt;9 × 10<sup>-7</sup></b>	90	1 MCCracken	15	CLAS	$\gamma p \rightarrow K^+ \Lambda$
<sup>1</sup> Uses $B(\Lambda \rightarrow p\pi^-) = (63.9 \pm 0.5)\%$ for normalization mode.					

**Λ DECAY PARAMETERS**

See the "Note on Baryon Decay Parameters" in the neutron Listings. Some early results have been omitted.

$\alpha_-$ FOR $\Lambda \rightarrow p\pi^-$					
VALUE	EVTS	DOCUMENT ID	TECN	COMMENT	
<b>0.732 ± 0.014 OUR AVERAGE</b>					Error includes scale factor of 2.3.
0.750 ± 0.009 ± 0.004	420k	ABLIKIM	19Bj	BES3	$J/\psi$ to $\Lambda \bar{\Lambda}$
0.721 ± 0.006 ± 0.005		1 IRELAND	19	CLAS	$K$ production
• • • We do not use the following data for averages, fits, limits, etc. • • •					
0.584 ± 0.046	8500	ASTBURY	75	SPEC	
0.649 ± 0.023	10325	CLELAND	72	OSPK	
0.67 ± 0.06	3520	DAUBER	69	HBC	From $\Xi$ decay
0.645 ± 0.017	10130	OVERSETH	67	OSPK	$\Lambda$ from $\pi^- p$
0.62 ± 0.07	1156	CRONIN	63	CNTR	$\Lambda$ from $\pi^- p$
<sup>1</sup> This is a new analysis based on existing kaon photoproduction data of the CLAS collaboration and using spin algebra constraints.					

$\alpha_+$ FOR $\bar{\Lambda} \rightarrow \bar{p}\pi^+$					
VALUE	EVTS	DOCUMENT ID	TECN	COMMENT	
<b>-0.758 ± 0.010 ± 0.007</b>	420k	ABLIKIM	19Bj	BES3	$J/\psi$ to $\Lambda \bar{\Lambda}$
• • • We do not use the following data for averages, fits, limits, etc. • • •					
-0.755 ± 0.083 ± 0.063	≈ 8.7k	ABLIKIM	10	BES	$J/\psi \rightarrow \Lambda \bar{\Lambda}$
-0.63 ± 0.13	770	TIXIER	88	DM2	$J/\psi \rightarrow \Lambda \bar{\Lambda}$

$\bar{\alpha}_0$ FOR $\bar{\Lambda} \rightarrow \bar{\pi}\pi^0$					
VALUE	EVTS	DOCUMENT ID	TECN	COMMENT	
<b>-0.692 ± 0.016 ± 0.006</b>	47k	ABLIKIM	19Bj	BES3	$J/\psi$ to $\Lambda \bar{\Lambda}$



$\Lambda(1405) 1/2^-$

$I(J^P) = 0(\frac{1}{2}^-)$  Status: \*\*\*\*

In the 1998 Note on the  $\Lambda(1405)$  in PDG 98, R.H. Dalitz discussed the S-shaped cusp behavior of the intensity at the  $N\bar{K}$  threshold observed in THOMAS 73 and HEMINGWAY 85. He commented that this behavior "is characteristic of S-wave coupling; the other below threshold hyperon, the  $\Sigma(1385)$ , has no such threshold distortion because its  $N\bar{K}$  coupling is P-wave. For  $\Lambda(1405)$  this asymmetry is the sole direct evidence that  $J^P = 1/2^-$ ."

A recent measurement by the CLAS collaboration, MORIYA 14, definitively established the long-assumed  $J^P = 1/2^-$  spin-parity assignment of the  $\Lambda(1405)$ . The experiment produced the  $\Lambda(1405)$  spin-polarized in the photoproduction process  $\gamma p \rightarrow K^+ \Lambda(1405)$  and measured the decay of the  $\Lambda(1405)$  (polarized)  $\rightarrow \Sigma^+$  (polarized)  $\pi^-$ . The observed isotropic decay of  $\Lambda(1405)$  is consistent with spin  $J = 1/2$ . The polarization transfer to the  $\Sigma^+$  (polarized) direction revealed negative parity, and thus established  $J^P = 1/2^-$ .

See the related review(s):  
Pole Structure of the  $\Lambda(1405)$  Region

$\Lambda(1405)$  POLE POSITION

REAL PART

VALUE (MeV)	DOCUMENT ID	TECN
••• We do not use the following data for averages, fits, limits, etc. •••		
$1429 \pm \frac{8}{7}$	<sup>1</sup> MAI	15 DPWA
$1434 \pm 2$	<sup>2</sup> MAI	15 DPWA
$1421 \pm \frac{3}{2}$	GUO	13 DPWA
$1424 \pm \frac{7}{23}$	IKEDA	12 DPWA

<sup>1</sup> Solution number 4.  
<sup>2</sup> Solution number 2.

-2xIMAGINARY PART

VALUE (MeV)	DOCUMENT ID	TECN
••• We do not use the following data for averages, fits, limits, etc. •••		
$24 \pm \frac{4}{6}$	<sup>1</sup> MAI	15 DPWA
$20 \pm \frac{4}{2}$	<sup>2</sup> MAI	15 DPWA
$38 \pm \frac{16}{10}$	GUO	13 DPWA
$52 \pm \frac{6}{28}$	IKEDA	12 DPWA

<sup>1</sup> Solution number 4.  
<sup>2</sup> Solution number 2.

$\Lambda(1405)$  MASS

PRODUCTION EXPERIMENTS

VALUE (MeV)	EVTS	DOCUMENT ID	TECN	COMMENT
<b>1405.1 <math>\pm</math> <math>\frac{1.3}{1.0}</math> OUR AVERAGE</b>				
$1405 \pm \frac{11}{9}$		HASSANVAND 13	SPEC	$pp \rightarrow p\Lambda(1405) K^+$
$1405 \pm \frac{1.4}{1.0}$		ESMAILI 10	RVUE	$^4\text{He } K^- \rightarrow \Sigma^\pm \pi^\mp X$ at rest
$1406.5 \pm 4.0$		<sup>1</sup> DALITZ 91		M-matrix fit
••• We do not use the following data for averages, fits, limits, etc. •••				
$1391 \pm 1$	700	<sup>1</sup> HEMINGWAY 85	HBC	$K^- p$ 4.2 GeV/c
$\sim 1405$	400	<sup>2</sup> THOMAS 73	HBC	$\pi^- p$ 1.69 GeV/c
1405	120	BARBARO... 68B	DBC	$K^- d$ 2.1-2.7 GeV/c
$1400 \pm 5$	67	BIRMINGHAM 66	HBC	$K^- p$ 3.5 GeV/c
$1382 \pm 8$		ENGLER 65	HDHC	$\pi^- p, \pi^+ d$ 1.68 GeV/c
$1400 \pm 24$		MUSGRAVE 65	HBC	$\bar{p}p$ 3-4 GeV/c
1410		ALEXANDER 62	HBC	$\pi^- p$ 2.1 GeV/c
1405		ALSTON 62	HBC	$K^- p$ 1.2-0.5 GeV/c
1405		ALSTON 61B	HBC	$K^- p$ 1.15 GeV/c

<sup>1</sup> DALITZ 91 fits the HEMINGWAY 85 data.  
<sup>2</sup> THOMAS 73 data is fit by CHAO 73 (see next section).

EXTRAPOLATIONS BELOW  $N\bar{K}$  THRESHOLD

VALUE (MeV)	DOCUMENT ID	TECN	COMMENT
••• We do not use the following data for averages, fits, limits, etc. •••			
1407.56 or 1407.50	<sup>1</sup> KIMURA 00		potential model
1411	<sup>2</sup> MARTIN 81		K-matrix fit
1406	<sup>3</sup> CHAO 73	DPWA	0-range fit (sol. B)
1421	MARTIN 70	RVUE	Constant K-matrix
$1416 \pm 4$	MARTIN 69	HBC	Constant K-matrix
$1403 \pm 3$	KIM 67	HBC	K-matrix fit
$1407.5 \pm 1.2$	<sup>4</sup> KITTEL 66	HBC	0-effective-range fit
$1410.7 \pm 1.0$	KIM 65	HBC	0-effective-range fit
$1409.6 \pm 1.7$	<sup>4</sup> SAKITT 65	HBC	0-effective-range fit

<sup>1</sup> The KIMURA 00 values are from fits A and B from a coupled-channel potential model using low-energy  $\bar{K}N$  and  $\Sigma\pi$  data, kaonic-hydrogen x-ray measurements, and our  $\Lambda(1405)$  mass and width. The results bear mainly on the nature of the  $\Lambda(1405)$ : three-quark state or  $\bar{K}N$  bound state.  
<sup>2</sup> The MARTIN 81 fit includes the  $K^\pm p$  forward scattering amplitudes and the dispersion relations they must satisfy.  
<sup>3</sup> See also the accompanying paper of THOMAS 73.  
<sup>4</sup> Data of SAKITT 65 are used in the fit by KITTEL 66.

$\Lambda(1405)$  WIDTH

PRODUCTION EXPERIMENTS

VALUE (MeV)	EVTS	DOCUMENT ID	TECN	COMMENT
<b>50.5 <math>\pm</math> 2.0 OUR AVERAGE</b>				
$62 \pm 10$		HASSANVAND 13	SPEC	$pp \rightarrow p\Lambda(1405) K^+$
$50 \pm 2$		<sup>1</sup> DALITZ 91		M-matrix fit
••• We do not use the following data for averages, fits, limits, etc. •••				
$24 \pm \frac{4}{3}$		ESMAILI 10	RVUE	$^4\text{He } K^- \rightarrow \Sigma^\pm \pi^\mp X$ at rest
$32 \pm 1$	700	<sup>1</sup> HEMINGWAY 85	HBC	$K^- p$ 4.2 GeV/c
45 to 55	400	<sup>2</sup> THOMAS 73	HBC	$\pi^- p$ 1.69 GeV/c
35	120	BARBARO... 68B	DBC	$K^- d$ 2.1-2.7 GeV/c
$50 \pm 10$	67	BIRMINGHAM 66	HBC	$K^- p$ 3.5 GeV/c
$89 \pm 20$		ENGLER 65	HDHC	
$60 \pm 20$		MUSGRAVE 65	HBC	
$35 \pm 5$		ALEXANDER 62	HBC	
50		ALSTON 62	HBC	
20		ALSTON 61B	HBC	

<sup>1</sup> DALITZ 91 fits the HEMINGWAY 85 data.  
<sup>2</sup> THOMAS 73 data is fit by CHAO 73 (see next section).

EXTRAPOLATIONS BELOW  $N\bar{K}$  THRESHOLD

VALUE (MeV)	DOCUMENT ID	TECN	COMMENT
••• We do not use the following data for averages, fits, limits, etc. •••			
50.24 or 50.26	<sup>1</sup> KIMURA 00		potential model
30	<sup>2</sup> MARTIN 81		K-matrix fit
55	<sup>3,4</sup> CHAO 73	DPWA	0-range fit (sol. B)
20	MARTIN 70	RVUE	Constant K-matrix
$29 \pm 6$	MARTIN 69	HBC	Constant K-matrix
$50 \pm 5$	KIM 67	HBC	K-matrix fit
$34.1 \pm 4.1$	<sup>5</sup> KITTEL 66	HBC	
$37.0 \pm 3.2$	KIM 65	HBC	
$28.2 \pm 4.1$	<sup>5</sup> SAKITT 65	HBC	

<sup>1</sup> The KIMURA 00 values are from fits A and B from a coupled-channel potential model using low-energy  $\bar{K}N$  and  $\Sigma\pi$  data, kaonic-hydrogen x-ray measurements, and our  $\Lambda(1405)$  mass and width. The results bear mainly on the nature of the  $\Lambda(1405)$ : three-quark state or  $\bar{K}N$  bound state.  
<sup>2</sup> The MARTIN 81 fit includes the  $K^\pm p$  forward scattering amplitudes and the dispersion relations they must satisfy.  
<sup>3</sup> An asymmetric shape, with  $\Gamma/2 = 41$  MeV below resonance, 14 MeV above.  
<sup>4</sup> See also the accompanying paper of THOMAS 73.  
<sup>5</sup> Data of SAKITT 65 are used in the fit by KITTEL 66.

$\Lambda(1405)$  DECAY MODES

Mode	Fraction ( $\Gamma_i/\Gamma$ )
$\Gamma_1 \Sigma\pi$	100 %
$\Gamma_2 \Lambda\gamma$	
$\Gamma_3 \Sigma^0\gamma$	
$\Gamma_4 N\bar{K}$	

$\Lambda(1405)$  PARTIAL WIDTHS

$\Gamma(\Lambda\gamma)$	VALUE (keV)	DOCUMENT ID	COMMENT	$\Gamma_2$
••• We do not use the following data for averages, fits, limits, etc. •••				
	$27 \pm 8$	BURKHARDT 91	Isobar model fit	
$\Gamma(\Sigma^0\gamma)$	VALUE (keV)	DOCUMENT ID	COMMENT	$\Gamma_3$
••• We do not use the following data for averages, fits, limits, etc. •••				
	$10 \pm 4$ or $23 \pm 7$	BURKHARDT 91	Isobar model fit	

$\Lambda(1405)$  BRANCHING RATIOS

$\Gamma(N\bar{K})/\Gamma(\Sigma\pi)$	VALUE	CL%	DOCUMENT ID	TECN	COMMENT	$\Gamma_4/\Gamma_1$
••• We do not use the following data for averages, fits, limits, etc. •••						
	<3	95	HEMINGWAY 85	HBC	$K^- p$ 4.2 GeV/c	



# Baryon Particle Listings

## $\Lambda(1405), \Lambda(1520)$

### $\Lambda(1405)$ REFERENCES

MAI	15	EPJ A51 30	M. Mai, U.-G. Meißner	(BONN, JULI)
MORIVA	14	PRL 112 082004	K. Morio et al.	(CLAS Collab.)JP
GUO	13	PR C87 035202	Z.-H. Guo, J. Oller	
HASSANVAND	13	PR C87 055202	M. Hassanvand et al.	
	Also	PR C88 019905 (errata.)	M. Hassanvand et al.	
IKEDA	12	NP A881 98	Y. Ikeda, T. Hyodo, W. Weise	(MUNT, RIKEN, TINT)
ESMALI	10	PL B686 23	J. Esmaili, Y. Akaishi, T. Yamazaki	(RIKEN, ISUT+)
KIMURA	00	PR C62 015206	M. Kimura et al.	
PDG	98	EPJ C3 1	C. Caso et al.	(PDG Collab.)
BURKHARDT	91	PR C44 607	H. Burkhardt, J. Lowe	(NOTT, UNM, BIRM)
DALITZ	91	JP G17 289	R.-H. Dalitz, A. Deloff	(OXFTP, WINR)
HENNINGWAY	85	NP B253 742	R.J. Hemingway	(CERN J)
MARTIN	81	NP B179 33	A.D. Martin	(DURH)
CHAO	73	NP B56 46	Y.A. Chao et al.	(RHEL, CMU, LOUC)
THOMAS	73	NP B56 15	D.W. Thomas et al.	(CMU)J
MARTIN	70	NP B16 479	A.D. Martin, G.G. Ross	(DURH)
MARTIN	69	PR 183 1352	B.R. Martin, M. Sakitt	(LOUC, BNL)
	Also	PR 183 1345	B.R. Martin, M. Sakitt	(LOUC, BNL)
BARBARO...	68B	PRL 21 573	A. Barbaro-Galtieri et al.	(LRL, SLAC)
KIM	67	PRL 19 1074	J.K. Kim	(YALE)
BIRMINGHAM	66	PR 152 1148	M. Haque et al.	(BIRM, GLAS, LOIC, OXF+)
KITTEL	66	PL 21 349	W. Kittel, G. Otter, I. Wacek	(VIEN)
ENGLER	65	PRL 15 224	A. Engler et al.	(CMU, BNL, IJ)
KIM	65	PRL 14 29	J.K. Kim	(COLU)
MUSGRAVE	65	NC 35 735	B. Musgrave et al.	(BIRM, CERN, EPOL+)
SAKITT	65	PR 139 8719	M. Sakitt et al.	(UMD, LRL)
ALEXANDER	62	PRL 8 447	G. Alexander et al.	(LRL)I
ALSTON	62	CERN Conf. 311	M.H. Alston et al.	(LRL)I
ALSTON	61B	PRL 6 698	M.H. Alston et al.	(LRL)I

### OTHER RELATED PAPERS

IWASAKI	97	PRL 78 3067	M. Iwasaki et al.	(KEK 228 Collab.)
FINK	90	PR C41 2720	P.J. Fink et al.	(IBMY, ORST, ANSM)
LEINWEBER	90	ANP 198 203	D.B. Leinweber	(MCMS)
MUELLER-GR...	90	NP A513 557	A. Mueller-Groeling, K. Holinde, J. Speth	(JULI)
BARRETT	89	NC 102A 179	R.C. Barrett	(SURR)
BATTY	89	NC 102A 255	C.J. Batty, A. Gal	(RAL, HEBR)
CAPSTICK	89	Excited Baryons 88, p.32	S. Capstick	(GUEL)
LOWE	89	NC 102A 167	J. Lowe	(BIRM)
WHITEHOUSE	89	PRL 63 1352	D.A. Whitehouse et al.	(BIRM, BOST, BRCO+)
SIEGEL	88	PR C38 2221	P.B. Siegel, W. Weise	(REGE)
WORKMAN	88	PR D37 3117	R.L. Workman, H.W. Fearing	(TRIU)
SCHNICK	87	PRL 58 1719	J. Schnick, R.H. Landau	(ORST)
CAPSTICK	86	PR D34 2809	S. Capstick, N. Isgur	(TNT0)
JENNINGS	86	PL B176 229	B.K. Jennings	(TRIU)
MALTMAN	86	PR D34 1372	K. Maltman, N. Isgur	(LANL, TNT0)
ZHONG	86	PL B171 471	Y.S. Zhong et al.	(ADLD, TRIU, SURR)
BURKHARDT	85	NP A440 653	H. Burkhardt, J. Lowe, A.S. Rosenthal	(NOTT+)
DAREWYCH	85	PR D32 1765	J.W. Darewych, R. Koniuk, N. Isgur	(YORKC, TNT0)
VEIT	85	PR D31 1033	E.A. Veit et al.	(TRIU, ADLD, SURR)
KIANG	84	PR C30 1638	D. Kiang et al.	(DALH, MCMS)
MILLER	84	Conference paper	D.J. Miller	(LOUC)
Conf. Intersections between Particle and Nuclear Physics, p. 783				
VANDUJK	84	PR D30 937	W. van Dijk	(MCMS)
VEIT	84	PL 137B 415	E.A. Veit et al.	(TRIU, SURR, CERN)
DALITZ	82	Heid. Conf.	R.H. Dalitz et al.	(OXFTP)
Heidelberg Conf., p. 201				
DALITZ	81	Kaon Conf.	R.H. Dalitz, J.G. McGinley	(OXFTP)
Low and Intermediate Energy Kaon-Nucleon Physics, p.381				
MARTIN	81B	Kaon Conf.	A.D. Martin	(DURH)
Low and Intermediate Energy Kaon-Nucleon Physics, p. 97				
OADES	77	NC 42A 462	G.C. Oades, G. Rasche	(AARH, ZURI)
SHAW	73	Purdue Conf. 417	G.L. Shaw	(UCI)
BARBARO...	72	LBL-555	A. Barbaro-Galtieri	(LBL)
DOBSON	72	PR D6 3256	P.N. Dobson, R. McEthaney	(HAWA)
RAJASEKA...	72	PR D5 610	G. Rajasekaran	(TATA)
Earlier papers also cited in RAJASEKARAN 72.				
CLINE	71	PRL 26 1194	D. Cline, R. Laumann, J. Mapp	(WIS C)
MARTIN	71	PL 35B 62	A.D. Martin, A.D. Martin, G.G. Ross	(DURH, LOUC+)
DALITZ	67	PR 153 1617	R.H. Dalitz, T.C. Wong, G. Rajasekaran	(OXFTP+)
DONALD	66	PL 22 711	R.A. Donald et al.	(LIVP)
KADYK	66	PRL 17 599	J.A. Kadyk et al.	(LRL)
ABRAMS	65	PR 139 B454	G.S. Abrams, B. Sechi-Zorn	(UMD)

## $\Lambda(1520) 3/2^-$

$$I(J^P) = 0(\frac{3}{2}^-) \text{ Status: } ***$$

Discovered by FERRO-LUZZI 62; the elaboration in WATSON 63 is the classic paper on the Breit-Wigner analysis of a multichannel resonance.

The measurements of the mass, width, and elasticity published before 1975 are now obsolete and have been omitted. They were last listed in our 1982 edition Physics Letters 111B 1 (1982).

Production and formation experiments agree quite well, so they are listed together here.

### $\Lambda(1520)$ POLE POSITION

#### REAL PART

VALUE (MeV)		DOCUMENT ID	TECN	COMMENT
<b>1517 to 1518 (<math>\approx</math> 1517.5) OUR ESTIMATE</b>				
<b>1517.5 <math>\pm</math> 0.4 OUR AVERAGE</b>				
1517.5 $\pm$ 0.4		SARANTSEV 19	DPWA	$\bar{K}N$ multichannel
1517 +4		1 KAMANO 15	DPWA	$\bar{K}N$ multichannel
1517 -4				
• • • We do not use the following data for averages, fits, limits, etc. • • •				
1518		ZHANG 13A	DPWA	$\bar{K}N$ multichannel
1518.8		QIANG 10	SPEC	$e p \rightarrow e' K^+ X$ (fit to X)
1 From the preferred solution A in KAMANO 15.				

### -2xIMAGINARY PART

VALUE (MeV)		DOCUMENT ID	TECN	COMMENT
<b>14 to 18 (<math>\approx</math> 16) OUR ESTIMATE</b>				
<b>15.3 <math>\pm</math> 0.9 OUR AVERAGE</b>				
15.3 $\pm$ 0.9		SARANTSEV 19	DPWA	$\bar{K}N$ multichannel
15 +10		1 KAMANO 15	DPWA	$\bar{K}N$ multichannel
15 -8				
• • • We do not use the following data for averages, fits, limits, etc. • • •				
16		ZHANG 13A	DPWA	$\bar{K}N$ multichannel
17.2		QIANG 10	SPEC	$e p \rightarrow e' K^+ X$ (fit to X)
1 From the preferred solution A in KAMANO 15.				

### $\Lambda(1520)$ POLE RESIDUES

The normalized residue is the residue divided by  $\Gamma_{pole}/2$ .

#### Normalized residue in $N\bar{K} \rightarrow \Lambda(1520) \rightarrow N\bar{K}$

MODULUS	PHASE ( $^\circ$ )	DOCUMENT ID	TECN	COMMENT
<b>0.45 <math>\pm</math> 0.01</b>	<b>-10 <math>\pm</math> 3</b>	SARANTSEV 19	DPWA	$\bar{K}N$ multichannel
• • • We do not use the following data for averages, fits, limits, etc. • • •				
0.431	-11	1 KAMANO 15	DPWA	$\bar{K}N$ multichannel
1 From the preferred solution A in KAMANO 15.				

#### Normalized residue in $N\bar{K} \rightarrow \Lambda(1520) \rightarrow \Sigma\pi$

MODULUS	PHASE ( $^\circ$ )	DOCUMENT ID	TECN	COMMENT
<b>0.44 <math>\pm</math> 0.01</b>	<b>-15 <math>\pm</math> 3</b>	SARANTSEV 19	DPWA	$\bar{K}N$ multichannel
• • • We do not use the following data for averages, fits, limits, etc. • • •				
0.435	-10	1 KAMANO 15	DPWA	$\bar{K}N$ multichannel
1 From the preferred solution A in KAMANO 15.				

#### Normalized residue in $N\bar{K} \rightarrow \Lambda(1520) \rightarrow \Lambda\eta$

MODULUS	PHASE ( $^\circ$ )	DOCUMENT ID	TECN	COMMENT
<b>0.013 <math>\pm</math> 0.003</b>	<b>116 <math>\pm</math> 3</b>	SARANTSEV 19	DPWA	$\bar{K}N$ multichannel

#### Normalized residue in $N\bar{K} \rightarrow \Lambda(1520) \rightarrow \Sigma(1385)\pi, S\text{-wave}$

MODULUS	PHASE ( $^\circ$ )	DOCUMENT ID	TECN	COMMENT
• • • We do not use the following data for averages, fits, limits, etc. • • •				
0.431	-123	1 KAMANO 15	DPWA	$\bar{K}N$ multichannel
1 From the preferred solution A in KAMANO 15.				

#### Normalized residue in $N\bar{K} \rightarrow \Lambda(1520) \rightarrow \Sigma(1385)\pi, D\text{-wave}$

MODULUS	PHASE ( $^\circ$ )	DOCUMENT ID	TECN	COMMENT
• • • We do not use the following data for averages, fits, limits, etc. • • •				
0.0141	122	1 KAMANO 15	DPWA	$\bar{K}N$ multichannel
1 From the preferred solution A in KAMANO 15.				

### $\Lambda(1520)$ MASS

VALUE (MeV)	EVTS	DOCUMENT ID	TECN	COMMENT
<b>1518 to 1520 (<math>\approx</math> 1519) OUR ESTIMATE</b>				
<b>1519.42 <math>\pm</math> 0.19 OUR AVERAGE</b>				
1518.5 $\pm$ 0.5		SARANTSEV 19	DPWA	$\bar{K}N$ multichannel
1519.6 $\pm$ 0.5		ZHANG 13A	DPWA	$\bar{K}N$ multichannel
1520.4 $\pm$ 0.6 $\pm$ 1.5		QIANG 10	SPEC	$e p \rightarrow e' K^+ X$ (fit to X)
1517.3 $\pm$ 1.5	300	BARBER 80D	SPEC	$\gamma p \rightarrow \Lambda(1520) K^+$
1517.8 $\pm$ 1.2	5k	BARLAG 79	HBC	$K^- p$ 4.2 GeV/c
1520.0 $\pm$ 0.5		ALSTON... 78	DPWA	$\bar{K}N \rightarrow \bar{K}N$
1519.7 $\pm$ 0.3	4k	CAMERON 77	HBC	$K^- p$ 0.96-1.36 GeV/c
1519 $\pm$ 1		GOPAL 77	DPWA	$\bar{K}N$ multichannel
1519.4 $\pm$ 0.3	2000	CORDEN 75	DBC	$K^- d$ 1.4-1.8 GeV/c

### $\Lambda(1520)$ WIDTH

VALUE (MeV)	EVTS	DOCUMENT ID	TECN	COMMENT
<b>15 to 17 (<math>\approx</math> 16) OUR ESTIMATE</b>				
<b>15.73 <math>\pm</math> 0.26 OUR AVERAGE</b>				
15.7 $\pm$ 1.0		SARANTSEV 19	DPWA	$\bar{K}N$ multichannel
17 $\pm$ 1		ZHANG 13A	DPWA	$\bar{K}N$ multichannel
18.6 $\pm$ 1.9 $\pm$ 1.0		QIANG 10	SPEC	$e p \rightarrow e' K^+ X$ (fit to X)
16.3 $\pm$ 3.3	300	BARBER 80D	SPEC	$\gamma p \rightarrow \Lambda(1520) K^+$
16 $\pm$ 1		GOPAL 80	DPWA	$\bar{K}N \rightarrow \bar{K}N$
14 $\pm$ 3	677	1 BARLAG 79	HBC	$K^- p$ 4.2 GeV/c
15.4 $\pm$ 0.5		ALSTON... 78	DPWA	$\bar{K}N \rightarrow \bar{K}N$
16.3 $\pm$ 0.5	4k	CAMERON 77	HBC	$K^- p$ 0.96-1.36 GeV/c
15.0 $\pm$ 0.5		GOPAL 77	DPWA	$\bar{K}N$ multichannel
15.5 $\pm$ 1.6	2000	CORDEN 75	DBC	$K^- d$ 1.4-1.8 GeV/c
1 From the best-resolution sample of $\Lambda\pi\pi$ events only.				

$\Lambda(1520)$  DECAY MODES

Mode	Fraction ( $\Gamma_i/\Gamma$ )
$\Gamma_1$ $N\bar{K}$	(45 ± 1 ) %
$\Gamma_2$ $\Sigma\pi$	(42 ± 1 ) %
$\Gamma_3$ $\Lambda\pi\pi$	(10 ± 1 ) %
$\Gamma_4$ $\Sigma(1385)\pi, S\text{-wave}$	
$\Gamma_5$ $\Sigma(1385)\pi, D\text{-wave}$	
$\Gamma_6$ $\Sigma(1385)\pi$	
$\Gamma_7$ $\Sigma(1385)\pi(\rightarrow\Lambda\pi\pi)$	
$\Gamma_8$ $\Lambda(\pi\pi)_{S\text{-wave}}$	
$\Gamma_9$ $\Sigma\pi\pi$	( 0.9 ± 0.1 ) %
$\Gamma_{10}$ $\Lambda\gamma$	( 0.85 ± 0.15 ) %
$\Gamma_{11}$ $\Sigma^0\gamma$	

$\Lambda(1520)$  BRANCHING RATIOS

See "Sign conventions for resonance couplings" in the Note on  $\Lambda$  and  $\Sigma$  Resonances.

$\Gamma(N\bar{K})/\Gamma_{\text{total}}$

VALUE	DOCUMENT ID	TECN	COMMENT
<b>0.45 to 0.47 OUR ESTIMATE</b>			
0.45 ± 0.01	SARANTSEV	19 DPWA	$\bar{K}N$ multichannel
0.47 ± 0.04	ZHANG	13A DPWA	$\bar{K}N$ multichannel
0.47 ± 0.02	GOPAL	80 DPWA	$\bar{K}N \rightarrow \bar{K}N$
0.45 ± 0.03	ALSTON...	78 DPWA	$\bar{K}N \rightarrow \bar{K}N$
0.448 ± 0.014	CORDEN	75 DBC	$K^-d$ 1.4-1.8 GeV/c
••• We do not use the following data for averages, fits, limits, etc. •••			
0.43	<sup>1</sup> KAMANO	15 DPWA	$\bar{K}N$ multichannel
0.47 ± 0.01	GOPAL	77 DPWA	See GOPAL 80
0.42	MAST	76 HBC	$K^-p \rightarrow \bar{K}^0n$

<sup>1</sup> From the preferred solution A in KAMANO 15.

$\Gamma(\Sigma\pi)/\Gamma_{\text{total}}$

VALUE	DOCUMENT ID	TECN	COMMENT
<b>0.42 to 0.46 OUR ESTIMATE</b>			
0.43 ± 0.01	SARANTSEV	19 DPWA	$\bar{K}N$ multichannel
0.47 ± 0.05	ZHANG	13A DPWA	$\bar{K}N$ multichannel
0.426 ± 0.014	CORDEN	75 DBC	$K^-d$ 1.4-1.8 GeV/c
0.418 ± 0.017	BARBARO...	69B HBC	$K^-p$ 0.28-0.45 GeV/c
••• We do not use the following data for averages, fits, limits, etc. •••			
0.446	<sup>1</sup> KAMANO	15 DPWA	$\bar{K}N$ multichannel
0.46	KIM	71 DPWA	K-matrix analysis

<sup>1</sup> From the preferred solution A in KAMANO 15.

$\Gamma(\Sigma\pi)/\Gamma(N\bar{K})$

VALUE	DOCUMENT ID	TECN	COMMENT
<b>0.9 to 1.0 OUR ESTIMATE</b>			
0.98 ± 0.03	<sup>1</sup> GOPAL	77 DPWA	$\bar{K}N$ multichannel
0.82 ± 0.08	BURKHARDT	69 HBC	$K^-p$ 0.8-1.2 GeV/c
1.06 ± 0.14	SCHEUER	68 DBC	$K^-N$ 3 GeV/c
0.96 ± 0.20	DAHL	67 HBC	$\pi^-p$ 1.6-4 GeV/c
0.73 ± 0.11	DAUBER	67 HBC	$K^-p$ 2 GeV/c
••• We do not use the following data for averages, fits, limits, etc. •••			
1.06 ± 0.12	BERTHON	74 HBC	Quasi-2-body $\sigma$
1.72 ± 0.78	MUSGRAVE	65 HBC	

<sup>1</sup> The  $\bar{K}N \rightarrow \Sigma\pi$  amplitude at resonance is +0.46 ± 0.01.

$\Gamma(\Lambda\pi\pi)/\Gamma_{\text{total}}$

VALUE	DOCUMENT ID	TECN	COMMENT
<b>0.09 to 0.11 OUR ESTIMATE</b>			
0.091 ± 0.006	CORDEN	75 DBC	$K^-d$ 1.4-1.8 GeV/c
0.11 ± 0.01	<sup>1</sup> MAST	73B IPWA	$K^-p \rightarrow \Lambda\pi\pi$

<sup>1</sup> Assumes  $\Gamma(N\bar{K})/\Gamma_{\text{total}} = 0.46 \pm 0.02$ .

$\Gamma(\Lambda\pi\pi)/\Gamma(N\bar{K})$

VALUE	DOCUMENT ID	TECN	COMMENT
<b>0.18 to 0.22 OUR ESTIMATE</b>			
0.22 ± 0.03	BURKHARDT	69 HBC	$K^-p$ 0.8-1.2 GeV/c
0.19 ± 0.04	SCHEUER	68 DBC	$K^-N$ 3 GeV/c
0.17 ± 0.05	DAHL	67 HBC	$\pi^-p$ 1.6-4 GeV/c
0.21 ± 0.18	DAUBER	67 HBC	$K^-p$ 2 GeV/c
••• We do not use the following data for averages, fits, limits, etc. •••			
0.27 ± 0.13	BERTHON	74 HBC	Quasi-2-body $\sigma$
0.2	KIM	71 DPWA	K-matrix analysis

$\Gamma(\Sigma\pi)/\Gamma(\Lambda\pi\pi)$

VALUE	DOCUMENT ID	TECN	COMMENT
<b>3.4 to 4.4 OUR ESTIMATE</b>			
3.9 ± 1.0	UHLIG	67 HBC	$K^-p$ 0.9-1.0 GeV/c
3.3 ± 1.1	BIRMINGHAM	66 HBC	$K^-p$ 3.5 GeV/c
4.5 ± 1.0	ARMENTEROS65c	HBC	

$\Gamma(\Sigma(1385)\pi, S\text{-wave})/\Gamma_{\text{total}}$

VALUE	DOCUMENT ID	TECN	COMMENT
••• We do not use the following data for averages, fits, limits, etc. •••			
0.121	<sup>1</sup> KAMANO	15 DPWA	$\bar{K}N$ multichannel

<sup>1</sup> From the preferred solution A in KAMANO 15.

$\Gamma(\Sigma(1385)\pi, D\text{-wave})/\Gamma_{\text{total}}$

VALUE	DOCUMENT ID	TECN	COMMENT
••• We do not use the following data for averages, fits, limits, etc. •••			
0.003	<sup>1</sup> KAMANO	15 DPWA	Multichannel

<sup>1</sup> From the preferred solution A in KAMANO 15.

$\Gamma(\Sigma(1385)\pi)/\Gamma_{\text{total}}$

VALUE	DOCUMENT ID	TECN	COMMENT
<b>0.041 ± 0.005</b>	CHAN	72 HBC	$K^-p \rightarrow \Lambda\pi\pi$

$\Gamma(\Sigma(1385)\pi(\rightarrow\Lambda\pi\pi))/\Gamma(\Lambda\pi\pi)$

The  $\Lambda\pi\pi$  mode is largely due to  $\Sigma(1385)\pi$ . Only the values of  $(\Sigma(1385)\pi)/(\Lambda\pi\pi)$  given by MAST 73B and CORDEN 75 are based on real 3-body partial-wave analyses. The discrepancy between the two results is essentially due to the different hypotheses made concerning the shape of the  $(\pi\pi)_{S\text{-wave}}$  state.

VALUE	CL%	DOCUMENT ID	TECN	COMMENT
0.58 ± 0.22		CORDEN	75 DBC	$K^-d$ 1.4-1.8 GeV/c
0.82 ± 0.10		<sup>1</sup> MAST	73B IPWA	$K^-p \rightarrow \Lambda\pi\pi$
••• We do not use the following data for averages, fits, limits, etc. •••				
<0.44	90	WIELAND	11 SPHR	$\gamma p \rightarrow K^+\Lambda(1520)$
0.39 ± 0.10		<sup>2</sup> BURKHARDT	71 HBC	$K^-p \rightarrow (\Lambda\pi\pi)\pi$

<sup>1</sup> Both  $\Sigma(1385)\pi DS_{03}$  and  $\Sigma(\pi\pi) DP_{03}$  contribute.  
<sup>2</sup> The central bin (1514-1524 MeV) gives  $0.74 \pm 0.10$ ; other bins are lower by 2-to-5 standard deviations.

$\Gamma(\Lambda(\pi\pi)_{S\text{-wave}})/\Gamma(\Lambda\pi\pi)$

VALUE	DOCUMENT ID	TECN	COMMENT
<b>0.20 ± 0.08</b>	CORDEN	75 DBC	$K^-d$ 1.4-1.8 GeV/c

$\Gamma(\Sigma\pi\pi)/\Gamma_{\text{total}}$

VALUE	DOCUMENT ID	TECN	COMMENT
<b>0.007 to 0.011 OUR ESTIMATE</b>			
0.007 ± 0.002	<sup>1</sup> CORDEN	75 DBC	$K^-d$ 1.4-1.8 GeV/c
0.0085 ± 0.0006	<sup>2</sup> MAST	73 MPWA	$K^-p \rightarrow \Sigma\pi\pi$
0.010 ± 0.0015	BARBARO...	69B HBC	$K^-p$ 0.28-0.45 GeV/c

<sup>1</sup> Much of the  $\Sigma\pi\pi$  decay proceeds via  $\Sigma(1385)\pi$ .  
<sup>2</sup> Assumes  $\Gamma(N\bar{K})/\Gamma_{\text{total}} = 0.46$ .

$\Gamma(\Lambda\gamma)/\Gamma_{\text{total}}$

VALUE (units $10^{-3}$ )	EVTS	DOCUMENT ID	TECN	COMMENT
<b>7 to 11 OUR ESTIMATE</b>				
10.7 ± 2.9 <sup>+1.5</sup> <sub>-0.4</sub>	32	TAYLOR	05 CLAS	$\gamma p \rightarrow K^+\Lambda\gamma$
10.2 ± 2.1 ± 1.5	290	ANTIP OV	04A SPNX	$pN(C) \rightarrow \Lambda(1520)K^+N(C)$
8.0 ± 1.4	238	MAST	68B HBC	Using $\Gamma(N\bar{K})/\Gamma_{\text{total}} = 0.45$

$\Gamma(\Sigma^0\gamma)/\Gamma_{\text{total}}$

VALUE	DOCUMENT ID	TECN	COMMENT
<b>0.02 ± 0.0035</b>	<sup>1</sup> MAST	68B HBC	Not measured; see note

<sup>1</sup> Calculated from  $\Gamma(\Lambda\gamma)/\Gamma_{\text{total}}$ , assuming SU(3). Needed to constrain the sum of all the branching ratios to be unity.

$\Lambda(1520)$  REFERENCES

SARANTSEV 19 EPJ A55 180	A.V. Sarantsev et al.	(BONN, PNPI)
KAMANO 15 PR C92 025205	H. Kamano et al.	(ANL, OSAK)
ZHANG 13A PR C88 035205	H. Zhang et al.	(KSU)
WIELAND 11 EPJ A47 47	F. Wieland et al.	(ELSA SAPHIR Collab.)
QIANG 10 PL B694 123	Y. Qiang et al.	(DUKE, JEFF, PNPI, GWU+)
TAYLOR 05 PR C71 054609	S. Taylor et al.	(JLab CLAS Collab.)
Also PR C72 039902 (errat.)	S. Taylor et al.	(JLab CLAS Collab.)
ANTIP OV 04A PL B604 22	Yu.M. Antipov et al.	(IHEP SPHINX Collab.)
PDG 82 PL 111B 1	M. Roos et al.	(HELS, CIT, CERN)
BARBER 80D ZPHY C7 17	D.P. Barber et al.	(DARE, LANC, SHEF)
GOPAL 80 Toronto Conf. 159	G.P. Gopal	(RHEL) IUP
BARLAG 79 NP B149 220	S.J.M. Barlag et al.	(AMST, CERN, NIJ+)
ALSTON... 78 PR D18 182	M. Alston-Garnjost et al.	(LBL, MTHO+IUP)
Also PRL 38 1007	M. Alston-Garnjost et al.	(LBL, MTHO+IUP)
CAMERON 77 NP B131 399	W. Cameron et al.	(RHEL, LOIC IUP)
GOPAL 77 NP B119 362	G.P. Gopal et al.	(RHEL) IUP
MAST 76 PR D14 13	T.S. Mast et al.	(LBL)
CORDEN 75 NP B84 306	M.J. Corden et al.	(BIRM)
BERTHON 74 NC 21A 146	A. Berthon et al.	(CDEF, RHEL, SACL+)
MAST 73 PR D7 3212	T.S. Mast et al.	(LBL) IUP
MAST 73B PR D7 5	T.S. Mast et al.	(LBL) IUP
CHAN 72 PRL 28 256	S.B. Chan et al.	(MASA, YALE)
BURKHARDT 71 NP B27 64	E. Burkhart et al.	(HEID, CERN, SACL)
KIM 71 PRL 27 356	J.K. Kim	(HARV) IUP
Also Duke Conf. 161	J.K. Kim	(HARV) IUP
Hyperon Resonances, 1970		
BARBARO... 69B Lund Conf. 352	A. Barbaro-Galtrieri et al.	(LRL)
Also Duke Conf. 95	R.D. Tripp	(LRL)
Hyperon Resonances 1970		
BURKHARDT 69 NP B14 106	E. Burkhart et al.	(HEID, EFI, CERN+)
MAST 68B PRL 21 1715	T.S. Mast et al.	(LRL)
SCHEUER 68 NP B8 503	J.C. Scheuer et al.	(SABRE Collab.)
DAHL 67 PR 163 1377	O.I. Dahl et al.	(LRL)
DAUBER 67 PL 24B 925	P.M. Dauber et al.	(UCLA)

## Baryon Particle Listings

 $\Lambda(1520), \Lambda(1600)$ 

UHLIG 67	PR 155 1448	R.P. Uhlig <i>et al.</i>	(UMD, NRL)
BIRMINGHAM 66	PR 152 1148	M. Haque <i>et al.</i>	(BIRM, GLAS, LOIC, OXF+)
ARMENTEROS 65C	PL 19 338	R. Armenteros <i>et al.</i>	(CERN, HEID, SAFL)
MUSGRAVE 65	NC 35 735	B. Musgrave <i>et al.</i>	(BIRM, CERN, EPOL+)
WATSON 63	PR 131 2248	M.B. Watson, M. Ferro-Luzzi, R.D. Tripp	(LRL) IJP
FERRO-LUZZI 62	PRL 8 28	M. Ferro-Luzzi, R.D. Tripp, M.B. Watson	(LRL) IJP

$$\Lambda(1600) \ 1/2^+$$

$$I(J^P) = 0(\frac{1}{2}^+) \text{ Status: } ****$$

 $\Lambda(1600)$  POLE POSITION

## REAL PART

VALUE (MeV) DOCUMENT ID TECN COMMENT

1540 to 1560 ( $\approx 1550$ ) OUR ESTIMATE

1546  $\pm$  6 OUR AVERAGE Error includes scale factor of 2.1.

1562 $\pm$ 8	SARANTSEV 19	DPWA	$\bar{K}N$ multichannel
1544 $\pm$ 3	<sup>1</sup> KAMANO 15	DPWA	Multichannel

••• We do not use the following data for averages, fits, limits, etc. •••

1572	ZHANG 13A	DPWA	Multichannel
------	-----------	------	--------------

<sup>1</sup> From the preferred solution A in KAMANO 15.

## -2xIMAGINARY PART

VALUE (MeV) DOCUMENT ID TECN COMMENT

120 to 240 ( $\approx 180$ ) OUR ESTIMATE

159  $\pm$  12 OUR AVERAGE Error includes scale factor of 6.2.

232 $\pm$ 15	SARANTSEV 19	DPWA	$\bar{K}N$ multichannel
112 $\pm$ 12	<sup>1</sup> KAMANO 15	DPWA	Multichannel

••• We do not use the following data for averages, fits, limits, etc. •••

138	ZHANG 13A	DPWA	Multichannel
-----	-----------	------	--------------

<sup>1</sup> From the preferred solution A in KAMANO 15.

 $\Lambda(1600)$  POLE RESIDUES

The normalized residue is the residue divided by  $\Gamma_{pole}/2$ .

Normalized residue in  $N\bar{K} \rightarrow \Lambda(1600) \rightarrow N\bar{K}$ 

MODULUS PHASE (°) DOCUMENT ID TECN COMMENT

0.36  $\pm$  0.07 -63  $\pm$  10 SARANTSEV 19 DPWA  $\bar{K}N$  multichannel

••• We do not use the following data for averages, fits, limits, etc. •••

0.105 -80 <sup>1</sup> KAMANO 15 DPWA Multichannel

<sup>1</sup> From the preferred solution A in KAMANO 15.

Normalized residue in  $N\bar{K} \rightarrow \Lambda(1600) \rightarrow \Sigma\pi$ 

MODULUS PHASE (°) DOCUMENT ID TECN COMMENT

0.39  $\pm$  0.08 148  $\pm$  10 SARANTSEV 19 DPWA  $\bar{K}N$  multichannel

••• We do not use the following data for averages, fits, limits, etc. •••

0.232 108 <sup>1</sup> KAMANO 15 DPWA Multichannel

<sup>1</sup> From the preferred solution A in KAMANO 15.

Normalized residue in  $N\bar{K} \rightarrow \Lambda(1600) \rightarrow \Lambda\eta$ 

MODULUS PHASE (°) DOCUMENT ID TECN COMMENT

0.22  $\pm$  0.13 180  $\pm$  20 SARANTSEV 19 DPWA  $\bar{K}N$  multichannel

Normalized residue in  $N\bar{K} \rightarrow \Lambda(1600) \rightarrow \Lambda\sigma$

MODULUS PHASE (°) DOCUMENT ID TECN COMMENT

0.30  $\pm$  0.06 -70  $\pm$  10 SARANTSEV 19 DPWA  $\bar{K}N$  multichannel

Normalized residue in  $N\bar{K} \rightarrow \Lambda(1600) \rightarrow \Sigma(1385)\pi$

MODULUS PHASE (°) DOCUMENT ID TECN COMMENT

0.37  $\pm$  0.07 103  $\pm$  12 SARANTSEV 19 DPWA  $\bar{K}N$  multichannel

••• We do not use the following data for averages, fits, limits, etc. •••

0.183 77 <sup>1</sup> KAMANO 15 DPWA Multichannel

<sup>1</sup> From the preferred solution A in KAMANO 15.

Normalized residue in  $N\bar{K} \rightarrow \Lambda(1600) \rightarrow N\bar{K}^*(892), S=1/2, P\text{-wave}$ 

MODULUS PHASE (°) DOCUMENT ID TECN COMMENT

0.02  $\pm$  0.01 126  $\pm$  45 SARANTSEV 19 DPWA  $\bar{K}N$  multichannel

Normalized residue in  $N\bar{K} \rightarrow \Lambda(1600) \rightarrow N\bar{K}^*(892), S=3/2, P\text{-wave}$

MODULUS PHASE (°) DOCUMENT ID TECN COMMENT

0.02  $\pm$  0.01 -135  $\pm$  45 SARANTSEV 19 DPWA  $\bar{K}N$  multichannel

 $\Lambda(1600)$  MASS

VALUE (MeV) DOCUMENT ID TECN COMMENT

1570 to 1630 ( $\approx 1600$ ) OUR ESTIMATE

1605 $\pm$ 8	SARANTSEV 19	DPWA	$\bar{K}N$ multichannel
1592 $\pm$ 10	ZHANG 13A	DPWA	Multichannel
1568 $\pm$ 20	GOPAL 80	DPWA	$\bar{K}N \rightarrow \bar{K}N$
1703 $\pm$ 100	ALSTON-... 78	DPWA	$\bar{K}N \rightarrow \bar{K}N$
1573 $\pm$ 25	GOPAL 77	DPWA	$\bar{K}N$ multichannel
1596 $\pm$ 6	KANE 74	DPWA	$K^-p \rightarrow \Sigma\pi$
1620 $\pm$ 10	LANGBEIN 72	IPWA	$\bar{K}N$ multichannel

••• We do not use the following data for averages, fits, limits, etc. •••

1572 or 1617	<sup>1</sup> MARTIN 77	DPWA	$\bar{K}N$ multichannel
1646 $\pm$ 7	<sup>2</sup> CARROLL 76	DPWA	Isospin-0 total $\sigma$
	KIM 71	DPWA	K-matrix analysis

<sup>1</sup> The two MARTIN 77 values are from a T-matrix pole and from a Breit-Wigner fit.

<sup>2</sup> A total cross-section bump with  $(J+1/2) \Gamma_{el} / \Gamma_{total} = 0.04$ .

 $\Lambda(1600)$  WIDTH

VALUE (MeV) DOCUMENT ID TECN COMMENT

150 to 250 ( $\approx 200$ ) OUR ESTIMATE

245 $\pm$ 15	SARANTSEV 19	DPWA	$\bar{K}N$ multichannel
150 $\pm$ 28	ZHANG 13A	DPWA	Multichannel
116 $\pm$ 20	GOPAL 80	DPWA	$\bar{K}N \rightarrow \bar{K}N$
593 $\pm$ 200	ALSTON-... 78	DPWA	$\bar{K}N \rightarrow \bar{K}N$
147 $\pm$ 50	GOPAL 77	DPWA	$\bar{K}N$ multichannel
175 $\pm$ 20	KANE 74	DPWA	$K^-p \rightarrow \Sigma\pi$
60 $\pm$ 10	LANGBEIN 72	IPWA	$\bar{K}N$ multichannel

••• We do not use the following data for averages, fits, limits, etc. •••

247 or 271	<sup>1</sup> MARTIN 77	DPWA	$\bar{K}N$ multichannel
20	<sup>2</sup> CARROLL 76	DPWA	Isospin-0 total $\sigma$
50	KIM 71	DPWA	K-matrix analysis

<sup>1</sup> The two MARTIN 77 values are from a T-matrix pole and from a Breit-Wigner fit.

<sup>2</sup> A total cross-section bump with  $(J+1/2) \Gamma_{el} / \Gamma_{total} = 0.04$ .

 $\Lambda(1600)$  DECAY MODES

Mode	Fraction ( $\Gamma_i/\Gamma$ )
$\Gamma_1$ $N\bar{K}$	15-30 %
$\Gamma_2$ $\Sigma\pi$	10-60 %
$\Gamma_3$ $\Lambda\sigma$	(19 $\pm$ 4) %
$\Gamma_4$ $\Sigma(1385)\pi$	(9 $\pm$ 4) %

 $\Lambda(1600)$  BRANCHING RATIOS

See "Sign conventions for resonance couplings" in the Note on  $\Lambda$  and  $\Sigma$  Resonances.

$\Gamma(N\bar{K})/\Gamma_{total}$   $\Gamma_1/\Gamma$

VALUE DOCUMENT ID TECN COMMENT

## 0.14 to 0.28 OUR ESTIMATE

0.29 $\pm$ 0.06	SARANTSEV 19	DPWA	$\bar{K}N$ multichannel
0.14 $\pm$ 0.04	ZHANG 13A	DPWA	Multichannel
0.23 $\pm$ 0.04	GOPAL 80	DPWA	$\bar{K}N \rightarrow \bar{K}N$
0.14 $\pm$ 0.05	ALSTON-... 78	DPWA	$\bar{K}N \rightarrow \bar{K}N$
0.25 $\pm$ 0.15	LANGBEIN 72	IPWA	$\bar{K}N$ multichannel

••• We do not use the following data for averages, fits, limits, etc. •••

0.064 <sup>1</sup> KAMANO 15 DPWA Multichannel

0.24  $\pm$  0.04 GOPAL 77 DPWA See GOPAL 80

0.30 or 0.29 <sup>2</sup> MARTIN 77 DPWA  $\bar{K}N$  multichannel

<sup>1</sup> From the preferred solution A in KAMANO 15.

<sup>2</sup> The two MARTIN 77 values are from a T-matrix pole and from a Breit-Wigner fit.

$\Gamma(\Sigma\pi)/\Gamma_{total}$   $\Gamma_2/\Gamma$

VALUE DOCUMENT ID TECN COMMENT

0.37  $\pm$  0.07 SARANTSEV 19 DPWA  $\bar{K}N$  multichannel

••• We do not use the following data for averages, fits, limits, etc. •••

0.851 <sup>1</sup> KAMANO 15 DPWA Multichannel

<sup>1</sup> From the preferred solution A in KAMANO 15.

$\Gamma(\Lambda\sigma)/\Gamma_{total}$   $\Gamma_3/\Gamma$

VALUE DOCUMENT ID TECN COMMENT

0.19  $\pm$  0.04 SARANTSEV 19 DPWA  $\bar{K}N$  multichannel

$\Gamma(\Sigma(1385)\pi)/\Gamma_{total}$   $\Gamma_4/\Gamma$

VALUE DOCUMENT ID TECN COMMENT

0.09  $\pm$  0.04 SARANTSEV 19 DPWA  $\bar{K}N$  multichannel

••• We do not use the following data for averages, fits, limits, etc. •••

0.085 <sup>1</sup> KAMANO 15 DPWA Multichannel

<sup>1</sup> From the preferred solution A in KAMANO 15.

$(\Gamma_i/\Gamma)^{1/2}/\Gamma_{total}$  in  $N\bar{K} \rightarrow \Lambda(1600) \rightarrow \Sigma\pi$   $(\Gamma_1\Gamma_2)^{1/2}/\Gamma$

VALUE DOCUMENT ID TECN COMMENT

-0.23  $\pm$  0.03 ZHANG 13A DPWA Multichannel

-0.16  $\pm$  0.04 GOPAL 77 DPWA  $\bar{K}N$  multichannel

-0.33  $\pm$  0.11 KANE 74 DPWA  $K^-p \rightarrow \Sigma\pi$

0.28  $\pm$  0.09 LANGBEIN 72 IPWA  $\bar{K}N$  multichannel

••• We do not use the following data for averages, fits, limits, etc. •••

-0.39 or -0.39 <sup>1</sup> MARTIN 77 DPWA  $\bar{K}N$  multichannel

not seen HEPP 76B DPWA  $K^-N \rightarrow \Sigma\pi$

<sup>1</sup> The two MARTIN 77 values are from a T-matrix pole and from a Breit-Wigner fit.

**$\Lambda(1600)$  REFERENCES**

SARANTSEV	19	EPJ A55 180	A.V. Sarantsev et al.	(BONN, PNPI)
KAMANO	15	PR C92 025205	H. Kamano et al.	(ANL, OSAK)
ZHANG	13A	PR C88 035205	H. Zhang et al.	(KSU)
GOPAL	80	Toronto Conf. 159	G.P. Gopal	(RHEL) IJP
ALSTON-...	78	PR D18 182	M. Alston-Garnjost et al.	(LBL, MTHO+) IJP
Also		PRL 38 1007	M. Alston-Garnjost et al.	(LBL, MTHO+) IJP
GOPAL	77	NP B119 362	G.P. Gopal et al.	(LOIC, RHEL) IJP
MARTIN	77	NP B127 349	B.R. Martin, M.K. Pldcock, R.G. Moorhouse	(LOUC+) IJP
Also		NP B126 266	B.R. Martin, M.K. Pldcock	(LOUC)
Also		NP B126 285	B.R. Martin, M.K. Pldcock	(LOUC) IJP
CARROLL	76	PRL 37 806	A.S. Carroll et al.	(BNL) I
HEPP	76B	PL 65B 487	V. Hepp et al.	(CERN, HEIDH, MPIM) IJP
KANE	74	LBL-2452	D.F. Kane	(LBL) IJP
LANGBEIN	72	NP B47 477	W. Langbein, F. Wagner	(MPIM) IJP
KIM	71	PRL 27 356	J.K. Kim	(HARV) IJP

**$\Lambda(1670) 1/2^-$**

$I(J^P) = 0(\frac{1}{2}^-)$  Status: \* \* \* \*

The measurements of the mass, width, and elasticity published before 1974 are now obsolete and have been omitted. They were last listed in our 1982 edition Physics Letters **111B** 1 (1982).

**$\Lambda(1670)$  POLE POSITIONS**

REAL PART				
VALUE (MeV)	DOCUMENT ID	TECN	COMMENT	
<b>1670 to 1678 (<math>\approx 1674</math>) OUR ESTIMATE</b>				
1676 $\pm 2$	SARANTSEV 19	DPWA	$\bar{K}N$ multichannel	
1669 $+3$ $-8$	<sup>1</sup> KAMANO 15	DPWA	$\bar{K}N$ multichannel	
1677.5 $\pm 0.8$	GARCIA-REC...03	DPWA	$\bar{K}N$ multichannel	
• • •	We do not use the following data for averages, fits, limits, etc. • • •			
1667	ZHANG 13A	DPWA	$\bar{K}N$ multichannel	
	<sup>1</sup> From the preferred solution A in KAMANO 15.			
<b>-2xIMAGINARY PART</b>				
VALUE (MeV)	DOCUMENT ID	TECN	COMMENT	
<b>28 to 36 (<math>\approx 32</math>) OUR ESTIMATE</b>				
33 $\pm 4$	SARANTSEV 19	DPWA	$\bar{K}N$ multichannel	
19 $+18$ $-2$	<sup>1</sup> KAMANO 15	DPWA	$\bar{K}N$ multichannel	
29.2 $\pm 1.4$	GARCIA-REC...03	DPWA	$\bar{K}N$ multichannel	
• • •	We do not use the following data for averages, fits, limits, etc. • • •			
26	ZHANG 13A	DPWA	$\bar{K}N$ multichannel	
	<sup>1</sup> From the preferred solution A in KAMANO 15.			

**$\Lambda(1670)$  POLE RESIDUES**

The normalized residue is the residue divided by  $\Gamma_{pole}/2$ .

Normalized residue in $\bar{K}N \rightarrow \Lambda(1670) \rightarrow \bar{K}N$				
MODULUS	PHASE ( $^\circ$ )	DOCUMENT ID	TECN	COMMENT
<b>0.30 <math>\pm 0.06</math></b>	<b>-145 <math>\pm 11</math></b>	SARANTSEV 19	DPWA	$\bar{K}N$ multichannel
• • •	We do not use the following data for averages, fits, limits, etc. • • •			
0.351	164	<sup>1</sup> KAMANO 15	DPWA	$\bar{K}N$ multichannel
	<sup>1</sup> From the preferred solution A in KAMANO 15.			
Normalized residue in $N\bar{K} \rightarrow \Lambda(1670) \rightarrow \Sigma\pi$				
MODULUS	PHASE ( $^\circ$ )	DOCUMENT ID	TECN	COMMENT
<b>0.19 <math>\pm 0.06</math></b>	<b>145 <math>\pm 14</math></b>	SARANTSEV 19	DPWA	$\bar{K}N$ multichannel
• • •	We do not use the following data for averages, fits, limits, etc. • • •			
0.327	125	<sup>1</sup> KAMANO 15	DPWA	$\bar{K}N$ multichannel
	<sup>1</sup> From the preferred solution A in KAMANO 15.			
Normalized residue in $N\bar{K} \rightarrow \Lambda(1670) \rightarrow \Lambda\eta$				
MODULUS	PHASE ( $^\circ$ )	DOCUMENT ID	TECN	COMMENT
<b>0.26 <math>\pm 0.09</math></b>	<b>104 <math>\pm 14</math></b>	SARANTSEV 19	DPWA	$\bar{K}N$ multichannel
• • •	We do not use the following data for averages, fits, limits, etc. • • •			
0.474	59	<sup>1</sup> KAMANO 15	DPWA	Multichannel
	<sup>1</sup> From the preferred solution A in KAMANO 15.			
Normalized residue in $N\bar{K} \rightarrow \Lambda(1670) \rightarrow \Xi K$				
MODULUS	PHASE ( $^\circ$ )	DOCUMENT ID	TECN	COMMENT
<b>0.02 <math>\pm 0.02</math></b>	<b>100 <math>\pm 25</math></b>	SARANTSEV 19	DPWA	$\bar{K}N$ multichannel
Normalized residue in $N\bar{K} \rightarrow \Lambda(1670) \rightarrow \Lambda\omega, S=1/2, S\text{-wave}$				
MODULUS	PHASE ( $^\circ$ )	DOCUMENT ID	TECN	COMMENT
<b>0.09 <math>\pm 0.04</math></b>	<b>-60 <math>\pm 35</math></b>	SARANTSEV 19	DPWA	$\bar{K}N$ multichannel
Normalized residue in $N\bar{K} \rightarrow \Lambda(1670) \rightarrow \Lambda\omega, S=3/2, D\text{-wave}$				
MODULUS	PHASE ( $^\circ$ )	DOCUMENT ID	TECN	COMMENT
<b>0.05 <math>\pm 0.04</math></b>		SARANTSEV 19	DPWA	$\bar{K}N$ multichannel

Normalized residue in $N\bar{K} \rightarrow \Lambda(1670) \rightarrow N\bar{K}^*(892), S=1/2, S\text{-wave}$				
MODULUS	PHASE ( $^\circ$ )	DOCUMENT ID	TECN	COMMENT
<b>0.31 <math>\pm 0.14</math></b>	<b>100 <math>\pm 45</math></b>	SARANTSEV 19	DPWA	$\bar{K}N$ multichannel
Normalized residue in $N\bar{K} \rightarrow \Lambda(1670) \rightarrow N\bar{K}^*(892), S=3/2, D\text{-wave}$				
MODULUS	PHASE ( $^\circ$ )	DOCUMENT ID	TECN	COMMENT
<b>0.06 <math>\pm 0.03</math></b>	<b>-85 <math>\pm 40</math></b>	SARANTSEV 19	DPWA	$\bar{K}N$ multichannel
Normalized residue in $N\bar{K} \rightarrow \Lambda(1670) \rightarrow \Lambda\sigma$				
MODULUS	PHASE ( $^\circ$ )	DOCUMENT ID	TECN	COMMENT
<b>0.25 <math>\pm 0.08</math></b>	<b>160 <math>\pm 15</math></b>	SARANTSEV 19	DPWA	$\bar{K}N$ multichannel
Normalized residue in $N\bar{K} \rightarrow \Lambda(1670) \rightarrow \Sigma(1385)\pi$				
MODULUS	PHASE ( $^\circ$ )	DOCUMENT ID	TECN	COMMENT
<b>0.13 <math>\pm 0.06</math></b>	<b>110 <math>\pm 12</math></b>	SARANTSEV 19	DPWA	$\bar{K}N$ multichannel
• • •	We do not use the following data for averages, fits, limits, etc. • • •			
0.0988	-104	<sup>1</sup> KAMANO 15	DPWA	Multichannel
	<sup>1</sup> From the preferred solution A in KAMANO 15.			

**$\Lambda(1670)$  MASS**

VALUE (MeV)	DOCUMENT ID	TECN	COMMENT
<b>1670 to 1678 (<math>\approx 1674</math>) OUR ESTIMATE</b>			
1677 $\pm 2$	SARANTSEV 19	DPWA	$\bar{K}N$ multichannel
1672 $\pm 3$	ZHANG 13A	DPWA	Multichannel
1670.8 $\pm 1.7$	KOISO 85	DPWA	$K^-p \rightarrow \Sigma\pi$
1667 $\pm 5$	GOPAL 80	DPWA	$\bar{K}N \rightarrow \bar{K}N$
1671 $\pm 3$	ALSTON-... 78	DPWA	$\bar{K}N \rightarrow \bar{K}N$
1675 $\pm 2$	HEPP 76B	DPWA	$K^-N \rightarrow \Sigma\pi$
1679 $\pm 1$	KANE 74	DPWA	$K^-p \rightarrow \Sigma\pi$
1665 $\pm 5$	PREVOST 74	DPWA	$K^-N \rightarrow \Sigma(1385)\pi$
• • •	We do not use the following data for averages, fits, limits, etc. • • •		
1673 $\pm 2$	MANLEY 02	DPWA	$\bar{K}N$ multichannel
1668.9 $\pm 2.0$	ABAEV 96	DPWA	$K^-p \rightarrow \Lambda\eta$
1670 $\pm 5$	GOPAL 77	DPWA	$\bar{K}N$ multichannel
1664	<sup>1</sup> MARTIN 77	DPWA	$\bar{K}N$ multichannel
	<sup>1</sup> MARTIN 77 obtains identical resonance parameters from a T-matrix pole and from a Breit-Wigner fit.		

**$\Lambda(1670)$  WIDTH**

VALUE (MeV)	DOCUMENT ID	TECN	COMMENT
<b>25 to 35 (<math>\approx 30</math>) OUR ESTIMATE</b>			
33 $\pm 4$	SARANTSEV 19	DPWA	$\bar{K}N$ multichannel
29 $\pm 5$	ZHANG 13A	DPWA	$\bar{K}N$ multichannel
34.1 $\pm 3.7$	KOISO 85	DPWA	$K^-p \rightarrow \Sigma\pi$
29 $\pm 5$	GOPAL 80	DPWA	$\bar{K}N \rightarrow \bar{K}N$
29 $\pm 5$	ALSTON-... 78	DPWA	$\bar{K}N \rightarrow \bar{K}N$
46 $\pm 5$	HEPP 76B	DPWA	$K^-N \rightarrow \Sigma\pi$
40 $\pm 3$	KANE 74	DPWA	$K^-p \rightarrow \Sigma\pi$
19 $\pm 5$	PREVOST 74	DPWA	$K^-N \rightarrow \Sigma(1385)\pi$
• • •	We do not use the following data for averages, fits, limits, etc. • • •		
23 $\pm 6$	MANLEY 02	DPWA	$\bar{K}N$ multichannel
21.1 $\pm 3.6$	ABAEV 96	DPWA	$K^-p \rightarrow \Lambda\eta$
45 $\pm 10$	GOPAL 77	DPWA	$\bar{K}N$ multichannel
12	<sup>1</sup> MARTIN 77	DPWA	$\bar{K}N$ multichannel
	<sup>1</sup> MARTIN 77 obtains identical resonance parameters from a T-matrix pole and from a Breit-Wigner fit.		

**$\Lambda(1670)$  DECAY MODES**

Mode	Fraction ( $\Gamma_i/\Gamma$ )
$\Gamma_1 N\bar{K}$	20-30 %
$\Gamma_2 \Sigma\pi$	25-55 %
$\Gamma_3 \Lambda\eta$	10-25 %
$\Gamma_4 \Sigma(1385)\pi, D\text{-wave}$	( 6.0 $\pm 2.0$ ) %
$\Gamma_5 N\bar{K}^*(892), S=1/2, S\text{-wave}$	
$\Gamma_6 N\bar{K}^*(892), S=3/2, D\text{-wave}$	( 5 $\pm 4$ ) %
$\Gamma_7 \Lambda\sigma$	( 20 $\pm 8$ ) %

**$\Lambda(1670)$  BRANCHING RATIOS**

See "Sign conventions for resonance couplings" in the Note on  $\Lambda$  and  $\Sigma$  Resonances.

$\Gamma(N\bar{K})/\Gamma_{total}$	DOCUMENT ID	TECN	COMMENT	$\Gamma_1/\Gamma$
<b>0.20 to 0.30 OUR ESTIMATE</b>				
0.33 $\pm 0.07$	SARANTSEV 19	DPWA	$\bar{K}N$ multichannel	
0.26 $\pm 0.25$	ZHANG 13A	DPWA	$\bar{K}N$ multichannel	
0.18 $\pm 0.03$	GOPAL 80	DPWA	$\bar{K}N \rightarrow \bar{K}N$	
0.17 $\pm 0.03$	ALSTON-... 78	DPWA	$\bar{K}N \rightarrow \bar{K}N$	



See key on page 999

Baryon Particle Listings  
 $\Lambda(1690)$

Normalized residue in  $N\bar{K} \rightarrow \Lambda(1690) \rightarrow \Sigma(1385)\pi$ , D-wave

MODULUS	PHASE (°)	DOCUMENT ID	TECN	COMMENT
<b>0.06 ± 0.04</b>	<b>164 ± 15</b>	SARANTSEV 19	DPWA	$\bar{K}N$ multichannel
0.319	-22	<sup>1</sup> KAMANO 15	DPWA	$\bar{K}N$ multichannel

••• We do not use the following data for averages, fits, limits, etc. •••

<sup>1</sup>From the preferred solution A in KAMANO 15.

Normalized residue in  $N\bar{K} \rightarrow \Lambda(1690) \rightarrow N\bar{K}^*(892)$ , S-wave

VALUE	DOCUMENT ID	TECN	COMMENT
<b>0.05 ± 0.04</b>	SARANTSEV 19	DPWA	$\bar{K}N$ multichannel

Normalized residue in  $N\bar{K} \rightarrow \Lambda(1690) \rightarrow N\bar{K}^*(892)$ , D-wave

VALUE	DOCUMENT ID	TECN	COMMENT
<b>0.18 ± 0.05 @ -110 ± 45</b>	SARANTSEV 19	DPWA	$\bar{K}N$ multichannel

$\Lambda(1690)$  MASS

VALUE (MeV)	DOCUMENT ID	TECN	COMMENT
<b>1685 to 1695 (≈ 1690) OUR ESTIMATE</b>			
1689 ± 3	SARANTSEV 19	DPWA	$\bar{K}N$ multichannel
1691 ± 3	ZHANG 13A	DPWA	$\bar{K}N$ multichannel
1695.7 ± 2.6	KOISO 85	DPWA	$K^-p \rightarrow \Sigma\pi$
1690 ± 5	GOPAL 80	DPWA	$\bar{K}N \rightarrow \bar{K}N$
1692 ± 5	ALSTON-... 78	DPWA	$\bar{K}N \rightarrow \bar{K}N$
1690 ± 3	HEPP 76B	DPWA	$K^-N \rightarrow \Sigma\pi$
1689 ± 1	KANE 74	DPWA	$K^-p \rightarrow \Sigma\pi$
••• We do not use the following data for averages, fits, limits, etc. •••			
1690 ± 5	GOPAL 77	DPWA	$\bar{K}N$ multichannel
1687 or 1689	<sup>1</sup> MARTIN 77	DPWA	$\bar{K}N$ multichannel
1692 ± 4	CARROLL 76	DPWA	Isospin-0 total $\sigma$

<sup>1</sup>The two MARTIN 77 values are from a T-matrix pole and from a Breit-Wigner fit. Another  $D_{03}$   $\Lambda$  at 1966 MeV is also suggested by MARTIN 77, but is very uncertain.

$\Lambda(1690)$  WIDTH

VALUE (MeV)	DOCUMENT ID	TECN	COMMENT
<b>60 to 80 (≈ 70) OUR ESTIMATE</b>			
75 ± 5	SARANTSEV 19	DPWA	$\bar{K}N$ multichannel
54 ± 5	ZHANG 13A	DPWA	$\bar{K}N$ multichannel
67.2 ± 5.6	KOISO 85	DPWA	$K^-p \rightarrow \Sigma\pi$
61 ± 5	GOPAL 80	DPWA	$\bar{K}N \rightarrow \bar{K}N$
64 ± 10	ALSTON-... 78	DPWA	$\bar{K}N \rightarrow \bar{K}N$
82 ± 8	HEPP 76B	DPWA	$K^-N \rightarrow \Sigma\pi$
60 ± 4	KANE 74	DPWA	$K^-p \rightarrow \Sigma\pi$
••• We do not use the following data for averages, fits, limits, etc. •••			
60 ± 5	GOPAL 77	DPWA	$\bar{K}N$ multichannel
62 or 62	<sup>1</sup> MARTIN 77	DPWA	$\bar{K}N$ multichannel
38	CARROLL 76	DPWA	Isospin-0 total $\sigma$

<sup>1</sup>The two MARTIN 77 values are from a T-matrix pole and from a Breit-Wigner fit. Another  $D_{03}$   $\Lambda$  at 1966 MeV is also suggested by MARTIN 77, but is very uncertain.

$\Lambda(1690)$  DECAY MODES

Mode	Fraction ( $\Gamma_i/\Gamma$ )
$\Gamma_1$ $N\bar{K}$	20-30 %
$\Gamma_2$ $\Sigma\pi$	20-40 %
$\Gamma_3$ $\Lambda\sigma$	(5.0 ± 2.0) %
$\Gamma_4$ $\Lambda\pi\pi$	~ 25 %
$\Gamma_5$ $\Sigma\pi\pi$	~ 20 %
$\Gamma_6$ $\Lambda\eta$	
$\Gamma_7$ $\Sigma(1385)\pi$ , S-wave	(9 ± 5) %
$\Gamma_8$ $\Sigma(1385)\pi$ , D-wave	(3.0 ± 2.0) %
$\Gamma_9$ $N\bar{K}^*(892)$ , S=1/2, D-wave	
$\Gamma_{10}$ $N\bar{K}^*(892)$ , S=3/2, S-wave	
$\Gamma_{11}$ $N\bar{K}^*(892)$ , S=3/2, D-wave	

$\Lambda(1690)$  BRANCHING RATIOS

$\Gamma(N\bar{K})/\Gamma_{total}$	DOCUMENT ID	TECN	COMMENT
<b>0.20 to 0.28 OUR ESTIMATE</b>			
0.23 ± 0.05	SARANTSEV 19	DPWA	$\bar{K}N$ multichannel
0.25 ± 0.04	ZHANG 13A	DPWA	$\bar{K}N$ multichannel
0.23 ± 0.03	GOPAL 80	DPWA	$\bar{K}N \rightarrow \bar{K}N$
0.22 ± 0.03	ALSTON-... 78	DPWA	$\bar{K}N \rightarrow \bar{K}N$
••• We do not use the following data for averages, fits, limits, etc. •••			
0.239	<sup>1</sup> KAMANO 15	DPWA	$\bar{K}N$ multichannel
0.24 ± 0.03	GOPAL 77	DPWA	See GOPAL 80
0.28 or 0.26	<sup>2</sup> MARTIN 77	DPWA	$\bar{K}N$ multichannel

<sup>1</sup>From the preferred solution A in KAMANO 15.  
<sup>2</sup>The two MARTIN 77 values are from a T-matrix pole and from a Breit-Wigner fit. Another  $D_{03}$   $\Lambda$  at 1966 MeV is also suggested by MARTIN 77, but is very uncertain.

$\Gamma(\Sigma\pi)/\Gamma_{total}$

VALUE	DOCUMENT ID	TECN	COMMENT
<b>0.50 ± 0.10</b>	SARANTSEV 19	DPWA	$\bar{K}N$ multichannel
0.387	<sup>1</sup> KAMANO 15	DPWA	$\bar{K}N$ multichannel

••• We do not use the following data for averages, fits, limits, etc. •••

<sup>1</sup>From the preferred solution A in KAMANO 15.

$\Gamma(\Lambda\eta)/\Gamma_{total}$

VALUE	DOCUMENT ID	TECN	COMMENT
~ 0.01	SARANTSEV 19	DPWA	$\bar{K}N$ multichannel
not seen	<sup>1</sup> KAMANO 15	DPWA	Multichannel

••• We do not use the following data for averages, fits, limits, etc. •••

<sup>1</sup>From the preferred solution A in KAMANO 15.

$\Gamma(\Lambda\sigma)/\Gamma_{total}$

VALUE	DOCUMENT ID	TECN	COMMENT
<b>0.05 ± 0.02</b>	SARANTSEV 19	DPWA	$\bar{K}N$ multichannel

$\Gamma(\Sigma(1385)\pi, S\text{-wave})/\Gamma_{total}$

VALUE	DOCUMENT ID	TECN	COMMENT
<b>0.09 ± 0.05</b>	SARANTSEV 19	DPWA	$\bar{K}N$ multichannel
0.062	<sup>1</sup> KAMANO 15	DPWA	$\bar{K}N$ multichannel

••• We do not use the following data for averages, fits, limits, etc. •••

<sup>1</sup>From the preferred solution A in KAMANO 15.

$\Gamma(\Sigma(1385)\pi, D\text{-wave})/\Gamma_{total}$

VALUE	DOCUMENT ID	TECN	COMMENT
<b>0.03 ± 0.02</b>	SARANTSEV 19	DPWA	$\bar{K}N$ multichannel
0.308	<sup>1</sup> KAMANO 15	DPWA	$\bar{K}N$ multichannel

••• We do not use the following data for averages, fits, limits, etc. •••

<sup>1</sup>From the preferred solution A in KAMANO 15.

$\Gamma(N\bar{K}^*(892), S=1/2, D\text{-wave})/\Gamma_{total}$

VALUE	DOCUMENT ID	TECN	COMMENT
not seen	SARANTSEV 19	DPWA	$\bar{K}N$ multichannel
not seen	<sup>1</sup> KAMANO 15	DPWA	$\bar{K}N$ multichannel

••• We do not use the following data for averages, fits, limits, etc. •••

<sup>1</sup>From the preferred solution A in KAMANO 15.

$\Gamma(N\bar{K}^*(892), S=3/2, S\text{-wave})/\Gamma_{total}$

VALUE	DOCUMENT ID	TECN	COMMENT
0.003	KAMANO 15	DPWA	Multichannel

••• We do not use the following data for averages, fits, limits, etc. •••

$\Gamma(N\bar{K}^*(892), S=3/2, D\text{-wave})/\Gamma_{total}$

VALUE	DOCUMENT ID	TECN	COMMENT
not seen	<sup>1</sup> KAMANO 15	DPWA	Multichannel

••• We do not use the following data for averages, fits, limits, etc. •••

<sup>1</sup>From the preferred solution A in KAMANO 15.

$(\Gamma_1\Gamma_7)^{1/2}/\Gamma_{total}$  in  $N\bar{K} \rightarrow \Lambda(1690) \rightarrow \Sigma\pi$

VALUE	DOCUMENT ID	TECN	COMMENT
-0.27 ± 0.03	ZHANG 13A	DPWA	Multichannel
-0.34 ± 0.02	KOISO 85	DPWA	$K^-p \rightarrow \Sigma\pi$
-0.25 ± 0.03	GOPAL 77	DPWA	$\bar{K}N$ multichannel
-0.29 ± 0.03	HEPP 76B	DPWA	$K^-N \rightarrow \Sigma\pi$
-0.28 ± 0.03	LONDON 75	HLBC	$K^-p \rightarrow \Sigma^0\pi^0$
-0.28 ± 0.02	KANE 74	DPWA	$K^-p \rightarrow \Sigma\pi$
••• We do not use the following data for averages, fits, limits, etc. •••			
-0.30 or -0.28	<sup>1</sup> MARTIN 77	DPWA	$\bar{K}N$ multichannel

<sup>1</sup>The two MARTIN 77 values are from a T-matrix pole and from a Breit-Wigner fit. Another  $D_{03}$   $\Lambda$  at 1966 MeV is also suggested by MARTIN 77, but is very uncertain.

$(\Gamma_1\Gamma_4)^{1/2}/\Gamma_{total}$  in  $N\bar{K} \rightarrow \Lambda(1690) \rightarrow \Lambda\pi\pi$

VALUE	DOCUMENT ID	TECN	COMMENT
0.25 ± 0.02	<sup>1</sup> BARTLEY 68	HDBC	$K^-p \rightarrow \Lambda\pi\pi$

••• We do not use the following data for averages, fits, limits, etc. •••

<sup>1</sup>BARTLEY 68 uses only cross-section data. The enhancement is not seen by PRE-VOST 71.

$(\Gamma_1\Gamma_5)^{1/2}/\Gamma_{total}$  in  $N\bar{K} \rightarrow \Lambda(1690) \rightarrow \Sigma\pi\pi$

VALUE	DOCUMENT ID	TECN	COMMENT
0.21	ARMENTEROS68c	HDBC	$K^-N \rightarrow \Sigma\pi\pi$

$(\Gamma_1\Gamma_6)^{1/2}/\Gamma_{total}$  in  $N\bar{K} \rightarrow \Lambda(1690) \rightarrow \Lambda\eta$

VALUE	DOCUMENT ID	TECN	COMMENT
0.00 ± 0.03	BAXTER 73	DPWA	$K^-p \rightarrow$ neutrals

# Baryon Particle Listings

## $\Lambda(1690)$ , $\Lambda(1710)$ , $\Lambda(1800)$

$(\Gamma_1 \Gamma_2)^{1/2} / \Gamma_{\text{total}}$ in $N\bar{K} \rightarrow \Lambda(1690) \rightarrow \Sigma(1385)\pi$ , S-wave		$(\Gamma_1 \Gamma_2)^{1/2} / \Gamma$	
VALUE	DOCUMENT ID	TECN	COMMENT
$-0.28 \pm 0.06$	ZHANG	13A	DPWA Multichannel
$+0.27 \pm 0.04$	PREVOST	74	DPWA $K^- N \rightarrow \Sigma(1385)\pi$

### $\Lambda(1690)$ REFERENCES

SARANTSEV	19	EPJ A55 180	A.V. Sarantsev et al.	(BONN, PNPI)
KAMANO	15	PR C92 025205	H. Kamano et al.	(ANL, OSAK)
ZHANG	13A	PR C88 035205	H. Zhang et al.	(KSU)
KOISO	85	NP A433 619	H. Koiso et al.	(TOKY, MASA)
PDG	82	PL 111B 1	M. Roos et al.	(HELS, CIT, CERN)
GOPAL	80	Toronto Conf. 159	G.P. Gopal	(RHEL) IJP
ALSTON...	78	PR D18 182	M. Alston-Garnjost et al.	(LBL, MTHO+) IJP
		PRL 38 1007	M. Alston-Garnjost et al.	(LBL, MTHO+) IJP
GOPAL	77	NP B119 362	G.P. Gopal et al.	(LOIC, RHEL) IJP
MARTIN	77	NP B127 349	B.R. Martin, M.K. Pidcock, R.G. Moorhouse	(LOUC+) IJP
		NP B126 266	B.R. Martin, M.K. Pidcock	(LOUC) IJP
		NP B126 285	B.R. Martin, M.K. Pidcock	(LOUC) IJP
CARROLL	76	PRL 37 806	A.S. Carroll et al.	(BNL) I
HEPP	76B	PL 65B 487	V. Hepp et al.	(CERN, HEIDH, MPIM) IJP
LONDON	75	NP B85 289	G.W. London et al.	(BNL, CERN, EPOL+) IJP
KANE	74	LBL-2452	D.F. Kane	(LBL) IJP
PREVOST	74	NP B69 246	J. Prevost et al.	(SACL, CERN, HEID)
BAXTER	73	NP B67 125	D.F. Baxter et al.	(OXF) IJP
PREVOST	71	Amsterdam Conf.	J. Prevost	(CERN, HEID, SACL)
ARMENTEROS	65C	NP B8 216	R. Armenteros et al.	(CERN, HEID, SACL) I
BARTLEY	68	PRL 21 1111	J.H. Bartley et al.	(TUFTS, FSU, BRAN)

$\Lambda(1710) 1/2^+$	$I(J^P) = 0(\frac{1}{2}^+)$ Status: *
-----------------------	---------------------------------------

OMITTED FROM SUMMARY TABLE

### $\Lambda(1710)$ MASS

VALUE (MeV)	DOCUMENT ID	TECN	COMMENT
$1713 \pm 13$	ZHANG	13A	DPWA Multichannel

### $\Lambda(1710)$ WIDTH

VALUE (MeV)	DOCUMENT ID	TECN	COMMENT
$180 \pm 42$	ZHANG	13A	DPWA Multichannel

### $\Lambda(1710)$ DECAY MODES

Mode	Fraction ( $\Gamma_i / \Gamma$ )
$\Gamma_1$ $N\bar{K}$	(43±4) %
$\Gamma_2$ $\Sigma\pi$	(21±5) %
$\Gamma_3$ $\Sigma^*(1385)\pi$ , P-wave	(20±8) %
$\Gamma_4$ $N\bar{K}^*(892)$	
$\Gamma_5$ $N\bar{K}^*(892)$ , S=1/2	(5±4) %
$\Gamma_6$ $N\bar{K}^*(892)$ , S=3/2, P-wave	(10±8) %

### $\Lambda(1710)$ BRANCHING RATIOS

$\Gamma(N\bar{K}) / \Gamma_{\text{total}}$	$\Gamma_1 / \Gamma$		
VALUE	DOCUMENT ID	TECN	COMMENT
$0.43 \pm 0.04$	ZHANG	13A	DPWA Multichannel
$\Gamma(\Sigma\pi) / \Gamma_{\text{total}}$	$\Gamma_2 / \Gamma$		
VALUE	DOCUMENT ID	TECN	COMMENT
$0.21 \pm 0.05$	ZHANG	13A	DPWA Multichannel
$\Gamma(\Sigma^*(1385)\pi, P\text{-wave}) / \Gamma_{\text{total}}$	$\Gamma_3 / \Gamma$		
VALUE	DOCUMENT ID	TECN	COMMENT
$0.20 \pm 0.08$	ZHANG	13A	DPWA Multichannel
$\Gamma(N\bar{K}^*(892), S=1/2) / \Gamma_{\text{total}}$	$\Gamma_5 / \Gamma$		
VALUE	DOCUMENT ID	TECN	COMMENT
$0.05 \pm 0.04$	ZHANG	13A	DPWA Multichannel
$\Gamma(N\bar{K}^*(892), S=3/2, P\text{-wave}) / \Gamma_{\text{total}}$	$\Gamma_6 / \Gamma$		
VALUE	DOCUMENT ID	TECN	COMMENT
$0.10 \pm 0.08$	ZHANG	13A	DPWA Multichannel

### $\Lambda(1710)$ REFERENCES

ZHANG	13A	PR C88 035205	H. Zhang et al.	(KSU)
-------	-----	---------------	-----------------	-------

## $\Lambda(1800) 1/2^-$

$I(J^P) = 0(\frac{1}{2}^-)$  Status: \*\*\*

### $\Lambda(1800)$ POLE POSITION

#### REAL PART

VALUE (MeV)	DOCUMENT ID	TECN	COMMENT
$1809 \pm 9$	SARANTSEV	19	DPWA $\bar{K}N$ multichannel
1729	ZHANG	13A	DPWA Multichannel

#### -2xIMAGINARY PART

VALUE (MeV)	DOCUMENT ID	TECN	COMMENT
$205 \pm 16$	SARANTSEV	19	DPWA $\bar{K}N$ multichannel
198	ZHANG	13A	DPWA Multichannel

### $\Lambda(1800)$ POLE RESIDUES

The normalized residue is the residue divided by  $\Gamma_{\text{pole}}/2$ .

#### Normalized residue in $N\bar{K} \rightarrow \Lambda(1800) \rightarrow N\bar{K}$

MODULUS	PHASE (°)	DOCUMENT ID	TECN	COMMENT
$0.34 \pm 0.07$	$103 \pm 8$	SARANTSEV	19	DPWA $\bar{K}N$ multichannel

#### Normalized residue in $N\bar{K} \rightarrow \Lambda(1800) \rightarrow \Sigma\pi$

MODULUS	PHASE (°)	DOCUMENT ID	TECN	COMMENT
$0.30 \pm 0.06$	$-123 \pm 8$	SARANTSEV	19	DPWA $\bar{K}N$ multichannel

#### Normalized residue in $N\bar{K} \rightarrow \Lambda(1800) \rightarrow \Lambda\eta$

MODULUS	PHASE (°)	DOCUMENT ID	TECN	COMMENT
$0.06 \pm 0.03$	$75 \pm 10$	SARANTSEV	19	DPWA $\bar{K}N$ multichannel

#### Normalized residue in $N\bar{K} \rightarrow \Lambda(1800) \rightarrow \Lambda\sigma$

MODULUS	PHASE (°)	DOCUMENT ID	TECN	COMMENT
$0.24 \pm 0.05$	$25 \pm 10$	SARANTSEV	19	DPWA $\bar{K}N$ multichannel

#### Normalized residue in $N\bar{K} \rightarrow \Lambda(1800) \rightarrow \Lambda\omega, S=1/2, S\text{-wave}$

MODULUS	PHASE (°)	DOCUMENT ID	TECN	COMMENT
$0.12 \pm 0.04$	$-114 \pm 30$	SARANTSEV	19	DPWA $\bar{K}N$ multichannel

#### Normalized residue in $N\bar{K} \rightarrow \Lambda(1800) \rightarrow \Lambda\omega, S=3/2, D\text{-wave}$

MODULUS	PHASE (°)	DOCUMENT ID	TECN	COMMENT
$0.08 \pm 0.03$	$-90 \pm 17$	SARANTSEV	19	DPWA $\bar{K}N$ multichannel

#### Normalized residue in $N\bar{K} \rightarrow \Lambda(1800) \rightarrow \Sigma(1385)\pi$

MODULUS	PHASE (°)	DOCUMENT ID	TECN	COMMENT
$0.16 \pm 0.06$	$-140 \pm 35$	SARANTSEV	19	DPWA $\bar{K}N$ multichannel

#### Normalized residue in $N\bar{K} \rightarrow \Lambda(1800) \rightarrow N\bar{K}^*(892), S=1/2, S\text{-wave}$

MODULUS	PHASE (°)	DOCUMENT ID	TECN	COMMENT
$0.18 \pm 0.06$	$65 \pm 40$	SARANTSEV	19	DPWA $\bar{K}N$ multichannel

#### Normalized residue in $N\bar{K} \rightarrow \Lambda(1800) \rightarrow N\bar{K}^*(892), S=3/2, D\text{-wave}$

MODULUS	PHASE (°)	DOCUMENT ID	TECN	COMMENT
$0.09 \pm 0.07$		SARANTSEV	19	DPWA $\bar{K}N$ multichannel

### $\Lambda(1800)$ MASS

VALUE (MeV)	DOCUMENT ID	TECN	COMMENT
<b>1750 to 1850 (<math>\approx 1800</math>) OUR ESTIMATE</b>			
1811±10	SARANTSEV	19	DPWA $\bar{K}N$ multichannel
1783±19	ZHANG	13A	DPWA $\bar{K}N$ multichannel
1841±10	GOPAL	80	DPWA $\bar{K}N \rightarrow \bar{K}N$
1725±20	ALSTON...	78	DPWA $\bar{K}N \rightarrow \bar{K}N$
1830±20	LANGBEIN	72	IPWA $\bar{K}N$ multichannel
••• We do not use the following data for averages, fits, limits, etc. •••			
1845±10	MANLEY	02	DPWA $\bar{K}N$ multichannel
1825±20	GOPAL	77	DPWA $\bar{K}N$ multichannel
1767 or 1842	MARTIN	77	DPWA $\bar{K}N$ multichannel
1780	KIM	71	DPWA K-matrix analysis
1872±10	BRICMAN	70B	DPWA $\bar{K}N \rightarrow \bar{K}N$

### $\Lambda(1800)$ WIDTH

VALUE (MeV)	DOCUMENT ID	TECN	COMMENT
<b>150 to 250 (<math>\approx 200</math>) OUR ESTIMATE</b>			
209±18	SARANTSEV	19	DPWA $\bar{K}N$ multichannel
256±35	ZHANG	13A	DPWA $\bar{K}N$ multichannel
228±20	GOPAL	80	DPWA $\bar{K}N \rightarrow \bar{K}N$
185±20	ALSTON...	78	DPWA $\bar{K}N \rightarrow \bar{K}N$
70±15	LANGBEIN	72	IPWA $\bar{K}N$ multichannel

# Baryon Particle Listings

## $\Lambda(1800), \Lambda(1810)$

• • • We do not use the following data for averages, fits, limits, etc. • • •

518±84	MANLEY	02	DPWA	$\bar{K}N$ multichannel
230±20	GOPAL	77	DPWA	$\bar{K}N$ multichannel
435 or 473	<sup>1</sup> MARTIN	77	DPWA	$\bar{K}N$ multichannel
40	KIM	71	DPWA	K-matrix analysis
100±20	BRICMAN	70B	DPWA	$\bar{K}N \rightarrow \bar{K}N$

### $\Lambda(1800)$ DECAY MODES

Mode	Fraction ( $\Gamma_i/\Gamma$ )
$\Gamma_1$ $N\bar{K}$	25–40 %
$\Gamma_2$ $\Sigma\pi$	seen
$\Gamma_3$ $\Lambda\sigma$	(15 ± 4) %
$\Gamma_4$ $\Sigma(1385)\pi$	seen
$\Gamma_5$ $\Lambda\eta$	0.01 to 0.10
$\Gamma_6$ $N\bar{K}^*(892)$	seen
$\Gamma_7$ $N\bar{K}^*(892), S=1/2, S\text{-wave}$	
$\Gamma_8$ $N\bar{K}^*(892), S=3/2, D\text{-wave}$	

### $\Lambda(1800)$ BRANCHING RATIOS

See “Sign conventions for resonance couplings” in the Note on  $\Lambda$  and  $\Sigma$  Resonances.

$\Gamma(N\bar{K})/\Gamma_{\text{total}}$	DOCUMENT ID	TECN	COMMENT	$\Gamma_1/\Gamma$
<b>0.35 ± 0.07</b>	SARANTSEV	19	DPWA $\bar{K}N$ multichannel	
0.13 ± 0.06	ZHANG	13A	DPWA $\bar{K}N$ multichannel	
0.36 ± 0.04	GOPAL	80	DPWA $\bar{K}N \rightarrow \bar{K}N$	
0.28 ± 0.05	ALSTON-...	78	DPWA $\bar{K}N \rightarrow \bar{K}N$	
0.35 ± 0.15	LANGBEIN	72	IPWA $\bar{K}N$ multichannel	

• • • We do not use the following data for averages, fits, limits, etc. • • •

0.24 ± 0.10	MANLEY	02	DPWA $\bar{K}N$ multichannel	
0.37 ± 0.05	GOPAL	77	DPWA See GOPAL 80	
1.21 or 0.70	<sup>1</sup> MARTIN	77	DPWA $\bar{K}N$ multichannel	
0.80	KIM	71	DPWA K-matrix analysis	
0.18 ± 0.02	BRICMAN	70B	DPWA $\bar{K}N \rightarrow \bar{K}N$	

$\Gamma(\Sigma\pi)/\Gamma_{\text{total}}$	DOCUMENT ID	TECN	COMMENT	$\Gamma_2/\Gamma$
<b>0.27 ± 0.06</b>	SARANTSEV	19	DPWA $\bar{K}N$ multichannel	

$\Gamma(\Lambda\sigma)/\Gamma_{\text{total}}$	DOCUMENT ID	TECN	COMMENT	$\Gamma_3/\Gamma$
<b>0.15 ± 0.04</b>	SARANTSEV	19	DPWA $\bar{K}N$ multichannel	

$\Gamma(\Sigma(1385)\pi)/\Gamma_{\text{total}}$	DOCUMENT ID	TECN	COMMENT	$\Gamma_4/\Gamma$
<b>0.09 ± 0.04</b>	SARANTSEV	19	DPWA $\bar{K}N$ multichannel	

$\Gamma(\Lambda\eta)/\Gamma_{\text{total}}$	DOCUMENT ID	TECN	COMMENT	$\Gamma_5/\Gamma$
<b>0.01 to 0.10 OUR ESTIMATE</b>				
0.010 ± 0.005	SARANTSEV	19	DPWA $\bar{K}N$ multichannel	
0.06 ± 0.05	ZHANG	13A	DPWA Multichannel	

$(\Gamma_1\Gamma_2)^{1/2}/\Gamma_{\text{total}}$ in $N\bar{K} \rightarrow \Lambda(1800) \rightarrow \Sigma\pi$	DOCUMENT ID	TECN	COMMENT	$(\Gamma_1\Gamma_2)^{1/2}/\Gamma$
–0.07 ± 0.02	ZHANG	13A	DPWA Multichannel	
–0.08 ± 0.05	GOPAL	77	DPWA $\bar{K}N$ multichannel	
• • • We do not use the following data for averages, fits, limits, etc. • • •				
–0.74 or –0.43	<sup>1</sup> MARTIN	77	DPWA $\bar{K}N$ multichannel	
0.24	KIM	71	DPWA K-matrix analysis	

$(\Gamma_1\Gamma_4)^{1/2}/\Gamma_{\text{total}}$ in $N\bar{K} \rightarrow \Lambda(1800) \rightarrow \Sigma(1385)\pi$	DOCUMENT ID	TECN	COMMENT	$(\Gamma_1\Gamma_4)^{1/2}/\Gamma$
–0.09 ± 0.05	ZHANG	13A	DPWA Multichannel	
+0.056 ± 0.028	<sup>2</sup> CAMERON	78	DPWA $K^-p \rightarrow \Sigma(1385)\pi$	

$(\Gamma_1\Gamma_7)^{1/2}/\Gamma_{\text{total}}$ in $N\bar{K} \rightarrow \Lambda(1800) \rightarrow N\bar{K}^*(892), S=1/2, S\text{-wave}$	DOCUMENT ID	TECN	COMMENT	$(\Gamma_1\Gamma_7)^{1/2}/\Gamma$
–0.13 ± 0.02	ZHANG	13A	DPWA Multichannel	
–0.17 ± 0.03	<sup>2</sup> CAMERON	78B	DPWA $K^-p \rightarrow N\bar{K}^*$	

$(\Gamma_1\Gamma_8)^{1/2}/\Gamma_{\text{total}}$ in $N\bar{K} \rightarrow \Lambda(1800) \rightarrow N\bar{K}^*(892), S=3/2, D\text{-wave}$	DOCUMENT ID	TECN	COMMENT	$(\Gamma_1\Gamma_8)^{1/2}/\Gamma$
–0.13 ± 0.04	CAMERON	78B	DPWA $K^-p \rightarrow N\bar{K}^*$	

### $\Lambda(1800)$ FOOTNOTES

<sup>1</sup>The two MARTIN 77 values are from a T-matrix pole and from a Breit-Wigner fit.  
<sup>2</sup>The published sign has been changed to be in accord with the baryon-first convention.

### $\Lambda(1800)$ REFERENCES

SARANTSEV	19	EPL A55 180	A.V. Sarantsev <i>et al.</i>	(BONN, PNPI)
ZHANG	13A	PR C88 035205	H. Zhang <i>et al.</i>	(KSU)
MANLEY	02	PRL 88 012002	D.M. Manley <i>et al.</i>	(BNL Crystal Ball Collab.)
GOPAL	80	Toronto Conf. 159	G.P. Gopal	(RHEL) IJP
ALSTON-...	78	PR D18 182	M. Alston-Garnjost <i>et al.</i>	(LBL, MTHO+) IJP
Also		PRL 38 1007	M. Alston-Garnjost <i>et al.</i>	(LBL, MTHO+) IJP
CAMERON	78	NP B143 189	W. Cameron <i>et al.</i>	(RHEL, LOIC) IJP
CAMERON	78B	NP B146 327	W. Cameron <i>et al.</i>	(RHEL, LOIC) IJP
GOPAL	77	NP B119 362	G.P. Gopal <i>et al.</i>	(LOIC, RHEL) IJP
MARTIN	77	NP B127 349	B.R. Martin, M.K. Pidcock, R.G. Moorhouse	(LOUC+) IJP
Also		NP B126 266	B.R. Martin, M.K. Pidcock	(LOUC) IJP
Also		NP B126 285	B.R. Martin, M.K. Pidcock	(LOUC) IJP
LANGBEIN	72	NP B47 477	W. Langbein, F. Wagner	(MFM) IJP
KIM	71	PRL 27 356	J.K. Kim	(HARV) IJP
Also		Duke Conf. 161	J.K. Kim	(HARV) IJP
Hyperon Resonances, 1970				
BRICMAN	70B	PL 33B 511	C. Bricman, M. Ferro-Luzzi, J.P. Lagnaux	(CERN) IJP

$$\Lambda(1810) 1/2^+$$

$$I(J^P) = 0(1/2^+) \text{ Status: } ***$$

### $\Lambda(1810)$ POLE POSITION

#### REAL PART

VALUE (MeV)	DOCUMENT ID	TECN	COMMENT
<b>1773 ± 7</b>	SARANTSEV	19	DPWA $\bar{K}N$ multichannel
• • • We do not use the following data for averages, fits, limits, etc. • • •			
2097 $^{+40}_{-1}$	<sup>1</sup> KAMANO	15	DPWA Multichannel
1780	ZHANG	13A	DPWA Multichannel
	<sup>1</sup> From the preferred solution A in KAMANO 15. Solution B reports $M = 1841^{+3}_{-4}$ MeV.		

#### –2xIMAGINARY PART

VALUE (MeV)	DOCUMENT ID	TECN	COMMENT
<b>38 ± 14</b>	SARANTSEV	19	DPWA $\bar{K}N$ multichannel
• • • We do not use the following data for averages, fits, limits, etc. • • •			
166 $^{+64}_{-12}$	<sup>1</sup> KAMANO	15	DPWA Multichannel
64	ZHANG	13A	DPWA Multichannel
	<sup>1</sup> From the preferred solution A in KAMANO 15. Solution B Reports $\Gamma = 62^{+6}_{-4}$ MeV.		

### $\Lambda(1810)$ POLE RESIDUES

The normalized residue is the residue divided by  $\Gamma_{\text{pole}}/2$ .

#### Normalized residue in $N\bar{K} \rightarrow \Lambda(1810) \rightarrow N\bar{K}$

MODULUS	PHASE (°)	DOCUMENT ID	TECN	COMMENT
<b>0.018 ± 0.008</b>	<b>65 ± 26</b>	SARANTSEV	19	DPWA $\bar{K}N$ multichannel
• • • We do not use the following data for averages, fits, limits, etc. • • •				
0.205	–63	<sup>1</sup> KAMANO	15	DPWA Multichannel
	<sup>1</sup> From the preferred solution A in KAMANO 15.			

#### Normalized residue in $N\bar{K} \rightarrow \Lambda(1810) \rightarrow \Sigma\pi$

MODULUS	PHASE (°)	DOCUMENT ID	TECN	COMMENT
<b>0.045 ± 0.020</b>	<b>–143 ± 24</b>	SARANTSEV	19	DPWA $\bar{K}N$ multichannel
• • • We do not use the following data for averages, fits, limits, etc. • • •				
0.0325	29	<sup>1</sup> KAMANO	15	DPWA Multichannel
	<sup>1</sup> From the preferred solution A in KAMANO 15.			

#### Normalized residue in $N\bar{K} \rightarrow \Lambda(1810) \rightarrow \Lambda\eta$

MODULUS	PHASE (°)	DOCUMENT ID	TECN	COMMENT
• • • We do not use the following data for averages, fits, limits, etc. • • •				
0.155	165	<sup>1</sup> KAMANO	15	DPWA Multichannel
	<sup>1</sup> From the preferred solution A in KAMANO 15.			

#### Normalized residue in $N\bar{K} \rightarrow \Lambda(1810) \rightarrow \Lambda\sigma$

MODULUS	PHASE (°)	DOCUMENT ID	TECN	COMMENT
<b>0.055 ± 0.020</b>	<b>30 ± 16</b>	SARANTSEV	19	DPWA $\bar{K}N$ multichannel

#### Normalized residue in $N\bar{K} \rightarrow \Lambda(1810) \rightarrow \Xi K$

MODULUS	PHASE (°)	DOCUMENT ID	TECN	COMMENT
• • • We do not use the following data for averages, fits, limits, etc. • • •				
0.0937	–64	<sup>1</sup> KAMANO	15	DPWA Multichannel
	<sup>1</sup> From the preferred solution A in KAMANO 15.			

#### Normalized residue in $N\bar{K} \rightarrow \Lambda(1810) \rightarrow \Sigma(1385)\pi$

MODULUS	PHASE (°)	DOCUMENT ID	TECN	COMMENT
<b>0.08 ± 0.03</b>	<b>–50 ± 30</b>	SARANTSEV	19	DPWA $\bar{K}N$ multichannel
• • • We do not use the following data for averages, fits, limits, etc. • • •				
0.244	–10	<sup>1</sup> KAMANO	15	DPWA Multichannel
	<sup>1</sup> From the preferred solution A in KAMANO 15.			



## Baryon Particle Listings

 $\Lambda(1810)$ Normalized residue in  $N\bar{K} \rightarrow \Lambda(1810) \rightarrow N\bar{K}^*(892)$ ,  $S=1/2$ ,  $P$ -wave

MODULUS	PHASE (°)	DOCUMENT ID	TECN	COMMENT
<b>0.03 ± 0.03</b>		SARANTSEV 19	DPWA	$\bar{K}N$ multichannel
0.159	-97	<sup>1</sup> KAMANO 15	DPWA	Multichannel

••• We do not use the following data for averages, fits, limits, etc. •••

<sup>1</sup> From the preferred solution A in KAMANO 15.

Normalized residue in  $N\bar{K} \rightarrow \Lambda(1810) \rightarrow N\bar{K}^*(892)$ ,  $S=3/2$ ,  $P$ -wave

MODULUS	PHASE (°)	DOCUMENT ID	TECN	COMMENT
<b>0.05 ± 0.04</b>		SARANTSEV 19	DPWA	$\bar{K}N$ multichannel
0.0497	2	<sup>1</sup> KAMANO 15	DPWA	Multichannel

••• We do not use the following data for averages, fits, limits, etc. •••

<sup>1</sup> From the preferred solution A in KAMANO 15.

 $\Lambda(1810)$  MASS

VALUE (MeV)	DOCUMENT ID	TECN	COMMENT
<b>1740 to 1840 (≈ 1790) OUR ESTIMATE</b>			
1773 ± 7	SARANTSEV 19	DPWA	$\bar{K}N$ multichannel
1821 ± 10	ZHANG 13A	DPWA	Multichannel
1841 ± 20	GOPAL 80	DPWA	$\bar{K}N \rightarrow \bar{K}N$
1735 ± 5	CARROLL 76	DPWA	Isospin-0 total $\sigma$
1746 ± 10	PREVOST 74	DPWA	$K^-N \rightarrow \Sigma(1385)\pi$
1780 ± 20	LANGBEIN 72	IPWA	$\bar{K}N$ multichannel
••• We do not use the following data for averages, fits, limits, etc. •••			
1853 ± 20	GOPAL 77	DPWA	$\bar{K}N$ multichannel
1861 or 1953	<sup>1</sup> MARTIN 77	DPWA	$\bar{K}N$ multichannel
1755	KIM 71	DPWA	K-matrix analysis
1800	ARMENTEROS70	HBC	$\bar{K}N \rightarrow \bar{K}N$
1750	ARMENTEROS70	HBC	$\bar{K}N \rightarrow \Sigma\pi$
1690 ± 10	BARBARO... 70	HBC	$\bar{K}N \rightarrow \Sigma\pi$
1740	BAILEY 69	DPWA	$\bar{K}N \rightarrow \bar{K}N$
1745	ARMENTEROS68B	HBC	$\bar{K}N \rightarrow \bar{K}N$

<sup>1</sup> The two MARTIN 77 values are from a T-matrix pole and from a Breit-Wigner fit.

 $\Lambda(1810)$  WIDTH

VALUE (MeV)	DOCUMENT ID	TECN	COMMENT
<b>50 to 170 (≈ 110) OUR ESTIMATE</b>			
39 ± 15	SARANTSEV 19	DPWA	$\bar{K}N$ multichannel
174 ± 50	ZHANG 13A	DPWA	Multichannel
164 ± 20	GOPAL 80	DPWA	$\bar{K}N \rightarrow \bar{K}N$
90 ± 20	CAMERON 78B	DPWA	$K^-p \rightarrow N\bar{K}^*$
46 ± 20	PREVOST 74	DPWA	$K^-N \rightarrow \Sigma(1385)\pi$
120 ± 10	LANGBEIN 72	IPWA	$\bar{K}N$ multichannel
••• We do not use the following data for averages, fits, limits, etc. •••			
166 ± 20	GOPAL 77	DPWA	$\bar{K}N$ multichannel
535 or 585	<sup>1</sup> MARTIN 77	DPWA	$\bar{K}N$ multichannel
28	CARROLL 76	DPWA	Isospin-0 total $\sigma$
35	KIM 71	DPWA	K-matrix analysis
30	ARMENTEROS70	HBC	$\bar{K}N \rightarrow \bar{K}N$
70	ARMENTEROS70	HBC	$\bar{K}N \rightarrow \Sigma\pi$
22	BARBARO... 70	HBC	$\bar{K}N \rightarrow \Sigma\pi$
300	BAILEY 69	DPWA	$\bar{K}N \rightarrow \bar{K}N$
147	ARMENTEROS68B	HBC	

<sup>1</sup> The two MARTIN 77 values are from a T-matrix pole and from a Breit-Wigner fit.

 $\Lambda(1810)$  DECAY MODES

Mode	Fraction ( $\Gamma_i/\Gamma$ )
$\Gamma_1$ $N\bar{K}$	0.05 to 0.35
$\Gamma_2$ $\Sigma\pi$	(16 ± 5) %
$\Gamma_3$ $\Lambda\eta$	
$\Gamma_4$ $\Xi K$	
$\Gamma_5$ $\Sigma(1385)\pi$	(40 ± 15) %
$\Gamma_6$ $N\bar{K}^*(892)$	30–60 %
$\Gamma_7$ $N\bar{K}^*(892)$ , $S=1/2$ , $P$ -wave	
$\Gamma_8$ $N\bar{K}^*(892)$ , $S=3/2$ , $P$ -wave	

 $\Lambda(1810)$  BRANCHING RATIOS

$\Gamma(N\bar{K})/\Gamma_{\text{total}}$	DOCUMENT ID	TECN	COMMENT	$\Gamma_1/\Gamma$
<b>0.05 to 0.35 OUR ESTIMATE</b>				
0.025 ± 0.013	SARANTSEV 19	DPWA	$\bar{K}N$ multichannel	
0.19 ± 0.08	ZHANG 13A	DPWA	$\bar{K}N$ multichannel	
0.24 ± 0.04	GOPAL 80	DPWA	$\bar{K}N \rightarrow \bar{K}N$	
0.36 ± 0.05	LANGBEIN 72	IPWA	$\bar{K}N$ multichannel	

••• We do not use the following data for averages, fits, limits, etc. •••

0.225	<sup>1</sup> KAMANO 15	DPWA	$\bar{K}N$ multichannel
0.21 ± 0.04	GOPAL 77	DPWA	See GOPAL 80
0.52 or 0.49	<sup>2</sup> MARTIN 77	DPWA	$\bar{K}N$ multichannel
0.30	KIM 71	DPWA	K-matrix analysis
0.15	ARMENTEROS70	DPWA	$\bar{K}N \rightarrow \bar{K}N$
0.55	BAILEY 69	DPWA	$\bar{K}N \rightarrow \bar{K}N$
0.4	ARMENTEROS68B	DPWA	$\bar{K}N \rightarrow \bar{K}N$

<sup>1</sup> From the preferred solution A in KAMANO 15.

<sup>2</sup> The two MARTIN 77 values are from a T-matrix pole and from a Breit-Wigner fit.

$\Gamma(\Sigma\pi)/\Gamma_{\text{total}}$	DOCUMENT ID	TECN	COMMENT	$\Gamma_2/\Gamma$
<b>0.16 ± 0.05</b>	SARANTSEV 19	DPWA	$\bar{K}N$ multichannel	

••• We do not use the following data for averages, fits, limits, etc. •••

0.009	<sup>1</sup> KAMANO 15	DPWA	Multichannel
-------	------------------------	------	--------------

<sup>1</sup> From the preferred solution A in KAMANO 15.

$\Gamma(\Lambda\eta)/\Gamma_{\text{total}}$	DOCUMENT ID	TECN	COMMENT	$\Gamma_3/\Gamma$
<b>0.111</b>	<sup>1</sup> KAMANO 15	DPWA	Multichannel	

<sup>1</sup> From the preferred solution A in KAMANO 15.

$\Gamma(\Xi K)/\Gamma_{\text{total}}$	DOCUMENT ID	TECN	COMMENT	$\Gamma_4/\Gamma$
<b>0.051</b>	<sup>1</sup> KAMANO 15	DPWA	Multichannel	

<sup>1</sup> From the preferred solution A in KAMANO 15.

$\Gamma(\Sigma(1385)\pi)/\Gamma_{\text{total}}$	DOCUMENT ID	TECN	COMMENT	$\Gamma_5/\Gamma$
<b>0.40 ± 0.15</b>	SARANTSEV 19	DPWA	$\bar{K}N$ multichannel	

••• We do not use the following data for averages, fits, limits, etc. •••

0.600	<sup>1</sup> KAMANO 15	DPWA	Multichannel
-------	------------------------	------	--------------

<sup>1</sup> From the preferred solution A in KAMANO 15.

$\Gamma(N\bar{K}^*(892), S=1/2, P\text{-wave})/\Gamma_{\text{total}}$	DOCUMENT ID	TECN	COMMENT	$\Gamma_7/\Gamma$
<b>0.003</b>	<sup>1</sup> KAMANO 15	DPWA	Multichannel	

••• We do not use the following data for averages, fits, limits, etc. •••

0.003	<sup>1</sup> KAMANO 15	DPWA	Multichannel
-------	------------------------	------	--------------

<sup>1</sup> From the preferred solution A in KAMANO 15.

$(\Gamma_1\Gamma_7)^{1/2}/\Gamma_{\text{total}}$ in $N\bar{K} \rightarrow \Lambda(1810) \rightarrow \Sigma\pi$	DOCUMENT ID	TECN	COMMENT	$(\Gamma_1\Gamma_2)^{1/2}/\Gamma$
-0.08 ± 0.05	ZHANG 13A	DPWA	Multichannel	
-0.24 ± 0.04	GOPAL 77	DPWA	$\bar{K}N$ multichannel	

••• We do not use the following data for averages, fits, limits, etc. •••

+0.25 or +0.23	<sup>1</sup> MARTIN 77	DPWA	$\bar{K}N$ multichannel
< 0.01	LANGBEIN 72	IPWA	$\bar{K}N$ multichannel
0.17	KIM 71	DPWA	K-matrix analysis
+0.20	<sup>2</sup> ARMENTEROS70	DPWA	$\bar{K}N \rightarrow \Sigma\pi$
-0.13 ± 0.03	BARBARO... 70	DPWA	$\bar{K}N \rightarrow \Sigma\pi$

<sup>1</sup> The two MARTIN 77 values are from a T-matrix pole and from a Breit-Wigner fit.

<sup>2</sup> The published sign has been changed to be in accord with the baryon-first convention.

$(\Gamma_1\Gamma_7)^{1/2}/\Gamma_{\text{total}}$ in $N\bar{K} \rightarrow \Lambda(1810) \rightarrow \Sigma(1385)\pi$	DOCUMENT ID	TECN	COMMENT	$(\Gamma_1\Gamma_5)^{1/2}/\Gamma$
+0.18 ± 0.10	PREVOST 74	DPWA	$K^-N \rightarrow \Sigma(1385)\pi$	

$(\Gamma_1\Gamma_7)^{1/2}/\Gamma_{\text{total}}$ in $N\bar{K} \rightarrow \Lambda(1810) \rightarrow N\bar{K}^*(892)$ , $S=1/2$ , $P$ -wave	DOCUMENT ID	TECN	COMMENT	$(\Gamma_1\Gamma_7)^{1/2}/\Gamma$
-0.14 ± 0.03	<sup>1</sup> CAMERON 78B	DPWA	$K^-p \rightarrow N\bar{K}^*$	

<sup>1</sup> The published sign has been changed to be in accord with the baryon-first convention.

$(\Gamma_1\Gamma_7)^{1/2}/\Gamma_{\text{total}}$ in $N\bar{K} \rightarrow \Lambda(1810) \rightarrow N\bar{K}^*(892)$ , $S=3/2$ , $P$ -wave	DOCUMENT ID	TECN	COMMENT	$(\Gamma_1\Gamma_8)^{1/2}/\Gamma$
+0.38 ± 0.06	ZHANG 13A	DPWA	Multichannel	
+0.35 ± 0.06	CAMERON 78B	DPWA	$K^-p \rightarrow N\bar{K}^*$	

 $\Lambda(1810)$  REFERENCES

SARANTSEV 19	EPJ A55 180	A.V. Sarantsev et al.	(BONN, PNPI)
KAMANO 15	PR C92 025205	H. Kamano et al.	(ANL, OSAK)
ZHANG 13A	PR C88 035205	H. Zhang et al.	(KSU)
GOPAL 80	Toronto Conf. 159	G.P. Gopal	(RHEL) IJP
CAMERON 78B	NP B146 327	W. Cameron et al.	(RHEL, LOIC) IJP
GOPAL 77	NP B119 362	G.P. Gopal et al.	(LOIC, RHEL) IJP
MARTIN 77	NP B127 349	B.R. Martin, M.K. Pidcock, R.G. Moorhouse	(LOUC+) IJP
Also	NP B126 266	B.R. Martin, M.K. Pidcock	(LOUC) IJP
Also	NP B126 285	B.R. Martin, M.K. Pidcock	(LOUC) IJP

See key on page 999

# Baryon Particle Listings

## $\Lambda(1810)$ , $\Lambda(1820)$

CARROLL 76	PRL 37 806	A.S. Carroll et al.	(BNL)1
PREVOST 74	NP B69 246	J. Prevost et al.	(SACL, CERN, HEID)
LANGBEIN 72	NP B47 477	W. Langbein, F. Wagner	(MPIM) IJP
KIM 71	PRL 27 356	J.K. Kim	(HARV) IJP
Also Duke Conf. 161		J.K. Kim	(HARV) IJP
Hyperon Resonances, 1970			
ARMENTEROS 70	Duke Conf. 123	R. Armenteros et al.	(CERN, HEID, SACL) IJP
Hyperon Resonances, 1970			
BARBARO... 70	Duke Conf. 173	A. Barbaro-Galtieri	(LRL) IJP
Hyperon Resonances, 1970			
BAILEY 69	Thesis UCRL 50617	J.M. Bailey	(LLL) IJP
ARMENTEROS 68B	NP B8 195	R. Armenteros et al.	(CERN, HEID, SACL) IJP

$\Lambda(1820) \ 5/2^+$

 $I(J^P) = 0(\frac{5}{2}^+)$  Status: \*\*\*

This resonance is the cornerstone for all partial-wave analyses in this region. Most of the results published before 1973 are now obsolete and have been omitted. They may be found in our 1982 edition Physics Letters **111B** 1 (1982).

### $\Lambda(1820)$ POLE POSITION

#### REAL PART

VALUE (MeV)	DOCUMENT ID	TECN	COMMENT
<b>1812 to 1825 (<math>\approx</math> 1818) OUR ESTIMATE</b>			
1813 $\pm$ 3	SARANTSEV 19	DPWA	$\bar{K}N$ multichannel
1824 $^{+2}_{-1}$	<sup>1</sup> KAMANO 15	DPWA	$\bar{K}N$ multichannel
••• We do not use the following data for averages, fits, limits, etc. •••			
1814	ZHANG 13A	DPWA	$\bar{K}N$ multichannel
<sup>1</sup> From the preferred solution A in KAMANO 15.			

#### -2xIMAGINARY PART

VALUE (MeV)	DOCUMENT ID	TECN	COMMENT
<b>75 to 80 (<math>\approx</math> 77) OUR ESTIMATE</b>			
78 $\pm$ 7	SARANTSEV 19	DPWA	$\bar{K}N$ multichannel
77 $\pm$ 2	<sup>1</sup> KAMANO 15	DPWA	$\bar{K}N$ multichannel
••• We do not use the following data for averages, fits, limits, etc. •••			
85	ZHANG 13A	DPWA	$\bar{K}N$ multichannel
<sup>1</sup> From the preferred solution A in KAMANO 15.			

### $\Lambda(1820)$ POLE RESIDUES

The normalized residue is the residue divided by  $\Gamma_{pole}/2$ .

#### Normalized residue in $N\bar{K} \rightarrow \Lambda(1820) \rightarrow N\bar{K}$

MODULUS	PHASE (°)	DOCUMENT ID	TECN	COMMENT
<b>0.60 <math>\pm</math> 0.12</b>	<b>-22 <math>\pm</math> 5</b>	SARANTSEV 19	DPWA	$\bar{K}N$ multichannel
••• We do not use the following data for averages, fits, limits, etc. •••				
0.558	-13	<sup>1</sup> KAMANO 15	DPWA	$\bar{K}N$ multichannel
<sup>1</sup> From the preferred solution A in KAMANO 15.				

#### Normalized residue in $N\bar{K} \rightarrow \Lambda(1820) \rightarrow \Sigma\pi$

MODULUS	PHASE (°)	DOCUMENT ID	TECN	COMMENT
<b>0.34 <math>\pm</math> 0.07</b>	<b>174 <math>\pm</math> 5</b>	SARANTSEV 19	DPWA	$\bar{K}N$ multichannel
••• We do not use the following data for averages, fits, limits, etc. •••				
0.357	168	<sup>1</sup> KAMANO 15	DPWA	$\bar{K}N$ multichannel
<sup>1</sup> From the preferred solution A in KAMANO 15.				

#### Normalized residue in $N\bar{K} \rightarrow \Lambda(1820) \rightarrow \Lambda\eta$

MODULUS	PHASE (°)	DOCUMENT ID	TECN	COMMENT
••• We do not use the following data for averages, fits, limits, etc. •••				
0.0184	-3	<sup>1</sup> KAMANO 15	DPWA	$\bar{K}N$ multichannel
<sup>1</sup> From the preferred solution A in KAMANO 15.				

#### Normalized residue in $N\bar{K} \rightarrow \Lambda(1820) \rightarrow \Xi K$

MODULUS	PHASE (°)	DOCUMENT ID	TECN	COMMENT
$\sim 0$		SARANTSEV 19	DPWA	$\bar{K}N$ multichannel
••• We do not use the following data for averages, fits, limits, etc. •••				
0.00111	70	<sup>1</sup> KAMANO 15	DPWA	$\bar{K}N$ multichannel
<sup>1</sup> From the preferred solution A in KAMANO 15.				

#### Normalized residue in $N\bar{K} \rightarrow \Lambda(1820) \rightarrow \Sigma(1385)\pi, P$ -wave

MODULUS	PHASE (°)	DOCUMENT ID	TECN	COMMENT
<b>0.07 <math>\pm</math> 0.02</b>	<b>-60 <math>\pm</math> 50</b>	SARANTSEV 19	DPWA	$\bar{K}N$ multichannel
••• We do not use the following data for averages, fits, limits, etc. •••				
0.340	161	<sup>1</sup> KAMANO 15	DPWA	$\bar{K}N$ multichannel
<sup>1</sup> From the preferred solution A in KAMANO 15.				

#### Normalized residue in $N\bar{K} \rightarrow \Lambda(1820) \rightarrow \Sigma(1385)\pi, F$ -wave

MODULUS	PHASE (°)	DOCUMENT ID	TECN	COMMENT
<b>0.11 <math>\pm</math> 0.04</b>	<b>5 <math>\pm</math> 45</b>	SARANTSEV 19	DPWA	$\bar{K}N$ multichannel
••• We do not use the following data for averages, fits, limits, etc. •••				
0.201	151	<sup>1</sup> KAMANO 15	DPWA	$\bar{K}N$ multichannel
<sup>1</sup> From the preferred solution A in KAMANO 15.				

#### Normalized residue in $N\bar{K} \rightarrow \Lambda(1820) \rightarrow N\bar{K}^*(892), S=1/2, F$ -wave

MODULUS	PHASE (°)	DOCUMENT ID	TECN	COMMENT
<b>0.02 <math>\pm</math> 0.02</b>		SARANTSEV 19	DPWA	$\bar{K}N$ multichannel
••• We do not use the following data for averages, fits, limits, etc. •••				
0.00750	41	<sup>1</sup> KAMANO 15	DPWA	$\bar{K}N$ multichannel
<sup>1</sup> From the preferred solution A in KAMANO 15.				

#### Normalized residue in $N\bar{K} \rightarrow \Lambda(1820) \rightarrow N\bar{K}^*(892), S=3/2, P$ -wave

MODULUS	PHASE (°)	DOCUMENT ID	TECN	COMMENT
<b>0.35 <math>\pm</math> 0.15</b>	<b>-30 <math>\pm</math> 45</b>	SARANTSEV 19	DPWA	$\bar{K}N$ multichannel
••• We do not use the following data for averages, fits, limits, etc. •••				
0.171	-139	<sup>1</sup> KAMANO 15	DPWA	$\bar{K}N$ multichannel
<sup>1</sup> From the preferred solution A in KAMANO 15.				

#### Normalized residue in $N\bar{K} \rightarrow \Lambda(1820) \rightarrow N\bar{K}^*(892), S=3/2, F$ -wave

MODULUS	PHASE (°)	DOCUMENT ID	TECN	COMMENT
<b>0.02 <math>\pm</math> 0.02</b>		SARANTSEV 19	DPWA	$\bar{K}N$ multichannel
••• We do not use the following data for averages, fits, limits, etc. •••				
0.000517	161	<sup>1</sup> KAMANO 15	DPWA	$\bar{K}N$ multichannel
<sup>1</sup> From the preferred solution A in KAMANO 15.				

### $\Lambda(1820)$ MASS

VALUE (MeV)	DOCUMENT ID	TECN	COMMENT
<b>1815 to 1825 (<math>\approx</math> 1820) OUR ESTIMATE</b>			
1822 $\pm$ 4	SARANTSEV 19	DPWA	$\bar{K}N$ multichannel
1823.5 $\pm$ 0.8	ZHANG 13A	DPWA	$\bar{K}N$ multichannel
1823 $\pm$ 3	GOPAL 80	DPWA	$\bar{K}N \rightarrow \bar{K}N$
1819 $\pm$ 2	ALSTON... 78	DPWA	$\bar{K}N \rightarrow \bar{K}N$
1821 $\pm$ 2	KANE 74	DPWA	$K^- p \rightarrow \Sigma\pi$
••• We do not use the following data for averages, fits, limits, etc. •••			
1830	DECLAIS 77	DPWA	$\bar{K}N \rightarrow \bar{K}N$
1822 $\pm$ 2	GOPAL 77	DPWA	$\bar{K}N$ multichannel
1817 or 1819	<sup>1</sup> MARTIN 77	DPWA	$\bar{K}N$ multichannel
<sup>1</sup> The two MARTIN 77 values are from a T-matrix pole and from a Breit-Wigner fit.			

### $\Lambda(1820)$ WIDTH

VALUE (MeV)	DOCUMENT ID	TECN	COMMENT
<b>70 to 90 (<math>\approx</math> 80) OUR ESTIMATE</b>			
80 $\pm$ 8	SARANTSEV 19	DPWA	$\bar{K}N$ multichannel
89 $\pm$ 2	ZHANG 13A	DPWA	$\bar{K}N$ multichannel
77 $\pm$ 5	GOPAL 80	DPWA	$\bar{K}N \rightarrow \bar{K}N$
72 $\pm$ 5	ALSTON... 78	DPWA	$\bar{K}N \rightarrow \bar{K}N$
87 $\pm$ 3	KANE 74	DPWA	$K^- p \rightarrow \Sigma\pi$
••• We do not use the following data for averages, fits, limits, etc. •••			
82	DECLAIS 77	DPWA	$\bar{K}N \rightarrow \bar{K}N$
81 $\pm$ 5	GOPAL 77	DPWA	$\bar{K}N$ multichannel
76 or 76	<sup>1</sup> MARTIN 77	DPWA	$\bar{K}N$ multichannel
<sup>1</sup> The two MARTIN 77 values are from a T-matrix pole and from a Breit-Wigner fit.			

### $\Lambda(1820)$ DECAY MODES

Mode	Fraction ( $\Gamma_i/\Gamma$ )
$\Gamma_1$ $N\bar{K}$	55-65 %
$\Gamma_2$ $\Sigma\pi$	8-14 %
$\Gamma_3$ $\Sigma(1385)\pi$	5-10 %
$\Gamma_4$ $\Sigma(1385)\pi, P$ -wave	
$\Gamma_5$ $\Sigma(1385)\pi, F$ -wave	(2.0 $\pm$ 1.0) %
$\Gamma_6$ $\Lambda\eta$	
$\Gamma_7$ $\Xi K$	
$\Gamma_8$ $\Sigma\pi\pi$	
$\Gamma_9$ $N\bar{K}^*(892), S=1/2, F$ -wave	
$\Gamma_{10}$ $N\bar{K}^*(892), S=3/2, P$ -wave	(3.0 $\pm$ 1.0) %
$\Gamma_{11}$ $N\bar{K}^*(892), S=3/2, F$ -wave	

### $\Lambda(1820)$ BRANCHING RATIOS

Errors quoted do not include uncertainties in the parametrizations used in the partial-wave analyses and are thus too small. See also "Sign conventions for resonance couplings" in the Note on  $\Lambda$  and  $\Sigma$  Resonances.

$\Gamma(N\bar{K})/\Gamma_{total}$	VALUE	DOCUMENT ID	TECN	COMMENT	$\Gamma_i/\Gamma$
<b>0.55 to 0.65 OUR ESTIMATE</b>					
0.58 $\pm$ 0.12		SARANTSEV 19	DPWA	$\bar{K}N$ multichannel	
0.54 $\pm$ 0.01		ZHANG 13A	DPWA	$\bar{K}N$ multichannel	
0.58 $\pm$ 0.02		GOPAL 80	DPWA	$\bar{K}N \rightarrow \bar{K}N$	
0.60 $\pm$ 0.03		ALSTON... 78	DPWA	$\bar{K}N \rightarrow \bar{K}N$	

# Baryon Particle Listings

## $\Lambda(1820), \Lambda(1830)$

••• We do not use the following data for averages, fits, limits, etc. •••

0.547	1	KAMANO	15	DPWA	$\bar{K}N$ multichannel
0.51		DECLAIS	77	DPWA	$\bar{K}N \rightarrow \bar{K}N$
0.57 ± 0.02		GOPAL	77	DPWA	See GOPAL 80
0.59 or 0.58	2	MARTIN	77	DPWA	$\bar{K}N$ multichannel

<sup>1</sup> From the preferred solution A in KAMANO 15.  
<sup>2</sup> The two MARTIN 77 values are from a T-matrix pole and from a Breit-Wigner fit.

$\Gamma(\Sigma\pi)/\Gamma_{total}$	DOCUMENT ID	TECN	COMMENT	$\Gamma_2/\Gamma$
<b>0.19 ± 0.04</b>	SARANTSEV 19	DPWA	$\bar{K}N$ multichannel	

••• We do not use the following data for averages, fits, limits, etc. •••

0.218	1	KAMANO	15	DPWA	$\bar{K}N$ multichannel
-------	---	--------	----	------	-------------------------

<sup>1</sup> From the preferred solution A in KAMANO 15.

$\Gamma(\Sigma(1385)\pi, P\text{-wave})/\Gamma_{total}$	DOCUMENT ID	TECN	COMMENT	$\Gamma_4/\Gamma$
~ 0.01	SARANTSEV 19	DPWA	$\bar{K}N$ multichannel	

••• We do not use the following data for averages, fits, limits, etc. •••

0.173	1	KAMANO	15	DPWA	$\bar{K}N$ multichannel
-------	---	--------	----	------	-------------------------

<sup>1</sup> From the preferred solution A in KAMANO 15.

$\Gamma(\Sigma(1385)\pi, F\text{-wave})/\Gamma_{total}$	DOCUMENT ID	TECN	COMMENT	$\Gamma_5/\Gamma$
<b>0.02 ± 0.01</b>	SARANTSEV 19	DPWA	$\bar{K}N$ multichannel	

••• We do not use the following data for averages, fits, limits, etc. •••

0.055	1	KAMANO	15	DPWA	$\bar{K}N$ multichannel
-------	---	--------	----	------	-------------------------

<sup>1</sup> From the preferred solution A in KAMANO 15.

$\Gamma(\Lambda\eta)/\Gamma_{total}$	DOCUMENT ID	TECN	COMMENT	$\Gamma_6/\Gamma$	
0.001	1	KAMANO	15	DPWA	Multichannel

<sup>1</sup> From the preferred solution A in KAMANO 15.

$\Gamma(\Xi K)/\Gamma_{total}$	DOCUMENT ID	TECN	COMMENT	$\Gamma_7/\Gamma$	
not seen	1	KAMANO	15	DPWA	Multichannel

••• We do not use the following data for averages, fits, limits, etc. •••

<sup>1</sup> From the preferred solution A in KAMANO 15.

$\Gamma(\Sigma\pi\pi)/\Gamma_{total}$	DOCUMENT ID	TECN	COMMENT	$\Gamma_8/\Gamma$
no clear signal	1	ARMENTEROS68C	HDBC $K^-N \rightarrow \Sigma\pi\pi$	

<sup>1</sup> There is a suggestion of a bump, enough to be consistent with what is expected from  $\Sigma(1385) \rightarrow \Sigma\pi$  decay.

$\Gamma(N\bar{K}^*(892), S=1/2, F\text{-wave})/\Gamma_{total}$	DOCUMENT ID	TECN	COMMENT	$\Gamma_9/\Gamma$	
not seen	1	KAMANO	15	DPWA	Multichannel

••• We do not use the following data for averages, fits, limits, etc. •••

<sup>1</sup> From the preferred solution A in KAMANO 15.

$\Gamma(N\bar{K}^*(892), S=3/2, P\text{-wave})/\Gamma_{total}$	DOCUMENT ID	TECN	COMMENT	$\Gamma_{10}/\Gamma$
<b>0.03 ± 0.01</b>	ZHANG 13A	DPWA	Multichannel	

••• We do not use the following data for averages, fits, limits, etc. •••

0.006	1	KAMANO	15	DPWA	Multichannel
-------	---	--------	----	------	--------------

<sup>1</sup> From the preferred solution A in KAMANO 15.

$\Gamma(N\bar{K}^*(892), S=3/2, F\text{-wave})/\Gamma_{total}$	DOCUMENT ID	TECN	COMMENT	$\Gamma_{11}/\Gamma$	
not seen	1	KAMANO	15	DPWA	Multichannel

••• We do not use the following data for averages, fits, limits, etc. •••

<sup>1</sup> From the preferred solution A in KAMANO 15.

$(\Gamma_1\Gamma_2)^{1/2}/\Gamma_{total}$ in $N\bar{K} \rightarrow \Lambda(1820) \rightarrow \Sigma\pi$	DOCUMENT ID	TECN	COMMENT	$(\Gamma_1\Gamma_2)^{1/2}/\Gamma$
-0.28 ± 0.01	ZHANG 13A	DPWA	Multichannel	
-0.28 ± 0.03	GOPAL 77	DPWA	$\bar{K}N$ multichannel	
-0.28 ± 0.01	KANE 74	DPWA	$K^-p \rightarrow \Sigma\pi$	

••• We do not use the following data for averages, fits, limits, etc. •••

-0.25 or -0.25	1	MARTIN	77	DPWA	$\bar{K}N$ multichannel
----------------	---	--------	----	------	-------------------------

<sup>1</sup> The two MARTIN 77 values are from a T-matrix pole and from a Breit-Wigner fit.

$(\Gamma_1\Gamma_2)^{1/2}/\Gamma_{total}$ in $N\bar{K} \rightarrow \Lambda(1820) \rightarrow \Sigma(1385)\pi, P\text{-wave}$	DOCUMENT ID	TECN	COMMENT	$(\Gamma_1\Gamma_4)^{1/2}/\Gamma$	
-0.20 ± 0.02	ZHANG 13A	DPWA	Multichannel		
-0.167 ± 0.054	1	CAMERON	78	DPWA	$K^-p \rightarrow \Sigma(1385)\pi$
+0.27 ± 0.03	PREVOST 74	DPWA	$K^-N \rightarrow \Sigma(1385)\pi$		

<sup>1</sup> The published sign has been changed to be in accord with the baryon-first convention.

$(\Gamma_1\Gamma_2)^{1/2}/\Gamma_{total}$ in $N\bar{K} \rightarrow \Lambda(1820) \rightarrow \Sigma(1385)\pi, F\text{-wave}$	DOCUMENT ID	TECN	COMMENT	$(\Gamma_1\Gamma_5)^{1/2}/\Gamma$	
+0.065 ± 0.029	1	CAMERON	78	DPWA	$K^-p \rightarrow \Sigma(1385)\pi$

<sup>1</sup> The published sign has been changed to be in accord with the baryon-first convention.

$(\Gamma_1\Gamma_2)^{1/2}/\Gamma_{total}$ in $N\bar{K} \rightarrow \Lambda(1820) \rightarrow \Lambda\eta$	DOCUMENT ID	TECN	COMMENT	$(\Gamma_1\Gamma_6)^{1/2}/\Gamma$
-0.096 ± 0.040 -0.020	RADER	73	MPWA	

### $\Lambda(1820)$ REFERENCES

SARANTSEV 19	EPJ A55 180	A.V. Sarantsev et al.	(BONN, PNPI)
KAMANO 15	PR C92 025205	H. Kamano et al.	(ANL, OSAK)
ZHANG 13A	PR C88 035205	H. Zhang et al.	(KSU)
PDG 82	PL 111B 1	M. Roos et al.	(HEL, CIT, CERN)
GOPAL 80	Toronto Conf. 159	G.P. Gopal	(RHEL) IJP
ALSTON... 78	PR D18 182	M. Alston-Garnjost et al.	(LBL, MTHO+) IJP
Also	PRL 38 1007	M. Alston-Garnjost et al.	(LBL, MTHO+) IJP
CAMERON 78	NP B143 189	W. Cameron et al.	(RHEL, LOIC) IJP
DECLAIS 77	CERN 77-16	Y. Declais et al.	(CAEN, CERN) IJP
GOPAL 77	NP B119 362	G.P. Gopal et al.	(LOIC, RHEL) IJP
MARTIN 77	NP B127 349	B.R. Martin, M.K. Pidcock, R.G. Moorhouse	(LOUC+) IJP
Also	NP B126 266	B.R. Martin, M.K. Pidcock	(LOUC)
Also	NP B126 285	B.R. Martin, M.K. Pidcock	(LOUC) IJP
KANE 74	LBL-2452	D.F. Kane	(LBL) IJP
PREVOST 74	NP B69 246	J. Prevost et al.	(SACL, CERN, HEID)
RADER 73	NC 16A 178	R.K. Rader et al.	(SACL, HEID, CERN+)
ARMENTEROS 68C	NP B8 216	R. Armenteros et al.	(CERN, HEID, SACL) I

### $\Lambda(1830) 5/2^-$

$I(J^P) = 0(\frac{5}{2}^-)$  Status: \* \* \* \*

For results published before 1973 (they are now obsolete), see our 1982 edition Physics Letters **111B** 1 (1982).

The best evidence for this resonance is in the  $\Sigma\pi$  channel.

### $\Lambda(1830)$ POLE POSITION

#### REAL PART

VALUE (MeV)	DOCUMENT ID	TECN	COMMENT		
<b>1800 to 1860 (≈ 1830) OUR ESTIMATE</b>					
1819.5 ± 3.0	SARANTSEV 19	DPWA	$\bar{K}N$ multichannel		
1899 ± 35 -37	1	KAMANO	15	DPWA	Multichannel
1766 ± 37 -34	2	KAMANO	15	DPWA	Multichannel
1809	ZHANG 13A	DPWA	Multichannel		

<sup>1</sup> The preferred solution A in KAMANO 15 reports two poles. This entry is from the preferred solution A.

<sup>2</sup> From the preferred solution A in KAMANO 15. Not seen in solution B.

#### -2xIMAGINARY PART

VALUE (MeV)	DOCUMENT ID	TECN	COMMENT		
<b>50 to 80 (≈ 65) OUR ESTIMATE</b>					
62 ± 5	SARANTSEV 19	DPWA	$\bar{K}N$ multichannel		
80 ± 100 34	1	KAMANO	15	DPWA	Multichannel
212 ± 94 62	2	KAMANO	15	DPWA	Multichannel
109	ZHANG 13A	DPWA	Multichannel		

<sup>1</sup> The preferred solution A in KAMANO 15 reports two poles. This entry is from the preferred solution A.

<sup>2</sup> From the preferred solution A in KAMANO 15. Not seen in solution B.

### $\Lambda(1830)$ POLE RESIDUES

The normalized residue is the residue divided by  $\Gamma_{pole}/2$ .

#### Normalized residue in $N\bar{K} \rightarrow \Lambda(1830) \rightarrow N\bar{K}$

MODULUS	PHASE (°)	DOCUMENT ID	TECN	COMMENT		
<b>0.055 ± 0.010 20 ± 14</b>		SARANTSEV 19	DPWA	$\bar{K}N$ multichannel		
0.00502	-80	1	KAMANO	15	DPWA	Multichannel

<sup>1</sup> From the preferred solution A in KAMANO 15.

#### Normalized residue in $N\bar{K} \rightarrow \Lambda(1830) \rightarrow \Sigma\pi$

MODULUS	PHASE (°)	DOCUMENT ID	TECN	COMMENT		
<b>0.15 ± 0.03 180 ± 10</b>		SARANTSEV 19	DPWA	$\bar{K}N$ multichannel		
0.00581	179	1	KAMANO	15	DPWA	Multichannel

<sup>1</sup> From the preferred solution A in KAMANO 15.

#### Normalized residue in $N\bar{K} \rightarrow \Lambda(1830) \rightarrow \Lambda\eta$

MODULUS	PHASE (°)	DOCUMENT ID	TECN	COMMENT		
0.00941	-65	1	KAMANO	15	DPWA	Multichannel

<sup>1</sup> From the preferred solution A in KAMANO 15.

Normalized residue in  $N\bar{K} \rightarrow \Lambda(1830) \rightarrow \Xi K$

MODULUS	PHASE (°)	DOCUMENT ID	TECN	COMMENT
<b>0.010 ± 0.005</b>	<b>65 ± 20</b>	SARANTSEV 19	DPWA	$\bar{K}N$ multichannel
0.0477	94	<sup>1</sup> KAMANO 15	DPWA	Multichannel

• • • We do not use the following data for averages, fits, limits, etc. • • •

<sup>1</sup> From the preferred solution A in KAMANO 15.

Normalized residue in  $N\bar{K} \rightarrow \Lambda(1830) \rightarrow \Sigma(1385)\pi, D\text{-wave}$

MODULUS	PHASE (°)	DOCUMENT ID	TECN	COMMENT
<b>0.10 ± 0.04</b>	<b>10 ± 25</b>	SARANTSEV 19	DPWA	$\bar{K}N$ multichannel
0.0237	113	<sup>1</sup> KAMANO 15	DPWA	Multichannel

• • • We do not use the following data for averages, fits, limits, etc. • • •

<sup>1</sup> From the preferred solution A in KAMANO 15.

Normalized residue in  $N\bar{K} \rightarrow \Lambda(1830) \rightarrow \Sigma(1385)\pi, G\text{-wave}$

MODULUS	PHASE (°)	DOCUMENT ID	TECN	COMMENT
<b>0.03 ± 0.02</b>		SARANTSEV 19	DPWA	$\bar{K}N$ multichannel
0.000726	127	<sup>1</sup> KAMANO 15	DPWA	Multichannel

• • • We do not use the following data for averages, fits, limits, etc. • • •

<sup>1</sup> From the preferred solution A in KAMANO 15.

Normalized residue in  $N\bar{K} \rightarrow \Lambda(1830) \rightarrow N\bar{K}^*(892), S=1/2, D\text{-wave}$

MODULUS	PHASE (°)	DOCUMENT ID	TECN	COMMENT
0.0278	-177	<sup>1</sup> KAMANO 15	DPWA	Multichannel

• • • We do not use the following data for averages, fits, limits, etc. • • •

<sup>1</sup> From the preferred solution A in KAMANO 15.

Normalized residue in  $N\bar{K} \rightarrow \Lambda(1830) \rightarrow N\bar{K}^*(892), S=3/2, D\text{-wave}$

MODULUS	PHASE (°)	DOCUMENT ID	TECN	COMMENT
0.0255	3	<sup>1</sup> KAMANO 15	DPWA	Multichannel

• • • We do not use the following data for averages, fits, limits, etc. • • •

<sup>1</sup> From the preferred solution A in KAMANO 15.

Normalized residue in  $N\bar{K} \rightarrow \Lambda(1830) \rightarrow N\bar{K}^*(892), S=3/2, G\text{-wave}$

MODULUS	PHASE (°)	DOCUMENT ID	TECN	COMMENT
0.00773	-17	<sup>1</sup> KAMANO 15	DPWA	Multichannel

• • • We do not use the following data for averages, fits, limits, etc. • • •

<sup>1</sup> From the preferred solution A in KAMANO 15.

Normalized residue in  $N\bar{K} \rightarrow \Lambda(1830) \rightarrow \Lambda\omega, S=1/2, D\text{-wave}$

MODULUS	PHASE (°)	DOCUMENT ID	TECN	COMMENT
<b>0.04 ± 0.03</b>		SARANTSEV 19	DPWA	$\bar{K}N$ multichannel

Normalized residue in  $N\bar{K} \rightarrow \Lambda(1830) \rightarrow \Lambda\omega, S=3/2, D\text{-wave}$

MODULUS	PHASE (°)	DOCUMENT ID	TECN	COMMENT
<b>0.05 ± 0.03</b>	<b>-110 ± 35</b>	SARANTSEV 19	DPWA	$\bar{K}N$ multichannel

$\Lambda(1830)$  MASS

VALUE (MeV)	DOCUMENT ID	TECN	COMMENT
<b>1820 to 1830 (≈ 1825) OUR ESTIMATE</b>			
1821 ± 3	SARANTSEV 19	DPWA	$\bar{K}N$ multichannel
1820 ± 4	ZHANG 13A	DPWA	Multichannel
1831 ± 10	GOPAL 80	DPWA	$\bar{K}N \rightarrow \bar{K}N$
1825 ± 10	GOPAL 77	DPWA	$\bar{K}N$ multichannel
1825 ± 1	KANE 74	DPWA	$K^- p \rightarrow \Sigma\pi$
• • • We do not use the following data for averages, fits, limits, etc. • • •			
1817 or 1818	<sup>1</sup> MARTIN 77	DPWA	$\bar{K}N$ multichannel

<sup>1</sup> The two MARTIN 77 values are from a T-matrix pole and from a Breit-Wigner fit.

$\Lambda(1830)$  WIDTH

VALUE (MeV)	DOCUMENT ID	TECN	COMMENT
<b>60 to 120 (≈ 90) OUR ESTIMATE</b>			
64 ± 7	SARANTSEV 19	DPWA	$\bar{K}N$ multichannel
114 ± 10	ZHANG 13A	DPWA	Multichannel
100 ± 10	GOPAL 80	DPWA	$\bar{K}N \rightarrow \bar{K}N$
94 ± 10	GOPAL 77	DPWA	$\bar{K}N$ multichannel
119 ± 3	KANE 74	DPWA	$K^- p \rightarrow \Sigma\pi$
• • • We do not use the following data for averages, fits, limits, etc. • • •			
56 or 56	<sup>1</sup> MARTIN 77	DPWA	$\bar{K}N$ multichannel

<sup>1</sup> The two MARTIN 77 values are from a T-matrix pole and from a Breit-Wigner fit.

$\Lambda(1830)$  DECAY MODES

Mode	Fraction ( $\Gamma_i/\Gamma$ )	Scale factor
$\Gamma_1$ $N\bar{K}$	0.04 to 0.08	
$\Gamma_2$ $\Sigma\pi$	35-75 %	
$\Gamma_3$ $\Xi K$		
$\Gamma_4$ $\Sigma(1385)\pi$	>15 %	
$\Gamma_5$ $\Sigma(1385)\pi, D\text{-wave}$	(40 ± 15) %	3.2
$\Gamma_6$ $\Sigma(1385)\pi, G\text{-wave}$		
$\Gamma_7$ $\Lambda\eta$		
$\Gamma_8$ $N\bar{K}^*(892), S=1/2, D\text{-wave}$		
$\Gamma_9$ $N\bar{K}^*(892), S=3/2, D\text{-wave}$		
$\Gamma_{10}$ $N\bar{K}^*(892), S=3/2, G\text{-wave}$		

$\Lambda(1830)$  BRANCHING RATIOS

See "Sign conventions for resonance couplings" in the Note on  $\Lambda$  and  $\Sigma$  Resonances.

$\Gamma(N\bar{K})/\Gamma_{\text{total}}$	VALUE	DOCUMENT ID	TECN	COMMENT	$\Gamma_1/\Gamma$
<b>0.04 to 0.08 OUR ESTIMATE</b>					
	0.055 ± 0.010	SARANTSEV 19	DPWA	$\bar{K}N$ multichannel	
	0.041 ± 0.005	ZHANG 13A	DPWA	Multichannel	
	0.08 ± 0.03	GOPAL 80	DPWA	$\bar{K}N \rightarrow \bar{K}N$	
	0.02 ± 0.02	ALSTON-... 78	DPWA	$\bar{K}N \rightarrow \bar{K}N$	
• • • We do not use the following data for averages, fits, limits, etc. • • •					
	0.006	<sup>1</sup> KAMANO 15	DPWA	Multichannel	
	0.04 ± 0.03	GOPAL 77	DPWA	See GOPAL 80	
	0.04 or 0.04	<sup>2</sup> MARTIN 77	DPWA	$\bar{K}N$ multichannel	

<sup>1</sup> From the preferred solution A in KAMANO 15.  
<sup>2</sup> The two MARTIN 77 values are from a T-matrix pole and from a Breit-Wigner fit.

$\Gamma(\Sigma\pi)/\Gamma_{\text{total}}$	VALUE	DOCUMENT ID	TECN	COMMENT	$\Gamma_2/\Gamma$
<b>0.42 ± 0.08</b>					
• • • We do not use the following data for averages, fits, limits, etc. • • •					
	0.017	<sup>1</sup> KAMANO 15	DPWA	Multichannel	

<sup>1</sup> From the preferred solution A in KAMANO 15.

$\Gamma(\Xi K)/\Gamma_{\text{total}}$	VALUE	DOCUMENT ID	TECN	COMMENT	$\Gamma_3/\Gamma$
• • • We do not use the following data for averages, fits, limits, etc. • • •					
	0.562	<sup>1</sup> KAMANO 15	DPWA	Multichannel	

<sup>1</sup> From the preferred solution A in KAMANO 15.

$\Gamma(\Sigma(1385)\pi, D\text{-wave})/\Gamma_{\text{total}}$	VALUE	DOCUMENT ID	TECN	COMMENT	$\Gamma_5/\Gamma$
<b>0.40 ± 0.15 OUR AVERAGE</b> Error includes scale factor of 3.2.					
	0.20 ± 0.08	SARANTSEV 19	DPWA	$\bar{K}N$ multichannel	
	0.52 ± 0.06	ZHANG 13A	DPWA	Multichannel	
• • • We do not use the following data for averages, fits, limits, etc. • • •					
	0.134	<sup>1</sup> KAMANO 15	DPWA	Multichannel	

<sup>1</sup> From the preferred solution A in KAMANO 15.

$\Gamma(\Sigma(1385)\pi, G\text{-wave})/\Gamma_{\text{total}}$	VALUE	DOCUMENT ID	TECN	COMMENT	$\Gamma_6/\Gamma$
	0.020 ± 0.015	SARANTSEV 19	DPWA	$\bar{K}N$ multichannel	

$\Gamma(\Lambda\eta)/\Gamma_{\text{total}}$	VALUE	DOCUMENT ID	TECN	COMMENT	$\Gamma_7/\Gamma$
• • • We do not use the following data for averages, fits, limits, etc. • • •					
	0.024	<sup>1</sup> KAMANO 15	DPWA	Multichannel	

<sup>1</sup> From the preferred solution A in KAMANO 15.

$\Gamma(N\bar{K}^*(892), S=1/2, D\text{-wave})/\Gamma_{\text{total}}$	VALUE	DOCUMENT ID	TECN	COMMENT	$\Gamma_8/\Gamma$
• • • We do not use the following data for averages, fits, limits, etc. • • •					
	0.134	<sup>1</sup> KAMANO 15	DPWA	Multichannel	

<sup>1</sup> From the preferred solution A in KAMANO 15.

$\Gamma(N\bar{K}^*(892), S=3/2, D\text{-wave})/\Gamma_{\text{total}}$	VALUE	DOCUMENT ID	TECN	COMMENT	$\Gamma_9/\Gamma$
• • • We do not use the following data for averages, fits, limits, etc. • • •					
	0.115	<sup>1</sup> KAMANO 15	DPWA	Multichannel	

<sup>1</sup> From the preferred solution A in KAMANO 15.

$\Gamma(N\bar{K}^*(892), S=3/2, G\text{-wave})/\Gamma_{\text{total}}$	VALUE	DOCUMENT ID	TECN	COMMENT	$\Gamma_{10}/\Gamma$
• • • We do not use the following data for averages, fits, limits, etc. • • •					
	0.009	<sup>1</sup> KAMANO 15	DPWA	Multichannel	

<sup>1</sup> From the preferred solution A in KAMANO 15.

# Baryon Particle Listings

## $\Lambda(1830), \Lambda(1890)$

**$(\Gamma_1 \Gamma_2)^{J^P} / \Gamma_{\text{total}}$  in  $N\bar{K} \rightarrow \Lambda(1830) \rightarrow \Sigma \pi$   $(\Gamma_1 \Gamma_2)^{J^P} / \Gamma$**

VALUE	DOCUMENT ID	TECN	COMMENT
$-0.13 \pm 0.01$	ZHANG	13A	DPWA Multichannel
$-0.17 \pm 0.03$	GOPAL	77	DPWA $\bar{K}N$ multichannel
$-0.15 \pm 0.01$	KANE	74	DPWA $K^- p \rightarrow \Sigma \pi$
••• We do not use the following data for averages, fits, limits, etc. •••			
$-0.17$ or $-0.17$	<sup>1</sup> MARTIN	77	DPWA $\bar{K}N$ multichannel

<sup>1</sup>The two MARTIN 77 values are from a T-matrix pole and from a Breit-Wigner fit.

**$(\Gamma_1 \Gamma_2)^{J^P} / \Gamma_{\text{total}}$  in  $N\bar{K} \rightarrow \Lambda(1830) \rightarrow \Sigma(1385)\pi$   $(\Gamma_1 \Gamma_2)^{J^P} / \Gamma$**

VALUE	DOCUMENT ID	TECN	COMMENT
<b>0.20 to 0.50 OUR ESTIMATE</b>			
$+0.141 \pm 0.014$	<sup>1</sup> CAMERON	78	DPWA $K^- p \rightarrow \Sigma(1385)\pi$
$+0.13 \pm 0.03$	PREVOST	74	DPWA $K^- N \rightarrow \Sigma(1385)\pi$

<sup>1</sup>The CAMERON 78 upper limit on G-wave decay is 0.03. The published sign has been changed to be in accord with the baryon-first convention.

**$(\Gamma_1 \Gamma_2)^{J^P} / \Gamma_{\text{total}}$  in  $N\bar{K} \rightarrow \Lambda(1830) \rightarrow \Lambda \eta$   $(\Gamma_1 \Gamma_2)^{J^P} / \Gamma$**

VALUE	DOCUMENT ID	TECN	COMMENT
$-0.044 \pm 0.020$	RADER	73	MPWA

### $\Lambda(1830)$ REFERENCES

SARANTSEV	19	EPJ A55 180	A.V. Sarantsev et al.	(BONN, PNPI)
KAMANO	15	PR C92 025205	H. Kamano et al.	(ANL, OSAK)
ZHANG	13A	PR C88 035205	H. Zhang et al.	(KSU)
PDG	82	PL 111B 1	M. Roos et al.	(HELS, CIT, CERN)
GOPAL	80	Toronto Conf. 159	G.P. Gopal	(RHEL) IJP
ALSTON-...	78	PR D18 182	M. Alston-Garnjost et al.	(LBL, MTHO+) IJP
Also		PR L 38 1007	M. Alston-Garnjost et al.	(LBL, MTHO+) IJP
CAMERON	78	NP B143 189	W. Cameron et al.	(RHEL, LOIC) IJP
GOPAL	77	NP B119 362	G.P. Gopal et al.	(LOIC, RHEL) IJP
MARTIN	77	NP B127 349	B.R. Martin, M.K. Pidcock, R.G. Moorhouse	(LOUC+) IJP
Also		NP B126 266	B.R. Martin, M.K. Pidcock	(LOUC) IJP
Also		NP B126 285	B.R. Martin, M.K. Pidcock	(LOUC) IJP
KANE	74	LBL-2452	D.F. Kane	(LBL) IJP
PREVOST	74	NP B69 246	J. Prevost et al.	(SACL, CERN, HEID)
RADER	73	NC 16A 178	R.K. Rader et al.	(SACL, HEID, CERN+)

**$\Lambda(1890) 3/2^+$**   $I(J^P) = 0(\frac{3}{2}^+)$  Status: \*\*\*\*

For results published before 1974 (they are now obsolete), see our 1982 edition Physics Letters **111B** 1 (1982).

### $\Lambda(1890)$ POLE POSITION

**REAL PART**

VALUE (MeV)	DOCUMENT ID	TECN	COMMENT
<b>1872±5</b>	SARANTSEV	19	DPWA $\bar{K}N$ multichannel

••• We do not use the following data for averages, fits, limits, etc. •••

$1859^{+5}_{-7}$	<sup>1</sup> KAMANO	15	DPWA Multichannel
1876	ZHANG	13A	DPWA Multichannel

<sup>1</sup>From the preferred solution A in KAMANO 15, incompatible with solution B.

**-2xIMAGINARY PART**

VALUE (MeV)	DOCUMENT ID	TECN	COMMENT
<b>101±10</b>	SARANTSEV	19	DPWA $\bar{K}N$ multichannel

••• We do not use the following data for averages, fits, limits, etc. •••

$113^{+20}_{-4}$	<sup>1</sup> KAMANO	15	DPWA $\bar{K}N$ multichannel
145	ZHANG	13A	DPWA $\bar{K}N$ multichannel

<sup>1</sup>From the preferred solution A in KAMANO 15, incompatible with solution B.

### $\Lambda(1890)$ POLE RESIDUE

The "normalized residue" is the residue divided by  $\Gamma_{\text{pole}}/2$ .

**Normalized residue in  $KN \rightarrow \Lambda(1890) \rightarrow KN$**

MODULUS	PHASE (°)	DOCUMENT ID	TECN	COMMENT
<b>0.30 ± 0.06</b>	<b>0 ± 10</b>	SARANTSEV	19	DPWA $\bar{K}N$ multichannel

••• We do not use the following data for averages, fits, limits, etc. •••

0.241	-23	<sup>1</sup> KAMANO	15	DPWA $\bar{K}N$ multichannel
-------	-----	---------------------	----	------------------------------

<sup>1</sup>From the preferred solution A in KAMANO 15.

**Normalized residue in  $N\bar{K} \rightarrow \Lambda(1890) \rightarrow \Sigma \pi$**

MODULUS	PHASE (°)	DOCUMENT ID	TECN	COMMENT
<b>0.14 ± 0.05</b>	<b>148 ± 12</b>	SARANTSEV	19	DPWA $\bar{K}N$ multichannel

••• We do not use the following data for averages, fits, limits, etc. •••

0.101	104	<sup>1</sup> KAMANO	15	DPWA $\bar{K}N$ multichannel
-------	-----	---------------------	----	------------------------------

<sup>1</sup>From the preferred solution A in KAMANO 15.

**Normalized residue in  $N\bar{K} \rightarrow \Lambda(1890) \rightarrow \Lambda \eta$**

MODULUS	PHASE (°)	DOCUMENT ID	TECN	COMMENT
0.0485	-54	<sup>1</sup> KAMANO	15	DPWA Multichannel

••• We do not use the following data for averages, fits, limits, etc. •••

<sup>1</sup>From the preferred solution A in KAMANO 15.

**Normalized residue in  $N\bar{K} \rightarrow \Lambda(1890) \rightarrow \Xi K$**

MODULUS	PHASE (°)	DOCUMENT ID	TECN	COMMENT
<b>0.065 ± 0.020</b>	<b>160 ± 30</b>	SARANTSEV	19	DPWA $\bar{K}N$ multichannel

••• We do not use the following data for averages, fits, limits, etc. •••

0.0562	-85	<sup>1</sup> KAMANO	15	DPWA $\bar{K}N$ multichannel
--------	-----	---------------------	----	------------------------------

<sup>1</sup>From the preferred solution A in KAMANO 15.

**Normalized residue in  $N\bar{K} \rightarrow \Lambda(1890) \rightarrow \Sigma(1385)\pi, P$ -wave**

MODULUS	PHASE (°)	DOCUMENT ID	TECN	COMMENT
<b>0.11 ± 0.05</b>	<b>-160 ± 45</b>	SARANTSEV	19	DPWA $\bar{K}N$ multichannel

••• We do not use the following data for averages, fits, limits, etc. •••

0.295	-40	<sup>1</sup> KAMANO	15	DPWA $\bar{K}N$ multichannel
-------	-----	---------------------	----	------------------------------

<sup>1</sup>From the preferred solution A in KAMANO 15.

**Normalized residue in  $N\bar{K} \rightarrow \Lambda(1890) \rightarrow \Sigma(1385)\pi, F$ -wave**

MODULUS	PHASE (°)	DOCUMENT ID	TECN	COMMENT
<b>0.10 ± 0.04</b>	<b>10 ± 50</b>	SARANTSEV	19	DPWA $\bar{K}N$ multichannel

••• We do not use the following data for averages, fits, limits, etc. •••

0.064	127	<sup>1</sup> KAMANO	15	DPWA $\bar{K}N$ multichannel
-------	-----	---------------------	----	------------------------------

<sup>1</sup>From the preferred solution A in KAMANO 15.

**Normalized residue in  $N\bar{K} \rightarrow \Lambda(1890) \rightarrow N\bar{K}^*(892), S=1/2, P$ -wave**

MODULUS	PHASE (°)	DOCUMENT ID	TECN	COMMENT
<b>0.03 ± 0.03</b>		SARANTSEV	19	DPWA $\bar{K}N$ multichannel

••• We do not use the following data for averages, fits, limits, etc. •••

0.188	-160	<sup>1</sup> KAMANO	15	DPWA $\bar{K}N$ multichannel
-------	------	---------------------	----	------------------------------

<sup>1</sup>From the preferred solution A in KAMANO 15.

**Normalized residue in  $N\bar{K} \rightarrow \Lambda(1890) \rightarrow N\bar{K}^*(892), S=3/2, P$ -wave**

MODULUS	PHASE (°)	DOCUMENT ID	TECN	COMMENT
<b>0.05 ± 0.03</b>	<b>180 ± 40</b>	SARANTSEV	19	DPWA $\bar{K}N$ multichannel

••• We do not use the following data for averages, fits, limits, etc. •••

0.209	15	<sup>1</sup> KAMANO	15	DPWA $\bar{K}N$ multichannel
-------	----	---------------------	----	------------------------------

<sup>1</sup>From the preferred solution A in KAMANO 15.

**Normalized residue in  $N\bar{K} \rightarrow \Lambda(1890) \rightarrow N\bar{K}^*(892), S=3/2, F$ -wave**

MODULUS	PHASE (°)	DOCUMENT ID	TECN	COMMENT
<b>0.0141</b>	129	<sup>1</sup> KAMANO	15	DPWA Multichannel

••• We do not use the following data for averages, fits, limits, etc. •••

<sup>1</sup>From the preferred solution A in KAMANO 15.

**Normalized residue in  $N\bar{K} \rightarrow \Lambda(1890) \rightarrow \Lambda \omega, S=1/2, P$ -wave**

MODULUS	PHASE (°)	DOCUMENT ID	TECN	COMMENT
<b>0.24 ± 0.06</b>	<b>15 ± 20</b>	SARANTSEV	19	DPWA $\bar{K}N$ multichannel

**Normalized residue in  $N\bar{K} \rightarrow \Lambda(1890) \rightarrow \Lambda \omega, S=3/2, P$ -wave**

MODULUS	PHASE (°)	DOCUMENT ID	TECN	COMMENT
<b>0.15 ± 0.08</b>	<b>-165 ± 20</b>	SARANTSEV	19	DPWA $\bar{K}N$ multichannel

### $\Lambda(1890)$ MASS

**1870 to 1910 (≈ 1890) OUR ESTIMATE**

VALUE (MeV)	DOCUMENT ID	TECN	COMMENT
1873 ± 5	SARANTSEV	19	DPWA $\bar{K}N$ multichannel
1900 ± 5	ZHANG	13A	DPWA $\bar{K}N$ multichannel
1897 ± 5	GOPAL	80	DPWA $\bar{K}N \rightarrow \bar{K}N$
1908 ± 10	ALSTON-...	78	DPWA $\bar{K}N \rightarrow \bar{K}N$
1894 ± 10	HEMINGWAY	75	DPWA $K^- p \rightarrow \bar{K}N$

••• We do not use the following data for averages, fits, limits, etc. •••

1900 ± 5	GOPAL	77	DPWA $\bar{K}N$ multichannel
1856 or 1868	<sup>1</sup> MARTIN	77	DPWA $\bar{K}N$ multichannel
1900	<sup>2</sup> NAKKASYAN	75	DPWA $K^- p \rightarrow \Lambda \omega$

<sup>1</sup>The two MARTIN 77 values are from a T-matrix pole and from a Breit-Wigner fit.

<sup>2</sup>Found in one of two best solutions.

### $\Lambda(1890)$ WIDTH

**80 to 160 (≈ 120) OUR ESTIMATE**

VALUE (MeV)	DOCUMENT ID	TECN	COMMENT
103 ± 10	SARANTSEV	19	DPWA $\bar{K}N$ multichannel
161 ± 15	ZHANG	13A	DPWA $\bar{K}N$ multichannel
74 ± 10	GOPAL	80	DPWA $\bar{K}N \rightarrow \bar{K}N$
119 ± 20	ALSTON-...	78	DPWA $\bar{K}N \rightarrow \bar{K}N$
107 ± 10	HEMINGWAY	75	DPWA $K^- p \rightarrow \bar{K}N$

• • • We do not use the following data for averages, fits, limits, etc. • • •

72 ± 10	GOPAL	77	DPWA	$\bar{K}N$ multichannel
191 or 193	<sup>1</sup> MARTIN	77	DPWA	$\bar{K}N$ multichannel
100	<sup>2</sup> NAKKASYAN	75	DPWA	$K^- p \rightarrow \Lambda\omega$

<sup>1</sup>The two MARTIN 77 values are from a T-matrix pole and from a Breit-Wigner fit.  
<sup>2</sup>Found in one of two best solutions.

**$\Lambda(1890)$  DECAY MODES**

Mode	Fraction ( $\Gamma_i/\Gamma$ )
$\Gamma_1$ $N\bar{K}$	0.24 to 0.36
$\Gamma_2$ $\Sigma\pi$	3-10 %
$\Gamma_3$ $\Lambda\eta$	
$\Gamma_4$ $\Xi K$	
$\Gamma_5$ $\Sigma(1385)\pi$	seen
$\Gamma_6$ $\Sigma(1385)\pi, P$ -wave	(6.0 ± 3.0) %
$\Gamma_7$ $\Sigma(1385)\pi, F$ -wave	(4.0 ± 2.0) %
$\Gamma_8$ $N\bar{K}^*(892)$	seen
$\Gamma_9$ $N\bar{K}^*(892), S=1/2$	
$\Gamma_{10}$ $N\bar{K}^*(892), S=1/2, P$ -wave	
$\Gamma_{11}$ $N\bar{K}^*(892), S=3/2, P$ -wave	
$\Gamma_{12}$ $N\bar{K}^*(892), S=3/2, F$ -wave	
$\Gamma_{13}$ $\Lambda\omega$	

**$\Lambda(1890)$  BRANCHING RATIOS**

See "Sign conventions for resonance couplings" in the Note on  $\Lambda$  and  $\Sigma$  Resonances.

**$\Gamma(N\bar{K})/\Gamma_{total}$**

VALUE	DOCUMENT ID	TECN	COMMENT	$\Gamma_1/\Gamma$
<b>0.24 to 0.36 OUR ESTIMATE</b>				
0.30 ± 0.06	SARANTSEV	19	DPWA $\bar{K}N$ multichannel	
0.37 ± 0.03	ZHANG	13A	DPWA $\bar{K}N$ multichannel	
0.20 ± 0.02	GOPAL	80	DPWA $\bar{K}N \rightarrow \bar{K}N$	
0.34 ± 0.05	ALSTON-...	78	DPWA $\bar{K}N \rightarrow \bar{K}N$	
0.24 ± 0.04	HEMINGWAY	75	DPWA $K^- p \rightarrow \bar{K}N$	
• • • We do not use the following data for averages, fits, limits, etc. • • •				
0.305	<sup>1</sup> KAMANO	15	DPWA $\bar{K}N$ multichannel	
0.18 ± 0.02	GOPAL	77	DPWA See GOPAL 80	
0.36 or 0.34	<sup>2</sup> MARTIN	77	DPWA $\bar{K}N$ multichannel	
<sup>1</sup> From the preferred solution A in KAMANO 15.				
<sup>2</sup> The two MARTIN 77 values are from a T-matrix pole and from a Breit-Wigner fit.				

**$\Gamma(\Sigma\pi)/\Gamma_{total}$**

VALUE	DOCUMENT ID	TECN	COMMENT	$\Gamma_2/\Gamma$
6 ± 2	SARANTSEV	19	DPWA $\bar{K}N$ multichannel	
<0.03	LANGBEIN	72	IPWA $\bar{K}N$ multichannel	
• • • We do not use the following data for averages, fits, limits, etc. • • •				
0.04	<sup>1</sup> KAMANO	15	DPWA $\bar{K}N$ multichannel	
<sup>1</sup> From the preferred solution A in KAMANO 15.				

**$\Gamma(\Lambda\eta)/\Gamma_{total}$**

VALUE	DOCUMENT ID	TECN	COMMENT	$\Gamma_3/\Gamma$
• • • We do not use the following data for averages, fits, limits, etc. • • •				
0.012	<sup>1</sup> KAMANO	15	DPWA $\bar{K}N$ multichannel	
<sup>1</sup> From the preferred solution A in KAMANO 15.				

**$\Gamma(\Xi K)/\Gamma_{total}$**

VALUE	DOCUMENT ID	TECN	COMMENT	$\Gamma_4/\Gamma$
~0.01	SARANTSEV	19	DPWA $\bar{K}N$ multichannel	
• • • We do not use the following data for averages, fits, limits, etc. • • •				
0.009	<sup>1</sup> KAMANO	15	DPWA $\bar{K}N$ multichannel	
<sup>1</sup> From the preferred solution A in KAMANO 15.				

**$\Gamma(\Sigma(1385)\pi, P$ -wave)/ $\Gamma_{total}$**

VALUE	DOCUMENT ID	TECN	COMMENT	$\Gamma_6/\Gamma$
<b>0.06 ± 0.03</b>	SARANTSEV	19	DPWA $\bar{K}N$ multichannel	
• • • We do not use the following data for averages, fits, limits, etc. • • •				
0.453	<sup>1</sup> KAMANO	15	DPWA $\bar{K}N$ multichannel	
<sup>1</sup> From the preferred solution A in KAMANO 15.				

**$\Gamma(\Sigma(1385)\pi, F$ -wave)/ $\Gamma_{total}$**

VALUE	DOCUMENT ID	TECN	COMMENT	$\Gamma_7/\Gamma$
<b>0.04 ± 0.02</b>	SARANTSEV	19	DPWA $\bar{K}N$ multichannel	
• • • We do not use the following data for averages, fits, limits, etc. • • •				
0.019	<sup>1</sup> KAMANO	15	DPWA $\bar{K}N$ multichannel	
<sup>1</sup> From the preferred solution A in KAMANO 15.				

**$\Gamma(N\bar{K}^*(892), S=1/2, P$ -wave)/ $\Gamma_{total}$**

VALUE	DOCUMENT ID	TECN	COMMENT	$\Gamma_{10}/\Gamma$
<0.01	SARANTSEV	19	DPWA $\bar{K}N$ multichannel	
• • • We do not use the following data for averages, fits, limits, etc. • • •				
0.073	<sup>1</sup> KAMANO	15	DPWA $\bar{K}N$ multichannel	
<sup>1</sup> From the preferred solution A in KAMANO 15.				

**$\Gamma(N\bar{K}^*(892), S=3/2, P$ -wave)/ $\Gamma_{total}$**

VALUE	DOCUMENT ID	TECN	COMMENT	$\Gamma_{11}/\Gamma$
~0.01	SARANTSEV	19	DPWA $\bar{K}N$ multichannel	
• • • We do not use the following data for averages, fits, limits, etc. • • •				
0.088	<sup>1</sup> KAMANO	15	DPWA $\bar{K}N$ multichannel	
<sup>1</sup> From the preferred solution A in KAMANO 15.				

**$\Gamma(N\bar{K}^*(892), S=3/2, F$ -wave)/ $\Gamma_{total}$**

VALUE	DOCUMENT ID	TECN	COMMENT	$\Gamma_{12}/\Gamma$
• • • We do not use the following data for averages, fits, limits, etc. • • •				
0.001	<sup>1</sup> KAMANO	15	DPWA $\bar{K}N$ multichannel	
<sup>1</sup> From the preferred solution A in KAMANO 15.				

**$(\Gamma_1\Gamma_7)^{1/2}/\Gamma_{total}$  in  $N\bar{K} \rightarrow \Lambda(1890) \rightarrow \Sigma\pi$**

VALUE	DOCUMENT ID	TECN	COMMENT	$(\Gamma_1\Gamma_2)^{1/2}/\Gamma$
-0.09 ± 0.02	ZHANG	13A	DPWA $\bar{K}N$ multichannel	
-0.09 ± 0.03	GOPAL	77	DPWA $\bar{K}N$ multichannel	
• • • We do not use the following data for averages, fits, limits, etc. • • •				
+0.15 or +0.14	<sup>1</sup> MARTIN	77	DPWA $\bar{K}N$ multichannel	
<sup>1</sup> The two MARTIN 77 values are from a T-matrix pole and from a Breit-Wigner fit.				

**$(\Gamma_1\Gamma_6)^{1/2}/\Gamma_{total}$  in  $N\bar{K} \rightarrow \Lambda(1890) \rightarrow \Sigma(1385)\pi, P$ -wave**

VALUE	DOCUMENT ID	TECN	COMMENT	$(\Gamma_1\Gamma_6)^{1/2}/\Gamma$
<0.03	CAMERON	78	DPWA $K^- p \rightarrow \Sigma(1385)\pi$	

**$(\Gamma_1\Gamma_7)^{1/2}/\Gamma_{total}$  in  $N\bar{K} \rightarrow \Lambda(1890) \rightarrow \Sigma(1385)\pi, F$ -wave**

VALUE	DOCUMENT ID	TECN	COMMENT	$(\Gamma_1\Gamma_7)^{1/2}/\Gamma$
-0.31 ± 0.04	ZHANG	13A	DPWA $\bar{K}N$ multichannel	
-0.126 ± 0.055	<sup>1</sup> CAMERON	78	DPWA $K^- p \rightarrow \Sigma(1385)\pi$	
<sup>1</sup> The published sign has been changed to be in accord with the baryon-first convention.				

**$(\Gamma_1\Gamma_9)^{1/2}/\Gamma_{total}$  in  $N\bar{K} \rightarrow \Lambda(1890) \rightarrow N\bar{K}^*(892), S=1/2$**

VALUE	DOCUMENT ID	TECN	COMMENT	$(\Gamma_1\Gamma_9)^{1/2}/\Gamma$
-0.17 ± 0.05	ZHANG	13A	DPWA $\bar{K}N$ multichannel	
-0.07 ± 0.03	<sup>1,2</sup> CAMERON	78B	DPWA $K^- p \rightarrow N\bar{K}^*$	
<sup>1</sup> Upper limits on the $P_3$ and $F_3$ waves are each 0.03.				
<sup>2</sup> The published sign has been changed to be in accord with the baryon-first convention.				

**$(\Gamma_1\Gamma_7)^{1/2}/\Gamma_{total}$  in  $N\bar{K} \rightarrow \Lambda(1890) \rightarrow N\bar{K}^*(892), S=3/2, F$ -wave**

VALUE	DOCUMENT ID	TECN	COMMENT	$(\Gamma_1\Gamma_{12})^{1/2}/\Gamma$
-0.11 ± 0.03	ZHANG	13A	DPWA $\bar{K}N$ multichannel	

**$(\Gamma_1\Gamma_7)^{1/2}/\Gamma_{total}$  in  $N\bar{K} \rightarrow \Lambda(1890) \rightarrow \Lambda\omega$**

VALUE	DOCUMENT ID	TECN	COMMENT	$(\Gamma_1\Gamma_{13})^{1/2}/\Gamma$
seen	BACCARI	77	IPWA $K^- p \rightarrow \Lambda\omega$	
0.032	<sup>1</sup> NAKKASYAN	75	DPWA $K^- p \rightarrow \Lambda\omega$	
<sup>1</sup> Found in one of two best solutions.				

**$\Lambda(1890)$  REFERENCES**

SARANTSEV	19	EPJ A55 180	A.V. Sarantsev <i>et al.</i>	(BONN, PNPI)
KAMANO	15	PR C92 025205	H. Kamano <i>et al.</i>	(ANL, OSAK)
ZHANG	13A	PR C68 035205	H. Zhang <i>et al.</i>	(KSU)
FDG	82	PL 111B 1	M. Roos <i>et al.</i>	(HELS, CIT, CERN)
GOPAL	80	Toronto Conf. 159	G.P. Gopal	(RHEL) IJP
ALSTON-...	78	PR D18 182	M. Alston-Garnjost <i>et al.</i>	(LBL, MTHO+) IJP
			Also	(LBL, MTHO+) IJP
CAMERON	78	NP B143 189	W. Cameron <i>et al.</i>	(RHEL, LOIC) IJP
CAMERON	78B	NP B146 327	W. Cameron <i>et al.</i>	(RHEL, LOIC) IJP
BACCARI	77	NC 41A 96	B. Baccari <i>et al.</i>	(SACL, CDEF) IJP
GOPAL	77	NP B119 362	G.P. Gopal <i>et al.</i>	(LOIC, RHEL) IJP
MARTIN	77	NP B127 349	B.R. Martin, M.K. Pidcock, R.G. Moorhouse	(LOUC+) IJP
			Also	(LOUC) IJP
			Also	(LOUC) IJP
HEMINGWAY	75	NP B91 12	B.R. Martin, M.K. Pidcock	(LOUC) IJP
NAKKASYAN	75	NP B93 85	R.J. Hemingway <i>et al.</i>	(CERN, HEIDH, MPIM) IJP
LANGBEIN	72	NP B47 477	A. Nakkasyan	(CERN) IJP
			W. Langbein, F. Wagner	(MPIM) IJP

## Baryon Particle Listings

 $\Lambda(1890)$ ,  $\Lambda(2000)$ ,  $\Lambda(2050)$ ,  $\Lambda(2070)$  **$\Lambda(2000)$**  $I(J^P) = 0(\frac{1}{2}^-)$  Status: \*

OMITTED FROM SUMMARY TABLE

BARBARO-GALTIERI 70 (in  $\Sigma\pi$ ) and BRANDSTETTER 72 (in  $\Lambda\omega$ ) proposed a state at about this mass. Those analyses are considered to be obsolete, see NAKKASYAN 75 and PDG 18.

 **$\Lambda(2000)$  MASS**

VALUE (MeV)	DOCUMENT ID	TECN	COMMENT
<b><math>\approx 2000</math> OUR ESTIMATE</b>			
2020 $\pm$ 16	ZHANG	13A	DPWA Multichannel
2030 $\pm$ 30	CAMERON	78B	DPWA $K^-p \rightarrow N\bar{K}^*$

 **$\Lambda(2000)$  WIDTH**

VALUE (MeV)	DOCUMENT ID	TECN	COMMENT
255 $\pm$ 63	ZHANG	13A	DPWA Multichannel
125 $\pm$ 25	CAMERON	78B	DPWA $K^-p \rightarrow N\bar{K}^*$

 **$\Lambda(2000)$  DECAY MODES**

Mode	Fraction ( $\Gamma_i/\Gamma$ )
$\Gamma_1$ $N\bar{K}$	(27 $\pm$ 6) %
$\Gamma_2$ $\Sigma\pi$	
$\Gamma_3$ $\Lambda\eta$	(16 $\pm$ 7) %
$\Gamma_4$ $N\bar{K}^*(892)$ , $S=1/2$ , $S$ -wave	
$\Gamma_5$ $N\bar{K}^*(892)$ , $S=3/2$ , $D$ -wave	

 **$\Lambda(2000)$  BRANCHING RATIOS**

See "Sign conventions for resonance couplings" in the Note on  $\Lambda$  and  $\Sigma$  Resonances.

$\Gamma(N\bar{K})/\Gamma_{\text{total}}$	DOCUMENT ID	TECN	COMMENT	$\Gamma_1/\Gamma$
<b>0.27 <math>\pm</math> 0.06</b>	ZHANG	13A	DPWA Multichannel	

$(\Gamma_1\Gamma_2)^{1/2}/\Gamma_{\text{total}}$ in $N\bar{K} \rightarrow \Lambda(2000) \rightarrow \Sigma\pi$	DOCUMENT ID	TECN	COMMENT	$(\Gamma_1\Gamma_2)^{1/2}/\Gamma$
-0.07 $\pm$ 0.03	ZHANG	13A	DPWA Multichannel	

$\Gamma(\Lambda\eta)/\Gamma_{\text{total}}$	DOCUMENT ID	TECN	COMMENT	$\Gamma_3/\Gamma$
<b>0.16 <math>\pm</math> 0.07</b>	ZHANG	13A	DPWA Multichannel	

$(\Gamma_1\Gamma_3)^{1/2}/\Gamma_{\text{total}}$ in $N\bar{K} \rightarrow \Lambda(2000) \rightarrow N\bar{K}^*(892)$ , $S=1/2$ , $S$ -wave	DOCUMENT ID	TECN	COMMENT	$(\Gamma_1\Gamma_3)^{1/2}/\Gamma$
-0.12 $\pm$ 0.03	<sup>1</sup> CAMERON	78B	DPWA $K^-p \rightarrow N\bar{K}^*$	

<sup>1</sup> The published sign has been changed to be in accord with the baryon-first convention.

$(\Gamma_1\Gamma_5)^{1/2}/\Gamma_{\text{total}}$ in $N\bar{K} \rightarrow \Lambda(2000) \rightarrow N\bar{K}^*(892)$ , $S=3/2$ , $D$ -wave	DOCUMENT ID	TECN	COMMENT	$(\Gamma_1\Gamma_5)^{1/2}/\Gamma$
+0.34 $\pm$ 0.05	ZHANG	13A	DPWA Multichannel	
+0.09 $\pm$ 0.03	CAMERON	78B	DPWA $K^-p \rightarrow N\bar{K}^*$	

 **$\Lambda(2000)$  REFERENCES**

PDG 18	PR D98 030001	M. Tanabashi et al.	(PDG Collab.)
ZHANG 13A	PR C88 035205	H. Zhang et al.	(KSU)
CAMERON 78B	NP B146 327	W. Cameron et al.	(RHEL, LOIC)JUP
NAKKASYAN 75	NP B93 05	A. Nakkasyan	(CERN)JUP
BRANDSTETTER 72	NP B39 13	A.A. Brandstetter et al.	(RHEL, CDF+)JUP
BARBARO-GALTIERI 70	Duke Conf. 173	A. Barbaro-Galtieri	(LRL)JUP

Hyperon Resonances, 1970

 **$\Lambda(2050)$  3/2<sup>-</sup>** $I(J^P) = 0(\frac{3}{2}^-)$  Status: \*

OMITTED FROM SUMMARY TABLE

 **$\Lambda(2050)$  MASS**

VALUE (MeV)	DOCUMENT ID	TECN	COMMENT
<b>2056 <math>\pm</math> 22</b>	ZHANG	13A	DPWA Multichannel

 **$\Lambda(2050)$  WIDTH**

VALUE (MeV)	DOCUMENT ID	TECN	COMMENT
<b>493 <math>\pm</math> 61</b>	ZHANG	13A	DPWA Multichannel

 **$\Lambda(2050)$  DECAY MODES**

Mode	Fraction ( $\Gamma_i/\Gamma$ )
$\Gamma_1$ $N\bar{K}$	(19 $\pm$ 4) %
$\Gamma_2$ $\Sigma\pi$	(6.0 $\pm$ 3.0) %
$\Gamma_3$ $\Sigma^*(1385)\pi$ , $S$ -wave	(8 $\pm$ 6) %
$\Gamma_4$ $\Sigma^*(1385)\pi$ , $D$ -wave	(4.0 $\pm$ 3.0) %
$\Gamma_5$ $N\bar{K}^*(892)$ , $S=1/2$	(23 $\pm$ 7) %

 **$\Lambda(2050)$  BRANCHING RATIOS**

$\Gamma(N\bar{K})/\Gamma_{\text{total}}$	DOCUMENT ID	TECN	COMMENT	$\Gamma_1/\Gamma$
<b>0.19 <math>\pm</math> 0.04</b>	ZHANG	13A	DPWA Multichannel	

$\Gamma(\Sigma\pi)/\Gamma_{\text{total}}$	DOCUMENT ID	TECN	COMMENT	$\Gamma_2/\Gamma$
<b>0.06 <math>\pm</math> 0.03</b>	ZHANG	13A	DPWA Multichannel	

$\Gamma(\Sigma^*(1385)\pi, S\text{-wave})/\Gamma_{\text{total}}$	DOCUMENT ID	TECN	COMMENT	$\Gamma_3/\Gamma$
<b>0.08 <math>\pm</math> 0.06</b>	ZHANG	13A	DPWA Multichannel	

$\Gamma(\Sigma^*(1385)\pi, D\text{-wave})/\Gamma_{\text{total}}$	DOCUMENT ID	TECN	COMMENT	$\Gamma_4/\Gamma$
<b>0.04 <math>\pm</math> 0.03</b>	ZHANG	13A	DPWA Multichannel	

$\Gamma(N\bar{K}^*(892), S=1/2)/\Gamma_{\text{total}}$	DOCUMENT ID	TECN	COMMENT	$\Gamma_5/\Gamma$
<b>0.23 <math>\pm</math> 0.07</b>	ZHANG	13A	DPWA Multichannel	

 **$\Lambda(2050)$  REFERENCES**

ZHANG 13A	PR C88 035205	H. Zhang et al.	(KSU)
-----------	---------------	-----------------	-------

 **$\Lambda(2070)$  3/2<sup>+</sup>** $J^P = \frac{3}{2}^+$  Status: \*

OMITTED FROM SUMMARY TABLE

 **$\Lambda(2070)$  POLE POSITION****REAL PART**

VALUE (MeV)	DOCUMENT ID	TECN	COMMENT
<b>2044 <math>\pm</math> 20</b>	SARANTSEV 19	DPWA	$\bar{K}N$ multichannel

**-2xIMAGINARY PART**

VALUE (MeV)	DOCUMENT ID	TECN	COMMENT
<b>360 <math>\pm</math> 45</b>	SARANTSEV 19	DPWA	$\bar{K}N$ multichannel

 **$\Lambda(2070)$  POLE RESIDUES****Normalized residue in  $N\bar{K} \rightarrow \Lambda(2070) \rightarrow N\bar{K}$** 

MODULUS	PHASE ( $^\circ$ )	DOCUMENT ID	TECN	COMMENT
<b>0.15 <math>\pm</math> 0.05</b>	<b>-37 <math>\pm</math> 10</b>	SARANTSEV 19	DPWA	$\bar{K}N$ multichannel

**Normalized residue in  $N\bar{K} \rightarrow \Lambda(2070) \rightarrow \Sigma\pi$** 

MODULUS	PHASE ( $^\circ$ )	DOCUMENT ID	TECN	COMMENT
<b>0.10 <math>\pm</math> 0.03</b>	<b>-47 <math>\pm</math> 8</b>	SARANTSEV 19	DPWA	$\bar{K}N$ multichannel

**Normalized residue in  $N\bar{K} \rightarrow \Lambda(2070) \rightarrow \Xi K$** 

MODULUS	PHASE ( $^\circ$ )	DOCUMENT ID	TECN	COMMENT
<b>0.11 <math>\pm</math> 0.03</b>	<b>0 <math>\pm</math> 25</b>	SARANTSEV 19	DPWA	$\bar{K}N$ multichannel

**Normalized residue in  $N\bar{K} \rightarrow \Lambda(2070) \rightarrow \Lambda\omega$ ,  $S=1/2$ ,  $P$ -wave**

MODULUS	PHASE ( $^\circ$ )	DOCUMENT ID	TECN	COMMENT
<b>0.10 <math>\pm</math> 0.04</b>	<b>150 <math>\pm</math> 17</b>	SARANTSEV 19	DPWA	$\bar{K}N$ multichannel

**Normalized residue in  $N\bar{K} \rightarrow \Lambda(2070) \rightarrow \Lambda\omega$ ,  $S=3/2$ ,  $P$ -wave**

MODULUS	PHASE ( $^\circ$ )	DOCUMENT ID	TECN	COMMENT
<b>0.08 <math>\pm</math> 0.04</b>	<b>20 <math>\pm</math> 30</b>	SARANTSEV 19	DPWA	$\bar{K}N$ multichannel

**Normalized residue in  $N\bar{K} \rightarrow \Lambda(2070) \rightarrow \Lambda\omega$ ,  $S=3/2$ ,  $F$ -wave**

MODULUS	PHASE ( $^\circ$ )	DOCUMENT ID	TECN	COMMENT
<b>0.04 <math>\pm</math> 0.02</b>	<b>-175 <math>\pm</math> 35</b>	SARANTSEV 19	DPWA	$\bar{K}N$ multichannel

**Normalized residue in  $N\bar{K} \rightarrow \Lambda(2070) \rightarrow \Sigma(1385)\pi$ ,  $P$ -wave**

MODULUS	PHASE ( $^\circ$ )	DOCUMENT ID	TECN	COMMENT
<b>0.12 <math>\pm</math> 0.07</b>	<b>-160 <math>\pm</math> 55</b>	SARANTSEV 19	DPWA	$\bar{K}N$ multichannel

**Normalized residue in  $N\bar{K} \rightarrow \Lambda(2070) \rightarrow \Sigma(1385)\pi$ ,  $F$ -wave**

MODULUS	PHASE ( $^\circ$ )	DOCUMENT ID	TECN	COMMENT
<b>0.07 <math>\pm</math> 0.04</b>	<b>-145 <math>\pm</math> 50</b>	SARANTSEV 19	DPWA	$\bar{K}N$ multichannel

**Normalized residue in  $N\bar{K} \rightarrow \Lambda(2070) \rightarrow N\bar{K}^*(892), S=1/2, P\text{-wave}$**

MODULUS	PHASE (°)	DOCUMENT ID	TECN	COMMENT
$0.36 \pm 0.07$	$-45 \pm 30$	SARANTSEV 19	DPWA	$\bar{K}N$ multichannel

**Normalized residue in  $N\bar{K} \rightarrow \Lambda(2070) \rightarrow N\bar{K}^*(892), S=3/2, P\text{-wave}$**

MODULUS	PHASE (°)	DOCUMENT ID	TECN	COMMENT
$0.16 \pm 0.05$	$150 \pm 35$	SARANTSEV 19	DPWA	$\bar{K}N$ multichannel

**Normalized residue in  $N\bar{K} \rightarrow \Lambda(2070) \rightarrow N\bar{K}^*(892), S=3/2, F\text{-wave}$**

MODULUS	PHASE (°)	DOCUMENT ID	TECN	COMMENT
$0.14 \pm 0.08$	$-50 \pm 30$	SARANTSEV 19	DPWA	$\bar{K}N$ multichannel

**$\Lambda(2070)$  MASS**

VALUE (MeV)	DOCUMENT ID	TECN	COMMENT
$2070 \pm 24$	SARANTSEV 19	DPWA	$\bar{K}N$ multichannel

**$\Lambda(2070)$  WIDTH**

VALUE (MeV)	DOCUMENT ID	TECN	COMMENT
$370 \pm 50$	SARANTSEV 19	DPWA	$\bar{K}N$ multichannel

**$\Lambda(2070)$  DECAY MODES**

Mode	Fraction ( $\Gamma_i/\Gamma$ )
$\Gamma_1 N\bar{K}$	(12 ± 5) %
$\Gamma_2 \Sigma \pi$	( 7.0 ± 3.0) %
$\Gamma_3 \Xi K$	( 7.0 ± 3.0) %
$\Gamma_4 \Lambda\omega, S=1/2, P\text{-wave}$	( 7 ± 4) %
$\Gamma_5 \Lambda\omega, S=3/2, P\text{-wave}$	( 3.0 ± 2.0) %
$\Gamma_6 \Lambda\omega, S=3/2, F\text{-wave}$	( 1.0 ± 1.0) %
$\Gamma_7 \Sigma(1385)\pi, P\text{-wave}$	(10 ± 5) %
$\Gamma_8 \Sigma(1385)\pi, F\text{-wave}$	( 2.0 ± 2.0) %
$\Gamma_9 N\bar{K}^*(892), S=1/2, P\text{-wave}$	(42 ± 8) %
$\Gamma_{10} N\bar{K}^*(892), S=3/2, P\text{-wave}$	(14 ± 6) %
$\Gamma_{11} N\bar{K}^*(892), S=3/2, F\text{-wave}$	(10 ± 6) %

**$\Lambda(2070)$  BRANCHING RATIOS**

$\Gamma(N\bar{K})/\Gamma_{\text{total}}$	DOCUMENT ID	TECN	COMMENT	$\Gamma_1/\Gamma$
$0.12 \pm 0.05$	SARANTSEV 19	DPWA	$\bar{K}N$ multichannel	

$\Gamma(\Sigma \pi)/\Gamma_{\text{total}}$	DOCUMENT ID	TECN	COMMENT	$\Gamma_2/\Gamma$
$0.07 \pm 0.03$	SARANTSEV 19	DPWA	$\bar{K}N$ multichannel	

$\Gamma(\Xi K)/\Gamma_{\text{total}}$	DOCUMENT ID	TECN	COMMENT	$\Gamma_3/\Gamma$
$0.07 \pm 0.03$	SARANTSEV 19	DPWA	$\bar{K}N$ multichannel	

$\Gamma(\Lambda\omega, S=1/2, P\text{-wave})/\Gamma_{\text{total}}$	DOCUMENT ID	TECN	COMMENT	$\Gamma_4/\Gamma$
$0.07 \pm 0.04$	SARANTSEV 19	DPWA	$\bar{K}N$ multichannel	

$\Gamma(\Lambda\omega, S=3/2, P\text{-wave})/\Gamma_{\text{total}}$	DOCUMENT ID	TECN	COMMENT	$\Gamma_5/\Gamma$
$0.03 \pm 0.02$	SARANTSEV 19	DPWA	$\bar{K}N$ multichannel	

$\Gamma(\Lambda\omega, S=3/2, F\text{-wave})/\Gamma_{\text{total}}$	DOCUMENT ID	TECN	COMMENT	$\Gamma_6/\Gamma$
$0.01 \pm 0.01$	SARANTSEV 19	DPWA	$\bar{K}N$ multichannel	

$\Gamma(\Sigma(1385)\pi, P\text{-wave})/\Gamma_{\text{total}}$	DOCUMENT ID	TECN	COMMENT	$\Gamma_7/\Gamma$
$0.10 \pm 0.05$	SARANTSEV 19	DPWA	$\bar{K}N$ multichannel	

$\Gamma(\Sigma(1385)\pi, F\text{-wave})/\Gamma_{\text{total}}$	DOCUMENT ID	TECN	COMMENT	$\Gamma_8/\Gamma$
$0.02 \pm 0.02$	SARANTSEV 19	DPWA	$\bar{K}N$ multichannel	

$\Gamma(N\bar{K}^*(892), S=1/2, P\text{-wave})/\Gamma_{\text{total}}$	DOCUMENT ID	TECN	COMMENT	$\Gamma_9/\Gamma$
$0.42 \pm 0.08$	SARANTSEV 19	DPWA	$\bar{K}N$ multichannel	

$\Gamma(N\bar{K}^*(892), S=3/2, P\text{-wave})/\Gamma_{\text{total}}$	DOCUMENT ID	TECN	COMMENT	$\Gamma_{10}/\Gamma$
$0.14 \pm 0.06$	SARANTSEV 19	DPWA	$\bar{K}N$ multichannel	

$\Gamma(N\bar{K}^*(892), S=3/2, F\text{-wave})/\Gamma_{\text{total}}$	DOCUMENT ID	TECN	COMMENT	$\Gamma_{11}/\Gamma$
$0.10 \pm 0.06$	SARANTSEV 19	DPWA	$\bar{K}N$ multichannel	

**$\Lambda(2070)$  REFERENCES**

SARANTSEV 19	EPI A55 180	A.V. Sarantsev et al.	(BONN, PNPI)
--------------	-------------	-----------------------	--------------

$\Lambda(2080) 5/2^-$

$J^P = \frac{5}{2}^-$  Status: \*

OMITTED FROM SUMMARY TABLE

**$\Lambda(2080)$  POLE POSITION**

**REAL PART**

VALUE (MeV)	DOCUMENT ID	TECN	COMMENT
$2070 \pm 15$	SARANTSEV 19	DPWA	$\bar{K}N$ multichannel

**-2xIMAGINARY PART**

VALUE (MeV)	DOCUMENT ID	TECN	COMMENT
$172 \pm 28$	SARANTSEV 19	DPWA	$\bar{K}N$ multichannel

**$\Lambda(2080)$  POLE RESIDUES**

**Normalized residue in  $N\bar{K} \rightarrow \Lambda(2080) \rightarrow N\bar{K}$**

MODULUS	PHASE (°)	DOCUMENT ID	TECN	COMMENT
$0.12 \pm 0.03$	$-35 \pm 22$	SARANTSEV 19	DPWA	$\bar{K}N$ multichannel

**Normalized residue in  $N\bar{K} \rightarrow \Lambda(2080) \rightarrow \Sigma \pi$**

MODULUS	PHASE (°)	DOCUMENT ID	TECN	COMMENT
$0.07 \pm 0.03$	$11 \pm 16$	SARANTSEV 19	DPWA	$\bar{K}N$ multichannel

**Normalized residue in  $N\bar{K} \rightarrow \Lambda(2080) \rightarrow \Xi K$**

MODULUS	PHASE (°)	DOCUMENT ID	TECN	COMMENT
$0.06 \pm 0.02$	$115 \pm 20$	SARANTSEV 19	DPWA	$\bar{K}N$ multichannel

**Normalized residue in  $N\bar{K} \rightarrow \Lambda(2080) \rightarrow \Lambda\omega, S=1/2, D\text{-wave}$**

MODULUS	PHASE (°)	DOCUMENT ID	TECN	COMMENT
$0.06 \pm 0.03$	$115 \pm 25$	SARANTSEV 19	DPWA	$\bar{K}N$ multichannel

**Normalized residue in  $N\bar{K} \rightarrow \Lambda(2080) \rightarrow \Lambda\omega, S=3/2, D\text{-wave}$**

MODULUS	PHASE (°)	DOCUMENT ID	TECN	COMMENT
$0.09 \pm 0.03$	$-10 \pm 35$	SARANTSEV 19	DPWA	$\bar{K}N$ multichannel

**Normalized residue in  $N\bar{K} \rightarrow \Lambda(2080) \rightarrow \Sigma(1385)\pi, D\text{-wave}$**

MODULUS	PHASE (°)	DOCUMENT ID	TECN	COMMENT
$0.14 \pm 0.04$	$155 \pm 45$	SARANTSEV 19	DPWA	$\bar{K}N$ multichannel

**Normalized residue in  $N\bar{K} \rightarrow \Lambda(2080) \rightarrow \Sigma(1385)\pi, G\text{-wave}$**

MODULUS	PHASE (°)	DOCUMENT ID	COMMENT
$0.05 \pm 0.03$	$30 \pm 45$	SARANTSEV 19	$\bar{K}N$ multichannel

**Normalized residue in  $N\bar{K} \rightarrow \Lambda(2080) \rightarrow N\bar{K}^*(892), S=1/2, D\text{-wave}$**

MODULUS	PHASE (°)	DOCUMENT ID	TECN	COMMENT
$0.16 \pm 0.08$	$-120 \pm 50$	SARANTSEV 19	DPWA	$\bar{K}N$ multichannel

**Normalized residue in  $N\bar{K} \rightarrow \Lambda(2080) \rightarrow N\bar{K}^*(892), S=3/2, D\text{-wave}$**

MODULUS	PHASE (°)	DOCUMENT ID	TECN	COMMENT
$0.20 \pm 0.14$	$60 \pm 50$	SARANTSEV 19	DPWA	$\bar{K}N$ multichannel

**$\Lambda(2080)$  MASS**

VALUE (MeV)	DOCUMENT ID	TECN	COMMENT
$2082 \pm 13$	SARANTSEV 19	DPWA	$\bar{K}N$ multichannel

**$\Lambda(2080)$  WIDTH**

VALUE (MeV)	DOCUMENT ID	TECN	COMMENT
$181 \pm 29$	SARANTSEV 19	DPWA	$\bar{K}N$ multichannel

**$\Lambda(2080)$  DECAY MODES**

Mode	Fraction ( $\Gamma_i/\Gamma$ )
$\Gamma_1 N\bar{K}$	(11.0 ± 3.0) %
$\Gamma_2 \Sigma \pi$	( 5.0 ± 2.0) %
$\Gamma_3 \Xi K$	( 4.0 ± 1.0) %
$\Gamma_4 \Lambda\omega, S=1/2, D\text{-wave}$	( 4.0 ± 2.0) %
$\Gamma_5 \Lambda\omega, S=3/2, D\text{-wave}$	( 8.0 ± 3.0) %
$\Gamma_6 \Sigma(1385)\pi, D\text{-wave}$	(15 ± 5) %
$\Gamma_7 \Sigma(1385)\pi, G\text{-wave}$	( 3.0 ± 2.0) %
$\Gamma_8 N\bar{K}^*(892), S=1/2, D\text{-wave}$	(17 ± 9) %
$\Gamma_9 N\bar{K}^*(892), S=3/2, D\text{-wave}$	(25 ± 16) %



## Baryon Particle Listings

 $\Lambda(2080)$ ,  $\Lambda(2085)$  $\Lambda(2080)$  BRANCHING RATIOS

$\Gamma(N\bar{K})/\Gamma_{\text{total}}$	DOCUMENT ID	TECN	COMMENT	$\Gamma_1/\Gamma$
0.11±0.03	SARANTSEV 19	DPWA	$\bar{K}N$ multichannel	
$\Gamma(\Sigma\pi)/\Gamma_{\text{total}}$	DOCUMENT ID	TECN	COMMENT	$\Gamma_2/\Gamma$
0.05±0.02	SARANTSEV 19	DPWA	$\bar{K}N$ multichannel	
$\Gamma(\Xi K)/\Gamma_{\text{total}}$	DOCUMENT ID	TECN	COMMENT	$\Gamma_3/\Gamma$
0.04±0.01	SARANTSEV 19	DPWA	$\bar{K}N$ multichannel	
$\Gamma(\Lambda\omega, S=1/2, D\text{-wave})/\Gamma_{\text{total}}$	DOCUMENT ID	TECN	COMMENT	$\Gamma_4/\Gamma$
0.04±0.02	SARANTSEV 19	DPWA	$\bar{K}N$ multichannel	
$\Gamma(\Lambda\omega, S=3/2, D\text{-wave})/\Gamma_{\text{total}}$	DOCUMENT ID	TECN	COMMENT	$\Gamma_5/\Gamma$
0.08±0.03	SARANTSEV 19	DPWA	$\bar{K}N$ multichannel	
$\Gamma(\Sigma(1385)\pi, D\text{-wave})/\Gamma_{\text{total}}$	DOCUMENT ID	TECN	COMMENT	$\Gamma_6/\Gamma$
0.15±0.05	SARANTSEV 19	DPWA	$\bar{K}N$ multichannel	
$\Gamma(\Sigma(1385)\pi, G\text{-wave})/\Gamma_{\text{total}}$	DOCUMENT ID	TECN	COMMENT	$\Gamma_7/\Gamma$
0.03±0.02	SARANTSEV 19	DPWA	$\bar{K}N$ multichannel	
$\Gamma(N\bar{K}^*(892), S=1/2, D\text{-wave})/\Gamma_{\text{total}}$	DOCUMENT ID	TECN	COMMENT	$\Gamma_8/\Gamma$
0.17±0.09	SARANTSEV 19	DPWA	$\bar{K}N$ multichannel	
$\Gamma(N\bar{K}^*(892), S=3/2, D\text{-wave})/\Gamma_{\text{total}}$	DOCUMENT ID	TECN	COMMENT	$\Gamma_9/\Gamma$
0.25±0.16	SARANTSEV 19	DPWA	$\bar{K}N$ multichannel	

 $\Lambda(2080)$  REFERENCES

SARANTSEV 19 EPJ A55 180 A.V. Sarantsev et al. (BONN, PNPI)

$$\Lambda(2085) 7/2^+ \quad I(J^P) = 0(\frac{7}{2}^+) \quad \text{Status: **}$$

OMITTED FROM SUMMARY TABLE  
was  $\Lambda(2020)$

In LITCHFIELD 71, need for the state rests solely on a possibly inconsistent polarization measurement at 1.784 GeV/c. HEMINGWAY 75 does not require this state. GOPAL 77 does not need it in either  $N\bar{K}$  or  $\Sigma\pi$ . With new  $K^-n$  angular distributions included, DECLAIS 77 sees it. However, this and other new data are included in GOPAL 80 and the state is not required. BACCARI 77 weakly supports it.

 $\Lambda(2085)$  POLE POSITION

## REAL PART

VALUE	DOCUMENT ID	TECN	COMMENT
1757	<sup>1</sup> KAMANO 15	DPWA	Multichannel
<sup>1</sup> From the preferred solution A in KAMANO 15. Solution B reports $M = 2041^{+80}_{-82}$ MeV.			

## -2xIMAGINARY PART

VALUE	DOCUMENT ID	TECN	COMMENT
146	<sup>1</sup> KAMANO 15	DPWA	Multichannel
<sup>1</sup> From the preferred solution A in KAMANO 15. Solution B reports $M = 238^{+114}_{-34}$ MeV.			

 $\Lambda(2085)$  POLE RESIDUES

The normalized residue is the residue divided by  $\Gamma_{\text{pole}}/2$ .

Normalized residue in  $N\bar{K} \rightarrow \Lambda(2085) \rightarrow N\bar{K}$ 

MODULUS	PHASE (°)	DOCUMENT ID	TECN	COMMENT
0.000145	-77	<sup>1</sup> KAMANO 15	DPWA	Multichannel
<sup>1</sup> From the preferred solution A in KAMANO 15.				

Normalized residue in  $N\bar{K} \rightarrow \Lambda(2085) \rightarrow \Sigma\pi$ 

MODULUS	PHASE (°)	DOCUMENT ID	TECN	COMMENT
0.0112	120	<sup>1</sup> KAMANO 15	DPWA	Multichannel
<sup>1</sup> From the preferred solution A in KAMANO 15.				

Normalized residue in  $N\bar{K} \rightarrow \Lambda(2085) \rightarrow \Lambda\eta$ 

MODULUS	PHASE (°)	DOCUMENT ID	TECN	COMMENT
0.000786	-100	<sup>1</sup> KAMANO 15	DPWA	Multichannel
<sup>1</sup> From the preferred solution A in KAMANO 15.				

Normalized residue in  $N\bar{K} \rightarrow \Lambda(2085) \rightarrow \Sigma(1385)\pi, F\text{-wave}$ 

MODULUS	PHASE (°)	DOCUMENT ID	TECN	COMMENT
0.00451	-82	<sup>1</sup> KAMANO 15	DPWA	Multichannel
<sup>1</sup> From the preferred solution A in KAMANO 15.				

Normalized residue in  $N\bar{K} \rightarrow \Lambda(2085) \rightarrow \Sigma(1385)\pi, H\text{-wave}$ 

MODULUS	PHASE (°)	DOCUMENT ID	TECN	COMMENT
0.0000298	-128	<sup>1</sup> KAMANO 15	DPWA	Multichannel
<sup>1</sup> From the preferred solution A in KAMANO 15.				

 $\Lambda(2085)$  MASS

VALUE (MeV)	DOCUMENT ID	TECN	COMMENT
$\approx 2020$ OUR ESTIMATE			
2043±22	ZHANG 13A	DPWA	Multichannel
2140	BACCARI 77	DPWA	$K^-p \rightarrow \Lambda\omega$
2117	DECLAIS 77	DPWA	$\bar{K}N \rightarrow \bar{K}N$
2100±30	LITCHFIELD 71	DPWA	$K^-p \rightarrow \bar{K}N$
2020±20	BARBARO... 70	DPWA	$K^-p \rightarrow \Sigma\pi$

 $\Lambda(2085)$  WIDTH

VALUE (MeV)	DOCUMENT ID	TECN	COMMENT
200±75	ZHANG 13A	DPWA	Multichannel
128	BACCARI 77	DPWA	$K^-p \rightarrow \Lambda\omega$
167	DECLAIS 77	DPWA	$\bar{K}N \rightarrow \bar{K}N$
120±30	LITCHFIELD 71	DPWA	$K^-p \rightarrow \bar{K}N$
160±30	BARBARO... 70	DPWA	$K^-p \rightarrow \Sigma\pi$

 $\Lambda(2085)$  DECAY MODES

Mode	Fraction ( $\Gamma_i/\Gamma$ )
$\Gamma_1$ $N\bar{K}$	
$\Gamma_2$ $\Sigma\pi$	
$\Gamma_3$ $\Lambda\eta$	
$\Gamma_4$ $\Sigma(1385)\pi, F\text{-wave}$	
$\Gamma_5$ $\Sigma(1385)\pi, H\text{-wave}$	
$\Gamma_6$ $N\bar{K}^*(892), S=1/2, F\text{-wave}$	
$\Gamma_7$ $N\bar{K}^*(892), S=3/2, F\text{-wave}$	
$\Gamma_8$ $N\bar{K}^*(892), S=3/2, H\text{-wave}$	
$\Gamma_9$ $\Lambda\omega$	
$\Gamma_{10}$ $N\bar{K}^*(892), S=1/2$	(30±9) %

 $\Lambda(2085)$  BRANCHING RATIOS

See "Sign conventions for resonance couplings" in the Note on  $\Lambda$  and  $\Sigma$  Resonances.

$\Gamma(N\bar{K})/\Gamma_{\text{total}}$	DOCUMENT ID	TECN	COMMENT	$\Gamma_1/\Gamma$
0.028±0.005	ZHANG 13A	DPWA	Multichannel	
0.05	DECLAIS 77	DPWA	$\bar{K}N \rightarrow \bar{K}N$	
0.05 ±0.02	LITCHFIELD 71	DPWA	$K^-p \rightarrow \bar{K}N$	
••• We do not use the following data for averages, fits, limits, etc. •••				
not seen	<sup>1</sup> KAMANO 15	DPWA	Multichannel	
<sup>1</sup> From the preferred solution A in KAMANO 15.				

$\Gamma(\Sigma\pi)/\Gamma_{\text{total}}$	DOCUMENT ID	TECN	COMMENT	$\Gamma_2/\Gamma$
0.891	<sup>1</sup> KAMANO 15	DPWA	Multichannel	
<sup>1</sup> From the preferred solution A in KAMANO 15.				

Baryon Particle Listings
Λ(2085), Λ(2100)

Γ(Λη)/Γtotal Γ3/Γ

Table with columns: VALUE, DOCUMENT ID, TECN, COMMENT. Row 1: 0.002, 1 KAMANO 15 DPWA Multichannel. Note: We do not use the following data for averages, fits, limits, etc.

Γ(Σ(1385)π, F-wave)/Γtotal Γ4/Γ

Table with columns: VALUE, DOCUMENT ID, TECN, COMMENT. Row 1: 0.105, 1 KAMANO 15 DPWA Multichannel. Note: We do not use the following data for averages, fits, limits, etc.

Γ(Σ(1385)π, H-wave)/Γtotal Γ5/Γ

Table with columns: VALUE, DOCUMENT ID, TECN, COMMENT. Row 1: not seen, 1 KAMANO 15 DPWA Multichannel. Note: We do not use the following data for averages, fits, limits, etc.

Γ(NK\*(892), S=1/2, F-wave)/Γtotal Γ6/Γ

Table with columns: VALUE, DOCUMENT ID, TECN, COMMENT. Row 1: not seen, 1 KAMANO 15 DPWA Multichannel. Note: We do not use the following data for averages, fits, limits, etc.

Γ(NK\*(892), S=3/2, F-wave)/Γtotal Γ7/Γ

Table with columns: VALUE, DOCUMENT ID, TECN, COMMENT. Row 1: 0.001, 1 KAMANO 15 DPWA Multichannel. Note: We do not use the following data for averages, fits, limits, etc.

Γ(NK\*(892), S=3/2, H-wave)/Γtotal Γ8/Γ

Table with columns: VALUE, DOCUMENT ID, TECN, COMMENT. Row 1: not seen, 1 KAMANO 15 DPWA Multichannel. Note: We do not use the following data for averages, fits, limits, etc.

Γ(NK\*(892), S=1/2)/Γtotal Γ10/Γ

Table with columns: VALUE, DOCUMENT ID, TECN, COMMENT. Row 1: 0.30±0.09, ZHANG 13A DPWA Multichannel.

(Γ1Γf)1/2/Γtotal in NK → Λ(2085) → Σπ (Γ1Γ2)1/2/Γ

Table with columns: VALUE, DOCUMENT ID, TECN, COMMENT. Row 1: +0.02±0.01, ZHANG 13A DPWA Multichannel. Row 2: -0.15±0.02, BARBARO... 70 DPWA K-ρ → Σπ.

(Γ1Γf)1/2/Γtotal in NK → Λ(2085) → Λω (Γ1Γ9)1/2/Γ

Table with columns: VALUE, DOCUMENT ID, TECN, COMMENT. Row 1: <0.05, BACCARI 77 DPWA K-ρ → Λω.

Λ(2085) REFERENCES

Reference list for Λ(2085) with columns: Author, Year, Conference/Journal, and other details.

Λ(2100) 7/2- I(JP) = 0(7/2-) Status: \*\*\*\*

Most of the results published before 1973 are now obsolete and have been omitted. They may be found in our 1982 edition Physics Letters 111B 1 (1982).

This entry only includes results from partial-wave analyses. Parameters of peaks seen in cross sections and in invariant-mass distributions around 2100 MeV used to be listed in a separate entry immediately following. It may be found in our 1986 edition Physics Letters 170B 1 (1986).

Λ(2100) POLE POSITION

REAL PART

Table with columns: VALUE (MeV), DOCUMENT ID, TECN, COMMENT. Row 1: 2040±14, SARANTSEV 19 DPWA KN multichannel.

-2xIMAGINARY PART

Table with columns: VALUE (MeV), DOCUMENT ID, TECN, COMMENT. Row 1: 215±29, SARANTSEV 19 DPWA KN multichannel.

Λ(2100) POLE RESIDUE

The "normalized residue" is the residue divided by Γpole/2.

Normalized residue in NK → Λ(2100) → NK

Table with columns: MODULUS, PHASE (°), DOCUMENT ID, TECN, COMMENT. Row 1: 0.28±0.06, -40±10, SARANTSEV 19 DPWA KN multichannel.

Normalized residue in NK → Λ(2100) → Σπ

Table with columns: MODULUS, PHASE (°), DOCUMENT ID, TECN, COMMENT. Row 1: 0.09±0.02, -35±15, SARANTSEV 19 DPWA KN multichannel.

Normalized residue in NK → Λ(2100) → Σ(1385)π, D-wave

Table with columns: MODULUS, PHASE (°), DOCUMENT ID, TECN, COMMENT. Row 1: 0.04±0.03, SARANTSEV 19 DPWA KN multichannel.

Normalized residue in NK → Λ(2100) → Σ(1385)π, G-wave

Table with columns: MODULUS, PHASE (°), DOCUMENT ID, TECN, COMMENT. Row 1: 0.06±0.03, -45±15, SARANTSEV 19 DPWA KN multichannel.

Normalized residue in NK → Λ(2100) → NK\*(892), S=3/2, D-wave

Table with columns: MODULUS, PHASE (°), DOCUMENT ID, TECN, COMMENT. Row 1: 0.11±0.06, -30±30, SARANTSEV 19 DPWA KN multichannel.

Λ(2100) MASS

Table with columns: VALUE (MeV), DOCUMENT ID, TECN, COMMENT. Section: 2090 to 2110 (≈ 2100) OUR ESTIMATE. Rows include SARANTSEV, ZHANG, GOPAL, DEBELLEFON, HEMINGWAY, KANE, BACCARI, DECLAIS, NAKKASYAN.

Λ(2100) WIDTH

Table with columns: VALUE (MeV), DOCUMENT ID, TECN, COMMENT. Section: 100 to 250 (≈ 200) OUR ESTIMATE. Rows include SARANTSEV, ZHANG, DEBELLEFON, GOPAL, HEMINGWAY, KANE, BACCARI, DECLAIS, NAKKASYAN.

Λ(2100) DECAY MODES

Table with columns: Mode, Fraction (Γi/Γ). Rows include NK, Σπ, Λη, ΣK, Λω, NK\*(892), Σ(1385)π, D-wave, Σ(1385)π, G-wave, NK\*(892), S=3/2, D-wave, NK\*(892), S=1/2, G-wave, NK\*(892), S=3/2, G-wave.

Λ(2100) BRANCHING RATIOS

See "Sign conventions for resonance couplings" in the Note on Λ and Σ Resonances.

Γ(NK)/Γtotal Γ1/Γ

Table with columns: VALUE, DOCUMENT ID, TECN, COMMENT. Row 1: 0.25 to 0.35 (≈ 0.30) OUR ESTIMATE.

Table with columns: VALUE, DOCUMENT ID, TECN, COMMENT. Row 1: 0.24±0.05, SARANTSEV 19 DPWA KN multichannel.

Table with columns: VALUE, DOCUMENT ID, TECN, COMMENT. Row 1: 0.23±0.01, ZHANG 13A DPWA Multichannel.

Table with columns: VALUE, DOCUMENT ID, TECN, COMMENT. Row 1: 0.34±0.03, GOPAL 80 DPWA KN → KN.

Table with columns: VALUE, DOCUMENT ID, TECN, COMMENT. Row 1: 0.24±0.06, DEBELLEFON 78 DPWA KN → KN.

Table with columns: VALUE, DOCUMENT ID, TECN, COMMENT. Row 1: 0.31±0.03, HEMINGWAY 75 DPWA K-ρ → KN.

## Baryon Particle Listings

 $\Lambda(2100)$ ,  $\Lambda(2110)$ 

0.29	DECLAIS	77	DPWA	$\bar{K}N \rightarrow \bar{K}N$
0.30±0.03	GOPAL	77	DPWA	See GOPAL 80

$\Gamma(\Sigma\pi)/\Gamma_{\text{total}}$	DOCUMENT ID	TECN	COMMENT	$\Gamma_2/\Gamma$
0.030±0.015	SARANTSEV	19	DPWA	$\bar{K}N$ multichannel

$\Gamma(\Sigma(1385)\pi, D\text{-wave})/\Gamma_{\text{total}}$	DOCUMENT ID	TECN	COMMENT	$\Gamma_7/\Gamma$
<0.01	SARANTSEV	19	DPWA	$\bar{K}N$ multichannel

$\Gamma(\Sigma(1385)\pi, G\text{-wave})/\Gamma_{\text{total}}$	DOCUMENT ID	TECN	COMMENT	$\Gamma_8/\Gamma$
0.01±0.01	SARANTSEV	19	DPWA	$\bar{K}N$ multichannel

$\Gamma(N\bar{K}^*(892), S=3/2, D\text{-wave})/\Gamma_{\text{total}}$	DOCUMENT ID	TECN	COMMENT	$\Gamma_9/\Gamma$
0.04±0.02	SARANTSEV	19	DPWA	$\bar{K}N$ multichannel

$(\Gamma_1\Gamma_2)^{1/2}/\Gamma_{\text{total}}$ in $N\bar{K} \rightarrow \Lambda(2100) \rightarrow \Sigma\pi$	DOCUMENT ID	TECN	COMMENT	$(\Gamma_1\Gamma_2)^{1/2}/\Gamma$
+0.03±0.01	ZHANG	13A	DPWA	Multichannel
+0.12±0.04	GOPAL	77	DPWA	$\bar{K}N$ multichannel
+0.11±0.01	KANE	74	DPWA	$K^-p \rightarrow \Sigma\pi$

$(\Gamma_1\Gamma_3)^{1/2}/\Gamma_{\text{total}}$ in $N\bar{K} \rightarrow \Lambda(2100) \rightarrow \Lambda\eta$	DOCUMENT ID	TECN	COMMENT	$(\Gamma_1\Gamma_3)^{1/2}/\Gamma$
-0.050±0.020	RADER	73	MPWA	$K^-p \rightarrow \Lambda\eta$

$(\Gamma_1\Gamma_4)^{1/2}/\Gamma_{\text{total}}$ in $N\bar{K} \rightarrow \Lambda(2100) \rightarrow \Xi K$	DOCUMENT ID	TECN	COMMENT	$(\Gamma_1\Gamma_4)^{1/2}/\Gamma$
0.035±0.018	LITCHFIELD	71	DPWA	$K^-p \rightarrow \Xi K$
••• We do not use the following data for averages, fits, limits, etc. •••				
0.003	MULLER	69B	DPWA	$K^-p \rightarrow \Xi K$
0.05	TRIPP	67	RVUE	$K^-p \rightarrow \Xi K$

$(\Gamma_1\Gamma_5)^{1/2}/\Gamma_{\text{total}}$ in $N\bar{K} \rightarrow \Lambda(2100) \rightarrow \Lambda\omega$	DOCUMENT ID	TECN	COMMENT	$(\Gamma_1\Gamma_5)^{1/2}/\Gamma$
-0.070	2 BACCARI	77	DPWA	$GD_{37}$ wave
+0.011	2 BACCARI	77	DPWA	$GG_{17}$ wave
+0.008	2 BACCARI	77	DPWA	$GG_{37}$ wave
0.122 or 0.154	1 NAKKASYAN	75	DPWA	$K^-p \rightarrow \Lambda\omega$

$(\Gamma_1\Gamma_9)^{1/2}/\Gamma_{\text{total}}$ in $N\bar{K} \rightarrow \Lambda(2100) \rightarrow N\bar{K}^*(892), S=3/2, D\text{-wave}$	DOCUMENT ID	TECN	COMMENT	$(\Gamma_1\Gamma_9)^{1/2}/\Gamma$
+0.16±0.02	ZHANG	13A	DPWA	Multichannel
+0.21±0.04	CAMERON	78B	DPWA	$K^-p \rightarrow N\bar{K}^*$

$(\Gamma_1\Gamma_{10})^{1/2}/\Gamma_{\text{total}}$ in $N\bar{K} \rightarrow \Lambda(2100) \rightarrow N\bar{K}^*(892), S=1/2, G\text{-wave}$	DOCUMENT ID	TECN	COMMENT	$(\Gamma_1\Gamma_{10})^{1/2}/\Gamma$
-0.03±0.02	ZHANG	13A	DPWA	Multichannel
-0.04±0.03	3 CAMERON	78B	DPWA	$K^-p \rightarrow N\bar{K}^*$

$(\Gamma_1\Gamma_{11})^{1/2}/\Gamma_{\text{total}}$ in $N\bar{K} \rightarrow \Lambda(2100) \rightarrow N\bar{K}^*(892), S=3/2, G\text{-wave}$	DOCUMENT ID	TECN	COMMENT	$(\Gamma_1\Gamma_{11})^{1/2}/\Gamma$
+0.08±0.02	ZHANG	13A	DPWA	Multichannel

 $\Lambda(2100)$  FOOTNOTES

<sup>1</sup> The NAKKASYAN 75 values are from the two best solutions found. Each has the  $\Lambda(2100)$  and one additional resonance ( $P_3$  or  $F_5$ ).

<sup>2</sup> Note that the three for BACCARI 77 entries are for three different waves.

<sup>3</sup> The published sign has been changed to be in accord with the baryon-first convention. The upper limit on the  $G_3$  wave is 0.03.

 $\Lambda(2100)$  REFERENCES

SARANTSEV	19	EPJ A55 180	A.V. Sarantsev et al.	(BONN, PNPI)
ZHANG	13A	PR C88 035205	H. Zhang et al.	(KSU)
PDG	86	PL 170B 1	M. Aguilar-Benitez et al.	(CERN, CIT+)
PDG	82	PL 111B 1	M. Roos et al.	(HELSE, CIT, CERN)
GOPAL	80	Toronto Conf. 159	G.P. Gopal	(RHEL) IJP
CAMERON	78B	NP B146 327	W. Cameron et al.	(RHEL, LOIC) IJP
DEBELLEFON	78	NC 42A 403	A. de Bellefon et al.	(CDEF, SAEL) IJP
BACCARI	77	NC 41A 96	B. Baccari et al.	(SAEL, CDEF) IJP
DECLAIS	77	CERN 77-16	Y. Declais et al.	(CAEN, CERN) IJP
GOPAL	77	NP B119 362	G.P. Gopal et al.	(LOIC, RHEL) IJP
HEMINGWAY	75	NP B91 12	R.J. Hemingway et al.	(CERN, HEIDH, MPIM) IJP
NAKKASYAN	75	NP B93 85	A. Nakkasyan	(CERN) IJP
KANE	74	LBL-2452	D.F. Kane	(LBL) IJP
RADER	73	NC 16A 178	R.K. Rader et al.	(SAEL, HEID, CERN+) IJP
LITCHFIELD	71	NP B30 125	P.J. Litchfield et al.	(RHEL, CDEF, SAEL) IJP
MULLER	69B	Thesis UCRL 19372	R.A. Muller	(LRL)
TRIPP	67	NP B3 10	R.D. Tripp et al.	(LRL, SLAC, CERN+)

 $\Lambda(2110) 5/2^+$ 

$$I(J^P) = 0(\frac{5}{2}^+) \text{ Status: } ***$$

For results published before 1974 (they are now obsolete), see our 1982 edition Physics Letters **111B** 1 (1982). All the references have been retained.

This resonance is in the Baryon Summary Table, but the evidence for it could be better.

 $\Lambda(2110)$  POLE POSITION

## REAL PART

VALUE (MeV)	DOCUMENT ID	TECN	COMMENT
2048±10	SARANTSEV	19	DPWA $\bar{K}N$ multichannel
••• We do not use the following data for averages, fits, limits, etc. •••			
1970	ZHANG	13A	DPWA $\bar{K}N$ multichannel

## -2xIMAGINARY PART

VALUE (MeV)	DOCUMENT ID	TECN	COMMENT
255±20	SARANTSEV	19	DPWA $\bar{K}N$ multichannel
••• We do not use the following data for averages, fits, limits, etc. •••			
350	ZHANG	13A	DPWA $\bar{K}N$ multichannel

 $\Lambda(2110)$  POLE RESIDUE

The "normalized residue" is the residue divided by  $\Gamma_{\text{pole}}/2$ .

Normalized residue in  $N\bar{K} \rightarrow \Lambda(2110) \rightarrow N\bar{K}$ 

MODULUS	PHASE (°)	DOCUMENT ID	TECN	COMMENT
0.020±0.005	5 ± 15	SARANTSEV	19	DPWA $\bar{K}N$ multichannel

Normalized residue in  $N\bar{K} \rightarrow \Lambda(2110) \rightarrow \Sigma\pi$ 

MODULUS	PHASE (°)	DOCUMENT ID	TECN	COMMENT
0.13±0.03	0 ± 15	SARANTSEV	19	DPWA $\bar{K}N$ multichannel

Normalized residue in  $N\bar{K} \rightarrow \Lambda(2110) \rightarrow \Xi K$ 

MODULUS	PHASE (°)	DOCUMENT ID	TECN	COMMENT
0.005±0.005		SARANTSEV	19	DPWA $\bar{K}N$ multichannel

Normalized residue in  $N\bar{K} \rightarrow \Lambda(2110) \rightarrow \Lambda\omega, S=1/2, P\text{-wave}$ 

MODULUS	PHASE (°)	DOCUMENT ID	TECN	COMMENT
0.01±0.01		SARANTSEV	19	DPWA $\bar{K}N$ multichannel

Normalized residue in  $N\bar{K} \rightarrow \Lambda(2110) \rightarrow \Lambda\omega, S=3/2, P\text{-wave}$ 

MODULUS	PHASE (°)	DOCUMENT ID	TECN	COMMENT
0.03±0.01	-7 ± 16	SARANTSEV	19	DPWA $\bar{K}N$ multichannel

Normalized residue in  $N\bar{K} \rightarrow \Lambda(2110) \rightarrow \Lambda\omega, S=3/2, F\text{-wave}$ 

MODULUS	PHASE (°)	DOCUMENT ID	TECN	COMMENT
0.01±0.01		SARANTSEV	19	DPWA $\bar{K}N$ multichannel

 $\Lambda(2110)$  MASS

VALUE (MeV)	DOCUMENT ID	TECN	COMMENT
<b>2050 to 2130 (≈ 2090) OUR ESTIMATE</b>			
2086±12	SARANTSEV	19	DPWA $\bar{K}N$ multichannel
2036±13	ZHANG	13A	DPWA $\bar{K}N$ multichannel
2092±25	GOPAL	80	DPWA $\bar{K}N \rightarrow \bar{K}N$
2125±25	CAMERON	78B	DPWA $K^-p \rightarrow N\bar{K}^*$
2106±50	DEBELLEFON	78	DPWA $\bar{K}N \rightarrow \bar{K}N$
2140±20	DEBELLEFON	77	DPWA $K^-p \rightarrow \Sigma\pi$
2100±50	GOPAL	77	DPWA $\bar{K}N$ multichannel
2112±7	KANE	74	DPWA $K^-p \rightarrow \Sigma\pi$
••• We do not use the following data for averages, fits, limits, etc. •••			
2137	BACCARI	77	DPWA $K^-p \rightarrow \Lambda\omega$
2103	1 NAKKASYAN	75	DPWA $K^-p \rightarrow \Lambda\omega$

 $\Lambda(2110)$  WIDTH

VALUE (MeV)	DOCUMENT ID	TECN	COMMENT
<b>200 to 300 (≈ 250) OUR ESTIMATE</b>			
274±25	SARANTSEV	19	DPWA $\bar{K}N$ multichannel
400±38	ZHANG	13A	DPWA $\bar{K}N$ multichannel
245±25	GOPAL	80	DPWA $\bar{K}N \rightarrow \bar{K}N$
160±30	CAMERON	78B	DPWA $K^-p \rightarrow N\bar{K}^*$
251±50	DEBELLEFON	78	DPWA $\bar{K}N \rightarrow \bar{K}N$
140±20	DEBELLEFON	77	DPWA $K^-p \rightarrow \Sigma\pi$
200±50	GOPAL	77	DPWA $\bar{K}N$ multichannel
190±30	KANE	74	DPWA $K^-p \rightarrow \Sigma\pi$
••• We do not use the following data for averages, fits, limits, etc. •••			
132	BACCARI	77	DPWA $K^-p \rightarrow \Lambda\omega$
391	1 NAKKASYAN	75	DPWA $K^-p \rightarrow \Lambda\omega$

# Baryon Particle Listings

## $\Lambda(2110), \Lambda(2325)$

### $\Lambda(2110)$ DECAY MODES

Mode	Fraction ( $\Gamma_i/\Gamma$ )
$\Gamma_1$ $N\bar{K}$	5–25 %
$\Gamma_2$ $\Sigma\pi$	10–40 %
$\Gamma_3$ $\Lambda\omega$	seen
$\Gamma_4$ $\Lambda\omega, S=1/2, P$ -wave	
$\Gamma_5$ $\Lambda\omega, S=3/2, P$ -wave	(5.0±2.0) %
$\Gamma_6$ $\Lambda\omega, S=3/2, F$ -wave	
$\Gamma_7$ $\Xi K$	
$\Gamma_8$ $\Sigma(1385)\pi$	seen
$\Gamma_9$ $\Sigma(1385)\pi, P$ -wave	
$\Gamma_{10}$ $N\bar{K}^*(892)$	10–60 %
$\Gamma_{11}$ $N\bar{K}^*(892), S=1/2$	
$\Gamma_{12}$ $N\bar{K}^*(892), S=3/2, P$ -wave	

### $\Lambda(2110)$ BRANCHING RATIOS

See “Sign conventions for resonance couplings” in the Note on  $\Lambda$  and  $\Sigma$  Resonances.

$\Gamma(N\bar{K})/\Gamma_{\text{total}}$	DOCUMENT ID	TECN	COMMENT	$\Gamma_1/\Gamma$
<b>0.05 to 0.25 OUR ESTIMATE</b>				
0.020±0.005	SARANTSEV 19	DPWA	$\bar{K}N$ multichannel	
0.083±0.005	ZHANG 13A	DPWA	$\bar{K}N$ multichannel	
0.07±0.03	GOPAL 80	DPWA	$\bar{K}N \rightarrow \bar{K}N$	
0.27±0.06	2 DEBELLEFON 78	DPWA	$\bar{K}N \rightarrow \bar{K}N$	
••• We do not use the following data for averages, fits, limits, etc. •••				
0.07±0.03	GOPAL 77	DPWA	See GOPAL 80	

$\Gamma(\Sigma\pi)/\Gamma_{\text{total}}$	DOCUMENT ID	TECN	COMMENT	$\Gamma_2/\Gamma$
<b>0.88±0.20</b>	SARANTSEV 19	DPWA	$\bar{K}N$ multichannel	

$\Gamma(\Lambda\omega, S=1/2, P\text{-wave})/\Gamma_{\text{total}}$	DOCUMENT ID	TECN	COMMENT	$\Gamma_4/\Gamma$
VALUE	DOCUMENT ID	TECN	COMMENT	
<0.01	SARANTSEV 19	DPWA	$\bar{K}N$ multichannel	

$\Gamma(\Lambda\omega, S=3/2, P\text{-wave})/\Gamma_{\text{total}}$	DOCUMENT ID	TECN	COMMENT	$\Gamma_5/\Gamma$
VALUE	DOCUMENT ID	TECN	COMMENT	
0.05±0.02	SARANTSEV 19	DPWA	$\bar{K}N$ multichannel	

$\Gamma(\Lambda\omega, S=3/2, F\text{-wave})/\Gamma_{\text{total}}$	DOCUMENT ID	TECN	COMMENT	$\Gamma_6/\Gamma$
VALUE	DOCUMENT ID	TECN	COMMENT	
<0.01	SARANTSEV 19	DPWA	$\bar{K}N$ multichannel	

$\Gamma(\Xi K)/\Gamma_{\text{total}}$	DOCUMENT ID	TECN	COMMENT	$\Gamma_7/\Gamma$
VALUE	DOCUMENT ID	TECN	COMMENT	
~ 0	SARANTSEV 19	DPWA	$\bar{K}N$ multichannel	

$(\Gamma_1\Gamma_2)^{1/2}/\Gamma_{\text{total}}$ in $N\bar{K} \rightarrow \Lambda(2110) \rightarrow \Sigma\pi$	DOCUMENT ID	TECN	COMMENT	$(\Gamma_1\Gamma_2)^{1/2}/\Gamma$
VALUE	DOCUMENT ID	TECN	COMMENT	
+0.04±0.01	ZHANG 13A	DPWA	Multichannel	
+0.14±0.01	DEBELLEFON 77	DPWA	$K^-p \rightarrow \Sigma\pi$	
+0.20±0.03	KANE 74	DPWA	$K^-p \rightarrow \Sigma\pi$	
••• We do not use the following data for averages, fits, limits, etc. •••				
+0.10±0.03	GOPAL 77	DPWA	$\bar{K}N$ multichannel	

$(\Gamma_1\Gamma_2)^{1/2}/\Gamma_{\text{total}}$ in $N\bar{K} \rightarrow \Lambda(2110) \rightarrow \Lambda\omega$	DOCUMENT ID	TECN	COMMENT	$(\Gamma_1\Gamma_2)^{1/2}/\Gamma$
VALUE	DOCUMENT ID	TECN	COMMENT	
<0.05	BACCARI 77	DPWA	$K^-p \rightarrow \Lambda\omega$	
0.112	1 NAKKASYAN 75	DPWA	$K^-p \rightarrow \Lambda\omega$	

$(\Gamma_1\Gamma_2)^{1/2}/\Gamma_{\text{total}}$ in $N\bar{K} \rightarrow \Lambda(2110) \rightarrow \Sigma(1385)\pi, P$ -wave	DOCUMENT ID	TECN	COMMENT	$(\Gamma_1\Gamma_2)^{1/2}/\Gamma$
VALUE	DOCUMENT ID	TECN	COMMENT	
+0.04±0.01	ZHANG 13A	DPWA	Multichannel	
+0.071±0.025	3 CAMERON 78	DPWA	$K^-p \rightarrow \Sigma(1385)\pi$	

$(\Gamma_1\Gamma_2)^{1/2}/\Gamma_{\text{total}}$ in $N\bar{K} \rightarrow \Lambda(2110) \rightarrow N\bar{K}^*(892), S=1/2$	DOCUMENT ID	TECN	COMMENT	$(\Gamma_1\Gamma_2)^{1/2}/\Gamma$
VALUE	DOCUMENT ID	TECN	COMMENT	
-0.09±0.01	ZHANG 13A	DPWA	Multichannel	
-0.17±0.04	4 CAMERON 78B	DPWA	$K^-p \rightarrow N\bar{K}^*$	

$(\Gamma_1\Gamma_2)^{1/2}/\Gamma_{\text{total}}$ in $N\bar{K} \rightarrow \Lambda(2110) \rightarrow N\bar{K}^*(892), S=3/2, P$ -wave	DOCUMENT ID	TECN	COMMENT	$(\Gamma_1\Gamma_2)^{1/2}/\Gamma$
VALUE	DOCUMENT ID	TECN	COMMENT	
0.24±0.01	ZHANG 13A	DPWA	Multichannel	

### $\Lambda(2110)$ FOOTNOTES

- 1 Found in one of two best solutions.
- 2 The published error of 0.6 was a misprint.
- 3 The CAMERON 78 upper limit on  $F$ -wave decay is 0.03. The sign here has been changed to be in accord with the baryon-first convention.
- 4 The published sign has been changed to be in accord with the baryon-first convention. The CAMERON 78B upper limits on the  $P_3$  and  $F_3$  waves are each 0.03.

### $\Lambda(2110)$ REFERENCES

SARANTSEV 19	EPJ A55 180	A.V. Sarantsev et al.	(BONN, PNPI)
ZHANG 13A	PR C88 035205	H. Zhang et al.	(KSU)
PDG 82	PL 111B 1	M. Roos et al.	(HELS, CIT, CERN)
GOPAL 80	Toronto Conf. 159	G.P. Gopal	(RHEL) IJP
CAMERON 78	NP B143 189	W. Cameron et al.	(RHEL, LOIC) IJP
CAMERON 78B	NP B146 327	W. Cameron et al.	(RHEL, LOIC) IJP
DEBELLEFON 78	NC 42A 403	A. de Bellefon et al.	(CDEF, SACL) IJP
BACCARI 77	NC 41A 96	B. Baccari et al.	(SACL, CDEF) IJP
DEBELLEFON 77	NC 37A 175	A. de Bellefon et al.	(CDEF, SACL) IJP
GOPAL 77	NP B119 362	G.P. Gopal et al.	(LOIC, RHEL) IJP
NAKKASYAN 75	NP B93 85	A. Nakkasyan	(CERN) IJP
KANE 74	LBL-2452	D.F. Kane	(LBL) IJP

## $\Lambda(2325) 3/2^-$

$$I(J^P) = 0(\frac{3}{2}^-) \text{ Status: } *$$

OMITTED FROM SUMMARY TABLE

BACCARI 77 finds this state with either  $J^P = 3/2^-$  or  $3/2^+$  in a energy-dependent partial-wave analyses of  $K^-p \rightarrow \Lambda\omega$  from 2070 to 2436 MeV. A subsequent semi-energy-independent analysis from threshold to 2436 MeV selects  $3/2^-$ . DEBELLEFON 78 (same group) also sees this state in an energy-dependent partial-wave analysis of  $K^-p \rightarrow \bar{K}N$  data, and finds  $J^P = 3/2^-$  or  $3/2^+$ . They again prefer  $J^P = 3/2^-$ , but only on the basis of model-dependent considerations.

### $\Lambda(2325)$ MASS

VALUE (MeV)	DOCUMENT ID	TECN	COMMENT
<b>≈ 2325 OUR ESTIMATE</b>			
2342±30	DEBELLEFON 78	DPWA	$\bar{K}N \rightarrow \bar{K}N$
2327±20	BACCARI 77	DPWA	$K^-p \rightarrow \Lambda\omega$

### $\Lambda(2325)$ WIDTH

VALUE (MeV)	DOCUMENT ID	TECN	COMMENT
177±40	DEBELLEFON 78	DPWA	$\bar{K}N \rightarrow \bar{K}N$
160±40	BACCARI 77	IPWA	$K^-p \rightarrow \Lambda\omega$

### $\Lambda(2325)$ DECAY MODES

Mode
$\Gamma_1$ $N\bar{K}$
$\Gamma_2$ $\Lambda\omega$

### $\Lambda(2325)$ BRANCHING RATIOS

$\Gamma(N\bar{K})/\Gamma_{\text{total}}$	DOCUMENT ID	TECN	COMMENT	$\Gamma_1/\Gamma$
VALUE	DOCUMENT ID	TECN	COMMENT	
0.19±0.06	DEBELLEFON 78	DPWA	$\bar{K}N \rightarrow \bar{K}N$	

$(\Gamma_1\Gamma_2)^{1/2}/\Gamma_{\text{total}}$ in $N\bar{K} \rightarrow \Lambda(2325) \rightarrow \Lambda\omega$	DOCUMENT ID	TECN	COMMENT	$(\Gamma_1\Gamma_2)^{1/2}/\Gamma$
VALUE	DOCUMENT ID	TECN	COMMENT	
0.06±0.02	1 BACCARI 77	IPWA	$DS_{33}$ wave	
0.05±0.02	1 BACCARI 77	DPWA	$DD_{13}$ wave	
0.08±0.03	1 BACCARI 77	DPWA	$DD_{33}$ wave	

### $\Lambda(2325)$ FOOTNOTES

- 1 Note that the three BACCARI 77 entries are for three different waves.

### $\Lambda(2325)$ REFERENCES

DEBELLEFON 78	NC 42A 403	A. de Bellefon et al.	(CDEF, SACL) IJP
BACCARI 77	NC 41A 96	B. Baccari et al.	(SACL, CDEF) IJP

## Baryon Particle Listings

 $\Lambda(2325)$ ,  $\Lambda(2350)$ ,  $\Lambda(2585)$  Bumps **$\Lambda(2350)$   $9/2^+$**  $I(J^P) = 0(\frac{9}{2}^+)$  Status: \*\*\*

DAUM 68 favors  $J^P = 7/2^-$  or  $9/2^+$ . BRICMAN 70 favors  $9/2^+$ . LASINSKI 71 suggests three states in this region using a Pomeron + resonances model. There are now also three formation experiments from the College de France-Saclay group, DEBELLEFON 77, BACCARI 77, and DEBELLEFON 78, which find  $9/2^+$  in energy-dependent partial-wave analyses of  $\bar{K}N \rightarrow \Sigma\pi$ ,  $\Lambda\omega$ , and  $N\bar{K}$ .

 **$\Lambda(2350)$  MASS**

VALUE (MeV)	DOCUMENT ID	TECN	COMMENT
<b>2340 to 2370 (<math>\approx 2350</math>) OUR ESTIMATE</b>			
2370 $\pm$ 50	DEBELLEFON 78	DPWA	$\bar{K}N \rightarrow \bar{K}N$
2365 $\pm$ 20	DEBELLEFON 77	DPWA	$K^-p \rightarrow \Sigma\pi$
2358 $\pm$ 6	BRICMAN 70	CNTR	Total, charge exchange
• • • We do not use the following data for averages, fits, limits, etc. • • •			
2372	BACCARI 77	DPWA	$K^-p \rightarrow \Lambda\omega$
2344 $\pm$ 15	COOL 70	CNTR	$K^-p$ , $K^-d$ total
2360 $\pm$ 20	LU 70	CNTR	$\gamma p \rightarrow K^+Y^*$
2340 $\pm$ 7	BUGG 68	CNTR	$K^-p$ , $K^-d$ total

 **$\Lambda(2350)$  WIDTH**

VALUE (MeV)	DOCUMENT ID	TECN	COMMENT
<b>100 to 250 (<math>\approx 150</math>) OUR ESTIMATE</b>			
204 $\pm$ 50	DEBELLEFON 78	DPWA	$\bar{K}N \rightarrow \bar{K}N$
110 $\pm$ 20	DEBELLEFON 77	DPWA	$K^-p \rightarrow \Sigma\pi$
324 $\pm$ 30	BRICMAN 70	CNTR	Total, charge exchange
• • • We do not use the following data for averages, fits, limits, etc. • • •			
257	BACCARI 77	DPWA	$K^-p \rightarrow \Lambda\omega$
190	COOL 70	CNTR	$K^-p$ , $K^-d$ total
55	LU 70	CNTR	$\gamma p \rightarrow K^+Y^*$
140 $\pm$ 20	BUGG 68	CNTR	$K^-p$ , $K^-d$ total

 **$\Lambda(2350)$  DECAY MODES**

Mode	Fraction ( $\Gamma_i/\Gamma$ )
$\Gamma_1$ $N\bar{K}$	$\sim 12\%$
$\Gamma_2$ $\Sigma\pi$	$\sim 10\%$
$\Gamma_3$ $\Lambda\omega$	

 **$\Lambda(2350)$  BRANCHING RATIOS**

See "Sign conventions for resonance couplings" in the Note on  $\Lambda$  and  $\Sigma$  Resonances.

$\Gamma(N\bar{K})/\Gamma_{\text{total}}$	DOCUMENT ID	TECN	COMMENT	$\Gamma_1/\Gamma$
<b><math>\sim 0.12</math> OUR ESTIMATE</b>				
0.12 $\pm$ 0.04	DEBELLEFON 78	DPWA	$\bar{K}N \rightarrow \bar{K}N$	
$(\Gamma_1\Gamma_2)^{1/2}/\Gamma_{\text{total}}$ in $N\bar{K} \rightarrow \Lambda(2350) \rightarrow \Sigma\pi$				$(\Gamma_1\Gamma_2)^{1/2}/\Gamma$
VALUE	DOCUMENT ID	TECN	COMMENT	
-0.11 $\pm$ 0.02	DEBELLEFON 77	DPWA	$K^-p \rightarrow \Sigma\pi$	
$(\Gamma_1\Gamma_3)^{1/2}/\Gamma_{\text{total}}$ in $N\bar{K} \rightarrow \Lambda(2350) \rightarrow \Lambda\omega$				$(\Gamma_1\Gamma_3)^{1/2}/\Gamma$
VALUE	DOCUMENT ID	TECN	COMMENT	
<0.05	BACCARI 77	DPWA	$K^-p \rightarrow \Lambda\omega$	

 **$\Lambda(2350)$  REFERENCES**

DEBELLEFON 78	NC 42A 403	A. de Bellefón et al.	(CDEF, SACL)JUP
BACCARI 77	NC 41A 96	B. Baccari et al.	(SACL, CDEF)JUP
DEBELLEFON 77	NC 37A 175	A. de Bellefón et al.	(CDEF, SACL)JUP
LASINSKI 71	NP B29 125	T.A. Lasinski	(EF)JUP
BRICMAN 70	PL 31B 152	C. Bricman et al.	(CERN, CAEN, SACL)
COOL 70	PR D1 1887	R.L. Cool et al.	(BNL)I
Also	PRL 16 1228	R.L. Cool et al.	(BNL)I
LU 70	PR D2 1846	D.C. Lu et al.	(YALE)
BUGG 68	PR 168 1466	D.V. Bugg et al.	(RHEL, BIRM, CAVE)I
DAUM 68	NP B7 19	C. Daum et al.	(CERN)JP

 **$\Lambda(2585)$  Bumps** $I(J^P) = 0(?^?)$  Status: \*\*

OMITTED FROM SUMMARY TABLE

 **$\Lambda(2585)$  MASS (BUMPS)**

VALUE (MeV)	DOCUMENT ID	TECN	COMMENT
<b><math>\approx 2585</math> OUR ESTIMATE</b>			
2585 $\pm$ 45	ABRAMS 70	CNTR	$K^-p$ , $K^-d$ total
2530 $\pm$ 25	LU 70	CNTR	$\gamma p \rightarrow K^+Y^*$

 **$\Lambda(2585)$  WIDTH (BUMPS)**

VALUE (MeV)	DOCUMENT ID	TECN	COMMENT
300	ABRAMS 70	CNTR	$K^-p$ , $K^-d$ total
150	LU 70	CNTR	$\gamma p \rightarrow K^+Y^*$

 **$\Lambda(2585)$  DECAY MODES (BUMPS)**

Mode	Fraction ( $\Gamma_i/\Gamma$ )
$\Gamma_1$ $N\bar{K}$	

 **$\Lambda(2585)$  BRANCHING RATIOS (BUMPS)**

$(J+\frac{1}{2}) \times \Gamma(N\bar{K})/\Gamma_{\text{total}}$   $\Gamma_1/\Gamma$   
 $J$  is not known, so only  $(J+\frac{1}{2}) \times \Gamma(N\bar{K})/\Gamma_{\text{total}}$  can be given.

VALUE	DOCUMENT ID	TECN	COMMENT
1	ABRAMS 70	CNTR	$K^-p$ , $K^-d$ total
0.12 $\pm$ 0.12	<sup>1</sup> BRICMAN 70	CNTR	Total, charge exchange

 **$\Lambda(2585)$  FOOTNOTES (BUMPS)**

<sup>1</sup>The resonance is at the end of the region analyzed — no clear signal.

 **$\Lambda(2585)$  REFERENCES (BUMPS)**

ABRAMS 70	PR D1 1917	R.J. Abrams et al.	(BNL)I
Also	PRL 16 1228	R.L. Cool et al.	(BNL)I
BRICMAN 70	PL 31B 152	C. Bricman et al.	(CERN, CAEN, SACL)
LU 70	PR D2 1846	D.C. Lu et al.	(YALE)

## $\Sigma$ BARYONS

### ( $S = -1, I = 1$ )

$\Sigma^+ = uus, \Sigma^0 = uds, \Sigma^- = dds$



$I(J^P) = 1(\frac{1}{2}^+)$  Status: \*\*\*\*

We have omitted some results that have been superseded by later experiments. See our earlier editions.

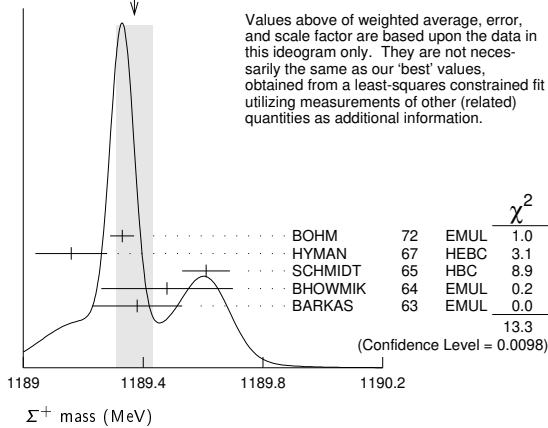
### $\Sigma^+$ MASS

The fit uses  $\Sigma^+, \Sigma^0, \Sigma^-$ , and  $\Lambda$  mass and mass-difference measurements.

VALUE (MeV)	EVTS	DOCUMENT ID	TECN	COMMENT
<b>1189.37 ± 0.07 OUR FIT</b>				Error includes scale factor of 2.2.
<b>1189.37 ± 0.06 OUR AVERAGE</b>				Error includes scale factor of 1.8. See the ideogram below.
1189.33 ± 0.04	607	<sup>1</sup> BOHM 72	EMUL	
1189.16 ± 0.12		HYMAN 67	HEBC	
1189.61 ± 0.08	4205	SCHMIDT 65	HBC	See note with $\Lambda$ mass
1189.48 ± 0.22	58	<sup>2</sup> BHOWMIK 64	EMUL	
1189.38 ± 0.15	144	<sup>2</sup> BARKAS 63	EMUL	

<sup>1</sup>BOHM 72 is updated with our 1973  $K^-, \pi^-,$  and  $\pi^0$  masses (Reviews of Modern Physics **45** S1 (1973)).  
<sup>2</sup>These masses have been raised 30 keV to take into account a 46 keV increase in the proton mass and a 21 keV decrease in the  $\pi^0$  mass (note added 1967 edition, Reviews of Modern Physics **39** 1 (1967)).

WEIGHTED AVERAGE  
1189.37±0.06 (Error scaled by 1.8)



### $\Sigma^+$ MEAN LIFE

Measurements with fewer than 1000 events have been omitted.

VALUE ( $10^{-10}$ s)	EVTS	DOCUMENT ID	TECN	COMMENT
<b>0.8018 ± 0.0026 OUR AVERAGE</b>				
0.8038 ± 0.0040 ± 0.0014		BARBOSA 00	E761	hyperons, 375 GeV
0.8043 ± 0.0080 ± 0.0014		<sup>1</sup> BARBOSA 00	E761	hyperons, 375 GeV
0.798 ± 0.005	30k	MARRAFFINO 80	HBC	$K^-\rho$ 0.42-0.5 GeV/c
0.807 ± 0.013	5719	CONFORTO 76	HBC	$K^-\rho$ 1-1.4 GeV/c
0.795 ± 0.010	20k	EISELE 70	HBC	$K^-\rho$ at rest
0.803 ± 0.008	10664	BARLOUTAUD 69	HBC	$K^-\rho$ 0.4-1.2 GeV/c
0.83 ± 0.032	1300	<sup>2</sup> CHANG 66	HBC	

<sup>1</sup>This is a measurement of the  $\Sigma^-$  lifetime. Here we assume  $CPT$  invariance; see below for the fractional  $\Sigma^+ - \Sigma^-$  lifetime difference obtained by BARBOSA 00.  
<sup>2</sup>We have increased the CHANG 66 error of 0.018; see our 1970 edition, Reviews of Modern Physics **42** 87 (1970).

$(\tau_{\Sigma^+} - \tau_{\Sigma^-}) / \tau_{\Sigma^+}$

A test of  $CPT$  invariance.

VALUE	DOCUMENT ID	TECN	COMMENT
<b><math>(-6 \pm 12) \times 10^{-4}</math></b>	BARBOSA 00	E761	hyperons, 375 GeV

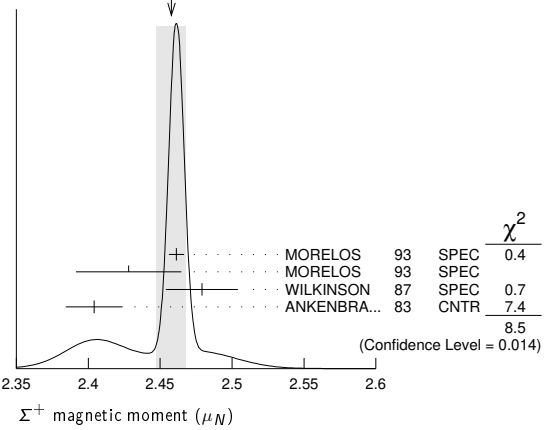
### $\Sigma^+$ MAGNETIC MOMENT

See the "Note on Baryon Magnetic Moments" in the  $\Lambda$  Listings. Measurements with an error  $\geq 0.1 \mu_N$  have been omitted.

VALUE ( $\mu_N$ )	EVTS	DOCUMENT ID	TECN	COMMENT
<b>2.458 ± 0.010 OUR AVERAGE</b>				Error includes scale factor of 2.1. See the ideogram below.
2.4613 ± 0.0034 ± 0.0040	250k	MORELOS 93	SPEC	$p$ Cu 800 GeV
2.428 ± 0.036 ± 0.007	12k	<sup>1</sup> MORELOS 93	SPEC	$p$ Cu 800 GeV
2.479 ± 0.012 ± 0.022	137k	WILKINSON 87	SPEC	$p$ Be 400 GeV
2.4040 ± 0.0198	44k	<sup>2</sup> ANKENBRA... 83	CNTR	$p$ Cu 400 GeV

<sup>1</sup>We assume  $CPT$  invariance: this is (minus) the  $\Sigma^-$  magnetic moment as measured by MORELOS 93. See below for the moment difference testing  $CPT$ .  
<sup>2</sup>ANKENBRANDT 83 gives the value  $2.38 \pm 0.02 \mu_N$ . MORELOS 93 uses the same hyperon magnet and channel and claims to determine the field integral better, leading to the revised value given here.

WEIGHTED AVERAGE  
2.458±0.010 (Error scaled by 2.1)



$(\mu_{\Sigma^+} + \mu_{\Sigma^-}) / \mu_{\Sigma^+}$

A test of  $CPT$  invariance.

VALUE	DOCUMENT ID	TECN	COMMENT
<b>0.014 ± 0.015</b>	<sup>1</sup> MORELOS 93	SPEC	$p$ Cu 800 GeV

<sup>1</sup>This is our calculation from the MORELOS 93 measurements of the  $\Sigma^+$  and  $\Sigma^-$  magnetic moments given above. The statistical error on  $\mu_{\Sigma^-}$  dominates the error here.

### $\Sigma^+$ DECAY MODES

Mode	Fraction ( $\Gamma_i/\Gamma$ )	Confidence level
$\Gamma_1$ $p\pi^0$	(51.57 ± 0.30) %	
$\Gamma_2$ $n\pi^+$	(48.31 ± 0.30) %	
$\Gamma_3$ $p\gamma$	(1.23 ± 0.05) × 10 <sup>-3</sup>	
$\Gamma_4$ $n\pi^+\gamma$	[a] (4.5 ± 0.5) × 10 <sup>-4</sup>	
$\Gamma_5$ $\Lambda e^+\nu_e$	(2.0 ± 0.5) × 10 <sup>-5</sup>	

### $\Delta S = \Delta Q$ ( $SQ$ ) violating modes or $\Delta S = 1$ weak neutral current ( $S1$ ) modes

Mode	Fraction	Confidence level
$\Gamma_6$ $n e^+\nu_e$	$SQ < 5 \times 10^{-6}$	90%
$\Gamma_7$ $n\mu^+\nu_\mu$	$SQ < 3.0 \times 10^{-5}$	90%
$\Gamma_8$ $p e^+ e^-$	$S1 < 7 \times 10^{-6}$	
$\Gamma_9$ $p\mu^+\mu^-$	$S1 (2.4 \pm 1.7) \times 10^{-8}$	

[a] See the Listings below for the pion momentum range used in this measurement.

### CONSTRAINED FIT INFORMATION

An overall fit to 2 branching ratios uses 14 measurements and one constraint to determine 3 parameters. The overall fit has a  $\chi^2 = 7.7$  for 12 degrees of freedom.

The following *off-diagonal* array elements are the correlation coefficients  $\langle \delta x_i \delta x_j \rangle / (\delta x_i \delta x_j)$ , in percent, from the fit to the branching fractions,  $x_i \equiv \Gamma_i / \Gamma_{\text{total}}$ . The fit constrains the  $x_i$  whose labels appear in this array to sum to one.

$x_2$	-100	
$x_3$	12	-14
	$x_1$	$x_2$

## Baryon Particle Listings

 $\Sigma^+$  $\Sigma^+$  BRANCHING RATIOS $\Gamma(n\pi^+)/\Gamma(N\pi)$ 

VALUE	EVTS	DOCUMENT ID	TECN	COMMENT
<b>0.4836 ± 0.0030 OUR FIT</b>				
<b>0.4836 ± 0.0030 OUR AVERAGE</b>				
0.4828 ± 0.0036	10k	<sup>1</sup> MARRAFFINO 80	HBC	$K^- p$ 0.42–0.5 GeV/c
0.488 ± 0.008	1861	NOWAK 78	HBC	
0.484 ± 0.015	537	TOVEE 71	EMUL	
0.488 ± 0.010	1331	BARLOUTAUD 69	HBC	$K^- p$ 0.4–1.2 GeV/c
0.46 ± 0.02	534	CHANG 66	HBC	
0.490 ± 0.024	308	HUMPHREY 62	HBC	

<sup>1</sup> MARRAFFINO 80 actually gives  $\Gamma(p\pi^0)/\Gamma(\text{total}) = 0.5172 \pm 0.0036$ . $\Gamma(p\gamma)/\Gamma(p\pi^0)$ 

VALUE (units $10^{-3}$ )	EVTS	DOCUMENT ID	TECN	COMMENT
<b>2.38 ± 0.10 OUR FIT</b>				
<b>2.38 ± 0.10 OUR AVERAGE</b>				
2.32 ± 0.11 ± 0.10	32k	TIMM 95	E761	$\Sigma^+$ 375 GeV
2.81 ± 0.39 <sup>+0.21</sup> <sub>-0.43</sub>	408	HESSEY 89	CNTR	$K^- p \rightarrow \Sigma^+ \pi^-$ at rest
2.52 ± 0.28	190	<sup>1</sup> KOBAYASHI 87	CNTR	$\pi^+ p \rightarrow \Sigma^+ K^+$
2.46 <sup>+0.30</sup> <sub>-0.35</sub>	155	BIAGI 85	CNTR	CERN hyperon beam
2.11 ± 0.38	46	MANZ 80	HBC	$K^- p \rightarrow \Sigma^+ \pi^-$
2.1 ± 0.3	45	ANG 69B	HBC	$K^- p$ at rest
2.76 ± 0.51	31	GERSHWIN 69B	HBC	$K^- p \rightarrow \Sigma^+ \pi^-$
3.7 ± 0.8	24	BAZIN 65	HBC	$K^- p$ at rest

<sup>1</sup> KOBAYASHI 87 actually gives  $\Gamma(p\gamma)/\Gamma(\text{total}) = (1.30 \pm 0.15) \times 10^{-3}$ . $\Gamma(n\pi^+\gamma)/\Gamma(n\pi^+)$ 

VALUE (units $10^{-3}$ )	EVTS	DOCUMENT ID	TECN	COMMENT
<b>0.93 ± 0.10</b>	180	EBENHOH 73	HBC	$\pi^+ < 150$ MeV/c
••• We do not use the following data for averages, fits, limits, etc. •••				
0.27 ± 0.05	29	ANG 69B	HBC	$\pi^+ < 110$ MeV/c
~1.8		BAZIN 65B	HBC	$\pi^+ < 116$ MeV/c

 $\Gamma(\Lambda e^+ \nu_e)/\Gamma_{\text{total}}$ 

VALUE (units $10^{-5}$ )	EVTS	DOCUMENT ID	TECN	COMMENT
<b>2.0 ± 0.5 OUR AVERAGE</b>				
1.6 ± 0.7	5	BALTAY 69	HBC	$K^- p$ at rest
2.9 ± 1.0	10	EISELE 69	HBC	$K^- p$ at rest
2.0 ± 0.8	6	BARASH 67	HBC	$K^- p$ at rest

 $\Gamma(n e^+ \nu_e)/\Gamma(n\pi^+)$ 

EFFECTIVE DENOM.	EVTS	DOCUMENT ID	TECN	COMMENT
<b>&lt; 1.1 × 10<sup>-5</sup> OUR LIMIT</b>				Our 90% CL limit = (2.3 events)/(effective denominator sum). [Number of events increased to 2.3 for a 90% confidence level.]
111000	0	<sup>1</sup> EBENHOH 74	HBC	$K^- p$ at rest
105000	0	<sup>1</sup> SECHI-ZORN 73	HBC	$K^- p$ at rest

<sup>1</sup> Effective denominator calculated by us. $\Gamma(n\mu^+ \nu_\mu)/\Gamma(n\pi^+)$ 

EFFECTIVE DENOM.	EVTS	DOCUMENT ID	TECN	COMMENT
<b>&lt; 6.2 × 10<sup>-5</sup> OUR LIMIT</b>				Our 90% CL limit = (6.7 events)/(effective denominator sum). [Number of events increased to 6.7 for a 90% confidence level.]
33800	0	BAGGETT 69B	HBC	
62000	2	<sup>1</sup> EISELE 69B	HBC	
10150	0	<sup>2</sup> COURANT 64	HBC	
1710	0	<sup>2</sup> NAUENBERG 64	HBC	
120	1	GALTIERI 62	EMUL	

<sup>1</sup> Effective denominator calculated by us.<sup>2</sup> Effective denominator taken from EISELE 67. $\Gamma(pe^+ e^-)/\Gamma_{\text{total}}$ 

VALUE (units $10^{-6}$ )	DOCUMENT ID	TECN	COMMENT
<b>&lt; 7</b>	<sup>1</sup> ANG 69B	HBC	$K^- p$ at rest

<sup>1</sup> ANG 69B found three  $pe^+ e^-$  events in agreement with  $\gamma \rightarrow e^+ e^-$  conversion from  $\Sigma^+ \rightarrow p\gamma$ . The limit given here is for neutral currents. $\Gamma(p\mu^+ \mu^-)/\Gamma_{\text{total}}$ 

VALUE (units $10^{-8}$ )	EVTS	DOCUMENT ID	TECN	COMMENT
<b>2.4 ± 1.7 ± 1.3 OUR AVERAGE</b>				
2.2 <sup>+0.9+1.5</sup> <sub>-0.8-1.1</sub>	10.2	<sup>1</sup> AAIJ 18E	LHCB	$pp$ at 7, 8 TeV
8.6 <sup>+6.6</sup> <sub>-5.4</sub> ± 5.5	3	<sup>2</sup> PARK 05	HYCP	$p$ Cu, 800 GeV

 $\Gamma_2/(\Gamma_1+\Gamma_2)$ 

<sup>1</sup> AAIJ 18E sees no structure in the dimuon mass distribution, contrary to PARK 05.  
<sup>2</sup> The masses of the three dimuons of PARK 05 are within 1 MeV of one another, perhaps indicating the existence of a new state  $P^0$  with mass  $214.3 \pm 0.5$  MeV. In that case, the decay is  $\Sigma^+ \rightarrow pP^0, P^0 \rightarrow \mu^+ \mu^-$ , with a branching fraction of  $(3.1^{+2.4}_{-1.9} \pm 1.5) \times 10^{-8}$ .

 $\Gamma(\Sigma^+ \rightarrow n e^+ \nu_e)/\Gamma(\Sigma^- \rightarrow n e^- \bar{\nu}_e)$ 

VALUE	CL%	EVTS	DOCUMENT ID	TECN	COMMENT
<b>&lt; 0.009 OUR LIMIT</b>					Our 90% CL limit, using $\Gamma(n e^+ \nu_e)/\Gamma(n\pi^+)$ above.
••• We do not use the following data for averages, fits, limits, etc. •••					
< 0.019	90	0	EBENHOH 74	HBC	$K^- p$ at rest
< 0.018	90	0	SECHI-ZORN 73	HBC	$K^- p$ at rest
< 0.12	95	0	COLE 71	HBC	$K^- p$ at rest
< 0.03	90	0	EISELE 69B	HBC	See EBENHOH 74

 $\Gamma(\Sigma^+ \rightarrow n\mu^+ \nu_\mu)/\Gamma(\Sigma^- \rightarrow n\mu^- \bar{\nu}_\mu)$ 

VALUE	EVTS	DOCUMENT ID	TECN	COMMENT
<b>&lt; 0.12 OUR LIMIT</b>				Our 90% CL limit, using $\Gamma(n\mu^+ \nu_\mu)/\Gamma(n\pi^+)$ above.
••• We do not use the following data for averages, fits, limits, etc. •••				
0.06 <sup>+0.045</sup> <sub>-0.03</sub>	2	EISELE 69B	HBC	$K^- p$ at rest

 $\Gamma(\Sigma^+ \rightarrow n\ell^+ \nu)/\Gamma(\Sigma^- \rightarrow n\ell^- \bar{\nu})$ 

VALUE	EVTS	DOCUMENT ID	TECN	COMMENT
<b>&lt; 0.043 OUR LIMIT</b>				Our 90% CL limit, using $[\Gamma(\Sigma^+ \rightarrow n\mu^+ \nu_\mu) + \Gamma(\Sigma^+ \rightarrow n e^+ \nu_e)]/\Gamma(\Sigma^+ \rightarrow n\pi^+)$ .
••• We do not use the following data for averages, fits, limits, etc. •••				
< 0.08	1	NORTON 69	HBC	
< 0.034	0	BAGGETT 67	HBC	

 $\Sigma^+$  DECAY PARAMETERS

See the "Note on Baryon Decay Parameters" in the neutron Listings. A few early results have been omitted.

 $\alpha_0$  FOR  $\Sigma^+ \rightarrow p\pi^0$ 

VALUE	EVTS	DOCUMENT ID	TECN	COMMENT
<b>-0.980 ± 0.017 ± 0.015 OUR FIT</b>				
<b>-0.980 ± 0.017 ± 0.013 OUR AVERAGE</b>				
-0.945 <sup>+0.055</sup> <sub>-0.042</sub>	1259	<sup>1</sup> LIPMAN 73	OSPK	$\pi^+ p \rightarrow \Sigma^+$
-0.940 ± 0.045	16k	BELLAMY 72	ASPK	$\pi^+ p \rightarrow \Sigma^+ K^+$
-0.98 <sup>+0.05</sup> <sub>-0.02</sub>	1335	<sup>2</sup> HARRIS 70	OSPK	$\pi^+ p \rightarrow \Sigma^+ K^+$
-0.999 ± 0.022	32k	BANGERTER 69	HBC	$K^- p$ 0.4 GeV/c

<sup>1</sup> Decay protons scattered off aluminum.<sup>2</sup> Decay protons scattered off carbon. $\phi_0$  ANGLE FOR  $\Sigma^+ \rightarrow p\pi^0$ 

VALUE (°)	EVTS	DOCUMENT ID	TECN	COMMENT
<b>36 ± 34 OUR AVERAGE</b>				
38.1 <sup>+35.7</sup> <sub>-37.1</sub>	1259	<sup>1</sup> LIPMAN 73	OSPK	$\pi^+ p \rightarrow \Sigma^+ K^+$
22 ± 90		<sup>2</sup> HARRIS 70	OSPK	$\pi^+ p \rightarrow \Sigma^+ K^+$

<sup>1</sup> Decay proton scattered off aluminum.<sup>2</sup> Decay protons scattered off carbon. $\alpha_+ / \alpha_0$ 

VALUE	EVTS	DOCUMENT ID	TECN	COMMENT
<b>-0.069 ± 0.013 OUR FIT</b>				
<b>-0.073 ± 0.021</b>	23k	MARRAFFINO 80	HBC	$K^- p$ 0.42–0.5 GeV/c

 $\alpha_+$  FOR  $\Sigma^+ \rightarrow n\pi^+$ 

VALUE	EVTS	DOCUMENT ID	TECN	COMMENT
<b>0.068 ± 0.013 OUR FIT</b>				
<b>0.066 ± 0.016 OUR AVERAGE</b>				
0.037 ± 0.049	4101	BERLEY 70B	HBC	
0.069 ± 0.017	35k	BANGERTER 69	HBC	$K^- p$ 0.4 GeV/c

 $\phi_+$  ANGLE FOR  $\Sigma^+ \rightarrow n\pi^+$ 

VALUE (°)	EVTS	DOCUMENT ID	TECN	COMMENT
<b>167 ± 20 OUR AVERAGE</b>				Error includes scale factor of 1.1.
184 ± 24	1054	<sup>1</sup> BERLEY 70B	HBC	
143 ± 29	560	BANGERTER 69B	HBC	$K^- p$ 0.4 GeV/c

<sup>1</sup> Changed from 176 to 184° to agree with our sign convention.





# Baryon Particle Listings

$\Sigma^-$



$$I(J^P) = 1(\frac{1}{2}^+) \text{ Status: } ****$$

We have omitted some results that have been superseded by later experiments. See our earlier editions.

## $\Sigma^-$ MASS

The fit uses  $\Sigma^+$ ,  $\Sigma^0$ ,  $\Sigma^-$ , and  $\Lambda$  mass and mass-difference measurements.

VALUE (MeV)	EVTS	DOCUMENT ID	TECN	COMMENT
<b>1197.449 ± 0.030 OUR FIT</b>				Error includes scale factor of 1.2.
<b>1197.45 ± 0.04 OUR AVERAGE</b>				Error includes scale factor of 1.2.
1197.417 ± 0.040		GUREV 93	SPEC	$\Sigma^-$ C atom, crystal diff.
1197.532 ± 0.057		GALL 88	CNTR	$\Sigma^-$ Pb, $\Sigma^-$ W atoms
1197.43 ± 0.08	3000	SCHMIDT 65	HBC	See note with $\Lambda$ mass
••• We do not use the following data for averages, fits, limits, etc. •••				
1197.24 ± 0.15		<sup>1</sup> DUGAN 75	CNTR	Exotic atoms
<sup>1</sup> GALL 88 concludes that the DUGAN 75 mass needs to be reevaluated.				

## $m_{\Sigma^-} - m_{\Sigma^+}$

VALUE (MeV)	EVTS	DOCUMENT ID	TECN	COMMENT
<b>8.08 ± 0.08 OUR FIT</b>				Error includes scale factor of 1.9.
<b>8.09 ± 0.16 OUR AVERAGE</b>				
7.91 ± 0.23	86	BOHM 72	EMUL	
8.25 ± 0.25	2500	DOSCH 65	HBC	
8.25 ± 0.40	87	BARKAS 63	EMUL	

## $m_{\Sigma^-} - m_{\Lambda}$

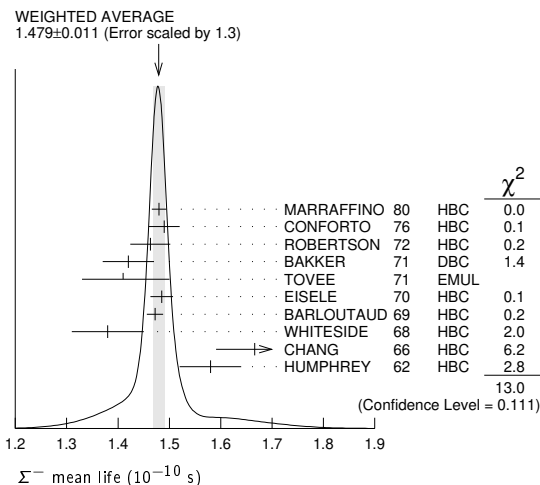
VALUE (MeV)	EVTS	DOCUMENT ID	TECN	COMMENT
<b>81.766 ± 0.030 OUR FIT</b>				Error includes scale factor of 1.2.
<b>81.69 ± 0.07 OUR AVERAGE</b>				
81.64 ± 0.09	2279	HEPP 68	HBC	
81.80 ± 0.13	85	SCHMIDT 65	HBC	See note with $\Lambda$ mass
81.70 ± 0.19		BURNSTEIN 64	HBC	

## $\Sigma^-$ MEAN LIFE

Measurements with an error  $\geq 0.2 \times 10^{-10}$  s have been omitted.

VALUE ( $10^{-10}$ s)	EVTS	DOCUMENT ID	TECN	COMMENT
<b>1.479 ± 0.011 OUR AVERAGE</b>				Error includes scale factor of 1.3. See the ideogram below.
1.480 ± 0.014	16k	MARRAFFINO 80	HBC	$K^- p$ 0.42–0.5 GeV/c
1.49 ± 0.03	8437	CONFORTO 76	HBC	$K^- p$ 1–1.4 GeV/c
1.463 ± 0.039	2400	ROBERTSON 72	HBC	$K^- p$ 0.25 GeV/c
1.42 ± 0.05	1383	BAKKER 71	DBC	$K^- N \rightarrow \Sigma^- \pi \pi$
1.41 +0.09 -0.08		TOVEE 71	EMUL	
1.485 ± 0.022	100k	EISELE 70	HBC	$K^- p$ at rest
1.472 ± 0.016	10k	BARLOUTAUD 69	HBC	$K^- p$ 0.4–1.2 GeV/c
1.38 ± 0.07	506	WHITESIDE 68	HBC	$K^- p$ at rest
1.666 ± 0.075	3267	<sup>2</sup> CHANG 66	HBC	$K^- p$ at rest
1.58 ± 0.06	1208	HUMPHREY 62	HBC	$K^- p$ at rest

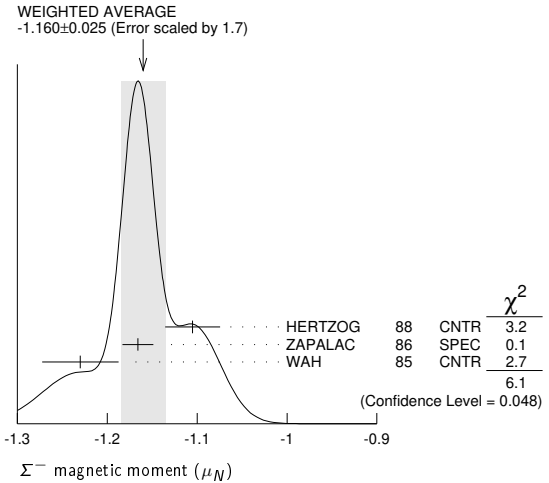
<sup>2</sup>We have increased the CHANG 66 error of 0.026; see our 1970 edition, Reviews of Modern Physics **42** 87 (1970).



## $\Sigma^-$ MAGNETIC MOMENT

See the "Note on Baryon Magnetic Moments" in the  $\Lambda$  Listings. Measurements with an error  $\geq 0.3 \mu_N$  have been omitted.

VALUE ( $\mu_N$ )	EVTS	DOCUMENT ID	TECN	COMMENT
<b>-1.160 ± 0.025 OUR AVERAGE</b>				Error includes scale factor of 1.7. See the ideogram below.
-1.105 ± 0.029 ± 0.010		HERTZOG 88	CNTR	$\Sigma^-$ Pb, $\Sigma^-$ W atoms
-1.166 ± 0.014 ± 0.010	671k	ZAPALAC 86	SPEC	$n e^- \nu, n \pi^-$ decays
-1.23 ± 0.03 ± 0.03		WAH 85	CNTR	$p \text{Cu} \rightarrow \Sigma^- X$
••• We do not use the following data for averages, fits, limits, etc. •••				
-0.89 ± 0.14	516k	DECK 83	SPEC	$p \text{Be} \rightarrow \Sigma^- X$



## $\Sigma^-$ CHARGE RADIUS

VALUE (fm)	DOCUMENT ID	TECN	COMMENT
<b>0.780 ± 0.080 ± 0.060</b>	<sup>3</sup> ESCHRICH 01	SELX	$\Sigma^- e \rightarrow \Sigma^- e$
<sup>3</sup> ESCHRICH 01 actually gives $\langle r^2 \rangle = (0.61 \pm 0.12 \pm 0.09) \text{ fm}^2$ .			

## $\Sigma^-$ DECAY MODES

Mode	Fraction ( $\Gamma_i/\Gamma$ )
$\Gamma_1$ $n \pi^-$	(99.848 ± 0.005) %
$\Gamma_2$ $n \pi^- \gamma$	[a] ( 4.6 ± 0.6 ) × 10 <sup>-4</sup>
$\Gamma_3$ $n e^- \bar{\nu}_e$	( 1.017 ± 0.034 ) × 10 <sup>-3</sup>
$\Gamma_4$ $n \mu^- \bar{\nu}_\mu$	( 4.5 ± 0.4 ) × 10 <sup>-4</sup>
$\Gamma_5$ $\Lambda e^- \bar{\nu}_e$	( 5.73 ± 0.27 ) × 10 <sup>-5</sup>

[a] See the Listings below for the pion momentum range used in this measurement.

## CONSTRAINED FIT INFORMATION

An overall fit to 3 branching ratios uses 16 measurements and one constraint to determine 4 parameters. The overall fit has a  $\chi^2 = 8.7$  for 13 degrees of freedom.

The following off-diagonal array elements are the correlation coefficients  $\langle \delta x_i \delta x_j \rangle / (\delta x_i \delta x_j)$ , in percent, from the fit to the branching fractions,  $x_i \equiv \Gamma_i/\Gamma_{\text{total}}$ . The fit constrains the  $x_i$  whose labels appear in this array to sum to one.

$x_3$	-64		
$x_4$	-77	0	
$x_5$	-5	0	0
	$x_1$	$x_3$	$x_4$

## $\Sigma^-$ BRANCHING RATIOS

$\Gamma(n \pi^- \gamma) / \Gamma(n \pi^-)$   $\Gamma_2 / \Gamma_1$   
 The  $\pi^+$  momentum cuts differ, so we do not average the results but simply use the latest value for the Summary Table.

VALUE (units 10 <sup>-3</sup> )	EVTS	DOCUMENT ID	TECN	COMMENT
<b>0.46 ± 0.06</b>	292	EBENHOH 73	HBC	$\pi^+ < 150 \text{ MeV/c}$
••• We do not use the following data for averages, fits, limits, etc. •••				
0.10 ± 0.02	23	ANG 69b	HBC	$\pi^- < 110 \text{ MeV/c}$
~ 1.1		BAZIN 65b	HBC	$\pi^- < 166 \text{ MeV/c}$

See key on page 999

# Baryon Particle Listings

$\Sigma^-$

## $\Gamma(ne^- \bar{\nu}_e)/\Gamma(n\pi^-)$ $\Gamma_3/\Gamma_1$

Measurements with an error  $\geq 0.2 \times 10^{-3}$  have been omitted.

VALUE (units $10^{-3}$ )	EVTS	DOCUMENT ID	TECN	COMMENT
<b>1.019 ± 0.031</b>				<b>OUR FIT</b>
<b>1.019 ± 0.031</b>				<b>OUR AVERAGE</b>
0.96 ± 0.05	2847	BOURQUIN	83c	SPEC SPS hyperon beam
1.09 $\begin{smallmatrix} +0.06 \\ -0.08 \end{smallmatrix}$	601	<sup>4</sup> EBENHOH	74	HBC $K^- p$ at rest
1.05 $\begin{smallmatrix} +0.07 \\ -0.13 \end{smallmatrix}$	455	<sup>4</sup> SECHI-ZORN	73	HBC $K^- p$ at rest
0.97 ± 0.15	57	COLE	71	HBC $K^- p$ at rest
1.11 ± 0.09	180	BIERMAN	68	HBC

<sup>4</sup> An additional negative systematic error is included for internal radiative corrections and latest form factors; see BOURQUIN 83c.

## $\Gamma(n\mu^- \bar{\nu}_\mu)/\Gamma(n\pi^-)$ $\Gamma_4/\Gamma_1$

VALUE (units $10^{-3}$ )	EVTS	DOCUMENT ID	TECN	COMMENT
<b>0.45 ± 0.04</b>				<b>OUR FIT</b>
<b>0.45 ± 0.04</b>				<b>OUR AVERAGE</b>
0.38 ± 0.11	13	COLE	71	HBC $K^- p$ at rest
0.43 ± 0.06	72	ANG	69	HBC $K^- p$ at rest
0.43 ± 0.09	56	BAGGETT	69	HBC $K^- p$ at rest
0.56 ± 0.20	11	BAZIN	65B	HBC $K^- p$ at rest
0.66 ± 0.15	22	COURANT	64	HBC

## $\Gamma(\Lambda e^- \bar{\nu}_e)/\Gamma(n\pi^-)$ $\Gamma_5/\Gamma_1$

VALUE (units $10^{-4}$ )	EVTS	DOCUMENT ID	TECN	COMMENT
<b>0.574 ± 0.027</b>				<b>OUR FIT</b>
<b>0.574 ± 0.027</b>				<b>OUR AVERAGE</b>
0.561 ± 0.031	1620	<sup>5</sup> BOURQUIN	82	SPEC SPS hyperon beam
0.63 ± 0.11	114	THOMPSON	80	ASPK Hyperon beam
0.52 ± 0.09	31	BALTAY	69	HBC $K^- p$ at rest
0.69 ± 0.12	31	EISELE	69	HBC $K^- p$ at rest
0.64 ± 0.12	35	BARASH	67	HBC $K^- p$ at rest
0.75 ± 0.28	11	COURANT	64	HBC $K^- p$ at rest

<sup>5</sup> The value is from BOURQUIN 83B, and includes radiation corrections and new acceptance.

## $\Sigma^-$ DECAY PARAMETERS

See the "Note on Baryon Decay Parameters" in the neutron Listings. Older, outdated results have been omitted.

### $\alpha_-$ FOR $\Sigma^- \rightarrow n\pi^-$

VALUE	EVTS	DOCUMENT ID	TECN	COMMENT
<b>-0.068 ± 0.008</b>				<b>OUR AVERAGE</b>
-0.062 ± 0.024	28k	HANSL	78	HBC $K^- p \rightarrow \Sigma^- \pi^+$
-0.067 ± 0.011	60k	BOGERT	70	HBC $K^- p$ 0.4 GeV/c
-0.071 ± 0.012	51k	BANGERTER	69	HBC $K^- p$ 0.4 GeV/c

### $\phi$ ANGLE FOR $\Sigma^- \rightarrow n\pi^-$

( $\tan\phi = \beta/\gamma$ )

VALUE (°)	EVTS	DOCUMENT ID	TECN	COMMENT
<b>10 ± 15</b>				<b>OUR AVERAGE</b>
+ 5 ± 23	1092	<sup>6</sup> BERLEY	70B	HBC $n$ rescattering
14 ± 19	1385	BANGERTER	69B	HBC $K^- p$ 0.4 GeV/c

<sup>6</sup> BERLEY 70B changed from -5 to +5° to agree with our sign convention.

### $g_A/g_V$ FOR $\Sigma^- \rightarrow ne^- \bar{\nu}_e$

Measurements with fewer than 500 events have been omitted. Where necessary, signs have been changed to agree with our conventions, which are given in the "Note on Baryon Decay Parameters" in the neutron Listings. What is actually listed is  $|g_1/f_1 - 0.237g_2/f_1|$ . This reduces to  $g_A/g_V \equiv g_1(0)/f_1(0)$  on making the usual assumption that  $g_2 = 0$ . See also the note on HSUEH 88.

VALUE	EVTS	DOCUMENT ID	TECN	COMMENT
<b>0.340 ± 0.017</b>				<b>OUR AVERAGE</b>
+0.327 ± 0.007 ± 0.019	50k	<sup>7</sup> HSUEH	88	SPEC $\Sigma^-$ 250 GeV
+0.34 ± 0.05	4456	<sup>8</sup> BOURQUIN	83c	SPEC SPS hyperon beam
0.385 ± 0.037	3507	<sup>9</sup> TANENBAUM	74	ASPK

• • • We do not use the following data for averages, fits, limits, etc. • • •

0.29 ± 0.07	25k	HSUEH	85	SPEC See HSUEH 88
0.17 $\begin{smallmatrix} +0.07 \\ -0.09 \end{smallmatrix}$	519	DECAMP	77	ELEC Hyperon beam

<sup>7</sup> The sign is, with our conventions, unambiguously positive. The value assumes, as usual, that  $g_2 = 0$ . If  $g_2$  is included in the fit, than (with our sign convention)  $g_2 = -0.56 \pm 0.37$ , with a corresponding reduction of  $g_A/g_V$  to  $+0.20 \pm 0.08$ .

<sup>8</sup> BOURQUIN 83c favors the positive sign by at least 2.6 standard deviations.

<sup>9</sup> TANENBAUM 74 gives  $0.435 \pm 0.035$ , assuming no  $q^2$  dependence in  $g_A$  and  $g_V$ . The listed result allows  $q^2$  dependence, and is taken from HSUEH 88.

### $f_2(0)/f_1(0)$ FOR $\Sigma^- \rightarrow ne^- \bar{\nu}_e$

The signs have been changed to be in accord with our conventions, given in the "Note on Baryon Decay Parameters" in the neutron Listings.

VALUE	EVTS	DOCUMENT ID	TECN	COMMENT
<b>0.97 ± 0.14</b>				<b>OUR AVERAGE</b>
+0.96 ± 0.07 ± 0.13	50k	HSUEH	88	SPEC $\Sigma^-$ 250 GeV
+1.02 ± 0.34	4456	BOURQUIN	83c	SPEC SPS hyperon beam

## TRIPLE CORRELATION COEFFICIENT $D$ for $\Sigma^- \rightarrow ne^- \bar{\nu}_e$

The coefficient  $D$  of the term  $D \mathbf{P} \cdot (\mathbf{p}_e \times \mathbf{p}_\nu)$  in the  $\Sigma^- \rightarrow ne^- \bar{\nu}$  decay angular distribution. A nonzero value would indicate a violation of time-reversal invariance.

VALUE	EVTS	DOCUMENT ID	TECN	COMMENT
<b>0.11 ± 0.10</b>	50k	HSUEH	88	SPEC $\Sigma^-$ 250 GeV

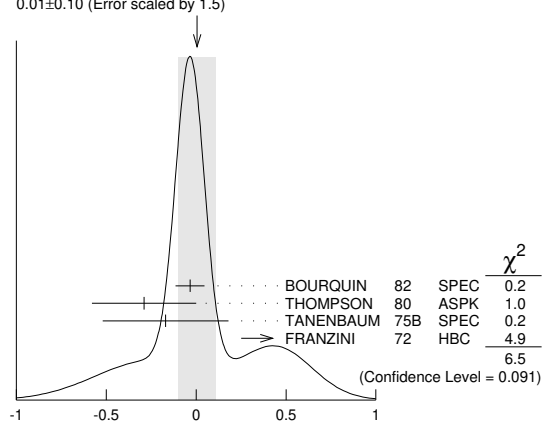
## $g_V/g_A$ FOR $\Sigma^- \rightarrow \Lambda e^- \bar{\nu}_e$

For the sign convention, see the "Note on Baryon Decay Parameters" in the neutron Listings. The value is predicted to be zero by conserved vector current theory. The values averaged assume CVC-SU(3) weak magnetism term.

VALUE	EVTS	DOCUMENT ID	TECN	COMMENT
<b>0.01 ± 0.10</b>				<b>OUR AVERAGE</b>
-0.034 ± 0.080	1620	<sup>10</sup> BOURQUIN	82	SPEC SPS hyperon beam
-0.29 ± 0.29	114	THOMPSON	80	ASPK BNL hyperon beam
-0.17 ± 0.35	55	TANENBAUM	75B	SPEC BNL hyperon beam
+0.45 ± 0.20	186	<sup>10,11</sup> FRANZINI	72	HBC

<sup>10</sup> The sign has been changed to agree with our convention.  
<sup>11</sup> The FRANZINI 72 value includes the events of earlier papers.

WEIGHTED AVERAGE  
 0.01 ± 0.10 (Error scaled by 1.5)



## $g_W/g_A$ FOR $\Sigma^- \rightarrow \Lambda e^- \bar{\nu}_e$

The values quoted assume the CVC prediction  $g_V = 0$ .

VALUE	EVTS	DOCUMENT ID	TECN	COMMENT
<b>2.4 ± 1.7</b>				<b>OUR AVERAGE</b>
1.75 ± 3.5	114	THOMPSON	80	ASPK BNL hyperon beam
3.5 ± 4.5	55	TANENBAUM	75B	SPEC BNL hyperon beam
2.4 ± 2.1	186	FRANZINI	72	HBC

## $\Sigma^-$ REFERENCES

We have omitted some papers that have been superseded by later experiments. See our earlier editions.

ESCHRICH 01	PL B522 233	I. Eschrich et al.	(FNAL SELEX Collab.)
GUREV 93	JETPL 57 400	M.P. Gurev et al.	(PNPI)
	Translated from ZETFP 57 389.		
GALL 88	PRL 60 186	K.P. Gall et al.	(BOST, MIT, WILL, CIT+)
HERTZOG 88	PR D37 1142	D.W. Hertzog et al.	(WILL, BOST, MIT+)
HSUEH 88	PR D38 2056	S.Y. Hsueh et al.	(CHIC, ELMT, FNAL+)
ZAPALAC 86	PRL 57 1526	G. Zapalac et al.	(EFI, ELMT, FNAL+)
HSUEH 85	PRL 54 2399	S.Y. Hsueh et al.	(CHIC, ELMT, FNAL+)
WAH 85	PRL 55 2551	Y.W. Wah et al.	(FNAL, IOWA, ISU)
BOURQUIN 83B	ZPHY C21 27	M.H. Bourquin et al.	(BRIS, GEVA, HEIDP+)
BOURQUIN 83C	ZPHY C21 17	M.H. Bourquin et al.	(BRIS, GEVA, HEIDP+)
DECK 83	PR D28 1	L. Deck et al.	(RUTG, WISC, MICH, MINN)
BOURQUIN 82	ZPHY C12 307	M.H. Bourquin et al.	(BRIS, GEVA, HEIDP+)
MARRAFFINO 80	PR D21 2501	J. Marraffino et al.	(VAND, MPIM)
THOMPSON 80	PR D21 25	J.A. Thompson et al.	(PITT, BNL)
HANSL 78	NP B132 45	T. Hansl et al.	(MPIM, VAND)
DECAMP 77	PL 66B 295	D. Decamp et al.	(LALO, EPOL)
CONFORTO 76	NP B105 189	B. Conforto et al.	(RHEL, LOIC)
DUGAN 75	NP A254 396	G. Dugan et al.	(COLU, YALE)
TANENBAUM 75B	PR D12 1871	W. Tanenbaum et al.	(YALE, FNAL, BNL)
EBENHOH 74	ZPHY 266 367	H. Ebenhoeh et al.	(HEIDT)
TANENBAUM 74	PRL 33 175	W. Tanenbaum et al.	(YALE, FNAL, BNL)
EBENHOH 73	ZPHY 264 413	W. Ebenhoeh et al.	(HEIDT)
SECHI-ZORN 73	PR D8 12	B. Sechi-Zorn, G.A. Snow	(UMD)
BOHM 72	NP B48 1	G. Bohm et al.	(BERL, KIDR, BRUX, IASD+)
FRANZINI 72	PR D6 2417	P. Franzini et al.	(COLU, HEID, UM+)
ROBERTSON 72	Thesis UMI 78-00877	R.M. Robertson	(IIT)
BAKKER 71	LNC 1 37	A.M. Bakker et al.	(SABRE Collab.)
COLE 71	PR D4 431	J. Cole et al.	(STON, COLU)
	Also	Thesis Nevis 175	(COLU)
TOVEE 71	NP B33 493	D.N. Tovee et al.	(LOUC, KIDR, BERL+)
BERLEY 70B	PR D1 2015	D. Berley et al.	(BNL, MASA, YALE)
BOGERT 70	PR D2 6	D.V. Bogert et al.	(BNL, MASA, YALE)
EISELE 70	ZPHY 238 372	F. Eisele et al.	(HEID)
PDG 70	RMP 42 87	A. Barbaro-Galtieri et al.	(LRL, BRAN+)
ANG 69	ZPHY 223 103	G. Ang et al.	(HEID)
ANG 69B	ZPHY 228 151	G. Ang et al.	(HEID)
BAGGETT 69	PRL 23 249	N.V. Baggett, B. Kehoe, G.A. Snow	(UMD)
BALTAY 69	PRL 22 615	C. Baltay et al.	(COLU, STON)
BANGERTER 69	Thesis UCRL 19244	R.O. Bangenter	(LRL)
BANGERTER 69B	PR 187 1821	R.O. Bangenter et al.	(LRL)

# Baryon Particle Listings

## $\Sigma^-, \Sigma(1385)$

BARLOUTAUD 69	NP B14 153	R. Barloutaud <i>et al.</i>	(SACL, CERN, HEID)
EISELE 69	ZPHY 221 1	F. Eisele <i>et al.</i>	(HEID)
BIERMAN 68	PRL 20 1459	E. Bierman <i>et al.</i>	(PRIN)
HEPP 68	ZPHY 214 71	V. Hepp, H. Schleich	(HEID)
WHITESIDE 68	NC 54A 537	H. Whiteside, J. Gollub	(OBER)
BARASH 67	PRL 19 181	N. Barash <i>et al.</i>	(UMD)
CHANG 66	PR 151 1081	C.Y. Chang	(COLU)
BAZIN 65B	PR 140 B1358	M. Bazin <i>et al.</i>	(PRIN, RUTG, COLU)
DOSCH 65	PL 14 239	H.C. Dosch <i>et al.</i>	(HEID)
Also	PR 151 1081	C.Y. Chang	(COLU)
SCHMIDT 65	PR 140 B1328	P. Schmidt	(COLU)
BURNSTEIN 64	PRL 13 66	R.A. Burnstein <i>et al.</i>	(UMD)
COURANT 64	PR 136 B1791	H. Courant <i>et al.</i>	(CERN, HEID, UMD+)
BARKAS 63	PRL 11 26	W.H. Barkas, J.N. Dyer, H.H. Heckman	(LRL)
HUMPHREY 62	PR 127 1305	W.E. Humphrey, R.R. Ross	(LRL)

### $\Sigma(1385) 3/2^+$

$$I(J^P) = 1(\frac{3}{2}^+) \text{ Status: } ****$$

Discovered by ALSTON 60. Early measurements of the mass and width for combined charge states have been omitted. They may be found in our 1984 edition Reviews of Modern Physics 56 S1 (1984).

We average only the most significant determinations. We do not average results from inclusive experiments with large backgrounds or results which are not accompanied by some discussion of experimental resolution. Nevertheless systematic differences between experiments remain. (See the ideograms in the Listings below.) These differences could arise from interference effects that change with production mechanism and/or beam momentum. They can also be accounted for in part by differences in the parametrizations employed. (See BORENSTEIN 74 for a discussion on this point.) Thus BORENSTEIN 74 uses a Breit-Wigner with energy-independent width, since a  $P$ -wave was found to give unsatisfactory fits. CAMERON 78 uses the same form. On the other hand HOLMGREN 77 obtains a good fit to their  $\Lambda\pi$  spectrum with a  $P$ -wave Breit-Wigner, but includes the partial width for the  $\Sigma\pi$  decay mode in the parametrization. AGUILAR-BENITEZ 81D gives masses and widths for five different Breit-Wigner shapes. The results vary considerably. Only the best-fit  $S$ -wave results are given here.

### $\Sigma(1385)$ POLE POSITIONS

#### $\Sigma(1385)^+$ REAL PART

VALUE	DOCUMENT ID	COMMENT
1379 ± 1	LICHTENBERG74	Extrapolates HABIBI 73

#### $\Sigma(1385)^+$ -IMAGINARY PART

VALUE	DOCUMENT ID	COMMENT
17.5 ± 1.5	LICHTENBERG74	Extrapolates HABIBI 73

#### $\Sigma(1385)^-$ REAL PART

VALUE	DOCUMENT ID	COMMENT
1383 ± 1	LICHTENBERG74	Extrapolates HABIBI 73

#### $\Sigma(1385)^-$ -IMAGINARY PART

VALUE	DOCUMENT ID	COMMENT
22.5 ± 1.5	LICHTENBERG74	Extrapolates HABIBI 73

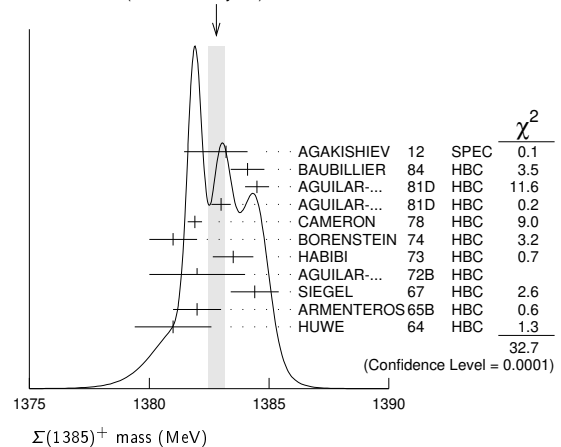
### $\Sigma(1385)$ MASSES

#### $\Sigma(1385)^+$ MASS

VALUE (MeV)	EVTS	DOCUMENT ID	TECN	COMMENT
<b>1382.80 ± 0.35 OUR AVERAGE</b>				Error includes scale factor of 1.9. See the ideogram below.
1383.2 ± 0.9	±0.1 -1.5	AGAKISHIEV 12	SPEC	$pp \rightarrow \Sigma(1385)^+ K^+ n$ , 3.5 GeV
1384.1 ± 0.7	1897	BAUBILLIER 84	HBC	$K^- p \rightarrow 8.25 \text{ GeV}/c$
1384.5 ± 0.5	5256	AGUILAR-... 81D	HBC	$K^- p \rightarrow \Lambda\pi\pi 4.2 \text{ GeV}/c$
1383.0 ± 0.4	9361	AGUILAR-... 81D	HBC	$K^- p \rightarrow \Lambda 3\pi 4.2 \text{ GeV}/c$
1381.9 ± 0.3	6900	CAMERON 78	HBC	$K^- p 0.96-1.36 \text{ GeV}/c$
1381 ± 1	6846	BORENSTEIN 74	HBC	$K^- p 2.18 \text{ GeV}/c$
1383.5 ± 0.85	2300	HABIBI 73	HBC	$K^- p \rightarrow \Lambda\pi\pi$
1382 ± 2	400	AGUILAR-... 72B	HBC	$K^- p \rightarrow \Lambda\pi's$
1384.4 ± 1.0	1260	SIEGEL 67	HBC	$K^- p 2.1 \text{ GeV}/c$
1382 ± 1	750	ARMENTEROS65B	HBC	$K^- p 0.9-1.2 \text{ GeV}/c$
1381.0 ± 1.6	859	HUWE 64	HBC	$K^- p 1.22 \text{ GeV}/c$
• • • We do not use the following data for averages, fits, limits, etc. • • •				
1385.1 ± 1.2	600	BAKER 80	HYBR	$\pi^+ p 7 \text{ GeV}/c$
1383.2 ± 1.0	750	BAKER 80	HYBR	$K^- p 7 \text{ GeV}/c$
1381 ± 2	7k	<sup>1</sup> BAUBILLIER 79B	HBC	$K^- p 8.25 \text{ GeV}/c$
1391 ± 2	2k	CAUTIS 79	HYBR	$\pi^+ p/K^- p 11.5 \text{ GeV}$
1390 ± 2	100	<sup>1</sup> SUGAHARA 79B	HBC	$\pi^- p 6 \text{ GeV}/c$
1385 ± 3	22k	<sup>1,2</sup> BARREIRO 77B	HBC	$K^- p 4.2 \text{ GeV}/c$
1385 ± 1	2594	HOLMGREN 77	HBC	See AGUILAR-BENITEZ 81D
1380 ± 2		<sup>1</sup> BARDADIN-... 75	HBC	$K^- p 14.3 \text{ GeV}/c$

1382 ± 1	3740	<sup>3</sup> BERTHON 74	HBC	$K^- p 1263-1843 \text{ MeV}/c$
1390 ± 6	46	AGUILAR-... 70B	HBC	$K^- p \rightarrow \Sigma\pi's 4 \text{ GeV}/c$
1383 ± 8	62	<sup>4</sup> BIRMINGHAM 66	HBC	$K^- p 3.5 \text{ GeV}/c$
1378 ± 5	135	LONDON 66	HBC	$K^- p 2.24 \text{ GeV}/c$
1384.3 ± 1.9	250	<sup>4</sup> SMITH 65	HBC	$K^- p 1.8 \text{ GeV}/c$
1382.6 ± 2.1	250	<sup>4</sup> SMITH 65	HBC	$K^- p 1.95 \text{ GeV}/c$
1375.0 ± 3.9	170	COOPER 64	HBC	$K^- p 1.45 \text{ GeV}/c$
1376.0 ± 3.9	154	<sup>4</sup> ELY 61	HLBC	$K^- p 1.11 \text{ GeV}/c$

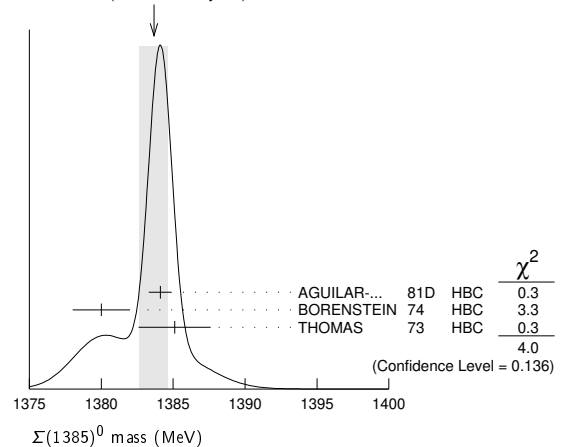
WEIGHTED AVERAGE  
1382.80±0.35 (Error scaled by 1.9)



#### $\Sigma(1385)^0$ MASS

VALUE (MeV)	EVTS	DOCUMENT ID	TECN	COMMENT
<b>1383.7 ± 1.0 OUR AVERAGE</b>				Error includes scale factor of 1.4. See the ideogram below.
1384.1 ± 0.8	5722	AGUILAR-... 81D	HBC	$K^- p \rightarrow \Lambda 3\pi 4.2 \text{ GeV}/c$
1380 ± 2	3100	<sup>5</sup> BORENSTEIN 74	HBC	$K^- p \rightarrow \Lambda 3\pi 2.18 \text{ GeV}/c$
1385.1 ± 2.5	240	<sup>4</sup> THOMAS 73	HBC	$\pi^- p \rightarrow \Lambda\pi^0 K^0$
• • • We do not use the following data for averages, fits, limits, etc. • • •				
1389 ± 3	500	<sup>6</sup> BAUBILLIER 79B	HBC	$K^- p 8.25 \text{ GeV}/c$

WEIGHTED AVERAGE  
1383.7±1.0 (Error scaled by 1.4)



#### $\Sigma(1385)^-$ MASS

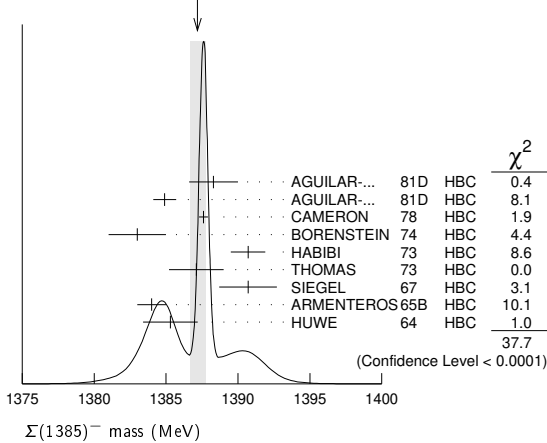
VALUE (MeV)	EVTS	DOCUMENT ID	TECN	COMMENT
<b>1387.2 ± 0.5 OUR AVERAGE</b>				Error includes scale factor of 2.2. See the ideogram below.
1388.3 ± 1.7	620	AGUILAR-... 81D	HBC	$K^- p \rightarrow \Lambda\pi\pi 4.2 \text{ GeV}/c$
1384.9 ± 0.8	3346	AGUILAR-... 81D	HBC	$K^- p \rightarrow \Lambda 3\pi 4.2 \text{ GeV}/c$
1387.6 ± 0.3	9720	CAMERON 78	HBC	$K^- p 0.96-1.36 \text{ GeV}/c$
1383 ± 2	2303	BORENSTEIN 74	HBC	$K^- p 2.18 \text{ GeV}/c$
1390.7 ± 1.2	1900	HABIBI 73	HBC	$K^- p \rightarrow \Lambda\pi\pi$
1387.1 ± 1.9	630	<sup>4</sup> THOMAS 73	HBC	$\pi^- p \rightarrow \Lambda\pi^- K^+$
1390.7 ± 2.0	370	SIEGEL 67	HBC	$K^- p 2.1 \text{ GeV}/c$
1384 ± 1	1380	ARMENTEROS65B	HBC	$K^- p 0.9-1.2 \text{ GeV}/c$
1385.3 ± 1.9	1086	<sup>4</sup> HUWE 64	HBC	$K^- p 1.15-1.30 \text{ GeV}/c$

Σ(1385)

••• We do not use the following data for averages, fits, limits, etc. •••

Table of experimental data for Σ(1385) mass, including columns for value, error, document ID, and comment.

WEIGHTED AVERAGE 1387.2±0.5 (Error scaled by 2.2)



mΣ(1385)- - mΣ(1385)+

Table of mass differences between Σ(1385)- and Σ(1385)+, including document IDs and comments.

mΣ(1385)0 - mΣ(1385)+

Table of mass differences between Σ(1385)0 and Σ(1385)+, including document IDs and comments.

mΣ(1385)- - mΣ(1385)0

Table of mass differences between Σ(1385)- and Σ(1385)0, including document IDs and comments.

Σ(1385) WIDTHS

Σ(1385)+ WIDTH

Table of widths for Σ(1385)+, including document IDs and comments.

••• We do not use the following data for averages, fits, limits, etc. •••

Table of experimental data for Σ(1385) width, including document IDs and comments.

Σ(1385)0 WIDTH

Table of widths for Σ(1385)0, including document IDs and comments.

••• We do not use the following data for averages, fits, limits, etc. •••

Table of experimental data for Σ(1385)- width, including document IDs and comments.

Σ(1385)- WIDTH

Table of widths for Σ(1385)-, including document IDs and comments.

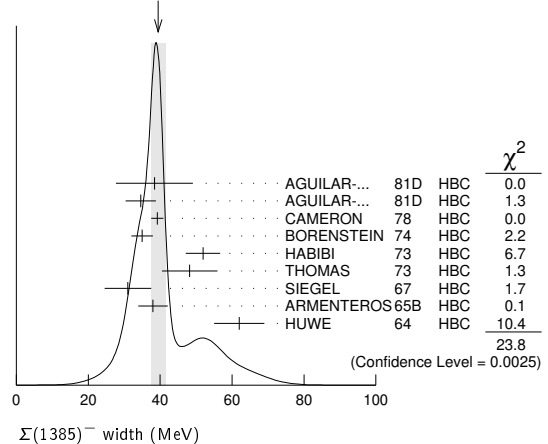
••• We do not use the following data for averages, fits, limits, etc. •••

Table of experimental data for Σ(1385)0 width, including document IDs and comments.

••• We do not use the following data for averages, fits, limits, etc. •••

Table of experimental data for Σ(1385)+ width, including document IDs and comments.

WEIGHTED AVERAGE 39.4±2.1 (Error scaled by 1.7)



# Baryon Particle Listings

## $\Sigma(1385), \Sigma(1580)$

### $\Sigma(1385)$ DECAY MODES

Mode	Fraction ( $\Gamma_i/\Gamma$ )	Confidence level
$\Gamma_1 \Lambda\pi$	(87.0 ± 1.5) %	
$\Gamma_2 \Sigma\pi$	(11.7 ± 1.5) %	
$\Gamma_3 \Lambda\gamma$	( 1.25 <sup>+0.13</sup> <sub>-0.12</sub> ) %	
$\Gamma_4 \Sigma^+\gamma$	( 7.0 ± 1.7 ) × 10 <sup>-3</sup>	
$\Gamma_5 \Sigma^-\gamma$	< 2.4	90%
$\Gamma_6 N\bar{K}$		

### $\Sigma(1385)$ BRANCHING RATIOS

$\Gamma(\Sigma\pi)/\Gamma(\Lambda\pi)$	DOCUMENT ID	TECN	CHG	COMMENT	$\Gamma_2/\Gamma_1$
<b>0.135 ± 0.011 OUR AVERAGE</b>					
0.20 ± 0.06	DIONISI	78B	HBC	± $K^-p \rightarrow Y^*K\bar{K}$	
0.16 ± 0.03	BERTHON	74	HBC	+ $K^-p$ 1.26–1.84 GeV/c	
0.11 ± 0.02	BERTHON	74	HBC	- $K^-p$ 1.26–1.84 GeV/c	
0.21 ± 0.05	BORENSTEIN	74	HBC	+ $K^-p \rightarrow \Lambda\pi^+\pi^-$ , $\Sigma^0\pi^+\pi^-$	
0.18 ± 0.04	MAST	73	MPWA	± $K^-p \rightarrow \Lambda\pi^+\pi^-$ , $\Sigma^0\pi^+\pi^-$	
0.10 ± 0.05	THOMAS	73	HBC	- $\pi^-p \rightarrow \Lambda K\pi, \Sigma K\pi$	
0.16 ± 0.07	AGUILAR...	72B	HBC	+ $K^-p$ 3.9, 4.6 GeV/c	
0.13 ± 0.04	COLLEY	71B	DBC	-0 $K^-N$ 1.5 GeV/c	
0.13 ± 0.04	PAN	69	HBC	+ $\pi^+p \rightarrow \Lambda K\pi, \Sigma K\pi$	
0.08 ± 0.06	LONDON	66	HBC	+ $K^-p$ 2.24 GeV/c	
0.163 ± 0.041	ARMENTEROS65B	HBC	±	$K^-p$ 0.95–1.20 GeV/c	
0.09 ± 0.04	HUWE	64	HBC	± $K^-p$ 1.2–1.7 GeV	
• • • We do not use the following data for averages, fits, limits, etc. • • •					
<0.04	ALSTON	62	HBC	±0 $K^-p$ 1.15 GeV/c	
0.04 ± 0.04	BASTIEN	61	HBC	±	

$\Gamma(\Lambda\gamma)/\Gamma(\Lambda\pi)$	DOCUMENT ID	TECN	COMMENT	$\Gamma_3/\Gamma_1$
This ratio is of course for $\Sigma(1385)^0 \rightarrow \Lambda\gamma$ and $\Lambda\pi^0$ .				
<b>1.43<sup>+0.15</sup><sub>-0.13</sub> OUR AVERAGE</b>				
1.42 ± 0.12 <sup>+0.11</sup> <sub>-0.07</sub>	624 ± 25	KELLER	11 CLAS $\gamma p \rightarrow K^+\Lambda\gamma, E_\gamma$ 1.6–3.8 GeV	
1.53 ± 0.39 <sup>+0.15</sup> <sub>-0.24</sub>	61	TAYLOR	05 CLAS $\gamma p \rightarrow K^+\Lambda\gamma$	

$\Gamma(\Sigma^+\gamma)/\Gamma(\Sigma\pi)$	DOCUMENT ID	TECN	COMMENT	$\Gamma_4/\Gamma_2$
This ratio is for $\Sigma(1385)^+ \rightarrow \Sigma^+\gamma$ over $\Sigma(1385)^+ \rightarrow \Sigma\pi$ .				
<b>5.98 ± 1.11<sup>+0.27</sup><sub>-0.61</sub></b>	11	KELLER	12 CLAS $\gamma p \rightarrow K^0\Sigma(1385)^+$	

$\Gamma(\Sigma^-\gamma)/\Gamma_{total}$	CL%	DOCUMENT ID	TECN	CHG	COMMENT	$\Gamma_5/\Gamma$
<b>&lt;2.4 × 10<sup>-4</sup></b>	90	12	MOLCHANOV	04 SELX	- $\Sigma^-p \rightarrow \Sigma(1385)^-p$ , 600 GeV	
• • • We do not use the following data for averages, fits, limits, etc. • • •						
<6.1 × 10 <sup>-4</sup>	90	13	ARIK	77 SPEC	- $\Sigma^-p \rightarrow \Sigma(1385)^-p$ , 23 GeV	

$(\Gamma_i/\Gamma_i)^{1/2}/\Gamma_{total}$ in $N\bar{K} \rightarrow \Sigma(1385) \rightarrow \Lambda\pi$	DOCUMENT ID	CHG	COMMENT	$(\Gamma_6/\Gamma_1)^{1/2}/\Gamma$
+0.586 ± 0.319	14	DEVENISH	74B 0	Fixed-t dispersion rel.

### $\Sigma(1385)$ FOOTNOTES

- From fit to inclusive  $\Lambda\pi$  spectrum.
- Includes data of HOLMGREN 77.
- The errors are statistical only. The resolution is not unfolded.
- The error is enlarged to  $\Gamma/\sqrt{N}$ . See the note on the  $K^*(892)$  mass in the 1984 edition.
- From a fit to  $\Lambda\pi^0$  with the width fixed at 34 MeV.
- From fit to inclusive  $\Lambda\pi^0$  spectrum with the width fixed at 40 MeV.
- Redundant with data in the mass Listings.
- Results from  $\Lambda\pi^+\pi^-$  and  $\Lambda\pi^+\pi^-\pi^0$  combined by us.
- The error is enlarged to  $\Gamma/\sqrt{N}$ . See the note on the  $K^*(892)$  mass in the 1984 edition.
- Consistent with +, 0, and - widths equal.
- KELLER 12 gives  $\Gamma(\Sigma^+\gamma)/\Gamma(\Sigma^+\pi^0) = (11.95 \pm 2.21 \pm 0.53 \pm 1.21)\%$ , using 1/2 our total  $\Sigma(1385) \rightarrow \Sigma\pi$  fraction for  $\Sigma^+\pi^0$ . We divide the KELLER 12 value by two.
- We calculate this from the MOLCHANOV 04 upper limit of 9.5 keV on the  $\Sigma^-\gamma$  width.
- We calculate this from the ARIK 77 upper limit of 24 keV on the  $\Sigma^-\gamma$  width.
- An extrapolation of the parametrized amplitude below threshold.

### $\Sigma(1385)$ REFERENCES

AGAKISHIEV	12	PR C05 035203	G. Agakishiev et al.	(HADES Collab.)
KELLER	12	PR D85 052004	D. Keller et al.	(JLab CLAS Collab.)
KELLER	11	PR D83 072004	D. Keller et al.	(JLab CLAS Collab.)
TAYLOR	05	PR C71 054609	S. Taylor et al.	(JLab CLAS Collab.)
		Also	PR C72 039902 (errat.)	(JLab CLAS Collab.)
MOLCHANOV	04	PL B590 161	V.V. Molchanov et al.	(FNAL SELEX Collab.)
BAUBILLIER	84	ZPHY C23 213	M. Baubillier et al.	(BIRM, CERN, GLAS+)
PDG	84	RMP 56 51	C.G. Wohl et al.	(LBL, CIT, CERN)
AGUILAR...	81D	AFIS A77 144	M. Aguilar-Benitez, J. Salicio	(MADR)
BAKER	80	NP B166 207	P.A. Baker et al.	(LOIC)
BAUBILLIER	79B	NP B148 18	M. Baubillier et al.	(BIRM, CERN, GLAS+)
CAUTIS	79	NP B156 507	C.V. Cautis et al.	(SLAC)
SUGAHARA	79B	NP B156 237	R. Sugahara et al.	(KEK, OSKC, KINK)
CAMERON	78	NP B143 189	W. Cameron et al.	(RHEL LOIC)
DIONISI	78B	PL 78B 154	C. Dionisi, R. Armenteros, J. Diaz	(CERN, AMST+)
ARIK	77	PRL 38 1000	E. Arik et al.	(PITT, BNL, MASA)
BARREIRO	77B	NP B126 319	F. Barreiro et al.	(CERN, AMST, NIJ)
HOLMGREN	77	NP B119 261	S.O. Holmgren et al.	(CERN, AMST, NIJ)
BARDADIN...	75	NP B98 418	M. Bardadin-Otwinowska et al.	(SACL, EPOL+)
BERTHON	74	NC 21A 146	A. Berthon et al.	(CDEF, RHEL, SACL+)
BORENSTEIN	74	PR D9 3006	S.R. Borenstein et al.	(BNL, MICH)
DEVENISH	74B	NP B81 330	R.C.E. Devenish, C.D. Froggatt, B.R. Martin	(DESY+)
LICHTENBERG	74	PR D10 3865	D.B. Lichtenberg	(IND)
		Also	Private Comm.	(IND)
HABIBI	73	Thesis Univ 199	M. Habibi	(COLU)
		Also	Purdue Conf. 387	(COLU, BING)
MAST	73	PR D7 3212	T.S. Mast et al.	(LBL) IJP
		Also	PR D7 5	(LBL) IJP
THOMAS	73	NP B56 15	D.W. Thomas et al.	(CMU) JIP
AGUILAR...	72B	PR D6 29	M. Aguilar-Benitez et al.	(BNL)
COLLEY	71B	NP B31 61	D.C. Colley et al.	(BIRM, EDIN, GLAS+)
AGUILAR...	70B	PRL 25 58	M. Aguilar-Benitez et al.	(BNL, SYR)
PAN	69	PRL 23 808	Y.L. Pan, F.L. Forman	(PENN) I
SIEGEL	67	Thesis UCRL 18041	D.M. Siegel	(LRL)
BIRMINGHAM	66	PR 152 1148	M. Haque et al.	(BIRM, GLAS, LOIC, OXF+)
LONDON	66	PR 143 1034	G.W. London et al.	(BNL, SYR) J
ARMENTEROS	65B	PL 19 75	R. Armenteros et al.	(CERN, HEID, SACL)
SMITH	65	Thesis UCLA	L.T. Smith	(UCLA)
COOPER	64	PL 8 365	W.A. Cooper et al.	(CERN, AMST)
HUWE	64	Thesis UCRL 11291	D.O. Huwe	(LRL) JIP
		Also	PR 181 1824	(LRL) J
CURTIS	63	PR 132 1771	L.J. Curtis et al.	(MICH) J
ALSTON	62	CERN Conf. 311	M.H. Alston et al.	(LRL)
BASTIEN	61	PRL 6 702	P.L. Bastien, M. Ferro-Luzzi, A.H. Rosenfeld	(LRL)
DAHL	61	PRL 6 142	O.H. Dahl et al.	(LRL)
ELY	61	PRL 7 461	R.P. Ely et al.	(LRL) J
ALSTON	60	PRL 5 520	M.H. Alston et al.	(LRL) I

$\Sigma(1580) 3/2^-$

 $I(J^P) = 1(\frac{3}{2}^-)$  Status: \*

OMITTED FROM SUMMARY TABLE  
 Seen in the isospin-1  $\bar{K}N$  cross section at BNL (LI 73, CARROLL 76) and in a partial-wave analysis of  $K^-p \rightarrow \Lambda\pi^0$  for c.m. energies 1560–1600 MeV by LITCHFIELD 74. LITCHFIELD 74 finds  $J^P = 3/2^-$ . Not seen by ENGLER 78, CAMERON 78C, OLMSTED 04, nor by PRAKHOV 04.

Neither ZHANG 13A nor SARANTSEV 19 see any evidence for this state.

### $\Sigma(1580)$ POLE POSITION

REAL PART	DOCUMENT ID	TECN	COMMENT
• • • We do not use the following data for averages, fits, limits, etc. • • •			
1607 <sup>+13</sup> <sub>-11</sub>	1	KAMANO	15 DPWA Multichannel
1 From the preferred solution A in KAMANO 15. Solution B reports $M = 1492 \pm 4$ MeV.			
<b>-2 × IMAGINARY PART</b>			
VALUE (MeV)	DOCUMENT ID	TECN	COMMENT
• • • We do not use the following data for averages, fits, limits, etc. • • •			
253 <sup>+30</sup> <sub>-18</sub>	2	KAMANO	15 DPWA Multichannel
2 From the preferred solution A in KAMANO 15. Solution B reports $M = 138 \pm 8$ MeV.			

### $\Sigma(1580)$ POLE RESIDUES

The "normalized residue" is the residue divided by  $\Gamma_{pole}/2$ .

Normalized residue in $N\bar{K} \rightarrow \Sigma(1580) \rightarrow N\bar{K}$	DOCUMENT ID	TECN	COMMENT
• • • We do not use the following data for averages, fits, limits, etc. • • •			
0.00778	3	KAMANO	15 DPWA Multichannel
3 From the preferred solution A in KAMANO 15.			
Normalized residue in $N\bar{K} \rightarrow \Sigma(1580) \rightarrow \Sigma\pi$	DOCUMENT ID	TECN	COMMENT
• • • We do not use the following data for averages, fits, limits, etc. • • •			
0.0625	4	KAMANO	15 DPWA Multichannel
4 From the preferred solution A in KAMANO 15.			

Baryon Particle Listings  
 $\Sigma(1580), \Sigma(1620)$

Normalized residue in  $N\bar{K} \rightarrow \Sigma(1580) \rightarrow \Lambda\pi$

MODULUS	PHASE (°)	DOCUMENT ID	TECN	COMMENT
0.059	156	<sup>5</sup> KAMANO	15	DPWA Multichannel

<sup>5</sup> From the preferred solution A in KAMANO 15.

Normalized residue in  $N\bar{K} \rightarrow \Sigma(1580) \rightarrow \Sigma(1385)\pi, S\text{-wave}$

MODULUS	PHASE (°)	DOCUMENT ID	TECN	COMMENT
0.0368	-18	<sup>6</sup> KAMANO	15	DPWA Multichannel

<sup>6</sup> From the preferred solution A in KAMANO 15.

Normalized residue in  $N\bar{K} \rightarrow \Sigma(1580) \rightarrow \Sigma(1385)\pi, D\text{-wave}$

MODULUS	PHASE (°)	DOCUMENT ID	TECN	COMMENT
0.0103	123	<sup>7</sup> KAMANO	15	DPWA Multichannel

<sup>7</sup> From the preferred solution A in KAMANO 15.

$\Sigma(1580)$  MASS

VALUE (MeV)	DOCUMENT ID	TECN	COMMENT
$\approx 1580$ OUR ESTIMATE			
1583 ± 4	<sup>8</sup> CARROLL	76	DPWA Isospin-1 total $\sigma$
1582 ± 4	<sup>9</sup> LITCHFIELD	74	DPWA $K^- p \rightarrow \Lambda\pi^0$

<sup>8</sup> CARROLL 76 sees a total-cross-section bump with  $(J+1/2) \Gamma_{el} / \Gamma_{total} = 0.06$ .  
<sup>9</sup> The main effect observed by LITCHFIELD 74 is in the  $\Lambda\pi$  final state; the  $\bar{K}N$  and  $\Sigma\pi$  couplings are estimated from a multichannel fit including total-cross-section data of LI 73.

$\Sigma(1580)$  WIDTH

VALUE (MeV)	DOCUMENT ID	TECN	COMMENT
15	<sup>10</sup> CARROLL	76	DPWA Isospin-1 total $\sigma$
11 ± 4	<sup>11</sup> LITCHFIELD	74	DPWA $K^- p \rightarrow \Lambda\pi^0$

<sup>10</sup> CARROLL 76 sees a total-cross-section bump with  $(J+1/2) \Gamma_{el} / \Gamma_{total} = 0.06$ .  
<sup>11</sup> The main effect observed by LITCHFIELD 74 is in the  $\Lambda\pi$  final state; the  $\bar{K}N$  and  $\Sigma\pi$  couplings are estimated from a multichannel fit including total-cross-section data of LI 73.

$\Sigma(1580)$  DECAY MODES

Mode
$\Gamma_1$ $N\bar{K}$
$\Gamma_2$ $\Lambda\pi$
$\Gamma_3$ $\Sigma\pi$
$\Gamma_4$ $\Sigma(1385)\pi, S\text{-wave}$
$\Gamma_5$ $\Sigma(1385)\pi, D\text{-wave}$
$\Gamma_6$ $N\bar{K}^*(892), S=1/2, D\text{-wave}$
$\Gamma_7$ $N\bar{K}^*(892), S=3/2, S\text{-wave}$
$\Gamma_8$ $N\bar{K}^*(892), S=3/2, D\text{-wave}$

$\Sigma(1580)$  BRANCHING RATIOS

See "Sign conventions for resonance couplings" in the Note on  $\Lambda$  and  $\Sigma$  Resonances.

$\Gamma(N\bar{K})/\Gamma_{total}$

VALUE	DOCUMENT ID	TECN	COMMENT
+0.03 ± 0.01	<sup>12</sup> LITCHFIELD	74	DPWA $\bar{K}N$ multichannel

<sup>12</sup> The main effect observed by LITCHFIELD 74 is in the  $\Lambda\pi$  final state; the  $\bar{K}N$  and  $\Sigma\pi$  couplings are estimated from a multichannel fit including total-cross-section data of LI 73.  
<sup>13</sup> From the preferred solution A in KAMANO 15.

$\Gamma(\Lambda\pi)/\Gamma_{total}$

VALUE	DOCUMENT ID	TECN	COMMENT
0.490	<sup>14</sup> KAMANO	15	DPWA Multichannel

<sup>14</sup> From the preferred solution A in KAMANO 15.

$\Gamma(\Sigma\pi)/\Gamma_{total}$

VALUE	DOCUMENT ID	TECN	COMMENT
0.387	<sup>15</sup> KAMANO	15	DPWA Multichannel

<sup>15</sup> From the preferred solution A in KAMANO 15.

$\Gamma(\Sigma(1385)\pi, S\text{-wave})/\Gamma_{total}$

VALUE	DOCUMENT ID	TECN	COMMENT
0.12	<sup>16</sup> KAMANO	15	DPWA Multichannel

<sup>16</sup> From the preferred solution A in KAMANO 15.

$\Gamma(\Sigma(1385)\pi, D\text{-wave})/\Gamma_{total}$

VALUE	DOCUMENT ID	TECN	COMMENT
0.001	<sup>17</sup> KAMANO	15	DPWA Multichannel

<sup>17</sup> From the preferred solution A in KAMANO 15.

$\Gamma(N\bar{K}^*(892), S=1/2, D\text{-wave})/\Gamma_{total}$

VALUE	DOCUMENT ID	TECN	COMMENT
not seen	<sup>18</sup> KAMANO	15	DPWA Multichannel

<sup>18</sup> From the preferred solution A in KAMANO 15.

$\Gamma(N\bar{K}^*(892), S=3/2, S\text{-wave})/\Gamma_{total}$

VALUE	DOCUMENT ID	TECN	COMMENT
not seen	<sup>19</sup> KAMANO	15	DPWA Multichannel

<sup>19</sup> From the preferred solution A in KAMANO 15.

$\Gamma(N\bar{K}^*(892), S=3/2, D\text{-wave})/\Gamma_{total}$

VALUE	DOCUMENT ID	TECN	COMMENT
not seen	<sup>20</sup> KAMANO	15	DPWA Multichannel

<sup>20</sup> From the preferred solution A in KAMANO 15.

$(\Gamma_i \Gamma_f)^{1/2} / \Gamma_{total}$  in  $N\bar{K} \rightarrow \Sigma(1580) \rightarrow \Lambda\pi$

VALUE	DOCUMENT ID	TECN	COMMENT
not seen	CAMERON	78c	HBC $K_L^0 p \rightarrow \Lambda\pi^+$
not seen	ENGLER	78	HBC $K_L^0 p \rightarrow \Lambda\pi^+$
+0.10 ± 0.02	<sup>21</sup> LITCHFIELD	74	DPWA $K^- p \rightarrow \Lambda\pi^0$

<sup>21</sup> The main effect observed by LITCHFIELD 74 is in the  $\Lambda\pi$  final state; the  $\bar{K}N$  and  $\Sigma\pi$  couplings are estimated from a multichannel fit including total-cross-section data of LI 73.

$(\Gamma_i \Gamma_f)^{1/2} / \Gamma_{total}$  in  $N\bar{K} \rightarrow \Sigma(1580) \rightarrow \Sigma\pi$

VALUE	DOCUMENT ID	TECN	COMMENT
not seen	CAMERON	78c	HBC $K_L^0 p \rightarrow \Sigma^0 \pi^+$
not seen	ENGLER	78	HBC $K_L^0 p \rightarrow \Sigma^0 \pi^+$
+0.03 ± 0.04	<sup>22</sup> LITCHFIELD	74	DPWA $\bar{K}N$ multichannel

<sup>22</sup> The main effect observed by LITCHFIELD 74 is in the  $\Lambda\pi$  final state; the  $\bar{K}N$  and  $\Sigma\pi$  couplings are estimated from a multichannel fit including total-cross-section data of LI 73.

$\Sigma(1580)$  REFERENCES

SARANTSEV	19	EPJ A55 180	A.V. Sarantsev et al.	(BONN, PNPI)
KAMANO	15	PR C92 025205	H. Kamano et al.	(ANL, OSAK)
ZHANG	13A	PR C88 035205	H. Zhang et al.	(KSU)
OLMSTED	04	PL B588 29	J. Olmsted et al.	(BNL Crystal Ball Collab.)
PRAKHOV	04	PR C69 042202	S. Prakhov et al.	(BNL Crystal Ball Collab.)
CAMERON	78c	NP B132 189	W. Cameron et al.	(BGNA, EDIN, GLAS+)
ENGLER	78	PR D18 3061	A. Engler et al.	(CMU, ANL)
CARROLL	76	PRL 37 306	A.S. Carroll et al.	(BNL)
LITCHFIELD	74	PL 51B 509	P.J. Litchfield	(CERN)UP
LI	73	Purdue Conf. 283	K.K. Li	(BNL)

$\Sigma(1620) 1/2^-$

$I(J^P) = 1(\frac{1}{2}^-)$  Status: \*

OMITTED FROM SUMMARY TABLE

The  $S_{11}$  state at 1697 MeV reported by VANHORN 75 is tentatively listed under the  $\Sigma(1750)$ . CARROLL 76 sees two bumps in the isospin-1 total cross section near this mass. GAO 12 sees no evidence for this resonance.

Production experiments are listed separately in the next entry.

$\Sigma(1620)$  POLE POSITION

REAL PART

VALUE (MeV)	DOCUMENT ID	TECN	COMMENT
1680 ± 8	SARANTSEV	19	DPWA $\bar{K}N$ multichannel

<sup>1501</sup> We do not use the following data for averages, fits, limits, etc. ●●●

1501	ZHANG	13A	DPWA $\bar{K}N$ multichannel
------	-------	-----	------------------------------

-2xIMAGINARY PART

VALUE (MeV)	DOCUMENT ID	TECN	COMMENT
39 ± 11	SARANTSEV	19	DPWA $\bar{K}N$ multichannel

<sup>171</sup> We do not use the following data for averages, fits, limits, etc. ●●●

171	ZHANG	13A	DPWA $\bar{K}N$ multichannel
-----	-------	-----	------------------------------

# Baryon Particle Listings

## $\Sigma(1620), \Sigma(1660)$

### $\Sigma(1620)$ POLE RESIDUE

The "normalized residue" is the residue divided by  $\Gamma_{pole}/2$ .

#### Normalized residue in $N\bar{K} \rightarrow \Sigma(1620) \rightarrow \Sigma\pi$

MODULUS	PHASE (°)	DOCUMENT ID	TECN	COMMENT
$0.14 \pm 0.03$	$-90 \pm 25$	SARANTSEV 19	DPWA	$\bar{K}N$ multichannel

#### Normalized residue in $N\bar{K} \rightarrow \Sigma(1620) \rightarrow \Lambda\pi$

MODULUS	PHASE (°)	DOCUMENT ID	TECN	COMMENT
$0.10 \pm 0.03$	$75 \pm 20$	SARANTSEV 19	DPWA	$\bar{K}N$ multichannel

#### Normalized residue in $N\bar{K} \rightarrow \Sigma(1620) \rightarrow \Xi K$

MODULUS	PHASE (°)	DOCUMENT ID	TECN	COMMENT
$0.02 \pm 0.01$	$120 \pm 20$	SARANTSEV 19	DPWA	$\bar{K}N$ multichannel

#### Normalized residue in $N\bar{K} \rightarrow \Sigma(1620) \rightarrow \Lambda(1520)\pi$

MODULUS	PHASE (°)	DOCUMENT ID	TECN	COMMENT
$0.12 \pm 0.05$	$140 \pm 40$	SARANTSEV 19	DPWA	$\bar{K}N$ multichannel

#### Normalized residue in $N\bar{K} \rightarrow \Sigma(1620) \rightarrow \Sigma(1385)\pi$

MODULUS	PHASE (°)	DOCUMENT ID	TECN	COMMENT
$0.015 \pm 0.010$	$155 \pm 40$	SARANTSEV 19	DPWA	$\bar{K}N$ multichannel

#### Normalized residue in $N\bar{K} \rightarrow \Sigma(1620) \rightarrow N\bar{K}^*(892), S\text{-wave}$

MODULUS	PHASE (°)	DOCUMENT ID	TECN	COMMENT
$0.05 \pm 0.04$		SARANTSEV 19	DPWA	$\bar{K}N$ multichannel

#### Normalized residue in $N\bar{K} \rightarrow \Sigma(1620) \rightarrow N\bar{K}^*(892), D\text{-wave}$

MODULUS	PHASE (°)	DOCUMENT ID	TECN	COMMENT
$0.01 \pm 0.01$		SARANTSEV 19	DPWA	$\bar{K}N$ multichannel

#### Normalized residue in $N\bar{K} \rightarrow \Sigma(1620) \rightarrow N\bar{K}$

VALUE	DOCUMENT ID	TECN	COMMENT
$0.11 + -0.03 @ 43 + -20$	SARANTSEV 19	DPWA	$\bar{K}N$ multichannel

### $\Sigma(1620)$ MASS

VALUE (MeV)	DOCUMENT ID	TECN	COMMENT
<b>1600 to 1650 (<math>\approx 1620</math>) OUR ESTIMATE</b>			
$1681 \pm 6$	SARANTSEV 19	DPWA	$\bar{K}N$ multichannel
$1600 \pm 15$	ZHANG 13A	DPWA	$\bar{K}N$ multichannel
$1600 \pm 6$	<sup>1</sup> MORRIS 78	DPWA	$K^- n \rightarrow \Lambda\pi^-$
$1608 \pm 5$	<sup>2</sup> CARROLL 76	DPWA	Isospin-1 total $\sigma$
$1630 \pm 10$	LANGBEIN 72	IPWA	$\bar{K}N$ multichannel
$1620$	KIM 71	DPWA	K-matrix analysis
$1633 \pm 10$	<sup>3</sup> CARROLL 76	DPWA	Isospin-1 total $\sigma$

• • • We do not use the following data for averages, fits, limits, etc. • • •

### $\Sigma(1620)$ WIDTH

VALUE (MeV)	DOCUMENT ID	TECN	COMMENT
<b>40 to 100 (<math>\approx 70</math>) OUR ESTIMATE</b>			
$40 \pm 12$	SARANTSEV 19	DPWA	$\bar{K}N$ multichannel
$400 \pm 152$	ZHANG 13A	DPWA	$\bar{K}N$ multichannel
$87 \pm 19$	<sup>1</sup> MORRIS 78	DPWA	$K^- n \rightarrow \Lambda\pi^-$
$15$	<sup>2</sup> CARROLL 76	DPWA	Isospin-1 total $\sigma$
$65 \pm 20$	LANGBEIN 72	IPWA	$\bar{K}N$ multichannel
$40$	KIM 71	DPWA	K-matrix analysis
$10$	<sup>3</sup> CARROLL 76	DPWA	Isospin-1 total $\sigma$

• • • We do not use the following data for averages, fits, limits, etc. • • •

### $\Sigma(1620)$ DECAY MODES

Mode	Fraction ( $\Gamma_i/\Gamma$ )
$\Gamma_1$ $N\bar{K}$	0.10 to 0.60
$\Gamma_2$ $\Lambda\pi$	( $9.0 \pm 3.0$ ) %
$\Gamma_3$ $\Sigma\pi$	( $17 \pm 5$ ) %
$\Gamma_4$ $\Xi K$	
$\Gamma_5$ $\Lambda(1520)\pi$	( $10 \pm 5$ ) %
$\Gamma_6$ $\Sigma(1385)\pi$	

### $\Sigma(1620)$ BRANCHING RATIOS

$\Gamma(N\bar{K})/\Gamma_{total}$	DOCUMENT ID	TECN	COMMENT	$\Gamma_1/\Gamma$
<b>0.10 to 0.60 OUR ESTIMATE</b>				
$0.11 \pm 0.03$	SARANTSEV 19	DPWA	$\bar{K}N$ multichannel	
$0.59 \pm 0.10$	ZHANG 13A	DPWA	$\bar{K}N$ multichannel	
$0.22 \pm 0.02$	LANGBEIN 72	IPWA	$\bar{K}N$ multichannel	
$0.05$	KIM 71	DPWA	K-matrix analysis	

### $\Gamma(\Sigma\pi)/\Gamma_{total}$

VALUE	DOCUMENT ID	TECN	COMMENT	$\Gamma_3/\Gamma$
$0.17 \pm 0.05$	SARANTSEV 19	DPWA	$\bar{K}N$ multichannel	

### $\Gamma(\Lambda\pi)/\Gamma_{total}$

VALUE	DOCUMENT ID	TECN	COMMENT	$\Gamma_2/\Gamma$
$0.09 \pm 0.03$	SARANTSEV 19	DPWA	$\bar{K}N$ multichannel	

### $\Gamma(\Xi K)/\Gamma_{total}$

VALUE	DOCUMENT ID	TECN	COMMENT	$\Gamma_4/\Gamma$
$\sim 0$	SARANTSEV 19	DPWA	$\bar{K}N$ multichannel	

### $\Gamma(\Lambda(1520)\pi)/\Gamma_{total}$

VALUE	DOCUMENT ID	TECN	COMMENT	$\Gamma_5/\Gamma$
$0.10 \pm 0.05$	SARANTSEV 19	DPWA	$\bar{K}N$ multichannel	

### $\Gamma(\Sigma(1385)\pi)/\Gamma_{total}$

VALUE	DOCUMENT ID	TECN	COMMENT	$\Gamma_6/\Gamma$
$< 0.01$	SARANTSEV 19	DPWA	$\bar{K}N$ multichannel	

### $(\Gamma_1\Gamma_2)^{1/2}/\Gamma_{total}$ in $N\bar{K} \rightarrow \Sigma(1620) \rightarrow \Lambda\pi$

VALUE	DOCUMENT ID	TECN	COMMENT	$(\Gamma_1\Gamma_2)^{1/2}/\Gamma$
$0.12 \pm 0.02$	<sup>1</sup> MORRIS 78	DPWA	$K^- n \rightarrow \Lambda\pi^-$	
not seen	BAILLON 75	IPWA	$\bar{K}N \rightarrow \Lambda\pi$	
$0.15$	KIM 71	DPWA	K-matrix analysis	

### $(\Gamma_1\Gamma_3)^{1/2}/\Gamma_{total}$ in $N\bar{K} \rightarrow \Sigma(1620) \rightarrow \Sigma\pi$

VALUE	DOCUMENT ID	TECN	COMMENT	$(\Gamma_1\Gamma_3)^{1/2}/\Gamma$
$+0.32 \pm 0.03$	ZHANG 13A	DPWA	Multichannel	
not seen	HEPP 76B	DPWA	$K^- N \rightarrow \Sigma\pi$	
$+0.40 \pm 0.06$	LANGBEIN 72	IPWA	$\bar{K}N$ multichannel	
$+0.08$	KIM 71	DPWA	K-matrix analysis	

### $\Sigma(1620)$ FOOTNOTES

- <sup>1</sup> MORRIS 78 obtains an equally good fit without including this resonance.
- <sup>2</sup> Total cross-section bump with  $(J+1/2) \Gamma_{el} / \Gamma_{total}$  is 0.06 seen by CARROLL 76.
- <sup>3</sup> Total cross-section bump with  $(J+1/2) \Gamma_{el} / \Gamma_{total}$  is 0.04 seen by CARROLL 76.

### $\Sigma(1620)$ REFERENCES

SARANTSEV 19	EPJ A55 180	A.V. Sarantsev et al.	(BONN, PNPI)
ZHANG 13A	PR C88 035205	H. Zhang et al.	(KSU)
GAO 12	PR C86 025201	P. Gao, J. Shi, B.S. Zou	(BHEP, BEIJT)
	NP A567 41	P. Gao, B.S. Zou, A. Sibirtsev	(BHEP, BEIJT+)
MORRIS 78	PR D17 55	W.A. Morris et al.	(FSU) IJP
CARROLL 76	PRL 37 806	A.S. Carroll et al.	(BNL) I
HEPP 76B	PL 65B 487	V. Hepp et al.	(CERN, HEIDH, MPIM) IJP
BAILLON 75	NP B94 39	P.H. Baillon, P.J. Litchfield	(CERN, RHEL) IJP
VANHORN 75	NP B87 145	A.J. van Horn	(LBL) IJP
	NP B87 157	A.J. van Horn	(LBL) IJP
LANGBEIN 72	NP B47 477	W. Langbein, F. Wagner	(MPIM) IJP
KIM 71	PRL 27 356	J.K. Kim	(HARV) IJP
	Duke Conf. 161	J.K. Kim	(HARV) IJP
	Hyperon Resonances, 1970		

$$\Sigma(1660) 1/2^+$$

$$I(J^P) = 1(\frac{1}{2}^+) \text{ Status: } ***$$

For results published before 1974 (they are now obsolete), see our 1982 edition Physics Letters **111B** 1 (1982).

### $\Sigma(1660)$ POLE POSITION

#### REAL PART

VALUE (MeV)	DOCUMENT ID	TECN	COMMENT
$1585 \pm 20$	SARANTSEV 19	DPWA	$\bar{K}N$ multichannel

• • • We do not use the following data for averages, fits, limits, etc. • • •

VALUE	DOCUMENT ID	TECN	COMMENT
$1547^{+111}_{-59}$	<sup>1</sup> KAMANO 15	DPWA	$\bar{K}N$ multichannel

<sup>1</sup> From the preferred solution A in KAMANO 15. Solution B reports  $M = 1457^{+5}_{-1}$  MeV.

#### -2xIMAGINARY PART

VALUE (MeV)	DOCUMENT ID	TECN	COMMENT
$290^{+140}_{-40}$	SARANTSEV 19	DPWA	$\bar{K}N$ multichannel

• • • We do not use the following data for averages, fits, limits, etc. • • •

VALUE	DOCUMENT ID	TECN	COMMENT
$183^{+86}_{-78}$	<sup>1</sup> KAMANO 15	DPWA	$\bar{K}N$ multichannel

<sup>1</sup> From the preferred solution A in KAMANO 15. Solution B reports  $\Gamma = 78^{+2}_{-8}$  MeV.

$\Sigma(1660)$  POLE RESIDUES

The normalized residue is the residue divided by  $\Gamma_{pole}/2$ .

Normalized residue in  $N\bar{K} \rightarrow \Sigma(1660) \rightarrow N\bar{K}$

MODULUS	PHASE (°)	DOCUMENT ID	TECN	COMMENT
<b>0.07 ± 0.03</b>	<b>-165 ± 35</b>	SARANTSEV 19	DPWA	$\bar{K}N$ multichannel
0.0247	168	<sup>1</sup> KAMANO 15	DPWA	$\bar{K}N$ multichannel

• • • We do not use the following data for averages, fits, limits, etc. • • •  
<sup>1</sup> From the preferred solution A in KAMANO 15.

Normalized residue in  $N\bar{K} \rightarrow \Sigma(1660) \rightarrow \Sigma\pi$

MODULUS	PHASE (°)	DOCUMENT ID	TECN	COMMENT
<b>0.17 ± 0.04</b>	<b>150 ± 20</b>	SARANTSEV 19	DPWA	$\bar{K}N$ multichannel
0.16	78	<sup>1</sup> KAMANO 15	DPWA	$\bar{K}N$ multichannel

• • • We do not use the following data for averages, fits, limits, etc. • • •  
<sup>1</sup> From the preferred solution A in KAMANO 15.

Normalized residue in  $N\bar{K} \rightarrow \Sigma(1660) \rightarrow \Lambda\pi$

MODULUS	PHASE (°)	DOCUMENT ID	TECN	COMMENT
<b>0.16 ± 0.05</b>	<b>0 ± 25</b>	SARANTSEV 19	DPWA	$\bar{K}N$ multichannel
0.0614	-84	<sup>1</sup> KAMANO 15	DPWA	$\bar{K}N$ multichannel

• • • We do not use the following data for averages, fits, limits, etc. • • •  
<sup>1</sup> From the preferred solution A in KAMANO 15.

Normalized residue in  $N\bar{K} \rightarrow \Sigma(1660) \rightarrow \Sigma\sigma$

MODULUS	PHASE (°)	DOCUMENT ID	TECN	COMMENT
<b>0.14 ± 0.06</b>	<b>-150 ± 30</b>	SARANTSEV 19	DPWA	$\bar{K}N$ multichannel

Normalized residue in  $N\bar{K} \rightarrow \Sigma(1660) \rightarrow \Sigma(1385)\pi$

MODULUS	PHASE (°)	DOCUMENT ID	TECN	COMMENT
0.0513	-44	<sup>1</sup> KAMANO 15	DPWA	Multichannel

• • • We do not use the following data for averages, fits, limits, etc. • • •  
<sup>1</sup> From the preferred solution A in KAMANO 15.

Normalized residue in  $N\bar{K} \rightarrow \Sigma(1660) \rightarrow \Lambda(1405)\pi$

MODULUS	PHASE (°)	DOCUMENT ID	TECN	COMMENT
<b>0.06 ± 0.03</b>	<b>-90 ± 25</b>	SARANTSEV 19	DPWA	$\bar{K}N$ multichannel

Normalized residue in  $N\bar{K} \rightarrow \Sigma(1660) \rightarrow \Lambda(1520)\pi$

MODULUS	PHASE (°)	DOCUMENT ID	TECN	COMMENT
<b>0.04 ± 0.02</b>	<b>5 ± 20</b>	SARANTSEV 19	DPWA	$\bar{K}N$ multichannel

$\Sigma(1660)$  MASS

VALUE (MeV)	DOCUMENT ID	TECN	COMMENT
<b>1640 to 1680 (≈ 1660) OUR ESTIMATE</b>			
1665 ± 20	SARANTSEV 19	DPWA	$\bar{K}N$ multichannel
1633 ± 3	GAO 12	DPWA	$\bar{K}N \rightarrow \Lambda\pi$
1665.1 ± 11.2	<sup>1</sup> KOISO 85	DPWA	$K^-p \rightarrow \Sigma\pi$
1670 ± 10	GOPAL 80	DPWA	$\bar{K}N \rightarrow \bar{K}N$
1679 ± 10	ALSTON-... 78	DPWA	$\bar{K}N \rightarrow \bar{K}N$
1668 ± 25	VANHORN 75	DPWA	$K^-p \rightarrow \Lambda\pi^0$
1670 ± 20	KANE 74	DPWA	$K^-p \rightarrow \Sigma\pi$
• • • We do not use the following data for averages, fits, limits, etc. • • •			
1676 ± 15	GOPAL 77	DPWA	$\bar{K}N$ multichannel
1565 or 1597	<sup>2</sup> MARTIN 77	DPWA	$\bar{K}N$ multichannel
1660 ± 30	<sup>3</sup> BAILLON 75	IPWA	$\bar{K}N \rightarrow \Lambda\pi$
1671 ± 2	<sup>4</sup> PONTE 75	DPWA	$K^-p \rightarrow \Lambda\pi^0$

<sup>1</sup> The evidence of KOISO 85 is weak.  
<sup>2</sup> The two MARTIN 77 values are from a T-matrix pole and from a Breit-Wigner fit.  
<sup>3</sup> From solution 1 of BAILLON 75; not present in solution 2.  
<sup>4</sup> From solution 2 of PONTE 75; not present in solution 1.

$\Sigma(1660)$  WIDTH

VALUE (MeV)	DOCUMENT ID	TECN	COMMENT
<b>100 to 300 (≈ 200) OUR ESTIMATE</b>			
300 +140 -40	SARANTSEV 19	DPWA	$\bar{K}N$ multichannel
121 + 4 - 7	GAO 12	DPWA	$\bar{K}N \rightarrow \Lambda\pi$
81.5 ± 22.2	<sup>1</sup> KOISO 85	DPWA	$K^-p \rightarrow \Sigma\pi$
152 ± 20	GOPAL 80	DPWA	$\bar{K}N \rightarrow \bar{K}N$
38 ± 10	ALSTON-... 78	DPWA	$\bar{K}N \rightarrow \bar{K}N$
230 +165 - 60	VANHORN 75	DPWA	$K^-p \rightarrow \Lambda\pi^0$
250 ± 110	KANE 74	DPWA	$K^-p \rightarrow \Sigma\pi$
• • • We do not use the following data for averages, fits, limits, etc. • • •			
120 ± 20	GOPAL 77	DPWA	$\bar{K}N$ multichannel
202 or 217	<sup>2</sup> MARTIN 77	DPWA	$\bar{K}N$ multichannel
80 ± 40	<sup>3</sup> BAILLON 75	IPWA	$\bar{K}N \rightarrow \Lambda\pi$
81 ± 10	<sup>4</sup> PONTE 75	DPWA	$K^-p \rightarrow \Lambda\pi^0$

<sup>1</sup> The evidence of KOISO 85 is weak.  
<sup>2</sup> The two MARTIN 77 values are from a T-matrix pole and from a Breit-Wigner fit.  
<sup>3</sup> From solution 1 of BAILLON 75; not present in solution 2.  
<sup>4</sup> From solution 2 of PONTE 75; not present in solution 1.

$\Sigma(1660)$  DECAY MODES

Mode	Fraction ( $\Gamma_i/\Gamma$ )
$\Gamma_1$ $N\bar{K}$	0.05 to 0.15 (≈ 010)
$\Gamma_2$ $\Lambda\pi$	(35 ± 12 ) %
$\Gamma_3$ $\Sigma\pi$	(37 ± 10 ) %
$\Gamma_4$ $\Sigma\sigma$	(20 ± 8 ) %
$\Gamma_5$ $\Sigma(1385)\pi$	
$\Gamma_6$ $\Lambda(1405)\pi$	( 4.0 ± 2.0 ) %
$\Gamma_7$ $\Lambda(1520)\pi$	

$\Sigma(1660)$  BRANCHING RATIOS

See "Sign conventions for resonance couplings" in the Note on  $\Lambda$  and  $\Sigma$  Resonances.

$\Gamma(N\bar{K})/\Gamma_{total}$   $\Gamma_1/\Gamma$

VALUE	DOCUMENT ID	TECN	COMMENT
<b>0.05 to 0.15 (≈ 010) OUR ESTIMATE</b>			
0.07 ± 0.03	SARANTSEV 19	DPWA	$\bar{K}N$ multichannel
0.12 ± 0.03	GOPAL 80	DPWA	$\bar{K}N \rightarrow \bar{K}N$
0.10 ± 0.05	ALSTON-... 78	DPWA	$\bar{K}N \rightarrow \bar{K}N$
• • • We do not use the following data for averages, fits, limits, etc. • • •			
0.005	<sup>1</sup> KAMANO 15	DPWA	$\bar{K}N$ multichannel
<0.04	GOPAL 77	DPWA	See GOPAL 80
0.27 or 0.29	<sup>2</sup> MARTIN 77	DPWA	$\bar{K}N$ multichannel

<sup>1</sup> From the preferred solution A in KAMANO 15.  
<sup>2</sup> The two MARTIN 77 values are from a T-matrix pole and from a Breit-Wigner fit.

$\Gamma(\Lambda\pi)/\Gamma_{total}$   $\Gamma_2/\Gamma$

VALUE	DOCUMENT ID	TECN	COMMENT
<b>0.35 ± 0.12</b>	SARANTSEV 19	DPWA	$\bar{K}N$ multichannel
• • • We do not use the following data for averages, fits, limits, etc. • • •			
0.128	<sup>1</sup> KAMANO 15	DPWA	$\bar{K}N$ multichannel

<sup>1</sup> From the preferred solution A in KAMANO 15.

$\Gamma(\Sigma\pi)/\Gamma_{total}$   $\Gamma_3/\Gamma$

VALUE	DOCUMENT ID	TECN	COMMENT
<b>0.37 ± 0.10</b>	SARANTSEV 19	DPWA	$\bar{K}N$ multichannel
• • • We do not use the following data for averages, fits, limits, etc. • • •			
0.865	<sup>1</sup> KAMANO 15	DPWA	$\bar{K}N$ multichannel

<sup>1</sup> From the preferred solution A in KAMANO 15.

$\Gamma(\Sigma\sigma)/\Gamma_{total}$   $\Gamma_4/\Gamma$

VALUE	DOCUMENT ID	TECN	COMMENT
<b>0.20 ± 0.08</b>	SARANTSEV 19	DPWA	$\bar{K}N$ multichannel

$\Gamma(\Sigma(1385)\pi)/\Gamma_{total}$   $\Gamma_5/\Gamma$

VALUE	DOCUMENT ID	TECN	COMMENT
0.001	<sup>1</sup> KAMANO 15	DPWA	Multichannel

• • • We do not use the following data for averages, fits, limits, etc. • • •  
<sup>1</sup> From the preferred solution A in KAMANO 15.

$\Gamma(\Lambda(1405)\pi)/\Gamma_{total}$   $\Gamma_6/\Gamma$

VALUE	DOCUMENT ID	TECN	COMMENT
<b>0.04 ± 0.02</b>	SARANTSEV 19	DPWA	$\bar{K}N$ multichannel

$\Gamma(\Lambda(1520)\pi)/\Gamma_{total}$   $\Gamma_7/\Gamma$

VALUE	DOCUMENT ID	TECN	COMMENT
<0.01	SARANTSEV 19	DPWA	$\bar{K}N$ multichannel

$(\Gamma_1\Gamma_7)^{1/2}/\Gamma_{total}$  in  $N\bar{K} \rightarrow \Sigma(1660) \rightarrow \Lambda\pi$   $(\Gamma_1\Gamma_2)^{1/2}/\Gamma$

VALUE	DOCUMENT ID	TECN	COMMENT
-0.064 + 0.005 - 0.003	GAO 12	DPWA	$\bar{K}N \rightarrow \Lambda\pi$
< 0.04	GOPAL 77	DPWA	$\bar{K}N$ multichannel
0.12 + 0.12 - 0.04	VANHORN 75	DPWA	$K^-p \rightarrow \Lambda\pi^0$

• • • We do not use the following data for averages, fits, limits, etc. • • •  
<sup>1</sup> MARTIN 77 values are from a T-matrix pole and from a Breit-Wigner fit.  
<sup>2</sup> BAILLON 75 values are from a T-matrix pole and from a Breit-Wigner fit.  
<sup>3</sup> From solution 1 of BAILLON 75; not present in solution 2.  
<sup>4</sup> From solution 2 of PONTE 75; not present in solution 1.

$(\Gamma_1\Gamma_7)^{1/2}/\Gamma_{total}$  in  $N\bar{K} \rightarrow \Sigma(1660) \rightarrow \Sigma\pi$   $(\Gamma_1\Gamma_3)^{1/2}/\Gamma$

VALUE	DOCUMENT ID	TECN	COMMENT
-0.13 ± 0.04	<sup>1</sup> KOISO 85	DPWA	$K^-p \rightarrow \Sigma\pi$
-0.16 ± 0.03	GOPAL 77	DPWA	$\bar{K}N$ multichannel
-0.11 ± 0.01	KANE 74	DPWA	$K^-p \rightarrow \Sigma\pi$



## Baryon Particle Listings

 $\Sigma(1660)$ ,  $\Sigma(1670)$ ,  $\Sigma(1670)$ 

••• We do not use the following data for averages, fits, limits, etc. •••

–0.34 or –0.37 <sup>2</sup> MARTIN 77 DPWA  $\bar{K}N$  multichannel  
not seen HEPP 76B DPWA  $K^-N \rightarrow \Sigma\pi$

<sup>1</sup>The evidence of KOISO 85 is weak.

<sup>2</sup>The two MARTIN 77 values are from a T-matrix pole and from a Breit-Wigner fit.

 $\Sigma(1660)$  REFERENCES

SARANTSEV	19	EPJ A55 180	A.V. Sarantsev <i>et al.</i>	(BONN, PNPI)
KAMANO	15	PR C92 025205	H. Kamano <i>et al.</i>	(ANL, OSAK)
GAO	12	PR C86 025201	P. Gao, J. Shi, B.S. Zou	(BHEP, BEIJT)
Also		NP A867 41	P. Gao, B.S. Zou, A. Sibirtsev	(BHEP, BEIJT+)
KOISO	85	NP A433 619	H. Koiso <i>et al.</i>	(TOKY, MASA)
PDG	82	PL 111B 1	M. Roos <i>et al.</i>	(HELSE, CIT, CERN)
GOPAL	80	Toronto Conf. 159	G.P. Gopal	(RHEL) IJP
ALSTON...	78	PR D38 182	M. Alston-Garnjost <i>et al.</i>	(LBL, MTHO+) IJP
Also		PRL 38 1007	M. Alston-Garnjost <i>et al.</i>	(LBL, MTHO+) IJP
GOPAL	77	NP B119 352	G.P. Gopal <i>et al.</i>	(LOIC, RHEL) IJP
MARTIN	77	NP B127 349	B.R. Martin, M.K. Piddcock, R.G. Moorhouse	(LOUC+) IJP
Also		NP B126 266	B.R. Martin, M.K. Piddcock	(LOUC) IJP
Also		NP B126 285	B.R. Martin, M.K. Piddcock	(LOUC) IJP
HEPP	76B	PL 65B 487	V. Hepp <i>et al.</i>	(CERN, HEIDH, MPIM) IJP
BAILLON	75	NP B94 39	P.H. Baillon, P.J. Litchfield	(CERN, RHEL) IJP
PONTE	75	PR D12 2597	R.A. Ponte <i>et al.</i>	(MASA, TENN, UCR) IJP
VANHORN	75	NP B87 145	A.J. van Horn	(LBL) IJP
Also		NP B87 157	A.J. van Horn	(LBL) IJP
KANE	74	LBL-2452	D.F. Kane	(LBL) IJP

THE  $\Sigma(1670)$  REGION

**Production experiments:** The measured  $\Sigma\pi/\Sigma\pi\pi$  branching ratio for the  $\Sigma(1670)$  produced in the reaction  $K^-p \rightarrow \pi^-\Sigma(1670)^+$  is strongly dependent on momentum transfer. This was first discovered by EBERHARD 69 [1], who suggested that there exist two  $\Sigma$  resonances with the same mass and quantum numbers: one with a large  $\Sigma\pi\pi$  (mainly  $\Lambda(1405)\pi$ ) branching fraction produced peripherally, and the other with a large  $\Sigma\pi$  branching fraction produced at larger angles. The experimental results have been confirmed by AGUILAR-BENITEZ 70 [2], APSELL 74 [3], ESTES 74 [4], and TIMMERMANS 76 [5]. If, in fact, there are two resonances, the most likely quantum numbers for both the  $\Sigma\pi$  and the  $\Lambda(1405)\pi$  states are  $D_{13}$ . There is also possibly a third  $\Sigma$  in this region, the  $\Sigma(1690)$  in the Listings, the main evidence for which is a large  $\Lambda\pi/\Sigma\pi$  branching ratio. These topics have been reviewed by EBERHARD 73 [6] and by MILLER 70 [7].

**Formation experiments:** Two states are also observed near this mass in formation experiments. One of these, the  $\Sigma(1670)D_{13}$ , has the same quantum numbers as those observed in production and has a large  $\Sigma\pi/\Sigma\pi\pi$  branching ratio; it may well be the  $\Sigma(1670)$  produced at larger angles (see TIMMERMANS 76 [5]). The other state, the  $\Sigma(1660)P_{11}$ , has different quantum numbers, its  $\Sigma\pi/\Sigma\pi\pi$  branching ratio is unknown, and its relation to the produced  $\Sigma(1670)$  states is obscure.

## References

1. P.H. Eberhard *et al.*, Phys. Rev. Lett. **22**, 200 (1969).
2. M. Aguilar-Benitez, *et al.*, Phys. Rev. Lett. **25**, 58 (1970).
3. S.P. Apsell, *et al.*, Phys. Rev. **D10**, 1419 (1974).
4. R.D. Estes, Thesis LBL-3827 (1974).
5. J.J.M. Timmermans, *et al.*, Nucl. Phys. **B112**, 77 (1976).
6. P.H. Eberhard, Purdue Conf. 247 (1973).
7. D.H. Miller, Duke Conf. 229 (1970).

 $\Sigma(1670) 3/2^-$ 

$$I(J^P) = 1(\frac{3}{2}^-) \text{ Status: } ***$$

For most results published before 1974 (they are now obsolete), see our 1982 edition Physics Letters **111B** 1 (1982).

Results from production experiments are listed separately in the next entry.

 $\Sigma(1670)$  POLE POSITION

## REAL PART

VALUE (MeV)	DOCUMENT ID	TECN	COMMENT
<b>1655 ± 3</b>	SARANTSEV 19	DPWA	$\bar{K}N$ multichannel
1669 ± $\frac{7}{7}$	<sup>1</sup> KAMANO 15	DPWA	$\bar{K}N$ multichannel

••• We do not use the following data for averages, fits, limits, etc. •••

1674	ZHANG 13A	DPWA	$\bar{K}N$ multichannel
------	-----------	------	-------------------------

<sup>1</sup> From the preferred solution A in KAMANO 15.

## –2×IMAGINARY PART

VALUE (MeV)	DOCUMENT ID	TECN	COMMENT
<b>45 to 65 (≈ 55) OUR ESTIMATE</b>			
52 ± 6	SARANTSEV 19	DPWA	$\bar{K}N$ multichannel
64 ± $\frac{10}{14}$	<sup>1</sup> KAMANO 15	DPWA	$\bar{K}N$ multichannel

••• We do not use the following data for averages, fits, limits, etc. •••

54	ZHANG 13A	DPWA	$\bar{K}N$ multichannel
----	-----------	------	-------------------------

<sup>1</sup> From the preferred solution A in KAMANO 15.

 $\Sigma(1670)$  POLE RESIDUES

The normalized residue is the residue divided by  $\Gamma_{pole}/2$ .

Normalized residue in  $N\bar{K} \rightarrow \Sigma(1670) \rightarrow N\bar{K}$ 

MODULUS	PHASE (°)	DOCUMENT ID	TECN	COMMENT
<b>0.10 ± 0.02</b>	<b>–31 ± 12</b>	SARANTSEV 19	DPWA	$\bar{K}N$ multichannel
0.129	–20	<sup>1</sup> KAMANO 15	DPWA	$\bar{K}N$ multichannel

<sup>1</sup> From the preferred solution A in KAMANO 15.

Normalized residue in  $N\bar{K} \rightarrow \Sigma(1670) \rightarrow \Sigma\pi$ 

MODULUS	PHASE (°)	DOCUMENT ID	TECN	COMMENT
<b>0.25 ± 0.05</b>	<b>–25 ± 10</b>	SARANTSEV 19	DPWA	$\bar{K}N$ multichannel
0.249	–21	<sup>1</sup> KAMANO 15	DPWA	$\bar{K}N$ multichannel

<sup>1</sup> From the preferred solution A in KAMANO 15.

Normalized residue in  $N\bar{K} \rightarrow \Sigma(1670) \rightarrow \Lambda\pi$ 

MODULUS	PHASE (°)	DOCUMENT ID	TECN	COMMENT
<b>0.09 ± 0.03</b>	<b>–52 ± 12</b>	SARANTSEV 19	DPWA	$\bar{K}N$ multichannel
0.0818	–7	<sup>1</sup> KAMANO 15	DPWA	$\bar{K}N$ multichannel

<sup>1</sup> From the preferred solution A in KAMANO 15.

Normalized residue in  $N\bar{K} \rightarrow \Sigma(1670) \rightarrow \Xi K$ 

MODULUS	PHASE (°)	DOCUMENT ID	TECN	COMMENT
<b>0.02 ± 0.01</b>	<b>160 ± 20</b>	SARANTSEV 19	DPWA	$\bar{K}N$ multichannel

Normalized residue in  $N\bar{K} \rightarrow \Sigma(1670) \rightarrow \Sigma\sigma$ 

MODULUS	PHASE (°)	DOCUMENT ID	TECN	COMMENT
<b>0.08 ± 0.03</b>	<b>–25 ± 15</b>	SARANTSEV 19	DPWA	$\bar{K}N$ multichannel

Normalized residue in  $N\bar{K} \rightarrow \Sigma(1670) \rightarrow \Sigma(1385)\pi, S\text{-wave}$ 

MODULUS	PHASE (°)	DOCUMENT ID	TECN	COMMENT
0.228	167	<sup>1</sup> KAMANO 15	DPWA	$\bar{K}N$ multichannel

<sup>1</sup> From the preferred solution A in KAMANO 15.

Normalized residue in  $N\bar{K} \rightarrow \Sigma(1670) \rightarrow \Sigma(1385)\pi, D\text{-wave}$ 

MODULUS	PHASE (°)	DOCUMENT ID	TECN	COMMENT
0.0915	141	KAMANO 15	DPWA	$\bar{K}N$ multichannel

Normalized residue in  $N\bar{K} \rightarrow \Sigma(1670) \rightarrow \Lambda(1405)\pi$ 

MODULUS	PHASE (°)	DOCUMENT ID	TECN	COMMENT
<b>0.03 ± 0.02</b>	<b>160 ± 15</b>	SARANTSEV 19	DPWA	$\bar{K}N$ multichannel

Normalized residue in  $N\bar{K} \rightarrow \Sigma(1670) \rightarrow \Lambda(1520)\pi, P\text{-wave}$ 

MODULUS	PHASE (°)	DOCUMENT ID	TECN	COMMENT
<b>0.04 ± 0.02</b>	<b>120 ± 20</b>	SARANTSEV 19	DPWA	$\bar{K}N$ multichannel

See key on page 999

Baryon Particle Listings  
 $\Sigma(1670)$

**Normalized residue in  $N\bar{K} \rightarrow \Sigma(1670) \rightarrow \Lambda(1520)\pi$ , F-wave**

MODULUS	PHASE (°)	DOCUMENT ID	TECN	COMMENT
0.01 ± 0.01		SARANTSEV 19	DPWA	$\bar{K}N$ multichannel

**Normalized residue in  $N\bar{K} \rightarrow \Sigma(1670) \rightarrow \Delta\bar{K}$ , S-wave**

MODULUS	PHASE (°)	DOCUMENT ID	TECN	COMMENT
0.01 ± 0.01		SARANTSEV 19	DPWA	$\bar{K}N$ multichannel

**Normalized residue in  $N\bar{K} \rightarrow \Sigma(1670) \rightarrow N\bar{K}^*(892)$ , S=3/2, S-wave**

VALUE	DOCUMENT ID	TECN	COMMENT
0.05 ± 0.03 @ 50 ± 60	SARANTSEV 19	DPWA	$\bar{K}N$ multichannel

**Normalized residue in  $N\bar{K} \rightarrow \Sigma(1670) \rightarrow N\bar{K}^*(892)$ , S=3/2, D-wave**

MODULUS	PHASE (°)	DOCUMENT ID	TECN	COMMENT
0.01 ± 0.01		SARANTSEV 19	DPWA	$\bar{K}N$ multichannel

**Normalized residue in  $N\bar{K} \rightarrow \Sigma(1670) \rightarrow N\bar{K}^*(892)$ , S=1/2, D-wave**

MODULUS	PHASE (°)	DOCUMENT ID	TECN	COMMENT
0.03 ± 0.02		SARANTSEV 19	DPWA	$\bar{K}N$ multichannel

**$\Sigma(1670)$  MASS**

VALUE (MeV)	DOCUMENT ID	TECN	COMMENT
<b>1665 to 1685 (≈ 1675) OUR ESTIMATE</b>			
1665 ± 3	SARANTSEV 19	DPWA	$\bar{K}N$ multichannel
1678 ± 2	ZHANG 13A	DPWA	$\bar{K}N$ multichannel
1673 ± 1	GAO 12	DPWA	$\bar{K}N \rightarrow \Lambda\pi$
1665.1 ± 4.1	KOISO 85	DPWA	$K^-p \rightarrow \Sigma\pi$
1682 ± 5	GOPAL 80	DPWA	$\bar{K}N \rightarrow \bar{K}N$
1679 ± 10	ALSTON-... 78	DPWA	$\bar{K}N \rightarrow \bar{K}N$
1670 ± 5	GOPAL 77	DPWA	$\bar{K}N$ multichannel
1670 ± 6	HEPP 76B	DPWA	$K^-N \rightarrow \Sigma\pi$
1685 ± 20	BAILLON 75	IPWA	$\bar{K}N \rightarrow \Lambda\pi$
1659 ± 12 - 5	VANHORN 75	DPWA	$K^-p \rightarrow \Lambda\pi^0$
1670 ± 2	KANE 74	DPWA	$K^-p \rightarrow \Sigma\pi$
••• We do not use the following data for averages, fits, limits, etc. •••			
1667 or 1668	<sup>1</sup> MARTIN 77	DPWA	$\bar{K}N$ multichannel
1650	DEBELLEFON 76	IPWA	$K^-p \rightarrow \Lambda\pi^0$
1671 ± 3	PONTE 75	DPWA	$K^-p \rightarrow \Lambda\pi^0$ (sol. 1)
1655 ± 2	PONTE 75	DPWA	$K^-p \rightarrow \Lambda\pi^0$ (sol. 2)
<sup>1</sup> The two MARTIN 77 values are from a T-matrix pole and from a Breit-Wigner fit.			

**$\Sigma(1670)$  WIDTH**

VALUE (MeV)	DOCUMENT ID	TECN	COMMENT
<b>40 to 100 (≈ 70) OUR ESTIMATE</b>			
54 ± 6	SARANTSEV 19	DPWA	$\bar{K}N$ multichannel
55 ± 4	ZHANG 13A	DPWA	$\bar{K}N$ multichannel
52 ± 5 - 2	GAO 12	DPWA	$\bar{K}N \rightarrow \Lambda\pi$
65.0 ± 7.3	KOISO 85	DPWA	$K^-p \rightarrow \Sigma\pi$
79 ± 10	GOPAL 80	DPWA	$\bar{K}N \rightarrow \bar{K}N$
56 ± 20	ALSTON-... 78	DPWA	$\bar{K}N \rightarrow \bar{K}N$
50 ± 5	GOPAL 77	DPWA	$\bar{K}N$ multichannel
56 ± 3	HEPP 76B	DPWA	$K^-N \rightarrow \Sigma\pi$
85 ± 25	BAILLON 75	IPWA	$\bar{K}N \rightarrow \Lambda\pi$
32 ± 11	VANHORN 75	DPWA	$K^-p \rightarrow \Lambda\pi^0$
79 ± 6	KANE 74	DPWA	$K^-p \rightarrow \Sigma\pi$
••• We do not use the following data for averages, fits, limits, etc. •••			
46 or 46	<sup>1</sup> MARTIN 77	DPWA	$\bar{K}N$ multichannel
80	DEBELLEFON 76	IPWA	$K^-p \rightarrow \Lambda\pi^0$
44 ± 11	PONTE 75	DPWA	$K^-p \rightarrow \Lambda\pi^0$ (sol. 1)
76 ± 5	PONTE 75	DPWA	$K^-p \rightarrow \Lambda\pi^0$ (sol. 2)
<sup>1</sup> The two MARTIN 77 values are from a T-matrix pole and from a Breit-Wigner fit.			

**$\Sigma(1670)$  DECAY MODES**

Mode	Fraction ( $\Gamma_i/\Gamma$ )
$\Gamma_1$ $N\bar{K}$	0.06 to 0.12
$\Gamma_2$ $\Lambda\pi$	5–15 %
$\Gamma_3$ $\Sigma\pi$	30–60 %
$\Gamma_4$ $\Lambda\pi\pi$	
$\Gamma_5$ $\Sigma\pi\pi$	
$\Gamma_6$ $\Sigma\sigma$	(7.0 ± 3.0) %
$\Gamma_7$ $\Sigma(1385)\pi$	
$\Gamma_8$ $\Sigma(1385)\pi$ , S-wave	
$\Gamma_9$ $\Sigma(1385)\pi$ , S-wave	
$\Gamma_{10}$ $\Sigma(1385)\pi$ , D-wave	
$\Gamma_{11}$ $N\bar{K}^*(892)$ , S=1/2, D-wave	
$\Gamma_{12}$ $N\bar{K}^*(892)$ , S=3/2, S-wave	
$\Gamma_{13}$ $N\bar{K}^*(892)$ , S=3/2, D-wave	

$\Gamma_{14}$	$\Lambda(1405)\pi$
$\Gamma_{15}$	$\Lambda(1520)\pi$

**$\Sigma(1670)$  BRANCHING RATIOS**

See "Sign conventions for resonance couplings" in the Note on  $\Lambda$  and  $\Sigma$  Resonances.

**$\Gamma(N\bar{K})/\Gamma_{total}$**

VALUE	DOCUMENT ID	TECN	COMMENT
<b>0.06 to 0.12 OUR ESTIMATE</b>			
0.10 ± 0.02	SARANTSEV 19	DPWA	$\bar{K}N$ multichannel
0.062 ± 0.007	ZHANG 13A	DPWA	$\bar{K}N$ multichannel
0.10 ± 0.03	GOPAL 80	DPWA	$\bar{K}N \rightarrow \bar{K}N$
0.11 ± 0.03	ALSTON-... 78	DPWA	$\bar{K}N \rightarrow \bar{K}N$
••• We do not use the following data for averages, fits, limits, etc. •••			
0.121	<sup>1</sup> KAMANO 15	DPWA	$\bar{K}N$ multichannel
0.08 ± 0.03	GOPAL 77	DPWA	See GOPAL 80
0.07 or 0.07	<sup>2</sup> MARTIN 77	DPWA	$\bar{K}N$ multichannel

<sup>1</sup> From the preferred solution A in KAMANO 15.

<sup>2</sup> The two MARTIN 77 values are from a T-matrix pole and from a Breit-Wigner fit.

**$\Gamma(\Lambda\pi)/\Gamma_{total}$**

VALUE	DOCUMENT ID	TECN	COMMENT
<b>0.09 ± 0.02</b>	SARANTSEV 19	DPWA	$\bar{K}N$ multichannel
••• We do not use the following data for averages, fits, limits, etc. •••			
0.058	<sup>1</sup> KAMANO 15	DPWA	$\bar{K}N$ multichannel
<sup>1</sup> From the preferred solution A in KAMANO 15.			

**$\Gamma(\Sigma\pi)/\Gamma_{total}$**

VALUE	DOCUMENT ID	TECN	COMMENT
<b>0.70 ± 0.15</b>	SARANTSEV 19	DPWA	$\bar{K}N$ multichannel
••• We do not use the following data for averages, fits, limits, etc. •••			
0.465	<sup>1</sup> KAMANO 15	DPWA	$\bar{K}N$ multichannel
<sup>1</sup> From the preferred solution A in KAMANO 15.			

**$\Gamma(\Lambda\pi\pi)/\Gamma_{total}$**

VALUE	DOCUMENT ID	TECN	COMMENT
••• We do not use the following data for averages, fits, limits, etc. •••			
< 0.11	ARMENTEROS68E HBC		$K^-p$ ( $\Gamma_1=0.09$ )

**$\Gamma(\Sigma\pi\pi)/\Gamma_{total}$**

VALUE	DOCUMENT ID	TECN	COMMENT
••• We do not use the following data for averages, fits, limits, etc. •••			
< 0.14	<sup>1</sup> ARMENTEROS68E HBC		$K^-p$ , $K^-d$ ( $\Gamma_1=0.09$ )
<sup>1</sup> Ratio only for $\Sigma 2\pi$ system in $l=1$ , which cannot be $\Sigma(1385)$ .			

**$\Gamma(\Sigma\sigma)/\Gamma_{total}$**

VALUE	DOCUMENT ID	TECN	COMMENT
<b>0.07 ± 0.03</b>	SARANTSEV 19	DPWA	$\bar{K}N$ multichannel

**$\Gamma(\Sigma(1385)\pi, S\text{-wave})/\Gamma_{total}$**

VALUE	DOCUMENT ID	TECN	COMMENT
••• We do not use the following data for averages, fits, limits, etc. •••			
0.309	<sup>1</sup> KAMANO 15	DPWA	Multichannel
<sup>1</sup> From the preferred solution A in KAMANO 15.			

**$\Gamma(\Sigma(1385)\pi, D\text{-wave})/\Gamma_{total}$**

VALUE	DOCUMENT ID	TECN	COMMENT
••• We do not use the following data for averages, fits, limits, etc. •••			
0.044	<sup>1</sup> KAMANO 15	DPWA	Multichannel
<sup>1</sup> From the preferred solution A in KAMANO 15.			

**$\Gamma(N\bar{K}^*(892), S=1/2, D\text{-wave})/\Gamma_{total}$**

VALUE	DOCUMENT ID	TECN	COMMENT
••• We do not use the following data for averages, fits, limits, etc. •••			
0.001	<sup>1</sup> KAMANO 15	DPWA	Multichannel
<sup>1</sup> From the preferred solution A in KAMANO 15.			

**$\Gamma(N\bar{K}^*(892), S=3/2, S\text{-wave})/\Gamma_{total}$**

VALUE	DOCUMENT ID	TECN	COMMENT
••• We do not use the following data for averages, fits, limits, etc. •••			
0.002	<sup>1</sup> KAMANO 15	DPWA	Multichannel
<sup>1</sup> From the preferred solution A in KAMANO 15.			

**$\Gamma(N\bar{K}^*(892), S=3/2, D\text{-wave})/\Gamma_{total}$**

VALUE	DOCUMENT ID	TECN	COMMENT
••• We do not use the following data for averages, fits, limits, etc. •••			
0.001	<sup>1</sup> KAMANO 15	DPWA	Multichannel
<sup>1</sup> From the preferred solution A in KAMANO 15.			

# Baryon Particle Listings

## $\Sigma(1670), \Sigma(1750)$

$\Gamma(\Lambda(1405)\pi)/\Gamma_{\text{total}}$	DOCUMENT ID	TECN	COMMENT	$\Gamma_{14}/\Gamma$
0.01 ± 0.01	SARANTSEV 19	DPWA	$\bar{K}N$ multichannel	
••• We do not use the following data for averages, fits, limits, etc. •••				
<0.06	ARMENTEROS68E	HBC	$K^-p, K^-d$ ( $\Gamma_1=0.09$ )	

$\Gamma(\Lambda(1405)\pi)/\Gamma(\Sigma(1385)\pi)$	DOCUMENT ID	TECN	COMMENT	$\Gamma_{14}/\Gamma_7$
0.23 ± 0.08	BRUCKER 70	DBC	$K^-N \rightarrow \Sigma\pi\pi$	

$(\Gamma_1\Gamma_7)^{1/2}/\Gamma_{\text{total}}$ in $N\bar{K} \rightarrow \Sigma(1670) \rightarrow \Lambda\pi$	DOCUMENT ID	TECN	COMMENT	$(\Gamma_1\Gamma_2)^{1/2}/\Gamma$
+0.08 ± 0.01	ZHANG 13A	DPWA	Multichannel	
+0.081 ± 0.002	GAO 12	DPWA	$\bar{K}N \rightarrow \Lambda\pi$	
-0.004				
+0.17 ± 0.03	<sup>1</sup> MORRIS 78	DPWA	$K^-n \rightarrow \Lambda\pi^-$	
+0.13 ± 0.02	<sup>1</sup> MORRIS 78	DPWA	$K^-n \rightarrow \Lambda\pi^-$	
+0.10 ± 0.02	GOPAL 77	DPWA	$\bar{K}N$ multichannel	
+0.06 ± 0.02	BAILLON 75	IPWA	$\bar{K}N \rightarrow \Lambda\pi$	
+0.09 ± 0.02	VANHORN 75	DPWA	$K^-p \rightarrow \Lambda\pi^0$	
+0.018 ± 0.060	DEVENISH 74B		Fixed- $t$ dispersion rel.	
••• We do not use the following data for averages, fits, limits, etc. •••				
+0.08 or +0.08	<sup>2</sup> MARTIN 77	DPWA	$\bar{K}N$ multichannel	
+0.05	DEBELLEFON 76	IPWA	$K^-p \rightarrow \Lambda\pi^0$	
+0.08 ± 0.01	PONTE 75	DPWA	$K^-p \rightarrow \Lambda\pi^0$ (sol. 1)	
+0.17 ± 0.01	PONTE 75	DPWA	$K^-p \rightarrow \Lambda\pi^0$ (sol. 2)	

<sup>1</sup> Results are with and without an  $S_{11}$   $\Sigma(1620)$  in the fit.  
<sup>2</sup> The two MARTIN 77 values are from a T-matrix pole and from a Breit-Wigner fit.

$(\Gamma_1\Gamma_7)^{1/2}/\Gamma_{\text{total}}$ in $N\bar{K} \rightarrow \Sigma(1670) \rightarrow \Sigma\pi$	DOCUMENT ID	TECN	COMMENT	$(\Gamma_1\Gamma_3)^{1/2}/\Gamma$
+0.20 ± 0.01	ZHANG 13A	DPWA	Multichannel	
+0.20 ± 0.02	KOISO 85	DPWA	$K^-p \rightarrow \Sigma\pi$	
+0.21 ± 0.02	GOPAL 77	DPWA	$\bar{K}N$ multichannel	
+0.20 ± 0.01	HEPP 76B	DPWA	$K^-N \rightarrow \Sigma\pi$	
+0.21 ± 0.03	KANE 74	DPWA	$K^-p \rightarrow \Sigma\pi$	
••• We do not use the following data for averages, fits, limits, etc. •••				
+0.18 or +0.17	<sup>1</sup> MARTIN 77	DPWA	$\bar{K}N$ multichannel	

<sup>1</sup> The two MARTIN 77 values are from a T-matrix pole and from a Breit-Wigner fit.

$(\Gamma_1\Gamma_7)^{1/2}/\Gamma_{\text{total}}$ in $N\bar{K} \rightarrow \Sigma(1670) \rightarrow \Sigma(1385)\pi, S\text{-wave}$	DOCUMENT ID	TECN	COMMENT	$(\Gamma_1\Gamma_8)^{1/2}/\Gamma$
+0.11 ± 0.03	PREVOST 74	DPWA	$K^-N \rightarrow \Sigma(1385)\pi$	
••• We do not use the following data for averages, fits, limits, etc. •••				
0.17 ± 0.02	<sup>1</sup> SIMS 68	DBC	$K^-N \rightarrow \Lambda\pi\pi$	

$\Gamma_1\Gamma_7/\Gamma_{\text{total}}^2$ in $N\bar{K} \rightarrow \Sigma(1670) \rightarrow \Lambda(1405)\pi$	DOCUMENT ID	TECN	COMMENT	$\Gamma_1\Gamma_{14}/\Gamma^2$
0.007 ± 0.002	<sup>1</sup> BRUCKER 70	DBC	$K^-N \rightarrow \Sigma\pi\pi$	
••• We do not use the following data for averages, fits, limits, etc. •••				
<0.03	BERLEY 69	HBC	$K^-p$ 0.6-0.82 GeV/c	

$(\Gamma_1\Gamma_7)^{1/2}/\Gamma_{\text{total}}$ in $N\bar{K} \rightarrow \Sigma(1670) \rightarrow \Lambda(1520)\pi$	DOCUMENT ID	TECN	COMMENT	$(\Gamma_1\Gamma_{15})^{1/2}/\Gamma$
0.081 ± 0.016	<sup>1</sup> CAMERON 77	DPWA	P-wave decay	

<sup>1</sup> The CAMERON 77 upper limit on F-wave decay is 0.03.

### $\Sigma(1670)$ REFERENCES

SARANTSEV 19	EPJ A55 180	A.V. Sarantsev et al.	(BONN, PNPI)
KAMANO 15	PR C92 025205	H. Kamano et al.	(ANL, OSAK)
ZHANG 13A	PR C88 035205	H. Zhang et al.	(KSU)
GAO 12	PR C86 025201	P. Gao, J. Shi, B.S. Zou	(BHEP, BEIJT)
Also	NP A867 41	P. Gao, B.S. Zou, A. Sibirtsev	(BHEP, BEIJT+)
KOISO 85	NP A433 619	H. Koiso et al.	(TOKY, MASA)
PDC 82	PL 111B 1	M. Roos et al.	(HELS, CIT, CERH)
GOPAL 80	Toronto Conf. 159	G.P. Gopal	(RHEL) IJP
ALSTON... 78	PR D18 182	M. Alston-Garnjost et al.	(LBL, MTHO+) IJP
Also	PRL 38 1007	M. Alston-Garnjost et al.	(LBL, MTHO+) IJP
MORRIS 78	PR D17 55	W.A. Morris et al.	(FSU) IJP
CAMERON 77	NP B131 399	W. Cameron et al.	(RHEL, LOIC) IJP
GOPAL 77	NP B119 362	G.P. Gopal et al.	(LOIC, RHEL) IJP
MARTIN 77	NP B127 349	B.R. Martin, M.K. Piddcock, R.G. Moorhouse	(LOUC+) IJP
Also	NP B126 266	B.R. Martin, M.K. Piddcock	(LOUC) IJP
Also	NP B126 285	B.R. Martin, M.K. Piddcock	(LOUC) IJP
DEBELLEFON 76	NP B109 129	A. de Bellefon, A. Berthon	(CDEF) IJP
HEPP 76B	PL 65B 487	V. Hepp et al.	(CERN, HEID, MPIM) IJP
BAILLON 75	NP B94 39	P.H. Baillon, P.J. Litchfield	(CERN, RHEL) IJP
PONTE 75	PR D12 2597	R.A. Ponte et al.	(MASA, TENN, UCR) IJP
VANHORN 75	NP B87 145	A.J. van Horn	(LBL) IJP
Also	NP B87 157	A.J. van Horn	(LBL) IJP
DEVENISH 74B	NP B81 330	R.C.E. Devenish, C.D. Froggatt, B.R. Martin	(DESY+) IJP
KANE 74	LBL-2452	D.F. Kane	(LBL) IJP
PREVOST 74	NP B69 246	J. Prevost et al.	(SACL, CERN, HEID)
BRUCKER 70	Duke Conf. 155	E.B. Brucker et al.	(FSU) I
Also	Hyperon Resonances, 1970		
BERLEY 69	PL 30B 430	D. Berley et al.	(BNL)
ARMENTEROS 65E	PL 28B 521	R. Armenteros et al.	(CERN, HEID, SACL) I
SIMS 68	PRL 21 1413	W.H. Sims et al.	(FSU, TUFTS, BRAN)

## $\Sigma(1750) 1/2^-$

$I(J^P) = 1(\frac{1}{2}^-)$  Status: \*\*\*

For most results published before 1974 (they are now obsolete), see our 1982 edition Physics Letters **111B** 1 (1982).

There is evidence for this state in many partial-wave analyses, but with wide variations in the mass, width, and couplings. The latest analyses indicated significant couplings to  $N\bar{K}$  and  $\Lambda\pi$ , as well as to  $\Sigma\eta$  whose threshold is at 1746 MeV (JONES 74).

### $\Sigma(1750)$ POLE POSITION

REAL PART	DOCUMENT ID	TECN	COMMENT
VALUE (MeV)			
<b>1689 ± 11</b>	SARANTSEV 19	DPWA	$\bar{K}N$ multichannel
••• We do not use the following data for averages, fits, limits, etc. •••			
$1704 \pm \frac{3}{6}$	<sup>1</sup> KAMANO 15	DPWA	$\bar{K}N$ multichannel
1708	ZHANG 13A	DPWA	$\bar{K}N$ multichannel
	<sup>1</sup> From the preferred solution A in KAMANO 15. Solution B reports two poles at $M = 1551 \pm \frac{2}{9}$ MeV and $1940 \pm \frac{2}{2}$ MeV.		

-2xIMAGINARY PART	DOCUMENT ID	TECN	COMMENT
VALUE (MeV)			
<b>206 ± 18</b>	SARANTSEV 19	DPWA	$\bar{K}N$ multichannel
••• We do not use the following data for averages, fits, limits, etc. •••			
$86 \pm \frac{14}{4}$	<sup>1</sup> KAMANO 15	DPWA	$\bar{K}N$ multichannel
158	ZHANG 13A	DPWA	$\bar{K}N$ multichannel
	<sup>1</sup> From the preferred solution A in KAMANO 15. Solution B Reports two poles with $\Gamma = 376 \pm \frac{12}{2}$ and $172 \pm \frac{4}{4}$ MeV.		

### $\Sigma(1750)$ POLE RESIDUES

The normalized residue is the residue divided by  $\Gamma_{\text{pole}}/2$ .

Normalized residue in $N\bar{K} \rightarrow \Sigma(1750) \rightarrow N\bar{K}$	DOCUMENT ID	TECN	COMMENT
MODULUS PHASE (°)			
<b>0.46 ± 0.09 -144 ± 15</b>	SARANTSEV 19	DPWA	$\bar{K}N$ multichannel
••• We do not use the following data for averages, fits, limits, etc. •••			
0.0982 178	<sup>1</sup> KAMANO 15	DPWA	$\bar{K}N$ multichannel
	<sup>1</sup> From the preferred solution A in KAMANO 15.		

Normalized residue in $N\bar{K} \rightarrow \Sigma(1750) \rightarrow \Sigma\pi$	DOCUMENT ID	TECN	COMMENT
MODULUS PHASE (°)			
<b>0.27 ± 0.05 100 ± 18</b>	SARANTSEV 19	DPWA	$\bar{K}N$ multichannel
••• We do not use the following data for averages, fits, limits, etc. •••			
0.192 137	<sup>1</sup> KAMANO 15	DPWA	Multichannel
	<sup>1</sup> From the preferred solution A in KAMANO 15.		

Normalized residue in $N\bar{K} \rightarrow \Sigma(1750) \rightarrow \Sigma\eta$	DOCUMENT ID	TECN	COMMENT
MODULUS PHASE (°)			
<b>0.05 ± 0.03</b>	SARANTSEV 19	DPWA	$\bar{K}N$ multichannel

Normalized residue in $N\bar{K} \rightarrow \Sigma(1750) \rightarrow \Lambda\pi$	DOCUMENT ID	TECN	COMMENT
MODULUS PHASE (°)			
<b>0.26 ± 0.06 115 ± 15</b>	SARANTSEV 19	DPWA	$\bar{K}N$ multichannel
••• We do not use the following data for averages, fits, limits, etc. •••			
0.207 169	<sup>1</sup> KAMANO 15	DPWA	$\bar{K}N$ multichannel
	<sup>1</sup> From the preferred solution A in KAMANO 15.		

Normalized residue in $N\bar{K} \rightarrow \Sigma(1750) \rightarrow \Xi K$	DOCUMENT ID	TECN	COMMENT
MODULUS PHASE (°)			
<b>0.02 ± 0.02</b>	SARANTSEV 19	DPWA	$\bar{K}N$ multichannel

Normalized residue in $N\bar{K} \rightarrow \Sigma(1750) \rightarrow \Sigma(1385)\pi, D\text{-wave}$	DOCUMENT ID	TECN	COMMENT
MODULUS PHASE (°)			
<b>0.04 ± 0.03</b>	SARANTSEV 19	DPWA	$\bar{K}N$ multichannel
••• We do not use the following data for averages, fits, limits, etc. •••			
0.0536 73	<sup>1</sup> KAMANO 15	DPWA	$\bar{K}N$ multichannel
	<sup>1</sup> From the preferred solution A in KAMANO 15.		

Normalized residue in $N\bar{K} \rightarrow \Sigma(1750) \rightarrow \Lambda(1520)\pi$	DOCUMENT ID	TECN	COMMENT
MODULUS PHASE (°)			
<b>0.15 ± 0.07 -25 ± 40</b>	SARANTSEV 19	DPWA	$\bar{K}N$ multichannel

Normalized residue in $N\bar{K} \rightarrow \Sigma(1750) \rightarrow N\bar{K}^*(892), S=1/2, S\text{-wave}$	DOCUMENT ID	TECN	COMMENT
MODULUS PHASE (°)			
<b>0.05 ± 0.03 -100 ± 35</b>	SARANTSEV 19	DPWA	$\bar{K}N$ multichannel

$\Sigma(1750)$  MASS

VALUE (MeV)	DOCUMENT ID	TECN	COMMENT
<b>1700 to 1800 (<math>\approx 1750</math>) OUR ESTIMATE</b>			
1692 ± 11	SARANTSEV 19	DPWA	$\bar{K}N$ multichannel
1739 ± 8	ZHANG 13A	DPWA	$\bar{K}N$ multichannel
1756 ± 10	GOPAL 80	DPWA	$\bar{K}N \rightarrow \bar{K}N$
1770 ± 10	ALSTON... 78	DPWA	$\bar{K}N \rightarrow \bar{K}N$
• • • We do not use the following data for averages, fits, limits, etc. • • •			
1770 ± 15	GOPAL 77	DPWA	$\bar{K}N$ multichannel
1800 or 1813	<sup>1</sup> MARTIN 77	DPWA	$\bar{K}N$ multichannel
1715 ± 10	<sup>2</sup> CARROLL 76	DPWA	Isospin-1 total $\sigma$
1730	DEBELLEFON 76	IPWA	$K^- p \rightarrow \Lambda \pi^0$
1780 ± 30	BAILLON 75	IPWA	$\bar{K}N \rightarrow \Lambda \pi$ (sol. 1)
1700 ± 30	BAILLON 75	IPWA	$\bar{K}N \rightarrow \Lambda \pi$ (sol. 2)
1697 +20 -10	VANHORN 75	DPWA	$K^- p \rightarrow \Lambda \pi^0$
1785 ± 12	CHU 74	DBC	Fits $\sigma(K^- n \rightarrow \Sigma^- \eta)$
1760 ± 5	<sup>3</sup> JONES 74	HBC	Fits $\sigma(K^- p \rightarrow \Sigma^0 \eta)$
1739 ± 10	PREVOST 74	DPWA	$K^- N \rightarrow \Sigma(1385) \pi$

<sup>1</sup> The two MARTIN 77 values are from a T-matrix pole and from a Breit-Wigner fit.  
<sup>2</sup> A total cross-section bump with  $(J+1/2) \Gamma_{el} / \Gamma_{total} = 0.30$ .  
<sup>3</sup> An S-wave Breit-Wigner fit to the threshold cross section with no background and errors statistical only.

$\Sigma(1750)$  WIDTH

VALUE (MeV)	DOCUMENT ID	TECN	COMMENT
<b>100 to 200 (<math>\approx 150</math>) OUR ESTIMATE</b>			
208 ± 18	SARANTSEV 19	DPWA	$\bar{K}N$ multichannel
182 ± 60	ZHANG 13A	DPWA	$\bar{K}N$ multichannel
64 ± 10	GOPAL 80	DPWA	$\bar{K}N \rightarrow \bar{K}N$
161 ± 20	ALSTON... 78	DPWA	$\bar{K}N \rightarrow \bar{K}N$
• • • We do not use the following data for averages, fits, limits, etc. • • •			
60 ± 10	GOPAL 77	DPWA	$\bar{K}N$ multichannel
117 or 119	<sup>1</sup> MARTIN 77	DPWA	$\bar{K}N$ multichannel
10	<sup>2</sup> CARROLL 76	DPWA	Isospin-1 total $\sigma$
110	DEBELLEFON 76	IPWA	$K^- p \rightarrow \Lambda \pi^0$
140 ± 30	BAILLON 75	IPWA	$\bar{K}N \rightarrow \Lambda \pi$ (sol. 1)
160 ± 50	BAILLON 75	IPWA	$\bar{K}N \rightarrow \Lambda \pi$ (sol. 2)
66 +14 -12	VANHORN 75	DPWA	$K^- p \rightarrow \Lambda \pi^0$
89 ± 33	CHU 74	DBC	Fits $\sigma(K^- n \rightarrow \Sigma^- \eta)$
92 ± 7	<sup>3</sup> JONES 74	HBC	Fits $\sigma(K^- p \rightarrow \Sigma^0 \eta)$
108 ± 20	PREVOST 74	DPWA	$K^- N \rightarrow \Sigma(1385) \pi$

<sup>1</sup> The two MARTIN 77 values are from a T-matrix pole and from a Breit-Wigner fit.  
<sup>2</sup> A total cross-section bump with  $(J+1/2) \Gamma_{el} / \Gamma_{total} = 0.30$ .  
<sup>3</sup> An S-wave Breit-Wigner fit to the threshold cross section with no background and errors statistical only.

$\Sigma(1750)$  DECAY MODES

Mode	Fraction ( $\Gamma_i/\Gamma$ )
$\Gamma_1$ $N\bar{K}$	0.06 to 0.12
$\Gamma_2$ $\Lambda \pi$	(14 ± 5) %
$\Gamma_3$ $\Sigma \pi$	(16 ± 4) %
$\Gamma_4$ $\Sigma \eta$	15-55 %
$\Gamma_5$ $\Sigma(1385) \pi, D$ -wave	< 1 %
$\Gamma_6$ $\Lambda(1520) \pi$	(2.0 ± 1.0) %
$\Gamma_7$ $N\bar{K}^*(892), S=1/2$	(8 ± 4) %
$\Gamma_8$ $N\bar{K}^*(892), S=3/2, D$ -wave	

$\Sigma(1750)$  BRANCHING RATIOS

See "Sign conventions for resonance couplings" in the Note on  $\Lambda$  and  $\Sigma$  Resonances.

$\Gamma(N\bar{K})/\Gamma_{total}$	DOCUMENT ID	TECN	COMMENT
<b>0.06 to 0.12 OUR ESTIMATE</b>			
0.46 ± 0.09	SARANTSEV 19	DPWA	$\bar{K}N$ multichannel
0.09 ± 0.07	ZHANG 13A	DPWA	Multichannel
0.14 ± 0.03	GOPAL 80	DPWA	$\bar{K}N \rightarrow \bar{K}N$
0.33 ± 0.05	ALSTON... 78	DPWA	$\bar{K}N \rightarrow \bar{K}N$
• • • We do not use the following data for averages, fits, limits, etc. • • •			
0.154	<sup>1</sup> KAMANO 15	DPWA	Multichannel
0.15 ± 0.03	GOPAL 77	DPWA	See GOPAL 80
0.06 or 0.05	<sup>2</sup> MARTIN 77	DPWA	$\bar{K}N$ multichannel

<sup>1</sup> From the preferred solution A in KAMANO 15.  
<sup>2</sup> The two MARTIN 77 values are from a T-matrix pole and from a Breit-Wigner fit.

$\Gamma(\Lambda \pi)/\Gamma_{total}$   $\Gamma_2/\Gamma$

VALUE	DOCUMENT ID	TECN	COMMENT
<b>0.14 ± 0.05</b>	SARANTSEV 19	DPWA	$\bar{K}N$ multichannel
• • • We do not use the following data for averages, fits, limits, etc. • • •			
0.435	<sup>1</sup> KAMANO 15	DPWA	$\bar{K}N$ multichannel

<sup>1</sup> From the preferred solution A in KAMANO 15.

$\Gamma(\Sigma \pi)/\Gamma_{total}$   $\Gamma_3/\Gamma$

VALUE	DOCUMENT ID	TECN	COMMENT
<b>0.16 ± 0.04</b>	SARANTSEV 19	DPWA	$\bar{K}N$ multichannel
• • • We do not use the following data for averages, fits, limits, etc. • • •			
0.373	<sup>1</sup> KAMANO 15	DPWA	$\bar{K}N$ multichannel

<sup>1</sup> From the preferred solution A in KAMANO 15.

$\Gamma(\Lambda(1520)\pi)/\Gamma_{total}$   $\Gamma_6/\Gamma$

VALUE	DOCUMENT ID	TECN	COMMENT
<b>0.02 ± 0.01</b>	SARANTSEV 19	DPWA	$\bar{K}N$ multichannel

$\Gamma(\Sigma(1385)\pi, D$ -wave)/ $\Gamma_{total}$   $\Gamma_5/\Gamma$

VALUE	DOCUMENT ID	TECN	COMMENT
<b>&lt; 0.01</b>	SARANTSEV 19	DPWA	$\bar{K}N$ multichannel
• • • We do not use the following data for averages, fits, limits, etc. • • •			
0.024	<sup>1</sup> KAMANO 15	DPWA	$\bar{K}N$ multichannel

<sup>1</sup> From the preferred solution A in KAMANO 15.

$\Gamma(N\bar{K}^*(892), S=1/2)/\Gamma_{total}$   $\Gamma_7/\Gamma$

VALUE	DOCUMENT ID	TECN	COMMENT
<b><math>\sim 0</math></b>	SARANTSEV 19	DPWA	$\bar{K}N$ multichannel
<b>0.08 ± 0.04</b>	ZHANG 13A	DPWA	$\bar{K}N$ multichannel
• • • We do not use the following data for averages, fits, limits, etc. • • •			
0.004	<sup>1</sup> KAMANO 15	DPWA	$\bar{K}N$ multichannel

<sup>1</sup> From the preferred solution A in KAMANO 15.

$\Gamma(N\bar{K}^*(892), S=3/2, D$ -wave)/ $\Gamma_{total}$   $\Gamma_8/\Gamma$

VALUE	DOCUMENT ID	TECN	COMMENT
• • • We do not use the following data for averages, fits, limits, etc. • • •			
0.01	<sup>1</sup> KAMANO 15	DPWA	Multichannel

<sup>1</sup> From the preferred solution A in KAMANO 15.

$(\Gamma_i \Gamma_j)^{1/2}/\Gamma_{total}$  in  $N\bar{K} \rightarrow \Sigma(1750) \rightarrow \Lambda \pi$   $(\Gamma_1 \Gamma_2)^{1/2}/\Gamma$

VALUE	DOCUMENT ID	TECN	COMMENT
+0.10 ± 0.04	ZHANG 13A	DPWA	Multichannel
0.04 ± 0.03	GOPAL 77	DPWA	$\bar{K}N$ multichannel
• • • We do not use the following data for averages, fits, limits, etc. • • •			
-0.10 or -0.09	<sup>1</sup> MARTIN 77	DPWA	$\bar{K}N$ multichannel
-0.12	DEBELLEFON 76	IPWA	$K^- p \rightarrow \Lambda \pi^0$
-0.12 ± 0.02	BAILLON 75	IPWA	$\bar{K}N \rightarrow \Lambda \pi$ (sol. 1)
-0.13 ± 0.03	BAILLON 75	IPWA	$\bar{K}N \rightarrow \Lambda \pi$ (sol. 2)
-0.13 ± 0.04	VANHORN 75	DPWA	$K^- p \rightarrow \Lambda \pi^0$
-0.120 ± 0.077	DEVENISH 74B		Fixed-t dispersion rel.

<sup>1</sup> The two MARTIN 77 values are from a T-matrix pole and from a Breit-Wigner fit.

$(\Gamma_i \Gamma_j)^{1/2}/\Gamma_{total}$  in  $N\bar{K} \rightarrow \Sigma(1750) \rightarrow \Sigma \pi$   $(\Gamma_1 \Gamma_3)^{1/2}/\Gamma$

VALUE	DOCUMENT ID	TECN	COMMENT
+0.17 ± 0.07	ZHANG 13A	DPWA	Multichannel
-0.09 ± 0.05	GOPAL 77	DPWA	$\bar{K}N$ multichannel
• • • We do not use the following data for averages, fits, limits, etc. • • •			
+0.06 or +0.06	<sup>1</sup> MARTIN 77	DPWA	$\bar{K}N$ multichannel
0.13 ± 0.02	LANGBEIN 72	IPWA	$\bar{K}N$ multichannel

<sup>1</sup> The two MARTIN 77 values are from a T-matrix pole and from a Breit-Wigner fit.

$(\Gamma_i \Gamma_j)^{1/2}/\Gamma_{total}$  in  $N\bar{K} \rightarrow \Sigma(1750) \rightarrow \Sigma \eta$   $(\Gamma_1 \Gamma_4)^{1/2}/\Gamma$

VALUE	DOCUMENT ID	TECN	COMMENT
0.23 ± 0.01	<sup>1</sup> JONES 74	HBC	Fits $\sigma(K^- p \rightarrow \Sigma^0 \eta)$
• • • We do not use the following data for averages, fits, limits, etc. • • •			
seen	CLINE 69	DBC	Threshold bump

<sup>1</sup> An S-wave Breit-Wigner fit to the threshold cross section with no background and errors statistical only.

$(\Gamma_i \Gamma_j)^{1/2}/\Gamma_{total}$  in  $N\bar{K} \rightarrow \Sigma(1750) \rightarrow \Sigma(1385)\pi, D$ -wave  $(\Gamma_1 \Gamma_5)^{1/2}/\Gamma$

VALUE	DOCUMENT ID	TECN	COMMENT
+0.17 ± 0.07	ZHANG 13A	DPWA	Multichannel
+0.18 ± 0.15	PREVOST 74	DPWA	$K^- N \rightarrow \Sigma(1385) \pi$

$(\Gamma_i \Gamma_j)^{1/2}/\Gamma_{total}$  in  $N\bar{K} \rightarrow \Sigma(1750) \rightarrow \Lambda(1520)\pi$   $(\Gamma_1 \Gamma_6)^{1/2}/\Gamma$

VALUE	DOCUMENT ID	TECN	COMMENT
• • • We do not use the following data for averages, fits, limits, etc. • • •			
0.032 ± 0.021	CAMERON 77	DPWA	P-wave decay

# Baryon Particle Listings

## $\Sigma(1750), \Sigma(1775)$

### $\Sigma(1750)$ REFERENCES

SARANTSEV	19	EPJ A55 180	A.V. Sarantsev <i>et al.</i>	(BONN, PNPI)
KAMANO	15	PR C92 025205	H. Kamano <i>et al.</i>	(ANL, OSAK)
ZHANG	13A	PR C88 035205	H. Zhang <i>et al.</i>	(KSU)
PDG	82	PL 111B 1	M. Roos <i>et al.</i>	(HEL5, CIT, CERN)
GOPAL	80	Toronto Conf. 159	G.P. Gopal	(RHEL) IJP
ALSTON-...	78	PR D18 182	M. Alston-Garnjost <i>et al.</i>	(LBL, MTHO+) IJP
Also		PRL 38 1007	M. Alston-Garnjost <i>et al.</i>	(LBL, MTHO+) IJP
CAMERON	77	NP B131 399	W. Cameron <i>et al.</i>	(RHEL, LOIC) IJP
GOPAL	77	NP B119 362	G.P. Gopal <i>et al.</i>	(LOIC, RHEL) IJP
MARTIN	77	NP B127 349	B.R. Martin, M.K. Pldcock, R.G. Moorhouse	(LOUC+) IJP
Also		NP B126 266	B.R. Martin, M.K. Pldcock	(LOUC) IJP
Also		NP B126 285	B.R. Martin, M.K. Pldcock	(LOUC) IJP
CARROLL	76	PRL 37 806	A.S. Carroll <i>et al.</i>	(BNL) I
DEBELLEFON	76	NP B109 129	A. de Bellefon, A. Berthon	(CDEF) IJP
BAILLON	75	NP B94 39	P.H. Baillon, P.J. Litchfield	(CERN, RHEL) IJP
VANHORN	75	NP B87 145	A.J. van Horn	(LBL) IJP
Also		NP B87 157	A.J. van Horn	(LBL) IJP
CHU	74	NC 20A 35	R.Y.L. Chu <i>et al.</i>	(PLAT, TUFTS, BRAN) IJP
DEVENISH	74B	NP B81 330	R.C.E. Devenish, C.D. Froggatt, B.R. Martin	(DESY+) IJP
JONES	74	NP B73 141	M.D. Jones	(CHIC) IJP
PREVOST	74	NP B69 246	J. Prevost <i>et al.</i>	(SACL, CERN, HEID) IJP
LANGBEIN	72	NP B47 477	W. Langbein, F. Wagner	(MPIM) IJP
CLINE	69	LNC 2 407	D. Cline, R. Laumann, J. Mapp	(WISC) IJP

### $\Sigma(1775) 5/2^-$

$$I(J^P) = 1(5/2^-) \text{ Status: } ****$$

Discovered by GALTIERI 63, this resonance plays the same role as cornerstone for isospin-1 analyses in this region as the  $\Lambda(1820)F_{05}$  does in the isospin-0 channel.

For most results published before 1974 (they are now obsolete), see our 1982 edition Physics Letters **111B** 1 (1982).

### $\Sigma(1775)$ POLE POSITION

#### REAL PART

VALUE (MeV)	DOCUMENT ID	TECN	COMMENT
<b>1760 to 1780 (<math>\approx 1770</math>) OUR ESTIMATE</b>			
$1767 \pm 4$	SARANTSEV 19	DPWA	$\bar{K}N$ multichannel
$1767^{+2}_{-2}$	<sup>1</sup> KAMANO 15	DPWA	$\bar{K}N$ multichannel
• • • We do not use the following data for averages, fits, limits, etc. • • •			
1759	ZHANG 13A	DPWA	$\bar{K}N$ multichannel
<sup>1</sup> From the preferred solution A in KAMANO 15.			

#### -2xIMAGINARY PART

VALUE (MeV)	DOCUMENT ID	TECN	COMMENT
<b>45 to 65 (<math>\approx 55</math>) OUR ESTIMATE</b>			
$122 \pm 8$	SARANTSEV 19	DPWA	$\bar{K}N$ multichannel
$128^{+4}_{-2}$	<sup>1</sup> KAMANO 15	DPWA	$\bar{K}N$ multichannel
• • • We do not use the following data for averages, fits, limits, etc. • • •			
118	ZHANG 13A	DPWA	$\bar{K}N$ multichannel
<sup>1</sup> From the preferred solution A in KAMANO 15.			

### $\Sigma(1775)$ POLE RESIDUES

The normalized residue is the residue divided by  $\Gamma_{pole}/2$ .

#### Normalized residue in $N\bar{K} \rightarrow \Sigma(1775) \rightarrow N\bar{K}$

MODULUS	PHASE ( $^\circ$ )	DOCUMENT ID	TECN	COMMENT
$0.44 \pm 0.09$	$-17 \pm 10$	SARANTSEV 19	DPWA	$\bar{K}N$ multichannel
• • • We do not use the following data for averages, fits, limits, etc. • • •				
0.371	-32	<sup>1</sup> KAMANO 15	DPWA	$\bar{K}N$ multichannel
<sup>1</sup> From the preferred solution A in KAMANO 15.				

#### Normalized residue in $N\bar{K} \rightarrow \Sigma(1775) \rightarrow \Sigma\pi$

MODULUS	PHASE ( $^\circ$ )	DOCUMENT ID	TECN	COMMENT
$0.13 \pm 0.03$	$10 \pm 12$	SARANTSEV 19	DPWA	$\bar{K}N$ multichannel
• • • We do not use the following data for averages, fits, limits, etc. • • •				
0.115	-24	<sup>1</sup> KAMANO 15	DPWA	$\bar{K}N$ multichannel
<sup>1</sup> From the preferred solution A in KAMANO 15.				

#### Normalized residue in $N\bar{K} \rightarrow \Sigma(1775) \rightarrow \Lambda\pi$

MODULUS	PHASE ( $^\circ$ )	DOCUMENT ID	TECN	COMMENT
$0.47 \pm 0.10$	$130 \pm 15$	SARANTSEV 19	DPWA	$\bar{K}N$ multichannel
• • • We do not use the following data for averages, fits, limits, etc. • • •				
0.325	157	<sup>1</sup> KAMANO 15	DPWA	$\bar{K}N$ multichannel
<sup>1</sup> From the preferred solution A in KAMANO 15.				

#### Normalized residue in $N\bar{K} \rightarrow \Sigma(1775) \rightarrow \Sigma(1385)\pi, D\text{-wave}$

MODULUS	PHASE ( $^\circ$ )	DOCUMENT ID	TECN	COMMENT
• • • We do not use the following data for averages, fits, limits, etc. • • •				
0.391	137	<sup>1</sup> KAMANO 15	DPWA	$\bar{K}N$ multichannel
<sup>1</sup> From the preferred solution A in KAMANO 15.				

#### Normalized residue in $N\bar{K} \rightarrow \Sigma(1775) \rightarrow \Sigma(1385)\pi, G\text{-wave}$

MODULUS	PHASE ( $^\circ$ )	DOCUMENT ID	TECN	COMMENT
• • • We do not use the following data for averages, fits, limits, etc. • • •				
0.0129	-58	<sup>1</sup> KAMANO 15	DPWA	$\bar{K}N$ multichannel
<sup>1</sup> From the preferred solution A in KAMANO 15.				

#### Normalized residue in $N\bar{K} \rightarrow \Sigma(1775) \rightarrow N\bar{K}^*(892), S=1/2, D\text{-wave}$

MODULUS	PHASE ( $^\circ$ )	DOCUMENT ID	TECN	COMMENT
$0.04 \pm 0.02$	$-100 \pm 60$	SARANTSEV 19	DPWA	$\bar{K}N$ multichannel

#### Normalized residue in $N\bar{K} \rightarrow \Sigma(1775) \rightarrow N\bar{K}^*(892), S=3/2, D\text{-wave}$

MODULUS	PHASE ( $^\circ$ )	DOCUMENT ID	TECN	COMMENT
$0.09 \pm 0.06$	$10 \pm 50$	SARANTSEV 19	DPWA	$\bar{K}N$ multichannel

#### Normalized residue in $N\bar{K} \rightarrow \Sigma(1775) \rightarrow N\bar{K}^*(892), S=3/2, G\text{-wave}$

MODULUS	PHASE ( $^\circ$ )	DOCUMENT ID	TECN	COMMENT
$0.04 \pm 0.02$	$-100 \pm 60$	SARANTSEV 19	DPWA	$\bar{K}N$ multichannel

#### Normalized residue in $N\bar{K} \rightarrow \Sigma(1775) \rightarrow \Xi K$

MODULUS	PHASE ( $^\circ$ )	DOCUMENT ID	TECN	COMMENT
$0.02 \pm 0.01$	$-90 \pm 35$	SARANTSEV 19	DPWA	$\bar{K}N$ multichannel

#### Normalized residue in $N\bar{K} \rightarrow \Sigma(1775) \rightarrow \Lambda(1520)\pi, P\text{-wave}$

MODULUS	PHASE ( $^\circ$ )	DOCUMENT ID	TECN	COMMENT
$0.09 \pm 0.03$	$10 \pm 30$	SARANTSEV 19	DPWA	$\bar{K}N$ multichannel

#### Normalized residue in $N\bar{K} \rightarrow \Sigma(1775) \rightarrow \Lambda(1520)\pi, F\text{-wave}$

VALUE	DOCUMENT ID	TECN	COMMENT
$0.01 \pm 0.01$	SARANTSEV 19	DPWA	$\bar{K}N$ multichannel

#### Normalized residue in $N\bar{K} \rightarrow \Sigma(1775) \rightarrow \Delta\bar{K}, D\text{-wave}$

VALUE	DOCUMENT ID	TECN	COMMENT
$0.02 \pm 0.02$	SARANTSEV 19	DPWA	$\bar{K}N$ multichannel

### $\Sigma(1775)$ MASS

VALUE (MeV)	DOCUMENT ID	TECN	COMMENT
<b>1770 to 1780 (<math>\approx 1775</math>) OUR ESTIMATE</b>			
$1776 \pm 4$	SARANTSEV 19	DPWA	$\bar{K}N$ multichannel
$1778 \pm 1$	ZHANG 13A	DPWA	$\bar{K}N$ multichannel
$1778 \pm 5$	GOPAL 80	DPWA	$\bar{K}N \rightarrow \bar{K}N$
$1777 \pm 5$	ALSTON-... 78	DPWA	$\bar{K}N \rightarrow \bar{K}N$
$1775 \pm 10$	BAILLON 75	IPWA	$\bar{K}N \rightarrow \Lambda\pi$
$1774 \pm 10$	VANHORN 75	DPWA	$K^- p \rightarrow \Lambda\pi^0$
$1772 \pm 6$	KANE 74	DPWA	$K^- p \rightarrow \Sigma\pi$
• • • We do not use the following data for averages, fits, limits, etc. • • •			
$1774 \pm 5$	GOPAL 77	DPWA	$\bar{K}N$ multichannel
$1772$ or $1777$	<sup>1</sup> MARTIN 77	DPWA	$\bar{K}N$ multichannel
1765	DEBELLEFON 76	IPWA	$K^- p \rightarrow \Lambda\pi^0$
<sup>1</sup> The two MARTIN 77 values are from a T-matrix pole and from a Breit-Wigner fit.			

### $\Sigma(1775)$ WIDTH

VALUE (MeV)	DOCUMENT ID	TECN	COMMENT
<b>105 to 135 (<math>\approx 120</math>) OUR ESTIMATE</b>			
$124 \pm 8$	SARANTSEV 19	DPWA	$\bar{K}N$ multichannel
$131 \pm 3$	ZHANG 13A	DPWA	$\bar{K}N$ multichannel
$137 \pm 10$	GOPAL 80	DPWA	$\bar{K}N \rightarrow \bar{K}N$
$116 \pm 10$	ALSTON-... 78	DPWA	$\bar{K}N \rightarrow \bar{K}N$
$125 \pm 15$	BAILLON 75	IPWA	$\bar{K}N \rightarrow \Lambda\pi$
$146 \pm 18$	VANHORN 75	DPWA	$K^- p \rightarrow \Lambda\pi^0$
$154 \pm 10$	KANE 74	DPWA	$K^- p \rightarrow \Sigma\pi$
• • • We do not use the following data for averages, fits, limits, etc. • • •			
$130 \pm 10$	GOPAL 77	DPWA	$\bar{K}N$ multichannel
$102$ or $103$	<sup>1</sup> MARTIN 77	DPWA	$\bar{K}N$ multichannel
120	DEBELLEFON 76	IPWA	$K^- p \rightarrow \Lambda\pi^0$
<sup>1</sup> The two MARTIN 77 values are from a T-matrix pole and from a Breit-Wigner fit.			

### $\Sigma(1775)$ DECAY MODES

Mode	Fraction ( $\Gamma_i/\Gamma$ )
$\Gamma_1$ $N\bar{K}$	37-43%
$\Gamma_2$ $\Lambda\pi$	14-20%
$\Gamma_3$ $\Sigma\pi$	2-5%
$\Gamma_4$ $\Sigma(1385)\pi$	8-12%
$\Gamma_5$ $\Sigma(1385)\pi, D\text{-wave}$	
$\Gamma_6$ $\Sigma(1385)\pi, D\text{-wave}$	
$\Gamma_7$ $\Sigma(1385)\pi, G\text{-wave}$	
$\Gamma_8$ $\Lambda(1520)\pi, P\text{-wave}$	17-23%
$\Gamma_9$ $\Sigma\pi\pi$	

$\Gamma_{10}$	$\Delta(1232)\bar{K}$ , $D$ -wave
$\Gamma_{11}$	$N\bar{K}^*(892)$ , $S=1/2$
$\Gamma_{12}$	$N\bar{K}^*(892)$ , $S=1/2$ , $D$ -wave
$\Gamma_{13}$	$N\bar{K}^*(892)$ , $S=3/2$ , $D$ -wave
$\Gamma_{14}$	$N\bar{K}^*(892)$ , $S=3/2$ , $G$ -wave

 **$\Sigma(1775)$  BRANCHING RATIOS**

See "Sign conventions for resonance couplings" in the Note on  $\Lambda$  and  $\Sigma$  Resonances. Also, the errors quoted do not include uncertainties due to the parametrization used in the partial-wave analyses and are thus too small.

$\Gamma(N\bar{K})/\Gamma_{\text{total}}$				$\Gamma_1/\Gamma$
VALUE	DOCUMENT ID	TECN	COMMENT	
<b>0.37 to 0.43 OUR ESTIMATE</b>				
0.43 $\pm$ 0.09	SARANTSEV	19	DPWA	$\bar{K}N$ multichannel
0.40 $\pm$ 0.01	ZHANG	13A	DPWA	$\bar{K}N$ multichannel
0.40 $\pm$ 0.02	GOPAL	80	DPWA	$\bar{K}N \rightarrow \bar{K}N$
0.37 $\pm$ 0.03	ALSTON-...	78	DPWA	$\bar{K}N \rightarrow \bar{K}N$
••• We do not use the following data for averages, fits, limits, etc. •••				
0.402	<sup>1</sup> KAMANO	15	DPWA	Multichannel
0.41 $\pm$ 0.03	GOPAL	77	DPWA	See GOPAL 80
0.37 or 0.36	<sup>2</sup> MARTIN	77	DPWA	$\bar{K}N$ multichannel

<sup>1</sup> From the preferred solution A in KAMANO 15.

<sup>2</sup> The two MARTIN 77 values are from a T-matrix pole and from a Breit-Wigner fit.

$\Gamma(\Lambda\pi)/\Gamma_{\text{total}}$				$\Gamma_2/\Gamma$
VALUE	DOCUMENT ID	TECN	COMMENT	
0.49 $\pm$ 0.10	SARANTSEV	19	DPWA	$\bar{K}N$ multichannel
••• We do not use the following data for averages, fits, limits, etc. •••				
0.244	<sup>1</sup> KAMANO	15	DPWA	$\bar{K}N$ multichannel
<sup>1</sup> From the preferred solution A in KAMANO 15.				

$\Gamma(\Lambda\pi)/\Gamma(N\bar{K})$				$\Gamma_2/\Gamma_1$
VALUE	DOCUMENT ID	TECN	COMMENT	
0.33 $\pm$ 0.05	UHLIG	67	HBC	$K^- p$ 0.9 GeV/c

$\Gamma(\Sigma\pi)/\Gamma_{\text{total}}$				$\Gamma_3/\Gamma$
VALUE	DOCUMENT ID	TECN	COMMENT	
0.035 $\pm$ 0.010	SARANTSEV	19	DPWA	$\bar{K}N$ multichannel
••• We do not use the following data for averages, fits, limits, etc. •••				
0.042	<sup>1</sup> KAMANO	15	DPWA	$\bar{K}N$ multichannel
<sup>1</sup> From the preferred solution A in KAMANO 15.				

$\Gamma(\Sigma(1385)\pi)/\Gamma(N\bar{K})$				$\Gamma_4/\Gamma_1$
VALUE	DOCUMENT ID	TECN	COMMENT	
0.25 $\pm$ 0.09	UHLIG	67	HBC	$K^- p$ 0.9 GeV/c

$\Gamma(\Sigma(1385)\pi, D\text{-wave})/\Gamma_{\text{total}}$				$\Gamma_6/\Gamma$
VALUE	DOCUMENT ID	TECN	COMMENT	
••• We do not use the following data for averages, fits, limits, etc. •••				
0.309	<sup>1</sup> KAMANO	15	DPWA	Multichannel
<sup>1</sup> From the preferred solution A in KAMANO 15.				

$\Gamma(\Sigma(1385)\pi, G\text{-wave})/\Gamma_{\text{total}}$				$\Gamma_7/\Gamma$
VALUE	DOCUMENT ID	TECN	COMMENT	
••• We do not use the following data for averages, fits, limits, etc. •••				
not seen	<sup>1</sup> KAMANO	15	DPWA	Multichannel
<sup>1</sup> From the preferred solution A in KAMANO 15.				

$\Gamma(\Lambda(1520)\pi, P\text{-wave})/\Gamma_{\text{total}}$				$\Gamma_8/\Gamma$
VALUE	DOCUMENT ID	TECN	COMMENT	
0.02 $\pm$ 0.01	SARANTSEV	19	DPWA	$\bar{K}N$ multichannel

$\Gamma(\Lambda(1520)\pi, P\text{-wave})/\Gamma(N\bar{K})$				$\Gamma_8/\Gamma_1$
VALUE	DOCUMENT ID	TECN	COMMENT	
0.28 $\pm$ 0.05	UHLIG	67	HBC	$K^- p$ 0.9 GeV/c

$\Gamma(\Sigma\pi\pi)/\Gamma_{\text{total}}$				$\Gamma_9/\Gamma$
VALUE	DOCUMENT ID	TECN	COMMENT	
••• We do not use the following data for averages, fits, limits, etc. •••				
0.12	<sup>1</sup> ARMENTEROS68c	HD8C	$K^- N \rightarrow \Sigma\pi\pi$	
<sup>1</sup> For about 3/4 of this, the $\Sigma\pi$ system has $l=0$ and is almost entirely $\Lambda(1520)$ . For the rest, the $\Sigma\pi$ has $l=1$ , which is about what is expected from the known $\Sigma(1775) \rightarrow \Sigma(1385)\pi$ rate, as seen in $\Lambda\pi\pi$ .				

$\Gamma(N\bar{K}^*(892), S=1/2, D\text{-wave})/\Gamma_{\text{total}}$				$\Gamma_{12}/\Gamma$
VALUE	DOCUMENT ID	TECN	COMMENT	
••• We do not use the following data for averages, fits, limits, etc. •••				
not seen	<sup>1</sup> KAMANO	15	DPWA	Multichannel
<sup>1</sup> From the preferred solution A in KAMANO 15.				

$\Gamma(N\bar{K}^*(892), S=3/2, D\text{-wave})/\Gamma_{\text{total}}$				$\Gamma_{13}/\Gamma$
VALUE	DOCUMENT ID	TECN	COMMENT	
••• We do not use the following data for averages, fits, limits, etc. •••				
0.003	<sup>1</sup> KAMANO	15	DPWA	Multichannel
<sup>1</sup> From the preferred solution A in KAMANO 15.				

$\Gamma(N\bar{K}^*(892), S=3/2, G\text{-wave})/\Gamma_{\text{total}}$				$\Gamma_{14}/\Gamma$
VALUE	DOCUMENT ID	TECN	COMMENT	
••• We do not use the following data for averages, fits, limits, etc. •••				
not seen	<sup>1</sup> KAMANO	15	DPWA	Multichannel
<sup>1</sup> From the preferred solution A in KAMANO 15.				

$(\Gamma_1\Gamma_7)^{1/2}/\Gamma_{\text{total}}$ in $N\bar{K} \rightarrow \Sigma(1775) \rightarrow \Lambda\pi$				$(\Gamma_1\Gamma_2)^{1/2}/\Gamma$
VALUE	DOCUMENT ID	TECN	COMMENT	
-0.31 $\pm$ 0.01	ZHANG	13A	DPWA	Multichannel
-0.28 $\pm$ 0.03	GOPAL	77	DPWA	$\bar{K}N$ multichannel
-0.25 $\pm$ 0.02	BAILLON	75	IPWA	$\bar{K}N \rightarrow \Lambda\pi$
-0.28 $\pm$ 0.04	VANHORN	75	DPWA	$K^- p \rightarrow \Lambda\pi^0$
-0.25 $\pm$ 0.048	DEVENISH	74B	Fixed- $t$ dispersion rel.	
••• We do not use the following data for averages, fits, limits, etc. •••				
-0.29 or -0.28	<sup>1</sup> MARTIN	77	DPWA	$\bar{K}N$ multichannel
-0.30	DEBELLEFON	76	IPWA	$K^- p \rightarrow \Lambda\pi^0$
<sup>1</sup> The two MARTIN 77 values are from a T-matrix pole and from a Breit-Wigner fit.				

$(\Gamma_1\Gamma_7)^{1/2}/\Gamma_{\text{total}}$ in $N\bar{K} \rightarrow \Sigma(1775) \rightarrow \Sigma\pi$				$(\Gamma_1\Gamma_3)^{1/2}/\Gamma$
VALUE	DOCUMENT ID	TECN	COMMENT	
+0.08 $\pm$ 0.01	ZHANG	13A	DPWA	Multichannel
+0.13 $\pm$ 0.02	GOPAL	77	DPWA	$\bar{K}N$ multichannel
0.09 $\pm$ 0.01	KANE	74	DPWA	$K^- p \rightarrow \Sigma\pi$
••• We do not use the following data for averages, fits, limits, etc. •••				
+0.08 or +0.08	<sup>1</sup> MARTIN	77	DPWA	$\bar{K}N$ multichannel
<sup>1</sup> The two MARTIN 77 values are from a T-matrix pole and from a Breit-Wigner fit.				

$(\Gamma_1\Gamma_7)^{1/2}/\Gamma_{\text{total}}$ in $N\bar{K} \rightarrow \Sigma(1775) \rightarrow \Sigma(1385)\pi, D\text{-wave}$				$(\Gamma_1\Gamma_5)^{1/2}/\Gamma$
VALUE	DOCUMENT ID	TECN	COMMENT	
-0.12 $\pm$ 0.01	ZHANG	13A	DPWA	Multichannel
-0.184 $\pm$ 0.011	<sup>1</sup> CAMERON	78	DPWA	$K^- p \rightarrow \Sigma(1385)\pi$
+0.20 $\pm$ 0.02	PREVOST	74	DPWA	$K^- N \rightarrow \Sigma(1385)\pi$
••• We do not use the following data for averages, fits, limits, etc. •••				
0.32 $\pm$ 0.06	SIMS	68	DBC	$K^- N \rightarrow \Lambda\pi\pi$
0.24 $\pm$ 0.03	ARMENTEROS67c	HBC	$K^- p \rightarrow \Lambda\pi\pi$	
<sup>1</sup> The CAMERON 78 upper limit on G-wave decay is 0.03.				

$(\Gamma_1\Gamma_7)^{1/2}/\Gamma_{\text{total}}$ in $N\bar{K} \rightarrow \Sigma(1775) \rightarrow \Lambda(1520)\pi, P\text{-wave}$				$(\Gamma_1\Gamma_8)^{1/2}/\Gamma$
VALUE	DOCUMENT ID	TECN	COMMENT	
-0.06 $\pm$ 0.01	ZHANG	13A	DPWA	Multichannel
-0.305 $\pm$ 0.010	<sup>1</sup> CAMERON	77	DPWA	$K^- p \rightarrow \Lambda(1520)\pi^0$
0.31 $\pm$ 0.02	BARLETTA	72	DPWA	$K^- p \rightarrow \Lambda(1520)\pi^0$
0.27 $\pm$ 0.03	ARMENTEROS65c	HBC	$K^- p \rightarrow \Lambda(1520)\pi^0$	
<sup>1</sup> This rate combines P-wave- and F-wave decays. The CAMERON 77 results for the separate P-wave- and F-wave decays are $-0.303 \pm 0.010$ and $-0.037 \pm 0.014$ . The published signs have been changed here to be in accord with the baryon-first convention.				

$(\Gamma_1\Gamma_7)^{1/2}/\Gamma_{\text{total}}$ in $N\bar{K} \rightarrow \Sigma(1775) \rightarrow \Delta(1232)\bar{K}, D\text{-wave}$				$(\Gamma_1\Gamma_{10})^{1/2}/\Gamma$
VALUE	DOCUMENT ID	TECN	COMMENT	
+0.06 $\pm$ 0.03	ZHANG	13A	DPWA	Multichannel

$(\Gamma_1\Gamma_7)^{1/2}/\Gamma_{\text{total}}$ in $N\bar{K} \rightarrow \Sigma(1775) \rightarrow N\bar{K}^*(892), S=1/2$				$(\Gamma_1\Gamma_{11})^{1/2}/\Gamma$
VALUE	DOCUMENT ID	TECN	COMMENT	
+0.04 $\pm$ 0.01	ZHANG	13A	DPWA	Multichannel

$(\Gamma_1\Gamma_7)^{1/2}/\Gamma_{\text{total}}$ in $N\bar{K} \rightarrow \Sigma(1775) \rightarrow N\bar{K}^*(892), S=3/2, D\text{-wave}$				$(\Gamma_1\Gamma_{13})^{1/2}/\Gamma$
VALUE	DOCUMENT ID	TECN	COMMENT	
+0.04 $\pm$ 0.01	ZHANG	13A	DPWA	Multichannel

 **$\Sigma(1775)$  REFERENCES**

SARANTSEV	19	EPJ A55 180	A.V. Sarantsev et al.	(BONN, PNPI)
KAMANO	15	PR C92 025205	H. Kamano et al.	(ANL, OSAK)
ZHANG	13A	PR C08 035205	H. Zhang et al.	(KSU)
PDC	82	PL 111B 1	M. Roos et al.	(HELS, CIT, CERN)
GOPAL	80	Toronto Conf. 159	G.P. Gopal	(RHEL) IJP
ALSTON-...	78	PR D18 182	M. Alston-Garnjost et al.	(LBL, MTHO+) IJP
Also		PRL 38 1007	M. Alston-Garnjost et al.	(LBL, MTHO+) IJP
CAMERON	78	NP B143 189	W. Cameron et al.	(RHEL, LOIC) IJP
CAMERON	77	NP B131 399	W. Cameron et al.	(RHEL, LOIC) IJP
GOPAL	77	NP B119 362	G.P. Gopal et al.	(LOIC, RHEL) IJP
MARTIN	77	NP B127 349	B.R. Martin, M.K. Pidcock, R.G. Moorhouse	(LOUC+) IJP
Also		NP B126 266	B.R. Martin, M.K. Pidcock	(LOUC) IJP
Also		NP B126 285	B.R. Martin, M.K. Pidcock	(LOUC) IJP
DEBELLEFON	76	NP B109 129	A. de Bellefon, A. Berthon	(CDFE) IJP
BAILLON	75	NP B94 39	P.H. Baillon, P.J. Litchfield	(CERN, RHEL) IJP

# Baryon Particle Listings

## $\Sigma(1775), \Sigma(1780), \Sigma(1880)$

VANHORN	75	NP B87 145	A.J. van Horn	(LBL) IJP
Also		NP B87 157	A.J. van Horn	(LBL) IJP
DEVENISH	74B	NP B81 330	R.C.E. Devenish, C.D. Froggatt, B.R. Martin	(DESY+)
KANE	74	LBL-2452	D.F. Kane	(LBL) IJP
PREVOST	74	NP B69 246	J. Prevost <i>et al.</i>	(SACL, CERN, HEID)
BARLETTA	72	NP B40 45	W.A. Barletta	(EFI) IJP
Also		PRL 17 841	S. Fenster <i>et al.</i>	(CHIC, ANL, CERN) IJP
ARMENTEROS	68C	NP B8 216	R. Armenteros <i>et al.</i>	(CERN, HEID, SAACL) I
SIMS	68	PRL 21 1413	W.H. Sims <i>et al.</i>	(FSU, TUFTS, BRAN)
ARMENTEROS	67C	ZPHY 202 486	R. Armenteros <i>et al.</i>	(CERN, HEID, SAACL)
UHLIG	67	PR 155 1448	R.P. Uhlig <i>et al.</i>	(UMD, NRL)
ARMENTEROS	65C	PL 19 338	R. Armenteros <i>et al.</i>	(CERN, HEID, SAACL) IJP
GALTIERI	63	PL 6 296	A. Galtieri, A. Hussain, R. Tripp	(LRL) IJ

**$\Sigma(1780) 3/2^+$**   $I(J^P) = 1(\frac{3}{2}^+)$  Status: \*  
 OMITTED FROM SUMMARY TABLE  
 was  $\Sigma(1730)$

### $\Sigma(1780)$ MASS

VALUE (MeV)	DOCUMENT ID	TECN	COMMENT
<b>1730 to 1830 (<math>\approx 1780</math>) OUR ESTIMATE</b>			
1727 $\pm$ 27	ZHANG	13A	DPWA Multichannel
1798 or 1802	<sup>1</sup> MARTIN	77	DPWA $\bar{K}N$ multichannel
1720 $\pm$ 30	<sup>2</sup> BAILLON	75	IPWA $\bar{K}N \rightarrow \Lambda\pi$
1840 $\pm$ 10	LANGBEIN	72	IPWA $\bar{K}N$ multichannel

<sup>1</sup> The two MARTIN 77 values are from a T-matrix pole and from a Breit-Wigner fit.  
<sup>2</sup> From solution 1 of BAILLON 75; not present in solution 2.

### $\Sigma(1780)$ WIDTH

VALUE (MeV)	DOCUMENT ID	TECN	COMMENT
<b>100 to 300 (<math>\approx 200</math>) OUR ESTIMATE</b>			
276 $\pm$ 87	ZHANG	13A	DPWA Multichannel
93 or 93	<sup>1</sup> MARTIN	77	DPWA $\bar{K}N$ multichannel
120 $\pm$ 30	<sup>2</sup> BAILLON	75	IPWA $\bar{K}N \rightarrow \Lambda\pi$
120 $\pm$ 10	LANGBEIN	72	IPWA $\bar{K}N$ multichannel

<sup>1</sup> The two MARTIN 77 values are from a T-matrix pole and from a Breit-Wigner fit.  
<sup>2</sup> From solution 1 of BAILLON 75; not present in solution 2.

### $\Sigma(1780)$ DECAY MODES

Mode	Fraction ( $\Gamma_i/\Gamma$ )
$\Gamma_1$ $N\bar{K}$	( 2.0 $\pm$ 1.0 ) %
$\Gamma_2$ $\Lambda\pi$	( 70 $\pm$ 17 ) %
$\Gamma_3$ $\Sigma\pi$	( 12 $\pm$ 6 ) %

### $\Sigma(1780)$ BRANCHING RATIOS

$\Gamma(N\bar{K})/\Gamma_{total}$	$\Gamma_1/\Gamma$
0.02 $\pm$ 0.01	

$\Gamma(\Lambda\pi)/\Gamma_{total}$	$\Gamma_2/\Gamma$
0.70 $\pm$ 0.17	

$\Gamma(\Sigma\pi)/\Gamma_{total}$	$\Gamma_3/\Gamma$
0.12 $\pm$ 0.06	

### $\Sigma(1780)$ REFERENCES

ZHANG	13A	PR C88 035205	H. Zhang <i>et al.</i>	(KSU)
MARTIN	77	NP B127 349	B.R. Martin, M.K. Pidcock, R.G. Moorhouse	(LOUC+)
BAILLON	75	NP B94 39	P.H. Baillon, P.J. Litchfield	(CERN, RHEL)
LANGBEIN	72	NP B47 477	W. Langbein, F. Wagner	(MPIM)

**$\Sigma(1880) 1/2^+$**   $I(J^P) = 1(\frac{1}{2}^+)$  Status: \*\*  
 OMITTED FROM SUMMARY TABLE

A  $P_{11}$  resonance is suggested by several partial-wave analyses, but with wide variations in the mass and other parameters. We list here all claims which lie well above the  $P_{11}$   $\Sigma(1770)$ .

### $\Sigma(1880)$ POLE POSITION

REAL PART	DOCUMENT ID	TECN	COMMENT
1776	ZHANG	13A	DPWA Multichannel

• • • We do not use the following data for averages, fits, limits, etc. • • •

### —2xIMAGINARY PART

VALUE (MeV)	DOCUMENT ID	TECN	COMMENT
270	ZHANG	13A	DPWA Multichannel

• • • We do not use the following data for averages, fits, limits, etc. • • •

### $\Sigma(1880)$ MASS

VALUE (MeV)	DOCUMENT ID	TECN	COMMENT
<b>1820 to 1940 (<math>\approx 1880</math>) OUR ESTIMATE</b>			
1821 $\pm$ 17	ZHANG	13A	DPWA Multichannel
1826 $\pm$ 20	GOPAL	80	DPWA $\bar{K}N \rightarrow \bar{K}N$
1870 $\pm$ 10	CAMERON	78B	DPWA $K^-p \rightarrow N\bar{K}^*$
1847 or 1863	<sup>1</sup> MARTIN	77	DPWA $\bar{K}N$ multichannel
1960 $\pm$ 30	<sup>2</sup> BAILLON	75	IPWA $\bar{K}N \rightarrow \Lambda\pi$
1985 $\pm$ 50	VANHORN	75	DPWA $K^-p \rightarrow \Lambda\pi^0$
1898	<sup>3</sup> LEA	73	DPWA Multichannel K-matrix
$\sim 1850$	ARMENTEROSTO	IPWA	$\bar{K}N \rightarrow \bar{K}N$
1950 $\pm$ 50	BARBARO...	70	DPWA $K^-N \rightarrow \Lambda\pi$
1920 $\pm$ 30	LITCHFIELD	70	DPWA $K^-N \rightarrow \Lambda\pi$
1850	BAILEY	69	DPWA $\bar{K}N \rightarrow \bar{K}N$
1882 $\pm$ 40	SMART	68	DPWA $K^-N \rightarrow \Lambda\pi$

### $\Sigma(1880)$ WIDTH

VALUE (MeV)	DOCUMENT ID	TECN	COMMENT
<b>100 to 300 (<math>\approx 200</math>) OUR ESTIMATE</b>			
300 $\pm$ 59	ZHANG	13A	DPWA Multichannel
86 $\pm$ 15	GOPAL	80	DPWA $\bar{K}N \rightarrow \bar{K}N$
80 $\pm$ 10	CAMERON	78B	DPWA $K^-p \rightarrow N\bar{K}^*$
216 or 220	<sup>1</sup> MARTIN	77	DPWA $\bar{K}N$ multichannel
260 $\pm$ 40	<sup>2</sup> BAILLON	75	IPWA $\bar{K}N \rightarrow \Lambda\pi$
220 $\pm$ 140	VANHORN	75	DPWA $K^-p \rightarrow \Lambda\pi^0$
222	<sup>3</sup> LEA	73	DPWA Multichannel K-matrix
$\sim 30$	ARMENTEROSTO	IPWA	$\bar{K}N \rightarrow \bar{K}N$
200 $\pm$ 50	BARBARO...	70	DPWA $K^-N \rightarrow \Lambda\pi$
170 $\pm$ 40	LITCHFIELD	70	DPWA $K^-N \rightarrow \Lambda\pi$
200	BAILEY	69	DPWA $\bar{K}N \rightarrow \bar{K}N$
222 $\pm$ 150	SMART	68	DPWA $K^-N \rightarrow \Lambda\pi$

### $\Sigma(1880)$ DECAY MODES

Mode	Fraction ( $\Gamma_i/\Gamma$ )
$\Gamma_1$ $N\bar{K}$	0.10 to 0.30 ( $\approx 0.20$ )
$\Gamma_2$ $\Lambda\pi$	
$\Gamma_3$ $\Sigma\pi$	
$\Gamma_4$ $\Lambda(1520)\pi, D$ -wave	( 2.0 $\pm$ 1.0 ) %
$\Gamma_5$ $N\bar{K}^*(892), S=1/2, P$ -wave	
$\Gamma_6$ $N\bar{K}^*(892), S=3/2, P$ -wave	
$\Gamma_7$ $\Delta(1232)\bar{K}, P$ -wave	( 39 $\pm$ 8 ) %

### $\Sigma(1880)$ BRANCHING RATIOS

See "Sign conventions for resonance couplings" in the Note on  $\Lambda$  and  $\Sigma$  Resonances.

$\Gamma(N\bar{K})/\Gamma_{total}$	$\Gamma_1/\Gamma$
0.10 to 0.30 ( $\approx 0.20$ ) OUR ESTIMATE	

VALUE	DOCUMENT ID	TECN	COMMENT
0.10 $\pm$ 0.03	ZHANG	13A	DPWA Multichannel
0.06 $\pm$ 0.02	GOPAL	80	DPWA $\bar{K}N \rightarrow \bar{K}N$
0.27 or 0.27	<sup>1</sup> MARTIN	77	DPWA $\bar{K}N$ multichannel
0.31	<sup>3</sup> LEA	73	DPWA Multichannel K-matrix
0.20	ARMENTEROSTO	IPWA	$\bar{K}N \rightarrow \bar{K}N$
0.22	BAILEY	69	DPWA $\bar{K}N \rightarrow \bar{K}N$

$(\Gamma_1\Gamma_2)^{1/2}/\Gamma_{total}$ in $N\bar{K} \rightarrow \Sigma(1880) \rightarrow \Lambda\pi$	$(\Gamma_1\Gamma_2)^{1/2}/\Gamma$
-0.24 or -0.24	
-0.12 $\pm$ 0.02	<sup>1</sup> MARTIN 77 DPWA $\bar{K}N$ multichannel
+0.05 $\pm$ 0.07	<sup>2</sup> BAILLON 75 IPWA $\bar{K}N \rightarrow \Lambda\pi$
-0.02	
+0.05 $\pm$ 0.07	VANHORN 75 DPWA $K^-p \rightarrow \Lambda\pi^0$
-0.169 $\pm$ 0.119	DEVENISH 74B Fixed-t dispersion rel.
-0.30	<sup>3</sup> LEA 73 DPWA Multichannel K-matrix
-0.09 $\pm$ 0.04	BARBARO... 70 DPWA $K^-N \rightarrow \Lambda\pi$
-0.14 $\pm$ 0.03	LITCHFIELD 70 DPWA $K^-N \rightarrow \Lambda\pi$
-0.11 $\pm$ 0.03	SMART 68 DPWA $K^-N \rightarrow \Lambda\pi$

$(\Gamma_1\Gamma_3)^{1/2}/\Gamma_{total}$ in $N\bar{K} \rightarrow \Sigma(1880) \rightarrow \Sigma\pi$	$(\Gamma_1\Gamma_3)^{1/2}/\Gamma$
+0.30 or +0.29	<sup>1</sup> MARTIN 77 DPWA $\bar{K}N$ multichannel
not seen	<sup>3</sup> LEA 73 DPWA Multichannel K-matrix

See key on page 999

# Baryon Particle Listings

## $\Sigma(1880), \Sigma(1900)$

$\Gamma(\Lambda(1520)\pi, D\text{-wave})/\Gamma_{\text{total}}$		$\Gamma_4/\Gamma$	
VALUE	DOCUMENT ID	TECN	COMMENT
<b>0.02±0.01</b>	ZHANG	13A	DPWA Multichannel

$(\Gamma_1/\Gamma_7)^{1/2}/\Gamma_{\text{total}}$ in $N\bar{K} \rightarrow \Sigma(1880) \rightarrow N\bar{K}^*(892), S=1/2, P\text{-wave } (\Gamma_1/\Gamma_5)^{1/2}/\Gamma$			
VALUE	DOCUMENT ID	TECN	COMMENT
-0.05±0.03	4 CAMERON	78B	DPWA $K^-p \rightarrow N\bar{K}^*$

$(\Gamma_1/\Gamma_7)^{1/2}/\Gamma_{\text{total}}$ in $N\bar{K} \rightarrow \Sigma(1880) \rightarrow N\bar{K}^*(892), S=3/2, P\text{-wave } (\Gamma_1/\Gamma_6)^{1/2}/\Gamma$			
VALUE	DOCUMENT ID	TECN	COMMENT
+0.11±0.03	CAMERON	78B	DPWA $K^-p \rightarrow N\bar{K}^*$

$\Gamma(\Delta(1232)\bar{K}, P\text{-wave})/\Gamma_{\text{total}}$		$\Gamma_7/\Gamma$	
VALUE	DOCUMENT ID	TECN	COMMENT
<b>0.39±0.08</b>	ZHANG	13A	DPWA Multichannel

### $\Sigma(1880)$ FOOTNOTES

- The two MARTIN 77 values are from a T-matrix pole and from a Breit-Wigner fit.
- From solution 1 of BAILLON 75; not present in solution 2.
- Only unconstrained states from table 1 of LEA 73 are listed.
- The published sign has been changed to be in accord with the baryon-first convention.

### $\Sigma(1880)$ REFERENCES

ZHANG 13A PR C88 035205	H. Zhang et al. (KSU)
GOPAL 80 Toronto Conf. 159	G.P. Gopal (RHEL) IJP
CAMERON 78B NP B146 327	W. Cameron et al. (RHEL, LOIC) IJP
MARTIN 77 NP B127 349	B.R. Martin, M.K. Pidcock, R.G. Moorhouse (LOUC+) IJP
Also NP B126 266	B.R. Martin, M.K. Pidcock (LOUC) IJP
Also NP B126 285	B.R. Martin, M.K. Pidcock (LOUC) IJP
BAILLON 75 NP B94 39	P.H. Baillon, P.J. Litchfield (CERN, RHEL) IJP
VANHORN 75 NP B87 145	A.J. van Horn (LBL) IJP
Also NP B87 157	A.J. van Horn (LBL) IJP
DEVENISH 74B NP B81 330	R.C.E. Devenish, C.D. Froggatt, B.R. Martin (DESY+) IJP
LEA 73 NP B56 77	A.T. Lea et al. (RHEL, LOUC, GLAS, AARH) IJP
ARMENTEROS 70 Duke Conf. 123	R. Armenteros et al. (CERN, HEID, SACL) IJP
Hyperon Resonances, 1970	
BARBARO... 70 Duke Conf. 173	A. Barbaro-Galteri (LRL) IJP
Hyperon Resonances, 1970	
LITCHFIELD 70 NP B22 269	P.J. Litchfield (RHEL) IJP
BAILEY 69 Thesis UCRL 50617	J.M. Bailey (LLL) IJP
SMART 68 PR 169 1330	W.M. Smart (LRL) IJP

$\Sigma(1900) 1/2^-$

 $I(J^P) = 1(\frac{1}{2}^-)$  Status: \*\*

OMITTED FROM SUMMARY TABLE

### $\Sigma(1900)$ POLE POSITION

REAL PART			
VALUE	DOCUMENT ID	TECN	COMMENT
<b>1936±10</b>	SARANTSEV	19	DPWA $\bar{K}N$ multichannel
-2×IMAGINARY PART			
VALUE	DOCUMENT ID	TECN	COMMENT
<b>150±25</b>	SARANTSEV	19	DPWA $\bar{K}N$ multichannel

### $\Sigma(1900)$ POLE RESIDUES

The normalized residue is the residue divided by  $\Gamma_{\text{pole}}/2$ .

Normalized residue in $N\bar{K} \rightarrow \Sigma(1900) \rightarrow N\bar{K}$			
MODULUS	PHASE (°)	DOCUMENT ID	TECN
<b>0.45±0.09</b>	<b>90 ± 25</b>	SARANTSEV	19
		DPWA	$\bar{K}N$ multichannel

Normalized residue in $N\bar{K} \rightarrow \Sigma(1900) \rightarrow \Sigma\pi$			
MODULUS	PHASE (°)	DOCUMENT ID	TECN
<b>0.38±0.08</b>	<b>95 ± 20</b>	SARANTSEV	19
		DPWA	$\bar{K}N$ multichannel

Normalized residue in $N\bar{K} \rightarrow \Sigma(1900) \rightarrow \Sigma\eta$			
MODULUS	PHASE (°)	DOCUMENT ID	TECN
<b>0.03±0.01</b>	<b>20 ± 20</b>	SARANTSEV	19
		DPWA	$\bar{K}N$ multichannel

Normalized residue in $N\bar{K} \rightarrow \Sigma(1900) \rightarrow \Lambda\pi$			
MODULUS	PHASE (°)	DOCUMENT ID	TECN
<b>0.14±0.05</b>	<b>-160 ± 50</b>	SARANTSEV	19
		DPWA	$\bar{K}N$ multichannel

Normalized residue in $N\bar{K} \rightarrow \Sigma(1900) \rightarrow \Xi K$			
MODULUS	PHASE (°)	DOCUMENT ID	TECN
<b>0.08±0.05</b>	<b>75 ± 25</b>	SARANTSEV	19
		DPWA	$\bar{K}N$ multichannel

Normalized residue in $N\bar{K} \rightarrow \Sigma(1900) \rightarrow \Sigma(1385)\pi$			
MODULUS	PHASE (°)	DOCUMENT ID	TECN
<b>0.16±0.05</b>	<b>40 ± 30</b>	SARANTSEV	19
		DPWA	$\bar{K}N$ multichannel

Normalized residue in $N\bar{K} \rightarrow \Sigma(1900) \rightarrow \Lambda(1520)\pi$			
MODULUS	PHASE (°)	DOCUMENT ID	TECN
<b>0.04±0.02</b>	<b>-25 ± 40</b>	SARANTSEV	19
		DPWA	$\bar{K}N$ multichannel

Normalized residue in $N\bar{K} \rightarrow \Sigma(1900) \rightarrow \Delta\bar{K}$			
MODULUS	PHASE (°)	DOCUMENT ID	TECN
<b>0.11±0.04</b>	<b>60 ± 30</b>	SARANTSEV	19
		DPWA	$\bar{K}N$ multichannel

Normalized residue in $N\bar{K} \rightarrow \Sigma(1900) \rightarrow N\bar{K}^*(892), S=1/2, S\text{-wave}$			
MODULUS	PHASE (°)	DOCUMENT ID	TECN
<b>0.17±0.06</b>	<b>50 ± 50</b>	SARANTSEV	19
		DPWA	$\bar{K}N$ multichannel

Normalized residue in $N\bar{K} \rightarrow \Sigma(1900) \rightarrow N\bar{K}^*(892), S=3/2, D\text{-wave}$			
MODULUS	PHASE (°)	DOCUMENT ID	TECN
<b>0.05±0.04</b>		SARANTSEV	19
		DPWA	$\bar{K}N$ multichannel

### $\Sigma(1900)$ MASS

VALUE (MeV)	DOCUMENT ID	TECN	COMMENT
<b>1900 to 1950 (≈ 1925) OUR ESTIMATE</b>			
1938±12	SARANTSEV	19	DPWA $\bar{K}N$ multichannel
1900±21	ZHANG	13A	DPWA $\bar{K}N$ multichannel
1944±15	GOPAL	80	DPWA $\bar{K}N \rightarrow \bar{K}N$
1755 or 1834	1 MARTIN	77	DPWA $\bar{K}N$ multichannel
2004±40	VANHORN	75	DPWA $K^-p \rightarrow \Lambda\pi^0$
•••	We do not use the following data for averages, fits, limits, etc. •••		
1955±15	GOPAL	77	DPWA $\bar{K}N$ multichannel
1	The two MARTIN 77 values are from a T-matrix pole and from a Breit-Wigner fit.		

### $\Sigma(1900)$ WIDTH

VALUE (MeV)	DOCUMENT ID	TECN	COMMENT
<b>140 to 190 (≈ 165) OUR ESTIMATE</b>			
155±30	SARANTSEV	19	DPWA $\bar{K}N$ multichannel
191±47	ZHANG	13A	DPWA $\bar{K}N$ multichannel
215±25	GOPAL	80	DPWA $\bar{K}N \rightarrow \bar{K}N$
413 or 450	1 MARTIN	77	DPWA $\bar{K}N$ multichannel
116±40	VANHORN	75	DPWA $K^-p \rightarrow \Lambda\pi^0$
•••	We do not use the following data for averages, fits, limits, etc. •••		
170±40	GOPAL	77	DPWA $\bar{K}N$ multichannel
1	The two MARTIN 77 values are from a T-matrix pole and from a Breit-Wigner fit.		

### $\Sigma(1900)$ DECAY MODES

Mode	Fraction ( $\Gamma_i/\Gamma$ )
$\Gamma_1 N\bar{K}$	0.40 to 0.70 (≈ 0.55)
$\Gamma_2 \Sigma\pi$	0.10 to 0.40 (≈ 0.25)
$\Gamma_3 \Sigma\eta$	(1.0 ± 1.0) %
$\Gamma_4 \Lambda\pi$	(6.0 ± 2.0) %
$\Gamma_5 \Xi K$	(3.0 ± 2.0) %
$\Gamma_6 \Sigma(1385)\pi$	(7.0 ± 3.0) %
$\Gamma_7 \Lambda(1520)\pi$	
$\Gamma_8 \Delta\bar{K}$	(2.5 ± 1.0) %
$\Gamma_9 N\bar{K}^*(892), S=1/2, S\text{-wave}$	(7.0 ± 3.0) %
$\Gamma_{10} N\bar{K}^*(892), S=3/2, D\text{-wave}$	

### $\Sigma(1900)$ BRANCHING RATIOS

$\Gamma(N\bar{K})/\Gamma_{\text{total}}$		$\Gamma_1/\Gamma$	
VALUE	DOCUMENT ID	TECN	COMMENT
<b>0.40 to 0.70 (≈ 0.55) OUR ESTIMATE</b>			
0.45±0.09	SARANTSEV	19	DPWA $\bar{K}N$ multichannel
0.67±0.17	ZHANG	13A	DPWA $\bar{K}N$ multichannel

$\Gamma(\Sigma\pi)/\Gamma_{\text{total}}$		$\Gamma_2/\Gamma$	
VALUE	DOCUMENT ID	TECN	COMMENT
<b>0.10 to 0.40 (≈ 0.25) OUR ESTIMATE</b>			
0.33±0.07	SARANTSEV	19	DPWA $\bar{K}N$ multichannel
0.10±0.05	ZHANG	13A	DPWA $\bar{K}N$ multichannel

$\Gamma(\Sigma\eta)/\Gamma_{\text{total}}$		$\Gamma_3/\Gamma$	
VALUE	DOCUMENT ID	TECN	COMMENT
<b>0.01±0.01</b>	SARANTSEV	19	DPWA $\bar{K}N$ multichannel

$\Gamma(\Lambda\pi)/\Gamma_{\text{total}}$		$\Gamma_4/\Gamma$	
VALUE	DOCUMENT ID	TECN	COMMENT
<b>0.06±0.02</b>	SARANTSEV	19	DPWA $\bar{K}N$ multichannel

$\Gamma(\Xi K)/\Gamma_{\text{total}}$		$\Gamma_5/\Gamma$	
VALUE	DOCUMENT ID	TECN	COMMENT
<b>0.03±0.02</b>	SARANTSEV	19	DPWA $\bar{K}N$ multichannel

$\Gamma(\Sigma(1385)\pi)/\Gamma_{\text{total}}$		$\Gamma_6/\Gamma$	
VALUE	DOCUMENT ID	TECN	COMMENT
<b>0.07±0.03</b>	SARANTSEV	19	DPWA $\bar{K}N$ multichannel



# Baryon Particle Listings

## $\Sigma(1900), \Sigma(1910)$

$\Gamma(\Lambda(1520)\pi)/\Gamma_{\text{total}}$				$\Gamma_7/\Gamma$
VALUE	DOCUMENT ID	TECN	COMMENT	
<0.01	SARANTSEV 19	DPWA	$\bar{K}N$ multichannel	

$\Gamma(\Delta\bar{K})/\Gamma_{\text{total}}$				$\Gamma_8/\Gamma$
VALUE	DOCUMENT ID	TECN	COMMENT	
<b>0.025 ± 0.010</b>	SARANTSEV 19	DPWA	$\bar{K}N$ multichannel	

$\Gamma(N\bar{K}^*(892), S=1/2, S\text{-wave})/\Gamma_{\text{total}}$				$\Gamma_9/\Gamma$
VALUE	DOCUMENT ID	TECN	COMMENT	
<b>0.07 ± 0.03</b>	SARANTSEV 19	DPWA	$\bar{K}N$ multichannel	

$\Gamma(N\bar{K}^*(892), S=3/2, D\text{-wave})/\Gamma_{\text{total}}$				$\Gamma_{10}/\Gamma$
VALUE	DOCUMENT ID	TECN	COMMENT	
<0.01	SARANTSEV 19	DPWA	$\bar{K}N$ multichannel	

### $\Sigma(1900)$ REFERENCES

SARANTSEV 19	EPJ A55 180	A.V. Sarantsev et al.	(BONN, PNPI)
ZHANG 13A	PR C88 035205	H. Zhang et al.	(KSU)
GOPAL 80	Toronto Conf. 159	G.P. Gopal	(RHEL)
GOPAL 77	NP B119 362	G.P. Gopal et al.	(LOIC, RHEL)
MARTIN 77	NP B127 349	B.R. Martin, M.K. Pittcock, R.G. Moorhouse	(LOUC+)
VANHORN 75	NP B87 145	A.J. van Horn	(LBL)

**$\Sigma(1910) 3/2^-$**   $I(J^P) = 1(\frac{3}{2}^-)$  Status: \*\*\*  
 was  $\Sigma(1940)$

For results published before 1974 (they are now obsolete), see our 1982 edition Physics Letters **111B** 1 (1982).

Not all analyses require this state. It is not required by the GOPAL 77 analysis of  $K^-n \rightarrow (\Sigma\pi)^-$  nor by the GOPAL 80 analysis of  $K^-n \rightarrow K^-n$ . See also HEMINGWAY 75.

### $\Sigma(1910)$ POLE RESIDUES

The normalized residue is the residue divided by  $\Gamma_{\text{pole}}/2$ .

Normalized residue in $N\bar{K} \rightarrow \Sigma(1910) \rightarrow N\bar{K}$			
MODULUS	PHASE (°)	DOCUMENT ID	TECN COMMENT
<b>0.03 ± 0.02</b>	<b>-95 ± 60</b>	SARANTSEV 19	DPWA $\bar{K}N$ multichannel

Normalized residue in $N\bar{K} \rightarrow \Sigma(1910) \rightarrow \Sigma\pi$			
MODULUS	PHASE (°)	DOCUMENT ID	TECN COMMENT
<b>0.16 ± 0.04</b>	<b>-160 ± 15</b>	SARANTSEV 19	DPWA $\bar{K}N$ multichannel

Normalized residue in $N\bar{K} \rightarrow \Sigma(1910) \rightarrow \Lambda\pi$			
MODULUS	PHASE (°)	DOCUMENT ID	TECN COMMENT
<b>0.04 ± 0.03</b>	<b>25 ± 25</b>	SARANTSEV 19	DPWA $\bar{K}N$ multichannel

Normalized residue in $N\bar{K} \rightarrow \Sigma(1910) \rightarrow \Xi\pi$			
MODULUS	PHASE (°)	DOCUMENT ID	TECN COMMENT
<b>0.01 ± 0.01</b>		SARANTSEV 19	DPWA $\bar{K}N$ multichannel

Normalized residue in $N\bar{K} \rightarrow \Sigma(1910) \rightarrow \Lambda(1520)\pi, P\text{-wave}$			
MODULUS	PHASE (°)	DOCUMENT ID	TECN COMMENT
<b>0.01 ± 0.01</b>		SARANTSEV 19	DPWA $\bar{K}N$ multichannel

Normalized residue in $N\bar{K} \rightarrow \Sigma(1910) \rightarrow \Lambda(1520)\pi, F\text{-wave}$			
MODULUS	PHASE (°)	DOCUMENT ID	TECN COMMENT
~ 0		SARANTSEV 19	DPWA $\bar{K}N$ multichannel

Normalized residue in $N\bar{K} \rightarrow \Sigma(1910) \rightarrow \Delta\bar{K}, S\text{-wave}$			
MODULUS	PHASE (°)	DOCUMENT ID	TECN COMMENT
<b>0.03 ± 0.01</b>	<b>120 ± 20</b>	SARANTSEV 19	DPWA $\bar{K}N$ multichannel

Normalized residue in $N\bar{K} \rightarrow \Sigma(1910) \rightarrow N\bar{K}^*(892), S=3/2, S\text{-wave}$			
MODULUS	PHASE (°)	DOCUMENT ID	TECN COMMENT
<b>0.03 ± 0.02</b>	<b>20 ± 35</b>	SARANTSEV 19	DPWA $\bar{K}N$ multichannel

Normalized residue in $N\bar{K} \rightarrow \Sigma(1910) \rightarrow N\bar{K}^*(892), S=1/2, D\text{-wave}$			
MODULUS	PHASE (°)	DOCUMENT ID	TECN COMMENT
<b>0.02 ± 0.01</b>		SARANTSEV 19	DPWA $\bar{K}N$ multichannel

Normalized residue in $N\bar{K} \rightarrow \Sigma(1910) \rightarrow N\bar{K}^*(892), S=3/2, D\text{-wave}$			
MODULUS	PHASE (°)	DOCUMENT ID	TECN COMMENT
<b>0.01 ± 0.01</b>		SARANTSEV 19	DPWA $\bar{K}N$ multichannel

### $\Sigma(1910)$ MASS

1870 to 1950 (≈ 1910) OUR ESTIMATE			
VALUE (MeV)	DOCUMENT ID	TECN	COMMENT
1878 ± 12	SARANTSEV 19	DPWA	$\bar{K}N$ multichannel
1920 ± 50	GOPAL 77	DPWA	$\bar{K}N$ multichannel
1950 ± 30	BAILLON 75	IPWA	$\bar{K}N \rightarrow \Lambda\pi$
1949 +40 -60	VANHORN 75	DPWA	$K^-p \rightarrow \Lambda\pi^0$
1935 ± 80	KANE 74	DPWA	$K^-p \rightarrow \Sigma\pi$
1940 ± 20	LITCHFIELD 74B	DPWA	$K^-p \rightarrow \Lambda(1520)\pi^0$
1950 ± 20	LITCHFIELD 74C	DPWA	$K^-p \rightarrow \Delta(1232)\bar{K}$
• • • We do not use the following data for averages, fits, limits, etc. • • •			
1886 or 1893	<sup>1</sup> MARTIN 77	DPWA	$\bar{K}N$ multichannel
1940	DEBELLEFON 76	IPWA	$K^-p \rightarrow \Lambda\pi^0, F_{17}$ wave

### $\Sigma(1910)$ WIDTH

150 to 300 (≈ 220) OUR ESTIMATE			
VALUE (MeV)	DOCUMENT ID	TECN	COMMENT
224 ± 25	SARANTSEV 19	DPWA	$\bar{K}N$ multichannel
170 ± 25	CAMERON 78B	DPWA	$K^-p \rightarrow N\bar{K}^*$
300 ± 80	GOPAL 77	DPWA	$\bar{K}N$ multichannel
150 ± 75	BAILLON 75	IPWA	$\bar{K}N \rightarrow \Lambda\pi$
160 +70 -40	VANHORN 75	DPWA	$K^-p \rightarrow \Lambda\pi^0$
330 ± 80	KANE 74	DPWA	$K^-p \rightarrow \Sigma\pi$
60 ± 20	LITCHFIELD 74B	DPWA	$K^-p \rightarrow \Lambda(1520)\pi^0$
70 +20 -30	LITCHFIELD 74C	DPWA	$K^-p \rightarrow \Delta(1232)\bar{K}$
• • • We do not use the following data for averages, fits, limits, etc. • • •			
157 or 159	<sup>1</sup> MARTIN 77	DPWA	$\bar{K}N$ multichannel

### $\Sigma(1910)$ DECAY MODES

Mode	Fraction ( $\Gamma_i/\Gamma$ )
$\Gamma_1 N\bar{K}$	0.01 to 0.05 (≈ 0.02)
$\Gamma_2 \Lambda\pi$	( 6 ± 4 ) %
$\Gamma_3 \Sigma\pi$	( 86 ± 21 ) %
$\Gamma_4 \Sigma(1385)\pi$	seen
$\Gamma_5 \Xi K$	
$\Gamma_6 \Sigma(1385)\pi, S\text{-wave}$	
$\Gamma_7 \Lambda(1520)\pi$	seen
$\Gamma_8 \Lambda(1520)\pi, P\text{-wave}$	
$\Gamma_9 \Lambda(1520)\pi, F\text{-wave}$	
$\Gamma_{10} \Delta(1232)\bar{K}$	( 3.0 ± 1.0 ) %
$\Gamma_{11} \Delta(1232)\bar{K}, S\text{-wave}$	
$\Gamma_{12} \Delta(1232)\bar{K}, D\text{-wave}$	
$\Gamma_{13} N\bar{K}^*(892)$	seen
$\Gamma_{14} N\bar{K}^*(892), S=3/2, S\text{-wave}$	
$\Gamma_{15} N\bar{K}^*(892), S=1/2, D\text{-wave}$	( 1.0 ± 1.0 ) %
$\Gamma_{16} N\bar{K}^*(892), S=3/2, D\text{-wave}$	

### $\Sigma(1910)$ BRANCHING RATIOS

See "Sign conventions for resonance couplings" in the Note on  $\Lambda$  and  $\Sigma$  Resonances.

$\Gamma(N\bar{K})/\Gamma_{\text{total}}$				$\Gamma_1/\Gamma$
VALUE	DOCUMENT ID	TECN	COMMENT	
<b>0.01 to 0.05 (≈ 0.02) OUR ESTIMATE</b>				
0.03 ± 0.02	SARANTSEV 19	DPWA	$\bar{K}N$ multichannel	
<0.04	GOPAL 77	DPWA	$\bar{K}N$ multichannel	
0.14 or 0.13	<sup>1</sup> MARTIN 77	DPWA	$\bar{K}N$ multichannel	

$\Gamma(\Lambda\pi)/\Gamma_{\text{total}}$				$\Gamma_2/\Gamma$
VALUE	DOCUMENT ID	TECN	COMMENT	
<b>0.06 ± 0.04</b>	SARANTSEV 19	DPWA	$\bar{K}N$ multichannel	

$\Gamma(\Sigma\pi)/\Gamma_{\text{total}}$				$\Gamma_3/\Gamma$
VALUE	DOCUMENT ID	TECN	COMMENT	
<b>0.86 ± 0.21</b>	SARANTSEV 19	DPWA	$\bar{K}N$ multichannel	

$\Gamma(\Xi K)/\Gamma_{\text{total}}$				$\Gamma_5/\Gamma$
VALUE	DOCUMENT ID	TECN	COMMENT	
~ 0	SARANTSEV 19	DPWA	$\bar{K}N$ multichannel	

$\Gamma(\Lambda(1520)\pi, P\text{-wave})/\Gamma_{\text{total}}$				$\Gamma_8/\Gamma$
VALUE	DOCUMENT ID	TECN	COMMENT	
~ 0	SARANTSEV 19	DPWA	$\bar{K}N$ multichannel	

$\Gamma(\Lambda(1520)\pi, F\text{-wave})/\Gamma_{\text{total}}$				$\Gamma_9/\Gamma$
VALUE	DOCUMENT ID	TECN	COMMENT	
$\sim 0$	SARANTSEV	19	DPWA $\bar{K}N$ multichannel	
$\Gamma(\Delta(1232)\bar{K})/\Gamma_{\text{total}}$				$\Gamma_{10}/\Gamma$
VALUE	DOCUMENT ID	TECN	COMMENT	
$0.03 \pm 0.01$	SARANTSEV	19	DPWA $\bar{K}N$ multichannel	
$\Gamma(N\bar{K}^*(892))/\Gamma_{\text{total}}$				$\Gamma_{13}/\Gamma$
VALUE	DOCUMENT ID	TECN	COMMENT	
$0.03 \pm 0.02$	SARANTSEV	19	DPWA $\bar{K}N$ multichannel	
$\Gamma(N\bar{K}^*(892), S=1/2, D\text{-wave})/\Gamma_{\text{total}}$				$\Gamma_{15}/\Gamma$
VALUE	DOCUMENT ID	TECN	COMMENT	
$0.01 \pm 0.01$	SARANTSEV	19	DPWA $\bar{K}N$ multichannel	
$\Gamma(N\bar{K}^*(892), S=3/2, D\text{-wave})/\Gamma_{\text{total}}$				$\Gamma_{16}/\Gamma$
VALUE	DOCUMENT ID	TECN	COMMENT	
$\sim 0$	SARANTSEV	19	DPWA $\bar{K}N$ multichannel	
$(\Gamma_1\Gamma_f)^{1/2}/\Gamma_{\text{total}}$ in $N\bar{K} \rightarrow \Sigma(1910) \rightarrow \Lambda\pi$				$(\Gamma_1\Gamma_2)^{1/2}/\Gamma$
VALUE	DOCUMENT ID	TECN	COMMENT	
$-0.06 \pm 0.03$	GOPAL	77	DPWA $\bar{K}N$ multichannel	
$-0.04 \pm 0.02$	BAILLON	75	IPWA $\bar{K}N \rightarrow \Lambda\pi$	
$-0.05 \pm 0.03$	VANHORN	75	DPWA $K^-p \rightarrow \Lambda\pi^0$	
$-0.153 \pm 0.070$	DEVENISH	74B	Fixed- $t$ dispersion rel.	
$\bullet \bullet \bullet$ We do not use the following data for averages, fits, limits, etc. $\bullet \bullet \bullet$				
$-0.15$ or $-0.14$	<sup>1</sup> MARTIN	77	DPWA $\bar{K}N$ multichannel	
$(\Gamma_1\Gamma_f)^{1/2}/\Gamma_{\text{total}}$ in $N\bar{K} \rightarrow \Sigma(1910) \rightarrow \Sigma\pi$				$(\Gamma_1\Gamma_3)^{1/2}/\Gamma$
VALUE	DOCUMENT ID	TECN	COMMENT	
$-0.08 \pm 0.04$	GOPAL	77	DPWA $\bar{K}N$ multichannel	
$-0.14 \pm 0.04$	KANE	74	DPWA $K^-p \rightarrow \Sigma\pi$	
$\bullet \bullet \bullet$ We do not use the following data for averages, fits, limits, etc. $\bullet \bullet \bullet$				
$+0.16$ or $+0.16$	<sup>1</sup> MARTIN	77	DPWA $\bar{K}N$ multichannel	
$(\Gamma_1\Gamma_f)^{1/2}/\Gamma_{\text{total}}$ in $N\bar{K} \rightarrow \Sigma(1910) \rightarrow \Sigma(1385)\pi$				$(\Gamma_1\Gamma_4)^{1/2}/\Gamma$
VALUE	DOCUMENT ID	TECN	COMMENT	
$+0.066 \pm 0.025$	<sup>2</sup> CAMERON	78	DPWA $K^-p \rightarrow \Sigma(1385)\pi$	
$(\Gamma_1\Gamma_f)^{1/2}/\Gamma_{\text{total}}$ in $N\bar{K} \rightarrow \Sigma(1910) \rightarrow \Lambda(1520)\pi, P\text{-wave}$				$(\Gamma_1\Gamma_8)^{1/2}/\Gamma$
VALUE	DOCUMENT ID	TECN	COMMENT	
$< 0.03$	CAMERON	77	DPWA $K^-p \rightarrow \Lambda(1520)\pi^0$	
$-0.11 \pm 0.04$	LITCHFIELD	74B	DPWA $K^-p \rightarrow \Lambda(1520)\pi^0$	
$(\Gamma_1\Gamma_f)^{1/2}/\Gamma_{\text{total}}$ in $N\bar{K} \rightarrow \Sigma(1910) \rightarrow \Lambda(1520)\pi, F\text{-wave}$				$(\Gamma_1\Gamma_9)^{1/2}/\Gamma$
VALUE	DOCUMENT ID	TECN	COMMENT	
$0.062 \pm 0.021$	CAMERON	77	DPWA $K^-p \rightarrow \Lambda(1520)\pi^0$	
$-0.08 \pm 0.04$	LITCHFIELD	74B	DPWA $K^-p \rightarrow \Lambda(1520)\pi^0$	
$(\Gamma_1\Gamma_f)^{1/2}/\Gamma_{\text{total}}$ in $N\bar{K} \rightarrow \Sigma(1910) \rightarrow \Delta(1232)\bar{K}, S\text{-wave}$				$(\Gamma_1\Gamma_{11})^{1/2}/\Gamma$
VALUE	DOCUMENT ID	TECN	COMMENT	
$-0.16 \pm 0.05$	LITCHFIELD	74C	DPWA $K^-p \rightarrow \Delta(1232)\bar{K}$	
$(\Gamma_1\Gamma_f)^{1/2}/\Gamma_{\text{total}}$ in $N\bar{K} \rightarrow \Sigma(1910) \rightarrow \Delta(1232)\bar{K}, D\text{-wave}$				$(\Gamma_1\Gamma_{12})^{1/2}/\Gamma$
VALUE	DOCUMENT ID	TECN	COMMENT	
$-0.14 \pm 0.05$	LITCHFIELD	74C	DPWA $K^-p \rightarrow \Delta(1232)\bar{K}$	
$(\Gamma_1\Gamma_f)^{1/2}/\Gamma_{\text{total}}$ in $N\bar{K} \rightarrow \Sigma(1910) \rightarrow N\bar{K}^*(892)$				$(\Gamma_1\Gamma_{13})^{1/2}/\Gamma$
VALUE	DOCUMENT ID	TECN	COMMENT	
$-0.09 \pm 0.02$	<sup>3</sup> CAMERON	78B	DPWA $K^-p \rightarrow N\bar{K}^*$	

$\Sigma(1910)$  FOOTNOTES

- The two MARTIN 77 values are from a T-matrix pole and from a Breit-Wigner fit.
- The published sign has been changed to be in accord with the baryon-first convention.
- Upper limits on the  $D_1$  and  $D_3$  waves are each 0.03.

$\Sigma(1910)$  REFERENCES

SARANTSEV 19	EPJ A55 180	A.V. Sarantsev et al.	(BONN, PNPI)
PDG 82	PL 111B 1	M. Roos et al.	(HEL5, CIT, CERN)
GOPAL 80	Toronto Conf. 159	G.P. Gopal	(RHEL)
CAMERON 78	NP B143 189	W. Cameron et al.	(RHEL, LOIC) IJP
CAMERON 78B	NP B146 327	W. Cameron et al.	(RHEL, LOIC) IJP
CAMERON 77	NP B131 399	W. Cameron et al.	(RHEL, LOIC) IJP
GOPAL 77	NP B119 362	G.P. Gopal et al.	(LOIC, RHEL) IJP
GOYAL 77	PR D16 2746	D.P. Goyal, A.V. Sodhi	(DELH)
MARTIN 77	NP B127 349	B.R. Martin, M.K. Pidcock, R.G. Moorhouse	(LOUC+) IJP
Also	NP B126 266	B.R. Martin, M.K. Pidcock	(LOUC)
Also	NP B126 285	B.R. Martin, M.K. Pidcock	(LOUC) IJP
DEBELLEFON 76	NP B109 129	A. de Bellefon, A. Berthon	(CDEF) IJP
BAILLON 75	NP B9 39	P.H. Baillon, P.J. Litchfield	(CERN, RHEL) IJP
HEMINGWAY 75	NP B9 12	R.J. Hemingway et al.	(CERN, HEIDH, MPIM) IJP
VANHORN 75	NP B87 145	A.J. van Horn	(LBL) IJP
Also	NP B87 157	A.J. van Horn	(LBL) IJP
DEVENISH 74B	NP B81 330	B.C.E. Devenish, C.D. Froggatt, B.R. Martin	(DESY+) IJP
KANE 74	LBL-2452	D.F. Kane	(LBL) IJP
LITCHFIELD 74B	NP B74 19	P.J. Litchfield et al.	(CERN, HEIDH) IJP
LITCHFIELD 74C	NP B74 39	P.J. Litchfield et al.	(CERN, HEIDH) IJP

$\Sigma(1915) 5/2^+$

$I(J^P) = 1(\frac{5}{2}^+)$  Status: \* \* \* \*

Discovered by COOL 66. For results published before 1974 (they are now obsolete), see our 1982 edition Physics Letters **111B** 1 (1982).

This entry only includes results from partial-wave analyses. Parameters of peaks seen in cross sections and invariant-mass distributions in this region used to be listed in a separate entry immediately following. They may be found in our 1986 edition Physics Letters **170B** 1 (1986).

$\Sigma(1915)$  POLE POSITION

REAL PART

VALUE (MeV)	DOCUMENT ID	TECN	COMMENT
<b>1885 to 1915 (<math>\approx 1900</math>) OUR ESTIMATE</b>			
$1908 \pm 7$	SARANTSEV	19	DPWA $\bar{K}N$ multichannel
$1890 \pm \frac{3}{2}$	<sup>1</sup> KAMANO	15	DPWA $\bar{K}N$ multichannel
$\bullet \bullet \bullet$ We do not use the following data for averages, fits, limits, etc. $\bullet \bullet \bullet$			
1897	ZHANG	13A	DPWA $\bar{K}N$ multichannel
<sup>1</sup> From the preferred solution A in KAMANO 15.			

$-2 \times$ IMAGINARY PART

VALUE (MeV)	DOCUMENT ID	TECN	COMMENT
<b>90 to 110 (<math>\approx 100</math>) OUR ESTIMATE</b>			
$98 \pm 12$	SARANTSEV	19	DPWA $\bar{K}N$ multichannel
$97 \pm \frac{4}{6}$	<sup>1</sup> KAMANO	15	DPWA $\bar{K}N$ multichannel
$\bullet \bullet \bullet$ We do not use the following data for averages, fits, limits, etc. $\bullet \bullet \bullet$			
133	ZHANG	13A	DPWA $\bar{K}N$ multichannel
<sup>1</sup> From the preferred solution A in KAMANO 15.			

$\Sigma(1915)$  POLE RESIDUES

The normalized residue is the residue divided by  $\Gamma_{\text{pole}}/2$ .

Normalized residue in  $N\bar{K} \rightarrow \Sigma(1915) \rightarrow N\bar{K}$

MODULUS	PHASE ( $^\circ$ )	DOCUMENT ID	TECN	COMMENT
$0.08 \pm 0.02$	$-33 \pm 15$	SARANTSEV	19	DPWA $\bar{K}N$ multichannel
$\bullet \bullet \bullet$ We do not use the following data for averages, fits, limits, etc. $\bullet \bullet \bullet$				
0.0391	-15	<sup>1</sup> KAMANO	15	DPWA $\bar{K}N$ multichannel
<sup>1</sup> From the preferred solution A in KAMANO 15.				

Normalized residue in  $N\bar{K} \rightarrow \Sigma(1915) \rightarrow \Sigma\pi$

MODULUS	PHASE ( $^\circ$ )	DOCUMENT ID	TECN	COMMENT
$0.09 \pm 0.02$	$180 \pm 12$	SARANTSEV	19	DPWA $\bar{K}N$ multichannel
$\bullet \bullet \bullet$ We do not use the following data for averages, fits, limits, etc. $\bullet \bullet \bullet$				
0.157	157	<sup>1</sup> KAMANO	15	DPWA $\bar{K}N$ multichannel
<sup>1</sup> From the preferred solution A in KAMANO 15.				

Normalized residue in  $N\bar{K} \rightarrow \Sigma(1915) \rightarrow \Lambda\pi$

MODULUS	PHASE ( $^\circ$ )	DOCUMENT ID	TECN	COMMENT
$0.07 \pm 0.02$	$-170 \pm 20$	SARANTSEV	19	DPWA $\bar{K}N$ multichannel
$\bullet \bullet \bullet$ We do not use the following data for averages, fits, limits, etc. $\bullet \bullet \bullet$				
0.0757	166	<sup>1</sup> KAMANO	15	DPWA $\bar{K}N$ multichannel
<sup>1</sup> From the preferred solution A in KAMANO 15.				

Normalized residue in  $N\bar{K} \rightarrow \Sigma(1915) \rightarrow \Xi K$

MODULUS	PHASE ( $^\circ$ )	DOCUMENT ID	TECN	COMMENT
$0.02 \pm 0.01$	$-65 \pm 35$	SARANTSEV	19	DPWA $\bar{K}N$ multichannel
$\bullet \bullet \bullet$ We do not use the following data for averages, fits, limits, etc. $\bullet \bullet \bullet$				
0.002	-88	<sup>1</sup> KAMANO	15	DPWA $\bar{K}N$ multichannel
<sup>1</sup> From the preferred solution A in KAMANO 15.				

Normalized residue in  $N\bar{K} \rightarrow \Lambda(1915) \rightarrow \Sigma(1385)\pi, P\text{-wave}$

MODULUS	PHASE ( $^\circ$ )	DOCUMENT ID	TECN	COMMENT
$0.02 \pm 0.02$		SARANTSEV	19	DPWA $\bar{K}N$ multichannel
$\bullet \bullet \bullet$ We do not use the following data for averages, fits, limits, etc. $\bullet \bullet \bullet$				
0.0724	161	<sup>1</sup> KAMANO	15	DPWA $\bar{K}N$ multichannel
<sup>1</sup> From the preferred solution A in KAMANO 15.				

Normalized residue in  $N\bar{K} \rightarrow \Lambda(1915) \rightarrow \Sigma(1385)\pi, F\text{-wave}$

MODULUS	PHASE ( $^\circ$ )	DOCUMENT ID	TECN	COMMENT
$0.05 \pm 0.03$	$-30 \pm 50$	SARANTSEV	19	DPWA $\bar{K}N$ multichannel
$\bullet \bullet \bullet$ We do not use the following data for averages, fits, limits, etc. $\bullet \bullet \bullet$				
0.0162	-163	<sup>1</sup> KAMANO	15	DPWA $\bar{K}N$ multichannel
<sup>1</sup> From the preferred solution A in KAMANO 15.				

Normalized residue in  $N\bar{K} \rightarrow \Sigma(1915) \rightarrow \Lambda(1520)\pi, D\text{-wave}$

MODULUS	PHASE ( $^\circ$ )	DOCUMENT ID	TECN	COMMENT
$0.08 \pm 0.02$	$-105 \pm 50$	SARANTSEV	19	DPWA $\bar{K}N$ multichannel

## Baryon Particle Listings

 $\Sigma(1915)$ Normalized residue in  $N\bar{K} \rightarrow \Sigma(1915) \rightarrow \Delta\bar{K}$ , *P*-wave

MODULUS	PHASE (°)	DOCUMENT ID	TECN	COMMENT
$0.12 \pm 0.03$	$-10 \pm 20$	SARANTSEV 19	DPWA	$\bar{K}N$ multichannel

Normalized residue in  $N\bar{K} \rightarrow \Sigma(1915) \rightarrow \Delta\bar{K}$ , *F*-wave

MODULUS	PHASE (°)	DOCUMENT ID	TECN	COMMENT
$0.07 \pm 0.02$	$-35 \pm 25$	SARANTSEV 19	DPWA	$\bar{K}N$ multichannel

Normalized residue in  $N\bar{K} \rightarrow \Sigma(1915) \rightarrow \Lambda(1520)\pi$ , *G*-wave

MODULUS	PHASE (°)	DOCUMENT ID	TECN	COMMENT
$0.01 \pm 0.01$		SARANTSEV 19	DPWA	$\bar{K}N$ multichannel

Normalized residue in  $N\bar{K} \rightarrow \Sigma(1915) \rightarrow N\bar{K}^*(892)$ , *S*=1/2, *F*-wave

MODULUS	PHASE (°)	DOCUMENT ID	TECN	COMMENT
$0.07 \pm 0.04$	$-60 \pm 45$	SARANTSEV 19	DPWA	$\bar{K}N$ multichannel

• • • We do not use the following data for averages, fits, limits, etc. • • •

0.00476	4	<sup>1</sup> KAMANO 15	DPWA	$\bar{K}N$ multichannel
---------	---	------------------------	------	-------------------------

<sup>1</sup> From the preferred solution A in KAMANO 15.

Normalized residue in  $N\bar{K} \rightarrow \Sigma(1915) \rightarrow N\bar{K}^*(892)$ , *S*=3/2, *P*-wave

MODULUS	PHASE (°)	DOCUMENT ID	TECN	COMMENT
$0.0494$	51	<sup>1</sup> KAMANO 15	DPWA	$\bar{K}N$ multichannel

• • • We do not use the following data for averages, fits, limits, etc. • • •

<sup>1</sup> From the preferred solution A in KAMANO 15.

Normalized residue in  $N\bar{K} \rightarrow \Sigma(1915) \rightarrow N\bar{K}^*(892)$ , *S*=3/2, *F*-wave

MODULUS	PHASE (°)	DOCUMENT ID	TECN	COMMENT
$0.07 \pm 0.03$	$-40 \pm 45$	SARANTSEV 19	DPWA	$\bar{K}N$ multichannel

• • • We do not use the following data for averages, fits, limits, etc. • • •

0.000314	16	<sup>1</sup> KAMANO 15	DPWA	$\bar{K}N$ multichannel
----------	----	------------------------	------	-------------------------

<sup>1</sup> From the preferred solution A in KAMANO 15.

 $\Sigma(1915)$  MASS

VALUE (MeV)	DOCUMENT ID	TECN	COMMENT
<b>1900 to 1935 (≈ 1915) OUR ESTIMATE</b>			
1918 ± 6	SARANTSEV 19	DPWA	$\bar{K}N$ multichannel
1920 ± 7	ZHANG 13A	DPWA	$\bar{K}N$ multichannel
1937 ± 20	ALSTON... 78	DPWA	$\bar{K}N \rightarrow \bar{K}N$
1894 ± 5	<sup>1</sup> CORDEN 77c		$K^- n \rightarrow \Sigma\pi$
1909 ± 5	<sup>1</sup> CORDEN 77c		$K^- n \rightarrow \Sigma\pi$
1920 ± 10	GOPAL 77	DPWA	$\bar{K}N$ multichannel
1920 ± 30	BAILLON 75	IPWA	$\bar{K}N \rightarrow \Lambda\pi$
1914 ± 10	HEMINGWAY 75	DPWA	$K^- p \rightarrow \bar{K}N$
1920 $^{+15}_{-20}$	VANHORN 75	DPWA	$K^- p \rightarrow \Lambda\pi^0$
1920 ± 5	KANE 74	DPWA	$K^- p \rightarrow \Sigma\pi$
• • • We do not use the following data for averages, fits, limits, etc. • • •			
not seen	DECLAIS 77	DPWA	$\bar{K}N \rightarrow \bar{K}N$
1925 or 1933	<sup>2</sup> MARTIN 77	DPWA	$\bar{K}N$ multichannel
1900 ± 4	<sup>3</sup> CORDEN 76	DPWA	$K^- n \rightarrow \Lambda\pi^-$
1915	DEBELLEFON 76	IPWA	$K^- p \rightarrow \Lambda\pi^0$

<sup>1</sup> The two entries for CORDEN 77c are from two different acceptable solutions.

<sup>2</sup> The two MARTIN 77 values are from a T-matrix pole and from a Breit-Wigner fit.

<sup>3</sup> Preferred solution 3; see CORDEN 76 for other possibilities.

 $\Sigma(1915)$  WIDTH

VALUE (MeV)	DOCUMENT ID	TECN	COMMENT
<b>80 to 160 (≈ 120) OUR ESTIMATE</b>			
102 ± 12	SARANTSEV 19	DPWA	$\bar{K}N$ multichannel
149 ± 17	ZHANG 13A	DPWA	Multichannel
161 ± 20	ALSTON... 78	DPWA	$\bar{K}N \rightarrow \bar{K}N$
107 ± 14	<sup>1</sup> CORDEN 77c		$K^- n \rightarrow \Sigma\pi$
85 ± 13	<sup>1</sup> CORDEN 77c		$K^- n \rightarrow \Sigma\pi$
130 ± 10	GOPAL 77	DPWA	$\bar{K}N$ multichannel
70 ± 20	BAILLON 75	IPWA	$\bar{K}N \rightarrow \Lambda\pi$
85 ± 15	HEMINGWAY 75	DPWA	$K^- p \rightarrow \bar{K}N$
102 ± 18	VANHORN 75	DPWA	$K^- p \rightarrow \Lambda\pi^0$
162 ± 25	KANE 74	DPWA	$K^- p \rightarrow \Sigma\pi$
• • • We do not use the following data for averages, fits, limits, etc. • • •			
171 or 173	<sup>2</sup> MARTIN 77	DPWA	$\bar{K}N$ multichannel
75 ± 14	<sup>3</sup> CORDEN 76	DPWA	$K^- n \rightarrow \Lambda\pi^-$
60	DEBELLEFON 76	IPWA	$K^- p \rightarrow \Lambda\pi^0$

<sup>1</sup> The two entries for CORDEN 77c are from two different acceptable solutions.

<sup>2</sup> The two MARTIN 77 values are from a T-matrix pole and from a Breit-Wigner fit.

<sup>3</sup> Preferred solution 3; see CORDEN 76 for other possibilities.

 $\Sigma(1915)$  DECAY MODES

Mode	Fraction ( $\Gamma_i/\Gamma$ )
$\Gamma_1$ $N\bar{K}$	0.05 to 0.15
$\Gamma_2$ $\Lambda\pi$	( 6.0 ± 2.0 ) %
$\Gamma_3$ $\Sigma\pi$	( 10.0 ± 2.0 ) %
$\Gamma_4$ $\Xi K$	
$\Gamma_5$ $\Sigma(1385)\pi$ , <i>P</i> -wave	( 2.0 ± 2.0 ) %
$\Gamma_6$ $\Sigma(1385)\pi$ , <i>F</i> -wave	( 4.0 ± 2.0 ) %
$\Gamma_7$ $\Sigma(1385)\pi$	< 5 %
$\Gamma_8$ $\Sigma(1385)\pi$ , <i>P</i> -wave	
$\Gamma_9$ $\Sigma(1385)\pi$ , <i>F</i> -wave	
$\Gamma_{10}$ $\Lambda(1520)\pi$ , <i>D</i> -wave	( 8.0 ± 2.0 ) %
$\Gamma_{11}$ $\Lambda(1520)\pi$ , <i>G</i> -wave	
$\Gamma_{12}$ $N\bar{K}^*(892)$ , <i>S</i> =1/2, <i>F</i> -wave	( 5.0 ± 3.0 ) %
$\Gamma_{13}$ $N\bar{K}^*(892)$ , <i>S</i> =3/2, <i>P</i> -wave	
$\Gamma_{14}$ $N\bar{K}^*(892)$ , <i>S</i> =3/2, <i>F</i> -wave	( 5.0 ± 2.0 ) %
$\Gamma_{15}$ $\Delta\bar{K}$ , <i>P</i> -wave	( 16 ± 5 ) %
$\Gamma_{16}$ $\Delta\bar{K}$ , <i>F</i> -wave	( 5.0 ± 3.0 ) %

 $\Sigma(1915)$  BRANCHING RATIOS

See "Sign conventions for resonance couplings" in the Note on  $\Lambda$  and  $\Sigma$  Resonances.

$\Gamma(N\bar{K})/\Gamma_{\text{total}}$	DOCUMENT ID	TECN	COMMENT	$\Gamma_1/\Gamma$
<b>0.05 to 0.15 OUR ESTIMATE</b>				
0.08 ± 0.02	SARANTSEV 19	DPWA	$\bar{K}N$ multichannel	
0.026 ± 0.004	ZHANG 13A	DPWA	$\bar{K}N$ multichannel	
0.03 ± 0.02	<sup>1</sup> GOPAL 80	DPWA	$\bar{K}N \rightarrow \bar{K}N$	
0.14 ± 0.05	ALSTON...	78	DPWA	$\bar{K}N \rightarrow \bar{K}N$
0.11 ± 0.04	HEMINGWAY 75	DPWA	$K^- p \rightarrow \bar{K}N$	
• • • We do not use the following data for averages, fits, limits, etc. • • •				
0.036	<sup>2</sup> KAMANO 15	DPWA	$\bar{K}N$ multichannel	
0.05 ± 0.03	GOPAL 77	DPWA	See GOPAL 80	
0.08 or 0.08	<sup>3</sup> MARTIN 77	DPWA	$\bar{K}N$ multichannel	
<sup>1</sup> The mass and width are fixed to the GOPAL 77 values due to the low elasticity.				
<sup>2</sup> From the preferred solution A in KAMANO 15.				
<sup>3</sup> The two MARTIN 77 values are from a T-matrix pole and from a Breit-Wigner fit.				

$\Gamma(\Lambda\pi)/\Gamma_{\text{total}}$	DOCUMENT ID	TECN	COMMENT	$\Gamma_2/\Gamma$
<b>0.06 ± 0.02</b>				
0.06 ± 0.02	SARANTSEV 19	DPWA	$\bar{K}N$ multichannel	
• • • We do not use the following data for averages, fits, limits, etc. • • •				
0.127	<sup>1</sup> KAMANO 15	DPWA	$\bar{K}N$ multichannel	
<sup>1</sup> From the preferred solution A in KAMANO 15.				

$\Gamma(\Sigma\pi)/\Gamma_{\text{total}}$	DOCUMENT ID	TECN	COMMENT	$\Gamma_3/\Gamma$
<b>0.10 ± 0.02</b>				
0.10 ± 0.02	SARANTSEV 19	DPWA	$\bar{K}N$ multichannel	
• • • We do not use the following data for averages, fits, limits, etc. • • •				
0.678	<sup>1</sup> KAMANO 15	DPWA	$\bar{K}N$ multichannel	
<sup>1</sup> From the preferred solution A in KAMANO 15.				

$\Gamma(\Xi K)/\Gamma_{\text{total}}$	DOCUMENT ID	TECN	COMMENT	$\Gamma_4/\Gamma$
<b>&lt; 0.01</b>				
< 0.01	SARANTSEV 19	DPWA	$\bar{K}N$ multichannel	
• • • We do not use the following data for averages, fits, limits, etc. • • •				
not seen	<sup>1</sup> KAMANO 15	DPWA	Multichannel	
<sup>1</sup> From the preferred solution A in KAMANO 15.				

$\Gamma(\Sigma(1385)\pi, P\text{-wave})/\Gamma_{\text{total}}$	DOCUMENT ID	TECN	COMMENT	$\Gamma_5/\Gamma$
<b>0.02 ± 0.02</b>				
0.02 ± 0.02	SARANTSEV 19	DPWA	$\bar{K}N$ multichannel	
• • • We do not use the following data for averages, fits, limits, etc. • • •				
0.112	<sup>1</sup> KAMANO 15	DPWA	$\bar{K}N$ multichannel	
<sup>1</sup> From the preferred solution A in KAMANO 15.				

$\Gamma(\Sigma(1385)\pi, F\text{-wave})/\Gamma_{\text{total}}$	DOCUMENT ID	TECN	COMMENT	$\Gamma_6/\Gamma$
<b>0.04 ± 0.02</b>				
0.04 ± 0.02	SARANTSEV 19	DPWA	$\bar{K}N$ multichannel	
• • • We do not use the following data for averages, fits, limits, etc. • • •				
0.004	<sup>1</sup> KAMANO 15	DPWA	$\bar{K}N$ multichannel	
<sup>1</sup> From the preferred solution A in KAMANO 15.				

$\Gamma(\Lambda(1520)\pi, D\text{-wave})/\Gamma_{\text{total}}$	DOCUMENT ID	TECN	COMMENT	$\Gamma_{10}/\Gamma$
<b>0.08 ± 0.02</b>				
0.08 ± 0.02	SARANTSEV 19	DPWA	$\bar{K}N$ multichannel	

See key on page 999

# Baryon Particle Listings

## $\Sigma(1915), \Sigma(1940), \Sigma(2010)$

$\Gamma(\Lambda(1520)\pi, G\text{-wave})/\Gamma_{\text{total}}$				$\Gamma_{11}/\Gamma$
VALUE	DOCUMENT ID	TECN	COMMENT	
def 0	SARANTSEV 19	DPWA	$\bar{K}N$ multichannel	

$\Gamma(N\bar{K}^*(892), S=1/2, F\text{-wave})/\Gamma_{\text{total}}$				$\Gamma_{12}/\Gamma$
VALUE	DOCUMENT ID	TECN	COMMENT	
<b>0.05 ± 0.03</b>	SARANTSEV 19	DPWA	$\bar{K}N$ multichannel	

• • • We do not use the following data for averages, fits, limits, etc. • • •  
 0.001 <sup>1</sup> KAMANO 15 DPWA Multichannel  
<sup>1</sup> From the preferred solution A in KAMANO 15.

$\Gamma(N\bar{K}^*(892), S=3/2, P\text{-wave})/\Gamma_{\text{total}}$				$\Gamma_{13}/\Gamma$
VALUE	DOCUMENT ID	TECN	COMMENT	
0.042	<sup>1</sup> KAMANO 15	DPWA	Multichannel	

• • • We do not use the following data for averages, fits, limits, etc. • • •  
<sup>1</sup> From the preferred solution A in KAMANO 15.

$\Gamma(N\bar{K}^*(892), S=3/2, F\text{-wave})/\Gamma_{\text{total}}$				$\Gamma_{14}/\Gamma$
VALUE	DOCUMENT ID	TECN	COMMENT	
<b>0.05 ± 0.02</b>	SARANTSEV 19	DPWA	$\bar{K}N$ multichannel	

• • • We do not use the following data for averages, fits, limits, etc. • • •  
 not seen <sup>1</sup> KAMANO 15 DPWA Multichannel  
<sup>1</sup> From the preferred solution A in KAMANO 15.

$\Gamma(\Delta\bar{K}, P\text{-wave})/\Gamma_{\text{total}}$				$\Gamma_{15}/\Gamma$
VALUE	DOCUMENT ID	TECN	COMMENT	
<b>0.16 ± 0.05</b>	SARANTSEV 19	DPWA	$\bar{K}N$ multichannel	

$\Gamma(\Delta\bar{K}, F\text{-wave})/\Gamma_{\text{total}}$				$\Gamma_{16}/\Gamma$
VALUE	DOCUMENT ID	TECN	COMMENT	
<b>0.05 ± 0.03</b>	SARANTSEV 19	DPWA	$\bar{K}N$ multichannel	

$(\Gamma_1\Gamma_f)^{1/2}/\Gamma_{\text{total}}$ in $N\bar{K} \rightarrow \Sigma(1915) \rightarrow \Lambda\pi$				$(\Gamma_1\Gamma_2)^{1/2}/\Gamma$
VALUE	DOCUMENT ID	TECN	COMMENT	
-0.09 ± 0.03	GOPAL 77	DPWA	$\bar{K}N$ multichannel	

-0.10 ± 0.01 <sup>1</sup> CORDEN 76 DPWA  $K^-n \rightarrow \Lambda\pi^-$   
 -0.06 ± 0.02 BAILLON 75 IPWA  $\bar{K}N \rightarrow \Lambda\pi$   
 -0.09 ± 0.02 VANHORN 75 DPWA  $K^-p \rightarrow \Lambda\pi^0$   
 -0.087 ± 0.056 DEVENISH 74B Fixed-t dispersion rel.

• • • We do not use the following data for averages, fits, limits, etc. • • •  
 -0.09 or -0.09 <sup>2</sup> MARTIN 77 DPWA  $\bar{K}N$  multichannel  
 -0.10 DEBELLEFON 76 IPWA  $K^-p \rightarrow \Lambda\pi^0$

<sup>1</sup> Preferred solution 3; see CORDEN 76 for other possibilities.  
<sup>2</sup> The two MARTIN 77 values are from a T-matrix pole and from a Breit-Wigner fit.

$(\Gamma_1\Gamma_f)^{1/2}/\Gamma_{\text{total}}$ in $N\bar{K} \rightarrow \Sigma(1915) \rightarrow \Sigma\pi$				$(\Gamma_1\Gamma_3)^{1/2}/\Gamma$
VALUE	DOCUMENT ID	TECN	COMMENT	
-0.14 ± 0.01	ZHANG 13A	DPWA	Multichannel	

-0.17 ± 0.01 <sup>1</sup> CORDEN 77c  $K^-n \rightarrow \Sigma\pi$   
 -0.15 ± 0.02 <sup>1</sup> CORDEN 77c  $K^-n \rightarrow \Sigma\pi$   
 -0.19 ± 0.03 GOPAL 77 DPWA  $\bar{K}N$  multichannel  
 -0.16 ± 0.03 KANE 74 DPWA  $K^-p \rightarrow \Sigma\pi$

• • • We do not use the following data for averages, fits, limits, etc. • • •  
 -0.05 or -0.05 <sup>2</sup> MARTIN 77 DPWA  $\bar{K}N$  multichannel

<sup>1</sup> The two entries for CORDEN 77c are from two different acceptable solutions.  
<sup>2</sup> The two MARTIN 77 values are from a T-matrix pole and from a Breit-Wigner fit.

$(\Gamma_1\Gamma_f)^{1/2}/\Gamma_{\text{total}}$ in $N\bar{K} \rightarrow \Sigma(1915) \rightarrow \Sigma(1385)\pi, P\text{-wave}$				$(\Gamma_1\Gamma_8)^{1/2}/\Gamma$
VALUE	DOCUMENT ID	TECN	COMMENT	
<0.01	CAMERON 78	DPWA	$K^-p \rightarrow \Sigma(1385)\pi$	

$(\Gamma_1\Gamma_f)^{1/2}/\Gamma_{\text{total}}$ in $N\bar{K} \rightarrow \Sigma(1915) \rightarrow \Sigma(1385)\pi, F\text{-wave}$				$(\Gamma_1\Gamma_9)^{1/2}/\Gamma$
VALUE	DOCUMENT ID	TECN	COMMENT	
+0.06 ± 0.02	ZHANG 13A	DPWA	Multichannel	

+0.039 ± 0.009 <sup>1</sup> CAMERON 78 DPWA  $K^-p \rightarrow \Sigma(1385)\pi$   
<sup>1</sup> The published sign has been changed to be in accord with the baryon-first convention.

### $\Sigma(1915)$ REFERENCES

SARANTSEV 19	EPJ A55 180	A.V. Sarantsev et al.	(BONN, PNPI)
KAMANO 15	PR C92 025205	H. Kamano et al.	(ANL, OSAK)
ZHANG 13A	PR C88 035205	H. Zhang et al.	(KSU)
PDG 86	PL 170B 1	M. Aguilar-Benitez et al.	(CERN, CIT+)
PDG 82	PL 111B 1	M. Roos et al.	(HEL5, CIT, CERN)
GOPAL 80	Toronto Conf. 159	G.P. Gopal et al.	(RHEL) IJP
ALSTON... 78	PR D18 182	M. Alston-Garnjost et al.	(LBL, MTHO+) IJP
Also	PRL 38 1007	M. Alston-Garnjost et al.	(LBL, MTHO+) IJP
CAMERON 78	NP B143 189	W. Cameron et al.	(RHEL, LOIC) IJP
CORDEN 77C	NP B125 61	M.J. Corden et al.	(BIRM) IJP
DECLAIS 77	CERN 77-16	Y. Declais et al.	(CAEN, CERN) IJP
GOPAL 77	NP B119 362	G.P. Gopal et al.	(LOIC, RHEL) IJP
MARTIN 77	NP B127 349	B.R. Martin, M.K. Pidcock, R.G. Moorhouse	(LOUC+) IJP
Also	NP B126 266	B.R. Martin, M.K. Pidcock	(LOUC) IJP
Also	NP B126 285	B.R. Martin, M.K. Pidcock	(LOUC) IJP

CORDEN 76	NP B104 382	M.J. Corden et al.	(BIRM) IJP
DEBELLEFON 76	NP B109 129	A. de Bellefon, A. Berthon	(CDEF) IJP
BAILLON 75	NP B94 39	P.H. Baillon, P.J. Litchfield	(CERN, RHEL) IJP
HEMINGWAY 75	NP B91 12	R.J. Hemingway et al.	(CERN, HEIDH, MPM) IJP
VANHORN 75	NP B87 145	A.J. van Horn	(LBL) IJP
Also	NP B87 157	A.J. van Horn	(LBL) IJP
DEVENISH 74B	NP B81 330	R.C.E. Devenish, C.D. Froggatt, B.R. Martin	(DESY+) IJP
KANE 74	LBL-2452	D.F. Kane	(LBL) IJP
COOL 66	PRL 16 1228	R.L. Cool et al.	(BNL)

## $\Sigma(1940) 3/2^+$

$I(J^P) = 1(\frac{3}{2}^+)$  Status: \*

OMITTED FROM SUMMARY TABLE

### $\Sigma(1940)$ MASS

VALUE (MeV)	DOCUMENT ID	TECN	COMMENT
<b>1920 to 1960 (<math>\approx 1940</math>) OUR ESTIMATE</b>			
1941 ± 18	ZHANG 13A	DPWA	$\bar{K}N$ multichannel
1925 ± 200	VANHORN 75	DPWA	$K^-p \rightarrow \Lambda\pi^0$

### $\Sigma(1940)$ WIDTH

VALUE (MeV)	DOCUMENT ID	TECN	COMMENT
<b>100 to 400 (<math>\approx 250</math>) OUR ESTIMATE</b>			
400 ± 49	ZHANG 13A	DPWA	$\bar{K}N$ multichannel
65 <sup>+5</sup> <sub>-20</sub>	VANHORN 75	DPWA	$K^-p \rightarrow \Lambda\pi^0$

### $\Sigma(1940)$ DECAY MODES

Mode	Fraction ( $\Gamma_i/\Gamma$ )
$\Gamma_1$ $N\bar{K}$	(13.0 ± 2.0) %
$\Gamma_2$ $\Sigma\pi$	( 4.0 ± 2.0) %
$\Gamma_3$ $\Sigma(1385)\pi, P\text{-wave}$	(22 ± 7) %
$\Gamma_4$ $\Lambda(1520)\pi, S\text{-wave}$	( 5.0 ± 2.0) %

### $\Sigma(1940)$ BRANCHING RATIOS

$\Gamma(N\bar{K})/\Gamma_{\text{total}}$	$\Gamma_1/\Gamma$		
VALUE	DOCUMENT ID	TECN	COMMENT
<b>0.13 ± 0.02</b>	ZHANG 13A	DPWA	$\bar{K}N$ multichannel

$\Gamma(\Sigma\pi)/\Gamma_{\text{total}}$	$\Gamma_2/\Gamma$		
VALUE	DOCUMENT ID	TECN	COMMENT
<b>0.04 ± 0.02</b>	ZHANG 13A	DPWA	$\bar{K}N$ multichannel

$\Gamma(\Sigma(1385)\pi, P\text{-wave})/\Gamma_{\text{total}}$	$\Gamma_3/\Gamma$		
VALUE	DOCUMENT ID	TECN	COMMENT
<b>0.22 ± 0.07</b>	ZHANG 13A	DPWA	$\bar{K}N$ multichannel

$\Gamma(\Lambda(1520)\pi, S\text{-wave})/\Gamma_{\text{total}}$	$\Gamma_4/\Gamma$		
VALUE	DOCUMENT ID	TECN	COMMENT
<b>0.05 ± 0.02</b>	ZHANG 13A	DPWA	$\bar{K}N$ multichannel

### $\Sigma(1940)$ REFERENCES

ZHANG 13A	PR C88 035205	H. Zhang et al.	(KSU)
VANHORN 75	NP B87 145	A.J. van Horn	(LBL)

## $\Sigma(2010) 3/2^-$

$I(J^P) = 1(\frac{3}{2}^-)$  Status: \*

OMITTED FROM SUMMARY TABLE

### $\Sigma(2010)$ POLE POSITION

<b>REAL PART</b>			
VALUE (MeV)	DOCUMENT ID	TECN	COMMENT
<b>1995 ± 12</b>	SARANTSEV 19	DPWA	$\bar{K}N$ multichannel

<b>-2×IMAGINARY PART</b>			
VALUE (MeV)	DOCUMENT ID	TECN	COMMENT
<b>175 ± 24</b>	SARANTSEV 19	DPWA	$\bar{K}N$ multichannel

### $\Sigma(2010)$ POLE RESIDUES

The normalized residue is the residue divided by  $\Gamma_{\text{pole}}/2$ .

<b>Normalized residue in <math>N\bar{K} \rightarrow \Sigma(2010) \rightarrow N\bar{K}</math></b>				
MODULUS	PHASE (°)	DOCUMENT ID	TECN	COMMENT
<b>0.07 ± 0.03</b>	<b>-115 ± 25</b>	SARANTSEV 19	DPWA	$\bar{K}N$ multichannel

# Baryon Particle Listings

## $\Sigma(2010)$ , $\Sigma(2030)$

Normalized residue in $N\bar{K} \rightarrow \Sigma(2010) \rightarrow \Sigma\pi$			
MODULUS	PHASE (°)	DOCUMENT ID	TECN COMMENT
0.04±0.02	130 ± 22	SARANTSEV 19	DPWA $\bar{K}N$ multichannel
Normalized residue in $N\bar{K} \rightarrow \Sigma(2010) \rightarrow \Lambda\pi$			
MODULUS	PHASE (°)	DOCUMENT ID	TECN COMMENT
0.06±0.03	170 ± 25	SARANTSEV 19	DPWA $\bar{K}N$ multichannel
Normalized residue in $N\bar{K} \rightarrow \Sigma(2010) \rightarrow \Xi K$			
MODULUS	PHASE (°)	DOCUMENT ID	TECN COMMENT
0.04±0.02	-120 ± 45	SARANTSEV 19	DPWA $\bar{K}N$ multichannel
Normalized residue in $N\bar{K} \rightarrow \Sigma(2010) \rightarrow \Lambda(1520)\pi, P\text{-wave}$			
MODULUS	PHASE (°)	DOCUMENT ID	TECN COMMENT
0.03±0.02	80 ± 35	SARANTSEV 19	DPWA $\bar{K}N$ multichannel
Normalized residue in $N\bar{K} \rightarrow \Sigma(2010) \rightarrow \Lambda(1520)\pi, F\text{-wave}$			
MODULUS	PHASE (°)	DOCUMENT ID	TECN COMMENT
0.08±0.05	150 ± 65	SARANTSEV 19	DPWA $\bar{K}N$ multichannel
Normalized residue in $N\bar{K} \rightarrow \Sigma(2010) \rightarrow \Sigma(1385)\pi, P\text{-wave}$			
VALUE	DOCUMENT ID	TECN	COMMENT
0.04+−0.02025+45	SARANTSEV 19	DPWA	$\bar{K}N$ multichannel
Normalized residue in $N\bar{K} \rightarrow \Sigma(2010) \rightarrow \Sigma(1385)\pi, F\text{-wave}$			
VALUE	DOCUMENT ID	TECN	COMMENT
0.02±0.02	SARANTSEV 19	DPWA	$\bar{K}N$ multichannel
Normalized residue in $N\bar{K} \rightarrow \Sigma(2010) \rightarrow \Delta\bar{K}, S\text{-wave}$			
MODULUS	PHASE (°)	DOCUMENT ID	TECN COMMENT
0.08±0.04	0 ± 30	SARANTSEV 19	DPWA $\bar{K}N$ multichannel
Normalized residue in $N\bar{K} \rightarrow \Sigma(2010) \rightarrow \Delta\bar{K}, D\text{-wave}$			
MODULUS	PHASE (°)	DOCUMENT ID	TECN COMMENT
0.02±0.02		SARANTSEV 19	DPWA $\bar{K}N$ multichannel
Normalized residue in $N\bar{K} \rightarrow \Sigma(2010) \rightarrow N\bar{K}^*(892), S\text{-wave}$			
VALUE	DOCUMENT ID	TECN	COMMENT
0.12+−0.030-60+−60	SARANTSEV 19	DPWA	$\bar{K}N$ multichannel
Normalized residue in $N\bar{K} \rightarrow \Sigma(2010) \rightarrow N\bar{K}^*(892), S=1/2, D\text{-wave}$			
MODULUS	PHASE (°)	DOCUMENT ID	TECN COMMENT
0.08±0.04	55 ± 60	SARANTSEV 19	DPWA $\bar{K}N$ multichannel
Normalized residue in $N\bar{K} \rightarrow \Sigma(2010) \rightarrow N\bar{K}^*(892), S=3/2, D\text{-wave}$			
MODULUS	PHASE (°)	DOCUMENT ID	TECN COMMENT
0.08±0.04	15 ± 60	SARANTSEV 19	DPWA $\bar{K}N$ multichannel

### $\Sigma(2010)$ MASS

VALUE (MeV)	DOCUMENT ID	TECN	COMMENT
2005±14	SARANTSEV 19	DPWA	$\bar{K}N$ multichannel

### $\Sigma(2010)$ WIDTH

VALUE (MeV)	DOCUMENT ID	TECN	COMMENT
178±23	SARANTSEV 19	DPWA	$\bar{K}N$ multichannel

### $\Sigma(2010)$ DECAY MODES

Mode	Fraction ( $\Gamma_i/\Gamma$ )
$\Gamma_1$ $N\bar{K}$	( 7.0±3.0 ) %
$\Gamma_2$ $\Lambda\pi$	( 5.0±2.0 ) %
$\Gamma_3$ $\Sigma\pi$	( 3.0±2.0 ) %
$\Gamma_4$ $\Xi K$	( 3.0±2.0 ) %
$\Gamma_5$ $\Sigma(1385)\pi, P\text{-wave}$	( 3.0±2.0 ) %
$\Gamma_6$ $\Sigma(1385)\pi, F\text{-wave}$	( 2.0±2.0 ) %
$\Gamma_7$ $\Lambda(1520)\pi, P\text{-wave}$	( 2.0±2.0 ) %
$\Gamma_8$ $\Lambda(1520)\pi, F\text{-wave}$	( 12 ± 6 ) %
$\Gamma_9$ $\Delta\bar{K}, S\text{-wave}$	( 11 ± 5 ) %
$\Gamma_{10}$ $\Delta\bar{K}, D\text{-wave}$	( 1.0±1.0 ) %
$\Gamma_{11}$ $N\bar{K}^*(892), S=1/2, S\text{-wave}$	( 27 ± 7 ) %
$\Gamma_{12}$ $N\bar{K}^*(892), S=1/2, D\text{-wave}$	( 13 ± 6 ) %
$\Gamma_{13}$ $N\bar{K}^*(892), S=3/2, D\text{-wave}$	( 13 ± 6 ) %

### $\Sigma(2010)$ BRANCHING RATIOS

See "Sign conventions for resonance couplings" in the Note on  $\Lambda$  and  $\Sigma$  Resonances.

$\Gamma(N\bar{K})/\Gamma_{\text{total}}$	DOCUMENT ID	TECN	COMMENT
0.07±0.03	SARANTSEV 19	DPWA	$\bar{K}N$ multichannel

$\Gamma(\Lambda\pi)/\Gamma_{\text{total}}$	DOCUMENT ID	TECN	COMMENT
0.05±0.02	SARANTSEV 19	DPWA	$\bar{K}N$ multichannel
$\Gamma(\Sigma\pi)/\Gamma_{\text{total}}$	DOCUMENT ID	TECN	COMMENT
0.03±0.02	SARANTSEV 19	DPWA	$\bar{K}N$ multichannel
$\Gamma(\Xi K)/\Gamma_{\text{total}}$	DOCUMENT ID	TECN	COMMENT
0.03±0.02	SARANTSEV 19	DPWA	$\bar{K}N$ multichannel
$\Gamma(\Sigma(1385)\pi, P\text{-wave})/\Gamma_{\text{total}}$	DOCUMENT ID	TECN	COMMENT
0.03±0.02	SARANTSEV 19	DPWA	$\bar{K}N$ multichannel
$\Gamma(\Sigma(1385)\pi, F\text{-wave})/\Gamma_{\text{total}}$	DOCUMENT ID	TECN	COMMENT
0.02±0.02	SARANTSEV 19	DPWA	$\bar{K}N$ multichannel
$\Gamma(\Lambda(1520)\pi, P\text{-wave})/\Gamma_{\text{total}}$	DOCUMENT ID	TECN	COMMENT
0.02±0.02	SARANTSEV 19	DPWA	$\bar{K}N$ multichannel
$\Gamma(\Lambda(1520)\pi, F\text{-wave})/\Gamma_{\text{total}}$	DOCUMENT ID	TECN	COMMENT
0.12±0.06	SARANTSEV 19	DPWA	$\bar{K}N$ multichannel
$\Gamma(\Delta\bar{K}, S\text{-wave})/\Gamma_{\text{total}}$	DOCUMENT ID	TECN	COMMENT
0.11±0.05	SARANTSEV 19	DPWA	$\bar{K}N$ multichannel
$\Gamma(\Delta\bar{K}, D\text{-wave})/\Gamma_{\text{total}}$	DOCUMENT ID	TECN	COMMENT
0.01±0.01	SARANTSEV 19	DPWA	$\bar{K}N$ multichannel
$\Gamma(N\bar{K}^*(892), S=1/2, S\text{-wave})/\Gamma_{\text{total}}$	DOCUMENT ID	TECN	COMMENT
0.27±0.07	SARANTSEV 19	DPWA	$\bar{K}N$ multichannel
$\Gamma(N\bar{K}^*(892), S=1/2, D\text{-wave})/\Gamma_{\text{total}}$	DOCUMENT ID	TECN	COMMENT
0.13±0.06	SARANTSEV 19	DPWA	$\bar{K}N$ multichannel
$\Gamma(N\bar{K}^*(892), S=3/2, D\text{-wave})/\Gamma_{\text{total}}$	DOCUMENT ID	TECN	COMMENT
0.13±0.06	SARANTSEV 19	DPWA	$\bar{K}N$ multichannel

### $\Sigma(2010)$ REFERENCES

SARANTSEV 19 EPJ A55 180 A.V. Sarantsev et al. (BONN, PNPI)

## $\Sigma(2030) 7/2^+$

$I(J^P) = 1(\frac{7}{2}^+)$  Status: \*\*\*

Discovered by COOL 66 and by WOHL 66. For most results published before 1974 (they are now obsolete), see our 1982 edition Physics Letters **111B** 1 (1982).

This entry only includes results from partial-wave analyses. Parameters of peaks seen in cross sections and invariant-mass distributions around 2030 MeV may be found in our 1984 edition, Reviews of Modern Physics **56** S1 (1984).

### $\Sigma(2030)$ POLE POSITION

#### REAL PART

VALUE (MeV)	DOCUMENT ID	TECN	COMMENT
<b>2010 to 2030 (≈ 2020) OUR ESTIMATE</b>			
2014 ± 6	SARANTSEV 19	DPWA	$\bar{K}N$ multichannel
2025 ± <sup>+10</sup> <sub>-5</sub>	<sup>1</sup> KAMANO 15	DPWA	$\bar{K}N$ multichannel

• • • We do not use the following data for averages, fits, limits, etc. • • •

1993	ZHANG 13A	DPWA	$\bar{K}N$ multichannel
------	-----------	------	-------------------------

<sup>1</sup> From the preferred solution A in KAMANO 15.

#### −2×IMAGINARY PART

VALUE (MeV)	DOCUMENT ID	TECN	COMMENT
<b>130 to 190 (≈ 160) OUR ESTIMATE</b>			
172±12	SARANTSEV 19	DPWA	$\bar{K}N$ multichannel
130+ <sub>-24</sub>	<sup>1</sup> KAMANO 15	DPWA	$\bar{K}N$ multichannel

• • • We do not use the following data for averages, fits, limits, etc. • • •

176	ZHANG 13A	DPWA	$\bar{K}N$ multichannel
-----	-----------	------	-------------------------

<sup>1</sup> From the preferred solution A in KAMANO 15.

$\Sigma(2030)$  POLE RESIDUES

The normalized residue is the residue divided by  $\Gamma_{pole}/2$ .

Normalized residue in  $N\bar{K} \rightarrow \Sigma(2030) \rightarrow N\bar{K}$

MODULUS	PHASE (°)	DOCUMENT ID	TECN	COMMENT
$0.20 \pm 0.04$	$-38 \pm 8$	SARANTSEV 19	DPWA	$\bar{K}N$ multichannel
0.220	-38	<sup>1</sup> KAMANO 15	DPWA	$\bar{K}N$ multichannel

<sup>1</sup> From the preferred solution A in KAMANO 15.

Normalized residue in  $N\bar{K} \rightarrow \Sigma(2030) \rightarrow \Sigma\pi$

MODULUS	PHASE (°)	DOCUMENT ID	TECN	COMMENT
$0.07 \pm 0.02$	$165 \pm 12$	SARANTSEV 19	DPWA	$\bar{K}N$ multichannel
0.0807	135	<sup>1</sup> KAMANO 15	DPWA	$\bar{K}N$ multichannel

<sup>1</sup> From the preferred solution A in KAMANO 15.

Normalized residue in  $N\bar{K} \rightarrow \Sigma(2030) \rightarrow \Lambda\pi$

MODULUS	PHASE (°)	DOCUMENT ID	TECN	COMMENT
$0.18 \pm 0.04$	$-22 \pm 12$	SARANTSEV 19	DPWA	$\bar{K}N$ multichannel
0.138	-24	<sup>1</sup> KAMANO 15	DPWA	$\bar{K}N$ multichannel

<sup>1</sup> From the preferred solution A in KAMANO 15.

Normalized residue in  $N\bar{K} \rightarrow \Sigma(2030) \rightarrow \Xi K$

MODULUS	PHASE (°)	DOCUMENT ID	TECN	COMMENT
$0.01 \pm 0.01$		SARANTSEV 19	DPWA	$\bar{K}N$ multichannel
0.0348	129	<sup>1</sup> KAMANO 15	DPWA	$\bar{K}N$ multichannel

<sup>1</sup> From the preferred solution A in KAMANO 15.

Normalized residue in  $N\bar{K} \rightarrow \Sigma(2030) \rightarrow \Sigma(1385)\pi, F\text{-wave}$

MODULUS	PHASE (°)	DOCUMENT ID	TECN	COMMENT
$0.04 \pm 0.03$		SARANTSEV 19	DPWA	$\bar{K}N$ multichannel
0.089	-23	<sup>1</sup> KAMANO 15	DPWA	$\bar{K}N$ multichannel

<sup>1</sup> From the preferred solution A in KAMANO 15.

Normalized residue in  $N\bar{K} \rightarrow \Sigma(2030) \rightarrow \Sigma(1385)\pi, H\text{-wave}$

MODULUS	PHASE (°)	DOCUMENT ID	TECN	COMMENT
0.0245	132	<sup>1</sup> KAMANO 15	DPWA	Multichannel

<sup>1</sup> From the preferred solution A in KAMANO 15.

Normalized residue in  $N\bar{K} \rightarrow \Sigma(2030) \rightarrow \Lambda(1520)\pi, D\text{-wave}$

MODULUS	PHASE (°)	DOCUMENT ID	TECN	COMMENT
$0.03 \pm 0.02$	$-100 \pm 40$	SARANTSEV 19	DPWA	$\bar{K}N$ multichannel

Normalized residue in  $N\bar{K} \rightarrow \Sigma(2030) \rightarrow \Lambda(1520)\pi, G\text{-wave}$

MODULUS	PHASE (°)	DOCUMENT ID	TECN	COMMENT
$0.02 \pm 0.02$		SARANTSEV 19	DPWA	$\bar{K}N$ multichannel

Normalized residue in  $N\bar{K} \rightarrow \Sigma(2030) \rightarrow \Delta\bar{K}, F\text{-wave}$

MODULUS	PHASE (°)	DOCUMENT ID	TECN	COMMENT
$0.16 \pm 0.06$	$-130 \pm 20$	SARANTSEV 19	DPWA	$\bar{K}N$ multichannel

Normalized residue in  $N\bar{K} \rightarrow \Sigma(2030) \rightarrow \Delta\bar{K}, H\text{-wave}$

MODULUS	PHASE (°)	DOCUMENT ID	TECN	COMMENT
$0.04 \pm 0.02$	$-130 \pm 35$	SARANTSEV 19	DPWA	$\bar{K}N$ multichannel

Normalized residue in  $N\bar{K} \rightarrow \Sigma(2030) \rightarrow N\bar{K}^*(892), S=1/2, F\text{-wave}$

MODULUS	PHASE (°)	DOCUMENT ID	TECN	COMMENT
$0.02 \pm 0.02$		SARANTSEV 19	DPWA	$\bar{K}N$ multichannel
0.193	38	<sup>1</sup> KAMANO 15	DPWA	$\bar{K}N$ multichannel

<sup>1</sup> From the preferred solution A in KAMANO 15.

Normalized residue in  $N\bar{K} \rightarrow \Sigma(2030) \rightarrow N\bar{K}^*(892), S=3/2, F\text{-wave}$

MODULUS	PHASE (°)	DOCUMENT ID	TECN	COMMENT
$0.16 \pm 0.09$	$-160 \pm 40$	SARANTSEV 19	DPWA	$\bar{K}N$ multichannel
0.320	37	<sup>1</sup> KAMANO 15	DPWA	$\bar{K}N$ multichannel

<sup>1</sup> From the preferred solution A in KAMANO 15.

Normalized residue in  $N\bar{K} \rightarrow \Sigma(2030) \rightarrow N\bar{K}^*(892), S=3/2, H\text{-wave}$

MODULUS	PHASE (°)	DOCUMENT ID	TECN	COMMENT
0.00358	22	<sup>1</sup> KAMANO 15	DPWA	Multichannel

<sup>1</sup> From the preferred solution A in KAMANO 15.

$\Sigma(2030)$  MASS

VALUE (MeV)	DOCUMENT ID	TECN	COMMENT
<b>2025 to 2040 (≈ 2030) OUR ESTIMATE</b>			
2032 ± 6	SARANTSEV 19	DPWA	$\bar{K}N$ multichannel
2030 ± 5	ZHANG 13A	DPWA	$\bar{K}N$ multichannel
2036 ± 5	GOPAL 80	DPWA	$\bar{K}N \rightarrow \bar{K}N$
2038 ± 10	CORDEN 77B		$K^-N \rightarrow N\bar{K}^*$
2030 ± 3	<sup>1</sup> CORDEN 76	DPWA	$K^-n \rightarrow \Lambda\pi^-$
2035 ± 15	BAILLON 75	IPWA	$\bar{K}N \rightarrow \Lambda\pi$
2038 ± 10	HEMINGWAY 75	DPWA	$K^-p \rightarrow \bar{K}N$
2042 ± 11	VANHORN 75	DPWA	$K^-p \rightarrow \Lambda\pi^0$
2020 ± 6	KANE 74	DPWA	$K^-p \rightarrow \Sigma\pi$
2035 ± 10	LITCFIELD 74B	DPWA	$K^-p \rightarrow \Lambda(1520)\pi^0$
2020 ± 30	LITCFIELD 74C	DPWA	$K^-p \rightarrow \Delta(1232)\bar{K}$
2025 ± 10	LITCFIELD 74D	DPWA	$K^-p \rightarrow \Lambda(1820)\pi^0$
••• We do not use the following data for averages, fits, limits, etc. •••			
2040 ± 5	GOPAL 77	DPWA	$\bar{K}N$ multichannel
2027 to 2057	GOYAL 77	DPWA	$K^-N \rightarrow \Sigma\pi$
2030	DEBELLEFON 76	IPWA	$K^-p \rightarrow \Lambda\pi^0$

<sup>1</sup> Preferred solution 3; see CORDEN 76 for other possibilities.

$\Sigma(2030)$  WIDTH

VALUE (MeV)	DOCUMENT ID	TECN	COMMENT
<b>150 to 200 (≈ 180) OUR ESTIMATE</b>			
177 ± 12	SARANTSEV 19	DPWA	$\bar{K}N$ multichannel
207 ± 17	ZHANG 13A	DPWA	$\bar{K}N$ multichannel
172 ± 10	GOPAL 80	DPWA	$\bar{K}N \rightarrow \bar{K}N$
137 ± 40	CORDEN 77B		$K^-N \rightarrow N\bar{K}^*$
201 ± 9	<sup>1</sup> CORDEN 76	DPWA	$K^-n \rightarrow \Lambda\pi^-$
180 ± 20	BAILLON 75	IPWA	$\bar{K}N \rightarrow \Lambda\pi$
172 ± 15	HEMINGWAY 75	DPWA	$K^-p \rightarrow \bar{K}N$
178 ± 13	VANHORN 75	DPWA	$K^-p \rightarrow \Lambda\pi^0$
111 ± 5	KANE 74	DPWA	$K^-p \rightarrow \Sigma\pi$
160 ± 20	LITCFIELD 74B	DPWA	$K^-p \rightarrow \Lambda(1520)\pi^0$
200 ± 30	LITCFIELD 74C	DPWA	$K^-p \rightarrow \Delta(1232)\bar{K}$
••• We do not use the following data for averages, fits, limits, etc. •••			
260	DECLAIS 77	DPWA	$\bar{K}N \rightarrow \bar{K}N$
190 ± 10	GOPAL 77	DPWA	$\bar{K}N$ multichannel
126 to 195	GOYAL 77	DPWA	$K^-N \rightarrow \Sigma\pi$
160	DEBELLEFON 76	IPWA	$K^-p \rightarrow \Lambda\pi^0$
70 to 125	LITCFIELD 74D	DPWA	$K^-p \rightarrow \Lambda(1820)\pi^0$

<sup>1</sup> Preferred solution 3; see CORDEN 76 for other possibilities.

$\Sigma(2030)$  DECAY MODES

Mode	Fraction ( $\Gamma_i/\Gamma$ )
$\Gamma_1$ $N\bar{K}$	17–23 %
$\Gamma_2$ $\Lambda\pi$	17–23 %
$\Gamma_3$ $\Sigma\pi$	5–10 %
$\Gamma_4$ $\Xi K$	<2 %
$\Gamma_5$ $\Sigma(1385)\pi$	5–15 %
$\Gamma_6$ $\Sigma(1385)\pi, F\text{-wave}$	
$\Gamma_7$ $\Sigma(1385)\pi, F\text{-wave}$	( 1.0 ± 1.0 ) %
$\Gamma_8$ $\Sigma(1385)\pi, H\text{-wave}$	
$\Gamma_9$ $\Lambda(1520)\pi$	10–20 %
$\Gamma_{10}$ $\Lambda(1520)\pi, D\text{-wave}$	
$\Gamma_{11}$ $\Lambda(1520)\pi, G\text{-wave}$	
$\Gamma_{12}$ $\Delta(1232)\bar{K}$	10–20 %
$\Gamma_{13}$ $\Delta(1232)\bar{K}, F\text{-wave}$	(15 ± 5) %
$\Gamma_{14}$ $\Delta(1232)\bar{K}, H\text{-wave}$	( 1.0 ± 1.0 ) %
$\Gamma_{15}$ $N\bar{K}^*(892)$	<5 %
$\Gamma_{16}$ $N\bar{K}^*(892), S=1/2, F\text{-wave}$	
$\Gamma_{17}$ $N\bar{K}^*(892), S=3/2, F\text{-wave}$	(14 ± 8) %
$\Gamma_{18}$ $N\bar{K}^*(892), S=3/2, H\text{-wave}$	
$\Gamma_{19}$ $\Lambda(1820)\pi, P\text{-wave}$	

# Baryon Particle Listings

## $\Sigma(2030)$

### $\Sigma(2030)$ BRANCHING RATIOS

See "Sign conventions for resonance couplings" in the Note on  $\Lambda$  and  $\Sigma$  Resonances.

$\Gamma(N\bar{K})/\Gamma_{total}$				$\Gamma_1/\Gamma$
VALUE	DOCUMENT ID	TECN	COMMENT	
<b>0.17 to 0.23 OUR ESTIMATE</b>				
0.20 ± 0.04	SARANTSEV 19	DPWA	$\bar{K}N$ multichannel	
0.13 ± 0.01	ZHANG 13A	DPWA	$\bar{K}N$ multichannel	
0.19 ± 0.03	GOPAL 80	DPWA	$\bar{K}N \rightarrow \bar{K}N$	
0.18 ± 0.03	HEMINGWAY 75	DPWA	$K^-p \rightarrow \bar{K}N$	
• • • We do not use the following data for averages, fits, limits, etc. • • •				
0.269	<sup>1</sup> KAMANO 15	DPWA	Multichannel	
0.15	DECLAIS 77	DPWA	$\bar{K}N \rightarrow \bar{K}N$	
0.24 ± 0.02	GOPAL 77	DPWA	See GOPAL 80	

<sup>1</sup> From the preferred solution A in KAMANO 15.

$\Gamma(\Lambda\pi)/\Gamma_{total}$				$\Gamma_2/\Gamma$
VALUE	DOCUMENT ID	TECN	COMMENT	
<b>0.17 ± 0.04</b>	SARANTSEV 19	DPWA	$\bar{K}N$ multichannel	
• • • We do not use the following data for averages, fits, limits, etc. • • •				
0.080	<sup>1</sup> KAMANO 15	DPWA	$\bar{K}N$ multichannel	

<sup>1</sup> From the preferred solution A in KAMANO 15.

$\Gamma(\Sigma\pi)/\Gamma_{total}$				$\Gamma_3/\Gamma$
VALUE	DOCUMENT ID	TECN	COMMENT	
<b>0.025 ± 0.008</b>	SARANTSEV 19	DPWA	$\bar{K}N$ multichannel	
• • • We do not use the following data for averages, fits, limits, etc. • • •				
0.037	<sup>1</sup> KAMANO 15	DPWA	$\bar{K}N$ multichannel	

<sup>1</sup> From the preferred solution A in KAMANO 15.

$\Gamma(\Xi K)/\Gamma_{total}$				$\Gamma_4/\Gamma$
VALUE	DOCUMENT ID	TECN	COMMENT	
<0.01	SARANTSEV 19	DPWA	$\bar{K}N$ multichannel	
• • • We do not use the following data for averages, fits, limits, etc. • • •				
0.006	<sup>1</sup> KAMANO 15	DPWA	$\bar{K}N$ multichannel	

<sup>1</sup> From the preferred solution A in KAMANO 15.

$\Gamma(\Lambda(1520)\pi, D\text{-wave})/\Gamma_{total}$				$\Gamma_{10}/\Gamma$
VALUE	DOCUMENT ID	TECN	COMMENT	
~ 0.01	SARANTSEV 19	DPWA	$\bar{K}N$ multichannel	

$\Gamma(\Lambda(1520)\pi, G\text{-wave})/\Gamma_{total}$				$\Gamma_{11}/\Gamma$
VALUE	DOCUMENT ID	TECN	COMMENT	
<0.01	SARANTSEV 19	DPWA	$\bar{K}N$ multichannel	

$\Gamma(\Sigma(1385)\pi, F\text{-wave})/\Gamma_{total}$				$\Gamma_7/\Gamma$
VALUE	DOCUMENT ID	TECN	COMMENT	
<b>0.01 ± 0.01</b>	SARANTSEV 19	DPWA	$\bar{K}N$ multichannel	
• • • We do not use the following data for averages, fits, limits, etc. • • •				
0.030	<sup>1</sup> KAMANO 15	DPWA	$\bar{K}N$ multichannel	

<sup>1</sup> From the preferred solution A in KAMANO 15.

$\Gamma(\Sigma(1385)\pi, H\text{-wave})/\Gamma_{total}$				$\Gamma_8/\Gamma$
VALUE	DOCUMENT ID	TECN	COMMENT	
• • • We do not use the following data for averages, fits, limits, etc. • • •				
0.003	<sup>1</sup> KAMANO 15	DPWA	Multichannel	

<sup>1</sup> From the preferred solution A in KAMANO 15.

$\Gamma(\Delta(1232)\bar{K}, F\text{-wave})/\Gamma_{total}$				$\Gamma_{13}/\Gamma$
VALUE	DOCUMENT ID	TECN	COMMENT	
<b>0.15 ± 0.05</b>	SARANTSEV 19	DPWA	$\bar{K}N$ multichannel	

$\Gamma(\Delta(1232)\bar{K}, H\text{-wave})/\Gamma_{total}$				$\Gamma_{14}/\Gamma$
VALUE	DOCUMENT ID	TECN	COMMENT	
<b>0.01 ± 0.01</b>	SARANTSEV 19	DPWA	$\bar{K}N$ multichannel	

$\Gamma(N\bar{K}^*(892), S=1/2, F\text{-wave})/\Gamma_{total}$				$\Gamma_{16}/\Gamma$
VALUE	DOCUMENT ID	TECN	COMMENT	
<0.01	SARANTSEV 19	DPWA	$\bar{K}N$ multichannel	
• • • We do not use the following data for averages, fits, limits, etc. • • •				
0.154	<sup>1</sup> KAMANO 15	DPWA	$\bar{K}N$ multichannel	

<sup>1</sup> From the preferred solution A in KAMANO 15.

$\Gamma(N\bar{K}^*(892), S=3/2, F\text{-wave})/\Gamma_{total}$				$\Gamma_{17}/\Gamma$
VALUE	DOCUMENT ID	TECN	COMMENT	
<b>0.14 ± 0.08</b>	SARANTSEV 19	DPWA	$\bar{K}N$ multichannel	
• • • We do not use the following data for averages, fits, limits, etc. • • •				
0.422	<sup>1</sup> KAMANO 15	DPWA	$\bar{K}N$ multichannel	

<sup>1</sup> From the preferred solution A in KAMANO 15.

$\Gamma(N\bar{K}^*(892), S=3/2, H\text{-wave})/\Gamma_{total}$				$\Gamma_{18}/\Gamma$
VALUE	DOCUMENT ID	TECN	COMMENT	
• • • We do not use the following data for averages, fits, limits, etc. • • •				
not seen	<sup>1</sup> KAMANO 15	DPWA	$\bar{K}N$ multichannel	

<sup>1</sup> From the preferred solution A in KAMANO 15.

$(\Gamma_1\Gamma_f)^{1/2}/\Gamma_{total}$ in $N\bar{K} \rightarrow \Sigma(2030) \rightarrow \Lambda\pi$				$(\Gamma_1\Gamma_2)^{1/2}/\Gamma$
VALUE	DOCUMENT ID	TECN	COMMENT	
+0.15 ± 0.01	ZHANG 13A	DPWA	Multichannel	
+0.18 ± 0.02	GOPAL 77	DPWA	$\bar{K}N$ multichannel	
+0.20 ± 0.01	<sup>1</sup> CORDEN 76	DPWA	$K^-n \rightarrow \Lambda\pi^-$	
+0.18 ± 0.02	BAILLON 75	IPWA	$\bar{K}N \rightarrow \Lambda\pi$	
+0.20 ± 0.01	VANHORN 75	DPWA	$K^-p \rightarrow \Lambda\pi^0$	
+0.195 ± 0.053	DEVENISH 74B		Fixed- $t$ dispersion rel.	
• • • We do not use the following data for averages, fits, limits, etc. • • •				
0.20	DEBELLEFON 76	IPWA	$K^-p \rightarrow \Lambda\pi^0$	

<sup>1</sup> Preferred solution 3; see CORDEN 76 for other possibilities.

$(\Gamma_1\Gamma_f)^{1/2}/\Gamma_{total}$ in $N\bar{K} \rightarrow \Sigma(2030) \rightarrow \Sigma\pi$				$(\Gamma_1\Gamma_3)^{1/2}/\Gamma$
VALUE	DOCUMENT ID	TECN	COMMENT	
-0.08 ± 0.01	ZHANG 13A	DPWA	Multichannel	
-0.09 ± 0.01	<sup>1</sup> CORDEN 77C		$K^-n \rightarrow \Sigma\pi$	
-0.06 ± 0.01	<sup>1</sup> CORDEN 77C		$K^-n \rightarrow \Sigma\pi$	
-0.15 ± 0.03	GOPAL 77	DPWA	$\bar{K}N$ multichannel	
-0.10 ± 0.01	KANE 74	DPWA	$K^-p \rightarrow \Sigma\pi$	
• • • We do not use the following data for averages, fits, limits, etc. • • •				
-0.085 ± 0.02	<sup>2</sup> GOYAL 77	DPWA	$K^-n \rightarrow \Sigma\pi$	

<sup>1</sup> The two entries for CORDEN 77C are from two different acceptable solutions.

<sup>2</sup> This coupling is extracted from unnormalized data.

$(\Gamma_1\Gamma_f)^{1/2}/\Gamma_{total}$ in $N\bar{K} \rightarrow \Sigma(2030) \rightarrow \Xi K$				$(\Gamma_1\Gamma_4)^{1/2}/\Gamma$
VALUE	DOCUMENT ID	TECN	COMMENT	
0.023	MULLER 69B	DPWA	$K^-p \rightarrow \Xi K$	
<0.05	BURGUN 68	DPWA	$K^-p \rightarrow \Xi K$	
<0.05	TRIPP 67	RVUE	$K^-p \rightarrow \Xi K$	

$(\Gamma_1\Gamma_f)^{1/2}/\Gamma_{total}$ in $N\bar{K} \rightarrow \Sigma(2030) \rightarrow \Sigma(1385)\pi, F\text{-wave}$				$(\Gamma_1\Gamma_6)^{1/2}/\Gamma$
VALUE	DOCUMENT ID	TECN	COMMENT	
+0.16 ± 0.01	ZHANG 13A	DPWA	Multichannel	
+0.153 ± 0.026	<sup>1</sup> CAMERON 78	DPWA	$K^-p \rightarrow \Sigma(1385)\pi$	

<sup>1</sup> The published sign has been changed to be in accord with the baryon-first convention.

$(\Gamma_1\Gamma_f)^{1/2}/\Gamma_{total}$ in $N\bar{K} \rightarrow \Sigma(2030) \rightarrow \Lambda(1520)\pi, D\text{-wave}$				$(\Gamma_1\Gamma_{10})^{1/2}/\Gamma$
VALUE	DOCUMENT ID	TECN	COMMENT	
+0.114 ± 0.010	<sup>1</sup> CAMERON 77	DPWA	$K^-p \rightarrow \Lambda(1520)\pi^0$	
0.14 ± 0.03	LITCHFIELD 74B	DPWA	$K^-p \rightarrow \Lambda(1520)\pi^0$	
• • • We do not use the following data for averages, fits, limits, etc. • • •				
0.10 ± 0.03	<sup>2</sup> CORDEN 75B	DBC	$K^-n \rightarrow N\bar{K}\pi^-$	

<sup>1</sup> The published sign has been changed to be in accord with the baryon-first convention.

<sup>2</sup> An upper limit.

$(\Gamma_1\Gamma_f)^{1/2}/\Gamma_{total}$ in $N\bar{K} \rightarrow \Sigma(2030) \rightarrow \Lambda(1520)\pi, G\text{-wave}$				$(\Gamma_1\Gamma_{11})^{1/2}/\Gamma$
VALUE	DOCUMENT ID	TECN	COMMENT	
+0.146 ± 0.010	<sup>1</sup> CAMERON 77	DPWA	$K^-p \rightarrow \Lambda(1520)\pi^0$	
0.02 ± 0.02	LITCHFIELD 74B	DPWA	$K^-p \rightarrow \Lambda(1520)\pi^0$	

<sup>1</sup> The published sign has been changed to be in accord with the baryon-first convention.

$(\Gamma_1\Gamma_f)^{1/2}/\Gamma_{total}$ in $N\bar{K} \rightarrow \Sigma(2030) \rightarrow \Delta(1232)\bar{K}, F\text{-wave}$				$(\Gamma_1\Gamma_{13})^{1/2}/\Gamma$
VALUE	DOCUMENT ID	TECN	COMMENT	
+0.12 ± 0.02	ZHANG 13A	DPWA	Multichannel	
0.16 ± 0.03	LITCHFIELD 74C	DPWA	$K^-p \rightarrow \Delta(1232)\bar{K}$	
• • • We do not use the following data for averages, fits, limits, etc. • • •				
0.17 ± 0.03	<sup>1</sup> CORDEN 75B	DBC	$K^-n \rightarrow N\bar{K}\pi^-$	

<sup>1</sup> An upper limit.

$(\Gamma_1\Gamma_f)^{1/2}/\Gamma_{total}$ in $N\bar{K} \rightarrow \Sigma(2030) \rightarrow \Delta(1232)\bar{K}, H\text{-wave}$				$(\Gamma_1\Gamma_{14})^{1/2}/\Gamma$
VALUE	DOCUMENT ID	TECN	COMMENT	
0.00 ± 0.02	LITCHFIELD 74C	DPWA	$K^-p \rightarrow \Delta(1232)\bar{K}$	

$(\Gamma_1\Gamma_f)^{1/2}/\Gamma_{total}$ in $N\bar{K} \rightarrow \Sigma(2030) \rightarrow N\bar{K}^*(892), S=1/2, F\text{-wave}$				$(\Gamma_1\Gamma_{16})^{1/2}/\Gamma$
VALUE	DOCUMENT ID	TECN	COMMENT	
+0.06 ± 0.02	ZHANG 13A	DPWA	Multichannel	
+0.06 ± 0.03	<sup>1</sup> CAMERON 78B	DPWA	$K^-p \rightarrow N\bar{K}^*$	
-0.02 ± 0.01	CORDEN 77B		$K^-d \rightarrow NN\bar{K}^*$	

<sup>1</sup> The published sign has been changed to be in accord with the baryon-first convention.

See key on page 999

# Baryon Particle Listings

## $\Sigma(2030), \Sigma(2070), \Sigma(2080)$

$(\Gamma_1 \Gamma_f)^{1/2} / \Gamma_{\text{total}}$  in  $N\bar{K} \rightarrow \Sigma(2030) \rightarrow N\bar{K}^*(892), S=3/2, F\text{-wave}$   $(\Gamma_1 \Gamma_f)^{1/2} / \Gamma$

VALUE	DOCUMENT ID	TECN	COMMENT
+0.05 ± 0.01	ZHANG	13A	DPWA Multichannel
+0.04 ± 0.03	<sup>1</sup> CAMERON	78B	DPWA $K^- p \rightarrow N\bar{K}^*$
-0.12 ± 0.02	CORDEN	77B	$K^- d \rightarrow NN\bar{K}^*$

<sup>1</sup> The upper limit on the  $G_3$  wave is 0.03.

$(\Gamma_1 \Gamma_f)^{1/2} / \Gamma_{\text{total}}$  in  $N\bar{K} \rightarrow \Sigma(2030) \rightarrow \Lambda(1820)\pi, P\text{-wave}$   $(\Gamma_1 \Gamma_f)^{1/2} / \Gamma$

VALUE	DOCUMENT ID	TECN	COMMENT
0.14 ± 0.02	CORDEN	75B	DBC $K^- n \rightarrow N\bar{K}\pi^-$
0.18 ± 0.04	LITCHFIELD	74D	DPWA $K^- p \rightarrow \Lambda(1820)\pi^0$

### $\Sigma(2030)$ REFERENCES

SARANTSEV	19	EPJ A55 180	A.V. Sarantsev et al.	(BONN, PNPI)
KAMANO	15	PR C92 025205	H. Kamano et al.	(ANL, OSAK)
ZHANG	13A	PR C88 035205	H. Zhang et al.	(KSU)
PDG	84	RMP 56 51	C.G. Wohl et al.	(LBL, CIT, CERN)
PDG	82	PL 111B 1	M. Roos et al.	(HELS, CIT, CERN)
GOPAL	80	Toronto Conf. 159	G.P. Gopal	(RHEL) IJP
CAMERON	78	NP B143 189	W. Cameron et al.	(RHEL, LOIC) IJP
CAMERON	75B	NP B146 327	W. Cameron et al.	(RHEL, LOIC) IJP
CAMERON	77	NP B131 399	W. Cameron et al.	(RHEL, LOIC) IJP
CORDEN	77B	NP B121 365	M.J. Corden et al.	(BIRM) IJP
CORDEN	77C	NP B125 61	M.J. Corden et al.	(BIRM) IJP
DECLAIS	77	CERN 77-16	Y. Declais et al.	(CAEN, CERN) IJP
GOPAL	77	NP B119 362	G.P. Gopal et al.	(LOIC, RHEL) IJP
GOYAL	77	PR D16 2746	D.P. Goyal, A.V. Sodhi	(DELH) IJP
CORDEN	76	NP B104 382	M.J. Corden et al.	(BIRM) IJP
DEBELLEFON	76	NP B109 129	A. de Bellefon, A. Berthon	(CDEF) IJP
BAILLON	75	NP B94 39	P.H. Baillon, P.J. Litchfield	(CERN, RHEL) IJP
CORDEN	75B	NP B92 365	M.J. Corden et al.	(BIRM) IJP
HEMINGWAY	75	NP B91 12	R.J. Hemingway et al.	(CERN, HEIDH, MPIM) IJP
VANHORN	75	NP B87 145	A.J. van Horn	(LBL) IJP
Also			A.J. van Horn	(LBL) IJP
DEVENISH	74B	NP B81 330	R.C.E. Devenish, C.D. Froggatt, B.R. Martin	(DESY+) IJP
KANE	74	LBL-2452	D.F. Kane	(LBL) IJP
LITCHFIELD	74B	NP B74 19	P.J. Litchfield et al.	(CERN, HEIDH) IJP
LITCHFIELD	74C	NP B74 39	P.J. Litchfield et al.	(CERN, HEIDH) IJP
LITCHFIELD	74D	NP B74 12	P.J. Litchfield et al.	(CERN, HEIDH) IJP
MULLER	69B	Thesis UCRL 19372	R.A. Muller	(LRL)
BURGUN	68	NP B8 447	G. Burigun et al.	(SACL, CDEF, RHEL)
TRIPP	67	NP B3 10	R.D. Tripp et al.	(LRL, SLAC, CERN+) IJP
COOL	66	PRL 16 1228	R.L. Cool et al.	(BNL)
WOHL	66	PRL 17 107	C.G. Wohl, F.T. Solmitz, M.L. Stevenson	(LRL) IJP

$\Sigma(2070) 5/2^+$   $I(J^P) = 1(5/2^+) \text{ Status: } *$

OMITTED FROM SUMMARY TABLE  
 This state suggested by BERTHON 70B finds support in GOPAL 80 with new  $K^- p$  polarization and  $K^- n$  angular distributions. The very broad state seen in KANE 72 is not required in the later (KANE 74) analysis of  $\bar{K} N \rightarrow \Sigma \pi$ .

### $\Sigma(2070)$ MASS

VALUE (MeV)	DOCUMENT ID	TECN	COMMENT
<b>2020 to 2100 (<math>\approx 2060</math>) OUR ESTIMATE</b>			
2051 ± 25	GOPAL	80	DPWA $\bar{K} N \rightarrow \bar{K} N$
2070 ± 10	BERTHON	70B	DPWA $K^- p \rightarrow \Sigma \pi$
• • • We do not use the following data for averages, fits, limits, etc. • • •			
2057	KANE	72	DPWA $K^- p \rightarrow \Sigma \pi$

### $\Sigma(2070)$ WIDTH

VALUE (MeV)	DOCUMENT ID	TECN	COMMENT
<b>100 to 300 (<math>\approx 200</math>) OUR ESTIMATE</b>			
300 ± 30	GOPAL	80	DPWA $\bar{K} N \rightarrow \bar{K} N$
140 ± 20	BERTHON	70B	DPWA $K^- p \rightarrow \Sigma \pi$
• • • We do not use the following data for averages, fits, limits, etc. • • •			
906	KANE	72	DPWA $K^- p \rightarrow \Sigma \pi$

### $\Sigma(2070)$ DECAY MODES

Mode	$\Gamma_1$	$\Gamma_2$
$N\bar{K}$	$\Gamma_1$	
$\Sigma \pi$		$\Gamma_2$

### $\Sigma(2070)$ BRANCHING RATIOS

See "Sign conventions for resonance couplings" in the Note on  $\Lambda$  and  $\Sigma$  Resonances.

$\Gamma(N\bar{K}) / \Gamma_{\text{total}}$   $\Gamma_1 / \Gamma$

VALUE	DOCUMENT ID	TECN	COMMENT
0.08 ± 0.03	GOPAL	80	DPWA $\bar{K} N \rightarrow \bar{K} N$

$(\Gamma_1 \Gamma_f)^{1/2} / \Gamma_{\text{total}}$  in  $N\bar{K} \rightarrow \Sigma(2070) \rightarrow \Sigma \pi$   $(\Gamma_1 \Gamma_f)^{1/2} / \Gamma$

VALUE	DOCUMENT ID	TECN	COMMENT
0.12 ± 0.02	BERTHON	70B	DPWA $K^- p \rightarrow \Sigma \pi$
• • • We do not use the following data for averages, fits, limits, etc. • • •			
0.104	KANE	72	DPWA $K^- p \rightarrow \Sigma \pi$

### $\Sigma(2070)$ REFERENCES

GOPAL	80	Toronto Conf. 159	G.P. Gopal	(RHEL) IJP
KANE	74	LBL-2452	D.F. Kane	(LBL)
KANE	72	PR D5 1583	D.F.J. Kane	(LBL)
BERTHON	70B	NP B24 417	A. Berthon et al.	(CDEF, RHEL, SACL) IJP

## $\Sigma(2080) 3/2^+$

$I(J^P) = 1(3/2^+) \text{ Status: } *$

OMITTED FROM SUMMARY TABLE  
 Suggested by some but not all partial-wave analyses across this region.

### $\Sigma(2080)$ MASS

VALUE (MeV)	DOCUMENT ID	TECN	COMMENT
<b>2060 to 2120 (<math>\approx 2090</math>) OUR ESTIMATE</b>			
2091 ± 7	<sup>1</sup> CORDEN	76	DPWA $K^- n \rightarrow \Lambda \pi^-$
2070 to 2120	DEBELLEFON	76	IPWA $K^- p \rightarrow \Lambda \pi^0$
2120 ± 40	BAILLON	75	IPWA $\bar{K} N \rightarrow \Lambda \pi$ (sol. 1)
2140 ± 40	BAILLON	75	IPWA $\bar{K} N \rightarrow \Lambda \pi$ (sol. 2)
2082 ± 4	COX	70	DPWA See CORDEN 76
2070 ± 30	LITCHFIELD	70	DPWA $K^- N \rightarrow \Lambda \pi$

### $\Sigma(2080)$ WIDTH

VALUE (MeV)	DOCUMENT ID	TECN	COMMENT
<b>100 to 240 (<math>\approx 170</math>) OUR ESTIMATE</b>			
186 ± 48	<sup>1</sup> CORDEN	76	DPWA $K^- n \rightarrow \Lambda \pi^-$
100	DEBELLEFON	76	IPWA $K^- p \rightarrow \Lambda \pi^0$
240 ± 50	BAILLON	75	IPWA $\bar{K} N \rightarrow \Lambda \pi$ (sol. 1)
200 ± 50	BAILLON	75	IPWA $\bar{K} N \rightarrow \Lambda \pi$ (sol. 2)
87 ± 20	COX	70	DPWA See CORDEN 76
250 ± 40	LITCHFIELD	70	DPWA $K^- N \rightarrow \Lambda \pi$

### $\Sigma(2080)$ DECAY MODES

Mode	$\Gamma_1$	$\Gamma_2$
$N\bar{K}$	$\Gamma_1$	
$\Lambda \pi$		$\Gamma_2$

### $\Sigma(2080)$ BRANCHING RATIOS

See "Sign conventions for resonance couplings" in the Note on  $\Lambda$  and  $\Sigma$  Resonances.

$(\Gamma_1 \Gamma_f)^{1/2} / \Gamma_{\text{total}}$  in  $N\bar{K} \rightarrow \Sigma(2080) \rightarrow \Lambda \pi$   $(\Gamma_1 \Gamma_f)^{1/2} / \Gamma$

VALUE	DOCUMENT ID	TECN	COMMENT
-0.10 ± 0.03	<sup>1</sup> CORDEN	76	DPWA $K^- n \rightarrow \Lambda \pi^-$
-0.10	DEBELLEFON	76	IPWA $K^- p \rightarrow \Lambda \pi^0$
-0.13 ± 0.04	BAILLON	75	IPWA $\bar{K} N \rightarrow \Lambda \pi$ (sol. 1 and 2)
-0.16 ± 0.03	COX	70	DPWA See CORDEN 76
-0.09 ± 0.03	LITCHFIELD	70	DPWA $K^- N \rightarrow \Lambda \pi$

### $\Sigma(2080)$ FOOTNOTES

<sup>1</sup> Preferred solution 3; see CORDEN 76 for other possibilities, including a  $D_{15}$  at this mass.

### $\Sigma(2080)$ REFERENCES

CORDEN	76	NP B104 382	M.J. Corden et al.	(BIRM) IJP
DEBELLEFON	76	NP B109 129	A. de Bellefon, A. Berthon	(CDEF) IJP
Also			A. de Bellefon et al.	(CDEF, SACL) IJP
BAILLON	75	NP B94 39	P.H. Baillon, P.J. Litchfield	(CERN, RHEL) IJP
COX	70	NP B19 61	G.F. Cox et al.	(BIRM, EDIN, GLAS, LOIC) IJP
LITCHFIELD	70	NP B22 269	P.J. Litchfield	(RHEL) IJP



# Baryon Particle Listings

## $\Sigma(2080), \Sigma(2100), \Sigma(2160)$

**$\Sigma(2100) 7/2^-$**

$I(J^P) = 1(\frac{7}{2}^-)$  Status: \*

OMITTED FROM SUMMARY TABLE

### $\Sigma(2100)$ POLE POSITION

REAL PART			
VALUE (MeV)	DOCUMENT ID	TECN	COMMENT
<b>2093 ± 16</b>	SARANTSEV	19	DPWA $\bar{K}N$ multichannel
-2xIMAGINARY PART			
VALUE (MeV)	DOCUMENT ID	TECN	COMMENT
<b>210 ± 35</b>	SARANTSEV	19	DPWA $\bar{K}N$ multichannel

### $\Sigma(2100)$ POLE RESIDUES

Normalized residue in $N\bar{K} \rightarrow \Sigma(2100) \rightarrow N\bar{K}$			
MODULUS	PHASE (°)	DOCUMENT ID	TECN COMMENT
<b>0.09 ± 0.02</b>	<b>-110 ± 15</b>	SARANTSEV	19 DPWA $\bar{K}N$ multichannel
Normalized residue in $N\bar{K} \rightarrow \Sigma(2100) \rightarrow \Sigma\pi$			
MODULUS	PHASE (°)	DOCUMENT ID	TECN COMMENT
<b>0.04 ± 0.02</b>	<b>-50 ± 20</b>	SARANTSEV	19 DPWA $\bar{K}N$ multichannel
Normalized residue in $N\bar{K} \rightarrow \Sigma(2100) \rightarrow \Lambda\pi$			
MODULUS	PHASE (°)	DOCUMENT ID	TECN COMMENT
<b>0.03 ± 0.02</b>	<b>-100 ± 25</b>	SARANTSEV	19 DPWA $\bar{K}N$ multichannel
Normalized residue in $N\bar{K} \rightarrow \Sigma(2100) \rightarrow \Xi K$			
MODULUS	PHASE (°)	DOCUMENT ID	TECN COMMENT
<b>0.010 ± 0.005</b>	<b>-120 ± 35</b>	SARANTSEV	19 DPWA $\bar{K}N$ multichannel
Normalized residue in $N\bar{K} \rightarrow \Sigma(2100) \rightarrow \Lambda(1520)\pi, F\text{-wave}$			
MODULUS	PHASE (°)	DOCUMENT ID	TECN COMMENT
<b>0.02 ± 0.01</b>	<b>-100 ± 30</b>	SARANTSEV	19 DPWA $\bar{K}N$ multichannel
Normalized residue in $N\bar{K} \rightarrow \Sigma(2100) \rightarrow \Lambda(1520)\pi, H\text{-wave}$			
MODULUS	PHASE (°)	DOCUMENT ID	TECN COMMENT
<b>0.01 ± 0.01</b>		SARANTSEV	19 DPWA $\bar{K}N$ multichannel
Normalized residue in $N\bar{K} \rightarrow \Sigma(2100) \rightarrow \Sigma(1385)\pi, D\text{-wave}$			
MODULUS	PHASE (°)	DOCUMENT ID	TECN COMMENT
<b>0.10 ± 0.03</b>	<b>-60 ± 30</b>	SARANTSEV	19 DPWA $\bar{K}N$ multichannel
Normalized residue in $N\bar{K} \rightarrow \Sigma(2100) \rightarrow \Sigma(1385)\pi, G\text{-wave}$			
MODULUS	PHASE (°)	DOCUMENT ID	TECN COMMENT
<b>0.03 ± 0.01</b>	<b>-50 ± 30</b>	SARANTSEV	19 DPWA $\bar{K}N$ multichannel
Normalized residue in $N\bar{K} \rightarrow \Sigma(2100) \rightarrow \Delta\bar{K}, G\text{-wave}$			
MODULUS	PHASE (°)	DOCUMENT ID	TECN COMMENT
<b>0.04 ± 0.02</b>	<b>75 ± 35</b>	SARANTSEV	19 DPWA $\bar{K}N$ multichannel
Normalized residue in $N\bar{K} \rightarrow \Sigma(2100) \rightarrow N\bar{K}^*(892), S=3/2, D\text{-wave}$			
MODULUS	PHASE (°)	DOCUMENT ID	TECN COMMENT
<b>0.08 ± 0.04</b>	<b>20 ± 50</b>	SARANTSEV	19 DPWA $\bar{K}N$ multichannel

### $\Sigma(2100)$ MASS

VALUE (MeV)	DOCUMENT ID	TECN	COMMENT
<b>≈ 2100 OUR ESTIMATE</b>			
2146 ± 17	SARANTSEV	19	DPWA $\bar{K}N$ multichannel
2060 ± 20	BARBARO...	70	DPWA $K^-p \rightarrow \Lambda\pi^0$
2120 ± 30	BARBARO...	70	DPWA $K^-p \rightarrow \Sigma\pi$

### $\Sigma(2100)$ WIDTH

VALUE (MeV)	DOCUMENT ID	TECN	COMMENT
260 ± 40	SARANTSEV	19	DPWA $\bar{K}N$ multichannel
70 ± 30	BARBARO...	70	DPWA $K^-p \rightarrow \Lambda\pi^0$
135 ± 30	BARBARO...	70	DPWA $K^-p \rightarrow \Sigma\pi$

### $\Sigma(2100)$ DECAY MODES

Mode	Fraction ( $\Gamma_i/\Gamma$ )
$\Gamma_1 N\bar{K}$	( 8.0 ± 2.0 ) %
$\Gamma_2 \Lambda\pi$	( 1.5 ± 1.0 ) %
$\Gamma_3 \Sigma\pi$	( 2.0 ± 1.0 ) %
$\Gamma_4 \Xi K$	
$\Gamma_5 \Sigma(1385)\pi, D\text{-wave}$	( 12 ± 6 ) %
$\Gamma_6 \Sigma(1385)\pi, G\text{-wave}$	
$\Gamma_7 \Lambda(1520)\pi, F\text{-wave}$	( 1.0 ± 1.0 ) %
$\Gamma_8 \Lambda(1520)\pi, H\text{-wave}$	
$\Gamma_9 N\bar{K}^*(892), S=3/2, D\text{-wave}$	( 6.0 ± 3.0 ) %
$\Gamma_{10} \Delta\bar{K}, G\text{-wave}$	( 1.0 ± 1.0 ) %

### $\Sigma(2100)$ BRANCHING RATIOS

See "Sign conventions for resonance couplings" in the Note on  $\Lambda$  and  $\Sigma$  Resonances.

$(\Gamma_i\Gamma_f)^{1/2}/\Gamma_{\text{total}}$ in $N\bar{K} \rightarrow \Sigma(2100) \rightarrow \Lambda\pi$	DOCUMENT ID	TECN	COMMENT	$(\Gamma_1\Gamma_2)^{1/2}/\Gamma$
VALUE -0.07 ± 0.02	BARBARO...	70	DPWA	$K^-p \rightarrow \Lambda\pi^0$
$(\Gamma_i\Gamma_f)^{1/2}/\Gamma_{\text{total}}$ in $N\bar{K} \rightarrow \Sigma(2100) \rightarrow \Sigma\pi$	DOCUMENT ID	TECN	COMMENT	$(\Gamma_1\Gamma_3)^{1/2}/\Gamma$
VALUE +0.13 ± 0.02	BARBARO...	70	DPWA	$K^-p \rightarrow \Sigma\pi$
$\Gamma(N\bar{K})/\Gamma_{\text{total}}$	DOCUMENT ID	TECN	COMMENT	$\Gamma_1/\Gamma$
VALUE <b>0.08 ± 0.02</b>	SARANTSEV	19	DPWA	$\bar{K}N$ multichannel
$\Gamma(\Lambda\pi)/\Gamma_{\text{total}}$	DOCUMENT ID	TECN	COMMENT	$\Gamma_2/\Gamma$
VALUE <b>0.015 ± 0.01</b>	SARANTSEV	19	DPWA	$\bar{K}N$ multichannel
$\Gamma(\Sigma\pi)/\Gamma_{\text{total}}$	DOCUMENT ID	TECN	COMMENT	$\Gamma_3/\Gamma$
VALUE <b>0.02 ± 0.01</b>	SARANTSEV	19	DPWA	$\bar{K}N$ multichannel
$\Gamma(\Xi K)/\Gamma_{\text{total}}$	DOCUMENT ID	TECN	COMMENT	$\Gamma_4/\Gamma$
VALUE <0.01	SARANTSEV	19	DPWA	$\bar{K}N$ multichannel
$\Gamma(\Sigma(1385)\pi, D\text{-wave})/\Gamma_{\text{total}}$	DOCUMENT ID	TECN	COMMENT	$\Gamma_5/\Gamma$
VALUE <b>0.12 ± 0.06</b>	SARANTSEV	19	DPWA	$\bar{K}N$ multichannel
$\Gamma(\Sigma(1385)\pi, G\text{-wave})/\Gamma_{\text{total}}$	DOCUMENT ID	TECN	COMMENT	$\Gamma_6/\Gamma$
VALUE ~0.01	SARANTSEV	19	DPWA	$\bar{K}N$ multichannel
$\Gamma(\Lambda(1520)\pi, F\text{-wave})/\Gamma_{\text{total}}$	DOCUMENT ID	TECN	COMMENT	$\Gamma_7/\Gamma$
VALUE <b>0.01 ± 0.01</b>	SARANTSEV	19	DPWA	$\bar{K}N$ multichannel
$\Gamma(\Lambda(1520)\pi, H\text{-wave})/\Gamma_{\text{total}}$	DOCUMENT ID	TECN	COMMENT	$\Gamma_8/\Gamma$
VALUE ~0	SARANTSEV	19	DPWA	$\bar{K}N$ multichannel
$\Gamma(N\bar{K}^*(892), S=3/2, D\text{-wave})/\Gamma_{\text{total}}$	DOCUMENT ID	TECN	COMMENT	$\Gamma_9/\Gamma$
VALUE <b>0.06 ± 0.03</b>	SARANTSEV	19	DPWA	$\bar{K}N$ multichannel
$\Gamma(\Delta\bar{K}, G\text{-wave})/\Gamma_{\text{total}}$	DOCUMENT ID	TECN	COMMENT	$\Gamma_{10}/\Gamma$
VALUE <b>0.01 ± 0.01</b>	SARANTSEV	19	DPWA	$\bar{K}N$ multichannel

### $\Sigma(2100)$ REFERENCES

SARANTSEV 19 EPJ A55 180 A.V. Sarantsev et al. (BONN, PNPI)  
 BARBARO... 70 Duke Conf. 173 A. Barbaro-Galsteri (LRL) IJP  
 Hyperon Resonances, 1970

**$\Sigma(2160) 1/2^-$**

$I(J^P) = 1(\frac{1}{2}^-)$  Status: \*

OMITTED FROM SUMMARY TABLE

### $\Sigma(2160)$ POLE POSITION

REAL PART			
VALUE (MeV)	DOCUMENT ID	TECN	COMMENT
<b>2158 ± 25</b>	SARANTSEV	19	DPWA $\bar{K}N$ multichannel
-2xIMAGINARY PART			
VALUE (MeV)	DOCUMENT ID	TECN	COMMENT
<b>300 ± 300 -60</b>	SARANTSEV	19	DPWA $\bar{K}N$ multichannel

### $\Sigma(2160)$ POLE RESIDUES

Normalized residue in $N\bar{K} \rightarrow \Sigma(2160) \rightarrow N\bar{K}$			
MODULUS	PHASE (°)	DOCUMENT ID	TECN COMMENT
<b>0.29 ± 0.08</b>	<b>-20 ± 35</b>	SARANTSEV	19 DPWA $\bar{K}N$ multichannel
Normalized residue in $N\bar{K} \rightarrow \Sigma(2160) \rightarrow \Sigma\pi$			
MODULUS	PHASE (°)	DOCUMENT ID	TECN COMMENT
<b>0.14 ± 0.04</b>	<b>-5 ± 35</b>	SARANTSEV	19 DPWA $\bar{K}N$ multichannel

See key on page 999

Baryon Particle Listings  
 $\Sigma(2160), \Sigma(2230)$

**Normalized residue in  $N\bar{K} \rightarrow \Sigma(2160) \rightarrow \Lambda\pi$**

MODULUS	PHASE (°)	DOCUMENT ID	TECN	COMMENT
$0.39 \pm 0.08$	$85 \pm 25$	SARANTSEV 19	DPWA	$\bar{K}N$ multichannel

**Normalized residue in  $N\bar{K} \rightarrow \Sigma(2160) \rightarrow \Xi K$**

MODULUS	PHASE (°)	DOCUMENT ID	TECN	COMMENT
$0.05 \pm 0.02$	$-85 \pm 35$	SARANTSEV 19	DPWA	$\bar{K}N$ multichannel

**Normalized residue in  $N\bar{K} \rightarrow \Sigma(2160) \rightarrow \Lambda(1520)\pi$**

MODULUS	PHASE (°)	DOCUMENT ID	TECN	COMMENT
$0.025 \pm 0.015$		SARANTSEV 19	DPWA	$\bar{K}N$ multichannel

**Normalized residue in  $N\bar{K} \rightarrow \Sigma(2160) \rightarrow \Sigma(1385)\pi$**

MODULUS	PHASE (°)	DOCUMENT ID	TECN	COMMENT
$0.03 \pm 0.02$		SARANTSEV 19	DPWA	$\bar{K}N$ multichannel

**Normalized residue in  $N\bar{K} \rightarrow \Sigma(2160) \rightarrow \Delta\bar{K}$**

MODULUS	PHASE (°)	DOCUMENT ID	TECN	COMMENT
$0.035 \pm 0.02$	$-30 \pm 40$	SARANTSEV 19	DPWA	$\bar{K}N$ multichannel

**Normalized residue in  $N\bar{K} \rightarrow \Sigma(2160) \rightarrow N\bar{K}^*(892), S\text{-wave}$**

MODULUS	PHASE (°)	DOCUMENT ID	TECN	COMMENT
$0.09 \pm 0.03$	$-40 \pm 50$	SARANTSEV 19	DPWA	$\bar{K}N$ multichannel

**Normalized residue in  $N\bar{K} \rightarrow \Sigma(2160) \rightarrow N\bar{K}^*(892), D\text{-wave}$**

MODULUS	PHASE (°)	DOCUMENT ID	TECN	COMMENT
$0.04 \pm 0.03$		SARANTSEV 19	DPWA	$\bar{K}N$ multichannel

**$\Sigma(2160)$  MASS**

VALUE (MeV)	DOCUMENT ID	TECN	COMMENT
$2105 \pm 50$ OUR AVERAGE	Error includes scale factor of 3.4.		
$2165 \pm 23$	SARANTSEV 19	DPWA	$\bar{K}N$ multichannel
$2060 \pm 20$	ZHANG 13A	DPWA	$\bar{K}N$ multichannel

**$\Sigma(2160)$  WIDTH**

VALUE (MeV)	DOCUMENT ID	TECN	COMMENT
$313^{+120}_{-50}$ OUR AVERAGE			
$320^{+300}_{-60}$	SARANTSEV 19	DPWA	$\bar{K}N$ multichannel
$300 \pm 134$	ZHANG 13A	DPWA	$\bar{K}N$ multichannel

**$\Sigma(2160)$  DECAY MODES**

Mode	Fraction ( $\Gamma_i/\Gamma$ )
$\Gamma_1 N\bar{K}$	$(29 \pm 7) \%$
$\Gamma_2 \Sigma\pi$	$(7.0 \pm 2.0) \%$
$\Gamma_3 \Lambda\pi$	$(54 \pm 12) \%$
$\Gamma_4 N\bar{K}^*(892), S\text{-wave}$	$(3.0 \pm 1.0) \%$
$\Gamma_5 N\bar{K}^*(892), D\text{-wave}$	

**$\Sigma(2160)$  BRANCHING RATIOS**

**$\Gamma(N\bar{K})/\Gamma_{\text{total}}$**

VALUE	DOCUMENT ID	TECN	COMMENT	$\Gamma_1/\Gamma$
$0.29 \pm 0.07$	SARANTSEV 19	DPWA	$\bar{K}N$ multichannel	

**$\Gamma(\Sigma\pi)/\Gamma_{\text{total}}$**

VALUE	DOCUMENT ID	TECN	COMMENT	$\Gamma_2/\Gamma$
$0.07 \pm 0.02$	SARANTSEV 19	DPWA	$\bar{K}N$ multichannel	

**$\Gamma(\Lambda\pi)/\Gamma_{\text{total}}$**

VALUE	DOCUMENT ID	TECN	COMMENT	$\Gamma_3/\Gamma$
$0.54 \pm 0.12$	SARANTSEV 19	DPWA	$\bar{K}N$ multichannel	

**$\Gamma(N\bar{K}^*(892), S\text{-wave})/\Gamma_{\text{total}}$**

VALUE	DOCUMENT ID	TECN	COMMENT	$\Gamma_4/\Gamma$
$0.03 \pm 0.01$	SARANTSEV 19	DPWA	$\bar{K}N$ multichannel	

**$\Gamma(N\bar{K}^*(892), D\text{-wave})/\Gamma_{\text{total}}$**

VALUE	DOCUMENT ID	TECN	COMMENT	$\Gamma_5/\Gamma$
$\sim 0.01$	SARANTSEV 19	DPWA	$\bar{K}N$ multichannel	

**$\Sigma(2160)$  REFERENCES**

SARANTSEV 19	EPJ A55 180	A.V. Sarantsev et al.	(BONN, PNPI)
ZHANG 13A	PR C88 035205	H. Zhang et al.	(KSU)

**$\Sigma(2230) 3/2^+$**

$I(J^P) = 1(\frac{3}{2}^+)$  Status: \*

OMITTED FROM SUMMARY TABLE

**$\Sigma(2230)$  POLE POSITION**

**REAL PART**

VALUE (MeV)	DOCUMENT ID	TECN	COMMENT
$2234 \pm 25$	SARANTSEV 19	DPWA	$\bar{K}N$ multichannel

**-2xIMAGINARY PART**

VALUE (MeV)	DOCUMENT ID	TECN	COMMENT
$340 \pm 45$	SARANTSEV 19	DPWA	$\bar{K}N$ multichannel

**$\Sigma(2230)$  POLE RESIDUES**

**Normalized residue in  $N\bar{K} \rightarrow \Sigma(2230) \rightarrow N\bar{K}$**

MODULUS	PHASE (°)	DOCUMENT ID	TECN	COMMENT
$0.07 \pm 0.02$	$25 \pm 15$	SARANTSEV 19	DPWA	$\bar{K}N$ multichannel

**Normalized residue in  $N\bar{K} \rightarrow \Sigma(2230) \rightarrow \Sigma\pi$**

MODULUS	PHASE (°)	DOCUMENT ID	TECN	COMMENT
$0.03 \pm 0.02$	$180 \pm 25$	SARANTSEV 19	DPWA	$\bar{K}N$ multichannel

**Normalized residue in  $N\bar{K} \rightarrow \Sigma(2030) \rightarrow \Lambda\pi$**

MODULUS	PHASE (°)	DOCUMENT ID	TECN	COMMENT
$0.11 \pm 0.05$	$-16 \pm 10$	SARANTSEV 19	DPWA	$\bar{K}N$ multichannel

**Normalized residue in  $N\bar{K} \rightarrow \Sigma(2230) \rightarrow \Xi K$**

MODULUS	PHASE (°)	DOCUMENT ID	TECN	COMMENT
$0.04 \pm 0.02$	$155 \pm 20$	SARANTSEV 19	DPWA	$\bar{K}N$ multichannel

**Normalized residue in  $N\bar{K} \rightarrow \Sigma(2230) \rightarrow \Lambda(1520)\pi, S\text{-wave}$**

MODULUS	PHASE (°)	DOCUMENT ID	TECN	COMMENT
$0.12 \pm 0.05$	$-80 \pm 25$	SARANTSEV 19	DPWA	$\bar{K}N$ multichannel

**Normalized residue in  $N\bar{K} \rightarrow \Sigma(2230) \rightarrow \Lambda(1520)\pi, D\text{-wave}$**

MODULUS	PHASE (°)	DOCUMENT ID	TECN	COMMENT
$0.03 \pm 0.02$	$160 \pm 30$	SARANTSEV 19	DPWA	$\bar{K}N$ multichannel

**Normalized residue in  $N\bar{K} \rightarrow \Sigma(2230) \rightarrow \Sigma(1385)\pi, P\text{-wave}$**

MODULUS	PHASE (°)	DOCUMENT ID	TECN	COMMENT
$0.05 \pm 0.02$	$60 \pm 25$	SARANTSEV 19	DPWA	$\bar{K}N$ multichannel

**Normalized residue in  $N\bar{K} \rightarrow \Sigma(2230) \rightarrow \Sigma(1385)\pi, F\text{-wave}$**

MODULUS	PHASE (°)	DOCUMENT ID	TECN	COMMENT
$0.05 \pm 0.03$	$-70 \pm 20$	SARANTSEV 19	DPWA	$\bar{K}N$ multichannel

**Normalized residue in  $N\bar{K} \rightarrow \Sigma(2230) \rightarrow \Delta\bar{K}, P\text{-wave}$**

MODULUS	PHASE (°)	DOCUMENT ID	TECN	COMMENT
$0.11 \pm 0.04$	$60 \pm 15$	SARANTSEV 19	DPWA	$\bar{K}N$ multichannel

**Normalized residue in  $N\bar{K} \rightarrow \Sigma(2230) \rightarrow \Delta\bar{K}, F\text{-wave}$**

MODULUS	PHASE (°)	DOCUMENT ID	TECN	COMMENT
$0.07 \pm 0.03$	$90 \pm 25$	SARANTSEV 19	DPWA	$\bar{K}N$ multichannel

**Normalized residue in  $N\bar{K} \rightarrow \Sigma(2230) \rightarrow N\bar{K}^*(892), S=1/2, P\text{-wave}$**

MODULUS	PHASE (°)	DOCUMENT ID	TECN	COMMENT
$0.08 \pm 0.04$	$40 \pm 45$	SARANTSEV 19	DPWA	$\bar{K}N$ multichannel

**Normalized residue in  $N\bar{K} \rightarrow \Sigma(2230) \rightarrow N\bar{K}^*(892), S=3/2, P\text{-wave}$**

MODULUS	PHASE (°)	DOCUMENT ID	TECN	COMMENT
$0.14 \pm 0.03$	$-40 \pm 45$	SARANTSEV 19	DPWA	$\bar{K}N$ multichannel

**Normalized residue in  $N\bar{K} \rightarrow \Sigma(2230) \rightarrow N\bar{K}^*(892), S=3/2, F\text{-wave}$**

MODULUS	PHASE (°)	DOCUMENT ID	TECN	COMMENT
$0.05 \pm 0.03$	$35 \pm 30$	SARANTSEV 19	DPWA	$\bar{K}N$ multichannel

**$\Sigma(2230)$  MASS**

VALUE (MeV)	DOCUMENT ID	TECN	COMMENT
$2240 \pm 27$	SARANTSEV 19	DPWA	$\bar{K}N$ multichannel

**$\Sigma(2230)$  WIDTH**

VALUE (MeV)	DOCUMENT ID	TECN	COMMENT
$345 \pm 50$	SARANTSEV 19	DPWA	$\bar{K}N$ multichannel

# Baryon Particle Listings

## $\Sigma(2230), \Sigma(2250)$

### $\Sigma(2230)$ DECAY MODES

Mode	Fraction ( $\Gamma_i/\Gamma$ )
$\Gamma_1 N\bar{K}$	( 6.0±2.0 ) %
$\Gamma_2 \Sigma \pi$	( 2.0±1.0 ) %
$\Gamma_3 \Lambda \pi$	( 12 ± 6 ) %
$\Gamma_4 \Xi K$	( 2.0±1.0 ) %
$\Gamma_5 \Lambda(1520)\pi, S\text{-wave}$	( 14 ± 5 ) %
$\Gamma_6 \Lambda(1520)\pi, D\text{-wave}$	
$\Gamma_7 \Sigma(1385)\pi, P\text{-wave}$	( 4 ± 4 ) %
$\Gamma_8 \Sigma(1385)\pi, F\text{-wave}$	( 3.0±2.0 ) %
$\Gamma_9 \Delta\bar{K}, P\text{-wave}$	( 14 ± 5 ) %
$\Gamma_{10} \Delta\bar{K}, F\text{-wave}$	( 8.0±2.0 ) %
$\Gamma_{11} N\bar{K}^*(892), S=1/2, F\text{-wave}$	( 8.0±3.0 ) %
$\Gamma_{12} N\bar{K}^*(892), S=3/2, F\text{-wave}$	( 26 ± 5 ) %

### $\Sigma(2230)$ BRANCHING RATIOS

$\Gamma(N\bar{K})/\Gamma_{\text{total}}$	DOCUMENT ID	TECN	COMMENT	$\Gamma_1/\Gamma$
VALUE <b>0.06±0.02</b>	SARANTSEV 19	DPWA	$\bar{K}N$ multichannel	
$\Gamma(\Sigma\pi)/\Gamma_{\text{total}}$	DOCUMENT ID	TECN	COMMENT	$\Gamma_2/\Gamma$
VALUE <b>0.02±0.01</b>	SARANTSEV 19	DPWA	$\bar{K}N$ multichannel	
$\Gamma(\Lambda\pi)/\Gamma_{\text{total}}$	DOCUMENT ID	TECN	COMMENT	$\Gamma_3/\Gamma$
VALUE <b>0.12±0.06</b>	SARANTSEV 19	DPWA	$\bar{K}N$ multichannel	
$\Gamma(\Xi K)/\Gamma_{\text{total}}$	DOCUMENT ID	TECN	COMMENT	$\Gamma_4/\Gamma$
VALUE <b>0.02±0.01</b>	SARANTSEV 19	DPWA	$\bar{K}N$ multichannel	
$\Gamma(\Lambda(1520)\pi, S\text{-wave})/\Gamma_{\text{total}}$	DOCUMENT ID	TECN	COMMENT	$\Gamma_5/\Gamma$
VALUE <b>0.14±0.05</b>	SARANTSEV 19	DPWA	$\bar{K}N$ multichannel	
$\Gamma(\Lambda(1520)\pi, D\text{-wave})/\Gamma_{\text{total}}$	DOCUMENT ID	TECN	COMMENT	$\Gamma_6/\Gamma$
••• We do not use the following data for averages, fits, limits, etc. ••• ~1	SARANTSEV 19	DPWA	$\bar{K}N$ multichannel	
$\Gamma(\Sigma(1385)\pi, P\text{-wave})/\Gamma_{\text{total}}$	DOCUMENT ID	TECN	COMMENT	$\Gamma_7/\Gamma$
VALUE <b>0.04±0.04</b>	SARANTSEV 19	DPWA	$\bar{K}N$ multichannel	
$\Gamma(\Sigma(1385)\pi, F\text{-wave})/\Gamma_{\text{total}}$	DOCUMENT ID	TECN	COMMENT	$\Gamma_8/\Gamma$
VALUE <b>0.03±0.02</b>	SARANTSEV 19	DPWA	$\bar{K}N$ multichannel	
$\Gamma(\Delta\bar{K}, P\text{-wave})/\Gamma_{\text{total}}$	DOCUMENT ID	TECN	COMMENT	$\Gamma_9/\Gamma$
VALUE <b>0.14±0.05</b>	SARANTSEV 19	DPWA	$\bar{K}N$ multichannel	
$\Gamma(\Delta\bar{K}, F\text{-wave})/\Gamma_{\text{total}}$	DOCUMENT ID	TECN	COMMENT	$\Gamma_{10}/\Gamma$
VALUE <b>0.08±0.02</b>	SARANTSEV 19	DPWA	$\bar{K}N$ multichannel	
$\Gamma(N\bar{K}^*(892), S=1/2, F\text{-wave})/\Gamma_{\text{total}}$	DOCUMENT ID	TECN	COMMENT	$\Gamma_{11}/\Gamma$
VALUE <b>0.08±0.03</b>	SARANTSEV 19	DPWA	$\bar{K}N$ multichannel	
$\Gamma(N\bar{K}^*(892), S=3/2, F\text{-wave})/\Gamma_{\text{total}}$	DOCUMENT ID	TECN	COMMENT	$\Gamma_{12}/\Gamma$
VALUE <b>0.26±0.05</b>	SARANTSEV 19	DPWA	$\bar{K}N$ multichannel	

### $\Sigma(2230)$ REFERENCES

SARANTSEV 19 EPJ A55 180 A.V. Sarantsev et al. (BONN, PNPI)

## $\Sigma(2250)$

$I(J^P) = 1(?)^?$  Status: \*\*\*

Results from partial-wave analyses are too weak to warrant separating them from the production and cross-section experiments. LASINSKI 71 in  $\bar{K}N$  using a Pomeron + resonances model, and DEBELLEFON 76, DEBELLEFON 77, and DEBELLEFON 78 in energy-dependent partial-wave analyses of  $\bar{K}N \rightarrow \Lambda\pi, \Sigma\pi$ , and  $N\bar{K}$ , respectively, suggest two resonances around this mass.

### $\Sigma(2250)$ MASS

VALUE (MeV)	DOCUMENT ID	TECN	COMMENT
<b>2210 to 2280 (<math>\approx 2250</math>) OUR ESTIMATE</b>			
2270±50	DEBELLEFON 78	DPWA	$D_5$ wave
2210±30	DEBELLEFON 78	DPWA	$G_9$ wave
2275±20	DEBELLEFON 77	DPWA	$D_5$ wave
2215±20	DEBELLEFON 77	DPWA	$G_9$ wave
2300±30	<sup>1</sup> DEBELLEFON 75B	HBC	$K^-p \rightarrow \Xi^*0 K^0$
2251 <sup>+30</sup> <sub>-20</sub>	VANHORN 75	DPWA	$K^-p \rightarrow \Lambda\pi^0, F_5$ wave
2280±14	AGUILAR-... 70B	HBC	$K^-p$ 3.9, 4.6 GeV/c
2237±11	BRICMAN 70	CNTR	Total, charge exchange
2255±10	COOL 70	CNTR	$K^-p, K^-d$ total
2250±7	BUGG 68	CNTR	$K^-p, K^-d$ total
••• We do not use the following data for averages, fits, limits, etc. •••			
2260	DEBELLEFON 76	IPWA	$D_5$ wave
2215	DEBELLEFON 76	IPWA	$G_9$ wave
2250±20	LU 70	CNTR	$\gamma p \rightarrow K^+ Y^*$
2245	BLANPIED 65	CNTR	$\gamma p \rightarrow K^+ Y^*$
2299±6	BOCK 65	HBC	$\bar{p}p$ 5.7 GeV/c

### $\Sigma(2250)$ WIDTH

VALUE (MeV)	DOCUMENT ID	TECN	COMMENT
<b>60 to 150 (<math>\approx 100</math>) OUR ESTIMATE</b>			
120±40	DEBELLEFON 78	DPWA	$D_5$ wave
80±20	DEBELLEFON 78	DPWA	$G_9$ wave
70±20	DEBELLEFON 77	DPWA	$D_5$ wave
60±20	DEBELLEFON 77	DPWA	$G_9$ wave
130±20	<sup>1</sup> DEBELLEFON 75B	HBC	$K^-p \rightarrow \Xi^*0 K^0$
192±30	VANHORN 75	DPWA	$K^-p \rightarrow \Lambda\pi^0, F_5$ wave
100±20	AGUILAR-... 70B	HBC	$K^-p$ 3.9, 4.6 GeV/c
164±50	BRICMAN 70	CNTR	Total, charge exchange
230±20	BUGG 68	CNTR	$K^-p, K^-d$ total
••• We do not use the following data for averages, fits, limits, etc. •••			
100	DEBELLEFON 76	IPWA	$D_5$ wave
140	DEBELLEFON 76	IPWA	$G_9$ wave
170	COOL 70	CNTR	$K^-p, K^-d$ total
125	LU 70	CNTR	$\gamma p \rightarrow K^+ Y^*$
150	BLANPIED 65	CNTR	$\gamma p \rightarrow K^+ Y^*$
21 <sup>+17</sup> <sub>-21</sub>	BOCK 65	HBC	$\bar{p}p$ 5.7 GeV/c

### $\Sigma(2250)$ DECAY MODES

Mode	Fraction ( $\Gamma_i/\Gamma$ )
$\Gamma_1 N\bar{K}$	<10 %
$\Gamma_2 \Lambda\pi$	seen
$\Gamma_3 \Sigma\pi$	seen
$\Gamma_4 N\bar{K}\pi$	
$\Gamma_5 \Xi(1530)K$	

### $\Sigma(2250)$ BRANCHING RATIOS

See "Sign conventions for resonance couplings" in the Note on  $\Lambda$  and  $\Sigma$  Resonances.

$\Gamma(N\bar{K})/\Gamma_{\text{total}}$	DOCUMENT ID	TECN	COMMENT	$\Gamma_1/\Gamma$
VALUE <b>&lt;0.1 OUR ESTIMATE</b>				
0.08±0.02	DEBELLEFON 78	DPWA	$D_5$ wave	
0.02±0.01	DEBELLEFON 78	DPWA	$G_9$ wave	

$(J+\frac{1}{2})\times\Gamma(N\bar{K})/\Gamma_{\text{total}}$	DOCUMENT ID	TECN	COMMENT	$\Gamma_1/\Gamma$
VALUE				
••• We do not use the following data for averages, fits, limits, etc. •••				
0.16±0.12	BRICMAN 70	CNTR	Total, charge exchange	
0.42	COOL 70	CNTR	$K^-p, K^-d$ total	
0.47	BUGG 68	CNTR		

See key on page 999

Baryon Particle Listings

$\Sigma(2250)$ ,  $\Sigma(2455)$  Bumps,  $\Sigma(2620)$  Bumps,  $\Sigma(3000)$  Bumps

$(\Gamma_1 \Gamma_f)^{1/2} / \Gamma_{\text{total}}$  in  $N\bar{K} \rightarrow \Sigma(2250) \rightarrow \Lambda\pi$   $(\Gamma_1 \Gamma_2)^{1/2} / \Gamma$

VALUE	DOCUMENT ID	TECN	COMMENT
-0.16 ± 0.03	VANHORN 75	DPWA	$K^- p \rightarrow \Lambda\pi^0, F_5$ wave

••• We do not use the following data for averages, fits, limits, etc. •••

+0.11	DEBELLEFON 76	IPWA	$D_5$ wave
-0.10	DEBELLEFON 76	IPWA	$G_9$ wave
-0.18	BARBARO... 70	DPWA	$K^- p \rightarrow \Lambda\pi^0, G_9$ wave

$(\Gamma_1 \Gamma_f)^{1/2} / \Gamma_{\text{total}}$  in  $N\bar{K} \rightarrow \Sigma(2250) \rightarrow \Sigma\pi$   $(\Gamma_1 \Gamma_3)^{1/2} / \Gamma$

VALUE	DOCUMENT ID	TECN	COMMENT
+0.06 ± 0.02	DEBELLEFON 77	DPWA	$D_5$ wave
-0.03 ± 0.02	DEBELLEFON 77	DPWA	$G_9$ wave
+0.07	BARBARO... 70	DPWA	$K^- p \rightarrow \Sigma\pi, G_9$ wave

$\Gamma(N\bar{K}) / \Gamma(\Sigma\pi)$   $\Gamma_1 / \Gamma_3$

VALUE	DOCUMENT ID	TECN	COMMENT
<0.18	BARNES 69	HBC	1 standard dev. limit

$\Gamma(\Lambda\pi) / \Gamma(\Sigma\pi)$   $\Gamma_2 / \Gamma_3$

VALUE	DOCUMENT ID	TECN	COMMENT
<0.18	BARNES 69	HBC	1 standard dev. limit

$(\Gamma_1 \Gamma_f)^{1/2} / \Gamma_{\text{total}}$  in  $N\bar{K} \rightarrow \Sigma(2250) \rightarrow \Xi(1530)K$   $(\Gamma_1 \Gamma_5)^{1/2} / \Gamma$

VALUE	DOCUMENT ID	TECN	COMMENT
0.18 ± 0.04	1 DEBELLEFON 75B	HBC	$K^- p \rightarrow \Xi^+ K^0$

$\Sigma(2250)$  FOOTNOTES

<sup>1</sup> Seen in the (initial and final state)  $D_5$  wave. Isospin not determined.

$\Sigma(2250)$  REFERENCES

DEBELLEFON 78	NC 42A 403	A. de Bellefon et al.	(CDEF, SACL) IJP
DEBELLEFON 77	NC 37A 175	A. de Bellefon et al.	(CDEF, SACL) IJP
DEBELLEFON 76	NP B109 129	A. de Bellefon, A. Berthon	(CDEF) IJP
Also	NP B90 1	A. de Bellefon et al.	(CDEF, SACL) IJP
DEBELLEFON 75B	NC 28A 289	A. de Bellefon et al.	(CDEF, SACL) IJP
VANHORN 75	NP B87 145	A.J. van Horn	(LBL) IJP
Also	NP B87 157	A.J. van Horn	(LBL) IJP
LASINSKI 71	NP B29 125	T.A. Lasinski	(EFI) IJP
AGUILAR... 70B	PRL 25 58	M. Aguilar-Benitez et al.	(BNL, SYRA)
BARBARO... 70	Duke Conf. 173	A. Barbaro-Galteri	(LRL) IJP
BRICMAN 70	PL 31B 152	C. Bricman et al.	(CERN, CAEN, SACL)
COOL 70	PR D1 1887	R.L. Cool et al.	(BNL) I
Also	PRL 16 1228	R.L. Cool et al.	(BNL) I
LU 70	PR D2 1846	D.C. Lu et al.	(YALE)
BARNES 69	PRL 22 479	V.E. Barnes et al.	(BNL, SYRA)
BUGG 68	PR 168 1466	D.V. Bugg et al.	(RHEL, BIRM, CAVE) I
BLANPIED 65	PRL 14 741	W.A. Blanpied et al.	(YALE, CEA)
BOCK 65	PL 17 166	R.K. Bock et al.	(CERN, SACL)

$\Sigma(2455)$  Bumps  $I(J^P) = 1(?)^?$  Status: \*\*

OMITTED FROM SUMMARY TABLE

There is also some slight evidence for  $Y^*$  states in this mass region from the reaction  $\gamma p \rightarrow K^+ X$  — see GREENBERG 68.

$\Sigma(2455)$  MASS

VALUE (MeV)	DOCUMENT ID	TECN	COMMENT
$\approx 2455$ OUR ESTIMATE			
2455 ± 10	ABRAMS 70	CNTR	$K^- p, K^- d$ total
2455 ± 7	BUGG 68	CNTR	$K^- p, K^- d$ total

$\Sigma(2455)$  WIDTH

VALUE (MeV)	DOCUMENT ID	TECN	COMMENT
140	ABRAMS 70	CNTR	$K^- p, K^- d$ total
100 ± 20	BUGG 68	CNTR	

$\Sigma(2455)$  DECAY MODES

Mode
$\Gamma_1$ $N\bar{K}$

$\Sigma(2455)$  BRANCHING RATIOS

$(J+\frac{1}{2}) \times \Gamma(N\bar{K}) / \Gamma_{\text{total}}$   $\Gamma_1 / \Gamma$

VALUE	DOCUMENT ID	TECN	COMMENT
0.39	ABRAMS 70	CNTR	$K^- p, K^- d$ total
0.05 ± 0.05	1 BRICMAN 70	CNTR	Total, charge exchange
0.3	BUGG 68	CNTR	

$\Sigma(2455)$  FOOTNOTES

<sup>1</sup> Fit of total cross section given by BRICMAN 70 is poor in this region.

$\Sigma(2455)$  REFERENCES

ABRAMS 70	PR D1 1917	R.J. Abrams et al.	(BNL) I
Also	PRL 19 678	R.J. Abrams et al.	(BNL)
BRICMAN 70	PL 31B 152	C. Bricman et al.	(CERN, CAEN, SACL)
BUGG 68	PR 168 1466	D.V. Bugg et al.	(RHEL, BIRM, CAVE) I
GREENBERG 68	PRL 20 221	J.S. Greenberg et al.	(YALE)

$\Sigma(2620)$  Bumps  $I(J^P) = 1(?)^?$  Status: \*\*

OMITTED FROM SUMMARY TABLE

$\Sigma(2620)$  MASS

VALUE (MeV)	DOCUMENT ID	TECN	COMMENT
$\approx 2620$ OUR ESTIMATE			
2542 ± 22	DIBIANCA 75	DBC	$K^- N \rightarrow \Xi K\pi$
2620 ± 15	ABRAMS 70	CNTR	$K^- p, K^- d$ total

$\Sigma(2620)$  WIDTH

VALUE (MeV)	DOCUMENT ID	TECN	COMMENT
221 ± 81	DIBIANCA 75	DBC	$K^- N \rightarrow \Xi K\pi$
175	ABRAMS 70	CNTR	$K^- p, K^- d$ total

$\Sigma(2620)$  DECAY MODES

Mode
$\Gamma_1$ $N\bar{K}$

$\Sigma(2620)$  BRANCHING RATIOS

$(J+\frac{1}{2}) \times \Gamma(N\bar{K}) / \Gamma_{\text{total}}$   $\Gamma_1 / \Gamma$

VALUE	DOCUMENT ID	TECN	COMMENT
0.32	ABRAMS 70	CNTR	$K^- p, K^- d$ total
0.36 ± 0.12	BRICMAN 70	CNTR	Total, charge exchange

$\Sigma(2620)$  REFERENCES

DIBIANCA 75	NP B98 137	F.A. Dibianca, R.J. Endorf	(CMU)
ABRAMS 70	PR D1 1917	R.J. Abrams et al.	(BNL) I
Also	PRL 19 678	R.J. Abrams et al.	(BNL)
BRICMAN 70	PL 31B 152	C. Bricman et al.	(CERN, CAEN, SACL)

$\Sigma(3000)$  Bumps  $I(J^P) = 1(?)^?$  Status: \*

OMITTED FROM SUMMARY TABLE

Seen as an enhancement in  $\Lambda\pi$  and  $\bar{K}N$  invariant mass spectra and in the missing mass of neutrals recoiling against a  $K^0$ .

$\Sigma(3000)$  MASS

VALUE (MeV)	DOCUMENT ID	TECN	CHG	COMMENT
$\approx 3000$ OUR ESTIMATE				
3000	EHRlich 66	HBC	0	$\pi^- p$ 7.91 GeV/c

$\Sigma(3000)$  DECAY MODES

Mode
$\Gamma_1$ $N\bar{K}$
$\Gamma_2$ $\Lambda\pi$

$\Sigma(3000)$  REFERENCES

EHRlich 66	PR 152 1194	R. Ehrlich, W. Selove, H. Yuta	(PENN) I
------------	-------------	--------------------------------	----------

## Baryon Particle Listings

 $\Sigma(3170)$  Bumps **$\Sigma(3170)$  Bumps** $I(J^P) = 1(?^?)$  Status: \*

OMITTED FROM SUMMARY TABLE

Seen by AMIRZADEH 79 as a narrow 6.5-standard-deviation enhancement in the reaction  $K^- p \rightarrow Y^{*+} \pi^-$  using data from independent high statistics bubble chamber experiments at 8.25 and 6.5 GeV/c. The dominant decay modes are multibody, multistrange final states and the production is via isospin-3/2 baryon exchange. Isospin 1 is favored.

Not seen in a  $K^- p$  experiment in LASS at 11 GeV/c (ASTON 85B).

 **$\Sigma(3170)$  MASS  
(PRODUCTION EXPERIMENTS)**

VALUE (MeV)	EVTS	DOCUMENT ID	TECN	COMMENT
$\approx 3170$ OUR ESTIMATE				
$3170 \pm 5$	35	AMIRZADEH 79	HBC	$K^- p \rightarrow Y^{*+} \pi^-$

 **$\Sigma(3170)$  WIDTH  
(PRODUCTION EXPERIMENTS)**

VALUE (MeV)	EVTS	DOCUMENT ID	TECN	COMMENT
<20	35	<sup>1</sup> AMIRZADEH 79	HBC	$K^- p \rightarrow Y^{*+} \pi^-$

 **$\Sigma(3170)$  DECAY MODES  
(PRODUCTION EXPERIMENTS)**

Mode	Fraction ( $\Gamma_i/\Gamma$ )
$\Gamma_1$ $\Lambda K \bar{K} \pi$ 's	seen
$\Gamma_2$ $\Sigma K \bar{K} \pi$ 's	seen
$\Gamma_3$ $\Xi K \pi$ 's	seen

 **$\Sigma(3170)$  BRANCHING RATIOS  
(PRODUCTION EXPERIMENTS)**

$\Gamma(\Lambda K \bar{K} \pi \text{'s})/\Gamma_{\text{total}}$	$\Gamma_1/\Gamma$		
VALUE	DOCUMENT ID	TECN	COMMENT
seen	AMIRZADEH 79	HBC	$K^- p \rightarrow Y^{*+} \pi^-$
$\Gamma(\Sigma K \bar{K} \pi \text{'s})/\Gamma_{\text{total}}$	$\Gamma_2/\Gamma$		
VALUE	DOCUMENT ID	TECN	COMMENT
seen	AMIRZADEH 79	HBC	$K^- p \rightarrow Y^{*+} \pi^-$
$\Gamma(\Xi K \pi \text{'s})/\Gamma_{\text{total}}$	$\Gamma_3/\Gamma$		
VALUE	DOCUMENT ID	TECN	COMMENT
seen	AMIRZADEH 79	HBC	$K^- p \rightarrow Y^{*+} \pi^-$

 **$\Sigma(3170)$  FOOTNOTES  
(PRODUCTION EXPERIMENTS)**

<sup>1</sup> Observed width consistent with experimental resolution.

 **$\Sigma(3170)$  REFERENCES  
(PRODUCTION EXPERIMENTS)**

ASTON 85B	PR D32 2270	D. Aston <i>et al.</i>	(SLAC, CARL, CNRC, CINC)
AMIRZADEH 79	PL 89B 125	J. Amirzadeh <i>et al.</i>	(BIRM, CERN, GLAS+) <sup>1</sup>
Also	Toronto Conf. 263	J.B. Kinson <i>et al.</i>	(BIRM, CERN, GLAS+) <sup>1</sup>

## $\Xi$ BARYONS

### $(S = -2, I = 1/2)$

$\Xi^0 = uss, \Xi^- = dss$

$\Xi^0$

$I(J^P) = \frac{1}{2}(\frac{1}{2}^+)$  Status: \*\*\*\*

The parity has not actually been measured, but + is of course expected.

### $\Xi^0$ MASS

The fit uses the  $\Xi^0, \Xi^-,$  and  $\Xi^+$  masses and the  $\Xi^- - \Xi^0$  mass difference. It assumes that the  $\Xi^-$  and  $\Xi^+$  masses are the same.

VALUE (MeV)	EVTS	DOCUMENT ID	TECN	COMMENT
<b>1314.86 ± 0.20 OUR FIT</b>				
<b>1314.82 ± 0.06 ± 0.20</b>	3120	FANTI	00 NA48	$p$ Be, 450 GeV
• • • We do not use the following data for averages, fits, limits, etc. • • •				
1315.2 ± 0.92	49	WILQUET	72 HLBC	
1313.4 ± 1.8	1	PALMER	68 HBC	

### $m_{\Xi^-} - m_{\Xi^0}$

The fit uses the  $\Xi^0, \Xi^-,$  and  $\Xi^+$  masses and the  $\Xi^- - \Xi^0$  mass difference. It assumes that the  $\Xi^-$  and  $\Xi^+$  masses are the same.

VALUE (MeV)	EVTS	DOCUMENT ID	TECN	COMMENT
<b>6.85 ± 0.21 OUR FIT</b>				
<b>6.3 ± 0.7 OUR AVERAGE</b>				
6.9 ± 2.2	29	LONDON	66 HBC	
6.1 ± 0.9	88	PJERROU	65B HBC	
6.8 ± 1.6	23	JAUNEAU	63 FBC	
• • • We do not use the following data for averages, fits, limits, etc. • • •				
6.1 ± 1.6	45	CARMONY	64B HBC	See PJERROU 65B

### $\Xi^0$ MEAN LIFE

VALUE ( $10^{-10}$ s)	EVTS	DOCUMENT ID	TECN	COMMENT
<b>2.90 ± 0.09 OUR AVERAGE</b>				
2.83 ± 0.16	6300	1 ZECH	77 SPEC	Neutral hyperon beam
2.86 <sup>+0.21</sup> <sub>-0.19</sub>	652	BALTAY	74 HBC	1.75 GeV/c $K^- p$
2.90 <sup>+0.32</sup> <sub>-0.27</sub>	157	2 MAYEUR	72 HLBC	2.1 GeV/c $K^-$
3.07 <sup>+0.22</sup> <sub>-0.20</sub>	340	DAUBER	69 HBC	
3.0 ± 0.5	80	PJERROU	65B HBC	
2.5 <sup>+0.4</sup> <sub>-0.3</sub>	101	HUBBARD	64 HBC	
3.9 <sup>+1.4</sup> <sub>-0.8</sub>	24	JAUNEAU	63 FBC	
• • • We do not use the following data for averages, fits, limits, etc. • • •				
3.5 <sup>+1.0</sup> <sub>-0.8</sub>	45	CARMONY	64B HBC	See PJERROU 65B

<sup>1</sup> The ZECH 77 result is  $\tau_{\Xi^0} = [2.77 - (\tau_A - 2.69)] \times 10^{-10}$  s, in which we use  $\tau_A = 2.63 \times 10^{-10}$  s.

<sup>2</sup> The MAYEUR 72 value is modified by the erratum.

### $\Xi^0$ MAGNETIC MOMENT

See the "Note on Baryon Magnetic Moments" in the  $\Lambda$  Listings.

VALUE ( $\mu_N$ )	EVTS	DOCUMENT ID	TECN	COMMENT
<b>-1.250 ± 0.014 OUR AVERAGE</b>				
-1.253 ± 0.014	270k	COX	81 SPEC	
-1.20 ± 0.06	42k	BUNCE	79 SPEC	

### $\Xi^0$ DECAY MODES

Mode	Fraction ( $\Gamma_i/\Gamma$ )	Confidence level
$\Gamma_1 \Lambda\pi^0$	(99.524 ± 0.012) %	
$\Gamma_2 \Lambda\gamma$	(1.17 ± 0.07) × 10 <sup>-3</sup>	
$\Gamma_3 \Lambda e^+ e^-$	(7.6 ± 0.6) × 10 <sup>-6</sup>	
$\Gamma_4 \Sigma^0 \gamma$	(3.33 ± 0.10) × 10 <sup>-3</sup>	
$\Gamma_5 \Sigma^+ e^- \bar{\nu}_e$	(2.52 ± 0.08) × 10 <sup>-4</sup>	
$\Gamma_6 \Sigma^+ \mu^- \bar{\nu}_\mu$	(2.33 ± 0.35) × 10 <sup>-6</sup>	

### $\Delta S = \Delta Q$ (SQ) violating modes or $\Delta S = 2$ forbidden ( $S_2$ ) modes

$\Gamma$	Mode	SQ	Value	Confidence level
$\Gamma_7$	$\Sigma^- e^+ \nu_e$	SQ	< 9	× 10 <sup>-4</sup> 90%
$\Gamma_8$	$\Sigma^- \mu^+ \nu_\mu$	SQ	< 9	× 10 <sup>-4</sup> 90%
$\Gamma_9$	$p \pi^-$	$S_2$	< 8	× 10 <sup>-6</sup> 90%
$\Gamma_{10}$	$p e^- \bar{\nu}_e$	$S_2$	< 1.3	× 10 <sup>-3</sup>
$\Gamma_{11}$	$p \mu^- \bar{\nu}_\mu$	$S_2$	< 1.3	× 10 <sup>-3</sup>

### CONSTRAINED FIT INFORMATION

An overall fit to 5 branching ratios uses 11 measurements and one constraint to determine 5 parameters. The overall fit has a  $\chi^2 = 7.5$  for 7 degrees of freedom.

The following *off-diagonal* array elements are the correlation coefficients  $\langle \delta x_i \delta x_j \rangle / (\delta x_i \delta x_j)$ , in percent, from the fit to the branching fractions,  $x_i \equiv \Gamma_i/\Gamma_{\text{total}}$ . The fit constrains the  $x_i$  whose labels appear in this array to sum to one.

$x_2$	-57			
$x_4$	-82	0		
$x_5$	-7	0	0	
$x_6$	0	0	0	1
	$x_1$	$x_2$	$x_4$	$x_5$

### $\Xi^0$ BRANCHING RATIOS

#### $\Gamma(\Lambda\gamma)/\Gamma(\Lambda\pi^0)$ $\Gamma_2/\Gamma_1$

VALUE (units 10 <sup>-3</sup> )	EVTS	DOCUMENT ID	TECN	COMMENT
<b>1.17 ± 0.07 OUR FIT</b>				
<b>1.17 ± 0.07 OUR AVERAGE</b>				
1.17 ± 0.05 ± 0.06	672	<sup>3</sup> LAI	04A NA48	$p$ Be, 450 GeV
1.91 ± 0.34 ± 0.19	31	<sup>4</sup> FANTI	00 NA48	$p$ Be, 450 GeV
1.06 ± 0.12 ± 0.11	116	JAMES	90 SPEC	FNAL hyperons
<sup>3</sup> LAI 04A used our 2002 value of 99.5% for the $\Xi^0 \rightarrow \Lambda\pi^0$ branching fraction to get $\Gamma(\Xi^0 \rightarrow \Lambda\gamma)/\Gamma_{\text{total}} = (1.16 \pm 0.05 \pm 0.06) \times 10^{-3}$ . We adjust slightly to go back to what was directly measured.				
<sup>4</sup> FANTI 00 used our 1998 value of 99.5% for the $\Xi^0 \rightarrow \Lambda\pi^0$ branching fraction to get $\Gamma(\Xi^0 \rightarrow \Lambda\gamma)/\Gamma_{\text{total}} = (1.90 \pm 0.34 \pm 0.19) \times 10^{-3}$ . We adjust slightly to go back to what was directly measured.				

#### $\Gamma(\Lambda e^+ e^-)/\Gamma_{\text{total}}$ $\Gamma_3/\Gamma$

VALUE (units 10 <sup>-6</sup> )	EVTS	DOCUMENT ID	TECN	COMMENT
<b>7.6 ± 0.4 ± 0.5</b>	397 ± 21	<sup>5</sup> BATLEY	07c NA48	$p$ Be, 400 GeV
<sup>5</sup> This BATLEY 07c result is consistent with internal bremsstrahlung.				

#### $\Gamma(\Sigma^0 \gamma)/\Gamma(\Lambda\pi^0)$ $\Gamma_4/\Gamma_1$

VALUE (units 10 <sup>-3</sup> )	EVTS	DOCUMENT ID	TECN	COMMENT
<b>3.35 ± 0.10 OUR FIT</b>				
<b>3.35 ± 0.10 OUR AVERAGE</b>				
3.34 ± 0.05 ± 0.09	4045	ALAVI-HARATI 01c	KTEV	$p$ nucleus, 800 GeV
3.16 ± 0.76 ± 0.32	17	<sup>6</sup> FANTI	00 NA48	$p$ Be, 450 GeV
3.56 ± 0.42 ± 0.10	85	TEIGE	89 SPEC	FNAL hyperons
<sup>6</sup> FANTI 00 used our 1998 value of 99.5% for the $\Xi^0 \rightarrow \Lambda\pi^0$ branching fraction to get $\Gamma(\Xi^0 \rightarrow \Sigma^0 \gamma)/\Gamma_{\text{total}} = (3.14 \pm 0.76 \pm 0.32) \times 10^{-3}$ . We adjust slightly to go back to what was directly measured.				

#### $\Gamma(\Sigma^+ e^- \bar{\nu}_e)/\Gamma_{\text{total}}$ $\Gamma_5/\Gamma$

VALUE (units 10 <sup>-4</sup> )	EVTS	DOCUMENT ID	TECN	COMMENT
<b>2.52 ± 0.08 OUR FIT</b>				
<b>2.53 ± 0.08 OUR AVERAGE</b>				
2.51 ± 0.03 ± 0.09	6101	BATLEY	07 NA48	$p$ Be, 400 GeV
2.55 ± 0.14 ± 0.10	419	<sup>7</sup> BATLEY	07 NA48	$p$ Be, 400 GeV
2.71 ± 0.22 ± 0.31	176	AFFOLDER	99 KTEV	$p$ nucleus, 800 GeV
<sup>7</sup> This BATLEY 07 result is for $\Xi^0 \rightarrow \Sigma^- e^+ \nu_e$ events.				

#### $\Gamma(\Sigma^+ \mu^- \bar{\nu}_\mu)/\Gamma_{\text{total}}$ $\Gamma_6/\Gamma$

VALUE (units 10 <sup>-6</sup> )	EVTS	DOCUMENT ID	TECN	COMMENT
<b>2.3 ± 0.4 OUR FIT</b>				
<b>2.17 ± 0.32 ± 0.17</b>				
2.17 ± 0.32 ± 0.17	66	<sup>8</sup> BATLEY	13 NA48	$p$ Be, 400 GeV
<sup>8</sup> BATLEY 13 used $\Xi^0 \rightarrow \Sigma^+ e^- \bar{\nu}_e$ decay as a normalization mode and its branching fraction value of $(2.51 \pm 0.03 \pm 0.09) \times 10^{-4}$ from BATLEY 07.				

#### $\Gamma(\Sigma^+ \mu^- \bar{\nu}_\mu)/\Gamma(\Sigma^+ e^- \bar{\nu}_e)$ $\Gamma_6/\Gamma_5$

VALUE	EVTS	DOCUMENT ID	TECN	COMMENT
<b>0.0092 ± 0.0015 OUR FIT</b>				
0.018 <sup>+0.007</sup> <sub>-0.005</sub> ± 0.002	9	ABOUZAID	05 KTEV	$p$ nucleus 800 GeV

## Baryon Particle Listings

=0

 $\Gamma(\Sigma^- e^+ \nu_e)/\Gamma(\Lambda\pi^0)$   $\Gamma_7/\Gamma_1$ Test of  $\Delta S = \Delta Q$  rule.

VALUE (units $10^{-3}$ )	CL%	EVTS	DOCUMENT ID	TECN	COMMENT
<0.9	90	0	YEH	74	HBC Effective denom.=2500
••• We do not use the following data for averages, fits, limits, etc. •••					
<1.5			DAUBER	69	HBC
<6			HUBBARD	66	HBC

 $\Gamma(\Sigma^- \mu^+ \nu_\mu)/\Gamma(\Lambda\pi^0)$   $\Gamma_8/\Gamma_1$ Test of  $\Delta S = \Delta Q$  rule.

VALUE (units $10^{-3}$ )	CL%	EVTS	DOCUMENT ID	TECN	COMMENT
<0.9	90	0	YEH	74	HBC Effective denom.=2500
••• We do not use the following data for averages, fits, limits, etc. •••					
<1.5			DAUBER	69	HBC
<6			HUBBARD	66	HBC

 $\Gamma(p\pi^-)/\Gamma(\Lambda\pi^0)$   $\Gamma_9/\Gamma_1$  $\Delta S=2$ . Forbidden in first-order weak interaction.

VALUE (units $10^{-6}$ )	CL%	EVTS	DOCUMENT ID	TECN	COMMENT
< 8.2	90		WHITE	05	HYCP $p$ Cu, 800 GeV
••• We do not use the following data for averages, fits, limits, etc. •••					
< 36	90		GEWENIGER	75	SPEC
<1800	90	0	YEH	74	HBC Effective denom.=1300
< 900			DAUBER	69	HBC
<5000			HUBBARD	66	HBC

 $\Gamma(p e^- \bar{\nu}_e)/\Gamma(\Lambda\pi^0)$   $\Gamma_{10}/\Gamma_1$  $\Delta S=2$ . Forbidden in first-order weak interaction.

VALUE (units $10^{-3}$ )	CL%	EVTS	DOCUMENT ID	TECN	COMMENT
<1.3			DAUBER	69	HBC
••• We do not use the following data for averages, fits, limits, etc. •••					
<3.4	90	0	YEH	74	HBC Effective denom.=670
<6			HUBBARD	66	HBC

 $\Gamma(p\mu^- \bar{\nu}_\mu)/\Gamma(\Lambda\pi^0)$   $\Gamma_{11}/\Gamma_1$  $\Delta S=2$ . Forbidden in first-order weak interaction.

VALUE (units $10^{-3}$ )	CL%	EVTS	DOCUMENT ID	TECN	COMMENT
<1.3			DAUBER	69	HBC
••• We do not use the following data for averages, fits, limits, etc. •••					
<3.5	90	0	YEH	74	HBC Effective denom.=664
<6			HUBBARD	66	HBC

 $\Xi^0$  DECAY PARAMETERS

See the "Note on Baryon Decay Parameters" in the neutron Listings.

 $\alpha(\Xi^0) \alpha_-(\Lambda)$ This is a product of the  $\Xi^0 \rightarrow \Lambda\pi^0$  and  $\Lambda \rightarrow p\pi^-$  asymmetries.

VALUE	EVTS	DOCUMENT ID	TECN	COMMENT
<b>-0.261 ± 0.006 OUR AVERAGE</b>				
-0.276 ± 0.001 ± 0.035	4M	BATLEY	10B	NA48 $p$ Be, 400 GeV
-0.260 ± 0.004 ± 0.005	300k	HANDLER	82	SPEC FNAL hyperons
••• We do not use the following data for averages, fits, limits, etc. •••				
-0.317 ± 0.027	6075	BUNCE	78	SPEC FNAL hyperons
-0.35 ± 0.06	505	BALTAY	74	HBC $K^- p$ 1.75 GeV/c
-0.28 ± 0.06	739	DAUBER	69	HBC $K^- p$ 1.7-2.6 GeV/c

 $\alpha$  FOR  $\Xi^0 \rightarrow \Lambda\pi^0$ The above average,  $\alpha(\Xi^0)\alpha_-(\Lambda) = -0.261 \pm 0.006$ , divided by our current average  $\alpha_-(\Lambda) = 0.732 \pm 0.014$ , gives the following value for  $\alpha(\Xi^0)$ :

VALUE	DOCUMENT ID
<b>-0.356 ± 0.011 OUR EVALUATION</b>	

 $\phi$  ANGLE FOR  $\Xi^0 \rightarrow \Lambda\pi^0$  ( $\tan\phi = \beta/\gamma$ )

VALUE (°)	EVTS	DOCUMENT ID	TECN	COMMENT
<b>21 ± 12 OUR AVERAGE</b>				
16 ± 17	652	BALTAY	74	HBC 1.75 GeV/c $K^- p$
38 ± 19	739	DAUBER	69	HBC
- 8 ± 30	146	BERGE	66	HBC

<sup>9</sup>DAUBER 69 uses  $\alpha_\Lambda = 0.647 \pm 0.020$ .<sup>10</sup>The errors have been multiplied by 1.2 due to approximations used for the  $\Xi$  polarization; see DAUBER 69 for a discussion.

## RADIATIVE HYPERON DECAYS

Revised July 2011 by J.D. Jackson (LBNL).

The weak radiative decays of spin-1/2 hyperons,  $B_i \rightarrow B_f\gamma$ , yield information about matrix elements (form factors) similar to that gained from weak hadronic decays. For a polarized spin-1/2 hyperon decaying radiatively via a  $\Delta Q = 0$ ,  $\Delta S = 1$

transition, the angular distribution of the direction  $\hat{p}$  of the final spin-1/2 baryon in the hyperon rest frame is

$$\frac{dN}{d\Omega} = \frac{N}{4\pi} (1 + \alpha_\gamma \mathbf{P}_i \cdot \hat{p}). \quad (1)$$

Here  $\mathbf{P}_i$  is the polarization of the decaying hyperon, and  $\alpha_\gamma$  is the asymmetry parameter. In terms of the form factors  $F_1(q^2)$ ,  $F_2(q^2)$ , and  $G(q^2)$  of the effective hadronic weak electromagnetic vertex,

$$F_1(q^2)\gamma_\lambda + iF_2(q^2)\sigma_{\lambda\mu}q^\mu + G(q^2)\gamma_\lambda\gamma_5,$$

 $\alpha_\gamma$  is

$$\alpha_\gamma = \frac{2 \operatorname{Re}[G(0)F_M^*(0)]}{|G(0)|^2 + |F_M(0)|^2}, \quad (2)$$

where  $F_M = (m_i - m_f)[F_2 - F_1/(m_i + m_f)]$ . If the decaying hyperon is unpolarized, the decay baryon has a longitudinal polarization given by  $P_f = -\alpha_\gamma$  [1].

The angular distribution for the weak hadronic decay,  $B_i \rightarrow B_f\pi$ , has the same form as Eq. (1), but of course with a different asymmetry parameter,  $\alpha_\pi$ . Now, however, if the decaying hyperon is unpolarized, the decay baryon has a longitudinal polarization given by  $P_f = +\alpha_\pi$  [2,3]. The difference of sign is because the spins of the pion and photon are different.

$\Xi^0 \rightarrow \Lambda\gamma$  decay—The radiative decay  $\Xi^0 \rightarrow \Lambda\gamma$  of an unpolarized  $\Xi^0$  uses the hadronic decay  $\Lambda \rightarrow p\pi^-$  as the analyzer. As noted above, the longitudinal polarization of the  $\Lambda$  will be  $P_\Lambda = -\alpha_{\Xi\Lambda\gamma}$ . Let  $\alpha_-$  be the  $\Lambda \rightarrow p\pi^-$  asymmetry parameter and  $\theta_{\Lambda p}$  be the angle, as seen in the  $\Lambda$  rest frame, between the  $\Lambda$  line of flight and the proton momentum. Then the hadronic version of Eq. (1) applied to the  $\Lambda \rightarrow p\pi^-$  decay gives

$$\frac{dN}{d \cos \theta_{\Lambda p}} = \frac{N}{2} (1 - \alpha_{\Xi\Lambda\gamma} \alpha_- \cos \theta_{\Lambda p}) \quad (3)$$

for the angular distribution of the proton in the  $\Lambda$  frame. Our current value, from the CERN NA48/1 experiment [4], is  $\alpha_{\Xi\Lambda\gamma} = -0.704 \pm 0.019 \pm 0.064$ .

$\Xi^0 \rightarrow \Sigma^0\gamma$  decay—The asymmetry parameter here,  $\alpha_{\Xi\Sigma\gamma}$ , is measured by following the decay chain  $\Xi^0 \rightarrow \Sigma^0\gamma$ ,  $\Sigma^0 \rightarrow \Lambda\gamma$ ,  $\Lambda \rightarrow p\pi^-$ . Again, for an unpolarized  $\Xi^0$ , the longitudinal polarization of the  $\Sigma^0$  will be  $P_\Sigma = -\alpha_{\Xi\Sigma\gamma}$ . In the  $\Sigma^0 \rightarrow \Lambda\gamma$  decay, a parity-conserving magnetic-dipole transition, the polarization of the  $\Sigma^0$  is transferred to the  $\Lambda$ , as may be seen as follows. Let  $\theta_{\Sigma\Lambda}$  be the angle seen in the  $\Sigma^0$  rest frame between the  $\Sigma^0$  line of flight and the  $\Lambda$  momentum. For  $\Sigma^0$  helicity +1/2, the probability amplitudes for positive and negative spin states of the  $\Sigma^0$  along the  $\Lambda$  momentum are  $\cos(\theta_{\Sigma\Lambda}/2)$  and  $\sin(\theta_{\Sigma\Lambda}/2)$ . Then the amplitude for a negative helicity photon and a negative helicity  $\Lambda$  is  $\cos(\theta_{\Sigma\Lambda}/2)$ , while the amplitude for positive helicities for the photon and  $\Lambda$  is  $\sin(\theta_{\Sigma\Lambda}/2)$ . For  $\Sigma^0$  helicity -1/2, the amplitudes are interchanged. If the  $\Sigma^0$  has longitudinal polarization  $P_\Sigma$ , the probabilities for  $\Lambda$  helicities  $\pm 1/2$  are therefore

$$p(\pm 1/2) = \frac{1}{2}(1 \mp P_\Sigma) \cos^2(\theta_{\Sigma\Lambda}/2) + \frac{1}{2}(1 \pm P_\Sigma) \sin^2(\theta_{\Sigma\Lambda}/2), \quad (4)$$

See key on page 999

Baryon Particle Listings

$\Xi^0, \Xi^-$

and the longitudinal polarization of the  $\Lambda$  is

$$P_\Lambda = -P_\Sigma \cos \theta_{\Sigma\Lambda} + \alpha_{\Xi\Sigma\gamma} \cos \theta_{\Sigma\Lambda} \quad (5)$$

Using Eq. (1) for the  $\Lambda \rightarrow p\pi^-$  decay again, we get for the joint angular distribution of the  $\Sigma^0 \rightarrow \Lambda\gamma, \Lambda \rightarrow p\pi^-$  chain,

$$\frac{d^2N}{d\cos\theta_{\Sigma\Lambda} d\cos\theta_{\Lambda p}} = \frac{N}{4} (1 + \alpha_{\Xi\Sigma\gamma} \cos\theta_{\Sigma\Lambda} \alpha_- \cos\theta_{\Lambda p}) \quad (6)$$

Our current average for  $\alpha_{\Xi\Sigma\gamma}$  is  $-0.69 \pm 0.06$  [4,5].

References

1. R.E. Behrends, Phys. Rev. **111**, 1691 (1958); see Eq. (7) or (8).
2. In ancient times, the signs of the asymmetry term in the angular distributions of radiative and hadronic decays of polarized hyperons were sometimes opposite. For roughly 50 years, however, the overwhelming convention has been to make them the same. The aim, not always achieved, is to remove ambiguities.
3. For the definition of  $\alpha_\pi$ , see the note on "Baryon Decay Parameters" in the Neutron Listings.
4. J.R. Batley *et al.*, Phys. Lett. **B693**, 241 (2010).
5. A. Alavi-Harati *et al.*, Phys. Rev. Lett. **86**, 3239 (2001).

$\alpha$  FOR  $\Xi^0 \rightarrow \Lambda\gamma$

See the note above on "Radiative Hyperon Decays."

VALUE	EVTS	DOCUMENT ID	TECN	COMMENT
<b><math>-0.704 \pm 0.019 \pm 0.064</math></b>	52k	11 BATLEY	10B NA48	$p$ Be, 400 GeV
•••				We do not use the following data for averages, fits, limits, etc. •••
$-0.78 \pm 0.18 \pm 0.06$	672	LAI	04A NA48	See BATLEY 10B
$-0.43 \pm 0.44$	87	12 JAMES	90 SPEC	FNAL hyperons

<sup>11</sup> BATLEY 10B also measured the  $\Xi^0 \rightarrow \bar{\Lambda}\gamma$  asymmetry to be  $-0.798 \pm 0.064$  (no systematic error given) with 4769 events.  
<sup>12</sup> The sign has been changed; see the erratum, JAMES 02.

$\alpha$  FOR  $\Xi^0 \rightarrow \Lambda e^+ e^-$

VALUE	EVTS	DOCUMENT ID	TECN	COMMENT
<b><math>-0.8 \pm 0.2</math></b>	397 ± 21	13 BATLEY	07c NA48	$p$ Be, 400 GeV
<sup>13</sup>				This BATLEY 07c result is consistent with the asymmetry $\alpha$ for $\Xi^0 \rightarrow \Lambda\gamma$ , as expected if the mechanism is internal bremsstrahlung.

$\alpha$  FOR  $\Xi^0 \rightarrow \Sigma^0\gamma$

See the note above on "Radiative Hyperon Decays."

VALUE	EVTS	DOCUMENT ID	TECN	COMMENT
<b><math>-0.69 \pm 0.06</math> OUR AVERAGE</b>				
$-0.729 \pm 0.030 \pm 0.076$	15k	14 BATLEY	10B NA48	$p$ Be, 400 GeV
$-0.63 \pm 0.08 \pm 0.05$	4045	ALAVI-HARATI 01c	KTEV	$p$ nucleus, 800 GeV
•••				We do not use the following data for averages, fits, limits, etc. •••
$+0.20 \pm 0.32 \pm 0.05$	85	15 TEIGE	89 SPEC	FNAL hyperons

<sup>14</sup> BATLEY 10B also measured the  $\Xi^0 \rightarrow \bar{\Sigma}^0\gamma$  asymmetry to be  $-0.786 \pm 0.104$  (no systematic error given) with 1404 events.  
<sup>15</sup> This result has been withdrawn, due to an error. See the erratum, TEIGE 02.

$g_1(0)/f_1(0)$  FOR  $\Xi^0 \rightarrow \Sigma^+ e^- \bar{\nu}_e$

VALUE	EVTS	DOCUMENT ID	TECN	COMMENT
<b><math>1.22 \pm 0.05</math> OUR AVERAGE</b>				
$1.21 \pm 0.05$		BATLEY	13 NA48	$p$ Be, 400 GeV
$1.32 \pm_{-0.17}^{+0.21} \pm 0.05$	487	16 ALAVI-HARATI 01i	KTEV	$p$ nucleus, 800 GeV
•••				We do not use the following data for averages, fits, limits, etc. •••
$1.20 \pm 0.04 \pm 0.03$	6520	17 BATLEY	07 NA48	See BATLEY 13

<sup>16</sup> ALAVI-HARATI 01i assumes here that the second-class current is zero and that the weak-magnetism term takes its exact SU(3) value.  
<sup>17</sup> This BATLEY 07 result uses our 2006 value of  $V_{US}$  from semileptonic kaon decays as input.

$g_2(0)/f_1(0)$  FOR  $\Xi^0 \rightarrow \Sigma^+ e^- \bar{\nu}_e$

VALUE	EVTS	DOCUMENT ID	TECN	COMMENT
<b><math>-1.7 \pm_{-2.0}^{+2.1} \pm 0.5</math></b>	487	18 ALAVI-HARATI 01i	KTEV	$p$ nucleus, 800 GeV

<sup>18</sup> ALAVI-HARATI 01i thus assumes that  $g_2 = 0$  in calculating  $g_1/f_1$ , above.

$f_2(0)/f_1(0)$  FOR  $\Xi^0 \rightarrow \Sigma^+ e^- \bar{\nu}_e$

VALUE	EVTS	DOCUMENT ID	TECN	COMMENT
<b><math>2.0 \pm 0.9</math> OUR AVERAGE</b>				
$2.0 \pm 1.3$		BATLEY	13 NA48	$p$ Be, 400 GeV
$2.0 \pm 1.2 \pm 0.5$	487	ALAVI-HARATI 01i	KTEV	$p$ nucleus, 800 GeV

$\Xi^0$  REFERENCES

BATLEY	13	PL B720 105	J.R. Batley <i>et al.</i>	(CERN NA48/1 Collab.)
BATLEY	10B	PL B693 241	J.R. Batley <i>et al.</i>	(CERN NA48/1 Collab.)
BATLEY	07	PL B645 36	J.R. Batley <i>et al.</i>	(CERN NA48/1 Collab.)
BATLEY	07C	PL B650 1	J.R. Batley <i>et al.</i>	(CERN NA48 Collab.)
ABOUZAID	05	PRL 95 081801	E. Abouzaid <i>et al.</i>	(FNAL KTeV Collab.)
WHITE	05	PRL 94 101804	C.G. White <i>et al.</i>	(FNAL HyperCP Collab.)
LAI	04A	PL B584 251	A. Lai <i>et al.</i>	(CERN NA48 Collab.)
JAMES	02	PRL 89 169901 (err.)	C. James <i>et al.</i>	(MINN, MICH, WISC, RUTG)
TEIGE	02	PRL 89 169902 (err.)	S. Teige <i>et al.</i>	(RUTG, MICH, MINN)
ALAVI-HARATI	01C	PRL 86 3239	A. Alavi-Harati <i>et al.</i>	(FNAL KTeV Collab.)
ALAVI-HARATI	01i	PRL 87 132001	A. Alavi-Harati <i>et al.</i>	(FNAL KTeV Collab.)
FANTI	00	EPJ C12 69	V. Fanti <i>et al.</i>	(CERN NA48 Collab.)
AFFOLDER	99	PRL 82 3751	A. Affolder <i>et al.</i>	(FNAL KTeV Collab.)
JAMES	90	PRL 64 843	C. James <i>et al.</i>	(MINN, MICH, WISC, RUTG)
TEIGE	89	PRL 63 2717	S. Teige <i>et al.</i>	(RUTG, MICH, MINN)
HANDLER	82	PR D25 639	R. Handler <i>et al.</i>	(WISC, MICH, MINN)
COX	81	PRL 46 877	P.T. Cox <i>et al.</i>	(MICH, WISC, RUTG, MINN+)
BUNCE	79	PL B68 386	G.R.M. Bunce <i>et al.</i>	(BNL, MICH, RUTG+)
BUNCE	78	PR D18 633	G.R.M. Bunce <i>et al.</i>	(WISC, MICH, RUTG)
ZECH	77	NP B124 413	G. Zech <i>et al.</i>	(SIEG, CERN, DORT, HEIDH)
GEWENIGER	75	PL B78 193	C. Geweniger <i>et al.</i>	(CERN, HEIDH)
BALTAY	74	PR D9 419	C. Baltay <i>et al.</i>	(COLU, BING, J)
YEH	74	PR D10 3545	N. Yeh <i>et al.</i>	(BING, COLU)
MAYEUR	72	NP B47 333	C. Mayeur <i>et al.</i>	(BRUX, CERN, TUFTS, LOUC)
Also		NP B53 268 (erratum)	C. Mayeur	
WILQUET	72	PL B42 372	G. Wilquet <i>et al.</i>	(BRUX, CERN, TUFTS+)
DAUBER	69	PR 179 1262	P.M. Dauber <i>et al.</i>	(LRL)
PALMER	68	PL B26 323	R.B. Palmer <i>et al.</i>	(BNL, SYRA)
BERGE	66	PR 147 945	J.P. Berge <i>et al.</i>	(LRL)
HUBBARD	66	Thesis UCRL 11510	J.R. Hubbard	(LRL)
LONDON	66	PR 143 1034	G.W. London <i>et al.</i>	(BNL, SYRA)
PJERROU	65B	PRL 14 275	G.M. Pjerrou <i>et al.</i>	(UCLA)
Also		Thesis	G.M. Pjerrou	(UCLA)
CARMONY	64B	PRL 12 482	D.D. Carmony <i>et al.</i>	(UCLA)
HUBBARD	64	PR 135 B183	J.R. Hubbard <i>et al.</i>	(LRL)
JAUNEAU	63	PL 4 49	L. Jauneau <i>et al.</i>	(EPOL, CERN, LOUC+)
Also		Siena Conf. 1 1	L. Jauneau <i>et al.</i>	(EPOL, CERN, LOUC+)



$I(J^P) = \frac{1}{2}(1^+)$  Status: \* \* \* \*

The parity has not actually been measured, but + is of course expected.

We have omitted some results that have been superseded by later experiments. See our earlier editions.

$\Xi^-$  MASS

The fit uses the  $\Xi^-$ ,  $\Xi^+$ , and  $\Xi^0$  masses and the  $\Xi^- - \Xi^+$  mass difference. It assumes that the  $\Xi^-$  and  $\Xi^+$  masses are the same.

VALUE (MeV)	EVTS	DOCUMENT ID	TECN	COMMENT
<b><math>1321.71 \pm 0.07</math> OUR FIT</b>				
<b><math>1321.70 \pm 0.08 \pm 0.05</math></b>	2478 ± 68	ABDALLAH	06E DLPH	from Z decays
•••				We do not use the following data for averages, fits, limits, etc. •••
$1321.46 \pm 0.34$	632	DIBIANCA	75 DBC	4.9 GeV/c $K^-$ d
$1321.12 \pm 0.41$	268	WILQUET	72 HLBC	
$1321.87 \pm 0.51$	195	<sup>1</sup> GOLDWASSER 70	HBC	5.5 GeV/c $K^-$ p
$1321.67 \pm 0.52$	6	CHIEN	66 HBC	6.9 GeV/c $\bar{p}$ p
$1321.4 \pm 1.1$	299	LONDON	66 HBC	
$1321.3 \pm 0.4$	149	PJERROU	65B HBC	
$1321.1 \pm 0.3$	241	<sup>2</sup> BADIER	64 HBC	
$1321.4 \pm 0.4$	517	<sup>2</sup> JAUNEAU	63D FBC	
$1321.1 \pm 0.65$	62	<sup>2</sup> SCHNEIDER	63 HBC	

<sup>1</sup> GOLDWASSER 70 uses  $m_\Lambda = 1115.58$  MeV.  
<sup>2</sup> These masses have been increased 0.09 MeV because the  $\Lambda$  mass increased.

$\Xi^+$  MASS

The fit uses the  $\Xi^-$ ,  $\Xi^+$ , and  $\Xi^0$  masses and the  $\Xi^- - \Xi^+$  mass difference. It assumes that the  $\Xi^-$  and  $\Xi^+$  masses are the same.

VALUE (MeV)	EVTS	DOCUMENT ID	TECN	COMMENT
<b><math>1321.71 \pm 0.07</math> OUR FIT</b>				
<b><math>1321.73 \pm 0.08 \pm 0.05</math></b>	2256 ± 63	ABDALLAH	06E DLPH	from Z decays
•••				We do not use the following data for averages, fits, limits, etc. •••
$1321.6 \pm 0.8$	35	VOTRUBA	72 HBC	10 GeV/c $K^+$ p
$1321.2 \pm 0.4$	34	STONE	70 HBC	
$1320.69 \pm 0.93$	5	CHIEN	66 HBC	6.9 GeV/c $\bar{p}$ p

$(m_{\Xi^-} - m_{\Xi^+}) / m_{\Xi^-}$

A test of CPT invariance.

VALUE	DOCUMENT ID	TECN	COMMENT
<b><math>(-2.5 \pm 8.7) \times 10^{-5}</math></b>	ABDALLAH	06E DLPH	from Z decays

Downloaded from https://academic.oup.com/ptep/article/2020/8/083C01/5891211 by guest on 12 November 2020



# Baryon Particle Listings



## Ξ<sup>-</sup> MEAN LIFE

Measurements with an error > 0.2 × 10<sup>-10</sup> s or with systematic errors not included have been omitted.

VALUE (10 <sup>-10</sup> s)	EVTS	DOCUMENT ID	TECN	COMMENT
<b>1.639 ± 0.015 OUR AVERAGE</b>				
1.65 ± 0.07 ± 0.12	2478 ± 68	ABDALLAH	06E	DLPH from Z decays
1.652 ± 0.051	32k	BOURQUIN	84	SPEC Hyperon beam
1.665 ± 0.065	41k	BOURQUIN	79	SPEC Hyperon beam
1.609 ± 0.028	4286	HEMINGWAY	78	HBC 4.2 GeV/c K <sup>-</sup> p
1.67 ± 0.08		DIBIANCA	75	DBC 4.9 GeV/c K <sup>-</sup> d
1.63 ± 0.03	4303	BALTAY	74	HBC 1.75 GeV/c K <sup>-</sup> p
1.73 <sup>+0.08</sup> / <sub>-0.07</sub>	680	MAYEUR	72	HLBC 2.1 GeV/c K <sup>-</sup>
1.61 ± 0.04	2610	DAUBER	69	HBC
1.80 ± 0.16	299	LONDON	66	HBC
1.70 ± 0.12	246	PJERROU	65B	HBC
1.69 ± 0.07	794	HUBBARD	64	HBC
1.86 <sup>+0.15</sup> / <sub>-0.14</sub>	517	JAUNEAU	63D	FBC

## Ξ<sup>+</sup> MEAN LIFE

VALUE (10 <sup>-10</sup> s)	EVTS	DOCUMENT ID	TECN	COMMENT
<b>1.70 ± 0.08 ± 0.12</b>	2256 ± 63	ABDALLAH	06E	DLPH from Z decays
• • • We do not use the following data for averages, fits, limits, etc. • • •				
1.55 <sup>+0.35</sup> / <sub>-0.20</sub>	35	<sup>3</sup> VOTRUBA	72	HBC 10 GeV/c K <sup>+</sup> p
1.6 ± 0.3	34	STONE	70	HBC
1.9 <sup>+0.7</sup> / <sub>-0.5</sub>	12	<sup>3</sup> SHEN	67	HBC
1.51 ± 0.55	5	<sup>3</sup> CHIEN	66	HBC 6.9 GeV/c $\bar{p}p$

$$(\tau_{\Xi^-} - \tau_{\Xi^+}) / \tau_{\Xi^-}$$

A test of CPT invariance.

VALUE	DOCUMENT ID	TECN	COMMENT
<b>-0.01 ± 0.07</b>	ABDALLAH	06E	DLPH from Z decays

## Ξ<sup>-</sup> MAGNETIC MOMENT

See the "Note on Baryon Magnetic Moments" in the *A* Listings.

VALUE (μ <sub>N</sub> )	EVTS	DOCUMENT ID	TECN	COMMENT
<b>-0.6507 ± 0.0025 OUR AVERAGE</b>				
-0.6505 ± 0.0025	4.36M	DURYEA	92	SPEC 800 GeV p Be
-0.661 ± 0.036 ± 0.036	44k	TROST	89	SPEC Ξ <sup>-</sup> ~ 250 GeV
-0.69 ± 0.04	218k	RAMEIKA	84	SPEC 400 GeV pBe
• • • We do not use the following data for averages, fits, limits, etc. • • •				
-0.674 ± 0.021 ± 0.020	122k	HO	90	SPEC See DURYEA 92
-2.1 ± 0.8	2436	COOL	74	OSPK 1.8 GeV/c K <sup>-</sup> p
-0.1 ± 2.1	2724	BINGHAM	70B	OSPK 1.8 GeV/c K <sup>-</sup> p

## Ξ<sup>+</sup> MAGNETIC MOMENT

See the "Note on Baryon Magnetic Moments" in the *A* Listings.

VALUE (μ <sub>N</sub> )	EVTS	DOCUMENT ID	TECN	COMMENT
<b>+0.657 ± 0.028 ± 0.020</b>	70k	HO	90	SPEC 800 GeV pBe

$$(\mu_{\Xi^-} + \mu_{\Xi^+}) / |\mu_{\Xi^-}|$$

A test of CPT invariance. We calculate this from the Ξ<sup>-</sup> and Ξ<sup>+</sup> magnetic moments above.

VALUE	DOCUMENT ID
<b>+0.01 ± 0.05 OUR EVALUATION</b>	

## Ξ<sup>-</sup> DECAY MODES

Mode	Fraction (Γ <sub><i>i</i></sub> /Γ)	Confidence level
Γ <sub>1</sub> Λπ <sup>-</sup>	(99.887 ± 0.035) %	
Γ <sub>2</sub> Σ <sup>-</sup> γ	(1.27 ± 0.23) × 10 <sup>-4</sup>	
Γ <sub>3</sub> Λe <sup>-</sup> $\bar{\nu}_e$	(5.63 ± 0.31) × 10 <sup>-4</sup>	
Γ <sub>4</sub> Λμ <sup>-</sup> $\bar{\nu}_\mu$	(3.5 <sup>+3.5</sup> / <sub>-2.2</sub> ) × 10 <sup>-4</sup>	
Γ <sub>5</sub> Σ <sup>0</sup> e <sup>-</sup> $\bar{\nu}_e$	(8.7 ± 1.7) × 10 <sup>-5</sup>	
Γ <sub>6</sub> Σ <sup>0</sup> μ <sup>-</sup> $\bar{\nu}_\mu$	< 8 × 10 <sup>-4</sup>	90%
Γ <sub>7</sub> Σ <sup>0</sup> e <sup>-</sup> $\bar{\nu}_e$	< 2.3 × 10 <sup>-3</sup>	90%

## ΔS = 2 forbidden (S2) modes

Γ <sub>8</sub> nπ <sup>-</sup>	S2	< 1.9	× 10 <sup>-5</sup>	90%
Γ <sub>9</sub> n e <sup>-</sup> $\bar{\nu}_e$	S2	< 3.2	× 10 <sup>-3</sup>	90%
Γ <sub>10</sub> n μ <sup>-</sup> $\bar{\nu}_\mu$	S2	< 1.5	%	90%
Γ <sub>11</sub> pπ <sup>-</sup> π <sup>-</sup>	S2	< 4	× 10 <sup>-4</sup>	90%
Γ <sub>12</sub> pπ <sup>-</sup> e <sup>-</sup> $\bar{\nu}_e$	S2	< 4	× 10 <sup>-4</sup>	90%
Γ <sub>13</sub> pπ <sup>-</sup> μ <sup>-</sup> $\bar{\nu}_\mu$	S2	< 4	× 10 <sup>-4</sup>	90%
Γ <sub>14</sub> pμ <sup>-</sup> μ <sup>-</sup>	L	< 4	× 10 <sup>-8</sup>	90%

## CONSTRAINED FIT INFORMATION

An overall fit to 4 branching ratios uses 5 measurements and one constraint to determine 5 parameters. The overall fit has a χ<sup>2</sup> = 1.0 for 1 degrees of freedom.

The following *off-diagonal* array elements are the correlation coefficients <δx<sub>*i*</sub>δx<sub>*j*</sub>> / (δx<sub>*i*</sub>δx<sub>*j*</sub>), in percent, from the fit to the branching fractions, x<sub>*i*</sub> ≡ Γ<sub>*i*</sub>/Γ<sub>total</sub>. The fit constrains the x<sub>*i*</sub> whose labels appear in this array to sum to one.

x <sub>2</sub>	-6			
x <sub>3</sub>	-8	0		
x <sub>4</sub>	-99	0	-1	
x <sub>5</sub>	-5	0	0	0
	x <sub>1</sub>	x <sub>2</sub>	x <sub>3</sub>	x <sub>4</sub>

## Ξ<sup>-</sup> BRANCHING RATIOS

A number of early results have been omitted.

Γ(Σ <sup>-</sup> γ)/Γ(Λπ <sup>-</sup> )	Γ <sub>2</sub> /Γ <sub>1</sub>
<b>1.27 ± 0.24 OUR FIT</b>	
<b>1.27 ± 0.23 OUR AVERAGE</b>	
1.22 ± 0.23 ± 0.06	211 <sup>4</sup> DUBBS 94 E761 Ξ <sup>-</sup> 375 GeV
2.27 ± 1.02	9 BIAGI 87B SPEC SPS hyperon beam

Γ(Λe <sup>-</sup> $\bar{\nu}_e$ )/Γ(Λπ <sup>-</sup> )	Γ <sub>3</sub> /Γ <sub>1</sub>
<b>0.564 ± 0.031 OUR FIT</b>	
<b>0.564 ± 0.031</b>	2857 BOURQUIN 83 SPEC SPS hyperon beam
• • • We do not use the following data for averages, fits, limits, etc. • • •	
0.30 ± 0.13	11 THOMPSON 80 ASPK Hyperon beam

Γ(Λμ <sup>-</sup> $\bar{\nu}_\mu$ )/Γ(Λπ <sup>-</sup> )	Γ <sub>4</sub> /Γ <sub>1</sub>
<b>0.35 <sup>+0.35</sup>/<sub>-0.22</sub> OUR FIT</b>	
<b>0.35 ± 0.35</b>	1 YEH 74 HBC Effective denom.=2859
• • • We do not use the following data for averages, fits, limits, etc. • • •	
< 2.3	90 0 THOMPSON 80 ASPK Effective denom.=1017
< 1.3	DAUBER 69 HBC
< 12	BERGE 66 HBC

Γ(Σ <sup>0</sup> e <sup>-</sup> $\bar{\nu}_e$ )/Γ(Λπ <sup>-</sup> )	Γ <sub>5</sub> /Γ <sub>1</sub>
<b>0.087 ± 0.017 OUR FIT</b>	
<b>0.087 ± 0.017</b>	154 BOURQUIN 83 SPEC SPS hyperon beam

[Γ(Λe <sup>-</sup> $\bar{\nu}_e$ ) + Γ(Σ <sup>0</sup> e <sup>-</sup> $\bar{\nu}_e$ )]/Γ(Λπ <sup>-</sup> )	(Γ <sub>3</sub> +Γ <sub>5</sub> )/Γ <sub>1</sub>
<b>0.651 ± 0.031</b>	3011 <sup>5</sup> BOURQUIN 83 SPEC SPS hyperon beam
0.68 ± 0.22	17 <sup>6</sup> DUCLOS 71 OSPK
• • • We do not use the following data for averages, fits, limits, etc. • • •	
<sup>5</sup> See the separate BOURQUIN 83 values for Γ(Λe <sup>-</sup> $\bar{\nu}_e$ )/Γ(Λπ <sup>-</sup> ) and Γ(Σ <sup>0</sup> e <sup>-</sup> $\bar{\nu}_e$ )/Γ(Λπ <sup>-</sup> ) above.	
<sup>6</sup> DUCLOS 71 cannot distinguish Σ <sup>0</sup> s from Λ's. The Cabibbo theory predicts the Σ <sup>0</sup> rate is about a factor 6 smaller than the Λ rate.	

Γ(Σ <sup>0</sup> μ <sup>-</sup> $\bar{\nu}_\mu$ )/Γ(Λπ <sup>-</sup> )	Γ <sub>6</sub> /Γ <sub>1</sub>
<b>&lt; 0.76</b>	90 0 YEH 74 HBC Effective denom.=3026
• • • We do not use the following data for averages, fits, limits, etc. • • •	
< 5	BERGE 66 HBC

Γ(Ξ <sup>0</sup> e <sup>-</sup> $\bar{\nu}_e$ )/Γ(Λπ <sup>-</sup> )	Γ <sub>7</sub> /Γ <sub>1</sub>
<b>&lt; 2.3</b>	90 0 YEH 74 HBC Effective denom.=1000

See key on page 999

# Baryon Particle Listings



**$\Gamma(n\pi^-)/\Gamma(\Lambda\pi^-)$**   **$\Gamma_8/\Gamma_1$**   
 $\Delta S=2$ . Forbidden in first-order weak interaction.

VALUE (units $10^{-3}$ )	CL%	EVTS	DOCUMENT ID	TECN	COMMENT
<0.019	90		BIAGI	82B	SPEC SPS hyperon beam
<3.0	90	0	YEH	74	HBC Effective denom.=760
<1.1			DAUBER	69	HBC
<5.0			FERRO-LUZZI	63	HBC

••• We do not use the following data for averages, fits, limits, etc. •••

**$\Gamma(ne^- \bar{\nu}_e)/\Gamma(\Lambda\pi^-)$**   **$\Gamma_9/\Gamma_1$**   
 $\Delta S=2$ . Forbidden in first-order weak interaction.

VALUE (units $10^{-3}$ )	CL%	EVTS	DOCUMENT ID	TECN	COMMENT
< 3.2	90	0	YEH	74	HBC Effective denom.=715
<10	90		BINGHAM	65	RVUE

••• We do not use the following data for averages, fits, limits, etc. •••

**$\Gamma(n\mu^- \bar{\nu}_\mu)/\Gamma(\Lambda\pi^-)$**   **$\Gamma_{10}/\Gamma_1$**   
 $\Delta S=2$ . Forbidden in first-order weak interaction.

VALUE (units $10^{-3}$ )	CL%	EVTS	DOCUMENT ID	TECN	COMMENT
<15.3	90	0	YEH	74	HBC Effective denom.=150

**$\Gamma(p\pi^-\pi^-)/\Gamma(\Lambda\pi^-)$**   **$\Gamma_{11}/\Gamma_1$**   
 $\Delta S=2$ . Forbidden in first-order weak interaction.

VALUE (units $10^{-4}$ )	CL%	EVTS	DOCUMENT ID	TECN	COMMENT
<3.7	90	0	YEH	74	HBC Effective denom.=6200

**$\Gamma(p\pi^-e^- \bar{\nu}_e)/\Gamma(\Lambda\pi^-)$**   **$\Gamma_{12}/\Gamma_1$**   
 $\Delta S=2$ . Forbidden in first-order weak interaction.

VALUE (units $10^{-4}$ )	CL%	EVTS	DOCUMENT ID	TECN	COMMENT
<3.7	90	0	YEH	74	HBC Effective denom.=6200

**$\Gamma(p\pi^-\mu^- \bar{\nu}_\mu)/\Gamma(\Lambda\pi^-)$**   **$\Gamma_{13}/\Gamma_1$**   
 $\Delta S=2$ . Forbidden in first-order weak interaction.

VALUE (units $10^{-4}$ )	CL%	EVTS	DOCUMENT ID	TECN	COMMENT
<3.7	90	0	YEH	74	HBC Effective denom.=6200

**$\Gamma(p\mu^-\mu^-)/\Gamma(\Lambda\pi^-)$**   **$\Gamma_{14}/\Gamma_1$**   
 $\Delta L=2$  decay, forbidden by total lepton number conservation.

VALUE (units $10^{-8}$ )	CL%	DOCUMENT ID	TECN	COMMENT
<4.0	90	RAJARAM 05	HYCP	p Cu, 800 GeV
<3.7 $\times 10^4$	90	LITTENBERG 92B	HBC	Uses YEH 74 data

••• We do not use the following data for averages, fits, limits, etc. •••

<sup>7</sup> This LITTENBERG 92B limit and the identical YEH 74 limits for the preceding three modes all result from nonobservance of any 3-prong decays of the  $\Xi^-$ . One could as well apply the limit to the *sum* of the four modes.

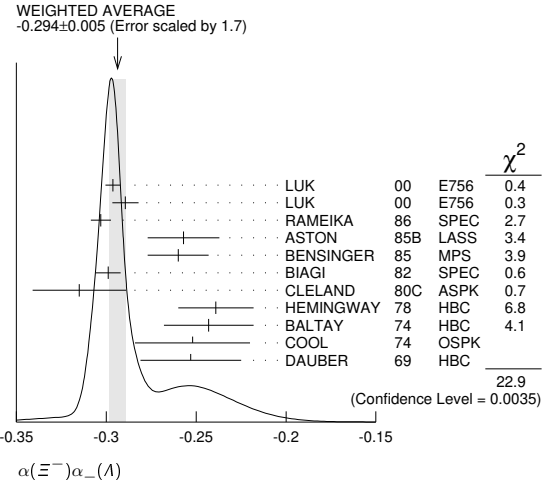
## $\Xi^-$ DECAY PARAMETERS

See the "Note on Baryon Decay Parameters" in the neutron Listings.

**$\alpha(\Xi^-)\alpha_-(\Lambda)$**

VALUE	EVTS	DOCUMENT ID	TECN	COMMENT
<b>-0.294 ± 0.005</b>	<b>OUR AVERAGE</b>			Error includes scale factor of 1.7. See the ideogram below.
-0.2963 ± 0.0042	189k	LUK	00	E756 p Be, 800 GeV
-0.2894 ± 0.0073	63k	<sup>8</sup> LUK	00	E756 p Be, 800 GeV
-0.303 ± 0.004 ± 0.004	192k	RAMEIKA	86	SPEC 400 GeV pBe
-0.257 ± 0.020	11k	ASTON	85B	LASS 11 GeV/c $K^-p$
-0.260 ± 0.017	21k	BENSINGER	85	MPS 5 GeV/c $K^-p$
-0.299 ± 0.007	150k	BIAGI	82	SPEC SPS hyperon beam
-0.315 ± 0.026	9046	CLELAND	80C	ASPK BNL hyperon beam
-0.239 ± 0.021	6599	HEMINGWAY	78	HBC 4.2 GeV/c $K^-p$
-0.243 ± 0.025	4303	BALTAY	74	HBC 1.75 GeV/c $K^-p$
-0.252 ± 0.032	2436	COOL	74	OSPK 1.8 GeV/c $K^-p$
-0.253 ± 0.028	2781	DAUBER	69	HBC

<sup>8</sup> This LUK 00 value is for  $\alpha(\Xi^+)\alpha_+(\bar{\Lambda})$ . We assume CP conservation here by including it in the average for  $\alpha(\Xi^-)\alpha_-(\Lambda)$ . But see the second data block below for the CP test.



**$\alpha$  FOR  $\Xi^- \rightarrow \Lambda\pi^-$**   
 The above average,  $\alpha(\Xi^-)\alpha_-(\Lambda) = -0.294 \pm 0.005$ , divided by our current average  $\alpha_-(\Lambda) = 0.732 \pm 0.014$ , gives the following value for  $\alpha(\Xi^-)$ :

VALUE	DOCUMENT ID
<b>-0.401 ± 0.010</b>	<b>OUR EVALUATION</b>

**$\frac{[\alpha(\Xi^-)\alpha_-(\Lambda) - \alpha(\Xi^+)\alpha_+(\bar{\Lambda})]}{[\alpha(\Xi^-)\alpha_-(\Lambda) + \alpha(\Xi^+)\alpha_+(\bar{\Lambda})]}$**   
 This is zero if CP is conserved. The  $\alpha$ 's are the decay-asymmetry parameters for  $\Xi^- \rightarrow \Lambda\pi^-$  and  $\Lambda \rightarrow p\pi^-$  and for  $\Xi^+ \rightarrow \bar{\Lambda}\pi^+$  and  $\bar{\Lambda} \rightarrow \bar{p}\pi^+$ .

VALUE (units $10^{-4}$ )	EVTS	DOCUMENT ID	TECN	COMMENT
<b>0.0 ± 5.1 ± 4.4</b>	158M	HOLMSTROM 04	HYCP	p Cu, 800 GeV
+120 ± 140	252k	LUK 00	E756	p Be, 800 GeV

••• We do not use the following data for averages, fits, limits, etc. •••

## $\phi$ ANGLE FOR $\Xi^- \rightarrow \Lambda\pi^-$ ( $\tan\phi = \beta/\gamma$ )

VALUE (°)	EVTS	DOCUMENT ID	TECN	COMMENT
<b>-2.1 ± 0.8</b>	<b>OUR AVERAGE</b>			
-2.39 ± 0.64 ± 0.64	144M	<sup>9</sup> HUANG 04	HYCP	p Cu, 800 GeV
-1.61 ± 2.66 ± 0.37	1.35M	<sup>10</sup> CHAKRAVORTY 03	E756	p Be, 800 GeV
5 ± 10	11k	ASTON 85B	LASS	$K^-p$
14.7 ± 16.0	21k	<sup>11</sup> BENSINGER 85	MPS	5 GeV/c $K^-p$
11 ± 9	4303	BALTAY 74	HBC	1.75 GeV/c $K^-p$
5 ± 16	2436	COOL 74	OSPK	1.8 GeV/c $K^-p$
-14 ± 11	2781	DAUBER 69	HBC	Uses $\alpha_\Lambda = 0.647 \pm 0.020$
0 ± 12	1004	<sup>12</sup> BERGE 66	HBC	
-26 ± 30	2724	BINGHAM 70B	OSPK	
0 ± 20.4	364	<sup>12</sup> LONDON 66	HBC	Using $\alpha_\Lambda = 0.62$
54 ± 30	356	<sup>12</sup> CARMONY 64B	HBC	

<sup>9</sup> From this result and  $\alpha_\Xi$ , HUANG 04 gets  $\beta_\Xi = -0.037 \pm 0.011 \pm 0.010$  and  $\gamma_\Xi = 0.888 \pm 0.0004 \pm 0.006$ . And the strong p-s phase difference for  $\Lambda\pi^-$  scattering is  $(4.6 \pm 1.4 \pm 1.2)^\circ$ .

<sup>10</sup> From this result and  $\alpha_\Xi$ , CHAKRAVORTY 03 obtains  $\beta_\Xi = -0.025 \pm 0.042 \pm 0.006$  and  $\gamma_\Xi = 0.889 \pm 0.001 \pm 0.007$ . And the strong p-s phase difference for  $\Lambda\pi^-$  scattering is  $(3.17 \pm 5.28 \pm 0.73)^\circ$ .

<sup>11</sup> BENSINGER 85 used  $\alpha_\Lambda = 0.642 \pm 0.013$ .

<sup>12</sup> The errors have been multiplied by 1.2 due to approximations used for the  $\Xi$  polarization; see DAUBER 69 for a discussion.

**$g_A/g_V$  FOR  $\Xi^- \rightarrow \Lambda e^- \bar{\nu}_e$**

VALUE	EVTS	DOCUMENT ID	TECN	COMMENT
<b>-0.25 ± 0.05</b>	1992	<sup>13</sup> BOURQUIN 83	SPEC	SPS hyperon beam

<sup>13</sup> BOURQUIN 83 assumes that  $g_2 = 0$ . Also, the sign has been changed to agree with our conventions, given in the "Note on Baryon Decay Parameters" in the neutron Listings.

## $\Xi^-$ REFERENCES

We have omitted those papers that have been superseded by later experiments. See our earlier editions.

ABDALLAH 06E	PL B639 179	J. Abdallah et al.	(DELPHI Collab.)
RAJARAM 05	PRL 94 181801	D. Rajaram et al.	(FNAL HyperCP Collab.)
HOLMSTROM 04	PRL 93 242001	T. Holmstrom et al.	(FNAL HyperCP Collab.)
HUANG 04	PRL 93 011802	M. Huang et al.	(FNAL HyperCP Collab.)
CHAKRAVORTY... 03	PRL 91 031601	A. Chakravorty et al.	(FNAL E756 Collab.)
LUK 00	PRL 85 4860	K.B. Luk et al.	(FNAL E756 Collab.)
DUBBS 94	PRL 72 808	T. Dubbs et al.	(FNAL E761 Collab.)
DURYEA 92	PRL 68 768	J. Duryea et al.	(MINN, FNAL, MICH, RUTG)
LITTENBERG 92B	PR D46 892	L.S. Littenberg, R.E. Shrock	(BNL, STON)
HO 90	PRL 65 1713	P.M. Ho et al.	(MICH, FNAL, MINN, RUTG)
Also	PR D44 3402	P.M. Ho et al.	(MICH, FNAL, MINN, RUTG)
TROST 89	PR D40 1703	L.H. Trost et al.	(FNAL-715 Collab.)
BIAGI 87B	ZPHY C35 143	S.F. Biagi et al.	(BRIS, CERN, GEVA+)
RAMEIKA 86	PR D33 3172	R. Rameika et al.	(RUTG, MICH, WISC+)
ASTON 85B	PR D32 2270	D. Aston et al.	(SLAC, CARL, CNRC, CINC)
BENSINGER 85	NP B252 561	J.R. Bensing et al.	(CHIC, ELMT, FNAL+)

# Baryon Particle Listings

## $\Xi^-, \Xi^0, \Xi(1530)$

BOURQUIN	84	NP B241 1	M.H. Bourquin <i>et al.</i>	(BRIS, GEVA, HEIDP+)
RAMEIKA	84	PRL 52 581	R. Rameika <i>et al.</i>	(RUTG, MICH, WISC+)
BOURQUIN	83	ZPHY C21 1	M.H. Bourquin <i>et al.</i>	(BRIS, GEVA, HEIDP+)
BIAGI	82	PL 112B 265	S.F. Biagi <i>et al.</i>	(BRIS, CAVE, GEVA+)
BIAGI	82B	PL 112B 277	S.F. Biagi <i>et al.</i>	(LOQM, GEVA, RL+)
CLELAND	80C	PR D21 12	W.E. Cleland <i>et al.</i>	(PITT, BNL)
THOMPSON	80	PR D21 25	J.A. Thompson <i>et al.</i>	(PITT, BNL)
BOURQUIN	79	PL 87B 297	M.H. Bourquin <i>et al.</i>	(BRIS, GEVA, HEIDP+)
HEMINGWAY	78	NP B142 205	R.J. Hemingway <i>et al.</i>	(CERN, ZEEM, NIJH+)
DIBIANCA	75	NP B99 137	F.A. Dibianca, R.J. Endorf	(CMU)
BALTAY	74	PR D9 49	C. Baltay <i>et al.</i>	(COLU, BING) J
COOL	74	PR D10 792	R.L. Cool <i>et al.</i>	(BNL)
Also		PRL 29 1630	R.L. Cool <i>et al.</i>	(BNL)
YEH	74	PR D10 3545	N. Yeh <i>et al.</i>	(BING, COLU)
MAYEUR	72	NP B47 333	C. Mayeur <i>et al.</i>	(BRUX, CERN, TUFTS, LOUC)
VOTRUBA	72	NP B45 77	M.F. Votruba, A. Saffder, T.M. Ratcliffe	(BIRM+)
WILQUET	72	PL 42B 372	G. Wilquet <i>et al.</i>	(BRUX, CERN, TUFTS+)
DUCCLOS	71	NP B32 493	J. Duclos <i>et al.</i>	(CERN)
BINGHAM	70B	PR D1 3010	G.M. Bingham <i>et al.</i>	(UCSD, WASH)
GOLDWASSER	70	PR D1 1960	E.L. Goldwasser, P.F. Schultz	(ILL)
STONE	70	PL 32B 515	S.L. Stone <i>et al.</i>	(ROCH)
DAUBER	69	PR 179 1262	P.H. Dauber <i>et al.</i>	(LRL) J
SHEN	67	PL 25B 443	B.C. Shen, A. Firestone, G. Goldhaber	(UCB+)
BERGE	66	PR 147 945	J.P. Berge <i>et al.</i>	(LRL)
CHIEN	66	PR 152 1171	C.Y. Chien <i>et al.</i>	(YALE, BNL)
LONDON	66	PR 143 1034	G.W. London <i>et al.</i>	(BNL, SYRA)
BINGHAM	65	PRSL 285 202	H.H. Bingham	(CERN)
PJERROU	65B	PRL 14 275	G.M. Pjerrou <i>et al.</i>	(UCLA)
Also		Thesis	G.M. Pjerrou	(UCLA)
BADIER	64	Dubna Conf. 1 593	J. Badier <i>et al.</i>	(EPOL, SACL, ZEEM)
CARMONY	64B	PRL 12 462	D.D. Carmony <i>et al.</i>	(UCLA) J
HUBBARD	64	PR 135 B183	J.R. Hubbard <i>et al.</i>	(LRL)
FERRO-LUZZI	63	PR 130 1568	M. Ferro-Luzzi <i>et al.</i>	(LRL)
JAUNEAU	63D	Siena Conf. 4	L. Jauneau <i>et al.</i>	(EPOL, CERN, LOUC+)
Also		PL 5 261	L. Jauneau <i>et al.</i>	(EPOL, CERN, LOUC+)
SCHNEIDER	63	PL 4 360	J. Schneider	(CERN)

### $\Xi$ RESONANCES

Revised 2004 by C.G. Wohl, (LBNL).

The accompanying table gives our evaluation of the present status of the  $\Xi$  resonances. Not much is known about  $\Xi$  resonances. This is because (1) they can only be produced as a part of a final state, and so the analysis is more complicated than if direct formation were possible, (2) the production cross sections are small (typically a few  $\mu\text{b}$ ), and (3) the final states are topologically complicated and difficult to study with electronic techniques. Thus early information about  $\Xi$  resonances came entirely from bubble chamber experiments, where the numbers of events are small, and only in the 1980's did electronic experiments make any significant contributions. However, nothing of significance on  $\Xi$  resonances has been added since our 1988 edition.

For a detailed earlier review, see Meadows [1].

Table 1. The status of the  $\Xi$  resonances. Only those with an overall status of \*\*\* or \*\*\*\* are included in the Baryon Summary Table.

Particle	$J^P$	Overall status	Status as seen in —				
			$\Xi\pi$	$\Lambda K$	$\Sigma K$	$\Xi(1530)\pi$	Other channels
$\Xi(1318)$	1/2+	****					Decays weakly
$\Xi(1530)$	3/2+	****	****				
$\Xi(1620)$	*	*	*				
$\Xi(1690)$	***	***		***	**		
$\Xi(1820)$	3/2-	***	**	***	**	**	
$\Xi(1950)$	***	**	**			*	
$\Xi(2030)$	***	***		**	***		
$\Xi(2120)$	*	*		*			
$\Xi(2250)$	**	**					3-body decays
$\Xi(2370)$	**	**					3-body decays
$\Xi(2500)$	*	*		*	*		3-body decays

\*\*\*\* Existence is certain, and properties are at least fairly well explored.  
 \*\*\* Existence ranges from very likely to certain, but further confirmation is desirable and/or quantum numbers, branching fractions, etc. are not well determined.  
 \*\* Evidence of existence is only fair.  
 \* Evidence of existence is poor.

### Reference

1. B.T. Meadows, in *Proceedings of the IV<sup>th</sup> International Conference on Baryon Resonances* (Toronto, 1980), ed. N. Isgur, p. 283.

## $\Xi(1530) 3/2^+$

$$I(J^P) = \frac{1}{2}(\frac{3}{2}^+) \text{ Status: } ***$$

This is the only  $\Xi$  resonance whose properties are all reasonably well known. Assuming that the  $\Lambda_C^+$  has  $J^P = 1/2^+$ , AUBERT 08AK, in a study of  $\Lambda_C^+ \rightarrow \Xi^- \pi^+ K^+$ , finds conclusively that the spin of the  $\Xi(1530)^0$  is 3/2. In conjunction with SCHLEIN 63B and BUTTON-SHAFFER 66, this proves also that the parity is +.

We use only those determinations of the mass and width that are accompanied by some discussion of systematics and resolution.

### $\Xi(1530)$ POLE POSITIONS

#### $\Xi(1530)^0$ REAL PART

VALUE	DOCUMENT ID	COMMENT
1531.6 ± 0.4	LICHTENBERG74	Using HABIB1 73

#### $\Xi(1530)^0$ IMAGINARY PART

VALUE	DOCUMENT ID	COMMENT
4.45 ± 0.35	LICHTENBERG74	Using HABIB1 73

#### $\Xi(1530)^-$ REAL PART

VALUE	DOCUMENT ID	COMMENT
1534.4 ± 1.1	LICHTENBERG74	Using HABIB1 73

#### $\Xi(1530)^-$ IMAGINARY PART

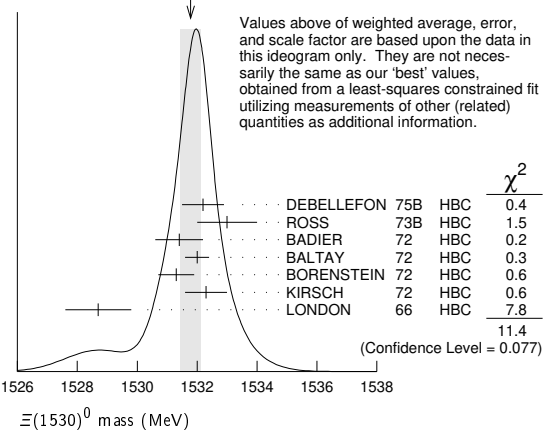
VALUE	DOCUMENT ID	COMMENT
3.9 ± 1.75 - 3.9	LICHTENBERG74	Using HABIB1 73

### $\Xi(1530)$ MASSES

#### $\Xi(1530)^0$ MASS

VALUE (MeV)	EVTS	DOCUMENT ID	TECN	COMMENT
<b>1531.80 ± 0.32 OUR FIT</b>		Error includes scale factor of 1.3.		
<b>1531.78 ± 0.34 OUR AVERAGE</b>		Error includes scale factor of 1.4. See the ideogram below.		
1532.2 ± 0.7		DEBELLEFON	75B HBC	$K^- p \rightarrow \Xi^- \bar{K} \pi$
1533 ± 1		ROSS	73B HBC	$K^- p \rightarrow \Xi \bar{K} \pi(\pi)$
1531.4 ± 0.8	59	BADIER	72 HBC	$K^- p$ 3.95 GeV/c
1532.0 ± 0.4	1262	BALTAY	72 HBC	$K^- p$ 1.75 GeV/c
1531.3 ± 0.6	324	BORENSTEIN	72 HBC	$K^- p$ 2.2 GeV/c
1532.3 ± 0.7	286	KIRSCH	72 HBC	$K^- p$ 2.87 GeV/c
1528.7 ± 1.1	76	LONDON	66 HBC	$K^- p$ 2.24 GeV/c
• • • We do not use the following data for averages, fits, limits, etc. • • •				
1532.1 ± 0.4	1244	ASTON	85B LASS	$K^- p$ 11 GeV/c
1532.1 ± 0.6	2700	1 BAUBILLIER	81B HBC	$K^- p$ 8.25 GeV/c
1530 ± 1	450	BIAGI	81 SPEC	SPS hyperon beam
1527 ± 6	80	SIXEL	79 HBC	$K^- p$ 10 GeV/c
1535 ± 4	100	SIXEL	79 HBC	$K^- p$ 16 GeV/c
1533.6 ± 1.4	97	BERTHON	74 HBC	Quasi-2-body $\sigma$

WEIGHTED AVERAGE  
1531.78±0.34 (Error scaled by 1.4)



See key on page 999

# Baryon Particle Listings

## $\Xi(1530)$ , $\Xi(1620)$ , $\Xi(1690)$

### $\Xi(1530)^-$ MASS

VALUE (MeV)	EVTS	DOCUMENT ID	TECN	COMMENT
<b>1535.0 ± 0.6 OUR FIT</b>				
<b>1535.2 ± 0.8 OUR AVERAGE</b>				
1534.5 ± 1.2		DEBELLEFON 75B	HBC	$K^- p \rightarrow \Xi^- \bar{K} \pi$
1535.3 ± 2.0		ROSS 73B	HBC	$K^- p \rightarrow \Xi^- \bar{K} \pi(\pi)$
1536.2 ± 1.6	185	KIRSCH 72	HBC	$K^- p$ 2.87 GeV/c
1535.7 ± 3.2	38	LONDON 66	HBC	$K^- p$ 2.24 GeV/c
• • • We do not use the following data for averages, fits, limits, etc. • • •				
1540 ± 3	48	BERTHON 74	HBC	Quasi-2-body $\sigma$
1534.7 ± 1.1	334	BALTAY 72	HBC	$K^- p$ 1.75 GeV/c

### $m_{\Xi(1530)^-} - m_{\Xi(1530)}$

VALUE (MeV)	DOCUMENT ID	TECN	COMMENT
<b>3.2 ± 0.6 OUR FIT</b>			
<b>2.9 ± 0.9 OUR AVERAGE</b>			
2.7 ± 1.0	BALTAY 72	HBC	$K^- p$ 1.75 GeV/c
2.0 ± 3.2	MERRILL 66	HBC	$K^- p$ 1.7-2.7 GeV/c
5.7 ± 3.0	PJERROU 65B	HBC	$K^- p$ 1.8-1.95 GeV/c
• • • We do not use the following data for averages, fits, limits, etc. • • •			
3.9 ± 1.8	<sup>2</sup> KIRSCH 72	HBC	$K^- p$ 2.87 GeV/c
7 ± 4	<sup>2</sup> LONDON 66	HBC	$K^- p$ 2.24 GeV/c

### $\Xi(1530)$ WIDTHS

#### $\Xi(1530)^0$ WIDTH

VALUE (MeV)	EVTS	DOCUMENT ID	TECN	COMMENT
<b>9.1 ± 0.5 OUR AVERAGE</b>				
9.5 ± 1.2		DEBELLEFON 75B	HBC	$K^- p \rightarrow \Xi^- \bar{K} \pi$
9.1 ± 2.4		ROSS 73B	HBC	$K^- p \rightarrow \Xi^- \bar{K} \pi(\pi)$
11 ± 2		BADIER 72	HBC	$K^- p$ 3.95 GeV/c
9.0 ± 0.7		BALTAY 72	HBC	$K^- p$ 1.75 GeV/c
8.4 ± 1.4		BORENSTEIN 72	HBC	$\Xi^- \pi^+$
11.0 ± 1.8		KIRSCH 72	HBC	$\Xi^- \pi^+$
7 ± 7		BERGE 66	HBC	$K^- p$ 1.5-1.7 GeV/c
8.5 ± 3.5		LONDON 66	HBC	$K^- p$ 2.24 GeV/c
7 ± 2		SCHLEIN 63B	HBC	$K^- p$ 1.8, 1.95 GeV/c
• • • We do not use the following data for averages, fits, limits, etc. • • •				
12.8 ± 1.0	2700	<sup>1</sup> BAUBILLIER 81B	HBC	$K^- p$ 8.25 GeV/c
19 ± 6	80	<sup>3</sup> SIXEL 79	HBC	$K^- p$ 10 GeV/c
14 ± 5	100	<sup>3</sup> SIXEL 79	HBC	$K^- p$ 16 GeV/c

#### $\Xi(1530)^-$ WIDTH

VALUE (MeV)	DOCUMENT ID	TECN	COMMENT
<b>9.9 ± 1.7 OUR AVERAGE</b>			
9.6 ± 2.8	DEBELLEFON 75B	HBC	$K^- p \rightarrow \Xi^- \bar{K} \pi$
8.3 ± 3.6	ROSS 73B	HBC	$K^- p \rightarrow \Xi^- \bar{K} \pi(\pi)$
7.8 ± 3.5	BALTAY 72	HBC	$K^- p$ 1.75 GeV/c
16.2 ± 4.6	KIRSCH 72	HBC	$\Xi^- \pi^0, \Xi^0 \pi^-$

### $\Xi(1530)$ DECAY MODES

Mode	Fraction ( $\Gamma_i/\Gamma$ )	Confidence level
$\Gamma_1 \Xi^- \pi$	100 %	
$\Gamma_2 \Xi^- \gamma$	<3.7 %	90%

### $\Xi(1530)$ BRANCHING RATIOS

$\Gamma(\Xi^- \gamma)/\Gamma_{\text{total}}$	CL%	DOCUMENT ID	TECN	COMMENT	$\Gamma_2/\Gamma$
<0.037	90	ABLIKIM 20	BES3	$J/\psi \rightarrow \Xi(1530)^- \Xi^+$	
<0.04	90	KALBFLEISCH 75	HBC	$K^- p$ 2.18 GeV/c	

### $\Xi(1530)$ FOOTNOTES

- <sup>1</sup> BAUBILLIER 81B is a fit to the inclusive spectrum. The resolution (5 MeV) is not unfolded.
- <sup>2</sup> Redundant with data in the mass Listings.
- <sup>3</sup> SIXEL 79 doesn't unfold the experimental resolution of 15 MeV.

### $\Xi(1530)$ REFERENCES

ABLIKIM 20	PR D101 012004	M. Ablikim et al.	(BESIII Collab.)
AUBERT 08AK	PR D78 034008	B. Aubert et al.	(BABAR Collab.)
ASTON 85B	PR D32 2270	D. Aston et al.	(SLAC, CARL, CNRC, CINC)
BAUBILLIER 81B	NP B192 1	M. Baubillier et al.	(BIRM, CERN, GLAS+)
BIAGI 81	ZPHY C9 305	S.F. Biagi et al.	(BRIS, CAVE, GEVA+)
SIXEL 79	NP B159 125	P. Sixel et al.	(AACH3, BERL, CERN, LOIC+)
DEBELLEFON 75B	NC 28A 289	A. de Bellefon et al.	(CDEF, SACL)
KALBFLEISCH 75	PR D11 987	G.R. Kalbfleisch, R.C. Strand, J.W. Chapman	(BNL+)
BERTHON 74	NC 21A 146	A. Berthon et al.	(CDEF, RHEL, SACL+)

LICHTENBERG 74	PR D10 3865	D.B. Lichtenberg	(IND)
Also	Private Comm.	D.B. Lichtenberg	(IND)
HABIBI 73	Thesis Nevis 199	M. Habibi	(COLU)
ROSS 73B	Purdue Conf. 355	R.T. Ross, J.L. Lloyd, D. Radojicic	(COXF)
BADIER 72	NP B37 429	J. Badier et al.	(EPOL)
BALTAY 72	PL 42B 129	C. Baltay et al.	(COLU, BING)
BORENSTEIN 72	PR D5 1559	S.R. Borenstein et al.	(BNL, MICH)1
KIRSCH 72	NP B40 349	L.E. Kirsch et al.	(BRAN, UMD, SYRA+)
BERGE 66	PR 147 945	J.P. Berge et al.	(LRL)1
BUTTON-... 66	PR 142 883	J. Button-Shafer et al.	(LRL)JP
LONDON 66	PR 143 1034	G.W. London et al.	(BNL, SYRA)1J
MERRILL 66	Thesis UCRL 16455	D.W. Merrill	(LRL)JP
PJERROU 65B	PRL 14 275	G.M. Pjerrou et al.	(UCLA)
SCHLEIN 63B	PRL 11 167	P.E. Schlein et al.	(UCLA)1JP

### OTHER RELATED PAPERS

MAZZUCATO 81	NP B178 1	M. Mazzucato et al.	(AMST, CERN, NUM+)
BRIEFEL 77	PR D16 2706	E. Briefel et al.	(BRAN, UMD, SYRA+)
BRIEFEL 75	PR D12 1859	E. Briefel et al.	(BRAN, UMD, SYRA+)
HUNGERBU... 74	PR D10 2051	V. Hungerbuehler et al.	(YALE, FNAL, BNL+)
BUTTON-... 66	PR 142 883	J. Button-Shafer et al.	(LRL)JP

## $\Xi(1620)$

$I(J^P) = \frac{1}{2}(?^?)$  Status: \*  
J, P need confirmation.

### OMITTED FROM SUMMARY TABLE

What little evidence there is consists of weak signals in the  $\Xi\pi$  channel. A number of other experiments (e.g., BORENSTEIN 72 and HASSALL 81) have looked for but not seen any effect.

### $\Xi(1620)$ MASS

VALUE (MeV)	EVTS	DOCUMENT ID	TECN	COMMENT
<b>≈ 1620 OUR ESTIMATE</b>				
1624 ± 3	31	BRIEFEL 77	HBC	$K^- p$ 2.87 GeV/c
1633 ± 12	34	DEBELLEFON 75B	HBC	$K^- p \rightarrow \Xi^- \bar{K} \pi$
1606 ± 6	29	ROSS 72	HBC	$K^- p$ 3.1-3.7 GeV/c

### $\Xi(1620)$ WIDTH

VALUE (MeV)	EVTS	DOCUMENT ID	TECN	COMMENT
22.5	31	<sup>1</sup> BRIEFEL 77	HBC	$K^- p$ 2.87 GeV/c
40 ± 15	34	DEBELLEFON 75B	HBC	$K^- p \rightarrow \Xi^- \bar{K} \pi$
21 ± 7	29	ROSS 72	HBC	$K^- p \rightarrow \Xi^- \pi^+ K^*(892)$

### $\Xi(1620)$ DECAY MODES

Mode
$\Gamma_1 \Xi^- \pi$

### $\Xi(1620)$ FOOTNOTES

- <sup>1</sup> The fit is insensitive to values between 15 and 30 MeV.

### $\Xi(1620)$ REFERENCES

HASSALL 81	NP B189 397	J.K. Hassall et al.	(CAVE, MSU)
BRIEFEL 77	PR D16 2706	E. Briefel et al.	(BRAN, UMD, SYRA+)
Also	Duke Conf. 317	E. Briefel et al.	(BRAN, UMD, SYRA+)
Also	Hyperon Resonances, 1970		
DEBELLEFON 75B	PR D12 1859	E. Briefel et al.	(BRAN, UMD, SYRA+)
BORENSTEIN 72	NC 28A 289	A. de Bellefon et al.	(CDEF, SACL)
ROSS 72	PL D5 1559	S.R. Borenstein et al.	(BNL, MICH)1
	PL 38B 177	R.T. Ross et al.	(COXF)1

### OTHER RELATED PAPERS

HUNGERBU... 74	PR D10 2051	V. Hungerbuehler et al.	(YALE, FNAL, BNL+)
SCHMIDT 73	Purdue Conf. 363	P.E. Schmidt	(BRAN)
KALBFLEISCH 70	Duke Conf. 331	G.R. Kalbfleisch	(BNL)1
Also	Hyperon Resonances 1970		
APSELL 69	PRL 23 884	S.P. Apsell et al.	(BRAN, UMD, SYRA+)
BARTSCH 69	PL 28B 439	J. Bartsch et al.	(AACH, BERL, CERN+)

## $\Xi(1690)$

$I(J^P) = \frac{1}{2}(?^?)$  Status: \*\* \*

AUBERT 08AK, in a study of  $\Lambda_c^+ \rightarrow \Xi^- \pi^+ K^+$ , finds some evidence that the  $\Xi(1690)$  has  $J^P = 1/2^-$ .

DIONISI 78 sees a threshold enhancement in both the neutral and negatively charged  $\Sigma \bar{K}$  mass spectra in  $K^- p \rightarrow (\Sigma \bar{K}) K \pi$  at 4.2 GeV/c. The data from the  $\Sigma \bar{K}$  channels alone cannot distinguish between a resonance and a large scattering length. Weaker evidence at the same mass is seen in the corresponding  $\Lambda \bar{K}$  channels, and a coupled-channel analysis yields results consistent with a new  $\Xi$ .

BIAGI 81 sees an enhancement at 1700 MeV in the diffractively produced  $\Lambda K^-$  system. A peak is also observed in the  $\Lambda \bar{K}^0$  mass spectrum at 1660 MeV that is consistent with a 1720 MeV resonance decaying to  $\Sigma^0 \bar{K}^0$ , with the  $\gamma$  from the  $\Sigma^0$  decay not detected.

# Baryon Particle Listings

## $\Xi(1690), \Xi(1820)$

BIAGI 87 provides further confirmation of this state in diffractive dissociation of  $\Xi^-$  into  $\Lambda K^-$ . The significance claimed is 6.7 standard deviations.

ADAMOVICH 98 sees a peak of  $1400 \pm 300$  events in the  $\Xi^- \pi^+$  spectrum produced by 345 GeV/c  $\Sigma^-$ -nucleus interactions.

### $\Xi(1690)$ MASSES

#### MIXED CHARGES

**1690 ± 10 OUR ESTIMATE** This is only an educated guess; the error given is larger than the error on the average of the published values.

#### $\Xi(1690)^0$ MASS

VALUE (MeV)	EVTS	DOCUMENT ID	TECN	COMMENT
1686 ± 4	1400	ADAMOVICH 98	WA89	$\Sigma^-$ nucleus, 345 GeV/c
1699 ± 5	175	<sup>1</sup> DIONISI 78	HBC	$K^- p$ 4.2 GeV/c
1684 ± 5	183	<sup>2</sup> DIONISI 78	HBC	$K^- p$ 4.2 GeV/c

#### $\Xi(1690)^-$ MASS

VALUE (MeV)	EVTS	DOCUMENT ID	TECN	COMMENT
1691.1 ± 1.9 ± 2.0	104	BIAGI 87	SPEC	$\Xi^-$ Be 116 GeV
1700 ± 10	150	<sup>3</sup> BIAGI 81	SPEC	$\Xi^-$ H 100, 135 GeV
1694 ± 6	45	<sup>4</sup> DIONISI 78	HBC	$K^- p$ 4.2 GeV/c

### $\Xi(1690)$ WIDTHS

#### MIXED CHARGES

**<30 OUR ESTIMATE**

#### $\Xi(1690)^0$ WIDTH

VALUE (MeV)	EVTS	DOCUMENT ID	TECN	COMMENT
10 ± 6	1400	ADAMOVICH 98	WA89	$\Sigma^-$ nucleus, 345 GeV/c
44 ± 23	175	<sup>1</sup> DIONISI 78	HBC	$K^- p$ 4.2 GeV/c
20 ± 4	183	<sup>2</sup> DIONISI 78	HBC	$K^- p$ 4.2 GeV/c

#### $\Xi(1690)^-$ WIDTH

VALUE (MeV)	CL%	EVTS	DOCUMENT ID	TECN	COMMENT
< 8	90	104	BIAGI 87	SPEC	$\Xi^-$ Be 116 GeV
47 ± 14		150	<sup>3</sup> BIAGI 81	SPEC	$\Xi^-$ H 100, 135 GeV
26 ± 6		45	<sup>4</sup> DIONISI 78	HBC	$K^- p$ 4.2 GeV/c

### $\Xi(1690)$ DECAY MODES

Mode	Fraction ( $\Gamma_i/\Gamma$ )
$\Gamma_1 \Lambda \bar{K}$	seen
$\Gamma_2 \Sigma \bar{K}$	seen
$\Gamma_3 \Xi \pi$	seen
$\Gamma_4 \Xi^- \pi^+ \pi^0$	
$\Gamma_5 \Xi^- \pi^+ \pi^-$	possibly seen
$\Gamma_6 \Xi(1530) \pi$	

### $\Xi(1690)$ BRANCHING RATIOS

$\Gamma(\Lambda \bar{K})/\Gamma_{\text{total}}$	$\Gamma_1/\Gamma$				
VALUE	EVTS	DOCUMENT ID	TECN	CHG	COMMENT
seen	104	BIAGI 87	SPEC	-	$\Xi^-$ Be 116 GeV

$\Gamma(\Sigma \bar{K})/\Gamma(\Lambda \bar{K})$	$\Gamma_2/\Gamma_1$				
VALUE	EVTS	DOCUMENT ID	TECN	CHG	COMMENT
0.75 ± 0.39	75	ABE 02c	BELL		$e^+ e^- \approx \tau(4S)$
2.7 ± 0.9		DIONISI 78	HBC	0	$K^- p$ 4.2 GeV/c
3.1 ± 1.4		DIONISI 78	HBC	-	$K^- p$ 4.2 GeV/c

$\Gamma(\Xi \pi)/\Gamma(\Sigma \bar{K})$	$\Gamma_3/\Gamma_2$			
VALUE	DOCUMENT ID	TECN	CHG	COMMENT
< 0.09	DIONISI 78	HBC	0	$K^- p$ 4.2 GeV/c

$\Gamma(\Xi \pi)/\Gamma_{\text{total}}$	$\Gamma_3/\Gamma$		
VALUE	DOCUMENT ID	TECN	COMMENT
seen	ADAMOVICH 98	WA89	$\Sigma^-$ nucleus, 345 GeV/c

$\Gamma(\Xi^- \pi^+ \pi^0)/\Gamma(\Sigma \bar{K})$	$\Gamma_4/\Gamma_2$			
VALUE	DOCUMENT ID	TECN	CHG	COMMENT
< 0.04	DIONISI 78	HBC	0	$K^- p$ 4.2 GeV/c

$\Gamma(\Xi^- \pi^+ \pi^-)/\Gamma_{\text{total}}$	$\Gamma_5/\Gamma$				
VALUE	EVTS	DOCUMENT ID	TECN	CHG	COMMENT
possibly seen	4	BIAGI 87	SPEC	-	$\Xi^-$ Be 116 GeV

$\Gamma(\Xi^- \pi^+ \pi^-)/\Gamma(\Sigma \bar{K})$	$\Gamma_5/\Gamma_2$			
VALUE	DOCUMENT ID	TECN	CHG	COMMENT
< 0.03	DIONISI 78	HBC	-	$K^- p$ 4.2 GeV/c

$\Gamma(\Xi(1530) \pi)/\Gamma(\Sigma \bar{K})$	$\Gamma_6/\Gamma_2$			
VALUE	DOCUMENT ID	TECN	CHG	COMMENT
< 0.06	DIONISI 78	HBC	-	$K^- p$ 4.2 GeV/c

### $\Xi(1690)$ FOOTNOTES

- <sup>1</sup> From a fit to the  $\Sigma^+ K^-$  spectrum.
- <sup>2</sup> From a coupled-channel analysis of the  $\Sigma^+ K^-$  and  $\Lambda \bar{K}^0$  spectra.
- <sup>3</sup> A fit to the inclusive spectrum from  $\Xi^- N \rightarrow \Lambda K^- X$ .
- <sup>4</sup> From a coupled-channel analysis of the  $\Sigma^0 K^-$  and  $\Lambda K^-$  spectra.

### $\Xi(1690)$ REFERENCES

AUBERT 08AK	PR D78 034008	B. Aubert <i>et al.</i>	(BABAR Collab.)
ABE 02c	PL B524 33	K. Abe <i>et al.</i>	(KEK BELLE Collab.)
ADAMOVICH 98	EPJ C5 621	M.L. Adamovich <i>et al.</i>	(CERN WA89 Collab.)
BIAGI 87	ZPHY C34 15	S.F. Biagi <i>et al.</i>	(BRIS, CERN, GEVA+)
BIAGI 81	ZPHY C9 305	S.F. Biagi <i>et al.</i>	(BRIS, CAVE, GEVA+)
DIONISI 78	PL 80B 145	C. Dionisi <i>et al.</i>	(CERN, AMST, NIJM+)

## $\Xi(1820) 3/2^-$

$$I(J^P) = \frac{1}{2}(\frac{3}{2}^-) \text{ Status: } ***$$

The clearest evidence is an 8-standard-deviation peak in  $\Lambda K^-$  seen by GAY 76C. TEODORO 78 favors  $J = 3/2$ , but cannot make a parity discrimination. BIAGI 87C is consistent with  $J = 3/2$  and favors negative parity for this  $J$  value.

### $\Xi(1820)$ MASS

We only average the measurements that appear to us to be most significant and best determined.

VALUE (MeV)	EVTS	DOCUMENT ID	TECN	CHG	COMMENT
<b>1823 ± 5 OUR ESTIMATE</b>					
<b>1823.5 ± 1.4 OUR AVERAGE</b>					
1825.5 ± 4.7 ± 4.7	288	ABLIKIM 20c	BES3	-	$e^+ e^- \rightarrow \Xi(1820)^- \Xi^+$
1819.4 ± 3.1 ± 2.0	280	<sup>1</sup> BIAGI 87	SPEC	0	$\Xi^- \text{Be} \rightarrow (\Lambda K^-) X$
1826 ± 3 ± 1	54	BIAGI 87c	SPEC	0	$\Xi^- \text{Be} \rightarrow (\Lambda \bar{K}^0) X$
1822 ± 6		JENKINS 83	MPS	-	$K^- p \rightarrow K^+ (\text{MM})$
1830 ± 6	300	BIAGI 81	SPEC	-	SPS hyperon beam
1823 ± 2	130	GAY 76c	HBC	-	$K^- p$ 4.2 GeV/c
• • • We do not use the following data for averages, fits, limits, etc. • • •					
1817 ± 3		ADAMOVICH 99b	WA89		$\Sigma^-$ nucleus, 345 GeV
1797 ± 19	74	BRIEFEL 77	HBC	0	$K^- p$ 2.87 GeV/c
1829 ± 9	68	BRIEFEL 77	HBC	-0	$\Xi(1530) \pi$
1860 ± 14	39	BRIEFEL 77	HBC	-	$\Sigma^- \bar{K}^0$
1870 ± 9	44	BRIEFEL 77	HBC	0	$\Lambda \bar{K}^0$
1813 ± 4	57	BRIEFEL 77	HBC	-	$\Lambda K^-$
1807 ± 27		DIBIANCA 75	DBC	-0	$\Xi \pi, \Xi^* \pi$
1762 ± 8	28	<sup>2</sup> BADIÉ 72	HBC	-0	$\Xi \pi, \Xi \pi \pi, Y K$
1838 ± 5	38	<sup>2</sup> BADIÉ 72	HBC	-0	$\Xi \pi, \Xi \pi \pi, Y K$
1830 ± 10	25	<sup>3</sup> CRENNELL 70b	DBC	-0	3.6, 3.9 GeV/c
1826 ± 12		<sup>4</sup> CRENNELL 70b	DBC	-0	3.6, 3.9 GeV/c
1830 ± 10	40	ALITTI 69	HBC	-	$\Lambda, \Sigma \bar{K}$
1814 ± 4	30	BADIÉ 65	HBC	0	$\Lambda \bar{K}^0$
1817 ± 7	29	SMITH 65c	HBC	-0	$\Lambda \bar{K}^0, \Lambda K^-$
1770		HALSTEINSLID63	FBC	-0	$K^-$ freon 3.5 GeV/c

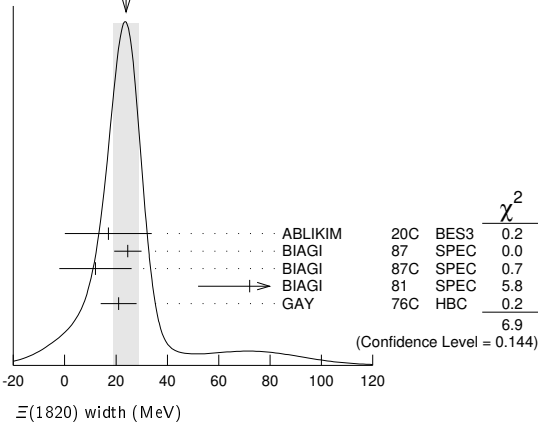
### $\Xi(1820)$ WIDTH

VALUE (MeV)	EVTS	DOCUMENT ID	TECN	CHG	COMMENT
<b>24 +15 -10 OUR ESTIMATE</b>					
<b>24 ± 5 OUR AVERAGE</b>					Error includes scale factor of 1.3. See the ideogram below.
17.0 ± 15.0 ± 7.9	288	ABLIKIM 20c	BES3	-	$e^+ e^- \rightarrow \Xi(1820)^- \Xi^+$
24.6 ± 5.3	280	<sup>1</sup> BIAGI 87	SPEC	0	$\Xi^- \text{Be} \rightarrow (\Lambda K^-) X$
12 ± 14 ± 1.7	54	BIAGI 87c	SPEC	0	$\Xi^- \text{Be} \rightarrow (\Lambda \bar{K}^0) X$
72 ± 20	300	BIAGI 81	SPEC	-	SPS hyperon beam
21 ± 7	130	GAY 76c	HBC	-	$K^- p$ 4.2 GeV/c
• • • We do not use the following data for averages, fits, limits, etc. • • •					
23 ± 13		ADAMOVICH 99b	WA89		$\Sigma^-$ nucleus, 345 GeV
99 ± 57	74	BRIEFEL 77	HBC	0	$K^- p$ 2.87 GeV/c
52 ± 34	68	BRIEFEL 77	HBC	-0	$\Xi(1530) \pi$
72 ± 17	39	BRIEFEL 77	HBC	-	$\Sigma^- \bar{K}^0$
44 ± 11	44	BRIEFEL 77	HBC	0	$\Lambda \bar{K}^0$
26 ± 11	57	BRIEFEL 77	HBC	-	$\Lambda K^-$
85 ± 58		DIBIANCA 75	DBC	-0	$\Xi \pi, \Xi^* \pi$
51 ± 13		<sup>2</sup> BADIÉ 72	HBC	-0	Lower mass

Baryon Particle Listings  
 $\Xi(1820), \Xi(1950)$

58 ± 13	2	BADIER	72	HBC	-0	Higher mass
103 <sup>+38</sup> <sub>-24</sub>	3	CRENNELL	70B	DBC	-0	3.6, 3.9 GeV/c
48 <sup>+36</sup> <sub>-19</sub>	4	CRENNELL	70B	DBC	-0	3.6, 3.9 GeV/c
55 <sup>+40</sup> <sub>-20</sub>		ALITTI	69	HBC	-	$\Lambda, \Sigma \bar{K}$
12 ± 4		BADIER	65	HBC	0	$\Lambda \bar{K}^0$
30 ± 7		SMITH	65B	HBC	-0	$\Lambda \bar{K}$
<80		HALSTEINSLID63	FBC	-0	-	$K^-$ freon 3.5 GeV/c

WEIGHTED AVERAGE  
 24±5 (Error scaled by 1.3)



$\Xi(1820)$  DECAY MODES

Mode	Fraction ( $\Gamma_i/\Gamma$ )
$\Gamma_1$ $\Lambda \bar{K}$	large
$\Gamma_2$ $\Sigma \bar{K}$	small
$\Gamma_3$ $\Xi \pi$	small
$\Gamma_4$ $\Xi(1530)\pi$	small
$\Gamma_5$ $\Xi \pi \pi$ (not $\Xi(1530)\pi$ )	

$\Xi(1820)$  BRANCHING RATIOS

The dominant modes seem to be  $\Lambda \bar{K}$  and (perhaps)  $\Xi(1530)\pi$ , but the branching fractions are very poorly determined.

$\Gamma(\Lambda \bar{K})/\Gamma_{total}$   $\Gamma_1/\Gamma$

VALUE	DOCUMENT ID	TECN	CHG	COMMENT
<b>0.25 ± 0.05 OUR AVERAGE</b>				
0.24 ± 0.05	ANISOVICH 12A	DPWA	-	Multichannel
0.30 ± 0.15	ALITTI 69	HBC	-	$K^- p$ 3.9-5 GeV/c

$\Gamma(\Xi \pi)/\Gamma_{total}$   $\Gamma_3/\Gamma$

VALUE	DOCUMENT ID	TECN	CHG	COMMENT
<b>0.10 ± 0.10</b>				
	ALITTI 69	HBC	-	$K^- p$ 3.9-5 GeV/c

$\Gamma(\Xi \pi)/\Gamma(\Lambda \bar{K})$   $\Gamma_3/\Gamma_1$

VALUE	CL%	DOCUMENT ID	TECN	CHG	COMMENT
<b>&lt;0.36</b>	95	GAY 76c	HBC	-	$K^- p$ 4.2 GeV/c
<b>0.20 ± 0.20</b>		BADIER 65	HBC	0	$K^- p$ 3 GeV/c

$\Gamma(\Xi \pi)/\Gamma(\Xi(1530)\pi)$   $\Gamma_3/\Gamma_4$

VALUE	DOCUMENT ID	TECN	CHG	COMMENT
<b>1.5 <sup>+0.6</sup><sub>-0.4</sub></b>	APSELL 70	HBC	0	$K^- p$ 2.87 GeV/c

$\Gamma(\Sigma \bar{K})/\Gamma_{total}$   $\Gamma_2/\Gamma$

VALUE	DOCUMENT ID	TECN	CHG	COMMENT
<b>0.30 ± 0.15</b>				
	ALITTI 69	HBC	-	$K^- p$ 3.9-5 GeV/c
••• We do not use the following data for averages, fits, limits, etc. •••				
<0.02	TRIPP 67	RVUE		Use SMITH 65c

$\Gamma(\Sigma \bar{K})/\Gamma(\Lambda \bar{K})$   $\Gamma_2/\Gamma_1$

VALUE	DOCUMENT ID	TECN	CHG	COMMENT
<b>0.24 ± 0.10</b>	GAY 76c	HBC	-	$K^- p$ 4.2 GeV/c

$\Gamma(\Xi(1530)\pi)/\Gamma_{total}$   $\Gamma_4/\Gamma$

VALUE	DOCUMENT ID	TECN	CHG	COMMENT
<b>0.30 ± 0.15</b>				
	ALITTI 69	HBC	-	$K^- p$ 3.9-5 GeV/c
••• We do not use the following data for averages, fits, limits, etc. •••				
seen	ASTON 85B	LASS		$K^- p$ 11 GeV/c
not seen	5 HASSALL 81	HBC		$K^- p$ 6.5 GeV/c
<0.25	6 DAUBER 69	HBC		$K^- p$ 2.7 GeV/c

$\Gamma(\Xi(1530)\pi)/\Gamma(\Lambda \bar{K})$   $\Gamma_4/\Gamma_1$

VALUE	DOCUMENT ID	TECN	CHG	COMMENT
<b>0.38 ± 0.27 OUR AVERAGE</b>				Error includes scale factor of 2.3.
1.0 ± 0.3	GAY 76c	HBC	-	$K^- p$ 4.2 GeV/c
0.26 ± 0.13	SMITH 65c	HBC	-0	$K^- p$ 2.45-2.7 GeV/c

$\Gamma(\Xi \pi \pi \text{ (not } \Xi(1530)\pi))/\Gamma(\Lambda \bar{K})$   $\Gamma_5/\Gamma_1$

VALUE	DOCUMENT ID	TECN	CHG	COMMENT
<b>0.30 ± 0.20</b>	BIAGI 87	SPEC	-	$\Xi^-$ Be 116 GeV
••• We do not use the following data for averages, fits, limits, etc. •••				
<0.14	7 BADIER 65	HBC	0	1 st. dev. limit
>0.1	SMITH 65c	HBC	-0	$K^- p$ 2.45-2.7 GeV/c

$\Gamma(\Xi \pi \pi \text{ (not } \Xi(1530)\pi))/\Gamma(\Xi(1530)\pi)$   $\Gamma_5/\Gamma_4$

VALUE	DOCUMENT ID	TECN	CHG	COMMENT
consistent with zero	GAY 76c	HBC	-	$K^- p$ 4.2 GeV/c
••• We do not use the following data for averages, fits, limits, etc. •••				
0.3 ± 0.5	8 APSELL 70	HBC	0	$K^- p$ 2.87 GeV/c

$\Xi(1820)$  FOOTNOTES

- BIAGI 87 also sees weak signals in the in the  $\Xi^- \pi^+ \pi^-$  channel at 1782.6 ± 1.4 MeV ( $\Gamma = 6.0 \pm 1.5$  MeV) and 1831.9 ± 2.8 MeV ( $\Gamma = 9.6 \pm 9.9$  MeV).
- BADIER 72 adds all channels and divides the peak into lower and higher mass regions. The data can also be fitted with a single Breit-Wigner of mass 1800 MeV and width 150 MeV.
- From a fit to inclusive  $\Xi \pi$ ,  $\Xi \pi \pi$ , and  $\Lambda K^-$  spectra.
- From a fit to inclusive  $\Xi \pi$  and  $\Xi \pi \pi$  spectra only.
- Including  $\Xi \pi \pi$ .
- DAUBER 69 uses in part the same data as SMITH 65c.
- For the decay mode  $\Xi^- \pi^+ \pi^0$  only. This limit includes  $\Xi(1530)\pi$ .
- Or less. Upper limit for the 3-body decay.

$\Xi(1820)$  REFERENCES

ABLIKIM	20C	PRL 124 032002	M. Ablikim et al.	(BESIII Collab.)
ANISOVICH	12A	EPL A48 15	A.V. Anisovich et al.	(BONN, FNPI)
ADAMOVIICH	99B	EPL C11 271	M.L. Adamovich et al.	(CERN WA89 Collab.)
BIAGI	87	ZPHY C34 15	S.F. Biagi et al.	(BRIS, CERN, GEVA+)
BIAGI	87C	ZPHY C34 175	S.F. Biagi et al.	(BRIS, CERN, GEVA+)
ASTON	85B	PR D32 2270	D. Aston et al.	(SLAC, CARL, CNRC, CINC)
JENKINS	83	PRL 51 951	C.M. Jenkins et al.	(FSU, BRAN, LBL+)
BIAGI	81	ZPHY C9 305	S.F. Biagi et al.	(BRIS, CAVE, GEVA+)
HASSALL	81	NP B189 397	J.K. Hassall et al.	(CAVE, MSU)
TEODORO	78	PL 77B 451	D. Teodoro et al.	(AMST, CERN, NIJM+)
BRIEFEL	77	PR D16 2706	E. Briefel et al.	(BRAN, UMD, SYRA+)
Also				
GAY	76C	PL 62B 477	S.P. Apse et al.	(BRAN, UMD, SYRA+)
DIBIANCA	75	NP B98 137	J.B. Gay et al.	(AMST, CERN, NIJM+)
BADIER	72	NP B37 429	F.A. Dibilanca, R.J. Endorf	(AMST, CERN, NIJM+)
APSELL	70	PRL 24 777	J. Badier et al.	(EPOL)
CRENNELL	70B	PR D1 847	S.P. Apse et al.	(BRAN, UMD, SYRA+)
ALITTI	69	PRL 22 79	D.J. Crennell et al.	(BNL)
DAUBER	69	PR 179 1262	J. Alitti et al.	(BNL, SYRA+)
TRIPP	67	NP B3 10	P.M. Dauber et al.	(LRL)
BADIER	65	PL 16 171	R.D. Tripp et al.	(LRL, SLAC, CERN+)
SMITH	65B	Athens Conf. 251	J. Badier et al.	(EPOL, SACL, AMST)
SMITH	65C	PRL 14 25	G.A. Smith, J.S. Lindsey	(LRL)
HALSTEINSLID	63	Siena Conf. 1 73	G.A. Smith et al.	(LRL)JJP
			A. Halsteinslid et al.	(BERG, CERN, EPOL+)

OTHER RELATED PAPERS

TEODORO	78	PL 77B 451	D. Teodoro et al.	(AMST, CERN, NIJM+)
BRIEFEL	75	PR D12 1859	E. Briefel et al.	(BRAN, UMD, SYRA+)
SCHMIDT	73	Purdue Conf. 363	P.E. Schmidt	(BRAN)
MERRILL	68	PR 167 1202	D.W. Merrill, J. Button-Shafer	(LRL)
SMITH	64	PRL 13 61	G.A. Smith et al.	(LRL)JJP

$\Xi(1950)$

$I(J^P) = \frac{1}{2}(?)$  Status: \*\*\*

We list here everything reported between 1875 and 2000 MeV. The accumulated evidence for a  $\Xi$  near 1950 MeV seems strong enough to include a  $\Xi(1950)$  in the main Baryon Table, but not much can be said about its properties. In fact, there may be more than one  $\Xi$  near this mass.

$\Xi(1950)$  MASS

VALUE (MeV)	EVTS	DOCUMENT ID	TECN	COMMENT
<b>1950 ± 15 OUR ESTIMATE</b>				
1955 ± 6		ADAMOVIICH 99B	WA89	$\Sigma^-$ nucleus, 345 GeV
1944 ± 9	129	BIAGI 87	SPEC	$\Xi^-$ Be → $(\Xi^- \pi^+) \pi^- X$
1963 ± 5 ± 2	63	BIAGI 87c	SPEC	$\Xi^-$ Be → $(\Lambda \bar{K}^0) X$
1937 ± 7	150	BIAGI 81	SPEC	SPS hyperon beam
1961 ± 18	139	BRIEFEL 77	HBC	2.87 $K^- p$ → $\Xi^- \pi^+ X$
1936 ± 22	44	BRIEFEL 77	HBC	2.87 $K^- p$ → $\Xi^0 \pi^- X$
1964 ± 10	56	BRIEFEL 77	HBC	$\Xi(1530)\pi$
1900 ± 12		DIBIANCA 75	DBC	$\Xi \pi$
1952 ± 11	25	ROSS 73c		$(\Xi \pi)^-$
1956 ± 6	29	BADIER 72	HBC	$\Xi \pi, \Xi \pi \pi, \gamma K$
1955 ± 14	21	GOLDWASSER 70	HBC	$\Xi \pi$

# Baryon Particle Listings

## $\Xi(1950), \Xi(2030)$

1894 ± 18	66	DAUBER	69	HBC	$\Xi\pi$
1930 ± 20	27	ALITTI	68	HBC	$\Xi^-\pi^+$
1933 ± 16	35	BADIER	65	HBC	$\Xi^-\pi^+$

### $\Xi(1950)$ WIDTH

VALUE (MeV)	EVTS	DOCUMENT ID	TECN	COMMENT
<b>60 ± 20 OUR ESTIMATE</b>				
68 ± 22		ADAMOVICH 99B	WA89	$\Sigma^-$ nucleus, 345 GeV
100 ± 31	129	BIAGI 87	SPEC	$\Xi^- \text{Be} \rightarrow (\Xi^- \pi^+) \pi^- X$
25 ± 15 ± 1.2	63	BIAGI 87c	SPEC	$\Xi^- \text{Be} \rightarrow (\Lambda \bar{K}^0) X$
60 ± 8	150	BIAGI 81	SPEC	SPS hyperon beam
159 ± 5.7	139	BRIEFEL 77	HBC	2.87 $K^- p \rightarrow \Xi^- \pi^+ X$
87 ± 26	44	BRIEFEL 77	HBC	2.87 $K^- p \rightarrow \Xi^0 \pi^- X$
60 ± 39	56	BRIEFEL 77	HBC	$\Xi(1530)\pi$
63 ± 78		DIBIANCA 75	DBC	$\Xi\pi$
38 ± 10		ROSS 73c		$(\Xi\pi)^-$
35 ± 11	29	BADIER 72	HBC	$\Xi\pi, \Xi\pi\pi, \Upsilon K$
56 ± 26	21	GOLDWASSER 70	HBC	$\Xi\pi$
98 ± 23	66	DAUBER 69	HBC	$\Xi\pi$
80 ± 40	27	ALITTI 68	HBC	$\Xi^-\pi^+$
140 ± 35	35	BADIER 65	HBC	$\Xi^-\pi^+$

### $\Xi(1950)$ DECAY MODES

Mode	Fraction ( $\Gamma_i/\Gamma$ )
$\Gamma_1 \Lambda \bar{K}$	seen
$\Gamma_2 \Sigma \bar{K}$	possibly seen
$\Gamma_3 \Xi\pi$	seen
$\Gamma_4 \Xi(1530)\pi$	
$\Gamma_5 \Xi\pi\pi$ (not $\Xi(1530)\pi$ )	

### $\Xi(1950)$ BRANCHING RATIOS

$\Gamma(\Sigma \bar{K})/\Gamma(\Lambda \bar{K})$			$\Gamma_2/\Gamma_1$		
VALUE	CL%	EVTS	DOCUMENT ID	TECN	COMMENT
<2.3	90	0	BIAGI 87c	SPEC	$\Xi^- \text{Be} 116 \text{ GeV}$
$\Gamma(\Sigma \bar{K})/\Gamma_{\text{total}}$			$\Gamma_2/\Gamma$		
VALUE	EVTS	DOCUMENT ID	TECN	COMMENT	
possibly seen	17	HASSALL 81	HBC	$K^- p 6.5 \text{ GeV/c}$	
$\Gamma(\Xi\pi)/\Gamma(\Xi(1530)\pi)$			$\Gamma_3/\Gamma_4$		
VALUE	DOCUMENT ID	TECN	COMMENT		
2.8 <sup>+0.7</sup> <sub>-0.6</sub>	APSELL 70	HBC			
$\Gamma(\Xi\pi\pi \text{ (not } \Xi(1530)\pi)/\Gamma(\Xi(1530)\pi)$			$\Gamma_5/\Gamma_4$		
VALUE	DOCUMENT ID	TECN	COMMENT		
0.0 ± 0.3	APSELL 70	HBC			

### $\Xi(1950)$ REFERENCES

ADAMOVICH 99B	EPJ C11 271	M.I. Adamovich et al.	(CERN WA89 Collab.)
BIAGI 87	ZPHY C34 15	S.F. Biagi et al.	(BRIS, CERN, GEVA+)
BIAGI 87c	ZPHY C34 175	S.F. Biagi et al.	(BRIS, CERN, GEVA+)
BIAGI 81	ZPHY C9 305	S.F. Biagi et al.	(BRIS, CAVE, GEVA+)
HASSALL 81	NP B189 397	J.K. Hassall et al.	(CAVE, MSU)
BRIEFEL 77	PR D16 2706	E. Briefel et al.	(BRAN, UMD, SYRA+)
	Duke Conf. 317	E. Briefel et al.	(BRAN, UMD, SYRA+)
Hyperon Resonances, 1970			
DIBIANCA 75	NP B98 137	F.A. Dibianca, R.J. Endorf	(CMU)
ROSS 73c	Purdue Conf. 345	R.T. Ross, J.L. Lloyd, D. Radojčić	(OXF)
BADIER 72	NP B37 429	J. Badier et al.	(EPOL)
APSELL 70	PRL 24 777	S.P. Appell et al.	(BRAN, UMD, SYRA+)
GOLDWASSER 70	PR D1 1960	E.L. Goldwasser, P.F. Schultzt	(ILL)
DAUBER 69	PR 179 1262	P.M. Dauber et al.	(LRL)
ALITTI 68	PRL 21 1119	J. Alitti et al.	(BNL, SYRA)
BADIER 65	PL 16 171	J. Badier et al.	(EPOL, SAFL, AMST)

## $\Xi(2030)$

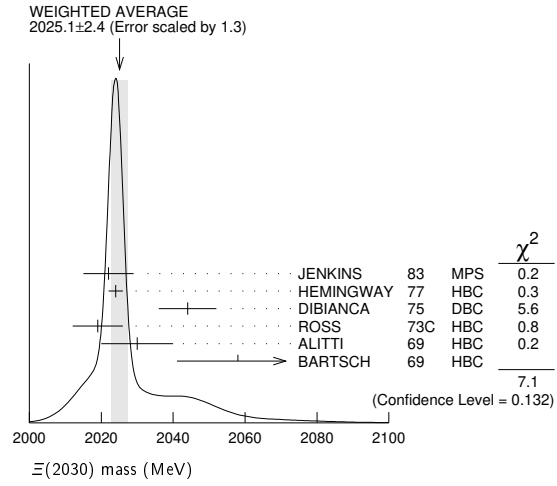
$$I(J^P) = \frac{1}{2} (\geq \frac{5}{2}?) \text{ status: } ***$$

The evidence for this state has been much improved by HEMINGWAY 77, who see an eight standard deviation enhancement in  $\Sigma \bar{K}$  and a weaker coupling to  $\Lambda \bar{K}$ . ALITTI 68 and HEMINGWAY 77 observe no signals in the  $\Xi\pi\pi$  (or  $\Xi(1530)\pi$ ) channel, in contrast to DIBIANCA 75. The decay  $(\Lambda/\Sigma)\bar{K}\pi$  reported by BARTSCH 69 is also not confirmed by HEMINGWAY 77.

A moments analysis of the HEMINGWAY 77 data indicates at a level of three standard deviations that  $J \geq 5/2$ .

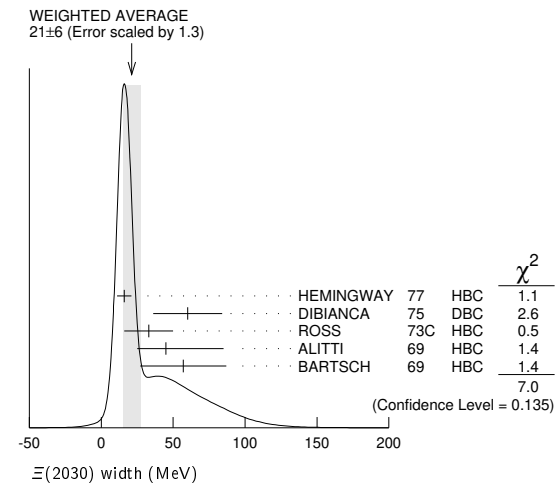
### $\Xi(2030)$ MASS

VALUE (MeV)	EVTS	DOCUMENT ID	TECN	CHG	COMMENT
<b>2025 ± 5 OUR ESTIMATE</b>					
<b>2025.1 ± 2.4 OUR AVERAGE</b> Error includes scale factor of 1.3. See the ideogram below.					
2022 ± 7		JENKINS 83	MPS	-	$K^- p \rightarrow K^+ \text{MM}$
2024 ± 2	200	HEMINGWAY 77	HBC	-	$K^- p 4.2 \text{ GeV/c}$
2044 ± 8		DIBIANCA 75	DBC	-0	$\Xi\pi\pi, \Xi^*\pi$
2019 ± 7	15	ROSS 73c	HBC	-0	$\Sigma \bar{K}$
2030 ± 10	42	ALITTI 69	HBC	-	$K^- p 3.9-5 \text{ GeV/c}$
2058 ± 17	40	BARTSCH 69	HBC	-0	$K^- p 10 \text{ GeV/c}$



### $\Xi(2030)$ WIDTH

VALUE (MeV)	EVTS	DOCUMENT ID	TECN	CHG	COMMENT
<b>20 ± 15 OUR ESTIMATE</b>					
<b>21 ± 6 OUR AVERAGE</b> Error includes scale factor of 1.3. See the ideogram below.					
16 ± 5	200	HEMINGWAY 77	HBC	-	$K^- p 4.2 \text{ GeV/c}$
60 ± 24		DIBIANCA 75	DBC	-0	$\Xi\pi\pi, \Xi^*\pi$
33 ± 17	15	ROSS 73c	HBC	-0	$\Sigma \bar{K}$
45 <sup>+40</sup> <sub>-20</sub>		ALITTI 69	HBC	-	$K^- p 3.9-5 \text{ GeV/c}$
57 ± 30		BARTSCH 69	HBC	-0	$K^- p 10 \text{ GeV/c}$



### $\Xi(2030)$ DECAY MODES

Mode	Fraction ( $\Gamma_i/\Gamma$ )
$\Gamma_1 \Lambda \bar{K}$	~ 20 %
$\Gamma_2 \Sigma \bar{K}$	~ 80 %
$\Gamma_3 \Xi\pi$	small
$\Gamma_4 \Xi(1530)\pi$	small
$\Gamma_5 \Xi\pi\pi$ (not $\Xi(1530)\pi$ )	small
$\Gamma_6 \Lambda \bar{K}\pi$	small
$\Gamma_7 \Sigma \bar{K}\pi$	small

See key on page 999

# Baryon Particle Listings

## $\Xi(2030)$ , $\Xi(2120)$ , $\Xi(2250)$

### $\Xi(2030)$ BRANCHING RATIOS

$$\frac{\Gamma(\Xi\pi)}{[\Gamma(\Lambda\bar{K}) + \Gamma(\Sigma\bar{K}) + \Gamma(\Xi\pi) + \Gamma(\Xi(1530)\pi)]} \quad \Gamma_3/(\Gamma_1+\Gamma_2+\Gamma_3+\Gamma_4)$$

VALUE	DOCUMENT ID	TECN	CHG	COMMENT
<0.30	ALITTI 69	HBC	—	1 standard dev. limit

$$\frac{\Gamma(\Xi\pi)/\Gamma(\Sigma\bar{K})}{\Gamma_3/\Gamma_2}$$

VALUE	CL%	DOCUMENT ID	TECN	CHG	COMMENT
<0.19	95	HEMINGWAY 77	HBC	—	$K^- p$ 4.2 GeV/c

$$\frac{\Gamma(\Lambda\bar{K})/[\Gamma(\Lambda\bar{K}) + \Gamma(\Sigma\bar{K}) + \Gamma(\Xi\pi) + \Gamma(\Xi(1530)\pi)]}{\Gamma_1/(\Gamma_1+\Gamma_2+\Gamma_3+\Gamma_4)}$$

VALUE	DOCUMENT ID	TECN	CHG	COMMENT
0.25 ± 0.15	ALITTI 69	HBC	—	$K^- p$ 3.9–5 GeV/c

$$\frac{\Gamma(\Lambda\bar{K})/\Gamma(\Sigma\bar{K})}{\Gamma_1/\Gamma_2}$$

VALUE	DOCUMENT ID	TECN	CHG	COMMENT
0.22 ± 0.09	HEMINGWAY 77	HBC	—	$K^- p$ 4.2 GeV/c

$$\frac{\Gamma(\Sigma\bar{K})/[\Gamma(\Lambda\bar{K}) + \Gamma(\Sigma\bar{K}) + \Gamma(\Xi\pi) + \Gamma(\Xi(1530)\pi)]}{\Gamma_2/(\Gamma_1+\Gamma_2+\Gamma_3+\Gamma_4)}$$

VALUE	DOCUMENT ID	TECN	CHG	COMMENT
0.75 ± 0.20	ALITTI 69	HBC	—	$K^- p$ 3.9–5 GeV/c

$$\frac{\Gamma(\Xi(1530)\pi)/[\Gamma(\Lambda\bar{K}) + \Gamma(\Sigma\bar{K}) + \Gamma(\Xi\pi) + \Gamma(\Xi(1530)\pi)]}{\Gamma_4/(\Gamma_1+\Gamma_2+\Gamma_3+\Gamma_4)}$$

VALUE	DOCUMENT ID	TECN	CHG	COMMENT
<0.15	ALITTI 69	HBC	—	1 standard dev. limit

$$\frac{[\Gamma(\Xi(1530)\pi) + \Gamma(\Xi\pi(\text{not } \Xi(1530)\pi))]/\Gamma(\Sigma\bar{K})}{(\Gamma_4+\Gamma_5)/\Gamma_2}$$

VALUE	CL%	DOCUMENT ID	TECN	CHG	COMMENT
<0.11	95	1 HEMINGWAY 77	HBC	—	$K^- p$ 4.2 GeV/c

$$\frac{\Gamma(\Lambda\bar{K}\pi)/\Gamma_{\text{total}}}{\Gamma_6/\Gamma_7}$$

VALUE	DOCUMENT ID	TECN	COMMENT
seen	BARTSCH 69	HBC	$K^- p$ 10 GeV

$$\frac{\Gamma(\Lambda\bar{K}\pi)/\Gamma(\Sigma\bar{K})}{\Gamma_6/\Gamma_2}$$

VALUE	CL%	DOCUMENT ID	TECN	CHG	COMMENT
<0.32	95	HEMINGWAY 77	HBC	—	$K^- p$ 4.2 GeV/c

$$\frac{\Gamma(\Sigma\bar{K}\pi)/\Gamma_{\text{total}}}{\Gamma_7/\Gamma_7}$$

VALUE	DOCUMENT ID	TECN	COMMENT
seen	BARTSCH 69	HBC	$K^- p$ 10 GeV

$$\frac{\Gamma(\Sigma\bar{K}\pi)/\Gamma(\Sigma\bar{K})}{\Gamma_7/\Gamma_2}$$

VALUE	CL%	DOCUMENT ID	TECN	CHG	COMMENT
<0.04	95	2 HEMINGWAY 77	HBC	—	$K^- p$ 4.2 GeV/c

### $\Xi(2030)$ FOOTNOTES

- For the decay mode  $\Xi^- \pi^+ \pi^-$  only.
- For the decay mode  $\Sigma^\pm K^- \pi^\mp$  only.

### $\Xi(2030)$ REFERENCES

JENKINS 83	PRL 51 951	C.M. Jenkins et al.	(FSU, BRAN, LBL+)
HEMINGWAY 77	PL 68B 197	R.J. Hemingway et al.	(AMST, CERN, NIJM+)
Also	PL 62B 477	J.B. Gay et al.	(AMST, CERN, NIJM)
DIBIANCA 75	NP B98 137	F.A. Dibianca, R.J. Endorf	(CMU)
ROSS 73C	Purdue Conf. 345	R.T. Ross, J.L. Lloyd, D. Radojčić	(OXF)
ALITTI 69	PRL 22 79	J. Alitti et al.	(BNL, SYRA)
BARTSCH 69	PL 28B 439	J. Bartsch et al.	(AACH, BERL, CERN+)
ALITTI 68	PRL 21 1119	J. Alitti et al.	(BNL, SYRA)

## $\Xi(2120)$

$$I(J^P) = \frac{1}{2}(?)^? \text{ Status: } * \\ J, P \text{ need confirmation.}$$

OMITTED FROM SUMMARY TABLE

### $\Xi(2120)$ MASS

VALUE (MeV)	EVTS	DOCUMENT ID	TECN	COMMENT
$\approx 2120$ OUR ESTIMATE				
2137 ± 4	18	1 CHLIAPNIK...	79 HBC	$K^+ p$ 32 GeV/c
2123 ± 7		2 GAY	76c HBC	$K^- p$ 4.2 GeV/c

### $\Xi(2120)$ WIDTH

VALUE (MeV)	EVTS	DOCUMENT ID	TECN	COMMENT
<20	18	1 CHLIAPNIK...	79 HBC	$K^+ p$ 32 GeV/c
25 ± 12		2 GAY	76c HBC	$K^- p$ 4.2 GeV/c

### $\Xi(2120)$ DECAY MODES

Mode	Fraction ( $\Gamma_i/\Gamma$ )
$\Gamma_1 \Lambda\bar{K}$	seen

### $\Xi(2120)$ BRANCHING RATIOS

$\Gamma(\Lambda\bar{K})/\Gamma_{\text{total}}$	DOCUMENT ID	TECN	COMMENT	$\Gamma_1/\Gamma$
seen	1 CHLIAPNIK...	79 HBC	$K^+ p \rightarrow (\bar{K} K^+) X$	
seen	2 GAY	76c HBC	$K^- p$ 4.2 GeV/c	

### $\Xi(2120)$ FOOTNOTES

- CHLIAPNIKOV 79 does not uniquely identify the  $K^+$  in the  $(\bar{K} K^+) X$  final state. It also reports bumps with fewer events at 2240, 2540, and 2830 MeV.
- GAY 76c sees a 4-standard deviation signal. However, HEMINGWAY 77, with more events from the same experiment points out that the signal is greatly reduced if a cut is made on the 4-momentum  $u$ . This suggests an anomalous production mechanism if the  $\Xi(2120)$  is real.

### $\Xi(2120)$ REFERENCES

CHLIAPNIK... 79	NP B158 253	P.V. Chliapnikov et al.	(CERN, BELG, MONS)
HEMINGWAY 77	PL 68B 197	R.J. Hemingway et al.	(AMST, CERN, NIJM+)
GAY 76c	PL 62B 477	J.B. Gay et al.	(AMST, CERN, NIJM)

## $\Xi(2250)$

$$I(J^P) = \frac{1}{2}(?)^? \text{ Status: } ** \\ J, P \text{ need confirmation.}$$

OMITTED FROM SUMMARY TABLE

The evidence for this state is mixed. BARTSCH 69 sees a bump of not much statistical significance in  $\Lambda\bar{K}\pi$ ,  $\Sigma\bar{K}\pi$ , and  $\Xi\pi\pi$  mass spectra. GOLDWASSER 70 sees a narrower bump in  $\Xi\pi\pi$  at a higher mass. Not seen by HASSALL 81 with 45 events/ $\mu\text{b}$  at 6.5 GeV/c. Seen by JENKINS 83. Perhaps seen by BIAGI 87.

### $\Xi(2250)$ MASS

VALUE (MeV)	EVTS	DOCUMENT ID	TECN	CHG	COMMENT
$\approx 2250$ OUR ESTIMATE					
2189 ± 7	66	BIAGI 87	SPEC	—	$\Xi^- \text{Be} \rightarrow (\Xi^- \pi^+ \pi^-) X$
2214 ± 5		JENKINS 83	MPS	—	$K^- p \rightarrow K^+ \text{MM}$
2295 ± 15	18	GOLDWASSER 70	HBC	—	$K^- p$ 5.5 GeV/c
2244 ± 52	35	BARTSCH 69	HBC	—	$K^- p$ 10 GeV/c

### $\Xi(2250)$ WIDTH

VALUE (MeV)	EVTS	DOCUMENT ID	TECN	CHG	COMMENT
46 ± 27	66	BIAGI 87	SPEC	—	$\Xi^- \text{Be} \rightarrow (\Xi^- \pi^+ \pi^-) X$
< 30		GOLDWASSER 70	HBC	—	$K^- p$ 5.5 GeV/c
130 ± 80		BARTSCH 69	HBC	—	

### $\Xi(2250)$ DECAY MODES

Mode	Fraction ( $\Gamma_i/\Gamma$ )
$\Gamma_1 \Xi\pi\pi$	
$\Gamma_2 \Lambda\bar{K}\pi$	
$\Gamma_3 \Sigma\bar{K}\pi$	

### $\Xi(2250)$ REFERENCES

BIAGI 87	ZPHY C34 15	S.F. Biagi et al.	(BRIS, CERN, GEVA+)
JENKINS 83	PRL 51 951	C.M. Jenkins et al.	(FSU, BRAN, LBL+)
HASSALL 81	NP B189 337	J.K. Hassall et al.	(CAVE, MSU)
GOLDWASSER 70	PR D1 1960	E.L. Goldwasser, P.F. Schultz	(ILL)
BARTSCH 69	PL 28B 439	J. Bartsch et al.	(AACH, BERL, CERN+)



## Baryon Particle Listings

 $\Xi(2250)$ ,  $\Xi(2370)$ ,  $\Xi(2500)$  $\Xi(2370)$  $I(J^P) = \frac{1}{2}(??)$  Status: \*\*  
J, P need confirmation.

OMITTED FROM SUMMARY TABLE

 $\Xi(2370)$  MASS

VALUE (MeV)	EVTS	DOCUMENT ID	TECN	CHG	COMMENT
<b><math>\approx 2370</math> OUR ESTIMATE</b>					
2356 $\pm$ 10		JENKINS 83	MPS	—	$K^- p \rightarrow K^+ \text{MM}$
2370	50	HASSALL 81	HBC	-0	$K^- p$ 6.5 GeV/c
2373 $\pm$ 8	94	AMIRZADEH 80	HBC	-0	$K^- p$ 8.25 GeV/c
2392 $\pm$ 27		DIBIANCA 75	DBC		$\Xi 2\pi$

 $\Xi(2370)$  WIDTH

VALUE (MeV)	EVTS	DOCUMENT ID	TECN	CHG	COMMENT
80	50	HASSALL 81	HBC	-0	$K^- p$ 6.5 GeV/c
80 $\pm$ 25	94	AMIRZADEH 80	HBC	-0	$K^- p$ 8.25 GeV/c
75 $\pm$ 69		DIBIANCA 75	DBC		$\Xi 2\pi$

 $\Xi(2370)$  DECAY MODES

Mode	Fraction ( $\Gamma_i/\Gamma$ )
$\Gamma_1$ $\Lambda \bar{K} \pi$ Includes $\Gamma_4 + \Gamma_6$ .	seen
$\Gamma_2$ $\Sigma \bar{K} \pi$ Includes $\Gamma_5 + \Gamma_6$ .	seen
$\Gamma_3$ $\Omega^- K$	
$\Gamma_4$ $\Lambda \bar{K}^*(892)$	
$\Gamma_5$ $\Sigma \bar{K}^*(892)$	
$\Gamma_6$ $\Sigma(1385) \bar{K}$	

 $\Xi(2370)$  BRANCHING RATIOS

$\Gamma(\Lambda \bar{K} \pi)/\Gamma_{\text{total}}$	$\Gamma_1/\Gamma$			
VALUE	DOCUMENT ID	TECN	CHG	COMMENT
seen	AMIRZADEH 80	HBC	-0	$K^- p$ 8.25 GeV/c

$\Gamma(\Sigma \bar{K} \pi)/\Gamma_{\text{total}}$	$\Gamma_2/\Gamma$			
VALUE	DOCUMENT ID	TECN	CHG	COMMENT
seen	AMIRZADEH 80	HBC	-0	$K^- p$ 8.25 GeV/c

$[\Gamma(\Lambda \bar{K} \pi) + \Gamma(\Sigma \bar{K} \pi)]/\Gamma_{\text{total}}$	$(\Gamma_1 + \Gamma_2)/\Gamma$				
VALUE	EVTS	DOCUMENT ID	TECN	CHG	COMMENT
seen	50	HASSALL 81	HBC	-0	$K^- p$ 6.5 GeV/c

$\Gamma(\Omega^- K)/\Gamma_{\text{total}}$	$\Gamma_3/\Gamma$			
VALUE	DOCUMENT ID	TECN	CHG	COMMENT
0.09 $\pm$ 0.04	<sup>1</sup> KINSON 80	HBC	—	$K^- p$ 8.25 GeV/c

$[\Gamma(\Lambda \bar{K}^*(892)) + \Gamma(\Sigma \bar{K}^*(892))]/\Gamma_{\text{total}}$	$(\Gamma_4 + \Gamma_5)/\Gamma$			
VALUE	DOCUMENT ID	TECN	CHG	COMMENT
0.22 $\pm$ 0.13	<sup>1</sup> KINSON 80	HBC	—	$K^- p$ 8.25 GeV/c

$\Gamma(\Sigma(1385) \bar{K})/\Gamma_{\text{total}}$	$\Gamma_6/\Gamma$			
VALUE	DOCUMENT ID	TECN	CHG	COMMENT
0.12 $\pm$ 0.08	<sup>1</sup> KINSON 80	HBC	—	$K^- p$ 8.25 GeV/c

 $\Xi(2370)$  FOOTNOTES<sup>1</sup> KINSON 80 is a reanalysis of AMIRZADEH 80 with 50% more events. $\Xi(2370)$  REFERENCES

JENKINS 83	PRL 51 951	C.M. Jenkins et al.	(FSU, BRAN, LBL+)
HASSALL 81	NP B189 397	J.K. Hassall et al.	(CAVE, MSU)
AMIRZADEH 80	PL 90B 324	J. Amirzadeh et al.	(BIRM, CERN, GLAS+) <sup>1</sup>
KINSON 80	Toronto Conf. 263	J.B. Kinson et al.	(BIRM, CERN, GLAS+) <sup>1</sup>
DIBIANCA 75	NP B98 137	F.A. Dibianna, R.J. Endorf	(CMU)

 $\Xi(2500)$  $I(J^P) = \frac{1}{2}(??)$  Status: \*  
J, P need confirmation.

OMITTED FROM SUMMARY TABLE

The ALITTI 69 peak might be instead the  $\Xi(2370)$  or might be neither the  $\Xi(2370)$  nor the  $\Xi(2500)$ . $\Xi(2500)$  MASS

VALUE (MeV)	EVTS	DOCUMENT ID	TECN	CHG	COMMENT
<b><math>\approx 2500</math> OUR ESTIMATE</b>					
2505 $\pm$ 10		JENKINS 83	MPS	—	$K^- p \rightarrow K^+ \text{MM}$
2430 $\pm$ 20	30	ALITTI 69	HBC	—	$K^- p$ 4.6-5 GeV/c
2500 $\pm$ 10	45	BARTSCH 69	HBC	-0	$K^- p$ 10 GeV/c

 $\Xi(2500)$  WIDTH

VALUE (MeV)	DOCUMENT ID	TECN	CHG
150 $\pm$ 40	ALITTI 69	HBC	—
59 $\pm$ 27	BARTSCH 69	HBC	-0

 $\Xi(2500)$  DECAY MODES

Mode	Fraction ( $\Gamma_i/\Gamma$ )
$\Gamma_1$ $\Xi \pi$	
$\Gamma_2$ $\Lambda \bar{K}$	
$\Gamma_3$ $\Sigma \bar{K}$	
$\Gamma_4$ $\Xi \pi \pi$	seen
$\Gamma_5$ $\Xi(1530) \pi$	
$\Gamma_6$ $\Lambda \bar{K} \pi + \Sigma \bar{K} \pi$	seen

 $\Xi(2500)$  BRANCHING RATIOS

$\Gamma(\Xi \pi)/[\Gamma(\Xi \pi) + \Gamma(\Lambda \bar{K}) + \Gamma(\Sigma \bar{K}) + \Gamma(\Xi(1530) \pi)]$	$\Gamma_1/(\Gamma_1 + \Gamma_2 + \Gamma_3 + \Gamma_5)$		
VALUE	DOCUMENT ID	TECN	COMMENT
<0.5	ALITTI 69	HBC	1 standard dev. limit

$\Gamma(\Lambda \bar{K})/[\Gamma(\Xi \pi) + \Gamma(\Lambda \bar{K}) + \Gamma(\Sigma \bar{K}) + \Gamma(\Xi(1530) \pi)]$	$\Gamma_2/(\Gamma_1 + \Gamma_2 + \Gamma_3 + \Gamma_5)$		
VALUE	DOCUMENT ID	TECN	CHG
0.5 $\pm$ 0.2	ALITTI 69	HBC	—

$\Gamma(\Sigma \bar{K})/[\Gamma(\Xi \pi) + \Gamma(\Lambda \bar{K}) + \Gamma(\Sigma \bar{K}) + \Gamma(\Xi(1530) \pi)]$	$\Gamma_3/(\Gamma_1 + \Gamma_2 + \Gamma_3 + \Gamma_5)$		
VALUE	DOCUMENT ID	TECN	CHG
0.5 $\pm$ 0.2	ALITTI 69	HBC	—

$\Gamma(\Xi(1530) \pi)/[\Gamma(\Xi \pi) + \Gamma(\Lambda \bar{K}) + \Gamma(\Sigma \bar{K}) + \Gamma(\Xi(1530) \pi)]$	$\Gamma_5/(\Gamma_1 + \Gamma_2 + \Gamma_3 + \Gamma_5)$		
VALUE	DOCUMENT ID	TECN	COMMENT
<0.2	ALITTI 69	HBC	1 standard dev. limit

$\Gamma(\Xi \pi \pi)/\Gamma_{\text{total}}$	$\Gamma_4/\Gamma$		
VALUE	DOCUMENT ID	TECN	CHG
seen	BARTSCH 69	HBC	-0

$[\Gamma(\Lambda \bar{K} \pi) + \Gamma(\Sigma \bar{K} \pi)]/\Gamma_{\text{total}}$	$\Gamma_6/\Gamma$		
VALUE	DOCUMENT ID	TECN	CHG
seen	BARTSCH 69	HBC	-0

 $\Xi(2500)$  REFERENCES

JENKINS 83	PRL 51 951	C.M. Jenkins et al.	(FSU, BRAN, LBL+)
ALITTI 69	PRL 22 79	J. Alitti et al.	(BNL, SYRA) <sup>1</sup>
BARTSCH 69	PL 28B 439	J. Bartsch et al.	(AACH, BERL, CERN+)

# $\Omega^-$ BARYONS

## ( $S = -3, I = 0$ )

$\Omega^- = sss$



$I(J^P) = 0(\frac{3}{2}^+)$  Status: \*\*\*\*

The unambiguous discovery in both production and decay was by BARNES 64. The quantum numbers follow from the assignment of the particle to the baryon decuplet. DEUTSCHMANN 78 and BAUBILLIER 78 rule out  $J = 1/2$  and find consistency with  $J = 3/2$ . AUBERT, BE 06 finds from the decay angular distributions of  $\Xi_c^0 \rightarrow \Omega^- K^+$  and  $\Omega_c^0 \rightarrow \Omega^- K^+$  that  $J = 3/2$ ; this depends on the spins of the  $\Xi_c^0$  and  $\Omega_c^0$  being  $J = 1/2$ , their supposed values.

We have omitted some results that have been superseded by later experiments. See our earlier editions.

### $\Omega^-$ MASS

The fit assumes the  $\Omega^-$  and  $\Omega^+$  masses are the same, and averages them together.

VALUE (MeV)	EVTS	DOCUMENT ID	TECN	COMMENT
<b>1672.45 ± 0.29 OUR FIT</b>				
<b>1672.43 ± 0.32 OUR AVERAGE</b>				
1673 ± 1	100	HARTOUNI 85	SPEC	80–280 GeV $K_L^0 C$
1673.0 ± 0.8	41	BAUBILLIER 78	HBC	8.25 GeV/c $K^- p$
1671.7 ± 0.6	27	HEMINGWAY 78	HBC	4.2 GeV/c $K^- p$
1673.4 ± 1.7	4	<sup>1</sup> DIBIANCA 75	DBC	4.9 GeV/c $K^- d$
1673.3 ± 1.0	3	PALMER 68	HBC	$K^- p$ 4.6, 5 GeV/c
1671.8 ± 0.8	3	SCHULTZ 68	HBC	$K^- p$ 5.5 GeV/c
1674.2 ± 1.6	5	SCOTTER 68	HBC	$K^- p$ 6 GeV/c
1672.1 ± 1.0	1	<sup>2</sup> FRY 55	EMUL	
••• We do not use the following data for averages, fits, limits, etc. •••				
1671.43 ± 0.78	13	<sup>3</sup> DEUTSCH... 73	HBC	$K^- p$ 10 GeV/c
1671.9 ± 1.2	6	<sup>3</sup> SPETH 69	HBC	See DEUTSCHMANN 73
1673.0 ± 8.0	1	ABRAMS 64	HBC	$\rightarrow \Xi^- \pi^0$
1670.6 ± 1.0	1	<sup>2</sup> FRY 55B	EMUL	
1615	1	<sup>4</sup> EISENBERG 54	EMUL	

- <sup>1</sup>DIBIANCA 75 gives a mass for each event. We quote the average.
- The FRY 55 and FRY 55B events were identified as  $\Omega^-$  by ALVAREZ 73. The masses assume decay to  $\Lambda K^-$  at rest. For FRY 55B, decay from an atomic orbit could Doppler shift the  $K^-$  energy and the resulting  $\Omega^-$  mass by several MeV. This shift is negligible for FRY 55 because the  $\Omega^-$  decay is approximately perpendicular to its orbital velocity, as is known because the  $\Lambda$  strikes the nucleus (L.Alvarez, private communication 1973). We have calculated the error assuming that the orbital n is 4 or larger.
- Excluded from the average; the  $\Omega^-$  lifetimes measured by the experiments differ significantly from other measurements.
- The EISENBERG 54 mass was calculated for decay in flight. ALVAREZ 73 has shown that the  $\Omega^-$  interacted with an Ag nucleus to give  $K^- \Xi Ag$ .

### $\Omega^+$ MASS

The fit assumes the  $\Omega^-$  and  $\Omega^+$  masses are the same, and averages them together.

VALUE (MeV)	EVTS	DOCUMENT ID	TECN	COMMENT
<b>1672.45 ± 0.29 OUR FIT</b>				
<b>1672.5 ± 0.7 OUR AVERAGE</b>				
1672 ± 1	72	HARTOUNI 85	SPEC	80–280 GeV $K_L^0 C$
1673.1 ± 1.0	1	FIRESTONE 71B	HBC	12 GeV/c $K^+ d$

$$(m_{\Omega^-} - m_{\Omega^+}) / m_{\Omega^-}$$

A test of  $CPT$  invariance.

VALUE	DOCUMENT ID	TECN	COMMENT
<b>(-1.44 ± 7.98) × 10<sup>-5</sup></b>	CHAN	98 E756	$p$ Be, 800 GeV

### $\Omega^-$ MEAN LIFE

Measurements with an error  $> 0.1 \times 10^{-10}$  s have been omitted. The fit assumes the  $\Omega^-$  and  $\Omega^+$  mean lives are the same, and averages them together.

VALUE (10 <sup>-10</sup> s)	EVTS	DOCUMENT ID	TECN	COMMENT
<b>0.821 ± 0.011 OUR FIT</b>				
<b>0.821 ± 0.011 OUR AVERAGE</b>				
0.817 ± 0.013 ± 0.018	6934	CHAN	98 E756	$p$ Be, 800 GeV
0.811 ± 0.037	1096	LUK	88 SPEC	$p$ Be 400 GeV
0.823 ± 0.013	12k	BOURQUIN 84	SPEC	SPS hyperon beam

••• We do not use the following data for averages, fits, limits, etc. •••  
 0.822 ± 0.028      2437      BOURQUIN 79B SPEC      See BOURQUIN 84

### $\Omega^+$ MEAN LIFE

The fit assumes the  $\Omega^-$  and  $\Omega^+$  mean lives are the same, and averages them together.

VALUE (10 <sup>-10</sup> s)	EVTS	DOCUMENT ID	TECN	COMMENT
<b>0.821 ± 0.011 OUR FIT</b>				
<b>0.823 ± 0.031 ± 0.022</b>	1801	CHAN	98 E756	$p$ Be, 800 GeV

$$(\tau_{\Omega^-} - \tau_{\Omega^+}) / \tau_{\Omega^-}$$

A test of  $CPT$  invariance. Our calculation, from the averages in the preceding two data blocks.

VALUE	DOCUMENT ID
<b>0.00 ± 0.05 OUR ESTIMATE</b>	

### $\Omega^-$ MAGNETIC MOMENT

VALUE ( $\mu_N$ )	EVTS	DOCUMENT ID	TECN	COMMENT
<b>-2.02 ± 0.05 OUR AVERAGE</b>				
-2.024 ± 0.056	235k	WALLACE 95	SPEC	$\Omega^-$ 300–550 GeV
-1.94 ± 0.17 ± 0.14	25k	DIEHL 91	SPEC	Spin-transfer production

### $\Omega^-$ DECAY MODES

Mode	Fraction ( $\Gamma_i/\Gamma$ )	Confidence level
$\Gamma_1 \Lambda K^-$	(67.8 ± 0.7) %	
$\Gamma_2 \Xi^0 \pi^-$	(23.6 ± 0.7) %	
$\Gamma_3 \Xi^- \pi^0$	(8.6 ± 0.4) %	
$\Gamma_4 \Xi^- \pi^+ \pi^-$	(3.7 <sup>+0.7</sup> <sub>-0.6</sub> ) × 10 <sup>-4</sup>	
$\Gamma_5 \Xi(1530)^0 \pi^-$	< 7 × 10 <sup>-5</sup>	90%
$\Gamma_6 \Xi^0 e^- \bar{\nu}_e$	(5.6 ± 2.8) × 10 <sup>-3</sup>	
$\Gamma_7 \Xi^- \gamma$	< 4.6 × 10 <sup>-4</sup>	90%
<b><math>\Delta S = 2</math> forbidden (<math>S_2</math>) modes</b>		
$\Gamma_8 \Lambda \pi^-$	$S_2$ < 2.9 × 10 <sup>-6</sup>	90%

### $\Omega^-$ BRANCHING RATIOS

The BOURQUIN 84 values (which include results of BOURQUIN 79B, a separate experiment) are much more accurate than any other results, and so the other results have been omitted.

$\Gamma(\Lambda K^-)/\Gamma_{total}$	EVTS	DOCUMENT ID	TECN	COMMENT
<b>0.678 ± 0.007</b>	14k	BOURQUIN 84	SPEC	SPS hyperon beam
••• We do not use the following data for averages, fits, limits, etc. •••				
0.686 ± 0.013	1920	BOURQUIN 79B	SPEC	See BOURQUIN 84

$\Gamma(\Xi^0 \pi^-)/\Gamma_{total}$	EVTS	DOCUMENT ID	TECN	COMMENT
<b>0.236 ± 0.007</b>	1947	BOURQUIN 84	SPEC	SPS hyperon beam
••• We do not use the following data for averages, fits, limits, etc. •••				
0.234 ± 0.013	317	BOURQUIN 79B	SPEC	See BOURQUIN 84

$\Gamma(\Xi^- \pi^0)/\Gamma_{total}$	EVTS	DOCUMENT ID	TECN	COMMENT
<b>0.086 ± 0.004</b>	759	BOURQUIN 84	SPEC	SPS hyperon beam
••• We do not use the following data for averages, fits, limits, etc. •••				
0.080 ± 0.008	145	BOURQUIN 79B	SPEC	See BOURQUIN 84

$\Gamma(\Xi^- \pi^+ \pi^-)/\Gamma_{total}$	EVTS	DOCUMENT ID	TECN	COMMENT
<b>3.74<sup>+0.67</sup><sub>-0.56</sub></b>	100	<sup>5</sup> KAMAEV 10	HYCP	$p$ Cu, 800 GeV
••• We do not use the following data for averages, fits, limits, etc. •••				
4.3 <sup>+3.4</sup> <sub>-1.3</sub>	4	BOURQUIN 84	SPEC	SPS hyperon beam

<sup>5</sup> This KAMAEV 10 value uses 76  $\Omega^- \rightarrow \Xi^- \pi^+ \pi^-$  and 24  $\Omega^+ \rightarrow \Xi^+ \pi^- \pi^+$  decays. The  $\Omega^-$  and  $\Omega^+$  branching fractions measurements are statistically equal. The errors given combine statistical and systematic contributions. The  $CP$  branching-fraction asymmetry,  $(\Omega^- - \Omega^+)/\text{sum}$ , is  $+0.12 \pm 0.20$ .



See key on page 999

Baryon Particle Listings  
 $\Omega(2250)^-, \Omega(2380)^-, \Omega(2470)^-$

**$\Omega(2250)^-$**   $I(J^P) = 0(?^?)$  Status: \*\*\*

**$\Omega(2250)^-$  MASS**

VALUE (MeV)	EVTS	DOCUMENT ID	TECN	COMMENT
<b>2252 ± 9 OUR AVERAGE</b>				
2253 ± 13	44	ASTON	87B LASS	$K^- p$ 11 GeV/c
2251 ± 9 ± 8	78	BIAGI	86B SPEC	SPS $\Xi^-$ beam

**$\Omega(2250)^-$  WIDTH**

VALUE (MeV)	EVTS	DOCUMENT ID	TECN	COMMENT
<b>55 ± 18 OUR AVERAGE</b>				
81 ± 38	44	ASTON	87B LASS	$K^- p$ 11 GeV/c
48 ± 20	78	BIAGI	86B SPEC	SPS $\Xi^-$ beam

**$\Omega(2250)^-$  DECAY MODES**

Mode	Fraction ( $\Gamma_i/\Gamma$ )
$\Gamma_1 \Xi^- \pi^+ K^-$	seen
$\Gamma_2 \Xi(1530)^0 K^-$	seen

**$\Omega(2250)^-$  BRANCHING RATIOS**

$\Gamma(\Xi(1530)^0 K^-)/\Gamma(\Xi^- \pi^+ K^-)$   $\Gamma_2/\Gamma_1$

VALUE	EVTS	DOCUMENT ID	TECN	COMMENT
~ 1.0	44	ASTON	87B LASS	$K^- p$ 11 GeV/c
0.70 ± 0.20	49	BIAGI	86B SPEC	$\Xi^-$ Be 116 GeV/c

**$\Omega(2250)^-$  REFERENCES**

ASTON	87B	PL B194 579	D. Aston <i>et al.</i>	(SLAC, NAGO, CINC, INUS)
BIAGI	86B	ZPHY C31 33	S.F. Biagi <i>et al.</i>	(LOQM, GEVA, RAL+)

**$\Omega(2380)^-$**  Status: \*\*

OMITTED FROM SUMMARY TABLE

**$\Omega(2380)^-$  MASS**

VALUE (MeV)	EVTS	DOCUMENT ID	TECN	COMMENT
<b>≈ 2380 OUR ESTIMATE</b>				
2384 ± 9 ± 8	45	BIAGI	86B SPEC	SPS $\Xi^-$ beam

**$\Omega(2380)^-$  WIDTH**

VALUE (MeV)	EVTS	DOCUMENT ID	TECN	COMMENT
26 ± 23	45	BIAGI	86B SPEC	SPS $\Xi^-$ beam

**$\Omega(2380)^-$  DECAY MODES**

Mode	Fraction ( $\Gamma_i/\Gamma$ )
$\Gamma_1 \Xi^- \pi^+ K^-$	seen
$\Gamma_2 \Xi(1530)^0 K^-$	
$\Gamma_3 \Xi^- \bar{K}^*(892)^0$	

**$\Omega(2380)^-$  BRANCHING RATIOS**

$\Gamma(\Xi(1530)^0 K^-)/\Gamma(\Xi^- \pi^+ K^-)$   $\Gamma_2/\Gamma_1$

VALUE	CL%	EVTS	DOCUMENT ID	TECN	COMMENT
< 0.44	90	9	BIAGI	86B SPEC	$\Xi^-$ Be 116 GeV/c

$\Gamma(\Xi^- \bar{K}^*(892)^0)/\Gamma(\Xi^- \pi^+ K^-)$   $\Gamma_3/\Gamma_1$

VALUE	EVTS	DOCUMENT ID	TECN	COMMENT
0.5 ± 0.3	21	BIAGI	86B SPEC	$\Xi^-$ Be 116 GeV/c

**$\Omega(2380)^-$  REFERENCES**

BIAGI	86B	ZPHY C31 33	S.F. Biagi <i>et al.</i>	(LOQM, GEVA, RAL+)
-------	-----	-------------	--------------------------	--------------------

**$\Omega(2470)^-$**  Status: \*\*

OMITTED FROM SUMMARY TABLE

A peak in the  $\Omega^- \pi^+ \pi^-$  mass spectrum with a signal significance claimed to be at least 5.5 standard deviations. There is no reason to seriously doubt the existence of this state, but unless the evidence is overwhelming we usually wait for confirmation from a second experiment before elevating peaks to the Summary Table.

**$\Omega(2470)^-$  MASS**

VALUE (MeV)	EVTS	DOCUMENT ID	TECN	COMMENT
<b>2474 ± 12</b>	59	ASTON	88G LASS	$K^- p$ 11 GeV/c

**$\Omega(2470)^-$  WIDTH**

VALUE (MeV)	EVTS	DOCUMENT ID	TECN	COMMENT
<b>72 ± 33</b>	59	ASTON	88G LASS	$K^- p$ 11 GeV/c

**$\Omega(2470)^-$  DECAY MODES**

Mode
$\Gamma_1 \Omega^- \pi^+ \pi^-$

**$\Omega(2470)^-$  REFERENCES**

ASTON	88G	PL B215 799	D. Aston <i>et al.</i>	(SLAC, NAGO, CINC, INUS)
-------	-----	-------------	------------------------	--------------------------

# Baryon Particle Listings

## Charmed Baryons, $\Lambda_c^+$

### CHARMED BARYONS ( $C = +1$ )

$$\Lambda_c^+ = udc, \Sigma_c^{++} = uuc, \Sigma_c^+ = udc, \Sigma_c^0 = ddc,$$

$$\Xi_c^+ = usc, \Xi_c^0 = dsc, \Omega_c^0 = ssc$$

See the related review(s):  
Charmed Baryons



$$I(J^P) = 0(\frac{1}{2}^+) \text{ Status: } ****$$

The parity of the  $\Lambda_c^+$  is defined to be positive (as are the parities of the proton, neutron, and  $\Lambda$ ). The quark content is  $udc$ . Results of an analysis of  $pK^-\pi^+$  decays (JEZABEK 92) are consistent with  $J = 1/2$ . Nobody doubts that the spin is indeed  $1/2$ .

We have omitted some results that have been superseded by later experiments. The omitted results may be found in earlier editions.

#### $\Lambda_c^+$ MASS

Our value in 2004,  $2284.9 \pm 0.6$  MeV, was the average of the measurements now filed below as "not used." The BABAR measurement is so much better that we use it alone. Note that it is about 2.6 (old) standard deviations above the 2004 value.

The fit also includes  $\Sigma_c^-\Lambda_c^+$  and  $\Lambda_c^{*+}-\Lambda_c^+$  mass-difference measurements, but this doesn't affect the  $\Lambda_c^+$  mass. The new (in 2006)  $\Lambda_c^+$  mass simply pushes all those other masses higher.

VALUE (MeV)	EVTS	DOCUMENT ID	TECN	COMMENT
<b>2286.46 ± 0.14</b>	<b>OUR FIT</b>			
<b>2286.46 ± 0.14</b>	4891	<sup>1</sup> AUBERT,B	05S BABR	$\Lambda_c^0 K^+$ and $\Sigma^0 K_S^0 K^+$
• • • We do not use the following data for averages, fits, limits, etc. • • •				
2284.7 ± 0.6 ± 0.7	1134	AVERY	91 CLEO	Six modes
2281.7 ± 2.7 ± 2.6	29	ALVAREZ	90B NA14	$pK^-\pi^+$
2285.8 ± 0.6 ± 1.2	101	BARLAG	89 NA32	$pK^-\pi^+$
2284.7 ± 2.3 ± 0.5	5	AGUILAR...	88B LEBE	$pK^-\pi^+$
2283.1 ± 1.7 ± 2.0	628	ALBRECHT	88C ARG	$pK^-\pi^+, p\bar{K}^0, \Lambda 3\pi$
2286.2 ± 1.7 ± 0.7	97	ANJOS	88B E691	$pK^-\pi^+$
2281 ± 3	2	JONES	87 HBC	$pK^-\pi^+$
2283 ± 3	3	BOSETTI	82 HBC	$pK^-\pi^+$
2290 ± 3	1	CALICCHIO	80 HYBR	$pK^-\pi^+$

<sup>1</sup>AUBERT,B 05S uses low-Q  $\Lambda_c^0 K^+$  and  $\Sigma^0 K_S^0 K^+$  decays to minimize systematic errors. The error above includes systematic as well as statistical errors. Many cross checks and adjustments to properties of the BABAR detector, as well as the large number of clean events, make this by far the best measurement of the  $\Lambda_c^+$  mass.

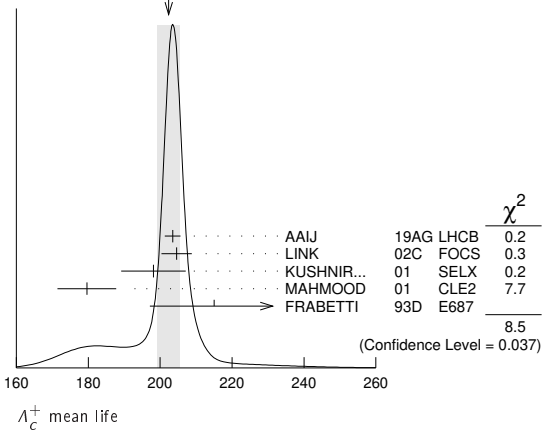
#### $\Lambda_c^+$ MEAN LIFE

Measurements with an error  $\geq 100 \times 10^{-15}$  s or with fewer than 20 events have been omitted from the Listings.

VALUE ( $10^{-15}$ s)	EVTS	DOCUMENT ID	TECN	COMMENT
<b>202.4 ± 3.1</b>	<b>OUR AVERAGE</b>			Error includes scale factor of 1.7. See the ideogram below.
203.5 ± 1.7 ± 1.4	304k	<sup>1</sup> AAIJ	19AG LHCB	$\Lambda_c^+ \rightarrow pK^-\pi^+$
204.6 ± 3.4 ± 2.5	8034	LINK	02C FOCS	$\Lambda_c^+ \rightarrow pK^-\pi^+$
198.1 ± 7.0 ± 5.6	1630	KUSHNIR...	01 SELX	$\Lambda_c^+ \rightarrow pK^-\pi^+$
179.6 ± 6.9 ± 4.4	4749	MAHMOOD	01 CLE2	$e^+e^- \approx \tau(4S)$
215 ± 16 ± 8	1340	FRABETTI	93D E687	$\gamma\text{Be}, \Lambda_c^+ \rightarrow pK^-\pi^+$
• • • We do not use the following data for averages, fits, limits, etc. • • •				
180 ± 30 ± 30	29	ALVAREZ	90 NA14	$\gamma, \Lambda_c^+ \rightarrow pK^-\pi^+$
200 ± 30 ± 30	90	FRABETTI	90 E687	$\gamma\text{Be}, \Lambda_c^+ \rightarrow pK^-\pi^+$
196 <sup>+23</sup> <sub>-20</sub>	101	BARLAG	89 NA32	$pK^-\pi^+$ + c.c.
220 ± 30 ± 20	97	ANJOS	88B E691	$pK^-\pi^+$ + c.c.

<sup>1</sup>AAIJ 19AG reports [ $\Lambda_c^+$  MEAN LIFE] / [ $D^\pm$  MEAN LIFE] =  $0.1956 \pm 0.0010 \pm 0.0013$  which we multiply by our best value  $D^\pm$  MEAN LIFE =  $(1.040 \pm 0.007) \times 10^{-12}$  s. Our first error is their experiment's error and our second error is the systematic error from using our best value.

WEIGHTED AVERAGE  
202.4±3.1 (Error scaled by 1.7)



#### $\Lambda_c^+$ DECAY MODES

Branching fractions marked with a footnote, e.g. [a], have been corrected for decay modes not observed in the experiments. For example, the sub-mode fraction  $\Lambda_c^+ \rightarrow p\bar{K}^*(892)^0$  seen in  $\Lambda_c^+ \rightarrow pK^-\pi^+$  has been multiplied up to include  $\bar{K}^*(892)^0 \rightarrow \bar{K}^0\pi^0$  decays.

Mode	Fraction ( $\Gamma_i/\Gamma$ )	Scale factor/ Confidence level
<b>Hadronic modes with a p or n: S = -1 final states</b>		
$\Gamma_1$ $pK_S^0$	(1.59 ± 0.08) %	S=1.1
$\Gamma_2$ $pK^-\pi^+$	(6.28 ± 0.32) %	S=1.4
$\Gamma_3$ $p\bar{K}^*(892)^0$	[a] (1.96 ± 0.27) %	
$\Gamma_4$ $\Delta(1232)^{++}K^-$	(1.08 ± 0.25) %	
$\Gamma_5$ $\Lambda(1520)\pi^+$	[a] (2.2 ± 0.5) %	
$\Gamma_6$ $pK^-\pi^+$ nonresonant	(3.5 ± 0.4) %	
$\Gamma_7$ $pK_S^0\pi^0$	(1.97 ± 0.13) %	S=1.1
$\Gamma_8$ $nK_S^0\pi^+$	(1.82 ± 0.25) %	
$\Gamma_9$ $p\bar{K}^0\eta$	(1.6 ± 0.4) %	
$\Gamma_{10}$ $pK_S^0\pi^+\pi^-$	(1.60 ± 0.12) %	S=1.1
$\Gamma_{11}$ $pK^-\pi^+\pi^0$	(4.46 ± 0.30) %	S=1.5
$\Gamma_{12}$ $pK^*(892)^-\pi^+$	[a] (1.4 ± 0.5) %	
$\Gamma_{13}$ $p(K^-\pi^+)_{\text{nonresonant}}\pi^0$	(4.6 ± 0.8) %	
$\Gamma_{14}$ $\Delta(1232)\bar{K}^*(892)$	seen	
$\Gamma_{15}$ $pK^-\pi^+\pi^-$	(1.4 ± 0.9) × 10 <sup>-3</sup>	
$\Gamma_{16}$ $pK^-\pi^+2\pi^0$	(1.0 ± 0.5) %	
<b>Hadronic modes with a p: S = 0 final states</b>		
$\Gamma_{17}$ $p\pi^0$	< 2.7 × 10 <sup>-4</sup>	CL=90%
$\Gamma_{18}$ $p\eta$	(1.24 ± 0.30) × 10 <sup>-3</sup>	
$\Gamma_{19}$ $p\omega(782)^0$	(9 ± 4) × 10 <sup>-4</sup>	
$\Gamma_{20}$ $p\pi^+\pi^-$	(4.61 ± 0.28) × 10 <sup>-3</sup>	
$\Gamma_{21}$ $p\eta(980)$	[a] (3.5 ± 2.3) × 10 <sup>-3</sup>	
$\Gamma_{22}$ $p2\pi^+2\pi^-$	(2.3 ± 1.4) × 10 <sup>-3</sup>	
$\Gamma_{23}$ $pK^+K^-$	(1.06 ± 0.06) × 10 <sup>-3</sup>	
$\Gamma_{24}$ $p\phi$	[a] (1.06 ± 0.14) × 10 <sup>-3</sup>	
$\Gamma_{25}$ $pK^+K^-\text{non-}\phi$	(5.3 ± 1.2) × 10 <sup>-4</sup>	
$\Gamma_{26}$ $p\phi\pi^0$	(10 ± 4) × 10 <sup>-5</sup>	
$\Gamma_{27}$ $pK^+K^-\pi^0$ nonresonant	< 6.3 × 10 <sup>-5</sup>	CL=90%
<b>Hadronic modes with a hyperon: S = -1 final states</b>		
$\Gamma_{28}$ $\Lambda\pi^+$	(1.30 ± 0.07) %	S=1.1
$\Gamma_{29}$ $\Lambda\pi^+\pi^0$	(7.1 ± 0.4) %	S=1.1
$\Gamma_{30}$ $\Lambda\rho^+$	< 6 %	CL=95%
$\Gamma_{31}$ $\Lambda\pi^-2\pi^+$	(3.64 ± 0.29) %	S=1.4
$\Gamma_{32}$ $\Sigma(1385)^+\pi^+\pi^-, \Sigma^{*+} \rightarrow \Lambda\pi^+$	(1.0 ± 0.5) %	
$\Gamma_{33}$ $\Sigma(1385)^-2\pi^+, \Sigma^{*-} \rightarrow \Lambda\pi^-$	(7.6 ± 1.4) × 10 <sup>-3</sup>	
$\Gamma_{34}$ $\Lambda\pi^+\rho^0$	(1.5 ± 0.6) %	
$\Gamma_{35}$ $\Sigma(1385)^+\rho^0, \Sigma^{*+} \rightarrow \Lambda\pi^+$	(5 ± 4) × 10 <sup>-3</sup>	
$\Gamma_{36}$ $\Lambda\pi^-2\pi^+$ nonresonant	< 1.1 %	CL=90%
$\Gamma_{37}$ $\Lambda\pi^-\pi^02\pi^+$ total	(2.3 ± 0.8) %	
$\Gamma_{38}$ $\Lambda\pi^+\eta$	[a] (1.84 ± 0.26) %	
$\Gamma_{39}$ $\Sigma(1385)^+\eta$	[a] (9.1 ± 2.0) × 10 <sup>-3</sup>	
$\Gamma_{40}$ $\Lambda\pi^+\omega$	[a] (1.5 ± 0.5) %	

Table of branching ratios for Lambda\_c+ decays. Includes entries for various final states like pi- pi0 2 pi+, K+ K-, etc. with associated branching fractions and constraints.

Hadronic modes with a hyperon: S = 0 final states

Table of branching ratios for hadronic modes with a hyperon and S = 0 final states. Includes entries for Lambda K+, Sigma K+, etc.

Doubly Cabibbo-suppressed modes

Table of branching ratios for doubly Cabibbo-suppressed modes, including p K+ pi-.

Semileptonic modes

Table of branching ratios for semileptonic modes, including Lambda e+ nu\_e and Lambda mu+ nu\_mu.

Inclusive modes

Table of inclusive branching ratios for e+ anything, p anything, n anything, Lambda anything, and 3prongs.

Delta C = 1 weak neutral current (CI) modes, or Lepton Family number (LF), or Lepton number (L), or Baryon number (B) violating modes

Table of branching ratios for Delta C = 1 weak neutral current and other violating modes.

[a] This branching fraction includes all the decay modes of the final-state resonance.

CONSTRAINED FIT INFORMATION

An overall fit to 41 branching ratios uses 62 measurements and one constraint to determine 21 parameters. The overall fit has a chi-squared = 47.4 for 42 degrees of freedom.

The following off-diagonal array elements are the correlation coefficients <delta x\_i delta x\_j> / (delta x\_i delta x\_j), in percent, from the fit to the branching fractions, x\_i = Gamma\_i / Gamma\_total. The fit constrains the x\_i whose labels appear in this array to sum to one.

Large table showing correlation coefficients between various decay modes, labeled X2 through X62.

Lambda\_c+ BRANCHING RATIOS

A few really obsolete results have been omitted.

Hadronic modes with a p: S = -1 final states

Table of branching ratios for hadronic modes with a p and S = -1 final states. Includes Gamma(p K\_S^0) / Gamma\_total and Gamma(p K\_S^0) / Gamma(p K^- pi^+).

Table of branching ratios for hadronic modes with a p and S = -1 final states, including Gamma(p K^- pi^+) / Gamma\_total.

Table of branching ratios for hadronic modes with a p and S = -1 final states, including Gamma(p K^- pi^+) / Gamma\_total.

1 This ZUPANC 14 value is the FIRST-EVER model-independent measurement of a Lambda\_c+ branching fraction. 2 See the note by P. Burchat, "Lambda\_c+ Branching Fractions," in any edition of the Review from 2002 through 2014 for how this value was obtained. It is now obsolete.

Gamma(p K\*(892)^0) / Gamma(p K^- pi^+)

Table of branching ratios for Gamma(p K\*(892)^0) / Gamma(p K^- pi^+).

1 AITALA 00 makes a coherent 5-dimensional amplitude analysis of 946 +/- 38 Lambda\_c+ -> p K^- pi^+ decays.







# Baryon Particle Listings

$\Lambda_c^+$

$\Gamma(\Sigma^+ \rho^0)/\Gamma(\rho K^- \pi^+)$		$\Gamma_{49}/\Gamma_2$	
VALUE	CL%	DOCUMENT ID	TECN COMMENT
<0.27	95	KUBOTA	93 CLE2 $e^+ e^- \approx \Upsilon(4S)$

$\Gamma(\Sigma^- 2\pi^+)/\Gamma_{total}$		$\Gamma_{50}/\Gamma$	
VALUE (%)	EVTS	DOCUMENT ID	TECN COMMENT
<b>1.87 ± 0.18 OUR FIT</b>			
<b>1.81 ± 0.17 ± 0.09</b>	161	ABLIKIM	17Y BES3 $e^+ e^-$ at 4.6 GeV

$\Gamma(\Sigma^- 2\pi^+)/\Gamma(\rho K^- \pi^+)$		$\Gamma_{50}/\Gamma_2$	
VALUE	EVTS	DOCUMENT ID	TECN COMMENT
<b>0.297 ± 0.030 OUR FIT</b>			Error includes scale factor of 1.1.
<b>0.314 ± 0.067</b>	30 ± 6	VAZQUEZ-JA...08	SELX $\Sigma^-$ nucleus, 600 GeV

$\Gamma(\Sigma^- 2\pi^+)/\Gamma(\Sigma^+ \pi^+ \pi^-)$		$\Gamma_{50}/\Gamma_{48}$	
VALUE	EVTS	DOCUMENT ID	TECN COMMENT
<b>0.42 ± 0.04 OUR FIT</b>			Error includes scale factor of 1.1.
<b>0.53 ± 0.15 ± 0.07</b>	56	FRABETTI	94E E687 $\gamma$ Be, $\bar{E}_\gamma$ 220 GeV

$\Gamma(\Sigma^0 \pi^+ \pi^0)/\Gamma(\rho K^- \pi^+)$		$\Gamma_{51}/\Gamma_2$	
VALUE	EVTS	DOCUMENT ID	TECN COMMENT
<b>0.56 ± 0.05 OUR AVERAGE</b>			Error includes scale factor of 1.5.
0.575 ± 0.005 ± 0.036	2.7M	BERGER	18 BELL $e^+ e^- \approx \Upsilon(4S)$
0.36 ± 0.09 ± 0.10	117	AVERY	94 CLE2 $e^+ e^- \approx \Upsilon(3S), \Upsilon(4S)$

$\Gamma(\Sigma^+ \pi^0 \pi^0)/\Gamma(\rho K^- \pi^+)$		$\Gamma_{52}/\Gamma_2$	
VALUE	EVTS	DOCUMENT ID	TECN COMMENT
<b>0.247 ± 0.006 ± 0.019</b>	925k	BERGER	18 BELL $e^+ e^- \approx \Upsilon(4S)$

$\Gamma(\Sigma^0 \pi^- 2\pi^+)/\Gamma(\rho K^- \pi^+)$		$\Gamma_{53}/\Gamma_2$	
VALUE	EVTS	DOCUMENT ID	TECN COMMENT
<b>0.18 ± 0.05 OUR FIT</b>			
<b>0.21 ± 0.05 ± 0.05</b>	90	AVERY	94 CLE2 $e^+ e^- \approx \Upsilon(3S), \Upsilon(4S)$

$\Gamma(\Sigma^0 \pi^- 2\pi^+)/\Gamma(\Lambda \pi^- 2\pi^+)$		$\Gamma_{53}/\Gamma_{31}$	
VALUE	EVTS	DOCUMENT ID	TECN COMMENT
<b>0.31 ± 0.08 OUR FIT</b>			
<b>0.26 ± 0.06 ± 0.09</b>	480	LINK	05F FOCS $\gamma$ nucleus, $\bar{E}_\gamma \approx 180$ GeV

$\Gamma(\Sigma^+ \omega)/\Gamma_{total}$		$\Gamma_{55}/\Gamma$	
VALUE (%)	EVTS	DOCUMENT ID	TECN COMMENT
<b>1.70 ± 0.21 OUR FIT</b>			
<b>1.56 ± 0.20 ± 0.07</b>	157	ABLIKIM	16 BES3 $e^+ e^- \rightarrow \Lambda_c \bar{\Lambda}_c, 4.599$ GeV

$\Gamma(\Sigma^+ \omega)/\Gamma(\rho K^- \pi^+)$		$\Gamma_{55}/\Gamma_2$	
VALUE	EVTS	DOCUMENT ID	TECN COMMENT
<b>0.271 ± 0.031 OUR FIT</b>			Unseen decay modes of the $\omega$ are included.
<b>0.54 ± 0.13 ± 0.06</b>	107	KUBOTA	93 CLE2 $e^+ e^- \approx \Upsilon(4S)$

$\Gamma(\Sigma^- \pi^0 2\pi^+)/\Gamma_{total}$		$\Gamma_{56}/\Gamma$	
VALUE (%)	EVTS	DOCUMENT ID	TECN COMMENT
<b>2.11 ± 0.33 ± 0.14</b>	88	ABLIKIM	17Y BES3 $e^+ e^-$ at 4.6 GeV

$\Gamma(\Sigma^+ K^+ K^-)/\Gamma(\rho K^- \pi^+)$		$\Gamma_{57}/\Gamma_2$	
VALUE	EVTS	DOCUMENT ID	TECN COMMENT
<b>0.056 ± 0.006 OUR FIT</b>			
<b>0.070 ± 0.011 ± 0.011</b>	59	AVERY	93 CLE2 $e^+ e^- \approx 10.5$ GeV

$\Gamma(\Sigma^+ K^+ K^-)/\Gamma(\Sigma^+ \pi^+ \pi^-)$		$\Gamma_{57}/\Gamma_{48}$	
VALUE	EVTS	DOCUMENT ID	TECN COMMENT
<b>0.078 ± 0.008 OUR FIT</b>			
<b>0.074 ± 0.009 OUR AVERAGE</b>			
0.076 ± 0.007 ± 0.009	246	ABE	02c BELL $e^+ e^- \approx \Upsilon(4S)$
0.071 ± 0.011 ± 0.011	103	LINK	02G FOCS $\gamma$ nucleus, $\approx 180$ GeV

$\Gamma(\Sigma^+ \phi)/\Gamma(\rho K^- \pi^+)$		$\Gamma_{58}/\Gamma_2$	
VALUE	EVTS	DOCUMENT ID	TECN COMMENT
<b>0.062 ± 0.009 OUR FIT</b>			Unseen decay modes of the $\phi$ are included.
<b>0.069 ± 0.023 ± 0.016</b>	26	AVERY	93 CLE2 $e^+ e^- \approx 10.5$ GeV

$\Gamma(\Sigma^+ \phi)/\Gamma(\Sigma^+ \pi^+ \pi^-)$		$\Gamma_{58}/\Gamma_{48}$	
VALUE	EVTS	DOCUMENT ID	TECN COMMENT
<b>0.087 ± 0.012 OUR FIT</b>			
<b>0.086 ± 0.012 OUR AVERAGE</b>			
0.085 ± 0.012 ± 0.012	129	ABE	02c BELL $e^+ e^- \approx \Upsilon(4S)$
0.087 ± 0.016 ± 0.006	57	LINK	02G FOCS $\gamma$ nucleus, $\approx 180$ GeV

$\Gamma(\Xi(1690)^0 K^+, \Xi^* \rightarrow \Sigma^+ K^-)/\Gamma(\Sigma^+ \pi^+ \pi^-)$		$\Gamma_{59}/\Gamma_{48}$	
VALUE	EVTS	DOCUMENT ID	TECN COMMENT
<b>0.023 ± 0.005 OUR AVERAGE</b>			
0.023 ± 0.005 ± 0.005	75	ABE	02c BELL $e^+ e^- \approx \Upsilon(4S)$
0.022 ± 0.006 ± 0.006	34	LINK	02G FOCS $\gamma$ nucleus, $\approx 180$ GeV

$\Gamma(\Sigma^+ K^+ K^- \text{ nonresonant})/\Gamma(\Sigma^+ \pi^+ \pi^-)$		$\Gamma_{60}/\Gamma_{48}$	
VALUE	CL%	DOCUMENT ID	TECN COMMENT
<0.018	90	ABE	02c BELL $e^+ e^- \approx \Upsilon(4S)$
<0.028	90	LINK	02G FOCS $\gamma$ nucleus, $\approx 180$ GeV

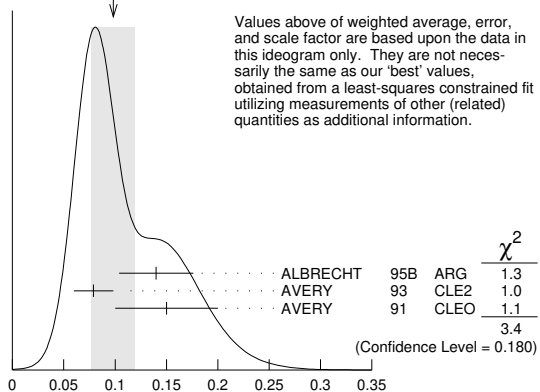
••• We do not use the following data for averages, fits, limits, etc. •••

$\Gamma(\Xi^0 K^+)/\Gamma_{total}$		$\Gamma_{61}/\Gamma$	
VALUE (units $10^{-3}$ )	EVTS	DOCUMENT ID	TECN COMMENT
<b>5.5 ± 0.7 OUR FIT</b>			
<b>5.90 ± 0.86 ± 0.39</b>	68	ABLIKIM	18Y BES3 $e^+ e^-$ at 4.6 GeV

$\Gamma(\Xi^0 K^+)/\Gamma(\rho K^- \pi^+)$		$\Gamma_{61}/\Gamma_2$	
VALUE	EVTS	DOCUMENT ID	TECN COMMENT
<b>0.088 ± 0.012 OUR FIT</b>			
<b>0.078 ± 0.013 ± 0.013</b>	56	AVERY	93 CLE2 $e^+ e^- \approx 10.5$ GeV

$\Gamma(\Xi^- K^+ \pi^+)/\Gamma(\rho K^- \pi^+)$		$\Gamma_{62}/\Gamma_2$	
VALUE	EVTS	DOCUMENT ID	TECN COMMENT
<b>0.099 ± 0.009 OUR FIT</b>			Error includes scale factor of 1.3. See the ideogram below.
<b>0.098 ± 0.021 OUR AVERAGE</b>			
0.14 ± 0.03 ± 0.02	34	ALBRECHT	95B ARG $e^+ e^- \approx 10.4$ GeV
0.079 ± 0.013 ± 0.014	60	AVERY	93 CLE2 $e^+ e^- \approx 10.5$ GeV
0.15 ± 0.04 ± 0.03	30	AVERY	91 CLEO $e^+ e^- 10.5$ GeV

WEIGHTED AVERAGE  
0.098 ± 0.021 (Error scaled by 1.3)



$\Gamma(\Xi^- K^+ \pi^+)/\Gamma(\Lambda \pi^+)$		$\Gamma_{62}/\Gamma_{28}$	
VALUE	EVTS	DOCUMENT ID	TECN COMMENT
<b>0.48 ± 0.04 OUR FIT</b>			
<b>0.480 ± 0.016 ± 0.039</b>	2665 ± 84	AUBERT	07U BABR $e^+ e^- \approx \Upsilon(4S)$

$\Gamma(\Xi(1530)^0 K^+)/\Gamma_{total}$		$\Gamma_{63}/\Gamma$	
VALUE (units $10^{-3}$ )	EVTS	DOCUMENT ID	TECN COMMENT
<b>4.3 ± 0.9 OUR FIT</b>			Error includes scale factor of 1.1.
<b>5.02 ± 0.99 ± 0.31</b>	60	ABLIKIM	18Y BES3 $e^+ e^-$ at 4.6 GeV

$\Gamma(\Xi(1530)^0 K^+)/\Gamma(\rho K^- \pi^+)$		$\Gamma_{63}/\Gamma_2$	
VALUE	EVTS	DOCUMENT ID	TECN COMMENT
<b>0.068 ± 0.014 OUR FIT</b>			Error includes scale factor of 1.
<b>0.053 ± 0.016 ± 0.010</b>	24	AVERY	93 CLE2 $e^+ e^- \approx 10.5$ GeV
0.05 ± 0.02 ± 0.01	11	ALBRECHT	95B ARG $e^+ e^- \approx 10.4$ GeV

Hadronic modes with a hyperon: S = 0 final states

$\Gamma(\Lambda K^+)/\Gamma(\Lambda \pi^+)$		$\Gamma_{64}/\Gamma_{28}$	
VALUE	EVTS	DOCUMENT ID	TECN COMMENT
<b>0.047 ± 0.009 OUR AVERAGE</b>			Error includes scale factor of 1.8.
0.044 ± 0.004 ± 0.003	1162 ± 101	AUBERT	07U BABR $e^+ e^- \approx \Upsilon(4S)$
0.074 ± 0.010 ± 0.012	265	ABE	02c BELL $e^+ e^- \approx \Upsilon(4S)$

$\Gamma(\Lambda K^+ \pi^+ \pi^-)/\Gamma(\Lambda \pi^+)$		$\Gamma_{65}/\Gamma_{28}$	
VALUE	CL%	DOCUMENT ID	TECN COMMENT
<4.1 × 10 <sup>-2</sup>	90	AUBERT	07U BABR $e^+ e^- \approx \Upsilon(4S)$

$\Gamma(\Sigma^0 K^+)/\Gamma(\Sigma^0 \pi^+)$		$\Gamma_{66}/\Gamma_{44}$	
VALUE	EVTS	DOCUMENT ID	TECN COMMENT
<b>0.040 ± 0.006 OUR AVERAGE</b>			
0.038 ± 0.005 ± 0.003	366 ± 52	AUBERT	07U BABR $e^+ e^- \approx \Upsilon(4S)$
0.056 ± 0.014 ± 0.008	75	ABE	02c BELL $e^+ e^- \approx \Upsilon(4S)$

See key on page 999

Baryon Particle Listings

$\Lambda_c^+$

$\Gamma(\Sigma^0 K^+ \pi^+ \pi^-)/\Gamma(\Sigma^0 \pi^+)$		$\Gamma_{67}/\Gamma_{44}$	
VALUE	CL%	DOCUMENT ID	TECN COMMENT
$<2.0 \times 10^{-2}$	90	AUBERT	07u BABR $e^+ e^- \approx \Upsilon(4S)$

$\Gamma(\Sigma^+ K^+ \pi^-)/\Gamma(\Sigma^+ \pi^+ \pi^-)$		$\Gamma_{68}/\Gamma_{48}$	
VALUE	EVTS	DOCUMENT ID	TECN COMMENT
$0.047 \pm 0.011 \pm 0.008$	105	ABE	02c BELL $e^+ e^- \approx \Upsilon(4S)$

$\Gamma(\Sigma^+ K^*(892)^0)/\Gamma(\Sigma^+ \pi^+ \pi^-)$		$\Gamma_{69}/\Gamma_{48}$	
VALUE	EVTS	DOCUMENT ID	TECN COMMENT
$0.078 \pm 0.018 \pm 0.013$	49	LINK	02g FOCS $\gamma$ nucleus, $\approx 180$ GeV

$\Gamma(\Sigma^- K^+ \pi^+)/\Gamma(\Sigma^+ K^*(892)^0)$		$\Gamma_{70}/\Gamma_{69}$	
VALUE	CL%	DOCUMENT ID	TECN COMMENT
$<0.35$	90	LINK	02g FOCS $\gamma$ nucleus, $\approx 180$ GeV

Doubly Cabibbo-suppressed modes

$\Gamma(\rho K^+ \pi^-)/\Gamma(\rho K^- \pi^+)$		$\Gamma_{71}/\Gamma_{2}$	
VALUE (units $10^{-3}$ )	EVTS	DOCUMENT ID	TECN COMMENT
$1.77 \pm 0.27$ OUR AVERAGE			Error includes scale factor of 1.9.
$1.65 \pm 0.15 \pm 0.05$	392	AAIJ	18v LHCB $\Lambda_b^0 \rightarrow \Lambda_c^+ \mu^- X$
$2.35 \pm 0.27 \pm 0.21$	3379	YANG	16 BELL At or near $\Upsilon$ 's

Semileptonic modes

$\Gamma(\Lambda e^+ \nu_e)/\Gamma_{total}$		$\Gamma_{72}/\Gamma$	
VALUE (%)	EVTS	DOCUMENT ID	TECN COMMENT
$3.63 \pm 0.38 \pm 0.20$	104	ABLIKIM	15y BES3 $567 \text{ pb}^{-1}$ , 4.599 GeV

$\Gamma(\Lambda e^+ \nu_e)/\Gamma(e^+ \text{ anything})$		$\Gamma_{72}/\Gamma_{74}$	
VALUE (%)	EVTS	DOCUMENT ID	TECN COMMENT
$91.9 \pm 12.5 \pm 5.4$	214	ABLIKIM	18AF BES3 $e^+ e^-$ 4.6 GeV

$\Gamma(\Lambda e^+ \nu_e)/\Gamma(\rho K^- \pi^+)$		$\Gamma_{72}/\Gamma_{2}$	
VALUE	DOCUMENT ID	TECN	COMMENT
$0.43 \pm 0.08$	1,2 BERGFELD 94	CLE2	$e^+ e^- \approx \Upsilon(4S)$
$0.38 \pm 0.14$	2,3 ALBRECHT 91g	ARG	$e^+ e^- \approx 10.4$ GeV

<sup>1</sup> BERGFELD 94 measures  $\sigma(e^+ e^- \rightarrow \Lambda_c^+ X) \cdot B(\Lambda_c^+ \rightarrow \Lambda e^+ \nu_e) = (4.87 \pm 0.28 \pm 0.69)$  pb.

<sup>2</sup> To extract  $\Gamma(\Lambda_c^+ \rightarrow \Lambda e^+ \nu_e)/\Gamma(\Lambda_c^+ \rightarrow \rho K^- \pi^+)$ , we use  $\sigma(e^+ e^- \rightarrow \Lambda_c^+ X) \cdot B(\Lambda_c^+ \rightarrow \rho K^- \pi^+) = (11.2 \pm 1.3)$  pb, which is the weighted average of measurements from ARGUS (ALBRECHT 96E) and CLEO (AVERY 91).

<sup>3</sup> ALBRECHT 91g measures  $\sigma(e^+ e^- \rightarrow \Lambda_c^+ X) \cdot B(\Lambda_c^+ \rightarrow \Lambda e^+ \nu_e) = (4.20 \pm 1.28 \pm 0.71)$  pb.

$\Gamma(\Lambda \mu^+ \nu_\mu)/\Gamma_{total}$		$\Gamma_{73}/\Gamma$	
VALUE (%)	EVTS	DOCUMENT ID	TECN COMMENT
$3.49 \pm 0.46 \pm 0.27$	79	ABLIKIM	17d BES3 $e^+ e^-$ at 4.6 GeV

$\Gamma(\Lambda \mu^+ \nu_\mu)/\Gamma(\rho K^- \pi^+)$		$\Gamma_{73}/\Gamma_{2}$	
VALUE	DOCUMENT ID	TECN	COMMENT
$0.40 \pm 0.09$	1,2 BERGFELD 94	CLE2	$e^+ e^- \approx \Upsilon(4S)$
$0.35 \pm 0.20$	2,3 ALBRECHT 91g	ARG	$e^+ e^- \approx 10.4$ GeV

<sup>1</sup> BERGFELD 94 measures  $\sigma(e^+ e^- \rightarrow \Lambda_c^+ X) \cdot B(\Lambda_c^+ \rightarrow \Lambda \mu^+ \nu_\mu) = (4.43 \pm 0.51 \pm 0.64)$  pb.

<sup>2</sup> To extract  $\Gamma(\Lambda_c^+ \rightarrow \Lambda \mu^+ \nu_\mu)/\Gamma(\Lambda_c^+ \rightarrow \rho K^- \pi^+)$ , we use  $\sigma(e^+ e^- \rightarrow \Lambda_c^+ X) \cdot B(\Lambda_c^+ \rightarrow \rho K^- \pi^+) = (11.2 \pm 1.3)$  pb, which is the weighted average of measurements from ARGUS (ALBRECHT 96E) and CLEO (AVERY 91).

<sup>3</sup> ALBRECHT 91g measures  $\sigma(e^+ e^- \rightarrow \Lambda_c^+ X) \cdot B(\Lambda_c^+ \rightarrow \Lambda \mu^+ \nu_\mu) = (3.91 \pm 2.02 \pm 0.90)$  pb.

$\Gamma(\Lambda \mu^+ \nu_\mu)/\Gamma(\Lambda e^+ \nu_e)$		$\Gamma_{73}/\Gamma_{72}$	
VALUE	DOCUMENT ID	TECN	COMMENT
$0.96 \pm 0.16 \pm 0.04$	1 ABLIKIM 17d	BES3	$e^+ e^-$ at 4.6 GeV

<sup>1</sup> This is the ratio of the ABLIKIM 17d  $\Lambda \mu^+ \nu_e$  branching fraction and the ABLIKIM 15y  $\Lambda e^+ \nu_e$  branching fraction (see above), and so is not an independent measurement.

Inclusive modes

$\Gamma(e^+ \text{ anything})/\Gamma_{total}$		$\Gamma_{74}/\Gamma$	
VALUE (%)	EVTS	DOCUMENT ID	TECN COMMENT
$3.95 \pm 0.34 \pm 0.09$	214	ABLIKIM	18AF BES3 $e^+ e^-$ 4.6 GeV

$\Gamma(p \text{ anything})/\Gamma_{total}$		$\Gamma_{75}/\Gamma$	
VALUE	DOCUMENT ID	TECN	COMMENT
$0.50 \pm 0.08 \pm 0.14$	1 CRAWFORD 92	CLEO	$e^+ e^-$ 10.5 GeV

<sup>1</sup> This CRAWFORD 92 value includes protons from  $\Lambda$  decay. The value is model dependent, but account is taken of this in the systematic error.

$\Gamma(n \text{ anything})/\Gamma_{total}$		$\Gamma_{76}/\Gamma$	
VALUE	DOCUMENT ID	TECN	COMMENT
$0.50 \pm 0.08 \pm 0.14$	1 CRAWFORD 92	CLEO	$e^+ e^-$ 10.5 GeV

<sup>1</sup> This CRAWFORD 92 value includes neutrons from  $\Lambda$  decay. The value is model dependent, but account is taken of this in the systematic error.

$\Gamma(\Lambda \text{ anything})/\Gamma_{total}$		$\Gamma_{77}/\Gamma$	
VALUE (%)	EVTS	DOCUMENT ID	TECN COMMENT
$38.2 \pm 2.8 \pm 0.9$	700	ABLIKIM	18E BES3 $e^+ e^-$ at 4.6 GeV

$\Gamma(3\text{prongs})/\Gamma_{total}$		$\Gamma_{78}/\Gamma$	
VALUE	DOCUMENT ID	TECN	COMMENT
$0.24 \pm 0.07 \pm 0.04$	KAYIS-TOPAK.03	CHRS	$\nu_\mu$ emulsion, $\bar{E} = 27$ GeV

Rare or forbidden modes

$\Gamma(\rho e^+ e^-)/\Gamma_{total}$		$\Gamma_{79}/\Gamma$		
VALUE	CL%	EVTS	DOCUMENT ID	TECN COMMENT
$<5.5 \times 10^{-6}$	90	$4.0 \pm 7.1$	LEES	11g BABR $e^+ e^- \approx \Upsilon(4S)$

$\Gamma(\rho \mu^+ \mu^- \text{ non-resonant})/\Gamma_{total}$		$\Gamma_{80}/\Gamma$	
VALUE	CL%	DOCUMENT ID	TECN COMMENT
$<7.7 \times 10^{-8}$	90	AAIJ	18w LHCB Ratio to $p\phi, \phi \rightarrow \mu^+ \mu^-$
$<4.4 \times 10^{-5}$	90	LEES	11g BABR $e^+ e^- \approx \Upsilon(4S)$
$<3.4 \times 10^{-4}$	90	KODAMA	95 E653 $\pi^-$ emulsion 600 GeV

$\Gamma(\rho e^+ \mu^-)/\Gamma_{total}$		$\Gamma_{81}/\Gamma$		
VALUE	CL%	EVTS	DOCUMENT ID	TECN COMMENT
$<9.9 \times 10^{-6}$	90	$-0.7 \pm 3.0$	LEES	11g BABR $e^+ e^- \approx \Upsilon(4S)$

$\Gamma(\rho e^- \mu^+)/\Gamma_{total}$		$\Gamma_{82}/\Gamma$		
VALUE	CL%	EVTS	DOCUMENT ID	TECN COMMENT
$<19 \times 10^{-6}$	90	$6.2 \pm 4.9$	LEES	11g BABR $e^+ e^- \approx \Upsilon(4S)$

$\Gamma(\bar{p} 2e^+)/\Gamma_{total}$		$\Gamma_{83}/\Gamma$		
VALUE	CL%	EVTS	DOCUMENT ID	TECN COMMENT
$<2.7 \times 10^{-6}$	90	$-1.5 \pm 4.5$	LEES	11g BABR $e^+ e^- \approx \Upsilon(4S)$

$\Gamma(\bar{p} 2\mu^+)/\Gamma_{total}$		$\Gamma_{84}/\Gamma$		
VALUE	CL%	EVTS	DOCUMENT ID	TECN COMMENT
$<9.4 \times 10^{-6}$	90	$0.0 \pm 2.2$	LEES	11g BABR $e^+ e^- \approx \Upsilon(4S)$

$\Gamma(\bar{p} e^+ \mu^+)/\Gamma_{total}$		$\Gamma_{85}/\Gamma$		
VALUE	CL%	EVTS	DOCUMENT ID	TECN COMMENT
$<16 \times 10^{-6}$	90	$10.1 \pm 6.8$	LEES	11g BABR $e^+ e^- \approx \Upsilon(4S)$

$\Gamma(\Sigma^- \mu^+ \mu^+)/\Gamma_{total}$		$\Gamma_{86}/\Gamma$		
VALUE	CL%	EVTS	DOCUMENT ID	TECN COMMENT
$<7.0 \times 10^{-4}$	90	0	KODAMA	95 E653 $\pi^-$ emulsion 600 GeV

$\Lambda_c^+$  DECAY PARAMETERS

See the note on "Baryon Decay Parameters" in the neutron Listings.

$\alpha$ FOR $\Lambda_c^+ \rightarrow \Lambda \pi^+$		$\Gamma_{87}/\Gamma$	
VALUE	EVTS	DOCUMENT ID	TECN COMMENT
$-0.84 \pm 0.09$ OUR AVERAGE			
$-0.80 \pm 0.11 \pm 0.02$		ABLIKIM	19ax BES3 $e^+ e^-$ at 4.6 GeV
$-0.78 \pm 0.16 \pm 0.19$		LINK	06a FOCS $\gamma A, \bar{E}_\gamma \approx 180$ GeV
$-0.94 \pm 0.21 \pm 0.12$	414	1 BISHAI	95 CLE2 $e^+ e^- \approx \Upsilon(4S)$
$-0.96 \pm 0.42$		ALBRECHT	92 ARG $e^+ e^- \approx 10.4$ GeV
$-1.1 \pm 0.4$	86	AVERY	90b CLEO $e^+ e^- \approx 10.6$ GeV

<sup>1</sup> BISHAI 95 actually gives  $\alpha = -0.94 \pm 0.21 \pm 0.12$ , chopping the errors at the physical limit  $-1.0$ . However, for  $\alpha \approx -1.0$ , some experiments should get unphysical values ( $\alpha < -1.0$ ), and for averaging with other measurements such values (or errors that extend below  $-1.0$ ) should not be chopped.

$\alpha$ FOR $\Lambda_c^+ \rightarrow \Sigma^+ \pi^0$		$\Gamma_{88}/\Gamma$	
VALUE	EVTS	DOCUMENT ID	TECN COMMENT
$-0.55 \pm 0.11$ OUR AVERAGE			
$-0.57 \pm 0.10 \pm 0.07$		ABLIKIM	19ax BES3 $e^+ e^-$ at 4.6 GeV
$-0.45 \pm 0.31 \pm 0.06$	89	BISHAI	95 CLE2 $e^+ e^- \approx \Upsilon(4S)$



$\Lambda_c(2595)^+$  DECAY MODES

$\Lambda_c^+ \pi \pi$  and its submode  $\Sigma_c(2455) \pi$  — the latter just barely — are the only strong decays allowed to an excited  $\Lambda_c^+$  having this mass; and the submode seems to dominate.

Mode	Fraction ( $\Gamma_i/\Gamma$ )
$\Gamma_1$ $\Lambda_c^+ \pi^+ \pi^-$	[a] —
$\Gamma_2$ $\Sigma_c(2455)^{++} \pi^-$	24 ± 7 %
$\Gamma_3$ $\Sigma_c(2455)^0 \pi^+$	24 ± 7 %
$\Gamma_4$ $\Lambda_c^+ \pi^+ \pi^-$ 3-body	18 ± 10 %
$\Gamma_5$ $\Lambda_c^+ \pi^0$	[b] not seen
$\Gamma_6$ $\Lambda_c^+ \gamma$	not seen

[a] See AALTONEN 11H, Fig. 8, for the calculated ratio of  $\Lambda_c^+ \pi^0 \pi^0$  and  $\Lambda_c^+ \pi^+ \pi^-$  partial widths as a function of the  $\Lambda_c(2595)^+ - \Lambda_c^+$  mass difference. At our value of the mass difference, the ratio is about 4.

[b] A test that the isospin is indeed 0, so that the particle is indeed a  $\Lambda_c^+$ .

$\Lambda_c(2595)^+$  BRANCHING RATIOS

$\Gamma(\Sigma_c(2455)^{++} \pi^-)/\Gamma(\Lambda_c^+ \pi^+ \pi^-)$				$\Gamma_2/\Gamma_1$
VALUE	DOCUMENT ID	TECN	COMMENT	
<b>0.36 ± 0.10 OUR AVERAGE</b>				
0.37 ± 0.12 ± 0.13	ALBRECHT 97	ARG	$e^+ e^- \approx 10$ GeV	
0.36 ± 0.09 ± 0.09	EDWARDS 95	CLE2	$e^+ e^- \approx 10.5$ GeV	

$\Gamma(\Sigma_c(2455)^0 \pi^+)/\Gamma(\Lambda_c^+ \pi^+ \pi^-)$				$\Gamma_3/\Gamma_1$
VALUE	DOCUMENT ID	TECN	COMMENT	
<b>0.37 ± 0.10 OUR AVERAGE</b>				
0.29 ± 0.10 ± 0.11	ALBRECHT 97	ARG	$e^+ e^- \approx 10$ GeV	
0.42 ± 0.09 ± 0.09	EDWARDS 95	CLE2	$e^+ e^- \approx 10.5$ GeV	

$[\Gamma(\Sigma_c(2455)^{++} \pi^-) + \Gamma(\Sigma_c(2455)^0 \pi^+)]/\Gamma(\Lambda_c^+ \pi^+ \pi^-)$				$(\Gamma_2 + \Gamma_3)/\Gamma_1$
VALUE	CL%	DOCUMENT ID	TECN	COMMENT
• • • We do not use the following data for averages, fits, limits, etc. • • •				
0.66 <sup>+0.13</sup> <sub>-0.16</sub> ± 0.07		ALBRECHT 97	ARG	$e^+ e^- \approx 10$ GeV
>0.51	90	FRABETTI 96	E687	$\gamma$ Be, $\bar{E}_\gamma \approx 220$ GeV

<sup>3</sup>The results of FRABETTI 96 are consistent with this ratio being 100%.

$\Gamma(\Lambda_c^+ \pi^0)/\Gamma(\Lambda_c^+ \pi^+ \pi^-)$				$\Gamma_5/\Gamma_1$
VALUE	CL%	DOCUMENT ID	TECN	COMMENT
<b>&lt;3.53</b>	90	EDWARDS 95	CLE2	$e^+ e^- \approx 10.5$ GeV

$\Lambda_c^+ \pi^0$  decay is forbidden by isospin conservation if this state is in fact a  $\Lambda_c$ .

$\Gamma(\Lambda_c^+ \gamma)/\Gamma(\Lambda_c^+ \pi^+ \pi^-)$				$\Gamma_6/\Gamma_1$
VALUE	CL%	DOCUMENT ID	TECN	COMMENT
<b>&lt;0.98</b>	90	EDWARDS 95	CLE2	$e^+ e^- \approx 10.5$ GeV

$\Lambda_c(2595)^+$  REFERENCES

AALTONEN 11H PR D84 012003	T. Aaltonen et al. (CDF Collab.)
BLECHMAN 03 PR D67 074033	A.E. Blechman et al. (JHU, FLOR)
ALBRECHT 97 PL B402 207	H. Albrecht et al. (ARGUS Collab.)
FRABETTI 96 PL B365 461	P.L. Frabetti et al. (FNAL E687 Collab.)
EDWARDS 95 PRL 74 3331	K.W. Edwards et al. (CLEO Collab.)

**$\Lambda_c(2625)^+$**   $I(J^P) = 0(\frac{3}{2}^-)$  Status: \*\*\*

The spin-parity has not been measured but is expected to be  $3/2^-$ : this is presumably the charm counterpart of the strange  $\Lambda(1520)$ .

$\Lambda_c(2625)^+$  MASS

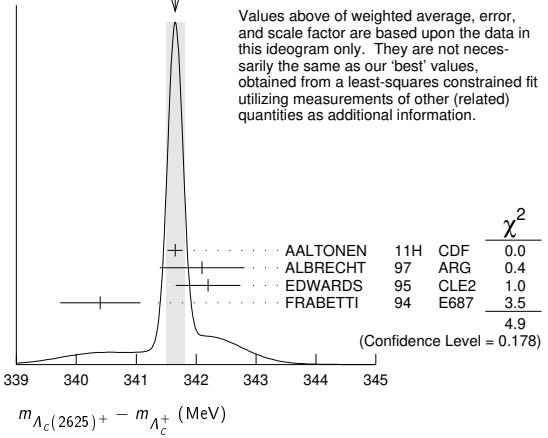
The mass is obtained from the  $\Lambda_c(2625)^+ - \Lambda_c^+$  mass-difference measurements below.

VALUE (MeV)	EVTS	DOCUMENT ID	TECN	COMMENT
<b>2628.11 ± 0.19 OUR FIT</b>				Error includes scale factor of 1.1.
• • • We do not use the following data for averages, fits, limits, etc. • • •				
2626.6 ± 0.5 ± 1.5	42 ± 9	ALBRECHT 93F	ARG	See ALBRECHT 97

$\Lambda_c(2625)^+ - \Lambda_c^+$  MASS DIFFERENCE

VALUE (MeV)	EVTS	DOCUMENT ID	TECN	COMMENT
<b>341.65 ± 0.13 OUR FIT</b>				Error includes scale factor of 1.1.
<b>341.65 ± 0.15 OUR AVERAGE</b>				Error includes scale factor of 1.3. See the ideogram below.
341.65 ± 0.04 ± 0.12	6.2k	AALTONEN 11H	CDF	$p\bar{p}$ at 1.96 TeV
342.1 ± 0.5 ± 0.5	51	ALBRECHT 97	ARG	$e^+ e^- \approx 10$ GeV
342.2 ± 0.2 ± 0.5	245 ± 19	EDWARDS 95	CLE2	$e^+ e^- \approx 10.5$ GeV
340.4 ± 0.6 ± 0.3	40 ± 9	FRABETTI 94	E687	$\gamma$ Be, $\bar{E}_\gamma = 220$ GeV

WEIGHTED AVERAGE  
341.65±0.15 (Error scaled by 1.3)



$\Lambda_c(2625)^+$  WIDTH

VALUE (MeV)	CL%	EVTS	DOCUMENT ID	TECN	COMMENT
<b>&lt;0.97</b>	90	6.2k	AALTONEN 11H	CDF	$p\bar{p}$ at 1.96 TeV
• • • We do not use the following data for averages, fits, limits, etc. • • •					
<1.9	90	245 ± 19	EDWARDS 95	CLE2	$e^+ e^- \approx 10.5$ GeV
<3.2	90		ALBRECHT 93F	ARG	$e^+ e^- \approx \Upsilon(4S)$

$\Lambda_c(2625)^+$  DECAY MODES

$\Lambda_c^+ \pi \pi$  and its submode  $\Sigma(2455) \pi$  are the only strong decays allowed to an excited  $\Lambda_c^+$  having this mass.

Mode	Fraction ( $\Gamma_i/\Gamma$ )	Confidence level
$\Gamma_1$ $\Lambda_c^+ \pi^+ \pi^-$	$\approx 67\%$	
$\Gamma_2$ $\Sigma_c(2455)^{++} \pi^-$	<5	90%
$\Gamma_3$ $\Sigma_c(2455)^0 \pi^+$	<5	90%
$\Gamma_4$ $\Lambda_c^+ \pi^+ \pi^-$ 3-body	large	
$\Gamma_5$ $\Lambda_c^+ \pi^0$	[a] not seen	
$\Gamma_6$ $\Lambda_c^+ \gamma$	not seen	

[a] A test that the isospin is indeed 0, so that the particle is indeed a  $\Lambda_c^+$ .

$\Lambda_c(2625)^+$  BRANCHING RATIOS

$\Gamma(\Sigma_c(2455)^{++} \pi^-)/\Gamma(\Lambda_c^+ \pi^+ \pi^-)$				$\Gamma_2/\Gamma_1$
VALUE	CL%	DOCUMENT ID	TECN	COMMENT
<b>&lt;0.08</b>	90	EDWARDS 95	CLE2	$e^+ e^- \approx 10.5$ GeV

$\Gamma(\Sigma_c(2455)^0 \pi^+)/\Gamma(\Lambda_c^+ \pi^+ \pi^-)$				$\Gamma_3/\Gamma_1$
VALUE	CL%	DOCUMENT ID	TECN	COMMENT
<b>&lt;0.07</b>	90	EDWARDS 95	CLE2	$e^+ e^- \approx 10.5$ GeV

$[\Gamma(\Sigma_c(2455)^{++} \pi^-) + \Gamma(\Sigma_c(2455)^0 \pi^+)]/\Gamma(\Lambda_c^+ \pi^+ \pi^-)$				$(\Gamma_2 + \Gamma_3)/\Gamma_1$	
VALUE	CL%	EVTS	DOCUMENT ID	TECN	COMMENT
• • • We do not use the following data for averages, fits, limits, etc. • • •					
<0.36	90		FRABETTI 94	E687	$\gamma$ Be, $\bar{E}_\gamma = 220$ GeV
0.46 ± 0.14		21	ALBRECHT 93F	ARG	$e^+ e^- \approx \Upsilon(4S)$

$\Gamma(\Lambda_c^+ \pi^+ \pi^- \text{ 3-body})/\Gamma(\Lambda_c^+ \pi^+ \pi^-)$				$\Gamma_4/\Gamma_1$
VALUE	EVTS	DOCUMENT ID	TECN	COMMENT
• • • We do not use the following data for averages, fits, limits, etc. • • •				
0.54 ± 0.14	16	ALBRECHT 93F	ARG	$e^+ e^- \approx \Upsilon(4S)$

## Baryon Particle Listings

 $\Lambda_c(2625)^+$ ,  $\Lambda_c(2765)^+$ ,  $\Lambda_c(2860)^+$ ,  $\Lambda_c(2880)^+$ 

$\Gamma(\Lambda_c^+ \pi^0)/\Gamma(\Lambda_c^+ \pi^+ \pi^-)$   $\Gamma_5/\Gamma_1$   
 $\Lambda_c^+ \pi^0$  decay is forbidden by isospin conservation if this state is in fact a  $\Lambda_c$ .

VALUE	CL%	DOCUMENT ID	TECN	COMMENT
<0.91	90	EDWARDS	95	CLE2 $e^+ e^- \approx 10.5$ GeV

$\Gamma(\Lambda_c^+ \gamma)/\Gamma(\Lambda_c^+ \pi^+ \pi^-)$   $\Gamma_6/\Gamma_1$

VALUE	CL%	DOCUMENT ID	TECN	COMMENT
<0.52	90	EDWARDS	95	CLE2 $e^+ e^- \approx 10.5$ GeV

 $\Lambda_c(2625)^+$  REFERENCES

AALTONEN	11H	PR D84 012003	T. Aaltonen et al.	(CDF Collab.)
ALBRECHT	97	PL B402 207	H. Albrecht et al.	(ARGUS Collab.)
EDWARDS	95	PRL 74 3331	K.W. Edwards et al.	(CLEO Collab.)
FRABETTI	94	PRL 72 961	P.L. Frabetti et al.	(FNAL E687 Collab.)
ALBRECHT	93F	PL B317 227	H. Albrecht et al.	(ARGUS Collab.)

$\Lambda_c(2765)^+$  or  $\Sigma_c(2765)$   $I(J^P) = ?(??)$  Status: \*

OMITTED FROM SUMMARY TABLE

A broad, statistically significant peak ( $997^{+141}_{-129}$  events) seen in  $\Lambda_c^+ \pi^+ \pi^-$ . However, nothing at all is known about its quantum numbers, including whether it is a  $\Lambda_c^+$  or a  $\Sigma_c$ , or whether the width might be due to overlapping states.

 $\Lambda_c(2765)^+$  MASS

The mass is obtained from the  $\Lambda_c(2765)^+ - \Lambda_c^+$  mass-difference measurement below.

VALUE (MeV)	DOCUMENT ID
<b>2766.6 ± 2.4 OUR FIT</b>	

 $\Lambda_c(2765)^+ - \Lambda_c^+$  MASS DIFFERENCE

VALUE (MeV)	EVTS	DOCUMENT ID	TECN	COMMENT
<b>480.1 ± 2.4 OUR FIT</b>				
<b>480.1 ± 2.4</b>	$997^{+141}_{-129}$	ARTUSO	01	CLE2 $e^+ e^- \approx \mathcal{T}(4S)$

 $\Lambda_c(2765)^+$  WIDTH

VALUE (MeV)	DOCUMENT ID	TECN	COMMENT
<b>50</b>	ARTUSO	01	CLE2 $e^+ e^- \approx \mathcal{T}(4S)$

 $\Lambda_c(2765)^+$  DECAY MODES

Mode	Fraction ( $\Gamma_i/\Gamma$ )
$\Gamma_1$ $\Lambda_c^+ \pi^+ \pi^-$	seen

 $\Lambda_c(2765)^+$  REFERENCES

ARTUSO	01	PRL 86 4479	M. Artuso et al.	(CLEO Collab.)
--------	----	-------------	------------------	----------------

$\Lambda_c(2860)^+$   $I(J^P) = 0(\frac{3}{2}^+)$  Status: \*\*\*

 $\Lambda_c(2860)^+$  MASS

VALUE (MeV)	DOCUMENT ID	TECN	COMMENT
<b>2856.1 ± 2.0 ± 0.5 ± 1.1 ± 1.7 ± 0.5 ± 5.6</b>	<sup>1</sup> AAIJ	17s	LHCB in $\Lambda_b^0 \rightarrow D^0 p \pi^-$

<sup>1</sup> The third AAIJ 17s uncertainty comes from modeling the resonant shape of the nearby  $\Lambda_c(2880)^+$  and the background (non-resonant) amplitudes.

 $\Lambda_c(2860)^+$  WIDTH

VALUE (MeV)	DOCUMENT ID	TECN	COMMENT
<b>67.6 ± 10.1 ± 8.1 ± 1.4 ± 5.9 ± 20.0</b>	<sup>1</sup> AAIJ	17s	LHCB in $\Lambda_b^0 \rightarrow D^0 p \pi^-$

<sup>1</sup> The third AAIJ 17s uncertainty comes from modeling the resonant shape of the nearby  $\Lambda_c(2880)^+$  and the background (non-resonant) amplitudes.

 $\Lambda_c(2860)^+$  DECAY MODES

Mode	Fraction ( $\Gamma_i/\Gamma$ )
$\Gamma_1$ $D^0 p$	seen

 $\Lambda_c(2860)^+$  BRANCHING RATIOS

$\Gamma(D^0 p)/\Gamma_{\text{total}}$	DOCUMENT ID	TECN	COMMENT	$\Gamma_1/\Gamma$
seen	AAIJ	17s	LHCB in $\Lambda_b^0 \rightarrow D^0 p \pi^-$	

 $\Lambda_c(2860)^+$  REFERENCES

AAIJ	17s	JHEP 1705 030	R. Aaij et al.	(LHCb Collab.) JP
------	-----	---------------	----------------	-------------------

$\Lambda_c(2880)^+$   $I(J^P) = 0(\frac{5}{2}^+)$  Status: \*\*\*

A narrow peak seen in  $\Lambda_c^+ \pi^+ \pi^-$  and in  $p D^0$ . It is not seen in  $p D^+$ , and therefore it is a  $\Lambda_c^+$  and not a  $\Sigma_c$ .

 $\Lambda_c(2880)^+$  MASS

VALUE (MeV)	EVTS	DOCUMENT ID	TECN	COMMENT
<b>2881.63 ± 0.24 OUR FIT</b>				
<b>2881.62 ± 0.24 OUR AVERAGE</b>				
$2881.75 \pm 0.29 \pm 0.07^{+0.14}_{-0.20}$	<sup>1</sup> AAIJ	17s	LHCB	in $\Lambda_b^0 \rightarrow D^0 p \pi^-$
$2881.9 \pm 0.1 \pm 0.5$	2.8k	AUBERT	07	BABR in $p D^0$
$2881.2 \pm 0.2 \pm 0.4$	690	MIZUK	07	BELL in $\Sigma_c(2455)^{0,++} \pi^\pm$

<sup>1</sup> The third AAIJ 17s uncertainty comes from modeling the resonant shape of the  $\Lambda_c(2880)^+$  and the background (non-resonant) amplitudes.

 $\Lambda_c(2880)^+ - \Lambda_c^+$  MASS DIFFERENCE

VALUE (MeV)	EVTS	DOCUMENT ID	TECN	COMMENT
<b>595.17 ± 0.28 OUR FIT</b>				
<b>596 ± 1 ± 2</b>	350	ARTUSO	01	CLE2 in $\Lambda_c^+ \pi^+ \pi^-$

 $\Lambda_c(2880)^+$  WIDTH

VALUE (MeV)	CL%	EVTS	DOCUMENT ID	TECN	COMMENT
<b>5.6 ± 0.8 ± 0.6 OUR AVERAGE</b>					
$5.43^{+0.77+0.81}_{-0.71-0.29}$		<sup>2</sup> AAIJ	17s	LHCB	in $\Lambda_b^0 \rightarrow D^0 p \pi^-$
$5.8 \pm 1.5 \pm 1.1$	2.8k	AUBERT	07	BABR	in $p D^0$
$5.8 \pm 0.7 \pm 1.1$	690	MIZUK	07	BELL	in $\Sigma_c(2455)^{0,++} \pi^\pm$
••• We do not use the following data for averages, fits, limits, etc. •••					
<8	90	ARTUSO	01	CLEO	in $\Lambda_c^+ \pi^+ \pi^-$

<sup>2</sup> AAIJ 17s reports  $5.43^{+0.77+0.81}_{-0.71-0.29} \pm 0.29^{+0.75}_{-0.00}$  MeV value where the third uncertainty comes from modeling the resonant shape of the  $\Lambda_c(2880)^+$  and the background (non-resonant) amplitudes. We have combined in quadrature the systematic uncertainties.

 $\Lambda_c(2880)^+$  DECAY MODES

Mode	Fraction ( $\Gamma_i/\Gamma$ )
$\Gamma_1$ $\Lambda_c^+ \pi^+ \pi^-$	seen
$\Gamma_2$ $\Sigma_c(2455)^{0,++} \pi^\pm$	seen
$\Gamma_3$ $\Sigma_c(2520)^{0,++} \pi^\pm$	seen
$\Gamma_4$ $p D^0$	seen

 $\Lambda_c(2880)^+$  BRANCHING RATIOS

$\Gamma(\Sigma_c(2455)^{0,++} \pi^\pm)/\Gamma(\Lambda_c^+ \pi^+ \pi^-)$	DOCUMENT ID	TECN	COMMENT	$\Gamma_2/\Gamma_1$
<b>0.392 ± 0.031 OUR AVERAGE</b>			Error includes scale factor of 1.3.	
$0.404 \pm 0.021 \pm 0.014$	MIZUK	07	BELL	in $\Sigma_c(2455)^{0,++} \pi^\pm$
$0.31 \pm 0.06 \pm 0.03$	96	ARTUSO	01	CLE2 $e^+ e^- \approx \mathcal{T}(4S)$

$\Gamma(\Sigma_c(2520)^{0,++} \pi^\pm)/\Gamma(\Lambda_c^+ \pi^+ \pi^-)$	DOCUMENT ID	TECN	COMMENT	$\Gamma_3/\Gamma_1$
<b>0.091 ± 0.025 ± 0.010</b>	MIZUK	07	BELL	in $\Sigma_c(2455)^{0,++} \pi^\pm$
••• We do not use the following data for averages, fits, limits, etc. •••				
<0.11	90	ARTUSO	01	CLE2 $e^+ e^- \approx \mathcal{T}(4S)$

See key on page 999

# Baryon Particle Listings

## $\Lambda_c(2880)^+, \Lambda_c(2940)^+, \Sigma_c(2455)$

### $\Gamma(\Sigma_c(2520)^{0,++}\pi^\pm)/\Gamma(\Sigma_c(2455)^{0,++}\pi^\pm)$ $\Gamma_3/\Gamma_2$

VALUE	DOCUMENT ID	TECN	COMMENT
0.225 ± 0.062 ± 0.025	<sup>3</sup> MIZUK	07	BELL in $\Sigma_c(2455)^{0,++}\pi^\pm$

<sup>3</sup>This MIZUK 07 ratio is redundant with MIZUK 07 ratios given above.

### $\Lambda_c(2880)^+$ REFERENCES

AAIJ	175	JHEP 1705 030	R. Aaij <i>et al.</i>	(LHCb Collab.) JP
AUBERT	07	PRL 98 012001	B. Aubert <i>et al.</i>	(BABAR Collab.)
MIZUK	07	PRL 98 262001	R. Mizuk <i>et al.</i>	(BELLE Collab.)
ARTUSO	01	PRL 86 4479	M. Artuso <i>et al.</i>	(CLEO Collab.)

### $\Lambda_c(2940)^+$

$$I(J^P) = 0(\frac{3}{2}^-) \text{ Status: } ***$$

A narrow peak seen in  $pD^0$  and in  $\Lambda_c^+\pi^+\pi^-$ . It is not seen in  $pD^+$ , and therefore it is a  $\Lambda_c^+$  and not a  $\Sigma_c$ .  $J^P = 3/2^-$  is favored, but not certain.

### $\Lambda_c(2940)^+$ MASS

VALUE (MeV)	EVTS	DOCUMENT ID	TECN	COMMENT
<b>2939.6<sup>+1.3</sup><sub>-1.5</sub> OUR AVERAGE</b>				
2944.8 <sup>+3.5</sup> <sub>-2.5</sub> ± 0.4 <sup>+0.1</sup> <sub>-4.6</sub>	1	AAIJ	17s	LHCB in $\Lambda_b^0 \rightarrow D^0 p \pi^-$
2939.8 ± 1.3 ± 1.0	2.2k	AUBERT	07	BABR in $pD^0$
2938.0 ± 1.3 <sup>+2.0</sup> <sub>-4.0</sub>	220	MIZUK	07	BELL in $\Sigma_c(2455)^{0,++}\pi^\pm$

<sup>1</sup>The third AAIJ 17s uncertainty comes from modeling the resonant shape of the nearby  $\Lambda_c(2880)^+$  and the background (non-resonant) amplitudes.

### $\Lambda_c(2940)^+$ WIDTH

VALUE (MeV)	EVTS	DOCUMENT ID	TECN	COMMENT
<b>20<sup>+6</sup><sub>-5</sub> OUR AVERAGE</b>				
27.7 <sup>+8.2</sup> <sub>-6.0</sub> ± 0.9 <sup>+5.2</sup> <sub>-10.4</sub>	2	AAIJ	17s	LHCB in $\Lambda_b^0 \rightarrow D^0 p \pi^-$
17.5 ± 5.2 ± 5.9	2.2k	AUBERT	07	BABR in $pD^0$
13 <sup>+8</sup> <sub>-5</sub> <sup>+27</sup> <sub>-7</sub>	220	MIZUK	07	BELL in $\Sigma_c(2455)^{0,++}\pi^\pm$

<sup>2</sup>The third AAIJ 17s uncertainty comes from modeling the resonant shape of the nearby  $\Lambda_c(2880)^+$  and the background (non-resonant) amplitudes.

### $\Lambda_c(2940)^+$ DECAY MODES

Mode	Fraction ( $\Gamma_i/\Gamma$ )
$\Gamma_1$ $pD^0$	seen
$\Gamma_2$ $\Sigma_c(2455)^{0,++}\pi^\pm$	seen

### $\Lambda_c(2940)^+$ REFERENCES

AAIJ	175	JHEP 1705 030	R. Aaij <i>et al.</i>	(LHCb Collab.) JP
AUBERT	07	PRL 98 012001	B. Aubert <i>et al.</i>	(BABAR Collab.)
MIZUK	07	PRL 98 262001	R. Mizuk <i>et al.</i>	(BELLE Collab.)

### $\Sigma_c(2455)$

$$I(J^P) = 1(\frac{1}{2}^+) \text{ Status: } ****$$

The angular distribution of  $B^- \rightarrow \Sigma_c(2455)^0 \bar{p}$  favors  $J = 1/2$  (as the quark model predicts).  $J = 3/2$  is excluded by more than four standard deviations; see AUBERT 08BN.

### $\Sigma_c(2455)$ MASSES

The masses are obtained from the mass-difference measurements that follow.

#### $\Sigma_c(2455)^{++}$ MASS

VALUE (MeV)	DOCUMENT ID
<b>2453.97 ± 0.14 OUR FIT</b>	

#### $\Sigma_c(2455)^+$ MASS

VALUE (MeV)	DOCUMENT ID
<b>2452.9 ± 0.4 OUR FIT</b>	

#### $\Sigma_c(2455)^0$ MASS

VALUE (MeV)	DOCUMENT ID
<b>2453.75 ± 0.14 OUR FIT</b>	

### $\Sigma_c(2455) - \Lambda_c^+$ MASS DIFFERENCES

#### $m_{\Sigma_c^{++}} - m_{\Lambda_c^+}$

VALUE (MeV)	EVTS	DOCUMENT ID	TECN	COMMENT
<b>167.510 ± 0.017 OUR FIT</b>				
<b>167.510 ± 0.022 OUR AVERAGE</b>				
167.51 ± 0.01 ± 0.02	36k	LEE	14	BELL $e^+e^-$ at $\Upsilon(4S)$
167.44 ± 0.04 ± 0.12	13.8k	AALTONEN	11H	CDF $p\bar{p}$ at 1.96 TeV
167.4 ± 0.1 ± 0.2	2k	ARTUSO	02	CLE2 $e^+e^- \approx \Upsilon(4S)$
167.35 ± 0.19 ± 0.12	461	LINK	00c	FOCS $\gamma A, \bar{E}_\gamma$ 180 GeV
167.76 ± 0.29 ± 0.15	122	AITALA	96B	E791 $\pi^- N, 500$ GeV
167.6 ± 0.6 ± 0.6	56	FRABETTI	96	E687 $\gamma Be, \bar{E}_\gamma \approx 220$ GeV
168.2 ± 0.3 ± 0.2	126	CRAWFORD	93	CLE2 $e^+e^- \approx \Upsilon(4S)$
167.8 ± 0.4 ± 0.3	54	BOWCOCK	89	CLEO $e^+e^- \approx 10$ GeV
168.2 ± 0.5 ± 1.6	92	ALBRECHT	88D	ARG $e^+e^- \approx 10$ GeV
167.4 ± 0.5 ± 2.0	46	DIESBURG	87	SPEC $nA \sim 600$ GeV
••• We do not use the following data for averages, fits, limits, etc. •••				
167 ± 1	2	JONES	87	HBC $\nu p$ in BEBC
166 ± 1	1	BOSETTI	82	HBC See JONES 87
168 ± 3	6	BALTAY	79	HLBC $\nu$ Ne-H in 15-ft
166 ± 15	1	CAZZOLI	75	HBC $\nu p$ in BNL 7-ft

#### $m_{\Sigma_c^+} - m_{\Lambda_c^+}$

VALUE (MeV)	EVTS	DOCUMENT ID	TECN	COMMENT
<b>166.4 ± 0.4 OUR FIT</b>				
<b>166.4 ± 0.2 ± 0.3</b>	661	AMMAR	01	CLE2 $e^+e^- \approx \Upsilon(4S)$
••• We do not use the following data for averages, fits, limits, etc. •••				
168.5 ± 0.4 ± 0.2	111	CRAWFORD	93	CLE2 See AMMAR 01
168 ± 3	1	CALICCHIO	80	HBC $\nu p$ in BEBC-TST

#### $m_{\Sigma_c^0} - m_{\Lambda_c^+}$

VALUE (MeV)	EVTS	DOCUMENT ID	TECN	COMMENT
<b>167.290 ± 0.017 OUR FIT</b>				
<b>167.290 ± 0.022 OUR AVERAGE</b>				
167.29 ± 0.01 ± 0.02	32k	LEE	14	BELL $e^+e^-$ at $\Upsilon(4S)$
167.28 ± 0.03 ± 0.12	15.9k	AALTONEN	11H	CDF $p\bar{p}$ at 1.96 TeV
167.2 ± 0.1 ± 0.2	2k	ARTUSO	02	CLE2 $e^+e^- \approx \Upsilon(4S)$
167.38 ± 0.21 ± 0.13	362	LINK	00c	FOCS $\gamma A, \bar{E}_\gamma$ 180 GeV
167.38 ± 0.29 ± 0.15	143	AITALA	96B	E791 $\pi^- N, 500$ GeV
167.8 ± 0.6 ± 0.2		ALEEV	96	SPEC $n$ nucleus, 50 GeV/c
166.6 ± 0.5 ± 0.6	69	FRABETTI	96	E687 $\gamma Be, \bar{E}_\gamma \approx 220$ GeV
167.1 ± 0.3 ± 0.2	124	CRAWFORD	93	CLE2 $e^+e^- \approx \Upsilon(4S)$
168.4 ± 1.0 ± 0.3	14	ANJOS	89D	E691 $\gamma Be$ 90–260 GeV
••• We do not use the following data for averages, fits, limits, etc. •••				
167.9 ± 0.5 ± 0.3	48	<sup>1</sup> BOWCOCK	89	CLEO $e^+e^-$ 10 GeV
167.0 ± 0.5 ± 1.6	70	<sup>1</sup> ALBRECHT	88D	ARG $e^+e^-$ 10 GeV
178.2 ± 0.4 ± 2.0	85	<sup>2</sup> DIESBURG	87	SPEC $nA \sim 600$ GeV
163 ± 2	1	AMMAR	86	EMUL $\nu A$

<sup>1</sup>This result enters the fit through  $m_{\Sigma_c^{++}} - m_{\Sigma_c^0}$  given below.

<sup>2</sup>See the note on DIESBURG 87 in the  $m_{\Sigma_c^{++}} - m_{\Sigma_c^0}$  section below.

### $\Sigma_c(2455)$ MASS DIFFERENCES

#### $m_{\Sigma_c^{++}} - m_{\Sigma_c^0}$

VALUE (MeV)	DOCUMENT ID	TECN	COMMENT
<b>0.220 ± 0.013 OUR FIT</b>			
<b>0.221 ± 0.014 OUR AVERAGE</b>			
0.22 ± 0.01 ± 0.01	LEE	14	BELL $e^+e^-$ at $\Upsilon(4S)$
0.2 ± 0.1 ± 0.1	ARTUSO	02	CLE2 $e^+e^- \approx \Upsilon(4S)$
-0.03 ± 0.28 ± 0.11	LINK	00c	FOCS $\gamma A, \bar{E}_\gamma$ 180 GeV
0.38 ± 0.40 ± 0.15	AITALA	96B	E791 $\pi^- N, 500$ GeV
1.1 ± 0.4 ± 0.1	CRAWFORD	93	CLE2 $e^+e^- \approx \Upsilon(4S)$
-0.1 ± 0.6 ± 0.1	BOWCOCK	89	CLEO $e^+e^- \approx 10$ GeV
1.2 ± 0.7 ± 0.3	ALBRECHT	88D	ARG $e^+e^- \approx 10$ GeV
••• We do not use the following data for averages, fits, limits, etc. •••			
-10.8 ± 2.9	<sup>3</sup> DIESBURG	87	SPEC $nA \sim 600$ GeV
<sup>3</sup> DIESBURG 87 is completely incompatible with the other experiments, which is surprising since it agrees with them about $m_{\Sigma_c(2455)^{++}} - m_{\Lambda_c^+}$ . We go with the majority here.			

#### $m_{\Sigma_c^+} - m_{\Sigma_c^0}$

VALUE (MeV)	DOCUMENT ID	TECN	COMMENT
<b>-0.9 ± 0.4 OUR FIT</b>			
••• We do not use the following data for averages, fits, limits, etc. •••			
1.4 ± 0.5 ± 0.3	CRAWFORD	93	CLE2 See AMMAR 01

# Baryon Particle Listings

## $\Sigma_c(2455), \Sigma_c(2520)$

### $\Sigma_c(2455)$ WIDTHS

#### $\Sigma_c(2455)^{++}$ WIDTH

VALUE (MeV)	EVTS	DOCUMENT ID	TECN	COMMENT
<b><math>1.89^{+0.09}_{-0.18}</math> OUR AVERAGE</b>		Error includes scale factor of 1.1.		
$1.84 \pm 0.04^{+0.07}_{-0.20}$	36k	LEE	14	BELL $e^+e^-$ at $\Upsilon(4S)$
$2.34 \pm 0.13 \pm 0.45$	13.8k	AALTONEN	11H	CDF $p\bar{p}$ at 1.96 TeV
$2.3 \pm 0.2 \pm 0.3$	2k	ARTUSO	02	CLE2 $e^+e^- \approx \Upsilon(4S)$
$2.05^{+0.41}_{-0.38} \pm 0.38$	1110	LINK	02	FOCS $\gamma A, \bar{E}_\gamma \approx 180$ GeV

#### $\Sigma_c(2455)^+$ WIDTH

VALUE (MeV)	CL%	EVTS	DOCUMENT ID	TECN	COMMENT
<b>&lt;4.6</b>	90	661	AMMAR	01	CLE2 $e^+e^- \approx \Upsilon(4S)$

#### $\Sigma_c(2455)^0$ WIDTH

VALUE (MeV)	EVTS	DOCUMENT ID	TECN	COMMENT
<b><math>1.83^{+0.11}_{-0.19}</math> OUR AVERAGE</b>		Error includes scale factor of 1.2.		
$1.76 \pm 0.04^{+0.09}_{-0.21}$	32k	LEE	14	BELL $e^+e^-$ at $\Upsilon(4S)$
$1.65 \pm 0.11 \pm 0.49$	15.9k	AALTONEN	11H	CDF $p\bar{p}$ at 1.96 TeV
$2.6 \pm 0.5 \pm 0.3$		AUBERT	08BN	BABR $B^- \rightarrow \bar{p}\Lambda_c^+\pi^-$
$2.5 \pm 0.2 \pm 0.3$	2k	ARTUSO	02	CLE2 $e^+e^- \approx \Upsilon(4S)$
$1.55^{+0.41}_{-0.37} \pm 0.38$	913	LINK	02	FOCS $\gamma A, \bar{E}_\gamma \approx 180$ GeV

### $\Sigma_c(2455)$ DECAY MODES

$\Lambda_c^+\pi$  is the only strong decay allowed to a  $\Sigma_c$  having this mass.

Mode	Fraction ( $\Gamma_i/\Gamma$ )
$\Gamma_1 \Lambda_c^+\pi$	$\approx 100\%$

### $\Sigma_c(2455)$ REFERENCES

LEE	14	PR D89 091102	S.-H. Lee <i>et al.</i>	(BELLE Collab.)
AALTONEN	11H	PR D84 012003	T. Aaltonen <i>et al.</i>	(CDF Collab.)
AUBERT	08BN	PR D78 112003	B. Aubert <i>et al.</i>	(BABAR Collab.)
ARTUSO	02	PR D65 071101	M. Artuso <i>et al.</i>	(CLEO Collab.)
LINK	02	PL B525 205	J.M. Link <i>et al.</i>	(FNAL FOCUS Collab.)
AMMAR	01	PRL 86 1167	R. Ammar <i>et al.</i>	(CLEO Collab.)
LINK	00C	PL B488 218	J.M. Link <i>et al.</i>	(FNAL FOCUS Collab.)
AITALA	96B	PL B379 292	E.M. Aitala <i>et al.</i>	(FNAL E791 Collab.)
ALEV	96	JINRRC 3-77 31	A.N. Alev <i>et al.</i>	(Serpukhov EXCHARM Collab.)
FRABETTI	96	PL B365 461	P.L. Frabetti <i>et al.</i>	(FNAL E687 Collab.)
CRAWFORD	93	PRL 71 3259	G. Crawford <i>et al.</i>	(CLEO Collab.)
ANJOS	89D	PRL 62 1721	J.C. Anjos <i>et al.</i>	(FNAL E691 Collab.)
BOWCOCK	89	PRL 62 1240	T.J.V. Bowcock <i>et al.</i>	(CLEO Collab.)
ALBRECHT	88D	PL B211 489	H. Albrecht <i>et al.</i>	(ARGUS Collab.)
DIESBURG	87	PRL 59 2711	M. Diesburg <i>et al.</i>	(FNAL E400 Collab.)
JONES	87	ZPHY C36 593	G.T. Jones <i>et al.</i>	(CERN WA21 Collab.)
AMMAR	86	JETPL 43 515	R. Ammar <i>et al.</i>	(ITEP)
BOSETTI	82	PL 109B 234	P.C. Bosetti <i>et al.</i>	(AACH3, BONN, CERN+)
CALICCHIO	80	PL 93B 521	M. Calicchio <i>et al.</i>	(BARI, BIRM, BRUX+)
BALTAY	79	PRL 42 1721	C. Baltay <i>et al.</i>	(COLU, BNL)
CAZZOLI	75	PRL 34 1125	E.G. Cazzoli <i>et al.</i>	(BNL)

## $\Sigma_c(2520)$

$$I(J^P) = 1(\frac{3}{2}^+) \text{ Status: } ***$$

Seen in the  $\Lambda_c^+\pi^\pm$  mass spectrum. The natural assignment is that this is the  $J^P = 3/2^+$  excitation of the  $\Sigma_c(2455)$ , the charm counterpart of the  $\Sigma(1385)$ , but neither  $J$  nor  $P$  has been measured.

### $\Sigma_c(2520)$ MASSES

The masses are obtained from the mass-difference measurements that follow.

#### $\Sigma_c(2520)^{++}$ MASS

VALUE (MeV)	EVTS	DOCUMENT ID	TECN	COMMENT
<b><math>2518.41 \pm 0.21_{-0.19}</math> OUR FIT</b>		Error includes scale factor of 1.1.		
••• We do not use the following data for averages, fits, limits, etc. •••				
$2530 \pm 5 \pm 5$	6	<sup>1</sup> AMMOSOV 93	HLBC	$\nu p \rightarrow \mu^- \Sigma_c(2530)^{++}$
<sup>1</sup> AMMOSOV 93 sees a cluster of 6 events and estimates the background to be 1 event.				

#### $\Sigma_c(2520)^+$ MASS

VALUE (MeV)	DOCUMENT ID
<b><math>2517.5 \pm 2.3</math> OUR FIT</b>	

#### $\Sigma_c(2520)^0$ MASS

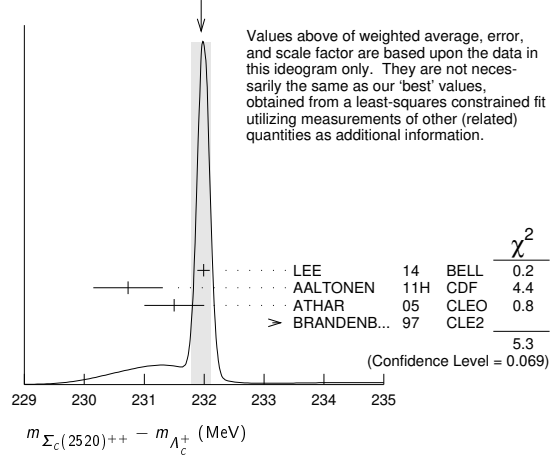
VALUE (MeV)	DOCUMENT ID
<b><math>2518.48 \pm 0.20</math> OUR FIT</b>	
Error includes scale factor of 1.1.	

### $\Sigma_c(2520)$ MASS DIFFERENCES

#### $m_{\Sigma_c(2520)^{++}} - m_{\Lambda_c^+}$

VALUE (MeV)	EVTS	DOCUMENT ID	TECN	COMMENT
<b><math>231.95 \pm 0.17_{-0.12}</math> OUR FIT</b>		Error includes scale factor of 1.3.		
<b><math>231.95 \pm 0.16</math> OUR AVERAGE</b>		Error includes scale factor of 1.6. See the ideogram below.		
$231.99 \pm 0.10 \pm 0.02$	44k	LEE	14	BELL $e^+e^-$ at $\Upsilon(4S)$
$230.73 \pm 0.56 \pm 0.16$	8.8k	AALTONEN	11H	CDF $p\bar{p}$ at 1.96 TeV
$231.5 \pm 0.4 \pm 0.3$	1.3k	ATHAR	05	CLEO $e^+e^-$ , 9.4-11.5 GeV
$234.5 \pm 1.1 \pm 0.8$	677	BRANDENB...	97	CLE2 $e^+e^- \approx \Upsilon(4S)$

WEIGHTED AVERAGE  
231.95±0.16 (Error scaled by 1.6)



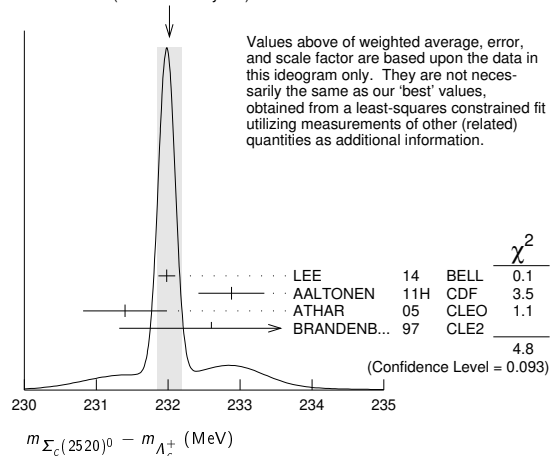
#### $m_{\Sigma_c(2520)^+} - m_{\Lambda_c^+}$

VALUE (MeV)	EVTS	DOCUMENT ID	TECN	COMMENT
<b><math>231.0 \pm 2.3</math> OUR FIT</b>		Error includes scale factor of 1.3.		
<b><math>231.0 \pm 1.1 \pm 2.0</math></b>	327	AMMAR	01	CLE2 $e^+e^- \approx \Upsilon(4S)$

#### $m_{\Sigma_c(2520)^0} - m_{\Lambda_c^+}$

VALUE (MeV)	EVTS	DOCUMENT ID	TECN	COMMENT
<b><math>232.02^{+0.15}_{-0.14}</math> OUR FIT</b>		Error includes scale factor of 1.3.		
<b><math>232.02 \pm 0.17</math> OUR AVERAGE</b>		Error includes scale factor of 1.5. See the ideogram below.		
$231.98 \pm 0.11 \pm 0.04$	41k	LEE	14	BELL $e^+e^-$ at $\Upsilon(4S)$
$232.88 \pm 0.43 \pm 0.16$	9.0k	AALTONEN	11H	CDF $p\bar{p}$ at 1.96 TeV
$231.4 \pm 0.5 \pm 0.3$	1.3k	ATHAR	05	CLEO $e^+e^-$ , 9.4-11.5 GeV
$232.6 \pm 1.0 \pm 0.8$	504	BRANDENB...	97	CLE2 $e^+e^- \approx \Upsilon(4S)$

WEIGHTED AVERAGE  
232.02±0.17 (Error scaled by 1.5)



#### $m_{\Sigma_c(2520)^{++}} - m_{\Sigma_c(2520)^0}$

VALUE (MeV)	EVTS	DOCUMENT ID	TECN	COMMENT
<b><math>0.01 \pm 0.15 \pm 0.03</math></b>	44/41k	LEE	14	BELL $e^+e^-$ at $\Upsilon(4S)$
••• We do not use the following data for averages, fits, limits, etc. •••				
$0.1 \pm 0.8 \pm 0.3$		<sup>2</sup> ATHAR	05	CLEO $e^+e^-$ , 9.4-11.5 GeV
$1.9 \pm 1.4 \pm 1.0$		<sup>3</sup> BRANDENB...	97	CLE2 $e^+e^- \approx \Upsilon(4S)$

<sup>2</sup>This ATHAR 05 result is redundant with measurements in earlier entries.  
<sup>3</sup>This BRANDENBURG 97 result is redundant with measurements in earlier entries.

See key on page 999

Baryon Particle Listings

$\Sigma_c(2520), \Sigma_c(2800), \Xi_c^+$

$\Sigma_c(2520)$  WIDTHS

$\Sigma_c(2520)^{++}$  WIDTH

VALUE (MeV)	EVTS	DOCUMENT ID	TECN	COMMENT
<b>14.78<sup>+0.30</sup><sub>-0.40</sub></b> OUR AVERAGE				
14.77 ± 0.25 <sup>+0.18</sup> <sub>-0.30</sub>	44k	LEE	14	BELL e <sup>+</sup> e <sup>-</sup> at $\Upsilon(4S)$
15.03 ± 2.12 ± 1.36	8.8k	AALTONEN	11H	CDF $p\bar{p}$ at 1.96 TeV
14.4 <sup>+1.6</sup> <sub>-1.5</sub> ± 1.4	1.3k	ATHAR	05	CLEO e <sup>+</sup> e <sup>-</sup> , 9.4–11.5 GeV
17.9 <sup>+3.8</sup> <sub>-3.2</sub> ± 4.0	677	BRANDENB...	97	CLE2 e <sup>+</sup> e <sup>-</sup> $\approx \Upsilon(4S)$

$\Sigma_c(2520)^+$  WIDTH

VALUE (MeV)	CL%	EVTS	DOCUMENT ID	TECN	COMMENT
<b>&lt;17</b>	90	327	AMMAR	01	CLE2 e <sup>+</sup> e <sup>-</sup> $\approx \Upsilon(4S)$

$\Sigma_c(2520)^0$  WIDTH

VALUE (MeV)	EVTS	DOCUMENT ID	TECN	COMMENT
<b>15.3<sup>+0.4</sup><sub>-0.5</sub></b> OUR AVERAGE				
15.41 ± 0.41 <sup>+0.20</sup> <sub>-0.32</sub>	41k	LEE	14	BELL e <sup>+</sup> e <sup>-</sup> at $\Upsilon(4S)$
12.51 ± 1.82 ± 1.37	9.0k	AALTONEN	11H	CDF $p\bar{p}$ at 1.96 TeV
16.6 <sup>+1.9</sup> <sub>-1.7</sub> ± 1.4	1.3k	ATHAR	05	CLEO e <sup>+</sup> e <sup>-</sup> , 9.4–11.5 GeV
13.0 <sup>+3.7</sup> <sub>-3.0</sub> ± 4.0	504	BRANDENB...	97	CLE2 e <sup>+</sup> e <sup>-</sup> $\approx \Upsilon(4S)$

$\Sigma_c(2520)$  DECAY MODES

$\Lambda_c^+ \pi$  is the only strong decay allowed to a  $\Sigma_c$  having this mass.

Mode	Fraction ( $\Gamma_i/\Gamma$ )
$\Gamma_1 \Lambda_c^+ \pi$	$\approx 100\%$

$\Sigma_c(2520)$  REFERENCES

LEE	14	PR D89 091102	S.-H. Lee <i>et al.</i>	(BELLE Collab.)
AALTONEN	11H	PR D84 012003	T. Aaltonen <i>et al.</i>	(CDF Collab.)
ATHAR	05	PR D71 051101	S.B. Athar <i>et al.</i>	(CLEO Collab.)
AMMAR	01	PRL 86 1167	R. Ammar <i>et al.</i>	(CLEO Collab.)
BRANDENB...	97	PRL 78 2304	G. Brandenburg <i>et al.</i>	(CLEO Collab.)
AMMOS OV	93	JETPL 58 247	V.V. Ammosov <i>et al.</i>	(SERP)
Translated from ZETFP 58 241.				

**$\Sigma_c(2800)$**   $I(J^P) = 1(?^?)$  Status: \*\*\*  
 Seen in the  $\Lambda_c^+ \pi^+$ ,  $\Lambda_c^+ \pi^0$ , and  $\Lambda_c^+ \pi^-$  mass spectra.

$\Sigma_c(2800)$  MASSES

The charged ++ and + masses are obtained from the mass-difference measurements that follow. The neutral mass is dominated by the mass-difference measurement, but is pulled up somewhat by the less well-determined but considerably higher direct-mass measurement. It is possible, in fact, that AUBERT 08BN is seeing a different  $\Sigma_c$ .

$\Sigma_c(2800)^{++}$  MASS

VALUE (MeV)	DOCUMENT ID
<b>2801<sup>+4</sup><sub>-6</sub></b> OUR FIT	

$\Sigma_c(2800)^+$  MASS

VALUE (MeV)	DOCUMENT ID
<b>2792<sup>+14</sup><sub>-5</sub></b> OUR FIT	

$\Sigma_c(2800)^0$  MASS

VALUE (MeV)	DOCUMENT ID	TECN	COMMENT
<b>2806<sup>+5</sup><sub>-7</sub></b> OUR FIT			Error includes scale factor of 1.3.
<b>2846 ± 8 ± 10</b>	AUBERT	08BN BABR	$B^- \rightarrow \bar{p} \Lambda_c^+ \pi^-$

$\Sigma_c(2800)$  MASS DIFFERENCES

$m_{\Sigma_c(2800)^{++}} - m_{\Lambda_c^+}$

VALUE (MeV)	EVTS	DOCUMENT ID	TECN	COMMENT
<b>514<sup>+4</sup><sub>-6</sub></b> OUR FIT				
<b>514.5<sup>+3.4</sup><sub>-3.1</sub> + 2.8<sub>-4.9</sub></b>	2810 <sup>+1090</sup> <sub>-775</sub>	MIZUK	05	BELL e <sup>+</sup> e <sup>-</sup> $\approx \Upsilon(4S)$

$m_{\Sigma_c(2800)^+} - m_{\Lambda_c^+}$

VALUE (MeV)	EVTS	DOCUMENT ID	TECN	COMMENT
<b>505<sup>+14</sup><sub>-5</sub></b> OUR FIT				
<b>505.4<sup>+5.8</sup><sub>-4.6</sub> + 12.4<sub>-2.0</sub></b>	1540 <sup>+1750</sup> <sub>-1050</sub>	MIZUK	05	BELL e <sup>+</sup> e <sup>-</sup> $\approx \Upsilon(4S)$

$m_{\Sigma_c(2800)^0} - m_{\Lambda_c^+}$

VALUE (MeV)	EVTS	DOCUMENT ID	TECN	COMMENT
<b>519<sup>+5</sup><sub>-7</sub></b> OUR FIT				Error includes scale factor of 1.3.
<b>515.4<sup>+3.2</sup><sub>-3.1</sub> + 2.1<sub>-6.0</sub></b>	2240 <sup>+1300</sup> <sub>-740</sub>	MIZUK	05	BELL e <sup>+</sup> e <sup>-</sup> $\approx \Upsilon(4S)$

$\Sigma_c(2800)$  WIDTHS

$\Sigma_c(2800)^{++}$  WIDTH

VALUE (MeV)	EVTS	DOCUMENT ID	TECN	COMMENT
<b>75<sup>+18</sup><sub>-13</sub> + 12<sub>-11</sub></b>	2810 <sup>+1090</sup> <sub>-775</sub>	MIZUK	05	BELL e <sup>+</sup> e <sup>-</sup> $\approx \Upsilon(4S)$

$\Sigma_c(2800)^+$  WIDTH

VALUE (MeV)	EVTS	DOCUMENT ID	TECN	COMMENT
<b>62<sup>+37</sup><sub>-23</sub> + 52<sub>-38</sub></b>	1540 <sup>+1750</sup> <sub>-1050</sub>	MIZUK	05	BELL e <sup>+</sup> e <sup>-</sup> $\approx \Upsilon(4S)$

$\Sigma_c(2800)^0$  WIDTH

VALUE (MeV)	EVTS	DOCUMENT ID	TECN	COMMENT
<b>72<sup>+22</sup><sub>-15</sub></b> OUR AVERAGE				
86 <sup>+33</sup> <sub>-22</sub> ± 12		AUBERT	08BN BABR	$B^- \rightarrow \bar{p} \Lambda_c^+ \pi^-$
61 <sup>+18</sup> <sub>-13</sub> + 22 <sub>-13</sub>	2240 <sup>+1300</sup> <sub>-740</sub>	MIZUK	05	BELL e <sup>+</sup> e <sup>-</sup> $\approx \Upsilon(4S)$

$\Sigma_c(2800)$  DECAY MODES

Mode	Fraction ( $\Gamma_i/\Gamma$ )
$\Gamma_1 \Lambda_c^+ \pi$	seen

$\Sigma_c(2800)$  REFERENCES

AUBERT	08BN	PR D78 112003	B. Aubert <i>et al.</i>	(BABAR Collab.)
MIZUK	05	PRL 94 122002	R. Mizuk <i>et al.</i>	(BELLE Collab.)

**$\Xi_c^+$**   $I(J^P) = \frac{1}{2}(\frac{1}{2}^+)$  Status: \*\*\*  
 Neither of  $J$  or  $P$  has actually been measured. Nor have any absolute branching fractions been measured.

$\Xi_c^+$  MASS

The fit uses the  $\Xi_c^+$  and  $\Xi_c^0$  mass and mass-difference measurements.

VALUE (MeV)	EVTS	DOCUMENT ID	TECN	COMMENT
<b>2467.94<sup>+0.17</sup><sub>-0.20</sub></b> OUR FIT				
<b>2467.95 ± 0.19</b> OUR AVERAGE				
2467.97 ± 0.14 ± 0.17	3.8k	<sup>1</sup> AAIJ	14Z	LHCB $p\bar{p}$ at 7, 8 TeV
2468.00 ± 0.18 ± 0.51	5.1k	AALTONEN	14B	CDF $p\bar{p}$ at 1.96 TeV
2468.1 ± 0.4 <sup>+0.2</sup> <sub>-1.4</sub>	4.9k	<sup>2</sup> LESIAK	05	BELL e <sup>+</sup> e <sup>-</sup> , $\Upsilon(4S)$
2465.8 ± 1.9 ± 2.5	90	FRABETTI	98	E687 $\gamma$ Be, $\bar{E}_\gamma = 220$ GeV
2467.0 ± 1.6 ± 2.0	147	EDWARDS	96	CLE2 e <sup>+</sup> e <sup>-</sup> $\approx \Upsilon(4S)$
2465.1 ± 3.6 ± 1.9	30	ALBRECHT	90F	ARG e <sup>+</sup> e <sup>-</sup> at $\Upsilon(4S)$
2467 ± 3 ± 4	23	ALAM	89	CLEO e <sup>+</sup> e <sup>-</sup> 10.6 GeV
2466.5 ± 2.7 ± 1.2	5	BARLAG	89c	ACCM $\pi^-$ Cu 230 GeV
••• We do not use the following data for averages, fits, limits, etc. •••				
2464.4 ± 2.0 ± 1.4	30	FRABETTI	93B	E687 See FRABETTI 98
2459 ± 5 ± 30	56	<sup>3</sup> COTEUS	87	SPEC $nA \approx 600$ GeV
2460 ± 25	82	BIAGI	83	SPEC $\Sigma^-$ Be 135 GeV

<sup>1</sup> AAIJ 14Z systematic error includes in quadrature the 0.14 MeV uncertainty from the  $m(\Lambda_c^+)$  mass value.  
<sup>2</sup> The systematic error was (wrongly) given the other way round in LESIAK 05; see the erratum.  
<sup>3</sup> Although COTEUS 87 claims to agree well with BIAGI 83 on the mass and width, there appears to be a discrepancy between the two experiments. BIAGI 83 sees a single peak (stated significance about 6 standard deviations) in the  $\Lambda K^- \pi^+ \pi^+$  mass spectrum. COTEUS 87 sees two peaks in the same spectrum, one at the  $\Xi_c^+$  mass, the other 75 MeV lower. The latter is attributed to  $\Xi_c^+ \rightarrow \Sigma^0 K^- \pi^+ \pi^+ \rightarrow (\Lambda \gamma) K^- \pi^+ \pi^+$ , with the  $\gamma$  unseen. The combined significance of the double peak is stated to be 5.5



# Baryon Particle Listings



standard deviations. But the absence of any trace of a lower peak in BIAGI 83 seems to us to throw into question the interpretation of the lower peak of COTEUS 87.

## $\Xi_c^+$ MEAN LIFE

VALUE ( $10^{-15}$ s)	EVTS	DOCUMENT ID	TECN	COMMENT
<b>456 ± 5 OUR AVERAGE</b>				
457 ± 5 ± 3	56k	1 AAIJ	19AG LHCB	$\Xi_c^+ \rightarrow pK^- \pi^+$
503 ± 47 ± 18	250	MAHMOOD	02 CLE2	$e^+ e^- \approx \Upsilon(4S)$
439 ± 22 ± 9	532	LINK	01D FOCS	$\gamma$ nucleus, $\bar{E}_\gamma \approx 180$ GeV
340 <sup>+</sup> <sub>-50</sub> ± 70 ± 20	56	FRABETTI	98 E687	$\gamma$ Be, $\bar{E}_\gamma = 220$ GeV
400 <sup>+</sup> <sub>-120</sub> ± 180 ± 100	102	COTEUS	87 SPEC	$nA \approx 600$ GeV
480 <sup>+</sup> <sub>-150</sub> ± 210 ± 200	53	BIAGI	85c SPEC	$\Sigma^-$ Be 135 GeV
• • • We do not use the following data for averages, fits, limits, etc. • • •				
410 <sup>+</sup> <sub>-80</sub> ± 110 ± 20	30	FRABETTI	93B E687	See FRABETTI 98
200 <sup>+</sup> <sub>-110</sub> ± 60	6	BARLAG	89c ACCM	$\pi^- (K^-)$ Cu 230 GeV

<sup>1</sup> AAIJ 19AG reports  $[\Xi_c^+ \text{ MEAN LIFE}] / [D^\pm \text{ MEAN LIFE}] = 0.4392 \pm 0.0034 \pm 0.0028$  which we multiply by our best value  $D^\pm \text{ MEAN LIFE} = (1.040 \pm 0.007) \times 10^{-12}$  s. Our first error is their experiment's error and our second error is the systematic error from using our best value.

## $\Xi_c^+$ DECAY MODES

Branching fractions marked with a footnote, e.g. [a], have been corrected for decay modes not observed in the experiments. For example, the sub-mode fraction  $\Xi_c^+ \rightarrow \Sigma^+ \bar{K}^*(892)^0$  seen in  $\Xi_c^+ \rightarrow \Sigma^+ K^- \pi^+$  has been multiplied up to include  $\bar{K}^*(892)^0 \rightarrow \bar{K}^0 \pi^0$  decays.

Mode	Fraction ( $\Gamma_i/\Gamma$ )	Confidence level
------	--------------------------------	------------------

**No absolute branching fractions have been measured. The following are branching ratios relative to  $\Xi_c^+ \rightarrow \Sigma^- 2\pi^+$ .**

### Cabibbo-favored ( $S = -2$ ) decays — relative to $\Xi_c^+ \rightarrow \Sigma^- 2\pi^+$

$\Gamma_1$	$p2K_S^0$	0.087 ± 0.021	
$\Gamma_2$	$\Lambda \bar{K}^0 \pi^+$	—	
$\Gamma_3$	$\Sigma(1385)^+ \bar{K}^0$	[a] 1.0 ± 0.5	
$\Gamma_4$	$\Lambda K^- 2\pi^+$	0.323 ± 0.033	
$\Gamma_5$	$\Lambda \bar{K}^*(892)^0 \pi^+$	[a] < 0.16	90%
$\Gamma_6$	$\Sigma(1385)^+ K^- \pi^+$	[a] < 0.23	90%
$\Gamma_7$	$\Sigma^+ K^- \pi^+$	0.94 ± 0.10	
$\Gamma_8$	$\Sigma^+ \bar{K}^*(892)^0$	[a] 0.81 ± 0.15	
$\Gamma_9$	$\Sigma^0 K^- 2\pi^+$	0.27 ± 0.12	
$\Gamma_{10}$	$\Xi^0 \pi^+$	0.55 ± 0.16	
$\Gamma_{11}$	$\Xi^- 2\pi^+$	<b>DEFINED AS 1</b>	
$\Gamma_{12}$	$\Xi(1530)^0 \pi^+$	[a] < 0.10	90%
$\Gamma_{13}$	$\Xi(1620)^0 \pi^+$	seen	
$\Gamma_{14}$	$\Xi(1690)^0 \pi^+$	seen	
$\Gamma_{15}$	$\Xi^0 \pi^+ \pi^0$	2.3 ± 0.7	
$\Gamma_{16}$	$\Xi^0 \pi^+ 2\pi^+$	1.7 ± 0.5	
$\Gamma_{17}$	$\Xi^0 e^+ \nu_e$	2.3 <sup>+</sup> <sub>-0.8</sub>	
$\Gamma_{18}$	$\Omega^- K^+ \pi^+$	0.07 ± 0.04	

### Cabibbo-suppressed decays — relative to $\Xi_c^+ \rightarrow \Sigma^- 2\pi^+$

$\Gamma_{19}$	$pK^- \pi^+$	0.0045 ± 0.0022	
$\Gamma_{20}$	$p\bar{K}^*(892)^0$	[a] 0.0024 ± 0.0013	
$\Gamma_{21}$	$\Sigma^+ \pi^+ \pi^-$	0.48 ± 0.20	
$\Gamma_{22}$	$\Sigma^- 2\pi^+$	0.18 ± 0.09	
$\Gamma_{23}$	$\Sigma^+ K^+ K^-$	0.15 ± 0.06	
$\Gamma_{24}$	$\Sigma^+ \phi$	[a] < 0.11	90%
$\Gamma_{25}$	$\Xi(1690)^0 K^+, \Xi^0 \rightarrow \Sigma^+ K^-$	< 0.05	90%
$\Gamma_{26}$	$p\phi(1020)$	(9 ± 4) × 10 <sup>-5</sup>	

[a] This branching fraction includes all the decay modes of the final-state resonance.

## $\Xi_c^+$ BRANCHING RATIOS

### Cabibbo-favored ( $S = -2$ ) decays

$\Gamma(p2K_S^0)/\Gamma(\Xi^- 2\pi^+)$		$\Gamma_1/\Gamma_{11}$		
VALUE	EVTS	DOCUMENT ID	TECN	COMMENT
<b>0.087 ± 0.016 ± 0.014</b>	168 ± 27	LESIAK	05 BELL	$e^+ e^-$ , $\Upsilon(4S)$

## $\Gamma(\Sigma(1385)^+ \bar{K}^0)/\Gamma(\Xi^- 2\pi^+)$

Unseen decay modes of the  $\Sigma(1385)^+$  are included.

VALUE	EVTS	DOCUMENT ID	TECN	COMMENT
<b>1.00 ± 0.49 ± 0.24</b>	20	LINK	03E FOCS	< 1.72, 90% CL

## $\Gamma(\Lambda K^- 2\pi^+)/\Gamma(\Xi^- 2\pi^+)$

VALUE	EVTS	DOCUMENT ID	TECN	COMMENT
<b>0.323 ± 0.033 OUR AVERAGE</b>				
0.32 ± 0.03 ± 0.02	1177 ± 55	LESIAK	05 BELL	$e^+ e^-$ , $\Upsilon(4S)$
0.28 ± 0.06 ± 0.06	58	LINK	03E FOCS	$\gamma$ nucleus, $\bar{E}_\gamma \approx 180$ GeV
0.58 ± 0.16 ± 0.07	61	BERGFELD	96 CLE2	$e^+ e^- \approx \Upsilon(4S)$

## $\Gamma(\Lambda \bar{K}^*(892)^0 \pi^+)/\Gamma(\Lambda K^- 2\pi^+)$

Unseen decay modes of the  $\bar{K}^*(892)^0$  are included.

VALUE	CL%	DOCUMENT ID	TECN	COMMENT
<b>&lt; 0.5</b>	90	BERGFELD	96 CLE2	$e^+ e^- \approx \Upsilon(4S)$

## $\Gamma(\Sigma(1385)^+ K^- \pi^+)/\Gamma(\Lambda K^- 2\pi^+)$

Unseen decay modes of the  $\Sigma(1385)^+$  are included.

VALUE	CL%	DOCUMENT ID	TECN	COMMENT
<b>&lt; 0.7</b>	90	BERGFELD	96 CLE2	$e^+ e^- \approx \Upsilon(4S)$

## $\Gamma(\Sigma^+ K^- \pi^+)/\Gamma(\Xi^- 2\pi^+)$

VALUE	EVTS	DOCUMENT ID	TECN	COMMENT
<b>0.94 ± 0.10 OUR AVERAGE</b>				
0.91 ± 0.11 ± 0.04	251	LINK	03E FOCS	$\gamma$ nucleus, $\bar{E}_\gamma \approx 180$ GeV
0.92 ± 0.20 ± 0.07		<sup>1</sup> JUN	00 SELX	$\Sigma^-$ nucleus, 600 GeV
1.18 ± 0.26 ± 0.17	119	BERGFELD	96 CLE2	$e^+ e^- \approx \Upsilon(4S)$

<sup>1</sup> This JUN 00 result is redundant with other results given below.

## $\Gamma(\Sigma^+ \bar{K}^*(892)^0 \pi^+)/\Gamma(\Xi^- 2\pi^+)$

Unseen decay modes of the  $\bar{K}^*(892)^0$  are included.

VALUE	EVTS	DOCUMENT ID	TECN	COMMENT
<b>0.81 ± 0.15 OUR AVERAGE</b>				
0.78 ± 0.16 ± 0.06	119	LINK	03E FOCS	$\gamma$ nucleus, $\bar{E}_\gamma \approx 180$ GeV
0.92 ± 0.27 ± 0.14	61	BERGFELD	96 CLE2	$e^+ e^- \approx \Upsilon(4S)$

## $\Gamma(\Sigma^0 K^- 2\pi^+)/\Gamma(\Lambda K^- 2\pi^+)$

VALUE	EVTS	DOCUMENT ID	TECN	COMMENT
<b>0.84 ± 0.36</b>	47	<sup>1</sup> COTEUS	87 SPEC	$nA \approx 600$ GeV

<sup>1</sup> See, however, the note on the COTEUS 87  $\Xi_c^+$  mass measurement.

## $\Gamma(\Xi^0 \pi^+)/\Gamma(\Xi^- 2\pi^+)$

VALUE	EVTS	DOCUMENT ID	TECN	COMMENT
<b>0.55 ± 0.13 ± 0.09</b>	39	EDWARDS	96 CLE2	$e^+ e^- \approx \Upsilon(4S)$

## $\Gamma(\Xi^- 2\pi^+)/\Gamma_{\text{total}}$

VALUE (units $10^{-2}$ )	EVTS	DOCUMENT ID	TECN	COMMENT
<b>2.86 ± 1.21 ± 0.38</b>	24	<sup>1</sup> LI	19c BELL	$e^+ e^- \approx \Upsilon(4S)$
• • • We do not use the following data for averages, fits, limits, etc. • • •				
seen	131	BERGFELD	96 CLE2	$e^+ e^- \approx \Upsilon(4S)$
seen	160	AVERY	95 CLE2	$e^+ e^- \approx \Upsilon(4S)$
seen	30	FRABETTI	93B E687	$\gamma$ Be, $\bar{E}_\gamma = 220$ GeV
seen	30	ALBRECHT	90F ARG	$e^+ e^-$ at $\Upsilon(4S)$
seen	23	ALAM	89 CLEO	$e^+ e^-$ 10.6 GeV

<sup>1</sup> LI 19c report a significance of 6.8  $\sigma$  for the observation of this decay mode, observed in  $\Xi_c^+$  from  $\bar{B}^0 \rightarrow \bar{\Lambda}_c^- \Xi_c^+$ .

## $\Gamma(\Xi(1530)^0 \pi^+)/\Gamma(\Xi^- 2\pi^+)$

Unseen decay modes of the  $\Xi(1530)^0$  are included.

VALUE	CL%	DOCUMENT ID	TECN	COMMENT
<b>&lt; 0.1</b>	90	LINK	03E FOCS	$\gamma$ nucleus, $\bar{E}_\gamma \approx 180$ GeV

• • • We do not use the following data for averages, fits, limits, etc. • • •

< 0.2	90	BERGFELD	96 CLE2	$e^+ e^- \approx \Upsilon(4S)$
-------	----	----------	---------	--------------------------------

## $\Gamma(\Xi(1620)^0 \pi^+)/\Gamma_{\text{total}}$

VALUE	DOCUMENT ID	TECN	COMMENT
seen	SUMIHAMA	19 BELL	$e^+ e^-$ mostly at $\Upsilon(4S)$

## $\Gamma(\Xi(1690)^0 \pi^+)/\Gamma_{\text{total}}$

VALUE	DOCUMENT ID	TECN	COMMENT
seen	SUMIHAMA	19 BELL	$e^+ e^-$ mostly at $\Upsilon(4S)$

## $\Gamma(\Xi^0 \pi^+ \pi^0)/\Gamma(\Xi^- 2\pi^+)$

VALUE	EVTS	DOCUMENT ID	TECN	COMMENT
<b>2.34 ± 0.57 ± 0.37</b>	81	EDWARDS	96 CLE2	$e^+ e^- \approx \Upsilon(4S)$

## $\Gamma(\Xi(1530)^0 \pi^+)/\Gamma(\Xi^0 \pi^+ \pi^0)$

VALUE	CL%	DOCUMENT ID	TECN	COMMENT
< 0.3	90	EDWARDS	96 CLE2	$e^+ e^- \approx \Upsilon(4S)$

• • • We do not use the following data for averages, fits, limits, etc. • • •



# Baryon Particle Listings

$$\Xi_c^0, \Xi_c^{\prime 0}, \Xi_c^{\prime +}$$

## CONSTRAINED FIT INFORMATION

An overall fit to 5 branching ratios uses 6 measurements and one constraint to determine 4 parameters. The overall fit has a  $\chi^2 = 1.4$  for 3 degrees of freedom.

The following *off-diagonal* array elements are the correlation coefficients  $\langle \delta x_i \delta x_j \rangle / (\delta x_i \delta x_j)$ , in percent, from the fit to the branching fractions,  $x_i \equiv \Gamma_i / \Gamma_{\text{total}}$ . The fit constrains the  $x_i$  whose labels appear in this array to sum to one.

$x_5$	68	
$x_8$	89	76
	$x_1$	$x_5$

## $\Xi_c^0$ BRANCHING RATIOS

### Cabibbo-favored (S = -2) decays

$\Gamma(pK^-K^-\pi^+) / \Gamma_{\text{total}}$	$\Gamma_1 / \Gamma$
VALUE (%)	EVTS
<b>0.48 ± 0.12 OUR FIT</b>	Error includes scale factor of 1.1.
<b>0.58 ± 0.23 ± 0.05</b>	17 ± 5 LI 19A BELL $e^+e^- \approx \mathcal{T}(4S)$

$\Gamma(pK^-K^-\pi^+) / \Gamma(\Xi^- \pi^+)$	$\Gamma_1 / \Gamma_8$
VALUE	EVTS
<b>0.339 ± 0.035 OUR FIT</b>	
<b>0.34 ± 0.04 OUR AVERAGE</b>	
0.33 ± 0.03 ± 0.03	1908 ± 62 LESIAK 05 BELL $e^+e^- \approx \mathcal{T}(4S)$
0.35 ± 0.06 ± 0.03	148 ± 18 DANKO 04 CLEO $e^+e^-$

$\Gamma(pK^-K^0(892)^0, K^{*0} \rightarrow K^-\pi^+) / \Gamma(\Xi^- \pi^+)$	$\Gamma_2 / \Gamma_8$
VALUE	EVTS
<b>0.14 ± 0.03 ± 0.01</b>	DANKO 04 CLEO $e^+e^-$

$\Gamma(pK^-K^-\pi^+(no K^{*0})) / \Gamma(\Xi^- \pi^+)$	$\Gamma_3 / \Gamma_8$
VALUE	EVTS
<b>0.21 ± 0.04 ± 0.02</b>	DANKO 04 CLEO $e^+e^-$

$\Gamma(\Lambda K^0) / \Gamma(\Xi^- \pi^+)$	$\Gamma_4 / \Gamma_8$
VALUE	EVTS
<b>0.21 ± 0.02 ± 0.02</b>	465 ± 37 LESIAK 05 BELL $e^+e^- \approx \mathcal{T}(4S)$

$\Gamma(\Lambda K^-\pi^+) / \Gamma_{\text{total}}$	$\Gamma_5 / \Gamma$
VALUE (%)	EVTS
<b>1.45 ± 0.33 OUR FIT</b>	Error includes scale factor of 1.1.
<b>1.17 ± 0.37 ± 0.09</b>	24 ± 6 LI 19A BELL $e^+e^- \approx \mathcal{T}(4S)$

$\Gamma(\Lambda K^-\pi^+) / \Gamma(\Xi^- \pi^+)$	$\Gamma_5 / \Gamma_8$
VALUE	EVTS
<b>1.02 ± 0.15 OUR FIT</b>	Error includes scale factor of 1.2.
<b>1.07 ± 0.12 ± 0.07</b>	2979 ± 211 LESIAK 05 BELL $e^+e^- \approx \mathcal{T}(4S)$

$\Gamma(\Lambda K^0 \pi^+ \pi^-) / \Gamma_{\text{total}}$	$\Gamma_6 / \Gamma$
VALUE	EVTS
seen	FRABETTI 98B E687 $\gamma$ Be, $\bar{E}_\gamma = 220$ GeV

$\Gamma(\Lambda K^-\pi^+ \pi^+ \pi^-) / \Gamma_{\text{total}}$	$\Gamma_7 / \Gamma$
VALUE	EVTS
seen	FRABETTI 98B E687 $\gamma$ Be, $\bar{E}_\gamma = 220$ GeV

$\Gamma(\Xi^- \pi^+) / \Gamma_{\text{total}}$	$\Gamma_8 / \Gamma$
VALUE (%)	EVTS
<b>1.43 ± 0.32 OUR FIT</b>	Error includes scale factor of 1.1.
<b>1.80 ± 0.50 ± 0.14</b>	45 ± 7 LI 19A BELL $e^+e^- \approx \mathcal{T}(4S)$

$\Gamma(\Xi^- \pi^+) / \Gamma(\Xi^- \pi^+ \pi^+ \pi^-)$	$\Gamma_8 / \Gamma_9$
VALUE	EVTS
<b>0.30 ± 0.12 ± 0.05</b>	ALBRECHT 90F ARG $e^+e^- \approx \mathcal{T}(4S)$

$\Gamma(\Omega^- K^+) / \Gamma(\Xi^- \pi^+)$	$\Gamma_{10} / \Gamma_8$
VALUE	EVTS
<b>0.294 ± 0.018 ± 0.016</b>	65.0 AUBERT,B 05M BABR $e^+e^- \approx \mathcal{T}(4S)$

$\Gamma(\Xi^- e^+ \nu_e) / \Gamma(\Xi^- \pi^+)$	$\Gamma_{11} / \Gamma_8$
VALUE	EVTS
<b>1.3 ± 0.8 OUR AVERAGE</b>	Error includes scale factor of 1.8.
3.1 ± 1.0 $\pm_{0.5}^{0.3}$	54 ALEXANDER 95B CLE2 $e^+e^- \approx \mathcal{T}(4S)$
0.96 ± 0.43 ± 0.18	<sup>1</sup> ALBRECHT 93B ARG $e^+e^- \approx 10.4$ GeV

<sup>1</sup>This ALBRECHT 93B value is the average of the  $(\Xi^- e^+ \text{ anything}) / \Xi^- \pi^+$  and  $(\Xi^- \mu^+ \text{ anything}) / \Xi^- \pi^+$  ratios. Here we average it with the  $\Xi^- e^+ \nu_e / \Xi^- \pi^+$  ratio.

## Cabibbo-suppressed decays

$\Gamma(\Xi^- K^+) / \Gamma(\Xi^- \pi^+)$	$\Gamma_{12} / \Gamma_8$
VALUE (units $10^{-2}$ )	EVTS
<b>2.75 ± 0.51 ± 0.25</b>	314 ± 58 CHISTOV 13 BELL $e^+e^- \approx \mathcal{T}(4S)$

$\Gamma(\Lambda K^+ K^- (no \phi)) / \Gamma(\Xi^- \pi^+)$	$\Gamma_{13} / \Gamma_8$
VALUE (units $10^{-2}$ )	EVTS
<b>2.86 ± 0.61 ± 0.37</b>	510 ± 110 CHISTOV 13 BELL $e^+e^- \approx \mathcal{T}(4S)$

$\Gamma(\Lambda \phi) / \Gamma(\Xi^- \pi^+)$	$\Gamma_{14} / \Gamma_8$
VALUE (units $10^{-2}$ )	EVTS
<b>3.43 ± 0.58 ± 0.32</b>	316 ± 54 CHISTOV 13 BELL $e^+e^- \approx \mathcal{T}(4S)$

## $\Xi_c^0$ DECAY PARAMETERS

See the note on "Baryon Decay Parameters" in the neutron Listings.

$\alpha$ FOR $\Xi_c^0 \rightarrow \Xi^- \pi^+$	VALUE	EVTS	DOCUMENT ID	TECN	COMMENT
	<b>-0.56 ± 0.39 <math>\pm_{0.09}^{0.10}</math></b>	138	CHAN	01	CLE2 $e^+e^- \approx \mathcal{T}(4S)$

## $\Xi_c^0$ REFERENCES

AALJ	19A	PR D100 032001	R. Aaij et al.	(LHCb Collab.)
LI	19A	PRL 122 082001	Y.B. Li et al.	(BELLE Collab.)
AALTONEN	14B	PR D89 072014	T. Aaltonen et al.	(CDF Collab.)
CHISTOV	13	PR D88 071103	R. Chistov et al.	(BELLE Collab.)
AUBERT,B	05M	PRL 95 142003	B. Aubert et al.	(BABAR Collab.)
LESLIAK	05	PL B605 237	T. Lesiak et al.	(BELLE Collab.)
		PL B617 198 (errata.)	T. Lesiak et al.	(BELLE Collab.)
DANKO	04	PR D69 052004	I. Danko et al.	(CLEO Collab.)
LINK	02H	PL B541 211	J.M. Link et al.	(FNAL FOCUS Collab.)
CHAN	01	PR D63 111102	S. Chan et al.	(CLEO Collab.)
FRABETTI	98B	PL B426 403	P.L. Frabetti et al.	(FNAL E687 Collab.)
ALEXANDER	95B	PRL 74 3113	J. Alexander et al.	(CLEO Collab.)
		PRL 75 4155 (erratum)	J. Alexander et al.	(CLEO Collab.)
ALBRECHT	93B	PL B303 368	H. Albrecht et al.	(ARGUS Collab.)
FRABETTI	93C	PRL 70 2058	P.L. Frabetti et al.	(FNAL E687 Collab.)
HENDERSON	92B	PL B283 161	S. Henderson et al.	(CLEO Collab.)
ALBRECHT	90F	PL B247 121	H. Albrecht et al.	(ARGUS Collab.)
BARLAG	90	PL B236 495	S. Barlag et al.	(ACCMOR Collab.)
ALAM	89	PL B226 401	M.S. Alam et al.	(CLEO Collab.)
AVERY	89	PRL 62 863	P. Avery et al.	(CLEO Collab.)

$$\Xi_c^{\prime 0}$$

$$I(J^P) = \frac{1}{2}(\frac{1}{2}^+)$$
 Status: \*\*\*

The  $\Xi_c^{\prime 0}$  and  $\Xi_c^0$  presumably complete the SU(3) sextet whose other members are the  $\Sigma_c^{\prime +}$ ,  $\Sigma_c^+$ ,  $\Sigma_c^0$ , and  $\Omega_c^0$ ; see Fig. 3 in the note on Charmed Baryons. The quantum numbers given above come from this presumption but have not been measured.

## $\Xi_c^{\prime +}$ MASS

The mass is obtained from the mass-difference measurement that follows.

VALUE (MeV)	DOCUMENT ID
<b>2578.4 ± 0.5 OUR FIT</b>	

## $\Xi_c^{\prime +} - \Xi_c^+$ MASS DIFFERENCE

VALUE (MeV)	EVTS	DOCUMENT ID	TECN	COMMENT
<b>110.5 ± 0.4 OUR FIT</b>				
<b>110.5 ± 0.1 ± 0.4</b>	7k	YELTON 16 BELL		$e^+e^-$ , $\mathcal{T}$ regions
••• We do not use the following data for averages, fits, limits, etc. •••				
107.8 ± 1.7 ± 2.5	25	JESSOP 99 CLE2		$e^+e^- \approx \mathcal{T}(4S)$

## $\Xi_c^{\prime +} - \Xi_c^{\prime 0}$ MASS DIFFERENCE

VALUE (MeV)	DOCUMENT ID	TECN	COMMENT
<b>-0.8 ± 0.6 OUR FIT</b>			
••• We do not use the following data for averages, fits, limits, etc. •••			
-0.8 ± 0.1 ± 0.5	YELTON 16 BELL		7055 and 11,560 evts

## $\Xi_c^{\prime +}$ DECAY MODES

The  $\Xi_c^{\prime +} - \Xi_c^+$  mass difference is too small for any strong decay to occur.

Mode	Fraction ( $\Gamma_i / \Gamma$ )
$\Gamma_1 \Xi_c^{\prime +} \gamma$	seen

## $\Xi_c^{\prime +}$ REFERENCES

YELTON	16	PR D94 052011	J. Yelton et al.	(BELLE Collab.)
JESSOP	99	PRL 82 492	C.P. Jessop et al.	(CLEO Collab.)

See key on page 999

Baryon Particle Listings

$\Xi_c^0, \Xi_c(2645), \Xi_c(2790)$

$\Xi_c^0$

$I(J^P) = \frac{1}{2}(\frac{1}{2}^+)$  Status: \*\*\*

The  $\Xi_c^0$  and  $\Xi_c^+$  presumably complete the SU(3) sextet whose other members are the  $\Sigma_c^{++}, \Sigma_c^+, \Sigma_c^0$ , and  $\Omega_c^0$ : see Fig. 3 in the note on Charmed Baryons. The quantum numbers given above come from this presumption but have not been measured.

$\Xi_c^0$  MASS

The mass is obtained from the mass-difference measurement that follows.

VALUE (MeV)	DOCUMENT ID
<b>2579.2 ± 0.5 OUR FIT</b>	

$\Xi_c^0 - \Xi_c^0$  MASS DIFFERENCE

VALUE (MeV)	EVTs	DOCUMENT ID	TECN	COMMENT
<b>108.3 ± 0.4 OUR FIT</b>				
<b>108.3 ± 0.1 ± 0.4</b>	11.5k	YELTON	16	BELL $e^+e^-$ , $\Upsilon$ regions
• • • We do not use the following data for averages, fits, limits, etc. • • •				
107.0 ± 1.4 ± 2.5	28	JESSOP	99	CLE2 $e^+e^- \approx \Upsilon(4S)$

$\Xi_c^0$  DECAY MODES

The  $\Xi_c^0 - \Xi_c^0$  mass difference is too small for any strong decay to occur.

Mode	Fraction ( $\Gamma_i/\Gamma$ )
$\Xi_c^0 \gamma$	seen

$\Xi_c^0$  REFERENCES

YELTON	16	PR D94 052011	J. Yelton <i>et al.</i>	(BELLE Collab.)
JESSOP	99	PRL 82 492	C.P. Jessop <i>et al.</i>	(CLEO Collab.)

$\Xi_c(2645)$

$I(J^P) = \frac{1}{2}(\frac{3}{2}^+)$  Status: \*\*\*

The natural assignment is that this is the  $J^P = 3/2^+$  excitation of the  $\Xi_c$  in the same SU(4) multiplet as the  $\Delta(1232)$ , but the quantum numbers have not been measured.

$\Xi_c(2645)$  MASSES

$\Xi_c(2645)^+$  MASS

VALUE (MeV)	EVTs	DOCUMENT ID	TECN	COMMENT
<b>2645.56 ± 0.24 ± 0.30 OUR FIT</b>				
<b>2645.6 ± 0.2 ± 0.6</b>	578 ± 32	LESIAK	08	BELL $e^+e^- \approx \Upsilon(4S)$

$\Xi_c(2645)^0$  MASS

VALUE (MeV)	EVTs	DOCUMENT ID	TECN	COMMENT
<b>2646.38 ± 0.20 ± 0.23 OUR FIT</b>				Error includes scale factor of 1.1.
<b>2645.7 ± 0.2 ± 0.6</b>	611 ± 32	LESIAK	08	BELL $e^+e^- \approx \Upsilon(4S)$

$\Xi_c(2645) - \Xi_c$  MASS DIFFERENCES

$m_{\Xi_c(2645)^+} - m_{\Xi_c^0}$

VALUE (MeV)	EVTs	DOCUMENT ID	TECN	COMMENT
<b>174.66 ± 0.09 OUR FIT</b>				
<b>174.66 ± 0.06 ± 0.07</b>	1260	YELTON	16	BELL $e^+e^-$ in $\Upsilon$ regions
• • • We do not use the following data for averages, fits, limits, etc. • • •				
177.1 ± 0.5 ± 1.1	47	FRABETTI	98b	E687 $\gamma$ Be, $\bar{E}_\gamma = 220$ GeV
174.3 ± 0.5 ± 1.0	34	GIBBONS	96	CLE2 $e^+e^- \approx \Upsilon(4S)$

$m_{\Xi_c(2645)^0} - m_{\Xi_c^+}$

VALUE (MeV)	EVTs	DOCUMENT ID	TECN	COMMENT
<b>178.44 ± 0.10 OUR FIT</b>				
<b>178.46 ± 0.07 ± 0.07</b>	975	YELTON	16	BELL $e^+e^-$ in $\Upsilon$ regions
• • • We do not use the following data for averages, fits, limits, etc. • • •				
178.2 ± 0.5 ± 1.0	55	AVERY	95	CLE2 $e^+e^- \approx \Upsilon(4S)$

$\Xi_c(2645)^+ - \Xi_c(2645)^0$  MASS DIFFERENCE

VALUE (MeV)	DOCUMENT ID	TECN	COMMENT
<b>-0.82 ± 0.26 OUR FIT</b>			
• • • We do not use the following data for averages, fits, limits, etc. • • •			
-0.85 ± 0.09 ± 0.49	YELTON	16	BELL 1260 and 975 evts
-0.1 ± 0.3 ± 0.6	LESIAK	08	BELL $\approx 600$ evts each

$\Xi_c(2645)$  WIDTHS

$\Xi_c(2645)^+$  WIDTH

VALUE (MeV)	CL%	EVTs	DOCUMENT ID	TECN	COMMENT
<b>2.14 ± 0.19 OUR AVERAGE</b>					Error includes scale factor of 1.1.
2.06 ± 0.13 ± 0.13		1260	YELTON	16	BELL $e^+e^-$ in $\Upsilon$ regions
2.6 ± 0.2 ± 0.4		3.7k	KATO	14	BELL $e^+e^- \Upsilon(1S)-\Upsilon(5S)$
• • • We do not use the following data for averages, fits, limits, etc. • • •					
<3.1		90	GIBBONS	96	CLE2 $e^+e^- \approx \Upsilon(4S)$

$\Xi_c(2645)^0$  WIDTH

VALUE (MeV)	CL%	EVTs	DOCUMENT ID	TECN	COMMENT	
<b>2.35 ± 0.18 ± 0.13</b>						
2.35 ± 0.18 ± 0.13		975	YELTON	16	BELL $e^+e^-$ in $\Upsilon$ regions	
• • • We do not use the following data for averages, fits, limits, etc. • • •						
<5.5		90	55	AVERY	95	CLE2 $e^+e^- \approx \Upsilon(4S)$

$\Xi_c(2645)$  DECAY MODES

$\Xi_c \pi$  is the only strong decay allowed to a  $\Xi_c$  resonance having this mass.

Mode	Fraction ( $\Gamma_i/\Gamma$ )
$\Xi_c^0 \pi^+$	seen
$\Xi_c^+ \pi^-$	seen

$\Xi_c(2645)$  REFERENCES

YELTON	16	PR D94 052011	J. Yelton <i>et al.</i>	(BELLE Collab.)
KATO	14	PR D89 052003	Y. Kato <i>et al.</i>	(BELLE Collab.)
LESIAK	08	PL B665 9	T. Lesiak <i>et al.</i>	(BELLE Collab.)
FRABETTI	98b	PL B426 403	P.L. Frabetti <i>et al.</i>	(FNAL E687 Collab.)
GIBBONS	96	PRL 77 810	L.K. Gibbons <i>et al.</i>	(CLEO Collab.)
AVERY	95	PRL 75 4364	P. Avery <i>et al.</i>	(CLEO Collab.)

$\Xi_c(2790)$

$I(J^P) = \frac{1}{2}(\frac{1}{2}^-)$  Status: \*\*\*

Seen in  $\Xi_c' \pi$  decays. The simplest assignment, based on the mass, width, and decay mode, is that this belongs in the same SU(4) multiplet as the  $\Lambda(1405)$  and the  $\Lambda_c(2595)^+$ , but the spin and parity have not been measured.

$\Xi_c(2790)$  MASSES

The masses are obtained from the mass-difference measurements that follow.

$\Xi_c(2790)^+$  MASS

VALUE (MeV)	DOCUMENT ID
<b>2792.4 ± 0.5 OUR FIT</b>	

$\Xi_c(2790)^0$  MASS

VALUE (MeV)	DOCUMENT ID
<b>2794.1 ± 0.5 OUR FIT</b>	

$\Xi_c(2790) - \Xi_c'$  MASS DIFFERENCES

$m_{\Xi_c(2790)^+} - m_{\Xi_c^0}$

VALUE (MeV)	EVTs	DOCUMENT ID	TECN	COMMENT
<b>213.20 ± 0.22 OUR FIT</b>				
<b>213.2 ± 0.2 ± 0.1</b>		YELTON	16	BELL 2231 and 11,560 evts
• • • We do not use the following data for averages, fits, limits, etc. • • •				
211.2 ± 1.3 ± 1.0	18	CSORNA	01	CLEO $e^+e^- \approx \Upsilon(4S)$

$m_{\Xi_c(2790)^0} - m_{\Xi_c^+}$

VALUE (MeV)	EVTs	DOCUMENT ID	TECN	COMMENT
<b>215.70 ± 0.22 OUR FIT</b>				
<b>215.7 ± 0.2 ± 0.1</b>		YELTON	16	BELL 1241 and 7055 evts
• • • We do not use the following data for averages, fits, limits, etc. • • •				
216.2 ± 1.3 ± 1.0	14	CSORNA	01	CLEO $e^+e^- \approx \Upsilon(4S)$

$\Xi_c(2790)^+ - \Xi_c(2790)^0$  MASS DIFFERENCE

VALUE (MeV)	DOCUMENT ID	TECN	COMMENT
<b>-1.7 ± 0.7 OUR FIT</b>			
• • • We do not use the following data for averages, fits, limits, etc. • • •			
-3.3 ± 0.4 ± 0.5	YELTON	16	BELL 2231 and 1241 evts

$\Xi_c(2790)$  WIDTHS

$\Xi_c(2790)^+$  WIDTH

VALUE (MeV)	CL%	EVTs	DOCUMENT ID	TECN	COMMENT
<b>8.9 ± 0.6 ± 0.8</b>					
8.9 ± 0.6 ± 0.8		2231	YELTON	16	BELL $e^+e^-$ , $\Upsilon$ regions

# Baryon Particle Listings

## $\Xi_c(2790), \Xi_c(2815), \Xi_c(2930)$

••• We do not use the following data for averages, fits, limits, etc. •••

<15 90 CSORNA 01 CLEO  $e^+e^- \approx \Upsilon(4S)$

### $\Xi_c(2790)^0$ WIDTH

VALUE (MeV)	CL%	EVTS	DOCUMENT ID	TECN	COMMENT
<b>10.0 ± 0.7 ± 0.8</b>		1241	YELTON	16	BELL $e^+e^-$ , $\Upsilon$ regions

••• We do not use the following data for averages, fits, limits, etc. •••

<12 90 CSORNA 01 CLEO  $e^+e^- \approx \Upsilon(4S)$

### $\Xi_c(2790)$ DECAY MODES

Mode	Fraction ( $\Gamma_i/\Gamma$ )
$\Gamma_1 \Xi_c' \pi$	seen

### $\Xi_c(2790)$ BRANCHING RATIOS

$\Gamma(\Xi_c' \pi)/\Gamma_{total}$	VALUE	DOCUMENT ID	TECN	COMMENT	$\Gamma_1/\Gamma$
seen		YELTON	16	BELL $e^+e^-$ , $\Upsilon$ regions	
seen		CSORNA	01	CLEO $e^+e^- \approx \Upsilon(4S)$	

### $\Xi_c(2790)$ REFERENCES

YELTON	16	PR D94 052011	J. Yelton et al.	(BELLE Collab.)
CSORNA	01	PRL 86 4243	S.E. Csorna et al.	(CLEO Collab.)

## $\Xi_c(2815)$

$$I(J^P) = \frac{1}{2}(\frac{3}{2}^-) \text{ Status: } ***$$

Seen in both  $\Xi_c' \pi$  and  $\Xi_c \pi \pi$  decays. The simplest assignment is that this belongs to the same SU(4) multiplet as the  $\Lambda(1520)$  and the  $\Lambda_c(2625)$ , but the spin and parity have not been measured.

### $\Xi_c(2815)$ MASSES

The masses are obtained from the mass-difference measurements that follow.

### $\Xi_c(2815)^+$ MASS

VALUE (MeV)	CL%	EVTS	DOCUMENT ID	TECN	COMMENT
<b>2816.74 ± 0.20 ± 0.23</b>					<b>OUR FIT</b>

••• We do not use the following data for averages, fits, limits, etc. •••

2817.0 ± 1.2 ± 0.7 ± 0.8 73 ± 10 LESIAK 08 BELL  $e^+e^- \approx \Upsilon(4S)$

### $\Xi_c(2815)^0$ MASS

VALUE (MeV)	CL%	EVTS	DOCUMENT ID	TECN	COMMENT
<b>2820.25 ± 0.25 ± 0.31</b>					<b>OUR FIT</b>

••• We do not use the following data for averages, fits, limits, etc. •••

2820.4 ± 1.4 ± 0.9 ± 1.0 48 ± 8 LESIAK 08 BELL  $e^+e^- \approx \Upsilon(4S)$

### $\Xi_c(2815) - \Xi_c$ MASS DIFFERENCES

#### $m_{\Xi_c(2815)^+} - m_{\Xi_c^+}$

VALUE (MeV)	CL%	EVTS	DOCUMENT ID	TECN	COMMENT
<b>348.80 ± 0.10</b>					<b>OUR FIT</b>
<b>348.80 ± 0.08 ± 0.06</b>		941	YELTON	16	BELL $e^+e^-$ , $\Upsilon$ regions
348.6 ± 0.6 ± 1.0		20	ALEXANDER	99b	CLE2 $e^+e^- \approx \Upsilon(4S)$

••• We do not use the following data for averages, fits, limits, etc. •••

#### $m_{\Xi_c(2815)^0} - m_{\Xi_c^0}$

VALUE (MeV)	CL%	EVTS	DOCUMENT ID	TECN	COMMENT
<b>349.35 ± 0.11</b>					<b>OUR FIT</b>
<b>349.35 ± 0.08 ± 0.07</b>		1258	YELTON	16	BELL $e^+e^-$ , $\Upsilon$ regions
347.2 ± 0.7 ± 2.0		9	ALEXANDER	99b	CLE2 $e^+e^- \approx \Upsilon(4S)$

••• We do not use the following data for averages, fits, limits, etc. •••

### $\Xi_c(2815)^+ - \Xi_c(2815)^0$ MASS DIFFERENCE

#### $m_{\Xi_c(2815)^+} - m_{\Xi_c(2815)^0}$

VALUE (MeV)	CL%	EVTS	DOCUMENT ID	TECN	COMMENT
<b>-3.51 ± 0.26</b>					<b>OUR FIT</b>
-3.47 ± 0.12 ± 0.48			YELTON	16	BELL 941 and 1258 evts
-3.4 ± 1.9 ± 0.9			LESIAK	08	BELL 73 & 48 events

••• We do not use the following data for averages, fits, limits, etc. •••

### $\Xi_c(2815)$ WIDTHS

#### $\Xi_c(2815)^+$ WIDTH

VALUE (MeV)	CL%	EVTS	DOCUMENT ID	TECN	COMMENT
<b>2.43 ± 0.20 ± 0.17</b>		941	YELTON	16	BELL $e^+e^-$ , $\Upsilon$ regions

••• We do not use the following data for averages, fits, limits, etc. •••

<3.5 90 ALEXANDER 99b CLE2  $e^+e^- \approx \Upsilon(4S)$

#### $\Xi_c(2815)^0$ WIDTH

VALUE (MeV)	CL%	EVTS	DOCUMENT ID	TECN	COMMENT
<b>2.54 ± 0.18 ± 0.17</b>		1258	YELTON	16	BELL $e^+e^-$ , $\Upsilon$ regions

••• We do not use the following data for averages, fits, limits, etc. •••

<6.5 90 ALEXANDER 99b CLE2  $e^+e^- \approx \Upsilon(4S)$

### $\Xi_c(2815)$ DECAY MODES

The  $\Xi_c \pi \pi$  modes are consistent with being entirely via  $\Xi_c(2645) \pi$ .

Mode	Fraction ( $\Gamma_i/\Gamma$ )
$\Gamma_1 \Xi_c' \pi$	seen
$\Gamma_2 \Xi_c(2645) \pi$	seen

### $\Gamma(\Xi_c' \pi)/\Gamma_{total}$

VALUE	DOCUMENT ID	TECN	COMMENT	$\Gamma_1/\Gamma$
seen	YELTON	16	BELL $e^+e^-$ , $\Upsilon$ regions	
seen	ALEXANDER	99b	CLE2 $e^+e^- \approx \Upsilon(4S)$	

### $\Gamma(\Xi_c(2645) \pi)/\Gamma_{total}$

VALUE	DOCUMENT ID	TECN	COMMENT	$\Gamma_2/\Gamma$
seen	YELTON	16	BELL $e^+e^-$ , $\Upsilon$ regions	
seen	LESIAK	08	BELL $e^+e^- \approx \Upsilon(4S)$	

### $\Xi_c(2815)$ REFERENCES

YELTON	16	PR D94 052011	J. Yelton et al.	(BELLE Collab.)
LESIAK	08	PL B665 9	T. Lesiak et al.	(BELLE Collab.)
ALEXANDER	99b	PRL 83 3390	J.P. Alexander et al.	(CLEO Collab.)

## $\Xi_c(2930)$

$$I(J^P) = ?(??) \text{ Status: } **$$

OMITTED FROM SUMMARY TABLE

### $\Xi_c(2930)$ MASSES

#### $\Xi_c(2930)^+$ MASS

VALUE (MeV)	CL%	EVTS	DOCUMENT ID	TECN	COMMENT
<b>2942.3 ± 4.4 ± 1.5</b>		21	LI	18D	BELL $e^+e^-$ at $\Upsilon(4S)$

#### $\Xi_c(2930)^0$ MASS

VALUE (MeV)	CL%	EVTS	DOCUMENT ID	TECN	COMMENT
<b>2929.7 ± 2.8 ± 5.0</b>					<b>OUR AVERAGE</b>

2928.9 ± 3.0 ± 0.9 ± 12.0 61 LI 18A BELL  $e^+e^-$  at  $\Upsilon(4S)$

2931 ± 3 ± 5 34 AUBERT 08H BABR  $\Upsilon(4S) \rightarrow B \bar{B}$

#### $\Xi_c(2930)^+ - \Xi_c(2930)^0$ MASS DIFFERENCE

VALUE (MeV)	CL%	EVTS	DOCUMENT ID	TECN	COMMENT
13.4 ± 5.3 ± 1.7 ± 12.1		21	<sup>1</sup> LI	18D	BELL $e^+e^-$ at $\Upsilon(4S)$

<sup>1</sup> This LI 18D value is not independent of the mass measurements.

### $\Xi_c(2930)$ WIDTHS

#### $\Xi_c(2930)^+$ WIDTH

VALUE (MeV)	CL%	EVTS	DOCUMENT ID	TECN	COMMENT
<b>14.8 ± 8.8 ± 2.5</b>		21	LI	18D	BELL $e^+e^-$ at $\Upsilon(4S)$

#### $\Xi_c(2930)^0$ WIDTH

VALUE (MeV)	CL%	EVTS	DOCUMENT ID	TECN	COMMENT
<b>26 ± 8</b>					<b>OUR AVERAGE</b>
19.5 ± 8.4 ± 5.9 ± 7.9		61	LI	18A	BELL $e^+e^-$ at $\Upsilon(4S)$
36 ± 7 ± 11		34	AUBERT	08H	BABR $\Upsilon(4S) \rightarrow B \bar{B}$

See key on page 999

Baryon Particle Listings

$\Xi_c(2930), \Xi_c(2970)$

$\Xi_c(2930)$  DECAY MODES

Mode	Fraction ( $\Gamma_i/\Gamma$ )
$\Gamma_1 \Lambda_c^+ K^-$	seen
$\Gamma_2 \Lambda_c^+ K_S^0$	seen

$\Xi_c(2930)$  BRANCHING RATIOS

$\Gamma(\Lambda_c^+ K^-)/\Gamma_{\text{total}}$					$\Gamma_1/\Gamma$
VALUE	EVTS	DOCUMENT ID	TECN	COMMENT	
seen	61	LI	18A	BELL	Significance 5.1 std
seen	34	AUBERT	08H	BABR	$e^+e^-$ at $\Upsilon(4S)$

$\Gamma(\Lambda_c^+ K_S^0)/\Gamma_{\text{total}}$					$\Gamma_2/\Gamma$
VALUE	EVTS	DOCUMENT ID	TECN	COMMENT	
seen	21	LI	18D	BELL	Significance 4.1 std

$\Xi_c(2930)$  REFERENCES

LI	18A	EPJ C78 252	Y.B. Li <i>et al.</i>	(BELLE Collab.)
LI	18D	EPJ C78 928	Y.B. Li <i>et al.</i>	(BELLE Collab.)
AUBERT	08H	PR D77 031101	B. Aubert <i>et al.</i>	(BABAR Collab.)

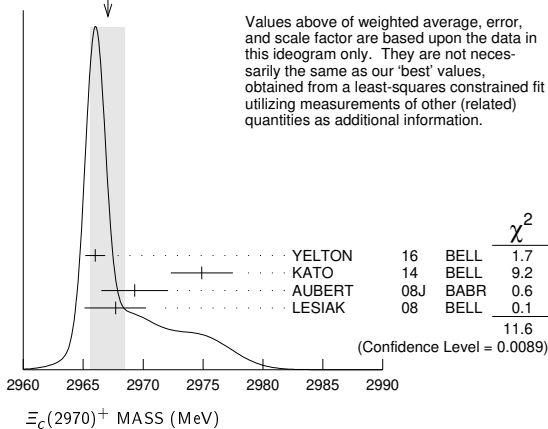
$\Xi_c(2970)$   $I(J^P) = \frac{1}{2}(?)^?$  Status: \*\*\*  
 was  $\Xi_c(2980)$

$\Xi_c(2970)$  MASSES

$\Xi_c(2970)^+$  MASS

VALUE (MeV)	EVTS	DOCUMENT ID	TECN	COMMENT
<b>2966.34 ± 0.17 OUR FIT</b>				
<b>2967.1 ± 1.4 OUR AVERAGE</b>				Error includes scale factor of 2.0. See the ideogram below.
2966.0 ± 0.8 ± 0.2	0.9k	YELTON	16	BELL $e^+e^- \rightarrow \Upsilon(4S), \Upsilon(5S)$ and continuum
2974.9 ± 1.5 ± 2.1	244 ± 39	KATO	14	BELL $e^+e^- \Upsilon(1S)$ to $\Upsilon(5S)$
2969.3 ± 2.2 ± 1.7	756 ± 206	AUBERT	08J	BABR $e^+e^- \approx 10.58$ GeV
2967.7 ± 2.3 ± 1.1 ± 1.2	78 ± 13	LESLIAK	08	BELL $e^+e^- \approx \Upsilon(4S)$
• • • We do not use the following data for averages, fits, limits, etc. • • •				
2978.5 ± 2.1 ± 2.0	405 ± 51	CHISTOV	06	BELL See KATO 14

WEIGHTED AVERAGE  
 2967.1 ± 1.4 (Error scaled by 2.0)



$\Xi_c(2970)^0$  MASS

The evidence is statistically weaker for this charge state.

VALUE (MeV)	EVTS	DOCUMENT ID	TECN	COMMENT
<b>2970.9 ± 0.4 OUR FIT</b>				
<b>2970.5 ± 1.3 OUR AVERAGE</b>				Error includes scale factor of 1.9.
2970.8 ± 0.7 ± 0.2	1.4k	YELTON	16	BELL $e^+e^- \rightarrow \Upsilon(4S), \Upsilon(5S)$ and continuum
2972.9 ± 4.4 ± 1.6	67 ± 44	AUBERT	08J	BABR $e^+e^- \approx 10.58$ GeV
2965.7 ± 2.4 ± 1.1 ± 1.2	57 ± 13	LESLIAK	08	BELL $e^+e^- \approx \Upsilon(4S)$
2977.1 ± 8.8 ± 3.5	42 ± 24	CHISTOV	06	BELL $e^+e^- \approx \Upsilon(4S)$

$\Xi_c(2970) - \Xi_c$  MASS DIFFERENCES

$m_{\Xi_c(2970)^+} - m_{\Xi_c^+}$		DOCUMENT ID	TECN	COMMENT
VALUE (MeV)	EVTS			
<b>498.40 ± 0.27 OUR FIT</b>				
498.1 ± 0.8 ± 0.2	916	YELTON	16	BELL $e^+e^-$ , $\Upsilon$ regions

$m_{\Xi_c(2970)^0} - m_{\Xi_c^0}$		DOCUMENT ID	TECN	COMMENT
VALUE (MeV)	EVTS			
<b>500.0 ± 0.4 OUR FIT</b>				
499.9 ± 0.7 ± 0.2	1.4k	YELTON	16	BELL $e^+e^-$ , $\Upsilon$ regions

$\Xi_c(2970)^+ - \Xi_c(2970)^0$  MASS DIFFERENCE

VALUE (MeV)	DOCUMENT ID	TECN	COMMENT
<b>-4.6 ± 0.4 OUR FIT</b>			
-4.8 ± 0.1 ± 0.5	YELTON	16	BELL 916 and 1443 evts

$\Xi_c(2970)$  WIDTHS

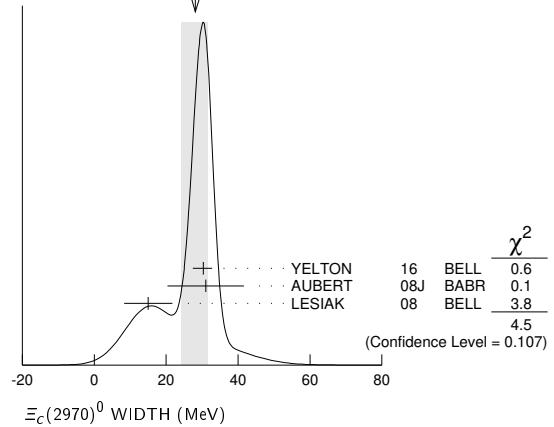
$\Xi_c(2970)^+$  WIDTH

VALUE (MeV)	EVTS	DOCUMENT ID	TECN	COMMENT
<b>20.9 ± 2.4 OUR AVERAGE</b>				Error includes scale factor of 1.2.
28.1 ± 2.4 ± 1.0 ± 5.0	916	YELTON	16	BELL $e^+e^-$ , $\Upsilon$ regions
14.8 ± 2.5 ± 4.1	244 ± 39	KATO	14	BELL $e^+e^- \Upsilon(1S)$ to $\Upsilon(5S)$
27 ± 8 ± 2	756 ± 206	AUBERT	08J	BABR $e^+e^- \approx 10.58$ GeV
18 ± 6 ± 3	78 ± 13	LESLIAK	08	BELL $e^+e^- \approx \Upsilon(4S)$
• • • We do not use the following data for averages, fits, limits, etc. • • •				
43.5 ± 7.5 ± 7.0	405 ± 51	CHISTOV	06	BELL See KATO 14

$\Xi_c(2970)^0$  WIDTH

VALUE (MeV)	EVTS	DOCUMENT ID	TECN	COMMENT
<b>28.1 ± 3.4 OUR AVERAGE</b>				Error includes scale factor of 1.5. See the ideogram below.
30.3 ± 2.3 ± 1.0 ± 1.8	1443	YELTON	16	BELL $e^+e^-$ , $\Upsilon$ regions
31 ± 7 ± 8	67 ± 44	AUBERT	08J	BABR $e^+e^- \approx 10.58$ GeV
15 ± 6 ± 3	57 ± 13	LESLIAK	08	BELL $e^+e^- \approx \Upsilon(4S)$

WEIGHTED AVERAGE  
 28.1 ± 3.4 ± 4.0 (Error scaled by 1.5)



$\Xi_c(2970)$  DECAY MODES

Mode	Fraction ( $\Gamma_i/\Gamma$ )
$\Gamma_1 \Lambda_c^+ \bar{K} \pi$	seen
$\Gamma_2 \Sigma_c(2455) \bar{K}$	seen
$\Gamma_3 \Lambda_c^+ \bar{K}$	not seen
$\Gamma_4 \Xi_c 2\pi$	seen
$\Gamma_5 \Xi_c \pi$	seen
$\Gamma_6 \Xi_c(2645) \pi$	seen

## Baryon Particle Listings

 $\Xi_c(2970)$ ,  $\Xi_c(3055)$ ,  $\Xi_c(3080)$ ,  $\Xi_c(3123)$  $\Xi_c(2970)$  BRANCHING RATIOS

$\Gamma(\Lambda_c^+ \bar{K} \pi) / \Gamma_{\text{total}}$				$\Gamma_1 / \Gamma$
VALUE	DOCUMENT ID	TECN	COMMENT	
seen	AUBERT 08J	BABR	$e^+ e^- \approx \Upsilon(4S)$	
seen	CHISTOV 06	BELL	$e^+ e^- \approx \Upsilon(4S)$	
$\Gamma(\Sigma_c(2455) \bar{K}) / \Gamma(\Lambda_c^+ \bar{K} \pi)$				$\Gamma_2 / \Gamma_1$
VALUE	DOCUMENT ID	TECN	COMMENT	
$0.55 \pm 0.07 \pm 0.13$	AUBERT 08J	BABR	$e^+ e^- \approx \Upsilon(4S)$	
$\Gamma(\Xi_c^0 \pi) / \Gamma_{\text{total}}$				$\Gamma_5 / \Gamma$
VALUE	DOCUMENT ID	TECN	COMMENT	
seen	YELTON 16	BELL	$e^+ e^-$ , $\Upsilon$ regions	
$\Gamma(\Xi_c(2645) \pi) / \Gamma_{\text{total}}$				$\Gamma_6 / \Gamma$
VALUE	DOCUMENT ID	TECN	COMMENT	
seen	LESIAK 08	BELL	$e^+ e^- \approx \Upsilon(4S)$	

 $\Xi_c(2970)$  REFERENCES

YELTON 16	PR D94 052011	J. Yelton <i>et al.</i>	(BELLE Collab.)
KATO 14	PR D89 052003	Y. Kato <i>et al.</i>	(BELLE Collab.)
AUBERT 08J	PR D77 012002	B. Aubert <i>et al.</i>	(BABAR Collab.)
LESIAK 08	PL B665 9	T. Lesiak <i>et al.</i>	(BELLE Collab.)
CHISTOV 06	PRL 97 162001	R. Chistov <i>et al.</i>	(BELLE Collab.)

 $\Xi_c(3055)$  $I(J^P) = ?(??)$  Status: \*\*\* $\Xi_c(3055)$  MASSES

$\Xi_c(3055)^+$ MASS				
VALUE (MeV)	EVTS	DOCUMENT ID	TECN	COMMENT
$3055.9 \pm 0.4$	894	KATO 16	BELL	$e^+ e^- \Upsilon$ region
••• We do not use the following data for averages, fits, limits, etc. •••				
$3058.1 \pm 1.0 \pm 2.1$	$199 \pm 46$	KATO 14	BELL	See KATO 16
$3054.2 \pm 1.2 \pm 0.5$	$218 \pm 95$	AUBERT 08J	BABR	$e^+ e^- \approx 10.58$ GeV

 $\Xi_c(3055)$  WIDTHS

$\Xi_c(3055)^+$ WIDTH				
VALUE (MeV)	EVTS	DOCUMENT ID	TECN	COMMENT
$7.8 \pm 1.2 \pm 1.5$		KATO 16	BELL	$e^+ e^- \Upsilon$ region
••• We do not use the following data for averages, fits, limits, etc. •••				
$9.7 \pm 3.4 \pm 3.3$	$199 \pm 46$	KATO 14	BELL	$e^+ e^- \Upsilon(1S)$ to $\Upsilon(5S)$
$17 \pm 6 \pm 11$	$218 \pm 95$	AUBERT 08J	BABR	$e^+ e^- \approx 10.58$ GeV

 $\Xi_c(3055)$  DECAY MODES

Mode	Fraction ( $\Gamma_i / \Gamma$ )
$\Gamma_1 \Sigma^{++} K^-$	seen
$\Gamma_2 \Lambda D^+$	seen

 $\Xi_c(3055)$  BRANCHING RATIOS

$\Gamma(\Lambda D^+) / \Gamma(\Sigma^{++} K^-)$				$\Gamma_2 / \Gamma_1$
VALUE	DOCUMENT ID	TECN	COMMENT	
$5.09 \pm 1.01 \pm 0.76$	KATO 16	BELL	721 and 103 evts	

 $\Xi_c(3055)$  REFERENCES

KATO 16	PR D94 032002	Y. Kato <i>et al.</i>	(BELLE Collab.)
KATO 14	PR D89 052003	Y. Kato <i>et al.</i>	(BELLE Collab.)
AUBERT 08J	PR D77 012002	B. Aubert <i>et al.</i>	(BABAR Collab.)

 $\Xi_c(3080)$  $I(J^P) = \frac{1}{2}(??)$  Status: \*\*\* $\Xi_c(3080)$  MASSES

$\Xi_c(3080)^+$ MASS				
VALUE (MeV)	EVTS	DOCUMENT ID	TECN	COMMENT
$3077.2 \pm 0.4$ OUR AVERAGE				
$3077.9 \pm 0.9$	596	KATO 16	BELL	$e^+ e^- \Upsilon$ region
$3077.0 \pm 0.4 \pm 0.2$	$403 \pm 60$	AUBERT 08J	BABR	$e^+ e^- \approx 10.58$ GeV

••• We do not use the following data for averages, fits, limits, etc. •••

$3076.9 \pm 0.3 \pm 0.2$	$210 \pm 30$	KATO 14	BELL	See KATO 16
$3076.7 \pm 0.9 \pm 0.5$	$326 \pm 40$	CHISTOV 06	BELL	See KATO 14

 $\Xi_c(3080)^0$  MASS

VALUE (MeV)	EVTS	DOCUMENT ID	TECN	COMMENT
$3079.9 \pm 1.4$ OUR AVERAGE	Error includes scale factor of 1.3.			
$3079.3 \pm 1.1 \pm 0.2$	$90 \pm 27$	AUBERT 08J	BABR	$e^+ e^- \approx 10.58$ GeV
$3082.8 \pm 1.8 \pm 1.5$	$67 \pm 20$	CHISTOV 06	BELL	$e^+ e^- \approx \Upsilon(4S)$

 $\Xi_c(3080)$  WIDTHS $\Xi_c(3080)^+$  WIDTH

VALUE (MeV)	EVTS	DOCUMENT ID	TECN	COMMENT
$3.6 \pm 1.1$ OUR AVERAGE	Error includes scale factor of 1.5.			
$3.0 \pm 0.7 \pm 0.4$	596	KATO 16	BELL	$e^+ e^- \Upsilon$ region
$5.5 \pm 1.3 \pm 0.6$	$403 \pm 60$	AUBERT 08J	BABR	$e^+ e^- \approx 10.58$ GeV
••• We do not use the following data for averages, fits, limits, etc. •••				
$2.4 \pm 0.9 \pm 1.6$	$210 \pm 30$	KATO 14	BELL	See KATO 16
$6.2 \pm 1.2 \pm 0.8$	$326 \pm 40$	CHISTOV 06	BELL	See KATO 14

 $\Xi_c(3080)^0$  WIDTH

VALUE (MeV)	EVTS	DOCUMENT ID	TECN	COMMENT
$5.6 \pm 2.2$ OUR AVERAGE				
$5.9 \pm 2.3 \pm 1.5$	$90 \pm 27$	AUBERT 08J	BABR	$e^+ e^- \approx 10.58$ GeV
$5.2 \pm 3.1 \pm 1.8$	$67 \pm 20$	CHISTOV 06	BELL	$e^+ e^- \approx \Upsilon(4S)$

 $\Xi_c(3080)$  DECAY MODES

Mode	Fraction ( $\Gamma_i / \Gamma$ )
$\Gamma_1 \Lambda_c^+ \bar{K} \pi$	seen
$\Gamma_2 \Sigma_c(2455) \bar{K}$	seen
$\Gamma_3 \Sigma_c(2455)^{++} K^-$	seen
$\Gamma_4 \Sigma_c(2520)^{++} K^-$	seen
$\Gamma_5 \Sigma_c(2455) \bar{K} + \Sigma_c(2520) \bar{K}$	seen
$\Gamma_6 \Lambda_c^+ \bar{K}$	not seen
$\Gamma_7 \Lambda_c^+ \bar{K} \pi^+ \pi^-$	not seen
$\Gamma_8 \Lambda D^+$	seen

 $\Xi_c(3080)$  BRANCHING RATIOS

$\Gamma(\Sigma_c(2455) \bar{K}) / \Gamma(\Lambda_c^+ \bar{K} \pi)$				$\Gamma_2 / \Gamma_1$
VALUE	DOCUMENT ID	TECN	COMMENT	
$0.45 \pm 0.06$ OUR AVERAGE				
$0.45 \pm 0.05 \pm 0.05$	AUBERT 08J	BABR	in $\Lambda_c^+ K^- \pi^+$	
$0.44 \pm 0.12 \pm 0.07$	AUBERT 08J	BABR	in $\Lambda_c^+ K_S^0 \pi^-$	

$\Gamma(\Sigma_c(2520)^{++} K^-) / \Gamma(\Sigma_c(2455)^{++} K^-)$				$\Gamma_4 / \Gamma_3$
VALUE	DOCUMENT ID	TECN	COMMENT	
$1.07 \pm 0.27 \pm 0.04$	KATO 16	BELL	234 and 176 evts	

$[\Gamma(\Sigma_c(2455) \bar{K}) + \Gamma(\Sigma_c(2520) \bar{K})] / \Gamma(\Lambda_c^+ \bar{K} \pi)$				$\Gamma_5 / \Gamma_1$
VALUE	DOCUMENT ID	TECN	COMMENT	
$0.89 \pm 0.12$ OUR AVERAGE				
$0.95 \pm 0.14 \pm 0.06$	AUBERT 08J	BABR	in $\Lambda_c^+ K^- \pi^+$	
$0.78 \pm 0.21 \pm 0.05$	AUBERT 08J	BABR	in $\Lambda_c^+ K_S^0 \pi^-$	

$\Gamma(\Lambda D^+) / \Gamma(\Sigma_c(2455)^{++} K^-)$				$\Gamma_8 / \Gamma_3$
VALUE	DOCUMENT ID	TECN	COMMENT	
$1.29 \pm 0.30 \pm 0.15$	KATO 16	BELL	186 and 176 evts	

 $\Xi_c(3080)$  REFERENCES

KATO 16	PR D94 032002	Y. Kato <i>et al.</i>	(BELLE Collab.)
KATO 14	PR D89 052003	Y. Kato <i>et al.</i>	(BELLE Collab.)
AUBERT 08J	PR D77 012002	B. Aubert <i>et al.</i>	(BABAR Collab.)
CHISTOV 06	PRL 97 162001	R. Chistov <i>et al.</i>	(BELLE Collab.)

 $\Xi_c(3123)$  $I(J^P) = ?(??)$  Status: \*

OMITTED FROM SUMMARY TABLE

A peak in the  $\Sigma_c(2520)^{++} K^- \rightarrow \Lambda_c^+ K^- \pi^+$  mass spectrum with a significance of 3.6 standard deviations. KATO 14 finds no evidence for this state.

$\Xi_c(3123), \Omega_c^0$

$\Xi_c(3123)$  MASSES

$\Xi_c(3123)^+$  MASS

VALUE (MeV)	EVTs	DOCUMENT ID	TECN	COMMENT
<b>3122.9 ± 1.3 ± 0.3</b>	101 ± 35	AUBERT	08J	BABR $e^+e^- \approx 10.58$ GeV

$\Xi_c(3123)$  WIDTHS

$\Xi_c(3123)^+$  WIDTH

VALUE (MeV)	EVTs	DOCUMENT ID	TECN	COMMENT
<b>4.4 ± 3.4 ± 1.7</b>	101 ± 35	AUBERT	08J	BABR $e^+e^- \approx 10.58$ GeV

$\Xi_c(3123)$  REFERENCES

KATO	14	PR D89 052003	Y. Kato <i>et al.</i>	(BELLE Collab.)
AUBERT	08J	PR D77 012002	B. Aubert <i>et al.</i>	(BABAR Collab.)



$I(J^P) = 0(\frac{1}{2}^+)$  Status: \*\*\*

The quantum numbers have not been measured, but are simply assigned in accord with the quark model, in which the  $\Omega_c^0$  is the *ssc* ground state. No absolute branching fractions have been measured.

$\Omega_c^0$  MASS

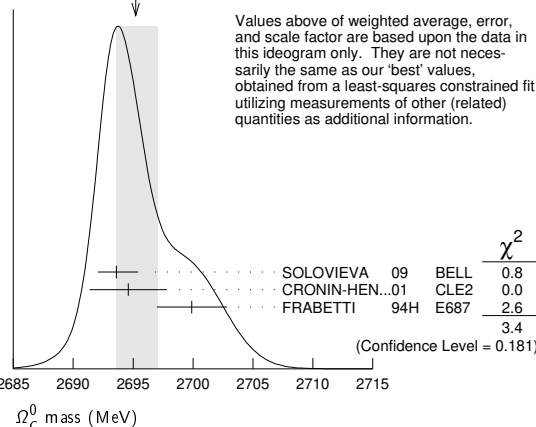
VALUE (MeV)	EVTs	DOCUMENT ID	TECN	COMMENT
<b>2695.2 ± 1.7 OUR FIT</b>	Error			includes scale factor of 1.3.

**2695.2 ± 1.8 OUR AVERAGE** Error includes scale factor of 1.3. See the ideogram below.

2693.6 ± 0.3 ± 1.8	725	SOLOVIEVA	09	BELL $\Omega^- \pi^+$ in $e^+e^- \rightarrow \Upsilon(4S)$
2694.6 ± 2.6 ± 1.9	40	<sup>1</sup> CRONIN-HEN..01	CLE2	$e^+e^- \approx 10.6$ GeV
2699.9 ± 1.5 ± 2.5	42	<sup>2</sup> FRABETTI	94H	E687 $\gamma$ Be, $\overline{E}_\gamma = 221$ GeV
• • • We do not use the following data for averages, fits, limits, etc. • • •				
2705.9 ± 3.3 ± 2.0	10	<sup>3</sup> FRABETTI	93	E687 $\gamma$ Be, $\overline{E}_\gamma = 221$ GeV
2719.0 ± 7.0 ± 2.5	11	<sup>4</sup> ALBRECHT	92H	ARG $e^+e^- \approx 10.6$ GeV
2740 ± 20	3	BIAGI	85B	SPEC $\Sigma^-$ Be 135 GeV/c

- <sup>1</sup> CRONIN-HENNESSY 01 sees  $40.4 \pm 9.0$  events in a sum over five channels.
- <sup>2</sup> FRABETTI 94H claims a signal of  $42.5 \pm 8.8$   $\Sigma^+ K^- K^- \pi^+$  events. The background is about 24 events.
- <sup>3</sup> FRABETTI 93 claims a signal of  $10.3 \pm 3.9$   $\Omega^- \pi^+$  events above a background of 5.8 events.
- <sup>4</sup> ALBRECHT 92H claims a signal of  $11.5 \pm 4.3$   $\Xi^- K^- \pi^+ \pi^+$  events. The background is about 5 events.

WEIGHTED AVERAGE  
2695.2 ± 1.8-1.6 (Error scaled by 1.3)



$\Omega_c^0$  MEAN LIFE

VALUE ( $10^{-15}$ s)	EVTs	DOCUMENT ID	TECN	COMMENT
<b>268 ± 24 ± 10</b>	978	<sup>1</sup> AAIJ	18J	LHCB $p K^- K^- \pi^+$
• • • We do not use the following data for averages, fits, limits, etc. • • •				
72 ± 11 ± 11	64	LINK	03c	FOCS $\Omega^- \pi^+, \Xi^- K^- \pi^+ \pi^+$
55 +13+18 -11-23	86	ADAMOVICH	95B	WA89 $\Omega^- \pi^- \pi^+ \pi^+, \Xi^- K^- \pi^+ \pi^+$
86 +27 -20	25	FRABETTI	95D	E687 $\Sigma^+ K^- K^- \pi^+$

<sup>1</sup> AAIJ 18J, with nearly five times more events than the previous three experiments combined, gets a lifetime that is nearly four times larger than the average of those experiments,  $(69 \pm 12) \times 10^{-15}$  s. We go with the larger data sample.

$\Omega_c^0$  DECAY MODES

Mode	Fraction ( $\Gamma_i/\Gamma$ )	Confidence level
------	--------------------------------	------------------

No absolute branching fractions have been measured. The following are branching ratios relative to  $\Omega^- \pi^+$ .

Cabibbo-favored ( $S = -3$ ) decays — relative to  $\Omega^- \pi^+$

$\Gamma_i$	Mode	Fraction ( $\Gamma_i/\Gamma$ )	Confidence level
$\Gamma_1$	$\Omega^- \pi^+$	<b>DEFINED AS 1</b>	
$\Gamma_2$	$\Omega^- \pi^+ \pi^0$	1.80 ± 0.33	
$\Gamma_3$	$\Omega^- \rho^+$	>1.3	90%
$\Gamma_4$	$\Omega^- \pi^- 2\pi^+$	0.31 ± 0.05	
$\Gamma_5$	$\Omega^- e^+ \nu_e$	2.4 ± 1.2	
$\Gamma_6$	$\Xi^0 \overline{K}^0$	1.64 ± 0.29	
$\Gamma_7$	$\Xi^0 K^- \pi^+$	1.20 ± 0.18	
$\Gamma_8$	$\Xi^0 \overline{K}^{*0}, \overline{K}^{*0} \rightarrow K^- \pi^+$	0.68 ± 0.16	
$\Gamma_9$	$\Xi^- \overline{K}^0 \pi^+$	2.12 ± 0.28	
$\Gamma_{10}$	$\Xi^- K^- 2\pi^+$	0.63 ± 0.09	
$\Gamma_{11}$	$\Xi(1530)^0 K^- \pi^+, \Xi^{*0} \rightarrow$	0.21 ± 0.06	
$\Gamma_{12}$	$\Xi^- \overline{K}^{*0} \pi^+$	0.34 ± 0.11	
$\Gamma_{13}$	$\Sigma^+ K^- K^- \pi^+$	<0.32	90%
$\Gamma_{14}$	$\Lambda \overline{K}^0 \overline{K}^0$	1.72 ± 0.35	

$\Omega_c^0$  BRANCHING RATIOS

A few early but now obsolete measurements have been omitted. See K.A. Olive, et al. (Particle Data Group), Chinese Physics **C38** 070001 (2014).

$\Gamma(\Omega^- \pi^+ \pi^0)/\Gamma(\Omega^- \pi^+)$	$\Gamma_2/\Gamma_1$
<b>1.80 ± 0.33 OUR AVERAGE</b>	Error includes scale factor of 1.9.
2.00 ± 0.17 ± 0.11	403 YELTON 18 BELL $e^+e^- \rightarrow \Upsilon(4S)$ , +higher
1.27 ± 0.31 ± 0.11	64 AUBERT 07AH BABR $e^+e^- \approx \Upsilon(4S)$

$\Gamma(\Omega^- \rho^+)/\Gamma(\Omega^- \pi^+ \pi^0)$	$\Gamma_3/\Gamma_2$
<b>&gt;0.71</b>	<sup>1</sup> YELTON 18 BELL $e^+e^- \rightarrow \Upsilon(4S)$ , +higher
<sup>1</sup> This submode fraction is evaluated from a background-subtracted signal in a mass plot. Result ignores interference effects and systematic uncertainties, which YELTON 18 claim are both small.	

$\Gamma(\Omega^- \pi^- 2\pi^+)/\Gamma(\Omega^- \pi^+)$	$\Gamma_4/\Gamma_1$
<b>0.31 ± 0.05 OUR AVERAGE</b>	
0.32 ± 0.05 ± 0.02	108 YELTON 18 BELL $e^+e^- \rightarrow \Upsilon(4S)$ , +higher
0.28 ± 0.09 ± 0.01	25 AUBERT 07AH BABR $e^+e^- \approx \Upsilon(4S)$

$\Gamma(\Omega^- \pi^+)/\Gamma(\Omega^- e^+ \nu_e)$	$\Gamma_1/\Gamma_5$
<b>0.41 ± 0.19 ± 0.04</b>	11 AMMAR 02 CLE2 $e^+e^- \approx \Upsilon(4S)$

$\Gamma(\Xi^0 \overline{K}^0)/\Gamma(\Omega^- \pi^+)$	$\Gamma_6/\Gamma_1$
<b>1.64 ± 0.26 ± 0.12</b>	98 YELTON 18 BELL $e^+e^- \rightarrow \Upsilon(4S)$ , +higher

$\Gamma(\Xi^0 K^- \pi^+)/\Gamma(\Omega^- \pi^+)$	$\Gamma_7/\Gamma_1$
<b>1.20 ± 0.16 ± 0.08</b>	168 YELTON 18 BELL $e^+e^- \rightarrow \Upsilon(4S)$ , +higher

$\Gamma(\Xi^0 \overline{K}^{*0}, \overline{K}^{*0} \rightarrow K^- \pi^+)/\Gamma(\Xi^0 K^- \pi^+)$	$\Gamma_8/\Gamma_7$
<b>0.57 ± 0.10</b>	95 <sup>1</sup> YELTON 18 BELL $e^+e^- \rightarrow \Upsilon(4S)$ , +higher
<sup>1</sup> This submode fraction is evaluated from a background-subtracted signal in a mass plot. Result ignores interference effects and systematic uncertainties, which YELTON 18 claim are both small.	

$\Gamma(\Xi^- \overline{K}^0 \pi^+)/\Gamma(\Omega^- \pi^+)$	$\Gamma_9/\Gamma_1$
<b>2.12 ± 0.24 ± 0.14</b>	349 YELTON 18 BELL $e^+e^- \rightarrow \Upsilon(4S)$ , +higher

$\Gamma(\Xi^- K^- 2\pi^+)/\Gamma(\Omega^- \pi^+)$	$\Gamma_{10}/\Gamma_1$
<b>0.63 ± 0.09 OUR AVERAGE</b>	Error includes scale factor of 1.4.
0.68 ± 0.07 ± 0.03	278 YELTON 18 BELL $e^+e^- \rightarrow \Upsilon(4S)$ , +higher
0.46 ± 0.13 ± 0.03	45 AUBERT 07AH BABR $e^+e^- \approx \Upsilon(4S)$

$\Gamma(\Xi(1530)^0 K^- \pi^+, \Xi^{*0} \rightarrow \Xi^- \pi^+)/\Gamma(\Xi^- K^- 2\pi^+)$	$\Gamma_{11}/\Gamma_{10}$
<b>0.33 ± 0.09</b>	74 <sup>1</sup> YELTON 18 BELL $e^+e^- \rightarrow \Upsilon(4S)$ , +higher
<sup>1</sup> This submode fraction is evaluated from a background-subtracted signal in a mass plot. Result ignores interference effects and systematic uncertainties, which YELTON 18 claim are both small.	



# Baryon Particle Listings

## $\Omega_c^0, \Omega_c(2770)^0, \Omega_c(3000)^0, \Omega_c(3050)^0, \Omega_c(3065)^0$

$\Gamma(\Xi^- \bar{K}^0 \pi^+)/\Gamma(\Xi^- K^- 2\pi^+)$   $\Gamma_{12}/\Gamma_{10}$

VALUE	EVTS	DOCUMENT ID	TECN	COMMENT
<b>0.55 ± 0.16</b>	136	<sup>1</sup> YELTON	18 BELL	$e^+ e^- \rightarrow \Upsilon(4S)$ , +higher

<sup>1</sup> This submode fraction is evaluated from a background-subtracted signal in a mass plot. Result ignores interference effects and systematic uncertainties, which YELTON 18 claim are both small.

$\Gamma(\Sigma^+ K^- K^- \pi^+)/\Gamma(\Omega^- \pi^+)$   $\Gamma_{13}/\Gamma_1$

VALUE	CL%	EVTS	DOCUMENT ID	TECN	COMMENT
<b>&lt;0.32</b>	90	17	YELTON	18 BELL	$e^+ e^- \rightarrow \Upsilon(4S)$ , +higher

$\Gamma(\Lambda \bar{K}^0 \bar{K}^0)/\Gamma(\Omega^- \pi^+)$   $\Gamma_{14}/\Gamma_1$

VALUE	EVTS	DOCUMENT ID	TECN	COMMENT
<b>1.72 ± 0.32 ± 0.14</b>	95	YELTON	18 BELL	$e^+ e^- \rightarrow \Upsilon(4S)$ , +higher

### $\Omega_c^0$ REFERENCES

AAIJ	18J	PRL 121 092003	R. Aaij et al.	(LHCb Collab.)
YELTON	18	PR D97 032001	J. Yelton et al.	(BELLE Collab.)
PDG	14	CP C38 070001	K. Olive et al.	(PDG Collab.)
SOLOVIEVA	09	PL B672 1	E. Solovieva et al.	(BELLE Collab.)
AUBERT	07AH	PRL 99 062001	B. Aubert et al.	(BABAR Collab.)
LINK	03C	PL B561 41	J.M. Link et al.	(FNAL FOCUS Collab.)
AMMAR	02	PRL 89 171803	R. Ammar et al.	(CLEO Collab.)
CRONIN-HENNESSY	01	PRL 86 3730	D. Cronin-Hennessy et al.	(CLEO Collab.)
ADAMOVICH	95B	PL B358 151	M.I. Adamovich et al.	(CERN WA89 Collab.)
FRABETTI	95D	PL B357 678	P.L. Frabetti et al.	(FNAL E687 Collab.)
FRABETTI	94H	PL B338 106	P.L. Frabetti et al.	(FNAL E687 Collab.)
FRABETTI	93	PL B300 190	P.L. Frabetti et al.	(FNAL E687 Collab.)
ALBRECHT	92H	PL B288 367	H. Albrecht et al.	(ARGUS Collab.)
BIAGI	85B	ZPHY C28 175	S.F. Biagi et al.	(CERN WA62 Collab.)

**$\Omega_c(2770)^0$**   $I(J^P) = 0(\frac{3}{2}^+)$  Status: \*\*\*

The natural assignment is that this goes with the  $\Sigma_c(2520)$  and  $\Xi_c(2645)$  to complete the lowest mass  $J^P = \frac{3}{2}^+$  SU(3) sextet, part of the SU(4) 20-plet that includes the  $\Delta(1232)$ . But  $J$  and  $P$  have not been measured.

### $\Omega_c(2770)^0$ MASS

The mass is obtained from the mass-difference measurement that follows.

VALUE (MeV)	DOCUMENT ID
<b>2765.9 ± 2.0 OUR FIT</b>	Error includes scale factor of 1.2.

### $\Omega_c(2770)^0 - \Omega_c^0$ MASS DIFFERENCE

VALUE (MeV)	EVTS	DOCUMENT ID	TECN	COMMENT
<b>70.7<sup>+0.8</sup><sub>-0.9</sub> OUR FIT</b>				
<b>70.7<sup>+0.8</sup><sub>-1.0</sub> OUR AVERAGE</b>				
70.7 ± 0.9 <sup>+0.1</sup> <sub>-0.9</sub>	54 ± 9	SOLOVIEVA 09	BELL	$\Omega_c^0 \gamma$ in $e^+ e^- \rightarrow \Upsilon(4S)$
70.8 ± 1.0 ± 1.1	105 ± 22	AUBERT, BE 06i	BABR	$e^+ e^- \approx \Upsilon(4S)$

### $\Omega_c(2770)^0$ DECAY MODES

The  $\Omega_c(2770)^0 - \Omega_c^0$  mass difference is too small for any strong decay to occur.

Mode	Fraction ( $\Gamma_i/\Gamma$ )
$\Gamma_1 \Omega_c^0 \gamma$	presumably 100%

### $\Omega_c(2770)^0$ REFERENCES

SOLOVIEVA	09	PL B672 1	E. Solovieva et al.	(BELLE Collab.)
AUBERT, BE	06i	PRL 97 232001	B. Aubert et al.	(BABAR Collab.)

**$\Omega_c(3000)^0$**   $I(J^P) = ?(?^?)$  Status: \*\*\*

### $\Omega_c(3000)^0$ MASS

VALUE (MeV)	EVTS	DOCUMENT ID	TECN	COMMENT
<b>3000.41 ± 0.22 OUR AVERAGE</b>				
3000.7 ± 1.0 ± 0.2	38	YELTON	18B BELL	$e^+ e^-$ at $\Upsilon(4S)$
3000.4 ± 0.2 ± 0.1	1.3k	AAIJ	17AH LHCb	$pp$ at 7, 8, 13 TeV

### $\Omega_c(3000)^0$ WIDTH

VALUE (MeV)	EVTS	DOCUMENT ID	TECN	COMMENT
<b>4.5 ± 0.6 ± 0.3</b>	1.3k	AAIJ	17AH LHCb	$pp$ at 7, 8, 13 TeV

### $\Omega_c(3000)^0$ DECAY MODES

Mode	Fraction ( $\Gamma_i/\Gamma$ )
$\Gamma_1 \Xi_c^+ K^-$	seen

### $\Omega_c(3000)^0$ BRANCHING RATIOS

$\Gamma(\Xi_c^+ K^-)/\Gamma_{\text{total}}$   $\Gamma_1/\Gamma$

VALUE	EVTS	DOCUMENT ID	TECN	COMMENT
seen	38	<sup>1</sup> YELTON	18B BELL	$e^+ e^-$ at $\Upsilon(4S)$
seen	1.3k	AAIJ	17AH LHCb	$pp$ at 7, 8, 13 TeV

<sup>1</sup> YELTON 18B report a significance of 3.9 $\sigma$

### $\Omega_c(3000)^0$ REFERENCES

YELTON	18B	PR D97 051102	J. Yelton et al.	(BELLE Collab.)
AAIJ	17AH	PRL 118 182001	R. Aaij et al.	(LHCb Collab.)

**$\Omega_c(3050)^0$**   $I(J^P) = ?(?^?)$  Status: \*\*\*

### $\Omega_c(3050)^0$ MASS

VALUE (MeV)	EVTS	DOCUMENT ID	TECN	COMMENT
<b>3050.20 ± 0.13 OUR AVERAGE</b>				
3050.2 ± 0.4 ± 0.2	28	YELTON	18B BELL	$e^+ e^-$ at $\Upsilon(4S)$
3050.2 ± 0.1 ± 0.1	970	AAIJ	17AH LHCb	$pp$ at 7, 8, 13 TeV

### $\Omega_c(3050)^0$ WIDTH

VALUE (MeV)	CL%	DOCUMENT ID	TECN	COMMENT
<b>&lt;1.2</b>	95	AAIJ	17AH LHCb	$pp$ at 7, 8, 13 TeV

### $\Omega_c(3050)^0$ DECAY MODES

Mode	Fraction ( $\Gamma_i/\Gamma$ )
$\Gamma_1 \Xi_c^+ K^-$	seen

### $\Omega_c(3050)^0$ BRANCHING RATIOS

$\Gamma(\Xi_c^+ K^-)/\Gamma_{\text{total}}$   $\Gamma_1/\Gamma$

VALUE	EVTS	DOCUMENT ID	TECN	COMMENT
seen	28	<sup>1</sup> YELTON	18B BELL	$e^+ e^-$ at $\Upsilon(4S)$
seen	970	AAIJ	17AH LHCb	$pp$ at 7, 8, 13 TeV

<sup>1</sup> YELTON 18B report a significance of 4.6 $\sigma$

### $\Omega_c(3050)^0$ REFERENCES

YELTON	18B	PR D97 051102	J. Yelton et al.	(BELLE Collab.)
AAIJ	17AH	PRL 118 182001	R. Aaij et al.	(LHCb Collab.)

**$\Omega_c(3065)^0$**   $I(J^P) = ?(?^?)$  Status: \*\*\*

### $\Omega_c(3065)^0$ MASS

VALUE (MeV)	EVTS	DOCUMENT ID	TECN	COMMENT
<b>3065.46 ± 0.28 OUR AVERAGE</b>				
3064.9 ± 0.6 ± 0.2	82	YELTON	18B BELL	$e^+ e^-$ at $\Upsilon(4S)$
3065.6 ± 0.1 ± 0.3	1.74k	AAIJ	17AH LHCb	$pp$ at 7, 8, 13 TeV

### $\Omega_c(3065)^0$ WIDTH

VALUE (MeV)	EVTS	DOCUMENT ID	TECN	COMMENT
<b>3.5 ± 0.4 ± 0.2</b>	1.74k	AAIJ	17AH LHCb	$pp$ at 7, 8, 13 TeV

### $\Omega_c(3065)^0$ DECAY MODES

Mode	Fraction ( $\Gamma_i/\Gamma$ )
$\Gamma_1 \Xi_c^+ K^-$	seen

See key on page 999

Baryon Particle Listings  
 $\Omega_c(3065)^0, \Omega_c(3090)^0, \Omega_c(3120)^0$

$\Omega_c(3065)^0$  BRANCHING RATIOS

$\Gamma(\Xi_c^+ K^-)/\Gamma_{\text{total}}$					$\Gamma_1/\Gamma$
VALUE	EVTS	DOCUMENT ID	TECN	COMMENT	
seen	82	YELTON	18B BELL	$e^+ e^-$ at $\Upsilon(4S)$	
seen	1.74k	AAIJ	17AH LHCB	$pp$ at 7, 8, 13 TeV	

$\Omega_c(3065)^0$  REFERENCES

YELTON	18B PR D97 051102	J. Yelton <i>et al.</i>	(BELLE Collab.)
AAIJ	17AH PRL 118 182001	R. Aaij <i>et al.</i>	(LHCb Collab.)

$\Omega_c(3090)^0$   $I(J^P) = ?(??)$  Status: \*\*\*

$\Omega_c(3090)^0$  MASS

VALUE (MeV)	EVTS	DOCUMENT ID	TECN	COMMENT
<b><math>3090.0 \pm 0.5</math> OUR AVERAGE</b>				
$3089.3 \pm 1.2 \pm 0.2$	87	YELTON	18B BELL	$e^+ e^-$ at $\Upsilon(4S)$
$3090.2 \pm 0.3 \pm 0.5$	2.0k	AAIJ	17AH LHCB	$pp$ at 7, 8, 13 TeV

$\Omega_c(3090)^0$  WIDTH

VALUE (MeV)	EVTS	DOCUMENT ID	TECN	COMMENT
<b><math>8.7 \pm 1.0 \pm 0.8</math></b>	2.0k	AAIJ	17AH LHCB	$pp$ at 7, 8, 13 TeV

$\Omega_c(3090)^0$  DECAY MODES

Mode	Fraction ( $\Gamma_i/\Gamma$ )
$\Gamma_1 \Xi_c^+ K^-$	seen

$\Omega_c(3090)^0$  BRANCHING RATIOS

$\Gamma(\Xi_c^+ K^-)/\Gamma_{\text{total}}$					$\Gamma_1/\Gamma$
VALUE	EVTS	DOCUMENT ID	TECN	COMMENT	
seen	87	YELTON	18B BELL	$e^+ e^-$ at $\Upsilon(4S)$	
seen	2.0k	AAIJ	17AH LHCB	$pp$ at 7, 8, 13 TeV	

$\Omega_c(3090)^0$  REFERENCES

YELTON	18B PR D97 051102	J. Yelton <i>et al.</i>	(BELLE Collab.)
AAIJ	17AH PRL 118 182001	R. Aaij <i>et al.</i>	(LHCb Collab.)

$\Omega_c(3120)^0$

$I(J^P) = ?(??)$  Status: \*\*\*

$\Omega_c(3120)^0$  MASS

VALUE (MeV)	EVTS	DOCUMENT ID	TECN	COMMENT
<b><math>3119.1 \pm 0.3 \pm 0.9 \pm 0.3</math></b>	480	<sup>1</sup> AAIJ	17AH LHCB	$pp$ at 7, 8, 13 TeV

<sup>1</sup> The third error is the uncertainty on the  $\Xi_c^+$  mass. (AAIJ 17AH gave  $+0.3$  MeV here, but as of 2018 it is  $\pm 0.3$ .)

$\Omega_c(3120)^0$  WIDTH

VALUE (MeV)	CL%	DOCUMENT ID	TECN	COMMENT
<b>&lt;2.6</b>	95	AAIJ	17AH LHCB	$pp$ at 7, 8, 13 TeV

$\Omega_c(3120)^0$  DECAY MODES

Mode	Fraction ( $\Gamma_i/\Gamma$ )
$\Gamma_1 \Xi_c^+ K^-$	seen

$\Omega_c(3120)^0$  BRANCHING RATIOS

$\Gamma(\Xi_c^+ K^-)/\Gamma_{\text{total}}$					$\Gamma_1/\Gamma$
VALUE	EVTS	DOCUMENT ID	TECN	COMMENT	
seen		AAIJ	17AH LHCB	$pp$ at 7, 8, 13 TeV	

$\Omega_c(3120)^0$  REFERENCES

AAIJ	17AH PRL 118 182001	R. Aaij <i>et al.</i>	(LHCb Collab.)
------	---------------------	-----------------------	----------------

# Baryon Particle Listings



## DOUBLY CHARMED BARYONS

### (C = +2)

$\Xi_{cc}^{++} = ucc, \Xi_{cc}^+ = dcc, \Omega_{cc}^+ = scc$



$I(J^P) = ?(??)$  Status: \*\*\*

### $\Xi_{cc}^{++}$ MASS

VALUE (MeV)	EVTS	DOCUMENT ID	TECN	COMMENT
<b>3621.2 ± 0.7 OUR AVERAGE</b>				
3620.6 ± 1.5 ± 0.4 ± 0.3	91	<sup>1</sup> AAIJ	18BA LHCb	pp at 13 TeV
3621.40 ± 0.72 ± 0.27 ± 0.14	313	<sup>2</sup> AAIJ	17Bc LHCb	pp at 13 TeV

<sup>1</sup> The third error in AAIJ 18BA value is from the uncertainty of the  $\Xi_{cc}^+$  mass.  
<sup>2</sup> The third error in AAIJ 17Bc value is from the uncertainty of the  $\Lambda_{cc}^+$  mass. The width of the signal is  $6.6 \pm 0.8$  MeV, consistent with the experimental resolution.

### $\Xi_{cc}^{++}$ MEAN LIFE

VALUE ( $10^{-15}$ s)	EVTS	DOCUMENT ID	TECN	COMMENT
<b><math>256_{-22}^{+24} \pm 14</math></b>	304	AAIJ	18G LHCb	pp at 13 TeV

### $\Xi_{cc}^{++}$ DECAY MODES

Mode	Fraction ( $\Gamma_i/\Gamma$ )
$\Gamma_1 \Lambda_c^+ K^- \pi^+ \pi^+$	seen
$\Gamma_2 \Xi_c^+ \pi^+, \Xi_c^+ \rightarrow \rho K^- \pi^+$	seen
$\Gamma_3 D^+ \rho K^- \pi^+$	

$\Gamma(\Lambda_c^+ K^- \pi^+ \pi^+)/\Gamma_{total}$	DOCUMENT ID	TECN	COMMENT
seen	AAIJ	17Bc LHCb	12 std significance

$\Gamma(\Xi_c^+ \pi^+, \Xi_c^+ \rightarrow \rho K^- \pi^+)/\Gamma_{total}$	DOCUMENT ID	TECN	COMMENT
seen	91	AAIJ	18BA LHCb 5.9 std significance

$\Gamma(\Xi_c^+ \pi^+, \Xi_c^+ \rightarrow \rho K^- \pi^+)/\Gamma(\Lambda_c^+ K^- \pi^+ \pi^+)$	DOCUMENT ID	TECN	COMMENT
<b><math>2.2 \pm 0.6 \pm 0.1</math></b>	<sup>3</sup> AAIJ	18BA LHCb	Ratio 91 over 289 events
<sup>3</sup> AAIJ 18BA reports $[\Gamma(\Xi_{cc}^{++} \rightarrow \Xi_c^+ \pi^+, \Xi_c^+ \rightarrow \rho K^- \pi^+)/\Gamma(\Xi_{cc}^{++} \rightarrow \Lambda_c^+ K^- \pi^+ \pi^+)] / [B(\Lambda_c^+ \rightarrow \rho K^- \pi^+)] = (3.5 \pm 0.9 \pm 0.3) \times 10^{-2}$ which we multiply by our best value $B(\Lambda_c^+ \rightarrow \rho K^- \pi^+) = (6.28 \pm 0.32) \times 10^{-2}$ . Our first error is their experiment's error and our second error is the systematic error from using our best value.			

$\Gamma(D^+ \rho K^- \pi^+)/\Gamma(\Lambda_c^+ K^- \pi^+ \pi^+)$	DOCUMENT ID	TECN	COMMENT
<b><math>&lt; 1.7 \times 10^{-2}</math></b>	90	AAIJ	19A0 LHCb pp at 13 TeV

### $\Xi_{cc}^{++}$ REFERENCES

AAIJ	19A0 JHEP 1910 124	R. Aaij <i>et al.</i>	(LHCb Collab.)
AAIJ	18BA PRL 121 162002	R. Aaij <i>et al.</i>	(LHCb Collab.)
AAIJ	18G PRL 121 052002	R. Aaij <i>et al.</i>	(LHCb Collab.)
AAIJ	17Bc PRL 119 112001	R. Aaij <i>et al.</i>	(LHCb Collab.)

See key on page 999

Baryon Particle Listings

$\Lambda_b^0$

**BOTTOM BARYONS**  
( $B = -1$ )

$\Lambda_b^0 = udb, \Xi_b^0 = usb, \Xi_b^- = dsb, \Omega_b^- = sss$

$\Lambda_b^0$

$I(J^P) = 0(\frac{1}{2}^+)$  Status: \*\*\*

In the quark model, a  $\Lambda_b^0$  is an isospin-0  $udb$  state. The lowest  $\Lambda_b^0$  ought to have  $J^P = 1/2^+$ . None of  $I, J,$  or  $P$  have actually been measured.

$\Lambda_b^0$  MASS

$m_{\Lambda_b^0}$	VALUE (MeV)	EVTs	DOCUMENT ID	TECN	COMMENT
<b>5619.60 ± 0.17 OUR AVERAGE</b>					
5619.62 ± 0.16 ± 0.13			1 AAIJ	17AM LHCb	$pp$ at 7, 8 TeV
5619.30 ± 0.34			2 AAIJ	14AA LHCb	$pp$ at 7 TeV
5620.15 ± 0.31 ± 0.47			3 AALTONEN	14B CDF	$p\bar{p}$ at 1.96 TeV
5619.7 ± 0.7 ± 1.1			4 AAD	13U ATLS	$pp$ at 7 TeV
5621 ± 4 ± 3			4 ABE	97B CDF	$p\bar{p}$ at 1.8 TeV
5668 ± 16 ± 8		4	5 ABREU	96N DLPH	$e^+e^- \rightarrow Z$
5614 ± 21 ± 4		4	5 BUSKULIC	96L ALEP	$e^+e^- \rightarrow Z$
5619.65 ± 0.17 ± 0.17			6 AAIJ	16V LHCb	Repl. by AAIJ 17AM
5619.44 ± 0.13 ± 0.38			3 AAIJ	13AV LHCb	Repl. by AAIJ 17AM
5619.19 ± 0.70 ± 0.30			3 AAIJ	12E LHCb	Repl. by AAIJ 13AV
5619.7 ± 1.2 ± 1.2			7 ACOSTA	06 CDF	Repl. by AALTONEN 14B
not seen			8 ABE	93B CDF	Repl. by ABE 97B
5640 ± 50 ± 30		16	9 ALBAJAR	91E UA1	$p\bar{p}$ 630 GeV
5640 $\begin{smallmatrix} +100 \\ -210 \end{smallmatrix}$		52	BARI	91 SFM	$\Lambda_b^0 \rightarrow pD^0\pi^-$
5650 $\begin{smallmatrix} +150 \\ -200 \end{smallmatrix}$		90	BARI	91 SFM	$\Lambda_b^0 \rightarrow \Lambda_c^+\pi^+\pi^-\pi^-$

- • • We do not use the following data for averages, fits, limits, etc. • • •
- 1 Uses  $\Lambda_b^0 \rightarrow \chi_{c1}pK^-, \Lambda_b^0 \rightarrow \chi_{c2}pK^-, \Lambda_b^0 \rightarrow J/\psi\Lambda, \Lambda_b^0 \rightarrow p\psi(2S)K^-, \Lambda_b^0 \rightarrow pJ/\psi\pi^+\pi^-K^-,$  and  $\Lambda_b^0 \rightarrow pJ/\psi K^-$  decays.
- 2 Uses exclusively reconstructed final states  $\Lambda_b^0 \rightarrow \Lambda_c^+D_s^-, \Lambda_c^+D^-$  and  $\bar{B}^0 \rightarrow D^+D_s^-$  decays. The uncertainty includes both statistical and systematic contributions.
- 3 Uses  $\Lambda_b^0 \rightarrow J/\psi\Lambda$  fully reconstructed decays.
- 4 ABE 97B observed 38 events with a background of  $18 \pm 1.6$  events in the mass range 5.60–5.65 GeV/ $c^2$ , a significance of  $> 3.4$  standard deviations.
- 5 Uses 4 fully reconstructed  $\Lambda_b^0$  events.
- 6 Uses  $\Lambda_b^0 \rightarrow p\psi(2S)K^-, \Lambda_b^0 \rightarrow pJ/\psi\pi^+\pi^-K^-,$  and  $\Lambda_b^0 \rightarrow pJ/\psi K^-$  decays.
- 7 Uses exclusively reconstructed final states containing a  $J/\psi \rightarrow \mu^+\mu^-$  decays.
- 8 ABE 93B states that, based on the signal claimed by ALBAJAR 91E, CDF should have found  $30 \pm 23 \Lambda_b^0 \rightarrow J/\psi(1S)\Lambda$  events. Instead, CDF found not more than 2 events.
- 9 ALBAJAR 91E claims  $16 \pm 5$  events above a background of  $9 \pm 1$  events, a significance of about 5 standard deviations.

$m_{\Lambda_b^0} - m_{B^0}$

VALUE (MeV)	DOCUMENT ID	TECN	COMMENT
<b>339.2 ± 1.4 ± 0.1</b>	1 ACOSTA	06 CDF	$p\bar{p}$ at 1.96 TeV

1 Uses exclusively reconstructed final states containing  $J/\psi \rightarrow \mu^+\mu^-$  decays.

$m_{\Lambda_b^0} - m_{B^+}$

VALUE (MeV)	DOCUMENT ID	TECN	COMMENT
<b>339.72 ± 0.28 OUR AVERAGE</b>			
339.72 ± 0.24 ± 0.18	1 AAIJ	14AA LHCb	$pp$ at 7 TeV
339.71 ± 0.71 ± 0.09	2 AAIJ	12E LHCb	$pp$ at 7 TeV

- 1 Uses exclusively reconstructed final states  $\Lambda_b^0 \rightarrow \Lambda_c^+D_s^-, \Lambda_c^+D^-$  and  $\bar{B}^0 \rightarrow D^+D_s^-$  decays.
- 2 Uses exclusively reconstructed final states containing  $J/\psi \rightarrow \mu^+\mu^-$  decays.

$\Lambda_b^0$  MEAN LIFE

See  $b$ -baryon Admixture section for data on  $b$ -baryon mean life average over species of  $b$ -baryon particles.

“OUR EVALUATION” is an average using rescaled values of the data listed below. The average and rescaling were performed by the Heavy Flavor Averaging Group (HFLAV) and are described at <https://hflav.web.cern.ch/>. The averaging/rescaling procedure takes into account correlations between the measurements and asymmetric lifetime errors.

VALUE ( $10^{-12}$ s)	EVTs	DOCUMENT ID	TECN	COMMENT
<b>1.471 ± 0.009 OUR EVALUATION</b>				
1.477 ± 0.027 ± 0.009	1	SIRUNYAN	18BY CMS	$pp$ at 8 TeV
1.415 ± 0.027 ± 0.006	2	AAIJ	14E LHCb	$pp$ at 7 TeV
1.479 ± 0.009 ± 0.010	3	AAIJ	14U LHCb	$pp$ at 7, 8 TeV
1.565 ± 0.035 ± 0.020	2	AALTONEN	14B CDF	$p\bar{p}$ at 1.96 TeV

1.449 ± 0.036 ± 0.017	2	AAD	13U ATLS	$pp$ at 7 TeV
1.503 ± 0.052 ± 0.031	2	CHATRCHYAN	13AC CMS	$pp$ at 7 TeV
1.303 ± 0.075 ± 0.035	2	ABAZOV	12U D0	$p\bar{p}$ at 1.96 TeV
1.401 ± 0.046 ± 0.035	4	AALTONEN	10B CDF	$p\bar{p}$ at 1.96 TeV
1.27 $\begin{smallmatrix} +0.35 \\ -0.29 \end{smallmatrix}$ ± 0.09		ABREU	95S DLPH	Excess $p\mu^-$ , decay lengths
• • • We do not use the following data for averages, fits, limits, etc. • • •				
1.482 ± 0.018 ± 0.012	5	AAIJ	13BB LHCb	Repl. by AAIJ 14U
1.537 ± 0.045 ± 0.014	2	AALTONEN	11 CDF	Repl. by AALTONEN 14B
1.218 $\begin{smallmatrix} +0.130 \\ -0.115 \end{smallmatrix}$ ± 0.042	2	ABAZOV	07S D0	Repl. by ABAZOV 12U
1.290 $\begin{smallmatrix} +0.119+0.087 \\ -0.110-0.091 \end{smallmatrix}$	6	ABAZOV	07U D0	$p\bar{p}$ at 1.96 TeV
1.593 $\begin{smallmatrix} +0.083 \\ -0.078 \end{smallmatrix}$ ± 0.033	2	ABULENCIA	07A CDF	Repl. by AALTONEN 11
1.22 $\begin{smallmatrix} +0.22 \\ -0.18 \end{smallmatrix}$ ± 0.04	2	ABAZOV	05C D0	Repl. by ABAZOV 07S
1.11 $\begin{smallmatrix} +0.19 \\ -0.18 \end{smallmatrix}$ ± 0.05	7	ABREU	99W DLPH	$e^+e^- \rightarrow Z$
1.29 $\begin{smallmatrix} +0.24 \\ -0.22 \end{smallmatrix}$ ± 0.06	7	ACKERSTAFF	98G OPAL	$e^+e^- \rightarrow Z$
1.21 ± 0.11	7	BARATE	98D ALEP	$e^+e^- \rightarrow Z$
1.32 ± 0.15 ± 0.07	8	ABE	96M CDF	$p\bar{p}$ at 1.8 TeV
1.19 $\begin{smallmatrix} +0.21+0.07 \\ -0.18-0.08 \end{smallmatrix}$		ABREU	96D DLPH	Repl. by ABREU 99W
1.14 $\begin{smallmatrix} +0.22 \\ -0.19 \end{smallmatrix}$ ± 0.07	69	AKERS	95K OPAL	Repl. by ACKERSTAFF 98G
1.02 $\begin{smallmatrix} +0.23 \\ -0.18 \end{smallmatrix}$ ± 0.06	44	BUSKULIC	95L ALEP	Repl. by BARATE 98D

- 1 Measured using  $\Lambda_b^0 \rightarrow J/\psi\Lambda$  decays.
- 2 Measured mean life using fully reconstructed  $\Lambda_b^0 \rightarrow J/\psi\Lambda$  decays.
- 3 Used  $\Lambda_b^0 \rightarrow J/\psi p K^-$  decays.
- 4 Measured mean life using fully reconstructed  $\Lambda_b^0 \rightarrow \Lambda_c^+\pi^-$  decays.
- 5 Measured the lifetime ratio of decays  $\Lambda_b^0 \rightarrow J/\psi p K^-$  to  $B^0 \rightarrow J/\psi\pi^+K^-$  to be  $0.976 \pm 0.012 \pm 0.006$  with  $\tau_{B^0} = 1.519 \pm 0.007$  ps.
- 6 Measured using semileptonic decays  $\Lambda_b^0 \rightarrow \Lambda_c^+\mu\nu X$  and  $\Lambda_c^+ \rightarrow K_S^0 p$ .
- 7 Measured using  $\Lambda_c \ell^-$  and  $\Lambda \ell^+ \ell^-$ .
- 8 Excess  $\Lambda_c \ell^-$ , decay lengths.

$\tau_{\Lambda_b^0}/\tau_{B^0}$

VALUE	DOCUMENT ID	TECN	COMMENT
<b>0.940 ± 0.035 ± 0.006</b>	1 AAIJ	14E LHCb	$pp$ at 7 TeV

1 Measured using  $\Lambda_b^0 \rightarrow J/\psi\Lambda$  decays.

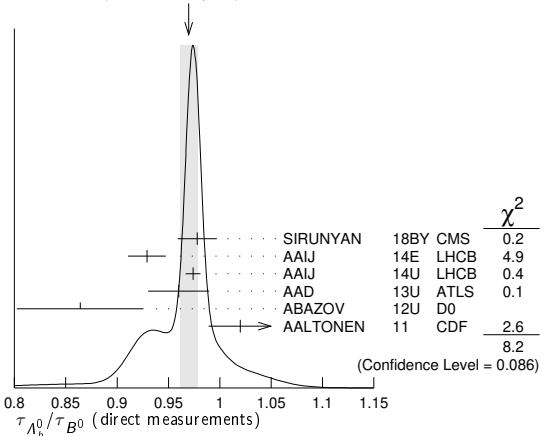
$\tau_{\Lambda_b^0}/\tau_{B^0}$  MEAN LIFE RATIO

$\tau_{\Lambda_b^0}/\tau_{B^0}$  (direct measurements)

“OUR EVALUATION” has been obtained by the Heavy Flavor Averaging Group (HFLAV) by including both  $B^0$  and  $B^+$  decays.

VALUE	DOCUMENT ID	TECN	COMMENT	
<b>0.964 ± 0.007 OUR EVALUATION</b>				
<b>0.970 ± 0.009 OUR AVERAGE</b>			Error includes scale factor of 1.4. See the ideogram below.	
0.978 ± 0.018 ± 0.006	1	SIRUNYAN	18BY CMS	$pp$ at 8 TeV
0.929 ± 0.018 ± 0.004	1	AAIJ	14E LHCb	$pp$ at 7 TeV
0.974 ± 0.006 ± 0.004	2	AAIJ	14U LHCb	$pp$ at 7, 8 TeV
0.960 ± 0.025 ± 0.016	3	AAD	13U ATLS	$pp$ at 7 TeV
0.864 ± 0.052 ± 0.033	4,5	ABAZOV	12U D0	$p\bar{p}$ at 1.96 TeV
1.020 ± 0.030 ± 0.008	4	AALTONEN	11 CDF	$p\bar{p}$ at 1.96 TeV
• • • We do not use the following data for averages, fits, limits, etc. • • •				
0.976 ± 0.012 ± 0.006	6	AAIJ	13BB LHCb	Repl. by AAIJ 14U
0.811 $\begin{smallmatrix} +0.096 \\ -0.087 \end{smallmatrix}$ ± 0.034	4,5	ABAZOV	07S D0	Repl. by ABAZOV 12U
1.041 ± 0.057	7	ABULENCIA	07A CDF	Repl. by AALTONEN 11
0.87 $\begin{smallmatrix} +0.17 \\ -0.14 \end{smallmatrix}$ ± 0.03	7	ABAZOV	05C D0	Repl. by ABAZOV 07S

WEIGHTED AVERAGE  
0.970 ± 0.009 (Error scaled by 1.4)



# Baryon Particle Listings

## $\Lambda_b^0$

- <sup>1</sup> Measured using  $\Lambda_b^0 \rightarrow J/\psi\Lambda$  and  $B^0 \rightarrow J/\psi K^*(892)^0$  decays.
- <sup>2</sup> Used  $\Lambda_b^0 \rightarrow J/\psi p K^-$  and  $B^0 \rightarrow J/\psi K^*(892)^0$  decays.
- <sup>3</sup> Measured with  $\Lambda_b^0 \rightarrow J/\psi(\mu^+\mu^-) \Lambda^0(p\pi^-)$  decays.
- <sup>4</sup> Uses fully reconstructed  $\Lambda_b \rightarrow J/\psi\Lambda$  decays.
- <sup>5</sup> Uses  $B^0 \rightarrow J/\psi K_S^0$  decays for denominator.
- <sup>6</sup> Measures  $1/\tau_{\Lambda_b^0} - 1/\tau_{B^0}$  and uses  $\tau_{B^0} = 1.519 \pm 0.007$  ps to extract lifetime ratio.
- <sup>7</sup> Measured mean life ratio using fully reconstructed decays.

### $\Lambda_b^0$ DECAY MODES

The branching fractions  $B(b\text{-baryon} \rightarrow \Lambda \ell^- \bar{\nu}_\ell \text{anything})$  and  $B(\Lambda_b^0 \rightarrow \Lambda_c^+ \ell^- \bar{\nu}_\ell \text{anything})$  are not pure measurements because the underlying measured products of these with  $B(b \rightarrow b\text{-baryon})$  were used to determine  $B(b \rightarrow b\text{-baryon})$ , as described in the note "Production and Decay of  $b$ -Flavored Hadrons."

For inclusive branching fractions, e.g.,  $\Lambda_b \rightarrow \bar{\Lambda}_c \text{anything}$ , the values usually are multiplicities, not branching fractions. They can be greater than one.

Mode	Fraction ( $\Gamma_i/\Gamma$ )	Scale factor/ Confidence level
$\Gamma_1$ $J/\psi(1S) \Lambda \times B(b \rightarrow \Lambda_b^0)$	$(5.8 \pm 0.8) \times 10^{-5}$	
$\Gamma_2$ $J/\psi(1S) \Lambda$		
$\Gamma_3$ $\psi(2S) \Lambda$		
$\Gamma_4$ $p D^0 \pi^-$	$(6.3 \pm 0.7) \times 10^{-4}$	
$\Gamma_5$ $\Lambda_c(2860)^+ \pi^-$ , $\Lambda_c^+ \rightarrow D^0 p$		
$\Gamma_6$ $\Lambda_c(2880)^+ \pi^-$ , $\Lambda_c^+ \rightarrow D^0 p$		
$\Gamma_7$ $\Lambda_c(2940)^+ \pi^-$ , $\Lambda_c^+ \rightarrow D^0 p$		
$\Gamma_8$ $p D^0 K^-$	$(4.6 \pm 0.8) \times 10^{-5}$	
$\Gamma_9$ $p J/\psi \pi^-$	$(2.6^{+0.5}_{-0.4}) \times 10^{-5}$	
$\Gamma_{10}$ $p \pi^- J/\psi$ , $J/\psi \rightarrow \mu^+ \mu^-$	$(1.6 \pm 0.8) \times 10^{-6}$	
$\Gamma_{11}$ $p J/\psi K^-$	$(3.2^{+0.6}_{-0.5}) \times 10^{-4}$	
$\Gamma_{12}$ $P_c(4380)^+ K^-$ , $P_c \rightarrow p J/\psi$ [a]	$(2.7 \pm 1.4) \times 10^{-5}$	
$\Gamma_{13}$ $P_c(4450)^+ K^-$ , $P_c \rightarrow p J/\psi$ [a]	$(1.3 \pm 0.4) \times 10^{-5}$	
$\Gamma_{14}$ $\chi_{c1}(1P) p K^-$	$(7.6^{+1.5}_{-1.3}) \times 10^{-5}$	
$\Gamma_{15}$ $\chi_{c2}(1P) p K^-$	$(7.9^{+1.6}_{-1.4}) \times 10^{-5}$	
$\Gamma_{16}$ $p J/\psi(1S) \pi^+ \pi^- K^-$	$(6.6^{+1.3}_{-1.1}) \times 10^{-5}$	
$\Gamma_{17}$ $p \psi(2S) K^-$	$(6.6^{+1.2}_{-1.0}) \times 10^{-5}$	
$\Gamma_{18}$ $\chi_{c1}(3872) p K^-$		
$\Gamma_{19}$ $\chi_{c1}(3872) p K^-$ , $\chi_{c1}(3872) \rightarrow J/\psi \pi^+ \pi^-$	$(1.23 \pm 0.33) \times 10^{-6}$	
$\Gamma_{20}$ $\chi_{c1}(3872) \Lambda(1520)$		
$\Gamma_{21}$ $\psi(2S) p \pi^-$	$(7.5^{+1.6}_{-1.4}) \times 10^{-6}$	
$\Gamma_{22}$ $p \bar{K}^0 \pi^-$	$(1.3 \pm 0.4) \times 10^{-5}$	
$\Gamma_{23}$ $p K^0 K^-$	$< 3.5 \times 10^{-6}$	CL=90%
$\Gamma_{24}$ $\Lambda_c^+ \pi^-$	$(4.9 \pm 0.4) \times 10^{-3}$	S=1.2
$\Gamma_{25}$ $\Lambda_c^+ K^-$	$(3.59 \pm 0.30) \times 10^{-4}$	S=1.2
$\Gamma_{26}$ $\Lambda_c^+ \bar{\Delta}_1(1260)^-$	seen	
$\Gamma_{27}$ $\Lambda_c^+ D^-$	$(4.6 \pm 0.6) \times 10^{-4}$	
$\Gamma_{28}$ $\Lambda_c^+ D_s^-$	$(1.10 \pm 0.10) \%$	
$\Gamma_{29}$ $\Lambda_c^+ \pi^+ \pi^- \pi^-$	$(7.7 \pm 1.1) \times 10^{-3}$	S=1.1
$\Gamma_{30}$ $\Lambda_c(2595)^+ \pi^-$ , $\Lambda_c(2595)^+ \rightarrow \Lambda_c^+ \pi^+ \pi^-$	$(3.4 \pm 1.5) \times 10^{-4}$	
$\Gamma_{31}$ $\Lambda_c(2625)^+ \pi^-$ , $\Lambda_c(2625)^+ \rightarrow \Lambda_c^+ \pi^+ \pi^-$	$(3.3 \pm 1.3) \times 10^{-4}$	
$\Gamma_{32}$ $\Sigma_c(2455)^0 \pi^+ \pi^-$ , $\Sigma_c^0 \rightarrow \Lambda_c^+ \pi^-$	$(5.7 \pm 2.2) \times 10^{-4}$	
$\Gamma_{33}$ $\Sigma_c(2455)^{++} \pi^- \pi^-$ , $\Sigma_c^{++} \rightarrow \Lambda_c^+ \pi^+$	$(3.2 \pm 1.6) \times 10^{-4}$	
$\Gamma_{34}$ $\Lambda_c^+ p \bar{p} \pi^-$	$(2.65 \pm 0.29) \times 10^{-4}$	
$\Gamma_{35}$ $\Sigma_c(2455)^0 p \bar{p}$ , $\Sigma_c(2455)^0 \rightarrow \Lambda_c^+ \pi^-$	$(2.4 \pm 0.5) \times 10^{-5}$	
$\Gamma_{36}$ $\Sigma_c(2520)^0 p \bar{p}$ , $\Sigma_c(2520)^0 \rightarrow \Lambda_c^+ \pi^-$	$(3.2 \pm 0.7) \times 10^{-5}$	
$\Gamma_{37}$ $\Lambda K^0 2\pi^+ 2\pi^-$		
$\Gamma_{38}$ $\Lambda_c^+ \ell^- \bar{\nu}_\ell \text{anything}$ [b]	$(10.9 \pm 2.2) \%$	
$\Gamma_{39}$ $\Lambda_c^+ \ell^- \bar{\nu}_\ell$	$(6.2^{+1.4}_{-1.3}) \%$	

$\Gamma_{40}$ $\Lambda_c^+ \pi^+ \pi^- \ell^- \bar{\nu}_\ell$	$(5.6 \pm 3.1) \%$	
$\Gamma_{41}$ $\Lambda_c(2595)^+ \ell^- \bar{\nu}_\ell$	$(7.9^{+4.0}_{-3.5}) \times 10^{-3}$	
$\Gamma_{42}$ $\Lambda_c(2625)^+ \ell^- \bar{\nu}_\ell$	$(1.3^{+0.6}_{-0.5}) \%$	
$\Gamma_{43}$ $\Sigma_c(2455)^0 \pi^+ \ell^- \bar{\nu}_\ell$		
$\Gamma_{44}$ $\Sigma_c(2455)^{++} \pi^- \ell^- \bar{\nu}_\ell$		
$\Gamma_{45}$ $p h^-$	$[c] < 2.3 \times 10^{-5}$	CL=90%
$\Gamma_{46}$ $p \pi^-$	$(4.5 \pm 0.8) \times 10^{-6}$	
$\Gamma_{47}$ $p K^-$	$(5.4 \pm 1.0) \times 10^{-6}$	
$\Gamma_{48}$ $p D_s^-$	$< 4.8 \times 10^{-4}$	CL=90%
$\Gamma_{49}$ $p \mu^- \bar{\nu}_\mu$	$(4.1 \pm 1.0) \times 10^{-4}$	
$\Gamma_{50}$ $\Lambda \mu^+ \mu^-$	$(1.08 \pm 0.28) \times 10^{-6}$	
$\Gamma_{51}$ $p \pi^- \mu^+ \mu^-$	$(6.9 \pm 2.5) \times 10^{-8}$	
$\Gamma_{52}$ $\Lambda \gamma$	$(7.1 \pm 1.7) \times 10^{-6}$	
$\Gamma_{53}$ $\Lambda \eta$	$(9^{+7}_{-5}) \times 10^{-6}$	
$\Gamma_{54}$ $\Lambda \eta'(958)$	$< 3.1 \times 10^{-6}$	CL=90%
$\Gamma_{55}$ $\Lambda \pi^+ \pi^-$	$(4.7 \pm 1.9) \times 10^{-6}$	
$\Gamma_{56}$ $\Lambda K^+ \pi^-$	$(5.7 \pm 1.3) \times 10^{-6}$	
$\Gamma_{57}$ $\Lambda K^+ K^-$	$(1.62 \pm 0.23) \times 10^{-5}$	
$\Gamma_{58}$ $\Lambda \phi$	$(9.8 \pm 2.6) \times 10^{-6}$	
$\Gamma_{59}$ $p \pi^- \pi^+ \pi^-$	$(2.11 \pm 0.23) \times 10^{-5}$	
$\Gamma_{60}$ $p K^- K^+ \pi^-$	$(4.1 \pm 0.6) \times 10^{-6}$	
$\Gamma_{61}$ $p K^- \pi^+ \pi^-$	$(5.1 \pm 0.5) \times 10^{-5}$	
$\Gamma_{62}$ $p K^- K^+ K^-$	$(1.27 \pm 0.14) \times 10^{-5}$	

[a]  $P_c^+$  is a pentaquark-charmonium state.

[b] Not a pure measurement. See note at head of  $\Lambda_b^0$  Decay Modes.

[c] Here  $h^-$  means  $\pi^-$  or  $K^-$ .

### CONSTRAINED FIT INFORMATION

An overall fit to 10 branching ratios uses 12 measurements and one constraint to determine 7 parameters. The overall fit has a  $\chi^2 = 10.7$  for 6 degrees of freedom.

The following *off-diagonal* array elements are the correlation coefficients  $\langle \delta x_i \delta x_j \rangle / (\delta x_i \delta x_j)$ , in percent, from the fit to the branching fractions,  $x_i \equiv \Gamma_i/\Gamma_{\text{total}}$ . The fit constrains the  $x_i$  whose labels appear in this array to sum to one.

$x_{25}$	94				
$x_{29}$	50	47			
$x_{39}$	14	14	7		
$x_{46}$	0	0	0	0	
$x_{47}$	0	0	0	0	82
	$x_{24}$	$x_{25}$	$x_{29}$	$x_{39}$	$x_{46}$

### $\Lambda_b^0$ BRANCHING RATIOS

$\Gamma(J/\psi(1S) \Lambda \times B(b \rightarrow \Lambda_b^0)) / \Gamma_{\text{total}}$   $\Gamma_1/\Gamma$

VALUE (units $10^{-5}$ )	EVTs	DOCUMENT ID	TECN	COMMENT
<b>5.8 ± 0.8 OUR AVERAGE</b>				
6.01 ± 0.60 ± 0.58 ± 0.28		<sup>1</sup> ABAZOV	11o D0	$p\bar{p}$ at 1.96 TeV
4.7 ± 2.3 ± 0.2		<sup>2</sup> ABE	97B CDF	$p\bar{p}$ at 1.8 TeV

• • • We do not use the following data for averages, fits, limits, etc. • • •

- 180 ± 60 ± 90 16 ALBAJAR 91E UA1  $p\bar{p}$  at 630 GeV
- <sup>1</sup> ABAZOV 11o uses  $B(B^0 \rightarrow J/\psi K_S^0) \times B(b \rightarrow B^0) = (1.74 \pm 0.08) \times 10^{-4}$  to obtain the result. The  $(\pm 0.08) \times 10^{-4}$  uncertainty of this product is listed as the last uncertainty of the measurement,  $(\pm 0.28) \times 10^{-5}$ .
- <sup>2</sup> ABE 97B reports  $[B(\Lambda_b^0 \rightarrow J/\psi \Lambda) \times B(b \rightarrow \Lambda_b^0)] / [B(B^0 \rightarrow J/\psi K_S^0) \times B(b \rightarrow B^0)] = 0.27 \pm 0.12 \pm 0.05$ . We multiply by our best value  $B(B^0 \rightarrow J/\psi K_S^0) \times B(b \rightarrow B^0) = (1.74 \pm 0.08) \times 10^{-4}$ . Our first error is their experiment error and our second error is the systematic error from using our best value.

$\Gamma(\psi(2S) \Lambda) / \Gamma(J/\psi(1S) \Lambda)$   $\Gamma_3/\Gamma_2$

VALUE	DOCUMENT ID	TECN	COMMENT
<b>0.508 ± 0.023 OUR AVERAGE</b>			
0.513 ± 0.023 ± 0.019	<sup>1</sup> AAIJ	19F LHCb	$p\bar{p}$ at 7, 8 TeV
0.50 ± 0.03 ± 0.02	<sup>2</sup> AAD	15CH ATLAS	$p\bar{p}$ at 8 TeV

- <sup>1</sup> AAIJ 19f uses  $B(J/\psi \rightarrow \mu^+ \mu^-) = (5.961 \pm 0.033) \times 10^{-2}$  and  $B(\psi(2S) \rightarrow e^+ e^-) = (7.93 \pm 0.17) \times 10^{-3}$  from PDG 18 with assumption of lepton universality. AAIJ 19f reports this result as  $0.513 \pm 0.023 \pm 0.016 \pm 0.011$ , where the last uncertainty is the contribution due to the external input of branching fractions used in the analysis.
- <sup>2</sup> AAD 15CH uses  $B(J/\psi \rightarrow \mu^+ \mu^-) = (5.961 \pm 0.033) \times 10^{-2}$  and  $B(\psi(2S) \rightarrow \mu^+ \mu^-) = (7.89 \pm 0.17) \times 10^{-3}$  from PDG 14 with assumption of lepton universality.



## Baryon Particle Listings

$\Lambda_b^0$			
$\Gamma(\Lambda_c^+ D_s^-)/\Gamma_{\text{total}}$ <span style="float:right">Γ<sub>28</sub>/Γ</span>			
<u>VALUE</u> (units 10 <sup>-2</sup> )	<u>DOCUMENT ID</u>	<u>TECN</u>	<u>COMMENT</u>
<b>1.1 ± 0.1</b>	1 AAIJ	14AA LHCb	$p\bar{p}$ at 7 TeV
1 Uses $B(\bar{B}^0 \rightarrow D^+ D_s^-) = (7.2 \pm 0.8) \times 10^{-3}$ and their measured $B(\Lambda_b^0 \rightarrow \Lambda_c^+ \pi^-)/B(\bar{B}^0 \rightarrow D^+ \pi^-)$ values.			
$\Gamma(\Lambda_c^+ D^-)/\Gamma(\Lambda_c^+ D_s^-)$ <span style="float:right">Γ<sub>27</sub>/Γ<sub>28</sub></span>			
<u>VALUE</u>	<u>DOCUMENT ID</u>	<u>TECN</u>	<u>COMMENT</u>
<b>0.042 ± 0.003 ± 0.003</b>	AAIJ	14AA LHCb	$p\bar{p}$ at 7 TeV
$\Gamma(\Lambda_c^+ \pi^+ \pi^- \pi^-)/\Gamma_{\text{total}}$ <span style="float:right">Γ<sub>29</sub>/Γ</span>			
<u>VALUE</u> (units 10 <sup>-3</sup> )	<u>EVTS</u>	<u>DOCUMENT ID</u>	<u>TECN</u>
<b>7.7 ± 1.1 OUR FIT</b>	Error includes scale factor of 1.1.		
<b>14.9 ± 3.8 ± 1.2</b>	1 AALTONEN	12A CDF	$p\bar{p}$ at 1.96 TeV
• • • We do not use the following data for averages, fits, limits, etc. • • •			
seen	90	BARI	91 SFM $\Lambda_c^+ \rightarrow p K^- \pi^+$
1 AALTONEN 12A reports $[\Gamma(\Lambda_b^0 \rightarrow \Lambda_c^+ \pi^+ \pi^- \pi^-)/\Gamma_{\text{total}}] / [B(\Lambda_b^0 \rightarrow \Lambda_c^+ \pi^-)] = 3.04 \pm 0.33^{+0.70}_{-0.55}$ which we multiply by our best value $B(\Lambda_b^0 \rightarrow \Lambda_c^+ \pi^-) = (4.9 \pm 0.4) \times 10^{-3}$ . Our first error is their experiment's error and our second error is the systematic error from using our best value.			
$\Gamma(\Lambda_c^+ \pi^+ \pi^- \pi^-)/\Gamma(\Lambda_c^+ \pi^-)$ <span style="float:right">Γ<sub>29</sub>/Γ<sub>24</sub></span>			
<u>VALUE</u>	<u>DOCUMENT ID</u>	<u>TECN</u>	<u>COMMENT</u>
<b>1.56 ± 0.21 OUR FIT</b>			
<b>1.43 ± 0.16 ± 0.13</b>	AAIJ	11E LHCb	$p\bar{p}$ at 7 TeV
$\Gamma(\Lambda_c(2595)^+ \pi^-, \Lambda_c(2595)^+ \rightarrow \Lambda_c^+ \pi^+ \pi^-)/\Gamma(\Lambda_c^+ \pi^+ \pi^- \pi^-)$ <span style="float:right">Γ<sub>30</sub>/Γ<sub>29</sub></span>			
<u>VALUE</u> (units 10 <sup>-2</sup> )	<u>DOCUMENT ID</u>	<u>TECN</u>	<u>COMMENT</u>
<b>4.4 ± 1.7 ± 0.6 ± 0.4</b>	AAIJ	11E LHCb	$p\bar{p}$ at 7 TeV
$\Gamma(\Lambda_c(2625)^+ \pi^-, \Lambda_c(2625)^+ \rightarrow \Lambda_c^+ \pi^+ \pi^-)/\Gamma(\Lambda_c^+ \pi^+ \pi^- \pi^-)$ <span style="float:right">Γ<sub>31</sub>/Γ<sub>29</sub></span>			
<u>VALUE</u> (units 10 <sup>-2</sup> )	<u>DOCUMENT ID</u>	<u>TECN</u>	<u>COMMENT</u>
<b>4.3 ± 1.5 ± 0.4</b>	AAIJ	11E LHCb	$p\bar{p}$ at 7 TeV
$\Gamma(\Sigma_c(2455)^0 \pi^+ \pi^-, \Sigma_c^0 \rightarrow \Lambda_c^+ \pi^-)/\Gamma(\Lambda_c^+ \pi^+ \pi^- \pi^-)$ <span style="float:right">Γ<sub>32</sub>/Γ<sub>29</sub></span>			
<u>VALUE</u> (units 10 <sup>-2</sup> )	<u>DOCUMENT ID</u>	<u>TECN</u>	<u>COMMENT</u>
<b>7.4 ± 2.4 ± 1.2</b>	AAIJ	11E LHCb	$p\bar{p}$ at 7 TeV
$\Gamma(\Sigma_c(2455)^{++} \pi^- \pi^-, \Sigma_c^{++} \rightarrow \Lambda_c^+ \pi^+)/\Gamma(\Lambda_c^+ \pi^+ \pi^- \pi^-)$ <span style="float:right">Γ<sub>33</sub>/Γ<sub>29</sub></span>			
<u>VALUE</u> (units 10 <sup>-2</sup> )	<u>DOCUMENT ID</u>	<u>TECN</u>	<u>COMMENT</u>
<b>4.2 ± 1.8 ± 0.7</b>	AAIJ	11E LHCb	$p\bar{p}$ at 7 TeV
$\Gamma(\Lambda_c^+ \rho \bar{p} \pi^-)/\Gamma(\Lambda_c^+ \pi^-)$ <span style="float:right">Γ<sub>34</sub>/Γ<sub>24</sub></span>			
<u>VALUE</u> (units 10 <sup>-2</sup> )	<u>DOCUMENT ID</u>	<u>TECN</u>	<u>COMMENT</u>
<b>5.40 ± 0.23 ± 0.32</b>	AAIJ	18AWLHCb	$p\bar{p}$ at 7 and 8 TeV
$\Gamma(\Sigma_c(2455)^0 \rho \bar{p}, \Sigma_c(2455)^0 \rightarrow \Lambda_c^+ \pi^-)/\Gamma(\Lambda_c^+ \rho \bar{p} \pi^-)$ <span style="float:right">Γ<sub>35</sub>/Γ<sub>34</sub></span>			
<u>VALUE</u> (units 10 <sup>-2</sup> )	<u>DOCUMENT ID</u>	<u>TECN</u>	<u>COMMENT</u>
<b>8.9 ± 1.5 ± 0.6</b>	AAIJ	18AWLHCb	$p\bar{p}$ at 7 and 8 TeV
$\Gamma(\Sigma_c(2520)^0 \rho \bar{p}, \Sigma_c(2520)^0 \rightarrow \Lambda_c^+ \pi^-)/\Gamma(\Lambda_c^+ \rho \bar{p} \pi^-)$ <span style="float:right">Γ<sub>36</sub>/Γ<sub>34</sub></span>			
<u>VALUE</u>	<u>DOCUMENT ID</u>	<u>TECN</u>	<u>COMMENT</u>
<b>0.119 ± 0.020 ± 0.014</b>	AAIJ	18AWLHCb	$p\bar{p}$ at 7 and 8 TeV
$\Gamma(\Lambda K^0 2\pi^+ 2\pi^-)/\Gamma_{\text{total}}$ <span style="float:right">Γ<sub>37</sub>/Γ</span>			
<u>VALUE</u>	<u>EVTS</u>	<u>DOCUMENT ID</u>	<u>TECN</u>
• • • We do not use the following data for averages, fits, limits, etc. • • •			
seen	4	1 ARENTON	86 FMPS $\Lambda K_S^0 2\pi^+ 2\pi^-$
1 See the footnote to the ARENTON 86 mass value.			
$\Gamma(\Lambda_c^+ \ell^- \bar{\nu}_\ell \text{ anything})/\Gamma_{\text{total}}$ <span style="float:right">Γ<sub>38</sub>/Γ</span>			
The values and averages in this section serve only to show what values result if one assumes our $B(b \rightarrow b\text{-baryon})$ . They cannot be thought of as measurements since the underlying product branching fractions were also used to determine $B(b \rightarrow b\text{-baryon})$ as described in the note on "Production and Decay of $b$ -Flavored Hadrons."			
<u>VALUE</u>	<u>EVTS</u>	<u>DOCUMENT ID</u>	<u>TECN</u>
<b>0.109 ± 0.022 OUR AVERAGE</b>			
0.102 ± 0.019 ± 0.013		1 BARATE	98D ALEP $e^+ e^- \rightarrow Z$
0.14 ± 0.05 ± 0.02	29	2 ABREU	95S DLPH $e^+ e^- \rightarrow Z$
• • • We do not use the following data for averages, fits, limits, etc. • • •			
0.090 ± 0.022 ± 0.012	55	3 BUSKULIC	95L ALEP Repl. by BARATE 98D
0.18 ± 0.07 ± 0.02	21	4 BUSKULIC	92E ALEP $\Lambda_c^+ \rightarrow p K^- \pi^+$
1 BARATE 98D reports $[\Gamma(\Lambda_b^0 \rightarrow \Lambda_c^+ \ell^- \bar{\nu}_\ell \text{ anything})/\Gamma_{\text{total}}] \times [B(\bar{b} \rightarrow b\text{-baryon})] = 0.0086 \pm 0.0007 \pm 0.0014$ which we divide by our best value $B(\bar{b} \rightarrow b\text{-baryon}) = (8.4 \pm 1.1) \times 10^{-2}$ . Our first error is their experiment's error and our second error is the systematic error from using our best value. Measured using $\Lambda_c \ell^-$ and $\Lambda \ell^+ \ell^-$ .			
2 ABREU 95S reports $[\Gamma(\Lambda_b^0 \rightarrow \Lambda_c^+ \ell^- \bar{\nu}_\ell \text{ anything})/\Gamma_{\text{total}}] \times [B(\bar{b} \rightarrow b\text{-baryon})] = 0.0118 \pm 0.0026^{+0.0031}_{-0.0021}$ which we divide by our best value $B(\bar{b} \rightarrow b\text{-baryon}) = (8.4 \pm 1.1) \times 10^{-2}$ . Our first error is their experiment's error and our second error is the systematic error from using our best value.			
3 BUSKULIC 95L reports $[\Gamma(\Lambda_b^0 \rightarrow \Lambda_c^+ \ell^- \bar{\nu}_\ell \text{ anything})/\Gamma_{\text{total}}] \times [B(\bar{b} \rightarrow b\text{-baryon})] = 0.00755 \pm 0.0014 \pm 0.0012$ which we divide by our best value $B(\bar{b} \rightarrow b\text{-baryon}) = (8.4 \pm 1.1) \times 10^{-2}$ . Our first error is their experiment's error and our second error is the systematic error from using our best value.			
4 BUSKULIC 92E reports $[\Gamma(\Lambda_b^0 \rightarrow \Lambda_c^+ \ell^- \bar{\nu}_\ell \text{ anything})/\Gamma_{\text{total}}] \times [B(\bar{b} \rightarrow b\text{-baryon})] = 0.015 \pm 0.0035 \pm 0.0045$ which we divide by our best value $B(\bar{b} \rightarrow b\text{-baryon}) = (8.4 \pm 1.1) \times 10^{-2}$ . Our first error is their experiment's error and our second error is the systematic error from using our best value. Superseded by BUSKULIC 95L.			
$\Gamma(\Lambda_c^+ \ell^- \bar{\nu}_\ell)/\Gamma_{\text{total}}$ <span style="float:right">Γ<sub>39</sub>/Γ</span>			
<u>VALUE</u>	<u>DOCUMENT ID</u>	<u>TECN</u>	<u>COMMENT</u>
<b>0.062 ± 0.014 ± 0.013 OUR FIT</b>			
<b>0.050 ± 0.011 ± 0.016 ± 0.008 ± 0.012</b>	1 ABDALLAH	04A DLPH	$e^+ e^- \rightarrow Z^0$
1 Derived from a combined likelihood and event rate fit to the distribution of the $I_{\text{sgur}}$ -Wise variable and using HQET. The slope of the form factor is measured to be $\rho^2 = 2.03 \pm 0.46^{+0.72}_{-1.00}$ .			
$\Gamma(\Lambda_c^+ \ell^- \bar{\nu}_\ell)/\Gamma(\Lambda_c^+ \pi^-)$ <span style="float:right">Γ<sub>39</sub>/Γ<sub>24</sub></span>			
<u>VALUE</u>	<u>DOCUMENT ID</u>	<u>TECN</u>	<u>COMMENT</u>
<b>12.7 ± 3.1 ± 2.7 OUR FIT</b>			
<b>16.6 ± 3.0 ± 2.8 ± 3.6</b>	AALTONEN	09E CDF	$p\bar{p}$ at 1.96 TeV
$\Gamma(\Lambda_c^+ \pi^+ \pi^- \ell^- \bar{\nu}_\ell)/\Gamma_{\text{total}}$ <span style="float:right">Γ<sub>40</sub>/Γ</span>			
<u>VALUE</u>	<u>DOCUMENT ID</u>	<u>TECN</u>	<u>COMMENT</u>
<b>0.056 ± 0.031 ± 0.030</b>	1 ABDALLAH	04A DLPH	$e^+ e^- \rightarrow Z^0$
1 Derived from the fraction of $\Gamma(\Lambda_b^0 \rightarrow \Lambda_c^+ \ell^- \bar{\nu}_\ell) / (\Gamma(\Lambda_b^0 \rightarrow \Lambda_c^+ \ell^- \bar{\nu}_\ell) + \Gamma(\Lambda_b^0 \rightarrow \Lambda_c^+ \pi^+ \pi^- \ell^- \bar{\nu}_\ell)) = 0.47^{+0.10+0.07}_{-0.08-0.06}$ .			
$\Gamma(\Lambda_c^+ \ell^- \bar{\nu}_\ell) / [\Gamma(\Lambda_c^+ \ell^- \bar{\nu}_\ell) + \Gamma(\Lambda_c^+ \pi^+ \pi^- \ell^- \bar{\nu}_\ell)]$ <span style="float:right">Γ<sub>39</sub>/(Γ<sub>39</sub>+Γ<sub>40</sub>)</span>			
<u>VALUE</u>	<u>DOCUMENT ID</u>	<u>TECN</u>	<u>COMMENT</u>
<b>0.47 ± 0.10 ± 0.07 ± 0.08 ± 0.06</b>	ABDALLAH	04A DLPH	$e^+ e^- \rightarrow Z^0$
$\Gamma(\Lambda_c(2595)^+ \ell^- \bar{\nu}_\ell)/\Gamma(\Lambda_c^+ \ell^- \bar{\nu}_\ell)$ <span style="float:right">Γ<sub>41</sub>/Γ<sub>39</sub></span>			
<u>VALUE</u>	<u>DOCUMENT ID</u>	<u>TECN</u>	<u>COMMENT</u>
<b>0.126 ± 0.033 ± 0.047 ± 0.038</b>	AALTONEN	09E CDF	$p\bar{p}$ at 1.96 TeV
$\Gamma(\Lambda_c(2625)^+ \ell^- \bar{\nu}_\ell)/\Gamma(\Lambda_c^+ \ell^- \bar{\nu}_\ell)$ <span style="float:right">Γ<sub>42</sub>/Γ<sub>39</sub></span>			
<u>VALUE</u>	<u>DOCUMENT ID</u>	<u>TECN</u>	<u>COMMENT</u>
<b>0.210 ± 0.042 ± 0.071 ± 0.050</b>	AALTONEN	09E CDF	$p\bar{p}$ at 1.96 TeV
$[\frac{1}{2}\Gamma(\Sigma_c(2455)^0 \pi^+ \ell^- \bar{\nu}_\ell) + \frac{1}{2}\Gamma(\Sigma_c(2455)^{++} \pi^- \ell^- \bar{\nu}_\ell)] / \Gamma(\Lambda_c^+ \ell^- \bar{\nu}_\ell)$ <span style="float:right">(1/2)Γ<sub>43</sub> + (1/2)Γ<sub>44</sub>/Γ<sub>39</sub></span>			
<u>VALUE</u>	<u>DOCUMENT ID</u>	<u>TECN</u>	<u>COMMENT</u>
<b>0.054 ± 0.022 ± 0.021 ± 0.018</b>	AALTONEN	09E CDF	$p\bar{p}$ at 1.96 TeV
$\Gamma(\rho h^-)/\Gamma_{\text{total}}$ <span style="float:right">Γ<sub>45</sub>/Γ</span>			
<u>VALUE</u>	<u>CL%</u>	<u>DOCUMENT ID</u>	<u>TECN</u>
<b>&lt; 2.3 × 10<sup>-5</sup></b>	90	1 ACOSTA	05o CDF $p\bar{p}$ at 1.96 TeV
1 Assumes $f_A / f_d = 0.25$ , and equal momentum distribution for $\Lambda_b$ and $B$ mesons.			
$\Gamma(\rho \pi^-)/\Gamma_{\text{total}}$ <span style="float:right">Γ<sub>46</sub>/Γ</span>			
<u>VALUE</u> (units 10 <sup>-6</sup> )	<u>CL%</u>	<u>DOCUMENT ID</u>	<u>TECN</u>
<b>4.5 ± 0.8 OUR FIT</b>			
<b>4.0 ± 0.9 ± 0.5</b>		1 AALTONEN	09c CDF $p\bar{p}$ at 1.96 TeV
• • • We do not use the following data for averages, fits, limits, etc. • • •			
< 50	90	2 BUSKULIC	96v ALEP $e^+ e^- \rightarrow Z$
1 AALTONEN 09c reports $[\Gamma(\Lambda_b^0 \rightarrow \rho \pi^-)/\Gamma_{\text{total}}] / [B(\bar{b} \rightarrow B^0)] = 0.042 \pm 0.007 \pm 0.006$ which we multiply or divide by our best values $B(B^0 \rightarrow K^+ \pi^-) = (1.96 \pm 0.05) \times 10^{-5}$ , $B(\bar{b} \rightarrow b\text{-baryon}) = (8.4 \pm 1.1) \times 10^{-2}$ , $B(\bar{b} \rightarrow B^0) = (40.8 \pm 0.7) \times 10^{-2}$ . Our first error is their experiment's error and our second error is the systematic error from using our best values.			
2 BUSKULIC 96v assumes PDG 96 production fractions for $B^0, B^+, B_s, b$ baryons.			
$\Gamma(\rho K^-)/\Gamma_{\text{total}}$ <span style="float:right">Γ<sub>47</sub>/Γ</span>			
<u>VALUE</u> (units 10 <sup>-6</sup> )	<u>CL%</u>	<u>DOCUMENT ID</u>	<u>TECN</u>
<b>5.4 ± 1.0 OUR FIT</b>			
<b>6.3 ± 1.1 ± 0.8</b>		1 AALTONEN	09c CDF $p\bar{p}$ at 1.96 TeV
• • • We do not use the following data for averages, fits, limits, etc. • • •			
< 360	90	2 ADAM	96D DLPH $e^+ e^- \rightarrow Z$
< 50	90	3 BUSKULIC	96v ALEP $e^+ e^- \rightarrow Z$





## Baryon Particle Listings

 $\Lambda_b^0$  $B(\Lambda_b \rightarrow \Lambda \mu^+ \mu^-) (2.0 < q^2 < 4.3 \text{ GeV}^2/c^4)$ 

VALUE (units $10^{-7}$ )	DOCUMENT ID	TECN	COMMENT
<b>0.28 <math>\pm</math> 0.28 -0.21</b> OUR AVERAGE			
0.253 $\pm$ 0.276 $\pm$ 0.046	<sup>1</sup> AAIJ	15AE LHCB	$pp$ at 7, 8 TeV
1.8 $\pm$ 1.7 $\pm$ 0.6	AALTONEN	11AI CDF	$p\bar{p}$ at 1.96 TeV
• • • We do not use the following data for averages, fits, limits, etc. • • •			
0.71 $\pm$ 0.60 $\pm$ 0.23	<sup>2</sup> AAIJ	13AJ LHCB	Repl. by AAIJ 15AE
<sup>1</sup> AAIJ 15AE measurement covers $2.0 < q^2 < 4.0 \text{ GeV}^2/c^4$ .			
<sup>2</sup> Uses $B(\Lambda_b^0 \rightarrow J/\psi \Lambda) = (6.2 \pm 1.4) \times 10^{-4}$ .			

 $B(\Lambda_b \rightarrow \Lambda \mu^+ \mu^-) (q^2 < 4.3 \text{ GeV}^2/c^4)$ 

VALUE (units $10^{-7}$ )	DOCUMENT ID	TECN	COMMENT
<b>2.7 <math>\pm</math> 2.5 <math>\pm</math> 0.9</b>	AALTONEN	11AI CDF	$p\bar{p}$ at 1.96 TeV

 $B(\Lambda_b \rightarrow \Lambda \mu^+ \mu^-) (4.0 < q^2 < 6.0 \text{ GeV}^2/c^4)$ 

VALUE (units $10^{-7}$ )	DOCUMENT ID	TECN	COMMENT
<b>0.04 <math>\pm</math> 0.18 -0.00 <math>\pm</math> 0.02</b>	AAIJ	15AE LHCB	$pp$ at 7, 8 TeV

 $B(\Lambda_b \rightarrow \Lambda \mu^+ \mu^-) (1.0 < q^2 < 6.0 \text{ GeV}^2/c^4)$ 

VALUE (units $10^{-7}$ )	DOCUMENT ID	TECN	COMMENT
<b>0.47 <math>\pm</math> 0.31 -0.27</b> OUR AVERAGE			
0.45 $\pm$ 0.30 $\pm$ 0.10	<sup>1</sup> AAIJ	15AE LHCB	$pp$ at 7 and 8 TeV
1.3 $\pm$ 2.1 $\pm$ 0.4	AALTONEN	11AI CDF	$p\bar{p}$ at 1.96 TeV
<sup>1</sup> AAIJ 15AE measurement covers $1.1 < q^2 < 6.0 \text{ GeV}^2/c^4$ .			

 $B(\Lambda_b \rightarrow \Lambda \mu^+ \mu^-) (6.0 < q^2 < 8.0 \text{ GeV}^2/c^4)$ 

VALUE (units $10^{-7}$ )	DOCUMENT ID	TECN	COMMENT
<b>0.50 <math>\pm</math> 0.24 -0.22 <math>\pm</math> 0.10</b>	AAIJ	15AE LHCB	$pp$ at 7, 8 TeV

 $B(\Lambda_b \rightarrow \Lambda \mu^+ \mu^-) (4.3 < q^2 < 8.68 \text{ GeV}^2/c^4)$ 

VALUE (units $10^{-7}$ )	DOCUMENT ID	TECN	COMMENT
<b>0.5 <math>\pm</math> 0.7</b> OUR AVERAGE			
0.66 $\pm$ 0.74 $\pm$ 0.18	<sup>1</sup> AAIJ	13AJ LHCB	$pp$ at 7 TeV
-0.2 $\pm$ 1.6 $\pm$ 0.1	AALTONEN	11AI CDF	$p\bar{p}$ at 1.96 TeV
<sup>1</sup> Uses $B(\Lambda_b^0 \rightarrow J/\psi \Lambda) = (6.2 \pm 1.4) \times 10^{-4}$ .			

 $B(\Lambda_b \rightarrow \Lambda \mu^+ \mu^-) (10.09 < q^2 < 12.86 \text{ GeV}^2/c^4)$ 

VALUE (units $10^{-7}$ )	DOCUMENT ID	TECN	COMMENT
<b>2.2 <math>\pm</math> 0.6</b> OUR AVERAGE			
2.08 $\pm$ 0.42 $\pm$ 0.35	<sup>1</sup> AAIJ	15AE LHCB	$pp$ at 7, 8 TeV
3.0 $\pm$ 1.5 $\pm$ 1.0	AALTONEN	11AI CDF	$p\bar{p}$ at 1.96 TeV
• • • We do not use the following data for averages, fits, limits, etc. • • •			
1.55 $\pm$ 0.58 $\pm$ 0.55	<sup>2</sup> AAIJ	13AJ LHCB	Repl. by AAIJ 15AE
<sup>1</sup> AAIJ 15AE measurement covers $11.0 < q^2 < 12.5 \text{ GeV}^2/c^4$ .			
<sup>2</sup> Uses $B(\Lambda_b^0 \rightarrow J/\psi \Lambda) = (6.2 \pm 1.4) \times 10^{-4}$ .			

 $B(\Lambda_b \rightarrow \Lambda \mu^+ \mu^-) (14.18 < q^2 < 16.0 \text{ GeV}^2/c^4)$ 

VALUE (units $10^{-7}$ )	DOCUMENT ID	TECN	COMMENT
<b>1.7 <math>\pm</math> 0.5</b> OUR AVERAGE			Error includes scale factor of 1.1.
2.04 $\pm$ 0.35 $\pm$ 0.33	<sup>1</sup> AAIJ	15AE LHCB	$pp$ at 7, 8 TeV
1.0 $\pm$ 0.7 $\pm$ 0.3	AALTONEN	11AI CDF	$p\bar{p}$ at 1.96 TeV
• • • We do not use the following data for averages, fits, limits, etc. • • •			
1.44 $\pm$ 0.44 $\pm$ 0.42	<sup>2</sup> AAIJ	13AJ LHCB	Repl. by AAIJ 15AE
<sup>1</sup> AAIJ 15AE measurement covers $15.0 < q^2 < 16.0 \text{ GeV}^2/c^4$ .			
<sup>2</sup> Uses $B(\Lambda_b^0 \rightarrow J/\psi \Lambda) = (6.2 \pm 1.4) \times 10^{-4}$ .			

 $B(\Lambda_b \rightarrow \Lambda \mu^+ \mu^-) (16.0 < q^2 < 20.0 \text{ GeV}^2/c^4)$ 

VALUE (units $10^{-7}$ )	DOCUMENT ID	TECN	COMMENT
<b>7.0 <math>\pm</math> 1.9 <math>\pm</math> 2.2</b>	AALTONEN	11AI CDF	$p\bar{p}$ at 1.96 TeV
• • • We do not use the following data for averages, fits, limits, etc. • • •			
4.73 $\pm$ 0.77 $\pm$ 1.25	<sup>1,2</sup> AAIJ	13AJ LHCB	Repl. by AAIJ 15AE
<sup>1</sup> Uses $B(\Lambda_b^0 \rightarrow J/\psi \Lambda) = (6.2 \pm 1.4) \times 10^{-4}$ .			
<sup>2</sup> Requires $16.00 < q^2 < 20.30 \text{ GeV}^2/c^4$ .			

 $B(\Lambda_b \rightarrow \Lambda \mu^+ \mu^-) (18.0 < q^2 < 20.0 \text{ GeV}^2/c^4)$ 

VALUE (units $10^{-7}$ )	DOCUMENT ID	TECN	COMMENT
<b>2.44 <math>\pm</math> 0.28 <math>\pm</math> 0.50</b>	AAIJ	15AE LHCB	$pp$ at 7, 8 TeV

 $B(\Lambda_b \rightarrow \Lambda \mu^+ \mu^-) (15.0 < q^2 < 20.0 \text{ GeV}^2/c^4)$ 

VALUE (units $10^{-7}$ )	DOCUMENT ID	TECN	COMMENT
<b>6.00 <math>\pm</math> 0.45 <math>\pm</math> 1.25</b>	AAIJ	15AE LHCB	$pp$ at 7, 8 TeV

## CP VIOLATION

 $A_{CP}$  is defined as

$$A_{CP} = \frac{B(\Lambda_b^0 \rightarrow f) - B(\bar{\Lambda}_b^0 \rightarrow \bar{f})}{B(\Lambda_b^0 \rightarrow f) + B(\bar{\Lambda}_b^0 \rightarrow \bar{f})},$$

the CP-violation asymmetry of exclusive  $\Lambda_b^0$  and  $\bar{\Lambda}_b^0$  decay. $A_{CP}(\Lambda_b \rightarrow p \pi^-)$ 

VALUE	DOCUMENT ID	TECN	COMMENT
<b>-0.025 <math>\pm</math> 0.029</b> OUR AVERAGE			Error includes scale factor of 1.2.
-0.035 $\pm$ 0.017 $\pm$ 0.020	AAIJ	18AX LHCB	$pp$ at 7 and 8 TeV
0.06 $\pm$ 0.07 $\pm$ 0.03	AALTONEN	14P CDF	$p\bar{p}$ at 1.96 TeV
• • • We do not use the following data for averages, fits, limits, etc. • • •			
0.03 $\pm$ 0.17 $\pm$ 0.05	AALTONEN	11N CDF	Repl. by AALTONEN 14P

 $A_{CP}(\Lambda_b \rightarrow p K^-)$ 

VALUE	DOCUMENT ID	TECN	COMMENT
<b>-0.025 <math>\pm</math> 0.022</b> OUR AVERAGE			
-0.020 $\pm$ 0.013 $\pm$ 0.019	AAIJ	18AX LHCB	$pp$ at 7 and 8 TeV
-0.10 $\pm$ 0.08 $\pm$ 0.04	AALTONEN	14P CDF	$p\bar{p}$ at 1.96 TeV
• • • We do not use the following data for averages, fits, limits, etc. • • •			
0.37 $\pm$ 0.17 $\pm$ 0.03	AALTONEN	11N CDF	Repl. by AALTONEN 14P

 $\Delta A_{CP}(p K^- / \pi^-)$ 

VALUE	DOCUMENT ID	TECN	COMMENT
$\Delta A_{CP} \equiv A_{CP}(p K^-) - A_{CP}(p \pi^-)$			
<b>0.014 <math>\pm</math> 0.022 <math>\pm</math> 0.010</b>	AAIJ	18AX LHCB	$pp$ at 7 and 8 TeV

 $A_{CP}(\Lambda_b \rightarrow p \bar{K}^0 \pi^-)$ 

VALUE	DOCUMENT ID	TECN	COMMENT
<b>0.22 <math>\pm</math> 0.13 <math>\pm</math> 0.03</b>	AAIJ	14Q LHCB	$pp$ at 7 TeV

 $\Delta A_{CP}(J/\psi p \pi^- / K^-)$ 

VALUE (units $10^{-2}$ )	DOCUMENT ID	TECN	COMMENT
$\Delta A_{CP} \equiv A_{CP}(J/\psi p \pi^-) - A_{CP}(J/\psi p K^-)$			
<b>5.7 <math>\pm</math> 2.4 <math>\pm</math> 1.2</b>	AAIJ	14K LHCB	$pp$ at 7, 8 TeV

 $A_{CP}(\Lambda_b \rightarrow \Lambda K^+ \pi^-)$ 

VALUE	DOCUMENT ID	TECN	COMMENT
<b>-0.53 <math>\pm</math> 0.23 <math>\pm</math> 0.11</b>	<sup>1</sup> AAIJ	16W LHCB	$pp$ at 7, 8 TeV
<sup>1</sup> Measured relative to $\Lambda_b^0 \rightarrow \Lambda_c^+ \pi^-$ decay.			

 $A_{CP}(\Lambda_b \rightarrow \Lambda K^+ K^-)$ 

VALUE	DOCUMENT ID	TECN	COMMENT
<b>-0.28 <math>\pm</math> 0.10 <math>\pm</math> 0.07</b>	<sup>1</sup> AAIJ	16W LHCB	$pp$ at 7, 8 TeV
<sup>1</sup> Measured relative to $\Lambda_b^0 \rightarrow \Lambda_c^+ \pi^-$ decay.			

 $\Delta A_{CP}(\Lambda_b^0 \rightarrow p K^- \mu^+ \mu^-)$ 

VALUE (units $10^{-2}$ )	DOCUMENT ID	TECN	COMMENT
$\Delta A_{CP} \equiv A_{CP}(p K^- \mu^+ \mu^-) - A_{CP}(p K^- J/\psi)$			
<b>-3.5 <math>\pm</math> 5.0 <math>\pm</math> 0.2</b>	AAIJ	17T LHCB	$pp$ at 7, 8 TeV

 $\Delta A_{CP}(\Lambda_b^0 \rightarrow p \pi^- \pi^+ \pi^-)$ 

VALUE (units $10^{-2}$ )	DOCUMENT ID	TECN	COMMENT
$\Delta A_{CP} \equiv A_{CP}(\Lambda_b^0 \rightarrow p \pi^- \pi^+ \pi^-) - A_{CP}(\Lambda_b^0 \rightarrow (\Lambda_c^+ \rightarrow p \pi^- \pi^+) \pi^-)$			
<b>1.1 <math>\pm</math> 2.5 <math>\pm</math> 0.6</b>	<sup>1</sup> AAIJ	19AH LHCB	$pp$ at 7 and 8 TeV
<sup>1</sup> Full phase space.			

 $\Delta A_{CP}(\Lambda_b^0 \rightarrow (p \pi^- \pi^+ \pi^-)_{LBM})$ 

VALUE (units $10^{-2}$ )	DOCUMENT ID	TECN	COMMENT
$\Delta A_{CP} \equiv A_{CP}(\Lambda_b^0 \rightarrow (p \pi^- \pi^+ \pi^-)_{LBM}) - A_{CP}(\Lambda_b^0 \rightarrow (\Lambda_c^+ \rightarrow p \pi^- \pi^+) \pi^-)$			Two-body low invariant-mass region (LBM): $m(p \pi^-) < 2000 \text{ MeV}$ and $m(\pi^+ \pi^-) < 1640 \text{ MeV}$ .
<b>3.7 <math>\pm</math> 4.1 <math>\pm</math> 0.5</b>	<sup>1</sup> AAIJ	19AH LHCB	$pp$ at 7 and 8 TeV
<sup>1</sup> Measurement done with $m(p \pi^-) < 2000 \text{ MeV}/c^2$ and $m(\pi^+ \pi^-) < 1640 \text{ MeV}/c^2$ .			

 $\Delta A_{CP}(\Lambda_b^0 \rightarrow p a_1(1260)^-)$ 

VALUE (units $10^{-2}$ )	DOCUMENT ID	TECN	COMMENT
$\Delta A_{CP} \equiv A_{CP}(\Lambda_b^0 \rightarrow p a_1(1260)^-) - A_{CP}(\Lambda_b^0 \rightarrow (\Lambda_c^+ \rightarrow p \pi^- \pi^+) \pi^-)$			419 $< m(\pi^+ \pi^- \pi^+) < 1500 \text{ MeV}$ .
<b>-1.5 <math>\pm</math> 4.2 <math>\pm</math> 0.6</b>	AAIJ	19AH LHCB	$pp$ at 7 and 8 TeV

 $\Delta A_{CP}(\Lambda_b^0 \rightarrow N(1520)^0 \rho(770)^0)$ 

VALUE (units $10^{-2}$ )	DOCUMENT ID	TECN	COMMENT
$\Delta A_{CP} \equiv A_{CP}(\Lambda_b^0 \rightarrow N(1520)^0 \rho(770)^0) - A_{CP}(\Lambda_b^0 \rightarrow (\Lambda_c^+ \rightarrow p \pi^- \pi^+) \pi^-)$			1078 $< m(p \pi^-) < 1800 \text{ MeV}$ and $m(\pi^+ \pi^-) < 1100 \text{ MeV}$ .
<b>2.0 <math>\pm</math> 4.9 <math>\pm</math> 0.4</b>	AAIJ	19AH LHCB	$pp$ at 7 and 8 TeV

$\Delta A_{CP}(\Lambda_b^0 \rightarrow \Delta(1232)^{++}\pi^-\pi^-)$ 

$$\Delta A_{CP} \equiv A_{CP}(\Lambda_b^0 \rightarrow \Delta(1232)^{++}\pi^-\pi^-) - A_{CP}(\Lambda_b^0 \rightarrow (\Lambda_c^+ \rightarrow p\pi^-\pi^+)\pi^-). 1078 < m(p\pi^+) < 1432 \text{ MeV.}$$

VALUE (units $10^{-2}$ )	DOCUMENT ID	TECN	COMMENT
<b><math>0.1 \pm 3.2 \pm 0.6</math></b>	AAIJ	19AH LHCb	$pp$ at 7 and 8 TeV

 $\Delta A_{CP}(\Lambda_b^0 \rightarrow pK^-\pi^+\pi^-)$ 

$$\Delta A_{CP} \equiv A_{CP}(\Lambda_b^0 \rightarrow pK^-\pi^+\pi^-) - A_{CP}(\Lambda_b^0 \rightarrow (\Lambda_c^+ \rightarrow pK^-\pi^+)\pi^-)$$

VALUE (units $10^{-2}$ )	DOCUMENT ID	TECN	COMMENT
<b><math>3.2 \pm 1.1 \pm 0.6</math></b>	<sup>1</sup> AAIJ	19AH LHCb	$pp$ at 7 and 8 TeV

<sup>1</sup> Full phase space. $\Delta A_{CP}(\Lambda_b^0 \rightarrow (pK^-\pi^+\pi^-)_{LBM})$ 

$$\Delta A_{CP} \equiv A_{CP}(\Lambda_b^0 \rightarrow (pK^-\pi^+\pi^-)_{LBM}) - A_{CP}(\Lambda_b^0 \rightarrow (\Lambda_c^+ \rightarrow pK^-\pi^+)\pi^-).$$

Two-body low invariant-mass region (LBM):  $m(pK^-) < 2000 \text{ MeV}$  and  $m(\pi^+\pi^-) < 1640 \text{ MeV}$ .

VALUE (units $10^{-2}$ )	DOCUMENT ID	TECN	COMMENT
<b><math>3.5 \pm 1.5 \pm 0.5</math></b>	<sup>1</sup> AAIJ	19AH LHCb	$pp$ at 7 and 8 TeV

<sup>1</sup> Measurement done with  $m(pK^-) < 2000 \text{ MeV}/c^2$  and  $m(\pi^+\pi^-) < 1640 \text{ MeV}/c^2$ . $\Delta A_{CP}(\Lambda_b^0 \rightarrow N(1520)^0 K^*(892)^0)$ 

$$\Delta A_{CP} \equiv A_{CP}(\Lambda_b^0 \rightarrow N(1520)^0 K^*(892)^0) - A_{CP}(\Lambda_b^0 \rightarrow (\Lambda_c^+ \rightarrow pK^-\pi^+)\pi^-).$$

$1078 < m(p\pi^+) < 1800 \text{ MeV}$  and  $750 < m(\pi^+K^-) < 1100 \text{ MeV}$ .

VALUE (units $10^{-2}$ )	DOCUMENT ID	TECN	COMMENT
<b><math>5.5 \pm 2.5 \pm 0.5</math></b>	AAIJ	19AH LHCb	$pp$ at 7 and 8 TeV

 $\Delta A_{CP}(\Lambda_b^0 \rightarrow \Lambda(1520)\rho(770)^0)$ 

$$\Delta A_{CP} \equiv A_{CP}(\Lambda_b^0 \rightarrow \Lambda(1520)\rho(770)^0) - A_{CP}(\Lambda_b^0 \rightarrow (\Lambda_c^+ \rightarrow pK^-\pi^+)\pi^-).$$

$1460 < m(pK^-) < 1580 \text{ MeV}$  and  $m(\pi^+\pi^-) < 1100 \text{ MeV}$ .

VALUE (units $10^{-2}$ )	DOCUMENT ID	TECN	COMMENT
<b><math>0.6 \pm 6.0 \pm 0.5</math></b>	AAIJ	19AH LHCb	$pp$ at 7 and 8 TeV

 $\Delta A_{CP}(\Lambda_b^0 \rightarrow \Delta(1232)^{++}K^-\pi^-)$ 

$$\Delta A_{CP} \equiv A_{CP}(\Lambda_b^0 \rightarrow \Delta(1232)^{++}K^-\pi^-) - A_{CP}(\Lambda_b^0 \rightarrow (\Lambda_c^+ \rightarrow pK^-\pi^+)\pi^-).$$

$1078 < m(p\pi^+) < 1432 \text{ MeV}$ .

VALUE (units $10^{-2}$ )	DOCUMENT ID	TECN	COMMENT
<b><math>4.4 \pm 2.6 \pm 0.6</math></b>	AAIJ	19AH LHCb	$pp$ at 7 and 8 TeV

 $\Delta A_{CP}(\Lambda_b^0 \rightarrow pK_1(1410)^-)$ 

$$\Delta A_{CP} \equiv A_{CP}(\Lambda_b^0 \rightarrow pK_1(1410)^-) - A_{CP}(\Lambda_b^0 \rightarrow (\Lambda_c^+ \rightarrow pK^-\pi^+)\pi^-).$$

$1200 < m(K^-\pi^+\pi^-) < 1600 \text{ MeV}$ .

VALUE (units $10^{-2}$ )	DOCUMENT ID	TECN	COMMENT
<b><math>4.7 \pm 3.5 \pm 0.8</math></b>	AAIJ	19AH LHCb	$pp$ at 7 and 8 TeV

 $\Delta A_{CP}(\Lambda_b^0 \rightarrow pK^-K^+\pi^-)$ 

$$\Delta A_{CP} \equiv A_{CP}(\Lambda_b^0 \rightarrow pK^-K^+\pi^-) - A_{CP}(\Lambda_b^0 \rightarrow (\Lambda_c^+ \rightarrow p\pi^-\pi^+)\pi^-)$$

VALUE (units $10^{-2}$ )	DOCUMENT ID	TECN	COMMENT
<b><math>-6.9 \pm 4.9 \pm 0.8</math></b>	<sup>1</sup> AAIJ	19AH LHCb	$pp$ at 7 and 8 TeV

<sup>1</sup> Full phase space. $\Delta A_{CP}(\Lambda_b^0 \rightarrow pK^-K^+K^-)$ 

$$\Delta A_{CP} \equiv A_{CP}(\Lambda_b^0 \rightarrow pK^-K^+K^-) - A_{CP}(\Lambda_b^0 \rightarrow (\Lambda_c^+ \rightarrow pK^-\pi^+)\pi^-)$$

VALUE (units $10^{-2}$ )	DOCUMENT ID	TECN	COMMENT
<b><math>0.2 \pm 1.8 \pm 0.6</math></b>	<sup>1</sup> AAIJ	19AH LHCb	$pp$ at 7 and 8 TeV

<sup>1</sup> Full phase space. $\Delta A_{CP}(\Lambda_b^0 \rightarrow \Lambda(1520)\phi(1020))$ 

$$\Delta A_{CP} \equiv A_{CP}(\Lambda_b^0 \rightarrow \Lambda(1520)\phi(1020)) - A_{CP}(\Lambda_b^0 \rightarrow (\Lambda_c^+ \rightarrow pK^-\pi^+)\pi^-).$$

$1460 < m(pK^-) < 1600 \text{ MeV}$  and  $1005 < m(K^+K^-) < 1040 \text{ MeV}$ .

VALUE (units $10^{-2}$ )	DOCUMENT ID	TECN	COMMENT
<b><math>4.3 \pm 5.6 \pm 0.4</math></b>	AAIJ	19AH LHCb	$pp$ at 7 and 8 TeV

 $\Delta A_{CP}(\Lambda_b^0 \rightarrow (pK^-)_{\text{highmass}}\phi(1020))$ 

$$\Delta A_{CP} \equiv A_{CP}(\Lambda_b^0 \rightarrow (pK^-)_{\text{highmass}}\phi(1020)) - A_{CP}(\Lambda_b^0 \rightarrow (\Lambda_c^+ \rightarrow pK^-\pi^+)\pi^-).$$

$m(pK^-) > 1600 \text{ MeV}$  and  $1005 < m(K^+K^-) < 1040 \text{ MeV}$ .

VALUE (units $10^{-2}$ )	DOCUMENT ID	TECN	COMMENT
<b><math>-0.7 \pm 3.3 \pm 0.7</math></b>	<sup>1</sup> AAIJ	19AH LHCb	$pp$ at 7 and 8 TeV

<sup>1</sup> Measurement done with  $m(pK^-) > 1600 \text{ MeV}/c^2$ . $\Delta A_{CP}(\Lambda_b^0 \rightarrow (pK^-K^+K^-)_{LBM})$ 

$$\Delta A_{CP} \equiv A_{CP}(\Lambda_b^0 \rightarrow (pK^-K^+K^-)_{LBM}) - A_{CP}(\Lambda_b^0 \rightarrow (\Lambda_c^+ \rightarrow pK^-\pi^+)\pi^-).$$

Two-body low invariant-mass region (LBM):  $m(pK^-) < 2000 \text{ MeV}$  and  $m(K^+K^-) < 1675 \text{ MeV}$ .

VALUE (units $10^{-2}$ )	DOCUMENT ID	TECN	COMMENT
<b><math>2.7 \pm 2.3 \pm 0.6</math></b>	<sup>1</sup> AAIJ	19AH LHCb	$pp$ at 7 and 8 TeV

<sup>1</sup> Measurement done with  $m(pK^-) < 2000 \text{ MeV}/c^2$  and  $m(K^+K^-) < 1675 \text{ MeV}/c^2$ .

## CP AND T VIOLATION PARAMETERS

Measured values of the triple-product asymmetry parameters, odd under time-reversal, are defined as  $A_{c(s)}(\Lambda/\phi) = (N_{c(s)}^+ - N_{c(s)}^-) / (\text{sum})$

where  $N_{c(s)}^+$ ,  $N_{c(s)}^-$  are the number of  $\Lambda$  or  $\phi$  candidates for which the  $\cos(\Phi)$  and  $\sin(\Phi)$  observables are positive and negative, respectively. Angles  $\cos(\Phi)$  and  $\sin(\Phi)$  are defined as in LEITNER 07.

 $A_c(\Lambda)$ 

VALUE	DOCUMENT ID	TECN	COMMENT
<b><math>-0.22 \pm 0.12 \pm 0.06</math></b>	AAIJ	16J LHCb	$pp$ at 7, 8 TeV

 $A_s(\Lambda)$ 

VALUE	DOCUMENT ID	TECN	COMMENT
<b><math>0.13 \pm 0.12 \pm 0.05</math></b>	AAIJ	16J LHCb	$pp$ at 7, 8 TeV

 $A_c(\phi)$ 

VALUE	DOCUMENT ID	TECN	COMMENT
<b><math>-0.01 \pm 0.12 \pm 0.03</math></b>	AAIJ	16J LHCb	$pp$ at 7, 8 TeV

 $A_s(\phi)$ 

VALUE	DOCUMENT ID	TECN	COMMENT
<b><math>-0.07 \pm 0.12 \pm 0.01</math></b>	AAIJ	16J LHCb	$pp$ at 7, 8 TeV

 $a_{CP}(\Lambda_b^0 \rightarrow p\pi^-\pi^+\pi^-)$ 

Observable calculated as half of the difference between triple products for  $\Lambda_b^0$  and  $\bar{\Lambda}_b^0$ , which is sensitive to CP violation.

VALUE (%)	DOCUMENT ID	TECN	COMMENT
<b><math>1.15 \pm 1.45 \pm 0.32</math></b>	<sup>1</sup> AAIJ	17H LHCb	$pp$ at 7, 8 TeV

<sup>1</sup> Measured over full phase space of the decay. $a_{CP}(\Lambda_b^0 \rightarrow pK^-\pi^+\pi^-)$ 

Observable calculated as half of the difference between triple products for  $\Lambda_b^0$  and  $\bar{\Lambda}_b^0$ , which is sensitive to CP violation.

VALUE (%)	DOCUMENT ID	TECN	COMMENT
<b><math>-0.81 \pm 0.84 \pm 0.31</math></b>	<sup>1</sup> AAIJ	18AG LHCb	$pp$ at 7, 8 TeV

<sup>1</sup> Measured over full phase space of the decay. $a_{CP}(\Lambda_b^0 \rightarrow pK^-K^+\pi^-)$ 

Observable calculated as half of the difference between triple products for  $\Lambda_b^0$  and  $\bar{\Lambda}_b^0$ , which is sensitive to CP violation.

VALUE (%)	DOCUMENT ID	TECN	COMMENT
<b><math>-0.93 \pm 4.54 \pm 0.42</math></b>	<sup>1</sup> AAIJ	17H LHCb	$pp$ at 7, 8 TeV

<sup>1</sup> Measured over full phase space of the decay. $a_{CP}(\Lambda_b^0 \rightarrow pK^-K^+K^-)$ 

Observable calculated as half of the difference between triple products for  $\Lambda_b^0$  and  $\bar{\Lambda}_b^0$ , which is sensitive to CP violation.

VALUE (%)	DOCUMENT ID	TECN	COMMENT
<b><math>1.12 \pm 1.51 \pm 0.32</math></b>	<sup>1</sup> AAIJ	18AG LHCb	$pp$ at 7, 8 TeV

<sup>1</sup> Measured over full phase space of the decay. $a_{CP}(\Lambda_b^0 \rightarrow pK^-\mu^+\mu^-)$ 

VALUE (%)	DOCUMENT ID	TECN	COMMENT
<b><math>1.2 \pm 5.0 \pm 0.7</math></b>	AAIJ	17T LHCb	$pp$ at 7, 8 TeV

## P VIOLATION PARAMETERS

Observables calculated as average of the triple products for  $\Lambda_b^0$  and  $\bar{\Lambda}_b^0$ , which is sensitive to parity violation.

 $a_P(\Lambda_b^0 \rightarrow p\pi^-\pi^+\pi^-)$ 

VALUE (%)	DOCUMENT ID	TECN	COMMENT
<b><math>-3.71 \pm 1.45 \pm 0.32</math></b>	<sup>1</sup> AAIJ	17H LHCb	$pp$ at 7, 8 TeV

<sup>1</sup> Measured over full phase space of the decay. $a_P(\Lambda_b^0 \rightarrow pK^-\pi^+\pi^-)$ 

VALUE (%)	DOCUMENT ID	TECN	COMMENT
<b><math>-0.60 \pm 0.84 \pm 0.31</math></b>	<sup>1</sup> AAIJ	18AG LHCb	$pp$ at 7, 8 TeV

<sup>1</sup> Measured over full phase space of the decay. $a_P(\Lambda_b^0 \rightarrow pK^-K^+\pi^-)$ 

VALUE (%)	DOCUMENT ID	TECN	COMMENT
<b><math>3.62 \pm 4.54 \pm 0.42</math></b>	<sup>1</sup> AAIJ	17H LHCb	$pp$ at 7, 8 TeV

<sup>1</sup> Measured over full phase space of the decay. $a_P(\Lambda_b^0 \rightarrow pK^-K^+K^-)$ 

VALUE (%)	DOCUMENT ID	TECN	COMMENT
<b><math>-1.56 \pm 1.51 \pm 0.32</math></b>	<sup>1</sup> AAIJ	18AG LHCb	$pp$ at 7, 8 TeV

<sup>1</sup> Measured over full phase space of the decay.



See key on page 999

Baryon Particle Listings

$\Lambda_b(5912)^0, \Lambda_b(5920)^0, \Lambda_b(6146)^0, \Lambda_b(6152)^0$

**$\Lambda_b(5912)^0$**   $J^P = \frac{1}{2}^-$  Status: \*\*\*  
 Quantum numbers are based on quark model expectations.

**$\Lambda_b(5912)^0$  MASS**

VALUE (MeV)	DOCUMENT ID	TECN	COMMENT
<b>5912.20 ± 0.13 ± 0.17</b>	<sup>1,2</sup> AAIJ	12AL LHCb	$pp$ at 7 TeV

<sup>1</sup> Observed in  $\Lambda_b(5912)^0 \rightarrow \Lambda_b^0 \pi^+ \pi^-$  decays with  $17.6 \pm 4.8$  candidates with a significance of 5.2 sigma.  
<sup>2</sup> AAIJ 12AL measures  $m(\Lambda_b(5912)^0) - m(\Lambda_b^0) = 292.60 \pm 0.12 \pm 0.04$  MeV. We have adjusted the measurement to our best value of  $m(\Lambda_b^0) = 5619.60 \pm 0.17$  MeV. Our first error is their experiment's error and our second error is the systematic error from using our best values.

**$\Lambda_b(5912)^0$  WIDTH**

VALUE (MeV)	CL%	DOCUMENT ID	TECN	COMMENT
<b>&lt;0.66</b>	90	AAIJ	12AL LHCb	$pp$ at 7 TeV

**$\Lambda_b(5912)^0$  DECAY MODES**

Mode	Fraction ( $\Gamma_i/\Gamma$ )
$\Gamma_1 \Lambda_b^0 \pi^+ \pi^-$	seen

**$\Lambda_b(5912)^0$  BRANCHING RATIOS**

$\Gamma(\Lambda_b^0 \pi^+ \pi^-)/\Gamma_{\text{total}}$	$\Gamma_1/\Gamma$
seen	seen

**$\Lambda_b(5912)^0$  REFERENCES**

AAIJ	12AL PRL 109 172003	R. Aaij et al.	(LHCb Collab.)
------	---------------------	----------------	----------------

**$\Lambda_b(5920)^0$**   $J^P = \frac{3}{2}^-$  Status: \*\*\*  
 Quantum numbers are based on quark model expectations.

**$\Lambda_b(5920)^0$  MASS**

VALUE (MeV)	DOCUMENT ID	TECN	COMMENT
<b>5919.92 ± 0.19 OUR AVERAGE</b>	Error includes scale factor of 1.1.		
5919.4 ± 0.5 ± 0.2	<sup>1,2</sup> AALTONEN	13v CDF	$p\bar{p}$ at 1.96 TeV
5920.00 ± 0.09 ± 0.17	<sup>3,4</sup> AAIJ	12AL LHCb	$pp$ at 7 TeV

<sup>1</sup> Measured in  $\Lambda_b(5920)^0 \rightarrow \Lambda_b^0 \pi^+ \pi^-$  decays with  $17.3^{+5.3}_{-4.6}$  events, with a significance of 3.5 sigma.  
<sup>2</sup> AALTONEN 13v measures  $m(\Lambda_b(5920)^0) - m(\Lambda_b^0) - 2m(\pi) = 20.68 \pm 0.35 \pm 0.30$  MeV. We have adjusted the measurement to our best values of  $m(\Lambda_b^0) = 5619.60 \pm 0.17$  MeV and  $m(\pi) = 139.57039 \pm 0.00018$  MeV. Our first error is their experiment's error and our second error is the systematic error from using our best values.  
<sup>3</sup> Observed in  $\Lambda_b(5920)^0 \rightarrow \Lambda_b^0 \pi^+ \pi^-$  decays with  $52.5 \pm 8.1$  candidates with a significance of 10.2 sigma.  
<sup>4</sup> AAIJ 12AL measures  $m(\Lambda_b(5920)^0) - m(\Lambda_b^0) = 300.40 \pm 0.08 \pm 0.04$  MeV. We have adjusted the measurement to our best value of  $m(\Lambda_b^0) = 5619.60 \pm 0.17$  MeV. Our first error is their experiment's error and our second error is the systematic error from using our best values.

**$\Lambda_b(5920)^0$  WIDTH**

VALUE (MeV)	CL%	DOCUMENT ID	TECN	COMMENT
<b>&lt;0.63</b>	90	AAIJ	12AL LHCb	$pp$ at 7 TeV

**$\Lambda_b(5920)^0$  DECAY MODES**

Mode	Fraction ( $\Gamma_i/\Gamma$ )
$\Gamma_1 \Lambda_b^0 \pi^+ \pi^-$	seen

**$\Lambda_b(5920)^0$  BRANCHING RATIOS**

$\Gamma(\Lambda_b^0 \pi^+ \pi^-)/\Gamma_{\text{total}}$	$\Gamma_1/\Gamma$
seen	seen

**$\Lambda_b(5920)^0$  REFERENCES**

AALTONEN	13V PR D88 071101	T. Aaltonen et al.	(CDF Collab.)
AAIJ	12AL PRL 109 172003	R. Aaij et al.	(LHCb Collab.)

**$\Lambda_b(6146)^0$**   $J^P = \frac{3}{2}^+$  Status: \*\*\*  
 Quantum numbers are based on quark model expectations.

**$\Lambda_b(6146)^0$  MASS**

VALUE (MeV)	DOCUMENT ID	TECN	COMMENT
<b>6146.17 ± 0.33 ± 0.27</b>	<sup>1</sup> AAIJ	19AJ LHCb	$pp$ at 7, 8, 13 TeV

<sup>1</sup> Observed in  $\Lambda_b^0 \pi^+ \pi^-$  mode.

**$\Lambda_b(6146)^0$  WIDTH**

VALUE (MeV)	DOCUMENT ID	TECN	COMMENT
<b>2.9 ± 1.3 ± 0.3</b>	<sup>1</sup> AAIJ	19AJ LHCb	$pp$ at 7, 8, 13 TeV

<sup>1</sup> Observed in  $\Lambda_b^0 \pi^+ \pi^-$  mode.

**$m_{\Lambda_b(6146)^0} - m_{\Lambda_b^0}$**

VALUE (MeV)	DOCUMENT ID	TECN	COMMENT
<b>526.55 ± 0.33 ± 0.10</b>	<sup>1</sup> AAIJ	19AJ LHCb	$pp$ at 7, 8, 13 TeV

<sup>1</sup> Observed in  $\Lambda_b^0 \pi^+ \pi^-$  mode.

**$\Lambda_b(6146)^0$  DECAY MODES**

Mode	Fraction ( $\Gamma_i/\Gamma$ )
$\Gamma_1 \Lambda_b^0 \pi^+ \pi^-$	seen

**$\Lambda_b(6146)^0$  BRANCHING RATIOS**

$\Gamma(\Lambda_b^0 \pi^+ \pi^-)/\Gamma_{\text{total}}$	$\Gamma_1/\Gamma$
seen	seen

**$\Lambda_b(6146)^0$  REFERENCES**

AAIJ	19AJ PRL 123 152001	R. Aaij et al.	(LHCb Collab.)
------	---------------------	----------------	----------------

**$\Lambda_b(6152)^0$**   $J^P = \frac{5}{2}^+$  Status: \*\*\*  
 Quantum numbers are based on quark model expectations.

**$\Lambda_b(6152)^0$  MASS**

VALUE (MeV)	DOCUMENT ID	TECN	COMMENT
<b>6152.51 ± 0.26 ± 0.27</b>	<sup>1</sup> AAIJ	19AJ LHCb	$pp$ at 7, 8, 13 TeV

<sup>1</sup> Observed in  $\Lambda_b^0 \pi^+ \pi^-$  mode.

**$\Lambda_b(6152)^0$  WIDTH**

VALUE (MeV)	DOCUMENT ID	TECN	COMMENT
<b>2.1 ± 0.8 ± 0.3</b>	<sup>1</sup> AAIJ	19AJ LHCb	$pp$ at 7, 8, 13 TeV

<sup>1</sup> Observed in  $\Lambda_b^0 \pi^+ \pi^-$  mode.

**$m_{\Lambda_b(6152)^0} - m_{\Lambda_b^0}$**

VALUE (MeV)	DOCUMENT ID	TECN	COMMENT
<b>532.89 ± 0.26 ± 0.10</b>	<sup>1</sup> AAIJ	19AJ LHCb	$pp$ at 7, 8, 13 TeV

<sup>1</sup> Observed in  $\Lambda_b^0 \pi^+ \pi^-$  mode.

**$m_{\Lambda_b(6152)^0} - m_{\Lambda_b(6146)^0}$**

VALUE (MeV)	DOCUMENT ID	TECN	COMMENT
<b>6.34 ± 0.32 ± 0.02</b>	AAIJ	19AJ LHCb	$pp$ at 7, 8, 13 TeV

**$\Lambda_b(6152)^0$  DECAY MODES**

Mode	Fraction ( $\Gamma_i/\Gamma$ )
$\Gamma_1 \Lambda_b^0 \pi^+ \pi^-$	seen

**$\Lambda_b(6152)^0$  BRANCHING RATIOS**

$\Gamma(\Lambda_b^0 \pi^+ \pi^-)/\Gamma_{\text{total}}$	$\Gamma_1/\Gamma$
seen	seen

**$\Lambda_b(6152)^0$  REFERENCES**

AAIJ	19AJ PRL 123 152001	R. Aaij et al.	(LHCb Collab.)
------	---------------------	----------------	----------------

# Baryon Particle Listings

$\Sigma_b, \Sigma_b^*$

$\Sigma_b$

$I(J^P) = 1(\frac{1}{2}^+)$  Status: \*\*\*  
I, J, P need confirmation.

In the quark model  $\Sigma_b^+, \Sigma_b^0, \Sigma_b^-$  are an isotriplet ( $uub, udb, ddb$ ) state. The lowest  $\Sigma_b$  ought to have  $J^P = 1/2^+$ . None of I, J, or P have actually been measured.

## $\Sigma_b$ MASS

### $\Sigma_b^+$ MASS

VALUE (MeV)	DOCUMENT ID	TECN	COMMENT
<b>5810.56 ± 0.25 OUR AVERAGE</b>			
5810.55 ± 0.11 ± 0.23	<sup>1</sup> AAIJ	19A	LHCB $pp$ at 7, 8 TeV
5811.3 $^{+0.9}_{-0.8}$ ± 1.7	<sup>2</sup> AALTONEN	12F	CDF $p\bar{p}$ at 1.96 TeV
• • • We do not use the following data for averages, fits, limits, etc. • • •			
5807.8 $^{+2.0}_{-2.2}$ ± 1.7	<sup>3</sup> AALTONEN	07K	CDF Repl. by AALTONEN 12F
<sup>1</sup> Measured using fully reconstructed $\Lambda_b^0 \rightarrow \Lambda_c^+ \pi^-$ and $\Lambda_c^+ \rightarrow p K^- \pi^+$ decays.			
<sup>2</sup> Measured using fully reconstructed $\Lambda_b^0 \rightarrow \Lambda_c^+ \pi^-$ and $\Lambda_c^+ \rightarrow K^- \pi^+$ decays.			
<sup>3</sup> Observed four $\Lambda_b^0 \pi^\pm$ resonances in the fully reconstructed decay mode $\Lambda_b^0 \rightarrow \Lambda_c^+ \pi^-$ , where $\Lambda_c^+ \rightarrow p K^- \pi^+$ .			

### $\Sigma_b^0$ MASS

VALUE (MeV)	DOCUMENT ID	TECN	COMMENT
<b>5815.64 ± 0.27 OUR AVERAGE</b>			
5815.64 ± 0.14 ± 0.24	<sup>1</sup> AAIJ	19A	LHCB $pp$ at 7, 8 TeV
5815.5 $^{+0.6}_{-0.5}$ ± 1.7	<sup>2</sup> AALTONEN	12F	CDF $p\bar{p}$ at 1.96 TeV
• • • We do not use the following data for averages, fits, limits, etc. • • •			
5815.2 ± 1.0 ± 1.7	<sup>3</sup> AALTONEN	07K	CDF Repl. by AALTONEN 12F
<sup>1</sup> Measured using fully reconstructed $\Lambda_b^0 \rightarrow \Lambda_c^+ \pi^-$ and $\Lambda_c^+ \rightarrow p K^- \pi^+$ decays.			
<sup>2</sup> Measured using fully reconstructed $\Lambda_b^0 \rightarrow \Lambda_c^+ \pi^-$ and $\Lambda_c^+ \rightarrow K^- \pi^+$ decays.			
<sup>3</sup> Observed four $\Lambda_b^0 \pi^\pm$ resonances in the fully reconstructed decay mode $\Lambda_b^0 \rightarrow \Lambda_c^+ \pi^-$ , where $\Lambda_c^+ \rightarrow p K^- \pi^+$ .			

### $m_{\Sigma_b^+} - m_{\Sigma_b^-}$

VALUE (MeV)	DOCUMENT ID	TECN	COMMENT
<b>-5.06 ± 0.18 OUR AVERAGE</b>			
-5.09 ± 0.18 ± 0.01	<sup>1</sup> AAIJ	19A	LHCB $pp$ at 7, 8 TeV
-4.2 $^{+1.1}_{-1.0}$ ± 0.1	<sup>2</sup> AALTONEN	12F	CDF $p\bar{p}$ at 1.96 TeV
<sup>1</sup> Measured using fully reconstructed $\Lambda_b^0 \rightarrow \Lambda_c^+ \pi^-$ and $\Lambda_c^+ \rightarrow p K^- \pi^+$ decays.			
<sup>2</sup> Measured using fully reconstructed $\Lambda_b^0 \rightarrow \Lambda_c^+ \pi^-$ and $\Lambda_c^+ \rightarrow K^- \pi^+$ decays.			

## $\Sigma_b$ WIDTH

### $\Sigma_b^+$ WIDTH

VALUE (MeV)	DOCUMENT ID	TECN	COMMENT
<b>5.0 ± 0.5 OUR AVERAGE</b>			
4.83 ± 0.31 ± 0.37	<sup>1</sup> AAIJ	19A	LHCB $pp$ at 7, 8 TeV
9.7 $^{+3.8}_{-2.8}$ $^{+1.2}_{-1.1}$	<sup>2</sup> AALTONEN	12F	CDF $p\bar{p}$ at 1.96 TeV
<sup>1</sup> Measured using fully reconstructed $\Lambda_b^0 \rightarrow \Lambda_c^+ \pi^-$ and $\Lambda_c^+ \rightarrow p K^- \pi^+$ decays.			
<sup>2</sup> Measured using fully reconstructed $\Lambda_b^0 \rightarrow \Lambda_c^+ \pi^-$ and $\Lambda_c^+ \rightarrow K^- \pi^+$ decays.			

### $\Sigma_b^0$ WIDTH

VALUE (MeV)	DOCUMENT ID	TECN	COMMENT
<b>5.3 ± 0.5 OUR AVERAGE</b>			
5.33 ± 0.42 ± 0.37	<sup>1</sup> AAIJ	19A	LHCB $pp$ at 7, 8 TeV
4.9 $^{+3.1}_{-2.1}$ ± 1.1	<sup>2</sup> AALTONEN	12F	CDF $p\bar{p}$ at 1.96 TeV
<sup>1</sup> Measured using fully reconstructed $\Lambda_b^0 \rightarrow \Lambda_c^+ \pi^-$ and $\Lambda_c^+ \rightarrow p K^- \pi^+$ decays.			
<sup>2</sup> Measured using fully reconstructed $\Lambda_b^0 \rightarrow \Lambda_c^+ \pi^-$ and $\Lambda_c^+ \rightarrow K^- \pi^+$ decays.			

## $\Sigma_b$ DECAY MODES

Mode	Fraction ( $\Gamma_i/\Gamma$ )
$\Gamma_1 \Lambda_b^0 \pi$	dominant

## $\Sigma_b$ BRANCHING RATIOS

$\Gamma(\Lambda_b^0 \pi)/\Gamma_{\text{total}}$	$\Gamma_1/\Gamma$		
<b>dominant</b>	<b>dominant</b>		
VALUE	DOCUMENT ID	TECN	COMMENT
dominant	AALTONEN	07K	CDF $p\bar{p}$ at 1.96 TeV

## $\Sigma_b$ REFERENCES

AAIJ	19A	PRL 122 012001	R. Aaij et al.	(LHCb Collab.)
AALTONEN	12F	PR D85 092011	T. Aaltonen et al.	(CDF Collab.)
AALTONEN	07K	PRL 99 202001	T. Aaltonen et al.	(CDF Collab.)

$\Sigma_b^*$

$I(J^P) = 1(\frac{3}{2}^+)$  Status: \*\*\*  
I, J, P need confirmation.

I, J, P need confirmation. Quantum numbers shown are quark-model predictions.

## $\Sigma_b^*$ MASS

### $\Sigma_b^{*+}$ MASS

VALUE (MeV)	DOCUMENT ID	TECN	COMMENT
<b>5830.32 ± 0.27 OUR AVERAGE</b>			
5830.28 ± 0.14 ± 0.24	<sup>1</sup> AAIJ	19A	LHCB $pp$ at 7, 8 TeV
5832.1 ± 0.7 $^{+1.7}_{-1.8}$	<sup>2</sup> AALTONEN	12F	CDF $p\bar{p}$ at 1.96 TeV
<sup>1</sup> Measured using fully reconstructed $\Lambda_b^0 \rightarrow \Lambda_c^+ \pi^-$ and $\Lambda_c^+ \rightarrow p K^- \pi^+$ decays.			
<sup>2</sup> Measured using fully reconstructed $\Lambda_b^0 \rightarrow \Lambda_c^+ \pi^-$ and $\Lambda_c^+ \rightarrow K^- \pi^+$ decays.			

### $\Sigma_b^{*0}$ MASS

VALUE (MeV)	DOCUMENT ID	TECN	COMMENT
<b>5834.74 ± 0.30 OUR AVERAGE</b>			
5834.73 ± 0.17 ± 0.25	<sup>1</sup> AAIJ	19A	LHCB $pp$ at 7, 8 TeV
5835.1 ± 0.6 $^{+1.7}_{-1.8}$	<sup>2</sup> AALTONEN	12F	CDF $p\bar{p}$ at 1.96 TeV
<sup>1</sup> Measured using fully reconstructed $\Lambda_b^0 \rightarrow \Lambda_c^+ \pi^-$ and $\Lambda_c^+ \rightarrow p K^- \pi^+$ decays.			
<sup>2</sup> Measured using fully reconstructed $\Lambda_b^0 \rightarrow \Lambda_c^+ \pi^-$ and $\Lambda_c^+ \rightarrow K^- \pi^+$ decays.			

### $m_{\Sigma_b^{*+}} - m_{\Sigma_b^{*-}}$

VALUE (MeV)	DOCUMENT ID	TECN	COMMENT
<b>-4.37 ± 0.33 OUR AVERAGE</b>			Error includes scale factor of 1.6.
-4.45 ± 0.22 ± 0.01	<sup>1</sup> AAIJ	19A	LHCB $pp$ at 7, 8 TeV
-3.0 $^{+1.0}_{-0.9}$ ± 0.1	<sup>2</sup> AALTONEN	12F	CDF $p\bar{p}$ at 1.96 TeV
<sup>1</sup> Measured using fully reconstructed $\Lambda_b^0 \rightarrow \Lambda_c^+ \pi^-$ and $\Lambda_c^+ \rightarrow p K^- \pi^+$ decays.			
<sup>2</sup> Measured using fully reconstructed $\Lambda_b^0 \rightarrow \Lambda_c^+ \pi^-$ and $\Lambda_c^+ \rightarrow K^- \pi^+$ decays.			

### $m_{\Sigma_b^{*+}} - m_{\Sigma_b^+}$

VALUE (MeV)	DOCUMENT ID	TECN	COMMENT
<b>19.73 ± 0.18 ± 0.01</b>			
19.73 ± 0.18 ± 0.01	<sup>1</sup> AAIJ	19A	LHCB $pp$ at 7, 8 TeV
<sup>1</sup> Measured using fully reconstructed $\Lambda_b^0 \rightarrow \Lambda_c^+ \pi^-$ and $\Lambda_c^+ \rightarrow p K^- \pi^+$ decays.			

### $m_{\Sigma_b^{*0}} - m_{\Sigma_b^0}$

VALUE (MeV)	DOCUMENT ID	TECN	COMMENT
<b>19.09 ± 0.22 ± 0.02</b>			
19.09 ± 0.22 ± 0.02	<sup>1</sup> AAIJ	19A	LHCB $pp$ at 7, 8 TeV
<sup>1</sup> Measured using fully reconstructed $\Lambda_b^0 \rightarrow \Lambda_c^+ \pi^-$ and $\Lambda_c^+ \rightarrow p K^- \pi^+$ decays.			

## $\Sigma_b^*$ WIDTH

### $\Sigma_b^{*+}$ WIDTH

VALUE (MeV)	DOCUMENT ID	TECN	COMMENT
<b>9.4 ± 0.5 OUR AVERAGE</b>			
9.34 ± 0.47 ± 0.26	<sup>1</sup> AAIJ	19A	LHCB $pp$ at 7, 8 TeV
11.5 $^{+2.7}_{-2.2}$ $^{+1.0}_{-1.5}$	<sup>2</sup> AALTONEN	12F	CDF $p\bar{p}$ at 1.96 TeV
<sup>1</sup> Measured using fully reconstructed $\Lambda_b^0 \rightarrow \Lambda_c^+ \pi^-$ and $\Lambda_c^+ \rightarrow p K^- \pi^+$ decays.			
<sup>2</sup> Measured using fully reconstructed $\Lambda_b^0 \rightarrow \Lambda_c^+ \pi^-$ and $\Lambda_c^+ \rightarrow K^- \pi^+$ decays.			

### $\Sigma_b^{*0}$ WIDTH

VALUE (MeV)	DOCUMENT ID	TECN	COMMENT
<b>10.4 ± 0.8 OUR AVERAGE</b>			Error includes scale factor of 1.3.
10.68 ± 0.60 ± 0.33	<sup>1</sup> AAIJ	19A	LHCB $pp$ at 7, 8 TeV
7.5 $^{+2.2}_{-1.8}$ $^{+0.9}_{-1.4}$	<sup>2</sup> AALTONEN	12F	CDF $p\bar{p}$ at 1.96 TeV
<sup>1</sup> Measured using fully reconstructed $\Lambda_b^0 \rightarrow \Lambda_c^+ \pi^-$ and $\Lambda_c^+ \rightarrow p K^- \pi^+$ decays.			
<sup>2</sup> Measured using fully reconstructed $\Lambda_b^0 \rightarrow \Lambda_c^+ \pi^-$ and $\Lambda_c^+ \rightarrow K^- \pi^+$ decays.			

### $m_{\Sigma_b^{*+}} - m_{\Sigma_b^+}$

VALUE (MeV)	DOCUMENT ID	TECN	COMMENT
<b>21.2 <math>^{+2.0+0.4}_{-1.9-0.3}</math></b>			
21.2 $^{+2.0+0.4}_{-1.9-0.3}$	<sup>1</sup> AALTONEN	07K	CDF $p\bar{p}$ at 1.96 TeV
<sup>1</sup> Observed four $\Lambda_b^0 \pi^\pm$ resonances in the fully reconstructed decay mode $\Lambda_b^0 \rightarrow \Lambda_c^+ \pi^-$ , where $\Lambda_c^+ \rightarrow p K^- \pi^+$ . Assumes $m_{\Sigma_b^{*+}} - m_{\Sigma_b^+} = m_{\Sigma_b^{*0}} - m_{\Sigma_b^0}$ .			

## $\Sigma_b^*$ DECAY MODES

Mode	Fraction ( $\Gamma_i/\Gamma$ )
$\Gamma_1 \Lambda_b^0 \pi$	dominant

See key on page 999

Baryon Particle Listings

$\Sigma_b^*$ ,  $\Sigma_b(6097)^+$ ,  $\Sigma_b(6097)^-$ ,  $\Xi_b^0$ ,  $\Xi_b^-$

$\Sigma_b^*$  BRANCHING RATIOS

$\Gamma(\Lambda_b^0 \pi)/\Gamma_{\text{total}}$	DOCUMENT ID	TECN	COMMENT	$\Gamma_1/\Gamma$	
dominant	AALTONEN	07K	CDF	$p\bar{p}$ at 1.96 TeV	

$\Sigma_b^*$  REFERENCES

AAIJ	19A	PRL 122 012001	R. Aaij <i>et al.</i>	(LHCb Collab.)
AALTONEN	12F	PR D85 092011	T. Aaltonen <i>et al.</i>	(CDF Collab.)
AALTONEN	07K	PRL 99 202001	T. Aaltonen <i>et al.</i>	(CDF Collab.)

$\Sigma_b(6097)^+$	$J^P = ?^?$	Status: ***
--------------------	-------------	-------------

$\Sigma_b(6097)^+$  MASS

VALUE (MeV)	DOCUMENT ID	TECN	COMMENT
<b>6095.8 ± 1.7 ± 0.4</b>	<sup>1</sup> AAIJ	19A	LHCB $pp$ at 7, 8 TeV
<sup>1</sup> Measured using fully reconstructed $\Lambda_b^0 \rightarrow \Lambda_c^+ \pi^-$ and $\Lambda_c^+ \rightarrow p K^- \pi^+$ decays.			

$m_{\Sigma_b(6097)^+} - m_{\Sigma_b(6097)^-}$	DOCUMENT ID	TECN	COMMENT
-2.2 +2.4 +0.3 MeV	<sup>1</sup> AAIJ	19A	LHCB $pp$ at 7, 8 TeV
<sup>1</sup> Measured using fully reconstructed $\Lambda_b^0 \rightarrow \Lambda_c^+ \pi^-$ and $\Lambda_c^+ \rightarrow p K^- \pi^+$ decays.			

$\Sigma_b(6097)^+$  WIDTH

VALUE (MeV)	DOCUMENT ID	TECN	COMMENT
<b>31.0 ± 5.5 ± 0.7</b>	<sup>1</sup> AAIJ	19A	LHCB $pp$ at 7, 8 TeV
<sup>1</sup> Measured using fully reconstructed $\Lambda_b^0 \rightarrow \Lambda_c^+ \pi^-$ and $\Lambda_c^+ \rightarrow p K^- \pi^+$ decays.			

$\Sigma_b(6097)^+$  DECAY MODES

Mode	Fraction ( $\Gamma_i/\Gamma$ )
$\Gamma_1 \Lambda_b \pi^+ \times B(b \rightarrow \Sigma_b(6097)^+)$	seen

$\Sigma_b(6097)^+$  BRANCHING RATIOS

$\Gamma(\Lambda_b \pi^+ \times B(b \rightarrow \Sigma_b(6097)^+))/\Gamma_{\text{total}}$	DOCUMENT ID	TECN	COMMENT	$\Gamma_1/\Gamma$	
seen	AAIJ	19A	LHCB	$pp$ at 7, 8 TeV	

$\Sigma_b(6097)^+$  REFERENCES

AAIJ	19A	PRL 122 012001	R. Aaij <i>et al.</i>	(LHCb Collab.)
------	-----	----------------	-----------------------	----------------

$\Sigma_b(6097)^-$	$J^P = ?^?$	Status: ***
--------------------	-------------	-------------

$\Sigma_b(6097)^-$  MASS

VALUE (MeV)	DOCUMENT ID	TECN	COMMENT
<b>6098.0 ± 1.7 ± 0.5</b>	<sup>1</sup> AAIJ	19A	LHCB $pp$ at 7, 8 TeV
<sup>1</sup> Measured using fully reconstructed $\Lambda_b^0 \rightarrow \Lambda_c^+ \pi^-$ and $\Lambda_c^+ \rightarrow p K^- \pi^+$ decays.			

$\Sigma_b(6097)^-$  WIDTH

VALUE (MeV)	DOCUMENT ID	TECN	COMMENT
<b>28.9 ± 4.2 ± 0.9</b>	<sup>1</sup> AAIJ	19A	LHCB $pp$ at 7, 8 TeV
<sup>1</sup> Measured using fully reconstructed $\Lambda_b^0 \rightarrow \Lambda_c^+ \pi^-$ and $\Lambda_c^+ \rightarrow p K^- \pi^+$ decays.			

$\Sigma_b(6097)^-$  DECAY MODES

Mode	Fraction ( $\Gamma_i/\Gamma$ )
$\Gamma_1 \Lambda_b \pi^- \times B(b \rightarrow \Sigma_b(6097)^-)$	seen

$\Sigma_b(6097)^-$  BRANCHING RATIOS

$\Gamma(\Lambda_b \pi^- \times B(b \rightarrow \Sigma_b(6097)^-))/\Gamma_{\text{total}}$	DOCUMENT ID	TECN	COMMENT	$\Gamma_1/\Gamma$	
seen	AAIJ	19A	LHCB	$pp$ at 7, 8 TeV	

$\Sigma_b(6097)^-$  REFERENCES

AAIJ	19A	PRL 122 012001	R. Aaij <i>et al.</i>	(LHCb Collab.)
------	-----	----------------	-----------------------	----------------

$\Xi_b^0, \Xi_b^-$

$I(J^P) = \frac{1}{2}(\frac{1}{2}^+)$  Status: \*\*\*  
I, J, P need confirmation.

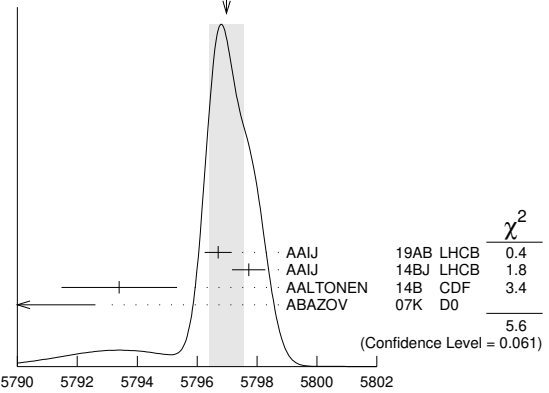
In the quark model,  $\Xi_b^0$  and  $\Xi_b^-$  are an isodoublet (*usb, dsb*) state; the lowest  $\Xi_b^0$  and  $\Xi_b^-$  ought to have  $J^P = 1/2^+$ . None of I, J, or P have actually been measured.

$\Xi_b$  MASSES

$\Xi_b^-$  MASS

VALUE (MeV)	DOCUMENT ID	TECN	COMMENT
<b>5797.0 ± 0.6 OUR AVERAGE</b>	Error includes scale factor of 1.7. See the ideogram below.		
5796.70 ± 0.39 ± 0.23	AAIJ	19AB	LHCB $pp$ at 7, 8 and 13 TeV
5797.72 ± 0.46 ± 0.31	<sup>1</sup> AAIJ	14BJ	LHCB $pp$ at 7, 8 TeV
5793.4 ± 1.8 ± 0.7	<sup>2</sup> AALTONEN	14B	CDF $p\bar{p}$ at 1.96 TeV
5774 ± 11 ± 15	<sup>3</sup> ABAZOV	07K	D0 $p\bar{p}$ at 1.96 TeV
••• We do not use the following data for averages, fits, limits, etc. •••			
5795.8 ± 0.9 ± 0.4	<sup>4</sup> AAIJ	13AV	LHCB Repl. by AAIJ 19AB
5796.7 ± 5.1 ± 1.4	<sup>5</sup> AALTONEN	11X	CDF Repl. by AALTONEN 14B
5790.9 ± 2.6 ± 0.8	<sup>6</sup> AALTONEN	09AP	CDF Repl. by AALTONEN 14B
5792.9 ± 2.5 ± 1.7	<sup>7</sup> AALTONEN	07A	CDF Repl. by AALTONEN 09AP
<sup>1</sup> Reconstructed in $\Xi_b^- \rightarrow \Xi_c^0 \pi^-$ , $\Xi_c^0 \rightarrow p K^- K^- \pi^+$ decays. Reference $\Lambda_b^0$ mass 5619.30 ± 0.34 MeV from AAIJ 14AA.			
<sup>2</sup> Uses $\Xi_b^- \rightarrow J/\psi \Xi^-$ and $\Xi_c^0 \pi^-$ decays.			
<sup>3</sup> Observed in $\Xi_b^- \rightarrow J/\psi \Xi^-$ decays with 15.2 ± 4.4 <sup>+1.9</sup> <sub>-0.4</sub> candidates, a significance of 5.5 sigma.			
<sup>4</sup> Measured in $\Xi_b^- \rightarrow J/\psi \Xi^-$ decays.			
<sup>5</sup> Measured in $\Xi_b^- \rightarrow \Xi_c^0 \pi^-$ with 25.8 <sup>+5.5</sup> <sub>-5.2</sub> candidates.			
<sup>6</sup> Measured in $\Xi_b^- \rightarrow J/\psi \Xi^-$ decays with 66 <sup>+14</sup> <sub>-9</sub> candidates.			
<sup>7</sup> Observed in $\Xi_b^- \rightarrow J/\psi \Xi^-$ decays with 17.5 ± 4.3 candidates, a significance of 7.7 sigma.			

WEIGHTED AVERAGE  
5797.0±0.6 (Error scaled by 1.7)



$\Xi_b^-$  MASS (MeV)

$\Xi_b^0$  MASS

VALUE (MeV)	DOCUMENT ID	TECN	COMMENT
<b>5791.9 ± 0.5 OUR AVERAGE</b>	Error includes scale factor of 1.6.		
5794.3 ± 2.4 ± 0.7	AAIJ	14H	LHCB $pp$ at 7 TeV
5791.80 ± 0.39 ± 0.31	<sup>1</sup> AAIJ	14Z	LHCB $pp$ at 7, 8 TeV
5788.7 ± 4.3 ± 1.4	<sup>2</sup> AALTONEN	14B	CDF $p\bar{p}$ at 1.96 TeV
••• We do not use the following data for averages, fits, limits, etc. •••			
5787.8 ± 5.0 ± 1.3	<sup>3</sup> AALTONEN	11X	CDF Repl. by AALTONEN 14B
<sup>1</sup> Uses $\Xi_b^0 \rightarrow \Xi_c^+ \pi^-$ and $\Xi_c^+ \rightarrow p K^- \pi^+$ decays. The measurement comes from the mass difference of $\Xi_b^0$ and $\Lambda_b^0$ .			
<sup>2</sup> Uses $\Xi_b^0 \rightarrow \Xi_c^+ \pi^-$ decays.			
<sup>3</sup> Measured in $\Xi_b^0 \rightarrow \Xi_c^+ \pi^-$ with 25.3 <sup>+5.6</sup> <sub>-5.4</sub> candidates.			

$m_{\Xi_b^-} - m_{\Lambda_b^0}$

VALUE (MeV)	DOCUMENT ID	TECN	COMMENT
<b>177.5 ± 0.5 OUR AVERAGE</b>	Error includes scale factor of 1.6.		
177.73 ± 0.33 ± 0.14	<sup>1</sup> AAIJ	17BE	LHCB $pp$ at 7, 8 TeV
176.2 ± 0.9 ± 0.1	<sup>2</sup> AAIJ	13AV	LHCB $pp$ at 7 TeV
••• We do not use the following data for averages, fits, limits, etc. •••			
177.08 ± 0.47 ± 0.16	<sup>3</sup> AAIJ	17BE	LHCB $pp$ at 7, 8 TeV
178.36 ± 0.46 ± 0.16	<sup>4,5</sup> AAIJ	14BJ	LHCB $pp$ at 7, 8 TeV
<sup>1</sup> Combination of the original statistically independent measurements of AAIJ 14BE and AAIJ 17BJ taking into account correlation between systematic uncertainties.			
<sup>2</sup> Reconstructed in $\Xi_b^- \rightarrow J/\psi \Xi^-$ decays.			
<sup>3</sup> Reconstructed in $\Xi_b^- \rightarrow J/\psi \Lambda K^-$ decays. Reference decays $\Lambda_b^0 \rightarrow J/\psi \Lambda$ were used.			
<sup>4</sup> Reconstructed in $\Xi_b^- \rightarrow \Xi_c^0 \pi^-$ , $\Xi_c^0 \rightarrow p K^- K^- \pi^+$ decays. Reference $\Lambda_b^0 \rightarrow \Lambda_c^+ \pi^-$ .			
<sup>5</sup> Combined with AAIJ 17BE.			

## Baryon Particle Listings

$$\Xi_b^0, \Xi_b^-$$

$$m_{\Xi_b^0} - m_{\Lambda_b^0}$$

VALUE (MeV)	DOCUMENT ID	TECN	COMMENT
<b>172.5 ± 0.4 OUR AVERAGE</b>			
174.8 ± 2.4 ± 0.5	<sup>1</sup> AAIJ	14H LHCb	$pp$ at 7 TeV
172.44 ± 0.39 ± 0.17	<sup>1</sup> AAIJ	14Z LHCb	$pp$ at 7, 8 TeV
<sup>1</sup> Uses $\Xi_b^0 \rightarrow \Xi_c^+ \pi^-$ and $\Xi_c^+ \rightarrow p K^- \pi^+$ decays.			

$$m_{\Xi_b^-} - m_{\Xi_b^0}$$

VALUE (MeV)	DOCUMENT ID	TECN	COMMENT
<b>5.9 ± 0.6 OUR AVERAGE</b>			
5.92 ± 0.60 ± 0.23	<sup>1</sup> AAIJ	14B LHCb	$pp$ at 7, 8 TeV
3.1 ± 5.6 ± 1.3	<sup>2</sup> AALTONEN	11X CDF	$p\bar{p}$ at 1.96 TeV
<sup>1</sup> Reconstructed in $\Xi_b^- \rightarrow \Xi_c^0 \pi^-$ , $\Xi_c^0 \rightarrow p K^- K^- \pi^+$ decays. Uses $m(\Xi_b^0) - m(\Lambda_b^0) = 172.44 \pm 0.39 \pm 0.17$ MeV from AAIJ 14Z.			
<sup>2</sup> Derived from measurements in $\Xi_b^- \rightarrow \Xi_c^+ \pi^-$ and $\Xi_b^- \rightarrow J/\psi \Xi^-$ from AALTONEN 09AP taking correlated systematic uncertainties into account.			

 $\Xi_b$  MEAN LIFE

"OUR EVALUATION" is an average using rescaled values of the data listed below. The average and rescaling were performed by the Heavy Flavor Averaging Group (HFLAV) and are described at <https://hflav.web.cern.ch/>. The averaging/rescaling procedure takes into account correlations between the measurements and asymmetric lifetime errors.

 $\Xi_b^-$  MEAN LIFE

VALUE ( $10^{-12}$ s)	DOCUMENT ID	TECN	COMMENT
<b>1.572 ± 0.040 OUR EVALUATION</b>			
<b>1.57 ± 0.04 OUR AVERAGE</b>			Error includes scale factor of 1.1.
1.599 ± 0.041 ± 0.022	<sup>1</sup> AAIJ	14B LHCb	$pp$ at 7, 8 TeV
1.55 $^{+0.10}_{-0.09}$ ± 0.03	<sup>2</sup> AAIJ	14T LHCb	$pp$ at 7, 8 TeV
1.36 ± 0.15 ± 0.02	AALTONEN	14B CDF	$p\bar{p}$ at 1.96 TeV
• • • We do not use the following data for averages, fits, limits, etc. • • •			
1.56 $^{+0.27}_{-0.25}$ ± 0.02	<sup>3</sup> AALTONEN	09AP CDF	Repl. by AALTONEN 14B
<sup>1</sup> Reconstructed in $\Xi_b^- \rightarrow \Xi_c^0 \pi^-$ , $\Xi_c^0 \rightarrow p K^- K^- \pi^+$ decays. Reference $\Lambda_b^0$ lifetime $1.479 \pm 0.009 \pm 0.010$ ps from AAIJ 14U.			
<sup>2</sup> Measured in $\Xi_b^- \rightarrow J/\psi \Xi^-$ decays.			
<sup>3</sup> Measured in $\Xi_b^- \rightarrow J/\psi \Xi^-$ decays with $66^{+14}_{-9}$ candidates.			

 $\Xi_b^0$  MEAN LIFE

VALUE ( $10^{-12}$ s)	DOCUMENT ID	TECN	COMMENT
<b>1.480 ± 0.030 OUR EVALUATION</b>			
<b>1.477 ± 0.026 ± 0.019</b>			
1.479 ± 0.009 ± 0.010	<sup>1</sup> AAIJ	14Z LHCb	$pp$ at 7, 8 TeV
<sup>1</sup> Uses $\Xi_b^0 \rightarrow \Xi_c^+ \pi^-$ and $\Xi_c^+ \rightarrow p K^- \pi^+$ decays. The measurement comes from the value of relative lifetime of $\Xi_b^0$ to $\Lambda_b^0$ .			

 $\Xi_b$  MEAN LIFE

VALUE ( $10^{-12}$ s)	DOCUMENT ID	TECN	COMMENT
• • • We do not use the following data for averages, fits, limits, etc. • • •			
1.48 $^{+0.40}_{-0.31}$ ± 0.12	<sup>1</sup> ABDALLAH	05c DLPH	$e^+ e^- \rightarrow Z^0$
1.35 $^{+0.37}_{-0.28}$ $^{+0.15}_{-0.17}$	<sup>2</sup> BUSKULIC	96T ALEP	$e^+ e^- \rightarrow Z$
1.5 $^{+0.7}_{-0.4}$ ± 0.3	<sup>3</sup> ABREU	95v DLPH	Repl. by ABDALLAH 05c
<sup>1</sup> Used the decay length of $\Xi^-$ accompanied by a lepton of the same sign.			
<sup>2</sup> Excess $\Xi^- \ell^-$ , impact parameters.			
<sup>3</sup> Excess $\Xi^- \ell^-$ , decay lengths.			

 $\tau_{mix}$  (1/2 $\pi$ ) times the oscillation period

VALUE (s)	DOCUMENT ID	TECN	COMMENT
$> 13 \times 10^{-12}$	<sup>1</sup> AAIJ	17B LHCb	$pp$ at 7, 8 TeV
<sup>1</sup> Uses $\Xi_b^{*-}$ and $\Xi_b^-$ decays to $\Xi_b^0 \pi^-$ , where $\Xi_b^0 \rightarrow \Xi_c^+ \pi^-$ , $\Xi_c^+ \rightarrow p K^- \pi^+$ .			

## MEAN LIFE RATIOS

 $\tau_{\Xi_b^-} / \tau_{\Lambda_b^0}$  mean life ratio

VALUE	DOCUMENT ID	TECN	COMMENT
<b>1.089 ± 0.026 ± 0.011</b>			
1.089 ± 0.026 ± 0.011	<sup>1</sup> AAIJ	14B LHCb	$pp$ at 7, 8 TeV
<sup>1</sup> Reconstructed in $\Xi_b^- \rightarrow \Xi_c^0 \pi^-$ , $\Xi_c^0 \rightarrow p K^- K^- \pi^+$ decays. Reference $\Lambda_b^0 \rightarrow \Lambda^+ \pi^-$ .			

 $\tau_{\Xi_b^0} / \tau_{\Xi_b^-}$  mean life ratio

VALUE	DOCUMENT ID	TECN	COMMENT
<b>1.083 ± 0.032 ± 0.016</b>			
1.083 ± 0.032 ± 0.016	<sup>1</sup> AAIJ	14B LHCb	$pp$ at 7, 8 TeV
<sup>1</sup> Reconstructed in $\Xi_b^- \rightarrow \Xi_c^0 \pi^-$ , $\Xi_c^0 \rightarrow p K^- K^- \pi^+$ decays. Uses $\Xi_b^0$ measurements from AAIJ 14Z.			

 $\Xi_b$  DECAY MODES

Mode	Fraction ( $\Gamma_i/\Gamma$ )	Scale factor/ Confidence level
$\Gamma_1$ $\Xi^- \ell^- \bar{\nu}_\ell X \times B(\bar{b} \rightarrow \Xi_b^-)$	$(3.9 \pm 1.2) \times 10^{-4}$	S=1.4
$\Gamma_2$ $J/\psi \Xi^- \times B(b \rightarrow \Xi_b^-)$	$(1.02^{+0.26}_{-0.21}) \times 10^{-5}$	
$\Gamma_3$ $J/\psi \Lambda K^- \times B(b \rightarrow \Xi_b^-)$	$(2.5 \pm 0.4) \times 10^{-6}$	
$\Gamma_4$ $\rho D^0 K^- \times B(\bar{b} \rightarrow \Xi_b^-)$	$(1.7 \pm 0.6) \times 10^{-6}$	
$\Gamma_5$ $\rho K^0 \pi^- \times B(\bar{b} \rightarrow \Xi_b^-)/B(\bar{b} \rightarrow \Xi_b^0)$	$< 1.6 \times 10^{-6}$	CL=90%
$\Gamma_6$ $\rho K^0 K^- \times B(\bar{b} \rightarrow \Xi_b^-)/B(\bar{b} \rightarrow \Xi_b^0)$	$< 1.1 \times 10^{-6}$	CL=90%
$\Gamma_7$ $\rho K^- K^- \times B(\bar{b} \rightarrow \Xi_b^-)$	$(3.7 \pm 0.8) \times 10^{-8}$	
$\Gamma_8$ $\rho K^- K^-$		
$\Gamma_9$ $\rho \pi^- \pi^-$		
$\Gamma_{10}$ $\rho K^- \pi^-$		
$\Gamma_{11}$ $\Lambda \pi^+ \pi^- \times B(b \rightarrow \Xi_b^0)/B(b \rightarrow \Lambda_b^0)$	$< 1.7 \times 10^{-6}$	CL=90%
$\Gamma_{12}$ $\Lambda K^- \pi^+ \times B(b \rightarrow \Xi_b^0)/B(b \rightarrow \Lambda_b^0)$	$< 8 \times 10^{-7}$	CL=90%
$\Gamma_{13}$ $\Lambda K^+ K^- \times B(b \rightarrow \Xi_b^0)/B(b \rightarrow \Lambda_b^0)$	$< 3 \times 10^{-7}$	CL=90%
$\Gamma_{14}$ $\Lambda_c^+ K^- \times B(\bar{b} \rightarrow \Xi_b^-)$	$(6 \pm 4) \times 10^{-7}$	
$\Gamma_{15}$ $\Lambda_b^0 \pi^- \times B(b \rightarrow \Xi_b^-)/B(b \rightarrow \Lambda_b^0)$	$(5.7 \pm 2.0) \times 10^{-4}$	
$\Gamma_{16}$ $\rho K^- \pi^+ \pi^- \times B(b \rightarrow \Xi_b^0)/B(b \rightarrow \Lambda_b^0)$	$(1.9 \pm 0.4) \times 10^{-6}$	
$\Gamma_{17}$ $\rho K^- K^- \pi^+ \times B(b \rightarrow \Xi_b^0)/B(b \rightarrow \Lambda_b^0)$	$(1.73 \pm 0.32) \times 10^{-6}$	
$\Gamma_{18}$ $\rho K^- K^+ K^- \times B(b \rightarrow \Xi_b^0)/B(b \rightarrow \Lambda_b^0)$	$(1.8 \pm 1.0) \times 10^{-7}$	

 $\Xi_b$  BRANCHING RATIOS

$\Gamma(\Xi^- \ell^- \bar{\nu}_\ell X \times B(\bar{b} \rightarrow \Xi_b^-))/\Gamma_{total}$	$\Gamma_1/\Gamma$
<b>3.9 ± 1.2 OUR AVERAGE</b>	Error includes scale factor of 1.4.
3.0 ± 1.0 ± 0.3	ABDALLAH 05c DLPH $e^+ e^- \rightarrow Z^0$
5.4 ± 1.1 ± 0.8	BUSKULIC 96T ALEP Excess $\Xi^- \ell^-$ over $\Xi^- \ell^+$
• • • We do not use the following data for averages, fits, limits, etc. • • •	
5.9 ± 2.1 ± 1.0	ABREU 95v DLPH Repl. by ABDALLAH 05c

$\Gamma(J/\psi \Xi^- \times B(b \rightarrow \Xi_b^-))/\Gamma_{total}$	$\Gamma_2/\Gamma$
<b>0.102 ± 0.026</b>	
$-0.021$	
0.098 $^{+0.023}_{-0.016}$ ± 0.014	<sup>1</sup> AALTONEN 09AP CDF $p\bar{p}$ at 1.96 TeV
0.16 ± 0.07 ± 0.02	<sup>2</sup> ABAZOV 07K D0 $p\bar{p}$ at 1.96 TeV

<sup>1</sup> AALTONEN 09AP reports  $[\Gamma(\Xi_b^- \rightarrow J/\psi \Xi^- \times B(b \rightarrow \Xi_b^-))/\Gamma_{total}] / [B(\Lambda_b^0 \rightarrow J/\psi(1S)\Lambda \times B(b \rightarrow \Lambda_b^0))] = 0.167^{+0.037}_{-0.025} \pm 0.012$  which we multiply by our best value  $B(\Lambda_b^0 \rightarrow J/\psi(1S)\Lambda \times B(b \rightarrow \Lambda_b^0)) = (5.8 \pm 0.8) \times 10^{-5}$ . Our first error is their experiment's error and our second error is the systematic error from using our best value.

<sup>2</sup> ABAZOV 07K reports  $[\Gamma(\Xi_b^- \rightarrow J/\psi \Xi^- \times B(b \rightarrow \Xi_b^-))/\Gamma_{total}] / [B(\Lambda_b^0 \rightarrow J/\psi(1S)\Lambda \times B(b \rightarrow \Lambda_b^0))] = 0.28 \pm 0.09^{+0.09}_{-0.08}$  which we multiply by our best value  $B(\Lambda_b^0 \rightarrow J/\psi(1S)\Lambda \times B(b \rightarrow \Lambda_b^0)) = (5.8 \pm 0.8) \times 10^{-5}$ . Our first error is their experiment's error and our second error is the systematic error from using our best value.

$\Gamma(J/\psi \Lambda K^- \times B(b \rightarrow \Xi_b^-))/\Gamma_{total}$	$\Gamma_3/\Gamma$
<b>2.45 ± 0.19 ± 0.35</b>	
2.45 ± 0.19 ± 0.35	<sup>1,2</sup> AAIJ 17B LHCb $pp$ at 7 and 8 TeV

<sup>1</sup> AAIJ 17B reports  $[\Gamma(\Xi_b^- \rightarrow J/\psi \Lambda K^- \times B(b \rightarrow \Xi_b^-))/\Gamma_{total}] / [B(\Lambda_b^0 \rightarrow J/\psi(1S)\Lambda \times B(b \rightarrow \Lambda_b^0))] = (4.19 \pm 0.29 \pm 0.15) \times 10^{-2}$  which we multiply by our best value  $B(\Lambda_b^0 \rightarrow J/\psi(1S)\Lambda \times B(b \rightarrow \Lambda_b^0)) = (5.8 \pm 0.8) \times 10^{-5}$ . Our first error is their experiment's error and our second error is the systematic error from using our best value.

<sup>2</sup> Integrated over the  $b$ -baryon transverse momentum  $p_T < 25$  GeV and rapidity  $2.0 < y < 4.5$ .

$\Gamma(\rho D^0 K^- \times B(\bar{b} \rightarrow \Xi_b^-))/\Gamma_{total}$	$\Gamma_4/\Gamma$
<b>(1.7 ± 0.4 ± 0.4) × 10<sup>-6</sup></b>	
(1.7 ± 0.4 ± 0.4) × 10 <sup>-6</sup>	<sup>1</sup> AAIJ 14H LHCb $pp$ at 7 TeV

<sup>1</sup> AAIJ 14H reports  $[\Gamma(\Xi_b^- \rightarrow \rho D^0 K^- \times B(\bar{b} \rightarrow \Xi_b^-))/\Gamma_{total}] / [B(\bar{b} \rightarrow b\text{-baryon})] / [B(\Lambda_b^0 \rightarrow \rho D^0 K^-)] = 0.44 \pm 0.09 \pm 0.06$  which we multiply by our best values  $B(\bar{b} \rightarrow b\text{-baryon}) = (8.4 \pm 1.1) \times 10^{-2}$ ,  $B(\Lambda_b^0 \rightarrow \rho D^0 K^-) = (4.6 \pm 0.8) \times 10^{-5}$ . Our first error is their experiment's error and our second error is the systematic error from using our best values.





## Baryon Particle Listings

 $\Xi'_b(5935)^-$ ,  $\Xi_b(5945)^0$ ,  $\Xi_b(5955)^-$ ,  $\Xi_b(6227)$ 

$$m_{\Xi'_b(5935)^-} - m_{\Xi_b^0} - m_{\pi^-}$$

VALUE (MeV)	DOCUMENT ID	TECN	COMMENT
<b>3.653 ± 0.018 ± 0.006</b>	<sup>2</sup> AAIJ	15H LHCb	$pp$ at 7, 8 TeV
<sup>2</sup> Observed in $\Xi_b^0 \pi^-$ channel with $\Xi_b^0 \rightarrow \Xi_c^+ \pi^-$ and $\Xi_c^+ \rightarrow p K^- \pi^+$ .			

 $\Xi'_b(5935)^-$  WIDTH

VALUE (MeV)	CL%	DOCUMENT ID	TECN	COMMENT
<b>&lt;0.08</b>	95	<sup>3</sup> AAIJ	15H LHCb	$pp$ at 7, 8 TeV
<sup>3</sup> Observed in $\Xi_b^0 \pi^-$ channel with $\Xi_b^0 \rightarrow \Xi_c^+ \pi^-$ and $\Xi_c^+ \rightarrow p K^- \pi^+$ .				

 $\Xi'_b(5935)^-$  DECAY MODES

Mode	Fraction ( $\Gamma_i/\Gamma$ )
$\Gamma_1$ $\Xi_b^0 \pi^- \times B(\bar{b} \rightarrow \Xi'_b(5935)^-)/B(\bar{b} \rightarrow \Xi_b^0)$	(11.8 ± 1.8) %

 $\Xi'_b(5935)^-$  BRANCHING RATIOS

$\Gamma(\Xi_b^0 \pi^- \times B(\bar{b} \rightarrow \Xi'_b(5935)^-)/B(\bar{b} \rightarrow \Xi_b^0))/\Gamma_{\text{total}}$	$\Gamma_1/\Gamma$
<b>0.118 ± 0.017 ± 0.007</b>	
<sup>4</sup> Observed in $\Xi_b^0 \pi^-$ channel with $\Xi_b^0 \rightarrow \Xi_c^+ \pi^-$ and $\Xi_c^+ \rightarrow p K^- \pi^+$ .	

 $\Xi'_b(5935)^-$  REFERENCES

AAIJ 15H PRL 114 062004 R. Aaij et al. (LHCb Collab.)

**$\Xi_b(5945)^0$**   $J^P = \frac{3}{2}^+$  Status: \*\*\*

Quantum numbers are based on quark model expectations.

 $\Xi_b(5945)^0$  MASS

VALUE (MeV)	DOCUMENT ID	TECN	COMMENT
<b>5952.3 ± 0.6 OUR AVERAGE</b>	<sup>1</sup> AAIJ	16AE LHCb	$pp$ at 7, 8 TeV
5952.3 ± 0.1 ± 0.6	<sup>2</sup> CHATRCHYAN12s	CMS	$pp$ at 7 TeV, 5.3 fb <sup>-1</sup>

- <sup>1</sup> AAIJ 16AE measures  $m(\Xi_b(5945)^0) - m(\Xi_b^-) - m(\pi^+) = 15.727 \pm 0.068 \pm 0.023$  MeV. We have adjusted the measurement to our best values of  $m(\Xi_b^-) = 5797.0 \pm 0.6$  MeV,  $m(\pi^+) = 139.57039 \pm 0.00018$  MeV. Our first error is their experiment's error and our second error is the systematic error from using our best values.
- <sup>2</sup> CHATRCHYAN 12s measures  $m(\Xi_b(5945)^0) - m(\Xi_b^-) - m(\pi^+) = 14.84 \pm 0.74 \pm 0.28$  MeV. We have adjusted the measurement to our best values of  $m(\Xi_b^-) = 5797.0 \pm 0.6$  MeV,  $m(\pi^+) = 139.57039 \pm 0.00018$  MeV. Our first error is their experiment's error and our second error is the systematic error from using our best values.

 $\Xi_b(5945)^0$  WIDTH

VALUE (MeV)	DOCUMENT ID	TECN	COMMENT
<b>0.90 ± 0.16 ± 0.08</b>	<sup>3</sup> AAIJ	16AE LHCb	$pp$ at 7, 8 TeV
• • • We do not use the following data for averages, fits, limits, etc. • • •			
2.1 ± 1.7	<sup>4</sup> CHATRCHYAN12s	CMS	$pp$ at 7 TeV, 5.3 fb <sup>-1</sup>
<sup>3</sup> Measured using $\Xi_b(5945)^0 \rightarrow \Xi_b^- \pi^+$ , $\Xi_b^- \rightarrow \Xi_c^0 \pi^-$ , $\Xi_c^0 \rightarrow p K^- K^- \pi^+$ decays.			
<sup>4</sup> Systematic uncertainty not evaluated.			

 $\Xi_b(5945)^0$  DECAY MODES

Mode	Fraction ( $\Gamma_i/\Gamma$ )
$\Gamma_1$ $\Xi_b^- \pi^+$	seen

 $\Xi_b(5945)^0$  BRANCHING RATIOS

$\Gamma(\Xi_b^- \pi^+)/\Gamma_{\text{total}}$	$\Gamma_1/\Gamma$
seen	
seen	
<sup>1</sup> AAIJ 16AE ATLAS $pp$ at 7, 8 TeV	
<sup>2</sup> CHATRCHYAN12s CMS $pp$ at 7 TeV, 5.3 fb <sup>-1</sup>	

 $\Xi_b(5945)^0$  REFERENCESAAIJ 16AE JHEP 1605 161 R. Aaij et al. (LHCb Collab.)  
CHATRCHYAN 12s PRL 108 252002 S. Chatrchyan et al. (CMS Collab.) **$\Xi_b(5955)^-$** 

$$J^P = \frac{3}{2}^+ \quad \text{Status: ***}$$

 $\Xi_b(5955)^-$  MASS

VALUE (MeV)	DOCUMENT ID	TECN	COMMENT
<b>5955.33 ± 0.12 ± 0.05</b>	<sup>1</sup> AAIJ	15H LHCb	$pp$ at 7, 8 TeV
<sup>1</sup> Not independent of the mass difference measurement below. Observed in $\Xi_b^0 \pi^-$ channel with $\Xi_b^0 \rightarrow \Xi_c^+ \pi^-$ and $\Xi_c^+ \rightarrow p K^- \pi^+$ .			

$$m_{\Xi_b(5955)^-} - m_{\Xi_b^0} - m_{\pi^-}$$

VALUE (MeV)	DOCUMENT ID	TECN	COMMENT
<b>23.96 ± 0.12 ± 0.06</b>	<sup>1</sup> AAIJ	15H LHCb	$pp$ at 7, 8 TeV
<sup>1</sup> Observed in $\Xi_b^0 \pi^-$ channel with $\Xi_b^0 \rightarrow \Xi_c^+ \pi^-$ and $\Xi_c^+ \rightarrow p K^- \pi^+$ .			

 $\Xi_b(5955)^-$  WIDTH

VALUE (MeV)	DOCUMENT ID	TECN	COMMENT
<b>1.65 ± 0.31 ± 0.10</b>	<sup>1</sup> AAIJ	15H LHCb	$pp$ at 7, 8 TeV
<sup>1</sup> Observed in $\Xi_b^0 \pi^-$ channel with $\Xi_b^0 \rightarrow \Xi_c^+ \pi^-$ and $\Xi_c^+ \rightarrow p K^- \pi^+$ .			

 $\Xi_b(5955)^-$  DECAY MODES

Mode	Fraction ( $\Gamma_i/\Gamma$ )
$\Gamma_1$ $\Xi_b^0 \pi^- \times B(\bar{b} \rightarrow \Xi_b(5955)^-)/B(\bar{b} \rightarrow \Xi_b^0)$	(20.7 ± 3.5) %

 $\Xi_b(5955)^-$  BRANCHING RATIOS

$\Gamma(\Xi_b^0 \pi^- \times B(\bar{b} \rightarrow \Xi_b(5955)^-)/B(\bar{b} \rightarrow \Xi_b^0))/\Gamma_{\text{total}}$	$\Gamma_1/\Gamma$
<b>0.207 ± 0.032 ± 0.015</b>	
<sup>1</sup> Observed in $\Xi_b^0 \pi^-$ channel with $\Xi_b^0 \rightarrow \Xi_c^+ \pi^-$ and $\Xi_c^+ \rightarrow p K^- \pi^+$ .	

 $\Xi_b(5955)^-$  REFERENCES

AAIJ 15H PRL 114 062004 R. Aaij et al. (LHCb Collab.)

 **$\Xi_b(6227)$** 

$$J^P = ?^? \quad \text{Status: ***}$$

 $\Xi_b(6227)$  MASS

VALUE (MeV)	DOCUMENT ID	TECN	COMMENT
<b>6226.9 ± 2.0 ± 0.4</b>	<sup>1,2</sup> AAIJ	18H LHCb	$pp$ at 7, 8, 13 TeV
<sup>1</sup> Uses $\Lambda_b^0 K^-$ and $\Xi_b^0 \pi^-$ modes.			
<sup>2</sup> Measures mass difference $m(\Xi_b(6227)^-) - m(\Lambda_b^0) = 607.3 \pm 2.0 \pm 0.3$ MeV and uses $m(\Lambda_b^0) = 5619.58 \pm 0.17$ MeV.			

 $\Xi_b(6227)$  WIDTH

VALUE (MeV)	DOCUMENT ID	TECN	COMMENT
<b>18.1 ± 5.4 ± 1.8</b>	<sup>1</sup> AAIJ	18H LHCb	$pp$ at 7, 8, 13 TeV
<sup>1</sup> Uses $\Lambda_b^0 K^-$ and $\Xi_b^0 \pi^-$ modes.			

 $\Xi_b(6227)$  DECAY MODES

Mode	Fraction ( $\Gamma_i/\Gamma$ )	Scale factor
$\Gamma_1$ $\Lambda_b^0 K^- \times B(b \rightarrow \Xi_b(6227)^-)/B(b \rightarrow \Lambda_b^0)$	(3.20 ± 0.35) × 10 <sup>-3</sup>	
$\Gamma_2$ $\Xi_b^0 \pi^- \times B(b \rightarrow \Xi_b(6227)^-)/B(b \rightarrow \Xi_b^0)$	(2.8 ± 1.1) %	1.8

 $\Xi_b(6227)$  BRANCHING RATIOS

$\Gamma(\Lambda_b^0 K^- \times B(b \rightarrow \Xi_b(6227)^-)/B(b \rightarrow \Lambda_b^0))/\Gamma_{\text{total}}$	$\Gamma_1/\Gamma$
<b>3.20 ± 0.35 OUR AVERAGE</b>	
3.0 ± 0.3 ± 0.4	AAIJ 18H LHCb $pp$ at 7, 8 TeV
3.4 ± 0.3 ± 0.4	AAIJ 18H LHCb $pp$ at 13 TeV

$\Xi_b(6227), \Omega_b^-, b$ -baryon ADMIXTURE ( $\Lambda_b, \Xi_b, \Omega_b$ )

$\Gamma(\Xi_b^0 \pi^- \times B(b \rightarrow \Xi_b(6227)) / B(b \rightarrow \Xi_b^0)) / \Gamma_{total}$				$\Gamma_2 / \Gamma$
VALUE (units $10^{-3}$ )	DOCUMENT ID	TECN	COMMENT	
<b>28 ± 11 OUR AVERAGE</b>	Error includes scale factor of 1.8.			
47 ± 10 ± 7	AAIJ	18H LHCb	$pp$ at 7, 8 TeV	
22 ± 6 ± 3	AAIJ	18H LHCb	$pp$ at 13 TeV	

$\Xi_b(6227)$  REFERENCES

AAIJ	18H PRL 121 072002	R. Aaij et al.	(LHCb Collab.)
------	--------------------	----------------	----------------



$I(J^P) = 0(\frac{1}{2}^+)$  Status: \*\*\*  
*I, J, P* need confirmation.

In the quark model  $\Omega_b^-$  is  $ssb$  ground state. None of its quantum numbers has been measured.

$\Omega_b^-$  MASS

VALUE (MeV)	DOCUMENT ID	TECN	COMMENT
<b>6046.1 ± 1.7 OUR AVERAGE</b>			
6045.1 ± 3.2 ± 0.8	1 AAIJ	16O LHCb	$pp$ at 7, 8 TeV
6047.5 ± 3.8 ± 0.6	2 AALTONEN	14B CDF	$p\bar{p}$ at 1.96 TeV
6046.0 ± 2.2 ± 0.5	3 AAIJ	13AV LHCb	$pp$ at 7 TeV

• • • We do not use the following data for averages, fits, limits, etc. • • •

6054.4 ± 6.8 ± 0.9	4 AALTONEN	09AP CDF	Repl. by AALTONEN 14B
6165 ± 10 ± 13	5 ABAZOV	08AL D0	$p\bar{p}$ at 1.96 TeV

- Reconstructed in  $\Omega_b^- \rightarrow \Omega_c^0 \pi^-, \Omega_c^0 \rightarrow pK^- K^- \pi^+$  decays. Reference  $\Xi_b^-$  mass 5797.72 ± 0.6 MeV from AAJ 14b.
- Uses  $\Omega_b^- \rightarrow J/\psi \Omega^-$  and  $\Omega_c^0 \pi^-$  decays, with the first evidence for  $\Omega_b^- \rightarrow \Omega_c^0 \pi^-$  at 3.3  $\sigma$  significance.
- Measured in  $\Omega_b^- \rightarrow J/\psi \Omega^-$  with 19 ± 5 events.
- Observed in  $\Omega_b^- \rightarrow J/\psi \Omega^-$  decays with 16 $^{+6}_{-4}$  candidates, a significance of 5.5 sigma from a combined mass-lifetime fit.
- Observed in  $\Omega_b^- \rightarrow J/\psi \Omega^-$  decays with 17.8 ± 4.9 ± 0.8 candidates, a significance of 5.4 sigma.

$m_{\Omega_b^-} - m_{\Lambda_b^0}$

VALUE (MeV)	DOCUMENT ID	TECN	COMMENT
<b>426.4 ± 2.2 ± 0.4</b>	AAIJ	13AV LHCb	$pp$ at 7 TeV

$m_{\Omega_b^-} - m_{\Xi_b^-}$

VALUE (MeV)	DOCUMENT ID	TECN	COMMENT
<b>247.3 ± 3.2 ± 0.5</b>	1 AAIJ	16O LHCb	$pp$ at 7, 8 TeV

- Uses  $\Omega_b^- \rightarrow \Omega_c^0 \pi^-, \Omega_c^0 \rightarrow pK^- K^- \pi^+$  and  $\Xi_b^- \rightarrow \Xi_c^0 \pi^-, \Xi_c^0 \rightarrow pK^- K^- \pi^+$  decays.

$\Omega_b^-$  MEAN LIFE

"OUR EVALUATION" has been provided by the Heavy Flavor Averaging Group (HFLAV, <https://hflav.web.cern.ch/>).

VALUE ( $10^{-12}$ s)	DOCUMENT ID	TECN	COMMENT
-----------------------	-------------	------	---------

**1.64 $^{+0.18}_{-0.17}$  OUR EVALUATION**

**1.65 $^{+0.18}_{-0.16}$  OUR AVERAGE**

1.78 ± 0.26 ± 0.05 ± 0.06	1 AAIJ	16O LHCb	$pp$ at 7, 8 TeV
1.54 $^{+0.26}_{-0.21}$ ± 0.05	2 AAIJ	14T LHCb	$pp$ at 7, 8 TeV
1.66 $^{+0.53}_{-0.40}$ ± 0.02	2 AALTONEN	14B CDF	$p\bar{p}$ at 1.96 TeV
1.13 $^{+0.53}_{-0.40}$ ± 0.02	3 AALTONEN	09AP CDF	Repl. by AALTONEN 14B

• • • We do not use the following data for averages, fits, limits, etc. • • •

- Measured in  $\Omega_b^- \rightarrow \Omega_c^0 \pi^-, \Omega_c^0 \rightarrow pK^- K^- \pi^+$  decays relative to  $\Xi_b^- \rightarrow \Xi_c^0 \pi^-, \Xi_c^0 \rightarrow pK^- K^- \pi^+$  decays with reference  $\Xi_b^-$  mean life 1.599 ± 0.06 ps from AAJ 14b.
- Measured in  $\Omega_b^- \rightarrow J/\psi \Omega^-$  decays.
- Observed in  $\Omega_b^- \rightarrow J/\psi \Omega^-$  decays with 16 $^{+6}_{-4}$  candidates, a significance of 5.5 sigma from a combined mass-lifetime fit.

$\tau(\Omega_b^-) / \tau(\Xi_b^-)$  mean life ratio

VALUE	DOCUMENT ID	TECN	COMMENT
<b>1.11 ± 0.16 ± 0.03</b>	1 AAIJ	16O LHCb	$pp$ at 7, 8 TeV

- Uses  $\Omega_b^- \rightarrow \Omega_c^0 \pi^-, \Omega_c^0 \rightarrow pK^- K^- \pi^+$  and  $\Xi_b^- \rightarrow \Xi_c^0 \pi^-, \Xi_c^0 \rightarrow pK^- K^- \pi^+$  decays.

$\Omega_b^-$  DECAY MODES

Mode	Fraction ( $\Gamma_i / \Gamma$ )	Confidence level
$\Gamma_1$ $J/\psi \Omega^- \times B(b \rightarrow \Omega_b)$	$(2.9^{+1.1}_{-0.8}) \times 10^{-6}$	
$\Gamma_2$ $\rho K^- K^- \times B(\bar{b} \rightarrow \Omega_b)$	< 2.5 × 10 <sup>-9</sup>	90%
$\Gamma_3$ $\rho \pi^- \pi^- \times B(\bar{b} \rightarrow \Omega_b)$	< 1.5 × 10 <sup>-8</sup>	90%
$\Gamma_4$ $\rho K^- \pi^- \times B(\bar{b} \rightarrow \Omega_b)$	< 7 × 10 <sup>-9</sup>	90%

$\Omega_b^-$  BRANCHING RATIOS

$\Gamma(J/\psi \Omega^- \times B(b \rightarrow \Omega_b)) / \Gamma_{total}$				$\Gamma_1 / \Gamma$
VALUE (units $10^{-4}$ )	DOCUMENT ID	TECN	COMMENT	

**0.029 $^{+0.011}_{-0.008}$  OUR AVERAGE**

0.026 $^{+0.010}_{-0.007}$ ± 0.004	1 AALTONEN	09AP CDF	$p\bar{p}$ at 1.96 TeV
0.08 ± 0.04 ± 0.02	2 ABAZOV	08AL D0	$p\bar{p}$ at 1.96 TeV

- AALTONEN 09AP reports  $[\Gamma(\Omega_b^- \rightarrow J/\psi \Omega^- \times B(b \rightarrow \Omega_b)) / \Gamma_{total}] / [B(\Lambda_b^0 \rightarrow J/\psi(1S) \Lambda \times B(b \rightarrow \Lambda_b^0))] = 0.045^{+0.017}_{-0.012} \pm 0.004$  which we multiply by our best value  $B(\Lambda_b^0 \rightarrow J/\psi(1S) \Lambda \times B(b \rightarrow \Lambda_b^0)) = (5.8 \pm 0.8) \times 10^{-5}$ . Our first error is their experiment's error and our second error is the systematic error from using our best value.
- ABAZOV 08AL reports  $[\Gamma(\Omega_b^- \rightarrow J/\psi \Omega^- \times B(b \rightarrow \Omega_b)) / \Gamma_{total}] / [B(\Xi_b^- \rightarrow J/\psi \Xi^- \times B(b \rightarrow \Xi_b^-))] = 0.80 \pm 0.32^{+0.14}_{-0.22}$  which we multiply by our best value  $B(\Xi_b^- \rightarrow J/\psi \Xi^- \times B(b \rightarrow \Xi_b^-)) = (1.02^{+0.26}_{-0.21}) \times 10^{-5}$ . Our first error is their experiment's error and our second error is the systematic error from using our best value.

$\Gamma(\rho K^- K^- \times B(\bar{b} \rightarrow \Omega_b)) / \Gamma_{total}$				$\Gamma_2 / \Gamma$
VALUE (units $10^{-5}$ )	CL%	DOCUMENT ID	TECN	COMMENT

**< 2.5 × 10<sup>-4</sup>**

- AAIJ 17F reports  $[\Gamma(\Omega_b^- \rightarrow \rho K^- K^- \times B(\bar{b} \rightarrow \Omega_b)) / \Gamma_{total}] / [B(B^+ \rightarrow K^+ K^- K^+)] / [B(\bar{b} \rightarrow B^+)] < 18 \times 10^{-5}$  which we multiply by our best values  $B(B^+ \rightarrow K^+ K^- K^+) = 3.40 \times 10^{-5}$ ,  $B(\bar{b} \rightarrow B^+) = 40.8 \times 10^{-2}$ .

$\Gamma(\rho \pi^- \pi^- \times B(\bar{b} \rightarrow \Omega_b)) / \Gamma_{total}$				$\Gamma_3 / \Gamma$
VALUE (units $10^{-5}$ )	CL%	DOCUMENT ID	TECN	COMMENT

**< 1.5 × 10<sup>-3</sup>**

- AAIJ 17F reports  $[\Gamma(\Omega_b^- \rightarrow \rho \pi^- \pi^- \times B(\bar{b} \rightarrow \Omega_b)) / \Gamma_{total}] / [B(B^+ \rightarrow K^+ K^- K^+) / [B(\bar{b} \rightarrow B^+)]] < 109 \times 10^{-5}$  which we multiply by our best values  $B(B^+ \rightarrow K^+ K^- K^+) = 3.40 \times 10^{-5}$ ,  $B(\bar{b} \rightarrow B^+) = 40.8 \times 10^{-2}$ .

$\Gamma(\rho K^- \pi^- \times B(\bar{b} \rightarrow \Omega_b)) / \Gamma_{total}$				$\Gamma_4 / \Gamma$
VALUE (units $10^{-5}$ )	CL%	DOCUMENT ID	TECN	COMMENT

**< 7 × 10<sup>-4</sup>**

- AAIJ 17F reports  $[\Gamma(\Omega_b^- \rightarrow \rho K^- \pi^- \times B(\bar{b} \rightarrow \Omega_b)) / \Gamma_{total}] / [B(B^+ \rightarrow K^+ K^- K^+) / [B(\bar{b} \rightarrow B^+)]] < 51 \times 10^{-5}$  which we multiply by our best values  $B(B^+ \rightarrow K^+ K^- K^+) = 3.40 \times 10^{-5}$ ,  $B(\bar{b} \rightarrow B^+) = 40.8 \times 10^{-2}$ .

$\Omega_b^-$  REFERENCES

AAIJ	17F PRL 118 071801	R. Aaij et al.	(LHCb Collab.)
AAIJ	16O PR D39 092007	R. Aaij et al.	(LHCb Collab.)
AAIJ	14B PL B728 234	R. Aaij et al.	(LHCb Collab.)
AAIJ	14T PL B736 154	R. Aaij et al.	(LHCb Collab.)
AALTONEN	14B PR D89 072014	T. Aaltonen et al.	(CDF Collab.)
AAIJ	13AV PRL 110 182001	R. Aaij et al.	(LHCb Collab.)
AALTONEN	09AP PR D80 072003	T. Aaltonen et al.	(CDF Collab.)
ABAZOV	08AL PRL 101 232002	V.M. Abazov et al.	(D0 Collab.)

$b$ -baryon ADMIXTURE ( $\Lambda_b, \Xi_b, \Omega_b$ )

$b$ -baryon ADMIXTURE MEAN LIFE

Each measurement of the  $b$ -baryon mean life is an average over an admixture of various  $b$  baryons which decay weakly. Different techniques emphasize different admixtures of produced particles, which could result in a different  $b$ -baryon mean life. More  $b$ -baryon flavor specific channels are not included in the measurement.

VALUE ( $10^{-12}$ s)	EVTS	DOCUMENT ID	TECN	COMMENT
-----------------------	------	-------------	------	---------

• • • We do not use the following data for averages, fits, limits, etc. • • •

1.218 $^{+0.130}_{-0.115}$ ± 0.042	1 ABAZOV	07S D0	Repl. by ABAZOV 12u
1.22 $^{+0.22}_{-0.18}$ ± 0.04	1 ABAZOV	05c D0	Repl. by ABAZOV 07s
1.16 ± 0.20 ± 0.08	2 ABREU	99w DLPH	$e^+ e^- \rightarrow Z$
1.19 ± 0.14 ± 0.07	3 ABREU	99w DLPH	$e^+ e^- \rightarrow Z$

## Baryon Particle Listings

 $b$ -baryon ADMIXTURE ( $\Lambda_b, \Xi_b, \Omega_b$ )

1.14 ± 0.08 ± 0.04	4	ABREU	99W	DLPH	$e^+e^- \rightarrow Z$
1.11 $^{+0.19}_{-0.18}$ ± 0.05	5	ABREU	99W	DLPH	$e^+e^- \rightarrow Z$
1.29 $^{+0.24}_{-0.22}$ ± 0.06	5	ACKERSTAFF	98G	OPAL	$e^+e^- \rightarrow Z$
1.20 ± 0.08 ± 0.06	6	BARATE	98D	ALEP	$e^+e^- \rightarrow Z$
1.21 ± 0.11	5	BARATE	98D	ALEP	$e^+e^- \rightarrow Z$
1.32 ± 0.15 ± 0.07	7	ABE	96M	CDF	$p\bar{p}$ at 1.8 TeV
1.46 $^{+0.22}_{-0.21}$ $^{+0.07}_{-0.09}$		ABREU	96D	DLPH	Repl. by ABREU 99W
1.10 $^{+0.19}_{-0.17}$ ± 0.09	5	ABREU	96D	DLPH	$e^+e^- \rightarrow Z$
1.16 ± 0.11 ± 0.06	5	AKERS	96	OPAL	$e^+e^- \rightarrow Z$
1.27 $^{+0.35}_{-0.29}$ ± 0.09		ABREU	95S	DLPH	Repl. by ABREU 99W
1.05 $^{+0.12}_{-0.11}$ ± 0.09	290	BUSKULIC	95L	ALEP	Repl. by BARATE 98D
1.04 $^{+0.48}_{-0.38}$ ± 0.10	11	8 ABREU	93F	DLPH	Excess $\Lambda\mu^-$ , decay lengths
1.05 $^{+0.23}_{-0.20}$ ± 0.08	157	9 AKERS	93	OPAL	Excess $\Lambda\ell^-$ , decay lengths
1.12 $^{+0.32}_{-0.29}$ ± 0.16	101	10 BUSKULIC	92I	ALEP	Excess $\Lambda\ell^-$ , impact parameters

<sup>1</sup> Measured mean life using fully reconstructed  $\Lambda_b^0 \rightarrow J/\psi\Lambda$  decays.

<sup>2</sup> Measured using  $\Lambda\ell^-$  decay length.

<sup>3</sup> Measured using  $p\ell^-$  decay length.

<sup>4</sup> This ABREU 99W result is the combined result of the  $\Lambda\ell^-$ ,  $p\ell^-$ , and excess  $\Lambda\mu^-$  impact parameter measurements.

<sup>5</sup> Measured using  $\Lambda_C\ell^-$  and  $\Lambda\ell^+\ell^-$ .

<sup>6</sup> Measured using the excess of  $\Lambda\ell^-$ , lepton impact parameter.

<sup>7</sup> Measured using  $\Lambda_C\ell^-$ .

<sup>8</sup> ABREU 93F superseded by ABREU 96D.

<sup>9</sup> AKERS 93 superseded by AKERS 96.

<sup>10</sup> BUSKULIC 92I superseded by BUSKULIC 95L.

### $b$ -baryon ADMIXTURE DECAY MODES ( $\Lambda_b, \Xi_b, \Omega_b$ )

These branching fractions are actually an average over weakly decaying  $b$ -baryons weighted by their production rates at the LHC, LEP, and Tevatron, branching ratios, and detection efficiencies. They scale with the  $b$ -baryon production fraction  $B(b \rightarrow b\text{-baryon})$ .

The branching fractions  $B(b\text{-baryon} \rightarrow \Lambda\ell^-\bar{\nu}_\ell\text{anything})$  and  $B(\Lambda_b^0 \rightarrow \Lambda_C^+\ell^-\bar{\nu}_\ell\text{anything})$  are not pure measurements because the underlying measured products of these with  $B(b \rightarrow b\text{-baryon})$  were used to determine  $B(b \rightarrow b\text{-baryon})$ , as described in the note "Production and Decay of  $b$ -Flavored Hadrons."

For inclusive branching fractions, e.g.,  $B \rightarrow D^\pm\text{anything}$ , the values usually are multiplicities, not branching fractions. They can be greater than one.

Mode	Fraction ( $\Gamma_i/\Gamma$ )
$\Gamma_1$ $p\mu^-\bar{\nu}$ anything	$(5.8^{+2.3}_{-2.0})\%$
$\Gamma_2$ $p\ell\bar{\nu}_\ell$ anything	$(5.6 \pm 1.2)\%$
$\Gamma_3$ $p$ anything	$(70 \pm 22)\%$
$\Gamma_4$ $\Lambda\ell^-\bar{\nu}_\ell$ anything	$(3.8 \pm 0.6)\%$
$\Gamma_5$ $\Lambda\ell^+\nu_\ell$ anything	$(3.2 \pm 0.8)\%$
$\Gamma_6$ $\Lambda$ anything	$(39 \pm 7)\%$
$\Gamma_7$ $\Xi^-\ell^-\bar{\nu}_\ell$ anything	$(6.6 \pm 1.6) \times 10^{-3}$

### $b$ -baryon ADMIXTURE ( $\Lambda_b, \Xi_b, \Omega_b$ ) BRANCHING RATIOS

$\Gamma(p\mu^-\bar{\nu}\text{anything})/\Gamma_{\text{total}}$	$\Gamma_1/\Gamma$
VALUE (%)	EVTS
<b><math>5.8^{+2.3}_{-1.5} \pm 0.8</math></b>	125

<sup>11</sup> ABREU 95s reports  $[\Gamma(b\text{-baryon} \rightarrow p\mu^-\bar{\nu}\text{anything})/\Gamma_{\text{total}}] \times [B(\bar{b} \rightarrow b\text{-baryon})] = 0.0049 \pm 0.0011^{+0.0015}_{-0.0011}$  which we divide by our best value  $B(\bar{b} \rightarrow b\text{-baryon}) = (8.4 \pm 1.1) \times 10^{-2}$ . Our first error is their experiment's error and our second error is the systematic error from using our best value.

$\Gamma(p\ell\bar{\nu}_\ell\text{anything})/\Gamma_{\text{total}}$	$\Gamma_2/\Gamma$
VALUE (%)	DOCUMENT ID
<b><math>5.6 \pm 0.9 \pm 0.7</math></b>	12 BARATE

<sup>12</sup> BARATE 98v reports  $[\Gamma(b\text{-baryon} \rightarrow p\ell\bar{\nu}_\ell\text{anything})/\Gamma_{\text{total}}] \times [B(\bar{b} \rightarrow b\text{-baryon})] = (4.72 \pm 0.66 \pm 0.44) \times 10^{-3}$  which we divide by our best value  $B(\bar{b} \rightarrow b\text{-baryon}) = (8.4 \pm 1.1) \times 10^{-2}$ . Our first error is their experiment's error and our second error is the systematic error from using our best value.

$\Gamma(p\ell\bar{\nu}_\ell\text{anything})/\Gamma(p\text{anything})$	$\Gamma_2/\Gamma_3$
VALUE (%)	DOCUMENT ID
<b><math>8.0 \pm 1.2 \pm 1.4</math></b>	BARATE

### $\Gamma(\Lambda\ell^-\bar{\nu}_\ell\text{anything})/\Gamma_{\text{total}}$

The values and averages in this section serve only to show what values result if one assumes our  $B(b \rightarrow b\text{-baryon})$ . They cannot be thought of as measurements since the underlying product branching fractions were also used to determine  $B(b \rightarrow b\text{-baryon})$  as described in the note on "Production and Decay of  $b$ -Flavored Hadrons."

VALUE (%)	EVTS	DOCUMENT ID	TECN	COMMENT
<b><math>3.8 \pm 0.6</math> OUR AVERAGE</b>				
$3.9 \pm 0.5 \pm 0.5$		13 BARATE	98D	ALEP $e^+e^- \rightarrow Z$
$3.5 \pm 0.4 \pm 0.5$		14 AKERS	96	OPAL Excess of $\Lambda\ell^-$ over $\Lambda\ell^+$
$3.6 \pm 0.9 \pm 0.5$	262	15 ABREU	95S	DLPH Excess of $\Lambda\ell^-$ over $\Lambda\ell^+$
$7.3 \pm 1.4 \pm 1.0$	290	16 BUSKULIC	95L	ALEP Excess of $\Lambda\ell^-$ over $\Lambda\ell^+$

••• We do not use the following data for averages, fits, limits, etc. •••  
seen 157 <sup>17</sup> AKERS 93 OPAL Excess of  $\Lambda\ell^-$  over  $\Lambda\ell^+$   
 $8.3 \pm 2.5 \pm 1.1$  101 <sup>18</sup> BUSKULIC 92I ALEP Excess of  $\Lambda\ell^-$  over  $\Lambda\ell^+$

<sup>13</sup> BARATE 98D reports  $[\Gamma(b\text{-baryon} \rightarrow \Lambda\ell^-\bar{\nu}_\ell\text{anything})/\Gamma_{\text{total}}] \times [B(\bar{b} \rightarrow b\text{-baryon})] = 0.00326 \pm 0.00016 \pm 0.00039$  which we divide by our best value  $B(\bar{b} \rightarrow b\text{-baryon}) = (8.4 \pm 1.1) \times 10^{-2}$ . Our first error is their experiment's error and our second error is the systematic error from using our best value. Measured using the excess of  $\Lambda\ell^-$ , lepton impact parameter.

<sup>14</sup> AKERS 96 reports  $[\Gamma(b\text{-baryon} \rightarrow \Lambda\ell^-\bar{\nu}_\ell\text{anything})/\Gamma_{\text{total}}] \times [B(\bar{b} \rightarrow b\text{-baryon})] = 0.00291 \pm 0.00023 \pm 0.00025$  which we divide by our best value  $B(\bar{b} \rightarrow b\text{-baryon}) = (8.4 \pm 1.1) \times 10^{-2}$ . Our first error is their experiment's error and our second error is the systematic error from using our best value.

<sup>15</sup> ABREU 95s reports  $[\Gamma(b\text{-baryon} \rightarrow \Lambda\ell^-\bar{\nu}_\ell\text{anything})/\Gamma_{\text{total}}] \times [B(\bar{b} \rightarrow b\text{-baryon})] = 0.0030 \pm 0.0006 \pm 0.0004$  which we divide by our best value  $B(\bar{b} \rightarrow b\text{-baryon}) = (8.4 \pm 1.1) \times 10^{-2}$ . Our first error is their experiment's error and our second error is the systematic error from using our best value.

<sup>16</sup> BUSKULIC 95L reports  $[\Gamma(b\text{-baryon} \rightarrow \Lambda\ell^-\bar{\nu}_\ell\text{anything})/\Gamma_{\text{total}}] \times [B(\bar{b} \rightarrow b\text{-baryon})] = 0.0061 \pm 0.0006 \pm 0.0010$  which we divide by our best value  $B(\bar{b} \rightarrow b\text{-baryon}) = (8.4 \pm 1.1) \times 10^{-2}$ . Our first error is their experiment's error and our second error is the systematic error from using our best value.

<sup>17</sup> AKERS 93 superseded by AKERS 96.

<sup>18</sup> BUSKULIC 92I reports  $[\Gamma(b\text{-baryon} \rightarrow \Lambda\ell^-\bar{\nu}_\ell\text{anything})/\Gamma_{\text{total}}] \times [B(\bar{b} \rightarrow b\text{-baryon})] = 0.0070 \pm 0.0010 \pm 0.0018$  which we divide by our best value  $B(\bar{b} \rightarrow b\text{-baryon}) = (8.4 \pm 1.1) \times 10^{-2}$ . Our first error is their experiment's error and our second error is the systematic error from using our best value. Superseded by BUSKULIC 95L.

### $\Gamma(\Lambda\ell^+\nu_\ell\text{anything})/\Gamma(\Lambda\text{anything})$

VALUE (units $10^{-2}$ )	DOCUMENT ID	TECN	COMMENT
<b><math>8.0 \pm 1.2 \pm 0.8</math></b>	ABBIENDI	99L	OPAL $e^+e^- \rightarrow Z$
••• We do not use the following data for averages, fits, limits, etc. •••			
$7.0 \pm 1.2 \pm 0.7$	ACKERSTAFF	97N	OPAL Repl. by ABBIENDI 99L

### $\Gamma(\Lambda\text{anything})/\Gamma_{\text{total}}$

VALUE (%)	DOCUMENT ID	TECN	COMMENT
<b><math>39 \pm 7</math> OUR AVERAGE</b>			
$42 \pm 6 \pm 5$	19 ABBIENDI	99L	OPAL $e^+e^- \rightarrow Z$
$27^{+15}_{-9} \pm 3$	20 ABREU	95C	DLPH $e^+e^- \rightarrow Z$

••• We do not use the following data for averages, fits, limits, etc. •••  
 $47 \pm 7 \pm 6$  <sup>21</sup> ACKERSTAFF 97N OPAL Repl. by ABBIENDI 99L

<sup>19</sup> ABBIENDI 99L reports  $[\Gamma(b\text{-baryon} \rightarrow \Lambda\text{anything})/\Gamma_{\text{total}}] \times [B(\bar{b} \rightarrow b\text{-baryon})] = 0.035 \pm 0.0032 \pm 0.0035$  which we divide by our best value  $B(\bar{b} \rightarrow b\text{-baryon}) = (8.4 \pm 1.1) \times 10^{-2}$ . Our first error is their experiment's error and our second error is the systematic error from using our best value.

<sup>20</sup> ABREU 95c reports  $0.28^{+0.17}_{-0.12}$  from a measurement of  $[\Gamma(b\text{-baryon} \rightarrow \Lambda\text{anything})/\Gamma_{\text{total}}] \times [B(\bar{b} \rightarrow b\text{-baryon})]$  assuming  $B(\bar{b} \rightarrow b\text{-baryon}) = 0.08 \pm 0.02$ , which we rescale to our best value  $B(\bar{b} \rightarrow b\text{-baryon}) = (8.4 \pm 1.1) \times 10^{-2}$ . Our first error is their experiment's error and our second error is the systematic error from using our best value.

<sup>21</sup> ACKERSTAFF 97N reports  $[\Gamma(b\text{-baryon} \rightarrow \Lambda\text{anything})/\Gamma_{\text{total}}] \times [B(\bar{b} \rightarrow b\text{-baryon})] = 0.0393 \pm 0.0046 \pm 0.0037$  which we divide by our best value  $B(\bar{b} \rightarrow b\text{-baryon}) = (8.4 \pm 1.1) \times 10^{-2}$ . Our first error is their experiment's error and our second error is the systematic error from using our best value.

### $\Gamma(\Xi^-\ell^-\bar{\nu}_\ell\text{anything})/\Gamma_{\text{total}}$

VALUE (units $10^{-3}$ )	DOCUMENT ID	TECN	COMMENT
<b><math>6.6 \pm 1.6</math> OUR AVERAGE</b>			
$6.4 \pm 1.6 \pm 0.8$	22 BUSKULIC	96T	ALEP Excess $\Xi^-\ell^-$ over $\Xi^-\ell^+$
$7.0 \pm 2.8 \pm 0.9$	23 ABREU	95V	DLPH Excess $\Xi^-\ell^-$ over $\Xi^-\ell^+$

<sup>22</sup> BUSKULIC 96T reports  $[\Gamma(b\text{-baryon} \rightarrow \Xi^-\ell^-\bar{\nu}_\ell\text{anything})/\Gamma_{\text{total}}] \times [B(\bar{b} \rightarrow b\text{-baryon})] = 0.00054 \pm 0.00011 \pm 0.00008$  which we divide by our best value  $B(\bar{b} \rightarrow b\text{-baryon}) = (8.4 \pm 1.1) \times 10^{-2}$ . Our first error is their experiment's error and our second error is the systematic error from using our best value.

<sup>23</sup> ABREU 95v reports  $[\Gamma(b\text{-baryon} \rightarrow \Xi^-\ell^-\bar{\nu}_\ell\text{anything})/\Gamma_{\text{total}}] \times [B(\bar{b} \rightarrow b\text{-baryon})] = 0.00059 \pm 0.00021 \pm 0.0001$  which we divide by our best value  $B(\bar{b} \rightarrow b\text{-baryon}) = (8.4 \pm 1.1) \times 10^{-2}$ . Our first error is their experiment's error and our second error is the systematic error from using our best value.

### $b$ -baryon ADMIXTURE ( $\Lambda_b, \Xi_b, \Omega_b$ ) REFERENCES

ABAZOV	12U	PR	D85	112003	V.M. Abazov et al.	(DO Collab.)
ABAZOV	07S	PRL	99	142001	V.M. Abazov et al.	(DO Collab.)
ABAZOV	05C	PRL	94	102001	V.M. Abazov et al.	(DO Collab.)
ABBIENDI	99L	EPJ	C9	1	G. Abbiendi et al.	(OPAL Collab.)
ABREU	99W	EPJ	C10	185	P. Abreu et al.	(DELPHI Collab.)
ACKERSTAFF	98G	PL	B426	161	K. Ackerstaff et al.	(OPAL Collab.)
BARATE	98D	EPJ	C2	197	R. Barate et al.	(ALEPH Collab.)
BARATE	98V	EPJ	C5	205	R. Barate et al.	(ALEPH Collab.)
ACKERSTAFF	97N	ZPHY	C74	423	K. Ackerstaff et al.	(OPAL Collab.)
ABE	96M	PRL	77	1439	F. Abe et al.	(CDF Collab.)

See key on page 999

## Baryon Particle Listings

### $b$ -baryon ADMIXTURE ( $\Lambda_b, \Xi_b, \Omega_b$ )

---

ABREU	96D	ZPHY C71 199	P. Abreu <i>et al.</i>	(DELPHI Collab.)	ABREU	95V	ZPHY C68 541	P. Abreu <i>et al.</i>	(DELPHI Collab.)
AKERS	96	ZPHY C69 195	R. Akers <i>et al.</i>	(OPAL Collab.)	BUSKULIC	95L	PL B357 685	D. Buskulic <i>et al.</i>	(ALEPH Collab.)
BUSKULIC	96T	PL B384 449	D. Buskulic <i>et al.</i>	(ALEPH Collab.)	ABREU	93F	PL B311 379	P. Abreu <i>et al.</i>	(DELPHI Collab.)
ABREU	95C	PL B347 447	P. Abreu <i>et al.</i>	(DELPHI Collab.)	AKERS	93	PL B316 435	R. Akers <i>et al.</i>	(OPAL Collab.)
ABREU	95S	ZPHY C68 375	P. Abreu <i>et al.</i>	(DELPHI Collab.)	BUSKULIC	92I	PL B297 449	D. Buskulic <i>et al.</i>	(ALEPH Collab.)

---

## Baryon Particle Listings

Pentaquarks,  $P_c(4312)^+$ ,  $P_c(4380)^+$ ,  $P_c(4440)^+$ ,  $P_c(4457)^+$ 

## EXOTIC BARYONS

See the related review(s):

## Pentaquarks

 $P_c(4312)^+$  Status: \* $P_c(4312)^+$  MASS

VALUE (MeV)	DOCUMENT ID	TECN	COMMENT
$4311.9 \pm 0.7^{+6.8}_{-0.6}$	AAIJ	19W LHCb	<i>pp</i> at 7, 8, 13 TeV

 $P_c(4312)^+$  WIDTH

VALUE (MeV)	DOCUMENT ID	TECN	COMMENT
$9.8 \pm 2.7^{+3.7}_{-4.5}$	AAIJ	19W LHCb	<i>pp</i> at 7, 8, 13 TeV

 $P_c(4312)^+$  DECAY MODES

Mode	Fraction ( $\Gamma_i/\Gamma$ )
$\Gamma_1$ $J/\psi p$	seen

 $P_c(4312)^+$  BRANCHING RATIOS

$\Gamma(J/\psi p)/\Gamma_{\text{total}}$	$\Gamma_1/\Gamma$		
VALUE	DOCUMENT ID	TECN	COMMENT
seen	AAIJ	19W LHCb	<i>pp</i> at 7, 8, 13 TeV

 $P_c(4312)^+$  REFERENCESAAIJ 19W PRL 122 222001 R. Aaij *et al.* (LHCb Collab.) $P_c(4380)^+$  Status: \*

A resonance seen in  $\Lambda_b^0 \rightarrow P_c^+ K^-$ , then  $P_c \rightarrow J/\psi p$ , with a significance of 9 standard deviations. The  $J/\psi p$  quark content is  $uudc\bar{c}$ , a pentaquark. See also the  $P_c(4450)^+$ . In the best amplitude fit, the two states have opposite parity, one having  $J = 3/2$ , the other  $J = 5/2$ .

Extraction of the pentaquark signals requires some understanding of the dominant  $K^- p$  background. AAIJ 15P used a model-dependent approach. AAIJ 16AG reanalyzed the data making minimal assumptions about the  $K^- p$  background, and thus confirmed the strong significance of the pentaquark signals.

 $P_c(4380)^+$  MASS

VALUE (MeV)	DOCUMENT ID	TECN	COMMENT
$4380 \pm 8 \pm 29$	AAIJ	15P LHCb	<i>pp</i> at 7, 8 TeV

 $P_c(4380)^+$  WIDTH

VALUE (MeV)	DOCUMENT ID	TECN	COMMENT
$205 \pm 18 \pm 86$	AAIJ	15P LHCb	<i>pp</i> at 7, 8 TeV

 $P_c(4380)^+$  DECAY MODES

Mode	Fraction ( $\Gamma_i/\Gamma$ )
$\Gamma_1$ $J/\psi p$	seen

 $P_c(4380)^+$  BRANCHING RATIOS

$\Gamma(J/\psi p)/\Gamma_{\text{total}}$	$\Gamma_1/\Gamma$		
VALUE	DOCUMENT ID	TECN	COMMENT
seen	AAIJ	15P LHCb	<i>pp</i> at 7, 8 TeV

 $P_c(4380)^+$  REFERENCESAAIJ 16AG PRL 117 082002 R. Aaij *et al.* (LHCb Collab.)  
AAIJ 15P PRL 115 072001 R. Aaij *et al.* (LHCb Collab.) $P_c(4440)^+$ 

Status: \*

 $P_c(4440)^+$  MASS

VALUE (MeV)	DOCUMENT ID	TECN	COMMENT
$4440.3 \pm 1.3^{+4.1}_{-4.7}$	AAIJ	19W LHCb	<i>pp</i> at 7, 8, 13 TeV

 $P_c(4440)^+$  WIDTH

VALUE (MeV)	DOCUMENT ID	TECN	COMMENT
$20.6 \pm 4.9^{+8.7}_{-10.1}$	AAIJ	19W LHCb	<i>pp</i> at 7, 8, 13 TeV

 $P_c(4440)^+$  DECAY MODES

Mode	Fraction ( $\Gamma_i/\Gamma$ )
$\Gamma_1$ $J/\psi p$	seen

 $P_c(4440)^+$  BRANCHING RATIOS

$\Gamma(J/\psi p)/\Gamma_{\text{total}}$	$\Gamma_1/\Gamma$		
VALUE	DOCUMENT ID	TECN	COMMENT
seen	AAIJ	19W LHCb	<i>pp</i> at 7, 8, 13 TeV

 $P_c(4440)^+$  REFERENCESAAIJ 19W PRL 122 222001 R. Aaij *et al.* (LHCb Collab.) $P_c(4457)^+$ 

Status: \*

was  $P_c(4450)$ 

A resonance seen in  $\Lambda_b^0 \rightarrow P_c^+ K^-$ , then  $P_c \rightarrow J/\psi p$ , with a significance of 12 standard deviations. The  $J/\psi p$  quark content is  $uudc\bar{c}$ , a pentaquark. See also the  $P_c(4380)^+$ . In the best amplitude fit, the two states have opposite parity, one having  $J = 3/2$ , the other  $J = 5/2$ .

Extraction of the pentaquark signals requires some understanding of the dominant  $K^- p$  background. AAIJ 15P used a model-dependent approach. AAIJ 16AG reanalyzed the data making minimal assumptions about the  $K^- p$  background, and thus confirmed the strong significance of the pentaquark signals.

 $P_c(4457)^+$  MASS

VALUE (MeV)	DOCUMENT ID	TECN	COMMENT
$4457.3 \pm 0.6^{+4.1}_{-1.7}$	AAIJ	19W LHCb	<i>pp</i> at 7, 8, 13 TeV

••• We do not use the following data for averages, fits, limits, etc. •••

4449.8  $\pm 1.7 \pm 2.5$  <sup>1</sup> AAIJ 15P LHCb Repl. by AAIJ 19W<sup>1</sup> Considering  $P_c(4440)$  and  $P_c(4457)$  as a single resonance. $P_c(4457)^+$  WIDTH

VALUE (MeV)	DOCUMENT ID	TECN	COMMENT
$6.4 \pm 2.0^{+5.7}_{-1.9}$	AAIJ	19W LHCb	<i>pp</i> at 7, 8, 13 TeV

••• We do not use the following data for averages, fits, limits, etc. •••

39  $\pm 5 \pm 19$  <sup>1</sup> AAIJ 15P LHCb Repl. by AAIJ 19W<sup>1</sup> Considering  $P_c(4440)$  and  $P_c(4457)$  as a single resonance. $P_c(4457)^+$  DECAY MODES

Mode	Fraction ( $\Gamma_i/\Gamma$ )
$\Gamma_1$ $J/\psi p$	seen

 $P_c(4457)^+$  BRANCHING RATIOS

$\Gamma(J/\psi p)/\Gamma_{\text{total}}$	$\Gamma_1/\Gamma$		
VALUE	DOCUMENT ID	TECN	COMMENT
seen	AAIJ	19W LHCb	<i>pp</i> at 7, 8, 13 TeV
seen	AAIJ	15P LHCb	<i>pp</i> at 7, 8 TeV

 $P_c(4457)^+$  REFERENCESAAIJ 19W PRL 122 222001 R. Aaij *et al.* (LHCb Collab.)  
AAIJ 16AG PRL 117 082002 R. Aaij *et al.* (LHCb Collab.)  
AAIJ 15P PRL 115 072001 R. Aaij *et al.* (LHCb Collab.)

## MISCELLANEOUS SEARCHES

Magnetic Monopole Searches . . . . .	2017
Supersymmetric Particle Searches . . . . .	2019
Technicolor . . . . .	2062
Quark and Lepton Compositeness . . . . .	2063
Extra Dimensions . . . . .	2067
WIMP and Dark Matter Searches . . . . .	2073
Other Particle Searches . . . . .	2085

## SEARCHES IN OTHER SECTIONS

Neutral Higgs Bosons, Searches for . . . . .	1056
Charged Higgs Bosons ( $H^\pm$ and $H^{\pm\pm}$ ), Searches for . . . . .	1065
New Heavy Bosons . . . . .	1068
Axions ( $A^0$ ) and Other Very Light Bosons . . . . .	1084
Heavy Charged Lepton Searches . . . . .	1134
Double- $\beta$ Decay . . . . .	1145
Heavy Neutral Leptons, Searches for . . . . .	1168
$b'$ (Fourth Generation) Quark . . . . .	1197
$t'$ (Fourth Generation) Quark . . . . .	1199
Free Quark Searches . . . . .	1201

## Related Reviews in Volume 1

86. Extra dimensions (rev.) . . . . .	889
87. $W'$ -boson searches (rev.) . . . . .	897
88. $Z'$ -boson searches (rev.) . . . . .	900
89. Supersymmetry: theory (rev.) . . . . .	905
90. Supersymmetry: experiment (rev.) . . . . .	923
91. Axions and other similar particles (rev.) . . . . .	939
92. Quark and lepton compositeness, searches for (rev.) . . . . .	953
93. Dynamical electroweak symmetry . . . . .	958
breaking: implications of the $H(0)$ (rev.) . . . . .	
94. Grand unified theories (rev.) . . . . .	971
95. Leptoquarks (rev.) . . . . .	986
96. Magnetic monopoles (rev.) . . . . .	989





SEARCHES  
not in other sections

Magnetic Monopole Searches

See the related review(s):  
Magnetic Monopoles

Monopole Production Cross Section — Accelerator Searches

Table with columns: X-SECT (cm²), MASS (GeV), CHG (g), ENERGY (GeV), BEAM, DOCUMENT ID, TECN. Lists various experimental searches for monopoles with different parameters and results.

••• We do not use the following data for averages, fits, limits, etc. •••

Table listing excluded data points with columns: MASS (GeV), ENERGY (GeV), BEAM, DOCUMENT ID, TECN.

- 1 The search was sensitive to monopoles which had stopped in aluminium trapping volumes. Monopoles with spins 0 and 1/2 were considered; mass-dependent spin 1/2 monopole limits are quoted here.
2 AAD 16AB model-independent 95% CL limits estimated using a fiducial region of approximately constant acceptance. Limits are mass-dependent.
3 ACHARYA 16 limits at 95% CL estimated using a Dreil-Yan-like production mechanism for scalar monopoles.
4 AAD 12Cs searched for monopoles as highly ionising objects. The cross section limits are based on an assumed Dreil-Yan-like production process for spin 1/2 monopoles. The limits are mass- and scenario-dependent.
5 ABBIENDI 08 assume production of spin 1/2 monopoles with effective charge gβ (n=1), via e+e- -> γ\* -> M M-bar, so that the cross section is proportional to (1 + cos²θ). There is no z information for such highly saturated tracks, so a parabolic track in the jet chamber is projected onto the xy plane. Charge per hit in the chamber produces a clean separation of signal and background.
6 ABULENCIA 06k searches for high-ionizing signals in CDF central outer tracker and time-of-flight detector. For Dreil-Yan M M-bar production, the cross section limit implies M > 360 GeV at 95% CL.
7 AKTAS 05A model-dependent limits as a function of monopole mass shown for arbitrary mass of 60 GeV. Based on search for stopped monopoles in the H1 Al beam pipe.
8 AKTAS 05A limits with assumed elastic spin 0 monopole pair production.
9 AKTAS 05A limits with assumed inelastic spin 1/2 monopole pair production.
10 KALBFLEISCH 04 reports searches for stopped magnetic monopoles in Be, Al, and Pb samples obtained from discarded material from the upgrading of DØ and CDF. A large-aperture warm-bore cryogenic detector was used. The approach was an extension of the methods of KALBFLEISCH 00. Cross section results moderately model dependent; interpretation as a mass lower limit depends on possibly invalid perturbation expansion.
11 KALBFLEISCH 00 used an induction method to search for stopped monopoles in pieces of the DØ (FNAL) beryllium beam pipe and in extensions to the drift chamber aluminium support cylinder. Results are model dependent.
12 KALBFLEISCH 00 result is for aluminum.
13 KALBFLEISCH 00 result is for beryllium.
14 HE 97 used a lead target and barium phosphate glass detectors. Cross-section limits are well below those predicted via the Dreil-Yan mechanism.
15 This work has also been reinterpreted in the framework of monopole production via the thermal Schwinger process (GOULD 17); this gives rise to lower mass limits.
16 Multiphoton events.
17 Cherenkov radiation polarization.
18 Re-examines CERN neutrino experiments.
19 AAD 20c give limits for Dreil-Yan production with spin-0 and spin-1/2 monopoles. The above limit is for spin = 0 at mass = 3 TeV.
20 ACHARYA 19b limits both β-dependent and β-independent on monopoles with spins 0, 1/2, and 1 and with magnetic charges ranging from one to five times the Dirac charge in mass ranges between 200 GeV and 5000 GeV.
21 ACHARYA 18A provide limits on monopoles with spins 0, 1/2, and 1 and with magnetic charges ranging from two to five times the Dirac charge.

Monopole Production — Other Accelerator Searches

Table with columns: MASS (GeV), CHG (g), SPIN, ENERGY (GeV), BEAM, DOCUMENT ID, TECN. Lists other accelerator searches for monopoles.

- 1 ABBOTT 98k search for heavy pointlike Dirac monopoles via central production of a pair of photons with high transverse energies.
2 ACCIARRI 95c finds a limit B(Z -> γγ) < 0.8 x 10^-5 (which is possible via a monopole loop) at 95% CL and sets the mass limit via a cross section model.

Monopole Flux — Cosmic Ray Searches

"Caty" in the charge column indicates a search for monopole-catalyzed nucleon decay.

Table with columns: FLUX (cm^-2sr^-1s^-1), MASS (GeV), CHG (g), COMMENTS (β = v/c), EVTS, DOCUMENT ID, TECN. Lists cosmic ray searches for monopoles.



# Searches Particle Listings

## Magnetic Monopole Searches

<3.7E-15	>E12	1	$\beta=1.E-4$	0	16	ORITO	91	PLAS
<3.2E-16	>E10	1	$\beta > 0.05$	0	16	ORITO	91	PLAS
<3.2E-16	>E10-E12	2,3		0	16	ORITO	91	PLAS
<3.8E-13		1	all $\beta$	0		BERMON	90	INDU
<5.E-16		Caty	$\beta < 1.E-3$	0	15	BEZUKOV	90	CHER
<1.8E-14		1	$\beta > 1.1E-4$	0	17	BUCKLAND	90	HEPT
<1E-18		1	$3.E-4 < \beta < 1.5E-3$	0	18	GHOSH	90	MICA
<7.2E-13		1	all $\beta$	0		HUBER	90	INDU
<5.E-12	>E7	1	$3.E-4 < \beta < 5.E-3$	0		BARISH	87	CNTR
<1.E-13		Caty	$1.E-5 < \beta < 1$	0	15	BARTELT	87	SOUJ
<1.E-10		1	all $\beta$	0		EBISU	87	INDU
<2.E-13		1	$1.E-4 < \beta < 6.E-4$	0		MASEK	87	HEPT
<2.E-14		1	$4.E-5 < \beta < 2.E-4$	0		NAKAMURA	87	PLAS
<2.E-14		1	$1.E-3 < \beta < 1$	0		NAKAMURA	87	PLAS
<5.E-14		1	$9.E-4 < \beta < 1.E-2$	0		SHEP KO	87	CNTR
<2.E-13		1	$4.E-4 < \beta < 1$	0		TSUKAMOTO	87	CNTR
<5.E-14		1	all $\beta$	1	19	CAPLIN	86	INDU
<5.E-12		1		0		CROMAR	86	INDU
<1.E-13		1	$7.E-4 < \beta$	0		HARA	86	CNTR
<7.E-11		1	all $\beta$	0		INCANDELA	86	INDU
<1.E-18		1	$4.E-4 < \beta < 1.E-3$	0	18	PRICE	86	MICA
<5.E-12		1		0		BERMON	85	INDU
<6.E-12		1		0		CAPLIN	85	INDU
<6.E-10		1		0		EBISU	85	INDU
<3.E-15		Caty	$5.E-5 \leq \beta \leq 1.E-3$	0	15	KAJITA	85	KAMI
<2.E-21		Caty	$\beta < 1.E-3$	0	15,20	KAJITA	85	KAMI
<3.E-15		Caty	$1.E-3 < \beta < 1.E-1$	0	15	PARK	85B	CNTR
<5.E-12		1	$1.E-4 < \beta < 1$	0		BATTISTONI	84	NUSX
<7.E-12		1		0		INCANDELA	84	INDU
<7.E-13		1	$3.E-4 < \beta$	0	17	KAJINO	84	CNTR
<2.E-12		1	$3.E-4 < \beta < 1.E-1$	0		KAJINO	84B	CNTR
<6.E-13		1	$5.E-4 < \beta < 1$	0		KAWAGOE	84	CNTR
<2.E-14		1	$1.E-3 < \beta$	0	15	KRISHNA...	84	CNTR
<4.E-13		1	$6.E-4 < \beta < 2.E-3$	0		LISS	84	CNTR
<1.E-16		1	$3.E-4 < \beta < 1.E-3$	0	18	PRICE	84	MICA
<1.E-13		1	$1.E-4 < \beta$	0		PRICE	84B	PLAS
<4.E-13		1	$6.E-4 < \beta < 2.E-3$	0		TARLE	84	CNTR
<4.E-13		1	$1.E-2 < \beta < 1.E-3$	0	21	ANDERSON	83	EMUL
<1.E-12		1	$7.E-3 < \beta < 1$	0		BARTELT	83B	CNTR
<3.E-13		1	$1.E-3 < \beta < 4.E-1$	0		BARWICK	83	PLAS
<3.E-12		Caty	$5.E-4 < \beta < 5.E-2$	0	15	BONARELLI	83	CNTR
<4.E-11		1		0	15	BOSETTI	83	CNTR
<5.E-15		1	$1.E-2 < \beta < 1$	0		CABRERA	83	INDU
<8.E-15		Caty	$1.E-4 < \beta < 1.E-1$	0	15	DOKE	83	PLAS
<5.E-12		1	$1.E-4 < \beta < 3.E-2$	0		ERREDE	83	IMB
<2.E-12		1	$6.E-4 < \beta < 1$	0		GROOM	83	CNTR
<1.E-13		1	$\beta=3.E-3$	0		MASHIMO	83	CNTR
<2.E-12		1	$7.E-3 < \beta < 6.E-1$	0		ALEXEYEV	82	CNTR
6.E-10		1	all $\beta$	1	22	BONARELLI	82	CNTR
<2.E-11		1	$1.E-2 < \beta < 1.E-1$	0		CABRERA	82	INDU
<2.E-15		concentrator		0		MASHIMO	82	CNTR
<1.E-13	>1	1	$1.E-3 < \beta$	0		BARTLETT	81	PLAS
<5.E-11	<E17	1	$3.E-4 < \beta < 1.E-3$	0		KINOSHITA	81B	PLAS
<2.E-11		concentrator		0		ULLMAN	81	CNTR
1.E-11	>200	2		1	23	BARTLETT	78	PLAS
<2.E-13	>2	0		0		PRICE	75	PLAS
<1.E-19	>2	obsidian, mica		0		FLEISCHER	71	PLAS
<5.E-15	<15	<3	concentrator	0		FLEISCHER	69C	PLAS
<2.E-11	<1-3	concentrator		0		CARITHERS	66	ELEC
				0		MALKUS	51	EMUL

- ALBERT 17 limits were estimated using a Cherenkov light in an array of optical modules under the Mediterranean Sea. The limits are for MM masses between  $10^{10}$  and  $10^{14}$  GeV. The limits are speed-dependent.
- AAB 16 search was made with a set of telescopes sampling the longitudinal profile of fluorescence light emitted by extensive air showers. Limits are speed dependent.
- AARTSEN 16b was based on a Cherenkov signature in an array of optical modules which were sunk in the Antarctic ice cap. Limits are speed-dependent.
- Beyond the monopole speed, the limits of AARTSEN 14 depend on the catalysis cross section ( $\sigma$ ) which corresponds to the monopole radiating 7 times the light per track length compared to the Cherenkov light from a single electrically charged, relativistic particle. The values quoted here correspond to  $\sigma = 1$  barn or  $l = 30$ .
- ABBASI 13 and ABBASI 10a were based on a Cherenkov signature in an array of optical modules which were sunk in the Antarctic ice cap. Limits are speed-dependent.
- ADRIAN-MARTINEZ 12a measurements were based on a Cherenkov signature in an underwater telescope in the Western Mediterranean Sea. Limits are speed-dependent.
- The limits from UENO 12 depend on the monopole speed and are also sensitive to assumed values of monopole mass and the catalysis cross section.
- HOGAN 08 and DETRIXHE 11 limits on relativistic monopoles are based on nonobservation of radio Cherenkov signals at the South Pole. Limits are speed-dependent.
- BALESTRA 08 exposed of nuclear track detector modules totaling  $400 \text{ m}^2$  for 4 years at the Chacaltaya Laboratory (5230 m) in search for intermediate-mass monopoles with  $\beta > 0.05$ . The analysis is mainly based on three CR39 modules. For  $M > 5 \times 10^{13}$  GeV there can be upward-going monopoles as well, hence the flux limit is half that obtained for less massive monopoles. Previous experiments (e.g. MACRO and OHYA (ORITO 91)) had set limits only for  $M > 1 \times 10^9$  GeV.
- AMBROSIO 02b direct search final result for  $m \geq 10^{17}$  GeV, based upon 4.2 to 9.5 years of running, depending upon the subsystem. Limit with CR39 track-etch detector extends the limit from  $\beta=4 \times 10^{-5}$  ( $3.1 \times 10^{-16} \text{ cm}^{-2} \text{ sr}^{-1} \text{ s}^{-1}$ ) to  $\beta=1 \times 10^{-4}$  ( $2.1 \times 10^{-16} \text{ cm}^{-2} \text{ sr}^{-1} \text{ s}^{-1}$ ). Limit curve in paper is piecewise continuous due to different detection techniques for different  $\beta$  ranges.

- AMBROSIO 02c limit for catalysis of nucleon decay with catalysis cross section of  $\approx 1$  mb. The flux limit increases by  $\sim 3$  at the higher  $\beta$  limit, and increases to  $1 \times 10^{-14} \text{ cm}^{-2} \text{ sr}^{-1} \text{ s}^{-1}$  if the catalysis cross section is 0.01 mb. Based upon 71193 hr of data with the streamer detector, with an acceptance of  $4250 \text{ m}^2 \text{ sr}$ .
- AMBROSIO 02b result for "more than two years of data." Ionization search using several subsystems. Limit curve as a function of  $\beta$  not given. Included in AMBROSIO 02b.
- AMBROSIO 97 global MACRO 90%CL is  $0.78 \times 10^{-15}$  at  $\beta=1.1 \times 10^{-4}$ , goes through a minimum at  $0.61 \times 10^{-15}$  near  $\beta=(1.1-2.7) \times 10^{-3}$ , then rises to  $0.84 \times 10^{-15}$  at  $\beta=0.1$ . The global limit in this region is below the Parker bound at  $10^{-15}$ . Less stringent limits are established for  $4 \times 10^{-5} < \beta < 1 \times 10^{-4}$ . Limits set by various triggers and different subdetectors are given in the paper. All limits assume a catalysis cross section smaller than a few mb.
- AHLEN 94 limit for dyons extends down to  $\beta=0.9E-4$  and a limit of  $1.3E-14$  extends to  $\beta = 0.8E-4$ . Also see comment by PRICE 94 and reply of BARISH 94. One loophole in the AHLEN 94 result is that in the case of monopoles catalyzing nucleon decay, relativistic particles could veto the events. See AMBROSIO 97 for additional results.
- Catalysis of nucleon decay; sensitive to assumed catalysis cross section.
- ORITO 91 limits are functions of velocity. Lowest limits are given here.
- Used DKMPR mechanism and Penning effect.
- Assumes monopole attaches fermion nucleus.
- Limit from combining data of CAPLIN 86, BERMON 85, INCANDELA 84, and CABRERA 83. For a discussion of controversy about CAPLIN 86 observed event, see GUY 87. Also see SCHOUTEN 87.
- Based on lack of high-energy solar neutrinos from catalysis in the sun.
- Anomalous long-range  $\alpha$  ( $^4\text{He}$ ) tracks.
- CABRERA 82 candidate event has single Dirac charge within  $\pm 5\%$ .
- ALVAREZ 75, FLEISCHER 75, and FRIEDLANDER 75 explain as fragmenting nucleus. EBERHARD 75 and ROSS 76 discuss conflict with other experiments. HAGSTROM 77 reinterprets as antineutrino. PRICE 78 reassesses.

### Monopole Flux — Astrophysics

FLUX ( $\text{cm}^{-2} \text{sr}^{-1} \text{s}^{-1}$ )	MASS (GeV)	CHG (g)	COMMENTS ( $\beta = v/c$ )	DOCUMENT ID	TECN
<1.3E-20			faint white dwarf	1	FREESE 99 ASTR
<1.E-16	E17	1	galactic field	2	ADAMS 93 COSM
<1.E-23			Jovian planets	1	ARAFUNE 85 ASTR
<1.E-16	E15		solar trapping	BRACCI 85B ASTR	
<1.E-18		1		1	HARVEY 84 COSM
<3.E-23			neutron stars	KOLB 84 ASTR	
<7.E-22			pulsars	1	FREESE 83B ASTR
<1.E-18	<E18	1	intergalactic field	1	REPHAELI 83 COSM
<1.E-23			neutron stars	1	DIMOPOUL... 82 COSM
<5.E-22			neutron stars	1	KOLB 82 COSM
<5.E-15	>E21		galactic halo	1	SALPETER 82 COSM
<1.E-12	E19	1	$\beta=3.E-3$	3	TURNER 82 COSM
<1.E-16		1	galactic field	PARKER 70 COSM	

- Catalysis of nucleon decay.
- ADAMS 93 limit based on "survival and growth of a small galactic seed field" is  $10^{-16} (m/10^{17} \text{ GeV}) \text{ cm}^{-2} \text{ s}^{-1} \text{ sr}^{-1}$ . Above  $10^{17}$  GeV, limit  $10^{-16} (10^{17} \text{ GeV}/m) \text{ cm}^{-2} \text{ s}^{-1} \text{ sr}^{-1}$  (from requirement that monopole density does not overclose the universe) is more stringent.
- Re-evaluates PARKER 70 limit for GUT monopoles.

### Monopole Density — Matter Searches

DENSITY	CHG (g)	MATERIAL	DOCUMENT ID	TECN
<9.8E-5/gram	$\geq 1$	Polar rock	BENDTZ 13	INDU
<6.9E-6/gram	>1/3	Meteorites and other	JEON 95	INDU
<2.E-7/gram	>0.6	Fe ore	1	EBISU 87 INDU
<4.6E-6/gram	>0.5	deep schist	KOVALIK 86	INDU
<1.6E-6/gram	>0.5	manganese nodules	2	KOVALIK 86 INDU
<1.3E-6/gram	>0.5	seawater	KOVALIK 86	INDU
>1.E+14/gram	>1/3	iron aerosols	MIKHAILOV 83	SPEC
>6.E-4/gram		air, seawater	CARRIGAN 76	CNTR
<5.E-1/gram	>0.04	11 materials	CABRERA 75	INDU
<2.E-4/gram	>0.05	moon rock	ROSS 73	INDU
<6.E-7/gram	<140	seawater	KOLM 71	CNTR
<1.E-2/gram	<120	manganese nodules	FLEISCHER 69	PLAS
<1.E-4/gram	>0	manganese	FLEISCHER 69B	PLAS
<2.E-3/gram	<1-3	magnetite, meteor	GOTO 63	EMUL
<2.E-2/gram		meteorite	PETUKHOV 63	CNTR

- Mass  $1 \times 10^{14} - 1 \times 10^{17}$  GeV.
- KOVALIK 86 examined 498 kg of schist from two sites which exhibited clear mineralogical evidence of having been buried at least 20 km deep and held below the Curie temperature.

### Monopole Density — Astrophysics

DENSITY	CHG (g)	MATERIAL	DOCUMENT ID	TECN
<1.E-9/gram	1	sun, catalysis	1	ARAFUNE 83 COSM
<6.E-33/nucl	1	moon wake	SCHATTEN 83	ELEC
<2.E-28/nucl		earth heat	CARRIGAN 80	COSM
<2.E-4/prot		42cm absorption	BRODERICK 79	COSM
<2.E-13/m <sup>3</sup>		moon wake	SCHATTEN 70	ELEC

- Catalysis of nucleon decay.

See key on page 999

Searches Particle Listings

Magnetic Monopole Searches, Supersymmetric Particle Searches

REFERENCES FOR Magnetic Monopole Searches

AAD 20G PRL 124 031802 G. Aad et al. (ATLAS Collab.)  
 ACHARYA 19B PRL 123 021802 B. Acharya et al. (MoEDAL Collab.)  
 ACHARYA 18A PL B782 510 B. Acharya et al. (MoEDAL Collab.)  
 ACHARYA 17 PRL 118 016801 B. Acharya et al. (MoEDAL Collab.)  
 ALBERT 17 JHEP 1707 054 A. Albert et al. (ANTARES Collab.)  
 GOULD 17 PRL 119 241601 A. Gould, A. Rajantie (Pierre Auger Collab.)  
 AAB 16 PR D94 082002 A. Aab et al. (ATLAS Collab.)  
 AAD 16AB PR D93 052009 G. Aad et al. (ATLAS Collab.)  
 AARTSEN 16B EPJ C76 133 M.G. Aartsen et al. (IceCube Collab.)  
 ACHARYA 16 JHEP 1608 067 B. Acharya et al. (MoEDAL Collab.)  
 AARTSEN 14 EPJ C74 2938 M.G. Aartsen et al. (IceCube Collab.)  
 Also EPJ C79 124 (erratum)  
 ABBASI 13 PR D87 022001 R. Abbasi et al. (IceCube Collab.)  
 BENDTZ 13 PRL 110 121803 K. Bendtz et al.  
 AAD 12CS PRL 109 261803 G. Aad et al. (ATLAS Collab.)  
 ADRIAN-MAR...12A ASP 35 634 S. Adrian-Martinez et al. (ANTARES Collab.)  
 UENO 12 ASP 36 131 K. Ueno et al. (Super-Kamiokande Collab.)  
 DETRIXHE 11 PR D83 023513 M. Detrixhe et al. (ANITA Collab.)  
 ABBASI 10A EPJ C69 361 R. Abbasi et al. (IceCube Collab.)  
 ABBIENDI 08 PL B663 37 G. Abbiendi et al. (OPAL Collab.)  
 BALESTRA 08 EPJ C55 57 S. Balestra et al. (SLIM Collab.)  
 HOGAN 08 PR D78 075031 D.P. Hogan et al. (KANS, NEBR, DELA Collab.)  
 ABULENCIA 06K PRL 96 201801 A. Abulencia et al. (CDF Collab.)  
 AKTAS 05A EPJ C41 133 A. Aktas et al. (HI Collab.)  
 KALBFLEISCH 04 PR D69 052002 G.R. Kalbfleisch et al. (OKLA Collab.)  
 AMBROSIO 02B EPJ C25 511 M. Ambrosio et al. (MACRO Collab.)  
 AMBROSIO 02C EPJ C26 163 M. Ambrosio et al. (MACRO Collab.)  
 AMBROSIO 02D ASP 18 27 M. Ambrosio et al. (MACRO Collab.)  
 KALBFLEISCH 00 PRL 85 5292 G.R. Kalbfleisch et al.  
 FREESE 99 PR D59 063007 K. Freese, E. Krasteva  
 ABBOTT 98K PRL 81 524 B. Abbott et al. (D0 Collab.)  
 AMBROSIO 97 PL B406 249 M. Ambrosio et al. (MACRO Collab.)  
 HE 97 PRL 79 3134 M. He (MACRO Collab.)  
 ACCIARRI 95C PRL B345 609 M. Acciari et al. (L3 Collab.)  
 JEON 95 PRL 75 1443 H. Jeon, M.J. Longo (MICH)  
 Also PRL 76 159 (erratum)  
 AHLEN 94 PRL 72 608 S.P. Ahlen et al. (MACRO Collab.)  
 BARISH 94 PRL 73 1306 B.C. Barish, G. Giacomelli, J.T. Hong (CIT+)  
 BECKER-SZ... 94 PR D49 2169 R.A. Becker-Szendy et al. (IMB Collab.)  
 PRICE 94 PRL 73 1305 P.B. Price (UCB)  
 ADAMS 93 PRL 70 2511 F.C. Adams et al. (MICH, FNAL)  
 PINFOLD 93 PL B316 407 J.L. Pinfold et al. (ALBE, HARV, MONT+)  
 KINOSHITA 92 PR D46 0801 K. Kinoshita et al. (HARV, BGNA, REHO)  
 THRON 92 PR D46 4846 J.L. Thron et al. (SOUAND-2 Collab.)  
 GARDNER 91 PR D44 622 D.D. Gardner et al. (STAN)  
 HUBER 91 PR D44 636 M.E. Huber et al. (STAN)  
 ORITO 91 PRL 66 1951 S. Orto et al. (ICEPP, WAS CR, NIHO, ICRR)  
 BERMON 90 PRL 64 839 S. Bermon et al. (IBM, BNL)  
 BERTANI 90 EPL 12 613 M. Bertani et al. (BGNA, INFN)  
 BEZRUKOV 90 SJNP 52 54 L.B. Bezrukov et al. (INRM)  
 Translated from YAF 52 86  
 BUCKLAND 90 PR D41 2726 K.N. Buckland et al. (UCSD)  
 GHOSH 90 EPL 12 25 D.C. Ghosh, S. Chatterjee (JADA)  
 HUBER 90 PRL 64 835 M.E. Huber et al. (STAN)  
 PRICE 90 PRL 65 149 P.B. Price, J. Guin, K. Kinoshita (UCB, HARV)  
 KINOSHITA 89 PL B228 543 K. Kinoshita et al. (HARV, TISA, KEK+)  
 BRAUNSCH... 88B ZPHY C38 543 R. Braunschweig et al. (TASSO Collab.)  
 KINOSHITA 88 PRL 60 1610 K. Kinoshita et al. (HARV, TISA, KEK+)  
 BARISH 87 PR D36 2641 B.C. Barish, G. Liu, C. Lane (CIT)  
 BARTELT 87 PR D36 1990 J.E. Bartelt et al. (Soudan Collab.)  
 Also PR D40 1701 (erratum) (Soudan Collab.)  
 EBISU 87 PR D36 3359 T. Ebisu, T. Watanabe (KOBE)  
 Also JP G11 883 T. Ebisu, T. Watanabe (KOBE)  
 GENTILE 87 PR D35 1081 T. Gentile et al. (CLEO Collab.)  
 GUY 87 NAT 325 463 J. Guy (LOIC)  
 MASEK 87 PR D35 2758 G.E. Masek et al. (UCSD)  
 NAKAMURA 87 PL B183 395 S. Nakamura et al. (INUS, WAS CR, NIHO)  
 PRICE 87 PRL 59 2523 P.B. Price, R. Guoxiao, K. Kinoshita (UCB, HARV)  
 SCHOUTEN 87 JP E20 850 J.C. Schouten et al. (LOIC)  
 SHEPKO 87 PR D35 2917 M.J. Shepko et al. (TAMU)  
 TSUKAMOTO 87 EPL 3 39 T. Tsukamoto et al. (ICRR)  
 CAPLIN 86 NAT 321 402 A.D. Caplin et al. (LOIC)  
 Also JP E20 850 J.C. Schouten et al. (LOIC)  
 Also NAT 325 463 J. Guy (LOIC)  
 CROMAR 86 PRL 56 2561 M.W. Cromar, A.F. Clark, F.R. Fickett (NBSB)  
 HARA 86 PR D36 553 T. Hara et al. (ICRR, KYOT, KEK, KOBE+)  
 INCANDELA 86 PR D34 2637 J. Incandela et al. (CHIC, FNAL, MICH)  
 KOVALIK 86 PR A33 1183 J.M. Kovalik, J.L. Kirschvink (CIT)  
 PRICE 86 PRL 56 1226 P.B. Price, M.H. Salamon (UCB)  
 ARAFUNE 85 PR D32 2586 J. Arafune, M. Fukugita, S. Yanagita (ICRR, KYOTU+)  
 BERMON 85 PRL 55 1850 S. Bermon et al. (IBM)  
 BRACCI 85B NP B258 726 L. Bracci, G. Fiorentini, G. Mezzorani (PISA+)  
 Also LNC 42 123 L. Bracci, G. Fiorentini (PISA)  
 CAPLIN 85 NAT 317 234 A.D. Caplin et al. (LOIC)  
 EBISU 85 JP G11 883 T. Ebisu, T. Watanabe (KOBE)  
 KAJITA 85 JPS J 54 4065 T. Kajita et al. (ICRR, KEK, MIIG)  
 PARK 85B NP B252 261 H.S. Park et al. (IMB Collab.)  
 BATTISTONI 84 PL 133B 454 G. Battistoni et al. (NUSEX Collab.)  
 FRYBERGER 84 PR D29 1524 D. Fryberger et al. (SLAC, UCB)  
 HARVEY 84 NP B236 255 J.A. Harvey (PRIN)  
 INCANDELA 84 PRL 53 2067 J. Incandela et al. (CHIC, FNAL, MICH)  
 KAJINO 84 PRL 52 1373 F. Kajino et al. (ICRR)  
 KAJINO 84B JP G10 447 F. Kajino et al. (ICRR)  
 KAWAGOE 84 LNC 41 315 K. Kawagoe et al. (TOKY)  
 KOLB 84 APJ 286 702 E.W. Kolb, M.S. Turner (FNAL, CHIC)  
 KRISHNA... 84 PL 142B 99 M.R. Krishnaswamy et al. (TATA, OSK+)  
 LISS 84 PR D30 804 T.M. Liss, S.P. Ahlen, G. Tarle (UCB, IND+)  
 PRICE 84 PRL 52 1265 P.B. Price et al. (ROMA, UCB, IND+)  
 PRICE 84B PL 140B 112 P.B. Price (CERN)  
 TARLE 84 PRL 52 90 G. Tarle, S.P. Ahlen, T.M. Liss (UCB, MICH+)  
 ANDERSON 83 PR D28 2308 S.N. Anderson et al. (WASH)  
 ARAFUNE 83 PL 133B 380 J. Arafune, M. Fukugita (ICRR, KYOTO)  
 AUBERT 83B PL 120B 465 B. Aubert et al. (CERN, LAPP)  
 BARTELT 83B PRL 50 655 J.E. Bartelt et al. (MINN, ANL)  
 BARWICK 83 PR D28 2338 S.W. Barwick, K. Kinoshita, P.B. Price (UCB)  
 BONARELLI 83 PL 126B 137 R. Bonarelli, P. Capiluppi, I. d'Antone (BGNA)  
 BOSETTI 83 PL 133B 265 P.C. Bosetti et al. (AACH3, HAWA, TOKY)  
 CABRERA 83 PRL 51 1933 B. Cabrera et al. (STAN)  
 DOKE 83 PL 129B 370 T. Doke et al. (WASU, RIKK, TTAM, RIKEN)  
 ERREDE 83 PRL 51 245 S.M. Errede et al. (IMB Collab.)  
 FREESE 83B PRL 51 1625 K. Freese, M.S. Turner, D.N. Schramm (CHIC)  
 GROOM 83 PRL 50 573 D.E. Groom et al. (UTAH, STAN)  
 MASHIMO 83 PL 128B 327 T. Mashimo et al. (ICEPP)  
 MIKHAILOV 83 PL 130B 331 V.F. Mikhailov (KAZA)  
 MUSSET 83 PL 128B 333 P. Musset, M. Price, E. Lohrmann (CERN, HAMB)  
 REPHAELI 83 PL 121B 115 Y. Rephaeli, M.S. Turner (CHIC)  
 SCHATTEN 83 PR D27 1525 K.H. Schatten (NASA)  
 ALEXEYEV 82 LNC 35 413 E.N. Alekseev et al. (INRM)  
 BONARELLI 82 PL 112B 100 R. Bonarelli et al. (BGNA)

CABRERA 82 PRL 48 1378 B. Cabrera (STAN)  
 DELL 82 NP B209 45 G.F. Dell et al. (BNL, ADEL, ROMA)  
 DIMOPOUL... 82 PL 119B 320 S. Dimopoulos, J. Preskill, F. Wilczek (HARV+)  
 KINOSHITA 82 PRL 48 77 K. Kinoshita, P.B. Price, D. Fryberger (UCB+)  
 KOLB 82 PRL 49 1373 E.W. Kolb, S.A. Colgatoe, J.A. Harvey (LASL, PRIN)  
 MASHIMO 82 JPS J 51 3067 T. Mashimo, K. Kawagoe, M. Koshiba (INUS)  
 SALPETER 82 PRL 49 1114 E.E. Salpeter, S.L. Shapiro, I. Wasserman (CORN)  
 TURNER 82 PR D26 1296 M.S. Turner, E.N. Parker, T.J. Bogdan (CHIC)  
 BARTLETT 81 PR D24 612 D.F. Bartlett et al. (COLO, GESC)  
 KINOSHITA 81B PR D24 1707 K. Kinoshita, P.B. Price (UCB)  
 ULLMAN 81 PRL 47 289 J.D. Ullman (LEHM, BNL)  
 CARRIGAN 80 NAT 288 348 R.A. Carrigan (FNAL)  
 BRODERICK 79 PR D19 1046 J.J. Broderick et al. (VPI)  
 BARTLETT 78 PR D18 2253 D.F. Bartlett, D. Soo, M.G. White (COLO, PRIN)  
 CARRIGAN 78 PR D17 1754 R.A. Carrigan, B.P. Strauss, G. Giacomelli (FNAL+)  
 HOFFMANN 78 LNC 23 357 H. Hoffmann et al. (CERN, ROMA)  
 PRICE 78 PR D18 1382 P.B. Price et al. (UCB, HOUS)  
 HAGSTROM 77 PRL 38 729 R. Hagstrom (LBL)  
 CARRIGAN 76 PR D13 1823 R.A. Carrigan, F.A. Nezrick, B.P. Strauss (FNAL)  
 DELL 76 LNC 15 269 G.F. Dell et al. (CERN, BNL, ROMA, ADEL)  
 ROSS 76 LBL-4665 R.R. Ross (LBL)  
 STEVENS 76B PR D14 2207 D.M. Stevens et al. (VPI, BNL)  
 ZRELOV 76 CZJP B26 1306 V.P. Zrelov et al. (JINR)  
 ALVAREZ 75 LBL-4260 L.W. Alvarez (LBL)  
 BURKE 75 PL 60B 113 D.L. Burke et al. (MICH)  
 CABRERA 75 Thesis B. Cabrera (STAN)  
 CARRIGAN 75 NP B91 279 R.A. Carrigan, F.A. Nezrick (FNAL)  
 Also PR D3 56 R.A. Carrigan, F.A. Nezrick (FNAL)  
 EBERHARD 75 PR D11 3099 P.H. Eberhard et al. (LBL, MPIM)  
 EBERHARD 75B LBL-4289 P.H. Eberhard (LBL)  
 FLEISCHER 75 PRL 35 1412 R.L. Fleischer, R.N.F. Walker (GESC, WUSL)  
 FRIEDLANDER 75 PRL 35 1167 M.W. Friedlander (WUSL)  
 GIACOMELLI 75 NC 28A 21 G. Giacomelli et al. (BGNA, CERN, SAUL+)  
 PRICE 75 PRL 35 487 P.B. Price et al. (UCB, HOUS)  
 CARRIGAN 74 PR D10 3867 R.A. Carrigan, F.A. Nezrick, B.P. Strauss (FNAL)  
 CARRIGAN 73 PR D8 3717 R.A. Carrigan, F.A. Nezrick, B.P. Strauss (FNAL)  
 ROSS 73 PR D8 698 R.R. Ross et al. (LBL, SLAC)  
 Also PR D4 3260 P.H. Eberhard et al. (LBL, SLAC)  
 Also SCI 167 701 L.W. Alvarez et al. (LBL, SLAC)  
 BARTLETT 72 PR D6 1817 D.F. Bartlett, M.D. Lahana (COLO)  
 GUREVICH 72 PL 38B 549 I.I. Gurevich et al. (KIAE, NOVO, SERP)  
 Also JETP 34 917 L.M. Barkov, I.I. Gurevich, M.S. Zolotarev (KIAE+)  
 Translated from ZETF 61 1721  
 Also PL 31B 394 I.I. Gurevich et al. (KIAE, NOVO, SERP)  
 FLEISCHER 71 PR D4 24 R.L. Fleischer et al. (GESC)  
 KOLM 71 PR D4 1285 H.H. Kolm, F. Villa, A. Odian (MIT, SLAC)  
 PARKER 70 APJ 160 383 E.N. Parker (CHIC)  
 SCHATTEN 70 PR D1 2245 K.H. Schatten (GESC, FSU)  
 FLEISCHER 69 PR 177 2029 R.L. Fleischer et al. (GESC, NASA)  
 FLEISCHER 69B PR 184 1393 R.L. Fleischer et al. (GESC, UNCS, GSCO)  
 FLEISCHER 69C PR 184 1398 R.L. Fleischer, P.B. Price, R.T. Woods (GESC)  
 Also JAP 41 958 R.L. Fleischer et al. (GESC)  
 CARITHERS 66 PR 149 1070 W.C.J. Carithers, R.J. Stefanski, R.K. Adair  
 AMALDI 63 NC 28 773 E. Amaldi et al. (ROMA, UCSD, CERN)  
 GOTO 63 PR 132 387 G. Goto, H.H. Kolm, K.W. Ford (TOKY, MIT, BRAN)  
 PETUKHOV 63 NP 49 87 V.A. Petukhov, M.N. Yakimenko (LEBD)  
 PURCELL 63 PR 129 2326 E.M. Purcell et al. (HARV, BNL)  
 FIDECARO 61 NC 22 657 M. Fiducaro, G. Finocchiaro, G. Giacomelli (CERN)  
 BRADNER 59 PR 114 603 H. Bradner, W.M. Isbell (LBL)  
 MALKUS 51 PR 83 899 W.V.R. Malkus (CHIC)

OTHER RELATED PAPERS

GROOM 86 PRPL 140 323 D.E. Groom (UTAH)  
 Review

Supersymmetric Particle Searches

The exclusion of particle masses within a mass range ( $m_1, m_2$ ) will be denoted with the notation "none  $m_1 - m_2$ " in the VALUE column of the following Listings. The latest unpublished results are described in the "Supersymmetry: Experiment" review.

See the related review(s):  
 Supersymmetry, Part I (Theory)  
 Supersymmetry, Part II (Experiment)

CONTENTS:

- $\tilde{\chi}_1^0$  (Lightest Neutralino) mass limit
  - Accelerator limits for stable  $\tilde{\chi}_1^0$
  - Bounds on  $\tilde{\chi}_1^0$  from dark matter searches
  - $\tilde{\chi}_1^0$ -p elastic cross section
    - Spin-dependent interactions
    - Spin-independent interactions
  - Other bounds on  $\tilde{\chi}_1^0$  from astrophysics and cosmology
  - Unstable  $\tilde{\chi}_1^0$  (Lightest Neutralino) mass limit
- $\tilde{\chi}_1^0, \tilde{\chi}_2^0, \tilde{\chi}_3^0$  (Neutralinos) mass limits
- $\tilde{\chi}_1^\pm, \tilde{\chi}_2^\pm$  (Charginos) mass limits
- Long-lived  $\tilde{\chi}^\pm$  (Chargino) mass limit
- $\tilde{\nu}$  (Sneutrino) mass limit
- Charged sleptons
  - R-parity conserving  $\tilde{e}$  (Selectron) mass limit
  - R-parity violating  $\tilde{e}$  (Selectron) mass limit
  - R-parity conserving  $\tilde{\mu}$  (Smuon) mass limit
  - R-parity violating  $\tilde{\mu}$  (Smuon) mass limit
  - R-parity conserving  $\tilde{\tau}$  (Stau) mass limit
  - R-parity violating  $\tilde{\tau}$  (Stau) mass limit
  - Long-lived  $\tilde{\ell}$  (Slepton) mass limit
- $\tilde{q}$  (Squark) mass limit
  - R-parity conserving  $\tilde{q}$  (Squark) mass limit
  - R-parity violating  $\tilde{q}$  (Squark) mass limit

# Searches Particle Listings

## Supersymmetric Particle Searches

Long-lived  $\tilde{q}$  (Squark) mass limit  
 $\tilde{b}$  (Sbottom) mass limit  
 – R-parity conserving  $\tilde{b}$  (Sbottom) mass limit  
 – R-parity violating  $\tilde{b}$  (Sbottom) mass limit  
 $\tilde{t}$  (Stop) mass limit  
 – R-parity conserving  $\tilde{t}$  (Stop) mass limit  
 – R-parity violating  $\tilde{t}$  (Stop) mass limit  
 Heavy  $\tilde{g}$  (Gluino) mass limit  
 – R-parity conserving heavy  $\tilde{g}$  (Gluino) mass limit  
 – R-parity violating heavy  $\tilde{g}$  (Gluino) mass limit  
 Long-lived  $\tilde{g}$  (Gluino) mass limit  
 Light  $\tilde{G}$  (Gravitino) mass limits from collider experiments  
 Supersymmetry miscellaneous results

Most of the results shown below, unless stated otherwise, are based on the Minimal Supersymmetric Standard Model (MSSM), as described in the Note on Supersymmetry. Unless otherwise indicated, this includes the assumption of common gaugino and scalar masses at the scale of Grand Unification (GUT), and use of the resulting relations in the spectrum and decay branching ratios. Unless otherwise indicated, it is also assumed that  $R$ -parity ( $R$ ) is conserved and that:

- 1) The  $\tilde{\chi}_1^0$  is the highest supersymmetric particle (LSP)
- 2)  $m_{\tilde{f}_L} = m_{\tilde{f}_R}$ , where  $\tilde{f}_{L,R}$  refer to the scalar partners of left- and right-handed fermions.

Limits involving different assumptions are identified in the Comments or in the Footnotes. We summarize here the notations used in this Chapter to characterize some of the most common deviations from the MSSM (for further details, see the Note on Supersymmetry).

Theories with  $R$ -parity violation ( $\mathcal{R}$ ) are characterized by a superpotential of the form:  $\lambda_{ijk} L_i L_j e_k^c + \lambda'_{ijk} L_i Q_j d_k^c + \lambda''_{ijk} u_i^c d_j^c d_k^c$ , where  $i, j, k$  are generation indices. The presence of any of these couplings is often identified in the following by the symbols  $L\tilde{L}\tilde{E}$ ,  $LQ\tilde{D}$ , and  $U\tilde{D}\tilde{D}$ . Mass limits in the presence of  $\mathcal{R}$  will often refer to “direct” and “indirect” decays. Direct refers to  $\mathcal{R}$  decays of the particle in consideration. Indirect refers to cases where  $\mathcal{R}$  appears in the decays of the LSP. The LSP need not be the  $\tilde{\chi}_1^0$ .

In several models, most notably in theories with so-called Gauge Mediated Supersymmetry Breaking (GMSB), the gravitino ( $\tilde{G}$ ) is the LSP. It is usually much lighter than any other massive particle in the spectrum, and  $m_{\tilde{G}}$  is then neglected in all decay processes involving gravitinos. In these scenarios, particles other than the neutralino are sometimes considered as the next-to-highest supersymmetric particle (NLSP), and are assumed to decay to their even- $R$  partner plus  $\tilde{G}$ . If the lifetime is short enough for the decay to take place within the detector,  $\tilde{G}$  is assumed to be undetected and to give rise to missing energy ( $\cancel{E}$ ) or missing transverse energy ( $\cancel{E}_T$ ) signatures.

When needed, specific assumptions on the eigenstate content of  $\tilde{\chi}^0$  and  $\tilde{\chi}^\pm$  states are indicated, using the notation  $\tilde{\gamma}$  (photino),  $\tilde{H}$  (higgsino),  $\tilde{W}$  (wino), and  $\tilde{Z}$  (zino) to signal that the limit of pure states was used. The terms gaugino is also used, to generically indicate wino-like charginos and zino-like neutralinos.

In the listings we have made use of the following abbreviations for simplified models employed by the experimental collaborations in supersymmetry searches published in the past year.

**WARNING:** Experimental lower mass limits determined within simplified models are to be treated with extreme care as they might not be directly applicable to realistic models. This is outlined in detail in the publications and we recommend consulting them before using bounds. For example, branching ratios, typically fixed to specific values in simplified models, can vary substantially in more elaborate models.

### Simplified Models Table

- Tglu1A:** gluino pair production with  $\tilde{g} \rightarrow q\bar{q}\tilde{\chi}_1^0$ .  
**Tglu1B:** gluino pair production with  $\tilde{g} \rightarrow q\bar{q}'\tilde{\chi}_1^\pm$ ,  $\tilde{\chi}_1^\pm \rightarrow W^\pm\tilde{\chi}_1^0$ .  
**Tglu1C:** gluino pair production with a 2/3 probability of having a  $\tilde{g} \rightarrow q\bar{q}'\tilde{\chi}_1^\pm$ ,  $\tilde{\chi}_1^\pm \rightarrow W^\pm\tilde{\chi}_1^0$  decay and a 1/3 probability of having a  $\tilde{g} \rightarrow q\bar{q}\tilde{\chi}_2^0$ ,  $\tilde{\chi}_2^0 \rightarrow Z^\pm\tilde{\chi}_1^0$  decay.  
**Tglu1D:** gluino pair production with one gluino decaying to  $q\bar{q}'\tilde{\chi}_1^\pm$  with  $\tilde{\chi}_1^\pm \rightarrow W^\pm + \tilde{G}$ , and the other gluino decaying to  $q\bar{q}\tilde{\chi}_1^0$  with  $\tilde{\chi}_1^0 \rightarrow \gamma + \tilde{G}$ .  
**Tglu1E:** gluino pair production with  $\tilde{g} \rightarrow q\bar{q}'\tilde{\chi}_1^\pm$ ,  $\tilde{\chi}_1^\pm \rightarrow W^\pm\tilde{\chi}_2^0$  and  $\tilde{\chi}_2^0 \rightarrow Z^\pm\tilde{\chi}_1^0$  where  $m_{\tilde{\chi}_1^\pm} = (m_{\tilde{g}} + m_{\tilde{\chi}_1^0})/2$ ,  $m_{\tilde{\chi}_2^0} = (m_{\tilde{\chi}_1^\pm} + m_{\tilde{\chi}_1^0})/2$ .  
**Tglu1F:** gluino pair production with  $\tilde{g} \rightarrow q\bar{q}'\tilde{\chi}_1^\pm$  or  $\tilde{g} \rightarrow q\bar{q}\tilde{\chi}_2^0$  with equal branching ratios, where  $\tilde{\chi}_1^\pm$  decays through an intermediate scalar tau lepton or sneutrino to  $\tau\nu\tilde{\chi}_1^0$  and where  $\tilde{\chi}_2^0$  decays through an intermediate scalar tau lepton or sneutrino to  $\tau^+\tau^-\tilde{\chi}_1^0$  or  $\nu\bar{\nu}\tilde{\chi}_1^0$ ; the mass hierarchy is such that  $m_{\tilde{\chi}_1^\pm} \sim m_{\tilde{\chi}_2^0} = (m_{\tilde{g}} + m_{\tilde{\chi}_1^0})/2$  and  $m_{\tilde{\tau},\tilde{\nu}} = (m_{\tilde{\chi}_1^\pm} + m_{\tilde{\chi}_1^0})/2$ .  
**Tglu1G:** gluino pair production with  $\tilde{g} \rightarrow q\bar{q}\tilde{\chi}_2^0$ , and  $\tilde{\chi}_2^0$  decaying through an intermediate slepton or sneutrino to  $l^{+l-}\tilde{\chi}_1^0$  or  $\nu\bar{\nu}\tilde{\chi}_1^0$  where  $m_{\tilde{\chi}_2^0} = (m_{\tilde{g}} + m_{\tilde{\chi}_1^0})/2$  and  $m_{\tilde{l},\tilde{\nu}} = (m_{\tilde{\chi}_2^0} + m_{\tilde{\chi}_1^0})/2$ .  
**Tglu1H:** gluino pair production with  $\tilde{g} \rightarrow q\bar{q}\tilde{\chi}_2^0$ , and  $\tilde{\chi}_2^0 \rightarrow \tilde{\chi}_1^0 Z^{0(*)}$ .  
**Tglu1I:** gluino pair production with  $\tilde{g} \rightarrow q\bar{q}\tilde{\chi}_2^0$ , and  $\tilde{\chi}_2^0 \rightarrow \tilde{\chi}_1^0 H$ .  
**Tglu1J:** gluino pair production with  $\tilde{g} \rightarrow q\bar{q}\tilde{\chi}_2^0$ , and  $\text{BR}(\tilde{\chi}_2^0 \rightarrow \tilde{\chi}_1^0 Z^{0(*)}) = \text{BR}(\tilde{\chi}_2^0 \rightarrow \tilde{\chi}_1^0 H) = 0.5$ .  
**Tglu1LL:** gluino pair production where  $\tilde{g} \rightarrow q\bar{q}\tilde{\chi}_1^0$  happens with 1/3 probability and  $\tilde{g} \rightarrow q\bar{q}'\tilde{\chi}_1^\pm$  happens with 2/3 probability. The  $\tilde{\chi}_1^\pm$  is assumed to be few hundreds of MeV heavier than the  $\tilde{\chi}_1^0$ , and decays to  $\tilde{\chi}_1^0$  via a pion.  
**Tglu2A:** gluino pair production with  $\tilde{g} \rightarrow b\bar{b}\tilde{\chi}_1^0$ .  
**Tglu3A:** gluino pair production with  $\tilde{g} \rightarrow t\bar{t}\tilde{\chi}_1^0$ .  
**Tglu3B:** gluino pair production with  $\tilde{g} \rightarrow t\bar{t}$  where  $\tilde{t}$  decays exclusively to  $t\tilde{\chi}_1^0$ .  
**Tglu3C:** gluino pair production with  $\tilde{g} \rightarrow t\bar{t}$  where  $\tilde{t}$  decays exclusively to  $c\tilde{\chi}_1^0$ .  
**Tglu3D:** gluino pair production with  $\tilde{g} \rightarrow t\bar{b}\tilde{\chi}_1^\pm$  with  $\tilde{\chi}_1^\pm \rightarrow W^\pm\tilde{\chi}_1^0$ .  
**Tglu3E:** gluino pair production where the gluino decays 25% of the time through  $\tilde{g} \rightarrow t\bar{t}\tilde{\chi}_1^0$ , 25% of the time through  $\tilde{g} \rightarrow b\bar{b}\tilde{\chi}_1^0$  and 50% of the time through  $\tilde{g} \rightarrow t\bar{b}\tilde{\chi}_1^\pm$  with  $\tilde{\chi}_1^\pm \rightarrow W^\pm\tilde{\chi}_1^0$ .  
**Tglu4A:** gluino pair production with one gluino decaying to  $q\bar{q}'\tilde{\chi}_1^\pm$  with  $\tilde{\chi}_1^\pm \rightarrow W^\pm + \tilde{G}$ , and the other gluino decaying to  $q\bar{q}\tilde{\chi}_1^0$  with  $\tilde{\chi}_1^0 \rightarrow \gamma + \tilde{G}$ .  
**Tglu4B:** gluino pair production with gluinos decaying to  $q\bar{q}\tilde{\chi}_1^0$  and  $\tilde{\chi}_1^0 \rightarrow \gamma + \tilde{G}$ .  
**Tglu4C:** gluino pair production with gluinos decaying to  $\tilde{g} \rightarrow q\bar{q}\tilde{\chi}_1^0$  and  $\tilde{\chi}_1^0 \rightarrow Z + \tilde{G}$ .  
**Tglu4D:** gluino pair production with  $\tilde{g} \rightarrow q\bar{q}\tilde{\chi}_1^0$  where the  $\tilde{\chi}_1^0$  decays with equal probability to  $\tilde{\chi}_1^0 \rightarrow \gamma + \tilde{G}$  or to  $\tilde{\chi}_1^0 \rightarrow H + \tilde{G}$ .  
**Tglu4E:** gluino pair production with  $\tilde{g} \rightarrow b\bar{b}\tilde{\chi}_1^0$  where the  $\tilde{\chi}_1^0$  decays with equal probability to  $\tilde{\chi}_1^0 \rightarrow \gamma + \tilde{G}$  or to  $\tilde{\chi}_1^0 \rightarrow Z + \tilde{G}$ .  
**Tglu4F:** gluino pair production with  $\tilde{g} \rightarrow t\bar{t}\tilde{\chi}_1^0$  where the  $\tilde{\chi}_1^0$  decays with equal probability to  $\tilde{\chi}_1^0 \rightarrow \gamma + \tilde{G}$  or to  $\tilde{\chi}_1^0 \rightarrow Z + \tilde{G}$ .  
**Tsqk1:** squark pair production with  $\tilde{q} \rightarrow q\tilde{\chi}_1^0$ .  
**Tsqk1LL:** squark pair production where  $\tilde{q} \rightarrow q\tilde{\chi}_1^0$  and  $\tilde{q} \rightarrow q'\tilde{\chi}_1^\pm$  each happen with 50% probability. The  $\tilde{\chi}_1^\pm$  is assumed to be few hundreds of MeV heavier than the  $\tilde{\chi}_1^0$ , and decays to  $\tilde{\chi}_1^0$  via a pion.  
**Tsqk2:** squark pair production with  $\tilde{q} \rightarrow q\tilde{\chi}_2^0$  and  $\tilde{\chi}_2^0 \rightarrow Z + \tilde{\chi}_1^0$ .  
**Tsqk3:** squark pair production with  $\tilde{q} \rightarrow q'\tilde{\chi}_1^\pm$ ,  $\tilde{\chi}_1^\pm \rightarrow W^\pm\tilde{\chi}_1^0$  (like Tglu1B but for squarks)

- Tsqk4:** squark pair production with squarks decaying to  $q\tilde{\chi}_1^0$  and  $\tilde{\chi}_1^0 \rightarrow \gamma + \tilde{G}$ .
- Tsqk4A:** squark pair production with one squark decaying to  $q\tilde{\chi}_1^\pm$  with  $\tilde{\chi}_1^\pm \rightarrow W^\pm + \tilde{G}$ , and the other squark decaying to  $q\tilde{\chi}_1^0$  with  $\tilde{\chi}_1^0 \rightarrow \gamma + \tilde{G}$ .
- Tsqk4B:** squark pair production with squarks decaying to  $q\tilde{\chi}_1^0$  and  $\tilde{\chi}_1^0 \rightarrow \gamma + \tilde{G}$ .
- Tstop1:** stop pair production with  $\tilde{t} \rightarrow t\tilde{\chi}_1^0$ .
- Tstop1LL:** stop pair production where  $\tilde{t} \rightarrow t\tilde{\chi}_1^0$  and  $\tilde{t} \rightarrow b\tilde{\chi}_1^\pm$  each happen with 50% probability. The  $\tilde{\chi}_1^\pm$  is assumed to be few hundreds of MeV heavier than the  $\tilde{\chi}_1^0$ , and decays to  $\tilde{\chi}_1^0$  via a pion.
- Tstop2:** stop pair production with  $\tilde{t} \rightarrow b\tilde{\chi}_1^\pm$  with  $\tilde{\chi}_1^\pm \rightarrow W^\pm\tilde{\chi}_1^0$ .
- Tstop3:** stop pair production with the subsequent four-body decay  $\tilde{t} \rightarrow bff'\tilde{\chi}_1^0$  where  $f$  represents a lepton or a quark.
- Tstop4:** stop pair production with  $\tilde{t} \rightarrow c\tilde{\chi}_1^0$ .
- Tstop5:** stop pair production with  $\tilde{t} \rightarrow b\tilde{\nu}\tilde{\tau}$  with  $\tilde{\tau} \rightarrow \tau\tilde{G}$ .
- Tstop6:** stop pair production with  $\tilde{t} \rightarrow t + \tilde{\chi}_2^0$ , where  $\tilde{\chi}_2^0 \rightarrow Z + \tilde{\chi}_1^0$  or  $H + \tilde{\chi}_1^0$  each with Br=50%.
- Tstop7:** stop pair production with  $\tilde{t}_2 \rightarrow \tilde{t}_1 + H/Z$ , where  $\tilde{t}_1 \rightarrow t + \tilde{\chi}_1^0$ .
- Tstop8:** stop pair production with equal probability of the stop decaying via  $\tilde{t} \rightarrow t\tilde{\chi}_1^0$  or via  $\tilde{t} \rightarrow b\tilde{\chi}_1^\pm$  with  $\tilde{\chi}_1^\pm \rightarrow W^\pm\tilde{\chi}_1^0$ .
- Tstop9:** stop pair production with equal probability of the stop decaying via  $\tilde{t} \rightarrow c\tilde{\chi}_1^0$  or via the four-body decay  $\tilde{t} \rightarrow bff'\tilde{\chi}_1^0$  where  $f$  represents a lepton or a quark.
- Tstop10:** stop pair production with  $\tilde{t} \rightarrow b\tilde{\chi}_1^\pm$  and  $\tilde{\chi}_1^\pm \rightarrow W^\pm\tilde{\chi}_1^0 \rightarrow (f\tilde{f}') + \tilde{\chi}_1^0$  with a virtual  $W$ -boson.
- Tstop11:** stop pair production with  $\tilde{t} \rightarrow b\tilde{\chi}_1^\pm$  with  $\tilde{\chi}_1^\pm$  decaying through an intermediate slepton to  $l\nu\tilde{\chi}_1^0$ .
- Tstop12:** stop pair production with  $\tilde{t} \rightarrow t\tilde{\chi}_1^0$  and  $\tilde{\chi}_1^0 \rightarrow \gamma + \tilde{G}$ .
- Tstop13:** stop pair production with  $\tilde{t} \rightarrow t\tilde{\chi}_1^0$  where the  $\tilde{\chi}_1^0$  can decay with equal probability to  $\tilde{\chi}_1^0 \rightarrow \gamma + \tilde{G}$  or to  $\tilde{\chi}_1^0 \rightarrow Z + \tilde{G}$ .
- Tstop1RPV:** stop pair production with  $\tilde{t} \rightarrow b\tilde{s}$  via RPV coupling  $\lambda_{323}$ .
- Tstop2RPV:** stop pair production with  $\tilde{t} \rightarrow b\tilde{t}$ , via RPV coupling  $\lambda_{t33}$ .
- Tsbot1:** sbottom pair production with  $\tilde{b} \rightarrow b\tilde{\chi}_1^0$ .
- Tsbot2:** sbottom pair production with  $\tilde{b} \rightarrow t\chi_1^-, \chi_1^- \rightarrow W^-\tilde{\chi}_1^0$ .
- Tsbot3:** sbottom pair production with  $\tilde{b} \rightarrow b\tilde{\chi}_2^0$ , where one of the  $\tilde{\chi}_2^0 \rightarrow Z^{(*)}\tilde{\chi}_1^0 \rightarrow f\tilde{f}\tilde{\chi}_1^0$  and the other  $\tilde{\chi}_2^0 \rightarrow \tilde{\ell}\ell^+ \rightarrow \ell^+\ell^-\tilde{\chi}_1^0$ .
- Tsbot4:** sbottom pair production with  $\tilde{b} \rightarrow b\tilde{\chi}_2^0$ , with  $\tilde{\chi}_2^0 \rightarrow H\tilde{\chi}_1^0$ .
- Tchi1chi1A:** electroweak pair and associated production of nearly mass-degenerate charginos  $\tilde{\chi}_1^\pm$  and neutralinos  $\tilde{\chi}_1^0$ , where  $\tilde{\chi}_1^\pm$  decays to  $\tilde{\chi}_1^0$  plus soft radiation, and where one of the  $\tilde{\chi}_1^0$  decays to  $\gamma + \tilde{G}$  while the other one decays to  $Z/H + \tilde{G}$  (with equal probability).
- Tchi1chi1B:** electroweak pair production of charginos  $\tilde{\chi}_1^\pm$ , where  $\tilde{\chi}_1^\pm$  decays through an intermediate slepton or sneutrino to  $l\nu\tilde{\chi}_1^0$  and where the slepton or sneutrino mass is 5%, 25%, 50%, 75% and 95% of the  $\tilde{\chi}_1^\pm$  mass.
- Tchi1chi1C:** electroweak pair production of charginos  $\tilde{\chi}_1^\pm$ , where  $\tilde{\chi}_1^\pm$  decays through an intermediate slepton or sneutrino to  $l\nu\tilde{\chi}_1^0$  and where  $m_{\tilde{\ell},\tilde{\nu}} = (m_{\tilde{\chi}_1^\pm} + m_{\tilde{\chi}_1^0})/2$ .
- Tchi1chi1D:** electroweak associated pair production of charginos  $\tilde{\chi}_1^\pm$ , where  $\tilde{\chi}_1^\pm$  decays through an intermediate scalar tau lepton or sneutrino to  $\tau\nu\tilde{\chi}_1^0$  and where  $m_{\tilde{\tau},\tilde{\nu}} = (m_{\tilde{\chi}_1^\pm} + m_{\tilde{\chi}_1^0})/2$ .
- Tchi1chi1F:** electroweak pair and associated production of nearly mass-degenerate charginos  $\tilde{\chi}_1^\pm$  and neutralinos  $\tilde{\chi}_1^0$  (i.e.  $\tilde{\chi}_1^\pm\tilde{\chi}_1^\pm$  and  $\tilde{\chi}_1^\pm\tilde{\chi}_1^0$  production) where the  $\tilde{\chi}_1^\pm$  decays exclusively to  $\tilde{\chi}_1^0$  plus soft radiation and the  $\tilde{\chi}_1^0$  decays to  $\gamma/Z + \tilde{G}$ .
- Tchi1chi1G:** electroweak pair production of charginos  $\tilde{\chi}_1^\pm$ , which are nearly mass-degenerate with neutralinos  $\tilde{\chi}_1^0$ . The  $\tilde{\chi}_1^\pm$  decays either to  $W^\pm + \tilde{G}$ , or to  $\tilde{\chi}_1^0$  plus soft radiation. The  $\tilde{\chi}_1^0$  decays exclusively to  $\gamma + \tilde{G}$ .
- Tchi1n1A:** electroweak associated production of mass-degenerate charginos  $\tilde{\chi}_1^\pm$  and neutralinos  $\tilde{\chi}_1^0$ , where  $\tilde{\chi}_1^\pm$  decays exclusively to  $W^\pm + \tilde{G}$  and  $\tilde{\chi}_1^0$  decays exclusively to  $\gamma + \tilde{G}$ .
- Tchi1n2A:** electroweak associated production of mass-degenerate charginos  $\tilde{\chi}_1^\pm$  and neutralinos  $\tilde{\chi}_2^0$ , where  $\tilde{\chi}_1^\pm$  decays through an intermediate slepton or sneutrino to  $l\nu\tilde{\chi}_1^0$  and where  $\tilde{\chi}_2^0$  decays through an intermediate slepton or sneutrino to  $l^+l^-\tilde{\chi}_1^0$  or  $\nu\bar{\nu}\tilde{\chi}_1^0$ .
- Tchi1n2B:** electroweak associated production of mass-degenerate charginos  $\tilde{\chi}_1^\pm$  and neutralinos  $\tilde{\chi}_2^0$ , where  $\tilde{\chi}_1^\pm$  decays through an intermediate slepton or sneutrino to  $l\nu\tilde{\chi}_1^0$  and where  $\tilde{\chi}_2^0$  decays through an intermediate slepton or sneutrino to  $l^+l^-\tilde{\chi}_1^0$  or  $\nu\bar{\nu}\tilde{\chi}_1^0$ .
- Tchi1n2C:** electroweak associated production of mass-degenerate charginos  $\tilde{\chi}_1^\pm$  and neutralinos  $\tilde{\chi}_2^0$ , where  $\tilde{\chi}_1^\pm$  decays through an intermediate slepton or sneutrino to  $l\nu\tilde{\chi}_1^0$  and where  $\tilde{\chi}_2^0$  decays through an intermediate slepton or sneutrino to  $l^+l^-\tilde{\chi}_1^0$  or  $\nu\bar{\nu}\tilde{\chi}_1^0$  and where  $m_{\tilde{\ell},\tilde{\nu}} = (m_{\tilde{\chi}_1^\pm} + m_{\tilde{\chi}_1^0})/2$ .
- Tchi1n2D:** electroweak associated production of mass-degenerate charginos  $\tilde{\chi}_1^\pm$  and neutralinos  $\tilde{\chi}_2^0$ , where  $\tilde{\chi}_1^\pm$  decays through an intermediate scalar tau lepton or sneutrino to  $\tau\nu\tilde{\chi}_1^0$  and where  $\tilde{\chi}_2^0$  decays through an intermediate scalar tau lepton or sneutrino to  $\tau^+\tau^-\tilde{\chi}_1^0$  or  $\nu\bar{\nu}\tilde{\chi}_1^0$  and where  $m_{\tilde{\tau},\tilde{\nu}} = (m_{\tilde{\chi}_1^\pm} + m_{\tilde{\chi}_1^0})/2$ .
- Tchi1n2E:** electroweak associated production of mass-degenerate charginos  $\tilde{\chi}_1^\pm$  and neutralinos  $\tilde{\chi}_2^0$ , where  $\tilde{\chi}_1^\pm \rightarrow W^\pm + \tilde{\chi}_1^0$  and  $\tilde{\chi}_2^0 \rightarrow H + \tilde{\chi}_1^0$ .
- Tchi1n2F:** electroweak associated production of mass-degenerate wino-like charginos  $\tilde{\chi}_1^\pm$  and neutralinos  $\tilde{\chi}_2^0$ , where  $\tilde{\chi}_1^\pm$  decays through an intermediate  $W^{**}$  to  $l\nu\tilde{\chi}_1^0$  and where  $\tilde{\chi}_2^0$  decays through an intermediate  $Z^*$  to  $l^+l^-\tilde{\chi}_1^0$  or  $\nu\bar{\nu}\tilde{\chi}_1^0$ .
- Tchi1n2G:** electroweak associated production of Higgsino-like charginos  $\tilde{\chi}_1^\pm$  and neutralinos  $\tilde{\chi}_2^0$ , and electroweak associated production of  $\tilde{\chi}_2^0$  and  $\tilde{\chi}_1^0$ , where  $m_{\tilde{\chi}_1^\pm} = (m_{\tilde{\chi}_2^0} + m_{\tilde{\chi}_1^0})/2$  and where  $\tilde{\chi}_1^\pm$  decays through an intermediate  $W^{**}$  to  $l\nu\tilde{\chi}_1^0$  and where  $\tilde{\chi}_2^0$  decays through an intermediate  $Z^*$  to  $l^+l^-\tilde{\chi}_1^0$ .
- Tchi1n2H:** electroweak associated production of mass-degenerate charginos  $\tilde{\chi}_1^\pm$  and neutralinos  $\tilde{\chi}_2^0$ , where  $\tilde{\chi}_1^\pm$  decays through an intermediate slepton or sneutrino to  $l\nu\tilde{\chi}_1^0$  and where  $\tilde{\chi}_2^0$  decays through an intermediate scalar tau lepton or sneutrino to  $\tau^+\tau^-\tilde{\chi}_1^0$  or  $\nu\bar{\nu}\tilde{\chi}_1^0$ .
- Tchi1n2I:** electroweak associated production of mass-degenerate charginos  $\tilde{\chi}_1^\pm$  and neutralinos  $\tilde{\chi}_2^0$ , where  $\tilde{\chi}_1^\pm$  decays to  $W^\pm + \tilde{\chi}_1^0$  and where  $\tilde{\chi}_2^0$  decays 50% of the time to  $Z + \tilde{\chi}_1^0$  and 50% of the time to  $H + \tilde{\chi}_1^0$ .
- Tchi1n2-GGM:** in the framework of General Gauge Mediation (GGM): electroweak pair and associated production of nearly mass-degenerate charginos  $\tilde{\chi}_1^\pm$  and neutralinos  $\tilde{\chi}_1^0, \tilde{\chi}_2^0$  (i.e.  $\tilde{\chi}_1^\pm\tilde{\chi}_1^\pm, \tilde{\chi}_1^\pm\tilde{\chi}_1^0$  and  $\tilde{\chi}_1^\pm\tilde{\chi}_2^0$  production) where the  $\tilde{\chi}_1^\pm$  decays exclusively to  $W^\pm + \tilde{G}$ , the  $\tilde{\chi}_2^0$  decays to  $Z/H + \tilde{G}$  and the  $\tilde{\chi}_1^0$  decays to  $\gamma/Z + \tilde{G}$ . The branching ratios depend on the composition of the gauge eigenstates of the neutralinos in the GGM scenario.
- Tn1n1A:** electroweak pair and associated production of nearly mass-degenerate Higgsino-like charginos  $\tilde{\chi}_1^\pm$  and neutralinos  $\tilde{\chi}_1^0$  and  $\tilde{\chi}_2^0$ , where  $\tilde{\chi}_1^\pm$  and  $\tilde{\chi}_2^0$  decay to  $\tilde{\chi}_1^0$  plus soft radiation and where both of the  $\tilde{\chi}_1^0$  decay to  $H + \tilde{G}$ .
- Tn1n1B:** electroweak pair and associated production of nearly mass-degenerate Higgsino-like charginos  $\tilde{\chi}_1^\pm$  and neutralinos  $\tilde{\chi}_1^0$  and  $\tilde{\chi}_2^0$ , where  $\tilde{\chi}_1^\pm$  and  $\tilde{\chi}_2^0$  decay to  $\tilde{\chi}_1^0$  plus soft radiation and where the  $\tilde{\chi}_1^0$  decays 50% of the time to  $H + \tilde{G}$  and 50% of the time to  $Z + \tilde{G}$ .
- Tn1n1C:** electroweak pair and associated production of nearly mass-degenerate Higgsino-like charginos  $\tilde{\chi}_1^\pm$  and neutralinos  $\tilde{\chi}_1^0$  and  $\tilde{\chi}_2^0$ , where  $\tilde{\chi}_1^\pm$  and  $\tilde{\chi}_2^0$  decay to  $\tilde{\chi}_1^0$  plus soft radiation and where both of the  $\tilde{\chi}_1^0$  decay to  $Z + \tilde{G}$ .
- Tn2n3A:** electroweak associated production of mass-degenerate neutralinos  $\tilde{\chi}_2^0$  and  $\tilde{\chi}_3^0$ , where  $\tilde{\chi}_2^0$  and  $\tilde{\chi}_3^0$  decay through intermediate sleptons to  $l^+l^-\tilde{\chi}_1^0$  and where the slepton mass is 5%, 25%, 50%, 75% and 95% of the  $\tilde{\chi}_2^0$  mass.
- Tn2n3B:** electroweak associated production of mass-degenerate neutralinos  $\tilde{\chi}_2^0$  and  $\tilde{\chi}_3^0$ , where  $\tilde{\chi}_2^0$  and  $\tilde{\chi}_3^0$  decay through intermediate sleptons to  $l^+l^-\tilde{\chi}_1^0$  and where  $m_{\tilde{\ell}} = (m_{\tilde{\chi}_2^0} + m_{\tilde{\chi}_1^0})/2$ .

# Searches Particle Listings

## Supersymmetric Particle Searches

### $\tilde{\chi}_1^0$ (Lightest Neutralino) mass limit

$\tilde{\chi}_1^0$  is often assumed to be the lightest supersymmetric particle (LSP). See also the  $\tilde{\chi}_2^0, \tilde{\chi}_3^0, \tilde{\chi}_4^0$  section below.

We have divided the  $\tilde{\chi}_1^0$  listings below into five sections:

- 1) Accelerator limits for stable  $\tilde{\chi}_1^0$ ,
- 2) Bounds on  $\tilde{\chi}_1^0$  from dark matter searches,
- 3)  $\tilde{\chi}_1^0 - p$  elastic cross section (spin-dependent, spin-independent interactions),
- 4) Other bounds on  $\tilde{\chi}_1^0$  from astrophysics and cosmology, and
- 5) Unstable  $\tilde{\chi}_1^0$  (Lightest Neutralino) mass limit.

### Accelerator limits for stable $\tilde{\chi}_1^0$

Unless otherwise stated, results in this section assume spectra, production rates, decay modes, and branching ratios as evaluated in the MSSM, with gaugino and sfermion mass unification at the GUT scale. These papers generally study production of  $\tilde{\chi}_i^0 \tilde{\chi}_j^0$  ( $i \geq 1, j \geq 2$ ),  $\tilde{\chi}_1^+ \tilde{\chi}_1^-$ , and (in the case of hadronic collisions)  $\tilde{\chi}_1^+ \tilde{\chi}_2^0$  pairs. The mass limits on  $\tilde{\chi}_1^0$  are either direct, or follow indirectly from the constraints set by the non-observation of  $\tilde{\chi}_1^\pm$  and  $\tilde{\chi}_2^0$  states on the gaugino and higgsino MSSM parameters  $M_2$  and  $\mu$ . In some cases, information is used from the nonobservation of slepton decays.

Obsolete limits obtained from  $e^+e^-$  collisions up to  $\sqrt{s}=184$  GeV have been removed from this compilation and can be found in the 2000 Edition (The European Physical Journal **C15** 1 (2000)) of this Review.  $\Delta m = m_{\tilde{\chi}_2^0} - m_{\tilde{\chi}_1^0}$ .

VALUE (GeV)	CL%	DOCUMENT ID	TECN	COMMENT
		1 DREINER	09 THEO	
>40	95	2 ABBIENDI	04H OPAL	all $\tan\beta$ , $\Delta m > 5$ GeV, $m_0 > 500$ GeV, $A_0 = 0$
>42.4	95	3 HEISTER	04 ALEP	all $\tan\beta$ , all $\Delta m$ , all $m_0$
>39.2	95	4 ABDALLAH	03M DLPH	all $\tan\beta$ , $m_{\tilde{\nu}} > 500$ GeV
>46	95	5 ABDALLAH	03M DLPH	all $\tan\beta$ , all $\Delta m$ , all $m_0$
>32.5	95	6 ACCIARRI	00D L3	$\tan\beta > 0.7$ , $\Delta m > 3$ GeV, all $m_0$
		7 AAD	14K ATLS	

• • • We do not use the following data for averages, fits, limits, etc. • • •

- 1 DREINER 09 show that in the general MSSM with non-universal gaugino masses there exists no model-independent laboratory bound on the mass of the lightest neutralino. An essentially massless  $\tilde{\chi}_1^0$  is allowed by the experimental and observational data, imposing some constraints on other MSSM parameters, including  $M_2$ ,  $\mu$  and the slepton and squark masses.
- 2 ABBIENDI 04H search for charginos and neutralinos in events with acoplanar leptons+jets and multi-jet final states in the 192–209 GeV data, combined with the results on leptonic final states from ABBIENDI 04. The results hold for a scan over the parameter space covering the region  $0 < M_2 < 5000$  GeV,  $-1000 < \mu < 1000$  GeV and  $\tan\beta$  from 1 to 40. This limit supersedes ABBIENDI 00H.
- 3 HEISTER 04 data collected up to 209 GeV. Updates earlier analysis of selectrons from HEISTER 02E, includes a new analysis of charginos and neutralinos decaying into stau and uses results on charginos with initial state radiation from HEISTER 02J. The limit is based on the direct search for charginos and neutralinos, the constraints from the slepton search and the Higgs mass limits from HEISTER 02 using a top mass of 175 GeV, interpreted in a framework with universal gaugino and sfermion masses. Assuming the mixing in the stau sector to be negligible, the limit improves to 43.1 GeV. Under the assumption of MSUGRA with unification of the Higgs and sfermion masses, the limit improves to 50 GeV, and reaches 53 GeV for  $A_0 = 0$ . These limits include and update the results of BARATE 01.
- 4 ABDALLAH 03M uses data from  $\sqrt{s} = 192$ –208 GeV. A limit on the mass of  $\tilde{\chi}_1^0$  is derived from direct searches for neutralinos combined with the chargino search. Neutralinos are searched in the production of  $\tilde{\chi}_1^0 \tilde{\chi}_2^0, \tilde{\chi}_1^0 \tilde{\chi}_3^0$ , as well as  $\tilde{\chi}_2^0 \tilde{\chi}_3^0$  and  $\tilde{\chi}_2^0 \tilde{\chi}_4^0$  giving rise to cascade decays, and  $\tilde{\chi}_1^0 \tilde{\chi}_2^0$  and  $\tilde{\chi}_1^0 \tilde{\chi}_3^0$ , followed by the decay  $\tilde{\chi}_2^0 \rightarrow \tilde{\tau} \tau$ . The results hold for the parameter space defined by values of  $M_2 < 1$  TeV,  $|\mu| \leq 2$  TeV with the  $\tilde{\chi}_1^0$  as LSP. The limit is obtained for  $\tan\beta = 1$  and large  $m_0$ , where  $\tilde{\chi}_2^0 \tilde{\chi}_3^0$  and chargino pair production are important. If the constraint from Higgs searches is also imposed, the limit improves to 49.0 GeV in the  $m_h^{\text{max}}$  scenario with  $m_t = 174.3$  GeV. These limits update the results of ABREU 00J.
- 5 ABDALLAH 03M uses data from  $\sqrt{s} = 192$ –208 GeV. An indirect limit on the mass of  $\tilde{\chi}_1^0$  is derived by constraining the MSSM parameter space by the results from direct searches for neutralinos (including cascade decays and  $\tilde{\tau} \tau$  final states), for charginos (for all  $\Delta m_{\pm}$ ) and for sleptons, stop and sbottom. The results hold for the full parameter space defined by values of  $M_2 < 1$  TeV,  $|\mu| \leq 2$  TeV with the  $\tilde{\chi}_1^0$  as LSP. Constraints from the Higgs search in the  $m_h^{\text{max}}$  scenario assuming  $m_t = 174.3$  GeV are included. The limit is obtained for  $\tan\beta \geq 5$  when stau mixing leads to mass degeneracy between  $\tilde{\tau}_1$  and  $\tilde{\chi}_1^0$  and the limit is based on  $\tilde{\chi}_2^0$  production followed by its decay to  $\tilde{\tau}_1 \tau$ . In the pathological scenario where  $m_0$  and  $|\mu|$  are large, so that the  $\tilde{\chi}_2^0$  production cross section is negligible, and where there is mixing in the stau sector but not in stop nor sbottom, the limit is based on charginos with soft decay products and an ISR photon. The limit then degrades to 39 GeV. See Figs. 40–42 for the dependence of the limit on  $\tan\beta$  and  $m_{\tilde{\nu}}$ . These limits update the results of ABREU 00W.
- 6 ACCIARRI 00D data collected at  $\sqrt{s}=189$  GeV. The results hold over the full parameter space defined by  $0.7 \leq \tan\beta \leq 60$ ,  $0 \leq M_2 \leq 2$  TeV,  $m_0 \leq 500$  GeV,  $|\mu| \leq 2$  TeV. The minimum mass limit is reached for  $\tan\beta=1$  and large  $m_0$ . The results of slepton

searches from ACCIARRI 99W are used to help set constraints in the region of small  $m_0$ . The limit improves to 48 GeV for  $m_0 \gtrsim 200$  GeV and  $\tan\beta \gtrsim 10$ . See their Figs. 6–8 for the  $\tan\beta$  and  $m_0$  dependence of the limits. Updates ACCIARRI 98F.

7 AAD 14K sets limits on the  $\chi$ -nucleon spin-dependent and spin-independent cross sections out to  $m_\chi = 10$  TeV.

### Bounds on $\tilde{\chi}_1^0$ from dark matter searches

These papers generally exclude regions in the  $M_2 - \mu$  parameter plane assuming that  $\tilde{\chi}_1^0$  is the dominant form of dark matter in the galactic halo. These limits are based on the lack of detection in laboratory experiments, telescopes, or by the absence of a signal in underground neutrino detectors. The latter signal is expected if  $\tilde{\chi}_1^0$  accumulates in the Sun or the Earth and annihilates into high-energy  $\nu$ 's.

VALUE	DOCUMENT ID	TECN
• • • We do not use the following data for averages, fits, limits, etc. • • •		
	1 DI-MAURO	19 FLAT
	2 JOHNSON	19 FLAT
	3 LI	19D FLAT
	4 ABDALLAH	18 HESS
	5 AHNEN	18 MGIC
	6 ALBERT	18B HAWC
	7 ALBERT	18C HAWC
	8 AARTSEN	17 ICCB
	9 AARTSEN	17A ICCB
	10 AARTSEN	17C ICCB
	11 ALBERT	17A ANTR
	12 ARCHAMBAU	17 VRTS
	13 AARTSEN	16D ICCB
	14 ABDALLAH	16A HESS
	15 ADRIAN-MAR	16 ANTR
	16 AHNEN	16 MGFL
	17 AVRORIN	16 BAIK
	18 CIRELLI	16 THEO
	18 LEITE	16 THEO
	19 ABRAMOWSKI	15 HESS
	20 ACKERMANN	15 FLAT
	21 ACKERMANN	15A FLAT
	22 ACKERMANN	15B FLAT
	23 BUCKLEY	15 THEO
	24 CHOI	15 SKAM
	25 ALEKSIC	14 MGIC
	26 AVRORIN	14 BAIK
	27 AARTSEN	13C ICCB
	28 ABRAMOWSKI	13 HESS
	29 BERGSTROM	13 COSM
	30 BOLIEV	13 BAKS
	29 JIN	13 ASTR
	29 KOPP	13 COSM
	31 ABBASI	12 ICCB
	32 ABRAMOWSKI	11 HESS
	33 ABDO	10 FLAT
	34 ACKERMANN	10 FLAT
	35 ACHTERBERG	06 AMND
	36 ACKERMANN	06 AMND
	37 DEBOER	06 RVUE
	38 DESAI	04 SKAM
	38 AMBROSIO	99 MCRO
	39 LOSECCO	95 RVUE
	40 MORI	93 KAMI
	41 BOTTINO	92 COSM
	42 BOTTINO	91 RVUE
	43 GELMINI	91 COSM
	44 KAMIONKOW	91B RVUE
	45 MORI	91B KAMI
	46 OLIVE	88 COSM

none 4–15 GeV

- 1 DI-MAURO 19 sets limits on the dark matter annihilation from gamma-ray searches in M31 and M33 galaxies using Fermi LAT data.
- 2 JOHNSON 19 sets limits on p-wave dark matter annihilations in the galactic center using Fermi data.
- 3 LI 19D sets limits on dark matter annihilation cross sections searching for line-like signals in the all-sky Fermi data.
- 4 ABDALLAH 18 places constraints on the dark matter annihilation cross section for annihilations into gamma-rays in the Galactic center for masses between 300 GeV to 70 TeV. This updates ABDALLAH 16.
- 5 AHNEN 18 uses observations of the dwarf satellite galaxy Ursa Major II to obtain upper limits on annihilation cross sections for dark matter in various channels for masses between 0.1–100 TeV.
- 6 ALBERT 18B sets limits on the annihilation cross section of dark matter with mass between 1 and 100 TeV from gamma-ray observations of the Andromeda galaxy.
- 7 ALBERT 18C sets limits on the spin-dependent coupling of dark matter to protons from dark matter annihilation in the Sun.
- 8 AARTSEN 17 is based on data collected during 327 days of detector livetime with IceCube. They looked for interactions of  $\nu$ 's resulting from neutralino annihilations in the Earth over a background of atmospheric neutrinos and set 90% CL limits on the spin independent neutralino-proton cross section for neutralino masses in the range 10–10000 GeV.
- 9 AARTSEN 17A is based on data collected during 532 days of livetime with the IceCube 86-string detector including the DeepCore sub-array. They looked for interactions of  $\nu$ 's

- from neutralino annihilations in the Sun over a background of atmospheric neutrinos and set 90% CL limits on the spin dependent neutralino-proton cross section for neutralino masses in the range 10–10000 GeV. This updates AARTSEN 16c.
- 10 AARTSEN 17c is based on 1005 days of running with the IceCube detector. They set a limit on the annihilation cross section for dark matter with masses between 10–1000 GeV annihilating in the Galactic center assuming an NFW profile. The limit is of  $1.2 \times 10^{23} \text{ cm}^3 \text{ s}^{-1}$  in the  $\tau^+ \tau^-$  channel. Supercedes AARTSEN 15e.
- 11 ALBERT 17A is based on data from the ANTARES neutrino telescope. They looked for interactions of  $\nu$ 's from neutralino annihilations in the Milky Way galaxy over a background of atmospheric neutrinos and set 90% CL limits on the muon neutrino flux. They also obtain limits on the thermally averaged cross section for neutralino masses in the range 50 to 100,000 GeV. This updates ADRIAN-MARTINEZ 15.
- 12 ARCHAMBAULT 17 performs a joint statistical analysis of four dwarf galaxies with VERITAS looking for gamma-ray emission from neutralino annihilation. They set limits on the neutralino annihilation cross section.
- 13 AARTSEN 16D is based on 329 live days of running with the DeepCore subdetector of the IceCube detector. They set a limit of  $10^{-23} \text{ cm}^3 \text{ s}^{-1}$  on the annihilation cross section to  $\nu\bar{\nu}$ . This updates AARTSEN 15c.
- 14 ABDALLAH 16A place upper limits on the annihilation cross section with final states in the energy range of 0.1 to 2 TeV. This complements ABRAMOWSKI 13.
- 15 ADRIAN-MARTINEZ 16 is based on data from the ANTARES neutrino telescope. They looked for interactions of  $\nu$ 's from neutralino annihilations in the Sun over a background of atmospheric neutrinos and set 90% CL limits on the muon neutrino flux. They also obtain limits on the spin dependent and spin independent neutralino-proton cross section for neutralino masses in the range 50 to 5,000 GeV. This updates ADRIAN-MARTINEZ 13.
- 16 AHNEN 16 combines 158 hours of Segue 1 observations with MAGIC with 6 year observations of 15 dwarf satellite galaxies by Fermi-LAT to set limits on annihilation cross sections for dark matter masses between 10 GeV and 100 TeV.
- 17 AVRORIN 16 is based on 2.76 years with Lake Baikal neutrino telescope. They derive 90% upper limits on the annihilation cross section from dark matter annihilations in the Galactic center.
- 18 CIRELLI 16 and LEITE 16 derive bounds on the annihilation cross section from radio observations.
- 19 ABRAMOWSKI 15 places constraints on the dark matter annihilation cross section for annihilations in the Galactic center for masses between 300 GeV to 10 TeV.
- 20 ACKERMANN 15 is based on 5.8 years of data with Fermi-LAT and search for monochromatic gamma-rays in the energy range of 0.2–500 GeV from dark matter annihilations. This updates ACKERMANN 13A.
- 21 ACKERMANN 15A is based on 50 months of data with Fermi-LAT and search for dark matter annihilation signals in the isotropic gamma-ray background as well as galactic subhalos in the energy range of a few GeV to a few tens of TeV.
- 22 ACKERMANN 15B is based on 6 years of data with Fermi-LAT observations of Milky Way dwarf spheroidal galaxies. Set limits on the annihilation cross section from  $m_\chi = 2 \text{ GeV}$  to 10 TeV. This updates ACKERMANN 14.
- 23 BUCKLEY 15 is based on 5 years of Fermi-LAT data searching for dark matter annihilation signals from Large Magellanic Cloud.
- 24 CHOI 15 is based on 3903 days of SuperKamiokande data searching for neutrinos produced from dark matter annihilations in the sun. They place constraints on the dark matter-nucleon scattering cross section for dark matter masses between 4–200 GeV.
- 25 ALEKSIC 14 is based on almost 160 hours of observations of Segue 1 satellite dwarf galaxy using the MAGIC telescopes between 2011 and 2013. Sets limits on the annihilation cross section out to  $m_\chi = 10 \text{ TeV}$ .
- 26 AVRORIN 14 is based on almost 2.76 years with Lake Baikal neutrino telescope. They derive 90% upper limits on the fluxes of muons and muon neutrinos from dark matter annihilations in the Sun.
- 27 AARTSEN 13c is based on data collected during 339.8 effective days with the IceCube 59-string detector. They looked for interactions of  $\nu_\mu$ 's from neutralino annihilations in nearby galaxies and galaxy clusters. They obtain limits on the neutralino annihilation cross section for neutralino masses in the range 30–100,000 GeV.
- 28 ABRAMOWSKI 13 place upper limits on the annihilation cross section with  $\gamma\gamma$  final states in the energy range of 0.5–25 TeV.
- 29 BERGSTROM 13, JIN 13, and KOPP 13 derive limits on the mass and annihilation cross section using AMS-02 data. JIN 13 also sets a limit on the lifetime of the dark matter particle.
- 30 BOLIEV 13 is based on data collected during 24.12 years of live time with the Bakon Underground Scintillator Telescope. They looked for interactions of  $\nu_\mu$ 's from neutralino annihilations in the Sun over a background of atmospheric neutrinos and set 90% CL limits on the muon flux. They also obtain limits on the spin dependent and spin independent neutralino-proton cross section for neutralino masses in the range 10–1000 GeV.
- 31 ABBASI 12 is based on data collected during 812 effective days with AMANDA II and 149 days of the IceCube 40-string detector combined with the data of ABBASI 09B. They looked for interactions of  $\nu_\mu$ 's from neutralino annihilations in the Sun over a background of atmospheric neutrinos and set 90% CL limits on the muon flux. No excess is observed. They also obtain limits on the spin dependent neutralino-proton cross section for neutralino masses in the range 50–5000 GeV.
- 32 ABRAMOWSKI 11 place upper limits on the annihilation cross section with  $\gamma\gamma$  final states.
- 33 ABDO 10 place upper limits on the annihilation cross section with  $\gamma\gamma$  or  $\mu^+ \mu^-$  final states.
- 34 ACKERMANN 10 place upper limits on the annihilation cross section with  $b\bar{b}$  or  $\mu^+ \mu^-$  final states.
- 35 ACHTERBERG 06 is based on data collected during 421.9 effective days with the AMANDA detector. They looked for interactions of  $\nu_\mu$ 's from the centre of the Earth over a background of atmospheric neutrinos and set 90% CL limits on the muon flux. Their limit is compared with the muon flux expected from neutralino annihilations into  $W^+ W^-$  and  $b\bar{b}$  at the centre of the Earth for MSSM parameters compatible with the relic dark matter density, see their Fig. 7.
- 36 ACKERMANN 06 is based on data collected during 143.7 days with the AMANDA-II detector. They looked for interactions of  $\nu_\mu$ 's from the Sun over a background of atmospheric neutrinos and set 90% CL limits on the muon flux. Their limit is compared with the muon flux expected from neutralino annihilations into  $W^+ W^-$  in the Sun for SUSY model parameters compatible with the relic dark matter density, see their Fig. 3.
- 37 DEBOER 06 interpret an excess of diffuse Galactic gamma rays observed with the EGRET satellite as originating from  $\pi^0$  decays from the annihilation of neutralinos into quark jets. They analyze the corresponding parameter space in a supergravity inspired MSSM

model with radiative electroweak symmetry breaking, see their Fig. 3 for the preferred region in the  $(m_0, m_{1/2})$  plane of a scenario with large  $\tan\beta$ .

- 38 AMBROSIO 99 and DESAI 04 set new neutrino flux limits which can be used to limit the parameter space in supersymmetric models based on neutralino annihilation in the Sun and the Earth.
- 39 LOSECO 95 reanalyzed the IMB data and places lower limit on  $m_{\tilde{\chi}_1^0}$  of 18 GeV if the LSP is a photino and 10 GeV if the LSP is a higgsino based on LSP annihilation in the sun producing high-energy neutrinos and the limits on neutrino fluxes from the IMB detector.
- 40 MORI 93 excludes some region in  $M_2 - \mu$  parameter space depending on  $\tan\beta$  and lightest scalar Higgs mass for neutralino dark matter  $m_{\tilde{\chi}_1^0} > m_W$ , using limits on upgoing muons produced by energetic neutrinos from neutralino annihilation in the Sun and the Earth.
- 41 BOTTINO 92 excludes some region  $M_2 - \mu$  parameter space assuming that the lightest neutralino is the dark matter, using upgoing muons at Kamiokande, direct searches by Ge detectors, and by LEP experiments. The analysis includes top radiative corrections on Higgs parameters and employs two different hypotheses for nucleon-Higgs coupling. Effects of rescaling in the local neutralino density according to the neutralino relic abundance are taken into account.
- 42 BOTTINO 91 excluded a region in  $M_2 - \mu$  plane using upgoing muon data from Kamioka experiment, assuming that the dark matter surrounding us is composed of neutralinos and that the Higgs boson is not too heavy.
- 43 GELMINI 91 exclude a region in  $M_2 - \mu$  plane using dark matter searches.
- 44 KAMIONKOWSKI 91 excludes a region in the  $M_2 - \mu$  plane using IMB limit on upgoing muons originated by energetic neutrinos from neutralino annihilation in the sun, assuming that the dark matter is composed of neutralinos and that  $m_{H_1^0} \lesssim 50 \text{ GeV}$ . See Fig. 8 in the paper.
- 45 MORI 91B exclude a part of the region in the  $M_2 - \mu$  plane with  $m_{\tilde{\chi}_1^0} \gtrsim 80 \text{ GeV}$  using a limit on upgoing muons originated by energetic neutrinos from neutralino annihilation in the earth, assuming that the dark matter surrounding us is composed of neutralinos and that  $m_{H_1^0} \lesssim 80 \text{ GeV}$ .
- 46 OLIVE 88 result assumes that photinos make up the dark matter in the galactic halo. Limit is based on annihilations in the sun and is due to an absence of high energy neutrinos detected in underground experiments. The limit is model dependent.

### $\tilde{\chi}_1^0 - p$ elastic cross section

Experimental results on the  $\tilde{\chi}_1^0 - p$  elastic cross section are evaluated at  $m_{\tilde{\chi}_1^0} = 100 \text{ GeV}$ . The experimental results on the cross section are often mass dependent. Therefore, the mass and cross section results are also given where the limit is strongest, when appropriate. Results are quoted separately for spin-dependent interactions (based on an effective 4-Fermi Lagrangian of the form  $\bar{\nu} \gamma^\mu \mu \gamma^5 \chi \bar{q} \gamma_\mu \gamma^5 q$ ) and spin-independent interactions ( $\bar{\nu} \chi \bar{q} q$ ). For calculational details see GRIEST 88b, ELLIS 88b, BARBIERI 89c, DREES 93b, ARNOWITT 96, BERGSTROM 96, and BAER 97 in addition to the theory papers listed in the Tables. For a description of the theoretical assumptions and experimental techniques underlying most of the listed papers, see the review on "Dark matter" in this "Review of Particle Physics," and references therein. Most of the following papers use galactic halo and nuclear interaction assumptions from (LEWIN 96).

### Spin-dependent interactions

••• We do not use the following data for averages, fits, limits, etc. •••

VALUE (pb)	CL%	DOCUMENT ID	TECN	COMMENT
< 4 × 10 <sup>-5</sup>	90	1 AMOLE	19 PICO	C <sub>3</sub> F <sub>8</sub>
< 5 × 10 <sup>-4</sup>	90	2 APRILE	19A XE1T	Xe
< 7 × 10 <sup>-4</sup>	90	3 XIA	19A PNDX	Xe
< 8 × 10 <sup>-4</sup>	90	4 AKERIB	17A LUX	Xe
< 0.28	90	5 BATTAT	17 DRFT	CS <sub>2</sub> ; CF <sub>4</sub>
< 0.027	90	6 BEHNKE	17 PICA	C <sub>4</sub> F <sub>10</sub>
< 5 × 10 <sup>-4</sup>	90	7 AMOLE	16 PICO	CF <sub>3</sub> I
< 6.8 × 10 <sup>-3</sup>	90	8 APRILE	16B X100	Xe
< 6.3 × 10 <sup>-3</sup>	90	9 FELIZARDO	14 SMPL	C <sub>2</sub> ClF <sub>5</sub>
< 0.01	90	10 AKIMOV	12 ZEP3	Xe
< 7 × 10 <sup>-3</sup>	90	11 BEHNKE	12 COUP	CF <sub>3</sub> I
< 8.5 × 10 <sup>-3</sup>	90	12 FELIZARDO	12 SMPL	C <sub>2</sub> ClF <sub>5</sub>
< 0.016	90	13 KIM	12 KIMS	Csl
5 × 10 <sup>-10</sup> to 10 <sup>-5</sup>	95	14 BUCHMUEL...	11B THEO	
< 1	90	15 ANGLE	08A XE10	Xe
< 0.055	90	16 BEDNYAKOV	08 HDMS	Ge
< 0.33	90	17 BEHNKE	08 COUP	CF <sub>3</sub> I
< 5	90	18 AKERIB	06 CDMS	Ge
< 2	90	19 SHIMIZU	06A CNTR	CaF <sub>2</sub>
< 0.4	90	20 ALNER	05 NAIA	NaI Spin Dep.
< 2	90	21 BARNABE-HE.	05 PICA	C
2 × 10 <sup>-11</sup> to 1 × 10 <sup>-4</sup>	90	22 ELLIS	04 THEO	$\mu > 0$
< 0.8	90	23 AHMED	03 NAIA	NaI Spin Dep.
< 40	90	24 TAKEDA	03 BOLO	NaF Spin Dep.
< 10	90	25 ANGLÖHER	02 CRES	Saphire
8 × 10 <sup>-7</sup> to 2 × 10 <sup>-5</sup>	90	26 ELLIS	01c THEO	$\tan\beta \leq 10$
< 3.8	90	27 BERNABE	00D DAMA	Xe
< 0.8	90	28 SPOONER	00 UKDM	NaI
< 4.8	90	29 BELLI	99c DAMA	F
< 100	90	30 OOTANI	99 BOLO	LIF
< 0.6	90	31 BERNABE	98c DAMA	Xe
< 5	90	32 BERNABE	97 DAMA	F

# Searches Particle Listings

## Supersymmetric Particle Searches

- 1 The strongest limit is  $< 2.5 \times 10^{-5}$  pb at  $m_{\chi} = 25$  GeV. This updates AMOLE 17.
- 2 The strongest limit is  $< 2 \times 10^{-4}$  pb at  $m_{\chi} = 30$  GeV. For scatterings on neutrons, the strongest limit is  $< 6.3 \times 10^{-6}$  at  $m_{\chi} = 30$  GeV.
- 3 The strongest limit is  $< 4.4 \times 10^{-4}$  pb at  $m_{\chi} = 40$  GeV. This updates FU 17.
- 4 The strongest limit is  $5 \times 10^{-4}$  pb at  $m_{\chi} = 35$  GeV. The limit for scattering on neutrons is  $3 \times 10^{-5}$  pb at 100 GeV and is  $1.6 \times 10^{-5}$  pb at 35 GeV. This updates AKERIB 16A.
- 5 Directional recoil detector. This updates DAW 12.
- 6 This result updates ARCHAMBAULT 12. The strongest limit is 0.013 pb at  $m_{\chi} = 20$  GeV.
- 7 The strongest limit is  $5 \times 10^{-4}$  pb at  $m_{\chi} = 80$  GeV.
- 8 The strongest limit is  $5.2 \times 10^{-3}$  pb at 50 GeV. The limit for scattering on neutrons is  $2.8 \times 10^{-4}$  pb at 100 GeV and the strongest limit is  $2.0 \times 10^{-4}$  pb at 50 GeV. This updates APRILE 13.
- 9 The strongest limit is 0.0043 pb and occurs at  $m_{\chi} = 35$  GeV. FELIZARDO 14 also presents limits for the scattering on neutrons. At  $m_{\chi} = 100$  GeV, the upper limit is 0.13 pb and the strongest limit is 0.066 pb at  $m_{\chi} = 35$  GeV.
- 10 This result updates LEBEDENKO 09A. The strongest limit is  $8 \times 10^{-3}$  pb at  $m_{\chi} = 50$  GeV. Limit applies to the neutralino neutron elastic cross section.
- 11 The strongest limit is  $6 \times 10^{-3}$  at  $m_{\chi} = 60$  GeV.
- 12 The strongest limit is  $5.7 \times 10^{-3}$  at  $m_{\chi} = 35$  GeV.
- 13 This result updates LEE 07A. The strongest limit is at  $m_{\chi} = 80$  GeV.
- 14 Predictions for the spin-dependent elastic cross section based on a frequentist approach to electroweak observables in the framework of  $N = 1$  supergravity models with radiative breaking of the electroweak gauge symmetry.
- 15 The strongest limit is 0.6 pb and occurs at  $m_{\chi} = 30$  GeV. The limit for scattering on neutrons is 0.01 pb at  $m_{\chi} = 100$  GeV, and the strongest limit is 0.0045 pb at  $m_{\chi} = 30$  GeV.
- 16 Limit applies to neutron elastic cross section.
- 17 The strongest upper limit is 0.25 pb and occurs at  $m_{\chi} \approx 40$  GeV.
- 18 The strongest upper limit is 4 pb and occurs at  $m_{\chi} \approx 60$  GeV. The limit on the neutron spin-dependent elastic cross section is 0.07 pb. This latter limit is improved in AHMED 09, where a limit of 0.02 pb is obtained at  $m_{\chi} = 100$  GeV. The strongest limit in AHMED 09 is 0.018 pb and occurs at  $m_{\chi} = 60$  GeV.
- 19 The strongest upper limit is 1.2 pb and occurs at  $m_{\chi} \approx 40$  GeV. The limit on the neutron spin-dependent cross section is 35 pb.
- 20 The strongest upper limit is 0.35 pb and occurs at  $m_{\chi} \approx 60$  GeV.
- 21 The strongest upper limit is 1.2 pb and occurs  $m_{\chi} \approx 30$  GeV.
- 22 ELLIS 04 calculates the  $\chi p$  elastic scattering cross section in the framework of  $N=1$  supergravity models with radiative breaking of the electroweak gauge symmetry, but without universal scalar masses. In the case of universal squark and slepton masses, but non-universal Higgs masses, the limit becomes  $2 \times 10^{-4}$ , see ELLIS 03E.
- 23 The strongest upper limit is 0.75 pb and occurs at  $m_{\chi} \approx 70$  GeV.
- 24 The strongest upper limit is 30 pb and occurs at  $m_{\chi} \approx 20$  GeV.
- 25 The strongest upper limit is 8 pb and occurs at  $m_{\chi} \approx 30$  GeV.
- 26 ELLIS 01C calculates the  $\chi p$  elastic scattering cross section in the framework of  $N=1$  supergravity models with radiative breaking of the electroweak gauge symmetry. In models with nonuniversal Higgs masses, the upper limit to the cross section is  $6 \times 10^{-4}$ .
- 27 The strongest upper limit is 3 pb and occurs at  $m_{\chi} \approx 60$  GeV. The limits are for inelastic scattering  $\chi^0 + {}^{129}\text{Xe} \rightarrow \chi^0 + {}^{129}\text{Xe}^* (39.58 \text{ keV})$ .
- 28 The strongest upper limit is 4.4 pb and occurs at  $m_{\chi} \approx 60$  GeV.
- 29 The strongest upper limit is about 35 pb and occurs at  $m_{\chi} \approx 15$  GeV.

### Spin-independent interactions

VALUE (pb)	CL%	DOCUMENT ID	TECN	COMMENT
• • • We do not use the following data for averages, fits, limits, etc. • • •				
$< 2.5 \times 10^{-8}$	90	1 ABE	19 XMAS	Xe
$< 3.9 \times 10^{-9}$	90	2 AJAJ	19 DEAP	Ar
$< 2 \times 10^{-8}$	90	3 AMOLE	19 PICO	C <sub>3</sub> F <sub>8</sub>
$< 2.25 \times 10^{-6}$	90	4 ADHIKARI	18 C100	Nal
$< 1.14 \times 10^{-8}$	90	5 AGNESE	18A DS50	Ar
$< 1.6 \times 10^{-8}$	90	6 AGNESE	18A CDMS	Ge
$< 9 \times 10^{-11}$	90	7 APRILE	18 XE1T	Xe
$< 1.8 \times 10^{-10}$	90	8 AKERIB	17 LUX	Xe
$< 1.4 \times 10^{-10}$	90	9 CUI	17A PNDX	Xe
$< 1.5 \times 10^{-9}$	90	10 APRILE	16B X100	Xe
$< 1.5 \times 10^{-9}$	90	11 AKERIB	14 LUX	Xe
$10^{-11}-10^{-7}$	95	12 BUCHMUEL...	14A THEO	
$< 4.6 \times 10^{-6}$	90	13 FELIZARDO	14 SMPL	C <sub>2</sub> ClF <sub>5</sub>
$10^{-11}-10^{-8}$	95	14 ROSZKOWSKI	14 THEO	
$< 2.2 \times 10^{-6}$	90	15 AGNESE	13 CDMS	Si
$< 5 \times 10^{-8}$	90	16 AKIMOV	12 ZEP3	Xe
$1.6 \times 10^{-6}; 3.7 \times 10^{-5}$		17 ANGLÖHER	12 CRES	CaWO <sub>4</sub>
$3 \times 10^{-12}$ to $3 \times 10^{-9}$	95	18 BECHTLE	12 THEO	
$< 1.6 \times 10^{-7}$		19 BEHNKE	12 COUP	CF <sub>3</sub> I
$< 2.3 \times 10^{-7}$	90	20 KIM	12 KIMS	Csl
$< 3.3 \times 10^{-8}$	90	21 AHMED	11A	Ge
$< 4.4 \times 10^{-8}$	90	22 ARMENGAUD	11 EDE2	Ge
$< 1 \times 10^{-7}$	90	23 ANGLE	08 XE10	Xe
$< 1 \times 10^{-6}$	90	BENETTI	08 WARP	Ar
$< 7.5 \times 10^{-7}$	90	24 ALNER	07A ZEP2	Xe
$< 2 \times 10^{-7}$		25 AKERIB	06A CDMS	Ge
$< 90 \times 10^{-7}$		ALNER	05 NAlA	Nal Spin Indep.
$< 12 \times 10^{-7}$		26 ALNER	05A ZEPL	

$< 14 \times 10^{-7}$		SANGLARD	05 EDEL	Ge
$< 4 \times 10^{-7}$		27 AKERIB	04 CDMS	Ge
$2 \times 10^{-11}$ to $1.5 \times 10^{-7}$	95	28 BALTZ	04 THEO	
$2 \times 10^{-11}$ to $8 \times 10^{-6}$		29,30 ELLIS	04 THEO	$\mu > 0$
$< 5 \times 10^{-8}$		31 PIERCE	04A THEO	
$< 2 \times 10^{-5}$		32 AHMED	03 NAlA	Nal Spin Indep.
$< 3 \times 10^{-6}$		33 AKERIB	03 CDMS	Ge
$2 \times 10^{-13}$ to $2 \times 10^{-7}$		34 BAER	03A THEO	
$< 1.4 \times 10^{-5}$		35 KLAPDOR-K...	03 HDMS	Ge
$< 6 \times 10^{-6}$		36 ABRAMS	02 CDMS	Ge
$1 \times 10^{-12}$ to $7 \times 10^{-6}$		29 KIM	02b THEO	
$< 3 \times 10^{-5}$		37 MORALES	02b CSME	Ge
$< 1 \times 10^{-5}$		38 MORALES	02c IGEX	Ge
$< 1 \times 10^{-6}$		BALTZ	01 THEO	
$< 3 \times 10^{-5}$		39 BAUDIS	01 HDMS	Ge
$< 7 \times 10^{-6}$		40 BOTTINO	01 THEO	
$< 1 \times 10^{-8}$		41 CORSETTI	01 THEO	$\tan\beta \leq 25$
$5 \times 10^{-10}$ to $1.5 \times 10^{-8}$		42 ELLIS	01c THEO	$\tan\beta \leq 10$
$< 4 \times 10^{-6}$		41 GOMEZ	01 THEO	
$2 \times 10^{-10}$ to $1 \times 10^{-7}$		41 LAHANAS	01 THEO	
$< 3 \times 10^{-6}$		ABUSAIDI	00 CDMS	Ge, Si
$< 6 \times 10^{-7}$		43 ACCOMANDO	00 THEO	
$2.5 \times 10^{-9}$ to $3.5 \times 10^{-8}$		44 BERNABEI	00 DAMA	Nal
$< 1.5 \times 10^{-5}$		49 FENG	00 THEO	$\tan\beta=10$
$< 4 \times 10^{-5}$		MORALES	00 IGEX	Ge
$< 7 \times 10^{-6}$		SPOONER	00 UKDM	Nal
$< 7 \times 10^{-6}$		BAUDIS	99 HDMO	<sup>76</sup> Ge
$< 7 \times 10^{-6}$		BERNABEI	98c DAMA	Xe

- 1 The strongest upper limit is  $2.2 \times 10^{-8}$  pb at 60 GeV.
- 2 This updates AMAUDRUZ 18.
- 3 This updates AMOLE 16.
- 4 The strongest limit is  $2.05 \times 10^{-6}$  at  $m = 60$  GeV.
- 5 The strongest limit is  $1.09 \times 10^{-8}$  pb at  $m_{\chi} = 126$  GeV. This updates AGNES 15.
- 6 The strongest limit is  $1.0 \times 10^{-8}$  pb at  $m_{\chi} = 46$  GeV. This updates AGNESE 15B.
- 7 Based on 278.8 days of data collection. The strongest limit is  $4.1 \times 10^{-11}$  pb at  $m_{\chi} = 30$  GeV. This updates APRILE 17G.
- 8 AKERIB 17. The strongest limit is  $1.1 \times 10^{-10}$  pb at 50 GeV. This updates AKERIB 16.
- 9 The strongest limit is  $8.6 \times 10^{-11}$  pb at 40 GeV. This updates TAN 16b.
- 10 The strongest limit is  $1.1 \times 10^{-9}$  pb at 50 GeV. This updates APRILE 12.
- 11 The strongest upper limit is  $7.6 \times 10^{-10}$  at  $m_{\chi} = 33$  GeV.
- 12 Predictions for the spin-independent elastic cross section based on a frequentist approach to electroweak observables in the framework of  $N = 1$  supergravity models with radiative breaking of the electroweak gauge symmetry using the 20 fb<sup>-1</sup> 8 TeV and the 5 fb<sup>-1</sup> 7 TeV LHC data and the LUX data.
- 13 The strongest limit is  $3.6 \times 10^{-6}$  pb and occurs at  $m_{\chi} = 35$  GeV. Felizardo 2014 updates Felizardo 2012.
- 14 Predictions for the spin-independent elastic cross section based on a Bayesian approach to electroweak observables in the framework of  $N = 1$  supergravity models with radiative breaking of the electroweak gauge symmetry using the 20 fb<sup>-1</sup> LHC data and LUX.
- 15 AGNESE 13 presents 90% CL limits on the elastic cross section for masses in the range 7–100 GeV using the Si based detector. The strongest upper limit is  $1.8 \times 10^{-6}$  pb at  $m_{\chi} = 50$  GeV. This limit is improved to  $7 \times 10^{-7}$  pb in AGNESE 13A.
- 16 This result updates LEBEDENKO 09. The strongest limit is  $3.9 \times 10^{-8}$  pb at  $m_{\chi} = 52$  GeV.
- 17 ANGLÖHER 12 presents results of 730 kg days from the CRESST-II dark matter detector. They find two maxima in the likelihood function corresponding to best fit WIMP masses of 25.3 and 11.6 GeV with elastic cross sections of  $1.6 \times 10^{-6}$  and  $3.7 \times 10^{-5}$  pb respectively, see their Table 4. The statistical significance is more than  $4\sigma$ . ANGLÖHER 12 updates ANGLÖHER 09
- 18 Predictions for the spin-independent elastic cross section based on a frequentist approach to electroweak observables in the framework of  $N = 1$  supergravity models with radiative breaking of the electroweak gauge symmetry using the 5 fb<sup>-1</sup> LHC data and XENON100.
- 19 The strongest limit is  $1.4 \times 10^{-7}$  at  $m_{\chi} = 60$  GeV.
- 20 This result updates LEE 07A. The strongest limit is  $2.1 \times 10^{-7}$  at  $m_{\chi} = 70$  GeV.
- 21 AHMED 11A gives combined results from CDMS and EDELWEISS. The strongest limit is at  $m_{\chi} = 90$  GeV.
- 22 ARMENGAUD 11 updates result of ARMENGAUD 10. Strongest limit at  $m_{\chi} = 85$  GeV.
- 23 The strongest upper limit is  $5.1 \times 10^{-8}$  pb and occurs at  $m_{\chi} \approx 30$  GeV. The values quoted here are based on the analysis performed in ANGLE 08 with the update from SORENSEN 09.
- 24 The strongest upper limit is  $6.6 \times 10^{-7}$  pb and occurs at  $m_{\chi} \approx 65$  GeV.
- 25 AKERIB 06A updates the results of AKERIB 05. The strongest upper limit is  $1.6 \times 10^{-7}$  pb and occurs at  $m_{\chi} \approx 60$  GeV.
- 26 The strongest upper limit is also close to  $1.0 \times 10^{-6}$  pb and occurs at  $m_{\chi} \approx 70$  GeV. BENOIT 06 claim that the discrimination power of ZEPLIN-I measurement (ALNER 05A) is not reliable enough to obtain a limit better than  $1 \times 10^{-3}$  pb. However, SMITH 06 do not agree with the criticisms of BENOIT 06.
- 27 AKERIB 04 is incompatible with BERNABEI 00 most likely value, under the assumption of standard WIMP-halo interactions. The strongest upper limit is  $4 \times 10^{-7}$  pb and occurs at  $m_{\chi} \approx 60$  GeV.
- 28 Predictions for the spin-independent elastic cross section in the framework of  $N = 1$  supergravity models with radiative breaking of the electroweak gauge symmetry.
- 29 KIM 02 and ELLIS 04 calculate the  $\chi p$  elastic scattering cross section in the framework of  $N=1$  supergravity models with radiative breaking of the electroweak gauge symmetry, but without universal scalar masses.

See key on page 999

# Searches Particle Listings Supersymmetric Particle Searches

- <sup>30</sup> In the case of universal squark and slepton masses, but non-universal Higgs masses, the limit becomes  $2 \times 10^{-6}$  ( $2 \times 10^{-11}$  when constraint from the BNL  $g-2$  experiment are included), see ELLIS 03E. ELLIS 05 display the sensitivity of the elastic scattering cross section to the  $\pi$ -Nucleon  $\Sigma$  term.
- <sup>31</sup> PIERCE 04A calculates the  $\chi p$  elastic scattering cross section in the framework of models with very heavy scalar masses. See Fig. 2 of the paper.
- <sup>32</sup> The strongest upper limit is  $1.8 \times 10^{-5}$  pb and occurs at  $m_\chi \approx 80$  GeV.
- <sup>33</sup> Under the assumption of standard WIMP-halo interactions, Akerib 03 is incompatible with BERNABEI 00 most likely value at the 99.98% CL. See Fig. 4.
- <sup>34</sup> BAER 03A calculates the  $\chi p$  elastic scattering cross section in several models including the framework of  $N=1$  supergravity models with radiative breaking of the electroweak gauge symmetry.
- <sup>35</sup> The strongest upper limit is  $7 \times 10^{-6}$  pb and occurs at  $m_\chi \approx 30$  GeV.
- <sup>36</sup> ABRAMS 02 is incompatible with the DAMA most likely value at the 99.9% CL. The strongest upper limit is  $3 \times 10^{-6}$  pb and occurs at  $m_\chi \approx 30$  GeV.
- <sup>37</sup> The strongest upper limit is  $2 \times 10^{-5}$  pb and occurs at  $m_\chi \approx 40$  GeV.
- <sup>38</sup> The strongest upper limit is  $7 \times 10^{-6}$  pb and occurs at  $m_\chi \approx 46$  GeV.
- <sup>39</sup> The strongest upper limit is  $1.8 \times 10^{-5}$  pb and occurs at  $m_\chi \approx 32$  GeV.
- <sup>40</sup> BOTTINO 01 calculates the  $\chi$ - $p$  elastic scattering cross section in the framework of the following supersymmetric models:  $N=1$  supergravity with the radiative breaking of the electroweak gauge symmetry,  $N=1$  supergravity with nonuniversal scalar masses and an effective MSSM model at the electroweak scale.
- <sup>41</sup> Calculates the  $\chi$ - $p$  elastic scattering cross section in the framework of  $N=1$  supergravity models with radiative breaking of the electroweak gauge symmetry.
- <sup>42</sup> ELLIS 01c calculates the  $\chi$ - $p$  elastic scattering cross section in the framework of  $N=1$  supergravity models with radiative breaking of the electroweak gauge symmetry. ELLIS 02B find a range  $2 \times 10^{-8}$ – $1.5 \times 10^{-7}$  at  $\tan\beta=50$ . In models with nonuniversal Higgs masses, the upper limit to the cross section is  $4 \times 10^{-7}$ .
- <sup>43</sup> ACCOMANDO 00 calculate the  $\chi$ - $p$  elastic scattering cross section in the framework of minimal  $N=1$  supergravity models with radiative breaking of the electroweak gauge symmetry. The limit is relaxed by at least an order of magnitude when models with nonuniversal scalar masses are considered. A subset of the authors in ARNOWITT 02 updated the limit to  $< 9 \times 10^{-8}$  ( $\tan\beta < 55$ ).
- <sup>44</sup> BERNABEI 00 search for annual modulation of the WIMP signal. The data favor the hypothesis of annual modulation at  $4\sigma$  and are consistent, for a particular model framework quoted there, with  $m_{\chi_0^0} = 44 \pm \frac{12}{9}$  GeV and a spin-independent  $X^0$ -proton cross section of  $(5.4 \pm 1.0) \times 10^{-6}$  pb. See also BERNABEI 01 and BERNABEI 00c.
- <sup>45</sup> FENG 00 calculate the  $\chi$ - $p$  elastic scattering cross section in the framework of  $N=1$  supergravity models with radiative breaking of the electroweak gauge symmetry with a particular emphasis on focus point models. At  $\tan\beta=50$ , the range is  $8 \times 10^{-8}$ – $4 \times 10^{-7}$ .

### Other bounds on $\chi_1^0$ from astrophysics and cosmology

Most of these papers generally exclude regions in the  $M_2$ - $\mu$  parameter plane by requiring that the  $\tilde{\chi}_1^0$  contribution to the overall cosmological density is less than some maximal value to avoid overclosure of the Universe. Those not based on the cosmological density are indicated. Many of these papers also include LEP and/or other bounds.

VALUE	DOCUMENT ID	TECN	COMMENT
>46 GeV	1 ELLIS 00	RVUE	
• • • We do not use the following data for averages, fits, limits, etc. • • •			
	2 BUCHMUEL... 14	COSM	
	3 BUCHMUEL... 14A	COSM	
	4 ROSZKOWSKI 14	COSM	
	5 CABRERA 13	COSM	
	6 ELLIS 13B	COSM	
	5 STREGE 13	COSM	
	2 AKULA 12	COSM	
	2 ARBEY 12A	COSM	
	2 BAER 12	COSM	
	7 BALAZS 12	COSM	
	8 BECHTLE 12	COSM	
	9 BESKIDT 12	COSM	
> 18 GeV	10 BOTTINO 12	COSM	
	2 BUCHMUEL... 12	COSM	
	2 CAO 12A	COSM	
	2 ELLIS 12B	COSM	
	11 FENG 12B	COSM	
	2 KADASTIK 12	COSM	
	7 STREGE 12	COSM	
	12 BUCHMUEL... 11	COSM	
	13 ROSZKOWSKI 11	COSM	
	14 ELLIS 10	COSM	
	15 BUCHMUEL... 09	COSM	
	16 DREINER 09	THEO	
	17 BUCHMUEL... 08	COSM	
	13 ELLIS 08	COSM	
	18 CALIBBI 07	COSM	
	19 ELLIS 07	COSM	
	20 ALLANACH 06	COSM	
	21 DE-AUSTRI 06	COSM	
	13 BAER 05	COSM	
	22 BALTZ 04	COSM	
> 6 GeV	10,23 BELANGER 04	THEO	
	24 ELLIS 04B	COSM	
	25 PIERCE 04A	COSM	
	26 BAER 03	COSM	

> 6 GeV	10 BOTTINO 03	COSM	
	26 CHATTOPAD...03	COSM	
	27 ELLIS 03	COSM	
	13 ELLIS 03B	COSM	
	26 ELLIS 03c	COSM	
	26 LAHANAS 03	COSM	
	28 LAHANAS 02	COSM	
	29 BARGER 01c	COSM	
	30 ELLIS 01B	COSM	
	27 BOEHM 00B	COSM	
	31 FENG 00	COSM	
< 600 GeV	32 ELLIS 98B	COSM	
	33 EDSJO 97	COSM	Co-annihilation
	34 BAER 96	COSM	
	13 BEREZINSKY 95	COSM	
	35 FALK 95	COSM	CP-violating phases
	36 DREES 93	COSM	Minimal supergravity
	37 FALK 93	COSM	Sfermion mixing
	36 KELLEY 93	COSM	Minimal supergravity
	38 MIZUTA 93	COSM	Co-annihilation
	39 LOPEZ 92	COSM	Minimal supergravity, $m_0=A=0$
	40 MCDONALD 92	COSM	
	41 GRIEST 91	COSM	
	42 NOJIRI 91	COSM	Minimal supergravity
	43 OLIVE 91	COSM	
	44 ROSZKOWSKI 91	COSM	
	45 GRIEST 90	COSM	
	43 OLIVE 89	COSM	
none 100 eV – 15 GeV	SREDNICKI 88	COSM	$\tilde{\gamma}; m_{\tilde{f}}=100$ GeV
none 100 eV–5 GeV	ELLIS 84	COSM	$\tilde{\gamma};$ for $m_{\tilde{f}}=100$ GeV
	GOLDBERG 83	COSM	$\tilde{\gamma}$
	46 KRAUSS 83	COSM	$\tilde{\gamma}$
	VYSOTSKII 83	COSM	$\tilde{\gamma}$

- <sup>1</sup> ELLIS 00 updates ELLIS 98. Uses LEP  $e^+e^-$  data at  $\sqrt{s}=202$  and 204 GeV to improve bound on neutralino mass to 51 GeV when scalar mass universality is assumed and 46 GeV when Higgs mass universality is relaxed. Limits on  $\tan\beta$  improve to  $> 2.7$  ( $\mu > 0$ ),  $> 2.2$  ( $\mu < 0$ ) when scalar mass universality is assumed and  $> 1.9$  (both signs of  $\mu$ ) when Higgs mass universality is relaxed.
- <sup>2</sup> Implications of the LHC result on the Higgs mass and on the SUSY parameter space in the framework of  $N=1$  supergravity models with radiative breaking of the electroweak gauge symmetry.
- <sup>3</sup> BUCHMUELLER 14A places constraints on the SUSY parameter space in the framework of  $N=1$  supergravity models with radiative breaking of the electroweak gauge symmetry using indirect experimental searches using the 20  $\text{fb}^{-1}$  8 TeV and the 5  $\text{fb}^{-1}$  7 TeV LHC and the LUX data.
- <sup>4</sup> ROSZKOWSKI 14 places constraints on the SUSY parameter space in the framework of  $N=1$  supergravity models with radiative breaking of the electroweak gauge symmetry using Bayesian statistics and indirect experimental searches using the 20  $\text{fb}^{-1}$  LHC and the LUX data.
- <sup>5</sup> CABRERA 13 and STREGE 13 place constraints on the SUSY parameter space in the framework of  $N=1$  supergravity models with radiative breaking of the electroweak gauge symmetry with and without non-universal Higgs masses using the 5.8  $\text{fb}^{-1}$ ,  $\sqrt{s}=7$  TeV ATLAS supersymmetry searches and XENON100 results.
- <sup>6</sup> ELLIS 13B place constraints on the SUSY parameter space in the framework of  $N=1$  supergravity models with radiative breaking of the electroweak gauge symmetry with and without Higgs mass universality. Models with universality below the GUT scale are also considered.
- <sup>7</sup> BALAZS 12 and STREGE 12 place constraints on the SUSY parameter space in the framework of  $N=1$  supergravity models with radiative breaking of the electroweak gauge symmetry using the 1  $\text{fb}^{-1}$  LHC supersymmetry searches, the 5  $\text{fb}^{-1}$  Higgs mass constraints, both with  $\sqrt{s}=7$  TeV, and XENON100 results.
- <sup>8</sup> BECHTLE 12 places constraints on the SUSY parameter space in the framework of  $N=1$  supergravity models with radiative breaking of the electroweak gauge symmetry using indirect experimental searches, using the 5  $\text{fb}^{-1}$  LHC and XENON100 data.
- <sup>9</sup> BESKIDT 12 places constraints on the SUSY parameter space in the framework of  $N=1$  supergravity models with radiative breaking of the electroweak gauge symmetry using indirect experimental searches, the 5  $\text{fb}^{-1}$  LHC and the XENON100 data.
- <sup>10</sup> BELANGER 04 and BOTTINO 12 (see also BOTTINO 03, BOTTINO 03A and BOTTINO 04) do not assume gaugino or scalar mass unification.
- <sup>11</sup> FENG 12B places constraints on the SUSY parameter space in the framework of  $N=1$  supergravity models with radiative breaking of the electroweak gauge symmetry and large sfermion masses using the 1  $\text{fb}^{-1}$  LHC supersymmetry searches, the 5  $\text{fb}^{-1}$  LHC Higgs mass constraints both with  $\sqrt{s}=7$  TeV, and XENON100 results.
- <sup>12</sup> BUCHMUELLER 11 places constraints on the SUSY parameter space in the framework of  $N=1$  supergravity models with radiative breaking of the electroweak gauge symmetry using indirect experimental searches and including supersymmetry breaking relations between A and B parameters.
- <sup>13</sup> Places constraints on the SUSY parameter space in the framework of  $N=1$  supergravity models with radiative breaking of the electroweak gauge symmetry but non-Universal Higgs masses.
- <sup>14</sup> ELLIS 10 places constraints on the SUSY parameter space in the framework of  $N=1$  supergravity models with radiative breaking of the electroweak gauge symmetry with universality above the GUT scale.
- <sup>15</sup> BUCHMUELLER 09 places constraints on the SUSY parameter space in the framework of  $N=1$  supergravity models with radiative breaking of the electroweak gauge symmetry using indirect experimental searches.
- <sup>16</sup> DREINER 09 show that in the general MSSM with non-universal gaugino masses there exists no model-independent laboratory bound on the mass of the lightest neutralino. An essentially massless  $\tilde{\chi}_1^0$  is allowed by the experimental and observational data, imposing some constraints on other MSSM parameters, including  $M_2$ ,  $\mu$  and the slepton and squark masses.



# Searches Particle Listings

## Supersymmetric Particle Searches

VALUE (GeV)	CL%	DOCUMENT ID	TECN	COMMENT
>525	95	1 SIRUNYAN	19CA CMS	$\tilde{\chi}_1^0 \rightarrow \gamma \tilde{G}$ , GMSB, SPS8, $\sigma_T = 1$ m
>290	95	2 SIRUNYAN	19CI CMS	$\geq 1 H (\rightarrow \gamma\gamma) + \text{jets} + \cancel{E}_T$ , Tn1n1A, GMSB
>230	95	2 SIRUNYAN	19CI CMS	$\geq 1 H (\rightarrow \gamma\gamma) + \text{jets} + \cancel{E}_T$ , Tn1n1B, GMSB
>930	95	3 SIRUNYAN	19K CMS	$\gamma + \text{lepton} + \cancel{E}_T$ , Tchi1n1A
none	95	4 AABOUD	18CK ATLS	$2H (\rightarrow bb) + \cancel{E}_T$ , Tn1n1A, GMSB
130–230, 290–880				
>295	95	5 AABOUD	18Z ATLS	$\geq 4\ell$ , GMSB, Tn1n1C
>180	95	6 SIRUNYAN	18AO CMS	$\ell^\pm \ell^\pm$ or $\geq 3\ell$ , Tn1n1A
>260	95	6 SIRUNYAN	18AO CMS	$\ell^\pm \ell^\pm$ or $\geq 3\ell$ , Tn1n1B
>450	95	6 SIRUNYAN	18AO CMS	$\ell^\pm \ell^\pm$ or $\geq 3\ell$ , Tn1n1C
>750	95	7 SIRUNYAN	18AP CMS	Combination of searches, GMSB, Tn1n1A
>650	95	7 SIRUNYAN	18AP CMS	Combination of searches, GMSB, Tn1n1B
>690	95	7 SIRUNYAN	18AP CMS	Combination of searches, GMSB, Tn1n1C
>500	95	8 SIRUNYAN	18AR CMS	$\ell^\pm \ell^\pm + \text{jets} + \cancel{E}_T$ , GMSB, Tn1n1B
>650	95	8 SIRUNYAN	18AR CMS	$\ell^\pm \ell^\pm + \text{jets} + \cancel{E}_T$ , GMSB, Tn1n1C
none	95	9 SIRUNYAN	18O CMS	$2H (\rightarrow bb) + \cancel{E}_T$ , Tn1n1A, GMSB
$^{230-770}$ >205	95	10 SIRUNYAN	18X CMS	$\geq 1 H (\rightarrow \gamma\gamma) + \text{jets} + \cancel{E}_T$ , Tn1n1A, GMSB
>130	95	10 SIRUNYAN	18X CMS	$\geq 1 H (\rightarrow \gamma\gamma) + \text{jets} + \cancel{E}_T$ , Tn1n1B, GMSB
>380	95	11 KHACHATRYAN	14L CMS	$\tilde{\chi}_1^0 \rightarrow Z \tilde{G}$ simplified models, GMSB, RPV
••• We do not use the following data for averages, fits, limits, etc. •••				
none	95	12 AABOUD	19G ATLS	$\tilde{\chi}_1^0 \rightarrow Z \tilde{G}$ from gluinos as in Tglu1A, GMSB, depending on $\sigma_T$
300–1000		13 AAIJ	17Z	displaced vertex with associated $\mu$
		14 KHACHATRYAN	16BX CMS	$\geq 3\ell^\pm$ , RPV, $\lambda$ or $\lambda'$ couplings, wino- or higgsino-like neutralinos
		15 AAD	14BH ATLS	$2\gamma + \cancel{E}_T$ , GMSB, SPS8
		16 AAD	13AP ATLS	$2\gamma + \cancel{E}_T$ , GMSB, SPS8
none	95	17 AAD	13Q ATLS	$\gamma + b + \cancel{E}_T$ , higgsino-like neutralino, GMSB
220–380		18 AAD	13R ATLS	$\tilde{\chi}_1^0 \rightarrow \mu j j$ , RPV, $\lambda'_{211} \neq 0$
		19 AALTONEN	13I CDF	$\tilde{\chi}_1^0 \rightarrow \gamma \tilde{G}$ , $\cancel{E}_T$ , GMSB
>220	95	20 CHATRCHYAN	13AH CMS	$\tilde{\chi}_1^0 \rightarrow \gamma \tilde{G}$ , GMSB, SPS8, $\sigma_T < 500$ mm
		21 AAD	12CP ATLS	$2\gamma + \cancel{E}_T$ , GMSB
		22 AAD	12CT ATLS	$\geq 4\ell^\pm$ , RPV
		23 AAD	12R ATLS	$\tilde{\chi}_1^0 \rightarrow \mu j j$ , RPV, $\lambda'_{211} \neq 0$
		24 ABAZOV	12AD D0	$\tilde{\chi}_1^0 \tilde{\chi}_1^0 \rightarrow \gamma Z \tilde{G}$ , GMSB
		25 CHATRCHYAN	12BK CMS	$2\gamma + \cancel{E}_T$ , GMSB
		26 CHATRCHYAN	11B CMS	$\tilde{W}^0 \rightarrow \gamma \tilde{G}$ , $\tilde{W}^\pm \rightarrow \ell^\pm \tilde{G}$ , GMSB
>149	95	27 AALTONEN	10 CDF	$p\bar{p} \rightarrow \tilde{\chi}\tilde{\chi}$ , $\tilde{\chi} = \tilde{\chi}_2^0, \tilde{\chi}_1^\pm, \tilde{\chi}_1^0 \rightarrow \gamma \tilde{G}$ , GMSB
>175	95	28 ABAZOV	10P D0	$\tilde{\chi}_1^0 \rightarrow \gamma \tilde{G}$ , GMSB
>125	95	29 ABAZOV	08F D0	$p\bar{p} \rightarrow \tilde{\chi}\tilde{\chi}$ , $\tilde{\chi} = \tilde{\chi}_2^0, \tilde{\chi}_1^\pm, \tilde{\chi}_1^0 \rightarrow \gamma \tilde{G}$ , GMSB
> 96.8	95	30 ABULENCIA	07H CDF	RPV, $LL\bar{E}$
		31 ABBIENDI	06B OPAL	$e^+ e^- \rightarrow \tilde{B}\tilde{B}$ , ( $\tilde{B} \rightarrow \tilde{G}\gamma$ )
		32 ABDALLAH	05B DLPH	$e^+ e^- \rightarrow \tilde{G}\tilde{\chi}_1^0$ , ( $\tilde{\chi}_1^0 \rightarrow \tilde{G}\gamma$ )
> 96	95	33 ABDALLAH	05B DLPH	$e^+ e^- \rightarrow \tilde{B}\tilde{B}$ , ( $\tilde{B} \rightarrow \tilde{G}\gamma$ )
1 SIRUNYAN 19CA searched in $77.4 \text{ fb}^{-1}$ of $pp$ collisions at $\sqrt{s} = 13 \text{ TeV}$ for events containing delayed photons in both single and diphoton plus $\cancel{E}_T$ final states. No excess is observed above the background expected from Standard Model processes. The results are used to set 95% C.L. exclusion limits in the context of GMSB, using the SPS8 benchmark model. For neutralino proper decay lengths of 0.1, 1, 10, and 100 m, masses up to about 320, 525, 360, and 215 GeV are excluded, respectively. See their Fig. 5. The searches involve the simplified models Tglu1D, Tglu4A,B,C, Tsqk4A,4B,4C.				
2 SIRUNYAN 19CI searched in $77.5 \text{ fb}^{-1}$ of $pp$ collisions at $\sqrt{s} = 13 \text{ TeV}$ for events with one or more high-momentum Higgs bosons, decaying to pairs of photons, jets and $\cancel{E}_T$ . No significant excess above the Standard Model expectations is observed. Limits are set on the sbottom mass in the Tsbot4 simplified model, see Figure 3, and on the wino mass in the Tchi1n2E simplified model, see their Figure 4. Limits are also set on the higgsino mass in the Tn1n1A and Tn1n1B simplified models, see their Figure 5.				
3 SIRUNYAN 19K searched in $35.9 \text{ fb}^{-1}$ of $pp$ collisions at $\sqrt{s} = 13 \text{ TeV}$ for events with a photon, an electron or muon, and large $\cancel{E}_T$ . No significant excess above the Standard Model expectations is observed. In the framework of GMSB, limits are set on the chargino and neutralino mass in the Tchi1n1A simplified model, see their Figure 6. Limits are also set on the gluino mass in the Tglu4A simplified model, and on the squark mass in the Tsqk4A simplified model, see their Figure 7.				
4 AABOUD 18CK searched for events with at least 3 $b$ -jets and large missing transverse energy in two datasets of $pp$ collisions at $\sqrt{s} = 13 \text{ TeV}$ of $36.1 \text{ fb}^{-1}$ and $24.3 \text{ fb}^{-1}$ depending on the trigger requirements. The analyses aimed to reconstruct two Higgs bosons decaying to pairs of $b$ -quarks. No significant excess above the Standard Model expectations is observed. Limits are set on the Higgsino mass in the Tn1n1A simplified model, see their Figure 15(a). Constraints are also presented as a function of the BR of Higgsino decaying into an higgs boson and a gravitino, see their Figure 15(b).				
5 AABOUD 18Z searched in $36.1 \text{ fb}^{-1}$ of $pp$ collisions at $\sqrt{s} = 13 \text{ TeV}$ for events containing four or more charged leptons (electrons, muons and up to two hadronically decaying taus). No significant deviation from the expected SM background is observed. Limits are set on the Higgsino mass in simplified models of general gauge mediated supersymmetry Tn1n1A/Tn1n1B/Tn1n1C, see their Figure 9. Limits are also set on the wino, slepton, sneutrino and gluino mass in a simplified model of N1SP pair production with R-parity violating decays of the LSP via $\lambda_{12k}$ or $\lambda_{j33}$ to charged leptons, see their Figures 7, 8.				
6 SIRUNYAN 18AO searched in $35.9 \text{ fb}^{-1}$ of $pp$ collisions at $\sqrt{s} = 13 \text{ TeV}$ for direct electroweak production of charginos and neutralinos in events with either two or more leptons (electrons or muons) of the same electric charge, or with three or more leptons, which can include up to two hadronically decaying tau leptons. No significant excess above the Standard Model expectations is observed. Limits are set on the chargino/neutralino mass in the Tchi1n2A, Tchi1n2H, Tchi1n2D, Tchi1n2E and Tchi1n2F simplified models, see their Figures 14, 15, 16, 17 and 18. Limits are also set on the higgsino mass in the Tn1n1A, Tn1n1B and Tn1n1C simplified models, see their Figure 19.				

### Unstable $\tilde{\chi}_1^0$ (Lightest Neutralino) mass limit

Unless otherwise stated, results in this section assume spectra and production rates as evaluated in the MSSM. Unless otherwise stated, the goldstino or gravitino mass  $m_{\tilde{G}}$  is assumed to be negligible relative to all other masses. In the following,  $\tilde{G}$  is assumed to be undetected and to give rise to a missing energy ( $\cancel{E}$ ) signature.

Some earlier papers are now obsolete and have been omitted. They were last listed in our PDG 14 edition: K. Olive, et al. (Particle Data Group), Chinese Physics **C38** 070001 (2014) (<http://pdg.lbl.gov>).

VALUE (GeV)	CL%	DOCUMENT ID	TECN	COMMENT
>525	95	1 SIRUNYAN	19CA CMS	$\tilde{\chi}_1^0 \rightarrow \gamma \tilde{G}$ , GMSB, SPS8, $\sigma_T = 1$ m
>290	95	2 SIRUNYAN	19CI CMS	$\geq 1 H (\rightarrow \gamma\gamma) + \text{jets} + \cancel{E}_T$ , Tn1n1A, GMSB
>230	95	2 SIRUNYAN	19CI CMS	$\geq 1 H (\rightarrow \gamma\gamma) + \text{jets} + \cancel{E}_T$ , Tn1n1B, GMSB
>930	95	3 SIRUNYAN	19K CMS	$\gamma + \text{lepton} + \cancel{E}_T$ , Tchi1n1A
none	95	4 AABOUD	18CK ATLS	$2H (\rightarrow bb) + \cancel{E}_T$ , Tn1n1A, GMSB
130–230, 290–880				
>295	95	5 AABOUD	18Z ATLS	$\geq 4\ell$ , GMSB, Tn1n1C

- 7 SIRUNYAN 18AP searched in  $35.9 \text{ fb}^{-1}$  of  $pp$  collisions at  $\sqrt{s} = 13 \text{ TeV}$  for direct electroweak production of charginos and neutralinos by combining a number of previous and new searches. No significant excess above the Standard Model expectations is observed. Limits are set on the chargino/neutralino mass in the Tchi1n2E, Tchi1n2F and Tchi1n2I simplified models, see their Figures 7, 8, 9 and 10. Limits are also set on the higgsino mass in the Tn1n1A, Tn1n1B and Tn1n1C simplified models, see their Figure 11, 12, 13 and 14.
- 8 SIRUNYAN 18AR searched in  $35.9 \text{ fb}^{-1}$  of  $pp$  collisions at  $\sqrt{s} = 13 \text{ TeV}$  for events containing two opposite-charge, same-flavour leptons (electrons or muons), jets and  $\cancel{E}_T$ . No significant excess above the Standard Model expectations is observed. Limits are set on the gluino mass in the Tglu4C simplified model, see their Figure 7. Limits are also set on the chargino/neutralino mass in the Tchi1n2F simplified models, see their Figure 8, and on the higgsino mass in the Tn1n1B and Tn1n1C simplified models, see their Figure 9. Finally, limits are set on the sbottom mass in the Tsb0t3 simplified model, see their Figure 10.
- 9 SIRUNYAN 18o searched in  $35.9 \text{ fb}^{-1}$  of  $pp$  collisions at  $\sqrt{s} = 13 \text{ TeV}$  for events with two Higgs bosons, decaying to pairs of  $b$ -quarks, and large  $\cancel{E}_T$ . No significant excess above the Standard Model expectations is observed. Limits are set on the Higgsino mass in the T1n1n1A simplified model, see their Figure 9.
- 10 SIRUNYAN 18x searched in  $35.9 \text{ fb}^{-1}$  of  $pp$  collisions at  $\sqrt{s} = 13 \text{ TeV}$  for events with one or more high-momentum Higgs bosons, decaying to pairs of photons, jets and  $\cancel{E}_T$ . The razor variables ( $M_R$  and  $R^2$ ) are used to categorise the events. No significant excess above the Standard Model expectations is observed. Limits are set on the sbottom mass in the Tsb0t4 simplified model and on the wino mass in the Tchi1n2E simplified model, see their Figure 5. Limits are also set on the higgsino mass in the Tn1n1A and Tn1n1B simplified models, see their Figure 6.
- 11 KHACHATRYAN 14L searched in  $19.5 \text{ fb}^{-1}$  of  $pp$  collisions at  $\sqrt{s} = 8 \text{ TeV}$  for evidence of direct pair production of neutralinos with Higgs or  $Z$ -bosons in the decay chain, leading to  $HH$ ,  $HZ$  and  $ZZ$  final states with missing transverse energy. The decays of 16–20. A Higgs boson to a  $b$ -quark pair, to a photon pair, and to final states with leptons are considered in conjunction with hadronic and leptonic decay modes of the  $Z$  and  $W$  bosons. No significant excesses over the expected SM backgrounds are observed. The results are interpreted in the context of GMSB simplified models where the decays  $\tilde{\chi}_1^0 \rightarrow H\bar{G}$  or  $\tilde{\chi}_1^0 \rightarrow Z\bar{G}$  take place either 100% or 50% of the time, see Figs. 16–20.
- 12 AABOUD 19g searched in  $32.9 \text{ fb}^{-1}$  of  $pp$  collisions at  $\sqrt{s} = 13 \text{ TeV}$  for evidence of neutralinos decaying into a  $Z$ -boson and a gravitino, in events characterized by the presence of dimuon vertices with displacements from the  $pp$  interaction point in the range of 1400 cm. Neutralinos are assumed to be produced in the decay chain of gluinos as in Tglu1A models. No significant excess is observed in the number of vertices relative to the predicted background. In GGM with a gluino mass of 1100 GeV, neutralino masses in the range 300–1000 GeV are excluded for certain values of  $c_T$ , see their Figure 7.
- 13 AAIJ 17z searched in  $1 \text{ fb}^{-1}$  of  $pp$  collisions at  $\sqrt{s} = 7 \text{ TeV}$  and in  $2 \text{ fb}^{-1}$  of  $pp$  collisions at  $\sqrt{s} = 8 \text{ TeV}$  for events containing a displaced vertex with one associated high transverse momentum  $\mu$ . No excess is observed above the background expected from Standard Model processes. The results are used to set 95% C.L. upper limits on the cross section times branching fractions of pair-produced neutralinos decaying non-promptly into a muon and two quarks. Long-lived particles in a mass range 23–198 GeV are considered, see their Fig. 5 and Fig. 6.
- 14 KHACHATRYAN 16BX searched in  $19.5 \text{ fb}^{-1}$  of  $pp$  collisions at  $\sqrt{s} = 8 \text{ TeV}$  for events containing 3 or more leptons coming from the electroweak production of wino- or higgsino-like neutralinos, assuming non-zero R-parity-violating leptonic couplings  $\lambda_{122}$ ,  $\lambda_{123}$ , and  $\lambda_{233}$  or semileptonic couplings  $\lambda_{131}^{\prime}$ ,  $\lambda_{233}^{\prime}$ ,  $\lambda_{331}^{\prime}$ , and  $\lambda_{333}^{\prime}$ . No excess over the expected background is observed and limits are derived on the neutralino mass, see Figs. 24 and 25.
- 15 AAD 14BH searched in  $20.3 \text{ fb}^{-1}$  of  $pp$  collisions at  $\sqrt{s} = 8 \text{ TeV}$  for events containing non-pointing photons in a diphoton plus missing transverse energy final state. No excess is observed above the background expected from Standard Model processes. The results are used to set 95% C.L. exclusion limits in the context of gauge-mediated supersymmetric breaking models, with the lightest neutralino being the next-to-lightest supersymmetric particle and decaying with a lifetime in the range from 0.25 ns to about 100 ns into a photon and a gravitino. For limits on the NLSP lifetime versus  $\Lambda$  plane, for the SPS8 model, see their Fig. 7.
- 16 AAD 13AP searched in  $4.8 \text{ fb}^{-1}$  of  $pp$  collisions at  $\sqrt{s} = 7 \text{ TeV}$  for events containing non-pointing photons in a diphoton plus missing transverse energy final state. No excess is observed above the background expected from Standard Model processes. The results are used to set 95% C.L. exclusion limits in the context of gauge-mediated supersymmetric breaking models, with the lightest neutralino being the next-to-lightest supersymmetric particle and decaying with a lifetime in excess of 0.25 ns into a photon and a gravitino. For limits in the NLSP lifetime versus  $\Lambda$  plane, for the SPS8 model, see their Fig. 8.
- 17 AAD 13Q searched in  $4.7 \text{ fb}^{-1}$  of  $pp$  collisions at  $\sqrt{s} = 7 \text{ TeV}$  for events containing a high- $p_T$  isolated photon, at least one jet identified as originating from a bottom quark, and high missing transverse momentum. Such signatures may originate from supersymmetric models with gauge-mediated supersymmetry breaking in events in which one of a pair of higgsino-like neutralinos decays into a photon and a gravitino while the other decays into a Higgs boson and a gravitino. No significant excess above the expected background was found and limits were set on the neutralino mass in a generalized GMSB model (GGM) with a higgsino-like neutralino NLSP, see their Fig. 4. Intermediate neutralino masses between 220 and 380 GeV are excluded at 95% C.L., regardless of the squark and gluino masses, purely on the basis of the expected weak production.
- 18 AAD 13R looked in  $4.4 \text{ fb}^{-1}$  of  $pp$  collisions at  $\sqrt{s} = 7 \text{ TeV}$  for events containing new, heavy particles that decay at a significant distance from their production point into a final state containing a high-momentum muon and charged hadrons. No excess over the expected background is observed and limits are placed on the production cross-section of neutralinos via squarks for various  $m_{\tilde{q}}$ ,  $m_{\tilde{\chi}_1^0}$  in an R-parity violating scenario with  $\lambda'_{211} \neq 0$ , as a function of the neutralino lifetime, see their Fig. 6.
- 19 AALTONEN 13i searched in  $6.3 \text{ fb}^{-1}$  of  $p\bar{p}$  collisions at  $\sqrt{s} = 1.96 \text{ TeV}$  for events containing  $\cancel{E}_T$  and a delayed photon that arrives late in the detector relative to the time expected from prompt production. No evidence of delayed photon production is observed.
- 20 CHATRCHYAN 13AH searched in  $4.9 \text{ fb}^{-1}$  of  $pp$  collisions at  $\sqrt{s} = 7 \text{ TeV}$  for events containing  $\cancel{E}_T$  and a delayed photon that arrives late in the detector relative to the time expected from prompt production. No significant excess above the expected background was found and limits were set on the pair production of  $\tilde{\chi}_1^0$  depending on the neutralino proper decay length, see Fig. 8. Supersedes CHATRCHYAN 12BK.
- 21 AAD 12CP searched in  $4.8 \text{ fb}^{-1}$  of  $pp$  collisions at  $\sqrt{s} = 7 \text{ TeV}$  for events with two photons and large  $\cancel{E}_T$  due to  $\tilde{\chi}_1^0 \rightarrow \gamma\bar{G}$  decays in a GMSB framework. No significant excess above the expected background was found and limits were set on the neutralino lifetime, see their Fig. 8. Superseded by AAD 13R.
- 22 AAD 12CT searched in  $4.7 \text{ fb}^{-1}$  of  $pp$  collisions at  $\sqrt{s} = 7 \text{ TeV}$  for events containing four or more leptons (electrons or muons) and either moderate values of missing transverse momentum or large effective mass. No significant excess is found in the data. Limits are presented in a simplified model of R-parity violating supersymmetry in which charginos are pair-produced and then decay into a  $W$ -boson and a  $\tilde{\chi}_1^0$ , which in turn decays through an RPV coupling into two charged leptons ( $e^\pm e^\mp$  or  $\mu^\pm \mu^\mp$ ) and a neutrino. In this model, limits are set on the neutralino mass as a function of the chargino mass, see Fig. 3a. Limits are also set in an R-parity violating mSUGRA model, see Fig. 3b.
- 23 AAD 12R looked in  $33 \text{ pb}^{-1}$  of  $pp$  collisions at  $\sqrt{s} = 7 \text{ TeV}$  for events containing new, heavy particles that decay at a significant distance from their production point into a final state containing a high-momentum muon and charged hadrons. No excess over the expected background is observed and limits are placed on the production cross-section of neutralinos via squarks for various  $(m_{\tilde{q}}, m_{\tilde{\chi}_1^0})$  in an R-parity violating scenario with  $\lambda'_{211} \neq 0$ , as a function of the neutralino lifetime, see their Fig. 8. Superseded by AAD 13R.
- 24 ABAZOV 12AD looked in  $6.2 \text{ fb}^{-1}$  of  $pp$  collisions at  $\sqrt{s} = 1.96 \text{ TeV}$  for events with a photon, a  $Z$ -boson, and large  $\cancel{E}_T$  in the final state. This topology corresponds to a GMSB model where pairs of neutralino NLSPs are either pair produced promptly or from decays of other supersymmetric particles and then decay to either  $Z\bar{G}$  or  $\gamma\bar{G}$ . No significant excess over the SM expectation is observed and a limit at 95% C.L. on the cross section is derived as a function of the effective SUSY breaking scale  $\Lambda$ , see Fig. 3. Assuming  $N_{mes} = 2$ ,  $M_{mes} = 3 \Lambda$ ,  $\tan\beta = 3$ ,  $\mu = 0.75 M_1$ , and  $C_{grav} = 1$ , the model is excluded at 95% C.L. for values of  $\Lambda < 87 \text{ TeV}$ .
- 25 CHATRCHYAN 12BK searched in  $2.23 \text{ fb}^{-1}$  of  $pp$  collisions at  $\sqrt{s} = 7 \text{ TeV}$  for events with two photons and large  $\cancel{E}_T$  due to  $\tilde{\chi}_1^0 \rightarrow \gamma\bar{G}$  decays in a GMSB framework. No significant excess above the expected background was found and limits were set on the pair production of  $\tilde{\chi}_1^0$  depending on the neutralino lifetime, see Fig. 6.
- 26 CHATRCHYAN 11B looked in  $35 \text{ pb}^{-1}$  of  $pp$  collisions at  $\sqrt{s} = 7 \text{ TeV}$  for events with an isolated lepton ( $e$  or  $\mu$ ), a photon and  $\cancel{E}_T$  which may arise in a generalized gauge mediated model from the decay of Wino-like NLSPs. No evidence for an excess over the expected background is observed. Limits are derived in the plane of squark/gluino mass versus Wino mass (see Fig. 4). Mass degeneracy of the produced squarks and gluinos is assumed.
- 27 AALTONEN 10 searched in  $2.6 \text{ fb}^{-1}$  of  $p\bar{p}$  collisions at  $\sqrt{s} = 1.96 \text{ TeV}$  for diphoton events with large  $\cancel{E}_T$ . They may originate from the production of  $\tilde{\chi}^\pm$  in pairs or associated to a  $\tilde{\chi}_1^0$ , decaying into  $\tilde{\chi}_1^0$  which itself decays in GMSB to  $\gamma\bar{G}$ . There is no excess of events beyond expectation. An upper limit on the cross section is calculated in the GMSB model as a function of the  $\tilde{\chi}_1^0$  mass and lifetime, see their Fig. 2. A limit is derived on the  $\tilde{\chi}_1^0$  mass of 149 GeV for  $\tau_{\tilde{\chi}_1^0} \ll 1 \text{ ns}$ , which improves the results of previous searches.
- 28 ABAZOV 10P looked in  $6.3 \text{ fb}^{-1}$  of  $p\bar{p}$  collisions at  $\sqrt{s} = 1.96 \text{ TeV}$  for events with at least two isolated  $\gamma$ s and large  $\cancel{E}_T$ . These could be the signature of  $\tilde{\chi}_2^0$  and  $\tilde{\chi}_1^\pm$  production, decaying to  $\tilde{\chi}_1^0$  and finally  $\tilde{\chi}_1^0 \rightarrow \gamma\bar{G}$  in a GMSB framework. No significant excess over the SM expectation is observed, and a limit at 95% C.L. on the cross section is derived for  $N_{mes} = 1$ ,  $\tan\beta = 15$  and  $\mu > 0$ , see their Fig. 2. This allows them to set a limit on the effective SUSY breaking scale  $\Lambda > 124 \text{ TeV}$ , from which the excluded  $\tilde{\chi}_1^0$  mass range is obtained.
- 29 ABAZOV 08F looked in  $1.1 \text{ fb}^{-1}$  of  $p\bar{p}$  collisions at  $\sqrt{s} = 1.96 \text{ TeV}$  for diphoton events with large  $\cancel{E}_T$ . They may originate from the production of  $\tilde{\chi}^\pm$  in pairs or associated to a  $\tilde{\chi}_1^0$ , decaying to a  $\tilde{\chi}_1^0$  which itself decays promptly in GMSB to  $\gamma\bar{G}$ . No significant excess was found compared to the background expectation. A limit is derived on the masses of SUSY particles in the GMSB framework for  $M = 2\Lambda$ ,  $N = 1$ ,  $\tan\beta = 15$  and  $\mu > 0$ , see Figure 2. It also excludes  $\Lambda < 91.5 \text{ TeV}$ . Supersedes the results of ABAZOV 05A. Superseded by ABAZOV 10P.
- 30 ABULENCIA 07H searched in  $346 \text{ pb}^{-1}$  of  $p\bar{p}$  collisions at  $\sqrt{s} = 1.96 \text{ TeV}$  for events with at least three leptons ( $e$  or  $\mu$ ) from the decay of  $\tilde{\chi}_1^0$  via  $L\bar{L}\bar{E}$  couplings. The results are consistent with the hypothesis of no signal. Upper limits on the cross-section are extracted and a limit is derived in the framework of mSUGRA on the masses of  $\tilde{\chi}_1^0$  and  $\tilde{\chi}_1^\pm$ , see e.g. their Fig. 3 and Tab. II.
- 31 ABBIENDI 06b use  $600 \text{ pb}^{-1}$  of data from  $\sqrt{s} = 189\text{--}209 \text{ GeV}$ . They look for events with diphotons +  $\cancel{E}$  final states originating from prompt decays of pair-produced neutralinos in a GMSB scenario with  $\tilde{\chi}_1^0$  NLSP. Limits on the cross-section are computed as a function of  $m(\tilde{\chi}_1^0)$ , see their Fig. 14. The limit on the  $\tilde{\chi}_1^0$  mass is for a pure Bino state assuming a prompt decay, with lifetimes up to  $10^{-9} \text{ s}$ . Supersedes the results of ABBIENDI 04n.
- 32 ABDALLAH 05B use data from  $\sqrt{s} = 180\text{--}209 \text{ GeV}$ . They look for events with single photons +  $\cancel{E}$  final states. Limits are computed in the plane  $(m(\tilde{G}), m(\tilde{\chi}_1^0))$ , shown in their Fig. 9b for a pure Bino state in the GMSB framework and in Fig. 9c for a no-scale supergravity model. Supersedes the results of ABREU 00z.
- 33 ABDALLAH 05b use data from  $\sqrt{s} = 130\text{--}209 \text{ GeV}$ . They look for events with diphotons +  $\cancel{E}$  final states and single photons not pointing to the vertex, expected in GMSB when the  $\tilde{\chi}_1^0$  is the NLSP. Limits are computed in the plane  $(m(\tilde{G}), m(\tilde{\chi}_1^0))$ , see their Fig. 10. The lower limit is derived on the  $\tilde{\chi}_1^0$  mass for a pure Bino state assuming a prompt decay and  $m_{\tilde{e}_R} = m_{\tilde{e}_L} = 2 m_{\tilde{\nu}_0}$ . It improves to 100 GeV for  $m_{\tilde{e}_R} = m_{\tilde{e}_L} = 1.1 m_{\tilde{\nu}_0}$ , and the limit in the plane  $(m(\tilde{\chi}_1^0), m(\tilde{e}_R))$  is shown in Fig. 10b. For long-lived neutralinos, cross-section limits are displayed in their Fig. 11. Supersedes the results of ABREU 00z.

# Searches Particle Listings

## Supersymmetric Particle Searches

### $\tilde{\chi}_2^0, \tilde{\chi}_3^0, \tilde{\chi}_4^0$ (Neutralinos) mass limits

Neutralinos are unknown mixtures of photinos, z-inos, and neutral higgsinos (the supersymmetric partners of photons and of Z and Higgs bosons). The limits here apply only to  $\tilde{\chi}_2^0, \tilde{\chi}_3^0$ , and  $\tilde{\chi}_4^0$ .  $\tilde{\chi}_1^0$  is the lightest supersymmetric particle (LSP); see  $\tilde{\chi}_1^0$  Mass Limits. It is not possible to quote rigorous mass limits because they are extremely model dependent; i.e. they depend on branching ratios of various  $\tilde{\chi}^0$  decay modes, on the masses of decay products ( $\tilde{e}, \tilde{\mu}, \tilde{\tau}, \tilde{g}$ ), and on the  $\tilde{e}$  mass exchanged in  $e^+e^- \rightarrow \tilde{\chi}_i^0 \tilde{\chi}_j^0$ . Limits arise either from direct searches, or from the MSSM constraints set on the gaugino and higgsino mass parameters  $M_2$  and  $\mu$  through searches for lighter charginos and neutralinos. Often limits are given as contour plots in the  $m_{\tilde{\chi}^0} - m_{\tilde{e}}$  plane vs other parameters. When specific assumptions are made, e.g. the neutralino is a pure photino ( $\tilde{\gamma}$ ), pure z-ino ( $\tilde{Z}$ ), or pure neutral higgsino ( $\tilde{H}^0$ ), the neutralinos will be labelled as such.

Limits obtained from  $e^+e^-$  collisions at energies up to 136 GeV, as well as other limits from different techniques, are now superseded and have not been included in this compilation. They can be found in the 1998 Edition (The European Physical Journal **C3** 1 (1998)) of this Review. Some later papers are now obsolete and have been omitted. They were last listed in our PDG 14 edition: K. Olive, et al. (Particle Data Group), Chinese Physics **C38** 070001 (2014) (<http://pdg.lbl.gov>).

VALUE (GeV)	CL%	DOCUMENT ID	TECN	COMMENT
> 680	95	1 AABOUD	19AU ATL	0, 1, 2 or more $\ell, H \rightarrow \gamma\gamma, b\bar{b}, WW^*, ZZ^*, \tau\tau$ (various searches), Tchi1n2E, $m_{\tilde{\chi}_1^0} = 0$ GeV
> 112	95	2 SIRUNYAN	19BU CMS	$pp \rightarrow \tilde{\chi}_1^+ \tilde{\chi}_2^0 + 2 \text{ jets}, \tilde{\chi}_2^0 \rightarrow \ell^+ \ell^- \tilde{\chi}_1^0$ , heavy sleptons, $m_{\tilde{\chi}_2^0} - m_{\tilde{\chi}_1^0} = 1$ GeV, $m_{\tilde{\chi}_2^0} = \tilde{m}_{\tilde{\chi}_1^+}$
> 215	95	2 SIRUNYAN	19BU CMS	$pp \rightarrow \tilde{\chi}_1^+ \tilde{\chi}_2^0 + 2 \text{ jets}, \tilde{\chi}_2^0 \rightarrow \ell^+ \ell^- \tilde{\chi}_1^0$ , heavy sleptons, $m_{\tilde{\chi}_2^0} - m_{\tilde{\chi}_1^0} = 30$ GeV, $m_{\tilde{\chi}_2^0} = \tilde{m}_{\tilde{\chi}_1^+}$
> 760	95	3 AABOUD	18AY ATLS	$2\tau + \cancel{E}_T$ , Tchi1n2D and $\tilde{\tau}_L$ -only, $m_{\tilde{\chi}_1^0} = 0$ GeV
> 1125	95	4 AABOUD	18BT ATLS	$2, 3\ell + \cancel{E}_T$ , Tchi1n2C, $m_{\tilde{\chi}_1^0} = 0$ GeV
> 580	95	5 AABOUD	18BT ATLS	$2, 3\ell + \cancel{E}_T$ , Tchi1n2F, $m_{\tilde{\chi}_1^0} = 0$ GeV
none 130–230, 290–880	95	6 AABOUD	18CK ATLS	$2H \rightarrow b\bar{b} + \cancel{E}_T$ , Tn1n1A, GMSB
none 220–600	95	7 AABOUD	18CO ATLS	$2, 3\ell + \cancel{E}_T$ , recursive jigsaw, Tchi1n2F, $m_{\tilde{\chi}_1^0} = 0$ GeV
> 145	95	8 AABOUD	18R ATLS	$2\ell$ (soft) + $\cancel{E}_T$ , Tchi1n2G, higgsino, $m_{\tilde{\chi}_2^0} - m_{\tilde{\chi}_1^0} = 5$ GeV
> 175	95	9 AABOUD	18R ATLS	$2\ell$ (soft) + $\cancel{E}_T$ , Tchi1n2F, wino, $m_{\tilde{\chi}_2^0} - m_{\tilde{\chi}_1^0} = 10$ GeV
> 1060	95	10 AABOUD	18U ATLS	$2\gamma + \cancel{E}_T$ , GGM, Tchi1chi1A, any NLSP mass
> 167	95	11 SIRUNYAN	18AJ CMS	$2\ell$ (soft) + $\cancel{E}_T$ , Tchi1n2G, higgsino, $m_{\tilde{\chi}_2^0} - m_{\tilde{\chi}_1^0} = 15$ GeV
> 710	95	12 SIRUNYAN	18DP CMS	$2\tau + \cancel{E}_T$ , Tchi1n2D, $m_{\tilde{\chi}_1^0} = 0$ GeV
none 220–490	95	13 SIRUNYAN	17AW CMS	$1\ell + 2 b\text{-jets} + \cancel{E}_T$ , Tchi1n2E, $m_{\tilde{\chi}_1^0} = 0$ GeV
> 600	95	14 AAD	16AA ATLS	$3, 4\ell + \cancel{E}_T$ , Tn2n3A, $m_{\tilde{\chi}_1^0} = 0$ GeV
> 670	95	14 AAD	16AA ATLS	$3, 4\ell + \cancel{E}_T$ , Tn2n3B, $m_{\tilde{\chi}_1^0} < 200$ GeV
> 250	95	15 AAD	15BA ATLS	$m_{\tilde{\chi}_1^+} = m_{\tilde{\chi}_2^0}, m_{\tilde{\chi}_1^0} = 0$ GeV
> 380	95	16 AAD	14H ATLS	$\tilde{\chi}_1^+ \tilde{\chi}_2^0 \rightarrow \tau^\pm \nu \tilde{\chi}_1^0 \tau^\pm \tau^\mp \tilde{\chi}_1^0$ , simplified model, $m_{\tilde{\chi}_1^+} = m_{\tilde{\chi}_2^0}, m_{\tilde{\chi}_1^0} = 0$ GeV
> 700	95	16 AAD	14H ATLS	$\tilde{\chi}_1^+ \tilde{\chi}_2^0 \rightarrow \ell^\pm \nu \tilde{\chi}_1^0 \ell^\pm \ell^\mp \tilde{\chi}_1^0$ , simplified model, $m_{\tilde{\chi}_1^+} = m_{\tilde{\chi}_2^0}, m_{\tilde{\chi}_1^0} = 0$ GeV
> 345	95	16 AAD	14H ATLS	$\tilde{\chi}_1^+ \tilde{\chi}_2^0 \rightarrow W_{\tilde{\chi}_1^0}^+ Z \tilde{\chi}_1^0$ , simplified model, $m_{\tilde{\chi}_1^+} = m_{\tilde{\chi}_2^0}, m_{\tilde{\chi}_1^0} = 0$ GeV
> 148	95	16 AAD	14H ATLS	$\tilde{\chi}_1^+ \tilde{\chi}_2^0 \rightarrow W_{\tilde{\chi}_1^0}^+ H \tilde{\chi}_1^0$ , simplified model, $m_{\tilde{\chi}_1^+} = m_{\tilde{\chi}_2^0}, m_{\tilde{\chi}_1^0} = 0$ GeV
> 620	95	17 AAD	14X ATLS	$\geq 4\ell^\pm, \tilde{\chi}_{2,3}^0 \rightarrow \ell^\pm \ell^\mp \tilde{\chi}_1^0, m_{\tilde{\chi}_1^0} = 0$ GeV
> 62.4	95	18 AAD	13 ATLS	$3\ell^\pm + \cancel{E}_T$ , pMSSM, SMS
> 99.9	95	19 CHATRCHYAN12BJ	CMS	$\geq 2\ell, \text{jets} + \cancel{E}_T, pp \rightarrow \tilde{\chi}_1^\pm \tilde{\chi}_2^0$
> 116.0	95	20 ABREU	00W DLPH	$\tilde{\chi}_2^0, 1 \leq \tan\beta \leq 40, \text{all } \Delta m, \text{all } m_0$
	95	20 ABREU	00W DLPH	$\tilde{\chi}_3^0, 1 \leq \tan\beta \leq 40, \text{all } \Delta m, \text{all } m_0$
	95	20 ABREU	00W DLPH	$\tilde{\chi}_4^0, 1 \leq \tan\beta \leq 40, \text{all } \Delta m, \text{all } m_0$

• • • We do not use the following data for averages, fits, limits, etc. • • •

none 180–355	95	21 AAD	14G ATLS	$\tilde{\chi}_1^+ \tilde{\chi}_2^0 \rightarrow W_{\tilde{\chi}_1^0}^+ Z \tilde{\chi}_1^0$ , simplified model, $m_{\tilde{\chi}_1^+} = m_{\tilde{\chi}_2^0}, m_{\tilde{\chi}_1^0} = 0$ GeV
		22 KHACHATRYAN14	CMS	$\tilde{\chi}_2^0 \rightarrow (Z, H) \tilde{\chi}_1^0 \tilde{\ell}\ell$ , simplified model
		23 AAD	12AS ATLS	$3\ell^\pm + \cancel{E}_T$ , pMSSM
		24 AAD	12T ATLS	$\ell^\pm \ell^\pm + \cancel{E}_T, pp \rightarrow \tilde{\chi}_1^\pm \tilde{\chi}_2^0$

- AABOUD 19AU searched in  $36.1 \text{ fb}^{-1}$  of  $pp$  collisions at  $\sqrt{s} = 13$  TeV for direct electroweak production of charginos and next-to-lightest neutralinos decaying into lightest neutralinos and a  $W$  and a Higgs boson, respectively. Fully hadronic, semileptonic, diphoton, and multilepton (electrons, muons) final states with missing transverse momentum are considered in this search. Observations are consistent with the Standard Model expectations, and 95% confidence-level limits of up to 680 GeV on the chargino/next-to-lightest neutralino masses are set (Tchi1n2E model). See their Figure 14 for an overlay of exclusion contours from all searches.
- SIRUNYAN 19BU searched for pair production of gauginos via vector boson fusion assuming the gaugino spectrum is compressed, in  $35.9 \text{ fb}^{-1}$  of  $pp$  collisions at  $\sqrt{s} = 13$  TeV. The final states explored included zero leptons plus two jets, one lepton plus two jets, and one hadronic tau plus two jets. A similar bound is obtained in the light slepton limit.
- AABOUD 18AY searched in  $36.1 \text{ fb}^{-1}$  of  $pp$  collisions at  $\sqrt{s} = 13$  TeV for direct electroweak production of charginos and neutralinos as in Tchi1n2D models, in events characterised by the presence of at least two hadronically decaying tau leptons and large missing transverse energy. No significant deviation from the expected SM background is observed. Assuming decays via intermediate  $\tilde{\tau}_1$  and  $m_{\tilde{\chi}_1^+} = m_{\tilde{\chi}_2^0}$ , the observed limits rule out  $\tilde{\chi}_2^0$  masses up to 760 GeV for a massless  $\tilde{\chi}_1^0$ . See their Fig.7 (right). Interpretations are also provided in Fig 8 (bottom) for different assumptions on the ratio between  $m_{\tilde{\tau}}$  and  $m_{\tilde{\chi}_2^0} + m_{\tilde{\chi}_1^0}$ .
- AABOUD 18BT searched in  $36.1 \text{ fb}^{-1}$  of  $pp$  collisions at  $\sqrt{s} = 13$  TeV for direct electroweak production of charginos, chargino and next-to-lightest neutralinos and sleptons in events with two or three leptons (electrons or muons), with or without jets, and large missing transverse energy. No significant excess above the Standard Model expectations is observed. Limits are set on the next-to-lightest neutralino mass up to 1100 GeV for massless  $\tilde{\chi}_1^0$  in the Tchi1n2C simplified model exploiting the  $3\ell$  signature, see their Figure 8(c).
- AABOUD 18BT searched in  $36.1 \text{ fb}^{-1}$  of  $pp$  collisions at  $\sqrt{s} = 13$  TeV for direct electroweak production of charginos, chargino and next-to-lightest neutralinos and sleptons in events with two or three leptons (electrons or muons), with or without jets, and large missing transverse energy. No significant excess above the Standard Model expectations is observed. Limits are set on the next-to-lightest neutralino mass up to 580 GeV for massless  $\tilde{\chi}_1^0$  in the Tchi1n2F simplified model exploiting the  $2\ell + 2$  jets and  $3\ell$  signatures, see their Figure 8(d).
- AABOUD 18CK searched for events with at least 3  $b$ -jets and large missing transverse energy in two datasets of  $pp$  collisions at  $\sqrt{s} = 13$  TeV of  $36.1 \text{ fb}^{-1}$  and  $24.3 \text{ fb}^{-1}$  depending on the trigger requirements. The analyses aimed to reconstruct two Higgs bosons decaying to pairs of  $b$ -quarks. No significant excess above the Standard Model expectations is observed. Limits are set on the Higgsino mass in the Tn1n1A simplified model, see their Figure 15(a). Constraints are also presented as a function of the BR of Higgsino decaying into a higgs boson and a gravitino, see their Figure 15(b).
- AABOUD 18CO searched in  $36.1 \text{ fb}^{-1}$  of  $pp$  collisions at  $\sqrt{s} = 13$  TeV for direct electroweak production of mass-degenerate charginos and next-to-lightest neutralinos in events with two or three leptons (electrons or muons), with or without jets, and large missing transverse energy. The search channels are based on recursive jigsaw reconstruction. Limits are set on the next-to-lightest neutralinos mass up to 600 GeV for massless neutralinos in the Tchi1n2F simplified model exploiting the statistical combination of  $2\ell + 2$  jets and  $3\ell$  channels. Next-to-lightest neutralinos masses below 220 GeV are not excluded due to an excess of events above the SM prediction in the dedicated regions. See their Figure 13(d).
- AABOUD 18R searched in  $36.1 \text{ fb}^{-1}$  of  $pp$  collisions at  $\sqrt{s} = 13$  TeV for electroweak production in scenarios with compressed mass spectra in final states with two low-momentum leptons and missing transverse momentum. The data are found to be consistent with the SM prediction. Results are interpreted in Tchi1n2G higgsino models, and  $\tilde{\chi}_2^0$  masses are excluded up to 145 GeV for  $m_{\tilde{\chi}_2^0} - m_{\tilde{\chi}_1^0} = 5$  GeV. The exclusion limits extend down to mass splittings of 2.5 GeV, see their Fig. 10 (top). Results are also interpreted in terms of exclusion bounds on the production cross-sections for the NUHM2 scenario as a function of the universal gaugino mass  $m_{1/2}$  and  $m_{\tilde{\chi}_2^0} - m_{\tilde{\chi}_1^0}$ , see their Fig. 12.
- AABOUD 18R searched in  $36.1 \text{ fb}^{-1}$  of  $pp$  collisions at  $\sqrt{s} = 13$  TeV for electroweak production in scenarios with compressed mass spectra in final states with two low-momentum leptons and missing transverse momentum. The data are found to be consistent with the SM prediction. Results are interpreted in Tchi1n2F wino models, and  $\tilde{\chi}_2^0$  masses are excluded up to 175 GeV for  $m_{\tilde{\chi}_2^0} - m_{\tilde{\chi}_1^0} = 10$  GeV. The exclusion limits extend down to mass splittings of 2 GeV, see their Fig. 10 (bottom). Results are also interpreted in terms of exclusion bounds on the production cross-sections for the NUHM2 scenario as a function of the universal gaugino mass  $m_{1/2}$  and  $m_{\tilde{\chi}_2^0} - m_{\tilde{\chi}_1^0}$ , see their Fig. 12.
- AABOUD 18U searched in  $36.1 \text{ fb}^{-1}$  of  $pp$  collisions at  $\sqrt{s} = 13$  TeV in events with at least one isolated photon, possibly jets and significant transverse momentum targeting generalised models of gauge-mediated SUSY breaking. No significant excess of events is observed above the SM prediction. Results of the diphoton channel are interpreted in terms of lower limits on the masses of gauginos Tchi1chi1A models, which reach as high as 1.3 TeV. Gaugino masses below 1060 GeV are excluded for any NLSP mass, see their Fig. 10.
- SIRUNYAN 18AJ searched in  $35.9 \text{ fb}^{-1}$  of  $pp$  collisions at  $\sqrt{s} = 13$  TeV for events containing two low-momentum, oppositely charged leptons (electrons or muons) and  $\cancel{E}_T$ . No excess over the expected background is observed. Limits are derived on the wino mass in the Tchi1n2F simplified model, see their Figure 5. Limits are also set on the stop mass in the Tstop10 simplified model, see their Figure 6. Finally, limits are set on the Higgsino mass in the Tchi1n2G simplified model, see Figure 8 and in the pMSSM, see Figure 7.

- 12 SIRUNYAN 18DP searched in 35.9 fb<sup>-1</sup> of pp collisions at  $\sqrt{s} = 13$  TeV for direct electroweak production of charginos and neutralinos or of chargino pairs in events with a tau lepton pair and significant missing transverse momentum. Both hadronic and leptonic decay modes are considered for the tau lepton. No significant excess above the Standard Model expectations is observed. Limits are set on the chargino mass in the Tchi1ch1D and Tchi1n2 simplified models, see their Figures 14 and 15. Also, excluded stau pair production cross sections are shown in Figures 11, 12, and 13.
- 13 SIRUNYAN 17AW searched in 35.9 fb<sup>-1</sup> of pp collisions at  $\sqrt{s} = 13$  TeV for events with a charged lepton (electron or muon), two jets identified as originating from a b-quark, and large  $E_T$ . No significant excess above the Standard Model expectations is observed. Limits are set on the mass of the chargino and the next-to-lightest neutralino in the Tchi1n2E simplified model, see their Figure 6.
- 14 AAD 16AA summarized and extended ATLAS searches for electroweak supersymmetry in final states containing several charged leptons,  $E_T$ , with or without hadronic jets, in 20 fb<sup>-1</sup> of pp collisions at  $\sqrt{s} = 8$  TeV. The paper reports the results of new interpretations and statistical combinations of previously published analyses, as well as new analyses. Exclusion limits at 95% C.L. are set on mass-degenerate  $\tilde{\chi}_2^0$  and  $\tilde{\chi}_3^0$  masses in the Tn2n3A and Tn2n3B simplified models. See their Fig. 15.
- 15 AAD 15BA searched in 20.3 fb<sup>-1</sup> of pp collisions at  $\sqrt{s} = 8$  TeV for electroweak production of charginos and neutralinos decaying to a final state containing a W boson and a 125 GeV Higgs boson, plus missing transverse momentum. No excess beyond the Standard Model expectation is observed. Exclusion limits are derived in simplified models of direct chargino and next-to-lightest neutralino production, with the decays  $\tilde{\chi}_1^\pm \rightarrow W^\pm \tilde{\chi}_1^0$  and  $\tilde{\chi}_2^0 \rightarrow H \tilde{\chi}_1^0$  having 100% branching fraction, see Fig. 8. A combination of the multiple final states for the Higgs decay yields the best limits (Fig. 8d).
- 16 AAD 14H searched in 20.3 fb<sup>-1</sup> of pp collisions at  $\sqrt{s} = 8$  TeV for electroweak production of charginos and neutralinos decaying to a final state with three leptons and missing transverse momentum. No excess beyond the Standard Model expectation is observed. Exclusion limits are derived in simplified models of direct chargino and next-to-lightest neutralino production, with decays to the lightest neutralino via either all three generations of leptons, staus only, gauge bosons, or Higgs bosons, see Fig. 7. An interpretation in the pMSSM is also given, see Fig. 8.
- 17 AAD 14X searched in 20.3 fb<sup>-1</sup> of pp collisions at  $\sqrt{s} = 8$  TeV for events with at least four leptons (electrons, muons, taus) in the final state. No significant excess above the Standard Model expectations is observed. Limits are set on the neutralino mass in an R-parity conserving simplified model where the decay  $\tilde{\chi}_{2,3}^0 \rightarrow \ell^\pm \ell^\mp \tilde{\chi}_1^0$  takes place with a branching ratio of 100%, see Fig. 10.
- 18 AAD 13 searched in 4.7 fb<sup>-1</sup> of pp collisions at  $\sqrt{s} = 7$  TeV for charginos and neutralinos decaying to a final state with three leptons (e and  $\mu$ ) and missing transverse energy. No excess beyond the Standard Model expectation is observed. Exclusion limits are derived in the phenomenological MSSM, see Fig. 2 and 3, and in simplified models, see Fig. 4. For the simplified models with intermediate slepton decays, degenerate  $\tilde{\chi}_1^\pm$  and  $\tilde{\chi}_2^0$  masses up to 500 GeV are excluded at 95% C.L. for very large mass differences with the  $\tilde{\chi}_1^0$ . Supersedes AAD 12As.
- 19 CHATRCHYAN 12BJ searched in 4.98 fb<sup>-1</sup> of pp collisions at  $\sqrt{s} = 7$  TeV for direct electroweak production of charginos and neutralinos in events with at least two leptons, jets and missing transverse momentum. No significant excesses over the expected SM backgrounds are observed and 95% C.L. limits on the production cross section of  $\tilde{\chi}_1^\pm \tilde{\chi}_2^0$  pair production were set in a number of simplified models, see Figs. 7 to 12. Most limits are for exactly 3 jets.
- 20 ABREU 00w combines data collected at  $\sqrt{s}=189$  GeV with results from lower energies. The mass limit is obtained by constraining the MSSM parameter space with gaugino and sfermion mass universality at the GUT scale, using the results of negative direct searches for neutralinos (including cascade decays and  $\tilde{\tau}\tau$  final states) from ABREU 01, for charginos from ABREU 00j and ABREU 00t (for all  $\Delta m_+$ ), and for charged sleptons from ABREU 01b. The results hold for the full parameter space defined by all values of  $M_2$  and  $|\mu| \leq 2$  TeV with the  $\tilde{\chi}_1^0$  as LSP.
- 21 AAD 14G searched in 20.3 fb<sup>-1</sup> of pp collisions at  $\sqrt{s} = 8$  TeV for electroweak production of chargino-neutralino pairs, decaying to a final state with two leptons (e and  $\mu$ ) and missing transverse momentum. No excess beyond the Standard Model expectation is observed. Exclusion limits are derived in simplified models of chargino and next-to-lightest neutralino production, with decays to the lightest neutralino via gauge bosons, see Fig. 7. An interpretation in the pMSSM is also given, see Fig. 10.
- 22 KHACHATRYAN 14t searched in 19.5 fb<sup>-1</sup> of pp collisions at  $\sqrt{s} = 8$  TeV for electroweak production of charginos and neutralinos decaying to a final state with three leptons (e or  $\mu$ ) and missing transverse momentum, or with a Z-boson, dijets and missing transverse momentum. No excess beyond the Standard Model expectation is observed. Exclusion limits are derived in simplified models, see Figs. 12–16.
- 23 AAD 12As searched in 2.06 fb<sup>-1</sup> of pp collisions at  $\sqrt{s} = 7$  TeV for charginos and neutralinos decaying to a final state with three leptons (e and  $\mu$ ) and missing transverse energy. No excess beyond the Standard Model expectation is observed. Exclusion limits are derived in the phenomenological MSSM, see Fig. 2 (top), and in simplified models, see Fig. 2 (bottom).
- 24 AAD 12T looked in 1 fb<sup>-1</sup> of pp collisions at  $\sqrt{s} = 7$  TeV for the production of supersymmetric particles decaying into final states with missing transverse momentum and exactly two isolated leptons (e or  $\mu$ ). Same-sign dilepton events were separately studied. Additionally, in opposite-sign events, a search was made for an excess of same-flavor over different-flavor lepton pairs. No excess over the expected background is observed and limits are placed on the effective production cross section of opposite-sign dilepton events with  $E_T > 250$  GeV and on same-sign dilepton events with  $E_T > 100$  GeV. The latter limit is interpreted in a simplified electroweak gaugino production model.

Unless otherwise stated, results in this section assume spectra, production rates, decay modes and branching ratios as evaluated in the MSSM, with gaugino and sfermion mass unification at the GUT scale. These papers generally study production of  $\tilde{\chi}_1^0 \tilde{\chi}_2^0$ ,  $\tilde{\chi}_1^\pm \tilde{\chi}_1^\mp$  and (in the case of hadronic collisions)  $\tilde{\chi}_1^\pm \tilde{\chi}_2^0$  pairs, including the effects of cascade decays. The mass limits on  $\tilde{\chi}_1^\pm$  are either direct, or follow indirectly from the constraints set by the non-observation of  $\tilde{\chi}_2^0$  states on the gaugino and higgsino MSSM parameters  $M_2$  and  $\mu$ . For generic values of the MSSM parameters, limits from high-energy  $e^+e^-$  collisions coincide with the highest value of the mass allowed by phase-space, namely  $m_{\tilde{\chi}_1^\pm} \lesssim \sqrt{s}/2$ . The still unpublished combination of the results of the four LEP collaborations from the 2000 run of LEP2 at  $\sqrt{s}$  up to  $\approx 209$  GeV yields a lower mass limit of 103.5 GeV valid for general MSSM models. The limits become however weaker in certain regions of the MSSM parameter space where the detection efficiencies or production cross sections are suppressed. For example, this may happen when: (i) the mass differences  $\Delta m_+ = m_{\tilde{\chi}_1^\pm} - m_{\tilde{\chi}_1^0}$  or  $\Delta m_\nu = m_{\tilde{\chi}_1^\pm} - m_{\tilde{\nu}}$  are very small, and the detection efficiency is reduced; (ii) the electron sneutrino mass is small, and the  $\tilde{\chi}_1^\pm$  production rate is suppressed due to a destructive interference between s and t channel exchange diagrams. The regions of MSSM parameter space where the following limits are valid are indicated in the comment lines or in the footnotes.

Some earlier papers are now obsolete and have been omitted. They were last listed in our PDG 14 edition: K. Olive, et al. (Particle Data Group), Chinese Physics **C38** 070001 (2014) (<http://pdg.lbl.gov>).

VALUE (GeV)	CL%	DOCUMENT ID	TECN	COMMENT
>1050	95	1 SIRUNYAN 20B	CMS	$\geq 1\gamma + E_T$ , Tchi1chi1F, $\tilde{\chi}_1^0 \rightarrow \gamma \tilde{G}$
> 825	95	1 SIRUNYAN 20B	CMS	$\geq 1\gamma + E_T$ , Tchi1chi1G, $\tilde{\chi}_1^\pm \rightarrow \tilde{\chi}_1^0 + \text{soft}$
> 840	95	1 SIRUNYAN 20B	CMS	$\geq 1\gamma + E_T$ , Tchi1n12-GGM, 120 GeV < $m_{\tilde{\chi}_1^0} < 720$ GeV
> 680	95	2 AABOUD 19AU	ATL	0, 1, 2 or more $\ell, H (\rightarrow \gamma\gamma, b\bar{b}, WW^*, ZZ^*, \tau\tau)$ (various searches), Tchi1n2E, $m_{\tilde{\chi}_1^0}=0$ GeV
> 112	95	3 SIRUNYAN 19BU	CMS	pp $\rightarrow \tilde{\chi}_1^\pm \tilde{\chi}_2^0 + 2$ jets, $\tilde{\chi}_1^\pm \rightarrow \ell^\pm \nu \tilde{\chi}_1^0$ , heavy sleptons, $m_{\tilde{\chi}_1^\pm} - m_{\tilde{\chi}_1^0} = 1$ GeV, $m_{\tilde{\chi}_1^0} = m_{\tilde{\chi}_2^0}$
> 215	95	3 SIRUNYAN 19BU	CMS	pp $\rightarrow \tilde{\chi}_1^\pm \tilde{\chi}_2^0 + 2$ jets, $\tilde{\chi}_1^\pm \rightarrow \ell^\pm \nu \tilde{\chi}_1^0$ , heavy sleptons, $m_{\tilde{\chi}_1^\pm} - m_{\tilde{\chi}_1^0} = 30$ GeV, $m_{\tilde{\chi}_1^0} = m_{\tilde{\chi}_2^0}$
> 235	95	4 SIRUNYAN 19CI	CMS	$\geq 1H (\rightarrow \gamma\gamma) + \text{jets} + E_T$ , Tchi1n2E, $m_{\tilde{\chi}_1^0} = 1$ GeV
> 930	95	5 SIRUNYAN 19K	CMS	$\gamma + \text{lepton} + E_T$ , Tchi1n1A
> 630	95	6 AABOUD 18AY	ATLS	$2\tau + E_T$ , Tchi1chi1D and $\tilde{\tau}_L$ -only, $m_{\tilde{\chi}_1^0} = 0$ GeV
> 760	95	7 AABOUD 18AY	ATLS	$2\tau + E_T$ , Tchi1n2D and $\tilde{\tau}_L$ -only, $m_{\tilde{\chi}_1^0} = 0$ GeV
> 740	95	8 AABOUD 18BT	ATLS	$2\ell + E_T$ , Tchi1chi1C, $m_{\tilde{\chi}_1^0}=0$ GeV
>1125	95	9 AABOUD 18BT	ATLS	$2,3\ell + E_T$ , Tchi1n2C, $m_{\tilde{\chi}_1^0}=0$ GeV
> 580	95	10 AABOUD 18BT	ATLS	$2,3\ell + E_T$ , Tchi1n2F, $m_{\tilde{\chi}_1^0}=0$ GeV
none	95	11 AABOUD 18CK	ATLS	$2H (\rightarrow b\bar{b}) + E_T$ , Tn1n1A, GMSB
130–230, 290–880	95	12 AABOUD 18CO	ATLS	$2,3\ell + E_T$ , recursive jigsaw, Tchi1n2F, $m_{\tilde{\chi}_1^0} = 0$ GeV
none	95	12 AABOUD 18CO	ATLS	$2,3\ell + E_T$ , recursive jigsaw, Tchi1n2F, $m_{\tilde{\chi}_1^0} = 0$ GeV
> 175	95	13 AABOUD 18R	ATLS	$2\ell (\text{soft}) + E_T$ , Tchi1n2F, wino, $m_{\tilde{\chi}_1^\pm} - m_{\tilde{\chi}_1^0} = 10$ GeV
> 145	95	14 AABOUD 18R	ATLS	$2\ell (\text{soft}) + E_T$ , Tchi1n2G, higgsino, $m_{\tilde{\chi}_1^\pm} - m_{\tilde{\chi}_1^0} = 5$ GeV
>1060	95	15 AABOUD 18U	ATLS	$2\gamma + E_T$ , GGM, Tchi1chi1A, any NLSP mass
>1400	95	16 AABOUD 18Z	ATLS	$\geq 4\ell$ , RPV, $\lambda_{12k} \neq 0$ , $m_{\tilde{\chi}_1^0} > 500$ GeV
>1320	95	16 AABOUD 18Z	ATLS	$\geq 4\ell$ , RPV, $\lambda_{12k} \neq 0$ , $m_{\tilde{\chi}_1^0} > 500$ GeV
> 980	95	16 AABOUD 18Z	ATLS	$\geq 4\ell$ , RPV, $\lambda_{133} \neq 0$ , 400 GeV < $m_{\tilde{\chi}_1^0} < 700$ GeV
> 980	95	17 SIRUNYAN 18AA	CMS	$\geq 1\gamma + E_T$ , GGM, wino-like $\tilde{\chi}_2^0 \tilde{\chi}_1^\pm$ pair production, nearly degenerate wino and bino masses
> 780	95	17 SIRUNYAN 18AA	CMS	$\geq 1\gamma + E_T$ , Tchi1n1A
> 950	95	17 SIRUNYAN 18AA	CMS	$\geq 1\gamma + E_T$ , Tchi1chi1A
> 230	95	18 SIRUNYAN 18AJ	CMS	$2\ell (\text{soft}) + E_T$ , Tchi1n2F, wino, $m_{\tilde{\chi}_2^0} - m_{\tilde{\chi}_1^0} = 20$ GeV

$\tilde{\chi}_1^\pm, \tilde{\chi}_2^0$  (Charginos) mass limits

Charginos are unknown mixtures of w-inos and charged higgsinos (the supersymmetric partners of W and Higgs bosons). A lower mass limit for the lightest chargino ( $\tilde{\chi}_1^\pm$ ) of approximately 45 GeV, independent of the field composition and of the decay mode, has been obtained by the LEP experiments from the analysis of the Z width and decays. These results, as well as other now superseded limits from  $e^+e^-$  collisions at energies below 136 GeV, and from hadronic collisions, can be found in the 1998 Edition (The European Physical Journal **C3** 1 (1998)) of this Review.

# Searches Particle Listings

## Supersymmetric Particle Searches

>1150	95	19 SIRUNYAN	18AO CMS	$\ell^\pm \ell^\pm$ or $\geq 3\ell$ , Tchi1n2A, $m_{\tilde{\ell}} = m_{\tilde{\nu}} = m_{\tilde{\chi}_1^0} + 0.5(m_{\tilde{\chi}_1^\pm} - m_{\tilde{\chi}_1^0})$ , $m_{\tilde{\chi}_1^0} = 0$ GeV		> 380	95	32 AAD	14H ATLS	$\tilde{\chi}_1^\pm \tilde{\chi}_2^0 \rightarrow \tau^\pm \nu \tilde{\chi}_1^0 \tau^\pm \tilde{\chi}_1^0$ , simplified model, $m_{\tilde{\chi}_1^\pm} = m_{\tilde{\chi}_2^0}$ , $m_{\tilde{\chi}_1^0} = 0$ GeV
>1120	95	19 SIRUNYAN	18AO CMS	$\ell^\pm \ell^\pm$ or $\geq 3\ell$ , Tchi1n2A, $m_{\tilde{\ell}} = m_{\tilde{\nu}} = m_{\tilde{\chi}_1^0} + 0.05(m_{\tilde{\chi}_1^\pm} - m_{\tilde{\chi}_1^0})$ , $m_{\tilde{\chi}_1^0} = 0$ GeV		> 750	95	33 AAD	14x ATLS	RPV, $\geq 4\ell^\pm$ , $\tilde{\chi}_1^\pm \rightarrow W^{(*)\pm} \tilde{\chi}_1^0$ , $\tilde{\chi}_1^0 \rightarrow \ell^\pm \tilde{\ell} \nu$
>1050	95	19 SIRUNYAN	18AO CMS	$\ell^\pm \ell^\pm$ or $\geq 3\ell$ , Tchi1n2A, $m_{\tilde{\ell}} = m_{\tilde{\nu}} = m_{\tilde{\chi}_1^0} + 0.95(m_{\tilde{\chi}_1^\pm} - m_{\tilde{\chi}_1^0})$ , $m_{\tilde{\chi}_1^0} = 0$ GeV		> 210	95	34 KHACHATRY..14L	CMS	$\tilde{\chi}_2^0 \rightarrow H \tilde{\chi}_1^0$ and $\tilde{\chi}_1^\pm \rightarrow W^\pm \tilde{\chi}_1^0$ simplified models, $m_{\tilde{\chi}_2^0} = m_{\tilde{\chi}_1^\pm}$ , $m_{\tilde{\chi}_1^0} = 0$ GeV
>1080	95	19 SIRUNYAN	18AO CMS	$\ell^\pm \ell^\pm$ or $\geq 3\ell$ , Tchi1n2H, $m_{\tilde{\ell}} = m_{\tilde{\nu}} = m_{\tilde{\chi}_1^0} + 0.5(m_{\tilde{\chi}_1^\pm} - m_{\tilde{\chi}_1^0})$ , $m_{\tilde{\chi}_1^0} = 0$ GeV		> 540	95	35 AAD	13 ATLS	$3\ell^\pm + \cancel{E}_T$ , pMSSM, SMS
>1030	95	19 SIRUNYAN	18AO CMS	$\ell^\pm \ell^\pm$ or $\geq 3\ell$ , Tchi1n2H, $m_{\tilde{\ell}} = m_{\tilde{\nu}} = m_{\tilde{\chi}_1^0} + 0.05(m_{\tilde{\chi}_1^\pm} - m_{\tilde{\chi}_1^0})$ , $m_{\tilde{\chi}_1^0} = 0$ GeV		> 540	95	36 AAD	13B ATLS	$2\ell^\pm + \cancel{E}_T$ , pMSSM, SMS
>1050	95	19 SIRUNYAN	18AO CMS	$\ell^\pm \ell^\pm$ or $\geq 3\ell$ , Tchi1n2H, $m_{\tilde{\ell}} = m_{\tilde{\nu}} = m_{\tilde{\chi}_1^0} + 0.95(m_{\tilde{\chi}_1^\pm} - m_{\tilde{\chi}_1^0})$ , $m_{\tilde{\chi}_1^0} = 0$ GeV		> 540	95	37 AAD	12CT ATLS	$\geq 4\ell^\pm$ , RPV, $m_{\tilde{\chi}_1^0} > 300$ GeV
> 625	95	19 SIRUNYAN	18AO CMS	$\ell^\pm \ell^\pm$ or $\geq 3\ell$ , Tchi1n2D, $m_{\tilde{\tau}} = m_{\tilde{\chi}_1^0} + 0.5(m_{\tilde{\chi}_1^\pm} - m_{\tilde{\chi}_1^0})$ , $m_{\tilde{\chi}_1^0} = 0$ GeV		> 94	95	38 CHATRCHYAN12BJ	CMS	$\geq 2\ell$ , jets + $\cancel{E}_T$ , $pp \rightarrow \tilde{\chi}_1^\pm \tilde{\chi}_2^0$
> 180	95	19 SIRUNYAN	18AO CMS	$\ell^\pm \ell^\pm$ or $\geq 3\ell$ , Tchi1n2E, $m_{\tilde{\chi}_1^0} = 0$ GeV		> 94	95	39 ABDALLAH	03M DLPH	$\tilde{\chi}_1^\pm$ , $\tan\beta \leq 40$ , $\Delta m_+ > 3$ GeV, all $m_0$
> 450	95	19 SIRUNYAN	18AO CMS	$\ell^\pm \ell^\pm$ or $\geq 3\ell$ , Tchi1n2F, $m_{\tilde{\chi}_1^0} = 0$ GeV		> 570	95	• • • We do not use the following data for averages, fits, limits, etc. • • •		
> 480	95	20 SIRUNYAN	18AP CMS	Combination of searches, Tchi1n2E, $m_{\tilde{\chi}_1^0} = 0$ GeV		> 680	95	40 KHACHATRY..16AA	CMS	$\geq 1\gamma + \text{jets} + \cancel{E}_T$ , Tchi1chi1A
> 650	95	20 SIRUNYAN	18AP CMS	Combination of searches, Tchi1n2F, $m_{\tilde{\chi}_1^0} = 0$ GeV		> 710	95	40 KHACHATRY..16AA	CMS	$\geq 1\gamma + \text{jets} + \cancel{E}_T$ , Tchi1n1A
> 535	95	20 SIRUNYAN	18AP CMS	Combination of searches, Tchi1n2I, $m_{\tilde{\chi}_1^0} = 0$ GeV		> 1000	95	40 KHACHATRY..16AA	CMS	$\geq 1\gamma + \text{jets} + \cancel{E}_T$ , GGM, $\tilde{\chi}_2^0 \tilde{\chi}_1^\pm$ pair production, wino-like NLSP
none 160-610	95	21 SIRUNYAN	18AR CMS	$\ell^\pm \ell^\pm + \text{jets} + \cancel{E}_T$ , Tchi1n2F, $m_{\tilde{\chi}_1^0} = 0$ GeV		> 307	95	41 KHACHATRY..16R	CMS	$\geq 1\gamma + 1e$ or $\mu + \cancel{E}_T$ , Tglu1F, $m_{\tilde{\chi}_1^\pm} = m_{\tilde{\chi}_2^0} > 200$ GeV
none 170-200	95	22 SIRUNYAN	18DN CMS	$\ell^\pm \ell^\pm$ , Tchi1chi1E, $m_{\tilde{\chi}_1^0} = 1$ GeV		> 410	95	42 KHACHATRY..16Y	CMS	1,2 soft $\ell^\pm + \text{jets} + \cancel{E}_T$ , Tchi1n2A, $m_{\tilde{\chi}_1^\pm} - m_{\tilde{\chi}_1^0} = 20$ GeV
> 810	95	22 SIRUNYAN	18DN CMS	$\ell^\pm \ell^\pm$ , Tchi1chi1C, $m_{\tilde{\chi}_1^0} = 0$ GeV		> 345	95	43 AAD	14AV ATLS	$\geq 2\tau + \cancel{E}_T$ , direct $\tilde{\chi}_1^\pm \tilde{\chi}_2^0$ , $\tilde{\chi}_1^\pm \tilde{\chi}_1^\mp$ production, $m_{\tilde{\chi}_2^0} = m_{\tilde{\chi}_1^\pm}$ , $m_{\tilde{\chi}_1^0} = 0$ GeV
> 630	95	23 SIRUNYAN	18DP CMS	$2\tau + \cancel{E}_T$ , Tchi1chi1D, $m_{\tilde{\chi}_1^0} = 0$ GeV		none	95	44 AAD	14AV ATLS	$\geq 2\tau + \cancel{E}_T$ , direct $\tilde{\chi}_1^\pm \tilde{\chi}_1^\mp$ production, $m_{\tilde{\chi}_1^0} = 0$ GeV
> 710	95	23 SIRUNYAN	18DP CMS	$2\tau + \cancel{E}_T$ , Tchi1n2D, $m_{\tilde{\chi}_1^0} = 0$ GeV		100-105, 120-135, 145-160	95	45 AAD	14G ATLS	$\tilde{\chi}_1^\pm \tilde{\chi}_1^\mp \rightarrow W^\pm \tilde{\chi}_1^0 W^- \tilde{\chi}_1^0$ , simplified model, $m_{\tilde{\chi}_1^0} = 0$ GeV
> 170	95	24 SIRUNYAN	18X CMS	$\geq 1H (\rightarrow \gamma\gamma) + \text{jets} + \cancel{E}_T$ , Tchi1n2E, $m_{\tilde{\chi}_1^0} < 25$ GeV		none	95	45 AAD	14G ATLS	$\tilde{\chi}_1^\pm \tilde{\chi}_1^\mp \rightarrow \ell^\pm \nu \tilde{\chi}_1^0 \ell^\mp \tilde{\chi}_1^0$ , simplified model, $m_{\tilde{\chi}_1^0} = 0$ GeV
> 420	95	25 KHACHATRY..17L	CMS	$2\tau + \cancel{E}_T$ , Tchi1chi1C and $\tilde{\tau}$ -only, $m_{\tilde{\chi}_1^0} = 0$ GeV		140-465	95	45 AAD	14G ATLS	$\tilde{\chi}_1^\pm \tilde{\chi}_2^0 \rightarrow W \tilde{\chi}_1^0 Z \tilde{\chi}_1^0$ , simplified model, $m_{\tilde{\chi}_1^\pm} = m_{\tilde{\chi}_2^0}$ , $m_{\tilde{\chi}_1^0} = 0$ GeV
none 220-490	95	26 SIRUNYAN	17AW CMS	$1\ell + 2b\text{-jets} + \cancel{E}_T$ , Tchi1n2E, $m_{\tilde{\chi}_1^0} = 0$ GeV		180-355	95	45 AAD	14G ATLS	$\tilde{\chi}_1^\pm \tilde{\chi}_2^0 \rightarrow W \tilde{\chi}_1^0 Z \tilde{\chi}_1^0$ , simplified model, $m_{\tilde{\chi}_1^\pm} = m_{\tilde{\chi}_2^0}$ , $m_{\tilde{\chi}_1^0} = 0$ GeV
> 500	95	27 AAD	16AA ATLS	$2\ell^\pm + \cancel{E}_T$ , Tchi1chi1B, $m_{\tilde{\chi}_1^0} = 0$ GeV		> 168	95	46 AALTONEN	14 CDF	$3\ell^\pm + \cancel{E}_T$ , $\tilde{\chi}_1^\pm \rightarrow \ell \nu \tilde{\chi}_1^0$ , mSUGRA with $m_0 = 60$ GeV
> 220	95	27 AAD	16AA ATLS	$2\ell^\pm + \cancel{E}_T$ , Tchi1chi1C, low $\Delta m$ for $\tilde{\chi}_1^\pm, \tilde{\chi}_1^0$		> 700	95	47 KHACHATRY..14I	CMS	$\tilde{\chi}_1^\pm \rightarrow W \tilde{\chi}_1^0, \tilde{\ell} \tilde{\nu}, \tilde{\ell} \nu$ , simplified model
> 700	95	28 AAD	16AA ATLS	$3,4\ell + \cancel{E}_T$ , Tchi1n2B, $m_{\tilde{\chi}_1^0} = 0$ GeV		> 710	95	48 AALTONEN	13Q CDF	$\tilde{\chi}_1^\pm \rightarrow \tau X$ , simplified gravity- and gauge-mediated models
> 700	95	28 AAD	16AA ATLS	$3,4\ell + \cancel{E}_T$ , Tchi1n2C, $m_{\tilde{\ell}} = m_{\tilde{\chi}_1^0} + 0.5$ (or 0.95) $(m_{\tilde{\chi}_1^\pm} - m_{\tilde{\chi}_1^0})$		> 420	95	49 AAD	12AS ATLS	$3\ell^\pm + \cancel{E}_T$ , pMSSM
> 400	95	28 AAD	16AA ATLS	2 hadronic $\tau + \cancel{E}_T$ & $3\ell + \cancel{E}_T$ combination, Tchi1n2D, $m_{\tilde{\chi}_1^0} = 0$ GeV		> 500	95	50 AAD	12T ATLS	$\ell^\pm \tilde{\ell} \tilde{\nu} + \cancel{E}_T, \ell^\pm \ell^\pm + \cancel{E}_T, pp \rightarrow \tilde{\chi}_1^\pm \tilde{\chi}_2^0$
> 540	95	29 KHACHATRY..16R	CMS	$\geq 1\gamma + 1e$ or $\mu + \cancel{E}_T$ , Tchi1n1A		none	95	51 CHATRCHYAN11B	CMS	$\tilde{W}^0 \rightarrow \gamma \tilde{G}, \tilde{W}^\pm \rightarrow \ell^\pm \tilde{G}$ , GMSB
> 250	95	30 AAD	15BA ATLS	$m_{\tilde{\chi}_1^\pm} = m_{\tilde{\chi}_2^0}, m_{\tilde{\chi}_1^0} = 0$ GeV		> 163	95	52 CHATRCHYAN11v	CMS	$\tan\beta = 3, m_0 = 60$ GeV, $A_0 = 0, \mu > 0$
> 590	95	31 AAD	15CA ATLS	$\geq 2\gamma + \cancel{E}_T$ , GGM, bino-like NLSP, any NLSP mass		1 SIRUNYAN 20b searched in 35.9 fb <sup>-1</sup> of pp collisions at $\sqrt{s} = 13$ TeV for events with at least one photon and large $\cancel{E}_T$ . No significant excess above the Standard Model expectations is observed. Limits are set on chargino masses in a general gauge-mediated SUSY breaking (GGM) scenario Tchi1n12-GGM, see Figure 4. Limits are also set on the NLSP mass in the Tchi1chi1F and Tchi1chi1G simplified models, see their Figure 5. Finally, limits are set on the gluino mass in the Tglu4A simplified model, see Figure 6.				
none 124-361	95	31 AAD	15CA ATLS	$\geq 1\gamma + e\mu + \cancel{E}_T$ , GGM, wino-like NLSP		2 AABOUD 19AU searched in 36.1 fb <sup>-1</sup> of pp collisions at $\sqrt{s} = 13$ TeV for direct production of charginos and next-to-lightest neutralinos decaying into lightest neutralinos and a W, and a Higgs boson, respectively. Fully hadronic, semileptonic, diphoton, and multilepton (electrons, muons) final states with missing transverse momentum are considered in this search. Observations are consistent with the Standard Model expectations, and 95% confidence-level limits of up to 680 GeV on the chargino/next-to-lightest neutralino masses are set (Tchi1n2E model). See their Figure 14 for an overlay of exclusion contours from all searches.				
> 700	95	32 AAD	14H ATLS	$\tilde{\chi}_1^\pm \tilde{\chi}_2^0 \rightarrow \ell^\pm \nu \tilde{\chi}_1^0 \ell^\mp \tilde{\chi}_1^0$ , simplified model, $m_{\tilde{\chi}_1^\pm} = m_{\tilde{\chi}_2^0}$ , $m_{\tilde{\chi}_1^0} = 0$ GeV		3 SIRUNYAN 19BU searched for pair production of gauginos via vector boson fusion assuming the gaugino spectrum is compressed, in 35.9 fb <sup>-1</sup> of pp collisions at $\sqrt{s} = 13$ TeV. The final states explored included zero leptons plus two jets, one lepton plus two jets, and one hadronic tau plus two jets. A similar bound is obtained in the light slepton limit.				
> 345	95	32 AAD	14H ATLS	$\tilde{\chi}_1^\pm \tilde{\chi}_2^0 \rightarrow W \tilde{\chi}_1^0 Z \tilde{\chi}_1^0$ , simplified model, $m_{\tilde{\chi}_1^\pm} = m_{\tilde{\chi}_2^0}, m_{\tilde{\chi}_1^0} = 0$ GeV		4 SIRUNYAN 19CI searched in 77.5 fb <sup>-1</sup> of pp collisions at $\sqrt{s} = 13$ TeV for events with one or more high-momentum Higgs bosons, decaying to pairs of photons, jets and $\cancel{E}_T$ . No significant excess above the Standard Model expectations is observed. Limits are set on the sbottom mass in the Tsbot4 simplified model, see Figure 3, and on the wino mass in the Tchi1n2E simplified model, see their Figure 4. Limits are also set on the higgsino mass in the Tn1n1A and Tn1n1B simplified models, see their Figure 5.				
> 148	95	32 AAD	14H ATLS	$\tilde{\chi}_1^\pm \tilde{\chi}_2^0 \rightarrow W \tilde{\chi}_1^0 H \tilde{\chi}_1^0$ , simplified model, $m_{\tilde{\chi}_1^\pm} = m_{\tilde{\chi}_2^0}, m_{\tilde{\chi}_1^0} = 0$ GeV		5 SIRUNYAN 19K searched in 35.9 fb <sup>-1</sup> of pp collisions at $\sqrt{s} = 13$ TeV for events with a photon, an electron or muon, and large $\cancel{E}_T$ . No significant excess above the Standard Model expectations is observed. In the framework of GMSB, limits are set on the chargino and neutralino mass in the Tchi1n1A simplified model, see their Figure 6. Limits are also set on the gluino mass in the Tglu4A simplified model, and on the squark mass in the Tsqk4A simplified model, see their Figure 7.				

- 6 AABOUD 18AY searched in  $36.1 \text{ fb}^{-1}$  of  $pp$  collisions at  $\sqrt{s} = 13 \text{ TeV}$  for direct electroweak production of charginos as in Tchi1ch1D models in events characterised by the presence of at least two hadronically decaying tau leptons and large missing transverse energy. No significant deviation from the expected SM background is observed. In the Tchi1ch1D model, assuming decays via intermediate  $\tilde{\tau}_L$ , the observed limits rule out  $\tilde{\chi}_1^\pm$  masses up to 630 GeV for a massless  $\tilde{\chi}_1^0$ . See their Fig.7 (left). Interpretations are also provided in Fig 8 (top) for different assumptions on the ratio between  $m_{\tilde{\tau}}$  and  $m_{\tilde{\chi}_1^\pm} + m_{\tilde{\chi}_1^0}$ .
- 7 AABOUD 18AY searched in  $36.1 \text{ fb}^{-1}$  of  $pp$  collisions at  $\sqrt{s} = 13 \text{ TeV}$  for direct electroweak production of charginos and neutralinos as in Tchi1n2D models, in events characterised by the presence of at least two hadronically decaying tau leptons and large missing transverse energy. No significant deviation from the expected SM background is observed. Assuming decays via intermediate  $\tilde{\tau}_L$  and  $m_{\tilde{\chi}_1^\pm} = m_{\tilde{\chi}_2^0}$ , the observed limits rule out  $\tilde{\chi}_1^\pm$  masses up to 760 GeV for a massless  $\tilde{\chi}_1^0$ . See their Fig.7 (right). Interpretations are also provided in Fig 8 (bottom) for different assumptions on the ratio between  $m_{\tilde{\tau}}$  and  $m_{\tilde{\chi}_1^\pm} + m_{\tilde{\chi}_1^0}$ .
- 8 AABOUD 18BT searched in  $36.1 \text{ fb}^{-1}$  of  $pp$  collisions at  $\sqrt{s} = 13 \text{ TeV}$  for direct electroweak production of charginos, chargino and next-to-lightest neutralinos and sleptons in events with two or three leptons (electrons or muons), with or without jets and large missing transverse energy. No significant excess above the Standard Model expectations is observed. Limits are set on the chargino mass up to 750 GeV for massless neutralinos in the Tchi1ch1C simplified model exploiting  $2\ell + 0$  jets signatures, see their Figure 8(a).
- 9 AABOUD 18BT searched in  $36.1 \text{ fb}^{-1}$  of  $pp$  collisions at  $\sqrt{s} = 13 \text{ TeV}$  for direct electroweak production of charginos, chargino and next-to-lightest neutralinos and sleptons in events with two or three leptons (electrons or muons), with or without jets, and large missing transverse energy. No significant excess above the Standard Model expectations is observed. Limits are set on the chargino mass up to 1100 GeV for massless neutralinos in the Tchi1n2C simplified model exploiting  $3\ell$  signature, see their Figure 8(c).
- 10 AABOUD 18BT searched in  $36.1 \text{ fb}^{-1}$  of  $pp$  collisions at  $\sqrt{s} = 13 \text{ TeV}$  for direct electroweak production of charginos, chargino and next-to-lightest neutralinos and sleptons in events with two or three leptons (electrons or muons), with or without jets, and large missing transverse energy. No significant excess above the Standard Model expectations is observed. Limits are set on the chargino mass up to 580 GeV for massless neutralinos in the Tchi1n2F simplified model exploiting  $2\ell + 2$  jets and  $3\ell$  signatures, see their Figure 8(d).
- 11 AABOUD 18CK searched for events with at least 3  $b$ -jets and large missing transverse energy in two datasets of  $pp$  collisions at  $\sqrt{s} = 13 \text{ TeV}$  of  $36.1 \text{ fb}^{-1}$  and  $24.3 \text{ fb}^{-1}$  depending on the trigger requirements. The analyses aimed to reconstruct two Higgs bosons decaying to pairs of  $b$ -quarks. No significant excess above the Standard Model expectations is observed. Limits are set on the Higgsino mass in the Tn1n1A simplified model, see their Figure 15(a). Constraints are also presented as a function of the BR of Higgsino decaying into an higgs boson and a gravitino, see their Figure 15(b).
- 12 AABOUD 18CO searched in  $36.1 \text{ fb}^{-1}$  of  $pp$  collisions at  $\sqrt{s} = 13 \text{ TeV}$  for direct electroweak production of mass-degenerate charginos and next-to-lightest neutralinos in events with two or three leptons (electrons or muons), with or without jets, and large missing transverse energy. The search channels are based on recursive jigsaw reconstruction. Limits are set on the chargino mass up to 600 GeV for massless neutralinos in the Tchi1n2F simplified model exploiting the statistical combination of  $2\ell + 2$  jets and  $3\ell$  channels. Chargino masses below 220 GeV are not excluded due to an excess of events above the SM prediction in the dedicated regions. See their Figure 13(d).
- 13 AABOUD 18R searched in  $36.1 \text{ fb}^{-1}$  of  $pp$  collisions at  $\sqrt{s} = 13 \text{ TeV}$  for electroweak production in scenarios with compressed mass spectra in final states with two low-momentum leptons and missing transverse momentum. The data are found to be consistent with the SM prediction. Results are interpreted in Tchi1n2G wino models and  $\tilde{\chi}_1^\pm$  masses are excluded up to 175 GeV for  $m_{\tilde{\chi}_1^\pm} - m_{\tilde{\chi}_1^0} = 10 \text{ GeV}$ . The exclusion limits extend down to mass splittings of 2 GeV, see their Fig. 10 (bottom).
- 14 AABOUD 18R searched in  $36.1 \text{ fb}^{-1}$  of  $pp$  collisions at  $\sqrt{s} = 13 \text{ TeV}$  for electroweak production in scenarios with compressed mass spectra in final states with two low-momentum leptons and missing transverse momentum. The data are found to be consistent with the SM prediction. Results are interpreted in Tchi1n2G higgsino models and  $\tilde{\chi}_1^\pm$  masses are excluded up to 145 GeV for  $m_{\tilde{\chi}_1^\pm} - m_{\tilde{\chi}_1^0} = 5 \text{ GeV}$ . The exclusion limits extend down to mass splittings of 2.5 GeV, see their Fig. 10 (top).
- 15 AABOUD 18U searched in  $36.1 \text{ fb}^{-1}$  of  $pp$  collisions at  $\sqrt{s} = 13 \text{ TeV}$  in events with at least one isolated photon, possibly jets and significant transverse momentum targeting generalised models of gauge-mediated SUSY breaking. No significant excess of events is observed above the SM prediction. Results of the diphoton channel are interpreted in terms of lower limits on the masses of gauginos Tchi1ch1A models, which reach as high as 1.3 TeV. Gaugino masses below 1060 GeV are excluded for any NLSP mass, see their Fig. 10.
- 16 AABOUD 18Z searched in  $36.1 \text{ fb}^{-1}$  of  $pp$  collisions at  $\sqrt{s} = 13 \text{ TeV}$  for events containing four or more charged leptons (electrons, muons and up to two hadronically decaying taus). No significant deviation from the expected SM background is observed. Limits are set on the Higgsino mass in simplified models of general gauge mediated supersymmetry Tn1n1A/Tn1n1B/Tn1n1C, see their Figure 9. Limits are also set on the wino, slepton, sneutrino and gluino mass in a simplified model of NLSP pair production with R-parity violating decays of the LSP via  $\lambda_{12c}$  or  $\lambda_{133}$  to charged leptons, see their Figures 7, 8.
- 17 SIRUNYAN 18AA searched in  $35.9 \text{ fb}^{-1}$  of  $pp$  collisions at  $\sqrt{s} = 13 \text{ TeV}$  for events with at least one photon and large  $E_T$ . No significant excess above the Standard Model expectations is observed. Limits are set on wino masses in a general gauge-mediated SUSY breaking (GGM) scenario with bino-like  $\tilde{\chi}_1^0$  and wino-like  $\tilde{\chi}_1^\pm$  and  $\tilde{\chi}_2^0$ , see Figure 7. Limits are also set on the NLSP mass in the Tchi1n1A and Tchi1ch1A simplified models, see their Figure 8. Finally, limits are set on the gluino mass in the Tglu4A and Tglu4B simplified models, see their Figure 9, and on the squark mass in the Tsq44A and Tsq44B simplified models, see their Figure 10.
- 18 SIRUNYAN 18AJ searched in  $35.9 \text{ fb}^{-1}$  of  $pp$  collisions at  $\sqrt{s} = 13 \text{ TeV}$  for events containing two low-momentum, oppositely charged leptons (electrons or muons) and  $E_T$ . No excess over the expected background is observed. Limits are derived on the wino mass in the Tchi1n2F simplified model, see their Figure 5. Limits are also set on the stop mass in the Tstop10 simplified model, see their Figure 6. Finally, limits are set on the Higgsino mass in the Tchi1n2G simplified model, see Figure 8 and in the pMSSM, see Figure 7.
- 19 SIRUNYAN 18AO searched in  $35.9 \text{ fb}^{-1}$  of  $pp$  collisions at  $\sqrt{s} = 13 \text{ TeV}$  for direct electroweak production of charginos and neutralinos in events with either two or more leptons (electrons or muons) of the same electric charge, or with three or more leptons, which can include up to two hadronically decaying tau leptons. No significant excess above the Standard Model expectations is observed. Limits are set on the chargino/neutralino mass in the Tchi1n2A, Tchi1n2H, Tchi1n2D, Tchi1n2E and Tchi1n2F simplified models, see their Figures 14, 15, 16, 17 and 18. Limits are also set on the higgsino mass in the Tn1n1A, Tn1n1B and Tn1n1C simplified models, see their Figure 19.
- 20 SIRUNYAN 18AP searched in  $35.9 \text{ fb}^{-1}$  of  $pp$  collisions at  $\sqrt{s} = 13 \text{ TeV}$  for direct electroweak production of charginos and neutralinos by combining a number of previous and new searches. No significant excess above the Standard Model expectations is observed. Limits are set on the chargino/neutralino mass in the Tchi1n2E, Tchi1n2F and Tchi1n2I simplified models, see their Figures 7, 8, 9 and 10. Limits are also set on the higgsino mass in the Tn1n1A, Tn1n1B and Tn1n1C simplified models, see their Figure 11, 12, 13 and 14.
- 21 SIRUNYAN 18AR searched in  $35.9 \text{ fb}^{-1}$  of  $pp$  collisions at  $\sqrt{s} = 13 \text{ TeV}$  for events containing two opposite-charge, same-flavour leptons (electrons or muons), jets and  $E_T$ . No significant excess above the Standard Model expectations is observed. Limits are set on the gluino mass in the Tglu4C simplified model, see their Figure 7. Limits are also set on the chargino/neutralino mass in the Tchi1n2F simplified models, see their Figure 8, and on the higgsino mass in the Tn1n1B and Tn1n1C simplified models, see their Figure 9. Finally, limits are set on the sbottom mass in the Tsb0t3 simplified model, see their Figure 10.
- 22 SIRUNYAN 18DN searched in  $35.9 \text{ fb}^{-1}$  of  $pp$  collisions at  $\sqrt{s} = 13 \text{ TeV}$  for direct electroweak production of charginos and for pair production of top squarks in events with two leptons (electrons or muons) of the opposite electric charge. No significant excess above the Standard Model expectations is observed. Limits are set on the chargino mass in the Tchi1ch1C and Tchi1ch1E simplified models, see their Figure 8. Limits are also set on the stop mass in the Tstop1 and Tstop2 simplified models, see their Figure 9.
- 23 SIRUNYAN 18DP searched in  $35.9 \text{ fb}^{-1}$  of  $pp$  collisions at  $\sqrt{s} = 13 \text{ TeV}$  for direct electroweak production of charginos and neutralinos or of chargino pairs in events with a tau lepton pair and significant missing transverse momentum. Both hadronic and leptonic decay modes are considered for the tau lepton. No significant excess above the Standard Model expectations is observed. Limits are set on the chargino mass in the Tchi1ch1D and Tchi1n2 simplified models, see their Figures 14 and 15. Also, excluded stau pair production cross sections are shown in Figures 11, 12, and 13.
- 24 SIRUNYAN 18X searched in  $35.9 \text{ fb}^{-1}$  of  $pp$  collisions at  $\sqrt{s} = 13 \text{ TeV}$  for events with one or more high-momentum Higgs bosons, decaying to pairs of photons, jets and  $E_T$ . The razor variables ( $M_R$  and  $R^2$ ) are used to categorise the events. No significant excess above the Standard Model expectations is observed. Limits are set on the sbottom mass in the Tsb0t4 simplified model and on the wino mass in the Tchi1n2E simplified model, see their Figure 5. Limits are also set on the higgsino mass in the Tn1n1A and Tn1n1B simplified models, see their Figure 6.
- 25 KHACHATRYAN 17L searched in about  $19 \text{ fb}^{-1}$  of  $pp$  collisions at  $\sqrt{s} = 8 \text{ TeV}$  for events with two  $\tau$  (at least one decaying hadronically) and  $E_T$ . In the Tchi1ch1C model, assuming decays via intermediate  $\tilde{\tau}$  or  $\tilde{\nu}_\tau$  with equivalent mass, the observed limits rule out  $\tilde{\chi}_1^\pm$  masses up to 420 GeV for a massless  $\tilde{\chi}_1^0$ . See their Fig.5.
- 26 SIRUNYAN 17AW searched in  $35.9 \text{ fb}^{-1}$  of  $pp$  collisions at  $\sqrt{s} = 13 \text{ TeV}$  for events with a charged lepton (electron or muon), two jets identified as originating from a  $b$ -quark, and large  $E_T$ . No significant excess above the Standard Model expectations is observed. Limits are set on the mass of the chargino and the next-to-lightest neutralino in the Tchi1n2E simplified model, see their Figure 6.
- 27 AAD 16AA summarized and extended ATLAS searches for electroweak supersymmetry in final states containing several charged leptons,  $E_T$ , with or without hadronic jets, in  $20 \text{ fb}^{-1}$  of  $pp$  collisions at  $\sqrt{s} = 8 \text{ TeV}$ . The paper reports the results of new interpretations and statistical combinations of previously published analyses, as well as new analyses. Exclusion limits at 95% C.L. are set on the  $\tilde{\chi}_1^\pm$  mass in the Tchi1ch1B and Tchi1ch1C simplified models. See their Fig. 13.
- 28 AAD 16AA summarized and extended ATLAS searches for electroweak supersymmetry in final states containing several charged leptons,  $E_T$ , with or without hadronic jets, in  $20 \text{ fb}^{-1}$  of  $pp$  collisions at  $\sqrt{s} = 8 \text{ TeV}$ . The paper reports the results of new interpretations and statistical combinations of previously published analyses, as well as new analyses. Exclusion limits at 95% C.L. are set on mass-degenerate  $\tilde{\chi}_1^\pm$  and  $\tilde{\chi}_2^0$  masses in the Tchi1n2B, Tchi1n2C, and Tchi1n2D simplified models. See their Figs. 16, 17, and 18. Interpretations in phenomenological-MSSM, two-parameter Non Universal Higgs Masses (NUHM2), and gauge-mediated symmetry breaking (GMSB) models are also given in their Figs. 20, 21 and 22.
- 29 KHACHATRYAN 16R searched in  $19.7 \text{ fb}^{-1}$  of  $pp$  collisions at  $\sqrt{s} = 8 \text{ TeV}$  for events with one or more photons, one electron or muon, and  $E_T$ . No significant excess above the Standard Model expectations is observed. Limits are set on wino masses in a general gauge-mediated SUSY breaking model (GGM), for a wino-like neutralino NLSP scenario, see Fig. 5. Limits are also set in the Tglu1D and Tchi1n1A simplified models, see Fig. 6. The Tchi1n1A limit is reduced to 340 GeV for a branching ratio reduced by the weak mixing angle.
- 30 AAD 15BA searched in  $20.3 \text{ fb}^{-1}$  of  $pp$  collisions at  $\sqrt{s} = 8 \text{ TeV}$  for electroweak production of charginos and neutralinos decaying to a final state containing a  $W$  boson and a 125 GeV Higgs boson, plus missing transverse momentum. No excess beyond the Standard Model expectation is observed. Exclusion limits are derived in simplified models of direct chargino and next-to-lightest neutralino production, with the decays  $\tilde{\chi}_1^\pm \rightarrow W^\pm \tilde{\chi}_1^0$  and  $\tilde{\chi}_2^0 \rightarrow H \tilde{\chi}_1^0$  having 100% branching fraction, see Fig. 8. A combination of the multiple final states for the Higgs decay yields the best limits (Fig. 8d).
- 31 AAD 15CA searched in  $20.3 \text{ fb}^{-1}$  of  $pp$  collisions at  $\sqrt{s} = 8 \text{ TeV}$  for events with one or more photons and  $E_T$ , with or without leptons ( $e, \mu$ ). No significant excess above the Standard Model expectations is observed. Limits are set on wino masses in the general gauge-mediated SUSY breaking model (GGM), for wino-like NLSP, see Fig. 9, 12.
- 32 AAD 14H searched in  $20.3 \text{ fb}^{-1}$  of  $pp$  collisions at  $\sqrt{s} = 8 \text{ TeV}$  for electroweak production of charginos and neutralinos decaying to a final state with three leptons and missing transverse momentum. No excess beyond the Standard Model expectation is observed.

# Searches Particle Listings

## Supersymmetric Particle Searches

- Exclusion limits are derived in simplified models of direct chargino and next-to-lightest neutralino production, with decays to the lightest neutralino via either all three generations of leptons, staus only, gauge bosons, or Higgs bosons, see Fig. 7. An interpretation in the pMSSM is also given, see Fig. 8.
- 33 AAD 14X searched in 20.3 fb<sup>-1</sup> of  $pp$  collisions at  $\sqrt{s} = 8$  TeV for events with at least four leptons (electrons, muons, taus) in the final state. No significant excess above the Standard Model expectations is observed. Limits are set on the wino-like chargino mass in the R-parity violating simplified model where the decay  $\tilde{\chi}_1^\pm \rightarrow W^{(*)\pm} \tilde{\chi}_1^0$ , with  $\tilde{\chi}_1^0 \rightarrow \ell^\pm \ell^\mp \nu$ , takes place with a branching ratio of 100%, see Fig. 8.
- 34 KHACHATRYAN 14L searched in 19.5 fb<sup>-1</sup> of  $pp$  collisions at  $\sqrt{s} = 8$  TeV for evidence of chargino-neutralino  $\tilde{\chi}_1^\pm \tilde{\chi}_2^0$  pair production with Higgs or  $W$ -bosons in the decay chain, leading to  $HW$  final states with missing transverse energy. The decays of a Higgs boson to a photon pair are considered in conjunction with hadronic and leptonic decay modes of the  $W$  bosons. No significant excesses over the expected SM backgrounds are observed. The results are interpreted in the context of simplified models where the decays  $\tilde{\chi}_2^0 \rightarrow H \tilde{\chi}_1^0$  and  $\tilde{\chi}_1^\pm \rightarrow W^\pm \tilde{\chi}_1^0$  take place 100% of the time, see Figs. 22–23.
- 35 AAD 13 searched in 4.7 fb<sup>-1</sup> of  $pp$  collisions at  $\sqrt{s} = 7$  TeV for charginos and neutralinos decaying to a final state with three leptons ( $e$  and  $\mu$ ) and missing transverse energy. No excess beyond the Standard Model expectation is observed. Exclusion limits are derived in the phenomenological MSSM, see Fig. 2 and 3, and in simplified models, see Fig. 4. For the simplified models with intermediate slepton decays, degenerate  $\tilde{\chi}_1^\pm$  and  $\tilde{\chi}_2^0$  masses up to 500 GeV are excluded at 95% C.L. for very large mass differences with the  $\tilde{\chi}_1^0$ . Supersedes AAD 12As.
- 36 AAD 13B searched in 4.7 fb<sup>-1</sup> of  $pp$  collisions at  $\sqrt{s} = 7$  TeV for gauginos decaying to a final state with two leptons ( $e$  and  $\mu$ ) and missing transverse energy. No excess beyond the Standard Model expectation is observed. Limits are derived in a simplified model of wino-like chargino pair production, where the chargino always decays to the lightest neutralino via an intermediate on-shell charged slepton, see Fig. 2(b). Chargino masses between 110 and 340 GeV are excluded at 95% C.L. for  $m_{\tilde{\chi}_1^0} = 10$  GeV. Exclusion limits are also derived in the phenomenological MSSM, see Fig. 3.
- 37 AAD 12CT searched in 4.7 fb<sup>-1</sup> of  $pp$  collisions at  $\sqrt{s} = 7$  TeV for events containing four or more leptons (electrons or muons) and either moderate values of missing transverse momentum or large effective mass. No significant excess is found in the data. Limits are presented in a simplified model of R-parity violating supersymmetry in which charginos are pair-produced and then decay into a  $W$ -boson and a  $\tilde{\chi}_1^0$ , which in turn decays through an RPV coupling into two charged leptons ( $e^\pm e^\mp$  or  $e^\pm \mu^\mp$ ) and a neutrino. In this model, chargino masses up to 540 GeV are excluded at 95% C.L. for  $m_{\tilde{\chi}_1^0}$  above 300 GeV, see Fig. 3a. The limit deteriorates for lighter  $\tilde{\chi}_1^0$ . Limits are also set in an R-parity violating mSUGRA model, see Fig. 3b.
- 38 CHATRCHYAN 12BJ searched in 4.98 fb<sup>-1</sup> of  $pp$  collisions at  $\sqrt{s} = 7$  TeV for direct electroweak production of charginos and neutralinos in events with at least two leptons, jets and missing transverse momentum. No significant excesses over the expected SM backgrounds are observed and 95% C.L. limits on the production cross section of  $\tilde{\chi}_1^\pm \tilde{\chi}_2^0$  pair production were set in a number of simplified models, see Figs. 7 to 12.
- 39 ABDALLAH 03M uses data from  $\sqrt{s} = 192$ –208 GeV to obtain limits in the framework of the MSSM with gaugino and sfermion mass universality at the GUT scale. An indirect limit on the mass of charginos is derived by constraining the MSSM parameter space by the results from direct searches for neutralinos (including cascade decays), for charginos and for sleptons. These limits are valid for values of  $M_2 < 1$  TeV,  $|\mu| \leq 2$  TeV with the  $\tilde{\chi}_1^0$  as LSP. Constraints from the Higgs search in the  $m_h^{\text{max}}$  scenario assuming  $m_t = 174.3$  GeV are included. The quoted limit applies if there is no mixing in the third family or when  $m_{\tilde{\tau}_1} - m_{\tilde{\chi}_1^0} > 6$  GeV. If mixing is included the limit degrades to 90 GeV. See Fig. 43 for the mass limits as a function of  $\tan\beta$ . These limits update the results of ABREU 00w.
- 40 KHACHATRYAN 16AA searched in 7.4 fb<sup>-1</sup> of  $pp$  collisions at  $\sqrt{s} = 8$  TeV for events with one or more photons, hadronic jets and  $\cancel{E}_T$ . No significant excess above the Standard Model expectations is observed. Limits are set on wino masses in the general gauge-mediated SUSY breaking model (GGM), for a wino-like neutralino NLSP scenario and with the wino mass fixed at 10 GeV above the bino mass, see Fig. 4. Limits are also set in the Tch1ch1A and Tch1n1A simplified models, see Fig. 3.
- 41 KHACHATRYAN 16R searched in 19.7 fb<sup>-1</sup> of  $pp$  collisions at  $\sqrt{s} = 8$  TeV for events with one or more photons, one electron or muon, and  $\cancel{E}_T$ . No significant excess above the Standard Model expectations is observed. Limits are also set in the TgluIF simplified model, see Fig. 6.
- 42 KHACHATRYAN 16Y searched in 19.7 fb<sup>-1</sup> of  $pp$  collisions at  $\sqrt{s} = 8$  TeV for events with one or two soft isolated leptons, hadronic jets, and  $\cancel{E}_T$ . No significant excess above the Standard Model expectations is observed. Limits are set on the  $\tilde{\chi}_1^\pm$  mass (which is degenerate with the  $\tilde{\chi}_2^0$ ) in the Tch1n2A simplified model, see Fig. 4.
- 43 AAD 14AV searched in 20.3 fb<sup>-1</sup> of  $pp$  collisions at  $\sqrt{s} = 8$  TeV for the direct production of charginos, neutralinos and staus in events containing at least two hadronically decaying  $\tau$ -leptons, large missing transverse momentum and low jet activity. The quoted limit was derived for direct  $\tilde{\chi}_1^\pm \tilde{\chi}_2^0$  and  $\tilde{\chi}_1^\pm \tilde{\chi}_1^0$  production with  $\tilde{\chi}_2^0 \rightarrow \tilde{\tau} \tau \rightarrow \tau \tau \tilde{\chi}_1^0$  and  $\tilde{\chi}_1^\pm \rightarrow \tilde{\tau} \nu(\tilde{\nu} \tau) \rightarrow \tau \nu \tilde{\chi}_1^0$ ,  $m_{\tilde{\chi}_1^0} = m_{\tilde{\chi}_1^\pm}$ ,  $m_{\tilde{\tau}} = 0.5(m_{\tilde{\chi}_1^\pm} + m_{\tilde{\chi}_1^0})$ ,  $m_{\tilde{\chi}_1^0} = 0$  GeV. No excess over the expected SM background is observed. Exclusion limits are set in simplified models of  $\tilde{\chi}_1^\pm \tilde{\chi}_1^0$  and  $\tilde{\chi}_1^\pm \tilde{\chi}_2^0$  pair production, see their Figure 7. Upper limits on the cross section and signal strength for direct di-stau production are derived, see Figures 8 and 9. Also, limits are derived in a pMSSM model where the only light slepton is the  $\tilde{\tau}_R$ , see Figure 10.
- 44 AAD 14AV searched in 20.3 fb<sup>-1</sup> of  $pp$  collisions at  $\sqrt{s} = 8$  TeV for the direct production of charginos, neutralinos and staus in events containing at least two hadronically decaying  $\tau$ -leptons, large missing transverse momentum and low jet activity. The quoted limit was derived for direct  $\tilde{\chi}_1^\pm \tilde{\chi}_1^0$  production with  $\tilde{\chi}_1^0 \rightarrow \tilde{\tau} \nu(\tilde{\nu} \tau) \rightarrow \tau \nu \tilde{\chi}_1^0$ ,  $m_{\tilde{\tau}} = 0.5(m_{\tilde{\chi}_1^\pm} + m_{\tilde{\chi}_1^0})$ ,  $m_{\tilde{\chi}_1^0} = 0$  GeV. No excess over the expected SM background is observed. Exclusion limits are set in simplified models of  $\tilde{\chi}_1^\pm \tilde{\chi}_1^0$  and  $\tilde{\chi}_1^\pm \tilde{\chi}_2^0$  pair production, see their Figure 7. Upper limits on the cross section and signal strength for direct di-stau production are derived, see Figures 8 and 9. Also, limits are derived in a pMSSM model where the only light slepton is the  $\tilde{\tau}_R$ , see Figure 10.
- 45 AAD 14G searched in 20.3 fb<sup>-1</sup> of  $pp$  collisions at  $\sqrt{s} = 8$  TeV for electroweak production of chargino pairs, or chargino-neutralino pairs, decaying to a final state with two leptons ( $e$  and  $\mu$ ) and missing transverse momentum. No excess beyond the Standard Model expectation is observed. Exclusion limits are derived in simplified models of chargino pair production, with chargino decays to the lightest neutralino via either sleptons or gauge bosons, see Fig 5; or in simplified models of chargino and next-to-lightest neutralino production, with decays to the lightest neutralino via gauge bosons, see Fig. 7. An interpretation in the pMSSM is also given, see Fig. 10.
- 46 AALTONEN 14 searched in 5.8 fb<sup>-1</sup> of  $p\bar{p}$  collisions at  $\sqrt{s} = 1.96$  TeV for evidence of chargino and next-to-lightest neutralino associated production in final states consisting of three leptons (electrons, muons or taus) and large missing transverse momentum. The results are consistent with the Standard Model predictions within 1.85  $\sigma$ . Limits on the chargino mass are derived in an mSUGRA model with  $m_0 = 60$  GeV,  $\tan\beta = 3$ ,  $A_0 = 0$  and  $\mu > 0$ , see their Fig. 2.
- 47 KHACHATRYAN 14I searched in 19.5 fb<sup>-1</sup> of  $pp$  collisions at  $\sqrt{s} = 8$  TeV for electroweak production of chargino pairs decaying to a final state with opposite-sign lepton pairs ( $e$  or  $\mu$ ) and missing transverse momentum. No excess beyond the Standard Model expectation is observed. Exclusion limits are derived in simplified models, see Fig. 18.
- 48 AALTONEN 13Q searched in 6.0 fb<sup>-1</sup> of  $p\bar{p}$  collisions at  $\sqrt{s} = 1.96$  TeV for evidence of chargino-neutralino associated production in like-sign dilepton final states. One lepton is identified as the hadronic decay of a tau lepton, while the other is an electron or muon. Good agreement with the Standard Model predictions is observed and limits are set on the chargino-neutralino cross section for simplified gravity- and gauge-mediated models, see their Figs. 2 and 3.
- 49 AAD 12As searched in 2.06 fb<sup>-1</sup> of  $pp$  collisions at  $\sqrt{s} = 7$  TeV for charginos and neutralinos decaying to a final state with three leptons ( $e$  and  $\mu$ ) and missing transverse energy. No excess beyond the Standard Model expectation is observed. Exclusion limits are derived in the phenomenological MSSM, see Fig. 2 (top), and in simplified models, see Fig. 2 (bottom).
- 50 AAD 12T looked in 1 fb<sup>-1</sup> of  $pp$  collisions at  $\sqrt{s} = 7$  TeV for the production of supersymmetric particles decaying into final states with missing transverse momentum and exactly two isolated leptons ( $e$  or  $\mu$ ). Opposite-sign and same-sign dilepton events were separately studied. Additionally, in opposite-sign events, a search was made for an excess of same-flavor over different-flavor lepton pairs. No excess over the expected background is observed and limits are placed on the effective production cross section of opposite-sign dilepton events with  $\cancel{E}_T > 250$  GeV and on same-sign dilepton events with  $\cancel{E}_T > 100$  GeV. The latter limit is interpreted in a simplified electroweak gaugino production model as a lower chargino mass limit.
- 51 CHATRCHYAN 11B looked in 35 pb<sup>-1</sup> of  $pp$  collisions at  $\sqrt{s} = 7$  TeV for events with an isolated lepton ( $e$  or  $\mu$ ), a photon and  $\cancel{E}_T$  which may arise in a generalized gauge mediated model from the decay of Wino-like NLSPs. No evidence for an excess over the expected background is observed. Limits are derived in the plane of squark/gluino mass versus Wino mass (see Fig. 4). Mass degeneracy of the produced squarks and gluinos is assumed.
- 52 CHATRCHYAN 11V looked in 35 pb<sup>-1</sup> of  $pp$  collisions at  $\sqrt{s} = 7$  TeV for events with  $\geq 3$  isolated leptons ( $e$ ,  $\mu$  or  $\tau$ ), with or without jets and  $\cancel{E}_T$ . No evidence for an excess over the expected background is observed. Limits are derived in the CMSSM ( $m_0, m_{1/2}$ ) plane for  $\tan\beta = 3$  (see Fig. 5).

### Long-lived $\tilde{\chi}^\pm$ (Chargino) mass limit

Limits on charginos which leave the detector before decaying.

VALUE (GeV)	CL%	DOCUMENT ID	TECN	COMMENT
>1090	95	1 AABOUD	19AT ATLS	long-lived $\tilde{\chi}_1^\pm$ mAMSB
> 460	95	2 AABOUD	18AS ATLS	$\tilde{\chi}^\pm \rightarrow \tilde{\chi}_1^0 \pi^\pm$ , lifetime 0.2 ns, $m_{\tilde{\chi}^\pm} - m_{\tilde{\chi}_1^0} = 160$ MeV
> 715	95	3 SIRUNYAN	18BR CMS	$\tilde{\chi}^\pm \rightarrow \tilde{\chi}_1^0 \pi^\pm$ , AMSB, $\tan\beta = 5$ and $\mu > 0$ , $\tau = 3$ ns
> 695	95	3 SIRUNYAN	18BR CMS	$\tilde{\chi}^\pm \rightarrow \tilde{\chi}_1^0 \pi^\pm$ , AMSB, $\tan\beta = 5$ and $\mu > 0$ , $\tau = 7$ ns
> 505	95	3 SIRUNYAN	18BR CMS	$\tilde{\chi}^\pm \rightarrow \tilde{\chi}_1^0 \pi^\pm$ , AMSB, $\tan\beta = 5$ , $\mu > 0$ , 0.5 ns $> \tau > 60$ ns
> 620	95	4 AAD	15AE ATLS	stable $\tilde{\chi}^\pm$
> 534	95	5 AAD	15BMATLS	stable $\tilde{\chi}^\pm$
> 239	95	5 AAD	15BMATLS	$\tilde{\chi}^\pm \rightarrow \tilde{\chi}_1^0 \pi^\pm$ , lifetime 1 ns, $m_{\tilde{\chi}^\pm} - m_{\tilde{\chi}_1^0} = 0.14$ GeV
> 482	95	5 AAD	15BMATLS	$\tilde{\chi}^\pm \rightarrow \tilde{\chi}_1^0 \pi^\pm$ , lifetime 15 ns, $m_{\tilde{\chi}^\pm} - m_{\tilde{\chi}_1^0} = 0.14$ GeV
> 103	95	6 AAD	13H ATLS	long-lived $\tilde{\chi}^\pm \rightarrow \tilde{\chi}_1^0 \pi^\pm$ , mAMSB, $\Delta m_{\tilde{\chi}_1^0} = 160$ MeV
> 92	95	7 AAD	12BJ ATLS	long-lived $\tilde{\chi}^\pm \rightarrow \pi^\pm \tilde{\chi}_1^0$ , mAMSB
> 171	95	8 ABAZOV	09M D0	$\tilde{H}$
> 102	95	9 ABBIENDI	03L OPAL	$m_{\tilde{H}^\pm} > 500$ GeV
none 2–93.0	95	10 ABREU	00T DLPH	$\tilde{H}^\pm$ or $m_{\tilde{H}^\pm} > m_{\tilde{\chi}^\pm}$
• • • We do not use the following data for averages, fits, limits, etc. • • •				
> 260	95	11 KHACHATRY...15AB	CMS	$\tilde{\chi}_1^\pm \rightarrow \tilde{\chi}_1^0 \pi^\pm, \tau_{\tilde{\chi}_1^\pm} = 0.2$ ns, AMSB
> 800	95	12 KHACHATRY...15A0	CMS	long-lived $\tilde{\chi}_1^\pm$ , mAMSB, $\tau > 100$ ns
> 100	95	12 KHACHATRY...15A0	CMS	long-lived $\tilde{\chi}_1^\pm$ , mAMSB, $\tau > 3$ ns
> 100	95	13 KHACHATRY...15W	CMS	long-lived $\tilde{\chi}^0, \tilde{q} \rightarrow q \tilde{\chi}^0, \tilde{\chi}^0 \rightarrow \ell^\pm \ell^\mp \nu$ , RPV
> 270	95	14 AAD	13BD ATLS	disappearing-track signature, AMSB
> 278	95	15 ABAZOV	13B D0	long-lived $\tilde{\chi}^\pm$ , gaugino-like
> 244	95	15 ABAZOV	13B D0	long-lived $\tilde{\chi}^\pm$ , higgsino-like

- <sup>1</sup> AABOUD 19AT searched in  $36.1 \text{ fb}^{-1}$  of  $pp$  collisions at  $\sqrt{s} = 13 \text{ TeV}$  for metastable  $R$ -hadrons. Multiple search strategies for a wide range of lifetimes, corresponding to path lengths of a few meters, are defined. No significant deviations from the expected Standard Model background are observed. Results are interpreted in terms of direct electroweak production of long-lived charginos in the context of mAMSB scenarios. Chargino masses are excluded at 95% C.L. below 1090 GeV. See their Figure 10 (right).
- <sup>2</sup> AABOUD 18AS searched in  $36.1 \text{ fb}^{-1}$  of  $pp$  collisions at  $\sqrt{s} = 13 \text{ TeV}$  for direct electroweak production of long-lived charginos in the context of AMSB or phenomenological MSSM scenarios with wino-like LSP. Events with a disappearing track due to a low-momentum pion accompanied by at least one jet with high transverse momentum from initial-state radiation are considered. No significant excess above the Standard Model expectations is observed. Exclusion limits are set at 95% confidence level on the mass of charginos for different chargino lifetimes. For a pure wino with a lifetime of about 0.2 ns, corresponding to a mass-splitting between the charged and neutral wino of around 160 MeV, chargino masses up to 460 GeV are excluded, see their Fig. 8.
- <sup>3</sup> SIRUNYAN 18BR searched in  $38.4 \text{ fb}^{-1}$  of  $pp$  collisions at  $\sqrt{s} = 13 \text{ TeV}$  for direct electroweak production of long-lived charginos in events containing isolated tracks with missing hits in the outer layer of the silicon tracker and little or no associated calorimetric energy deposits (disappearing tracks). No significant excess above the Standard Model expectations is observed. In an AMSB context, limits are set on the cross section of direct chargino production through  $pp \rightarrow \tilde{\chi}^{\pm} \tilde{\chi}^{\mp}$  and  $pp \rightarrow \tilde{\chi}^{\pm} \tilde{\chi}_1^0$ , assuming  $\text{BR}(\tilde{\chi}^{\pm} \rightarrow \tilde{\chi}_1^0 \pi^{\pm}) = 100\%$ , as a function of the chargino mass and mean proper lifetime, see Figures 3, 4 and 5.
- <sup>4</sup> AAD 15AE searched in  $19.1 \text{ fb}^{-1}$  of  $pp$  collisions at  $\sqrt{s} = 8 \text{ TeV}$  for heavy long-lived charged particles, measured through their specific ionization energy loss in the ATLAS pixel detector or their time-of-flight in the ALTAS muon system. In the absence of an excess of events above the expected backgrounds, limits are set on stable charginos, see Fig. 10.
- <sup>5</sup> AAD 15BM searched in  $18.4 \text{ fb}^{-1}$  of  $pp$  collisions at  $\sqrt{s} = 8 \text{ TeV}$  for stable and metastable non-relativistic charged particles through their anomalous specific ionization energy loss in the ATLAS pixel detector. In absence of an excess of events above the expected backgrounds, limits are set on stable charginos (see Table 5) and on metastable charginos decaying to  $\tilde{\chi}_1^0 \pi^{\pm}$ , see Fig. 11.
- <sup>6</sup> AAD 13H searched in  $4.7 \text{ fb}^{-1}$  of  $pp$  collisions at  $\sqrt{s} = 7 \text{ TeV}$  for direct electroweak production of long-lived charginos in the context of AMSB scenarios. The search is based on the signature of a high-momentum isolated track with few associated hits in the outer part of the tracking system, arising from a chargino decay into a neutralino and a low-momentum pion. The  $p_T$  spectrum of the tracks was found to be consistent with the SM expectations. Constraints on the lifetime and the production cross section were obtained, see Fig. 6. In the minimal AMSB framework with  $\tan\beta = 5$ , and  $\mu > 0$ , a chargino having a mass below 103 (85) GeV for a chargino-neutralino mass splitting  $\Delta m_{\tilde{\chi}_1^{\pm}} = 160$  (170) MeV is excluded at the 95% C.L. See Fig. 7 for more precise bounds.
- <sup>7</sup> AAD 12BJ looked in  $1.02 \text{ fb}^{-1}$  of  $pp$  collisions at  $\sqrt{s} = 7 \text{ TeV}$  for signatures of decaying charginos resulting in isolated tracks with few associated hits in the outer region of the tracking system. The  $p_T$  spectrum of the tracks was found to be consistent with the SM expectations. Constraints on the lifetime and the production cross section were obtained. In the minimal AMSB framework with  $m_{3/2} < 32 \text{ TeV}$ ,  $m_0 < 1.5 \text{ TeV}$ ,  $\tan\beta = 5$ , and  $\mu > 0$ , a chargino having a mass below 92 GeV and a lifetime between 0.5 ns and 2 ns is excluded at the 95% C.L. See their Fig. 8 for more precise bounds.
- <sup>8</sup> ABAZOV 09M searched in  $1.1 \text{ fb}^{-1}$  of  $p\bar{p}$  collisions at  $\sqrt{s} = 1.96 \text{ TeV}$  for events with direct production of a pair of charged massive stable particles identified by their TOF. The number of the observed events is consistent with the predicted background. The data are used to constrain the production cross section as a function of the  $\tilde{\chi}_1^{\pm}$  mass, see their Fig. 2. The quoted limit improves to 206 GeV for gaugino-like charginos.
- <sup>9</sup> ABBIENDI 03L used  $e^+e^-$  data at  $\sqrt{s} = 130\text{--}209 \text{ GeV}$  to select events with two high momentum tracks with anomalous  $dE/dx$ . The excluded cross section is compared to the theoretical expectation as a function of the heavy particle mass in their Fig. 3. The bounds are valid for colorless fermions with lifetime longer than  $10^{-6} \text{ s}$ . Supersedes the results from ACKERSTAFF 98P.
- <sup>10</sup> ABREU 00T searches for the production of heavy stable charged particles, identified by their ionization or Cherenkov radiation, using data from  $\sqrt{s} = 130$  to 189 GeV. These limits include and update the results of ABREU 98P.
- <sup>11</sup> KHACHATRYAN 15AB searched in  $19.5 \text{ fb}^{-1}$  of  $pp$  collisions at  $\sqrt{s} = 8 \text{ TeV}$  for events containing tracks with little or no associated calorimeter energy deposits and with missing hits in the outer layers of the tracking system (disappearing-track signature). Such disappearing tracks can result from the decay of charginos that are nearly mass degenerate with the lightest neutralino. The number of observed events is in agreement with the background expectation. Limits are set on the cross section of electroweak chargino production in terms of the chargino mass and mean proper lifetime, see Fig. 4. In the minimal AMSB model, a chargino mass below 260 GeV is excluded at 95% C.L., see their Fig. 5.
- <sup>12</sup> KHACHATRYAN 15O searched in  $18.8 \text{ fb}^{-1}$  of  $pp$  collisions at  $\sqrt{s} = 8 \text{ TeV}$  for evidence of long-lived charginos in the context of AMSB and pMSSM scenarios. The results are based on a previously published search for heavy stable charged particles at 7 and 8 TeV. In the minimal AMSB framework with  $\tan\beta = 5$  and  $\mu \geq 0$ , constraints on the chargino mass and lifetime were placed, see Fig. 5. Charginos with a mass below 800 (100) GeV are excluded at the 95% C.L. for lifetimes above 100 ns (3 ns). Constraints are also placed on the pMSSM parameter space, see Fig. 3.
- <sup>13</sup> KHACHATRYAN 15W searched in up to  $20.5 \text{ fb}^{-1}$  of  $pp$  collisions at  $\sqrt{s} = 8 \text{ TeV}$  for evidence of long-lived neutralinos produced through  $\tilde{q}\text{-pair}$  production, with  $\tilde{q} \rightarrow q\tilde{\chi}^0$  and  $\tilde{\chi}^0 \rightarrow \ell^+ \ell^- \nu$  (RPV:  $\lambda_{121}, \lambda_{122} \neq 0$ ). 95% C.L. exclusion limits on cross section times branching ratio are set as a function of mean proper decay length of the neutralino, see Figs. 6 and 9.
- <sup>14</sup> AAD 13BD searched in  $20.3 \text{ fb}^{-1}$  of  $pp$  collisions at  $\sqrt{s} = 8 \text{ TeV}$  for events containing tracks with no associated hits in the outer region of the tracking system resulting from the decay of charginos that are nearly mass degenerate with the lightest neutralino, as is often the case in AMSB scenarios. No significant excess above the background expectation is observed for candidate tracks with large transverse momentum. Constraints on chargino properties are obtained and in the minimal AMSB model, a chargino mass below 270 GeV is excluded at 95% C.L., see their Fig. 7.
- <sup>15</sup> ABAZOV 13b looked in  $6.3 \text{ fb}^{-1}$  of  $p\bar{p}$  collisions at  $\sqrt{s} = 1.96 \text{ TeV}$  for charged massive long-lived particles in events with muon-like particles that have both speed and ionization energy loss inconsistent with muons produced in beam collisions. In the absence of an excess, limits are set at 95% C.L. on gaugino- and higgsino-like charginos, see their Table 20 and Fig. 23.

 **$\tilde{\nu}$  (Sneutrino) mass limit**

The limits may depend on the number,  $N(\tilde{\nu})$ , of sneutrinos assumed to be degenerate in mass. Only  $\tilde{\nu}_L$  (not  $\tilde{\nu}_R$ ) is assumed to exist. It is possible that  $\tilde{\nu}$  could be the lightest supersymmetric particle (LSP).

We report here, but do not include in the Listings, the limits obtained from the fit of the final results obtained by the LEP Collaborations on the invisible width of the Z boson ( $\Delta\Gamma_{\text{inv.}} < 2.0 \text{ MeV}$ , LEP-SLC 06):  $m_{\tilde{\nu}} > 43.7 \text{ GeV}$  ( $N(\tilde{\nu})=1$ ) and  $m_{\tilde{\nu}} > 44.7 \text{ GeV}$  ( $N(\tilde{\nu})=3$ ).

Some earlier papers are now obsolete and have been omitted. They were last listed in our PDG 14 edition: K. Olive, et al. (Particle Data Group), Chinese Physics **C38** 070001 (2014) (<http://pdg.lbl.gov>).

VALUE (GeV)	CL%	DOCUMENT ID	TECN	COMMENT
<b>&gt;3400</b>	95	<sup>1</sup> AABOUD	18CM ATLS	RPV, $\tilde{\nu}_\tau \rightarrow e\mu$ , $\lambda_{312} = \lambda_{321} = 0.07$ , $\lambda'_{311} = 0.11$
>2900	95	<sup>2</sup> AABOUD	18CM ATLS	RPV, $\tilde{\nu}_\tau \rightarrow e\tau$ , $\lambda_{313} = \lambda_{331} = 0.07$ , $\lambda'_{311} = 0.11$
>2600	95	<sup>3</sup> AABOUD	18CM ATLS	RPV, $\tilde{\nu}_\tau \rightarrow \mu\tau$ , $\lambda_{323} = \lambda_{332} = 0.07$ , $\lambda'_{311} = 0.11$
>1060	95	<sup>4</sup> AABOUD	18Z ATLS	RPV, $\geq 4\ell$ , $\lambda_{12k} \neq 0$ , $m_{\tilde{\chi}_1^0} = 600 \text{ GeV}$ (mass-degenerate left-handed sleptons and sneutrinos of all 3 generations)
> 780	95	<sup>4</sup> AABOUD	18Z ATLS	RPV, $\geq 4\ell$ , $\lambda_{133} \neq 0$ , $m_{\tilde{\chi}_1^0} = 300 \text{ GeV}$ (mass-degenerate left-handed sleptons and sneutrinos of all 3 generations)
>1700	95	<sup>5</sup> SIRUNYAN	18AT CMS	RPV, $\tilde{\nu}_\tau \rightarrow e\mu$ , $\lambda_{132} = \lambda_{231} = \lambda'_{311} = 0.01$
>3800	95	<sup>5</sup> SIRUNYAN	18AT CMS	RPV, $\tilde{\nu}_\tau \rightarrow e\mu$ , $\lambda_{132} = \lambda_{231} = \lambda'_{311} = 0.1$
>2300	95	<sup>6</sup> AABOUD	16P ATLS	RPV, $\tilde{\nu}_\tau \rightarrow e\mu$ , $\lambda'_{311} = 0.11$
>2200	95	<sup>6</sup> AABOUD	16P ATLS	RPV, $\tilde{\nu}_\tau \rightarrow e\tau$ , $\lambda_{311} = 0.11$
>1900	95	<sup>6</sup> AABOUD	16P ATLS	RPV, $\tilde{\nu}_\tau \rightarrow \mu\tau$ , $\lambda'_{311} = 0.11$
> 400	95	<sup>7</sup> AAD	14X ATLS	RPV, $\geq 4\ell^{\pm}$ , $\tilde{\nu} \rightarrow \nu\tilde{\chi}_1^0$ , $\tilde{\chi}_1^0 \rightarrow \ell^{\pm} \ell^{\mp} \nu$
> 94	95	<sup>8</sup> AAD	11Z ATLS	RPV, $\tilde{\nu}_\tau \rightarrow e\mu$
> 84	95	<sup>9</sup> ABDALLAH	03M DLPH	$1 \leq \tan\beta \leq 40$ , $m_{\tilde{e}_R} - m_{\tilde{\chi}_1^0} > 10 \text{ GeV}$
> 41	95	<sup>10</sup> HEISTER	02N ALEP	$\tilde{\nu}_e$ , any $\Delta m$
		<sup>11</sup> DECAMP	92 ALEP	$\Gamma(Z \rightarrow \text{invisible})$ ; $N(\tilde{\nu})=3$ , model independent
• • • We do not use the following data for averages, fits, limits, etc. • • •				
>1280	95	<sup>12</sup> SIRUNYAN	19A0	RPV, $\mu^{\pm} \mu^{\pm} + \geq 2\text{jets}$ , $\lambda'_{211} \neq 0$ , $\tilde{\nu}_\mu \rightarrow \mu\tilde{\chi}_1^{\pm}$ , $\tilde{\chi}_1^{\pm} \rightarrow \mu q \bar{q} q \bar{q}$
>2300	95	<sup>13</sup> KHACHATRY...16BE	CMS	RPV, $\tilde{\nu}_\tau \rightarrow e\mu$ , $\lambda_{132} = \lambda_{231} = \lambda_{311} = 0.01$
>2000	95	<sup>13</sup> KHACHATRY...16BE	CMS	RPV, $\tilde{\nu}_\tau \rightarrow e\mu$ , $\lambda_{132} = \lambda_{231} = 0.07$ , $\lambda'_{311} = 0.11$
>1700	95	<sup>14</sup> AAD	15O ATLS	RPV ( $e\mu$ ), $\tilde{\nu}_\tau$ , $\lambda'_{311} = 0.11$ , $\lambda_{i3k} = 0.07$
		<sup>14</sup> AAD	15O ATLS	RPV ( $\tau\mu$ , $e\tau$ ), $\tilde{\nu}_\tau$ , $\lambda'_{311} = 0.11$ , $\lambda_{i3k} = 0.07$
> 95	95	<sup>15</sup> AAD	13A1 ATLS	RPV, $\tilde{\nu}_\tau \rightarrow e\mu$ , $e\tau$ , $\mu\tau$
> 37.1	95	<sup>16</sup> AAD	11H ATLS	RPV, $\tilde{\nu}_\tau \rightarrow e\mu$
> 36	95	<sup>17</sup> AALTONEN	10Z CDF	RPV, $\tilde{\nu}_\tau \rightarrow e\mu$ , $e\tau$ , $\mu\tau$
> 31.2	95	<sup>18</sup> ABAZOV	10M D0	RPV, $\tilde{\nu}_\tau \rightarrow e\mu$
		<sup>19</sup> ABDALLAH	04H DLPH	AMSB, $\mu > 0$
		<sup>20</sup> ADRIANI	93M L3	$\Gamma(Z \rightarrow \text{invisible})$ ; $N(\tilde{\nu})=1$
		<sup>21</sup> ABREU	91F DLPH	$\Gamma(Z \rightarrow \text{invisible})$ ; $N(\tilde{\nu})=1$
		<sup>21</sup> ALEXANDER	91F OPAL	$\Gamma(Z \rightarrow \text{invisible})$ ; $N(\tilde{\nu})=1$

<sup>1</sup> AABOUD 18CM searched in  $36.1 \text{ fb}^{-1}$  of  $pp$  collisions at  $\sqrt{s} = 13 \text{ TeV}$  for heavy particles decaying into an  $e\mu$ ,  $e\tau$ ,  $\mu\tau$  final state. No significant deviation from the expected SM background is observed. Limits are set on the mass of a stau neutrino with R-parity-violating couplings. For  $\tilde{\nu}_\tau \rightarrow e\mu$ , masses below 3.4 TeV are excluded at 95% CL, see their Figure 4(b). Upper limits on the RPV couplings  $|\lambda_{312}|$  versus  $|\lambda'_{311}|$  are also performed, see their Figure 8(a-b).

<sup>2</sup> AABOUD 18CM searched in  $36.1 \text{ fb}^{-1}$  of  $pp$  collisions at  $\sqrt{s} = 13 \text{ TeV}$  for heavy particles decaying into an  $e\mu$ ,  $e\tau$ ,  $\mu\tau$  final state. No significant deviation from the expected SM background is observed. Limits are set on the mass of a stau neutrino with R-parity-violating couplings. For  $\tilde{\nu}_\tau \rightarrow e\tau$ , masses below 2.9 TeV are excluded at 95% CL, see their Figure 5(b). Upper limits on the RPV couplings  $|\lambda_{313}|$  versus  $|\lambda'_{311}|$  are also performed, see their Figure 8(c).

<sup>3</sup> AABOUD 18CM searched in  $36.1 \text{ fb}^{-1}$  of  $pp$  collisions at  $\sqrt{s} = 13 \text{ TeV}$  for heavy particles decaying into an  $e\mu$ ,  $e\tau$ ,  $\mu\tau$  final state. No significant deviation from the expected SM background is observed. Limits are set on the mass of a stau neutrino with R-parity-violating couplings. For  $\tilde{\nu}_\tau \rightarrow \mu\tau$ , masses below 2.6 TeV are excluded at 95% CL, see their Figure 6(b). Upper limits on the RPV couplings  $|\lambda_{323}|$  versus  $|\lambda'_{311}|$  are also performed, see their Figure 8(d).



# Searches Particle Listings

## Supersymmetric Particle Searches

- 4 AABOUD 18z searched in  $36.1 \text{ fb}^{-1}$  of  $pp$  collisions at  $\sqrt{s} = 13 \text{ TeV}$  for events containing four or more charged leptons (electrons, muons and up to two hadronically decaying taus). No significant deviation from the expected SM background is observed. Limits are set on the Higgsino mass in simplified models of general gauge mediated supersymmetry  $\text{Tn1n1A/Tn1n1B/Tn1n1C}$ , see their Figure 9. Limits are also set on the wino, slepton, sneutrino and gluino mass in a simplified model of NLSP pair production with R-parity violating decays of the LSP via  $\lambda_{12k}$  or  $\lambda_{133}$  to charged leptons, see their Figures 7, 8.
- 5 SIRUNYAN 18AT searched in  $35.9 \text{ fb}^{-1}$  of  $pp$  collisions at  $\sqrt{s} = 13 \text{ TeV}$  for heavy resonances decaying into  $e\mu$  final states. No significant excess above the Standard Model expectation is observed and 95% C.L. exclusions are placed on the cross section times branching ratio for the R-parity-violating production and decay of a supersymmetric tau sneutrino, see their Fig. 3.
- 6 AABOUD 16P searched in  $3.2 \text{ fb}^{-1}$  of  $pp$  collisions at  $\sqrt{s} = 13 \text{ TeV}$  for events with different flavour dilepton pairs ( $e\mu, e\tau, \mu\tau$ ) from the production of  $\tilde{\nu}_\tau$  via an RPV  $\lambda'_{311}$  coupling and followed by a decay via  $\lambda_{312} = \lambda_{321} = 0.07$  for  $e + \mu$ , via  $\lambda_{313} = \lambda_{331} = 0.07$  for  $e + \tau$  and via  $\lambda_{323} = \lambda_{332} = 0.07$  for  $\mu + \tau$ . No evidence for a dilepton resonance over the SM expectation is observed, and limits are derived on  $m_{\tilde{\nu}_\tau}$  at 95% CL, see their Figs. 2(b), 3(b), 4(b), and Table 3.
- 7 AAD 14x searched in  $20.3 \text{ fb}^{-1}$  of  $pp$  collisions at  $\sqrt{s} = 8 \text{ TeV}$  for events with at least four leptons (electrons, muons, taus) in the final state. No significant excess above the Standard Model expectations is observed. Limits are set on the sneutrino mass in an R-parity violating simplified model where the decay  $\tilde{\nu}_\tau \rightarrow \nu \tilde{\chi}_1^0$ , with  $\tilde{\chi}_1^0 \rightarrow \ell^\pm \ell^\mp \nu$ , takes place with a branching ratio of 100%, see Fig. 9.
- 8 AAD 11z looked in  $1.07 \text{ fb}^{-1}$  of  $pp$  collisions at  $\sqrt{s} = 7 \text{ TeV}$  for events with one electron and one muon of opposite charge from the production of  $\tilde{\nu}_\tau$  via an RPV  $\lambda'_{311}$  coupling and followed by a decay via  $\lambda_{312}$  into  $e + \mu$ . No evidence for an  $(e, \mu)$  resonance over the SM expectation is observed, and a limit is derived in the plane of  $\lambda'_{311}$  versus  $m_{\tilde{\nu}_\tau}$  for three values of  $\lambda_{312}$ , see their Fig. 2. Masses  $m_{\tilde{\nu}_\tau} < 1.32 (1.45) \text{ TeV}$  are excluded for  $\lambda'_{311} = 0.10$  and  $\lambda_{312} = 0.05 (\lambda'_{311} = 0.11$  and  $\lambda_{312} = 0.07)$ .
- 9 ABDALLAH 03M uses data from  $\sqrt{s} = 192\text{--}208 \text{ GeV}$  to obtain limits in the framework of the MSSM with gaugino and sfermion mass universality at the GUT scale. An indirect limit on the mass is derived by constraining the MSSM parameter space by the results from direct searches for neutralinos (including cascade decays) and for sleptons. These limits are valid for values of  $M_2 < 1 \text{ TeV}$ ,  $|\mu| \leq 1 \text{ TeV}$  with the  $\tilde{\chi}_1^0$  as LSP. The quoted limit is obtained when there is no mixing in the third family. See Fig. 43 for the mass limits as a function of  $\tan\beta$ . These limits update the results of ABREU 00w.
- 10 HEISTER 02N derives a bound on  $m_{\tilde{\nu}_e}$  by exploiting the mass relation between the  $\tilde{\nu}_e$  and  $\tilde{e}$ , based on the assumption of universal GUT scale gaugino and scalar masses  $m_{1/2}$  and  $m_0$  and the search described in the  $\tilde{e}$  section. In the MSUGRA framework with radiative electroweak symmetry breaking, the limit improves to  $m_{\tilde{\nu}_e} > 130 \text{ GeV}$ , assuming a trilinear coupling  $A_0=0$  at the GUT scale. See Figs. 5 and 7 for the dependence of the limits on  $\tan\beta$ .
- 11 DECAMP 2J limit is from  $\Gamma(\text{invisible})/\Gamma(\ell\ell) = 5.91 \pm 0.15$  ( $N_p = 2.97 \pm 0.07$ ).
- 12 SIRUNYAN 19A0 searched in  $35.9 \text{ fb}^{-1}$  of  $pp$  collisions at  $\sqrt{s} = 13 \text{ TeV}$  for events containing two same-sign muons and at last two jets, originating from resonant production of second-generation sleptons ( $\tilde{\mu}_L, \tilde{\nu}_\mu$ ) via the R-parity violating coupling  $\lambda_{211}$  to quarks. No significant excess above the Standard Model expectations is observed. Upper limits on cross sections are derived in the context of two simplified models, see their Figure 4. The cross section limits are translated into limits on  $\lambda'_{211}$  for a modified CMSSM, see their Figure 5.
- 13 KHACHATRYAN 16BE searched in  $19.7 \text{ fb}^{-1}$  of  $pp$  collisions at  $\sqrt{s} = 8 \text{ TeV}$  for evidence of narrow resonances decaying into  $e\mu$  final states. No significant excess above the Standard Model expectation is observed and 95% C.L. exclusions are placed on the cross section times branching ratio for the production of an R-parity-violating supersymmetric tau sneutrino, see their Fig. 3.
- 14 AAD 15o searched in  $20.3 \text{ fb}^{-1}$  of  $pp$  collisions at  $\sqrt{s} = 8 \text{ TeV}$  for evidence of heavy particles decaying into  $e\mu, e\tau$  or  $\mu\tau$  final states. No significant excess above the Standard Model expectation is observed, and 95% C.L. exclusions are placed on the cross section times branching ratio for the production of an R-parity-violating supersymmetric tau sneutrino, applicable to any sneutrino flavour, see their Fig. 2.
- 15 AAD 13Al searched in  $4.6 \text{ fb}^{-1}$  of  $pp$  collisions at  $\sqrt{s} = 7 \text{ TeV}$  for evidence of heavy particles decaying into  $e\mu, e\tau$  or  $\mu\tau$  final states. No significant excess above the Standard Model expectation is observed, and 95% C.L. exclusions are placed on the cross section times branching ratio for the production of an R-parity-violating supersymmetric tau sneutrino, see their Fig. 2. For couplings  $\lambda'_{311} = 0.10$  and  $\lambda_{33k} = 0.05$ , the lower limits on the  $\tilde{\nu}_\tau$  mass are 1610, 1110, 1100 GeV in the  $e\mu, e\tau$ , and  $\mu\tau$  channels, respectively.
- 16 AAD 11h looked in  $35 \text{ pb}^{-1}$  of  $pp$  collisions at  $\sqrt{s} = 7 \text{ TeV}$  for events with one electron and one muon of opposite charge from the production of  $\tilde{\nu}_\tau$  via an RPV  $\lambda'_{311}$  coupling and followed by a decay via  $\lambda_{312}$  into  $e + \mu$ . No evidence for an excess over the SM expectation is observed, and a limit is derived in the plane of  $\lambda'_{311}$  versus  $m_{\tilde{\nu}_\tau}$  for several values of  $\lambda_{312}$ , see their Fig. 2. Superseded by AAD 11z.
- 17 AALTONEN 10Z searched in  $1 \text{ fb}^{-1}$  of  $p\bar{p}$  collisions at  $\sqrt{s} = 1.96 \text{ TeV}$  for events from the production  $d\bar{d} \rightarrow \tilde{\nu}_\tau$  with the subsequent decays  $\tilde{\nu}_\tau \rightarrow e\mu, \mu\tau, e\tau$  in the MSSM framework with RPV. Two isolated leptons of different flavor and opposite charges are required, with  $\tau$ s identified by their hadronic decay. No statistically significant excesses are observed over the SM background. Upper limits on  $\lambda'_{311}$  times the branching ratio are listed in their Table III for various  $\tilde{\nu}_\tau$  masses. Limits on the cross section times branching ratio for  $\lambda'_{311} = 0.10$  and  $\lambda_{33k} = 0.05$ , displayed in Fig. 2, are used to set limits on the  $\tilde{\nu}_\tau$  mass of 558 GeV for the  $e\mu$ , 441 GeV for the  $\mu\tau$  and 442 GeV for the  $e\tau$  channels.
- 18 ABAZOV 10M looked in  $5.3 \text{ fb}^{-1}$  of  $p\bar{p}$  collisions at  $\sqrt{s} = 1.96 \text{ TeV}$  for events with exactly one pair of high  $p_T$  isolated  $e\mu$  and a veto against hard jets. No evidence for an excess over the SM expectation is observed, and a limit at 95% C.L. on the cross section times branching ratio is derived, see their Fig. 3. These limits are translated into limits on couplings as a function of  $m_{\tilde{\nu}_\tau}$  as shown on their Fig. 4. As an example, for  $m_{\tilde{\nu}_\tau} = 100 \text{ GeV}$  and  $\lambda_{312} \leq 0.07$ , couplings  $\lambda'_{311} > 7.7 \times 10^{-4}$  are excluded.
- 19 ABDALLAH 04H use data from LEP 1 and  $\sqrt{s} = 192\text{--}208 \text{ GeV}$ . They re-use results or re-analyze the data from ABDALLAH 03M to put limits on the parameter space of anomaly-mediated supersymmetry breaking (AMSB), which is scanned in the region  $1 < m_{3/2} < 50 \text{ TeV}$ ,  $0 < m_0 < 1000 \text{ GeV}$ ,  $1.5 < \tan\beta < 35$ , both signs of  $\mu$ . The constraints

are obtained from the searches for mass degenerate chargino and neutralino, for SM-like and invisible Higgs, for leptonically decaying charginos and from the limit on non-SM Z width of 3.2 MeV. The limit is for  $m_t = 174.3 \text{ GeV}$  (see Table 2 for other  $m_t$  values). The limit improves to 114 GeV for  $\mu < 0$ .

20 ADRIANI 93M limit from  $\Delta\Gamma(Z)(\text{invisible}) < 16.2 \text{ MeV}$ .

21 ALEXANDER 91F limit is for one species of  $\tilde{\nu}$  and is derived from  $\Gamma(\text{invisible, new})/\Gamma(\ell\ell) < 0.38$ .

### Charged sleptons

This section contains limits on charged scalar leptons ( $\tilde{\ell}$ , with  $\ell=e, \mu, \tau$ ). Studies of width and decays of the Z boson (use is made here of  $\Delta\Gamma_{\text{inv}} < 2.0 \text{ MeV}$ , LEP 00) conclusively rule out  $m_{\tilde{\ell}_R} < 40 \text{ GeV}$  (41 GeV for  $\tilde{\ell}_L$ ), independently of decay modes, for each individual slepton. The limits improve to 43 GeV (43.5 GeV for  $\tilde{\ell}_L$ ) assuming all 3 flavors to be degenerate. Limits on higher mass sleptons depend on model assumptions and on the mass splitting  $\Delta m = m_{\tilde{\ell}} - m_{\tilde{\chi}_1^0}$ . The mass and composition

of  $\tilde{\chi}_1^0$  may affect the selectron production rate in  $e^+e^-$  collisions through  $t$ -channel exchange diagrams. Production rates are also affected by the potentially large mixing angle of the lightest mass eigenstate  $\tilde{\ell}_1 = \tilde{\ell}_R \sin\theta_\ell + \tilde{\ell}_L \cos\theta_\ell$ . It is generally assumed that only  $\tilde{\tau}$  may have significant mixing. The coupling to the Z vanishes for  $\theta_\ell=0.82$ . In the high-energy limit of  $e^+e^-$  collisions the interference between  $\gamma$  and Z exchange leads to a minimal cross section for  $\theta_\ell=0.91$ , a value which is sometimes used in the following entries relative to data taken at LEP2. When limits on  $m_{\tilde{\ell}_R}$  are quoted, it is understood that limits on  $m_{\tilde{\ell}_L}$  are usually at least as strong.

Possibly open decays involving gauginos other than  $\tilde{\chi}_1^0$  will affect the detection efficiencies. Unless otherwise stated, the limits presented here result from the study of  $\tilde{\ell}^+\tilde{\ell}^-$  production, with production rates and decay properties derived from the MSSM. Limits made obsolete by the recent analyses of  $e^+e^-$  collisions at high energies can be found in previous Editions of this Review.

For decays with final state gravitinos ( $\tilde{G}$ ),  $m_{\tilde{G}}$  is assumed to be negligible relative to all other masses.

### R-parity conserving $\tilde{e}$ (Selectron) mass limit

Some earlier papers are now obsolete and have been omitted. They were last listed in our PDG 14 edition: K. Olive, et al. (Particle Data Group), Chinese Physics **C38** 070001 (2014) (<http://pdg.lbl.gov>).

VALUE (GeV)	CL%	DOCUMENT ID	TECN	COMMENT
>250	95	1 SIRUNYAN	19AW CMS	$\ell^\pm \ell^\mp + \cancel{E}_T, \tilde{e}_R, m_{\tilde{\chi}_1^0} = 0 \text{ GeV}$
>310	95	1 SIRUNYAN	19AW CMS	$\ell^\pm \ell^\mp + \cancel{E}_T, \tilde{e}_L, m_{\tilde{\chi}_1^0} = 0 \text{ GeV}$
>350	95	1 SIRUNYAN	19AW CMS	$\ell^\pm \ell^\mp + \cancel{E}_T, m_{\tilde{e}_R} = m_{\tilde{e}_L}, m_{\tilde{\chi}_1^0} = 0 \text{ GeV}$
>290	95	1 SIRUNYAN	19AW CMS	$\ell^\pm \ell^\mp + \cancel{E}_T, \tilde{e}_R, \tilde{e}_L$ and $\tilde{e} = \tilde{e}, \tilde{\mu}$ , $m_{\tilde{\chi}_1^0} = 0 \text{ GeV}$
>400	95	1 SIRUNYAN	19AW CMS	$\ell^\pm \ell^\mp + \cancel{E}_T, \tilde{e}_L$ and $\tilde{e} = \tilde{e}, \tilde{\mu}$ , $m_{\tilde{\chi}_1^0} = 0 \text{ GeV}$
>450	95	1 SIRUNYAN	19AW CMS	$\ell^\pm \ell^\mp + \cancel{E}_T, m_{\tilde{e}_R} = m_{\tilde{e}_L}$ and $\tilde{e} = \tilde{e}, \tilde{\mu}$ , $m_{\tilde{\chi}_1^0} = 0 \text{ GeV}$
>500	95	2 AABOUD	18BT ATLS	$2\ell + \cancel{E}_T, m_{\tilde{e}_R} = m_{\tilde{e}_L}$ and $\tilde{e} = \tilde{e}, \tilde{\mu}, \tilde{\tau}$ , with $m_{\tilde{\chi}_1^0} = 0 \text{ GeV}$
>190	95	3 AABOUD	18R ATLS	$2\ell(\text{soft}) + \cancel{E}_T, m_{\tilde{e}} = m_{\tilde{\mu}}, m_{\tilde{e}} - m_{\tilde{\mu}} = 5 \text{ GeV}$
		4 CHATRCHYAN14R	CMS	$\geq 3\ell^\pm, \tilde{e} \rightarrow \ell^\pm \tau^\mp \tau^\mp \tilde{G}$ simplified model, GMSB, stau (N)NLSP scenario
		5 AAD	13B ATLS	$2\ell^\pm + \cancel{E}_T, \text{SMS, pMSSM}$
> 97.5		6 ABBIENDI	04 OPAL	$\tilde{e}_R, \Delta m > 11 \text{ GeV},  \mu  > 100 \text{ GeV}, \tan\beta=1.5$
> 94.4		7 ACHARD	04 L3	$\tilde{e}_R, \Delta m > 10 \text{ GeV},  \mu  > 200 \text{ GeV}, \tan\beta \geq 2$
> 71.3		7 ACHARD	04 L3	$\tilde{e}_R$ , all $\Delta m$
none 30–94	95	8 ABDALLAH	03M DLPH	$\Delta m > 15 \text{ GeV}, \tilde{e}_R^+ \tilde{e}_R^-$
> 94	95	9 ABDALLAH	03M DLPH	$\tilde{e}_R, 1 \leq \tan\beta \leq 40, \Delta m > 10 \text{ GeV}$
> 95	95	10 HEISTER	02E ALEP	$\Delta m > 15 \text{ GeV}, \tilde{e}_R^+ \tilde{e}_R^-$
> 73	95	11 HEISTER	02N ALEP	$\tilde{e}_R$ , any $\Delta m$
>107	95	11 HEISTER	02N ALEP	$\tilde{e}_L$ , any $\Delta m$
none 90–325	95	12 AAD	14G ATLS	$\tilde{e}\tilde{e} \rightarrow \ell^+ \tilde{\chi}_1^0 \ell^- \tilde{\chi}_1^0$ , simplified model, $m_{\tilde{e}_L} = m_{\tilde{e}_R}, m_{\tilde{\chi}_1^0} = 0 \text{ GeV}$
		13 KHACHATRY..14I	CMS	$\tilde{e} \rightarrow \ell \tilde{\chi}_1^0$ , simplified model

1 SIRUNYAN 19AW searched in  $35.9 \text{ fb}^{-1}$  of  $pp$  collisions at  $\sqrt{s} = 13 \text{ TeV}$  for direct electroweak pair production of selectrons or smuons in events with two leptons (electrons or muons) of the opposite electric charge and same flavour, no jets and large  $\cancel{E}_T$ . No significant excess above the Standard Model expectations is observed. Limits are set on the selectron mass assuming left-handed, right-handed or both left- and right-handed (mass degenerate) production, see their Figure 6. Similarly, limits are set on the smuon mass, see their Figure 7. Limits are also set on slepton masses under the assumption that the selectron and smuon are mass degenerate, see their Figure 5.

- 2 AABOUD 18B searched in  $36.1 \text{ fb}^{-1}$  of  $pp$  collisions at  $\sqrt{s} = 13 \text{ TeV}$  for direct electroweak production of charginos, chargino and next-to-lightest neutralinos and sleptons in events with two or three leptons (electrons or muons), with or without jets, and large missing transverse energy. No significant excess above the Standard Model expectations is observed. Limits are set on the slepton mass up to 500 GeV for massless  $\tilde{\chi}_1^0$ , assuming degeneracy of  $\tilde{e}$ ,  $\tilde{\mu}$ , and  $\tilde{\tau}$  and exploiting the  $2\ell$  signature, see their Figure 8(b).
- 3 AABOUD 18R searched in  $36.1 \text{ fb}^{-1}$  of  $pp$  collisions at  $\sqrt{s} = 13 \text{ TeV}$  for electroweak production in scenarios with compressed mass spectra in final states with two low-momentum leptons and missing transverse momentum. The data are found to be consistent with the SM prediction. Results are interpreted in slepton pair production models with a fourfold degeneracy assumed in selectron and smuon masses. The  $\tilde{e}$  masses are excluded up to 190 GeV for  $m_{\tilde{e}} - m_{\tilde{\chi}_1^0} = 5 \text{ GeV}$ . The exclusion limits extend down to mass splittings of 1 GeV, see their Fig. 11.
- 4 CHATRCHYAN 14R searched in  $19.5 \text{ fb}^{-1}$  of  $pp$  collisions at  $\sqrt{s} = 8 \text{ TeV}$  for events with at least three leptons (electrons, muons, taus) in the final state. No significant excess above the Standard Model expectations is observed. Limits are set on the slepton mass in a stau (N)NLSP simplified model (GMSB) where the decay  $\tilde{e} \rightarrow e^\pm \tau^\pm \mp \tilde{G}$  takes place with a branching ratio of 100%, see Fig. 8.
- 5 AAD 13B searched in  $4.7 \text{ fb}^{-1}$  of  $pp$  collisions at  $\sqrt{s} = 7 \text{ TeV}$  for sleptons decaying to a final state with two leptons ( $e$  and  $\mu$ ) and missing transverse energy. No excess beyond the Standard Model expectation is observed. Limits are derived in a simplified model of direct left-handed slepton pair production, where left-handed slepton masses between 85 and 195 GeV are excluded at 95% C.L. for  $m_{\tilde{\chi}_1^0} = 20 \text{ GeV}$ . See also Fig. 2(a). Exclusion limits are also derived in the phenomenological MSSM, see Fig. 3.
- 6 ABBIENDI 04 search for  $\tilde{e}_R \tilde{e}_R$  production in acoplanar di-electron final states in the 183–208 GeV data. See Fig. 13 for the dependence of the limits on  $m_{\tilde{\chi}_1^0}$  and for the limit at  $\tan\beta=35$ . This limit supersedes ABBIENDI 00g.
- 7 ACHARD 04 search for  $\tilde{e}_R \tilde{e}_L$  and  $\tilde{e}_R \tilde{e}_R$  production in single- and acoplanar di-electron final states in the 192–209 GeV data. Absolute limits on  $m_{\tilde{e}_R}$  are derived from a scan over the MSSM parameter space with universal GUT scale gaugino and scalar masses  $m_{1/2}$  and  $m_0$ ,  $1 \leq \tan\beta \leq 60$  and  $-2 \leq \mu \leq 2 \text{ TeV}$ . See Fig. 4 for the dependence of the limits on  $m_{\tilde{\chi}_1^0}$ . This limit supersedes ACCIARRI 99w.
- 8 ABDALLAH 03M looked for acoplanar dielectron +  $\cancel{E}$  final states at  $\sqrt{s} = 189\text{--}208 \text{ GeV}$ . The limit assumes  $\mu = -200 \text{ GeV}$  and  $\tan\beta = 1.5$  in the calculation of the production cross section and  $B(\tilde{e} \rightarrow e \tilde{\chi}_1^0)$ . See Fig. 15 for limits in the  $(m_{\tilde{e}_R}, m_{\tilde{\chi}_1^0})$  plane. These limits include and update the results of ABREU 01.
- 9 ABDALLAH 03M uses data from  $\sqrt{s} = 192\text{--}208 \text{ GeV}$  to obtain limits in the framework of the MSSM with gaugino and sfermion mass universality at the GUT scale. An indirect limit on the mass is derived by constraining the MSSM parameter space by the results from direct searches for neutralinos (including cascade decays) and for sleptons. These limits are valid for values of  $M_2 < 1 \text{ TeV}$ ,  $|\mu| \leq 1 \text{ TeV}$  with the  $\tilde{\chi}_1^0$  as LSP. The quoted limit is obtained when there is no mixing in the third family. See Fig. 43 for the mass limits as a function of  $\tan\beta$ . These limits update the results of ABREU 00w.
- 10 HEISTER 02E looked for acoplanar dielectron +  $\cancel{E}$  final states from  $e^+e^-$  interactions between 183 and 209 GeV. The mass limit assumes  $\mu < -200 \text{ GeV}$  and  $\tan\beta = 2$  for the production cross section and  $B(\tilde{e} \rightarrow e \tilde{\chi}_1^0) = 1$ . See their Fig. 4 for the dependence of the limit on  $\Delta m$ . These limits include and update the results of BARATE 01.
- 11 HEISTER 02N search for  $\tilde{e}_R \tilde{e}_L$  and  $\tilde{e}_R \tilde{e}_R$  production in single- and acoplanar di-electron final states in the 183–208 GeV data. Absolute limits on  $m_{\tilde{e}_R}$  are derived from a scan over the MSSM parameter space with universal GUT scale gaugino and scalar masses  $m_{1/2}$  and  $m_0$ ,  $1 \leq \tan\beta \leq 50$  and  $-10 \leq \mu \leq 10 \text{ TeV}$ . The region of small  $|\mu|$ , where cascade decays are important, is covered by a search for  $\tilde{\chi}_1^0 \tilde{\chi}_3^0$  in final states with leptons and possibly photons. Limits on  $m_{\tilde{e}_L}$  are derived by exploiting the mass relation between the  $\tilde{e}_L$  and  $\tilde{e}_R$ , based on universal  $m_0$  and  $m_{1/2}$ . When the constraint from the mass limit of the lightest Higgs from HEISTER 02 is included, the bounds improve to  $m_{\tilde{e}_R} > 77(75) \text{ GeV}$  and  $m_{\tilde{e}_L} > 115(115) \text{ GeV}$  for a top mass of 175(180) GeV. In the MSUGRA framework with radiative electroweak symmetry breaking, the limits improve further to  $m_{\tilde{e}_R} > 95 \text{ GeV}$  and  $m_{\tilde{e}_L} > 152 \text{ GeV}$ , assuming a trilinear coupling  $A_0 = 0$  at the GUT scale. See Figs. 4, 5, 7 for the dependence of the limits on  $\tan\beta$ .
- 12 AAD 14G searched in  $20.3 \text{ fb}^{-1}$  of  $pp$  collisions at  $\sqrt{s} = 8 \text{ TeV}$  for electroweak production of slepton pairs, decaying to a final state with two leptons ( $e$  and  $\mu$ ) and missing transverse momentum. No excess beyond the Standard Model expectation is observed. Exclusion limits are derived in simplified models of slepton pair production, see Fig. 8. An interpretation in the pMSSM is also given, see Fig. 10.
- 13 KHACHATRYAN 14I searched in  $19.5 \text{ fb}^{-1}$  of  $pp$  collisions at  $\sqrt{s} = 8 \text{ TeV}$  for electroweak production of slepton pairs decaying to a final state with opposite-sign lepton pairs ( $e$  or  $\mu$ ) and missing transverse momentum. No excess beyond the Standard Model expectation is observed. Exclusion limits are derived in simplified models, see Fig. 18.

**R-parity violating  $\tilde{e}$  (Selectron) mass limit**

Some earlier papers are now obsolete and have been omitted. They were last listed in our PDG 14 edition: K. Olive, et al. (Particle Data Group), Chinese Physics **C38** 070001 (2014) (<http://pdg.lbl.gov>).

VALUE (GeV)	CL%	DOCUMENT ID	TECN	COMMENT
>1065	95	1 AABOUD 18Z ATLS		$\geq 4\ell, \lambda_{12k} \neq 0, m_{\tilde{\chi}_1^0} = 600 \text{ GeV}$ (mass-degenerate left-handed sleptons and sneutrinos of all 3 generations)
> 780	95	1 AABOUD 18Z ATLS		$\geq 4\ell, \lambda_{133} \neq 0, m_{\tilde{\chi}_1^0} = 300 \text{ GeV}$ (mass-degenerate left-handed sleptons and sneutrinos of all 3 generations)
> 410	95	2 AAD 14X ATLS	RPV, $\tilde{e} \rightarrow \ell^\pm \tau^\pm \mp \tilde{G}$	$\geq 4\ell^\pm, \tilde{e} \rightarrow \ell^\pm \tau^\pm \mp \tilde{G}$
• • • We do not use the following data for averages, fits, limits, etc. • • •				
> 89	95	3 ABBIENDI 04F OPAL	RPV, $\tilde{e}_L$	
> 92	95	4 ABDALLAH 04M DLPH	RPV, $\tilde{e}_R$ , indirect, $\Delta m > 5 \text{ GeV}$	

- 1 AABOUD 18Z searched in  $36.1 \text{ fb}^{-1}$  of  $pp$  collisions at  $\sqrt{s} = 13 \text{ TeV}$  for events containing four or more charged leptons (electrons, muons and up to two hadronically decaying taus). No significant deviation from the expected SM background is observed. Limits are set on the Higgsino mass in simplified models of general gauge mediated supersymmetry Tn1nA/Tn1nB/Tn1nC, see their Figure 9. Limits are also set on the wino, slepton, sneutrino and gluino mass in a simplified model of NLSP pair production with R-parity violating decays of the LSP via  $\lambda_{12k}$  or  $\lambda_{133}$  to charged leptons, see their Figures 7, 8.
- 2 AAD 14X searched in  $20.3 \text{ fb}^{-1}$  of  $pp$  collisions at  $\sqrt{s} = 8 \text{ TeV}$  for events with at least four leptons (electrons, muons, taus) in the final state. No significant excess above the Standard Model expectations is observed. Limits are set on the slepton mass in an R-parity violating simplified model where the decay  $\tilde{e} \rightarrow \ell^\pm \tilde{\chi}_1^0$ , with  $\tilde{\chi}_1^0 \rightarrow \ell^\pm \ell^\mp \nu$ , takes place with a branching ratio of 100%, see Fig. 9.
- 3 ABBIENDI 04F use data from  $\sqrt{s} = 189\text{--}209 \text{ GeV}$ . They derive limits on sparticle masses under the assumption of RPV with  $LL\tilde{E}$  or  $LQ\tilde{D}$  couplings. The results are valid for  $\tan\beta = 1.5$ ,  $\mu = -200 \text{ GeV}$ , with, in addition,  $\Delta m > 5 \text{ GeV}$  for indirect decays via  $LQ\tilde{D}$ . The limit quoted applies to direct decays via  $LL\tilde{E}$  or  $LQ\tilde{D}$  couplings. For indirect decays, the limits on the  $\tilde{e}_R$  mass are respectively 99 and 92 GeV for  $LL\tilde{E}$  and  $LQ\tilde{D}$  couplings and  $m_{\tilde{\chi}_1^0} = 10 \text{ GeV}$  and degrade slightly for larger  $\tilde{\chi}_1^0$  mass. Supersedes the results of ABBIENDI 00.
- 4 ABDALLAH 04M use data from  $\sqrt{s} = 192\text{--}208 \text{ GeV}$  to derive limits on sparticle masses under the assumption of RPV with  $LL\tilde{E}$  or  $UD\tilde{D}$  couplings. The results are valid for  $\mu = -200 \text{ GeV}$ ,  $\tan\beta = 1.5$ ,  $\Delta m > 5 \text{ GeV}$  and assuming a BR of 1 for the given decay. The limit quoted is for indirect  $UD\tilde{D}$  decays using the neutralino constraint of 39.5 GeV for  $LL\tilde{E}$  and of 38.0 GeV for  $UD\tilde{D}$  couplings, also derived in ABDALLAH 04M. For indirect decays via  $LL\tilde{E}$  the limit improves to 95 GeV if the constraint from the neutralino is used and to 94 GeV if it is not used. For indirect decays via  $UD\tilde{D}$  couplings it remains unchanged when the neutralino constraint is not used. Supersedes the result of ABREU 00u.

**R-parity conserving  $\tilde{\mu}$  (Smuon) mass limit**

VALUE (GeV)	CL%	DOCUMENT ID	TECN	COMMENT
>210	95	1 SIRUNYAN 19AW CMS		$\ell^\pm \ell^\mp + \cancel{E}_T, \tilde{\mu}_R, m_{\tilde{\chi}_1^0} = 0 \text{ GeV}$
>280	95	1 SIRUNYAN 19AW CMS		$\ell^\pm \ell^\mp + \cancel{E}_T, \tilde{\mu}_L, m_{\tilde{\chi}_1^0} = 0 \text{ GeV}$
>290	95	1 SIRUNYAN 19AW CMS		$\ell^\pm \ell^\mp + \cancel{E}_T, \tilde{\mu}_R$ and $\tilde{e} = \tilde{e}, \tilde{\mu}, m_{\tilde{\chi}_1^0} = 0 \text{ GeV}$
>400	95	1 SIRUNYAN 19AW CMS		$\ell^\pm \ell^\mp + \cancel{E}_T, \tilde{\mu}_L$ and $\tilde{e} = \tilde{e}, \tilde{\mu}, m_{\tilde{\chi}_1^0} = 0 \text{ GeV}$
>450	95	1 SIRUNYAN 19AW CMS		$\ell^\pm \ell^\mp + \cancel{E}_T, m_{\tilde{e}_R} = m_{\tilde{e}_L}$ and $\tilde{e} = \tilde{e}, \tilde{\mu}, m_{\tilde{\chi}_1^0} = 0 \text{ GeV}$
>310	95	1 SIRUNYAN 19AW CMS		$\ell^\pm \ell^\mp + \cancel{E}_T, m_{\tilde{\mu}_R} = m_{\tilde{\mu}_L}, m_{\tilde{\chi}_1^0} = 0 \text{ GeV}$
>190	95	2 AABOUD 18R ATLS		$2\ell$ (soft) + $\cancel{E}_T, m_{\tilde{e}} = m_{\tilde{\mu}}, m_{\tilde{\mu}} - m_{\tilde{\chi}_1^0} = 5 \text{ GeV}$
		3 CHATRCHYAN 14R CMS		$\geq 3\ell^\pm, \tilde{e} \rightarrow \ell^\pm \tau^\mp \mp \tilde{G}$ simplified model, GMSB, stau (N)NLSP scenario
		4 AAD 13B ATLS		$2\ell^\pm + \cancel{E}_T, \text{SMS, pMSSM}$
> 91.0		5 ABBIENDI 04 OPAL		$\Delta m > 3 \text{ GeV}, \tilde{\mu}_R^+ \tilde{\mu}_R^-,  \mu  > 100 \text{ GeV}, \tan\beta = 1.5$
> 86.7		6 ACHARD 04 L3		$\Delta m > 10 \text{ GeV}, \tilde{\mu}_R^+ \tilde{\mu}_R^-,  \mu  > 200 \text{ GeV}, \tan\beta \geq 2$
none 30–88	95	7 ABDALLAH 03M DLPH		$\Delta m > 5 \text{ GeV}, \tilde{\mu}_R^+ \tilde{\mu}_R^-$
> 94	95	8 ABDALLAH 03M DLPH		$\tilde{\mu}_R^+ \tilde{\mu}_R^-, 1 \leq \tan\beta \leq 40, \Delta m > 10 \text{ GeV}$
> 88	95	9 HEISTER 02E ALEP		$\Delta m > 15 \text{ GeV}, \tilde{\mu}_R^+ \tilde{\mu}_R^-$
• • • We do not use the following data for averages, fits, limits, etc. • • •				
>500	95	10 AABOUD 18BT ATLS		$2\ell + \cancel{E}_T, m_{\tilde{e}_R} = m_{\tilde{e}_L}$ and $\tilde{e} = \tilde{e}, \tilde{\mu}, \tilde{\tau}$ , with $m_{\tilde{\chi}_1^0} = 0 \text{ GeV}$
none 90–325	95	11 AAD 14G ATLS		$\tilde{e}\tilde{e} \rightarrow \ell^\pm \tilde{\chi}_1^0 \ell^\mp \tilde{\chi}_1^0$ , simplified model, $m_{\tilde{e}_L} = m_{\tilde{e}_R}, m_{\tilde{\chi}_1^0} = 0 \text{ GeV}$
		12 KHACHATRYAN 14I CMS		$\tilde{e} \rightarrow \ell \tilde{\chi}_1^0$ , simplified model
> 80	95	13 ABREU 00V DLPH		$\tilde{\mu}_R \tilde{\mu}_R (\tilde{\mu}_R \rightarrow \mu \tilde{G}), m_{\tilde{G}} > 8 \text{ eV}$

- 1 SIRUNYAN 19AW searched in  $35.9 \text{ fb}^{-1}$  of  $pp$  collisions at  $\sqrt{s} = 13 \text{ TeV}$  for direct electroweak pair production of selectrons or smuons in events with two leptons (electrons or muons) of the opposite electric charge and same flavour, no jets and large  $\cancel{E}_T$ . No significant excess above the Standard Model expectations is observed. Limits are set on the selectron mass assuming left-handed, right-handed or both left- and right-handed (mass degenerate) production, see their Figure 6. Similarly, limits are set on the smuon mass, see their Figure 7. Limits are also set on slepton masses under the assumption that the selectron and smuon are mass degenerate, see their Figure 5.
- 2 AABOUD 18R searched in  $36.1 \text{ fb}^{-1}$  of  $pp$  collisions at  $\sqrt{s} = 13 \text{ TeV}$  for electroweak production in scenarios with compressed mass spectra in final states with two low-momentum leptons and missing transverse momentum. The data are found to be consistent with the SM prediction. Results are interpreted in slepton pair production models with a fourfold degeneracy assumed in selectron and smuon masses. The  $\tilde{\mu}$  masses are excluded up to 190 GeV for  $m_{\tilde{\mu}} - m_{\tilde{\chi}_1^0} = 5 \text{ GeV}$ . The exclusion limits extend down to mass splittings of 1 GeV, see their Fig. 11.
- 3 CHATRCHYAN 14R searched in  $19.5 \text{ fb}^{-1}$  of  $pp$  collisions at  $\sqrt{s} = 8 \text{ TeV}$  for events with at least three leptons (electrons, muons, taus) in the final state. No significant excess above the Standard Model expectations is observed. Limits are set on the slepton mass in a stau (N)NLSP simplified model (GMSB) where the decay  $\tilde{e} \rightarrow \ell^\pm \tau^\pm \mp \tilde{G}$  takes place with a branching ratio of 100%, see Fig. 8.
- 4 AAD 13B searched in  $4.7 \text{ fb}^{-1}$  of  $pp$  collisions at  $\sqrt{s} = 7 \text{ TeV}$  for sleptons decaying to a final state with two leptons ( $e$  and  $\mu$ ) and missing transverse energy. No excess beyond

# Searches Particle Listings

## Supersymmetric Particle Searches

the Standard Model expectation is observed. Limits are derived in a simplified model of direct left-handed slepton pair production, where left-handed slepton masses between 85 and 195 GeV are excluded at 95% C.L. for  $m_{\tilde{\chi}_1^0} = 20$  GeV. See also Fig. 2(a). Exclusion limits are also derived in the phenomenological MSSM, see Fig. 3.

- <sup>5</sup> ABBIENDI 04 search for  $\tilde{\mu}_R \tilde{\mu}_R$  production in acoplanar di-muon final states in the 183–208 GeV data. See Fig. 14 for the dependence of the limits on  $m_{\tilde{\chi}_1^0}$  and for the limit at  $\tan\beta=35$ . Under the assumption of 100% branching ratio for  $\tilde{\mu}_R \rightarrow \mu \tilde{\chi}_1^0$ , the limit improves to 94.0 GeV for  $\Delta m > 4$  GeV. See Fig. 11 for the dependence of the limits on  $m_{\tilde{\chi}_1^0}$  at several values of the branching ratio. This limit supersedes ABBIENDI 00G.
- <sup>6</sup> ACHARD 04 search for  $\tilde{\mu}_R \tilde{\mu}_R$  production in acoplanar di-muon final states in the 192–209 GeV data. Limits on  $m_{\tilde{\mu}_R}$  are derived from a scan over the MSSM parameter space with universal GUT scale gaugino and scalar masses  $m_{1/2}$  and  $m_0$ ,  $1 \leq \tan\beta \leq 60$  and  $-2 \leq \mu \leq 2$  TeV. See Fig. 4 for the dependence of the limits on  $m_{\tilde{\chi}_1^0}$ . This limit supersedes ACCIARRI 99w.
- <sup>7</sup> ABDALLAH 03M looked for acoplanar dimuon +  $\cancel{E}$  final states at  $\sqrt{s} = 189$ –208 GeV. The limit assumes  $B(\tilde{\mu} \rightarrow \mu \tilde{\chi}_1^0) = 100\%$ . See Fig. 16 for limits on the  $(m_{\tilde{\mu}_R}, m_{\tilde{\chi}_1^0})$  plane. These limits include and update the results of ABREU 01.
- <sup>8</sup> ABDALLAH 03M uses data from  $\sqrt{s} = 192$ –208 GeV to obtain limits in the framework of the MSSM with gaugino and sfermion mass universality at the GUT scale. An indirect limit on the mass is derived by constraining the MSSM parameter space by the results from direct searches for neutralinos (including cascade decays) and for sleptons. These limits are valid for values of  $M_2 < 1$  TeV,  $|\mu| \leq 1$  TeV with the  $\tilde{\chi}_1^0$  as LSP. The quoted limit is obtained when there is no mixing in the third family. See Fig. 43 for the mass limits as a function of  $\tan\beta$ . These limits update the results of ABREU 00w.
- <sup>9</sup> HEISTER 02E looked for acoplanar dimuon +  $\cancel{E}_T$  final states from  $e^+e^-$  interactions between 183 and 209 GeV. The mass limit assumes  $B(\tilde{\mu} \rightarrow \mu \tilde{\chi}_1^0) = 1$ . See their Fig. 4 for the dependence of the limit on  $\Delta m$ . These limits include and update the results of BARATE 01.
- <sup>10</sup> ABOUD 18BT searched in  $36.1 \text{ fb}^{-1}$  of  $pp$  collisions at  $\sqrt{s} = 13$  TeV for direct electroweak production of charginos, chargino and next-to-lightest neutralinos and sleptons in events with two or three leptons (electrons or muons), with or without jets, and large missing transverse energy. No significant excess above the Standard Model expectations is observed. Limits are set on the slepton mass up to 500 GeV for massless  $\tilde{\chi}_1^0$ , assuming degeneracy of  $\tilde{e}$ ,  $\tilde{\mu}$ , and  $\tilde{\tau}$  and exploiting the  $2\ell$  signature, see their Figure 8(b).
- <sup>11</sup> AAD 14G searched in 20.3  $\text{fb}^{-1}$  of  $pp$  collisions at  $\sqrt{s} = 8$  TeV for electroweak production of slepton pairs, decaying to a final state with two leptons ( $e$  and  $\mu$ ) and missing transverse momentum. No excess beyond the Standard Model expectation is observed. Exclusion limits are derived in simplified models of slepton pair production, see Fig. 8. An interpretation in the pMSSM is also given, see Fig. 10.
- <sup>12</sup> KHACHATRYAN 14i searched in 19.5  $\text{fb}^{-1}$  of  $pp$  collisions at  $\sqrt{s} = 8$  TeV for electroweak production of slepton pairs decaying to a final state with opposite-sign lepton pairs ( $e$  or  $\mu$ ) and missing transverse momentum. No excess beyond the Standard Model expectation is observed. Exclusion limits are derived in simplified models, see Fig. 18.
- <sup>13</sup> ABREU 00v use data from  $\sqrt{s} = 130$ –189 GeV to search for tracks with large impact parameter or visible decay vertices. Limits are obtained as function of  $m_{\tilde{G}}$ , after combining these results with the search for slepton pair production in the SUGRA framework from ABREU 01 to cover prompt decays and on stable particle searches from ABREU 00q. For limits at different  $m_{\tilde{G}}$ , see their Fig. 12.

### R-parity violating $\tilde{\mu}$ (Smuon) mass limit

VALUE (GeV)	CL%	DOCUMENT ID	TECN	COMMENT
> 780	95	<sup>1</sup> ABOUD 18z ATLS	18z ATLS	$\geq 4\ell, \lambda_{133} \neq 0, m_{\tilde{\chi}_1^0} = 300$ GeV (mass-degenerate left-handed sleptons and sneutrinos of all 3 generations)
>1060	95	<sup>1</sup> ABOUD 18z ATLS	18z ATLS	$\geq 4\ell, \lambda_{12k} \neq 0, m_{\tilde{\chi}_1^0} = 600$ GeV (mass-degenerate left-handed sleptons and sneutrinos of all 3 generations)
> 410	95	<sup>2</sup> AAD 14x ATLS	14x ATLS	RPV, $\geq 4\ell^{\pm}, \tilde{\ell} \rightarrow \ell \tilde{\chi}_1^0, \tilde{\chi}_1^0 \rightarrow \ell^{\pm} \tilde{\ell} \nu$
••• We do not use the following data for averages, fits, limits, etc. •••				
		<sup>3</sup> SIRUNYAN 19A0	19A0	$\mu^{\pm} \mu^{\pm} + \geq 2\text{jets}, \lambda'_{211} \neq 0, \tilde{\mu}_L \rightarrow \mu \tilde{\chi}_1^0, \tilde{\chi}_1^0 \rightarrow \mu q \bar{q}$
> 87	95	<sup>4</sup> ABDALLAH 04M DLPH	04M DLPH	RPV, $\tilde{\mu}_R$ , indirect, $\Delta m > 5$ GeV
> 81	95	<sup>5</sup> HEISTER 03G ALEP	03G ALEP	RPV, $\tilde{\mu}_L$

- <sup>1</sup> ABOUD 18z searched in  $36.1 \text{ fb}^{-1}$  of  $pp$  collisions at  $\sqrt{s} = 13$  TeV for events containing four or more charged leptons (electrons, muons and up to two hadronically decaying taus). No significant deviation from the expected SM background is observed. Limits are set on the Higgsino mass in simplified models of general gauge mediated supersymmetry Tn1n1A/Tn1n1B/Tn1n1C, see their Figure 9. Limits are also set on the wino, slepton, sneutrino and gluino mass in a simplified model of NLSP pair production with R-parity violating decays of the LSP via  $\lambda_{12k}$  or  $\lambda_{133}$  to charged leptons, see their Figures 7, 8.
- <sup>2</sup> AAD 14x searched in 20.3  $\text{fb}^{-1}$  of  $pp$  collisions at  $\sqrt{s} = 8$  TeV for events with at least four leptons (electrons, muons, taus) in the final state. No significant excess above the Standard Model expectations is observed. Limits are set on the slepton mass in an R-parity violating simplified model where the decay  $\tilde{\ell} \rightarrow \ell \tilde{\chi}_1^0$ , with  $\tilde{\chi}_1^0 \rightarrow \ell^{\pm} \tilde{\ell} \nu$ , takes place with a branching ratio of 100%, see Fig. 9.
- <sup>3</sup> SIRUNYAN 19A0 searched in 35.9  $\text{fb}^{-1}$  of  $pp$  collisions at  $\sqrt{s} = 13$  TeV for events containing two same-sign muons and at last two jets, originating from resonant production of second-generation sleptons ( $\tilde{\mu}_L, \tilde{\nu}_\mu$ ) via the R-parity violating coupling  $\lambda'_{211}$  to quarks. No significant excess above the Standard Model expectations is observed. Upper limits on cross sections are derived in the context of two simplified models, see their Figure 4. The cross section limits are translated into limits on  $\lambda'_{211}$  for a modified CMSSM, see their Figure 5.
- <sup>4</sup> ABDALLAH 04M use data from  $\sqrt{s} = 192$ –208 GeV to derive limits on sparticle masses under the assumption of RPV with  $L\tilde{L}\tilde{E}$  or  $U\tilde{D}\tilde{D}$  couplings. The results are valid for  $\mu$

$= -200$  GeV,  $\tan\beta = 1.5$ ,  $\Delta m \geq 5$  GeV and assuming a BR of 1 for the given decay. The limit quoted is for indirect  $U\tilde{D}\tilde{D}$  decays using the neutralino constraint of 39.5 GeV for  $L\tilde{L}\tilde{E}$  and of 38.0 GeV for  $U\tilde{D}\tilde{D}$  couplings, also derived in ABDALLAH 04M. For indirect decays via  $L\tilde{L}\tilde{E}$  the limit improves to 90 GeV if the constraint from the neutralino is used and remains at 87 GeV if it is not used. For indirect decays via  $U\tilde{D}\tilde{D}$  couplings it degrades to 85 GeV when the neutralino constraint is not used. Supersedes the result of ABREU 00U.

- <sup>5</sup> HEISTER 03G searches for the production of smuons in the case of RPV prompt decays with  $L\tilde{L}\tilde{E}$ ,  $L\tilde{Q}\tilde{D}$  or  $U\tilde{D}\tilde{D}$  couplings at  $\sqrt{s} = 189$ –209 GeV. The search is performed for direct and indirect decays, assuming one coupling at a time to be non-zero. The limit holds for direct decays mediated by RPV  $L\tilde{Q}\tilde{D}$  couplings and improves to 90 GeV for indirect decays (for  $\Delta m > 10$  GeV). Limits are also given for  $L\tilde{L}\tilde{E}$  direct ( $m_{\tilde{\mu}_R} > 87$  GeV) and indirect decays ( $m_{\tilde{\mu}_R} > 96$  GeV for  $m(\tilde{\chi}_1^0) > 23$  GeV from BARATE 98s) and for  $U\tilde{D}\tilde{D}$  indirect decays ( $m_{\tilde{\mu}_R} > 85$  GeV for  $\Delta m > 10$  GeV). Supersedes the results from BARATE 01b.

### R-parity conserving $\tilde{\tau}$ (Stau) mass limit

Some earlier papers are now obsolete and have been omitted. They were last listed in our PDG 14 edition: K. Olive, et al. (Particle Data Group), Chinese Physics **C38** 070001 (2014) (<http://pdg.lbl.gov>).

VALUE (GeV)	CL%	DOCUMENT ID	TECN	COMMENT
> 85.2		<sup>1</sup> ABBIENDI 04 OPAL	04 OPAL	$\Delta m > 6$ GeV, $\theta_r = \pi/2,  \mu  > 100$ GeV, $\tan\beta = 1.5$
> 78.3		<sup>2</sup> ACHARD 04 L3	04 L3	$\Delta m > 15$ GeV, $\theta_r = \pi/2,  \mu  > 200$ GeV, $\tan\beta \geq 2$
> 81.9	95	<sup>3</sup> ABDALLAH 03M DLPH	03M DLPH	$\Delta m > 15$ GeV, all $\theta_r$
> 79	95	<sup>4</sup> HEISTER 02E ALEP	02E ALEP	$\Delta m > 15$ GeV, $\theta_r = \pi/2$
> 76	95	<sup>4</sup> HEISTER 02E ALEP	02E ALEP	$\Delta m > 15$ GeV, $\theta_r = 0.91$
••• We do not use the following data for averages, fits, limits, etc. •••				
>500	95	<sup>5</sup> ABOUD 18BT ATLS	18BT ATLS	$2\ell + \cancel{E}_T, m_{\tilde{e}_R} = m_{\tilde{\ell}_L}, \tilde{\ell} = \tilde{e}, \tilde{\mu}, \tilde{\tau}, m_{\tilde{\chi}_1^0} = 0$ GeV
none 109	95	<sup>6</sup> KHACHATRY..17L CMS	17L CMS	$2\tau + \cancel{E}_T, \tilde{\tau}_L \rightarrow \tau \tilde{\chi}_1^0, m_{\tilde{\chi}_1^0} = 0$ GeV
none 109	95	<sup>7</sup> AAD 16AA ATLS	16AA ATLS	2 hadronic $\tau + \cancel{E}_T, \tilde{\tau}_{R/L} \rightarrow \tau \tilde{\chi}_1^0, m_{\tilde{\chi}_1^0} = 0$ GeV
		<sup>8</sup> AAD 12AF ATLS	12AF ATLS	$2\tau + \text{jets} + \cancel{E}_T, \text{GMSB}$
		<sup>9</sup> AAD 12AG ATLS	12AG ATLS	$\geq 1\tau_h + \text{jets} + \cancel{E}_T, \text{GMSB}$
		<sup>10</sup> AAD 12CM ATLS	12CM ATLS	$\geq 1\tau + \text{jets} + \cancel{E}_T, \text{GMSB}$
> 87.4	95	<sup>11</sup> ABBIENDI 06B OPAL	06B OPAL	$\tilde{\tau}_R \rightarrow \tau \tilde{G}, \text{all } \tau(\tilde{\tau}_R)$
> 68	95	<sup>12</sup> ABDALLAH 04H DLPH	04H DLPH	AMSB, $\mu > 0$
none $m_{\tilde{\tau}} - 26.3$	95	<sup>3</sup> ABDALLAH 03M DLPH	03M DLPH	$\Delta m > m_{\tilde{\tau}}, \text{all } \theta_r$

- <sup>1</sup> ABBIENDI 04 search for  $\tilde{\tau}\tilde{\tau}$  production in acoplanar di-tau final states in the 183–208 GeV data. See Fig. 15 for the dependence of the limits on  $m_{\tilde{\chi}_1^0}$  and for the limit

at  $\tan\beta=35$ . Under the assumption of 100% branching ratio for  $\tilde{\tau}_R \rightarrow \tau \tilde{\chi}_1^0$ , the limit improves to 89.8 GeV for  $\Delta m > 8$  GeV. See Fig. 12 for the dependence of the limits on  $m_{\tilde{\chi}_1^0}$  at several values of the branching ratio and for their dependence on  $\theta_r$ . This limit supersedes ABBIENDI 00G.

- <sup>2</sup> ACHARD 04 search for  $\tilde{\tau}\tilde{\tau}$  production in acoplanar di-tau final states in the 192–209 GeV data. Limits on  $m_{\tilde{\tau}_R}$  are derived from a scan over the MSSM parameter space with universal GUT scale gaugino and scalar masses  $m_{1/2}$  and  $m_0$ ,  $1 \leq \tan\beta \leq 60$  and  $-2 \leq \mu \leq 2$  TeV. See Fig. 4 for the dependence of the limits on  $m_{\tilde{\chi}_1^0}$ .

- <sup>3</sup> ABDALLAH 03M looked for acoplanar ditau +  $\cancel{E}$  final states at  $\sqrt{s} = 130$ –208 GeV. A dedicated search was made for low mass  $\tilde{\tau}$ s decoupling from the  $Z^0$ . The limit assumes  $B(\tilde{\tau} \rightarrow \tau \tilde{\chi}_1^0) = 100\%$ . See Fig. 20 for limits on the  $(m_{\tilde{\tau}}, m_{\tilde{\chi}_1^0})$  plane and as function

of the  $\tilde{\chi}_1^0$  mass and of the branching ratio. The limit in the low-mass region improves to 29.6 and 31.1 GeV for  $\tilde{\tau}_R$  and  $\tilde{\tau}_L$ , respectively, at  $\Delta m > m_{\tilde{\tau}}$ . The limit in the high-mass region improves to 84.7 GeV for  $\tilde{\tau}_R$  and  $\Delta m > 15$  GeV. These limits include and update the results of ABREU 01.

- <sup>4</sup> HEISTER 02E looked for acoplanar ditau +  $\cancel{E}_T$  final states from  $e^+e^-$  interactions between 183 and 209 GeV. The mass limit assumes  $B(\tilde{\tau} \rightarrow \tau \tilde{\chi}_1^0) = 1$ . See their Fig. 4 for the dependence of the limit on  $\Delta m$ . These limits include and update the results of BARATE 01.

- <sup>5</sup> ABOUD 18BT searched in  $36.1 \text{ fb}^{-1}$  of  $pp$  collisions at  $\sqrt{s} = 13$  TeV for direct electroweak production of charginos, chargino and next-to-lightest neutralinos and sleptons in events with two or three leptons (electrons or muons), with or without jets, and large missing transverse energy. No significant excess above the Standard Model expectations is observed. Limits are set on the slepton mass up to 500 GeV for massless  $\tilde{\chi}_1^0$ , assuming degeneracy of  $\tilde{e}$ ,  $\tilde{\mu}$ , and  $\tilde{\tau}$  and exploiting the  $2\ell$  signature, see their Figure 8(b).

- <sup>6</sup> KHACHATRYAN 17L searched in about 19  $\text{fb}^{-1}$  of  $pp$  collisions at  $\sqrt{s} = 8$  TeV for events with two  $\tau$  (at least one decaying hadronically) and  $\cancel{E}_T$ . Results were interpreted to set constraints on the cross section for production of  $\tilde{\tau}_L$  pairs for  $m_{\tilde{\chi}_1^0} = 1$  GeV. No mass constraints are set, see their Fig. 7.

- <sup>7</sup> AAD 16AA summarized and extended ATLAS searches for electroweak supersymmetry in final states containing several charged leptons,  $\cancel{E}_T$ , with or without hadronic jets, in  $20 \text{ fb}^{-1}$  of  $pp$  collisions at  $\sqrt{s} = 8$  TeV. The paper reports 95% C.L. exclusion limits on the cross-section for production of  $\tilde{\tau}_R$  and  $\tilde{\tau}_L$  pairs for various  $m_{\tilde{\chi}_1^0}$ , using the 2 hadronic  $\tau + \cancel{E}_T$  analysis. The  $m_{\tilde{\tau}_{R/L}} = 109$  GeV is excluded for  $m_{\tilde{\chi}_1^0} = 0$  GeV, with the constraints being stronger for  $\tilde{\tau}_R$ . See their Fig. 12.

- <sup>8</sup> AAD 12AF searched in 2  $\text{fb}^{-1}$  of  $pp$  collisions at  $\sqrt{s} = 7$  TeV for events with two tau leptons, jets and large  $\cancel{E}_T$  in a GMSB framework. No significant excess above the expected background was found and an upper limit on the visible cross section for new phenomena is set. A 95% C.L. lower limit of 32 TeV on the mGMSB breaking scale  $A$  is set for  $M_{\text{mess}} = 250$  TeV,  $N_5 = 3$ ,  $\mu > 0$  and  $C_{\text{grav}} = 1$ , independent of  $\tan\beta$ .

See key on page 999

# Searches Particle Listings Supersymmetric Particle Searches

- <sup>9</sup> AAD 12AG searched in 2.05 fb<sup>-1</sup> of pp collisions at  $\sqrt{s} = 7$  TeV for events with at least one hadronically decaying tau lepton, jets, and large  $E_T$  in a GMSB framework. No significant excess above the expected background was found and an upper limit on the visible cross section for new phenomena is set. A 95% C.L. lower limit of 30 TeV on the mGMSB breaking scale  $\Lambda$  is set for  $M_{mess} = 250$  TeV,  $N_S = 3$ ,  $\mu > 0$  and  $C_{grav} = 1$ , independent of  $\tan\beta$ . For large values of  $\tan\beta$ , the limit on  $\Lambda$  increases to 43 TeV.
- <sup>10</sup> AAD 12CM searched in 4.7 fb<sup>-1</sup> of pp collisions at  $\sqrt{s} = 7$  TeV for events with at least one tau lepton, zero or one additional light lepton ( $e/\mu$ ) jets, and large  $E_T$  in a GMSB framework. No significant excess above the expected background was found and an upper limit on the visible cross section for new phenomena is set. A 95% C.L. lower limit of 54 TeV on the mGMSB breaking scale  $\Lambda$  is set for  $M_{mess} = 250$  TeV,  $N_S = 3$ ,  $\mu > 0$  and  $C_{grav} = 1$ , for  $\tan\beta > 20$ . Here the  $\tilde{\tau}_1$  is the NLSP.
- <sup>11</sup> ABBIENDI 06B use 600 pb<sup>-1</sup> of data from  $\sqrt{s} = 189$ –209 GeV. They look for events from pair-produced staus in a GMSB scenario with  $\tilde{\tau}$  NLSP including prompt  $\tilde{\tau}$  decays to ditau +  $\cancel{E}$  final states, large impact parameters, kinked tracks and heavy stable charged particles. Limits on the cross-section are computed as a function of  $m(\tilde{\tau})$  and the lifetime, see their Fig. 7. The limit is compared to the  $\sigma \cdot BR^2$  from a scan over the GMSB parameter space.
- <sup>12</sup> ABDALLAH 04H use data from LEP 1 and  $\sqrt{s} = 192$ –208 GeV. They re-use results or re-analyze the data from ABDALLAH 03M to put limits on the parameter space of anomaly-mediated supersymmetry breaking (AMSB), which is scanned in the region  $1 < m_{3/2} < 50$  TeV,  $0 < m_0 < 1000$  GeV,  $1.5 < \tan\beta < 35$ , both signs of  $\mu$ . The constraints are obtained from the searches for mass degenerate chargino and neutralino, for SM-like and invisible Higgs, for leptonically decaying charginos and from the limit on non-SM Z width of 3.2 MeV. The limit is for  $m_{\tilde{t}} = 174.3$  GeV (see Table 2 for other  $m_{\tilde{t}}$  values). The limit improves to 75 GeV for  $\mu < 0$ .

### R-parity violating $\tilde{\tau}$ (Stau) mass limit

Some earlier papers are now obsolete and have been omitted. They were last listed in our PDG 14 edition: K. Olive, et al. (Particle Data Group), Chinese Physics C38 070001 (2014) (<http://pdg.lbl.gov>).

VALUE (GeV)	CL%	DOCUMENT ID	TECN	COMMENT
>1060	95	<sup>1</sup> AABOUD	18z ATLS	$\geq 4\ell$ , RPV, $\lambda_{12k} \neq 0$ , $m_{\tilde{\chi}_1^0} = 600$ GeV (mass-degenerate left-handed sleptons and sneutrinos of all 3 generations)
> 780	95	<sup>1</sup> AABOUD	18z ATLS	$\geq 4\ell$ , RPV, $\lambda_{133} \neq 0$ , $m_{\tilde{\chi}_1^0} = 300$ GeV (mass-degenerate left-handed sleptons and sneutrinos of all 3 generations)

- • • We do not use the following data for averages, fits, limits, etc. • • •
- > 74 95 <sup>2</sup> ABBIENDI 04F OPAL RPV,  $\tilde{\tau}_L$
- > 90 95 <sup>3</sup> ABDALLAH 04M DLPH RPV,  $\tilde{\tau}_R$ , indirect,  $\Delta m > 5$  GeV
- <sup>1</sup> AABOUD 18z searched in 36.1 fb<sup>-1</sup> of pp collisions at  $\sqrt{s} = 13$  TeV for events containing four or more charged leptons (electrons, muons and up to two hadronically decaying taus). No significant deviation from the expected SM background is observed. Limits are set on the Higgsino mass in simplified models of general gauge mediated supersymmetry Tn1n1A/Tn1n1B/Tn1n1C, see their Figure 9. Limits are also set on the wino, slepton, sneutrino and gluino mass in a simplified model of NLSP pair production with R-parity violating decays of the LSP via  $\lambda_{12k}$  or  $\lambda_{133}$  to charged leptons, see their Figures 7, 8.
- <sup>2</sup> ABBIENDI 04F use data from  $\sqrt{s} = 189$ –209 GeV. They derive limits on sparticle masses under the assumption of RPV with  $LL\tilde{E}$  or  $LQ\tilde{D}$  couplings. The results are valid for  $\tan\beta = 1.5$ ,  $\mu = -200$  GeV, with, in addition,  $\Delta m > 5$  GeV for indirect decays via  $LQ\tilde{D}$ . The limit quoted applies to direct decays with  $LL\tilde{E}$  couplings and improves to 75 GeV for  $LQ\tilde{D}$  couplings. The limit on the  $\tilde{\tau}_R$  mass for indirect decays is 92 GeV for  $LL\tilde{E}$  couplings at  $m_{\tilde{\chi}_1^0} = 10$  GeV and no exclusion is obtained for  $LQ\tilde{D}$  couplings. Supersedes the results of ABBIENDI 00.
- <sup>3</sup> ABDALLAH 04M use data from  $\sqrt{s} = 192$ –208 GeV to derive limits on sparticle masses under the assumption of RPV with  $LL\tilde{E}$  couplings. The results are valid for  $\mu = -200$  GeV,  $\tan\beta = 1.5$ ,  $\Delta m > 5$  GeV and assuming a BR of 1 for the given decay. The limit quoted is for indirect decays using the neutralino constraint of 39.5 GeV, also derived in ABDALLAH 04M. For indirect decays via  $LL\tilde{E}$  the limit decreases to 86 GeV if the constraint from the neutralino is not used. Supersedes the result of ABREU 00U.

### Long-lived $\tilde{\ell}$ (Slepton) mass limit

Limits on scalar leptons which leave detector before decaying. Limits from Z decays are independent of lepton flavor. Limits from continuum  $e^+e^-$  annihilation are also independent of flavor for smuons and staus. Selection limits from  $e^+e^-$  collisions in the continuum depend on MSSM parameters because of the additional neutralino exchange contribution.

VALUE (GeV)	CL%	DOCUMENT ID	TECN	COMMENT
>430	95	<sup>1</sup> AABOUD	19AT ATLS	long-lived $\tilde{\tau}$ , GMSB
>490	95	<sup>2</sup> KHACHATRYAN	16BW CMS	long-lived $\tilde{\tau}$ from inclusive production, mGMSB SPS line 7 scenario
>240	95	<sup>2</sup> KHACHATRYAN	16BW CMS	long-lived $\tilde{\tau}$ from direct pair production, mGMSB SPS line 7 scenario
>440	95	<sup>3</sup> AAD	15AE ATLS	mGMSB, $M_{mess} = 250$ TeV, $N_S = 3$ , $\mu > 0$ , $C_{grav} = 5000$ , $\tan\beta = 10$
>385	95	<sup>3</sup> AAD	15AE ATLS	mGMSB, $M_{mess} = 250$ TeV, $N_S = 3$ , $\mu > 0$ , $C_{grav} = 5000$ , $\tan\beta = 50$
>286	95	<sup>3</sup> AAD	15AE ATLS	direct $\tilde{\tau}$ production
none 124–309	95	<sup>4</sup> AAIJ	15BD LHCB	long-lived $\tilde{\tau}$ , mGMSB, SP57
> 98	95	<sup>5</sup> ABBIENDI	03L OPAL	$\tilde{\mu}_R, \tilde{\tau}_R$
none 2–87.5	95	<sup>6</sup> ABREU	00Q DLPH	$\tilde{\mu}_R, \tilde{\tau}_R$
> 81.2	95	<sup>7</sup> ACCIARRI	99H L3	$\tilde{\mu}_R, \tilde{\tau}_R$
> 81	95	<sup>8</sup> BARATE	98K ALEP	$\tilde{\mu}_R, \tilde{\tau}_R$

- • • We do not use the following data for averages, fits, limits, etc. • • •
- >300 95 <sup>9</sup> AAD 13AA ATLS long-lived  $\tilde{\tau}$ , GMSB,  $\tan\beta = 5$ –20
- >339 95 <sup>10</sup> ABAZOV 13B D0 long-lived  $\tilde{\tau}$ , 100  $< m_{\tilde{\tau}} < 300$  GeV
- >500 95 <sup>11,12</sup> CHATRCHYAN 13AB CMS long-lived  $\tilde{\tau}$ , direct  $\tilde{\tau}_1$  pair prod., minimal GMSB, SPS line 7
- >314 95 <sup>11,13</sup> CHATRCHYAN 13AB CMS long-lived  $\tilde{\tau}$ ,  $\tilde{\tau}_1$  from direct pair prod. and from decay of heavier SUSY particles, minimal GMSB, SPS line 7
- >136 95 <sup>14</sup> CHATRCHYAN 12L CMS long-lived  $\tilde{\tau}$ ,  $\tilde{\tau}_1$  from decay of heavier SUSY particles, minimal GMSB, SPS line 7
- <sup>15</sup> AAD 11P ATLS stable  $\tilde{\tau}$ , GMSB scenario,  $\tan\beta=5$
- <sup>1</sup> AABOUD 19AT searched in 36.1 fb<sup>-1</sup> of pp collisions at  $\sqrt{s} = 13$  TeV for metastable and stable R-hadrons. Multiple search strategies for a wide range of lifetimes, corresponding to path lengths of a few meters, are defined. No significant deviations from the expected Standard Model background are observed. Results are interpreted in terms of exclusion limits on long-lived stau in the context of GMSB models. Lower limits on the mass for direct production of staus are set at 430 GeV, see their Fig. 10 (left).
- <sup>2</sup> KHACHATRYAN 16BW searched in 2.5 fb<sup>-1</sup> of pp collisions at  $\sqrt{s} = 13$  TeV for events with heavy stable charged particles, identified by their anomalously high energy deposits in the silicon tracker and/or long time-of-flight measurements by the muon system. No evidence for an excess over the expected background is observed. Limits are derived for pair production of tau sleptons as a function of mass, depending on their direct or inclusive production in a minimal GMSB scenario along the Snowmass Points and Slopes (SPS) line 7, see Fig. 4 and Table 7.
- <sup>3</sup> AAD 15AE searched in 19.1 fb<sup>-1</sup> of pp collisions at  $\sqrt{s} = 8$  TeV for heavy long-lived charged particles, measured through their specific ionization energy loss in the ATLAS pixel detector or their time-of-flight in the ATLAS muon system. In the absence of an excess of events above the expected backgrounds, limits are set on stable  $\tilde{\tau}$  sleptons in various scenarios, see Figs. 5–7.
- <sup>4</sup> AAIJ 15BD searched in 3.0 fb<sup>-1</sup> of pp collisions at  $\sqrt{s} = 7$  and 8 TeV for evidence of Drell-Yan pair production of long-lived  $\tilde{\tau}$  particles. No evidence for such particles is observed and 95% C.L. upper limits on the cross section of  $\tilde{\tau}$  pair production are derived, see Fig. 7. In the mGMSB, assuming the SP57 benchmark scenario  $\tilde{\tau}$  masses between 124 and 309 GeV are excluded at 95% C.L.
- <sup>5</sup> ABBIENDI 03L used  $e^+e^-$  data at  $\sqrt{s} = 130$ –209 GeV to select events with two high momentum tracks with anomalous dE/dx. The excluded cross section is compared to the theoretical expectation as a function of the heavy particle mass in their Fig. 3. The limit improves to 98.5 GeV for  $\tilde{\mu}_L$  and  $\tilde{\tau}_L$ . The bounds are valid for colorless spin 0 particles with lifetimes longer than  $10^{-6}$  s. Supersedes the results from ACKERSTAFF 98P.
- <sup>6</sup> ABREU 00Q searches for the production of pairs of heavy, charged stable particles in  $e^+e^-$  annihilation at  $\sqrt{s} = 130$ –189 GeV. The upper bound improves to 88 GeV for  $\tilde{\mu}_L, \tilde{\tau}_L$ . These limits include and update the results of ABREU 98P.
- <sup>7</sup> ACCIARRI 99H searched for production of pairs of back-to-back heavy charged particles at  $\sqrt{s} = 130$ –183 GeV. The upper bound improves to 82.2 GeV for  $\tilde{\mu}_L, \tilde{\tau}_L$ .
- <sup>8</sup> The BARATE 98k mass limit improves to 82 GeV for  $\tilde{\mu}_L, \tilde{\tau}_L$ . Data collected at  $\sqrt{s} = 161$ –184 GeV.
- <sup>9</sup> AAD 13AA searched in 4.7 fb<sup>-1</sup> of pp collisions at  $\sqrt{s} = 7$  TeV for events containing long-lived massive particles in a GMSB framework. No significant excess above the expected background was found. A 95% C.L. lower limit of 300 GeV is placed on long-lived  $\tilde{\tau}$ 's in the GMSB model with  $M_{mess} = 250$  TeV,  $N_S = 3$ ,  $\mu > 0$ , for  $\tan\beta = 5$ –20. The lower limit on the GMSB breaking scale  $\Lambda$  was found to be 99–110 TeV, for  $\tan\beta$  values between 5 and 40, see Fig. 4 (top). Also, directly produced long-lived sleptons, or sleptons decaying to long-lived ones, are excluded at 95% C.L. up to a  $\tilde{\tau}$  mass of 278 GeV for models with slepton splittings smaller than 50 GeV.
- <sup>10</sup> ABAZOV 13b looked in 6.3 fb<sup>-1</sup> of p $\bar{p}$  collisions at  $\sqrt{s} = 1.96$  TeV for charged massive long-lived particles in events with muon-like particles that have both speed and ionization energy loss inconsistent with muons produced in beam collisions. In the absence of an excess, limits are set at 95% C.L. on the production cross section of stau leptons in the mass range 100–300 GeV, see their Table 20 and Fig. 23.
- <sup>11</sup> CHATRCHYAN 13AB looked in 5.0 fb<sup>-1</sup> of pp collisions at  $\sqrt{s} = 7$  TeV and in 18.8 fb<sup>-1</sup> of pp collisions at  $\sqrt{s} = 8$  TeV for events with heavy stable particles, identified by their anomalous dE/dx in the tracker and additionally requiring that it be identified as muon in the muon chambers, from pair production of  $\tilde{\tau}_1$ 's. No evidence for an excess over the expected background is observed. Supersedes CHATRCHYAN 12L.
- <sup>12</sup> CHATRCHYAN 13AB limits are derived for pair production of  $\tilde{\tau}_1$  as a function of mass in minimal GMSB scenarios along the Snowmass Points and Slopes (SPS) line 7 (see Fig. 8 and Table 7). The limit given here is valid for direct pair  $\tilde{\tau}_1$  production.
- <sup>13</sup> CHATRCHYAN 13AB limits are derived for the production of  $\tilde{\tau}_1$  as a function of mass in minimal GMSB scenarios along the Snowmass Points and Slopes (SPS) line 7 (see Fig. 8 and Table 7). The limit given here is valid for the production of  $\tilde{\tau}_1$  from both direct pair production and from the decay of heavier supersymmetric particles.
- <sup>14</sup> CHATRCHYAN 12L looked in 5.0 fb<sup>-1</sup> of pp collisions at  $\sqrt{s} = 7$  TeV for events with heavy stable particles, identified by their anomalous dE/dx in the tracker or additionally requiring that it be identified as muon in the muon chambers, from pair production of  $\tilde{\tau}_1$ 's. No evidence for an excess over the expected background is observed. Limits are derived for the production of  $\tilde{\tau}_1$  as a function of mass in minimal GMSB scenarios along the Snowmass Points and Slopes (SPS) line 7 (see Fig. 3). The limit given here is valid for the production of  $\tilde{\tau}_1$  in the decay of heavier supersymmetric particles.
- <sup>15</sup> AAD 11P looked in 37 pb<sup>-1</sup> of pp collisions at  $\sqrt{s} = 7$  TeV for events with two heavy stable particles, reconstructed in the Inner tracker and the Muon System and identified by their time of flight in the Muon System. No evidence for an excess over the SM expectation is observed. Limits on the mass are derived, see Fig. 3, for  $\tilde{\tau}$  in a GMSB scenario and for sleptons produced by electroweak processes only, in which case the limit degrades to 110 GeV.

# Searches Particle Listings

## Supersymmetric Particle Searches

### $\tilde{q}$ (Squark) mass limit

For  $m_{\tilde{q}} > 60\text{--}70$  GeV, it is expected that squarks would undergo a cascade decay via a number of neutralinos and/or charginos rather than undergo a direct decay to photinos as assumed by some papers. Limits obtained when direct decay is assumed are usually higher than limits when cascade decays are included.

Limits from  $e^+e^-$  collisions depend on the mixing angle of the lightest mass eigenstate  $\tilde{q}_1 = \tilde{q}_R \sin\theta_q + \tilde{q}_L \cos\theta_q$ . It is usually assumed that only the sbottom and stop squarks have non-trivial mixing angles (see the stop and sbottom sections). Here, unless otherwise noted, squarks are always taken to be either left/right degenerate, or purely of left or right type. Data from  $Z$  decays have set squark mass limits above 40 GeV, in the case of  $\tilde{q} \rightarrow q\tilde{\chi}_1^0$  decays if  $\Delta m = m_{\tilde{q}} - m_{\tilde{\chi}_1^0} \gtrsim 5$  GeV. For smaller values of  $\Delta m$ , current constraints on the invisible width of the  $Z$  ( $\Delta\Gamma_{\text{inv}} < 2.0$  MeV, LEP 00) exclude  $m_{\tilde{u}_{L,R}} < 44$  GeV,  $m_{\tilde{d}_R} < 33$  GeV,  $m_{\tilde{t}} < 44$  GeV and, assuming all squarks degenerate,  $m_{\tilde{q}} < 45$  GeV.

Some earlier papers are now obsolete and have been omitted. They were last listed in our PDG 14 edition: K. Olive, *et al.* (Particle Data Group), Chinese Physics **C38** 070001 (2014) (<http://pdg.lbl.gov>).

### R-parity conserving $\tilde{q}$ (Squark) mass limit

VALUE (GeV)	CL%	DOCUMENT ID	TECN	COMMENT
>1590	95	1 SIRUNYAN	19AG CMS	$2\gamma + \cancel{E}_T$ , Tsqk4B, 5.00 GeV $< m_{\tilde{\chi}_1^0} < 1500$ GeV
>1130	95	2 SIRUNYAN	19CH CMS	$\text{jets} + \cancel{E}_T$ , Tsqk1, 1 light flavour, $m_{\tilde{\chi}_1^0} = 0$ GeV
>1630	95	2 SIRUNYAN	19CH CMS	$\text{jets} + \cancel{E}_T$ , Tsqk1, 8 degenerate light flavours, $m_{\tilde{\chi}_1^0} = 0$ GeV
>1430	95	3 SIRUNYAN	19K CMS	$\gamma + \ell + \cancel{E}_T$ , Tsqk4A, $m_{\tilde{\chi}_1^0} = 1200$ GeV
>1200	95	4 AABOUD	18BJ ATLS	$\ell^\pm \ell^\mp + \text{jets} + \cancel{E}_T$ , Tsqk2, $m_{\tilde{\chi}_1^0} = 1$ GeV, any $m_{\tilde{\chi}_2^0}$
> 850	95	5 AABOUD	18BV ATLS	$c\text{-jets} + \cancel{E}_T$ , Tsqk1 (charm only), $m_{\tilde{\chi}_1^0} = 0$ GeV
> 710	95	6 AABOUD	18I ATLS	$\geq 1 \text{ jets} + \cancel{E}_T$ , Tsqk1, $m_{\tilde{q}} \sim m_{\tilde{\chi}_1^0}$
>1820	95	7 AABOUD	18U ATLS	$2\gamma + \cancel{E}_T$ , GGM, Tsqk4B, any NLSP mass
>1550	95	8 AABOUD	18V ATLS	$\text{jets} + \cancel{E}_T$ , Tsqk1, $m_{\tilde{\chi}_1^0} = 0$ GeV
>1150	95	9 AABOUD	18V ATLS	$\text{jets} + \cancel{E}_T$ , Tsqk3, $m_{\tilde{\chi}_1^\pm} = 0.5$ ( $m_{\tilde{q}} + m_{\tilde{\chi}_1^0}$ ), $m_{\tilde{\chi}_1^0} = 0$ GeV
>1650	95	10 SIRUNYAN	18AA CMS	$\geq 1\gamma + \cancel{E}_T$ , Tsqk4A
>1750	95	10 SIRUNYAN	18AA CMS	$\geq 1\gamma + \cancel{E}_T$ , Tsqk4B
> 675	95	11 SIRUNYAN	18AY CMS	$\text{jets} + \cancel{E}_T$ , Tsqk1, 1 light flavor state, $m_{\tilde{\chi}_1^0} = 0$ GeV
>1320	95	11 SIRUNYAN	18AY CMS	$\text{jets} + \cancel{E}_T$ , Tsqk1, 8 degenerate light flavor states, $m_{\tilde{\chi}_1^0} = 0$ GeV
>1220	95	12 AABOUD	17AR ATLS	$1\ell + \text{jets} + \cancel{E}_T$ , Tsqk3, $m_{\tilde{\chi}_1^0} = 0$ GeV
>1000	95	13 AABOUD	17N ATLS	2 same-flavour, opposite-sign $\ell + \text{jets} + \cancel{E}_T$ , Tsqk2, $m_{\tilde{\chi}_1^0} = 0$ GeV
>1150	95	14 KHACHATRY...17P	CMS	1 or more $\text{jets} + \cancel{E}_T$ , Tsqk1, 4(flavor) x 2(isospin) = 8 mass degenerate states, $m_{\tilde{\chi}_1^0} = 0$ GeV
> 575	95	14 KHACHATRY...17P	CMS	1 or more $\text{jets} + \cancel{E}_T$ , Tsqk1, one light flavor state, $m_{\tilde{\chi}_1^0} = 0$ GeV
>1370	95	15 KHACHATRY...17V	CMS	$2\gamma + \cancel{E}_T$ , GGM, Tsqk4, any NLSP mass
>1600	95	16 SIRUNYAN	17AY CMS	$\gamma + \text{jets} + \cancel{E}_T$ , Tsqk4B, $m_{\tilde{\chi}_1^0} = 0$ GeV
>1370	95	16 SIRUNYAN	17AY CMS	$\gamma + \text{jets} + \cancel{E}_T$ , Tsqk4A, $m_{\tilde{\chi}_1^0} = 0$ GeV
>1050	95	17 SIRUNYAN	17AZ CMS	$\geq 1 \text{ jets} + \cancel{E}_T$ , Tsqk1, single light flavor state, $m_{\tilde{\chi}_1^0} = 0$ GeV
>1550	95	17 SIRUNYAN	17AZ CMS	$\geq 1 \text{ jets} + \cancel{E}_T$ , Tsqk1, 4(flavor) x 2(isospin) = 8 degenerate mass states, $m_{\tilde{\chi}_1^0} = 0$ GeV
>1390	95	18 SIRUNYAN	17P CMS	$\text{jets} + \cancel{E}_T$ , Tsqk1, 4(flavor) x 2(isospin) = 8 degenerate mass states, $m_{\tilde{\chi}_1^0} = 0$ GeV
> 950	95	18 SIRUNYAN	17P CMS	$\text{jets} + \cancel{E}_T$ , Tsqk1, one light flavor state, $m_{\tilde{\chi}_1^0} = 0$ GeV
> 608	95	19 AABOUD	16D ATLS	$\geq 1 \text{ jet} + \cancel{E}_T$ , Tsqk1, $m_{\tilde{q}} - m_{\tilde{\chi}_1^0} = 5$ GeV

>1030	95	20 AABOUD	16N ATLS	$\geq 2 \text{ jets} + \cancel{E}_T$ , Tsqk1, $m_{\tilde{\chi}_1^0} = 0$ GeV
> 600	95	21 KHACHATRY...16Bs	CMS	$\text{jets} + \cancel{E}_T$ , Tsqk1, single light squark, $m_{\tilde{\chi}_1^0} = 0$ GeV
>1260	95	21 KHACHATRY...16Bs	CMS	$\text{jets} + \cancel{E}_T$ , Tsqk1, 8 degenerate light squarks, $m_{\tilde{\chi}_1^0} = 0$ GeV
> 850	95	22 AAD	15BV ATLS	$\text{jets} + \cancel{E}_T$ , $\tilde{q} \rightarrow q\tilde{\chi}_1^0$ , $m_{\tilde{\chi}_1^0} = 100$ GeV
> 250	95	23 AAD	15Cs ATLS	photon $+ \cancel{E}_T$ , $p\bar{p} \rightarrow \tilde{q}\tilde{q}^*\gamma$ , $\tilde{q} \rightarrow q\tilde{\chi}_1^0$ , $m_{\tilde{q}} - m_{\tilde{\chi}_1^0} = m_c$
> 490	95	24 AAD	15K ATLS	$\tilde{c} \rightarrow c\tilde{\chi}_1^0$ , $m_{\tilde{\chi}_1^0} < 200$ GeV
> 875	95	25 KHACHATRY...15AF	CMS	$\tilde{q} \rightarrow q\tilde{\chi}_1^0$ , simplified model, 8 degenerate light $\tilde{q}$ , $m_{\tilde{\chi}_1^0} = 0$
> 520	95	25 KHACHATRY...15AF	CMS	$\tilde{q} \rightarrow q\tilde{\chi}_1^0$ , simplified model, single light squark, $m_{\tilde{\chi}_1^0} = 0$
>1450	95	25 KHACHATRY...15AF	CMS	CMSSM, $\tan\beta = 30$ , $A_0 = -2\max(m_0, m_{1/2})$ , $\mu > 0$
> 850	95	26 AAD	14AE ATLS	$\text{jets} + \cancel{E}_T$ , $\tilde{q} \rightarrow q\tilde{\chi}_1^0$ simplified model, mass degenerate first and second generation squarks, $m_{\tilde{\chi}_1^0} = 0$ GeV
> 440	95	26 AAD	14AE ATLS	$\text{jets} + \cancel{E}_T$ , $\tilde{q} \rightarrow q\tilde{\chi}_1^0$ simplified model, single light-flavour squark, $m_{\tilde{\chi}_1^0} = 0$ GeV
>1700	95	26 AAD	14AE ATLS	$\text{jets} + \cancel{E}_T$ , mSUGRA/CMSSM, $m_{\tilde{q}} = m_{\tilde{g}}$
> 800	95	27 CHATRCHYAN14AH	CMS	$\text{jets} + \cancel{E}_T$ , $\tilde{q} \rightarrow q\tilde{\chi}_1^0$ simplified model, $m_{\tilde{\chi}_1^0} = 50$ GeV
> 780	95	28 CHATRCHYAN14I	CMS	multijets $+ \cancel{E}_T$ , $\tilde{q} \rightarrow q\tilde{\chi}_1^0$ simplified model, $m_{\tilde{\chi}_1^0} < 200$ GeV
>1360	95	29 AAD	13L ATLS	$\text{jets} + \cancel{E}_T$ , CMSSM, $m_{\tilde{g}} = m_{\tilde{q}}$
>1200	95	30 AAD	13Q ATLS	$\gamma + b + \cancel{E}_T$ , higgsino-like neutralino, $m_{\tilde{\chi}_1^0} > 220$ GeV, GMSB
>1250	95	31 CHATRCHYAN13	CMS	$\ell^\pm \ell^\mp + \text{jets} + \cancel{E}_T$ , CMSSM
>1430	95	32 CHATRCHYAN13G	CMS	$0,1,2, \geq 3 b\text{-jets} + \cancel{E}_T$ , CMSSM, $m_{\tilde{q}} = m_{\tilde{g}}$
> 750	95	33 CHATRCHYAN13H	CMS	$2\gamma + \geq 4 \text{ jets} + \text{low } \cancel{E}_T$ , stealth SUSY model
> 820	95	34 CHATRCHYAN13T	CMS	$\text{jets} + \cancel{E}_T$ , $\tilde{q} \rightarrow q\tilde{\chi}_1^0$ simplified model, $m_{\tilde{\chi}_1^0} = 0$ GeV
>1200	95	35 AAD	12AX ATLS	$\ell + \text{jets} + \cancel{E}_T$ , CMSSM, $m_{\tilde{q}} = m_{\tilde{g}}$
> 870	95	36 AAD	12CJ ATLS	$\ell^\pm + \text{jets} + \cancel{E}_T$ , CMSSM, $m_{\tilde{q}} = m_{\tilde{g}}$
> 950	95	37 AAD	12CP ATLS	$2\gamma + \cancel{E}_T$ , GMSB, bino NLSP, $m_{\tilde{\chi}_1^0} > 50$ GeV
> 760	95	38 AAD	12W ATLS	$\text{jets} + \cancel{E}_T$ , CMSSM, $m_{\tilde{q}} = m_{\tilde{g}}$
>1110	95	39 CHATRCHYAN12	CMS	$e, \mu, \text{jets, razor}$ , CMSSM
>1180	95	40 CHATRCHYAN12AE	CMS	$\text{jets} + \cancel{E}_T$ , $\tilde{q} \rightarrow q\tilde{\chi}_1^0$ , $m_{\tilde{\chi}_1^0} < 200$ GeV
>1080	95	41 CHATRCHYAN12AT	CMS	$\text{jets} + \cancel{E}_T$ , CMSSM
> 300	95	41 CHATRCHYAN12AT	CMS	$\text{jets} + \cancel{E}_T$ , CMSSM, $m_{\tilde{q}} = m_{\tilde{g}}$
> 300	95	42 AABOUD	18v ATLS	$\text{jets} + \cancel{E}_T$ , Tsqk5, $(m_{\tilde{\chi}_2^0} - m_{\tilde{\chi}_1^0}) / (m_{\tilde{q}} - m_{\tilde{\chi}_1^0}) < 0.95$ , $m_{\tilde{\chi}_1^0} = 60$ GeV
> 790	95	43 KHACHATRY...16BT	CMS	19-parameter pMSSM model, global Bayesian analysis, flat prior
> 820	95	44 AAD	15AI ATLS	$\ell^\pm + \text{jets} + \cancel{E}_T$
> 700	95	22 AAD	15BV ATLS	$\text{jets} + \cancel{E}_T$ , $m_{\tilde{g}} = m_{\tilde{q}}$ , $m_{\tilde{\chi}_1^0} = 1$ GeV
> 820	95	22 AAD	15BV ATLS	$\text{jets} + \cancel{E}_T$ , $\tilde{q} \rightarrow qW\tilde{\chi}_1^0$ , $m_{\tilde{\chi}_1^0} = 100$ GeV
> 850	95	22 AAD	15BV ATLS	2 or 3 leptons + jets, $\tilde{q}$ decays via sleptons, $m_{\tilde{\chi}_1^0} = 100$ GeV
> 700	95	22 AAD	15BV ATLS	$\tau, \tilde{q}$ decays via staus, $m_{\tilde{\chi}_1^0} = 50$ GeV
> 550	95	45 KHACHATRY...15AR	CMS	$\tilde{q} \rightarrow q\tilde{\chi}_1^0, \tilde{\chi}_1^0 \rightarrow \tilde{3}g, \tilde{3} \rightarrow S\tilde{G}, S \rightarrow gg, m_{\tilde{S}} = 100$ GeV, $m_{\tilde{S}} = 90$ GeV
> 1500	95	45 KHACHATRY...15AR	CMS	$\ell^\pm, \tilde{q} \rightarrow q\tilde{\chi}_1^\pm, \tilde{\chi}_1^\pm \rightarrow \tilde{3}W^\pm, \tilde{3} \rightarrow S\tilde{G}, S \rightarrow gg, m_{\tilde{S}} = 100$ GeV, $m_{\tilde{S}} = 90$ GeV
>1500	95	46 KHACHATRY...15AZ	CMS	$\geq 2\gamma, \geq 1 \text{ jet}$ , (Razor), bino-like NLSP, $m_{\tilde{\chi}_1^0} = 375$ GeV
>1000	95	46 KHACHATRY...15AZ	CMS	$\geq 1\gamma, \geq 2 \text{ jet}$ , wino-like NLSP, $m_{\tilde{\chi}_1^0} = 375$ GeV

••• We do not use the following data for averages, fits, limits, etc. •••

> 670	95	47 AAD	14E ATLS	$\ell^\pm \ell^\pm (\ell^\mp) + \text{jets}, \tilde{q} \rightarrow q' \tilde{\chi}_1^\pm, \tilde{\chi}_1^\pm \rightarrow W^{(*)} \tilde{\chi}_2^0, \tilde{\chi}_2^0 \rightarrow Z^{(*)} \tilde{\chi}_1^0$ simplified model, $m_{\tilde{\chi}_1^0} < 300$ GeV
> 780	95	47 AAD	14E ATLS	$\ell^\pm \ell^\pm (\ell^\mp) + \text{jets}, \tilde{q} \rightarrow q' \tilde{\chi}_1^\pm / \tilde{\chi}_2^0, \tilde{\chi}_1^\pm \rightarrow \ell^\pm \nu \tilde{\chi}_1^0, \tilde{\chi}_2^0 \rightarrow \ell^\pm \tilde{\chi}_1^0$ simplified model
> 700	95	48 CHATRCHYAN13Ao	CMS	$\ell^\pm \ell^\mp + \text{jets} + \cancel{E}_T$ , CMSSM, $m_0 < 700$ GeV
>1350	95	49 CHATRCHYAN13AV	CMS	jets (+ leptons) + $\cancel{E}_T$ , CMSSM, $m_{\tilde{g}} = m_{\tilde{q}}$
> 800	95	50 CHATRCHYAN13W	CMS	$\geq 1$ photons + jets + $\cancel{E}_T$ , GGM, wino-like NLSP, $m_{\tilde{\chi}_1^0} = 375$ GeV
>1000	95	50 CHATRCHYAN13W	CMS	$\geq 2$ photons + jets + $\cancel{E}_T$ , GGM, bino-like NLSP, $m_{\tilde{\chi}_1^0} = 375$ GeV
> 340	95	51 DREINER	12A THEO	$m_{\tilde{q}} \sim m_{\tilde{\chi}_1^0}$
> 650	95	52 DREINER	12A THEO	$m_{\tilde{q}} = m_{\tilde{g}} \sim m_{\tilde{\chi}_1^0}$

- <sup>1</sup> SIRUNYAN 19AG searched in  $35.9 \text{ fb}^{-1}$  of  $pp$  collisions at  $\sqrt{s} = 13 \text{ TeV}$  for events with two photons and large  $\cancel{E}_T$ . No significant excess above the Standard Model expectations is observed. Limits are set on the gluino mass in the Tglu4B simplified model and on the squark mass in the Tsqk4B simplified model, see their Figure 3.
- <sup>2</sup> SIRUNYAN 19CH searched in  $137 \text{ fb}^{-1}$  of  $pp$  collisions at  $\sqrt{s} = 13 \text{ TeV}$  for events containing multiple jets and large  $\cancel{E}_T$ . No significant excess above the Standard Model expectations is observed. Limits are set on the gluino mass in the Tglu1A, Tglu1C, Tglu2A and Tglu3A simplified models, see their Figure 13. Limits are also set on squark, sbottom and stop masses in the Tsqk1, Tsb0t1, Tstop1 simplified models, see their Figure 14.
- <sup>3</sup> SIRUNYAN 19K searched in  $35.9 \text{ fb}^{-1}$  of  $pp$  collisions at  $\sqrt{s} = 13 \text{ TeV}$  for events with a photon, an electron or muon, and large  $\cancel{E}_T$ . No significant excess above the Standard Model expectations is observed. In the framework of GMSB, limits are set on the chargino and neutralino mass in the Tch1n1A simplified model, see their Figure 6. Limits are also set on the gluino mass in the Tglu4A simplified model, and on the squark mass in the Tsqk4A simplified model, see their Figure 7.
- <sup>4</sup> AABOUD 18BJ searched in  $36.1 \text{ fb}^{-1}$  of  $pp$  collisions at  $\sqrt{s} = 13 \text{ TeV}$  in events with two opposite-sign charged leptons (electrons and muons), jets and missing transverse momentum, with various requirements to be sensitive to signals with different kinematic endpoint values in the dilepton invariant mass distribution. The data are found to be consistent with the SM expectation. Results are interpreted in the Tsqk2 model in case of  $m_{\tilde{\chi}_1^0} = 1 \text{ GeV}$ : for any  $m_{\tilde{\chi}_2^0}$ , squark masses below  $1200 \text{ GeV}$  are excluded, see their Fig. 14(b).
- <sup>5</sup> AABOUD 18BV searched in  $36.1 \text{ fb}^{-1}$  of  $pp$  collisions at  $\sqrt{s} = 13 \text{ TeV}$  for events with at least one jet identified as  $c$ -jet, large missing transverse energy and no leptons. Good agreement is observed between the number of events in data and Standard Model predictions. The results are translated into exclusion limits in Tsqk1 models considering only  $\tilde{c}_1$ . In scenarios with massless neutralinos, scharm masses below  $850 \text{ GeV}$  are excluded. If the differences of the  $\tilde{c}_1$  and  $\tilde{\chi}_1^0$  masses is below  $100 \text{ GeV}$ , scharm masses below  $500 \text{ GeV}$  are excluded. See their Fig. 6 and Fig. 7.
- <sup>6</sup> AABOUD 18I searched in  $36.1 \text{ fb}^{-1}$  of  $pp$  collisions at  $\sqrt{s} = 13 \text{ TeV}$  for events with at least one jet with a transverse momentum above  $250 \text{ GeV}$  and no leptons. Good agreement is observed between the number of events in data and Standard Model predictions. The results are translated into exclusion limits in Tsqk1 models. In the compressed scenario with similar squark and neutralino masses, squark masses below  $710 \text{ GeV}$  are excluded. See their Fig. 10(b).
- <sup>7</sup> AABOUD 18U searched in  $36.1 \text{ fb}^{-1}$  of  $pp$  collisions at  $\sqrt{s} = 13 \text{ TeV}$  in events with at least one isolated photon, possibly jets and significant transverse momentum targeting generalised models of gauge-mediated SUSY breaking. No significant excess of events is observed above the SM prediction. Results are interpreted in terms of lower limits on the masses of squark in Tsqk4B models. Masses below  $1820 \text{ GeV}$  are excluded for any NLSP mass, see their Fig. 9.
- <sup>8</sup> AABOUD 18V searched in  $36.1 \text{ fb}^{-1}$  of  $pp$  collisions at  $\sqrt{s} = 13 \text{ TeV}$  in events with no charged leptons, jets and missing transverse momentum. The data are found to be consistent with the SM expectation. Results are interpreted in the Tsqk1 model: squark masses below  $1550 \text{ GeV}$  are excluded for massless LSP, see their Fig. 13(a).
- <sup>9</sup> AABOUD 18V searched in  $36.1 \text{ fb}^{-1}$  of  $pp$  collisions at  $\sqrt{s} = 13 \text{ TeV}$  in events with no charged leptons, jets and missing transverse momentum. The data are found to be consistent with the SM expectation. Results are interpreted in the Tsqk3 model. Assuming that  $m_{\tilde{\chi}_1^\pm} = 0.5 (m_{\tilde{q}} + m_{\tilde{\chi}_1^0})$ , squark masses below  $1150 \text{ GeV}$  are excluded for massless LSP, see their Fig. 14(a). Exclusions are also shown assuming  $m_{\tilde{\chi}_1^0} = 60 \text{ GeV}$ , see their Fig. 14(b).
- <sup>10</sup> SIRUNYAN 18AA searched in  $35.9 \text{ fb}^{-1}$  of  $pp$  collisions at  $\sqrt{s} = 13 \text{ TeV}$  for events with at least one photon and large  $\cancel{E}_T$ . No significant excess above the Standard Model expectations is observed. Limits are set on wino masses in a general gauge-mediated SUSY breaking (GGM) scenario with bino-like  $\tilde{\chi}_1^\pm$  and wino-like  $\tilde{\chi}_1^0$  and  $\tilde{\chi}_2^0$ , see Figure 7. Limits are also set on the NLSP mass in the Tch1n1A and Tch1ch1A simplified models, see their Figure 8. Finally, limits are set on the gluino mass in the Tglu4A and Tglu4B simplified models, see their Figure 9, and on the squark mass in the Tsqk4A and Tsqk4B simplified models, see their Figure 10.
- <sup>11</sup> SIRUNYAN 18AY searched in  $35.9 \text{ fb}^{-1}$  of  $pp$  collisions at  $\sqrt{s} = 13 \text{ TeV}$  for events containing one or more jets and significant  $\cancel{E}_T$ . No significant excess above the Standard Model expectations is observed. Limits are set on the gluino mass in the Tglu1A, Tglu2A and Tglu3A simplified models, see their Figure 3. Limits are also set on squark, sbottom and stop masses in the Tsqk1, Tsb0t1, Tstop1 and Tstop4 simplified models, see their Figure 3. Finally, limits are set on long-lived gluino masses in a Tglu1A simplified model where the gluino is metastable or long-lived with proper decay lengths in the range  $10^{-3} \text{ mm} < c\tau < 10^5 \text{ mm}$ , see their Figure 4.

- <sup>12</sup> AABOUD 17AR searched in  $36.1 \text{ fb}^{-1}$  of  $pp$  collisions at  $\sqrt{s} = 13 \text{ TeV}$  for events with one isolated lepton, at least two jets and large missing transverse momentum. No significant excess above the Standard Model expectations is observed. Limits up to  $1.25 \text{ TeV}$  are set on the 1st and 2nd generation squark masses in Tsqk3 simplified models, with  $x = (m_{\tilde{\chi}_1^\pm} - m_{\tilde{\chi}_1^0}) / (m_{\tilde{q}} - m_{\tilde{\chi}_1^0}) = 1/2$ . Similar limits are obtained for variable  $x$  and fixed neutralino mass,  $m_{\tilde{\chi}_1^0} = 60 \text{ GeV}$ . See their Figure 13.
- <sup>13</sup> AABOUD 17N searched in  $14.7 \text{ fb}^{-1}$  of  $pp$  collisions at  $\sqrt{s} = 13 \text{ TeV}$  for events with 2 same-flavour, opposite-sign leptons (electrons or muons), jets and large missing transverse momentum. The results are interpreted as 95% C.L. limits in Tsqk2 models, assuming  $m_{\tilde{\chi}_1^0} = 0 \text{ GeV}$  and  $m_{\tilde{\chi}_2^0} = 600 \text{ GeV}$ . See their Fig. 12 for exclusion limits as a function of  $m_{\tilde{\chi}_2^0}$ .
- <sup>14</sup> KHACHATRYAN 17P searched in  $2.3 \text{ fb}^{-1}$  of  $pp$  collisions at  $\sqrt{s} = 13 \text{ TeV}$  for events with one or more jets and large  $\cancel{E}_T$ . No significant excess above the Standard Model expectations is observed. Limits are set on the gluino mass in the Tglu1A, Tglu2A, Tglu3A, Tglu3B, Tglu3C and Tglu3D simplified models, see their Figures 7 and 8. Limits are also set on the squark mass in the Tsqk1 simplified model, see their Fig. 7, and on the sbottom mass in the Tsb0t1 simplified model, see Fig. 8. Finally, limits are set on the stop mass in the Tstop1, Tstop3, Tstop4, Tstop6 and Tstop7 simplified models, see Fig. 8.
- <sup>15</sup> KHACHATRYAN 17V searched in  $2.3 \text{ fb}^{-1}$  of  $pp$  collisions at  $\sqrt{s} = 13 \text{ TeV}$  for events with two photons and large  $\cancel{E}_T$ . No significant excess above the Standard Model expectations is observed. Limits are set on the gluino and squark mass in the context of general gauge mediation models Tglu4B and Tsqk4, see their Fig. 4.
- <sup>16</sup> SIRUNYAN 17AY searched in  $35.9 \text{ fb}^{-1}$  of  $pp$  collisions at  $\sqrt{s} = 13 \text{ TeV}$  for events with at least one photon, jets and large  $\cancel{E}_T$ . No significant excess above the Standard Model expectations is observed. Limits are set on the gluino mass in the Tglu4A and Tglu4B simplified models, and on the squark mass in the Tsqk4A and Tsqk4B simplified models, see their Figure 6.
- <sup>17</sup> SIRUNYAN 17AZ searched in  $35.9 \text{ fb}^{-1}$  of  $pp$  collisions at  $\sqrt{s} = 13 \text{ TeV}$  for events with one or more jets and large  $\cancel{E}_T$ . No significant excess above the Standard Model expectations is observed. Limits are set on the gluino mass in the Tglu1A, Tglu2A, Tglu3A simplified models, see their Figures 6. Limits are also set on the squark mass in the Tsqk1 simplified model (for single light squark and for 8 degenerate light squarks), on the sbottom mass in the Tsb0t1 simplified model and on the stop mass in the Tstop1 simplified model, see their Fig. 7. Finally, limits are set on the stop mass in the Tstop2, Tstop4 and Tstop8 simplified models, see Fig. 8.
- <sup>18</sup> SIRUNYAN 17P searched in  $35.9 \text{ fb}^{-1}$  of  $pp$  collisions at  $\sqrt{s} = 13 \text{ TeV}$  for events with multiple jets and large  $\cancel{E}_T$ . No significant excess above the Standard Model expectations is observed. Limits are set on the gluino mass in the Tglu1A, Tglu1C, Tglu2A, Tglu3A and Tglu3D simplified models, see their Fig. 12. Limits are also set on the squark mass in the Tsqk1 simplified model, on the stop mass in the Tstop1 simplified model, and on the sbottom mass in the Tsb0t1 simplified model, see Fig. 13.
- <sup>19</sup> AABOUD 16D searched in  $3.2 \text{ fb}^{-1}$  of  $pp$  collisions at  $\sqrt{s} = 13 \text{ TeV}$  for events with an energetic jet and large missing transverse momentum. The results are interpreted as 95% C.L. limits on masses of first and second generation squarks decaying into a quark and the lightest neutralino in scenarios with  $m_{\tilde{q}} - m_{\tilde{\chi}_1^0} < 25 \text{ GeV}$ . See their Fig. 6.
- <sup>20</sup> AABOUD 16N searched in  $3.2 \text{ fb}^{-1}$  of  $pp$  collisions at  $\sqrt{s} = 13 \text{ TeV}$  for events containing hadronic jets, large  $\cancel{E}_T$ , and no electrons or muons. No significant excess above the Standard Model expectations is observed. First- and second-generation squark masses below  $1030 \text{ GeV}$  are excluded at the 95% C.L. decaying to quarks and a massless lightest neutralino. See their Fig. 7a.
- <sup>21</sup> KHACHATRYAN 16BS searched in  $2.3 \text{ fb}^{-1}$  of  $pp$  collisions at  $\sqrt{s} = 13 \text{ TeV}$  for events with at least one energetic jet, no isolated leptons, and significant  $\cancel{E}_T$ , using the transverse mass variable  $M_{T2}$  to discriminate between signal and background processes. No significant excess above the Standard Model expectations is observed. Limits are set on the squark mass in the Tsqk1 simplified model, both in the assumption of a single light squark and of 8 degenerate squarks, see Fig. 11 and Table 3.
- <sup>22</sup> AAD 15BV summarized and extended ATLAS searches for gluinos and first- and second-generation squarks in final states containing jets and missing transverse momentum, with or without leptons or  $b$ -jets in the  $\sqrt{s} = 8 \text{ TeV}$  data set collected in 2012. The paper reports the results of new interpretations and statistical combinations of previously published analyses, as well as new analyses. Exclusion limits at 95% C.L. are set on the squark mass in several R-parity conserving models. See their Figs. 9, 11, 18, 22, 24, 27, 28.
- <sup>23</sup> AAD 15CS searched in  $20.3 \text{ fb}^{-1}$  of  $pp$  collisions at  $\sqrt{s} = 8 \text{ TeV}$  for evidence of pair production of squarks, decaying into a quark and a neutralino, where a photon was radiated either from an initial-state quark, from an intermediate squark, or from a final-state quark. No evidence was found for an excess above the expected level of Standard Model background and a 95% C.L. exclusion limit was set on the squark mass as a function of the squark-neutralino mass difference, see Fig. 19.
- <sup>24</sup> AAD 15K searched in  $20.3 \text{ fb}^{-1}$  of  $pp$  collisions at  $\sqrt{s} = 8 \text{ TeV}$  for events containing at least two jets, where the two leading jets are each identified as originating from  $c$ -quarks, and large missing transverse momentum. No excess of events above the expected level of Standard Model background was found. Exclusion limits at 95% C.L. are set on the mass of superpartners of charm quarks ( $\tilde{c}$ ). Assuming that the decay  $\tilde{c} \rightarrow c \tilde{\chi}_1^0$  takes place 100% of the time, a scalar charm mass below  $490 \text{ GeV}$  is excluded for  $m_{\tilde{\chi}_1^0} < 200 \text{ GeV}$ . For more details, see their Fig. 2.
- <sup>25</sup> KHACHATRYAN 15AF searched in  $19.5 \text{ fb}^{-1}$  of  $pp$  collisions at  $\sqrt{s} = 8 \text{ TeV}$  for events with at least two energetic jets and significant  $\cancel{E}_T$ , using the transverse mass variable  $M_{T2}$  to discriminate between signal and background processes. No significant excess above the Standard Model expectations is observed. Limits are set on the squark mass in simplified models where the decay  $\tilde{q} \rightarrow q \tilde{\chi}_1^0$  takes place with a branching ratio of 100%, both for the case of a single light squark or 8 degenerate squarks, see Fig. 12. See also Table 5. Exclusions in the CMSSM, assuming  $\tan\beta = 30$ ,  $A_0 = -2 \max(m_0, m_{1/2})$  and  $\mu > 0$ , are also presented, see Fig. 15.
- <sup>26</sup> AAD 14AE searched in  $20.3 \text{ fb}^{-1}$  of  $pp$  collisions at  $\sqrt{s} = 8 \text{ TeV}$  for strongly produced supersymmetric particles in events containing jets and large missing transverse momentum, and no electrons or muons. No excess over the expected SM background is observed. Exclusion limits are derived in simplified models containing squarks that decay via  $\tilde{q} \rightarrow q \tilde{\chi}_1^0$ , where either a single light state or two degenerate generations of squarks are assumed, see Fig. 10.
- <sup>27</sup> CHATRCHYAN 14AH searched in  $4.7 \text{ fb}^{-1}$  of  $pp$  collisions at  $\sqrt{s} = 7 \text{ TeV}$  for events with at least two energetic jets and significant  $\cancel{E}_T$ , using the razor variables ( $M_R$  and

# Searches Particle Listings

## Supersymmetric Particle Searches

- $R^2$ ) to discriminate between signal and background processes. No significant excess above the Standard Model expectations is observed. Limits are set on squark masses in simplified models where the decay  $\tilde{q} \rightarrow q\tilde{\chi}_1^0$  takes place with a branching ratio of 100%, see Fig. 28. Exclusions in the CMSSM, assuming  $\tan\beta = 10$ ,  $A_0 = 0$  and  $\mu > 0$ , are also presented, see Fig. 26.
- 28 CHATRCHYAN 14i searched in  $19.5 \text{ fb}^{-1}$  of  $pp$  collisions at  $\sqrt{s} = 8 \text{ TeV}$  for events containing multijets and large  $\cancel{E}_T$ . No excess over the expected SM background is observed. Exclusion limits are derived in simplified models containing squarks that decay via  $\tilde{q} \rightarrow q\tilde{\chi}_1^0$ , where either a single light state or two degenerate generations of squarks are assumed, see Fig. 7a.
- 29 AAD 13l searched in  $4.7 \text{ fb}^{-1}$  of  $pp$  collisions at  $\sqrt{s} = 7 \text{ TeV}$  for the production of squarks and gluinos in events containing jets, missing transverse momentum and no high- $p_T$  electrons or muons. No excess over the expected SM background is observed. In mSUGRA/CMSSM models with  $\tan\beta = 10$ ,  $A_0 = 0$  and  $\mu > 0$ , squarks and gluinos of equal mass are excluded for masses below 1360 GeV at 95% C.L. In a simplified model containing only squarks of the first two generations, a gluino octet and a massless neutralino, squark masses below 1320 GeV are excluded at 95% C.L. for gluino masses below 2 TeV. See Figures 10–15 for more precise bounds.
- 30 AAD 13q searched in  $4.7 \text{ fb}^{-1}$  of  $pp$  collisions at  $\sqrt{s} = 7 \text{ TeV}$  for events containing a high- $p_T$  isolated photon, at least one jet identified as originating from a bottom quark, and high missing transverse momentum. Such signatures may originate from supersymmetric models with gauge-mediated supersymmetry breaking in events in which one of a pair of higgsino-like neutralinos decays into a photon and a gravitino while the other decays into a Higgs boson and a gravitino. No significant excess above the expected background was found and limits were set on the squark mass as a function of the neutralino mass in a generalized GMSB model (GGM) with a higgsino-like neutralino NLSP, see their Fig. 4. For neutralino masses greater than 220 GeV, squark masses below 1020 GeV are excluded at 95% C.L.
- 31 CHATRCHYAN 13 looked in  $4.98 \text{ fb}^{-1}$  of  $pp$  collisions at  $\sqrt{s} = 7 \text{ TeV}$  for events with two opposite-sign leptons ( $e, \mu, \tau$ ), jets and missing transverse energy. No excess beyond the Standard Model expectation is observed. Exclusion limits are derived in the mSUGRA/CMSSM model with  $\tan\beta = 10$ ,  $A_0 = 0$  and  $\mu > 0$ , see Fig. 6.
- 32 CHATRCHYAN 13c searched in  $4.98 \text{ fb}^{-1}$  of  $pp$  collisions at  $\sqrt{s} = 7 \text{ TeV}$  for the production of squarks and gluinos in events containing 0,1,2,  $\geq 3$   $b$ -jets, missing transverse momentum and no electrons or muons. No excess over the expected SM background is observed. In mSUGRA/CMSSM models with  $\tan\beta = 10$ ,  $A_0 = 0$ , and  $\mu > 0$ , squarks and gluinos of equal mass are excluded for masses below 1250 GeV at 95% C.L. Exclusions are also derived in various simplified models, see Fig. 7.
- 33 CHATRCHYAN 13h searched in  $4.96 \text{ fb}^{-1}$  of  $pp$  collisions at  $\sqrt{s} = 7 \text{ TeV}$  for events with two photons,  $\geq 4$  jets and low  $\cancel{E}_T$  due to  $\tilde{q} \rightarrow \gamma\tilde{\chi}_1^0$  decays in a stealth SUSY framework, where the  $\tilde{\chi}_1^0$  decays through a singlino ( $\tilde{S}$ ) intermediate state to  $\gamma S\tilde{G}$ , with the singlet state  $S$  decaying to two jets. No significant excess above the expected background was found and limits were set in a particular  $R$ -parity conserving stealth SUSY model. The model assumes  $m_{\tilde{\chi}_1^0} = 0.5 m_{\tilde{q}}$ ,  $m_S = 100 \text{ GeV}$  and  $m_S = 90 \text{ GeV}$ . Under these assumptions, squark masses less than 1430 GeV were excluded at the 95% C.L.
- 34 CHATRCHYAN 13t searched in  $11.7 \text{ fb}^{-1}$  of  $pp$  collisions at  $\sqrt{s} = 8 \text{ TeV}$  for events with at least two energetic jets and significant  $\cancel{E}_T$ , using the  $\alpha_T$  variable to discriminate between processes with genuine and misreconstructed  $\cancel{E}_T$ . No significant excess above the Standard Model expectations is observed. Limits are set on squark masses in simplified models where the decay  $\tilde{q} \rightarrow q\tilde{\chi}_1^0$  takes place with a branching ratio of 100%, assuming an eightfold degeneracy of the masses of the first two generation squarks, see Fig. 8 and Table 9. Also limits in the case of a single light squark are given.
- 35 AAD 12ax searched in  $1.04 \text{ fb}^{-1}$  of  $pp$  collisions at  $\sqrt{s} = 7 \text{ TeV}$  for supersymmetry in events containing jets, missing transverse momentum and one isolated electron or muon. No excess over the expected SM background is observed and model-independent limits are set on the cross section of new physics contributions to the signal regions. In mSUGRA/CMSSM models with  $\tan\beta = 10$ ,  $A_0 = 0$  and  $\mu > 0$ , squarks and gluinos of equal mass are excluded for masses below 820 GeV at 95% C.L. Limits are also set on simplified models for squark production and decay via an intermediate chargino and on supersymmetric models with bilinear  $R$ -parity violation. Supersedes AAD 11g.
- 36 AAD 12c searched in  $4.7 \text{ fb}^{-1}$  of  $pp$  collisions at  $\sqrt{s} = 7 \text{ TeV}$  for events containing one or more isolated leptons (electrons or muons), jets and  $\cancel{E}_T$ . The observations are in good agreement with the SM expectations and exclusion limits have been set in number of SUSY models. In the mSUGRA/CMSSM model with  $\tan\beta = 10$ ,  $A_0 = 0$ , and  $\mu > 0$ , 95% C.L. exclusion limits have been derived for  $m_{\tilde{q}} < 1200 \text{ GeV}$ , assuming equal squark and gluino masses. In minimal GMSB, values of the effective SUSY breaking scale  $\Lambda < 50 \text{ TeV}$  are excluded at 95% C.L. for  $\tan\beta < 45$ . Also exclusion limits in a number of simplified models have been presented, see Figs. 10 and 12.
- 37 AAD 12cp searched in  $4.8 \text{ fb}^{-1}$  of  $pp$  collisions at  $\sqrt{s} = 7 \text{ TeV}$  for events with two photons and large  $\cancel{E}_T$  due to  $\tilde{\chi}_1^0 \rightarrow \gamma\tilde{G}$  decays in a GMSB framework. No significant excess above the expected background was found and limits were set on the squark mass as a function of the neutralino mass in a generalized GMSB model (GGM) with a bino-like neutralino NLSP. The other sparticle masses were decoupled,  $\tan\beta = 2$  and  $c\tau_{NLSP} < 0.1 \text{ mm}$ . Also, in the framework of the SPS8 model, a 95% C.L. lower limit was set on the breaking scale  $\Lambda$  of 196 TeV.
- 38 AAD 12w searched in  $1.04 \text{ fb}^{-1}$  of  $pp$  collisions at  $\sqrt{s} = 7 \text{ TeV}$  for the production of squarks and gluinos in events containing jets, missing transverse momentum and no electrons or muons. No excess over the expected SM background is observed. In mSUGRA/CMSSM models with  $\tan\beta = 10$ ,  $A_0 = 0$  and  $\mu > 0$ , squarks and gluinos of equal mass are excluded for masses below 950 GeV at 95% C.L. In a simplified model containing only squarks of the first two generations, a gluino octet and a massless neutralino, squark masses below 875 GeV are excluded at 95% C.L.
- 39 CHATRCHYAN 12 looked in  $35 \text{ pb}^{-1}$  of  $pp$  collisions at  $\sqrt{s} = 7 \text{ TeV}$  for events with  $e$  and/or  $\mu$  and/or jets, a large total transverse energy, and  $\cancel{E}_T$ . The event selection is based on the dimensionless razor variable  $R$ , related to the  $\cancel{E}_T$  and  $M_R$ , an indicator of the heavy particle mass scale. No evidence for an excess over the expected background is observed. Limits are derived in the CMSSM ( $m_0, m_{1/2}$ ) plane for  $\tan\beta = 3, 10$  and 50 (see Fig. 7 and 8). Limits are also obtained for Simplified Model Spectra.
- 40 CHATRCHYAN 12ae searched in  $4.98 \text{ fb}^{-1}$  of  $pp$  collisions at  $\sqrt{s} = 7 \text{ TeV}$  for events with at least three jets and large missing transverse momentum. No significant excesses over the expected SM backgrounds are observed and 95% C.L. limits on the production cross section of squarks in a scenario where  $\tilde{q} \rightarrow q\tilde{\chi}_1^0$  with a 100% branching ratio, see Fig. 3. For  $m_{\tilde{\chi}_1^0} < 200 \text{ GeV}$ , values of  $m_{\tilde{q}}$  below 760 GeV are excluded at 95% C.L. Also limits in the CMSSM are presented, see Fig. 2.
- 41 CHATRCHYAN 12at searched in  $4.73 \text{ fb}^{-1}$  of  $pp$  collisions at  $\sqrt{s} = 7 \text{ TeV}$  for the production of squarks and gluinos in events containing jets, missing transverse momentum and no electrons or muons. No excess over the expected SM background is observed. In mSUGRA/CMSSM models with  $\tan\beta = 10$ ,  $A_0 = 0$  and  $\mu > 0$ , squarks with masses below 1110 GeV are excluded at 95% C.L. Squarks and gluinos of equal mass are excluded for masses below 1180 GeV at 95% C.L. Exclusions are also derived in various simplified models, see Fig. 6.
- 42 AABOU 18v searched in  $36.1 \text{ fb}^{-1}$  of  $pp$  collisions at  $\sqrt{s} = 13 \text{ TeV}$  in events with no charged leptons, jets and missing transverse momentum. The data are found to be consistent with the SM expectation. Results are interpreted in the Tsqk5 model. Squark masses below 1100 GeV are excluded if  $(m_{\tilde{\chi}_2^0} - m_{\tilde{\chi}_1^0})/(m_{\tilde{q}} - m_{\tilde{\chi}_1^0}) < 0.95$  and  $m_{\tilde{\chi}_1^0} = 60 \text{ GeV}$ , see their Fig. 16(a).
- 43 KHACHATRYAN 16bt performed a global Bayesian analysis of a wide range of CMS results obtained with data samples corresponding to  $5.0 \text{ fb}^{-1}$  of  $pp$  collisions at  $\sqrt{s} = 7 \text{ TeV}$  and in  $19.5 \text{ fb}^{-1}$  of  $pp$  collisions at  $\sqrt{s} = 8 \text{ TeV}$ . The set of searches considered, both individually and in combination, includes those with all-hadronic final states, same-sign and opposite-sign dileptons, and multi-lepton final states. An interpretation was given in a scan of the 19-parameter pMSSM. No scan points with a gluino mass less than 500 GeV survived and 98% of models with a squark mass less than 300 GeV were excluded.
- 44 AAD 15ai searched in  $20 \text{ fb}^{-1}$  of  $pp$  collisions at  $\sqrt{s} = 8 \text{ TeV}$  for events containing at least one isolated lepton (electron or muon), jets, and large missing transverse momentum. No excess of events above the expected level of Standard Model background was found. Exclusion limits at 95% C.L. are set on the squark masses in the CMSSM/mSUGRA, see Fig. 15, in the NUHM2, see Fig. 16, and in various simplified models, see Figs. 19–21.
- 45 KHACHATRYAN 15ar searched in  $19.7 \text{ fb}^{-1}$  of  $pp$  collisions at  $\sqrt{s} = 8 \text{ TeV}$  for events containing jets, either a charged lepton or a photon, and low missing transverse momentum. No significant excess above the Standard Model expectations is observed. Limits are set on the squark mass in a stealth SUSY model where the decays  $\tilde{q} \rightarrow q\tilde{\chi}_1^\pm$ ,  $\tilde{\chi}_1^\pm \rightarrow \tilde{S} W^\pm$ ,  $\tilde{S} \rightarrow S\tilde{G}$  and  $S \rightarrow gg$ , with  $m_{\tilde{S}} = 100 \text{ GeV}$  and  $m_S = 90 \text{ GeV}$ , take place with a branching ratio of 100%. See Fig. 6 for  $\gamma$  or Fig. 7 for  $e^\pm$  analyses.
- 46 KHACHATRYAN 15az searched in  $19.7 \text{ fb}^{-1}$  of  $pp$  collisions at  $\sqrt{s} = 8 \text{ TeV}$  for events with either at least one photon, hadronic jets and  $\cancel{E}_T$  (single photon channel) or with at least two photons and at least one jet and using the razor variables. No significant excess above the Standard Model expectations is observed. Limits are set on gluino masses in the general gauge-mediated SUSY breaking model (GGM), for both a bino-like and wino-like neutralino NLSP scenario, see Fig. 8 and 9.
- 47 AAD 14e searched in  $20.3 \text{ fb}^{-1}$  of  $pp$  collisions at  $\sqrt{s} = 8 \text{ TeV}$  for strongly produced supersymmetric particles in events containing jets and two same-sign leptons or three leptons. The search also utilizes jets originating from  $b$ -quarks, missing transverse momentum and other variables. No excess over the expected SM background is observed. Exclusion limits are derived in simplified models containing gluinos and squarks, see Figures 5 and 6. In the  $\tilde{q} \rightarrow q'\tilde{\chi}_1^\pm$ ,  $\tilde{\chi}_1^\pm \rightarrow W^{(*)}\tilde{\chi}_2^0$ ,  $\tilde{\chi}_2^0 \rightarrow Z^{(*)}\tilde{\chi}_1^0$  simplified model, the following assumptions have been made:  $m_{\tilde{\chi}_1^\pm} = 0.5 m_{\tilde{\chi}_2^0} + m_{\tilde{g}}$ ,  $m_{\tilde{\chi}_2^0} = 0.5 (m_{\tilde{\chi}_1^\pm} + m_{\tilde{q}})$ . In the  $\tilde{q} \rightarrow q'\tilde{\chi}_1^\pm$  or  $\tilde{q} \rightarrow q'\tilde{\chi}_2^0$ ,  $\tilde{\chi}_1^\pm \rightarrow e^\pm \nu_{\chi_1^0}$  or  $\tilde{\chi}_2^0 \rightarrow e^\pm e^\mp (\nu\nu)\tilde{\chi}_1^0$  simplified model, the following assumptions have been made:  $m_{\tilde{\chi}_1^\pm} = m_{\tilde{\chi}_2^0} = 0.5 (m_{\tilde{\chi}_1^\pm} + m_{\tilde{q}})$ ,  $m_{\tilde{\chi}_2^0} < 460 \text{ GeV}$ . Limits are also derived in the mSUGRA/CMSSM, bRPV and GMSB models, see their Fig. 8.
- 48 CHATRCHYAN 13ao searched in  $4.98 \text{ fb}^{-1}$  of  $pp$  collisions at  $\sqrt{s} = 7 \text{ TeV}$  for events with two opposite-sign isolated leptons accompanied by hadronic jets and  $\cancel{E}_T$ . No significant excesses over the expected SM backgrounds are observed and 95% C.L. exclusion limits are derived in the mSUGRA/CMSSM model with  $\tan\beta = 10$ ,  $A_0 = 0$  and  $\mu > 0$ , see Fig. 8.
- 49 CHATRCHYAN 13av searched in  $4.7 \text{ fb}^{-1}$  of  $pp$  collisions at  $\sqrt{s} = 7 \text{ TeV}$  for new heavy particle pairs decaying into jets (possibly  $b$ -tagged), leptons and  $\cancel{E}_T$  using the Razor variables. No significant excesses over the expected SM backgrounds are observed and 95% C.L. exclusion limits are derived in the mSUGRA/CMSSM model with  $\tan\beta = 10$ ,  $A_0 = 0$  and  $\mu > 0$ , see Fig. 3. The results are also interpreted in various simplified models, see Fig. 4.
- 50 CHATRCHYAN 13w searched in  $4.93 \text{ fb}^{-1}$  of  $pp$  collisions at  $\sqrt{s} = 7 \text{ TeV}$  for events with one or more photons, hadronic jets and  $\cancel{E}_T$ . No significant excess above the Standard Model expectations is observed. Limits are set on squark masses in the general gauge-mediated SUSY breaking model (GGM), for both a wino-like and bino-like neutralino NLSP scenario, see Fig. 5.
- 51 DREINER 12a reassesses constraints from CMS (at 7 TeV,  $\sim 4.4 \text{ fb}^{-1}$ ) under the assumption that the first and second generation squarks and the lightest SUSY particle are quasi-degenerate in mass (compressed spectrum).
- 52 DREINER 12a reassesses constraints from CMS (at 7 TeV,  $\sim 4.4 \text{ fb}^{-1}$ ) under the assumption that the first and second generation squarks, the gluino, and the lightest SUSY particle are quasi-degenerate in mass (compressed spectrum).

### R-parity violating $\tilde{q}$ (Squark) mass limit

VALUE (GeV)	CL%	DOCUMENT ID	TECN	COMMENT
none 100–720	95	1 SIRUNYAN	18EA CMS	2 large jets with four-parton substructure, $\tilde{q} \rightarrow 4q$
>1600	95	2 KHACHATRYAN 16bx	CMS	$\tilde{q} \rightarrow q\tilde{\chi}_1^0, \tilde{\chi}_1^0 \rightarrow \ell\ell\nu, \lambda_{121}$ or $\lambda_{122} \neq 0, m_{\tilde{g}} = 2400 \text{ GeV}$
>1000	95	3 AAD	15CB ATLS	jets, $\tilde{q} \rightarrow q\tilde{\chi}_1^0, \tilde{\chi}_1^0 \rightarrow \ell q q, m_{\tilde{\chi}_1^0} = 108 \text{ GeV}$ and $2.5 < c\tau_{\tilde{\chi}_1^0} < 200 \text{ mm}$
		4 AAD	12AX ATLS	$\ell + \text{jets} + \cancel{E}_T$ , CMSSM, $m_{\tilde{q}} = m_{\tilde{g}}$
		5 CHATRCHYAN 12al	CMS	$\geq 3\ell^\pm$

- 1 SIRUNYAN 18ea searched in  $38.2 \text{ fb}^{-1}$  of  $pp$  collisions at  $\sqrt{s} = 13 \text{ TeV}$  for the pair production of resonances, each decaying to at least four quarks. Reconstructed particles are clustered into two large jets of similar mass, each consistent with four-parton substructure. No statistically significant excess over the Standard Model expectation is observed. Limits are set on the squark and gluino mass in RPV supersymmetry models where squarks (gluinos) decay, through intermediate higgsinos, to four (five) quarks, see their Figure 4.

- <sup>2</sup> KHACHATRYAN 16BX searched in  $19.5 \text{ fb}^{-1}$  of  $pp$  collisions at  $\sqrt{s} = 8 \text{ TeV}$  for events containing 4 leptons coming from R-parity-violating decays of  $\tilde{\chi}_1^0 \rightarrow \ell\ell\nu$  with  $\lambda_{121} \neq 0$  or  $\lambda_{122} \neq 0$ . No excess over the expected background is observed. Limits are derived on the gluino, squark and stop masses, see Fig. 23.
- <sup>3</sup> AAD 15CB searched for events containing at least one long-lived particle that decays at a significant distance from its production point (displaced vertex, DV) into two leptons or into five or more charged particles in  $20.3 \text{ fb}^{-1}$  of  $pp$  collisions at  $\sqrt{s} = 8 \text{ TeV}$ . The dilepton signature is characterised by DV formed from at least two lepton candidates. Four different final states were considered for the multitrack signature, in which the DV must be accompanied by a high-transverse momentum muon or electron candidate that originates from the DV, jets or missing transverse momentum. No events were observed in any of the signal regions. Results were interpreted in SUSY scenarios involving R-parity violation, split supersymmetry, and gauge mediation. See their Fig. 14–20.
- <sup>4</sup> AAD 12AX searched in  $1.04 \text{ fb}^{-1}$  of  $pp$  collisions at  $\sqrt{s} = 7 \text{ TeV}$  for supersymmetry in events containing jets, missing transverse momentum and one isolated electron or muon. No excess over the expected SM background is observed and model-independent limits are set on the cross section of new physics contributions to the signal regions. In mSUGRA/CMSSM models with  $\tan\beta = 10$ ,  $A_0 = 0$  and  $\mu > 0$ , squarks and gluinos of equal mass are excluded for masses below  $820 \text{ GeV}$  at 95% C.L. Limits are also set on simplified models for squark production and decay via an intermediate chargino and on supersymmetric models with bilinear R-parity violation. Supersedes AAD 11G.
- <sup>5</sup> CHATRCHYAN 12AL looked in  $4.98 \text{ fb}^{-1}$  of  $pp$  collisions at  $\sqrt{s} = 7 \text{ TeV}$  for anomalous production of events with three or more isolated leptons. Limits on squark and gluino masses are set in RPV SUSY models with leptonic  $L\tilde{L}E$  couplings,  $\lambda_{123} > 0.05$ , and hadronic  $U\tilde{D}\tilde{D}$  couplings,  $\lambda_{112}^U > 0.05$ , see their Fig. 5. In the  $U\tilde{D}\tilde{D}$  case the leptons arise from supersymmetric cascade decays. A very specific supersymmetric spectrum is assumed. All decays are prompt.

### Long-lived $\tilde{q}$ (Squark) mass limit

The following are bounds on long-lived scalar quarks, assumed to hadronise into hadrons with lifetime long enough to escape the detector prior to a possible decay. Limits may depend on the mixing angle of mass eigenstates:  $\tilde{q}_1 = \tilde{q}_L \cos\theta_q + \tilde{q}_R \sin\theta_q$ .

The coupling to the  $Z^0$  boson vanishes for up-type squarks when  $\theta_u = 0.98$ , and for down type squarks when  $\theta_d = 1.17$ .

VALUE (GeV)	CL%	DOCUMENT ID	TECN	COMMENT
>1250	95	<sup>1</sup> AABOUD 19AT ATLS	19AT ATLS	$\tilde{b}$ R-hadrons
>1340	95	<sup>2</sup> AABOUD 19AT ATLS	19AT ATLS	$\tilde{t}$ R-hadrons
>1600	95	<sup>3</sup> SIRUNYAN 19BH CMS	19BH CMS	long-lived $\tilde{t}$ , RPV, $\tilde{t} \rightarrow \tilde{d}\tilde{d}$ , $10 \text{ mm} < c\tau < 110 \text{ mm}$
>1350	95	<sup>3</sup> SIRUNYAN 19BH CMS	19BH CMS	long-lived $\tilde{t}$ , RPV, $\tilde{t} \rightarrow b\tilde{l}$ , $7 \text{ mm} < c\tau < 110 \text{ mm}$
> 805	95	<sup>4</sup> AABOUD 16B ATLS	16B ATLS	$\tilde{b}$ R-hadrons
> 890	95	<sup>5</sup> AABOUD 16B ATLS	16B ATLS	$\tilde{t}$ R-hadrons
>1040	95	<sup>6</sup> KHACHATRYAN 16BWCMS	16BWCMS	$\tilde{t}$ R-hadrons, cloud interaction model
>1000	95	<sup>6</sup> KHACHATRYAN 16BWCMS	16BWCMS	$\tilde{t}$ R-hadrons, charge-suppressed interaction model
> 845	95	<sup>7</sup> AAD 15AE ATLS	15AE ATLS	$\tilde{b}$ R-hadron, stable, Regge model
> 900	95	<sup>7</sup> AAD 15AE ATLS	15AE ATLS	$\tilde{t}$ R-hadron, stable, Regge model
>1500	95	<sup>7</sup> AAD 15AE ATLS	15AE ATLS	$\tilde{g}$ decaying to 300 GeV stable sleptons, LeptoSUSY model
> 751	95	<sup>8</sup> AAD 15BM ATLS	15BM ATLS	$\tilde{b}$ R-hadron, stable, Regge model
> 766	95	<sup>8</sup> AAD 15BM ATLS	15BM ATLS	$\tilde{t}$ R-hadron, stable, Regge model
> 525	95	<sup>9</sup> KHACHATRYAN 15AK CMS	15AK CMS	$\tilde{t}$ R-hadrons, $10 \mu\text{s} < \tau < 1000 \text{ s}$
> 470	95	<sup>9</sup> KHACHATRYAN 15AK CMS	15AK CMS	$\tilde{t}$ R-hadrons, $1 \mu\text{s} < \tau < 1000 \text{ s}$
• • • We do not use the following data for averages, fits, limits, etc. • • •				
> 683	95	<sup>10</sup> AAD 13AA ATLS	13AA ATLS	$\tilde{t}$ , R-hadrons, generic interaction model
> 612	95	<sup>11</sup> AAD 13AA ATLS	13AA ATLS	$\tilde{b}$ , R-hadrons, generic interaction model
> 344	95	<sup>12</sup> AAD 13BC ATLS	13BC ATLS	R-hadrons, $\tilde{t} \rightarrow b\tilde{\chi}_1^0$ , Regge model, lifetime between $10^{-5}$ and $10^3 \text{ s}$ , $m_{\tilde{\chi}_1^0} = 100 \text{ GeV}$
> 379	95	<sup>13</sup> AAD 13BC ATLS	13BC ATLS	R-hadrons, $\tilde{t} \rightarrow t\tilde{\chi}_1^0$ , Regge model, lifetime between $10^{-5}$ and $10^3 \text{ s}$ , $m_{\tilde{\chi}_1^0} = 100 \text{ GeV}$
> 935	95	<sup>14</sup> CHATRCHYAN 13AB CMS	13AB CMS	long-lived $\tilde{t}$ forming R-hadrons, cloud interaction model

- <sup>1</sup> AABOUD 19AT searched in  $36.1 \text{ fb}^{-1}$  of  $pp$  collisions at  $\sqrt{s} = 13 \text{ TeV}$  for metastable and stable R-hadrons. Multiple search strategies for a wide range of lifetimes, corresponding to path lengths of a few meters, are defined. No significant deviations from the expected Standard Model background are observed. Sbottom R-hadrons are excluded at 95% C.L. for masses below  $1250 \text{ GeV}$ . Less stringent constraints are achieved with the muon-spectrometer agnostic analysis. See their Figure 9 (bottom-left).
- <sup>2</sup> AABOUD 19AT searched in  $36.1 \text{ fb}^{-1}$  of  $pp$  collisions at  $\sqrt{s} = 13 \text{ TeV}$  for metastable and stable R-hadrons. Multiple search strategies for a wide range of lifetimes, corresponding to path lengths of a few meters, are defined. No significant deviations from the expected Standard Model background are observed. Stop R-hadrons are excluded at 95% C.L. for masses below  $1340 \text{ GeV}$ . Similar constraints are achieved with the muon-spectrometer agnostic analysis. See their Figure 9 (bottom-right).
- <sup>3</sup> SIRUNYAN 19BH searched in  $35.9 \text{ fb}^{-1}$  of  $pp$  collisions at  $\sqrt{s} = 13 \text{ TeV}$  for long-lived particles decaying into jets, with each long-lived particle having a decay vertex well displaced from the production vertex. The selected events are found to be consistent with standard model predictions. Limits are set on the gluino mass in a GMSB model where the gluino is decaying via  $\tilde{g} \rightarrow g\tilde{G}$ , see their Figure 4 and in an RPV model of supersymmetry where the gluino is decaying via  $\tilde{g} \rightarrow \tilde{t}\tilde{b}\tilde{s}$ , see their Figures 5. Limits are also set on the stop mass in two RPV models, see their Figure 6 (for  $\tilde{t} \rightarrow b\tilde{l}$  decays) and Figure 7 (for  $\tilde{t} \rightarrow \tilde{d}\tilde{d}$  decays).
- <sup>4</sup> AABOUD 16B searched in  $3.2 \text{ fb}^{-1}$  of  $pp$  collisions at  $\sqrt{s} = 13 \text{ TeV}$  for long-lived R-hadrons using observables related to large ionization losses and slow propagation velocities, which are signatures of heavy charged particles traveling significantly slower than

the speed of light. Exclusion limits at 95% C.L. are set on the long-lived sbottom masses exceeding  $805 \text{ GeV}$ . See their Fig. 5.

- <sup>5</sup> AABOUD 16B searched in  $3.2 \text{ fb}^{-1}$  of  $pp$  collisions at  $\sqrt{s} = 13 \text{ TeV}$  for long-lived R-hadrons using observables related to large ionization losses and slow propagation velocities, which are signatures of heavy charged particles traveling significantly slower than the speed of light. Exclusion limits at 95% C.L. are set on the long-lived stop masses exceeding  $890 \text{ GeV}$ . See their Fig. 5.
- <sup>6</sup> KHACHATRYAN 16BW searched in  $2.5 \text{ fb}^{-1}$  of  $pp$  collisions at  $\sqrt{s} = 13 \text{ TeV}$  for events with heavy stable charged particles, identified by their anomalously high energy deposits in the silicon tracker and/or long time-of-flight measurements by the muon system. No evidence for an excess over the expected background is observed. Limits are derived for pair production of top squarks as a function of mass, depending on the interaction model, see Fig. 4 and Table 7.
- <sup>7</sup> AAD 15AE searched in  $19.1 \text{ fb}^{-1}$  of  $pp$  collisions at  $\sqrt{s} = 8 \text{ TeV}$  for heavy long-lived charged particles, measured through their specific ionization energy loss in the ATLAS pixel detector or their time-of-flight in the ALTAS muon system. In the absence of an excess of events above the expected backgrounds, limits are set R-hadrons in various scenarios, see Fig. 11. Limits are also set in LeptoSUSY models where the gluino decays to stable  $300 \text{ GeV}$  leptons, see Fig. 9.
- <sup>8</sup> AAD 15BM searched in  $18.4 \text{ fb}^{-1}$  of  $pp$  collisions at  $\sqrt{s} = 8 \text{ TeV}$  for stable and metastable non-relativistic charged particles through their anomalously specific ionization energy loss in the ATLAS pixel detector. In absence of an excess of events above the expected backgrounds, limits are set on stable bottom and top squark R-hadrons, see Table 5.
- <sup>9</sup> KHACHATRYAN 15AK looked in a data set corresponding to  $\text{fb}^{-1}$  of  $pp$  collisions at  $\sqrt{s} = 8 \text{ TeV}$ , and a search interval corresponding to 281 h of trigger lifetime, for long-lived particles that have stopped in the CMS detector. No evidence for an excess over the expected background in a cloud interaction model is observed. Assuming the decay  $\tilde{t} \rightarrow t\tilde{\chi}_1^0$  and lifetimes between  $1 \mu\text{s}$  and  $1000 \text{ s}$ , limits are derived on  $\tilde{t}$  production as a function of  $m_{\tilde{\chi}_1^0}$ , see Figs. 4 and 7. The exclusions require that  $m_{\tilde{\chi}_1^0}$  is kinematically consistent with the minimum values of the jet energy thresholds used.
- <sup>10</sup> AAD 13AA searched in  $4.7 \text{ fb}^{-1}$  of  $pp$  collisions at  $\sqrt{s} = 7 \text{ TeV}$  for events containing colored long-lived particles that hadronize forming R-hadrons. No significant excess above the expected background was found. Long-lived R-hadrons containing a  $\tilde{t}$  are excluded for masses up to  $683 \text{ GeV}$  at 95% C.L. in a general interaction model. Also, limits independent of the fraction of R-hadrons that arrive charged in the muon system were derived, see Fig. 6.
- <sup>11</sup> AAD 13AA searched in  $4.7 \text{ fb}^{-1}$  of  $pp$  collisions at  $\sqrt{s} = 7 \text{ TeV}$  for events containing colored long-lived particles that hadronize forming R-hadrons. No significant excess above the expected background was found. Long-lived R-hadrons containing a  $\tilde{b}$  are excluded for masses up to  $612 \text{ GeV}$  at 95% C.L. in a general interaction model. Also, limits independent of the fraction of R-hadrons that arrive charged in the muon system were derived, see Fig. 6.
- <sup>12</sup> AAD 13BC searched in  $5.0 \text{ fb}^{-1}$  of  $pp$  collisions at  $\sqrt{s} = 7 \text{ TeV}$  and in  $22.9 \text{ fb}^{-1}$  of  $pp$  collisions at  $\sqrt{s} = 8 \text{ TeV}$  for bottom squark R-hadrons that have come to rest within the ATLAS calorimeter and decay at some later time to hadronic jets and a neutralino. In absence of an excess of events above the expected backgrounds, limits are set on sbottom masses for the decay  $\tilde{b} \rightarrow b\tilde{\chi}_1^0$ , for different lifetimes, and for a neutralino mass of  $100 \text{ GeV}$ , see their Table 6 and Fig. 10.
- <sup>13</sup> AAD 13BC searched in  $5.0 \text{ fb}^{-1}$  of  $pp$  collisions at  $\sqrt{s} = 7 \text{ TeV}$  and in  $22.9 \text{ fb}^{-1}$  of  $pp$  collisions at  $\sqrt{s} = 8 \text{ TeV}$  for bottom squark R-hadrons that have come to rest within the ATLAS calorimeter and decay at some later time to hadronic jets and a neutralino. In absence of an excess of events above the expected backgrounds, limits are set on stop masses for the decay  $\tilde{t} \rightarrow t\tilde{\chi}_1^0$ , for different lifetimes, and for a neutralino mass of  $100 \text{ GeV}$ , see their Table 6 and Fig. 10.
- <sup>14</sup> CHATRCHYAN 13AB looked in  $5.0 \text{ fb}^{-1}$  of  $pp$  collisions at  $\sqrt{s} = 7 \text{ TeV}$  and in  $18.8 \text{ fb}^{-1}$  of  $pp$  collisions at  $\sqrt{s} = 8 \text{ TeV}$  for events with heavy stable particles, identified by their anomalous  $dE/dx$  in the tracker or additionally requiring that it be identified as muon in the muon chambers, for pair production of  $\tilde{t}_1$ 's. No evidence for an excess over the expected background is observed. Limits are derived for pair production of stops as a function of mass in the cloud interaction model (see Fig. 8 and Table 6). In the charge-suppressed model, the limit decreases to  $818 \text{ GeV}$ .

### $\tilde{b}$ (Sbottom) mass limit

Limits in  $e^+e^-$  depend on the mixing angle of the mass eigenstate  $\tilde{b}_1 = \tilde{b}_L \cos\theta_b + \tilde{b}_R \sin\theta_b$ . Coupling to the Z vanishes for  $\theta_b \sim 1.17$ . As a consequence, no absolute constraint in the mass region  $\lesssim 40 \text{ GeV}$  is available in the literature at this time from  $e^+e^-$  collisions. In the Listings below, we use  $\Delta m = m_{\tilde{b}_1} - m_{\tilde{\chi}_1^0}$ .

Some earlier papers are now obsolete and have been omitted. They were last listed in our PDG 14 edition: K. Olive, *et al.* (Particle Data Group), Chinese Physics **C38** 070001 (2014) (<http://pdg.lbl.gov>).

### R-parity conserving $\tilde{b}$ (Sbottom) mass limit

VALUE (GeV)	CL%	DOCUMENT ID	TECN	COMMENT
>1500	95	<sup>1</sup> AAD 19H ATLS	19H ATLS	$\geq 3$ b-jets + $E_T$ , Tsbot4, $\geq 1$ $h(\rightarrow b\tilde{b})$ , $m_{\tilde{\chi}_1^0} = 60 \text{ GeV}$
>1300	95	<sup>2</sup> AAD 19H ATLS	19H ATLS	$\geq 3$ b-jets + $E_T$ , Tsbot4, $\geq 1$ $h(\rightarrow b\tilde{b})$ , $m_{\tilde{\chi}_2^0} = m_{\tilde{\chi}_1^0} + 130 \text{ GeV}$
>1220	95	<sup>3</sup> SIRUNYAN 19CH CMS	19CH CMS	jets + $E_T$ , Tsbot1, $m_{\tilde{\chi}_1^0} = 0 \text{ GeV}$
> 530	95	<sup>4</sup> SIRUNYAN 19CI CMS	19CI CMS	$\geq 1$ H ( $\rightarrow \gamma\gamma$ ) + jets + $E_T$ , Tsbot4, $m_{\tilde{\chi}_2^0} = m_{\tilde{\chi}_1^0} + 130 \text{ GeV}$ , $m_{\tilde{\chi}_1^0} = 1 \text{ GeV}$
> 430	95	<sup>5</sup> AABOUD 18I ATLS	18I ATLS	$\geq 1$ jets + $E_T$ , Tsbot1, $m_{\tilde{b}} - m_{\tilde{\chi}_1^0} \sim m_b$



# Searches Particle Listings

## Supersymmetric Particle Searches

> 840	95	6	SIRUNYAN	18AL CMS	$\geq 3\ell^\pm + \text{jets} + \cancel{E}_T$ , Tsb02, $m_{\tilde{\chi}_1^0} = 50$ GeV	> 500	95	36	CHATRCHYAN14H CMS	same-sign $\ell^\pm \ell^\pm, \tilde{b} \rightarrow t \tilde{\chi}_1^\pm, \tilde{\chi}_1^\pm \rightarrow W^\pm \tilde{\chi}_1^0$ simplified model, $m_{\tilde{\chi}_1^\pm} = 2$ GeV, $m_{\tilde{\chi}_1^0} = 100$ GeV
> 975	95	7	SIRUNYAN	18AR CMS	$\ell^\pm \ell^\mp + \text{jets} + \cancel{E}_T$ , Tsb03, $m_{\tilde{\chi}_1^\pm} = (m_{\tilde{\chi}_2^0} + m_{\tilde{\chi}_1^0})/2, m_{\tilde{\chi}_1^0} = 100$ GeV	> 620	95	37	AAD 13AU ATLS	2 $b$ -jets + $\cancel{E}_T, \tilde{b}_1 \rightarrow b \tilde{\chi}_1^0, m_{\tilde{\chi}_1^0} < 120$ GeV
>1060	95	8	SIRUNYAN	18AY CMS	jets + $\cancel{E}_T$ , Tsb01, $m_{\tilde{\chi}_1^0} = 0$ GeV	> 550	95	38	CHATRCHYAN13AT CMS	jets + $\cancel{E}_T, \tilde{b} \rightarrow b \tilde{\chi}_1^0$ simplified model, $m_{\tilde{\chi}_1^0} = 50$ GeV
>1230	95	9	SIRUNYAN	18B CMS	jets + $\cancel{E}_T$ , Tsb01, $m_{\tilde{\chi}_1^0} = 0$ GeV	> 600	95	39	CHATRCHYAN13T CMS	jets + $\cancel{E}_T, \tilde{b} \rightarrow b \tilde{\chi}_1^0$ simplified model, $m_{\tilde{\chi}_1^0} = 0$ GeV
> 420	95	10	SIRUNYAN	18X CMS	$\geq 1 H (\rightarrow \gamma\gamma) + \text{jets} + \cancel{E}_T$ , Tsb04, $m_{\tilde{\chi}_2^0} = m_{\tilde{\chi}_1^0} + 130$ GeV, $m_{\tilde{\chi}_1^0} < 225$ GeV	> 450	95	40	CHATRCHYAN13v CMS	same-sign $\ell^\pm \ell^\pm + \geq 2$ $b$ -jets, $\tilde{b} \rightarrow t \tilde{\chi}_1^\pm, \tilde{\chi}_1^\pm \rightarrow W^\pm \tilde{\chi}_1^0$ simplified model, $m_{\tilde{\chi}_1^0} = 50$ GeV
> 700	95	11	AABOUD	17AJ ATLS	same-sign $\ell^\pm \ell^\pm + 3\ell + \text{jets} + \cancel{E}_T$ , Tsb02, $m_{\tilde{\chi}_1^0} = 0$ GeV	> 390	95	41	AAD 12AN ATLS	$\tilde{b}_1 \rightarrow b \tilde{\chi}_1^0$ , simplified model, $m_{\tilde{\chi}_1^0} < 60$ GeV
> 950	95	12	AABOUD	17AX ATLS	2 $b$ -jets + $\cancel{E}_T$ , Tsb01, $m_{\tilde{\chi}_1^0} = 0$ GeV	> 410	95	42	CHATRCHYAN12AI CMS	$\ell^\pm \ell^\pm + b$ -jets + $\cancel{E}_T$
> 880	95	13	AABOUD	17AX ATLS	2 $b$ -jets + $\cancel{E}_T$ , mixture Tsb01 and Tsb02 BR=50%, $m_{\tilde{\chi}_1^0} = 0$ GeV, $m_{\tilde{\chi}_1^\pm} - m_{\tilde{\chi}_1^0} = 1$ GeV	> 294	95	43	CHATRCHYAN12Bo CMS	$\tilde{b}_1 \rightarrow b \tilde{\chi}_1^0$ , simplified model, $m_{\tilde{\chi}_1^0} = 50$ GeV
> 315	95	14	KHACHATRY...17A	CMS	2 VBF jets + $\cancel{E}_T$ , Tsb01, $m_{\tilde{b}} - m_{\tilde{\chi}_1^0} = 5$ GeV	> 230	95	44	AAD 11K ATLS	stable $b$
> 450	95	15	KHACHATRY...17AW	CMS	$\geq 3\ell^\pm, 2$ jets, Tsb02, $m_{\tilde{\chi}_1^0} = 50$ GeV, $m_{\tilde{\chi}_1^\pm} = 200$ GeV	> 247	95	45	AAD 11o ATLS	$\tilde{g} \rightarrow \tilde{b}_1 b, \tilde{b}_1 \rightarrow b \tilde{\chi}_1^0, m_{\tilde{\chi}_1^0} = 60$ GeV
> 800	95	16	KHACHATRY...17P	CMS	1 or more jets + $\cancel{E}_T$ , Tsb01, $m_{\tilde{\chi}_1^0} = 0$ GeV	> 230	95	46	CHATRCHYAN11D CMS	$\tilde{b}, \tilde{t} \rightarrow b$
>1175	95	17	SIRUNYAN	17AZ CMS	$\geq 1$ jets + $\cancel{E}_T$ , Tsb01, $m_{\tilde{\chi}_1^0} = 0$ GeV	> 247	95	47	AALTONEN 10R CDF	$\tilde{b}_1 \rightarrow b \tilde{\chi}_1^0, m_{\tilde{\chi}_1^0} < 70$ GeV
> 890	95	18	SIRUNYAN	17K CMS	jets + $\cancel{E}_T$ , Tsb01, $m_{\tilde{\chi}_1^0} = 0$ GeV	> 247	95	48	ABAZOV 10L D0	$\tilde{b}_1 \rightarrow b \tilde{\chi}_1^0, m_{\tilde{\chi}_1^0} = 0$ GeV
> 810	95	19	SIRUNYAN	17s CMS	same-sign $\ell^\pm \ell^\pm + \text{jets} + \cancel{E}_T$ , Tsb02, $m_{\tilde{\chi}_1^0} = 50$ GeV, $m_{\tilde{\chi}_1^\pm} = 100$ GeV					
> 323	95	20	AABOUD	16D ATLS	$\geq 1$ jet + $\cancel{E}_T$ , Tsb01, $m_{\tilde{b}} - m_{\tilde{\chi}_1^0} = 5$ GeV					
> 840	95	21	AABOUD	16Q ATLS	2 $b$ -jets + $\cancel{E}_T$ , Tsb01, $m_{\tilde{\chi}_1^0} = 100$ GeV					
> 540	95	22	AAD	16BB ATLS	2 same-sign $3\ell + \text{jets} + \cancel{E}_T$ , Tsb02, $m_{\tilde{\chi}_1^0} < 55$ GeV					
> 680	95	23	KHACHATRY...16BJ	CMS	same-sign $\ell^\pm \ell^\pm$ , Tsb02, $m_{\tilde{\chi}_1^\pm} < 550$ GeV, $m_{\tilde{\chi}_1^0} = 50$ GeV					
> 500	95	23	KHACHATRY...16BJ	CMS	same-sign $\ell^\pm \ell^\pm$ , Tsb02, $m_{\tilde{b}} - m_{\tilde{\chi}_1^0} < 100$ GeV, $m_{\tilde{\chi}_1^0} = 50$ GeV					
> 880	95	24	KHACHATRY...16BS	CMS	jets + $\cancel{E}_T$ , Tsb01, $m_{\tilde{\chi}_1^0} = 0$ GeV					
> 550	95	25	KHACHATRY...16BY	CMS	opposite-sign $\ell^\pm \ell^\pm$ , Tsb03, $m_{\tilde{\chi}_1^0} = 100$ GeV					
> 600	95	26	AAD	15CJ ATLS	$\tilde{b} \rightarrow b \tilde{\chi}_1^0, m_{\tilde{\chi}_1^0} < 250$ GeV					
> 440	95	26	AAD	15CJ ATLS	$\tilde{b} \rightarrow t \tilde{\chi}_1^\pm, \tilde{\chi}_1^\pm \rightarrow W^{(*)} \tilde{\chi}_1^0, m_{\tilde{\chi}_1^0} = 60$ GeV, $m_{\tilde{b}} - m_{\tilde{\chi}_1^\pm} < m_t$					
none 300-650	95	26	AAD	15CJ ATLS	$\tilde{b} \rightarrow \tilde{b} \tilde{\chi}_2^0, \tilde{\chi}_2^0 \rightarrow h \tilde{\chi}_1^0, m_{\tilde{\chi}_1^0} = 60$ GeV, $m_{\tilde{\chi}_2^0} > 250$ GeV					
> 640	95	27	KHACHATRY...15AF	CMS	$\tilde{b} \rightarrow b \tilde{\chi}_1^0, m_{\tilde{\chi}_1^0} = 0$					
> 650	95	28	KHACHATRY...15AH	CMS	$\tilde{b} \rightarrow b \tilde{\chi}_1^0, m_{\tilde{\chi}_1^0} = 0$					
> 250	95	28	KHACHATRY...15AH	CMS	$\tilde{b} \rightarrow b \tilde{\chi}_1^0, m_{\tilde{b}} - m_{\tilde{\chi}_1^0} < 10$ GeV					
> 570	95	29	KHACHATRY...15I	CMS	$\tilde{b} \rightarrow t \tilde{\chi}_1^\pm, \tilde{\chi}_1^\pm \rightarrow W^\pm \tilde{\chi}_1^0, m_{\tilde{\chi}_1^0} = 50$ GeV, $150 < m_{\tilde{\chi}_1^\pm} < 300$ GeV					
> 255	95	30	AAD	14T ATLS	$\tilde{b}_1 \rightarrow b \tilde{\chi}_1^0, m_{\tilde{b}_1} - m_{\tilde{\chi}_1^0} \approx m_b$					
> 400	95	31	CHATRCHYAN14AH	CMS	jets + $\cancel{E}_T, \tilde{b} \rightarrow b \tilde{\chi}_1^0$ simplified model, $m_{\tilde{\chi}_1^0} = 50$ GeV					
		32	CHATRCHYAN14R	CMS	$\geq 3\ell^\pm, \tilde{b} \rightarrow t \tilde{\chi}_1^\pm, \tilde{\chi}_1^\pm \rightarrow W^\pm \tilde{\chi}_1^0$ simplified model, $m_{\tilde{\chi}_1^0} = 50$ GeV					
••• We do not use the following data for averages, fits, limits, etc. •••		33	KHACHATRY...15AD	CMS	$\ell^\pm \ell^\mp + \text{jets} + \cancel{E}_T, \tilde{b} \rightarrow b \ell^\pm \ell^\mp \tilde{\chi}_1^0$					
none 340-600	95	34	AAD	14AX ATLS	$\geq 3$ $b$ -jets + $\cancel{E}_T, \tilde{b} \rightarrow b \tilde{\chi}_2^0$ simplified model with $\tilde{\chi}_2^0 \rightarrow h \tilde{\chi}_1^0, m_{\tilde{\chi}_1^0} = 60$ GeV, $m_{\tilde{\chi}_2^0} = 300$ GeV					
> 440	95	35	AAD	14E ATLS	$\ell^\pm \ell^\pm (\ell^\mp) + \text{jets}, \tilde{b}_1 \rightarrow t \tilde{\chi}_1^\pm$ with $\tilde{\chi}_1^\pm \rightarrow W^{(*)} \tilde{\chi}_1^0$ simplified model, $m_{\tilde{\chi}_1^\pm} = 2 m_{\tilde{\chi}_1^0}$					

- 11 AABOUD 17AJ searched in  $36.1 \text{ fb}^{-1}$  of  $pp$  collisions at  $\sqrt{s} = 13 \text{ TeV}$  for events with two same-sign or three leptons, jets and large missing transverse momentum. No significant excess above the Standard Model expectations is observed. Limits up to 700 GeV are set on the bottom squark mass in Tsb02 simplified models assuming  $m_{\tilde{\chi}_1^0} = 0 \text{ GeV}$ . See their Figure 4(d).
- 12 AABOUD 17AX searched in  $36 \text{ fb}^{-1}$  of  $pp$  collisions at  $\sqrt{s} = 13 \text{ TeV}$  for events containing two jets identified as originating from  $b$ -quarks and large missing transverse momentum. No excess of events above the expected level of Standard Model background was found. Exclusion limits at 95% C.L. are set on the masses of bottom squarks. In the Tsb01 simplified model, a  $\tilde{b}_1$  mass below 950 GeV is excluded for  $m_{\tilde{\chi}_1^0} = 0$  (<420) GeV. See their Fig. 7(a).
- 13 AABOUD 17AX searched in  $36 \text{ fb}^{-1}$  of  $pp$  collisions at  $\sqrt{s} = 13 \text{ TeV}$  for events containing two jets identified as originating from  $b$ -quarks and large missing transverse momentum, with or without leptons. No excess of events above the expected level of Standard Model background was found. Exclusion limits at 95% C.L. are set on the masses of bottom squarks. Assuming 50% BR for Tsb01 and Tsb02 simplified models, a  $\tilde{b}_1$  mass below 880 (860) GeV is excluded for  $m_{\tilde{\chi}_1^0} = 0$  (<250) GeV. See their Fig. 7(b).
- 14 KHACHATRYAN 17A searched in  $18.5 \text{ fb}^{-1}$  of  $pp$  collisions at  $\sqrt{s} = 8 \text{ TeV}$  for events with two forward jets, produced through vector boson fusion, and missing transverse momentum. No significant excess above the Standard Model expectations is observed. A limit is set on sbottom masses in the Tsb01 simplified model, see Fig. 3.
- 15 KHACHATRYAN 17AW searched in  $2.3 \text{ fb}^{-1}$  of  $pp$  collisions at  $\sqrt{s} = 13 \text{ TeV}$  for events with at least three charged leptons, in any combination of electrons and muons, and significant  $\cancel{E}_T$ . No significant excess above the Standard Model expectations is observed. Limits are set on the gluino mass in the Tglu3A and Tglu1C simplified models, and on the sbottom mass in the Tsb02 simplified model, see their Figure 4.
- 16 KHACHATRYAN 17P searched in  $2.3 \text{ fb}^{-1}$  of  $pp$  collisions at  $\sqrt{s} = 13 \text{ TeV}$  for events with one or more jets and large  $\cancel{E}_T$ . No significant excess above the Standard Model expectations is observed. Limits are set on the gluino mass in the Tglu1A, Tglu2A, Tglu3A, Tglu3B, Tglu3C and Tglu3D simplified models, see their Figures 7 and 8. Limits are also set on the squark mass in the Tsqk1 simplified model, see their Fig. 7, and on the sbottom mass in the Tsb01 simplified model, see Fig. 8. Finally, limits are set on the stop mass in the Tstop1, Tstop3, Tstop4, Tstop6 and Tstop7 simplified models, see Fig. 8.
- 17 SIRUANYAN 17AZ searched in  $35.9 \text{ fb}^{-1}$  of  $pp$  collisions at  $\sqrt{s} = 13 \text{ TeV}$  for events with one or more jets and large  $\cancel{E}_T$ . No significant excess above the Standard Model expectations is observed. Limits are set on the gluino mass in the Tglu1A, Tglu2A, Tglu3A simplified models, see their Figures 6. Limits are also set on the squark mass in the Tsqk1 simplified model (for single light squark and for 8 degenerate light squarks), on the sbottom mass in the Tsb01 simplified model and on the stop mass in the Tstop1 simplified model, see their Fig. 7. Finally, limits are set on the stop mass in the Tstop2, Tstop4 and Tstop8 simplified models, see Fig. 8.
- 18 SIRUANYAN 17K searched in  $2.3 \text{ fb}^{-1}$  of  $pp$  collisions at  $\sqrt{s} = 13 \text{ TeV}$  for direct production of stop or sbottom pairs in events with multiple jets and significant  $\cancel{E}_T$ . A second search also requires an isolated lepton and is combined with the all-hadronic search. No significant excess above the Standard Model expectations is observed. Limits are set on the stop mass in the Tstop1, Tstop8 and Tstop4 simplified models, see their Figures 7, 8 and 9 (for the Tstop4 limits, only the results of the all-hadronic search are used). Limits are also set on the sbottom mass in the Tsb01 simplified model, see Fig. 10 (also here, only the results of the all-hadronic search are used).
- 19 SIRUANYAN 17S searched in  $35.9 \text{ fb}^{-1}$  of  $pp$  collisions at  $\sqrt{s} = 13 \text{ TeV}$  for events with two isolated same-sign leptons, jets, and large  $\cancel{E}_T$ . No significant excess above the Standard Model expectations is observed. Limits are set on the mass of the gluino mass in the Tglu3A, Tglu3B, Tglu3C, Tglu3D and Tglu1B simplified models, see their Figures 5 and 6, and on the sbottom mass in the Tsb02 simplified model, see their Figure 6.
- 20 AABOUD 16D searched in  $3.2 \text{ fb}^{-1}$  of  $pp$  collisions at  $\sqrt{s} = 13 \text{ TeV}$  for events with an energetic jet and large missing transverse momentum. The results are interpreted as 95% C.L. limits on mass of sbottom decaying into a  $b$ -quark and the lightest neutralino in scenarios with  $m_{\tilde{b}_1} - m_{\tilde{\chi}_1^0}$  between 5 and 20 GeV. See their Fig. 6.
- 21 AABOUD 16Q searched in  $3.2 \text{ fb}^{-1}$  of  $pp$  collisions at  $\sqrt{s} = 13 \text{ TeV}$  for events containing two jets identified as originating from  $b$ -quarks and large missing transverse momentum. No excess of events above the expected level of Standard Model background was found. Exclusion limits at 95% C.L. are set on the masses of third-generation squarks. Assuming that the decay  $\tilde{b}_1 \rightarrow b\tilde{\chi}_1^0$  (Tsb01) takes place 100% of the time, a  $\tilde{b}_1$  mass below 840 (800) GeV is excluded for  $m_{\tilde{\chi}_1^0} < 100$  (360) GeV. Differences in mass above 100 GeV between the  $\tilde{b}_1$  and the  $\tilde{\chi}_1^0$  are excluded up to a  $\tilde{b}_1$  mass of 500 GeV. For more details, see their Fig. 4.
- 22 AAD 16BB searched in  $3.2 \text{ fb}^{-1}$  of  $pp$  collisions at  $\sqrt{s} = 13 \text{ TeV}$  for events with exactly two same-sign leptons or at least three leptons, multiple hadronic jets,  $b$ -jets, and  $\cancel{E}_T$ . No significant excess over the Standard Model expectation is found. Exclusion limits at 95% C.L. are set on the sbottom mass for the Tsb02 model, assuming  $m_{\tilde{\chi}_1^\pm} = m_{\tilde{\chi}_1^0} + 100 \text{ GeV}$ . See their Fig. 4c.
- 23 KHACHATRYAN 16BJ searched in  $2.3 \text{ fb}^{-1}$  of  $pp$  collisions at  $\sqrt{s} = 13 \text{ TeV}$  for events with two isolated same-sign dileptons and jets in the final state. No significant excess above the Standard Model expectations is observed. Limits are set on the sbottom mass in the Tsb02 simplified model, see Fig. 6.
- 24 KHACHATRYAN 16BS searched in  $2.3 \text{ fb}^{-1}$  of  $pp$  collisions at  $\sqrt{s} = 13 \text{ TeV}$  for events with at least one energetic jet, no isolated leptons, and significant  $\cancel{E}_T$ , using the transverse mass variable  $M_{T2}$  to discriminate between signal and background processes. No significant excess above the Standard Model expectations is observed. Limits are set on the sbottom mass in the Tsb01 simplified model, see Fig. 11 and Table 3.
- 25 KHACHATRYAN 16BY searched in  $2.3 \text{ fb}^{-1}$  of  $pp$  collisions at  $\sqrt{s} = 13 \text{ TeV}$  for events with two opposite-sign, same-flavour leptons, jets, and missing transverse momentum. No significant excess above the Standard Model expectations is observed. Limits are set on the gluino mass in the Tglu4C simplified model, see Fig. 4, and on sbottom masses in the Tsb03 simplified model, see Fig. 5.
- 26 AAD 15CJ searched in  $20 \text{ fb}^{-1}$  of  $pp$  collisions at  $\sqrt{s} = 8 \text{ TeV}$  for evidence of third generation squarks by combining a large number of searches covering various final states. Limits on the sbottom mass are shown, either assuming the  $\tilde{b} \rightarrow b\tilde{\chi}_1^0$  decay, see Fig. 11, or assuming the  $\tilde{b} \rightarrow t\tilde{\chi}_1^\pm$  decay, with  $\tilde{\chi}_1^\pm \rightarrow W^{(*)}\tilde{\chi}_1^0$ , see Fig. 12a, or assuming the  $\tilde{b} \rightarrow b\tilde{\chi}_1^0$  decay, with  $\tilde{\chi}_1^0 \rightarrow h\tilde{\chi}_1^0$ , see Fig. 12b. Interpretations in the pMSSM are also discussed, see Figures 13–15.
- 27 KHACHATRYAN 15AF searched in  $19.5 \text{ fb}^{-1}$  of  $pp$  collisions at  $\sqrt{s} = 8 \text{ TeV}$  for events with at least two energetic jets and significant  $\cancel{E}_T$ , using the transverse mass variable  $M_{T2}$  to discriminate between signal and background processes. No significant excess above the Standard Model expectations is observed. Limits are set on the sbottom mass in simplified models where the decay  $\tilde{b} \rightarrow b\tilde{\chi}_1^0$  takes place with a branching ratio of 100%, see Fig. 12. See also Table 5. Exclusions in the CMSSM, assuming  $\tan\beta = 30$ ,  $A_0 = -2 \max(m_0, m_{1/2})$  and  $\mu > 0$ , are also presented, see Fig. 15.
- 28 KHACHATRYAN 15AH searched in  $19.4$  or  $19.7 \text{ fb}^{-1}$  of  $pp$  collisions at  $\sqrt{s} = 8 \text{ TeV}$  for events containing either a fully reconstructed top quark, or events containing dijets requiring one or both jets to originate from  $b$ -quarks, or events containing a mono-jet. No significant excess above the Standard Model expectations is observed. Limits are set on the sbottom mass in simplified models where the decay  $\tilde{b} \rightarrow b\tilde{\chi}_1^0$  takes place with a branching ratio of 100%, see Fig. 12. Limits are also set in a simplified model where the decay  $\tilde{b} \rightarrow c\tilde{\chi}_1^0$  takes place with a branching ratio of 100%, see Fig. 12.
- 29 KHACHATRYAN 15I searched in  $19.5 \text{ fb}^{-1}$  of  $pp$  collisions at  $\sqrt{s} = 8 \text{ TeV}$  for events in which  $b$ -jets and four  $W$ -bosons are produced. Five individual search channels are combined (fully hadronic, single lepton, same-sign dilepton, opposite-sign dilepton, multi-lepton). No significant excess above the Standard Model expectations is observed. Limits are set on the sbottom mass in a simplified model where the decay  $\tilde{b} \rightarrow t\tilde{\chi}_1^\pm$ , with  $\tilde{\chi}_1^\pm \rightarrow W^\pm\tilde{\chi}_1^0$ , takes place with a branching ratio of 100%, see Fig. 7.
- 30 AAD 14T searched in  $20.3 \text{ fb}^{-1}$  of  $pp$  collisions at  $\sqrt{s} = 8 \text{ TeV}$  for monojet-like events. No excess of events above the expected level of Standard Model background was found. Exclusion limits at 95% C.L. are set on the masses of third-generation squarks in simplified models which assume that the decay  $\tilde{b}_1 \rightarrow b\tilde{\chi}_1^0$  takes place 100% of the time, see Fig. 12.
- 31 CHATRCHYAN 14AH searched in  $4.7 \text{ fb}^{-1}$  of  $pp$  collisions at  $\sqrt{s} = 7 \text{ TeV}$  for events with at least two energetic jets and significant  $\cancel{E}_T$ , using the razor variables ( $M_R$  and  $R^2$ ) to discriminate between signal and background processes. A second analysis requires at least one of the jets to be originating from a  $b$ -quark. No significant excess above the Standard Model expectations is observed. Limits are set on sbottom masses in simplified models where the decay  $\tilde{b} \rightarrow b\tilde{\chi}_1^0$  takes place with a branching ratio of 100%, see Figs. 28 and 29. Exclusions in the CMSSM, assuming  $\tan\beta = 10$ ,  $A_0 = 0$  and  $\mu > 0$ , are also presented, see Fig. 26.
- 32 CHATRCHYAN 14R searched in  $19.5 \text{ fb}^{-1}$  of  $pp$  collisions at  $\sqrt{s} = 8 \text{ TeV}$  for events with at least three leptons (electrons, muons, taus) in the final state. No significant excess above the Standard Model expectations is observed. Limits are set on the gluino mass in a simplified model where the decay  $\tilde{b} \rightarrow t\tilde{\chi}_1^\pm$ , with  $\tilde{\chi}_1^\pm \rightarrow W^\pm\tilde{\chi}_1^0$ , takes place with a branching ratio of 100%, see Fig. 11.
- 33 KHACHATRYAN 15AD searched in  $19.4 \text{ fb}^{-1}$  of  $pp$  collisions at  $\sqrt{s} = 8 \text{ TeV}$  for events with two opposite-sign same flavor isolated leptons featuring either a kinematic edge, or a peak at the  $Z$ -boson mass, in the invariant mass spectrum. No evidence for a statistically significant excess over the expected SM backgrounds is observed and 95% C.L. exclusion limits are derived in a simplified model of sbottom pair production where the sbottom decays into a  $b$ -quark, two opposite-sign dileptons and a neutralino LSP, through an intermediate state containing either an off-shell  $Z$ -boson or a slepton, see Fig. 8.
- 34 AAD 14AX searched in  $20.1 \text{ fb}^{-1}$  of  $pp$  collisions at  $\sqrt{s} = 8 \text{ TeV}$  for the strong production of supersymmetric particles in events containing either zero or at least one high  $p_T$  lepton, large missing transverse momentum, high jet multiplicity and at least three jets identified as originating from  $b$ -quarks. No excess over the expected SM background is observed. Limits are derived in mSUGRA/CMSSM models with  $\tan\beta = 30$ ,  $A_0 = -2 m_0$  and  $\mu > 0$ , see their Fig. 14. Also, exclusion limits are set in simplified models containing scalar bottom quarks, where the decay  $\tilde{b} \rightarrow b\tilde{\chi}_2^0$  and  $\tilde{\chi}_2^0 \rightarrow h\tilde{\chi}_1^0$  takes place with a branching ratio of 100%, see their Figures 11.
- 35 AAD 14E searched in  $20.3 \text{ fb}^{-1}$  of  $pp$  collisions at  $\sqrt{s} = 8 \text{ TeV}$  for strongly produced supersymmetric particles in events containing jets and two same-sign leptons or three leptons. The search also utilizes jets originating from  $b$ -quarks, missing transverse momentum and other variables. No excess over the expected SM background is observed. Exclusion limits are derived in simplified models containing bottom, see Fig. 7. Limits are also derived in the mSUGRA/CMSSM, bRPV and GMSB models, see their Fig. 8.
- 36 CHATRCHYAN 14H searched in  $19.5 \text{ fb}^{-1}$  of  $pp$  collisions at  $\sqrt{s} = 8 \text{ TeV}$  for events with two isolated same-sign dileptons and jets in the final state. No significant excess above the Standard Model expectations is observed. Limits are set on the sbottom mass in a simplified models where the decay  $\tilde{b} \rightarrow t\tilde{\chi}_1^\pm$ ,  $\tilde{\chi}_1^\pm \rightarrow W^\pm\tilde{\chi}_1^0$  takes place with a branching ratio of 100%, with varying mass of the  $\tilde{\chi}_1^\pm$ , for  $m_{\tilde{\chi}_1^0} = 50 \text{ GeV}$ , see Fig. 6.
- 37 AAD 13AU searched in  $20.1 \text{ fb}^{-1}$  of  $pp$  collisions at  $\sqrt{s} = 8 \text{ TeV}$  for events containing two jets identified as originating from  $b$ -quarks and large missing transverse momentum. No excess of events above the expected level of Standard Model background was found. Exclusion limits at 95% C.L. are set on the masses of third-generation squarks. Assuming that the decay  $\tilde{b}_1 \rightarrow b\tilde{\chi}_1^0$  takes place 100% of the time, a  $\tilde{b}_1$  mass below 620 GeV is excluded for  $m_{\tilde{\chi}_1^0} < 120 \text{ GeV}$ . For more details, see their Fig. 5.
- 38 CHATRCHYAN 13AT provides interpretations of various searches for supersymmetry by the CMS experiment based on  $4.73$ – $4.98 \text{ fb}^{-1}$  of  $pp$  collisions at  $\sqrt{s} = 7 \text{ TeV}$  in the framework of simplified models. Limits are set on the sbottom mass in a simplified models where sbottom quarks are pair-produced and the decay  $\tilde{b} \rightarrow b\tilde{\chi}_1^0$  takes place with a branching ratio of 100%, see Fig. 4.
- 39 CHATRCHYAN 13T searched in  $11.7 \text{ fb}^{-1}$  of  $pp$  collisions at  $\sqrt{s} = 8 \text{ TeV}$  for events with at least two energetic jets and significant  $\cancel{E}_T$ , using the  $\alpha_T$  variable to discriminate between processes with genuine and misreconstructed  $\cancel{E}_T$ . No significant excess above the Standard Model expectations is observed. Limits are set on sbottom masses in simplified models where the decay  $\tilde{b} \rightarrow b\tilde{\chi}_1^0$  takes place with a branching ratio of 100%, see Fig. 8 and Table 9.
- 40 CHATRCHYAN 13V searched in  $10.5 \text{ fb}^{-1}$  of  $pp$  collisions at  $\sqrt{s} = 8 \text{ TeV}$  for events with two isolated same-sign dileptons and at least two  $b$ -jets in the final state. No significant excess above the Standard Model expectations is observed. Limits are set on the bottom mass in a simplified models where the decay  $\tilde{b} \rightarrow t\tilde{\chi}_1^\pm$ ,  $\tilde{\chi}_1^\pm \rightarrow W^\pm\tilde{\chi}_1^0$  takes place with a branching ratio of 100%, with varying mass of the  $\tilde{\chi}_1^\pm$ , for  $m_{\tilde{\chi}_1^0} = 50 \text{ GeV}$ , see Fig. 4.

# Searches Particle Listings

## Supersymmetric Particle Searches

41 AAD 12AN searched in 2.05 fb <sup>-1</sup> of $pp$ collisions at $\sqrt{s} = 7$ TeV for scalar bottom quarks in events with large missing transverse momentum and two $b$ -jets in the final state. The data are found to be consistent with the Standard Model expectations. Limits are set in an R-parity conserving minimal supersymmetric scenario, assuming $B(\bar{b}_1 \rightarrow b\tilde{\chi}_1^0) = 100\%$ , see their Fig. 2.	>1190	95	<sup>2</sup> SIRUNYAN	19CH CMS	jets + $\cancel{E}_T$ , Tstop1, $m_{\tilde{\chi}_1^0} = 0$ GeV
42 CHATRCHYAN 12AI looked in 4.98 fb <sup>-1</sup> of $pp$ collisions at $\sqrt{s} = 7$ TeV for events with two same-sign leptons ( $e, \mu$ ), but not necessarily same flavor, at least 2 $b$ -jets and missing transverse energy. No excess beyond the Standard Model expectation is observed. Exclusion limits are derived in a simplified model for sbottom pair production, where the sbottom decays through $\bar{b}_1 \rightarrow t\tilde{\chi}_1^- W$ , see Fig. 8.	>1140	95	<sup>3</sup> SIRUNYAN	19S CMS	1 or 2 $\ell +$ jets + $\cancel{E}_T$ , Tstop1, $m_{\tilde{\chi}_1^0} < 200$ GeV
43 CHATRCHYAN 12BO searched in 4.7 fb <sup>-1</sup> of $pp$ collisions at $\sqrt{s} = 7$ TeV for scalar bottom quarks in events with large missing transverse momentum and two $b$ -jets in the final state. The data are found to be consistent with the Standard Model expectations. Limits are set in an R-parity conserving minimal supersymmetric scenario, assuming $B(\bar{b}_1 \rightarrow b\tilde{\chi}_1^0) = 100\%$ , see their Fig. 2.	> 208	95	<sup>4</sup> SIRUNYAN	19U CMS	$e^\pm \mu^\mp + \geq 1b$ -jet, Tstop1, $m_{\tilde{\chi}_1^0} = 175$ GeV
44 AAD 11K looked in 34 pb <sup>-1</sup> of $pp$ collisions at $\sqrt{s} = 7$ TeV for events with heavy stable particles, identified by their anomalous $dE/dx$ in the tracker or time of flight in the tile calorimeter, from pair production of $\tilde{b}$ . No evidence for an excess over the SM expectation is observed and limits on the mass are derived for pair production of sbottom, see Fig. 4.	> 235	95	<sup>4</sup> SIRUNYAN	19U CMS	$e^\pm \mu^\mp + \geq 1b$ -jet, Tstop1, $m_{\tilde{\chi}_1^0} = 182.5$ GeV
45 AAD 11O looked in 35 pb <sup>-1</sup> of $pp$ collisions at $\sqrt{s} = 7$ TeV for events with jets, of which at least one is a $b$ -jet, and $\cancel{E}_T$ . No excess above the Standard Model was found. Limits are derived in the $(m_{\tilde{g}}, m_{\tilde{b}_1})$ plane (see Fig. 2) under the assumption of 100% branching ratios and $\tilde{b}_1$ being the lightest squark. The quoted limit is valid for $m_{\tilde{b}_1} < 500$ GeV. A similar approach for $\tilde{t}_1$ as the lightest squark with $\tilde{g} \rightarrow \tilde{t}_1 t$ and $\tilde{t}_1 \rightarrow b\tilde{\chi}_1^\pm$ with 100% branching ratios leads to a gluino mass limit of 520 GeV for $130 < m_{\tilde{t}_1} < 300$ GeV. Limits are also derived in the CMSSM $(m_0, m_{1/2})$ plane for $\tan\beta = 40$ , see Fig. 4, and in scenarios based on the gauge group SO(10).	> 242	95	<sup>4</sup> SIRUNYAN	19U CMS	$e^\pm \mu^\mp + \geq 1b$ -jet, Tstop1, $m_{\tilde{\chi}_1^0} = 167.5$ GeV
46 CHATRCHYAN 11D looked in 35 pb <sup>-1</sup> of $pp$ collisions at $\sqrt{s} = 7$ TeV for events with $\geq 2$ jets, at least one of which is $b$ -tagged, and $\cancel{E}_T$ , where the $b$ -jets are decay products of $\tilde{t}$ or $\tilde{b}$ . No evidence for an excess over the expected background is observed. Limits are derived in the CMSSM $(m_0, m_{1/2})$ plane for $\tan\beta = 50$ (see Fig. 2).	> 270	95	<sup>5</sup> AABOUD	18AQ ATLS	1 $\ell$ +jets+ $\cancel{E}_T$ , Tstop1, $m_{\tilde{\chi}_1^0} = 0$
47 AALTONEN 10R searched in 2.65 fb <sup>-1</sup> of $p\bar{p}$ collisions at $\sqrt{s} = 1.96$ TeV for events with $\cancel{E}_T$ and exactly two jets, at least one of which is $b$ -tagged. The results are in agreement with the SM prediction, and a limit on the cross section of 0.1 pb is obtained for the range of masses $80 < m_{\tilde{b}_1} < 280$ GeV assuming that the sbottom decays exclusively to $b\tilde{\chi}_1^0$ . The excluded mass region in the framework of conserved $R_p$ is shown in a plane of $(m_{\tilde{b}_1}, m_{\tilde{\chi}_1^0})$ , see their Fig. 2.	> 840	95	<sup>6</sup> AABOUD	18AQ ATLS	1 $\ell$ +jets+ $\cancel{E}_T$ , Tstop3, $m_{\tilde{t}_1^-} - m_{\tilde{\chi}_1^0} = 20$ GeV
48 ABAZOV 10I looked in 5.2 fb <sup>-1</sup> of $p\bar{p}$ collisions at $\sqrt{s} = 1.96$ TeV for events with at least 2 $b$ -jets and $\cancel{E}_T$ from the production of $\tilde{b}_1 \tilde{b}_1^*$ . No evidence for an excess over the SM expectation is observed, and a limit on the cross section is derived under the assumption of 100% branching ratio. The excluded mass region in the framework of conserved $R_p$ is shown in a plane of $(m_{\tilde{b}_1}, m_{\tilde{\chi}_1^0})$ , see their Fig. 3b. The exclusion also extends to $m_{\tilde{\chi}_1^0} = 110$ GeV for $160 < m_{\tilde{b}_1} < 200$ GeV.	> 500	95	<sup>7</sup> AABOUD	18AQ ATLS	1 $\ell$ +jets+ $\cancel{E}_T$ , Tstop2, $m_{\tilde{t}_1^-} - m_{\tilde{\chi}_1^0} = 10$ GeV
	> 500	95	<sup>8</sup> AABOUD	18BV ATLS	$c$ -jets+ $\cancel{E}_T$ , Tstop4, $m_{\tilde{t}_1^-} - m_{\tilde{\chi}_1^0} < 100$ GeV
	> 390	95	<sup>9</sup> AABOUD	18BV ATLS	$c$ -jets+ $\cancel{E}_T$ , Tstop4, $m_{\tilde{\chi}_1^0} = 0$
	> 430	95	<sup>10</sup> AABOUD	18I ATLS	$\geq 1$ jets+ $\cancel{E}_T$ , Tstop3, $m_{\tilde{t}_1^-} - m_{\tilde{\chi}_1^0} \sim 50$ GeV
	> 1160	95	<sup>11</sup> AABOUD	18I ATLS	$\geq 1$ jets+ $\cancel{E}_T$ , Tstop4, $m_{\tilde{t}_1^-} - m_{\tilde{\chi}_1^0} = 5$ GeV
	> 450	95	<sup>12</sup> AABOUD	18Y ATLS	2 $\ell$ ( $\geq 1$ hadronic $\tau$ ) + $b$ -jets + $\cancel{E}_T$ , Tstop5, $m_{\tilde{t}_1^-} \sim 800$ GeV
	> 720	95	<sup>13</sup> SIRUNYAN	18AJ CMS	2 $\ell$ (soft) + $\cancel{E}_T$ , Tstop10, $m_{\tilde{\chi}_1^\pm} = (m_{\tilde{t}_1} + m_{\tilde{\chi}_1^0})/2$ , $m_{\tilde{t}_1^-} - m_{\tilde{\chi}_1^0} = 40$ GeV
	> 780	95	<sup>14</sup> SIRUNYAN	18AL CMS	$\geq 3\ell^\pm +$ jets + $\cancel{E}_T$ , Tstop7, $m_{\tilde{t}_1^-} - m_{\tilde{\chi}_1^0} = 175$ GeV, $m_{\tilde{t}_1} = 200$ GeV, BR( $\tilde{t}_2 \rightarrow \tilde{t}_1 H$ ) = 100%
	> 710	95	<sup>14</sup> SIRUNYAN	18AL CMS	$\geq 3\ell^\pm +$ jets + $\cancel{E}_T$ , Tstop7, $m_{\tilde{t}_1^-} - m_{\tilde{\chi}_1^0} = 175$ GeV, $m_{\tilde{t}_1} = 200$ GeV, BR( $\tilde{t}_2 \rightarrow \tilde{t}_1 Z$ ) = 100%
	> 730	95	<sup>15</sup> SIRUNYAN	18AN CMS	$\geq 3\ell^\pm +$ jets + $\cancel{E}_T$ , Tstop7, $m_{\tilde{t}_1^-} - m_{\tilde{\chi}_1^0} = 175$ GeV, $m_{\tilde{t}_1} = 200$ GeV, BR( $\tilde{t}_2 \rightarrow \tilde{t}_1 H$ ) = 50%
	> 650	95	<sup>15</sup> SIRUNYAN	18AN CMS	1 or 2 $\gamma + \ell +$ jets, GGM, Tstop12, $m_{\tilde{\chi}_1^0} = 150$ GeV
	> 1000	95	<sup>16</sup> SIRUNYAN	18AY CMS	1 or 2 $\gamma + \ell +$ jets, GGM, Tstop12, $m_{\tilde{\chi}_1^0} = 500$ GeV
	> 500	95	<sup>16</sup> SIRUNYAN	18AY CMS	jets+ $\cancel{E}_T$ , Tstop1, $m_{\tilde{\chi}_1^0} = 0$ GeV
	> 510	95	<sup>17</sup> SIRUNYAN	18B CMS	jets+ $\cancel{E}_T$ , Tstop4, $m_{\tilde{t}_1^-} - m_{\tilde{\chi}_1^0} = 10$ GeV
	> 800	95	<sup>18</sup> SIRUNYAN	18C CMS	$\ell^\pm \ell^\mp + b$ -jets + $\cancel{E}_T$ , Tstop1, $m_{\tilde{\chi}_1^0} = 0$
	> 750	95	<sup>18</sup> SIRUNYAN	18C CMS	$\ell^\pm \ell^\mp + b$ -jets + $\cancel{E}_T$ , Tstop2, $m_{\tilde{\chi}_1^\pm} = (m_{\tilde{t}_1} + m_{\tilde{\chi}_1^0})/2$ , $m_{\tilde{\chi}_1^0} = 0$
	>1050	95	<sup>18</sup> SIRUNYAN	18C CMS	Combination of all-hadronic, 1 $\ell^\pm$ and $\ell^\pm \ell^\mp$ searches, Tstop1, $m_{\tilde{\chi}_1^0} = 0$
	>1000	95	<sup>18</sup> SIRUNYAN	18C CMS	Combination of all-hadronic, 1 $\ell^\pm$ and $\ell^\pm \ell^\mp$ searches, Tstop2, $m_{\tilde{\chi}_1^\pm} = (m_{\tilde{t}_1} + m_{\tilde{\chi}_1^0})/2$ , $m_{\tilde{\chi}_1^0} = 0$
	>1200	95	<sup>18</sup> SIRUNYAN	18C CMS	$\ell^\pm \ell^\mp + b$ -jets + $\cancel{E}_T$ , Tstop11, $m_{\tilde{\chi}_1^\pm} = 0.5(m_{\tilde{t}_1} + m_{\tilde{\chi}_1^0})$ , $m_{\tilde{\ell}} = 0.5 m_{\tilde{\chi}_1^\pm}$ , $m_{\tilde{\chi}_1^0} = 0$
	>1300	95	<sup>18</sup> SIRUNYAN	18C CMS	$\ell^\pm \ell^\mp + b$ -jets + $\cancel{E}_T$ , Tstop11, $m_{\tilde{\chi}_1^\pm} = 0.5(m_{\tilde{t}_1} + m_{\tilde{\chi}_1^0})$ , $m_{\tilde{\ell}} = 0.95 m_{\tilde{\chi}_1^\pm}$ , $m_{\tilde{\chi}_1^0} = 0$
	none 460–1060	95	<sup>18</sup> SIRUNYAN	18C CMS	$\ell^\pm \ell^\mp + b$ -jets + $\cancel{E}_T$ , Tstop11, $m_{\tilde{\chi}_1^\pm} = 0.5(m_{\tilde{t}_1} + m_{\tilde{\chi}_1^0})$ , $m_{\tilde{\ell}} = 0.05 m_{\tilde{\chi}_1^\pm}$ , $m_{\tilde{\chi}_1^0} = 0$
	>1020	95	<sup>19</sup> SIRUNYAN	18D CMS	top quark (hadronically decaying) + jets + $\cancel{E}_T$ , Tstop1, $m_{\tilde{\chi}_1^0} = 0$ GeV

### R-parity violating $\tilde{b}$ (Sbottm) mass limit

VALUE (GeV)	CL%	DOCUMENT ID	TECN	COMMENT
>307	95	<sup>1</sup> KHACHATRYAN...16BX CMS	RPV, $\tilde{b} \rightarrow td$ or $ts$ , $\lambda_{332}'$ or $\lambda_{331}'$ coupling	

• • • We do not use the following data for averages, fits, limits, etc. • • •

	>1000	95	<sup>2</sup> AAD	14E ATLS	$\ell^\pm \ell^\pm (\ell^\mp) +$ jets, $\tilde{b}_1 \rightarrow t\tilde{\chi}_1^\pm$ with $\tilde{\chi}_1^\pm \rightarrow W(\ast)\tilde{\chi}_1^0$ simplified model, $m_{\tilde{\chi}_1^\pm} = 2 m_{\tilde{\chi}_1^0}$
	> 500	95			
	> 510	95			
	> 800	95	<sup>1</sup> KHACHATRYAN 16BX searched in 19.5 fb <sup>-1</sup> of $pp$ collisions at $\sqrt{s} = 8$ TeV for events containing 2 leptons coming from R-parity-violating decays of supersymmetric particles. No excess over the expected background is observed. Limits are derived on the sbottom mass, assuming the RPV $\tilde{b} \rightarrow td$ or $\tilde{b} \rightarrow ts$ decay, see Fig. 15.		
	> 750	95	<sup>2</sup> AAD 14E searched in 20.3 fb <sup>-1</sup> of $pp$ collisions at $\sqrt{s} = 8$ TeV for strongly produced supersymmetric particles in events containing jets and two same-sign leptons or three leptons. The search also utilises jets originating from $b$ -quarks, missing transverse momentum and other variables. No excess over the expected SM background is observed. Exclusion limits are derived in simplified models containing sbottom, see Fig. 7. Limits are also derived in the mSUGRA/CMSSM, bRPV and GMSB models, see their Fig. 8.		

### $\tilde{t}$ (Stop) mass limit

Limits depend on the decay mode. In  $e^+e^-$  collisions they also depend on the mixing angle of the mass eigenstate  $\tilde{t}_1 = \tilde{t}_L \cos\theta_t + \tilde{t}_R \sin\theta_t$ . The coupling to the  $Z$  vanishes when  $\theta_t = 0.98$ . In the Listings below, we use  $\Delta m \equiv m_{\tilde{t}_1} - m_{\tilde{\chi}_1^0}$  or  $\Delta m \equiv m_{\tilde{t}_1} - m_{\tilde{\nu}_\tau}$ , depending on relevant decay mode. See also bounds in “ $\tilde{q}$  (Squark) MASS LIMIT.”

Some earlier papers are now obsolete and have been omitted. They were last listed in our PDG 14 edition: K. Olive, et al. (Particle Data Group), Chinese Physics **C38** 070001 (2014) (<http://pdg.lbl.gov>).

### R-parity conserving $\tilde{t}$ (Stop) mass limit

VALUE (GeV)	CL%	DOCUMENT ID	TECN	COMMENT
>1110	95	<sup>1</sup> SIRUNYAN	19AU CMS	$\gamma +$ jets + $b$ -jets + $\cancel{E}_T$ , Tstop13, $m_{\tilde{\chi}_1^0} = 1$ GeV
>1230	95	<sup>1</sup> SIRUNYAN	19AU CMS	$\gamma +$ jets + $b$ -jets + $\cancel{E}_T$ , Tstop13, $m_{\tilde{\chi}_1^0} = 800$ GeV

> 420	95	20	SIRUNYAN	18DI	CMS	$\ell^\pm + \text{jet} + \cancel{E}_T, T_{\text{stop3}}, m_{\tilde{t}_1} - m_{\tilde{\chi}_1^0} = 10 \text{ GeV}$	>1000	95	39	SIRUNYAN	17AS	CMS	$1\ell + \text{jets} + \cancel{E}_T, T_{\text{stop2}}, m_{\tilde{\chi}_1^\pm} = (m_{\tilde{t}} + m_{\tilde{\chi}_1^0})/2, m_{\tilde{\chi}_1^0} = 0$
> 560	95	20	SIRUNYAN	18DI	CMS	$\ell^\pm + \text{jet} + \cancel{E}_T, T_{\text{stop3}}, m_{\tilde{t}_1} - m_{\tilde{\chi}_1^0} = 80 \text{ GeV}$	> 980	95	39	SIRUNYAN	17AS	CMS	$1\ell + \text{jets} + \cancel{E}_T, T_{\text{stop8}}, m_{\tilde{\chi}_1^\pm} - m_{\tilde{\chi}_1^0} = 5 \text{ GeV}, m_{\tilde{\chi}_1^0} = 0 \text{ GeV}$
> 540	95	20	SIRUNYAN	18DI	CMS	$\ell^\pm, T_{\text{stop10}}, m_{\tilde{\chi}_1^\pm} = (m_{\tilde{t}} + m_{\tilde{\chi}_1^0})/2, m_{\tilde{t}_1} - m_{\tilde{\chi}_1^0} = 40 \text{ GeV}$	>1040	95	40	SIRUNYAN	17AT	CMS	$\text{jets} + \cancel{E}_T, T_{\text{stop1}}, m_{\tilde{\chi}_1^0} = 0 \text{ GeV}$
> 590	95	20	SIRUNYAN	18DI	CMS	Combination of all-hadronic and 1 $\ell^\pm$ searches, $T_{\text{stop3}}, m_{\tilde{t}_1} - m_{\tilde{\chi}_1^0} = 30 \text{ GeV}$	> 750	95	40	SIRUNYAN	17AT	CMS	$\text{jets} + \cancel{E}_T, T_{\text{stop2}}, m_{\tilde{\chi}_1^\pm} = (m_{\tilde{t}} + m_{\tilde{\chi}_1^0})/2, m_{\tilde{\chi}_1^0} = 0 \text{ GeV}$
> 670	95	20	SIRUNYAN	18DI	CMS	Combination of all-hadronic and 1 $\ell^\pm$ searches, $T_{\text{stop10}}, m_{\tilde{\chi}_1^\pm} = (m_{\tilde{t}} + m_{\tilde{\chi}_1^0})/2, m_{\tilde{t}_1} - m_{\tilde{\chi}_1^0} = 60 \text{ GeV}$	> 940	95	40	SIRUNYAN	17AT	CMS	$\text{jets} + \cancel{E}_T, T_{\text{stop8}}, m_{\tilde{\chi}_1^\pm} - m_{\tilde{\chi}_1^0} = 5 \text{ GeV}, m_{\tilde{\chi}_1^0} = 100 \text{ GeV}$
> 450	95	21	SIRUNYAN	18DN	CMS	$\ell^\pm \ell^\mp, T_{\text{stop1}}, m_{\tilde{t}_1} - m_{\tilde{\chi}_1^0} = m_{W^0}$	> 480	95	40	SIRUNYAN	17AT	CMS	$\text{jets} + \cancel{E}_T, T_{\text{stop4}}, 10 \text{ GeV} < m_{\tilde{t}_1} - m_{\tilde{\chi}_1^0} < 80 \text{ GeV}$
none 225-325	95	21	SIRUNYAN	18DN	CMS	$\ell^\pm \ell^\mp, T_{\text{stop2}}, m_{\tilde{\chi}_1^\pm} = (m_{\tilde{t}} + m_{\tilde{\chi}_1^0})/2, m_{\tilde{t}_1} - m_{\tilde{\chi}_1^0} = 2 m_{W^0}$	> 530	95	40	SIRUNYAN	17AT	CMS	$\text{jets} + \cancel{E}_T, T_{\text{stop10}}, m_{\tilde{\chi}_1^\pm} = (m_{\tilde{t}} + m_{\tilde{\chi}_1^0})/2, 10 \text{ GeV} < m_{\tilde{t}_1} - m_{\tilde{\chi}_1^0} < 80 \text{ GeV}$
none 210-690	95	21	SIRUNYAN	18DN	CMS	$\ell^\pm \ell^\mp, T_{\text{stop1}}, m_{\tilde{\chi}_1^0} = 0 \text{ GeV}$	>1070	95	41	SIRUNYAN	17AZ	CMS	$\geq 1 \text{ jets} + \cancel{E}_T, T_{\text{stop1}}, m_{\tilde{\chi}_1^0} = 0 \text{ GeV}$
none 250-600	95	21	SIRUNYAN	18DN	CMS	$\ell^\pm \ell^\mp, T_{\text{stop2}}, m_{\tilde{\chi}_1^\pm} = (m_{\tilde{t}} + m_{\tilde{\chi}_1^0})/2, m_{\tilde{\chi}_1^0} = 0 \text{ GeV}$	> 900	95	41	SIRUNYAN	17AZ	CMS	$\geq 1 \text{ jets} + \cancel{E}_T, T_{\text{stop2}}, m_{\tilde{\chi}_1^\pm} = (m_{\tilde{t}} + m_{\tilde{\chi}_1^0})/2, m_{\tilde{\chi}_1^0} = 0 \text{ GeV}$
> 700	95	22	AABOUD	17AJ	ATLS	same-sign $\ell^\pm \ell^\pm / 3 \ell + \text{jets} + \cancel{E}_T, T_{\text{stop11}}, m_{\tilde{\chi}_1^0} = m_{\tilde{\chi}_1^0} + 100 \text{ GeV}$	>1020	95	41	SIRUNYAN	17AZ	CMS	$\geq 1 \text{ jets} + \cancel{E}_T, T_{\text{stop8}}, m_{\tilde{\chi}_1^\pm} - m_{\tilde{\chi}_1^0} = 5 \text{ GeV}, m_{\tilde{\chi}_1^0} = 100 \text{ GeV}$
> 880	95	23	AABOUD	17AX	ATLS	$b\text{-jets} + \cancel{E}_T, \text{mixture } T_{\text{stop1}} \text{ and } T_{\text{stop2}} \text{ with BR}=50\%, m_{\tilde{\chi}_1^0} = 0 \text{ GeV}, m_{\tilde{\chi}_1^\pm} - m_{\tilde{\chi}_1^0} = 1 \text{ GeV}$	> 540	95	41	SIRUNYAN	17AZ	CMS	$\geq 1 \text{ jets} + \cancel{E}_T, T_{\text{stop4}}, 10 \text{ GeV} < m_{\tilde{t}_1} - m_{\tilde{\chi}_1^0} < 80 \text{ GeV}$
none 250-1000	95	24	AABOUD	17AY	ATLS	$\text{jets} + \cancel{E}_T, T_{\text{stop1}}, m_{\tilde{\chi}_1^0} = 0 \text{ GeV}$	none 280-830	95	42	SIRUNYAN	17K	CMS	$0, 1 \ell^\pm + \text{jets} + \cancel{E}_T \text{ (combination)}, T_{\text{stop1}}, m_{\tilde{\chi}_1^0} = 0 \text{ GeV}$
none 450-850	95	25	AABOUD	17AY	ATLS	$\text{jets} + \cancel{E}_T, \text{mixture of } T_{\text{stop1}} \text{ and } T_{\text{stop2}} \text{ with BR}=50\%, m_{\tilde{\chi}_1^\pm} - m_{\tilde{\chi}_1^0} = 1 \text{ GeV}$	> 700	95	42	SIRUNYAN	17K	CMS	$0, 1 \ell^\pm + \text{jets} + \cancel{E}_T \text{ (combination)}, T_{\text{stop8}}, m_{\tilde{\chi}_1^\pm} - m_{\tilde{\chi}_1^0} = 5 \text{ GeV}, m_{\tilde{\chi}_1^0} = 100 \text{ GeV}$
> 720	95	26	AABOUD	17BE	ATLS	$\ell^\pm \ell^\mp + \cancel{E}_T, T_{\text{stop1}}, m_{\tilde{\chi}_1^0} = 0 \text{ GeV}$	> 160	95	42	SIRUNYAN	17K	CMS	$\text{jets} + \cancel{E}_T, T_{\text{stop4}}, 10 < m_{\tilde{t}} - m_{\tilde{\chi}_1^0} < 80 \text{ GeV}$
> 400	95	27	AABOUD	17BE	ATLS	$\ell^\pm \ell^\mp + \cancel{E}_T, T_{\text{stop3}}, m_{\tilde{t}_1} - m_{\tilde{\chi}_1^0} = 40 \text{ GeV}$	none 230-960	95	43	SIRUNYAN	17P	CMS	$\text{jets} + \cancel{E}_T, T_{\text{stop1}}, m_{\tilde{\chi}_1^0} = 0 \text{ GeV}$
> 430	95	28	AABOUD	17BE	ATLS	$\ell^\pm \ell^\mp + \cancel{E}_T, T_{\text{stop1}} \text{ (offshell } t), m_{\tilde{t}_1} - m_{\tilde{\chi}_1^0} \sim m_{W^0}$	> 990	95	43	SIRUNYAN	17P	CMS	$\text{jets} + \cancel{E}_T, T_{\text{stop1}}, m_{\tilde{\chi}_1^0} = 0 \text{ GeV}$
> 700	95	29	AABOUD	17BE	ATLS	$\ell^\pm \ell^\mp + \cancel{E}_T, T_{\text{stop2}}, m_{\tilde{t}_1} - m_{\tilde{\chi}_1^0} = 10 \text{ GeV}, m_{\tilde{\chi}_1^0} = 0 \text{ GeV}$	> 323	95	44	AABOUD	16D	ATLS	$\geq 1 \text{ jet} + \cancel{E}_T, T_{\text{stop4}}, m_{\tilde{t}_1} - m_{\tilde{\chi}_1^0} = 5 \text{ GeV}$
> 750	95	30	KHACHATRY...17	CMS	$\text{jets} + \cancel{E}_T, T_{\text{stop1}}, m_{\tilde{\chi}_1^0} = 100 \text{ GeV}$	none, 745-780	95	45	AABOUD	16J	ATLS	$1 \ell^\pm + \geq 4 \text{ jets} + \cancel{E}_T, T_{\text{stop1}}, m_{\tilde{\chi}_1^0} = 0 \text{ GeV}$	
none 250-740	95	31	KHACHATRY...17AD	CMS	$\text{jets} + b\text{-jets} + \cancel{E}_T, T_{\text{stop1}}, m_{\tilde{\chi}_1^0} = 0 \text{ GeV}$	> 490-650	95	46	AAD	16AY	ATLS	$2\ell \text{ (including hadronic } \tau) + \cancel{E}_T, T_{\text{stop5}}, 87 \text{ GeV} < m_{\tilde{\tau}} < m_{\tilde{t}_1}$	
> 610	95	32	KHACHATRY...17AD	CMS	$\text{jets} + b\text{-jets} + \cancel{E}_T, \text{mixture } T_{\text{stop1}} \text{ and } T_{\text{stop2}} \text{ with BR}=50\%, m_{\tilde{\chi}_1^0} = 60 \text{ GeV}$	> 700	95	47	KHACHATRY...16AV	CMS	$1 \text{ or } 2 \ell^\pm + \text{jets} + b\text{-jets} + \cancel{E}_T, T_{\text{stop1}}, m_{\tilde{\chi}_1^0} < 250 \text{ GeV}$		
> 590	95	33	KHACHATRY...17P	CMS	$1 \text{ or more jets} + \cancel{E}_T, T_{\text{stop8}}, m_{\tilde{\chi}_1^\pm} - m_{\tilde{\chi}_1^0} = 5 \text{ GeV}, m_{\tilde{\chi}_1^0} = 100 \text{ GeV}$	> 700	95	47	KHACHATRY...16AV	CMS	$1 \text{ or } 2 \ell^\pm + \text{jets} + b\text{-jets } \cancel{E}_T, T_{\text{stop2}}, m_{\tilde{\chi}_1^0} = 0 \text{ GeV}, m_{\tilde{\chi}_1^\pm} = 0.75 m_{\tilde{t}_1} + 0.25 m_{\tilde{\chi}_1^0}$		
none 280-640	95	33	KHACHATRY...17P	CMS	$1 \text{ or more jets} + \cancel{E}_T, T_{\text{stop1}}, m_{\tilde{\chi}_1^0} = 0 \text{ GeV}$	> 775	95	48	KHACHATRY...16BK	CMS	$\text{jets} + \cancel{E}_T, T_{\text{stop1}}, m_{\tilde{\chi}_1^0} < 200 \text{ GeV}$		
> 350	95	33	KHACHATRY...17P	CMS	$1 \text{ or more jets} + \cancel{E}_T, T_{\text{stop4}}, 10 \text{ GeV} < m_{\tilde{t}_1} - m_{\tilde{\chi}_1^0} < 80 \text{ GeV}$	> 620	95	48	KHACHATRY...16BK	CMS	$\text{jets} + \cancel{E}_T, T_{\text{stop2}}, m_{\tilde{\chi}_1^0} = 0 \text{ GeV}$		
> 280	95	33	KHACHATRY...17P	CMS	$1 \text{ or more jets} + \cancel{E}_T, T_{\text{stop3}}, 10 \text{ GeV} < m_{\tilde{t}_1} - m_{\tilde{\chi}_1^0} < 80 \text{ GeV}$	> 800	95	49	KHACHATRY...16BS	CMS	$\text{jets} + \cancel{E}_T, T_{\text{stop1}}, m_{\tilde{\chi}_1^0} = 0 \text{ GeV}$		
> 320	95	33	KHACHATRY...17P	CMS	$1 \text{ or more jets} + \cancel{E}_T, T_{\text{stop9}}, 10 \text{ GeV} < m_{\tilde{t}_1} - m_{\tilde{\chi}_1^0} < 80 \text{ GeV}$	> 316	95	50	KHACHATRY...16Y	CMS	$1 \text{ or } 2 \text{ soft } \ell^\pm + \text{jets} + \cancel{E}_T, T_{\text{stop3}}, m_{\tilde{t}} - m_{\tilde{\chi}_1^0} = 25 \text{ GeV}$		
> 240	95	34	KHACHATRY...17s	CMS	$\text{jets} + \cancel{E}_T, T_{\text{stop4}}, m_{\tilde{t}} - m_{\tilde{\chi}_1^0} = 10 \text{ GeV}$	> 270	95	51	AAD	15CJ	ATLS	$B(\tilde{t} \rightarrow c\tilde{\chi}_1^0) + B(\tilde{t} \rightarrow b\tilde{f}'\tilde{\chi}_1^0) = 1, m_{\tilde{t}} - m_{\tilde{\chi}_1^0} = 10 \text{ GeV}$	
> 225	95	35	KHACHATRY...17s	CMS	$\text{jets} + \cancel{E}_T, T_{\text{stop3}}, m_{\tilde{t}} - m_{\tilde{\chi}_1^0} = 10 \text{ GeV}$	none, 200-700	95	51	AAD	15CJ	ATLS	$\tilde{t} \rightarrow t\tilde{\chi}_1^0, m_{\tilde{\chi}_1^0} = 0$	
> 325	95	36	KHACHATRY...17s	CMS	$\text{jets} + \cancel{E}_T, T_{\text{stop2}}, m_{\tilde{\chi}_1^\pm} = 0.25 m_{\tilde{t}} + 0.75 m_{\tilde{\chi}_1^0}, m_{\tilde{\chi}_1^0} = 225 \text{ GeV}$	> 500	95	51	AAD	15CJ	ATLS	$B(\tilde{t} \rightarrow t\tilde{\chi}_1^0) + B(\tilde{t} \rightarrow b\tilde{\chi}_1^\pm) = 1, \tilde{\chi}_1^\pm \rightarrow W^{(*)}\tilde{\chi}_1^0, m_{\tilde{\chi}_1^\pm} = 2m_{\tilde{\chi}_1^0}, m_{\tilde{\chi}_1^0} < 160 \text{ GeV}$	
> 400	95	37	KHACHATRY...17s	CMS	$\text{jets} + \cancel{E}_T, T_{\text{stop2}}, m_{\tilde{\chi}_1^\pm} = 0.75 m_{\tilde{t}} + 0.25 m_{\tilde{\chi}_1^0}, m_{\tilde{\chi}_1^0} = 0 \text{ GeV}$	> 600	95	51	AAD	15CJ	ATLS	$\tilde{t}_2 \rightarrow Z\tilde{t}_1, m_{\tilde{t}_1} - m_{\tilde{\chi}_1^0} = 180 \text{ GeV}, m_{\tilde{\chi}_1^0} = 0$	
> 500	95	38	KHACHATRY...17s	CMS	$\text{jets} + \cancel{E}_T, T_{\text{stop1}}, m_{\tilde{\chi}_1^0} = 0 \text{ GeV}$	> 600	95	51	AAD	15CJ	ATLS	$\tilde{t}_2 \rightarrow h\tilde{t}_1, m_{\tilde{t}_1} - m_{\tilde{\chi}_1^0} = 180 \text{ GeV}, m_{\tilde{\chi}_1^0} = 0$	
>1120	95	39	SIRUNYAN	17AS	CMS	$1\ell + \text{jets} + \cancel{E}_T, T_{\text{stop1}}, m_{\tilde{\chi}_1^0} = 0 \text{ GeV}$	none, 172.5-191	95	52	AAD	15J	ATLS	$\tilde{t} \rightarrow t\tilde{\chi}_1^0, m_{\tilde{\chi}_1^0} = 1 \text{ GeV}$

# Searches Particle Listings

## Supersymmetric Particle Searches

> 450	95	53	KHACHATRY...15AF CMS	$\tilde{t} \rightarrow t\tilde{\chi}_1^0, m_{\tilde{\chi}_1^0} = 0, m_{\tilde{t}} > m_t + m_{\tilde{\chi}_1^0}$	2	SIRUNYAN 19CH searched in 137 fb <sup>-1</sup> of $pp$ collisions at $\sqrt{s} = 13$ TeV for events containing multiple jets and large $E_T$ . No significant excess above the Standard Model expectations is observed. Limits are set on the gluino mass in the Tglu1A, Tglu1C, Tglu2A and Tglu3A simplified models, see their Figure 13. Limits are also set on squark, sbottom and stop masses in the Tsqk1, Tstot1, Tstop1 simplified models, see their Figure 14.
> 560	95	54	KHACHATRY...15AH CMS	$\tilde{t} \rightarrow t\tilde{\chi}_1^0, m_{\tilde{\chi}_1^0} = 0, m_{\tilde{t}} > m_t + m_{\tilde{\chi}_1^0}$	3	SIRUNYAN 19s searched in 35.9 fb <sup>-1</sup> of $pp$ collisions at $\sqrt{s} = 13$ TeV for events with zero or one charged leptons, jets and $E_T$ . The razor variables ( $M_R$ and $R^2$ ) are used to categorize the events. No significant excess above the Standard Model expectations is observed. Limits are set on the gluino mass in the Tglu3A and Tglu3C simplified models, see Figures 22 and 23, and on the stop mass in the Tstop1 simplified model, see their Figure 24.
> 250	95	55	KHACHATRY...15AH CMS	$\tilde{t} \rightarrow c\tilde{\chi}_1^0, m_{\tilde{\chi}_1^0} = 0, m_{\tilde{t}} < 100$ GeV	4	SIRUNYAN 19u searched in 35.9 fb <sup>-1</sup> of $pp$ collisions at $\sqrt{s} = 13$ TeV for events containing one electron-muon pair with opposite charge. The search targets a region of parameter space where the kinematics of top squark pair production and top quark pair production is very similar, due to the mass difference between the top squark and the neutralino being close to the top quark mass. No excess above the Standard Model expectations is observed. Limits are set on the stop mass in the Tstop1 model, with $m_{\tilde{t}} - m_{\tilde{\chi}_1^0}$ close to $m_t$ , see Figure 5.
none, 200–350	95	56	KHACHATRY...15L CMS	$\tilde{t} \rightarrow qq, \text{RPV}, \lambda_{\beta 12}'' \neq 0$	5	AABOUD 18AQ searched in 36.1 fb <sup>-1</sup> of $pp$ collisions at $\sqrt{s} = 13$ TeV for top squark pair production in final states with one isolated electron or muon, several energetic jets, and missing transverse momentum. No significant excess over the Standard Model prediction is observed. In case of Tstop1 models, top squark masses up to 940 GeV are excluded assuming $m_{\tilde{\chi}_1^0} = 0$ GeV, see their Fig. 20. If the top quark is not on-shell (3-body) decay, exclusions up to 500 GeV are obtained for $m_{\tilde{\chi}_1^0} = 300$ GeV. Exclusions as a function of $m_{\tilde{t}} - m_{\tilde{\chi}_1^0}$ are given in their Fig. 21.
none, 200–385	95	56	KHACHATRY...15L CMS	$\tilde{t} \rightarrow qb, \text{RPV}, \lambda_{323}'' \neq 0$	6	AABOUD 18AQ searched in 36.1 fb <sup>-1</sup> of $pp$ collisions at $\sqrt{s} = 13$ TeV for top squark pair production in final states with one isolated electron or muon, several energetic jets, and missing transverse momentum. No significant excess over the Standard Model prediction is observed. In case of Tstop3 models (4-body), top squark masses up to 370 GeV are excluded for $m_{\tilde{t}} - m_{\tilde{\chi}_1^0}$ as low as 20 GeV. Top squark masses below 195 GeV are excluded for all $m_{\tilde{\chi}_1^0}$ , see their Fig. 20 and Fig. 21.
> 730	95	57	KHACHATRY...15X CMS	$\tilde{t} \rightarrow t\tilde{\chi}_1^0, m_{\tilde{\chi}_1^0} = 100$ GeV, $m_{\tilde{t}} > m_t + m_{\tilde{\chi}_1^0}$	7	AABOUD 18AQ searched in 36.1 fb <sup>-1</sup> of $pp$ collisions at $\sqrt{s} = 13$ TeV for top squark pair production in final states with one isolated electron or muon, several energetic jets, and missing transverse momentum. No significant excess over the Standard Model prediction is observed. In case of Tstop2 models, top squark masses up to 840 GeV are excluded for $m_{\tilde{t}} - m_{\tilde{\chi}_1^0} = 10$ GeV. See their Fig. 23. Exclusion limits for this decay mode are presented also in the context of Higgsino-LSP phenomenological MSSM models, where $m_{\tilde{\chi}_1^0} = 5$ GeV, see their Fig 26.
none 400–645	95	57	KHACHATRY...15X CMS	$\tilde{t} \rightarrow t\tilde{\chi}_1^0$ or $\tilde{t} \rightarrow b\tilde{\chi}_1^\pm, m_{\tilde{\chi}_1^0} = 100$ GeV, $m_{\tilde{\chi}_1^\pm} - m_{\tilde{\chi}_1^0} = 5$ GeV	8	AABOUD 18BV searched in 36.1 fb <sup>-1</sup> of $pp$ collisions at $\sqrt{s} = 13$ TeV for events with at least one jet identified as $c$ -jet, large missing transverse energy and no leptons. Good agreement is observed between the number of events in data and Standard Model predictions. The results are translated into exclusion limits in Tstop4 models. In scenarios with differences of the stop and neutralino masses below 100 GeV, stop masses below 500 GeV are excluded. See their Fig.6 and Fig.7.
none 270–645	95	58	AAD	14AJ ATLS $\geq 4$ jets + $E_T, \tilde{t}_1 \rightarrow t\tilde{\chi}_1^0, m_{\tilde{\chi}_1^0} < 30$ GeV	9	AABOUD 18BV searched in 36.1 fb <sup>-1</sup> of $pp$ collisions at $\sqrt{s} = 13$ TeV for events with at least one jet identified as $c$ -jet, large missing transverse energy and no leptons. Good agreement is observed between the number of events in data and Standard Model predictions. The results are translated into exclusion limits in Tstop1 models. In scenarios with massless neutralinos, top squark masses below 850 GeV are excluded. See their Fig.6.
none 250–550	95	58	AAD	14AJ ATLS $\geq 4$ jets + $E_T, B(\tilde{t}_1 \rightarrow b\tilde{\chi}_1^\pm) = 50\%, m_{\tilde{\chi}_1^\pm} = 2 m_{\tilde{\chi}_1^0}, m_{\tilde{\chi}_1^0} < 60$ GeV	10	AABOUD 18i searched in 36.1 fb <sup>-1</sup> of $pp$ collisions at $\sqrt{s} = 13$ TeV for events with at least one jet with a transverse momentum above 250 GeV and no leptons. Good agreement is observed between the number of events in data and Standard Model predictions. The results are translated into exclusion limits in Tstop3 models. Stop masses below 390 GeV are excluded for $m_{\tilde{t}} - m_{\tilde{\chi}_1^0} = m_b$ . See their Fig.9(b).
none 210–640	95	59	AAD	14BD ATLS $\ell^\pm + \text{jets} + E_T, \tilde{t}_1 \rightarrow t\tilde{\chi}_1^0, m_{\tilde{\chi}_1^0} = 0$ GeV	11	AABOUD 18i searched in 36.1 fb <sup>-1</sup> of $pp$ collisions at $\sqrt{s} = 13$ TeV for events with at least one jet with a transverse momentum above 250 GeV and no leptons. Good agreement is observed between the number of events in data and Standard Model predictions. The results are translated into exclusion limits in Tstop4 models. In scenarios with differences of the stop and neutralino masses around 5 GeV, stop masses below 430 GeV are excluded. See their Fig.9(a).
> 500	95	59	AAD	14BD ATLS $\ell^\pm + \text{jets} + E_T, \tilde{t}_1 \rightarrow b\tilde{\chi}_1^\pm, m_{\tilde{\chi}_1^\pm} = 2 m_{\tilde{\chi}_1^0}, 100$ GeV < $m_{\tilde{\chi}_1^0} < 150$ GeV	12	AABOUD 18Y searched in 36.1 fb <sup>-1</sup> of $pp$ collisions at $\sqrt{s} = 13$ TeV for direct pair production of top squarks in final states with two tau leptons, $b$ -jets, and missing transverse momentum. At least one hadronic $\tau$ is required. No significant deviation from the SM predictions is observed in the data. The analysis results are interpreted in Tstop5 models with a nearly massless gravitino. Top squark masses up to 1.16 TeV and tau slepton masses up to 1 TeV are excluded, see their Fig. 7.
none 150–445	95	60	AAD	14F ATLS $\ell^\pm \ell^\mp$ final state, $\tilde{t}_1 \rightarrow b\tilde{\chi}_1^\pm, m_{\tilde{t}} - m_{\tilde{\chi}_1^\pm} = 10$ GeV, $m_{\tilde{\chi}_1^0} = 1$ GeV	13	SIRUNYAN 18AJ searched in 35.9 fb <sup>-1</sup> of $pp$ collisions at $\sqrt{s} = 13$ TeV for events containing two low-momentum, oppositely charged leptons (electrons or muons) and $E_T$ . No excess over the expected background is observed. Limits are derived on the wino mass in the Tch1n2F simplified model, see their Figure 5. Limits are also set on the stop mass in the Tstop10 simplified model, see their Figure 6. Finally, limits are set on the Higgsino mass in the Tch1n2G simplified model, see Figure 8 and in the pMSSM, see Figure 7.
none 215–530	95	60	AAD	14F ATLS $\ell^\pm \ell^\mp$ final state, $\tilde{t}_1 \rightarrow t\tilde{\chi}_1^0, m_{\tilde{\chi}_1^0} = 1$ GeV	14	SIRUNYAN 18AL searched in 35.9 fb <sup>-1</sup> of $pp$ collisions at $\sqrt{s} = 13$ TeV for events with at least three charged leptons, in any combination of electrons and muons, jets and significant $E_T$ . No significant excess above the Standard Model expectations is observed. Limits are set on the gluino mass in the Tglu3A and Tglu1C simplified models, see their Figure 5. Limits are also set on the sbottom mass in the Tstot2 simplified model, see their Figure 6, and on the stop mass in the Tstop7 simplified model, see their Figure 7.
> 270	95	61	AAD	14T ATLS $\tilde{t}_1 \rightarrow c\tilde{\chi}_1^0, m_{\tilde{\chi}_1^0} = 200$ GeV	15	SIRUNYAN 18AN searched in 19.7 fb <sup>-1</sup> of $pp$ collisions at $\sqrt{s} = 8$ TeV for events containing one or two photons and a pair of top quarks from the decay of a pair of top squark in a natural gauge-mediated scenario. The final state consists of a lepton (electron or muon), jets and one or two photons. No significant excess above the Standard Model expectations is observed. Limits are set on the stop mass in the Tstop12 simplified model, see their Figure 6.
> 240	95	61	AAD	14T ATLS $\tilde{t}_1 \rightarrow c\tilde{\chi}_1^0, m_{\tilde{\chi}_1^0} - m_{\tilde{\chi}_1^0} < 85$ GeV		
> 255	95	61	AAD	14T ATLS $\tilde{t}_1 \rightarrow b f f' \tilde{\chi}_1^0, m_{\tilde{t}} - m_{\tilde{\chi}_1^0} \approx m_b$		
> 400	95	62	CHATRCHYAN14AH CMS	jets + $E_T, \tilde{t} \rightarrow t\tilde{\chi}_1^0$ simplified model, $m_{\tilde{\chi}_1^0} = 50$ GeV		
> 740	95	64	KHACHATRY...14T CMS	$\tau + b$ -jets, RPV, $LQ\tilde{D}, \lambda_{333}'' \neq 0, \tilde{t} \rightarrow \tau b$ simplified model		
> 580	95	64	KHACHATRY...14T CMS	$\tau + b$ -jets, RPV, $LQ\tilde{D}, \lambda_{3jk}'' \neq 0 (j \neq 3), \tilde{t} \rightarrow \tilde{\chi}_1^\pm b, \tilde{\chi}_1^\pm \rightarrow qq\tau^\pm$ simplified model		
••• We do not use the following data for averages, fits, limits, etc. •••						
> 850	95	65	AABOUD	17AF ATLS $2\ell + \text{jets} + b\text{-jets} + E_T, \text{Tstop6}, m_{\tilde{\chi}_1^0} = 0$		
> 800	95	66	AABOUD	17AF ATLS $2\ell + \text{jets} + b\text{-jets} + E_T, \text{Tstop7}$ with 100% decays via $Z, m_{\tilde{\chi}_1^0} = 50$ GeV		
> 880	95	67	AABOUD	17AF ATLS $2\ell + \text{jets} + b\text{-jets} + E_T, \text{Tstop7}$ with 100% decays via higgs, $m_{\tilde{\chi}_1^0} = 50$ GeV		
> 230	95	68	AABOUD ROLBIECKI	17AY ATLS 15 THEO jets + $E_T$ , pMSSM-inspired $WW$ xsection, $\tilde{t}_1 \rightarrow bW\tilde{\chi}_1^0, m_{\tilde{t}} \approx m_b + m_W + m_{\tilde{\chi}_1^0}$		
> 600	95	69	AAD	14B ATLS $Z + b E_T, \tilde{t}_2 \rightarrow Z\tilde{\chi}_1^0, \tilde{t}_1 \rightarrow t\tilde{\chi}_1^0, m_{\tilde{\chi}_1^0} < 200$ GeV		
> 540	95	69	AAD	14B ATLS $Z + b E_T, \tilde{t}_1 \rightarrow t\tilde{\chi}_1^0, \tilde{\chi}_1^0 \rightarrow Z\tilde{G}$ , natural GMSB, 100 GeV < $m_{\tilde{\chi}_1^0} < m_{\tilde{t}} - 10$ GeV		
> 360	95	70	CHATRCHYAN14U CMS	$\tilde{t}_1 \rightarrow b\tilde{\chi}_1^\pm r, \tilde{\chi}_1^\pm \rightarrow f f' \tilde{\chi}_1^0, \tilde{\chi}_1^0 \rightarrow H\tilde{G}$ simplified model, $m_{\tilde{\chi}_1^\pm} - m_{\tilde{\chi}_1^0} = 5$ GeV, GMSB		
> 215	95		CZAKON	14 $\tilde{t} \rightarrow t\tilde{\chi}_1^0, m_{\tilde{\chi}_1^0} < 10$ GeV		
		71	KHACHATRY...14c CMS	$\tilde{t}_2 \rightarrow H\tilde{t}_1$ or $\tilde{t}_2 \rightarrow Z\tilde{t}_1$ simplified model		

<sup>1</sup> SIRUNYAN 19AU searched in 35.9 fb<sup>-1</sup> of  $pp$  collisions at  $\sqrt{s} = 13$  TeV for events with at least one photon, jets, some of which are identified as originating from  $b$ -quarks, and large  $E_T$ . No significant excess above the Standard Model expectations is observed. In the framework of GMSB, limits are set on the gluino mass in the Tglu4C, Tglu4D and Tglu4E simplified models, and on the top squark mass in the Tstop13 simplified model, see their Figure 5.

- 16 SIRUNYAN 18AY searched in  $35.9 \text{ fb}^{-1}$  of  $pp$  collisions at  $\sqrt{s} = 13 \text{ TeV}$  for events containing one or more jets and significant  $E_{\cancel{T}}$ . No significant excess above the Standard Model expectations is observed. Limits are set on the gluino mass in the Tglu1A, Tglu2A and Tglu3A simplified models, see their Figure 3. Limits are also set on squark, sbottom and stop masses in the Tsqk1, Tsb0t1, Tstop1 and Tstop4 simplified models, see their Figure 3. Finally, limits are set on long-lived gluino masses in a Tglu1A simplified model where the gluino is metastable or long-lived with proper decay lengths in the range  $10^{-3} \text{ mm} < c\tau < 10^5 \text{ mm}$ , see their Figure 4.
- 17 SIRUNYAN 18B searched in  $35.9 \text{ fb}^{-1}$  of  $pp$  collisions at  $\sqrt{s} = 13 \text{ TeV}$  for the pair production of third-generation squarks in events with jets and large  $E_{\cancel{T}}$ . No significant excess above the Standard Model expectations is observed. Limits are set on the sbottom mass in the Tsb0t1 simplified model, see their Figure 5, and on the stop mass in the Tstop4 simplified model, see their Figure 6.
- 18 SIRUNYAN 18C searched in  $35.9 \text{ fb}^{-1}$  of  $pp$  collisions at  $\sqrt{s} = 13 \text{ TeV}$  for the pair production of top squarks in events with two oppositely charged leptons (electrons or muons), jets identified as originating from a  $b$ -quark and large  $E_{\cancel{T}}$ . No significant excess above the Standard Model expectations is observed. Limits are set on the stop mass in the Tstop1, Tstop2 and Tstop11 simplified models, see their Figures 11 and 12. The Tstop1 and Tstop2 results are combined with complementary searches in the all-hadronic and single lepton channels, see their Figures 13 and 14.
- 19 SIRUNYAN 18D searched in  $35.9 \text{ fb}^{-1}$  of  $pp$  collisions at  $\sqrt{s} = 13 \text{ TeV}$  for events containing identified hadronically decaying top quarks, no leptons, and  $E_{\cancel{T}}$ . No significant excess above the Standard Model expectations is observed. Limits are set on the stop mass in the Tstop1 simplified model, see their Figure 8, and on the gluino mass in the Tglu3A, Tglu3B, Tglu3C and Tglu3E simplified models, see their Figure 9.
- 20 SIRUNYAN 18Di searched in  $35.9 \text{ fb}^{-1}$  of  $pp$  collisions at  $\sqrt{s} = 13 \text{ TeV}$  for pair production of top squarks in events with a low transverse momentum lepton (electron or muon), a high-momentum jet and significant missing transverse momentum. No significant excess above the Standard Model expectations is observed. Limits are set on the stop mass in the Tstop3 and Tstop10 simplified models, see their Figures 7 and 8. A combination of this search with the all-hadronic search is presented in Figure 9.
- 21 SIRUNYAN 18DN searched in  $35.9 \text{ fb}^{-1}$  of  $pp$  collisions at  $\sqrt{s} = 13 \text{ TeV}$  for direct electroweak production of charginos and for pair production of top squarks in events with two leptons (electrons or muons) of the opposite electric charge. No significant excess above the Standard Model expectations is observed. Limits are set on the chargino mass in the Tch1Ch1C and Tch1Ch1E simplified models, see their Figure 8. Limits are also set on the stop mass in the Tstop1 and Tstop2 simplified models, see their Figure 9.
- 22 ABOUD 17AJ searched in  $36.1 \text{ fb}^{-1}$  of  $pp$  collisions at  $\sqrt{s} = 13 \text{ TeV}$  for events with two same-sign or three leptons, jets and large missing transverse momentum. No significant excess above the Standard Model expectations is observed. Limits up to 700 GeV are set on the top squark mass in Tstop11 simplified models, assuming  $m_{\tilde{\chi}_1^0} = m_{\tilde{t}} - 275 \text{ GeV}$  and  $m_{\tilde{\chi}_2^0} = m_{\tilde{\chi}_1^0} + 100 \text{ GeV}$ . See their Figure 4(e).
- 23 ABOUD 17AX searched in  $36 \text{ fb}^{-1}$  of  $pp$  collisions at  $\sqrt{s} = 13 \text{ TeV}$  for events containing two jets identified as originating from  $b$ -quarks and large missing transverse momentum, with or without leptons. No excess of events above the expected level of Standard Model background was found. Exclusion limits at 95% C.L. are set on the masses of top squarks. Assuming 50% BR for Tstop1 and Tstop2 simplified models, a  $\tilde{t}_1$  mass below 880 (860) GeV is excluded for  $m_{\tilde{\chi}_1^0} = 0$  (<250) GeV. See their Fig. 7(b).
- 24 ABOUD 17AY searched in  $36.1 \text{ fb}^{-1}$  of  $pp$  collisions at  $\sqrt{s} = 13 \text{ TeV}$  for events with at least four jets and large missing transverse momentum. No significant excess above the Standard Model expectations is observed. Limits in the range 250–1000 GeV are set on the top squark mass in Tstop1 simplified models. For the first time, additional constraints are set for the region  $m_{\tilde{t}_1} \sim m_{\tilde{t}} + m_{\tilde{\chi}_1^0}$ , with exclusion of the  $\tilde{t}_1$  mass range 235–590 GeV. See their Figure 8.
- 25 ABOUD 17AZ searched in  $36.1 \text{ fb}^{-1}$  of  $pp$  collisions at  $\sqrt{s} = 13 \text{ TeV}$  for events with at least four jets and large missing transverse momentum. No significant excess above the Standard Model expectations is observed. Limits in the range 450–850 GeV are set on the top squark mass in a mixture of Tstop1 and Tstop2 simplified models with BR=50% and assuming  $m_{\tilde{\chi}_1^\pm} - m_{\tilde{\chi}_1^0} = 1 \text{ GeV}$  and  $m_{\tilde{\chi}_1^0} < 240 \text{ GeV}$ . Constraints are given for various values of the BR. See their Figure 9.
- 26 ABOUD 17BE searched in  $36.1 \text{ fb}^{-1}$  of  $pp$  collisions at  $\sqrt{s} = 13 \text{ TeV}$  for events with two opposite-charge leptons (electrons and muons) and large missing transverse momentum. No significant excess above the Standard Model expectations is observed. Limits up to 720 GeV are set on the top squark mass in Tstop1 simplified models, assuming massless neutralinos. See their Figure 9 (2-body area).
- 27 ABOUD 17BE searched in  $36.1 \text{ fb}^{-1}$  of  $pp$  collisions at  $\sqrt{s} = 13 \text{ TeV}$  for events with two opposite-charge leptons (electrons and muons) and large missing transverse momentum. No significant excess above the Standard Model expectations is observed. Limits up to 400 GeV are set on the top squark mass in Tstop3 simplified models, assuming  $m_{\tilde{t}_1} - m_{\tilde{\chi}_1^0} = 40 \text{ GeV}$ . See their Figure 9 (4-body area).
- 28 ABOUD 17BE searched in  $36.1 \text{ fb}^{-1}$  of  $pp$  collisions at  $\sqrt{s} = 13 \text{ TeV}$  for events with two opposite-charge leptons (electrons and muons) and large missing transverse momentum. No significant excess above the Standard Model expectations is observed. Limits up to 430 GeV are set on the top squark mass in Tstop1 simplified models where top quarks are offshell, assuming  $m_{\tilde{t}_1} - m_{\tilde{\chi}_1^0}$  close to the  $W$  mass. See their Figure 9 (3-body area).
- 29 ABOUD 17BE searched in  $36.1 \text{ fb}^{-1}$  of  $pp$  collisions at  $\sqrt{s} = 13 \text{ TeV}$  for events with two opposite-charge leptons (electrons and muons) and large missing transverse momentum. No significant excess above the Standard Model expectations is observed. Limits up to 700 GeV are set on the top squark mass in Tstop2 simplified models, assuming  $m_{\tilde{t}_1} - m_{\tilde{\chi}_1^0} = 10 \text{ GeV}$  and massless neutralinos. See their Figure 10.
- 30 KHACHATRYAN 17 searched in  $2.3 \text{ fb}^{-1}$  of  $pp$  collisions at  $\sqrt{s} = 13 \text{ TeV}$  for events containing four or more jets, no more than one lepton, and missing transverse momentum, using the razor variables ( $M_P$  and  $R^2$ ) to discriminate between signal and background processes. No evidence for an excess over the expected background is observed. Limits are derived on the stop mass in the Tstop1 simplified model, see Fig. 17.
- 31 KHACHATRYAN 17AD searched in  $2.3 \text{ fb}^{-1}$  of  $pp$  collisions at  $\sqrt{s} = 13 \text{ TeV}$  for events containing at least four jets (including  $b$ -jets), missing transverse momentum and tagged top quarks. No evidence for an excess over the expected background is observed. Top squark masses in the range 250–740 GeV and neutralino masses up to 240 GeV are excluded at 95% C.L. See Fig. 12.
- 32 KHACHATRYAN 17AD searched in  $2.3 \text{ fb}^{-1}$  of  $pp$  collisions at  $\sqrt{s} = 13 \text{ TeV}$  for events containing at least four jets (including  $b$ -jets), missing transverse momentum and tagged top quarks. No evidence for an excess over the expected background is observed. Limits are derived on the  $\tilde{t}$  mass in simplified models that are a mixture of Tstop1 and Tstop2 with branching fractions 50% for each of the two decay modes: top squark masses of up to 610 GeV and neutralino masses up to 190 GeV are excluded at 95% C.L. The  $\tilde{\chi}_1^\pm$  and the  $\tilde{\chi}_1^0$  are assumed to be nearly degenerate in mass, with a 5 GeV difference between their masses. See Fig. 12.
- 33 KHACHATRYAN 17P searched in  $2.3 \text{ fb}^{-1}$  of  $pp$  collisions at  $\sqrt{s} = 13 \text{ TeV}$  for events with one or more jets and large  $E_{\cancel{T}}$ . No significant excess above the Standard Model expectations is observed. Limits are set on the gluino mass in the Tglu1A, Tglu2A, Tglu3A, Tglu3B, Tglu3C and Tglu3D simplified models, see their Figures 7 and 8. Limits are also set on the squark mass in the Tsqk1 simplified model, see their Fig. 7, and on the sbottom mass in the Tsb0t1 simplified model, see Fig. 8. Finally, limits are set on the stop mass in the Tstop1, Tstop3, Tstop4, Tstop6 and Tstop7 simplified models, see Fig. 8.
- 34 KHACHATRYAN 17s searched in  $18.5 \text{ fb}^{-1}$  of  $pp$  collisions at  $\sqrt{s} = 8 \text{ TeV}$  for events containing multiple jets and missing transverse momentum, using the  $\alpha_T$  variable to discriminate between signal and background processes. No evidence for an excess over the expected background is observed. Limits are derived on the stop mass in the Tstop4 model: for  $\Delta m = m_{\tilde{t}} - m_{\tilde{\chi}_1^0}$  equal to 10 and 80 GeV, masses of stop below 240 and 260 GeV are excluded, respectively. See their Fig. 3.
- 35 KHACHATRYAN 17s searched in  $18.5 \text{ fb}^{-1}$  of  $pp$  collisions at  $\sqrt{s} = 8 \text{ TeV}$  for events containing multiple jets and missing transverse momentum, using the  $\alpha_T$  variable to discriminate between signal and background processes. No evidence for an excess over the expected background is observed. Limits are derived on the stop mass in the Tstop3 model: for  $\Delta m = m_{\tilde{t}} - m_{\tilde{\chi}_1^0}$  equal to 10 and 80 GeV, masses of stop below 225 and 130 GeV are excluded, respectively. See their Fig. 3.
- 36 KHACHATRYAN 17s searched in  $18.5 \text{ fb}^{-1}$  of  $pp$  collisions at  $\sqrt{s} = 8 \text{ TeV}$  for events containing multiple jets and missing transverse momentum, using the  $\alpha_T$  variable to discriminate between signal and background processes. No evidence for an excess over the expected background is observed. Limits are derived on the stop mass in the Tstop2 model: assuming  $m_{\tilde{\chi}_1^\pm} = 0.25 m_{\tilde{t}} + 0.75 m_{\tilde{\chi}_1^0}$ , masses of stop up to 325 GeV and masses of the neutralino up to 225 GeV are excluded. See their Fig. 3.
- 37 KHACHATRYAN 17s searched in  $18.5 \text{ fb}^{-1}$  of  $pp$  collisions at  $\sqrt{s} = 8 \text{ TeV}$  for events containing multiple jets and missing transverse momentum, using the  $\alpha_T$  variable to discriminate between signal and background processes. No evidence for an excess over the expected background is observed. Limits are derived on the stop mass in the Tstop2 model: assuming  $m_{\tilde{\chi}_1^\pm} = 0.75 m_{\tilde{t}} + 0.25 m_{\tilde{\chi}_1^0}$ , masses of stop up to 400 GeV are excluded for low neutralino masses. See their Fig. 3.
- 38 KHACHATRYAN 17s searched in  $18.5 \text{ fb}^{-1}$  of  $pp$  collisions at  $\sqrt{s} = 8 \text{ TeV}$  for events containing multiple jets and missing transverse momentum, using the  $\alpha_T$  variable to discriminate between signal and background processes. No evidence for an excess over the expected background is observed. Limits are derived on the stop mass in the Tstop1 model: assuming masses of stop up to 500 GeV and masses of the neutralino up to 105 GeV are excluded. See their Fig. 3.
- 39 SIRUNYAN 17As searched in  $35.9 \text{ fb}^{-1}$  of  $pp$  collisions at  $\sqrt{s} = 13 \text{ TeV}$  for events with a single lepton (electron or muon), jets, and large  $E_{\cancel{T}}$ . No significant excess above the Standard Model expectations is observed. Limits are set on the stop mass in the Tstop1, Tstop2 and Tstop8 simplified models, see their Figures 5, 6 and 7.
- 40 SIRUNYAN 17AT searched in  $35.9 \text{ fb}^{-1}$  of  $pp$  collisions at  $\sqrt{s} = 13 \text{ TeV}$  for direct production of top squarks in events with jets and large  $E_{\cancel{T}}$ . No significant excess above the Standard Model expectations is observed. Limits are set on the stop mass in the Tstop1, Tstop2, Tstop3, Tstop4, Tstop8 and Tstop10 simplified models, see their Figures 9 to 14.
- 41 SIRUNYAN 17AZ searched in  $35.9 \text{ fb}^{-1}$  of  $pp$  collisions at  $\sqrt{s} = 13 \text{ TeV}$  for events with one or more jets and large  $E_{\cancel{T}}$ . No significant excess above the Standard Model expectations is observed. Limits are set on the gluino mass in the Tglu1A, Tglu2A, Tglu3A simplified models, see their Figures 6. Limits are also set on the squark mass in the Tsqk1 simplified model (for single light squark and for 8 degenerate light squarks), on the sbottom mass in the Tsb0t1 simplified model and on the stop mass in the Tstop1 simplified model, see their Fig. 7. Finally, limits are set on the stop mass in the Tstop2, Tstop4 and Tstop8 simplified models, see Fig. 8.
- 42 SIRUNYAN 17k searched in  $2.3 \text{ fb}^{-1}$  of  $pp$  collisions at  $\sqrt{s} = 13 \text{ TeV}$  for direct production of stop or sbottom pairs in events with multiple jets and significant  $E_{\cancel{T}}$ . A second search also requires an isolated lepton and is combined with the all-hadronic search. No significant excess above the Standard Model expectations is observed. Limits are set on the stop mass in the Tstop1, Tstop8 and Tstop4 simplified models, see their Figures 7, 8 and 9 (for the Tstop4 limits, only the results of the all-hadronic search are used). Limits are also set on the sbottom mass in the Tsb0t1 simplified model, see Fig. 10 (also here, only the results of the all-hadronic search are used).
- 43 SIRUNYAN 17P searched in  $35.9 \text{ fb}^{-1}$  of  $pp$  collisions at  $\sqrt{s} = 13 \text{ TeV}$  for events with multiple jets and large  $E_{\cancel{T}}$ . No significant excess above the Standard Model expectations is observed. Limits are set on the gluino mass in the Tglu1A, Tglu1C, Tglu2A, Tglu3A and Tglu3D simplified models, see their Fig. 12. Limits are also set on the squark mass in the Tsqk1 simplified model, on the stop mass in the Tstop1 simplified model, and on the sbottom mass in the Tsb0t1 simplified model, see Fig. 13.
- 44 ABOUD 16D searched in  $3.2 \text{ fb}^{-1}$  of  $pp$  collisions at  $\sqrt{s} = 13 \text{ TeV}$  in events with an energetic jet and large missing transverse momentum. The results are interpreted as 95% C.L. limits on mass of stop decaying into a charm-quark and the lightest neutralino in scenarios with  $m_{\tilde{t}_1} - m_{\tilde{\chi}_1^0}$  between 5 and 20 GeV. See their Fig. 5.
- 45 ABOUD 16J searched in  $3.2 \text{ fb}^{-1}$  of  $pp$  collisions at  $\sqrt{s} = 13 \text{ TeV}$  in final states with one isolated electron or muon, jets, and missing transverse momentum. For the direct stop pair production model where the stop decays via top and lightest neutralino, the results exclude at 95% C.L. stop masses between 745 GeV and 780 GeV for a massless  $\tilde{\chi}_1^0$ . See their Fig. 8.
- 46 AAD 16AY searched in  $20 \text{ fb}^{-1}$  of  $pp$  collisions at  $\sqrt{s} = 8 \text{ TeV}$  for events with either two hadronically decaying tau leptons, one hadronically decaying tau and one light lepton, or two light leptons. No significant excess over the Standard Model expectation is found. Exclusion limits at 95% C.L. on the mass of top squarks decaying via  $\tilde{\tau}$  to a nearly massless gravitino are placed depending on  $m_{\tilde{\tau}}$  which is ranging from the 87 GeV LEP limit to  $m_{\tilde{t}_1}$ . See their Figs. 9 and 10.

# Searches Particle Listings

## Supersymmetric Particle Searches

- 47 KHACHATRYAN 16AV searched in  $19.7 \text{ fb}^{-1}$  of  $pp$  collisions at  $\sqrt{s} = 8 \text{ TeV}$  for events with one or two isolated leptons, hadronic jets,  $b$ -jets and  $\cancel{E}_T$ . No significant excess above the Standard Model expectations is observed. Limits are set on the stop mass in the Tstop1 and Tstop2 simplified models, see Fig. 11.
- 48 KHACHATRYAN 16BK searched in  $18.9 \text{ fb}^{-1}$  of  $pp$  collisions at  $\sqrt{s} = 8 \text{ TeV}$  for events with hadronic jets and  $\cancel{E}_T$ . No significant excess above the Standard Model expectations is observed. Limits are set on the stop mass in the Tstop1 and Tstop2 simplified models, see Fig. 16.
- 49 KHACHATRYAN 16BS searched in  $2.3 \text{ fb}^{-1}$  of  $pp$  collisions at  $\sqrt{s} = 13 \text{ TeV}$  for events with at least one energetic jet, no isolated leptons, and significant  $\cancel{E}_T$ , using the transverse mass variable  $M_{T2}$  to discriminate between signal and background processes. No significant excess above the Standard Model expectations is observed. Limits are set on the stop mass in the Tstop1 simplified model, see Fig. 11 and Table 3.
- 50 KHACHATRYAN 16V searched in  $19.7 \text{ fb}^{-1}$  of  $pp$  collisions at  $\sqrt{s} = 8 \text{ TeV}$  for events with one or two soft isolated leptons, hadronic jets, and  $\cancel{E}_T$ . No significant excess above the Standard Model expectations is observed. Limits are set on the stop mass in the Tstop3 simplified model, see Fig. 3.
- 51 AAD 15CJ searched in  $20 \text{ fb}^{-1}$  of  $pp$  collisions at  $\sqrt{s} = 8 \text{ TeV}$  for evidence of third generation squarks by combining a large number of searches covering various final states. Stop decays with and without charginos in the decay chain are considered and summaries of all ATLAS Run 1 searches for direct stop production can be found in Fig. 4 (no intermediate charginos) and Fig. 7 (intermediate charginos). Limits are set on stop masses in compressed mass regions, with  $B(\bar{t} \rightarrow c\bar{\chi}_1^0) + B(\bar{t} \rightarrow bff'\bar{\chi}_1^0) = 1$ , see Fig. 5. Limits are also set on stop masses assuming that both the decay  $\bar{t} \rightarrow t\bar{\chi}_1^0$  and  $\bar{t} \rightarrow b\bar{\chi}_1^\pm$  are possible, with both their branching ratios summing up to 1, assuming  $\bar{\chi}_1^\pm \rightarrow W^{(*)}\bar{\chi}_1^0$  and  $m_{\bar{\chi}_1^\pm} = 2m_{\bar{\chi}_1^0}$ , see Fig. 6. Limits on the mass of the next-to-lightest stop  $\bar{t}_2$ , decaying either to  $Z\bar{t}_1$ ,  $h\bar{t}_1$  or  $t\bar{\chi}_1^0$ , are also presented, see Figs. 9 and 10. Interpretations in the pMSSM are also discussed, see Figs 13–15.
- 52 AAD 15J interpreted the measurement of spin correlations in  $t\bar{t}$  production using  $20.3 \text{ fb}^{-1}$  of  $pp$  collisions at  $\sqrt{s} = 8 \text{ TeV}$  in exclusion limits on the pair production of light  $\bar{t}_1$  squarks with masses similar to the top quark mass. The  $\bar{t}_1$  is assumed to decay through  $\bar{t}_1 \rightarrow t\bar{\chi}_1^0$  with predominantly right-handed top and a 100% branching ratio. The data are found to be consistent with the Standard Model expectations and masses between the top quark mass and 191 GeV are excluded, see their Fig. 2
- 53 KHACHATRYAN 15AF searched in  $19.5 \text{ fb}^{-1}$  of  $pp$  collisions at  $\sqrt{s} = 8 \text{ TeV}$  for events with at least two energetic jets and significant  $\cancel{E}_T$ , using the transverse mass variable  $M_{T2}$  to discriminate between signal and background processes. No significant excess above the Standard Model expectations is observed. Limits are set on the stop mass in simplified models where the decay  $\bar{t} \rightarrow t\bar{\chi}_1^0$  takes place with a branching ratio of 100%, see Fig. 12. See also Table 5. Exclusions in the CMSSM, assuming  $\tan\beta = 30$ ,  $A_0 = -2 \max(m_0, m_{1/2})$  and  $\mu > 0$ , are also presented, see Fig. 15.
- 54 KHACHATRYAN 15AH searched in  $19.4$  or  $19.7 \text{ fb}^{-1}$  of  $pp$  collisions at  $\sqrt{s} = 8 \text{ TeV}$  for events containing either a fully reconstructed top quark, or events containing dijets requiring one or both jets to originate from  $b$ -quarks, or events containing a mono-jet. No significant excess above the Standard Model expectations is observed. Limits are set on the stop mass in simplified models where the decay  $\bar{t} \rightarrow t\bar{\chi}_1^0$  takes place with a branching ratio of 100%, see Fig. 9. Limits are also set in simplified models where the decays  $\bar{t} \rightarrow t\bar{\chi}_1^0$  and  $\bar{t} \rightarrow b\bar{\chi}_1^\pm$ , with  $m_{\bar{\chi}_1^\pm} - m_{\bar{\chi}_1^0} = 5 \text{ GeV}$ , each take place with a branching ratio of 50%, see Fig. 10, or with other fractions, see Fig. 11. Finally, limits are set in a simplified model where the decay  $\bar{t} \rightarrow c\bar{\chi}_1^0$  takes place with a branching ratio of 100%, see Figs. 9, 10 and 11.
- 55 KHACHATRYAN 15AH searched in  $19.4$  or  $19.7 \text{ fb}^{-1}$  of  $pp$  collisions at  $\sqrt{s} = 8 \text{ TeV}$  for events containing either a fully reconstructed top quark, or events containing dijets requiring one or both jets to originate from  $b$ -quarks, or events containing a mono-jet. No significant excess above the Standard Model expectations is observed. Limits are set on the stop mass in simplified models where the decay  $\bar{t} \rightarrow t\bar{\chi}_1^0$  takes place with a branching ratio of 100%, see Fig. 9. Limits are also set in simplified models where the decays  $\bar{t} \rightarrow t\bar{\chi}_1^0$  and  $\bar{t} \rightarrow b\bar{\chi}_1^\pm$ , with  $m_{\bar{\chi}_1^\pm} - m_{\bar{\chi}_1^0} = 5 \text{ GeV}$ , each take place with a branching ratio of 50%, see Fig. 10, or with other fractions, see Fig. 11. Finally, limits are set in a simplified model where the decay  $\bar{t} \rightarrow c\bar{\chi}_1^0$  takes place with a branching ratio of 100%, see Figs. 9, 10, and 11.
- 56 KHACHATRYAN 15L searched in  $19.4 \text{ fb}^{-1}$  of  $pp$  collisions at  $\sqrt{s} = 8 \text{ TeV}$  for pair production of heavy resonances decaying to pairs of jets in four jet events. No significant excess above the Standard Model expectations is observed. Limits are set on the stop mass in  $R$ -parity-violating supersymmetry models where  $\bar{t} \rightarrow qq$  ( $\lambda_{323} \neq 0$ ), see Fig. 6 (top) and  $\bar{t} \rightarrow qb$  ( $\lambda_{323} \neq 0$ ), see Fig. 6 (bottom).
- 57 KHACHATRYAN 15x searched in  $19.3 \text{ fb}^{-1}$  of  $pp$  collisions at  $\sqrt{s} = 8 \text{ TeV}$  for events with at least two energetic jets, at least one of which is required to originate from a  $b$  quark, possibly a lepton, and significant  $\cancel{E}_T$ , using the razor variables ( $M_R$  and  $R_2$ ) to discriminate between signal and background processes. No significant excess above the Standard Model expectations is observed. Limits are set on the stop mass in simplified models where the decay  $\bar{t} \rightarrow t\bar{\chi}_1^0$  and the decay  $\bar{t} \rightarrow b\bar{\chi}_1^\pm$ , with  $m_{\bar{\chi}_1^\pm} - m_{\bar{\chi}_1^0} = 5 \text{ GeV}$ , take place with branching ratios varying between 0 and 100%, see Figs. 15, 16 and 17.
- 58 AAD 14AJ searched in  $20.1 \text{ fb}^{-1}$  of  $pp$  collisions at  $\sqrt{s} = 8 \text{ TeV}$  for events containing four or more jets and large missing transverse momentum. No excess of events above the expected level of Standard Model background was found. Exclusion limits at 95% C.L. are set on the masses of third-generation squarks in simplified models which either assume that the decay  $\bar{t}_1 \rightarrow t\bar{\chi}_1^0$  takes place 100% of the time, see Fig. 8, or that this decay takes place 50% of the time, while the decay  $\bar{t}_1 \rightarrow b\bar{\chi}_1^\pm$  takes place the other 50% of the time, see Fig. 9.
- 59 AAD 14BD searched in  $20 \text{ fb}^{-1}$  of  $pp$  collisions at  $\sqrt{s} = 8 \text{ TeV}$  for events containing one isolated lepton, jets and large missing transverse momentum. No excess of events above the expected level of Standard Model background was found. Exclusion limits at 95% C.L. are set on the masses of third-generation squarks in simplified models which either assume that the decay  $\bar{t}_1 \rightarrow t\bar{\chi}_1^0$  takes place 100% of the time, see Fig. 15, or the decay  $\bar{t}_1 \rightarrow b\bar{\chi}_1^\pm$  takes place 100% of the time, see Fig. 16–22. For the mixed decay scenario, see Fig. 23.
- 60 AAD 14F searched in  $20.3 \text{ fb}^{-1}$  of  $pp$  collisions at  $\sqrt{s} = 8 \text{ TeV}$  for events containing two leptons ( $e$  or  $\mu$ ), and possibly jets and missing transverse momentum. No excess of events above the expected level of Standard Model background was found. Exclusion limits at 95% C.L. are set on the masses of third-generation squarks in simplified models which either assume that the decay  $\bar{t}_1 \rightarrow b\bar{\chi}_1^\pm$  takes place 100% of the time, see Figs. 14–17 and 20, or that the decay  $\bar{t}_1 \rightarrow t\bar{\chi}_1^0$  takes place 100% of the time, see Figs. 18 and 19.
- 61 AAD 14T searched in  $20.3 \text{ fb}^{-1}$  of  $pp$  collisions at  $\sqrt{s} = 8 \text{ TeV}$  for monojet-like and  $c$ -tagged events. No excess of events above the expected level of Standard Model background was found. Exclusion limits at 95% C.L. are set on the masses of third-generation squarks in simplified models which assume that the decay  $\bar{t}_1 \rightarrow c\bar{\chi}_1^0$  takes place 100% of the time, see Fig. 9 and 10. The results of the monojet-like analysis are also interpreted in terms of stop pair production in the four-body decay  $\bar{t}_1 \rightarrow bff'\bar{\chi}_1^0$ , see Fig. 11.
- 62 CHATRCHYAN 14AH searched in  $4.7 \text{ fb}^{-1}$  of  $pp$  collisions at  $\sqrt{s} = 7 \text{ TeV}$  for events with at least two energetic jets and significant  $\cancel{E}_T$ , using the razor variables ( $M_R$  and  $R_2$ ) to discriminate between signal and background processes. A second analysis requires at least one of the jets to be originating from a  $b$ -quark. No significant excess above the Standard Model expectations is observed. Limits are set on bottom masses in simplified models where the decay  $\bar{t} \rightarrow t\bar{\chi}_1^0$  takes place with a branching ratio of 100%, see Figs. 28 and 29. Exclusions in the CMSSM, assuming  $\tan\beta = 10$ ,  $A_0 = 0$  and  $\mu > 0$ , are also presented, see Fig. 26.
- 63 CHATRCHYAN 14R searched in  $19.5 \text{ fb}^{-1}$  of  $pp$  collisions at  $\sqrt{s} = 8 \text{ TeV}$  for events with at least three leptons (electrons, muons, taus) in the final state. No significant excess above the Standard Model expectations is observed. Limits are set on the stop mass in a natural higgsino NLSP simplified model (GMSB) where the decay  $\bar{t} \rightarrow b\bar{\chi}_1^\pm$ , with  $\bar{\chi}_1^\pm \rightarrow (qq'/\ell\nu)H$ ,  $Z\bar{G}$ , takes place with a branching ratio of 100% (the particles between brackets have a soft  $p_T$  spectrum), see Figs. 4–6.
- 64 KHACHATRYAN 14T searched in  $19.7 \text{ fb}^{-1}$  of  $pp$  collisions at  $\sqrt{s} = 8 \text{ TeV}$  for events with  $\tau$ -leptons and  $b$ -quark jets, possibly with extra light-flavour jets. No excess above the Standard Model expectations is observed. Limits are set on stop masses in RPV SUSY models with  $LQ\bar{D}$  couplings, in two simplified models. In the first model, the decay  $\bar{t} \rightarrow \tau b$  is considered, with  $\lambda_{333}^b \neq 0$ , see Fig. 3. In the second model, the decay  $\bar{t} \rightarrow \bar{\chi}^\pm b$ , with the subsequent decay  $\bar{\chi}^\pm \rightarrow qq\tau^\pm$  is considered, with  $\lambda_{3jk}^b \neq 0$  and the mass splitting between the top squark and the chargino chosen to be 100 GeV, see Fig. 4.
- 65 AABOUD 17AF searched in  $36 \text{ fb}^{-1}$  of  $pp$  collisions at  $\sqrt{s} = 13 \text{ TeV}$  for evidence of top squarks in events containing 2 leptons, jets,  $b$ -jets and  $\cancel{E}_T$ . In Tstop6 model, assuming  $m_{\bar{\chi}_1^0} = 0 \text{ GeV}$ ,  $\bar{t}_1$  masses up to 850 GeV are excluded for  $m_{\bar{\chi}_2^0} > 200 \text{ GeV}$ .
- 66 AABOUD 17AF searched in  $36 \text{ fb}^{-1}$  of  $pp$  collisions at  $\sqrt{s} = 13 \text{ TeV}$  for evidence of  $\bar{t}_2$  in events containing 2 leptons, jets,  $b$ -jets and  $\cancel{E}_T$ . In Tstop7 model, assuming  $m_{\bar{\chi}_1^0} = 50 \text{ GeV}$  and 100% decays via  $Z$  boson,  $\bar{t}_2$  masses up to 800 GeV are excluded. Exclusion limits are also shown as a function of the  $\bar{t}_2$  branching ratios in their Figure 7.
- 67 AABOUD 17AF searched in  $36 \text{ fb}^{-1}$  of  $pp$  collisions at  $\sqrt{s} = 13 \text{ TeV}$  for evidence of  $\bar{t}_2$  in events containing 2 leptons, jets,  $b$ -jets and  $\cancel{E}_T$ . In Tstop7 model, assuming  $m_{\bar{\chi}_1^0} = 50 \text{ GeV}$  and 100% decays via higgs boson,  $\bar{t}_2$  masses up to 880 GeV are excluded. Exclusion limits are also shown as a function of the  $\bar{t}_2$  branching ratios in their Figure 7.
- 68 AABOUD 17AY searched in  $36.1 \text{ fb}^{-1}$  of  $pp$  collisions at  $\sqrt{s} = 13 \text{ TeV}$  for events with at least four jets and large missing transverse momentum. No significant excess above the Standard Model expectations is observed. Limits are set on the top squark mass assuming three pMSSM-inspired models. The first one, referred to as Higgsino LSP model, assumes  $m_{\bar{\chi}_1^\pm} - m_{\bar{\chi}_1^0} = 5 \text{ GeV}$  and  $m_{\bar{\chi}_2^0} - m_{\bar{\chi}_1^0} = 10 \text{ GeV}$ , with a mixture of decay modes as in Tstop1, Tstop2 and Tstop6. See their Figure 10. The second and third models are referred to as Wino NLSP and well-tempered pMSSM models, respectively. See their Figure 11 and Figure 12, and text for details on assumptions.
- 69 AAD 14B searched in  $20.3 \text{ fb}^{-1}$  of  $pp$  collisions at  $\sqrt{s} = 8 \text{ TeV}$  for events containing a  $Z$  boson, with or without additional leptons, plus jets originating from  $b$ -quarks and significant missing transverse momentum. No excess over the expected SM background is observed. Limits are derived in simplified models featuring  $\bar{t}_2$  production, with  $\bar{t}_2 \rightarrow Z\bar{t}_1$ ,  $\bar{t}_1 \rightarrow t\bar{\chi}_1^0$  with a 100% branching ratio, see Fig. 4, and in the framework of natural GMSB, see Fig. 6.
- 70 CHATRCHYAN 14U searched in  $19.7 \text{ fb}^{-1}$  of  $pp$  collisions at  $\sqrt{s} = 8 \text{ TeV}$  for evidence of direct pair production of top squarks, with Higgs bosons in the decay chain. The search is performed using a selection of events containing two Higgs bosons, each decaying to a photon pair, missing transverse energy and possibly  $b$ -quark jets. No significant excesses over the expected SM backgrounds are observed. The results are interpreted in the context of a “natural SUSY” simplified model where the decays  $\bar{t}_1 \rightarrow b\bar{\chi}_1^\pm$ , with  $\bar{\chi}_1^\pm \rightarrow ff'\bar{\chi}_1^0$ , and  $\bar{\chi}_1^0 \rightarrow H\bar{G}$ , all happen with 100% branching ratio, see Fig. 4.
- 71 KHACHATRYAN 14C searched in  $19.5 \text{ fb}^{-1}$  of  $pp$  collisions at  $\sqrt{s} = 8 \text{ TeV}$  for evidence of direct pair production of top squarks, with Higgs or  $Z$ -bosons in the decay chain. The search is performed using a selection of events containing leptons and  $b$ -quark jets. No significant excesses over the expected SM backgrounds are observed. The results are interpreted in the context of a simplified model with pair production of a heavier top-squark mass eigenstate  $\bar{t}_2$  decaying to a lighter top-squark eigenstate  $\bar{t}_1$  via either  $\bar{t}_2 \rightarrow H\bar{t}_1$  or  $\bar{t}_2 \rightarrow Z\bar{t}_1$ , followed in both cases by  $\bar{t}_1 \rightarrow t\bar{\chi}_1^0$ . The interpretation is performed in the region where the mass difference between the  $\bar{t}_1$  and  $\bar{\chi}_1^0$  is approximately equal to the top-quark mass, which is not probed by searches for direct  $\bar{t}_1$  pair production, see Figs. 5 and 6. The analysis excludes top squarks with masses  $m_{\bar{t}_2} < 575 \text{ GeV}$  and  $m_{\bar{t}_1} < 400 \text{ GeV}$  at 95% C.L.

R-parity violating  $\tilde{t}$  (Stop) mass limit

VALUE (GeV)	CL%	DOCUMENT ID	TECN	COMMENT
>1150	95	1 SIRUNYAN	19BI ATLS	$\tilde{t} \rightarrow b\mu$ , long-lived, Tstop2RPV, $c\tau = 0.1$ cm
>1100	95	2 SIRUNYAN	19BJ CMS	$\tilde{t} \rightarrow be$ , Tstop2RPV, prompt
none 100-410	95	3 AABOUD	18BB ATLS	4 jets, Tstop1RPV with $\tilde{t} \rightarrow ds, \lambda''_{312}$ coupling
none 100-470, 480-610	95	4 AABOUD	18BB ATLS	4 jets, Tstop1RPV, $\lambda''_{323}$ coupling
$\geq 600-1500$	95	5 AABOUD	18P ATLS	$2\ell + b$ -jets, Tstop2RPV, depending on $\lambda''_{333}$ coupling ( $i = 1, 2, 3$ )
>1130	95	6 SIRUNYAN	18AD CMS	$\tilde{t} \rightarrow b\ell$ , long-lived, $c\tau = 70-100$ mm
> 550	95	6 SIRUNYAN	18AD CMS	$\tilde{t} \rightarrow b\ell$ , long-lived, $c\tau = 1-1000$ mm
>1400	95	7 SIRUNYAN	18DV CMS	long-lived $\tilde{t}$ , RPV, $\tilde{t} \rightarrow \bar{d}\bar{d}$ , 0.6 mm $< c\tau < 80$ mm
none 80-520	95	8 SIRUNYAN	18DY CMS	2, 4 jets, Tstop3RPV, $\lambda''_{312}$ coupling
none 80-270, 285-340, 400-525	95	8 SIRUNYAN	18DY CMS	2, 4 jets, Tstop1RPV, $\lambda''_{323}$ coupling
>1200	95	9 AABOUD	17AI ATLS	$\geq 1\ell + \geq 8$ jets, Tstop1 with $\tilde{\chi}_1^0 \rightarrow tbs, \lambda''_{323}$ coupling, $m_{\tilde{\chi}_1^0} = 500$ GeV
none, 100-315	95	10 AAD	16AMATLS	2 large-radius jets, Tstop1RPV

• • • We do not use the following data for averages, fits, limits, etc. • • •

1 SIRUNYAN 19BI searched in 35.9 fb<sup>-1</sup> of  $pp$  collisions at  $\sqrt{s} = 13$  TeV in final states with two muons and two jets, or with one muon, two jets, and missing transverse momentum. Limits are set in a model of pair-produced, prompt or long-lived top squarks with R-parity violating decays to a  $b$ -quark and a lepton (Tstop2RPV), branching fraction of  $\tilde{t} \rightarrow b\mu$  equal to 1/3 and  $c\tau$  between 0.1 cm and 10 cm in the case of long-lived top squarks. See their Fig. 10.

2 SIRUNYAN 19BJ searched in 35.9 fb<sup>-1</sup> of  $pp$  collisions at  $\sqrt{s} = 13$  TeV in final states with two electrons and two jets, or with one electron, two jets, and missing transverse momentum. Limits are set in a model of pair-produced, prompt top squarks with R-parity violating decays to a  $b$ -quark and a lepton (Tstop2RPV), assuming branching fraction of  $\tilde{t} \rightarrow be$  equal to 1/3 and  $c\tau = 0$  cm. See their Fig.10.

3 AABOUD 18BB searched in 36.7 fb<sup>-1</sup> of  $pp$  collisions at  $\sqrt{s} = 13$  TeV for massive colored resonances which are pair-produced and decay into two jets. No significant deviation from the background prediction is observed. Results are interpreted in a SUSY simplified model as Tstop1RPV with  $\tilde{t} \rightarrow ds$ . Top squarks with masses in the range 100-410 GeV are excluded, see their Figure 9(a). The  $\lambda''_{312}$  coupling is assumed to be sufficiently large for the decays to be prompt, but small enough to neglect the single-top-squark resonant production through RPV couplings.

4 AABOUD 18BB searched in 36.7 fb<sup>-1</sup> of  $pp$  collisions at  $\sqrt{s} = 13$  TeV for massive coloured resonances which are pair-produced and decay into two jets. No significant deviation from the background prediction is observed. Results are interpreted in Tstop1RPV. Top squarks with masses in the range 100-470 GeV or 480-610 GeV are excluded, see their Figure 9(b). The  $\lambda''_{323}$  coupling is assumed to be sufficiently large for the decays to be prompt, but small enough to neglect the single-top-squark resonant production through RPV couplings.

5 AABOUD 18P searched in 36.1 fb<sup>-1</sup> of  $pp$  collisions at  $\sqrt{s} = 13$  TeV for pair-produced top squarks that decay through RPV  $\lambda''_{333}$  ( $i = 1, 2, 3$ ) couplings to a final state with two leptons and two jets, at least one of which is identified as a  $b$ -jet. No significant excess is observed over the SM background. In the Tstop2RPV model, lower limits on the top squark masses between 600 and 1500 GeV are set depending on the branching fraction to  $be, b\mu$ , and  $b\tau$  final states. See their Figs 6 and 7.

6 SIRUNYAN 18AD searched in 2.6 fb<sup>-1</sup> of  $pp$  collisions at  $\sqrt{s} = 13$  TeV for long-lived particles by exploiting the multiplicity of displaced jets to search for the presence of signal decays occurring at distances between 1 and 1000 mm. Limits are set in a model of pair-produced, long-lived top squarks with R-parity violating decays to a  $b$ -quark and a lepton, see their Figure 3.

7 SIRUNYAN 18DV searched in 38.5 fb<sup>-1</sup> of  $pp$  collisions at  $\sqrt{s} = 13$  TeV for long-lived particles in events with multiple jets and two displaced vertices composed of many tracks. No events with two well-separated high-track-multiplicity vertices were observed. Limits are set on the stop and the gluino mass in RPV models of supersymmetry where the stop (gluino) is decaying solely into dijet (multijet) final states, see their Figures 6 and 7.

8 SIRUNYAN 18DY searched in 35.9 fb<sup>-1</sup> of  $pp$  collisions at  $\sqrt{s} = 13$  TeV for the pair production of resonances, each decaying to two quarks. The search is conducted separately in a boosted (two-jet) and resolved (four-jet) jet topology. The mass spectra are found to be consistent with the Standard Model expectations. Limits are set on the stop mass in the Tstop3RPV and Tstop1RPV simplified models, see their Figure 11.

9 AABOUD 17AI searched in 36.1 fb<sup>-1</sup> of  $pp$  collisions at  $\sqrt{s} = 13$  TeV for events with one or more isolated lepton, at least eight jets, either zero or many  $b$ -jets, for evidence of R-parity violating decays of the top squark. No significant excess above the Standard Model expectations is observed. Limits up to 1.25 (1.10) TeV are set on the top squark mass in R-parity-violating supersymmetry models where  $\tilde{t}_1$  decays for a bino LSP as:  $\tilde{t} \rightarrow t\tilde{\chi}_1^0$  and for a higgsino LSP as  $\tilde{t} \rightarrow t\tilde{\chi}_{1,2}^0/b\tilde{\chi}_1^+$ . This is followed by the decays through the non-zero  $\lambda''_{323}$  coupling  $\tilde{\chi}_{1,2}^0 \rightarrow tbs, \tilde{\chi}_1^\pm \rightarrow bbs$ . See their Figure 10 and text for details on model assumptions.

10 AAD 16AM searched in 17.4 fb<sup>-1</sup> of  $pp$  collisions at  $\sqrt{s} = 8$  TeV for events containing two large-radius hadronic jets. No deviation from the background prediction is observed. Top squarks with masses between 100 and 315 GeV are excluded at 95% C.L. in the hypothesis that they both decay via R-parity violating coupling  $\lambda''_{323}$  to  $b$ - and  $s$ -quarks. See their Fig. 10.

11 KHACHATRYAN 16AC searched in 19.7 fb<sup>-1</sup> of  $pp$  collisions at  $\sqrt{s} = 8$  TeV for events with low missing transverse momentum, two oppositely charged electrons or muons, and at least five jets, at least one of which is a  $b$ -jet, for evidence of R-parity violating, charging-mediated decays of the top squark. No significant excess above the Standard Model expectations is observed. Limits are set on the stop mass in R-parity-violating supersymmetry models where  $\tilde{t} \rightarrow b\tilde{\chi}_1^\pm$  with  $\tilde{\chi}_1^\pm \rightarrow \ell^\pm jj, \lambda'_{ijk} \neq 0$  ( $i, j, k \leq 2$ ), and with  $m_{\tilde{t}} - m_{\tilde{\chi}_1^\pm} = 100$  GeV, see Fig. 3.

12 KHACHATRYAN 16BX searched in 19.5 fb<sup>-1</sup> of  $pp$  collisions at  $\sqrt{s} = 8$  TeV for events containing 4 leptons coming from R-parity-violating decays of  $\tilde{\chi}_1^0 \rightarrow \ell\ell\nu$  with  $\lambda_{121} \neq 0$  or  $\lambda_{122} \neq 0$ . No excess over the expected background is observed. Limits are derived on the gluino, squark and stop masses, see Fig. 23.

13 KHACHATRYAN 15E searched for long-lived particles decaying to leptons in 19.7 fb<sup>-1</sup> of  $pp$  collisions at  $\sqrt{s} = 8$  TeV. Events were selected with an electron and muon with opposite charges and each with transverse impact parameter values between 0.02 and 2 cm. Limits are set on SUSY benchmark models with pair production of top squarks decaying into an  $e\mu$  final state via RPV interactions. See their Fig. 2

Heavy  $\tilde{g}$  (Gluino) mass limit

For  $m_{\tilde{g}} > 60-70$  GeV, it is expected that gluinos would undergo a cascade decay via a number of neutralinos and/or charginos rather than undergo a direct decay to photinos as assumed by some papers. Limits obtained when direct decay is assumed are usually higher than limits when cascade decays are included.

Some earlier papers are now obsolete and have been omitted. They were last listed in our PDG 14 edition: K. Olive, et al. (Particle Data Group), Chinese Physics C38 070001 (2014) (<http://pdg.lbl.gov>).

R-parity conserving heavy  $\tilde{g}$  (Gluino) mass limit

VALUE (GeV)	CL%	DOCUMENT ID	TECN	COMMENT
>1975	95	1 SIRUNYAN	20B CMS	$\geq 1\gamma + \cancel{E}_T, Tglu4A, BR(\tilde{g} \rightarrow qq\tilde{\chi}_1^\pm) = 0.5, m_{\tilde{g}} \simeq m_{\tilde{\chi}_1^\pm}$
>2000	95	2 AABOUD	19I ATL	$\geq 2$ jets + 1 or 2 $\tau + \cancel{E}_T, Tglu1F, m_{\tilde{g}} = 100$ GeV
>1860	95	3 SIRUNYAN	19AG CMS	$2\gamma + \cancel{E}_T, Tglu4B, 500$ GeV $< m_{\tilde{g}} < 1500$ GeV
>1920	95	4 SIRUNYAN	19AU CMS	$\gamma$ + jets + $b$ -jets + $\cancel{E}_T, Tglu4D, m_{\tilde{g}} = 127$ GeV
>1950	95	4 SIRUNYAN	19AU CMS	$\gamma$ + jets + $b$ -jets + $\cancel{E}_T, Tglu4E, m_{\tilde{g}} = 1$ GeV
>1800	95	4 SIRUNYAN	19AU CMS	$\gamma$ + jets + $b$ -jets + $\cancel{E}_T, Tglu4F, m_{\tilde{g}} = 1$ GeV
>2090	95	4 SIRUNYAN	19AU CMS	$\gamma$ + jets + $b$ -jets + $\cancel{E}_T, Tglu4D, m_{\tilde{g}} = 1200$ GeV
>2120	95	4 SIRUNYAN	19AU CMS	$\gamma$ + jets + $b$ -jets + $\cancel{E}_T, Tglu4E, m_{\tilde{g}} = 1200$ GeV
>1970	95	4 SIRUNYAN	19AU CMS	$\gamma$ + jets + $b$ -jets + $\cancel{E}_T, Tglu4F, m_{\tilde{g}} = 1200$ GeV
>1700	95	5 SIRUNYAN	19CE CMS	2 jets, Stealth SUSY, Tglu1A and $\tilde{\chi}_1^0 \rightarrow \tilde{S}\gamma$ ( $\tilde{S} \rightarrow S\tilde{G}$ ), $m_{\tilde{\chi}_1^0} = 200$ GeV
>2000	95	6 SIRUNYAN	19CH CMS	jets + $\cancel{E}_T, Tglu1A, m_{\tilde{g}} = 0$ GeV
>2030	95	6 SIRUNYAN	19CH CMS	jets + $\cancel{E}_T, Tglu1C, m_{\tilde{g}} = m_{\tilde{\chi}_2^0} = 0.5(m_{\tilde{g}} + m_{\tilde{\chi}_1^0}), m_{\tilde{\chi}_1^0} = 0$ GeV
>2270	95	6 SIRUNYAN	19CH CMS	jets + $\cancel{E}_T, Tglu2A, m_{\tilde{g}} = 0$ GeV
>2180	95	6 SIRUNYAN	19CH CMS	jets + $\cancel{E}_T, Tglu3A, m_{\tilde{g}} = 0$ GeV
>1750	95	7 SIRUNYAN	19K CMS	$\gamma + \ell + \cancel{E}_T, Tglu4A, m_{\tilde{g}} = 1500$ GeV
>2000	95	8 SIRUNYAN	19S CMS	1 or 2 $\ell +$ jets + $\cancel{E}_T, Tglu3A, m_{\tilde{g}} < 700$ GeV
>1900	95	8 SIRUNYAN	19S CMS	1 or 2 $\ell +$ jets + $\cancel{E}_T, Tglu3C, 150$ GeV $< m_{\tilde{g}} < 950$ GeV
>1970	95	9 AABOUD	18AR ATLS	jets + $\geq 3b$ -jets + $\cancel{E}_T, Tglu3A, m_{\tilde{g}} < 300$ GeV
>1920	95	10 AABOUD	18AR ATLS	jets + $\geq 3b$ -jets + $\cancel{E}_T, Tglu2A, m_{\tilde{g}} < 600$ GeV
>1650	95	11 AABOUD	18AS ATLS	$\geq 4$ jets and disappearing tracks from $\tilde{\chi}^\pm \rightarrow \tilde{\chi}_1^0 \pi^\pm$ , modified Tglu1A or Tglu1B, $\tilde{\chi}^\pm$ lifetime 0.2 ns, $m_{\tilde{\chi}^\pm} = 460$ GeV
>1850	95	12 AABOUD	18BJ ATLS	$\ell^\pm \cancel{E}_T +$ jets + $\cancel{E}_T, Tglu1G, m_{\tilde{g}} = 100$ GeV



# Searches Particle Listings

## Supersymmetric Particle Searches

>1650	95	13	AABOUD	18BJ ATLS	$\ell^\pm \ell^\mp + \text{jets} + \cancel{E}_T, T_{\text{glu1H}}, m_{\tilde{\chi}_1^0} = 100 \text{ GeV}$	>1700	95	36	AABOUD	17N ATLS	2 same-flavor, opposite-sign $\ell + \text{jets} + \cancel{E}_T, T_{\text{glu1G}}, m_{\tilde{\chi}_1^0} \sim 1 \text{ GeV}$
>2150	95	14	AABOUD	18U ATLS	$2\gamma + \cancel{E}_T, \text{GGM}, T_{\text{glu4B}}, \text{any NLSP mass}$	>1400	95	37	KHACHATRY...17	CMS	$\text{jets} + \cancel{E}_T, T_{\text{glu1A}}, m_{\tilde{\chi}_1^0} = 200 \text{ GeV}$
>1600	95	15	AABOUD	18U ATLS	$\gamma + \text{jets} + \cancel{E}_T, \text{GGM higgsino-bino, mix of Tglu4B and Tglu4C, any NLSP mass}$	>1650	95	37	KHACHATRY...17	CMS	$\text{jets} + \cancel{E}_T, T_{\text{glu2A}}, m_{\tilde{\chi}_1^0} = 200 \text{ GeV}$
>2030	95	16	AABOUD	18V ATLS	$\text{jets} + \cancel{E}_T, T_{\text{glu1A}}, m_{\tilde{\chi}_1^0} = 0 \text{ GeV}$	>1600	95	37	KHACHATRY...17	CMS	$\text{jets} + \cancel{E}_T, T_{\text{glu3A}}, m_{\tilde{\chi}_1^0} = 200 \text{ GeV}$
>1980	95	17	AABOUD	18V ATLS	$\text{jets} + \cancel{E}_T, T_{\text{glu1B}}, m_{\tilde{\chi}_1^\pm} = 0.5(m_{\tilde{g}} + m_{\tilde{\chi}_1^0}), m_{\tilde{\chi}_1^0} = 0 \text{ GeV}$	>1550	95	38	KHACHATRY...17AD	CMS	$\text{jets} + b\text{-jets} + \cancel{E}_T, T_{\text{glu3A}}, m_{\tilde{\chi}_1^0} = 0 \text{ GeV}$
>1750	95	18	AABOUD	18V ATLS	$\text{jets} + \cancel{E}_T, T_{\text{glu1C}}, m_{\tilde{\chi}_1^0} = 1 \text{ GeV}, \text{any } m_{\tilde{\chi}_2^0} > 100 \text{ GeV}$	>1450	95	39	KHACHATRY...17AD	CMS	$\text{jets} + b\text{-jets} + \cancel{E}_T, T_{\text{glu3C}}, 200 < m_{\tilde{\chi}_1^0} < 400 \text{ GeV}$
>2000	95	19	SIRUNYAN	18AA CMS	$\geq 1\gamma + \cancel{E}_T, T_{\text{glu4A}}$	>1570	95	40	KHACHATRY...17As	CMS	$1\ell, T_{\text{glu3A}}, m_{\tilde{\chi}_1^0} < 600 \text{ GeV}$
>2100	95	19	SIRUNYAN	18AA CMS	$\geq 1\gamma + \cancel{E}_T, T_{\text{glu4B}}$	>1500	95	40	KHACHATRY...17As	CMS	$1\ell, T_{\text{glu3A}}, m_{\tilde{\chi}_1^0} < 775 \text{ GeV}$
>1800	95	20	SIRUNYAN	18AC CMS	$1\ell + \text{jets}, T_{\text{glu3A}}, m_{\tilde{\chi}_1^0} < 650 \text{ GeV}$	>1400	95	40	KHACHATRY...17As	CMS	$1\ell, T_{\text{glu1B}}, m_{\tilde{\chi}_1^\pm} = (m_{\tilde{g}} + m_{\tilde{\chi}_1^0})/2, m_{\tilde{\chi}_1^0} < 725 \text{ GeV}$
>1700	95	20	SIRUNYAN	18AC CMS	$1\ell + \text{jets}, T_{\text{glu3A}}, m_{\tilde{\chi}_1^0} < 1040 \text{ GeV}$	none	95	40	KHACHATRY...17As	CMS	$1\ell, T_{\text{glu1B}}, m_{\tilde{\chi}_1^\pm} = (m_{\tilde{g}} + m_{\tilde{\chi}_1^0})/2, m_{\tilde{\chi}_1^0} < 850 \text{ GeV}$
>1900	95	20	SIRUNYAN	18AC CMS	$1\ell + \text{jets}, T_{\text{glu1B}}, m_{\tilde{\chi}_1^\pm} = (m_{\tilde{g}} + m_{\tilde{\chi}_1^0})/2, m_{\tilde{\chi}_1^0} < 300 \text{ GeV}$	1050-1350	95	40	KHACHATRY...17As	CMS	$\geq 3\ell^\pm, 2 \text{ jets}, T_{\text{glu3A}}, m_{\tilde{\chi}_1^0} = 0 \text{ GeV}$
>1250	95	20	SIRUNYAN	18AC CMS	$1\ell + \text{jets}, T_{\text{glu1B}}, m_{\tilde{\chi}_1^\pm} = (m_{\tilde{g}} + m_{\tilde{\chi}_1^0})/2, m_{\tilde{\chi}_1^0} < 950 \text{ GeV}$	>1175	95	41	KHACHATRY...17AW	CMS	$\geq 3\ell^\pm, 2 \text{ jets}, T_{\text{glu1C}}, m_{\tilde{\chi}_1^\pm} = (m_{\tilde{g}} + m_{\tilde{\chi}_1^0})/2, m_{\tilde{\chi}_1^0} = 0 \text{ GeV}$
>1610	95	21	SIRUNYAN	18AL CMS	$\geq 3\ell^\pm + \text{jets} + \cancel{E}_T, T_{\text{glu3A}}, m_{\tilde{\chi}_1^0} = 0 \text{ GeV}$	> 825	95	41	KHACHATRY...17AW	CMS	$1 \text{ or more jets} + \cancel{E}_T, T_{\text{glu1A}}, m_{\tilde{\chi}_1^0} = 0 \text{ GeV}$
>1160	95	21	SIRUNYAN	18AL CMS	$\geq 3\ell^\pm + \text{jets} + \cancel{E}_T, T_{\text{glu1C}}, m_{\tilde{\chi}_2^0} = m_{\tilde{\chi}_1^\pm} = (m_{\tilde{g}} + m_{\tilde{\chi}_1^0})/2, m_{\tilde{\chi}_1^0} = 0 \text{ GeV}$	>1350	95	42	KHACHATRY...17P	CMS	$1 \text{ or more jets} + \cancel{E}_T, T_{\text{glu2A}}, m_{\tilde{\chi}_1^0} = 0 \text{ GeV}$
>1500	95	22	SIRUNYAN	18AR CMS	$\ell^\pm \ell^\mp + \text{jets} + \cancel{E}_T, \text{GMSB}, T_{\text{glu4C}}, m_{\tilde{\chi}_1^0} = 100 \text{ GeV}$	>1545	95	42	KHACHATRY...17P	CMS	$1 \text{ or more jets} + \cancel{E}_T, T_{\text{glu3A}}, m_{\tilde{\chi}_1^0} = 0 \text{ GeV}$
>1770	95	22	SIRUNYAN	18AR CMS	$\ell^\pm \ell^\mp + \text{jets} + \cancel{E}_T, \text{GMSB}, T_{\text{glu4C}}, m_{\tilde{\chi}_1^0} = 1400 \text{ GeV}$	>1120	95	42	KHACHATRY...17P	CMS	$1 \text{ or more jets} + \cancel{E}_T, T_{\text{glu3D}}, m_{\tilde{\chi}_1^\pm} = m_{\tilde{\chi}_1^0} + 5 \text{ GeV}, m_{\tilde{\chi}_1^0} = 100 \text{ GeV}$
>1625	95	23	SIRUNYAN	18AY CMS	$\text{jets} + \cancel{E}_T, T_{\text{glu1A}}, m_{\tilde{\chi}_1^0} = 0 \text{ GeV}$	> 780	95	42	KHACHATRY...17P	CMS	$1 \text{ or more jets} + \cancel{E}_T, T_{\text{glu3B}}, m_{\tilde{\tau}_1} - m_{\tilde{\chi}_1^0} = 175 \text{ GeV}, m_{\tilde{\chi}_1^0} = 50 \text{ GeV}$
>1825	95	23	SIRUNYAN	18AY CMS	$\text{jets} + \cancel{E}_T, T_{\text{glu2A}}, m_{\tilde{\chi}_1^0} = 0 \text{ GeV}$	> 790	95	42	KHACHATRY...17P	CMS	$1 \text{ or more jets} + \cancel{E}_T, T_{\text{glu3C}}, m_{\tilde{\tau}_1} - m_{\tilde{\chi}_1^0} = 20 \text{ GeV}, m_{\tilde{\chi}_1^0} = 0 \text{ GeV}$
>1625	95	23	SIRUNYAN	18AY CMS	$\text{jets} + \cancel{E}_T, T_{\text{glu3A}}, m_{\tilde{\chi}_1^0} = 0 \text{ GeV}$	>1650	95	43	KHACHATRY...17V	CMS	$2\gamma + \cancel{E}_T, \text{GGM}, T_{\text{glu4B}}, \text{any NLSP mass}$
>2040	95	24	SIRUNYAN	18D CMS	top quark (hadronically decaying) + jets + $\cancel{E}_T, T_{\text{glu3A}}, m_{\tilde{\chi}_1^0} = 0 \text{ GeV}$	>1900	95	44	SIRUNYAN	17AF CMS	$1\ell + \text{jets} + b\text{-jets} + \cancel{E}_T, T_{\text{glu3A}}, m_{\tilde{\chi}_1^0} = 0 \text{ GeV}$
>1930	95	24	SIRUNYAN	18D CMS	top quark (hadronically decaying) + jets + $\cancel{E}_T, T_{\text{glu3B}}, m_{\tilde{\tau}_1} - m_{\tilde{\chi}_1^0} = 175 \text{ GeV}, m_{\tilde{\chi}_1^0} = 200 \text{ GeV}$	>1600	95	44	SIRUNYAN	17AF CMS	$1\ell + \text{jets} + b\text{-jets} + \cancel{E}_T, T_{\text{glu3B}}, m_{\tilde{\tau}_1} - m_{\tilde{\chi}_1^0} = 175 \text{ GeV}, m_{\tilde{\chi}_1^0} = 50 \text{ GeV}$
>1690	95	24	SIRUNYAN	18D CMS	top quark (hadronically decaying) + jets + $\cancel{E}_T, T_{\text{glu3C}}, m_{\tilde{\tau}_1} - m_{\tilde{\chi}_1^0} = 20 \text{ GeV}, m_{\tilde{\chi}_1^0} = 0 \text{ GeV}$	>1800	95	45	SIRUNYAN	17AY CMS	$\gamma + \text{jets} + \cancel{E}_T, T_{\text{glu4B}}, m_{\tilde{\chi}_1^0} = 0 \text{ GeV}$
>1990	95	24	SIRUNYAN	18D CMS	top quark (hadronically decaying) + jets + $\cancel{E}_T, T_{\text{glu3E}}, m_{\tilde{\chi}_1^\pm} = m_{\tilde{\chi}_1^0} + 5 \text{ GeV}, m_{\tilde{\chi}_1^0} = 100 \text{ GeV}$	>1600	95	45	SIRUNYAN	17AY CMS	$\gamma + \text{jets} + \cancel{E}_T, T_{\text{glu4A}}, m_{\tilde{\chi}_1^0} = 0 \text{ GeV}$
>2010	95	25	SIRUNYAN	18M CMS	$\geq 1 H (\rightarrow bb) + \cancel{E}_T, T_{\text{glu1I}}$	>1860	95	46	SIRUNYAN	17AZ CMS	$\geq 1 \text{ jets} + \cancel{E}_T, T_{\text{glu1A}}, m_{\tilde{\chi}_1^0} = 0 \text{ GeV}$
>1825	95	25	SIRUNYAN	18M CMS	$\geq 1 H (\rightarrow bb) + \cancel{E}_T, T_{\text{glu1J}}$	>2025	95	46	SIRUNYAN	17AZ CMS	$\geq 1 \text{ jets} + \cancel{E}_T, T_{\text{glu2A}}, m_{\tilde{\chi}_1^0} = 0 \text{ GeV}$
>1750	95	26	AABOUD	17AJ ATLS	same-sign $\ell^\pm \ell^\pm / 3\ell + \text{jets} + \cancel{E}_T, T_{\text{glu3A}}, m_{\tilde{\chi}_1^0} = 100 \text{ GeV}$	>1900	95	46	SIRUNYAN	17AZ CMS	$\geq 1 \text{ jets} + \cancel{E}_T, T_{\text{glu3A}}, m_{\tilde{\chi}_1^0} = 0 \text{ GeV}$
>1570	95	27	AABOUD	17AJ ATLS	same-sign $\ell^\pm \ell^\pm / 3\ell + \text{jets} + \cancel{E}_T, T_{\text{glu1E}}, m_{\tilde{\chi}_1^0} = 100 \text{ GeV}$	>1825	95	47	SIRUNYAN	17P CMS	$\text{jets} + \cancel{E}_T, T_{\text{glu1A}}, m_{\tilde{\chi}_1^0} = 0 \text{ GeV}$
>1860	95	28	AABOUD	17AJ ATLS	same-sign $\ell^\pm \ell^\pm / 3\ell + \text{jets} + \cancel{E}_T, T_{\text{glu1G}}, m_{\tilde{\chi}_1^0} = 200 \text{ GeV}$	>1950	95	47	SIRUNYAN	17P CMS	$\text{jets} + \cancel{E}_T, T_{\text{glu2A}}, m_{\tilde{\chi}_1^0} = 0 \text{ GeV}$
>2100	95	29	AABOUD	17AR ATLS	$1\ell + \text{jets} + \cancel{E}_T, T_{\text{glu1B}}, m_{\tilde{\chi}_1^0} = 0 \text{ GeV}$	>1960	95	47	SIRUNYAN	17P CMS	$\text{jets} + \cancel{E}_T, T_{\text{glu3A}}, m_{\tilde{\chi}_1^0} = 0 \text{ GeV}$
>1740	95	30	AABOUD	17AR ATLS	$1\ell + \text{jets} + \cancel{E}_T, T_{\text{glu1E}}, m_{\tilde{\chi}_1^0} = 0 \text{ GeV}$	>1800	95	47	SIRUNYAN	17P CMS	$\text{jets} + \cancel{E}_T, T_{\text{glu1C}}, m_{\tilde{\chi}_1^\pm} = m_{\tilde{\chi}_2^0} = (m_{\tilde{g}} + m_{\tilde{\chi}_1^0})/2, m_{\tilde{\chi}_1^0} = 0 \text{ GeV}$
>1800	95	31	AABOUD	17AY ATLS	$\text{jets} + \cancel{E}_T, T_{\text{glu3A}}, m_{\tilde{\tau}_1} - m_{\tilde{\chi}_1^0} = 5 \text{ GeV}$	>1870	95	47	SIRUNYAN	17P CMS	$\text{jets} + \cancel{E}_T, T_{\text{glu3D}}, m_{\tilde{\chi}_1^\pm} = m_{\tilde{\chi}_1^0} + 5 \text{ GeV}, m_{\tilde{\chi}_1^0} = 1000 \text{ GeV}$
>1800	95	32	AABOUD	17AZ ATLS	$\geq 7 \text{ jets} + \cancel{E}_T, \text{large R-jets and/or } b\text{-jets}, T_{\text{glu1E}}, m_{\tilde{\chi}_1^0} = 100 \text{ GeV}$	>1520	95	48	SIRUNYAN	17S CMS	same-sign $\ell^\pm \ell^\pm + \text{jets} + \cancel{E}_T, T_{\text{glu3A}}, m_{\tilde{\chi}_1^0} = 0 \text{ GeV}$
>1540	95	33	AABOUD	17AZ ATLS	$\geq 7 \text{ jets} + \cancel{E}_T, \text{large R-jets and/or } b\text{-jets}, T_{\text{glu3A}}, m_{\tilde{\chi}_1^0} = 0 \text{ GeV}$	>1200	95	48	SIRUNYAN	17S CMS	same-sign $\ell^\pm \ell^\pm + \text{jets} + \cancel{E}_T, T_{\text{glu3D}}, m_{\tilde{\chi}_1^\pm} = m_{\tilde{\chi}_1^0} + 5 \text{ GeV}, m_{\tilde{\chi}_1^0} = 100 \text{ GeV}$
>1340	95	34	AABOUD	17N ATLS	2 same-flavor, opposite-sign $\ell + \text{jets} + \cancel{E}_T, T_{\text{glu1H}}, m_{\tilde{\chi}_1^0} = 0 \text{ GeV}$	>1370	95	48	SIRUNYAN	17S CMS	same-sign $\ell^\pm \ell^\pm + \text{jets} + \cancel{E}_T, T_{\text{glu3B}}, m_{\tilde{\tau}_1} - m_{\tilde{\chi}_1^0} = 175 \text{ GeV}, m_{\tilde{\chi}_1^0} = 50 \text{ GeV}$
>1310	95	35	AABOUD	17N ATLS	2 same-flavor, opposite-sign $\ell + \text{jets} + \cancel{E}_T, T_{\text{glu1H}}, m_{\tilde{\chi}_2^0} = (m_{\tilde{g}} + m_{\tilde{\chi}_1^0})/2, m_{\tilde{\chi}_1^0} < 400 \text{ GeV}$	>1180	95	48	SIRUNYAN	17S CMS	same-sign $\ell^\pm \ell^\pm + \text{jets} + \cancel{E}_T, T_{\text{glu3C}}, m_{\tilde{\tau}_1} - m_{\tilde{\chi}_1^0} = 20 \text{ GeV}, m_{\tilde{\chi}_1^0} = 0 \text{ GeV}$

See key on page 999

# Searches Particle Listings

## Supersymmetric Particle Searches

>1280	95	48	SIRUNYAN	17s	CMS	same-sign $\ell^\pm \ell^\pm + \text{jets} + \cancel{E}_T$ , Tglu1B, $m_{\tilde{\chi}_1^\pm} = (m_{\tilde{g}} + m_{\tilde{\chi}_1^0})/2$ , $m_{\tilde{\chi}_1^0} = 0$ GeV	> 850	95	64	AAD	15Bg ATLS	GGM, $\tilde{g} \rightarrow q\bar{q}Z\tilde{G}$ , $\tan\beta = 1.5$ , $\mu > 450$ GeV
>1300	95	48	SIRUNYAN	17s	CMS	same-sign $\ell^\pm \ell^\pm + \text{jets} + \cancel{E}_T$ , Tglu1B, $m_{\tilde{t}_1} - m_{\tilde{\chi}_1^0} = 20$ GeV, $m_{\tilde{\chi}_1^0} = 100$ GeV	> 700	95	65	AAD	15Bv ATLS	general RPC $\tilde{g}$ decays, $m_{\tilde{\chi}_1^0} < 100$ GeV
>1570	95	49	AABOUD	16Ac	ATLS	$\geq 2$ jets + 1 or 2 $\tau + \cancel{E}_T$ , Tglu1F, $m_{\tilde{\chi}_1^0} = 100$ GeV	>1290	95	66	AAD	15Bx ATLS	$\tilde{g} \rightarrow X\tilde{\chi}_1^0$ , independent of $m_{\tilde{\chi}_1^0}$
>1460	95	50	AABOUD	16j	ATLS	$1 \ell^\pm + \geq 4$ jets + $\cancel{E}_T$ , Tglu3C, $m_{\tilde{t}_1} - m_{\tilde{\chi}_1^0} = 5$ GeV	>1260	95	67	AAD	15Ca ATLS	$\geq 2 \gamma + \cancel{E}_T$ , GGM, bino-like NLSP, any NLSP mass
>1650	95	51	AABOUD	16M	ATLS	$2 \gamma + \cancel{E}_T$ , Tglu1D, any NLSP mass	>1140	95	67	AAD	15Ca ATLS	$\geq 1 \gamma + b$ -jets + $\cancel{E}_T$ , GGM, higgsino-bino admix. NLSP and $\mu < 0$ , $m(\text{NLSP}) > 450$ GeV
>1510	95	52	AABOUD	16N	ATLS	$\geq 4$ jets + $\cancel{E}_T$ , Tglu1A, $m_{\tilde{\chi}_1^0} = 0$ GeV	>1225	95	68	KHACHATRY...15AF	CMS	$\tilde{g} \rightarrow q\bar{q}\tilde{\chi}_1^0$ , $m_{\tilde{\chi}_1^0} = 0$
>1500	95	53	AABOUD	16N	ATLS	$\geq 4$ jets + $\cancel{E}_T$ , Tglu1B, $m_{\tilde{\chi}_1^\pm} = (m_{\tilde{g}} + m_{\tilde{\chi}_1^0})/2$ , $m_{\tilde{\chi}_1^0} = 200$ GeV	>1300	95	68	KHACHATRY...15AF	CMS	$\tilde{g} \rightarrow b\bar{b}\tilde{\chi}_1^0$ , $m_{\tilde{\chi}_1^0} = 0$
>1780	95	54	AAD	16AD	ATLS	$0\ell$ , $\geq 3$ b-jets + $\cancel{E}_T$ , Tglu2A, $m_{\tilde{\chi}_1^0} < 800$ GeV	>1225	95	68	KHACHATRY...15AF	CMS	$\tilde{g} \rightarrow t\bar{t}\tilde{\chi}_1^0$ , $m_{\tilde{\chi}_1^0} = 0$
>1760	95	55	AAD	16AD	ATLS	$1\ell$ , $\geq 3$ b-jets + $\cancel{E}_T$ , Tglu3A, $m_{\tilde{\chi}_1^0} < 700$ GeV	>1550	95	68	KHACHATRY...15AF	CMS	CMSSM, $\tan\beta = 30$ , $m_{\tilde{g}} = m_{\tilde{q}}$ , $A_0 = -2\max(m_0, m_{1/2})$ , $\mu > 0$
>1300	95	56	AAD	16BB	ATLS	2 same-sign/ $3\ell + \text{jets} + \cancel{E}_T$ , Tglu1D, $m_{\tilde{\chi}_1^0} < 600$ GeV	>1150	95	68	KHACHATRY...15AF	CMS	CMSSM, $\tan\beta = 30$ , $A_0 = -2\max(m_0, m_{1/2})$ , $\mu > 0$
>1100	95	56	AAD	16BB	ATLS	2 same-sign/ $3\ell + \text{jets} + \cancel{E}_T$ , Tglu1E, $m_{\tilde{\chi}_1^0} < 300$ GeV	>1280	95	69	KHACHATRY...15f	CMS	$\tilde{g} \rightarrow t\bar{t}\tilde{\chi}_1^0$ , $m_{\tilde{\chi}_1^0} = 0$
>1200	95	56	AAD	16BB	ATLS	2 same-sign/ $3\ell + \text{jets} + \cancel{E}_T$ , Tglu3A, $m_{\tilde{\chi}_1^0} < 600$ GeV	>1310	95	70	KHACHATRY...15X	CMS	$\tilde{g} \rightarrow b\bar{b}\tilde{\chi}_1^0$ , $m_{\tilde{\chi}_1^0} = 100$ GeV
>1600	95	57	AAD	16Bg	ATLS	$1\ell$ , $\geq 4$ jets, $\cancel{E}_T$ , Tglu1B, $m_{\tilde{\chi}_1^\pm} = (m_{\tilde{g}} + m_{\tilde{\chi}_1^0})/2$ , $m_{\tilde{\chi}_1^0} = 100$ GeV	>1175	95	70	KHACHATRY...15X	CMS	$\tilde{g} \rightarrow t\bar{t}\tilde{\chi}_1^0$ , $m_{\tilde{\chi}_1^0} = 100$ GeV
>1400	95	58	AAD	16v	ATLS	$\geq 7$ to $\geq 10$ jets + $\cancel{E}_T$ , Tglu1E, $m_{\tilde{\chi}_1^0} < 200$ GeV	>1330	95	71	AAD	14AE ATLS	jets + $\cancel{E}_T$ , $\tilde{g} \rightarrow q\bar{q}\tilde{\chi}_1^0$ simplified model, $m_{\tilde{\chi}_1^0} = 0$ GeV
>1400	95	58	AAD	16v	ATLS	$\geq 7$ to $\geq 10$ jets + $\cancel{E}_T$ , pMSSM $M_1 = 60$ GeV, $M_2 = 3$ TeV, $\tan\beta = 10$ , $\mu < 0$	>1700	95	71	AAD	14AE ATLS	jets + $\cancel{E}_T$ , mSUGRA/CMSSM, $m_{\tilde{q}} = m_{\tilde{g}}$
>1100	95	59	KHACHATRY...16AM	CMS	boosted $W+b$ , Tglu3C, $m_{\tilde{t}_1} - m_{\tilde{\chi}_1^0} < 80$ GeV, $m_{\tilde{\chi}_1^0} < 400$ GeV	>1090	95	72	AAD	14AG ATLS	$\tau + \text{jets} + \cancel{E}_T$ , natural Gauge Mediation	
> 700	95	59	KHACHATRY...16AM	CMS	boosted $W+b$ , Tglu3B, $m_{\tilde{t}_1} - m_{\tilde{\chi}_1^0} = 175$ GeV, $m_{\tilde{\chi}_1^0} = 0$ GeV	>1600	95	72	AAD	14AG ATLS	$\tau + \text{jets} + \cancel{E}_T$ , mGMSB, $M_{\text{mess}} = 250$ GeV, $N_5 = 3$ , $\mu > 0$ , $C_{\text{grav}} = 1$	
>1050	95	60	KHACHATRY...16BJ	CMS	same-sign $\ell^\pm \ell^\pm$ , Tglu3A, $m_{\tilde{\chi}_1^0} < 800$ GeV	> 640	95	73	AAD	14x ATLS	$\geq 4\ell^\pm$ , $\tilde{g} \rightarrow q\bar{q}\tilde{\chi}_1^0$ , $\tilde{\chi}_1^0 \rightarrow \ell^\pm \ell^\mp \tilde{G}$ , $\tan\beta = 30$ , GGM	
>1300	95	60	KHACHATRY...16BJ	CMS	same-sign $\ell^\pm \ell^\pm$ , Tglu3A, $m_{\tilde{\chi}_1^0} = 0$	>1000	95	74	CHATRCHYAN14AH	CMS	jets + $\cancel{E}_T$ , $\tilde{g} \rightarrow q\bar{q}\tilde{\chi}_1^0$ simplified model, $m_{\tilde{\chi}_1^0} = 50$ GeV	
>1140	95	60	KHACHATRY...16BJ	CMS	same-sign $\ell^\pm \ell^\pm$ , Tglu3B, $m_{\tilde{t}_1} - m_{\tilde{\chi}_1^0} = 20$ GeV, $m_{\tilde{\chi}_1^0} = 0$	>1350	95	74	CHATRCHYAN14AH	CMS	jets + $\cancel{E}_T$ , CMSSM, $m_{\tilde{g}} = m_{\tilde{q}}$	
> 850	95	60	KHACHATRY...16BJ	CMS	same-sign $\ell^\pm \ell^\pm$ , Tglu3B, $m_{\tilde{t}_1} - m_{\tilde{\chi}_1^0} = 20$ GeV, $m_{\tilde{\chi}_1^0} < 700$ GeV	>1000	95	75	CHATRCHYAN14AH	CMS	jets + $\cancel{E}_T$ , $\tilde{g} \rightarrow b\bar{b}\tilde{\chi}_1^0$ simplified model, $m_{\tilde{\chi}_1^0} = 50$ GeV	
> 950	95	60	KHACHATRY...16BJ	CMS	same-sign $\ell^\pm \ell^\pm$ , Tglu3D, $m_{\tilde{\chi}_1^\pm} = m_{\tilde{\chi}_1^0} + 5$ GeV	>1000	95	76	CHATRCHYAN14AH	CMS	jets + $\cancel{E}_T$ , $\tilde{g} \rightarrow t\bar{t}\tilde{\chi}_1^0$ simplified model, $m_{\tilde{\chi}_1^0} = 50$ GeV	
>1100	95	60	KHACHATRY...16BJ	CMS	same-sign $\ell^\pm \ell^\pm$ , Tglu1B, $m_{\tilde{\chi}_1^\pm} = 0.5(m_{\tilde{g}} + m_{\tilde{\chi}_1^0})$ , $m_{\tilde{\chi}_1^0} < 400$ GeV	>1160	95	77	CHATRCHYAN14I	CMS	jets + $\cancel{E}_T$ , $\tilde{g} \rightarrow q\bar{q}\tilde{\chi}_1^0$ simplified model, $m_{\tilde{\chi}_1^0} < 100$ GeV	
> 830	95	60	KHACHATRY...16BJ	CMS	same-sign $\ell^\pm \ell^\pm$ , Tglu1B, $m_{\tilde{\chi}_1^\pm} = 0.5(m_{\tilde{g}} + m_{\tilde{\chi}_1^0})$ , $m_{\tilde{\chi}_1^0} < 700$ GeV	>1130	95	77	CHATRCHYAN14I	CMS	multijets + $\cancel{E}_T$ , $\tilde{g} \rightarrow t\bar{t}\tilde{\chi}_1^0$ simplified model, $m_{\tilde{\chi}_1^0} < 100$ GeV	
>1300	95	60	KHACHATRY...16BJ	CMS	same-sign $\ell^\pm \ell^\pm$ , Tglu3B, $m_{\tilde{t}_1} - m_{\tilde{\chi}_1^0} = m_t$ , $m_{\tilde{\chi}_1^0} = 0$	>1210	95	77	CHATRCHYAN14I	CMS	multijets + $\cancel{E}_T$ , $\tilde{g} \rightarrow q\bar{q}W/Z\tilde{\chi}_1^0$ simplified model, $m_{\tilde{\chi}_1^0} < 100$ GeV	
>1050	95	60	KHACHATRY...16BJ	CMS	same-sign $\ell^\pm \ell^\pm$ , Tglu3B, $m_{\tilde{t}_1} - m_{\tilde{\chi}_1^0} = m_t$ , $m_{\tilde{\chi}_1^0} < 800$ GeV	>1260	95	78	CHATRCHYAN14N	CMS	$1\ell^\pm + \text{jets} + \geq 2b$ -jets, $\tilde{g} \rightarrow t\bar{t}\tilde{\chi}_1^0$ simplified model, $m_{\tilde{\chi}_1^0} = 0$ GeV, $m_{\tilde{\tau}} > m_{\tilde{g}}$	
>1725	95	61	KHACHATRY...16Bs	CMS	jets + $\cancel{E}_T$ , Tglu1A, $m_{\tilde{\chi}_1^0} = 0$	...	95	79	CHATRCHYAN14R	CMS	$\geq 3\ell^\pm$ , $(\tilde{g}/\tilde{q}) \rightarrow q\ell^\pm \ell^\mp \tilde{G}$ simplified model, GMSB, slepton co-NLSP scenario	
>1750	95	61	KHACHATRY...16Bs	CMS	jets + $\cancel{E}_T$ , Tglu2A, $m_{\tilde{\chi}_1^0} = 0$	>1500	95	80	CHATRCHYAN14R	CMS	$\geq 3\ell^\pm$ , $\tilde{g} \rightarrow t\bar{t}\tilde{\chi}_1^0$ simplified model	
>1550	95	61	KHACHATRY...16Bs	CMS	jets + $\cancel{E}_T$ , Tglu3A, $m_{\tilde{\chi}_1^0} = 0$	>1770	95	81	AABOUD	18BJ ATLS	$\ell^\pm \ell^\mp + \text{jets} + \cancel{E}_T$ , Tglu1H, $m_{\tilde{\chi}_1^0} = 1$ GeV, any $m_{\tilde{\chi}_2^0}$	
>1280	95	62	KHACHATRY...16BY	CMS	opposite-sign $\ell^\pm \ell^\pm$ , Tglu4C, $m_{\tilde{\chi}_1^0} = 1000$ GeV	>1600	95	82	AABOUD	18v ATLS	jets + $\cancel{E}_T$ , Tglu1C-like, 1/2 BR per decay mode, any $m_{\tilde{\chi}_2^0} - m_{\tilde{\chi}_1^0}$ , $m_{\tilde{\chi}_1^0} = 60$ GeV	
>1030	95	62	KHACHATRY...16BY	CMS	opposite-sign $\ell^\pm \ell^\pm$ , Tglu4C, $m_{\tilde{\chi}_1^0} = 0$ GeV	>1600	95	83	AABOUD	17AZ ATLS	$\geq 7$ jets + $\cancel{E}_T$ , large R-jets and/or b-jets, pMSSM, $m_{\tilde{\chi}_1^\pm} = 200$ GeV	
>1440	95	63	KHACHATRY...16v	CMS	jets + $\cancel{E}_T$ , Tglu1A, $m_{\tilde{\chi}_1^0} = 0$	> 500	95	84	KHACHATRY...16AY	CMS	$1\ell^\pm + \text{jets} + b$ -jets + $\cancel{E}_T$ , Tglu3A, $m_{\tilde{\chi}_1^0} = 0$ GeV	
>1600	95	63	KHACHATRY...16v	CMS	jets + $\cancel{E}_T$ , Tglu2A, $m_{\tilde{\chi}_1^0} = 0$		95	85	KHACHATRY...16BT	CMS	19-parameter pMSSM model, global Bayesian analysis, flat prior	
>1550	95	63	KHACHATRY...16v	CMS	jets + $\cancel{E}_T$ , Tglu3A, $m_{\tilde{\chi}_1^0} = 0$		95	86	AAD	15AB ATLS	$\tilde{g} \rightarrow \tilde{S}g$ , $cr = 1$ m, $\tilde{S} \rightarrow \tilde{S} \tilde{G}$ and $\tilde{S} \rightarrow gg$ , BR = 100%	
>1450	95	63	KHACHATRY...16v	CMS	jets + $\cancel{E}_T$ , Tglu1C, $m_{\tilde{\chi}_1^0} = 0$	>1600	95	87	AAD	15AI ATLS	$\ell^\pm + \text{jets} + \cancel{E}_T$	
> 820	95	64	AAD	15Bg	ATLS	GGM, $\tilde{g} \rightarrow q\bar{q}Z\tilde{G}$ , $\tan\beta = 30$ , $\mu > 600$ GeV	>1280	95	65	AAD	15Bv ATLS	pMSSM, $M_1 = 60$ GeV, $m_{\tilde{q}} < 1500$ GeV
							>1100	95	65	AAD	15Bv ATLS	mSUGRA, $m_0 > 2$ TeV
							>1330	95	65	AAD	15Bv ATLS	via $\tilde{\tau}$ , natural GMSB, all $m_{\tilde{\tau}}$
								95	65	AAD	15Bv ATLS	jets + $\cancel{E}_T$ , $\tilde{g} \rightarrow q\bar{q}\tilde{\chi}_1^0$ , $m_{\tilde{\chi}_1^0} = 1$ GeV

• • • We do not use the following data for averages, fits, limits, etc. • • •

# Searches Particle Listings

## Supersymmetric Particle Searches

>1500	95	65	AAD	15BV ATLS	jets + $\cancel{E}_T$ , $\tilde{g} \rightarrow \tilde{q}q, \tilde{q} \rightarrow q\tilde{\chi}_1^0$ , $m_{\tilde{\chi}_1^0} = 1$ GeV	> 640	95	92	AAD	14E ATLS	$\ell^\pm \ell^\pm (\ell^\mp) + \text{jets}, \tilde{g} \rightarrow t\tilde{t}_1$ with $\tilde{t}_1 \rightarrow c\tilde{\chi}_1^0$ simplified model, $m_{\tilde{t}_1} = m_{\tilde{\chi}_1^0} + 20$ GeV
>1650	95	65	AAD	15BV ATLS	jets + $\cancel{E}_T$ , $m_{\tilde{g}} = m_{\tilde{q}}, m_{\tilde{\chi}_1^0} = 1$ GeV	> 860	95	92	AAD	14E ATLS	$\ell^\pm \ell^\pm (\ell^\mp) + \text{jets}, \tilde{g} \rightarrow q\cancel{q}\tilde{\chi}_1^\pm$ , $\tilde{\chi}_1^\pm \rightarrow W^{(*)\pm}\tilde{\chi}_1^0$ simplified model, $m_{\tilde{\chi}_1^\pm} = 2m_{\tilde{\chi}_1^0}$ , $m_{\tilde{\chi}_1^0} < 400$ GeV
> 850	95	65	AAD	15BV ATLS	jets + $\cancel{E}_T$ , $\tilde{g} \rightarrow g\tilde{\chi}_1^0$ , $m_{\tilde{\chi}_1^0} < 550$ GeV	>1040	95	92	AAD	14E ATLS	$\ell^\pm \ell^\pm (\ell^\mp) + \text{jets}, \tilde{g} \rightarrow q\cancel{q}\tilde{\chi}_1^\pm$ , $\tilde{\chi}_1^\pm \rightarrow W^{(*)\pm}\tilde{\chi}_2^0, \tilde{\chi}_2^0 \rightarrow Z^{(*)}\tilde{\chi}_1^0$ simplified model, $m_{\tilde{\chi}_1^0} < 520$ GeV
>1270	95	65	AAD	15BV ATLS	jets + $\cancel{E}_T$ , $\tilde{g} \rightarrow q\tilde{q}W\tilde{\chi}_1^0$ , $m_{\tilde{\chi}_1^0} = 100$ GeV	>1200	95	92	AAD	14E ATLS	$\ell^\pm \ell^\pm (\ell^\mp) + \text{jets}, \tilde{g} \rightarrow q\cancel{q}\tilde{\chi}_1^\pm$ , $\tilde{\chi}_1^\pm \rightarrow W^{(*)\pm}\tilde{\chi}_2^0, \tilde{\chi}_2^0 \rightarrow Z^{(*)}\tilde{\chi}_1^0$ simplified model, $m_{\tilde{\chi}_1^0} < 520$ GeV
>1150	95	65	AAD	15BV ATLS	jets + $\ell^\pm \ell^\pm, \tilde{g}$ decays via sleptons, $m_{\tilde{\chi}_1^0} = 100$ GeV	>1050	95	93	CHATRCHYAN14H	CMS	same-sign $\ell^\pm \ell^\pm, \tilde{g} \rightarrow t\tilde{t}_1$ simplified model, massless $\tilde{\chi}_1^0$
>1320	95	65	AAD	15BV ATLS	$\tau, \tilde{q}$ decays via staus, $m_{\tilde{\chi}_1^0} = 100$ GeV	> 900	95	94	CHATRCHYAN14H	CMS	same-sign $\ell^\pm \ell^\pm, \tilde{g} \rightarrow q\cancel{q}\tilde{\chi}_1^\pm$ , $\tilde{\chi}_1^\pm \rightarrow W^\pm\tilde{\chi}_1^0$ simplified model, $m_{\tilde{\chi}_1^\pm} = 0.5m_{\tilde{g}}$ , mass-less $\tilde{\chi}_1^0$
>1220	95	65	AAD	15BV ATLS	$b$ -jets, $\tilde{g} \rightarrow t\tilde{t}_1$ , $m_{\tilde{\chi}_1^0} < 400$ GeV	>1050	95	95	CHATRCHYAN14H	CMS	same-sign $\ell^\pm \ell^\pm, \tilde{g} \rightarrow b\tilde{t}_1$ , $\tilde{\chi}_1^\pm \rightarrow W^\pm\tilde{\chi}_1^0$ simplified model, $m_{\tilde{\chi}_1^\pm} = 300$ GeV, $m_{\tilde{\chi}_1^0} = 50$ GeV
>1310	95	65	AAD	15BV ATLS	$b$ -jets, $\tilde{g} \rightarrow \tilde{t}_1 t$ and $\tilde{t}_1 \rightarrow t\tilde{\chi}_1^0$ , $m_{\tilde{t}_1} < 1000$ GeV	>1260	95	65	AAD	15BV ATLS	$b$ -jets, $\tilde{g} \rightarrow \tilde{t}_1 t$ and $\tilde{g} \rightarrow c\tilde{\chi}_1^0$
>1220	95	65	AAD	15BV ATLS	$b$ -jets, $\tilde{g} \rightarrow \tilde{t}_1 t$ and $\tilde{t}_1 \rightarrow t\tilde{\chi}_1^0$ , $m_{\tilde{t}_1} < 1000$ GeV	>1200	95	65	AAD	15BV ATLS	$b$ -jets, $\tilde{g} \rightarrow \tilde{b}_1 b$ and $\tilde{b}_1 \rightarrow b\tilde{\chi}_1^0$ , $m_{\tilde{b}_1} < 1000$ GeV
>1180	95	65	AAD	15BV ATLS	$b$ -jets, $\tilde{g} \rightarrow \tilde{t}_1 t$ and $\tilde{t}_1 \rightarrow b\tilde{\chi}_1^\pm$ , $m_{\tilde{t}_1} < 1000$ GeV, $m_{\tilde{\chi}_1^0} = 60$ GeV	>1250	95	65	AAD	15BV ATLS	$b$ -jets, $\tilde{g} \rightarrow b\tilde{b}\tilde{\chi}_1^0$ , $m_{\tilde{\chi}_1^0} < 400$ GeV
>1260	95	65	AAD	15BV ATLS	$b$ -jets, $\tilde{g} \rightarrow \tilde{t}_1 t$ and $\tilde{g} \rightarrow c\tilde{\chi}_1^0$	none,	95	65	AAD	15BV ATLS	$b$ -jets, $\tilde{g}$ decay via offshell $\tilde{t}_1$ and $\tilde{b}_1$ , $m_{\tilde{\chi}_1^0} < 500$ GeV
>1200	95	65	AAD	15BV ATLS	$b$ -jets, $\tilde{g} \rightarrow \tilde{b}_1 b$ and $\tilde{b}_1 \rightarrow b\tilde{\chi}_1^0$ , $m_{\tilde{b}_1} < 1000$ GeV	>1100	95	88	AAD	15CB ATLS	jets, $\tilde{g} \rightarrow q\cancel{q}\tilde{\chi}_1^0, \tilde{\chi}_1^0 \rightarrow Z\tilde{G}$ , GGM, $m_{\tilde{\chi}_1^0} = 400$ GeV and $3 < c\tau_{\tilde{\chi}_1^0} < 500$ mm
>1250	95	65	AAD	15BV ATLS	$b$ -jets, $\tilde{g} \rightarrow b\tilde{b}\tilde{\chi}_1^0$ , $m_{\tilde{\chi}_1^0} < 400$ GeV	>1400	95	88	AAD	15CB ATLS	jets or $\cancel{E}_T$ , $\tilde{g} \rightarrow q\cancel{q}\tilde{\chi}_1^0$ . Split SUSY, $m_{\tilde{\chi}_1^0} = 100$ GeV and $15 < c\tau < 300$ mm
none,	95	65	AAD	15BV ATLS	$b$ -jets, $\tilde{g}$ decay via offshell $\tilde{t}_1$ and $\tilde{b}_1$ , $m_{\tilde{\chi}_1^0} < 500$ GeV	>1500	95	88	AAD	15CB ATLS	$\cancel{E}_T, \tilde{g} \rightarrow q\cancel{q}\tilde{\chi}_1^0$ . Split SUSY, $m_{\tilde{\chi}_1^0} = 100$ GeV and $20 < c\tau < 250$ mm
>1100	95	88	AAD	15CB ATLS	jets, $\tilde{g} \rightarrow q\cancel{q}\tilde{\chi}_1^0, \tilde{\chi}_1^0 \rightarrow Z\tilde{G}$ , GGM, $m_{\tilde{\chi}_1^0} = 400$ GeV and $3 < c\tau_{\tilde{\chi}_1^0} < 500$ mm	>1300	95	90	KHACHATRY...15AZ	CMS	$\ell^\pm \ell^\pm + \text{jets} + \cancel{E}_T$ , GMSB, $\tilde{g} \rightarrow q\tilde{q}Z\tilde{G} \geq 2\gamma, \geq 1$ jet, (Razor), binonlike NLSP, $m_{\tilde{\chi}_1^0} = 375$ GeV
>1400	95	88	AAD	15CB ATLS	jets or $\cancel{E}_T$ , $\tilde{g} \rightarrow q\cancel{q}\tilde{\chi}_1^0$ . Split SUSY, $m_{\tilde{\chi}_1^0} = 100$ GeV and $15 < c\tau < 300$ mm	> 800	95	90	KHACHATRY...15AZ	CMS	$\geq 1\gamma, \geq 2$ jet, wino-like NLSP, $m_{\tilde{\chi}_1^0} = 375$ GeV
>1500	95	88	AAD	15CB ATLS	$\cancel{E}_T, \tilde{g} \rightarrow q\cancel{q}\tilde{\chi}_1^0$ . Split SUSY, $m_{\tilde{\chi}_1^0} = 100$ GeV and $20 < c\tau < 250$ mm	>1280	95	91	AAD	14AX ATLS	$\geq 3$ $b$ -jets + $\cancel{E}_T$ , CMSSM
>1300	95	90	KHACHATRY...15AZ	CMS	$\geq 2\gamma, \geq 1$ jet, (Razor), binonlike NLSP, $m_{\tilde{\chi}_1^0} = 375$ GeV	>1250	95	91	AAD	14AX ATLS	$\geq 3$ $b$ -jets + $\cancel{E}_T, \tilde{g} \rightarrow \tilde{b}_1 b\tilde{\chi}_1^0$ simplified model, $\tilde{b}_1 \rightarrow b\tilde{\chi}_1^0$ , $m_{\tilde{\chi}_1^0} = 60$ GeV, $m_{\tilde{b}_1} < 900$ GeV
> 800	95	90	KHACHATRY...15AZ	CMS	$\geq 1\gamma, \geq 2$ jet, wino-like NLSP, $m_{\tilde{\chi}_1^0} = 375$ GeV	>1190	95	91	AAD	14AX ATLS	$\geq 3$ $b$ -jets + $\cancel{E}_T, \tilde{g} \rightarrow \tilde{t}_1 t\tilde{\chi}_1^0$ simplified model, $\tilde{t}_1 \rightarrow t\tilde{\chi}_1^0$ , $m_{\tilde{\chi}_1^0} = 60$ GeV, $m_{\tilde{t}_1} < 1000$ GeV
>1280	95	91	AAD	14AX ATLS	$\geq 3$ $b$ -jets + $\cancel{E}_T$ , CMSSM	>1180	95	91	AAD	14AX ATLS	$\geq 3$ $b$ -jets + $\cancel{E}_T, \tilde{g} \rightarrow \tilde{t}_1 t\tilde{\chi}_1^0$ simplified model, $\tilde{t}_1 \rightarrow b\tilde{\chi}_1^\pm$ , $m_{\tilde{\chi}_1^\pm} = 2m_{\tilde{\chi}_1^0}, m_{\tilde{\chi}_1^0} = 60$ GeV, $m_{\tilde{t}_1} < 1000$ GeV
>1250	95	91	AAD	14AX ATLS	$\geq 3$ $b$ -jets + $\cancel{E}_T, \tilde{g} \rightarrow \tilde{b}_1 b\tilde{\chi}_1^0$ simplified model, $m_{\tilde{\chi}_1^0} < 400$ GeV	>1250	95	91	AAD	14AX ATLS	$\geq 3$ $b$ -jets + $\cancel{E}_T, \tilde{g} \rightarrow b\tilde{b}\tilde{\chi}_1^0$ simplified model, $m_{\tilde{\chi}_1^0} < 400$ GeV
>1340	95	91	AAD	14AX ATLS	$\geq 3$ $b$ -jets + $\cancel{E}_T, \tilde{g} \rightarrow t\tilde{t}_1$ simplified model, $m_{\tilde{\chi}_1^0} < 400$ GeV	>1340	95	91	AAD	14AX ATLS	$\geq 3$ $b$ -jets + $\cancel{E}_T, \tilde{g} \rightarrow t\tilde{t}_1$ simplified model, $m_{\tilde{\chi}_1^0} < 400$ GeV
>1300	95	91	AAD	14AX ATLS	$\geq 3$ $b$ -jets + $\cancel{E}_T, \tilde{g} \rightarrow t\tilde{b}\tilde{\chi}_1^\pm$ simplified model, $\tilde{\chi}_1^\pm \rightarrow f\tilde{f}\tilde{\chi}_1^0, m_{\tilde{\chi}_1^\pm} - m_{\tilde{\chi}_1^0} = 2$ GeV, $m_{\tilde{\chi}_1^0} < 300$ GeV	>950	95	92	AAD	14E ATLS	$\ell^\pm \ell^\pm (\ell^\mp) + \text{jets}, \tilde{g} \rightarrow t\tilde{t}_1$ simplified model
> 950	95	92	AAD	14E ATLS	$\ell^\pm \ell^\pm (\ell^\mp) + \text{jets}, \tilde{g} \rightarrow t\tilde{t}_1$ simplified model	>1000	95	92	AAD	14E ATLS	$\ell^\pm \ell^\pm (\ell^\mp) + \text{jets}, \tilde{g} \rightarrow t\tilde{t}_1$ with $\tilde{t}_1 \rightarrow b\tilde{\chi}_1^\pm$ simplified model, $m_{\tilde{t}_1} < 200$ GeV, $m_{\tilde{\chi}_1^\pm} = 118$ GeV, $m_{\tilde{\chi}_1^0} = 60$ GeV

1 SIRUNYAN 20b searched in 35.9 fb<sup>-1</sup> of pp collisions at  $\sqrt{s} = 13$  TeV for events with at least one photon and large  $\cancel{E}_T$ . No significant excess above the Standard Model expectations is observed. Limits are set on chargino masses in a general gauge-mediated SUSY breaking (GGM) scenario Tchi1n12-GGM, see Figure 4. Limits are also set on the NLSP mass in the Tchi1chi1F and Tchi1chi1G simplified models, see their Figure 5. Finally, limits are set on the gluino mass in the Tglu4A simplified model, see Figure 6.

2 AABOUD 19f searched in 36.1 fb<sup>-1</sup> of pp collisions at  $\sqrt{s} = 13$  TeV in final states with hadronic jets, 1 or two hadronically decaying  $\tau$  and  $\cancel{E}_T$ . In Tglu1F, gluino masses are excluded at 95% C.L. up to 2000 GeV for neutralino masses of 100 GeV or below. Neutralino masses up to 1000 GeV are excluded for all gluino masses below 1400 GeV. See their Fig. 9. Limits are also presented in the context of Gauge-Mediated Symmetry Breaking models: in this case, values of  $\Lambda$  below 110 TeV are excluded at the 95% CL for all values of  $\tan\beta$  in the range  $2 < \tan\beta < 60$ , see their Fig 10.

3 SIRUNYAN 19AG searched in 35.9 fb<sup>-1</sup> of pp collisions at  $\sqrt{s} = 13$  TeV for events with two photons and large  $\cancel{E}_T$ . No significant excess above the Standard Model expectations is observed. Limits are set on the gluino mass in the Tglu4B simplified model and on the squark mass in the Tsqk4B simplified model, see their Figure 3.

4 SIRUNYAN 19AU searched in 35.9 fb<sup>-1</sup> of pp collisions at  $\sqrt{s} = 13$  TeV for events with at least one photon, jets, some of which are identified as originating from  $b$ -quarks, and large  $\cancel{E}_T$ . No significant excess above the Standard Model expectations is observed. In the framework of GMSB, limits are set on the gluino mass in the Tglu4C, Tglu4D and Tglu4E simplified models, and on the top squark mass in the Tstop13 simplified model, see their Figure 5.

5 SIRUNYAN 19CE searched in 35.9 fb<sup>-1</sup> of pp collisions at  $\sqrt{s} = 13$  TeV for new particles decaying to a photon and two gluons in events with at least three large-radius jets of which two have substructure and are composed of a photon and two gluons. No statistically significant excess is observed above the SM background expectation. Upper limits at 95% confidence level on the cross section for gluino pair production are set, using a simplified Tglu1A-like stealth SUSY model. Gluino masses up to 1500-1700 GeV are excluded, depending on the neutralino mass, with the highest exclusion set for  $m_{\tilde{\chi}_1^0} = 200$  GeV. See their Fig 4.

6 SIRUNYAN 19CH searched in 137 fb<sup>-1</sup> of pp collisions at  $\sqrt{s} = 13$  TeV for events containing multiple jets and large  $\cancel{E}_T$ . No significant excess above the Standard Model expectations is observed. Limits are set on the gluino mass in the Tglu1A, Tglu1C, Tglu2A and Tglu3A simplified models, see their Figure 13. Limits are also set on squark, sbottom and stop masses in the Tsqk1, Tstop1, Tstop1 simplified models, see their Figure 14.

7 SIRUNYAN 19K searched in 35.9 fb<sup>-1</sup> of pp collisions at  $\sqrt{s} = 13$  TeV for events with a photon, an electron or muon, and large  $\cancel{E}_T$ . No significant excess above the Standard Model expectations is observed. In the framework of GMSB, limits are set on the chargino and neutralino mass in the Tchi1n1A simplified model, see their Figure 6. Limits are also set on the gluino mass in the Tglu4A simplified model, and on the squark mass in the Tsqk4A simplified model, see their Figure 7.

8 SIRUNYAN 19s searched in 35.9 fb<sup>-1</sup> of pp collisions at  $\sqrt{s} = 13$  TeV for events with zero or one charged leptons, jets and  $\cancel{E}_T$ . The razor variables ( $M_R$  and  $R^2$ ) are used to categorize the events. No significant excess above the Standard Model expectations is observed. Limits are set on the gluino mass in the Tglu3A and Tglu3C simplified models, see Figures 22 and 23, and on the stop mass in the Tstop1 simplified model, see their Figure 24.

9 AABOUD 18AR searched in 36.1 fb<sup>-1</sup> of pp collisions at  $\sqrt{s} = 13$  TeV for gluino pair production in events containing large missing transverse momentum and several energetic jets, at least three of which must be identified as originating from  $b$ -quarks. No excess is found above the predicted background. In Tglu3A models, gluino masses of less than 1.97 TeV are excluded for  $m_{\tilde{\chi}_1^0}$  below 300 GeV, see their Fig. 10(a). Interpretations are also provided for scenarios where Tglu3A modes mix with Tglu2A and Tglu3D, see their Fig 11.

See key on page 999

# Searches Particle Listings

## Supersymmetric Particle Searches

- 10 AABOUD 18AR searched in  $36.1 \text{ fb}^{-1}$  of  $pp$  collisions at  $\sqrt{s} = 13 \text{ TeV}$  for gluino pair production in events containing large missing transverse momentum and several energetic jets, at least three of which must be identified as originating from  $b$ -quarks. No excess is found above the predicted background. In Tglu2A models, gluino masses of less than 1.92 TeV are excluded for  $m_{\tilde{\chi}_1^0}$  below 600 GeV, see their Fig. 10(b). Interpretations are also provided for scenarios where Tglu2A modes mix with Tglu3A and Tglu3D, see their Fig. 11.
- 11 AABOUD 18AS searched for in  $36.1 \text{ fb}^{-1}$  of  $pp$  collisions at  $\sqrt{s} = 13 \text{ TeV}$  for gluino pair production in the context of AMSB or phenomenological MSSM scenarios with wino-like LSP and long-lived charginos. Events with a disappearing track due to a low-momentum pion accompanied by at least four jets are considered. No significant excess above the Standard Model expectations is observed. Exclusion limits are set at 95% confidence level on the mass of gluinos for different chargino lifetimes. Gluino masses up to 1.65 TeV are excluded assuming a chargino mass of 460 GeV and lifetime of 0.2 ns, corresponding to a mass-splitting between the charged and neutral wino of around 160 MeV. See their Fig. 9.
- 12 AABOUD 18BJ searched in  $36.1 \text{ fb}^{-1}$  of  $pp$  collisions at  $\sqrt{s} = 13 \text{ TeV}$  in events with two opposite-sign charged leptons (electrons and muons), jets and missing transverse momentum, with various requirements to be sensitive to signals with different kinematic endpoint values in the dilepton invariant mass distribution. The data are found to be consistent with the SM expectation. Results are interpreted in the Tglu1G model: gluino masses below 1850 GeV are excluded for  $m_{\tilde{\chi}_1^0} = 100 \text{ GeV}$ , see their Fig. 12(a).
- 13 AABOUD 18BJ searched in  $36.1 \text{ fb}^{-1}$  of  $pp$  collisions at  $\sqrt{s} = 13 \text{ TeV}$  in events with two opposite-sign charged leptons (electrons and muons), jets and missing transverse momentum, with various requirements to be sensitive to signals with different kinematic endpoint values in the dilepton invariant mass distribution. The data are found to be consistent with the SM expectation. Results are interpreted in the Tglu1H model: gluino masses below 1650 GeV are excluded for  $m_{\tilde{\chi}_1^0} = 100 \text{ GeV}$ , see their Fig. 13(a).
- 14 AABOUD 18U searched in  $36.1 \text{ fb}^{-1}$  of  $pp$  collisions at  $\sqrt{s} = 13 \text{ TeV}$  in events with at least one isolated photon, possibly jets and significant transverse momentum targeting generalised models of gauge-mediated SUSY breaking. No significant excess of events is observed above the SM prediction. Results for the di-photon channel are interpreted in terms of lower limits on the masses of gluinos in Tglu4B models, which reach as high as 2.3 TeV. Gluinos with masses below 2.15 TeV are excluded for any NLSP mass, see their Fig. 8.
- 15 AABOUD 18U searched in  $36.1 \text{ fb}^{-1}$  of  $pp$  collisions at  $\sqrt{s} = 13 \text{ TeV}$  in events with at least one isolated photon, possibly jets and significant transverse momentum targeting generalised models of gauge-mediated SUSY breaking. No significant excess of events is observed above the SM prediction. Results of the  $\gamma + \text{jets} + \cancel{E}_T$  channel are interpreted in terms of lower limits on the masses of gluinos in GGM higgsino-bino models (mix of Tglu4B and Tglu4C), which reach as high as 2050 GeV. Gluino masses below 1600 GeV are excluded for any NLSP mass provided that  $m_{\tilde{g}} - m_{\tilde{\chi}_1^0} > 50 \text{ GeV}$ . See their Fig. 11.
- 16 AABOUD 18V searched in  $36.1 \text{ fb}^{-1}$  of  $pp$  collisions at  $\sqrt{s} = 13 \text{ TeV}$  in events with no charged leptons, jets and missing transverse momentum. The data are found to be consistent with the SM expectation. Results are interpreted in the Tglu1A model: gluino masses below 2030 GeV are excluded for massless LSP, see their Fig. 13(b).
- 17 AABOUD 18V searched in  $36.1 \text{ fb}^{-1}$  of  $pp$  collisions at  $\sqrt{s} = 13 \text{ TeV}$  in events with no charged leptons, jets and missing transverse momentum. The data are found to be consistent with the SM expectation. Results are interpreted in the Tglu1B model. Assuming that  $m_{\tilde{\chi}_1^\pm} = 0.5(m_{\tilde{g}} + m_{\tilde{\chi}_1^0})$ , gluino masses below 1980 GeV are excluded for massless LSP, see their Fig. 14(c). Exclusions are also shown assuming  $m_{\tilde{\chi}_1^0} = 60 \text{ GeV}$ , see their Fig. 14(d).
- 18 AABOUD 18V searched in  $36.1 \text{ fb}^{-1}$  of  $pp$  collisions at  $\sqrt{s} = 13 \text{ TeV}$  in events with no charged leptons, jets and missing transverse momentum. The data are found to be consistent with the SM expectation. Results are interpreted in the Tglu1E model: gluino masses below 1750 GeV are excluded for  $m_{\tilde{\chi}_1^0} = 1 \text{ GeV}$  and any  $m_{\tilde{\chi}_2^0}$  above 100 GeV, see their Fig. 15. Gluino mass exclusion up to 2 TeV is found for  $m_{\tilde{\chi}_2^0} = 1 \text{ TeV}$ .
- 19 SIRUNYAN 18AA searched in  $35.9 \text{ fb}^{-1}$  of  $pp$  collisions at  $\sqrt{s} = 13 \text{ TeV}$  for events with at least one photon and large  $\cancel{E}_T$ . No significant excess above the Standard Model expectations is observed. Limits are set on wino masses in a general gauge-mediated SUSY breaking (GGM) scenario with bino-like  $\tilde{\chi}_1^0$  and wino-like  $\tilde{\chi}_1^\pm$  and  $\tilde{\chi}_2^0$ , see Figure 7. Limits are also set on the NLSP mass in the Tch1n1A and Tch1ch1A simplified models, see their Figure 8. Finally, limits are set on the gluino mass in the Tglu4A and Tglu4B simplified models, see their Figure 9, and on the squark mass in the Tsk4A and Tsk4B simplified models, see their Figure 10.
- 20 SIRUNYAN 18AC searched in  $35.9 \text{ fb}^{-1}$  of  $pp$  collisions at  $\sqrt{s} = 13 \text{ TeV}$  for events with a single electron or muon and multiple jets. No significant excess above the Standard Model expectations is observed. Limits are set on the gluino mass in the Tglu3A and Tglu1B simplified models, see their Figure 5.
- 21 SIRUNYAN 18AL searched in  $35.9 \text{ fb}^{-1}$  of  $pp$  collisions at  $\sqrt{s} = 13 \text{ TeV}$  for events with at least three charged leptons, in any combination of electrons and muons, jets and significant  $\cancel{E}_T$ . No significant excess above the Standard Model expectations is observed. Limits are set on the gluino mass in the Tglu3A and Tglu1C simplified models, see their Figure 5. Limits are also set on the sbottom mass in the Tstot2 simplified model, see their Figure 6, and on the stop mass in the Tstot7 simplified model, see their Figure 7.
- 22 SIRUNYAN 18AR searched in  $35.9 \text{ fb}^{-1}$  of  $pp$  collisions at  $\sqrt{s} = 13 \text{ TeV}$  for events containing two opposite-charge, same-flavour leptons (electrons or muons), jets and  $\cancel{E}_T$ . No significant excess above the Standard Model expectations is observed. Limits are set on the gluino mass in the Tglu4C simplified model, see their Figure 7. Limits are also set on the chargino/neutralino mass in the Tch1n2F simplified models, see their Figure 8, and on the higgsino mass in the Tn1n1B and Tn1n1C simplified models, see their Figure 9. Finally, limits are set on the sbottom mass in the Tstot3 simplified model, see their Figure 10.
- 23 SIRUNYAN 18AY searched in  $35.9 \text{ fb}^{-1}$  of  $pp$  collisions at  $\sqrt{s} = 13 \text{ TeV}$  for events containing one or more jets and significant  $\cancel{E}_T$ . No significant excess above the Standard Model expectations is observed. Limits are set on the gluino mass in the Tglu1A, Tglu2A and Tglu3A simplified models, see their Figure 3. Limits are also set on squark, sbottom and stop masses in the Tsk1, Tstot1, Tstot1 and Tstot4 simplified models, see their Figure 3. Finally, limits are set on long-lived gluino masses in a Tglu1A simplified model where the gluino is metastable or long-lived with proper decay lengths in the range  $10^{-3} \text{ mm} < c\tau < 10^5 \text{ mm}$ , see their Figure 4.
- 24 SIRUNYAN 18D searched in  $35.9 \text{ fb}^{-1}$  of  $pp$  collisions at  $\sqrt{s} = 13 \text{ TeV}$  for events containing identified hadronically decaying top quarks, no leptons, and  $\cancel{E}_T$ . No significant excess above the Standard Model expectations is observed. Limits are set on the stop mass in the Tstot1 simplified model, see their Figure 8, and on the gluino mass in the Tglu3A, Tglu3B, Tglu3C and Tglu3E simplified models, see their Figure 9.
- 25 SIRUNYAN 18M searched in  $35.9 \text{ fb}^{-1}$  of  $pp$  collisions at  $\sqrt{s} = 13 \text{ TeV}$  for events with one or more high-momentum Higgs bosons, decaying to pairs of  $b$ -quarks, and large  $\cancel{E}_T$ . No significant excess above the Standard Model expectations is observed. Limits are set on the gluino mass in the Tglu1I and Tglu1J simplified models, see their Figure 3.
- 26 AABOUD 17AJ searched in  $36.1 \text{ fb}^{-1}$  of  $pp$  collisions at  $\sqrt{s} = 13 \text{ TeV}$  for events with two same-sign or three leptons, jets and large missing transverse momentum. No significant excess above the Standard Model expectations is observed. Limits up to 1.75 TeV are set on the gluino mass in Tglu3A simplified models in case of off-shell top squarks and for  $m_{\tilde{\chi}_1^0} = 100 \text{ GeV}$ . See their Figure 4(a).
- 27 AABOUD 17AJ searched in  $36.1 \text{ fb}^{-1}$  of  $pp$  collisions at  $\sqrt{s} = 13 \text{ TeV}$  for events with two same-sign or three leptons, jets and large missing transverse momentum. No significant excess above the Standard Model expectations is observed. Limits up to 1.57 TeV are set on the gluino mass in Tglu1E simplified models (2-step models) for  $m_{\tilde{\chi}_1^0} = 100 \text{ GeV}$ . See their Figure 4(b).
- 28 AABOUD 17AJ searched in  $36.1 \text{ fb}^{-1}$  of  $pp$  collisions at  $\sqrt{s} = 13 \text{ TeV}$  for events with two same-sign or three leptons, jets and large missing transverse momentum. No significant excess above the Standard Model expectations is observed. Limits up to 1.86 TeV are set on the gluino mass in Tglu1G simplified models for  $m_{\tilde{\chi}_1^0} = 200 \text{ GeV}$ . See their Figure 4(c).
- 29 AABOUD 17AR searched in  $36.1 \text{ fb}^{-1}$  of  $pp$  collisions at  $\sqrt{s} = 13 \text{ TeV}$  for events with one isolated lepton, at least two jets and large missing transverse momentum. No significant excess above the Standard Model expectations is observed. Limits up to 2.1 TeV are set on the gluino mass in Tglu1B simplified models, with  $x = (m_{\tilde{\chi}_1^\pm} - m_{\tilde{\chi}_1^0}) / (m_{\tilde{g}} - m_{\tilde{\chi}_1^0}) = 1/2$ . Similar limits are obtained for variable  $x$  and fixed neutralino mass,  $m_{\tilde{\chi}_1^0} = 60 \text{ GeV}$ . See their Figure 13.
- 30 AABOUD 17AR searched in  $36.1 \text{ fb}^{-1}$  of  $pp$  collisions at  $\sqrt{s} = 13 \text{ TeV}$  for events with one isolated lepton, at least two jets and large missing transverse momentum. No significant excess above the Standard Model expectations is observed. Limits up to 1.74 TeV are set on the gluino mass in Tglu1E simplified model. Limits up to 1.7 TeV are also set on pMSSM models leading to similar signal event topologies. See their Figure 13.
- 31 AABOUD 17AY searched in  $36.1 \text{ fb}^{-1}$  of  $pp$  collisions at  $\sqrt{s} = 13 \text{ TeV}$  for events with at least four jets and large missing transverse momentum. No significant excess above the Standard Model expectations is observed. Limits up to 1.8 TeV are set on the gluino mass in Tglu3A simplified models assuming  $m_{\tilde{\tau}_1} - m_{\tilde{\chi}_1^0} = 5 \text{ GeV}$ . See their Figure 13.
- 32 AABOUD 17AZ searched in  $36.1 \text{ fb}^{-1}$  of  $pp$  collisions at  $\sqrt{s} = 13 \text{ TeV}$  for events with at least seven jets and large missing transverse momentum. Selected events are further classified based on the presence of large R-jets or  $b$ -jets and no leptons. No significant excess above the Standard Model expectations is observed. Limits up to 1.8 TeV are set on the gluino mass in Tglu1E simplified models. See their Figure 6b.
- 33 AABOUD 17AZ searched in  $36.1 \text{ fb}^{-1}$  of  $pp$  collisions at  $\sqrt{s} = 13 \text{ TeV}$  for events with at least seven jets and large missing transverse momentum. Selected events are further classified based on the presence of large R-jets or  $b$ -jets and no leptons. No significant excess above the Standard Model expectations is observed. Limits up to 1.54 TeV are set on the gluino mass in Tglu3A simplified models. See their Figure 7a.
- 34 AABOUD 17N searched in  $14.7 \text{ fb}^{-1}$  of  $pp$  collisions at  $\sqrt{s} = 13 \text{ TeV}$  in final states with 2 same-flavor, opposite-sign leptons (electrons or muons), jets and large missing transverse momentum. In Tglu1J models, gluino masses are excluded at 95% C.L. up to 1300 GeV for  $m_{\tilde{\chi}_1^0} = 0 \text{ GeV}$  and  $m_{\tilde{\chi}_2^0} = 1100 \text{ GeV}$ . See their Fig. 12 for exclusion limits as a function of  $m_{\tilde{\chi}_2^0}$ . Limits are also presented assuming  $m_{\tilde{\chi}_2^0} = m_{\tilde{\chi}_1^0} + 100 \text{ GeV}$ , see their Fig. 13.
- 35 AABOUD 17N searched in  $14.7 \text{ fb}^{-1}$  of  $pp$  collisions at  $\sqrt{s} = 13 \text{ TeV}$  in final states with 2 same-flavor, opposite-sign leptons (electrons or muons), jets and large missing transverse momentum. In Tglu1H models, gluino masses are excluded at 95% C.L. up to 1310 GeV for  $m_{\tilde{\chi}_1^0} < 400 \text{ GeV}$  and assuming  $m_{\tilde{\chi}_2^0} = (m_{\tilde{g}} + m_{\tilde{\chi}_1^0})/2$ . See their Fig. 15.
- 36 AABOUD 17N searched in  $14.7 \text{ fb}^{-1}$  of  $pp$  collisions at  $\sqrt{s} = 13 \text{ TeV}$  in final states with 2 same-flavor, opposite-sign leptons (electrons or muons), jets and large missing transverse momentum. In Tglu1G models, gluino masses are excluded at 95% C.L. up to 1700 GeV for small  $m_{\tilde{\chi}_1^0}$ . The results probe kinematic endpoints as small as  $m_{\tilde{\chi}_2^0} - m_{\tilde{\chi}_1^0} = (m_{\tilde{g}} - m_{\tilde{\chi}_1^0})/2 = 50 \text{ GeV}$ . See their Fig. 14.
- 37 KHACHATRYAN 17 searched in  $2.3 \text{ fb}^{-1}$  of  $pp$  collisions at  $\sqrt{s} = 13 \text{ TeV}$  for events containing four or more jets, no more than one lepton, and missing transverse momentum, using the razor variables ( $M_R$  and  $R^2$ ) to discriminate between signal and background processes. No evidence for an excess over the expected background is observed. Limits are derived on the gluino mass in the Tglu1A, Tglu2A and Tglu3A simplified models, see Figs. 16 and 17. Also, assuming gluinos decay only via three-body processes involving third-generation quarks plus a neutralino/chargino, and assuming  $m_{\tilde{\chi}_1^\pm} = m_{\tilde{\chi}_1^0} + 5 \text{ GeV}$ , a branching ratio-independent limit on the gluino mass is given, see Fig. 16.
- 38 KHACHATRYAN 17AD searched in  $2.3 \text{ fb}^{-1}$  of  $pp$  collisions at  $\sqrt{s} = 13 \text{ TeV}$  for events containing at least four jets (including  $b$ -jets), missing transverse momentum and tagged top quarks. No evidence for an excess over the expected background is observed. Gluino masses up to 1550 GeV and neutralino masses up to 900 GeV are excluded at 95% C.L. See Fig. 13.
- 39 KHACHATRYAN 17AD searched in  $2.3 \text{ fb}^{-1}$  of  $pp$  collisions at  $\sqrt{s} = 13 \text{ TeV}$  for events containing at least four jets (including  $b$ -jets), missing transverse momentum and tagged top quarks. No evidence for an excess over the expected background is observed. Gluino masses up to 1450 GeV and neutralino masses up to 820 GeV are excluded at 95% C.L. See Fig. 13.
- 40 KHACHATRYAN 17AS searched in  $2.3 \text{ fb}^{-1}$  of  $pp$  collisions at  $\sqrt{s} = 13 \text{ TeV}$  for events with a single electron or muon and multiple jets. No significant excess above the Standard Model expectations is observed. Limits are set on the gluino mass in the Tglu3A and Tglu1B simplified models, see their Fig. 7.
- 41 KHACHATRYAN 17AW searched in  $2.3 \text{ fb}^{-1}$  of  $pp$  collisions at  $\sqrt{s} = 13 \text{ TeV}$  for events with at least three charged leptons, in any combination of electrons and muons, and

# Searches Particle Listings

## Supersymmetric Particle Searches

- significant  $\mathcal{E}_T$ . No significant excess above the Standard Model expectations is observed. Limits are set on the gluino mass in the Tglu3A and Tglu1C simplified models, and on the sbottom mass in the Tsb02 simplified model, see their Figure 4.
- 42 KHACHATRYAN 17P searched in  $2.3 \text{ fb}^{-1}$  of  $pp$  collisions at  $\sqrt{s} = 13 \text{ TeV}$  for events with one or more jets and large  $\mathcal{E}_T$ . No significant excess above the Standard Model expectations is observed. Limits are set on the gluino mass in the Tglu1A, Tglu2A, Tglu3A, Tglu3B, Tglu3C and Tglu3D simplified models, see their Figures 7 and 8. Limits are also set on the squark mass in the Tsqk1 simplified model, see their Fig. 7, and on the sbottom mass in the Tsb01 simplified model, see Fig. 8. Finally, limits are set on the stop mass in the Tstop1, Tstop3, Tstop4, Tstop6 and Tstop7 simplified models, see Fig. 8.
- 43 KHACHATRYAN 17V searched in  $2.3 \text{ fb}^{-1}$  of  $pp$  collisions at  $\sqrt{s} = 13 \text{ TeV}$  for events with two photons and large  $\mathcal{E}_T$ . No significant excess above the Standard Model expectations is observed. Limits are set on the gluino and squark mass in the context of general gauge mediation models Tglu4B and Tsqk4, see their Fig. 4.
- 44 SIRUNYAN 17AF searched in  $35.9 \text{ fb}^{-1}$  of  $pp$  collisions at  $\sqrt{s} = 13 \text{ TeV}$  for events with a single lepton (electron or muon), jets, including at least one jet originating from a  $b$ -quark, and large  $\mathcal{E}_T$ . No significant excess above the Standard Model expectations is observed. Limits are set on the gluino mass in the Tglu3A and Tglu3B simplified models, see their Figure 2.
- 45 SIRUNYAN 17AV searched in  $35.9 \text{ fb}^{-1}$  of  $pp$  collisions at  $\sqrt{s} = 13 \text{ TeV}$  for events with at least one photon, jets and large  $\mathcal{E}_T$ . No significant excess above the Standard Model expectations is observed. Limits are set on the gluino mass in the Tglu4A and Tglu4B simplified models, and on the squark mass in the Tsqk4A and Tsqk4B simplified models, see their Figure 6.
- 46 SIRUNYAN 17AZ searched in  $35.9 \text{ fb}^{-1}$  of  $pp$  collisions at  $\sqrt{s} = 13 \text{ TeV}$  for events with one or more jets and large  $\mathcal{E}_T$ . No significant excess above the Standard Model expectations is observed. Limits are set on the gluino mass in the Tglu1A, Tglu2A, Tglu3A simplified models, see their Figures 6. Limits are also set on the squark mass in the Tsqk1 simplified model (for single light squark and for 8 degenerate light squarks), on the sbottom mass in the Tsb01 simplified model and on the stop mass in the Tstop1 simplified model, see their Fig. 7. Finally, limits are set on the stop mass in the Tstop2, Tstop4 and Tstop8 simplified models, see Fig. 8.
- 47 SIRUNYAN 17P searched in  $35.9 \text{ fb}^{-1}$  of  $pp$  collisions at  $\sqrt{s} = 13 \text{ TeV}$  for events with multiple jets and large  $\mathcal{E}_T$ . No significant excess above the Standard Model expectations is observed. Limits are set on the gluino mass in the Tglu1A, Tglu1C, Tglu2A, Tglu3A and Tglu3D simplified models, see their Fig. 12. Limits are also set on the squark mass in the Tsqk1 simplified model, on the stop mass in the Tstop1 simplified model, and on the sbottom mass in the Tsb01 simplified model, see Fig. 13.
- 48 SIRUNYAN 17S searched in  $35.9 \text{ fb}^{-1}$  of  $pp$  collisions at  $\sqrt{s} = 13 \text{ TeV}$  for events with two isolated same-sign leptons, jets, and large  $\mathcal{E}_T$ . No significant excess above the Standard Model expectations is observed. Limits are set on the mass of the gluino mass in the Tglu3A, Tglu3B, Tglu3C, Tglu3D and Tglu1B simplified models, see their Figures 5 and 6, and on the sbottom mass in the Tsb02 simplified model, see their Figure 6.
- 49 AABOUD 16AC searched in  $3.2 \text{ fb}^{-1}$  of  $pp$  collisions at  $\sqrt{s} = 13 \text{ TeV}$  in final states with hadronic jets, 1 or two hadronically decaying  $\tau$  and  $\mathcal{E}_T$ . In Tglu1F, gluino masses are excluded at 95% C.L. up to 1570 GeV for neutralino masses of 100 GeV or below. Neutralino masses up to 700 GeV are excluded for all gluino masses between 800 GeV and 1500 GeV, while the strongest neutralino-mass exclusion of 750 GeV is achieved for gluino masses around 1400 GeV. See their Fig. 8. Limits are also presented in the context of Gauge-Mediated Symmetry Breaking models: in this case, values of  $A$  below 92 TeV are excluded at the 95% C.L. corresponding to gluino masses below 2000 GeV. See their Fig. 9.
- 50 AABOUD 16I searched in  $3.2 \text{ fb}^{-1}$  of  $pp$  collisions at  $\sqrt{s} = 13 \text{ TeV}$  in final states with one isolated electron or muon, hadronic jets, and  $\mathcal{E}_T$ . Gluino-mediated pair production of stops with a nearly mass-degenerate stop and neutralino are targeted and gluino masses are excluded at 95% C.L. up to 1460 GeV. A 100% of stops decaying via charm + neutralino is assumed. The results are also valid in case of 4-body decays  $\tilde{t}_1 \rightarrow f f' b \tilde{\chi}_1^0$ . See their Fig. 8.
- 51 AABOUD 16M searched in  $3.2 \text{ fb}^{-1}$  of  $pp$  collisions at  $\sqrt{s} = 13 \text{ TeV}$  for events with two photons, hadronic jets and  $\mathcal{E}_T$ . No significant excess above the Standard Model expectations is observed. Exclusion limits at 95% C.L. are set on gluino masses in the general gauge-mediated SUSY breaking model (GGM), for bino-like NLSP. See their Fig. 3.
- 52 AABOUD 16N searched in  $3.2 \text{ fb}^{-1}$  of  $pp$  collisions at  $\sqrt{s} = 13 \text{ TeV}$  for events containing hadronic jets, large  $\mathcal{E}_T$ , and no electrons or muons. No significant excess above the Standard Model expectations is observed. Gluino masses below 1510 GeV are excluded at the 95% C.L. in a simplified model with only gluinos and the lightest neutralino. See their Fig. 7b.
- 53 AABOUD 16N searched in  $3.2 \text{ fb}^{-1}$  of  $pp$  collisions at  $\sqrt{s} = 13 \text{ TeV}$  for events containing hadronic jets, large  $\mathcal{E}_T$ , and no electrons or muons. No significant excess above the Standard Model expectations is observed. Gluino masses below 1500 GeV are excluded at the 95% C.L. in a simplified model with gluinos decaying via an intermediate  $\tilde{\chi}_1^\pm$  to two quarks, a  $W$  boson and a  $\tilde{\chi}_1^0$  for  $m_{\tilde{\chi}_1^0} = 200 \text{ GeV}$ . See their Fig. 8.
- 54 AAD 16AD searched in  $3.2 \text{ fb}^{-1}$  of  $pp$  collisions at  $\sqrt{s} = 13 \text{ TeV}$  for events containing several energetic jets, of which at least three must be identified as  $b$ -jets, large  $\mathcal{E}_T$  and no electrons or muons. No significant excess above the Standard Model expectations is observed. For  $\tilde{\chi}_1^0$  below 800 GeV, gluino masses below 1780 GeV are excluded at 95% C.L. for gluinos decaying via bottom squarks. See their Fig. 7a.
- 55 AAD 16AD searched in  $3.2 \text{ fb}^{-1}$  of  $pp$  collisions at  $\sqrt{s} = 13 \text{ TeV}$  for events containing several energetic jets, of which at least three must be identified as  $b$ -jets, large  $\mathcal{E}_T$  and one electron or muon. Large-radius jets with a high mass are also used to identify highly boosted top quarks. No significant excess above the Standard Model expectations is observed. For  $\tilde{\chi}_1^0$  below 700 GeV, gluino masses below 1760 GeV are excluded at 95% C.L. for gluinos decaying via top squarks. See their Fig. 7b.
- 56 AAD 16BB searched in  $3.2 \text{ fb}^{-1}$  of  $pp$  collisions at  $\sqrt{s} = 13 \text{ TeV}$  for events with exactly two same-sign leptons or at least three leptons, multiple hadronic jets,  $b$ -jets, and  $\mathcal{E}_T$ . No significant excess over the Standard Model expectation is found. Exclusion limits at 95% C.L. are set on the gluino mass in various simplified models (Tglu1D, Tglu1E, Tglu3A). See their Figs. 4a, 4b, and 4d.
- 57 AAD 16BG searched in  $3.2 \text{ fb}^{-1}$  of  $pp$  collisions at  $\sqrt{s} = 13 \text{ TeV}$  in final states with one isolated electron or muon, hadronic jets, and  $\mathcal{E}_T$ . The data agree with the SM background expectation in the six signal selections defined in the search, and the largest deviation is a 2.1 standard deviation excess. Gluinos are excluded at 95% C.L. up to 1600 GeV assuming they decay via the lightest chargino to the lightest neutralino as in the model Tglu1B for  $m_{\tilde{\chi}_1^0} = 100 \text{ GeV}$ , assuming  $m_{\tilde{\chi}_1^\pm} = (m_{\tilde{g}} + m_{\tilde{\chi}_1^0})/2$ . See their Fig. 6.
- 58 AAD 16V searched in  $3.2 \text{ fb}^{-1}$  of  $pp$  collisions at  $\sqrt{s} = 13 \text{ TeV}$  for events with  $\mathcal{E}_T$  various hadronic jet multiplicities from  $\geq 7$  to  $\geq 10$  and with various  $b$ -jet multiplicity requirements. No significant excess over the Standard Model expectation is found. Exclusion limits at 95% C.L. are set on the gluino mass in one simplified model (Tglu1E) and a pMSSM-inspired model. See their Fig. 5.
- 59 KHACHATRYAN 16AM searched in  $19.7 \text{ fb}^{-1}$  of  $pp$  collisions at  $\sqrt{s} = 8 \text{ TeV}$  for events with highly boosted  $W$ -bosons and  $b$ -jets, using the razor variables ( $M_R$  and  $R^2$ ) to discriminate between signal and background processes. No significant excess above the Standard Model expectations is observed. Limits are set on the gluino mass in the Tglu3C and Tglu3B simplified models, see Fig. 12.
- 60 KHACHATRYAN 16BJ searched in  $2.3 \text{ fb}^{-1}$  of  $pp$  collisions at  $\sqrt{s} = 13 \text{ TeV}$  for events with two isolated same-sign dileptons and jets in the final state. No significant excess above the Standard Model expectations is observed. Limits are set on the gluino mass in the following simplified models: Tglu3A and Tglu3D, see Fig. 4, Tglu3B and Tglu3C, see Fig. 5, and Tglu1B, see Fig. 7.
- 61 KHACHATRYAN 16BS searched in  $2.3 \text{ fb}^{-1}$  of  $pp$  collisions at  $\sqrt{s} = 13 \text{ TeV}$  for events with at least one energetic jet, no isolated leptons, and significant  $\mathcal{E}_T$ , using the transverse mass variable  $M_{T2}$  to discriminate between signal and background processes. No significant excess above the Standard Model expectations is observed. Limits are set on the gluino mass in the Tglu1A, Tglu2A and Tglu3A simplified models, see Fig. 10 and Table 3.
- 62 KHACHATRYAN 16BY searched in  $2.3 \text{ fb}^{-1}$  of  $pp$  collisions at  $\sqrt{s} = 13 \text{ TeV}$  for events with two opposite-sign, same-flavour leptons, jets, and missing transverse momentum. No significant excess above the Standard Model expectations is observed. Limits are set on the gluino mass in the Tglu4C simplified model, see Fig. 4, and on sbottom masses in the Tsb03 simplified model, see Fig. 5.
- 63 KHACHATRYAN 16V searched in  $2.3 \text{ fb}^{-1}$  of  $pp$  collisions at  $\sqrt{s} = 13 \text{ TeV}$  for events with at least four energetic jets and significant  $\mathcal{E}_T$ , no identified isolated electron or muon or charged track. No significant excess above the Standard Model expectations is observed. Limits are set on the gluino mass in the Tglu1A, Tglu1C, Tglu2A, and Tglu3A simplified models, see Fig. 8.
- 64 AAD 15BG searched in  $20.3 \text{ fb}^{-1}$  of  $pp$  collisions at  $\sqrt{s} = 8 \text{ TeV}$  for events with jets, missing  $\mathcal{E}_T$ , and two opposite-sign same flavor isolated leptons featuring either a kinematic edge, or a peak at the  $Z$ -boson mass, in the invariant mass spectrum. No evidence for a statistically significant excess over the expected SM backgrounds are observed and 95% C.L. exclusion limits are derived in a GGM simplified model of gluino pair production where the gluino decays into quarks, a  $Z$ -boson, and a massless gravitino LSP, see Fig. 12. Also, limits are set in simplified models with slepton/sneutrino intermediate states, see Fig. 13.
- 65 AAD 15BV summarized and extended ATLAS searches for gluinos and first- and second-generation squarks in final states containing jets and missing transverse momentum, with or without leptons or  $b$ -jets in the  $\sqrt{s} = 8 \text{ TeV}$  data set collected in 2012. The paper reports the results of new interpretations and statistical combinations of previously published analyses, as well as new analyses. Exclusion limits at 95% C.L. are set on the gluino mass in several R-parity conserving models, leading to a generalized constraint on gluino masses exceeding 1150 GeV for lightest supersymmetric particle masses below 100 GeV. See their Figs. 10, 19, 20, 21, 23, 25, 26, 29-37.
- 66 AAD 15BX interpreted the results of a wide range of ATLAS direct searches for supersymmetry, during the first run of the LHC using the  $\sqrt{s} = 7 \text{ TeV}$  and  $\sqrt{s} = 8 \text{ TeV}$  data set collected in 2012, within the wider framework of the phenomenological mSMM (pMSSM). The integrated luminosity was up to  $20.3 \text{ fb}^{-1}$ . From an initial random sampling of 500 million pMSSM points, generated from the 19-parameter pMSSM, a total of 310,327 model points with  $\tilde{\chi}_1^0$  LSP were selected each of which satisfies constraints from previous collider searches, precision measurements, cold dark matter energy density measurements and direct dark matter searches. The impact of the ATLAS Run 1 searches on this space was presented, considering the fraction of model points surviving, after projection into two-dimensional spaces of sparticle masses. Good complementarity is observed between different ATLAS analyses, with almost all showing regions of unique sensitivity. ATLAS searches have good sensitivity at LSP mass below 800 GeV.
- 67 AAD 15CA searched in  $20.3 \text{ fb}^{-1}$  of  $pp$  collisions at  $\sqrt{s} = 8 \text{ TeV}$  for events with one or more photons, hadronic jets or  $b$ -jets and  $\mathcal{E}_T$ . No significant excess above the Standard Model expectations is observed. Limits are set on gluino masses in the general gauge-mediated SUSY breaking model (GGM), for bino-like or higgsino-bino admixtures NLSP, see Fig. 8, 10, 11.
- 68 KHACHATRYAN 15AF searched in  $19.5 \text{ fb}^{-1}$  of  $pp$  collisions at  $\sqrt{s} = 8 \text{ TeV}$  for events with at least two energetic jets and significant  $\mathcal{E}_T$ , using the transverse mass variable  $M_{T2}$  to discriminate between signal and background processes. No significant excess above the Standard Model expectations is observed. Limits are set on the gluino mass in simplified models where the decay  $\tilde{g} \rightarrow q\bar{q}\tilde{\chi}_1^0$  takes place with a branching ratio of 100%, see Fig. 13(a), or where the decay  $\tilde{g} \rightarrow b\bar{b}\tilde{\chi}_1^0$  takes place with a branching ratio of 100%, see Fig. 13(b), or where the decay  $\tilde{g} \rightarrow t\bar{t}\tilde{\chi}_1^0$  takes place with a branching ratio of 100%, see Fig. 13(c). See also Table 5. Exclusions in the CMSSM, assuming  $\tan\beta = 30$ ,  $A_0 = -2 \max(m_0, m_{1/2})$  and  $\mu > 0$ , are also presented, see Fig. 15.
- 69 KHACHATRYAN 15I searched in  $19.5 \text{ fb}^{-1}$  of  $pp$  collisions at  $\sqrt{s} = 8 \text{ TeV}$  for events in which  $b$ -jets and four  $W$ -bosons are produced. Five individual search channels are combined (fully hadronic, single lepton, same-sign dilepton, opposite-sign dilepton, multi-lepton). No significant excess above the Standard Model expectations is observed. Limits are set on the gluino mass in a simplified model where the decay  $\tilde{g} \rightarrow t\bar{t}\tilde{\chi}_1^0$  takes place with a branching ratio of 100%, see Fig. 5. Also a simplified model with gluinos decaying into on-shell top squarks is considered, see Fig. 6.
- 70 KHACHATRYAN 15X searched in  $19.3 \text{ fb}^{-1}$  of  $pp$  collisions at  $\sqrt{s} = 8 \text{ TeV}$  for events with at least two energetic jets, at least one of which is required to originate from a  $b$  quark, and significant  $\mathcal{E}_T$ , using the razor variables ( $M_R$ ) and  $R^2$  to discriminate between signal and background processes. No significant excess above the Standard Model expectations is observed. Limits are set on the gluino mass in simplified models where the decay  $\tilde{g} \rightarrow b\bar{b}\tilde{\chi}_1^0$  and the decay  $\tilde{g} \rightarrow t\bar{t}\tilde{\chi}_1^0$  take place with branching ratios varying between 0, 50 and 100%, see Figs. 13 and 14.
- 71 AAD 14AE searched in  $20.3 \text{ fb}^{-1}$  of  $pp$  collisions at  $\sqrt{s} = 8 \text{ TeV}$  for strongly produced supersymmetric particles in events containing jets and large missing transverse momentum, and no electrons or muons. No excess over the expected SM background is observed. Exclusion limits are derived in simplified models containing gluinos and squarks, see Figures 5, 6 and 7. Limits are also derived in the mSUGRA/CMSSM with parameters  $\tan\beta = 30$ ,  $A_0 = -2 m_0$  and  $\mu > 0$ , see their Fig. 8.

- <sup>72</sup> AAD 14AG searched in 20.3 fb<sup>-1</sup> of  $pp$  collisions at  $\sqrt{s} = 8$  TeV for events containing one hadronically decaying  $\tau$ -lepton, zero or one additional light leptons (electrons or muons), jets and large missing transverse momentum. No excess of events above the expected level of Standard Model background was found. Exclusion limits at 95% C.L. are set in several SUSY scenarios. For an interpretation in the minimal GMSB model, see their Fig. 8. For an interpretation in the mSUGRA/CMSSM with parameters  $\tan\beta = 30$ ,  $A_0 = -2m_0$  and  $\mu > 0$ , see their Fig. 9. For an interpretation in the framework of natural Gauge Mediation, see Fig. 10. For an interpretation in the bRPV scenario, see their Fig. 11.
- <sup>73</sup> AAD 14X searched in 20.3 fb<sup>-1</sup> of  $pp$  collisions at  $\sqrt{s} = 8$  TeV for events with at least four leptons (electrons, muons, taus) in the final state. No significant excess above the Standard Model expectations is observed. Limits are set on the gluino mass in a general gauge-mediation model (GGM) where the decay  $\tilde{g} \rightarrow q\bar{q}\tilde{\chi}_1^0$ , with  $\tilde{\chi}_1^0 \rightarrow \ell^\pm \ell^\mp \tilde{G}$ , takes place with a branching ratio of 100%, for two choices of  $\tan\beta = 1.5$  and 30, see Fig. 11. Also some constraints on the higgsino mass parameter  $\mu$  are discussed.
- <sup>74</sup> CHATRCHYAN 14AH searched in 4.7 fb<sup>-1</sup> of  $pp$  collisions at  $\sqrt{s} = 7$  TeV for events with at least two energetic jets and significant  $\cancel{E}_T$ , using the razor variables ( $M_R$  and  $R^2$ ) to discriminate between signal and background processes. No significant excess above the Standard Model expectations is observed. Limits are set on sbottom masses in simplified models where the decay  $\tilde{g} \rightarrow q\bar{q}\tilde{\chi}_1^0$  takes place with a branching ratio of 100%, see Fig. 28. Exclusions in the CMSSM, assuming  $\tan\beta = 10$ ,  $A_0 = 0$  and  $\mu > 0$ , are also presented, see Fig. 26.
- <sup>75</sup> CHATRCHYAN 14AH searched in 4.7 fb<sup>-1</sup> of  $pp$  collisions at  $\sqrt{s} = 7$  TeV for events with at least two energetic jets and significant  $\cancel{E}_T$ , using the razor variables ( $M_R$  and  $R^2$ ) to discriminate between signal and background processes. A second analysis requires at least one of the jets to be originating from a  $b$ -quark. No significant excess above the Standard Model expectations is observed. Limits are set on sbottom masses in simplified models where the decay  $\tilde{g} \rightarrow b\bar{b}\tilde{\chi}_1^0$  takes place with a branching ratio of 100%, see Figs. 28 and 29. Exclusions in the CMSSM, assuming  $\tan\beta = 10$ ,  $A_0 = 0$  and  $\mu > 0$ , are also presented, see Fig. 26.
- <sup>76</sup> CHATRCHYAN 14AH searched in 4.7 fb<sup>-1</sup> of  $pp$  collisions at  $\sqrt{s} = 7$  TeV for events with at least two energetic jets and significant  $\cancel{E}_T$ , using the razor variables ( $M_R$  and  $R^2$ ) to discriminate between signal and background processes. A second analysis requires at least one of the jets to be originating from a  $b$ -quark. No significant excess above the Standard Model expectations is observed. Limits are set on sbottom masses in simplified models where the decay  $\tilde{g} \rightarrow t\bar{t}\tilde{\chi}_1^0$  takes place with a branching ratio of 100%, see Figs. 28 and 29. Exclusions in the CMSSM, assuming  $\tan\beta = 10$ ,  $A_0 = 0$  and  $\mu > 0$ , are also presented, see Fig. 26.
- <sup>77</sup> CHATRCHYAN 14I searched in 19.5 fb<sup>-1</sup> of  $pp$  collisions at  $\sqrt{s} = 8$  TeV for events containing multijets and large  $\cancel{E}_T$ . No excess over the expected SM background is observed. Exclusion limits are derived in simplified models containing gluinos that decay via  $\tilde{g} \rightarrow q\bar{q}\tilde{\chi}_1^0$  with a 100% branching ratio, see Fig. 7b, or via  $\tilde{g} \rightarrow t\bar{t}\tilde{\chi}_1^0$  with a 100% branching ratio, see Fig. 7c, or via  $\tilde{g} \rightarrow q\bar{q}W/Z\tilde{\chi}_1^0$ , see Fig. 7d.
- <sup>78</sup> CHATRCHYAN 14N searched in 19.3 fb<sup>-1</sup> of  $pp$  collisions at  $\sqrt{s} = 8$  TeV for events containing a single isolated electron or muon and multiple jets, at least two of which are identified as originating from a  $b$ -quark. No significant excesses over the expected SM backgrounds are observed. The results are interpreted in three simplified models of gluino pair production with subsequent decay into virtual or on-shell top squarks, where each of the top squarks decays in turn into a top quark and a  $\tilde{\chi}_1^0$ , see Fig. 4. The models differ in which masses are allowed to vary.
- <sup>79</sup> CHATRCHYAN 14R searched in 19.5 fb<sup>-1</sup> of  $pp$  collisions at  $\sqrt{s} = 8$  TeV for events with at least three leptons (electrons, muons, taus) in the final state. No significant excess above the Standard Model expectations is observed. Limits are set on the gluino mass in a slepton co-NLSP simplified model (GMSB) where the decay  $\tilde{g} \rightarrow q\bar{q}\ell\ell\tilde{G}$  takes place with a branching ratio of 100%, see Fig. 8.
- <sup>80</sup> CHATRCHYAN 14R searched in 19.5 fb<sup>-1</sup> of  $pp$  collisions at  $\sqrt{s} = 8$  TeV for events with at least three leptons (electrons, muons, taus) in the final state. No significant excess above the Standard Model expectations is observed. Limits are set on the gluino mass in a simplified model where the decay  $\tilde{g} \rightarrow t\bar{t}\tilde{\chi}_1^0$  takes place with a branching ratio of 100%, see Fig. 11.
- <sup>81</sup> AABOUD 18BJ searched in 36.1 fb<sup>-1</sup> of  $pp$  collisions at  $\sqrt{s} = 13$  TeV in events with two opposite-sign charged leptons (electrons and muons), jets and missing transverse momentum, with various requirements to be sensitive to signals with different kinematic endpoint values in the dilepton invariant mass distribution. The data are found to be consistent with the SM expectation. Results are interpreted in the Tglu1H model in case of  $m_{\tilde{\chi}_1^0} = 1$  GeV: for any  $m_{\tilde{\chi}_2^0}$ , gluino masses below 1500 GeV are excluded, see their Fig. 14(a).
- <sup>82</sup> AABOUD 18v searched in 36.1 fb<sup>-1</sup> of  $pp$  collisions at  $\sqrt{s} = 13$  TeV in events with no charged leptons, jets and missing transverse momentum. The data are found to be consistent with the SM expectation. Results are interpreted in a Tglu1C-like model, assuming 50% BR for each gluino decay mode. Gluino masses below 1770 GeV are excluded for any  $m_{\tilde{\chi}_2^0} - m_{\tilde{\chi}_1^0}$  and  $m_{\tilde{\chi}_1^0} = 60$  GeV, see their Fig. 16(b).
- <sup>83</sup> AABOUD 17AZ searched in 36.1 fb<sup>-1</sup> of  $pp$  collisions at  $\sqrt{s} = 13$  TeV for events with at least seven jets and large missing transverse momentum. Selected events are further classified based on the presence of large  $R$ -jets or  $b$ -jets and no leptons. No significant excess above the Standard Model expectations is observed. Limits are set for pMSSM models with  $M_1 = 60$  GeV,  $\tan(\beta) = 10$ ,  $\mu < 0$  varying the soft-breaking parameters  $M_3$  and  $\mu$ . Gluino masses up to 1600 GeV are excluded for  $m_{\tilde{\chi}_1^\pm} = 200$  GeV. See their Figure 6a and text for details on the model.
- <sup>84</sup> KHACHATRYAN 16AY searched in 2.3 fb<sup>-1</sup> of  $pp$  collisions at  $\sqrt{s} = 13$  TeV for events with one isolated high transverse momentum lepton ( $e$  or  $\mu$ ), hadronic jets of which at least one is identified as coming from a  $b$ -quark, and large  $\cancel{E}_T$ . No significant excess above the Standard Model expectations is observed. Limits are set on the gluino mass in the Tglu3A simplified model, see Fig. 10, and in the Tglu3B model, see Fig. 11.
- <sup>85</sup> KHACHATRYAN 16BT performed a global Bayesian analysis of a wide range of CMS results obtained with data samples corresponding to 5.0 fb<sup>-1</sup> of  $pp$  collisions at  $\sqrt{s} = 7$  TeV and in 19.5 fb<sup>-1</sup> of  $pp$  collisions at  $\sqrt{s} = 8$  TeV. The set of searches considered, both individually and in combination, includes those with all-hadronic final states, same-sign and opposite-sign dileptons, and multi-lepton final states. An interpretation was given in a scan of the 19-parameter pMSSM. No scan points with a gluino mass less than 500 GeV survived and 98% of models with a squark mass less than 300 GeV were excluded.
- <sup>86</sup> AAD 15AB searched for the decay of neutral, weakly interacting, long-lived particles in 20.3 fb<sup>-1</sup> of  $pp$  collisions at  $\sqrt{s} = 8$  TeV. Signal events require at least two reconstructed vertices possibly originating from long-lived particles decaying to jets in the inner tracking detector and muon spectrometer. No significant excess of events over the expected background was found. Results were interpreted in Stealth SUSY benchmark models where a pair of gluinos decay to long-lived singlinos,  $S$ , which in turn each decay to a low-mass gravitino and a pair of jets. The 95% confidence-level limits are set on the cross section  $\times$  branching ratio for the decay  $\tilde{g} \rightarrow \tilde{S}g$ , as a function of the singlino proper lifetime ( $c\tau$ ). See their Fig. 10(f).
- <sup>87</sup> AAD 15AI searched in 20 fb<sup>-1</sup> of  $pp$  collisions at  $\sqrt{s} = 8$  TeV for events containing at least one isolated lepton (electron or muon), jets, and large missing transverse momentum. No excess of events above the expected level of Standard Model background was found. Exclusion limits at 95% C.L. are set on the gluino mass in the CMSSM/mSUGRA, see Fig. 15, in the NUHM2, see Fig. 16, and in various simplified models, see Figs. 18–22.
- <sup>88</sup> AAD 15CB searched for events containing at least one long-lived particle that decays at a significant distance from its production point (displaced vertex, DV) into two leptons or into five or more charged particles in 20.3 fb<sup>-1</sup> of  $pp$  collisions at  $\sqrt{s} = 8$  TeV. The dilepton signature is characterised by DV formed from at least two lepton candidates. Four different final states were considered for the multitrack signature, in which the DV must be accompanied by a high-transverse momentum muon or electron candidate that originates from the DV, jets or missing transverse momentum. No events were observed in any of the signal regions. Results were interpreted in SUSY scenarios involving  $R$ -parity violation, split supersymmetry, and gauge mediation. See their Fig. 12–20.
- <sup>89</sup> KHACHATRYAN 15AD searched in 19.4 fb<sup>-1</sup> of  $pp$  collisions at  $\sqrt{s} = 8$  TeV for events with two opposite-sign same flavor isolated leptons featuring either a kinematic edge, or a peak at the  $Z$ -boson mass, in the invariant mass spectrum. No evidence for a statistically significant excess over the expected SM backgrounds is observed and 95% C.L. exclusion limits are derived in a simplified model of gluino pair production where the gluino decays into quarks, a  $Z$ -boson, and a massless gravitino LSP, see Fig. 9.
- <sup>90</sup> KHACHATRYAN 15AZ searched in 19.7 fb<sup>-1</sup> of  $pp$  collisions at  $\sqrt{s} = 8$  TeV for events with either at least one photon, hadronic jets and  $\cancel{E}_T$  (single photon channel) or with at least two photons and at least one jet and using the razor variables. No significant excess above the Standard Model expectations is observed. Limits are set on gluino masses in the general gauge-mediated SUSY breaking model (GGM), for both a bino-like and wino-like neutralino NLSP scenario, see Fig. 8 and 9.
- <sup>91</sup> AAD 14AX searched in 20.1 fb<sup>-1</sup> of  $pp$  collisions at  $\sqrt{s} = 8$  TeV for the strong production of supersymmetric particles in events containing either zero or at least one high- $p_T$  lepton, large missing transverse momentum, high jet multiplicity and at least three jets identified as originating from  $b$ -quarks. No excess over the expected SM background is observed. Limits are derived in mSUGRA/CMSSM models with  $\tan\beta = 30$ ,  $A_0 = -2m_0$  and  $\mu > 0$ , see their Fig. 14. Also, exclusion limits in simplified models containing gluinos and scalar top and bottom quarks are set, see their Figures 12, 13.
- <sup>92</sup> AAD 14E searched in 20.3 fb<sup>-1</sup> of  $pp$  collisions at  $\sqrt{s} = 8$  TeV for strongly produced supersymmetric particles in events containing jets and two same-sign leptons or three leptons. The search also utilises jets originating from  $b$ -quarks, missing transverse momentum and other variables. No excess over the expected SM background is observed. Exclusion limits are derived in simplified models containing gluinos and squarks, see Figs. 5 and 6. In the  $\tilde{g} \rightarrow q\bar{q}\tilde{\chi}_1^\pm, \tilde{\chi}_1^\pm \rightarrow W^{(*)}\tilde{\chi}_2^0, \tilde{\chi}_2^0 \rightarrow Z^{(*)}\tilde{\chi}_1^0$  simplified model, the following assumptions have been made:  $m_{\tilde{\chi}_1^\pm} = 0.5 m_{\tilde{\chi}_1^0} + m_{\tilde{g}}$ ,  $m_{\tilde{\chi}_2^0} = 0.5 (m_{\tilde{\chi}_1^0} + m_{\tilde{\chi}_1^\pm})$ ,  $m_{\tilde{\chi}_1^0} < 520$  GeV. In the  $\tilde{g} \rightarrow q\bar{q}\tilde{\chi}_1^\pm, \tilde{\chi}_1^\pm \rightarrow \ell^\pm\nu\tilde{\chi}_1^0$  or  $\tilde{g} \rightarrow q\bar{q}\tilde{\chi}_2^0, \tilde{\chi}_2^0 \rightarrow \ell^\pm\ell^\mp(\nu\nu)\tilde{\chi}_1^0$  simplified model, the following assumptions have been made:  $m_{\tilde{\chi}_1^\pm} = m_{\tilde{\chi}_2^0} = 0.5 (m_{\tilde{\chi}_1^0} + m_{\tilde{g}})$ ,  $m_{\tilde{\chi}_1^0} < 660$  GeV. Limits are also derived in the mSUGRA/CMSSM, bRPV and GMSB models, see their Fig. 8.
- <sup>93</sup> CHATRCHYAN 14H searched in 19.5 fb<sup>-1</sup> of  $pp$  collisions at  $\sqrt{s} = 8$  TeV for events with two isolated same-sign dileptons and jets in the final state. No significant excess above the Standard Model expectations is observed. Limits are set on the gluino mass in simplified models where the decay  $\tilde{g} \rightarrow t\bar{t}\tilde{\chi}_1^0$  takes place with a branching ratio of 100%, or where the decay  $\tilde{g} \rightarrow \tilde{t}t, \tilde{t} \rightarrow t\tilde{\chi}_1^0$  takes place with a branching ratio of 100%, with varying mass of the  $\tilde{\chi}_1^0$ , or where the decay  $\tilde{g} \rightarrow b\bar{b}, \tilde{b} \rightarrow t\tilde{\chi}_1^\pm, \tilde{\chi}_1^\pm \rightarrow W^\pm\tilde{\chi}_1^0$  takes place with a branching ratio of 100%, with varying mass of the  $\tilde{\chi}_1^\pm$ , see Fig. 5.
- <sup>94</sup> CHATRCHYAN 14H searched in 19.5 fb<sup>-1</sup> of  $pp$  collisions at  $\sqrt{s} = 8$  TeV for events with two isolated same-sign dileptons and jets in the final state. No significant excess above the Standard Model expectations is observed. Limits are set on the gluino mass in simplified models where the decay  $\tilde{g} \rightarrow q\bar{q}\tilde{\chi}_1^\pm, \tilde{\chi}_1^\pm \rightarrow W^\pm\tilde{\chi}_1^0$  takes place with a branching ratio of 100%, with varying mass of the  $\tilde{\chi}_1^\pm$  and  $\tilde{\chi}_1^0$ , see Fig. 7.
- <sup>95</sup> CHATRCHYAN 14H searched in 19.5 fb<sup>-1</sup> of  $pp$  collisions at  $\sqrt{s} = 8$  TeV for events with two isolated same-sign dileptons and jets in the final state. No significant excess above the Standard Model expectations is observed. Limits are set on the gluino mass in simplified models where the decay  $\tilde{g} \rightarrow b\bar{b}\tilde{\chi}_1^\pm, \tilde{\chi}_1^\pm \rightarrow W^\pm\tilde{\chi}_1^0$  takes place with a branching ratio of 100%, for two choices of  $m_{\tilde{\chi}_1^\pm}$  and fixed  $m_{\tilde{\chi}_1^0}$ , see Fig. 6.

R-parity violating heavy  $\tilde{g}$  (Gluino) mass limit

VALUE (GeV)	CL%	DOCUMENT ID	TECN	COMMENT
>1500	95	1 SIRUNYAN	19F CMS	$\tilde{g} \rightarrow jjj$
>2260	95	2 AABOUD	18Z ATLS	$\geq 4\ell, \lambda_{12k} \neq 0, m_{\tilde{\chi}_1^0} > 1000$ GeV
>1650	95	2 AABOUD	18Z ATLS	$\geq 4\ell, \lambda_{133} \neq 0, m_{\tilde{\chi}_1^0} > 500$ GeV
>1610	95	3 SIRUNYAN	18AK CMS	$\tilde{g} \rightarrow tbs, \lambda''_{332}$ coupling
>1690	95	4 SIRUNYAN	18D CMS	top quark (hadronically decaying) + jets + $\cancel{E}_T$ , Tglu3C, $m_{\tilde{t}_1} - m_{\tilde{\chi}_1^0} = 20$ GeV, $m_{\tilde{\chi}_1^0} = 0$ GeV

# Searches Particle Listings

## Supersymmetric Particle Searches

Search ID	Year	Author(s)	Experiment	Search Description	Mass Range (GeV)	Significance (%)	Model	Search Description
none 100-1410	95	5 SIRUNYAN	18EA CMS	2 large jets with four-parton substructure, $\tilde{g} \rightarrow 5q$	> 600	95	23 AAD	15CB ATLS $\ell\ell/Z, \tilde{g} \rightarrow (e\bar{e}/\mu\bar{\mu}/e\bar{\nu})qq, m_{\tilde{\chi}_1^0} = 400 \text{ GeV}$ and $0.7 <$
>2100	95	6 AABOUD	17AI ATLS	$\geq 1\ell+$ $\geq 8$ jets, Tglu3A and $\tilde{\chi}_1^0 \rightarrow uds, \lambda''_{112}$ coupling, $m_{\tilde{\chi}_1^0}=1000 \text{ GeV}$	>1000	95	24 AAD	15X ATLS $\geq 10$ jets, $\tilde{g} \rightarrow q\bar{q}\tilde{\chi}_1^0, \tilde{\chi}_1^0 \rightarrow qq\bar{q}, m_{\tilde{\chi}_1^0}=500 \text{ GeV}$
>1650	95	7 AABOUD	17AI ATLS	$\geq 1\ell+$ $\geq 8$ jets, $\tilde{g} \rightarrow t\bar{t}, \tilde{t} \rightarrow b\bar{s}, \lambda''_{323}$ coupling, $m_{\tilde{t}}=1000 \text{ GeV}$	> 917	95	24 AAD	15X ATLS $\geq 6,7$ jets, $\tilde{g} \rightarrow qq\bar{q}$ , (light-quark, $\lambda'$ couplings)
>1800	95	8 AABOUD	17AI ATLS	$\geq 1\ell+$ $\geq 8$ jets, Tglu1A and $\tilde{\chi}_1^0 \rightarrow qq\ell, \lambda'$ coupling, $m_{\tilde{\chi}_1^0}=1000 \text{ GeV}$	> 929	95	24 AAD	15X ATLS $\geq 6,7$ jets, $\tilde{g} \rightarrow qq\bar{q}$ , (b-quark, $\lambda''$ couplings)
>1800	95	9 AABOUD	17AJ ATLS	same-sign $\ell^\pm\ell^\pm / 3\ell + \text{jets} + \cancel{E}_T$ , Tglu3A, $\lambda''_{112}$ coupling, $m_{\tilde{\chi}_1^0} = 50 \text{ GeV}$	>1180	95	25 AAD	14AX ATLS $\geq 3$ b-jets + $\cancel{E}_T, \tilde{g} \rightarrow \tilde{t}_1 t \tilde{\chi}_1^0$ simplified model, $\tilde{t}_1 \rightarrow b\tilde{\chi}_1^\pm, m_{\tilde{\chi}_1^\pm}=2m_{\tilde{\chi}_1^0}, m_{\tilde{\chi}_1^0}=60 \text{ GeV}, m_{\tilde{t}_1} < 1000 \text{ GeV}$
>1750	95	10 AABOUD	17AJ ATLS	same-sign $\ell^\pm\ell^\pm / 3\ell + \text{jets} + \cancel{E}_T$ , Tglu1A and $\tilde{\chi}_1^0 \rightarrow qq\ell, \lambda'$ coupling	> 850	95	26 AAD	14E ATLS $\ell^\pm\ell^\pm(\ell\bar{\nu}) + \text{jets}, \tilde{g} \rightarrow t\tilde{t}_1$ with $\tilde{t}_1 \rightarrow b\bar{s}$ simplified model
>1450	95	11 AABOUD	17AJ ATLS	same-sign $\ell^\pm\ell^\pm / 3\ell + \text{jets} + \cancel{E}_T, \tilde{g} \rightarrow t\tilde{t}_1$ and $\tilde{t}_1 \rightarrow sd, \lambda''_{321}$ coupling	> 900	95	27 CHATRCHYAN14H	CMS same-sign $\ell^\pm\ell^\pm, \tilde{g} \rightarrow tbs$ simplified model
>1450	95	12 AABOUD	17AJ ATLS	same-sign $\ell^\pm\ell^\pm / 3\ell + \text{jets} + \cancel{E}_T, \tilde{g} \rightarrow t\tilde{t}_1$ and $\tilde{t}_1 \rightarrow bd, \lambda''_{313}$ coupling				
> 400	95	13 AABOUD	17AJ ATLS	same-sign $\ell^\pm\ell^\pm / 3\ell + \text{jets} + \cancel{E}_T, \tilde{d}_R \rightarrow tb(t\bar{s}), \lambda''_{313}(\lambda''_{321})$ coupling				
none 625-1375	95	14 AABOUD	17AZ ATLS	$\geq 7$ jets + $\cancel{E}_T$ , large R-jets and/or b-jets, $\tilde{g} \rightarrow t\tilde{t}_1$ and $\tilde{t}_1 \rightarrow b\bar{s}, \lambda''_{323}$ coupling				
none 600-650	95	15 KHACHATRY...17Y	CMS	$\tilde{g} \rightarrow qq\bar{q}\bar{q}, \lambda''_{212}$ coupling, $m_{\tilde{q}} = 100 \text{ GeV}$				
none 600-1030	95	15 KHACHATRY...17Y	CMS	$\tilde{g} \rightarrow qq\bar{q}\bar{q}, \lambda''_{212}$ coupling, $m_{\tilde{q}} = 900 \text{ GeV}$				
none 600-650	95	15 KHACHATRY...17Y	CMS	$\tilde{g} \rightarrow qq\bar{q}b, \lambda''_{213}$ coupling, $m_{\tilde{q}} = 100 \text{ GeV}$				
none 600-1080	95	15 KHACHATRY...17Y	CMS	$\tilde{g} \rightarrow qq\bar{q}b, \lambda''_{213}$ coupling, $m_{\tilde{q}} = 900 \text{ GeV}$				
none 600-680	95	15 KHACHATRY...17Y	CMS	$\tilde{g} \rightarrow qq\bar{q}bb, \lambda''_{212}$ coupling, $m_{\tilde{q}} = 100 \text{ GeV}$				
none 600-1080	95	15 KHACHATRY...17Y	CMS	$\tilde{g} \rightarrow qq\bar{q}bb, \lambda''_{212}$ coupling, $m_{\tilde{q}} = 900 \text{ GeV}$				
none 600-650	95	15 KHACHATRY...17Y	CMS	$\tilde{g} \rightarrow qq\bar{q}bb, \lambda''_{213}$ coupling, $m_{\tilde{q}} = 100 \text{ GeV}$				
none 600-1100	95	15 KHACHATRY...17Y	CMS	$\tilde{g} \rightarrow qq\bar{q}bb, \lambda''_{213}$ coupling, $m_{\tilde{q}} = 900 \text{ GeV}$				
>1050	95	16 KHACHATRY...16BJ	CMS	same-sign $\ell^\pm\ell^\pm, \text{Tglu3A}, m_{\tilde{\chi}_1^0} < 800 \text{ GeV}$				
>1140	95	16 KHACHATRY...16BJ	CMS	same-sign $\ell^\pm\ell^\pm, \text{Tglu3B}, m_{\tilde{t}} - m_{\tilde{\chi}_1^0} = 20 \text{ GeV}, m_{\tilde{\chi}_1^0} = 0$				
>1030	95	17 KHACHATRY...16BX	CMS	$\tilde{g} \rightarrow tbs, \lambda''_{332}$ coupling				
>1150	95	18 AAD	15BV ATLS	general RPC $\tilde{g}$ decays, $m_{\tilde{\chi}_1^0} < 100 \text{ GeV}$				
>1350	95	19 AAD	14X ATLS	$\geq 4\ell^\pm, \tilde{g} \rightarrow q\bar{q}\tilde{\chi}_1^0, \tilde{\chi}_1^0 \rightarrow \ell^\pm\ell\bar{\nu}$				
> 650	95	20 CHATRCHYAN14P	CMS	$\tilde{g} \rightarrow jjj$				
none 200-835	95	20 CHATRCHYAN14P	CMS	$\tilde{g} \rightarrow bjj$				
••• We do not use the following data for averages, fits, limits, etc. •••								
>1875	95	21 AABOUD	18CF ATLS	jets and large R-jets, Tglu2RPV and $\tilde{\chi}_1^0 \rightarrow qq\bar{q}, \lambda''$ coupling, $m_{\tilde{\chi}_1^0}=1000 \text{ GeV}$				
>1400	95	22 KHACHATRY...16BX	CMS	$\tilde{g} \rightarrow qq\tilde{\chi}_1^0, \tilde{\chi}_1^0 \rightarrow \ell\ell\nu, \lambda_{121}$ or $\lambda_{122} \neq 0, m_{\tilde{\chi}_1^0} > 400 \text{ GeV}$				
>1600	95	18 AAD	15BV ATLS	pMSSM, $M_1 = 60 \text{ GeV}, m_{\tilde{q}} < 1500 \text{ GeV}$				
>1280	95	18 AAD	15BV ATLS	mSUGRA, $m_0 > 2 \text{ TeV}$				
>1100	95	18 AAD	15BV ATLS	via $\tilde{\tau}$ , natural GMSB, all $m_{\tilde{\tau}}$				
>1220	95	18 AAD	15BV ATLS	b-jets, $\tilde{g} \rightarrow \tilde{t}_1 t$ and $\tilde{t}_1 \rightarrow t\tilde{\chi}_1^0, m_{\tilde{t}_1} < 1000 \text{ GeV}$				
>1180	95	18 AAD	15BV ATLS	b-jets, $\tilde{g} \rightarrow \tilde{t}_1 t$ and $\tilde{t}_1 \rightarrow b\tilde{\chi}_1^\pm, m_{\tilde{t}_1} < 1000 \text{ GeV}, m_{\tilde{\chi}_1^0} = 60 \text{ GeV}$				
> 880	95	18 AAD	15BV ATLS	jets, $\tilde{g} \rightarrow \tilde{t}_1 t$ and $\tilde{t}_1 \rightarrow sb, 400 < m_{\tilde{t}_1} < 1000 \text{ GeV}$				
		23 AAD	15CB ATLS	$\ell, \tilde{g} \rightarrow (e/\mu)qq$ , benchmark gluino, neutralino masses				

Downloaded from https://academic.oup.com/ptep/article/2020/8/083C01/5891211 by guest on 12 November 2020

1 SIRUNYAN 19F searched in  $35.9 \text{ fb}^{-1}$  of  $pp$  collisions at  $\sqrt{s} = 13 \text{ TeV}$  for three-jet resonances produced in the decay of a gluino in R-parity violating supersymmetric models. The mass range from 200 to 2000GeV is explored in four separate mass regions. The observations show agreement with standard model expectations. The results are interpreted within the framework of R-parity violating SUSY, where pair-produced gluinos decay to a six quark final state. Gluino masses below 1500GeV are excluded at 95% C.L. See their Fig.5.

2 AABOUD 18Z searched in  $36.1 \text{ fb}^{-1}$  of  $pp$  collisions at  $\sqrt{s} = 13 \text{ TeV}$  for events containing four or more charged leptons (electrons, muons and up to two hadronically decaying taus). No significant deviation from the expected SM background is observed. Limits are set on the Higgsino mass in simplified models of general gauge mediated supersymmetry Tn1n1A/Tn1n1B/Tn1n1C, see their Figure 9. Limits are also set on the wino, slepton, sneutrino and gluino mass in a simplified model of NLSP pair production with R-parity violating decays of the LSP via  $\lambda_{12k}$  or  $\lambda_{j33}$  to charged leptons, see their Figures 7, 8.

3 SIRUNYAN 18AK searched in  $35.9 \text{ fb}^{-1}$  of  $pp$  collisions at  $\sqrt{s} = 13 \text{ TeV}$  for events containing a single lepton, large jet and b-quark jet multiplicities, coming from R-parity-violating decays of gluinos. No excess over the expected background is observed. Limits are derived on the gluino mass, assuming the RPV  $\tilde{g} \rightarrow t\bar{s}$  decay, see their Figure 9.

4 SIRUNYAN 18D searched in  $35.9 \text{ fb}^{-1}$  of  $pp$  collisions at  $\sqrt{s} = 13 \text{ TeV}$  for events containing identified hadronically decaying top quarks, no leptons, and  $\cancel{E}_T$ . No significant excess above the Standard Model expectations is observed. Limits are set on the stop mass in the Tstop1 simplified model, see their Figure 8, and on the gluino mass in the Tglu3A, Tglu3B, Tglu3C and Tglu3E simplified models, see their Figure 9.

5 SIRUNYAN 18EA searched in  $38.2 \text{ fb}^{-1}$  of  $pp$  collisions at  $\sqrt{s} = 13 \text{ TeV}$  for the pair production of resonances, each decaying to at least four quarks. Reconstructed particles are clustered into two large jets of similar mass, each consistent with four-parton substructure. No statistically significant excess over the Standard Model expectation is observed. Limits are set on the squark and gluino mass in RPV supersymmetry models where squarks (gluinos) decay, through intermediate higgsinos, to four (five) quarks, see their Figure 4.

6 AABOUD 17AI searched in  $36.1 \text{ fb}^{-1}$  of  $pp$  collisions at  $\sqrt{s} = 13 \text{ TeV}$  for events with one or more isolated lepton, at least eight jets, either zero or many b-jets, for evidence of R-parity violating decays of the gluino. No significant excess above the Standard Model expectations is observed. Limits up to 2.1 TeV are set on the gluino mass in R-parity-violating supersymmetry models as Tglu3A with LSP decay through the non-zero  $\lambda''_{112}$  coupling as  $\tilde{\chi}_1^0 \rightarrow uds$ . See their Figure 9.

7 AABOUD 17AI searched in  $36.1 \text{ fb}^{-1}$  of  $pp$  collisions at  $\sqrt{s} = 13 \text{ TeV}$  for events with one or more isolated lepton, at least eight jets, either zero or many b-jets, for evidence of R-parity violating decays of the gluino. No significant excess above the Standard Model expectations is observed. Limits up to 1.65 TeV are set on the gluino mass in R-parity-violating supersymmetry models with  $\tilde{g} \rightarrow t\bar{t}, \tilde{t} \rightarrow b\bar{s}$  through the non-zero  $\lambda''_{323}$  coupling. See their Figure 9.

8 AABOUD 17AI searched in  $36.1 \text{ fb}^{-1}$  of  $pp$  collisions at  $\sqrt{s} = 13 \text{ TeV}$  for events with one or more isolated lepton, at least eight jets, either zero or many b-jets, for evidence of R-parity violating decays of the gluino. No significant excess above the Standard Model expectations is observed. Limits up to 1.8 TeV are set on the gluino mass in R-parity-violating supersymmetry models as Tglu1A with the LSP decay through the non-zero  $\lambda'$  coupling as  $\tilde{\chi}_1^0 \rightarrow qq\ell$ . See their Figure 9.

9 AABOUD 17AJ searched in  $36.1 \text{ fb}^{-1}$  of  $pp$  collisions at  $\sqrt{s} = 13 \text{ TeV}$  for events with two same-sign or three leptons, jets and large missing transverse momentum. No significant excess above the Standard Model expectations is observed. Limits up to 1.8 TeV are set on the gluino mass in R-parity-violating supersymmetry models as Tglu3A with LSP decay through the non-zero  $\lambda''_{112}$  coupling as  $\tilde{\chi}_1^0 \rightarrow uds$ . See their Figure 5(d).

10 AABOUD 17AJ searched in  $36.1 \text{ fb}^{-1}$  of  $pp$  collisions at  $\sqrt{s} = 13 \text{ TeV}$  for events with two same-sign or three leptons, jets and large missing transverse momentum. No significant excess above the Standard Model expectations is observed. Limits up to 1.75 TeV are set on the gluino mass in R-parity-violating supersymmetry models as Tglu1A with LSP decay through the non-zero  $\lambda'$  coupling as  $\tilde{\chi}_1^0 \rightarrow qq\ell$ . See their Figure 5(c).

11 AABOUD 17AJ searched in  $36.1 \text{ fb}^{-1}$  of  $pp$  collisions at  $\sqrt{s} = 13 \text{ TeV}$  for events with two same-sign or three leptons, jets and large missing transverse momentum. No significant excess above the Standard Model expectations is observed. Limits up to 1.45 TeV are set on the gluino mass in R-parity-violating supersymmetry models where  $\tilde{g} \rightarrow t\tilde{t}_1$  and  $\tilde{t}_1 \rightarrow sd$  through the non-zero  $\lambda''_{321}$  coupling. See their Figure 5(b).

12 AABOUD 17AJ searched in  $36.1 \text{ fb}^{-1}$  of  $pp$  collisions at  $\sqrt{s} = 13 \text{ TeV}$  for events with two same-sign or three leptons, jets and large missing transverse momentum. No significant excess above the Standard Model expectations is observed. Limits up to 1.45 TeV are set on the gluino mass in R-parity-violating supersymmetry models where  $\tilde{g} \rightarrow t\tilde{t}_1$  and  $\tilde{t}_1 \rightarrow bd$  through the non-zero  $\lambda''_{313}$  coupling. See their Figure 5(a).

13 AABOUD 17AJ searched in  $36.1 \text{ fb}^{-1}$  of  $pp$  collisions at  $\sqrt{s} = 13 \text{ TeV}$  for events with two same-sign or three leptons, jets and large missing transverse momentum. No significant

- excess above the Standard Model expectations is observed. Limits up to 400 GeV are set on the down type squark ( $\tilde{d}_R$  mass in R-parity-violating supersymmetry models where  $\tilde{d}_R \rightarrow tb$  through the non-zero  $\lambda''_{313}$  coupling or  $\tilde{d}_R \rightarrow ts$  through the non-zero  $\lambda''_{321}$ . See their Figure 5(e) and 5(f).
- 14 AABOUD 17AZ searched in  $36.1 \text{ fb}^{-1}$  of  $pp$  collisions at  $\sqrt{s} = 13 \text{ TeV}$  for events with at least seven jets and large missing transverse momentum. Selected events are further classified based on the presence of large R-jets or  $b$ -jets and no leptons. No significant excess above the Standard Model expectations is observed. Limits are set for R-parity violating decays of the gluino assuming  $\tilde{g} \rightarrow t\bar{t}_1$  and  $\tilde{t}_1 \rightarrow bs$  through the non-zero  $\lambda''_{323}$  couplings. The range 625–1375 GeV is excluded for  $m_{\tilde{t}_1} = 400 \text{ GeV}$ . See their Figure 7b.
- 15 KHACHATRYAN 17Y searched in  $19.7 \text{ fb}^{-1}$  of  $pp$  collisions at  $\sqrt{s} = 8 \text{ TeV}$  for events containing at least 8 or 10 jets, possibly  $b$ -tagged, coming from R-parity-violating decays of supersymmetric particles. No excess over the expected background is observed. Limits are derived on the gluino mass, assuming various RPV decay modes, see Fig. 7.
- 16 KHACHATRYAN 16BJ searched in  $2.3 \text{ fb}^{-1}$  of  $pp$  collisions at  $\sqrt{s} = 13 \text{ TeV}$  for events with two isolated same-sign dileptons and jets in the final state. No significant excess above the Standard Model expectations is observed. Limits are set on the gluino mass in the following simplified models: Tglu3A and Tglu3D, see Fig. 4, Tglu3B and Tglu3C, see Fig. 5, and Tglu1B, see Fig. 7.
- 17 KHACHATRYAN 16BX searched in  $19.5 \text{ fb}^{-1}$  of  $pp$  collisions at  $\sqrt{s} = 8 \text{ TeV}$  for events containing 0 or 1 leptons and  $b$ -tagged jets, coming from R-parity-violating decays of supersymmetric particles. No excess over the expected background is observed. Limits are derived on the gluino mass, assuming the RPV  $\tilde{g} \rightarrow tbs$  decay, see Fig. 7 and 10.
- 18 AAD 15BV summarized and extended ATLAS searches for gluinos and first- and second-generation squarks in final states containing jets and missing transverse momentum, with or without leptons or  $b$ -jets in the  $\sqrt{s} = 8 \text{ TeV}$  data set collected in 2012. The paper reports the results of new interpretations and statistical combinations of previously published analyses, as well as new analyses. Exclusion limits at 95% C.L. are set on the gluino mass in several R-parity conserving models, leading to a generalized constraint on gluino masses exceeding 1150 GeV for lightest supersymmetric particle masses below 100 GeV. See their Figs. 10, 19, 20, 21, 23, 25, 26, 29–37.
- 19 AAD 14X searched in  $20.3 \text{ fb}^{-1}$  of  $pp$  collisions at  $\sqrt{s} = 8 \text{ TeV}$  for events with at least four leptons (electrons, muons, taus) in the final state. No significant excess above the Standard Model expectations is observed. Limits are set on the gluino mass in an R-parity violating simplified model where the decay  $\tilde{g} \rightarrow q\bar{q}\tilde{\chi}_1^0$ , with  $\tilde{\chi}_1^0 \rightarrow \ell^\pm \ell^\mp \nu$ , takes place with a branching ratio of 100%, see Fig. 8.
- 20 CHATRCHYAN 14P searched in  $19.4 \text{ fb}^{-1}$  of  $pp$  collisions at  $\sqrt{s} = 8 \text{ TeV}$  for three-jet resonances produced in the decay of a gluino in R-parity violating supersymmetric models. No excess over the expected SM background is observed. Assuming a 100% branching ratio for the gluino decay into three light-flavour jets, limits are set on the cross section of gluino pair production, see Fig. 7, and gluino masses below 650 GeV are excluded at 95% C.L. Assuming a 100% branching ratio for the gluino decaying to one  $b$ -quark jet and two light-flavour jets, gluino masses between 200 GeV and 835 GeV are excluded at 95% C.L.
- 21 AABOUD 18cf searched in  $36.1 \text{ fb}^{-1}$  of  $pp$  collisions at  $\sqrt{s} = 13 \text{ TeV}$  for events with several jets, possibly  $b$ -jets, and large-radius jets for evidence of R-parity violating decays of the gluino. No significant excess above the Standard Model expectations is observed. Limits between 1000 and 1875 GeV are set on the gluino mass in R-parity-violating supersymmetry models as Tglu2RPV with the LSP decay through the non-zero  $\lambda''$  coupling as  $\tilde{\chi}_1^0 \rightarrow qq\bar{q}$ . The most stringent limit is obtained for  $m_{\tilde{\chi}_1^0} = 1000 \text{ GeV}$ , the weakest for  $m_{\tilde{\chi}_1^0} = 50 \text{ GeV}$ . See their Figure 7(b). Figure 7(a) presents results for gluinos directly decaying into 3 quarks, Tglu1RPV.
- 22 KHACHATRYAN 16BX searched in  $19.5 \text{ fb}^{-1}$  of  $pp$  collisions at  $\sqrt{s} = 8 \text{ TeV}$  for events containing 4 leptons coming from R-parity-violating decays of  $\tilde{\chi}_1^0 \rightarrow \ell\ell\nu$  with  $\lambda_{121} \neq 0$  or  $\lambda_{122} \neq 0$ . No excess over the expected background is observed. Limits are derived on the gluino, squark and stop masses, see Fig. 23.
- 23 AAD 15CB searched for events containing at least one long-lived particle that decays at a significant distance from its production point (displaced vertex, DV) into two leptons or into five or more charged particles in  $20.3 \text{ fb}^{-1}$  of  $pp$  collisions at  $\sqrt{s} = 8 \text{ TeV}$ . The dilepton signature is characterised by DV formed from at least two lepton candidates. Four different final states were considered for the multitrak signature, in which the DV must be accompanied by a high-transverse momentum muon or electron candidate that originates from the DV, jets or missing transverse momentum. No events were observed in any of the signal regions. Results were interpreted in SUSY scenarios involving R-parity violation, split supersymmetry, and gauge mediation. See their Fig. 12–20.
- 24 AAD 15X searched in  $20.3 \text{ fb}^{-1}$  of  $pp$  collisions at  $\sqrt{s} = 8 \text{ TeV}$  for events containing large number of jets, no requirements on missing transverse momentum and no isolated electrons or muons. The sensitivity of the search is enhanced by considering the number of  $b$ -tagged jets and the scalar sum of masses of large-radius jets in an event. No evidence was found for excesses above the expected level of Standard Model background. Exclusion limits at 95% C.L. are set on the gluino mass assuming the gluino decays to various quark flavors, and for various neutralino masses. See their Fig. 11–16.
- 25 AAD 14AX searched in  $20.1 \text{ fb}^{-1}$  of  $pp$  collisions at  $\sqrt{s} = 8 \text{ TeV}$  for the strong production of supersymmetric particles in events containing either zero or at last one high- $p_T$  lepton, large missing transverse momentum, high jet multiplicity and at least three jets identified as originating from  $b$ -quarks. No excess over the expected SM background is observed. Limits are derived in mSUGRA/CMSSM models with  $\tan\beta = 30$ ,  $A_0 = -2m_0$  and  $\mu > 0$ , see their Fig. 14. Also, exclusion limits in simplified models containing gluinos and scalar top and bottom quarks are set, see their Figures 12, 13.
- 26 AAD 14E searched in  $20.3 \text{ fb}^{-1}$  of  $pp$  collisions at  $\sqrt{s} = 8 \text{ TeV}$  for strongly produced supersymmetric particles in events containing jets and two same-sign leptons or three leptons. The search also utilises jets originating from  $b$ -quarks, missing transverse momentum and other variables. No excess over the expected SM background is observed. Exclusion limits are derived in simplified models containing gluinos and squarks, see Figures 5 and 6. In the  $\tilde{g} \rightarrow q\bar{q}\tilde{\chi}_1^\pm, \tilde{\chi}_1^\pm \rightarrow W^{(*)}\tilde{\chi}_2^0, \tilde{\chi}_2^0 \rightarrow Z^{(*)}\tilde{\chi}_1^0$  simplified model, the following assumptions have been made:  $m_{\tilde{\chi}_1^\pm} = 0.5 m_{\tilde{\chi}_2^0} + m_{\tilde{g}}$ ,  $m_{\tilde{\chi}_2^0} = 0.5 (m_{\tilde{\chi}_1^0} + m_{\tilde{\chi}_1^\pm})$ ,  $m_{\tilde{\chi}_1^0} < 520 \text{ GeV}$ . In the  $\tilde{g} \rightarrow q\bar{q}\tilde{\chi}_1^\pm, \tilde{\chi}_1^\pm \rightarrow \ell^\pm\nu\tilde{\chi}_1^0$  or  $\tilde{g} \rightarrow q\bar{q}\tilde{\chi}_2^0, \tilde{\chi}_2^0 \rightarrow \ell^\pm\ell^\mp(\nu\nu)\tilde{\chi}_1^0$  simplified model, the following assumptions have been made:  $m_{\tilde{\chi}_1^\pm} = m_{\tilde{\chi}_2^0} = 0.5 (m_{\tilde{\chi}_1^0} + m_{\tilde{g}})$ ,  $m_{\tilde{\chi}_1^0} < 660 \text{ GeV}$ . Limits are also derived in the mSUGRA/CMSSM, bRPV and GMSB models, see their Fig. 8.

27 CHATRCHYAN 14H searched in  $19.5 \text{ fb}^{-1}$  of  $pp$  collisions at  $\sqrt{s} = 8 \text{ TeV}$  for events with two isolated same-sign dileptons and jets in the final state. No significant excess above the Standard Model expectations is observed. Limits are set on the gluino mass in simplified models where the R-parity violating decay  $\tilde{g} \rightarrow tbs$  takes place with a branching ratio of 100%, see Fig. 8.

Long-lived  $\tilde{g}$  (Gluino) mass limit

Limits on light gluinos ( $m_{\tilde{g}} < 5 \text{ GeV}$ ) were last listed in our PDG 14 edition: K. Olive, et al. (Particle Data Group), Chinese Physics C38 070001 (2014) (<http://pdg.lbl.gov>).

VALUE (GeV)	CL%	DOCUMENT ID	TECN	COMMENT
>1980	95	1 AABOUD	19AT ATLS	R-hadrons, Tglu1A, metastable
>2060	95	2 AABOUD	19C ATLS	R-hadrons, Tglu1A, $\tau > 10 \text{ ns}$ , $m_{\tilde{\chi}_1^0} = 100 \text{ GeV}$
>1890	95	2 AABOUD	19C ATLS	R-hadrons, Tglu1A, stable
>2400	95	3 SIRUNYAN	19BH CMS	long-lived $\tilde{g}$ , RPV, $\tilde{g} \rightarrow \bar{t}\bar{b}\bar{s}$ , $10 \text{ mm} < cr < 250 \text{ mm}$
>2300	95	3 SIRUNYAN	19BH CMS	long-lived $\tilde{g}$ , GMSB, $\tilde{g} \rightarrow g\bar{G}$ , $20 \text{ mm} < cr < 110 \text{ mm}$
>2100	95	4 SIRUNYAN	19BT CMS	long-lived $\tilde{g}$ , GMSB, $\tilde{g} \rightarrow g\bar{G}$ , $0.3 \text{ m} < cr < 30 \text{ m}$
>2500	95	4 SIRUNYAN	19BT CMS	long-lived $\tilde{g}$ , GMSB, $\tilde{g} \rightarrow g\bar{G}$ , $cr = 1 \text{ m}$
>1900	95	4 SIRUNYAN	19BT CMS	long-lived $\tilde{g}$ , GMSB, $\tilde{g} \rightarrow g\bar{G}$ , $cr = 100 \text{ m}$
>2370	95	5 AABOUD	18s ATLS	displaced vertex + $E_{\text{TR}}$ , long-lived Tglu1A, $m_{\tilde{\chi}_1^0} = 100 \text{ GeV}$ , and $\tau = 0.17 \text{ ns}$
>1600	95	6 SIRUNYAN	18AY CMS	jets + $E_{\text{TR}}$ , Tglu1A, $cr < 0.1 \text{ mm}$ , $m_{\tilde{\chi}_1^0} = 100 \text{ GeV}$
>1750	95	6 SIRUNYAN	18AY CMS	jets + $E_{\text{TR}}$ , Tglu1A, $cr = 1 \text{ mm}$ , $m_{\tilde{\chi}_1^0} = 100 \text{ GeV}$
>1640	95	6 SIRUNYAN	18AY CMS	jets + $E_{\text{TR}}$ , Tglu1A, $cr = 10 \text{ mm}$ , $m_{\tilde{\chi}_1^0} = 100 \text{ GeV}$
>1490	95	6 SIRUNYAN	18AY CMS	jets + $E_{\text{TR}}$ , Tglu1A, $cr = 100 \text{ mm}$ , $m_{\tilde{\chi}_1^0} = 100 \text{ GeV}$
>1300	95	6 SIRUNYAN	18AY CMS	jets + $E_{\text{TR}}$ , Tglu1A, $cr = 1 \text{ m}$ , $m_{\tilde{\chi}_1^0} = 100 \text{ GeV}$
> 960	95	6 SIRUNYAN	18AY CMS	jets + $E_{\text{TR}}$ , Tglu1A, $cr = 10 \text{ m}$ , $m_{\tilde{\chi}_1^0} = 100 \text{ GeV}$
> 900	95	6 SIRUNYAN	18AY CMS	jets + $E_{\text{TR}}$ , Tglu1A, $cr = 100 \text{ m}$ , $m_{\tilde{\chi}_1^0} = 100 \text{ GeV}$
>2200	95	7 SIRUNYAN	18DV CMS	long-lived $\tilde{g}$ , RPV, $\tilde{g} \rightarrow \bar{t}\bar{b}\bar{s}$ , $0.6 \text{ mm} < cr < 80 \text{ mm}$
>1000	95	8 KHACHATRYAN 17AR	CMS	long-lived $\tilde{g}$ , RPV, $\tilde{g} \rightarrow t\bar{b}\bar{s}$ , $cr = 0.3 \text{ mm}$
>1300	95	8 KHACHATRYAN 17AR	CMS	long-lived $\tilde{g}$ , RPV, $\tilde{g} \rightarrow t\bar{b}\bar{s}$ , $cr = 1.0 \text{ mm}$
>1400	95	8 KHACHATRYAN 17AR	CMS	long-lived $\tilde{g}$ , RPV, $\tilde{g} \rightarrow t\bar{b}\bar{s}$ , $2 \text{ mm} < cr < 30 \text{ mm}$
>1580	95	9 AABOUD	16B ATLS	long-lived R-hadrons
> 740–1590	95	10 AABOUD	16C ATLS	R-hadrons, Tglu1A, $\tau > 0.4 \text{ ns}$ , $m_{\tilde{\chi}_1^0} = 100 \text{ GeV}$
>1570	95	10 AABOUD	16C ATLS	R-hadrons, Tglu1A, stable
>1610	95	11 KHACHATRYAN 16BW	CMS	long-lived $\tilde{g}$ forming R-hadrons, $f = 0.1$ , cloud interaction model
>1580	95	11 KHACHATRYAN 16BW	CMS	long-lived $\tilde{g}$ forming R-hadrons, $f = 0.1$ , charge-suppressed interaction model
>1520	95	11 KHACHATRYAN 16BW	CMS	long-lived $\tilde{g}$ forming R-hadrons, $f = 0.5$ , cloud interaction model
>1540	95	11 KHACHATRYAN 16BW	CMS	long-lived $\tilde{g}$ forming R-hadrons, $f = 0.5$ , charge-suppressed interaction model
>1270	95	12 AAD	15AE ATLS	$\tilde{g}$ R-hadron, generic R-hadron model
>1360	95	12 AAD	15AE ATLS	$\tilde{g}$ decaying to 300 GeV stable sleptons, LeptoSUSY model
>1115	95	13 AAD	15BM ATLS	$\tilde{g}$ R-hadron, stable
>1185	95	13 AAD	15BM ATLS	$\tilde{g} \rightarrow (g/q\bar{q})\tilde{\chi}_1^0$ , lifetime 10 ns, $m_{\tilde{\chi}_1^0} = 100 \text{ GeV}$
>1099	95	13 AAD	15BM ATLS	$\tilde{g} \rightarrow (g/q\bar{q})\tilde{\chi}_1^0$ , lifetime 10 ns, $m_{\tilde{g}} - m_{\tilde{\chi}_1^0} = 100 \text{ GeV}$
>1182	95	13 AAD	15BM ATLS	$\tilde{g} \rightarrow t\bar{t}\tilde{\chi}_1^0$ , lifetime 10 ns, $m_{\tilde{\chi}_1^0} = 100 \text{ GeV}$
>1157	95	13 AAD	15BM ATLS	$\tilde{g} \rightarrow t\bar{t}\tilde{\chi}_1^0$ , lifetime 10 ns, $m_{\tilde{g}} - m_{\tilde{\chi}_1^0} = 480 \text{ GeV}$
> 869	95	13 AAD	15BM ATLS	$\tilde{g} \rightarrow (g/q\bar{q})\tilde{\chi}_1^0$ , lifetime 1 ns, $m_{\tilde{\chi}_1^0} = 100 \text{ GeV}$
> 821	95	13 AAD	15BM ATLS	$\tilde{g} \rightarrow (g/q\bar{q})\tilde{\chi}_1^0$ , lifetime 1 ns, $m_{\tilde{g}} - m_{\tilde{\chi}_1^0} = 100 \text{ GeV}$



# Searches Particle Listings

## Supersymmetric Particle Searches

> 836	95	13	AAD	15BMATLS	$\tilde{g} \rightarrow t\bar{t}\tilde{\chi}_1^0$ , lifetime 1 ns, $m_{\tilde{\chi}_1^0} = 100$ GeV
> 836	95	13	AAD	15BMATLS	$\tilde{g} \rightarrow t\bar{t}\tilde{\chi}_1^0$ , lifetime 10 ns, $m_{\tilde{g}} - m_{\tilde{\chi}_1^0} = 480$ GeV
>1000	95	14	KHACHATRYAN...15AK	CMS	$\tilde{g}$ R-hadrons, $10 \mu\text{s} < \tau < 1000$ s
> 880	95	14	KHACHATRYAN...15AK	CMS	$\tilde{g}$ R-hadrons, $1 \mu\text{s} < \tau < 1000$ s
••• We do not use the following data for averages, fits, limits, etc. •••					
> 985	95	15	AAD	13AA ATLS	$\tilde{g}$ , R-hadrons, generic interaction model
> 832	95	16	AAD	13BC ATLS	R-hadrons, $\tilde{g} \rightarrow g/q\bar{q}\tilde{\chi}_1^0$ , generic R-hadron model, lifetime between $10^{-5}$ and $10^3$ s, $m_{\tilde{\chi}_1^0} = 100$ GeV
>1322	95	17	CHATRCHYAN13AB	CMS	long-lived $\tilde{g}$ forming R-hadrons, $f = 0.1$ , cloud interaction model
none 200–341	95	18	AAD	12P ATLS	long-lived $\tilde{g} \rightarrow g\tilde{\chi}_1^0$ , $m_{\tilde{\chi}_1^0} = 100$ GeV
> 640	95	19	CHATRCHYAN12AN	CMS	long-lived $\tilde{g} \rightarrow g\tilde{\chi}_1^0$
>1098	95	20	CHATRCHYAN12L	CMS	long-lived $\tilde{g}$ forming R-hadrons, $f = 0.1$
> 586	95	21	AAD	11K ATLS	stable $\tilde{g}$
> 544	95	22	AAD	11P ATLS	stable $\tilde{g}$ , GMSB scenario, $\tan\beta=5$
> 370	95	23	KHACHATRYAN...11	CMS	long lived $\tilde{g}$
> 398	95	24	KHACHATRYAN...11C	CMS	stable $\tilde{g}$

- <sup>1</sup> AABOUD 19AT searched in  $36.1 \text{ fb}^{-1}$  of  $pp$  collisions at  $\sqrt{s} = 13 \text{ TeV}$  for metastable and stable R-hadrons. Multiple search strategies for a wide range of lifetimes, corresponding to path lengths of a few meters, are defined. No significant deviations from the expected Standard Model background are observed. Gluino R-hadrons with lifetimes of the order of 50 ns are excluded at 95% C.L. for masses below 1980 GeV using the muon-spectrometer agnostic analysis. Using the full-detector search, the observed lower limits on the mass are 2000 GeV. See their Figure 9 (top).
- <sup>2</sup> AABOUD 19c searched in  $36.1 \text{ fb}^{-1}$  of  $pp$  collisions at  $\sqrt{s} = 13 \text{ TeV}$  for metastable and stable R-hadrons arising as excesses in the mass distribution of reconstructed tracks with high transverse momentum and large  $dE/dx$ . Gluino R-hadrons with lifetimes above 10 ns are excluded at 95% C.L. with lower mass limit range between 1000 GeV and 2060 GeV, see their Figure 5(a). Masses smaller than 1290 GeV are excluded for a lifetime of 1 ns, see their Figure 6. In the case of stable R-hadrons, the lower mass limit is 1890 GeV, see their Figure 5(b).
- <sup>3</sup> SIRUANYAN 19BH searched in  $35.9 \text{ fb}^{-1}$  of  $pp$  collisions at  $\sqrt{s} = 13 \text{ TeV}$  for long-lived particles decaying into jets, with each long-lived particle having a decay vertex well displaced from the production vertex. The selected events are found to be consistent with standard model predictions. Limits are set on the gluino mass in a GMSB model where the gluino is decaying via  $\tilde{g} \rightarrow g\tilde{G}$ , see their Figure 4 and in an RPV model of supersymmetry where the gluino is decaying via  $\tilde{g} \rightarrow t\bar{b}s$ , see their RPV 5. Limits are also set on the stop mass in two RPV models, see their Figure 6 (for  $t \rightarrow b\bar{l}$  decays) and Figure 7 (for  $\tilde{t} \rightarrow \bar{d}\bar{d}$  decays).
- <sup>4</sup> SIRUANYAN 19BT searched in  $137 \text{ fb}^{-1}$  of  $pp$  collisions at  $\sqrt{s} = 13 \text{ TeV}$  for long-lived particles decaying to displaced, nonprompt jets and missing transverse momentum. Candidate signal events are identified using the timing capabilities of the CMS electromagnetic calorimeter. The results of the search are found to be consistent with the background predictions. Limits are set on the gluino mass in a GMSB model where long-lived gluinos are pair produced and decaying via  $\tilde{g} \rightarrow g\tilde{G}$ , see their Figures 4 and 5.
- <sup>5</sup> AABOUD 18s searched in  $32.8 \text{ fb}^{-1}$  of  $pp$  collisions at  $\sqrt{s} = 13 \text{ TeV}$  for long-lived gluinos in final states with large missing transverse momentum and at least one high-mass displaced vertex with five or more tracks. The observed yield is consistent with the expected background. Exclusion limits are derived for Tglu1A models predicting the existence of long-lived gluinos reaching roughly  $m(\tilde{g}) = 2000 \text{ GeV}$  to  $2370 \text{ GeV}$  for  $m(\tilde{\chi}_1^0) = 100 \text{ GeV}$  and gluino lifetimes between 0.02 and 10 ns, see their Fig. 8. Limits are presented also as a function of the lifetime (for a fixed gluino-neutralino mass difference of 100 GeV) and of the gluino and neutralino masses (for a fixed lifetime of 1 ns). See their Fig. 9 and 10 respectively.
- <sup>6</sup> SIRUANYAN 18AY searched in  $35.9 \text{ fb}^{-1}$  of  $pp$  collisions at  $\sqrt{s} = 13 \text{ TeV}$  for events containing one or more jets and significant  $\cancel{E}_T$ . No significant excess above the Standard Model expectations is observed. Limits are set on the gluino mass in the Tglu1A, Tglu2A and Tglu3A simplified models, see their Figure 3. Limits are also set on squark, sbottom and stop masses in the Tsqk1, Tsb0t1, Tstop1 and Tstop4 simplified models, see their Figure 3. Finally, limits are set on long-lived gluino masses in a Tglu1A simplified model where the gluino is metastable or long-lived with proper decay lengths in the range  $10^{-3} \text{ mm} < c\tau < 10^5 \text{ mm}$ , see their Figure 4.
- <sup>7</sup> SIRUANYAN 18bv searched in  $38.5 \text{ fb}^{-1}$  of  $pp$  collisions at  $\sqrt{s} = 13 \text{ TeV}$  for long-lived particles in events with multiple jets and two displaced vertices composed of many tracks. No events with two well-separated high-track-multiplicity vertices were observed. Limits are set on the stop and the gluino mass in RPV models of supersymmetry where the stop (gluino) is decaying solely into dijet (multijet) final states, see their Figures 6 and 7.
- <sup>8</sup> KHACHATRYAN 17AR searched in  $17.6 \text{ fb}^{-1}$  of  $pp$  collisions at  $\sqrt{s} = 8 \text{ TeV}$  for R-parity-violating SUSY in which long-lived neutralinos or gluinos decay into multijet final states. No significant excess above the Standard Model expectations is observed. Limits are set on the gluino mass for a range of mean proper decay lengths ( $c\tau$ ), see their Fig. 7. The upper limits on the production cross section times branching ratio squared (Fig. 7) are also applicable to long-lived neutralinos.
- <sup>9</sup> AABOUD 16b searched in  $3.2 \text{ fb}^{-1}$  of  $pp$  collisions at  $\sqrt{s} = 13 \text{ TeV}$  for long-lived R-hadrons using observables related to large ionization losses and slow propagation velocities, which are signatures of heavy charged particles traveling significantly slower than the speed of light. Exclusion limits at 95% C.L. are set on the long-lived gluino masses exceeding 1580 GeV. See their Fig. 5.
- <sup>10</sup> AABOUD 16c searched in  $3.2 \text{ fb}^{-1}$  of  $pp$  collisions at  $\sqrt{s} = 13 \text{ TeV}$  for long-lived and stable R-hadrons identified by anomalously specific ionization energy loss in the ATLAS Pixel detector. Gluino R-hadrons with lifetimes above 0.4 ns are excluded at 95% C.L. with lower mass limit range between 740 GeV and 1590 GeV. In the case of stable R-hadrons, the lower mass limit is 1570 GeV. See their Figs. 5 and 6.

- <sup>11</sup> KHACHATRYAN 16BW searched in  $2.5 \text{ fb}^{-1}$  of  $pp$  collisions at  $\sqrt{s} = 13 \text{ TeV}$  for events with heavy stable charged particles, identified by their anomalously high energy deposits in the silicon tracker and/or long time-of-flight measurements by the muon system. No evidence for an excess over the expected background is observed. Limits are derived for pair production of gluinos as a function of mass, depending on the interaction model and on the fraction  $f$ , of produced gluinos hadronizing into a  $\tilde{g}$ -gluon state, see Fig. 4 and Table 7.
- <sup>12</sup> AAD 15AE searched in  $19.1 \text{ fb}^{-1}$  of  $pp$  collisions at  $\sqrt{s} = 8 \text{ TeV}$  for heavy long-lived charged particles, measured through their specific ionization energy loss in the ATLAS pixel detector or their time-of-flight in the ALTAS muon system. In the absence of an excess of events above the expected backgrounds, limits are set R-hadrons in various scenarios, see Fig. 11. Limits are also set in LeptoSUSY models where the gluino decays to stable 300 GeV leptons, see Fig. 9.
- <sup>13</sup> AAD 15BM searched in  $18.4 \text{ fb}^{-1}$  of  $pp$  collisions at  $\sqrt{s} = 8 \text{ TeV}$  for stable and metastable non-relativistic charged particles through their anomalous specific ionization energy loss in the ATLAS pixel detector. In absence of an excess of events above the expected backgrounds, limits are set within a generic R-hadron model, on stable gluino R-hadrons (see Table 5) and on metastable gluino R-hadrons decaying to  $(g/q\bar{q})$  plus a light  $\tilde{\chi}_1^0$  (see Fig. 7) and decaying to  $t\bar{t}$  plus a light  $\tilde{\chi}_1^0$  (see Fig. 9).
- <sup>14</sup> KHACHATRYAN 15AK looked in a data set corresponding to  $18.6 \text{ fb}^{-1}$  of  $pp$  collisions at  $\sqrt{s} = 8 \text{ TeV}$ , and a search interval corresponding to 281 h of trigger lifetime, for long-lived particles that have stopped in the CMS detector. No evidence for an excess over the expected background in a cloud interaction model is observed. Assuming the decay  $\tilde{g} \rightarrow g\tilde{\chi}_1^0$  and lifetimes between 1  $\mu\text{s}$  and 1000 s, limits are derived on  $\tilde{g}$  production as a function of  $m_{\tilde{\chi}_1^0}$ , see Figs. 4 and 6. The exclusions require that  $m_{\tilde{\chi}_1^0}$  is kinematically consistent with the minimum values of the jet energy thresholds used.
- <sup>15</sup> AAD 13AA searched in  $4.7 \text{ fb}^{-1}$  of  $pp$  collisions at  $\sqrt{s} = 7 \text{ TeV}$  for events containing colored long-lived particles that hadronize forming R-hadrons. No significant excess above the expected background was found. Long-lived R-hadrons containing a  $\tilde{g}$  are excluded for masses up to 985 GeV at 95% C.L. in a general interaction model. Also, limits independent of the fraction of R-hadrons that arrive charged in the muon system were derived, see Fig. 6.
- <sup>16</sup> AAD 13BC searched in  $5.0 \text{ fb}^{-1}$  of  $pp$  collisions at  $\sqrt{s} = 7 \text{ TeV}$  and in  $22.9 \text{ fb}^{-1}$  of  $pp$  collisions at  $\sqrt{s} = 8 \text{ TeV}$  for bottom squark R-hadrons that have come to rest within the ATLAS calorimeter and decay at some later time to hadronic jets and a neutralino. In absence of an excess of events above the expected backgrounds, limits are set on gluino masses for different decays, lifetimes, and neutralino masses, see their Table 6 and Fig. 10.
- <sup>17</sup> CHATRCHYAN 13AB looked in  $5.0 \text{ fb}^{-1}$  of  $pp$  collisions at  $\sqrt{s} = 7 \text{ TeV}$  and in  $18.8 \text{ fb}^{-1}$  of  $pp$  collisions at  $\sqrt{s} = 8 \text{ TeV}$  for events with heavy stable particles, identified by their anomalously  $dE/dx$  in the tracker or additionally requiring that it be identified as muon in the muon chambers, from pair production of  $\tilde{g}$ 's. No evidence for an excess over the expected background is observed. Limits are derived for pair production of gluinos as a function of mass (see Fig. 8 and Table 5), depending on the fraction,  $f$ , of formation of  $\tilde{g}$ - $\tilde{g}$  (R-gluonball) states. The quoted limit is for  $f = 0.1$ , while for  $f = 0.5$  it degrades to 1276 GeV. In the conservative scenario where every hadronic interaction causes it to become neutral, the limit decreases to 928 GeV for  $f = 0.1$ .
- <sup>18</sup> AAD 12P looked in  $31 \text{ pb}^{-1}$  of  $pp$  collisions at  $\sqrt{s} = 7 \text{ TeV}$  for events with pair production of long-lived gluinos. The hadronization of the gluinos leads to R-hadrons which may stop inside the detector and later decay via  $\tilde{g} \rightarrow g\tilde{\chi}_1^0$  during gaps between the proton bunches. No significant excess over the expected background is observed. From a counting experiment, a limit at 95% C.L. on the cross section as a function of  $m_{\tilde{g}}$  is derived for  $m_{\tilde{\chi}_1^0} = 100 \text{ GeV}$ , see Fig. 4. The limit is valid for lifetimes between  $10^{-5}$  and  $10^3$  seconds and assumes the Generic matter interaction model for the production cross section.
- <sup>19</sup> CHATRCHYAN 12AN looked in  $4.0 \text{ fb}^{-1}$  of  $pp$  collisions at  $\sqrt{s} = 7 \text{ TeV}$  for events with pair production of long-lived gluinos. The hadronization of the gluinos leads to R-hadrons which may stop inside the detector and later decay via  $\tilde{g} \rightarrow g\tilde{\chi}_1^0$  during gaps between the proton bunches. No significant excess over the expected background is observed. From a counting experiment, a limit at 95% C.L. on the cross section as a function of  $m_{\tilde{g}}$  is derived, see Fig. 3. The mass limit is valid for lifetimes between  $10^{-5}$  and  $10^3$  seconds, for what they call "the daughter gluon energy  $E_g > 100 \text{ GeV}$  and assuming the cloud interaction model for R-hadrons. Supersedes KHACHATRYAN 11.
- <sup>20</sup> CHATRCHYAN 12L looked in  $5.0 \text{ fb}^{-1}$  of  $pp$  collisions at  $\sqrt{s} = 7 \text{ TeV}$  for events with heavy stable particles, identified by their anomalously  $dE/dx$  in the tracker or additionally requiring that it be identified as muon in the muon chambers, from pair production of  $\tilde{g}$ 's. No evidence for an excess over the expected background is observed. Limits are derived for pair production of gluinos as a function of mass (see Fig. 3), depending on the fraction,  $f$ , of formation of  $\tilde{g}$ - $\tilde{g}$  (R-gluonball) states. The quoted limit is for  $f = 0.1$ , while for  $f = 0.5$  it degrades to 1046 GeV. In the conservative scenario where every hadronic interaction causes it to become neutral, the limit decreases to 928 GeV for  $f = 0.1$ . Supersedes KHACHATRYAN 11c.
- <sup>21</sup> AAD 11K looked in  $34 \text{ pb}^{-1}$  of  $pp$  collisions at  $\sqrt{s} = 7 \text{ TeV}$  for events with heavy stable particles, identified by their anomalously  $dE/dx$  in the tracker or time of flight in the tile calorimeter, from pair production of  $\tilde{g}$ . No evidence for an excess over the SM expectation is observed. Limits are derived for pair production of gluinos as a function of mass (see Fig. 4), for a fraction,  $f = 10\%$ , of formation of  $\tilde{g}$ - $\tilde{g}$  (R-gluonball). If instead of a phase space driven approach for the hadronic scattering of the R-hadrons, a triple-Regge model or a bag-model is used, the limit degrades to 566 and 562 GeV, respectively.
- <sup>22</sup> AAD 11P looked in  $37 \text{ pb}^{-1}$  of  $pp$  collisions at  $\sqrt{s} = 7 \text{ TeV}$  for events with heavy stable particles, reconstructed and identified by their time of flight in the Muon System. There is no requirement on their observation in the tracker to increase the sensitivity to cases where gluinos have a large fraction,  $f$ , of formation of neutral  $\tilde{g}$ - $\tilde{g}$  (R-gluonball). No evidence for an excess over the SM expectation is observed. Limits are derived as a function of mass (see Fig. 4), for  $f = 0.1$ . For fractions  $f = 0.5$  and 1.0 the limit degrades to 537 and 530 GeV, respectively.
- <sup>23</sup> KHACHATRYAN 11 looked in  $10 \text{ pb}^{-1}$  of  $pp$  collisions at  $\sqrt{s} = 7 \text{ TeV}$  for events with pair production of long-lived gluinos. The hadronization of the gluinos leads to R-hadrons which may stop inside the detector and later decay via  $\tilde{g} \rightarrow g\tilde{\chi}_1^0$  during gaps between the proton bunches. No significant excess over the expected background is observed. From a counting experiment, a limit at 95% C.L. on the cross section times branching ratio is derived for  $m_{\tilde{g}} - m_{\tilde{\chi}_1^0} > 100 \text{ GeV}$ , see their Fig. 2. Assuming 100% branching

ratio, lifetimes between 75 ns and  $3 \times 10^5$  s are excluded for  $m_{\tilde{g}} = 300$  GeV. The  $\tilde{g}$  mass exclusion is obtained with the same assumptions for lifetimes between 10  $\mu$ s and 1000 s, but shows some dependence on the model for R-hadron interactions with matter, illustrated in Fig. 3. From a time-profile analysis, the mass exclusion is 382 GeV for a lifetime of 10  $\mu$ s under the same assumptions as above.

24 KHACHATRYAN 11c looked in  $3.1 \text{ pb}^{-1}$  of  $pp$  collisions at  $\sqrt{s} = 7$  TeV for events with heavy stable particles, identified by their anomalous dE/dx in the tracker or additionally requiring that it be identified as muon in the muon chambers, from pair production of  $\tilde{g}$ . No evidence for an excess over the expected background is observed. Limits are derived for pair production of gluinos as a function of mass (see Fig. 3), depending on the fraction,  $f$ , of formation of  $\tilde{g} - g$  (R-gluonball). The quoted limit is for  $f=0.1$ , while for  $f=0.5$  it degrades to 357 GeV. In the conservative scenario where every hadronic interaction causes it to become neutral, the limit decreases to 311 GeV for  $f=0.1$ .

Light  $\tilde{G}$  (Gravitino) mass limits from collider experiments

The following are bounds on light ( $\ll 1$  eV) gravitino indirectly inferred from its coupling to matter suppressed by the gravitino decay constant.

Unless otherwise stated, all limits assume that other supersymmetric particles besides the gravitino are too heavy to be produced. The gravitino is assumed to be undetected and to give rise to a missing energy ( $\cancel{E}$ ) signature.

Some earlier papers are now obsolete and have been omitted. They were last listed in our PDG 14 edition: K. Olive, et al. (Particle Data Group), Chinese Physics **C38** 070001 (2014) (<http://pdg.lbl.gov>).

Table with 5 columns: VALUE (eV), CL%, DOCUMENT ID, TECN, COMMENT. Includes rows for AAD 15BH ATLS, ABDALLAH 05B DLPH, ACHARD 04E L3, HEISTER 03c ALEP, ACOSTA 02H CDF, and ABBIENDI, G 00D OPAL.

1 AAD 15BH searched in 20.3  $\text{fb}^{-1}$  of  $pp$  collisions at  $\sqrt{s} = 8$  TeV for associated production of a light gravitino and a squark or gluino. The squark (gluino) is assumed to decay exclusively to a quark (gluon) and a gravitino. No evidence was found for an excess above the expected level of Standard Model background and 95% C.L. lower limits were set on the gravitino mass as a function of the squark/gluino mass, both in the case of degenerate and non-degenerate squark/gluino masses, see Figs. 14 and 15.

2 ABDALLAH 05B use data from  $\sqrt{s} = 180-208$  GeV. They look for events with a single photon +  $\cancel{E}$  final states from which a cross section limit of  $\sigma < 0.18 \text{ pb}$  at 80 GeV is obtained, allowing a limit on the mass to be set. Supersedes the results of ABREU 00Z.

3 ACHARD 04E use data from  $\sqrt{s} = 189-209$  GeV. They look for events with a single photon +  $\cancel{E}$  final states from which a limit on the Gravitino mass is set corresponding to  $\sqrt{\mathcal{F}} > 238$  GeV. Supersedes the results of ACCIARRI 99R.

4 HEISTER 03c use the data from  $\sqrt{s} = 189-209$  GeV to search for  $\gamma \cancel{E}$  final states.

5 ACOSTA 02H looked in 87  $\text{pb}^{-1}$  of  $p\bar{p}$  collisions at  $\sqrt{s}=1.8$  TeV for events with a high- $E_T$  photon and  $\cancel{E}_T$ . They compared the data with a GMSB model where the final state could arise from  $q\bar{q} \rightarrow \tilde{G} G \gamma$ . Since the cross section for this process scales as  $1/|F|^4$ , a limit at 95% CL is derived on  $|F|^{1/2} > 221$  GeV. A model independent limit for the above topology is also given in the paper.

6 ABBIENDI, G 00D searches for  $\gamma \cancel{E}$  final states from  $\sqrt{s}=189$  GeV.

Supersymmetry miscellaneous results

Results that do not appear under other headings or that make nonminimal assumptions.

Some earlier papers are now obsolete and have been omitted. They were last listed in our PDG 14 edition: K. Olive, et al. (Particle Data Group), Chinese Physics **C38** 070001 (2014) (<http://pdg.lbl.gov>).

Table with 5 columns: VALUE, CL%, DOCUMENT ID, TECN, COMMENT. Includes rows for habemus MSSM, selected ATLAS searches on EVK sector, dark photon,  $\gamma_{\text{Higgs}}$  in SUSY-portal models, hidden-valley Higgs, scalar gluons, and  $\mu\mu$  resonances.

1 AAD 20c uses a statistical combination of six final states  $b\bar{b}b\bar{b}$ ,  $b\bar{b}WW$ ,  $b\bar{b}\tau\tau$ ,  $WWWW$ ,  $b\bar{b}\gamma\gamma$ , and  $WW\gamma\gamma$  to search for non-resonant and resonant production of Higgs boson pairs. The search uses  $36.1 \text{ fb}^{-1}$  of  $pp$  collisions data at  $\sqrt{s} = 13$  TeV. Constraints in the habemus Minimal Supersymmetric Standard Model in the  $(m_A, \tan\beta)$  parameter space are placed, see their Figure 7(b).

2 ABOUD 16AF uses a selection of searches by ATLAS for the electroweak production of SUSY particles studying resulting constraints on dark matter candidates. They use  $20 \text{ fb}^{-1}$  of  $pp$  collisions at  $\sqrt{s} = 8$  TeV. A likelihood-driven scan of an effective model focusing on the gaugino-higgsino and Higgs sector of the pMSSM is performed. The ATLAS searches impact models where  $m_{\chi_1^0} < 65$  GeV, excluding 86% of them. See their Figs. 2, 4, and 6.

3 AAD 16AG searches for prompt lepton-jets using  $20 \text{ fb}^{-1}$  of  $pp$  collisions at  $\sqrt{s} = 8$  TeV collected with the ATLAS detector. Lepton-jets are expected from decays of low-mass dark photons in SUSY-portal and Higgs-portal models. No significant excess of events is observed and 95% CL upper limits are computed on the production cross section times branching ratio for two prompt lepton-jets in models predicting 2 or 4  $\gamma_{\text{D}}$  via SUSY-portal topologies, for  $\gamma_{\text{D}}$  mass values between 0 and 2 GeV. See their Figs 9 and 10. The results are also interpreted in terms of a 90% CL exclusion region in kinetic mixing and dark-photon mass parameter space. See their Fig. 13.

4 AAD 13P searched in  $5 \text{ fb}^{-1}$  of  $pp$  collisions at  $\sqrt{s} = 7$  TeV for single lepton-jets with at least four muons; pairs of lepton-jets, each with two or more muons; and pairs of lepton-jets with two or more electrons. All of these could be signatures of Hidden Valley supersymmetric models. No statistically significant deviations from the Standard Model expectations are found. 95% C.L. limits are placed on the production cross section times branching ratio of dark photons for several parameter sets of a Hidden Valley model.

5 AALTONEN 12AB looked in  $5.1 \text{ fb}^{-1}$  of  $p\bar{p}$  collisions at  $\sqrt{s} = 1.96$  TeV for anomalous production of multiple low-energy leptons in association with a  $W$  or  $Z$  boson. Such events may occur in hidden valley models in which a supersymmetric Higgs boson is produced in association with a  $W$  or  $Z$  boson, with  $H \rightarrow \tilde{\chi}_1^0 \chi_1^0$  pair and with the  $\tilde{\chi}_1^0$  further decaying into a dark photon ( $\gamma_{\text{D}}$ ) and the unobservable lightest SUSY particle of the hidden sector. As the  $\gamma_{\text{D}}$  is expected to be light, it may decay into a lepton pair. No significant excess over the SM expectation is observed and a limit at 95% C.L. is set on the cross section for a benchmark model of supersymmetric hidden-valley Higgs production.

6 AAD 11AA looked in  $34 \text{ pb}^{-1}$  of  $pp$  collisions at  $\sqrt{s} = 7$  TeV for events with  $\geq 4$  jets originating from pair production of scalar gluons, each decaying to two gluons. No two-jet resonances are observed over the SM background. Limits are derived on the cross section times branching ratio (see Fig. 3). Assuming 100% branching ratio for the decay to two gluons, the quoted exclusion range is obtained, except for a 5 GeV mass window around 140 GeV.

7 CHATRYAN 11E looked in  $35 \text{ pb}^{-1}$  of  $pp$  collisions at  $\sqrt{s} = 7$  TeV for events with collimated  $\mu$  pairs (leptonic jets) from the decay of hidden sector states. No evidence for new resonance production is found. Limits are derived and compared to various SUSY models (see Fig. 4) where the LSP, either the  $\tilde{\chi}_1^0$  or a  $\tilde{q}$ , decays to dark sector particles.

8 ABAZOV 10N looked in  $5.8 \text{ fb}^{-1}$  of  $p\bar{p}$  collisions at  $\sqrt{s} = 1.96$  TeV for events from hidden valley models in which a  $\tilde{\chi}_1^0$  decays into a dark photon,  $\gamma_{\text{D}}$ , and the unobservable lightest SUSY particle of the hidden sector. As the  $\gamma_{\text{D}}$  is expected to be light, it may decay into a tightly collimated lepton pair, called lepton jet. They searched for events with  $\cancel{E}_T$  and two isolated lepton jets observable by an opposite charged lepton pair  $e, e, e\mu$  or  $\mu\mu$ . No significant excess over the SM expectation is observed, and a limit at 95% C.L. on the cross section times branching ratio is derived, see their Table 1. They also examined the invariant mass of the lepton jets for a narrow resonance, see their Fig. 4, but found no evidence for a signal.

REFERENCES FOR Supersymmetric Particle Searches

List of references for supersymmetric particle searches, including ATLAS, CMS, LHC, and various experimental collaborations like AAD, ABOUD, ABREU, etc.

Downloaded from <https://academic.oup.com/ptep/article/2020/8/083C01/5891211> by guest on 12 November 2020



See key on page 999

Searches Particle Listings  
Supersymmetric Particle Searches

Table with columns for author names, journal abbreviations, volume numbers, page numbers, and search terms. Includes entries like AAD 12AF PL B714 180, AAD 12AG PL B714 197, AAD 12AN PRL 108 181802, etc.







See key on page 999

# Searches Particle Listings Quark and Lepton Compositeness

## Limits for Excited $e$ ( $e^*$ ) from $e^+e^- \rightarrow \gamma\gamma$

These limits are derived from indirect effects due to  $e^*$  exchange in the  $t$  channel and depend on transition magnetic coupling between  $e$  and  $e^*$ . All limits are for  $\lambda_\gamma = 1$ . All limits except ABE 89j and ACHARD 02d are for nonchiral coupling with  $\eta_L = \eta_R = 1$ . We choose the chiral coupling limit as the best limit and list it in the Summary Table.

For limits prior to 1987, see our 1992 edition (Physical Review **D45** S1 (1992)).

VALUE (GeV)	CL%	DOCUMENT ID	TECN	COMMENT
>356	95	<sup>1</sup> ABDALLAH 04N	DLPH	$\sqrt{s} = 161\text{--}208$ GeV
•••		We do not use the following data for averages, fits, limits, etc. •••		
>310	95	ACHARD 02d	L3	$\sqrt{s} = 192\text{--}209$ GeV

<sup>1</sup> ABDALLAH 04N also obtain a limit on the excited electron mass with  $e^*e^*$  chiral coupling,  $m_{e^*} > 295$  GeV at 95% CL.

## Indirect Limits for Excited $e$ ( $e^*$ )

These limits make use of loop effects involving  $e^*$  and are therefore subject to theoretical uncertainty.

VALUE (GeV)	DOCUMENT ID	TECN	COMMENT
•••	We do not use the following data for averages, fits, limits, etc. •••		
	<sup>1</sup> DORENBOS... 89	CHRM	$\mathcal{T}_{\mu e} \rightarrow \mathcal{T}_{\mu e}, \nu_{\mu e} \rightarrow \nu_{\mu e}$
	<sup>2</sup> GRIFOLS 86	THEO	$\nu_{\mu e} \rightarrow \nu_{\mu e}$
	<sup>3</sup> RENARD 82	THEO	$g-2$ of electron

<sup>1</sup> DORENBOSCH 89 obtain the limit  $\lambda_{\text{cut}}^2 \Lambda_{\text{cut}}^2 / m_{e^*}^2 < 2.6$  (95% CL), where  $\Lambda_{\text{cut}}$  is the cutoff scale, based on the one-loop calculation by GRIFOLS 86. If one assumes that  $\Lambda_{\text{cut}} = 1$  TeV and  $\lambda_\gamma = 1$ , one obtains  $m_{e^*} > 620$  GeV. However, one generally expects  $\lambda_\gamma \approx m_{e^*} / \Lambda_{\text{cut}}$  in composite models.

<sup>2</sup> GRIFOLS 86 uses  $\nu_{\mu e} \rightarrow \nu_{\mu e}$  and  $\mathcal{T}_{\mu e} \rightarrow \mathcal{T}_{\mu e}$  data from CHARM Collaboration to derive mass limits which depend on the scale of compositeness.

<sup>3</sup> RENARD 82 derived from  $g-2$  data limits on mass and couplings of  $e^*$  and  $\mu^*$ . See figures 2 and 3 of the paper.

## MASS LIMITS for Excited $\mu$ ( $\mu^*$ )

### Limits for Excited $\mu$ ( $\mu^*$ ) from Pair Production

These limits are obtained from  $e^+e^- \rightarrow \mu^*\mu^*$  and thus rely only on the (electroweak) charge of  $\mu^*$ . Form factor effects are ignored unless noted. For the case of limits from  $Z$  decay, the  $\mu^*$  coupling is assumed to be of sequential type. All limits assume a dominant  $\mu^* \rightarrow \mu\gamma$  decay except the limits from  $\Gamma(Z)$ .

For limits prior to 1987, see our 1992 edition (Physical Review **D45** S1 (1992)).

VALUE (GeV)	CL%	DOCUMENT ID	TECN	COMMENT
>103.2	95	<sup>1</sup> ABBIENDI 02G	OPAL	$e^+e^- \rightarrow \mu^*\mu^*$ Homodoublet type
•••	We do not use the following data for averages, fits, limits, etc. •••			
>102.8	95	<sup>2</sup> ACHARD 03B	L3	$e^+e^- \rightarrow \mu^*\mu^*$ Homodoublet type

<sup>1</sup> From  $e^+e^-$  collisions at  $\sqrt{s} = 183\text{--}209$  GeV.  $f = f'$  is assumed.

<sup>2</sup> From  $e^+e^-$  collisions at  $\sqrt{s} = 189\text{--}209$  GeV.  $f = f'$  is assumed. ACHARD 03B also obtain limit for  $f = -f'$ :  $m_{\mu^*} > 96.6$  GeV.

### Limits for Excited $\mu$ ( $\mu^*$ ) from Single Production

These limits are from  $e^+e^- \rightarrow \mu^*\mu$  and depend on transition magnetic coupling between  $\mu$  and  $\mu^*$ . All limits assume  $\mu^* \rightarrow \mu\gamma$  decay. Limits from LEP are for chiral coupling, whereas all other limits are for nonchiral coupling,  $\eta_L = \eta_R = 1$ . In most papers, the limit is expressed in the form of an excluded region in the  $\lambda\text{--}m_{\mu^*}$  plane. See the original papers.

For limits prior to 1987, see our 1992 edition (Physical Review **D45** S1 (1992)).

VALUE (GeV)	CL%	DOCUMENT ID	TECN	COMMENT
>3800	95	<sup>1</sup> SIRUNYAN 19Z	CMS	$pp \rightarrow \mu\mu^*X$
•••	We do not use the following data for averages, fits, limits, etc. •••			
>2800	95	<sup>2</sup> AAD 16BM	ATLS	$pp \rightarrow \mu\mu^*X$
>2470	95	<sup>3</sup> KHACHATRYAN...16AQ	CMS	$pp \rightarrow \mu\mu^*X$
>3000	95	<sup>4</sup> AAD 15AP	ATLS	$pp \rightarrow \mu^{(*)}\mu^*X$
>2200	95	<sup>5</sup> AAD 13BB	ATLS	$pp \rightarrow \mu\mu^*X$
>1900	95	<sup>6</sup> CHATRCHYAN13AE	CMS	$pp \rightarrow \mu\mu^*X$
>1750	95	<sup>7</sup> AAD 12AZ	ATLS	$pp \rightarrow \mu^{(*)}\mu^*X$

<sup>1</sup> SIRUNYAN 19Z search for  $\mu^*$  production in  $\ell\ell\gamma$  final states in  $pp$  collisions at  $\sqrt{s} = 13$  TeV. The quoted limit assumes  $\Lambda = m_{\mu^*}$ ,  $f = f' = 1$ . The contact interaction is included in the  $\mu^*$  production and decay amplitudes.

<sup>2</sup> AAD 16BM search for  $\mu^*$  production in  $\mu\mu jj$  events in  $pp$  collisions at  $\sqrt{s} = 8$  TeV. Both the production and decay are assumed to occur via a contact interaction with  $\Lambda = m_{\mu^*}$ .

<sup>3</sup> KHACHATRYAN 16AQ search for single  $\mu^*$  production in  $pp$  collisions at  $\sqrt{s} = 8$  TeV. The limit above is from the  $\mu^* \rightarrow \mu\gamma$  search channel assuming  $f = f' = 1$ ,  $m_{\mu^*} = \Lambda$ . See their Table 7 for limits in other search channels or with different assumptions.

<sup>4</sup> AAD 15AP search for  $\mu^*$  production in events with three or more charged leptons in  $pp$  collisions at  $\sqrt{s} = 8$  TeV. The quoted limit assumes  $\Lambda = m_{\mu^*}$ ,  $f = f' = 1$ . The contact interaction is included in the  $\mu^*$  production and decay amplitudes.

<sup>5</sup> AAD 13BB search for single  $\mu^*$  production in  $pp$  collisions with  $\mu^* \rightarrow \mu\gamma$  decay.  $f = f' = 1$ , and  $\mu^*$  production via contact interaction with  $\Lambda = m_{\mu^*}$  are assumed.

<sup>6</sup> CHATRCHYAN 13AE search for single  $\mu^*$  production in  $pp$  collisions with  $\mu^* \rightarrow \mu\gamma$  decay.  $f = f' = 1$ , and  $\mu^*$  production via contact interaction with  $\Lambda = m_{\mu^*}$  are assumed.

<sup>7</sup> AAD 12AZ search for  $\mu^*$  production via four-fermion contact interaction in  $pp$  collisions with  $\mu^* \rightarrow \mu\gamma$  decay. The quoted limit assumes  $\Lambda = m_{\mu^*}$ . See their Fig. 8 for the exclusion plot in the mass-coupling plane.

## Indirect Limits for Excited $\mu$ ( $\mu^*$ )

These limits make use of loop effects involving  $\mu^*$  and are therefore subject to theoretical uncertainty.

VALUE (GeV)	DOCUMENT ID	TECN	COMMENT
•••	We do not use the following data for averages, fits, limits, etc. •••		
	<sup>1</sup> RENARD 82	THEO	$g-2$ of muon

<sup>1</sup> RENARD 82 derived from  $g-2$  data limits on mass and couplings of  $e^*$  and  $\mu^*$ . See figures 2 and 3 of the paper.

## MASS LIMITS for Excited $\tau$ ( $\tau^*$ )

### Limits for Excited $\tau$ ( $\tau^*$ ) from Pair Production

These limits are obtained from  $e^+e^- \rightarrow \tau^*\tau^*$  and thus rely only on the (electroweak) charge of  $\tau^*$ . Form factor effects are ignored unless noted. For the case of limits from  $Z$  decay, the  $\tau^*$  coupling is assumed to be of sequential type. All limits assume a dominant  $\tau^* \rightarrow \tau\gamma$  decay except the limits from  $\Gamma(Z)$ .

For limits prior to 1987, see our 1992 edition (Physical Review **D45** S1 (1992)).

VALUE (GeV)	CL%	DOCUMENT ID	TECN	COMMENT
>103.2	95	<sup>1</sup> ABBIENDI 02G	OPAL	$e^+e^- \rightarrow \tau^*\tau^*$ Homodoublet type
•••	We do not use the following data for averages, fits, limits, etc. •••			
>102.8	95	<sup>2</sup> ACHARD 03B	L3	$e^+e^- \rightarrow \tau^*\tau^*$ Homodoublet type

<sup>1</sup> From  $e^+e^-$  collisions at  $\sqrt{s} = 183\text{--}209$  GeV.  $f = f'$  is assumed.

<sup>2</sup> From  $e^+e^-$  collisions at  $\sqrt{s} = 189\text{--}209$  GeV.  $f = f'$  is assumed. ACHARD 03B also obtain limit for  $f = -f'$ :  $m_{\tau^*} > 96.6$  GeV.

### Limits for Excited $\tau$ ( $\tau^*$ ) from Single Production

These limits are from  $e^+e^- \rightarrow \tau^*\tau$  and depend on transition magnetic coupling between  $\tau$  and  $\tau^*$ . All limits assume  $\tau^* \rightarrow \tau\gamma$  decay. Limits from LEP are for chiral coupling, whereas all other limits are for nonchiral coupling,  $\eta_L = \eta_R = 1$ . In most papers, the limit is expressed in the form of an excluded region in the  $\lambda\text{--}m_{\tau^*}$  plane. See the original papers.

VALUE (GeV)	CL%	DOCUMENT ID	TECN	COMMENT
>2500	95	<sup>1</sup> AAD 15AP	ATLS	$pp \rightarrow \tau^{(*)}\tau^*X$
•••	We do not use the following data for averages, fits, limits, etc. •••			
> 180	95	<sup>2</sup> ACHARD 03B	L3	$e^+e^- \rightarrow \tau\tau^*$
> 185	95	<sup>3</sup> ABBIENDI 02G	OPAL	$e^+e^- \rightarrow \tau\tau^*$

<sup>1</sup> AAD 15AP search for  $\tau^*$  production in events with three or more charged leptons in  $pp$  collisions at  $\sqrt{s} = 8$  TeV. The quoted limit assumes  $\Lambda = m_{\tau^*}$ ,  $f = f' = 1$ . The contact interaction is included in the  $\tau^*$  production and decay amplitudes.

<sup>2</sup> ACHARD 03B result is from  $e^+e^-$  collisions at  $\sqrt{s} = 189\text{--}209$  GeV.  $f = f' = \Lambda / m_{\tau^*}$  is assumed. See their Fig. 4 for the exclusion plot in the mass-coupling plane.

<sup>3</sup> ABBIENDI 02G result is from  $e^+e^-$  collisions at  $\sqrt{s} = 183\text{--}209$  GeV.  $f = f' = \Lambda / m_{\tau^*}$  is assumed for  $\tau^*$  coupling. See their Fig. 4c for the exclusion limit in the mass-coupling plane.

## MASS LIMITS for Excited Neutrino ( $\nu^*$ )

### Limits for Excited $\nu$ ( $\nu^*$ ) from Pair Production

These limits are obtained from  $e^+e^- \rightarrow \nu^*\nu^*$  and thus rely only on the (electroweak) charge of  $\nu^*$ . Form factor effects are ignored unless noted. The  $\nu^*$  coupling is assumed to be of sequential type unless otherwise noted. All limits assume a dominant  $\nu^* \rightarrow \nu\gamma$  decay except the limits from  $\Gamma(Z)$ .

VALUE (GeV)	CL%	DOCUMENT ID	TECN	COMMENT
>1600	95	<sup>1</sup> AAD 15AP	ATLS	$pp \rightarrow \nu^*\nu^*X$
•••	We do not use the following data for averages, fits, limits, etc. •••			
> 102.6	95	<sup>2</sup> ABBIENDI 04N	OPAL	
		<sup>3</sup> ACHARD 03B	L3	$e^+e^- \rightarrow \nu^*\nu^*$ Homodoublet type

<sup>1</sup> AAD 15AP search for  $\nu^*$  pair production in events with three or more charged leptons in  $pp$  collisions at  $\sqrt{s} = 8$  TeV. The quoted limit assumes  $\Lambda = m_{\nu^*}$ ,  $f = f' = 1$ . The contact interaction is included in the  $\nu^*$  production and decay amplitudes.

<sup>2</sup> From  $e^+e^-$  collisions at  $\sqrt{s} = 192\text{--}209$  GeV, ABBIENDI 04N obtain limit on  $\sigma(e^+e^- \rightarrow \nu^*\nu^*) B^2(\nu^* \rightarrow \nu\gamma)$ . See their Fig.2. The limit ranges from 20 to 45 fb for  $m_{\nu^*} > 45$  GeV.

<sup>3</sup> From  $e^+e^-$  collisions at  $\sqrt{s} = 189\text{--}209$  GeV.  $f = -f'$  is assumed. ACHARD 03B also obtain limit for  $f = f'$ :  $m_{\nu_e^*} > 101.7$  GeV,  $m_{\nu_\mu^*} > 101.8$  GeV, and  $m_{\nu_\tau^*} > 92.9$  GeV.

See their Fig. 4 for the exclusion plot in the mass-coupling plane.



# Searches Particle Listings

## Quark and Lepton Compositeness

### Limits for Excited $\nu$ ( $\nu^*$ ) from Single Production

These limits are from  $e^+e^- \rightarrow \nu\nu^*$ ,  $Z \rightarrow \nu\nu^*$ , or  $ep \rightarrow \nu^*X$  and depend on transition magnetic coupling between  $\nu/e$  and  $\nu^*$ . Assumptions about  $\nu^*$  decay mode are given in footnotes.

VALUE (GeV)	CL%	DOCUMENT ID	TECN	COMMENT
>213	95	1 AARON 08 H1	H1	$ep \rightarrow \nu^*X$
•••		••• We do not use the following data for averages, fits, limits, etc. •••		
>190	95	2 ACHARD 03B L3	L3	$e^+e^- \rightarrow \nu\nu^*$
none 50–150	95	3 ADLOFF 02 H1	H1	$ep \rightarrow \nu^*X$
>158	95	4 CHEKANOV 02D ZEUS	ZEUS	$ep \rightarrow \nu^*X$

- AARON 08 search for single  $\nu^*$  production in  $ep$  collisions with the decays  $\nu^* \rightarrow \nu\gamma$ ,  $\nu Z$ ,  $eW$ . The quoted limit assumes  $f = -f' = \Lambda/m_{\nu^*}$ . See their Fig. 3 and Fig. 4 for the exclusion plots in the mass-coupling plane.
- ACHARD 03B result is from  $e^+e^-$  collisions at  $\sqrt{s} = 189\text{--}209$  GeV. The quoted limit is for  $\nu_e^*$ .  $f = -f' = \Lambda/m_{\nu^*}$  is assumed. See their Fig. 4 for the exclusion plot in the mass-coupling plane.
- ADLOFF 02 search for single  $\nu^*$  production in  $ep$  collisions with the decays  $\nu^* \rightarrow \nu\gamma$ ,  $\nu Z$ ,  $eW$ . The quoted limit assumes  $f = -f' = \Lambda/m_{\nu^*}$ . See their Fig. 1 for the exclusion plots in the mass-coupling plane.
- CHEKANOV 02D search for single  $\nu^*$  production in  $ep$  collisions with the decays  $\nu^* \rightarrow \nu\gamma$ ,  $\nu Z$ ,  $eW$ .  $f = -f' = \Lambda/m_{\nu^*}$  is assumed for the  $e^*$  coupling. CHEKANOV 02D also obtain limit for  $f = f' = \Lambda/m_{\nu^*}$ :  $m_{\nu^*} > 135$  GeV. See their Fig. 5c and Fig. 5d for the exclusion plot in the mass-coupling plane.

### MASS LIMITS for Excited $q$ ( $q^*$ )

#### Limits for Excited $q$ ( $q^*$ ) from Pair Production

These limits are mostly obtained from  $e^+e^- \rightarrow q^*q^*$  and thus rely only on the (electroweak) charge of the  $q^*$ . Form factor effects are ignored unless noted. Assumptions about the  $q^*$  decay are given in the comments and footnotes.

VALUE (GeV)	CL%	DOCUMENT ID	TECN	COMMENT
>338	95	1 AALTONEN 10H CDF	CDF	$q^* \rightarrow tW^-$
•••		••• We do not use the following data for averages, fits, limits, etc. •••		
none 700–1200	95	2 SIRUNYAN 18v CMS	CMS	$pp \rightarrow t^*_{3/2} \bar{t}^*_{3/2} \rightarrow t\bar{t}gg$
> 45.6	95	3 BARATE 98U ALEP	ALEP	$Z \rightarrow q^*q^*$
> 41.7	95	4 ADRIANI 93M L3	L3	$u$ or $d$ type, $Z \rightarrow q^*q^*$
> 44.7	95	5 BARDADIN... 92 RVUE	RVUE	$u$ -type, $\Gamma(Z)$
> 40.6	95	6 BARDADIN... 92 RVUE	RVUE	$d$ -type, $\Gamma(Z)$
> 44.2	95	7 DECAMP 92 ALEP	ALEP	$u$ -type, $\Gamma(Z)$
> 45	95	8 DECAMP 92 ALEP	ALEP	$d$ -type, $\Gamma(Z)$
> 45	95	9 DECAMP 92 ALEP	ALEP	$u$ or $d$ type, $Z \rightarrow q^*q^*$
> 45	95	10 ABREU 91F DLPH	DLPH	$u$ -type, $\Gamma(Z)$
> 45	95	11 ABREU 91F DLPH	DLPH	$d$ -type, $\Gamma(Z)$

- AALTONEN 10H obtain limits on the  $q^*q^*$  production cross section in  $p\bar{p}$  collisions. See their Fig. 3.
- SIRUNYAN 18v search for pair production of spin  $3/2$  excited top quarks.  $B(t^*_{3/2} \rightarrow t\bar{g}) = 1$  is assumed.
- BARATE 98U obtain limits on the form factor. See their Fig. 16 for limits in mass-form factor plane.
- ADRIANI 93M limit is valid for  $B(q^* \rightarrow qg) > 0.25$  (0.17) for up (down) type.
- BARDADIN-OTWINOWSKA 92 limit based on  $\Delta\Gamma(Z) < 36$  MeV.
- These limits are independent of decay modes.
- Limit is for  $B(q^* \rightarrow qg) + B(q^* \rightarrow q\gamma) = 1$ .

#### Limits for Excited $q$ ( $q^*$ ) from Single Production

These limits are from  $e^+e^- \rightarrow q^*q$ ,  $p\bar{p} \rightarrow q^*X$ , or  $pp \rightarrow q^*X$  and depend on transition magnetic couplings between  $q$  and  $q^*$ . Assumptions about  $q^*$  decay mode are given in the footnotes and comments.

VALUE (GeV)	CL%	DOCUMENT ID	TECN	COMMENT
none 1500–2600	95	1 AABOUD 18AB ATLS	ATLS	$pp \rightarrow b^*X$ , $b^* \rightarrow b\bar{g}$
none 1500–5300	95	2 AABOUD 18BA ATLS	ATLS	$pp \rightarrow q^*X$ , $q^* \rightarrow q\bar{g}$
none 1000–5500	95	3 SIRUNYAN 18AG CMS	CMS	$pp \rightarrow q^*X$ , $q^* \rightarrow q\bar{g}$
none 1000–1800	95	4 SIRUNYAN 18AG CMS	CMS	$pp \rightarrow b^*X$ , $b^* \rightarrow b\bar{g}$
none 600–6000	95	5 SIRUNYAN 18BO CMS	CMS	$pp \rightarrow q^*X$ , $q^* \rightarrow q\bar{g}$
none 1200–5000	95	6 SIRUNYAN 18P CMS	CMS	$pp \rightarrow q^*X$ , $q^* \rightarrow qW$
none 1200–4700	95	7 SIRUNYAN 18P CMS	CMS	$pp \rightarrow q^*X$ , $q^* \rightarrow qZ$
>6000	95	8 AABOUD 17AK ATLS	ATLS	$pp \rightarrow q^*X$ , $q^* \rightarrow q\bar{g}$
•••		••• We do not use the following data for averages, fits, limits, etc. •••		
none 600–5400	95	9 KHACHATRY...17W CMS	CMS	$pp \rightarrow q^*X$ , $q^* \rightarrow q\bar{g}$
none 1100–2100	95	10 AABOUD 16 ATLS	ATLS	$pp \rightarrow b^*X$ , $b^* \rightarrow b\bar{g}$
>1500	95	11 AAD 16AH ATLS	ATLS	$pp \rightarrow b^*X$ , $b^* \rightarrow tW$
>4400	95	12 AAD 16AI ATLS	ATLS	$pp \rightarrow q^*X$ , $q^* \rightarrow q\bar{g}$
>5200	95	13 AAD 16AV ATLS	ATLS	$pp \rightarrow q^*X$ , $q^* \rightarrow Wb$
>1390	95	14 AAD 16S ATLS	ATLS	$pp \rightarrow q^*X$ , $q^* \rightarrow q\bar{g}$
>5000	95	15 KHACHATRY...16I CMS	CMS	$pp \rightarrow b^*X$ , $b^* \rightarrow tW$
none 500–1600	95	16 KHACHATRY...16K CMS	CMS	$pp \rightarrow q^*X$ , $q^* \rightarrow q\bar{g}$
>4060	95	17 KHACHATRY...16L CMS	CMS	$pp \rightarrow q^*X$ , $q^* \rightarrow q\bar{g}$
>3500	95	18 AAD 15V ATLS	ATLS	$pp \rightarrow q^*X$ , $q^* \rightarrow q\bar{g}$
>3500	95	19 KHACHATRY...15V CMS	CMS	$pp \rightarrow q^*X$ , $q^* \rightarrow q\bar{g}$
>3200	95	20 AAD 14A ATLS	ATLS	$pp \rightarrow q^*X$ , $q^* \rightarrow q\bar{g}$
>2900	95	21 KHACHATRY...14 CMS	CMS	$pp \rightarrow q^*X$ , $q^* \rightarrow qW$
none 700–3500	95	22 KHACHATRY...14J CMS	CMS	$pp \rightarrow q^*X$ , $q^* \rightarrow qZ$
>2380	95	23 KHACHATRY...14J CMS	CMS	$pp \rightarrow q^*X$ , $q^* \rightarrow q\bar{g}$
>2150	95	24 CHATRCHYAN 13AJ CMS	CMS	$pp \rightarrow q^*X$ , $q^* \rightarrow qW$

- AABOUD 18AB assume  $\Lambda = m_{b^*}$ ,  $f_5 = f = f' = 1$ . The contact interactions are not included in  $b^*$  production and decay amplitudes.
- AABOUD 18BA search for first-generation excited quarks ( $u^*$  and  $d^*$ ) with degenerate mass, assuming  $\Lambda = m_{q^*}$ ,  $f_5 = f = f' = 1$ . The contact interactions are not included in  $q^*$  production and decay amplitudes.
- SIRUNYAN 18AG search for first-generation excited quarks ( $u^*$  and  $d^*$ ) with degenerate mass, assuming  $\Lambda = m_{q^*}$ ,  $f_5 = f = f' = 1$ .
- SIRUNYAN 18AG search for excited  $b$  quark assuming  $\Lambda = m_{q^*}$ ,  $f_5 = f = f' = 1$ .
- SIRUNYAN 18BO assume  $\Lambda = m_{q^*}$ ,  $f_5 = f = f' = 1$ . The contact interactions are not included in  $q^*$  production and decay amplitudes.
- SIRUNYAN 18P use the hadronic decay of  $W$  or  $Z$ , assuming  $\Lambda = m_{q^*}$ ,  $f_5 = f = f' = 1$ .
- AABOUD 17AK assume  $\Lambda = m_{q^*}$ ,  $f_5 = f = f' = 1$ . The contact interactions are not included in  $q^*$  production and decay amplitudes. Only the decay of  $q^* \rightarrow gW$  and  $q^* \rightarrow gZ$  is simulated as the benchmark signals in the analysis.
- KHACHATRYAN 17W assume  $\Lambda = m_{q^*}$ ,  $f_5 = f = f' = 1$ . The contact interactions are not included in  $q^*$  production and decay amplitudes.
- AABOUD 16 assume  $\Lambda = m_{b^*}$ ,  $f_5 = f = f' = 1$ . The contact interactions are not included in the  $b^*$  production and decay amplitudes.
- AAD 16AH search for  $b^*$  decaying to  $tW$  in  $pp$  collisions at  $\sqrt{s} = 8$  TeV.  $f_g = f_L = f_R = 1$  are assumed. See their Fig. 12b for limits on  $\sigma \cdot B$ .
- AAD 16AI assume  $\Lambda = m_{q^*}$ ,  $f_5 = f = f' = 1$ .
- AAD 16AV search for single production of vector-like quarks decaying to  $Wb$  in  $pp$  collisions. See their Fig. 8 for the limits on couplings and mixings.
- AAD 16S assume  $\Lambda = m_{q^*}$ ,  $f_5 = f = f' = 1$ . The contact interactions are not included in  $q^*$  production and decay amplitudes.
- KHACHATRYAN 16I search for  $b^*$  decaying to  $tW$  in  $pp$  collisions at  $\sqrt{s} = 8$  TeV.  $\kappa_L^b = g_L = 1$ ,  $\kappa_R^b = g_R = 0$  are assumed. See their Fig. 8 for limits on  $\sigma \cdot B$ .
- KHACHATRYAN 16K assume  $\Lambda = m_{q^*}$ ,  $f_5 = f = f' = 1$ . The contact interactions are not included in  $q^*$  production and decay amplitudes.
- KHACHATRYAN 16L search for resonances decaying to dijets in  $pp$  collisions at  $\sqrt{s} = 8$  TeV using the data scouting technique which increases the sensitivity to the low mass resonances.
- AAD 15V assume  $\Lambda = m_{q^*}$ ,  $f_5 = f = f' = 1$ . The contact interactions are not included in  $q^*$  production and decay amplitudes.
- KHACHATRYAN 15V assume  $\Lambda = m_{q^*}$ ,  $f_5 = f = f' = 1$ . The contact interactions are not included in  $q^*$  production and decay amplitudes.
- AAD 14A assume  $\Lambda = m_{q^*}$ ,  $f_5 = f = f' = 1$ .
- KHACHATRYAN 14 use the hadronic decay of  $W$ , assuming  $\Lambda = m_{q^*}$ ,  $f_5 = f = f' = 1$ .
- KHACHATRYAN 14 use the hadronic decay of  $Z$ , assuming  $\Lambda = m_{q^*}$ ,  $f_5 = f = f' = 1$ .
- KHACHATRYAN 14J assume  $f_5 = f = f' = \Lambda / m_{q^*}$ .
- CHATRCHYAN 13AJ use the hadronic decay of  $W$ .
- CHATRCHYAN 13AJ use the hadronic decay of  $Z$ .

### MASS LIMITS for Color Sextet Quarks ( $q_6$ )

VALUE (GeV)	CL%	DOCUMENT ID	TECN	COMMENT
>84	95	1 ABE 89D CDF	CDF	$p\bar{p} \rightarrow q_6\bar{q}_6$

- ABE 89D look for pair production of unit-charged particles which leave the detector before decaying. In the above limit the color sextet quark is assumed to fragment into a unit-charged or neutral hadron with equal probability and to have long enough lifetime not to decay within the detector. A limit of 121 GeV is obtained for a color decuplet.

### MASS LIMITS for Color Octet Charged Leptons ( $\ell_8$ )

$\lambda \equiv m_{\ell_8}/\Lambda$

VALUE (GeV)	CL%	DOCUMENT ID	TECN	COMMENT
>86	95	1 ABE 89D CDF	CDF	Stable $\ell_8$ : $p\bar{p} \rightarrow \ell_8\bar{\ell}_8$

- We do not use the following data for averages, fits, limits, etc. •••
- | VALUE (GeV) | CL% | DOCUMENT ID | TECN | COMMENT                     |
|-------------|-----|-------------|------|-----------------------------|
|             |     | 2 ABT 93 H1 | H1   | $e\bar{p} \rightarrow e_8X$ |
- ABE 89D look for pair production of unit-charged particles which leave the detector before decaying. In the above limit the color octet lepton is assumed to fragment into a unit-charged or neutral hadron with equal probability and to have long enough lifetime not to decay within the detector. The limit improves to 99 GeV if it always fragments into a unit-charged hadron.
  - ABT 93 search for  $e_8$  production via  $e$ -gluon fusion in  $ep$  collisions with  $e_8 \rightarrow e\bar{g}$ . See their Fig. 3 for exclusion plot in the  $m_{e_8}$ - $\lambda$  plane for  $m_{e_8} = 35\text{--}220$  GeV.

### MASS LIMITS for Color Octet Neutrinos ( $\nu_8$ )

$\lambda \equiv m_{\ell_8}/\Lambda$

VALUE (GeV)	CL%	DOCUMENT ID	TECN	COMMENT
>110	90	1 BARGER 89 RVUE	RVUE	$\nu_8$ : $p\bar{p} \rightarrow \nu_8\bar{\nu}_8$

- We do not use the following data for averages, fits, limits, etc. •••
- | VALUE (GeV)   | CL% | DOCUMENT ID       | TECN | COMMENT                                       |
|---------------|-----|-------------------|------|---|
| none 3.8–29.8 | 95  | 2 KIM 90 AMY      | AMY  | $\nu_8$ : $e^+e^- \rightarrow$ acoplanar jets |
| none 9–21.9   | 95  | 3 BARTEL 87B JADE | JADE | $\nu_8$ : $e^+e^- \rightarrow$ acoplanar jets |

See key on page 999

# Searches Particle Listings

## Quark and Lepton Compositeness, Extra Dimensions

- <sup>1</sup> BARGER 89 used ABE 89B limit for events with large missing transverse momentum. Two-body decay  $\nu_g \rightarrow \nu g$  is assumed.
- <sup>2</sup> KIM 90 is at  $E_{cm} = 50\text{--}60.8$  GeV. The same assumptions as in BARTEL 87b are used.
- <sup>3</sup> BARTEL 87b is at  $E_{cm} = 46.3\text{--}46.78$  GeV. The limit assumes the  $\nu g$  pair production cross section to be eight times larger than that of the corresponding heavy neutrino pair production. This assumption is not valid in general for the weak couplings, and the limit can be sensitive to its  $SU(2)_L \times U(1)_Y$  quantum numbers.

### MASS LIMITS for $W_8$ (Color Octet $W$ Boson)

VALUE (GeV)	DOCUMENT ID	TECN	COMMENT
• • • We do not use the following data for averages, fits, limits, etc. • • •			
	<sup>1</sup> ALBAJAR 89 UA1	$p\bar{p} \rightarrow W_8 X, W_8 \rightarrow W g$	
<sup>1</sup> ALBAJAR 89 give $\sigma(W_8 \rightarrow W + \text{jet})/\sigma(W) < 0.019$ (90% CL) for $m_{W_8} > 220$ GeV.			

### REFERENCES FOR Searches for Quark and Lepton Compositeness

ABOUD 19AZ	EPL 79 803	M. Aaboud et al.	(ATLAS Collab.)
ABRAMOWICZ 19	PR D99 092006	H. Abramowicz et al.	(ZEUS Collab.)
SIRUNYAN 19AC	JHEP 1904 114	A.M. Sirunyan et al.	(CMS Collab.)
SIRUNYAN 19Z	JHEP 1904 015	A.M. Sirunyan et al.	(CMS Collab.)
AABOUD 18AB	PR D98 032016	M. Aaboud et al.	(ATLAS Collab.)
AABOUD 18AV	JHEP 1807 089	M. Aaboud et al.	(ATLAS Collab.)
AABOUD 18BA	EPL 78 102	M. Aaboud et al.	(ATLAS Collab.)
SIRUNYAN 18AG	PL B781 390	A.M. Sirunyan et al.	(CMS Collab.)
SIRUNYAN 18BO	JHEP 1808 130	A.M. Sirunyan et al.	(CMS Collab.)
SIRUNYAN 18DD	EPL 78 789	A.M. Sirunyan et al.	(CMS Collab.)
SIRUNYAN 18P	PR D97 072006	A.M. Sirunyan et al.	(CMS Collab.)
SIRUNYAN 18V	PL B778 349	A.M. Sirunyan et al.	(CMS Collab.)
AABOUD 17AK	PR D96 052004	M. Aaboud et al.	(ATLAS Collab.)
AABOUD 17AT	JHEP 1710 182	M. Aaboud et al.	(ATLAS Collab.)
KHACHATRYAN 17W	PL B769 520	V. Khachatryan et al.	(CMS Collab.)
SIRUNYAN 17F	JHEP 1707 013	A.M. Sirunyan et al.	(CMS Collab.)
AABOUD 16	PL B759 229	M. Aaboud et al.	(ATLAS Collab.)
AABOUD 16U	PL B761 372	M. Aaboud et al.	(ATLAS Collab.)
AAD 16AH	JHEP 1602 110	G. Aad et al.	(ATLAS Collab.)
AAD 16AI	JHEP 1603 041	G. Aad et al.	(ATLAS Collab.)
AAD 16AV	EPL 76 442	G. Aad et al.	(ATLAS Collab.)
AAD 16BM	NJP 18 073021	G. Aad et al.	(ATLAS Collab.)
AAD 16S	PL B754 302	G. Aad et al.	(ATLAS Collab.)
KHACHATRYAN 16AQ	JHEP 1603 125	V. Khachatryan et al.	(CMS Collab.)
KHACHATRYAN 16I	JHEP 1601 166	V. Khachatryan et al.	(CMS Collab.)
KHACHATRYAN 16K	PRL 116 071801	V. Khachatryan et al.	(CMS Collab.)
KHACHATRYAN 16L	PRL 117 031802	V. Khachatryan et al.	(CMS Collab.)
AAD 15AP	JHEP 1508 138	G. Aad et al.	(ATLAS Collab.)
AAD 15AR	JHEP 1508 105	G. Aad et al.	(ATLAS Collab.)
AAD 15BY	JHEP 1510 150	G. Aad et al.	(ATLAS Collab.)
AAD 15L	PRL 114 221802	G. Aad et al.	(ATLAS Collab.)
AAD 15V	PR D91 052007	G. Aad et al.	(ATLAS Collab.)
KHACHATRYAN 15AE	JHEP 1504 025	V. Khachatryan et al.	(CMS Collab.)
KHACHATRYAN 15J	JHEP 1508 79	V. Khachatryan et al.	(CMS Collab.)
KHACHATRYAN 15V	PR D91 052009	V. Khachatryan et al.	(CMS Collab.)
AAD 14A	PL B728 562	G. Aad et al.	(ATLAS Collab.)
AAD 14BE	EPL 74 3134	G. Aad et al.	(ATLAS Collab.)
FABBRICHESI 14	PR D89 074028	M. Fabbrichesi, M. Pinamonti, A. Tonerò	
KHACHATRYAN 14	JHEP 1408 173	V. Khachatryan et al.	(CMS Collab.)
KHACHATRYAN 14J	PL B738 274	V. Khachatryan et al.	(CMS Collab.)
AAD 13BB	NJP 15 093011	G. Aad et al.	(ATLAS Collab.)
AAD 13E	PR D87 015010	G. Aad et al.	(ATLAS Collab.)
CHATRCHYAN 13AE	PL B720 309	S. Chatrchyan et al.	(CMS Collab.)
CHATRCHYAN 13AJ	PL B723 280	S. Chatrchyan et al.	(CMS Collab.)
CHATRCHYAN 13K	PR D87 032001	S. Chatrchyan et al.	(CMS Collab.)
AAD 12AB	PL B712 40	G. Aad et al.	(ATLAS Collab.)
AAD 12AZ	PR D85 072003	G. Aad et al.	(ATLAS Collab.)
AARON 11C	PL B705 52	F. D. Aaron et al.	(HI Collab.)
ABDALLAH 11	EPL 71 1555	J. Abdallah et al.	(DELPHI Collab.)
AALTONEN 10H	PRL 104 091801	T. Aaltonen et al.	(CDF Collab.)
ABDALLAH 09	EPL 60 1	J. Abdallah et al.	(DELPHI Collab.)
AARON 08	PL B663 382	F.D. Aaron et al.	(HI Collab.)
SCHAEEL 07A	EPL 69 411	S. Schaeel et al.	(ALEPH Collab.)
ABDALLAH 06C	EPL 65 589	J. Abdallah et al.	(DELPHI Collab.)
ABULENCIA 06L	PRL 96 211801	A. Abulencia et al.	(CDF Collab.)
ABBIENDI 04G	EPL 63 173	G. Abbiendi et al.	(OPAL Collab.)
ABBIENDI 04N	PL B602 167	G. Abbiendi et al.	(OPAL Collab.)
ABDALLAH 04N	EPL 63 405	J. Abdallah et al.	(DELPHI Collab.)
ACHARD 03B	PL B568 23	P. Achard et al.	(L3 Collab.)
BABICH 03	EPL 62 103	A.A. Babich et al.	
ABBIENDI 02G	PL B544 57	G. Abbiendi et al.	(OPAL Collab.)
ACHARD 02D	PL B531 28	P. Achard et al.	(L3 Collab.)
ADLOFF 02	PL B525 9	C. Adloff et al.	(HI Collab.)
CHEKANOV 02D	PL B549 32	S. Chekanov et al.	(ZEUS Collab.)
AFFOLDER 01L	PR 87 231803	T. Affolder et al.	(CDF Collab.)
BOURLIKOV 01	PR D64 071701	D. Bourlikov	
CHEUNG 01B	PL B517 167	K. Cheung	
ACCIARRI 00P	PL B489 81	M. Acciari et al.	(L3 Collab.)
AFFOLDER 00I	PR D62 012004	T. Affolder et al.	(CDF Collab.)
BARATE 98U	EPL 64 571	R. Barate et al.	(ALEPH Collab.)
BARGER 98E	PR D57 391	V. Barger et al.	
MCFARLAND 98	EPL 61 509	K.S. McFarland et al.	(CCFR/NuTeV Collab.)
DIAZCRUZ 94	PR D49 2149	J.L. Diaz Cruz, O.A. Sampayo	(CINV)
ABT 93	NP B396 3	I. Abt et al.	(HI Collab.)
ADRIANIN 93M	PRPL 236 1	O. Adriani et al.	(L3 Collab.)
BARDADIN 92	ZPHY C95 163	M. Bardadin-Otinowska	(CLER)
DECAMP 92	PRPL 216 253	D. Decamp et al.	(ALEPH Collab.)
PDG 92	PR D45 51	K. Hikasa et al.	(KEK, LBL, BOST+)
ABREU 91F	NP B347 511	P. Abreu et al.	(DELPHI Collab.)
KIM 90	PL B240 243	G.N. Kim et al.	(AMY Collab.)
KIM 89B	PRL 62 1825	F. Abe et al.	(CDF Collab.)
ABE 89D	PRL 63 1447	F. Abe et al.	(CDF Collab.)
ABE 89J	ZPHY C45 175	K. Abe et al.	(VENUS Collab.)
ALBAJAR 89	ZPHY C44 15	C. Albajar et al.	(UA1 Collab.)
BARGER 89	PL B220 464	V. Barger et al.	(WIS, KEK)
DORENBOSCH 89	ZPHY C41 567	J. Dorenbosch et al.	(CHARM Collab.)
BARTEL 87B	ZPHY C36 15	W. Bartel et al.	(JADE Collab.)
GRIFOLS 86	PL 168B 264	J.A. Griñols, S. Peris	(BARC)
JODIDIO 86	PR D34 1967	A. Jodidio et al.	(LBL, NWES, TRIU)
Also	PR D37 237 (erratum)	A. Jodidio et al.	(LBL, NWES, TRIU)
RENARD 82	PL 116B 264	F.M. Renard	(CERN)

### Extra Dimensions

For explanation of terms used and discussion of significant model dependence of following limits, see the "Extra Dimensions" review. Footnotes describe originally quoted limit.  $\delta$  indicates the number of extra dimensions.

Limits not encoded here are summarized in the "Extra Dimensions" review, where the latest unpublished results are also described.

### See the related review(s): Extra Dimensions

#### CONTENTS:

- Limits on  $R$  from Deviations in Gravitational Force Law
- Limits on  $R$  from On-Shell Production of Gravitons:  $\delta = 2$
- Mass Limits on  $M_{TT}$
- Limits on  $1/R = M_C$
- Limits on Kaluza-Klein Gravitons in Warped Extra Dimensions
- Limits on Kaluza-Klein Gluons in Warped Extra Dimensions
- Black Hole Production Limits
  - Semiclassical Black Holes
  - Quantum Black Holes

#### Limits on $R$ from Deviations in Gravitational Force Law

This section includes limits on the size of extra dimensions from deviations in the Newtonian ( $1/r^2$ ) gravitational force law at short distances. Deviations are parametrized by a gravitational potential of the form  $V = -(G m m'/r) [1 + \alpha \exp(-r/R)]$ . For  $\delta$  toroidal extra dimensions of equal size,  $\alpha = 8\delta/3$ . Quoted bounds are for  $\delta = 2$  unless otherwise noted.

VALUE ( $\mu\text{m}$ )	CL%	DOCUMENT ID	TECN	COMMENT
$< 30$	95	<sup>1</sup> KAPNER 07	07	Torsion pendulum
• • • We do not use the following data for averages, fits, limits, etc. • • •				
		<sup>2</sup> BERGE 18	MICR	Space accelerometer
		<sup>3</sup> FAYET 18A	MICR	Space accelerometer
		<sup>4</sup> HADDOCK 18		Neutron scattering
		<sup>5</sup> KLIMCHITSKAYA 17A		Torsion oscillator
		<sup>6</sup> XU 13		Nuclei properties
		<sup>7</sup> BEZERRA 11		Torsion oscillator
		<sup>8</sup> SUSHKOV 11		Torsion pendulum
		<sup>9</sup> BEZERRA 10		Microcantilever
		<sup>10</sup> MASUDA 09		Torsion pendulum
		<sup>11</sup> GERACI 08		Microcantilever
		<sup>12</sup> TRENKEL 08		Newton's constant
		<sup>13</sup> DECCA 07A		Torsion oscillator
$< 47$	95	<sup>14</sup> TU 07		Torsion pendulum
		<sup>15</sup> SMULLIN 05		Microcantilever
$< 130$	95	<sup>16</sup> HOYLE 04		Torsion pendulum
		<sup>17</sup> CHIAVERINI 03		Microcantilever
$\lesssim 200$	95	<sup>18</sup> LONG 03		Microcantilever
$< 190$	95	<sup>19</sup> HOYLE 01		Torsion pendulum
		<sup>20</sup> HOSKINS 85		Torsion pendulum

- <sup>1</sup> KAPNER 07 search for new forces, probing a range of  $\alpha \approx 10^{-3}\text{--}10^5$  and length scales  $R \approx 10\text{--}1000$   $\mu\text{m}$ . For  $\delta = 1$  the bound on  $R$  is 44  $\mu\text{m}$ . For  $\delta = 2$ , the bound is expressed in terms of  $M_*$ , here translated to a bound on the radius. See their Fig. 6 for details on the bound.
- <sup>2</sup> BERGE 18 uses results from the MICROSCOPE experiment to obtain constraints on non-Newtonian forces with strengths  $10^{-11} \lesssim |\alpha| \lesssim 10^{-7}$  and length scales  $R \gtrsim 10^5$  m. See their Figure 1 for more details. These constraints do not place limits on the size of extra flat dimensions.
- <sup>3</sup> FAYET 18A uses results from the MICROSCOPE experiment to obtain constraints on an EP-violating force possibly arising from a new  $U(1)$  gauge boson. For  $R \gtrsim 10^7$  m the limits are  $|\alpha| \lesssim$  a few  $10^{-13}$  to a few  $10^{-11}$  depending on the coupling, corresponding to  $|\epsilon| \lesssim 10^{-24}$  for the coupling of the new spin-1 or spin-0 mediator. These constraints do not place limits on the size of extra flat dimensions. This extends the results of FAYET 18.
- <sup>4</sup> HADDOCK 18 obtain constraints on non-Newtonian forces with strengths  $10^{22} \lesssim |\alpha| \lesssim 10^{24}$  and length scales  $R \approx 0.01\text{--}10$  nm. See their Figure 8 for more details. These constraints do not place limits on the size of extra flat dimensions.
- <sup>5</sup> KLIMCHITSKAYA 17A uses an experiment that measures the difference of Casimir forces to obtain bounds on non-Newtonian forces with strengths  $|\alpha| \approx 10^5\text{--}10^{17}$  and length scales  $R = 0.03\text{--}10$   $\mu\text{m}$ . See their Fig. 3. These constraints do not place limits on the size of extra flat dimensions.
- <sup>6</sup> XU 13 obtain constraints on non-Newtonian forces with strengths  $|\alpha| \approx 10^{34}\text{--}10^{36}$  and length scales  $R \approx 1\text{--}10$  fm. See their Fig. 4 for more details. These constraints do not place limits on the size of extra flat dimensions.
- <sup>7</sup> BEZERRA 11 obtain constraints on non-Newtonian forces with strengths  $10^{11} \lesssim |\alpha| \lesssim 10^{18}$  and length scales  $R = 30\text{--}1260$  nm. See their Fig. 2 for more details. These constraints do not place limits on the size of extra flat dimensions.
- <sup>8</sup> SUSHKOV 11 obtain improved limits on non-Newtonian forces with strengths  $10^7 \lesssim |\alpha| \lesssim 10^{11}$  and length scales  $0.4$   $\mu\text{m} < R < 4$   $\mu\text{m}$  (95% CL). See their Fig. 2. These bounds do not place limits on the size of extra flat dimensions. However, a model dependent bound of  $M_* > 70$  TeV is obtained assuming gauge bosons that couple to baryon number also propagate in  $(4 + \delta)$  dimensions.
- <sup>9</sup> BEZERRA 10 obtain improved constraints on non-Newtonian forces with strengths  $10^{19} \lesssim |\alpha| \lesssim 10^{29}$  and length scales  $R = 1.6\text{--}14$  nm (95% CL). See their Fig. 1. This bound does not place limits on the size of extra flat dimensions.

# Searches Particle Listings

## Extra Dimensions

- <sup>10</sup> MASUDA 09 obtain improved constraints on non-Newtonian forces with strengths  $10^9 \lesssim |\alpha| \lesssim 10^{11}$  and length scales  $R = 1.0\text{--}2.9 \mu\text{m}$  (95% CL). See their Fig. 3. This bound does not place limits on the size of extra flat dimensions.
- <sup>11</sup> GERACI 08 obtain improved constraints on non-Newtonian forces with strengths  $|\alpha| > 14,000$  and length scales  $R = 5\text{--}15 \mu\text{m}$ . See their Fig. 9. This bound does not place limits on the size of extra flat dimensions.
- <sup>12</sup> TRENKEL 08 uses two independent measurements of Newton's constant  $G$  to constrain new forces with strength  $|\alpha| \simeq 10^{-4}$  and length scales  $R = 0.02\text{--}1 \text{ m}$ . See their Fig. 1. This bound does not place limits on the size of extra flat dimensions.
- <sup>13</sup> DECCA 07A search for new forces and obtain bounds in the region with strengths  $|\alpha| \simeq 10^{13}\text{--}10^{18}$  and length scales  $R = 20\text{--}86 \text{ nm}$ . See their Fig. 6. This bound does not place limits on the size of extra flat dimensions.
- <sup>14</sup> TU 07 search for new forces probing a range of  $|\alpha| \simeq 10^{-1}\text{--}10^5$  and length scales  $R \simeq 20\text{--}1000 \mu\text{m}$ . For  $\delta = 1$  the bound on  $R$  is  $53 \mu\text{m}$ . See their Fig. 3 for details on the bound.
- <sup>15</sup> SMULLIN 05 search for new forces, and obtain bounds in the region with strengths  $\alpha \simeq 10^3\text{--}10^8$  and length scales  $R = 6\text{--}20 \mu\text{m}$ . See their Figs. 1 and 16 for details on the bound. This work does not place limits on the size of extra flat dimensions.
- <sup>16</sup> HOYLE 04 search for new forces, probing  $\alpha$  down to  $10^{-2}$  and distances down to  $10 \mu\text{m}$ . Quoted bound on  $R$  is for  $\delta = 2$ . For  $\delta = 1$ , bound goes to  $160 \mu\text{m}$ . See their Fig. 34 for details on the bound.
- <sup>17</sup> CHIAVERINI 03 search for new forces, probing  $\alpha$  above  $10^4$  and  $\lambda$  down to  $3 \mu\text{m}$ , finding no signal. See their Fig. 4 for details on the bound. This bound does not place limits on the size of extra flat dimensions.
- <sup>18</sup> LONG 03 search for new forces, probing  $\alpha$  down to 3, and distances down to about  $10 \mu\text{m}$ . See their Fig. 4 for details on the bound.
- <sup>19</sup> HOYLE 01 search for new forces, probing  $\alpha$  down to  $10^{-2}$  and distances down to  $20 \mu\text{m}$ . See their Fig. 4 for details on the bound. The quoted bound is for  $\alpha \geq 3$ .
- <sup>20</sup> HOSKINS 85 search for new forces, probing distances down to 4 mm. See their Fig. 13 for details on the bound. This bound does not place limits on the size of extra flat dimensions.

### Limits on $R$ from On-Shell Production of Gravitons: $\delta = 2$

This section includes limits on on-shell production of gravitons in collider and astrophysical processes. Bounds quoted are on  $R$ , the assumed common radius of the flat extra dimensions, for  $\delta = 2$  extra dimensions. Studies often quote bounds in terms of derived parameter; experiments are actually sensitive to the masses of the KK gravitons:  $m_{\vec{n}} = |\vec{n}|/R$ . See the Review on "Extra Dimensions" for details. Bounds are given in  $\mu\text{m}$  for  $\delta = 2$ .

VALUE ( $\mu\text{m}$ )	CL%	DOCUMENT ID	TECN	COMMENT
< 4.8	95	<sup>1</sup> SIRUNYAN	18s CMS	$pp \rightarrow jG$
< 0.00016	95	<sup>2</sup> HANNESTAD	03	Neutron star heating
• • • We do not use the following data for averages, fits, limits, etc. • • •				
< 8.0	95	<sup>3</sup> AABOUD	18f ATLS	$pp \rightarrow jG$
< 89	95	<sup>4</sup> SIRUNYAN	18bv CMS	$pp \rightarrow ZG$
		<sup>5</sup> SIRUNYAN	17aq CMS	$pp \rightarrow \gamma G$
< 90	95	<sup>6</sup> AABOUD	16f ATLS	$pp \rightarrow \gamma G$
		<sup>7</sup> KHACHATRYAN	16n CMS	$pp \rightarrow \gamma G$
		<sup>8</sup> AAD	15cs ATLS	$pp \rightarrow \gamma G$
< 127	95	<sup>9</sup> AAD	13c ATLS	$pp \rightarrow \gamma G$
< 34.4	95	<sup>10</sup> AAD	13d ATLS	$pp \rightarrow jj$
< 0.0087	95	<sup>11</sup> AJELLO	12 FLAT	Neutron star $\gamma$ sources
< 245	95	<sup>12</sup> AALTONEN	08ac CDF	$p\bar{p} \rightarrow \gamma G, jG$
< 615	95	<sup>13</sup> ABAZOV	08s D0	$p\bar{p} \rightarrow \gamma G, jG$
< 0.916	95	<sup>14</sup> DAS	08	Supernova cooling
< 350	95	<sup>15</sup> ABULENCIA,A	06 CDF	$p\bar{p} \rightarrow jG$
< 270	95	<sup>16</sup> ABDALLAH	05b DLPH	$e^+e^- \rightarrow \gamma G$
< 210	95	<sup>17</sup> ACHARD	04e L3	$e^+e^- \rightarrow \gamma G$
< 480	95	<sup>18</sup> ACOSTA	04c CDF	$p\bar{p} \rightarrow jG$
< 0.00038	95	<sup>19</sup> CASSE	04	Neutron star $\gamma$ sources
< 610	95	<sup>20</sup> ABAZOV	03 D0	$p\bar{p} \rightarrow jG$
< 0.96	95	<sup>21</sup> HANNESTAD	03	Supernova cooling
< 0.096	95	<sup>22</sup> HANNESTAD	03	Diffuse $\gamma$ background
< 0.051	95	<sup>23</sup> HANNESTAD	03	Neutron star $\gamma$ sources
< 300	95	<sup>24</sup> HEISTER	03c ALEP	$e^+e^- \rightarrow \gamma G$
		<sup>25</sup> FAIRBAIRN	01	Cosmology
< 0.66	95	<sup>26</sup> HANHART	01	Supernova cooling
		<sup>27</sup> CASSISI	00	Red giants
< 1300	95	<sup>28</sup> ACCIARRI	99s L3	$e^+e^- \rightarrow ZG$

- <sup>1</sup> SIRUNYAN 18s search for  $pp \rightarrow jG$ , using  $35.9 \text{ fb}^{-1}$  of data at  $\sqrt{s} = 13 \text{ TeV}$  to place lower limits on  $M_D$  for two to six extra dimensions (see their Table VII), from which this bound on  $R$  is derived. This limit supersedes that in KHACHATRYAN 15AL.
- <sup>2</sup> HANNESTAD 03 obtain a limit on  $R$  from the heating of old neutron stars by the surrounding cloud of trapped KK gravitons. Limits for all  $\delta \leq 7$  are given in their Tables V and VI. These limits supersede those in HANNESTAD 02.
- <sup>3</sup> AABOUD 18f search for  $pp \rightarrow jG$ , using  $36.1 \text{ fb}^{-1}$  of data at  $\sqrt{s} = 13 \text{ TeV}$  to place lower limits on  $M_D$  for two to six extra dimensions (see their Table 7), from which this bound on  $R$  is derived. This limit supersedes that in AABOUD 16f.
- <sup>4</sup> SIRUNYAN 18bv search for  $pp \rightarrow ZG$ , using  $35.9 \text{ fb}^{-1}$  of data at  $\sqrt{s} = 13 \text{ TeV}$  to place lower limits on  $M_D$  for two to seven extra dimensions (see their Figure 11), from which this bound on  $R$  is derived.
- <sup>5</sup> SIRUNYAN 17aq search for  $pp \rightarrow \gamma G$ , using  $12.9 \text{ fb}^{-1}$  of data at  $\sqrt{s} = 13 \text{ TeV}$  to place limits on  $M_D$  for three to six extra dimensions (see their Table 3).
- <sup>6</sup> AABOUD 16f search for  $pp \rightarrow \gamma G$ , using  $3.2 \text{ fb}^{-1}$  of data at  $\sqrt{s} = 13 \text{ TeV}$  to place limits on  $M_D$  for two to six extra dimensions (see their Figure 9), from which this bound on  $R$  is derived.
- <sup>7</sup> KHACHATRYAN 16n search for  $pp \rightarrow \gamma G$ , using  $19.6 \text{ fb}^{-1}$  of data at  $\sqrt{s} = 8 \text{ TeV}$  to place limits on  $M_D$  for three to six extra dimensions (see their Table 5).
- <sup>8</sup> AAD 15cs search for  $pp \rightarrow \gamma G$ , using  $20.3 \text{ fb}^{-1}$  of data at  $\sqrt{s} = 8 \text{ TeV}$  to place lower limits on  $M_D$  for two to six extra dimensions (see their Fig. 18).

- <sup>9</sup> AAD 13c search for  $pp \rightarrow \gamma G$ , using  $4.6 \text{ fb}^{-1}$  of data at  $\sqrt{s} = 7 \text{ TeV}$  to place bounds on  $M_D$  for two to six extra dimensions, from which this bound on  $R$  is derived.
- <sup>10</sup> AAD 13d search for the dijet decay of quantum black holes in  $4.8 \text{ fb}^{-1}$  of data produced in  $pp$  collisions at  $\sqrt{s} = 7 \text{ TeV}$  to place bounds on  $M_D$  for two to seven extra dimensions, from which these bounds on  $R$  are derived. Limits on  $M_D$  for all  $\delta \leq 7$  are given in their Table 3.
- <sup>11</sup> AJELLO 12 obtain a limit on  $R$  from the gamma-ray emission of point  $\gamma$  sources that arise from the photon decay of KK gravitons which are gravitationally bound around neutron stars. Limits for all  $\delta \leq 7$  are given in their Table 7.
- <sup>12</sup> AALTONEN 08ac search for  $p\bar{p} \rightarrow \gamma G$  and  $p\bar{p} \rightarrow jG$  at  $\sqrt{s} = 1.96 \text{ TeV}$  with  $2.0 \text{ fb}^{-1}$  and  $1.1 \text{ fb}^{-1}$  respectively, in order to place bounds on the fundamental scale and size of the extra dimensions. See their Table III for limits on all  $\delta \leq 6$ .
- <sup>13</sup> ABAZOV 08s search for  $p\bar{p} \rightarrow \gamma G$ , using  $1 \text{ fb}^{-1}$  of data at  $\sqrt{s} = 1.96 \text{ TeV}$  to place bounds on  $M_D$  for two to eight extra dimensions, from which these bounds on  $R$  are derived. See their paper for intermediate values of  $\delta$ .
- <sup>14</sup> DAS 08 obtain a limit on  $R$  from Kaluza-Klein graviton cooling of SN1987A due to plasmon-plasmon annihilation.
- <sup>15</sup> ABULENCIA,A 06 search for  $p\bar{p} \rightarrow jG$  using  $368 \text{ pb}^{-1}$  of data at  $\sqrt{s} = 1.96 \text{ TeV}$ . See their Table II for bounds for all  $\delta \leq 6$ .
- <sup>16</sup> ABDALLAH 05b search for  $e^+e^- \rightarrow \gamma G$  at  $\sqrt{s} = 180\text{--}209 \text{ GeV}$  to place bounds on the size of extra dimensions and the fundamental scale. Limits for all  $\delta \leq 6$  are given in their Table 6. These limits supersede those in ABREU 00z.
- <sup>17</sup> ACHARD 04 search for  $e^+e^- \rightarrow \gamma G$  at  $\sqrt{s} = 189\text{--}209 \text{ GeV}$  to place bounds on the size of extra dimensions and the fundamental scale. See their Table 8 for limits with  $\delta \leq 8$ . These limits supersede those in ACCIARRI 99r.
- <sup>18</sup> ACOSTA 04c search for  $p\bar{p} \rightarrow jG$  at  $\sqrt{s} = 1.8 \text{ TeV}$  to place bounds on the size of extra dimensions and the fundamental scale. See their paper for bounds on  $\delta = 4, 6$ .
- <sup>19</sup> CASSE 04 obtain a limit on  $R$  from the gamma-ray emission of point  $\gamma$  sources that arises from the photon decay of gravitons around newly born neutron stars, applying the technique of HANNESTAD 03 to neutron stars in the galactic bulge. Limits for all  $\delta \leq 7$  are given in their Table I.
- <sup>20</sup> ABAZOV 03 search for  $p\bar{p} \rightarrow jG$  at  $\sqrt{s} = 1.8 \text{ TeV}$  to place bounds on  $M_D$  for 2 to 7 extra dimensions, from which these bounds on  $R$  are derived. See their paper for bounds on intermediate values of  $\delta$ . We quote results without the approximate NLO scaling introduced in the paper.
- <sup>21</sup> HANNESTAD 03 obtain a limit on  $R$  from graviton cooling of supernova SN1987A. Limits for all  $\delta \leq 7$  are given in their Tables V and VI.
- <sup>22</sup> HANNESTAD 03 obtain a limit on  $R$  from gravitons emitted in supernovae and which subsequently decay, contaminating the diffuse cosmic  $\gamma$  background. Limits for all  $\delta \leq 7$  are given in their Tables V and VI. These limits supersede those in HANNESTAD 02.
- <sup>23</sup> HANNESTAD 03 obtain a limit on  $R$  from gravitons emitted in two recent supernovae and which subsequently decay, creating point  $\gamma$  sources. Limits for all  $\delta \leq 7$  are given in their Tables V and VI. These limits are corrected in the published erratum.
- <sup>24</sup> HEISTER 03c use the process  $e^+e^- \rightarrow \gamma G$  at  $\sqrt{s} = 189\text{--}209 \text{ GeV}$  to place bounds on the size of extra dimensions and the scale of gravity. See their Table 4 for limits with  $\delta \leq 6$  for derived limits on  $M_D$ .
- <sup>25</sup> FAIRBAIRN 01 obtains bounds on  $R$  from over production of KK gravitons in the early universe. Bounds are quoted in paper in terms of fundamental scale of gravity. Bounds depend strongly on temperature of QCD phase transition and range from  $R < 0.13 \mu\text{m}$  to  $0.001 \mu\text{m}$  for  $\delta=2$ ; bounds for  $\delta=3,4$  can be derived from Table 1 in the paper.
- <sup>26</sup> HANHART 01 obtain bounds on  $R$  from limits on graviton cooling of supernova SN 1987a using numerical simulations of proto-neutron star neutrino emission.
- <sup>27</sup> CASSISI 00 obtain rough bounds on  $M_D$  (and thus  $R$ ) from red giant cooling for  $\delta=2,3$ . See their paper for details.
- <sup>28</sup> ACCIARRI 99s search for  $e^+e^- \rightarrow ZG$  at  $\sqrt{s}=189 \text{ GeV}$ . Limits on the gravity scale are found in their Table 2, for  $\delta \leq 4$ .

### Mass Limits on $M_{TT}$

This section includes limits on the cut-off mass scale,  $M_{TT}$ , of dimension-8 operators from KK graviton exchange in models of large extra dimensions. Ambiguities in the UV-divergent summation are absorbed into the parameter  $\lambda$ , which is taken to be  $\lambda = \pm 1$  in the following analyses. Bounds for  $\lambda = -1$  are shown in parenthesis after the bound for  $\lambda = +1$ , if appropriate. Different papers use slightly different definitions of the mass scale. The definition used here is related to another popular convention by  $M_{TT}^4 = (2/\pi) \Lambda_{\text{Pl}}^4$ , as discussed in the above Review on "Extra Dimensions."

VALUE (TeV)	CL%	DOCUMENT ID	TECN	COMMENT
> 9.02	95	<sup>1</sup> SIRUNYAN	18dd CMS	$pp \rightarrow$ dijet, ang. distrib.
> 20.6	(> 15.7)	<sup>2</sup> GIUDICE	03 RVUE	Dim-6 operators
• • • We do not use the following data for averages, fits, limits, etc. • • •				
> 6.9	95	<sup>3</sup> SIRUNYAN	19ac CMS	$pp \rightarrow e^+e^-, \mu^+\mu^-, \gamma\gamma$
> 7.0	(> 5.6)	<sup>4</sup> SIRUNYAN	18du CMS	$pp \rightarrow \gamma\gamma$
> 6.5	95	<sup>5</sup> AABOUD	17ap ATLS	$pp \rightarrow \gamma\gamma$
> 3.8	95	<sup>6</sup> AAD	14be ATLS	$pp \rightarrow e^+e^-, \mu^+\mu^-$
> 3.2	95	<sup>7</sup> AAD	13e ATLS	$pp \rightarrow e^+e^-, \mu^+\mu^-, \gamma\gamma$
		<sup>8</sup> BAAK	12 RVUE	Electroweak
> 0.90	(> 0.92)	<sup>9</sup> AARON	11c H1	$e^{\pm}p \rightarrow e^{\pm}X$
> 1.48	95	<sup>10</sup> ABAZOV	09ae D0	$p\bar{p} \rightarrow$ dijet, ang. distrib.
> 1.45	95	<sup>11</sup> ABAZOV	09d D0	$p\bar{p} \rightarrow e^+e^-, \gamma\gamma$
> 1.1	(> 1.0)	<sup>12</sup> SCHAEEL	07a ALEP	$e^+e^- \rightarrow e^+e^-$
> 0.898	(> 0.998)	<sup>13</sup> ABDALLAH	06c DLPH	$e^+e^- \rightarrow \ell^+\ell^-$
> 0.853	(> 0.939)	<sup>14</sup> GERDES	06	$p\bar{p} \rightarrow e^+e^-, \gamma\gamma$
> 0.96	(> 0.93)	<sup>15</sup> ABAZOV	05v D0	$p\bar{p} \rightarrow \mu^+\mu^-$
> 0.78	(> 0.79)	<sup>16</sup> CHEKANOV	04b ZEUS	$e^{\pm}p \rightarrow e^{\pm}X$
> 0.805	(> 0.956)	<sup>17</sup> ABBIENDI	03d OPAL	$e^+e^- \rightarrow \gamma\gamma$
> 0.7	(> 0.7)	<sup>18</sup> ACHARD	03d L3	$e^+e^- \rightarrow ZZ$
> 0.82	(> 0.78)	<sup>19</sup> ADLOFF	03 H1	$e^{\pm}p \rightarrow e^{\pm}X$
> 1.28	(> 1.25)	<sup>20</sup> GIUDICE	03 RVUE	
> 0.80	(> 0.85)	<sup>21</sup> HEISTER	03c ALEP	$e^+e^- \rightarrow \gamma\gamma$

> 0.84	(> 0.99)	95	22	ACHARD	02D L3	$e^+e^- \rightarrow \gamma\gamma$
> 1.2	(> 1.1)	95	23	ABBOTT	01 D0	$p\bar{p} \rightarrow e^+e^-, \gamma\gamma$
> 0.60	(> 0.63)	95	24	ABBIENDI	00R OPAL	$e^+e^- \rightarrow \mu^+\mu^-$
> 0.63	(> 0.50)	95	24	ABBIENDI	00R OPAL	$e^+e^- \rightarrow \tau^+\tau^-$
> 0.68	(> 0.61)	95	24	ABBIENDI	00R OPAL	$e^+e^- \rightarrow \mu^+\mu^-, \tau^+\tau^-$
			25	ABREU	00A DLPH	$e^+e^- \rightarrow \gamma\gamma$
> 0.680	(> 0.542)	95	26	ABREU	00S DLPH	$e^+e^- \rightarrow \mu^+\mu^-, \tau^+\tau^-$
> 15-28		99.7	27	CHANG	00B RVUE	Electroweak
> 0.98		95	28	CHEUNG	00 RVUE	$e^+e^- \rightarrow \gamma\gamma$
> 0.29-0.38		95	29	GRAESSER	00 RVUE	$(g-2)_\mu$
> 0.50-1.1		95	30	HAN	00 RVUE	Electroweak
> 2.0	(> 2.0)	95	31	MATHEWS	00 RVUE	$p\bar{p} \rightarrow jj$
> 1.0	(> 1.1)	95	32	MELE	00 RVUE	$e^+e^- \rightarrow VV$
			33	ABBIENDI	99P OPAL	
			34	ACCIARRI	99M L3	
			35	ACCIARRI	99S L3	
> 1.412	(> 1.077)	95	36	BOURILKOV	99	$e^+e^- \rightarrow e^+e^-$

- 1 SIRUNYAN 18DD use dijet angular distributions in  $35.9 \text{ fb}^{-1}$  of data from  $pp$  collisions at  $\sqrt{s} = 13 \text{ TeV}$  to place a lower bound on  $\Lambda_T$ , here converted to  $M_{TT}$ . This updates the results of SIRUNYAN 17F.
- 2 GIUDICE 03 place bounds on  $\Lambda_6$ , the coefficient of the gravitationally-induced dimension-6 operator  $(2\pi\lambda/\Lambda_6^2)(\sum \bar{T}_i \gamma_i^5 \eta)(\sum \bar{T}_i \gamma_i^5 \eta)$ , using data from a variety of experiments. Results are quoted for  $\lambda = \pm 1$  and are independent of  $\delta$ .
- 3 SIRUNYAN 19AC use  $35.9 (36.3) \text{ fb}^{-1}$  of data from  $pp$  collisions at  $\sqrt{s} = 13 \text{ TeV}$  in the dielectron (dimuon) channels to place a lower limit on  $\Lambda_T$ , here converted to  $M_{TT}$ . The dielectron and dimuon channels are combined with previous results in the diphoton channel to set the best limit. Bounds on individual channels and different priors can be found in their Table 2. This updates the results in KHACHATRYAN 15AE.
- 4 SIRUNYAN 18DU use  $35.9 \text{ fb}^{-1}$  of data from  $pp$  collisions at  $\sqrt{s} = 13 \text{ TeV}$  to place lower limits on  $M_{TT}$  (equivalent to their  $M_S$ ). This updates the results of CHATRCHYAN 12R.
- 5 ABOUD 17AP use  $36.7 \text{ fb}^{-1}$  of data from  $pp$  collisions at  $\sqrt{s} = 13 \text{ TeV}$  to place lower limits on  $M_{TT}$  (equivalent to their  $M_S$ ). This updates the results of AAD 13As.
- 6 AAD 14BE use  $20 \text{ fb}^{-1}$  of data from  $pp$  collisions at  $\sqrt{s} = 8 \text{ TeV}$  in the dielectron channel to place lower limits on  $M_{TT}$  (equivalent to their  $M_S$ ).
- 7 AAD 13E use  $4.9$  and  $5.0 \text{ fb}^{-1}$  of data from  $pp$  collisions at  $\sqrt{s} = 7 \text{ TeV}$  in the dielectron and dimuon channels, respectively, to place lower limits on  $M_{TT}$  (equivalent to their  $M_S$ ). The dielectron and dimuon channels are combined with previous results in the diphoton channel to set the best limit. Bounds on individual channels and different priors can be found in their Table VIII.
- 8 BAAK 12 use electroweak precision observables to place bounds on the ratio  $\Lambda_T/M_D$  as a function of  $M_D$ . See their Fig. 22 for constraints with a Higgs mass of  $120 \text{ GeV}$ .
- 9 AARON 11C search for deviations in the differential cross section of  $e^\pm p \rightarrow e^\pm X$  in  $446 \text{ pb}^{-1}$  of data taken at  $\sqrt{s} = 301$  and  $319 \text{ GeV}$  to place a bound on  $M_{TT}$ .
- 10 ABZOV 09AE use dijet angular distributions in  $0.7 \text{ fb}^{-1}$  of data from  $p\bar{p}$  collisions at  $\sqrt{s} = 1.96 \text{ TeV}$  to place lower bounds on  $\Lambda_T$  (equivalent to their  $M_S$ ), here converted to  $M_{TT}$ .
- 11 ABZOV 09B use  $1.05 \text{ fb}^{-1}$  of data from  $p\bar{p}$  collisions at  $\sqrt{s} = 1.96 \text{ TeV}$  to place lower bounds on  $\Lambda_T$  (equivalent to their  $M_S$ ), here converted to  $M_{TT}$ .
- 12 SCHAEEL 07A use  $e^+e^-$  collisions at  $\sqrt{s} = 189-209 \text{ GeV}$  to place lower limits on  $\Lambda_T$ , here converted to limits on  $M_{TT}$ .
- 13 ABDALLAH 06C use  $e^+e^-$  collisions at  $\sqrt{s} \sim 130-207 \text{ GeV}$  to place lower limits on  $M_{TT}$ , which is equivalent to their definition of  $M_S$ . Bound shown includes all possible final state leptons,  $\ell = e, \mu, \tau$ . Bounds on individual leptonic final states can be found in their Table 31.
- 14 GERDES 06 use  $100$  to  $110 \text{ pb}^{-1}$  of data from  $p\bar{p}$  collisions at  $\sqrt{s} = 1.8 \text{ TeV}$ , as recorded by the CDF Collaboration during Run I of the Tevatron. Bound shown includes a  $K$ -factor of  $1.3$ . Bounds on individual  $e^+e^-$  and  $\gamma\gamma$  final states are found in their Table I.
- 15 ABZOV 05V use  $246 \text{ pb}^{-1}$  of data from  $p\bar{p}$  collisions at  $\sqrt{s} = 1.96 \text{ TeV}$  to search for deviations in the differential cross section to  $\mu^+\mu^-$  from graviton exchange.
- 16 CHEKANOV 04B search for deviations in the differential cross section of  $e^\pm p \rightarrow e^\pm X$  with  $130 \text{ pb}^{-1}$  of combined data and  $Q^2$  values up to  $40,000 \text{ GeV}^2$  to place a bound on  $M_{TT}$ .
- 17 ABBIENDI 03D use  $e^+e^-$  collisions at  $\sqrt{s} = 181-209 \text{ GeV}$  to place bounds on the ultraviolet scale  $M_{TT}$ , which is equivalent to their definition of  $M_S$ .
- 18 ACHARD 03D look for deviations in the cross section for  $e^+e^- \rightarrow ZZ$  from  $\sqrt{s} = 200-209 \text{ GeV}$  to place a bound on  $M_{TT}$ .
- 19 ADLOFF 03 search for deviations in the differential cross section of  $e^\pm p \rightarrow e^\pm X$  at  $\sqrt{s} = 301$  and  $319 \text{ GeV}$  to place bounds on  $M_{TT}$ .
- 20 GIUDICE 03 review existing experimental bounds on  $M_{TT}$  and derive a combined limit.
- 21 HEISTER 03C use  $e^+e^-$  collisions at  $\sqrt{s} = 189-209 \text{ GeV}$  to place bounds on the scale of dim-8 gravitational interactions. Their  $M_S^\pm$  is equivalent to our  $M_{TT}$  with  $\lambda = \pm 1$ .
- 22 ACHARD 02 search for s-channel graviton exchange effects in  $e^+e^- \rightarrow \gamma\gamma$  at  $E_{cm} = 192-209 \text{ GeV}$ .
- 23 ABBOTT 01 search for variations in differential cross sections to  $e^+e^-$  and  $\gamma\gamma$  final states at the Tevatron.
- 24 ABBIENDI 00R uses  $e^+e^-$  collisions at  $\sqrt{s} = 189 \text{ GeV}$ .
- 25 ABREU 00A search for s-channel graviton exchange effects in  $e^+e^- \rightarrow \gamma\gamma$  at  $E_{cm} = 189-202 \text{ GeV}$ .
- 26 ABREU 00S uses  $e^+e^-$  collisions at  $\sqrt{s} = 183$  and  $189 \text{ GeV}$ . Bounds on  $\mu$  and  $\tau$  individual final states given in paper.
- 27 CHANG 00B derive  $3\sigma$  limit on  $M_{TT}$  of  $(28, 19, 15) \text{ TeV}$  for  $\delta = (2, 4, 6)$  respectively assuming the presence of a torsional coupling in the gravitational action. Highly model dependent.
- 28 CHEUNG 00 obtains limits from anomalous diphoton production at OPAL due to graviton exchange. Original limit for  $\delta = 4$ . However, unknown UV theory renders  $\delta$  dependence unreliable. Original paper works in HLZ convention.
- 29 GRAESSER 00 obtains a bound from graviton contributions to  $g-2$  of the muon through loops of  $0.29 \text{ TeV}$  for  $\delta = 2$  and  $0.38 \text{ TeV}$  for  $\delta = 4, 6$ . Limits scale as  $\lambda^{1/2}$ . However

calculational scheme not well-defined without specification of high-scale theory. See the "Extra Dimensions Review."

- 30 HAN 00 calculates corrections to gauge boson self-energies from KK graviton loops and constrain them using  $S$  and  $T$ . Bounds on  $M_{TT}$  range from  $0.5 \text{ TeV}$  ( $\delta = 6$ ) to  $1.1 \text{ TeV}$  ( $\delta = 2$ ); see text. Limits have strong dependence,  $\lambda^{\delta+2}$ , on unknown  $\lambda$  coefficient.
- 31 MATHEWS 00 search for evidence of graviton exchange in CDF and D0 dijet production data. See their Table 2 for slightly stronger  $\delta$ -dependent bounds. Limits expressed in terms of  $\bar{M}_S^4 = M_{TT}^4/8$ .
- 32 MELE 00 obtains bound from KK graviton contributions to  $e^+e^- \rightarrow VV$  ( $V = \gamma, W, Z$ ) at LEP. Authors use Hewett conventions.
- 33 ABBIENDI 99P search for s-channel graviton exchange effects in  $e^+e^- \rightarrow \gamma\gamma$  at  $E_{cm} = 189 \text{ GeV}$ . The limits  $G_\pm > 660 \text{ GeV}$  and  $G_- > 634 \text{ GeV}$  are obtained from combined  $E_{cm} = 183$  and  $189 \text{ GeV}$  data, where  $G_\pm$  is a scale related to the fundamental gravity scale.
- 34 ACCIARRI 99M search for the reaction  $e^+e^- \rightarrow \gamma G$  and s-channel graviton exchange effects in  $e^+e^- \rightarrow \gamma\gamma, W^+W^-, ZZ, e^+e^-, \mu^+\mu^-, \tau^+\tau^-, q\bar{q}$  at  $E_{cm} = 183 \text{ GeV}$ . Limits on the gravity scale are listed in their Tables 1 and 2.
- 35 ACCIARRI 99S search for the reaction  $e^+e^- \rightarrow ZG$  and s-channel graviton exchange effects in  $e^+e^- \rightarrow \gamma\gamma, W^+W^-, ZZ, e^+e^-, \mu^+\mu^-, \tau^+\tau^-, q\bar{q}$  at  $E_{cm} = 189 \text{ GeV}$ . Limits on the gravity scale are listed in their Tables 1 and 2.
- 36 BOURILKOV 99 performs global analysis of LEP data on  $e^+e^-$  collisions at  $\sqrt{s} = 183$  and  $189 \text{ GeV}$ . Bound is on  $\Lambda_T$ .

### Limits on $1/R = M_C$

This section includes limits on  $1/R = M_C$ , the compactification scale in models with one TeV-sized extra dimension, due to exchange of Standard Model KK excitations. Bounds assume fermions are not in the bulk, unless stated otherwise. See the "Extra Dimensions" review for discussion of model dependence.

VALUE (TeV)	CL%	DOCUMENT ID	TECN	COMMENT
>4.16	95	1 AAD	12CC ATLS	$pp \rightarrow t\bar{t}$
>6.1		2 BARBIERI	04 RVUE	Electroweak
		••• We do not use the following data for averages, fits, limits, etc. •••		
		3 ABOUD	18AV ATLS	$pp \rightarrow t\bar{t}t\bar{t}$
		4 ABOUD	18CE ATLS	$pp \rightarrow t\bar{t}t\bar{t}$
>3.8	95	5 ACCOMANDO 15	RVUE	Electroweak
>3.40	95	6 KHACHATRY...15T	CMS	$pp \rightarrow \ell X$
		7 CHATRCHYAN13AQ	CMS	$pp \rightarrow \ell X$
>1.38	95	8 CHATRCHYAN13W	CMS	$pp \rightarrow \gamma\gamma, \delta=6, M_D=5 \text{ TeV}$
>0.715	95	9 EDELHAUSER 13	RVUE	$pp \rightarrow \ell\bar{\ell} + X$
>1.40	95	10 AAD	12CP ATLS	$pp \rightarrow \gamma\gamma, \delta=6, M_D=5 \text{ TeV}$
>1.23	95	11 AAD	12X ATLS	$pp \rightarrow \gamma\gamma, \delta=6, M_D=5 \text{ TeV}$
>0.26	95	12 ABZOV	12M D0	$p\bar{p} \rightarrow \mu\mu$
>0.75	95	13 BAAK	12 RVUE	Electroweak
		14 FLACKE	12 RVUE	Electroweak
>0.43	95	15 NISHIWAKI	12 RVUE	$H \rightarrow WW, \gamma\gamma$
>0.729	95	16 AAD	11F ATLS	$pp \rightarrow \gamma\gamma, \delta=6, M_D=5 \text{ TeV}$
>0.961	95	17 AAD	11X ATLS	$pp \rightarrow \gamma\gamma, \delta=6, M_D=5 \text{ TeV}$
>0.477	95	18 ABZOV	10P D0	$p\bar{p} \rightarrow \gamma\gamma, \delta=6, M_D=5 \text{ TeV}$
>1.59	95	19 ABZOV	09AE D0	$p\bar{p} \rightarrow$ dijet, angular dist.
>0.6	95	20 HAISCH	07 RVUE	$\bar{B} \rightarrow X_S \gamma$
>0.6	90	21 GOGOLADZE	06 RVUE	Electroweak
>3.3	95	22 CORNET	00 RVUE	Electroweak
> 3.3-3.8	95	23 RIZZO	00 RVUE	Electroweak

- 1 AAD 12cc use  $4.9$  and  $5.0 \text{ fb}^{-1}$  of data from  $pp$  collisions at  $\sqrt{s} = 7 \text{ TeV}$  in the dielectron and dimuon channels, respectively, to place a lower bound on the mass of the lightest KK  $Z/\gamma$  boson (equivalent to  $1/R = M_C$ ). The limit quoted here assumes a flat prior corresponding to when the pure  $Z/\gamma$  KK cross section term dominates. See their Section 15 for more details.
- 2 BARBIERI 04 use electroweak precision observables to place a lower bound on the compactification scale  $1/R$ . Both the gauge bosons and the Higgs boson are assumed to propagate in the bulk.
- 3 ABOUD 18AV use  $36.1 \text{ fb}^{-1}$  of data from  $pp$  collisions at  $\sqrt{s} = 13 \text{ TeV}$  in final states with multiple b-jets, to place a lower bound on the compactification scale in a model with two universal extra dimensions. Assuming the radii of the two extra dimensions are equal, a lower limit of  $1.8 \text{ TeV}$  for the Kaluza-Klein mass is obtained.
- 4 ABOUD 18CE use  $36.1 \text{ fb}^{-1}$  of data from  $pp$  collisions at  $\sqrt{s} = 13 \text{ TeV}$  in final states with same-charge leptons and b-jets, to place a lower bound on the compactification scale in a model with two universal extra dimensions. Assuming the radii of the two extra dimensions are equal, a lower limit of  $1.45 \text{ TeV}$  for the Kaluza-Klein mass is obtained.
- 5 ACCOMANDO 15 use electroweak precision observables to place a lower bound on the compactification scale  $1/R$ . See their Fig. 2 for the bound as a function of  $\sin\beta$ , which parametrizes the VEV contribution from brane and bulk Higgs fields. The quoted value is for the minimum bound which occurs at  $\sin\beta = 0.45$ .
- 6 KHACHATRYAN 15T use  $19.7 \text{ fb}^{-1}$  of data from  $pp$  collisions at  $\sqrt{s} = 8 \text{ TeV}$  to place a lower bound on the compactification scale  $1/R$ .
- 7 CHATRCHYAN 13AQ use  $5.0 \text{ fb}^{-1}$  of data from  $pp$  collisions at  $\sqrt{s} = 7 \text{ TeV}$  and a further  $3.7 \text{ fb}^{-1}$  of data at  $\sqrt{s} = 8 \text{ TeV}$  to place a lower bound on the compactification scale  $1/R$ , in models with universal extra dimensions and Standard Model fields propagating in the bulk. See their Fig. 5 for the bound as a function of the universal bulk fermion mass parameter  $\mu$ .
- 8 CHATRCHYAN 13W use diphoton events with large missing transverse momentum in  $4.93 \text{ fb}^{-1}$  of data produced from  $pp$  collisions at  $\sqrt{s} = 7 \text{ TeV}$  to place a lower bound on the compactification scale in a universal extra dimension model with gravitational decays. The bound assumes that the cutoff scale  $\Lambda$ , for the radiative corrections to the Kaluza-Klein masses, satisfies  $\Lambda/M_C = 20$ . The model parameters are chosen such that the decay  $\gamma^* \rightarrow G\gamma$  occurs with an appreciable branching fraction.
- 9 EDELHAUSER 13 use  $19.6$  and  $20.6 \text{ fb}^{-1}$  of data from  $pp$  collisions at  $\sqrt{s} = 8 \text{ TeV}$  analyzed by the CMS Collaboration in the dielectron and dimuon channels, respectively,

Reference	Process	Model	Bound	Model	Process
to place a lower bound on the mass of the second lightest Kaluza-Klein $Z/\gamma$ boson (converted to a limit on $1/R = M_C$ ). The bound assumes Standard Model fields propagating in the bulk and that the cutoff scale $\Lambda$ , for the radiative corrections to the Kaluza-Klein masses, satisfies $\Lambda/M_C = 20$ .					
10 AAD 12CP use diphoton events with large missing transverse momentum in 4.8 fb <sup>-1</sup> of data produced from $pp$ collisions at $\sqrt{s} = 7$ TeV to place a lower bound on the compactification scale in a universal extra dimension model with gravitational decays. The bound assumes that the cutoff scale $\Lambda$ , for the radiative corrections to the Kaluza-Klein masses, satisfies $\Lambda/M_C = 20$ . The model parameters are chosen such that the decay $\gamma^* \rightarrow G\gamma$ occurs with an appreciable branching fraction.	$pp \rightarrow G \rightarrow ZZ$		>1.8	95	19 SIRUNYAN 18Bk CMS
11 AAD 12X use diphoton events with large missing transverse momentum in 1.07 fb <sup>-1</sup> of data produced from $pp$ collisions at $\sqrt{s} = 7$ TeV to place a lower bound on the compactification scale in a universal extra dimension model with gravitational decays. The bound assumes that the cutoff scale $\Lambda$ , for the radiative corrections to the Kaluza-Klein masses, satisfies $\Lambda/M_C = 20$ . The model parameters are chosen such that the decay $\gamma^* \rightarrow G\gamma$ occurs with an appreciable branching fraction.	$pp \rightarrow G \rightarrow jj$		>4.1	95	20 SIRUNYAN 18Bo CMS
12 ABAZOV 12M use same-sign dimuon events in 7.3 fb <sup>-1</sup> of data from $p\bar{p}$ collisions at $\sqrt{s} = 1.96$ TeV to place a lower bound on the compactification scale $1/R$ , in models with universal extra dimensions where all Standard Model fields propagate in the bulk.	$pp \rightarrow G \rightarrow HH$		>4.1	95	21 SIRUNYAN 18cw CMS
13 BAAK 12 use electroweak precision observables to place a lower bound on the compactification scale $1/R$ , in models with universal extra dimensions and Standard Model fields propagating in the bulk. Bound assumes a 125 GeV Higgs mass. See their Fig. 25 for the bound as a function of the Higgs mass.	$pp \rightarrow G \rightarrow ZZ$		>2.68	95	22 SIRUNYAN 18DJ CMS
14 FLACKE 12 use electroweak precision observables to place a lower bound on the compactification scale $1/R$ , in models with universal extra dimensions and Standard Model fields propagating in the bulk. See their Fig. 1 for the bound as a function of the universal bulk fermion mass parameter $\mu$ .	$pp \rightarrow G \rightarrow \gamma\gamma$		>1.23 (>0.84)	95	23 SIRUNYAN 18DU CMS
15 NISHIWAKI 12 use up to 2 fb <sup>-1</sup> of data from the ATLAS and CMS experiments that constrains the production cross section of a Higgs-like particle to place a lower bound on the compactification scale $1/R$ in universal extra dimension models. The quoted bound assumes Standard Model fields propagating in the bulk and a 125 GeV Higgs mass. See their Fig. 1 for the bound as a function of the Higgs mass.	$pp \rightarrow G \rightarrow HH$		>0.94 (>0.71)	95	24 SIRUNYAN 18F CMS
16 AAD 11F use diphoton events with large missing transverse energy in 3.1 pb <sup>-1</sup> of data produced from $pp$ collisions at $\sqrt{s} = 7$ TeV to place a lower bound on the compactification scale in a universal extra dimension model with gravitational decays. The bound assumes that the cutoff scale $\Lambda$ , for the radiative corrections to the Kaluza-Klein masses, satisfies $\Lambda/M_C = 20$ . The model parameters are chosen such that the decay $\gamma^* \rightarrow G\gamma$ occurs with an appreciable branching fraction.	$pp \rightarrow G \rightarrow b\bar{b}$		>2.23	95	25 SIRUNYAN 18I CMS
17 AAD 11X use diphoton events with large missing transverse energy in 36 pb <sup>-1</sup> of data produced from $pp$ collisions at $\sqrt{s} = 7$ TeV to place a lower bound on the compactification scale in a universal extra dimension model with gravitational decays. The bound assumes that the cutoff scale $\Lambda$ , for the radiative corrections to the Kaluza-Klein masses, satisfies $\Lambda/M_C = 20$ . The model parameters are chosen such that the decay $\gamma^* \rightarrow G\gamma$ occurs with an appreciable branching fraction.	$pp \rightarrow G \rightarrow W\bar{W}, ZZ$		>0.845	95	26 SIRUNYAN 18P CMS
18 ABAZOV 10P use diphoton events with large missing transverse energy in 6.3 fb <sup>-1</sup> of data produced from $p\bar{p}$ collisions at $\sqrt{s} = 1.96$ TeV to place a lower bound on the compactification scale in a universal extra dimension model with gravitational decays. The bound assumes that the cutoff scale $\Lambda$ , for the radiative corrections to the Kaluza-Klein masses, satisfies $\Lambda/M_C = 20$ . The model parameters are chosen such that the decay $\gamma^* \rightarrow G\gamma$ occurs with an appreciable branching fraction.	$pp \rightarrow G \rightarrow \gamma\gamma$		>1.058	95	27 AABOUD 17AP ATLS
19 ABAZOV 09AE use dijet angular distributions in 0.7 fb <sup>-1</sup> of data from $p\bar{p}$ collisions at $\sqrt{s} = 1.96$ TeV to place a lower bound on the compactification scale.	$pp \rightarrow G \rightarrow W\bar{W}, ZZ$		>0.754	95	28 AAD 16R ATLS
20 HAISCH 07 use inclusive $B$ -meson decays to place a Higgs mass independent bound on the compactification scale $1/R$ in the minimal universal extra dimension model.	$pp \rightarrow G \rightarrow ZZ$		>0.607	95	29 AAD 15AU ATLS
21 GOGOLADZE 06 use electroweak precision observables to place a lower bound on the compactification scale in models with universal extra dimensions. Bound assumes a 115 GeV Higgs mass. See their Fig. 3 for the bound as a function of the Higgs mass.	$pp \rightarrow G \rightarrow WW$		>1.05	95	30 AAD 15AZ ATLS
22 CORNET 00 translates a bound on the coefficient of the 4-fermion operator $(\bar{\ell}\gamma_\mu\tau^a\ell)(\bar{\ell}\gamma^\mu\tau^a\ell)$ derived by Hagiwara and Matsumoto into a limit on the mass scale of KK $W$ bosons.	$pp \rightarrow G \rightarrow W\bar{W}, ZZ$		>0.90	95	31 AAD 15CT ATLS
23 RIZZO 00 obtains limits from global electroweak fits in models with a Higgs in the bulk (3.8 TeV) or on the standard brane (3.3 TeV).	$pp \rightarrow G \rightarrow e^+e^-, \mu^+\mu^-$		>0.889	95	32 AAD 14V ATLS
	$pp \rightarrow G \rightarrow WW$		>0.785	95	33 AAD 13A ATLS
	$pp \rightarrow G \rightarrow WW$		>0.71	95	34 AAD 13AO ATLS
	$pp \rightarrow G \rightarrow WW$			95	35 AAD 13AS ATLS
	$pp \rightarrow G \rightarrow ZZ$			95	36 AAD 12AD ATLS
	$p\bar{p} \rightarrow G \rightarrow ZZ$			95	37 AALTONEN 12V CDF
	Electroweak			95	38 BAAK 12 RVUE
	$p\bar{p} \rightarrow G \rightarrow ZZ$			95	39 AALTONEN 11G CDF
	$p\bar{p} \rightarrow G \rightarrow e^+e^-, \gamma\gamma$			95	40 AALTONEN 11R CDF
	$p\bar{p} \rightarrow G \rightarrow WW$			95	41 ABAZOV 11H D0
	$p\bar{p} \rightarrow G \rightarrow WW$			95	42 AALTONEN 10N CDF
	$p\bar{p} \rightarrow G \rightarrow e^+e^-, \gamma\gamma$			95	43 ABAZOV 10F D0
	$p\bar{p} \rightarrow G \rightarrow ZZ$			95	44 AALTONEN 08S CDF
	$p\bar{p} \rightarrow G \rightarrow e^+e^-, \gamma\gamma$			95	45 ABAZOV 08J D0
	$p\bar{p} \rightarrow G \rightarrow \gamma\gamma$			95	46 AALTONEN 07G CDF
	$p\bar{p} \rightarrow G \rightarrow e\bar{e}$			95	47 AALTONEN 07H CDF
	$p\bar{p} \rightarrow G \rightarrow \ell\ell, \gamma\gamma$			95	48 ABAZOV 05N D0
	$p\bar{p} \rightarrow G \rightarrow \ell\bar{\ell}$			95	49 ABULENCIA 05A CDF

### Limits on Kaluza-Klein Gravitons in Warped Extra Dimensions

This section places limits on the mass of the first Kaluza-Klein (KK) excitation of the graviton in the warped extra dimension model of Randall and Sundrum. Bounds in parenthesis assume Standard Model fields propagate in the bulk. Experimental bounds depend strongly on the warp parameter,  $k$ . See the "Extra Dimensions" review for a full discussion.

Here we list limits for the value of the warp parameter  $k/\bar{M}_P = 0.1$ .

VALUE (TeV)	CL%	DOCUMENT ID	TECN	COMMENT
>4.25	95	1 SIRUNYAN 18BB CMS	$pp \rightarrow G \rightarrow e^+e^-, \mu^+\mu^-$	
• • • We do not use the following data for averages, fits, limits, etc. • • •				
2 AAD 20C ATLS		$pp \rightarrow G \rightarrow HH$		
3 AABOUD 19A ATLS		$pp \rightarrow G \rightarrow HH$		
4 AABOUD 19O ATLS		$pp \rightarrow G \rightarrow HH$		
5 AAD 19D ATLS		$pp \rightarrow G \rightarrow W\bar{W}, ZZ$		
6 SIRUNYAN 19I CMS		$pp \rightarrow G \rightarrow HH$		
7 SIRUNYAN 19BE CMS		$pp \rightarrow G \rightarrow HH$		
8 SIRUNYAN 19CF CMS		$pp \rightarrow G \rightarrow HH$		
9 AABOUD 18AK ATLS		$pp \rightarrow G \rightarrow WW$		
10 AABOUD 18AL ATLS		$pp \rightarrow G \rightarrow ZZ$		
11 AABOUD 18BF ATLS		$pp \rightarrow G \rightarrow ZZ$		
12 AABOUD 18BI ATLS		$pp \rightarrow G \rightarrow t\bar{t}$		
13 AABOUD 18CJ ATLS		$pp \rightarrow G \rightarrow V, V, V, H, \ell\bar{\ell}$		
14 AABOUD 18CQ ATLS		$pp \rightarrow G \rightarrow HH$		
15 AABOUD 18CW ATLS		$pp \rightarrow G \rightarrow HH$		
16 SIRUNYAN 18AF CMS		$pp \rightarrow G \rightarrow HH$		
17 SIRUNYAN 18AS CMS		$pp \rightarrow G \rightarrow ZZ$		
18 SIRUNYAN 18AX CMS		$pp \rightarrow G \rightarrow WW$		

1 SIRUNYAN 18BB use 35.9 (36.3) fb<sup>-1</sup> of data from  $pp$  collisions at  $\sqrt{s} = 13$  TeV to search for dilepton resonances in the dilepton (dimuon) channel. See their paper for other limits with warp parameter values  $k/\bar{M}_P = 0.01$  and 0.05. This updates the results of KHACHATRYAN 17T.

2 AAD 20C use 36.1 fb<sup>-1</sup> of data from  $pp$  collisions at  $\sqrt{s} = 13$  TeV to search for Higgs boson pair production in the  $b\bar{b}b\bar{b}, b\bar{b}W^+W^-$ , and  $b\bar{b}\tau^+\tau^-$  final states. See their Figure 5(b)(c) for limits on the cross section as a function of the KK graviton mass. In the case of  $k/\bar{M}_P = 1$  and 2, gravitons are excluded in the mass range 260–3000 GeV and 260–1760 GeV, respectively.

3 AABOUD 19A use 36.1 fb<sup>-1</sup> of data from  $pp$  collisions at  $\sqrt{s} = 13$  TeV to search for Higgs boson pair production in the  $b\bar{b}b\bar{b}$  final state. See their Figure 9 for limits on the cross section times branching fraction as a function of the KK graviton mass. Assuming  $k/\bar{M}_P = 1$ , gravitons in the mass range 313–1362 GeV are excluded. This updates the results of AABOUD 16I.

4 AABOUD 19O use 36.1 fb<sup>-1</sup> of data from  $pp$  collisions at  $\sqrt{s} = 13$  TeV to search for Higgs boson pair production in the  $b\bar{b}W^+W^-$  final state. See their Figure 12 for limits on the cross section times branching fraction as a function of the KK graviton mass for  $k/\bar{M}_P = 1$  and  $k/\bar{M}_P = 2$ .

5 AAD 19D use 139 fb<sup>-1</sup> of data from  $pp$  collisions at  $\sqrt{s} = 13$  TeV to search for diboson resonances in the all-hadronic final state. See their Figure 9(b) for the limit on the cross section times branching fraction as a function of the KK graviton mass, including theoretical values for  $k/\bar{M}_P = 1$ . This updates the results of AABOUD 18F.

6 SIRUNYAN 19I use 35.9 fb<sup>-1</sup> of data from  $pp$  collisions at  $\sqrt{s} = 13$  TeV to search for Higgs boson pair production in the  $\gamma\gamma b\bar{b}$  final state. See their Figure 9 for limits on the cross section times branching fraction as a function of the KK graviton mass. Assuming  $k/\bar{M}_P = 1$ , gravitons in the mass range 290–810 GeV are excluded. This updates the result of KHACHATRYAN 16BQ.

7 SIRUNYAN 19BE use 35.9 fb<sup>-1</sup> of data from  $pp$  collisions at  $\sqrt{s} = 13$  TeV to search for Higgs boson pair production by combining the results from four final states:  $b\bar{b}\gamma\gamma, b\bar{b}\tau^+\tau^-, b\bar{b}b\bar{b}$ , and  $b\bar{b}VV$ . See their Figure 7 for limits on the cross section times branching fraction as a function of the KK graviton mass.

8 SIRUNYAN 19CF use 35.9 fb<sup>-1</sup> of data from  $pp$  collisions at  $\sqrt{s} = 13$  TeV to search for Higgs boson pair production in the  $b\bar{b}q\bar{q}\ell\nu$  final state. See their Figure 7 for limits on the cross section times branching fraction as a function of the KK graviton mass, including theoretical values for  $k/\bar{M}_P = 0.1$  and 0.3.

9 AABOUD 18AK use 36.1 fb<sup>-1</sup> of data from  $pp$  collisions at  $\sqrt{s} = 13$  TeV to search for  $WW$  resonances in  $\ell\nu qq$  final states ( $\ell = e, \mu$ ). See their Figure 7(d) for the limit on the cross section times branching fraction as a function of the KK graviton mass, including theoretical values for  $k/\bar{M}_P = 1$ . This updates the results of AABOUD 16AE.

10 AABOUD 18AL use 36.1 fb<sup>-1</sup> of data from  $pp$  collisions at  $\sqrt{s} = 13$  TeV to search for diboson resonances in the  $\ell\ell q\bar{q}$  and  $\nu\tau q\bar{q}$  final states. See their Figure 14 for the limit on cross section times branching fraction as a function of the KK graviton mass, including theoretical values for  $k/\bar{M}_P = 0.5$  and 1. This updates the results of AABOUD 16AE.

11 AABOUD 18BF use 36.1 fb<sup>-1</sup> of data from  $pp$  collisions at  $\sqrt{s} = 13$  TeV to search for  $ZZ$  resonances in the  $\ell\ell\ell\ell$  and  $\ell\nu\nu\bar{\nu}$  final states ( $\ell = e, \mu$ ). See their Figure 10 for the limit on the cross section times branching fraction as a function of the KK graviton mass, including theoretical values for  $k/\bar{M}_P = 1$ .

12 AABOUD 18BI use 36.1 fb<sup>-1</sup> of data from  $pp$  collisions at  $\sqrt{s} = 13$  TeV to search for top-quark pairs decaying into the lepton-plus jets topology. See their Figure 16 for the limit on the KK graviton mass as a function of the cross section times branching fraction, including theoretical values for  $k/\bar{M}_P = 1$ .

13 AABOUD 18CJ combine the searches for heavy resonances decaying into bosonic and leptonic final states from 36.1 fb<sup>-1</sup> of  $pp$  collision data at  $\sqrt{s} = 13$  TeV. The lower limit on the KK graviton mass, with  $k/\bar{M}_P = 1$ , is 2.3 TeV.

14 AABOUD 18CQ use 36.1 fb<sup>-1</sup> of data from  $pp$  collisions at  $\sqrt{s} = 13$  TeV to search for Higgs boson pair production in the  $b\bar{b}\tau^+\tau^-$  final state. See their Figure 2 for limits on the cross section times branching fraction as a function of the KK graviton mass. Assuming  $k/\bar{M}_P = 1$ , gravitons in the mass range 325–885 GeV are excluded.

- 15 AABOUD 18CW use  $36.1 \text{ fb}^{-1}$  of data from  $pp$  collisions at  $\sqrt{s} = 13 \text{ TeV}$  to search for Higgs boson pair production in the  $\gamma\gamma b\bar{b}$  final state. See their Figure 7 for limits on the cross section times branching fraction as a function of the KK graviton mass.
- 16 SIRUNYAN 18AF use  $35.9 \text{ fb}^{-1}$  of data from  $pp$  collisions at  $\sqrt{s} = 13 \text{ TeV}$  to search for Higgs boson pair production in the  $b\bar{b}b\bar{b}$  final state. See their Figure 9 for limits on the cross section times branching fraction as a function of the KK graviton mass, including theoretical values for  $k/\overline{M}_P = 0.5$ . This updates the results of KHACHATRYAN 15R.
- 17 SIRUNYAN 18AS use  $35.9 \text{ fb}^{-1}$  of data from  $pp$  collisions at  $\sqrt{s} = 13 \text{ TeV}$  to search for ZZ resonances in the  $\ell\ell\nu\bar{\nu}$  final state ( $\ell = e, \mu$ ). See their Figure 5 for the limit on the KK graviton mass as a function of the cross section times branching fraction, including theoretical values for  $k/\overline{M}_P = 0.1, 0.5, \text{ and } 1.0$ .
- 18 SIRUNYAN 18AX use  $35.9 \text{ fb}^{-1}$  of data from  $pp$  collisions at  $\sqrt{s} = 13 \text{ TeV}$  to search for WW resonances in  $\ell\nu q\bar{q}$  final states ( $\ell = e, \mu$ ). See their Figure 6 for the limit on the KK graviton mass as a function of the cross section times branching fraction, including theoretical values for  $k/\overline{M}_P = 0.5$ . This updates the results of KHACHATRYAN 14A.
- 19 SIRUNYAN 18BK use  $35.9 \text{ fb}^{-1}$  of data from  $pp$  collisions at  $\sqrt{s} = 13 \text{ TeV}$  to search for ZZ resonances in the  $\nu\bar{\nu}q\bar{q}$  final state. See their Figure 4 for the limit on the KK graviton mass as a function of the cross section times branching fraction, including theoretical values for  $k/\overline{M}_P = 0.5$ .
- 20 SIRUNYAN 18BO use up to  $36 \text{ fb}^{-1}$  of data from  $pp$  collisions at  $\sqrt{s} = 13 \text{ TeV}$  to search for dijet resonances. Besides the quoted bound, KK graviton masses between 1.9 TeV and 2.5 TeV are also excluded. See their Figure 11 for the limit on the product of the cross section, branching fraction and acceptance as a function of the KK graviton mass. This updates the results of KHACHATRYAN 17W.
- 21 SIRUNYAN 18CW use  $35.9 \text{ fb}^{-1}$  of data from  $pp$  collisions at  $\sqrt{s} = 13 \text{ TeV}$  to search for Higgs boson pair production in the  $b\bar{b}b\bar{b}$  final state. See their Figure 8 for limits on the cross section times branching fraction as a function of the KK graviton mass, including theoretical values for  $k/\overline{M}_P = 0.5$ .
- 22 SIRUNYAN 18DJ use  $35.9 \text{ fb}^{-1}$  of data from  $pp$  collisions at  $\sqrt{s} = 13 \text{ TeV}$  to search for ZZ resonances in  $2\ell q\bar{q}$  final states ( $\ell = e, \mu$ ). See their Figure 6 for the limit on the KK graviton mass as a function of the cross section times branching fraction. Assuming  $k/\overline{M}_P = 0.5$ , a graviton mass is excluded below 925 GeV.
- 23 SIRUNYAN 18DU use  $35.9 \text{ fb}^{-1}$  of data from  $pp$  collisions at  $\sqrt{s} = 13 \text{ TeV}$ , in the diphoton channel to place a lower limit on the mass of the lightest KK graviton. See their paper for limits with other warp parameter values  $k/\overline{M}_P = 0.01 \text{ and } 0.2$ . This updates the results of KHACHATRYAN 16M.
- 24 SIRUNYAN 18F use  $35.9 \text{ fb}^{-1}$  of data from  $pp$  collisions at  $\sqrt{s} = 13 \text{ TeV}$  to search for Higgs boson pair production in the  $b\bar{b}\ell\nu\ell\nu$  final state. See their Figure 7 for limits on the cross section times branching fraction as a function of the KK graviton mass, including theoretical values for  $k/\overline{M}_P = 0.1$ .
- 25 SIRUNYAN 18I use  $19.7 \text{ fb}^{-1}$  of data from  $pp$  collisions at  $\sqrt{s} = 8 \text{ TeV}$  to search for narrow resonances decaying to bottom quark pairs. See their Figure 3 for the limit on the KK graviton mass as a function of the cross section times branching fraction in the mass range of 325–1200 GeV.
- 26 SIRUNYAN 18P use  $35.9 \text{ fb}^{-1}$  of data from  $pp$  collisions at  $\sqrt{s} = 13 \text{ TeV}$  to search for diboson resonances with dijet final states. See their Figure 6 for the limit on the KK graviton mass as a function of the cross section times branching fraction, including theoretical values for  $k/\overline{M}_P = 0.5$ . This updates the results of SIRUNYAN 17AK.
- 27 AABOUD 17AP use  $36.7 \text{ fb}^{-1}$  of data from  $pp$  collisions at  $\sqrt{s} = 13 \text{ TeV}$  in the diphoton channel to place a lower limit on the mass of the lightest KK graviton. This updates the results of AABOUD 16H.
- 28 AAD 16R use  $20.3 \text{ fb}^{-1}$  of data from  $pp$  collisions at  $\sqrt{s} = 8 \text{ TeV}$  to place a lower bound on the mass of the lightest KK graviton. See their Figure 4 for the limit on the KK graviton mass as a function of the cross section times branching fraction.
- 29 AAD 15AU use  $20 \text{ fb}^{-1}$  of data from  $pp$  collisions at  $\sqrt{s} = 8 \text{ TeV}$  to search for KK gravitons in a warped extra dimension decaying to ZZ dibosons. See their Figure 2 for limits on the KK graviton mass as a function of the cross section times branching fraction.
- 30 AAD 15AZ use  $20.3 \text{ fb}^{-1}$  of data from  $pp$  collisions at  $\sqrt{s} = 8 \text{ TeV}$  to place a lower bound on the mass of the lightest KK graviton. See their Figure 2 for limits on the KK graviton mass as a function of the cross section times branching ratio.
- 31 AAD 15CT use  $20.3 \text{ fb}^{-1}$  of data from  $pp$  collisions at  $\sqrt{s} = 8 \text{ TeV}$  to place a lower bound on the mass of the lightest KK graviton. See their Figures 6b and 6c for the limit on the KK graviton mass as a function of the cross section times branching fraction.
- 32 AAD 14V use  $20.3 (20.5) \text{ fb}^{-1}$  of data from  $pp$  collisions at  $\sqrt{s} = 8 \text{ TeV}$  in the dielectron (dimuon) channels to place a lower bound on the mass of the lightest KK graviton. This updates the results of AAD 12CC.
- 33 AAD 13A use  $4.7 \text{ fb}^{-1}$  of data from  $pp$  collisions at  $\sqrt{s} = 7 \text{ TeV}$  in the  $\ell\nu\ell\nu$  channel, to place a lower bound on the mass of the lightest KK graviton.
- 34 AAD 13AO use  $4.7 \text{ fb}^{-1}$  of data from  $pp$  collisions at  $\sqrt{s} = 7 \text{ TeV}$  in the  $\ell\nu jj$  channel, to place a lower bound on the mass of the lightest KK graviton.
- 35 AAD 13AS use  $4.9 \text{ fb}^{-1}$  of data from  $pp$  collisions at  $\sqrt{s} = 7 \text{ TeV}$  in the diphoton channel to place lower limits on the mass of the lightest KK graviton. The diphoton channel is combined with previous results in the dielectron and dimuon channels to set the best limit. See their Table 2 for warp parameter values  $k/\overline{M}_P$  between 0.01 and 0.1. This updates the results of AAD 12V.
- 36 AAD 12AD use  $1.02 \text{ fb}^{-1}$  of data from  $pp$  collisions at  $\sqrt{s} = 7 \text{ TeV}$  to search for KK gravitons in a warped extra dimension decaying to ZZ dibosons in the  $lljj$  and  $llll$  channels ( $\ell = e, \mu$ ). The limit is quoted for the combined  $lljj + llll$  channels. See their Figure 5 for limits on the cross section  $\sigma(G \rightarrow ZZ)$  as a function of the graviton mass.
- 37 AALTONEN 12V use  $6 \text{ fb}^{-1}$  of data from  $p\bar{p}$  collisions at  $\sqrt{s} = 1.96 \text{ TeV}$  to search for KK gravitons in a warped extra dimension decaying to ZZ dibosons in the  $lljj$  and  $llll$  channels ( $\ell = e, \mu$ ). It provides improved limits over the previous analysis in AALTONEN 11G. See their Figure 16 for limits from all channels combined on the cross section times branching ratio  $\sigma(p\bar{p} \rightarrow G^* \rightarrow ZZ)$  as a function of the graviton mass.
- 38 BAAK 12 use electroweak precision observables to place a lower bound on the compactification scale  $k e^{-\pi k R}$ , assuming Standard Model fields propagate in the bulk and the Higgs is confined to the IR brane. See their Fig. 27 for more details.
- 39 AALTONEN 11G use  $2.5\text{--}2.9 \text{ fb}^{-1}$  of data from  $p\bar{p}$  collisions at  $\sqrt{s} = 1.96 \text{ TeV}$  to search for KK gravitons in a warped extra dimension decaying to ZZ dibosons via the  $e\bar{e}e, e\bar{e}\mu\mu, \mu\bar{\mu}\mu\mu, e\bar{e}jj, \text{ and } \mu\bar{\mu}jj$  channels. See their Fig. 20 for limits on the cross section  $\sigma(G \rightarrow ZZ)$  as a function of the graviton mass.
- 40 AALTONEN 11R uses  $5.7 \text{ fb}^{-1}$  of data from  $p\bar{p}$  collisions at  $\sqrt{s} = 1.96 \text{ TeV}$  in the dielectron channel to place a lower bound on the mass of the lightest graviton. It provides combined limits with the diphoton channel analysis of AALTONEN 11U. For

warp parameter values  $k/\overline{M}_P$  between 0.01 to 0.1 the lower limit on the mass of the lightest graviton is between 612 and 1058 GeV. See their Table 1 for more details.

- 41 ABAZOV 11H use  $5.4 \text{ fb}^{-1}$  of data from  $p\bar{p}$  collisions at  $\sqrt{s} = 1.96 \text{ TeV}$  to place a lower bound on the mass of the lightest graviton. Their 95% C.L. exclusion limit does not include masses less than 300 GeV.
- 42 AALTONEN 10N use  $2.9 \text{ fb}^{-1}$  of data from  $p\bar{p}$  collisions at  $\sqrt{s} = 1.96 \text{ TeV}$  to place a lower bound on the mass of the lightest graviton.
- 43 ABAZOV 10F use  $5.4 \text{ fb}^{-1}$  of data from  $p\bar{p}$  collisions at  $\sqrt{s} = 1.96 \text{ TeV}$  to place a lower bound on the mass of the lightest graviton. For warp parameter values of  $k/\overline{M}_P$  between 0.01 and 0.1 the lower limit on the mass of the lightest graviton is between 560 and 1050 GeV. See their Fig. 3 for more details.
- 44 AALTONEN 08s use  $p\bar{p}$  collisions at  $\sqrt{s} = 1.96 \text{ TeV}$  to search for KK gravitons in warped extra dimensions. They search for graviton resonances decaying to four electrons via two Z bosons using  $1.1 \text{ fb}^{-1}$  of data. See their Fig. 8 for limits on  $\sigma \cdot \text{B}(G \rightarrow ZZ)$  versus the graviton mass.
- 45 ABAZOV 08j use  $p\bar{p}$  collisions at  $\sqrt{s} = 1.96 \text{ TeV}$  to search for KK gravitons in warped extra dimensions. They search for graviton resonances decaying to electrons and photons using  $1 \text{ fb}^{-1}$  of data. For warp parameter values of  $k/\overline{M}_P$  between 0.01 and 0.1 the lower limit on the mass of the lightest excitation is between 300 and 900 GeV. See their Fig. 4 for more details.
- 46 AALTONEN 07G use  $p\bar{p}$  collisions at  $\sqrt{s} = 1.96 \text{ TeV}$  to search for KK gravitons in warped extra dimensions. They search for graviton resonances decaying to photons using  $1.2 \text{ fb}^{-1}$  of data. For warp parameter values of  $k/\overline{M}_P = 0.1, 0.05, \text{ and } 0.01$  the bounds on the graviton mass are 850, 694, and 230 GeV, respectively. See their Fig. 3 for more details. See also AALTONEN 07H.
- 47 AALTONEN 07H use  $p\bar{p}$  collisions at  $\sqrt{s} = 1.96 \text{ TeV}$  to search for KK gravitons in warped extra dimensions. They search for graviton resonances decaying to electrons using  $1.3 \text{ fb}^{-1}$  of data. For a warp parameter value of  $k/\overline{M}_P = 0.1$  the bound on the graviton mass is 807 GeV. See their Fig. 4 for more details. A combined analysis with the diphoton data of AALTONEN 07G yields for  $k/\overline{M}_P = 0.1$  a graviton mass lower bound of 889 GeV.
- 48 ABAZOV 05n use  $p\bar{p}$  collisions at  $\sqrt{s} = 1.96 \text{ TeV}$  to search for KK gravitons in warped extra dimensions. They search for graviton resonances decaying to muons, electrons or photons, using  $260 \text{ pb}^{-1}$  of data. For warp parameter values of  $k/\overline{M}_P = 0.1, 0.05, \text{ and } 0.01$ , the bounds on the graviton mass are 785, 650 and 250 GeV respectively. See their Fig. 3 for more details.
- 49 ABULENCIA 05A use  $p\bar{p}$  collisions at  $\sqrt{s} = 1.96 \text{ TeV}$  to search for KK gravitons in warped extra dimensions. They search for graviton resonances decaying to muons or electrons, using  $200 \text{ pb}^{-1}$  of data. For warp parameter values of  $k/\overline{M}_P = 0.1, 0.05, \text{ and } 0.01$ , the bounds on the graviton mass are 710, 510 and 170 GeV respectively.

### Limits on Kaluza-Klein Gluons in Warped Extra Dimensions

This section places limits on the mass of the first Kaluza-Klein (KK) excitation of the gluon in warped extra dimension models with Standard Model fields propagating in the bulk. Bounds are given for a specific benchmark model with  $\Gamma/m = 15.3\%$  where  $\Gamma$  is the width and  $m$  the mass of the KK gluon. See the "Extra Dimensions" review for more discussion.

VALUE (TeV)	CL%	DOCUMENT ID	TECN	COMMENT
>3.8	95	1 AABOUD	18BI ATLS	$g_{KK} \rightarrow t\bar{t} \rightarrow \ell j$
• • •		We do not use the following data for averages, fits, limits, etc. • • •		
		2 AABOUD	19AS ATLS	$g_{KK} \rightarrow t\bar{t} \rightarrow jj$
		3 SIRUNYAN	19AL CMS	$g_{KK} \rightarrow t\bar{t}$
>2.5	95	4 CHATRCHYAN	13BM CMS	$g_{KK} \rightarrow t\bar{t}$
		5 CHEN	13A	$B \rightarrow X_S \gamma$
>1.5	95	6 AAD	12BV ATLS	$g_{KK} \rightarrow t\bar{t} \rightarrow \ell j$

- 1 AABOUD 18BI use  $36.1 \text{ fb}^{-1}$  of data from  $pp$  collisions at  $\sqrt{s} = 13 \text{ TeV}$ . This result updates AAD 13AQ.
- 2 AABOUD 19AS use  $36.1 \text{ fb}^{-1}$  of data from  $pp$  collisions at  $\sqrt{s} = 13 \text{ TeV}$ . An upper bound of 3.4 TeV is placed on the KK gluon mass for  $\Gamma/m = 30\%$ .
- 3 SIRUNYAN 19AL use  $35.9 \text{ fb}^{-1}$  of data from  $pp$  collisions at  $\sqrt{s} = 13 \text{ TeV}$  to place limits on a KK gluon decaying to a top quark and a heavy vector-like fermion, T. KK gluon masses between 1.5 and 2.3 TeV and between 2.0 and 2.4 TeV are excluded for T masses of 1.2 and 1.5 TeV, respectively.
- 4 CHATRCHYAN 13BM use  $19.7 \text{ fb}^{-1}$  of data from  $pp$  collisions at  $\sqrt{s} = 8 \text{ TeV}$ . Bound is for a width of approximately 15–20% of the KK gluon mass.
- 5 CHEN 13A place limits on the KK mass scale for a specific warped model with custodial symmetry and bulk fermions. See their Figures 4 and 5.
- 6 AAD 12BV use  $2.05 \text{ fb}^{-1}$  of data from  $pp$  collisions at  $\sqrt{s} = 7 \text{ TeV}$ .

### Black Hole Production Limits

#### Semiclassical Black Holes

VALUE (GeV)	DOCUMENT ID	TECN	COMMENT
• • •	We do not use the following data for averages, fits, limits, etc. • • •		
	1 SIRUNYAN	18DA CMS	$pp \rightarrow \text{multijet}$
	2 AAD	16N ATLS	$pp \rightarrow \text{multijet}$
	3 AAD	16O ATLS	$pp \rightarrow \ell + (\ell\ell/\ell j/jj)$
	4 AAD	13AW ATLS	$pp \rightarrow \mu\mu$
1	SIRUNYAN 18DA		use $35.9 \text{ fb}^{-1}$ of data from $pp$ collisions at $\sqrt{s} = 13 \text{ TeV}$ to search for semiclassical black holes decaying to multijet final states. No excess of events above the expected level of standard model background was observed. Exclusions at 95% CL are set on the mass threshold for black hole production as a function of the higher-dimensional Planck scale for rotating and nonrotating black holes under several model assumptions (ADD, 2, 4, 6 extra dimensions model) in the 7.1–10.3 TeV range. These limits supersede those in SIRUNYAN 17CP.
2	AAD 16N		use $3.6 \text{ fb}^{-1}$ of data from $pp$ collisions at $\sqrt{s} = 13 \text{ TeV}$ to search for semiclassical black hole decays to multijet final states. No excess of events above the expected level of Standard Model background was observed. Exclusion contours at 95% C.L. are set on the mass threshold for black hole production versus higher-dimensional Planck scale for rotating black holes (ADD, 6 extra dimensions model).

## Searches Particle Listings

## Extra Dimensions

- <sup>3</sup> AAD 16o use 3.2 fb<sup>-1</sup> of data from  $pp$  collisions at  $\sqrt{s} = 13$  TeV to search for semi-classical black hole decays to high-mass final states with leptons and jets. No excess of events above the expected level of Standard Model background was observed. Exclusion contours at 95% C.L. are set on the mass threshold for black hole production versus higher-dimensional Planck scale for rotating black holes (ADD, 2 to 6 extra dimensions).
- <sup>4</sup> AAD 13aw use 20.3 fb<sup>-1</sup> of data from  $pp$  collisions at  $\sqrt{s} = 8$  TeV to search for semi-classical black hole decays to like-sign dimuon final states using large track multiplicity. No excess of events above the expected level of Standard Model background was observed. Exclusion contours at 95% C.L. are set on the mass threshold for black hole production versus higher-dimensional Planck scale in various extra dimensions, rotating and non-rotating models.

## Quantum Black Holes

VALUE (GeV)	DOCUMENT ID	TECN	COMMENT
•••			We do not use the following data for averages, fits, limits, etc. •••
<sup>1</sup>	AABOUD 18BA ATLS	$pp \rightarrow \gamma j$	
<sup>2</sup>	AABOUD 18CM ATLS	$pp \rightarrow e\mu, e\tau, \mu\tau$	
<sup>3</sup>	SIRUNYAN 18AT CMS	$pp \rightarrow e\mu$	
<sup>4</sup>	SIRUNYAN 18DD CMS	$pp \rightarrow$ dijet, ang. distrib.	
<sup>5</sup>	AABOUD 17AK ATLS	$pp \rightarrow jj$	
<sup>6</sup>	SIRUNYAN 17CP CMS	$pp \rightarrow jj$	
<sup>7</sup>	KHACHATRYAN...16BE CMS	$pp \rightarrow e\mu$	
<sup>8</sup>	KHACHATRYAN...15V CMS	$pp \rightarrow jj$	
<sup>9</sup>	AAD 14AL ATLS	$pp \rightarrow \ell j$	
<sup>10</sup>	AAD 14V ATLS	$pp \rightarrow ee, \mu\mu$	
<sup>11</sup>	CHATRCHYAN13A CMS	$pp \rightarrow jj$	

- <sup>1</sup> AABOUD 18BA use 36.7 fb<sup>-1</sup> of data from  $pp$  collisions at  $\sqrt{s} = 13$  TeV to search for quantum black hole decays to final states with a photon and a jet. No excess of events above the expected level of Standard Model background was observed. Exclusion limits at 95% C.L. are set on mass thresholds for black hole production in ADD (6 extra dimensions) and RS1 models. Assuming the black hole mass threshold is equal to the Planck scale, mass thresholds below 7.1 TeV and 4.4 TeV are excluded for the ADD and RS1 models, respectively. These limits supersede those in AAD 16A1.
- <sup>2</sup> AABOUD 18CM use 36.1 fb<sup>-1</sup> of data from  $pp$  collisions at  $\sqrt{s} = 13$  TeV to search for quantum black hole decays with different-flavor high-mass dilepton final states. No excess of events above the expected level of Standard Model background was observed. Exclusion limits at 95% C.L. are set on mass thresholds for black hole production in ADD (6 extra dimensions) and RS1 models. Assuming the black hole mass threshold is equal to the higher-dimensional Planck scale, mass thresholds below 5.6 (3.4), 4.9 (2.9), and 4.5 (2.6) TeV are excluded in the  $e\mu, e\tau$  and  $\mu\tau$  channels for the ADD (RS1) models, respectively. These limits supersede those in AABOUD 16P.
- <sup>3</sup> SIRUNYAN 18AT use 35.9 fb<sup>-1</sup> of data from  $pp$  collisions at  $\sqrt{s} = 13$  TeV to search for quantum black hole decays to  $e\mu$  final states. In Figure 4, lower mass limits of 5.3, 5.5 and 5.6 TeV are placed in a model with 4, 5 and 6 extra dimensions, respectively, and a lower mass limit of 3.6 TeV is found for a single warped dimension.
- <sup>4</sup> SIRUNYAN 18DD use 35.9 fb<sup>-1</sup> of data from  $pp$  collisions at  $\sqrt{s} = 13$  TeV to search for quantum black hole decays in dijet angular distributions. A lower mass limit of 5.9 (8.2) TeV is placed in the RS (ADD) model with one (six) extra dimension(s).
- <sup>5</sup> AABOUD 17AK use 37 fb<sup>-1</sup> of data from  $pp$  collisions at  $\sqrt{s} = 13$  TeV to search for quantum black hole decays to final states with dijets. No excess of events above the expected level of Standard Model background was observed. Exclusion limits at 95% C.L. are set on mass thresholds for black hole production in an ADD (6 extra dimensions) model. Assuming the black hole mass threshold is equal to the higher-dimensional Planck scale, mass thresholds below 8.9 TeV are excluded.
- <sup>6</sup> SIRUNYAN 17CP use 2.3 fb<sup>-1</sup> of data from  $pp$  collisions at  $\sqrt{s} = 13$  TeV to search for quantum black holes decaying to dijet final states. No excess of events above the expected level of standard model background was observed. Limits on the quantum black hole mass threshold are set as a function of the higher-dimensional Planck scale, under the assumption that the mass threshold must exceed the above Planck scale. Depending on the model, mass thresholds in the range up to 5.1–9.0 TeV are excluded.
- <sup>7</sup> KHACHATRYAN 16BE use 19.7 fb<sup>-1</sup> of data from  $pp$  collisions at  $\sqrt{s} = 8$  TeV to search for quantum black holes undergoing lepton flavor violating decay to the  $e\mu$  final state. No excess of events above the expected level of standard model background was observed. Exclusion limits at 95% C.L. are set on mass thresholds for black hole production in the ADD (2–6 flat extra dimensions), RS1 (1 warped extra dimension), and a model with a Planck scale at the TeV scale from a renormalization of the gravitational constant (no extra dimensions). Limits on the black hole mass threshold are set assuming that it is equal to the higher-dimensional Planck scale. Mass thresholds for quantum black holes in the range up to 3.15–3.63 TeV are excluded in the ADD model. In the RS1 model, mass thresholds below 2.81 TeV are excluded in the PDG convention for the Schwarzschild radius. In the model with no extra dimensions, mass thresholds below 1.99 TeV are excluded.
- <sup>8</sup> KHACHATRYAN 15V use 19.7 fb<sup>-1</sup> of data from  $pp$  collisions at  $\sqrt{s} = 8$  TeV to search for quantum black holes decaying to dijet final states. No excess of events above the expected level of standard model background was observed. Exclusion limits at 95% C.L. are set on mass thresholds for black hole production in the ADD (2–6 flat extra dimensions) and RS1 (1 warped extra dimension) model. Limits on the black hole mass threshold are set as a function of the higher-dimensional Planck scale, under the assumption that the mass threshold must exceed the above Planck scale. Depending on the model, mass thresholds in the range up to 5.0–6.3 TeV are excluded. This paper supersedes CHATRCHYAN 13AD.
- <sup>9</sup> AAD 14AL use 20.3 fb<sup>-1</sup> of data from  $pp$  collisions at  $\sqrt{s} = 8$  TeV to search for quantum black hole decays to final states with high-invariant-mass lepton + jet. No excess of events above the expected level of Standard Model background was observed. Exclusion limits at 95% C.L. are set on mass thresholds for black hole production in ADD (6 extra dimensions) model. Assuming the black hole mass threshold is equal to the higher-dimensional Planck scale, mass thresholds below 5.3 TeV are excluded.
- <sup>10</sup> AAD 14V use 20.3 (20.5) fb<sup>-1</sup> of data in the dielectron (dimuon) channels from  $pp$  collisions at  $\sqrt{s} = 8$  TeV to search for quantum black hole decays involving high-mass dilepton resonances. No excess of events above the expected level of Standard Model background was observed. Exclusion limits at 95% C.L. are set on mass thresholds for black hole production in ADD (6 extra dimensions) and RS1 models. Assuming the black hole mass threshold is equal to the higher-dimensional Planck scale, mass thresholds below 3.65 TeV and 2.24 TeV are excluded for the ADD and RS1 models, respectively.

- <sup>11</sup> CHATRCHYAN 13A use 5 fb<sup>-1</sup> of data from  $pp$  collisions at  $\sqrt{s} = 7$  TeV to search for quantum black holes decaying to dijet final states. No excess of events above the expected level of standard model background was observed. Exclusion limits at 95% C.L. are set on mass thresholds for black hole production in the ADD (2–6 flat extra dimensions) and RS (1 warped extra dimension) model. Limits on the black hole mass threshold are set as a function of the higher-dimensional Planck scale, under assumption that the mass threshold must exceed the above Planck scale. Depending on the model, mass thresholds in the range up to 4.0–5.3 TeV are excluded.

## REFERENCES FOR Extra Dimensions

AAD 20C	PL B800 135103	G. Aad et al.	(ATLAS Collab.)
AABOUD 19A	JHEP 1901 030	M. Aaboud et al.	(ATLAS Collab.)
AABOUD 19AS	PR D99 092004	M. Aaboud et al.	(ATLAS Collab.)
AABOUD 19O	JHEP 1904 092	M. Aaboud et al.	(ATLAS Collab.)
AAD 19D	JHEP 1909 091	G. Aad et al.	(ATLAS Collab.)
SIRUNYAN 19	PL B788 7	A.M. Sirunyan et al.	(CMS Collab.)
SIRUNYAN 19AC	JHEP 1904 114	A.M. Sirunyan et al.	(CMS Collab.)
SIRUNYAN 19AL	EPJ C79 208	A.M. Sirunyan et al.	(CMS Collab.)
SIRUNYAN 19BE	PRL 122 121803	A.M. Sirunyan et al.	(CMS Collab.)
SIRUNYAN 19CF	JHEP 1910 125	A.M. Sirunyan et al.	(CMS Collab.)
AABOUD 18AK	JHEP 1803 042	M. Aaboud et al.	(ATLAS Collab.)
AABOUD 18AL	JHEP 1803 009	M. Aaboud et al.	(ATLAS Collab.)
AABOUD 18AV	JHEP 1807 089	M. Aaboud et al.	(ATLAS Collab.)
AABOUD 18BA	EPJ C78 102	M. Aaboud et al.	(ATLAS Collab.)
AABOUD 18BF	EPJ C78 293	M. Aaboud et al.	(ATLAS Collab.)
AABOUD 18BI	EPJ C78 565	M. Aaboud et al.	(ATLAS Collab.)
AABOUD 18CE	JHEP 1812 039	M. Aaboud et al.	(ATLAS Collab.)
AABOUD 18CJ	PR D98 052008	M. Aaboud et al.	(ATLAS Collab.)
AABOUD 18CM	PR D98 092008	M. Aaboud et al.	(ATLAS Collab.)
AABOUD 18CQ	PRL 121 191801	M. Aaboud et al.	(ATLAS Collab.)
AABOUD 18CW	JHEP 1811 040	M. Aaboud et al.	(ATLAS Collab.)
AABOUD 18FI	PL B777 31	M. Aaboud et al.	(ATLAS Collab.)
BERGE 18	PRL 120 141101	J. Berge et al.	(MICROSCOPE Collab.)
FAYET 18	PR D97 055039	P. Fayet	(EPOL)
FAYET 18A	PR D99 055043	P. Fayet	(ENSP, EPOL)
HADDOCK 18	PR D97 062002	C. Haddock et al.	(NAGO, KEK, OSAK+)
SIRUNYAN 18AF	PL B781 244	A.M. Sirunyan et al.	(CMS Collab.)
SIRUNYAN 18AS	JHEP 1803 003	A.M. Sirunyan et al.	(CMS Collab.)
SIRUNYAN 18AT	JHEP 1804 073	A.M. Sirunyan et al.	(CMS Collab.)
SIRUNYAN 18AX	JHEP 1805 088	A.M. Sirunyan et al.	(CMS Collab.)
SIRUNYAN 18BB	JHEP 1806 120	A.M. Sirunyan et al.	(CMS Collab.)
SIRUNYAN 18BK	JHEP 1807 075	A.M. Sirunyan et al.	(CMS Collab.)
SIRUNYAN 18BO	JHEP 1808 130	A.M. Sirunyan et al.	(CMS Collab.)
SIRUNYAN 18BV	EPJ C78 291	A.M. Sirunyan et al.	(CMS Collab.)
SIRUNYAN 18CW	JHEP 1808 152	A.M. Sirunyan et al.	(CMS Collab.)
SIRUNYAN 18DA	JHEP 1811 042	A.M. Sirunyan et al.	(CMS Collab.)
SIRUNYAN 18DD	EPJ C78 789	A.M. Sirunyan et al.	(CMS Collab.)
SIRUNYAN 18DJ	JHEP 1809 101	A.M. Sirunyan et al.	(CMS Collab.)
SIRUNYAN 18DU	PR D98 092001	A.M. Sirunyan et al.	(CMS Collab.)
SIRUNYAN 18F	JHEP 1801 054	A.M. Sirunyan et al.	(CMS Collab.)
SIRUNYAN 18I	PRL 120 201801	A.M. Sirunyan et al.	(CMS Collab.)
SIRUNYAN 18P	PR D97 072006	A.M. Sirunyan et al.	(CMS Collab.)
SIRUNYAN 18S	PR D97 092005	A.M. Sirunyan et al.	(CMS Collab.)
AABOUD 17AK	PR D96 052004	M. Aaboud et al.	(ATLAS Collab.)
AABOUD 17AP	PL B775 105	M. Aaboud et al.	(ATLAS Collab.)
KHACHATRYAN...17T	PL B768 57	V. Khachatryan et al.	(CMS Collab.)
KHACHATRYAN...17A	PL B769 520	V. Khachatryan et al.	(CMS Collab.)
KLIMCHITSKAYA...17A	PR D95 123013	G.L. Klimchitskaya, V.M. Mostepanenko	(CMS Collab.)
SIRUNYAN 17AK	PL B774 533	A.M. Sirunyan et al.	(CMS Collab.)
SIRUNYAN 17AJ	JHEP 1710 073	A.M. Sirunyan et al.	(CMS Collab.)
SIRUNYAN 17CP	PL B774279	A.M. Sirunyan et al.	(CMS Collab.)
SIRUNYAN 17F	JHEP 1707 013	A.M. Sirunyan et al.	(CMS Collab.)
AABOUD 16AE	JHEP 1609 173	M. Aaboud et al.	(ATLAS Collab.)
AABOUD 16D	PR D94 032005	M. Aaboud et al.	(ATLAS Collab.)
AABOUD 16F	JHEP 1606 059	M. Aaboud et al.	(ATLAS Collab.)
AABOUD 16H	JHEP 1609 001	M. Aaboud et al.	(ATLAS Collab.)
AABOUD 16I	PR D94 052002	M. Aaboud et al.	(ATLAS Collab.)
AABOUD 16P	EPJ C76 541	M. Aaboud et al.	(ATLAS Collab.)
AAD 16A1	JHEP 1603 041	G. Aad et al.	(ATLAS Collab.)
AAD 16N	JHEP 1603 026	G. Aad et al.	(ATLAS Collab.)
AAD 16O	PL B760 520	G. Aad et al.	(ATLAS Collab.)
AAD 16R	PL B755 285	G. Aad et al.	(ATLAS Collab.)
KHACHATRYAN...16BE	EPJ C76 317	V. Khachatryan et al.	(CMS Collab.)
KHACHATRYAN...16BQ	PR D94 052012	V. Khachatryan et al.	(CMS Collab.)
KHACHATRYAN...16M	PRL 117 051802	V. Khachatryan et al.	(CMS Collab.)
KHACHATRYAN...16N	PL B755 102	V. Khachatryan et al.	(ATLAS Collab.)
AAD 15AU	EPJ C75 69	G. Aad et al.	(ATLAS Collab.)
AAD 15AZ	EPJ C75 209	G. Aad et al.	(ATLAS Collab.)
Also	EPJ C75 370 (err.)	G. Aad et al.	(ATLAS Collab.)
AAD 15CS	PR D91 012008	G. Aad et al.	(ATLAS Collab.)
Also	PR D92 059903 (err.)	G. Aad et al.	(ATLAS Collab.)
AAD 15CT	JHEP 1512 055	G. Aad et al.	(ATLAS Collab.)
ACCOMANDO 15	MPL A30 1540010	E. Accomando	(SHMP)
KHACHATRYAN...15AE	JHEP 1504 025	V. Khachatryan et al.	(CMS Collab.)
KHACHATRYAN...15AL	EPJ C75 235	V. Khachatryan et al.	(CMS Collab.)
KHACHATRYAN...15R	PL B749 560	V. Khachatryan et al.	(CMS Collab.)
KHACHATRYAN...15T	PR D91 022005	V. Khachatryan et al.	(CMS Collab.)
KHACHATRYAN...15V	PR D91 052009	V. Khachatryan et al.	(CMS Collab.)
AAD 14AL	PRL 112 091804	G. Aad et al.	(ATLAS Collab.)
AAD 14BE	EPJ C74 3134	G. Aad et al.	(ATLAS Collab.)
AAD 14V	PR D90 052005	G. Aad et al.	(ATLAS Collab.)
KHACHATRYAN...14A	JHEP 1408 174	V. Khachatryan et al.	(CMS Collab.)
AAD 13A	PL B718 860	G. Aad et al.	(ATLAS Collab.)
AAD 13AO	PR D87 112006	G. Aad et al.	(ATLAS Collab.)
AAD 13AQ	PR D88 012004	G. Aad et al.	(ATLAS Collab.)
AAD 13AS	NJP 15 043007	G. Aad et al.	(ATLAS Collab.)
AAD 13AW	PR D88 072001	G. Aad et al.	(ATLAS Collab.)
AAD 13C	PRL 110 011802	G. Aad et al.	(ATLAS Collab.)
AAD 13D	JHEP 1301 029	G. Aad et al.	(ATLAS Collab.)
AAD 13E	PR D87 015010	G. Aad et al.	(ATLAS Collab.)
CHATRCHYAN 13A	JHEP 1301 013	S. Chatrchyan et al.	(CMS Collab.)
CHATRCHYAN 13AD	JHEP 1307 178	S. Chatrchyan et al.	(CMS Collab.)
CHATRCHYAN 13AQ	PR D87 072005	S. Chatrchyan et al.	(CMS Collab.)
CHATRCHYAN 13BM	PRL 111 211804	S. Chatrchyan et al.	(CMS Collab.)
Also	PRL 112 119903 (err.)	S. Chatrchyan et al.	(CMS Collab.)
CHATRCHYAN 13W	JHEP 1303 111	S. Chatrchyan et al.	(CMS Collab.)
CHEN 13A	CP C37 06302	J.-B. Chen et al.	(DALI)
EDELHAUSER 13	JHEP 1308 091	L. Edelhauser, T. Flacke, M. Kramer	(AACH, KAIST)
XU 12	JP G40 035107	J. Xu et al.	(CMS Collab.)
AAD 12AD	PL B712 331	G. Aad et al.	(ATLAS Collab.)
AAD 12BV	JHEP 1209 041	G. Aad et al.	(ATLAS Collab.)
AAD 12CC	JHEP 1211 138	G. Aad et al.	(ATLAS Collab.)
AAD 12CP	PL B718 411	G. Aad et al.	(ATLAS Collab.)
AAD 12X	PL B710 519	G. Aad et al.	(ATLAS Collab.)
AAD 12Y	PL B710 538	G. Aad et al.	(ATLAS Collab.)
AALTONEN 12M	PR D85 012008	T. Aaltonen et al.	(CDF)
ABAZOV 12V	PRL 108 131802	V.M. Abazov et al.	(DO Collab.)

See key on page 999

# Searches Particle Listings

## Extra Dimensions, WIMP and Dark Matter Searches

AJELLO	12	JCAP 1202 012	M. Ajello et al.	(Fermi-LAT Collab.)
BAAK	12	EPJ C72 2003	M. Baak et al.	(Glitter Group)
CHATRCHYAN	12R	PRL 108 111801	S. Chattrchyan et al.	(CMS Collab.)
FLACKE	12	PR D85 126007	T. Flacke, C. Pasold	(WURZ)
NISHIWAKI	12	PL B707 506	K. Nishiwaki et al.	(KOBÉ, OSAK)
AAD	11F	PRL 106 121803	G. Aad et al.	(ATLAS Collab.)
AAD	11X	EPJ C71 1744	G. Aad et al.	(ATLAS Collab.)
AALTONEN	11G	PR D83 112008	T. Aaltonen et al.	(CDF Collab.)
AALTONEN	11R	PRL 107 051801	T. Aaltonen et al.	(CDF Collab.)
AALTONEN	11U	PR D83 011102	T. Aaltonen et al.	(CDF Collab.)
AARON	11C	PL B705 52	F. D. Aaron et al.	(HI Collab.)
ABAZOV	11H	PRL 107 011801	V.M. Abazov et al.	(DO Collab.)
BEZERRA	11	PR D83 075004	V.B. Bezerra et al.	(CDF Collab.)
SUSHKOV	11	PRL 107 171101	A.O. Sushkov et al.	(CDF Collab.)
AALTONEN	10N	PRL 104 241801	T. Aaltonen et al.	(CDF Collab.)
ABAZOV	10F	PRL 104 241802	V.M. Abazov et al.	(DO Collab.)
ABAZOV	10P	PRL 105 221802	V.M. Abazov et al.	(DO Collab.)
BEZERRA	10	PR D81 055003	V.B. Bezerra et al.	(DO Collab.)
ABAZOV	09AE	PRL 103 191803	V.M. Abazov et al.	(DO Collab.)
ABAZOV	09D	PRL 102 051601	V.M. Abazov et al.	(DO Collab.)
MASUDA	09	PRL 102 171101	M. Masuda, M. Sasaki	(ICRR)
AALTONEN	08AC	PRL 101 181602	T. Aaltonen et al.	(CDF Collab.)
AALTONEN	08S	PR D78 012008	T. Aaltonen et al.	(CDF Collab.)
ABAZOV	08J	PRL 100 091802	V.M. Abazov et al.	(DO Collab.)
ABAZOV	08S	PRL 101 011601	V.M. Abazov et al.	(DO Collab.)
DAS	08	PR D78 063011	P.K. Das, V.H.S. Kumar, P.K. Suresh	(STAN)
GERACI	08	PR D78 022002	A.A. Geraci et al.	(STAN)
TRENKEL	08	PR D77 122001	C. Trenkel	(CDF Collab.)
AALTONEN	07G	PRL 99 171801	T. Aaltonen et al.	(CDF Collab.)
AALTONEN	07H	PRL 99 171802	T. Aaltonen et al.	(CDF Collab.)
DECCA	07A	EPJ C51 963	R. Decca et al.	(CDF Collab.)
HAISSCH	07	PR D76 034014	U. Haisch, A. Weiler	(CDF Collab.)
KAPNER	07	PRL 98 021101	D.J. Kapner et al.	(CDF Collab.)
SCHAEF	07A	EPJ C49 411	S. Schaefer et al.	(ALEPH Collab.)
TU	07	PRL 98 201101	L.-C. Tu et al.	(CDF Collab.)
ABDALLAH	06C	EPJ C45 589	J. Abdallah et al.	(DELPHI Collab.)
ABULENCIA	06	PRL 97 171802	A. Abulencia et al.	(CDF Collab.)
GERDES	06	PR D73 112008	D. Gerdes et al.	(CDF Collab.)
GOGOLADZE	06	PR D74 093012	I. Gogoladze, C. Macesanu	(CDF Collab.)
ABAZOV	05N	PRL 95 091801	V.M. Abazov et al.	(DO Collab.)
ABAZOV	05V	PRL 95 161602	V.M. Abazov et al.	(DO Collab.)
ABDALLAH	05B	EPJ C38 395	J. Abdallah et al.	(DELPHI Collab.)
ABULENCIA	05A	PRL 95 252001	A. Abulencia et al.	(CDF Collab.)
SMULLIN	05	PR D72 122001	S.J. Smullin et al.	(CDF Collab.)
ACHARD	04E	PL B587 16	P. Achard et al.	(L3 Collab.)
ACOSTA	04C	PRL 92 121802	D. Acosta et al.	(CDF Collab.)
BARBIERI	04	NP B703 127	R. Barbieri et al.	(CDF Collab.)
CASSE	04	PRL 92 111102	M. Casse et al.	(CDF Collab.)
CHEKANOV	04B	PL B591 23	S. Chekanov et al.	(ZEUS Collab.)
HOYLE	04	PR D70 042004	C.D. Hoyle et al.	(WASH)
ABAZOV	03	PRL 90 251802	V.M. Abazov et al.	(DO Collab.)
ABBIENDI	03D	EPJ C26 331	G. Abbiendi et al.	(OPAL Collab.)
ACHARD	03D	PL B572 133	P. Achard et al.	(L3 Collab.)
ADLOFF	03	PL B568 35	C. Adloff et al.	(HI Collab.)
CHIAVERINI	03	PRL 90 151101	J. Chilverini et al.	(CDF Collab.)
GIUDICE	03	NP B663 377	G.F. Giudice, A. Strumia	(CDF Collab.)
HANNESSTAD	03	PR D67 125008	S. Hannestad, G.G. Raffelt	(CDF Collab.)
Also		PR D69 029901(errat.)	S. Hannestad, G.G. Raffelt	(CDF Collab.)
HEISTER	03C	EPJ C28 1	A. Heister et al.	(ALEPH Collab.)
LONG	03	Nature 421 922	J.C. Long et al.	(CDF Collab.)
ACHARD	02	PL B524 65	P. Achard et al.	(L3 Collab.)
ACHARD	02D	PL B531 28	P. Achard et al.	(L3 Collab.)
HANNESSTAD	02	PRL 88 071301	S. Hannestad, G. Raffelt	(CDF Collab.)
ABBOTT	01	PRL 86 1156	B. Abbott et al.	(DO Collab.)
FAIRBAIRN	01	PL B508 335	M. Fairbairn et al.	(CDF Collab.)
HANHART	01	PL B509 1	C. Hanhart et al.	(CDF Collab.)
HOYLE	01	PRL 86 1418	C.D. Hoyle et al.	(CDF Collab.)
ABBIENDI	00R	EPJ C13 553	G. Abbiendi et al.	(OPAL Collab.)
ABREU	00A	PL B491 67	P. Abreu et al.	(DELPHI Collab.)
ABREU	00S	PL B485 45	P. Abreu et al.	(DELPHI Collab.)
ABREU	00Z	EPJ C17 53	P. Abreu et al.	(DELPHI Collab.)
CASSISI	00	PL B481 323	S. Cassisi et al.	(CDF Collab.)
CHANG	00B	PRL 85 3765	L.N. Chang et al.	(CDF Collab.)
CHEUNG	00	PR D61 015005	K. Cheung	(CDF Collab.)
CORNET	00	PR D61 037701	F. Cornet, M. Relano, J. Rico	(CDF Collab.)
GRAESSER	00	PR D61 074019	M.L. Graesser	(CDF Collab.)
HAN	00	PR D62 125018	T. Han, D. Marfatia, R.-J. Zhang	(CDF Collab.)
MATHEWS	00	JHEP 0007 008	P. Mathews, S. Raychaudhuri, K. Sridhar	(CDF Collab.)
MELE	00	PR D61 117901	S. Mele, E. Sanchez	(CDF Collab.)
RIZZO	00	PR D61 016007	T.G. Rizzo, J.D. Wells	(CDF Collab.)
ABBIENDI	99P	PL B465 303	G. Abbiendi et al.	(OPAL Collab.)
ACCIARRI	99M	PL B464 135	M. Acciari et al.	(L3 Collab.)
ACCIARRI	99R	PL B470 268	M. Acciari et al.	(L3 Collab.)
ACCIARRI	99S	PL B470 281	M. Acciari et al.	(L3 Collab.)
BOURLIKOV	99	JHEP 9908 006	D. Bourlikov	(CDF Collab.)
HOSKINS	85	PR D32 3084	J.K. Hoskins et al.	(CDF Collab.)

### WIMP and Dark Matter Searches

We omit papers on CHAMP's, millicharged particles, and other exotic particles.

#### GALACTIC WIMP SEARCHES

These limits are for weakly-interacting stable particles that may constitute the invisible mass in the galaxy. Unless otherwise noted, a local mass density of  $0.3 \text{ GeV}/\text{cm}^3$  is assumed; see each paper for velocity distribution assumptions. In the papers the limit is given as a function of the  $\chi^0$  mass. Here we list limits only for typical mass values of sub-GeV, GeV, 20 GeV, 100 GeV, and 1 TeV. Specific limits on supersymmetric dark matter particles may be found in the Supersymmetry section.

### Spin-Independent Cross Section Limits for Dark Matter Particle ( $\chi^0$ ) on Nucleon

#### For $m_{\chi^0}$ in GeV range

We provide here limits for  $m_{\chi^0} < 5 \text{ GeV}$

VALUE (pb)	CL%	DOCUMENT ID	TECN	COMMENT
● ● ● We do not use the following data for averages, fits, limits, etc. ● ● ●				
$< 1 \times 10^{-2}$	90	1 ABDELHAME...19A	CRES	CaWO <sub>4</sub>
$< 5.4 \times 10^{-6}$	90	2 AGNESE	19A	SCDM GeV-scale WIMPs on Ge
$< 1$	90	3 AKERIB	19	LUX light DM on Xe via Migdal/brem effect
$< 1 \times 10^{-6}$	90	4 AMOLE	19	PICO C <sub>3</sub> F <sub>8</sub>
$< 1.6 \times 10^{-3}$	90	5 APRILE	19c	XE1T DM on Xe
$< 1 \times 10^{-7}$	90	6 APRILE	19d	XE1T DM on Xe
$< 0.1$	90	7 ARMENGAUD	19	EDEL GeV-scale WIMPs on Ge
$< 1.6 \times 10^3$	90	8 KOBAYASHI	19	XMAS annual modulation Xe
$< 7 \times 10^2$	90	9 LIU	19b	CDEX Ge; sub-GeV DM via Migdal
$< 7 \times 10^{-7}$	90	10 AGNES	18	DS50 GeV-scale WIMPs on Ar
$< 1.5 \times 10^{-5}$	95	11 AGNESE	18	SCDM GeV-scale WIMPs on Ge
$< 2 \times 10^{-8}$	90	12 APRILE	18	XE1T Xe, Si
$< 4.5 \times 10^{-3}$	90	13 ARNAUD	18	NEWS low mass WIMP, Ne
$< 8 \times 10^{-6}$	90	14 JIANG	18	CDEX GeV-scale WIMPs on Ge
$< 3 \times 10^{-5}$	90	15 YANG	18	CDEX WIMPs on Ge
$< 1 \times 10^{-6}$	90	16 AKERIB	17	LUX Xe
$< 1 \times 10^2$	90	17 ANGLOTHER	17A	CRES GeV-scale WIMPs
$< 7 \times 10^{-5}$	90	18 ANGLOTHER	16	CRES CaWO <sub>4</sub>
$< 3 \times 10^{-5}$	90	19 APRILE	16	X100 Xe
$< 4.3 \times 10^{-4}$	90	20 ARMENGAUD	16	EDE3 GeV-scale WIMPs on Ge
$< 7 \times 10^{-5}$	90	21 HEHN	16	EDE3 SI WIMP on Ge
$< 6 \times 10^{-5}$	90	22 ZHAO	16	CDEX GeV-scale WIMPs on Ge
$< 1 \times 10^{-4}$	90	23 AMOLE	15	PICO C <sub>3</sub> F <sub>8</sub>
$< 8 \times 10^{-5}$	90	24 XIAO	15	PNDX WIMPs on Xe
$< 3 \times 10^{-5}$	90	25 AGNESE	14	SCDM GeV-scale WIMPs
$< 1 \times 10^{-3}$	90	26 AKERIB	14	LUX WIMP on Xe
$< 9 \times 10^{-4}$	90	27 LI	13b	TEXO WIMPs on Ge
$< 3 \times 10^{-4}$	90	28 ARCHAMBAU.12	12	PICA C <sub>4</sub> F <sub>10</sub>
$< 2 \times 10^{-4}$	90	29 AALSETH	11	CGNT GeV WIMPs on Ge
$< 5 \times 10^{-4}$	90	30 AHMED	11b	CDM2 GeV-scale WIMPs on Ge
$< 8 \times 10^{-5}$	90	31 ANGLE	11	XE10 Xe
$< 5 \times 10^{-4}$	90	32 AKERIB	10	CDM2 WIMPs on Ge/Si

- 1 ABDELHAMEED 19A search for GeV scale dark matter SI scatter on CaWO<sub>4</sub>; no signal, limits placed in  $\sigma$  vs. mass plane for  $m(\text{DM}) \sim 0.1\text{--}10 \text{ GeV}$ . The listed limit is for  $m(\text{DM}) = 1 \text{ GeV}$ .
- 2 AGNESE 19A search for 1.5–10 GeV WIMP scatter on Ge in CDMSlite dataset. Limits set in a likelihood analysis. No signal was observed. Limit reported for  $m(\chi) = 5 \text{ GeV}$ .
- 3 AKERIB 19 search for 0.4–5 GeV DM using bremsstrahlung photons and "Migdal" electrons;  $1.4 \times 10^4 \text{ kg d}$  exposure of liquid Xe; constraint  $\sigma^{SI}(\chi, N) < 1 \text{ pb}$  for  $m(\chi) = 5 \text{ GeV}$  in light scalar mediator model.
- 4 AMOLE 19 search for SI WIMP scatter on C<sub>3</sub>F<sub>8</sub> in PICO-60 bubble chamber; no signal; set limit for spin independent coupling  $\sigma^{SI}(\chi, N) < 1 \times 10^{-6} \text{ pb}$  for  $m(\chi) = 5 \text{ GeV}$ .
- 5 APRILE 19c search for light DM scatter on Xe via atomic excitation, ionization (Migdal effect) or bremsstrahlung; no signal, limits placed in  $\sigma$  vs.  $m(\text{DM})$  plane for  $m(\text{DM}) \sim 0.085\text{--}2 \text{ GeV}$ . The listed limit is for  $m(\text{DM}) = 1 \text{ GeV}$ .
- 6 APRILE 19d search for light DM scatter on Xe via ionization to probe SI, SD, and  $\chi$  e cross sections; with 22 t d exposure, limits placed in various  $\sigma$  vs.  $m(\text{DM})$  planes. Quoted limit is for  $m(\text{DM}) = 5 \text{ GeV}$ .
- 7 ARMENGAUD 19 search for GeV scale WIMP scatter on Ge; limits placed in  $\sigma^{SI}(\chi, N)$  vs.  $m(\chi)$  plane for  $m(\chi) \sim 0.045\text{--}10 \text{ GeV}$ ; quoted limit is for  $m(\chi) = 5 \text{ GeV}$ .
- 8 KOBAYASHI 19 search for sub-GeV WIMP annual modulation in Xe via brems; no signal; limits placed in  $\sigma^{SI}(\chi, N)$  vs.  $m(\chi)$  plane for  $m \sim 0.3\text{--}1 \text{ GeV}$ ; quoted limit is for  $m(\chi) = 0.5 \text{ GeV}$ .
- 9 LIU 19b search for sub-GeV DM using Migdal effect on Ge at CDEX-IB; no signal, require  $\sigma^{SI}(\chi, N) < 7 \times 10^2 \text{ pb}$  for  $m(\chi) = 0.1 \text{ GeV}$ .
- 10 AGNES 18 search for 1.8–20 GeV WIMP SI scatter on Ar; quoted limit is for  $m(\chi) = 5 \text{ GeV}$ .
- 11 AGNESE 18 search for GeV scale WIMPs using CDMSlite; limits placed in  $\sigma^{SI}(\chi, N)$  vs.  $m(\chi)$  plane for  $m \sim 1.5\text{--}20 \text{ GeV}$ ; quoted limit is for  $m(\chi) = 5 \text{ GeV}$ .
- 12 APRILE 18 search for WIMP scatter on 1 t yr Xe; no signal, limits set in  $\sigma(\chi, N)$  vs.  $m(\chi)$  plane for  $m(\chi) \sim 6\text{--}1000 \text{ GeV}$ ; quoted limit is for  $m = 6 \text{ GeV}$ .
- 13 ARNAUD 18 search for low mass WIMP scatter on Ne via SPC at NEWS-G; limits set in  $\sigma^{SI}(\chi, N)$  vs.  $m(\chi)$  plane for  $m \sim 0.5\text{--}20 \text{ GeV}$ ; quoted limit is for  $m = 5 \text{ GeV}$ .
- 14 JIANG 18 search for GeV scale WIMP scatter on Ge; limits placed in  $\sigma^{SI}(\chi, N)$  vs.  $m(\chi)$  plane for  $m(\chi) \sim 3\text{--}10 \text{ GeV}$ ; quoted limit is for  $m(\chi) = 5 \text{ GeV}$ .
- 15 YANG 18 search for WIMP scatter on Ge; limits placed in  $\sigma^{SI}(\chi, N)$  vs.  $m(\chi)$  plane for  $m(\chi) \sim 2\text{--}10 \text{ GeV}$ ; quoted limit is for  $m(\chi) = 5 \text{ GeV}$ .
- 16 AKERIB 17 search for WIMP scatter on Xe; limits placed in  $\sigma^{SI}(\chi, N)$  vs.  $m(\chi)$  plane for  $m(\chi) \sim 5\text{--}1 \times 10^5 \text{ GeV}$ ; quoted limit is for  $m(\chi) = 5 \text{ GeV}$ .
- 17 ANGLOTHER 17A search for GeV scale WIMP scatter on Al<sub>2</sub>O<sub>3</sub> crystal; limits placed in  $\sigma^{SI}(\chi, N)$  vs.  $m(\chi)$  plane for  $m(\chi) \sim 0.15\text{--}10 \text{ GeV}$ ; quoted limit is for  $m(\chi) = 5 \text{ GeV}$ .
- 18 ANGLOTHER 16 search for GeV scale WIMP scatter on CaWO<sub>4</sub>; limits placed in  $\sigma^{SI}(\chi, N)$  vs.  $m(\chi)$  plane for  $m(\chi) \sim 0.5\text{--}30 \text{ GeV}$ ; quoted limit is for  $m(\chi) = 5 \text{ GeV}$ .
- 19 APRILE 16 search for low mass WIMPs via ionization at XENON100; limits placed in  $\sigma^{SI}(\chi, N)$  vs.  $m(\chi)$  plane for  $m \sim 3.5\text{--}20 \text{ GeV}$ ; quoted limit is for  $m(\chi) = 5 \text{ GeV}$ .
- 20 ARMENGAUD 16 search for GeV scale WIMP scatter on Ge; limits placed in  $\sigma^{SI}(\chi, N)$  vs.  $m(\chi)$  plane for  $m(\chi) \sim 4\text{--}30 \text{ GeV}$ ; quoted limit is for  $m(\chi) = 5 \text{ GeV}$ .
- 21 HEHN 16 search for low mass WIMPs via SI scatter on Ge target using profile likelihood analysis; limits placed in  $\sigma^{SI}(\chi, N)$  vs.  $m(\chi)$  plane for  $m(\chi) \sim 4\text{--}30 \text{ GeV}$ ; quoted limit is for  $m(\chi) = 5 \text{ GeV}$ .



# Searches Particle Listings

## WIMP and Dark Matter Searches

- 22 ZHAO 16 search for GeV-scale WIMP scatter on Ge; limits placed in  $\sigma^{SI}(\chi N)$  vs.  $m(\chi)$  plane for  $m(\chi) \sim 4\text{--}30$  GeV; quoted limit is for  $m(\chi) = 5$  GeV.
- 23 AMOLE 15 search for WIMP scatter on  $C_3F_8$  in PICO-2L; limits placed in  $\sigma^{SI}(\chi N)$  vs.  $m(\chi)$  plane for  $m(\chi) \sim 4\text{--}25$  GeV; quoted limit is for  $m(\chi) = 5$  GeV.
- 24 XIAO 15 search for WIMP scatter on Xe with PandaX-I; limits placed in  $\sigma^{SI}(\chi N)$  vs.  $m(\chi)$  plane for  $m(\chi) \sim 5\text{--}100$  GeV; quoted limit is for  $m(\chi) = 5$  GeV.
- 25 AGNESE 14 search for GeV scale WIMPs SI scatter at SuperCDMS; no signal, limits placed in  $\sigma^{SI}(\chi N)$  vs.  $m(\chi)$  plane for  $m(\chi) \sim 3.5\text{--}30$  GeV; quoted limit is for  $m(\chi) = 5$  GeV.
- 26 AKERIB 14 search for WIMP scatter on Xe; limits placed in  $\sigma^{SI}(\chi N)$  vs.  $m(\chi)$  plane for  $m(\chi) \sim 5\text{--}5000$  GeV. Limit given for  $m(\chi) = 5$  GeV.
- 27 LI 13b search for WIMP scatter on Ge; limits placed in  $\sigma^{SI}(\chi N)$  vs.  $m(\chi)$  plane for  $m(\chi) \sim 4\text{--}100$  GeV; quoted limit is for  $m(\chi) = 5$  GeV.
- 28 ARCHAMBAULT 12 search for low mass WIMP scatter on  $C_4F_{10}$ ; limits set in  $\sigma^{SI}(\chi N)$  vs.  $m(\chi)$  plane for  $m \sim 4\text{--}12$  GeV; quoted limit is for  $m = 5$  GeV.
- 29 AALSETH 11 search for GeV-scale SI WIMP scatter on Ge; limits placed on  $\sigma^{SI}(\chi N)$  for  $m(\chi) \sim 3.5\text{--}100$  GeV; quoted limit is for  $m(\chi) = 5$  GeV.
- 30 AHMED 11b search for GeV scale WIMP scatter on Ge in CDMS II; limits placed in  $\sigma^{SD}(\chi n)$  vs.  $m(\chi)$  plane for  $m \sim 4\text{--}12$  GeV.
- 31 ANGLE 11 search for GeV scale WIMPs in Xenon-10; limits placed in  $\sigma^{SI}(\chi N)$  vs.  $m(\chi)$  plane for  $m(\chi) \sim 4\text{--}20$  GeV; quoted limit is for  $m(\chi) = 5$  GeV.
- 32 AKERIB 10 search for WIMP scatter on Ge/Si in CDMS2; limits place in  $\sigma^{SI}(\chi N)$  vs.  $m(\chi)$  plane for  $m 3\text{--}100$  GeV. Limit given for  $m(\text{DM})=5$  GeV

### For $m_{\chi 0} = 20$ GeV

For limits from  $X^0$  annihilation in the Sun, the assumed annihilation final state is shown in parenthesis in the comment.

VALUE (pb)	CL%	DOCUMENT ID	TECN	COMMENT
$<7 \times 10^{-5}$	90	1 ANGLOHER 19	CRES	CaWO <sub>4</sub>
$<3 \times 10^{-7}$	90	2 KIM 19A	KIMS	Nal
$<3.5 \times 10^{-5}$	90	3 KOBAYASHI 19	XMAS	SI WIMP on Xe
$<2 \times 10^{-7}$	90	4 SEONG 19	BELL	$\tau \rightarrow \gamma A, A \rightarrow \chi\chi$
$<1.44 \times 10^{-5}$	90	5 YANG 19	CDEX	annual modulation Ge
$<3 \times 10^{-7}$	90	6 ABE 18c	XMAS	$X^0$ -Xe modulation
$<5 \times 10^{-6}$	95	7 ADHIKARI 18	C100	Nal
$<4 \times 10^{-8}$	90	8 AGNESE 18	DS50	$X^0$ -Ar
$<6 \times 10^{-11}$	90	9 AGNESE 18	SCDM	Ge
$<4.5 \times 10^{-3}$	90	10 AGNESE 18a	SCDM	Ge
$<2 \times 10^{-6}$	90	11 APRILE 18	XE1T	Xe, Si
$<2 \times 10^{-10}$	90	12 ARNAUD 18	NEWS	GeV WIMPs on Ne
$<1 \times 10^{-3}$	90	13 AARTSEN 17	ICCB	$\nu$ , earth
$<1.7 \times 10^{-10}$	90	14 AKERIB 17	LUX	Xe
$<7.3 \times 10^{-7}$	90	15 BARBOSA-D... 17	ICCB	Nal
$<1 \times 10^{-5}$	90	16 CUI 17a	PNDX	WIMPs on Xe
$<2 \times 10^{-4}$	90	17 AGNESE 16	DS50	Ar
$<4.5 \times 10^{-5}$	90	18 AGUILAR-AR... 16	DMIC	Si CCDs
$<2 \times 10^{-6}$	90	19 ANGLOHER 16	CRES	CaWO <sub>4</sub>
$<9.4 \times 10^{-8}$	90	20 APRILE 16	X100	Xe
$<1.0 \times 10^{-7}$	90	21 ARMENGAUD 16	EDE3	Ge
$<5 \times 10^{-6}$	90	22 HEHN 16	EDE3	Ge
$<1 \times 10^{-5}$	90	23 ZHAO 16	CDEX	Ge
$<1.5 \times 10^{-6}$	90	24 AGNESE 15a	CDM2	Ge
$<1.5 \times 10^{-7}$	90	25 AGNESE 15b	CDM2	Ge
$<2 \times 10^{-6}$	90	26 AMOLE 15	PICO	$C_3F_8$
$<1.2 \times 10^{-5}$	90	27 XIAO 15	SKAM	H, solar $\nu$ ( $b\bar{b}$ )
$<1.19 \times 10^{-6}$	90	28 AGNESE 14a	SCDM	Ge
$<2 \times 10^{-8}$	90	29 AGNESE 14a	SCDM	Ge
$<2.0 \times 10^{-7}$	90	30 AKERIB 14	LUX	Xe
$<3.7 \times 10^{-5}$	90	31 ANGLOHER 14	CRES	CaWO <sub>4</sub>
$<1 \times 10^{-9}$	90	32 LEE 14a	KIMS	Csl
$<5 \times 10^{-6}$	90	33 LIU 14a	CDEX	Ge
$<8 \times 10^{-6}$	90	34 YUE 14	CDEX	Ge
$<1 \times 10^{-5}$	90	35 AARTSEN 13	ICCB	H, solar $\nu$ ( $\tau^+ \tau^-$ )
$<1.08 \times 10^{-4}$	90	36 ABE 13b	XMAS	Xe
$<1.5 \times 10^{-5}$	90	37 AGNESE 13	CDM2	Si
$<3.1 \times 10^{-6}$	90	38 AGNESE 13a	CDM2	Si
$<3.4 \times 10^{-6}$	90	39 AGNESE 13a	CDM2	Si
$<2.2 \times 10^{-6}$	90	40 BERNABEI 13a	DAMA	Nal modulation
$<1.2 \times 10^{-4}$	90	41 LI 13b	TEXO	Ge
$<1.2 \times 10^{-7}$	90	42 ZHAO 13	CDEX	Ge
$<8 \times 10^{-6}$	90	43 ANGLOHER 12	CRES	CaWO <sub>4</sub>
$<7 \times 10^{-9}$	90	44 ANGLOHER 12	CRES	CaWO <sub>4</sub>
$<7 \times 10^{-7}$	90	45 APRILE 12	X100	Xe
$<2 \times 10^{-6}$	90	46 ARMENGAUD 12	EDE2	Ge
$<7 \times 10^{-6}$	90	47 BARRETO 12	DMIC	CCD
$<1.5 \times 10^{-6}$	90	48 FELIZARDO 12	SMPPL	$C_2ClF_5$
$<1.7 \times 10^{-6}$	90	49 AALSETH 11	KIMS	Csl
$<5 \times 10^{-5}$	90	50 AALSETH 11a	CGNT	Ge
$<5 \times 10^{-7}$	90	51 AHMED 11	CDM2	Ge, inelastic
$<2.7 \times 10^{-7}$	90	52 AHMED 11a	RVUE	Ge
$<3 \times 10^{-6}$	90	53 ANGLE 11	XE10	Xe
$<7 \times 10^{-8}$	90	54 APRILE 11	X100	Xe
$<2 \times 10^{-8}$	90	55 APRILE 11a	X100	Xe, inelastic
$<2 \times 10^{-7}$	90	56 HORN 11	ZEP3	Xe
$<1 \times 10^{-5}$	90	57 AKERIB 10	CDM2	Si, Ge, low threshold
$<1 \times 10^{-7}$	90	58 AHMED 09	CDM2	Ge
$<2 \times 10^{-6}$	90	59 LIN 09	TEXO	Ge
$<4 \times 10^{-5}$	90	60 AALSETH 08	CGNT	Ge

- 1 ANGLOHER 19 search for low mass WIMP scatter on CaWO<sub>4</sub>; no signal; limits placed on Wilson coefficients for  $m(\chi) = 0.6\text{--}60$  GeV.
- 2 KIM 19a search for WIMP scatter in Nal KIMS experiment; no signal; require  $\sigma^{SI}(\chi n) < 7 \times 10^{-5}$  pb for  $m(\chi) = 20$  GeV.
- 3 KOBAYASHI 19 search for WIMP scatter in XMASS single-phase liquid Xe detector; no signal; require  $\sigma^{SI}(\chi N) < 3 \times 10^{-7}$  pb for  $m(\chi) = 20$  GeV.
- 4 SEONG 19 search for  $\tau \rightarrow \gamma A, A \rightarrow \chi\chi$  via CP-odd Higgs; no signal; limits on BF set; model dependent conversion to WIMP-nucleon scattering cross section limits  $\sigma^{SI} < 10^{-36}$  cm<sup>2</sup> for  $m(\chi) = 0.01\text{--}1$  GeV.
- 5 YANG 19 search for low mass wimps via annual modulation in Ge; no signal; require  $\sigma^{SI}(\chi N) < 3.5 \times 10^{-5}$  pb for  $m(\chi) = 20$  GeV.
- 6 ABE 18c search for WIMP annual modulation signal for  $m(\text{WIMP})$ : 6–20 GeV; limits set on SI WIMP-nucleon cross section: see Fig. 6.
- 7 ADHIKARI 18 search for WIMP scatter on Nal; no signal; require  $\sigma^{SI} < 1.44 \times 10^{-5}$  pb for  $m(\text{WIMP}) = 20$  GeV; inconsistent with DAMA/LIBRA result.
- 8 AGNESE 18 search low mass  $m(\text{WIMP})$ : 1.8–20 GeV scatter on Ar; limits on SI WIMP-nucleon cross section set in Fig. 8.
- 9 AGNESE 18 give limits for  $\sigma^{SI}(\chi N)$  for  $m(\text{WIMP})$  between 1.5 and 20 GeV using CDMSlite mode data.
- 10 AGNESE 18a search for WIMP scatter on Ge at SuperCDMS; 1 event, consistent with expected background; set limit in  $\sigma^{SI}(\chi N)$  vs.  $m(\chi)$  plane for  $m \sim 10\text{--}250$  GeV.
- 11 APRILE 18 search for WIMP scatter on 1 t yr Xe; no signal, limits placed in  $\sigma^{SI}(\chi N)$  vs.  $m(\chi)$  plane for  $m(\chi) \sim 6\text{--}1000$  GeV.
- 12 ARNAUD 18 search for low mass WIMP scatter on Ne via SPC at NEWS-G; limits set in  $\sigma^{SI}(\chi N)$  vs.  $m(\chi)$  plane for  $m \sim 0.5\text{--}20$  GeV.
- 13 AARTSEN 17 obtain  $\sigma(\text{Si}) < 6 \times 10^{-6}$  pb for  $m(\text{wimp}) = 20$  GeV from  $\nu$  from earth.
- 14 AKERIB 17 search for WIMP scatter on Xe; limits placed in  $\sigma^{SI}(\chi N)$  vs.  $m(\chi)$  plane for  $m(\chi) \sim 5\text{--}1 \times 10^5$  GeV.
- 15 BARBOSA-DE-SOUZA 17 search for annual modulation of WIMP scatter on Nal using an exposure of 61 kg yr of DM-Ice17 for recoil energy in the 4–20 keV range (DAMA found modulation for recoil energy  $< 5$  keV). No modulation seen. Sensitivity insufficient to distinguish DAMA signal from null.
- 16 CUI 17a search for SI WIMP scatter; limits placed in  $\sigma^{SI}(\chi N)$  vs.  $m(\chi)$  plane for  $m \sim 10\text{--}1 \times 10^4$  GeV using 54 ton-day exposure of Xe.
- 17 AGNESE 16 CDMSlite excludes low mass WIMPs 1.6–5.5 GeV and SI scattering cross section depending on  $m(\text{WIMP})$ ; see Fig. 4.
- 18 AGUILAR-AREVALO 16 search low mass 1–10 GeV WIMP scatter on Si CCDs; set limits Fig. 11.
- 19 ANGLOHER 16 search for GeV scale WIMP scatter on CaWO<sub>4</sub>; limits placed in  $\sigma^{SI}(\chi N)$  vs.  $m(\chi)$  plane for  $m(\chi) \sim 0.5\text{--}30$  GeV.
- 20 APRILE 16 search for low mass WIMPs via ionization at XENON100; limits placed in  $\sigma^{SI}(\chi N)$  vs.  $m(\chi)$  plane for  $m \sim 3.5\text{--}20$  GeV.
- 21 ARMENGAUD 16 search for GeV scale WIMP scatter on Ge; limits placed in  $\sigma^{SI}(\chi N)$  vs.  $m(\chi)$  plane for  $m(\chi) \sim 4\text{--}30$  GeV.
- 22 HEHN 16 search for low mass WIMPs via Si scatter on Ge target using profile likelihood analysis; limits placed in  $\sigma^{SI}(\chi N)$  vs.  $m(\chi)$  plane for  $m(\chi) \sim 4\text{--}30$  GeV.
- 23 ZHAO 16 search for GeV-scale WIMP scatter on Ge; limits placed in  $\sigma^{SI}(\chi N)$  vs.  $m(\chi)$  plane for  $m(\chi) \sim 4\text{--}30$  GeV.
- 24 AGNESE 15a reanalyse AHMED 11b low threshold data. See their Fig. 12 (left) for improved limits extending down to 5 GeV.
- 25 AGNESE 15b reanalyse AHMED 10 data.
- 26 See their Fig. 7 for limits extending down to 4 GeV.
- 27 XIAO 15 search for WIMP scatter on Xe with PandaX-I; limits placed in  $\sigma^{SI}(\chi N)$  vs.  $m(\chi)$  plane for  $m(\chi) \sim 5\text{--}100$  GeV.
- 28 This limit value is provided by the authors. See their Fig. 4 for limits extending down to  $m_{\chi 0} = 3.5$  GeV.
- 29 This limit value is provided by the authors. AGNESE 14a result is from CDMSlite mode operation with enhanced sensitivity to low mass  $m_{\chi 0}$ . See their Fig. 3 for limits extending down to  $m_{\chi 0} = 3.5$  GeV (see also Fig. 4 in AGNESE 14).
- 30 See their Fig. 5 for limits extending down to  $m_{\chi 0} = 5.5$  GeV.
- 31 See their Fig. 5 for limits extending down to  $m_{\chi 0} = 1$  GeV.
- 32 See their Fig. 5 for limits extending down to  $m_{\chi 0} = 5$  GeV.
- 33 LIU 14a result is based on prototype CDEX-0 detector. See their Fig. 13 for limits extending down to  $m_{\chi 0} = 2$  GeV.
- 34 See their Fig. 4 for limits extending down to  $m_{\chi 0} = 4.5$  GeV.
- 35 AARTSEN 13 search for neutrinos from the Sun arising from the pair annihilation of  $X^0$  trapped by the sun in data taken between June 2010 and May 2011.
- 36 See their Fig. 8 for limits extending down to  $m_{\chi 0} = 7$  GeV.
- 37 This limit value is provided by the authors. AGNESE 13 use data taken between Oct. 2006 and July 2007. See their Fig. 4 for limits extending down to  $m_{\chi 0} = 7$  GeV.

- <sup>38</sup>This limit value is provided by the authors. AGNESE 13A use data taken between July 2007 and Sep. 2008. Three candidate events are seen. Assuming these events are real, the best fit parameters are  $m_{\chi^0} = 8.6$  GeV and  $\sigma = 1.9 \times 10^{-5}$  pb.
- <sup>39</sup>This limit value is provided by the authors. Limit from combined data of AGNESE 13 and AGNESE 13A. See their Fig. 4 for limits extending down to  $m_{\chi^0} = 5.5$  GeV.
- <sup>40</sup>BERNABEI 13A search for annual modulation of counting rate in the 2–6 keV recoil energy interval, in a 14 yr live time exposure of 1.33 t yr. Find a modulation of 0.0112 ± 0.0012 counts/(day kg keV) with 9.3 sigma C.L. Find period and phase in agreement with expectations from DM particles.
- <sup>41</sup>LI 13b search for WIMP scatter on Ge; limits placed in  $\sigma^{SI}(\chi N)$  vs.  $m(\chi)$  plane for  $m(\chi) \sim 4$ –100 GeV.
- <sup>42</sup>See their Fig. 5 for limits for  $m_{\chi^0} = 4$ –12 GeV.
- <sup>43</sup>ANGLOHER 12 observe excess events above the expected background which are consistent with  $\chi^0$  with mass  $\sim 25$  GeV (or 12 GeV) and spin-independent  $\chi^0$ -nucleon cross section of  $2 \times 10^{-6}$  pb (or  $4 \times 10^{-5}$  pb).
- <sup>44</sup>Reanalysis of ANGLOHER 09 data with all three nuclides. See also BROWN 12.
- <sup>45</sup>See also APRILE 14A.
- <sup>46</sup>See their Fig. 4 for limits extending down to  $m_{\chi^0} = 7$  GeV.
- <sup>47</sup>See their Fig. 13 for cross section limits for  $m_{\chi^0}$  between 1.2 and 10 GeV.
- <sup>48</sup>See also DAHL 12 for a criticism.
- <sup>49</sup>See their Fig. 4 for limits extending to  $m_{\chi^0} = 3.5$  GeV.
- <sup>50</sup>AALSETH 11A find indications of annual modulation of the data, the energy spectrum being compatible with  $\chi^0$  mass around 8 GeV. See also AALSETH 13.
- <sup>51</sup>AHMED 11 search for  $\chi^0$  inelastic scattering. See their Fig. 8–10 for limits. The inelastic cross section reduces to the elastic cross section at the limit of zero mass splitting (Fig. 8, left).
- <sup>52</sup>AHMED 11A combine CDMS II and EDELWEISS data.
- <sup>53</sup>ANGLE 11 show limits down to  $m_{\chi^0} = 4$  GeV on Fig. 3.
- <sup>54</sup>APRILE 11 reanalyze APRILE 10 data.
- <sup>55</sup>APRILE 11A search for  $\chi^0$  inelastic scattering. See their Fig. 2 and 3 for limits. See also APRILE 14A.
- <sup>56</sup>HORN 11 perform detector calibration by neutrons. Earlier results are only marginally affected.
- <sup>57</sup>See their Fig. 10 and 12 for limits extending to  $\chi^0$  mass of 1 GeV.
- <sup>58</sup>Superseded by AHMED 10.
- <sup>59</sup>See their Fig. 6(a) for cross section limits for  $m_{\chi^0}$  extending down to 2 GeV.
- <sup>60</sup>See their Fig. 2 for cross section limits for  $m_{\chi^0}$  between 4 and 10 GeV.

**For  $m_{\chi^0} = 100$  GeV**

For limits from  $\chi^0$  annihilation in the Sun, the assumed annihilation final state is shown in parenthesis in the comment.

VALUE (pb)	CL%	DOCUMENT ID	TECN	COMMENT
•••	•••	•••	•••	•••
$<4 \times 10^{-8}$	90	1 ABE	19 XMAS	Xe
$<3.9 \times 10^{-9}$	90	2 AJAJ	19 DEAP	Ar
$<2.3 \times 10^{-6}$	90	3 ADHIKARI	18 C100	Nal
$<1.14 \times 10^{-8}$	90	4 AGNES	18A DS50	Ar
$<2 \times 10^{-8}$	90	5 AGNESE	18A CDMS	Ge
$<1.2 \times 10^{-8}$	90	6 AMAUDRUZ	18 DEAP	Ar
$<9.12 \times 10^{-11}$	90	7 APRILE	18 XE1T	Xe
		8 REN	18 PNDX	SIDM at PDX-II
$<1.7 \times 10^{-10}$	90	9 AKERIB	17 LUX	Xe
$<1.2 \times 10^{-10}$	90	10 APRILE	17G XE1T	Xe
$<1.2 \times 10^{-10}$	90	11 CUI	17A PNDX	Xe
$<2.0 \times 10^{-8}$	90	AGNES	16 DS50	Ar
$<1 \times 10^{-9}$	90	12 AKERIB	16 LUX	Xe
$<1 \times 10^{-9}$	90	13 APRILE	16B X100	Xe
$<2 \times 10^{-8}$	90	14 TAN	16 PNDX	Xe
$<4 \times 10^{-10}$	90	15 TAN	16B PNDX	Xe
$<6 \times 10^{-8}$	90	AGNES	15 DS50	Ar
$<4 \times 10^{-8}$	90	16 AGNESE	15B CDM2	Ge
$<7.13 \times 10^{-6}$	90	CHOI	15 SKAM	H, solar $\nu$ ( $b\bar{b}$ )
$<6.26 \times 10^{-7}$	90	CHOI	15 SKAM	H, solar $\nu$ ( $W^+ W^-$ )
$<2.76 \times 10^{-7}$	90	CHOI	15 SKAM	H, solar $\nu$ ( $\tau^+ \tau^-$ )
$<1.5 \times 10^{-8}$	90	17 XIAO	15 PNDX	Xe
$<1 \times 10^{-9}$	90	AKERIB	14 LUX	Xe
$<4.0 \times 10^{-6}$	90	18 AVROBIN	14 BAIK	H, solar $\nu$ ( $W^+ W^-$ )
$<1.0 \times 10^{-4}$	90	18 AVROBIN	14 BAIK	H, solar $\nu$ ( $b\bar{b}$ )
$<1.6 \times 10^{-6}$	90	18 AVROBIN	14 BAIK	H, solar $\nu$ ( $\tau^+ \tau^-$ )
$<5 \times 10^{-6}$	90	FELIZARDO	14 SMPPL	$C_2ClF_5$
$<6.01 \times 10^{-7}$	90	19 AARTSEN	13 ICCB	H, solar $\nu$ ( $W^+ W^-$ )
$<3.30 \times 10^{-5}$	90	19 AARTSEN	13 ICCB	H, solar $\nu$ ( $b\bar{b}$ )
$<1.9 \times 10^{-6}$	90	20 ADRIAN-MAR.13	ANTR	H, solar $\nu$ ( $W^+ W^-$ )
$<1.2 \times 10^{-4}$	90	20 ADRIAN-MAR.13	ANTR	H, solar $\nu$ ( $b\bar{b}$ )
$<7.6 \times 10^{-7}$	90	20 ADRIAN-MAR.13	ANTR	H, solar $\nu$ ( $\tau^+ \tau^-$ )
$<2 \times 10^{-6}$	90	21 AGNESE	13 CDM2	Si
$<1.6 \times 10^{-6}$	90	22 BOLIEV	13 BAKS	H, solar $\nu$ ( $W^+ W^-$ )
$<1.9 \times 10^{-5}$	90	22 BOLIEV	13 BAKS	H, solar $\nu$ ( $b\bar{b}$ )
$<7.1 \times 10^{-7}$	90	22 BOLIEV	13 BAKS	H, solar $\nu$ ( $\tau^+ \tau^-$ )
$<3.2 \times 10^{-4}$	90	23 LI	13B TEXO	WIMPs on Ge
$<1.67 \times 10^{-6}$	90	24 ABBASI	12 ICCB	H, solar $\nu$ ( $W^+ W^-$ )
$<1.07 \times 10^{-4}$	90	24 ABBASI	12 ICCB	H, solar $\nu$ ( $b\bar{b}$ )
$<4 \times 10^{-8}$	90	AKIMOV	12 ZEP3	Xe
$<1.4 \times 10^{-6}$	90	25 ANGLOHER	12 CRES	CaWO <sub>4</sub>

$<3 \times 10^{-9}$	90	26 APRILE	12 X100	Xe
$<3 \times 10^{-7}$	90	BEHNKE	12 COUP	CF <sub>3</sub> I
$<7 \times 10^{-6}$		FELIZARDO	12 SMPPL	C <sub>2</sub> ClF <sub>5</sub>
$<2.5 \times 10^{-7}$	90	27 KIM	12 KIMS	Csl
$<2 \times 10^{-4}$	90	AALSETH	11 CGNT	Ge
		28 AHMED	11 CDM2	Ge, inelastic
$<3.3 \times 10^{-8}$	90	29 AHMED	11A RVUE	Ge
		30 AJELLO	11 FLAT	
$<3 \times 10^{-8}$	90	31 APRILE	11 X100	Xe
		32 APRILE	11A X100	Xe, inelastic
$<1 \times 10^{-8}$	90	26 APRILE	11B X100	Xe
$<5 \times 10^{-8}$	90	33 ARMENGAUD	11 EDE2	Ge
		34 HORN	11 ZEP3	Xe
$<4 \times 10^{-8}$	90	AHMED	10 CDM2	Ge
$<9 \times 10^{-6}$	90	AKERIB	10 CDM2	Si, Ge, low threshold
		35 AKIMOV	10 ZEP3	Xe, inelastic
$<5 \times 10^{-8}$	90	APRILE	10 X100	Xe
$<1 \times 10^{-7}$	90	ARMENGAUD	10 EDE2	Ge
$<3 \times 10^{-5}$	90	FELIZARDO	10 SMPPL	C <sub>2</sub> ClF <sub>3</sub>
$<5 \times 10^{-8}$	90	36 AHMED	09 CDM2	Ge
		37 ANGLE	09 XE10	Xe, inelastic
		LIN	09 TEXO	Ge
$<3 \times 10^{-4}$	90	38 GIULIANI	05 RVUE	

- <sup>1</sup>ABE 19 search for SI DD in single phase Xe; no signal; require  $\sigma^{SI}(\chi p) < 4 \times 10^{-8}$  pb for  $m(\chi) \sim 100$  GeV.
- <sup>2</sup>AJAJ 19 search for SI WIMP-nucleon scatter with 758 tonne day exposure of single phase liquid Ar; no signal; require  $\sigma^{SI}(\chi N) < 3.9 \times 10^{-9}$  pb for  $m(\chi) = 100$  GeV.
- <sup>3</sup>ADHIKARI 18 search for WIMP scatter on NaI; limit set  $\sigma^{SI}(\chi p) < 2.3 \times 10^{-6}$  pb for  $m(\chi) = 100$  GeV.
- <sup>4</sup>AGNES 18A search for WIMP scatter on 46.4 kg Ar; no signal; require  $\sigma^{SI}(\chi N) < 1.4 \times 10^{-8}$  pb for  $m(\chi) = 100$  GeV.
- <sup>5</sup>AGNESE 18A set limit  $\sigma^{SI}(\chi N) < 2 \times 10^{-8}$  pb for  $m(\text{WIMP}) = 100$  GeV.
- <sup>6</sup>AMAUDRUZ 18 search for WIMP scatter on Ar with DEAP-3600; limits set:  $\sigma^{SI}(\chi p) < 1.2 \times 10^{-8}$  pb for  $m(\text{WIMP}) = 100$  GeV.
- <sup>7</sup>APRILE 18 search for WIMP scatter on 1.3 t liquid Xe; no signal; require  $\sigma^{SI}(\chi p) < 9.12 \times 10^{-11}$  pb for  $m(\chi) = 100$  GeV.
- <sup>8</sup>REN 18 search for self-interacting DM at PandaX-II with a total exposure of 54 ton day; limits set in  $m(\text{DM})$  vs.  $m(\text{mediator})$  plane.
- <sup>9</sup>AKERIB 17 exclude SI cross section  $> 1.7 \times 10^{-10}$  pb for  $m(\text{WIMP}) = 100$  GeV. Uses complete LUX data set.
- <sup>10</sup>APRILE 17G set limit  $\sigma^{SI}(\chi p) < 1.2 \times 10^{-10}$  pb for  $m(\text{WIMP}) = 100$  GeV using 1 ton fiducial mass Xe TPC. Exposure is 34.2 live days.
- <sup>11</sup>CUI 17A search for SI WIMP scatter; limits placed in  $\sigma^{SI}(\chi N)$  vs.  $m(\chi)$  plane for  $m \sim 10$ – $1 \times 10^4$  GeV using 54 ton-day exposure of Xe.
- <sup>12</sup>AKERIB 16 re-analysis of 2013 data exclude SI cross section  $> 1 \times 10^{-9}$  pb for  $m(\text{WIMP}) = 100$  GeV on Xe target.
- <sup>13</sup>APRILE 16B combined 447 live days using Xe target exclude  $\sigma(\text{SI}) > 1.1 \times 10^{-9}$  pb for  $m(\text{WIMP}) = 50$  GeV.
- <sup>14</sup>TAN 16 search for WIMP scatter off Xe target; see SI exclusion plot Fig. 6.
- <sup>15</sup>TAN 16B search for WIMP-p scatter off Xe target; see Fig. 5 for SI exclusion.
- <sup>16</sup>AGNESE 15B reanalyze AHMED 10 data.
- <sup>17</sup>XIAO 15 search for WIMP scatter on Xe with PandaX-I; limits placed in  $\sigma^{SI}(\chi N)$  vs.  $m(\chi)$  plane for  $m(\chi) \sim 5$ –100 GeV.
- <sup>18</sup>AVROBIN 14 search for neutrinos from the Sun arising from the pair annihilation of  $\chi^0$  trapped by the Sun in data taken between 1998 and 2003. See their Table 1 for limits assuming annihilation into neutrino pairs.
- <sup>19</sup>AARTSEN 13 search for neutrinos from the Sun arising from the pair annihilation of  $\chi^0$  trapped by the sun in data taken between June 2010 and May 2011.
- <sup>20</sup>ADRIAN-MARTINEZ 13 search for neutrinos from the Sun arising from the pair annihilation of  $\chi^0$  trapped by the sun in data taken between Jan. 2007 and Dec. 2008.
- <sup>21</sup>AGNESE 13 use data taken between Oct. 2006 and July 2007.
- <sup>22</sup>BOLIEV 13 search for neutrinos from the Sun arising from the pair annihilation of  $\chi^0$  trapped by the sun in data taken from 1978 to 2009. See also SUVOROVA 13 for an older analysis of the same data.
- <sup>23</sup>LI 13b search for WIMP scatter on Ge; limits placed in  $\sigma^{SI}(\chi N)$  vs.  $m(\chi)$  plane for  $m(\chi) \sim 4$ –100 GeV.
- <sup>24</sup>ABBASI 12 search for neutrinos from the Sun arising from the pair annihilation of  $\chi^0$  trapped by the Sun. The amount of  $\chi^0$  depends on the  $\chi^0$ -proton cross section.
- <sup>25</sup>Reanalysis of ANGLOHER 09 data with all three nuclides. See also BROWN 12.
- <sup>26</sup>See also APRILE 14A.
- <sup>27</sup>See their Fig. 6 for a limit on inelastically scattering  $\chi^0$  for  $m_{\chi^0} = 70$  GeV.
- <sup>28</sup>AHMED 11 search for  $\chi^0$  inelastic scattering. See their Fig. 8–10 for limits.
- <sup>29</sup>AHMED 11A combine CDMS and EDELWEISS data.
- <sup>30</sup>AJELLO 11 search for  $e^\pm$  flux from  $\chi^0$  annihilations in the Sun. Models in which  $\chi^0$  annihilates into an intermediate long-lived weakly interacting particles or  $\chi^0$  scatters inelastically are constrained. See their Fig. 6–8 for limits.
- <sup>31</sup>APRILE 11 reanalyze APRILE 10 data.
- <sup>32</sup>APRILE 11A search for  $\chi^0$  inelastic scattering. See their Fig. 2 and 3 for limits. See also APRILE 14A.
- <sup>33</sup>Supersedes ARMENGAUD 10. A limit on inelastic cross section is also given.
- <sup>34</sup>HORN 11 perform detector calibration by neutrons. Earlier results are only marginally affected.
- <sup>35</sup>AKIMOV 10 give cross section limits for inelastically scattering dark matter. See their Fig. 4.
- <sup>36</sup>Superseded by AHMED 10.
- <sup>37</sup>ANGLE 09 search for  $\chi^0$  inelastic scattering. See their Fig. 4 for limits.
- <sup>38</sup>GIULIANI 05 analyzes the spin-independent  $\chi^0$ -nucleon cross section limits with both isoscalar and isovector couplings. See their Fig. 3 and 4 for limits on the couplings.

# Searches Particle Listings

## WIMP and Dark Matter Searches

### For $m_{\chi^0} = 1$ TeV

For limits from  $X^0$  annihilation in the Sun, the assumed annihilation final state is shown in parenthesis in the comment.

VALUE (pb)	CL%	DOCUMENT ID	TECN	COMMENT
<3 × 10 <sup>-6</sup>	90	1 YAGUNA 19	Ar	I-spin viol DM
<3.8 × 10 <sup>-8</sup>	90	2 AGNES 18A	DS50 Ar	
<8.24 × 10 <sup>-10</sup>	90	3 APRILE 18	XE1T Xe	
<2 × 10 <sup>-9</sup>	90	4 AKERIB 17	LUX Xe	
<0.3	90	5 CHEN 17E	PNDX $\chi N \rightarrow \chi^* \rightarrow \chi \gamma$	
<1.2 × 10 <sup>-9</sup>	90	6 CUI 17A	PNDX Si WIMPs on Xe	
<8.6 × 10 <sup>-8</sup>	90	AGNES 16	DS50 Ar	
<2 × 10 <sup>-7</sup>	90	AGNES 15	DS50 Ar	
<2 × 10 <sup>-7</sup>	90	7 AGNESE 15B	CDM2 Ge	
<1 × 10 <sup>-8</sup>	90	AKERIB 14	LUX Xe	
<2.2 × 10 <sup>-6</sup>	90	8 AVRORIN 14	BAIK H, solar $\nu (W^+ W^-)$	
<5.5 × 10 <sup>-5</sup>	90	8 AVRORIN 14	BAIK H, solar $\nu (b\bar{b})$	
<6.8 × 10 <sup>-7</sup>	90	8 AVRORIN 14	BAIK H, solar $\nu (\tau^+ \tau^-)$	
<3.46 × 10 <sup>-7</sup>	90	9 AARTSEN 13	ICCB H, solar $\nu (W^+ W^-)$	
<7.75 × 10 <sup>-6</sup>	90	9 AARTSEN 13	ICCB H, solar $\nu (b\bar{b})$	
<6.9 × 10 <sup>-7</sup>	90	10 ADRIAN-MAR.13	ANTR H, solar $\nu (W^+ W^-)$	
<1.5 × 10 <sup>-5</sup>	90	10 ADRIAN-MAR.13	ANTR H, solar $\nu (b\bar{b})$	
<1.8 × 10 <sup>-7</sup>	90	10 ADRIAN-MAR.13	ANTR H, solar $\nu (\tau^+ \tau^-)$	
<4.3 × 10 <sup>-6</sup>	90	11 BOLIEV 13	BAKS H, solar $\nu (W^+ W^-)$	
<3.4 × 10 <sup>-5</sup>	90	11 BOLIEV 13	BAKS H, solar $\nu (b\bar{b})$	
<1.2 × 10 <sup>-6</sup>	90	11 BOLIEV 13	BAKS H, solar $\nu (\tau^+ \tau^-)$	
<2.12 × 10 <sup>-7</sup>	90	12 ABBASI 12	ICCB H, solar $\nu (W^+ W^-)$	
<6.56 × 10 <sup>-6</sup>	90	12 ABBASI 12	ICCB H, solar $\nu (b\bar{b})$	
<4 × 10 <sup>-7</sup>	90	AKIMOV 12	ZEP3 Xe	
<1.1 × 10 <sup>-5</sup>	90	13 ANGIOHER 12	CRES CaWO <sub>4</sub>	
<2 × 10 <sup>-8</sup>	90	14 APRILE 12	X100 Xe	
<2 × 10 <sup>-6</sup>	90	BEHNKE 12	COUP CF <sub>3</sub> I	
<4 × 10 <sup>-6</sup>	90	FELIZARDO 12	SMP L C <sub>2</sub> ClF <sub>5</sub>	
<1.5 × 10 <sup>-6</sup>	90	KIM 12	KIMS Csl	
		15 AHMED 11	CDM2 Ge, inelastic	
<1.5 × 10 <sup>-7</sup>	90	16 AHMED 11A	RVUE Ge	
<2 × 10 <sup>-7</sup>	90	17 APRILE 11	X100 Xe	
<8 × 10 <sup>-8</sup>	90	14 APRILE 11B	X100 Xe	
<2 × 10 <sup>-7</sup>	90	18 ARMENGAUD 11	EDE2 Ge	
		19 HORN 11	ZEP3 Xe	
<2 × 10 <sup>-7</sup>	90	AHMED 10	CDM2 Ge	
<4 × 10 <sup>-7</sup>	90	APRILE 10	X100 Xe	
<6 × 10 <sup>-7</sup>	90	ARMENGAUD 10	EDE2 Ge	
<3.5 × 10 <sup>-7</sup>	90	20 AHMED 09	CDM2 Ge	

- 1 YAGUNA 19 recasts DEAP-3600 single-phase liquid argon results in limit for isospin violating DM; for  $f_n/f_p = -0.69$ , requires  $\sigma^{SI}(\chi p) < 3 \times 10^{-6}$  pb for  $m(\chi) = 1$  TeV.
- 2 AGNES 18A search for WIMP scatter on 46.4 kg Ar; no signal; require  $\sigma^{SI}(\chi N) < 3.8 \times 10^{-8}$  pb for  $m(\chi) = 1$  TeV.
- 3 APRILE 18 search for WIMP scatter on 1.3 t Xe; no signal seen; require  $\sigma^{SI}(\chi p) < 8.24 \times 10^{-10}$  pb for  $m(\chi) = 1$  TeV.
- 4 AKERIB 17 search for WIMP scatter on Xe using complete LUX data set; limits placed in  $\sigma^{SI}(\chi N)$  vs.  $m(\chi)$  plane for  $m(\chi) \sim 5-1 \times 10^5$  GeV.
- 5 CHEN 17E search for inelastic WIMP scatter on Xe; require  $\sigma^{SI}(\chi N) < 0.3$  pb for  $m(\chi) = 1$  TeV and (mass difference) = 300 keV.
- 6 CUI 17A search for WIMP scatter using 54 ton-day exposure of Xe; limits placed in  $\sigma^{SI}(\chi N)$  vs.  $m(\chi)$  plane for  $m \sim 10-1 \times 10^4$  GeV.
- 7 AGNESE 15B reanalyse AHMED 10 data.
- 8 AVRORIN 14 search for neutrinos from the Sun arising from the pair annihilation of  $X^0$  trapped by the Sun in data taken between 1998 and 2003. See their Table 1 for limits assuming annihilation into neutrino pairs.
- 9 AARTSEN 13 search for neutrinos from the Sun arising from the pair annihilation of  $X^0$  trapped by the sun in data taken between June 2010 and May 2011.
- 10 ADRIAN-MARTINEZ 13 search for neutrinos from the Sun arising from the pair annihilation of  $X^0$  trapped by the sun in data taken between Jan. 2007 and Dec. 2008.
- 11 BOLIEV 13 search for neutrinos from the Sun arising from the pair annihilation of  $X^0$  trapped by the sun in data taken from 1978 to 2009. See also SUVOROVA 13 for an older analysis of the same data.
- 12 ABBASI 12 search for neutrinos from the Sun arising from the pair annihilation of  $X^0$  trapped by the Sun. The amount of  $X^0$  depends on the  $X^0$ -proton cross section.
- 13 Reanalysis of ANGIOHER 09 data with all three nuclides. See also BROWN 12. See also APRILE 14A.
- 14 AHMED 11 search for  $X^0$  inelastic scattering. See their Fig. 8-10 for limits.
- 16 AHMED 11A combine CDM2 and EDELWEISS data.
- 17 APRILE 11 reanalyse APRILE 10 data.
- 18 Supersedes ARMENGAUD 10. A limit on inelastic cross section is also given.
- 19 HORN 11 perform detector calibration by neutrons. Earlier results are only marginally affected.
- 20 Superseded by AHMED 10.

### Spin-Dependent Cross Section Limits for Dark Matter Particle ( $X^0$ ) on Proton

#### For $m_{\chi^0}$ in GeV range

We provide here limits for  $m_{\chi^0} < 5$  GeV

VALUE (pb)	CL%	DOCUMENT ID	TECN	COMMENT
< 1 × 10 <sup>6</sup>	95	1 ABDELHAME...19	CRES	GeV-scale WIMPs on Li
< 3 × 10 <sup>-4</sup>	90	2 AMOLE 19	PICO	C <sub>3</sub> F <sub>8</sub>
< 1.7 × 10 <sup>4</sup>	90	3 APRILE 19c	XE1T	light DM on Xe via Migdal/brem effect
< 8 × 10 <sup>6</sup>	90	4 ARMENGAUD 19	EDEL	GeV-scale WIMPs on Ge
< 70	90	5 XIA 19A	PNDX	SD WIMP on Xe
<100	90	6 AGNESE 18	SCDM	GeV-scale WIMPs on Ge
< 1	90	7 AKERIB 17A	LUX	Xe
< 0.6	90	8 FU 17	PNDX	SD WIMP on Xe
< 0.2	90	9 AMOLE 15	PICO	C <sub>3</sub> F <sub>8</sub>
< 1.6 × 10 <sup>-1</sup>	90	10 ARCHAMBAU.12	PICA	<sup>19</sup> F

• • • We do not use the following data for averages, fits, limits, etc. • • •

1 ABDELHAMEED 19 search for SD WIMP scatter on <sup>7</sup>Li; limits placed on  $\sigma^{SD}(\chi p)$  for  $m(\chi) \sim 0.8-20$  GeV; quoted limit is for  $m(\chi) = 1$  GeV.

2 AMOLE 19 search for SD WIMP scatter on C<sub>3</sub>F<sub>8</sub> in PICO-60 bubble chamber; no signal; set limit for spin dependent coupling  $\sigma^{SD}(\chi p) < 2 \times 10^{-4}$  pb for  $m(\chi) = 5$  GeV.

3 APRILE 19c search for light DM on Xe via Migdal/brem effect; no signal, require  $\sigma^{SD}(\chi p) < 1.7 \times 10^4$  pb for  $m(\chi) = 1$  GeV.

4 ARMENGAUD 19 search for GeV scale WIMP scatter on Ge; limits placed in  $\sigma^{SD}(\chi p)$  vs.  $m(\chi)$  plane for  $m(\chi) \sim 0.5-10$  GeV; quoted limit is for  $m(\chi) = 5$  GeV.

5 XIA 19A search for WIMP scatter on Xe in PandaX-II; limits placed in  $\sigma^{SD}(\chi p)$  vs.  $m(\chi)$  plane for  $m(\chi) \sim 5-1 \times 10^5$  GeV; quoted limit is for  $m(\chi) = 5$  GeV.

6 AGNESE 18 search for GeV scale WIMPs with CDM2lite; limits placed in  $\sigma^{SD}(\chi p)$  vs.  $m(\chi)$  plane for  $m(\chi) \sim 1.5-20$  GeV; quoted limit is for  $m(\chi) = 5$  GeV.

7 AKERIB 17A search for SD WIMP scatter on Xe using 129.5 kg yr exposure; limits placed in  $\sigma^{SD}(\chi p)$  vs.  $m(\chi)$  plane for  $m(\chi) \sim 6-1 \times 10^5$  GeV.

8 FU 17 search for SD WIMP scatter on Xe; limits set in  $\sigma^{SD}(\chi p)$  vs.  $m(\chi)$  plane for  $m(\chi) \sim 4-1 \times 10^3$  GeV; quoted limit is for  $m(\chi) = 5$  GeV.

9 AMOLE 15 search for WIMP scatter on C<sub>3</sub>F<sub>8</sub> in PICO-2L; limits placed in  $\sigma^{SD}(\chi p)$  vs.  $m(\chi)$  plane for  $m(\chi) \sim 4-1 \times 10^4$  GeV; quoted limit is for  $m(\chi) = 5$  GeV.

10 ARCHAMBAULT 12 search for SD WIMP scatter in <sup>19</sup>F with PICASSO; limits set in  $\sigma^{SD}(\chi p)$  vs.  $m(\chi)$  plane for  $m \sim 4-500$  GeV; quoted limit is for  $m(\chi) = 5$  GeV.

#### For $m_{\chi^0} = 20$ GeV

For limits from  $X^0$  annihilation in the Sun, the assumed annihilation final state is shown in parenthesis in the comment.

VALUE (pb)	CL%	DOCUMENT ID	TECN	COMMENT
< 3 × 10 <sup>5</sup>	95	1 ABDELHAME...19	CRES	<sup>7</sup> Li
< 2.5 × 10 <sup>-5</sup>	90	2 AMOLE 19	PICO	C <sub>3</sub> F <sub>8</sub>
< 2.5 × 10 <sup>-4</sup>	90	3 APRILE 19A	XE1T	Xe, SD
< 1 × 10 <sup>-3</sup>	90	4 XIA 19A	PNDX	SD WIMP on Xe
< 30	95	5 AGNESE 18	SCDM	Ge
< 1 × 10 <sup>-3</sup>	90	6 AKERIB 17A	LUX	Xe
< 1.32 × 10 <sup>-2</sup>	90	7 BEHNKE 17	PICA	C <sub>4</sub> F <sub>10</sub>
< 2 × 10 <sup>-3</sup>	90	8 FU 17	PNDX	SD WIMP on Xe
< 5 × 10 <sup>-4</sup>	90	9 AMOLE 16A	PICO	C <sub>3</sub> F <sub>8</sub>
< 2 × 10 <sup>-6</sup>	90	10 KHACHATRY...16A	CMS	8 TeV $pp \rightarrow Z + \cancel{e} \tau$ ; $Z \rightarrow \ell \bar{\ell}$
< 1.2 × 10 <sup>-3</sup>	90	AMOLE 15	PICO	C <sub>3</sub> F <sub>8</sub>
< 1.43 × 10 <sup>-3</sup>	90	CHOI 15	SKAM	H, solar $\nu (b\bar{b})$
< 1.42 × 10 <sup>-4</sup>	90	CHOI 15	SKAM	H, solar $\nu (\tau^+ \tau^-)$
< 5 × 10 <sup>-3</sup>	90	FELIZARDO 14	SMP L	C <sub>2</sub> ClF <sub>5</sub>
< 1.29 × 10 <sup>-2</sup>	90	11 AARTSEN 13	ICCB	H, solar $\nu (\tau^+ \tau^-)$
< 3.17 × 10 <sup>-2</sup>	90	12 APRILE 13	X100	Xe
< 3 × 10 <sup>-2</sup>	90	13 ARCHAMBAU.12	PICA	F (C <sub>4</sub> F <sub>10</sub> )
< 6 × 10 <sup>-2</sup>	90	BEHNKE 12	COUP	CF <sub>3</sub> I
< 20	90	DAW 12	DRFT	F (CF <sub>4</sub> )
< 7 × 10 <sup>-3</sup>	90	FELIZARDO 12	SMP L	C <sub>2</sub> ClF <sub>5</sub>
< 0.15	90	KIM 12	KIMS	Csl
< 1 × 10 <sup>5</sup>	90	14 AHLEN 11	DMTP	F (CF <sub>4</sub> )
< 0.1	90	14 BEHNKE 11	COUP	CF <sub>3</sub> I
< 1.5 × 10 <sup>-2</sup>	90	15 TANAKA 11	SKAM	H, solar $\nu (b\bar{b})$
< 0.2	90	ARCHAMBAU..09	PICA	F
< 4	90	LEBEDENKO 09A	ZEP3	Xe
< 0.6	90	ANGLE 08A	XE10	Xe
<100	90	ALNER 07	ZEP2	Xe
< 1	90	LEE 07A	KIMS	Csl
< 20	90	16 AKERIB 06	CDMS	<sup>73</sup> Ge, <sup>29</sup> Si
< 2	90	SHIMIZU 06A	CNTR	F (CaF <sub>2</sub> )
< 0.5	90	ALNER 05	NAIA	NaI
< 1.5	90	BARNABE-HE.05	PICA	F (C <sub>4</sub> F <sub>10</sub> )
< 1.5	90	GIRARD 05	SMP L	F (C <sub>2</sub> ClF <sub>5</sub> )
< 35	90	MIUCHI 03	BOLO	LiF
< 30	90	TAKEDA 03	BOLO	NaF

- 1 ABDELHAMEED 19 uses  $\text{Li}_2\text{MoO}_4$  target to set limit for spin dependent coupling  $\sigma^{SD}(\chi p) < 3. \times 10^5$  pb for  $m(\chi) = 20$  GeV.
- 2 AMOLE 19 search for SD WIMP scatter on  $\text{C}_3\text{F}_8$  in PICO-60 bubble chamber; no signal: set limit for spin dependent coupling  $\sigma^{SD}(\chi p) < 2.5 \times 10^{-5}$  pb for  $m(\chi) = 20$  GeV.
- 3 APRILE 19A search for SD WIMP scatter on 1 t yr Xe; no signal, limits placed in  $\sigma^{SD}(\chi p)$  vs.  $m(\chi)$  plane for  $m \sim 6\text{--}1000$  GeV.
- 4 XIA 19A search for WIMP scatter on Xe in PandaX-II; limits placed in  $\sigma^{SD}(\chi p)$  vs.  $m(\chi)$  plane for  $m(\chi) \sim 5\text{--}1 \times 10^5$  GeV.
- 5 AGNESE 18 give limits for  $\sigma^{SD}(\rho \chi)$  for  $m(\text{WIMP})$  between 1.5 and 20 GeV using CDMSlite mode data.
- 6 AKERIB 17A search for SD WIMP scatter on Xe using 129.5 kg yr exposure; limits placed in  $\sigma^{SD}(\chi p)$  vs.  $m(\chi)$  plane for  $m(\chi) \sim 6\text{--}1 \times 10^5$  GeV.
- 7 BEHNKE 17 show final Picasso results based on 231.4 kg d exposure at SNOLab for WIMP scatter on  $\text{C}_4\text{F}_{10}$  search via superheated droplet; require  $\sigma(\text{SD}) < 1.32 \times 10^{-2}$  pb for  $m(\text{WIMP}) = 20$  GeV.
- 8 FU 17 search for SD WIMP scatter on Xe; limits set in  $\sigma^{SD}(\chi p)$  vs.  $m(\chi)$  plane for  $m(\chi) \sim 4\text{--}1 \times 10^3$  GeV.
- 9 AMOLE 16A require SD WIMP- $p$  scattering  $< 5 \times 10^{-4}$  pb for  $m(\text{WIMP}) = 20$  GeV; bubbles from  $\text{C}_3\text{F}_8$  target.
- 10 KHACHATRYAN 16AJ require SD WIMP- $p < 2 \times 10^{-6}$  pb for  $m(\text{WIMP}) = 20$  GeV from  $pp \rightarrow Z + \cancel{E}_T$ ;  $Z \rightarrow \ell\bar{\ell}$  signal.
- 11 AARTSEN 13 search for neutrinos from the Sun arising from the pair annihilation of  $X^0$  trapped by the sun in data taken between June 2010 and May 2011.
- 12 The value has been provided by the authors. APRILE 13 note that the proton limits on Xe are highly sensitive to the theoretical model used. See also APRILE 14A.
- 13 ARCHAMBAULT 12 search for WIMP scatter on  $\text{C}_4\text{F}_{10}$ ; limits set in  $\sigma^{SD}(\chi p)$  vs.  $m(\chi)$  plane for  $m \sim 4\text{--}500$  GeV.
- 14 Use a direction-sensitive detector.
- 15 TANAKA 11 search for neutrinos from the Sun arising from the pair annihilation of  $X^0$  trapped by the Sun. The amount of  $X^0$  depends on the  $X^0$ -proton cross section.
- 16 See also AKERIB 05.

For  $m_{X^0} = 100$  GeV

For limits from  $X^0$  annihilation in the Sun, the assumed annihilation final state is shown in parenthesis in the comment.

VALUE (pb)	CL%	DOCUMENT ID	TECN	COMMENT
• • • We do not use the following data for averages, fits, limits, etc. • • •				
$< 4 \times 10^{-5}$	90	1 AMOLE 19	PICO	$\text{C}_3\text{F}_8$
$< 4 \times 10^{-4}$	90	2 APRILE 19A	XE1T	Xe, SD
$< 8 \times 10^{-4}$	90	3 XIA 19A	PNDX	SD WIMP on Xe
$< 8 \times 10^{-4}$	90	4 AKERIB 17A	LUX	Xe
$< 5 \times 10^{-5}$	90	5 AMOLE 17	PICO	$\text{C}_3\text{F}_8$
$< 3.3 \times 10^{-2}$	90	6 APRILE 17A	X100	Xe inelastic
$< 2.8 \times 10^{-1}$	90	7 BATTAT 17	DRFT	$\text{CS}_2$
$< 1.5 \times 10^{-3}$	90	8 FU 17	PNDX	Xe
$< 0.553\text{--}0.019$	95	9 AABOUD 16D	ATLS	$pp \rightarrow j + \cancel{E}_T$
$< 1 \times 10^{-5}$	90	10 AABOUD 16F	ATLS	$pp \rightarrow \gamma + \cancel{E}_T$
$< 1 \times 10^{-4}$	90	11 AARTSEN 16C	ICCB	solar $\nu (W^+ W^-)$
$< 2 \times 10^{-4}$	90	12 ADRIAN-MAR.16	ANTR	solar $\nu (W W, b\bar{b}, \tau\bar{\tau})$
$< 3 \times 10^{-3}$	90	13 AKERIB 16A	LUX	Xe
$< 5 \times 10^{-4}$	90	14 AMOLE 16	PICO	$\text{CF}_3\text{I}$
$< 1.5 \times 10^{-3}$	90	AMOLE 15	PICO	$\text{C}_3\text{F}_8$
$< 3.19 \times 10^{-3}$	90	CHOI 15	SKAM	H, solar $\nu (b\bar{b})$
$< 2.80 \times 10^{-4}$	90	CHOI 15	SKAM	H, solar $\nu (W^+ W^-)$
$< 1.24 \times 10^{-4}$	90	CHOI 15	SKAM	H, solar $\nu (\tau^+ \tau^-)$
$< 8 \times 10^2$	90	15 NAKAMURA 15	NAGE	$\text{CF}_4$
$< 1.7 \times 10^{-3}$	90	16 AVRORIN 14	BAIK	H, solar $\nu (W^+ W^-)$
$< 4.5 \times 10^{-2}$	90	16 AVRORIN 14	BAIK	H, solar $\nu (b\bar{b})$
$< 7.1 \times 10^{-4}$	90	16 AVRORIN 14	BAIK	H, solar $\nu (\tau^+ \tau^-)$
$< 6 \times 10^{-3}$	90	FELIZARDO 14	SMPL	$\text{C}_2\text{ClF}_5$
$< 2.68 \times 10^{-4}$	90	17 AARTSEN 13	ICCB	H, solar $\nu (W^+ W^-)$
$< 1.47 \times 10^{-2}$	90	17 AARTSEN 13	ICCB	H, solar $\nu (b\bar{b})$
$< 8.5 \times 10^{-4}$	90	18 ADRIAN-MAR.13	ANTR	H, solar $\nu (W^+ W^-)$
$< 5.5 \times 10^{-2}$	90	18 ADRIAN-MAR.13	ANTR	H, solar $\nu (b\bar{b})$
$< 3.4 \times 10^{-4}$	90	18 ADRIAN-MAR.13	ANTR	H, solar $\nu (\tau^+ \tau^-)$
$< 1.00 \times 10^{-2}$	90	19 APRILE 13	X100	Xe
$< 7.1 \times 10^{-4}$	90	20 BOLIEV 13	BAKS	H, solar $\nu (W^+ W^-)$
$< 8.4 \times 10^{-3}$	90	20 BOLIEV 13	BAKS	H, solar $\nu (b\bar{b})$
$< 3.1 \times 10^{-4}$	90	20 BOLIEV 13	BAKS	H, solar $\nu (\tau^+ \tau^-)$
$< 7.07 \times 10^{-4}$	90	21 ABBASI 12	ICCB	H, solar $\nu (W^+ W^-)$
$< 4.53 \times 10^{-2}$	90	21 ABBASI 12	ICCB	H, solar $\nu (b\bar{b})$
$< 7 \times 10^{-2}$	90	22 ARCHAMBAU.12	PICA	$\text{F} (\text{C}_4\text{F}_{10})$
$< 1 \times 10^{-2}$	90	BEHNKE 12	COUP	$\text{CF}_3\text{I}$
$< 1.8$	90	DAW 12	DRFT	$\text{F} (\text{CF}_4)$
$< 9 \times 10^{-3}$	90	FELIZARDO 12	SMPL	$\text{C}_2\text{ClF}_5$
$< 2 \times 10^{-2}$	90	KIM 12	KIMS	Csl
$< 2 \times 10^3$	90	15 AHLEN 11	DMPF	$\text{F} (\text{CF}_4)$
$< 7 \times 10^{-2}$	90	BEHNKE 11	COUP	$\text{CF}_3\text{I}$
$< 2.7 \times 10^{-4}$	90	23 TANAKA 11	SKAM	H, solar $\nu (W^+ W^-)$
$< 4.5 \times 10^{-3}$	90	23 TANAKA 11	SKAM	H, solar $\nu (b\bar{b})$
$< 6 \times 10^3$	90	24 FELIZARDO 10	SMPL	$\text{C}_2\text{ClF}_3$
$< 6 \times 10^3$	90	15 MIUCHI 10	NAGE	$\text{CF}_4$
$< 0.4$	90	ARCHAMBAU.09	PICA	F
$< 0.8$	90	LEBEDENKO 09A	ZEP3	Xe
$< 1.0$	90	ANGLE 08A	XE10	Xe

$< 15$	90	ALNER 07	ZEP2	Xe
$< 0.2$	90	LEE 07A	KIMS	Csl
$< 1 \times 10^4$	90	15 MIUCHI 07	NAGE	$\text{F} (\text{CF}_4)$
$< 5$	90	25 AKERIB 06	CDMS	$^{73}\text{Ge}, ^{29}\text{Si}$
$< 2$	90	SHIMIZU 06A	CNTR	$\text{F} (\text{CaF}_2)$
$< 0.3$	90	ALNER 05	NAIA	NaI
$< 2$	90	BARNABE-HE.05	PICA	$\text{F} (\text{C}_4\text{F}_{10})$
$< 100$	90	BENOIT 05	EDEL	$^{73}\text{Ge}$
$< 1.5$	90	GIRARD 05	SMPL	$\text{F} (\text{C}_2\text{ClF}_5)$
$< 0.7$	26	GIULIANI 05A	RVUE	
	27	GIULIANI 04	RVUE	
	28	GIULIANI 04A	RVUE	
$< 35$	90	MIUCHI 03	BOLO	LIF
$< 40$	90	TAKEDA 03	BOLO	NaF

- 1 AMOLE 19 search for SD WIMP scatter on  $\text{C}_3\text{F}_8$  in PICO-60 bubble chamber; no signal: set limit for spin dependent coupling  $\sigma^{SD}(\chi p) < 4 \times 10^{-5}$  pb for  $m(\chi) = 100$  GeV.
- 2 APRILE 19A search for SD WIMP scatter on 1 t yr Xe; no signal, limits placed in  $\sigma^{SD}(\chi p)$  vs.  $m(\chi)$  plane for  $m \sim 6\text{--}1000$  GeV.
- 3 XIA 19A search for WIMP scatter on Xe in PandaX-II; limits placed in  $\sigma^{SD}(\chi p)$  vs.  $m(\chi)$  plane for  $m(\chi) \sim 5\text{--}1 \times 10^5$  GeV.
- 4 AKERIB 17A search for SD WIMP scatter on Xe using 129.5 kg yr exposure; limits placed in  $\sigma^{SD}(\chi p)$  vs.  $m(\chi)$  plane for  $m(\chi) \sim 6\text{--}1 \times 10^5$  GeV.
- 5 AMOLE 17 require  $\sigma(\text{WIMP-}p)^{SD} < 5 \times 10^{-5}$  pb for  $m(\text{WIMP}) = 100$  GeV using PICO-60 1167 kg-days exposure at SNOLab.
- 6 APRILE 17A require require  $\sigma(\text{WIMP-}p)(\text{inelastic})^{SD} < 3.3 \times 10^{-2}$  pb for  $m(\text{WIMP}) = 100$  GeV, based on 7640 kg day exposure at LNGS.
- 7 BATTAT 17 use directional detection of  $\text{CS}_2$  ions to require  $\sigma(\text{SD}) < 2.8 \times 10^{-1}$  pb for 100 GeV WIMP with a 55 days exposure at the Bouby Underground Science Facility.
- 8 FU 17 from a 33000 kg d exposure at CJPL, PANDAX II derive for  $m(\text{DM}) = 100$  GeV,  $\sigma^{SD}(\text{WIMP-}p) < 2 \times 10^{-3}$  pb.
- 9 AABOUD 16D use ATLAS 13 TeV 3.2 fb $^{-1}$  of data to search for monojet plus missing  $E_T$ ; agree with SM rates; present limits on large extra dimensions, compressed SUSY spectra and wimp pair production.
- 10 AABOUD 16F search for monophoton plus missing  $E_T$  events at ATLAS with 13 TeV and 3.2 fb $^{-1}$ ; signal agrees with SM background; place limits on SD WIMP-proton scattering vs. mediator mass and large extra dimension models.
- 11 AARTSEN 16C search for high energy  $\nu$ s from WIMP annihilation in solar core; limits set on SD WIMP- $p$  scattering (Fig. 8).
- 12 ADRIAN-MARTINEZ 16 search for WIMP annihilation into  $\nu$ s from solar core; exclude SD cross section  $< \text{few } 10^{-4}$  depending on  $m(\text{WIMP})$ .
- 13 AKERIB 16A using 2013 data exclude SD WIMP-proton scattering  $> 3 \times 10^{-3}$  pb for  $m(\text{WIMP}) = 100$  GeV.
- 14 AMOLE 16 use bubble technique on  $\text{CF}_3\text{I}$  target to exclude SD WIMP- $p$  scattering  $> 5 \times 10^{-4}$  pb for  $m(\text{WIMP}) = 100$  GeV.
- 15 Use a direction-sensitive detector.
- 16 AVRORIN 14 search for neutrinos from the Sun arising from the pair annihilation of  $X^0$  trapped by the Sun in data taken between 1998 and 2003. See their Table 1 for limits assuming annihilation into neutrino pairs.
- 17 AARTSEN 13 search for neutrinos from the Sun arising from the pair annihilation of  $X^0$  trapped by the sun in data taken between June 2010 and May 2011.
- 18 ADRIAN-MARTINEZ 13 search for neutrinos from the Sun arising from the pair annihilation of  $X^0$  trapped by the sun in data taken between Jan. 2007 and Dec. 2008.
- 19 The value has been provided by the authors. APRILE 13 note that the proton limits on Xe are highly sensitive to the theoretical model used. See also APRILE 14A.
- 20 BOLIEV 13 search for neutrinos from the Sun arising from the pair annihilation of  $X^0$  trapped by the sun in data taken from 1978 to 2009. See also SUVOROVA 13 for an older analysis of the same data.
- 21 ABBASI 12 search for neutrinos from the Sun arising from the pair annihilation of  $X^0$  trapped by the Sun. The amount of  $X^0$  depends on the  $X^0$ -proton cross section.
- 22 ARCHAMBAULT 12 search for WIMP scatter on  $\text{C}_4\text{F}_{10}$ ; limits set in  $\sigma^{SD}(\chi p)$  vs.  $m(\chi)$  plane for  $m \sim 4\text{--}500$  GeV.
- 23 TANAKA 11 search for neutrinos from the Sun arising from the pair annihilation of  $X^0$  trapped by the Sun. The amount of  $X^0$  depends on the  $X^0$ -proton cross section.
- 24 See their Fig. 3 for limits on spin-dependent proton couplings for  $X^0$  mass of 50 GeV.
- 25 See also AKERIB 05.
- 26 GIULIANI 05A analyze available data and give combined limits.
- 27 GIULIANI 04 reanalyze COLLAR 00 data and give limits for spin-dependent  $X^0$ -proton coupling.
- 28 GIULIANI 04A give limits for spin-dependent  $X^0$ -proton couplings from existing data.

For  $m_{X^0} = 1$  TeV

For limits from  $X^0$  annihilation in the Sun, the assumed annihilation final state is shown in parenthesis in the comment.

VALUE (pb)	CL%	DOCUMENT ID	TECN	COMMENT
• • • We do not use the following data for averages, fits, limits, etc. • • •				
$< 3 \times 10^{-4}$	90	1 AMOLE 19	PICO	$\text{C}_3\text{F}_8$
$< 4 \times 10^{-3}$	90	2 APRILE 19A	XE1T	Xe, SD
$< 5 \times 10^{-3}$	90	3 XIA 19A	PNDX	SD WIMP on Xe
		4 ALBERT 18C	HAWC	DM annihilation in Sun to long-lived mediator
$< 2.05 \times 10^{-5}$	90	5 AARTSEN 17A	ICCB	$\nu, \text{sun}$
$< 7 \times 10^{-3}$	90	6 AKERIB 17A	LUX	Xe

# Searches Particle Listings

## WIMP and Dark Matter Searches

$< 2 \times 10^{-2}$	90	7 FU	17 PNDX	SD WIMP on Xe
$< 1 \times 10^{-2}$	90	8 ADRIAN-MAR.16B	ANTR	solar $\mu$ from WIMP annih.
$< 1.5 \times 10^3$	90	AMOLE	15 PICO	$C_3F_8$
$< 2.7 \times 10^{-3}$	90	NAKAMURA	15 NAGE	$CF_4$
$< 6.9 \times 10^{-2}$	90	9 AVROTORIN	14 BAIK	H, solar $\nu$ ( $W^+ W^-$ )
$< 8.4 \times 10^{-4}$	90	9 AVROTORIN	14 BAIK	H, solar $\nu$ ( $b\bar{b}$ )
$< 4.48 \times 10^{-4}$	90	10 AARTSEN	13 ICCB	H, solar $\nu$ ( $W^+ W^-$ )
$< 1.00 \times 10^{-2}$	90	10 AARTSEN	13 ICCB	H, solar $\nu$ ( $b\bar{b}$ )
$< 8.9 \times 10^{-4}$	90	11 ADRIAN-MAR.13	ANTR	H, solar $\nu$ ( $W^+ W^-$ )
$< 2.0 \times 10^{-2}$	90	11 ADRIAN-MAR.13	ANTR	H, solar $\nu$ ( $b\bar{b}$ )
$< 2.3 \times 10^{-4}$	90	11 ADRIAN-MAR.13	ANTR	H, solar $\nu$ ( $\tau^+ \tau^-$ )
$< 7.57 \times 10^{-2}$	90	12 APRILE	13 X100	Xe
$< 5.4 \times 10^{-3}$	90	13 BOLIEV	13 BAKS	H, solar $\nu$ ( $W^+ W^-$ )
$< 4.2 \times 10^{-2}$	90	13 BOLIEV	13 BAKS	H, solar $\nu$ ( $b\bar{b}$ )
$< 1.5 \times 10^{-3}$	90	13 BOLIEV	13 BAKS	H, solar $\nu$ ( $\tau^+ \tau^-$ )
$< 2.50 \times 10^{-4}$	90	14 ABBASI	12 ICCB	H, solar $\nu$ ( $W^+ W^-$ )
$< 7.86 \times 10^{-3}$	90	14 ABBASI	12 ICCB	H, solar $\nu$ ( $b\bar{b}$ )
$< 8 \times 10^{-2}$	90	BEHNKE	12 COUP	$CF_3I$
$< 8$	90	DAW	12 DRFT	F ( $CF_4$ )
$< 6 \times 10^{-2}$	90	FELIZARDO	12 SMPL	$C_2ClF_5$
$< 8 \times 10^{-2}$	90	KIM	12 KIMS	Csl
$< 8 \times 10^3$	90	15 AHLEN	11 DMTP	F ( $CF_4$ )
$< 0.4$	90	BEHNKE	11 COUP	$CF_3I$
$< 2 \times 10^{-3}$	90	16 TANAKA	11 SKAM	H, solar $\nu$ ( $b\bar{b}$ )
$< 2 \times 10^{-2}$	90	16 TANAKA	11 SKAM	H, solar $\nu$ ( $W^+ W^-$ )
$< 1 \times 10^{-3}$	90	17 ABBASI	10 ICCB	KK dark matter
$< 2 \times 10^4$	90	15 MIUCHI	10 NAGE	$CF_4$
$< 8.7 \times 10^{-4}$	90	ABBASI	09B ICCB	H, solar $\nu$ ( $W^+ W^-$ )
$< 2.2 \times 10^{-2}$	90	ABBASI	09B ICCB	H, solar $\nu$ ( $b\bar{b}$ )
$< 3$	90	ARCHAMBAU.09	PICA	F
$< 6$	90	LEBEDENKO	09A ZEP3	Xe
$< 9$	90	ANGLE	08A XE10	Xe
$< 100$	90	ALNER	07 ZEP2	Xe
$< 0.8$	90	LEE	07A KIMS	Csl
$< 4 \times 10^4$	90	15 MIUCHI	07 NAGE	F ( $CF_4$ )
$< 30$	90	18 AKERIB	06 CDMS	$^{73}Ge$ , $^{29}Si$
$< 1.5$	90	ALNER	05 NAIA	NaI
$< 15$	90	BARNABE-HE.05	PICA	F ( $C_4F_{10}$ )
$< 60$	90	BENOIT	05 EDEL	$^{73}Ge$
$< 10$	90	GIRARD	05 SMPL	F ( $C_2ClF_5$ )
$< 260$	90	MIUCHI	03 BOLO	LiF
$< 150$	90	TAKEDA	03 BOLO	NaF

- 1 AMOLE 19 search for SD WIMP scatter on  $C_3F_8$  in PICO-60 bubble chamber; no signal: set limit for spin dependent coupling  $\sigma_{SD}^{SD}(\chi p) < 3 \times 10^{-4}$  pb for  $m(\chi) = 1000$  GeV.
- 2 APRILE 19a search for SD WIMP scatter on 1 t yr Xe; no signal, limits placed in  $\sigma_{SD}^{SD}(\chi p)$  vs.  $m(\chi)$  plane for  $m \sim 6-1000$  GeV.
- 3 XIA 19a search for WIMP scatter on Xe in PandaX-II; limits placed in  $\sigma_{SD}^{SD}(\chi p)$  vs.  $m(\chi)$  plane for  $m(\chi) \sim 5-1 \times 10^5$  GeV.
- 4 ALBERT 18c search for DM annihilation in Sun to long-lived mediator (LLM) which decays outside Sun, for DM masses above 1 TeV; assuming LLM, limits set on  $\sigma_{SD}^{SD}(\chi p)$ .
- 5 AARTSEN 17a search for neutrinos from solar WIMP annihilation into  $\tau^+ \tau^-$  in 532 days of live time.
- 6 AKERIB 17a search for SD WIMP scatter on Xe using 129.5 kg yr exposure; limits placed in  $\sigma_{SD}^{SD}(\chi p)$  vs.  $m(\chi)$  plane for  $m(\chi) \sim 6-1 \times 10^5$  GeV.
- 7 FU 17 search for SD WIMP scatter on Xe; limits set in  $\sigma_{SD}^{SD}(\chi p)$  vs.  $m(\chi)$  plane for  $m(\chi) \sim 4-1 \times 10^3$  GeV.
- 8 ADRIAN-MARTINEZ 16b search for secluded DM via WIMP annihilation in solar core into light mediator which later decays to  $\mu$  or  $\nu$ s; limits presented in Figures 3 and 4.
- 9 AVROTORIN 14 search for neutrinos from the Sun arising from the pair annihilation of  $X^0$  trapped by the Sun in data taken between 1998 and 2003. See their Table 1 for limits assuming annihilation into neutrino pairs.
- 10 AARTSEN 13 search for neutrinos from the Sun arising from the pair annihilation of  $X^0$  trapped by the sun in data taken between June 2010 and May 2011.
- 11 ADRIAN-MARTINEZ 13 search for neutrinos from the Sun arising from the pair annihilation of  $X^0$  trapped by the sun in data taken between Jan. 2007 and Dec. 2008.
- 12 The value has been provided by the authors. APRILE 13 note that the proton limits on Xe are highly sensitive to the theoretical model used. See also APRILE 14a.
- 13 BOLIEV 13 search for neutrinos from the Sun arising from the pair annihilation of  $X^0$  trapped by the sun in data taken from 1978 to 2009. See also SUVOROVA 13 for an older analysis of the same data.
- 14 ABBASI 12 search for neutrinos from the Sun arising from the pair annihilation of  $X^0$  trapped by the Sun. The amount of  $X^0$  depends on the  $X^0$ -proton cross section.
- 15 Use a direction-sensitive detector.
- 16 TANAKA 11 search for neutrinos from the Sun arising from the pair annihilation of  $X^0$  trapped by the Sun. The amount of  $X^0$  depends on the  $X^0$ -proton cross section.
- 17 ABBASI 10 search for  $\nu_\mu$  from annihilations of Kaluza-Klein photon dark matter in the Sun.
- 18 See also AKERIB 05.

### Spin-Dependent Cross Section Limits for Dark Matter Particle ( $X^0$ ) on Neutron

#### For $m_{\chi_0}$ in GeV range

We provide here limits for  $m_{\chi_0} < 5$  GeV

VALUE (pb)	CL %	DOCUMENT ID	TECN	COMMENT
$< 1 \times 10^{10}$	95	1 ABDELHAMEE.19	CRES	SD low mass DM on Li
$< 2.3 \times 10^2$	90	2 APRILE	19c	light DM on Xe via Migdal/brem effect
$< 1 \times 10^{-2}$	90	3 APRILE	19b	light DM on Xe via ionization
$< 4 \times 10^4$	90	4 ARMENGAUD	19	EDEL GeV-scale WIMPs on Ge
$< 8 \times 10^{-2}$	90	5 XIA	19A	PNDX SD WIMP on Xe
$< 3$	90	6 AGNESE	18	CDM GeV-scale WIMPs on Ge
$< 3$	90	7 JIANG	18	CDEX GeV-scale WIMPs on Ge
$< 10$	90	8 YANG	18	CDEX WIMPs on Ge
$< 1 \times 10^{-1}$	90	9 AKERIB	17A	LUX Xe
$< 0.1$	90	10 FU	17	PNDX SD WIMP on Xe
$< 20$	90	11 ZHAO	16	CDEX GeV-scale WIMPs on Ge
$< 150$	90	12 AHMED	11B	CDM2 GeV-scale WIMPs on Ge

- 1 ABDELHAMEEED 19 search for GeV-scale WIMP SD scatter on  $^7Li$  crystal; set limit  $\sigma_{SD}^{SD}(\chi n)$  for  $m(\chi) \sim 0.8-20$  GeV; quoted limit for  $m(\chi) = 1$  GeV.
- 2 APRILE 19c search for light DM on Xe via Migdal/bremstrahlung effect; no signal, require  $\sigma_{SD}^{SD}(\chi n) < 230$  pb for  $m(\chi) = 1$  GeV.
- 3 APRILE 19b search for light DM scatter on Xe via ionization; no signal, limits placed in  $\sigma$  vs.  $m(DM) \sim 3-6$  GeV; quoted limit is for  $m(DM) = 5$  GeV.
- 4 ARMENGAUD 19 search for GeV scale WIMP scatter on Ge; limits placed in  $\sigma_{SD}^{SD}(\chi n)$  vs.  $m(\chi)$  plane for  $m(\chi) \sim 0.5-10$  GeV; quoted limit is for  $m(\chi) = 5$  GeV.
- 5 XIA 19a search for WIMP scatter on Xe in PandaX-II; limits placed in  $\sigma_{SD}^{SD}(\chi n)$  vs.  $m(\chi)$  plane for  $m(\chi) \sim 5-1 \times 10^5$  GeV; quoted limit is for  $m(\chi) = 5$  GeV.
- 6 AGNESE 18 search for GeV scale WIMPs scatter at CDMsite; limits placed in  $\sigma_{SD}^{SD}(\chi n)$  vs.  $m(\chi)$  plane for  $m \sim 1.5-20$  GeV; quoted limit is for  $m(\chi) = 5$  GeV.
- 7 JIANG 18 search for GeV scale WIMP scatter on Ge; limits placed in  $\sigma_{SD}^{SD}(\chi n)$  vs.  $m(\chi)$  plane for  $m(\chi) \sim 3-10$  GeV; quoted limit is for  $m(\chi) = 5$  GeV.
- 8 YANG 18 search for WIMP scatter on Ge; limits placed in  $\sigma_{SD}^{SD}(\chi n)$  vs.  $m(\chi)$  plane for  $m(\chi) \sim 2-10$  GeV; quoted limit is for  $m(\chi) = 5$  GeV.
- 9 AKERIB 17a search for SD WIMP scatter on Xe with 129.5 kg yr exposure; limits placed in  $\sigma_{SD}^{SD}(\chi n)$  vs.  $m(\chi)$  plane for  $m(\chi) \sim 5-1 \times 10^5$  GeV; quoted limit is for  $m(\chi) = 5$  GeV.
- 10 FU 17 search for SD WIMP scatter on Xe; limits set in  $\sigma_{SD}^{SD}(\chi n)$  vs.  $m(\chi)$  plane for  $m(\chi) \sim 4-1 \times 10^3$  GeV; quoted limit is for  $m(\chi) = 5$  GeV.
- 11 ZHAO 16 search for GeV-scale WIMP scatter on Ge; limits placed in  $\sigma_{SD}^{SD}(\chi n)$  vs.  $m(\chi)$  plane for  $m(\chi) \sim 4-30$  GeV; quoted limit is for  $m(\chi) = 5$  GeV.
- 12 AHMED 11b search for GeV scale WIMP scatter on Ge in CDMS II; limits placed in  $\sigma_{SD}^{SD}(\chi n)$  vs.  $m(\chi)$  plane for  $m \sim 4-12$  GeV. Limit given for  $m(\chi) = 5$  GeV.

#### For $m_{\chi_0} = 20$ GeV

VALUE (pb)	CL %	DOCUMENT ID	TECN	COMMENT
$< 8 \times 10^{-6}$	90	1 APRILE	19A	XE1T Xe, SD
$< 3 \times 10^{-5}$	90	2 XIA	19A	PNDX SD WIMP on Xe
$< 1.5$	95	3 AGNESE	18	SCDM Ge
$< 2.5 \times 10^{-5}$	90	4 AKERIB	17A	LUX Xe
$< 7 \times 10^{-5}$	90	5 FU	17	PNDX SD WIMP on Xe
$< 2$	90	6 ZHAO	16	CDEX GeV-scale WIMPs on Ge
$< 0.09$	90	FELIZARDO	14	SMPL $C_2ClF_5$
$< 8$	90	7 UCHIDA	14	XMAS $^{129}Xe$ , inelastic
$< 1.13 \times 10^{-3}$	90	8 APRILE	13	X100 Xe
$< 0.02$	90	AKIMOV	12	ZEP3 Xe
$< 0.06$	90	AHMED	09	CDM2 Ge
$< 0.04$	90	LEBEDENKO	09A	ZEP3 Xe
$< 50$	90	LIN	09	TEXO Ge
$< 6 \times 10^{-3}$	90	ANGLE	08A	XE10 Xe
$< 0.5$	90	ALNER	07	ZEP2 Xe
$< 25$	90	LEE	07A	KIMS Csl
$< 0.3$	90	10 AKERIB	06	CDMS $^{73}Ge$ , $^{29}Si$
$< 30$	90	SHIMIZU	06A	CNTR F ( $CaF_2$ )
$< 60$	90	ALNER	05	NAIA NaI
$< 20$	90	BARNABE-HE.05	PICA	F ( $C_4F_{10}$ )
$< 10$	90	BENOIT	05	EDEL $^{73}Ge$
$< 4$	90	KLAPDOR-K...	05	HDMS $^{73}Ge$ (enriched)
$< 600$	90	TAKEDA	03	BOLO NaF

- 1 APRILE 19a search for SD WIMP scatter on 1 t yr Xe; no signal: limits placed in  $\sigma_{SD}^{SD}(\chi n)$  vs.  $m(\chi)$  plane for  $m \sim 6-1000$  GeV.
- 2 XIA 19a search for WIMP scatter on Xe in PandaX-II; limits placed in  $\sigma_{SD}^{SD}(\chi n)$  vs.  $m(\chi)$  plane for  $m(\chi) \sim 5-1 \times 10^5$  GeV.
- 3 AGNESE 18 give limits for  $\sigma_{SD}^{SD}(n\chi)$  for  $m(WIMP)$  between 1.5 and 20 GeV using CDMSlite mode data.
- 4 AKERIB 17a search for SD WIMP scatter on Xe with 129.5 kg yr exposure; limits placed in  $\sigma_{SD}^{SD}(\chi n)$  vs.  $m(\chi)$  plane for  $m(\chi) \sim 5-1 \times 10^5$  GeV.
- 5 FU 17 search for SD WIMP scatter on Xe; limits set in  $\sigma_{SD}^{SD}(\chi n)$  vs.  $m(\chi)$  plane for  $m(\chi) \sim 4-1 \times 10^3$  GeV.
- 6 ZHAO 16 search for GeV-scale WIMP scatter on Ge; limits placed in  $\sigma_{SD}^{SD}(\chi n)$  vs.  $m(\chi)$  plane for  $m(\chi) \sim 4-30$  GeV.
- 7 Derived limit from search for inelastic scattering  $X^0 + ^{129}Xe \rightarrow X^0 + ^{129}Xe^*(39.58$  keV).
- 8 The value has been provided by the authors. See also APRILE 14a.
- 9 See their Fig. 6(b) for cross section limits for  $m_{\chi_0}$  extending down to 2 GeV.
- 10 See also AKERIB 05.

See key on page 999

Searches Particle Listings
WIMP and Dark Matter Searches

For m\_chi0 = 100 GeV

Table with columns: VALUE (pb), CL%, DOCUMENT ID, TECN, COMMENT. Lists search results for m\_chi0 = 100 GeV.

- 1 APRILE 19A search for SD WIMP scatter on 1 t yr Xe; no signal, limits placed in sigma^SD(chi n) vs. m(chi) plane for m ~ 6-1000 GeV.
2 SUZUKI 19 search in single phase liquid xenon detector for inelastic scattering X0 + 129Xe -> X0 + 129Xe\* (39.58 keV); no signal; require sigma(chi n)^SD < 4 x 10^-3 pb for m(chi) = 100 GeV.

For m\_chi0 = 1 TeV

Table with columns: VALUE (pb), CL%, DOCUMENT ID, TECN, COMMENT. Lists search results for m\_chi0 = 1 TeV.

- 1 APRILE 19A search for SD WIMP scatter on 1 t yr Xe; no signal, limits placed in sigma^SD(chi n) vs. m(chi) plane for m ~ 6-1000 GeV.
2 XIA 19A search for WIMP scatter on Xe in PandaX-II; limits placed in sigma^SD(chi n) vs. m(chi) plane for m(chi) ~ 5-1 x 10^5 GeV.

- 4 FU 17 search for SD WIMP scatter on Xe; limits set in sigma^SD(chi n) vs. m(chi) plane for m(chi) ~ 4-1 x 10^3 GeV.
5 Derived limit from search for inelastic scattering X0 + 129Xe\* -> X0 + 129Xe\* (39.58 keV).
6 The value has been provided by the authors. See also APRILE 14A.

Cross-Section Limits for Dark Matter Particles (X0) on electron

For m\_chi0 in GeV range

We provide here limits for m\_chi0 < 5 GeV

Table with columns: VALUE (pb), CL%, DOCUMENT ID, TECN, COMMENT. Lists search results for m\_chi0 in GeV range on electron.

- 1 AKERIB 20 search for mirror DM with LUX 95 d x 118 kg data for mirror e scatter from Xe; no signal, limits placed in kinetic mixing parameter vs. mirror e temperature T ~ 0.1-0.9 keV plane.
2 ABRAMOFF 19 search for MeV-scale WIMP scatter from Si skipper-CCD; limits placed on sigma(chi e) for m(chi) ~ 0.5-100 MeV depending on DM form factors. Limit given for m(DM) = 1 MeV.

Cross-Section Limits for Dark Matter Particles (X0) on Nuclei

For m\_chi0 in GeV range

We provide here limits for m\_chi0 < 5 GeV

Table with columns: VALUE (nb), CL%, DOCUMENT ID, TECN, COMMENT. Lists search results for m\_chi0 in GeV range on nuclei.

- 1 UCHIDA 14 limit is for inelastic scattering X0 + 129Xe\* -> X0 + 129Xe\* (39.58 keV).
2 ANGLOHER 02 limit is for spin-dependent WIMP-Aluminum cross section.
3 BENOIT 00 find four event categories in Ge detectors and suggest that low-energy surface nuclear recoils can explain anomalous events reported by UKDMC and Saclay NaI experiments.

# Searches Particle Listings

## WIMP and Dark Matter Searches

- <sup>9</sup> SMITH 96 use pulse shape discrimination to enhance the possible signal. A dark matter density of  $0.4 \text{ GeV cm}^{-3}$  is assumed.
- <sup>10</sup> GARCIA 95 limit is from the event rate. A weaker limit is obtained from searches for diurnal and annual modulation.
- <sup>11</sup> SNOWDEN-IFFT 95 look for recoil tracks in an ancient mica crystal. Similar limits are also given for  $^{27}\text{Al}$  and  $^{28}\text{Si}$ . See COLLAR 96 and SNOWDEN-IFFT 96 for discussion on potential backgrounds.
- <sup>12</sup> REUSSER 91 limit here is changed from published (0.04) after reanalysis by authors. J.L. Vuilleumier, private communication, March 29, 1996.

### For $m_{\chi^0} = 100 \text{ GeV}$

VALUE (nb)	CL%	DOCUMENT ID	TECN	COMMENT
• • • We do not use the following data for averages, fits, limits, etc. • • •				
< 3 $\times 10^{-3}$	90	1 UCHIDA	14 XMAS	$^{129}\text{Xe}$ , inelastic
< 0.3	90	2 ANGIOHER	02 CRES	Al
		3 BELLI	02 RVUE	
		4 BERNABEI	02c DAMA	
		5 GREEN	02 RVUE	
		6 ULLIO	01 RVUE	
		7 BENOIT	00 EDEL	Ge
< 4 $\times 10^{-3}$	90	8 BERNABEI	00D	$^{129}\text{Xe}$ , inel.
		9 AMBROSIO	99 MCRO	
		10 BRHLIK	99 RVUE	
< 8 $\times 10^{-3}$	95	11 KLIMENKO	98 CNTR	$^{73}\text{Ge}$ , inel.
< 0.08	95	12 KLIMENKO	98 CNTR	$^{73}\text{Ge}$ , inel.
< 4		ALESSAND...	96 CNTR	O
< 25		ALESSAND...	96 CNTR	Te
< 6 $\times 10^{-3}$	90	13 BELLI	96 CNTR	$^{129}\text{Xe}$ , inel.
		14 BELLI	96c CNTR	$^{129}\text{Xe}$
< 1 $\times 10^{-3}$	90	15 BERNABEI	96 CNTR	Na
< 0.3	90	15 BERNABEI	96 CNTR	I
< 0.7	95	16 SARSA	96 CNTR	Na
< 0.03	90	17 SMITH	96 CNTR	Na
< 0.8	90	17 SMITH	96 CNTR	I
< 0.35	95	18 GARCIA	95 CNTR	Natural Ge
< 0.6	95	QUENBY	95 CNTR	Na
< 3	95	QUENBY	95 CNTR	I
< 1.5 $\times 10^2$	90	19 SNOWDEN...	95 MICA	$^{16}\text{O}$
< 4 $\times 10^2$	90	19 SNOWDEN...	95 MICA	$^{39}\text{K}$
< 0.08	90	20 BECK	94 CNTR	$^{76}\text{Ge}$
< 2.5	90	BACCI	92 CNTR	Na
< 3	90	BACCI	92 CNTR	I
< 0.9	90	21 REUSSER	91 CNTR	Natural Ge
< 0.7	95	CALDWELL	88 CNTR	Natural Ge

- <sup>1</sup> UCHIDA 14 limit is for inelastic scattering  $\chi^0 + ^{129}\text{Xe}^* \rightarrow \chi^0 + ^{129}\text{Xe}^*$  (39.58 keV).
- <sup>2</sup> ANGIOHER 02 limit is for spin-dependent WIMP-Aluminum cross section.
- <sup>3</sup> BELLI 02 discuss dependence of the extracted WIMP cross section on the assumptions of the galactic halo structure.
- <sup>4</sup> BERNABEI 02c analyze the DAMA data in the scenario in which  $\chi^0$  scatters into a slightly heavier state as discussed by SMITH 01.
- <sup>5</sup> GREEN 02 discusses dependence of extracted WIMP cross section limits on the assumptions of the galactic halo structure.
- <sup>6</sup> ULLIO 01 disfavor the possibility that the BERNABEI 99 signal is due to spin-dependent WIMP coupling.
- <sup>7</sup> BENOIT 00 find four event categories in Ge detectors and suggest that low-energy surface nuclear recoils can explain anomalous events reported by UKDMC and Saclay Nal experiments.
- <sup>8</sup> BERNABEI 00D limit is for inelastic scattering  $\chi^0 ^{129}\text{Xe} \rightarrow \chi^0 ^{129}\text{Xe}$  (39.58 keV).
- <sup>9</sup> AMBROSIO 99 search for upgoing muon events induced by neutrinos originating from WIMP annihilations in the Sun and Earth.
- <sup>10</sup> BRHLIK 99 discuss the effect of astrophysical uncertainties on the WIMP interpretation of the BERNABEI 99 signal.
- <sup>11</sup> KLIMENKO 98 limit is for inelastic scattering  $\chi^0 ^{73}\text{Ge} \rightarrow \chi^0 ^{73}\text{Ge}^*$  (13.26 keV).
- <sup>12</sup> KLIMENKO 98 limit is for inelastic scattering  $\chi^0 ^{73}\text{Ge} \rightarrow \chi^0 ^{73}\text{Ge}^*$  (66.73 keV).
- <sup>13</sup> BELLI 96 limit for inelastic scattering  $\chi^0 ^{129}\text{Xe} \rightarrow \chi^0 ^{129}\text{Xe}^*$  (39.58 keV).
- <sup>14</sup> BELLI 96c use background subtraction and obtain  $\sigma < 0.35 \text{ pb}$  ( $< 0.15 \text{ fb}$ ) (90% CL) for spin-dependent (independent)  $\chi^0$ -proton cross section. The confidence level is from R. Bernabei, private communication, May 20, 1999.
- <sup>15</sup> BERNABEI 96 use pulse shape discrimination to enhance the possible signal. The limit here is from R. Bernabei, private communication, September 19, 1997.
- <sup>16</sup> SARSA 96 search for annual modulation of WIMP signal. See SARSA 97 for details of the analysis. The limit here is from M.L. Sarsa, private communication, May 26, 1997.
- <sup>17</sup> SMITH 96 use pulse shape discrimination to enhance the possible signal. A dark matter density of  $0.4 \text{ GeV cm}^{-3}$  is assumed.
- <sup>18</sup> GARCIA 95 limit is from the event rate. A weaker limit is obtained from searches for diurnal and annual modulation.
- <sup>19</sup> SNOWDEN-IFFT 95 look for recoil tracks in an ancient mica crystal. Similar limits are also given for  $^{27}\text{Al}$  and  $^{28}\text{Si}$ . See COLLAR 96 and SNOWDEN-IFFT 96 for discussion on potential backgrounds.
- <sup>20</sup> BECK 94 uses enriched  $^{76}\text{Ge}$  (86% purity).
- <sup>21</sup> REUSSER 91 limit here is changed from published (0.3) after reanalysis by authors. J.L. Vuilleumier, private communication, March 29, 1996.

### For $m_{\chi^0} = 1 \text{ TeV}$

VALUE (nb)	CL%	DOCUMENT ID	TECN	COMMENT
• • • We do not use the following data for averages, fits, limits, etc. • • •				
< 0.03	90	1 UCHIDA	14 XMAS	$^{129}\text{Xe}$ , inelastic
< 3	90	2 ANGIOHER	02 CRES	Al
		3 BENOIT	00 EDEL	Ge
		4 BERNABEI	99D CNTR	SIMP
		5 DERBIN	99 CNTR	SIMP
< 0.06	95	6 KLIMENKO	98 CNTR	$^{73}\text{Ge}$ , inel.
< 0.4	95	7 KLIMENKO	98 CNTR	$^{73}\text{Ge}$ , inel.
< 40		ALESSAND...	96 CNTR	O
< 700		ALESSAND...	96 CNTR	Te
< 0.05	90	8 BELLI	96 CNTR	$^{129}\text{Xe}$ , inel.
< 1.5	90	9 BELLI	96 CNTR	$^{129}\text{Xe}$ , inel.
		10 BELLI	96c CNTR	$^{129}\text{Xe}$
< 0.01	90	11 BERNABEI	96 CNTR	Na
< 9	90	11 BERNABEI	96 CNTR	I
< 7	95	12 SARSA	96 CNTR	Na
< 0.3	90	13 SMITH	96 CNTR	Na
< 6	90	13 SMITH	96 CNTR	I
< 6	95	14 GARCIA	95 CNTR	Natural Ge
< 8	95	QUENBY	95 CNTR	Na
< 50	95	QUENBY	95 CNTR	I
< 700	90	15 SNOWDEN...	95 MICA	$^{16}\text{O}$
< 1 $\times 10^3$	90	15 SNOWDEN...	95 MICA	$^{39}\text{K}$
< 0.8	90	16 BECK	94 CNTR	$^{76}\text{Ge}$
< 30	90	BACCI	92 CNTR	Na
< 30	90	BACCI	92 CNTR	I
< 15	90	17 REUSSER	91 CNTR	Natural Ge
< 6	95	CALDWELL	88 CNTR	Natural Ge

- <sup>1</sup> UCHIDA 14 limit is for inelastic scattering  $\chi^0 + ^{129}\text{Xe}^* \rightarrow \chi^0 + ^{129}\text{Xe}^*$  (39.58 keV).
- <sup>2</sup> ANGIOHER 02 limit is for spin-dependent WIMP-Aluminum cross section.
- <sup>3</sup> BENOIT 00 find four event categories in Ge detectors and suggest that low-energy surface nuclear recoils can explain anomalous events reported by UKDMC and Saclay Nal experiments.
- <sup>4</sup> BERNABEI 99D search for SIMPs (Strongly Interacting Massive Particles) in the mass range  $10^3$ - $10^{16}$  GeV. See their Fig. 3 for cross-section limits.
- <sup>5</sup> DERBIN 99 search for SIMPs (Strongly Interacting Massive Particles) in the mass range  $10^2$ - $10^{14}$  GeV. See their Fig. 3 for cross-section limits.
- <sup>6</sup> KLIMENKO 98 limit is for inelastic scattering  $\chi^0 ^{73}\text{Ge} \rightarrow \chi^0 ^{73}\text{Ge}^*$  (13.26 keV).
- <sup>7</sup> KLIMENKO 98 limit is for inelastic scattering  $\chi^0 ^{73}\text{Ge} \rightarrow \chi^0 ^{73}\text{Ge}^*$  (66.73 keV).
- <sup>8</sup> BELLI 96 limit for inelastic scattering  $\chi^0 ^{129}\text{Xe} \rightarrow \chi^0 ^{129}\text{Xe}^*$  (39.58 keV).
- <sup>9</sup> BELLI 96 limit for inelastic scattering  $\chi^0 ^{129}\text{Xe} \rightarrow \chi^0 ^{129}\text{Xe}^*$  (236.14 keV).
- <sup>10</sup> BELLI 96c use background subtraction and obtain  $\sigma < 0.7 \text{ pb}$  ( $< 0.7 \text{ fb}$ ) (90% CL) for spin-dependent (independent)  $\chi^0$ -proton cross section. The confidence level is from R. Bernabei, private communication, May 20, 1999.
- <sup>11</sup> BERNABEI 96 use pulse shape discrimination to enhance the possible signal. The limit here is from R. Bernabei, private communication, September 19, 1997.
- <sup>12</sup> SARSA 96 search for annual modulation of WIMP signal. See SARSA 97 for details of the analysis. The limit here is from M.L. Sarsa, private communication, May 26, 1997.
- <sup>13</sup> SMITH 96 use pulse shape discrimination to enhance the possible signal. A dark matter density of  $0.4 \text{ GeV cm}^{-3}$  is assumed.
- <sup>14</sup> GARCIA 95 limit is from the event rate. A weaker limit is obtained from searches for diurnal and annual modulation.
- <sup>15</sup> SNOWDEN-IFFT 95 look for recoil tracks in an ancient mica crystal. Similar limits are also given for  $^{27}\text{Al}$  and  $^{28}\text{Si}$ . See COLLAR 96 and SNOWDEN-IFFT 96 for discussion on potential backgrounds.
- <sup>16</sup> BECK 94 uses enriched  $^{76}\text{Ge}$  (86% purity).
- <sup>17</sup> REUSSER 91 limit here is changed from published (5) after reanalysis by authors. J.L. Vuilleumier, private communication, March 29, 1996.

### Miscellaneous Results from Underground Dark Matter Searches

VALUE	CL%	DOCUMENT ID	TECN	COMMENT
• • • We do not use the following data for averages, fits, limits, etc. • • •				
		1 ABRAMOFF	19 SENS	MeV DM e-Si; dark photon Si absorption
		2 ADHIKARI	19 C100	annual modulation Nal
		3 AMARE	19 ANAI	annual modulation Nal
		4 APRILE	19 XE1T	$\pi$ (Xe)
		5 BRINGMANN	19	cosmic ray DM
		6 BRUNE	19	Majoran DM
		7 CHOI	19 THEO	290 TeV IceCube $\nu$
		8 HA	19 C100	inelastic boosted dark $\gamma$
		9 KLOPF	19	$n \rightarrow \chi e^+ e^-$
		10 AARTSEN	18D ICCB	relic WIMP $\chi \rightarrow \nu X$
		11 ABE	18F XMAS	$A'e \rightarrow A'e$
		12 AGNES	18B DS50	Ar
		13 AGNESE	18B SCDM	MeV DM e-Si; dark photon Si absorption
		14 AKERIB	18A LUX	Xe
		15 ARMENGAUD	18 EDE3	Ge

Searches Particle Listings  
WIMP and Dark Matter Searches

<1 × 10<sup>-12</sup> 90 16 KACHULIS 18 SKAM boosted DM on e  
17 AGUILAR-AR...17 DMIC γ' on Si  
18 APRILE 17 X100 Xe  
19 APRILE 17D X100 Xe  
20 APRILE 17H X100 keV bosonic DM search  
21 APRILE 17K X100 χN → χ\* → χγ  
<4 × 10<sup>-3</sup> 90 22 ANGLOHER 16A CRES CaWO<sub>4</sub>  
23 APRILE 15 X100 Event rate modulation  
24 APRILE 15A X100 Electron scattering

1 ABRAMOFF 19 search for MeV scale DM via DM–e scattering and dark photon DM via absorption in Si; limits set in coupling vs. m(χ) plane and on dark photon in m(A) vs. kinetic mixing parameter plane.  
2 ADHIKARI 19 search for annual modulation signal from WIMP scatter on NaI with 1.7 yr exposure; result consistent with both DAMA/LIBRA and null hypothesis.  
3 AMARE 19 is ANAIS-112 search for WIMP scatter annual modulation on NaI; 157.55 kg yr exposure; result compatible with null hypothesis; confirm goal of reaching sensitivity at 3σ to DAMA/LIBRA result in 5 years.  
4 APRILE 19 search for WIMP-pion scattering in Xe; no signal: require σ(χπ) < 6.4 × 10<sup>-10</sup> pb for m(χ) = 30 GeV.  
5 BRINGMANN 19 derive theoretically limits on GeV and sub-GeV mass dark matter, in its high energy component generated by interaction with cosmic rays; place limits on σ<sup>SI</sup> and σ<sup>SD</sup> < 10<sup>5</sup> pb.  
6 BRUNE 19 examine possibility of Majoron dark matter; limits placed on Majoron mass vs. coupling from SN1987a and ν-less double beta decay.  
7 CHOI 19 from multimessenger observation finds limit on σ(νχ)/m(DM) < 5.1 × 10<sup>-23</sup> cm<sup>2</sup>/GeV based on 290 TeV IceCube neutrino event.  
8 HA 19 search for inelastic boosted MeV scale dark photon using COSINE-100 data; limits placed in m vs. epsilon plane for various mediators.  
9 KLOPF 19 search for DM via n → χe<sup>+</sup>e<sup>-</sup>; no signal: limits placed in branching fraction vs. m(e<sup>+</sup>e<sup>-</sup>) plane.  
10 AARTSEN 18D search for long-lived DM particles decaying χ → νX; no excess seen; for DM masses above 10 TeV, excluding lifetimes shorter than 10<sup>28</sup> s.  
11 ABE 18r search for keV mass ALPs and hidden photons (HP) scatter on electrons; limits set on mass vs. coupling.  
12 AGNES 18b search for MeV-scale DM scatter on electrons in Ar; no signal; require σ(χe) < 9 × 10<sup>-3</sup> pb for DM form factor F(DM) = 1 and < 300 pb for F(DM) proportional to 1/q<sup>2</sup> for m(χ) = 100 MeV.  
13 AGNESE 18a search for MeV scale DM via DM-e scattering and dark photon DM via absorption in Si; limits set on MeV DM in coupling vs. m(χ) plane and on dark photon in m(A') vs. kinetic mixing plane.  
14 AKERIB 18A search for annual and diurnal modulation of DM scattering rate on electrons for recoil energy between 2 and 6 keVee; no signal found.  
15 ARMENGAUD 18 search for ALP from the Sun and galactic bosonic DM, interacting in Ge; no signal; limits set for 0.8–500 keV DM particles.  
16 KACHULIS 18 search for an excess of elastically scattered electrons above the atmospheric neutrino background in Super-K; limits placed for simple annihilation or decay in the Sun or galactic center producing "boosted" dark matter.  
17 AGUILAR-AREVALO 17 search for hidden photon DM scatter on Si target CCD; limit kinetic mixing κ < 1 × 10<sup>-12</sup> for m = 10 eV.  
18 APRILE 17 search for WIMP-e annual modulation signal for recoil energy in the 2.0–5.8 keV interval using 4 years data with Xe. No significant effect seen.  
19 APRILE 17D set limits on 14 WIMP-nucleon different interaction operators. No deviations found using 225 live days in the 6.6–240 keV recoil energy range.  
20 APRILE 17H search for keV bosonic DM via eχ → e, looking for electronic recoils with 224.6 live days of data and 34 kg of LXe. Limits set on χee coupling for m(χ) = 8–125 keV.  
21 APRILE 17K search for magnetic inelastic DM via χN → χ\* → χγ. Limits set in DM magnetic moment vs. mass splitting plane for two DM masses corresponding to the DAMA/LIBRA best fit values.  
22 ANGLOHER 16A require q<sup>2</sup> dependent scattering < 8 × 10<sup>-3</sup> pb for asymmetric DM m(WIMP) = 3 GeV on CaWO<sub>4</sub> target. It uses a local dark matter density of 0.38 GeV/cm<sup>3</sup>.  
23 APRILE 15 search for periodic variation of electronic recoil event rate in the data between Feb. 2011 and Mar. 2012. No significant modulation is found for periods up to 500 days.  
24 APRILE 15A search for X<sup>0</sup> scattering off electrons. See their Fig. 4 for limits on cross section through axial-vector coupling for m<sub>χ<sup>0</sup></sub> between 0.6 GeV and 1 TeV. For m<sub>χ<sup>0</sup></sub> = 2 GeV, σ < 60 pb (90%CL) is obtained.

— X<sup>0</sup> Annihilation Cross Section —

Limits are on σv for X<sup>0</sup> pair annihilation at threshold.

VALUE (cm <sup>3</sup> s <sup>-1</sup> )	CL%	DOCUMENT ID	TECN	COMMENT
<0.8 × 10 <sup>-22</sup>	95	1 ABEYSEKARA 19	HAWC	DM annihilation to γs within galactic substructure
<4 × 10 <sup>-26</sup>	95	2 ALBERT 19b	HAWC	annihilation/decay to γ in M31
<7 × 10 <sup>-27</sup>	95	3 CHEUNG 19	FLAT	χχ → e <sup>+</sup> e <sup>-</sup> and b <b>̄</b> b
<2 × 10 <sup>-26</sup>	95	4 DI-MAURO 19	FLAT	Fermi-LAT M31 and M33
<1 × 10 <sup>-32</sup>	95	5 JOHNSON 19	FLAT	P-wave DM; Fermi-LAT
<4 × 10 <sup>-28</sup>	95	6 LI 19d	FLAT	χχ → γ
<1 × 10 <sup>-23</sup>	95	7 NG 19	FLAT	sterile ν decay/annihilation
<1 × 10 <sup>-22</sup>	95	8 QUEIROZ 19	FLAT	semi-annihilating DM
<1 × 10 <sup>-26</sup>	95	9 ABDALLAH 18	HESS	X <sup>0</sup> X <sup>0</sup> → γX; galactic halo
<1 × 10 <sup>-22</sup>	95	10 AHNEN 18	MGIC	X <sup>0</sup> X <sup>0</sup> → γX; Ursa Major II
<1 × 10 <sup>-26</sup>	95	11 ALBERT 18b	HAWC	X <sup>0</sup> X <sup>0</sup> → γX; Andromeda
<1 × 10 <sup>-26</sup>	95	12 CHANG 18A	HAWC	χχ → b <b>̄</b> b → γ
		13 LISANTI 18	THEO	Fermi, γ; galaxy groups

• • • We do not use the following data for averages, fits, limits, etc. • • •

<1.2 × 10<sup>-23</sup> 95 14 MAZZIOTTA 18 FLAT Fermi-LAT CRE data  
<1 × 10<sup>-23</sup> 90 15 AARTSEN 17C ICCB χχ → neutrinos  
<1.32 × 10<sup>-25</sup> 95 16 ALBERT 17A ANTR ν, DM annihilation  
<7 × 10<sup>-21</sup> 90 17 ARCHAMBAU.17 VRTS γ dwarf galaxies  
<1 × 10<sup>-28</sup> 90 18 AVRORIN 17 BAIK cosmic ν  
19 BOUDAUD 17 MeV DM to e<sup>+</sup>e<sup>-</sup>  
20 AARTSEN 16D ICCB ν, galactic center  
21 ABDALLAH 16 HESS Central Galactic Halo  
22 ABDALLAH 16A HESS WIMP+WIMP → γγ; galactic center  
23 AHNEN 16 MGFL Satellite galaxy, m(WIMP)=100 GeV  
<1.9 × 10<sup>-21</sup> 90 24 AVRORIN 16 BAIK νs from galactic center  
<3 × 10<sup>-26</sup> 95 25 CAPUTO 16 FLAT small Magellanic cloud  
<1 × 10<sup>-25</sup> 95 26 FORNUSA 16 FLAT Fermi-LAT γ-ray anisotropy  
<5 × 10<sup>-27</sup> 95 27 LEITE 16 WIMP, radio  
<2 × 10<sup>-26</sup> 95 28 LI 16 FLAT dwarf galaxies  
<1 × 10<sup>-25</sup> 95 29 LI 16A FLAT Fermi-LAT; M31  
<1 × 10<sup>-26</sup> 95 30 LIANG 16 FLAT Fermi-LAT, gamma line  
<1 × 10<sup>-25</sup> 95 31 LU 16 FLAT Fermi-LAT and AMS-02  
<1 × 10<sup>-23</sup> 95 32 SHIRASAKI 16 FLAT extra galactic  
33 AARTSEN 15C ICCB ν, Galactic halo  
34 AARTSEN 15E ICCB ν, Galactic center  
35 ABRAMOWSKI15 HESS Galactic center  
36 ACKERMANN 15 FLAT monochromatic γ  
37 ACKERMANN 15A FLAT isotropic γ background  
38 ACKERMANN 15B FLAT Satellite galaxy  
39 ADRIAN-MAR.15 ANTR ν, Galactic center  
40,41 ACKERMANN 14 FLAT Satellite galaxy, m = 10 GeV  
40,42 ACKERMANN 14 FLAT Satellite galaxy, m = 100 GeV  
40,42 ACKERMANN 14 FLAT Satellite galaxy, m = 1 TeV  
43 ALEKSIC 14 MGIC Segue 1, m = 1.35 TeV  
44 AARTSEN 13C ICCB Galaxies  
45 ABRAMOWSKI13 HESS Central Galactic Halo  
46 ACKERMANN 13A FLAT Galaxy  
47 ABRAMOWSKI12 HESS Fornax Cluster  
48 ACKERMANN 12 FLAT Galaxy  
49 ACKERMANN 12 FLAT Galaxy  
50 ALIU 12 VRTS Segue 1  
51 ABBASI 11C ICCB Galactic halo, m=1 TeV  
<1 × 10<sup>-22</sup> 90 52 ABRAMOWSKI11 HESS Near Galactic center, m=1 TeV  
<3 × 10<sup>-25</sup> 95 53 ACKERMANN 11 FLAT Satellite galaxy, m=10 GeV  
<1 × 10<sup>-26</sup> 95 53 ACKERMANN 11 FLAT Satellite galaxy, m=100 GeV  
<1 × 10<sup>-24</sup> 95 53 ACKERMANN 11 FLAT Satellite galaxy, m=1 TeV

1 ABEYSEKARA 19 search for γs from DM annihilation in galactic substructures with HAWC; no signal, limits placed in J(σv) vs. declination plane for m(DM) ~ 1–108 TeV.  
2 ALBERT 19b search for DM signal from M31 galaxy in μ, τ, t, b, W channels using HAWC for m(DM) ~ 1–100 TeV; no signal, limits placed in (σv) vs. m(DM) plane.  
3 CHEUNG 19 derive model-dependent bounds on ⟨σv⟩ from EDGES data: < 4 × 10<sup>-26</sup> cm<sup>3</sup>/s for e<sup>+</sup>e<sup>-</sup> and b**̄**b for m(χ) = 100 GeV (including boost factor).  
4 DI-MAURO 19 place limits on WIMP annihilation via Fermi-LAT observation of M31 and M33 galaxies: ⟨σv⟩ < 7 × 10<sup>-27</sup> cm<sup>3</sup>/s for m(χ) = 20 GeV from M31.  
5 JOHNSON 19 search for γ-rays, 10–600 GeV energy, from P-wave annihilating DM around SgrA\* BH using Fermi-LAT; limits set for various models.  
6 LI 19d search for χχ → γ in Fermi-LAT data; no signal, require ⟨σv⟩ < 2 × 10<sup>-26</sup> cm<sup>3</sup>/s for m(χ) = 100 GeV.  
7 NG 19 search for X-ray line from sterile ν decay/annihilation using NuStar M-31; no signal: limits placed in m(ν) vs mixing angle and ⟨σv⟩ vs m(ν).  
8 QUEIROZ 19 examine χχ → χSM semi-annihilation of DM reaction; limits placed for various assumed SM particles in ⟨σv⟩ vs. m(χ) plane.  
9 ABDALLAH 18 search for WIMP WIMP → γX in central galactic halo, 10 years of data; limits placed in ⟨σv⟩ vs. m(WIMP) plane for m(WIMP): 0.3–70 TeV.  
10 AHNEN 18 search for WIMP WIMP → γX from Ursa Major II; limits set in ⟨σv⟩ vs. m(WIMP) plane for b**̄**b, W<sup>+</sup>W<sup>-</sup>, τ<sup>+</sup>τ<sup>-</sup>, and μ<sup>+</sup>μ<sup>-</sup> annihilation modes.  
11 ALBERT 18b search for TeV-scale WIMPs with WIMP WIMP → γX in Andromeda galaxy using HAWC Observatory; limits set in ⟨σv⟩ vs m(WIMP) plane.  
12 CHANG 18A examine χχ → b**̄**b → γ using Fermi Pass 8 data; no signal; require ⟨σv⟩ < 10<sup>-26</sup> cm<sup>3</sup>/s for m(χ) = 50 GeV.  
13 LISANTI 18 examine Fermi Pass 8 γ-ray data from galaxy groups; report m(WIMP) > 30 GeV for annihilation in b**̄**b channel.  
14 MAZZIOTTA 18 examine Fermi-LAT electron and positron spectra searching for features originating from DM particles annihilation into e<sup>+</sup>e<sup>-</sup> pairs, from 45 GeV to 2 TeV; no signal found, limits are obtained.  
15 AARTSEN 17C use 1005 days of IceCube data to search for χχ → neutrinos via various annihilation channels. Limits set.  
16 ALBERT 17A search for DM annihilation to νs using ANTARES data from 2007–2015. No signal. Limits set in ⟨σv⟩ vs. m(DM) plane for m(DM) ~ 10–10 × 10<sup>5</sup> GeV. The listed limit is for m(DM) = 100 TeV.  
17 ARCHAMBAULT 17 set limits for WIMP mass between 100 GeV and 1 TeV on ⟨σv⟩ for W<sup>+</sup>W<sup>-</sup>, ZZ, b**̄**b, s**̄**s, u**̄**u, d**̄**d, t**̄**t, e<sup>+</sup>e<sup>-</sup>, gg, c**̄**c, hh, γγ, μ<sup>+</sup>μ<sup>-</sup>, τ<sup>+</sup>τ<sup>-</sup> annihilation channels.  
18 AVRORIN 17 find upper limits for the annihilation cross section in various channels for DM particle mass between 30 GeV and 10 TeV. Strongest upper limits coming from the two neutrino channel require ⟨σv⟩ < 6 × 10<sup>-20</sup> cm<sup>3</sup>/s in dwarf galaxies and ⟨σv⟩ < 7 × 10<sup>-21</sup> cm<sup>3</sup>/s in LMC for 5 TeV WIMP mass.

Downloaded from https://academic.oup.com/ptep/article/2020/8/083C01/5891211 by guest on 12 November 2020



# Searches Particle Listings

## WIMP and Dark Matter Searches

- 19 BOUDAUD 17 use data from the spacecraft Voyager 1, beyond the heliopause, and from AMS02 on  $\chi\chi \rightarrow e^+e^-$  to require  $\langle\sigma v\rangle < 1. \times 10^{-28} \text{ cm}^3/\text{s}$  for  $m(\chi) = 10 \text{ MeV}$ .
- 20 AARTSEN 16d search for GeV  $\nu$ s from WIMP annihilation in galaxy; limits set on  $\langle\sigma v\rangle$  in Fig. 6, 7.
- 21 ABDALLAH 16 require  $\langle\sigma v\rangle < 6 \times 10^{-26} \text{ cm}^3/\text{s}$  for  $m(\text{WIMP}) = 1.5 \text{ TeV}$  from 254 hours observation ( $WW$  channel) and  $< 2 \times 10^{-26} \text{ cm}^3/\text{s}$  for  $m(\text{WIMP}) = 1.0 \text{ TeV}$  in  $\tau^+\tau^-$  channel.
- 22 ABDALLAH 16a search for line spectra from  $WIMP + WIMP \rightarrow \gamma\gamma$  in 18 hr HESS data; rule out previous 130 GeV WIMP hint from Fermi-LAT data.
- 23 AHNEN 16 require  $\langle\sigma v\rangle < 3 \times 10^{-26} \text{ cm}^3/\text{s}$  for  $m(\text{WIMP}) = 100 \text{ GeV}$  ( $WW$  channel).
- 24 AVRORIN 16 require  $\langle s.v\rangle < 1.91 \times 10^{-21} \text{ cm}^3/\text{s}$  from WIMP annihilation to  $\nu$ s via  $W$  channel for  $m(\text{WIMP}) = 1 \text{ TeV}$ .
- 25 CAPUTO 16 place limits on WIMPs from annihilation to gamma rays in Small Magellanic Cloud using Fermi-LAT data:  $\langle\sigma v\rangle < 3 \times 10^{-26} \text{ cm}^3/\text{s}$  for  $m(\text{WIMP}) = 10 \text{ GeV}$ .
- 26 FORNASA 16 use anisotropies in the  $\gamma$ -ray diffuse emission detected by Fermi-LAT to bound  $\langle\sigma v\rangle < 10^{-25} \text{ cm}^3/\text{s}$  for  $m(\text{WIMP}) = 100 \text{ GeV}$  in  $b\bar{b}$  channel: see Fig. 28. The limit is driven by dark-matter subhalos in the Milky Way and it refers to their Most Constraining Scenario.
- 27 LEITE 16 constrain WIMP annihilation via search for radio emissions from Smith cloud;  $\langle\sigma v\rangle < 5 \times 10^{-27} \text{ cm}^3/\text{s}$  in  $ee$  channel for  $m(\text{WIMP}) = 5 \text{ GeV}$ .
- 28 LI 16 re-analyze Fermi-LAT data on 8 dwarf spheroidal; set limit  $\langle\sigma v\rangle < 2 \times 10^{-26} \text{ cm}^3/\text{s}$  for  $m(\text{WIMP}) = 100 \text{ GeV}$  in  $b\bar{b}$  mode with substructures included.
- 29 LI 16a constrain  $\langle\sigma v\rangle < 10^{-25} \text{ cm}^3/\text{s}$  in  $b\bar{b}$  channel for  $m(\text{WIMP}) = 100 \text{ GeV}$  using Fermi-LAT data from M31; see Fig. 6.
- 30 LIANG 16 search dwarf spheroidal galaxies, Large Magellanic Cloud, and Small Magellanic Cloud for  $\gamma$ -line in Fermi-LAT data.
- 31 LU 16 re-analyze Fermi-LAT and AMS-02 data; require  $\langle\sigma v\rangle < 10^{-25} \text{ cm}^3/\text{s}$  for  $m_m(\text{WIMP}) = 1 \text{ TeV}$  in  $b\bar{b}$  channel.
- 32 SHIRASAKI 16 re-analyze Fermi-LAT extra-galactic data; require  $\langle\sigma v\rangle < 10^{-23} \text{ cm}^3/\text{s}$  for  $m(\text{WIMP}) = 1 \text{ TeV}$  in  $b\bar{b}$  channel; see Fig. 8.
- 33 AARTSEN 15c search for neutrinos from  $X^0$  annihilation in the Galactic halo. See their Figs. 16 and 17, and Table 5 for limits on  $\sigma \cdot v$  for  $X^0$  mass between 100 GeV and 100 TeV.
- 34 AARTSEN 15e search for neutrinos from  $X^0$  annihilation in the Galactic center. See their Figs. 7 and 9, and Table 3 for limits on  $\sigma \cdot v$  for  $X^0$  mass between 30 GeV and 10 TeV.
- 35 ABRAMOWSKI 15 search for  $\gamma$  from  $X^0$  annihilation in the Galactic center. See their Fig. 4 for limits on  $\sigma \cdot v$  for  $X^0$  mass between 250 GeV and 10 TeV.
- 36 ACKERMANN 15 search for monochromatic  $\gamma$  from  $X^0$  annihilation in the Galactic halo. See their Fig. 8 and Tables 2-4 for limits on  $\sigma \cdot v$  for  $X^0$  mass between 0.2 GeV and 500 GeV.
- 37 ACKERMANN 15a search for  $\gamma$  from  $X^0$  annihilation (both Galactic and extragalactic) in the isotropic  $\gamma$  background. See their Fig. 7 for limits on  $\sigma \cdot v$  for  $X^0$  mass between 10 GeV and 30 TeV.
- 38 ACKERMANN 15b search for  $\gamma$  from  $X^0$  annihilation in 15 dwarf spheroidal satellite galaxies of the Milky Way. See their Figs. 1 and 2 for limits on  $\sigma \cdot v$  for  $X^0$  mass between 2 GeV and 10 TeV.
- 39 ADRIAN-MARTINEZ 15 search for neutrinos from  $X^0$  annihilation in the Galactic center. See their Figs. 10 and 11 and Tables 1 and 2 for limits on  $\sigma \cdot v$  for  $X^0$  mass between 25 GeV and 10 TeV.
- 40 ACKERMANN 14 search for  $\gamma$  from  $X^0$  annihilation in 25 dwarf spheroidal satellite galaxies of the Milky Way. See their Tables II-VII for limits assuming annihilation into  $e^+e^-$ ,  $\mu^+\mu^-$ ,  $\tau^+\tau^-$ ,  $u\bar{u}$ ,  $b\bar{b}$ , and  $W^+W^-$ , for  $X^0$  mass ranging from 2 GeV to 10 TeV.
- 41 Limit assuming  $X^0$  pair annihilation into  $b\bar{b}$ .
- 42 Limit assuming  $X^0$  pair annihilation into  $W^+W^-$ .
- 43 ALEKSIC 14 search for  $\gamma$  from  $X^0$  annihilation in the dwarf spheroidal galaxy Segue 1. The listed limit assumes annihilation into  $W^+W^-$ . See their Figs. 6, 7, and 16 for limits on  $\sigma \cdot v$  for annihilation channels  $\mu^+\mu^-$ ,  $\tau^+\tau^-$ ,  $b\bar{b}$ ,  $t\bar{t}$ ,  $\gamma\gamma$ ,  $\gamma Z$ ,  $W^+W^-$ ,  $ZZ$  for  $X^0$  mass between  $10^2$  and  $10^4 \text{ GeV}$ .
- 44 AARTSEN 13c search for neutrinos from  $X^0$  annihilation in nearby galaxies and galaxy clusters. See their Figs. 5-7 for limits on  $\sigma \cdot v$  for  $X^0 X^0 \rightarrow \nu\bar{\nu}$ ,  $\mu^+\mu^-$ ,  $\tau^+\tau^-$ , and  $W^+W^-$  for  $X^0$  mass between 300 GeV and 100 TeV.
- 45 ABRAMOWSKI 13 search for monochromatic  $\gamma$  from  $X^0$  annihilation in the Milky Way halo in the central region. Limit on  $\sigma \cdot v$  between  $10^{-28}$  and  $10^{-25} \text{ cm}^3 \text{ s}^{-1}$  (95% CL) is obtained for  $X^0$  mass between 500 GeV and 20 TeV for  $X^0 X^0 \rightarrow \gamma\gamma$ .  $X^0$  density distribution in the Galaxy by Einasto is assumed. See their Fig. 4.
- 46 ACKERMANN 13a search for monochromatic  $\gamma$  from  $X^0$  annihilation in the Milky Way. Limit on  $\sigma \cdot v$  for the process  $X^0 X^0 \rightarrow \gamma\gamma$  in the range  $10^{-29}$ - $10^{-27} \text{ cm}^3 \text{ s}^{-1}$  (95% CL) is obtained for  $X^0$  mass between 5 and 300 GeV. The limit depends slightly on the assumed density profile of  $X^0$  in the Galaxy. See their Tables VII-X and Fig.10. Supersedes ACKERMANN 12.
- 47 ABRAMOWSKI 12 search for  $\gamma$ 's from  $X^0$  annihilation in the Fornax galaxy cluster. See their Fig. 7 for limits on  $\sigma \cdot v$  for  $X^0$  mass between 0.1 and 100 TeV for the annihilation channels  $\tau^+\tau^-$ ,  $b\bar{b}$ , and  $W^+W^-$ .
- 48 ACKERMANN 12 search for monochromatic  $\gamma$  from  $X^0$  annihilation in the Milky Way. Limit on  $\sigma \cdot v$  in the range  $10^{-28}$ - $10^{-26} \text{ cm}^3 \text{ s}^{-1}$  (95% CL) is obtained for  $X^0$  mass between 7 and 200 GeV if  $X^0$  annihilates into  $\gamma\gamma$ . The limit depends slightly on the assumed density profile of  $X^0$  in the Galaxy. See their Table III and Fig. 15.
- 49 ACKERMANN 12 search for  $\gamma$  from  $X^0$  annihilation in the Milky Way in the diffuse  $\gamma$  background. Limit on  $\sigma \cdot v$  of  $10^{-24} \text{ cm}^3 \text{ s}^{-1}$  or larger is obtained for  $X^0$  mass between 5 GeV and 10 TeV for various annihilation channels including  $W^+W^-$ ,  $b\bar{b}$ ,  $g\bar{g}$ ,  $e^+e^-$ ,  $\mu^+\mu^-$ ,  $\tau^+\tau^-$ . The limit depends slightly on the assumed density profile of  $X^0$  in the Galaxy. See their Figs. 17-20.
- 50 ALIU 12 search for  $\gamma$ 's from  $X^0$  annihilation in the dwarf spheroidal galaxy Segue 1. Limit on  $\sigma \cdot v$  in the range  $10^{-24}$ - $10^{-20} \text{ cm}^3 \text{ s}^{-1}$  (95% CL) is obtained for  $X^0$  mass between 10 GeV and 2 TeV for annihilation channels  $e^+e^-$ ,  $\mu^+\mu^-$ ,  $\tau^+\tau^-$ ,  $b\bar{b}$ , and  $W^+W^-$ . See their Fig. 3.

- 51 ABBASI 11c search for  $\nu_\mu$  from  $X^0$  annihilation in the outer halo of the Milky Way. The limit assumes annihilation into  $\nu\nu$ . See their Fig. 9 for limits with other annihilation channels.
- 52 ABRAMOWSKI 11 search for  $\gamma$  from  $X^0$  annihilation near the Galactic center. The limit assumes Einasto DM density profile.
- 53 ACKERMANN 11 search for  $\gamma$  from  $X^0$  annihilation in ten dwarf spheroidal satellite galaxies of the Milky Way. The limit for  $m = 10 \text{ GeV}$  assumes annihilation into  $b\bar{b}$ , the others  $W^+W^-$ . See their Fig. 2 for limits with other final states. See also GERINGER-SAMETH 11 for a different analysis of the same data.

### Dark Matter Particle ( $X^0$ ) Production in Hadron Collisions

Searches for  $X^0$  production in association with observable particles ( $\gamma$ , jets, ...) in high energy hadron collisions. If a specific form of effective interaction Lagrangian is assumed, the limits may be translated into limits on  $X^0$ -nucleon scattering cross section.

VALUE	DOCUMENT ID	TECN	COMMENT
• • •	We do not use the following data for averages, fits, limits, etc.	• • •	
1	AABOUD	19AA ATLS	multi-channel BSM search
2	AABOUD	19AI ATLS	$H \rightarrow \chi\chi$
3	AABOUD	19AL ATLS	$H \rightarrow \chi\chi$
4	AABOUD	19Q ATLS	single $t+\cancel{E}_T$
5	AABOUD	19V ATLS	review mediator based DM searches
6	BANERJEE	19 NA64	$eN \rightarrow eN+\cancel{E}$
7	SIRUNYAN	19AN CMS	$H\chi\chi \rightarrow b\bar{b}\cancel{E}_T$
8	SIRUNYAN	19BC CMS	$LQ LQ \rightarrow \mu j \cancel{E}_T$
9	SIRUNYAN	19Bo CMS	$VV \rightarrow Hqq; H \rightarrow DM$
10	SIRUNYAN	19C CMS	$pp \rightarrow t\bar{t}\chi\chi$
11	SIRUNYAN	19o CMS	$pp \rightarrow \gamma \cancel{E}_T$
12	SIRUNYAN	19X CMS	$pp \rightarrow t\bar{t} + \cancel{p}\cancel{T}; pp \rightarrow t(\bar{t}) + \cancel{p}\cancel{T}$
13	AABOUD	18 ATLS	$pp \rightarrow Z\chi\chi; Z \rightarrow \ell\ell$
14	AABOUD	18A ATLS	$pp \rightarrow t\bar{t}\cancel{E}_T; pp \rightarrow b\bar{b}\cancel{E}_T$
15	AABOUD	18ca ATLS	$pp \rightarrow V\chi\chi; V \rightarrow jj$
16	AABOUD	18i ATLS	$pp \rightarrow \text{jet}(s) + \cancel{E}_T$
17	AGUILAR-AR...18B	MBNE	$pN \rightarrow \chi\chi, \chi = e, \pi, \text{ or } N$
18	KHACHATRY...18	CMS	$pp \rightarrow Z(\ell\ell) + \cancel{E}_T$
19	SIRUNYAN	18BF CMS	$pp \rightarrow t\cancel{E}_T$
20	SIRUNYAN	18Bo CMS	dijet resonance search
21	SIRUNYAN	18BV CMS	$pp \rightarrow Z\cancel{E}_T$
22	SIRUNYAN	18c CMS	$pp \rightarrow t\bar{t}\cancel{E}_T$
23	SIRUNYAN	18cu CMS	$pp \rightarrow Z\cancel{E}_T$
24	SIRUNYAN	18DH CMS	$pp \rightarrow \chi\chi h; h \rightarrow \gamma\gamma \text{ or } \tau\bar{\tau}$
25	SIRUNYAN	18s CMS	$pp \rightarrow \text{jets } \cancel{E}_T$
26	AABOUD	17A ATLS	$pp(H \rightarrow b\bar{b} + WIMP \text{ pair})$
27	AABOUD	17AMATLS	$pp \rightarrow Z' \rightarrow Ah \rightarrow h(b\bar{b}) + \cancel{E}_T$
28	AABOUD	17AQ ATLS	$pp \rightarrow h(\gamma\gamma) + \cancel{E}_T$
29	AABOUD	17BD ATLS	$pp \rightarrow \text{jet}(s) + \cancel{E}_T$
30	AABOUD	17R ATLS	$pp \rightarrow \gamma\cancel{E}_T$
31	AGUILAR-AR...17A	MBNE	$pN \rightarrow \chi\chi X; \chi N \rightarrow \chi N$
32	BANERJEE	17 NA64	$eN \rightarrow eN\gamma'$
33	KHACHATRY...17A	CMS	forward jets + $\cancel{E}_T$
34	KHACHATRY...17F	CMS	$H \rightarrow \text{invisibles}$
35	SIRUNYAN	17 CMS	$Z + \cancel{E}_T$
36	SIRUNYAN	17AP CMS	$pp \rightarrow Z' \rightarrow Ah \rightarrow h+\text{MET}$
37	SIRUNYAN	17AQ CMS	$pp \rightarrow \gamma+\text{MET}$
38	SIRUNYAN	17BB CMS	$pp \rightarrow t\bar{t}+\cancel{E}_T; pp \rightarrow b\bar{b}+\cancel{E}_T$
39	SIRUNYAN	17G CMS	$pp \rightarrow j + \cancel{E}_T$
40	SIRUNYAN	17U CMS	$pp \rightarrow Z\chi\chi; Z \rightarrow \ell\bar{\ell}$
41	AABOUD	16AD ATLS	$(W \text{ or } Z \rightarrow \text{jets}) + \cancel{E}_T$
42	AAD	16AF ATLS	$VV \rightarrow \text{forward jets } + \cancel{E}_T$
43	AAD	16AG ATLS	$\ell + \text{jets}$
44	AAD	16M ATLS	$pp \rightarrow H + \cancel{E}_T, H \rightarrow b\bar{b}$
45	KHACHATRY...16BZ	CMS	$\text{jet}(s) + \cancel{E}_T$
46	KHACHATRY...16CA	CMS	$\text{jets } + \cancel{E}_T$
47	KHACHATRY...16N	CMS	$pp \rightarrow \gamma + \cancel{E}_T$
48	AAD	15AS ATLS	$b(\bar{b}) + \cancel{E}_T, t\bar{t} + \cancel{E}_T$
49	AAD	15BH ATLS	$\text{jet } + \cancel{E}_T$
50	AAD	15CF ATLS	$H^0 + \cancel{E}_T$
51	AAD	15CS ATLS	$\gamma + \cancel{E}_T$
52	KHACHATRY...15AG	CMS	$t\bar{t} + \cancel{E}_T$
53	KHACHATRY...15AL	CMS	$\text{jet } + \cancel{E}_T$
54	KHACHATRY...15T	CMS	$\ell + \cancel{E}_T$
55	AAD	14AI ATLS	$W + \cancel{E}_T$
56	AAD	14BK ATLS	$W, Z + \cancel{E}_T$
57	AAD	14K ATLS	$Z + \cancel{E}_T$
58	AAD	14o ATLS	$Z + \cancel{E}_T$
59	AAD	13AD ATLS	$\text{jet } + \cancel{E}_T$
60	AAD	13C ATLS	$\gamma + \cancel{E}_T$
61	AALTONEN	12K CDF	$t + \cancel{E}_T$
62	AALTONEN	12M CDF	$\text{jet } + \cancel{E}_T$
63	CHATRCHYAN12AP	CMS	$\text{jet } + \cancel{E}_T$
64	CHATRCHYAN12T	CMS	$\gamma + \cancel{E}_T$

- 1 AABOUD 19AA searches for BSM physics in more than 700 event classes with more than  $10^5$  regions at 13 TeV with  $3.2 \text{ fb}^{-1}$ ; no significant signal.
- 2 AABOUD 19AI searches for vector boson fusion  $pp \rightarrow Hq\bar{q}$ ,  $H \rightarrow$  invisible at 13 TeV with  $36.1 \text{ fb}^{-1}$ ; no signal; require  $B(H \rightarrow \text{invisible}) < 0.37$  (0.28 expected).
- 3 AABOUD 19AL perform search in three different channels for  $H \rightarrow \chi\chi$  at 7, 8 and 13 TeV; combined result  $\text{BF}(H \rightarrow \text{invisible}) < 0.26$  (0.17 expected).
- 4 AABOUD 19Q search for single  $t + \cancel{E}_T$  at 13 TeV with  $36.1 \text{ fb}^{-1}$  of data; no signal; limits set in  $\sigma$  or coupling vs. mass plane for simplified models.
- 5 AABOUD 19V review ATLAS results from 7, 8 and 13 TeV searches for mediator-based DM and DE scalar which couples to gravity; no signal; limits set for large variety of simplified models.
- 6 BANERJEE 19 search for dark photon via  $eN \rightarrow eN + \cancel{E}$  in NA64; no signal, limits placed in kinetic mixing  $\epsilon$  vs.  $m(\text{DM})$  plane for  $m(\text{DM}) \sim 0.001\text{--}1 \text{ GeV}$ .
- 7 SIRUNYAN 19AN search at 13 TeV with  $35.9 \text{ fb}^{-1}$  for  $pp \rightarrow H\chi\chi \rightarrow b\bar{b}\cancel{E}_T$ ; no signal; limits set in the context of a 2HDM + pseudoscalar (*a*) model and a baryonic  $Z'$  model.
- 8 SIRUNYAN 19BC search for DM via LeptoQuark pair annihilation  $LQ \rightarrow \mu j\chi\chi \rightarrow \mu j \cancel{E}_T$  with  $77.4 \text{ fb}^{-1}$ , 13 TeV; no signal; limits placed in  $m(\chi)$  vs.  $m(LQ)$  plane. Model dependent limits on DM mass up to 600 GeV depending on  $m(LQ)$  placed.
- 9 SIRUNYAN 19BO search for vector boson fusion  $VV \rightarrow q\bar{q}H$  with  $H \rightarrow \chi\chi$  at 13 TeV with  $38.2 \text{ fb}^{-1}$ ; no signal; limits placed for several models. Also search for  $H \rightarrow$  invisible at 7, 8, and 13 TeV; no signal; limit placed on  $\text{BF} < 0.19$ .
- 10 SIRUNYAN 19C search for DM via  $pp \rightarrow t\bar{t}\chi\chi$  at 13 TeV,  $35.9 \text{ fb}^{-1}$ ; no signal; limits placed on coupling vs. mediator mass for various simplified models.
- 11 SIRUNYAN 19O search for  $pp \rightarrow \gamma$  at 13 TeV with  $35.9 \text{ fb}^{-1}$ ; no signal; limits placed on parameters of various models.
- 12 SIRUNYAN 19X search for  $pp \rightarrow t\bar{t}\cancel{E}_T$  and  $pp \rightarrow t\cancel{E}_T + \dots$  at 13 TeV with  $35.9 \text{ fb}^{-1}$ ; no signal; limits placed on  $\chi$  production  $\sigma$  for various simplified models with  $m(\chi) = 1 \text{ GeV}$ .
- 13 AABOUD 18 search for  $pp \rightarrow Z + \cancel{E}_T$  with  $Z \rightarrow \ell\ell$  at 13 TeV with  $36.1 \text{ fb}^{-1}$  of data. Limits set for simplified models.
- 14 AABOUD 18A search for  $pp \rightarrow t\bar{t}\cancel{E}_T$  or  $pp \rightarrow b\bar{b}\cancel{E}_T$  at 13 TeV,  $36.1 \text{ fb}^{-1}$  of data. Limits set for simplified models.
- 15 AABOUD 18CA search for  $pp \rightarrow V\chi\chi$  with  $V \rightarrow jj$  at 13 TeV,  $36.1 \text{ fb}^{-1}$ ; no signal; limits set in  $m(\text{DM})$  vs  $m(\text{mediator})$  simplified model plane.
- 16 AABOUD 18I search for  $pp \rightarrow j + \cancel{E}_T$  at 13 TeV with  $36.1 \text{ fb}^{-1}$  of data. Limits set for simplified models with pair-produced weakly interacting dark-matter candidates.
- 17 AGUILAR-AREVALO 18B search for WIMP production in MiniBooNE *p* beam dump; no signal; limits set for  $m(\chi) \sim 5\text{--}50 \text{ MeV}$  in vector portal DM model.
- 18 KHACHATRYAN 18 search for  $pp \rightarrow Z(\ell\ell) + \cancel{E}_T$ ; no signal; limits set on effective dark matter interactions and other exotic physics models.
- 19 SIRUNYAN 18BF search for  $pp \rightarrow t\cancel{E}_T$  at 13 TeV and  $36 \text{ fb}^{-1}$ ; no signal; limits placed on DM models involving a flavor changing neutral current, scalar resonance decaying to top quark and DM.
- 20 SIRUNYAN 18BO search for high mass dijet resonances at 13 TeV and  $36 \text{ fb}^{-1}$ ; no signal; limits placed on various models, including simplified DM models involving a spin  $= 1$   $Z'$  mediator.
- 21 SIRUNYAN 18BV search for  $pp \rightarrow Z\cancel{E}_T$  at 13 TeV; no signal, limits placed for various exotic physics models including DM.
- 22 SIRUNYAN 18C search for new physics in  $pp \rightarrow$  final states with two oppositely charged leptons at 13 TeV with  $35.9 \text{ fb}^{-1}$ . Limits placed on  $m(\text{mediator})$  and top squark for various simplified models.
- 23 SIRUNYAN 18CU search for  $pp \rightarrow Z\cancel{E}_T$  at 13 TeV and  $2.3 \text{ fb}^{-1}$ ; no signal; limits placed for various exotic models including D5.
- 24 SIRUNYAN 18BH search for  $pp \rightarrow \chi\chi h$ ;  $h \rightarrow \gamma\gamma$  or  $\tau\tau$  at 13 TeV,  $35.9 \text{ fb}^{-1}$ ; no signal; limits placed on massive boson mediator  $Z'$  in the context of  $Z'+2\text{HDM}$  and baryonic  $Z'$  models. Limits also cast in terms of spin-independent WIMP-nucleon cross section for masses 1–200 GeV.
- 25 SIRUNYAN 18S search for  $pp \rightarrow$  jets  $\cancel{E}_T$  at 13 TeV; no signal; limits placed on simplified dark matter models, on the branching ratio of the Higgs boson to invisible particles, and on several other exotic physics models including fermion portal DM.
- 26 AABOUD 17A search for  $H \rightarrow b\bar{b} + \cancel{E}_T$ . See Fig. 4b for limits set on VB mediator vs WIMP mass.
- 27 AABOUD 17AM search for  $pp \rightarrow Z' \rightarrow Ah \rightarrow h(b\bar{b}) + \cancel{E}_T$  at 13 TeV. Limits set in  $m(Z')$  vs.  $m(A)$  plane and on the visible cross section of  $h(b\bar{b}) + \cancel{E}_T$  events in bins of  $\cancel{E}_T$ .
- 28 AABOUD 17AQ search for WIMP in  $pp \rightarrow h(\gamma\gamma) + \cancel{E}_T$  in  $36.1 \text{ fb}^{-1}$  of data. Limits on the visible cross section are also provided. Model dependent limits on spin independent DM - Nucleon cross-section are also presented, which are more stringent than those from direct searches for DM mass smaller than  $2.5 \text{ GeV}$ .
- 29 AABOUD 17BD search for  $pp \rightarrow \text{jet}(s) + \cancel{E}_T$  at 13 TeV with  $3.2 \text{ fb}^{-1}$  of data. Limits set for simplified models. Observables corrected for detector effects can be used to constrain other models.
- 30 AABOUD 17R, for an axial vector mediator in the *s*-channel, excludes  $m(\text{mediator}) < 750\text{--}1200 \text{ GeV}$  for  $m(\text{DM}) < 230\text{--}480 \text{ GeV}$ , depending on the couplings.
- 31 AGUILAR-AREVALO 17A search for DM produced in 8 GeV proton collisions with steel beam dump followed by DM-nucleon scattering in MiniBooNE detector. Limit placed on DM cross section parameter  $Y < 2 \times 10^{-8}$  for  $\alpha_D = 0.5$  and for  $0.01 < m(\text{DM}) < 0.3 \text{ GeV}$ .
- 32 BANERJEE 17 search for dark photon invisible decay via *eN* scattering; exclude  $m(\gamma')$   $< 100 \text{ MeV}$  as an explanation of  $(g_{\mu} - 2)$  muon anomaly.
- 33 KHACHATRYAN 17A search for WIMPs in forward jets +  $\cancel{E}_T$  channel with  $18.5 \text{ fb}^{-1}$  at 8 TeV; limits set in effective theory model, Fig. 3.
- 34 KHACHATRYAN 17F search for  $H \rightarrow$  invisibles in  $pp$  collisions at 7, 8, and 13 TeV; place limits on Higgs portal DM.
- 35 SIRUNYAN 17 search for  $pp \rightarrow Z + \cancel{E}_T$  with  $2.3 \text{ fb}^{-1}$  at 13 TeV; no signal seen; limits placed on WIMPs and unparticles.
- 36 SIRUNYAN 17AP search for  $pp \rightarrow Z' \rightarrow Ah \rightarrow h + \text{MET}$  with  $h \rightarrow b\bar{b}$  or  $\gamma\gamma$  and  $A \rightarrow \chi\chi$  with  $2.3 \text{ fb}^{-1}$  at 13 TeV. Limits set in  $m(Z')$  vs.  $m(A)$  plane.
- 37 SIRUNYAN 17AQ search for  $pp \rightarrow \gamma + \text{MET}$  at 13 TeV with  $12.9 \text{ fb}^{-1}$ . Limits derived for simplified DM models, effective electroweak-DM interaction and Extra Dimensions models.

- 38 SIRUNYAN 17BB search for WIMPs via  $pp \rightarrow t\bar{t} + \cancel{E}_T$ ,  $pp \rightarrow b\bar{b} + \cancel{E}_T$  at 13 TeV with  $2.2 \text{ fb}^{-1}$ . Limits derived for various simplified models.
- 39 SIRUNYAN 17G search for  $pp \rightarrow j + \cancel{E}_T$  with  $12.9 \text{ fb}^{-1}$  at 13 TeV; limits placed on WIMP mass/mediators in DM simplified models.
- 40 SIRUNYAN 17U search for WIMPs/unparticles via  $pp \rightarrow Z\chi\chi$ ,  $Z \rightarrow \ell\bar{\ell}$  at 13 TeV with  $2.3 \text{ fb}^{-1}$ . Limits derived for various simplified models.
- 41 AABOUD 16AD place limits on  $VVX$  effective theory via search for hadronic *W* or *Z* plus WIMP pair production. See Fig. 5.
- 42 AAD 16AF search for  $VV \rightarrow (H \rightarrow \text{WIMP pair}) +$  forward jets with  $20.3 \text{ fb}^{-1}$  at 8 TeV; set limits in Higgs portal model, Fig. 8.
- 43 AAD 16AG search for lepton jets with  $20.3 \text{ fb}^{-1}$  of data at 8 TeV; Fig. 13 excludes dark photons around 0.1–1 GeV for kinetic mixing  $10^{-6}\text{--}10^{-2}$ .
- 44 AAD 16M search with  $20.3 \text{ fb}^{-1}$  of data at 8 TeV  $pp$  collisions; limits placed on EFT model (Fig. 7) and simplified  $Z'$  model (Fig. 6).
- 45 KHACHATRYAN 16BZ search for jet(s) +  $\cancel{E}_T$  in  $19.7 \text{ fb}^{-1}$  at 8 TeV; limits set for variety of simplified models.
- 46 KHACHATRYAN 16CA search for WIMPs via jet(s) +  $\cancel{E}_T$  using razor variable; require mediator scale  $> 1 \text{ TeV}$  for various effective theories.
- 47 KHACHATRYAN 16N search for  $\gamma + \text{WIMPs}$  in  $19.6 \text{ fb}^{-1}$  at 8 TeV; limits set on SI and SD WIMP-*p* scattering in Fig. 3.
- 48 AAD 15AS search for events with one or more bottom quark and missing  $\cancel{E}_T$ , and also events with a top quark pair and missing  $\cancel{E}_T$  in  $pp$  collisions at  $E_{\text{cm}} = 8 \text{ TeV}$  with  $L = 20.3 \text{ fb}^{-1}$ . See their Figs. 5 and 6 for translated limits on  $X^0$ -nucleon cross section for  $m = 1\text{--}700 \text{ GeV}$ .
- 49 AAD 15BH search for events with a jet and missing  $\cancel{E}_T$  in  $pp$  collisions at  $E_{\text{cm}} = 8 \text{ TeV}$  with  $L = 20.3 \text{ fb}^{-1}$ . See their Fig. 12 for translated limits on  $X^0$ -nucleon cross section for  $m = 1\text{--}1200 \text{ GeV}$ .
- 50 AAD 15CF search for events with a  $H^0$  ( $\rightarrow \gamma\gamma$ ) and missing  $\cancel{E}_T$  in  $pp$  collisions at  $E_{\text{cm}} = 8 \text{ TeV}$  with  $L = 20.3 \text{ fb}^{-1}$ . See paper for limits on the strength of some contact interactions containing  $X^0$  and the Higgs fields.
- 51 AAD 15CS search for events with a photon and missing  $\cancel{E}_T$  in  $pp$  collisions at  $E_{\text{cm}} = 8 \text{ TeV}$  with  $L = 20.3 \text{ fb}^{-1}$ . See their Fig. 13 (see also erratum) for translated limits on  $X^0$ -nucleon cross section for  $m = 1\text{--}1000 \text{ GeV}$ .
- 52 KHACHATRYAN 15AG search for events with a top quark pair and missing  $\cancel{E}_T$  in  $pp$  collisions at  $E_{\text{cm}} = 8 \text{ TeV}$  with  $L = 19.7 \text{ fb}^{-1}$ . See their Fig. 8 for translated limits on  $X^0$ -nucleon cross section for  $m = 1\text{--}200 \text{ GeV}$ .
- 53 KHACHATRYAN 15AL search for events with a jet and missing  $\cancel{E}_T$  in  $pp$  collisions at  $E_{\text{cm}} = 8 \text{ TeV}$  with  $L = 19.7 \text{ fb}^{-1}$ . See their Figs. 5 and Tables 4–6 for translated limits on  $X^0$ -nucleon cross section for  $m = 1\text{--}1000 \text{ GeV}$ .
- 54 KHACHATRYAN 15T search for events with a lepton and missing  $\cancel{E}_T$  in  $pp$  collisions at  $E_{\text{cm}} = 8 \text{ TeV}$  with  $L = 19.7 \text{ fb}^{-1}$ . See their Fig. 17 for translated limits on  $X^0$ -proton cross section for  $m = 1\text{--}1000 \text{ GeV}$ .
- 55 AAD 14AI search for events with a *W* and missing  $\cancel{E}_T$  in  $pp$  collisions at  $E_{\text{cm}} = 8 \text{ TeV}$  with  $L = 20.3 \text{ fb}^{-1}$ . See their Fig. 4 for translated limits on  $X^0$ -nucleon cross section for  $m = 1\text{--}1500 \text{ GeV}$ .
- 56 AAD 14BK search for hadronically decaying *W*, *Z* in association with  $\cancel{E}_T$  in  $20.3 \text{ fb}^{-1}$  at 8 TeV  $pp$  collisions. Fig. 5 presents exclusion results for SI and SD scattering cross section. In addition, cross section limits on the anomalous production of *W* or *Z* bosons with large missing transverse momentum are also set in two fiducial regions.
- 57 AAD 14K search for events with a *Z* and missing  $\cancel{E}_T$  in  $pp$  collisions at  $E_{\text{cm}} = 8 \text{ TeV}$  with  $L = 20.3 \text{ fb}^{-1}$ . See their Fig. 5 and 6 for translated limits on  $X^0$ -nucleon cross section for  $m = 1\text{--}10^3 \text{ GeV}$ .
- 58 AAD 14O search for  $ZH^0$  production with  $H^0$  decaying to invisible final states. See their Fig. 4 for translated limits on  $X^0$ -nucleon cross section for  $m = 1\text{--}60 \text{ GeV}$  in Higgs-portal  $X^0$  scenario.
- 59 AAD 13AD search for events with a jet and missing  $\cancel{E}_T$  in  $pp$  collisions at  $E_{\text{cm}} = 7 \text{ TeV}$  with  $L = 4.7 \text{ fb}^{-1}$ . See their Figs. 5 and 6 for translated limits on  $X^0$ -nucleon cross section for  $m = 1\text{--}1300 \text{ GeV}$ .
- 60 AAD 13C search for events with a photon and missing  $\cancel{E}_T$  in  $pp$  collisions at  $E_{\text{cm}} = 7 \text{ TeV}$  with  $L = 4.6 \text{ fb}^{-1}$ . See their Fig. 3 for translated limits on  $X^0$ -nucleon cross section for  $m = 1\text{--}1000 \text{ GeV}$ .
- 61 AALTONEN 12K search for events with a top quark and missing  $\cancel{E}_T$  in  $p\bar{p}$  collisions at  $E_{\text{cm}} = 1.96 \text{ TeV}$  with  $L = 7.7 \text{ fb}^{-1}$ . Upper limits on  $\sigma(tX^0)$  in the range 0.4–2 pb (95% CL) is given for  $m_{X^0} = 0\text{--}150 \text{ GeV}$ .
- 62 AALTONEN 12M search for events with a jet and missing  $\cancel{E}_T$  in  $p\bar{p}$  collisions at  $E_{\text{cm}} = 1.96 \text{ TeV}$  with  $L = 6.7 \text{ fb}^{-1}$ . Upper limits on the cross section in the range 2–10 pb (90% CL) is given for  $m_{X^0} = 1\text{--}300 \text{ GeV}$ . See their Fig. 2 for translated limits on  $X^0$ -nucleon cross section.
- 63 CHATRCHYAN 12AP search for events with a jet and missing  $\cancel{E}_T$  in  $pp$  collisions at  $E_{\text{cm}} = 7 \text{ TeV}$  with  $L = 5.0 \text{ fb}^{-1}$ . See their Fig. 4 for translated limits on  $X^0$ -nucleon cross section for  $m_{X^0} = 0.1\text{--}1000 \text{ GeV}$ .
- 64 CHATRCHYAN 12T search for events with a photon and missing  $\cancel{E}_T$  in  $pp$  collisions at  $E_{\text{cm}} = 7 \text{ TeV}$  with  $L = 5.0 \text{ fb}^{-1}$ . Upper limits on the cross section in the range 13–15 fb (90% CL) is given for  $m_{X^0} = 1\text{--}1000 \text{ GeV}$ . See their Fig. 2 for translated limits on  $X^0$ -nucleon cross section.

## REFERENCES FOR WIMP AND Dark Matter Searches

AKERIB	20	PR D101 012003	D.S. Akhmed et al.	(LUX Collab.)
AABOUD	19AA	EPJ C79 120	M. Aaboud et al.	(ATLAS Collab.)
AABOUD	19AI	PL B793 499	M. Aaboud et al.	(ATLAS Collab.)
AABOUD	19AL	PRL 122 231801	M. Aaboud et al.	(ATLAS Collab.)
AABOUD	19Q	JHEP 1905 041	M. Aaboud et al.	(ATLAS Collab.)
AABOUD	19V	JHEP 1905 142	M. Aaboud et al.	(ATLAS Collab.)
ABDELHAMEED	19	EPJ C79 630	A.H. Abdelhameed et al.	(CREST Collab.)
ABDELHAMEED	19A	PR D100 102002	A.H. Abdelhameed et al.	(CREST Collab.)
ABE	19	PL B789 45	K. Abe et al.	(XMASS Collab.)
ABEYSEKARA	19	JCAP 1907 022	A.U. Abeysekara et al.	(HAWC Collab.)
ABRAMOFF	19	PRL 122 161801	O. Abramoff et al.	(SENSEI Collab.)
ADHIKARI	19	PRL 123 031302	G. Adhikari et al.	(COSINE-100 Collab.)
AGNESE	19A	PR D99 062001	R. Agnese et al.	(CDMS Collab.)
AGUILAR-AR.	19A	PRL 123 181802	A. Aguilar-Arevalo et al.	(DMIC Collab.)



AALSETH	11	PRL 106 131301	C.E. Aalseth <i>et al.</i>	(CoGeNT Collab.)
AALSETH	11A	PRL 107 141301	C.E. Aalseth <i>et al.</i>	(CoGeNT Collab.)
ABBASI	11C	PR D84 022004	R. Abbasi <i>et al.</i>	(IceCube Collab.)
ABRAMOWSKI	11	PRL 106 161301	A. Abramowski <i>et al.</i>	(H.E.S.S. Collab.)
ACKERMANN	11	PRL 107 241302	M. Ackermann <i>et al.</i>	(Fermi-LAT Collab.)
AHLEN	11	PL B695 124	S. Ahlen <i>et al.</i>	(DMTPC Collab.)
AHMED	11	PR D83 112002	Z. Ahmed <i>et al.</i>	(CDMS Collab.)
AHMED	11A	PR D84 011102	Z. Ahmed <i>et al.</i>	(CDMS and EDELWEISS Collabs.)
AHMED	11B	PRL 106 131302	Z. Ahmed <i>et al.</i>	(CDMS Collab.)
AJELLO	11	PR D84 032007	M. Ajello <i>et al.</i>	(Fermi-LAT Collab.)
ANGLE	11	PRL 107 051301	J. Angle <i>et al.</i>	(XENON10 Collab.)
Also		PRL 110 249901 (err.)	J. Angle <i>et al.</i>	(XENON10 Collab.)
APRILE	11	PR D84 052003	E. Aprile <i>et al.</i>	(XENON100 Collab.)
APRILE	11A	PR D84 061101	E. Aprile <i>et al.</i>	(XENON100 Collab.)
APRILE	11B	PRL 107 131302	E. Aprile <i>et al.</i>	(XENON100 Collab.)
ARMENGAUD	11	PL B702 329	E. Armengaud <i>et al.</i>	(EDELWEISS-II Collab.)
BEHNKE	11	PRL 106 021303	E. Behnke <i>et al.</i>	(COUPP Collab.)
GERINGER-SA...	11	PRL 107 241303	A. Gerlinger-Sameth, S.M. Koushappas	(ZEPLIN-III Collab.)
HORN	11	PL B705 471	M. Horn <i>et al.</i>	(CDMS Collab.)
TANAKA	11	APJ 742 78	T. Tanaka <i>et al.</i>	(Super-Kamiokande Collab.)
ABBASI	10	PR D81 057101	R. Abbasi <i>et al.</i>	(IceCube Collab.)
AHMED	10	SCI 327 1619	Z. Ahmed <i>et al.</i>	(CDMS II Collab.)
AKERIB	10	PR D82 122004	D.S. Akerib <i>et al.</i>	(CDMS II Collab.)
AKIMOV	10	PL B692 180	D.Yu. Akimov <i>et al.</i>	(ZEPLIN-III Collab.)
APRILE	10	PRL 105 131302	E. Aprile <i>et al.</i>	(XENON100 Collab.)
ARMENGAUD	10	PL B687 294	E. Armengaud <i>et al.</i>	(EDELWEISS-II Collab.)
FELIZARDO	10	PRL 105 211301	M. Felizardo <i>et al.</i>	(The SIMPLE Collab.)
MIUCHI	10	PL B686 11	K. Miuchi <i>et al.</i>	(NEWAGE Collab.)
ABBASI	09B	PRL 102 201302	R. Abbasi <i>et al.</i>	(IceCube Collab.)
AHMED	09	PRL 102 011301	Z. Ahmed <i>et al.</i>	(CDMS Collab.)
ANGLE	09	PR D80 115005	J. Angle <i>et al.</i>	(XENON10 Collab.)
ANGLOHER	09	ASP 31 270	G. Angloher <i>et al.</i>	(CREST Collab.)
ARCHAMBAU...	09	PL B682 185	S. Archambault <i>et al.</i>	(PICASSO Collab.)
LEBEDENKO	09A	PRL 103 151302	V.N. Lebedenko <i>et al.</i>	(ZEPLIN-III Collab.)
LIN	09	PR D79 061101	S.T. Lin <i>et al.</i>	(TEXONO Collab.)
AALSETH	08	PRL 101 251301	C.E. Aalseth <i>et al.</i>	(CoGeNT Collab.)
Also		PRL 102 109903 (err.)	C.E. Aalseth <i>et al.</i>	(CoGeNT Collab.)
ANGLE	08A	PRL 101 091301	J. Angle <i>et al.</i>	(XENON10 Collab.)
BEDNYAKOV	08	PAN 71 111	V.A. Bednyakov, H.P. Klapdor-Kleingrothaus, I.V. Krivosheina	
Translated from YAF		71 112		
ALNER	07	PL B653 161	G.J. Alner <i>et al.</i>	(ZEPLIN-II Collab.)
LEE	07A	PRL 99 091301	H.S. Lee <i>et al.</i>	(KIMS Collab.)
MIUCHI	07	PL B654 58	K. Miuchi <i>et al.</i>	
AKERIB	06	PR D73 011102	D.S. Akerib <i>et al.</i>	(CDMS Collab.)
SHIMIZU	06A	PL B633 195	Y. Shimizu <i>et al.</i>	
AKERIB	05	PR D72 052009	D.S. Akerib <i>et al.</i>	(CDMS Collab.)
ALNER	05	PL B616 17	G.J. Alner <i>et al.</i>	(UK Dark Matter Collab.)
BARNABE-HE...	05	PL B624 186	M. Barnabe-Heider <i>et al.</i>	(PICASSO Collab.)
BERNOIT	05	PL B616 25	A. Bernoit <i>et al.</i>	(EDELWEISS Collab.)
GIRARD	05	PL B621 233	T.A. Girard <i>et al.</i>	(SIMPLE Collab.)
GIULIANI	05	PRL 95 101301	F. Giuliani	
GIULIANI	05A	PR D71 123503	F. Giuliani, T.A. Girard	
KLAPDOR-K...	05	PL B609 226	H.V. Klapdor-Kleingrothaus, I.V. Krivosheina, C. Tomei	
GIULIANI	04	PL B588 151	F. Giuliani, T.A. Girard	
GIULIANI	04A	PRL 93 161301	F. Giuliani	
MIUCHI	03	ASP 19 135	K. Miuchi <i>et al.</i>	
TAKEDA	03	PL B572 145	A. Takeda <i>et al.</i>	
ANGLOHER	02	ASP 18 43	G. Angloher <i>et al.</i>	(CREST Collab.)
BELLI	02	PR D66 043503	P. Belli <i>et al.</i>	
BERNABE	02C	EPJ C23 61	R. Bernabei <i>et al.</i>	(DAMA Collab.)
GREEN	02	PR D66 083003	A.M. Green	
BAUDIS	01	PR D63 022001	L. Baudis <i>et al.</i>	(Heidelberg-Moscow Collab.)
SMITH	01	PR D64 043502	D. Smith, N. Weiner	
ULLIO	01	JHEP 0107 044	P. Ullio, M. Kamionkowski, P. Vogel	
BERNOIT	00	PL B479 8	A. Bernoit <i>et al.</i>	(EDELWEISS Collab.)
BERNABE	00D	NJP 2 15	R. Bernabei <i>et al.</i>	(DAMA Collab.)
COLLAR	00	PRL 85 3083	J.J. Collar <i>et al.</i>	(SIMPLE Collab.)
AMBROSIO	99	PR D60 082002	M. Ambrosio <i>et al.</i>	(Macro Collab.)
BERNABE	99	PL B450 448	R. Bernabei <i>et al.</i>	(DAMA Collab.)
BERNABE	99D	PRL 83 4918	R. Bernabei <i>et al.</i>	(DAMA Collab.)
BRHLIK	99	PL B464 303	M. Brikhik, L. Roszkowski	
DERBIN	99	PAN 62 1886	A.V. Derbin <i>et al.</i>	
Translated from YAF		62 2034		
KLIMENKO	98	JETPL 67 875	A.A. Klimenko <i>et al.</i>	
Translated from ZETFP		67 835		
SARSA	97	PR D56 1856	M.L. Sarsa <i>et al.</i>	(ZARA Collab.)
ALESSAND...	96	PL B384 316	A. Alessandrello <i>et al.</i>	(MILA, MILAI, SASSO Collabs.)
BELLI	96	PL B387 222	P. Belli <i>et al.</i>	(DAMA Collab.)
Also		PL B389 783 (erratum)	P. Belli <i>et al.</i>	(DAMA Collab.)
BELLI	96C	PL C19 537	P. Belli <i>et al.</i>	(DAMA Collab.)
BERNABE	96	PL B389 757	R. Bernabei <i>et al.</i>	(DAMA Collab.)
COLLAR	96	PRL 76 331	J.J. Collar <i>et al.</i>	(SCUC Collab.)
SARSA	96	PL B386 458	M.L. Sarsa <i>et al.</i>	(ZARA Collab.)
Also		PR D56 1856	M.L. Sarsa <i>et al.</i>	(ZARA Collab.)
SMITH	96	PL B379 299	P.F. Smith <i>et al.</i>	(RAL, SHEF, LOIC+ Collabs.)
SNOWDEN-...	96	PRL 76 332	D.P. Snowden-Hift, E.S. Freeman, P.B. Price	(UCB Collab.)
GARCIA	95	PR D51 1458	E. Garcia <i>et al.</i>	(ZARA, SUC, PNL Collabs.)
QUENBY	95	PL B351 70	J.J. Quenby <i>et al.</i>	(LOIC, RAL, SHEF+ Collabs.)
SNOWDEN-...	95	PRL 74 4133	D.P. Snowden-Hift, E.S. Freeman, P.B. Price	(UCB Collab.)
Also		PRL 76 331	J.J. Collar <i>et al.</i>	(SCUC Collab.)
Also		PRL 76 332	D.P. Snowden-Hift, E.S. Freeman, P.B. Price	(UCB Collab.)
BECK	94	PL B336 141	M. Beck <i>et al.</i>	(MPIH, KIAE, SASSO Collabs.)
BACCI	92	PL B293 460	C. Bacci <i>et al.</i>	(Beijing-Rom-Saclay Collab.)
REUSSER	91	PL B255 143	D. Reusser <i>et al.</i>	(NEUC, CIT, PSI Collabs.)
CALDWELL	88	PRL 61 510	D.O. Caldwell <i>et al.</i>	(UCSB, UCB, LBL Collabs.)

- Limits on charged particles in  $e^+e^-$  collisions
- Limits on charged particles in hadron reactions
- Limits on charged particles in cosmic rays
- Searches for quantum black hole production

Note that searches appear in separate sections elsewhere for Higgs bosons (and technipions), other heavy bosons (including  $W_R$ ,  $W'$ ,  $Z'$ , leptoquarks, axiglons), axions (including pseudo-Goldstone bosons, Majorons, familons), WIMPs, heavy leptons, heavy neutrinos, free quarks, monopoles, supersymmetric particles, and compositeness.

We no longer list for limits on tachyons and centauros. See our 1994 edition for these limits.

### CONCENTRATION OF STABLE PARTICLES IN MATTER

#### Concentration of Heavy (Charge +1) Stable Particles in Matter

VALUE	CL%	DOCUMENT ID	TECN	COMMENT
$<4 \times 10^{-17}$	95	1 YAMAGATA	93 SPEC	Deep sea water, $M=5-1600 m_p$
$<6 \times 10^{-15}$	95	2 VERKERK	92 SPEC	Water, $M=10^5$ to $3 \times 10^7$ GeV
$<7 \times 10^{-15}$	95	2 VERKERK	92 SPEC	Water, $M=10^4$ , $6 \times 10^7$ GeV
$<9 \times 10^{-15}$	95	2 VERKERK	92 SPEC	Water, $M=10^8$ GeV
$<3 \times 10^{-23}$	90	3 HEMMICK	90 SPEC	Water, $M=1000 m_p$
$<2 \times 10^{-21}$	90	3 HEMMICK	90 SPEC	Water, $M=5000 m_p$
$<3 \times 10^{-20}$	90	3 HEMMICK	90 SPEC	Water, $M=10000 m_p$
$<1 \times 10^{-29}$		SMITH	82B SPEC	Water, $M=30-400 m_p$
$<2 \times 10^{-28}$		SMITH	82B SPEC	Water, $M=12-1000 m_p$
$<1 \times 10^{-14}$		SMITH	82B SPEC	Water, $M>1000 m_p$
$<(0.2-1) \times 10^{-21}$		SMITH	79 SPEC	Water, $M=6-350 m_p$

- • • We do not use the following data for averages, fits, limits, etc. • • •
- 1 YAMAGATA 93 used deep sea water at 4000 m since the concentration is enhanced in deep sea due to gravity.
- 2 VERKERK 92 looked for heavy isotopes in sea water and put a bound on concentration of stable charged massive particle in sea water. The above bound can be translated into a bound on charged dark matter particle ( $5 \times 10^6$  GeV), assuming the local density,  $\rho=0.3$  GeV/cm<sup>3</sup>, and the mean velocity ( $v$ )=300 km/s.
- 3 See HEMMICK 90 Fig. 7 for other masses 100-10000  $m_p$ .

#### Concentration of Heavy Stable Particles Bound to Nuclei

VALUE	CL%	DOCUMENT ID	TECN	COMMENT
$<1.2 \times 10^{-11}$	95	1 JAVORSEK	01 SPEC	Au, $M=3$ GeV
$<6.9 \times 10^{-10}$	95	1 JAVORSEK	01 SPEC	Au, $M=144$ GeV
$<1 \times 10^{-11}$	95	2 JAVORSEK	01B SPEC	Au, $M=188$ GeV
$<1 \times 10^{-8}$	95	2 JAVORSEK	01B SPEC	Au, $M=1669$ GeV
$<6 \times 10^{-9}$	95	2 JAVORSEK	01B SPEC	Fe, $M=188$ GeV
$<1 \times 10^{-8}$	95	2 JAVORSEK	01B SPEC	Fe, $M=647$ GeV
$<4 \times 10^{-20}$	90	3 HEMMICK	90 SPEC	C, $M=100 m_p$
$<8 \times 10^{-20}$	90	3 HEMMICK	90 SPEC	C, $M=1000 m_p$
$<2 \times 10^{-16}$	90	3 HEMMICK	90 SPEC	C, $M=10000 m_p$
$<6 \times 10^{-13}$	90	3 HEMMICK	90 SPEC	Li, $M=1000 m_p$
$<1 \times 10^{-11}$	90	3 HEMMICK	90 SPEC	Be, $M=1000 m_p$
$<6 \times 10^{-14}$	90	3 HEMMICK	90 SPEC	B, $M=1000 m_p$
$<4 \times 10^{-17}$	90	3 HEMMICK	90 SPEC	O, $M=1000 m_p$
$<4 \times 10^{-15}$	90	3 HEMMICK	90 SPEC	F, $M=1000 m_p$
$<1.5 \times 10^{-13}$ /nucleon	68	4 NORMAN	89 SPEC	$206\text{PbX}^-$
$<1.2 \times 10^{-12}$ /nucleon	68	4 NORMAN	87 SPEC	$56,58\text{FeX}^-$

- • • We do not use the following data for averages, fits, limits, etc. • • •
- 1 JAVORSEK 01 search for (neutral) SIMPs (strongly interacting massive particles) bound to Au nuclei. Here  $M$  is the effective SIMP mass.
- 2 JAVORSEK 01B search for (neutral) SIMPs (strongly interacting massive particles) bound to Au and Fe nuclei from various origins with exposures on the earth's surface, in a satellite, heavy ion collisions, etc. Here  $M$  is the mass of the anomalous nucleus. See also JAVORSEK 02.
- 3 See HEMMICK 90 Fig. 7 for other masses 100-10000  $m_p$ .
- 4 Bound valid up to  $m_{X^-} \sim 100$  TeV.

## Other Particle Searches

### OMITTED FROM SUMMARY TABLE OTHER PARTICLE SEARCHES

Revised February 2018 by K. Hikasa (Tohoku University).

We collect here those searches which do not appear in any other search categories. These are listed in the following order:

- Concentration of stable particles in matter
- General new physics searches
- Limits on jet-jet resonance in hadron collisions
- Limits on neutral particle production at accelerators

## GENERAL NEW PHYSICS SEARCHES

This subsection lists some of the search experiments which look for general signatures characteristic of new physics, independent of the framework of a specific model.

The observed events are compatible with Standard Model expectation, unless noted otherwise.

VALUE	DOCUMENT ID	TECN	COMMENT
• • • We do not use the following data for averages, fits, limits, etc. • • •			
1	SIRUNYAN 20A	CMS	SUSY/LQ search with mT2 or long-lived charged particles
2	ALCANTARA 19		Auger, superheavy DM
3	PORAYKO 18	PPTA	pulsar timing fuzzy DM search
4	AAD 15AT	ATLS	$t + \cancel{E}_T$
5	KHACHATRYAN 15F	CMS	$t + \cancel{E}_T$
6	AALTONEN 14J	CDF	$W + 2$ jets
7	AAD 13A	ATLS	$WW \rightarrow \ell\nu\ell'\nu$
8	AAD 13C	ATLS	$\gamma + \cancel{E}_T$
9	AALTONEN 13I	CDF	Delayed $\gamma + \cancel{E}_T$
10	CHATRCHYAN 13	CMS	$\ell^+\ell^- + \text{jets} + \cancel{E}_T$
11	AAD 12C	ATLS	$t\bar{t} + \cancel{E}_T$
12	AALTONEN 12M	CDF	jet + $\cancel{E}_T$
13	CHATRCHYAN 12AP	CMS	jet + $\cancel{E}_T$
14	CHATRCHYAN 12Q	CMS	$Z + \text{jets} + \cancel{E}_T$
15	CHATRCHYAN 12T	CMS	$\gamma + \cancel{E}_T$
16	AAD 11S	ATLS	jet + $\cancel{E}_T$
17	AALTONEN 11AF	CDF	$\ell^\pm\ell^\pm$
18	CHATRCHYAN 11C	CMS	$\ell^+\ell^- + \text{jets} + \cancel{E}_T$
19	CHATRCHYAN 11U	CMS	jet + $\cancel{E}_T$
20	AALTONEN 10AF	CDF	$\gamma\gamma + \ell, \cancel{E}_T$
21	AALTONEN 09AF	CDF	$\ell\gamma b \cancel{E}_T$
22	AALTONEN 09G	CDF	$\ell\ell\ell \cancel{E}_T$
1	SIRUNYAN 20A		search for SUSY and LQ production using mT2 or presence of long-lived charged particle; no signal, limits placed in various mass planes for different BSM scenarios and various assumed lifetimes.
2	ALCANTARA 19		19 place limits on m(WIMPZilla=X) vs lifetime from upper bound on ultra high energy cosmic rays at Auger experiment: e.g. $\tau(X) < 4 \times 10^{22}$ yr for m(X) = $10^{16}$ GeV.
3	PORAYKO 18		search for deviations in the residuals of pulsar timing data using PPTA. No signal observed. Limits set on fuzzy DM with $3 \times 10^{-24} < m(\text{DM}) < 2 \times 10^{-22}$ eV.
4	AAD 15AT		search for events with a top quark and missing $E_T$ in $pp$ collisions at $E_{\text{cm}} = 8$ TeV with $L = 20.3 \text{ fb}^{-1}$ .
5	KHACHATRYAN 15F		search for events with a top quark and missing $E_T$ in $pp$ collisions at $E_{\text{cm}} = 8$ TeV with $L = 19.7 \text{ fb}^{-1}$ .
6	AALTONEN 14J		examine events with a $W$ and two jets in $p\bar{p}$ collisions at $E_{\text{cm}} = 1.96$ TeV with $L = 8.9 \text{ fb}^{-1}$ . Invariant mass distributions of the two jets are consistent with the Standard Model expectation.
7	AAD 13A		search for resonant $WW$ production in $pp$ collisions at $E_{\text{cm}} = 7$ TeV with $L = 4.7 \text{ fb}^{-1}$ .
8	AAD 13C		search for events with a photon and missing $E_T$ in $pp$ collisions at $E_{\text{cm}} = 7$ TeV with $L = 4.6 \text{ fb}^{-1}$ .
9	AALTONEN 13I		search for events with a photon and missing $E_T$ , where the photon is detected after the expected timing, in $p\bar{p}$ collisions at $E_{\text{cm}} = 1.96$ TeV with $L = 6.3 \text{ fb}^{-1}$ . The data are consistent with the Standard Model expectation.
10	CHATRCHYAN 13		search for events with an opposite-sign lepton pair, jets, and missing $E_T$ in $pp$ collisions at $E_{\text{cm}} = 7$ TeV with $L = 4.98 \text{ fb}^{-1}$ .
11	AAD 12C		search for events with a $t\bar{t}$ pair and missing $E_T$ in $pp$ collisions at $E_{\text{cm}} = 7$ TeV with $L = 1.04 \text{ fb}^{-1}$ .
12	AALTONEN 12M		search for events with a jet and missing $E_T$ in $p\bar{p}$ collisions at $E_{\text{cm}} = 1.96$ TeV with $L = 6.7 \text{ fb}^{-1}$ .
13	CHATRCHYAN 12AP		search for events with a jet and missing $E_T$ in $pp$ collisions at $E_{\text{cm}} = 7$ TeV with $L = 5.0 \text{ fb}^{-1}$ .
14	CHATRCHYAN 12Q		search for events with a $Z$ , jets, and missing $E_T$ in $pp$ collisions at $E_{\text{cm}} = 7$ TeV with $L = 4.98 \text{ fb}^{-1}$ .
15	CHATRCHYAN 12T		search for events with a photon and missing $E_T$ in $pp$ collisions at $E_{\text{cm}} = 7$ TeV with $L = 5.0 \text{ fb}^{-1}$ .
16	AAD 11S		search for events with one jet and missing $E_T$ in $pp$ collisions at $E_{\text{cm}} = 7$ TeV with $L = 33 \text{ pb}^{-1}$ .
17	AALTONEN 11AF		search for high- $p_T$ like-sign dileptons in $p\bar{p}$ collisions at $E_{\text{cm}} = 1.96$ TeV with $L = 6.1 \text{ fb}^{-1}$ .
18	CHATRCHYAN 11C		search for events with an opposite-sign lepton pair, jets, and missing $E_T$ in $pp$ collisions at $E_{\text{cm}} = 7$ TeV with $L = 34 \text{ pb}^{-1}$ .
19	CHATRCHYAN 11U		search for events with one jet and missing $E_T$ in $pp$ collisions at $E_{\text{cm}} = 7$ TeV with $L = 36 \text{ pb}^{-1}$ .
20	AALTONEN 10AF		search for $\gamma\gamma$ events with $e, \mu, \tau$ , or missing $E_T$ in $p\bar{p}$ collisions at $E_{\text{cm}} = 1.96$ TeV with $L = 1.1\text{--}2.0 \text{ fb}^{-1}$ .
21	AALTONEN 09AF		search for $\ell\gamma b$ events with missing $E_T$ in $p\bar{p}$ collisions at $E_{\text{cm}} = 1.96$ TeV with $L = 1.9 \text{ fb}^{-1}$ . The observed events are compatible with Standard Model expectation including $t\bar{t}\gamma$ production.
22	AALTONEN 09G		search for $\mu\mu\mu$ and $\mu\mu e$ events with missing $E_T$ in $p\bar{p}$ collisions at $E_{\text{cm}} = 1.96$ TeV with $L = 976 \text{ pb}^{-1}$ .

## LIMITS ON JET-JET RESONANCES

## Heavy Particle Production Cross Section

Limits are for a particle decaying to two hadronic jets.

Units(pb)	CL%	Mass(GeV)	DOCUMENT ID	TECN	COMMENT
• • • We do not use the following data for averages, fits, limits, etc. • • •					
			1 AABOUD 19AJ	ATLS	$pp \rightarrow \gamma X, X \rightarrow jj$
			2 SIRUNYAN 19B	CMS	$pp \rightarrow jA, A \rightarrow b\bar{b}$
			3 SIRUNYAN 19CD	CMS	$pp \rightarrow Z'\gamma, Z' \rightarrow jj$
			4 AABOUD 18AD	ATLS	$pp \rightarrow Y \rightarrow HX \rightarrow (bb) + (qq)$
			5 AABOUD 18CK	ATLS	$pp \rightarrow bbb + \cancel{E}_T$
			6 AABOUD 18CL	ATLS	$pp \rightarrow$ vector-like quarks
			7 AABOUD 18N	ATLS	$pp \rightarrow jj$ resonance
			8 SIRUNYAN 18DJ	CMS	$pp \rightarrow ZZ$ or $WZ \rightarrow \ell\bar{\ell}jj$
			9 SIRUNYAN 18DY	CMS	$pp \rightarrow RR; R \rightarrow jj$
			10 KHACHATRYAN 17W	CMS	$pp \rightarrow jj$ resonance
			11 KHACHATRYAN 17Y	CMS	$pp \rightarrow (8\text{--}10) j + \cancel{E}_T$
			12 SIRUNYAN 17F	CMS	$pp \rightarrow jj$ angular distribution
			13 AABOUD 16	ATLS	$pp \rightarrow b + \text{jet}$
			14 AAD 16N	ATLS	$pp \rightarrow 3$ high $E_T$ jets
			15 AAD 16S	ATLS	$pp \rightarrow jj$ resonance
			16 KHACHATRYAN 16K	CMS	$pp \rightarrow jj$ resonance
			17 KHACHATRYAN 16L	CMS	$pp \rightarrow jj$ resonance
			18 AAD 13D	ATLS	7 TeV $pp \rightarrow 2$ jets
			19 AALTONEN 13R	CDF	1.96 TeV $p\bar{p} \rightarrow 4$ jets
			20 CHATRCHYAN 13A	CMS	7 TeV $pp \rightarrow 2$ jets
			21 CHATRCHYAN 13A	CMS	7 TeV $pp \rightarrow b\bar{b}X$
			22 AAD 12S	ATLS	7 TeV $pp \rightarrow 2$ jets
			23 CHATRCHYAN 12BL	CMS	7 TeV $pp \rightarrow t\bar{t}X$
			24 AAD 11AG	ATLS	7 TeV $pp \rightarrow 2$ jets
			25 AALTONEN 11M	CDF	1.96 TeV $p\bar{p} \rightarrow W + 2$ jets
			26 ABAZOV 11I	D0	1.96 TeV $p\bar{p} \rightarrow W + 2$ jets
			27 AAD 10	ATLS	7 TeV $pp \rightarrow 2$ jets
			28 KHACHATRYAN 10	CMS	7 TeV $pp \rightarrow 2$ jets
			29 ABE 99F	CDF	1.8 TeV $p\bar{p} \rightarrow b\bar{b} + \text{anything}$
			30 ABE 97G	CDF	1.8 TeV $p\bar{p} \rightarrow 2$ jets
			31 ABE 93G	CDF	1.8 TeV $p\bar{p} \rightarrow 2$ jets
			31 ABE 93G	CDF	1.8 TeV $p\bar{p} \rightarrow 2$ jets
			31 ABE 93G	CDF	1.8 TeV $p\bar{p} \rightarrow 2$ jets
< 2603	95	200			
< 44	95	400			
< 7	95	600			

- AABOUD 19AJ search for low mass dijet resonance in  $pp \rightarrow \gamma X, X \rightarrow jj$  at 13 TeV with 79.8 fb<sup>-1</sup> of data; no signal found; limits placed on  $Z'$  model in coupling vs. m( $Z'$ ) plane.
- SIRUNYAN 19B search for low mass resonance  $pp \rightarrow jA, A \rightarrow b\bar{b}$  at 13 TeV using 35.9 fb<sup>-1</sup>; no signal; exclude resonances 50–350 GeV depending on production and decay.
- SIRUNYAN 19CD search for  $pp \rightarrow Z'\gamma, Z' \rightarrow jj$  with fat jet ( $jj$ ); no signal, limits placed in m( $Z'$ ) vs. coupling plane for  $Z'$  masses from 10 to 125 GeV.
- AABOUD 18AD search for new heavy particle  $Y \rightarrow HX \rightarrow (bb) + (qq)$ . No signal observed. Limits set on m(Y) vs. m(X) in the ranges of m(Y) in 1–4 TeV and m(X) in 50–1000 GeV.
- AABOUD 18CK search for SUSY Higgsinos in gauge-mediation via  $pp \rightarrow bbb + \cancel{E}_T$  at 13 TeV using two complementary analyses with 24.3/36.1 fb<sup>-1</sup>; no signal is found and Higgsinos with masses between 130 and 230 GeV and between 290 and 880 GeV are excluded at the 95% confidence level.
- AABOUD 18CL search for  $pp \rightarrow$  vector-like quarks  $\rightarrow$  jets at 13 TeV with 36 fb<sup>-1</sup>; no signal seen; limits set on various VLQ scenarios. For pure  $B \rightarrow Hb$  or  $T \rightarrow Ht$ , set the mass limit  $m > 1010$  GeV.
- AABOUD 18N search for dijet resonance at Atlas with 13 TeV and 29.3 fb<sup>-1</sup>; limits set on m( $Z'$ ) in the mass range of 450–1800 GeV.
- SIRUNYAN 18DJ search for  $pp \rightarrow ZZ$  or  $WZ \rightarrow \ell\bar{\ell}jj$  resonance at 13 TeV, 35.9 fb<sup>-1</sup>; no signal; limits set in the 400–4500 GeV mass range, exclusion of  $W'$  up to 2270 GeV in the HVT model A, and up to 2330 GeV for HVT model B. WED bulk graviton exclusion up to 925 GeV.
- SIRUNYAN 18DY search for  $pp \rightarrow RR; R \rightarrow jj$  two dijet resonances at 13 TeV 35.9 fb<sup>-1</sup>; no signal; limits placed on RPV top-squark pair production.
- KHACHATRYAN 17W search for dijet resonance in 12.9 fb<sup>-1</sup> data at 13 TeV; see Fig. 2 for limits on axiguons, diquarks, dark matter mediators etc.
- KHACHATRYAN 17Y search for  $pp \rightarrow (8\text{--}10) j$  in 19.7 fb<sup>-1</sup> at 8 TeV. No signal seen. Limits set on colorons, axiguons, RPV, and SUSY.
- SIRUNYAN 17F measure  $pp \rightarrow jj$  angular distribution in 2.6 fb<sup>-1</sup> at 13 TeV; limits set on LEDs and quantum black holes.
- AABOUD 16 search for resonant dijets including one or two  $b$ -jets with 3.2 fb<sup>-1</sup> at 13 TeV; exclude excited  $b^*$  quark from 1.1–2.1 TeV; exclude leptophilic  $Z'$  with SM couplings from 1.1–1.5 TeV.
- AAD 16N search for  $\geq 3$  jets with 3.6 fb<sup>-1</sup> at 13 TeV; limits placed on micro black holes (Fig. 10) and string balls (Fig. 11).
- AAD 16S search for high mass jet-jet resonance with 3.6 fb<sup>-1</sup> at 13 TeV; exclude portions of excited quarks,  $W'$ ,  $Z'$  and contact interaction parameter space.
- KHACHATRYAN 16K search for dijet resonance in 2.4 fb<sup>-1</sup> data at 13 TeV; see Fig. 3 for limits on axiguons, diquarks etc.
- KHACHATRYAN 16L use data scouting technique to search for  $jj$  resonance on 18.8 fb<sup>-1</sup> of data at 8 TeV. Limits on the coupling of a leptophobic  $Z'$  to quarks are set, improving on the results by other experiments in the mass range between 500–800 GeV.
- AAD 13D search for dijet resonances in  $pp$  collisions at  $E_{\text{cm}} = 7$  TeV with  $L = 4.8$  fb<sup>-1</sup>. The observed events are compatible with Standard Model expectation. See their Fig. 6 and Table 2 for limits on resonance cross section in the range  $m = 1.0\text{--}4.0$  TeV.
- AALTONEN 13R search for production of a pair of jet-jet resonances in  $p\bar{p}$  collisions at  $E_{\text{cm}} = 1.96$  TeV with  $L = 6.6 \text{ fb}^{-1}$ . See their Fig. 5 and Tables 1, II for cross section limits.

See key on page 999

Searches Particle Listings
Other Particle Searches

- 20 CHATRCHYAN 13A search for qq, qg, and gg resonances in pp collisions at Ecm = 7 TeV with L = 4.8 fb^-1. See their Fig. 3 and Table 1 for limits on resonance cross section in the range m = 1.0-4.3 TeV.
21 CHATRCHYAN 13A search for b-bbar resonances in pp collisions at Ecm = 7 TeV with L = 4.8 fb^-1. See their Fig. 8 and Table 4 for limits on resonance cross section in the range m = 1.0-4.0 TeV.
22 AAD 12s search for dijet resonances in pp collisions at Ecm = 7 TeV with L = 1.0 fb^-1. See their Fig. 3 and Table 2 for limits on resonance cross section in the range m = 0.9-4.0 TeV.
23 CHATRCHYAN 12BL search for t-tbar resonances in pp collisions at Ecm = 7 TeV with L = 4.4 fb^-1. See their Fig. 4 for limits on resonance cross section in the range m = 0.5-3.0 TeV.
24 AAD 11AG search for dijet resonances in pp collisions at Ecm = 7 TeV with L = 36 pb^-1. Limits on number of events for m = 0.6-4 TeV are given in their Table 3.
25 AALTONEN 11M find a peak in two jet invariant mass distribution around 140 GeV in W + 2 jet events in pp collisions at Ecm = 1.96 TeV with L = 4.3 fb^-1.
26 ABAZOV 11i search for two-jet resonances in W + 2 jet events in pp collisions at Ecm = 1.96 TeV with L = 4.3 fb^-1 and give limits sigma < (2.6-1.3) pb (95% CL) for m = 110-170 GeV. The result is incompatible with AALTONEN 11M.
27 AAD 10 search for narrow dijet resonances in pp collisions at Ecm = 7 TeV with L = 315 nb^-1. Limits on the cross section in the range 10-10^3 pb is given for m = 0.3-1.7 TeV.
28 KHACHATRYAN 10 search for narrow dijet resonances in pp collisions at Ecm = 7 TeV with L = 2.9 pb^-1. Limits on the cross section in the range 1-300 pb is given for m = 0.5-2.6 TeV separately in the final states qq, qg, and gg.
29 ABE 99F search for narrow b-bbar resonances in pp collisions at Ecm=1.8 TeV. Limits on sigma(pp -> X + anything) x B(X -> b-bbar) in the range 3-10^3 pb (95%CL) are given for mX=200-750 GeV. See their Table I.
30 ABE 97G search for narrow dijet resonances in pp collisions with 106 pb^-1 of data at Ecm = 1.8 TeV. Limits on sigma(pp -> X + anything) x B(X -> jj) in the range 10^4-10^-1 pb (95%CL) are given for dijet mass m=200-1150 GeV with both jets having |eta| < 2.0 and the dijet system having |cos(theta\*)| < 0.67. See their Table I for the list of limits. Supersedes ABE 93c.
31 ABE 93c give cross section times branching ratio into light (d, u, s, c, b) quarks for Gamma = 0.02 M. Their Table II gives limits for M = 200-900 GeV and Gamma = (0.02-0.2) M.

Table with 5 columns: ID, Author, Experiment, Process, and Limit. Rows include searches for Z' to l+l-, Black Hole, string ball, sphaleron, jj, b-mu-pi, gamma-gamma, V to Wh; h to b-bbar; W to l-nu, WH, ZH resonance, pi-nu-pi-nu, pi-nu to jj, l + (ls or jets), WW, WZ, ZZ resonance, p7Li to 8Be to X(17)N, X(17) to e+e-, e+e- collisions, m = 1.2-5 GeV, m = 0.5-20 GeV, m = 0-5 GeV, tau = (0.05-1.) x 10^-8 s, tau > 10^-7 s.

< 10^-36-10^-33 90
<(4-0.3) x 10^-31 95
<2 x 10^-36 90
<2.5 x 10^-35

- 1 AABOUD 19H searches for di-photon-jet resonance at 13 TeV and 36.7 fb^-1 of data; no signal found and limits placed on sigma-BR vs. mass plane for various simplified models.
2 AABOUD 19v review ATLAS searches for mediator-based DM at 7, 8, and 13 TeV with up to 37 fb^-1 of data; no signal found and limits set for wide variety of simplified models of dark matter.
3 SIRUNYAN 19o search for pp -> gamma ET at 13 TeV with 36.1 fb^-1; no signal found and limits set for various simplified models.
4 AABOUD 18CJ make multichannel search for pp -> VV/ll/ell-nu, V = W, Z, h at 13 TeV, 36.1 fb^-1; no signal found; limits placed for several BSM models.
5 AABOUD 18CM search for lepton-flavor violating resonance in pp -> e mu/ e tau/ mu tau at 13 TeV, 36.1 fb^-1; no signal is found and limits placed for various BSM models.
6 AAIJ 18AJ search for prompt and delayed dark photon decay A' -> mu+ mu- at LHCb detector using 1.6 fb^-1 of pp collisions at 13 TeV; limits on m(A') vs. kinetic mixing are set.
7 BANERJEE 18 search for dark photon A'/16.7 MeV boson X at NA64 via eZ -> eZX(A'); no signal found and limits set on the X-e- coupling ee in the range 1.3 x 10^-4 <= ee <= 4.2 x 10^-4 excluding part of the allowed parameter space.
8 BANERJEE 18A search for invisibly decaying dark photons in eZ -> eZA', A' -> invisible; no signal found and limits set on mixing for m(A') < 1 GeV.
9 MARSICANO 18 search for dark photon e+e- -> A'(gamma) visible decay in SLAC E137 e beam dump data. No signal observed and limits set in e coupling vs m(A') plane, see their figure 7.
10 SIRUNYAN 18BB search for high mass dilepton resonance; no signal found and exclude portions of p-space of Z', KK graviton models.
11 SIRUNYAN 18DA search for pp -> Black Hole, string ball, sphaleron via high multiplicity events at 13 TeV, 35.9 fb^-1; no signal, require e.g. m(BH) > 10.1 TeV.
12 SIRUNYAN 18DD search for pp -> jj deviations in dijet angular distribution. No signal observed. Set limits on large extra dimensions, black holes and DM mediators e.g. m(BH) > 5.9-8.2 TeV.
13 SIRUNYAN 18DR search for dimuon resonance in pp -> b mu pi at 8 and 13 TeV. Slight excess seen at m(mu pi) ~ 28 GeV in some channels.
14 SIRUNYAN 18DU search for high mass diphoton resonance in pp -> gamma gamma at 13 TeV using 35.9 fb^-1; no signal; limits placed on RS Graviton, LED, and clockwork.
15 SIRUNYAN 18ED search for pp -> V -> Wh; h -> b-bbar; W -> l-nu at 13 TeV with 35.9 fb^-1; no signal; limits set on m(W') > 2.9 TeV.
16 AABOUD 17B exclude m(W', Z') < 1.49-2.31 TeV depending on the couplings and W'/Z' degeneracy assumptions via WH, ZH search in pp collisions at 13 TeV with 3.2 fb^-1 of data.
17 AAIJ 17BR search for long-lived hidden valley pions from Higgs decay. Limits are set on the signal strength as a function of the mass and lifetime of the long-lived particle in their Fig. 4 and Tab. 4.
18 AAD 16o search for high ET, l + (ls or jets) with 3.2 fb^-1 at 13 TeV; exclude micro black holes mass < 8 TeV (Fig. 3) for models with two extra dimensions.
19 AAD 16r search for WW, WZ, ZZ resonance in 20.3 fb^-1 at 8 TeV data; limits placed on massive RS graviton (Fig. 4).
20 KRASZNAHORKAY 16 report pLi -> Be -> e e-bar N 5 sigma resonance at 16.7 MeV- possible evidence for nuclear interference or new light boson. However, such nuclear interference was ruled out already by ZANG 17.
21 LEES 15E search for long-lived neutral particles produced in e+e- collisions in the Upsilon region, which decays into e+e-, mu+mu-, e+mu-, pi+pi-, K+K-, or pi+K-. See their Fig. 2 for cross section limits.
22 ADAMS 97b search for a hadron-like neutral particle produced in pN interactions, which decays into a p0 and a weakly interacting massive particle. Upper limits are given for the ratio to Kp production for the mass range 1.2-5 GeV and lifetime 10^-9-10^-4 s. See also our Light Gluino Section.
23 GALLAS 95 limit is for a weakly interacting neutral particle produced in 800 GeV/c pN interactions decaying with a lifetime of 10^-4-10^-8 s. See their Figs. 8 and 9. Similar limits are obtained for a stable particle with interaction cross section 10^-29-10^-33 cm^2. See Fig. 10.
24 AKESSON 91 limit is from weakly interacting neutral long-lived particles produced in pN reaction at 450 GeV/c performed at CERN SPS. Bourquin-Gaillard formula is used as the production model. The above limit is for tau > 10^-7 s. For tau > 10^-9 s, sigma < 10^-30 cm^2/nucleon is obtained.
25 BADIER 86 looked for long-lived particles at 300 GeV pi- beam dump. The limit applies for nonstrongly interacting neutral or charged particles with mass > 2 GeV. The limit applies for particle modes, mu+pi-, mu+mu-, pi+pi-X, pi+pi-pi+ etc. See their figure 5 for the contours of limits in the mass-tau plane for each mode.

LIMITS ON NEUTRAL PARTICLE PRODUCTION

Production Cross Section of Radiatively-Decaying Neutral Particle

Table with 5 columns: VALUE (pb), CL%, DOCUMENT ID, TECN, COMMENT. Rows include searches for gamma from Sun, Z-gamma resonance, pp -> gamma + jet, e+e- -> X0 Y0, e+e- -> X0 gamma, e+e- -> X0 X0, e+e- -> X0 gamma, e+e- -> X0 Y0, e+e- -> X0 X0, e+e- -> Y0 gamma.

- 1 ALBERT 18c search for WIMP annihilation in Sun to long-lived, radiatively decaying mediator; no signal; limits set on sigma^SD(Xp) assuming long-lived mediator.
2 KHACHATRYAN 17D search for new scalar resonance decaying to Z gamma with Z -> e+e-, mu+mu- in pp collisions at 8 and 13 TeV; no signal seen.
3 AAD 16AI search for excited quarks (EQ) and quantum black holes (QBH) in 3.2 fb^-1 at 13 TeV of data; exclude EQ below 4.4 TeV and QBH below 3.8 (6.2) TeV for RS1 (AD3) models. The visible cross section limit was obtained for 5 TeV resonance with sigmaG/MG = 2%.
4 KHACHATRYAN 16M search for gamma-gamma resonance using 19.7 fb^-1 at 8 TeV and 3.3 fb^-1 at 13 TeV; slight excess at 750 GeV noted; limit set on RS graviton.
5 ABBIENDI 00d associated production limit is for mX0 = 90-188 GeV, mY0 = 0 at Ecm = 189 GeV. See also their Fig. 9.
6 ABBIENDI 00d pair production limit is for mX0 = 45-94 GeV, mY0 = 0 at Ecm = 189 GeV. See also their Fig. 12.
7 ACKERSTAFF 97b associated production limit is for mX0 = 80-160 GeV, mY0 = 0 from 10.0 pb^-1 at Ecm = 161 GeV. See their Fig. 3(a).
8 ACKERSTAFF 97b pair production limit is for mX0 = 40-80 GeV, mY0 = 0 from 10.0 pb^-1 at Ecm = 161 GeV. See their Fig. 3(b).

Heavy Particle Production Cross Section

Table with 5 columns: VALUE (cm^2/N), CL%, DOCUMENT ID, TECN, COMMENT. Rows include di-photon-jet resonance, ATLAS review, mediator-based DM, pp -> gamma ET, pp -> VV/ll/ell-nu, V = W, Z, h, pp -> e mu/ e tau/ mu tau, pp -> A' -> mu+mu-; dark photon, eZ -> eZX(A'), eZ -> eZA', A' -> XX, e+e- -> A'(gamma) visible decay.

# Searches Particle Listings

## Other Particle Searches

<sup>26</sup> GUSTAFSON 76 is a 300 GeV FNAL experiment looking for heavy ( $m > 2$  GeV) long-lived neutral hadrons in the M4 neutral beam. The above typical value is for  $m = 3$  GeV and assumes an interaction cross section of 1 mb. Values as a function of mass and interaction cross section are given in figure 2.

### Production of New Penetrating Non- $\nu$ Like States in Beam Dump

VALUE	CL%	DOCUMENT ID	TECN	COMMENT
$\dots$	$\dots$	$\dots$	$\dots$	$\dots$
$\dots$	$\dots$	$\dots$	$\dots$	$\dots$

<sup>1</sup> No excess neutral-current events leads to  $\sigma(\text{production}) \times \sigma(\text{interaction}) \times \text{acceptance} < 2.26 \times 10^{-71} \text{ cm}^4/\text{nucleon}^2$  (CL = 90%) for light neutrals. Acceptance depends on models (0.1 to 4.  $\times 10^{-4}$ ).

## LIMITS ON CHARGED PARTICLES IN $e^+e^-$

### Heavy Particle Production Cross Section in $e^+e^-$

Ratio to  $\sigma(e^+e^- \rightarrow \mu^+\mu^-)$  unless noted. See also entries in Free Quark Search and Magnetic Monopole Searches.

VALUE	CL%	DOCUMENT ID	TECN	COMMENT
$<1 \times 10^{-3}$	90	1 KILE	18 ALEP	$e^+e^- \rightarrow 4$ jets
$<2 \times 10^{-5}$	95	2 ABLIKIM	17AA BES3	$e^+e^- \rightarrow \ell\bar{\ell}\gamma$
$<1.1 \times 10^{-3}$	95	3 ACKERSTAFF	98P OPAL	$Q=1,2/3, m=45-89.5$ GeV
$<1.4 \times 10^{-3}$	95	4 ABREU	97D DLPH	$Q=1,2/3, m=45-84$ GeV
$<1.7 \times 10^{-2}$	90	5 BARATE	97K ALEP	$Q=1, m=45-85$ GeV
$<2 \times 10^{-5}$	95	6 AKERS	95R OPAL	$Q=1, m=5-45$ GeV
$<1 \times 10^{-5}$	95	6 AKERS	95R OPAL	$Q=2, m=5-45$ GeV
$<2 \times 10^{-3}$	90	7 BUSKULIC	93C ALEP	$Q=1, m=32-72$ GeV
$<(10^{-2}-1)$	95	8 ADACHI	90C TOPZ	$Q=1, m=1-16, 18-27$ GeV
$<7 \times 10^{-2}$	90	9 ADACHI	90E TOPZ	$Q=1, m=5-25$ GeV
$<1.6 \times 10^{-2}$	95	10 KINOSHITA	82 PLAS	$Q=3-180, m < 14.5$ GeV
$<5.0 \times 10^{-2}$	90	11 BARTEL	80 JADE	$Q=(3,4,5)/3$ 2-12 GeV

- KILE 18 investigate archived ALEPH  $e^+e^- \rightarrow 4$  jets data and see 4-5  $\sigma$  excess at 110 GeV.
- ABLIKIM 17AA search for dark photon  $A \rightarrow \ell\bar{\ell}$  at 3.773 GeV with 2.93  $\text{fb}^{-1}$ . Limits are set in  $\epsilon$  vs  $m(A)$  plane.
- ACKERSTAFF 98P search for pair production of long-lived charged particles at  $E_{\text{cm}}$  between 130 and 183 GeV and give limits  $\sigma < (0.05-0.2)$  pb (95%CL) for spin-0 and spin-1/2 particles with  $m=45-89.5$  GeV, charge 1 and 2/3. The limit is translated to the cross section at  $E_{\text{cm}}=183$  GeV with the  $s$  dependence described in the paper. See their Figs. 2-4.
- ABREU 97D search for pair production of long-lived particles and give limits  $\sigma < (0.4-2.3)$  pb (95%CL) for various center-of-mass energies  $E_{\text{cm}}=130-136, 161,$  and 172 GeV, assuming an almost flat production distribution in  $\cos\theta$ .
- BARATE 97K search for pair production of long-lived charged particles at  $E_{\text{cm}} = 130, 136, 161,$  and 172 GeV and give limits  $\sigma < (0.2-0.4)$  pb (95%CL) for spin-0 and spin-1/2 particles with  $m=45-85$  GeV. The limit is translated to the cross section at  $E_{\text{cm}}=172$  GeV with the  $E_{\text{cm}}$  dependence described in the paper. See their Figs. 2 and 3 for limits on  $J = 1/2$  and  $J = 0$  cases.
- AKERS 95R is a CERN-LEP experiment with  $W_{\text{cm}} \sim m_Z$ . The limit is for the production of a stable particle in multihadron events normalized to  $\sigma(e^+e^- \rightarrow \text{hadrons})$ . Constant phase space distribution is assumed. See their Fig. 3 for bounds for  $Q = \pm 2/3, \pm 4/3$ .
- BUSKULIC 93C is a CERN-LEP experiment with  $W_{\text{cm}} = m_Z$ . The limit is for a pair or single production of heavy particles with unusual ionization loss in TPC. See their Fig. 5 and Table 1.
- ADACHI 90C is a KEK-TRISTAN experiment with  $W_{\text{cm}} = 52-60$  GeV. The limit is for pair production of a scalar or spin-1/2 particle. See Figs. 3 and 4.
- ADACHI 90E is KEK-TRISTAN experiment with  $W_{\text{cm}} = 52-61.4$  GeV. The above limit is for inclusive production cross section normalized to  $\sigma(e^+e^- \rightarrow \mu^+\mu^-) \cdot \beta(3-\beta^2)/2$ , where  $\beta = (1 - 4m^2/W_{\text{cm}}^2)^{1/2}$ . See the paper for the assumption about the production mechanism.
- KINOSHITA 82 is SLAC PEP experiment at  $W_{\text{cm}} = 29$  GeV using lexan and  $^{39}\text{Cr}$  plastic sheets sensitive to highly ionizing particles.
- BARTEL 80 is DESY-PETRA experiment with  $W_{\text{cm}} = 27-35$  GeV. Above limit is for inclusive pair production and ranges between  $1. \times 10^{-1}$  and  $1. \times 10^{-2}$  depending on mass and production momentum distributions. (See their figures 9, 10, 11).

### Branching Fraction of $Z^0$ to a Pair of Stable Charged Heavy Fermions

VALUE	CL%	DOCUMENT ID	TECN	COMMENT
$<5 \times 10^{-6}$	95	1 AKERS	95R OPAL	$m = 40.4-45.6$ GeV
$<1 \times 10^{-3}$	95	AKRAWY	90O OPAL	$m = 29-40$ GeV

<sup>1</sup> AKERS 95R give the 95% CL limit  $\sigma(X\bar{X})/\sigma(\mu\mu) \leq 1.8 \times 10^{-4}$  for the pair production of singly- or doubly-charged stable particles. The limit applies for the mass range 40.4-45.6 GeV for  $X^\pm$  and  $< 45.6$  GeV for  $X^{\pm\pm}$ . See the paper for bounds for  $Q = \pm 2/3, \pm 4/3$ .

## LIMITS ON CHARGED PARTICLES IN HADRONIC REACTIONS

### MASS LIMITS for Long-Lived Charged Heavy Fermions

Limits are for spin 1/2 particles with no color and  $SU(2)_L$  charge. The electric charge  $Q$  of the particle (in the unit of  $e$ ) is therefore equal to its weak hypercharge. Pair production by Drell-Yan like  $\gamma$  and  $Z$  exchange is assumed to derive the limits.

VALUE (GeV)	CL%	DOCUMENT ID	TECN	COMMENT
$>660$	95	1 AAD	15BJ ATLS	$ Q  = 2$
$>200$	95	2 CHATRCHYAN	13AB CMS	$ Q  = 1/3$
$>480$	95	2 CHATRCHYAN	13AB CMS	$ Q  = 2/3$
$>574$	95	2 CHATRCHYAN	13AB CMS	$ Q  = 1$
$>685$	95	2 CHATRCHYAN	13AB CMS	$ Q  = 2$
$>140$	95	3 CHATRCHYAN	13AR CMS	$ Q  = 1/3$
$>310$	95	3 CHATRCHYAN	13AR CMS	$ Q  = 2/3$

- <sup>1</sup> AAD 15BJ use 20.3  $\text{fb}^{-1}$  of  $pp$  collisions at  $E_{\text{cm}} = 8$  TeV. See paper for limits for  $|Q| = 3, 4, 5, 6$ .
- <sup>2</sup> CHATRCHYAN 13AB use 5.0  $\text{fb}^{-1}$  of  $pp$  collisions at  $E_{\text{cm}} = 7$  TeV and 18.8  $\text{fb}^{-1}$  at  $E_{\text{cm}} = 8$  TeV. See paper for limits for  $|Q| = 3, 4, \dots, 8$ .
- <sup>3</sup> CHATRCHYAN 13AR use 5.0  $\text{fb}^{-1}$  of  $pp$  collisions at  $E_{\text{cm}} = 7$  TeV.

### Heavy Particle Production Cross Section

VALUE (nb)	CL%	DOCUMENT ID	TECN	COMMENT
$<1.2 \times 10^{-3}$	95	10 AAD	11I ATLS	$ q =10e, m=0.2-1$ TeV
$<1.0 \times 10^{-5}$	95	11,12 AALTONEN	09Z CDF	$m > 100$ GeV, noncolored
$<4.8 \times 10^{-5}$	95	11,13 AALTONEN	09Z CDF	$m > 100$ GeV, colored
$<0.31-0.04 \times 10^{-3}$	95	14 ABAZOV	09M D0	pair production
$<0.19$	95	15 AKTAS	04C H1	$m=3-10$ GeV
$<0.05$	95	16 ABE	92J CDF	$m=50-200$ GeV
$<30-130$	95	17 CARROLL	78 SPEC	$m=2-2.5$ GeV
$<100$	95	18 LEIPUNER	73 CNTR	$m=3-11$ GeV

- <sup>1</sup> AABOUD 19AA search for BSM physics at 13 TeV with 3.2  $\text{fb}^{-1}$  in  $> 10^5$  regions of  $> 700$  event classes; no significant signal found.
- <sup>2</sup> AABOUD 19Q search for single top+MET events at 13 TeV with 36.1  $\text{fb}^{-1}$  of data; no signal found and limits set in  $\sigma$  or coupling vs. mass plane for variety of simplified models including DM and vector-like top quark  $T$ .
- <sup>3</sup> AABOUD 17D search for  $W\bar{W}jj, WZjj$  in  $pp$  collisions at 8 TeV with 3.2  $\text{fb}^{-1}$ ; set limits on anomalous couplings.
- <sup>4</sup> AABOUD 17L search for the pair production of heavy vector-like  $T$  quarks in the  $Z(\rightarrow \nu\nu)TX$  final state.
- <sup>5</sup> SIRUNYAN 17B search for vector-like quark  $pp \rightarrow TX \rightarrow tHX$  in 2.3  $\text{fb}^{-1}$  at 13 TeV; no signal seen; limits placed.
- <sup>6</sup> SIRUNYAN 17C search for vector-like quark  $pp \rightarrow TX \rightarrow Z + (t \text{ or } b)$  in 2.3  $\text{fb}^{-1}$  at 13 TeV; no signal seen; limits placed.
- <sup>7</sup> SIRUNYAN 17J search for  $pp \rightarrow X_5/3 X_5/3 \rightarrow tWtW$  with 2.3  $\text{fb}^{-1}$  at 13 TeV. No signal seen:  $m(X) > 1020$  (990) GeV for RH (LH) new charge 5/3 quark.
- <sup>8</sup> AAIJ 15BD search for production of long-lived particles in  $pp$  collisions at  $E_{\text{cm}} = 7$  and 8 TeV. See their Table 6 for cross section limits.
- <sup>9</sup> AAD 13AH search for production of long-lived particles with  $|q|=(2-6)e$  in  $pp$  collisions at  $E_{\text{cm}} = 7$  TeV with 4.4  $\text{fb}^{-1}$ . See their Fig. 8 for cross section limits.
- <sup>10</sup> AAD 11I search for production of highly ionizing massive particles in  $pp$  collisions at  $E_{\text{cm}} = 7$  TeV with  $L = 3.1$   $\text{pb}^{-1}$ . See their Table 5 for similar limits for  $|q| = 6e$  and 17e, Table 6 for limits on pair production cross section.
- <sup>11</sup> AALTONEN 09Z search for long-lived charged particles in  $p\bar{p}$  collisions at  $E_{\text{cm}} = 1.96$  TeV with  $L = 1.0$   $\text{fb}^{-1}$ . The limits are on production cross section for a particle of mass above 100 GeV in the region  $|\eta| \lesssim 0.7, p_T > 40$  GeV, and  $0.4 < \beta < 1.0$ .
- <sup>12</sup> Limit for weakly interacting charge-1 particle.
- <sup>13</sup> Limit for up-quark like particle.
- <sup>14</sup> ABAZOV 09M search for pair production of long-lived charged particles in  $p\bar{p}$  collisions at  $E_{\text{cm}} = 1.96$  TeV with  $L = 1.1$   $\text{fb}^{-1}$ . Limit on the cross section of (0.31-0.04) pb (95% CL) is given for the mass range of 60-300 GeV, assuming the kinematics of stau pair production.
- <sup>15</sup> AKTAS 04C look for charged particle photoproduction at HERA with mean c.m. energy of 200 GeV.
- <sup>16</sup> ABE 92J look for pair production of unit-charged particles which leave detector before decaying. Limit shown here is for  $m=50$  GeV. See their Fig. 5 for different charges and stronger limits for higher mass.
- <sup>17</sup> CARROLL 78 look for neutral,  $S = -2$  dihyperon resonance in  $pp \rightarrow 2K^+X$ . Cross section varies within above limits over mass range and  $p_{\text{lab}} = 5.1-5.9$  GeV/c.
- <sup>18</sup> LEIPUNER 73 is an NAL 300 GeV  $p$  experiment. Would have detected particles with lifetime greater than 200 ns.

### Heavy Particle Production Differential Cross Section

VALUE ( $\text{cm}^2\text{sr}^{-1}\text{GeV}^{-1}$ )	CL%	DOCUMENT ID	TECN	CHG	COMMENT
$<2.6 \times 10^{-36}$	90	1 BALDIN	76 CNTR	-	$Q = 1, m=2.1-9.4$ GeV
$<2.2 \times 10^{-33}$	90	2 ALBROW	75 SPEC	$\pm$	$Q = \pm 1, m=4-15$ GeV
$<1.1 \times 10^{-33}$	90	2 ALBROW	75 SPEC	$\pm$	$Q = \pm 2, m=6-27$ GeV
$<8. \times 10^{-35}$	90	3 JOVANOVA...	75 CNTR	$\pm$	$m=15-26$ GeV
$<1.5 \times 10^{-34}$	90	3 JOVANOVA...	75 CNTR	$\pm$	$Q = \pm 2, m=3-10$ GeV
$<6. \times 10^{-35}$	90	3 JOVANOVA...	75 CNTR	$\pm$	$Q = \pm 2, m=10-26$ GeV
$<1. \times 10^{-31}$	90	4 APPEL	74 CNTR	$\pm$	$m=3.2-7.2$ GeV

$\dots$  We do not use the following data for averages, fits, limits, etc.  $\dots$

See key on page 999

Searches Particle Listings  
Other Particle Searches

$<5.8 \times 10^{-34}$	90	5	ALPER	73	SPEC	$\pm$	$m=1.5-24$ GeV
$<1.2 \times 10^{-35}$	90	6	ANTIPOV	71B	CNTR	$-$	$Q=-, m=2.2-2.8$
$<2.4 \times 10^{-35}$	90	7	ANTIPOV	71C	CNTR	$-$	$Q=-, m=1.2-1.7, 2.1-4$
$<2.4 \times 10^{-35}$	90		BINON	69	CNTR	$-$	$Q=-, m=1-1.8$ GeV
$<1.5 \times 10^{-36}$		8	DORFAN	65	CNTR	$-$	Be target $m=3-7$ GeV
$<3.0 \times 10^{-36}$		8	DORFAN	65	CNTR	$-$	Fe target $m=3-7$ GeV

9	SIRUNYAN	19BT	CMS	LLP via displaced jets+MET
10	SIRUNYAN	19CA	CMS	LLP $\rightarrow \gamma$ search
11	SIRUNYAN	19Q	CMS	$pp \rightarrow j +$ displaced dark quark jet
12	SIRUNYAN	18AW	CMS	Long-lived particle search
13	AAIJ	16AR	LHCB	$H \rightarrow XX$ long-lived particles
14	KHACHATRYAN	16BW	CMS	direct production: HSCPs
15	BADIER	86	BDMP	$\tau = (0.05-1.) \times 10^{-8}$ s

- BALDIN 76 is a 70 GeV Serpukhov experiment. Value is per Al nucleus at  $\theta = 0$ . For other charges in range  $-0.5$  to  $-3.0$ , CL = 90% limit is  $(2.6 \times 10^{-36})/|(charge)|$  for mass range  $(2.1-9.4$  GeV)  $\times |(charge)|$ . Assumes stable particle interacting with matter as do antiprotons.
- ALBROW 75 is a CERN ISR experiment with  $E_{cm} = 53$  GeV.  $\theta = 40$  mr. See figure 5 for mass ranges up to 35 GeV.
- JOVANOVICH 75 is a CERN ISR 26+26 and 15+15 GeV pp experiment. Figure 4 covers ranges  $Q = 1/3$  to 2 and  $m = 3$  to 26 GeV. Value is per GeV momentum.
- APPEL 74 is NAL 300 GeV pW experiment. Studies forward production of heavy (up to 24 GeV) charged particles with momenta 24-200 GeV (-charge) and 40-150 GeV (+charge). Above typical value is for 75 GeV and is per GeV momentum per nucleon.
- ALPER 73 is CERN ISR 26+26 GeV p experiment.  $p > 0.9$  GeV,  $0.2 < \beta < 0.65$ .
- ANTIPOV 71B is from same 70 GeV p experiment as ANTIPOV 71C and BINON 69.
- ANTIPOV 71C limit inferred from flux ratio. 70 GeV p experiment.
- DORFAN 65 is a 30 GeV/c p experiment at BNL. Units are per GeV momentum per nucleus.

- AAD 20b search for opposite-sign dileptons originating from long-lived particles in pp collisions at 13 TeV with  $32.8 \text{ fb}^{-1}$ ; limits placed in squark cross section vs.  $c\tau$  plane for RPV SUSY.
- AABOUD 19AE search for long-lived particles via displaced jets using  $10.8 \text{ fb}^{-1}$  or  $33.0 \text{ fb}^{-1}$  data (depending on a trigger) at 13 TeV; no signal found and limits set in branching ratio vs. decay length plane.
- AABOUD 19AK searches for long-lived particle  $Z_d$  via  $pp \rightarrow \Phi \rightarrow ZZ_d$  at 13 TeV with  $36.1 \text{ fb}^{-1}$ ; no signal found and limits set in  $\sigma \times BR$  vs. lifetime plane for simplified model.
- AABOUD 19AM search for Drell-Yan (DY) production of long-lived multi-charge particles at 13 TeV with  $36.1 \text{ fb}^{-1}$  of data; no signal found and exclude  $50 \text{ GeV} < m(\text{LLMCP}) < 980-1220$  GeV for electric charge  $|q| = (2-7)e$ .
- AABOUD 19AO search for neutral long-lived particles producing displaced jets at 13 TeV with  $36.1 \text{ fb}^{-1}$  of data; no signal found and exclude regions of  $\sigma \times BR$  vs. lifetime plane for various models.
- AABOUD 19AT search for heavy, charged long-lived particles at 13 TeV with  $36.1 \text{ fb}^{-1}$ ; no signal found and upper limits set on masses of various hypothetical particles.
- AABOUD 19G search for long-lived particle with decay to  $\mu^+\mu^-$  at 13 TeV with  $32.9 \text{ fb}^{-1}$ ; no signal found and limits set in combinations of lifetime, mass and coupling planes for various simplified models.
- SIRUNYAN 19BH search for long-lived SUSY particles via displaced jets at 13 TeV with  $35.9 \text{ fb}^{-1}$ ; no signal found and limits placed in mass vs lifetime plane for various hypothetical models.
- SIRUNYAN 19BT search for displaced jet(s)+ $E_T$  at 13 TeV with  $137 \text{ fb}^{-1}$ ; no signal found and limits placed in mass vs lifetime plane for gauge mediated SUSY breaking models.
- SIRUNYAN 19CA search for gluino/squark decay to long-lived neutralino, decay to  $\gamma$  in GMSB; no signal, limits placed in  $m(\chi)$  vs. lifetime plane for SPS8 GMSB benchmark point.
- SIRUNYAN 19Q search for  $pp \rightarrow j +$  displaced jet via dark quark with 13 TeV at  $16.1 \text{ fb}^{-1}$ ; no signal found and limits set in mass vs lifetime plane for dark quark/dark pion model.
- SIRUNYAN 18AW search for very long lived particles (LLPs) decaying hadronically or to  $\mu\tau$  in CMS detector; none seen/limits set on lifetime vs. cross section.
- AAIJ 16AR search for long lived particles from  $H \rightarrow XX$  with displaced X decay vertex using  $0.62 \text{ fb}^{-1}$  at 7 TeV; limits set in Fig. 7.
- KHACHATRYAN 16BW search for heavy stable charged particles via ToF with  $2.5 \text{ fb}^{-1}$  at 13 TeV; required stable  $m(\text{gluino}) > 1610$  GeV.
- BADIER 86 looked for long-lived particles at 300 GeV  $\pi^-$  beam dump. The limit applies for nonstrongly interacting neutral or charged particles with mass  $> 2$  GeV. The limit applies for particle modes,  $\mu^+\pi^-, \mu^+\mu^-, \pi^+\pi^-, \pi^+\pi^+X, \pi^+\pi^-\pi^\pm$  etc. See their figure 5 for the contours of limits in the mass- $\tau$  plane for each mode.

Long-Lived Heavy Particle Invariant Cross Section

VALUE ( $\text{cm}^2/\text{GeV}^2/N$ )	CL%	DOCUMENT ID	TECN	CHG	COMMENT		
$<5-700 \times 10^{-35}$	90	1	BERNSTEIN	88	CNTR		
$<5-700 \times 10^{-37}$	90	1	BERNSTEIN	88	CNTR		
$<2.5 \times 10^{-36}$	90	2	THRON	85	CNTR	$-$	$Q = 1, m=4-12$ GeV
$<1. \times 10^{-35}$	90	2	THRON	85	CNTR	$+$	$Q = 1, m=4-12$ GeV
$<6. \times 10^{-33}$	90	3	ARMITAGE	79	SPEC		$m=1.87$ GeV
$<1.5 \times 10^{-33}$	90	3	ARMITAGE	79	SPEC		$m=1.5-3.0$ GeV
$<1.1 \times 10^{-37}$	90	5	CUTTS	78	CNTR		$Q = (2/3, 1, 4/3, 2)$
$<3.0 \times 10^{-37}$	90	6	VIDAL	78	CNTR		$m=4-10$ GeV

- BERNSTEIN 88 limits apply at  $x = 0.2$  and  $p_T = 0$ . Mass and lifetime dependence of limits are shown in the regions:  $m = 1.5-7.5$  GeV and  $\tau = 10^{-8}-2 \times 10^{-6}$  s. First number is for hadrons; second is for weakly interacting particles.
- THRON 85 is FNAL 400 GeV proton experiment. Mass determined from measured velocity and momentum. Limits are for  $\tau > 3 \times 10^{-9}$  s.
- ARMITAGE 79 is CERN-ISR experiment at  $E_{cm} = 53$  GeV. Value is for  $x = 0.1$  and  $p_T = 0.15$ . Observed particles at  $m = 1.87$  GeV are found all consistent with being antideuteron.
- BOZZOLI 79 is CERN-SPS 200 GeV pN experiment. Looks for particle with  $\tau$  larger than  $10^{-8}$  s. See their figure 11-18 for production cross-section upper limits vs mass.
- CUTTS 78 is pBe experiment at FNAL sensitive to particles of  $\tau > 5 \times 10^{-8}$  s. Value is for  $-0.3 < x < 0$  and  $p_T = 0.175$ .
- VIDAL 78 is FNAL 400 GeV proton experiment. Value is for  $x = 0$  and  $p_T = 0$ . Puts lifetime limit of  $< 5 \times 10^{-8}$  s on particle in this mass range.

Long-Lived Heavy Particle Production

$(\sigma(\text{Heavy Particle}) / \sigma(p))$

VALUE	EVTS	DOCUMENT ID	TECN	CHG	COMMENT		
$<10^{-8}$		1	NAKAMURA	89	SPEC	$\pm$	$Q = (-5/3, \pm 2)$
	0	2	BUSSIERE	80	CNTR	$\pm$	$Q = (2/3, 1, 4/3, 2)$

- NAKAMURA 89 is KEK experiment with 12 GeV protons on Pt target. The limit applies for mass  $\lesssim 1.6$  GeV and lifetime  $\gtrsim 10^{-7}$  s.
- BUSSIERE 80 is CERN-SPS experiment with 200-240 GeV protons on Be and Al target. See their figures 6 and 7 for cross-section ratio vs mass.

Production and Capture of Long-Lived Massive Particles

VALUE ( $10^{-36} \text{ cm}^2$ )	DOCUMENT ID	TECN	COMMENT		
$<20$ to 800	1	ALEKSEEV	76	ELEC	$\tau=5$ ms to 1 day
$<200$ to 2000	1	ALEKSEEV	76B	ELEC	$\tau=100$ ms to 1 day
$<1.4$ to 9	2	FRANKEL	75	CNTR	$\tau=50$ ms to 10 hours
$<0.1$ to 9	3	FRANKEL	74	CNTR	$\tau=1$ to 1000 hours

- ALEKSEEV 76 and ALEKSEEV 76B are 61-70 GeV p Serpukhov experiment. Cross section is per Pb nucleus.
- FRANKEL 75 is extension of FRANKEL 74.
- FRANKEL 74 looks for particles produced in thick Al targets by 300-400 GeV/c protons.

Long-Lived Particle (LLP) Search at Hadron Collisions

Limits are for cross section times branching ratio.

VALUE ( $\text{pb/nucleon}$ )	DOCUMENT ID	TECN	COMMENT		
$<20$	1	AAD	20D	ATLS	$pp \rightarrow$ LLPs at 13 TeV
$<2$	2	AABOUD	19AE	ATLS	$pp$ at 13 TeV
$<3$	3	AABOUD	19AK	ATLS	$pp \rightarrow \Phi \rightarrow ZZ_d$
$<4$	4	AABOUD	19AM	ATLS	DY multi-charged LLP production
$<5$	5	AABOUD	19AO	ATLS	LLP via displaced jets
$<6$	6	AABOUD	19AT	ATLS	heavy, charged long-lived particles
$<7$	7	AABOUD	19G	ATLS	LLP decay to $\mu^+\mu^-$
$<8$	8	SIRUNYAN	19BH	CMS	LLP via displaced jets

Long-Lived Heavy Particle Cross Section

VALUE (pb/sr)	CL%	DOCUMENT ID	TECN	COMMENT		
$<34$	95	1	RAM	94	SPEC	$1015 < m_{X^{++}} < 1085$ MeV
$<75$	95	1	RAM	94	SPEC	$920 < m_{X^{++}} < 1025$ MeV

- RAM 94 search for a long-lived doubly-charged fermion  $X^{++}$  with mass between  $m_N$  and  $m_N+m_\pi$  and baryon number  $+1$  in the reaction  $pp \rightarrow X^{++}n$ . No candidate is found. The limit is for the cross section at  $15^\circ$  scattering angle at 460 MeV incident energy and applies for  $\tau(X^{++}) \gtrsim 0.1 \mu\text{s}$ .

LIMITS ON CHARGED PARTICLES IN COSMIC RAYS

Heavy Particle Flux in Cosmic Rays

VALUE ( $\text{cm}^{-2}\text{sr}^{-1}\text{s}^{-1}$ )	CL%	EVTS	DOCUMENT ID	TECN	COMMENT			
$<1$	$\times 10^{-8}$	90	0	1	ALVIS	18	MAJD	Fractionally charged
$\sim 6$	$\times 10^{-9}$		2	2	AGNESE	15	CDM2	$Q = 1/6$
$<1.4$	$\times 10^{-12}$	90	0	3	SAITO	90		$Q \approx 14, m \approx 370m_p$
$<1.7$	$\times 10^{-11}$	99	0	4	MINCER	85	CALO	$m \geq 1$ TeV
$<1.$	$\times 10^{-9}$	90	0	5	SAKUYAMA	83B	PLAS	$m \sim 1$ TeV
$2.$	$\times 10^{-9}$		3	6	BHAT	82	CC	
$3.0$	$\times 10^{-9}$		3	7	MARINI	82	CNTR	$Q=1, m \sim 4.5m_p$
$(4 \pm 1) \times 10^{-11}$			3	8	YOCK	81	SPRK	$Q=1, m \sim 4.5m_p$
$<1.3$	$\times 10^{-9}$	90	0	8	YOCK	81	SPRK	Fractionally charged
$<1.0$	$\times 10^{-9}$		0	9	YOCK	80	SPRK	$m \sim 4.5 m_p$
$<7.$	$\times 10^{-10}$	90	0	3	GOODMAN	79	ELEC	$m \geq 5$ GeV
$>6.$	$\times 10^{-9}$		5	10	BHAT	78	CNTR	$m > 1$ GeV
$<3.0$	$\times 10^{-8}$		0		BRIATORE	76	ELEC	
$<1.5$	$\times 10^{-9}$		0		YOCK	75	ELEC	$Q > 7e$ or $< -7e$
$<3.0$	$\times 10^{-10}$		0	11	YOCK	74	CNTR	$m > 6$ GeV
$<3.0$	$\times 10^{-10}$		0		DARDO	72	CNTR	
$<5.0$	$\times 10^{-11}$	90	0		TONWAR	72	CNTR	$m > 10$ GeV
			0		BJORNBOE	68	CNTR	$m > 5$ GeV
			0		JONES	67	ELEC	$m=5-15$ GeV

- We do not use the following data for averages, fits, limits, etc.
  - 1 ALVIS 18 MAJD Fractionally charged
  - 2 AGNESE 15 CDM2  $Q = 1/6$
  - 3 SAITO 90  $Q \approx 14, m \approx 370m_p$
  - 4 MINCER 85 CALO  $m \geq 1$  TeV
  - 5 SAKUYAMA 83B PLAS  $m \sim 1$  TeV
  - 6 BHAT 82 CC
  - 7 MARINI 82 CNTR  $Q=1, m \sim 4.5m_p$
  - 8 YOCK 81 SPRK  $Q=1, m \sim 4.5m_p$
  - 8 YOCK 81 SPRK Fractionally charged
  - 9 YOCK 80 SPRK  $m \sim 4.5 m_p$
  - 3 Goodman 79 ELEC  $m \geq 5$  GeV
  - 10 BHAT 78 CNTR  $m > 1$  GeV
  - 11 YOCK 74 CNTR  $m > 6$  GeV
  - DARDO 72 CNTR
  - TONWAR 72 CNTR  $m > 10$  GeV
  - BJORNBOE 68 CNTR  $m > 5$  GeV
  - JONES 67 ELEC  $m=5-15$  GeV

Downloaded from https://academic.oup.com/ptep/article/2020/8/083C01/5891211 by guest on 12 November 2020



## Other Particle Searches

- ALVIS 18 search for fractional charged flux of cosmic matter at Majorana demonstrator; no signal observed and limits are set on the flux of lightly ionizing particles for charge as low as  $e/1000$ .
- See AGNESE 15 Fig. 6 for limits extending down to  $Q = 1/200$ .
- SAITO 90 candidates carry about 450 MeV/nucleon. Cannot be accounted for by conventional backgrounds. Consistent with strange quark matter hypothesis.
- MINCER 85 is high statistics study of calorimeter signals delayed by 20–200 ns. Calibration with AGS beam shows they can be accounted for by rare fluctuations in signals from low-energy hadrons in the shower. Claim that previous delayed signals including BJORNBOE 68, DARDO 72, BHAT 82, SAKUYAMA 83b below may be due to this fake effect.
- SAKUYAMA 83b analyzed 6000 extended air shower events. Increase of delayed particles and change of lateral distribution above  $10^{17}$  eV may indicate production of very heavy parent at top of atmosphere.
- BHAT 82 observed 12 events with delay  $> 2 \times 10^{-8}$  s and with more than 40 particles. 1 eV has good hadron shower. However all events are delayed in only one of two detectors in cloud chamber, and could not be due to strongly interacting massive particle.
- MARINI 82 applied PEP-counter for TOF. Above limit is for velocity  $= 0.54$  of light. Limit is inconsistent with YOCK 80 YOCK 81 events if isotropic dependence on zenith angle is assumed.
- YOCK 81 saw another 3 events with  $Q = \pm 1$  and  $m$  about  $4.5m_p$  as well as 2 events with  $m > 5.3m_p$ ,  $Q = \pm 0.75 \pm 0.05$  and  $m > 2.8m_p$ ,  $Q = \pm 0.70 \pm 0.05$  and 1 event with  $m = (9.3 \pm 3.)m_p$ ,  $Q = \pm 0.89 \pm 0.06$  as possible heavy candidates.
- YOCK 80 events are with charge exactly or approximately equal to unity.
- BHAT 78 is at Kolar gold fields. Limit is for  $\tau > 10^{-6}$  s.
- YOCK 74 events could be tritons.

### Superheavy Particle (Quark Matter) Flux in Cosmic Rays

VALUE ( $\text{cm}^{-2}\text{s}^{-1}\text{s}^{-1}$ )	CL%	DOCUMENT ID	TECN	COMMENT
••• We do not use the following data for averages, fits, limits, etc. •••				
		1 ADRIANI	15 PMLA	$4 < m < 1.2 \times 10^5 m_p$
$< 5 \times 10^{-16}$	90	2 AMBROSIO	00B MCRO	$m > 5 \times 10^{14}$ GeV
$< 1.8 \times 10^{-12}$	90	3 ASTONE	93 CNTR	$m \geq 1.5 \times 10^{-13}$ gram
$< 1.1 \times 10^{-14}$	90	4 AHLEN	92 MCRO	$10^{-10} < m < 0.1$ gram
$< 2.2 \times 10^{-14}$	90	5 NAKAMURA	91 PLAS	$m > 10^{11}$ GeV
$< 6.4 \times 10^{-16}$	90	6 ORITO	91 PLAS	$m > 10^{12}$ GeV
$< 2.0 \times 10^{-11}$	90	7 LIU	88 BOLO	$m > 1.5 \times 10^{-13}$ gram
$< 4.7 \times 10^{-12}$	90	8 BARISH	87 CNTR	$1.4 \times 10^8 < m < 10^{12}$ GeV
$< 3.2 \times 10^{-11}$	90	9 NAKAMURA	85 CNTR	$m > 1.5 \times 10^{-13}$ gram
$< 3.5 \times 10^{-11}$	90	10 ULLMAN	81 CNTR	Planck-mass $10^{19}$ GeV
$< 7. \times 10^{-11}$	90	10 ULLMAN	81 CNTR	$m \leq 10^{16}$ GeV

- ADRIANI 15 search for relatively light quark matter with charge  $Z = 1-8$ . See their Figs. 2 and 3 for flux upper limits.
- AMBROSIO 00B searched for quark matter ("nuclearites") in the velocity range  $(10^{-5}-1)$  c. The listed limit is for  $2 \times 10^{-3}$  c.
- ASTONE 93 searched for quark matter ("nuclearites") in the velocity range  $(10^{-3}-1)$  c. Their Table 1 gives a compilation of searches for nuclearites.
- AHLEN 92 searched for quark matter ("nuclearites"). The bound applies to velocity  $< 2.5 \times 10^{-3}$  c. See their Fig. 3 for other velocity/c and heavier mass range.
- NAKAMURA 91 searched for quark matter in the velocity range  $(4 \times 10^{-5}-1)$  c.
- ORITO 91 searched for quark matter. The limit is for the velocity range  $(10^{-4}-10^{-3})$  c.
- LIU 88 searched for quark matter ("nuclearites") in the velocity range  $(2.5 \times 10^{-3}-1)$  c. A less stringent limit of  $5.8 \times 10^{-11}$  applies for  $(1-2.5) \times 10^{-3}$  c.
- BARISH 87 searched for quark matter ("nuclearites") in the velocity range  $(2.7 \times 10^{-4}-5 \times 10^{-3})$  c.
- NAKAMURA 85 at KEK searched for quark-matter. These might be lumps of strange quark matter with roughly equal numbers of  $u$ ,  $d$ ,  $s$  quarks. These lumps or nuclearites were assumed to have velocity of  $(10^{-4}-10^{-3})$  c.
- ULLMAN 81 is sensitive for heavy slow singly charge particle reaching earth with vertical velocity 100–350 km/s.

### Highly Ionizing Particle Flux

VALUE ( $\text{m}^{-2}\text{yr}^{-1}$ )	CL%	EVTs	DOCUMENT ID	TECN	COMMENT
••• We do not use the following data for averages, fits, limits, etc. •••					
$< 0.4$	95	0	KINOSHITA	81b PLAS	$Z/\beta$ 30–100

### SEARCHES FOR BLACK HOLE PRODUCTION

VALUE	DOCUMENT ID	TECN	COMMENT
••• We do not use the following data for averages, fits, limits, etc. •••			
not seen	1 AABOUD	16P ATLS	13 TeV $pp \rightarrow e\mu, e\tau, \mu\tau$
	2 AAD	15AN ATLS	8 TeV $pp \rightarrow$ multijets
	3 AAD	14A ATLS	8 TeV $pp \rightarrow \gamma + \text{jet}$
	4 AAD	14AL ATLS	8 TeV $pp \rightarrow \ell + \text{jet}$
	5 AAD	14C ATLS	8 TeV $pp \rightarrow 2 \ell + (\ell \text{ or jets})$
	6 AAD	13D ATLS	7 TeV $pp \rightarrow 2 \text{ jets}$
	7 CHATRCHYAN 13A	CMS	7 TeV $pp \rightarrow 2 \text{ jets}$
	8 CHATRCHYAN 13AD	CMS	8 TeV $pp \rightarrow$ multijets
	9 AAD	12AK ATLS	7 TeV $pp \rightarrow \ell + (\ell \text{ or jets})$
	10 CHATRCHYAN 12W	CMS	7 TeV $pp \rightarrow$ multijets
	11 AAD	11AG ATLS	7 TeV $pp \rightarrow 2 \text{ jets}$

- AABOUD 16P set limits on quantum BH production in  $n = 6$  ADD or  $n = 1$  RS models.
- AAD 15AN search for black hole or string ball formation followed by its decay to multijet final states, in  $pp$  collisions at  $E_{\text{cm}} = 8$  TeV with  $L = 20.3 \text{ fb}^{-1}$ . See their Figs. 6–8 for limits.

- ADD 14A search for quantum black hole formation followed by its decay to a  $\gamma$  and a jet, in  $pp$  collisions at  $E_{\text{cm}} = 8$  TeV with  $L = 20 \text{ fb}^{-1}$ . See their Fig. 3 for limits.
- ADD 14AL search for quantum black hole formation followed by its decay to a lepton and a jet, in  $pp$  collisions at  $E_{\text{cm}} = 8$  TeV with  $L = 20.3 \text{ fb}^{-1}$ . See their Fig. 2 for limits.
- ADD 14C search for microscopic (semiclassical) black hole formation followed by its decay to final states with a lepton and  $\geq 2$  (leptons or jets), in  $pp$  collisions at  $E_{\text{cm}} = 8$  TeV with  $L = 20.3 \text{ fb}^{-1}$ . See their Figures 8–11, Tables 7, 8 for limits.
- ADD 13D search for quantum black hole formation followed by its decay to two jets, in  $pp$  collisions at  $E_{\text{cm}} = 7$  TeV with  $L = 4.8 \text{ fb}^{-1}$ . See their Fig. 8 and Table 3 for limits.
- CHATRCHYAN 13A search for quantum black hole formation followed by its decay to two jets, in  $pp$  collisions at  $E_{\text{cm}} = 7$  TeV with  $L = 5 \text{ fb}^{-1}$ . See their Figs. 5 and 6 for limits.
- CHATRCHYAN 13AD search for microscopic (semiclassical) black hole formation followed by its evaporation to multiparticle final states, in multijet (including  $\gamma, \ell$ ) events in  $pp$  collisions at  $E_{\text{cm}} = 8$  TeV with  $L = 12 \text{ fb}^{-1}$ . See their Figs. 5–7 for limits.
- ADD 12AK search for microscopic (semiclassical) black hole formation followed by its decay to final states with a lepton and  $\geq 2$  (leptons or jets), in  $pp$  collisions at  $E_{\text{cm}} = 7$  TeV with  $L = 1.04 \text{ fb}^{-1}$ . See their Fig. 4 and 5 for limits.
- CHATRCHYAN 12W search for microscopic (semiclassical) black hole formation followed by its evaporation to multiparticle final states, in multijet (including  $\gamma, \ell$ ) events in  $pp$  collisions at  $E_{\text{cm}} = 7$  TeV with  $L = 4.7 \text{ fb}^{-1}$ . See their Figs. 5–8 for limits.
- ADD 11AG search for quantum black hole formation followed by its decay to two jets, in  $pp$  collisions at  $E_{\text{cm}} = 7$  TeV with  $L = 36 \text{ pb}^{-1}$ . See their Fig. 11 and Table 4 for limits.

### REFERENCES FOR Other Particle Searches

AAD 20D PL B801 135114	G. Aad et al.	(ATLAS Collab.)
SIRUNYAN 20A EPJ C80 3	A.M. Sirunyan et al.	(CMS Collab.)
AABOUD 19AA EPJ C79 120	M. Aaboud et al.	(ATLAS Collab.)
AABOUD 19AE EPJ C79 481	M. Aaboud et al.	(ATLAS Collab.)
AABOUD 19AJ PL B795 56	M. Aaboud et al.	(ATLAS Collab.)
AABOUD 19AK PRL 122 151801	M. Aaboud et al.	(ATLAS Collab.)
AABOUD 19AM PR D99 052003	M. Aaboud et al.	(ATLAS Collab.)
AABOUD 19AO PR D99 052005	M. Aaboud et al.	(ATLAS Collab.)
AABOUD 19AT PR D99 092007	M. Aaboud et al.	(ATLAS Collab.)
AABOUD 19G PR D99 012001	M. Aaboud et al.	(ATLAS Collab.)
AABOUD 19H PR D99 012008	M. Aaboud et al.	(ATLAS Collab.)
AABOUD 19Q JHEP 1905 041	M. Aaboud et al.	(ATLAS Collab.)
AABOUD 19V JHEP 1905 142	M. Aaboud et al.	(ATLAS Collab.)
ALCANTARA 19B PR D99 103016	E. Alcantara, L.A. Anchordoqui, J.F. Soriano	
SIRUNYAN 19B PR D99 012005	A.M. Sirunyan et al.	(CMS Collab.)
SIRUNYAN 19BH PR D99 032011	A.M. Sirunyan et al.	(CMS Collab.)
SIRUNYAN 19BT PL B797 134876	A.M. Sirunyan et al.	(CMS Collab.)
SIRUNYAN 19CA PR D100 112003	A.M. Sirunyan et al.	(CMS Collab.)
SIRUNYAN 19CD PRL 123 231803	A.M. Sirunyan et al.	(CMS Collab.)
SIRUNYAN 19O JHEP 1902 074	A.M. Sirunyan et al.	(CMS Collab.)
SIRUNYAN 19Q JHEP 1902 179	A.M. Sirunyan et al.	(CMS Collab.)
AABOUD 18AD PL B779 24	M. Aaboud et al.	(ATLAS Collab.)
AABOUD 18CJ PR D98 052008	M. Aaboud et al.	(ATLAS Collab.)
AABOUD 18CK PR D98 092002	M. Aaboud et al.	(ATLAS Collab.)
AABOUD 18CL PR D98 092005	M. Aaboud et al.	(ATLAS Collab.)
AABOUD 18CM PR D98 092008	M. Aaboud et al.	(ATLAS Collab.)
AABOUD 18N PRL 121 091801	M. Aaboud et al.	(ATLAS Collab.)
AAJ 18P JHEP 1810 061801	R. Ajij et al.	(LHC Collab.)
ALBERT 18C PR D98 123012	A. Albert et al.	(HAWC Collab.)
ALVIS 18 PRL 120 211804	S.I. Alvis et al.	(MAJORANA Collab.)
BANERJEE 18 PR D99 022002	D. Banerjee et al.	(NA64 Collab.)
BANERJEE 18A PR D97 072002	D. Banerjee et al.	(NA64 Collab.)
KILE 18 JHEP 1810 116	J. Kile, J. von Wimmersperg-Toeller	(LISBT)
MARSICANO 18 PR D98 015031	L. Marsicano et al.	
PORAYKO 18 PR D98 102002	N.K. Porayako et al.	(PPTA Collab.)
SIRUNYAN 18AW JHEP 1805 127	A.M. Sirunyan et al.	(CMS Collab.)
SIRUNYAN 18BB JHEP 1806 120	A.M. Sirunyan et al.	(CMS Collab.)
SIRUNYAN 18DA JHEP 1811 042	A.M. Sirunyan et al.	(CMS Collab.)
SIRUNYAN 18DD EPJ C78 789	A.M. Sirunyan et al.	(CMS Collab.)
SIRUNYAN 18DJ JHEP 1809 101	A.M. Sirunyan et al.	(CMS Collab.)
SIRUNYAN 18DR JHEP 1811 161	A.M. Sirunyan et al.	(CMS Collab.)
SIRUNYAN 18DU PR D98 092001	A.M. Sirunyan et al.	(CMS Collab.)
SIRUNYAN 18DY PR D98 112014	A.M. Sirunyan et al.	(CMS Collab.)
SIRUNYAN 18ED JHEP 1811 172	A.M. Sirunyan et al.	(CMS Collab.)
AABOUD 17B PL B765 32	M. Aaboud et al.	(ATLAS Collab.)
AABOUD 17D PR D95 032001	M. Aaboud et al.	(ATLAS Collab.)
AABOUD 17L JHEP 1708 052	M. Aaboud et al.	(ATLAS Collab.)
AAJ 17BR EPJ C77 812	R. Ajij et al.	(LHC Collab.)
ABLIKIM 17AA PL B774 252	M. Ablikim et al.	(BESIII Collab.)
KHACHATRYAN... 17D JHEP 1701 076	V. Khachatryan et al.	(CMS Collab.)
KHACHATRYAN... 17W PL B769 520	V. Khachatryan et al.	(CMS Collab.)
KHACHATRYAN... 17Y PL B770 257	V. Khachatryan et al.	(CMS Collab.)
SIRUNYAN 17B JHEP 1704 136	A.M. Sirunyan et al.	(CMS Collab.)
SIRUNYAN 17C JHEP 1705 029	A.M. Sirunyan et al.	(CMS Collab.)
SIRUNYAN 17F JHEP 1707 013	A.M. Sirunyan et al.	(CMS Collab.)
SIRUNYAN 17J JHEP 1708 073	A.M. Sirunyan et al.	(CMS Collab.)
ZANG 17 PL B773 159	X. Zang, G.A. Miller	(WASH)
AABOUD 16P PL B759 229	M. Aaboud et al.	(ATLAS Collab.)
AABOUD 16P EPJ C76 541	M. Aaboud et al.	(ATLAS Collab.)
AAD 16AI JHEP 1603 041	G. Aad et al.	(ATLAS Collab.)
AAD 16N JHEP 1603 026	G. Aad et al.	(ATLAS Collab.)
AAD 16O PL B760 520	G. Aad et al.	(ATLAS Collab.)
AAD 16R PL B765 285	G. Aad et al.	(ATLAS Collab.)
AAD 16S PL B754 302	G. Aad et al.	(ATLAS Collab.)
AAJ 16AR EPJ C76 664	R. Ajij et al.	(LHC Collab.)
KHACHATRYAN... 16BW PR D94 112004	V. Khachatryan et al.	(CMS Collab.)
KHACHATRYAN... 16K PRL 116 071801	V. Khachatryan et al.	(CMS Collab.)
KHACHATRYAN... 16L PRL 117 031802	V. Khachatryan et al.	(CMS Collab.)
KHACHATRYAN... 16M PRL 117 051802	V. Khachatryan et al.	(CMS Collab.)
KRASZNHAKO... 16P PRL 116 042501	A.J. Krasznahorkay et al.	(HNHR, ANIK+)
AAD 15AN JHEP 1507 032	G. Aad et al.	(ATLAS Collab.)
AAD 15AT EPJ C75 79	G. Aad et al.	(ATLAS Collab.)
AAD 15BJ EPJ C75 362	G. Aad et al.	(ATLAS Collab.)
AAJ 15BD EPJ C75 595	R. Ajij et al.	(LHC Collab.)
ADRIANI 15 PRL 115 111101	O. Adriani et al.	(PAMELA Collab.)
AGNESE 15 PRL 114 111302	R. Agnese et al.	(CDMS Collab.)
KHACHATRYAN... 15F PRL 114 101801	V. Khachatryan et al.	(CMS Collab.)
LEES 15E PRL 114 171801	J.P. Lees et al.	(BABAR Collab.)
AAD 14A PL B728 562	G. Aad et al.	(ATLAS Collab.)
AAD 14AL PRL 112 091804	G. Aad et al.	(ATLAS Collab.)
AAD 14C JHEP 1408 103	G. Aad et al.	(ATLAS Collab.)
AALTONEN 14J PR D89 092001	T. Aaltonen et al.	(CDF Collab.)
AAD 13A PL B718 860	G. Aad et al.	(ATLAS Collab.)
AAD 13AH PL B722 305	G. Aad et al.	(ATLAS Collab.)

Downloaded from https://academic.oup.com/ptep/article/2020/8/083C01/5891211 by guest on 12 November 2020

See key on page 999

Searches Particle Listings  
Other Particle Searches

AAD	13C	PRL 110 011802	G. Aad et al.	(ATLAS Collab.)	AKRAWY	90O	PL B252 290	M.Z. Akrawy et al.	(OPAL Collab.)
AAD	13D	JHEP 1301 029	G. Aad et al.	(ATLAS Collab.)	HEMMICK	90	PR D41 2074	T.K. Hemmick et al.	(ROCH, MICH, OHIO+)
AALTONEN	131	PR D88 031103	T. Aaltonen et al.	(CDF Collab.)	SAITO	90	PRL 65 2094	T. Saito et al.	(ICRR, KOBE)
AALTONEN	13R	PRL 111 031802	T. Aaltonen et al.	(CDF Collab.)	NAKAMURA	89	PR D39 1261	T.T. Nakamura et al.	(KYOT, TMT C)
CHATRCHYAN	13	PL B718 815	S. Chatrchyan et al.	(CMS Collab.)	NORMAN	89	PR D39 2499	E.B. Norman et al.	(LBL)
CHATRCHYAN	13A	JHEP 1301 013	S. Chatrchyan et al.	(CMS Collab.)	BERNSTEIN	88	PR D37 3103	R.M. Bernstein et al.	(STAN, WISC)
CHATRCHYAN	13AB	JHEP 1307 122	S. Chatrchyan et al.	(CMS Collab.)	LIU	88	PRL 61 271	G. Liu, B. Barish	(CIT)
CHATRCHYAN	13AD	JHEP 1307 178	S. Chatrchyan et al.	(CMS Collab.)	BARISH	87	PR D36 2641	B.C. Barish, G. Liu, C. Lane	(CIT)
CHATRCHYAN	13AR	PR D87 092008	S. Chatrchyan et al.	(CMS Collab.)	NORMAN	87	PRL 58 1403	E.B. Norman, S.B. Gazes, D.A. Bennett	(LBL)
AAD	12AK	PL B716 122	G. Aad et al.	(ATLAS Collab.)	BADIER	86	ZPHY C31 21	J. Badier et al.	(NA3 Collab.)
AAD	12C	PRL 108 041805	G. Aad et al.	(ATLAS Collab.)	MINCER	85	PR D32 541	A. Mincer et al.	(UMD, GMAS, NSF)
AAD	12S	PL B708 37	G. Aad et al.	(ATLAS Collab.)	NAKAMURA	85	PL 161B 417	K. Nakamura et al.	(KEK, INUS)
AALTONEN	12M	PRL 108 211804	T. Aaltonen et al.	(CDF Collab.)	THRON	85	PR D31 451	J.L. Thron et al.	(YALE, FNAL, IOWA)
CHATRCHYAN	12AP	JHEP 1209 094	S. Chatrchyan et al.	(CMS Collab.)	SAKUYAMA	83B	LNC 37 17	H. Sakuyama, N. Suzuki	(MEIS)
CHATRCHYAN	12BL	JHEP 1212 015	S. Chatrchyan et al.	(CMS Collab.)	Also		LNC 36 389	H. Sakuyama, K. Watanabe	(MEIS)
CHATRCHYAN	12Q	PL B716 260	S. Chatrchyan et al.	(CMS Collab.)	Also		NC 78A 147	H. Sakuyama, K. Watanabe	(MEIS)
CHATRCHYAN	12T	PRL 108 261803	S. Chatrchyan et al.	(CMS Collab.)	Also		NC 6C 371	H. Sakuyama, K. Watanabe	(MEIS)
CHATRCHYAN	12W	JHEP 1204 061	S. Chatrchyan et al.	(CMS Collab.)	BHAT	82	PR D25 2820	P.N. Bhat et al.	(TATA)
AAD	11AG	NJP 13 053044	G. Aad et al.	(ATLAS Collab.)	KINOSHITA	82	PRL 48 77	K. Kinoshita, P.B. Price, D. Fryberger	(UCB+)
AAD	11I	PL B698 353	G. Aad et al.	(ATLAS Collab.)	MARINI	82	PR D26 1777	A. Marini et al.	(FRAS, LBL, NWES, STAN+)
AAD	11S	PL B705 294	G. Aad et al.	(ATLAS Collab.)	SMITH	82B	NP B206 333	P.F. Smith et al.	(RAL)
AALTONEN	11AF	PRL 107 181801	T. Aaltonen et al.	(CDF Collab.)	KINOSHITA	81B	PR D24 1707	K. Kinoshita, P.B. Price	(UCB)
AALTONEN	11M	PRL 106 171801	T. Aaltonen et al.	(CDF Collab.)	LOSECCO	81	PL 102B 209	J.M. LoSecco et al.	(MICH, PENN, BNL)
ABAZOV	11I	PRL 107 011804	V.M. Abazov et al.	(DO Collab.)	ULLMAN	81	PRL 47 289	J.D. Ullman	(LEHM, BNL)
CHATRCHYAN	11C	JHEP 1106 026	S. Chatrchyan et al.	(CMS Collab.)	YOCK	81	PR D23 1207	P.C.M. Yock	(AUCK)
CHATRCHYAN	11U	PRL 107 201804	S. Chatrchyan et al.	(CMS Collab.)	BARTEL	80	ZPHY C6 295	W. Bartel et al.	(JADE Collab.)
AAD	10	PRL 105 161801	G. Aad et al.	(ATLAS Collab.)	BUSSIERE	80	NP B174 1	A. Bussiere et al.	(BGNA, SACL, LAPP)
AALTONEN	10AF	PR D82 052005	T. Aaltonen et al.	(CDF Collab.)	YOCK	80	PR D22 61	P.C.M. Yock	(AUCK)
KHACHATRYAN	10	PRL 105 211801	V. Khachatryan et al.	(CMS Collab.)	ARMITAGE	79	NP B150 87	J.C.M. Armitage et al.	(CERN, DARE, FOM+)
Also		PRL 106 029802	V. Khachatryan et al.	(CMS Collab.)	BOZZOLI	79	NP B159 363	W. Bozzoli et al.	(BGNA, LAPP, SACL+)
AALTONEN	09AF	PR D80 011102	T. Aaltonen et al.	(CDF Collab.)	GOODMAN	79	PR D19 2572	J.A. Goodman et al.	(UMD)
AALTONEN	09G	PR D79 052004	T. Aaltonen et al.	(CDF Collab.)	SMITH	79	NP B149 525	P.F. Smith, J.R.J. Bennett	(RHEL)
AALTONEN	09Z	PRL 103 021802	T. Aaltonen et al.	(CDF Collab.)	BHAT	78	PRAM 10 115	P.N. Bhat, P.V. Ramana Murthy	(TATA)
ABAZOV	09M	PRL 102 161802	V.M. Abazov et al.	(DO Collab.)	CARROLL	78	PRL 41 777	A.S. Carroll et al.	(BNL, PRIN)
AKTAS	04C	EPJ C36 413	A. Aktas et al.	(HI Collab.)	CUTTS	78	PRL 41 363	D. Cutts et al.	(BROW, FNAL, ILL, BARI+)
JAVORSEK	02	PR D65 072003	D. Javorsek II et al.		VIDAL	78	PL 77B 344	R.A. Vidal et al.	(COLU, FNAL, STON+)
JAVORSEK	01	PR D64 012005	D. Javorsek II et al.		ALEKSEEV	76	SJNP 22 531	G.D. Alekseev et al.	(JINR)
JAVORSEK	01B	PRL 87 231804	D. Javorsek II et al.		ALEKSEEV	76B	SJNP 23 633	Translated from YAF 22 1021.	(JINR)
ABBIENDI	00D	EPJ C13 197	G. Abbiendi et al.	(OPAL Collab.)	BALDIN	76	SJNP 22 264	Translated from YAF 23 1190.	(JINR)
AMBROSIO	00B	EPJ C13 453	M. Ambrosio et al.	(MACRO Collab.)	BRIATORE	76	NC 31A 553	L. Briatore et al.	(LCGT, FRAS, FREIB)
ABE	99F	PRL 82 2038	F. Abe et al.	(CDF Collab.)	GUSTAFSON	76	PRL 37 474	H.R. Gustafson et al.	(MICH)
ACKERSTAFF	98P	PL B433 195	K. Ackerstaff et al.	(OPAL Collab.)	ALBROW	75	NP B97 189	M.G. Albrow et al.	(CERN, DARE, FOM+)
ABE	97G	PR D55 5263	F. Abe et al.	(CDF Collab.)	FRANKEL	75	PR D12 2561	S. Frankel et al.	(PENN, FNAL)
ABREU	97D	PL B396 315	P. Abreu et al.	(DELPHI Collab.)	JOVANOVI...	75	PL 56B 105	J.V. Jovanovich et al.	(MANI, AACH, CERN+)
ACKERSTAFF	97B	PL B391 210	K. Ackerstaff et al.	(OPAL Collab.)	YOCK	75	NP B56 216	P.C.M. Yock	(AUCK, SLAC)
ADAMS	97B	PRL 79 4083	J. Adams et al.	(FNAL KTeV Collab.)	APPEL	74	PRL 32 428	J.A. Appel et al.	(COLU, FNAL)
BARATE	97K	PL B405 379	R. Barate et al.	(ALEPH Collab.)	FRANKEL	74	PR D9 1932	S. Frankel et al.	(PENN, FNAL)
AKERS	95R	ZPHY C67 203	R. Akers et al.	(OPAL Collab.)	YOCK	74	NP B76 175	P.C.M. Yock	(AUCK)
GALLAS	95	PR D52 6	E. Gallas et al.	(MSU, FNAL, MIT, FLOR)	ALPER	73	PL 46B 265	B. Alper et al.	(CERN, LIVP, LUND, BOHR+)
RAM	94	PR D49 3120	S. Ram et al.	(TELA, TRIU)	LEIPUNER	73	PRL 31 1226	L.B. Leipuner et al.	(BNL, YALE)
ABE	93G	PRL 71 2542	F. Abe et al.	(CDF Collab.)	DARDO	72	NC 9A 319	M. Dardo et al.	(TORI)
ASTONE	93	PR D47 4770	P. Astone et al.	(ROMA, ROMA, CATA, FRAS)	TONWAR	72	JP A5 569	S.C. Tonwar, S. Naranan, B.V. Sreekantan	(TATA)
BUSKULIC	93C	PL B303 198	D. Buskulic et al.	(ALEPH Collab.)	ANTIPOV	71B	NP B31 235	Y.M. Antipov et al.	(SERP)
YAMAGATA	93	PR D47 1231	T. Yamagata, Y. Takamori, H. Utsunomiya	(ALEPH Collab.)	ANTIPPOV	71C	PL 34B 164	Y.M. Antipov et al.	(SERP)
ABE	92J	PR D46 1889	F. Abe et al.	(CDF Collab.)	BINON	69	PL 30B 530	F.G. Binon et al.	(SERP)
AHLEN	92	PRL 69 1860	S.P. Ahlen et al.	(MACRO Collab.)	BJORNBOE	68	NC B53 241	J. Bjornboe et al.	(BOHR, TATA, BERN+)
VERKERK	92	PRL 68 1116	P. Verkerk et al.	(ENSP, SACL, PAST)	JONES	67	PR 164 1584	L.W. Jones	(MICH, WISC, LBL, UCLA, MINN+)
AKESSON	91	ZPHY C52 219	T. Akesson et al.	(HELIOS Collab.)	DORFAN	65	PRL 14 999	D.E. Dorfan et al.	(COLU)
NAKAMURA	91	PL B263 529	S. Nakamura et al.	(ICEPP, WASCR, NIHO, ICRR)					
ORITO	91	PRL 66 1951	S. Orito et al.	(TOPAZ Collab.)					
ADACHI	90C	PL B244 352	I. Adachi et al.	(TOPAZ Collab.)					
ADACHI	90E	PL B249 336	I. Adachi et al.	(TOPAZ Collab.)					

Downloaded from https://academic.oup.com/ptep/article/2020/8/083C01/5891211 by guest on 12 November 2020

